UC Santa Cruz
UC Santa Cruz Previously Published Works

Title
Review of Particle Physics*

Permalink
https://escholarship.org/uc/item/8733j9tn

Journal
International Journal of Modern Physics A, 41(22)

ISSN
0217-751X

Authors
Group, Particle Data
Takahashi, F
Hikasa, K
et al.

Publication Date
2026-08-10

DOI
10.1142/s0217751x26300115

Copyright Information
This work is made available under the terms of a Creative Commons Attribution License, available at https://creativecommons.org/licenses/by/4.0/

Peer reviewed

eScholarship.org Powered by the California Digital Library
University of California

Int. J. Mod. Phys. A 2026.41. Downloaded from www.worldscientific.com
by UNIVERSITY OF CALIFORNIA @ BERKELEY on 09/16/26. Re-use and distribution is strictly not permitted, except for Open Access articles.

REVIEW OF PARTICLE PHYSICS*

Particle Data Group

Abstract

The *Review* summarizes much of particle physics and cosmology. Using data from previous editions, plus 3,200 new measurements from 903 papers, we list, evaluate, and average measured properties of gauge bosons and the recently discovered Higgs boson, leptons, quarks, mesons, and baryons. We summarize searches for hypothetical particles such as supersymmetric particles, heavy bosons, axions, dark photons, etc. Particle properties and search limits are listed in Summary Tables. We give numerous tables, figures, formulae, and reviews of topics such as Higgs Boson Physics, Supersymmetry, Grand Unified Theories, Neutrino Mixing, Dark Energy, Dark Matter, Cosmology, Particle Detectors, Colliders, Probability and Statistics. Most of the 118 reviews are updated, including many that are heavily revised.

The *Review* is divided into two volumes. Volume 1 includes the Summary Tables and 96 review articles. Volume 2 consists of the Particle Listings and contains also 22 reviews that address specific aspects of the data presented in the Listings.

The complete *Review* (both volumes) is published online on the website of the Particle Data Group (pdg.lbl.gov) and in a journal. Volume 1 is available in print as the *PDG Book*. A *Particle Physics Booklet* with the Summary Tables and essential tables, figures, and equations from selected review articles is available in print, as a web version optimized for use on phones, and as an Android app. The PDG API (Application Programming Interface) provides access to the data published in the *Review* in machine-readable format.

The 2026 edition of the *Review of Particle Physics* should be cited as:
F. Takahashi *et al.* (Particle Data Group), Int. J. Mod. Phys. A **41**, 2630011 (2026)

DOI: 10.1142/S0217751X26300115

For the online version see pdg.lbl.gov:

© 2026

Except where otherwise noted, content of this work (the *Review of Particle Physics*) is licensed under a Creative Commons Attribution 4.0 International (CC BY 4.0) license.

*The publication of the *Review of Particle Physics* is supported by the Director, Office of Science, Office of High Energy Physics of the U.S. Department of Energy under Contract No. DE–AC02–05CH11231; by an implementing arrangement between the governments of Japan (MEXT: Ministry of Education, Culture, Sports, Science and Technology, and KEK: High Energy Accelerator Research Organization) and the United States (DOE) on cooperative research and development; by the Italian National Institute of Nuclear Physics (INFN); and by the European Laboratory for Particle Physics (CERN). Individual collaborators receive support for their PDG activities from their respective institutes or funding agencies.

Int. J. Mod. Phys. A 2026.41. Downloaded from www.worldscientific.com
by UNIVERSITY OF CALIFORNIA @ BERKELEY on 09/16/26. Re-use and distribution is strictly not permitted, except for Open Access articles.

Particle Data Group

F. Takahashi,[1] K. Hikasa,[2,3,1] Y. Sumino,[1] M. Tanabashi,[4,5] J. Tanaka,[6] M. Yokoyama,[7,8] K. Agashe,[9] G. Aielli,[10] B.C. Allanach,[11] J. Alvarez-Muñiz,[12] C. Amsler,[13] M. Antonelli,[14] E.C. Aschenauer,[15] D.M. Asner,[16] K. Assamagan,[15] H. Baer,[17] Sw. Banerjee,[18] R.M. Barnett,[19] L. Baudis,[20] C.W. Bauer,[19] J. Beringer,[19] A. Bettini*,[21] O. Biebel,[22] K.M. Black,[23] E. Blucher,[24] R. Bonventre,[19] R.A. Briere,[25] A. Buckley,[26] V.D. Burkert,[27] M.A. Bychkov,[28] G. Cacciapaglia,[29,30] R.N. Cahn,[19] F. Canelli,[20] J. Cao,[31] Z. Cao,[31] M. Carena,[32,24,33] G. Casarosa,[34,35] A. Ceccucci,[36] M. Cepeda,[37] A. Cerri,[38,35,39] R.S. Chivukula,[40] M. Cortês,[41] G. Cowan,[42] V. Crede,[43] O. Cremonesi,[44] G. D'Ambrosio,[45] T. Damour,[46] C.T.H. Davies,[47] J. de Blas,[48] D. de Florian,[49] A. de Gouvêa,[50] T. DeGrand,[51] Z. Demiragli,[52] S. Dittmaier,[53] B.A. Dobrescu,[32] M. D'Onofrio,[54] M. Dorigo,[55] H.K. Dreiner,[56] J.M. Duarte,[40] P. Eerola,[57] U. Egede,[58] A.X. El-Khadra,[59] J. Ellis,[60,36] S.C. Eno,[9] J. Erler,[61] A. Fava,[32] W. Fetscher,[62] B.D. Fields,[63,59] A. Freitas,[64] H. Gallagher,[65] P. Gasik,[66,67,68] T. Gershon,[69] T. Gherghetta,[70] S. Giovannella,[14] M.C. Gonzalez-Garcia,[71,72,73] M. Goodman,[74] C. Grab,[62] A.V. Gritsan,[75] C. Grojean,[76,77] D.E. Groom,[19] M. Grünewald,[78] A. Gurtu,[36,79] T. Gutsche,[80] H.E. Haber,[81] M. Hamel,[82] C. Hanhart,[83] S. Hashimoto,[84] Y. Hayato,[85,8] A. Hebecker,[86] S. Heinemeyer,[87] J.J. Hernández-Rey†,[88] D.W. Hertzog,[89] J. Hisano,[4,5] A. Höcker,[36] M. Hoferichter,[90] W. Hofmann,[91] J. Holder,[92,93] L. Hsu,[32] J. Huston,[94] T. Hyodo,[95,96] Al. Ianni,[97] M. Kado,[98] J. Kaplon,[36] M. Karliner,[99] U.F. Katz,[100] M. Kenzie,[101] V.A. Khoze,[102] S.R. Klein,[103,104] A. Knue,[105] R. Kogler,[76] G. Kramberger,[106] M. Kramer,[19] F. Krauss,[102] M. Kreps,[69] J. Kretzschmar,[54] P. Križan,[107,106] Y. Kwon,[108] O. Lahav,[109] L.P. Lellouch,[110] J. Lesgourgues,[111] A.R. Liddle,[41] Z. Ligeti,[19] C.-J. Lin,[19] C. Lippmann,[66] T.M. Liss,[112] L. Lista,[113,45] A. Lister,[114] L. Littenberg,[15] C. Lourenço,[36] K.S. Lugovsky,[19] S.B. Lugovsky,[115] A. Lusiani,[35,116] Y. Makida,[84] F. Maltoni,[117,118] A.V. Manohar,[40] A. Masoni,[119] S. Meinel,[120] U.-G. Meißner,[121,83] I.-A. Melzer-Pellmann,[76] P. Mertsch,[111] M. Mikhasenko,[122] D.J. Miller,[26] D. Milstead,[123] R.E. Mitchell,[124] K. Mönig,[125] P. Molaro,[126,127] F. Moortgat,[36,128] N. Nagata,[7] K. Nakamura‡,[84,8] P. Nason,[44,129] S. Navas†,[48] A. Nelles,[125,100] M. Neubert,[130] Y. Nir,[131] H.B. O'Connell,[32] C.A.J. O'Hare,[132] K.A. Olive,[70] C. Patrignani,[118] J.A. Peacock,[133] K. Peters,[66,134] E. Pianori,[19] A. Pich,[88] A. Piepke,[135] F. Pietropaolo,[36,136] A. Pomarol,[137,138] S. Profumo,[81] A. Quadt,[139] K. Rabbertz,[140] J. Rademacker,[141] G. Raffelt,[98] M. Ramsey-Musolf,[142,143,144] L. Reina,[43] P. Richardson,[102] D.J. Robinson,[19] S. Roesler,[36] S. Rolli,[145] A. Romaniouk,[146,147] L.J Rosenberg,[89] G. Rybka,[89] M.G. Ryskin,[115] B. Safdi,[104] Y. Sakai,[84] F. Salamida,[148,97] N. Saoulidou,[149] S. Sarkar,[150] F. Sauli§,[36] P. Savard,[151,152] O. Schneider,[153] S. Schönert,[154] K. Scholberg,[155] C. Schwanda,[13] A.J. Schwartz,[156] J. Schwiening,[66] D. Scott,[114] F. Sefkow,[76] U. Seljak,[104,19] V. Sharma,[40] S.R. Sharpe,[89] V. Shiltsev,[157] G. Signorelli,[34,35] M. Silari,[36] F. Simon,[140] P. Skands,[58] T. Skwarnicki,[158] G.F. Smoot‡,[159,104,19,160,161] A. Soffer,[99] M.S. Sozzi,[34,35] S. Spanier,[162] C. Spiering,[125] A. Stahl,[163] M. Taševský,[164] K. Terao,[165,166] K. Terashi,[6] J. Terning,[167] U. Thoma,[121] R.S. Thorne,[109] L. Tiator,[61] M. Titov,[168] D.R. Tovey,[169] K. Trabelsi,[170] P. Urquijo,[171] G. Valencia,[58] R. Van de Water,[32] N. Varelas,[172] G. Venanzoni¶,[54,35] V. Vennin,[173,30] L. Verde,[73,72] I. Vivarelli,[118] W. Vogelsang,[80] W. Walkowiak,[174] C.W. Walter,[155] D. Wands,[175] D.H. Weinberg,[176] E.J. Weinberg,[177] R. Wendell,[178] N. Wermes,[56] M. White,[104,19] L.R. Wiencke,[179] S. Willocq,[144] L. Winslow,[180] C.L. Woody,[15] R.L. Workman,[181] W.-M. Yao,[19] R. Yoshida,[74] C. Z. Yuan,[31] G. Zanderighi,[98,154] G.P. Zeller,[32] R.-Y. Zhu,[182] S.-L. Zhu,[183] F. Zimmermann,[36] P.A. Zyla[19]

Technical Associates: J. Anderson,[19] V.K.S. Kashyap,[184] B. Mohanty,[184] A. Ozerov,[185] S. Rohr,[36] P. Schaffner,[19] G.A. Valdiviesso,[186] W. Zheng[31]

1. *Tohoku University, Department of Physics, Sendai, Japan*
2. *Division for Interdisciplinary Advanced Research and Education, Tohoku University, Sendai, Japan*
3. *Institute of Liberal Arts and Sciences, Tohoku University, Sendai, Japan*
4. *Department of Physics, Nagoya University, Nagoya, Japan*
5. *Nagoya University, Kobayashi-Maskawa Institute, Nagoya, Japan*
6. *International Center for Elementary Particle Physics (ICEPP), The University of Tokyo, Tokyo, Japan*
7. *The University of Tokyo, Department of Physics, Tokyo, Japan*
8. *The University of Tokyo, Kavli IPMU (WPI), The University of Tokyo Institutes for Advanced Study, Kashiwa, Japan*
9. *University of Maryland, Department of Physics, College Park, MD, USA*
10. *Università degli Studi di Roma "Tor Vergata", Rome, Italy*

*Coordination activities supported directly by INFN.
†Support from Projects PID2024-156285NB-C41 and -C42, funded by MICIU/AEI/10.13039/501100011033 and FEDER/EU
‡Deceased.
§Retired.
¶Supported by the Leverhulme Trust (grant LIP-2021-014).

11. *Department of Applied Mathematics and Theoretical Physics, University of Cambridge, Cambridge, UK*
12. *Instituto Galego de Física de Altas Enerxías (IGFAE) & Dept. Física de Partículas, Universidade de Santiago de Compostela, Santiago de Compostela, Spain*
13. *Marietta Blau Institute for Particle Physics, Austrian Academy of Sciences, Vienna, Austria*
14. *Lab. Nazionali di Frascati dell'INFN, Frascati, Italy*
15. *Brookhaven National Laboratory, Nuclear and Particle Physics Directorate, Upton, NY, USA*
16. *SNOLAB, Lively, Ontario, Canada*
17. *University of Oklahoma, Department of Physics and Astronomy, Norman, OK, USA*
18. *University of Louisville, Louisville, KY, USA*
19. *Physics Division, Lawrence Berkeley National Laboratory, Berkeley, CA, USA*
20. *Universität Zürich, Physik-Institut, Zürich, Switzerland*
21. *INFN and Dipartimento di Fisica e Astronomia, Università di Padova, Padova, Italy*
22. *Ludwig-Maximilians-Universität, Fakultät für Physik, München, Germany*
23. *University of Wisconsin, Department of Physics, Madison, WI, USA*
24. *University of Chicago, Enrico Fermi Institute and Department of Physics, Chicago, IL, USA*
25. *Department of Physics, Carnegie Mellon University, Pittsburgh, PA, USA*
26. *University of Glasgow, School of Physics and Astronomy, Glasgow, UK*
27. *Jefferson Lab, Newport News, VA, USA*
28. *University of Virginia, Department of Physics, Charlottesville, VA, USA*
29. *Laboratoire de Physique Théorique et Hautes Energies, Paris, France*
30. *Centre National de la Recherche Scientifique, France*
31. *Institute of High Energy Physics, Chinese Academy of Sciences, Beijing, China*
32. *Fermi National Accelerator Laboratory, Batavia, IL, USA*
33. *University of Chicago, Kavli Institute for Cosmological Physics, Chicago, IL, USA*
34. *University of Pisa, Pisa, Italy*
35. *INFN Sezione di Pisa, Pisa, Italy*
36. *CERN, European Organization for Nuclear Research, Genève, Switzerland*
37. *CIEMAT, Centro de Investigaciones Energéticas Medioambientales y Tecnológicas, Madrid, Spain*
38. *Dipartimento Scienze fisiche, della Terra e dell'ambiente, Università degli Studi di Siena, Siena, Italy*
39. *Department of Physics and Astronomy, University of Sussex, Brighton, UK*
40. *Department of Physics, University of California at San Diego, La Jolla, CA, USA*
41. *Instituto de Astrofísica e Ciências do Espaço, Universidade de Lisboa, Lisbon, Portugal*
42. *Department of Physics, Royal Holloway, University of London, London, UK*
43. *Florida State University, Department of Physics, Tallahassee, FL, USA*
44. *INFN Sezione di Milano-Bicocca, Piazza della Scienza, Milano, Italy*
45. *INFN Sezione di Napoli, Napoli, Italy*
46. *Institut des Hautes Etudes Scientifiques, Bures-sur-Yvette, France*
47. *University of Glasgow, Department of Physics and Astronomy, Glasgow, UK*
48. *Universidad de Granada, Dpto. de Física Teórica y del Cosmos, Granada, Spain*
49. *UNSAM - Universidad Nacional de San Martin, International Center for Advanced Studies (ICAS) and Instituto de Ciencias Físicas (ICIFI), Buenos Aires, Argentina*
50. *Northwestern University, Department of Physics and Astronomy, Evanston, IL, USA*
51. *University of Colorado at Boulder, Department of Physics, Boulder, CO, USA*
52. *Boston University, Department of Physics, Boston, MA, USA*
53. *University of Freiburg, Freiburg, Germany*
54. *University of Liverpool, Department of Physics, Liverpool, UK*
55. *INFN Sezione di Trieste, Trieste, Italy*
56. *Universität Bonn, Physikalisches Institut, Bonn, Germany*
57. *Research Council of Finland, Helsinki, Finland*
58. *Monash University, School of Physics and Astronomy, Melbourne, Australia*
59. *University of Illinois, Department of Physics, Urbana, IL, USA*
60. *King's College London, Department of Physics, London, UK*
61. *Institut für Kernphysik, Johannes Gutenberg University, Mainz, Germany*
62. *ETH Zurich, Institute for Particle Physics and Astrophysics, Zurich, Switzerland*
63. *University of Illinois, Department of Astronomy, Urbana, IL, USA*

Int. J. Mod. Phys. A 2026.41. Downloaded from www.worldscientific.com
by UNIVERSITY OF CALIFORNIA @ BERKELEY on 09/16/26. Re-use and distribution is strictly not permitted, except for Open Access articles.

Int. J. Mod. Phys. A 2026.41. Downloaded from www.worldscientific.com
by UNIVERSITY OF CALIFORNIA @ BERKELEY on 09/16/26. Re-use and distribution is strictly not permitted, except for Open Access articles.

64. *University of Pittsburgh, Department of Physics and Astronomy, Pittsburgh, PA, USA*
65. *Tufts University, Department of Physics and Astronomy, Medford, MA, USA*
66. *GSI, Helmholtzzentrum für Schwerionenforschung, Darmstadt, Germany*
67. *FAIR, Facility for Antiproton and Ion Research in Europe, Darmstadt, Germany*
68. *Fachbereich Physik, Technische Universität Darmstadt, Darmstadt, Germany*
69. *University of Warwick, Department of Physics, Coventry, UK*
70. *University of Minnesota, School of Physics and Astronomy, Minneapolis, MN, USA*
71. *CN Yang Institute for Theoretical Physics, Stony Brook University, Stony Brook, NY, USA*
72. *Institució Catalana de Recerca i Estudis Avancats, Barcelona, Spain*
73. *Instituto de ciencias del Cosmos, University of Barcelona, Barcelona, Spain*
74. *Argonne National Laboratory, Argonne, IL, USA*
75. *Johns Hopkins University, Baltimore, MD, USA*
76. *Deutsches Elektronen-Synchrotron DESY, Hamburg, Germany*
77. *Institut für Physik, Humboldt-Universität zu Berlin, Berlin, Germany*
78. *University College Dublin, School of Physics, Dublin, Ireland*
79. *TIFR, Mumbai, India*
80. *Universität Tübingen, Institut für Theoretische Physik, Tübingen, Germany*
81. *Santa Cruz Institute for Particle Physics, University of California, Santa Cruz, CA, USA*
82. *Université Paris-Saclay, CEA, LIST, F-91120 Palaiseau, France*
83. *Forschungszentrum Jülich, Institute for Advanced Simulation, Jülich, Germany*
84. *KEK, High Energy Accelerator Research Organization, Tsukuba, Japan*
85. *Kamioka Observatory, ICRR, The University of Tokyo, Tokyo, Japan*
86. *Heidelberg University, Institute for Theoretical Physics, Heidelberg, Germany*
87. *Instituto de Física Teórica (UAM/CSIC), Universidad Autónoma de Madrid, Madrid, Spain*
88. *IFIC — Instituto de Física Corpuscular, Universitat de València — C.S.I.C., Valencia, Spain*
89. *University of Washington, Department of Physics, Seattle, WA, USA*
90. *University of Bern, Albert Einstein Center for Fundamental Physics, Institute for Theoretical Physics, Bern, Switzerland*
91. *Max-Planck-Institut für Kernphysik, Heidelberg, Germany*
92. *University of Delaware, Department of Physics and Astronomy, Newark, DE, USA*
93. *University of Delaware, Bartol Research Institute, Newark, DE, USA*
94. *Michigan State University, Dept. of Physics and Astronomy, East Lansing, MI, USA*
95. *Research Center for Nuclear Physics, The University of Osaka, Osaka, Japan*
96. *Department of Physics, Tokyo Metropolitan University, Tokyo, Japan*
97. *INFN - Laboratori Nazionali del Gran Sasso, Assergi, Italy*
98. *Max-Planck-Institut für Physik (Werner-Heisenberg-Institut), Garching, Germany*
99. *Department of Particle Physics, Tel-Aviv University, Tel Aviv, Israel*
100. *Friedrich-Alexander-Universität Erlangen-Nürnberg, Erlangen Centre for Astroparticle Physics, Erlangen, Germany*
101. *University of Cambridge, Cambridge, UK*
102. *University of Durham, Institute for Particle Physics Phenomenology, Department of Physics, Durham, UK*
103. *Nuclear Science Division, Lawrence Berkeley National Laboratory, Berkeley, CA, USA*
104. *University of California, Department of Physics, Berkeley, CA, USA*
105. *Technische Universität, Dortmund, Germany*
106. *Jozef Stefan Institute, Ljubljana, Slovenia*
107. *Faculty of Mathematics and Physics, University of Ljubljana, Ljubljana, Slovenia*
108. *Yonsei University, Department of Physics, Seoul, Republic of Korea*
109. *University College London, Department of Physics and Astronomy, London, UK*
110. *Aix-Marseille Univ, Université de Toulon, CNRS, CPT, Marseille, France*
111. *Institute for Theoretical Particle Physics and Cosmology (TTK), RWTH Aachen University, Aachen, Germany*
112. *The City College of New York, New York, NY, USA*
113. *Università degli Studi di Napoli Federico II, Napoli, Italy*
114. *University of British Columbia, Department of Physics and Astronomy, Vancouver, BC, Canada*
115. *Affiliation provided upon request*
116. *Scuola Normale Superiore, Pisa, Italy*

Int. J. Mod. Phys. A 2026.41. Downloaded from www.worldscientific.com
by UNIVERSITY OF CALIFORNIA @ BERKELEY on 09/16/26. Re-use and distribution is strictly not permitted, except for Open Access articles.

117. Universitè catholique de Louvain, Centre for Cosmology, Particle Physics and Phenomenology (CP3), Louvain-la-Neuve, Belgium
118. Università di Bologna and INFN, Dipartimento di Fisica e Astronomia, Bologna, Italy
119. INFN Sezione di Cagliari, Monserrato, Italy
120. University of Arizona, Tucson, AZ, USA
121. Universität Bonn, Helmholtz-Institut für Strahlen- und Kernphysik, Bonn, Germany
122. Institut für Experimentalphysik 1, Ruhr-Universität Bochum, Bochum, Germany
123. Stockholms Universitet, AlbaNova University Centre, Fysikum, Stockholm, Sweden
124. Indiana University, Department of Physics, Bloomington, IN, USA
125. Deutsches Elektronen-Synchrotron DESY, Zeuthen, Germany
126. INAF-OATS, Trieste, Italy
127. Institute for Fundamental Physics of the Universe, Trieste, Italy
128. University of Ghent, Dept. of Physics and Astronomy, Ghent, Belgium
129. Dip. di Fisica "G. Occhialini", Università di Milano-Bicocca, Milano, Italy
130. Johannes Gutenberg University, PRISMA Cluster of Excellence and Mainz Institute for Theoretical Physics, Mainz, Germany
131. Department of Particle Physics and Astrophysics, Weizmann Institute of Science, Rehovot, Israel
132. University of Sydney, Sydney, Australia
133. University of Edinburgh, Royal Observatory, Institute for Astronomy, Edinburgh, UK
134. University of Frankfurt, Frankfurt, Germany
135. University of Alabama, Department of Physics and Astronomy, Tuscaloosa, AL, USA
136. INFN Sezione di Padova, Padua, Italy
137. Universitat Autònoma de Barcelona, Departament de Física, Barcelona, Spain
138. IFAE, Universitat Autònoma de Barcelona, Barcelona, Spain
139. Georg-August-Universität Göttingen, II. Physikalisches Institut, Göttingen, Germany
140. Karlsruhe Institute of Technology, Karlsruhe, Germany
141. University of Bristol, HH Wills Physics Laboratory, Bristol, UK
142. Tsung-Dao Lee Institute, Shanghai Jiao Tong University, Shanghai, China
143. Shanghai Jiao Tong University, Shanghai, China
144. University of Massachusetts, Department of Physics, Amherst, MA, USA
145. DOE, Washington, DC, USA
146. Universität Innsbruck, Department of Astro and Particle Physics, Innsbruck, Austria
147. Istinye University, Sariyer, Istanbul, Turkey
148. Dipartimento di Scienze Fisiche e Chimiche, Università dell'Aquila, L'Aquila, Italy
149. University of Athens, Athens, Greece
150. University of Oxford, Rudolf Peierls Centre for Theoretical Physics, Oxford, UK
151. University of Toronto, Toronto, Canada
152. TRIUMF, Vancouver, Canada
153. Institute of Physics, Ecole Polytechnique Fédérale de Lausanne (EPFL), Lausanne, Switzerland
154. Department of Physics, Technical University Munich, Munich, Germany
155. Duke University, Physics Department, Durham, NC, USA
156. University of Cincinnati, Department of Physics, Cincinnati, OH, USA
157. Northern Illinois University, Department of Physics, DeKalb, IL, USA
158. Syracuse University, Department of Physics, Syracuse, NY, USA
159. The Hong Kong University of Science and Technology, Kowloon, Hong Kong
160. Donostia International Physics Center (DIPC), Donostia-San Sebastián, Spain
161. Paris Centre for Cosmological Physics, APC (CNRS), Université de Paris, Paris, France
162. University of Tennessee, Department of Physics and Astronomy, Knoxville, TN, USA
163. III. Physikalisches Institut, Physikzentrum, RWTH Aachen University, Aachen, Germany
164. Institute of Physics, Czech Academy of Sciences, Prague, Czech Republic
165. SLAC National Accelerator Laboratory, Menlo Park, CA, USA
166. Stanford University, Stanford, CA, USA
167. Department of Physics, University of California, Davis, CA, USA
168. IRFU, CEA, Université Paris-Saclay, F-91191 Gif-sur-Yvette, France
169. University of Sheffield, School of Mathematical and Physical Sciences, Sheffield, UK

170. Centre de Physique des Particules de Marseille, Marseille, France
171. University of Melbourne, School of Physics, Victoria, Australia
172. University of Illinois at Chicago, Chicago, IL, USA
173. Laboratoire de Physique de l'Ecole Normale Supérieure de Paris, Paris, France
174. Universität Siegen, Department für Physik, Siegen, Germany
175. University of Portsmouth, Institute of Cosmology and Gravitation, Portsmouth, UK
176. Ohio State University, Department of Astronomy and CCAPP, Columbus, OH, USA
177. Columbia University, Department of Physics, New York, NY, USA
178. Kyoto University, Kyoto, Japan
179. Dept. of Physics, Colorado School of Mines, Golden, CO, USA
180. Massachusetts Institute of Technology, Cambridge, CA, USA
181. George Washington University, Department of Physics, Washington, D.C., USA
182. California Institute of Technology, High Energy Physics, Pasadena, CA, USA
183. School of Physics, Peking University, Beijing, China
184. National Institute of Science Education and Research, Jatni, India
185. Department of Statistics, University of California, Berkeley, CA, USA
186. Universidade Federal de Alfenas UNIFAL-MG, Poços de Caldas, Brazil

Int. J. Mod. Phys. A 2026.41. Downloaded from www.worldscientific.com
by UNIVERSITY OF CALIFORNIA @ BERKELEY on 09/16/26. Re-use and distribution is strictly not permitted, except for Open Access articles.

Int. J. Mod. Phys. A 2026.41. Downloaded from www.worldscientific.com
by UNIVERSITY OF CALIFORNIA @ BERKELEY on 09/16/26. Re-use and distribution is strictly not permitted, except for Open Access articles.

HIGHLIGHTS OF THE 2026 EDITION OF THE REVIEW OF PARTICLE PHYSICS

All PDG data and review articles are available online at **pdg.lbl.gov**.

903 new papers with 3,200 new measurements

- 339 new measurements from *LHC* experiments (ATLAS, CMS and LHCb).
- Extensive *Higgs boson* coverage: 92 new papers and 250 measurements, including the latest results on mass, couplings, decay width, constraints on the Higgs self-coupling, and searches for other new scalar bosons.
- *Supersymmetry*: 40 new papers with 143 measurements with major exclusions.
- *Top quark*: 32 new papers with 71 measurements provide latest results on mass, coupling, and the discovery of quantum entanglement between pairs of top quarks at LHC.
- *W mass and Electroweak measurements*: The LHC-Tevatron M_W Working Group reports a new combination that provides a more precise world average. New measurements for the leptonic effective electroweak mixing angle are also reported.
- *c-, b-hadron physics*: 170 papers and 717 measurements provide world-leading data on lifetimes, mixing, CP violation, CKM angles, semileptonic and hadronic branching fractions, including rare processes, and constraints on new physics.
- *Neutrino Physics*: 58 new papers with 126 measurements on neutrino mass, mixing, and CP-violation.
- *Meson resonances*: 171 papers with 618 measurements provide substantial improvements, including new cross particle fits involving $J/\psi(1S)$, $\psi(2S)$ and $\eta_c(1S)$; emerging evidence for existence of additional scalar mesons in the 1700 - 1800 MeV region led to revamping of the $f_0(1710)$, $f_0(1810)$ entries; complex pole positions quoted when available in addition to Breit-Wigner masses and widths; many decay branching fractions re-adjusted with current PDG values; and recently observed states now considered established added to Summary Tables.
- Data from both Summary Tables and Particle Listings are now available in machine-readable format via the PDG API.

118 reviews (most are revised)

- New review on Muon Anomalous Magnetic moment (g-2), covering the latest experimental and theoretical results.
- Major revision of *Higgs Physics* review with a renewed focus on the SM Higgs theory and phenomenology.
- Major revision of *EWK* review includes a pedagogical introduction to the renormalization procedure, updated *EWK* fits based on the HEPFit and GFitter frameworks, and the addition of an SMEFT fit to electroweak precision observables.
- Major revision of *Top Quark* review summarizes latest LHC results and constraints on new physics from top quark.
- Major revision of *Machine Learning* review, with new discussions of self-supervised learning, foundation models, and other recent developments.
- Major revision of various sections in the Particle Detectors for:
  - Accelerator physics in particular on *Gaseous detectors*, *Low-noise detector readout*, and *Semiconductor detectors*.
  - Non-accelerator physics in particular on *Atmospheric fluorescence detectors*, *Atmospheric Cherenkov telescopes*, and *Deep liquid detectors*.
- Major revision of the *Statistics* review, which has been updated and restructured for clarity.
- *Semileptonic B Hadron Decays, Determination of V_{cb} and V_{ub}* summarizes the latest results and discusses long-standing issues with inclusive and exclusive measurements.
- The *Quark Model* review has been updated to include new charmed baryons observed by LHCb and CMS.
- The *Monte Carlo Particle Numbering Scheme* has been extended to better incorporate tentative states, tetraquarks, and pentaquarks.

Int. J. Mod. Phys. A 2026.41. Downloaded from www.worldscientific.com
by UNIVERSITY OF CALIFORNIA @ BERKELEY on 09/16/26. Re-use and distribution is strictly not permitted, except for Open Access articles.

Int. J. Mod. Phys. A 2026.41. Downloaded from www.worldscientific.com
by UNIVERSITY OF CALIFORNIA @ BERKELEY on 09/16/26. Re-use and distribution is strictly not permitted, except for Open Access articles.

VOLUME 1: SUMMARY TABLES AND REVIEWS

Highlights (rev.) 6
Introduction (rev.) 13
History plots 21
Online particle physics information (rev.) 22

SUMMARY TABLES

Gauge and Higgs bosons 27
Leptons 30
Quarks 34
Mesons 35
Meson quick reference table 97
Baryon quick reference table 98
Baryons 99
Searches not in Other Sections 119
Tests of conservation laws 121

REVIEWS, TABLES, AND PLOTS

Constants, Units, Atomic and Nuclear Properties

1. Physical constants (rev.) 145
2. Astrophysical constants and parameters (rev.) 146
3. International system of units (SI) 148
4. Periodic table of the elements 149
5. Electronic structure of the elements 150
6. Atomic and nuclear properties of materials 152
7. Electromagnetic relations (rev.) 153
8. Naming scheme for hadrons (rev.) 155

Standard Model and Related Topics

9. Quantum chromodynamics (rev.) 161
10. Electroweak model and constraints on new physics (rev.) 196
11. Higgs boson physics, status of (rev.) 226
12. CKM quark-mixing matrix (rev.) 273
13. CP violation in the quark sector (rev.) 283
14. Neutrino masses, mixing, and oscillations (rev.) 297
15. Quark model (rev.) 324
16. Heavy-quark & soft-collinear effective theory 343
17. Lattice quantum chromodynamics (rev.) 352
18. Structure functions (rev.) 373
19. Fragmentation functions in e^+e^-, ep and pp collisions 396
20. High Energy Soft QCD and Diffraction (rev.) 413

Astrophysics and Cosmology

21. Experimental tests of gravitational theory (rev.) 437
22. Big-Bang cosmology (rev.) 450
23. Inflation (rev.) 463
24. Big-Bang nucleosynthesis (rev.) 480
25. Cosmological parameters (rev.) 488
26. Neutrinos in cosmology (rev.) 497
27. Dark matter (rev.) 505
28. Dark energy (rev.) 523
29. Cosmic microwave background (rev.) 531
30. Cosmic rays (rev.) 542

Experimental Methods and Colliders

31. Accelerator physics of colliders (rev.) 569
32. High-energy collider parameters (rev.) 580
33. Neutrino beam lines at high-energy proton synchrotrons (rev.) 585
34. Passage of particles through matter 586
35. Particle detectors at accelerators (rev.) 602
36. Particle detectors for non-accelerator phys. (rev.) 661
37. Radioactivity and radiation protection (rev.) 695
38. Commonly used radioactive sources 701

Mathematical Tools

39. Probability (rev.) 705
40. Statistics (rev.) 710
41. Machine Learning (rev.) 727
42. Monte Carlo techniques (rev.) 768
43. Monte Carlo event generators (rev.) 772
44. Monte Carlo neutrino event generators (rev.) 784
45. Monte Carlo particle numbering scheme (rev.) 789
46. Clebsch-Gordan coefficients, spherical harmonics, and d functions 794
47. SU(3) isoscalar factors and representation matrices 795
48. SU(n) multiplets and Young diagrams 796

Kinematics, Cross-Section Formulae, and Plots

49. Kinematics 799
50. Resonances (rev.) 803
51. Cross-section formulae for specific processes 815
52. Neutrino cross section measurements (rev.) 824
53. Plots of cross sections and related quantities 831

Particle Properties

Gauge Bosons

54. Mass and width of the W boson (rev.) 839
55. Z boson (rev.) 841

Charged Leptons

56. Muon anomalous magnetic moment (rev.) 846
57. Muon decay parameters 853
58. τ branching fractions (rev.) 856
59. τ-lepton decay parameters 859

Quarks

60. Quark masses 861
61. Top quark (rev.) 871

(Continued on next page.)

Int. J. Mod. Phys. A 2026.41. Downloaded from www.worldscientific.com
by UNIVERSITY OF CALIFORNIA @ BERKELEY on 09/16/26. Re-use and distribution is strictly not permitted, except for Open Access articles.

Mesons
62. Form factors for semileptonic kaon ($K_{\ell 3}$), radiative pion ($\pi_{\ell 2\gamma}$) & kaon ($K_{\ell 2\gamma}$) decays (rev.) 911
63. Spectroscopy of light meson resonances (rev.) 914
64. Scalar mesons below 1 GeV (rev.) 928
65. Rare kaon decays (rev.) 937
66. CPT invariance tests in neutral kaon decay 943
67. V_{ud}, V_{us}, Cabibbo angle, and CKM unitarity (rev.) 945
68. CP-violation in K_L decays 949
69. Review of multibody charm analyses (rev.) 952
70. D^0–$\overline{D}^0$ mixing (rev.) 958
71. Leptonic decays of charged pseudoscalar mesons (rev.) 969
72. Production and decay of b-flavored hadrons (rev.) 980
73. Polarization in B decays (rev.) 992
74. B^0–$\overline{B}^0$ mixing (rev.) 996
75. Semileptonic B-hadron decays, V_{cb} and V_{ub} (rev.) 1003
76. CKM angles from B hadrons, determination of (rev.) 1021
77. Spectroscopy of mesons containing two heavy quarks (rev.) 1026
78. Heavy non-$q\overline{q}$ mesons (rev.) 1035

Baryons
79. Baryon decay parameters 1046
80. N and Δ resonances 1047
81. Λ and Σ resonances 1052
82. Pole structure of the $\Lambda(1405)$ region (rev.) 1055
83. Pentaquarks (rev.) 1057

Hypothetical Particles and Concepts
84. Extra dimensions (rev.) 1067
85. W'-boson searches (rev.) 1076
86. Z'-boson searches (rev.) 1080
87. Supersymmetry: theory (rev.) 1086
88. Supersymmetry: experiment (rev.) 1108
89. Axions and other similar particles (rev.) 1130
90. Quark and lepton compositeness, searches for (rev.) 1150
91. Dynamical electroweak symmetry breaking: implications of the H^0 (rev.) 1156
92. Grand unified theories (rev.) 1171
93. Leptoquarks (rev.) 1189
94. Magnetic monopoles (rev.) 1194

INDEX (Volumes 1 and 2 combined) 1201

VOLUME 2: PARTICLE LISTINGS (available online only)

Illustrative key and abbreviations
Illustrative key 1227
Abbreviations 1228

Gauge and Higgs bosons
(γ, gluon, graviton, W, Z, Higgs, Axions) 1241

Leptons
(e, μ, τ, Heavy-charged lepton searches, Neutrino properties, Number of neutrino types Double-β decay, Neutrino mixing, Heavy-neutral lepton searches) 1369

Quarks
(u, d, s, c, b, t, b', t' (4th gen.), Free quarks) 1447

Mesons
Light unflavored (π, ρ, a, b) (η, ω, f, ϕ, h) 1491
Strange (K, K^*) 1623
Charmed (D, D^*) 1677
Charmed, strange (D_s, D_s^*, D_{sJ}) 1749
Bottom (B, V_{cb}/V_{ub}, B^*, B_J^*) 1775
Bottom, strange (B_s, B_s^*, B_{sJ}^*) 1965
Bottom, charmed (B_c) 1996
$c\overline{c}$ (η_c, $J/\psi(1S)$, χ_c, h_c, ψ) 2002
$b\overline{b}$ (η_b, Υ, χ_b, h_b) 2142
Other mesons (T_c, T_b tetraquarks) 2183

Baryons
N 2203
Δ 2263
Λ 2289
Σ 2315
Ξ 2347
Ω 2361
Charmed (Λ_c, Σ_c, Ξ_c, Ω_c) 2364
Doubly charmed (Ξ_{cc}) 2396
Bottom (Λ_b, Σ_b, Ξ_b, Ω_b, b-baryon admixture) 2398
Exotic baryons (P_c pentaquarks) 2423

Searches not in Other Sections
Magnetic monopole searches 2429
Supersymmetric particle searches 2432
Technicolor 2493
Searches for quark and lepton compositeness 2494
Extra dimensions 2499
WIMP and dark matter searches 2505
Other particle searches 2523

Int. J. Mod. Phys. A 2026.41. Downloaded from www.worldscientific.com
by UNIVERSITY OF CALIFORNIA @ BERKELEY on 09/16/26. Re-use and distribution is strictly not permitted, except for Open Access articles.

INTRODUCTION

1. Overview . . . 13
2. Particle Listings responsibilities . . . 13
3. Consultants . . . 14
4. Naming scheme for hadrons . . . 17
5. Procedures . . . 17
   5.1 Selection and treatment of data . . . 17
   5.2 Averages and fits . . . 18
      5.2.1 Treatment of errors . . . 18
      5.2.2 Unconstrained averaging . . . 18
      5.2.3 Constrained fits . . . 19
   5.3 Rounding . . . 19
   5.4 Discussion . . . 19
History plots . . . 21

ONLINE PARTICLE PHYSICS INFORMATION

1. Introduction . . . 22
2. Particle Data Group (PDG) resources . . . 22
3. Particle physics information platform . . . 22
4. Literature databases . . . 22
5. Journals . . . 23
6. Conference and seminars databases . . . 23
7. Research institutions . . . 23
8. People . . . 23
9. Experiments . . . 23
10. Jobs . . . 23
11. Software packages and repositories . . . 24
12. Data repositories and preservation . . . 24
13. Particle physics education and outreach . . . 24
14. Regional HEP efforts . . . 24

Int. J. Mod. Phys. A 2026.41. Downloaded from www.worldscientific.com
by UNIVERSITY OF CALIFORNIA @ BERKELEY on 09/16/26. Re-use and distribution is strictly not permitted, except for Open Access articles.

Int. J. Mod. Phys. A 2026.41. Downloaded from www.worldscientific.com
by UNIVERSITY OF CALIFORNIA @ BERKELEY on 09/16/26. Re-use and distribution is strictly not permitted, except for Open Access articles.

Introduction

1 Overview

The *Review of Particle Physics* is a comprehensive review of the field of Particle Physics and of related areas in Cosmology. It is divided into two volumes. Volume 1 includes the "Summary Tables" and "Reviews, Tables, and Plots". Volume 2 consists of the "Particle Listings".

The *Review* is updated each year and made available on the PDG website (pdg.lbl.gov). In even-numbered years, the *Review* is also published in a journal and printed as the *PDG Book* together with an abridged *Particle Physics Booklet* containing Summary Tables and essential tables, figures, and equations from selected review articles. This edition is an updating through January 2026.

The Summary Tables give our best values and limits for particle properties such as masses, widths or lifetimes, and branching fractions, as well as an extensive summary of searches for hypothetical particles and a summary of experimental tests of conservation laws.

The 94 review articles in Reviews, Tables and Plots cover a wide variety of theoretical and experimental topics. Together with the Summary Tables they provide an exhaustive reference for the practicing particle physicist. Two more review articles, Online Particle Physics Information and Tests of Conservation Laws, can be found in the introduction and Summary Tables, respectively.

The Particle Listings are a compilation/evaluation of data on particle properties. They contain all the data used to get the values given in the Summary Tables. They also give information on unconfirmed particles and particle searches. In this edition, the Particle Listings include 3,200 new measurements from 903 papers, in addition to the 49,555 measurements from 13,778 papers that first appeared in previous editions [1]. 22 review articles are part of the Particle Listings and address specific aspects of the data presented in the Listings. Because of the large quantity of data, the Particle Listings are not an archive of all published data on particle properties. We refer interested readers to earlier editions for data now considered to be obsolete.

We organize the particles into six categories:

- Gauge and Higgs bosons
- Leptons
- Quarks
- Mesons
- Baryons
- Searches not in other sections

The last category only includes searches for particles that do not belong to the previous groups. For example, it includes searches for supersymmetric particles, compositeness and extra dimensions, while searches for heavy charged leptons are with the leptons.

In Sec. 2 of this Introduction, we list the main areas of responsibility of the authors of the Particle Listings. Our many consultants, without whom we would not have been able to produce this *Review*, are acknowledged in Sec. 3. In Sec. 4, we mention briefly the naming scheme for hadrons, and in Sec. 5, we discuss our procedures for choosing among measurements of particle properties and for obtaining best values of the properties from the measurements.

The accuracy and usefulness of this *Review* depend in large part on interaction between its users and the authors. We appreciate comments, criticisms, and suggestions for improvements of any kind. Please send them to pdg@lbl.gov from where they will be forwarded to the appropriate author according to the list of responsibilities in Sec. 2 below.

In addition to the online publication at pdg.lbl.gov, the *Review* is available in different formats:

- The printed *PDG Book* includes volume 1 only, *i.e.* it contains the Summary Tables and most review articles. Since the 2016 edition [2] the detailed tables from the Particle Listings are no longer printed.
- The *Particle Physics Booklet* includes the Summary Tables plus essential tables, figures, and equations from selected review articles. Starting with the Booklets of the 2018 edition, we have excluded most text and explanations in order to revert back to a more pocket-sized format. The Booklet is available in print, as a web version optimized for use on phones, and as an Android app (see pdg.lbl.gov/booklet).
- *pdgLive* (pdgLive.lbl.gov) is a web application giving more interactive access to PDG data than the static web pages and PDF files that are also available.
- Files that can be downloaded from the PDG website include a table of masses, widths, and PDG Monte Carlo particle ID numbers; PDF files of volume 1 (PDG Book), volume 2 (Particle Listings) and Booklet; individual review articles; all figures; and an archive file containing the complete PDG website (except for pdgLive).
- The data published in the *Review of Particle Physics* is available in machine-readable format through the PDG API (Application Programming Interface). See pdg.lbl.gov/api for details.

Copies of the *PDG Book* or the *Particle Physics Booklet* can be ordered from our website or directly at pdg.lbl.gov/order. For special requests only, please email pdg@lbl.gov in North and South America, Australia, and the Far East, and pdg-products@cern.ch in all other areas.

This *Review* is considered to be a single comprehensive review of particle physics and related areas. Therefore we prefer that it be cited as a whole, rather than citing *e.g.* an individual review article that is part of this *Review*. For the 2026 edition, the proper citation is:

F. Takahashi *et al.* (Particle Data Group), Int. J. Mod. Phys. A **41**, 2630011 (2026).

If you wish to refer to a specific part of the *Review*, for example to the Higgs boson review article, the following form should be used:

"Status of Higgs Boson Physics" in F. Takahashi *et al.* (Particle Data Group), Int. J. Mod. Phys. A **41**, 2630011 (2026).

2 Particle Listings responsibilities

* Asterisk indicates the people to contact with questions or comments about Particle Listings sections. Please contact them by e-mail to pdg@lbl.gov.

- Gauge and Higgs bosons

γ	A. Bettini, D.E. Groom*
Gluons	R.M. Barnett,* A.V. Manohar
Graviton	A. Bettini,* D.E. Groom
W, Z	M. Grünewald,* A. Gurtu*, J. Kretzschmar
Higgs bosons	S. Heinemeyer,* K. Hikasa, J. Tanaka
Heavy bosons	R. Bonventre,* K.A. Olive, M. Tanabashi
Axions	C. O'Hare, K.A. Olive, F. Takahashi

- Leptons

Neutrinos	C.-J. Lin,* K.A. Olive, A. Piepke, M. Yokoyama
Double-β decay	A. Bettini*, A. Piepke
e, μ	A. Bettini,* C. Grab
τ	A. Lusiani, K. Mönig*

- Quarks

Quarks	R.M. Barnett,* A.V. Manohar
Top quark	Y. Sumino, W.-M. Yao*
b', t'	Y. Sumino, W.-M. Yao*
Free quark	A. Bettini,* C.-J. Lin

- Mesons

π, η	A. Bettini,* C. Grab
K (stable)	G. D'Ambrosio, C.-J. Lin*
D (stable)	G. Casarosa, J. Rademacker, D. Robinson*
B (stable)	A. Cerri,* P. Eerola, M. Kreps, Y. Kwon, W.-M. Yao*

Int. J. Mod. Phys. A 2026.41. Downloaded from www.worldscientific.com
by UNIVERSITY OF CALIFORNIA @ BERKELEY on 09/16/26. Re-use and distribution is strictly not permitted, except for Open Access articles.

Unstable mesons	C. Amsler,*, S. Giovannella, T. Gutsche, C. Hanhart, J.J. Hernández-Rey, C. Lourenco, A. Masoni, M. Mikhasenko, R.E. Mitchell, S. Navas, C. Patrignani, K. Peters, C. Schwanda, S. Spanier, G. Venanzoni, C.Z. Yuan

- Baryons

Stable baryons	C. Grab, D. Robinson*
Unstable baryons	V. Crede, U. Thoma, L. Tiator, R.L. Workman*
Charmed baryons	G. Casarosa, J. Rademacker, D. Robinson*
Bottom baryons	A. Cerri,* P. Eerola, M. Kreps, Y. Kwon, W.-M. Yao*

- Miscellanoues searches

Monopole	A. Bettini,* D. Milstead
Supersymmetry	H.K. Dreiner,* A. de Gouvêa, I.-A. Melzer-Pellmann, K.A. Olive, I. Vivarelli
Technicolor	K. Agashe,* K.A. Olive, M. Tanabashi
Compositeness	M. Tanabashi, J. Terning*
Extra Dimensions	T. Gherghetta, K.A. Olive, D. Robinson*
WIMP, DM, Other	H. Baer, A. Bettini,* W.-M. Yao*

3 Consultants

The Particle Data Group benefits greatly from the assistance of hundreds of physicists who are asked to referee review articles and verify every piece of data entered into this *Review*. Of special value is the advice of the PDG International Advisory Committee, which meets biennially and thoroughly reviews all aspects of our operation. The members of the 2026 committee are:

S. Demers (Yale)
D. d'Enterria (CERN)
J. Frieman (FNAL)
S. Gori (UCSC)
M. Ishitsuka (Tokyo)

We have especially relied on the expertise of the following people for advice on particular topics:

- I. Abt (MPP, Garching)
- M. Achasov (Budker Inst., Novosibirsk)
- S. Adachi (Kyoto U.)
- C. Adams (Columbia U.)
- D. Adan (RWTH Aachen U.)
- E. Adli (Oslo U.)
- Y. Afik (Chicago U.)
- S. Alderweireldt (Edinburgh U.)
- M. Aleksa (CERN)
- M. Alpízar (IF-UNAM)
- G. Alves (USP; FNAL)
- A. Antognini (ETH Zurich)
- E. Aprile (Columbia U.)
- S. Arguedas Cuendis (ICC, U. of Barcelona)
- M. Artuso (Syracuse U.)
- N. Asbah (CERN)
- P. Athron (Nanjing U.)
- E. Auffray (CERN)
- G. Azuelos (U. de Montreal)
- S. Bahinipati (IIT Bhubaneswar)
- X. Bai (Yale U.)
- A.B. Balantekin (Wisconsin U.)
- A. Baldini (INFN, Pisa)
- A. Barabash (ITEP)
- E. Barriga (Florida State U.)
- V. Baru (Ruhr U. Bochum)
- R. Battiston (Trento U.)
- G. Bell (Siegen U.)
- J. Bellido Caceres (Adelaide U.)
- V. Belyaev (ITEP)
- J. Bendavid (CERN)
- X. Benhou (IHEP Beijing)
- J. Bennett (Mississippi U.)
- F. Betti (INFN, Bologna)
- F. Bianchini (SLAC)
- T. Biekotter (KIT)
- P. Bisio (INFN, Genova)
- F. Blanc (CERN)
- P. Blasi (GSSI)
- M. Blaskiewicz (BNL)
- O. Boente (CERN)
- M. Bona (QMUL)
- A. Bondar (Budker Inst., Novosibirsk)
- C. Bonifazi (ICAS and ICIFI, UNSAM)
- M. Boonekamp (CEA/IRFU Saclay)
- M. Borsato (CERN)
- S. Bressler (Weizmann Inst.)
- F. Brizioli (CERN)
- R. Bruce (CERN)
- O. Bruning (CERN)
- J. Butter (Cavendish Lab.)
- M. Cadeddu (INFN, Cagliari)
- C. Caillol (CERN)
- R. Camacho (CERN)
- S. Camarda (CERN)
- F. Caola (Rudolf Peierls, Oxford U.)
- L. Capriotti (INFN, Ferrara)
- A. Caputo (CERN)
- B. Carlo (INFN, LNGS)
- V. Carretero (IFIC, Valencia)
- G. Cavoto (Rome U.; INFN, Rome)
- S. Cebrian Guajardo (U. de Zaragoza)
- M. Cermeno (UAM/CSIC, U. Autónoma de Madrid)
- R. Cervantes (FNAL)
- C. Chen (CPPM Marseille)
- D. Chen (SEU)
- M. Chen (Queen's U.)
- Y. Chenghui (IHEP Beijing)
- G. Chiarelli (INFN, Pisa)
- V. Chobanova (CERN)
- J. Choi (Seoul National U.)
- I. Cholis (Oakland U.)
- V. Cirigliano (U. Washington)
- S. Clayton (LANL)
- G. Colangelo (U. Bern)
- J.I. Collar (Chicago U.)
- L. Corpe (Clermont-Ferrand U.)
- A. Cortes Gonzalez (Physik, Humboldt U.)
- P. Crivelli (ETH Zurich)
- A. Czarnecki (Alberta U.)
- W. Dabrowski (AGH-UST)
- T. Dado (CERN)
- D. Daniil (Russian Academy of Sciences)
- D. Dannheim (CERN)

Int. J. Mod. Phys. A 2026.41. Downloaded from www.worldscientific.com
by UNIVERSITY OF CALIFORNIA @ BERKELEY on 09/16/26. Re-use and distribution is strictly not permitted, except for Open Access articles.

- A. De Angelis (INFN, Padova)
- P. Decowski (NIKHEF)
- G. Degrassi (Roma Tre U.; INFN, Rome)
- G. de Lellis (INFN, Napoli)
- M. Delmastro (CERN; LAPP)
- D. d'Enterria (CERN)
- A. Derbin (NRC Kurchatov Inst. PNPI)
- S. Derenzo (LBNL)
- B. Dev (WashU)
- M. Di Carlo (CERN)
- C. Diez (Siegen U.)
- E. Di Marco (INFN, Rome)
- A. Dixit (Chicago U.)
- S. Dobbs (Florida State U.)
- B. Dobrich (MPP, Garching)
- M. Dolan (School of Phys. U. of Melbourne)
- S. Dolan (CERN)
- L. Dong (IHEP Beijing)
- M. Drewes (TU Munich)
- G. Drexlin (KIT)
- J.J. Dudek (IReS)
- V. Dutta (UC Santa Barbara)
- W. East (Perimeter Inst.)
- S.R. Elliott (LANL)
- R. Essig (YITP, Stony Brook)
- J. Fan (Brown U.)
- J. Fan (Henan U.)
- G. Fedotovich (Budker Inst., Novosibirsk)
- J. Feng (UC Irvine)
- A. Ferrari (CERN)
- C. Finley (Stockholm U.)
- W. Fischer (BNL)
- J. Flynn (Southampton U.)
- J. Formaggio (MIT)
- P. Francavilla (CERN)
- D. Franco (Paris U.)
- M. Frank (Concordia U.)
- T. Fujii (OMU Osaka)
- S. Funk (Erlangen U.)
- J. Gao (IHEP Beijing)
- I. Garcia Garcia (U. Washington)
- M. Garcia-Sciveres (LBNL)
- C. Gatti (INFN, LNF)
- P. Gauzzi (INFN, Rome; Rome U. Sapienza)
- A. Gaz (INFN, Padua)
- X. Geng (Tsinghua U.)
- B. Geoffrey (Wits U.)
- G. Gerbier (CEA Saclay, DSM/IRFU/SPP)
- F. Geurts (Rice U.)
- M. Giovannozzi (CERN)
- V. Gligorov (CNRS)
- J. Gomez Cadenas (DIPC)
- G. Gomez-Ceballos (CERN)
- M. Goodsell (LPTHE, Paris)
- S. Gori (UC Santa Cruz)
- S. Gozzini (IFIC, Valencia)
- P. Grabmayr (Tübingen U.)
- N. Grieser (CERN)
- G. Grilli (INFN, LNGS)
- A. Grohsjean (DESY, Hamburg)
- F. Guo (ITP)
- W. Guo (USTC)
- G. Gustavino (Rome U. Sapienza)
- P. Guzowski (Manchester U.)
- U. Haisch (MPP, Garching)
- F. Halzen (Wisconsin U.)
- K. Harigaya (Chicago U.)
- F.A. Harris (Hawaii U.)
- P. Harris (MIT)
- F. Hartmann (KIT)
- D. Hayden (Michigan State U.)
- C. Hays (Oxford U.)
- K.M. Heeger (Yale U.)
- A. Heijboen (NIKHEF)
- G. Heinrich (KIT)
- J. Heitger (WWU)
- T. Herbermann (MPIK)
- S. Hernández (SJTU)
- C. Hill (Ohio State U.)
- A. Hinzmann (Hamburg U.)
- J. Hirschauer (FNAL)
- J. Hogan (Bethel U.)
- N. Houston (BJUT)
- T. Huege (KIT)
- T. Humair (DESY, Hamburg)
- N. Ilic (Toronto U.)
- K. Inoue (Tohoku U.)
- M. Ivanov (MIT)
- C. James (CIRA)
- A. Kagan (U. of Cincinnati)
- A. Kalweit (CERN)
- A. Kar (LTHE, Sorbonne U.)
- D. Kar (Wits U.)
- G. Karathanasis (CERN)
- G. Kasieczka (Hamburg U.)
- V. Kekelidze (JINR, Dubna)
- I. Kim (LLNL)
- J. Kim (Utah U.)
- Y. Kim (IBS, Daejeon)
- K. Kirch (ETH Zurich)
- E. Klempt (Bonn U.)
- S. Knirck (FAS, Harvard U.)
- K. Knoepfle (MPIK)
- T. Kobayashi (SISSA/INFN, Trieste)
- B. Kopf (Ruhr U. Bochum)
- T. Koseki (KEK)
- M. Koshimizu (Shizuoka U.)
- E. Kou (LAL Orsay)
- A. Kramida (NIST)
- S. Kraml (LPSC, Grenoble)
- W. Krzemien (NCNR, HEP)
- A. Kulik (INR, Moscow)
- G. Landsberg (Brown U.)
- V. Lebedev (JINR, Dubna)
- P. Leng (Columbia U.)
- A. Lenz (Siegen U.)
- O. Leroy (CPPM Marseille)
- H. Li (IHEP Beijing)
- C. Li (Liaoning Normal U.)
- Y. Liang (Guangxi U.)
- A. Libanov (Physics Department, MSU)
- J. Libby (Indian Inst. Tech., Madras)

Int. J. Mod. Phys. A 2026.41. Downloaded from www.worldscientific.com
by UNIVERSITY OF CALIFORNIA @ BERKELEY on 09/16/26. Re-use and distribution is strictly not permitted, except for Open Access articles.

- C. Lin (NYCU)
- T. Linden (Stockholm U.)
- E. Lisi (INFN, Bari)
- H. Liu (Lanzhou U.)
- J. Liu (SJTU)
- T. Liu (Guangxi U.)
- I. Logashenko (Budker Inst., Novosibirsk)
- H. Ma (IHEP Beijing)
- S. Maccolini (TU Dortmund)
- M. Madhavacheril (Pennsilvania U.)
- F. Mahmoudi (IP2I, Lyon)
- B. Maier (KIT)
- P. Malta (IFRJ)
- B. Mandelli (CERN)
- V. Mantovani (TU Munich)
- D. Manuzzi (CERN)
- R. Manzoni (ETH Zurich)
- Y. Maravin (CERN)
- M. Margoni (INFN, Padova)
- L. Mariscano (INFN, Genova)
- D. Marsh (King's Coll. London)
- R. Maruyama (Yale U.)
- N. Mavromatos (King's Coll. London)
- A. Mcdaniel (Clemson U.)
- J. Mcfayden (CERN)
- C. Melcher (Ticke College of Engineering, UT)
- R. Meril (Siegen U.)
- C.A. Meyer (Carnegie Mellon U.)
- C. Milardi (INFN, LNF)
- V. Mitsou (IFIC, Valencia)
- R. Mizuk (U. Paris-Saclay)
- R.N. Mohapatra (U. Maryland)
- P. Mohr (NIST)
- C. Mondino (CERN)
- G. Montefalcone (Texas U.)
- S. Moriyama (ICRR)
- B. Nachman (Stanford U.)
- S. Narison (Montpellier U.)
- I. Nasteva (CERN)
- K. Ng (CUHK)
- A. Nicholson (North Carolina U.)
- V. Nikolaenko (CERN)
- S. Nishida (KEK)
- T. Nomura (KEK)
- R. Novotny (CERN)
- A. Nucciotti (INFN, Milano-Bicocca)
- V. Obraztsov (IHEP, Protvino)
- O. Ozcelik (CERN)
- T. Pajero (Oxford U.)
- S. Pandey (MIT)
- D. Paneque (MPP, Garching)
- I. Papaphilippou (CERN)
- P. Pedroni (INFN, Pavia)
- J.R. Pelaez (UCM, Madrid)
- C. Pena (FNAL)
- A. Pereiro (Santiago de Compostela U.)
- S. Perez (UC Davis)
- F. Piccini (INFN, Pavia)
- A. Pilkington (Manchester U.)
- P. Piminov (Budker Inst., Novosibirsk)
- E. Pinetti (FNAL)
- A. Pinto Pinoargote (CEA/IRFU Saclay; LPNHE Paris)
- T. Plehn (Heidelberg U.)
- S. Polikarpov (MEPhI Moscow)
- A. Pompili (INFN, Bari)
- W. Porod (Würzburg U.)
- T. Potter (Cambridge U.)
- J. Pradler (HEPHY, Vienna)
- S. Prakhov (UC Los Angeles)
- S.A. Prell (Iowa State U.)
- M. Prim (CERN)
- P. Privitera (Chicago U.)
- S. Qian (IHEP Beijing)
- W. Qian (IHEP Beijing)
- A. Reimers (DESY, Hamburg)
- Z. Ren (CERN)
- F. Resnati (ETH Zurich)
- A. Rettaroli (INFN, LNF)
- J. Richard (IP2I, Lyon)
- J. Rico (ICREA, Barcelona; SISSA/INFN, Trieste)
- E. Rizvi (CERN)
- N. Rodd (LBNL)
- C. Rogers (STFC, Rutherford Appleton Lab.)
- Y. Rogovsky (Budker Inst., Novosibirsk)
- A. Romero Jorge (ITP, Frankfurt)
- G. Ruggiero (Lancaster U.)
- T. Saab (Florida State U.)
- K. Sakashita (KEK)
- R. Salerno (CNRS)
- S. Sanchez Cruz (CERN)
- J. Santiago (Granada U.)
- M. Sarsa (U. de Zaragoza)
- A. Schmidt (CERN)
- P. Schmidt-Wellenburg (PSI)
- R. Schoefbeck (HEPHY, Vienna)
- B. Schwingenheur (MPIK)
- S. Scorza (LPSC, Grenoble)
- T. Seifen (Bonn U.)
- S. Sekmen (CERN)
- S. Seo (FNAL)
- S. Serednyakov (Budker Inst., Novosibirsk)
- A.G. Shamov (Budker Inst., Novosibirsk)
- M. Shiozawa (ICRR)
- Y. Shirman (UC Irvine)
- J. Shu (School of Physics, Peking U.)
- D. Shwartz (Budker Inst., Novosibirsk)
- H. Sieber (ETH Zurich)
- M. Smy (UC Irvine)
- E. Spadaro (INFN, Milano-Bicocca)
- T. Spadaro (INFN, LNF)
- N. Spooner (Sheffield U.)
- M. Spurio (INFN, Bologna)
- I.W. Stewart (MIT)
- D. Stratakis (FNAL)
- A. Suzuki (LBNL)
- R. Tenchini (INFN, Pisa)
- R. Tesarek (FNAL)
- V. Tishchenko (BNL)
- M. Tobar (UWA, Perth)
- E. Todarello (Turin U.)
- S. Tolmachev (Kurchatov Inst.)
- D. Tonelli (Trieste U.)

Int. J. Mod. Phys. A 2026.41. Downloaded from www.worldscientific.com
by UNIVERSITY OF CALIFORNIA @ BERKELEY on 09/16/26. Re-use and distribution is strictly not permitted, except for Open Access articles.

- S. Troitsky (INR, Moscow)
- B. Tuchming (CEA/IRFU Saclay)
- G. Tuci (Heidelberg U.)
- J. Tyson (UC Davis)
- Y. Unno (KEK)
- P.L. Vahle (William and Mary Coll.)
- Z. Vallari (Ohio State U.)
- R. Van Kooten (Indiana U.)
- A. Vaquero (U. de Zaragoza)
- W. Verkerke (NIKHEF)
- M. Vesterinen (Warwick U.)
- M. Vieites (CERN)
- T. Virdee (Imperial Coll. Physics Dep.)
- E. Vitagliano (Padova U.)
- J. Vogel (CERN)
- M. Volpe (APC, Paris)
- K. Vos (Maastricht U.)
- M. Vos (IFIC, Valencia)
- E. Vryonidou (Manchester U.)
- A.P. Walker-Loud (LBNL)
- H. Wang (Stanford U.)
- J. Wang (MIT)
- M. Wang (INFN, Milano-Bicocca)
- S. Wang (IHEP Beijing)
- S. Wang (SWUST)
- Z. Wang (PMO, Nanjing)
- A. Watson (Leeds U.)
- F. Wietfeldt (Tulane U.)
- P. Winter (ANL)
- Y. Wu (CERN)
- M. Xiao (Zhejiang U.)
- Z. Xu (Columbia U.)
- K. Yamauchi (Tokyo U. of Science)
- H. Yan (Ningbo U.)
- H. Yang (USTC)
- L. Yang (Tsinghua U.)
- Q. Yang (Shenzhen U.)
- H. Yin (CERN)
- P. Yin (Nanjing U.)
- P. Yin (IHEP Beijing)
- W. Yin (Tokyo Metropolitan U.)
- K. Yokoya (KEK)
- S. Youn (IBS, Daejeon)
- A. Young (NCSU)
- D. Yu (Tsinghua U.)
- Q. Yue (Tsinghua U.)
- E. Zakharov (IKI RAS)
- Y. Zeng (IHEP Beijing)
- D. Zerwas (LAL Orsay)
- Z. Zhang (Wuhan U.)
- P. Zhao (TU Munich)
- N. Zhou (SJTU)
- Y. Zhu (USTC)
- K. Zioutas (CERN)

4 Naming scheme for hadrons

We introduced in the 1986 edition [3] a new naming scheme for the hadrons. Changes from older terminology affected mainly the heavier mesons made of u, d, and s quarks. Otherwise, the only important change to known hadrons was that the $F^{\pm}$ became the $D_s^{\pm}$. None of the lightest pseudoscalar or vector mesons changed names, nor did the $c\bar{c}$ or $b\bar{b}$ mesons (we do, however, now use χ_c for the $c\bar{c}$ χ states), nor did any of the established baryons. The Summary Tables give both the new and old names whenever a change has occurred.

In the 2018 edition [4], the naming scheme was extended to address the naming of charmonium and bottomonium states that were commonly referred to as X, Y, or Z states in the literature. The further discovery of various exotic hadron states — including in particular tetraquarks and pentaquarks containing $qq\bar{q}\bar{q}$ and $q\bar{q}qqq$ minimal quark content, respectively — rendered the 2018 extension insufficient. In the 2024 edition, the naming scheme was again revised and extended to cover all experimentally-known states. The current scheme is described in "Naming Scheme for Hadrons" (p. 155) of this *Review*. A table details the correspondence between the names newly adopted by the PDG and those that have previously appeared in the literature.

We give here our conventions on typesetting style. Particle symbols are italic (or slanted) characters: e^-, p, Λ, π^0, K_L, D_s^+, b. Charge is indicated by a superscript: B^-, Δ^{++}. Charge is not normally indicated for p, n, or the quarks, and is optional for neutral isosinglets: η or η^0. Antiparticles and particles are distinguished by charge for charged leptons and mesons: τ^+, K^-. Otherwise, distinct antiparticles are indicated by a bar (overline): $\overline{\nu}_\mu$, $\bar{t}$, $\overline{p}$, $\overline{K}^0$, and $\overline{\Sigma}^+$ (the antiparticle of the Σ^-).

5 Procedures

5.1 *Selection and treatment of data*

The Particle Listings contain all relevant data known to us that are published in journals. With very few exceptions, we do not include results from preprints or conference reports. Nor do we include data that are of historical importance only (the Listings are not an archival record). We search every volume of 30 journals through our cutoff date for relevant data. We also include later published papers that are sent to us by the authors (or others).

In the Particle Listings, we clearly separate measurements that are used to calculate or estimate values given in the Summary Tables from measurements that are not used. We give explanatory comments in many such cases. Among the reasons a measurement might be excluded are the following:

- It is superseded by or included in later results.
- No error is given.
- It involves assumptions we question.
- It has a poor signal-to-noise ratio, low statistical significance, or is otherwise of poorer quality than other data available.
- It is clearly inconsistent with other results that appear to be more reliable. Usually we then state the criterion, which sometimes is quite subjective, for selecting "more reliable" data for averaging. See Sec. 5.4.
- It is not independent of other results.
- It is not the best limit (see below).
- It is quoted from a preprint or a conference report.

In some cases, *none* of the measurements is entirely reliable and no average is calculated. For example, the masses of many of the baryon resonances, obtained from partial-wave analyses, are quoted as estimated ranges thought to probably include the true values, rather than as averages with errors. This is discussed in the Baryon Particle Listings.

For upper limits, we normally quote in the Summary Tables the strongest limit. We do not average or combine upper limits except in a very few cases where they may be re-expressed as measured numbers with Gaussian errors.

As is customary, we assume that particle and antiparticle share the same spin, mass, and mean life. The Tests of Conservation Laws table, following the Summary Tables, lists tests of CPT as well as other conservation laws.

We use the following indicators in the Particle Listings to tell how we get values from the tabulated measurements:

- OUR AVERAGE —From a weighted average of selected data.
- OUR FIT —From a constrained or overdetermined multiparameter fit of selected data.

Int. J. Mod. Phys. A 2026.41. Downloaded from www.worldscientific.com
by UNIVERSITY OF CALIFORNIA @ BERKELEY on 09/16/26. Re-use and distribution is strictly not permitted, except for Open Access articles.

- OUR EVALUATION —Not from a direct measurement, but evaluated from measurements of related quantities.
- OUR ESTIMATE —Based on the observed range of the data. Not from a formal statistical procedure.
- OUR LIMIT —For special cases where the limit is evaluated by us from measured ratios or other data. Not from a direct measurement.

An experimentalist who sees indications of new a particle will of course want to know what has been seen in that region in the past. Hence, we include in the Particle Listings all reported states that, in our opinion, have sufficient statistical merit and that have not been disproved by more reliable data. However, we promote to the Summary Tables only those states that we feel are well-established. This judgment is, of course, somewhat subjective and no precise criteria can be given. For more detailed discussions, see the reviews section on Particle Properties.

5.2 *Averages and fits*

We divide this discussion on obtaining averages and errors into three sections: (1) treatment of errors; (2) unconstrained averaging; (3) constrained fits.

5.2.1 *Treatment of errors*

In what follows, the "error" δx means that the range $x \pm \delta x$ is intended to be a 68.3% confidence interval about the central value x. We treat this error as if it were Gaussian. Thus, when the error *is* Gaussian, δx is the usual one standard deviation (1σ). Many experimenters now give statistical and systematic errors separately, in which case we usually quote both errors, with the statistical error first. For averages and fits, we then add the two errors in quadrature and use this combined error for δx.

When experimenters quote asymmetric errors $(\delta x)^+$ and $(\delta x)^-$ for a measurement x, the error that we use for that measurement in making an average or a fit with other measurements is a continuous function of these three quantities. When the resultant average or fit $\overline{x}$ is less than $x - (\delta x)^-$, we use $(\delta x)^-$; when it is greater than $x + (\delta x)^+$, we use $(\delta x)^+$. In between, the error we use is a linear function of x. Since the errors we use are functions of the result, we iterate to get the final result. Asymmetric output errors are determined from the input errors assuming a linear relation between the input and output quantities.

In fitting or averaging, we usually do not include correlations between different measurements, but we try to select data in such a way as to reduce correlations. Correlated errors are, however, treated explicitly when there are a number of results of the form $A_i \pm \sigma_i \pm \Delta$ that have identical systematic errors Δ. In this case, one can first average the $A_i \pm \sigma_i$ and then combine the resulting statistical error with Δ. One obtains, however, the same result by averaging $A_i \pm (\sigma_i^2 + \Delta_i^2)^{1/2}$, where $\Delta_i = \sigma_i \Delta [\sum (1/\sigma_j^2)]^{1/2}$. This procedure has the advantage that, with the modified systematic errors Δ_i, each measurement may be treated as independent and averaged in the usual way with other data. Therefore, when appropriate, we adopt this procedure. We tabulate Δ and invoke an automated procedure that computes Δ_i before averaging.

Another common case of correlated errors occurs when experimenters measure two quantities and then quote the two and their difference, *e.g.*, m_1, m_2, and $\Delta = m_2 - m_1$. We cannot enter all of m_1, m_2 and Δ into a constrained fit because they are not independent. In some cases, it is a good approximation to ignore the quantity with the largest error and put the other two into the fit. However, in some cases correlations are such that the errors on m_1, m_2 and Δ are comparable and none of the three values can be ignored. In this case, we put all three values into the fit and invoke an automated procedure to increase the errors prior to fitting such that the three quantities can be treated as independent measurements in the constrained fit. We include a note saying that this has been done.

5.2.2 *Unconstrained averaging*

To average data, we use a standard weighted least-squares procedure and in some cases, discussed below, increase the errors with a "scale factor." We begin by assuming that measurements of a given quantity are uncorrelated, and calculate a weighted average and error as

$$\overline{x} \pm \delta\overline{x} = \frac{\sum_i w_i\, x_i}{\sum_i w_i} \pm \left(\sum_i w_i\right)^{-1/2} , \qquad (1)$$

where

$$w_i = 1/(\delta x_i)^2 .$$

Here x_i and δx_i are the value and error reported by the ith experiment, and the sums run over the N experiments. We then calculate $\chi^2 = \sum w_i(\overline{x} - x_i)^2$ and compare it with $N-1$, which is the expectation value of χ^2 if the measurements are from a Gaussian distribution.

If $\chi^2/(N-1)$ is less than or equal to 1, and there are no known problems with the data, we accept the results.

If $\chi^2/(N-1)$ is very large, we may choose not to use the average at all. Alternatively, we may quote the calculated average, but then make an educated guess of the error, a conservative estimate designed to take into account known problems with the data.

Finally, if $\chi^2/(N-1)$ is greater than 1, but not greatly so, we still average the data, but then also do the following:

(a) We increase our quoted error, $\delta\overline{x}$ in Eq. (1), by a scale factor S defined as

$$S = \left[\chi^2/(N-1)\right]^{1/2} . \qquad (2)$$

Our reasoning is as follows. The large value of the χ^2 is likely to be due to underestimation of errors in at least one of the experiments. Not knowing which of the errors are underestimated, we assume they are all underestimated by the same factor S. If we scale up all the input errors by this factor, the χ^2 becomes $N-1$, and of course the output error $\delta\overline{x}$ scales up by the same factor. See Ref. [5].

When combining data with widely varying errors, we modify this procedure slightly. We evaluate S using only the experiments with smaller errors. Our cutoff or ceiling on δx_i is arbitrarily chosen to be

$$\delta_0 = 3N^{1/2}\, \delta\overline{x} ,$$

where $\delta\overline{x}$ is the unscaled error of the mean of all the experiments. Our reasoning is that although the low-precision experiments have little influence on the values $\overline{x}$ and $\delta\overline{x}$, they can make significant contributions to the χ^2, and the contribution of the high-precision experiments thus tends to be obscured. Note that if each experiment has the same error δx_i, then $\delta\overline{x}$ is $\delta x_i/N^{1/2}$, so each δx_i is well below the cutoff. (More often, however, we simply exclude measurements with relatively large errors from averages and fits: new, precise data chase out old, imprecise data.)

Our scaling procedure has the property that if there are two values with comparable errors separated by much more than their stated errors (with or without a number of other values of lower accuracy), the scaled-up error $\delta\,\overline{x}$ is approximately half the interval between the two discrepant values.

We emphasize that our scaling procedure for *errors* in no way affects central values. And if you wish to recover the unscaled error $\delta\overline{x}$, simply divide the quoted error by S.

(b) If the number M of experiments with an error smaller than δ_0 is at least three, and if $\chi^2/(M-1)$ is greater than 1.25, we show in the Particle Listings an ideogram of the data. Figure 1 is an example. Sometimes one or two data points lie apart from the main body; other times the data split into two or more groups. We extract no numbers from these ideograms; they are simply visual aids, which the reader may use as they see fit.

Each measurement in an ideogram is represented by a Gaussian with a central value x_i, error δx_i, and area proportional to $1/\delta x_i$. The choice of $1/\delta x_i$ for the area is somewhat arbitrary. With this choice, the center of gravity of the ideogram corresponds to an average that uses weights $1/\delta x_i$ rather than the $(1/\delta x_i)^2$ actually used in the averages. This may be appropriate when some of the experiments have seriously underestimated systematic errors. However, since for this choice of area the height of the Gaussian for each measurement is proportional to $(1/\delta\, x_i)^2$, the peak position of the ideogram will often favor the high-precision measurements at least as much as does the least-squares average. See our 1986 edition [3] for a detailed discussion of the use of ideograms.

Int. J. Mod. Phys. A 2026.41. Downloaded from www.worldscientific.com
by UNIVERSITY OF CALIFORNIA @ BERKELEY on 09/16/26. Re-use and distribution is strictly not permitted, except for Open Access articles.

5.2.3 *Constrained fits*

In some cases, such as branching ratios or masses and mass differences, a constrained fit may be needed to obtain the best values of a set of parameters. For example, most branching ratios and rate measurements are analyzed by making a simultaneous least-squares fit to all the data and extracting the partial decay fractions P_i, the partial widths Γ_i, the full width Γ (or mean life), and the associated error matrix.

Assume, for example, that a state has m partial decay fractions P_i, where $\sum P_i = 1$. These have been measured in N_r different ratios R_r, where, e.g., $R_1 = P_1/P_2$, $R_2 = P_1/P_3$, *etc.* [We can handle any ratio R of the form $\sum \alpha_i P_i / \sum \beta_i P_i$, where α_i and β_i are constants, usually 1 or 0. The forms $R = P_i P_j$ and $R = (P_i P_j)^{1/2}$ are also allowed.] Further, assume that *each* ratio R has been measured by N_k experiments (we designate each experiment with a subscript k, e.g., R_{1k}). We then find the best values of the fractions P_i by minimizing the χ^2 as a function of the $m-1$ independent parameters:

$$\chi^2 = \sum_{r=1}^{N_r} \sum_{k=1}^{N_k} \left(\frac{R_{rk} - R_r}{\delta R_{rk}} \right)^2 , \tag{3}$$

where the R_{rk} are the measured values and R_r are the fitted values of the branching ratios.

In addition to the fitted values $\overline{P}_i$, we calculate an error matrix $\langle \delta \overline{P}_i \ \delta \overline{P}_j \rangle$. We tabulate the diagonal elements of $\delta \overline{P}_i = \langle \delta \overline{P}_i \ \delta \overline{P}_i \rangle^{1/2}$ (except that some errors are scaled as discussed below). In the Particle Listings, we give the complete correlation matrix; we also calculate the fitted value of each ratio, for comparison with the input data, and list it above the relevant input, along with a simple unconstrained average of the same input.

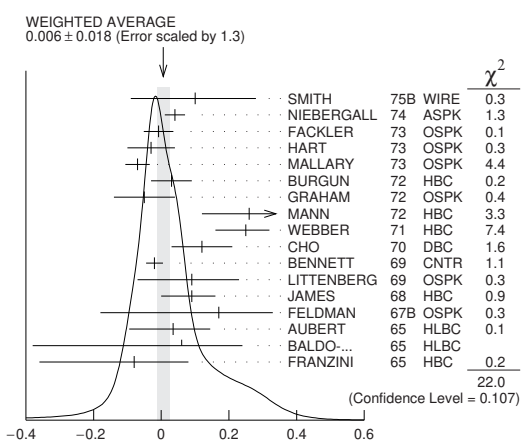

Figure 1: A typical ideogram. The arrow at the top shows the position of the weighted average, while the width of the shaded pattern shows the error in the average after scaling by the factor S. The column on the right gives the χ^2 contribution of each of the experiments. Note that the next-to-last experiment, denoted by the incomplete error flag ($\perp$), is not used in the calculation of S (see the text).

Three comments on the example above:

(1) There was no connection assumed between measurements of the full width and the branching ratios. But often we also have information on partial widths Γ_i as well as the total width Γ. In this case we must introduce Γ as a parameter in the fit, along with the P_i, and we give correlation matrices for the widths in the Particle Listings.

(2) We try to pick those ratios and widths that are as independent and as close to the original data as possible. When one experiment measures all the branching fractions and constrains their sum to be one, we leave one of them (usually the least well-determined one) out of the fit to make the set of input data more nearly independent. We now do allow for correlations between input data.

(3) We calculate scale factors for both the R_r and P_i when the measurements for any R give a larger-than-expected contribution to the χ^2. According to Eq. (3), the double sum for χ^2 is first summed over experiments $k = 1$ to N_k, leaving a single sum over ratios $\chi^2 = \sum \chi_r^2$. One is tempted to define a scale factor for the ratio r as $S_r^2 = \chi_r^2 / \langle \chi_r^2 \rangle$. However, since $\langle \chi_r^2 \rangle$ is not a fixed quantity (it is somewhere between N_k and N_{k-1}), we do not know how to evaluate this expression. Instead, we define

$$S_r^2 = \frac{1}{N_k} \sum_{k=1}^{N_k} \frac{\left(R_{rk} - \overline{R}_r \right)^2}{\langle (R_{rk} - \overline{R}_r)^2 \rangle}. \tag{4}$$

With this definition the expected value of S_r^2 is one. We can show that

$$\langle (R_{rk} - \overline{R}_r)^2 \rangle = \langle (\delta R_{rk})^2 \rangle - (\delta \overline{R}_r)^2, \tag{5}$$

where $\delta \overline{R}_r$ is the fitted error for ratio r.

The fit is redone using errors for the branching ratios that are scaled by the larger of S_r and unity, from which new and often larger errors $\delta \overline{P}_i{}'$ are obtained. The scale factors we finally list in such cases are defined by $S_i = \delta \overline{P}_i{}' / \delta \overline{P}_i$. However, in line with our policy of not letting S affect the central values, we give the values of $\overline{P}_i$ obtained from the original (unscaled) fit.

There is one special case in which the errors that are obtained by the preceding procedure may be changed. When a fitted branching ratio (or rate) $\overline{P}_i$ turns out to be less than three standard deviations ($\delta \overline{P}_i{}'$) from zero, a new smaller error $(\delta \overline{P}_i{}'')^-$ is calculated on the low side by requiring the area under the Gaussian between $\overline{P}_i - (\delta \overline{P}_i{}'')^-$ and $\overline{P}_i$ to be 68.3% of the area between zero and $\overline{P}_i$. A similar correction is made for branching fractions that are within three standard deviations of one. This keeps the quoted errors from overlapping the boundary of the physical region.

5.3 *Rounding*

While the results shown in the Particle Listings are usually exactly those published by the experiments, the numbers that appear in the Summary Tables (means, averages and limits) are subject to a set of rounding rules.

The basic rule states that if the three highest order digits of the error lie between 100 and 354, we round to two significant digits. If they lie between 355 and 949, we round to one significant digit. Finally, if they lie between 950 and 999, we round up to 1000 and keep two significant digits. In all cases, the central value is given with a precision that matches that of the error. So, for example, the result (coming from an average) 0.827 ± 0.119 would appear as 0.83 ± 0.12, while 0.827 ± 0.367 would turn into 0.8 ± 0.4.

In cases where there are asymmetric errors, if these errors differ by less than 10 percent of the average of the two errors, the average is instead used as a symmetric error in the displayed result and the rounding is determined by this average. Otherwise, the narrower of the two asymmetric errors is used to determine the rounding on both.

Rounding of this form is also performed on the value of limits that come from calculations (but not on limits that are directly taken from a single source).

Finally, we should point out that in several instances, when a group of results come from a single fit to a set of data, we have chosen to keep two significant digits for all the results. This happens, for instance, for several properties of the W and Z bosons and the τ lepton.

5.4 *Discussion*

The problem of averaging data containing discrepant values is nicely discussed by Taylor in Ref. [6]. He considers a number of algorithms that attempt to incorporate inconsistent data into a meaningful average. However, it is difficult to develop a procedure that handles simultaneously in a reasonable way two basic types of situations: (a) data that lie apart from the main body of the data are incorrect (contain unreported errors); and (b) the opposite—it is the main body of data that is incorrect. Unfortunately, as Taylor shows, case (b) is not infrequent. He concludes that the

Int. J. Mod. Phys. A 2026.41. Downloaded from www.worldscientific.com
by UNIVERSITY OF CALIFORNIA @ BERKELEY on 09/16/26. Re-use and distribution is strictly not permitted, except for Open Access articles.

choice of procedure is less significant than the initial choice of data to include or exclude.

We place much emphasis on this choice of data. Often we solicit the help of outside experts (consultants). Sometimes, however, it is simply impossible to determine which of a set of discrepant measurements are correct. Our scale-factor technique is an attempt to address this ignorance by increasing the error. In effect, we are saying that present experiments do not allow a precise determination of this quantity because of unresolvable discrepancies, and one must await further measurements. The reader is warned of this situation by the size of the scale factor, and if they desire can go back to the literature (via the Particle Listings) and redo the average with a different choice of data.

Our situation is less severe than most of the cases Taylor considers, such as estimates of the fundamental constants like $\hbar$, *etc.* Most of the errors in his case are dominated by systematic effects. For our data, statistical errors are often at least as large as systematic errors, and statistical errors are usually easier to estimate. A notable exception occurs in partial-wave analyses, where different techniques applied to the same data yield different results. In this case, as stated earlier, we often do not make an average but just quote a range of values.

A brief history of early Particle Data Group averages is given in Ref. [5]. Our History Plots show the time evolution of some of our values of a few particle properties. Sometimes large changes occur. These usually reflect the introduction of significant new data or the discarding of older data. Older data are discarded in favor of newer data when it is felt that the newer data have smaller systematic errors, or have more checks on systematic errors, or have made corrections unknown at the time of the older experiments, or simply have much smaller errors. Sometimes, the scale factor becomes large near the time at which a large jump takes place, reflecting the uncertainty introduced by the new and inconsistent data. By and large, however, a full scan of our history plots shows a dull progression toward greater precision at central values quite consistent with the first data points shown.

We conclude that the reliability of the combination of experimental data and our averaging procedures is usually good, but it is important to be aware that fluctuations outside of the quoted errors can and do occur.

ACKNOWLEDGMENTS

The publication of the *Review of Particle Physics* is supported by the Director, Office of Science, Office of High Energy Physics of the U.S. Department of Energy under Contract No. DE–AC02–05CH11231; by an implementing arrangement between the governments of Japan (MEXT: Ministry of Education, Culture, Sports, Science and Technology, and KEK: High Energy Accelerator Research Organization) and the United States (DOE) on cooperative research and development; by the Italian National Institute of Nuclear Physics (INFN); and by the European Laboratory for Particle Physics (CERN). Individual collaborators receive support for their PDG activities from their respective institutes or funding agencies.

We thank all those who have assisted in the many phases of preparing this *Review*. We particularly thank the many who have responded to our requests for verification of data entered in the Listings, and those who have made suggestions or pointed out errors.

We are grateful to the staff at CERN, DESY, IHEP Beijing, KEK, LBNL, NISER and UNIFAL who take care of the mailing and distribution of our products.

This work used resources of the National Energy Research Scientific Computing Center, a DOE Office of Science User Facility supported by the Office of Science of the U.S. Department of Energy under Contract No. DE-AC02-05CH11231.

References

[1] The previous edition was: S. Navas *et al.* (Particle Data Group), Phys. Rev. **D110**, 030001 (2024).

[2] C. Patrignani *et al.* (Particle Data Group), Chin. Phys. **C40**, 10, 100001 (2016).

[3] M. Aguilar-Benitez *et al.* (Particle Data Group), Phys. Lett. **170B**, 1 (1986).

[4] M. Tanabashi *et al.* (Particle Data Group), Phys. Rev. D **98**, 3, 030001 (2018).

[5] A. H. Rosenfeld, Ann. Rev. Nucl. Part. Sci. **25**, 555 (1975).

[6] B.N. Taylor, "Numerical Comparisons of Several Algorithms for Treating Inconsistent Data in a Least-Squares Adjustment of the Fundamental Constants," U.S. National Bureau of Standards NBSIR 81-2426 (1982).

Int. J. Mod. Phys. A 2026.41. Downloaded from www.worldscientific.com
by UNIVERSITY OF CALIFORNIA @ BERKELEY on 09/16/26. Re-use and distribution is strictly not permitted, except for Open Access articles.

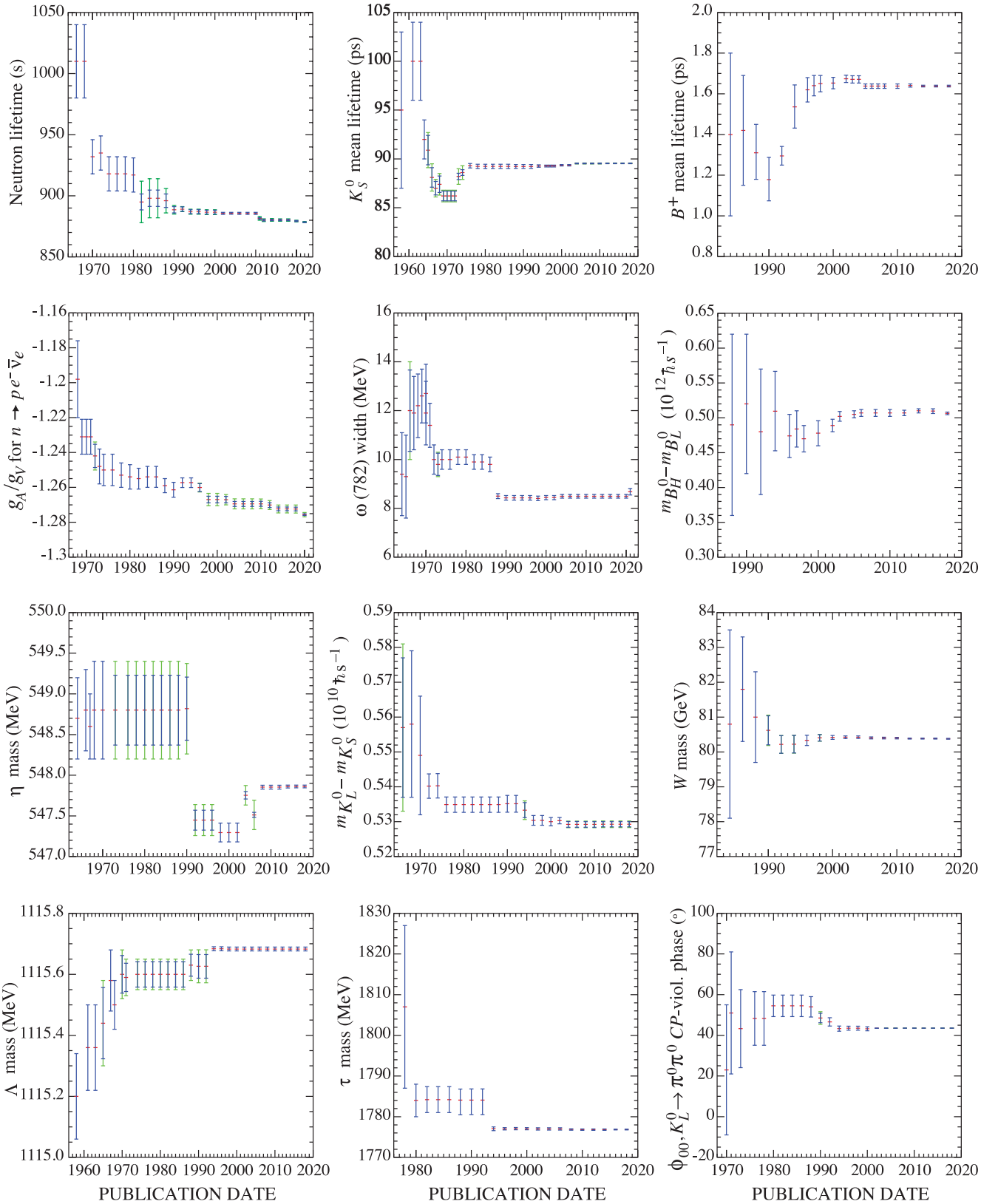

Figure 1: A historical perspective of values of a few particle properties tabulated in this *Review* as a function of date of publication of the *Review*. A full error bar indicates the quoted error; a thick-lined portion indicates the same but without the "scale factor."

Int. J. Mod. Phys. A 2026.41. Downloaded from www.worldscientific.com
by UNIVERSITY OF CALIFORNIA @ BERKELEY on 09/16/26. Re-use and distribution is strictly not permitted, except for Open Access articles.

Online Particle Physics Information

Revised March 2026 by K. Assamagan (BNL) and H.B. O'Connell (FNAL).

1	Introduction	22
2	Particle Data Group (PDG) resources	22
3	Particle physics information platform	22
4	Literature databases	22
5	Journals	23
6	Conference and seminars databases	23
7	Research institutions	23
8	People	23
9	Experiments	23
10	Jobs	23
11	Software packages and repositories	24
12	Data repositories and preservation	24
13	Particle physics education and outreach	24
14	Regional HEP efforts	24

1 Introduction

Online resources are used in a diverse and expanding set of ways in particle physics. Many of these resources have become central to our collective work. We provide a brief curated selection of the major resources here. An expanded and regularly updated online repository is referred to below and can be found at

`https://github.com/particledatagroup/hep-resources`

By contrast, it is meant to be inclusive and catalog all useful resources related to particle physics. The community is warmly invited to contribute in order to ensure a broad and up to date coverage of relevant resources. Practical details are available online.

2 Particle Data Group (PDG) resources

- **Review of Particle Physics (RPP):** A comprehensive report on the fields of particle physics and related areas of cosmology and astrophysics, including both review articles and a compilation/evaluation of data on particle properties. The review section includes articles, tables and plots on a wide variety of theoretical and experimental topics of interest to particle physicists and astrophysicists. The particle properties section provides tables of published measurements as well as the Particle Data Group's best values and limits for particle properties such as masses, widths, lifetimes, and branching fractions, as well as an extensive summary of searches for hypothetical particles. RPP is published as a large book every two years, with partial updates made available once each year on the web.

  All the contents of the book version of RPP are available online:

  `https://pdg.lbl.gov`

  The printed book can be ordered:

  `https://pdg.lbl.gov/order`

  Of historical interest is the complete RPP collection which can be found online:

  `https://pdg.lbl.gov/publications`

- **Particle Physics booklet:** An abridged version of the Review of Particle Physics, available as a pocket-sized 250-page booklet. It is one of the most useful summaries of physics data. The booklet contains an abbreviated set of reviews and the summary tables from the most recent edition of the Review of Particle Physics.

  The PDF file of the booklet can be downloaded:

  `https://pdg.lbl.gov/current/booklet.pdf`

  The printed booklet can be ordered:

  `https://pdg.lbl.gov/order`

  A mobile version of the booklet is also available:

  `https://pdg.lbl.gov/booklet`

- **PDGLive:** A web application for browsing the contents of the PDG database that contains the information published in the Review of Particle Physics. It allows one to navigate to a particle of interest, see a summary of the information available, and then proceed to the detailed information published in the Review of Particle Physics. Data entries are directly linked to the corresponding bibliographic information in INSPIRE.

  `https://pdglive.lbl.gov`

- **Computer-readable files:** Data files that can be downloaded from the PDG include tables of particle masses and widths, PDG Monte Carlo particle numbers, and cross-section data. The files are updated with each new edition of the Review of Particle Physics.

  `https://pdg.lbl.gov/files`

- **PDG API:** In addition to the fixed-format data files that have been available for many years, PDG is developing new tools to access PDG data in machine-readable format (currently available as beta versions).

  `https://pdg.lbl.gov/api`

3 Particle physics information platform

INSPIRE: INSPIRE serves as a one-stop information platform for the particle physics community, comprising interlinked databases on literature, authors, jobs, seminars, conferences, institutions and experiments (each described in more detail below). Run in collaboration by CERN (which hosts INSPIRE), DESY, Fermilab, IHEP, IN2P3, SLAC and TIB, it has been serving the scientific community for almost 60 years. Previously hosted at SLAC and known as SPIRES, in December 1991 it became the first website outside Europe and the first database on the web. Close interaction with the user community and with arXiv, ADS, HEPData, ORCID, PDG, ROR and publishers is the backbone of INSPIRE's evolution. Since 2020, it is running on a modernized platform that is continually being improved.

`https://inspirehep.net/`

4 Literature databases

Most research articles in the field of high-energy physics are first made available on the arXiv eprint server, where researchers can learn about the latest developments by browsing through the new announcements five days a week. They are indexed, together with all other publications in high-energy physics and related fields, in the INSPIRE literature collection. For neighboring fields such as astrophysics or mathematics, other databases are more exhaustive.

- **ADS:** The SAO/NASA Astrophysics Data System is a Digital Library portal that maintains four bibliographic collections covering astronomy and astrophysics (including heliophysics and planetary science), physics, Earth science, and general science, containing more than 28 million records, including all arXiv e-prints. The ADS search engine also indexes the full-text for many publications in this collection and tracks citations. The system also provides access and links to a wealth of external resources, including electronic articles hosted by publishers and arXiv, data catalogs and a variety of data products hosted by the astronomy archives worldwide. The ADS can be accessed at:

  `http://ads.harvard.edu/`

- **arXiv.org:** A repository of full-text articles in physics, astronomy, mathematics, computer science, statistics, nonlinear sciences, quantitative finance, quantitative biology, electrical engineering and systems science, and economics. Papers are submitted by registered authors to arXiv, often as preprints in advance of submission to a journal for publication; includes postprints, working papers, and other relevant material. Established in 1991, the repository is interlinked with ADS and INSPIRE, among others. Readers can browse subject categories or search by author, title, abstract, date, and other fields. Receive daily update alerts for subfields by email or RSS.

  `https://arXiv.org`

- **INSPIRE Literature:** The literature collection, the flagship of the INSPIRE suite. Its almost 2 million literature records cover high energy physics, astrophysics, gravitation and cosmology, nuclear physics, quantum information science

Int. J. Mod. Phys. A 2026.41. Downloaded from www.worldscientific.com
by UNIVERSITY OF CALIFORNIA @ BERKELEY on 09/16/26. Re-use and distribution is strictly not permitted, except for Open Access articles.

and other related fields. Records offer a growing number of full-text articles attached and metadata including author affiliations, abstracts, references, experiments, keywords as well as links to arXiv, ADS, PDG, HEPData, publisher platforms and other servers. It provides fast metadata searches that can be easily refined using facets, plots extracted from full text, author disambiguation, author profile pages and citation analysis.

`https://inspirehep.net/literature`

- **MathSciNet:** This database of almost 4 million items provides reviews, abstracts and bibliographic information for much of the mathematical sciences literature. Over 125,000 new items, most of them classified according to the Mathematics Subject Classification, and more than 90,000 reviews of the current published literature are added each year. Author identification allows users to search for publications by author and citation data allows users to track the history and influence of research publications.

  `https://www.ams.org/mathscinet`

  OSTI.GOV: A portal to free, publicly available DOE-sponsored R&D results including technical reports, bibliographic citations, journal articles, conference papers, books, multimedia and data information. It consolidates OSTI's home page and the now-retired primary search tool SciTech Connect. It contains over 4 million records, including records for 2 million journal articles, 1 million of which have digital object identifiers (DOIs) linking to full-text articles on publishers' websites.

  `https://www.osti.gov/`

5 Journals

- **CERN Journal List:** This list of journals and conference series publishing particle physics content provides information on Open Access, copyright policies and terms of use for CERN authors.

  `https://scientific-info.cern/submit-and-publish/publish-open-access`

- **INSPIRE Journals:** A database of almost 4,000 journals relevant to HEP and related fields. Each entry displays the papers published in the journal that are included in the INSPIRE Literature database.

  `https://inspirehep.net/journals`

- **SCOAP^3 Journals:** A list of journals currently financed by the SCOAP^3 consortium. All HEP publications in those journals are made freely available under Open Access conditions at no cost for the authors.

  `https://scoap3.org/journals-2025-2027/`

6 Conference and seminars databases

- **INSPIRE Conferences:** The database of more than 31,000 past, present, and future conferences, schools, and meetings relevant to high-energy physics and related fields is searchable by title, acronym, series, date and location. Included are information about published proceedings, links to conference contributions in the INSPIRE HEP database, and links to the conference website when available. New conferences can be submitted from the entry page.

  `https://inspirehep.net/conferences`

- **INSPIRE Seminars:** Created to support the surge of online seminars during the COVID-19 pandemic, this database already contains more than 3,400 seminars in high-energy physics and related fields. Seminars can be filtered by date, series and subject and exported to a calendar. Direct links to join the online seminar and external resources are included. All seminars are community-maintained and can be submitted from the entry page.

  `https://inspirehep.net/seminars`

- **researchseminars.org:** A list of research seminars and conferences, organized by topic and seminars series or conference.

  `https://researchseminars.org/`

7 Research institutions

- **INSPIRE Institutions:** INSPIRE Institutions contains over 12,000 institutes, laboratories, and universities, where research on particle physics and astrophysics is led. Every record includes, whenever possible, as detailed information, such as address, web links, experiments, and links to INSPIRE papers authored by people affiliated to that institution. One can search for a particular institution by name, acronym, and location.

  `https://inspirehep.net/institutions`

- **Research Organization Registry (ROR):** The Research Organization Registry (ROR) is a global, community-led registry of open persistent identifiers for research organizations. It includes IDs and metadata for more than 120,000 organizations and counting. Registry updates are curated through a community process and released on a rolling basis.

  `https://ror.org/`

8 People

- **INSPIRE Authors:** Searchable worldwide database of more than a hundred thousand active, departed, retired, and deceased people associated with particle physics and related fields. The affiliation history of these researchers, their e-mail addresses, ORCIDs, web pages, experiments they participated in, PhD advisor, information on their graduate students and links to their papers and seminars are provided, as well as a user interface to update this information.

  `https://inspirehep.net/authors`

- **ORCID**: Registry providing persistent digital identifiers allowing to unambiguously identify researchers. Through integration in key research workflows such as manuscript and grant submission, it supports automated linkages between scientists and their professional activities ensuring that their work is recognized.

  `https://orcid.org`

9 Experiments

- **INSPIRE Experiments:** Contains almost 4,000 past, present, and future experiments in particle physics. It lists and classifies both accelerator and non-accelerator experiments as well as theory collaborations. Includes official experiment name and number, location, and collaboration lists. Simple searches by participant, title, experiment number, institution, date approved, accelerator, or detector, return a description of the experiment, including a complete list of authors, title, overview of the experiment's goals and methods, and a link to the experiment's web page if available. Recently, it has expanded its scope to include particle accelerators besides experiments and to link them together.

  `https://inspirehep.net/experiments`

- **Cosmic ray/Gamma ray/Neutrino and similar experiments:** This extensive collection of experiment websites is organized by focus of study and by location. Additional sections link to educational materials, organizations, and other useful resources. The site is maintained at the Max Planck Institute for Nuclear Physics, Heidelberg.

  `https://www.mpi-hd.mpg.de/hfm/CosmicRay/CosmicRaySites.html`

- **Wikipedia particle experiments:** A list of particle experiments with Wikipedia pages.

  `https://en.wikipedia.org/wiki/Category:Particle_experiments`

10 Jobs

- **AAS Job Register:** The American Astronomical Society publishes once a month graduate, postgraduate, faculty and other positions mainly in astronomy and astrophysics.

  `https://jobregister.aas.org/`

- **Academic Jobs Online:** A full-service online recruiting site for academic institutions worldwide in all disciplines and areas.

  `https://academicjobsonline.org/`

Int. J. Mod. Phys. A 2026.41. Downloaded from www.worldscientific.com
by UNIVERSITY OF CALIFORNIA @ BERKELEY on 09/16/26. Re-use and distribution is strictly not permitted, except for Open Access articles.

- **APS Careers:** A gateway for physicists, students, and physics enthusiasts to information about physics jobs and careers. It contains Physics job listings, career advice, upcoming workshops and meetings, and career and job-related resources provided by the American Physical Society.
  `https://www.aps.org/careers`
- **INSPIRE Jobs:** Lists academic and research jobs in high energy physics, nuclear physics, accelerator physics and astrophysics with the option to post a job or to receive email notices of new job listings. Several hundreds of jobs are listed all year round, with more activity during the application season.
  `https://inspirehep.net/jobs`
- **IOP Careers:** Career information and resources primarily aimed at university students are provided by the UK Institute of Physics.
  `https://www.iop.org/careers-physics/your-future-with-physics`
- **Physics Today Jobs:** Online recruitment advertising website for Physics Today magazine, published by the American Institute of Physics. Physics Today Jobs is the managing partner of the AIP Career Network, an online job board network for the physical science, engineering, and computing disciplines. Over 6,000 resumes are currently available, and nearly 5,000 jobs were posted in 2018.
  `https://jobs.physicstoday.org/`
- **Physicsworld Jobs:** A recruitment service run by IOP Publishing that connects employers from different industry sectors with jobseekers who have a background in physics and engineering.
  `https://www.physicsworldjobs.com/`

11 Software packages and repositories

A vast number of software tools are used for various aspects of high-energy physics research. Due to their number, their often specialized purpose and the quickly-changing nature of software, no attempt has been made to present them in this chapter. The accompanying online version contains an extensive categorized list of software.

12 Data repositories and preservation

Initiatives to preserve and disseminate data produced during different stages of research, from Monte Carlo events to machine-readable versions of tables in papers, have grown in recent years. Unfortunately, there currently exists no central resource aggregating all these data as is the case for the more established means of scholarly communication. Instead, there are a number of repositories targeting different types of data and research subjects. They are listed in the online version.

13 Particle physics education and outreach

Particle physics public engagement efforts are widespread, with laboratories, experiments, universities and individual researchers engaged in a range of efforts. The online version of this chapter provides links to resources for particle physicists wanting to become engaged in public education as well as resources that physicists can provide directly to students, teachers or lay people. There are classroom activities, interactive websites, films, and direct links to education offices at institutions and experiments. Many researchers also engage the public via a variety of social media platforms. Additionally, a selection of news sites relevant for experts and for the general public are provided.

14 Regional HEP efforts

The online version of this chapter provides links to summaries of regional HEP activities across Europe, Japan, the US, Africa, Latin America, and other regions that may be classified as developing or emerging. This list of summaries is not exhaustive and is based on the expert knowledge of the authors at the time of information gathering; the narrative was developed in July 2023 and will require periodic updates as the HEP landscape changes.

SUMMARY TABLES OF PARTICLE PHYSICS

Gauge and Higgs bosons 27
Leptons 30
Quarks 34
Mesons 35
Baryons 99
Searches not in Other Sections* 119
Tests of conservation laws 121

Meson Quick Reference Table 97
Baryon Quick Reference Table 98

Int. J. Mod. Phys. A 2026.41. Downloaded from www.worldscientific.com
by UNIVERSITY OF CALIFORNIA @ BERKELEY on 09/16/26. Re-use and distribution is strictly not permitted, except for Open Access articles.

* There are also search limits in the Summary Tables for the Gauge and Higgs Bosons, the Leptons, the Quarks, and the Mesons.

Int. J. Mod. Phys. A 2026.41. Downloaded from www.worldscientific.com
by UNIVERSITY OF CALIFORNIA @ BERKELEY on 09/16/26. Re-use and distribution is strictly not permitted, except for Open Acces

Int. J. Mod. Phys. A 2026.41. Downloaded from www.worldscientific.com
by UNIVERSITY OF CALIFORNIA @ BERKELEY on 09/16/26. Re-use and distribution is strictly not permitted, except for Open Access articles.

SUMMARY TABLES OF PARTICLE PROPERTIES

Extracted from the Particle Listings of the
Review of Particle Physics
F. Takahashi *et al.* (Particle Data Group),
Int. J. Mod. Phys. A **41**, 2630011 (2026)
Available at `https://pdg.lbl.gov`

Particle Data Group

F. Takahashi, K. Hikasa, Y. Sumino, M. Tanabashi, J. Tanaka, M. Yokoyama, K. Agashe, G. Aielli, B.C. Allanach, J. Alvarez-Muñiz, C. Amsler, M. Antonelli, E.C. Aschenauer, D.M. Asner, K. Assamagan, H. Baer, Sw. Banerjee, R.M. Barnett, L. Baudis, C.W. Bauer, J. Beringer, A. Bettini, O. Biebel, K.M. Black, E. Blucher, R. Bonventre, R.A. Briere, A. Buckley, V.D. Burkert, M.A. Bychkov, G. Cacciapaglia, R.N. Cahn, F. Canelli, J. Cao, Z. Cao, M. Carena, G. Casarosa, A. Ceccucci, M. Cepeda, A. Cerri, R.S. Chivukula, M. Cortês, G. Cowan, V. Crede, O. Cremonesi, G. D'Ambrosio, T. Damour, C.T.H. Davies, J. de Blas, D. de Florian, A. de Gouvêa, T. DeGrand, Z. Demiragli, S. Dittmaier, B.A. Dobrescu, M. D'Onofrio, M. Dorigo, H.K. Dreiner, J.M. Duarte, P. Eerola, U. Egede, A.X. El-Khadra, J. Ellis, S.C. Eno, J. Erler, A. Fava, W. Fetscher, B.D. Fields, A. Freitas, H. Gallagher, P. Gasik, T. Gershon, T. Gherghetta, S. Giovannella, M.C. Gonzalez-Garcia, M. Goodman, C. Grab, A.V. Gritsan, C. Grojean, D.E. Groom, M. Grünewald, A. Gurtu, T. Gutsche, H.E. Haber, M. Hamel, C. Hanhart, S. Hashimoto, Y. Hayato, A. Hebecker, S. Heinemeyer, J.J. Hernández-Rey, D.W. Hertzog, J. Hisano, A. Höcker, M. Hoferichter, W. Hofmann, J. Holder, L. Hsu, J. Huston, T. Hyodo, Al. Ianni, M. Kado, J. Kaplon, M. Karliner, U.F. Katz, M. Kenzie, V.A. Khoze, S.R. Klein, A. Knue, R. Kogler, G. Kramberger, M. Kramer, F. Krauss, M. Kreps, J. Kretzschmar, P. Krian, Y. Kwon, O. Lahav, L.P. Lellouch, J. Lesgourgues, A.R. Liddle, Z. Ligeti, C.-J. Lin, C. Lippmann, T.M. Liss, L. Lista, A. Lister, L. Littenberg, C. Lourenço, K.S. Lugovsky, S.B. Lugovsky, A. Lusiani, Y. Makida, F. Maltoni, A.V. Manohar, A. Masoni, S. Meinel, U.-G. Meißner, I.-A. Melzer-Pellmann, P. Mertsch, M. Mikhasenko, D.J. Miller, D. Milstead, R.E. Mitchell, K. Mönig, P. Molaro, F. Moortgat, N. Nagata, K. Nakamura, P. Nason, S. Navas, A. Nelles, M. Neubert, Y. Nir, H.B. O'Connell, C.A.J. O'Hare, K.A. Olive, C. Patrignani, J.A. Peacock, K. Peters, E. Pianori, A. Pich, A. Piepke, F. Pietropaolo, A. Pomarol, S. Profumo, A. Quadt, K. Rabbertz, J. Rademacker, G. Raffelt, M. Ramsey-Musolf, L. Reina, P. Richardson, D.J. Robinson, S. Roesler, S. Rolli, A. Romaniouk, L.J Rosenberg, G. Rybka, M.G. Ryskin, B. Safdi, Y. Sakai, F. Salamida, N. Saoulidou, S. Sarkar, F. Sauli, P. Savard, O. Schneider, S. Schönert, K. Scholberg, C. Schwanda, A.J. Schwartz, J. Schwiening, D. Scott, F. Sefkow, U. Seljak, V. Sharma, S.R. Sharpe, V. Shiltsev, G. Signorelli, M. Silari, F. Simon, P. Skands, T. Skwarnicki, G.F. Smoot, A. Soffer, M.S. Sozzi, S. Spanier, C. Spiering, A. Stahl, M. Taševský, K. Terao, K. Terashi, J. Terning, U. Thoma, R.S. Thorne, L. Tiator, M. Titov, D.R. Tovey, K. Trabelsi, P. Urquijo, G. Valencia, R. Van de Water, N. Varelas, G. Venanzoni, V. Vennin, L. Verde, I. Vivarelli, W. Vogelsang, W. Walkowiak, C.W. Walter, D. Wands, D.H. Weinberg, E.J. Weinberg, R. Wendell, N. Wermes, M. White, L.R. Wiencke, S. Willocq, L. Winslow, C.L. Woody, R.L. Workman, W.-M. Yao, R. Yoshida, C. Z. Yuan, G. Zanderighi, G.P. Zeller, R.-Y. Zhu, S.-L. Zhu, F. Zimmermann, P.A. Zyla

Technical Associates:

J. Anderson, V.K.S. Kashyap, B. Mohanty, A. Ozerov, S. Rohr, P. Schaffner, G.A. Valdiviesso, W. Zheng

©2026 (CC BY 4.0)
(Approximate closing date for data: January 15, 2026)

GAUGE AND HIGGS BOSONS

γ (photon)

$I(J^{PC}) = 0,1(1^{--})$

Mass $m < 1 \times 10^{-18}$ eV
Charge $q < 1 \times 10^{-46}\ e$ (mixed charge)
Charge $q < 1 \times 10^{-35}\ e$ (single charge)
Mean life τ = Stable

g (gluon)

$I(J^P) = 0(1^-)$

Mass $m = 0$ [a]
SU(3) color octet

graviton

$J = 2$

Mass $m < 1.76 \times 10^{-23}$ eV

W

$J = 1$

Charge = $\pm 1\ e$
Mass $m = 80.3625 \pm 0.0077$ GeV [b]
W/Z mass ratio = 0.88136 ± 0.00015
$m_Z - m_W = 10.818 \pm 0.013$ GeV
$m_{W^+} - m_{W^-} = -0.029 \pm 0.028$ GeV
Full width $\Gamma = 2.14 \pm 0.05$ GeV (S = 1.7)
$\langle N_{\pi^\pm} \rangle = 15.70 \pm 0.35$
$\langle N_{K^\pm} \rangle = 2.20 \pm 0.19$
$\langle N_p \rangle = 0.92 \pm 0.14$
$\langle N_{\rm charged} \rangle = 19.39 \pm 0.08$

W^- modes are charge conjugates of the modes below.

W^+ DECAY MODES		Fraction (Γ_i/Γ)	Confidence level	p (MeV/c)
$\ell^+\nu$	[c]	(10.86 ± 0.09) %		–
$e^+\nu$		(10.71 ± 0.16) %		40181
$\mu^+\nu$		(10.63 ± 0.15) %		40181
$\tau^+\nu$		(11.38 ± 0.21) %		40162
hadrons		(67.41 ± 0.27) %		–
$\pi^+\gamma$		$< 1.9 \times 10^{-6}$	95%	40181
$\rho^+\gamma$		$< 5.2 \times 10^{-6}$	95%	40178
$K^+\gamma$		$< 1.7 \times 10^{-6}$	95%	40180
$D_s^+\gamma$		$< 6 \times 10^{-4}$	95%	40157
cX		(33.0 ± 1.2) %		–
$c\overline{s}$		$(31\ ^{+13}_{-11})$ %		–
invisible	[d]	(1.4 ± 2.8) %		–
$\pi^+\pi^+\pi^-$		$< 1.01 \times 10^{-6}$	95%	40181

Z

$J = 1$

Charge = 0
Mass $m = 91.1879 \pm 0.0020$ GeV [e]
Full width $\Gamma = 2.4955 \pm 0.0023$ GeV
$\Gamma(\ell^+\ell^-) = 83.984 \pm 0.086$ MeV [c]
$\Gamma(\text{invisible}) = 499.3 \pm 1.5$ MeV [f]
$\Gamma(\text{hadrons}) = 1744.4 \pm 2.0$ MeV
$\Gamma(\mu^+\mu^-)/\Gamma(e^+e^-) = 1.0001 \pm 0.0024$
$\Gamma(\tau^+\tau^-)/\Gamma(e^+e^-) = 1.0020 \pm 0.0032$ [g]

Average charged multiplicity

$\langle N_{charged} \rangle = 20.76 \pm 0.16$ (S = 2.1)

Couplings to quarks and leptons

$g_V^\ell = -0.03783 \pm 0.00041$
$g_V^u = 0.266 \pm 0.034$
$g_V^d = -0.38^{+0.04}_{-0.05}$
$g_A^\ell = -0.50123 \pm 0.00026$
$g_A^u = 0.519^{+0.028}_{-0.033}$
$g_A^d = -0.527^{+0.040}_{-0.028}$
$g^{\nu_\ell} = 0.5008 \pm 0.0008$
$g^{\nu_e} = 0.53 \pm 0.09$
$g^{\nu_\mu} = 0.502 \pm 0.017$

Int. J. Mod. Phys. A 2026.41. Downloaded from www.worldscientific.com
by UNIVERSITY OF CALIFORNIA @ BERKELEY on 09/16/26. Re-use and distribution is strictly not permitted, except for Open Acce

Asymmetry parameters [h]

$A_e = 0.1515 \pm 0.0019$
$A_\mu = 0.142 \pm 0.015$
$A_\tau = 0.143 \pm 0.004$
$A_s = 0.90 \pm 0.09$
$A_c = 0.670 \pm 0.027$
$A_b = 0.923 \pm 0.020$

Charge asymmetry (%) at Z pole

$A_{FB}^{(0\ell)} = 1.71 \pm 0.10$
$A_{FB}^{(0u)} = 4 \pm 7$
$A_{FB}^{(0s)} = 9.8 \pm 1.1$
$A_{FB}^{(0c)} = 7.07 \pm 0.35$
$A_{FB}^{(0b)} = 9.92 \pm 0.16$
$\sin^2(\theta_{\rm eff}) = 0.23148 \pm 0.00012$

Z DECAY MODES		Fraction (Γ_i/Γ)	Scale factor/ Confidence level	p (MeV/c)
e^+e^-		(3.3632 ± 0.0042) %		45594
$\mu^+\mu^-$		(3.3662 ± 0.0066) %		45594
$\tau^+\tau^-$		(3.3696 ± 0.0083) %		45559
$\ell^+\ell^-$	[c]	(3.3658 ± 0.0023) %		–
$\ell^+\ell^-\ell^+\ell^-$	[i]	$(4.55 \pm 0.17) \times 10^{-6}$		45594
invisible		(20.000 ± 0.055) %		–
hadrons		(69.911 ± 0.056) %		–
$(u\overline{u}+c\overline{c})/2$		(11.6 ± 0.6) %		–
$(d\overline{d}+s\overline{s}+b\overline{b})/3$		(15.6 ± 0.4) %		–
$c\overline{c}$		(12.03 ± 0.21) %		–
$b\overline{b}$		(15.12 ± 0.05) %		–
$b\overline{b}b\overline{b}$		$(3.6 \pm 1.3) \times 10^{-4}$		–
ggg		< 1.1 %	CL=95%	–
$\pi^0\gamma$		$< 2.01 \times 10^{-5}$	CL=95%	45594
$\eta\gamma$		$< 5.1 \times 10^{-5}$	CL=95%	45592
$\rho^0\gamma$		$< 4.0 \times 10^{-6}$	CL=95%	45591
$\omega\gamma$		$< 3.9 \times 10^{-6}$	CL=95%	45591
$\eta'(958)\gamma$		$< 4.2 \times 10^{-5}$	CL=95%	45589
$\phi\gamma$		$< 7 \times 10^{-7}$	CL=95%	45588
$\gamma\gamma$		$< 1.46 \times 10^{-5}$	CL=95%	45594
$\pi^0\pi^0$		$< 1.52 \times 10^{-5}$	CL=95%	45594
$\gamma\gamma\gamma$		$< 2.2 \times 10^{-6}$	CL=95%	45594
$\pi^\pm W^\mp$	[j]	$< 7 \times 10^{-5}$	CL=95%	10182
$\rho^\pm W^\mp$	[j]	$< 8.3 \times 10^{-5}$	CL=95%	10157
$J/\psi(1S)X$		$(3.51 {}^{+0.23}_{-0.25}) \times 10^{-3}$	S=1.1	–
$J/\psi(1S)\gamma$		$< 6 \times 10^{-7}$	CL=95%	45541
$\psi(2S)X$		$(1.60 \pm 0.29) \times 10^{-3}$		–
$\psi(2S)\gamma$		$< 1.3 \times 10^{-6}$	CL=95%	45519
$J/\psi(1S)J/\psi(1S)$		$< 2.2 \times 10^{-6}$	CL=95%	45489
$\chi_{c1}(1P)X$		$(2.9 \pm 0.7) \times 10^{-3}$		–
$\chi_{c2}(1P)X$		$< 3.2 \times 10^{-3}$	CL=90%	–
$\Upsilon(1S)X + \Upsilon(2S)X + \Upsilon(3S)X$		$(1.0 \pm 0.5) \times 10^{-4}$		–
$\Upsilon(1S)X$		$< 4.4 \times 10^{-5}$	CL=95%	–
$\Upsilon(1S)\gamma$		$< 1.1 \times 10^{-6}$	CL=95%	45103
$\Upsilon(2S)X$		$< 1.39 \times 10^{-4}$	CL=95%	–
$\Upsilon(2S)\gamma$		$< 1.3 \times 10^{-6}$	CL=95%	45043
$\Upsilon(3S)X$		$< 9.4 \times 10^{-5}$	CL=95%	–
$\Upsilon(3S)\gamma$		$< 2.4 \times 10^{-6}$	CL=95%	45006
$\Upsilon(1,2,3S)\Upsilon(1,2,3S)$		$< 1.5 \times 10^{-6}$	CL=95%	–
$K^0_S\gamma$		$< 3.1 \times 10^{-6}$	CL=95%	45593
$D^0\gamma$		$< 4.0 \times 10^{-6}$	CL=95%	45575
$(D^0/\overline{D}^0)X$		(20.7 ± 2.0) %		–
$D^\pm X$		(12.2 ± 1.7) %		–
$D^*(2010)^\pm X$	[j]	(11.4 ± 1.3) %		–
$D_{s1}(2536)^\pm X$		$(3.6 \pm 0.8) \times 10^{-3}$		–
$D_{sJ}(2573)^\pm X$		$(5.8 \pm 2.2) \times 10^{-3}$		–
$D^{*\prime}(2629)^\pm X$		searched for		–
B^+X	[k]	(6.08 ± 0.13) %		–
B^0_sX	[k]	(1.59 ± 0.13) %		–
B^+_cX		searched for		–
Λ^+_cX		(1.54 ± 0.33) %		–
Ξ^0_cX		seen		–
Ξ_bX		seen		–
b-baryon X	[k]	(1.38 ± 0.22) %		–
anomalous $\gamma+$ hadrons	[l]	$< 3.2 \times 10^{-3}$	CL=95%	–
$e^+e^-\gamma$	[l]	$< 5.2 \times 10^{-4}$	CL=95%	45594
$\mu^+\mu^-\gamma$	[l]	$< 5.6 \times 10^{-4}$	CL=95%	45594
$\tau^+\tau^-\gamma$	[l]	$< 7.3 \times 10^{-4}$	CL=95%	45559
$\ell^+\ell^-\gamma\gamma$	[n]	$< 6.8 \times 10^{-6}$	CL=95%	–
$q\overline{q}\gamma\gamma$	[n]	$< 5.5 \times 10^{-6}$	CL=95%	–
$\nu\overline{\nu}\gamma\gamma$	[n]	$< 3.1 \times 10^{-6}$	CL=95%	45594
$e^\pm\mu^\mp$	LF [j]	$< 1.9 \times 10^{-7}$	CL=95%	45594
$e^\pm\tau^\mp$	LF [j]	$< 5.0 \times 10^{-6}$	CL=95%	45577
$\mu^\pm\tau^\mp$	LF [j]	$< 6.5 \times 10^{-6}$	CL=95%	45577
pe	L,B	$< 1.8 \times 10^{-6}$	CL=95%	45589
$p\mu$	L,B	$< 1.8 \times 10^{-6}$	CL=95%	45589

H

was H^0

$J = 0$

Mass $m = 125.13 \pm 0.11$ GeV (S = 1.5)
Full width $\Gamma = 3.0^{+1.5}_{-0.7}$ MeV (assumes equal on-shell and off-shell effective couplings)

H Signal Strengths in Different Channels

Combined final state $= 1.03 \pm 0.04$
$WW^* = 1.00 \pm 0.08$
$ZZ^* = 1.02 \pm 0.08$
$\gamma\gamma = 1.10 \pm 0.06$
$c\overline{c}$ final state $= -0.5 \pm 3.4$
$b\overline{b} = 0.94 \pm 0.11$
$\mu^+\mu^- = 1.31 \pm 0.29$
$\tau^+\tau^- = 0.91 \pm 0.09$
$Z\gamma = 2.2 \pm 0.7$
$\gamma^*\gamma$ final state $= 1.5 \pm 0.5$
Fermion coupling $(\kappa_F) = 0.94 \pm 0.05$
Gauge boson coupling $(\kappa_V) = 1.023 \pm 0.026$
$t\overline{t}H$ production $= 0.91^{+0.20}_{-0.18}$ (S = 1.6)
$b\overline{b}H$ production < 3.7, CL = 95%
tH production $= 7.1 \pm 2.5$
HH production < 2.4, CL = 95%
HHH production < 760, CL = 95%
Higgs trilinear self coupling modifier $\kappa_\lambda = 3.8^{+2.1}_{-4.0}$
Higgs-gauge boson quartic coupling modifier $\kappa_{2V} = 1.02 \pm 0.23$
H production cross section in pp collisions at $\sqrt{s} = 13$ TeV $= 56.8 \pm 3.4$ pb
H production cross section in pp collisions at $\sqrt{s} = 13.6$ TeV $= 58 \pm 9$ pb

H DECAY MODES		Fraction (Γ_i/Γ)	Confidence level	p (MeV/c)
WW^*		(25.7 ± 2.5) %		–
ZZ^*		(2.80 ± 0.30) %		–
$\gamma\gamma$		$(2.50 \pm 0.20) \times 10^{-3}$		62565
$b\overline{b}$		(53 ± 8) %		–
e^+e^-		$< 3.0 \times 10^{-4}$	95%	62565
$\mu^+\mu^-$		$(3.0 \pm 0.9) \times 10^{-4}$		62565
$\tau^+\tau^-$		$(6.0 {}^{+0.8}_{-0.7})$ %		62540
$Z\gamma$		$(3.4 \pm 1.1) \times 10^{-3}$		29339
$Z\rho(770)$		< 1.21 %	95%	29332
$Z\phi(1020)$		$< 3.6 \times 10^{-3}$	95%	29326
ZJ/ψ		$< 1.9 \times 10^{-3}$	95%	29214
$Z\psi(2S)$		$< 6.6 \times 10^{-3}$	95%	29162
$J/\psi\gamma$		$< 2.0 \times 10^{-4}$	95%	62527
$J/\psi J/\psi$		$< 3.8 \times 10^{-4}$	95%	62489
$\psi(2S)\gamma$		$< 9.9 \times 10^{-4}$	95%	62511
$\psi(2S)J/\psi$		$< 2.1 \times 10^{-3}$	95%	62473
$\psi(2S)\psi(2S)$		$< 3.0 \times 10^{-3}$	95%	62457
$\Upsilon(1S)\gamma$		$< 2.5 \times 10^{-4}$	95%	62208
$\Upsilon(1S)\Upsilon(1S)$		$< 1.7 \times 10^{-3}$	95%	61846
$\Upsilon(2S)\gamma$		$< 4.2 \times 10^{-4}$	95%	62164
$\Upsilon(3S)\gamma$		$< 3.4 \times 10^{-4}$	95%	62137
$\Upsilon(nS)\Upsilon(mS)$		$< 3.5 \times 10^{-4}$	95%	–
$D^*\gamma$		$< 1.0 \times 10^{-3}$	95%	62549
$\rho(770)\gamma$		$< 3.7 \times 10^{-4}$	95%	62563
$\omega(782)\gamma$		$< 5.5 \times 10^{-4}$	95%	62563
$K^*(892)\gamma$		$< 2.2 \times 10^{-4}$	95%	62562
$\phi(1020)\gamma$		$< 3.0 \times 10^{-4}$	95%	62561
$e\mu$	LF	$< 4.4 \times 10^{-5}$	95%	62565
$e\tau$	LF	$< 2.0 \times 10^{-3}$	95%	62553

$\mu\tau$	LF	< 1.5	$\times 10^{-3}$	95%	6255 3
invisible		< 10.7	%	95%	–
γ invisible		< 1.3	%	95%	–

Neutral Higgs Bosons, Searches for

Mass limits for heavy neutral Higgs bosons (H_2^0, A^0) in the MSSM

The results have been obtained in the M_h^{125} benchmark scenario

m > 1121 GeV, CL = 95% (tanβ = 10)
m > 1475 GeV, CL = 95% (tanβ = 20)
m > 1677 GeV, CL = 95% (tanβ = 30)
m > 1826 GeV, CL = 95% (tanβ = 40)
m > 1950 GeV, CL = 95% (tanβ = 50)
m > 2062 GeV, CL = 95% (tanβ = 60)

Charged Higgs Bosons ($H^\pm$ and $H^{\pm\pm}$), Searches for

Mass limits for m_{H^+} < m(top) in the MSSM

m > 155 GeV, CL = 95%

Mass limits for m_{H^+} > m(top) in the MSSM

The results have been obtained in the m_h^{mod-} benchmark scenario

m > 181 GeV, CL = 95% (tanβ = 10)
m > 249 GeV, CL = 95% (tanβ = 20)
m > 390 GeV, CL = 95% (tanβ = 30)
m > 894 GeV, CL = 95% (tanβ = 40)
m > 1017 GeV, CL = 95% (tanβ = 50)
m > 1103 GeV, CL = 95% (tanβ = 60)

New Heavy Bosons (W', Z', leptoquarks, etc.), Searches for

Additional W Bosons

W' with standard couplings
Mass $m >$ 6000 GeV, CL = 95% (pp direct search)
W_R (Right-handed W Boson)
Mass $m >$ 715 GeV, CL = 90% (electroweak fit)

Additional Z Bosons

Z'_{SM} with standard couplings
Mass $m >$ 5150 GeV, CL = 95% (pp direct search)
Z_{LR} of SU(2)$_L$×SU(2)$_R$×U(1) (with $g_L = g_R$)
Mass $m >$ 630 GeV, CL = 95% ($p\overline{p}$ direct search)
Mass $m >$ 1162 GeV, CL = 95% (electroweak fit)
Z_χ of SO(10) → SU(5)×U(1)$_\chi$ (with $g_\chi = e/\cos\theta_W$)
Mass $m >$ 4800 GeV, CL = 95% (pp direct search)
Z_ψ of E_6 → SO(10)×U(1)$_\psi$ (with $g_\psi = e/\cos\theta_W$)
Mass $m >$ 4560 GeV, CL = 95% (pp direct search)
Z_η of E_6 → SU(3)×SU(2)×U(1)×U(1)$_\eta$ (with $g_\eta = e/\cos\theta_W$)
Mass $m >$ 3.900 × 10^3 GeV, CL = 95% (pp direct search)

Scalar Leptoquarks

$m >$ 1800 GeV, CL = 95% (1st gen., pair prod., B(eq)=1)
$m >$ 3400 GeV, CL = 95% (1st gen., single prod., g_{de}=1)
$m >$ 1700 GeV, CL = 95% (2nd gen., pair prod., B(μq)=1)
$m >$ 660 GeV, CL = 95% (2nd gen., single prod., B(μq)=1)
$m >$ 1520 GeV, CL = 95% (3rd gen., pair prod., B(τt)=1)
$m >$ 1280 GeV, CL = 95% (3rd gen., single prod., B(τb)=1)
(See the Particle Listings for assumptions on leptoquark quantum numbers and branching fractions.)

Diquarks

Mass $m >$ 7200 GeV, CL = 95% (E_6 diquark)

Axigluon

Mass $m >$ 6600 GeV, CL = 95%

Axions (A^0) and Other Very Light Bosons, Searches for

See the review on "Axions and other similar particles."

The best limit for the half-life of neutrinoless double beta decay with Majoron emission is > 7.2 × 10^{24} years (CL = 90%).

NOTES

In this Summary Table:

When a quantity has "(S = ...)" to its right, the error on the quantity has been enlarged by the "scale factor" S, defined as S = $\sqrt{\chi^2/(N-1)}$, where N is the number of measurements used in calculating the quantity. We do this when S > 1, which often indicates that the measurements are inconsistent. When S > 1.25, we also show in the Particle Listings an ideogram of the measurements. For more about S, see the Introduction.

A decay momentum p is given for each decay mode. For a 2-body decay, p is the momentum of each decay product in the rest frame of the decaying particle. For a 3-or-more-body decay, p is the largest momentum any of the products can have in this frame.

[a] Theoretical value. A mass as large as a few MeV may not be precluded.
[b] This value does not include the AALTONEN 22 measurement by CDF. See the W mass section in the listings for details.
[c] ℓ indicates each type of lepton (e, μ, and τ), not sum over them.
[d] This represents the width for the decay of the W boson into a charged particle with momentum below detectability, p< 200 MeV.
[e] The Z-boson mass listed here corresponds to a Breit-Wigner resonance parameter. It lies approximately 34 MeV above the real part of the position of the pole (in the energy-squared plane) in the Z-boson propagator.
[f] This partial width takes into account Z decays into $\nu\overline{\nu}$ and any other possible undetected modes.
[g] This ratio has not been corrected for the τ mass.
[h] Here $A \equiv 2g_V g_A/(g_V^2+g_A^2)$.
[i] Here ℓ indicates e or μ.
[j] The value is for the sum of the charge states or particle/antiparticle states indicated.
[k] This value is updated using the product of (i) the $Z \to b\overline{b}$ fraction from this listing and (ii) the b-hadron fraction in an unbiased sample of weakly decaying b-hadrons produced in Z-decays provided by the Heavy Flavor Averaging Group (HFLAV, http://www.slac.stanford.edu/xorg/hflav/osc/PDG_2009/#FRACZ).
[l] See the Z Particle Listings for the γ energy range used in this measurement.
[n] For $m_{\gamma\gamma}$ = (60 ± 5) GeV.

Int. J. Mod. Phys. A 2026.41. Downloaded from www.worldscientific.com
by UNIVERSITY OF CALIFORNIA @ BERKELEY on 09/16/26. Re-use and distribution is strictly not permitted, except for Open Access articles.

Int. J. Mod. Phys. A 2026.41. Downloaded from www.worldscientific.com
by UNIVERSITY OF CALIFORNIA @ BERKELEY on 09/16/26. Re-use and distribution is strictly not permitted, except for Open Acce

LEPTONS

e

$J = \frac{1}{2}$

Mass $m = (548.579909044 \pm 0.000000010) \times 10^{-6}$ u
Mass $m = 0.51099895069 \pm 0.00000000016$ MeV
$|m_{e^+} - m_{e^-}|/m < 8 \times 10^{-9}$, CL = 90%
$|q_{e^+} + q_{e^-}|/e < 4 \times 10^{-8}$
Magnetic moment anomaly
$(g-2)/2 = (1159.65218062 \pm 0.00000012) \times 10^{-6}$
$(g_{e^+} - g_{e^-}) / g_{\rm average} = (-0.5 \pm 2.1) \times 10^{-12}$
Electric dipole moment $d < 0.041 \times 10^{-28}$ $e$cm, CL = 90%
Mean life $\tau > 6.6 \times 10^{28}$ yr, CL = 90% [a]

μ

$J = \frac{1}{2}$

Mass $m = 0.1134289257 \pm 0.0000000025$ u
Mass $m = 105.6583755 \pm 0.0000023$ MeV
Mean life $\tau = (2.1969811 \pm 0.0000022) \times 10^{-6}$ s
$\tau_{\mu^+}/\tau_{\mu^-} = 1.00002 \pm 0.00008$
$c\tau = 658.6384$ m
Magnetic moment anomaly $(g-2)/2 = (11659207.2 \pm 1.5) \times 10^{-10}$
$(g_{\mu^+} - g_{\mu^-}) / g_{\rm average} = (-0.11 \pm 0.12) \times 10^{-8}$
Electric dipole moment $|d| < 1.8 \times 10^{-19}$ $e$cm, CL = 95%

Decay parameters [b]

$\rho = 0.74979 \pm 0.00026$
$\eta = 0.057 \pm 0.034$
$\delta = 0.75047 \pm 0.00034$
$\xi P_\mu = 1.0009^{+0.0016}_{-0.0007}$ [c]
$\xi P_\mu \delta/\rho = 1.0018^{+0.0016}_{-0.0007}$ [c]
$\xi' = 1.00 \pm 0.04$
$\xi'' = 0.98 \pm 0.04$
$\alpha/A = (0 \pm 4) \times 10^{-3}$
$\alpha'/A = (-10 \pm 20) \times 10^{-3}$
$\beta/A = (4 \pm 6) \times 10^{-3}$
$\beta'/A = (2 \pm 7) \times 10^{-3}$
$\overline{\eta} = 0.02 \pm 0.08$

μ^+ modes are charge conjugates of the modes below.

μ^- DECAY MODES		Fraction (Γ_i/Γ)	Confidence level	p (MeV/c)
$e^- \overline{\nu}_e \nu_\mu$		$\approx 100\%$		53
$e^- \overline{\nu}_e \nu_\mu \gamma$	[d]	$(6.0 \pm 0.5) \times 10^{-8}$		53
$e^- \overline{\nu}_e \nu_\mu e^+ e^-$	[e]	$(3.4 \pm 0.4) \times 10^{-5}$		53
Lepton Family number (*LF*) violating modes				
$e^- \nu_e \overline{\nu}_\mu$	*LF*	[f] < 1.2 %	90%	53
$e^- \gamma$	*LF*	$< 1.5 \times 10^{-13}$	90%	53
$e^- e^+ e^-$	*LF*	$< 1.0 \times 10^{-12}$	90%	53
$e^- 2\gamma$	*LF*	$< 7.2 \times 10^{-11}$	90%	53

τ

$J = \frac{1}{2}$

Mass $m = 1776.93 \pm 0.09$ MeV
$(m_{\tau^+} - m_{\tau^-})/m_{\rm average} < 2.8 \times 10^{-4}$, CL = 90%
Mean life $\tau = (290.3 \pm 0.5) \times 10^{-15}$ s
$c\tau = 87.03$ μm
Magnetic moment anomaly $= -0.0024$ to 0.0047, CL = 95%
$\mathrm{Re}(d_\tau) = -0.185$ to 0.061×10^{-16} $e$cm, CL = 95%
$\mathrm{Im}(d_\tau) = -0.103$ to 0.023×10^{-16} $e$cm, CL = 95%

Weak dipole moment

$\mathrm{Re}(d_\tau^w) < 0.50 \times 10^{-17}$ $e$cm, CL = 95%
$\mathrm{Im}(d_\tau^w) < 1.1 \times 10^{-17}$ $e$cm, CL = 95%

Weak anomalous magnetic dipole moment

$\mathrm{Re}(\alpha_\tau^w) < 1.1 \times 10^{-3}$, CL = 95%
$\mathrm{Im}(\alpha_\tau^w) < 2.7 \times 10^{-3}$, CL = 95%
$\tau^\pm \to \pi^\pm K^0_S \nu_\tau$ (RATE DIFFERENCE) / (RATE SUM) = (-0.36 ± 0.25)%

Decay parameters

See the τ Particle Listings for a note concerning τ-decay parameters.

$\rho(e \text{ or } \mu) = 0.745 \pm 0.008$
$\rho(e) = 0.747 \pm 0.010$
$\rho(\mu) = 0.763 \pm 0.020$
$\xi(e \text{ or } \mu) = 0.985 \pm 0.030$
$\xi(e) = 0.994 \pm 0.040$
$\xi(\mu) = 1.030 \pm 0.059$
$\eta(e \text{ or } \mu) = 0.013 \pm 0.020$
$\eta(\mu) = 0.094 \pm 0.073$
$(\delta\xi)(e \text{ or } \mu) = 0.746 \pm 0.021$
$(\delta\xi)(e) = 0.734 \pm 0.028$
$(\delta\xi)(\mu) = 0.778 \pm 0.037$
$\xi(\pi) = 0.993 \pm 0.022$
$\xi(\rho) = 0.994 \pm 0.008$
$\xi(a_1) = 1.001 \pm 0.027$
ξ(all hadronic modes) $= 0.995 \pm 0.007$
$\xi'(\mu) = 0.2 \pm 1.0$
$\overline{\eta}(\mu) = -1.3 \pm 1.7$
$(\xi\kappa)(e \text{ or } \mu) = 0.5 \pm 0.4$
$(\xi\kappa)(e) = -0.4 \pm 1.2$
$(\xi\kappa)(\mu) = 0.8 \pm 0.6$

τ^+ modes are charge conjugates of the modes below. "$h^\pm$" stands for $\pi^\pm$ or $K^\pm$. "ℓ" stands for e or μ. "Neutrals" stands for γ's and/or π^0's.

τ^- DECAY MODES		Fraction (Γ_i/Γ)	Scale factor/ Confidence level	p (MeV/c)
Modes with one charged particle				
particle$^- \geq 0$ neutrals $\geq 0K^0 \nu_\tau$ ("1-prong")		(85.24 ± 0.06) %		–
particle$^- \geq 0$ neutrals $\geq 0K^0_L \nu_\tau$		(84.58 ± 0.06) %		–
$\mu^- \overline{\nu}_\mu \nu_\tau$	[g]	(17.37 ± 0.04) %		885
$\mu^- \overline{\nu}_\mu \nu_\tau \gamma$	[e]	$(3.67 \pm 0.08) \times 10^{-3}$		885
$e^- \overline{\nu}_e \nu_\tau$	[g]	(17.85 ± 0.04) %		888
$e^- \overline{\nu}_e \nu_\tau \gamma$	[e]	(1.83 ± 0.05) %		888
$h^- \geq 0K^0_L \nu_\tau$		(12.03 ± 0.05) %		883
$h^- \nu_\tau$		(11.51 ± 0.05) %		883
$\pi^- \nu_\tau$	[g]	(10.82 ± 0.05) %		883
$K^- \nu_\tau$	[g]	$(6.97 \pm 0.10) \times 10^{-3}$		820
$h^- \geq 1$ neutrals ν_τ		(37.00 ± 0.09) %		–
$h^- \geq 1\pi^0 \nu_\tau$ (ex.K^0)		(36.50 ± 0.09) %		–
$h^- \pi^0 \nu_\tau$		(25.93 ± 0.09) %		878
$\pi^- \pi^0 \nu_\tau$	[g]	(25.49 ± 0.09) %		878
$\pi^- \pi^0$ non-$\rho(770) \nu_\tau$		$(3.0 \pm 3.2) \times 10^{-3}$		878
$K^- \pi^0 \nu_\tau$	[g]	$(4.33 \pm 0.15) \times 10^{-3}$		814
$h^- \geq 2\pi^0 \nu_\tau$		(10.81 ± 0.09) %		–
$h^- 2\pi^0 \nu_\tau$		(9.48 ± 0.10) %		862
$h^- 2\pi^0 \nu_\tau$ (ex.K^0)		(9.32 ± 0.10) %		862
$\pi^- 2\pi^0 \nu_\tau$ (ex.K^0)	[g]	(9.26 ± 0.10) %		862
$\pi^- 2\pi^0 \nu_\tau$ (ex.K^0), scalar		< 9	$\times 10^{-3}$ CL=95%	862
$\pi^- 2\pi^0 \nu_\tau$ (ex.K^0), vector		< 7	$\times 10^{-3}$ CL=95%	862
$K^- 2\pi^0 \nu_\tau$ (ex.K^0)	[g]	$(6.5 \pm 2.2) \times 10^{-4}$		796
$h^- \geq 3\pi^0 \nu_\tau$		(1.34 ± 0.07) %		–
$h^- \geq 3\pi^0 \nu_\tau$ (ex. K^0)		(1.26 ± 0.07) %		–
$h^- 3\pi^0 \nu_\tau$		(1.18 ± 0.07) %		836
$\pi^- 3\pi^0 \nu_\tau$ (ex.K^0)	[g]	(1.04 ± 0.07) %		836
$K^- 3\pi^0 \nu_\tau$ (ex.K^0, η)	[g]	$(4.8 \pm 2.1) \times 10^{-4}$		766
$h^- 4\pi^0 \nu_\tau$ (ex.K^0)		$(1.6 \pm 0.4) \times 10^{-3}$		800
$h^- 4\pi^0 \nu_\tau$ (ex.K^0,η)	[g]	$(1.1 \pm 0.4) \times 10^{-3}$		800
$a_1(1260) \nu_\tau \to \pi^- \gamma \nu_\tau$		$(4.0 \pm 1.5) \times 10^{-4}$		–
$K^- \geq 0\pi^0 \geq 0K^0 \geq 0\gamma \nu_\tau$		(1.552 ± 0.029) %		820
$K^- \geq 1$ (π^0 or K^0 or γ) ν_τ		$(8.59 \pm 0.28) \times 10^{-3}$		–
Modes with K^0's				
K^0_S(particles)$^- \nu_\tau$		$(9.43 \pm 0.28) \times 10^{-3}$		–
$h^- \overline{K}^0 \nu_\tau$		$(9.87 \pm 0.14) \times 10^{-3}$		812
$\pi^- \overline{K}^0 \nu_\tau$	[g]	$(8.38 \pm 0.14) \times 10^{-3}$		812
$\pi^- \overline{K}^0$ (non-$K^*(892)^-$) ν_τ		$(5.4 \pm 2.1) \times 10^{-4}$		812
$K^- K^0 \nu_\tau$	[g]	$(1.486 \pm 0.034) \times 10^{-3}$		737
$K^- K^0 \geq 0\pi^0 \nu_\tau$		$(2.99 \pm 0.07) \times 10^{-3}$		737
$h^- \overline{K}^0 \pi^0 \nu_\tau$		$(5.32 \pm 0.13) \times 10^{-3}$		794

Int. J. Mod. Phys. A 2026.41. Downloaded from www.worldscientific.com
by UNIVERSITY OF CALIFORNIA @ BERKELEY on 09/16/26. Re-use and distribution is strictly not permitted, except for Open Access articles.

$\pi^- \overline{K}^0 \pi^0 \nu_\tau$	[g]	$(3.82 \pm 0.13) \times 10^{-3}$			794
$\overline{K}^0 \rho^- \nu_\tau$		$(2.2 \pm 0.5) \times 10^{-3}$			612
$K^- K^0 \pi^0 \nu_\tau$	[g]	$(1.50 \pm 0.07) \times 10^{-3}$			685
$\pi^- \overline{K}^0 \geq 1\pi^0 \nu_\tau$		$(4.08 \pm 0.25) \times 10^{-3}$			–
$\pi^- \overline{K}^0 \pi^0 \pi^0 \nu_\tau$ (ex.K^0)	[g]	$(2.6 \pm 2.3) \times 10^{-4}$			763
$K^- K^0 \pi^0 \pi^0 \nu_\tau$		$< 1.6 \times 10^{-4}$	CL=95%		619
$\pi^- K^0 \overline{K}^0 \nu_\tau$		$(1.55 \pm 0.24) \times 10^{-3}$			682
$\pi^- K^0_S K^0_S \nu_\tau$	[g]	$(2.35 \pm 0.06) \times 10^{-4}$			682
$\pi^- K^0_S K^0_L \nu_\tau$	[g]	$(1.08 \pm 0.24) \times 10^{-3}$			682
$\pi^- K^0_L K^0_L \nu_\tau$		$(2.35 \pm 0.06) \times 10^{-4}$			682
$\pi^- K^0 \overline{K}^0 \pi^0 \nu_\tau$		$(3.6 \pm 1.2) \times 10^{-4}$			614
$\pi^- K^0_S K^0_S \pi^0 \nu_\tau$	[g]	$(1.82 \pm 0.21) \times 10^{-5}$			614
$K^{*-} K^0 \pi^0 \nu_\tau \to \pi^- K^0_S K^0_S \pi^0 \nu_\tau$		$(1.08 \pm 0.21) \times 10^{-5}$			–
$f_1(1285) \pi^- \nu_\tau \to \pi^- K^0_S K^0_S \pi^0 \nu_\tau$		$(6.8 \pm 1.5) \times 10^{-6}$			–
$f_1(1420) \pi^- \nu_\tau \to \pi^- K^0_S K^0_S \pi^0 \nu_\tau$		$(2.4 \pm 0.8) \times 10^{-6}$			–
$\pi^- K^0_S K^0_L \pi^0 \nu_\tau$	[g]	$(3.2 \pm 1.2) \times 10^{-4}$			614
$\pi^- K^0_L K^0_L \pi^0 \nu_\tau$		$(1.82 \pm 0.21) \times 10^{-5}$			614
$K^- K^0_S K^0_S \nu_\tau$		$< 6.3 \times 10^{-7}$	CL=90%		466
$K^- K^0_S K^0_S \pi^0 \nu_\tau$		$< 4.0 \times 10^{-7}$	CL=90%		337
$K^0 h^+ h^- h^- \geq 0$ neutrals ν_τ		$< 1.7 \times 10^{-3}$	CL=95%		760
$K^0 h^+ h^- h^- \nu_\tau$	[g]	$(2.5 \pm 2.0) \times 10^{-4}$			760

Modes with three charged particles

$h^- h^- h^+ \geq 0$ neutrals $\geq 0 K^0_L \nu_\tau$		(15.20 ± 0.06) %			861
$h^- h^- h^+ \geq 0$ neutrals ν_τ (ex. $K^0_S \to \pi^+ \pi^-$) ("3-prong")		(14.55 ± 0.06) %			861
$h^- h^- h^+ \nu_\tau$		(9.80 ± 0.05) %			861
$h^- h^- h^+ \nu_\tau$ (ex.K^0)		(9.45 ± 0.05) %			861
$h^- h^- h^+ \nu_\tau$ (ex.K^0,ω)		(9.42 ± 0.05) %			861
$\pi^- \pi^+ \pi^- \nu_\tau$		(9.31 ± 0.05) %			861
$\pi^- \pi^+ \pi^- \nu_\tau$ (ex.K^0)		(9.02 ± 0.05) %			861
$\pi^- \pi^+ \pi^- \nu_\tau$ (ex.K^0), non-axial vector		< 2.4 %	CL=95%		861
$\pi^- \pi^+ \pi^- \nu_\tau$ (ex.K^0,ω)	[g]	(8.99 ± 0.05) %			861
$h^- h^- h^+ \geq 1$ neutrals ν_τ		(5.29 ± 0.05) %			–
$h^- h^- h^+ \geq 1\pi^0 \nu_\tau$ (ex. K^0)		(5.09 ± 0.05) %			–
$h^- h^- h^+ \pi^0 \nu_\tau$		(4.76 ± 0.05) %			834
$h^- h^- h^+ \pi^0 \nu_\tau$ (ex.K^0)		(4.57 ± 0.05) %			834
$h^- h^- h^+ \pi^0 \nu_\tau$ (ex. K^0, ω)		(2.79 ± 0.07) %			834
$\pi^- \pi^+ \pi^- \pi^0 \nu_\tau$		(4.62 ± 0.05) %			834
$\pi^- \pi^+ \pi^- \pi^0 \nu_\tau$ (ex.K^0)		(4.49 ± 0.05) %			834
$\pi^- \pi^+ \pi^- \pi^0 \nu_\tau$ (ex.K^0,ω)	[g]	(2.74 ± 0.07) %			834
$h^- h^- h^+ \geq 2\pi^0 \nu_\tau$ (ex. K^0)		$(5.17 \pm 0.31) \times 10^{-3}$			–
$h^- h^- h^+ 2\pi^0 \nu_\tau$		$(5.05 \pm 0.31) \times 10^{-3}$			797
$h^- h^- h^+ 2\pi^0 \nu_\tau$ (ex.K^0)		$(4.95 \pm 0.31) \times 10^{-3}$			797
$h^- h^- h^+ 2\pi^0 \nu_\tau$ (ex.K^0,ω,η)	[g]	$(10 \pm 4) \times 10^{-4}$			797
$h^- h^- h^+ 3\pi^0 \nu_\tau$		$(2.13 \pm 0.30) \times 10^{-4}$			749
$2\pi^- \pi^+ 3\pi^0 \nu_\tau$ (ex.K^0)		$(1.94 \pm 0.30) \times 10^{-4}$			749
$2\pi^- \pi^+ 3\pi^0 \nu_\tau$ (ex.K^0, η, $f_1(1285)$)		$(1.7 \pm 0.4) \times 10^{-4}$			–
$2\pi^- \pi^+ 3\pi^0 \nu_\tau$ (ex.K^0, η, ω, $f_1(1285)$)	[g]	$(1.4 \pm 2.7) \times 10^{-5}$			–
$K^- h^+ h^- \geq 0$ neutrals ν_τ		$(6.29 \pm 0.14) \times 10^{-3}$			794
$K^- h^+ \pi^- \nu_\tau$ (ex.K^0)		$(4.37 \pm 0.07) \times 10^{-3}$			794
$K^- h^+ \pi^- \pi^0 \nu_\tau$ (ex.K^0)		$(8.6 \pm 1.2) \times 10^{-4}$			763
$K^- \pi^+ \pi^- \geq 0$ neutrals ν_τ		$(4.77 \pm 0.14) \times 10^{-3}$			794
$K^- \pi^+ \pi^- \geq 0\pi^0 \nu_\tau$ (ex.K^0)		$(3.73 \pm 0.13) \times 10^{-3}$			794
$K^- \pi^+ \pi^- \nu_\tau$		$(3.45 \pm 0.07) \times 10^{-3}$			794
$K^- \pi^+ \pi^- \nu_\tau$ (ex.K^0)		$(2.93 \pm 0.07) \times 10^{-3}$			794
$K^- \pi^+ \pi^- \nu_\tau$ (ex.K^0,ω)	[g]	$(2.93 \pm 0.07) \times 10^{-3}$			794
$K^- \rho^0 \nu_\tau \to K^- \pi^+ \pi^- \nu_\tau$		$(1.4 \pm 0.5) \times 10^{-3}$			–
$K^- \pi^+ \pi^- \pi^0 \nu_\tau$		$(1.31 \pm 0.12) \times 10^{-3}$			763
$K^- \pi^+ \pi^- \pi^0 \nu_\tau$ (ex.K^0)		$(8.0 \pm 1.2) \times 10^{-4}$			763
$K^- \pi^+ \pi^- \pi^0 \nu_\tau$ (ex.K^0,η)		$(7.6 \pm 1.2) \times 10^{-4}$			763
$K^- \pi^+ \pi^- \pi^0 \nu_\tau$ (ex.K^0,ω)		$(3.7 \pm 0.9) \times 10^{-4}$			763
$K^- \pi^+ \pi^- \pi^0 \nu_\tau$ (ex.K^0,ω,η)	[g]	$(3.9 \pm 1.4) \times 10^{-4}$			763
$K^- \pi^+ K^- \geq 0$ neut. ν_τ		$< 9 \times 10^{-4}$	CL=95%		685
$K^- K^+ \pi^- \geq 0$ neut. ν_τ		$(1.496 \pm 0.033) \times 10^{-3}$			685
$K^- K^+ \pi^- \nu_\tau$	[g]	$(1.435 \pm 0.027) \times 10^{-3}$			685
$K^- K^+ \pi^- \pi^0 \nu_\tau$	[g]	$(6.1 \pm 1.8) \times 10^{-5}$			618
$K^- K^+ K^- \nu_\tau$		$(2.2 \pm 0.8) \times 10^{-5}$	S=5.4		472
$K^- K^+ K^- \nu_\tau$ (ex. ϕ)		$< 2.5 \times 10^{-6}$	CL=90%		–
$K^- K^+ K^- \pi^0 \nu_\tau$		$< 4.8 \times 10^{-6}$	CL=90%		346
$\pi^- K^+ \pi^- \geq 0$ neut. ν_τ		$< 2.5 \times 10^{-3}$	CL=95%		794
$e^- e^- e^+ \overline{\nu}_e \nu_\tau$		$(2.8 \pm 1.5) \times 10^{-5}$			888
$\mu^- e^- e^+ \overline{\nu}_\mu \nu_\tau$		$< 3.2 \times 10^{-5}$	CL=90%		885
$\pi^- e^- e^+ \nu_\tau$		seen			883
$\pi^- \mu^- \mu^+ \nu_\tau$		$< 1.14 \times 10^{-5}$	CL=90%		870

Modes with five charged particles

$3h^- 2h^+ \geq 0$ neutrals ν_τ (ex. $K^0_S \to \pi^- \pi^+$) ("5-prong")		$(9.9 \pm 0.4) \times 10^{-4}$			794
$3h^- 2h^+ \nu_\tau$ (ex.K^0)		$(8.29 \pm 0.31) \times 10^{-4}$			794
$3\pi^- 2\pi^+ \nu_\tau$ (ex.K^0, ω)		$(8.27 \pm 0.31) \times 10^{-4}$			794
$3\pi^- 2\pi^+ \nu_\tau$ (ex.K^0, ω, $f_1(1285)$)	[g]	$(7.75 \pm 0.30) \times 10^{-4}$			–
$K^- 2\pi^- 2\pi^+ \nu_\tau$ (ex.K^0)	[g]	$(6 \pm 12) \times 10^{-7}$			716
$K^+ 3\pi^- \pi^+ \nu_\tau$		$< 5.0 \times 10^{-6}$	CL=90%		716
$K^+ K^- 2\pi^- \pi^+ \nu_\tau$		$< 4.5 \times 10^{-7}$	CL=90%		528
$3h^- 2h^+ \pi^0 \nu_\tau$ (ex.K^0)		$(1.65 \pm 0.11) \times 10^{-4}$			746
$3\pi^- 2\pi^+ \pi^0 \nu_\tau$ (ex.K^0)		$(1.64 \pm 0.11) \times 10^{-4}$			746
$3\pi^- 2\pi^+ \pi^0 \nu_\tau$ (ex.K^0, η, $f_1(1285)$)		$(1.11 \pm 0.10) \times 10^{-4}$			–
$3\pi^- 2\pi^+ \pi^0 \nu_\tau$ (ex.K^0, η, ω, $f_1(1285)$)	[g]	$(3.8 \pm 0.9) \times 10^{-5}$			–
$K^- 2\pi^- 2\pi^+ \pi^0 \nu_\tau$ (ex.K^0)	[g]	$(1.1 \pm 0.6) \times 10^{-6}$			657
$K^+ 3\pi^- \pi^+ \pi^0 \nu_\tau$		$< 8 \times 10^{-7}$	CL=90%		657
$3h^- 2h^+ 2\pi^0 \nu_\tau$		$< 3.4 \times 10^{-6}$	CL=90%		687

Miscellaneous other allowed modes

$(5\pi)^- \nu_\tau$		$(7.8 \pm 0.5) \times 10^{-3}$			800
$4h^- 3h^+ \geq 0$ neutrals ν_τ ("7-prong")		$< 3.0 \times 10^{-7}$	CL=90%		682
$4h^- 3h^+ \nu_\tau$		$< 4.3 \times 10^{-7}$	CL=90%		682
$4h^- 3h^+ \pi^0 \nu_\tau$		$< 2.5 \times 10^{-7}$	CL=90%		612
$X^-(S{=}-1) \nu_\tau$		(2.92 ± 0.04) %			–
$K^*(892)^- \geq 0$ neutrals $\geq 0 K^0_L \nu_\tau$		(1.42 ± 0.18) %		S=1.4	665
$K^*(892)^- \nu_\tau$		(1.20 ± 0.07) %		S=1.8	665
$K^*(892)^- \nu_\tau \to \pi^- \overline{K}^0 \nu_\tau$		$(7.82 \pm 0.26) \times 10^{-3}$			–
$K^*(892)^0 K^- \geq 0$ neutrals ν_τ		$(3.2 \pm 1.4) \times 10^{-3}$			542
$K^*(892)^0 K^- \nu_\tau$		$(2.1 \pm 0.4) \times 10^{-3}$			542
$\overline{K}^*(892)^0 \pi^- \geq 0$ neutrals ν_τ		$(3.8 \pm 1.7) \times 10^{-3}$			655
$\overline{K}^*(892)^0 \pi^- \nu_\tau$		$(2.2 \pm 0.5) \times 10^{-3}$			655
$(\overline{K}^*(892)\pi)^- \nu_\tau \to \pi^- \overline{K}^0 \pi^0 \nu_\tau$		$(1.0 \pm 0.4) \times 10^{-3}$			–
$K_1(1270)^- \nu_\tau$		$(4.7 \pm 1.1) \times 10^{-3}$			445
$K_1(1400)^- \nu_\tau$		$(1.7 \pm 2.6) \times 10^{-3}$		S=1.7	335
$K^*(1410)^- \nu_\tau$		$(1.5 {}^{+1.4}_{-1.0}) \times 10^{-3}$			326
$K^*_0(1430)^- \nu_\tau$		$< 5 \times 10^{-4}$	CL=95%		317
$K^*_2(1430)^- \nu_\tau$		$< 3 \times 10^{-3}$	CL=95%		315
$\eta \pi^- \nu_\tau$		$< 9.9 \times 10^{-5}$	CL=95%		797
$\eta \pi^- \pi^0 \nu_\tau$	[g]	$(1.39 \pm 0.07) \times 10^{-3}$			778
$\eta \pi^- \pi^0 \pi^0 \nu_\tau$	[g]	$(1.9 \pm 0.4) \times 10^{-4}$			746
$\eta K^- \nu_\tau$	[g]	$(1.55 \pm 0.08) \times 10^{-4}$			720
$\eta K^*(892)^- \nu_\tau$		$(1.38 \pm 0.15) \times 10^{-4}$			511
$\eta K^- \pi^0 \nu_\tau$	[g]	$(4.8 \pm 1.2) \times 10^{-5}$			665
$\eta K^- \pi^0$ (non-$K^*(892)$) ν_τ		$< 3.5 \times 10^{-5}$	CL=90%		–
$\eta \overline{K}^0 \pi^- \nu_\tau$	[g]	$(9.4 \pm 1.5) \times 10^{-5}$			661
$\eta \overline{K}^0 \pi^- \pi^0 \nu_\tau$		$< 5.0 \times 10^{-5}$	CL=90%		590
$\eta K^- K^0 \nu_\tau$		$< 9.0 \times 10^{-6}$	CL=90%		430
$\eta \pi^+ \pi^- \pi^- \geq 0$ neutrals ν_τ		$< 3 \times 10^{-3}$	CL=90%		744
$\eta \pi^- \pi^+ \pi^- \nu_\tau$ (ex.K^0)	[g]	$(2.20 \pm 0.13) \times 10^{-4}$			744
$\eta \pi^- \pi^+ \pi^- \nu_\tau$ (ex.K^0,$f_1(1285)$)		$(9.9 \pm 1.6) \times 10^{-5}$			–
$\eta a_1(1260)^- \nu_\tau \to \eta \pi^- \rho^0 \nu_\tau$		$< 3.9 \times 10^{-4}$	CL=90%		–
$\eta \eta \pi^- \nu_\tau$		$< 7.4 \times 10^{-6}$	CL=90%		637
$\eta \eta \pi^- \pi^0 \nu_\tau$		$< 2.0 \times 10^{-4}$	CL=95%		559
$\eta \eta K^- \nu_\tau$		$< 3.0 \times 10^{-6}$	CL=90%		382
$\eta'(958) \pi^- \nu_\tau$		$< 4.0 \times 10^{-6}$	CL=90%		620
$\eta'(958) \pi^- \pi^0 \nu_\tau$		$< 1.2 \times 10^{-5}$	CL=90%		591
$\eta'(958) K^- \nu_\tau$		$< 2.4 \times 10^{-6}$	CL=90%		495
$\phi \pi^- \nu_\tau$		$(3.4 \pm 0.6) \times 10^{-5}$			585
$\phi K^- \nu_\tau$	[g]	$(4.4 \pm 1.6) \times 10^{-5}$			445
$f_1(1285) \pi^- \nu_\tau$		$(3.9 \pm 0.5) \times 10^{-4}$		S=1.9	408
$f_1(1285) \pi^- \nu_\tau \to \eta \pi^- \pi^+ \pi^- \nu_\tau$		$(1.18 \pm 0.07) \times 10^{-4}$		S=1.3	–

Int. J. Mod. Phys. A 2026.41. Downloaded from www.worldscientific.com
by UNIVERSITY OF CALIFORNIA @ BERKELEY on 09/16/26. Re-use and distribution is strictly not permitted, except for Open Acce

$f_1(1285)\pi^-\nu_\tau \to 3\pi^-2\pi^+\nu_\tau$	[g]	$(5.2 \pm 0.4)\times10^{-5}$		–
$\pi(1300)^-\nu_\tau \to (\rho\pi)^-\nu_\tau \to (3\pi)^-\nu_\tau$		<1.0	$\times10^{-4}$ CL=90%	–
$\pi(1300)^-\nu_\tau \to ((\pi\pi)_{S-\text{wave}}\,\pi)^-\nu_\tau \to (3\pi)^-\nu_\tau$		<1.9	$\times10^{-4}$ CL=90%	–
$h^-\omega \geq 0$ neutrals ν_τ		(2.40 ± 0.08) %		708
$h^-\omega\nu_\tau$		(1.99 ± 0.06) %		708
$\pi^-\omega\nu_\tau$	[g]	(1.95 ± 0.06) %		708
$K^-\omega\nu_\tau$	[g]	$(4.1 \pm 0.9)\times10^{-4}$		610
$h^-\omega\pi^0\nu_\tau$	[g]	$(4.1 \pm 0.4)\times10^{-3}$		684
$h^-\omega 2\pi^0\nu_\tau$		$(1.4 \pm 0.5)\times10^{-4}$		644
$\pi^-\omega 2\pi^0\nu_\tau$	[g]	$(7.2 \pm 1.6)\times10^{-5}$		644
$h^-2\omega\nu_\tau$		<5.4	$\times10^{-7}$ CL=90%	250
$2h^-h^+\omega\nu_\tau$		$(1.20 \pm 0.22)\times10^{-4}$		641
$2\pi^-\pi^+\omega\nu_\tau$ (ex.K^0)	[g]	$(8.4 \pm 0.6)\times10^{-5}$		641

Lepton Family number (LF), Lepton number (L), or Baryon number (B) violating modes

L means lepton number violation (*e.g.* $\tau^- \to e^+\pi^-\pi^-$). Following common usage, LF means lepton family violation *and not* lepton number violation (*e.g.* $\tau^- \to e^-\pi^+\pi^-$). B means baryon number violation.

$e^-\gamma$	LF	<3.3	$\times10^{-8}$ CL=90%	888
$e^-\gamma\gamma$	LF	<2.5	$\times10^{-4}$ CL=90%	888
$\mu^-\gamma$	LF	<4.2	$\times10^{-8}$ CL=90%	885
$\mu^-\gamma\gamma$	LF	<5.8	$\times10^{-4}$ CL=90%	885
$e^-\pi^0$	LF	<8.0	$\times10^{-8}$ CL=90%	883
$\mu^-\pi^0$	LF	<1.1	$\times10^{-7}$ CL=90%	880
$e^-K^0_S$	LF	<8	$\times10^{-9}$ CL=90%	819
$\mu^-K^0_S$	LF	<1.2	$\times10^{-8}$ CL=90%	815
$e^-\eta$	LF	<9.2	$\times10^{-8}$ CL=90%	804
$\mu^-\eta$	LF	<6.5	$\times10^{-8}$ CL=90%	800
$e^-\rho^0$	LF	<2.2	$\times10^{-8}$ CL=90%	719
$\mu^-\rho^0$	LF	<1.7	$\times10^{-8}$ CL=90%	715
$e^-\omega$	LF	<2.4	$\times10^{-8}$ CL=90%	716
$\mu^-\omega$	LF	<3.9	$\times10^{-8}$ CL=90%	711
$e^-K^*(892)^0$	LF	<1.9	$\times10^{-8}$ CL=90%	665
$\mu^-K^*(892)^0$	LF	<2.9	$\times10^{-8}$ CL=90%	659
$e^-\overline{K}^*(892)^0$	LF	<1.7	$\times10^{-8}$ CL=90%	665
$\mu^-\overline{K}^*(892)^0$	LF	<4.3	$\times10^{-8}$ CL=90%	659
$e^-\eta'(958)$	LF	<1.6	$\times10^{-7}$ CL=90%	630
$\mu^-\eta'(958)$	LF	<1.3	$\times10^{-7}$ CL=90%	625
$e^-f_0(980) \to e^-\pi^+\pi^-$	LF	<3.2	$\times10^{-8}$ CL=90%	–
$\mu^-f_0(980) \to \mu^-\pi^+\pi^-$	LF	<3.4	$\times10^{-8}$ CL=90%	–
$e^-\phi$	LF	<2.0	$\times10^{-8}$ CL=90%	596
$\mu^-\phi$	LF	<2.3	$\times10^{-8}$ CL=90%	590
$e^-e^+e^-$	LF	<2.5	$\times10^{-8}$ CL=90%	888
$e^-\mu^+\mu^-$	LF	<2.4	$\times10^{-8}$ CL=90%	882
$e^+\mu^-\mu^-$	LF	<1.3	$\times10^{-8}$ CL=90%	882
$\mu^-e^+e^-$	LF	<1.6	$\times10^{-8}$ CL=90%	885
$\mu^+e^-e^-$	LF	<1.5	$\times10^{-8}$ CL=90%	885
$\mu^-\mu^+\mu^-$	LF	<1.9	$\times10^{-8}$ CL=90%	873
$e^-\pi^+\pi^-$	LF	<2.3	$\times10^{-8}$ CL=90%	877
$e^+\pi^-\pi^-$	L	<2.0	$\times10^{-8}$ CL=90%	877
$\mu^-\pi^+\pi^-$	LF	<2.1	$\times10^{-8}$ CL=90%	866
$\mu^+\pi^-\pi^-$	L	<3.9	$\times10^{-8}$ CL=90%	866
$e^-\pi^+K^-$	LF	<3.7	$\times10^{-8}$ CL=90%	813
$e^-\pi^-K^+$	LF	<3.1	$\times10^{-8}$ CL=90%	813
$e^+\pi^-K^-$	L	<3.2	$\times10^{-8}$ CL=90%	813
$e^-K^0_SK^0_S$	LF	<7.1	$\times10^{-8}$ CL=90%	736
$e^-K^+K^-$	LF	<3.4	$\times10^{-8}$ CL=90%	739
$e^+K^-K^-$	L	<3.3	$\times10^{-8}$ CL=90%	739
$\mu^-\pi^+K^-$	LF	<8.6	$\times10^{-8}$ CL=90%	800
$\mu^-\pi^-K^+$	LF	<4.5	$\times10^{-8}$ CL=90%	800
$\mu^+\pi^-K^-$	L	<4.8	$\times10^{-8}$ CL=90%	800
$\mu^-K^0_SK^0_S$	LF	<8.0	$\times10^{-8}$ CL=90%	696
$\mu^-K^+K^-$	LF	<4.4	$\times10^{-8}$ CL=90%	699
$\mu^+K^-K^-$	L	<4.7	$\times10^{-8}$ CL=90%	699
$e^-\pi^0\pi^0$	LF	<6.5	$\times10^{-6}$ CL=90%	878
$\mu^-\pi^0\pi^0$	LF	<1.4	$\times10^{-5}$ CL=90%	867
$e^-\eta\eta$	LF	<3.5	$\times10^{-5}$ CL=90%	699
$\mu^-\eta\eta$	LF	<6.0	$\times10^{-5}$ CL=90%	653
$e^-\pi^0\eta$	LF	<2.4	$\times10^{-5}$ CL=90%	798
$\mu^-\pi^0\eta$	LF	<2.2	$\times10^{-5}$ CL=90%	784
pe^-e^-	L,B	<3.0	$\times10^{-8}$ CL=90%	641
$\overline{p}e^+e^-$	L,B	<3.0	$\times10^{-8}$ CL=90%	641
$\overline{p}e^+\mu^-$	L,B	<2.0	$\times10^{-8}$ CL=90%	635
$\overline{p}e^-\mu^+$	L,B	<1.8	$\times10^{-8}$ CL=90%	635
$p\mu^-\mu^-$	L,B	<4.0	$\times10^{-8}$ CL=90%	618
$\overline{p}\mu^+\mu^-$	L,B	<1.8	$\times10^{-8}$ CL=90%	618
$\overline{p}\gamma$	L,B	<3.5	$\times10^{-6}$ CL=90%	641
$\overline{p}\pi^0$	L,B	<1.5	$\times10^{-5}$ CL=90%	632
$\overline{p}2\pi^0$	L,B	<3.3	$\times10^{-5}$ CL=90%	604
$\overline{p}\eta$	L,B	<8.9	$\times10^{-6}$ CL=90%	475
$\overline{p}\pi^0\eta$	L,B	<2.7	$\times10^{-5}$ CL=90%	360
$\Lambda\pi^-$	L,B	<4.7	$\times10^{-8}$ CL=90%	525
$\overline{\Lambda}\pi^-$	L,B	<4.3	$\times10^{-8}$ CL=90%	525
e^-light boson	LF	<4.5	$\times10^{-4}$ CL=90%	–
μ^-light boson	LF	<2.8	$\times10^{-4}$ CL=90%	–

Heavy Charged Lepton Searches

$L^\pm$ – charged lepton

Mass $m >$ 100.8 GeV, CL = 95% [h] Decay to νW.

$L^\pm$ – stable charged heavy lepton

Mass $m >$ 102.6 GeV, CL = 95%

Neutrino Properties

See the note on "Neutrino properties listings" in the Particle Listings.

Mass $m <$ 0.45 eV, CL = 90% (tritium decay)
Mean life/mass, $\tau/m >$ 300 s/eV, CL = 90% (reactor)
Mean life/mass, $\tau/m > 7\times10^9$ s/eV (solar)
Mean life/mass, $\tau/m >$ 15.4 s/eV, CL = 90% (accelerator)
Magnetic moment $\mu < 0.064\times10^{-10}\ \mu_B$, CL = 90% (solar + radiochemical)

Number of Neutrino Types

Number $N = 2.996 \pm 0.007$ (Standard Model fits to LEP-SLC data)
Number $N = 2.92 \pm 0.05$ (S = 1.2) (Direct measurement of invisible Z width)

Neutrino Mixing

The following values are obtained through data analyses based on the 3-neutrino mixing scheme described in the review "Neutrino Masses, Mixing, and Oscillations."

$\sin^2(\theta_{12}) = 0.307 \pm 0.012$
$\Delta m^2_{21} = (7.60 \pm 0.17)\times10^{-5}$ eV^2
$\sin^2(\theta_{23}) = 0.523^{+0.031}_{-0.027}$ (S = 1.3) (Inverted order)
$\sin^2(\theta_{23}) = 0.533 \pm 0.018$ (Normal order)
$\Delta m^2_{32} = (-2.52 \pm 0.04)\times10^{-3}$ eV^2 (S = 1.3) (Inverted order)
$\Delta m^2_{32} = (2.445 \pm 0.023)\times10^{-3}$ eV^2 (Normal order)
$\sin^2(\theta_{13}) = (2.17 \pm 0.07)\times10^{-2}$ (S = 1.4)
δ, CP violating phase $= 1.21^{+0.19}_{-0.17}\ \pi$ rad (S = 1.2)
$\langle \Delta m^2_{21} - \Delta\overline{m}^2_{21}\rangle < 1.1\times10^{-4}$ eV^2, CL = 99.7%
$\langle \Delta m^2_{32} - \Delta\overline{m}^2_{32}\rangle = (-0.12 \pm 0.25)\times10^{-3}$ eV^2

NOTES

In this Summary Table:

When a quantity has "(S = ...)" to its right, the error on the quantity has been enlarged by the "scale factor" S, defined as $S = \sqrt{\chi^2/(N-1)}$, where N is the number of measurements used in calculating the quantity. We do this when S > 1, which often indicates that the measurements are inconsistent. When S > 1.25, we also show in the Particle Listings an ideogram of the measurements. For more about S, see the Introduction.

A decay momentum p is given for each decay mode. For a 2-body decay, p is the momentum of each decay product in the rest frame of the decaying particle. For a 3-or-more-body decay, p is the largest momentum any of the products can have in this frame.

[a] This is the best limit for the mode $e^- \to \nu\gamma$.

[*b*] See the review on "Muon Decay Parameters" for definitions and details.

[*c*] P_μ is the longitudinal polarization of the muon from pion decay. For $V-A$ coupling, $P_\mu = 1$ and $\rho = \delta = 3/4$.

[*d*] This only includes events with energy of $e > 45$ MeV and energy of $\gamma > 40$ MeV. Since the $e^- \overline{\nu}_e \nu_\mu$ and $e^- \overline{\nu}_e \nu_\mu \gamma$ modes cannot be clearly separated, we regard the latter mode as a subset of the former.

[*e*] See the relevant Particle Listings for the energy limits used in this measurement.

[*f*] A test of additive vs. multiplicative lepton family number conservation.

[*g*] Basis mode for the τ.

[*h*] $L^\pm$ mass limit depends on decay assumptions; see the Full Listings.

Int. J. Mod. Phys. A 2026.41. Downloaded from www.worldscientific.com
by UNIVERSITY OF CALIFORNIA @ BERKELEY on 09/16/26. Re-use and distribution is strictly not permitted, except for Open Access articles.

Int. J. Mod. Phys. A 2026.41. Downloaded from www.worldscientific.com
by UNIVERSITY OF CALIFORNIA @ BERKELEY on 09/16/26. Re-use and distribution is strictly not permitted, except for Open Acce

QUARKS

The u-, d-, and s-quark masses are the $\overline{\text{MS}}$ masses at the scale μ = 2 GeV. The c- and b-quark masses are the $\overline{\text{MS}}$ masses renormalized at the $\overline{\text{MS}}$ mass, i.e. $\overline{m} = \overline{m}(\mu = \overline{m})$. The t-quark mass is extracted from event kinematics (see the review "The Top Quark").

u

$I(J^P) = \frac{1}{2}(\frac{1}{2}^+)$

$m_u = 2.16 \pm 0.07$ MeV, CL = 90% Charge = $\frac{2}{3}$ e $I_z = +\frac{1}{2}$
$m_u/m_d = 0.462 \pm 0.020$, CL = 90%

d

$I(J^P) = \frac{1}{2}(\frac{1}{2}^+)$

$m_d = 4.70 \pm 0.07$ MeV, CL = 90% Charge = $-\frac{1}{3}$ e $I_z = -\frac{1}{2}$
m_s/m_d = 17–22
$\overline{m} = (m_u+m_d)/2 = 3.49 \pm 0.07$ MeV, CL = 90%

s

$I(J^P) = 0(\frac{1}{2}^+)$

$m_s = 92.9 \pm 0.7$ MeV, CL = 90% Charge = $-\frac{1}{3}$ e Strangeness = -1
m_s / $((m_u + m_d)/2) = 27.33^{+0.18}_{-0.14}$, CL = 90%

c

$I(J^P) = 0(\frac{1}{2}^+)$

$m_c = 1.2729 \pm 0.0045$ GeV, CL = 90% Charge = $\frac{2}{3}$ e Charm = $+1$
$m_b - m_c = 3.45 \pm 0.05$ GeV

b

$I(J^P) = 0(\frac{1}{2}^+)$

$m_b = 4.186 \pm 0.006$ GeV, CL = 90% Charge = $-\frac{1}{3}$ e Bottom = -1

t

$I(J^P) = 0(\frac{1}{2}^+)$

Charge = $\frac{2}{3}$ e Top = $+1$

Mass (direct measurements) $m = 172.60 \pm 0.27$ GeV [a,b] (S = 1.5)
Mass (from cross-section measurements) $m = 162.5^{+2.1}_{-1.5}$ GeV [a]
Mass (Pole from cross-section measurements) $m = 172.1 \pm 0.6$ GeV
$m_t - m_{\overline{t}} = -0.15 \pm 0.20$ GeV (S = 1.1)
Full width $\Gamma = 1.42^{+0.19}_{-0.15}$ GeV (S = 1.4)
$\Gamma(Wb)/\Gamma(Wq(q = b, s, d)) = 0.957 \pm 0.034$ (S = 1.5)

t-quark EW Couplings

$F_0 = 0.693 \pm 0.013$
$F_- = 0.315 \pm 0.010$
$F_+ = -0.005 \pm 0.007$
$F_{V+A} < 0.29$, CL = 95%

t DECAY MODES		Fraction (Γ_i/Γ)	Confidence level	p (MeV/c)
$Wq(q = b, s, d)$				–
Wb				–
$e\nu_e b$		(11.10 ± 0.30) %		–
$\mu\nu_\mu b$		(11.40 ± 0.20) %		–
$\tau\nu_\tau b$		(10.7 ± 0.5) %		–
$q\overline{q}b$		(66.5 ± 1.4) %		–
$\gamma q(q=u,c)$	[c]	$< 9.5 \times 10^{-6}$	95%	–
$aq(q=u, c)$		$< 1 \times 10^{-3}$	95%	–
$\Delta T = 1$ weak neutral current ($T1$) modes				
$Zq(q=u,c)$	$T1$	[d] $< 1.2 \times 10^{-4}$	95%	–
Hu	$T1$	$< 1.9 \times 10^{-4}$	95%	–
Hc	$T1$	$< 3.4 \times 10^{-4}$	95%	–
$\ell^+\overline{q}q'(q=d,s,b;\ q'=u,c)$	$T1$	$< 1.6 \times 10^{-3}$	95%	–
Lepton Family number (LF) violating modes				
$e^\pm\mu^\mp c$	LF	$< 2.16 \times 10^{-7}$	95%	–
$e^\pm\mu^\mp u$	LF	$< 1.2 \times 10^{-8}$	95%	–

b′ (4th Generation) Quark, Searches for

Mass $m >$ 190 GeV, CL = 95% ($p\overline{p}$, quasi-stable b')
Mass $m >$ 1390 GeV, CL = 95% (B($b' \to Zb$) = 1)
Mass $m >$ 1350 GeV, CL = 95% (B($b' \to Wt$) = 1)
Mass $m >$ 1570 GeV, CL = 95% (B($b' \to Hb$) = 1)
Mass $m >$ 46.0 GeV, CL = 95% (e^+e^-, all decays)

t′ (4th Generation) Quark, Searches for

$m(t'(2/3)) >$ 1280 GeV, CL = 95% (B($t' \to Zt$) = 1)
$m(t'(2/3)) >$ 1295 GeV, CL = 95% (B($t' \to Wb$) = 1)
$m(t'(2/3)) >$ 1310 GeV, CL = 95% (singlet t')
$m(t'(2/3)) >$ 1350 GeV, CL = 95% (t' in a weak isospin doublet (t',b'))
$m(t'(5/3)) > 1.460 \times 10^3$ GeV, CL = 95% ($t'(5/3) \to tW^+$)

Free Quark Searches

All searches since 1977 have had negative results.

NOTES

[a] A discussion of the definition of the top quark mass in these measurements can be found in the review "The Top Quark."

[b] Based on published top mass measurements using data from Tevatron Run-I and Run-II and LHC at $\sqrt{s} = 7$ TeV. Including the most recent unpublished results from Tevatron Run-II, the Tevatron Electroweak Working Group reports a top mass of 173.2 ± 0.9 GeV. See the note "The Top Quark' in the Quark Particle Listings of this *Review*.

[c] This limit is for $\Gamma(t \to \gamma q)/\Gamma(t \to Wb)$.

[d] This limit is for $\Gamma(t \to Zq)/\Gamma(t \to Wb)$.

Int. J. Mod. Phys. A 2026.41. Downloaded from www.worldscientific.com
by UNIVERSITY OF CALIFORNIA @ BERKELEY on 09/16/26. Re-use and distribution is strictly not permitted, except for Open Access articles.

LIGHT UNFLAVORED MESONS ($S = C = B = 0$)

For $I = 1$ (π, b, ρ, a): $u\overline{d}$, $(u\overline{u}-d\overline{d})/\sqrt{2}$, $d\overline{u}$;
for $I = 0$ (η, η', h, h', ω, ϕ, f, f'): $c_1(u\overline{u} + d\overline{d}) + c_2(s\overline{s})$

$\pi^\pm$

$I^G(J^P) = 1^-(0^-)$

Mass $m = 139.57039 \pm 0.00018$ MeV (S = 1.8)
Mean life $\tau = (2.6033 \pm 0.0005) \times 10^{-8}$ s (S = 1.2)
$c\tau = 7.8045$ m

$\pi^\pm \to \ell^\pm \nu\gamma$ form factors [a]

$F_V = 0.0254 \pm 0.0017$
$F_A = 0.0119 \pm 0.0001$
F_V slope parameter $a = 0.10 \pm 0.06$
$R = 0.059^{+0.009}_{-0.008}$

π^- modes are charge conjugates of the modes below.

For decay limits to particles which are not established, see the section on Searches for Axions and Other Very Light Bosons.

π^+ DECAY MODES		Fraction (Γ_i/Γ)	Confidence level	p (MeV/c)
$\mu^+\nu_\mu$	[b]	(99.98770 ± 0.00004) %		30
$\mu^+\nu_\mu\gamma$	[c]	$(2.00 \pm 0.25) \times 10^{-4}$		30
$e^+\nu_e$	[b]	$(1.230 \pm 0.004) \times 10^{-4}$		70
$e^+\nu_e\gamma$	[c]	$(7.39 \pm 0.05) \times 10^{-7}$		70
$e^+\nu_e\pi^0$		$(1.036 \pm 0.006) \times 10^{-8}$		4
$e^+\nu_e e^+e^-$		$(3.2 \pm 0.5) \times 10^{-9}$		70
$\mu^+\nu_\mu\nu\overline{\nu}$		$< 9 \times 10^{-6}$	90%	30
$e^+\nu_e\nu\overline{\nu}$		$< 1.6 \times 10^{-7}$	90%	70
Lepton Family number (LF) or Lepton number (L) violating modes				
$\mu^+\overline{\nu}_e$	L [d]	$< 1.5 \times 10^{-3}$	90%	30
$\mu^+\nu_e$	LF [d]	$< 8.0 \times 10^{-3}$	90%	30
$\mu^-e^+e^+\nu$	LF	$< 1.6 \times 10^{-6}$	90%	30

π^0

$I^G(J^{PC}) = 1^-(0^{-+})$

Mass $m = 134.9768 \pm 0.0005$ MeV (S = 1.1)
$m_{\pi^\pm} - m_{\pi^0} = 4.5936 \pm 0.0005$ MeV
Mean life $\tau = (8.43 \pm 0.13) \times 10^{-17}$ s (S = 1.2)
$c\tau = 25.3$ nm

For decay limits to particles which are not established, see the appropriate Search sections (A^0 (axion) and Other Light Boson (X^0) Searches, etc.).

π^0 DECAY MODES		Fraction (Γ_i/Γ)	Scale factor/ Confidence level	p (MeV/c)
2γ		(98.823 ± 0.034) %	S=1.5	67
$e^+e^-\gamma$		(1.174 ± 0.035) %	S=1.5	67
γpositronium		$(1.82 \pm 0.29) \times 10^{-9}$		67
$e^+e^+e^-e^-$		$(3.34 \pm 0.16) \times 10^{-5}$		67
e^+e^-		$(6.46 \pm 0.33) \times 10^{-8}$		67
4γ		$< 2 \times 10^{-8}$	CL=90%	67
invisible		$< 4.4 \times 10^{-9}$	CL=90%	–
$\nu_e\overline{\nu}_e$		$< 1.7 \times 10^{-6}$	CL=90%	67
$\nu_\mu\overline{\nu}_\mu$		$< 1.6 \times 10^{-6}$	CL=90%	67
$\nu_\tau\overline{\nu}_\tau$		$< 2.1 \times 10^{-6}$	CL=90%	67
$\gamma\nu\overline{\nu}$		$< 1.9 \times 10^{-7}$	CL=90%	67
Charge conjugation (C) or Lepton Family number (LF) violating modes				
3γ	C	$< 3.1 \times 10^{-8}$	CL=90%	67
μ^+e^-	LF	$< 3.8 \times 10^{-10}$	CL=90%	26
μ^-e^+	LF	$< 3.2 \times 10^{-10}$	CL=90%	26
$\mu^+e^- + \mu^-e^+$	LF	$< 3.6 \times 10^{-10}$	CL=90%	26

η

$I^G(J^{PC}) = 0^+(0^{-+})$

Mass $m = 547.862 \pm 0.017$ MeV
Full width $\Gamma = 1.31 \pm 0.05$ keV

C-nonconserving decay parameters

$\pi^+\pi^-\pi^0$ left-right asymmetry $= (0.09^{+0.11}_{-0.12}) \times 10^{-2}$
$\pi^+\pi^-\pi^0$ sextant asymmetry $= (0.12^{+0.10}_{-0.11}) \times 10^{-2}$
$\pi^+\pi^-\pi^0$ quadrant asymmetry $= (-0.09 \pm 0.09) \times 10^{-2}$
$\pi^+\pi^-\gamma$ left-right asymmetry $= (0.9 \pm 0.4) \times 10^{-2}$
$\pi^+\pi^-\gamma$ β (D-wave) $= -0.02 \pm 0.07$ (S = 1.3)

CP-nonconserving decay parameters

$\pi^+\pi^-e^+e^-$ decay-plane asymmetry $A_\phi = (-1.6 \pm 2.6) \times 10^{-2}$

Other decay parameters

$\pi^0\pi^0\pi^0$ Dalitz plot $\alpha = -0.0296 \pm 0.0016$ (S = 1.7)
Parameter Λ in $\eta \to \ell^+\ell^-\gamma$ decay $= 0.731 \pm 0.013$ GeV/c^2 (S = 1.3)

η DECAY MODES		Fraction (Γ_i/Γ)	Scale factor/ Confidence level	p (MeV/c)
Neutral modes				
neutral modes		(71.95 ± 0.29) %	S=1.3	–
2γ		(39.36 ± 0.18) %	S=1.1	274
$3\pi^0$		(32.56 ± 0.21) %	S=1.2	179
$\pi^0 2\gamma$		$(2.55 \pm 0.22) \times 10^{-4}$		257
$2\pi^0 2\gamma$		$< 1.2 \times 10^{-3}$	CL=90%	238
4γ		$< 2.8 \times 10^{-4}$	CL=90%	274
invisible		$< 2.4 \times 10^{-5}$	CL=90%	–
Charged modes				
charged modes		(28.05 ± 0.29) %	S=1.3	–
$\pi^+\pi^-\pi^0$		(23.02 ± 0.25) %	S=1.2	174
$\pi^+\pi^-\gamma$		(4.28 ± 0.07) %	S=1.1	236
$e^+e^-\gamma$		$(6.96 \pm 0.18) \times 10^{-3}$		274
$\mu^+\mu^-\gamma$		$(2.98 \pm 0.13) \times 10^{-4}$		253
e^+e^-		$< 7 \times 10^{-7}$	CL=90%	274
$\mu^+\mu^-$		$(5.8 \pm 0.8) \times 10^{-6}$		253
$2e^+2e^-$		$(2.40 \pm 0.22) \times 10^{-5}$		274
$\pi^+\pi^-e^+e^-(\gamma)$		$(2.76 \pm 0.16) \times 10^{-4}$	S=1.5	235
$e^+e^-\mu^+\mu^-$		$< 6.88 \times 10^{-6}$	CL=90%	253
$2\mu^+2\mu^-$		$(5.0 \pm 1.3) \times 10^{-9}$		161
$\mu^+\mu^-\pi^+\pi^-$		$< 4.0 \times 10^{-7}$	CL=90%	113
$\pi^+e^-\overline{\nu}_e$ + c.c.		$< 1.7 \times 10^{-4}$	CL=90%	256
$\pi^+\pi^-2\gamma$		$< 2.1 \times 10^{-3}$		236
$\pi^+\pi^-\pi^0\gamma$		$< 6 \times 10^{-4}$	CL=90%	174
$\pi^0\mu^+\mu^-\gamma$		$< 3 \times 10^{-6}$	CL=90%	210
Charge conjugation (C), Parity (P), Charge conjugation × Parity (CP), or Lepton Family number (LF) violating modes				
$\pi^0\gamma$	C	[e] $< 9 \times 10^{-5}$	CL=90%	257
$\pi^+\pi^-$	P,CP	$< 4.4 \times 10^{-6}$	CL=90%	236
$2\pi^0$	P,CP	$< 3.5 \times 10^{-4}$	CL=90%	238
$2\pi^0\gamma$	C	$< 5 \times 10^{-4}$	CL=90%	238
$3\pi^0\gamma$	C	$< 6 \times 10^{-5}$	CL=90%	179
3γ	C	$< 1.6 \times 10^{-5}$	CL=90%	274
$4\pi^0$	P,CP	$< 6.9 \times 10^{-7}$	CL=90%	40
$\pi^0e^+e^-$	C	[f] $< 8 \times 10^{-6}$	CL=90%	257
$\pi^0\mu^+\mu^-$	C	[f] $< 5 \times 10^{-6}$	CL=90%	210
$\mu^+e^- + \mu^-e^+$	LF	$< 6 \times 10^{-6}$	CL=90%	264
$\pi^+\pi^+e^-e^-$ + c.c.	LF	$< 4.6 \times 10^{-6}$	CL=90%	235

$f_0(500)$

$I^G(J^{PC}) = 0^+(0^{++})$

also known as σ; was $f_0(600)$, $f_0(400\text{–}1200)$

See the review on "Scalar Mesons below 1 GeV."

Mass (T-Matrix Pole $\sqrt{s}$) = (400–550)$-i$(200–350) MeV
Mass (Breit-Wigner) = 400 to 800 MeV
Full width (Breit-Wigner) = 100 to 800 MeV

$f_0(500)$ DECAY MODES	Fraction (Γ_i/Γ)	p (MeV/c)
$\pi\pi$	seen	–
$\gamma\gamma$	seen	–

$\rho(770)$

$I^G(J^{PC}) = 1^+(1^{--})$

See the review on "Spectroscopy of Light Meson Resonances."

T-Matrix Pole $\sqrt{s} = (761\text{–}765) - i\,(71\text{–}74)$ MeV
ρ^0 mass (Breit-Wigner) = 775.26 ± 0.23 MeV [g]
$\rho^\pm$ mass (Breit-Wigner) = 775.11 ± 0.34 MeV [h]
ρ^0 full width (Breit-Wigner) = 147.4 ± 0.8 MeV [g] (S = 2.0)
$\rho^\pm$ full width (Breit-Wigner) = 149.1 ± 0.8 MeV [h]

Int. J. Mod. Phys. A 2026.41. Downloaded from www.worldscientific.com
by UNIVERSITY OF CALIFORNIA @ BERKELEY on 09/16/26. Re-use and distribution is strictly not permitted, except for Open Acce

$\rho(770)$ DECAY MODES	Fraction (Γ_i/Γ)	Scale factor/ Confidence level	p (MeV/c)
$\pi\pi$	~ 100 %		363
$\rho(770)^\pm$ decays			
$\pi^\pm\gamma$	$(4.5 \pm 0.5) \times 10^{-4}$	S=2.2	375
$\pi^\pm\eta$	$< 6 \times 10^{-3}$	CL=84%	152
$\pi^\pm\pi^+\pi^-\pi^0$	$< 2.0 \times 10^{-3}$	CL=84%	254
$\rho(770)^0$ decays			
$\pi^+\pi^-\gamma$	$(9.9 \pm 1.6) \times 10^{-3}$		362
$\pi^0\gamma$	$(4.7 \pm 0.8) \times 10^{-4}$	S=1.7	376
$\eta\gamma$	$(3.00 \pm 0.21) \times 10^{-4}$		194
$\pi^0\pi^0\gamma$	$(4.5 \pm 0.8) \times 10^{-5}$		363
$\mu^+\mu^-$	[i] $(4.55 \pm 0.28) \times 10^{-5}$		373
e^+e^-	[i] $(4.72 \pm 0.05) \times 10^{-5}$		388
$\pi^+\pi^-\pi^0$	$(9 \pm 4) \times 10^{-5}$		323
$\pi^+\pi^-\pi^+\pi^-$	$(1.8 \pm 0.9) \times 10^{-5}$		251
$\pi^+\pi^-\pi^0\pi^0$	$(1.6 \pm 0.8) \times 10^{-5}$		256
$\pi^0 e^+e^-$	$< 1.2 \times 10^{-5}$	CL=90%	376

$\omega(782)$

$I^G(J^{PC}) = 0^-(1^{--})$

Mass $m = 782.66 \pm 0.13$ MeV (S = 2.0)
Full width $\Gamma = 8.68 \pm 0.13$ MeV

$\omega(782)$ DECAY MODES	Fraction (Γ_i/Γ)	Scale factor/ Confidence level	p (MeV/c)
$\pi^+\pi^-\pi^0$	(89.2 ± 0.7) %		327
$\pi^0\gamma$	(8.33 ± 0.25) %	S=2.1	380
$\pi^+\pi^-$	(1.53 ± 0.12) %	S=1.2	366
neutrals (excluding $\pi^0\gamma$)	$(7 \pm^{7}_{5}) \times 10^{-3}$	S=1.1	–
$\eta\gamma$	$(4.5 \pm 0.4) \times 10^{-4}$	S=1.1	200
$\pi^0 e^+e^-$	$(7.7 \pm 0.6) \times 10^{-4}$		380
$\pi^0\mu^+\mu^-$	$(1.34 \pm 0.18) \times 10^{-4}$	S=1.5	349
e^+e^-	$(7.41 \pm 0.19) \times 10^{-5}$	S=1.8	391
$\pi^+\pi^-\pi^0\pi^0$	$< 2 \times 10^{-4}$	CL=90%	262
$\pi^+\pi^-e^+e^-$	$< 2.8 \times 10^{-6}$	CL=90%	365
$\pi^+\pi^-\gamma$	$< 3.6 \times 10^{-3}$	CL=95%	366
$\pi^+\pi^-\pi^+\pi^-$	$< 1 \times 10^{-3}$	CL=90%	256
$\pi^0\pi^0\gamma$	$(6.7 \pm 1.1) \times 10^{-5}$		367
$\eta\pi^0\gamma$	$< 3.3 \times 10^{-5}$	CL=90%	162
$\mu^+\mu^-$	$(7.4 \pm 1.8) \times 10^{-5}$		377
3γ	$< 1.9 \times 10^{-4}$	CL=95%	391
Charge conjugation (C) violating modes			
$\eta\pi^0$ C	$< 2.1 \times 10^{-4}$	CL=90%	162
$2\pi^0$ C	$< 2.2 \times 10^{-4}$	CL=90%	367
$3\pi^0$ C	$< 2.3 \times 10^{-4}$	CL=90%	330
invisible	$< 7 \times 10^{-5}$	CL=90%	–

$\eta'(958)$

$I^G(J^{PC}) = 0^+(0^{-+})$

Mass $m = 957.78 \pm 0.06$ MeV
Full width $\Gamma = 0.188 \pm 0.006$ MeV

$\eta'(958)$ DECAY MODES	Fraction (Γ_i/Γ)	Confidence level	p (MeV/c)
$\pi^+\pi^-\eta$	(42.5 ± 0.5) %		232
$\rho^0\gamma$ (including non-resonant $\pi^+\pi^-\gamma$)	(29.48 ± 0.35) %		165
$\pi^0\pi^0\eta$	(22.4 ± 0.5) %		239
$\omega\gamma$	(2.52 ± 0.07) %		159
ωe^+e^-	$(2.0 \pm 0.4) \times 10^{-4}$		159
$\gamma\gamma$	(2.307 ± 0.033) %		479
$3\pi^0$	$(2.50 \pm 0.17) \times 10^{-3}$		430
$\mu^+\mu^-\gamma$	$(1.13 \pm 0.28) \times 10^{-4}$		467
$\pi^+\pi^-\mu^+\mu^-$	$(2.13 \pm 0.13) \times 10^{-5}$		401
$\pi^+\pi^-\pi^0$	$(3.61 \pm 0.17) \times 10^{-3}$		428
$(\pi^+\pi^-\pi^0)$ S-wave	$(3.8 \pm 0.5) \times 10^{-3}$		428
$\pi^\mp\rho^\pm$	$(7.4 \pm 2.3) \times 10^{-4}$		106
$2(\pi^+\pi^-)$	$(8.51 \pm 0.33) \times 10^{-5}$		372
$\pi^+\pi^-2\pi^0$	$(2.11 \pm 0.15) \times 10^{-4}$		376
$2(\pi^+\pi^-)$ neutrals	< 1 %	95%	–
$2(\pi^+\pi^-)\pi^0$	$< 1.8 \times 10^{-3}$	90%	298
$2(\pi^+\pi^-)2\pi^0$	< 1 %	95%	197
$3(\pi^+\pi^-)$	$< 3.1 \times 10^{-5}$	90%	189
$K^\pm\pi^\mp$	$< 4 \times 10^{-5}$	90%	334
$\pi^+\pi^-e^+e^-$	$(2.43 \pm 0.06) \times 10^{-3}$		458
$\pi^+e^-\nu_e +$ c.c.	$< 2.1 \times 10^{-4}$	90%	469
γe^+e^-	$(4.80 \pm 0.15) \times 10^{-4}$		479
$\pi^0\gamma\gamma$	$(3.20 \pm 0.24) \times 10^{-3}$		469
$\pi^0\gamma\gamma$ (non resonant)	$(6.2 \pm 0.9) \times 10^{-4}$		–
$\eta\gamma\gamma$	$< 1.33 \times 10^{-4}$	90%	322
$4\pi^0$	$< 1.2 \times 10^{-5}$	90%	380
e^+e^-	$< 5.6 \times 10^{-9}$	90%	479
$e^+e^-e^+e^-$	$(4.5 \pm 1.1) \times 10^{-6}$		479
$e^+e^-\mu^+\mu^-$	$< 1.8 \times 10^{-6}$	90%	467
$\mu^+\mu^-\mu^+\mu^-$	$< 5 \times 10^{-7}$	90%	419
invisible	$< 2.1 \times 10^{-4}$	90%	–
γ Dark Photon	5×10^{-7} to 3.5×10^{-6}	90%	–
Charge conjugation (C), Parity (P), Lepton family number (LF) violating modes			
$\pi^+\pi^-$ P,CP	$< 1.8 \times 10^{-5}$	90%	458
$\pi^0\pi^0$ P,CP	$< 4 \times 10^{-4}$	90%	459
$\pi^0 e^+e^-$ C	[f] $< 1.4 \times 10^{-3}$	90%	469
$\pi^0\rho^0$ C	< 4 %	90%	111
ηe^+e^- C	[f] $< 2.4 \times 10^{-3}$	90%	322
3γ C	$< 1.0 \times 10^{-4}$	90%	479
$\mu^+\mu^-\pi^0$ C	[f] $< 6.0 \times 10^{-5}$	90%	445
$\mu^+\mu^-\eta$ C	[f] $< 1.5 \times 10^{-5}$	90%	273
$e\mu$ LF	$< 4.7 \times 10^{-4}$	90%	473
$\pi^+\pi^-$ALP $\to \pi^+\pi^-e^+e^-$	$< 1.9 \times 10^{-5}$	90%	–

$f_0(980)$

$I^G(J^{PC}) = 0^+(0^{++})$

See the review on "Scalar Mesons below 1 GeV."
T-matrix pole $\sqrt{s} = (980\text{–}1010) - i\,(20\text{–}35)$ MeV [j]
Mass (Breit-Wigner) = 990 ± 20 MeV [j]
Full width (Breit-Wigner) = 10 to 100 MeV [j]

$f_0(980)$ DECAY MODES	Fraction (Γ_i/Γ)	p (MeV/c)
$\pi\pi$	seen	476
$K\overline{K}$	seen	36
$\gamma\gamma$	seen	495

$a_0(980)$

$I^G(J^{PC}) = 1^-(0^{++})$

See the review on "Scalar Mesons below 1 GeV."
T-matrix pole $\sqrt{s} = (970\text{–}1020) - i\,(30\text{–}70)$ MeV [j]
Mass $m = 980 \pm 20$ MeV [j]
Full width $\Gamma = 50$ to 100 MeV [j]

$a_0(980)$ DECAY MODES	Fraction (Γ_i/Γ)	p (MeV/c)
$\eta\pi$	seen	319
$K\overline{K}$	seen	†
$\eta'\pi$	seen	†
$\rho\pi$	not seen	138
$\gamma\gamma$	seen	490

$\phi(1020)$

$I^G(J^{PC}) = 0^-(1^{--})$

Mass $m = 1019.460 \pm 0.016$ MeV
Full width $\Gamma = 4.249 \pm 0.013$ MeV (S = 1.1)

$\phi(1020)$ DECAY MODES	Fraction (Γ_i/Γ)	Scale factor/ Confidence level	p (MeV/c)
K^+K^-	(50.1 ± 0.6) %	S=1.6	127
$K^0_L K^0_S$	(33.6 ± 0.4) %	S=1.3	110
$\rho\pi + \pi^+\pi^-\pi^0$	(14.7 ± 0.4) %	S=1.5	–
$\eta\gamma$	(1.306 ± 0.024) %	S=1.2	363
$\pi^0\gamma$	$(1.33 \pm 0.05) \times 10^{-3}$		501
$\ell^+\ell^-$	—		510
e^+e^-	$(2.963 \pm 0.034) \times 10^{-4}$	S=1.4	510
$\mu^+\mu^-$	$(2.86 \pm 0.22) \times 10^{-4}$	S=1.2	499
ηe^+e^-	$(1.08 \pm 0.04) \times 10^{-4}$		363
$\pi^+\pi^-$	$(9.5 \pm 1.9) \times 10^{-5}$	S=2.0	490
$\omega\pi^0$	$(4.7 \pm 0.5) \times 10^{-5}$		171
$\omega\gamma$	< 5 %	CL=84%	209
$\rho\gamma$	$< 1.2 \times 10^{-5}$	CL=90%	215

Int. J. Mod. Phys. A 2026.41. Downloaded from www.worldscientific.com
by UNIVERSITY OF CALIFORNIA @ BERKELEY on 09/16/26. Re-use and distribution is strictly not permitted, except for Open Access articles.

$\pi^+\pi^-\gamma$	$(4.1 \pm 1.3) \times 10^{-5}$			490
$f_0(980)\gamma$	$(3.22 \pm 0.19) \times 10^{-4}$		S=1.1	29
$\pi^0\pi^0\gamma$	$(1.13 \pm 0.06) \times 10^{-4}$			492
$\pi^+\pi^-\pi^+\pi^-$	$(3.9 \,^{+2.8}_{-2.2}) \times 10^{-6}$			410
$\pi^+\pi^+\pi^-\pi^-\pi^0$	$< 4.6 \times 10^{-6}$	CL=90%		342
$\pi^0 e^+ e^-$	$(1.33 \,^{+0.07}_{-0.10}) \times 10^{-5}$			501
$\pi^0\eta\gamma$	$(7.27 \pm 0.30) \times 10^{-5}$		S=1.5	346
$a_0(980)\gamma$	$(7.6 \pm 0.6) \times 10^{-5}$			39
$K^0\overline{K}^0\gamma$	$< 1.9 \times 10^{-8}$	CL=90%		110
$\eta'(958)\gamma$	$(6.23 \pm 0.21) \times 10^{-5}$			60
$\eta\pi^0\pi^0\gamma$	$< 2 \times 10^{-5}$	CL=90%		293
$\mu^+\mu^-\gamma$	$(1.4 \pm 0.5) \times 10^{-5}$			499
$\rho\gamma\gamma$	$< 1.2 \times 10^{-4}$	CL=90%		215
$\eta\pi^+\pi^-$	$< 1.8 \times 10^{-5}$	CL=90%		288
$\eta\mu^+\mu^-$	$< 9.4 \times 10^{-6}$	CL=90%		321
$\eta U \to \eta e^+ e^-$	$< 1 \times 10^{-6}$	CL=90%		–
invisible	$< 1.7 \times 10^{-4}$	CL=90%		–
Lepton Family number (*LF*) violating modes				
$e^\pm\mu^\mp$ *LF*	$< 2 \times 10^{-6}$	CL=90%		504
$\pi^+\pi^+e^-e^-$ *L*	$< 1.3 \times 10^{-5}$	CL=90%		490

$h_1(1170)$

$I^G(J^{PC}) = 0^-(1^{+-})$

Mass $m = 1166 \pm 6$ MeV
Full width $\Gamma = 375 \pm 35$ MeV

$h_1(1170)$ DECAY MODES	Fraction (Γ_i/Γ)	p (MeV/c)
$\rho\pi$	seen	305

$b_1(1235)$

$I^G(J^{PC}) = 1^+(1^{+-})$

Mass $m = 1229.5 \pm 3.2$ MeV (S = 1.6)
Full width $\Gamma = 142 \pm 9$ MeV (S = 1.2)

$b_1(1235)$ DECAY MODES	Fraction (Γ_i/Γ)	Confidence level	p (MeV/c)
$\omega\pi$	seen		348
[D/S amplitude ratio $= 0.277 \pm 0.027$]			
$\pi^\pm\gamma$	$(1.6 \pm 0.4) \times 10^{-3}$		607
$\eta\rho$	seen		†
$\pi^+\pi^+\pi^-\pi^0$	< 50 %	84%	535
$K^*(892)^\pm K^\mp$	seen		†
$(K\overline{K})^\pm\pi^0$	< 8 %	90%	248
$K^0_S K^0_L \pi^\pm$	< 6 %	90%	235
$K^0_S K^0_S \pi^\pm$	< 2 %	90%	235
$\phi\pi$	< 1.5 %	84%	147

$a_1(1260)$ [k]

$I^G(J^{PC}) = 1^-(1^{++})$

T-Matrix Pole $\sqrt{s} = (1209^{+13}_{-10}) - i(288^{+45}_{-12})$ MeV
Mass (Breit-Wigner) = 1230 ± 40 MeV [j]
Full width (Breit-Wigner) = 250 to 600 MeV [j]

$a_1(1260)$ DECAY MODES	Fraction (Γ_i/Γ)	p (MeV/c)
3π	seen	577
$(\rho\pi)_{S-\text{wave}}$, $\rho \to \pi\pi$	seen	353
$(\rho\pi)_{D-\text{wave}}$, $\rho \to \pi\pi$	seen	353
$(\rho(1450)\pi)_{S-\text{wave}}$, $\rho \to \pi\pi$	seen	†
$(\rho(1450)\pi)_{D-\text{wave}}$, $\rho \to \pi\pi$	seen	†
$f_0(500)\pi$, $f_0 \to \pi\pi$	seen	–
$f_0(980)\pi$, $f_0 \to \pi\pi$	seen	179
$f_0(1370)\pi$, $f_0 \to \pi\pi$	seen	†
$f_2(1270)\pi$, $f_2 \to \pi\pi$	seen	†
$\pi^+\pi^-\pi^0$	seen	576
$\pi^0\pi^0\pi^0$	not seen	577
$KK\pi$	seen	250
$K^*(892)K$	seen	†
$\pi\gamma$	seen	608

$f_2(1270)$

$I^G(J^{PC}) = 0^+(2^{++})$

T-Matrix Pole $\sqrt{s} = (1260\text{–}1283) - i\,(90\text{–}110)$ MeV
Mass (Breit-Wigner) = 1275.4 ± 0.8 MeV (S = 1.1)
Full width (Breit-Wigner) = $186.6^{+2.8}_{-2.2}$ MeV (S = 1.5)

$f_2(1270)$ DECAY MODES	Fraction (Γ_i/Γ)	Scale factor/ Confidence level	p (MeV/c)
$\pi\pi$	$(84.3 \,^{+2.8}_{-1.0})$ %	S=1.2	623
$\pi^+\pi^-2\pi^0$	$(7.7 \,^{+1.2}_{-3.1})$ %	S=1.2	563
$K\overline{K}$	(4.6 ± 0.4) %	S=2.7	404
$2\pi^+2\pi^-$	(2.8 ± 0.4) %	S=1.2	559
$\eta\eta$	$(4.0 \pm 0.8) \times 10^{-3}$	S=2.1	326
$4\pi^0$	$(3.0 \pm 1.0) \times 10^{-3}$		565
$\gamma\gamma$	$(1.42 \pm 0.24) \times 10^{-5}$	S=1.4	638
$\eta\pi\pi$	$< 8 \times 10^{-3}$	CL=95%	478
$K^0K^-\pi^+ +$ c.c.	$< 3.4 \times 10^{-3}$	CL=95%	293
e^+e^-	$< 6 \times 10^{-10}$	CL=90%	638

$f_1(1285)$

$I^G(J^{PC}) = 0^+(1^{++})$

Mass $m = 1281.8 \pm 0.5$ MeV (S = 1.7)
Full width $\Gamma = 23.0 \pm 1.0$ MeV (S = 1.5)

$f_1(1285)$ DECAY MODES	Fraction (Γ_i/Γ)	Scale factor/ Confidence level	p (MeV/c)
4π	(32.7 ± 1.8) %	S=1.2	568
$\pi^0\pi^0\pi^+\pi^-$	(21.8 ± 1.2) %	S=1.2	566
$2\pi^+2\pi^-$	(10.9 ± 0.6) %	S=1.2	563
$\rho^0\pi^+\pi^-$	(10.9 ± 0.6) %	S=1.2	336
$\rho^0\rho^0$	seen		†
$4\pi^0$	$< 7 \times 10^{-4}$	CL=90%	568
$\eta\pi^+\pi^-$	(35 ± 15) %		479
$\eta\pi\pi$	(52.2 ± 1.9) %	S=1.2	482
$a_0(980)\pi$ [ignoring $a_0(980) \to K\overline{K}$]	(38 ± 4) %		238
$\eta\pi\pi$ [excluding $a_0(980)\pi$]	(14 ± 4) %		482
$K\overline{K}\pi$	(9.0 ± 0.4) %	S=1.1	308
$K\overline{K}^*(892)$	not seen		†
$\pi^+\pi^-\pi^0$	$(3.0 \pm 0.9) \times 10^{-3}$		603
$\rho^\pm\pi^\mp$	$< 3.1 \times 10^{-3}$	CL=95%	390
$\gamma\rho^0$	(6.1 ± 1.0) %	S=1.7	407
$\phi\gamma$	seen		236
e^+e^-	$< 9.4 \times 10^{-9}$	CL=90%	641

$\eta(1295)$

$I^G(J^{PC}) = 0^+(0^{-+})$

See the review on "Spectroscopy of Light Meson Resonances."
Mass $m = 1294 \pm 4$ MeV (S = 1.6)
Full width $\Gamma = 55 \pm 5$ MeV

$\eta(1295)$ DECAY MODES	Fraction (Γ_i/Γ)	p (MeV/c)
$\eta\pi^+\pi^-$	seen	487
$a_0(980)\pi$	seen	248
$\eta\pi^0\pi^0$	seen	490
$\eta(\pi\pi)_{S\text{-wave}}$	seen	–
$\sigma\eta$	seen	–
$K\overline{K}\pi$	seen	320

$\pi(1300)$

$I^G(J^{PC}) = 1^-(0^{-+})$

Mass $m = 1300 \pm 100$ MeV [j]
Full width $\Gamma = 200$ to 600 MeV [j]

$\pi(1300)$ DECAY MODES	Fraction (Γ_i/Γ)	p (MeV/c)
$\rho\pi$	seen	404
$\pi(\pi\pi)_{S\text{-wave}}$	seen	–

$a_2(1320)$

$I^G(J^{PC}) = 1^-(2^{++})$

T-Matrix Pole $\sqrt{s} = (1305\text{–}1321) - i(52\text{–}58)$ MeV
Mass (Breit-Wigner) = 1318.2 ± 0.6 MeV (S = 1.2)
Full width $\Gamma = 107 \pm 5$ MeV

Int. J. Mod. Phys. A 2026.41. Downloaded from www.worldscientific.com
by UNIVERSITY OF CALIFORNIA @ BERKELEY on 09/16/26. Re-use and distribution is strictly not permitted, except for Open Acce

$a_2(1320)$ DECAY MODES	Fraction (Γ_i/Γ)	Scale factor/ Confidence level	p (MeV/c)
3π	(70.1 ± 2.7) %	S=1.2	624
$\eta\pi$	(14.5 ± 1.2) %		535
$\omega\pi\pi$	(10.6 ± 3.2) %	S=1.3	366
$K\overline{K}$	(4.9 ± 0.8) %		437
$\eta'(958)\pi$	$(5.5 \pm 0.9) \times 10^{-3}$		288
$\pi^{\pm}\gamma$	$(2.91 \pm 0.27) \times 10^{-3}$		652
$\gamma\gamma$	$(9.4 \pm 0.7) \times 10^{-6}$		659
e^+e^-	$< 5 \times 10^{-9}$	CL=90%	659

$f_0(1370)$

$I^G(J^{PC}) = 0^+(0^{++})$

See the review on "Spectroscopy of Light Meson Resonances."
T-Matrix Pole $\sqrt{s} = (1250\text{–}1440) - i\,(60\text{–}300)$ MeV
Mass (Breit-Wigner) = 1200 to 1500 MeV
Full width (Breit-Wigner) = 200 to 500 MeV

$f_0(1370)$ DECAY MODES	Fraction (Γ_i/Γ)	p (MeV/c)
$\pi\pi$	seen	672
4π	seen	617
$4\pi^0$	seen	617
$2\pi^+2\pi^-$	seen	612
$\pi^+\pi^-2\pi^0$	seen	615
$\rho\rho$	seen	†
$2(\pi\pi)$ s-wave	seen	–
$\pi(1300)\pi$	seen	†
$a_1(1260)\pi$	seen	35
$\eta\eta$	seen	411
$K\overline{K}$	seen	475
$K\overline{K}n\pi$	not seen	†
6π	not seen	508
$\omega\omega$	not seen	†
$\gamma\gamma$	seen	685
e^+e^-	not seen	685

$\eta(1405)$

$I^G(J^{PC}) = 0^+(0^{-+})$

See the review on "Spectroscopy of Light Meson Resonances." See also $\eta(1475)$.
Mass $m = 1408.0^{+1.8}_{-1.2}$ MeV (S = 2.1)
Full width $\Gamma = 49.8^{+2.3}_{-2.0}$ MeV (S = 1.6)

$\eta(1405)$ DECAY MODES	Fraction (Γ_i/Γ)	Confidence level	p (MeV/c)
$K\overline{K}\pi$	seen		423
$\eta\pi\pi$	seen		562
$a_0(980)\pi$	seen		344
$\eta(\pi\pi)$ s-wave	seen		–
$f_0(980)\eta$	seen		†
4π	seen		638
$\rho\rho$	<58 %	99.85%	†
$\rho^0\gamma$	seen		491
$\phi\gamma$	seen		335
$K^*(892)K$	seen		120

$h_1(1415)$

$I^G(J^{PC}) = 0^-(1^{+-})$

Mass $m = 1409^{+9}_{-8}$ MeV (S = 1.9)
Full width $\Gamma = 78 \pm 11$ MeV

$f_1(1420)$

$I^G(J^{PC}) = 0^+(1^{++})$

See the review on "Spectroscopy of Light Meson Resonances."
Mass $m = 1427.7^{+1.7}_{-1.4}$ MeV (S = 2.1)
Full width $\Gamma = 55.4 \pm 3.2$ MeV (S = 1.3)

$f_1(1420)$ DECAY MODES	Fraction (Γ_i/Γ)	p (MeV/c)
$K\overline{K}\pi$	seen	439
$K\overline{K}^*(892)+$ c.c.	seen	165
$\eta\pi\pi$	possibly seen	574
$\phi\gamma$	seen	350

$\omega(1420)$ [l]

$I^G(J^{PC}) = 0^-(1^{--})$

Mass $m = 1410 \pm 60$ MeV [j]
Full width $\Gamma = 290 \pm 190$ MeV [j]

$\omega(1420)$ DECAY MODES	Fraction (Γ_i/Γ)	p (MeV/c)
$\rho\pi$	seen	480
$\rho(1450)\pi$	possibly seen	†
$\omega\pi\pi$	seen	437
$\omega\eta$	possibly seen	230
$b_1(1235)\pi$	seen	112
e^+e^-	seen	705

$a_0(1450)$

$I^G(J^{PC}) = 1^-(0^{++})$

See the review on "Spectroscopy of Light Meson Resonances."
T-Matrix Pole $\sqrt{s} = (1290\text{–}1500) - i\,(30\text{–}140)$ MeV
Mass (Breit-Wigner) = 1439 ± 34 MeV (S = 1.8)
Full width (Breit-Wigner) = 258 ± 14 MeV

Branching fractions are given relative to the one **DEFINED AS 1**.

$a_0(1450)$ DECAY MODES	Fraction (Γ_i/Γ)	p (MeV/c)
$\pi\eta$	0.093 ± 0.020	607
$\pi\eta'(958)$	0.033 ± 0.017	384
$K\overline{K}$	0.082 ± 0.028	523
$\omega\pi\pi$	**DEFINED AS 1**	458
$a_0(980)\pi\pi$	seen	310
$\gamma\gamma$	seen	719

$\rho(1450)$

$I^G(J^{PC}) = 1^+(1^{--})$

See the review on "Spectroscopy of Light Meson Resonances."
Mass $m = 1465 \pm 25$ MeV [j]
Full width $\Gamma = 400 \pm 60$ MeV [j]

$\rho(1450)$ DECAY MODES	Fraction (Γ_i/Γ)	p (MeV/c)
$\pi\pi$	seen	720
$\pi^+\pi^-$	seen	719
4π	seen	669
e^+e^-	seen	732
$\eta\rho$	seen	311
$a_2(1320)\pi$	not seen	55
$K\overline{K}$	seen	541
K^+K^-	seen	541
$K\overline{K}^*(892)+$ c.c.	possibly seen	229
$\pi^0\gamma$	seen	726
$\eta\gamma$	seen	630
$f_0(500)\gamma$	not seen	–
$f_0(980)\gamma$	not seen	398
$f_0(1370)\gamma$	not seen	92
$f_2(1270)\gamma$	not seen	177

$\eta(1475)$

$I^G(J^{PC}) = 0^+(0^{-+})$

See the review on "Spectroscopy of Light Meson Resonances." See also $\eta(1405)$.
Mass $m = 1476 \pm 4$ MeV (S = 1.4)
Full width $\Gamma = 96 \pm 9$ MeV (S = 1.7)

$\eta(1475)$ DECAY MODES	Fraction (Γ_i/Γ)	p (MeV/c)
$K\overline{K}\pi$	seen	477
$K\overline{K}^*(892)+$ c.c.	seen	244
$a_0(980)\pi$	seen	396
$\gamma\gamma$	seen	738
$K^0_S K^0_S \eta$	possibly seen	†
$\gamma\phi(1020)$	possibly seen	386

Int. J. Mod. Phys. A 2026.41. Downloaded from www.worldscientific.com
by UNIVERSITY OF CALIFORNIA @ BERKELEY on 09/16/26. Re-use and distribution is strictly not permitted, except for Open Access articles.

$f_0(1500)$

$I^G(J^{PC}) = 0^+(0^{++})$

See the review on "Spectroscopy of Light Meson Resonances."
T-Matrix Pole $\sqrt{s}$ = (1430–1530) − i (40–90) MeV
Mass (Breit-Wigner) = 1522 ± 25 MeV
Full width (Breit-Wigner) = 108 ± 33 MeV

$f_0(1500)$ DECAY MODES	Fraction (Γ_i/Γ)	Scale factor	p (MeV/c)
$\pi\pi$	(34.5±2.2) %	1.2	749
$\pi^+\pi^-$	seen		748
$2\pi^0$	seen		749
4π	(48.9±3.3) %	1.2	700
$4\pi^0$	seen		700
$2\pi^+2\pi^-$	seen		696
$2(\pi\pi)_{S\text{-wave}}$	seen		–
$\rho\rho$	seen		†
$\pi(1300)\pi$	seen		163
$a_1(1260)\pi$	seen		234
$\eta\eta$	(6.0±0.9) %	1.1	528
$\eta\eta'(958)$	(2.2±0.8) %	1.4	107
$K\overline{K}$	(8.5±1.0) %	1.1	579
$\gamma\gamma$	not seen		761

$f_2'(1525)$

$I^G(J^{PC}) = 0^+(2^{++})$

Mass m = 1517.3 ± 2.4 MeV (S = 2.8)
Full width $\Gamma = 72^{+7}_{-6}$ MeV

$f_2'(1525)$ DECAY MODES	Fraction (Γ_i/Γ)	p (MeV/c)
$K\overline{K}$	(88.8 ±2.2) %	576
$\eta\eta$	(10.3 ±2.2) %	525
$\pi\pi$	(8.2 ±1.5) $\times 10^{-3}$	747
$\gamma\phi$	seen	416
$\gamma\gamma$	(1.12±0.15) $\times 10^{-6}$	759

$f_2(1565)$

$I^G(J^{PC}) = 0^+(2^{++})$

See the review on "Spectroscopy of Light Meson Resonances."
T-Matrix Pole $\sqrt{s}$ = (1495–1560) − i (40–110) MeV
Mass (Breit-Wigner) = 1571 ± 13 MeV
Full width (Breit-Wigner) = 132 ± 23 MeV (S = 1.1)

$f_2(1565)$ DECAY MODES	Fraction (Γ_i/Γ)	p (MeV/c)
$\pi\pi$	seen	774
$\pi^+\pi^-$	seen	773
$\pi^0\pi^0$	seen	774
$\rho^0\rho^0$	seen	126
$2\pi^+2\pi^-$	seen	722
$\eta\eta$	seen	563
$\omega\omega$	seen	64
$K\overline{K}$	seen	611
$\gamma\gamma$	seen	785

$\pi_1(1600)$

$I^G(J^{PC}) = 1^-(1^{-+})$

See the review on "Spectroscopy of Light Meson Resonances."
Mass (T-Matrix Pole $\sqrt{s}$) = (1480–1680) − i (150–300) MeV
Mass (Breit-Wigner, $\eta\pi$ mode) = 1354 ± 25 MeV (S = 1.8)
Mass (Breit-Wigner, non-$\eta\pi$ mode) = 1645^{+40}_{-17} MeV (S = 1.3)
Full width (Breit-Wigner, $\eta\pi$ mode) = 330 ± 35 MeV
Full width (Breit-Wigner, non-$\eta\pi$ mode) = 370^{+50}_{-60} MeV

$\pi_1(1600)$ DECAY MODES	Fraction (Γ_i/Γ)	p (MeV/c)
$\pi\pi\pi$	seen	795
$\rho^0\pi^-$	seen	631
$f_2(1270)\pi^-$	not seen	304
$b_1(1235)\pi$	seen	343
$\eta'(958)\pi^-$	seen	532
$\eta\pi$	seen	725
$f_1(1285)\pi$	seen	300

$a_1(1640)$

$I^G(J^{PC}) = 1^-(1^{++})$

Mass m = 1655 ± 16 MeV (S = 1.2)
Full width Γ = 250 ± 40 MeV (S = 1.8)

$a_1(1640)$ DECAY MODES	Fraction (Γ_i/Γ)	p (MeV/c)
$\pi\pi\pi$	seen	800
$f_2(1270)\pi$	seen	314
$\sigma\pi$	seen	–
$\rho\pi_{S-wave}$	seen	638
$\rho\pi_{D-wave}$	seen	638
$\omega\pi\pi$	seen	607
$f_1(1285)\pi$	seen	309
$a_1(1260)\eta$	not seen	†

$\eta_2(1645)$

$I^G(J^{PC}) = 0^+(2^{-+})$

Mass m = 1617 ± 5 MeV
Full width Γ = 181 ± 11 MeV

$\eta_2(1645)$ DECAY MODES	Fraction (Γ_i/Γ)	p (MeV/c)
$a_2(1320)\pi$	seen	242
$K\overline{K}\pi$	seen	580
$K^*\overline{K}$	seen	404
$\eta\pi^+\pi^-$	seen	685
$a_0(980)\pi$	seen	499
$f_2(1270)\eta$	not seen	†

$\omega(1650)$ [n]

$I^G(J^{PC}) = 0^-(1^{--})$

Mass m = 1670 ± 30 MeV [j]
Full width Γ = 150 ± 50 MeV [j]

$\omega(1650)$ DECAY MODES	Fraction (Γ_i/Γ)	p (MeV/c)
$\rho\pi$	seen	647
$\rho(1450)\pi$	seen	145
$\omega\pi\pi$	seen	617
$\omega\eta$	seen	500
e^+e^-	seen	835
$\pi^0\gamma$	not seen	830

$\omega_3(1670)$

$I^G(J^{PC}) = 0^-(3^{--})$

Mass m = 1667 ± 4 MeV
Full width Γ = 168 ± 10 MeV

$\omega_3(1670)$ DECAY MODES	Fraction (Γ_i/Γ)	p (MeV/c)
$\rho\pi$	seen	645
$\omega\pi\pi$	seen	615
$b_1(1235)\pi$	possibly seen	361

$\pi_2(1670)$

$I^G(J^{PC}) = 1^-(2^{-+})$

Mass $m = 1670.6^{+2.9}_{-1.2}$ MeV (S = 1.3)
Full width $\Gamma = 258^{+8}_{-9}$ MeV (S = 1.2)

$\pi_2(1670)$ DECAY MODES	Fraction (Γ_i/Γ)	Confidence level	p (MeV/c)
3π	(95.8±1.4) %		808
$f_2(1270)\pi$	(56.3±3.2) %		327
$\rho\pi$	(31 ±4) %		647
$\sigma\pi$	(10 ±4) %		–
$\pi(\pi\pi)_{S\text{-wave}}$	(8.7±3.4) %		–
$\pi^\pm\pi^+\pi^-$	(53 ±4) %		806
$K\overline{K}^*(892)+$ c.c.	(4.2±1.4) %		453
$\omega\rho$	(2.7±1.1) %		302
$\pi^\pm\gamma$	(7.0±1.2) $\times 10^{-4}$		829
$\gamma\gamma$	< 2.8 $\times 10^{-7}$	90%	835
$\eta\pi$	< 5 %		739
$\pi^\pm 2\pi^+2\pi^-$	< 5 %		735
$\rho(1450)\pi$	< 3.6 $\times 10^{-3}$	97.7%	145
$b_1(1235)\pi$	< 1.9 $\times 10^{-3}$	97.7%	364

Int. J. Mod. Phys. A 2026.41. Downloaded from www.worldscientific.com
by UNIVERSITY OF CALIFORNIA @ BERKELEY on 09/16/26. Re-use and distribution is strictly not permitted, except for Open Acce

$f_1(1285)\pi$	possibly seen	322
$a_2(1320)\pi$	not seen	291

$\phi(1680)$

$I^G(J^{PC}) = 0^-(1^{--})$

Mass $m = 1680 \pm 20$ MeV [j]
Full width $\Gamma = 150 \pm 50$ MeV [j]

$\phi(1680)$ DECAY MODES	Fraction (Γ_i/Γ)	p (MeV/c)
$K\overline{K}^*(892)+$ c.c.	seen	461
$K^0_S K\pi$	seen	621
$K\overline{K}$	seen	680
e^+e^-	seen	840
$\omega\pi\pi$	not seen	623
$K^+K^-\pi^+\pi^-$	seen	544
$\eta\phi$	seen	290
$\eta\gamma$	seen	751
$\rho(770)\pi$	not seen	653
$f'_2(1525)\gamma$	not seen	155

$\rho_3(1690)$

$I^G(J^{PC}) = 1^+(3^{--})$

Mass $m = 1688.8 \pm 2.1$ MeV
Full width $\Gamma = 161 \pm 10$ MeV (S = 1.5)

$\rho_3(1690)$ DECAY MODES	Fraction (Γ_i/Γ)	Scale factor	p (MeV/c)
4π	(71.1 ± 1.9) %		790
$\pi^\pm\pi^+\pi^-\pi^0$	(67 ±22) %		787
$\omega\pi$	(16 ± 6) %		655
$\pi\pi$	(23.6 ± 1.3) %		834
$K\overline{K}\pi$	(3.8 ± 1.2) %		629
$K\overline{K}$	(1.58± 0.26) %	1.2	685
$\eta\pi^+\pi^-$	seen		727
$\rho(770)\eta$	seen		520
$\pi\pi\rho$	seen		633
$a_2(1320)\pi$	seen		307
$\rho\rho$	seen		335

$\rho(1700)$

$I^G(J^{PC}) = 1^+(1^{--})$

See the review on "Spectroscopy of Light Meson Resonances."
Mass $m = 1720 \pm 20$ MeV [j] ($\eta\rho^0$ and $\pi^+\pi^-$ modes)
Full width $\Gamma = 250 \pm 100$ MeV [j] ($\eta\rho^0$ and $\pi^+\pi^-$ modes)

$\rho(1700)$ DECAY MODES	Fraction (Γ_i/Γ)	p (MeV/c)
$2(\pi^+\pi^-)$	seen	803
$\rho\pi\pi$	seen	653
$\rho^0\pi^+\pi^-$	seen	651
$\rho^\pm\pi^\mp\pi^0$	seen	652
$a_1(1260)\pi$	seen	404
$h_1(1170)\pi$	seen	450
$\pi(1300)\pi$	seen	349
$\rho\rho$	seen	373
$\pi^+\pi^-$	seen	849
$\pi\pi$	seen	849
$K\overline{K}^*(892)+$ c.c.	seen	496
$\eta\rho$	seen	545
$a_2(1320)\pi$	not seen	334
$K\overline{K}$	seen	704
e^+e^-	seen	860
$\pi^0\omega$	seen	674
$\pi^0\gamma$	not seen	855
$f_0(1500)\gamma$	not seen	187

$a_2(1700)$

$I^G(J^{PC}) = 1^-(2^{++})$

T-Matrix Pole $\sqrt{s} = (1630\text{–}1780) - i\,(60\text{–}250)$ MeV
Mass $m = 1706 \pm 14$ MeV (S = 1.2)
Full width $\Gamma = 380^{+60}_{-50}$ MeV (S = 3.9)

$a_2(1700)$ DECAY MODES	Fraction (Γ_i/Γ)	p (MeV/c)
$\eta\pi$	(2.5 ± 0.6) %	758
$\eta'\pi$	seen	574
$\gamma\gamma$	$(7.9 \pm 1.7) \times 10^{-7}$	853
$\rho\pi$	seen	669
$f_2(1270)\pi$	seen	357
$K\overline{K}$	(1.3 ± 0.8) %	695
$\omega\pi^-\pi^0$	seen	639
$\omega\rho$	seen	347

$f_0(1710)$

$I^G(J^{PC}) = 0^+(0^{++})$

See the review on "Spectroscopy of Light Meson Resonances."
T-matrix pole $\sqrt{s} = (1680\text{–}1820) - i\,(50\text{–}180)$ MeV
Mass (Breit-Wigner) = 1723^{+7}_{-6} MeV (S = 1.3)
Full width (Breit-Wigner) = 149 ± 10 MeV (S = 1.4)

$f_0(1710)$ DECAY MODES	Fraction (Γ_i/Γ)	p (MeV/c)
$K\overline{K}$	seen	706
$\eta\eta$	seen	665
$\eta\eta'$	not seen	407
$\pi\pi$	seen	851
$\gamma\gamma$	seen	862
$\omega\omega$	seen	360

$\pi(1800)$

$I^G(J^{PC}) = 1^-(0^{-+})$

See the review on "Spectroscopy of Light Meson Resonances."
Mass $m = 1810^{+9}_{-11}$ MeV (S = 2.2)
Full width $\Gamma = 215^{+7}_{-8}$ MeV

$\pi(1800)$ DECAY MODES	Fraction (Γ_i/Γ)	p (MeV/c)
$\pi^+\pi^-\pi^-$	seen	878
$f_0(500)\pi^-$	seen	–
$f_0(980)\pi^-$	seen	624
$f_0(1370)\pi^-$	seen	366
$f_0(1500)\pi^-$	not seen	232
$\rho\pi^-$	not seen	731
$\eta\eta\pi^-$	seen	660
$a_0(980)\eta$	seen	471
$a_2(1320)\eta$	not seen	†
$f_2(1270)\pi$	not seen	441
$f_0(1370)\pi^-$	not seen	366
$f_0(1500)\pi^-$	seen	232
$\eta\eta'(958)\pi^-$	seen	373
$K^*_0(1430)K^-$	seen	†
$K^*(892)K^-$	not seen	568

$\phi_3(1850)$

$I^G(J^{PC}) = 0^-(3^{--})$

Mass $m = 1854 \pm 7$ MeV
Full width $\Gamma = 87^{+28}_{-23}$ MeV (S = 1.2)

$\phi_3(1850)$ DECAY MODES	Fraction (Γ_i/Γ)	p (MeV/c)
$K\overline{K}$	seen	785
$K\overline{K}^*(892)+$ c.c.	seen	602

$\eta_2(1870)$

$I^G(J^{PC}) = 0^+(2^{-+})$

Mass $m = 1842 \pm 8$ MeV
Full width $\Gamma = 225 \pm 14$ MeV

$\eta_2(1870)$ DECAY MODES	Fraction (Γ_i/Γ)	p (MeV/c)
$\eta\pi\pi$	seen	816
$a_2(1320)\pi$	seen	434
$f_2(1270)\eta$	seen	119
$a_0(980)\pi$	seen	651
$\gamma\gamma$	seen	921

Int. J. Mod. Phys. A 2026.41. Downloaded from www.worldscientific.com
by UNIVERSITY OF CALIFORNIA @ BERKELEY on 09/16/26. Re-use and distribution is strictly not permitted, except for Open Access articles.

$\pi_2(1880)$

$I^G(J^{PC}) = 1^-(2^{-+})$

Mass $m = 1874^{+26}_{-5}$ MeV (S = 1.6)
Full width $\Gamma = 237^{+33}_{-30}$ MeV (S = 1.2)

$\pi_2(1880)$ DECAY MODES	Fraction (Γ_i/Γ)	p (MeV/c)
$\eta\eta\pi^-$	seen	702
$a_0(980)\eta$	seen	528
$a_2(1320)\eta$	seen	76
$f_0(1500)\pi$	seen	294
$f_1(1285)\pi$	seen	485
$\omega\pi^-\pi^0$	seen	744

$f_2(1950)$

$I^G(J^{PC}) = 0^+(2^{++})$

T-Matrix Pole $\sqrt{s} = (1830\text{–}2020) - i\,(110\text{–}220)$ MeV
Mass (Breit-Wigner) = 1936 ± 12 MeV (S = 1.3)
Full width (Breit-Wigner) = 464 ± 24 MeV

$f_2(1950)$ DECAY MODES	Fraction (Γ_i/Γ)	p (MeV/c)
$K^*(892)\overline{K}^*(892)$	seen	377
$\pi^+\pi^-$	seen	958
$\pi^0\pi^0$	seen	959
4π	seen	921
$\eta\eta$	seen	798
$K\overline{K}$	seen	833
$\gamma\gamma$	seen	968
$\gamma\phi$	seen	700
$p\overline{p}$	seen	238

$a_4(1970)$

$I^G(J^{PC}) = 1^-(4^{++})$

Mass $m = 1967 \pm 16$ MeV (S = 2.1)
Full width $\Gamma = 324^{+15}_{-18}$ MeV

$a_4(1970)$ DECAY MODES	Fraction (Γ_i/Γ)	p (MeV/c)
$K\overline{K}$	seen	851
$\pi^+\pi^-\pi^0$	seen	959
$\rho\pi$	seen	825
$f_2(1270)\pi$	seen	559
$\omega\pi^-\pi^0$	seen	801
$\omega\rho$	seen	601
$\eta\pi$	seen	902
$\eta'(958)\pi$	seen	743

$f_2(2010)$

$I^G(J^{PC}) = 0^+(2^{++})$

Mass $m = 2010^{+60}_{-80}$ MeV
Full width $\Gamma = 200 \pm 60$ MeV

$f_2(2010)$ DECAY MODES	Fraction (Γ_i/Γ)	p (MeV/c)
$\phi\phi$	seen	†
$K\overline{K}$	seen	876
$\gamma\phi$	seen	747

$f_0(2020)$

$I^G(J^{PC}) = 0^+(0^{++})$

T-Matrix Pole $\sqrt{s} = (1870\text{–}2080) - i\,(120\text{–}240)$ MeV
Mass (Breit-Wigner) = $1982^{+54.1}_{-3.0}$ MeV
Full width (Breit-Wigner) = 440 ± 50 MeV

$f_0(2020)$ DECAY MODES	Fraction (Γ_i/Γ)	p (MeV/c)
$\rho\pi\pi$	seen	814
$\pi^0\pi^0$	seen	982
$\rho\rho$	seen	617
$\omega\omega$	seen	608
$\eta\eta$	seen	826
$\eta'\eta'$	seen	254

$f_4(2050)$

$I^G(J^{PC}) = 0^+(4^{++})$

Mass $m = 2018 \pm 11$ MeV (S = 2.1)
Full width $\Gamma = 237 \pm 18$ MeV (S = 1.9)

$f_4(2050)$ DECAY MODES	Fraction (Γ_i/Γ)	p (MeV/c)
$\omega\omega$	seen	637
$\pi\pi$	(17.0 ± 1.5) %	1000
$K\overline{K}$	$(6.8^{+3.4}_{-1.8})\times10^{-3}$	880
$\eta\eta$	$(2.1\pm0.8)\times10^{-3}$	848
$4\pi^0$	< 1.2 %	964
$\gamma\gamma$	seen	1009
$a_2(1320)\pi$	seen	567

$f_2(2150)$

$I^G(J^{PC}) = 0^+(2^{++})$

Mass $m = 2157 \pm 12$ MeV
Full width $\Gamma = 152 \pm 30$ MeV (S = 1.4)

$f_2(2150)$ DECAY MODES	Fraction (Γ_i/Γ)	p (MeV/c)
$\eta\eta$	seen	929
$K\overline{K}$	seen	959
$f_2(1270)\eta$	seen	542
$a_2(1320)\pi$	seen	666
$p\overline{p}$	seen	532

$\phi(2170)$

$I^G(J^{PC}) = 0^-(1^{--})$

Mass $m = 2164 \pm 5$ MeV
Full width $\Gamma = 88^{+26}_{-21}$ MeV (S = 2.5)

$\phi(2170)$ DECAY MODES	Fraction (Γ_i/Γ)	p (MeV/c)
e^+e^-	seen	1082
$\phi\eta$	seen	728
$\phi\eta'$	seen	439
$\phi\pi\pi$	seen	815
$\phi f_0(980)$	seen	401
$K^+K^-f_0(980) \to K^+K^-\pi^+\pi^-$	seen	–
$K^+K^-f_0(980) \to K^+K^-\pi^0\pi^0$	seen	–
$K^{*0}K^\pm\pi^\mp$	not seen	762
$K^*(892)^0\overline{K}^*(892)^0$	not seen	612

$f_2(2300)$

$I^G(J^{PC}) = 0^+(2^{++})$

Mass $m = 2297 \pm 28$ MeV
Full width $\Gamma = 150 \pm 40$ MeV

$f_2(2300)$ DECAY MODES	Fraction (Γ_i/Γ)	p (MeV/c)
$\phi\phi$	seen	529
$K\overline{K}$	seen	1037
$\gamma\gamma$	seen	1149
$\Lambda\overline{\Lambda}$	seen	273

$f_2(2340)$

$I^G(J^{PC}) = 0^+(2^{++})$

Mass $m = 2346^{+21}_{-10}$ MeV
Full width $\Gamma = 331^{+27}_{-18}$ MeV

$f_2(2340)$ DECAY MODES	Fraction (Γ_i/Γ)	p (MeV/c)
$\phi\phi$	seen	580
$\eta\eta$	seen	1037
$\eta'\eta'$	seen	677

Int. J. Mod. Phys. A 2026.41. Downloaded from www.worldscientific.com
by UNIVERSITY OF CALIFORNIA @ BERKELEY on 09/16/26. Re-use and distribution is strictly not permitted, except for Open Acce

STRANGE MESONS
($S = \pm 1$, $C = B = 0$)

$K^+ = u\overline{s}$, $K^0 = d\overline{s}$, $\overline{K}^0 = \overline{d}s$, $K^- = \overline{u}s$, similarly for K^*'s

$K^\pm$

$I(J^P) = \frac{1}{2}(0^-)$

Mass $m = 493.677 \pm 0.015$ MeV [o] (S = 2.8)
Mean life $\tau = (1.2380 \pm 0.0020) \times 10^{-8}$ s (S = 1.8)
$c\tau = 3.711$ m

CP violation parameters (Δ = rate difference/sum)

$\Delta(K^\pm \to \mu^\pm \nu_\mu) = (-0.27 \pm 0.21)\%$
$\Delta(K^\pm \to \pi^\pm \pi^0) = (0.4 \pm 0.6)\%$ [p]
$\Delta(K^\pm \to \pi^\pm e^+ e^-) = (-2.2 \pm 1.6) \times 10^{-2}$
$\Delta(K^\pm \to \pi^\pm \mu^+ \mu^-) = 0.010 \pm 0.023$
$\Delta(K^\pm \to \pi^\pm \pi^0 \gamma) = (0.0 \pm 1.2) \times 10^{-3}$
$\Delta(K^\pm \to \pi^\pm \pi^+ \pi^-) = (0.04 \pm 0.06)\%$
$\Delta(K^\pm \to \pi^\pm \pi^0 \pi^0) = (-0.02 \pm 0.28)\%$

T violation parameters

$K^+ \to \pi^0 \mu^+ \nu_\mu \quad P_T = (-1.7 \pm 2.5) \times 10^{-3}$
$K^+ \to \mu^+ \nu_\mu \gamma \quad P_T = (-0.6 \pm 1.9) \times 10^{-2}$
$K^+ \to \pi^0 \mu^+ \nu_\mu \quad \mathrm{Im}(\xi) = -0.006 \pm 0.008$

Slope parameter g [q]

(See Particle Listings for quadratic coefficients and alternative parametrization related to $\pi\pi$ scattering)

$K^\pm \to \pi^\pm \pi^+ \pi^- \quad g = -0.21134 \pm 0.00017$
$(g_+ - g_-) / (g_+ + g_-) = (-1.5 \pm 2.2) \times 10^{-4}$
$K^\pm \to \pi^\pm \pi^0 \pi^0 \quad g = 0.626 \pm 0.007$
$(g_+ - g_-) / (g_+ + g_-) = (1.8 \pm 1.8) \times 10^{-4}$

$K^\pm$ decay form factors [a,r]

Assuming μ-e universality
$\lambda_+(K^+_{\mu 3}) = \lambda_+(K^+_{e3}) = (2.959 \pm 0.025) \times 10^{-2}$
$\lambda_0(K^+_{\mu 3}) = (1.76 \pm 0.25) \times 10^{-2}$ (S = 2.7)

Not assuming μ-e universality
$\lambda_+(K^+_{e3}) = (2.956 \pm 0.025) \times 10^{-2}$
$\lambda_+(K^+_{\mu 3}) = (3.09 \pm 0.25) \times 10^{-2}$ (S = 1.5)
$\lambda_0(K^+_{\mu 3}) = (1.73 \pm 0.27) \times 10^{-2}$ (S = 2.6)

K_{e3} form factor quadratic fit
$\lambda'_+ (K^\pm_{e3})$ linear coeff. $= (2.59 \pm 0.04) \times 10^{-2}$
$\lambda''_+ (K^\pm_{e3})$ quadratic coeff. $= (0.186 \pm 0.021) \times 10^{-2}$

λ'_+ (LINEAR $K^\pm_{\mu 3}$ FORM FACTOR FROM QUADRATIC FIT) $= (24 \pm 4) \times 10^{-3}$
λ''_+ (QUADRATIC $K^\pm_{\mu 3}$ FORM FACTOR) $= (1.8 \pm 1.5) \times 10^{-3}$
M_V (VECTOR POLE MASS FOR $K^\pm_{e3}$ DECAY) $= 890.3 \pm 2.8$ MeV
M_V (VECTOR POLE MASS FOR $K^\pm_{\mu 3}$ DECAY) $= 878 \pm 12$ MeV
M_S (SCALAR POLE MASS FOR $K^\pm_{\mu 3}$ DECAY) $= 1210 \pm 50$ MeV
Λ_+ (DISPERSIVE VECTOR FORM FACTOR IN $K^\pm_{e3}$ DECAY) $= (2.460 \pm 0.017) \times 10^{-2}$
Λ_+ (DISPERSIVE VECTOR FORM FACTOR IN $K^\pm_{\mu 3}$ DECAY) $= (25.4 \pm 0.9) \times 10^{-3}$
$\ln(C)$ (DISPERSIVE SCALAR FORM FACTOR in $K^\pm_{\mu 3}$ decays) $= (182 \pm 16) \times 10^{-3}$
$K^+_{e3} \quad |f_S/f_+| = (-0.08^{+0.34}_{-0.40}) \times 10^{-2}$
$K^+_{e3} \quad |f_T/f_+| = (-1.2^{+1.3}_{-1.1}) \times 10^{-2}$
$K^+_{\mu 3} \quad |f_S/f_+| = (0.2 \pm 0.6) \times 10^{-2}$
$K^+_{\mu 3} \quad |f_T/f_+| = (-0.1 \pm 0.7) \times 10^{-2}$
$K^+ \to e^+ \nu_e \gamma \quad |F_A + F_V| = 0.133 \pm 0.008$ (S = 1.3)
$K^+ \to \mu^+ \nu_\mu \gamma \quad |F_A + F_V| = 0.165 \pm 0.013$
$K^+ \to e^+ \nu_e \gamma \quad |F_A - F_V| < 0.49$, CL = 90%
$K^+ \to \mu^+ \nu_\mu \gamma \quad |F_A - F_V| = -0.153 \pm 0.033$ (S = 1.1)

Charge radius

$\langle r \rangle = 0.560 \pm 0.031$ fm

Forward-backward asymmetry

$A_{FB}(K^\pm_{\pi\mu\mu}) = \frac{\Gamma(cos(\theta_{K\mu})>0) - \Gamma(cos(\theta_{K\mu})<0)}{\Gamma(cos(\theta_{K\mu})>0) + \Gamma(cos(\theta_{K\mu})<0)} < 0.9 \times 10^{-2}$, CL = 90%

K^- modes are charge conjugates of the modes below.

K^+ DECAY MODES		Fraction (Γ_i/Γ)	Scale factor/ Confidence level	p (MeV/c)
Leptonic and semileptonic modes				
$e^+ \nu_e$		$(1.582 \pm 0.007) \times 10^{-5}$		247
$\mu^+ \nu_\mu$		(63.56 ± 0.11) %	S=1.2	236
$\pi^0 e^+ \nu_e$ Called K^+_{e3}.		(5.07 ± 0.04) %	S=2.1	228
$\pi^0 \mu^+ \nu_\mu$ Called $K^+_{\mu 3}$.		(3.352 ± 0.034) %	S=1.9	215
$\pi^0 \pi^0 e^+ \nu_e$		$(2.55 \pm 0.04) \times 10^{-5}$	S=1.1	206
$\pi^0 \pi^0 \mu^+ \nu_\mu$		$(3.45 \pm 0.16) \times 10^{-6}$		156
$\pi^+ \pi^- e^+ \nu_e$		$(4.247 \pm 0.024) \times 10^{-5}$		203
$\pi^+ \pi^- \mu^+ \nu_\mu$		$(1.4 \pm 0.9) \times 10^{-5}$		151
$\pi^0 \pi^0 \pi^0 e^+ \nu_e$		$< 5.4 \times 10^{-8}$	CL=90%	135
Hadronic modes				
$\pi^+ \pi^0$		(20.67 ± 0.08) %	S=1.2	205
$\pi^+ \pi^0 \pi^0$		(1.760 ± 0.023) %	S=1.1	133
$\pi^+ \pi^+ \pi^-$		(5.583 ± 0.024) %		125
Leptonic and semileptonic modes with photons				
$\mu^+ \nu_\mu \gamma$	[s,t]	$(6.2 \pm 0.8) \times 10^{-3}$		236
$\mu^+ \nu_\mu \gamma (SD^+)$	[a,u]	$(1.33 \pm 0.22) \times 10^{-5}$		–
$\mu^+ \nu_\mu \gamma (SD^+ INT)$	[a,u]	$< 2.7 \times 10^{-5}$	CL=90%	–
$\mu^+ \nu_\mu \gamma (SD^- + SD^- INT)$	[a,u]	$< 2.6 \times 10^{-4}$	CL=90%	–
$e^+ \nu_e \gamma$		$(1.03 \pm 0.14) \times 10^{-5}$		247
$\pi^0 e^+ \nu_e \gamma$	[s,t]	$(2.698 \pm 0.033) \times 10^{-4}$		228
$\pi^0 e^+ \nu_e \gamma (SD)$	[a,u]	$< 5.3 \times 10^{-5}$	CL=90%	228
$\pi^0 \mu^+ \nu_\mu \gamma$	[s,t]	$(1.25 \pm 0.25) \times 10^{-5}$		215
$\pi^0 \pi^0 e^+ \nu_e \gamma$		$< 5 \times 10^{-6}$	CL=90%	206
Hadronic modes with photons or $\ell\overline{\ell}$ pairs				
$\pi^+ \pi^0 \gamma (INT)$		$(-4.2 \pm 0.9) \times 10^{-6}$		–
$\pi^+ \pi^0 \gamma (DE)$	[s,v]	$(6.0 \pm 0.4) \times 10^{-6}$		205
$\pi^+ \pi^0 e^+ e^-$		$(4.24 \pm 0.14) \times 10^{-6}$		205
$\pi^+ \pi^0 \pi^0 \gamma$	[s,t]	$(4.0 \pm 1.1) \times 10^{-6}$		133
$\pi^+ \pi^+ \pi^- \gamma$	[s,t]	$(7.1 \pm 0.5) \times 10^{-6}$		125
$\pi^+ \gamma \gamma$	[s]	$(9.65 \pm 0.16) \times 10^{-7}$		227
$\pi^+ 3\gamma$	[s]	$< 1.0 \times 10^{-4}$	CL=90%	227
$\pi^+ e^+ e^- \gamma$		$(1.19 \pm 0.13) \times 10^{-8}$		227
Leptonic modes with $\ell\overline{\ell}$ pairs				
$e^+ \nu_e \nu\overline{\nu}$		$< 6 \times 10^{-5}$	CL=90%	247
$\mu^+ \nu_\mu \nu\overline{\nu}$		$< 1.0 \times 10^{-6}$	CL=90%	236
$e^+ \nu_e e^+ e^-$		$(2.48 \pm 0.20) \times 10^{-8}$		247
$\mu^+ \nu_\mu e^+ e^-$		$(7.06 \pm 0.31) \times 10^{-8}$		236
$e^+ \nu_e \mu^+ \mu^-$		$(1.7 \pm 0.5) \times 10^{-8}$		223
$\mu^+ \nu_\mu \mu^+ \mu^-$		$< 4.1 \times 10^{-7}$	CL=90%	185
Lepton family number (LF), Lepton number (L), $\Delta S = \Delta Q$ (SQ) violating modes, or $\Delta S = 1$ weak neutral current ($S1$) modes				
$\pi^+ \pi^+ e^- \overline{\nu}_e$	SQ	$< 1.3 \times 10^{-8}$	CL=90%	203
$\pi^+ \pi^+ \mu^- \overline{\nu}_\mu$	SQ	$< 3.0 \times 10^{-6}$	CL=95%	151
$\pi^+ e^+ e^-$	$S1$	$(3.00 \pm 0.09) \times 10^{-7}$		227
$\pi^+ \mu^+ \mu^-$	$S1$	$(9.17 \pm 0.14) \times 10^{-8}$	S=1.8	172
$\pi^+ e^+ e^- e^+ e^-$	$S1$	$< 1.4 \times 10^{-8}$	CL=90%	227
$\pi^+ \nu\overline{\nu}$	$S1$	$(1.33 \pm 0.30) \times 10^{-10}$		227
$\pi^+ \pi^0 \nu\overline{\nu}$	$S1$	$< 4.3 \times 10^{-5}$	CL=90%	205
$\mu^- \nu e^+ e^+$	LF	$< 8.1 \times 10^{-11}$	CL=90%	236
$\mu^+ \nu_e$	LF [d]	$< 4 \times 10^{-3}$	CL=90%	236
$\pi^+ \mu^+ e^-$	LF	$< 1.3 \times 10^{-11}$	CL=90%	214
$\pi^0 \pi^+ \mu^+ e^-$	LF	$< 5.0 \times 10^{-10}$	CL=90%	154
$\pi^+ \mu^- e^+$	LF	$< 6.6 \times 10^{-11}$	CL=90%	214
$\pi^0 \pi^+ \mu^- e^+$	LF	$< 3.1 \times 10^{-10}$	CL=90%	154
$\pi^- \mu^+ e^+$	L	$< 4.2 \times 10^{-11}$	CL=90%	214
$\pi^0 \pi^- \mu^+ e^+$	L	$< 2.9 \times 10^{-10}$	CL=90%	154
$\pi^- e^+ e^+$	L	$< 5.3 \times 10^{-11}$	CL=90%	227
$\pi^- \mu^+ \mu^+$	L	$< 4.2 \times 10^{-11}$	CL=90%	172
$\pi^- \pi^0 e^+ e^+$	L	$< 8.5 \times 10^{-10}$	CL=90%	205
$\mu^+ \overline{\nu}_e$	L [d]	$< 3.3 \times 10^{-3}$	CL=90%	236

Int. J. Mod. Phys. A 2026.41. Downloaded from www.worldscientific.com
by UNIVERSITY OF CALIFORNIA @ BERKELEY on 09/16/26. Re-use and distribution is strictly not permitted, except for Open Access articles.

$\pi^0 e^+ \overline{\nu}_e$	L	$<$	3	$\times 10^{-3}$	CL=90%	228
$\pi^+ \gamma$		[x] $<$	2.3	$\times 10^{-9}$	CL=90%	227

K^0

$I(J^P) = \frac{1}{2}(0^-)$

50% K_S, 50% K_L

Mass $m = 497.611 \pm 0.013$ MeV (S = 1.2)

$m_{K^0} - m_{K^\pm} = 3.934 \pm 0.020$ MeV (S = 1.6)

Mean square charge radius

$\langle r^2 \rangle = -0.077 \pm 0.010$ fm^2

***T*-violation parameters in K^0-$\overline{K}^0$ mixing** [r]

Asymmetry A_T in K^0-$\overline{K}^0$ mixing $= (6.6 \pm 1.6) \times 10^{-3}$

***CP*-violation parameters**

$\mathrm{Re}(\epsilon) = (1.596 \pm 0.013) \times 10^{-3}$

***CPT*-violation parameters** [r]

$\mathrm{Re}\ \delta = (2.5 \pm 2.3) \times 10^{-4}$

$\mathrm{Im}\ \delta = (-1.5 \pm 1.6) \times 10^{-5}$

Re(y), K_{e3} parameter $= (0.4 \pm 2.5) \times 10^{-3}$

Re(x_-), K_{e3} parameter $= (-2.9 \pm 2.0) \times 10^{-3}$

$|m_{K^0} - m_{\overline{K}^0}| \ / \ m_{\mathrm{average}} < 6 \times 10^{-19}$, CL = 90% [y]

$(\Gamma_{K^0} - \Gamma_{\overline{K}^0})/m_{\mathrm{average}} = (8 \pm 8) \times 10^{-18}$

Tests of $\Delta S = \Delta Q$

Re(x_+), K_{e3} parameter $= (-0.9 \pm 3.0) \times 10^{-3}$

K^0_S

$I(J^P) = \frac{1}{2}(0^-)$

Mean life $\tau = (0.8954 \pm 0.0004) \times 10^{-10}$ s (S = 1.1) Assuming *CPT*

Mean life $\tau = (0.89564 \pm 0.00033) \times 10^{-10}$ s Not assuming *CPT*

$c\tau = 2.6844$ cm Assuming *CPT*

***CP*-violation parameters** [z]

$\mathrm{Im}(\eta_{+-0}) = -0.002 \pm 0.009$

$\mathrm{Im}(\eta_{000}) = -0.001 \pm 0.016$

$|\eta_{000}| = |A(K^0_S \to 3\pi^0)/A(K^0_L \to 3\pi^0)| < 0.0088$, CL = 90%

CP asymmetry A in $\pi^+\pi^- e^+ e^- = (-0.4 \pm 0.8)$%

K^0_S DECAY MODES		Fraction (Γ_i/Γ)	Scale factor/ Confidence level	p (MeV/c)
Hadronic modes				
$\pi^0\pi^0$		(30.69 ± 0.05) %		209
$\pi^+\pi^-$		(69.20 ± 0.05) %		206
$\pi^+\pi^-\pi^0$		$(3.5\ ^{+1.1}_{-0.9}) \times 10^{-7}$		133
Modes with photons or $\ell\overline{\ell}$ pairs				
$\pi^+\pi^-\gamma$	[t,aa]	$(1.79 \pm 0.05) \times 10^{-3}$		206
$\pi^+\pi^- e^+ e^-$		$(4.79 \pm 0.15) \times 10^{-5}$		206
$\pi^0\gamma\gamma$	[aa]	$(4.9 \pm 1.8) \times 10^{-8}$		230
$\gamma\gamma$		$(2.63 \pm 0.17) \times 10^{-6}$	S=3.1	249
$\mu^+\mu^-\mu^+\mu^-$		$< 5.1 \times 10^{-12}$	CL=90%	119
Semileptonic modes				
$\pi^\pm e^\mp \nu_e$	[bb]	$(7.14 \pm 0.06) \times 10^{-4}$		229
***CP* violating (*CP*) and $\Delta S = 1$ weak neutral current (*S1*) modes**				
$3\pi^0$	*CP*	$< 2.6 \times 10^{-8}$	CL=90%	139
$\mu^+\mu^-$	*S1*	$< 2.1 \times 10^{-10}$	CL=90%	225
e^+e^-	*S1*	$< 9 \times 10^{-9}$	CL=90%	249
$\pi^0 e^+ e^-$	*S1* [aa]	$(3.0\ ^{+1.5}_{-1.2}) \times 10^{-9}$		230
$\pi^0\mu^+\mu^-$	*S1*	$(2.9\ ^{+1.5}_{-1.2}) \times 10^{-9}$		177
invisible		$< 8.4 \times 10^{-4}$	CL=90%	–

K^0_L

$I(J^P) = \frac{1}{2}(0^-)$

$m_{K_L} - m_{K_S}$

$= (0.5293 \pm 0.0009) \times 10^{10}\ \hbar\ \mathrm{s}^{-1}$ (S = 1.3) Assuming *CPT*

$= (3.484 \pm 0.006) \times 10^{-12}$ MeV Assuming *CPT*

$= (0.5289 \pm 0.0010) \times 10^{10}\ \hbar\ \mathrm{s}^{-1}$ Not assuming *CPT*

Mean life $\tau = (5.116 \pm 0.021) \times 10^{-8}$ s (S = 1.1)

$c\tau = 15.34$ m

Slope parameters [q]

(See Particle Listings for other linear and quadratic coefficients)

$K^0_L \to \pi^+\pi^-\pi^0$: $g = 0.678 \pm 0.008$ (S = 1.5)

$K^0_L \to \pi^+\pi^-\pi^0$: $h = 0.076 \pm 0.006$

$K^0_L \to \pi^+\pi^-\pi^0$: $k = 0.0099 \pm 0.0015$

$K^0_L \to \pi^0\pi^0\pi^0$: $h = (0.6 \pm 1.2) \times 10^{-3}$

K_L decay form factors [r]

Linear parametrization assuming μ-e universality

$\lambda_+(K^0_{\mu3}) = \lambda_+(K^0_{e3}) = (2.82 \pm 0.04) \times 10^{-2}$ (S = 1.1)

$\lambda_0(K^0_{\mu3}) = (1.38 \pm 0.18) \times 10^{-2}$ (S = 2.2)

Quadratic parametrization assuming μ-e universality

$\lambda'_+(K^0_{\mu3}) = \lambda'_+(K^0_{e3}) = (2.40 \pm 0.12) \times 10^{-2}$ (S = 1.2)

$\lambda''_+(K^0_{\mu3}) = \lambda''_+(K^0_{e3}) = (0.20 \pm 0.05) \times 10^{-2}$ (S = 1.2)

$\lambda_0(K^0_{\mu3}) = (1.16 \pm 0.09) \times 10^{-2}$ (S = 1.2)

Pole parametrization assuming μ-e universality

$M^\mu_V\ (K^0_{\mu3}) = M^e_V\ (K^0_{e3}) = 878 \pm 6$ MeV (S = 1.1)

$M^\mu_S\ (K^0_{\mu3}) = 1252 \pm 90$ MeV (S = 2.6)

Dispersive parametrization assuming μ-e universality

$\Lambda_+ = (2.51 \pm 0.06) \times 10^{-2}$ (S = 1.5)

$\ln(C) = (1.75 \pm 0.18) \times 10^{-1}$ (S = 2.0)

K^0_{e3} $|f_S/f_+| = (1.5\ ^{+1.4}_{-1.6}) \times 10^{-2}$

K^0_{e3} $|f_T/f_+| = (5\ ^{+4}_{-5}) \times 10^{-2}$

$K^0_{\mu3}$ $|f_T/f_+| = (12 \pm 12) \times 10^{-2}$

$K_L \to \ell^+\ell^-\gamma$, $K_L \to \ell^+\ell^-\ell'^+\ell'^-$: $\alpha_{K^*} = -0.205 \pm 0.022$ (S = 1.8)

$K^0_L \to \ell^+\ell^-\gamma$, $K^0_L \to \ell^+\ell^-\ell'^+\ell'^-$: $\alpha_{DIP} = -1.69 \pm 0.08$ (S = 1.7)

$K_L \to \pi^+\pi^- e^+ e^-$: $a_1/a_2 = -0.737 \pm 0.014$ GeV^2

$K_L \to \pi^0 2\gamma$: $a_V = -0.43 \pm 0.06$ (S = 1.5)

***CP*-violation parameters** [z]

$A_L = (0.332 \pm 0.006)$%

$|\eta_{00}| = (2.222 \pm 0.012) \times 10^{-3}$ (S = 1.7)

$|\eta_{+-}| = (2.233 \pm 0.012) \times 10^{-3}$ (S = 1.7)

$|\epsilon| = (2.229 \pm 0.012) \times 10^{-3}$ (S = 1.7)

$|\eta_{00}/\eta_{+-}| = 0.9950 \pm 0.0007$ [cc] (S = 1.6)

$\mathrm{Re}(\epsilon'/\epsilon) = (1.67 \pm 0.23) \times 10^{-3}$ [cc] (S = 1.6)

Assuming *CPT*

$\phi_{+-} = (43.51 \pm 0.05)^\circ$ (S = 1.2)

$\phi_{00} = (43.52 \pm 0.05)^\circ$ (S = 1.2)

$\phi_\epsilon = \phi_{SW} = (43.52 \pm 0.04)^\circ$ (S = 1.2)

$\mathrm{Im}(\epsilon'/\epsilon) = -(\phi_{00} - \phi_{+-})/3 = (-0.002 \pm 0.005)^\circ$ (S = 1.7)

Not assuming *CPT*

$\phi_{+-} = (43.4 \pm 0.5)^\circ$ (S = 1.2)

$\phi_{00} = (43.7 \pm 0.6)^\circ$ (S = 1.2)

$\phi_\epsilon = (43.5 \pm 0.5)^\circ$ (S = 1.3)

CP asymmetry A in $K^0_L \to \pi^+\pi^- e^+ e^- = (13.7 \pm 1.5)$%

β_{CP} from $K^0_L \to e^+e^-e^+e^- = -0.19 \pm 0.07$

γ_{CP} from $K^0_L \to e^+e^-e^+e^- = 0.01 \pm 0.11$ (S = 1.6)

j for $K^0_L \to \pi^+\pi^-\pi^0 = 0.0012 \pm 0.0008$

f for $K^0_L \to \pi^+\pi^-\pi^0 = 0.004 \pm 0.006$

$|\eta_{+-\gamma}| = (2.35 \pm 0.07) \times 10^{-3}$

$\phi_{+-\gamma} = (44 \pm 4)^\circ$

$|\epsilon'_{+-\gamma}|/\epsilon < 0.3$, CL = 90%

$|g_{E1}|$ for $K^0_L \to \pi^+\pi^-\gamma < 0.21$, CL = 90%

***T*-violation parameters**

$\mathrm{Im}(\xi)$ in $K^0_{\mu3} = -0.007 \pm 0.026$

***CPT* invariance tests**

$\phi_{00} - \phi_{+-} = (0.34 \pm 0.32)^\circ$

Int. J. Mod. Phys. A 2026.41. Downloaded from www.worldscientific.com
by UNIVERSITY OF CALIFORNIA @ BERKELEY on 09/16/26. Re-use and distribution is strictly not permitted, except for Open Acce

$\mathrm{Re}(\frac{2}{3}\eta_{+-} + \frac{1}{3}\eta_{00}) - \frac{A_L}{2} = (-3 \pm 35) \times 10^{-6}$

$\Delta S = -\Delta Q$ in $K^0_{\ell 3}$ decay

Re $x = -0.002 \pm 0.006$
Im $x = 0.0012 \pm 0.0021$

K^0_L DECAY MODES		Fraction (Γ_i/Γ)	Scale factor/ Confidence level	p (MeV/c)
Semileptonic modes				
$\pi^\pm e^\mp \nu_e$ Called K^0_{e3}.	[bb]	(40.55 ± 0.11) %	S=1.7	229
$\pi^\pm \mu^\mp \nu_\mu$ Called $K^0_{\mu 3}$.	[bb]	(27.04 ± 0.07) %	S=1.1	216
$(\pi\mu\mathrm{atom})\nu$		$(1.05 \pm 0.11) \times 10^{-7}$		188
$\pi^0 \pi^\pm e^\mp \nu$	[bb]	$(5.20 \pm 0.11) \times 10^{-5}$		207
$\pi^\pm e^\mp \nu e^+ e^-$	[bb]	$(1.26 \pm 0.04) \times 10^{-5}$		229
Hadronic modes, including Charge conjugation × Parity Violating (*CPV*) modes				
$3\pi^0$		(19.52 ± 0.12) %	S=1.6	139
$\pi^+ \pi^- \pi^0$		(12.54 ± 0.05) %		133
$\pi^+ \pi^-$	*CPV* [dd]	$(1.967 \pm 0.010) \times 10^{-3}$	S=1.5	206
$\pi^0 \pi^0$	*CPV*	$(8.64 \pm 0.06) \times 10^{-4}$	S=1.8	209
Semileptonic modes with photons				
$\pi^\pm e^\mp \nu_e \gamma$	[t,bb,ee]	$(3.79 \pm 0.06) \times 10^{-3}$		229
$\pi^\pm \mu^\mp \nu_\mu \gamma$		$(5.65 \pm 0.23) \times 10^{-4}$		216
Hadronic modes with photons or $\ell\overline{\ell}$ pairs				
$\pi^0 \pi^0 \gamma$		$< 2.43 \times 10^{-7}$	CL=90%	209
$\pi^+ \pi^- \gamma$	[t,ee]	$(4.15 \pm 0.15) \times 10^{-5}$	S=2.8	206
$\pi^+ \pi^- \gamma$(DE)		$(2.84 \pm 0.11) \times 10^{-5}$	S=2.0	206
$\pi^0 2\gamma$	[ee]	$(1.273 \pm 0.033) \times 10^{-6}$		230
$\pi^0 \gamma e^+ e^-$		$(1.62 \pm 0.17) \times 10^{-8}$		230
Other modes with photons or $\ell\overline{\ell}$ pairs				
2γ		$(5.47 \pm 0.04) \times 10^{-4}$	S=1.1	249
3γ		$< 7.4 \times 10^{-8}$	CL=90%	249
$e^+ e^- \gamma$		$(9.4 \pm 0.4) \times 10^{-6}$	S=2.0	249
$\mu^+ \mu^- \gamma$		$(3.59 \pm 0.11) \times 10^{-7}$	S=1.3	225
$\mu^+ \mu^- \mu^+ \mu^-$		$< 2.3 \times 10^{-9}$	CL=90%	119
$e^+ e^- \gamma\gamma$	[ee]	$(5.95 \pm 0.33) \times 10^{-7}$		249
$\mu^+ \mu^- \gamma\gamma$	[ee]	$(1.0 {}^{+0.8}_{-0.6}) \times 10^{-8}$		225
Charge conjugation × Parity (*CP*) or Lepton Family number (*LF*) violating modes, or $\Delta S = 1$ weak neutral current (*S1*) modes				
$\mu^+ \mu^-$	*S1*	$(6.84 \pm 0.11) \times 10^{-9}$		225
$e^+ e^-$	*S1*	$(9 {}^{+6}_{-4}) \times 10^{-12}$		249
$\pi^+ \pi^- e^+ e^-$	*S1* [ee]	$(3.11 \pm 0.19) \times 10^{-7}$		206
$\pi^0 \pi^0 e^+ e^-$	*S1*	$< 6.6 \times 10^{-9}$	CL=90%	209
$\pi^0 \pi^0 \mu^+ \mu^-$	*S1*	$< 9.2 \times 10^{-11}$	CL=90%	57
$\mu^+ \mu^- e^+ e^-$	*S1*	$(2.69 \pm 0.27) \times 10^{-9}$		225
$e^+ e^- e^+ e^-$	*S1*	$(3.56 \pm 0.21) \times 10^{-8}$		249
$\pi^0 \mu^+ \mu^-$	*CP,S1* [ff]	$< 3.8 \times 10^{-10}$	CL=90%	177
$\pi^0 e^+ e^-$	*CP,S1* [ff]	$< 2.8 \times 10^{-10}$	CL=90%	230
$\pi^0 \nu\overline{\nu}$	*CP,S1* [gg]	$< 2.2 \times 10^{-9}$	CL=90%	230
$\pi^0 \pi^0 \nu\overline{\nu}$	*S1*	$< 8.1 \times 10^{-7}$	CL=90%	209
$e^\pm \mu^\mp$	*LF* [bb]	$< 4.7 \times 10^{-12}$	CL=90%	238
$e^\pm e^\pm \mu^\mp \mu^\mp$	*LF* [bb]	$< 4.12 \times 10^{-11}$	CL=90%	225
$\pi^0 \mu^\pm e^\mp$	*LF* [bb]	$< 7.6 \times 10^{-11}$	CL=90%	217
$\pi^0 \pi^0 \mu^\pm e^\mp$	*LF*	$< 1.7 \times 10^{-10}$	CL=90%	159
Lorentz invariance violating modes				
$\pi^0 \gamma$		$< 1.7 \times 10^{-7}$	CL=90%	230

$K^*_0(700)$

$I(J^P) = \frac{1}{2}(0^+)$

also known as κ; was $K^*_0(800)$

See the review on "Scalar Mesons below 1 GeV."

Mass (T-Matrix Pole $\sqrt{s}$) = (630–730) $- i$ (260–340) MeV
Mass (Breit-Wigner) = 838 ± 11 MeV
Full width (Breit-Wigner) = 463 ± 27 MeV

$K^*_0(700)$ DECAY MODES	Fraction (Γ_i/Γ)	p (MeV/c)
$K\pi$	100 %	250

$K^*(892)$

$I(J^P) = \frac{1}{2}(1^-)$

Mass (T-Matrix Pole $\sqrt{s}$) = $(890 \pm 14) - i\,(26 \pm 6)$ MeV
$K^*(892)^\pm$ hadroproduced mass $m = 891.88 \pm 0.23$ MeV
$K^*(892)^\pm$ in τ decays mass $m = 895.5 \pm 0.8$ MeV
$K^*(892)^0$ mass $m = 895.56 \pm 0.20$ MeV (S = 1.7)
$K^*(892)^\pm$ hadroproduced full width $\Gamma = 48.5 \pm 1.2$ MeV (S = 2.1)
$K^*(892)^\pm$ in τ decays full width $\Gamma = 46.2 \pm 1.3$ MeV
$K^*(892)^0$ full width $\Gamma = 47.1 \pm 0.5$ MeV (S = 2.0)

$K^*(892)$ DECAY MODES	Fraction (Γ_i/Γ)	Confidence level	p (MeV/c)
$K\pi$	~ 100 %		290
$K^0\gamma$	$(2.47 \pm 0.21) \times 10^{-3}$		307
$K^\pm\gamma$	$(1.04 \pm 0.10) \times 10^{-3}$		309
$K\pi\pi$	$< 7 \times 10^{-4}$	95%	223

$K_1(1270)$

$I(J^P) = \frac{1}{2}(1^+)$

Mass $m = 1256 \pm 6$ MeV (S = 2.2)
Full width $\Gamma = 90 \pm 20$ MeV [j]

$K_1(1270)$ DECAY MODES	Fraction (Γ_i/Γ)	Scale factor	p (MeV/c)
$K\rho$	(53 ± 8) %	2.1	†
$K^*_0(1430)\pi$	(14 ± 8) %	4.0	†
$K^*(892)\pi$	(18 ± 4) %	1.2	288
$K\omega$	(9.6 ± 2.1) %	1.3	†
$Kf_0(1370)$	(3.0 ± 2.0) %		†
γK^0	seen		529

$K_1(1400)$

$I(J^P) = \frac{1}{2}(1^+)$

Mass $m = 1403 \pm 7$ MeV
Full width $\Gamma = 174 \pm 13$ MeV (S = 1.6)

$K_1(1400)$ DECAY MODES	Fraction (Γ_i/Γ)	p (MeV/c)
$K^*(892)\pi$	(94 ± 6) %	402
$K\rho$	(3.0 ± 3.0) %	293
$Kf_0(1370)$	(2.0 ± 2.0) %	†
$K\omega$	(1.0 ± 1.0) %	284
$K^*_0(1430)\pi$	not seen	†
γK^0	seen	613
$K\phi$	seen	†

$K^*(1410)$

$I(J^P) = \frac{1}{2}(1^-)$

T-matrix pole $\sqrt{s} = (1368 \pm 38) - i\,(106 {}^{+48}_{-59})$ MeV
Mass $m = 1414 \pm 15$ MeV (S = 1.3)
Full width $\Gamma = 232 \pm 21$ MeV (S = 1.1)

$K^*(1410)$ DECAY MODES	Fraction (Γ_i/Γ)	Confidence level	p (MeV/c)
$K^*(892)\pi$	> 40 %	95%	410
$K\pi$	(6.6 ± 1.3) %		612
$K\rho$	< 7 %	95%	306
γK^0	$< 2.3 \times 10^{-4}$	90%	619
$K\phi$	seen		†

$K^*_0(1430)$

$I(J^P) = \frac{1}{2}(0^+)$

T-matrix pole $\sqrt{s} = (1431 \pm 6) - i\,(110 \pm 19)$ MeV
Mass $m = 1425 \pm 50$ MeV [j]
Full width $\Gamma = 270 \pm 80$ MeV [j]

$K^*_0(1430)$ DECAY MODES	Fraction (Γ_i/Γ)	p (MeV/c)
$K\pi$	(93 ± 10) %	619
$K\eta$	$(8.6 {}^{+2.7}_{-3.4})$ %	486
$K\eta'(958)$	seen	†

Int. J. Mod. Phys. A 2026.41. Downloaded from www.worldscientific.com
by UNIVERSITY OF CALIFORNIA @ BERKELEY on 09/16/26. Re-use and distribution is strictly not permitted, except for Open Access articles.

$K_2^*(1430)$ $I(J^P) = \frac{1}{2}(2^+)$

T-matrix pole $\sqrt{s} = (1424 \pm 4) - i\,(66 \pm 2)$ MeV
$K_2^*(1430)^\pm$ mass $m = 1427.3 \pm 1.5$ MeV (S = 1.3)
$K_2^*(1430)^0$ mass $m = 1432.4 \pm 1.3$ MeV
$K_2^*(1430)^\pm$ full width $\Gamma = 100.0 \pm 2.2$ MeV (S = 1.1)
$K_2^*(1430)^0$ full width $\Gamma = 109 \pm 5$ MeV (S = 1.9)

$K_2^*(1430)$ DECAY MODES	Fraction (Γ_i/Γ)	Scale factor/ Confidence level	p (MeV/c)
$K\pi$	(49.9±1.2) %		620
$K^*(892)\pi$	(24.7±1.5) %		420
$K^*(892)\pi\pi$	(13.4±2.2) %		373
$K\rho$	(8.7±0.8) %	S=1.2	320
$K\omega$	(2.9±0.8) %		313
$K^+\gamma$	$(2.4\pm0.5)\times10^{-3}$	S=1.1	628
$K\eta$	$(1.5^{+3.4}_{-1.0})\times10^{-3}$	S=1.3	488
$K\omega\pi$	$< 7.2 \times10^{-4}$	CL=95%	106
$K^0\gamma$	$< 9 \times10^{-4}$	CL=90%	627

$K(1460)$ $I(J^P) = \frac{1}{2}(0^-)$

$K(1460)$ DECAY MODES	Fraction (Γ_i/Γ)	p (MeV/c)
$K^*(892)\pi$	seen	–
$K\rho$	seen	–
$K_0^*(1430)\pi$	seen	–
$K\phi$	seen	–

$K_1(1650)$ $I(J^P) = \frac{1}{2}(1^+)$

Mass $m = 1650 \pm 50$ MeV
Full width $\Gamma = 150 \pm 50$ MeV

$K^*(1680)$ $I(J^P) = \frac{1}{2}(1^-)$

Mass $m = 1718 \pm 18$ MeV
Full width $\Gamma = 320 \pm 110$ MeV (S = 4.2)

$K^*(1680)$ DECAY MODES	Fraction (Γ_i/Γ)	p (MeV/c)
$K\pi$	(38.7±2.5) %	782
$K\rho$	$(31.4^{+5.0}_{-2.1})$ %	571
$K^*(892)\pi$	$(29.9^{+2.2}_{-5.0})$ %	618
$K\phi$	seen	387
$K\eta$	$(1.4^{+1.0}_{-0.8})$ %	683

$K_2(1770)$ [hh] $I(J^P) = \frac{1}{2}(2^-)$

Mass $m = 1773 \pm 8$ MeV
Full width $\Gamma = 186 \pm 14$ MeV

$K_2(1770)$ DECAY MODES	Fraction (Γ_i/Γ)	p (MeV/c)
$K\pi\pi$		794
$K_2^*(1430)\pi$	seen	287
$K^*(892)\pi$	seen	654
$Kf_2(1270)$	seen	53
$Kf_0(980)$	possibly seen	466
$K\phi$	seen	441
$K\omega$	seen	607

$K_3^*(1780)$ $I(J^P) = \frac{1}{2}(3^-)$

T-matrix pole $\sqrt{s} = (1754 \pm 13) - i\,(119 \pm 14)$ MeV
Mass $m = 1779 \pm 8$ MeV (S = 1.2)
Full width $\Gamma = 161 \pm 17$ MeV (S = 1.1)

$K_3^*(1780)$ DECAY MODES	Fraction (Γ_i/Γ)	Confidence level	p (MeV/c)
$K\rho$	(31 ± 9) %		616
$K^*(892)\pi$	(20 ± 5) %		657
$K\pi$	(18.8± 1.0) %		815
$K\eta$	(30 ±13) %		721
$K_2^*(1430)\pi$	< 16 %	95%	292

$K_2(1820)$ [hh] $I(J^P) = \frac{1}{2}(2^-)$

Mass $m = 1819 \pm 12$ MeV
Full width $\Gamma = 264 \pm 34$ MeV

$K_2(1820)$ DECAY MODES	Fraction (Γ_i/Γ)	p (MeV/c)
$K\pi\pi$	seen	819
$K_2^*(1430)\pi$	seen	328
$K^*(892)\pi$	seen	683
$Kf_2(1270)$	seen	191
$K\omega$	seen	640
$K\phi$	seen	483

$K_0^*(1950)$ $I(J^P) = \frac{1}{2}(0^+)$

Mass $m = 1957 \pm 14$ MeV
Full width $\Gamma = 170 \pm 50$ MeV (S = 2.2)

$K_0^*(1950)$ DECAY MODES	Fraction (Γ_i/Γ)	p (MeV/c)
$K^-\pi^+$	(52±14) %	911

$K_2^*(1980)$ $I(J^P) = \frac{1}{2}(2^+)$

Mass $m = 1990^{+60}_{-50}$ MeV (S = 2.8)
Full width $\Gamma = 348^{+50}_{-30}$ MeV (S = 1.3)

$K_2^*(1980)$ DECAY MODES	Fraction (Γ_i/Γ)	p (MeV/c)
$K^*(892)\pi$	possibly seen	791
$K\rho$	possibly seen	762
$Kf_2(1270)$	possibly seen	424
$K\phi$	seen	627
$K\eta$	seen	850

$K_4^*(2045)$ $I(J^P) = \frac{1}{2}(4^+)$

Mass $m = 2048^{+8}_{-9}$ MeV (S = 1.1)
Full width $\Gamma = 199^{+27}_{-19}$ MeV

$K_4^*(2045)$ DECAY MODES	Fraction (Γ_i/Γ)	p (MeV/c)
$K\pi$	(9.9±1.2) %	960
$K^*(892)\pi\pi$	(9 ±5) %	804
$K^*(892)\pi\pi\pi$	(7 ±5) %	770
$\rho K\pi$	(5.7±3.2) %	744
$\omega K\pi$	(5.0±3.0) %	740
$\phi K\pi$	(2.8±1.4) %	597
$\phi K^*(892)$	(1.4±0.7) %	367

CHARMED MESONS ($C = \pm1$)

$D^+ = c\overline{d}$, $D^0 = c\overline{u}$, $\overline{D}^0 = \overline{c}u$, $D^- = \overline{c}d$, similarly for D^*'s

$D^\pm$ $I(J^P) = \frac{1}{2}(0^-)$

Mass $m = 1869.66 \pm 0.05$ MeV
Mean life $\tau = (1033 \pm 5) \times 10^{-15}$ s
$c\tau = 309.8\ \mu$m

c-quark decays

$\Gamma(c \to \ell^+ \text{anything})/\Gamma(c \to \text{anything}) = 0.096 \pm 0.004$ [ii]
$\Gamma(c \to D^*(2010)^+ \text{anything})/\Gamma(c \to \text{anything}) = 0.255 \pm 0.017$

CP-violation decay-rate asymmetries

$A_{CP}(\mu^\pm\nu) = (8 \pm 8)\%$

Int. J. Mod. Phys. A 2026.41. Downloaded from www.worldscientific.com
by UNIVERSITY OF CALIFORNIA @ BERKELEY on 09/16/26. Re-use and distribution is strictly not permitted, except for Open Acce

$A_{CP}(K_L^0 e^{\pm}\nu) = (-0.6 \pm 1.6)\%$
$A_{CP}(K_S^0 \pi^{\pm}) = (-0.41 \pm 0.09)\%$
$A_{CP}(K_L^0 K^{\pm})$ in $D^{\pm} \to K_L^0 K^{\pm} = (-4.2 \pm 3.4) \times 10^{-2}$
$A_{CP}(K^{\mp} 2\pi^{\pm}) = (-0.18 \pm 0.16)\%$
$A_{CP}(K^{\mp}\pi^{\pm}\pi^{\pm}\pi^0) = (-0.3 \pm 0.7)\%$
$A_{CP}(K_S^0 \pi^{\pm}\pi^0) = (-0.1 \pm 0.7)\%$
$A_{CP}(K_S^0 \pi^{\pm}\eta)$ in $D^{\pm} \to K_S^0 \pi^{\pm}\eta = (-0.9 \pm 3.1) \times 10^{-2}$
$A_{CP}(K_S^0 \pi^{\pm}\pi^{+}\pi^{-}) = (0.0 \pm 1.2)\%$
$A_{CP}(K^{\pm}\pi^{+}\pi^{-}\pi^0)$ in $D^{\pm} \to K^{\pm}\pi^{+}\pi^{-}\pi^0 = -0.04 \pm 0.06$
$A_{CP}(\pi^{\pm}\pi^0) = (-0.5 \pm 1.0)\%$ (S = 1.7)
$A_{CP}(\pi^{\pm}\eta) = (0.3 \pm 0.5)\%$
$A_{CP}(\pi^{\pm}\pi^0\eta)$ in $D^{\pm} \to \pi^{\pm}\pi^0\eta = (-6 \pm 7) \times 10^{-2}$
$A_{CP}(\pi^{\pm}\eta\eta)$ in $D^{\pm} \to \pi^{\pm}\eta\eta = (8 \pm 9) \times 10^{-2}$
$A_{CP}(\pi^{\pm}\eta'(958)) = (0.41 \pm 0.23)\%$ (S = 1.2)
$A_{CP}(\overline{K}^0/K^0 K^{\pm}) = (0.11 \pm 0.17)\%$
$A_{CP}(K_S^0 K^{\pm}) = (-0.01 \pm 0.07)\%$
$A_{CP}(K_S^0 K^{\pm}\pi^0)$ in $D^{\pm} \to K_S^0 K^{\pm}\pi^0 = (1 \pm 4) \times 10^{-2}$
$A_{CP}(K_L^0 K^{\pm}\pi^0)$ in $D^{\pm} \to K_L^0 K^{\pm}\pi^0 = (-1 \pm 4) \times 10^{-2}$
$A_{CP}(K^{+}K^{-}\pi^{\pm}) = (0.37 \pm 0.29)\%$
$A_{CP}(K^{\pm}K^{*0}) = (-0.3 \pm 0.4)\%$
$A_{CP|S}(K^{+}\overline{K}^{*0})$ in $D^{\pm} \to K^{-}K^{+}\pi^{\pm} = (-0.3 \pm 0.6) \times 10^{-3}$
$A_{CP}(\phi\pi^{\pm}) = (0.01 \pm 0.09)\%$ (S = 1.8)
$A_{CP|S}(\phi\pi^{+})$ in $D^{\pm} \to K^{-}K^{+}\pi^{\pm} = (1.0 \pm 0.5) \times 10^{-3}$
$A_{CP}(K^{\pm}K_0^*(1430)^0) = (8^{+7}_{-6})\%$
$A_{CP}(K^{\pm}K_2^*(1430)^0) = (43^{+20}_{-26})\%$
$A_{CP}(K^{\pm}K_0^*(700)) = (-12^{+18}_{-13})\%$
$A_{CP}(a_0(1450)^0\pi^{\pm}) = (-19^{+14}_{-16})\%$
$A_{CP}(\phi(1680)\pi^{\pm}) = (-9 \pm 26)\%$
$A_{CP}(\pi^{\pm}2\pi^0)$ in $D^{\pm} \to \pi^{\pm}2\pi^0 = (5.6 \pm 2.7)\%$
$A_{CP}(\pi^{+}\pi^{-}\pi^{\pm}) = (0.5 \pm 2.0)\%$
$A_{CP}(2\pi^{\pm}\pi^{\mp}\pi^0)$ in $D^{\pm} \to 2\pi^{\pm}\pi^{\mp}\pi^0 = (0.3 \pm 2.0)\%$
$A_{CP}(2\pi^{\pm}\pi^{\mp}2\pi^0)$ in $D^{\pm} \to 2\pi^{\pm}\pi^{\mp}2\pi^0 = (-4 \pm 4)\%$
$A_{CP}(\pi^{+}\pi^{-}\pi^{\pm}\eta)$ in $D^{\pm} \to \pi^{+}\pi^{-}\pi^{\pm}\eta = (3 \pm 5) \times 10^{-2}$
$A_{CP}(K_S^0 K^{\pm}\pi^{+}\pi^{-}) = (-4 \pm 7)\%$
$A_{CP}(K^{\pm}\pi^0) = (-3 \pm 5)\%$
$A_{CP}(K^{\pm}\eta)$ in $D^{\pm} \to K^{\pm}\eta = (-6 \pm 11) \times 10^{-2}$

χ^2 tests of *CP*-violation (*CPV*)

Local *CPV* in $D^{\pm} \to \pi^{+}\pi^{-}\pi^{\pm} = 78.1\%$
Local *CPV* in $D^{\pm} \to K^{+}K^{-}\pi^{\pm} = 31\%$
Local *CPV* in $D^{\pm} \to K^{+}K^{-}K^{\pm} = 31.6\%$

CP violating asymmetries of *P*-odd (*T*-odd) moments

$A_T(K_S^0 K^{\pm}\pi^{+}\pi^{-}) = (-3 \pm 8) \times 10^{-3}$ [jj] (S = 1.1)
$A_{Tviol}(K_S^0 K^{\mp}\pi^{\pm}\pi^{\pm})$ in $D^{\pm} \to K_S^0 K^{\mp}\pi^{\pm}\pi^{\pm} = (-2 \pm 5) \times 10^{-3}$
$A_{Tviol}(K^{+}K^{-}K_S^0\pi^{\pm})$ in $D^{\pm} \to K^{+}K^{-}K_S^0\pi^{\pm} = (-3.3 \pm 2.7)\%$

D^+ form factors

$f_+(0)|V_{cs}|$ in $\overline{K}^0\ell^{+}\nu_\ell = 0.7163 \pm 0.0033$
$r_1 \equiv a_1/a_0$ in $\overline{K}^0\ell^{+}\nu_\ell = -2.13 \pm 0.14$
$r_2 \equiv a_2/a_0$ in $\overline{K}^0\ell^{+}\nu_\ell = -3 \pm 12$ (S = 1.5)
$f_+(0)|V_{cd}|$ in $\pi^0\ell^{+}\nu_\ell = 0.1407 \pm 0.0025$
$r_1 \equiv a_1/a_0$ in $\pi^0\ell^{+}\nu_\ell = -2.00 \pm 0.13$
$r_2 \equiv a_2/a_0$ in $\pi^0\ell^{+}\nu_\ell = -4 \pm 5$
$f_+(0)|V_{cd}|$ in $D^{+} \to \eta\ell^{+}\nu_\ell$ ($\ell = e$ or ν) $= (8.4 \pm 0.4) \times 10^{-2}$
$f_+^{\eta'}(0)|V_{cd}|$ in $D^{+} \to \eta'\ell^{+}\nu_\ell$ ($\ell = e, \nu$) $= (5.9 \pm 0.6) \times 10^{-2}$
$r_1 \equiv a_1/a_0$ in $D^{+} \to \eta e^{+}\nu_e = -5.3 \pm 2.7$ (S = 1.9)
$r_v \equiv V(0)/A_1(0)$ in $D^{+} \to \omega e^{+}\nu_e = 1.24 \pm 0.11$
$r_2 \equiv A_2(0)/A_1(0)$ in $D^{+} \to \omega e^{+}\nu_e = 1.06 \pm 0.16$
$r_v \equiv V(0)/A_1(0)$ in $D^{+}, D^0 \to \rho e^{+}\nu_e = 1.53 \pm 0.08$
$r_2 \equiv A_2(0)/A_1(0)$ in $D^{+}, D^0 \to \rho e^{+}\nu_e = 0.82 \pm 0.05$
$r_v \equiv V(0)/A_1(0)$ in $\overline{K}^*(892)^0\ell^{+}\nu_\ell = 1.47 \pm 0.04$ (S = 2.0)
$r_2 \equiv A_2(0)/A_1(0)$ in $\overline{K}^*(892)^0\ell^{+}\nu_\ell = 0.786 \pm 0.018$
$r_3 \equiv A_3(0)/A_1(0)$ in $\overline{K}^*(892)^0\ell^{+}\nu_\ell = 0.0 \pm 0.4$
Γ_L/Γ_T in $\overline{K}^*(892)^0\ell^{+}\nu_\ell = 1.13 \pm 0.08$
Γ_+/Γ_- in $\overline{K}^*(892)^0\ell^{+}\nu_\ell = 0.22 \pm 0.06$ (S = 1.6)
$r_V \equiv V_2(0)/V_1(0)$ in $D \to K_1(1270)e^{+}\nu_e = (-4.3 \pm 2.7) \times 10^{-2}$
$r_A \equiv A(0)/V_1(0)$ in $D \to K_1(1270)e^{+}\nu_e = (-11.2 \pm 1.3) \times 10^{-2}$

Most decay modes (other than the semileptonic modes) that involve a neutral K meson are now given as K_S^0 modes, not as $\overline{K}^0$ modes. Nearly always it is a K_S^0 that is measured, and interference between Cabibbo-allowed and doubly Cabibbo-suppressed modes can invalidate the assumption that $2\Gamma(K_S^0) = \Gamma(\overline{K}^0)$.

D^+ DECAY MODES	Fraction (Γ_i/Γ)	Scale factor/ Confidence level	p (MeV/c)
Inclusive modes			
e^{+} semileptonic	(16.07 ± 0.30) %		–
μ^{+} anything	(17.6 ± 3.2) %		–
K^{-} anything	(25.7 ± 1.4) %		–
K_S^0 anything	(33.1 ± 0.4) %		–
K^{+} anything	(5.9 ± 0.8) %		–
$K^*(892)^{-}$ anything	(6 ± 5) %		–
$\overline{K}^*(892)^0$ anything	(23 ± 5) %		–
$K^*(892)^0$ anything	< 6.6 %	CL=90%	–
η anything	(6.3 ± 0.7) %		–
η' anything	(1.04 ± 0.18) %		–
ϕ anything	(1.12 ± 0.04) %		–
$\pi^{+}\pi^{+}\pi^{-}$ anything	(15.25 ± 0.20) %		–
Leptonic and semileptonic modes			
$e^{+}\nu_e$	$< 9.7 \times 10^{-7}$	CL=90%	935
$\gamma e^{+}\nu_e$	$< 1.2 \times 10^{-5}$	CL=90%	935
$\mu^{+}\nu_\mu$	$(4.02 \pm 0.09) \times 10^{-4}$		932
$\tau^{+}\nu_\tau$	$(9.9 \pm 1.2) \times 10^{-4}$		90
$\overline{K}^0 e^{+}\nu_e$	(8.81 ± 0.07) %		869
$\overline{K}^0\mu^{+}\nu_\mu$	(8.68 ± 0.10) %		865
$K_S^0\pi^0 e^{+}\nu_e$	$(9.43 \pm 0.16) \times 10^{-3}$		863
$(K_S^0\pi^0)_{S-wave} e^{+}\nu_e$	$(6.03 \pm 0.23) \times 10^{-4}$		863
$\overline{K}^*(892)^0 e^{+}\nu_e$, $\overline{K}^{*0} \to K_S^0\pi^0$	$(8.82 \pm 0.15) \times 10^{-3}$		–
$K^{-}\pi^{+} e^{+}\nu_e$	(4.00 ± 0.17) %	S=3.1	864
$\overline{K}^*(892)^0 e^{+}\nu_e$, $\overline{K}^*(892)^0 \to K^{-}\pi^{+}$	(3.75 ± 0.16) %		722
$(K^{-}\pi^{+})_{[0.8-1.0]\mathrm{GeV}} e^{+}\nu_e$	(3.39 ± 0.09) %		864
$(K^{-}\pi^{+})_{S-wave} e^{+}\nu_e$	$(2.28 \pm 0.11) \times 10^{-3}$		–
$\overline{K}^*(1410)^0 e^{+}\nu_e$, $\overline{K}^*(1410)^0 \to K^{-}\pi^{+}$	$< 6 \times 10^{-3}$	CL=90%	–
$\overline{K}_2^*(1430)^0 e^{+}\nu_e$, $\overline{K}_2^*(1430)^0 \to K^{-}\pi^{+}$	$< 5 \times 10^{-4}$	CL=90%	–
$K^{-}\pi^{+} e^{+}\nu_e$ nonresonant	$< 7 \times 10^{-3}$	CL=90%	864
$\overline{K}^*(892)^0 e^{+}\nu_e$	(5.40 ± 0.10) %	S=1.1	722
$K_S^0\pi^0\mu^{+}\nu_\mu$	$(8.96 \pm 0.19) \times 10^{-3}$		851
$(K_S^0\pi^0)_{S-wave}\mu^{+}\nu_\mu$	$(6.4 \pm 0.7) \times 10^{-4}$		851
$\overline{K}^*(892)^0\mu^{+}\nu_\mu$, $\overline{K}^{*0} \to K_S^0\pi^0$	$(8.32 \pm 0.19) \times 10^{-3}$		–
$K^{-}\pi^{+}\mu^{+}\nu_\mu$	(3.62 ± 0.33) %		851
$\overline{K}^*(892)^0\mu^{+}\nu_\mu$, $\overline{K}^*(892)^0 \to K^{-}\pi^{+}$	(3.52 ± 0.10) %		717
$K^{-}\pi^{+}\mu^{+}\nu_\mu$ nonresonant	$(1.9 \pm 0.5) \times 10^{-3}$		851
$\overline{K}^*(892)^0\mu^{+}\nu_\mu$	(5.26 ± 0.15) %	S=1.1	717
$\overline{K}_1(1270)^0 e^{+}\nu_e$, $\overline{K}_1^0 \to K^{-}\pi^{+}\pi^0$	$(1.23 \pm 0.08) \times 10^{-3}$	S=1.3	–
$\overline{K}_1(1270)^0 e^{+}\nu_e$, $\overline{K}_1^0 \to K_S^0\pi^{+}\pi^{-}$	$(1.5 {}^{+0.5}_{-0.4}) \times 10^{-4}$		–
$K^{-}\pi^{+}\pi^0\mu^{+}\nu_\mu$	$< 1.5 \times 10^{-3}$	CL=90%	825
$\overline{K}_1(1270)^0\mu^{+}\nu_\mu$, $\overline{K}_1^0 \to K^{-}\pi^{+}\pi^0$	$(1.09 {}^{+0.12}_{-0.16}) \times 10^{-3}$		–
$\overline{K}_1(1400)^0 e^{+}\nu_e$	$< 1.4 \times 10^{-4}$	CL=90%	409
$\overline{K}_0^*(1430)^0\mu^{+}\nu_\mu$	$< 2.3 \times 10^{-4}$	CL=90%	380
$\overline{K}^*(1680)^0\mu^{+}\nu_\mu$	$< 1.4 \times 10^{-3}$	CL=90%	105
$\pi^0 e^{+}\nu_e$	$(3.72 \pm 0.17) \times 10^{-3}$	S=2.0	930
$\pi^0\mu^{+}\nu_\mu$	$(3.50 \pm 0.15) \times 10^{-3}$		927
$\eta e^{+}\nu_e$	$(1.11 \pm 0.07) \times 10^{-3}$		855
$\eta\mu^{+}\nu_\mu$	$(1.04 \pm 0.11) \times 10^{-3}$		851
$\pi^{-}\pi^{+} e^{+}\nu_e$	$(2.45 \pm 0.08) \times 10^{-3}$		924
$f_0(500)^0 e^{+}\nu_e$, $f_0(500)^0 \to \pi^{+}\pi^{-}$	$(6.2 \pm 0.4) \times 10^{-4}$		–
$\rho^0 e^{+}\nu_e$	$(1.87 \pm 0.06) \times 10^{-3}$		774
$f_0(500)^0\mu^{+}\nu_\mu$, $f_0^0 \to \pi^{+}\pi^{-}$	$(7.2 \pm 1.5) \times 10^{-4}$		–
$\rho^0\mu^{+}\nu_\mu$	$(1.64 \pm 0.16) \times 10^{-3}$		770
$\omega e^{+}\nu_e$	$(1.69 \pm 0.11) \times 10^{-3}$		771

Int. J. Mod. Phys. A 2026.41. Downloaded from www.worldscientific.com
by UNIVERSITY OF CALIFORNIA @ BERKELEY on 09/16/26. Re-use and distribution is strictly not permitted, except for Open Access articles.

$\omega\mu^+\nu_\mu$		$(1.77 \pm 0.21) \times 10^{-3}$		767
$\eta'(958)\,e^+\nu_e$		$(1.84 \pm 0.19) \times 10^{-4}$		690
$\eta'(958)\,\mu^+\nu_\mu$		$(1.92 \pm 0.29) \times 10^{-4}$		684
$a(980)^0 e^+\nu_e,\ a(980)^0 \to \eta\pi^0$		$(1.7\ {}^{+0.8}_{-0.7}) \times 10^{-4}$		–
$K^0_S K^0_S e^+\nu_e$		$< 1.54 \times 10^{-5}$ CL=90%		791
$K^0_S \eta e^+\nu_e$		$< 2.0 \times 10^{-4}$ CL=90%		775
$\eta\eta e^+\nu_e$		$< 1.0 \times 10^{-4}$ CL=90%		757
$K^+K^-e^+\nu_e$		$< 2.10 \times 10^{-5}$ CL=90%		794
$b_1(1235)^0 e^+\nu_e,\ b_1^0 \to \omega\pi^0$		$< 1.75 \times 10^{-4}$ CL=90%		–
$\phi e^+\nu_e$		$< 1.3 \times 10^{-5}$ CL=90%		657
$D^0 e^+\nu_e$		$< 1.0 \times 10^{-4}$ CL=90%		5

Hadronic modes with a $\overline{K}$ or $\overline{K}K\overline{K}$

$K^0_S\pi^+$		(1.554 ± 0.033) %	S=1.8	863
$K^0_L\pi^+$		(1.46 ± 0.05) %		863
$K^-2\pi^+$	[kk]	(9.31 ± 0.14) %	S=1.4	846
$(K^-\pi^+)_{S-\text{wave}}\pi^+$		(7.46 ± 0.16) %		846
$\overline{K}^*_0(1430)^0\pi^+,\ \overline{K}^*_0(1430)^0 \to K^-\pi^+$	[ll]	(1.24 ± 0.06) %		382
$\overline{K}^*(892)^0\pi^+,\ \overline{K}^*(892)^0 \to K^-\pi^+$		(1.03 ± 0.11) %		714
$\overline{K}^*(1410)^0\pi^+,\ \overline{K}^{*0} \to K^-\pi^+$		not seen		381
$\overline{K}^*_2(1430)^0\pi^+,\ \overline{K}^*_2(1430)^0 \to K^-\pi^+$	[ll]	$(2.2 \pm 0.7) \times 10^{-4}$		371
$\overline{K}^*(1680)^0\pi^+,\ \overline{K}^*(1680)^0 \to K^-\pi^+$	[ll]	$(2.2 \pm 1.1) \times 10^{-4}$		58
$K^-(2\pi^+)_{I=2}$		(1.44 ± 0.26) %		–
$K^0_S\pi^+\pi^0$	[kk]	(7.31 ± 0.20) %		845
$K^0_S\rho^+$		$(6.10\ {}^{+0.60}_{-0.35})$ %		677
$K^0_S\rho(1450)^+,\ \rho^+ \to \pi^+\pi^0$		$(1.5\ {}^{+1.2}_{-1.4}) \times 10^{-3}$		–
$\overline{K}^*(892)^0\pi^+,\ \overline{K}^*(892)^0 \to K^0_S\pi^0$		$(2.62 \pm 0.32) \times 10^{-3}$		714
$\overline{K}^*_0(1430)^0\pi^+,\ \overline{K}^{*0}_0 \to K^0_S\pi^0$		$(2.7 \pm 0.9) \times 10^{-3}$		–
$\overline{K}^*_0(1680)^0\pi^+,\ \overline{K}^{*0}_0 \to K^0_S\pi^0$		$(10\ {}^{+7}_{-10}) \times 10^{-4}$		–
$\overline{\kappa}^0\pi^+,\ \overline{\kappa}^0 \to K^0_S\pi^0$		$(6\ {}^{+5}_{-4}) \times 10^{-3}$		–
$K^0_S\pi^+\pi^0$ nonresonant		$(3 \pm 4) \times 10^{-3}$		845
$K^0_S\pi^+\pi^0$ nonresonant and $\overline{\kappa}^0\pi^+$		$(1.36\ {}^{+0.21}_{-0.40})$ %		–
$(K^0_S\pi^0)_{S-\text{wave}}\pi^+$		$(1.26\ {}^{+0.27}_{-0.33})$ %		845
$K^0_S\pi^+\omega$		$(7.1 \pm 0.5) \times 10^{-3}$		606
$K^0_S\pi^+\eta$		(1.27 ± 0.05) %		722
$K^0_S a_0(980)^+,\ a_0^+ \to \pi^+\eta$		(1.33 ± 0.06) %		–
$\overline{K}^*_0(1430)^0\pi^+,\ \overline{K}^*_0 \to K^0_S\eta$		$(1.38 \pm 0.26) \times 10^{-3}$		–
$K^0_S\pi^+\eta'(958)$		$(1.90 \pm 0.21) \times 10^{-3}$		481
$K^-2\pi^+\pi^0$	[nn]	(6.35 ± 0.08) %		817
$\overline{K}^*(892)^0\rho(770)^+,\ \overline{K}^{*0} \to K^-\pi^+,\ \rho^+ \to \pi^0\pi^+$		(4.34 ± 0.19) %		–
$\overline{K}_1(1270)^0\pi^+,\ \overline{K}^0_1 \to K^-\rho(770)^+,\ \rho^+ \to \pi^+\pi^0$		$(2.41 \pm 0.27) \times 10^{-3}$		–
$\overline{K}_1(1400)^0\pi^+,\ \overline{K}^0_1 \to \overline{K}^*(892)\pi,\ \overline{K}^* \to K^-\pi$		$(4.64 \pm 0.24) \times 10^{-3}$		–
$\overline{K}(1460)^0\pi^+,\ \overline{K}(1460)^0 \to \overline{K}^*(892)\pi,\ \overline{K}^* \to K^-\pi$		$(3.24 \pm 0.23) \times 10^{-3}$		–
$\overline{K}^*(1680)^0\pi^+,\ \overline{K}^{*0} \to \overline{K}^*(892)\pi,\ \overline{K}^* \to K^-\pi$		$(2.4 \pm 0.6) \times 10^{-3}$		–
$(K^-\pi^+)_{S-wave}\rho(770)^+,\ \rho^+ \to \pi^+\pi^0$		(1.16 ± 0.06) %		–
$\overline{K}(1460)^0\pi^+,\ \overline{K}(1460)^0 \to K^-(\pi^+\pi^0)_{L=1}$		$(5.5 \pm 0.6) \times 10^{-3}$		–
$\overline{K}(1460)^0\pi^+,\ \overline{K}(1460)^0 \to (K^-\pi)_{L=1}\pi$		$(2.2 \pm 0.4) \times 10^{-3}$		–
$(K^-\rho(770)^+)_{L=1}\pi^+,\ \rho^+ \to \pi^+\pi^0$		$(1.14 \pm 0.09) \times 10^{-3}$		–
$(\overline{K}^*(892)\pi)_{L=1}\pi^+,\ \overline{K}^* \to K^-\pi$		$(5.1 \pm 0.9) \times 10^{-4}$		–
$(\overline{K}^*(892)^0\pi^+)_{L=1}\pi^0,\ \overline{K}^{*0} \to K^-\pi^+$		$(5.1 \pm 2.8) \times 10^{-4}$		–
$(K^-(\pi^+\pi^0)_{L=0})_{L=1}\pi^+$		$(5.1 \pm 1.8) \times 10^{-4}$		–
$(K^-\pi^+)_{L=1}\rho(770)^+,\ \rho^+ \to \pi^+\pi^0$		$(3.2 \pm 0.9) \times 10^{-4}$		–
$K^0_S 2\pi^+\pi^-$	[nn]	(3.08 ± 0.08) %		814
$K^0_S\pi^+2\pi^0$		(2.89 ± 0.09) %		817
$K^0_S a_1(1260)^+,\ a_1^+ \to \rho(770)^+\pi^0$		$(8.7 \pm 1.6) \times 10^{-3}$		–
$K^0_S a_1(1260)^+,\ a_1^+ \to f_0(500)\pi^+,\ f_0 \to \pi^0\pi^0$		$(1.0 \pm 0.6) \times 10^{-3}$		–
$\overline{K}_1(1400)^0\pi^+,\ \overline{K}^0_1 \to \overline{K}^*(892)^0\pi^0,\ \overline{K}^{*0} \to K^0_S\pi^0$		$(2.3 \pm 0.4) \times 10^{-3}$		–
$\overline{K}^*(892)^0\rho^+,\ \overline{K}^{*0} \to K^0_S\pi^0$		$(9.7 \pm 0.9) \times 10^{-3}$		–
$\overline{K}^*(892)^0\pi^+\pi^0$ non-resonant, $\overline{K}^{*0} \to K^0_S\pi^0$		$(2.6 \pm 0.7) \times 10^{-3}$		–
$K^0_S\rho^+\pi^0$ non-resonant		$(4.8 \pm 0.5) \times 10^{-3}$		–
$K^-2\pi^+\eta$		$(1.35 \pm 0.12) \times 10^{-3}$		657
$K^0_S\pi^+\pi^0\eta$		$(1.22 \pm 0.25) \times 10^{-3}$		657
$K^-3\pi^+\pi^-$	[kk]	$(5.7 \pm 0.5) \times 10^{-3}$	S=1.1	772
$\overline{K}^*(892)^0 2\pi^+\pi^-,\ \overline{K}^*(892)^0 \to K^-\pi^+$		$(1.2 \pm 0.4) \times 10^{-3}$		645
$\overline{K}^*(892)^0\rho^0\pi^+,\ \overline{K}^*(892)^0 \to K^-\pi^+$		$(2.3 \pm 0.4) \times 10^{-3}$		239
$\overline{K}^*(892)^0 a_1(1260)^+$	[oo]	$(9.2 \pm 1.8) \times 10^{-3}$		†
$K^-\rho^0 2\pi^+$		$(1.70 \pm 0.28) \times 10^{-3}$		524
$K^-3\pi^+\pi^-$ nonresonant		$(4.0 \pm 2.9) \times 10^{-4}$		772
$K^0_S 2\pi^+\pi^-\pi^0$		(1.53 ± 0.08) %		773
$K^0_S\pi^+3\pi^0$		$(5.5 \pm 0.5) \times 10^{-3}$		776
$K^-2\pi^+2\pi^0$		$(4.95 \pm 0.32) \times 10^{-3}$		776
$K^-3\pi^+\pi^-\pi^0$		$(6.6 \pm 0.8) \times 10^{-4}$		718
$K^+2K^0_S$		$(2.54 \pm 0.13) \times 10^{-3}$		545
$K^+K^-K^0_S\pi^+$		$(2.4 \pm 0.5) \times 10^{-4}$		436

Pionic modes

$\pi^+\pi^0$		$(1.243 \pm 0.033) \times 10^{-3}$		925
$2\pi^+\pi^-$		$(3.27 \pm 0.09) \times 10^{-3}$		909
$\rho^0\pi^+$		$(8.4 \pm 0.8) \times 10^{-4}$		767
$\pi^+(\pi^+\pi^-)_{S-\text{wave}}$		$(2.01 \pm 0.06) \times 10^{-3}$		909
$\sigma\pi^+,\ \sigma \to \pi^+\pi^-$		$(1.38 \pm 0.10) \times 10^{-3}$		–
$f_0(980)\pi^+,\ f_0 \to \pi^+\pi^-$		$(1.57 \pm 0.32) \times 10^{-4}$		669
$f_0(1370)\pi^+,\ f_0 \to \pi^+\pi^-$		$(8 \pm 4) \times 10^{-5}$		–
$\omega\pi^+,\ \omega \to \pi^+\pi^-$		$(3.4 \pm 0.5) \times 10^{-6}$		–
$f_2(1270)\pi^+,\ f_2 \to \pi^+\pi^-$		$(4.58 \pm 0.28) \times 10^{-4}$		485
$\rho(1450)^0\pi^+,\ \rho^0 \to \pi^+\pi^-$		$(1.8 \pm 0.5) \times 10^{-4}$		338
$\rho(1700)^0\pi^+,\ \rho^0 \to \pi^+\pi^-$		$(1.9 \pm 0.5) \times 10^{-4}$		–
$f_0(1500)\pi^+,\ f_0 \to \pi^+\pi^-$		$(1.1 \pm 0.4) \times 10^{-4}$		–
$f_0(1710)\pi^+,\ f_0 \to \pi^+\pi^-$		$< 5 \times 10^{-5}$ CL=95%		–
$f_0(1790)\pi^+,\ f_0 \to \pi^+\pi^-$		$< 7 \times 10^{-5}$ CL=95%		–
$(\pi^+\pi^+)_{S-\text{wave}}\pi^-$		$< 1.2 \times 10^{-4}$ CL=95%		909
$2\pi^+\pi^-$ nonresonant		$< 1.1 \times 10^{-4}$ CL=95%		909
$\pi^+2\pi^0$		$(4.61 \pm 0.15) \times 10^{-3}$		910
$2\pi^+\pi^-\pi^0$		(1.165 ± 0.030) %		883
$\pi^+3\pi^0$		$(4.17 \pm 0.26) \times 10^{-3}$		885
$\pi^+4\pi^0$		$(1.9 \pm 0.4) \times 10^{-3}$		851
$2\pi^+\pi^-2\pi^0$		(1.07 ± 0.05) %		848
$3\pi^+2\pi^-$		$(1.64 \pm 0.16) \times 10^{-3}$	S=1.1	845
$2\pi^+\pi^-3\pi^0$		$(3.42 \pm 0.35) \times 10^{-3}$		803
$3\pi^+2\pi^-\pi^0$		$(2.34 \pm 0.27) \times 10^{-3}$		799
$\eta\pi^+$		$(3.75 \pm 0.09) \times 10^{-3}$		848
$\eta\pi^+\pi^0$		$(2.05 \pm 0.35) \times 10^{-3}$	S=2.2	831
$\rho(770)^+\eta,\ \rho^+ \to \pi^+\pi^0$		$(1.9 \pm 0.8) \times 10^{-4}$		–
$a_0(980)^+\pi^0,\ a_0^+ \to \pi^+\eta$		$(9.0 \pm 1.9) \times 10^{-4}$		–
$a_0(980)^0\pi^+,\ a_0^0 \to \pi^0\eta$		$(3.5 \pm 1.1) \times 10^{-4}$		–
$a_2(1700)^+\pi^0,\ a_2^+ \to \pi^+\eta$		$(9 \pm 5) \times 10^{-5}$		–
$a_0(1450)^+\pi^0,\ a_0^+ \to \pi^+\eta$		$(1.4 \pm 0.6) \times 10^{-4}$		–
$\eta 2\pi^+\pi^-$		$(3.41 \pm 0.20) \times 10^{-3}$		798
$\eta\pi^+2\pi^0$		$(3.20 \pm 0.33) \times 10^{-3}$		801
$\eta\pi^+3\pi^0$		$(2.9 \pm 0.5) \times 10^{-3}$		759
$\eta 2\pi^+\pi^-\pi^0$		$(3.88 \pm 0.34) \times 10^{-3}$		755
$\eta\eta\pi^+$		$(2.96 \pm 0.26) \times 10^{-3}$		700
$\omega\pi^+$		$(2.8 \pm 0.6) \times 10^{-4}$		764
$\omega\pi^+\pi^0$		$(3.9 \pm 0.9) \times 10^{-3}$		742
$\eta'(958)\pi^+$		$(4.96 \pm 0.18) \times 10^{-3}$		681
$\eta'(958)\pi^+\pi^0$		$(1.6 \pm 0.5) \times 10^{-3}$		654

Hadronic modes with a $K\overline{K}$ pair

$K^0_S K^+$		$(3.02 \pm 0.09) \times 10^{-3}$	S=2.2	793
$K^0_L K^+$		$(3.21 \pm 0.16) \times 10^{-3}$		793

Int. J. Mod. Phys. A 2026.41. Downloaded from www.worldscientific.com
by UNIVERSITY OF CALIFORNIA @ BERKELEY on 09/16/26. Re-use and distribution is strictly not permitted, except for Open Acce

$K^0_S K^+ \pi^0$		$(5.07 \pm 0.30) \times 10^{-3}$		744
$K^*(892)^+ K^0_S$, $K^{*+} \to K^+ \pi^0$		$(2.89 \pm 0.30) \times 10^{-3}$		612
$\overline{K}^*(892)^0 K^+$, $\overline{K}^{*0} \to K^0_S \pi^0$		$(5.2 \pm 1.4) \times 10^{-4}$		613
$K^0_L K^+ \pi^0$		$(5.24 \pm 0.31) \times 10^{-3}$		744
$K^+ K^- \pi^+$	[kk]	$(9.61 \pm 0.17) \times 10^{-3}$		744
$K^+ \overline{K}^*(892)^0$, $\overline{K}^*(892)^0 \to K^- \pi^+$		$(2.47 {}^{+0.08}_{-0.13}) \times 10^{-3}$		613
$K^+ \overline{K}^*_0(1430)^0$, $\overline{K}^*_0(1430)^0 \to K^- \pi^+$		$(1.81 \pm 0.34) \times 10^{-3}$		–
$K^+ \overline{K}^*_2(1430)^0$, $\overline{K}^*_2 \to K^- \pi^+$		$(1.6 {}^{+1.2}_{-0.8}) \times 10^{-4}$		–
$K^+ \overline{K}^*_0(700)$, $\overline{K}^*_0 \to K^- \pi^+$		$(6.7 {}^{+3.5}_{-2.1}) \times 10^{-4}$		–
$a_0(1450)^0 \pi^+$, $a^0_0 \to K^+ K^-$		$(4.4 {}^{+7.0}_{-1.8}) \times 10^{-4}$		–
$\phi(1680) \pi^+$, $\phi \to K^+ K^-$		$(4.9 {}^{+4.0}_{-1.9}) \times 10^{-5}$		–
$\phi \pi^+$, $\phi \to K^+ K^-$		$(2.67 {}^{+0.06}_{-0.08}) \times 10^{-3}$		647
$\phi \pi^+$		$(5.70 \pm 0.14) \times 10^{-3}$		647
$K^+ K^- \pi^+ \pi^0$		$(6.62 \pm 0.32) \times 10^{-3}$		682
$K^0_S K^0_S \pi^+$		$(2.97 \pm 0.10) \times 10^{-3}$		741
$K^0_S K^*(892)^+$, $K^{*+} \to K^0_S \pi^+$		$(2.90 \pm 0.11) \times 10^{-3}$		–
$K^0_S (K^0_S \pi^+) \to K^0_S K^0_S \pi^+$		$(1.31 \pm 0.34) \times 10^{-4}$		–
$K^0_S K^0_S \pi^+ \pi^0$		$(1.34 \pm 0.21) \times 10^{-3}$		679
$K^0_S K^+ \pi^+ \pi^- \pi^0$		$(2.5 \pm 0.4) \times 10^{-4}$		602
$K^0_S K^+ \omega$		$(2.0 \pm 0.4) \times 10^{-4}$		293
$K^0_S K^+ \eta$		$(2.27 \pm 0.23) \times 10^{-4}$		516
$K^+ K^0_S \pi^+ \pi^-$		$(1.89 \pm 0.13) \times 10^{-3}$		678
$K^0_S K^+ \pi^0 \pi^0$		$(5.8 \pm 1.3) \times 10^{-4}$		683
$K^0_S K^- 2\pi^+$		$(2.27 \pm 0.13) \times 10^{-3}$		678
$K^+ K^- 2\pi^+ \pi^-$		$(6.7 \pm 1.1) \times 10^{-5}$		601
$\phi 2\pi^+ \pi^-$		$(5.4 \pm 1.9) \times 10^{-5}$		566
A few poorly measured branching fractions:				
$\phi \pi^+ \pi^0$		(2.3 ± 1.0) %		619
$\phi \rho^+$		< 1.5 %	CL=90%	260
$K^+ K^- \pi^+ \pi^0$ non-ϕ		$(1.5 {}^{+0.7}_{-0.6})$ %		682
Radiative modes				
$\rho(770)^+ \gamma$		$< 1.3 \times 10^{-5}$	CL=90%	–
$K^*(892)^+ \gamma$		$< 1.8 \times 10^{-5}$	CL=90%	722
Doubly Cabibbo-suppressed modes				
$K^+ \pi^0$		$(1.54 \pm 0.13) \times 10^{-4}$	S=1.4	864
$K^+ \eta$		$(1.16 \pm 0.09) \times 10^{-4}$		776
$K^+ \eta'(958)$		$(1.88 \pm 0.14) \times 10^{-4}$		571
$K^+ 2\pi^0$		$(2.1 \pm 0.4) \times 10^{-4}$		847
$K^*(892)^+ \pi^0$		$(3.4 \pm 1.4) \times 10^{-4}$		714
$K^+ \pi^+ \pi^-$		$(4.88 \pm 0.08) \times 10^{-4}$	S=1.4	846
$K^+ \rho^0$		$(1.9 \pm 0.4) \times 10^{-4}$		679
$K^+ \eta \pi^0$		$(2.1 \pm 0.5) \times 10^{-4}$		726
$K^*(892)^+ \eta$		$(4.4 {}^{+1.8}_{-1.5}) \times 10^{-4}$		586
$K^*(892)^0 \pi^+$, $K^*(892)^0 \to K^+ \pi^-$		$(2.3 \pm 0.4) \times 10^{-4}$		714
$K^+ f_0(980)$, $f_0(980) \to \pi^+ \pi^-$		$(4.4 \pm 2.6) \times 10^{-5}$		–
$K^*_2(1430)^0 \pi^+$, $K^*_2(1430)^0 \to K^+ \pi^-$		$(3.9 \pm 2.6) \times 10^{-5}$		–
$K^+ \pi^+ \pi^-$ nonresonant		not seen		846
$K^+ \pi^+ \pi^- \pi^0$		$(1.21 \pm 0.09) \times 10^{-3}$		817
$K^+ \pi^+ \pi^- \pi^0$ nonresonant		$(1.10 \pm 0.07) \times 10^{-3}$		817
$K^+ \pi^+ \pi^- \eta$		$(1.56 \pm 0.22) \times 10^{-4}$		657
$K^+ (\pi^+ \pi^- \eta)_{non-\eta'}$		$(6.7 \pm 1.8) \times 10^{-5}$		–
$K^+ \omega$		$(5.7 {}^{+2.5}_{-2.1}) \times 10^{-5}$		675
$K^+ \eta \eta$		$(5.9 \pm 2.3) \times 10^{-5}$		475
$2K^+ K^-$		$(6.09 \pm 0.10) \times 10^{-5}$	S=1.3	550
$\phi(1020)^0 K^+$		$< 2.1 \times 10^{-5}$	CL=90%	–
$K^+ \phi(1020)$, $\phi \to K^+ K^-$		$(4.3 \pm 0.6) \times 10^{-6}$		–
$K^+ (K^+ K^-)_{S-wave}$		$(5.72 \pm 0.11) \times 10^{-5}$		550
$\Delta C = 1$ weak neutral current ($C1$) modes, or Lepton Family number (LF), or Lepton number (L), or Baryon number (B) violating modes				
$\pi^+ e^+ e^-$	$C1$	$< 1.1 \times 10^{-6}$	CL=90%	930
$\pi^+ \pi^0 e^+ e^-$		$< 1.4 \times 10^{-5}$	CL=90%	925
$\pi^+ \phi$, $\phi \to e^+ e^-$	[pp]	$(1.7 {}^{+1.4}_{-0.9}) \times 10^{-6}$		–
$\pi^+ \mu^+ \mu^-$	$C1$	$< 6.7 \times 10^{-8}$	CL=90%	918
$\pi^+ \phi$, $\phi \to \mu^+ \mu^-$	[pp]	$(1.8 \pm 0.8) \times 10^{-6}$		–
$\rho^+ \mu^+ \mu^-$	$C1$	$< 5.6 \times 10^{-4}$	CL=90%	757
$K^+ e^+ e^-$	[qq]	$< 8.5 \times 10^{-7}$	CL=90%	870
$K^+ \pi^0 e^+ e^-$		$< 1.5 \times 10^{-5}$	CL=90%	864
$K^0_S \pi^+ e^+ e^-$		$< 2.6 \times 10^{-5}$	CL=90%	–
$K^0_S K^+ e^+ e^-$		$< 1.1 \times 10^{-5}$	CL=90%	792
$K^+ \mu^+ \mu^-$	[qq]	$< 5.4 \times 10^{-8}$	CL=90%	856
$\pi^+ e^+ \mu^-$	LF	$< 2.1 \times 10^{-7}$	CL=90%	927
$\pi^+ e^- \mu^+$	LF	$< 2.2 \times 10^{-7}$	CL=90%	927
$K^+ e^+ \mu^-$	LF	$< 7.5 \times 10^{-8}$	CL=90%	866
$K^+ e^- \mu^+$	LF	$< 1.0 \times 10^{-7}$	CL=90%	866
$\pi^- 2e^+$	L	$< 5.3 \times 10^{-7}$	CL=90%	930
$\pi^- 2\mu^+$	L	$< 1.4 \times 10^{-8}$	CL=90%	918
$\pi^- e^+ \mu^+$	L	$< 1.3 \times 10^{-7}$	CL=90%	927
$\rho^- 2\mu^+$	L	$< 5.6 \times 10^{-4}$	CL=90%	757
$K^- 2e^+$	L	$< 9 \times 10^{-7}$	CL=90%	870
$K^0_S \pi^- 2e^+$	L	$< 3.3 \times 10^{-6}$	CL=90%	863
$K^- \pi^0 2e^+$	L	$< 8.5 \times 10^{-6}$	CL=90%	864
$K^- 2\mu^+$	L	$< 1.0 \times 10^{-5}$	CL=90%	856
$K^- e^+ \mu^+$	L	$< 1.9 \times 10^{-6}$	CL=90%	866
$K^*(892)^- 2\mu^+$	L	$< 8.5 \times 10^{-4}$	CL=90%	703
Λe^+	L,B	$< 1.1 \times 10^{-6}$	CL=90%	602
$\overline{\Lambda} e^+$	L,B	$< 6.5 \times 10^{-7}$	CL=90%	602
$\Sigma^0 e^+$	L,B	$< 1.7 \times 10^{-6}$	CL=90%	554
$\overline{\Sigma}^0 e^+$	L,B	$< 1.3 \times 10^{-6}$	CL=90%	554
$\overline{n} e^+$		$< 1.43 \times 10^{-5}$	CL=90%	699
$n e^+$		$< 2.91 \times 10^{-5}$	CL=90%	699

D^0

$I(J^P) = \frac{1}{2}(0^-)$

Mass $m = 1864.84 \pm 0.04$ MeV
$m_{D^\pm} - m_{D^0} = 4.822 \pm 0.015$ MeV
Mean life $\tau = (410.3 \pm 1.0) \times 10^{-15}$ s
$c\tau = 123.01\ \mu$m

Mixing and related parameters

$|m_{D^0_1} - m_{D^0_2}| = (0.997 \pm 0.116) \times 10^{10}\ \hbar\ \mathrm{s}^{-1}$
$(\Gamma_{D^0_1} - \Gamma_{D^0_2})/\Gamma = 2y = (1.394 \pm 0.056) \times 10^{-2}$
$|q/p| = 0.995 \pm 0.016$
$A_\Gamma = (0.89 \pm 1.13) \times 10^{-4}$
$\phi^{K^0_S \pi\pi} = 0.02 {}^{+0.04}_{-0.05}$
$\delta(K\pi)$ - relative strong phase $= 191 {}^{+6}_{-7}$ degrees
$K^- \pi^+ \pi^0$ coherence factor $R_{K\pi\pi^0} = 0.792 \pm 0.033$
$K^- \pi^+ \pi^0$ average relative strong phase $\delta^{K\pi\pi^0} = (198 \pm 10)^\circ$
$K^- \pi^- 2\pi^+$ coherence factor $R_{K3\pi} = (45 \pm 4) \times 10^{-2}$
$K^- \pi^- 2\pi^+$ average relative strong phase $\delta^{K3\pi} = (156 {}^{+12}_{-10})^\circ$ (S = 1.1)
$D^0 \to K^- \pi^- 2\pi^+$, $R_{K3\pi}$ (y $\cos\delta^{K3\pi}$ − x $\sin\delta^{K3\pi}$) $= (-3.0 \pm 0.7) \times 10^{-3}$ TeV^{-1}
$K^0_S K^+ \pi^-$ coherence factor $R_{K^0_S K\pi} = 0.70 \pm 0.08$
$K^0_S K^+ \pi^-$ average relative strong phase $\delta^{K^0_S K\pi} = (0 \pm 16)^\circ$
$K^* K$ coherence factor $R_{K^* K} = 0.94 \pm 0.12$
$K^* K$ average relative strong phase $\delta^{K^* K} = (-17 \pm 18)^\circ$

***CP*-even fractions (labeled by the D^0 decay)**

CP-even fraction in $D^0 \to K^0_S \pi^+ \pi^- \pi^0$ decays $= (23.6 \pm 0.9)$%
CP-even fraction in $D^0 \to \pi^+ \pi^- \pi^0$ decays $= (94.2 \pm 0.7)$% (S = 1.9)
CP-even fraction in $D^0 \to \pi^+ \pi^- \pi^+ \pi^-$ decays $= (74.6 \pm 0.8)$%
CP-even fraction in $D^0 \to \pi^+ \pi^- 2\pi^0$ decays $= 0.68 \pm 0.08$
CP-even fraction in $D^0 \to 2\pi^+ 2\pi^- \pi^0$ decays $= 0.44 \pm 0.10$
CP-even fraction in $D^0 \to \pi^+ \pi^- 3\pi^0$ decays $= 0.52 {}^{+0.34}_{-0.27}$
CP-even fraction in $D^0 \to 2\pi^+ 2\pi^- 2\pi^0$ decays $= 0.79 \pm 0.26$
CP-even fraction in $D^0 \to K^+ K^- \pi^0$ decays $= (64.1 \pm 3.0)$% (S = 1.7)
CP-even fraction in $D^0 \to K^+ K^- \pi^+ \pi^-$ decays $= (74.1 \pm 3.0)$%

***CP*-violation decay-rate asymmetries (labeled by the D^0 decay)**

$A_{CP}(K^+ K^-) = (4 \pm 5) \times 10^{-4}$

Int. J. Mod. Phys. A 2026.41. Downloaded from www.worldscientific.com
by UNIVERSITY OF CALIFORNIA @ BERKELEY on 09/16/26. Re-use and distribution is strictly not permitted, except for Open Access articles.

$A_{CP}(2K^0_S) = (-0.9 \pm 1.2)\%$ (S = 1.7)
$A_{CP}(\pi^+\pi^-) = (0.13 \pm 0.14)\%$
$A_{CP}(\pi^0\pi^0) = (0.1 \pm 0.5)\%$
$A_{CP}(\rho\gamma) = (6 \pm 15) \times 10^{-2}$
$A_{CP}(\phi\gamma) = (-9 \pm 7) \times 10^{-2}$
$A_{CP}(\overline{K}^*(892)^0\gamma) = (-0.3 \pm 2.0) \times 10^{-2}$
$A_{CP}(\pi^+\pi^-\pi^0) = (0.4 \pm 0.4)\%$
$A_{CP}(\eta\pi^+\pi^-)$ in $D^0, \overline{D}^0 \to \eta\pi^+\pi^- = (0.9 \pm 1.3) \times 10^{-2}$
$A_{CP}(\rho(770)^+\pi^- \to \pi^+\pi^-\pi^0) = (1.2 \pm 0.9)\%$ [rr]
$A_{CP}(\rho(770)^0\pi^0 \to \pi^+\pi^-\pi^0) = (-3.1 \pm 3.0)\%$ [rr]
$A_{CP}(\rho(770)^-\pi^+ \to \pi^+\pi^-\pi^0) = (-1.0 \pm 1.7)\%$ [rr]
$A_{CP}(\rho(1450)^+\pi^- \to \pi^+\pi^-\pi^0) = (0 \pm 70)\%$ [rr]
$A_{CP}(\rho(1450)^0\pi^0 \to \pi^+\pi^-\pi^0) = (-20 \pm 40)\%$ [rr]
$A_{CP}(\rho(1450)^-\pi^+ \to \pi^+\pi^-\pi^0) = (6 \pm 9)\%$ [rr]
$A_{CP}(\rho(1700)^+\pi^- \to \pi^+\pi^-\pi^0) = (-5 \pm 14)\%$ [rr]
$A_{CP}(\rho(1700)^0\pi^0 \to \pi^+\pi^-\pi^0) = (13 \pm 9)\%$ [rr]
$A_{CP}(\rho(1700)^-\pi^+ \to \pi^+\pi^-\pi^0) = (8 \pm 11)\%$ [rr]
$A_{CP}(f_0(980)\pi^0 \to \pi^+\pi^-\pi^0) = (0 \pm 35)\%$ [rr]
$A_{CP}(f_0(1370)\pi^0 \to \pi^+\pi^-\pi^0) = (25 \pm 18)\%$ [rr]
$A_{CP}(f_0(1500)\pi^0 \to \pi^+\pi^-\pi^0) = (0 \pm 18)\%$ [rr]
$A_{CP}(f_0(1710)\pi^0 \to \pi^+\pi^-\pi^0) = (0 \pm 24)\%$ [rr]
$A_{CP}(f_2(1270)\pi^0 \to \pi^+\pi^-\pi^0) = (-4 \pm 6)\%$ [rr]
$A_{CP}(\sigma(400)\pi^0 \to \pi^+\pi^-\pi^0) = (6 \pm 8)\%$ [rr]
$A_{CP}(\text{nonresonant } \pi^+\pi^-\pi^0) = (-13 \pm 23)\%$ [rr]
$A_{CP}(\pi^+\pi^-2\pi^0)$ in $D^0, \overline{D}^0 \to \pi^+\pi^-2\pi^0 = (-2.5 \pm 2.0)\%$
$A_{CP}(a_1(1260)^+\pi^- \to 2\pi^+2\pi^-) = (5 \pm 6)\%$
$A_{CP}(a_1(1260)^-\pi^+ \to 2\pi^+2\pi^-) = (14 \pm 18)\%$
$A_{CP}(\pi(1300)^+\pi^- \to 2\pi^+2\pi^-) = (-2 \pm 15)\%$
$A_{CP}(\pi(1300)^-\pi^+ \to 2\pi^+2\pi^-) = (-6 \pm 30)\%$
$A_{CP}(a_1(1640)^+\pi^- \to 2\pi^+2\pi^-) = (9 \pm 26)\%$
$A_{CP}(\pi_2(1670)^+\pi^- \to 2\pi^+2\pi^-) = (7 \pm 18)\%$
$A_{CP}(\sigma f_0(1370) \to 2\pi^+2\pi^-) = (-15 \pm 19)\%$
$A_{CP}(\sigma\rho(770)^0 \to 2\pi^+2\pi^-) = (3 \pm 27)\%$
$A_{CP}(2\rho(770)^0 \to 2\pi^+2\pi^-) = (-6 \pm 6)\%$
$A_{CP}(2f_2(1270) \to 2\pi^+2\pi^-) = (-28 \pm 24)\%$
$A_{CP}(\pi^+\pi^-\pi^0\eta)$ in $D^0, \overline{D}^0 \to \pi^+\pi^-\pi^0\eta = (-6 \pm 6) \times 10^{-2}$
$A_{CP}(K^+K^-\pi^0) = (-1.0 \pm 1.7)\%$
$A_{CP}(K^*(892)^+K^- \to K^+K^-\pi^0) = (-0.9 \pm 1.3)\%$ [rr]
$A_{CP}(K^*(1410)^+K^- \to K^+K^-\pi^0) = (-21 \pm 24)\%$ [rr]
$A_{CP}((K^+\pi^0)_{S-wave}K^- \to K^+K^-\pi^0) = (7 \pm 15)\%$ [rr]
$A_{CP}(\phi(1020)\pi^0 \to K^+K^-\pi^0) = (1.1 \pm 2.2)\%$ [rr]
$A_{CP}(f_0(980)\pi^0 \to K^+K^-\pi^0) = (-3 \pm 19)\%$ [rr]
$A_{CP}(a_0(980)^0\pi^0 \to K^+K^-\pi^0) = (-5 \pm 16)\%$ [rr]
$A_{CP}(f'_2(1525)\pi^0 \to K^+K^-\pi^0) = (0 \pm 160)\%$ [rr]
$A_{CP}(K^*(892)^-K^+ \to K^+K^-\pi^0) = (-5 \pm 4)\%$ [rr]
$A_{CP}(K^*(1410)^-K^+ \to K^+K^-\pi^0) = (-17 \pm 29)\%$ [rr]
$A_{CP}((K^-\pi^0)_{S-wave}K^+ \to K^+K^-\pi^0) = (-10 \pm 40)\%$ [rr]
$A_{CP}(K^+K^-\eta)$ in $D^0, \overline{D}^0 \to K^+K^-\eta = (-1.4 \pm 3.5) \times 10^{-2}$
$A_{CP}(\phi(1020)\eta \to K^+K^-\eta)$ in $D^0, \overline{D}^0 \to \phi(1020)\eta = (-2 \pm 4) \times 10^{-2}$
$A_{CP}(K^0_S\pi^0) = (-0.20 \pm 0.17)\%$
$A_{CP}(K^0_S\eta) = (0.5 \pm 0.5)\%$
$A_{CP}(K^0_S\eta') = (1.0 \pm 0.7)\%$
$A_{CP}(K^0_S\phi) = (-3 \pm 9)\%$
$A_{CP}(K^-\pi^+) = (0.2 \pm 0.5)\%$
$A_{CP}(K^+\pi^-) = (-0.4 \pm 0.7)\%$ (S = 1.3)
$A_{CP}(D_{CP(\pm1)} \to K^\mp\pi^\pm) = (13.1 \pm 1.0)\%$
$A_{CP}(K^-\pi^+\pi^0) = (0.1 \pm 0.5)\%$
$A_{CP}(K^+\pi^-\pi^0) = (0 \pm 5)\%$
$A_{CP}(K^0_S\pi^+\pi^-) = (-0.1 \pm 0.8)\%$
$A_{CP}(K^\mp\pi^\pm\eta)$ in $D^0, \overline{D}^0 \to K^\mp\pi^\pm\eta = (-1.9 \pm 1.6) \times 10^{-2}$
$A_{CP}(K^0_S\pi^0\eta)$ in $D^0, \overline{D}^0 \to K^0_S\pi^0\eta = (-3.9 \pm 3.3) \times 10^{-2}$
$A_{CP}(K^\mp\pi^\pm\pi^0\eta)$ in $D^0, \overline{D}^0 \to K^\mp\pi^\pm\pi^0\eta = (-8 \pm 5) \times 10^{-2}$
$A_{CP}(K^*(892)^-\pi^+ \to K^0_S\pi^+\pi^-) = (0.4 \pm 0.5)\%$
$A_{CP}(K^*(892)^+\pi^- \to K^0_S\pi^+\pi^-) = (1 \pm 6)\%$
$A_{CP}(\overline{K}^0\rho^0 \to K^0_S\pi^+\pi^-) = (-0.1 \pm 0.5)\%$
$A_{CP}(\overline{K}^0\omega \to K^0_S\pi^+\pi^-) = (-13 \pm 7)\%$
$A_{CP}(\overline{K}^0 f_0(980) \to K^0_S\pi^+\pi^-) = (-0.4 \pm 2.7)\%$
$A_{CP}(\overline{K}^0 f_2(1270) \to K^0_S\pi^+\pi^-) = (-4 \pm 5)\%$
$A_{CP}(\overline{K}^0 f_0(1370) \to K^0_S\pi^+\pi^-) = (-1 \pm 9)\%$
$A_{CP}(\overline{K}^0\rho^0(1450) \to K^0_S\pi^+\pi^-) = (-4 \pm 10)\%$
$A_{CP}(\overline{K}^0 f_0(600) \to K^0_S\pi^+\pi^-) = (-3 \pm 5)\%$
$A_{CP}(K^*(1410)^-\pi^+ \to K^0_S\pi^+\pi^-) = (-2 \pm 9)\%$
$A_{CP}(K^*_0(1430)^-\pi^+ \to K^0_S\pi^+\pi^-) = (4 \pm 4)\%$
$A_{CP}(K^*_0(1430)^+\pi^- \to K^0_S\pi^+\pi^-) = (12 \pm 15)\%$
$A_{CP}(K^*_2(1430)^-\pi^+ \to K^0_S\pi^+\pi^-) = (3 \pm 6)\%$
$A_{CP}(K^*_2(1430)^+\pi^- \to K^0_S\pi^+\pi^-) = (-10 \pm 32)\%$
$A_{CP}(K^-\pi^+\pi^+\pi^-) = (0.2 \pm 0.5)\%$
$A_{CP}(K^+\pi^-\pi^+\pi^-) = (-2 \pm 4)\%$
$A_{CP}(K^+K^-\pi^+\pi^-) = (1.3 \pm 1.7)\%$
$A_{CP}(2K^0_S\pi^+\pi^-)$ in $D^0, \overline{D}^0 \to 2K^0_S\pi^+\pi^- = (-2.5 \pm 1.4) \times 10^{-2}$
$A_{CP}(K^*_1(1270)^+K^- \to K^+K^-\pi^+\pi^-) = (-2.3 \pm 1.7)\%$
$A_{CP}(K^*_1(1270)^+K^- \to K^{*0}\pi^+K^-) = (-1 \pm 10)\%$
$A_{CP}(K^*_1(1270)^-K^+ \to \overline{K}^{*0}\pi^-K^+) = (-10 \pm 32)\%$
$A_{CP}(K^*_1(1270)^-K^+ \to K^+K^-\pi^+\pi^-) = (1.7 \pm 3.5)\%$
$A_{CP}(K^*_1(1270)^+K^- \to \rho^0K^+K^-) = (-7 \pm 17)\%$
$A_{CP}(K^*_1(1270)^-K^+ \to \rho^0K^-K^+) = (10 \pm 13)\%$
$A_{CP}(K_1(1400)^+K^- \to K^+K^-\pi^+\pi^-) = (-4.4 \pm 2.1)\%$
$A_{CP}(K^*(1410)^+K^- \to K^{*0}\pi^+K^-) = (-20 \pm 17)\%$
$A_{CP}(K^*(1410)^-K^+ \to \overline{K}^{*0}\pi^-K^+) = (-1 \pm 14)\%$
$A_{CP}(K^*(1680)^+K^- \to K^+K^-\pi^+\pi^-) = (-17 \pm 29)\%$
$A_{CP}(K^{*0}\overline{K}^{*0})$ in $D^0, \overline{D}^0 \to K^{*0}\overline{K}^{*0} = (-5 \pm 14)\%$
$A_{CP}(K^{*0}\overline{K}^{*0}$ S-wave$) = (-3.9 \pm 2.2)\%$
$A_{CP}(\phi\rho^0)$ in $D^0, \overline{D}^0 \to \phi\rho^0 = (1 \pm 9)\%$
$A_{CP}(\phi\rho^0$ S-wave$) = (-3 \pm 5)\%$
$A_{CP}(\phi\rho^0$ D-wave$) = (-37 \pm 19)\%$
$A_{CP}(\phi(\pi^+\pi^-)_{S-wave}) = (6 \pm 6)\%$
$A_{CP}(K^*(892)^0(K^-\pi^+)_{S-wave}) = (-10 \pm 40)\%$
$A_{CP}(K^+K^-\pi^+\pi^-$ non-resonant$) = (8 \pm 20)\%$
$A_{CP}((K^-\pi^+)_{P-wave}(K^+\pi^-)_{S-wave}) = (3 \pm 11)\%$
$A_{CP}(K^+K^-\mu^+\mu^-)$ in $D^0, \overline{D}^0 \to K^+K^-\mu^+\mu^- = (-2 \pm 6)\%$
$A_{CP}(\pi^+\pi^-\mu^+\mu^-)$ in $D^0, \overline{D}^0 \to \pi^+\pi^-\mu^+\mu^- = (2.9 \pm 2.1)\%$

CP-violation asymmetry difference

$\Delta A_{CP} = A_{CP}(K^+K^-) - A_{CP}(\pi^+\pi^-) = (-0.154 \pm 0.029)\%$

χ^2 tests of CP-violation (CPV) p-values

Local CPV in $D^0, \overline{D}^0 \to \pi^+\pi^-\pi^0 = 10.6\%$
Local CPV in $D^0, \overline{D}^0 \to \pi^+\pi^-\pi^+\pi^- = (0.6 \pm 0.2)\%$
Local CPV in $D^0, \overline{D}^0 \to K^0_S\pi^+\pi^- = 96\%$
Local CPV in $D^0, \overline{D}^0 \to K^+K^-\pi^0 = 16.6\%$
Local CPV in $D^0, \overline{D}^0 \to K^+K^-\pi^+\pi^- = 9.1\%$

T-violation decay-rate asymmetry

$A_T(K^+K^-\pi^+\pi^-) = (2.9 \pm 2.2) \times 10^{-3}$ [jj]
$A_{Tviol}(2K^0_S\pi^+\pi^-)$ in $D^0, \overline{D}^0 \to 2K^0_S\pi^+\pi^- = (-1.9 \pm 1.4) \times 10^{-2}$
$A_{\mathrm{Tviol}}(K^0_S\pi^+\pi^-\pi^0)$ in $D^0, \overline{D}^0 \to K^0_S\pi^+\pi^-\pi^0 = (-0.3^{+1.4}_{-1.6}) \times 10^{-3}$

CPT-violation decay-rate asymmetry

$A_{CPT}(K^\mp\pi^\pm) = -1.46 \times 10^{-4}$ to 6.6×10^{-5}, CL = 95%

Form factors

$r_V \equiv V(0)/A_1(0)$ in $D^0 \to K^*(892)^-\ell^+\nu_\ell = 1.45 \pm 0.04$
$r_2 \equiv A_2(0)/A_1(0)$ in $D^0 \to K^*(892)^-\ell^+\nu_\ell = 0.720 \pm 0.033$
$r_V \equiv V(0)/A_1(0)$ in $D^0 \to \rho^-\ell^+\nu_\ell = 1.55 \pm 0.09$
$r_2 \equiv A_2(0)/A_1(0)$ in $D^0 \to \rho^-\ell^+\nu_\ell = 0.82 \pm 0.06$
$f_+(0)$ in $D^0 \to K^-\ell^+\nu_\ell = 0.736 \pm 0.004$
$f_+(0)|V_{cs}|$ in $D^0 \to K^-\ell^+\nu_\ell = 0.7176 \pm 0.0018$
$r_1 \equiv a_1/a_0$ in $D^0 \to K^-\ell^+\nu_\ell = -2.40 \pm 0.16$
$r_2 \equiv a_2/a_0$ in $D^0 \to K^-\ell^+\nu_\ell = 5 \pm 4$
$f_+(0)$ in $D^0 \to \pi^-\ell^+\nu_\ell = 0.637 \pm 0.009$
$f_+(0)|V_{cd}|$ in $D^0 \to \pi^-\ell^+\nu_\ell = 0.1436 \pm 0.0026$ (S = 1.5)
$r_1 \equiv a_1/a_0$ in $D^0 \to \pi^-\ell^+\nu_\ell = -1.97 \pm 0.28$ (S = 1.4)
$r_2 \equiv a_1/a_0$ in $D^0 \to \pi^-\ell^+\nu_\ell = -0.2 \pm 2.2$ (S = 1.7)
$f_+^{a_0}(0)|V_{cd}|$ in $D^0 \to a_0(980)^-e^+\nu_e = 0.126 \pm 0.013$

Most decay modes (other than the semileptonic modes) that involve a neutral K meson are now given as K^0_S modes, not as $\overline{K}^0$ modes. Nearly always it is a K^0_S that is measured, and interference between Cabibbo-allowed and doubly Cabibbo-suppressed modes can invalidate the assumption that $2\Gamma(K^0_S) = \Gamma(\overline{K}^0)$.

D^0 DECAY MODES	Fraction (Γ_i/Γ)	Scale factor/ Confidence level	p (MeV/c)
Topological modes			
0-prongs	[ss] (15 ± 6) %		–
2-prongs	(71 ± 6) %		–

Int. J. Mod. Phys. A 2026.41. Downloaded from www.worldscientific.com
by UNIVERSITY OF CALIFORNIA @ BERKELEY on 09/16/26. Re-use and distribution is strictly not permitted, except for Open Acce

4-prongs	[tt]	(14.6 ± 0.5) %		–
6-prongs	[uu]	$(6.5 \pm 1.3) \times 10^{-4}$		–

Inclusive modes

e^+ anything	[vv]	(6.49 ± 0.11) %		–
μ^+ anything		(6.8 ± 0.6) %		–
K^- anything		(54.7 ± 2.8) %	S=1.3	–
K^0_S anything		(20.75 ± 0.23) %		–
K^+ anything		(3.4 ± 0.4) %		–
$K^*(892)^-$ anything		(15 ± 9) %		–
$\overline{K}^*(892)^0$ anything		(9 ± 4) %		–
$K^*(892)^+$ anything		< 3.6 %	CL=90%	–
$K^*(892)^0$ anything		(2.8 ± 1.3) %		–
η anything		(9.5 ± 0.9) %		–
η' anything		(2.48 ± 0.27) %		–
ϕ anything		(1.08 ± 0.04) %		–
$\pi^+\pi^+\pi^-$ anything		(17.60 ± 0.25) %		–
invisibles		$< 9.4 \times 10^{-5}$	CL=90%	–

Semileptonic modes

$K^- e^+ \nu_e$		(3.537 ± 0.017) %	S=1.1	867
$K^- \mu^+ \nu_\mu$		(3.418 ± 0.019) %		864
$K^*(892)^- e^+ \nu_e$		(2.16 ± 0.16) %		719
$K^*(892)^- \mu^+ \nu_\mu$		(2.01 ± 0.06) %	S=1.7	714
$K^- \pi^0 e^+ \nu_e$		$(1.6 {}^{+1.3}_{-0.5})$ %		861
$\overline{K}^0 \pi^- e^+ \nu_e$		(1.447 ± 0.033) %		860
$(\overline{K}^0 \pi^-)_{S-wave} e^+ \nu_e$		$(8.5 \pm 0.6) \times 10^{-4}$		860
$K^- \pi^0 \mu^+ \nu_\mu$		$(7.10 \pm 0.21) \times 10^{-3}$	S=1.7	849
$(K^- \pi^0)_{S-wave} \mu^+ \nu_\mu$		$(4.09 \pm 0.35) \times 10^{-4}$		849
$\overline{K}^0 \pi^- \mu^+ \nu_\mu$		(1.40 ± 0.04) %	S=1.7	847
$(\overline{K}^0 \pi^-)_{S-wave} \mu^+ \nu_\mu$		$(7.5 \pm 1.6) \times 10^{-4}$		847
$K^- \eta e^+ \nu_e$		$(8 \pm 4) \times 10^{-5}$		773
$K^- \pi^+ \pi^- e^+ \nu_e$		$(2.8 {}^{+1.4}_{-1.1}) \times 10^{-4}$		843
$K_1(1270)^- e^+ \nu_e$, $K_1^- \to K^- \pi^+ \pi^-$		$(3.23 \pm 0.25) \times 10^{-4}$		511
$K_1(1270)^- e^+ \nu_e$, $K_1^- \to K^0_S \pi^- \pi^0$		$(1.7 {}^{+0.6}_{-0.5}) \times 10^{-4}$		–
$K^- \pi^+ \pi^- \mu^+ \nu_\mu$		$< 1.3 \times 10^{-3}$	CL=90%	821
$(\overline{K}^*(892)\pi)^- \mu^+ \nu_\mu$		$< 1.5 \times 10^{-3}$	CL=90%	692
$K_1(1270)^- \mu^+ \nu_\mu$, $K_1^- \to K^- \pi^+ \pi^-$		$(2.6 {}^{+0.4}_{-0.5}) \times 10^{-4}$		–
$K_1(1400)^- e^+ \nu_e$		$< 7 \times 10^{-5}$	CL=90%	405
$\pi^- e^+ \nu_e$		$(2.91 \pm 0.04) \times 10^{-3}$		927
$\pi^- \mu^+ \nu_\mu$		$(2.67 \pm 0.12) \times 10^{-3}$	S=1.3	924
$\pi^- \pi^0 e^+ \nu_e$		$(1.45 \pm 0.07) \times 10^{-3}$		922
$\rho^- e^+ \nu_e$		$(1.46 \pm 0.08) \times 10^{-3}$	S=2.0	771
$\rho^- \mu^+ \nu_\mu$		$(1.35 \pm 0.13) \times 10^{-3}$		767
$a(980)^- e^+ \nu_e$, $a^- \to \eta \pi^-$		$(8.6 \pm 1.8) \times 10^{-5}$		–
$K^0_S K^- e^+ \nu_e$		$< 2.13 \times 10^{-5}$	CL=90%	790
$b_1(1235)^- e^+ \nu_e$, $b_1^- \to \omega \pi^-$		$< 1.12 \times 10^{-4}$	CL=90%	–

Hadronic modes with one $\overline{K}$

$K^- \pi^+$		(3.936 ± 0.030) %	S=1.3	861
$K^0_S \pi^0$		(1.239 ± 0.022) %		860
$K^0_L \pi^0$		$(9.76 \pm 0.32) \times 10^{-3}$		860
$K^0_L \eta$		$(4.34 \pm 0.16) \times 10^{-3}$		772
$K^0_L \eta'$		$(8.12 \pm 0.35) \times 10^{-3}$	S=1.3	565
$K^0_L \omega$		(1.16 ± 0.04) %		670
$K^0_S \pi^+ \pi^-$	[kk]	(2.84 ± 0.16) %	S=1.1	842
$K^0_S \rho^0$		$(6.3 {}^{+0.6}_{-0.8}) \times 10^{-3}$		674
$K^0_S \omega$, $\omega \to \pi^+ \pi^-$		$(2.1 \pm 0.6) \times 10^{-4}$		670
$K^0_S (\pi^+ \pi^-)_{S-wave}$		$(3.4 \pm 0.8) \times 10^{-3}$		842
$K^0_S f_0(980)$, $f_0 \to \pi^+ \pi^-$		$(1.22 {}^{+0.40}_{-0.23}) \times 10^{-3}$		549
$K^0_S f_0(1370)$, $f_0 \to \pi^+ \pi^-$		$(2.8 {}^{+0.9}_{-1.3}) \times 10^{-3}$		†
$K^0_S f_2(1270)$, $f_2 \to \pi^+ \pi^-$		$(9 {}^{+10}_{-6}) \times 10^{-5}$		262
$K^*(892)^- \pi^+$, $K^{*-} \to K^0_S \pi^-$		$(1.67 {}^{+0.13}_{-0.16})$ %		711
$K^*_0(1430)^- \pi^+$, $K^{*-}_0 \to K^0_S \pi^-$		$(2.71 {}^{+0.40}_{-0.32}) \times 10^{-3}$		378
$K^*_2(1430)^- \pi^+$, $K^{*-}_2 \to K^0_S \pi^-$		$(3.4 {}^{+1.9}_{-1.0}) \times 10^{-4}$		367
$K^*(1680)^- \pi^+$, $K^{*-} \to K^0_S \pi^-$		$(4 \pm 4) \times 10^{-4}$		46
$K^*(892)^+ \pi^-$, $K^{*+} \to K^0_S \pi^+$	[xx]	$(1.14 {}^{+0.60}_{-0.34}) \times 10^{-4}$		711
$K^*_0(1430)^+ \pi^-$, $K^{*+}_0 \to K^0_S \pi^+$	[xx]	$< 1.4 \times 10^{-5}$	CL=95%	–
$K^*_2(1430)^+ \pi^-$, $K^{*+}_2 \to K^0_S \pi^+$	[xx]	$< 3.4 \times 10^{-5}$	CL=95%	–
$K^0_S \pi^+ \pi^-$ nonresonant		$(2.6 {}^{+6.0}_{-1.6}) \times 10^{-4}$		842
$K^- \pi^+ \pi^0$	[kk]	(14.4 ± 0.5) %	S=2.0	844
$K^- \rho^+$		(11.2 ± 0.7) %		676
$K^- \rho(1700)^+$, $\rho^+ \to \pi^+ \pi^0$		$(8.2 \pm 1.8) \times 10^{-3}$		†
$K^*(892)^- \pi^+$, $K^*(892)^- \to K^- \pi^0$		$(2.30 {}^{+0.40}_{-0.20})$ %		711
$\overline{K}^*(892)^0 \pi^0$, $\overline{K}^*(892)^0 \to K^- \pi^+$		(1.95 ± 0.24) %		711
$K^*_0(1430)^- \pi^+$, $K^{*-}_0 \to K^- \pi^0$		$(4.7 \pm 2.2) \times 10^{-3}$		378
$\overline{K}^*_0(1430)^0 \pi^0$, $\overline{K}^{*0}_0 \to K^- \pi^+$		$(5.9 {}^{+5.0}_{-1.6}) \times 10^{-3}$		379
$K^*(1680)^- \pi^+$, $K^{*-} \to K^- \pi^0$		$(1.9 \pm 0.7) \times 10^{-3}$		46
$K^- \pi^+ \pi^0$ nonresonant		$(1.15 {}^{+0.60}_{-0.20})$ %		844
$K^0_S 2\pi^0$		$(9.1 \pm 1.1) \times 10^{-3}$	S=2.2	843
$K^0_L \pi^0 \pi^0$		(1.26 ± 0.06) %		843
$K^0_S (2\pi^0)_{S-wave}$		$(2.6 \pm 0.7) \times 10^{-3}$		–
$\overline{K}^*(892)^0 \pi^0$, $\overline{K}^{*0} \to K^0_S \pi^0$		$(6.0 \pm 0.9) \times 10^{-3}$		711
$\overline{K}^*(1430)^0 \pi^0$, $\overline{K}^{*0} \to K^0_S \pi^0$		$(4 \pm 23) \times 10^{-5}$		–
$\overline{K}^*(1680)^0 \pi^0$, $\overline{K}^{*0} \to K^0_S \pi^0$		$(1.0 \pm 0.4) \times 10^{-3}$		–
$K^0_S f_2(1270)$, $f_2 \to 2\pi^0$		$(2.3 \pm 1.1) \times 10^{-4}$		–
$2K^0_S$, one $K^0_S \to 2\pi^0$		$(3.2 \pm 1.1) \times 10^{-4}$		–
$K^0_S 3\pi^0$		$(7.6 \pm 0.4) \times 10^{-3}$		815
$K^- 2\pi^+ \pi^-$	[kk]	(8.20 ± 0.14) %	S=1.2	813
$K^- \pi^+ \rho^0$ total		(6.85 ± 0.31) %		609
$K^- \pi^+ \rho^0$ 3-body		$(6.1 \pm 1.6) \times 10^{-3}$		609
$\overline{K}^*(892)^0 \rho^0$, $\overline{K}^{*0} \to K^- \pi^+$		(1.01 ± 0.05) %		416
$\overline{K}^*(892)^0 \rho^0$ transverse, $\overline{K}^{*0} \to K^- \pi^+$		(1.2 ± 0.4) %		417
$K^- a_1(1260)^+$, $a_1^+ \to \rho^0 \pi^+$		(4.31 ± 0.32) %		327
$K_1(1270)^- \pi^+$, $K_1^- \to K^- \pi^+ \pi^-$ total		$(3.9 \pm 0.4) \times 10^{-3}$		–
$K_1(1270)^- \pi^+$, $K_1^- \to \overline{K}^*(892)^0 \pi^-$, $\overline{K}^{*0} \to K^- \pi^+$		$(6.6 \pm 2.3) \times 10^{-4}$		484
$K^- 2\pi^+ \pi^-$ nonresonant		(1.80 ± 0.07) %		813
$K^0_S \pi^+ \pi^- \pi^0$	[yy]	(5.2 ± 0.6) %		813
$K^0_S \eta$, $\eta \to \pi^+ \pi^- \pi^0$		$(1.17 \pm 0.03) \times 10^{-3}$		772
$K^0_S \omega$, $\omega \to \pi^+ \pi^- \pi^0$		$(9.9 \pm 0.6) \times 10^{-3}$		670
$K^- \pi^+ 2\pi^0$		(8.86 ± 0.23) %		815
$K^- \pi^+ 3\pi^0$		$(9.5 \pm 0.4) \times 10^{-3}$		774
$K^0_S \pi^+ \pi^- 2\pi^0$		(1.27 ± 0.06) %		771
$K^- 2\pi^+ \pi^- \pi^0$		(4.3 ± 0.4) %		771
$\overline{K}^*(892)^0 \pi^+ \pi^- \pi^0$, $\overline{K}^{*0} \to K^- \pi^+$		(1.3 ± 0.6) %		643
$\overline{K}^*(892)^0 \omega$, $\overline{K}^{*0} \to K^- \pi^+$, $\omega \to \pi^+ \pi^- \pi^0$		$(6.5 \pm 3.0) \times 10^{-3}$		410
$K^- \pi^+ \omega$		(3.39 ± 0.10) %		605
$\overline{K}^*(892)^0 \omega$		(1.1 ± 0.5) %		410
$K^0_S \pi^0 \omega$		$(8.5 \pm 0.6) \times 10^{-3}$		605
$K^0_S \eta \pi^0$		(1.01 ± 0.05) %		721
$K^0_S a_0(980)$, $a_0 \to \eta \pi^0$		(1.20 ± 0.28) %		–
$\overline{K}^*(892)^0 \eta$, $\overline{K}^{*0} \to K^0_S \pi^0$		$(2.9 \pm 0.7) \times 10^{-3}$		–
$K^- \pi^+ \eta$		(1.88 ± 0.05) %	S=1.4	721
$K^*(892)^0 \eta$, $K^{*0} \to K^- \pi^+$		$(8.9 {}^{+0.8}_{-0.6}) \times 10^{-3}$		–
$a_0(980)^+ K^-$, $a_0^+ \to \eta \pi^+$		$(7.4 {}^{+0.9}_{-0.7}) \times 10^{-3}$		–
$K^*_2(1980)^- \pi^+$, $K^{*-}_2 \to K^- \eta$		$(2.2 {}^{+1.7}_{-1.9}) \times 10^{-4}$		–
$K^- \pi^+ \pi^0 \eta$		$(4.49 \pm 0.27) \times 10^{-3}$		656
$K^0_S \pi^+ \pi^- \eta$		$(2.80 \pm 0.21) \times 10^{-3}$		651

Int. J. Mod. Phys. A 2026.41. Downloaded from www.worldscientific.com
by UNIVERSITY OF CALIFORNIA @ BERKELEY on 09/16/26. Re-use and distribution is strictly not permitted, except for Open Access articles.

$K^0_S 2\pi^0 \eta$	$(1.76 \pm 0.26) \times 10^{-3}$		656
$K^0_S 2\pi^+ 2\pi^-$	$(2.70 \pm 0.29) \times 10^{-3}$		768
$K^0_S \rho^0 \pi^+ \pi^-$, no $K^*(892)^-$	$(1.1 \pm 0.7) \times 10^{-3}$		–
$K^*(892)^- 2\pi^+ \pi^-$, $K^*(892)^- \to K^0_S \pi^-$, no ρ^0	$(5 \pm 8) \times 10^{-4}$		642
$K^*(892)^- \rho^0 \pi^+$, $K^*(892)^- \to K^0_S \pi^-$	$(1.6 \pm 0.6) \times 10^{-3}$		230
$K^0_S 2\pi^+ 2\pi^-$ nonresonant	$< 1.2 \times 10^{-3}$	CL=90%	768
$K^- 3\pi^+ 2\pi^-$	$(1.48 \pm 0.32) \times 10^{-4}$	S=1.4	713
$K^- 2\pi^+ \pi^- 2\pi^0$	$(1.90 \pm 0.19) \times 10^{-3}$		717

Fractions of some of the following modes with resonances have already appeared above as submodes of particular charged-particle modes. These nine modes below are all corrected for unseen decays of the resonances.

$K^0_S \eta$	$(5.08 \pm 0.13) \times 10^{-3}$		772
$K^0_S \omega$	(1.11 ± 0.06) %		670
$K^0_S \eta'(958)$	$(9.49 \pm 0.32) \times 10^{-3}$		565
$\overline{K}^*(892)^0 \pi^+ \pi^- \pi^0$	(1.9 ± 0.9) %		643
$\overline{K}^*(892)^0 \eta$	(1.41 ± 0.12) %		582
$K^- \pi^+ \eta'(958)$	$(6.43 \pm 0.34) \times 10^{-3}$		479
$K^0_S \eta'(958) \pi^0$	$(2.52 \pm 0.27) \times 10^{-3}$		479
$\overline{K}^*(892)^0 \eta'(958)$	$< 1.0 \times 10^{-3}$	CL=90%	119

Hadronic modes with three K's

$K^0_S K^+ K^-$	$(4.49 \pm 0.29) \times 10^{-3}$		544
$K^0_S a_0(980)^0$, $a^0_0 \to K^+ K^-$	$(3.0 \pm 0.4) \times 10^{-3}$		–
$K^- a_0(980)^+$, $a^+_0 \to K^+ K^0_S$	$(6.0 \pm 1.8) \times 10^{-4}$		–
$K^+ a_0(980)^-$, $a^-_0 \to K^- K^0_S$	$< 1.1 \times 10^{-4}$	CL=95%	–
$K^0_S f_0(980)$, $f_0 \to K^+ K^-$	$< 9 \times 10^{-5}$	CL=95%	–
$K^0_S \phi$, $\phi \to K^+ K^-$	$(2.06 \pm 0.14) \times 10^{-3}$		520
$K^0_L \phi$	$(4.06 \pm 0.23) \times 10^{-3}$		521
$K^0_S f_0(1370)$, $f_0 \to K^+ K^-$	$(1.7 \pm 1.1) \times 10^{-4}$		–
$3K^0_S$	$(7.6 \pm 0.7) \times 10^{-4}$	S=1.4	539
$K^+ 2K^- \pi^+$	$(2.24 \pm 0.32) \times 10^{-4}$		434
$K^+ K^- \overline{K}^*(892)^0$, $\overline{K}^{*0} \to K^- \pi^+$	$(4.5 \pm 1.8) \times 10^{-5}$		†
$K^- \pi^+ \phi$, $\phi \to K^+ K^-$	$(4.0 \pm 1.7) \times 10^{-5}$		422
$\phi \overline{K}^*(892)^0$, $\phi \to K^+ K^-$, $\overline{K}^{*0} \to K^- \pi^+$	$(1.08 \pm 0.20) \times 10^{-4}$		†
$K^+ 2K^- \pi^+$ nonresonant	$(3.4 \pm 1.5) \times 10^{-5}$		434
$2K^0_S K^\pm \pi^\mp$	$(6.0 \pm 1.3) \times 10^{-4}$		427

Pionic modes

$\pi^+ \pi^-$	$(1.451 \pm 0.024) \times 10^{-3}$	S=1.4	922
$2\pi^0$	$(8.25 \pm 0.25) \times 10^{-4}$		923
$\pi^+ \pi^- \pi^0$	(1.49 ± 0.06) %	S=2.1	907
$\rho^+ \pi^-$	(1.01 ± 0.04) %		764
$\rho^0 \pi^0$	$(3.85 \pm 0.23) \times 10^{-3}$		764
$\rho^- \pi^+$	$(5.14 \pm 0.25) \times 10^{-3}$		764
$\rho(1450)^+ \pi^-$, $\rho^+ \to \pi^+ \pi^0$	$(1.6 \pm 2.1) \times 10^{-5}$		–
$\rho(1450)^0 \pi^0$, $\rho^0 \to \pi^+ \pi^-$	$(4.5 \pm 1.9) \times 10^{-5}$		–
$\rho(1450)^- \pi^+$, $\rho^- \to \pi^- \pi^0$	$(2.7 \pm 0.4) \times 10^{-4}$		–
$\rho(1700)^+ \pi^-$, $\rho^+ \to \pi^+ \pi^0$	$(6.1 \pm 1.5) \times 10^{-4}$		–
$\rho(1700)^0 \pi^0$, $\rho^0 \to \pi^+ \pi^-$	$(7.4 \pm 1.8) \times 10^{-4}$		–
$\rho(1700)^- \pi^+$, $\rho^- \to \pi^- \pi^0$	$(4.8 \pm 1.1) \times 10^{-4}$		–
$f_0(980) \pi^0$, $f_0 \to \pi^+ \pi^-$	$(3.7 \pm 0.9) \times 10^{-5}$		–
$f_0(500) \pi^0$, $f_0 \to \pi^+ \pi^-$	$(1.22 \pm 0.22) \times 10^{-4}$		–
$f_0(1370) \pi^0$, $f_0 \to \pi^+ \pi^-$	$(5.5 \pm 2.1) \times 10^{-5}$		–
$f_0(1500) \pi^0$, $f_0 \to \pi^+ \pi^-$	$(5.8 \pm 1.6) \times 10^{-5}$		–
$f_0(1710) \pi^0$, $f_0 \to \pi^+ \pi^-$	$(4.6 \pm 1.6) \times 10^{-5}$		–
$f_2(1270) \pi^0$, $f_2 \to \pi^+ \pi^-$	$(1.96 \pm 0.21) \times 10^{-4}$		–
$\pi^+ \pi^- \pi^0$ nonresonant	$(1.2 \pm 0.4) \times 10^{-4}$		907
$3\pi^0$	$(2.0 \pm 0.5) \times 10^{-4}$		908
$2\pi^+ 2\pi^-$	$(7.15 \pm 0.25) \times 10^{-3}$	S=2.2	880
$a_1(1260)^+ \pi^-$, $a^+_1 \to 2\pi^+ \pi^-$ total	$(4.37 \pm 0.31) \times 10^{-3}$		–
$a_1(1260)^+ \pi^-$, $a^+_1 \to \rho^0 \pi^+$ S-wave	$(2.97 \pm 0.21) \times 10^{-3}$		–
$a_1(1260)^+ \pi^-$, $a^+_1 \to \rho^0 \pi^+$ D-wave	$(1.8 \pm 0.5) \times 10^{-4}$		–
$a_1(1260)^+ \pi^-$, $a^+_1 \to \sigma \pi^+$	$(6.0 \pm 0.7) \times 10^{-4}$		–
$a_1(1260)^- \pi^+$, $a^-_1 \to 2\pi^- \pi^+$ total	$(7.4 \pm 2.1) \times 10^{-4}$		–
$a_1(1260)^- \pi^+$, $a^-_1 \to \rho^0 \pi^-$ S-wave	$(2.2 \pm 0.8) \times 10^{-4}$		–
$a_1(1260)^- \pi^+$, $a^-_1 \to \sigma \pi^-$	$(5.7 \pm 3.2) \times 10^{-5}$		–
$\pi(1300)^+ \pi^-$, $\pi(1300)^+ \to 2\pi^+ \pi^-$ total	$(2.3 \pm 0.4) \times 10^{-3}$		–
$\pi(1300)^+ \pi^-$, $\pi(1300)^+ \to \sigma \pi^+$	$(4.9 \pm 2.5) \times 10^{-4}$		–
$\pi(1300)^- \pi^+$, $\pi(1300)^- \to 2\pi^- \pi^+$ total	$(1.68 \pm 0.33) \times 10^{-3}$		–
$\pi(1300)^- \pi^+$, $\pi(1300)^- \to \sigma \pi^-$	$(2.1 \pm 2.0) \times 10^{-4}$		–
$a_2(1320)^+ \pi^-$, $a^+_2 \to \rho^0 \pi^+$ D-wave	$(1.4 \pm 1.0) \times 10^{-5}$		–
$a_2(1320)^- \pi^+$, $a^-_2 \to \rho^0 \pi^-$ D-wave	$(2.9 \pm 1.0) \times 10^{-5}$		–
$a_1(1420)^+ \pi^-$, $a^+_1 \to f_0(980) \pi^+$ P-wave, $f_0 \to \pi^+ \pi^-$	$(4.3 \pm 2.0) \times 10^{-5}$		–
$a_1(1640)^+ \pi^-$, $a^+_1 \to \rho^0 \pi^+$ S-wave	$(1.2 \pm 0.7) \times 10^{-4}$		–
$a_1(1640)^+ \pi^-$, $a^+_1 \to \rho^0 \pi^+$ D-wave	$(3.0 \pm 1.5) \times 10^{-4}$		–
$a_1(1640)^+ \pi^-$, $a^+_1 \to \sigma \pi^+$	$(1.7 \pm 1.3) \times 10^{-4}$		–
$a_1(1640)^- \pi^+$, $a^-_1 \to \rho^0 \pi^-$ S-wave	$(4 \pm 4) \times 10^{-5}$		–
$\pi_2(1670)^+ \pi^-$, $\pi^+_2 \to f_2(1270)^0 \pi^+$, $f^0_2 \to \pi^+ \pi^-$	$(1.9 \pm 0.9) \times 10^{-4}$		–
$\pi_2(1670)^+ \pi^-$, $\pi^+_2 \to \sigma \pi^+$	$(2.5 \pm 1.0) \times 10^{-4}$		–
$2\rho(770)^0$ total	$(1.79 \pm 0.12) \times 10^{-3}$		518
$2\rho^0$, parallel helicities	$(7.9 \pm 3.0) \times 10^{-5}$		–
$2\rho^0$, perpendicular helicities	$(4.6 \pm 0.6) \times 10^{-4}$		–
$2\rho^0$, longitudinal helicities	$(1.20 \pm 0.10) \times 10^{-3}$		–
$2\rho(770)^0$, S-wave	$(1.3 \pm 0.5) \times 10^{-4}$		–
$2\rho(770)^0$, P-wave	$(6.2 \pm 1.0) \times 10^{-4}$		–
$2\rho(770)^0$, D-wave	$(1.2 \pm 0.5) \times 10^{-3}$		–
$\rho(770)^0 \rho(1450)^0$, $\rho(1450)^0 \to \pi^+ \pi^-$	$(1.8 \pm 1.1) \times 10^{-4}$		–
$\rho(770)^0 \rho(1450)^0$ P-wave, $\rho(1450)^0 \to \pi^+ \pi^-$	$(7 \pm 5) \times 10^{-5}$		–
$\rho(770)^0 \rho(1450)^0$ D-wave, $\rho(1450)^0 \to \pi^+ \pi^-$	$(1.1 \pm 1.0) \times 10^{-4}$		–
Resonant $(\pi^+ \pi^-) \pi^+ \pi^-$ 3-body total	$(1.43 \pm 0.12) \times 10^{-3}$		–
$(\pi^+ \pi^-)_{S-wave}$	$(4.5 \pm 0.8) \times 10^{-3}$		880
$(\pi^+ \pi^-)_{S-wave}$ $\sigma \pi^+ \pi^-$	$(5.9 \pm 0.8) \times 10^{-4}$		–
$f_0(980) \pi^+ \pi^-$, $f_0 \to \pi^+ \pi^-$	$(1.7 \pm 0.5) \times 10^{-4}$		–
$\rho(770)^0 (\pi^+ \pi^-)_{S-wave}$	$(1.9 \pm 1.3) \times 10^{-4}$		–
$\sigma \rho(770)^0$	$(4.7 \pm 2.4) \times 10^{-4}$		–
$f_2(1270) \pi^+ \pi^-$, $f_2 \to \pi^+ \pi^-$	$(3.5 \pm 0.6) \times 10^{-4}$		–
$f_2(1270)^0 (\pi^+ \pi^-)_{S-wave}$, $f_2(1270)^0 \to \pi^+ \pi^-$	$(1.3 \pm 1.0) \times 10^{-4}$		–
$f_2(1270) f_2(1270)$, $f_2 \to \pi^+ \pi^-$	$(1.5 \pm 1.7) \times 10^{-4}$		–
$f_0(1370) \sigma$, $f_0 \to \pi^+ \pi^-$	$(1.5 \pm 0.5) \times 10^{-3}$		–
$\pi^+ \pi^- 2\pi^0$	(1.002 ± 0.031) %		882
$\pi^+ \pi^- 2\pi^0$ (non-η)	$(9.51 \pm 0.33) \times 10^{-3}$		–
$a_1(1260)^+ \pi^-$, $a^+_1 \to \pi^+ 2\pi^0$ total	$(5.8 \pm 0.8) \times 10^{-3}$		–
$a_1(1260)^- \pi^+$, $a^-_1 \to \pi^- 2\pi^0$ total	$(7.2 \pm 2.5) \times 10^{-4}$		–
$a_1(1260)^0 \pi^0$, $a^0_1 \to \pi^+ \pi^- \pi^0$ total	$(3.3 \pm 0.9) \times 10^{-3}$		–
$a_1(1420)^+ \pi^-$, $a^+_1 \to f_0(980) \pi^+$ P-wave, $f_0 \to \pi^0 \pi^0$	$(3.0 \pm 1.4) \times 10^{-5}$		–
$a_1(1640)^- \pi^+$, $a^-_1 \to \rho^- \pi^0$ S-wave	$(3.0 \pm 2.8) \times 10^{-5}$		–
$a_1(1640)^+ \pi^-$, $a^+_1 \to \rho^+ \pi^0$ S-wave	$(1.1 \pm 0.7) \times 10^{-4}$		–
$a_2(1320)^+ \pi^-$, $a^+_2 \to \rho^+ \pi^0$ D-wave	$(2.0 \pm 1.4) \times 10^{-5}$		–
$a_2(1320)^- \pi^+$, $a^-_2 \to \rho^- \pi^0$ D-wave	$(3.0 \pm 1.4) \times 10^{-5}$		–

Int. J. Mod. Phys. A 2026.41. Downloaded from www.worldscientific.com
by UNIVERSITY OF CALIFORNIA @ BERKELEY on 09/16/26. Re-use and distribution is strictly not permitted, except for Open Acce

$h_1(1170)^0\pi^0$, $h_1^0 \to \rho\pi$		$(1.3 \pm 1.3)\times10^{-4}$		–
$\pi(1300)^-\pi^+$, $\pi(1300)^- \to \pi^-2\pi^0$ total		$(1.14 \pm 0.27)\times10^{-3}$		–
$\pi(1300)^+\pi^-$, $\pi(1300)^+ \to \pi^+2\pi^0$ total		$(1.56 \pm 0.30)\times10^{-3}$		–
$\pi(1300)^0\pi^0$, $\pi(1300)^0 \to \pi^+\pi^-\pi^0$ total		$(2.3 \pm 0.4)\times10^{-3}$		–
$\pi_2(1670)^0\pi^0$, $\pi_2(1670)^0 \to \pi^+\pi^-\pi^0$ total		$(1.1 \pm 0.4)\times10^{-4}$		–
$\rho(770)^+\rho(770)^-$		$(9.1 \pm 0.9)\times10^{-3}$		–
$\rho(770)^+\rho(770)^-$ S-wave		$(1.3 \pm 0.4)\times10^{-3}$		–
$\rho(770)^+\rho(770)^-$ P-wave		$(1.96 \pm 0.23)\times10^{-3}$		–
$\rho(770)^+\rho(770)^-$ D-wave		$(3.6 \pm 0.4)\times10^{-3}$		–
$\rho(770)^+\rho(1450)^-$ D-wave, $\rho(1450)^- \to \pi^-\pi^0$		$(1.7 \pm 2.0)\times10^{-4}$		–
$\rho(770)^0(\pi^0\pi^0)_{S-wave}$		$(1.0 \pm 0.4)\times10^{-4}$		–
$(\pi^+\pi^-)_{S-wave}(\pi^0\pi^0)_{S-wave}$		$(3.7 \pm 0.6)\times10^{-3}$		882
$\omega(782)\pi^0$, $\omega \to \pi^+\pi^-\pi^0$		$(9 \pm 4)\times10^{-5}$		–
$\phi(1020)\pi^0$, $\phi(1020) \to \pi^+\pi^-\pi^0$		$(1.5 \pm 0.5)\times10^{-4}$		–
$4\pi^0$		$(7.6 \pm 1.1)\times10^{-4}$		883
$\eta\pi^0$	[zz]	$(6.3 \pm 0.5)\times10^{-4}$	S=1.1	846
$\omega\pi^0$	[zz]	$(1.17 \pm 0.35)\times10^{-4}$		761
$\omega\eta$		$(1.98 \pm 0.18)\times10^{-3}$	S=1.1	648
$2\pi^+2\pi^-\pi^0$		$(3.46 \pm 0.21)\times10^{-3}$		844
$\pi^+\pi^-3\pi^0$		$(1.53 \pm 0.21)\times10^{-3}$		847
$2\pi^+2\pi^-2\pi^0$		$(4.8 \pm 0.4)\times10^{-3}$		798
$\eta\pi^+\pi^-$	[zz]	$(1.16 \pm 0.07)\times10^{-3}$		827
$\rho(770)^0\eta$, $\rho^0 \to \pi^+\pi^-$		$(1.77 \pm 0.25)\times10^{-4}$		–
$a_0(980)^-\pi^+$, $a_0^- \to \pi^-\eta$		$(6.9 \pm 1.9)\times10^{-5}$		–
$a_0(980)^+\pi^-$, $a_0^+ \to \pi^+\eta$		$(5.1 \pm 0.8)\times10^{-4}$		–
$a_2(1320)^+\pi^-$, $a_2^+ \to \pi^+\eta$		$(2.4 \pm 1.4)\times10^{-5}$		–
$a_2(1700)^+\pi^-$, $a_2^+ \to \pi^+\eta$		$(6 \pm 4)\times10^{-5}$		–
$(\pi^+\pi^-)_{S-wave}\eta$		$(4.5 \pm 3.2)\times10^{-5}$		827
$\omega\pi^+\pi^-$	[zz]	$(1.33 \pm 0.20)\times10^{-3}$		738
$\omega\pi^0\pi^0$		$< 1.10 \times10^{-3}$	CL=90%	740
$\eta2\pi^0$		$(3.8 \pm 1.3)\times10^{-4}$		829
$\pi^+\pi^-\pi^0\eta$		$(3.23 \pm 0.22)\times10^{-3}$		797
$\eta3\pi^0$		$(2.36 \pm 0.28)\times10^{-3}$		799
$\eta2\pi^+2\pi^-$		$(6.0 \pm 1.2)\times10^{-4}$		751
$3\pi^+3\pi^-$		$(4.3 \pm 1.2)\times10^{-4}$		795
$\eta'(958)\pi^0$		$(9.2 \pm 1.0)\times10^{-4}$		678
$\eta'(958)\pi^+\pi^-$		$(4.5 \pm 1.7)\times10^{-4}$		650
2η		$(2.11 \pm 0.19)\times10^{-3}$	S=2.3	754
$2\eta\pi^0$		$(7.3 \pm 2.2)\times10^{-4}$		699
$2\eta\pi^+\pi^-$		$(8.5 \pm 1.4)\times10^{-4}$		623
3η		$< 1.3 \times10^{-4}$	CL=90%	421
$\eta\eta'(958)$		$(1.01 \pm 0.19)\times10^{-3}$		537

Hadronic modes with a $K\overline{K}$ pair

K^+K^-		$(4.07 \pm 0.06)\times10^{-3}$	S=1.6	791
$2K_S^0$		$(1.41 \pm 0.05)\times10^{-4}$	S=1.1	789
$K_S^0K^-\pi^+$		$(3.4 \pm 0.5)\times10^{-3}$	S=1.1	739
$\overline{K}^*(892)^0K_S^0$, $\overline{K}^{*0} \to K^-\pi^+$		$(8.3 \pm 1.6)\times10^{-5}$		608
$K^*(892)^+K^-$, $K^{*+} \to K_S^0\pi^+$		$(1.91 \pm 0.30)\times10^{-3}$		–
$\overline{K}^*(1410)^0K_S^0$, $\overline{K}^{*0} \to K^-\pi^+$		$(1.3 \pm 1.9)\times10^{-4}$		–
$K^*(1410)^+K^-$, $K^{*+} \to K_S^0\pi^+$		$(3.2 \pm 1.9)\times10^{-4}$		–
$(K^-\pi^+)_{S-wave}K_S^0$		$(6.0 \pm 2.9)\times10^{-4}$		739
$(K_S^0\pi^+)_{S-wave}K^-$		$(3.9 \pm 1.0)\times10^{-4}$		739
$a_0(980)^-\pi^+$, $a_0^- \to K_S^0K^-$		$(1.3 \pm 1.4)\times10^{-4}$		–
$a_0(1450)^-\pi^+$, $a_0^- \to K_S^0K^-$		$(2.5 \pm 2.0)\times10^{-5}$		–
$a_2(1320)^-\pi^+$, $a_2^- \to K_S^0K^-$		$(5 \pm 5)\times10^{-6}$		–
$\rho(1450)^-\pi^+$, $\rho^- \to K_S^0K^-$		$(4.7 \pm 2.5)\times10^{-5}$		–
$K_S^0K^+\pi^-$		$(2.19 \pm 0.34)\times10^{-3}$	S=1.1	739
$K^*(892)^0K_S^0$, $K^{*0} \to K^+\pi^-$		$(1.13 \pm 0.21)\times10^{-4}$		608
$K^*(892)^-K^+$, $K^{*-} \to K_S^0\pi^-$		$(6.3 \pm 1.0)\times10^{-4}$		–
$K^*(1410)^0K_S^0$, $K^{*0} \to K^+\pi^+$		$(5 \pm 8)\times10^{-5}$		–
$K^*(1410)^-K^+$, $K^{*-} \to K_S^0\pi^-$		$(2.6 \pm 2.1)\times10^{-4}$		–
$(K^+\pi^-)_{S-wave}K_S^0$		$(3.7 \pm 1.9)\times10^{-4}$		739
$(K_S^0\pi^-)_{S-wave}K^+$		$(1.4 \pm 0.6)\times10^{-4}$		739
$a_0(980)^+\pi^-$, $a_0^+ \to K_S^0K^+$		$(6 \pm 4)\times10^{-4}$		–
$a_0(1450)^+\pi^-$, $a_0^+ \to K_S^0K^+$		$(3.3 \pm 2.6)\times10^{-5}$		–
$\rho(1700)^+\pi^-$, $\rho^+ \to K_S^0K^+$		$(1.2 \pm 0.6)\times10^{-5}$		–
$K^+K^-\pi^0$		$(3.41 \pm 0.14)\times10^{-3}$		743
$K^*(892)^+K^-$, $K^*(892)^+ \to K^+\pi^0$		$(1.51 \pm 0.07)\times10^{-3}$		–
$K^*(892)^-K^+$, $K^*(892)^- \to K^-\pi^0$		$(5.4 \pm 0.4)\times10^{-4}$		–
$(K^+\pi^0)_{S-wave}K^-$		$(2.42 \pm 0.17)\times10^{-3}$		743
$(K^-\pi^0)_{S-wave}K^+$		$(1.3 \pm 0.5)\times10^{-4}$		743
$f_0(980)\pi^0$, $f_0 \to K^+K^-$		$(3.6 \pm 0.6)\times10^{-4}$		–
$\phi\pi^0$, $\phi \to K^+K^-$		$(6.6 \pm 0.4)\times10^{-4}$		–
$2K_S^0\pi^0$		$< 1.45 \times10^{-4}$	CL=90%	740
$K^+K^-\eta$		$(5.9 \pm 1.9)\times10^{-5}$		514
$\phi(1020)\eta$		$(1.80 \pm 0.12)\times10^{-4}$		489
$K^+K^-\eta$ nonresonant		$(9.9 {}^{+0.9}_{-0.8})\times10^{-5}$		514
$2K_S^0\eta$		$(1.3 \pm 0.6)\times10^{-4}$		508
$K^+K^-\pi^0\pi^0$		$(6.9 \pm 0.8)\times10^{-4}$		681
$K^+K^-\pi^+\pi^-$		$(2.78 \pm 0.17)\times10^{-3}$	S=3.6	677
$\phi(\pi^+\pi^-)_{S-wave}$, $\phi \to K^+K^-$		$(1.1 \pm 0.6)\times10^{-4}$		614
$(\phi\rho^0)_{S-wave}$, $\phi \to K^+K^-$		$(7.8 \pm 0.8)\times10^{-4}$		250
$(\phi\rho^0)_{P-wave}$, $\phi \to K^+K^-$		$(4.4 \pm 2.1)\times10^{-5}$		–
$(\phi\rho^0)_{D-wave}$, $\phi \to K^+K^-$		$(4.7 \pm 1.6)\times10^{-5}$		–
$(K^*(892)^0\overline{K}^*(892)^0)_{S-wave}$, $K^{*0} \to K^\pm\pi^\mp$		$(2.52 \pm 0.18)\times10^{-4}$		–
$(K^*(892)^0\overline{K}^*(892)^0)_{P-wave}$, $K^* \to K^\pm\pi^\mp$		$(1.35 \pm 0.11)\times10^{-4}$		–
$(K^*(892)^0\overline{K}^*(892)^0)_{D-wave}$, $K^* \to K^\pm\pi^\mp$		$(5.3 \pm 0.5)\times10^{-5}$		–
$K^*(892)^0(K^-\pi^+)_{S-wave}$ 3-body, $K^{*0} \to K^+\pi^-$		$(1.6 \pm 0.7)\times10^{-4}$		–
$K_1(1270)^+K^-$, $K_1^+ \to K^{*0}\pi^+$		$(1.5 \pm 1.0)\times10^{-4}$		–
$K_1(1270)^+K^-$, $K_1^+ \to K^*(1430)^0\pi^+$, $K^{*0} \to K^+\pi^-$		$(1.7 \pm 0.6)\times10^{-4}$		–
$K_1(1270)^+K^-$, $K_1^+ \to \rho^0K^+$		$(2.5 \pm 0.7)\times10^{-4}$		–
$K_1(1270)^+K^-$, $K_1^+ \to \omega(782)K^+$, $\omega \to \pi^+\pi^-$		$(1.7 \pm 1.4)\times10^{-5}$		–
$K_1(1270)^-K^+$, $K_1^- \to \rho^0K^-$		$(1.5 \pm 0.4)\times10^{-4}$		–
$K_1(1400)^+K^-$, $K_1^+ \to K^*(892)^0\pi^+$, $K^{*0} \to K^+\pi^-$		$(5.2 \pm 0.5)\times10^{-4}$		–
$K^*(1410)^-K^+$, $K^{*-} \to \overline{K}^{*0}\pi^-$		$(7.8 \pm 1.3)\times10^{-5}$		–
$K_1(1680)^+K^-$, $K_1^+ \to K^{*0}\pi^+$, $K^{*0} \to K^+\pi^-$		$(1.0 \pm 0.4)\times10^{-4}$		–
$K^+K^-\pi^+\pi^-$ non-resonant		$(3.1 \pm 0.7)\times10^{-4}$		–
$2K_S^0\pi^+\pi^-$		$(5.3 \pm 0.9)\times10^{-4}$		673
$K_S^0K^-\pi^+\pi^0$		$(1.32 \pm 0.16)\times10^{-3}$		677
$K_S^0K^+\pi^-\pi^0$		$(6.5 \pm 0.7)\times10^{-4}$		677
$K_S^0K^-2\pi^+\pi^-$		$< 1.5 \times10^{-4}$	CL=90%	595
$K^+K^-\pi^+\pi^-\pi^0$		$(3.1 \pm 2.0)\times10^{-3}$		600

Other $K\overline{K}X$ modes. They include all decay modes of the ϕ, η, and ω.

$\phi\pi^0$		$(1.17 \pm 0.04)\times10^{-3}$		645
$\phi\eta$		$(1.8 \pm 0.5)\times10^{-4}$		489
$\phi\omega$		$(6.5 \pm 1.0)\times10^{-4}$		238

Radiative modes

$\rho^0\gamma$		$(1.81 \pm 0.31)\times10^{-5}$		771
$\omega\gamma$		$< 2.4 \times10^{-4}$	CL=90%	768
$\phi\gamma$		$(2.80 \pm 0.19)\times10^{-5}$		654
$\overline{K}^*(892)^0\gamma$		$(4.1 \pm 0.7)\times10^{-4}$		719

Doubly Cabibbo suppressed (DC) modes or $\Delta C = 2$ forbidden via mixing ($C2M$) modes

$K^+\ell^-\overline{\nu}_\ell$ via $\overline{D}^0$	[aaa]	$< 2.2 \times10^{-5}$	CL=90%	–
K^+ or $K^*(892)^+e^-\overline{\nu}_e$ via $\overline{D}^0$		$< 6 \times10^{-5}$	CL=90%	–

Int. J. Mod. Phys. A 2026.41. Downloaded from www.worldscientific.com
by UNIVERSITY OF CALIFORNIA @ BERKELEY on 09/16/26. Re-use and distribution is strictly not permitted, except for Open Access articles.

$K^+\pi^-$	DC	$(1.48 \pm 0.07) \times 10^{-4}$		S=3.1	861
$K^+\pi^-$ via DCS		$(1.359 \pm 0.025) \times 10^{-4}$			–
$K^+\pi^-$ via $\overline{D}^0$		$< 1.6 \times 10^{-5}$		CL=95%	861
$K^0_S\pi^+\pi^-$ in $D^0 \to \overline{D}^0$		$< 1.8 \times 10^{-4}$		CL=95%	–
$K^*(892)^+\pi^-$, $K^{*+} \to K^0_S\pi^+$	DC	$(1.14 {}^{+0.60}_{-0.34}) \times 10^{-4}$			711
$K^*_0(1430)^+\pi^-$, $K^{*+}_0 \to K^0_S\pi^+$	DC	$< 1.4 \times 10^{-5}$			–
$K^*_2(1430)^+\pi^-$, $K^{*+}_2 \to K^0_S\pi^+$	DC	$< 3.4 \times 10^{-5}$			–
$K^+\pi^-\pi^0$	DC	$(3.05 \pm 0.13) \times 10^{-4}$		S=1.3	844
$K^+\pi^-\pi^0$ via $\overline{D}^0$		$(7.6 \pm 0.5) \times 10^{-4}$			–
$K^+\pi^-\eta$		$(1.04 \pm 0.18) \times 10^{-4}$			721
$K^+\pi^-2\pi^0$		$(1.40 \pm 0.28) \times 10^{-4}$			815
$K^+\pi^+2\pi^-$ via DCS		$(2.48 \pm 0.07) \times 10^{-4}$			–
$K^+\pi^+2\pi^-$	DC	$(2.64 \pm 0.06) \times 10^{-4}$		S=1.1	813
$K^+\pi^+2\pi^-$ via $\overline{D}^0$		$(7.9 \pm 3.0) \times 10^{-6}$			812
$K^+\pi^-\pi^0\eta$		$< 7 \times 10^{-5}$		CL=90%	656
μ^- anything via $\overline{D}^0$		$< 4 \times 10^{-4}$		CL=90%	–

$\Delta C = 1$ weak neutral current ($C1$) modes, Lepton Family number (LF) violating modes, Lepton (L) or Baryon (B) number violating modes

$\gamma\gamma$	$C1$	$< 8.5 \times 10^{-7}$		CL=90%	932
e^+e^-	$C1$	$< 7.9 \times 10^{-8}$		CL=90%	932
$\mu^+\mu^-$	$C1$	$< 2.1 \times 10^{-9}$		CL=90%	926
$\pi^0e^+e^-$	$C1$	$< 4 \times 10^{-6}$		CL=90%	928
$\pi^0\mu^+\mu^-$	$C1$	$< 1.8 \times 10^{-4}$		CL=90%	915
$\pi^0\nu\overline{\nu}$		$< 2.1 \times 10^{-4}$		CL=90%	928
ηe^+e^-	$C1$	$< 3 \times 10^{-6}$		CL=90%	852
$\eta\mu^+\mu^-$	$C1$	$< 5.3 \times 10^{-4}$		CL=90%	838
$\pi^+\pi^-e^+e^-$	$C1$	$< 7 \times 10^{-6}$		CL=90%	922
$\rho^0e^+e^-$	$C1$	$< 1.0 \times 10^{-4}$		CL=90%	771
$\pi^+\pi^-\mu^+\mu^-$	$C1$	$(9.6 \pm 1.2) \times 10^{-7}$			894
$\pi^+\pi^-\mu^+\mu^-$ (non-res)		$< 5.5 \times 10^{-7}$		CL=90%	–
$\rho^0\mu^+\mu^-$	$C1$	$< 2.2 \times 10^{-5}$		CL=90%	754
ωe^+e^-	$C1$	$< 6 \times 10^{-6}$		CL=90%	768
$\omega\mu^+\mu^-$	$C1$	$< 8.3 \times 10^{-4}$		CL=90%	751
$K^-K^+e^+e^-$	$C1$	$< 1.1 \times 10^{-5}$		CL=90%	791
ϕe^+e^-	$C1$	$< 5.2 \times 10^{-5}$		CL=90%	654
$K^-K^+\mu^+\mu^-$	$C1$	$(1.54 \pm 0.32) \times 10^{-7}$			710
$K^-K^+\mu^+\mu^-$ (non-res)		$< 3.3 \times 10^{-5}$		CL=90%	–
$\phi\mu^+\mu^-$	$C1$	$< 3.1 \times 10^{-5}$		CL=90%	631
$\overline{K}^0e^+e^-$	$[qq]$	$< 2.4 \times 10^{-5}$		CL=90%	866
$\overline{K}^0\mu^+\mu^-$	$[qq]$	$< 2.6 \times 10^{-4}$		CL=90%	852
$K^-\pi^+e^+e^-$, $675 < m_{ee} < 875$ MeV		$(4.0 \pm 0.4) \times 10^{-6}$			–
$K^-\pi^+e^+e^-$, $1.005 < m_{ee} < 1.035$ GeV		$< 5 \times 10^{-7}$		CL=90%	–
$\overline{K}^*(892)^0e^+e^-$	$[qq]$	$< 4.7 \times 10^{-5}$		CL=90%	719
$K^-\pi^+\mu^+\mu^-$	$C1$	$< 3.59 \times 10^{-4}$		CL=90%	829
$K^-\pi^+\mu^+\mu^-$, $675 < m_{\mu\mu} < 875$ MeV		$(4.2 \pm 0.4) \times 10^{-6}$			–
$\overline{K}^*(892)^0\mu^+\mu^-$	$[qq]$	$< 2.4 \times 10^{-5}$		CL=90%	700
$\pi^+\pi^-\pi^0\mu^+\mu^-$	$C1$	$< 8.1 \times 10^{-4}$		CL=90%	863
$\mu^\pm e^\mp$	LF	$[bb]$ $< 1.3 \times 10^{-8}$		CL=90%	929
$\pi^0e^\pm\mu^\mp$	LF	$[bb]$ $< 8.0 \times 10^{-7}$		CL=90%	924
$\eta e^\pm\mu^\mp$	LF	$[bb]$ $< 2.25 \times 10^{-6}$		CL=90%	848
$\pi^+\pi^-e^\pm\mu^\mp$	LF	$[bb]$ $< 1.71 \times 10^{-6}$		CL=90%	911
$\rho^0e^\pm\mu^\mp$	LF	$[bb]$ $< 5.0 \times 10^{-7}$		CL=90%	767
$\omega e^\pm\mu^\mp$	LF	$[bb]$ $< 1.71 \times 10^{-6}$		CL=90%	764
$K^-K^+e^\pm\mu^\mp$	LF	$[bb]$ $< 1.00 \times 10^{-6}$		CL=90%	754
$\phi e^\pm\mu^\mp$	LF	$[bb]$ $< 5.1 \times 10^{-7}$		CL=90%	648
$\overline{K}^0e^\pm\mu^\mp$	LF	$[bb]$ $< 1.74 \times 10^{-6}$		CL=90%	863
$K^-\pi^+e^\pm\mu^\mp$	LF	$[bb]$ $< 1.90 \times 10^{-6}$		CL=90%	848
$\overline{K}^*(892)^0e^\pm\mu^\mp$	LF	$[bb]$ $< 1.25 \times 10^{-6}$		CL=90%	714
$2\pi^-2e^+$	L	$< 9.1 \times 10^{-7}$		CL=90%	922
$2\pi^-2\mu^+$	L	$< 1.52 \times 10^{-6}$		CL=90%	894
$K^-\pi^-2e^+$	L	$< 5.0 \times 10^{-7}$		CL=90%	861
$K^-\pi^-2\mu^+$	L	$< 5.3 \times 10^{-7}$		CL=90%	829
$2K^-2e^+$	L	$< 3.4 \times 10^{-7}$		CL=90%	791
$2K^-2\mu^+$	L	$< 1.0 \times 10^{-7}$		CL=90%	710
$\pi^-\pi^-e^+\mu^+$	L	$< 3.06 \times 10^{-6}$		CL=90%	911
$K^-\pi^-e^+\mu^+$	L	$< 2.10 \times 10^{-6}$		CL=90%	848
$2K^-e^+\mu^+$	L	$< 5.8 \times 10^{-7}$		CL=90%	754
pe^-	L,B	$< 5.5 \times 10^{-7}$		CL=90%	696
$\overline{p}e^+$	L,B	$< 6.9 \times 10^{-7}$		CL=90%	696
$p\mu^-$	L,B	$< 5.1 \times 10^{-7}$		CL=90%	691
$\overline{p}\mu^+$	L,B	$< 6.3 \times 10^{-7}$		CL=90%	691

Exotic modes

$\gamma\gamma_D$	$[bbb]$	$< 2.0 \times 10^{-6}$		CL=90%	–
$\omega\gamma_D$	$[bbb]$	$< 1.1 \times 10^{-5}$		CL=90%	–

$D^*(2007)^0$

$I(J^P) = \frac{1}{2}(1^-)$

Mass $m = 2006.86 \pm 0.05$ MeV (S = 1.1)
$m_{D^{*0}} - m_{D^0} = 142.014 \pm 0.030$ MeV (S = 1.5)
Full width $\Gamma < 2.1$ MeV, CL = 90%

$\overline{D}^*(2007)^0$ modes are charge conjugates of modes below.

$D^*(2007)^0$ DECAY MODES	Fraction (Γ_i/Γ)	Confidence level	p (MeV/c)
$D^0\pi^0$	(64.7 ± 0.9) %		43
$D^0\gamma$	(35.3 ± 0.9) %		137
$D^0e^+e^-$	$(3.91 \pm 0.33) \times 10^{-3}$		137
$\mu^+\mu^-$	$< 2.5 \times 10^{-8}$	90%	998
e^+e^-	$< 1.7 \times 10^{-6}$	90%	1003

$D^*(2010)^\pm$

$I(J^P) = \frac{1}{2}(1^-)$

Mass $m = 2010.27 \pm 0.04$ MeV
$m_{D^*(2010)^+} - m_{D^+} = 140.603 \pm 0.015$ MeV
$m_{D^*(2010)^+} - m_{D^0} = 145.4257 \pm 0.0017$ MeV
Full width $\Gamma = 83.4 \pm 1.8$ keV

$D^*(2010)^-$ modes are charge conjugates of the modes below.

$D^*(2010)^\pm$ DECAY MODES	Fraction (Γ_i/Γ)	Confidence level	p (MeV/c)
$D^0\pi^+$	(67.7 ± 0.5) %		39
$D^+\pi^0$	(30.7 ± 0.5) %		38
$D^+\gamma$	(1.6 ± 0.4) %		136
$e^+\nu_e$	$< 1.1 \times 10^{-5}$	90%	1005
$\mu^+\nu_\mu$	$< 4.3 \times 10^{-6}$	90%	1002

$D^*_0(2300)$

$I(J^P) = \frac{1}{2}(0^+)$

was $D^*_0(2400)$

Mass $m = 2343 \pm 10$ MeV (S = 1.5)
Full width $\Gamma = 229 \pm 16$ MeV

$D^*_0(2300)$ DECAY MODES	Fraction (Γ_i/Γ)	p (MeV/c)
$D\pi^\pm$	seen	411

$D_1(2420)$

$I(J^P) = \frac{1}{2}(1^+)$

Mass $m = 2422.1 \pm 0.6$ MeV (S = 1.7)
$m_{D_1(2420)^0} - m_{D^{*+}} = 411.8 \pm 0.6$ MeV (S = 1.7)
$m_{D_1(2420)^\pm} - m_{D_1(2420)^0} = 4 \pm 4$ MeV
Full width $\Gamma = 31.3 \pm 1.9$ MeV (S = 2.8)

$\overline{D}_1(2420)$ modes are charge conjugates of modes below.

$D_1(2420)$ DECAY MODES	Fraction (Γ_i/Γ)	p (MeV/c)
$D^*(2007)^0\pi$	seen	359

$D_1(2430)^0$

$I(J^P) = \frac{1}{2}(1^+)$

Mass $m = 2412 \pm 9$ MeV
Full width $\Gamma = 314 \pm 29$ MeV

$D_1(2430)^0$ DECAY MODES	Fraction (Γ_i/Γ)	p (MeV/c)
$D^*(2010)^+\pi^-$	seen	345

Int. J. Mod. Phys. A 2026.41. Downloaded from www.worldscientific.com
by UNIVERSITY OF CALIFORNIA @ BERKELEY on 09/16/26. Re-use and distribution is strictly not permitted, except for Open Acce

$D_2^*(2460)$

$I(J^P) = \frac{1}{2}(2^+)$

Mass $m = 2461.1 \pm 0.8$ MeV (S = 6.3)
$m_{D_2^*(2460)^0} - m_{D^+} = 591.5 \pm 0.8$ MeV (S = 6.0)
$m_{D_2^*(2460)^0} - m_{D^{*+}} = 450.9 \pm 0.8$ MeV (S = 6.0)
$m_{D_2^*(2460)^\pm} - m_{D_2^*(2460)^0} = 2.4 \pm 1.7$ MeV
Full width $\Gamma = 47.3 \pm 0.8$ MeV (S = 1.5)

$\overline{D}_2^*(2460)$ modes are charge conjugates of modes below.

$D_2^*(2460)$ DECAY MODES	Fraction (Γ_i/Γ)	p (MeV/c)
$D\pi^-$	seen	509
$D^*(2010)\pi^-$	seen	389

$D_3^*(2750)$

$I(J^P) = \frac{1}{2}(3^-)$

Mass $m = 2763.1 \pm 3.2$ MeV (S = 2.1)
Full width $\Gamma = 66 \pm 5$ MeV

$D_3^*(2750)$ DECAY MODES	Fraction (Γ_i/Γ)	p (MeV/c)
$D\pi$	seen	743
$D^+\pi^-$	seen	739
$D^0\pi^\pm$	seen	743
$D^*\pi$	seen	639
$D^{*+}\pi^-$	seen	639

CHARMED, STRANGE MESONS ($C = \pm1$, $S = \pm1$) (including possibly non-$q\overline{q}$ states)

$D_s^+ = c\overline{s}$, $D_s^- = \overline{c}s$, similarly for D_s^*'s

$D_s^\pm$

$I(J^P) = 0(0^-)$

Mass $m = 1968.35 \pm 0.07$ MeV
$m_{D_s^\pm} - m_{D^\pm} = 98.69 \pm 0.05$ MeV
Mean life $\tau = (501.2 \pm 2.2) \times 10^{-15}$ s (S = 1.3)
$c\tau = 150.3\ \mu$m

CP-violating decay-rate asymmetries

$A_{CP}(\mu^\pm\nu) = (-0.2 \pm 2.5)\%$
$A_{CP}(\tau^\pm\nu)$ in $D_s^+ \to \tau^+\nu_\tau$, $D_s^- \to \tau^-\overline{\nu}_\tau = (3 \pm 5)\%$
$A_{CP}(K^\pm K_S^0) = (0.07 \pm 0.24)\%$
$A_{CP}(K^\pm K_L^0)$ in $D_s^\pm \to K^\pm K_L^0 = (-1.1 \pm 2.7) \times 10^{-2}$
$A_{CP}(K^+K^-\pi^\pm) = (0.35 \pm 0.34)\%$
$A_{CP}(\phi\pi^\pm) = (-0.38 \pm 0.27)\%$
$A_{CP}(K^\pm K_S^0\pi^0) = (-0.9 \pm 1.9)\%$
$A_{CP}(2K_S^0\pi^\pm) = (1.3 \pm 1.6)\%$
$A_{CP}(K^+K^-\pi^\pm\pi^0) = (-0.6 \pm 0.9)\%$
$A_{CP}(K^\pm K_S^0\pi^+\pi^-) = (0.7 \pm 2.9)\%$ (S = 1.3)
$A_{CP}(K_S^0K^\mp 2\pi^\pm) = (0.7 \pm 1.8)\%$ (S = 1.3)
$A_{CP}(\pi^+\pi^-\pi^\pm) = (-0.9 \pm 1.1)\%$
$A_{CP}(\pi^\pm\eta) = (0.24 \pm 0.29)\%$
$A_{CP}(\pi^\pm\pi^+\pi^-\eta) = (2.4 \pm 3.0)\%$
$A_{CP}(\pi^\pm\eta') = (-0.08 \pm 0.17)\%$ (S = 1.2)
$A_{CP}(\eta\pi^\pm\pi^0) = (0.9 \pm 1.5)\%$
$A_{CP}(\eta'\pi^\pm\pi^0) = (-1.5 \pm 2.5)\%$
$A_{CP}(K^\pm\pi^0) = (2 \pm 4)\%$ (S = 1.2)
$A_{CP}(\overline{K}^0/K^0\pi^\pm) = (0.4 \pm 0.5)\%$
$A_{CP}(K_S^0\pi^\pm) = (0.20 \pm 0.18)\%$
$A_{CP}(K^\pm\pi^+\pi^-) = (2.2 \pm 1.9)\%$
$A_{CP}(K_S^0\pi^+\pi^0)$ in $D_s^\pm \to K_S^0\pi^\pm\pi^0 = (-2 \pm 5)\%$
$A_{CP}(K^\pm\pi^+\pi^-\pi^0)$ in $D_s^\pm \to K^\pm\pi^+\pi^-\pi^0 = (7 \pm 5) \times 10^{-2}$
$A_{CP}(K^\pm\eta) = (1.8 \pm 1.9)\%$
$A_{CP}(K^\pm\eta'(958)) = (6 \pm 19)\%$

CP violating asymmetries of *P*-odd (*T*-odd) moments

$A_T(K_S^0K^\pm\pi^+\pi^-) = (-8 \pm 6) \times 10^{-3}$ [*jj*]
$A_{Tviol}(K_S^0K^\mp\pi^\pm\pi^\pm)$ in $D_s^\pm \to K_S^0K^\mp\pi^\pm\pi^\pm = (0.2 \pm 2.5) \times 10^{-3}$

$D_s^+ \to \phi\ell^+\nu_\ell$ form factors

$r_2 = 0.83 \pm 0.08$ (S = 1.8)
$r_v = 1.76 \pm 0.07$ (S = 1.1)
$\Gamma_L/\Gamma_T = 0.72 \pm 0.18$
$f_+(0)\,|V_{cs}|$ in $D_s^+ \to \eta e^+\nu_e = 0.449 \pm 0.009$
$f_+(0)\,|V_{cs}|$ in $D_s^+ \to \eta\mu^+\nu_\mu = 0.452 \pm 0.012$
$r_1 \equiv a_1/a_0$ in $D_s^+ \to \eta\mu^+\nu_\mu = -2.9 \pm 0.6$
$\langle A_{FB}^\eta\rangle$ in $D_s^+ \to \eta\mu^+\nu_\mu = (-5.9 \pm 3.1) \times 10^{-2}$
$f_+(0)\,|V_{cs}|$ in $D_s^+ \to \eta' e^+\nu_e = 0.527 \pm 0.024$
$r_1 \equiv a_1/a_0$ in $D_s^+ \to \eta'\mu^+\nu_\mu = -11 \pm 5$
$\langle A_{FB}^{\eta'}\rangle$ in $D_s^+ \to \eta'\mu^+\nu_\mu = (-6 \pm 8) \times 10^{-2}$
$f_+(0)\,|V_{cs}|$ in $D_s^+ \to \eta'\mu^+\nu_\mu = 0.50 \pm 0.04$
$f_+(0)\,|V_{cs}|$ in $D_s^+ \to f_0(980)\,e^+\nu_e = 0.50 \pm 0.04$
$f_+(0)|V_{cd}|$ in $D_s^+ \to K^0 e^+\nu_e = 0.145 \pm 0.010$
$r_v \equiv V(0)/A_1(0)$ in $D_s^+ \to K^*(892)^0 e^+\nu_e = 1.7 \pm 0.4$
$r_2 \equiv A_2(0)/A_1(0)$ in $D_s^+ \to K^*(892)^0 e^+\nu_e = 0.77 \pm 0.29$
$f_{D_s^+}\,|V_{cs}|$ in $D_s^+ \to \mu^+\nu_\mu = 242.7 \pm 3.0$ MeV
$f_{D_s^+}\,|V_{cs}|$ in $D_s^+ \to \tau^+\nu_\tau = 247.5 \pm 2.3$ MeV

Unless otherwise noted, the branching fractions for modes with a resonance in the final state include all the decay modes of the resonance. D_s^- modes are charge conjugates of the modes below.

D_s^+ DECAY MODES		Fraction (Γ_i/Γ)	Scale factor/ Confidence level	p (MeV/c)
Inclusive modes				
e^+ semileptonic	[*ccc*]	(6.33 ± 0.15) %		–
π^+ anything		(119.3 ± 1.4) %		–
π^- anything		(43.2 ± 0.9) %		–
π^0 anything		(123 ± 7) %		–
K^- anything		(18.7 ± 0.5) %		–
K^+ anything		(28.9 ± 0.7) %		–
K_S^0 anything		(19.0 ± 1.1) %		–
η anything	[*ddd*]	(29.9 ± 2.8) %		–
ω anything		(6.1 ± 1.4) %		–
η' anything	[*eee*]	(10.3 ± 1.4) %	S=1.1	–
$f_0(980)$ anything, $f_0 \to \pi^+\pi^-$		< 1.3 %	CL=90%	–
ϕ anything		(15.7 ± 1.0) %		–
K^+K^- anything		(15.8 ± 0.7) %		–
$K_S^0K^+$ anything		(5.8 ± 0.5) %		–
$K_S^0K^-$ anything		(1.9 ± 0.4) %		–
$2K_S^0$ anything		(1.70 ± 0.32) %		–
$2K^+$ anything		$< 2.6 \times 10^{-3}$	CL=90%	–
$2K^-$ anything		$< 6 \times 10^{-4}$	CL=90%	–
$2\pi^+\pi^-$ + anything		(32.8 ± 0.7) %		–
Leptonic and semileptonic modes				
$e^+\nu_e$		$< 8.3 \times 10^{-5}$	CL=90%	984
$\mu^+\nu_\mu$		$(5.37 \pm 0.11) \times 10^{-3}$		981
$\tau^+\nu_\tau$		(5.39 ± 0.09) %		182
$\gamma e^+\nu_e$		$< 1.3 \times 10^{-4}$	CL=90%	984
$K^+K^-e^+\nu_e$		—		851
$K_S^0K_S^0e^+\nu_e$		$< 3.8 \times 10^{-4}$	CL=90%	849
$\phi e^+\nu_e$	[*fff*]	(2.34 ± 0.12) %	S=1.2	720
$K_1(1270)^0 e^+\nu_e$		$< 4.1 \times 10^{-4}$	CL=90%	584
$b_1(1235)^0 e^+\nu_e$, $b_1^0 \to \omega\pi^0$		$< 6.4 \times 10^{-4}$	CL=90%	–
$\phi\mu^+\nu_\mu$		(2.24 ± 0.11) %		715
$\eta e^+\nu_e$	[*fff*]	(2.27 ± 0.06) %		908
$\eta'(958)\,e^+\nu_e$	[*fff*]	$(8.1 \pm 0.4) \times 10^{-3}$		751
$\eta\mu^+\nu_\mu$		(2.24 ± 0.07) %		905
$\eta'(958)\,\mu^+\nu_\mu$		$(8.0 \pm 0.6) \times 10^{-3}$		747
$\omega e^+\nu_e$	[*ggg*]	$< 2.0 \times 10^{-3}$	CL=90%	829
$K^0 e^+\nu_e$		$(2.88 \pm 0.26) \times 10^{-3}$	S=1.2	921
$K^*(892)^0 e^+\nu_e$	[*fff*]	$(2.05 \pm 0.20) \times 10^{-3}$		782
$f_0(500)\,e^+\nu_e$, $f_0 \to \pi^0\pi^0$		$< 7.3 \times 10^{-4}$	CL=90%	–
$f_0(500)\,e^+\nu_e$, $f_0 \to \pi^+\pi^-$		$< 3.3 \times 10^{-4}$	CL=90%	–
$f_0(980)\,e^+\nu_e$, $f_0 \to \pi^0\pi^0$		$(7.9 \pm 1.5) \times 10^{-4}$		–
$f_0(980)\,e^+\nu_e$, $f_0 \to \pi^+\pi^-$		$(1.64 \pm 0.13) \times 10^{-3}$		–
$f_0(980)\,\mu^+\nu_\mu$, $f_0 \to K^+K^-$		$< 5.45 \times 10^{-4}$	CL=90%	–
$a_0(980)^0 e^+\nu_e$, $a_0^0 \to \pi^0\eta$		$< 1.2 \times 10^{-4}$	CL=90%	–
$\pi^0 e^+\nu_e$		$< 6.4 \times 10^{-5}$	CL=90%	980

Int. J. Mod. Phys. A 2026.41. Downloaded from www.worldscientific.com
by UNIVERSITY OF CALIFORNIA @ BERKELEY on 09/16/26. Re-use and distribution is strictly not permitted, except for Open Access articles.

Hadronic modes with a $K\overline{K}$ pair

$K^+ K^0_S$		(1.500 ± 0.014) %		850
$K^+ K^0_L$		(1.49 ± 0.06) %		850
$K^0_S K^0_L \pi^+$		(1.86 ± 0.07) %		802
$\phi(1020)\pi^+$, $\phi \to K^0_L K^0_S$		(1.31 ± 0.06) %		–
$K^0_L K^*(892)^+$, $K^{*+} \to K^0_S \pi^+$		$(3.59 \pm 0.32) \times 10^{-3}$		–
$K^0_S K^*(892)^+$, $K^{*+} \to K^0_L \pi^+$		$(2.68 \pm 0.33) \times 10^{-3}$		–
$\phi(1680)\pi^+$, $\phi \to K^0_L K^0_S$		$(6.1 \pm 2.1) \times 10^{-4}$		–
$K^+ \overline{K}^0$		(2.95 ± 0.14) %		850
$K^+ K^- \pi^+$	[kk]	(5.45 ± 0.08) %	S=1.3	805
$\phi\pi^+$	[fff,hhh]	(4.5 ± 0.4) %		712
$\phi\pi^+$, $\phi \to K^+ K^-$	[hhh]	(2.25 ± 0.05) %		712
$K^+ \overline{K}^*(892)^0$		$(12.7 {}^{+4.0}_{-3.1})$ %		685
$K^+ \overline{K}^*(892)^0$, $\overline{K}^{*0} \to K^- \pi^+$		(2.61 ± 0.05) %		416
$K^+ \overline{K}^*(892)^0$, $\overline{K}^{*0} \to K^0_S \pi^0$		$(4.8 \pm 0.4) \times 10^{-3}$		–
$f_0(980)\pi^+$, $f_0 \to K^+ K^-$		(1.12 ± 0.19) %		732
$f_0(1370)\pi^+$, $f_0 \to K^+ K^-$		$(7.2 \pm 3.0) \times 10^{-4}$		–
$f_0(1710)\pi^+$, $f_0 \to K^+ K^-$		$(6.8 \pm 2.8) \times 10^{-4}$		198
$a_0(980)^+ \pi^0$, $a_0^+ \to K^+ K^0_S$		$(1.1 \pm 0.4) \times 10^{-3}$		–
$a_0(1710)^+ \pi^0$, $a_0^+ \to K^+ K^0_S$		$(3.5 \pm 0.6) \times 10^{-3}$		–
$K^+ \overline{K}^*_0(1430)^0$, $\overline{K}^*_0 \to K^- \pi^+$		$(1.79 \pm 0.26) \times 10^{-3}$		218
$K^+ \overline{K}^*(1410)^0$, $\overline{K}^*_0 \to K^0_S \pi^0$		$(8.8 \pm 2.8) \times 10^{-4}$		–
$K^+ K^0_S \pi^0$		(1.471 ± 0.028) %		805
$K^*(892)^+ K^0_S$, $K^{*+} \to K^+ \pi^0$		$(2.04 \pm 0.32) \times 10^{-3}$		–
$2K^0_S \pi^+$		$(7.32 \pm 0.14) \times 10^{-3}$		802
$f_0(980)\pi^+$, $f_0 \to K^0_S K^0_S$		$< 1.8 \times 10^{-4}$ CL=90%		–
$f_0(1710)\pi^+$, $f_0 \to K^0_S K^0_S$		$(3.39 \pm 0.31) \times 10^{-3}$		–
$K^*(892)^+ K^0_S$, $K^{*+} \to K^0_S \pi^+$		$(3.19 \pm 0.29) \times 10^{-3}$		683
$K^0 \overline{K}^0 \pi^+$		—		802
$K^*(892)^+ \overline{K}^0$	[fff]	(5.4 ± 1.2) %		683
$\phi\rho^+$		(4.9 ± 0.8) %	S=3.0	401
$K^+ K^- \pi^+ \pi^0$		(5.53 ± 0.15) %	S=1.3	748
$\overline{K}_1(1270)^0 K^+$, $\overline{K}_1(1270)^0 \to K^- \rho^+$		$(5.7 \pm 0.6) \times 10^{-3}$		–
$\overline{K}_1(1270)^0 K^+$, $\overline{K}_1(1270)^0 \to K^*(892)\pi$		(1.31 ± 0.25) %		–
$\overline{K}_1(1400)^0 K^+$, $\overline{K}_1(1400)^0 \to K^*(892)\pi$		(2.0 ± 0.4) %		–
$a_0(980)^0 \rho^+$, $a_0^0 \to K^+ K^-$		$(1.9 \pm 0.4) \times 10^{-3}$		–
$f_1(1420)^0 \pi^+$, $f_1(1420)^0 \to K^*(892)^\mp K^\pm$		$(3.9 \pm 0.7) \times 10^{-3}$		–
$f_1(1420)^0 \pi^+$, $f_1^0 \to a_0(980)^0 \pi^0$, $a_0^0 \to K^+ K^-$		$(4.0 \pm 1.4) \times 10^{-4}$		–
$\eta(1475)\pi^+$, $\eta \to a_0(980)^0 \pi^0$, $a_0^0 \to K^+ K^-$		$(7.0 \pm 2.8) \times 10^{-4}$		–
$K^0_S K^- 2\pi^+$		(1.569 ± 0.028) %		744
$K^+ K^- K^0_S \pi^+$		$(1.27 \pm 0.15) \times 10^{-4}$		527
$K^*(892)^+ \overline{K}^*(892)^0$	[fff]	(5.64 ± 0.35) %		416
$\eta(1475) K^0_S$, $\eta \to K^*(892)^0 \pi^+$, $K^{*0} \to K^- \pi^+$		$(3.5 \pm 1.0) \times 10^{-4}$		–
$\eta(1475)\pi^+$, $\eta \to \overline{K}^*(892)^+ K^-$, $\overline{K}^{*+} \to K^0_S \pi^+$		$(3.5 \pm 1.0) \times 10^{-4}$		–
$\eta(1475)\pi^+$, $\eta \to a_0(980)^- \pi^+$, $a_0^- \to K^0_S K^-$		$(1.7 \pm 0.9) \times 10^{-3}$		–
$f_1(1285)\pi^+$, $f_1 \to a_0(980)^- \pi^+$, $a_0^- \to K^0_S K^-$		$(3.5 \pm 0.8) \times 10^{-4}$		–
$K^+ K^0_S \pi^+ \pi^-$		$(9.34 \pm 0.22) \times 10^{-3}$		744
$K^+ K^- 2\pi^+ \pi^-$		$(6.6 \pm 0.6) \times 10^{-3}$		673
$\phi 2\pi^+ \pi^-$	[fff]	(1.21 ± 0.16) %		640
$\phi\rho^0 \pi^+$, $\phi \to K^+ K^-$		$(4.9 \pm 0.7) \times 10^{-3}$		181
$\phi a_1(1260)^+$, $\phi \to K^+ K^-$, $a_1^+ \to \rho^0 \pi^+$		$(7.5 \pm 1.2) \times 10^{-3}$		†
$\phi 2\pi^+ \pi^-$ non-ρ, $\phi \to K^+ K^-$		$(1.4 \pm 0.5) \times 10^{-3}$		–
$K^+ K^- \rho^0 \pi^+$ non-ϕ		$< 2.0 \times 10^{-4}$ CL=90%		249
$K^+ K^- 2\pi^+ \pi^-$ nonresonant		$(1.0 \pm 0.4) \times 10^{-3}$		673
$2K^0_S 2\pi^+ \pi^-$		$(8.0 \pm 3.3) \times 10^{-4}$		669

Hadronic modes without K's

$\pi^+ \pi^0$		$< 1.2 \times 10^{-4}$ CL=90%		975
$2\pi^+ \pi^-$		(1.090 ± 0.014) %		959
$\rho^0 \pi^+$		$(1.14 \pm 0.16) \times 10^{-4}$		825
$\omega\pi^+$, $\omega \to \pi^+ \pi^-$		$(3.9 \pm 0.4) \times 10^{-5}$		–
$\pi^+ (\pi^+ \pi^-)_{S-\text{wave}}$	[iii]	$(9.23 \pm 0.13) \times 10^{-3}$		959
$f_2(1270)\pi^+$, $f_2 \to \pi^+ \pi^-$		$(1.42 \pm 0.10) \times 10^{-3}$		559
$f'_2(1525)^0 \pi^+$, $f'_2 \to \pi^+ \pi^-$		$(5.8 \pm 2.0) \times 10^{-6}$		–
$\rho(1450)^0 \pi^+$, $\rho^0 \to \pi^+ \pi^-$		$(1.8 \pm 0.6) \times 10^{-4}$		421
$\rho(1700)^0 \pi^+$, $\rho^0 \to \pi^+ \pi^-$		$(4 \pm 4) \times 10^{-5}$		–
$\pi^+ 2\pi^0$		$(5.2 \pm 0.5) \times 10^{-3}$	S=1.1	961
$f_0(980)\pi^+$, $f_0 \to \pi^0 \pi^0$		$(2.9 \pm 0.6) \times 10^{-3}$		–
$f_0(1370)\pi^+$, $f_0 \to \pi^0 \pi^0$		$(1.3 \pm 0.6) \times 10^{-3}$		–
$f_2(1270)\pi^+$, $f_2 \to \pi^0 \pi^0$		$(5.0 \pm 3.5) \times 10^{-4}$		–
$2\pi^+ \pi^- \pi^0$		—		935
$\omega\pi^+$	[fff]	$(1.93 \pm 0.30) \times 10^{-3}$		822
$\eta\pi^+$	[fff]	(1.686 ± 0.027) %		902
$(2\pi^+ \pi^- \pi^0)_{\text{non}-\eta}$		(2.04 ± 0.09) %		–
$f_0(1370)\rho^+$, $f_0 \rho^+ \to 2\pi^+ \pi^- \pi^0$		$(5.1 \pm 0.9) \times 10^{-3}$		–
$f_0(980)^0 \rho^+$, $f_0^0 \rho^+ \to 2\pi^+ \pi^- \pi^0$		$(2.6 \pm 0.5) \times 10^{-3}$		–
$f_2(1270)^0 \rho^+$, $f_2(1270)^0 \rho^+ \to 2\pi^+ \pi^- \pi^0$		$(1.9 \pm 0.4) \times 10^{-3}$		–
$(\rho^+ \rho^0)_{S-wave} \to 2\pi^+ \pi^- \pi^0$		$(7.1 \pm 2.8) \times 10^{-4}$		–
$(\rho(1450)^+ \rho^0)_{S-wave} \to 2\pi^+ \pi^- \pi^0$		$(9.4 \pm 3.1) \times 10^{-4}$		–
$(\rho^+ \rho(1450)^0)_{P-wave} \to 2\pi^+ \pi^- \pi^0$		$(1.75 \pm 0.29) \times 10^{-3}$		–
$\phi\pi^+$, $\phi \to \rho\pi$		$(5.08 \pm 0.35) \times 10^{-3}$		–
$\omega\pi^+$, $\omega \to \rho\pi$		$(1.41 \pm 0.19) \times 10^{-3}$		–
$a_1(1260)^+ \pi^0$, $a_1^+ \to (\rho^0 \pi^+)_{S-wave}$		$(2.6 \pm 0.4) \times 10^{-3}$		–
$a_1(1260)^0 \pi^+$, $a_1^0 \to (\rho\pi)_{S-wave}$		$(1.3 \pm 0.5) \times 10^{-3}$		–
$\pi(1300)^0 \pi^+$, $\pi^0 \to (\rho\pi)_{P-wave}$		$(2.4 \pm 0.7) \times 10^{-3}$		–
$3\pi^+ 2\pi^-$		$(8.0 \pm 0.8) \times 10^{-3}$		899
$2\pi^+ \pi^- 2\pi^0$		(4.41 ± 0.20) %		902
$\omega\rho^+$, $\omega \to \pi^+ \pi^- \pi^0$		$(8.8 \pm 0.9) \times 10^{-3}$		602
$\phi\rho^+$, $\phi \to \pi^+ \pi^- \pi^0$		$(6.1 \pm 0.6) \times 10^{-3}$		–
$\rho(1450)^+ \pi^0$, $\rho(1450)^+ \to \omega\pi^+$, $\omega \to \pi^+ \pi^- \pi^0$		$(3.5 \pm 0.5) \times 10^{-3}$		–
$a_1(1260)^0 \rho^+$, $a_1(1260)^0 \to \rho^+ \pi^-$		$(5.0 \pm 0.4) \times 10^{-3}$		–
$a_1(1260)^0 \rho^+$, $a_1(1260)^0 \to \rho^- \pi^+$		$(3.26 \pm 0.27) \times 10^{-3}$		–
$a_1(1260)^+ \rho^0$, $a_1(1260)^+ \to \rho^+ \pi^0$		$(7.3 \pm 1.0) \times 10^{-3}$		–
$b_1(1235)^+ \pi^0$, $b_1(1235)^+ \to \omega\pi^+$, $\omega \to \pi^+ \pi^- \pi^0$		$(4.8 \pm 0.6) \times 10^{-3}$		–
$b_1(1235)^0 \pi^+$, $b_1(1235)^0 \to \omega\pi^0$, $\omega \to \pi^+ \pi^- \pi^0$		$(6.4 \pm 0.6) \times 10^{-3}$		–
$\eta\rho^+$	[fff]	(8.9 ± 0.8) %		724
$\eta\pi^+ \pi^0$		(9.10 ± 0.17) %		885
$\eta(\pi^+ \pi^0)_{P-wave}$		$(4.9 \pm 3.0) \times 10^{-3}$		885
$a_0(980)^{+0} \pi^{0+}$, $a_0(980)^{+0} \to \eta\pi^{+0}$		(2.1 ± 0.4) %		–
$\omega\pi^+ \pi^0$	[fff]	(2.8 ± 0.7) %		802
$2\pi^+ \pi^- \eta$		(3.08 ± 0.08) %		855
$a_1(1260)^+ \eta$, $a_1^+ \to \rho(770)^0 \pi^+$, $\rho^0 \to \pi^+ \pi^-$		(1.71 ± 0.14) %		–
$a_1(1260)^+ \eta$, $a_1^+ \to f_0(500)\pi^+$, $f_0 \to \pi^+ \pi^-$		$(2.5 \pm 0.9) \times 10^{-3}$		–
$a_0(980)^+ \rho(770)^0$, $a_0^+ \to \eta\pi^+$		$(2.1 \pm 0.9) \times 10^{-3}$		–

Int. J. Mod. Phys. A 2026.41. Downloaded from www.worldscientific.com
by UNIVERSITY OF CALIFORNIA @ BERKELEY on 09/16/26. Re-use and distribution is strictly not permitted, except for Open Acce

$\eta(1405)\pi^+$, $\eta \to a_0(980)^-\pi^+$, $a_0^- \to \eta\pi^-$		$(2.2 \pm 0.7) \times 10^{-4}$		–
$\eta(1405)\pi^+$, $\eta \to a_0(980)^+\pi^-$, $a_0^+ \to \eta\pi^+$		$(2.2 \pm 0.7) \times 10^{-4}$		–
$f_1(1420)\pi^+$, $f_1 \to a_0(980)^-\pi^+$, $a_0^- \to \eta\pi^-$		$(5.9 \pm 1.8) \times 10^{-4}$		–
$f_1(1420)\pi^+$, $f_1 \to a_0(980)^+\pi^-$, $a_0^+ \to \eta\pi^+$		$(5.2 \pm 1.8) \times 10^{-4}$		–
$3\pi^+ 2\pi^- \pi^0$		(4.9 ± 3.2) %		856
$\omega 2\pi^+\pi^-$	[fff]	(1.6 ± 0.5) %		766
$\eta'(958)\pi^+$	[eee, fff]	(3.95 ± 0.08) %		743
$3\pi^+ 2\pi^- 2\pi^0$		—		803
$\omega\eta\pi^+$	[fff]	$(5.4 \pm 1.3) \times 10^{-3}$		654
$\eta'(958)\rho^+$	[eee, fff]	(5.8 ± 1.5) %		465
$\eta'(958)\pi^+\pi^0$		(6.14 ± 0.18) %		720
$\eta'(958)\pi^+\pi^0$ nonresonant		< 5.1 %	CL=90%	720

Modes with one or three K's

$K^+\pi^0$		$(7.5 \pm 0.5) \times 10^{-4}$		917
$K^0_S\pi^+$		$(1.22 \pm 0.04) \times 10^{-3}$		916
$K^+\eta$	[fff]	$(1.76 \pm 0.08) \times 10^{-3}$		835
$K^+\omega$	[fff]	$(9.9 \pm 1.5) \times 10^{-4}$		741
$K^+\eta'(958)$	[fff]	$(2.68 \pm 0.24) \times 10^{-3}$		646
$K^+\pi^+\pi^-$		$(6.23 \pm 0.10) \times 10^{-3}$		900
$K^+\rho^0$		$(2.18 \pm 0.25) \times 10^{-3}$		745
$K^+\rho(1450)^0$, $\rho^0 \to \pi^+\pi^-$		$(7.3 \pm 1.7) \times 10^{-4}$		–
$K^+ f_0(500)$, $f_0 \to \pi^+\pi^-$		$(4.5 \pm 3.0) \times 10^{-4}$		–
$K^+ f_0(980)$, $f_0 \to \pi^+\pi^-$		$(2.8 \pm 1.1) \times 10^{-4}$		–
$K^+ f_0(1370)$, $f_0 \to \pi^+\pi^-$		$(1.2 \pm 0.6) \times 10^{-3}$		–
$K^*(892)^0\pi^+$, $K^{*0} \to K^+\pi^-$		$(1.68 \pm 0.26) \times 10^{-3}$		775
$K^*(1410)^0\pi^+$, $K^{*0} \to K^+\pi^-$		$(6 \pm 4) \times 10^{-4}$		–
$K^*(1430)^0\pi^+$, $K^{*0} \to K^+\pi^-$		$(9.4 \pm 3.2) \times 10^{-4}$		–
$K^+\pi^+\pi^-$ nonresonant		$(9.9 \pm 3.2) \times 10^{-4}$		900
$K^0_S\pi^+\pi^0$		$(5.09 \pm 0.22) \times 10^{-3}$		899
$K^0_S\rho(770)^+$, $\rho^+ \to \pi^+\pi^0$		$(2.6 \pm 0.4) \times 10^{-3}$		–
$K^0_S\rho(1450)^+$, $\rho^+ \to \pi^+\pi^0$		$(1.04 \pm 0.32) \times 10^{-3}$		–
$K^*(892)^0\pi^+$, $K^{*0} \to K^0_S\pi^0$		$(4.3 \pm 1.2) \times 10^{-4}$		–
$K^*(892)^+\pi^0$, $K^{*+} \to K^0_S\pi^+$		$(2.3 \pm 0.7) \times 10^{-4}$		–
$K^*(1410)^0\pi^+$, $K^{*0} \to K^0_S\pi^0$		$(1.7 \pm 0.9) \times 10^{-4}$		–
$K^0_S 2\pi^+\pi^-$		$(2.8 \pm 1.0) \times 10^{-3}$		870
$K^+\pi^+\pi^-\pi^0$		$(9.7 \pm 0.6) \times 10^{-3}$		873
$K^*(892)^0\rho^+$, $K^{*0} \to K^+\pi^-$		$(3.9 \pm 0.4) \times 10^{-3}$		–
$K^*(892)^+\rho^0$, $K^{*+} \to K^+\pi^0$		$(4.2 \pm 1.2) \times 10^{-4}$		–
$K_1(1270)^0\pi^+$, $K_1^0 \to K^+\rho^-$		$(3.9 \pm 1.3) \times 10^{-4}$		†
$K_1(1400)^0\pi^+$, $K_1^0 \to K^*(890)^+\pi^-$, $K^{*+} \to K^+\pi^0$		$(5.4 \pm 0.9) \times 10^{-4}$		–
$K_1(1400)^0\pi^+$, $K_1^0 \to K^*(890)^0\pi^0$, $K^{*0} \to K^+\pi^-$		$(5.9 \pm 1.0) \times 10^{-4}$		–
$K^+ a_1(1260)^0$, $a_1 \to \rho^+\pi^-$		$(1.8 \pm 1.1) \times 10^{-4}$		–
$K^+ a_1(1260)^0$, $a_1 \to \rho^-\pi^+$		$(1.8 \pm 1.1) \times 10^{-4}$		–
$K^+\pi^+\pi^-\pi^0$ nonresonant		$(9.2 \pm 2.4) \times 10^{-4}$		873
$(K^+\pi^0)_{P-wave}\rho^0$		$(1.01 \pm 0.21) \times 10^{-3}$		688
$K^+\omega\pi^0$	[fff]	$< 8.2 \times 10^{-3}$	CL=90%	684
$K^+\omega\pi^+\pi^-$	[fff]	$< 5.4 \times 10^{-3}$	CL=90%	603
$K^+\omega\eta$	[fff]	$< 7.9 \times 10^{-3}$	CL=90%	366
$2K^+K^-$		$(2.18 \pm 0.20) \times 10^{-4}$		628
ϕK^+, $\phi \to K^+K^-$		$(8.9 \pm 2.0) \times 10^{-5}$		–

Radiative decays

$\rho(770)^+\gamma$		$< 6.1 \times 10^{-4}$	CL=90%	–

Doubly Cabibbo-suppressed modes

$2K^+\pi^-$		$(1.293 \pm 0.027) \times 10^{-4}$	S=1.1	805
$K^+K^*(892)^0$, $K^{*0} \to K^+\pi^-$		$(6.1 \pm 3.4) \times 10^{-5}$		–
$2K^+\pi^-\pi^0$		$< 1.7 \times 10^{-4}$	CL=90%	748

Baryon-antibaryon mode

$p\overline{n}$		$(1.22 \pm 0.11) \times 10^{-3}$		295
$p\overline{p}e^+\nu_e$		$< 2.0 \times 10^{-4}$	CL=90%	296

$\Delta C = 1$ weak neutral current ($C1$) modes, Lepton family number (LF), or Lepton number (L) violating modes

$\pi^+e^+e^-$	[qq]	$< 5.5 \times 10^{-6}$	CL=90%	979
$\pi^+\phi$, $\phi \to e^+e^-$	[pp]	$(1.17 \pm 0.22) \times 10^{-5}$		–
$\pi^+\pi^0e^+e^-$		$< 7.0 \times 10^{-5}$	CL=90%	974
$\rho^+\phi$, $\phi \to e^+e^-$		$(2.4 \pm 0.7) \times 10^{-5}$		–
$\pi^+\mu^+\mu^-$	[qq]	$< 1.8 \times 10^{-7}$	CL=90%	968
$K^+e^+e^-$	$C1$	$< 3.7 \times 10^{-6}$	CL=90%	922
$K^+\pi^0e^+e^-$		$< 7.1 \times 10^{-5}$	CL=90%	917
$K^0_S\pi^+e^+e^-$		$< 8.1 \times 10^{-5}$	CL=90%	916
$K^+\mu^+\mu^-$	$C1$	$< 1.4 \times 10^{-7}$	CL=90%	909
$K^*(892)^+\mu^+\mu^-$	$C1$	$< 1.4 \times 10^{-3}$	CL=90%	765
$\pi^+e^+\mu^-$	LF	$< 1.1 \times 10^{-6}$	CL=90%	976
$\pi^+e^-\mu^+$	LF	$< 9.4 \times 10^{-7}$	CL=90%	976
$K^+e^+\mu^-$	LF	$< 7.9 \times 10^{-7}$	CL=90%	919
$K^+e^-\mu^+$	LF	$< 5.6 \times 10^{-7}$	CL=90%	919
π^-2e^+	L	$< 1.4 \times 10^{-6}$	CL=90%	979
$\pi^-2\mu^+$	L	$< 8.6 \times 10^{-8}$	CL=90%	968
$\pi^-e^+\mu^+$	L	$< 6.3 \times 10^{-7}$	CL=90%	976
K^-2e^+	L	$< 7.7 \times 10^{-7}$	CL=90%	922
$\pi^-\pi^0e^+e^+$		$< 2.9 \times 10^{-5}$	CL=90%	974
$K^-\pi^0e^+e^+$		$< 3.4 \times 10^{-5}$	CL=90%	917
$K^0_S\pi^-e^+e^+$		$< 1.3 \times 10^{-5}$	CL=90%	916
$K^0_S K^-e^+e^+$		$< 2.9 \times 10^{-5}$	CL=90%	850
$\phi\pi^-e^+e^+$		$< 6.9 \times 10^{-5}$	CL=90%	711
$\phi K^-e^+e^+$		$< 9.9 \times 10^{-5}$	CL=90%	606
$K^-2\mu^+$	L	$< 2.6 \times 10^{-8}$	CL=90%	909
$K^-e^+\mu^+$	L	$< 2.6 \times 10^{-7}$	CL=90%	919
$K^*(892)^-2\mu^+$	L	$< 1.4 \times 10^{-3}$	CL=90%	765

$D_s^{*\pm}$

$I(J^P) = 0(1^-)$

Mass $m = 2112.2 \pm 0.4$ MeV
$m_{D_s^{*\pm}} - m_{D_s^\pm} = 143.8 \pm 0.4$ MeV
Full width $\Gamma < 1.9$ MeV, CL = 90%

D_s^{*-} modes are charge conjugates of the modes below.

D_s^{*+} DECAY MODES	Fraction (Γ_i/Γ)	p (MeV/c)
$D_s^+\gamma$	(93.6 ± 0.4) %	139
$D_s^+\pi^0$	(5.77 ± 0.35) %	48
$D_s^+e^+e^-$	$(6.7 \pm 1.6) \times 10^{-3}$	139
$e^+\nu_e$	$(2.1 {}^{+1.2}_{-0.9}) \times 10^{-5}$	1056

$D_{s0}^*(2317)^\pm$

$I(J^P) = 0(0^+)$
J, P need confirmation.
J^P is natural, low mass consistent with 0^+.

See the review on "Heavy Non-$q\overline{q}$ Mesons."
Mass $m = 2317.8 \pm 0.5$ MeV
$m_{D_{s0}^*(2317)^\pm} - m_{D_s^\pm} = 349.4 \pm 0.5$ MeV
Full width $\Gamma < 3.8$ MeV, CL = 95%

$D_{s0}^*(2317)^-$ modes are charge conjugates of modes below.

$D_{s0}^*(2317)^\pm$ DECAY MODES	Fraction (Γ_i/Γ)	Confidence level	p (MeV/c)
$D_s^+\pi^0$	$(100 {}^{+0}_{-20})$ %		298
$D_s^+\gamma$	< 5 %	90%	323
$D_s^*(2112)^+\gamma$	< 6 %	90%	–
$D_s^+\gamma\gamma$	< 18 %	95%	323
$D_s^*(2112)^+\pi^0$	< 11 %	90%	–
$D_s^+\pi^+\pi^-$	$< 4 \times 10^{-3}$	90%	194
$D_s^+\pi^0\pi^0$	not seen		205

Int. J. Mod. Phys. A 2026.41. Downloaded from www.worldscientific.com
by UNIVERSITY OF CALIFORNIA @ BERKELEY on 09/16/26. Re-use and distribution is strictly not permitted, except for Open Access articles.

$D_{s1}(2460)^{\pm}$

$I(J^P) = 0(1^+)$

See the review on "Heavy Non-$q\overline{q}$ Mesons."

Mass $m = 2459.5 \pm 0.6$ MeV (S = 1.1)
$m_{D_{s1}(2460)^{\pm}} - m_{D_s^{*\pm}} = 347.3 \pm 0.7$ MeV (S = 1.2)
$m_{D_{s1}(2460)^{\pm}} - m_{D_s^{\pm}} = 491.1 \pm 0.6$ MeV (S = 1.1)
Full width $\Gamma < 3.5$ MeV, CL = 95%

$D_{s1}(2460)^-$ modes are charge conjugates of the modes below.

$D_{s1}(2460)^+$ DECAY MODES	Fraction (Γ_i/Γ)	Scale factor/ Confidence level	p (MeV/c)
$D_s^{*+}\pi^0$	(48 ±11) %		297
$D_s^+\gamma$	(18 ± 4) %		442
$D_s^+\pi^+\pi^-$	(4.3± 1.3) %	S=1.1	363
$D_s^{*+}\gamma$	< 8 %	CL=90%	323
$D_{s0}^*(2317)^+\gamma$	$(3.7^{+5.0}_{-2.4})$ %		138

$D_{s1}(2536)^{\pm}$

$I(J^P) = 0(1^+)$
J, P need confirmation.

Mass $m = 2535.12 \pm 0.06$ MeV
$m_{D_{s1}(2536)^{\pm}} - m_{D_s^*(2111)} = 422.9 \pm 0.4$ MeV
$m_{D_{s1}(2536)^{\pm}} - m_{D^*(2010)^{\pm}} = 524.85 \pm 0.04$ MeV
$m_{D_{s1}(2536)^{\pm}} - m_{D^*(2007)^0} = 528.26 \pm 0.05$ MeV (S = 1.1)
Full width $\Gamma = 0.92 \pm 0.05$ MeV

Branching fractions are given relative to the one **DEFINED AS 1**.
$D_{s1}(2536)^-$ modes are charge conjugates of the modes below.

$D_{s1}(2536)^+$ DECAY MODES	Fraction (Γ_i/Γ)	Confidence level	p (MeV/c)
$D^*(2010)^+K^0$	(31 ±7) %		149
$(D^*(2010)^+K^0)_{S-wave}$	(22 ±5) %		149
$K_S^0 D^*(2010)^+$	(17 ±4) %		149
$D^+\pi^-K^+$	$(10.0\pm2.5)\times10^{-3}$		176
$D^*(2007)^0K^+$	(36 ±6) %		167
D^+K^0	< 12 %	90%	381
D^0K^+	< 4 %	90%	391
$D_s^{*+}\gamma$	possibly seen		388
$D_s^+\pi^+\pi^-$	seen		437

$D_{s2}^*(2573)$

$I(J^P) = 0(2^+)$

Mass $m = 2569.1 \pm 0.8$ MeV (S = 2.4)
$m_{D_{s2}^*(2573)} - m_{D^0} = 704 \pm 3.2$ MeV
Full width $\Gamma = 16.9 \pm 0.7$ MeV

$D_{s2}^*(2573)^-$ modes are charge conjugates of the modes below.

$D_{s2}^*(2573)^+$ DECAY MODES	Fraction (Γ_i/Γ)	p (MeV/c)
D^0K^+	(37±6) %	431
$D^*(2007)^0K^+$	not seen	238
$D^+K_S^0$	seen	422
$D^{*+}K_S^0$	seen	225

$D_{s1}^*(2700)^{\pm}$

$I(J^P) = 0(1^-)$

Mass $m = 2714 \pm 5$ MeV (S = 1.5)
Full width $\Gamma = 122 \pm 10$ MeV

$D_{s1}^*(2700)^{\pm}$ DECAY MODES	Fraction (Γ_i/Γ)	p (MeV/c)
D^0K^+	seen	579
$D^+K_S^0$	seen	573
$D^{*0}K^+$	seen	438
$D^{*+}K_S^0$	seen	431

$D_{s3}^*(2860)^{\pm}$

$I(J^P) = 0(3^-)$

Mass $m = 2860 \pm 7$ MeV
Full width $\Gamma = 53 \pm 10$ MeV

$D_{s3}^*(2860)^{\pm}$ DECAY MODES	Fraction (Γ_i/Γ)	p (MeV/c)
D^0K^+	seen	710
$D^+K_S^0$	seen	704
$D^{*0}K^+$	seen	589
$D^{*+}K_S^0$	seen	584

BOTTOM MESONS
($B = \pm1$)

$B^+ = u\overline{b}$, $B^0 = d\overline{b}$, $\overline{B}^0 = \overline{d}b$, $B^- = \overline{u}b$, similarly for B^*'s

B-particle organization

Many measurements of B decays involve admixtures of B hadrons. Previously we arbitrarily included such admixtures in the $B^{\pm}$ section, but because of their importance we have created two new sections: "$B^{\pm}/B^0$ Admixture" for $\Upsilon(4S)$ results and "$B^{\pm}/B^0/B_s^0/b$-baryon Admixture" for results at higher energies. Most inclusive decay branching fractions and χ_b at high energy are found in the Admixture sections. B^0-$\overline{B}^0$ mixing data are found in the B^0 section, while B_s^0-$\overline{B}_s^0$ mixing data and B-$\overline{B}$ mixing data for a B^0/B_s^0 admixture are found in the B_s^0 section. CP-violation data are found in the $B^{\pm}$, B^0, and $B^{\pm}$ B^0 Admixture sections. b-baryons are found near the end of the Baryon section.

The organization of the B sections is now as follows, where bullets indicate particle sections and brackets indicate reviews.

- $B^{\pm}$
  mass, mean life, CP violation, branching fractions
- B^0
  mass, mean life, B^0-$\overline{B}^0$ mixing, CP violation, branching fractions
- $B^{\pm}/B^0$ Admixtures
  CP violation, branching fractions
- $B^{\pm}/B^0/B_s^0/b$-baryon Admixtures
  mean life, production fractions, branching fractions
- B^*, $B_1(5721)$, $B_2^*(5747)$, $B_J(5970)$
  mass, width
- B_s^0
  mass, mean life, B_s^0-$\overline{B}_s^0$ mixing, CP violation, branching fractions
- B_s^*, $B_{s1}(5830)^0$, $B_{s2}^*(5840)^0$
  mass, width
- $B_c^{\pm}$
  mass, mean life, branching fractions
- $B_c(2S)^{\pm}$
  mass

At the end of Baryon Listings:

- Λ_b
  mass, mean life, branching fractions
- $\Lambda_b(5912)^0$, $\Lambda_b(5920)^0$, $\Lambda_b(6070)^0$, $\Lambda_b(6146)^0$, $\Lambda_b(6152)^0$
  mass, width
- Σ_b
  mass
- Σ_b^*, $\Sigma_b(6097)^+$, $\Sigma_b(6097)^-$
  mass, width
- Ξ_b^0, Ξ_b^-
  mass, mean life, branching fractions
- $\Xi_b'(5935)^-$, $\Xi_b(5945)^0$, $\Xi_b(5955)^-$, $\Xi_b(6100)^-$, $\Xi_b(6227)^-$, $\Xi_b(6227)^0$, $\Xi_b(6327)^0$, $\Xi_b(6333)^0$

mass, width

- Ω_b^-
  mass, mean life, branching fractions
- $\Omega_b(6316)^-$, $\Omega_b(6330)^-$, $\Omega_b(6340)^-$, $\Omega_b(6350)^-$
  mass
- b-baryon Admixture
  mean life, branching fractions

$B^\pm$ $\quad I(J^P) = \frac{1}{2}(0^-)$

I, J, P need confirmation. Quantum numbers shown are quark-model predictions.

Mass $m_{B^\pm} = 5279.41 \pm 0.07$ MeV
Mean life $\tau_{B^\pm} = (1.637 \pm 0.004) \times 10^{-12}$ s
$c\tau = 490.8\ \mu$m

CP violation

$A_{CP}(B^+ \to J/\psi(1S)K^+) = (1.8 \pm 3.0) \times 10^{-3}$ (S = 1.5)
$A_{CP}(B^+ \to J/\psi(1S)\pi^+) = (1.5 \pm 0.5) \times 10^{-2}$
$A_{CP}(B^+ \to J/\psi\rho^+) = -0.05 \pm 0.05$
$A_{CP}(B^+ \to J/\psi K^*(892)^+) = -0.048 \pm 0.033$
$A_{CP}(B^+ \to \eta_c K^+) = -0.05 \pm 0.05$ (S = 1.5)
$A_{CP}(B^+ \to \psi(2S)\pi^+) = 0.03 \pm 0.06$
$A_{CP}(B^+ \to \psi(2S)K^+) = 0.004 \pm 0.020$ (S = 1.5)
$A_{CP}(B^+ \to \psi(2S)K^*(892)^+) = 0.08 \pm 0.21$
$A_{CP}(B^+ \to \chi_{c1}(1P)\pi^+) = 0.07 \pm 0.18$
$A_{CP}(B^+ \to \chi_{c0}K^+) = -0.20 \pm 0.18$ (S = 1.5)
$A_{CP}(B^+ \to \chi_{c1}K^+) = -0.009 \pm 0.033$
$A_{CP}(B^+ \to \chi_{c1}K^*(892)^+) = 0.5 \pm 0.5$
$A_{CP}(B^+ \to D^0\ell^+\nu_\ell) = (-0.14 \pm 0.20) \times 10^{-2}$
$A_{CP}(B^+ \to \overline{D}^0\pi^+) = (-3.2 \pm 3.5) \times 10^{-3}$
$A_{CP}(B^+ \to D_{CP(+1)}\pi^+) = -0.0088 \pm 0.0024$
$A_{CP}(B^+ \to D_{CP(-1)}\pi^+) = -0.003 \pm 0.012$
$A_{CP}([K^\mp\pi^\pm\pi^+\pi^-]_D\pi^+) = 0.070 \pm 0.020$
$A_{CP}(B^+ \to [\pi^+\pi^+\pi^-\pi^-]_D K^+) = 0.061 \pm 0.013$
$A_{CP}(B^+ \to [\pi^+\pi^-\pi^+\pi^-]_D K^*(892)^+) = 0.02 \pm 0.11$
$A_{CP}(B^+ \to [K^+K^-\pi^+\pi^-]_D K^+) = 0.095 \pm 0.023$
$A_{CP}(B^+ \to [K^+K^-\pi^+\pi^-]_D\pi^+) = -0.009 \pm 0.006$
$A_{CP}(B^+ \to \overline{D}^0K^+) = -0.018 \pm 0.004$
$A_{CP}([K^\mp\pi^\pm\pi^+\pi^-]_D K^+) = -0.32 \pm 0.04$
$A_{CP}(B^+ \to [\pi^+\pi^+\pi^-\pi^-]_D\pi^+) = (-8.2 \pm 3.2) \times 10^{-3}$
$A_{CP}(B^+ \to [K^-\pi^+]_D K^+) = -0.58 \pm 0.21$
$A_{CP}(B^+ \to [K^-\pi^+\pi^0]_D K^+) = -0.27 \pm 0.27$ (S = 2.4)
$A_{CP}(B^+ \to [K^+\pi^-\pi^0]_D K^+) = -0.024 \pm 0.013$
$A_{CP}(B^+ \to [K^+K^-\pi^0]_D K^+) = 0.07 \pm 0.07$
$A_{CP}(B^+ \to [\pi^+\pi^-\pi^0]_D K^+) = 0.11 \pm 0.04$
$A_{CP}(B^+ \to \overline{D}^0K^*(892)^+) = -0.007 \pm 0.019$
$A_{CP}(B^+ \to [K^-\pi^+]_{\overline{D}}K^*(892)^+) = -0.75 \pm 0.16$
$A_{CP}(B^+ \to [K^-\pi^+\pi^-\pi^+]_{\overline{D}}K^*(892)^+) = -0.45 \pm 0.25$
$A_{CP}(B^+ \to [K^-\pi^+]_D\pi^+) = 0.00 \pm 0.09$
$A_{CP}(B^+ \to [K^-\pi^+\pi^0]_D\pi^+) = 0.08 \pm 0.09$
$A_{CP}(B^+ \to [K^+K^-\pi^0]_D\pi^+) = -0.001 \pm 0.019$
$A_{CP}(B^+ \to [\pi^+\pi^-\pi^0]_D\pi^+) = 0.001 \pm 0.010$
$A_{CP}(B^+ \to [K^-\pi^+]_{(D\pi)}\pi^+) = -0.09 \pm 0.27$
$A_{CP}(B^+ \to [K^-\pi^+]_{(D\gamma)}\pi^+) = -0.7 \pm 0.6$
$A_{CP}(B^+ \to [K^-\pi^+]_{(D\pi)}K^+) = 0.8 \pm 0.4$
$A_{CP}(B^+ \to [K^-\pi^+]_{(D\gamma)}K^+) = 0.4 \pm 1.0$
$A_{CP}(B^+ \to [\pi^+\pi^-\pi^0]_D K^+) = -0.02 \pm 0.15$
$A_{CP}(B^+ \to [K^0_S K^+\pi^-]_D K^+) = 0.00 \pm 0.09$ (S = 1.4)
$A_{CP}(B^+ \to [K^0_S K^-\pi^+]_D K^+) = 0.00 \pm 0.07$
$A_{CP}(B^+ \to [K^0_S K^-\pi^+]_D\pi^+) = -0.003 \pm 0.014$
$A_{CP}(B^+ \to [K^0_S K^+\pi^-]_D\pi^+) = -0.016 \pm 0.025$ (S = 1.5)
$A_{CP}(B^+ \to [K^*(892)^-K^+]_D K^+) = 0.08 \pm 0.05$
$A_{CP}(B^+ \to [K^*(892)^+K^-]_D K^+) = 0.07 \pm 0.09$
$A_{CP}(B^+ \to [K^*(892)^+K^-]_D\pi^+) = 0.007 \pm 0.016$
$A_{CP}(B^+ \to [K^*(892)^-K^+]_D\pi^+) = -0.013 \pm 0.020$ (S = 1.9)
$\boldsymbol{A_{CP}(B^+ \to D_{CP(+1)}K^+)} = 0.132 \pm 0.015$ (S = 1.8)
$A_{ADS}(B^+ \to DK^+) = -0.451 \pm 0.026$
$A_{ADS}(B^+ \to D\pi^+) = 0.129 \pm 0.014$
$A_{ADS}(B^+ \to [D\gamma]_{D^*}K^+) = -0.6 \pm 1.3$
$A_{ADS}(B^+ \to [D\pi^0]_{D^*}K^+) = 0.72 \pm 0.29$
$A_{ADS}(B^+ \to [D\gamma]_{D^*}\pi^+) = 0.08 \pm 0.13$
$A_{ADS}(B^+ \to [D\pi^0]_{D^*}\pi^+) = -0.14 \pm 0.06$
$A_{ADS}(B^+ \to [K^-\pi^+]_D K^+\pi^-\pi^+) = -0.33 \pm 0.35$
$A_{ADS}(B^+ \to [K^-\pi^+]_D\pi^+\pi^-\pi^+) = -0.01 \pm 0.09$
$A_{CP}(B^+ \to D_{CP(-1)}K^+) = -0.14 \pm 0.05$
$A_{CP}(B^+ \to [K^+K^-]_D K^+\pi^-\pi^+) = -0.04 \pm 0.06$
$A_{CP}(B^+ \to [\pi^+\pi^-]_D K^+\pi^-\pi^+) = -0.05 \pm 0.10$
$A_{CP}(B^+ \to [K^-\pi^+]_D K^+\pi^-\pi^+) = 0.013 \pm 0.023$
$A_{CP}(B^+ \to [K^+K^-]_D\pi^+\pi^-\pi^+) = -0.019 \pm 0.015$
$A_{CP}(B^+ \to [\pi^+\pi^-]_D\pi^+\pi^-\pi^+) = -0.013 \pm 0.019$
$A_{CP}(B^+ \to [K^-\pi^+]_D\pi^+\pi^-\pi^+) = -0.002 \pm 0.011$
$A_{CP}(B^+ \to [\overline{D}^0\gamma]_{\overline{D}^*}\pi^+) = -0.004 \pm 0.004$
$A_{CP}(B^+ \to [\overline{D}^0\pi^0]_{\overline{D}^*}\pi^+) = 0.0007 \pm 0.0022$
$A_{CP}(B^+ \to [\overline{D}^0\gamma]_{\overline{D}^{*0}_{CP(-1)}}\pi^+) = 0.000 \pm 0.015$
$A_{CP}(B^+ \to [\overline{D}^0\pi^0]_{D^{*0}_{CP(+1)}}\pi^+) = 0.012 \pm 0.008$
$A_{CP}(B^+ \to [\overline{D}^0\pi^0]_{D^{*0}_{CP(-1)}}\pi^+) = -0.09 \pm 0.05$
$A_{CP}(B^+ \to [\overline{D}^0\gamma]_{\overline{D}^{*0}}K^+) = -0.004 \pm 0.014$
$A_{CP}(B^+ \to [\overline{D}^0\pi^0]_{\overline{D}^{*0}}K^+) = 0.017 \pm 0.007$
$A_{CP}(B^+ \to [\overline{D}^0\gamma]_{\overline{D}^{*0}_{CP(-1)}}K^+) = 0.12 \pm 0.06$
$A_{CP}(B^+ \to [D^0\pi^0]_{D^{*0}_{CP(+1)}}K^+) = -0.115 \pm 0.020$
$A_{CP}(B^+ \to [D^0\pi^0]_{D^{*0}_{CP(-1)}}K^+) = 0.07 \pm 0.10$
$A_{CP}(B^+ \to D_{CP(+1)}K^*(892)^+) = 0.08 \pm 0.06$
$A_{CP}(B^+ \to D_{CP(-1)}K^*(892)^+) = -0.23 \pm 0.22$
$A_{CP}(B^+ \to D_s^+\phi) = 0.0 \pm 0.4$
$A_{CP}(B^+ \to D_s^+\overline{D}^0) = (0.5 \pm 0.6)\%$
$A_{CP}(B^+ \to D_s^{*+}\overline{D}^0) = (-0.5 \pm 1.5) \times 10^{-2}$
$A_{CP}(B^+ \to D_s^+\overline{D}^{*0}) = (1.1 \pm 1.1) \times 10^{-2}$
$A_{CP}(B^+ \to D^{*+}\overline{D}^{*0}) = (1.3 \pm 2.6) \times 10^{-2}$
$A_{CP}(B^+ \to D^{*+}\overline{D}^0) = (3.1 \pm 1.7) \times 10^{-2}$
$A_{CP}(B^+ \to D^+\overline{D}^{*0}) = (0.0 \pm 2.4) \times 10^{-2}$
$A_{CP}(B^+ \to D^+\overline{D}^0) = (2.4 \pm 1.1) \times 10^{-2}$
$A_{CP}(B^+ \to K^0_S\pi^+) = -0.003 \pm 0.015$ (S = 1.1)
$A_{CP}(B^+ \to K^+\pi^0) = 0.027 \pm 0.012$
$A_{CP}(B^+ \to \eta' K^+) = 0.004 \pm 0.011$
$A_{CP}(B^+ \to \eta' K^*(892)^+) = -0.26 \pm 0.27$
$A_{CP}(B^+ \to \eta' K^*_0(1430)^+) = 0.06 \pm 0.20$
$A_{CP}(B^+ \to \eta' K^*_2(1430)^+) = 0.15 \pm 0.13$
$\boldsymbol{A_{CP}(B^+ \to \eta K^+)} = -0.37 \pm 0.08$
$A_{CP}(B^+ \to \eta K^*(892)^+) = 0.02 \pm 0.06$
$A_{CP}(B^+ \to \eta K^*_0(1430)^+) = 0.05 \pm 0.13$
$A_{CP}(B^+ \to \eta K^*_2(1430)^+) = -0.45 \pm 0.30$
$A_{CP}(B^+ \to \omega K^+) = -0.02 \pm 0.04$
$A_{CP}(B^+ \to \omega K^{*+}) = 0.29 \pm 0.35$
$A_{CP}(B^+ \to \omega(K\pi)^{*+}_0) = -0.10 \pm 0.09$
$A_{CP}(B^+ \to \omega K^*_2(1430)^+) = 0.14 \pm 0.15$
$A_{CP}(B^+ \to K^{*0}\pi^+) = -0.021 \pm 0.032$ (S = 1.5)
$A_{CP}(B^+ \to K^*(892)^+\pi^0) = -0.39 \pm 0.21$ (S = 1.6)
$\boldsymbol{A_{CP}(B^+ \to K^+\pi^-\pi^+)} = 0.015 \pm 0.006$ (S = 1.4)
$A_{CP}(B^+ \to K^+K^-K^+$ nonresonant$) = 0.06 \pm 0.05$
$A_{CP}(B^+ \to f(980)^0K^+) = -0.08 \pm 0.09$
$\boldsymbol{A_{CP}(B^+ \to f_2(1270)K^+)} = -0.68^{+0.19}_{-0.17}$
$A_{CP}(B^+ \to f_0(1500)K^+) = 0.28 \pm 0.30$
$A_{CP}(B^+ \to f'_2(1525)^0K^+) = -0.08^{+0.05}_{-0.04}$
$\boldsymbol{A_{CP}(B^+ \to \rho^0K^+)} = 0.160 \pm 0.021$
$A_{CP}(B^+ \to K^0\pi^+\pi^0) = 0.07 \pm 0.06$
$A_{CP}(B^+ \to K^*_0(1430)^0\pi^+) = 0.061 \pm 0.032$
$A_{CP}(B^+ \to K^*_0(1430)^+\pi^0) = 0.26^{+0.18}_{-0.14}$
$A_{CP}(B^+ \to K^*_2(1430)^0\pi^+) = 0.05^{+0.29}_{-0.24}$
$A_{CP}(B^+ \to K^+\pi^0\pi^0) = -0.06 \pm 0.07$
$A_{CP}(B^+ \to K^0\rho^+) = -0.03 \pm 0.15$
$A_{CP}(B^+ \to K^{*+}\pi^+\pi^-) = 0.07 \pm 0.08$
$A_{CP}(B^+ \to \rho^0K^*(892)^+) = 0.31 \pm 0.13$
$A_{CP}(B^+ \to K^*(892)^+f_0(980)) = -0.15 \pm 0.12$
$A_{CP}(B^+ \to a_1^+K^0) = 0.12 \pm 0.11$
$A_{CP}(B^+ \to b_1^+K^0) = -0.03 \pm 0.15$
$A_{CP}(B^+ \to K^*(892)^0\rho^+) = -0.01 \pm 0.16$
$A_{CP}(B^+ \to b_1^0K^+) = -0.46 \pm 0.20$

Int. J. Mod. Phys. A 2026.41. Downloaded from www.worldscientific.com
by UNIVERSITY OF CALIFORNIA @ BERKELEY on 09/16/26. Re-use and distribution is strictly not permitted, except for Open Acce

Int. J. Mod. Phys. A 2026.41. Downloaded from www.worldscientific.com
by UNIVERSITY OF CALIFORNIA @ BERKELEY on 09/16/26. Re-use and distribution is strictly not permitted, except for Open Access articles.

$A_{CP}(B^+ \to K^0 K^+) = 0.04 \pm 0.14$
$A_{CP}(B^+ \to K^0_S K^+) = -0.21 \pm 0.14$
$A_{CP}(B^+ \to K^+ K^0_S K^0_S) = 0.025 \pm 0.031$
$\boldsymbol{A_{CP}(B^+ \to K^+ K^- \pi^+)} = -0.115 \pm 0.008$
$A_{CP}(B^+ \to K^+ K^- \pi^+ \text{ nonresonant}) = -0.11 \pm 0.06$
$A_{CP}(B^+ \to \pi^+ K^+ K^-,\ m_{K^+K^-} < 1.1 \text{ GeV}) = -0.17 \pm 0.07$
$A_{CP}(B^+ \to K^+ \overline{K}^*(892)^0) = 0.04 \pm 0.05$
$A_{CP}(B^+ \to K^+ \overline{K}^*_0(1430)^0) = 0.10 \pm 0.17$
$A_{CP}(B^+ \to \phi\pi^+) = 0.1 \pm 0.5$
$A_{CP}(B^+ \to \pi^+ (K^+ K^-)_{S-wave}) = -0.66 \pm 0.04$
$\boldsymbol{A_{CP}(B^+ \to K^+ K^- K^+)} = -0.036 \pm 0.004$
$A_{CP}(B^+ \to \phi K^+) = 0.017 \pm 0.017 \quad (S = 1.8)$
$A_{CP}(B^+ \to X_0(1550) K^+) = -0.04 \pm 0.07$
$A_{CP}(B^+ \to K^{*+} K^+ K^-) = 0.11 \pm 0.09$
$A_{CP}(B^+ \to \phi K^*(892)^+) = -0.01 \pm 0.08$
$A_{CP}(B^+ \to \phi (K\pi)^{*+}_0) = 0.04 \pm 0.16$
$A_{CP}(B^+ \to \phi K_1(1270)^+) = 0.15 \pm 0.20$
$A_{CP}(B^+ \to \phi K^*_2(1430)^+) = -0.23 \pm 0.20$
$A_{CP}(B^+ \to K^+ \phi\phi) = -0.08 \pm 0.07$
$A_{CP}(B^+ \to K^+ [\phi\phi]_{\eta_c}) = 0.10 \pm 0.08$
$A_{CP}(B^+ \to K^*(892)^+ \gamma) = 0.008 \pm 0.015$
$A_{CP}(B^+ \to X_s \gamma) = 0.028 \pm 0.019$
$A_{CP}(B^+ \to \eta K^+ \gamma) = -0.12 \pm 0.07$
$A_{CP}(B^+ \to \phi K^+ \gamma) = -0.13 \pm 0.11 \quad (S = 1.1)$
$A_{CP}(B^+ \to \rho^+ \gamma) = (-9 \pm 14) \times 10^{-2}$
$A_{CP}(B^+ \to \pi^+ \pi^0) = -0.01 \pm 0.04 \quad (S = 1.1)$
$\boldsymbol{A_{CP}(B^+ \to \pi^+ \pi^- \pi^+)} = 0.076 \pm 0.008 \quad (S = 1.5)$
$A_{CP}(B^+ \to \pi^+ \pi^0 \pi^0) = (9 \pm 7) \times 10^{-2}$
$A_{CP}(B^+ \to \rho^0 \pi^+) = 0.003 \pm 0.014$
$A_{CP}(B^+ \to f_2(1270) \pi^+) = 0.40 \pm 0.06$
$A_{CP}(B^+ \to \rho^0(1450) \pi^+) = -0.11 \pm 0.05$
$A_{CP}(B^+ \to \rho_3(1690) \pi^+) = -0.80 \pm 0.28$
$\boldsymbol{A_{CP}(B^+ \to f_0(1370) \pi^+)} = 0.72 \pm 0.22$
$A_{CP}(B^+ \to \pi^+ \pi^- \pi^+ \text{ nonresonant}) = -0.14^{+0.23}_{-0.16}$
$A_{CP}(B^+ \to \rho^+ \pi^0) = 0.03 \pm 0.10$
$A_{CP}(B^+ \to X \pi^+,\ X \to \pi^0 \pi^0) = 0.18 \pm 0.12$
$A_{CP}(B^+ \to \rho^+ \rho^0) = -0.05 \pm 0.05$
$A_{CP}(B^+ \to \omega \pi^+) = -0.04 \pm 0.05$
$A_{CP}(B^+ \to \omega \rho^+) = -0.20 \pm 0.09$
$A_{CP}(B^+ \to \eta \pi^+) = -0.14 \pm 0.07 \quad (S = 1.4)$
$A_{CP}(B^+ \to \eta \rho^+) = 0.11 \pm 0.11$
$A_{CP}(B^+ \to \eta' \pi^+) = 0.06 \pm 0.16$
$A_{CP}(B^+ \to \eta' \rho^+) = 0.26 \pm 0.17$
$A_{CP}(B^+ \to b^0_1 \pi^+) = 0.05 \pm 0.16$
$A_{CP}(B^+ \to p\overline{p}\pi^+) = 0.021 \pm 0.030$
$A_{CP}(B^+ \to p\overline{p}K^+) = -0.02 \pm 0.04 \quad (S = 1.9)$
$A_{CP}(B^+ \to p\overline{p}K^*(892)^+) = 0.21 \pm 0.16 \quad (S = 1.4)$
$A_{CP}(B^+ \to p\overline{\Lambda}\gamma) = 0.17 \pm 0.17$
$A_{CP}(B^+ \to p\overline{\Lambda}\pi^0) = 0.01 \pm 0.17$
$A_{CP}(B^+ \to \overline{\Lambda} p \overline{p} p) = (5 \pm 16)\%$
$A_{CP}(B^+ \to K^+ \ell^+ \ell^-) = -0.02 \pm 0.08$
$A_{CP}(B^+ \to K^+ e^+ e^-) = 0.14 \pm 0.14$
$A_{CP}(B^+ \to K^+ \mu^+ \mu^-) = 0.011 \pm 0.017$
$A_{CP}(B^+ \to \pi^+ \mu^+ \mu^-) = -0.11 \pm 0.12$
$A_{CP}(B^+ \to K^{*+} \ell^+ \ell^-) = -0.09 \pm 0.14$
$A_{CP}(B^+ \to K^* e^+ e^-) = -0.14 \pm 0.23$
$A_{CP}(B^+ \to K^* \mu^+ \mu^-) = -0.12 \pm 0.24$
$\boldsymbol{\gamma} = (66.4^{+2.7}_{-2.8})^\circ$
$\boldsymbol{r_B(B^+ \to D^0 K^+)} = (9.88^{+0.22}_{-0.21}) \times 10^{-2}$
$\boldsymbol{\delta_B(B^+ \to D^0 K^+)} = (128.5^{+2.8}_{-3.0})^\circ$
$r_B(B^+ \to D^0 \pi^+) = (17 \pm 5) \times 10^{-3}$
$\delta_B(B^+ \to D^0 \pi^+) = (347 \pm 9)^\circ$
$\boldsymbol{r_B(B^+ \to D^0 K^{*+})} = 0.101^{+0.016}_{-0.036}$
$\boldsymbol{\delta_B(B^+ \to D^0 K^{*+})} = (47^{+61}_{-16})^\circ$
$\boldsymbol{r_B(B^+ \to D^{*0} K^+)} = 0.103^{+0.010}_{-0.011}$
$\boldsymbol{\delta_B(B^+ \to D^{*0} K^+)} = (312.2^{+6.3}_{-7.1})^\circ$

B^- modes are charge conjugates of the modes below. Modes which do not identify the charge state of the B are listed in the $B^\pm/B^0$ ADMIXTURE section.

The branching fractions listed below assume 50% $B^0\overline{B}^0$ and 50% B^+B^- production at the $\Upsilon(4S)$. We have attempted to bring older measurements up to date by rescaling their assumed $\Upsilon(4S)$ production ratio to 50:50 and their assumed D, D_s, D^*, and ψ branching ratios to current values whenever this would affect our averages and best limits significantly.

Indentation is used to indicate a subchannel of a previous reaction. All resonant subchannels have been corrected for resonance branching fractions to the final state so the sum of the subchannel branching fractions can exceed that of the final state.

For inclusive branching fractions, *e.g.*, $B \to D^\pm X$, the values usually are multiplicities, not branching fractions. They can be greater than one.

B^+ DECAY MODES		Fraction (Γ_i/Γ)	Scale factor/ Confidence level	p (MeV/c)
Semileptonic and leptonic modes				
$\ell^+ \nu_\ell X$	[jjj]	(10.99 ± 0.28) %		–
$e^+ \nu_e X_c$		(10.8 ± 0.4) %		–
$e^+ \nu_e X$		(10.8 ± 2.7) %		–
$\mu^+ \nu_\mu X$		(11.3 ± 3.5) %		–
$\ell^+ \nu_\ell X_u$	[jjj]	$(1.65 \pm 0.21) \times 10^{-3}$		–
$D \ell^+ \nu_\ell X$	[jjj]	(9.5 ± 0.7) %		–
$\overline{D}^0 \ell^+ \nu_\ell$	[jjj]	(2.21 ± 0.06) %		2310
$\tau^+ \nu_\tau X$		(2.5 ± 0.4) %		–
$\overline{D}^0 \tau^+ \nu_\tau$		$(7.7 \pm 2.5) \times 10^{-3}$		1911
$\overline{D}^*(2007)^0 \ell^+ \nu_\ell$	[jjj]	(5.53 ± 0.22) %		2258
$\overline{D}^*(2007)^0 \tau^+ \nu_\tau$		(1.88 ± 0.20) %		1839
$D^{(*)} n \pi \ell^+ \nu_\ell (n \geq 1)$	[jjj]	(1.83 ± 0.25) %		–
$D^- \pi^+ \ell^+ \nu_\ell$	[jjj]	$(3.82 \pm 0.20) \times 10^{-3}$		2306
$\overline{D}^*_2(2460)^0 \ell^+ \nu_\ell$, $\overline{D}^*_2{}^0 \to D^- \pi^+$	[jjj]	$(1.59 \pm 0.10) \times 10^{-3}$		2065
$\overline{D}^*_0(2420)^0 \ell^+ \nu_\ell$, $\overline{D}^*_0{}^0 \to D^- \pi^+$	[jjj]	$(9 \pm 5) \times 10^{-4}$	S=2.6	–
$D^{*-} \pi^+ \ell^+ \nu_\ell$	[jjj]	$(5.42 \pm 0.28) \times 10^{-3}$		2254
$\overline{D}_1(2420)^0 \ell^+ \nu_\ell$, $\overline{D}^0_1 \to D^{*-} \pi^+$	[jjj]	$(2.84 \pm 0.17) \times 10^{-3}$	S=1.1	2084
$\overline{D}'_1(2430)^0 \ell^+ \nu_\ell$, $\overline{D}'^0_1 \to D^{*-} \pi^+$	[jjj]	$(1.7 \pm 0.6) \times 10^{-3}$	S=1.8	–
$\overline{D}^*_2(2460)^0 \ell^+ \nu_\ell$, $\overline{D}^*_2{}^0 \to D^{*-} \pi^+$	[jjj]	$(1.06 \pm 0.18) \times 10^{-3}$	S=1.7	2065
$\overline{D}^0 \pi^+ \pi^- \ell^+ \nu_\ell$	[jjj]	$(1.73 \pm 0.19) \times 10^{-3}$		2301
$\overline{D}_1(2420)^0 \ell^+ \nu_\ell$, $\overline{D}^0_1 \to \overline{D}^0 \pi^+ \pi^-$	[jjj]	$(1.05 \pm 0.14) \times 10^{-3}$		–
$\overline{D}^{*0} \pi^+ \pi^- \ell^+ \nu_\ell$	[jjj]	$(7.0 \pm 1.7) \times 10^{-4}$		2248
$D_s^{(*)-} K^+ \ell^+ \nu_\ell$	[jjj]	$(6.1 \pm 1.0) \times 10^{-4}$		–
$D_s^- K^+ \ell^+ \nu_\ell$	[jjj]	$(3.0 {}^{+1.4}_{-1.2}) \times 10^{-4}$		2242
$D_s^{*-} K^+ \ell^+ \nu_\ell$	[jjj]	$(2.9 \pm 1.9) \times 10^{-4}$		2185
$\pi^0 \ell^+ \nu_\ell$	[jjj]	$(7.80 \pm 0.27) \times 10^{-5}$		2638
$\eta \ell^+ \nu_\ell$	[jjj]	$(3.5 \pm 0.4) \times 10^{-5}$		2611
$\eta' \ell^+ \nu_\ell$	[jjj]	$(2.4 \pm 0.7) \times 10^{-5}$		2553
$\omega \ell^+ \nu_\ell$	[jjj]	$(1.19 \pm 0.09) \times 10^{-4}$		2582
$\rho^0 \ell^+ \nu_\ell$	[jjj]	$(1.58 \pm 0.11) \times 10^{-4}$		2583
$\pi^+ \pi^- \ell^+ \nu_\ell$	[jjj]	$(2.3 \pm 0.4) \times 10^{-4}$		2636
$p \overline{p} \ell^+ \nu_\ell$	[jjj]	$(5.8 {}^{+2.6}_{-2.3}) \times 10^{-6}$		2467
$p \overline{p} \mu^+ \nu_\mu$		$(5.32 \pm 0.33) \times 10^{-6}$		2446
$p \overline{p} e^+ \nu_e$		$(8.2 {}^{+4.0}_{-3.3}) \times 10^{-6}$		2467
$e^+ \nu_e$		$< 9.8 \times 10^{-7}$	CL=90%	2640
$\mu^+ \nu_\mu$		$< 8.6 \times 10^{-7}$	CL=90%	2639
$\tau^+ \nu_\tau$		$(1.12 \pm 0.19) \times 10^{-4}$		2341
$\ell^+ \nu_\ell \gamma$	[jjj]	$< 3.0 \times 10^{-6}$	CL=90%	2640
$e^+ \nu_e \gamma$		$< 4.3 \times 10^{-6}$	CL=90%	2640
$\mu^+ \nu_\mu \gamma$		$< 3.4 \times 10^{-6}$	CL=90%	2639
$\mu^+ \mu^- \mu^+ \nu_\mu$		$< 1.6 \times 10^{-8}$	CL=95%	2634
Inclusive modes				
$D^0 X$		(8.6 ± 0.7) %		–
$\overline{D}^0 X$		(79 ± 4) %		–
$D^+ X$		(2.5 ± 0.5) %		–
$D^- X$		(9.9 ± 1.2) %		–
$D_s^+ X$		$(7.9 {}^{+1.4}_{-1.3})$ %		–
$D_s^- X$		$(1.10 {}^{+0.40}_{-0.32})$ %		–
$\Lambda_c^+ X$		$(2.1 {}^{+0.9}_{-0.6})$ %		–
$\overline{\Lambda}_c^- X$		$(2.8 {}^{+1.1}_{-0.9})$ %		–
$\overline{c} X$		(97 ± 4) %		–
$c X$		$(23.4 {}^{+2.2}_{-1.8})$ %		–
$c/\overline{c} X$		(120 ± 6) %		–

Int. J. Mod. Phys. A 2026.41. Downloaded from www.worldscientific.com
by UNIVERSITY OF CALIFORNIA @ BERKELEY on 09/16/26. Re-use and distribution is strictly not permitted, except for Open Acce

D, D^*, or D_s modes

$\overline{D}^0 \pi^+$		$(4.61 \pm 0.10) \times 10^{-3}$		2308
$D_{CP(+1)} \pi^+$	[kkk]	$(2.04 \pm 0.20) \times 10^{-3}$		–
$D_{CP(-1)} \pi^+$	[kkk]	$(2.1 \pm 0.4) \times 10^{-3}$		–
$\overline{D}^0 \rho^+$		$(9.7 \pm 1.1) \times 10^{-3}$	S=2.1	2237
$\overline{D}^0 K^+$		$(3.64 \pm 0.15) \times 10^{-4}$		2281
$D_{CP(+1)} K^+$	[kkk]	$(1.81 \pm 0.08) \times 10^{-4}$		–
$D_{CP(-1)} K^+$	[kkk]	$(2.04 \pm 0.13) \times 10^{-4}$		–
$D^0 K^+$		$(3.60 \pm 0.24) \times 10^{-6}$		2281
$[K^- \pi^+]_D K^+$	[lll]	$< 2.8 \times 10^{-7}$	CL=90%	–
$[K^+ \pi^-]_D K^+$	[lll]	$< 1.6 \times 10^{-5}$	CL=90%	–
$[K^- \pi^+ \pi^0]_D K^+$		seen		–
$[K^+ \pi^- \pi^0]_D K^+$		seen		–
$[K^- \pi^+ \pi^+ \pi^-]_D K^+$		seen		–
$[K^+ \pi^- \pi^+ \pi^-]_D K^+$		seen		–
$[K^- \pi^+]_D \pi^+$	[lll]	$(6.3 \pm 1.1) \times 10^{-7}$		–
$[K^+ \pi^-]_D \pi^+$		$(1.72 \pm 0.30) \times 10^{-4}$		–
$[K^- \pi^+ \pi^0]_D \pi^+$		seen		–
$[K^+ \pi^- \pi^0]_D \pi^+$		seen		–
$[K^- \pi^+ \pi^+ \pi^-]_D \pi^+$		seen		–
$[K^+ \pi^- \pi^+ \pi^-]_D \pi^+$		seen		–
$[\pi^+ \pi^- \pi^0]_D K^-$		$(4.6 \pm 0.9) \times 10^{-6}$		–
$[K^0_S K^+ \pi^-]_D K^+$		seen		–
$[K^0_S K^- \pi^+]_D K^+$		seen		–
$[K^*(892)^+ K^-]_D K^+$		seen		–
$[K^0_S K^- \pi^+]_D \pi^+$		seen		–
$[K^*(892)^+ K^-]_D \pi^+$		seen		–
$[K^0_S K^+ \pi^-]_D \pi^+$		seen		–
$[K^*(892)^- K^+]_D \pi^+$		seen		–
$\overline{D}^0 K^*(892)^+$		$(5.3 \pm 0.4) \times 10^{-4}$		2213
$D_{CP(-1)} K^*(892)^+$	[kkk]	$(2.7 \pm 0.8) \times 10^{-4}$		–
$D_{CP(+1)} K^*(892)^+$	[kkk]	$(6.2 \pm 0.7) \times 10^{-4}$		–
$D^0 K^*(892)^+$		$(5.4 {}^{+1.8}_{-4.0}) \times 10^{-6}$		2213
$\overline{D}^0 K^+ \pi^+ \pi^-$		$(5.2 \pm 2.1) \times 10^{-4}$		2237
$\overline{D}^0 K^+ \overline{K}^0$		$(3.75 \pm 0.35) \times 10^{-4}$		2189
$\overline{D}^0 K^+ \overline{K}^*(892)^0$		$(7.2 \pm 0.5) \times 10^{-4}$		2071
$\overline{D}^0 \pi^+ \pi^+ \pi^-$		$(5.5 \pm 2.0) \times 10^{-3}$	S=3.6	2289
$\overline{D}^0 \pi^+ \pi^+ \pi^-$ nonresonant		$(5 \pm 4) \times 10^{-3}$		2289
$\overline{D}^0 \pi^+ \rho^0$		$(4.2 \pm 3.0) \times 10^{-3}$		2208
$\overline{D}^0 a_1(1260)^+$		$(4 \pm 4) \times 10^{-3}$		2123
$\overline{D}^0 \omega \pi^+$		$(4.1 \pm 0.9) \times 10^{-3}$		2206
$D^*(2010)^- \pi^+ \pi^+$		$(1.35 \pm 0.22) \times 10^{-3}$		2247
$D^*(2010)^- K^+ \pi^+$		$(8.2 \pm 1.4) \times 10^{-5}$		2206
$\overline{D}_1(2420)^0 \pi^+$, $\overline{D}^0_1 \to D^*(2010)^- \pi^+$		$(8.4 \pm 1.5) \times 10^{-4}$		2081
$D^- \pi^+ \pi^+$		$(1.07 \pm 0.05) \times 10^{-3}$		2299
$D^- K^+ \pi^+$		$(7.7 \pm 0.5) \times 10^{-5}$		2260
$D^*_0(2300)^0 K^+$, $D^{*0}_0 \to D^- \pi^+$		$(6.1 \pm 2.4) \times 10^{-6}$		–
$D^*_2(2460)^0 K^+$, $D^{*0}_2 \to D^- \pi^+$		$(2.32 \pm 0.23) \times 10^{-5}$		–
$D^*_1(2760)^0 K^+$, $D^{*0}_1 \to D^- \pi^+$		$(3.6 \pm 1.2) \times 10^{-6}$		–
$D^+ K^0$		$< 2 \times 10^{-6}$	CL=90%	2278
$D^+ K^+ \pi^-$		$(5.6 \pm 1.1) \times 10^{-6}$		2260
$D^+ \eta$		$< 1.2 \times 10^{-5}$	CL=90%	2272
$D^*_2(2460)^0 K^+$, $D^{*0}_2 \to D^+ \pi^-$		$< 6.3 \times 10^{-7}$	CL=90%	–
$D^+ K^{*0}$		$< 4.9 \times 10^{-7}$	CL=90%	2211
$D^+ \overline{K}^{*0}$		$< 1.4 \times 10^{-6}$	CL=90%	2211
$\overline{D}^*(2007)^0 \pi^+$		$(5.17 \pm 0.15) \times 10^{-3}$		2256
$\overline{D}^{*0}_{CP(+1)} \pi^+$	[nnn]	$(2.9 \pm 0.6) \times 10^{-3}$		–
$D^{*0}_{CP(-1)} \pi^+$	[nnn]	$(2.6 \pm 1.0) \times 10^{-3}$		–
$\overline{D}^*(2007)^0 \omega \pi^+$		$(4.5 \pm 1.2) \times 10^{-3}$		2149
$\overline{D}^*(2007)^0 \rho^+$		$(9.8 \pm 1.7) \times 10^{-3}$		2182
$\overline{D}^*(2007)^0 K^+$		$(4.19 {}^{+0.31}_{-0.28}) \times 10^{-4}$		2227
$\overline{D}^{*0}_{CP(+1)} K^+$	[nnn]	$(2.75 \pm 0.35) \times 10^{-4}$		–
$\overline{D}^{*0}_{CP(-1)} K^+$	[nnn]	$(2.31 \pm 0.31) \times 10^{-4}$		–
$D^*(2007)^0 K^+$		$(4.5 \pm 1.2) \times 10^{-6}$		2227
$\overline{D}^*(2007)^0 K^*(892)^+$		$(8.1 \pm 1.4) \times 10^{-4}$		2156
$\overline{D}^*(2007)^0 K^+ \overline{K}^0$		$(2.9 \pm 0.6) \times 10^{-4}$		2132
$\overline{D}^*(2007)^0 K^+ \overline{K}^*(892)^0$		$(1.23 \pm 0.14) \times 10^{-3}$		2009
$\overline{D}^*(2007)^0 \pi^+ \pi^+ \pi^-$		(1.03 ± 0.12) %		2236
$\overline{D}^*(2007)^0 a_1(1260)^+$		(1.9 ± 0.5) %		2063
$\overline{D}^*(2007)^0 \pi^- \pi^+ \pi^+ \pi^0$		(1.8 ± 0.4) %		2219
$\overline{D}^{*0} 3\pi^+ 2\pi^-$		$(5.7 \pm 1.2) \times 10^{-3}$		2196
$D^*(2010)^+ \pi^0$		$< 3.6 \times 10^{-6}$		2255
$D^*(2010)^+ K^0$		$< 9.0 \times 10^{-6}$	CL=90%	2225
$D^*(2010)^- \pi^+ \pi^+ \pi^0$		(1.5 ± 0.7) %		2235
$D^*(2010)^- \pi^+ \pi^+ \pi^+ \pi^-$		$(2.6 \pm 0.4) \times 10^{-3}$		2217
$\overline{D}^{**0} \pi^+$	[ooo]	$(5.6 \pm 1.2) \times 10^{-3}$		–
$\overline{D}^*_1(2420)^0 \pi^+$		$(1.5 \pm 0.6) \times 10^{-3}$	S=1.3	2081
$\overline{D}_1(2420)^0 \pi^+ \times B(\overline{D}^0_1 \to \overline{D}^0 \pi^+ \pi^-)$		$(2.5 {}^{+1.6}_{-1.4}) \times 10^{-4}$	S=3.8	2081
$\overline{D}_1(2420)^0 \pi^+ \times B(\overline{D}^0_1 \to \overline{D}^0 \pi^+ \pi^-$ (nonresonant))		$(2.2 \pm 0.9) \times 10^{-4}$		2081
$\overline{D}_1(2430)^0 \pi^+$, $\overline{D}^0_1 \to D^*(2010)^- \pi^+$		$(3.5 \pm 0.6) \times 10^{-4}$		2079
$\overline{D}(2550)^0 \pi^+$, $\overline{D}^0 \to D^*(2010)^- \pi^+$		$(7.2 \pm 1.4) \times 10^{-5}$		–
$\overline{D}^*_J(2600)^0 \pi^+$, $\overline{D}^{*0}_J \to D^*(2010)^- \pi^+$		$(6.8 \pm 1.3) \times 10^{-5}$		–
$\overline{D}^*_2(2462)^0 \pi^+$, $\overline{D}^{*0}_2 \to D^- \pi^+$		$(3.56 \pm 0.24) \times 10^{-4}$		–
$\overline{D}^*_2(2462)^0 \pi^+$, $\overline{D}^{*0}_2 \to \overline{D}^0 \pi^- \pi^+$		$(2.2 \pm 1.0) \times 10^{-4}$		–
$\overline{D}^*_2(2462)^0 \pi^+$, $\overline{D}^{*0}_2 \to \overline{D}^0 \pi^- \pi^+$ (nonresonant)		$< 1.6 \times 10^{-4}$	CL=90%	–
$\overline{D}^*_2(2462)^0 \pi^+$, $\overline{D}^{*0}_2 \to D^*(2010)^- \pi^+$		$(2.1 \pm 1.0) \times 10^{-4}$		–
$\overline{D}^*_0(2400)^0 \pi^+ \times B(\overline{D}^*_0(2400)^0 \to D^- \pi^+)$		$(6.4 \pm 1.4) \times 10^{-4}$		2136
$\overline{D}_1(2421)^0 \pi^+$, $\overline{D}^0_1 \to D^{*-} \pi^+$		$(7.4 \pm 1.0) \times 10^{-4}$		–
$\overline{D}^*_2(2462)^0 \pi^+$, $\overline{D}^{*0}_2 \to D^{*-} \pi^+$		$(1.98 \pm 0.30) \times 10^{-4}$		–
$\overline{D}'_1(2427)^0 \pi^+$, $\overline{D}'^0_1 \to D^{*-} \pi^+$		$(3.5 \pm 0.9) \times 10^{-4}$	S=1.5	–
$\overline{D}_1(2420)^0 \pi^+ \times B(\overline{D}^0_1 \to \overline{D}^{*0} \pi^+ \pi^-)$		$< 6 \times 10^{-6}$	CL=90%	2081
$\overline{D}^*_1(2420)^0 \rho^+$		$< 1.4 \times 10^{-3}$	CL=90%	1996
$\overline{D}^*_2(2460)^0 \pi^+$		$< 1.3 \times 10^{-3}$	CL=90%	2063
$\overline{D}^*_2(2460)^0 \pi^+ \times B(\overline{D}^{*0}_2 \to \overline{D}^{*0} \pi^+ \pi^-)$		$< 2.2 \times 10^{-5}$	CL=90%	2063
$\overline{D}^*_1(2680)^0 \pi^+$, $\overline{D}^*_1(2680)^0 \to D^- \pi^+$		$(8.4 \pm 2.1) \times 10^{-5}$		–
$\overline{D}(2740)^0 \pi^+$, $\overline{D}^0 \to D^*(2010)^- \pi^+$		$(3.3 \pm 1.5) \times 10^{-5}$		–
$\overline{D}^*_3(2750)^0 \pi^+$, $\overline{D}^{*0}_3 \to D^*(2010)^- \pi^+$		$(1.10 \pm 0.32) \times 10^{-5}$		1913
$\overline{D}^*_3(2760)^0 \pi^+$, $\overline{D}^*_3(2760)^0 \pi^+ \to D^- \pi^+$		$(1.00 \pm 0.22) \times 10^{-5}$		–
$\overline{D}^*_2(3000)^0 \pi^+$, $\overline{D}^*_2(3000)^0 \pi^+ \to D^- \pi^+$		$(2.0 \pm 1.4) \times 10^{-6}$		–
$\overline{D}^*_2(2460)^0 \rho^+$		$< 4.7 \times 10^{-3}$	CL=90%	1977
$\overline{D}^0 D^+_s$		$(9.3 \pm 0.6) \times 10^{-3}$		1815
$D^*_{s0}(2317)^+ \overline{D}^0$, $D^{*+}_{s0} \to D^+_s \pi^0$		$(7.9 {}^{+1.5}_{-1.3}) \times 10^{-4}$		1605
$D_{s0}(2317)^+ \overline{D}^0 \times B(D_{s0}(2317)^+ \to D^{*+}_s \gamma)$		$< 7.6 \times 10^{-4}$	CL=90%	1605
$D_{s0}(2317)^+ \overline{D}^*(2007)^0 \times B(D_{s0}(2317)^+ \to D^+_s \pi^0)$		$(9 \pm 7) \times 10^{-4}$		1511
$D_{sJ}(2457)^+ \overline{D}^0$		$(3.1 {}^{+1.0}_{-0.9}) \times 10^{-3}$		–
$D_{sJ}(2457)^+ \overline{D}^0 \times B(D_{sJ}(2457)^+ \to D^+_s \gamma)$		$(4.6 {}^{+1.3}_{-1.1}) \times 10^{-4}$		–
$D_{sJ}(2457)^+ \overline{D}^0 \times B(D_{sJ}(2457)^+ \to D^+_s \pi^+ \pi^-)$		$< 2.2 \times 10^{-4}$	CL=90%	–
$D_{sJ}(2457)^+ \overline{D}^0 \times B(D_{sJ}(2457)^+ \to D^+_s \pi^0)$		$< 2.7 \times 10^{-4}$	CL=90%	–
$D_{sJ}(2457)^+ \overline{D}^0 \times B(D_{sJ}(2457)^+ \to D^{*+}_s \gamma)$		$< 9.8 \times 10^{-4}$	CL=90%	–
$D_{sJ}(2457)^+ \overline{D}^*(2007)^0$		(1.20 ± 0.30) %		–
$D_{sJ}(2457)^+ \overline{D}^*(2007)^0 \times B(D_{sJ}(2457)^+ \to D^+_s \gamma)$		$(1.4 {}^{+0.7}_{-0.6}) \times 10^{-3}$		–

$\overline{D}^0 D_{s1}(2536)^+ \times$ B($D_{s1}(2536)^+ \to D^*(2007)^0 K^+ + D^*(2010)^+ K^0$)	$(4.0 \pm 1.0) \times 10^{-4}$			1447
$\overline{D}^0 D_{s1}(2536)^+ \times$ B($D_{s1}(2536)^+ \to D^*(2007)^0 K^+$)	$(2.2 \pm 0.7) \times 10^{-4}$			1447
$\overline{D}^*(2007)^0 D_{s1}(2536)^+ \times$ B($D_{s1}(2536)^+ \to D^*(2007)^0 K^+$)	$(5.5 \pm 1.6) \times 10^{-4}$			1339
$\overline{D}^0 D_{s1}(2536)^+ \times$ B($D_{s1}(2536)^+ \to D^{*+} K^0$)	$(2.3 \pm 1.1) \times 10^{-4}$			1447
$\overline{D}^0 D_{sJ}(2700)^+ \times$ B($D_{sJ}(2700)^+ \to D^0 K^+$)	$(5.6 \pm 1.8) \times 10^{-4}$	S=1.7		–
$\overline{D}^{*0} D_{s1}(2536)^+,\ D^+_{s1} \to D^{*+} K^0$	$(3.9 \pm 2.6) \times 10^{-4}$			1339
$\overline{D}^0 D_{sJ}(2573)^+,\ D^+_{sJ} \to D^0 K^+$	$(8 \pm 15) \times 10^{-6}$			–
$\overline{D}^{*0} D_{sJ}(2573),\ D^+_{sJ} \to D^0 K^+$	$< 2 \times 10^{-4}$	CL=90%		1306
$\overline{D}^*(2007)^0 D_{sJ}(2573),\ D^+_{sJ} \to D^0 K^+$	$< 5 \times 10^{-4}$	CL=90%		1306
$\overline{D}^0 D_s^{*+}$	$(7.6 \pm 1.6) \times 10^{-3}$			1734
$\overline{D}^*(2007)^0 D_s^+$	$(7.0 \pm 1.0) \times 10^{-3}$			1737
$\overline{D}^*(2007)^0 D_s^{*+}$	(1.71 ± 0.24) %			1651
$D_s^{(*)+} \overline{D}^{**0}$	(2.7 ± 1.2) %			–
$\overline{D}^*(2007)^0 D^*(2010)^+$	$(8.1 \pm 1.7) \times 10^{-4}$			1713
$\overline{D}^0 D^*(2010)^+ + \overline{D}^*(2007)^0 D^+$	< 1.30 %	CL=90%		1792
$\overline{D}^0 D^*(2010)^+$	$(3.9 \pm 0.5) \times 10^{-4}$			1792
$\overline{D}^0 D^+$	$(3.8 \pm 0.4) \times 10^{-4}$			1866
$\overline{D}^0 D^+ K^0$	$(1.55 \pm 0.21) \times 10^{-3}$			1571
$D^+ \overline{D}^*(2007)^0$	$(6.3 \pm 1.7) \times 10^{-4}$			1791
$\overline{D}^*(2007)^0 D^+ K^0$	$(2.1 \pm 0.5) \times 10^{-3}$			1475
$\overline{D}^0 D^*(2010)^+ K^0$	$(3.8 \pm 0.4) \times 10^{-3}$			1476
$\overline{D}^*(2007)^0 D^*(2010)^+ K^0$	$(9.2 \pm 1.2) \times 10^{-3}$			1362
$\overline{D}^0 D^0 K^+$	$(1.45 \pm 0.33) \times 10^{-3}$	S=2.6		1577
$\overline{D}^*(2007)^0 D^0 K^+$	$(2.26 \pm 0.23) \times 10^{-3}$			1481
$\overline{D}^0 D^*(2007)^0 K^+$	$(6.3 \pm 0.5) \times 10^{-3}$			1481
$\overline{D}^*(2007)^0 D^*(2007)^0 K^+$	(1.12 ± 0.13) %			1368
$D^- D^+ K^+$	$(2.2 \pm 0.7) \times 10^{-4}$			1571
$T^*_{cs0}(2870)^0 D^+,\ T^{*0}_{cs0} \to D^- K^+$	$(1.2 \pm 0.5) \times 10^{-5}$			–
$T^*_{cs1}(2900)^0 D^+,\ T^{*0}_{cs1} \to D^- K^+$	$(6.7 \pm 2.3) \times 10^{-5}$			–
$D^- D^+ K^+$ nonresonant	$(5.3 \pm 1.8) \times 10^{-5}$			1571
$D^- D^*(2010)^+ K^+$	$(6.3 \pm 1.1) \times 10^{-4}$			1475
$D^*(2010)^- D^+ K^+$	$(6.0 \pm 1.3) \times 10^{-4}$			1475
EFF $K+$, EFF $\to D^*(2010)^\mp D^\pm$	$(1.5 \pm 0.4) \times 10^{-4}$			1475
$\eta_c(3945) K^+,\ \eta_c \to D^*(2010)^\mp D^\pm$	$(4.6 {}^{+2.7}_{-1.7}) \times 10^{-5}$			–
$\chi_{c2}(3930) K^+,\ \chi_{c2} \to D^*(2010)^\mp D^\pm$	$(2.4 {}^{+1.0}_{-1.7}) \times 10^{-5}$			–
$h_c(4000) K^+,\ h_c \to D^*(2010)^\mp D^\pm$	$(7.0 {}^{+2.5}_{-1.6}) \times 10^{-5}$			–
$\chi_{c1}(4010) K^+,\ \chi_{c1} \to D^*(2010)^\mp D^\pm$	$(1.38 {}^{+0.31}_{-0.28}) \times 10^{-4}$			–
$\psi(4040) K^+,\ \psi \to D^*(2010)^\mp D^\pm$	$(3.8 {}^{+1.1}_{-0.9}) \times 10^{-5}$			–
$h_c(4300) K^+,\ h_c \to D^*(2010)^\mp D^\pm$	$(1.6 {}^{+0.4}_{-0.7}) \times 10^{-5}$			–
$T^*_{\overline{c}s0}(2870)^0 K^+,\ T^{*0}_{\overline{c}s0} \to D^*(2010)^\mp D^\pm$	$(4.5 {}^{+1.2}_{-1.4}) \times 10^{-5}$			–
$T^*_{\overline{c}s1}(2900)^0 K^+,\ T^{*0}_{\overline{c}s1} \to D^*(2010)^\mp D^\pm$	$(3.8 {}^{+1.7}_{-1.6}) \times 10^{-5}$			–
NR K^+, NR $\to D^*(2010)^\mp D^\pm$	$(2.8 {}^{+0.5}_{-0.4}) \times 10^{-4}$			–
NR K^+, NR $\to D^*(2010)^\mp D^\pm$	$(1.6 {}^{+1.3}_{-0.8}) \times 10^{-5}$			–
NR K^+, NR $\to D^*(2010)^\mp D^\pm$	$(2.4 {}^{+0.6}_{-0.4}) \times 10^{-4}$			–
NR K^+, NR $\to D^*(2010)^\mp D^\pm$	$(2.2 {}^{+0.7}_{-0.5}) \times 10^{-4}$			–
$D^*(2010)^- D^*(2010)^+ K^+$	$(1.32 \pm 0.18) \times 10^{-3}$			1363
$(\overline{D} + \overline{D}^*)(D + D^*) K$	(4.05 ± 0.30) %			–
$D_s^- D_s^+ K^+$	$(1.2 \pm 0.4) \times 10^{-4}$			1429
$D_s^+ \pi^0$	$(1.6 \pm 0.5) \times 10^{-5}$			2270
$D_s^{*+} \pi^0$	$< 2.6 \times 10^{-4}$	CL=90%		2215
$D_s^+ \eta$	$< 1.4 \times 10^{-5}$	CL=90%		2235
$D_s^{*+} \eta$	$< 1.7 \times 10^{-5}$	CL=90%		2178
$D_s^+ \rho^0$	$< 3.0 \times 10^{-4}$	CL=90%		2197
$D_s^{*+} \rho^0$	$< 4 \times 10^{-4}$	CL=90%		2138
$D_s^+ \omega$	$< 4 \times 10^{-4}$	CL=90%		2195
$D_s^{*+} \omega$	$< 6 \times 10^{-4}$	CL=90%		2136
$D_s^+ a_1(1260)^0$	$< 1.8 \times 10^{-3}$	CL=90%		2080
$D_s^{*+} a_1(1260)^0$	$< 1.3 \times 10^{-3}$	CL=90%		2015
$D_s^+ K^+ K^-$	$(7.5 \pm 1.0) \times 10^{-6}$			2149
$D_s^+ \phi$	$< 4.2 \times 10^{-7}$	CL=90%		2141
$D_s^{*+} \phi$	$< 1.2 \times 10^{-5}$	CL=90%		2079
$D_s^+ \overline{K}^0$	$< 3 \times 10^{-6}$	CL=90%		2242
$D_s^{*+} \overline{K}^0$	$< 6 \times 10^{-6}$	CL=90%		2185
$D_s^+ \overline{K}^*(892)^0$	$< 4.4 \times 10^{-6}$	CL=90%		2172
$D_s^+ K^{*0}$	$< 3.5 \times 10^{-6}$	CL=90%		2172
$D_s^{*+} \overline{K}^*(892)^0$	$< 3.5 \times 10^{-4}$	CL=90%		2112
$D_s^- \pi^+ K^+$	$(1.80 \pm 0.22) \times 10^{-4}$			2222
$D_s^{*-} \pi^+ K^+$	$(1.45 \pm 0.24) \times 10^{-4}$			2164
$D_s^- \pi^+ K^*(892)^+$	$< 5 \times 10^{-3}$	CL=90%		2138
$D_s^{*-} \pi^+ K^*(892)^+$	$< 7 \times 10^{-3}$	CL=90%		2076
$D_s^- K^+ K^+$	$(9.7 \pm 2.1) \times 10^{-6}$			2149
$D_s^{*-} K^+ K^+$	$< 1.5 \times 10^{-5}$	CL=90%		2088

Charmonium modes

$\eta_c K^+$	$(1.20 \pm 0.08) \times 10^{-3}$	S=1.3		1751
$\eta_c K^*(892)^+$	$(1.4 {}^{+0.7}_{-0.5}) \times 10^{-3}$			1646
$\eta_c K^+ \pi^+ \pi^-$	$< 3.9 \times 10^{-4}$	CL=90%		1684
$\eta_c K^+ \omega(782)$	$< 5.3 \times 10^{-4}$	CL=90%		1475
$\eta_c K^+ \eta$	$< 2.2 \times 10^{-4}$	CL=90%		1588
$\eta_c K^+ \pi^0$	$< 6.2 \times 10^{-5}$	CL=90%		1723
$\eta_c(2S) K^+$	$(4.4 \pm 1.0) \times 10^{-4}$			1320
$\eta_c(2S) K^+,\ \eta_c \to p\overline{p}$	$(3.5 \pm 0.8) \times 10^{-8}$			–
$\eta_c(2S) K^+,\ \eta_c \to K^0_S K^\mp \pi^\pm$	$(3.4 {}^{+2.3}_{-1.6}) \times 10^{-6}$			–
$\eta_c(2S) K^+,\ \eta_c \to p\overline{p}\pi^+\pi^-$	$(1.12 \pm 0.18) \times 10^{-6}$			–
$h_c(1P) K^+,\ h_c \to J/\psi \pi^+ \pi^-$	$< 3.4 \times 10^{-6}$	CL=90%		1401
$X(3730)^0 K^+,\ X^0 \to \eta_c \eta$	$< 4.6 \times 10^{-5}$	CL=90%		–
$X(3730)^0 K^+,\ X^0 \to \eta_c \pi^0$	$< 5.7 \times 10^{-6}$	CL=90%		–
$\eta_{c2}(1D) K^+,\ \eta_{c2} \to h_c \gamma$	$< 3.7 \times 10^{-5}$	CL=90%		–
$\eta_{c2}(1D) \pi^+ K^0_S,\ \eta_{c2} \to h_c \gamma$	$< 1.1 \times 10^{-4}$	CL=90%		–
$\psi_2(3823) K^+,\ \psi_2 \to J/\psi \pi^+ \pi^-$	$(2.8 \pm 0.6) \times 10^{-7}$			–
$\psi_2(3823) K^+,\ \psi_2 \to J/\psi \eta$	$(1.2 {}^{+0.7}_{-0.5}) \times 10^{-6}$			–
$\psi_3(3842) K^+,\ \psi_3 \to J/\psi \eta$	$< 6.1 \times 10^{-7}$	CL=90%		–
$\chi_{c1}(3872) K^+$	$(1.9 \pm 0.6) \times 10^{-4}$			1141
$\chi_{c0}(3915) K^+$	$< 2.8 \times 10^{-4}$	CL=90%		1100
$\chi_{c0}(3915) K^+,\ \chi_{c0} \to D^+ D^-$	$(8.1 \pm 3.3) \times 10^{-6}$			–
$\chi_{c0}(3915) K^+,\ \chi_{c0} \to \eta_c \eta$	$< 4.7 \times 10^{-5}$	CL=90%		–
$\chi_{c0}(3915) K^+,\ \chi_{c0} \to \eta_c \pi^0$	$< 1.7 \times 10^{-5}$	CL=90%		–
$X(4014)^0 K^+,\ X^0 \to \eta_c \eta$	$< 3.9 \times 10^{-5}$	CL=90%		–
$X(4014)^0 K^+,\ X^0 \to \eta_c \pi^0$	$< 1.2 \times 10^{-5}$	CL=90%		–
$T_{c\overline{c}1}(3900)^0 K^+,\ T^0_{c\overline{c}1} \to \eta_c \pi^+ \pi^-$	$< 4.7 \times 10^{-5}$	CL=90%		–
$T_{c\overline{c}1}(3900)^0 K^+,\ T^0_{c\overline{c}1} \to J/\psi \eta$	$< 4.3 \times 10^{-7}$	CL=90%		–
$T_{c\overline{c}}(4020)^0 K^+,\ T^0_{c\overline{c}} \to \eta_c \pi^+ \pi^-$	$< 1.6 \times 10^{-5}$	CL=90%		–
$\chi_{c1}(3872) K^*(892)^+$	$< 5 \times 10^{-4}$	CL=90%		939
$\chi_{c1}(3872)^+ K^0,\ \chi^+_{c1} \to J/\psi(1S) \pi^+ \pi^0$ [ppp]	$< 6.1 \times 10^{-6}$	CL=90%		–
$\chi_{c1}(3872) K^0 \pi^+$	$(2.4 \pm 1.1) \times 10^{-4}$			1085
$T_{c\overline{c}1}(4430)^+ K^0,\ T^+_{c\overline{c}1} \to J/\psi \pi^+$	$< 1.5 \times 10^{-5}$	CL=95%		–
$T_{c\overline{c}1}(4430)^+ K^0,\ T^+_{c\overline{c}1} \to \psi(2S) \pi^+$	$< 4.7 \times 10^{-5}$	CL=95%		–

Int. J. Mod. Phys. A 2026.41. Downloaded from www.worldscientific.com
by UNIVERSITY OF CALIFORNIA @ BERKELEY on 09/16/26. Re-use and distribution is strictly not permitted, except for Open Access articles.

Int. J. Mod. Phys. A 2026.41. Downloaded from www.worldscientific.com
by UNIVERSITY OF CALIFORNIA @ BERKELEY on 09/16/26. Re-use and distribution is strictly not permitted, except for Open Acce

$T_{c\overline{c}1}(4430)^0 K^+$, $T^0_{c\overline{c}1} \to J/\psi\eta$	$< 1.27 \times 10^{-6}$	CL=90%		–
$\psi(4230)^0 K^+$, $\psi^0 \to J/\psi\pi^+\pi^-$	$< 1.56 \times 10^{-5}$	CL=95%		–
$\psi(4230) K^+$, $\psi \to J/\psi\eta$	$< 3.9 \times 10^{-7}$	CL=90%		–
$\psi(4360) K^+$, $\psi \to J/\psi\eta$	$< 1.24 \times 10^{-6}$	CL=90%		–
$\psi(4360) K^+$, $\psi(4360) \to \psi(2S)\pi^+\pi^-$	$(2.8 \pm 0.9) \times 10^{-6}$			–
$\psi(4390) K^+$, $\psi \to J/\psi\eta$	$< 2.41 \times 10^{-6}$	CL=90%		–
$\chi_{c0}(3915) K^+$, $\chi_{c0} \to J/\psi\gamma$	$< 1.4 \times 10^{-5}$	CL=90%		–
$\chi_{c0}(3915) K^+$, $\chi_{c0} \to \chi_{c1}(1P)\pi^0$	$< 3.8 \times 10^{-5}$	CL=90%		–
$X(3930)^0 K^+$, $X^0 \to J/\psi\gamma$	$< 2.5 \times 10^{-6}$	CL=90%		–
$J/\psi(1S) K^+$	$(1.019 \pm 0.019) \times 10^{-3}$			1684
$J/\psi(1S) K^0\pi^+$	$(1.13 \pm 0.11) \times 10^{-3}$			1651
$J/\psi(1S) K^+\pi^+\pi^-$	$(8.1 \pm 1.3) \times 10^{-4}$	S=2.5		1612
$J/\psi(1S) K^+K^-K^+$	$(3.37 \pm 0.29) \times 10^{-5}$			1252
$\chi_{c0}(3915) K^+$, $\chi_{c0} \to p\overline{p}$	$< 7.1 \times 10^{-8}$	CL=95%		–
$J/\psi(1S) K^*(892)^+$	$(1.43 \pm 0.08) \times 10^{-3}$			1571
$J/\psi(1S) K(1270)^+$	$(1.8 \pm 0.5) \times 10^{-3}$			1400
$J/\psi(1S) K(1400)^+$	$< 5 \times 10^{-4}$	CL=90%		1308
$J/\psi(1S)\eta K^+$	$(1.24 \pm 0.14) \times 10^{-4}$			1510
$\chi_{c1-odd}(3872) K^+$, $\chi_{c1-odd} \to J/\psi\eta$	$< 3.8 \times 10^{-6}$	CL=90%		–
$\psi(4160) K^+$, $\psi \to J/\psi\eta$	$< 8.7 \times 10^{-7}$	CL=90%		–
$J/\psi(1S)\eta' K^+$	$(3.1 \pm 0.4) \times 10^{-5}$			1273
$J/\psi(1S)\phi K^+$	$(5.0 \pm 0.4) \times 10^{-5}$			1227
$J/\psi(1S) K_1(1650)$, $K_1 \to \phi K^+$	$(6 {}^{+10}_{-6}) \times 10^{-6}$			–
$J/\psi(1S) K^*(1680)^+$, $K^* \to \phi K^+$	$(3.4 {}^{+1.9}_{-2.2}) \times 10^{-6}$			–
$J/\psi(1S) K_2^*(1980)$, $K_2^* \to \phi K^+$	$(1.5 {}^{+0.9}_{-0.5}) \times 10^{-6}$			–
$J/\psi(1S) K(1830)^+$, $K(1830)^+ \to \phi K^+$	$(1.3 {}^{+1.3}_{-1.1}) \times 10^{-6}$			–
$\chi_{c1}(4140) K^+$, $\chi_{c1} \to J/\psi(1S)\phi$	$(10 \pm 4) \times 10^{-6}$			–
$\chi_{c1}(4274) K^+$, $\chi_{c1} \to J/\psi(1S)\phi$	$(3.6 {}^{+2.2}_{-1.8}) \times 10^{-6}$			–
$\chi_{c0}(4500) K^+$, $\chi_{c0} \to J/\psi(1S)\phi$	$(3.3 {}^{+2.1}_{-1.7}) \times 10^{-6}$			–
$\chi_{c0}(4700) K^+$, $\chi_{c0} \to J/\psi(1S)\phi$	$(6 {}^{+5}_{-4}) \times 10^{-6}$			–
$J/\psi(1S)\omega K^+$	$(3.20 {}^{+0.60}_{-0.32}) \times 10^{-4}$			1388
$\chi_{c0}(3915) K^+$, $\chi_{c0} \to J/\psi\omega$	$(3.0 {}^{+0.9}_{-0.7}) \times 10^{-5}$			1103
$J/\psi(1S)\pi^+$	$(4.1 \pm 0.4) \times 10^{-5}$	S=2.5		1728
$J/\psi(1S)\pi^+\pi^+\pi^+\pi^-\pi^-$	$(1.17 \pm 0.13) \times 10^{-5}$			1635
$\psi(2S)\pi^+\pi^+\pi^-$	$(1.9 \pm 0.4) \times 10^{-5}$			1304
$J/\psi(1S)\rho^+$	$(4.1 \pm 0.5) \times 10^{-5}$	S=1.4		1612
$J/\psi(1S)\pi^+\pi^0$ nonresonant	$< 7.3 \times 10^{-6}$	CL=90%		1717
$J/\psi(1S) a_1(1260)^+$	$< 1.2 \times 10^{-3}$	CL=90%		1415
$J/\psi(1S) p\overline{p}\pi^+$	$< 5.0 \times 10^{-7}$	CL=90%		644
$J/\psi(1S) p\overline{\Lambda}$	$(1.46 \pm 0.12) \times 10^{-5}$			568
$J/\psi(1S)\overline{\Sigma}^0 p$	$< 1.1 \times 10^{-5}$	CL=90%		–
$J/\psi(1S) D^+$	$< 1.2 \times 10^{-4}$	CL=90%		871
$J/\psi(1S)\overline{D}^0\pi^+$	$< 2.5 \times 10^{-5}$	CL=90%		665
$J/\psi(1S) D_s^+$	$< 2.8 \times 10^{-7}$	CL=90%		727
$\psi(2S)\pi^+$	$(2.44 \pm 0.30) \times 10^{-5}$			1348
$\psi(2S) K^+$	$(6.25 \pm 0.21) \times 10^{-4}$			1284
$\psi(2S) K^*(892)^+$	$(6.7 \pm 1.4) \times 10^{-4}$	S=1.3		1116
$\psi(2S) K^+\pi^+\pi^-$	$(4.3 \pm 0.5) \times 10^{-4}$			1179
$\chi_{c0}(4500) K^+$, $\chi_{c0}(4500) \to \psi(2S)\pi^+\pi^-$	$(8.0 \pm 1.7) \times 10^{-5}$			–
$\chi_{c1}(4685) K^+$, $\chi_{c1}(4685) \to \psi(2S)\pi^+\pi^-$	$(1.25 \pm 0.32) \times 10^{-5}$			–
$\chi_{c0}(4700) K^+$, $\chi_{c0}(4700) \to \psi(2S)\pi^+\pi^-$	$(7.5 \pm 2.3) \times 10^{-6}$			–
$\psi(2S) K^*(1410)^+$, $K^*(1410)^+ \to K^+\pi^+\pi^-$	$(8 \pm 4) \times 10^{-6}$			–
$\psi(2S) K^*(1680)^+$, $K^*(1680)^+ \to K^+\pi^+\pi^-$	$(3.5 \pm 1.7) \times 10^{-5}$			–
$\psi(2S) K_1(1270)^+$, $K_1(1270)^+ \to K^+\pi^+\pi^-$	$(3.3 \pm 0.8) \times 10^{-5}$			–
$[\psi(2S) K_1(1270)^+$, $K_1(1270)^+ \to K^+\pi^+\pi^-]_{P-wave}$	$(3.3 \pm 0.7) \times 10^{-5}$			–
$[\psi(2S) K_1(1270)^+$, $K_1(1270)^+ \to K^+\pi^+\pi^-]_{D-wave}$	$(3.0 \pm 0.7) \times 10^{-5}$			–
$\psi(2S) K_1(1400)^+$, $K_1(1400)^+ \to K^+\pi^+\pi^-$	$(2.5 \pm 0.6) \times 10^{-5}$			–
$[\psi(2S) K_1(1400)^+$, $K_1(1400)^+ \to K^+\pi^+\pi^-]_{P-wave}$	$(2.1 \pm 1.9) \times 10^{-6}$			–
$\psi(2S) K_1(1460)^+$, $K_1(1460)^+ \to K^+\pi^+\pi^-$	$(2.3 \pm 0.5) \times 10^{-5}$			–
$\psi(2S) K_2^*(1430)^+$, $K_2^*(1430)^+ \to K^+\pi^+\pi^-$	$(1.89 \pm 0.29) \times 10^{-5}$			–
$T_{c\overline{c}1}(4200)^+ K^*(892)^0 \to \psi(2S) K^+\pi^+\pi^-$	$(1.7 \pm 0.6) \times 10^{-5}$			–
$[T_{c\overline{c}1}(4200)^+ K^*(892)^0 \to \psi(2S) K^+\pi^+\pi^-]_{P-wave}$	$(2.0 \pm 1.0) \times 10^{-5}$			–
$[T_{c\overline{c}1}(4200)^+ K^*(892)^0 \to \psi(2S) K^+\pi^+\pi^-]_{D-wave}$	$(1.21 \pm 0.34) \times 10^{-5}$			–
$T_{c\overline{c}1}(4430)^+ K^*(892)^0 \to \psi(2S) K^+\pi^+\pi^-$	$(3 \pm 10) \times 10^{-6}$			–
$T_{c\overline{c}1}(4430)^+ [K^+\pi^-]_{S-wave} \to \psi(2S) K^+\pi^+\pi^-$	$(1.5 \pm 0.5) \times 10^{-5}$			–
$T_{c\overline{c}s1}(4600)^0\pi^+$, $T_{c\overline{c}s1}(4600)^0 \to \psi(2S) K^+\pi^-$	$(1.9 \pm 1.1) \times 10^{-5}$			–
$T_{c\overline{c}s1}(4900)^0\pi^+$, $T_{c\overline{c}s1}(4900)^0 \to \psi(2S) K^+\pi^-$	$(1.1 \pm 0.9) \times 10^{-5}$			–
$\psi(2S)\phi(1020) K^+$	$(3.4 \pm 0.5) \times 10^{-6}$			418
$\psi(3770) K^+$	$(4.3 \pm 1.1) \times 10^{-4}$			1218
$\psi(3770) K+, \psi \to D^0\overline{D}^0$	$(1.5 \pm 0.5) \times 10^{-4}$	S=1.4		1218
$\psi(3770) K+, \psi \to D^+D^-$	$(9.4 \pm 3.5) \times 10^{-5}$			1218
$\psi(3770) K^+$, $\psi \to p\overline{p}$	$< 2 \times 10^{-7}$	CL=95%		–
$\psi(3770) K^+$, $\psi \to J/\psi\eta$	$< 4.6 \times 10^{-7}$	CL=90%		–
$\psi(4040) K^+$	$(1.6 \pm 0.5) \times 10^{-3}$			1002
$\psi(4040) K^+$, $\psi \to D^+D^-$	$(1.1 \pm 0.5) \times 10^{-5}$			–
$\psi(4160) K^+$	$(5.1 \pm 2.7) \times 10^{-4}$			869
$\psi(4160) K^+$, $\psi \to \overline{D}^0 D^0$	$(8 \pm 5) \times 10^{-5}$			–
$\psi(4160) K^+$, $\psi \to D^+D^-$	$(1.5 \pm 0.6) \times 10^{-5}$			–
$\psi(4415) K^+$, $\psi \to D^+D^-$	$(2.0 \pm 0.8) \times 10^{-5}$			–
$\psi(4415) K^+$, $\psi \to J/\psi\eta$	$< 9.6 \times 10^{-7}$	CL=90%		–
$\chi_{c0}\pi^+$, $\chi_{c0} \to \pi^+\pi^-$	$< 1 \times 10^{-7}$	CL=90%		1531
$\chi_{c0}\pi^+$, $\chi_{c0} \to \pi^0\pi^0$	$< 5 \times 10^{-7}$	CL=90%		–
$\chi_{c0} K^+$	$(1.49 {}^{+0.15}_{-0.14}) \times 10^{-4}$			1478
$\chi_{c0} K^0\pi^+$	$(1.45 \pm 0.21) \times 10^{-3}$			1439
$\chi_{c0} K^*(892)^+$	$< 2.1 \times 10^{-4}$	CL=90%		1341
$\chi_{c1}(1P)\pi^+$	$(2.2 \pm 0.5) \times 10^{-5}$			1468
$\chi_{c1}(1P) K^+$	$(4.74 \pm 0.22) \times 10^{-4}$			1412
$\chi_{c1}(1P) K^*(892)^+$	$(3.0 \pm 0.6) \times 10^{-4}$	S=1.1		1265
$\chi_{c1}(1P) K^0\pi^+$	$(5.8 \pm 0.4) \times 10^{-4}$			1370
$\chi_{c1}(1P) K^+\pi^0$	$(3.29 \pm 0.35) \times 10^{-4}$			1373
$\chi_{c1}(1P) K^+\pi^+\pi^-$	$(3.74 \pm 0.30) \times 10^{-4}$			1319
$\chi_{c1}(2P) K^+$, $\chi_{c1}(2P) \to \pi^+\pi^-\chi_{c1}(1P)$	$< 1.1 \times 10^{-5}$	CL=90%		–
$\chi_{c2}\pi^+$, $\chi_{c2} \to \pi^0\pi^0$	$< 7 \times 10^{-7}$	CL=90%		–
$\chi_{c2} K^+$	$(1.1 \pm 0.4) \times 10^{-5}$			1379
$\chi_{c2} K^+$, $\chi_{c2} \to p\overline{p}\pi^+\pi^-$	$< 1.9 \times 10^{-7}$			–
$\chi_{c2} K^*(892)^+$	$< 1.2 \times 10^{-4}$	CL=90%		1228
$\chi_{c2} K^0\pi^+$	$(1.24 \pm 0.25) \times 10^{-4}$			1336
$\chi_{c2} K^+\pi^0$	$< 6.2 \times 10^{-5}$	CL=90%		1339
$\chi_{c2} K^+\pi^+\pi^-$	$(1.34 \pm 0.19) \times 10^{-4}$			1284
$\chi_{c2}(3930) K^+$, $\chi_{c2} \to D^+D^-$	$(1.6 \pm 0.6) \times 10^{-5}$			–
$\chi_{c2}(3930)\pi^+$, $\chi_{c2} \to \pi^+\pi^-$	$< 1 \times 10^{-7}$	CL=90%		1437
$h_c(1P) K^+$	$(3.7 \pm 1.2) \times 10^{-5}$			1401
$h_c(1P) K^+$, $h_c \to p\overline{p}$	$< 6.4 \times 10^{-8}$	CL=95%		–
K* or *K modes				
$K^0\pi^+$	$(2.39 \pm 0.06) \times 10^{-5}$			2614
$K^+\pi^0$	$(1.32 \pm 0.04) \times 10^{-5}$			2615
$\eta' K^+$	$(7.04 \pm 0.25) \times 10^{-5}$			2528
$\eta' K^*(892)^+$	$(4.8 {}^{+1.8}_{-1.6}) \times 10^{-6}$			2472
$\eta' K_0^*(1430)^+$	$(5.2 \pm 2.1) \times 10^{-6}$			–
$\eta' K_2^*(1430)^+$	$(2.8 \pm 0.5) \times 10^{-5}$			2346

Int. J. Mod. Phys. A 2026.41. Downloaded from www.worldscientific.com
by UNIVERSITY OF CALIFORNIA @ BERKELEY on 09/16/26. Re-use and distribution is strictly not permitted, except for Open Access articles.

ηK^+	$(2.4 \pm 0.4) \times 10^{-6}$	S=1.7	2588
$\eta K^*(892)^+$	$(1.93 \pm 0.16) \times 10^{-6}$		2534
$\eta K_0^*(1430)^+$	$(1.8 \pm 0.4) \times 10^{-5}$		–
$\eta K_2^*(1430)^+$	$(9.1 \pm 3.0) \times 10^{-6}$		2414
$\eta(1295) K^+,\ \eta \to \eta\pi\pi$	$(2.9 {}^{+0.8}_{-0.7}) \times 10^{-6}$		2455
$\eta(1405) K^+,\ \eta \to \eta\pi\pi$	$< 1.3 \times 10^{-6}$	CL=90%	2425
$\eta(1405) K^+,\ \eta \to K^* K$	$< 1.2 \times 10^{-6}$	CL=90%	2425
$\eta(1405) K^+,\ \eta \to K^0 K\pi$	$(8.0 \pm 1.1) \times 10^{-6}$		–
$\eta(1475) K^+,\ \eta \to K^* K$	$(1.42 \pm 0.13) \times 10^{-5}$		2406
$\eta(1475) K^+,\ \eta \to a_0(980)\pi$	$(2.2 \pm 0.5) \times 10^{-6}$		–
$\eta(1475) K^+,\ \eta \to K^0 K\pi$	$(1.51 \pm 0.31) \times 10^{-5}$		–
$\eta(1760) K^+,\ \eta \to K^* \overline{K}$	$(3.4 \pm 0.6) \times 10^{-6}$		–
$\eta(1760) K^+,\ \eta \to a_0(980)\pi$	$(2.6 \pm 0.5) \times 10^{-6}$		–
$\eta(1760) K^+,\ \eta \to K^0 K\pi$	$(2.2 \pm 0.4) \times 10^{-5}$		–
$f_1(1285) K^+$	$< 2.0 \times 10^{-6}$	CL=90%	2458
$f_1(1285) K^+,\ f_1 \to a_0(980)\pi$	$(2.8 \pm 0.4) \times 10^{-6}$		–
$f_1(1420) K^+,\ f_1 \to \eta\pi\pi$	$< 2.9 \times 10^{-6}$	CL=90%	2420
$f_1(1420) K^+,\ f_1 \to K^* K$	$< 4.1 \times 10^{-6}$	CL=90%	2420
$f_1(1510) K^+,\ f_1 \to K^* \overline{K}$	$(3.8 \pm 1.5) \times 10^{-6}$		–
$h_1(1415) K^+,\ h_1 \to K^* \overline{K}$	$(2.22 \pm 0.27) \times 10^{-5}$		–
$h_1(1595) K^+,\ h_1 \to K^* \overline{K}$	$(1.04 \pm 0.16) \times 10^{-5}$		–
$\eta_2(1645) K^+,\ \eta_2 \to K^* \overline{K}$	$(1.50 \pm 0.28) \times 10^{-6}$		–
$\phi(1680) K^+,\ \phi \to K^* K$	$< 3.4 \times 10^{-6}$	CL=90%	2344
$f_0(1500) K^+$	$(3.7 \pm 2.2) \times 10^{-6}$		2393
ωK^+	$(6.5 \pm 0.4) \times 10^{-6}$		2558
$\omega K^*(892)^+$	$< 7.4 \times 10^{-6}$	CL=90%	2503
$\omega (K\pi)_0^{*+}$	$(2.8 \pm 0.4) \times 10^{-5}$		–
$\omega K_0^*(1430)^+$	$(2.4 \pm 0.5) \times 10^{-5}$		–
$\omega K_2^*(1430)^+$	$(2.1 \pm 0.4) \times 10^{-5}$		2379
$a_0(980)^+ K^0,\ a_0^+ \to \eta\pi^+$	$< 3.9 \times 10^{-6}$	CL=90%	–
$a_0(980)^0 K^+,\ a_0^0 \to \eta\pi^0$	$< 2.5 \times 10^{-6}$	CL=90%	–
$K^*(892)^0 \pi^+$	$(1.01 \pm 0.08) \times 10^{-5}$		2562
$K^*(892)^+ \pi^0$	$(6.8 \pm 0.9) \times 10^{-6}$		2563
$K^+ \pi^- \pi^+$	$(5.10 \pm 0.29) \times 10^{-5}$		2609
$K^+ \pi^- \pi^+$ nonresonant	$(1.63 {}^{+0.21}_{-0.15}) \times 10^{-5}$		2609
$\omega(782) K^+$	$(6 \pm 9) \times 10^{-6}$		2558
$K^+ f_0(980) \times B(f_0(980) \to \pi^+\pi^-)$	$(9.4 {}^{+1.0}_{-1.2}) \times 10^{-6}$		2522
$f_2(1270)^0 K^+$	$(1.07 \pm 0.27) \times 10^{-6}$		–
$f_0(1370)^0 K^+ \times B(f_0(1370)^0 \to \pi^+\pi^-)$	$< 1.07 \times 10^{-5}$	CL=90%	–
$\rho(14500) K^+ \times B(\rho(1450)^0 \to \pi^+\pi^-)$	$< 1.17 \times 10^{-5}$	CL=90%	–
$f_2'(1525) K^+ \times B(f_2'(1525) \to \pi^+\pi^-)$	$< 3.4 \times 10^{-6}$	CL=90%	2394
$K^+ \rho^0$	$(3.7 \pm 0.5) \times 10^{-6}$		2559
$K_0^*(1430)^0 \pi^+$	$(3.9 {}^{+0.6}_{-0.5}) \times 10^{-5}$	S=1.4	2445
$K_2^*(1430)^0 \pi^+$	$(5.6 {}^{+2.2}_{-1.5}) \times 10^{-6}$		2445
$K^*(1410)^0 \pi^+$	$< 4.5 \times 10^{-5}$	CL=90%	2448
$K^*(1680)^0 \pi^+$	$< 1.2 \times 10^{-5}$	CL=90%	2358
$K^+ \pi^0 \pi^0$	$(1.62 \pm 0.19) \times 10^{-5}$		2610
$f_0(980) K^+ \times B(f_0 \to \pi^0\pi^0)$	$(2.8 \pm 0.8) \times 10^{-6}$		2522
$K^- \pi^+ \pi^+$	$< 4.6 \times 10^{-8}$	CL=90%	2609
$K^- \pi^+ \pi^+$ nonresonant	$< 5.6 \times 10^{-5}$	CL=90%	2609
$K_1(1270)^0 \pi^+$	$< 4.0 \times 10^{-5}$	CL=90%	2488
$K_1(1400)^0 \pi^+$	$< 3.9 \times 10^{-5}$	CL=90%	2451
$K^0 \pi^+ \pi^0$	$< 6.6 \times 10^{-5}$	CL=90%	2609
$K_0^*(1430)^+ \pi^0$	$(1.19 {}^{+0.20}_{-0.23}) \times 10^{-5}$		–
$K^0 \rho^+$	$(7.3 {}^{+1.0}_{-1.2}) \times 10^{-6}$		2558
$K^*(892)^+ \pi^+ \pi^-$	$(7.5 \pm 1.0) \times 10^{-5}$		2557
$K^*(892)^+ \rho^0$	$(4.6 \pm 1.1) \times 10^{-6}$		2504
$K^*(892)^+ f_0(980)$	$(4.2 \pm 0.7) \times 10^{-6}$		2466
$a_1^+ K^0$	$(3.5 \pm 0.7) \times 10^{-5}$		–
$b_1^+ K^0 \times B(b_1^+ \to \omega\pi^+)$	$(9.6 \pm 1.9) \times 10^{-6}$		–
$K^*(892)^0 \rho^+$	$(9.2 \pm 1.5) \times 10^{-6}$		2504
$K_1(1400)^+ \rho^0$	$< 7.8 \times 10^{-4}$	CL=90%	2388
$K_2^*(1430)^+ \rho^0$	$< 1.5 \times 10^{-3}$	CL=90%	2381
$b_1^0 K^+ \times B(b_1^0 \to \omega\pi^0)$	$(9.1 \pm 2.0) \times 10^{-6}$		–
$b_1^+ K^{*0} \times B(b_1^+ \to \omega\pi^+)$	$< 5.9 \times 10^{-6}$	CL=90%	–
$b_1^0 K^{*+} \times B(b_1^0 \to \omega\pi^0)$	$< 6.7 \times 10^{-6}$	CL=90%	–
$K^+ \overline{K}^0$	$(1.32 \pm 0.17) \times 10^{-6}$	S=1.2	2593
$\overline{K}^0 K^+ \pi^0$	$< 2.4 \times 10^{-5}$	CL=90%	2578
$K^+ K_S^0 K_S^0$	$(1.05 \pm 0.04) \times 10^{-5}$		2521
$f_0(980) K^+,\ f_0 \to K_S^0 K_S^0$	$(1.47 \pm 0.33) \times 10^{-5}$		–
$f_0(1710) K^+,\ f_0 \to K_S^0 K_S^0$	$(4.8 {}^{+4.0}_{-2.6}) \times 10^{-7}$		–
$K^+ K_S^0 K_S^0$ nonresonant	$(2.0 \pm 0.4) \times 10^{-5}$		2521
$K_S^0 K_S^0 \pi^+$	$< 5.1 \times 10^{-7}$	CL=90%	2577
$K^+ K^- \pi^+$	$(5.2 \pm 0.4) \times 10^{-6}$		2578
$K^+ K^- \pi^+$ nonresonant	$(1.68 \pm 0.26) \times 10^{-6}$		2578
$K^+ \overline{K}^*(892)^0$	$(5.9 \pm 0.8) \times 10^{-7}$		2540
$K^+ \overline{K}_0^*(1430)^0$	$(3.8 \pm 1.3) \times 10^{-7}$		2421
$\pi^+ (K^+ K^-)_{S-wave}$	$(8.5 \pm 0.9) \times 10^{-7}$		2578
$\pi^+ K^+ K^-$, $m_{K^+K^-} < 1.1$ GeV	$(5.4 \pm 0.5) \times 10^{-6}$		–
$K^+ K^+ \pi^-$	$< 1.1 \times 10^{-8}$	CL=90%	2578
$K^+ K^+ \pi^-$ nonresonant	$< 8.79 \times 10^{-5}$	CL=90%	2578
$f_2'(1525) K^+$	$(1.8 \pm 0.5) \times 10^{-6}$	S=1.1	2394
$K^{*+} \pi^+ K^-$	$< 1.18 \times 10^{-5}$	CL=90%	2524
$K^*(892)^+ K^*(892)^0$	$(9.1 \pm 2.9) \times 10^{-7}$		2484
$K^{*+} K^+ \pi^-$	$< 6.1 \times 10^{-6}$	CL=90%	2524
$K^+ K^- K^+$	$(3.40 \pm 0.14) \times 10^{-5}$	S=1.4	2523
$K^+ \phi$	$(8.8 {}^{+0.7}_{-0.6}) \times 10^{-6}$	S=1.1	2516
$f_0(980) K^+ \times B(f_0(980) \to K^+ K^-)$	$(9.4 \pm 3.2) \times 10^{-6}$		2522
$a_2(1320) K^+ \times B(a_2(1320) \to K^+ K^-)$	$< 1.1 \times 10^{-6}$	CL=90%	2449
$X_0(1550) K^+ \times B(X_0(1550) \to K^+ K^-)$	$(4.3 \pm 0.7) \times 10^{-6}$		–
$\phi(1680) K^+ \times B(\phi(1680) \to K^+ K^-)$	$< 8 \times 10^{-7}$	CL=90%	2344
$f_0(1710) K^+ \times B(f_0(1710) \to K^+ K^-)$	$(1.1 \pm 0.6) \times 10^{-6}$		2330
$K^+ K^- K^+$ nonresonant	$(2.38 {}^{+0.28}_{-0.50}) \times 10^{-5}$		2523
$K^*(892)^+ K^+ K^-$	$(3.6 \pm 0.5) \times 10^{-5}$		2466
$K^*(892)^+ \phi$	$(10.0 \pm 2.0) \times 10^{-6}$	S=1.7	2460
$K^0 K^+ K^- \pi^+$	$(3.40 \pm 0.33) \times 10^{-4}$		2494
$J/\psi K^+,\ J/\psi \to K^0 K^- \pi^+$	$(5.4 \pm 1.2) \times 10^{-6}$		–
$\chi_{c1} K^+,\ \chi_{c1} \to K^0 K^- \pi^+$	$(2.25 \pm 0.25) \times 10^{-6}$		–
$\eta_c K^+,\ \eta_c \to K^0 K^- \pi^+$	$(2.83 \pm 0.30) \times 10^{-5}$		–
$\eta_c(2S) K^+,\ \eta_c(2S) \to K^0 K^- \pi^+$	$(3.3 \pm 0.4) \times 10^{-6}$		–
$K^0 K^+ K^+ \pi^-$	$(2.80 \pm 0.30) \times 10^{-4}$		2494
$J/\psi K^+,\ J/\psi \to K^0 K^+ \pi^-$	$(5.4 \pm 1.3) \times 10^{-6}$		–
$\chi_{c1} K^+,\ \chi_{c1} \to K^0 K^+ \pi^-$	$(2.06 \pm 0.32) \times 10^{-6}$		–
$\eta_c K^+,\ \eta_c \to K^0 K^+ \pi^-$	$(3.00 \pm 0.34) \times 10^{-5}$		–
$\eta_c(2S) K^+,\ \eta_c(2S) \to K^0 K^+ \pi^-$	$(3.1 \pm 0.6) \times 10^{-6}$		–
$\phi (K\pi)_0^{*+}$	$(8.3 \pm 1.6) \times 10^{-6}$		–
$\phi K_1(1270)^+$	$(6.1 \pm 1.9) \times 10^{-6}$		2380
$\phi K_1(1400)^+$	$< 3.2 \times 10^{-6}$	CL=90%	2339
$\phi K^*(1410)^+$	$< 4.3 \times 10^{-6}$	CL=90%	–
$\phi K_0^*(1430)^+$	$(7.0 \pm 1.6) \times 10^{-6}$		–
$\phi K_2^*(1430)^+$	$(8.4 \pm 2.1) \times 10^{-6}$		2332
$\phi K_2^*(1770)^+$	$< 1.50 \times 10^{-5}$	CL=90%	–
$\phi K_2^*(1820)^+$	$< 1.63 \times 10^{-5}$	CL=90%	–
$a_1^+ K^{*0}$	$< 3.6 \times 10^{-6}$	CL=90%	–
$K^+ \phi\phi$	$(4.2 \pm 0.8) \times 10^{-6}$	S=2.2	2306
$\eta'\eta' K^+$	$< 2.5 \times 10^{-5}$	CL=90%	2339
$\omega\phi K^+$	$< 1.9 \times 10^{-6}$	CL=90%	2374
$X(1812) K^+ \times B(X \to \omega\phi)$	$< 3.2 \times 10^{-7}$	CL=90%	–
$K^*(892)^+ \gamma$	$(3.95 \pm 0.13) \times 10^{-5}$	S=1.3	2564
$K_1(1270)^+ \gamma$	$(4.4 {}^{+0.7}_{-0.6}) \times 10^{-5}$		2490
$\eta K^+ \gamma$	$(7.9 \pm 0.9) \times 10^{-6}$		2588
$\eta' K^+ \gamma$	$(2.9 {}^{+1.0}_{-0.9}) \times 10^{-6}$		2528
$\phi K^+ \gamma$	$(2.7 \pm 0.4) \times 10^{-6}$	S=1.2	2516
$K^+ \pi^- \pi^+ \gamma$	$(2.58 \pm 0.15) \times 10^{-5}$	S=1.3	2609
$K^*(892)^0 \pi^+ \gamma$	$(2.33 \pm 0.12) \times 10^{-5}$		2562
$K^+ \rho^0 \gamma$	$(8.2 \pm 0.9) \times 10^{-6}$		2559
$(K^+ \pi^-)_{NR} \pi^+ \gamma$	$(9.9 {}^{+1.7}_{-2.0}) \times 10^{-6}$		2609
$K^0 \pi^+ \pi^0 \gamma$	$(4.6 \pm 0.5) \times 10^{-5}$		2609
$K_1(1400)^+ \gamma$	$(10 {}^{+5}_{-4}) \times 10^{-6}$		2453
$K^*(1410)^+ \gamma$	$(2.7 {}^{+0.8}_{-0.6}) \times 10^{-5}$		–
$K_0^*(1430)^0 \pi^+ \gamma$	$(1.32 {}^{+0.26}_{-0.32}) \times 10^{-6}$		2445
$K_2^*(1430)^+ \gamma$	$(1.4 \pm 0.4) \times 10^{-5}$		2447

Int. J. Mod. Phys. A 2026.41. Downloaded from www.worldscientific.com
by UNIVERSITY OF CALIFORNIA @ BERKELEY on 09/16/26. Re-use and distribution is strictly not permitted, except for Open Acce

$K^*(1680)^+\gamma$		$(6.7 \pm^{1.7}_{1.4})\times10^{-5}$			2360
$K_3^*(1780)^+\gamma$		$<3.9\times10^{-5}$	CL=90%		2340
$K_4^*(2045)^+\gamma$		$<9.9\times10^{-3}$	CL=90%		2242

Light unflavored meson modes

$\rho^+\gamma$		$(1.16\pm0.17)\times10^{-6}$			2583
$\pi^+\pi^0$		$(5.31\pm0.26)\times10^{-6}$			2636
$\pi^+\pi^+\pi^-$		$(1.52\pm0.14)\times10^{-5}$			2630
$\rho^0\pi^+$		$(8.3\pm1.2)\times10^{-6}$			2581
$\pi^+ f_0(980)$, $f_0\to\pi^+\pi^-$		$<1.5\times10^{-6}$	CL=90%		2545
$\pi^+ f_2(1270)$		$(2.2\pm^{0.7}_{0.4})\times10^{-6}$			2484
$\rho(1450)^0\pi^+$, $\rho^0\to\pi^+\pi^-$		$(1.4\pm^{0.6}_{0.9})\times10^{-6}$			2434
$\rho(1450)^0\pi^+$, $\rho^0\to K^+K^-$		$(1.60\pm0.14)\times10^{-6}$			–
$f_0(1370)\pi^+$, $f_0\to\pi^+\pi^-$		$<4.0\times10^{-6}$	CL=90%		2460
$f_0(1370)\pi^+$, $f_0\to\pi^0\pi^0$		$<1.1\times10^{-6}$	CL=90%		–
$f_0(500)\pi^+$, $f_0\to\pi^+\pi^-$		$<4.1\times10^{-6}$	CL=90%		–
$\pi^+\pi^-\pi^+$ nonresonant		$(5.3\pm^{1.5}_{1.1})\times10^{-6}$			2630
$\pi^+\pi^0\pi^0$		$(1.90\pm0.21)\times10^{-5}$			2631
$\rho^+\pi^0$		$(1.06\pm^{0.12}_{0.13})\times10^{-5}$			2581
$\rho(1450)^+\pi^0$, $\rho^+\to\pi^+\pi^0$		$(1.2\pm0.6)\times10^{-6}$			–
$\pi^+\pi^0\pi^0$ nonresonant		$<6\times10^{-7}$	CL=90%		2631
$X\,pi+, X\to\pi^0\pi^0$		$(6.9\pm1.1)\times10^{-6}$			–
$\pi^+\pi^-\pi^+\pi^0$		$<4.0\times10^{-3}$	CL=90%		2622
$\rho^+\rho^0$		$(2.40\pm0.19)\times10^{-5}$			2523
$\rho^+ f_0(980)$, $f_0\to\pi^+\pi^-$		$<2.0\times10^{-6}$	CL=90%		2486
$a_1(1260)^+\pi^0$		$(2.6\pm0.7)\times10^{-5}$			2494
$a_1(1260)^0\pi^+$		$(2.0\pm0.6)\times10^{-5}$			2494
$\omega\pi^+$		$(6.9\pm0.5)\times10^{-6}$			2580
$\omega\rho^+$		$(1.59\pm0.21)\times10^{-5}$			2522
$\eta\pi^+$		$(4.02\pm0.27)\times10^{-6}$			2609
$\eta\rho^+$		$(7.0\pm2.9)\times10^{-6}$		S=2.8	2553
$\eta'\pi^+$		$(2.7\pm0.9)\times10^{-6}$		S=1.9	2551
$\eta'\rho^+$		$(9.7\pm2.2)\times10^{-6}$			2492
$\phi\pi^+$		$(3.2\pm1.5)\times10^{-8}$			2539
$\phi\rho^+$		$<3.0\times10^{-6}$	CL=90%		2480
$a_0(980)^0\pi^+$, $a_0^0\to\eta\pi^0$		$<5.8\times10^{-6}$	CL=90%		–
$a_0(980)^+\pi^0$, $a_0^+\to\eta\pi^+$		$<1.4\times10^{-6}$	CL=90%		–
$\pi^+\pi^+\pi^+\pi^-\pi^-$		$<8.6\times10^{-4}$	CL=90%		2608
$\rho^0 a_1(1260)^+$		$<6.2\times10^{-4}$	CL=90%		2433
$\rho^0 a_2(1320)^+$		$<7.2\times10^{-4}$	CL=90%		2410
$b_1^0\pi^+$, $b_1^0\to\omega\pi^0$		$(6.7\pm2.0)\times10^{-6}$			–
$b_1^+\pi^0$, $b_1^+\to\omega\pi^+$		$<3.3\times10^{-6}$	CL=90%		–
$\pi^+\pi^+\pi^+\pi^-\pi^-\pi^0$		$<6.3\times10^{-3}$	CL=90%		2592
$b_1^+\rho^0$, $b_1^+\to\omega\pi^+$		$<5.2\times10^{-6}$	CL=90%		–
$a_1(1260)^+ a_1(1260)^0$		<1.3 %	CL=90%		2336
$b_1^0\rho^+$, $b_1^0\to\omega\pi^0$		$<3.3\times10^{-6}$	CL=90%		–

Charged particle ($h^\pm$) modes

$h^\pm = K^\pm$ or $\pi^\pm$

$h^+\pi^0$		$(1.6\pm^{0.7}_{0.6})\times10^{-5}$			2636
ωh^+		$(1.38\pm^{0.27}_{0.24})\times10^{-5}$			2580
h^+X^0 (Familon)		$<4.9\times10^{-5}$	CL=90%		–
K^+X^0, $X^0\to\mu^+\mu^-$		$<1\times10^{-7}$	CL=95%		–

Baryon modes

$p\overline{p}\pi^+$		$(1.62\pm0.20)\times10^{-6}$			2439
$p\overline{p}\pi^+$ nonresonant		$<5.3\times10^{-5}$	CL=90%		2439
$p\overline{p}\pi^+\pi^0$		$(4.6\pm1.3)\times10^{-6}$			2407
$p\overline{p}K^+$		$(5.9\pm0.5)\times10^{-6}$		S=1.5	2348
$\Theta(1710)^{++}\overline{p}$, $\Theta^{++}\to pK^+$	[qqq]	$<9.1\times10^{-8}$	CL=90%		–
$f_J(2220)K^+$, $f_J\to p\overline{p}$	[qqq]	$<4.1\times10^{-7}$	CL=90%		2135
$p\overline{n}\pi^0$		$<6.3\times10^{-6}$	CL=90%		2440
$p\overline{\Lambda}(1520)$		$(3.1\pm0.6)\times10^{-7}$			2322
$p\overline{p}K^+$ nonresonant		$<8.9\times10^{-5}$	CL=90%		2348
$p\overline{p}K^*(892)^+$		$(3.6\pm^{0.8}_{0.7})\times10^{-6}$			2215
$f_J(2220)K^{*+}$, $f_J\to p\overline{p}$		$<7.7\times10^{-7}$	CL=90%		2059
$p\overline{\Lambda}$		$(2.4\pm^{1.0}_{0.9})\times10^{-7}$			2430
$p\overline{\Lambda}\gamma$		$(2.4\pm^{0.5}_{0.4})\times10^{-6}$			2430
$p\overline{\Lambda}\pi^0$		$(3.0\pm^{0.7}_{0.6})\times10^{-6}$			2402
$p\overline{\Sigma}(1385)^0$		$<4.7\times10^{-7}$	CL=90%		2362
$\Delta^+\overline{\Lambda}$		$<8.2\times10^{-7}$	CL=90%		–
$p\overline{\Sigma}\gamma$		$<4.6\times10^{-6}$	CL=90%		2413
$p\overline{\Lambda}\pi^+\pi^-$		$(1.13\pm0.13)\times10^{-5}$			2368
$p\overline{\Lambda}\pi^+\pi^-$ nonresonant		$(5.9\pm1.1)\times10^{-6}$			2368
$p\overline{\Lambda}\rho^0$, $\rho^0\to\pi^+\pi^-$		$(4.8\pm0.9)\times10^{-6}$			2214
$p\overline{\Lambda}f_2(1270)$, $f_2\to\pi^+\pi^-$		$(2.0\pm0.8)\times10^{-6}$			2026
$p\overline{\Lambda}K^+K^-$		$(4.1\pm0.7)\times10^{-6}$			2132
$p\overline{\Lambda}\phi$		$(8.0\pm2.2)\times10^{-7}$			2119
$\overline{p}\Lambda K^+K^-$		$(3.7\pm0.6)\times10^{-6}$			2132
$\Lambda\overline{\Lambda}\pi^+$		$<9.4\times10^{-7}$	CL=90%		2358
$\Lambda\overline{\Lambda}K^+$		$(3.4\pm0.6)\times10^{-6}$			2251
$\Lambda\overline{\Lambda}K^{*+}$		$(2.2\pm^{1.2}_{0.9})\times10^{-6}$			2098
$\Lambda(1520)\overline{\Lambda}K^+$		$(2.2\pm0.7)\times10^{-6}$			2126
$\Lambda\overline{\Lambda}(1520)K^+$		$<2.08\times10^{-6}$			2126
$\overline{\Delta}^0 p$		$<1.38\times10^{-6}$	CL=90%		2403
$\overline{\Delta}^{++}\overline{p}$		$<1.4\times10^{-7}$	CL=90%		2403
$\overline{\Lambda}p\overline{p}p$		$(2.1\pm0.5)\times10^{-7}$			1669
$\overline{\Lambda}p\eta_c$		$<1.9\times10^{-5}$	CL=90%		777
$D^+p\overline{p}$		$<1.5\times10^{-5}$	CL=90%		1860
$D^*(2010)^+p\overline{p}$		$<1.5\times10^{-5}$	CL=90%		1786
$\overline{D}^0 p\overline{p}\pi^+$		$(3.72\pm0.27)\times10^{-4}$			1789
$\overline{D}^{*0} p\overline{p}\pi^+$		$(3.73\pm0.32)\times10^{-4}$			1709
$D^-p\overline{p}\pi^+\pi^-$		$(1.66\pm0.30)\times10^{-4}$			1705
$D^{*-}p\overline{p}\pi^+\pi^-$		$(1.86\pm0.25)\times10^{-4}$			1621
$p\overline{\Lambda}^0\overline{D}^0$		$(1.43\pm0.32)\times10^{-5}$			–
$p\overline{\Lambda}^0\overline{D}^*(2007)^0$		$<5\times10^{-5}$	CL=90%		–
$\overline{\Lambda}_c^- p\pi^+$		$(2.2\pm0.4)\times10^{-4}$		S=2.7	1980
$\overline{\Lambda}_c^- pK^+$		$(8.8\pm1.6)\times10^{-6}$			1849
$\overline{\Lambda}_c^-\Delta(1232)^{++}$		$<1.9\times10^{-5}$	CL=90%		1928
$\overline{\Lambda}_c^-\Delta_X(1600)^{++}$		$(4.6\pm0.9)\times10^{-5}$			–
$\overline{\Lambda}_c^-\Delta_X(2420)^{++}$		$(3.7\pm0.8)\times10^{-5}$			–
$(\overline{\Lambda}_c^- p)_s\pi^+$	[rrr]	$(3.1\pm^{0.7}_{0.6})\times10^{-5}$			–
$\overline{\Sigma}_c(2520)^0 p$		$<3\times10^{-6}$	CL=90%		1904
$\overline{\Sigma}_c(2800)^0 p$		$(2.6\pm0.9)\times10^{-5}$			–
$\overline{\Lambda}_c^- p\pi^+\pi^0$		$(1.8\pm0.6)\times10^{-3}$			1935
$\overline{\Lambda}_c^- p\pi^+\pi^+\pi^-$		$(2.2\pm0.7)\times10^{-3}$			1880
$\overline{\Lambda}_c^- p\pi^+\pi^+\pi^-\pi^0$		<1.34 %	CL=90%		1823
$\Lambda_c^+\Lambda_c^- K^+$		$(4.9\pm0.7)\times10^{-4}$			739
$\Xi_c(2930)\Lambda_c^+$, $\Xi_c\to K^+\Lambda_c^-$		$(1.7\pm0.5)\times10^{-4}$			–
$\overline{\Sigma}_c(2455)^0 p$		$(2.9\pm0.6)\times10^{-5}$			1938
$\overline{\Sigma}_c(2455)^0 p\pi^0$		$(3.5\pm1.1)\times10^{-4}$			1896
$\overline{\Sigma}_c(2455)^0 p\pi^-\pi^+$		$(3.5\pm1.0)\times10^{-4}$			1845
$\overline{\Sigma}_c(2455)^{--}p\pi^+\pi^+$		$(2.33\pm0.17)\times10^{-4}$			1845
$\Sigma_c(2455)^{++}\overline{\Xi}_c^-$		$(5.7\pm^{2.7}_{1.9})\times10^{-4}$			957
$\overline{\Lambda}_c(2593)^-/\overline{\Lambda}_c(2625)^- p\pi^+$		$<1.9\times10^{-4}$	CL=90%		–
$\overline{\Xi}_c^0\Lambda_c^+$		$(9.5\pm2.3)\times10^{-4}$			1144
$\Xi_c^0\Lambda_c^+$		$<2.6\times10^{-5}$	CL=95%		1144
$\overline{\Xi}_c^0\Lambda_c^+$, $\overline{\Xi}_c^0\to\overline{\Xi}^+\pi^-$		$(1.76\pm0.29)\times10^{-5}$			1144
$\overline{\Xi}_c^0\Lambda_c^+$, $\overline{\Xi}_c^0\to\Lambda K^+\pi^-$		$(1.14\pm0.26)\times10^{-5}$			1144
$\overline{\Xi}_c^0\Lambda_c^+$, $\overline{\Xi}_c^0\to pK^-K^-\pi^+$		$(5.5\pm1.9)\times10^{-6}$			–
$\Lambda_c^+\overline{\Xi}_c'^0$		$<6.5\times10^{-4}$	CL=90%		1023
$\Lambda_c^+\overline{\Xi}_c(2645)^0$		$<7.9\times10^{-4}$	CL=90%		–
$\Lambda_c^+\overline{\Xi}_c(2790)^0$		$(1.1\pm0.4)\times10^{-3}$			–

Lepton Family number (LF) or Lepton number (L) or Baryon number (B) violating modes, or/and $\Delta B=1$ weak neutral current ($B1$) modes

$\pi^+\ell^+\ell^-$	$B1$	[jjj]	$<4.9\times10^{-8}$	CL=90%		2638
$\pi^+e^+e^-$	$B1$		$<5.4\times10^{-8}$	CL=90%		2638
$\pi^+\mu^+\mu^-$	$B1$		$(1.78\pm0.22)\times10^{-8}$			2634
$\rho(770)^+e^+e^-$	$B1$		$<4.67\times10^{-7}$	CL=90%		–
$\rho(770)^+\mu^+\mu^-$	$B1$		$<3.81\times10^{-7}$	CL=90%		–
$\rho(770)^+\ell^+\ell^-$	$B1$		$<1.89\times10^{-7}$	CL=90%		–
$\pi^+\nu\overline{\nu}$	$B1$		$<1.4\times10^{-5}$	CL=90%		2638
$K^+\ell^+\ell^-$	$B1$	[jjj]	$(4.7\pm0.5)\times10^{-7}$		S=2.3	2617
$K^+e^+e^-$	$B1$		$(5.6\pm0.6)\times10^{-7}$			2617
$K^+\mu^+\mu^-$	$B1$		$(4.53\pm0.35)\times10^{-7}$		S=1.8	2612
$K^+\mu^+\mu^-$ nonresonant	$B1$		$(4.37\pm0.27)\times10^{-7}$			2612
$K^+\tau^+\tau^-$	$B1$		$<2.25\times10^{-3}$	CL=90%		1687
$K^+\overline{\nu}\nu$	$B1$		$(2.3\pm0.7)\times10^{-5}$			2617
$\rho^+\nu\overline{\nu}$	$B1$		$<3.0\times10^{-5}$	CL=90%		2583
$K^*(892)^+\ell^+\ell^-$	$B1$	[jjj]	$(1.01\pm0.11)\times10^{-6}$		S=1.1	2564
$K^*(892)^+e^+e^-$	$B1$		$(1.55\pm^{0.40}_{0.31})\times10^{-6}$			2564
$K^*(892)^+\mu^+\mu^-$	$B1$		$(9.6\pm1.0)\times10^{-7}$			2560

Int. J. Mod. Phys. A 2026.41. Downloaded from www.worldscientific.com
by UNIVERSITY OF CALIFORNIA @ BERKELEY on 09/16/26. Re-use and distribution is strictly not permitted, except for Open Access articles.

$K^*(892)^+ \nu\overline{\nu}$	B1	< 4.0	$\times 10^{-5}$	CL=90%	2564
$K^+ \pi^+ \pi^- \mu^+ \mu^-$	B1	(4.3 ± 0.4) $\times 10^{-7}$			2593
$D_s^+ \mu^+ \mu^-$	B1	< 2.4	$\times 10^{-8}$	CL=90%	2267
$\phi K^+ \mu^+ \mu^-$	B1	(7.9 $^{+2.1}_{-1.7}$) $\times 10^{-8}$			2490
$\overline{\Lambda} p \nu\overline{\nu}$	B1	< 3.0	$\times 10^{-5}$	CL=90%	2430
$\pi^+ e^+ \mu^-$	LF	< 6.4	$\times 10^{-3}$	CL=90%	2637
$\pi^+ e^- \mu^+$	LF	< 6.4	$\times 10^{-3}$	CL=90%	2637
$\pi^+ e^\pm \mu^\mp$	LF	< 1.7	$\times 10^{-7}$	CL=90%	2637
$\pi^+ e^+ \tau^-$	LF	< 7.4	$\times 10^{-5}$	CL=90%	2338
$\pi^+ e^- \tau^+$	LF	< 2.0	$\times 10^{-5}$	CL=90%	2338
$\pi^+ e^\pm \tau^\mp$	LF	< 7.5	$\times 10^{-5}$	CL=90%	2338
$\pi^+ \mu^+ \tau^-$	LF	< 6.2	$\times 10^{-5}$	CL=90%	2334
$\pi^+ \mu^- \tau^+$	LF	< 4.5	$\times 10^{-5}$	CL=90%	2334
$\pi^+ \mu^\pm \tau^\mp$	LF	< 7.2	$\times 10^{-5}$	CL=90%	2334
$K^+ e^+ \mu^-$	LF	< 7.0	$\times 10^{-9}$	CL=90%	2616
$K^+ e^- \mu^+$	LF	< 6.4	$\times 10^{-9}$	CL=90%	2616
$K^+ e^\pm \mu^\mp$	LF	< 9.1	$\times 10^{-8}$	CL=90%	2616
$K^+ e^+ \tau^-$	LF	< 1.53	$\times 10^{-5}$	CL=90%	2312
$K^+ e^- \tau^+$	LF	< 1.5	$\times 10^{-5}$	CL=90%	2312
$K^+ e^\pm \tau^\mp$	LF	< 3.0	$\times 10^{-5}$	CL=90%	2312
$K^+ \mu^+ \tau^-$	LF	< 2.45	$\times 10^{-5}$	CL=90%	2298
$K^+ \mu^- \tau^+$	LF	< 5.9	$\times 10^{-6}$	CL=90%	2298
$K^+ \mu^\pm \tau^\mp$	LF	< 4.8	$\times 10^{-5}$	CL=90%	2298
$K^*(892)^+ e^+ \mu^-$	LF	< 1.3	$\times 10^{-6}$	CL=90%	2563
$K^*(892)^+ e^- \mu^+$	LF	< 9.9	$\times 10^{-7}$	CL=90%	2563
$K^*(892)^+ e^\pm \mu^\mp$	LF	< 1.4	$\times 10^{-6}$	CL=90%	2563
$\pi^- e^+ e^+$	L	< 2.3	$\times 10^{-8}$	CL=90%	2638
$\pi^- \mu^+ \mu^+$	L	< 4.0	$\times 10^{-9}$	CL=95%	2634
$\pi^- e^+ \mu^+$	L	< 1.5	$\times 10^{-7}$	CL=90%	2637
$\rho^- e^+ e^+$	L	< 1.7	$\times 10^{-7}$	CL=90%	2583
$\rho^- \mu^+ \mu^+$	L	< 4.2	$\times 10^{-7}$	CL=90%	2578
$\rho^- e^+ \mu^+$	L	< 4.7	$\times 10^{-7}$	CL=90%	2582
$K^- e^+ e^+$	L	< 3.0	$\times 10^{-8}$	CL=90%	2617
$K^- \mu^+ \mu^+$	L	< 4.1	$\times 10^{-8}$	CL=90%	2612
$K^- e^+ \mu^+$	L	< 1.6	$\times 10^{-7}$	CL=90%	2616
$K^*(892)^- e^+ e^+$	L	< 4.0	$\times 10^{-7}$	CL=90%	2564
$K^*(892)^- \mu^+ \mu^+$	L	< 5.9	$\times 10^{-7}$	CL=90%	2560
$K^*(892)^- e^+ \mu^+$	L	< 3.0	$\times 10^{-7}$	CL=90%	2563
$D^- e^+ e^+$	L	< 2.6	$\times 10^{-6}$	CL=90%	2309
$D^- e^+ \mu^+$	L	< 1.8	$\times 10^{-6}$	CL=90%	2307
$D^- \mu^+ \mu^+$	L	< 6.9	$\times 10^{-7}$	CL=95%	2303
$D^{*-} \mu^+ \mu^+$	L	< 2.4	$\times 10^{-6}$	CL=95%	2251
$D_s^- \mu^+ \mu^+$	L	< 5.8	$\times 10^{-7}$	CL=95%	2267
$\overline{D}^0 \pi^- \mu^+ \mu^+$	L	< 1.5	$\times 10^{-6}$	CL=95%	2295
$\Lambda^0 \mu^+$	L,B	< 6	$\times 10^{-8}$	CL=90%	–
$\Lambda^0 e^+$	L,B	< 3.2	$\times 10^{-8}$	CL=90%	–
$\overline{\Lambda}^0 \mu^+$	L,B	< 6	$\times 10^{-8}$	CL=90%	–
$\overline{\Lambda}^0 e^+$	L,B	< 8	$\times 10^{-8}$	CL=90%	–

B^0

$I(J^P) = \frac{1}{2}(0^-)$

I, J, P need confirmation. Quantum numbers shown are quark-model predictions.

Mass $m_{B^0} = 5279.72 \pm 0.08$ MeV
$m_{B^0} - m_{B^\pm} = 0.31 \pm 0.05$ MeV
Mean life $\tau_{B^0} = (1.5113 \pm 0.0027) \times 10^{-12}$ s
$c\tau = 453.1\ \mu$m
$\tau_{B^+}/\tau_{B^0} = 1.0832 \pm 0.0034$ (direct measurements)

B^0-$\overline{B}^0$ mixing parameters

χ_d (B^0-$\overline{B}^0$ mixing probability) $= 0.1849 \pm 0.0010$
$\Delta m_{B^0} = m_{B^0_H} - m_{B^0_L} = (0.5068 \pm 0.0019) \times 10^{12}\ \hbar\ \mathrm{s}^{-1}$
$= (3.336 \pm 0.013) \times 10^{-10}$ MeV
$x_d = \Delta m_{B^0}/\Gamma_{B^0} = 0.7659 \pm 0.0032$
$\mathrm{Re}(\lambda_{CP}\ /\ |\lambda_{CP}|)\ \mathrm{Re}(z) = 0.047 \pm 0.022$
$\Delta\Gamma\ \mathrm{Re}(z) = -0.007 \pm 0.004\ \mathrm{ps}^{-1}$
$\mathrm{Re}(z) = (-4 \pm 4) \times 10^{-2}$ (S = 1.4)
$\mathrm{Im}(z) = (-0.8 \pm 0.4) \times 10^{-2}$

CP violation parameters

$\mathrm{Re}(\epsilon_{B^0})/(1+|\epsilon_{B^0}|^2) = (-0.5 \pm 0.4) \times 10^{-3}$
$A_{T/CP}(B^0 \leftrightarrow \overline{B}^0) = 0.005 \pm 0.018$
$A_{CP}(B^0 \to D^*(2010)^+ D^-) = 0.013 \pm 0.014$
$A_{CP}(B^0 \to \overline{D}^0 \pi^0) = (0.4 \pm 2.4) \times 10^{-2}$
$A_{CP}(B^0 \to [K^+ K^-]_D K^*(892)^0) = -0.05 \pm 0.06$
$A_{CP}(B^0 \to [K^+ \pi^-]_D K^*(892)^0) = 0.031 \pm 0.023$
$A_{CP}(B^0 \to [K^+ \pi^- \pi^+ \pi^-]_D K^*(892)^0) = -0.012 \pm 0.024$
$A_{CP}(B^0 \to [K^- \pi^+]_D K^*(892)^0) = 0.19 \pm 0.19$
$A_{CP}(B^0 \to [K^- \pi^+ \pi^+ \pi^-]_D K^*(892)^0) = -0.01 \pm 0.24$
$R_d^+ = \Gamma(B^0 \to [\pi^+ K^-]_D K^{*0})\ /\ \Gamma(B^0 \to [\pi^- K^+]_D K^{*0}) = 0.069 \pm 0.014$
$R_d^- = \Gamma(\overline{B}^0 \to [\pi^- K^+]_D K^{*0})\ /\ \Gamma(\overline{B}^0 \to [\pi^+ K^-]_D K^{*0}) = 0.093 \pm 0.014$
$A_{CP}(B^0 \to [\pi^+ \pi^-]_D K^*(892)^0) = -0.03 \pm 0.10$
$A_{CP}(B^0 \to [\pi^+ \pi^- \pi^+ \pi^-]_D K^*(892)^0) = 0.02 \pm 0.09$
$R_d^+ = \Gamma(B^0 \to [\pi^+ K^- \pi^+ \pi^-]_D K^{*0})\ /\ \Gamma(B^0 \to [\pi^- K^+ \pi^+ \pi^-]_D K^{*0}) = 0.060 \pm 0.015$
$R_d^- = \Gamma(\overline{B}^0 \to [\pi^- K^+ \pi^+ \pi^-]_D K^{*0})\ /\ \Gamma(\overline{B}^0 \to [\pi^+ K^- \pi^+ \pi^-]_D K^{*0}) = 0.038 \pm 0.015$
$\boldsymbol{A_{CP}\ (B^0 \to K^+ \pi^-)} = -0.0831 \pm 0.0031$
$A_{CP}(B^0 \to \eta' K^*(892)^0) = -0.07 \pm 0.18$
$A_{CP}(B^0 \to \eta' K_0^*(1430)^0) = -0.19 \pm 0.17$
$A_{CP}(B^0 \to \eta' K_2^*(1430)^0) = 0.14 \pm 0.18$
$\boldsymbol{A_{CP}(B^0 \to \eta K^*(892)^0)} = 0.19 \pm 0.05$
$A_{CP}(B^0 \to \eta K_0^*(1430)^0) = 0.06 \pm 0.13$
$A_{CP}(B^0 \to \eta K_2^*(1430)^0) = -0.07 \pm 0.19$
$A_{CP}(B^0 \to b_1 K^+) = -0.07 \pm 0.12$
$A_{CP}(B^0 \to \omega K^{*0}) = 0.45 \pm 0.25$
$A_{CP}(B^0 \to \omega (K\pi)_0^{*0}) = -0.07 \pm 0.09$
$A_{CP}(B^0 \to \omega K_2^*(1430)^0) = -0.37 \pm 0.17$
$A_{CP}(B^0 \to K^+ \pi^- \pi^0) = (0 \pm 6) \times 10^{-2}$
$A_{CP}(B^0 \to \rho^- K^+) = 0.20 \pm 0.11$
$A_{CP}(B^0 \to \rho(1450)^- K^+) = -0.10 \pm 0.33$
$A_{CP}(B^0 \to \rho(1700)^- K^+) = -0.4 \pm 0.6$
$A_{CP}(B^0 \to K^+ \pi^- \pi^0\ \mathrm{nonresonant}) = 0.10 \pm 0.18$
$A_{CP}(B^0 \to K^0 \pi^+ \pi^-) = -0.01 \pm 0.05$
$\boldsymbol{A_{CP}(B^0 \to K^*(892)^+ \pi^-)} = -0.27 \pm 0.04$
$A_{CP}(B^0 \to (K\pi)_0^{*+} \pi^-) = 0.02 \pm 0.04$
$A_{CP}(B^0 \to K_2^*(1430)^+ \pi^-) = -0.29 \pm 0.24$
$A_{CP}(B^0 \to K^*(1680)^+ \pi^-) = -0.07 \pm 0.14$
$A_{CP}(B^0 \to f_0(980)\ K_S^0) = 0.28 \pm 0.31$
$A_{CP}(B^0 \to (K\pi)_0^{*0} \pi^0) = -0.15 \pm 0.11$
$A_{CP}(B^0 \to K^{*0} \pi^0) = -0.15 \pm 0.13$
$A_{CP}(B^0 \to K^*(892)^0 \pi^+ \pi^-) = 0.07 \pm 0.05$
$A_{CP}(B^0 \to K^*(892)^0 \rho^0) = -0.06 \pm 0.09$
$A_{CP}(B^0 \to K^{*0} f_0(980)) = 0.07 \pm 0.10$
$A_{CP}(B^0 \to K^{*+} \rho^-) = 0.21 \pm 0.15$
$A_{CP}(B^0 \to K^*(892)^0 K^+ K^-) = 0.01 \pm 0.05$
$A_{CP}(B^0 \to a_1^- K^+) = -0.16 \pm 0.12$
$A_{CP}(B^0 \to K^0 K^0) = -0.6 \pm 0.7$
$A_{CP}(B^0 \to K^*(892)^0 \phi) = 0.00 \pm 0.04$
$A_{CP}(B^0 \to K^*(892)^0 K^- \pi^+) = 0.2 \pm 0.4$
$A_{CP}(B^0 \to \phi (K\pi)_0^{*0}) = 0.12 \pm 0.08$
$A_{CP}(B^0 \to \phi K_2^*(1430)^0) = -0.11 \pm 0.10$
$A_{CP}(B^0 \to K^*(892)^0 \gamma) = -0.012 \pm 0.010$
$A_{CP}(B^0 \to K_2^*(1430)^0 \gamma) = -0.08 \pm 0.15$
$A_{CP}(B^0 \to X_s \gamma) = -0.009 \pm 0.018$
$A_{CP}(B^0 \to \rho^+ \pi^-) = 0.13 \pm 0.06$ (S = 1.1)
$A_{CP}(B^0 \to \rho^- \pi^+) = -0.08 \pm 0.08$
$A_{CP}(B^0 \to \omega\omega) = -0.4 \pm 0.4$
$A_{CP}(B^0 \to a_1(1260)^\pm \pi^\mp) = -0.07 \pm 0.06$
$A_{CP}(B^0 \to b_1^- \pi^+) = -0.05 \pm 0.10$
$A_{CP}(B^0 \to p\overline{p} K^*(892)^0) = 0.05 \pm 0.12$
$A_{CP}(B^0 \to p\overline{\Lambda} \pi^-) = 0.04 \pm 0.07$
$A_{CP}(B^0 \to K^{*0} \ell^+ \ell^-) = -0.05 \pm 0.10$
$A_{CP}(B^0 \to K^{*0} e^+ e^-) = -0.21 \pm 0.19$
$A_{CP}(B^0 \to K^{*0} \mu^+ \mu^-) = -0.034 \pm 0.024$
$C_{D^{*-}D^+}\ (B^0 \to D^*(2010)^- D^+) = -0.02 \pm 0.08$
$\boldsymbol{S_{D^{*-}D^+}\ (B^0 \to D^*(2010)^- D^+)} = -0.83 \pm 0.09$
$C_{D^{*+}D^-}\ (B^0 \to D^*(2010)^+ D^-) = -0.03 \pm 0.09$ (S = 1.1)
$\boldsymbol{S_{D^{*+}D^-}\ (B^0 \to D^*(2010)^+ D^-)} = -0.80 \pm 0.09$
$C_{D^{*+}D^{*-}}\ (B^0 \to D^{*+} D^{*-}) = 0.01 \pm 0.09$ (S = 1.6)
$\boldsymbol{S_{D^{*+}D^{*-}}\ (B^0 \to D^{*+} D^{*-})} = -0.59 \pm 0.14$ (S = 1.8)
$C_+\ (B^0 \to D^{*+} D^{*-}) = 0.00 \pm 0.10$ (S = 1.6)
$\boldsymbol{S_+\ (B^0 \to D^{*+} D^{*-})} = -0.73 \pm 0.09$
$C_-\ (B^0 \to D^{*+} D^{*-}) = 0.19 \pm 0.31$
$S_-\ (B^0 \to D^{*+} D^{*-}) = -1.6 \pm 0.5$
$C\ (B^0 \to D^*(2010)^+ D^*(2010)^- K_S^0) = 0.01 \pm 0.29$

Int. J. Mod. Phys. A 2026.41. Downloaded from www.worldscientific.com
by UNIVERSITY OF CALIFORNIA @ BERKELEY on 09/16/26. Re-use and distribution is strictly not permitted, except for Open Acce

$S\,(B^0 \to D^*(2010)^+ D^*(2010)^- K^0_S) = 0.1 \pm 0.4$
$C_{D^+D^-}\,(B^0 \to D^+ D^-) = -0.06 \pm 0.18$ (S = 2.5)
$\boldsymbol{S_{D^+D^-}\,(B^0 \to D^+ D^-)} = -0.64 \pm 0.09$ (S = 1.3)
$C_{J/\psi(1S)\pi^0}\,(B^0 \to J/\psi(1S)\pi^0) = 0.07 \pm 0.09$ (S = 1.1)
$\boldsymbol{S_{J/\psi(1S)\pi^0}\,(B^0 \to J/\psi(1S)\pi^0)} = -0.88 \pm 0.17$ (S = 1.6)
$C(B^0 \to J/\psi(1S)\rho^0) = -0.06 \pm 0.06$
$\boldsymbol{S(B^0 \to J/\psi(1S)\rho^0)} = -0.66^{+0.16}_{-0.12}$
$C_{D^{(*)}_{CP}h^0}\,(B^0 \to D^{(*)}_{CP}h^0) = -0.02 \pm 0.08$
$\boldsymbol{S_{D^{(*)}_{CP}h^0}\,(B^0 \to D^{(*)}_{CP}h^0)} = -0.66 \pm 0.12$
$C_{K^0\pi^0}\,(B^0 \to K^0\pi^0) = 0.00 \pm 0.08$
$\boldsymbol{S_{K^0\pi^0}\,(B^0 \to K^0\pi^0)} = 0.64 \pm 0.13$
$C_{\eta'(958)K^0_S}\,(B^0 \to \eta'(958)K^0_S) = -0.04 \pm 0.20$ (S = 2.5)
$S_{\eta'(958)K^0_S}\,(B^0 \to \eta'(958)K^0_S) = 0.43 \pm 0.17$ (S = 1.5)
$C_{\eta' K^0}\,(B^0 \to \eta' K^0) = -0.08 \pm 0.04$ (S = 1.1)
$\boldsymbol{S_{\eta' K^0}\,(B^0 \to \eta' K^0)} = 0.64 \pm 0.05$
$C_{\omega K^0_S}\,(B^0 \to \omega K^0_S) = 0.0 \pm 0.4$ (S = 3.0)
$S_{\omega K^0_S}\,(B^0 \to \omega K^0_S) = 0.70 \pm 0.21$
$C\,(B^0 \to K^0_S\pi^0\pi^0) = -0.21 \pm 0.20$
$S\,(B^0 \to K^0_S\pi^0\pi^0) = 0.89^{+0.27}_{-0.30}$
$C_{\rho^0 K^0_S}\,(B^0 \to \rho^0 K^0_S) = -0.04 \pm 0.20$
$S_{\rho^0 K^0_S}\,(B^0 \to \rho^0 K^0_S) = 0.50^{+0.17}_{-0.21}$
$C_{f_0 K^0_S}\,(B^0 \to f_0(980)K^0_S) = 0.29 \pm 0.20$
$\boldsymbol{S_{f_0 K^0_S}\,(B^0 \to f_0(980)K^0_S)} = -0.50 \pm 0.16$
$S_{f_2 K^0_S}\,(B^0 \to f_2(1270)K^0_S) = -0.5 \pm 0.5$
$C_{f_2 K^0_S}\,(B^0 \to f_2(1270)K^0_S) = 0.3 \pm 0.4$
$S_{f_x K^0_S}\,(B^0 \to f_x(1300)K^0_S) = -0.2 \pm 0.5$
$C_{f_x K^0_S}\,(B^0 \to f_x(1300)K^0_S) = 0.13 \pm 0.35$
$S_{K^0\pi^+\pi^-}\,(B^0 \to K^0\pi^+\pi^-\text{ nonresonant}) = -0.01 \pm 0.33$
$C_{K^0\pi^+\pi^-}\,(B^0 \to K^0\pi^+\pi^-\text{ nonresonant}) = 0.01 \pm 0.26$
$C_{K^0_S K^0_S}\,(B^0 \to K^0_S K^0_S) = 0.0 \pm 0.4$ (S = 1.4)
$S_{K^0_S K^0_S}\,(B^0 \to K^0_S K^0_S) = -0.8 \pm 0.5$
$C_{K^+K^-K^0_S}\,(B^0 \to K^+K^-K^0_S\text{ nonresonant}) = 0.06 \pm 0.08$
$\boldsymbol{S_{K^+K^-K^0_S}\,(B^0 \to K^+K^-K^0_S\text{ nonresonant})} = -0.66 \pm 0.11$
$C_{K^+K^-K^0_S}\,(B^0 \to K^+K^-K^0_S\text{ inclusive}) = 0.01 \pm 0.09$
$\boldsymbol{S_{K^+K^-K^0_S}\,(B^0 \to K^+K^-K^0_S\text{ inclusive})} = -0.65 \pm 0.12$
$C_{\phi K^0_S}\,(B^0 \to \phi K^0_S) = -0.09 \pm 0.12$
$\boldsymbol{S_{\phi K^0_S}\,(B^0 \to \phi K^0_S)} = 0.58 \pm 0.12$
$C_{K_S K_S K_S}(B^0 \to K_S K_S K_S) = -0.14 \pm 0.12$
$S_{K_S K_S K_S}(B^0 \to K_S K_S K_S) = -0.82 \pm 0.17$
$C_{K^0_S\pi^+\pi^-\gamma}(B^0 \to K^0_S\pi^+\pi^-\gamma) = -0.39 \pm 0.20$
$S_{K^0_S\pi^+\pi^-\gamma}(B^0 \to K^0_S\pi^+\pi^-\gamma) = 0.14 \pm 0.25$
$C_{K^{*0}\gamma}\,(B^0 \to K^*(892)^0\gamma) = 0.03 \pm 0.10$
$S_{K^{*0}\gamma}\,(B^0 \to K^*(892)^0\gamma) = -0.08 \pm 0.17$
$C_{\eta K^0\gamma}\,(B^0 \to \eta K^0\gamma) = 0.1 \pm 0.4$ (S = 1.4)
$S_{\eta K^0\gamma}\,(B^0 \to \eta K^0\gamma) = -0.5 \pm 0.5$ (S = 1.2)
$C_{K^0\phi\gamma}\,(B^0 \to K^0\phi\gamma) = -0.3 \pm 0.6$
$S_{K^0\phi\gamma}\,(B^0 \to K^0\phi\gamma) = 0.7^{+0.7}_{-1.1}$
$C(B^0 \to K^0_S\rho^0\gamma) = -0.05 \pm 0.19$
$S(B^0 \to K^0_S\rho^0\gamma) = -0.04 \pm 0.23$
$C\,(B^0 \to \rho^0\gamma) = 0.4 \pm 0.5$
$S\,(B^0 \to \rho^0\gamma) = -0.8 \pm 0.7$
$\boldsymbol{C_{\pi\pi}\,(B^0 \to \pi^+\pi^-)} = -0.314 \pm 0.030$
$\boldsymbol{S_{\pi\pi}\,(B^0 \to \pi^+\pi^-)} = -0.670 \pm 0.030$
$C_{\pi^0\pi^0}(B^0 \to \pi^0\pi^0) = -0.23 \pm 0.18$
$C_{\rho\pi}\,(B^0 \to \rho^+\pi^-) = -0.03 \pm 0.07$ (S = 1.2)
$S_{\rho\pi}\,(B^0 \to \rho^+\pi^-) = 0.05 \pm 0.07$
$\boldsymbol{\Delta C_{\rho\pi}\,(B^0 \to \rho^+\pi^-)} = 0.27 \pm 0.06$
$\Delta S_{\rho\pi}\,(B^0 \to \rho^+\pi^-) = 0.01 \pm 0.08$
$C_{\rho^0\pi^0}\,(B^0 \to \rho^0\pi^0) = 0.27 \pm 0.24$
$S_{\rho^0\pi^0}\,(B^0 \to \rho^0\pi^0) = -0.23 \pm 0.34$
$C_{a_1\pi}\,(B^0 \to a_1(1260)^+\pi^-) = -0.05 \pm 0.11$
$S_{a_1\pi}\,(B^0 \to a_1(1260)^+\pi^-) = -0.2 \pm 0.4$ (S = 3.2)
$\boldsymbol{\Delta C_{a_1\pi}\,(B^0 \to a_1(1260)^+\pi^-)} = 0.43 \pm 0.14$ (S = 1.3)
$\Delta S_{a_1\pi}\,(B^0 \to a_1(1260)^+\pi^-) = -0.11 \pm 0.12$
$C\,(B^0 \to b_1^- K^+) = -0.22 \pm 0.24$
$\boldsymbol{\Delta C\,(B^0 \to b_1^-\pi^+)} = -1.04 \pm 0.24$
$C_{\rho^0\rho^0}\,(B^0 \to \rho^0\rho^0) = 0.2 \pm 0.9$
$S_{\rho^0\rho^0}\,(B^0 \to \rho^0\rho^0) = 0.3 \pm 0.7$
$C_{\rho\rho}\,(B^0 \to \rho^+\rho^-) = 0.00 \pm 0.08$
$S_{\rho\rho}\,(B^0 \to \rho^+\rho^-) = -0.18 \pm 0.11$
$|\lambda|\,(B^0 \to J/\psi K^*(892)^0) < 0.25$, CL = 95%
$\cos 2\beta\,(B^0 \to J/\psi K^*(892)^0) = 1.7^{+0.7}_{-0.9}$ (S = 1.6)
$\cos 2\beta\,(B^0 \to [K^0_S\pi^+\pi^-]_{D^{(*)}}\,h^0) = 0.91 \pm 0.25$
$(S_+ + S_-)/2\,(B^0 \to D^{*-}\pi^+) = -0.039 \pm 0.011$
$(S_- - S_+)/2\,(B^0 \to D^{*-}\pi^+) = -0.009 \pm 0.015$
$(S_+ + S_-)/2\,(B^0 \to D^-\pi^+) = -0.046 \pm 0.023$
$(S_- - S_+)/2\,(B^0 \to D^-\pi^+) = -0.022 \pm 0.021$
$S_+\,(B^0 \to D^-\pi^+) = 0.058 \pm 0.023$
$S_-\,(B^0 \to D^+\pi^-) = 0.038 \pm 0.021$
$(S_+ + S_-)/2\,(B^0 \to D^-\rho^+) = -0.024 \pm 0.032$
$(S_- - S_+)/2\,(B^0 \to D^-\rho^+) = -0.10 \pm 0.06$
$C_{\eta_c K^0_S}\,(B^0 \to \eta_c K^0_S) = 0.08 \pm 0.13$
$\boldsymbol{S_{\eta_c K^0_S}\,(B^0 \to \eta_c K^0_S)} = 0.93 \pm 0.17$
$C_{c\overline{c}K^{(*)0}}\,(B^0 \to c\overline{c}K^{(*)0}) = (0.4 \pm 1.0) \times 10^{-2}$
$\boldsymbol{\sin(2\beta)} = 0.710 \pm 0.011$
$C_{J/\psi(nS)K^0}\,(B^0 \to J/\psi(nS)K^0) = (0.2 \pm 1.0) \times 10^{-2}$
$\boldsymbol{S_{J/\psi(nS)K^0}\,(B^0 \to J/\psi(nS)K^0)} = 0.711 \pm 0.011$
$C_{J/\psi K^{*0}}\,(B^0 \to J/\psi K^{*0}) = 0.03 \pm 0.10$
$S_{J/\psi K^{*0}}\,(B^0 \to J/\psi K^{*0}) = 0.60 \pm 0.25$
$C_{\chi_{c0}K^0_S}\,(B^0 \to \chi_{c0}K^0_S) = -0.3^{+0.5}_{-0.4}$
$S_{\chi_{c0}K^0_S}\,(B^0 \to \chi_{c0}K^0_S) = -0.7 \pm 0.5$
$C_{\chi_{c1}K^0_S}\,(B^0 \to \chi_{c1}K^0_S) = 0.06 \pm 0.07$
$\boldsymbol{S_{\chi_{c1}K^0_S}\,(B^0 \to \chi_{c1}K^0_S)} = 0.63 \pm 0.10$
$\sin(2\beta_{\rm eff})(B^0 \to \phi K^0) = 0.22 \pm 0.30$
$\sin(2\beta_{\rm eff})(B^0 \to \phi K^*_0(1430)^0) = 0.97^{+0.03}_{-0.52}$
$\boldsymbol{\sin(2\beta_{\rm eff})(B^0 \to K^+K^-K^0_S)} = 0.77^{+0.13}_{-0.12}$
$\sin(2\beta_{\rm eff})(B^0 \to [K^0_S\pi^+\pi^-]_{D^{(*)}}\,h^0) = 0.80 \pm 0.16$
$\beta_{\rm eff}(B^0 \to [K^0_S\pi^+\pi^-]_{D^{(*)}}\,h^0) = (22 \pm 5)^\circ$
$2\beta_{\rm eff}(B^0 \to J/\psi\rho^0) = (42^{+10}_{-11})^\circ$
$|\lambda|\,(B^0 \to [K^0_S\pi^+\pi^-]_{D^{(*)}}\,h^0) = 1.01 \pm 0.08$
$|\sin(2\beta+\gamma)| > 0.40$, CL = 90%
$2\beta + \gamma = (80 \pm 60)^\circ$
$\boldsymbol{\alpha} = (84.1^{+3.7}_{-3.0})^\circ$
$x_+(B^0 \to DK^{*0}) = 0.07 \pm 0.08$
$x_-(B^0 \to DK^{*0}) = -0.18 \pm 0.08$
$y_+(B^0 \to DK^{*0}) = -0.35 \pm 0.10$
$y_-(B^0 \to DK^{*0}) = -0.03 \pm 0.13$
$\boldsymbol{r_{B^0}(B^0 \to DK^{*0})} = 0.250 \pm 0.022$
$\boldsymbol{\delta_{B^0}(B^0 \to DK^{*0})} = (202.8^{+10.3}_{-9.0})^\circ$
$a_{CP}(B^0 \to p\overline{p}K^+\pi^-) = (0.5 \pm 0.9)\%$
$a_P(B^0 \to p\overline{p}K^+\pi^-) = (1.5 \pm 0.9)\%$

$\overline{B}^0$ modes are charge conjugates of the modes below. Reactions indicate the weak decay vertex and do not include mixing. Modes which do not identify the charge state of the B are listed in the $B^\pm/B^0$ ADMIXTURE section.

The branching fractions listed below assume 50% $B^0\overline{B}^0$ and 50% B^+B^- production at the $\Upsilon(4S)$. We have attempted to bring older measurements up to date by rescaling their assumed $\Upsilon(4S)$ production ratio to 50:50 and their assumed D, D_s, D^*, and ψ branching ratios to current values whenever this would affect our averages and best limits significantly.

Indentation is used to indicate a subchannel of a previous reaction. All resonant subchannels have been corrected for resonance branching fractions to the final state so the sum of the subchannel branching fractions can exceed that of the final state.

For inclusive branching fractions, *e.g.*, $B \to D^\pm X$, the values usually are multiplicities, not branching fractions. They can be greater than one.

Int. J. Mod. Phys. A 2026.41. Downloaded from www.worldscientific.com
by UNIVERSITY OF CALIFORNIA @ BERKELEY on 09/16/26. Re-use and distribution is strictly not permitted, except for Open Access articles.

B^0 DECAY MODES		Fraction (Γ_i/Γ)	Scale factor/ Confidence level	p (MeV/c)
$\ell^+ \nu_\ell X$	[jjj]	(10.33 ± 0.28) %		–
$e^+ \nu_e X_c$		(10.1 ± 0.4) %		–
$\ell^+ \nu_\ell X_u$	[jjj]	$(1.51 \pm 0.19) \times 10^{-3}$		–
$D \ell^+ \nu_\ell X$	[jjj]	(9.1 ± 0.8) %		–
$D^- \ell^+ \nu_\ell$	[jjj]	(2.12 ± 0.06) %		2309
$D^- \tau^+ \nu_\tau$		$(7.2 \pm 1.5) \times 10^{-3}$		1909
$D^*(2010)^- \ell^+ \nu_\ell$	[jjj]	(4.90 ± 0.12) %		2257
$D^*(2010)^- \tau^+ \nu_\tau$		(1.50 ± 0.08) %	S=1.1	1838
$\overline{D}^{(*)} n \pi \ell^+ \nu_\ell (n \geq 1)$	[jjj]	(2.3 ± 0.5) %		–
$\overline{D}^0 \pi^- \ell^+ \nu_\ell$	[jjj]	$(3.64 \pm 0.20) \times 10^{-3}$		2308
$D_0^*(2300)^- \ell^+ \nu_\ell$, $D_0^{*-} \to \overline{D}^0 \pi^-$	[jjj]	$< 4.4 \times 10^{-4}$	CL=90%	–
$D_2^*(2460)^- \ell^+ \nu_\ell$, $D_2^{*-} \to \overline{D}^0 \pi^-$	[jjj]	$(1.41 \pm 0.20) \times 10^{-3}$	S=1.7	2065
$\overline{D}^{*0} \pi^- \ell^+ \nu_\ell$	[jjj]	$(5.44 \pm 0.28) \times 10^{-3}$		2256
$D_1(2420)^- \ell^+ \nu_\ell$, $D_1^- \to \overline{D}^{*0} \pi^-$	[jjj]	$(2.85 \pm 0.25) \times 10^{-3}$		–
$D_1(2420)^- \ell^+ \nu_\ell$, $D_1^- \to D^- \pi^+ \pi^-$	[jjj]	$(1.02 \pm 0.16) \times 10^{-3}$		–
$D_1'(2430)^- \ell^+ \nu_\ell$, $D_1'^- \to \overline{D}^{*0} \pi^-$	[jjj]	$(2.5 \pm 0.6) \times 10^{-3}$		–
$D_2^*(2460)^- \ell^+ \nu_\ell$, $D_2^{*-} \to \overline{D}^{*0} \pi^-$	[jjj]	$(6.6 \pm 1.1) \times 10^{-4}$		2065
$D^- \pi^+ \pi^- \ell^+ \nu_\ell$	[jjj]	$(1.45 \pm 0.22) \times 10^{-3}$		2299
$D^{*-} \pi^+ \pi^- \ell^+ \nu_\ell$	[jjj]	$(5.1 \pm 2.3) \times 10^{-4}$		2247
$\rho^- \ell^+ \nu_\ell$	[jjj]	$(2.94 \pm 0.21) \times 10^{-4}$		2583
$\pi^- \ell^+ \nu_\ell$	[jjj]	$(1.50 \pm 0.05) \times 10^{-4}$		2638
$\pi^- \tau^+ \nu_\tau$		$< 2.5 \times 10^{-4}$	CL=90%	2339
Inclusive modes				
$K^\pm X$		(78 ± 8) %		–
$D^0 X$		(8.1 ± 1.5) %		–
$\overline{D}^0 X$		(47.4 ± 2.8) %		–
$D^+ X$		< 3.9 %	CL=90%	–
$D^- X$		(36.9 ± 3.3) %		–
$D_s^+ X$		$(10.3 \pm^{2.1}_{1.8})$ %		–
$D_s^- X$		< 2.6 %	CL=90%	–
$\Lambda_c^+ X$		< 3.1 %	CL=90%	–
$\overline{\Lambda}_c^- X$		$(5.0 \pm^{2.1}_{1.5})$ %		–
$\overline{c} X$		(95 ± 5) %		–
$c X$		(24.6 ± 3.1) %		–
$\overline{c}/c X$		(119 ± 6) %		–
***D*, *D**, or D_s modes**				
$D^- \pi^+$		$(2.51 \pm 0.08) \times 10^{-3}$		2306
$D^- \rho^+$		$(7.6 \pm 1.3) \times 10^{-3}$		2235
$D^- K^0 \pi^+$		$(4.9 \pm 0.9) \times 10^{-4}$		2259
$D^- K^*(892)^+$		$(4.5 \pm 0.7) \times 10^{-4}$		2211
$D^- \omega \pi^+$		$(2.8 \pm 0.6) \times 10^{-3}$		2204
$D^- K^+$		$(2.05 \pm 0.08) \times 10^{-4}$		2279
$D^- K^+ \pi^+ \pi^-$		$(3.5 \pm 0.8) \times 10^{-4}$		2236
$D^- K^+ \overline{K}^0$		$(1.64 \pm 0.26) \times 10^{-4}$		2188
$D^- K^+ \overline{K}^*(892)^0$		$(7.7 \pm 0.6) \times 10^{-4}$		2070
$\overline{D}^0 \pi^+ \pi^-$		$(8.8 \pm 0.5) \times 10^{-4}$		2301
$D^*(2010)^- \pi^+$		$(2.66 \pm 0.07) \times 10^{-3}$		2255
$\overline{D}^0 K^+ K^-$		$(6.1 \pm 0.5) \times 10^{-5}$		2191
$D^- \pi^+ \pi^+ \pi^-$		$(6.0 \pm 0.6) \times 10^{-3}$		2287
$(D^- \pi^+ \pi^+ \pi^-)$ nonresonant		$(3.9 \pm 1.9) \times 10^{-3}$		2287
$D^- \pi^+ \rho^0$		$(1.1 \pm 1.0) \times 10^{-3}$		2206
$D^- a_1(1260)^+$		$(6.0 \pm 3.3) \times 10^{-3}$		2121
$D^*(2010)^- \pi^+ \pi^0$		(1.5 ± 0.5) %		2248
$D^*(2010)^- \rho^+$		$(6.8 \pm 0.9) \times 10^{-3}$		2180
$D^*(2010)^- K^+$		$(2.16 \pm 0.08) \times 10^{-4}$		2226
$D^*(2010)^- K^0 \pi^+$		$(3.0 \pm 0.8) \times 10^{-4}$		2205
$D^*(2010)^- K^*(892)^+$		$(3.3 \pm 0.6) \times 10^{-4}$		2155
$D^*(2010)^- K^+ \overline{K}^0$		$(1.8 \pm 0.4) \times 10^{-4}$		2131
$D^*(2010)^- K^+ \overline{K}^*(892)^0$		$(1.31 \pm 0.13) \times 10^{-3}$		2007
$D^*(2010)^- \pi^+ \pi^+ \pi^-$		$(7.21 \pm 0.29) \times 10^{-3}$		2235
$(D^*(2010)^- \pi^+ \pi^+ \pi^-)$ nonresonant		$(0.0 \pm 2.5) \times 10^{-3}$		2235
$D^*(2010)^- \pi^+ \rho^0$		$(5.7 \pm 3.2) \times 10^{-3}$		2150
$D^*(2010)^- a_1(1260)^+$		(1.30 ± 0.27) %		2061
$\overline{D}_1(2420)^0 \pi^- \pi^+$, $\overline{D}_1^0 \to D^{*-} \pi^+$		$(1.47 \pm 0.35) \times 10^{-4}$		–
$D^*(2010)^- K^+ \pi^- \pi^+$		$(4.7 \pm 0.4) \times 10^{-4}$		2181
$D^*(2010)^- \pi^+ \pi^+ \pi^- \pi^0$		(1.76 ± 0.27) %		2218
$D^{*-} 3\pi^+ 2\pi^-$		$(4.7 \pm 0.9) \times 10^{-3}$		2195
$D^*(2010)^- \omega \pi^+$		$(2.46 \pm 0.18) \times 10^{-3}$	S=1.2	2148
$\overline{D}_1(2430)^0 \omega$, $\overline{D}_1^0 \to D^{*-} \pi^+$		$(2.7 \pm^{0.8}_{0.4}) \times 10^{-4}$		1992
$D^{*-} \rho(1450)^+$, $\rho^+ \to \omega \pi^+$		$(1.07 \pm^{0.40}_{0.34}) \times 10^{-3}$		–
$\overline{D}_1(2420)^0 \omega$, $\overline{D}_1^0 \to D^{*-} \pi^+$		$(7.0 \pm 2.2) \times 10^{-5}$		1995
$\overline{D}_2^*(2460)^0 \omega$, $\overline{D}_2^0 \to D^{*-} \pi^+$		$(4.0 \pm 1.4) \times 10^{-5}$		1975
$D^{*-} b_1(1235)^+$, $b_1^+ \to \omega \pi^+$		$< 7 \times 10^{-5}$	CL=90%	–
$\overline{D}^{**-} \pi^+$	[ooo]	$(1.9 \pm 0.9) \times 10^{-3}$		–
$D_1(2420)^- \pi^+$, $D_1^- \to D^- \pi^+ \pi^-$		$(9.9 \pm^{2.0}_{2.5}) \times 10^{-5}$		–
$D_1(2420)^- \pi^+$, $D_1^- \to D^{*-} \pi^+ \pi^-$		$< 3.3 \times 10^{-5}$	CL=90%	–
$\overline{D}_2^*(2460)^- \pi^+$, $D_2^{*-} \to D^0 \pi^-$		$(2.38 \pm 0.16) \times 10^{-4}$		2062
$\overline{D}_0^*(2400)^- \pi^+$, $D_0^{*-} \to D^0 \pi^-$		$(7.6 \pm 0.8) \times 10^{-5}$		2090
$D_2^*(2460)^- \pi^+$, $D_2^{*-} \to D^{*-} \pi^+ \pi^-$		$< 2.4 \times 10^{-5}$	CL=90%	–
$\overline{D}_2^*(2460)^- \rho^+$		$< 4.9 \times 10^{-3}$	CL=90%	1974
$D^0 \overline{D}^0$		$(1.4 \pm 0.7) \times 10^{-5}$		1868
$D^{*0} \overline{D}^0$		$< 2.9 \times 10^{-4}$	CL=90%	1794
$D^- D^+$		$(2.11 \pm 0.18) \times 10^{-4}$		1864
$D^\pm D^{*\mp}$ (CP-averaged)		$(6.1 \pm 0.6) \times 10^{-4}$		–
$D^- D_s^+$		$(8.1 \pm 0.6) \times 10^{-3}$	S=1.1	1812
$D^*(2010)^- D_s^+$		$(8.2 \pm 0.8) \times 10^{-3}$		1735
$D^- D_s^{*+}$		$(7.4 \pm 1.6) \times 10^{-3}$		1732
$D^*(2010)^- D_s^{*+}$		(1.77 ± 0.14) %		1649
$D_{s0}(2317)^- K^+$, $D_{s0}^- \to D_s^- \pi^0$		$(4.2 \pm 1.4) \times 10^{-5}$		2097
$D_{s0}(2317)^- \pi^+$, $D_{s0}^- \to D_s^- \pi^0$		$< 2.5 \times 10^{-5}$	CL=90%	2128
$D_{sJ}(2457)^- K^+$, $D_{sJ}^- \to D_s^- \pi^0$		$< 9.4 \times 10^{-6}$	CL=90%	–
$D_{sJ}(2457)^- \pi^+$, $D_{sJ}^- \to D_s^- \pi^0$		$< 4.0 \times 10^{-6}$	CL=90%	–
$D_s^- D_s^+$		$< 3.6 \times 10^{-5}$	CL=90%	1759
$D_s^{*-} D_s^+$		$< 1.3 \times 10^{-4}$	CL=90%	1675
$D_s^{*-} D_s^{*+}$		$< 2.4 \times 10^{-4}$	CL=90%	1583
$D_{s0}^*(2317)^+ D^-$, $D_{s0}^{*+} \to D_s^+ \pi^0$		$(1.05 \pm 0.16) \times 10^{-3}$	S=1.1	1602
$D_{s0}(2317)^+ D^-$, $D_{s0}^+ \to D_s^{*+} \gamma$		$< 9.5 \times 10^{-4}$	CL=90%	–
$D_{s0}(2317)^+ D^*(2010)^-$, $D_{s0}^+ \to D_s^+ \pi^0$		$(1.5 \pm 0.6) \times 10^{-3}$		1509
$D_{sJ}(2457)^+ D^-$		$(3.5 \pm 1.1) \times 10^{-3}$		–
$D_{sJ}(2457)^+ D^-$, $D_{sJ}^+ \to D_s^+ \gamma$		$(6.5 \pm^{1.7}_{1.4}) \times 10^{-4}$		–
$D_{sJ}(2457)^+ D^-$, $D_{sJ}^+ \to D_s^{*+} \gamma$		$< 6.0 \times 10^{-4}$	CL=90%	–
$D_{sJ}(2457)^+ D^-$, $D_{sJ}^+ \to D_s^+ \pi^+ \pi^-$		$< 2.0 \times 10^{-4}$	CL=90%	–
$D_{sJ}(2457)^+ D^-$, $D_{sJ}^+ \to D_s^+ \pi^0$		$< 3.6 \times 10^{-4}$	CL=90%	–
$D^*(2010)^- D_{sJ}(2457)^+$		$(9.3 \pm 2.2) \times 10^{-3}$		–
$D_{sJ}(2457)^+ D^*(2010)$, $D_{sJ}^+ \to D_s^+ \gamma$		$(2.3 \pm^{0.9}_{0.7}) \times 10^{-3}$		–
$D^- D_{s1}(2536)^+$, $D_{s1}^+ \to D^{*0} K^+ + D^{*+} K^0$		$(2.8 \pm 0.7) \times 10^{-4}$		1444
$D^- D_{s1}(2536)^+$, $D_{s1}^+ \to D^{*0} K^+$		$(1.7 \pm 0.6) \times 10^{-4}$		1444
$D^- D_{s1}(2536)^+$, $D_{s1}^+ \to D^{*+} K^0$		$(2.6 \pm 1.1) \times 10^{-4}$		1444

Int. J. Mod. Phys. A 2026.41. Downloaded from www.worldscientific.com
by UNIVERSITY OF CALIFORNIA @ BERKELEY on 09/16/26. Re-use and distribution is strictly not permitted, except for Open Acce

$D^*(2010)^- D_{s1}(2536)^+$, $D_{s1}^+ \to D^{*0} K^+ + D^{*+} K^0$	$(5.0 \pm 1.4) \times 10^{-4}$			1336
$D^*(2010)^- D_{s1}(2536)^+$, $D_{s1}^+ \to D^{*0} K^+$	$(3.3 \pm 1.1) \times 10^{-4}$			1336
$D^{*-} D_{s1}(2536)^+$, $D_{s1}^+ \to D^{*+} K^0$	$(5.0 \pm 1.7) \times 10^{-4}$			1336
$D^- D_{sJ}(2573)^+$, $D_{sJ}^+ \to D^0 K^+$	$(3.4 \pm 1.8) \times 10^{-5}$			1414
$D^*(2010)^- D_{sJ}(2573)^+$, $D_{sJ}^+ \to D^0 K^+$	$< 2 \times 10^{-4}$	CL=90%		1304
$D^- D_{sJ}(2700)^+$, $D_{sJ}^+ \to D^0 K^+$	$(7.1 \pm 1.2) \times 10^{-4}$			–
$D^+ \pi^-$	$(7.3 \pm 1.2) \times 10^{-7}$			2306
$D_s^+ \pi^-$	$(2.03 \pm 0.18) \times 10^{-5}$			2271
$D_s^{*+} \pi^-$	$(2.1 \pm 0.4) \times 10^{-5}$	S=1.4		2215
$D_s^+ \rho^-$	$< 2.4 \times 10^{-5}$	CL=90%		2197
$D_s^{*+} \rho^-$	$(4.1 \pm 1.3) \times 10^{-5}$			2138
$D_s^+ a_0^-$	$< 1.9 \times 10^{-5}$	CL=90%		–
$D_s^{*+} a_0^-$	$< 3.6 \times 10^{-5}$	CL=90%		–
$D_s^+ a_1(1260)^-$	$< 2.1 \times 10^{-3}$	CL=90%		2080
$D_s^{*+} a_1(1260)^-$	$< 1.7 \times 10^{-3}$	CL=90%		2015
$D_s^+ a_2^-$	$< 1.9 \times 10^{-4}$	CL=90%		–
$D_s^{*+} a_2^-$	$< 2.0 \times 10^{-4}$	CL=90%		–
$D_s^- K^+$	$(2.7 \pm 0.5) \times 10^{-5}$	S=2.7		2242
$D_s^{*-} K^+$	$(2.19 \pm 0.30) \times 10^{-5}$			2185
$D_{s1}(2536)^\mp K^\pm$, $D_{s1}^- \to \overline{D}^*(2007)^0 K^-$	$(5.1 \pm 0.6) \times 10^{-6}$			–
$D_s^- K^*(892)^+$	$(3.5 \pm 1.0) \times 10^{-5}$			2172
$D_s^{*-} K^*(892)^+$	$(3.2 {}^{+1.5}_{-1.3}) \times 10^{-5}$			2112
$D_s^- \pi^+ K^0$	$(9.7 \pm 1.4) \times 10^{-5}$			2222
$D_s^{*-} \pi^+ K^0$	$< 1.10 \times 10^{-4}$	CL=90%		2164
$D_s^- K^+ \pi^+ \pi^-$	$(1.7 \pm 0.5) \times 10^{-4}$			2198
$D_s^- \pi^+ K^*(892)^0$	$< 3.0 \times 10^{-3}$	CL=90%		2138
$D_s^{*-} \pi^+ K^*(892)^0$	$< 1.6 \times 10^{-3}$	CL=90%		2076
$\overline{D}^0 K^0$	$(5.5 \pm 0.4) \times 10^{-5}$			2280
$\overline{D}^0 K^+ \pi^-$	$(8.8 \pm 1.7) \times 10^{-5}$			2262
$\overline{D}^0 K^*(892)^0$	$(4.5 \pm 0.6) \times 10^{-5}$			2213
$\overline{D}^0 K^*(1410)^0$	$< 6.7 \times 10^{-5}$	CL=90%		2062
$\overline{D}^0 K_0^*(1430)^0$	$(7 \pm 7) \times 10^{-6}$			2058
$\overline{D}^0 K_2^*(1430)^0$	$(2.1 \pm 0.9) \times 10^{-5}$			2057
$D_0^*(2300)^- K^+$, $D_0^{*-} \to \overline{D}^0 \pi^-$	$(1.9 \pm 0.9) \times 10^{-5}$			–
$D_2^*(2460)^- K^+$, $D_2^{*-} \to \overline{D}^0 \pi^-$	$(2.03 \pm 0.35) \times 10^{-5}$			2029
$D_3^*(2760)^- K^+$, $D_3^{*-} \to \overline{D}^0 \pi^-$	$< 1.0 \times 10^{-6}$	CL=90%		–
$\overline{D}^0 K^+ \pi^-$ nonresonant	$< 3.7 \times 10^{-5}$	CL=90%		2262
$[K^+ K^-]_D K^*(892)^0$	$(3.7 \pm 0.5) \times 10^{-5}$			–
$[\pi^+ \pi^-]_D K^*(892)^0$	$(5.0 \pm 0.8) \times 10^{-5}$			–
$[\pi^+ \pi^- \pi^+ \pi^-]_D K^{*0}$	$(4.0 \pm 0.6) \times 10^{-5}$			–
$\overline{D}^0 \pi^0$	$(2.67 \pm 0.09) \times 10^{-4}$			2308
$\overline{D}^0 \rho^0$	$(3.21 \pm 0.21) \times 10^{-4}$			2237
$\overline{D}^0 f_2$	$(1.56 \pm 0.21) \times 10^{-4}$			–
$\overline{D}^0 \eta$	$(2.56 \pm 0.12) \times 10^{-4}$			2274
$\overline{D}^0 \eta'$	$(1.38 \pm 0.16) \times 10^{-4}$	S=1.3		2198
$\overline{D}^0 \omega$	$(2.54 \pm 0.16) \times 10^{-4}$			2235
$\overline{D}^0 \phi$	$(7.7 \pm 2.3) \times 10^{-7}$			2183
$D^0 K^+ \pi^-$	$(5.3 \pm 3.2) \times 10^{-6}$			2262
$D^0 K^*(892)^0$	$(3.0 \pm 0.6) \times 10^{-6}$			2213
$\overline{D}^{*0} \gamma$	$< 2.5 \times 10^{-5}$	CL=90%		2258
$\overline{D}^*(2007)^0 \pi^0$	$(2.2 \pm 0.6) \times 10^{-4}$	S=2.6		2256
$\overline{D}^*(2007)^0 \rho^0$	$< 5.1 \times 10^{-4}$	CL=90%		2182
$\overline{D}^*(2007)^0 \eta$	$(2.3 \pm 0.6) \times 10^{-4}$	S=2.8		2220
$\overline{D}^*(2007)^0 \eta'$	$(1.40 \pm 0.22) \times 10^{-4}$			2141
$\overline{D}^*(2007)^0 \pi^+ \pi^-$	$(6.2 \pm 2.2) \times 10^{-4}$			2249
$\overline{D}^*(2007)^0 K^+ \pi^-$	$(5.2 \pm 1.9) \times 10^{-5}$			2207
$\overline{D}^*(2007)^0 K^0$	$(3.6 \pm 1.2) \times 10^{-5}$			2227
$\overline{D}^*(2007)^0 K^*(892)^0$	$< 6.9 \times 10^{-5}$	CL=90%		2157
$\overline{D}^*(2007)^0 \phi$	$(2.2 \pm 0.6) \times 10^{-6}$			2125
$D^*(2007)^0 K^*(892)^0$	$< 4.0 \times 10^{-5}$	CL=90%		2157
$D^*(2007)^0 \pi^+ \pi^+ \pi^- \pi^-$	$(2.7 \pm 0.5) \times 10^{-3}$			2219
$D^*(2010)^+ D^*(2010)^-$	$(8.0 \pm 0.6) \times 10^{-4}$			1711
$\overline{D}^*(2007)^0 \omega$	$(3.6 \pm 1.1) \times 10^{-4}$	S=3.1		2180
$D^*(2010)^+ D^-$	$(6.1 \pm 1.5) \times 10^{-4}$	S=1.6		1790
$D^*(2007)^0 \overline{D}^*(2007)^0$	$< 9 \times 10^{-5}$	CL=90%		1715
$D^- D^0 K^+$	$(1.07 \pm 0.11) \times 10^{-3}$			1574
$D^- D^*(2007)^0 K^+$	$(3.5 \pm 0.4) \times 10^{-3}$			1478
$D^*(2010)^- D^0 K^+$	$(2.47 \pm 0.21) \times 10^{-3}$			1479
$D^*(2010)^- D^*(2007)^0 K^+$	(1.06 ± 0.09) %			1366
$D^- D^+ K^0$	$(7.5 \pm 1.7) \times 10^{-4}$			1568
$D^*(2010)^- D^+ K^0 + D^- D^*(2010)^+ K^0$	$(6.4 \pm 0.5) \times 10^{-3}$			1473
$D^*(2010)^- D^*(2010)^+ K^0$	$(8.1 \pm 0.7) \times 10^{-3}$			1360
$D^{*-} D_{s1}(2536)^+$, $D_{s1}^+ \to D^{*+} K^0$	$(8.0 \pm 2.4) \times 10^{-4}$			1336
$\overline{D}^0 D^0 K^0$	$(2.7 \pm 1.1) \times 10^{-4}$			1575
$D^0 \overline{D}^0 K^+ \pi^-$	$(3.5 \pm 0.5) \times 10^{-4}$			1476
$\overline{D}^0 D^*(2007)^0 K^0 + \overline{D}^*(2007)^0 D^0 K^0$	$(1.1 \pm 0.5) \times 10^{-3}$			1478
$\overline{D}^*(2007)^0 D^*(2007)^0 K^0$	$(2.4 \pm 0.9) \times 10^{-3}$			1365
$(\overline{D} + \overline{D}^*)(D + D^*) K$	(3.68 ± 0.26) %			–

Charmonium modes

$\eta_c K^0$	$(1.04 \pm 0.13) \times 10^{-3}$			1751
$\eta_c(1S) K^+ \pi^-$	$(7.8 \pm 1.0) \times 10^{-4}$			1722
$\eta_c(1S) K^+ \pi^-$ (NR)	$(8.1 \pm 1.7) \times 10^{-5}$			–
$T_{c\overline{c}}(4100)^- K^+$, $T_{c\overline{c}}^- \to \eta_c \pi^-$	$(2.6 \pm 1.3) \times 10^{-5}$			–
$\eta_c(1S) K^*(1410)^0$	$(2.5 \pm 1.9) \times 10^{-4}$			1395
$\eta_c(1S) K_0^*(1430)^0$	$(2.1 \pm 0.5) \times 10^{-4}$			1387
$\eta_c(1S) K_2^*(1430)^0$	$(6.4 {}^{+2.9}_{-3.5}) \times 10^{-5}$			1386
$\eta_c(1S) K^*(1680)^0$	$(4 \pm 5) \times 10^{-5}$			1166
$\eta_c(1S) K_0^*(1950)^0$	$(6 {}^{+4}_{-5}) \times 10^{-5}$			–
$\eta_c K^*(892)^0$	$(5.3 {}^{+1.0}_{-1.2}) \times 10^{-4}$	S=2.0		1646
$\eta_c(2S) K_S^0$, $\eta_c \to p\overline{p}\pi^+\pi^-$	$(4.2 {}^{+1.4}_{-1.2}) \times 10^{-7}$			–
$\eta_c(2S) K^{*0}$	$< 3.9 \times 10^{-4}$	CL=90%		1158
$h_c(1P) K_S^0$	$< 1.4 \times 10^{-5}$			1401
$h_c(1P) K^{*0}$	$< 3.4 \times 10^{-4}$	CL=90%		1253
$J/\psi(1S) K^0$	$(8.91 \pm 0.21) \times 10^{-4}$			1683
$J/\psi(1S) K^+ \pi^-$	$(1.15 \pm 0.05) \times 10^{-3}$			1652
$J/\psi(1S) K^*(892)^0$	$(1.27 \pm 0.05) \times 10^{-3}$			1571
$J/\psi(1S) \eta K_S^0$	$(5.4 \pm 0.9) \times 10^{-5}$			1508
$J/\psi(1S) \eta' K_S^0$	$< 2.5 \times 10^{-5}$	CL=90%		1271
$J/\psi(1S) \phi K^0$	$(4.9 \pm 1.0) \times 10^{-5}$	S=1.3		1224
$J/\psi(1S) \omega K^0$	$(2.3 \pm 0.4) \times 10^{-4}$			1386
$\chi_{c0}(3915)$, $\chi_{c0} \to J/\psi\omega$	$(2.1 \pm 0.9) \times 10^{-5}$			1102
$J/\psi(1S) K(1270)^0$	$(1.3 \pm 0.5) \times 10^{-3}$			1400
$J/\psi(1S) \pi^0$	$(1.73 \pm 0.09) \times 10^{-5}$	S=1.2		1728
$J/\psi(1S) \eta$	$(1.23 \pm 0.19) \times 10^{-5}$			1673
$J/\psi(1S) \pi^+ \pi^-$	$(3.99 \pm 0.15) \times 10^{-5}$			1716
$J/\psi(1S) \pi^+ \pi^-$ nonresonant	$< 1.2 \times 10^{-5}$	CL=90%		1716
$J/\psi(1S) f_0(500)$, $f_0 \to \pi\pi$	$(8.8 {}^{+1.2}_{-1.6}) \times 10^{-6}$			–
$J/\psi(1S) f_2$	$(3.3 {}^{+0.5}_{-0.6}) \times 10^{-6}$	S=1.5		–
$J/\psi(1S) \rho^0$	$(2.55 {}^{+0.18}_{-0.16}) \times 10^{-5}$			1612
$J/\psi(1S) f_0(980)$, $f_0 \to \pi^+\pi^-$	$< 1.1 \times 10^{-6}$	CL=90%		–
$J/\psi(1S) \rho(1450)^0$, $\rho^0 \to \pi\pi$	$(2.9 {}^{+1.6}_{-0.7}) \times 10^{-6}$			–
$J/\psi \rho(1700)^0$, $\rho^0 \to \pi^+\pi^-$	$(2.0 \pm 1.3) \times 10^{-6}$			–
$J/\psi(1S) \omega$	$(2.08 \pm 0.29) \times 10^{-5}$			1609
$J/\psi(1S) K^+ K^-$	$(2.53 \pm 0.35) \times 10^{-6}$			1534
$J/\psi(1S) a_0(980)$, $a_0 \to K^+ K^-$	$(4.7 \pm 3.4) \times 10^{-7}$			–
$J/\psi(1S) \phi$	$< 1.1 \times 10^{-7}$	CL=90%		1520
$J/\psi(1S) \eta'(958)$	$(5.9 \pm 1.2) \times 10^{-6}$			1546
$J/\psi(1S) K^0 \pi^+ \pi^-$	$(4.5 \pm 0.4) \times 10^{-4}$			1611
$J/\psi(1S) K^0 K^- \pi^+ + \text{c.c.}$	$< 2.1 \times 10^{-5}$	CL=90%		1468
$J/\psi(1S) K^0 K^+ K^-$	$(2.5 \pm 0.7) \times 10^{-5}$	S=1.8		1249
$J/\psi(1S) K^0 \rho^0$	$(5.4 \pm 3.0) \times 10^{-4}$			1390
$J/\psi(1S) K^*(892)^+ \pi^-$	$(8 \pm 4) \times 10^{-4}$			1514
$J/\psi(1S) \pi^+ \pi^- \pi^+ \pi^-$	$(1.44 \pm 0.12) \times 10^{-5}$			1670
$J/\psi(1S) f_1(1285)$	$(8.4 \pm 2.1) \times 10^{-6}$			1385
$J/\psi(1S) K^*(892)^0 \pi^+ \pi^-$	$(6.6 \pm 2.2) \times 10^{-4}$			1447
$\eta_{c2}(1D) K_S^0$, $\eta_{c2} \to h_c \gamma$	$< 3.5 \times 10^{-5}$	CL=90%		–
$\eta_{c2}(1D) \pi^- K^+$, $\eta_{c2} \to h_c \gamma$	$< 1.0 \times 10^{-4}$	CL=90%		–
$\chi_{c1}(3872)^- K^+$	$< 5 \times 10^{-4}$	CL=90%		–

Int. J. Mod. Phys. A 2026.41. Downloaded from www.worldscientific.com
by UNIVERSITY OF CALIFORNIA @ BERKELEY on 09/16/26. Re-use and distribution is strictly not permitted, except for Open Access articles.

$\chi_{c1}(3872)^- K^+$, $\chi_{c1}(3872)^- \to J/\psi(1S)\pi^-\pi^0$	[ppp]	$< 4.2 \times 10^{-6}$	CL=90%	–
$\chi_{c1}(3872) K^0$		$(1.1 \pm 0.4) \times 10^{-4}$		1140
$\chi_{c1}(3872) K^*(892)^0$		$(9 \pm 5) \times 10^{-5}$		940
$\chi_{c1}(3872) K^+\pi^-$		$(1.8 \pm 0.7) \times 10^{-4}$		1087
$\chi_{c1}(3872)\gamma$		$< 1.2 \times 10^{-5}$	CL=90%	1220
$T_{c\overline{c}1}(4430)^\pm K^\mp$, $T^\pm_{c\overline{c}1} \to \psi(2S)\pi^\pm$		$(6.0 {}^{+3.0}_{-2.4}) \times 10^{-5}$		583
$T_{c\overline{c}1}(4430)^\pm K^\mp$, $T^\pm_{c\overline{c}1} \to J/\psi\pi^\pm$		$(5.4 {}^{+4.0}_{-1.2}) \times 10^{-6}$		583
$T_{c\overline{c}1}(3900)^\pm K^\mp$, $T^\pm_{c\overline{c}1} \to J/\psi\pi^\pm$		$< 9 \times 10^{-7}$		–
$T_{c\overline{c}1}(4200)^\pm K^\mp$, $T^\pm_{c\overline{c}1} \to J/\psi\pi^\pm$		$(2.2 {}^{+1.3}_{-0.8}) \times 10^{-5}$		–
$J/\psi(1S) p\overline{p}$		$(4.5 \pm 0.6) \times 10^{-7}$		862
$J/\psi(1S)\gamma$		$< 1.5 \times 10^{-6}$	CL=90%	1732
$J/\psi\mu^+\mu^-$, $J/\psi \to \mu^+\mu^-$		$< 1.0 \times 10^{-9}$	CL=95%	–
$J/\psi(1S)\overline{D}^0$		$< 9.6 \times 10^{-7}$	CL=90%	877
$\psi(2S)\pi^0$		$(1.17 \pm 0.19) \times 10^{-5}$		1348
$\psi(2S) K^0$		$(5.8 \pm 0.5) \times 10^{-4}$		1283
$\psi(2S) K^0\pi^+\pi^-$		$(2.81 \pm 0.30) \times 10^{-4}$		1177
$\psi(3770) K^0$, $\psi \to \overline{D}^0 D^0$		$< 1.23 \times 10^{-4}$	CL=90%	1217
$\psi(3770) K^0$, $\psi \to D^- D^+$		$< 1.88 \times 10^{-4}$	CL=90%	1217
$\psi(2S)\pi^+\pi^-$		$(2.24 \pm 0.35) \times 10^{-5}$		1332
$\psi(2S) K^+\pi^-$		$(5.8 \pm 0.4) \times 10^{-4}$		1239
$\psi(2S) K^*(892)^0$		$(5.9 \pm 0.4) \times 10^{-4}$		1116
$\chi_{c0} K^0$		$(1.9 \pm 0.4) \times 10^{-4}$		1477
$\chi_{c0} K^*(892)^0$		$(1.7 \pm 0.4) \times 10^{-4}$		1341
$\chi_{c1}\pi^0$		$(1.12 \pm 0.28) \times 10^{-5}$		1468
$\chi_{c1} K^0$		$(3.95 \pm 0.27) \times 10^{-4}$		1411
$\chi_{c1}\pi^- K^+$		$(4.97 \pm 0.30) \times 10^{-4}$		1372
$\chi_{c1} K^*(892)^0$		$(2.38 \pm 0.19) \times 10^{-4}$	S=1.2	1265
$T_{c\overline{c}}(4050)^- K^+$, $T^-_{c\overline{c}} \to \chi_{c1}\pi^-$		$(3.0 {}^{+4.0}_{-1.8}) \times 10^{-5}$		–
$T_{c\overline{c}}(4250)^- K^+$, $T^-_{c\overline{c}} \to \chi_{c1}\pi^-$		$(4.0 {}^{+20.0}_{-1.0}) \times 10^{-5}$		–
$\chi_{c1}\pi^+\pi^- K^0$		$(3.2 \pm 0.5) \times 10^{-4}$		1318
$\chi_{c1}\pi^-\pi^0 K^+$		$(3.5 \pm 0.6) \times 10^{-4}$		1321
$\chi_{c2} K^0$		$< 1.5 \times 10^{-5}$	CL=90%	1379
$\chi_{c2} K^*(892)^0$		$(4.9 \pm 1.2) \times 10^{-5}$	S=1.1	1228
$\chi_{c2}\pi^- K^+$		$(7.2 \pm 1.0) \times 10^{-5}$		1338
$\chi_{c2}\pi^+\pi^- K^0$		$< 1.70 \times 10^{-4}$	CL=90%	1282
$\chi_{c2}\pi^-\pi^0 K^+$		$< 7.4 \times 10^{-5}$	CL=90%	1286
$\psi(4660) K^0$, $\psi \to \Lambda_c^+\Lambda_c^-$		$< 2.3 \times 10^{-4}$	CL=90%	–
$\psi(4230)^0 K^0$, $\psi^0 \to J/\psi\pi^+\pi^-$		$< 1.7 \times 10^{-5}$	CL=90%	–

K or *K** modes

$K^+\pi^-$		$(2.00 \pm 0.04) \times 10^{-5}$		2615
$K^0\pi^0$		$(1.01 \pm 0.04) \times 10^{-5}$		2615
$\eta' K^0$		$(6.6 \pm 0.4) \times 10^{-5}$	S=1.4	2528
$\eta' K^*(892)^0$		$(2.8 \pm 0.6) \times 10^{-6}$		2472
$\eta' K_0^*(1430)^0$		$(6.3 \pm 1.6) \times 10^{-6}$		2346
$\eta' K_2^*(1430)^0$		$(1.37 \pm 0.32) \times 10^{-5}$		2346
ηK^0		$(1.23 {}^{+0.27}_{-0.24}) \times 10^{-6}$		2587
$\eta K^*(892)^0$		$(1.59 \pm 0.10) \times 10^{-5}$		2534
$\eta K_0^*(1430)^0$		$(1.10 \pm 0.22) \times 10^{-5}$		2415
$\eta K_2^*(1430)^0$		$(9.6 \pm 2.1) \times 10^{-6}$		2414
ωK^0		$(4.8 \pm 0.4) \times 10^{-6}$		2557
$a_0(980)^0 K^0$, $a_0^0 \to \eta\pi^0$		$< 7.8 \times 10^{-6}$	CL=90%	–
$b_1^0 K^0$, $b_1^0 \to \omega\pi^0$		$< 7.8 \times 10^{-6}$	CL=90%	–
$a_0(980)^\pm K^\mp$, $a_0^\pm \to \eta\pi^\pm$		$< 1.9 \times 10^{-6}$	CL=90%	–
$b_1^- K^+$, $b_1^- \to \omega\pi^-$		$(7.4 \pm 1.4) \times 10^{-6}$		–
$b_1^0 K^{*0}$, $b_1^0 \to \omega\pi^0$		$< 8.0 \times 10^{-6}$	CL=90%	–
$b_1^- K^{*+}$, $b_1^- \to \omega\pi^-$		$< 5.0 \times 10^{-6}$	CL=90%	–
$a_0(1450)^\pm K^\mp$, $a_0^\pm \to \eta\pi^\pm$		$< 3.1 \times 10^{-6}$	CL=90%	–
$K_S^0 X^0$ (Familon)		$< 5.3 \times 10^{-5}$	CL=90%	–
$\omega K^*(892)^0$		$(2.0 \pm 0.5) \times 10^{-6}$		2503
$\omega(K\pi)_0^{*0}$		$(1.84 \pm 0.25) \times 10^{-5}$		–
$\omega K_0^*(1430)^0$		$(1.60 \pm 0.34) \times 10^{-5}$		2380
$\omega K_2^*(1430)^0$		$(1.01 \pm 0.23) \times 10^{-5}$		2380
$\omega K^+\pi^-$ nonresonant		$(5.1 \pm 1.0) \times 10^{-6}$		2542
$K^+\pi^-\pi^0$		$(3.78 \pm 0.32) \times 10^{-5}$		2610
$K^+\rho^-$		$(7.0 \pm 0.9) \times 10^{-6}$		2559
$K^+\rho(1450)^-$		$(2.4 \pm 1.2) \times 10^{-6}$		–
$K^+\rho(1700)^-$		$(6 \pm 7) \times 10^{-7}$		–
$(K^+\pi^-\pi^0)$ nonresonant		$(2.8 \pm 0.6) \times 10^{-6}$		2610
$(K\pi)_0^{*+}\pi^-$, $(K\pi)_0^{*+} \to K^+\pi^0$		$(3.4 \pm 0.5) \times 10^{-5}$		–
$(K\pi)_0^{*0}\pi^0$, $(K\pi)_0^{*0} \to K^+\pi^-$		$(8.6 \pm 1.7) \times 10^{-6}$		–
$K_2^*(1430)^0\pi^0$		$< 4.0 \times 10^{-6}$	CL=90%	2445
$K^*(1680)^0\pi^0$		$< 7.5 \times 10^{-6}$	CL=90%	2358
$K_x^{*0}\pi^0$	[sss]	$(6.1 \pm 1.6) \times 10^{-6}$		–
$K^0\pi^+\pi^-$		$(4.97 \pm 0.18) \times 10^{-5}$		2609
$K^0\pi^+\pi^-$ nonresonant		$(1.39 {}^{+0.26}_{-0.18}) \times 10^{-5}$	S=1.6	2609
$K^0\rho^0$		$(3.4 \pm 1.1) \times 10^{-6}$	S=2.3	2558
$K^*(892)^+\pi^-$		$(7.5 \pm 0.4) \times 10^{-6}$		2563
$K_0^*(1430)^+\pi^-$		$(3.3 \pm 0.7) \times 10^{-5}$	S=2.0	–
$K_x^{*+}\pi^-$	[sss]	$(5.1 \pm 1.6) \times 10^{-6}$		–
$K^*(1410)^+\pi^-$, $K^{*+} \to K^0\pi^+$		$< 3.8 \times 10^{-6}$	CL=90%	–
$(K\pi)_0^{*+}\pi^-$, $(K\pi)_0^{*+} \to K^0\pi^+$		$(1.62 \pm 0.13) \times 10^{-5}$		–
$f_0(980) K^0$, $f_0 \to \pi^+\pi^-$		$(8.1 \pm 0.8) \times 10^{-6}$	S=1.3	2522
$K^0 f_0(500)$		$(1.6 {}^{+2.5}_{-1.6}) \times 10^{-7}$		–
$K^0 f_0(1500)$		$(1.3 \pm 0.8) \times 10^{-6}$		2393
$f_2(1270) K^0$		$(2.7 {}^{+1.3}_{-1.2}) \times 10^{-6}$		2459
$f_x(1300) K0, f_x \to \pi^+\pi^-$		$(1.8 \pm 0.7) \times 10^{-6}$		–
$K^*(892)^0\pi^0$		$(3.3 \pm 0.6) \times 10^{-6}$		2563
$K_2^*(1430)^+\pi^-$		$(3.65 \pm 0.34) \times 10^{-6}$		2445
$K^*(1680)^+\pi^-$		$(1.41 \pm 0.10) \times 10^{-5}$		2358
$K^+\pi^-\pi^+\pi^-$	[ttt]	$< 2.3 \times 10^{-4}$	CL=90%	2600
$\rho^0 K^+\pi^-$		$(2.8 \pm 0.7) \times 10^{-6}$		2543
$f_0(980) K^+\pi^-$, $f_0 \to \pi\pi$		$(1.4 {}^{+0.5}_{-0.6}) \times 10^{-6}$		2506
$K^+\pi^-\pi^+\pi^-$ nonresonant		$< 2.1 \times 10^{-6}$	CL=90%	2600
$K^*(892)^0\pi^+\pi^-$		$(5.5 \pm 0.5) \times 10^{-5}$		2557
$K^*(892)^0\rho^0$		$(3.9 \pm 1.3) \times 10^{-6}$	S=1.9	2504
$K^*(892)^0 f_0(980)$, $f_0 \to \pi\pi$		$(3.9 {}^{+2.1}_{-1.8}) \times 10^{-6}$	S=3.9	2466
$K_1(1270)^+\pi^-$		$< 3.0 \times 10^{-5}$	CL=90%	2488
$K_1(1400)^+\pi^-$		$< 2.7 \times 10^{-5}$	CL=90%	2451
$a_1(1260)^- K^+$	[ttt]	$(1.6 \pm 0.4) \times 10^{-5}$		2471
$K^*(892)^+\rho^-$		$(1.03 \pm 0.26) \times 10^{-5}$		2504
$K_0^*(1430)^+\rho^-$		$(2.8 \pm 1.2) \times 10^{-5}$		–
$K_1(1400)^0\rho^0$		$< 3.0 \times 10^{-3}$	CL=90%	2388
$K_0^*(1430)^0\rho^0$		$(2.7 \pm 0.6) \times 10^{-5}$		2381
$K_0^*(1430)^0 f_0(980)$, $f_0 \to \pi\pi$		$(2.7 \pm 0.9) \times 10^{-6}$		–
$K_2^*(1430)^0 f_0(980)$, $f_0 \to \pi\pi$		$(8.6 \pm 2.0) \times 10^{-6}$		–
K^+K^-		$(7.8 \pm 1.5) \times 10^{-8}$		2593
$K^0\overline{K}^0$		$(1.21 \pm 0.16) \times 10^{-6}$		2593
$K^0 K^-\pi^+$		$(6.7 \pm 0.5) \times 10^{-6}$		2578
$K^*(892)^\pm K^\mp$		$< 4 \times 10^{-7}$	CL=90%	2540
$\overline{K}^{*0} K^0 + K^{*0}\overline{K}^0$		$< 9.6 \times 10^{-7}$	CL=90%	–
$K^+K^-\pi^0$		$(2.2 \pm 0.6) \times 10^{-6}$		2579
$K_S^0 K_S^0\pi^0$		$< 9 \times 10^{-7}$	CL=90%	2578
$K_S^0 K_S^0\eta$		$< 1.0 \times 10^{-6}$	CL=90%	2516
$K_S^0 K_S^0\eta'$		$< 2.0 \times 10^{-6}$	CL=90%	2453
$K^0 K^+K^-$		$(2.68 \pm 0.11) \times 10^{-5}$		2522
$K^0\phi$		$(7.3 \pm 0.7) \times 10^{-6}$		2516
$f_0(980) K^0$, $f_0 \to K^+K^-$		$(7.0 {}^{+3.5}_{-3.0}) \times 10^{-6}$		–
$f_0(1500) K^0$		$(1.3 {}^{+0.7}_{-0.5}) \times 10^{-5}$		2393
$f_2'(1525)^0 K^0$		$(3 {}^{+5}_{-4}) \times 10^{-7}$		–
$f_0(1710) K^0$, $f_0 \to K^+K^-$		$(4.4 \pm 0.9) \times 10^{-6}$		–
$K^0 K^+K^-$ nonresonant		$(3.3 \pm 1.0) \times 10^{-5}$		2522
$K_S^0 K_S^0 K_S^0$		$(6.0 \pm 0.5) \times 10^{-6}$	S=1.1	2521
$f_0(980) K^0$, $f_0 \to K_S^0 K_S^0$		$(2.7 \pm 1.8) \times 10^{-6}$		–
$f_0(1710) K^0$, $f_0 \to K_S^0 K_S^0$		$(5.0 {}^{+5.0}_{-2.6}) \times 10^{-7}$		–
$f_2(2010) K^0$, $f_2 \to K_S^0 K_S^0$		$(5 \pm 6) \times 10^{-7}$		–
$K_S^0 K_S^0 K_S^0$ nonresonant		$(1.33 \pm 0.31) \times 10^{-5}$		2521
$K_S^0 K_S^0 K_L^0$		$< 1.6 \times 10^{-5}$	CL=90%	2521
$K^*(892)^0 K^+K^-$		$(2.75 \pm 0.26) \times 10^{-5}$		2467
$K^*(892)^0\phi$		$(1.00 \pm 0.05) \times 10^{-5}$		2460
$K^+K^-\pi^+\pi^-$ nonresonant		$< 7.17 \times 10^{-5}$	CL=90%	2559

Meson Summary Table

$K^*(892)^0 K^- \pi^+$		$(4.5 \pm 1.3) \times 10^{-6}$			2524
$K^*(892)^0 \overline{K}^*(892)^0$		$(8.3 \pm 2.4) \times 10^{-7}$	S=1.5		2485
$K^+ K^+ \pi^- \pi^-$ nonresonant		$< 6.0 \times 10^{-6}$	CL=90%		2559
$K^*(892)^0 K^+ \pi^-$		$< 2.2 \times 10^{-6}$	CL=90%		2524
$K^*(892)^0 K^*(892)^0$		$< 2 \times 10^{-7}$	CL=90%		2485
$K^*(892)^+ K^*(892)^-$		$< 2.0 \times 10^{-6}$	CL=90%		2485
$K_1(1400)^0 \phi$		$< 5.0 \times 10^{-3}$	CL=90%		2340
$\phi(K\pi)_0^{*0}$		$(4.3 \pm 0.4) \times 10^{-6}$			–
$\phi(K\pi)_0^{*0}$ $(1.60 < m_{K\pi} < 2.15)$	[uuu]	$< 1.7 \times 10^{-6}$	CL=90%		–
$K_0^*(1430)^0 K^- \pi^+$		$< 3.18 \times 10^{-5}$	CL=90%		2404
$K_0^*(1430)^0 \overline{K}^*(892)^0$		$< 3.3 \times 10^{-6}$	CL=90%		2360
$K_0^*(1430)^0 \overline{K}_0^*(1430)^0$		$< 8.4 \times 10^{-6}$	CL=90%		2222
$K_0^*(1430)^0 \phi$		$(3.9 \pm 0.8) \times 10^{-6}$			2333
$K_0^*(1430)^0 K^*(892)^0$		$< 1.7 \times 10^{-6}$	CL=90%		2360
$K_0^*(1430)^0 K_0^*(1430)^0$		$< 4.7 \times 10^{-6}$	CL=90%		2222
$K^*(1680)^0 \phi$		$< 3.5 \times 10^{-6}$	CL=90%		2238
$K^*(1780)^0 \phi$		$< 2.7 \times 10^{-6}$	CL=90%		–
$K^*(2045)^0 \phi$		$< 1.53 \times 10^{-5}$	CL=90%		–
$K_2^*(1430)^0 \rho^0$		$< 1.1 \times 10^{-3}$	CL=90%		2381
$K_2^*(1430)^0 \phi$		$(6.8 \pm 0.9) \times 10^{-6}$	S=1.2		2332
$K^0 \phi\phi$		$(3.7 \pm 0.7) \times 10^{-6}$	S=1.3		2305
$\eta' \eta' K^0$		$< 3.1 \times 10^{-5}$	CL=90%		2338
$\eta K^0 \gamma$		$(7.6 \pm 1.8) \times 10^{-6}$			2587
$\eta' K^0 \gamma$		$< 6.4 \times 10^{-6}$	CL=90%		2528
$K^0 \phi\gamma$		$(2.7 \pm 0.7) \times 10^{-6}$			2516
$K^+ \pi^- \gamma$		$(4.6 \pm 1.4) \times 10^{-6}$			2615
$K^*(892)^0 \gamma$		$(4.21 \pm 0.24) \times 10^{-5}$	S=2.0		2565
$K^*(1410)\gamma$		$< 1.3 \times 10^{-4}$	CL=90%		2451
$K^+ \pi^- \gamma$ nonresonant		$< 2.6 \times 10^{-6}$	CL=90%		2615
$K^*(892)^0 X(214)$, $X \to \mu^+ \mu^-$	[vvv]	$< 2.26 \times 10^{-8}$	CL=90%		–
$K^0 \pi^+ \pi^- \gamma$		$(1.99 \pm 0.18) \times 10^{-5}$			2609
$K^+ \pi^- \pi^0 \gamma$		$(4.1 \pm 0.4) \times 10^{-5}$			2610
$K_1(1270)^0 \gamma$		$< 5.8 \times 10^{-5}$	CL=90%		2491
$K_1(1400)^0 \gamma$		$< 1.2 \times 10^{-5}$	CL=90%		2454
$K_2^*(1430)^0 \gamma$		$(1.24 \pm 0.24) \times 10^{-5}$			2447
$K^*(1680)^0 \gamma$		$< 2.0 \times 10^{-3}$	CL=90%		2360
$K_3^*(1780)^0 \gamma$		$< 8.3 \times 10^{-5}$	CL=90%		2340
$K_4^*(2045)^0 \gamma$		$< 4.3 \times 10^{-3}$	CL=90%		2243

Light unflavored meson modes

$\rho^0 \gamma$		$(8.0 \pm 0.6) \times 10^{-7}$	S=1.4		2583
$\rho^0 X(214)$, $X \to \mu^+ \mu^-$	[vvv]	$< 1.73 \times 10^{-8}$	CL=90%		–
$\omega\gamma$		$(4.4 {}^{+1.8}_{-1.6}) \times 10^{-7}$			2582
$\phi\gamma$		$< 1.0 \times 10^{-7}$	CL=90%		2541
$f_2(1270)\gamma$, $f_2 \to (KS)^0(KS)^0$		$< 3.1 \times 10^{-7}$			–
$f_2'(1525)\gamma$, $f_2' \to (KS)^0(KS)^0$		$< 2.1 \times 10^{-7}$			–
$\pi^+ \pi^-$		$(5.37 \pm 0.20) \times 10^{-6}$	S=1.3		2636
$\pi^0 \pi^0$		$(1.46 \pm 0.19) \times 10^{-6}$	S=1.3		2636
$\eta\pi^0$		$(4.1 \pm 1.7) \times 10^{-7}$			2610
$\eta\eta$		$< 1.0 \times 10^{-6}$	CL=90%		2582
$\eta' \pi^0$		$(1.2 \pm 0.6) \times 10^{-6}$	S=1.7		2551
$\eta' \eta'$		$< 1.7 \times 10^{-6}$	CL=90%		2460
$\eta' \eta$		$< 1.2 \times 10^{-6}$	CL=90%		2523
$\eta' \rho^0$		$< 1.3 \times 10^{-6}$	CL=90%		2492
$\eta' f_0(980)$, $f_0 \to \pi^+ \pi^-$		$< 9 \times 10^{-7}$	CL=90%		2454
$\eta\rho^0$		$< 1.5 \times 10^{-6}$	CL=90%		2553
$\eta f_0(980)$, $f_0 \to \pi^+ \pi^-$		$< 4 \times 10^{-7}$	CL=90%		2516
$\omega\eta$		$(9.4 {}^{+4.0}_{-3.1}) \times 10^{-7}$			2552
$\omega\eta'$		$(1.0 {}^{+0.5}_{-0.4}) \times 10^{-6}$			2491
$\omega\rho^0$		$< 1.6 \times 10^{-6}$	CL=90%		2522
$\omega f_0(980)$, $f_0 \to \pi^+ \pi^-$		$< 1.5 \times 10^{-6}$	CL=90%		2485
$\omega\omega$		$(1.40 \pm 0.25) \times 10^{-6}$			2521
$\phi\pi^0$		$< 1.5 \times 10^{-7}$	CL=90%		2540
$\phi\eta$		$< 5 \times 10^{-7}$	CL=90%		2511
$\phi\eta'$		$< 5 \times 10^{-7}$	CL=90%		2448
$\phi\pi^+ \pi^-$		$(1.8 \pm 0.5) \times 10^{-7}$			2533
$\phi\rho^0$		$< 3.3 \times 10^{-7}$	CL=90%		2480
$\phi f_0(980)$, $f_0 \to \pi^+ \pi^-$		$< 3.8 \times 10^{-7}$	CL=90%		2441
$\phi\omega$		$< 7 \times 10^{-7}$	CL=90%		2479
$\phi\phi$		$< 1.3 \times 10^{-8}$	CL=90%		2435
$a_0(980)^\pm \pi^\mp$, $a_0^\pm \to \eta\pi^\pm$		$< 3.1 \times 10^{-6}$	CL=90%		–
$a_0(1450)^\pm \pi^\mp$, $a_0^\pm \to \eta\pi^\pm$		$< 2.3 \times 10^{-6}$	CL=90%		–
$\pi^+ \pi^- \pi^0$		$< 7.2 \times 10^{-4}$	CL=90%		2631
$\rho^0 \pi^0$		$(2.0 \pm 0.5) \times 10^{-6}$			2581
$\rho^\mp \pi^\pm$	[bb]	$(2.30 \pm 0.23) \times 10^{-5}$			2581
$\pi^+ \pi^- \pi^+ \pi^-$		$< 1.12 \times 10^{-5}$	CL=90%		2621
$\rho^0 \pi^+ \pi^-$		$< 8.8 \times 10^{-6}$	CL=90%		2575
$\rho^0 \rho^0$		$(9.6 \pm 1.5) \times 10^{-7}$			2524
$f_0(980)\pi^+ \pi^-$, $f_0 \to \pi^+ \pi^-$		$< 3.0 \times 10^{-6}$	CL=90%		–
$\rho^0 f_0(980)$, $f_0 \to \pi^+ \pi^-$		$(7.8 \pm 2.5) \times 10^{-7}$			2486
$f_0(980) f_0(980)$, $f_0 \to \pi^+ \pi^-$, $f_0 \to \pi^+ \pi^-$		$< 1.9 \times 10^{-7}$	CL=90%		2447
$f_0(980) f_0(980)$, $f_0 \to \pi^+ \pi^-$, $f_0 \to K^+ K^-$		$< 2.3 \times 10^{-7}$	CL=90%		2447
$a_1(1260)^\mp \pi^\pm$	[bb]	$(2.6 \pm 0.5) \times 10^{-5}$	S=1.9		2495
$a_2(1320)^\mp \pi^\pm$	[bb]	$< 6.3 \times 10^{-6}$	CL=90%		2473
$\pi^+ \pi^- \pi^0 \pi^0$		$< 3.1 \times 10^{-3}$	CL=90%		2622
$\rho^+ \rho^-$		$(2.80 \pm 0.17) \times 10^{-5}$			2524
$a_1(1260)^0 \pi^0$		$< 1.1 \times 10^{-3}$	CL=90%		2495
$\omega\pi^0$		$< 5 \times 10^{-7}$	CL=90%		2580
$\pi^+ \pi^+ \pi^- \pi^- \pi^0$		$< 9.0 \times 10^{-3}$	CL=90%		2609
$a_1(1260)^+ \rho^-$		$< 6.1 \times 10^{-5}$	CL=90%		2433
$a_1(1260)^0 \rho^0$		$< 2.4 \times 10^{-3}$	CL=90%		2433
$b_1^\mp \pi^\pm$, $b_1^\mp \to \omega\pi^\mp$		$(1.09 \pm 0.15) \times 10^{-5}$			–
$b_1^0 \pi^0$, $b_1^0 \to \omega\pi^0$		$< 1.9 \times 10^{-6}$	CL=90%		–
$b_1^- \rho^+$, $b_1^- \to \omega\pi^-$		$< 1.4 \times 10^{-6}$	CL=90%		–
$b_1^0 \rho^0$, $b_1^0 \to \omega\pi^0$		$< 3.4 \times 10^{-6}$	CL=90%		–
$\pi^+ \pi^+ \pi^+ \pi^- \pi^- \pi^-$		$< 3.0 \times 10^{-3}$	CL=90%		2592
$a_1(1260)^+ a_1(1260)^-$, $a_1^+ \to 2\pi^+ \pi^-$, $a_1^- \to 2\pi^- \pi^+$		$(1.18 \pm 0.31) \times 10^{-5}$			2336
$\pi^+ \pi^+ \pi^+ \pi^- \pi^- \pi^- \pi^0$		< 1.1 %	CL=90%		2572

Baryon modes

$p\overline{p}$		$(1.27 \pm 0.14) \times 10^{-8}$			2467
$p\overline{p}\pi^+ \pi^-$		$(2.87 \pm 0.19) \times 10^{-6}$			2406
$p\overline{p}K^+ \pi^-$		$(6.3 \pm 0.5) \times 10^{-6}$			2306
$p\overline{p}K^0$		$(2.79 \pm 0.16) \times 10^{-6}$			2347
$\Theta(1540)^+ \overline{p}$, $\Theta^+ \to p K_S^0$	[xxx]	$< 5 \times 10^{-8}$	CL=90%		2318
$f_J(2220) K^0$, $f_J \to p\overline{p}$		$< 4.5 \times 10^{-7}$	CL=90%		2135
$p\overline{p}K^*(892)^0$		$(1.24 {}^{+0.28}_{-0.25}) \times 10^{-6}$			2216
$f_J(2220) K_0^*$, $f_J \to p\overline{p}$		$< 1.5 \times 10^{-7}$	CL=90%		–
$p\overline{p}K^+ K^-$		$(1.21 \pm 0.32) \times 10^{-7}$			2179
$p\overline{p}\pi^0$		$(5.0 \pm 1.9) \times 10^{-7}$			2440
$p\overline{p}p\overline{p}$		$(2.2 \pm 0.4) \times 10^{-8}$			1735
$p\overline{\Lambda}\pi^-$		$(3.16 \pm 0.24) \times 10^{-6}$			2401
$p\overline{\Lambda}\pi^- \gamma$		$< 6.5 \times 10^{-7}$	CL=90%		2401
$p\overline{\Sigma}(1385)^-$		$< 2.6 \times 10^{-7}$	CL=90%		2363
$\Delta(1232)^+ \overline{p} + \Delta(1232)^- p$		$< 1.6 \times 10^{-6}$			–
$\Delta^0 \overline{\Lambda}$		$< 9.3 \times 10^{-7}$	CL=90%		2364
$p\overline{\Lambda}K^-$		$< 8.2 \times 10^{-7}$	CL=90%		2308
$p\overline{\Lambda}D^-$		$(2.5 \pm 0.4) \times 10^{-5}$			1765
$p\overline{\Lambda}D^{*-}$		$(3.4 \pm 0.8) \times 10^{-5}$			1685
$p\overline{\Sigma}^0 \pi^-$		$(1.2 \pm 0.4) \times 10^{-6}$			2383
$\overline{\Lambda}\Lambda$		$< 3.2 \times 10^{-7}$	CL=90%		2393
$\overline{\Lambda}\Lambda K^0$		$(4.8 {}^{+1.0}_{-0.9}) \times 10^{-6}$			2250
$\overline{\Lambda}\Lambda K^{*0}$		$(2.5 {}^{+0.9}_{-0.8}) \times 10^{-6}$			2098
$\overline{\Lambda}\Lambda D^0$		$(1.00 {}^{+0.30}_{-0.26}) \times 10^{-5}$			1662
$D^0 \Sigma^0 \overline{\Lambda}$ + c.c.		$< 3.1 \times 10^{-5}$	CL=90%		1611
$\Delta^0 \overline{\Delta}^0$		$< 1.5 \times 10^{-3}$	CL=90%		2335
$\Delta^{++} \overline{\Delta}^{--}$		$< 1.1 \times 10^{-4}$	CL=90%		2335
$\overline{D}^0 p\overline{p}$		$(1.04 \pm 0.07) \times 10^{-4}$			1863
$D_s^- \overline{\Lambda}p$		$(2.8 \pm 0.9) \times 10^{-5}$			1710
$\overline{D}^*(2007)^0 p\overline{p}$		$(9.9 \pm 1.1) \times 10^{-5}$			1788
$D^*(2010)^- p\overline{n}$		$(1.4 \pm 0.4) \times 10^{-3}$			1785
$D^- p\overline{p}\pi^+$		$(3.32 \pm 0.31) \times 10^{-4}$			1786
$D^*(2010)^- p\overline{p}\pi^+$		$(4.7 \pm 0.5) \times 10^{-4}$	S=1.2		1708
$\overline{D}^0 p\overline{p}\pi^+ \pi^-$		$(3.0 \pm 0.5) \times 10^{-4}$			1708
$\overline{D}^{*0} p\overline{p}\pi^+ \pi^-$		$(1.9 \pm 0.5) \times 10^{-4}$			1623
$\Theta_c \overline{p}\pi^+$, $\Theta_c \to D^- p$		$< 9 \times 10^{-6}$	CL=90%		–
$\Theta_c \overline{p}\pi^+$, $\Theta_c \to D^{*-} p$		$< 1.4 \times 10^{-5}$	CL=90%		–
$\overline{\Sigma}_c^{--} \Delta^{++}$		$< 8 \times 10^{-4}$	CL=90%		1839
$\overline{\Lambda}_c^- p\pi^+ \pi^-$		$(1.00 \pm 0.14) \times 10^{-3}$	S=1.4		1934
$\overline{\Lambda}_c^- p$		$(1.51 \pm 0.17) \times 10^{-5}$			2021
$\overline{\Lambda}_c^- p\pi^0$		$(1.52 \pm 0.17) \times 10^{-4}$			1982
$\Sigma_c(2455)^- p$		$< 2.4 \times 10^{-5}$			–

Int. J. Mod. Phys. A 2026.41. Downloaded from www.worldscientific.com
by UNIVERSITY OF CALIFORNIA @ BERKELEY on 09/16/26. Re-use and distribution is strictly not permitted, except for Open Acce

Int. J. Mod. Phys. A 2026.41. Downloaded from www.worldscientific.com
by UNIVERSITY OF CALIFORNIA @ BERKELEY on 09/16/26. Re-use and distribution is strictly not permitted, except for Open Access articles.

$\overline{\Lambda}_c^- p \pi^+ \pi^- \pi^0$		$< 5.07 \times 10^{-3}$	CL=90%	1883
$\overline{\Lambda}_c^- p \pi^+ \pi^- \pi^+ \pi^-$		$< 2.74 \times 10^{-3}$	CL=90%	1821
$\overline{\Lambda}_c^- p \pi^+ \pi^-$ (nonresonant)		$(5.4 \pm 1.0) \times 10^{-4}$	S=1.3	1934
$\overline{\Sigma}_c(2520)^{--} p \pi^+$		$(1.01 \pm 0.18) \times 10^{-4}$		1860
$\overline{\Sigma}_c(2520)^0 p \pi^-$		$< 3.1 \times 10^{-5}$	CL=90%	1860
$\overline{\Sigma}_c(2455)^0 p \pi^-$		$(1.08 \pm 0.09) \times 10^{-4}$		1895
$\overline{\Sigma}_c(2455)^0 N^0$, $N^0 \to p \pi^-$		$(6.3 \pm 1.6) \times 10^{-5}$		–
$\overline{\Sigma}_c(2455)^{--} p \pi^+$		$(1.89 \pm 0.15) \times 10^{-4}$		1895
$\Lambda_c^- p K^+ \pi^-$		$(3.4 \pm 0.7) \times 10^{-5}$		1786
$\overline{\Sigma}_c(2455)^{--} p K^+$, $\overline{\Sigma}_c^{--} \to \overline{\Lambda}_c^- \pi^-$		$(8.7 \pm 2.5) \times 10^{-6}$		1754
$\Sigma_c(2455)^0 \overline{\Xi}_c^0$		$(4.8 \pm 1.4) \times 10^{-4}$		954
$\Lambda_c^- p K^*(892)^0$		$< 2.42 \times 10^{-5}$	CL=90%	1647
$\Lambda_c^- p K^+ K^-$		$(2.0 \pm 0.4) \times 10^{-5}$		1588
$\Lambda_c^- p \phi$		$< 9 \times 10^{-6}$	CL=90%	1567
$\Lambda_c^- p \overline{p} p$		$< 2.8 \times 10^{-6}$		677
$\overline{\Lambda}_c^- \Lambda K^+$		$(4.9 \pm 1.1) \times 10^{-5}$		1767
$\overline{\Lambda}_c^- \Lambda_c^+$		$< 1.6 \times 10^{-5}$	CL=95%	1319
$\overline{\Lambda}_c(2593)^-$ / $\overline{\Lambda}_c(2625)^- p$		$< 1.1 \times 10^{-4}$	CL=90%	–
$\overline{\Xi}_c^- \Lambda_c^+$		$(1.1 \pm 0.8) \times 10^{-3}$		1147
$\overline{\Xi}_c^- \Lambda_c^+$, $\overline{\Xi}_c^- \to \overline{\Xi}^+ \pi^- \pi^-$		$(2.3 \pm 1.0) \times 10^{-5}$	S=1.8	1147
$\overline{\Xi}_c^- \Lambda_c^+$, $\overline{\Xi}_c^- \to \overline{p} K^+ \pi^-$		$(5.2 \pm 1.6) \times 10^{-6}$		–
$\Lambda_c^+ \Lambda_c^- K^0$		$(4.0 \pm 0.9) \times 10^{-4}$		732
$\overline{\Lambda}_c(2910)^- p$, $\overline{\Lambda}_c^- \to \overline{\Sigma}_c(2455)^{--} \pi^+$		$(1.2 \pm 0.4) \times 10^{-5}$		–
$\overline{\Lambda}_c(2910)^- p$, $\overline{\Lambda}_c^- \to \overline{\Sigma}_c(2455)^0 \pi^-$		$(9 \pm 4) \times 10^{-6}$		–
$\overline{\Xi}_c(2930)^- \Lambda_c^+$, $\overline{\Xi}_c^- \to \Lambda_c^- K^0$		$(2.4 \pm 0.6) \times 10^{-4}$		–
$\Omega_c^0 \overline{\Lambda}$, $\Omega_c^0 \to \Omega^- \pi^+$		$< 9.7 \times 10^{-8}$	CL=95%	–
$\Omega_c(2770)^0 \overline{\Lambda}$, $\Omega_c^0 \to \Omega^- \pi^+$		$< 3.12 \times 10^{-7}$	CL=95%	–
$\Omega_c^0 \Lambda$, $\Omega_c^0 \to \Omega^- \pi^+$		$< 9.5 \times 10^{-8}$	CL=95%	–
$\Omega_c(2770)^0 \Lambda$, $\Omega_c^0 \to \Omega^- \pi^+$		$< 1.00 \times 10^{-7}$	CL=95%	–
$\Lambda \psi_{DS}$	[yyy]	< 0.13–5.2×10^{-5}		–

Lepton Family number (*LF*) or Lepton number (*L*) or Baryon number (*B*) violating modes, or/and $\Delta B = 1$ weak neutral current (*B1*) modes

$\gamma\gamma$	*B1*		$< 6.4 \times 10^{-8}$	CL=90%	2640
$e^+ e^-$	*B1*		$< 2.5 \times 10^{-9}$	CL=90%	2640
$e^+ e^-\gamma$	*B1*		$< 1.2 \times 10^{-7}$	CL=90%	2640
$\mu^+ \mu^-$	*B1*		$< 1.5 \times 10^{-10}$	CL=90%	2638
$\mu^+ \mu^- \mu^+ \mu^-$	*B1*		$< 1.8 \times 10^{-10}$	CL=95%	2629
SP, $S \to \mu^+ \mu^-$, $P \to \mu^+ \mu^-$	*B1*	[zzz]	$< 6.0 \times 10^{-10}$	CL=95%	–
aa, $a \to \mu^+ \mu^-$	*B1*		$< 2.3 \times 10^{-10}$	CL=95%	–
$\tau^+ \tau^-$	*B1*		$< 2.1 \times 10^{-3}$	CL=95%	1952
$\pi^0 \ell^+ \ell^-$	*B1*	[jjj]	$< 3.8 \times 10^{-8}$	CL=90%	2638
$\pi^0 e^+ e^-$	*B1*		$< 7.9 \times 10^{-8}$	CL=90%	2638
$\pi^0 \mu^+ \mu^-$	*B1*		$< 5.9 \times 10^{-8}$	CL=90%	2634
$\eta \ell^+ \ell^-$	*B1*	[jjj]	$< 4.8 \times 10^{-8}$	CL=90%	2611
$\eta e^+ e^-$	*B1*		$< 1.05 \times 10^{-7}$	CL=90%	2611
$\eta \mu^+ \mu^-$	*B1*		$< 9.4 \times 10^{-8}$	CL=90%	2607
$\rho(770)^0 e^+ e^-$	*B1*		$< 4.55 \times 10^{-7}$	CL=90%	–
$\omega e^+ e^-$	*B1*		$< 3.07 \times 10^{-7}$	CL=90%	2582
$\omega \mu^+ \mu^-$	*B1*		$< 2.49 \times 10^{-7}$	CL=90%	2577
$\omega \ell^+ \ell^-$	*B1*		$< 2.20 \times 10^{-7}$	CL=90%	2582
$\pi^0 \nu \overline{\nu}$	*B1*		$< 9 \times 10^{-6}$	CL=90%	2638
$K^0 \ell^+ \ell^-$	*B1*	[jjj]	$(3.3 \pm 0.6) \times 10^{-7}$		2616
$K^0 e^+ e^-$	*B1*		$(2.5 {}^{+1.1}_{-0.9}) \times 10^{-7}$	S=1.3	2616
$K^0 \mu^+ \mu^-$	*B1*		$(3.39 \pm 0.35) \times 10^{-7}$	S=1.1	2612
$K^0 \nu \overline{\nu}$	*B1*		$< 2.6 \times 10^{-5}$	CL=90%	2616
$\rho^0 \nu \overline{\nu}$	*B1*		$< 4.0 \times 10^{-5}$	CL=90%	2583
$K^*(892)^0 \ell^+ \ell^-$	*B1*	[jjj]	$(9.9 {}^{+1.2}_{-1.1}) \times 10^{-7}$		2565
$K^*(892)^0 e^+ e^-$	*B1*		$(1.03 {}^{+0.19}_{-0.17}) \times 10^{-6}$		2565
$K^*(892)^0 \mu^+ \mu^-$	*B1*		$(9.4 \pm 0.5) \times 10^{-7}$		2560
$K^*(892)^0 \tau^+ \tau^-$	*B1*		$< 1.8 \times 10^{-3}$	CL=90%	1404
$\overline{D}^0 \mu^+ \mu^-$	*B1*		$< 4.0 \times 10^{-8}$	CL=90%	2305
$\pi^+ \pi^- \mu^+ \mu^-$	*B1*		$(2.1 \pm 0.5) \times 10^{-8}$		2626
$K^*(892)^0 \nu \overline{\nu}$	*B1*		$< 1.8 \times 10^{-5}$	CL=90%	2565
invisible	*B1*		$< 2.4 \times 10^{-5}$	CL=90%	–
$\nu \overline{\nu} \gamma$	*B1*		$< 1.6 \times 10^{-5}$	CL=90%	2640
$\phi \mu^+ \mu^-$	*B1*		$< 3.2 \times 10^{-9}$	CL=90%	2537
$\phi \nu \overline{\nu}$	*B1*		$< 1.27 \times 10^{-4}$	CL=90%	2541
$e^\pm \mu^\mp$	*LF*	[bb]	$< 1.0 \times 10^{-9}$	CL=90%	2639
$\pi^0 e^\pm \mu^\mp$	*LF*		$< 1.4 \times 10^{-7}$	CL=90%	2637
$K^0 e^\pm \mu^\mp$	*LF*		$< 3.8 \times 10^{-8}$	CL=90%	2615
$K^0_S \tau^+ e^-$			$< 1.5 \times 10^{-5}$	CL=90%	2311
$K^0_S \tau^- e^+$			$< 8 \times 10^{-6}$	CL=90%	2311
$K^0_S \tau^+ \mu^-$			$< 1.1 \times 10^{-5}$	CL=90%	2297
$K^0_S \tau^- \mu^+$			$< 3.6 \times 10^{-5}$	CL=90%	2297
$K^*(892)^0 e^+ \mu^-$	*LF*		$< 6.8 \times 10^{-9}$	CL=90%	2563
$K^*(892)^0 e^- \mu^+$	*LF*		$< 5.7 \times 10^{-9}$	CL=90%	2563
$K^*(892)^0 e^\pm \mu^\mp$	*LF*		$< 1.01 \times 10^{-8}$	CL=90%	2563
$K^*(892)^0 \tau^+ e^-$			$< 4.9 \times 10^{-6}$	CL=90%	2245
$K^*(892)^0 \tau^- e^+$			$< 5.9 \times 10^{-6}$	CL=90%	2245
$K^*(892)^0 \tau^+ \mu^-$	*LF*		$< 1.0 \times 10^{-5}$	CL=90%	2221
$K^*(892)^0 \tau^- \mu^+$	*LF*		$< 8.2 \times 10^{-6}$	CL=90%	2221
$e^\pm \tau^\mp$	*LF*	[bb]	$< 1.6 \times 10^{-5}$	CL=90%	2341
$\mu^\pm \tau^\mp$	*LF*	[bb]	$< 1.4 \times 10^{-5}$	CL=95%	2340
$p \mu^-$	*L,B*		$< 2.6 \times 10^{-9}$	CL=90%	2555
$\Lambda_c^+ \mu^-$	*L,B*		$< 1.4 \times 10^{-6}$	CL=90%	2143
$\Lambda_c^+ e^-$	*L,B*		$< 4 \times 10^{-6}$	CL=90%	2145

$B^\pm/B^0$ ADMIXTURE

CP violation

$A_{CP}(B \to K^*(892)\gamma) = -0.003 \pm 0.011$
$A_{CP}(B \to s\gamma) = 0.015 \pm 0.011$
$A_{CP}(B \to (s+d)\gamma) = 0.010 \pm 0.031$
$A_{CP}(B \to X_s \ell^+ \ell^-) = 0.04 \pm 0.11$
$A_{CP}(B \to X_s \ell^+ \ell^-)$ $(1.0 < q^2 < 6.0\ \mathrm{GeV}^2/c^4) = -0.06 \pm 0.22$
$A_{CP}(B \to X_s \ell^+ \ell^-)$ $(10.1 < q^2 < 12.9$ or $q^2 > 14.2\ \mathrm{GeV}^2/c^4)$ $= 0.19 \pm 0.18$
$A_{CP}(B \to K^* e^+ e^-) = -0.18 \pm 0.15$
$A_{CP}(B \to K^* \mu^+ \mu^-) = -0.03 \pm 0.13$
$A_{CP}(B \to K^* \ell^+ \ell^-) = -0.04 \pm 0.07$
$A_{CP}(B \to \eta \text{anything}) = -0.13 {}^{+0.04}_{-0.05}$
$\Delta A_{CP}(X_s\gamma) = A_{CP}(B^\pm \to X_s\gamma) - A_{CP}(B^0 \to X_s\gamma) = 0.041 \pm 0.023$
$\overline{A}_{CP}(B \to X_s\gamma) = (A_{CP}(B^+ \to X_s\gamma) + A_{CP}(B^0 \to X_s\gamma))/2 = 0.009 \pm 0.012$
$\Delta A_{CP}(B \to K^*\gamma) = A_{CP}(B^+ \to K^{*+}\gamma) - A_{CP}(B^0 \to K^{*0}\gamma) = 0.025 \pm 0.023$
$\overline{A}_{CP}(B \to K^*\gamma) = (A_{CP}(B^+ \to K^{*+}\gamma) + A_{CP}(B^0 \to K^{*0}\gamma))/2 = -0.009 \pm 0.011$

The branching fraction measurements are for an admixture of B mesons at the $\Upsilon(4S)$. The values quoted assume that $B(\Upsilon(4S) \to B\overline{B}) = 100\%$.

For inclusive branching fractions, *e.g.*, $B \to D^\pm$ *anything*, the treatment of multiple D's in the final state must be defined. One possibility would be to count the number of events with one-or-more D's and divide by the total number of B's. Another possibility would be to count the total number of D's and divide by the total number of B's, which is the definition of average multiplicity. The two definitions are identical if only one D is allowed in the final state. Even though the "one-or-more" definition seems sensible, for practical reasons inclusive branching fractions are almost always measured using the multiplicity definition. For heavy final state particles, authors call their results inclusive branching fractions while for light particles some authors call their results multiplicities. In the B sections, we list all results as inclusive branching fractions, adopting a multiplicity definition. This means that inclusive branching fractions can exceed 100% and that inclusive partial widths can exceed total widths, just as inclusive cross sections can exceed total cross section.

$\overline{B}$ modes are charge conjugates of the modes below. Reactions indicate the weak decay vertex and do not include mixing.

***B* DECAY MODES**		Fraction (Γ_i/Γ)	Scale factor/ Confidence level	p (MeV/c)
Semileptonic and leptonic modes				
$\ell^+ \nu_\ell$ anything	[jjj,aaaa]	(10.82 ± 0.15) %		–
$D^- \ell^+ \nu_\ell$ anything	[jjj]	(2.6 ± 0.5) %		–
$\overline{D}^0 \ell^+ \nu_\ell$ anything	[jjj]	(7.2 ± 1.5) %		–
$\overline{D} \ell^+ \nu_\ell$		(2.41 ± 0.12) %		2311
$\overline{D} e^+ \nu_e$		seen		2311
$\overline{D} \mu^+ \nu_\mu$		seen		2309
$D^{*-} \ell^+ \nu_\ell$ anything	[bbaa]	$(6.7 \pm 1.3) \times 10^{-3}$		–
$\overline{D}^* \ell^+ \nu_\ell$	[ccaa]	(4.95 ± 0.11) %		2257
$\overline{D}^{**} \ell^+ \nu_\ell$	[jjj,ddaa]	(2.7 ± 0.7) %		–
$\overline{D}_1(2420) \ell^+ \nu_\ell$ anything		$(3.8 \pm 1.3) \times 10^{-3}$	S=2.4	–

Int. J. Mod. Phys. A 2026.41. Downloaded from www.worldscientific.com
by UNIVERSITY OF CALIFORNIA @ BERKELEY on 09/16/26. Re-use and distribution is strictly not permitted, except for Open Acce

$\overline{D}\pi\ell^+\nu_\ell$ anything + $\overline{D}^*\pi\ell^+\nu_\ell$ anything		(2.6 ± 0.5) %	S=1.5		–
$\overline{D}\pi\ell^+\nu_\ell$ anything		(1.5 ± 0.6) %			–
$\overline{D}^*\pi\ell^+\nu_\ell$ anything		(1.9 ± 0.4) %			–
$\overline{D}_2^*(2460)\ell^+\nu_\ell$ anything		(4.4 ± 1.6) $\times 10^{-3}$			–
$D^{*-}\pi^+\ell^+\nu_\ell$ anything		(1.00 ± 0.34) %			–
$\overline{D}\pi^+\pi^-\ell^+\nu_\ell$		(1.62 ± 0.32) $\times 10^{-3}$			2301
$\overline{D}^*\pi^+\pi^-\ell^+\nu_\ell$		(9.4 ± 3.2) $\times 10^{-4}$			2247
$D_s^-\ell^+\nu_\ell$ anything	[jjj]	< 7 $\times 10^{-3}$	CL=90%		–
$D_s^-\ell^+\nu_\ell K^+$ anything	[jjj]	< 5 $\times 10^{-3}$	CL=90%		–
$D_s^-\ell^+\nu_\ell K^0$ anything	[jjj]	< 7 $\times 10^{-3}$	CL=90%		–
$X_c\ell^+\nu_\ell$		(10.63 ± 0.15) %			–
$X_u\ell^+\nu_\ell$		(1.88 ± 0.27) $\times 10^{-3}$			–
$X_u e^+\nu_e$		(1.57 ± 0.19) $\times 10^{-3}$			–
$X_u\mu^+\nu_\mu$		(1.62 ± 0.21) $\times 10^{-3}$			–
$K^+\ell^+\nu_\ell$ anything	[jjj]	(6.3 ± 0.5) %			–
$K^-\ell^+\nu_\ell$ anything	[jjj]	(10 ± 4) $\times 10^{-3}$			–
$K^0/\overline{K}^0\ell^+\nu_\ell$ anything	[jjj]	(4.6 ± 0.5) %			–
$\overline{D}\tau^+\nu_\tau$		(8.4 ± 0.7) $\times 10^{-3}$			1911
$\overline{D}^*\tau^+\nu_\tau$		(1.43 ± 0.07) %			1838

D, D^*, or D_s modes

$D^\pm$ anything		(23.3 ± 1.2) %			–
$D^0/\overline{D}^0$ anything		(64.6 ± 2.0) %	S=1.5		–
$D^*(2010)^\pm$ anything		(22.5 ± 1.5) %			–
$\overline{D}^*(2007)^0$ anything		(26.0 ± 2.7) %			–
$D_s^\pm$ anything	[bb]	(10.6 ± 0.6) %	S=1.7		–
$D_s^{*\pm}$ anything		(6.3 ± 1.0) %			–
$D_s^{*\pm}\overline{D}^{(*)}$		(3.4 ± 0.6) %			–
$\overline{D}D_{s0}(2317)$		seen			1605
$\overline{D}D_{s,J}(2457)$		seen			–
$D^{(*)}\overline{D}^{(*)}K^0$ + $D^{(*)}\overline{D}^{(*)}K^\pm$	[bb,eeaa]	(7.1 $^{+2.7}_{-1.7}$) %			–
$b\to c\overline{c}s$		(22 ± 4) %			–
$D_s^{(*)}\overline{D}^{(*)}$	[bb,eeaa]	(5.0 ± 0.4) %			–
$D^*D^*(2010)^\pm$	[bb]	< 5.9 $\times 10^{-3}$	CL=90%		1711
$DD^*(2010)^\pm$ + $D^*D^\pm$	[bb]	< 5.5 $\times 10^{-3}$	CL=90%		–
$DD^\pm$	[bb]	< 3.1 $\times 10^{-3}$	CL=90%		1866
$D_s^{(*)\pm}\overline{D}^{(*)}X\,(n\pi^\pm)$	[bb,eeaa]	(9 $^{+5}_{-4}$) %			–
$\overline{D}^*(2010)\gamma$		< 1.1 $\times 10^{-3}$	CL=90%		2257
$D_s^+\pi^-$, $D_s^{*+}\pi^-$, $D_s^+\rho^-$, $D_s^{*+}\rho^-$, $D_s^+\pi^0$, $D_s^{*+}\pi^0$, $D_s^+\eta$, $D_s^{*+}\eta$, $D_s^+\rho^0$, $D_s^{*+}\rho^0$, $D_s^+\omega$, $D_s^{*+}\omega$	[bb]	< 4 $\times 10^{-4}$	CL=90%		–
$D_{s1}(2536)^+$ anything		< 9.5 $\times 10^{-3}$	CL=90%		–

Charmonium modes

$J/\psi(1S)$ anything		(1.094 ± 0.032) %	S=1.1		–
$J/\psi(1S)$ (direct) anything		(7.8 ± 0.4) $\times 10^{-3}$	S=1.1		–
$\psi(2S)$ anything		(3.07 ± 0.21) $\times 10^{-3}$			–
$\chi_{c1}(1P)$ anything		(3.55 ± 0.27) $\times 10^{-3}$	S=1.3		–
$\chi_{c1}(1P)$ (direct) anything		(3.09 ± 0.19) $\times 10^{-3}$			–
$\chi_{c2}(1P)$ anything		(10.0 ± 1.7) $\times 10^{-4}$	S=1.6		–
$\chi_{c2}(1P)$ (direct) anything		(7.5 ± 1.1) $\times 10^{-4}$			–
$\eta_c(1S)$ anything		< 9 $\times 10^{-3}$	CL=90%		–
$K\chi_{c1}(3872)$		(1.9 ± 0.7) $\times 10^{-4}$			1141
$KX(3940)$, $X\to D^*0D^0$		< 6.7 $\times 10^{-5}$	CL=90%		1084
$K\chi_{c0}(3915)$, $\chi_{c0}\to\omega J/\psi$	[ffaa]	(7.1 ± 3.4) $\times 10^{-5}$			1103

K or K^* modes

$K^\pm$ anything	[bb]	(78.9 ± 2.5) %			–
K^+ anything		(66 ± 5) %			–
K^- anything		(13 ± 4) %			–
$K^0/\overline{K}^0$ anything	[bb]	(64 ± 4) %			–
$K^*(892)^\pm$ anything		(18 ± 6) %			–
$K^*(892)^0/\overline{K}^*(892)^0$ anything	[bb]	(14.6 ± 2.6) %			–
$K^*(892)\gamma$		(4.10 ± 0.12) $\times 10^{-5}$			2565
$\eta K\gamma$		(8.5 $^{+1.8}_{-1.6}$) $\times 10^{-6}$			2588
$K_1(1400)\gamma$		< 1.27 $\times 10^{-4}$	CL=90%		2454
$K_2^*(1430)\gamma$		(1.7 $^{+0.6}_{-0.5}$) $\times 10^{-5}$			2447
$K_2(1770)\gamma$		< 1.2 $\times 10^{-3}$	CL=90%		2342
$K_3^*(1780)\gamma$		< 3.7 $\times 10^{-5}$	CL=90%		2340
$K_4^*(2045)\gamma$		< 1.0 $\times 10^{-3}$	CL=90%		2243
$K\eta'(958)$		(8.3 ± 1.1) $\times 10^{-5}$			2528
$K^*(892)\eta'(958)$		(4.1 ± 1.1) $\times 10^{-6}$			2472
$K\eta$		< 5.2 $\times 10^{-6}$	CL=90%		2588
$K^*(892)\eta$		(1.8 ± 0.5) $\times 10^{-5}$			2534
$K\phi\phi$		(2.3 ± 0.9) $\times 10^{-6}$			2306
$\overline{b}\to\overline{s}\gamma$		(3.49 ± 0.19) $\times 10^{-4}$			–
$\overline{b}\to\overline{d}\gamma$		(9.2 ± 3.0) $\times 10^{-6}$			–
$\overline{b}\to\overline{s}$gluon		< 6.8 %	CL=90%		–
η anything		(2.6 $^{+0.5}_{-0.8}$) $\times 10^{-4}$			–
η' anything		(4.2 ± 0.9) $\times 10^{-4}$			–
K^+gluon (charmless)		< 1.87 $\times 10^{-4}$	CL=90%		–
K^0gluon (charmless)		(1.9 ± 0.7) $\times 10^{-4}$			–

Light unflavored meson modes

$\rho\gamma$		(1.39 ± 0.25) $\times 10^{-6}$	S=1.2		2583
$\rho/\omega\gamma$		(1.30 ± 0.23) $\times 10^{-6}$	S=1.2		–
$\pi^\pm$ anything	[bb,ggaa]	(358 ± 7) %			–
π^0 anything		(235 ±11) %			–
η anything		(17.6 ± 1.6) %			–
ρ^0 anything		(21 ± 5) %			–
ω anything		< 81 %	CL=90%		–
ϕ anything		(3.43 ± 0.12) %			–
$\phi K^*(892)$		< 2.2 $\times 10^{-5}$	CL=90%		2460
π^+ gluon (charmless)		(3.7 ± 0.8) $\times 10^{-4}$			–

Baryon modes

Λ_c^+ / $\overline{\Lambda}_c^-$ anything		(3.53 ± 0.34) %			–
Λ_c^+ anything		< 1.3 %	CL=90%		–
$\overline{\Lambda}_c^-$ anything		< 7 %	CL=90%		–
$\overline{\Lambda}_c^-\ell^+$ anything		< 9 $\times 10^{-4}$	CL=90%		–
$\overline{\Lambda}_c^-e^+$ anything		< 1.8 $\times 10^{-3}$	CL=90%		–
$\overline{\Lambda}_c^-\mu^+$ anything		< − 1.4 $\times 10^{-3}$	CL=90%		–
$\overline{\Lambda}_c^-p$ anything		(2.01 ± 0.31) %			–
$\overline{\Lambda}_c^-pe^+\nu_e$		< 8 $\times 10^{-4}$	CL=90%		2021
$\overline{\Sigma}_c^{--}$ anything		(3.3 ± 1.7) $\times 10^{-3}$			–
$\overline{\Sigma}_c^-$ anything		< 8 $\times 10^{-3}$	CL=90%		–
$\overline{\Sigma}_c^0$ anything		(3.6 ± 1.7) $\times 10^{-3}$			–
$\overline{\Sigma}_c^0N(N=p$ or $n)$		< 1.1 $\times 10^{-3}$	CL=90%		1938
Ξ_c^0 anything, $\Xi_c^0\to\Xi^-\pi^+$		(1.93 ± 0.30) $\times 10^{-4}$	S=1.1		–
Ξ_c^+, $\Xi_c^+\to\Xi^-\pi^+\pi^+$		(4.5 $^{+1.3}_{-1.2}$) $\times 10^{-4}$			–
$p/\overline{p}$ anything	[bb]	(8.0 ± 0.4) %			–
$p/\overline{p}$ (direct) anything	[bb]	(5.5 ± 0.5) %			–
$\overline{p}e^+\nu_e$ anything		< 5.9 $\times 10^{-4}$	CL=90%		–
$\Lambda/\overline{\Lambda}$ anything	[bb]	(4.0 ± 0.5) %			–
Λ anything		seen			–
$\overline{\Lambda}$ anything		seen			–
$\Xi^-/\overline{\Xi}^+$ anything	[bb]	(2.7 ± 0.6) $\times 10^{-3}$			–
baryons anything		(6.8 ± 0.6) %			–
$p\overline{p}$ anything		(2.47 ± 0.23) %			–
$\Lambda\overline{p}/\overline{\Lambda}p$ anything	[bb]	(2.5 ± 0.4) %			–
$\Lambda\overline{\Lambda}$ anything		< 5 $\times 10^{-3}$	CL=90%		–

Lepton Family number (LF) violating modes or $\Delta B = 1$ weak neutral current ($B1$) modes

se^+e^-	$B1$		(6.7 ± 1.7) $\times 10^{-6}$	S=2.0		–
$s\mu^+\mu^-$	$B1$		(4.3 ± 1.0) $\times 10^{-6}$			–
$s\ell^+\ell^-$	$B1$	[jjj]	(5.8 ± 1.3) $\times 10^{-6}$	S=1.8		–
$\pi\ell^+\ell^-$	$B1$		< 5.9 $\times 10^{-8}$	CL=90%		2638
πe^+e^-	$B1$		< 1.10 $\times 10^{-7}$	CL=90%		2638
$\pi\mu^+\mu^-$	$B1$		< 5.0 $\times 10^{-8}$	CL=90%		2634
Ke^+e^-	$B1$		(4.4 ± 0.6) $\times 10^{-7}$			2617
$K^*(892)e^+e^-$	$B1$		(1.19 ± 0.20) $\times 10^{-6}$	S=1.2		2565
$K\mu^+\mu^-$	$B1$		(4.4 ± 0.4) $\times 10^{-7}$			2612
$K^*(892)\mu^+\mu^-$	$B1$		(1.06 ± 0.09) $\times 10^{-6}$			2560
$K\ell^+\ell^-$	$B1$		(4.8 ± 0.4) $\times 10^{-7}$			2617
$K^*(892)\ell^+\ell^-$	$B1$		(1.05 ± 0.10) $\times 10^{-6}$			2565
$K\nu\overline{\nu}$	$B1$		< 1.6 $\times 10^{-5}$	CL=90%		2617
$K^*\nu\overline{\nu}$	$B1$		< 2.7 $\times 10^{-5}$	CL=90%		–
$\pi\nu\overline{\nu}$	$B1$		< 8 $\times 10^{-6}$	CL=90%		2638
$\rho\nu\overline{\nu}$	$B1$		< 2.8 $\times 10^{-5}$	CL=90%		2583
$se^\pm\mu^\mp$	LF	[bb]	< 2.2 $\times 10^{-5}$	CL=90%		–
$\pi e^\pm\mu^\mp$	LF		< 9.2 $\times 10^{-8}$	CL=90%		2637
$\rho e^\pm\mu^\mp$	LF		< 3.2 $\times 10^{-6}$	CL=90%		2582
$Ke^\pm\mu^\mp$	LF		< 3.8 $\times 10^{-8}$	CL=90%		2616
$K^*(892)e^\pm\mu^\mp$	LF		< 5.1 $\times 10^{-7}$	CL=90%		2563

Int. J. Mod. Phys. A 2026.41. Downloaded from www.worldscientific.com
by UNIVERSITY OF CALIFORNIA @ BERKELEY on 09/16/26. Re-use and distribution is strictly not permitted, except for Open Access articles.

$B^{\pm}/B^0/B^0_s/b$-baryon ADMIXTURE

These measurements are for an admixture of bottom particles at high energy (LHC, LEP, Tevatron, $Sp\overline{p}S$).

Mean life $\tau = (1.5673 \pm 0.0029) \times 10^{-12}$ s

Mean life $\tau = (1.72 \pm 0.10) \times 10^{-12}$ s Charged b-hadron admixture

Mean life $\tau = (1.58 \pm 0.14) \times 10^{-12}$ s Neutral b-hadron admixture

$\tau_{\text{charged } b\text{-hadron}}/\tau_{\text{neutral } b\text{-hadron}} = 1.09 \pm 0.13$

$|\Delta\tau_b|/\tau_{b,\overline{b}} = -0.001 \pm 0.014$

The branching fraction measurements are for an admixture of B mesons and baryons at energies above the $\Upsilon(4S)$. Only the highest energy results (LHC, LEP, Tevatron, $Sp\overline{p}S$) are used in the branching fraction averages. In the following, the production fractions are provided separately at three different colliders (LEP, $p\overline{p}$ Tevatron, and pp LHC) and are used for the subsequent measurements accordingly.

For inclusive branching fractions, *e.g.*, $B \to D^{\pm}$ anything, the values usually are multiplicities, not branching fractions. They can be greater than one.

The modes below are listed for a $\overline{b}$ initial state. b modes are their charge conjugates. Reactions indicate the weak decay vertex and do not include mixing.

$\overline{b}$ DECAY MODES	Fraction (Γ_i/Γ)	Scale factor/ Confidence level	p (MeV/c)

PRODUCTION FRACTIONS

The production fractions for weakly decaying b-hadrons at high energy have been calculated from the best values of mean lives, mixing parameters, and branching fractions in this edition by the Heavy Flavor Averaging Group (HFLAV) as described in the note "B^0-$\overline{B}^0$ Mixing" in the B^0 Particle Listings. We no longer provide world averages of the b-hadron production fractions, where results from LEP, Tevatron and LHC are averaged together; indeed the available data (from CDF and LHCb) shows that the fractions depend on the kinematics (in particular the p_T) of the produced b hadron. Hence, we would like to list the fractions at LEP Z decays, at $p\overline{p}$ collision at the Tevatron, and at pp collision at LHC, separately, when they are available.

Values assume:

$B(\overline{b} \to B^+) = B(\overline{b} \to B^0)$

$B(\overline{b} \to B^+) + B(\overline{b} \to B^0) + B(\overline{b} \to B^0_s) + B(b \to b\text{-baryon}) = 100\%$.

The notation for production fractions varies in the literature (f_d, d_{B^0}, $f(b \to \overline{B}^0)$, $Br(b \to \overline{B}^0)$). We use our own branching fraction notation here, $B(\overline{b} \to B^0 \text{ at } Z)$ at LEP, $B(\overline{b} \to B^0 \text{ at } p\overline{p})$ at Tevatron, $B(\overline{b} \to B^0 \text{ at } pp)$ at LHC. The $B(\overline{b} \to B^+_c)$ is a placeholder for the future measurements, and is negligible in the $\overline{b}$-production fractions.

Note these production fractions are b-hadronization fractions, not the conventional branching fractions of b-quark to a B-hadron, which may have considerable dependence on the initial and final state kinematic and production environment.

Production fractions at Z

The correlation coefficients between the reported production fractions are:

$cor(B^0_s \text{ at } Z, b\text{-baryon at } Z) = 0.064$

$cor(B^0_s \text{ at } Z, B^{\pm}{=}B^0 \text{ at } Z) = -0.633$

$cor(b\text{-baryon at } Z, B^{\pm}{=}B^0 \text{ at } Z) = -0.813$.

B^+ at Z		(40.8 ± 0.7) %	–
B^0 at Z		(40.8 ± 0.7) %	–
B^0_s at Z		(10.0 ± 0.8) %	–
b-baryon at Z		(8.4 ± 1.1) %	–

Production fractions at $p\overline{p}$

The correlation coefficients between the reported production fractions are:

$cor(B^0_s \text{ at } p\overline{p}, b\text{-baryon at } p\overline{p}) = -0.429$

$cor(B^0_s \text{ at } p\overline{p}, B^{\pm}{=}B^0 \text{ at } p\overline{p}) = +0.159$

$cor(b\text{-baryon at } p\overline{p}, B^{\pm}{=}B^0 \text{ at } p\overline{p}) = -0.960$.

as obtained with the Tevatron average of time-integrated mixing parameter $\overline{\chi} = 0.147 \pm 0.011$.

B^+ at $p\overline{p}$		(34.4 ± 2.1) %	–
B^0 at $p\overline{p}$		(34.4 ± 2.1) %	–
B^0_s at $p\overline{p}$		(11.5 ± 1.3) %	–
b-baryon at $p\overline{p}$		(19.8 ± 4.6) %	–

Production fractions at pp

B^+ at pp		(36.0 ± 0.5) %	–
B^0 at pp		(36.0 ± 0.5) %	–
B^0_s at pp		(9.04 ± 0.25) %	–
b-baryon at pp		(18.7 ± 1.1) %	–
B^+_c at pp		(2.7 ± 0.5) $\times 10^{-3}$	–

DECAY MODES

Semileptonic and leptonic modes

ν anything		(23.1 ± 1.5) %	–
$\ell^+ \nu_\ell$ anything	[*jj*]	(10.69 ± 0.22) %	–
$e^+ \nu_e$ anything		(10.86 ± 0.35) %	–
$\mu^+ \nu_\mu$ anything		(10.95 $^{+0.29}_{-0.25}$) %	–
$D^- \ell^+ \nu_\ell$ anything	[*jj*]	(2.2 ± 0.4) % S=1.8	–
$D^- \pi^+ \ell^+ \nu_\ell$ anything		(4.9 ± 1.9) $\times 10^{-3}$	–
$D^- \pi^- \ell^+ \nu_\ell$ anything		(2.6 ± 1.6) $\times 10^{-3}$	–
$\overline{D}^0 \ell^+ \nu_\ell$ anything	[*jj*]	(6.80 ± 0.34) %	–
$\overline{D}^0 \pi^- \ell^+ \nu_\ell$ anything		(1.07 ± 0.27) %	–
$\overline{D}^0 \pi^+ \ell^+ \nu_\ell$ anything		(2.3 ± 1.6) $\times 10^{-3}$	–
$D^{*-} \ell^+ \nu_\ell$ anything	[*jj*]	(2.75 ± 0.19) %	–
$D^{*-} \pi^- \ell^+ \nu_\ell$ anything		(6 ± 7) $\times 10^{-4}$	–
$D^{*-} \pi^+ \ell^+ \nu_\ell$ anything		(4.8 ± 1.0) $\times 10^{-3}$	–
$\overline{D}^0_j \ell^+ \nu_\ell$ anything $\times$ B($\overline{D}^0_j \to D^{*+} \pi^-$)	[*jj,hhaa*]	(2.6 ± 0.9) $\times 10^{-3}$	–
$D^-_j \ell^+ \nu_\ell$ anything $\times$ B($D^-_j \to D^0 \pi^-$)	[*jj,hhaa*]	(7.0 ± 2.3) $\times 10^{-3}$	–
$\overline{D}^*_2(2460)^0 \ell^+ \nu_\ell$ anything $\times$ B($\overline{D}^*_2(2460)^0 \to D^{*-} \pi^+$)		< 1.4 $\times 10^{-3}$ CL=90%	–
$D^*_2(2460)^- \ell^+ \nu_\ell$ anything $\times$ B($D^*_2(2460)^- \to D^0 \pi^-$)		(4.2 $^{+1.5}_{-1.8}$) $\times 10^{-3}$	–
$\overline{D}^*_2(2460)^0 \ell^+ \nu_\ell$ anything $\times$ B($\overline{D}^*_2(2460)^0 \to D^- \pi^+$)		(1.6 ± 0.8) $\times 10^{-3}$	–
charmless $\ell \overline{\nu}_\ell$	[*jj*]	(1.7 ± 0.5) $\times 10^{-3}$	–
$\tau^+ \nu_\tau$ anything		(2.41 ± 0.23) %	–
$D^{*-} \tau \nu_\tau$ anything		(9 ± 4) $\times 10^{-3}$	–
$\overline{c} \to \ell^- \overline{\nu}_\ell$ anything	[*jj*]	(8.02 ± 0.19) %	–
$c \to \ell^+ \nu$ anything		(1.6 $^{+0.4}_{-0.5}$) %	–

Charmed meson and baryon modes

$\overline{D}^0$ anything		(58.9 ± 2.8) %	–
$D^0 D^{\pm}_s$ anything	[*bb*]	(9.1 $^{+4.0}_{-2.8}$) %	–
$D^{\mp} D^{\pm}_s$ anything	[*bb*]	(4.0 $^{+2.3}_{-1.8}$) %	–
$\overline{D}^0 D^0$ anything	[*bb*]	(5.1 $^{+2.0}_{-1.8}$) %	–
$D^0 D^{\pm}$ anything	[*bb*]	(2.7 $^{+1.8}_{-1.6}$) %	–
$D^{\pm} D^{\mp}$ anything	[*bb*]	< 9 $\times 10^{-3}$ CL=90%	–
D^- anything		(22.9 ± 1.6) %	–
$D^*(2010)^+$ anything		(17.3 ± 2.0) %	–
$D_1(2420)^0$ anything		(5.0 ± 1.5) %	–
$D^*(2010)^{\mp} D^{\pm}_s$ anything	[*bb*]	(3.3 $^{+1.6}_{-1.3}$) %	–
$D^0 D^*(2010)^{\pm}$ anything	[*bb*]	(3.0 $^{+1.1}_{-0.9}$) %	–
$D^*(2010)^{\pm} D^{\mp}$ anything	[*bb*]	(2.5 $^{+1.2}_{-1.0}$) %	–
$D^*(2010)^{\pm} D^*(2010)^{\mp}$ anything	[*bb*]	(1.2 ± 0.4) %	–
$\overline{D} D$ anything		(10 $^{+11}_{-10}$) %	–
$D^*_2(2460)^0$ anything		(4.7 ± 2.7) %	–
D^-_s anything		(14.7 ± 2.1) %	–
D^+_s anything		(10.1 ± 3.1) %	–
Λ^+_c anything		(7.6 ± 1.1) %	–
$\overline{c}/c$ anything	[*ggaa*]	(116.2 ± 3.2) %	–

Charmonium modes

$J/\psi(1S)$ anything		(1.16 ± 0.10) %	–
$\psi(2S)$ anything		(3.06 ± 0.30) $\times 10^{-3}$	–
$\chi_{c0}(1P)$ anything		(2.9 ± 0.6) $\times 10^{-3}$	–
$\chi_{c1}(1P)$ anything		(5.6 ± 1.5) $\times 10^{-3}$ S=1.3	–
$\chi_{c2}(1P)$ anything		(1.4 ± 1.0) $\times 10^{-3}$	–
$\chi_c(2P)$ anything, $\chi_c \to \phi\phi$		< 2.8 $\times 10^{-7}$ CL=95%	–
$\eta_c(1S)$ anything		(5.7 ± 0.7) $\times 10^{-3}$	–
$\eta_c(2S)$ anything, $\eta_c \to \phi\phi$		(3.3 ± 1.4) $\times 10^{-7}$	–
$\chi_{c1}(3872)$ anything, $\chi_{c1} \to \phi\phi$		< 4.5 $\times 10^{-7}$ CL=95%	–
$\chi_{c0}(3915)$ anything, $\chi_{c0} \to \phi\phi$		< 3.1 $\times 10^{-7}$ CL=95%	–

Int. J. Mod. Phys. A 2026.41. Downloaded from www.worldscientific.com
by UNIVERSITY OF CALIFORNIA @ BERKELEY on 09/16/26. Re-use and distribution is strictly not permitted, except for Open Acce

K or K^* modes				
$\overline{s}\gamma$		$(3.1 \pm 1.1) \times 10^{-4}$		–
$\overline{s}\overline{\nu}\nu$	*B1*	$< 6.4 \times 10^{-4}$	CL=90%	–
$K^{\pm}$ anything		(74 ± 6) %		–
K^0_S anything		(29.0 ± 2.9) %		–
Pion modes				
$\pi^{\pm}$ anything		(397 ± 21) %		–
π^0 anything	[*ggaa*]	(280 ± 60) %		–
ϕ anything		(2.82 ± 0.23) %		–
Baryon modes				
$p/\overline{p}$ anything		(13.1 ± 1.1) %		–
$\Lambda/\overline{\Lambda}$ anything		(5.9 ± 0.6) %		–
b-baryon anything		(10.2 ± 2.8) %		–
Other modes				
charged anything	[*ggaa*]	(497 ± 7) %		–
hadron$^+$ hadron$^-$		$(1.7 {}^{+1.0}_{-0.7}) \times 10^{-5}$		–
charmless		$(7 \pm 21) \times 10^{-3}$		–
$\Delta B = 1$ weak neutral current ($B1$) modes				
$\mu^+\mu^-$ anything	*B1*	$< 3.2 \times 10^{-4}$	CL=90%	–

B^*

$I(J^P) = \frac{1}{2}(1^-)$
I, J, P need confirmation.

Quantum numbers shown are quark-model predictions.

Mass $m_{B^*} = 5324.75 \pm 0.20$ MeV
$m_{B^*} - m_B = 45.18 \pm 0.20$ MeV
$m_{B^{*+}} - m_{B^+} = 45.34 \pm 0.20$ MeV

B^* DECAY MODES	Fraction (Γ_i/Γ)	p (MeV/c)
$B\gamma$	seen	45

$B_1(5721)$

$I(J^P) = \frac{1}{2}(1^+)$
I, J, P need confirmation.

$B_1(5721)^+$ mass $= 5726.0^{+2.5}_{-2.7}$ MeV
$m_{B_1^+} - m_{B^{*0}} = 401.2^{+2.4}_{-2.7}$ MeV
$B_1(5721)^0$ mass $= 5726.1 \pm 1.2$ MeV (S = 1.2)
$m_{B_1^0} - m_{B^+} = 446.7 \pm 1.2$ MeV (S = 1.2)
$m_{B_1^0} - m_{B^{*+}} = 401.4 \pm 1.2$ MeV (S = 1.2)
Full width $\Gamma(B_1(5721)^+) = 31 \pm 6$ MeV (S = 1.1)
Full width $\Gamma(B_1(5721)^0) = 27.5 \pm 3.4$ MeV (S = 1.1)

$B_1(5721)$ DECAY MODES	Fraction (Γ_i/Γ)	p (MeV/c)
$B^*\pi$	seen	365

$B_2^*(5747)$

$I(J^P) = \frac{1}{2}(2^+)$
I, J, P need confirmation.

$B_2^*(5747)^+$ mass $= 5737.3 \pm 0.7$ MeV
$m_{B_2^{*+}} - m_{B^0} = 457.5 \pm 0.7$ MeV
$B_2^*(5747)^0$ mass $= 5739.6 \pm 0.7$ MeV (S = 1.4)
$m_{B_2^{*0}} - m_{B_1^0} = 13.5 \pm 1.4$ MeV (S = 1.3)
$m_{B_2^{*0}} - m_{B^+} = 460.2 \pm 0.6$ MeV (S = 1.4)
Full width $\Gamma(B_2^*(5747)^+) = 20 \pm 5$ MeV (S = 2.2)
Full width $\Gamma(B_2^*(5747)^0) = 24.2 \pm 1.7$ MeV

$B_2^*(5747)$ DECAY MODES	Fraction (Γ_i/Γ)	p (MeV/c)
$B\pi$	seen	420
$B^*\pi$	seen	376

$B_J(5970)$

$I(J^P) = \frac{1}{2}(?^?)$
I, J, P need confirmation.

$B_J(5970)^+$ mass $m = 5965 \pm 5$ MeV
$m_{B_J(5970)^+} - m_{B^0} = 685 \pm 5$ MeV
$B_J(5970)^0$ mass $m = 5971 \pm 5$ MeV
$m_{B_J(5970)^0} - m_{B^+} = 691 \pm 5$ MeV
$B_J(5970)^+$ full width $\Gamma = 62 \pm 20$ MeV
$B_J(5970)^0$ full width $\Gamma = 81 \pm 12$ MeV

$B_J(5970)$ DECAY MODES	Fraction (Γ_i/Γ)	p (MeV/c)
$B\pi$	possibly seen	633
$B^*\pi$	seen	592

BOTTOM, STRANGE MESONS ($B = \pm 1$, $S = \mp 1$)

$B_s^0 = s\overline{b}$, $\overline{B}_s^0 = \overline{s}b$, similarly for B_s^*'s

B_s^0

$I(J^P) = 0(0^-)$

I, J, P need confirmation. Quantum numbers shown are quark-model predictions.

Mass $m_{B_s^0} = 5366.93 \pm 0.10$ MeV
$m_{B_s^0} - m_B = 87.37 \pm 0.12$ MeV
Mean life $\tau = (1.515 \pm 0.006) \times 10^{-12}$ s
$c\tau = 454.2\ \mu$m
$\Delta\Gamma_{B_s^0} = \Gamma_{B_{sL}^0} - \Gamma_{B_{sH}^0} = (0.0783 \pm 0.0035) \times 10^{12}$ s^{-1}

B_s^0-$\overline{B}_s^0$ mixing parameters

$\Delta m_{B_s^0} = m_{B_{sH}^0} - m_{B_{sL}^0} = (17.766 \pm 0.006) \times 10^{12}\ \hbar$ s^{-1}
$= (1.1694 \pm 0.0004) \times 10^{-8}$ MeV
$x_s = \Delta m_{B_s^0}/\Gamma_{B_s^0} = 26.91 \pm 0.11$
χ_s (B_s^0-$\overline{B}_s^0$ mixing parameter) $= 0.499313 \pm 0.000006$

CP violation parameters in B_s^0

$\mathrm{Re}(\epsilon_{B_s^0}) / (1 + |\epsilon_{B_s^0}|^2) = (-0.15 \pm 0.70) \times 10^{-3}$
$C_{KK}(B_s^0 \to K^+K^-) = 0.162 \pm 0.035$
$S_{KK}(B_s^0 \to K^+K^-) = 0.14 \pm 0.05$ (S = 1.3)
$r_B(B_s^0 \to D_s^{\mp} K^{\pm}) = 0.318 \pm 0.034$
$r_B(B_s^0 \to D_s^{\mp} K^{\pm}\pi^{\pm}\pi^{\mp}) = 0.47 \pm 0.08$
$\delta_B(B_s^0 \to D_s^{\pm} K^{\mp}) = (348 \pm 6)^\circ$
$\delta_B(B_s^0 \to D_s^{\pm} K^{\mp}\pi^{\pm}\pi^{\mp}) = (-6 {}^{+10}_{-13})^\circ$
CP Violation phase β_s ($b \to c\overline{c}s$) $= (2.7 \pm 0.7) \times 10^{-2}$ rad
CP Violation phase β_s ($b \to s\overline{s}s$) $= (3.7 \pm 3.5) \times 10^{-2}$ rad
CP Violation phase β_s ($B_s^0 \to J/\psi(1S)\phi$) $= (3.0 \pm 0.7) \times 10^{-2}$ rad
$|\lambda|$ ($B_s^0 \to J/\psi(1S)\phi$) $= 0.995 \pm 0.009$
$|\lambda|$ ($b \to c\overline{c}s$) $= 0.989 \pm 0.008$
A, CP violation parameter $= -0.79 \pm 0.08$
C, CP violation parameter $= 0.19 \pm 0.06$
S, CP violation parameter $= 0.17 \pm 0.06$
$A^L_{CP}(B_s \to J/\psi\overline{K}^*(892)^0) = 0.021 \pm 0.027$
$A^{\parallel}_{CP}(B_s \to J/\psi\overline{K}^*(892)^0) = -0.07 \pm 0.06$
$A^{\perp}_{CP}(B_s \to J/\psi\overline{K}^*(892)^0) = 0.06 \pm 0.05$
$\boldsymbol{A_{CP}(B_s \to \pi^+K^-)} = 0.224 \pm 0.012$
$A_{CP}(B_s^0 \to [K^+K^-]_D\overline{K}^*(892)^0) = 0.06 \pm 0.04$
$A_{CP}(B_s^0 \to [\pi^+K^-]_D K^*(892)^0) = -0.009 \pm 0.023$
$A_{CP}(B_s^0 \to [\pi^+\pi^-]_D K^*(892)^0) = 0.00 \pm 0.06$
$A_{CP}(B_s^0 \to [K^+\pi^-\pi^+\pi^-]_D\overline{K}^*(892)^0) = -0.029 \pm 0.024$
$A_{CP}(B_s^0 \to [\pi^+\pi^-\pi^+\pi^-]_D\overline{K}^*(892)^0) = 0.02 \pm 0.05$
$R_s^+ = \Gamma(B_s^0 \to [\pi^-K^+]_D\overline{K}^{*0}) / \Gamma(B_s^0 \to [\pi^+K^-]_D\overline{K}^{*0}) = 0.004 \pm 0.006$
$R_s^- = \Gamma(\overline{B}_s^0 \to [\pi^+K^-]_D K^{*0}) / \Gamma(\overline{B}_s^0 \to [\pi^-K^+]_D K^{*0}) = 0.004 \pm 0.006$
$R_s^+ = \Gamma(B_s^0 \to [\pi^-K^+\pi^+\pi^-]_D\overline{K}^{*0}) / \Gamma(B_s^0 \to [\pi^+K^-\pi^+\pi^-]_D\overline{K}^{*0}) = 0.019 \pm 0.008$
$R_s^- = \Gamma(\overline{B}_s^0 \to [\pi^+K^-\pi^+\pi^-]_D K^{*0}) / \Gamma(\overline{B}_s^0 \to [\pi^-K^+\pi^+\pi^-]_D K^{*0}) = 0.015 \pm 0.008$
$S(B_s^0 \to \phi\gamma) = 0.43 \pm 0.32$
$C(B_s^0 \to \phi\gamma) = 0.11 \pm 0.31$
$A^{\Delta}(B_s^0 \to \phi\gamma) = -0.7 \pm 0.4$
$\Delta a_{\perp} < 1.2 \times 10^{-12}$ GeV, CL = 95%
$\Delta a_{\parallel} = (-0.9 \pm 1.5) \times 10^{-14}$ GeV
$\Delta a_X = (1.0 \pm 2.2) \times 10^{-14}$ GeV
$\Delta a_Y = (-3.8 \pm 2.2) \times 10^{-14}$ GeV
$\mathrm{Re}(\xi) = -0.022 \pm 0.033$

Int. J. Mod. Phys. A 2026.41. Downloaded from www.worldscientific.com
by UNIVERSITY OF CALIFORNIA @ BERKELEY on 09/16/26. Re-use and distribution is strictly not permitted, except for Open Access articles.

$\mathrm{Im}(\xi) = 0.004 \pm 0.011$

These branching fractions all scale with $B(\overline{b} \to B_s^0)$.

The branching fraction $B(B_s^0 \to D_s^- \ell^+ \nu_\ell \text{anything})$ is not a pure measurement since the measured product branching fraction $B(\overline{b} \to B_s^0) \times B(B_s^0 \to D_s^- \ell^+ \nu_\ell \text{anything})$ was used to determine $B(\overline{b} \to B_s^0)$, as described in the note on "B^0-$\overline{B}^0$ Mixing"

For inclusive branching fractions, *e.g.*, $B \to D^\pm$ anything, the values usually are multiplicities, not branching fractions. They can be greater than one.

B_s^0 DECAY MODES		Fraction (Γ_i/Γ)	Scale factor/ Confidence level	p (MeV/c)
$D_s^\pm$ anything		(65 ± 5) %		–
$D^0/\overline{D}^0$ anything		(24 ± 4) %		–
$D^\pm$ anything		(13 ± 5) %		–
$\ell \nu_\ell X$		(9.6 ± 0.8) %		–
$e^+ \nu X^-$		(9.1 ± 0.8) %		–
$\mu^+ \nu X^-$		(10.2 ± 1.0) %		–
$D_s^- \ell^+ \nu_\ell$ anything	[*iiaa*]	(8.1 ± 1.3) %		–
$D_s^{*-} \ell^+ \nu_\ell$ anything		(5.4 ± 1.1) %		–
$D_s^- \mu^+ \nu_\mu$		(2.31 ± 0.21) %		2321
$D_s^{*-} \mu^+ \nu_\mu$		(5.2 ± 0.5) %		2266
$D_{s1}(2536)^- \mu^+ \nu_\mu$, $D_{s1}^- \to D^{*-} K_S^0$		$(2.7 \pm 0.7) \times 10^{-3}$		–
$D_{s1}(2536)^- X \mu^+ \nu$, $D_{s1}^- \to \overline{D}^0 K^+$		$(4.4 \pm 1.3) \times 10^{-3}$		–
$D_{s2}(2573)^- X \mu^+ \nu$, $D_{s2}^- \to \overline{D}^0 K^+$		$(2.7 \pm 1.0) \times 10^{-3}$		–
$K^- \mu^+ \nu_\mu$		$(1.06 \pm 0.09) \times 10^{-4}$		2660
$D_s^- \pi^+$		$(2.98 \pm 0.13) \times 10^{-3}$		2320
$D_s^- \rho^+$		$(6.9 \pm 1.4) \times 10^{-3}$		2249
$D_s^- \pi^+ \pi^+ \pi^-$		$(6.1 \pm 1.0) \times 10^{-3}$		2301
$D_{s1}(2536)^- \pi^+$, $D_{s1}^- \to D_s^- \pi^+ \pi^-$		$(2.4 \pm 0.8) \times 10^{-5}$		–
$D_s^\mp K^\pm$		$(2.25 \pm 0.12) \times 10^{-4}$		2293
$D_{s1}(2536)^\mp K^\pm$, $D_{s1}^- \to \overline{D}^*(2007)^0 K^-$		$(2.48 \pm 0.28) \times 10^{-5}$		–
$D_s^- K^+ \pi^+ \pi^-$		$(3.2 \pm 0.6) \times 10^{-4}$		2249
$D_s^+ D_s^-$		$(4.5 \pm 0.6) \times 10^{-3}$	S=1.3	1824
$D_s^- D^+$		$(3.1 \pm 0.5) \times 10^{-4}$		1875
$D^+ D^-$		$(2.2 \pm 0.6) \times 10^{-4}$		1925
$D^{*+} D^{*-}$		$(2.14 \pm 0.32) \times 10^{-4}$		1778
$D^0 \overline{D}^0$		$(1.9 \pm 0.5) \times 10^{-4}$		1930
$D_s^{*-} \pi^+$		$(1.9 {}^{+0.5}_{-0.4}) \times 10^{-3}$		2265
$D_s^{*\mp} K^\pm$		$(1.32 {}^{+0.40}_{-0.32}) \times 10^{-4}$		–
$D_s^{*-} \rho^+$		$(9.5 \pm 2.0) \times 10^{-3}$		2191
$D_s^{*+} D_s^- + D_s^{*-} D_s^+$		(1.51 ± 0.13) %		1742
$D_s^{*+} D_s^{*-}$		(1.58 ± 0.20) %	S=1.3	1655
$D_s^{(*)+} D_s^{(*)-}$		(4.5 ± 1.4) %		–
$D^{*-} D_s^+$		$(4.0 \pm 0.7) \times 10^{-4}$		1801
$\overline{D}^{*0} \overline{K}^0$		$(2.8 \pm 1.1) \times 10^{-4}$		2278
$\overline{D}^0 \overline{K}^0$		$(4.3 \pm 0.9) \times 10^{-4}$		2330
$\overline{D}^0 K^- \pi^+$		$(1.04 \pm 0.13) \times 10^{-3}$		2312
$\overline{D}^*(2007)^0 K^- \pi^+$		$(7.3 \pm 2.6) \times 10^{-4}$		2259
$\overline{D}^0 \overline{K}^*(892)^0$		$(4.4 \pm 0.6) \times 10^{-4}$		2264
$\overline{D}^0 \overline{K}^*(1410)$		$(3.9 \pm 3.5) \times 10^{-4}$		2117
$\overline{D}^0 \overline{K}_0^*(1430)$		$(3.0 \pm 0.7) \times 10^{-4}$		2113
$\overline{D}^0 \overline{K}_2^*(1430)$		$(1.1 \pm 0.4) \times 10^{-4}$		2112
$\overline{D}^0 \overline{K}^*(1680)$		$< 7.8 \times 10^{-5}$	CL=90%	1997
$\overline{D}^0 \overline{K}_0^*(1950)$		$< 1.1 \times 10^{-4}$	CL=90%	1884
$\overline{D}^0 \overline{K}_3^*(1780)$		$< 2.6 \times 10^{-5}$	CL=90%	1970
$\overline{D}^0 \overline{K}_4^*(2045)$		$< 3.1 \times 10^{-5}$	CL=90%	1835
$\overline{D}^0 K^- \pi^+$ (non-resonant)		$(2.1 \pm 0.8) \times 10^{-4}$		2312
$[K^+ K^-]_D \overline{K}^*(892)^0$		$(4.4 \pm 0.6) \times 10^{-4}$		–
$[\pi^+ \pi^-]_D \overline{K}^*(892)^0$		$(4.4 \pm 0.6) \times 10^{-4}$		–
$[\pi^+ \pi^- \pi^+ \pi^-]_D \overline{K}^*(892)^0$		$(4.4 \pm 0.6) \times 10^{-4}$		–
$D_{s2}^*(2573)^- \pi^+$, $D_{s2}^* \to \overline{D}^0 K^-$		$(2.6 \pm 0.4) \times 10^{-4}$		–
$D_{s1}^*(2700)^- \pi^+$, $D_{s1}^* \to \overline{D}^0 K^-$		$(1.6 \pm 0.8) \times 10^{-5}$		–
$D_{s1}^*(2860)^- \pi^+$, $D_{s1}^* \to \overline{D}^0 K^-$		$(5 \pm 4) \times 10^{-5}$		–
$D_{s3}^*(2860)^- \pi^+$, $D_{s3}^* \to \overline{D}^0 K^-$		$(2.2 \pm 0.6) \times 10^{-5}$		–
$\overline{D}^0 K^+ K^-$		$(5.6 \pm 0.9) \times 10^{-5}$		2243
$\overline{D}^0 f_0(980)$		$< 3.1 \times 10^{-6}$	CL=90%	2242
$\overline{D}^0 \phi$		$(2.30 \pm 0.25) \times 10^{-5}$		2235
$\overline{D}^{*0} \phi$		$(3.2 \pm 0.4) \times 10^{-5}$		2178
$D^{*\mp} \pi^\pm$		$< 6.1 \times 10^{-6}$	CL=90%	–
$\eta_c \phi$		$(5.0 \pm 0.9) \times 10^{-4}$		1663
$\eta_c \pi^+ \pi^-$		$(1.8 \pm 0.7) \times 10^{-4}$		1840
$J/\psi(1S) \phi$		$(1.01 \pm 0.04) \times 10^{-3}$		1588
$J/\psi(1S) \phi\phi$		$(1.17 {}^{+0.14}_{-0.16}) \times 10^{-5}$		764
$J/\psi(1S) \pi^0$		$< 1.21 \times 10^{-5}$	CL=90%	1787
$J/\psi(1S) \eta$		$(4.45 \pm 0.25) \times 10^{-4}$	S=1.1	1733
$J/\psi(1S) K_S^0$		$(1.92 \pm 0.14) \times 10^{-5}$		1743
$J/\psi(1S) \overline{K}^*(892)^0$		$(3.95 \pm 0.24) \times 10^{-5}$		1637
$J/\psi(1S) \eta'$		$(3.53 \pm 0.22) \times 10^{-4}$	S=1.1	1612
$J/\psi(1S) \pi^+ \pi^-$		$(2.00 \pm 0.17) \times 10^{-4}$	S=1.7	1775
$J/\psi(1S) f_0(500)$, $f_0 \to \pi^+ \pi^-$		$< 4 \times 10^{-6}$	CL=90%	–
$J/\psi(1S) \rho$, $\rho \to \pi^+ \pi^-$		$< 3.4 \times 10^{-6}$	CL=90%	–
$J/\psi(1S) f_0(980)$, $f_0 \to \pi^+ \pi^-$		$(1.23 \pm 0.15) \times 10^{-4}$	S=2.1	–
$J/\psi(1S) f_2(1270)$, $f_2 \to \pi^+ \pi^-$		$(1.0 \pm 0.4) \times 10^{-6}$		–
$J/\psi(1S) f_2(1270)_0$, $f_2 \to \pi^+ \pi^-$		$(7.2 \pm 1.6) \times 10^{-7}$		–
$J/\psi(1S) f_2(1270)_\parallel$, $f_2 \to \pi^+ \pi^-$		$(1.04 \pm 0.32) \times 10^{-6}$		–
$J/\psi(1S) f_2(1270)_\perp$, $f_2 \to \pi^+ \pi^-$		$(1.3 \pm 0.7) \times 10^{-6}$		–
$J/\psi(1S) f_0(1370)$, $f_0 \to \pi^+ \pi^-$		$(4.4 {}^{+0.6}_{-4.0}) \times 10^{-5}$		–
$J/\psi(1S) f_0(1500)$, $f_0 \to \pi^+ \pi^-$		$(2.02 {}^{+0.32}_{-0.24}) \times 10^{-5}$		–
$J/\psi(1S) f_2'(1525)_0$, $f_2' \to \pi^+ \pi^-$		$(1.02 \pm 0.22) \times 10^{-6}$		–
$J/\psi(1S) f_2'(1525)_\parallel$, $f_2' \to \pi^+ \pi^-$		$(1.2 {}^{+2.6}_{-0.8}) \times 10^{-7}$		–
$J/\psi(1S) f_2'(1525)_\perp$, $f_2' \to \pi^+ \pi^-$		$(5 \pm 4) \times 10^{-7}$		–
$J/\psi(1S) f_0(1790)$, $f_0 \to \pi^+ \pi^-$		$(4.8 {}^{+10.0}_{-1.0}) \times 10^{-6}$		–
$J/\psi(1S) \pi^+ \pi^-$ (nonresonant)		$(1.72 {}^{+1.00}_{-0.34}) \times 10^{-5}$		1775
$J/\psi(1S) \overline{K}^0 \pi^+ \pi^-$		$< 4.4 \times 10^{-5}$	CL=90%	1675
$J/\psi(1S) K^+ K^-$		$(7.9 \pm 0.7) \times 10^{-4}$		1601
$J/\psi(1S) K^0 K^- \pi^+ + \text{c.c.}$		$(9.5 \pm 1.3) \times 10^{-4}$		1538
$J/\psi(1S) \overline{K}^0 K^+ K^-$		$< 1.2 \times 10^{-5}$	CL=90%	1333
$J/\psi K^*(892)^0 \overline{K}^*(892)^0$		$(1.07 \pm 0.09) \times 10^{-4}$		1082
$J/\psi(1S) f_2'(1525)$		$(2.6 \pm 0.6) \times 10^{-4}$		1310
$J/\psi(1S) p\overline{p}$		$(3.6 \pm 0.4) \times 10^{-6}$		982
$J/\psi(1S) \gamma$		$< 7.3 \times 10^{-6}$	CL=90%	1790
$J/\psi \mu^+ \mu^-$, $J/\psi \to \mu^+ \mu^-$		$< 2.6 \times 10^{-9}$	CL=95%	–
$J/\psi(1S) \pi^+ \pi^- \pi^+ \pi^-$		$(7.4 \pm 0.8) \times 10^{-5}$		1731
$J/\psi(1S) f_1(1285)$		$(7.2 \pm 1.4) \times 10^{-5}$		1460
$J/\psi(1S) \overline{D}^0$		$< 1.0 \times 10^{-6}$	CL=90%	996
$\psi(2S) \eta$		$(3.7 \pm 0.8) \times 10^{-4}$		1338
$\psi(2S) \eta'$		$(1.37 \pm 0.33) \times 10^{-4}$		1158
$\psi(2S) \pi^+ \pi^-$		$(6.8 \pm 1.2) \times 10^{-5}$		1397
$\psi(2S) \phi$		$(5.1 \pm 0.4) \times 10^{-4}$		1120
$\psi(2S) K^0$		$(1.9 \pm 0.5) \times 10^{-5}$		1352
$\psi(2S) K^- \pi^+$		$(3.1 \pm 0.4) \times 10^{-5}$		1310
$\psi(2S) \overline{K}^*(892)^0$		$(3.3 \pm 0.5) \times 10^{-5}$		1196
$\chi_{c1} \phi$		$(1.92 \pm 0.25) \times 10^{-4}$		1275
$\chi_{c1}(3872) \phi$		$(9.6 \pm 3.2) \times 10^{-5}$		936
$\chi_{c1}(3872) (K^+ K^-)_{non-\phi}$		$(7.6 \pm 3.0) \times 10^{-5}$		961
$\chi_{c1}(3872) \pi^+ \pi^-$		$(3.7 \pm 1.5) \times 10^{-5}$		1264
$\pi^+ \pi^-$		$(7.1 \pm 0.8) \times 10^{-7}$		2680
$\pi^0 \pi^0$		$< 7.7 \times 10^{-6}$	CL=90%	2680
$\eta \pi^0$		$< 1.0 \times 10^{-3}$	CL=90%	2654
$\eta \eta$		$< 1.43 \times 10^{-4}$	CL=90%	2627
$\rho^0 \rho^0$		$< 3.20 \times 10^{-4}$	CL=90%	2569
$\eta' K_S^0$		$< 8.16 \times 10^{-6}$	CL=90%	2573
$\eta' \eta$		$< 6.5 \times 10^{-5}$	CL=90%	2568
$\eta' \eta'$		$(3.3 \pm 0.7) \times 10^{-5}$		2507
$\eta' \phi$		$< 8.2 \times 10^{-7}$	CL=90%	2495
$\phi f_0(980)$, $f_0(980) \to \pi^+ \pi^-$		$(1.12 \pm 0.21) \times 10^{-6}$		–

Int. J. Mod. Phys. A 2026.41. Downloaded from www.worldscientific.com
by UNIVERSITY OF CALIFORNIA @ BERKELEY on 09/16/26. Re-use and distribution is strictly not permitted, except for Open Acce

$\phi f_2(1270)$, $f_2(1270) \to \pi^+\pi^-$	$(6.1 {}^{+1.8}_{-1.5}) \times 10^{-7}$		–
$\phi\rho^0$	$(2.7 \pm 0.8) \times 10^{-7}$		2526
$\phi\pi^+\pi^-$	$(3.5 \pm 0.5) \times 10^{-6}$		2579
$\phi\phi$	$(1.83 \pm 0.14) \times 10^{-5}$		2482
$\phi\phi\phi$	$(2.1 \pm 0.6) \times 10^{-6}$		2165
π^+K^-	$(5.9 \pm 0.6) \times 10^{-6}$		2659
K^+K^-	$(2.61 \pm 0.16) \times 10^{-5}$		2638
$K^0\overline{K}^0$	$(1.76 \pm 0.31) \times 10^{-5}$		2637
$K^0\pi^+\pi^-$	$(9.5 \pm 2.1) \times 10^{-6}$		2653
$K^0K^\pm\pi^\mp$	$(8.4 \pm 0.9) \times 10^{-5}$		2622
$K^*(892)^-\pi^+$	$(2.9 \pm 1.1) \times 10^{-6}$		2607
$K^*(892)^\pm K^\mp$	$(1.9 \pm 0.5) \times 10^{-5}$		2585
$K_0^*(1430)^\pm K^\mp$	$(3.1 \pm 2.5) \times 10^{-5}$		–
$K_2^*(1430)^\pm K^\mp$	$(1.0 \pm 1.7) \times 10^{-5}$		–
$K^*(892)^0\overline{K}^0$ + c.c.	$(2.0 \pm 0.6) \times 10^{-5}$		2585
$K_0^*(1430)\overline{K}^0$ + c.c.	$(3.3 \pm 1.0) \times 10^{-5}$		2468
$K_2^*(1430)^0\overline{K}^0$ + c.c.	$(1.7 \pm 2.2) \times 10^{-5}$		2467
$K_S^0\overline{K}^*(892)^0$ + c.c.	$(1.6 \pm 0.4) \times 10^{-5}$		2585
$K^0K^+K^-$	$(1.3 \pm 0.6) \times 10^{-6}$		2568
$\overline{K}^*(892)^0\rho^0$	$< 7.67 \times 10^{-4}$	CL=90%	2550
$\overline{K}^*(892)^0K^*(892)^0$	$(1.11 \pm 0.27) \times 10^{-5}$		2531
$\phi K^*(892)^0$	$(1.14 \pm 0.30) \times 10^{-6}$		2507
$p\overline{p}$	$< 4.4 \times 10^{-9}$	CL=90%	2514
$p\overline{p}K^0$	$(9.1 \pm 2.0) \times 10^{-7}$		2396
$p\overline{p}K^+K^-$	$(4.5 \pm 0.5) \times 10^{-6}$		2231
$p\overline{p}K^+\pi^-$	$(1.39 \pm 0.26) \times 10^{-6}$		2355
$p\overline{p}\pi^+\pi^-$	$(4.3 \pm 2.0) \times 10^{-7}$		2454
$p\overline{p}p\overline{p}$	$(2.3 \pm 1.0) \times 10^{-8}$		1797
$p\overline{\Lambda}K^-$ + c.c.	$(5.5 \pm 1.0) \times 10^{-6}$		2358
$\Lambda_c^-\Lambda\pi^+$	$(3.6 \pm 1.6) \times 10^{-4}$		1979
$\Lambda_c^-\Lambda_c^+$	$< 8.0 \times 10^{-5}$	CL=95%	1405

Lepton family (LF), lepton (L), baryon (B) number violating modes or $\Delta B = 1$ weak neutral current ($B1$) modes

$\gamma\gamma$	$B1$		$< 3.1 \times 10^{-6}$	CL=90%	2683
$\phi\gamma$	$B1$		$(3.4 \pm 0.4) \times 10^{-5}$		2587
$f_2(1270)\gamma$	$B1$		$(9 {}^{+4}_{-5}) \times 10^{-6}$		2532
$f_2'(1525)\gamma$	$B1$		$(6.7 {}^{+0.9}_{-0.8}) \times 10^{-6}$		2469
$\phi(1680)\gamma$, $\phi \to K^+K^-$	$B1$		$(9.3 \pm 2.4) \times 10^{-7}$		–
$\phi_3(1850)\gamma$, $\phi_3 \to K^+K^-$	$B1$		$(7 {}^{+6}_{-5}) \times 10^{-8}$		–
$f_2(2010)\gamma$, $f_2 \to K^+K^-$	$B1$		$(1.0 {}^{+0.7}_{-0.5}) \times 10^{-7}$		–
$\mu^+\mu^-$	$B1$		$(3.34 \pm 0.27) \times 10^{-9}$		2681
e^+e^-	$B1$		$< 9.4 \times 10^{-9}$	CL=90%	2683
$\tau^+\tau^-$	$B1$		$< 6.8 \times 10^{-3}$	CL=95%	2011
$\mu^+\mu^-\gamma$	$B1$		$< 4.2 \times 10^{-8}$	CL=95%	2681
$\mu^+\mu^-\mu^+\mu^-$	$B1$		$< 8.6 \times 10^{-10}$	CL=95%	2673
SP, $S \to \mu^+\mu^-$, $P \to \mu^+\mu^-$	$B1$	[zzz]	$< 2.2 \times 10^{-9}$	CL=95%	–
aa, $a \to \mu^+\mu^-$	$B1$		$< 5.8 \times 10^{-10}$	CL=95%	–
$\phi(1020)\mu^+\mu^-$	$B1$		$(8.2 \pm 0.4) \times 10^{-7}$		2582
$f_2'(1525)\mu^+\mu^-$	$B1$		$(1.57 \pm 0.22) \times 10^{-7}$		2464
$\overline{K}^*(892)^0\mu^+\mu^-$	$B1$		$(2.9 \pm 1.1) \times 10^{-8}$		2605
$\pi^+\pi^-\mu^+\mu^-$	$B1$		$(8.4 \pm 1.7) \times 10^{-8}$		2670
$\overline{D}^0\mu^+\mu^-$	$B1$		$< 1.2 \times 10^{-7}$	CL=90%	2354
$\phi\nu\overline{\nu}$	$B1$		$< 5.4 \times 10^{-3}$	CL=90%	2587
$e^\pm\mu^\mp$	LF	[bb]	$< 5.4 \times 10^{-9}$	CL=90%	2682
$e^\pm\tau^\mp$	LF		$< 1.4 \times 10^{-3}$	CL=90%	2389
$\mu^\pm\tau^\mp$	LF		$< 4.2 \times 10^{-5}$	CL=95%	2388
$\phi\mu^\pm e^\mp$	LF		$< 1.6 \times 10^{-8}$	CL=90%	2586
$\phi\mu^\pm\tau^\mp$	LF		$< 1.0 \times 10^{-5}$	CL=90%	2241
$p\mu^-$	L,B		$< 1.21 \times 10^{-8}$	CL=90%	2600

B_s^*

$I(J^P) = 0(1^-)$

I, J, P need confirmation. Quantum numbers shown are quark-model predictions.

Mass $m = 5415.4 \pm 1.4$ MeV (S = 2.6)
$m_{B_s^*} - m_{B_s} = 48.5 \pm 1.4$ MeV (S = 2.6)

B_s^* DECAY MODES	Fraction (Γ_i/Γ)	p (MeV/c)
$B_s\gamma$	seen	48

$B_{s1}(5830)^0$

$I(J^P) = 0(1^+)$
I, J, P need confirmation.

Mass $m = 5828.73 \pm 0.20$ MeV
$m_{B_{s1}^0} - m_{B^{*+}} = 503.98 \pm 0.17$ MeV
Full width $\Gamma = 0.5 \pm 0.4$ MeV

$B_{s1}(5830)^0$ DECAY MODES	Fraction (Γ_i/Γ)	p (MeV/c)
$B^{*+}K^-$	seen	97

$B_{s2}^*(5840)^0$

$I(J^P) = 0(2^+)$
I, J, P need confirmation.

Mass $m = 5839.88 \pm 0.12$ MeV
$m_{B_{s2}^{*0}} - m_{B^+} = 560.48 \pm 0.12$ MeV
Full width $\Gamma = 1.49 \pm 0.27$ MeV

Branching fractions are given relative to the one **DEFINED AS 1**.

$B_{s2}^*(5840)^0$ DECAY MODES	Fraction (Γ_i/Γ)	p (MeV/c)
B^+K^-	**DEFINED AS 1**	252
$B^{*+}K^-$	0.093 ± 0.018	141
$B^0K_S^0$	0.43 ± 0.11	245
$B^{*0}K_S^0$	0.04 ± 0.04	–

BOTTOM, CHARMED MESONS ($B = C = \pm 1$)

$B_c^+ = c\overline{b}$, $B_c^- = \overline{c}b$, similarly for B_c^*'s

B_c^+

$I(J^P) = 0(0^-)$
I, J, P need confirmation.

Quantum numbers shown are quark-model predictions.

Mass $m = 6274.47 \pm 0.32$ MeV
$m_{B_c^+} - m_{B_s^0} = 907.8 \pm 0.5$ MeV
Mean life $\tau = (0.510 \pm 0.009) \times 10^{-12}$ s

The following quantities are not pure branching ratios; rather the fractions $\Gamma_i/\Gamma \times B(\overline{b} \to B_c)$. B_c^- modes are charge conjugates of the modes below.

B_c^+ DECAY MODES × $B(\overline{b} \to B_c)$	Fraction (Γ_i/Γ)	Confidence level	p (MeV/c)
$J/\psi(1S)\ell^+\nu_\ell$ anything	seen		–
$J/\psi(1S)\mu^+\nu_\mu$	seen		2372
$J/\psi(1S)\tau^+\nu_\tau$	seen		1932
$J/\psi(1S)\pi^+$	seen		2370
$J/\psi(1S)K^+$	seen		2341
$J/\psi(1S)\pi^+\pi^+\pi^-$	seen		2350
$J/\psi(1S)a_1(1260)$	not seen		2169
$J/\psi(1S)K^+K^-\pi^+$	seen		2203
$J/\psi(1S)\pi^+\pi^+\pi^+\pi^-\pi^-$	seen		2309
$\psi(2S)\pi^+$	seen		2051
$J/\psi(1S)D^0K^+$	seen		1539
$J/\psi(1S)D^*(2007)^0K^+$	seen		1411
$J/\psi(1S)D^*(2010)^+K^{*0}$	seen		919
$J/\psi(1S)D^+K^{*0}$	seen		1122
$J/\psi(1S)D_s^+$	seen		1821
$J/\psi(1S)D_s^{*+}$	seen		1727
$J/\psi(1S)p\overline{p}\pi^+$	seen		1791
$p\overline{p}\pi^+$	not seen		2970
D^0K^+	seen		2837
$D^0\pi^+$	not seen		2858
$D^{*0}\pi^+$	not seen		2814
$D^{*0}K^+$	not seen		2792
$D_s^+\overline{D}^0$	$< 7.2 \times 10^{-4}$	90%	2483
$D_s^+D^0$	$< 3.0 \times 10^{-4}$	90%	2483
$D^+\overline{D}^0$	$< 1.9 \times 10^{-4}$	90%	2521
D^+D^0	$< 1.4 \times 10^{-4}$	90%	2521
$D_s^{*+}\overline{D}^0$	$< 5.3 \times 10^{-4}$	90%	2425
$D_s^+\overline{D}^*(2007)^0$	$< 4.6 \times 10^{-4}$	90%	2427

Int. J. Mod. Phys. A 2026.41. Downloaded from www.worldscientific.com
by UNIVERSITY OF CALIFORNIA @ BERKELEY on 09/16/26. Re-use and distribution is strictly not permitted, except for Open Access articles.

$D_s^{*+} D^0$	$<9 \times 10^{-4}$	90%	2425
$D_s^{+} D^*(2007)^0$	$<6.6 \times 10^{-4}$	90%	2427
$D^*(2010)^+ \overline{D}^0$	$<3.8 \times 10^{-4}$	90%	2467
$D^*(2010)^+ \overline{D}^0$, $D^{*+} \to D^+ \pi^0/\gamma$	not seen		–
$D^+ \overline{D}^*(2007)^0$	$<6.5 \times 10^{-4}$	90%	2466
$D^*(2007)^+ D^0$	$<2.0 \times 10^{-4}$	90%	–
$D^*(2010)^+ D^0$, $D^{*+} \to D^+ \pi^0/\gamma$	not seen		2467
$D^+ D^*(2007)^0$	$<3.7 \times 10^{-4}$	90%	2466
$D_s^{*+} \overline{D}^*(2007)^0$	$<1.3 \times 10^{-3}$	90%	2366
$D_s^{*+} D^*(2007)^0$	$<1.3 \times 10^{-3}$	90%	2366
$D^*(2010)^+ \overline{D}^*(2007)^0$	$<1.0 \times 10^{-3}$	90%	2410
$D^*(2010)^+ D^*(2007)^0$	$<7.7 \times 10^{-4}$	90%	2410
$D^+ K^{*0}$	not seen		2783
$D^+ \overline{K}^{*0}$	not seen		2783
$D_s^+ K^{*0}$	not seen		2751
$D_s^+ \overline{K}^{*0}$	not seen		2751
$D_s^+ \phi$	not seen		2727
$K^+ K^0$	not seen		3098
$B_s^0 \pi^+$ / $B(\overline{b} \to B_s)$	seen		–

$B_c(2S)^\pm$

$I(J^P) = 0(0^-)$

Mass $m = 6871.2 \pm 1.0$ MeV

The following quantities are not pure branching ratios; rather the fractions $\Gamma_i/\Gamma \times B(\overline{b} \to B_c(2S))$.

$B_c(2S)^\pm$ DECAY MODES × $B(\overline{b} \to B_c(2S))$	Fraction (Γ_i/Γ)	p (MeV/c)
$B_c^+ \pi^+ \pi^-$	seen	504

$c\overline{c}$ MESONS (including possibly non-$q\overline{q}$ states)

$\eta_c(1S)$

$I^G(J^{PC}) = 0^+(0^{-+})$

Mass $m = 2984.09 \pm 0.30$ MeV (S = 1.2)
Full width $\Gamma = 30.0 \pm 0.5$ MeV (S = 1.2)

$\eta_c(1S)$ DECAY MODES	Fraction (Γ_i/Γ)	Scale factor/ Confidence level	p (MeV/c)
Decays involving hadronic resonances			
$\eta'(958)\pi\pi$	(1.59 ± 0.34) %	S=1.7	1323
$\eta'(958)K\overline{K}$	(1.37 ± 0.31) %		1131
$\eta'(958)\eta\eta$	$(2.7 \pm 0.5) \times 10^{-3}$		1081
$\rho\rho$	(1.41 ± 0.34) %		1275
$K^*(892)^0 K^- \pi^+$ + c.c.	(1.43 ± 0.35) %		1278
$K^*(892)\overline{K}^*(892)$	$(5.5 \pm 1.1) \times 10^{-3}$	S=1.2	1196
$K^*(892)^0 \overline{K}^*(892)^0 \pi^+\pi^-$	(1.1 ± 0.4) %		1073
$\phi K^+ K^-$	$(3.0 {}^{+1.2}_{-1.0}) \times 10^{-3}$		1104
$\phi\phi$	$(1.4 \pm 0.4) \times 10^{-3}$	S=2.9	1089
$\phi 2(\pi^+\pi^-)$	$< 3.3 \times 10^{-3}$	CL=90%	1251
$a_0(980)\pi$	seen		1327
$a_2(1320)\pi$	seen		1196
$K^*(892)\overline{K}$ + c.c.	< 1.28 %	CL=90%	1310
$f_2(1270)\eta$	seen		1146
$f_2(1270)\eta'$	seen		984
$\omega\omega$	$(2.1 \pm 0.8) \times 10^{-3}$	S=2.4	1270
$\omega\phi$	$(3.0 \pm 0.8) \times 10^{-5}$		1185
$f_2(1270) f_2(1270)$	$(8.4 \pm 2.4) \times 10^{-3}$	S=1.2	774
$f_2(1270) f_2'(1525)$	$(7.7 \pm 2.5) \times 10^{-3}$		524
$f_0(500)\eta$	seen		–
$f_0(500)\eta'$	seen		–
$f_0(980)\eta$	seen		1265
$f_0(980)\eta'$	seen		1130
$f_0(1500)\eta$	seen		1016
$f_0(1710)\eta'$	seen		633
$f_0(2100)\eta'$	seen		†
$f_0(2200)\eta$	seen		499
$a_0(1320)\pi$	seen		–
$a_0(1450)\pi$	seen		1140
$a_2(1700)\pi$	seen		999
$a_0(1710)\pi$	seen		994
$a_0(1950)\pi$	seen		860
$K_0^*(1430)\overline{K}$ + c.c.	seen		1086
$K_2^*(1430)\overline{K}$ + c.c.	seen		1084
$K_0^*(1950)\overline{K}$ + c.c.	seen		742
$K_0^*(2600)\overline{K}$ + c.c.	seen		–
Decays into stable hadrons			
$K\overline{K}\pi$	(5.9 ± 0.5) %	S=1.8	1381
$K\overline{K}\eta$	(1.11 ± 0.15) %	S=1.3	1265
$\eta\pi^+\pi^-$	(1.5 ± 0.4) %		1428
$\eta 2(\pi^+\pi^-)$	(4.0 ± 1.2) %		1386
$K^+K^-\pi^+\pi^-$	$(6.7 \pm 1.8) \times 10^{-3}$	S=2.4	1345
$K^+K^-\pi^+\pi^-\pi^0$	(2.8 ± 0.5) %		1305
$K^0K^-\pi^+\pi^-\pi^+$ + c.c.	(5.1 ± 1.4) %		1302
$K^+K^-2(\pi^+\pi^-)$	$(6.9 \pm 2.0) \times 10^{-3}$		1254
$2(K^+K^-)$	$(1.2 \pm 0.4) \times 10^{-3}$	S=1.6	1056
$\pi^+\pi^-\pi^0$	$< 4 \times 10^{-4}$	CL=90%	1476
$\pi^+\pi^-\pi^0\pi^0$	(4.3 ± 1.0) %		1461
$2(\pi^+\pi^-)$	$(7.5 \pm 1.3) \times 10^{-3}$	S=1.6	1459
$2(\pi^+\pi^-\pi^0)$	(15.5 ± 2.0) %		1409
$3(\pi^+\pi^-)$	(1.55 ± 0.28) %		1407
$p\overline{p}$	$(1.11 \pm 0.12) \times 10^{-3}$	S=1.4	1160
$p\overline{p}\pi^0$	$(3.2 \pm 1.2) \times 10^{-3}$		1101
$p\overline{p}\pi^+\pi^-$	$(3.4 \pm 0.5) \times 10^{-3}$	S=1.2	1027
$\Lambda\overline{\Lambda}$	$(9.4 \pm 1.8) \times 10^{-4}$	S=1.2	991
$K^+\overline{p}\Lambda$ + c.c.	$(2.26 \pm 0.34) \times 10^{-3}$		773
$\overline{\Lambda}(1520)\Lambda$ + c.c.	$(2.8 \pm 1.2) \times 10^{-3}$		694
$\Sigma^+\overline{\Sigma}^-$	$(1.98 \pm 0.35) \times 10^{-3}$		901
$\Xi^-\overline{\Xi}^+$	$(8.3 \pm 1.8) \times 10^{-4}$		692
Radiative decays			
$\gamma\gamma$	$(2.13 \pm 0.15) \times 10^{-4}$	S=1.5	1492
$\gamma\phi$	$(1.15 {}^{+0.33}_{-0.40}) \times 10^{-5}$		1318
Charge conjugation (C), Parity (P), Lepton Family number (LF) violating modes			
$\pi^+\pi^-$	P,CP $< 1.0 \times 10^{-4}$	CL=90%	1486
$\pi^0\pi^0$	P,CP $< 3.3 \times 10^{-5}$	CL=90%	1486
K^+K^-	P,CP $< 5 \times 10^{-4}$	CL=90%	1408
$K_S^0 K_S^0$	P,CP $< 2.9 \times 10^{-4}$	CL=90%	1407

$J/\psi(1S)$

$I^G(J^{PC}) = 0^-(1^{--})$

Mass $m = 3096.900 \pm 0.006$ MeV
Full width $\Gamma = 92.6 \pm 1.7$ keV (S = 1.1)

$J/\psi(1S)$ DECAY MODES	Fraction (Γ_i/Γ)	Scale factor/ Confidence level	p (MeV/c)
hadrons	(87.7 ± 0.5) %		–
virtual $\gamma \to$ hadrons	(13.46 ± 0.07) %		–
ggg	(64.1 ± 1.0) %		–
γgg	(8.8 ± 1.1) %		–
e^+e^-	(5.971 ± 0.032) %		1548
$e^+e^-\gamma$ [jjaa]	$(8.8 \pm 1.4) \times 10^{-3}$		1548
$\mu^+\mu^-$	(5.961 ± 0.033) %		1545
$e^+e^-e^+e^-$	$(5.5 \pm 0.5) \times 10^{-5}$		1548
$e^+e^-\mu^+\mu^-$	$(3.53 \pm 0.26) \times 10^{-5}$		1545
$\mu^+\mu^-\mu^+\mu^-$	$(1.11 \pm 0.11) \times 10^{-6}$		1530
Decays involving hadronic resonances			
$\rho\pi$	(1.88 ± 0.12) %	S=2.6	1448
$\rho^0\pi^0$	$(6.2 \pm 0.6) \times 10^{-3}$		1448
$a_2(1320)^0\pi^+\pi^- \to 2(\pi^+\pi^-)\pi^0$	$(2.8 \pm 0.6) \times 10^{-3}$		–
$a_2(1320)^+\pi^-\pi^0$ + c.c $\to 2(\pi^+\pi^-)\pi^0$	$(3.7 \pm 0.7) \times 10^{-3}$		–
$a_2(1320)\rho$	(1.09 ± 0.22) %		1123
$\eta\pi^+\pi^-$	$(3.8 \pm 0.7) \times 10^{-4}$		1487
$\eta\rho$	$(1.93 \pm 0.23) \times 10^{-4}$		1396
$\eta\pi^+\pi^-\pi^0$	(1.17 ± 0.20) %		1470
$\eta\pi^+\pi^-3\pi^0$	$(4.9 \pm 1.0) \times 10^{-3}$		1419
$\eta\phi(2170) \to \eta\phi f_0(980) \to \eta\phi\pi^+\pi^-$	$(1.2 \pm 0.4) \times 10^{-4}$		628
$\eta\phi(2170) \to \eta K^*(892)^0\overline{K}^*(892)^0$	$< 2.52 \times 10^{-4}$	CL=90%	–

Meson Summary Table

$\eta K^+ K^-$		$(8.6 \pm 3.0) \times 10^{-4}$			1331
$\eta K^\pm K^0_S \pi^\mp$	[bb]	$(2.2 \pm 0.4) \times 10^{-3}$			1278
$\eta K^*(892)^0 \overline{K}^*(892)^0$		$(1.15 \pm 0.26) \times 10^{-3}$			1003
$\rho\eta'(958)$		$(8.1 \pm 0.8) \times 10^{-5}$		S=1.6	1281
$\rho^\pm \pi^\mp \pi^+ \pi^- 2\pi^0$		(2.8 ± 0.8) %			1364
$\rho^+ \rho^- \pi^+ \pi^- \pi^0$		$(6 \pm 4) \times 10^{-3}$			1186
$\rho^+ K^+ K^- \pi^- +$ c.c. $\to$ $K^+ K^- \pi^+ \pi^- \pi^0$		$(3.5 \pm 0.8) \times 10^{-3}$			–
$\rho^\mp K^\pm K^0_S$		$(1.9 \pm 0.4) \times 10^{-3}$			1269
$\rho(1450)\pi$		seen			1197
$\rho(1450)\pi \to \pi^+ \pi^- \pi^0$		$(2.2 \pm 1.1) \times 10^{-4}$			–
$\rho(1450)^\pm \pi^\mp \to K^0_S K^\pm \pi^\mp$		$(3.3 \pm 0.6) \times 10^{-4}$			–
$\rho(1450)^0 \pi^0 \to K^+ K^- \pi^0$		$(2.7 \pm 0.6) \times 10^{-4}$			–
$\rho(1450)\eta'(958) \to \pi^+ \pi^- \eta'(958)$		$(3.3 \pm 0.7) \times 10^{-6}$			–
$\rho(1700)\pi$		seen			1065
$\rho(1700)\pi \to \pi^+ \pi^- \pi^0$		$(1.6 \pm 1.1) \times 10^{-4}$			–
$\rho(2150)\pi$		seen			790
$\rho(2150)\pi \to \pi^+ \pi^- \pi^0$		$(10 \pm 40) \times 10^{-6}$			–
$\omega\pi^0$		$(4.5 \pm 0.5) \times 10^{-4}$		S=1.4	1446
$\omega\pi^0 \to \pi^+ \pi^- \pi^0$		$(1.6 \pm 0.7) \times 10^{-5}$			–
$\omega\pi^+ \pi^-$		$(8.5 \pm 1.0) \times 10^{-3}$		S=1.3	1435
$\omega\pi^0 \pi^0$		$(3.4 \pm 0.8) \times 10^{-3}$			1436
$\omega 3\pi^0$		$(1.9 \pm 0.6) \times 10^{-3}$			1419
$\omega f_2(1270)$		$(4.3 \pm 0.6) \times 10^{-3}$			1142
$\omega\eta$		$(1.74 \pm 0.20) \times 10^{-3}$		S=1.6	1394
$\omega\pi^+ \pi^- \pi^0$		$(4.0 \pm 0.7) \times 10^{-3}$			1418
$\omega\pi^0 \eta$		$(3.4 \pm 1.7) \times 10^{-4}$			1363
$\omega\pi^+ \pi^+ \pi^- \pi^-$		$(8.5 \pm 3.4) \times 10^{-3}$			1392
$\omega\pi^+ \pi^- 2\pi^0$		(3.3 ± 0.5) %			1394
$\omega\eta' \pi^+ \pi^-$		$(1.12 \pm 0.13) \times 10^{-3}$			1173
$\omega\eta'(958)$		$(1.89 \pm 0.18) \times 10^{-4}$			1279
$\omega f_0(980)$		$(1.4 \pm 0.5) \times 10^{-4}$			1267
$\omega f_0(1710) \to \omega K \overline{K}$		$(4.8 \pm 1.1) \times 10^{-4}$			878
$\omega f_1(1420)$		$(6.8 \pm 2.4) \times 10^{-4}$			1061
$\omega f'_2(1525)$		$< 2.2 \times 10^{-4}$		CL=90%	1007
$\omega X(1835) \to \omega p \overline{p}$		$< 3.9 \times 10^{-6}$		CL=95%	–
$\omega K^+ K^- \eta$		$(3.33 \pm 0.12) \times 10^{-4}$			996
$\omega X(1835),\ X \to \eta' \pi^+ \pi^-$		$< 6.2 \times 10^{-5}$			–
$\omega K^+ K^-$		$(1.52 \pm 0.31) \times 10^{-3}$			1268
$\omega K^\pm K^0_S \pi^\mp$	[bb]	$(3.4 \pm 0.5) \times 10^{-3}$			1210
$\omega K \overline{K}$		$(1.9 \pm 0.4) \times 10^{-3}$			1268
$\omega K^*(892)\overline{K}+$ c.c.		$(6.1 \pm 0.9) \times 10^{-3}$			1097
$\eta' K^{*\pm} K^\mp$		$(1.48 \pm 0.13) \times 10^{-3}$			–
$\eta' K^{*0} \overline{K}^0+$ c.c.		$(1.66 \pm 0.21) \times 10^{-3}$			1000
$\eta' h_1(1415) \to \eta' K^* \overline{K}+$ c.c.		$(2.16 \pm 0.31) \times 10^{-4}$			–
$\eta' h_1(1415) \to \eta' K^{*\pm} K^\mp$		$(1.51 \pm 0.23) \times 10^{-4}$			–
$\eta' h_1(1415) \to \gamma\eta'\eta'$		$(4.7 \pm^{1.1}_{2.0}) \times 10^{-7}$			–
$\overline{K} K^*(892)+$c.c.		seen			1373
$\overline{K} K^*(892)+$c.c. $\to$ $K^0_S K^\pm \pi^\mp$		$(4.8 \pm 0.5) \times 10^{-3}$			–
$K^+ K^*(892)^-+$ c.c.		$(6.0 \pm^{0.8}_{1.0}) \times 10^{-3}$		S=2.9	1373
$K^+ K^*(892)^-+$ c.c. $\to$ $K^+ K^- \pi^0$		$(2.69 \pm^{0.13}_{0.20}) \times 10^{-3}$			–
$K^+ K^*(892)^-+$ c.c. $\to$ $K^0 K^\pm \pi^\mp+$ c.c.		$(3.0 \pm 0.4) \times 10^{-3}$			–
$K^0 \overline{K}^*(892)^0+$ c.c.		$(4.2 \pm 0.4) \times 10^{-3}$			1373
$K^0 \overline{K}^*(892)^0+$ c.c. $\to$ $K^0 K^\pm \pi^\mp+$ c.c.		$(3.2 \pm 0.4) \times 10^{-3}$			–
$\overline{K}^*(892)^0 K^+ \pi^-+$ c.c.		$(5.7 \pm 0.8) \times 10^{-3}$			1343
$K^*(892)^\pm K^\mp \pi^0$		$(4.1 \pm 1.3) \times 10^{-3}$			1344
$K^*(892)^+ K^0_S \pi^-+$ c.c.		$(2.0 \pm 0.5) \times 10^{-3}$			1342
$K^*(892)^+ K^0_S \pi^-+$ c.c. $\to$ $K^0_S K^0_S \pi^+ \pi^-$		$(6.7 \pm 2.2) \times 10^{-4}$			–
$K^*(892)^0 K^- \pi^++$ c.c. $\to$ $K^+ K^- \pi^+ \pi^-$		$(3.8 \pm 0.5) \times 10^{-3}$			–
$K^*(892)^0 K^0_S \to \gamma K^0_S K^0_S$		$(6.3 \pm^{0.6}_{0.5}) \times 10^{-6}$			–
$K^*(892)^0 K^0_S \pi^0$		$(7 \pm 4) \times 10^{-4}$			1343
$K^*(892)^\pm K^*(700)^\mp$		$(1.1 \pm^{1.0}_{0.6}) \times 10^{-3}$			–
$K^*(892)^0 \overline{K}^*(892)^0$		$(2.3 \pm 0.6) \times 10^{-4}$			1266
$K^*(892)^\pm K^*(892)^\mp$		$(1.00 \pm^{0.22}_{0.40}) \times 10^{-3}$			1266
$K_1(1400)^\pm K^\mp$		$(3.8 \pm 1.4) \times 10^{-3}$			1170
$K^*(1410)\overline{K}+$c.c.		seen			1165
$K^*(1410)\overline{K}+$c.c $\to$ $K^\pm K^\mp \pi^0$		$(7 \pm 4) \times 10^{-5}$			–
$K^*(1410)\overline{K}+$ c.c. $\to$ $K^0_S K^\pm \pi^\mp$		$(8 \pm 5) \times 10^{-5}$			–
$K^*_2(1430)\overline{K}+$c.c.		seen			1158
$K^*_2(1430)\overline{K}+$c.c. $\to$ $K^\pm K^\mp \pi^0$		$(1.0 \pm 0.5) \times 10^{-4}$			–
$K^*_2(1430)\overline{K}+$ c.c. $\to$ $K^0_S K^\pm \pi^\mp$		$(3.8 \pm 1.0) \times 10^{-4}$			–
$\overline{K}^*_2(1430) K+$ c.c.		$< 4.0 \times 10^{-3}$		CL=90%	1158
$K^*_2(1430)^+ K^-+$ c.c. $\to$ $K^+ K^- \pi^0$		$(2.69 \pm^{0.25}_{0.19}) \times 10^{-4}$			–
$K^*_2(1430)^0 K^- \pi^++$ c.c. $\to$ $K^+ K^- \pi^+ \pi^-$		$(2.6 \pm 0.9) \times 10^{-3}$			–
$K^*_2(1430)^+ K^0_S \pi^-+$ c.c.		$(3.6 \pm 1.8) \times 10^{-3}$			1116
$\overline{K}^*_2(1430)^0 K^*(892)^0+$ c.c.		$(4.67 \pm 0.29) \times 10^{-3}$			1011
$K^*_2(1430)^- K^*(892)^++$ c.c.		$(3.4 \pm 2.9) \times 10^{-3}$			1011
$K^*_2(1430)^- K^*(892)^++$ c.c. $\to$ $K^*(892)^+ K^0_S \pi^-+$ c.c.		$(4 \pm 4) \times 10^{-4}$			–
$K^*_2(1430)^0 \overline{K}^*_2(1430)^0$		$< 2.9 \times 10^{-3}$		CL=90%	601
$\overline{K}_2(1770)^0 K^*(892)^0+$ c.c. $\to$ $K^*(892)^0 K^- \pi^++$ c.c.		$(6.9 \pm 0.9) \times 10^{-4}$			–
$K^*_2(1980)^+ K^-+$ c.c. $\to$ $K^+ K^- \pi^0$		$(1.10 \pm^{0.60}_{0.14}) \times 10^{-5}$			–
$K^*_4(2045)^+ K^-+$ c.c. $\to$ $K^+ K^- \pi^0$		$(6.2 \pm^{2.9}_{1.6}) \times 10^{-6}$			–
$K_1(1270)^\pm K^\mp$		$< 3.0 \times 10^{-3}$		CL=90%	1238
$K_1(1270) K^0_S \to \gamma K^0_S K^0_S$		$(8.5 \pm 2.5) \times 10^{-7}$			–
$a_2(1320)^\pm \pi^\mp$	[bb]	$< 4.3 \times 10^{-3}$		CL=90%	1263
$\phi\pi^0$		3×10^{-6} or 1×10^{-7}			1377
$\phi\pi^+ \pi^-$		$(9.4 \pm 1.5) \times 10^{-4}$		S=1.7	1365
$\phi\pi^0 \pi^0$		$(4.9 \pm 1.0) \times 10^{-4}$			1366
$\phi 2(\pi^+ \pi^-)$		$(1.60 \pm 0.32) \times 10^{-3}$			1318
$\phi\eta$		$(7.4 \pm 0.6) \times 10^{-4}$		S=1.2	1320
$\phi\eta'(958)$		$(4.6 \pm 0.5) \times 10^{-4}$		S=2.2	1192
$\phi\eta\eta'$		$(2.32 \pm 0.17) \times 10^{-4}$			885
$\phi f_0(980)$		$(3.2 \pm 0.9) \times 10^{-4}$		S=1.9	1178
$\phi f_0(980) \to \phi\pi^+ \pi^-$		$(2.57 \pm 0.34) \times 10^{-4}$			–
$\phi f_0(980) \to \phi\pi^0 \pi^0$		$(1.7 \pm 0.5) \times 10^{-4}$			–
$\phi\pi^0 f_0(980) \to \phi\pi^0 \pi^+ \pi^-$		$(4.5 \pm 1.0) \times 10^{-6}$			–
$\phi\pi^0 f_0(980) \to \phi\pi^0 p^0 \pi^0$		$(1.7 \pm 0.6) \times 10^{-6}$			1045
$\phi f_0(980)\eta \to \eta\phi\pi^+ \pi^-$		$(3.2 \pm 1.0) \times 10^{-4}$			–
$\phi(1680)^0 \pi^0 \to \phi\eta\pi^0$		$(6.7 \pm 1.1) \times 10^{-6}$			–
$X(2000)^0 \pi^0 \to \phi\eta\pi^0$		$(1.70 \pm^{0.50}_{0.23}) \times 10^{-6}$			–
$h_1(1900)^0 \pi^0 \to \phi\eta\pi^0$		$(8.4 \pm^{1.4}_{1.3}) \times 10^{-6}$			–
$\phi f_2(1270)$		$(3.2 \pm 0.6) \times 10^{-4}$			1036
$\phi f_1(1285)$		$(2.6 \pm 0.5) \times 10^{-4}$			1032
$\phi f_1(1285) \to \phi\pi^0 f_0(980) \to \phi\pi^0 \pi^+ \pi^-$		$(9.4 \pm 2.8) \times 10^{-7}$			952
$\phi f_1(1285) \to \phi\pi^0 f_0(980) \to \phi 3\pi^0$		$(2.1 \pm 2.2) \times 10^{-7}$			955
$\phi\eta(1405) \to \phi\eta\pi^+ \pi^-$		$(2.0 \pm 1.0) \times 10^{-5}$			946
$\phi f'_2(1525)$		$(8 \pm 4) \times 10^{-4}$		S=2.7	877
$\phi X(1835) \to \phi p \overline{p}$		$< 2.1 \times 10^{-7}$		CL=90%	–
$\phi X(1835) \to \phi\eta\pi^+ \pi^-$		$< 2.8 \times 10^{-4}$		CL=90%	578
$\phi X(1870) \to \phi\eta\pi^+ \pi^-$		$< 6.13 \times 10^{-5}$		CL=90%	–
$\phi K \overline{K}$		$(1.77 \pm 0.16) \times 10^{-3}$		S=1.3	1179
$\phi f_0(1710) \to \phi K \overline{K}$		$(3.6 \pm 0.6) \times 10^{-4}$			875
$\phi K^+ K^-$		$(8.2 \pm 1.1) \times 10^{-4}$			1179
$\phi K^0_S K^0_S$		$(5.8 \pm 1.5) \times 10^{-4}$			1176
$\phi K^\pm K^0_S \pi^\mp$	[bb]	$(7.2 \pm 0.8) \times 10^{-4}$			1114
$\phi K^*(892)\overline{K}+$ c.c.		$(2.18 \pm 0.23) \times 10^{-3}$			969
$b_1(1235)^\pm \pi^\mp$	[bb]	$(3.0 \pm 0.5) \times 10^{-3}$			1300
$b_1(1235)^0 \pi^0$		$(2.3 \pm 0.6) \times 10^{-3}$			1300
$f'_2(1525) K^+ K^-$		$(1.04 \pm 0.35) \times 10^{-3}$			897
$\Delta(1232)^+ \overline{p}$		$< 1 \times 10^{-4}$		CL=90%	1100
$\Delta(1232)^{++} \overline{p}\pi^-$		$(1.6 \pm 0.5) \times 10^{-3}$			1030
$\Delta(1232)^{++} \overline{\Delta}(1232)^{--}$		$(1.10 \pm 0.29) \times 10^{-3}$			938
$\overline{\Sigma}(1385)^0 p K^-$		$(5.1 \pm 3.2) \times 10^{-4}$			646
$\Sigma(1385)^0 \overline{\Lambda}+$ c.c.		$< 8.2 \times 10^{-6}$		CL=90%	911
$\Sigma(1385)^- \overline{\Sigma}^++$ c.c.	[bb]	$(3.0 \pm 0.7) \times 10^{-4}$			855
$\Sigma(1385)^+ \overline{\Sigma}^-+$ c.c.		$(3.3 \pm 0.8) \times 10^{-4}$			861
$\Sigma(1385)^- \overline{\Sigma}(1385)^++$ c.c.	[bb]	$(1.08 \pm 0.06) \times 10^{-3}$			697

Int. J. Mod. Phys. A 2026.41. Downloaded from www.worldscientific.com
by UNIVERSITY OF CALIFORNIA @ BERKELEY on 09/16/26. Re-use and distribution is strictly not permitted, except for Open Acce

Int. J. Mod. Phys. A 2026.41. Downloaded from www.worldscientific.com
by UNIVERSITY OF CALIFORNIA @ BERKELEY on 09/16/26. Re-use and distribution is strictly not permitted, except for Open Access articles.

$\Sigma(1385)^+\overline{\Sigma}(1385)^- +$ c.c.		$(1.25 \pm 0.07) \times 10^{-3}$			697
$\Sigma(1385)^0\overline{\Sigma}(1385)^0$		$(1.07 \pm 0.08) \times 10^{-3}$			697
$\Lambda(1520)\overline{\Lambda} +$ c.c. $\to \gamma\Lambda\overline{\Lambda}$		$< 4.1 \times 10^{-6}$	CL=90%		–
$\overline{\Lambda}(1520)\Lambda +$ c.c.		$< 1.80 \times 10^{-3}$	CL=90%		807
$\Xi^0\overline{\Xi}^0$		$(1.17 \pm 0.04) \times 10^{-3}$			818
$\Xi(1530)^-\overline{\Xi}^+ +$ c.c.		$(3.18 \pm 0.08) \times 10^{-4}$			600
$\Xi(1530)^0\overline{\Xi}^0$		$(3.2 \pm 1.4) \times 10^{-4}$			608
$\Theta(1540)\overline{\Theta}(1540) \to K^0_S p K^- \overline{n} +$ c.c.	[kkaa]	$< 1.1 \times 10^{-5}$	CL=90%		–
$\Theta(1540) K^- \overline{n} \to K^0_S p K^- \overline{n}$	[kkaa]	$< 2.1 \times 10^{-5}$	CL=90%		–
$\Theta(1540) K^0_S \overline{p} \to K^0_S \overline{p} K^+ n$	[kkaa]	$< 1.6 \times 10^{-5}$	CL=90%		–
$\overline{\Theta}(1540) K^+ n \to K^0_S \overline{p} K^+ n$	[kkaa]	$< 5.6 \times 10^{-5}$	CL=90%		–
$\overline{\Theta}(1540) K^0_S p \to K^0_S p K^- \overline{n}$	[kkaa]	$< 1.1 \times 10^{-5}$	CL=90%		–

Decays into stable hadrons

$2(\pi^+\pi^-)\pi^0$		(4.2 ± 0.4) %		S=2.1	1496
$3(\pi^+\pi^-)\pi^0$		(2.9 ± 0.6) %			1433
$\pi^+\pi^- 3\pi^0$		(1.9 ± 0.9) %			1497
$\rho^\pm\pi^\mp\pi^0\pi^0$		(1.41 ± 0.22) %			1421
$\rho^+\rho^-\pi^0$		$(6.0 \pm 1.1) \times 10^{-3}$			1298
$\pi^+\pi^- 4\pi^0$		$(6.5 \pm 1.3) \times 10^{-3}$			1470
$\pi^+\pi^-\pi^0$		(2.00 ± 0.07) %		S=2.0	1533
$2(\pi^+\pi^-\pi^0)$		(1.61 ± 0.20) %			1468
$\pi^+\pi^-\pi^0 K^+K^-$		(1.52 ± 0.27) %		S=1.4	1368
$\pi^+\pi^-$		$(1.47 \pm 0.14) \times 10^{-4}$			1542
$2(\pi^+\pi^-)$		$(3.20 \pm 0.25) \times 10^{-3}$		S=1.2	1517
$3(\pi^+\pi^-)$		$(4.3 \pm 0.4) \times 10^{-3}$			1466
$2(\pi^+\pi^-)3\pi^0$		(6.2 ± 0.9) %			1435
$4(\pi^+\pi^-)\pi^0$		$(9.0 \pm 3.0) \times 10^{-3}$			1345
$2(\pi^+\pi^-)\eta$		$(2.29 \pm 0.28) \times 10^{-3}$			1446
$3(\pi^+\pi^-)\eta$		$(7.2 \pm 1.5) \times 10^{-4}$			1379
$2(\pi^+\pi^-\pi^0)\eta$		$(1.6 \pm 0.5) \times 10^{-3}$			1381
$\pi^+\pi^-\pi^0\pi^0\eta$		$(2.4 \pm 0.5) \times 10^{-3}$			1448
$\rho^\pm\pi^\mp\pi^0\eta$		$(1.9 \pm 0.8) \times 10^{-3}$			1326
K^+K^-		$(3.06 \pm 0.05) \times 10^{-4}$			1468
$K^0_S K^0_L$		$(1.95 \pm 0.11) \times 10^{-4}$		S=2.4	1466
$K^0_S K^0_S$		$< 4.7 \times 10^{-9}$	CL=90%		1466
$K\overline{K}\pi$		$(6.1 \pm 1.0) \times 10^{-3}$			1442
$K^+K^-\pi^0$		$(2.88 \pm 0.12) \times 10^{-3}$			1442
$K^0_S K^\pm\pi^\mp$		$(5.3 \pm 0.5) \times 10^{-3}$			1440
$K^0_S K^0_L \pi^0$		$(2.06 \pm 0.26) \times 10^{-3}$			1440
$K^*(892)^0\overline{K}^0 +$ c.c. $\to K^0_S K^0_L \pi^0$		$(1.21 \pm 0.18) \times 10^{-3}$			–
$K^*_2(1430)^0\overline{K}^0 +$ c.c. $\to K^0_S K^0_L \pi^0$		$(4.3 \pm 1.3) \times 10^{-4}$			–
$K^+K^-\pi^+\pi^-$		$(7.0 \pm 1.0) \times 10^{-3}$			1407
$K^+K^-\pi^0\pi^0$		$(2.13 \pm 0.22) \times 10^{-3}$			1410
$K^+K^-\pi^0\pi^0\pi^0$		$(1.61 \pm 0.29) \times 10^{-3}$			1371
$K^0_S K^\pm\pi^\mp\pi^0\pi^0$		$(5.3 \pm 0.7) \times 10^{-3}$			1369
$K^0_S K^\pm\pi^\mp\pi^+\pi^-$		$(6.3 \pm 0.4) \times 10^{-3}$			1366
$K^0_S K^\pm\rho(770)^\pm\pi^0$		$(2.9 \pm 0.8) \times 10^{-3}$			–
$K^0_S K^0_L \pi^+\pi^-$		$(3.8 \pm 0.6) \times 10^{-3}$			1406
$K^0_S K^0_L \pi^0\pi^0$		$(1.9 \pm 0.4) \times 10^{-3}$			1408
$K^0_S K^0_L \eta$		$(1.45 \pm 0.33) \times 10^{-3}$			1328
$K^0_S K^0_S \pi^+\pi^-$		$(1.68 \pm 0.19) \times 10^{-3}$			1406
$K^\mp K^0_S \pi^\pm\pi^0$		$(5.7 \pm 0.5) \times 10^{-3}$			1408
$K^0_S K^\pm\pi^\mp\rho(770)^0$		$(3.1 \pm 0.5) \times 10^{-3}$			–
$K^+K^-2(\pi^+\pi^-)$		$(3.1 \pm 1.3) \times 10^{-3}$			1320
$K^+K^-\pi^+\pi^-\eta$		$(4.7 \pm 0.7) \times 10^{-3}$			1221
$2(K^+K^-)$		$(7.2 \pm 0.8) \times 10^{-4}$			1131
$K^+K^-K^0_S K^0_S$		$(4.2 \pm 0.7) \times 10^{-4}$			1127
$K^0_S K^*(892)^0\pi^+\pi^-$		$(1.7 \pm 0.6) \times 10^{-3}$			1304
$K^0_S K^*(892)^0\pi^0\pi^0$		$(1.01 \pm 0.18) \times 10^{-3}$			1306
$K^\mp K^*(892)^\pm\pi^+\pi^-$		$(3.4 \pm 1.2) \times 10^{-3}$			1305
$K^*(892)^\pm K^*(892)^0\pi^\mp$		$(4.8 \pm 1.0) \times 10^{-3}$			1212
$K^\mp K^*(892)^\pm\pi^0\pi^0$		$(1.57 \pm 0.32) \times 10^{-3}$			1308
$K^*(892)^+K^*(892)^-\pi^0$		(1.12 ± 0.23) %			1214
$p\overline{p}$		$(2.121 \pm 0.029) \times 10^{-3}$			1232
$p\overline{p}\pi^0$		$(1.19 \pm 0.08) \times 10^{-3}$		S=1.1	1176
$p\overline{p}\pi^+\pi^-$		$(6.0 \pm 0.5) \times 10^{-3}$		S=1.3	1107
$p\overline{p}\pi^+\pi^-\pi^0$	[llaa]	$(2.3 \pm 0.9) \times 10^{-3}$		S=1.9	1033
$p\overline{p}\eta$		$(1.513 \pm 0.023) \times 10^{-3}$			948
$p\overline{p}\rho$		$< 3.1 \times 10^{-4}$	CL=90%		774
$p\overline{p}\omega$		$(9.8 \pm 1.0) \times 10^{-4}$		S=1.3	768
$p\overline{p}\eta'(958)$		$(1.29 \pm 0.14) \times 10^{-4}$		S=2.0	596
$p\overline{p}a_0(980) \to p\overline{p}\pi^0\eta$		$(6.8 \pm 1.8) \times 10^{-5}$			–
$p\overline{p}\phi$		$(5.19 \pm 0.33) \times 10^{-5}$			527
$p\overline{n}\pi^-$		$(2.12 \pm 0.09) \times 10^{-3}$			1174
$n\overline{n}$		$(2.09 \pm 0.16) \times 10^{-3}$			1231
$n\overline{n}\pi^+\pi^-$		$(4 \pm 4) \times 10^{-3}$			1106
$nN(1440)$		seen			978
$nN(1520)$		seen			928
$nN(1535)$		seen			917
$\Lambda\overline{\Lambda}$		$(1.88 \pm 0.08) \times 10^{-3}$		S=2.6	1074
$\Lambda\overline{\Lambda}\pi^0$		$(3.8 \pm 0.4) \times 10^{-5}$			998
$\Lambda\overline{\Lambda}\pi^+\pi^-$		$(4.3 \pm 1.0) \times 10^{-3}$			903
$\Lambda\overline{\Lambda}\eta$		$(1.62 \pm 0.17) \times 10^{-4}$			672
$\Lambda\overline{\Sigma}^-\pi^+ +$ c.c.	[bb]	$(1.26 \pm 0.05) \times 10^{-3}$		S=1.2	950
$\Lambda\overline{\Sigma}^+\pi^- +$ c.c.		$(1.21 \pm 0.07) \times 10^{-3}$		S=1.8	945
$pK^-\overline{\Lambda} +$c.c.		$(8.6 \pm 1.1) \times 10^{-4}$			876
$pK^-\overline{\Sigma}^0$		$(2.9 \pm 0.8) \times 10^{-4}$			819
$pK^0_S\overline{\Sigma}^- +$c.c.		$(2.73 \pm 0.05) \times 10^{-4}$			819
$\overline{\Lambda}nK^0_S +$ c.c.		$(6.5 \pm 1.1) \times 10^{-4}$			872
$\Lambda\overline{\Sigma} +$ c.c.		$(2.83 \pm 0.23) \times 10^{-5}$			1034
$\Sigma^+\overline{\Sigma}^-$		$(1.07 \pm 0.04) \times 10^{-3}$			992
$\Sigma^0\overline{\Sigma}^0$		$(1.172 \pm 0.032) \times 10^{-3}$		S=1.4	988
$\Sigma^+\overline{\Sigma}^-\eta$		$(6.3 \pm 0.4) \times 10^{-5}$			498
$\Xi^-\overline{\Xi}^+$		$(9.7 \pm 0.8) \times 10^{-4}$		S=1.4	807
$\Xi^0\overline{\Sigma}^- K^+ +$ c.c		$(5.64 \pm 0.33) \times 10^{-5}$			–
$\Xi^0\overline{\Sigma}^0 K^0_S +$ c.c		$(2.2 \pm 0.4) \times 10^{-5}$			–
$\Xi^0\overline{\Lambda}K^0_S +$ c.c		$(3.76 \pm 0.27) \times 10^{-5}$			–

Radiative decays

$\gamma\eta_c(1S)$		(1.82 ± 0.15) %		S=1.6	111
$\gamma\eta_c(1S) \to 3\gamma$		seen			–
$\gamma\eta_c(1S) \to \gamma\eta\eta\eta'$		seen			–
3γ		$(1.16 \pm 0.22) \times 10^{-5}$			1548
4γ		$< 9 \times 10^{-6}$	CL=90%		1548
5γ		$< 1.5 \times 10^{-5}$	CL=90%		1548
$\gamma\pi^0$		$(3.39 \pm 0.08) \times 10^{-5}$			1546
$\gamma\pi^0\pi^0$		$(1.15 \pm 0.05) \times 10^{-3}$			1543
$\gamma 2\pi^+ 2\pi^-$		$(2.8 \pm 0.5) \times 10^{-3}$		S=1.9	1517
$\gamma f_2(1270) f_2(1270)$		$(9.5 \pm 1.7) \times 10^{-4}$			878
$\gamma f_2(1270) f_2(1270)$ (non resonant)		$(8.2 \pm 1.9) \times 10^{-4}$			–
$\gamma\pi^+\pi^- 2\pi^0$		$(8.3 \pm 3.1) \times 10^{-3}$			1518
$\gamma K^0_S K^0_S$		$(8.1 \pm 0.4) \times 10^{-4}$			1466
$\gamma(K\overline{K}\pi)$ $[J^{PC} = 0^{-+}]$		$(7 \pm 4) \times 10^{-4}$		S=2.1	1442
$\gamma K^+K^-\pi^+\pi^-$		$(2.1 \pm 0.6) \times 10^{-3}$			1407
$\gamma K^*(892)\overline{K}^*(892)$		$(4.0 \pm 1.3) \times 10^{-3}$			1266
$\gamma\eta$		$(1.090 \pm 0.013) \times 10^{-3}$			1500
$\gamma\eta\pi^0$		$(2.14 \pm 0.31) \times 10^{-5}$			1497
$\gamma a_0(980)^0 \to \gamma\eta\pi^0$		$< 2.5 \times 10^{-6}$	CL=95%		–
$\gamma a_2(1320)^0 \to \gamma\eta\pi^0$		$< 6.6 \times 10^{-6}$	CL=95%		–
$\gamma\eta\pi\pi$		$(6.1 \pm 1.0) \times 10^{-3}$			1487
$\gamma\eta_2(1870) \to \gamma\eta\pi^+\pi^-$		$(6.2 \pm 2.4) \times 10^{-4}$			–
$\gamma\eta'(958)$		$(5.28 \pm 0.06) \times 10^{-3}$		S=1.3	1400
$\gamma\rho\rho$		$(4.5 \pm 0.8) \times 10^{-3}$			1340
$\gamma\rho\omega$		$< 5.4 \times 10^{-4}$	CL=90%		1338
$\gamma\rho\phi$		$< 8.8 \times 10^{-5}$	CL=90%		1258
$\gamma\omega\omega$		$(1.61 \pm 0.33) \times 10^{-3}$			1336
$\gamma\phi\phi$		$(4.0 \pm 1.2) \times 10^{-4}$		S=2.1	1166
$\gamma\eta(1405/1475) \to \gamma K\overline{K}\pi$		$(2.8 \pm 0.6) \times 10^{-3}$		S=1.6	1223
$\gamma\eta(1405/1475) \to \gamma\gamma\rho^0$		$(7.8 \pm 2.0) \times 10^{-5}$		S=1.8	1223
$\gamma\eta(1405/1475) \to \gamma\eta\pi^+\pi^-$		$(3.0 \pm 0.5) \times 10^{-4}$			–
$\gamma\eta(1405/1475) \to \gamma\rho^0\rho^0$		$(1.7 \pm 0.4) \times 10^{-3}$		S=1.3	1223
$\gamma\eta(1405/1475) \to \gamma\gamma\phi$		$(3.6 \pm 0.6) \times 10^{-6}$			–
$\gamma\eta(1405) \to \gamma f_0(980)\pi^0 \to \gamma\pi^+\pi^-\pi^0$		$(1.50 \pm 0.16) \times 10^{-5}$			–
$\gamma\eta(1405) \to \gamma f_0(980)\pi^0 \to \gamma\pi^0\pi^0\pi^0$		$(6.64 {}^{+1.10}_{-0.23}) \times 10^{-6}$			–
$\gamma\eta(1405) \to \gamma\gamma\gamma$		$< 2.63 \times 10^{-6}$	CL=90%		–
$\gamma\eta(1475) \to \gamma\gamma\gamma$		$< 1.86 \times 10^{-6}$	CL=90%		–
$\gamma\eta(1760) \to \gamma\rho^0\rho^0$		$(1.3 \pm 0.9) \times 10^{-4}$			1048
$\gamma\eta(1760) \to \gamma\omega\omega$		$(1.98 \pm 0.33) \times 10^{-3}$			–
$\gamma\eta(1760) \to \gamma\gamma\gamma$		$< 4.80 \times 10^{-6}$	CL=90%		–
$\gamma\eta(2225)$		$(3.14 {}^{+0.50}_{-0.19}) \times 10^{-4}$			752
$\gamma f_2(1270)$		$(1.63 \pm 0.12) \times 10^{-3}$		S=1.3	1286
$\gamma f_2(1270) \to \gamma K^0_S K^0_S$		$(2.58 {}^{+0.60}_{-0.22}) \times 10^{-5}$			–
$\gamma f_1(1285)$		$(6.1 \pm 0.8) \times 10^{-4}$			1283
$\gamma f_1(1285) \to \gamma\gamma\phi$		$(2.9 {}^{+1.1}_{-0.9}) \times 10^{-7}$			–

Int. J. Mod. Phys. A 2026.41. Downloaded from www.worldscientific.com
by UNIVERSITY OF CALIFORNIA @ BERKELEY on 09/16/26. Re-use and distribution is strictly not permitted, except for Open Acce

$\gamma f_1(1285) \to \gamma \pi^0 f_0(980) \to \gamma \pi^0 \pi^0 \pi^0$	$(5.6 {}^{+0.9}_{-3.1}) \times 10^{-7}$			–
$\gamma f_1(1285) \to \gamma a_0(980)^0 \pi^0 \to \gamma K^0_S K^0_S \pi^0$	$(8.6 {}^{+3.4}_{-1.1}) \times 10^{-6}$			–
$\gamma f_0(1370) \to \gamma K \overline{K}$	$(4.2 \pm 1.5) \times 10^{-4}$			–
$\gamma f_0(1370) \to \gamma K^0_S K^0_S$	$(1.1 \pm 0.4) \times 10^{-5}$			–
$\gamma f_1(1420) \to \gamma K \overline{K} \pi$	$(7.9 \pm 1.3) \times 10^{-4}$			1220
$\gamma f_1(1420) \to \gamma K^*(892)^0 K^0_S \to \gamma K^0_S K^0_S \pi^0$	$(7.2 {}^{+0.7}_{-1.3}) \times 10^{-5}$			–
$\gamma f_1(1420) \to \gamma a_0(980)^0 \pi^0 \to \gamma K^0_S K^0_S \pi^0$	$(4.6 {}^{+2.4}_{-2.0}) \times 10^{-6}$			–
$\gamma f_1(1420) \to \gamma \gamma \phi$	$(5.5 \pm 1.9) \times 10^{-7}$			–
$\gamma f_1(1420) \to \gamma \pi^0 f_0(980) \to \gamma \pi^0 \pi^0 \pi^0$	$(2.23 {}^{+0.26}_{-1.20}) \times 10^{-6}$			–
$\gamma f_0(1500) \to \gamma \pi \pi$	$(1.09 \pm 0.24) \times 10^{-4}$			1183
$\gamma f_0(1500) \to \gamma \eta \eta$	$(1.7 {}^{+0.6}_{-1.4}) \times 10^{-5}$			–
$\gamma f_0(1500) \to \gamma K^0_S K^0_S$	$(1.59 {}^{+0.24}_{-0.60}) \times 10^{-5}$			–
$\gamma f_1(1510) \to \gamma \eta \pi^+ \pi^-$	$(4.5 \pm 1.2) \times 10^{-4}$			–
$\gamma f_1(1510) \to \gamma \gamma \phi$	$(7.8 {}^{+3.5}_{-3.1}) \times 10^{-7}$			–
$\gamma f'_2(1525)$	$(5.7 {}^{+0.8}_{-0.5}) \times 10^{-4}$		S=1.5	1177
$\gamma f'_2(1525) \to \gamma K^0_S K^0_S$	$(8.0 {}^{+0.7}_{-0.5}) \times 10^{-5}$			–
$\gamma f'_2(1525) \to \gamma K^*(892)^0 K^0_S \to \gamma K^0_S K^0_S \pi^0$	$(9.5 {}^{+1.6}_{-0.8}) \times 10^{-6}$			–
$\gamma f'_2(1525) \to \gamma \eta \eta$	$(3.4 \pm 1.4) \times 10^{-5}$			–
$\gamma f'_2(1525) \to \gamma \gamma \phi$	$(2.8 {}^{+0.9}_{-0.6}) \times 10^{-6}$			–
$\gamma f_2(1640) \to \gamma \omega \omega$	$(2.8 \pm 1.8) \times 10^{-4}$			–
$\gamma f_0(1710) \to \gamma \pi \pi$	$(3.8 \pm 0.5) \times 10^{-4}$			–
$\gamma f_0(1710) \to \gamma K \overline{K}$	$(9.5 {}^{+0.9}_{-0.5}) \times 10^{-4}$		S=1.4	1075
$\gamma f_0(1710) \to \gamma \omega \omega$	$(3.1 \pm 1.0) \times 10^{-4}$			–
$\gamma f_0(1710) \to \gamma \eta \eta$	$(2.4 {}^{+1.2}_{-0.7}) \times 10^{-4}$			–
$\gamma f_0(1710) \to \gamma \omega \phi$	$(2.5 \pm 0.6) \times 10^{-4}$			–
$\gamma f_0(1810) \to \gamma K^0_S K^0_S$	$(1.11 {}^{+0.20}_{-0.33}) \times 10^{-5}$			–
$\gamma f_2(1810) \to \gamma \eta \eta$	$(5.4 {}^{+3.5}_{-2.4}) \times 10^{-5}$			–
$\gamma \eta_1(1855) \to \gamma \eta \eta'$	$(2.7 {}^{+0.4}_{-0.5}) \times 10^{-6}$			–
$\gamma f_2(1910) \to \gamma \omega \omega$	$(2.0 \pm 1.4) \times 10^{-4}$			–
$\gamma f_2(1950) \to \gamma K^*(892) \overline{K}^*(892)$	$(7.0 \pm 2.2) \times 10^{-4}$			–
$\gamma f_2(1950) \to \gamma \gamma \phi$	$(10.0 {}^{+3.5}_{-2.2}) \times 10^{-6}$			–
$\gamma f_2(2010) \to \gamma \gamma \phi$	$(4.6 \pm 1.5) \times 10^{-6}$			–
$\gamma f_0(2020) \to \gamma \eta' \eta'$	$(2.63 {}^{+0.32}_{-0.50}) \times 10^{-4}$			–
$\gamma f_4(2050)$	$(2.7 \pm 0.7) \times 10^{-3}$			891
$\gamma f_0(2100) \to \gamma \eta \eta$	$(1.13 {}^{+0.60}_{-0.30}) \times 10^{-4}$			–
$\gamma f_0(2100) \to \gamma \pi \pi$	$(6.2 \pm 1.0) \times 10^{-4}$			–
$\gamma f_0(2200)$	seen			776
$\gamma f_0(2200) \to \gamma K \overline{K}$	$(5.9 \pm 1.3) \times 10^{-4}$			–
$\gamma f_0(2200) \to \gamma K^0_S K^0_S$	$(2.72 {}^{+0.19}_{-0.50}) \times 10^{-4}$			–
$\gamma f_0(2200) \to \gamma \gamma \phi$	$(2.0 {}^{+0.6}_{-0.8}) \times 10^{-7}$			–
$\gamma f_J(2220)$	seen			745
$\gamma f_J(2220) \to \gamma \pi \pi$	$< 3.9 \times 10^{-5}$		CL=90%	–
$\gamma f_J(2220) \to \gamma K \overline{K}$	$< 4.1 \times 10^{-5}$		CL=90%	–
$\gamma f_J(2220) \to \gamma p \overline{p}$	$(1.5 \pm 0.8) \times 10^{-5}$			–
$\gamma f_0(2330) \to \gamma K^0_S K^0_S$	$(4.9 \pm 0.7) \times 10^{-5}$			–
$\gamma f_0(2330) \to \gamma \eta' \eta'$	$(6.1 {}^{+4.0}_{-1.8}) \times 10^{-6}$			–
$\gamma f_2(2340) \to \gamma \eta \eta$	$(5.6 {}^{+2.4}_{-2.2}) \times 10^{-5}$			–
$\gamma f_2(2340) \to \gamma K^0_S K^0_S$	$(5.5 {}^{+4.0}_{-1.5}) \times 10^{-5}$			–
$\gamma f_2(2340) \to \gamma \eta' \eta'$	$(8.7 {}^{+0.9}_{-1.8}) \times 10^{-6}$			–
$\gamma f_0(2470) \to \gamma \eta' \eta'$	$(8.2 {}^{+4.0}_{-2.8}) \times 10^{-7}$			–
$\gamma X(1835) \to \gamma \pi^+ \pi^- \eta'$	$(2.7 {}^{+0.6}_{-0.8}) \times 10^{-4}$		S=1.6	1006
$\gamma X(1835) \to \gamma p \overline{p}$	$(7.7 {}^{+1.5}_{-0.9}) \times 10^{-5}$			–
$\gamma X(1835) \to \gamma K^0_S K^0_S \eta$	$(3.3 {}^{+2.0}_{-1.3}) \times 10^{-5}$			–
$\gamma X(1835) \to \gamma \gamma \phi(1020)$	$(3.4 {}^{+0.8}_{-1.1}) \times 10^{-6}$			–
$\gamma X(1835) \to \gamma \gamma \gamma$	$< 3.56 \times 10^{-6}$		CL=90%	–
$\gamma X(1835) \to \gamma 3(\pi^+ \pi^-)$	$(2.4 {}^{+0.7}_{-0.8}) \times 10^{-5}$			–
$\gamma \eta(2370) \to \gamma K^+ K^- \eta'$	$(1.8 \pm 0.7) \times 10^{-5}$			–
$\gamma \eta(2370) \to \gamma K^0_S K^0_S \eta'$	$(1.2 \pm 0.5) \times 10^{-5}$			–
$\gamma \eta(2370) \to \gamma \eta \eta \eta'$	$< 9.2 \times 10^{-6}$		CL=90%	–
$\gamma D^0 +$c.c.	$< 9.1 \times 10^{-8}$		CL=90%	987
$\gamma p \overline{p}$	$(3.8 \pm 1.0) \times 10^{-4}$			1232
$\gamma p \overline{p} \pi^+ \pi^-$	$< 7.9 \times 10^{-4}$		CL=90%	1107
$\gamma \Lambda \overline{\Lambda}$	$< 1.3 \times 10^{-4}$		CL=90%	1074
$\gamma A^0 \to \gamma$invisible	[*nnaa*] $< 1.7 \times 10^{-6}$		CL=90%	–
$\gamma A^0 \to \gamma \gamma \gamma$	$< 4.9 \times 10^{-7}$		CL=95%	–
$\gamma A^0 \to \gamma \mu^+ \mu^-$	[*ooaa*] $< 7.8 \times 10^{-7}$		CL=90%	–
Dalitz decays				
$\pi^0 e^+ e^-$	$(8.1 \pm 0.5) \times 10^{-7}$			1546
$\eta e^+ e^-$	$(1.42 \pm 0.08) \times 10^{-5}$			1500
$\eta'(958) e^+ e^-$	$(6.59 \pm 0.18) \times 10^{-5}$			1400
$\eta(1405) e^+ e^- \to f_0(980) \pi^0 e^+ e^- \to \pi^+ \pi^- \pi^0 e^+ e^-$	$(2.04 \pm 0.22) \times 10^{-7}$			–
$X(1835) e^+ e^-,\ X \to \pi^+ \pi^- \eta'$	$(3.58 \pm 0.25) \times 10^{-6}$			–
$X(2120) e^+ e^-,\ X \to \pi^+ \pi^- \eta'$	$(8.2 \pm 1.3) \times 10^{-7}$			–
$\eta(2370) e^+ e^-,\ \eta \to \pi^+ \pi^- \eta'$	$(1.08 \pm 0.17) \times 10^{-6}$			–
$\eta U \to \eta e^+ e^-$	[*ppaa*] $< 9.11 \times 10^{-7}$		CL=90%	–
$\eta'(958) U \to \eta'(958) e^+ e^-$	[*ppaa*] $< 2.0 \times 10^{-7}$		CL=90%	–
$\phi e^+ e^-$	$< 1.2 \times 10^{-7}$		CL=90%	1381
Weak decays				
$D^- e^+ \nu_e +$ c.c.	$< 7.1 \times 10^{-8}$		CL=90%	984
$D^- \mu^+ \nu_\mu +$ c.c.	$< 5.6 \times 10^{-7}$		CL=90%	980
$\overline{D}^0 e^+ e^-+$ c.c.	$< 8.5 \times 10^{-8}$		CL=90%	987
$D^0 \mu^+ \mu^-+$ c.c.	$< 1.1 \times 10^{-7}$		CL=90%	971
$D^-_s e^+ \nu_e +$ c.c.	$< 1.3 \times 10^{-6}$		CL=90%	923
$D^{*-}_s e^+ \nu_e +$ c.c.	$< 1.8 \times 10^{-6}$		CL=90%	828
$D^- \pi^+ +$ c.c.	$< 7.0 \times 10^{-8}$		CL=90%	977
$D^- \rho^+ +$ c.c	$< 6.0 \times 10^{-7}$		CL=90%	–
$\overline{D}^0 \pi^0 +$ c.c	$< 4.7 \times 10^{-7}$		CL=90%	–
$\overline{D}^0 \overline{K}^0 +$ c.c.	$< 1.7 \times 10^{-4}$		CL=90%	898
$\overline{D}^0 \overline{K}^{*0} +$ c.c.	$< 2.5 \times 10^{-6}$		CL=90%	670
$\overline{D}^0 \eta +$ c.c	$< 6.8 \times 10^{-7}$		CL=90%	–
$\overline{D}^0 \rho^0 +$ c.c	$< 5.2 \times 10^{-7}$		CL=90%	–
$D^-_s \pi^+ +$ c.c.	$< 4.1 \times 10^{-7}$		CL=90%	915
$D^-_s \rho^+ +$ c.c.	$< 8.0 \times 10^{-7}$		CL=90%	663
Charge conjugation (C), Parity (P), Lepton Family number (LF) violating modes				
$\gamma \gamma$	C $< 2.7 \times 10^{-7}$		CL=90%	1548
$\gamma \phi$	C $< 1.4 \times 10^{-6}$		CL=90%	1381
$e^\pm \mu^\mp$	LF $< 1.6 \times 10^{-7}$		CL=90%	1547
$e^\pm \tau^\mp$	LF $< 7.5 \times 10^{-8}$		CL=90%	1039
$\mu^\pm \tau^\mp$	LF $< 2.0 \times 10^{-6}$		CL=90%	1035
$K^+ K^+ e^- e^-+$ c.c.	L $< 2.1 \times 10^{-9}$		CL=90%	1467
$p e^-+$ c.c.	L,B $< 3.1 \times 10^{-8}$		CL=90%	1406
$\Lambda^+_c e^-+$c.c.	$< 6.9 \times 10^{-8}$		CL=90%	704
Other decays				
invisible	$< 7 \times 10^{-4}$		CL=90%	–

$\chi_{c0}(1P)$

$I^G(J^{PC}) = 0^+(0^{++})$

Mass $m = 3415.50 \pm 0.19$ MeV (S = 1.7)
Full width $\Gamma = 12.40 \pm 0.27$ MeV (S = 1.6)

$\chi_{c0}(1P)$ DECAY MODES	Fraction (Γ_i/Γ)	Scale factor/ Confidence level	p (MeV/c)
Hadronic decays			
$2(\pi^+ \pi^-)$	(2.10 ± 0.10) %	S=1.2	1679
$\rho^0 \pi^+ \pi^-$	$(8.2 \pm 2.6) \times 10^{-3}$		1607
$f_0(980) f_0(980)$	$(6.5 \pm 2.1) \times 10^{-4}$		1392
$\pi^+ \pi^- \pi^0 \pi^0$	(3.2 ± 0.4) %		1680
$\rho^+ \pi^- \pi^0 +$ c.c.	(2.8 ± 0.4) %		1608
$4\pi^0$	$(3.2 \pm 0.4) \times 10^{-3}$		1681

Int. J. Mod. Phys. A 2026.41. Downloaded from www.worldscientific.com
by UNIVERSITY OF CALIFORNIA @ BERKELEY on 09/16/26. Re-use and distribution is strictly not permitted, except for Open Access articles.

$\pi^+\pi^-K^+K^-$	(1.73 ± 0.15) %	S=1.1	1581
$K_0^*(1430)^0\overline{K}_0^*(1430)^0 \to \pi^+\pi^-K^+K^-$	$(9.6\ ^{+3.5}_{-2.8})\times10^{-4}$		–
$K_0^*(1430)^0\overline{K}_2^*(1430)^0+$ c.c. $\to \pi^+\pi^-K^+K^-$	$(7.8\ ^{+1.9}_{-2.4})\times10^{-4}$		–
$K_1(1270)^+K^-+$ c.c. $\to \pi^+\pi^-K^+K^-$	$(6.1\ \pm1.8)\times10^{-3}$		–
$K_1(1400)^+K^-+$ c.c. $\to \pi^+\pi^-K^+K^-$	$<2.6\ \times10^{-3}$	CL=90%	–
$f_0(980)f_0(980)$	$(1.6\ ^{+1.0}_{-0.9})\times10^{-4}$		1392
$f_0(980)f_0(2200)$	$(7.7\ ^{+2.0}_{-2.4})\times10^{-4}$		587
$f_0(1370)f_0(1370)$	$<2.7\ \times10^{-4}$	CL=90%	1020
$f_0(1370)f_0(1500)$	$<1.7\ \times10^{-4}$	CL=90%	908
$f_0(1370)f_0(1710)$	$(6.5\ ^{+3.4}_{-2.3})\times10^{-4}$		720
$f_0(1500)f_0(1370)$	$<1.3\ \times10^{-4}$	CL=90%	908
$f_0(1500)f_0(1500)$	$<5\ \times10^{-5}$	CL=90%	775
$f_0(1500)f_0(1710)$	$<7\ \times10^{-5}$	CL=90%	532
$K^+K^-\pi^+\pi^-\pi^0$	$(8.6\ \pm0.9)\times10^{-3}$		1546
$K_S^0K^\pm\pi^\mp\pi^+\pi^-$	$(4.1\ \pm0.4)\times10^{-3}$		1544
$K^+K^-\pi^0\pi^0$	$(5.4\ \pm0.9)\times10^{-3}$		1583
$K^+\pi^-\overline{K}^0\pi^0+$ c.c.	(2.42 ± 0.32) %		1581
$\rho^+K^-K^0+$ c.c.	(1.17 ± 0.20) %		1459
$K^*(892)^-K^+\pi^0 \to K^+\pi^-\overline{K}^0\pi^0+$ c.c.	$(4.5\ \pm1.1)\times10^{-3}$		–
$K_S^0K_S^0\pi^+\pi^-$	$(5.5\ \pm1.0)\times10^{-3}$		1579
$K^+K^-\eta\pi^0$	$(2.9\ \pm0.7)\times10^{-3}$		1468
$3(\pi^+\pi^-)$	(1.97 ± 0.22) %	S=3.0	1633
$K^+\overline{K}^*(892)^0\pi^-+$ c.c.	$(7.0\ \pm1.5)\times10^{-3}$		1524
$K^*(892)^0\overline{K}^*(892)^0$	$(1.7\ \pm0.6)\times10^{-3}$		1456
$\pi\pi$	$(8.76\pm0.26)\times10^{-3}$	S=1.4	1702
$\pi^0\eta$	$<1.7\ \times10^{-4}$		1661
$\pi^0\eta'$	$<1.1\ \times10^{-3}$		1570
$\pi^0\eta_c$	$<1.6\ \times10^{-3}$	CL=90%	384
$\eta\eta$	$(2.94\pm0.22)\times10^{-3}$	S=1.2	1617
$\eta\eta'$	$(8.9\ \pm1.1)\times10^{-5}$		1522
$\eta'\eta'$	$(2.11\pm0.12)\times10^{-3}$		1414
$\omega\omega$	$(1.02\pm0.05)\times10^{-3}$		1518
$\omega\phi$	$(1.21\pm0.10)\times10^{-4}$	S=1.4	1447
ωK^+K^-	$(1.87\pm0.20)\times10^{-3}$		1458
K^+K^-	$(6.15\pm0.19)\times10^{-3}$	S=1.4	1635
$K_S^0K_S^0$	$(3.08\pm0.18)\times10^{-3}$	S=1.1	1634
$\pi^+\pi^-\eta$	$<1.9\ \times10^{-4}$	CL=90%	1652
$2\pi^+2\pi^-\eta$	$(4.4\ \pm0.4)\times10^{-3}$		1616
$\pi^+\pi^-\eta'$	$<3.5\ \times10^{-4}$	CL=90%	1560
$\eta\eta\eta'$	$<2.5\ \times10^{-5}$	CL=90%	1364
$\overline{K}^0K^+\pi^-+$ c.c.	$<9\ \times10^{-5}$	CL=90%	1610
$K^+K^-\pi^0$	$<6\ \times10^{-5}$	CL=90%	1612
$K^+K^-\eta$	$<2.2\ \times10^{-4}$	CL=90%	1513
$K^+K^-K_S^0K_S^0$	$(1.4\ \pm0.5)\times10^{-3}$		1331
$K_S^0K_S^0K_S^0K_S^0$	$(5.6\ \pm0.5)\times10^{-4}$		1328
$K^+K^-K^+K^-$	$(2.7\ \pm0.4)\times10^{-3}$	S=1.5	1334
$K^+K^-\phi$	$(9.4\ \pm2.4)\times10^{-4}$		1382
$\overline{K}^0K^+\pi^-\phi+$ c.c.	$(3.7\ \pm0.6)\times10^{-3}$		1326
$K^+K^-\pi^0\phi$	$(1.90\pm0.35)\times10^{-3}$		1330
$K_S^0K_S^0K_S^0K^\pm\pi^\mp$	$(7.7\ \pm0.8)\times10^{-5}$		1261
$3(K^+K^-)$	$(1.04\pm0.21)\times10^{-5}$		694
$\phi\pi^+\pi^-\pi^0$	$(1.14\pm0.14)\times10^{-3}$		1525
$\phi\phi$	$(8.3\ \pm0.4)\times10^{-4}$	S=1.1	1370
$\phi\phi\eta$	$(8.2\ \pm0.9)\times10^{-4}$		1101
$p\overline{p}$	$(2.35\pm0.12)\times10^{-4}$	S=1.9	1427
$p\overline{p}\pi^0$	$(6.8\ \pm0.7)\times10^{-4}$	S=1.3	1379
$p\overline{p}\eta$	$(3.4\ \pm0.4)\times10^{-4}$		1187
$p\overline{p}\omega$	$(5.1\ \pm0.6)\times10^{-4}$		1043
$p\overline{p}\pi^+\pi^-$	$(1.9\ \pm1.1)\times10^{-3}$	S=2.3	1320
$p\overline{p}\pi^0\pi^0$	$(1.01\pm0.27)\times10^{-3}$		1324
$p\overline{p}\eta\pi^0$	$(2.35\pm0.20)\times10^{-4}$		1108
$p\overline{p}\eta\eta$	$(5.6\ \pm0.7)\times10^{-5}$		797
$p\overline{p}K^+K^-$	$(2.48\pm0.17)\times10^{-4}$		891
$p\overline{p}K^+K^-$ (non-resonant)	$(1.19\pm0.26)\times10^{-4}$		891
$K^+\overline{p}\Lambda(1520)+$ c.c.	$(2.9\ \pm0.7)\times10^{-4}$		860
$\Lambda(1520)\overline{\Lambda}(1520)$	$(3.0\ \pm1.2)\times10^{-4}$		780
$p\overline{p}\phi$	$(5.9\ \pm1.4)\times10^{-5}$		876
$p\overline{p}K_S^0K_S^0$	$<8\ \times10^{-4}$	CL=90%	884
$p\overline{p}K_S^0K^-\pi^++$ c.c.	$(2.5\ \pm0.4)\times10^{-5}$		764
$p\overline{n}\pi^-$	$(1.23\pm0.11)\times10^{-3}$		1377
$\overline{p}n\pi^+$	$(1.33\pm0.12)\times10^{-3}$		1377
$p\overline{n}\pi^-\pi^0$	$(2.28\pm0.20)\times10^{-3}$		1322
$\overline{p}n\pi^+\pi^0$	$(2.15\pm0.18)\times10^{-3}$		1322
$\Lambda\overline{\Lambda}$	$(3.50\pm0.17)\times10^{-4}$	S=1.1	1293
$\Lambda\overline{\Lambda}\pi^+\pi^-$	$(1.15\pm0.12)\times10^{-3}$		1154
$\Lambda\overline{\Lambda}\pi^+\pi^-$ (non-resonant)	$<5\ \times10^{-4}$	CL=90%	1154
$\Sigma(1385)^+\overline{\Lambda}\pi^-+$ c.c.	$<5\ \times10^{-4}$	CL=90%	1084
$\Sigma(1385)^-\overline{\Lambda}\pi^++$ c.c.	$<5\ \times10^{-4}$	CL=90%	1084
$\Lambda\overline{\Lambda}\eta$	$(2.2\ \pm0.4)\times10^{-4}$		980
$\Lambda\overline{\Lambda}\eta'$	$(7.3\ \pm1.6)\times10^{-5}$		587
$\Lambda\overline{\Lambda}\omega$	$(2.31\pm0.33)\times10^{-4}$		782
$\Lambda\overline{\Lambda}\phi$	$(2.9\ \pm1.2)\times10^{-5}$		500
$K^+\overline{p}\Lambda+$ c.c.	$(1.21\pm0.12)\times10^{-3}$	S=1.3	1133
$nK_S^0\overline{\Lambda}+$ c.c.	$(6.5\ \pm0.5)\times10^{-4}$		1129
$K^*(892)^+\overline{p}\Lambda+$ c.c.	$(4.7\ \pm0.9)\times10^{-4}$		845
$\overline{p}\Lambda(1520)K_S^0\pi^++$ c.c.	$(1.6\ \pm0.7)\times10^{-5}$		723
$\Sigma^0\overline{\Sigma}^0$	$(4.56\pm0.32)\times10^{-4}$		1222
$\Sigma^+\overline{p}K_S^0+$ c.c.	$(3.43\pm0.27)\times10^{-4}$		1090
$\Sigma^0\overline{p}K^++$ c.c.	$(2.95\pm0.20)\times10^{-4}$		1090
$\Sigma^+\overline{\Sigma}^-$	$(4.5\ \pm0.8)\times10^{-4}$	S=2.6	1225
$\Sigma^+\overline{\Sigma}^-\eta$	$(1.23\pm0.23)\times10^{-4}$		869
$\Sigma^-\overline{\Sigma}^+$	$(5.0\ \pm0.5)\times10^{-4}$		1218
$\Sigma(1385)^+\overline{\Sigma}(1385)^-$	$(1.6\ \pm0.6)\times10^{-4}$		1002
$\Sigma(1385)^-\overline{\Sigma}(1385)^+$	$(2.3\ \pm0.6)\times10^{-4}$		1002
$K^-\Lambda\overline{\Xi}^++$ c.c.	$(1.89\pm0.34)\times10^{-4}$		874
$\Xi^0\overline{\Xi}^0$	$(4.3\ \pm0.5)\times10^{-4}$	S=1.7	1090
$\Xi^-\overline{\Xi}^+$	$(4.34\pm0.20)\times10^{-4}$		1081
$\Omega^-\overline{\Omega}^+$	$(3.4\ \pm0.6)\times10^{-5}$		345
$\eta_c\pi^+\pi^-$	$<7\ \times10^{-4}$	CL=90%	308
Radiative decays			
$\gamma J/\psi(1S)$	(1.35 ± 0.09) %	S=1.8	304
$\gamma\rho^0$	$<9\ \times10^{-6}$	CL=90%	1620
$\gamma\omega$	$<8\ \times10^{-6}$	CL=90%	1618
$\gamma\phi$	$<6\ \times10^{-6}$	CL=90%	1556
$\gamma\gamma$	$(1.96\pm0.08)\times10^{-4}$	S=1.1	1708
$e^+e^-J/\psi(1S)$	$(1.29\pm0.29)\times10^{-4}$		304
$\mu^+\mu^-J/\psi(1S)$	$<1.8\ \times10^{-5}$	CL=90%	227

$\chi_{c1}(1P)$

$I^G(J^{PC}) = 0^+(1^{++})$

Mass $m = 3510.67 \pm 0.05$ MeV (S = 1.2)
Full width $\Gamma = 0.82 \pm 0.04$ MeV (S = 1.1)

$\chi_{c1}(1P)$ DECAY MODES	Fraction (Γ_i/Γ)	Scale factor/ Confidence level	p (MeV/c)
e^+e^-	$(1.5\ ^{+1.6}_{-1.0})\times10^{-7}$		1755
Hadronic decays			
$3(\pi^+\pi^-)$	(1.06 ± 0.11) %	S=3.0	1683
$2(\pi^+\pi^-)$	$(6.6\ \pm0.7)\times10^{-3}$	S=2.4	1728
$\rho^0\pi^+\pi^-$	$(1.6\ \pm1.3)\times10^{-3}$		1658
$\pi^+\pi^-\pi^0\pi^0$	(1.18 ± 0.15) %		1729
$\rho^+\pi^-\pi^0+$ c.c.	(1.44 ± 0.24) %		1658
$4\pi^0$	$(5.3\ \pm0.8)\times10^{-4}$		1729
$\pi^+\pi^-K^+K^-$	$(4.5\ \pm1.0)\times10^{-3}$		1632
$K^+K^-\pi^0\pi^0$	$(1.10\pm0.27)\times10^{-3}$		1634
$K^+K^-\pi^+\pi^-\pi^0$	(1.07 ± 0.12) %		1598
$K_S^0K^\pm\pi^\mp\pi^+\pi^-$	$(7.0\ \pm0.7)\times10^{-3}$		1596
$K^+\pi^-\overline{K}^0\pi^0+$ c.c.	$(8.5\ \pm1.3)\times10^{-3}$		1632
$\rho^-K^+\overline{K}^0+$ c.c.	$(5.0\ \pm1.2)\times10^{-3}$		1514
$K^*(892)^0\overline{K}^0\pi^0 \to K^+\pi^-\overline{K}^0\pi^0+$ c.c.	$(2.3\ \pm0.6)\times10^{-3}$		–
$K^+K^-\eta\pi^0$	$(1.10\pm0.34)\times10^{-3}$		1523
$\pi^+\pi^-K_S^0K_S^0$	$(6.8\ \pm2.9)\times10^{-4}$		1630
$K^+K^-\eta$	$(3.1\ \pm1.0)\times10^{-4}$		1566
$\overline{K}^0K^+\pi^-+$ c.c.	$(6.9\ \pm0.6)\times10^{-3}$	S=1.1	1661
$K^*(892)^0\overline{K}^0+$ c.c.	$(1.04\pm0.15)\times10^{-3}$		1602
$K^*(892)^+K^-+$ c.c.	$(1.22\pm0.23)\times10^{-3}$		1602
$K_J^*(1430)^0\overline{K}^0+$ c.c. $\to K_S^0K^+\pi^-+$ c.c.	$<8\ \times10^{-4}$	CL=90%	–
$K_J^*(1430)^+K^-+$ c.c. $\to K_S^0K^+\pi^-+$ c.c.	$<2.1\ \times10^{-3}$	CL=90%	–
$K^+K^-\pi^0$	$(1.80\pm0.24)\times10^{-3}$		1662
$\eta\pi^+\pi^-$	$(4.57\pm0.23)\times10^{-3}$		1701
$a_0(980)^+\pi^-+$ c.c. $\to \eta\pi^+\pi^-$	$(3.2\ \pm0.4)\times10^{-3}$	S=2.1	–
$a_2(1320)^+\pi^-+$ c.c. $\to \eta\pi^+\pi^-$	$(1.74\pm0.24)\times10^{-4}$		–

Int. J. Mod. Phys. A 2026.41. Downloaded from www.worldscientific.com
by UNIVERSITY OF CALIFORNIA @ BERKELEY on 09/16/26. Re-use and distribution is strictly not permitted, except for Open Acce

$a_2(1700)^+\pi^- +$ c.c. $\to \eta\pi^+\pi^-$	$(4.6 \pm 0.7) \times 10^{-5}$		–
$f_2(1270)\eta \to \eta\pi^+\pi^-$	$(3.5 \pm 0.6) \times 10^{-4}$		–
$f_4(2050)\eta \to \eta\pi^+\pi^-$	$(2.5 \pm 0.9) \times 10^{-5}$		–
$\pi_1(1400)^+\pi^- +$ c.c. $\to \eta\pi^+\pi^-$	$< 4 \times 10^{-5}$	CL=90%	–
$\pi_1(1600)^+\pi^- +$ c.c. $\to \eta\pi^+\pi^-$	$< 1.5 \times 10^{-5}$	CL=90%	–
$\pi_1(2015)^+\pi^- +$ c.c. $\to \eta\pi^+\pi^-$	$< 8 \times 10^{-6}$	CL=90%	–
$2\pi^+2\pi^-\eta$	$(8.0 \pm 0.8) \times 10^{-3}$		1666
$f_2(1270)\eta$	$(6.6 \pm 1.1) \times 10^{-4}$		1467
$\pi^+\pi^-\eta'$	$(2.2 \pm 0.4) \times 10^{-3}$		1612
$K^+K^-\eta'(958)$	$(8.4 \pm 0.5) \times 10^{-4}$		1461
$K_0^*(1430)^+K^-$ + c.c. $\to K^+K^-\eta'(958)$	$(6.4\ ^{+2.2}_{-2.8}) \times 10^{-4}$		–
$f_0(980)\eta'(958) \to K^+K^-\eta'(958)$	$(1.6\ ^{+1.4}_{-0.7}) \times 10^{-4}$		–
$f_0(1710)\eta'(958) \to K^+K^-\eta'(958)$	$(7\ ^{+7}_{-5}) \times 10^{-5}$		–
$f_2'(1525)\eta'(958) \to K^+K^-\eta'(958)$	$(9 \pm 6) \times 10^{-5}$		–
$\eta\eta\eta'$	$(1.39 \pm 0.16) \times 10^{-4}$		1423
$K_2^*(1430)^+K^-$ + c.c.	$(1.63 \pm 0.31) \times 10^{-3}$		1416
$K_2^*(1430)\overline{K}^0$ + c.c.	$(1.18 \pm 0.20) \times 10^{-3}$		1416
$\pi^0 f_0(980) \to \pi^0\pi^+\pi^-$	$(3.5 \pm 0.9) \times 10^{-7}$		–
$K^+\overline{K}^*(892)^0\pi^-$ + c.c.	$(1.6 \pm 0.9) \times 10^{-3}$		1577
$K^*(892)^0\overline{K}^*(892)^0$	$(1.4 \pm 0.4) \times 10^{-3}$		1512
$K^+K^-K^0_SK^0_S$	$< 4 \times 10^{-4}$	CL=90%	1390
$K^0_SK^0_SK^0_SK^0_S$	$(3.5 \pm 1.0) \times 10^{-5}$		1387
$K^+K^-K^+K^-$	$(5.3 \pm 1.1) \times 10^{-4}$		1393
$K^+K^-\phi$	$(4.1 \pm 1.5) \times 10^{-4}$		1440
$\overline{K}^0K^+\pi^-\phi$ + c.c.	$(3.3 \pm 0.5) \times 10^{-3}$		1387
$K^+K^-\pi^0\phi$	$(1.62 \pm 0.30) \times 10^{-3}$		1390
$K^0_SK^0_SK^0_SK^\pm\pi^\mp$	$(2.60 \pm 0.22) \times 10^{-4}$		1322
$3(K^+K^-)$	$(4.2 \pm 1.1) \times 10^{-6}$		779
$\phi\pi^+\pi^-\pi^0$	$(7.0 \pm 0.9) \times 10^{-4}$		1578
$\omega\omega$	$(6.25 \pm 0.30) \times 10^{-4}$		1571
ωK^+K^-	$(7.3 \pm 0.8) \times 10^{-4}$		1513
$\omega\phi$	$(2.13 \pm 0.30) \times 10^{-5}$	S=1.5	1503
$\phi\phi$	$(4.22 \pm 0.20) \times 10^{-4}$		1429
$\phi\phi\eta$	$(2.9 \pm 0.5) \times 10^{-4}$		1172
$p\overline{p}$	$(7.97 \pm 0.29) \times 10^{-5}$	S=1.3	1484
$p\overline{p}\pi^0$	$(1.54 \pm 0.18) \times 10^{-4}$		1438
$p\overline{p}\eta$	$(1.44 \pm 0.24) \times 10^{-4}$		1254
$p\overline{p}\omega$	$(2.10 \pm 0.30) \times 10^{-4}$		1117
$p\overline{p}\pi^+\pi^-$	$(5.0 \pm 1.9) \times 10^{-4}$		1381
$p\overline{p}\pi^0\pi^0$	$< 5 \times 10^{-4}$	CL=90%	1385
$p\overline{p}\eta\pi^0$	$(1.93 \pm 0.13) \times 10^{-4}$		1179
$p\overline{p}\eta\eta$	$(1.4 \pm 0.4) \times 10^{-5}$		887
$p\overline{p}K^+K^-$	$(1.86 \pm 0.12) \times 10^{-4}$		974
$p\overline{p}K^+K^-$ (non-resonant)	$(1.26 \pm 0.22) \times 10^{-4}$		974
$K^+\overline{p}\Lambda(1520)$ + c.c.	$(1.7 \pm 0.4) \times 10^{-4}$		951
$\Lambda(1520)\overline{\Lambda}(1520)$	$< 9 \times 10^{-5}$	CL=90%	880
$p\overline{p}\phi$	$< 1.7 \times 10^{-5}$	CL=90%	962
$p\overline{p}K^0_SK^0_S$	$< 4 \times 10^{-4}$	CL=90%	968
$p\overline{p}K^0_SK^-\pi^+$ + c.c.	$(4.1 \pm 0.5) \times 10^{-5}$		857
$p\overline{n}\pi^-$	$(3.8 \pm 0.5) \times 10^{-4}$		1435
$\overline{p}n\pi^+$	$(3.9 \pm 0.5) \times 10^{-4}$		1435
$p\overline{n}\pi^-\pi^0$	$(1.02 \pm 0.12) \times 10^{-3}$		1383
$\overline{p}n\pi^+\pi^0$	$(9.9 \pm 1.2) \times 10^{-4}$		1383
$\Lambda\overline{\Lambda}$	$(1.26 \pm 0.09) \times 10^{-4}$	S=1.1	1355
$\Lambda\overline{\Lambda}\pi^+\pi^-$	$(2.9 \pm 0.5) \times 10^{-4}$		1223
$\Lambda\overline{\Lambda}\pi^+\pi^-$ (non-resonant)	$(2.4 \pm 0.6) \times 10^{-4}$		1223
$\Sigma(1385)^+\overline{\Lambda}\pi^-$ + c.c.	$< 1.3 \times 10^{-4}$	CL=90%	1157
$\Sigma(1385)^-\overline{\Lambda}\pi^+$ + c.c.	$< 1.3 \times 10^{-4}$	CL=90%	1157
$\Lambda\overline{\Lambda}\eta$	$(5.8 \pm 1.5) \times 10^{-5}$		1059
$\Lambda\overline{\Lambda}\eta'$	$(1.5 \pm 0.5) \times 10^{-5}$		706
$\Lambda\overline{\Lambda}\omega$	$(9.9 \pm 1.5) \times 10^{-5}$		877
$\Lambda\overline{\Lambda}\phi$	$(5.9 \pm 1.0) \times 10^{-5}$		634
$K^+\overline{p}\Lambda$+c.c.	$(4.1 \pm 0.4) \times 10^{-4}$	S=1.2	1203
$nK^0_S\overline{\Lambda}$ + c.c.	$(1.64 \pm 0.17) \times 10^{-4}$		1200
$\overline{p}\Lambda(1520)K^0_S\pi^+$ + c.c.	$(4.0 \pm 0.9) \times 10^{-5}$		829
$K^*(892)^+\overline{p}\Lambda$ + c.c.	$(4.9 \pm 0.7) \times 10^{-4}$		935
$\Sigma^0\overline{\Sigma}^0$	$(4.2 \pm 0.6) \times 10^{-5}$		1288
$\Sigma^+\overline{p}K^0_S$ + c.c.	$(1.51 \pm 0.12) \times 10^{-4}$		1163
$\Sigma^0\overline{p}K^+$ + c.c.	$(1.44 \pm 0.10) \times 10^{-4}$		1163
$\Sigma^+\overline{\Sigma}^-$	$(3.6 \pm 0.6) \times 10^{-5}$		1291
$\Sigma^+\overline{\Sigma}^-\eta$	$(5.0 \pm 1.4) \times 10^{-5}$		958
$\Sigma^-\overline{\Sigma}^+$	$(5.6 \pm 1.5) \times 10^{-5}$		1283
$\Sigma(1385)^+\overline{\Sigma}(1385)^-$	$< 9 \times 10^{-5}$	CL=90%	1081
$\Sigma(1385)^-\overline{\Sigma}(1385)^+$	$< 5 \times 10^{-5}$	CL=90%	1081
$K^-\Lambda\overline{\Xi}^+$ + c.c.	$(1.34 \pm 0.24) \times 10^{-4}$		963
$\Xi^0\overline{\Xi}^0$	$(7.4 \pm 1.2) \times 10^{-5}$		1163
$\Xi^-\overline{\Xi}^+$	$(5.9 \pm 0.6) \times 10^{-5}$		1155
$\Omega^-\overline{\Omega}^+$	$(1.47 \pm 0.25) \times 10^{-5}$		533
$\pi^+\pi^- + K^+K^-$	$< 1.5 \times 10^{-3}$	CL=90%	–
$K^0_SK^0_S$	$< 6 \times 10^{-5}$	CL=90%	1683
$\eta_c\pi^+\pi^-$	$< 3.1 \times 10^{-4}$	CL=90%	413
Radiative decays			
$\gamma J/\psi(1S)$	(33.9 ± 1.2) %	S=1.3	389
$\gamma\rho^0$	$(2.14 \pm 0.17) \times 10^{-4}$		1670
$\gamma\omega$	$(6.7 \pm 0.8) \times 10^{-5}$		1668
$\gamma\phi$	$(2.4 \pm 0.5) \times 10^{-5}$		1607
$\gamma\gamma$	$< 6 \times 10^{-6}$	CL=90%	1755
$e^+e^-J/\psi(1S)$	$(3.42 \pm 0.23) \times 10^{-3}$		389
$\mu^+\mu^-J/\psi(1S)$	$(2.30 \pm 0.29) \times 10^{-4}$		335

$h_c(1P)$

$I^G(J^{PC}) = 0^-(1^{+-})$

Mass $m = 3525.37 \pm 0.14$ MeV (S = 1.2)
Full width $\Gamma = 0.78 \pm 0.28$ MeV

$h_c(1P)$ DECAY MODES	Fraction (Γ_i/Γ)	Scale factor/ Confidence level	p (MeV/c)
$J/\psi(1S)\pi^0$	$< 5 \times 10^{-4}$	CL=90%	382
$J/\psi(1S)\pi\pi$	$< 9 \times 10^{-5}$	CL=90%	312
$J/\psi(1S)\pi^+\pi^-$	$< 9 \times 10^{-4}$	CL=90%	305
$p\overline{p}$	$< 4 \times 10^{-5}$	CL=90%	1492
$p\overline{p}\pi^0$	$< 8 \times 10^{-4}$	CL=90%	1447
$p\overline{p}\pi^+\pi^-$	$(3.3 \pm 0.6) \times 10^{-3}$		1390
$p\overline{p}\pi^0\pi^0$	$< 6 \times 10^{-4}$	CL=90%	1394
$p\overline{p}\pi^+\pi^-\pi^0$	$(4.4 \pm 1.3) \times 10^{-3}$		1331
$p\overline{p}\eta$	$(7.4 \pm 2.2) \times 10^{-4}$		1264
$\pi^+\pi^-\pi^0$	$(1.57 \pm 0.13) \times 10^{-3}$		1749
$\pi^+\pi^-\eta$	$< 5 \times 10^{-4}$	CL=90%	1709
$\pi^+\pi^-\pi^0\eta$	$(8.3 \pm 2.4) \times 10^{-3}$		1695
$2\pi^+2\pi^-\pi^0\eta$	$(7.2 \pm 1.7) \times 10^{-3}$		1648
$2\pi^+2\pi^-\pi^0$	$(9.4 \pm 1.7) \times 10^{-3}$		1716
$2\pi^+2\pi^-\eta$	$< 6 \times 10^{-4}$	CL=90%	1674
$3\pi^+3\pi^-\pi^0$	$(9.1 \pm 1.5) \times 10^{-3}$		1661
$2\pi^+2\pi^-\omega$	$(3.9 \pm 1.0) \times 10^{-3}$		1627
$K^+K^-\pi^+\pi^-$	$< 7 \times 10^{-4}$	CL=90%	1640
$K^+K^-\pi^+\pi^-\pi^0$	$(3.8 \pm 0.8) \times 10^{-3}$		1606
$K^+K^-\pi^+\pi^-\eta$	$< 2.7 \times 10^{-3}$	CL=90%	1480
$K^+K^-\pi^0$	$(3.8 \pm 0.9) \times 10^{-4}$		1670
$K^+K^-\pi^0\eta$	$< 2.4 \times 10^{-3}$	CL=90%	1532
$K^+K^-\eta$	$(3.6 \pm 1.2) \times 10^{-4}$		1574
$2K^+2K^-\pi^0$	$< 2.8 \times 10^{-4}$	CL=90%	1339
$K^0_SK^\pm\pi^\mp$	$(7.1 \pm 1.9) \times 10^{-4}$		1668
$K^0_SK^\pm\pi^\mp\pi^+\pi^-$	$(3.2 \pm 1.0) \times 10^{-3}$		1604
Radiative decays			
$\gamma\eta$	$(3.8 \pm 0.6) \times 10^{-4}$		1720
$\gamma\eta'(958)$	$(1.41 \pm 0.15) \times 10^{-3}$		1633
$\gamma\pi^0$	$< 5 \times 10^{-5}$		1760
$\gamma\eta_c(1S)$	(64 ± 5) %	S=1.2	500
$\gamma\pi^+\pi^-$	$(3.0 \pm 0.7) \times 10^{-4}$		1757
$\gamma\pi^+\pi^-\eta$	$(3.5 \pm 0.6) \times 10^{-3}$		1709
$\gamma 2\pi^+2\pi^-$	$(2.18 \pm 0.30) \times 10^{-3}$		1735
$\gamma p\overline{p}$	$(3.3 \pm 0.7) \times 10^{-4}$		1492
$e^+e^-\eta_c(1S)$	$(3.8 \pm 0.8) \times 10^{-3}$		500
$\gamma f_2(1270) \to \gamma\pi^+\pi^-$	$(1.8 \pm 0.4) \times 10^{-4}$		–

$\chi_{c2}(1P)$

$I^G(J^{PC}) = 0^+(2^{++})$

Mass $m = 3556.17 \pm 0.07$ MeV
Full width $\Gamma = 1.94 \pm 0.09$ MeV (S = 1.1)

$\chi_{c2}(1P)$ DECAY MODES	Fraction (Γ_i/Γ)	Scale factor/ Confidence level	p (MeV/c)
Hadronic decays			
$2(\pi^+\pi^-)$	(1.11 ± 0.07) %	S=1.2	1751
$\pi^+\pi^-\pi^0\pi^0$	(1.81 ± 0.23) %		1752

Int. J. Mod. Phys. A 2026.41. Downloaded from www.worldscientific.com
by UNIVERSITY OF CALIFORNIA @ BERKELEY on 09/16/26. Re-use and distribution is strictly not permitted, except for Open Access articles.

$\rho^+\pi^-\pi^0$ + c.c.	(2.16 ± 0.34) %		1682
$4\pi^0$	$(1.10\pm0.15)\times10^{-3}$		1752
$K^+K^-\pi^0\pi^0$	$(2.0\pm0.4)\times10^{-3}$		1658
$K^+\pi^-\overline{K}^0\pi^0$ + c.c.	(1.37 ± 0.19) %		1657
$\rho^-K^+\overline{K}^0$ + c.c.	$(4.1\pm1.2)\times10^{-3}$		1540
$K^*(892)^0K^-\pi^+\to K^-\pi^+K^0\pi^0$ + c.c.	$(2.9\pm0.8)\times10^{-3}$		–
$K^*(892)^0\overline{K}^0\pi^0\to K^+\pi^-\overline{K}^0\pi^0$ + c.c.	$(3.8\pm0.9)\times10^{-3}$		–
$K^*(892)^-K^+\pi^0\to K^+\pi^-\overline{K}^0\pi^0$ + c.c.	$(3.7\pm0.8)\times10^{-3}$		–
$K^*(892)^+\overline{K}^0\pi^-\to K^+\pi^-\overline{K}^0\pi^0$ + c.c.	$(2.9\pm0.8)\times10^{-3}$		–
$K^+K^-\eta\pi^0$	$(1.3\pm0.4)\times10^{-3}$		1549
$K^+K^-\pi^+\pi^-$	$(8.4\pm1.1)\times10^{-3}$	S=1.2	1656
$K^+K^-\pi^+\pi^-\pi^0$	(1.06 ± 0.11) %		1623
$K^0_SK^\pm\pi^\mp\pi^+\pi^-$	$(6.6\pm0.7)\times10^{-3}$		1621
$K^+\overline{K}^*(892)^0\pi^-$ + c.c.	$(2.1\pm1.1)\times10^{-3}$		1602
$K^*(892)^0\overline{K}^*(892)^0$	$(2.3\pm0.9)\times10^{-3}$	S=2.1	1538
$3(\pi^+\pi^-)$	(1.51 ± 0.17) %	S=3.3	1707
$\phi\phi$	$(1.22\pm0.07)\times10^{-3}$	S=1.6	1457
$\phi\phi\eta$	$(5.3\pm0.6)\times10^{-4}$		1206
$\omega\omega$	$(8.6\pm0.4)\times10^{-4}$		1597
ωK^+K^-	$(6.6\pm0.8)\times10^{-4}$		1540
$\omega\phi$	$(9.8\pm1.3)\times10^{-6}$		1529
$\pi\pi$	$(2.33\pm0.06)\times10^{-3}$	S=1.2	1773
$\rho^0\pi^+\pi^-$	$(3.9\pm1.6)\times10^{-3}$		1682
$\pi^+\pi^-\pi^0$ (non-resonant)	$(2.0\pm0.4)\times10^{-5}$		1765
$\rho(770)^\pm\pi^\mp$	$(6\pm4)\times10^{-6}$		–
$\pi^+\pi^-\eta$	$(4.7\pm1.3)\times10^{-4}$		1724
$2\pi^+2\pi^-\eta$	$(5.7\pm0.6)\times10^{-3}$		1690
$\pi^+\pi^-\eta'$	$(4.9\pm1.8)\times10^{-4}$		1636
$\eta\eta$	$(5.4\pm0.4)\times10^{-4}$		1692
K^+K^-	$(1.16\pm0.05)\times10^{-3}$	S=1.7	1708
$K^0_SK^0_S$	$(5.2\pm0.4)\times10^{-4}$		1707
$K^*(892)^\pm K^\mp$	$(1.42\pm0.21)\times10^{-4}$		1627
$K^*(892)^0\overline{K}^0$ + c.c.	$(1.23\pm0.27)\times10^{-4}$		1627
$K^*_2(1430)^\pm K^\mp$	$(1.47\pm0.12)\times10^{-3}$		–
$K^*_2(1430)^0\overline{K}^0$ + c.c.	$(1.23\pm0.17)\times10^{-3}$		1443
$K^*_3(1780)^\pm K^\mp$	$(5.1\pm0.8)\times10^{-4}$		–
$K^*_3(1780)^0\overline{K}^0$ + c.c.	$(5.6\pm2.1)\times10^{-4}$		1274
$a_2(1320)^0\pi^0$	$(1.28\pm0.34)\times10^{-3}$		–
$a_2(1320)^\pm\pi^\mp$	$(1.7\pm0.6)\times10^{-3}$		1530
$\overline{K}^0K^+\pi^-$ + c.c.	$(1.27\pm0.18)\times10^{-3}$		1685
$K^+K^-\pi^0$	$(3.0\pm0.8)\times10^{-4}$		1686
$K^+K^-\eta$	$<3.2\times10^{-4}$	CL=90%	1592
$K^+K^-\eta'(958)$	$(1.51\pm0.09)\times10^{-4}$		1488
$\eta\eta'$	$(2.1\pm0.5)\times10^{-5}$		1600
$\eta'\eta'$	$(4.5\pm0.6)\times10^{-5}$		1498
$\eta\eta\eta'$	$(4.1\pm0.9)\times10^{-5}$		1451
$\pi^+\pi^-K^0_SK^0_S$	$(2.2\pm0.5)\times10^{-3}$		1655
$K^+K^-K^0_SK^0_S$	$<4\times10^{-4}$	CL=90%	1418
$K^0_SK^0_SK^0_SK^0_S$	$(1.12\pm0.18)\times10^{-4}$		1415
$K^+K^-K^+K^-$	$(1.64\pm0.22)\times10^{-3}$	S=1.1	1421
$K^+K^-\phi$	$(1.41\pm0.29)\times10^{-3}$		1468
$\overline{K}^0K^+\pi^-\phi$ + c.c.	$(4.8\pm0.7)\times10^{-3}$		1416
$K^+K^-\pi^0\phi$	$(2.7\pm0.5)\times10^{-3}$		1419
$K^0_SK^0_SK^0_SK^\pm\pi^\mp$	$(1.70\pm0.16)\times10^{-4}$		1351
$3(K^+K^-)$	$(7.1\pm1.4)\times10^{-6}$		818
$\phi\pi^+\pi^-\pi^0$	$(8.4\pm1.0)\times10^{-4}$		1603
$p\overline{p}$	$(8.06\pm0.33)\times10^{-5}$	S=1.6	1510
$p\overline{p}\pi^0$	$(4.6\pm0.4)\times10^{-4}$		1465
$p\overline{p}\eta$	$(1.72\pm0.25)\times10^{-4}$		1285
$p\overline{p}\omega$	$(3.6\pm0.4)\times10^{-4}$		1152
$p\overline{p}\pi^+\pi^-$	$(1.32\pm0.34)\times10^{-3}$		1410
$p\overline{p}\pi^0\pi^0$	$(7.8\pm2.3)\times10^{-4}$		1414
$p\overline{p}\eta\pi^0$	$(1.29\pm0.09)\times10^{-4}$		1212
$p\overline{p}\eta\eta$	$(2.6\pm0.5)\times10^{-5}$		929
$p\overline{p}K^+K^-$	$(2.52\pm0.17)\times10^{-4}$		1013
$p\overline{p}K^+K^-$ (non-resonant)	$(1.89\pm0.32)\times10^{-4}$		1013
$K^+\overline{p}\Lambda(1520)$ + c.c.	$(2.8\pm0.7)\times10^{-4}$		992
$\Lambda(1520)\overline{\Lambda}(1520)$	$(4.6\pm1.4)\times10^{-4}$		924
$p\overline{p}\phi$	$(2.8\pm0.9)\times10^{-5}$		1002
$p\overline{p}K^0_SK^0_S$	$<8\times10^{-4}$	CL=90%	1007
$p\overline{p}K^0_SK^-\pi^+$ + c.c.	$(5.6\pm0.5)\times10^{-5}$		900
$p\overline{n}\pi^-$	$(8.4\pm0.9)\times10^{-4}$		1463
$\overline{p}n\pi^+$	$(8.8\pm0.8)\times10^{-4}$		1463
$p\overline{n}\pi^-\pi^0$	$(2.15\pm0.18)\times10^{-3}$		1411
$\overline{p}n\pi^+\pi^0$	$(2.09\pm0.18)\times10^{-3}$		1411
$\Lambda\overline{\Lambda}$	$(1.81\pm0.16)\times10^{-4}$		1384
$\Lambda\overline{\Lambda}\pi^+\pi^-$	$(1.24\pm0.15)\times10^{-3}$		1255
$\Lambda\overline{\Lambda}\pi^+\pi^-$ (non-resonant)	$(6.5\pm1.5)\times10^{-4}$		1255
$\Sigma(1385)^+\overline{\Lambda}\pi^-$ + c.c.	$<4\times10^{-4}$	CL=90%	1192
$\Sigma(1385)^-\overline{\Lambda}\pi^+$ + c.c.	$<6\times10^{-4}$	CL=90%	1192
$\Lambda\overline{\Lambda}\eta$	$(1.04\pm0.25)\times10^{-4}$		1096
$\Lambda\overline{\Lambda}\eta'$	$(3.0\pm0.7)\times10^{-5}$		758
$\Lambda\overline{\Lambda}\omega$	$(1.38\pm0.21)\times10^{-4}$		921
$\Lambda\overline{\Lambda}\phi$	$(7.1\pm0.9)\times10^{-5}$		691
$K^+\overline{p}\Lambda$ + c.c.	$(7.7\pm0.5)\times10^{-4}$		1236
$nK^0_S\overline{\Lambda}$ + c.c.	$(3.54\pm0.28)\times10^{-4}$		1233
$K^*(892)^+\overline{p}\Lambda$ + c.c.	$(8.1\pm1.1)\times10^{-4}$		976
$\overline{p}\Lambda(1520)K^0_S\pi^+$ + c.c.	$(4.0\pm0.9)\times10^{-5}$		876
$\Sigma^0\overline{\Sigma}^0$	$(3.6\pm0.6)\times10^{-5}$		1319
$\Sigma^+\overline{p}K^0_S$ + c.c.	$(8.2\pm0.9)\times10^{-5}$		1197
$\Sigma^0\overline{p}K^+$ + c.c.	$(9.0\pm0.8)\times10^{-5}$		1197
$\Sigma^+\overline{\Sigma}^-$	$(3.3\pm0.7)\times10^{-5}$		1322
$\Sigma^+\overline{\Sigma}^-\eta$	$(5.4\pm1.3)\times10^{-5}$		998
$\Sigma^-\overline{\Sigma}^+$	$(4.4\pm1.8)\times10^{-5}$		1314
$\Sigma(1385)^+\overline{\Sigma}(1385)^-$	$<1.5\times10^{-4}$	CL=90%	1118
$\Sigma(1385)^-\overline{\Sigma}(1385)^+$	$<8\times10^{-5}$	CL=90%	1118
$K^-\Lambda\overline{\Xi}^+$ + c.c.	$(1.75\pm0.31)\times10^{-4}$		1004
$\Xi^0\overline{\Xi}^0$	$(1.81\pm0.22)\times10^{-4}$		1197
$\Xi^-\overline{\Xi}^+$	$(1.42\pm0.12)\times10^{-4}$		1189
$\Omega^-\overline{\Omega}^+$	$(4.47\pm0.30)\times10^{-5}$		604
$J/\psi(1S)\pi^+\pi^-\pi^0$	<1.5 %	CL=90%	185
$\pi^0\eta_c$	$<3.2\times10^{-3}$	CL=90%	511
$\eta_c(1S)\pi^+\pi^-$	$<5\times10^{-3}$	CL=90%	459
Radiative decays			
$\gamma J/\psi(1S)$	(19.0 ± 0.8) %	S=1.5	430
$\gamma\rho^0$	$<1.9\times10^{-5}$	CL=90%	1694
$\gamma\omega$	$<6\times10^{-6}$	CL=90%	1692
$\gamma\phi$	$<7\times10^{-6}$	CL=90%	1632
$\gamma\gamma$	$(2.88\pm0.10)\times10^{-4}$	S=1.1	1778
$e^+e^-J/\psi(1S)$	$(2.14\pm0.15)\times10^{-3}$		430
$\mu^+\mu^-J/\psi(1S)$	$(2.01\pm0.33)\times10^{-4}$		381

$\eta_c(2S)$

$I^G(J^{PC}) = 0^+(0^{-+})$

Quantum numbers are quark model predictions.

Mass $m = 3637.8 \pm 0.6$ MeV (S = 1.1)
Full width $\Gamma = 11.6 \pm 1.4$ MeV

$\eta_c(2S)$ DECAY MODES	Fraction (Γ_i/Γ)	Confidence level	p (MeV/c)
hadrons	seen		–
$K\overline{K}\pi$	$(1.9^{+1.2}_{-1.0})$ %		1729
$K\overline{K}\eta$	$(7^{+5}_{-4})\times10^{-3}$		1637
$K\overline{K}\eta'$	$(2.1\pm1.6)\times10^{-3}$		1537
$2\pi^+2\pi^-$	$<2.6\times10^{-3}$	90%	1792
$a_0(1450)\pi$	seen		1531
$a_2(1700)\pi$	seen		1415
$a_0(1710)\pi$	seen		1412
$\rho^0\rho^0$	$<2.3\times10^{-3}$	90%	1645
$3\pi^+3\pi^-$	$(1.7^{+0.9}_{-1.1})$ %		1749
$K^+K^-\pi^+\pi^-$	$<2.5\times10^{-3}$	90%	1700
$K^{*0}\overline{K}^{*0}$	$<4\times10^{-3}$	90%	1585
$K^+K^-\pi^+\pi^-\pi^0$	$(1.5^{+1.0}_{-0.9})$ %		1668
$K^+K^-2\pi^+2\pi^-$	<1.8 %	90%	1627
$K^0_SK^-2\pi^+\pi^-$ + c.c.	$(1.4^{+0.8}_{-1.0})$ %		1666
$2K^+2K^-$	$<1.4\times10^{-3}$	90%	1470
$K^*_2(1430)\overline{K}$ + c.c.	seen		1493
$K^*_0(1950)\overline{K}$ + c.c.	seen		1231
$K^*_0(2600)\overline{K}$ + c.c.	seen		–
$\phi\phi$	$<1.4\times10^{-3}$	90%	1506
$\omega\omega$	$<1.9\times10^{-3}$	90%	1642
$\omega\phi$	$<3.4\times10^{-4}$	90%	1577
$p\overline{p}$	$<3.2\times10^{-4}$	90%	1558
$p\overline{p}\pi^+\pi^-$	seen		1461
$p\overline{p}K^+K^-$	$(3.6\pm2.9)\times10^{-4}$		1079

Int. J. Mod. Phys. A 2026.41. Downloaded from www.worldscientific.com
by UNIVERSITY OF CALIFORNIA @ BERKELEY on 09/16/26. Re-use and distribution is strictly not permitted, except for Open Acce

$\gamma\gamma$	$(1.8^{+1.0}_{-1.1}) \times 10^{-4}$		1819
$\gamma J/\psi(1S)$	< 1.8 %	90%	501
$\pi^+\pi^-\eta$	$(5.5^{+3.3}_{-4.0}) \times 10^{-3}$		1766
$2\pi^+2\pi^-\eta$	$(1.6^{+0.9}_{-1.0})$ %		1733
$\pi^+\pi^-\eta'$	$(2.7^{+2.0}_{-1.8}) \times 10^{-3}$		1680
$\pi^+\pi^-\eta_c(1S)$	< 4 %	90%	537

$\psi(2S)$

$I^G(J^{PC}) = 0^-(1^{--})$

Mass $m = 3686.097 \pm 0.011$ MeV (S = 1.1)
Full width $\Gamma = 293 \pm 9$ keV (S = 1.2)

$\psi(2S)$ DECAY MODES	Fraction (Γ_i/Γ)	Scale factor/ Confidence level	p (MeV/c)
hadrons	(97.85 ± 0.13) %		–
virtual $\gamma \to$ hadrons	(1.79 ± 0.04) %		–
ggg	(10.6 ± 1.6) %		–
γgg	(1.03 ± 0.29) %		–
light hadrons	(15.4 ± 1.5) %		–
K^0_S anything	(16.1 ± 1.1) %		–
e^+e^-	$(7.95 \pm 0.22) \times 10^{-3}$	S=1.3	1843
$\mu^+\mu^-$	$(8.0 \pm 0.6) \times 10^{-3}$		1840
$\tau^+\tau^-$	$(3.1 \pm 0.4) \times 10^{-3}$		489
Decays into $J/\psi(1S)$ and anything			
$J/\psi(1S)$ anything	(61.6 ± 0.7) %	S=1.3	–
$J/\psi(1S)$ neutrals	(25.4 ± 0.5) %	S=1.6	–
$J/\psi(1S)\pi^+\pi^-$	(34.78 ± 0.33) %	S=1.1	477
$J/\psi(1S)\pi^0\pi^0$	(18.3 ± 0.5) %	S=1.6	481
$J/\psi(1S)\eta$	(3.38 ± 0.06) %	S=1.2	199
$J/\psi(1S)\pi^0$	$(1.268 \pm 0.032) \times 10^{-3}$		528
Hadronic decays			
$\pi^+\pi^-$	$(7.8 \pm 2.6) \times 10^{-6}$		1838
$\pi^+\pi^-\pi^0$	$(2.01 \pm 0.17) \times 10^{-4}$	S=1.7	1830
$\rho(770)\pi \to \pi^+\pi^-\pi^0$	$(3.2 \pm 1.2) \times 10^{-5}$	S=1.8	–
$\rho(2150)\pi \to \pi^+\pi^-\pi^0$	$(1.9 {}^{+1.2}_{-0.4}) \times 10^{-4}$		–
$2(\pi^+\pi^-)$	$(2.4 \pm 0.6) \times 10^{-4}$	S=2.2	1817
$\rho^0\pi^+\pi^-$	$(2.2 \pm 0.6) \times 10^{-4}$	S=1.4	1750
$2(\pi^+\pi^-)\pi^0$	$(2.9 \pm 1.0) \times 10^{-3}$	S=4.7	1799
$\rho a_2(1320)$	$(2.6 \pm 0.9) \times 10^{-4}$		1500
$\pi^+\pi^-\pi^0\pi^0\pi^0$	$(5.3 \pm 1.0) \times 10^{-3}$		1800
$\rho^\pm\pi^\mp\pi^0\pi^0$	$< 2.7 \times 10^{-3}$	CL=90%	1737
$\pi^+\pi^-4\pi^0$	$(1.4 \pm 1.0) \times 10^{-3}$		1778
$3(\pi^+\pi^-)$	$(3.5 \pm 2.0) \times 10^{-4}$	S=2.8	1774
$2(\pi^+\pi^-\pi^0)$	$(4.8 \pm 1.5) \times 10^{-3}$		1776
$3(\pi^+\pi^-)\pi^0$	$(3.5 \pm 1.6) \times 10^{-3}$		1746
$2(\pi^+\pi^-)3\pi^0$	(1.42 ± 0.31) %		1748
$\eta\pi^+\pi^-$	$< 1.6 \times 10^{-4}$	CL=90%	1791
$\eta\pi^+\pi^-\pi^0$	$(9.5 \pm 1.7) \times 10^{-4}$		1778
$\eta 2(\pi^+\pi^-)$	$(1.2 \pm 0.6) \times 10^{-3}$		1758
$\eta\pi^+\pi^-\pi^0\pi^0$	$< 4 \times 10^{-4}$	CL=90%	1760
$\eta\pi^+\pi^-3\pi^0$	$< 2.1 \times 10^{-3}$	CL=90%	1736
$\eta 2(\pi^+\pi^-\pi^0)$	$< 2.1 \times 10^{-3}$	CL=90%	1705
$\rho\eta$	$(2.2 \pm 0.6) \times 10^{-5}$	S=1.1	1717
$\eta'\pi^+\pi^-\pi^0$	$(4.5 \pm 2.1) \times 10^{-4}$		1692
$\eta'\rho$	$(1.9 {}^{+1.7}_{-1.2}) \times 10^{-5}$		1625
$\omega\pi^0$	$(2.1 \pm 0.6) \times 10^{-5}$		1757
$\omega\pi^+\pi^-$	$(7.3 \pm 1.2) \times 10^{-4}$	S=2.1	1748
$\omega\pi^+\pi^-2\pi^0$	$(8.7 \pm 2.4) \times 10^{-3}$		1715
$b_1^\pm\pi^\mp$	$(4.0 \pm 0.6) \times 10^{-4}$	S=1.1	1635
$\omega f_2(1270)$	$(2.2 \pm 0.4) \times 10^{-4}$		1515
$\omega\pi^0\pi^0$	$(1.11 \pm 0.35) \times 10^{-3}$		1749
$\omega 3\pi^0$	$< 8 \times 10^{-4}$	CL=90%	1736
$b_1^0\pi^0$	$(2.4 \pm 0.6) \times 10^{-4}$		–
$\omega\eta$	$< 1.1 \times 10^{-5}$	CL=90%	1715
$\omega\eta'$	$(3.2 {}^{+2.5}_{-2.1}) \times 10^{-5}$		1623
$\omega(782)\eta\eta$	$(1.65 \pm 0.21) \times 10^{-5}$		1580
$\phi\pi^0$	$< 4 \times 10^{-7}$	CL=90%	1699
$\phi\pi^+\pi^-$	$(1.18 \pm 0.26) \times 10^{-4}$	S=1.5	1690
$\phi f_0(980) \to \pi^+\pi^-$	$(7.5 \pm 3.3) \times 10^{-5}$	S=1.6	–
$\phi\eta$	$(3.10 \pm 0.31) \times 10^{-5}$		1654
$\eta\phi(2170)$, $\phi(2170) \to \phi f_0(980)$, $f_0 \to \pi^+\pi^-$	$< 2.2 \times 10^{-6}$	CL=90%	–
$\phi\eta'$	$(1.54 \pm 0.20) \times 10^{-5}$		1555
$\phi\eta\eta'$	$(3.14 \pm 0.29) \times 10^{-5}$		1331
$h_1(1900)\eta \to \phi\eta\eta'$	$(3.8 \pm 2.1) \times 10^{-6}$		–
$\phi(2170)\eta \to \phi\eta\eta'$	$(3.3 \pm 1.8) \times 10^{-6}$		–
$\phi(2170)\eta' \to \phi\eta\eta'$	$(3.8 \pm 1.0) \times 10^{-6}$		–
$h_1(2300)\eta \to \phi\eta\eta'$	$(2.2 \pm 1.0) \times 10^{-6}$		–
$h_1(2300)\eta' \to \phi\eta\eta'$	$(4.8 \pm 1.5) \times 10^{-6}$		–
$\phi\phi\phi$	$(1.46 \pm 0.18) \times 10^{-5}$		989
$\phi f_1(1285)$	$(3.0 \pm 1.3) \times 10^{-5}$		1436
$\phi\eta(1405) \to \phi\pi^+\pi^-\eta$	$(8.5 \pm 1.7) \times 10^{-6}$		–
$\phi f_2'(1525)$	$(4.4 \pm 1.6) \times 10^{-5}$		1325
K^+K^-	$(7.5 \pm 0.5) \times 10^{-5}$		1776
$K^+K^-\pi^+\pi^-$	$(7.3 \pm 0.5) \times 10^{-4}$		1726
$K^+K^-\pi^0$	$(4.07 \pm 0.31) \times 10^{-5}$		1754
$K^0_S K^0_S$	$< 1.1 \times 10^{-8}$	CL=90%	1775
$K^0_S K^0_L$	$(5.34 \pm 0.33) \times 10^{-5}$		1775
$K^0_S K^0_L \pi^0$	$< 3.0 \times 10^{-4}$	CL=90%	1753
$K^+K^-\pi^0\pi^0$	$(2.6 \pm 1.3) \times 10^{-4}$		1728
$K^+K^-\pi^0\pi^0\pi^0$	$(6.6 \pm 2.8) \times 10^{-4}$		1696
$K^0_S K^\pm\pi^\mp\pi^0\pi^0$	$(1.7 \pm 0.6) \times 10^{-3}$		1694
$K^0_S K^\pm\pi^\mp\pi^+\pi^-$	$(2.2 \pm 0.4) \times 10^{-3}$		1692
$K^+K^-\pi^+\pi^-\pi^0$	$(1.26 \pm 0.09) \times 10^{-3}$		1694
$\omega f_0(1710) \to \omega K^+K^-$	$(5.9 \pm 2.2) \times 10^{-5}$		–
$K^*(892)^0K^-\pi^+\pi^0$ + c.c.	$(8.6 \pm 2.2) \times 10^{-4}$		–
$K^*(892)^+K^-\pi^+\pi^-$ + c.c.	$(9.6 \pm 2.8) \times 10^{-4}$		–
$K^*(892)^+K^-\rho^0$ + c.c.	$(7.3 \pm 2.6) \times 10^{-4}$		–
$K^*(892)^0K^-\rho^+$ + c.c.	$(6.1 \pm 1.8) \times 10^{-4}$		–
$K^0_S K^0_S \pi^+\pi^-$	$(2.2 \pm 0.4) \times 10^{-4}$		1724
$K^0_S K^0_L \pi^0\pi^0$	$(1.3 \pm 0.6) \times 10^{-3}$		1726
$K^0_S K^*(892)^0\pi^0\pi^0$	$(3.1 \pm 1.3) \times 10^{-4}$		1645
$K^0_S K^\pm\rho(770)^\mp\pi^0$	$< 7 \times 10^{-4}$	CL=90%	–
$K^0_S K^\pm\pi^\mp\rho(770)^0$	$< 7 \times 10^{-4}$	CL=90%	–
$K^\mp K^*(892)^\pm\pi^0\pi^0$	$(7.0 \pm 2.9) \times 10^{-4}$		1646
$K^*(892)^+K^*(892)^-\pi^0$	$(3.6 \pm 1.8) \times 10^{-3}$		1573
$K^0_S K^0_L \eta$	$(1.3 \pm 0.5) \times 10^{-3}$		1661
$K^+K^-\rho^0$	$(2.2 \pm 0.4) \times 10^{-4}$		1616
$K^*(892)^0\overline{K}^*_2(1430)^0$	$(1.9 \pm 0.5) \times 10^{-4}$		1417
$K^+K^-\pi^+\pi^-\eta$	$(1.3 \pm 0.7) \times 10^{-3}$		1574
$K^+K^-2(\pi^+\pi^-)$	$(1.9 \pm 0.9) \times 10^{-3}$		1654
$K^+K^-2(\pi^+\pi^-)\pi^0$	$(1.00 \pm 0.31) \times 10^{-3}$		1611
$K^+K^*(892)^-$ + c.c.	$(2.9 \pm 0.4) \times 10^{-5}$	S=1.2	1698
$2(K^+K^-)$	$(6.3 \pm 1.3) \times 10^{-5}$		1499
$2(K^+K^-)\pi^0$	$(1.10 \pm 0.28) \times 10^{-4}$		1440
$K^+K^-\phi$	$(7.0 \pm 1.6) \times 10^{-5}$		1546
$K^0_S K^0_S \phi$	$(3.53 \pm 0.29) \times 10^{-5}$		1543
$K_1(1270)^\pm K^\mp$	$(1.00 \pm 0.28) \times 10^{-3}$		1587
$K^+\overline{K}^*(892)^0\pi^-$ + c.c.	$(6.7 \pm 2.5) \times 10^{-4}$		1674
ηK^+K^-, no $\eta\phi$	$(3.49 \pm 0.17) \times 10^{-5}$		1664
ηK^+K^-	$< 2.6 \times 10^{-4}$	CL=90%	1664
$X(1750)\eta \to K^+K^-\eta$	$(4.8 \pm 2.8) \times 10^{-6}$		–
$K_1(1400)^\pm K^\mp$	$< 3.1 \times 10^{-4}$	CL=90%	1532
$K^*_2(1430)^\pm K^\mp$	$(7.1 {}^{+1.3}_{-0.9}) \times 10^{-5}$		–
$K^*(892)^0\overline{K}^0$ + c.c.	$(1.09 \pm 0.20) \times 10^{-4}$		1697
ωK^+K^-	$(1.62 \pm 0.11) \times 10^{-4}$	S=1.1	1614
$\omega K^0_S K^0_S$	$(7.0 \pm 0.5) \times 10^{-5}$		1612
$\omega K^*(892)^+K^-$ + c.c.	$(2.07 \pm 0.26) \times 10^{-4}$		1482
$\omega K^*_2(1430)^+K^-$ + c.c.	$(6.1 \pm 1.2) \times 10^{-5}$		1252
$\omega\overline{K}^*(892)^0K^0$	$(1.68 \pm 0.30) \times 10^{-4}$		1481
$\omega\overline{K}^*_2(1430)^0K^0$	$(5.8 \pm 2.2) \times 10^{-5}$		1250
$\omega X(1440) \to \omega K^0_S K^-\pi^+$ + c.c.	$(1.6 \pm 0.4) \times 10^{-5}$		–
$\omega X(1440) \to \omega K^+K^-\pi^0$	$(1.09 \pm 0.26) \times 10^{-5}$		–
$\omega f_1(1285) \to \omega K^0_S K^-\pi^+$ + c.c.	$(3.0 \pm 1.0) \times 10^{-6}$		–
$\omega f_1(1285) \to \omega K^+K^-\pi^0$	$(1.2 \pm 0.7) \times 10^{-6}$		–
$p\overline{p}$	$(2.95 \pm 0.09) \times 10^{-4}$	S=1.3	1586
$n\overline{n}$	$(3.06 \pm 0.15) \times 10^{-4}$		1586
$p\overline{p}\pi^0$	1.2×10^{-4} to 2.4×10^{-4}		1543
$N(940)\overline{p}$ + c.c. $\to p\overline{p}\pi^0$	$(1.14 \pm 0.12) \times 10^{-4}$		–
$N(1440)\overline{p}$ + c.c. $\to p\overline{p}\pi^0$	$(7.5 \pm 1.1) \times 10^{-5}$	S=1.7	–
$N(1520)\overline{p}$ + c.c. $\to p\overline{p}\pi^0$	$(6.6 \pm 2.0) \times 10^{-6}$		–
$N(1535)\overline{p}$ + c.c. $\to p\overline{p}\pi^0$	$(1.7 \pm 0.4) \times 10^{-5}$		–
$N(1650)\overline{p}$ + c.c. $\to p\overline{p}\pi^0$	$(9.1 \pm 3.3) \times 10^{-6}$		–
$N(1710)\overline{p}$ + c.c. $\to p\overline{p}\pi^0$	$(4 \pm 4) \times 10^{-6}$		–
$N(1720)\overline{p}$ + c.c. $\to p\overline{p}\pi^0$	$(6.2 \pm 2.5) \times 10^{-6}$		–
$N(2100)\overline{p}$ + c.c. $\to p\overline{p}\pi^0$	$(8 \pm 4) \times 10^{-6}$		–

Int. J. Mod. Phys. A 2026.41. Downloaded from www.worldscientific.com
by UNIVERSITY OF CALIFORNIA @ BERKELEY on 09/16/26. Re-use and distribution is strictly not permitted, except for Open Access articles.

$N(2300)\overline{p}+$ c.c. $\to$ $p\overline{p}\pi^0$		$(3.6 \pm 3.1) \times 10^{-6}$		–
$N(2570)\overline{p}+$ c.c. $\to$ $p\overline{p}\pi^0$		$(1.9 \pm 1.5) \times 10^{-5}$		–
$p\overline{p}\pi^+\pi^-$		$(6.0 \pm 0.4) \times 10^{-4}$		1491
$p\overline{p}K^+K^-$		$(2.7 \pm 0.7) \times 10^{-5}$		1118
$p\overline{p}\eta$		5.5×10^{-5} to 9.1×10^{-5}		1373
$N(1535)\overline{p}+$ c.c. $\to$ $p\overline{p}\eta$		$(4.7 \pm 0.5) \times 10^{-5}$		–
$N(1710)\overline{p}+$ c.c. $\to$ $p\overline{p}\eta$		$(7.8 \pm 3.2) \times 10^{-6}$		–
$p\overline{p}\pi^+\pi^-\pi^0$		$(7.3 \pm 0.7) \times 10^{-4}$		1435
$p\overline{p}\rho^0$		$(5.0 \pm 2.2) \times 10^{-5}$		1252
$p\overline{p}\omega$		$(6.9 \pm 2.1) \times 10^{-5}$		1247
$p\overline{p}\eta'$		$(1.10 \pm 0.13) \times 10^{-5}$		1141
$p\overline{p}\phi$		$(6.1 \pm 0.6) \times 10^{-6}$		1109
$\phi X(1835) \to p\overline{p}\phi$		$< 1.82 \times 10^{-7}$	CL=90%	–
$p\overline{n}\pi^-$ or c.c.		$(2.48 \pm 0.17) \times 10^{-4}$		–
$p\overline{n}\pi^-\pi^0$		$(3.2 \pm 0.7) \times 10^{-4}$		1492
$\Lambda\overline{\Lambda}$		$(3.81 \pm 0.13) \times 10^{-4}$	S=1.4	1467
$\Lambda\overline{\Lambda}\pi^0$		$(1.4 \pm 0.7) \times 10^{-6}$		1412
$\Lambda\overline{\Lambda}\eta$		$(2.43 \pm 0.32) \times 10^{-5}$		1197
$\Lambda(1670)\overline{\Lambda} \to \Lambda\overline{\Lambda}\eta$		$(1.3 \pm 0.7) \times 10^{-5}$		–
$\Lambda\overline{\Lambda}\eta'$		$(7.3 \pm 1.0) \times 10^{-6}$		892
$\Lambda\overline{\Lambda}\omega(782)$		$(3.3 \pm 0.4) \times 10^{-5}$		1037
$\Lambda\overline{\Lambda}\pi^+\pi^-$		$(2.8 \pm 0.6) \times 10^{-4}$		1346
$\Lambda\overline{p}K^+$		$(1.00 \pm 0.14) \times 10^{-4}$		1327
$\Lambda\overline{p}K^*(892)^+$ + c.c.		$(6.3 \pm 0.7) \times 10^{-5}$		1087
$\Lambda\overline{p}K^+\pi^+\pi^-$		$(1.8 \pm 0.4) \times 10^{-4}$		1167
$\overline{\Lambda}nK^0_S$ + c.c.		$(8.1 \pm 1.8) \times 10^{-5}$		1324
$\Delta^{++}\overline{\Delta}^{--}$		$(1.28 \pm 0.35) \times 10^{-4}$		1371
$\Lambda\overline{\Sigma}^+\pi^-$ + c.c.		$(1.40 \pm 0.13) \times 10^{-4}$		1376
$\Lambda\overline{\Sigma}^-\pi^+$ + c.c.		$(1.54 \pm 0.14) \times 10^{-4}$		1379
$\Lambda\overline{\Sigma}^0$ + c.c.		$(1.6 \pm 0.7) \times 10^{-6}$		1437
$\Lambda\overline{\Sigma}^0\pi^0$ + c.c.		$(1.54 \pm 0.07) \times 10^{-4}$		1380
$\Lambda(1520)\overline{\Xi}^+K^-$ + c.c., $\Lambda(1520) \to pK^-$		$(9.5 \pm 1.2) \times 10^{-7}$		–
$\Sigma^0\overline{p}K^+$ + c.c.		$(1.67 \pm 0.18) \times 10^{-5}$		1291
$\Sigma^+\overline{\Sigma}^-$		$(2.43 \pm 0.10) \times 10^{-4}$	S=1.4	1408
$\Sigma^0\overline{\Sigma}^0$		$(2.35 \pm 0.09) \times 10^{-4}$	S=1.1	1405
$\Sigma^-\overline{\Sigma}^+$		$(2.82 \pm 0.09) \times 10^{-4}$		1401
$\Sigma^+\overline{\Sigma}^-\eta$		$(9.6 \pm 2.4) \times 10^{-6}$		1108
$\Sigma^+\overline{\Sigma}^-\omega$		$(1.89 \pm 0.28) \times 10^{-5}$		926
$\Sigma^0\overline{\Sigma}^0\omega(782)$		$(1.24 \pm 0.19) \times 10^{-5}$		921
$\Sigma^+\overline{\Sigma}^-\phi$		$(3.0 \pm 0.7) \times 10^{-6}$		686
$\Sigma^0\overline{\Sigma}^0\phi$		$(2.64 \pm 0.34) \times 10^{-6}$		679
$\Sigma(1385)^+\overline{\Sigma}(1385)^-$		$(8.5 \pm 0.7) \times 10^{-5}$		1218
$\Sigma(1385)^-\overline{\Sigma}(1385)^+$		$(8.5 \pm 0.8) \times 10^{-5}$		1218
$\Sigma(1385)^0\overline{\Sigma}(1385)^0$		$(6.9 \pm 0.7) \times 10^{-5}$		1218
$\Xi^-\overline{\Xi}^+$		$(2.87 \pm 0.11) \times 10^{-4}$	S=1.1	1284
$\Xi^0\overline{\Xi}^0$		$(2.3 \pm 0.4) \times 10^{-4}$	S=4.2	1291
$\Xi(1530)^0\overline{\Xi}(1530)^0$		$(6.8 \pm 0.4) \times 10^{-5}$		1025
$\Lambda\overline{\Xi}^+K^-$ + c.c.		$(3.67 \pm 0.22) \times 10^{-5}$		1114
$\Xi(1690)^-\overline{\Xi}^+ \to K^-\Lambda\overline{\Xi}^+$ + c.c.		$(6.2 \pm 2.1) \times 10^{-6}$	S=1.5	–
$\Xi(1820)^-\overline{\Xi}^+ \to K^-\Lambda\overline{\Xi}^+$ + c.c.		$(1.48 \pm 0.29) \times 10^{-5}$	S=1.2	–
$\Xi(1530)^-\overline{\Xi}(1530)^+$		$(1.15 \pm 0.07) \times 10^{-4}$		1025
$\Xi(1530)^-\overline{\Xi}^+$		$(7.0 \pm 1.2) \times 10^{-6}$		1165
$\Xi(1530)^0\overline{\Xi}^0$		$(5.3 \pm 0.5) \times 10^{-6}$		1169
$\Sigma^0\overline{\Xi}^+K^-$ + c.c.		$(3.7 \pm 0.4) \times 10^{-5}$		1060
$\Omega^-K^+\overline{\Xi}^0$ + c.c.		$(2.8 \pm 0.4) \times 10^{-6}$		606
$\overline{\Omega}^+K^0_S\Xi^-$ + c.c.		$(2.9 \pm 0.6) \times 10^{-6}$		590
$\Omega^-\overline{\Omega}^+$		$(5.66 \pm 0.30) \times 10^{-5}$	S=1.3	774
$\eta_c\pi^+\pi^-\pi^0$		$< 1.0 \times 10^{-3}$	CL=90%	512
$h_c(1P)\pi^0$		$(7.4 \pm 0.5) \times 10^{-4}$		85
$\Lambda_c^+\overline{p}e^+e^-$ + c.c.		$< 1.7 \times 10^{-6}$	CL=90%	830
$\Theta(1540)\overline{\Theta}(1540) \to K^0_S pK^-\overline{n}$ + c.c.	[kkaa]	$< 8.8 \times 10^{-6}$	CL=90%	–
$\Theta(1540)K^-\overline{n} \to K^0_S pK^-\overline{n}$	[kkaa]	$< 1.0 \times 10^{-5}$	CL=90%	–
$\Theta(1540)K^0_S\overline{p} \to K^0_S\overline{p}K^+n$	[kkaa]	$< 7.0 \times 10^{-6}$	CL=90%	–
$\overline{\Theta}(1540)K^+n \to K^0_S\overline{p}K^+n$	[kkaa]	$< 2.6 \times 10^{-5}$	CL=90%	–
$\overline{\Theta}(1540)K^0_S p \to K^0_S pK^-\overline{n}$	[kkaa]	$< 6.0 \times 10^{-6}$	CL=90%	–
Radiative decays				
$\gamma\chi_{c0}(1P)$		(10.06 ± 0.27) %	S=1.4	261
$\gamma\chi_{c1}(1P)$		(9.85 ± 0.26) %	S=1.2	171
$\gamma\chi_{c2}(1P)$		(9.63 ± 0.23) %	S=1.2	128
$\gamma\eta_c(1S)$		$(3.6 \pm 0.5) \times 10^{-3}$	S=1.3	635
$\gamma\eta_c(2S)$		$(5.4 {}^{+3.4}_{-2.9}) \times 10^{-4}$		48
$\gamma 2(\pi^+\pi^-)$		$(4.0 \pm 0.6) \times 10^{-4}$		1817
$\gamma 3(\pi^+\pi^-)$		$< 1.7 \times 10^{-4}$	CL=90%	1774
$\gamma\eta'(958)$		$(1.24 \pm 0.04) \times 10^{-4}$		1719
$\gamma f_2(1270)$		$(2.73 {}^{+0.29}_{-0.25}) \times 10^{-4}$	S=1.8	1622
$\gamma f_2(1270) \to \gamma K^0_S K^0_S$		$(2.1 \pm 0.9) \times 10^{-6}$		–
$\gamma f_0(1370) \to \gamma K\overline{K}$		$(3.1 \pm 1.7) \times 10^{-5}$		1588
$\gamma f_0(1370) \to \gamma K^0_S K^0_S$		$(1.2 {}^{+3.2}_{-1.7}) \times 10^{-6}$		–
$\gamma f_0(1500)$		$(9.3 \pm 1.9) \times 10^{-5}$		1529
$\gamma f_0(1500) \to \gamma K^0_S K^0_S$		$(1.7 {}^{+1.7}_{-1.2}) \times 10^{-6}$		–
$\gamma f'_2(1525)$		$(3.3 \pm 0.8) \times 10^{-5}$		1531
$\gamma f'_2(1525) \to \gamma K^0_S K^0_S$		$(1.4 \pm 0.6) \times 10^{-6}$		–
$\gamma f_0(1710)$		seen		1440
$\gamma f_0(1710) \to \gamma\pi\pi$		$(3.5 \pm 0.6) \times 10^{-5}$		–
$\gamma f_0(1710) \to \gamma K\overline{K}$		$(6.6 \pm 0.7) \times 10^{-5}$		–
$\gamma f_0(1710) \to \gamma K^0_S K^0_S$		$(1.83 {}^{+0.32}_{-0.27}) \times 10^{-5}$		–
$\gamma f_2(1950) \to \gamma K^0_S K^0_S$		$(1.2 {}^{+1.0}_{-0.8}) \times 10^{-6}$		–
$\gamma f_0(2020) \to \gamma K^0_S K^0_S$		$(4.6 \pm 1.5) \times 10^{-6}$		–
$\gamma f_0(2100) \to \gamma\pi\pi$		$(4.8 \pm 1.0) \times 10^{-6}$		1244
$\gamma f_0(2200) \to \gamma K\overline{K}$		$(3.2 \pm 1.0) \times 10^{-6}$		1193
$\gamma f_J(2220) \to \gamma\pi\pi$		$< 5.8 \times 10^{-6}$	CL=90%	1168
$\gamma f_J(2220) \to \gamma K\overline{K}$		$< 9.5 \times 10^{-6}$	CL=90%	1168
$\gamma\eta$		$(9.2 \pm 1.8) \times 10^{-7}$		1802
$\gamma\eta\pi^+\pi^-$		$(8.7 \pm 2.1) \times 10^{-4}$		1791
$\gamma\eta(1405)$		seen		1574
$\gamma\eta(1405) \to \gamma K\overline{K}\pi$		$< 9 \times 10^{-5}$	CL=90%	1569
$\gamma\eta(1405) \to \gamma\eta\pi^+\pi^-$		$(3.6 \pm 2.5) \times 10^{-5}$		–
$\gamma\eta(1405) \to \gamma f_0(980)\pi^0 \to \gamma\pi^+\pi^-\pi^0$		$< 5.0 \times 10^{-7}$	CL=90%	–
$\gamma\eta(1475)$		seen		1548
$\gamma\eta(1475) \to \gamma K\overline{K}\pi$		$< 1.4 \times 10^{-4}$	CL=90%	–
$\gamma\eta(1475) \to \gamma\eta\pi^+\pi^-$		$< 8.8 \times 10^{-5}$	CL=90%	–
$\gamma K^{*0}K^+\pi^-$ + c.c.		$(3.7 \pm 0.9) \times 10^{-4}$		1674
$\gamma K^{*0}\overline{K}^{*0}$		$(2.4 \pm 0.7) \times 10^{-4}$		1613
$\gamma K^0_S K^+\pi^-$ + c.c.		$(2.6 \pm 0.5) \times 10^{-4}$		1753
$\gamma K^+K^-\pi^+\pi^-$		$(1.9 \pm 0.5) \times 10^{-4}$		1726
$\gamma K^+K^-2(\pi^+\pi^-)$		$< 2.2 \times 10^{-4}$	CL=90%	1654
$\gamma 2(K^+K^-)$		$< 4 \times 10^{-5}$	CL=90%	1499
$\gamma p\overline{p}$		$(3.9 \pm 0.5) \times 10^{-5}$	S=2.0	1586
$\gamma f_2(1950) \to \gamma p\overline{p}$		$(1.20 \pm 0.22) \times 10^{-5}$		–
$\gamma f_2(2150) \to \gamma p\overline{p}$		$(7.2 \pm 1.8) \times 10^{-6}$		–
$\gamma X(1835) \to \gamma p\overline{p}$		$(4.6 {}^{+1.8}_{-4.0}) \times 10^{-6}$		–
$\gamma X \to \gamma p\overline{p}$	[qqaa]	$< 2 \times 10^{-6}$	CL=90%	–
$\gamma p\overline{p}\pi^+\pi^-$		$(2.8 \pm 1.4) \times 10^{-5}$		1491
$\gamma\gamma$		$< 1.5 \times 10^{-4}$	CL=90%	1843
$\gamma\gamma J/\psi$		$(3.1 {}^{+1.0}_{-1.2}) \times 10^{-4}$		542
$e^+e^-\eta'$		$(1.90 \pm 0.26) \times 10^{-6}$		1719
$e^+e^-\eta_c(1S)$		$(3.8 \pm 0.4) \times 10^{-5}$		635
$e^+e^-\chi_{c0}(1P)$		$(1.10 \pm 0.26) \times 10^{-3}$		261
$e^+e^-\chi_{c1}(1P)$		$(8.6 \pm 0.7) \times 10^{-4}$		171
$e^+e^-\chi_{c2}(1P)$		$(7.0 \pm 0.8) \times 10^{-4}$		128
Weak decays				
$D^0e^+e^-$ + c.c.		$< 1.4 \times 10^{-7}$	CL=90%	1371
$\Lambda_c^+\overline{\Sigma}^-$ + c.c.		$< 1.4 \times 10^{-5}$	CL=90%	586
Other decays				
invisible		< 1.6 %	CL=90%	–

$\psi(3770)$

$I^G(J^{PC}) = 0^-(1^{--})$

Mass $m = 3773.7 \pm 0.7$ MeV (S = 2.3)
Full width $\Gamma = 27.2 \pm 1.0$ MeV

$\psi(3770)$ DECAY MODES	Fraction (Γ_i/Γ)	Scale factor/ Confidence level	p (MeV/c)
$D\overline{D}$	$(93 {}^{+8}_{-9})$ %	S=2.0	287
$D^0\overline{D}^0$	$(52 {}^{+4}_{-5})$ %	S=2.0	287
D^+D^-	(41 ± 4) %	S=2.0	254
$J/\psi X$	$(5.0 \pm 2.2) \times 10^{-3}$		–
$J/\psi\pi^+\pi^-$	$(1.93 \pm 0.28) \times 10^{-3}$		561
$J/\psi\pi^0\pi^0$	$(8.0 \pm 3.0) \times 10^{-4}$		565
$J/\psi\eta$	$(8.7 \pm 1.2) \times 10^{-4}$		361
$J/\psi\pi^0$	$< 2.8 \times 10^{-4}$	CL=90%	604

Int. J. Mod. Phys. A 2026.41. Downloaded from www.worldscientific.com
by UNIVERSITY OF CALIFORNIA @ BERKELEY on 09/16/26. Re-use and distribution is strictly not permitted, except for Open Acce

$e^+ e^-$	$(9.6 \pm 0.7) \times 10^{-6}$	S=1.3	1887
Decays to light hadrons			
$b_1(1235)\pi$	$< 1.4 \times 10^{-5}$	CL=90%	1684
$\phi\eta'$	$< 2.3 \times 10^{-5}$	CL=90%	1607
$\omega\eta'$	$< 4 \times 10^{-4}$	CL=90%	1672
$\rho^0\eta'$	$< 6 \times 10^{-4}$	CL=90%	1674
$\phi\eta$	$(3.1 \pm 0.7) \times 10^{-4}$		1703
$\omega\eta$	$< 1.4 \times 10^{-5}$	CL=90%	1762
$\rho^0\eta$	$< 5 \times 10^{-4}$	CL=90%	1764
$\phi\pi^0$	$< 3 \times 10^{-5}$	CL=90%	1746
$\omega\pi^0$	$< 6 \times 10^{-4}$	CL=90%	1803
$\pi^+\pi^-\pi^0$	$< 5 \times 10^{-6}$	CL=90%	1874
$\rho\pi$	$< 5 \times 10^{-6}$	CL=90%	1805
K^+K^-	not seen		1821
$K^*(892)^+K^- +$ c.c.	$< 1.4 \times 10^{-5}$	CL=90%	1745
$K^*(892)^0\overline{K}^0 +$ c.c.	$< 1.2 \times 10^{-3}$	CL=90%	1745
$K^0_S K^0_L$	$(2.6\ ^{+1.4}_{-1.6}) \times 10^{-5}$		1820
$2(\pi^+\pi^-)$	$< 1.12 \times 10^{-3}$	CL=90%	1861
$2(\pi^+\pi^-)\pi^0$	$< 1.06 \times 10^{-3}$	CL=90%	1844
$2(\pi^+\pi^-\pi^0)$	< 5.85 %	CL=90%	1821
$\omega\pi^+\pi^-$	$< 6.0 \times 10^{-4}$	CL=90%	1794
$3(\pi^+\pi^-)$	$< 9.1 \times 10^{-3}$	CL=90%	1820
$3(\pi^+\pi^-)\pi^0$	< 1.37 %	CL=90%	1792
$3(\pi^+\pi^-)2\pi^0$	< 11.74 %	CL=90%	1760
$\eta\pi^+\pi^-$	$< 1.24 \times 10^{-3}$	CL=90%	1836
$\pi^+\pi^-2\pi^0$	$< 8.9 \times 10^{-3}$	CL=90%	1862
$\rho^0\pi^+\pi^-$	$< 6.9 \times 10^{-3}$	CL=90%	1796
$\eta 3\pi$	$< 1.34 \times 10^{-3}$	CL=90%	1824
$\eta 2(\pi^+\pi^-)$	< 2.43 %	CL=90%	1804
$\eta\rho^0\pi^+\pi^-$	< 1.45 %	CL=90%	1708
$\eta' 3\pi$	$< 2.44 \times 10^{-3}$	CL=90%	1741
$K^+K^-\pi^+\pi^-$	$< 9.0 \times 10^{-4}$	CL=90%	1773
$\phi\pi^+\pi^-$	$< 4.1 \times 10^{-4}$	CL=90%	1737
$K^+K^-2\pi^0$	$< 4.2 \times 10^{-3}$	CL=90%	1774
$4(\pi^+\pi^-)$	< 1.67 %	CL=90%	1757
$4(\pi^+\pi^-)\pi^0$	< 3.06 %	CL=90%	1720
$\phi f_0(980)$	$< 4.5 \times 10^{-4}$	CL=90%	1597
$K^+K^-\pi^+\pi^-\pi^0$	$< 2.36 \times 10^{-3}$	CL=90%	1741
$K^+K^-\rho^0\pi^0$	$< 8 \times 10^{-4}$	CL=90%	1624
$K^+K^-\rho^+\pi^-$	< 1.46 %	CL=90%	1623
ωK^+K^-	$< 3.4 \times 10^{-4}$	CL=90%	1664
$\phi\pi^+\pi^-\pi^0$	$< 3.8 \times 10^{-3}$	CL=90%	1723
$K^{*0}K^-\pi^+\pi^0 +$ c.c.	< 1.62 %	CL=90%	1694
$K^{*+}K^-\pi^+\pi^- +$ c.c.	< 3.23 %	CL=90%	1692
$K^+K^-\pi^+\pi^-2\pi^0$	< 2.67 %	CL=90%	1705
$K^+K^-2(\pi^+\pi^-)$	< 1.03 %	CL=90%	1702
$K^+K^-2(\pi^+\pi^-)\pi^0$	< 3.60 %	CL=90%	1661
ηK^+K^-	$< 4.1 \times 10^{-4}$	CL=90%	1712
$\eta K^+K^-\pi^+\pi^-$	< 1.24 %	CL=90%	1624
$\rho^0K^+K^-$	$< 5.0 \times 10^{-3}$	CL=90%	1666
$2(K^+K^-)$	$< 6.0 \times 10^{-4}$	CL=90%	1552
ϕK^+K^-	$< 7.5 \times 10^{-4}$	CL=90%	1598
$2(K^+K^-)\pi^0$	$< 2.9 \times 10^{-4}$	CL=90%	1494
$2(K^+K^-)\pi^+\pi^-$	$< 3.2 \times 10^{-3}$	CL=90%	1426
$K^0_S K^-\pi^+$	$< 3.2 \times 10^{-3}$	CL=90%	1799
$K^0_S K^-\pi^+\pi^0$	< 1.33 %	CL=90%	1773
$K^0_S K^-\rho^+$	$< 6.6 \times 10^{-3}$	CL=90%	1665
$K^0_S K^-2\pi^+\pi^-$	$< 8.7 \times 10^{-3}$	CL=90%	1740
$K^0_S K^-\pi^+\rho^0$	< 1.6 %	CL=90%	1621
$K^0_S K^-\pi^+\eta$	< 1.3 %	CL=90%	1670
$K^0_S K^-2\pi^+\pi^-\pi^0$	< 4.18 %	CL=90%	1703
$K^0_S K^-2\pi^+\pi^-\eta$	< 4.8 %	CL=90%	1570
$K^0_S K^-\pi^+2(\pi^+\pi^-)$	< 1.22 %	CL=90%	1658
$K^0_S K^-\pi^+2\pi^0$	< 2.65 %	CL=90%	1742
$K^0_S K^-K^+K^-\pi^+$	$< 4.9 \times 10^{-3}$	CL=90%	1491
$K^0_S K^-K^+K^-\pi^+\pi^0$	< 3.0 %	CL=90%	1427
$K^0_S K^-K^+K^-\pi^+\eta$	< 2.2 %	CL=90%	1214
$K^{*0}K^-\pi^+ +$ c.c.	$< 9.7 \times 10^{-3}$	CL=90%	1722
$p\overline{p}$	not seen		1637
$p\overline{p}\pi^0$	$< 4 \times 10^{-5}$	CL=90%	1595
$p\overline{p}\pi^+\pi^-$	$< 5.8 \times 10^{-4}$	CL=90%	1544
$\Lambda\overline{\Lambda}$	$< 1.2 \times 10^{-4}$	CL=90%	1522
$p\overline{p}\pi^+\pi^-\pi^0$	$< 1.85 \times 10^{-3}$	CL=90%	1490
$\omega p\overline{p}$	$< 2.9 \times 10^{-4}$	CL=90%	1310
$\Lambda\overline{\Lambda}\pi^0$	$< 7 \times 10^{-5}$	CL=90%	1469
$p\overline{p}2(\pi^+\pi^-)$	$< 2.6 \times 10^{-3}$	CL=90%	1426
$\eta p\overline{p}$	$< 5.4 \times 10^{-4}$	CL=90%	1431
$\eta p\overline{p}\pi^+\pi^-$	$< 3.3 \times 10^{-3}$	CL=90%	1284
$\rho^0 p\overline{p}$	$< 1.7 \times 10^{-3}$	CL=90%	1314
$p\overline{p}K^+K^-$	$< 3.2 \times 10^{-4}$	CL=90%	1186
$\eta p\overline{p}K^+K^-$	$< 6.9 \times 10^{-3}$	CL=90%	737
$\pi^0 p\overline{p}K^+K^-$	$< 1.2 \times 10^{-3}$	CL=90%	1094
$\phi p\overline{p}$	$< 1.3 \times 10^{-4}$	CL=90%	1178
$\Lambda\overline{\Lambda}\pi^+\pi^-$	$< 2.5 \times 10^{-4}$	CL=90%	1405
$\Lambda\overline{p}K^+$	$< 2.8 \times 10^{-4}$	CL=90%	1387
$\Lambda\overline{p}K^+\pi^+\pi^-$	$< 6.3 \times 10^{-4}$	CL=90%	1234
$\Lambda\overline{\Lambda}\eta$	$< 1.9 \times 10^{-4}$	CL=90%	1263
$\Sigma^+\overline{\Sigma}^-$	$< 1.0 \times 10^{-4}$	CL=90%	1465
$\Sigma^0\overline{\Sigma}^0$	$< 4 \times 10^{-5}$	CL=90%	1462
$\Xi^0\overline{\Xi}^0$	$< 3.4 \times 10^{-4}$	CL=90%	1353
$\Xi^-\overline{\Xi}^+$	$(1.4 \pm 0.4) \times 10^{-4}$		1347
$\Lambda\overline{\Xi}^+K^- +$ c.c.	$< 1.0 \times 10^{-4}$	CL=90%	1185
$\Sigma^0\overline{\Xi}^+K^- +$ c.c.	$< 3.4 \times 10^{-4}$	CL=90%	1134
$pK^-K^-\overline{\Xi}^+ +$ c.c.	$< 7 \times 10^{-5}$	CL=90%	949
Radiative decays			
$\gamma\chi_{c2}$	$< 6.4 \times 10^{-4}$	CL=90%	211
$\gamma\chi_{c1}$	$(2.49 \pm 0.23) \times 10^{-3}$		254
$\gamma\chi_{c0}$	$(7.1 \pm 0.6) \times 10^{-3}$		341
$\gamma\eta_c$	$< 8 \times 10^{-4}$	CL=90%	707
$\gamma\eta_c(2S)$	$< 9 \times 10^{-4}$	CL=90%	133
$\gamma\eta'$	$< 1.8 \times 10^{-4}$	CL=90%	1765
$\gamma\eta$	$< 1.5 \times 10^{-4}$	CL=90%	1847
$\gamma\pi^0$	$< 2 \times 10^{-4}$	CL=90%	1884

$\psi_2(3823)$

$I^G(J^{PC}) = 0^-(2^{--})$
I, J, P need confirmation.

was $\psi(3823)$, $X(3823)$

Mass $m = 3823.51 \pm 0.34$ MeV
Full width $\Gamma < 2.9$ MeV, CL = 90%

Branching fractions are given relative to the one **DEFINED AS 1**.

$\psi_2(3823)$ DECAY MODES	Fraction (Γ_i/Γ)	Confidence level	p (MeV/c)
$J/\psi(1S)\pi^+\pi^-$	<0.06	90%	607
$J/\psi(1S)\pi^0\pi^0$	<0.11	90%	610
$J/\psi(1S)\pi^0$	<0.030	90%	646
$J/\psi(1S)\eta$	<0.14	90%	431
$\chi_{c0}\gamma$	<0.24	90%	386
$\chi_{c1}\gamma$	**DEFINED AS 1**		300
$\chi_{c2}\gamma$	$0.28\ ^{+0.14}_{-0.11}$		258

$\psi_3(3842)$

$I^G(J^{PC}) = 0^-(3^{--})$
J, P need confirmation.

Mass $m = 3842.71 \pm 0.20$ MeV
Full width $\Gamma = 2.8 \pm 0.6$ MeV

$\psi_3(3842)$ DECAY MODES	Fraction (Γ_i/Γ)	p (MeV/c)
D^+D^-	seen	443
$D^0\overline{D}^0$	seen	463

$\chi_{c1}(3872)$

$I^G(J^{PC}) = 0^+(1^{++})$

also known as $X(3872)$

T-Matrix Pole $\sqrt{s}$ relative to D^0D^{*+} threshold $= (0.01 \pm 0.15^{+0.07}_{-0.08} \pm 0.07) - i(0.19 \pm 0.08^{+0.14}_{-0.19})$ MeV
T-Matrix Pole $\sqrt{s} = (3871.70 \pm 0.15^{+0.07}_{-0.08}) - i(0.19 \pm 0.08^{+0.14}_{-0.19})$ MeV
Mass $m = 3871.64 \pm 0.06$ MeV
Full width $\Gamma = 1.19 \pm 0.21$ MeV (S = 1.1)

$\chi_{c1}(3872)$ DECAY MODES	Fraction (Γ_i/Γ)	Confidence level	p (MeV/c)
e^+e^-	$< 2.7 \times 10^{-7}$	90%	1936
$\pi^+\pi^-\pi^0$	< 1.0 %	90%	1924
$\pi^+\pi^-J/\psi(1S)$	(4.3 ± 1.4) %		650
$\pi^+\pi^-\pi^0J/\psi(1S)$	not seen		588
$\omega\eta_c(1S)$	< 40 %	90%	368
$\rho(770)^0J/\psi(1S)$	(3.4 ± 1.1) %		–

Int. J. Mod. Phys. A 2026.41. Downloaded from www.worldscientific.com
by UNIVERSITY OF CALIFORNIA @ BERKELEY on 09/16/26. Re-use and distribution is strictly not permitted, except for Open Access articles.

$\omega J/\psi(1S)$	(5.0 ± 1.9)	%		†
$\phi\phi$	not seen			1646
$D^0\overline{D}^0\pi^0$	(55 ± 28)	%		116
$\overline{D}^{*0}D^0$	(46 ± 16)	%		†
$\gamma\gamma$	< 13	%	90%	1936
$D^0\overline{D}^0$	< 32	%	90%	519
D^+D^-	< 22	%	90%	502
$\pi^0\chi_{c2}$	< 5	%	90%	273
$\pi^0\chi_{c1}$	$(3.8^{+1.9}_{-1.7})$	%		319
$\pi^0\chi_{c0}$	< 16	%	90%	410
$\pi^+\pi^-\eta_c(1S)$	< 16	%	90%	745
$\pi^0\pi^0\chi_{c0}$	< 7	%	90%	346
$\pi^0\pi^0\chi_{c1}$	< 5	%	90%	228
$\pi^0\pi^0\chi_{c2}$	< 2.2	%	90%	156
$\pi^+\pi^-\chi_{c0}$	< 2.4	%	90%	339
$\pi^+\pi^-\chi_{c1}$	< 8	$\times 10^{-3}$	90%	218
$p\overline{p}$	< 2.7	$\times 10^{-5}$	95%	1693
$\pi^+\pi^-\eta$	< 5	$\times 10^{-3}$	90%	1887
Radiative decays				
γD^+D^-	< 4	%	90%	502
$\gamma\overline{D}^0D^0$	< 7	%	90%	519
$\gamma J/\psi$	$(10 \pm 4) \times 10^{-3}$			697
$\gamma\chi_{c1}$	< 1.0	%	90%	344
$\gamma\chi_{c2}$	< 4	%	90%	303
$\gamma\psi(2S)$	possibly seen			181
$\gamma\psi_2(3823)$	< 3.3	$\times 10^{-3}$	90%	48
***C*-violating decays**				
$\eta J/\psi$	< 2.1	%	90%	491

$\chi_{c0}(3915)$

$I^G(J^{PC}) = 0^+(0^{++})$

was $X(3915)$

Mass $m = 3922.1 \pm 1.8$ MeV (S = 1.5)
Full width $\Gamma = 20 \pm 4$ MeV (S = 1.1)

$\chi_{c0}(3915)$ DECAY MODES	Fraction (Γ_i/Γ)	p (MeV/c)
$\omega J/\psi$	seen	232
$\overline{D}^{*0}D^0$	not seen	313
D^+D^-	seen	592
$D_s^+D_s^-$	seen	†
$\pi^+\pi^-\eta_c(1S)$	not seen	788
$\eta_c\eta$	not seen	668
$\eta_c\pi^0$	not seen	817
$K\overline{K}$	not seen	1898
$\gamma\gamma$	seen	1961
$\gamma\psi(2S)$	not seen	229
$\pi^0\chi_{c1}$	not seen	368

$\chi_{c2}(3930)$

$I^G(J^{PC}) = 0^+(2^{++})$

Mass $m = 3922.5 \pm 1.0$ MeV (S = 1.7)
Full width $\Gamma = 35.2 \pm 2.2$ MeV (S = 1.2)

$\chi_{c2}(3930)$ DECAY MODES	Fraction (Γ_i/Γ)	p (MeV/c)
$\gamma\gamma$	seen	1961
$K\overline{K}\pi$	not seen	1878
$K^+K^-\pi^+\pi^-\pi^0$	not seen	1822
$D\overline{D}$	seen	607
D^+D^-	seen	592
$D^0\overline{D}^0$	seen	607
$\pi^+\pi^-\eta_c(1S)$	not seen	788
$K\overline{K}$	not seen	1898

$\psi(4040)$ [rraa]

$I^G(J^{PC}) = 0^-(1^{--})$

Mass $m = 4040 \pm 4$ MeV
Full width $\Gamma = 84 \pm 12$ MeV

Due to the complexity of the $c\overline{c}$ threshold region, in this listing, "seen" ("not seen") means that a cross section for the mode in question has been measured at effective $\sqrt{s}$ near this particle's central mass value, more (less) than 2σ above zero, without regard to any peaking behavior in $\sqrt{s}$ or absence thereof. See mode listing(s) for details and references.

$\psi(4040)$ DECAY MODES	Fraction (Γ_i/Γ)	Confidence level	p (MeV/c)
e^+e^-	$(1.02 \pm 0.17) \times 10^{-5}$		2020
$D\overline{D}$	seen		776
$D^0\overline{D}^0$	seen		776
D^+D^-	seen		764
$D^*\overline{D}$ + c.c.	seen		570
$D^*(2007)^0\overline{D}^0$ + c.c.	seen		576
$D^*(2010)^+D^-$ + c.c.	seen		562
$D^*\overline{D}^*$	seen		196
$D^*(2007)^0\overline{D}^*(2007)^0$	seen		228
$D^*(2010)^+D^*(2010)^-$	seen		196
$D\overline{D}\pi$ (excl. $D^*\overline{D}$)	not seen		–
$D^0D^-\pi^+$ + c.c. (excl. $D^*(2010)^+D^-$ + c.c.)	not seen		–
$D\overline{D}^*\pi$ (excl. $D^*\overline{D}^*$)	not seen		–
$D^0\overline{D}^{*-}\pi^+$ + c.c. (excl. $D^*(2010)^+D^*(2010)^-$)	seen		–
$D_s^+D_s^-$	seen		453
$\pi^+\pi^+\pi^-\pi^-\pi^0$	seen		1979
$J/\psi(1S)$ hadrons	seen		–
$J/\psi\pi^+\pi^-$	$< 4 \times 10^{-3}$	90%	795
$J/\psi\pi^0\pi^0$	$< 2 \times 10^{-3}$	90%	797
$J/\psi\eta$	$(5.2 \pm 0.7) \times 10^{-3}$		676
$J/\psi\pi^0$	$< 2.8 \times 10^{-4}$	90%	824
$J/\psi\pi^+\pi^-\pi^0$	$< 2 \times 10^{-3}$	90%	747
$\chi_{c1}\gamma$	$< 3.4 \times 10^{-3}$	90%	494
$\chi_{c2}\gamma$	$< 5 \times 10^{-3}$	90%	455
$\chi_{c1}\pi^+\pi^-\pi^0$	< 1.1 %	90%	307
$\chi_{c2}\pi^+\pi^-\pi^0$	< 3.2 %	90%	234
$h_c(1P)\pi^+\pi^-$	$< 3 \times 10^{-3}$	90%	404
$\phi\pi^+\pi^-$	$< 3 \times 10^{-3}$	90%	1880
$\Lambda\overline{\Lambda}\pi^+\pi^-$	$< 2.9 \times 10^{-4}$	90%	1579
$\Lambda\overline{\Lambda}\pi^0$	$< 9 \times 10^{-5}$	90%	1636
$\Lambda\overline{\Lambda}\eta$	$< 3.0 \times 10^{-4}$	90%	1452
$\Lambda\overline{\Lambda}$	$< 6 \times 10^{-6}$	90%	1684
$\Sigma^+\overline{\Sigma}^-$	$< 1.3 \times 10^{-4}$	90%	1632
$\Sigma^0\overline{\Sigma}^0$	$< 7 \times 10^{-5}$	90%	1630
$\Xi^+\overline{\Xi}^-$	$< 1.6 \times 10^{-4}$	90%	1527
$\Xi^0\overline{\Xi}^0$	$< 1.8 \times 10^{-4}$	90%	1533
$\Xi^-\overline{\Xi}^+$	$< 6 \times 10^{-5}$	90%	1527
$\Lambda\overline{\Xi}^+K^-$ + c.c.	$< 7 \times 10^{-5}$	90%	1386
$\Sigma^0\overline{\Xi}^+K^-$ + c.c.	$< 1.5 \times 10^{-5}$	90%	1343
$pK^-K^-\overline{\Xi}^+$ + c.c.	$< 4 \times 10^{-5}$	90%	1188
$\mu^+\mu^-$	$(9 \pm 6) \times 10^{-6}$		2017

$\chi_{c1}(4140)$

$I^G(J^{PC}) = 0^+(1^{++})$

was $X(4140)$

Mass $m = 4146.5 \pm 3.0$ MeV (S = 1.3)
Full width $\Gamma = 19^{+7}_{-5}$ MeV

$\chi_{c1}(4140)$ DECAY MODES	Fraction (Γ_i/Γ)	p (MeV/c)
$J/\psi\phi$	seen	216
$\gamma\gamma$	not seen	2073

$\psi(4160)$ [rraa]

$I^G(J^{PC}) = 0^-(1^{--})$

Mass $m = 4191 \pm 5$ MeV
Full width $\Gamma = 69 \pm 10$ MeV

Due to the complexity of the $c\overline{c}$ threshold region, in this listing, "seen" ("not seen") means that a cross section for the mode in question has been measured at effective $\sqrt{s}$ near this particle's central mass value, more (less) than 2σ above zero, without regard to any peaking behavior in $\sqrt{s}$ or absence thereof. See mode listing(s) for details and references.

$\psi(4160)$ DECAY MODES	Fraction (Γ_i/Γ)	Confidence level	p (MeV/c)
e^+e^-	$(6.9 \pm 3.3) \times 10^{-6}$		2096
$\mu^+\mu^-$	seen		2093
$D\overline{D}$	seen		956
$D^0\overline{D}^0$	seen		956
D^+D^-	seen		947
$D^*\overline{D}$ + c.c.	seen		798
$D^*(2007)^0\overline{D}^0$ + c.c.	seen		802

Int. J. Mod. Phys. A 2026.41. Downloaded from www.worldscientific.com
by UNIVERSITY OF CALIFORNIA @ BERKELEY on 09/16/26. Re-use and distribution is strictly not permitted, except for Open Acce

$D^*(2010)^+ D^- +$ c.c.	seen			792
$D^* \overline{D}^*$	seen			592
$D^*(2007)^0 \overline{D}^*(2007)^0$	seen			604
$D^*(2010)^+ D^*(2010)^-$	seen			592
$D^0 D^- \pi^+ +$c.c. (excl. $D^*(2010)^+ D^- +$c.c.)	not seen			–
$D \overline{D}^* \pi +$c.c. (excl. $D^* \overline{D}^*$)	seen			–
$D^0 D^{*-} \pi^+ +$c.c. (excl. $D^*(2010)^+ D^*(2010)^-$)	not seen			–
$D_s^+ D_s^-$	not seen			719
$D_s^{*+} D_s^- +$c.c.	seen			478
$J/\psi \pi^+ \pi^-$	< 3	$\times 10^{-3}$	90%	919
$J/\psi \pi^0 \pi^0$	< 3	$\times 10^{-3}$	90%	921
$J/\psi K^+ K^-$	< 2	$\times 10^{-3}$	90%	407
$J/\psi \eta$	< 8	$\times 10^{-3}$	90%	821
$J/\psi \pi^0$	< 1	$\times 10^{-3}$	90%	944
$J/\psi \eta'$	< 5	$\times 10^{-3}$	90%	456
$J/\psi \pi^+ \pi^- \pi^0$	< 1	$\times 10^{-3}$	90%	879
$\psi(2S) \pi^+ \pi^-$	< 4	$\times 10^{-3}$	90%	395
$\chi_{c1} \gamma$	< 5	$\times 10^{-3}$	90%	625
$\chi_{c2} \gamma$	< 1.3	%	90%	587
$\chi_{c1} \pi^+ \pi^- \pi^0$	< 2	$\times 10^{-3}$	90%	496
$\chi_{c2} \pi^+ \pi^- \pi^0$	< 8	$\times 10^{-3}$	90%	444
$h_c(1P) \pi^+ \pi^-$	< 5	$\times 10^{-3}$	90%	556
$h_c(1P) \pi^0 \pi^0$	< 2	$\times 10^{-3}$	90%	560
$h_c(1P) \eta$	< 2	$\times 10^{-3}$	90%	348
$h_c(1P) \pi^0$	< 4	$\times 10^{-4}$	90%	600
$\omega \pi^+ \pi^-$	seen			2013
$\phi \pi^+ \pi^-$	< 2	$\times 10^{-3}$	90%	1961
$\gamma \chi_{c1}(3872)$	< 1.6	$\times 10^{-3}$	90%	307
$\gamma \chi_{c0}(3915) \to \gamma J/\psi \pi^+ \pi^-$	< 1.36	$\times 10^{-4}$	90%	–
$\gamma X(3930) \to \gamma J/\psi \pi^+ \pi^-$	< 1.18	$\times 10^{-4}$	90%	–
$\gamma X(3940) \to \gamma J/\psi \pi^+ \pi^-$	< 1.47	$\times 10^{-4}$	90%	–
$\gamma \chi_{c0}(3915) \to \gamma \gamma J/\psi$	< 1.26	$\times 10^{-4}$	90%	–
$\gamma X(3930) \to \gamma \gamma J/\psi$	< 8.8	$\times 10^{-5}$	90%	–
$\gamma X(3940) \to \gamma \gamma J/\psi$	< 1.79	$\times 10^{-4}$	90%	–
$\omega \pi^0$	not seen			2020
$\omega \eta$	not seen			1984
$K^+ K^-$	not seen			2037
$K_S^0 K^\pm \pi^\mp$	seen			2017
$p \overline{p} p \overline{p}$	not seen			834
$\Lambda \overline{\Lambda}$	< 1.5	$\times 10^{-6}$	90%	1774
$\Sigma^+ \overline{\Sigma}^-$	< 2.0	$\times 10^{-4}$	90%	1725
$\Sigma^0 \overline{\Sigma}^0$	< 5	$\times 10^{-5}$	90%	1723
$\Xi^0 \overline{\Xi}^0$	< 1.4	$\times 10^{-4}$	90%	1632
$\Xi^- \overline{\Xi}^+$	< 8	$\times 10^{-5}$	90%	1626
$p K^- \overline{\Lambda} +$ c.c.	< 6	$\times 10^{-6}$	90%	1659
$\Lambda \overline{\Xi}^+ K^- +$ c.c.	seen			1494
$\Sigma^0 \overline{\Xi}^+ K^- +$ c.c.	< 3.1	$\times 10^{-6}$	90%	1454
$p K^- K^- \overline{\Xi}^+ +$ c.c.	< 1.1	$\times 10^{-4}$	90%	1311

$\psi(4230)$

$I^G(J^{PC}) = 0^-(1^{--})$

also known as $Y(4230)$; was $\psi(4260)$

Mass $m = 4221.7 \pm 2.5$ MeV (S = 1.9)
Full width $\Gamma = 51 \pm 7$ MeV (S = 3.4)

$\psi(4230)$ DECAY MODES	Fraction (Γ_i/Γ)	p (MeV/c)
$\mu^+ \mu^-$	$(3.0 \pm 2.7) \times 10^{-5}$	2107
$\eta_c(1S) \pi^+ \pi^-$	not seen	1027
$\eta_c(1S) \pi^+ \pi^- \pi^0$	seen	992
$J/\psi \pi^+ \pi^-$	seen	942
$J/\psi f_0(980)$, $f_0(980) \to \pi^+ \pi^-$	seen	–
$T_{c\overline{c}1}(3900)^\pm \pi^\mp$, $T^\pm_{c\overline{c}1} \to J/\psi \pi^\pm$	seen	–
$J/\psi \pi^0 \pi^0$	seen	944
$J/\psi K^+ K^-$	seen	460
$J/\psi K_S^0 K_S^0$	not seen	447
$J/\psi \eta$	seen	848
$J/\psi \pi^0$	not seen	966
$J/\psi \eta'$	seen	504
$J/\psi \pi^+ \pi^- \pi^0$	not seen	904
$J/\psi \eta \pi^0$	not seen	770
$J/\psi \eta \eta$	not seen	211
$\psi(2S) \pi^+ \pi^-$	seen	426
$\psi(2S) \eta$	not seen	†
$\chi_{c0} \omega$	seen	168
$\chi_{c1} \pi^+ \pi^- \pi^0$	not seen	527
$\chi_{c2} \pi^+ \pi^- \pi^0$	not seen	477
$h_c(1P) \pi^+ \pi^-$	seen	583
$h_c(1P) \eta$	seen	391
$\phi \pi^+ \pi^-$	not seen	1976
$\phi f_0(980) \to \phi \pi^+ \pi^-$	not seen	–
$\phi K^+ K^-$	not seen	1856
$\phi K_S^0 K_S^0$	not seen	1854
$\phi \eta$	not seen	1947
$\phi \eta'$	not seen	1864
$D \overline{D}$	not seen	987
$D^0 \overline{D}^0$	possibly seen	987
$D^+ D^-$	possibly seen	978
$D^* \overline{D} +$c.c.	not seen	835
$D^*(2007)^0 \overline{D}^0 +$c.c.	not seen	839
$D^*(2010)^+ D^- +$c.c.	not seen	829
$D^* \overline{D}^*$	not seen	641
$D^*(2007)^0 \overline{D}^*(2007)^0$	not seen	652
$D^*(2010)^+ D^*(2010)^-$	not seen	641
$D \overline{D} \pi +$c.c.	not seen	847
$D^0 D^- \pi^+ +$c.c. (excl. $D^*(2007)^0 \overline{D}^{*0} +$c.c., $D^*(2010)^+ D^- +$c.c.)	not seen	–
$D \overline{D}^* \pi +$c.c. (excl. $D^* \overline{D}^*$)	not seen	723
$D^0 D^*(2010)^- \pi^+ +$c.c.	seen	650
$D_1(2420) \overline{D} +$ c.c.	not seen	†
$D^* \overline{D}^* \pi$	seen	367
$D^{*0} D^{*-} \pi^+$	seen	364
$D_s^+ D_s^-$	not seen	760
$D_s^{*+} D_s^- +$c.c.	not seen	538
$D_s^{*+} D_s^{*-}$	not seen	†
$p \overline{p}$	not seen	1890
$p \overline{p} \pi^0$	not seen	1854
$p \overline{p} \eta$	not seen	1712
$\omega \pi^+ \pi^-$	seen	2028
$p \overline{p} \omega$	not seen	1610
$\Xi^- \overline{\Xi}^+$	not seen	1645
$\pi^+ \pi^+ \pi^- \pi^-$	not seen	2087
$\pi^+ \pi^+ \pi^- \pi^- \pi^0$	not seen	2071
$\omega \pi^0$	not seen	2035
$\omega \eta$	not seen	1999
$K_S^0 K^\pm \pi^\mp$	not seen	2032
$K_S^0 K^\pm \pi^\mp \pi^0$	not seen	2009
$K_S^0 K^\pm \pi^\mp \eta$	not seen	1917
$K^+ K^- \pi^0$	not seen	2033
$K^+ K^- \pi^+ \pi^-$	not seen	2008
$K^+ K^- \pi^+ \pi^- \pi^0$	not seen	1981
$K^+ K^+ K^- K^-$	not seen	1813
$K^+ K^+ K^- K^- \pi^0$	not seen	1762
$p \overline{p} \pi^+ \pi^-$	not seen	1810
$p \overline{p} \pi^+ \pi^- \pi^0$	not seen	1764
$p \overline{p} p \overline{p}$	not seen	864
$\Lambda \overline{\Lambda}$	not seen	1791
$\Sigma^+ \overline{\Sigma}^-$	not seen	1743
$p K^- \overline{\Lambda} +$ c.c.	not seen	1677
$\Lambda \overline{\Xi}^+ K^- +$ c.c.	not seen	1514
$\Sigma^0 \overline{\Xi}^+ K^- +$ c.c.	not seen	1474
Radiative decays		
$\eta_c(1S) \gamma$	possibly seen	1055
$\eta_c(1S) \pi^0 \gamma$	not seen	1048
$\eta_c(1S) \eta \gamma$	not seen	943
$\eta_c(1S) \eta' \gamma$	not seen	661
$\chi_{c1} \gamma$	not seen	650
$\chi_{c2} \gamma$	not seen	612
$\chi_{c1}(3872) \gamma$	seen	334

$\chi_{c1}(4274)$

$I^G(J^{PC}) = 0^+(1^{++})$

was $X(4274)$

Mass $m = 4290 \pm 6$ MeV (S = 1.5)
Full width $\Gamma = 54 \pm 8$ MeV (S = 1.2)

Int. J. Mod. Phys. A 2026.41. Downloaded from www.worldscientific.com
by UNIVERSITY OF CALIFORNIA @ BERKELEY on 09/16/26. Re-use and distribution is strictly not permitted, except for Open Access articles.

$\chi_{c1}(4274)$ DECAY MODES	Fraction (Γ_i/Γ)	p (MeV/c)
$J/\psi\phi$	seen	529

$\psi(4360)$

$I^G(J^{PC}) = 0^-(1^{--})$

also known as $Y(4360)$; was $X(4360)$

Mass $m = 4373 \pm 7$ MeV (S = 2.3)
Full width $\Gamma = 124 \pm 13$ MeV (S = 2.4)

$\psi(4360)$ DECAY MODES	Fraction (Γ_i/Γ)	p (MeV/c)
e^+e^-	seen	2187
$h_c\pi^+\pi^-$	seen	722
$J/\psi\pi^+\pi^-$	seen	1063
$\psi(2S)\pi^+\pi^-$	seen	578
$\psi(3770)\pi^+\pi^-$	possibly seen	494
$\psi_2(3823)\pi^+\pi^-$	seen	443
$J/\psi\eta$	seen	982
$D^0D^{*-}\pi^+$	not seen	867
$D^+D^-\pi^+\pi^-$	seen	861
$D_1(2420)\overline{D}+$ c.c.	possibly seen	429
$\phi\eta$	not seen	2029
$\omega\pi^0$	not seen	2114
$\omega\eta$	not seen	2080
$p\overline{p}\eta$	not seen	1805
$p\overline{p}\omega$	not seen	1708
$\chi_{c1}\gamma$	not seen	777
$\chi_{c2}\gamma$	not seen	741
$\Sigma^+\overline{\Sigma}^-$	not seen	1835
$\Xi^-\overline{\Xi}^+$	not seen	1742
$pK^-\overline{\Lambda}+$ c.c.	not seen	1772
$\Lambda\overline{\Xi}^+K^-+$ c.c.	not seen	1619
$\Sigma^0\overline{\Xi}^+K^-+$ c.c.	not seen	1582

$\psi(4415)$ [rraa]

$I^G(J^{PC}) = 0^-(1^{--})$

Mass $m = 4415 \pm 5$ MeV
Full width $\Gamma = 110 \pm 13$ MeV (S = 1.6)

Due to the complexity of the $c\overline{c}$ threshold region, in this listing, "seen" ("not seen") means that a cross section for the mode in question has been measured at effective $\sqrt{s}$ near this particle's central mass value, more (less) than 2σ above zero, without regard to any peaking behavior in $\sqrt{s}$ or absence thereof. See mode listing(s) for details and references.

$\psi(4415)$ DECAY MODES	Fraction (Γ_i/Γ)	Confidence level	p (MeV/c)
$D\overline{D}$	seen		1181
$D^0\overline{D}^0$	seen		1181
D^+D^-	seen		1173
$D^*\overline{D}+$ c.c.	seen		1057
$D^*(2007)^0\overline{D}^0+$ c.c.	seen		1060
$D^*(2010)^+D^-+$ c.c.	seen		1052
$D^*\overline{D}^*$	seen		911
$D^*(2007)^0\overline{D}^*(2007)^0+$ c.c.	seen		919
$D^*(2010)^+D^*(2010)^-+$ c.c.	seen		911
$D^0D^-\pi^+$(excl. $D^*(2010)^+D^-$ +c.c.	< 2.3 %	90%	–
$D\overline{D}_2^*(2460) \to D^0D^-\pi^+$+c.c.	(10 ± 4) %		–
$D^0D^{*-}\pi^+$+c.c.	< 31 %	90%	918
$D_1(2420)\overline{D}+$ c.c.	possibly seen		523
$D_s^+D_s^-$	not seen		999
$\omega\chi_{c2}$	$(9 \pm 4) \times 10^{-3}$		317
$D_s^{*+}D_s^-$+c.c.	seen		842
$D_s^{*+}D_s^{*-}$	seen		641
$\psi_2(3823)\pi^+\pi^-$	possibly seen		486
$\psi(3770)\pi^+\pi^-$	possibly seen		535
$J/\psi\eta$	< 1.0 %	90%	1017
$\chi_{c1}\gamma$	$< 1.3 \times 10^{-3}$	90%	811
$\chi_{c2}\gamma$	$< 7 \times 10^{-3}$	90%	775
$\Lambda\overline{\Lambda}$	$< 5 \times 10^{-6}$	90%	1905
$\Sigma^+\overline{\Sigma}^-$	$< 1.8 \times 10^{-4}$	90%	1859
$\Sigma^0\overline{\Sigma}^0$	$< 4 \times 10^{-5}$	90%	1857
$\Xi^0\overline{\Xi}^0$	$< 1.4 \times 10^{-4}$	90%	1773
$\Xi^-\overline{\Xi}^+$	$< 6 \times 10^{-5}$	90%	1768
$pK^-\overline{\Lambda}+$ c.c.	$< 1.0 \times 10^{-5}$	90%	1798
$\Lambda\overline{\Xi}^+K^-+$ c.c.	$< 4 \times 10^{-5}$	90%	1647
$\Sigma^0\overline{\Xi}^+K^-+$ c.c.	$< 2.5 \times 10^{-4}$	90%	1610
$pK^-K^-\overline{\Xi}^++$ c.c.	$< 8 \times 10^{-5}$	90%	1481
$\omega\pi^0$	not seen		2136
$\omega\eta$	not seen		2102
e^+e^-	$(3.2 \pm 1.2) \times 10^{-6}$		2207
$\mu^+\mu^-$	$(1.1 \pm 0.4) \times 10^{-5}$		2205

$\chi_{c0}(4500)$

$I^G(J^{PC}) = 0^+(0^{++})$

was $X(4500)$

Mass $m = 4484 \pm 12$ MeV (S = 3.4)
Full width $\Gamma = 87^{+30}_{-24}$ MeV (S = 2.9)

$\chi_{c0}(4500)$ DECAY MODES	Fraction (Γ_i/Γ)	p (MeV/c)
$J/\psi\phi$	seen	788
$\psi(2S)\pi^+\pi^-$	seen	681

$\psi(4660)$

$I^G(J^{PC}) = 0^-(1^{--})$

also known as $Y(4660)$; was $X(4660)$

Mass $m = 4623 \pm 10$ MeV (S = 3.7)
Full width $\Gamma = 55 \pm 9$ MeV (S = 1.9)

$\psi(4660)$ DECAY MODES	Fraction (Γ_i/Γ)	p (MeV/c)
e^+e^-	not seen	2311
$\psi(2S)\pi^+\pi^-$	seen	803
$J/\psi\eta$	not seen	1186
$D^0D^{*-}\pi^+$	not seen	1146
$D^{*0}D^{*-}\pi^+$	seen	1011
$\psi_2(3823)\pi^+\pi^-$	seen	684
$\chi_{c0}\phi$	not seen	557
$\chi_{c1}\gamma$	not seen	978
$\chi_{c1}\phi$	not seen	387
$\chi_{c2}\gamma$	not seen	943
$\chi_{c2}\phi$	seen	275
$\Lambda_c^+\Lambda_c^-$	seen	338
$D_s^+D_{s1}(2536)^-$	seen	517
$D_s^+D_{s2}^*(2573)^-$	seen	–
$\omega\pi^0$	not seen	2243
$\omega\eta$	not seen	2211
$\Sigma^+\overline{\Sigma}^-$	not seen	1982
$\Xi^0\overline{\Xi}^0$	not seen	1901
$\Xi^-\overline{\Xi}^+$	not seen	1896
$pK^-\overline{\Lambda}+$ c.c.	not seen	1924
$\Lambda\overline{\Xi}^+K^-+$ c.c.	not seen	1784
$\Sigma^0\overline{\Xi}^+K^-+$ c.c.	not seen	1749

$b\overline{b}$ MESONS (including possibly non-$q\overline{q}$ states)

$\eta_b(1S)$

$I^G(J^{PC}) = 0^+(0^{-+})$

Mass $m = 9398.7 \pm 2.0$ MeV (S = 1.5)
Full width $\Gamma = 10^{+5}_{-4}$ MeV

$\eta_b(1S)$ DECAY MODES	Fraction (Γ_i/Γ)	Confidence level	p (MeV/c)
hadrons	seen		–
$3h^+3h^-$	not seen		4672
$2h^+2h^-$	not seen		4689
$4h^+4h^-$	not seen		4648
$\gamma\gamma$	not seen		4699
$\mu^+\mu^-$	$< 9 \times 10^{-3}$	90%	4698
$\tau^+\tau^-$	< 8 %	90%	4350

Int. J. Mod. Phys. A 2026.41. Downloaded from www.worldscientific.com
by UNIVERSITY OF CALIFORNIA @ BERKELEY on 09/16/26. Re-use and distribution is strictly not permitted, except for Open Acce

$\Upsilon(1S)$

$I^G(J^{PC}) = 0^-(1^{--})$

Mass $m = 9460.40 \pm 0.10$ MeV
Full width $\Gamma = 54.02 \pm 1.25$ keV

$\Upsilon(1S)$ DECAY MODES	Fraction (Γ_i/Γ)	Scale factor/ Confidence level	p (MeV/c)
$\tau^+\tau^-$	(2.60 ± 0.10) %		4384
e^+e^-	(2.39 ± 0.08) %		4730
$\mu^+\mu^-$	(2.48 ± 0.04) %		4729
Hadronic decays			
ggg	(81.7 ± 0.7) %		–
γgg	(2.2 ± 0.6) %		–
$\eta'(958)$ anything	(2.94 ± 0.24) %		–
$J/\psi(1S)$ anything	$(5.4 \pm 0.4) \times 10^{-4}$	S=1.4	4223
$J/\psi(1S)\eta_c$	$< 2.2 \times 10^{-6}$	CL=90%	3623
$J/\psi(1S)\chi_{c0}$	$< 3.4 \times 10^{-6}$	CL=90%	3429
$J/\psi(1S)\chi_{c1}$	$(3.9 \pm 1.2) \times 10^{-6}$		3382
$J/\psi(1S)\chi_{c2}$	$< 1.4 \times 10^{-6}$	CL=90%	3359
$J/\psi(1S)\eta_c(2S)$	$< 2.2 \times 10^{-6}$	CL=90%	3317
$J/\psi(1S)X(3940)$	$< 5.4 \times 10^{-6}$	CL=90%	3148
$J/\psi(1S)X(4160)$	$< 5.4 \times 10^{-6}$	CL=90%	3020
$X(4350)$ anything, $X \to J/\psi(1S)\phi$	$< 8.1 \times 10^{-6}$	CL=90%	–
$T_{c\overline{c}1}(3900)^\pm$ anything, $T_{c\overline{c}1} \to J/\psi(1S)\pi^\pm$	$< 1.3 \times 10^{-5}$	CL=90%	–
$T_{c\overline{c}1}(4200)^\pm$ anything, $Z_c \to J/\psi(1S)\pi^\pm$	$< 6.0 \times 10^{-5}$	CL=90%	–
$T_{c\overline{c}1}(4430)^\pm$ anything, $T_{c\overline{c}1} \to J/\psi(1S)\pi^\pm$	$< 4.9 \times 10^{-5}$	CL=90%	–
$P_{c\overline{c}s}(4459)/\overline{P}_{c\overline{c}s}(4459)$ anything	$(3.5 \pm 2.0) \times 10^{-6}$		–
$P_{c\overline{c}s}(4338)/\overline{P}_{c\overline{c}s}(4338)$ anything	$< 1.8 \times 10^{-6}$	CL=90%	–
$P_c(4312)$ anything, $P_c(4312) \to pJ/\psi(1S)$	$< 5.7 \times 10^{-6}$	CL=90%	–
$P_c(4440)$ anything, $P_c(4440) \to pJ/\psi(1S)$	$< 1.00 \times 10^{-5}$	CL=90%	–
$P_c(4457)$ anything, $P_c(4457) \to pJ/\psi(1S)$	$< 7.6 \times 10^{-6}$	CL=90%	–
$p/\overline{p}J/\psi(1S)$ anything	$(8.1 \pm 0.8) \times 10^{-5}$		–
$J/\psi(1S)\Lambda/\overline{\Lambda}$ anything	$(3.7 \pm 0.6) \times 10^{-5}$		–
$X_{cs}^\pm$ anything, $X \to J/\psi K^\pm$	$< 5.7 \times 10^{-6}$	CL=90%	–
$\psi(4230)$ anything, $\psi \to J/\psi(1S)\pi^+\pi^-$	$< 3.8 \times 10^{-5}$	CL=90%	–
$\psi(4230)$ anything, $\psi \to J/\psi(1S)K^+K^-$	$< 7.5 \times 10^{-6}$	CL=90%	–
$\chi_{c1}(4140)$ anything, $\chi_{c1} \to J/\psi(1S)\phi$	$< 5.2 \times 10^{-6}$	CL=90%	–
χ_{c0} anything	$< 4 \times 10^{-3}$	CL=90%	–
χ_{c1} anything	$(1.90 \pm 0.35) \times 10^{-4}$		–
$\chi_{c1}(1P)X_{tetra}$	$< 3.78 \times 10^{-5}$	CL=90%	–
χ_{c2} anything	$(2.8 \pm 0.8) \times 10^{-4}$		–
$\psi(2S)$ anything	$(1.23 \pm 0.20) \times 10^{-4}$		–
$\psi(2S)\eta_c$	$< 3.6 \times 10^{-6}$	CL=90%	3345
$\psi(2S)\chi_{c0}$	$< 6.5 \times 10^{-6}$	CL=90%	3124
$\psi(2S)\chi_{c1}$	$< 4.5 \times 10^{-6}$	CL=90%	3070
$\psi(2S)\chi_{c2}$	$< 2.1 \times 10^{-6}$	CL=90%	3043
$\psi(2S)\eta_c(2S)$	$< 3.2 \times 10^{-6}$	CL=90%	2994
$\psi(2S)X(3940)$	$< 2.9 \times 10^{-6}$	CL=90%	2797
$\psi(2S)X(4160)$	$< 2.9 \times 10^{-6}$	CL=90%	2645
$\psi(4230)$ anything, $\psi \to \psi(2S)\pi^+\pi^-$	$< 7.9 \times 10^{-5}$	CL=90%	–
$\psi(4360)$ anything, $\psi \to \psi(2S)\pi^+\pi^-$	$< 5.2 \times 10^{-5}$	CL=90%	–
$\psi(4660)$ anything, $\psi \to \psi(2S)\pi^+\pi^-$	$< 2.2 \times 10^{-5}$	CL=90%	–
$T_{c\overline{c}}(4050)^\pm$ anything, $X \to \psi(2S)\pi^\pm$	$< 8.8 \times 10^{-5}$	CL=90%	–
$T_{c\overline{c}1}(4430)^\pm$ anything, $T_{c\overline{c}1} \to \psi(2S)\pi^\pm$	$< 6.7 \times 10^{-5}$	CL=90%	–
$\chi_{c1}(3872)$ anything	$< 2.2 \times 10^{-4}$	CL=90%	–
$T_{c\overline{c}1}(4200)^+T_{c\overline{c}1}(4200)^-$	$< 2.23 \times 10^{-5}$	CL=90%	–
$T_{c\overline{c}1}(3900)^\pm T_{c\overline{c}1}(4200)^\mp$	$< 8.1 \times 10^{-6}$	CL=90%	–
$T_{c\overline{c}1}(3900)^+T_{c\overline{c}1}(3900)^-$	$< 1.8 \times 10^{-6}$	CL=90%	–
$T_{c\overline{c}}(4050)^+T_{c\overline{c}}(4050)^-$	$< 1.58 \times 10^{-5}$	CL=90%	–
$T_{c\overline{c}}(4250)^+T_{c\overline{c}}(4250)^-$	$< 2.66 \times 10^{-5}$	CL=90%	–
$T_{c\overline{c}}(4050)^\pm T_{c\overline{c}}(4250)^\mp$	$< 4.42 \times 10^{-5}$	CL=90%	–
$T_{c\overline{c}1}(4430)^+T_{c\overline{c}1}(4430)^-$	$< 2.03 \times 10^{-5}$	CL=90%	–
$T_{c\overline{c}}(4055)^\pm T_{c\overline{c}}(4055)^\mp$	$< 2.33 \times 10^{-5}$	CL=90%	–
$T_{c\overline{c}}(4055)^\pm T_{c\overline{c}1}(4430)^\mp$	$< 4.55 \times 10^{-5}$	CL=90%	–
$\rho\pi$	$< 3.68 \times 10^{-6}$	CL=90%	4697
$\omega\pi^0$	$< 3.90 \times 10^{-6}$	CL=90%	4697
$\pi^+\pi^-$	$< 5 \times 10^{-4}$	CL=90%	4728
K^+K^-	$< 5 \times 10^{-4}$	CL=90%	4704
$p\overline{p}$	$< 5 \times 10^{-4}$	CL=90%	4636
$\pi^+\pi^-\pi^0$	$(2.1 \pm 0.8) \times 10^{-6}$		4725
ϕK^+K^-	$(2.4 \pm 0.5) \times 10^{-6}$		4623
$\omega\pi^+\pi^-$	$(4.5 \pm 1.0) \times 10^{-6}$		4694
$K^*(892)^0K^-\pi^+ +$ c.c.	$(4.4 \pm 0.8) \times 10^{-6}$		4667
$\phi f_2'(1525)$	$< 1.63 \times 10^{-6}$	CL=90%	4551
$\omega f_2(1270)$	$< 1.79 \times 10^{-6}$	CL=90%	4611
$\rho(770)a_2(1320)$	$< 2.24 \times 10^{-6}$	CL=90%	4605
$K^*(892)^0\overline{K}_2^*(1430)^0 +$ c.c.	$(3.0 \pm 0.8) \times 10^{-6}$		4579
$K_1(1270)^\pm K^\mp$	$< 2.41 \times 10^{-6}$	CL=90%	4634
$K_1(1400)^\pm K^\mp$	$(1.0 \pm 0.4) \times 10^{-6}$		4613
$b_1(1235)^\pm\pi^\mp$	$< 1.25 \times 10^{-6}$	CL=90%	4649
$\pi^+\pi^-\pi^0\pi^0$	$(1.28 \pm 0.30) \times 10^{-5}$		4720
$K_S^0K^+\pi^- +$ c.c.	$(1.6 \pm 0.4) \times 10^{-6}$		4696
$K^*(892)^0\overline{K}^0 +$ c.c.	$(2.9 \pm 0.9) \times 10^{-6}$		4675
$K^*(892)^-K^+ +$ c.c.	$< 1.11 \times 10^{-6}$	CL=90%	4675
$f_1(1285)$ anything	$(4.6 \pm 3.1) \times 10^{-3}$		–
$D^*(2010)^\pm$ anything	(2.52 ± 0.20) %		–
$f_1(1285)X_{tetra}$	$< 6.24 \times 10^{-5}$	CL=90%	–
^2H anything	$(2.85 \pm 0.25) \times 10^{-5}$		–
Sum of 100 exclusive modes	(1.200 ± 0.017) %		–
Radiative decays			
$\gamma\pi^+\pi^-$	$(6.3 \pm 1.8) \times 10^{-5}$		4728
$\gamma\pi^0\pi^0$	$(1.7 \pm 0.7) \times 10^{-5}$		4728
$\gamma\pi\pi$ (S-wave)	$(4.6 \pm 0.7) \times 10^{-5}$		4728
$\gamma\pi^0\eta$	$< 2.4 \times 10^{-6}$	CL=90%	4713
γK^+K^-	[ssaa] $(1.14 \pm 0.13) \times 10^{-5}$		4704
$\gamma p\overline{p}$	[ttaa] $< 6 \times 10^{-6}$	CL=90%	4636
$\gamma 2h^+2h^-$	$(7.0 \pm 1.5) \times 10^{-4}$		4720
$\gamma 3h^+3h^-$	$(5.4 \pm 2.0) \times 10^{-4}$		4703
$\gamma 4h^+4h^-$	$(7.4 \pm 3.5) \times 10^{-4}$		4679
$\gamma\pi^+\pi^-K^+K^-$	$(2.9 \pm 0.9) \times 10^{-4}$		4686
$\gamma 2\pi^+2\pi^-$	$(2.5 \pm 0.9) \times 10^{-4}$		4720
$\gamma 3\pi^+3\pi^-$	$(2.5 \pm 1.2) \times 10^{-4}$		4703
$\gamma 2\pi^+2\pi^-K^+K^-$	$(2.4 \pm 1.2) \times 10^{-4}$		4659
$\gamma\pi^+\pi^-p\overline{p}$	$(1.5 \pm 0.6) \times 10^{-4}$		4604
$\gamma 2\pi^+2\pi^-p\overline{p}$	$(4 \pm 6) \times 10^{-5}$		4563
$\gamma 2K^+2K^-$	$(2.0 \pm 2.0) \times 10^{-5}$		4601
$\gamma\eta'(958)$	$< 1.9 \times 10^{-6}$	CL=90%	4682
$\gamma\eta$	$< 1.0 \times 10^{-6}$	CL=90%	4714
$\gamma f_0(980)$	$< 3 \times 10^{-5}$	CL=90%	4678
$\gamma f_2'(1525)$	$(2.9 \pm 0.6) \times 10^{-5}$		4609
$\gamma f_2(1270)$	$(1.01 \pm 0.06) \times 10^{-4}$		4644
$\gamma\eta(1405)$	$< 8.2 \times 10^{-5}$	CL=90%	4625
$\gamma f_0(1500)$	$< 1.5 \times 10^{-5}$	CL=90%	4608
$\gamma f_0(1500) \to \gamma K^+K^-$	$(1.0 \pm 0.4) \times 10^{-5}$		–
$\gamma f_0(1710)$	$< 2.6 \times 10^{-4}$	CL=90%	4573
$\gamma f_0(1710) \to \gamma K^+K^-$	$(1.01 \pm 0.32) \times 10^{-5}$		–
$\gamma f_0(1710) \to \gamma\pi^+\pi^-$	$(5.3 \pm 2.0) \times 10^{-6}$		–
$\gamma f_0(1710) \to \gamma\pi^0\pi^0$	$< 1.4 \times 10^{-6}$	CL=90%	–
$\gamma f_0(1710) \to \gamma\eta\eta$	$< 1.8 \times 10^{-6}$	CL=90%	–
$\gamma f_4(2050)$	$< 5.3 \times 10^{-5}$	CL=90%	4515
$\gamma f_0(2200) \to \gamma K^+K^-$	$< 2 \times 10^{-4}$	CL=90%	4475
$\gamma f_J(2220) \to \gamma K^+K^-$	$< 8 \times 10^{-7}$	CL=90%	4469
$\gamma f_J(2220) \to \gamma\pi^+\pi^-$	$< 6 \times 10^{-7}$	CL=90%	–
$\gamma f_J(2220) \to \gamma p\overline{p}$	$< 1.1 \times 10^{-6}$	CL=90%	–
$\gamma\eta(2225) \to \gamma\phi\phi$	$< 3 \times 10^{-3}$	CL=90%	4469
$\gamma\eta_c(1S)$	$< 2.9 \times 10^{-5}$	CL=90%	4260
$\gamma\eta_c(2S)$	$< 4 \times 10^{-4}$	CL=90%	4031
$\gamma\chi_{c0}$	$< 6.6 \times 10^{-5}$	CL=90%	4114
$\gamma\chi_{c1}$	$(4.7 {}^{+2.4}_{-1.9}) \times 10^{-5}$		4079
$\gamma\chi_{c2}$	$< 7.6 \times 10^{-6}$	CL=90%	4062
$\gamma\chi_{c1}(3872)$	$< 4 \times 10^{-5}$	CL=90%	3938
$\gamma\chi_{c1}(3872)$, $\chi_{c1} \to \pi^+\pi^-\pi^0J/\psi$	$< 2.8 \times 10^{-6}$	CL=90%	–
$\gamma\chi_{c0}(3915) \to \omega J/\psi$	$< 3.0 \times 10^{-6}$	CL=90%	–
$\gamma\chi_{c1}(4140) \to \phi J/\psi$	$< 2.2 \times 10^{-6}$	CL=90%	–

Int. J. Mod. Phys. A 2026.41. Downloaded from www.worldscientific.com
by UNIVERSITY OF CALIFORNIA @ BERKELEY on 09/16/26. Re-use and distribution is strictly not permitted, except for Open Access articles.

$\gamma X \overline{X}(m_X < 3.1$ GeV)	[uuaa]	< 1	$\times 10^{-3}$	CL=90%	–
$\gamma X \overline{X}(m_X < 4.5$ GeV)	[vvaa]	< 2.4	$\times 10^{-4}$	CL=90%	–
$\gamma X \to \gamma + \geq 4$ prongs	[xxaa]	< 1.78	$\times 10^{-4}$	CL=95%	–
$\gamma A^0 \to \gamma \mu^+ \mu^-$	[yyaa]	< 9	$\times 10^{-6}$	CL=90%	–
$\gamma A^0 \to \gamma \tau^+ \tau^-$	[ssaa]	< 1.30	$\times 10^{-4}$	CL=90%	–
$\gamma A^0 \to \gamma g g$	[zzaa]	< 1	%	CL=90%	–
$\gamma A^0 \to \gamma s \overline{s}$	[zzaa]	< 1	$\times 10^{-3}$	CL=90%	–
Lepton Family number (*LF*) violating modes					
$e^\pm \mu^\mp$	*LF*	< 3.9	$\times 10^{-7}$	CL=90%	4730
$\mu^\pm \tau^\mp$	*LF*	< 2.7	$\times 10^{-6}$	CL=90%	4563
$e^\pm \tau^\mp$	*LF*	< 2.7	$\times 10^{-6}$	CL=90%	4563
$\gamma e^\pm \mu^\mp$	*LF*	< 4.2	$\times 10^{-7}$	CL=90%	4730
$\gamma \mu^\pm \tau^\mp$	*LF*	< 6.1	$\times 10^{-6}$	CL=90%	4563
$\gamma e^\pm \tau^\mp$	*LF*	< 6.5	$\times 10^{-6}$	CL=90%	4563
Other decays					
invisible		< 3.0	$\times 10^{-4}$	CL=90%	–
hadrons		(96 ± 4) %			–

$\chi_{b0}(1P)$

$I^G(J^{PC}) = 0^+(0^{++})$
J needs confirmation.

Mass $m = 9859.44 \pm 0.42 \pm 0.31$ MeV

$\chi_{b0}(1P)$ DECAY MODES	Fraction (Γ_i/Γ)		Confidence level	p (MeV/c)
$\gamma \Upsilon(1S)$	(1.94 ± 0.27) %			391
$D^0 X$	< 10.4	%	90%	–
$\pi^+ \pi^- K^+ K^- \pi^0$	< 1.6	$\times 10^{-4}$	90%	4875
$2\pi^+ \pi^- K^- K^0_S$	< 5	$\times 10^{-5}$	90%	4875
$2\pi^+ \pi^- K^- K^0_S 2\pi^0$	< 5	$\times 10^{-4}$	90%	4846
$2\pi^+ 2\pi^- 2\pi^0$	< 2.1	$\times 10^{-4}$	90%	4905
$2\pi^+ 2\pi^- K^+ K^-$	$(1.1 \pm 0.6) \times 10^{-4}$			4861
$2\pi^+ 2\pi^- K^+ K^- \pi^0$	< 2.7	$\times 10^{-4}$	90%	4846
$2\pi^+ 2\pi^- K^+ K^- 2\pi^0$	< 5	$\times 10^{-4}$	90%	4828
$3\pi^+ 2\pi^- K^- K^0_S \pi^0$	< 1.6	$\times 10^{-4}$	90%	4827
$3\pi^+ 3\pi^-$	< 8	$\times 10^{-5}$	90%	4904
$3\pi^+ 3\pi^- 2\pi^0$	< 6	$\times 10^{-4}$	90%	4881
$3\pi^+ 3\pi^- K^+ K^-$	$(2.4 \pm 1.2) \times 10^{-4}$			4827
$3\pi^+ 3\pi^- K^+ K^- \pi^0$	< 1.0	$\times 10^{-3}$	90%	4808
$4\pi^+ 4\pi^-$	< 8	$\times 10^{-5}$	90%	4880
$4\pi^+ 4\pi^- 2\pi^0$	< 2.1	$\times 10^{-3}$	90%	4850
$J/\psi J/\psi$	< 7	$\times 10^{-5}$	90%	3836
$J/\psi \psi(2S)$	< 1.2	$\times 10^{-4}$	90%	3571
$\psi(2S) \psi(2S)$	< 3.1	$\times 10^{-5}$	90%	3273
$J/\psi(1S)$ anything	< 2.3	$\times 10^{-3}$	90%	–

$\chi_{b1}(1P)$

$I^G(J^{PC}) = 0^+(1^{++})$
J needs confirmation.

Mass $m = 9892.78 \pm 0.26 \pm 0.31$ MeV
$m_{\chi_{b1}(1P)} - m_{\Upsilon(1S)} = 432.10 \pm 0.28$ MeV

$\chi_{b1}(1P)$ DECAY MODES	Fraction (Γ_i/Γ)		Confidence level	p (MeV/c)
$\gamma \Upsilon(1S)$	(35.2 ± 2.0) %			423
$D^0 X$	(12.6 ± 2.2) %			–
$\pi^+ \pi^- K^+ K^- \pi^0$	$(2.0 \pm 0.6) \times 10^{-4}$			4892
$2\pi^+ \pi^- K^- K^0_S$	$(1.3 \pm 0.5) \times 10^{-4}$			4892
$2\pi^+ \pi^- K^- K^0_S 2\pi^0$	< 6	$\times 10^{-4}$	90%	4863
$2\pi^+ 2\pi^- 2\pi^0$	$(8.0 \pm 2.5) \times 10^{-4}$			4921
$2\pi^+ 2\pi^- K^+ K^-$	$(1.5 \pm 0.5) \times 10^{-4}$			4878
$2\pi^+ 2\pi^- K^+ K^- \pi^0$	$(3.5 \pm 1.2) \times 10^{-4}$			4863
$2\pi^+ 2\pi^- K^+ K^- 2\pi^0$	$(8.6 \pm 3.2) \times 10^{-4}$			4845
$3\pi^+ 2\pi^- K^- K^0_S \pi^0$	$(9.3 \pm 3.3) \times 10^{-4}$			4844
$3\pi^+ 3\pi^-$	$(1.9 \pm 0.6) \times 10^{-4}$			4921
$3\pi^+ 3\pi^- 2\pi^0$	$(1.7 \pm 0.5) \times 10^{-3}$			4898
$3\pi^+ 3\pi^- K^+ K^-$	$(2.6 \pm 0.8) \times 10^{-4}$			4844
$3\pi^+ 3\pi^- K^+ K^- \pi^0$	$(7.5 \pm 2.6) \times 10^{-4}$			4825
$4\pi^+ 4\pi^-$	$(2.6 \pm 0.9) \times 10^{-4}$			4897
$4\pi^+ 4\pi^- 2\pi^0$	$(1.4 \pm 0.6) \times 10^{-3}$			4867
ω anything	(4.9 ± 1.4) %			–
ωX_{tetra}	< 4.44	$\times 10^{-4}$	90%	–
$J/\psi J/\psi$	< 2.7	$\times 10^{-5}$	90%	3857
$J/\psi \psi(2S)$	< 1.7	$\times 10^{-5}$	90%	3594
$\psi(2S) \psi(2S)$	< 6	$\times 10^{-5}$	90%	3298
$J/\psi(1S)$ anything	< 1.1	$\times 10^{-3}$	90%	–
$J/\psi(1S) X_{tetra}$	< 2.27	$\times 10^{-4}$	90%	–

$h_b(1P)$

$I^G(J^{PC}) = 0^-(1^{+-})$

Mass $m = 9899.3 \pm 0.8$ MeV

$h_b(1P)$ DECAY MODES	Fraction (Γ_i/Γ)	Confidence level	p (MeV/c)
$\eta_b(1S)\gamma$	(52^{+6}_{-5}) %		488
$\Upsilon(1S)\pi^0$	$< 1.8 \times 10^{-3}$	90%	408

$\chi_{b2}(1P)$

$I^G(J^{PC}) = 0^+(2^{++})$
J needs confirmation.

Mass $m = 9912.21 \pm 0.26 \pm 0.31$ MeV

$\chi_{b2}(1P)$ DECAY MODES	Fraction (Γ_i/Γ)		Confidence level	p (MeV/c)
$\gamma \Upsilon(1S)$	(18.0 ± 1.0) %			442
$D^0 X$	< 7.9	%	90%	–
$\pi^+ \pi^- K^+ K^- \pi^0$	$(8 \pm 5) \times 10^{-5}$			4902
$2\pi^+ \pi^- K^- K^0_S$	< 1.0	$\times 10^{-4}$	90%	4901
$2\pi^+ \pi^- K^- K^0_S 2\pi^0$	$(5.3 \pm 2.4) \times 10^{-4}$			4873
$2\pi^+ 2\pi^- 2\pi^0$	$(3.5 \pm 1.4) \times 10^{-4}$			4931
$2\pi^+ 2\pi^- K^+ K^-$	$(1.1 \pm 0.4) \times 10^{-4}$			4888
$2\pi^+ 2\pi^- K^+ K^- \pi^0$	$(2.1 \pm 0.9) \times 10^{-4}$			4872
$2\pi^+ 2\pi^- K^+ K^- 2\pi^0$	$(3.9 \pm 1.8) \times 10^{-4}$			4855
$3\pi^+ 2\pi^- K^- K^0_S \pi^0$	< 5	$\times 10^{-4}$	90%	4854
$3\pi^+ 3\pi^-$	$(7.0 \pm 3.1) \times 10^{-5}$			4931
$3\pi^+ 3\pi^- 2\pi^0$	$(1.0 \pm 0.4) \times 10^{-3}$			4908
$3\pi^+ 3\pi^- K^+ K^-$	< 8	$\times 10^{-5}$	90%	4854
$3\pi^+ 3\pi^- K^+ K^- \pi^0$	$(3.6 \pm 1.5) \times 10^{-4}$			4835
$4\pi^+ 4\pi^-$	$(8 \pm 4) \times 10^{-5}$			4907
$4\pi^+ 4\pi^- 2\pi^0$	$(1.8 \pm 0.7) \times 10^{-3}$			4877
$J/\psi J/\psi$	< 4	$\times 10^{-5}$	90%	3869
$J/\psi \psi(2S)$	< 5	$\times 10^{-5}$	90%	3608
$\psi(2S) \psi(2S)$	< 1.6	$\times 10^{-5}$	90%	3313
$J/\psi(1S)$ anything	$(1.5 \pm 0.4) \times 10^{-3}$			–

$\Upsilon(2S)$

$I^G(J^{PC}) = 0^-(1^{--})$

Mass $m = 10023.4 \pm 0.5$ MeV
$m_{\Upsilon(2S)} - m_{\Upsilon(1S)} = 562.81 \pm 0.11$ MeV
Full width $\Gamma = 31.98 \pm 2.63$ keV

$\Upsilon(2S)$ DECAY MODES	Fraction (Γ_i/Γ)		Scale factor/ Confidence level	p (MeV/c)
$\Upsilon(1S)\pi^+\pi^-$	(17.85 ± 0.26) %			475
$\Upsilon(1S)\pi^0\pi^0$	(8.6 ± 0.4) %			480
$\tau^+\tau^-$	(2.00 ± 0.21) %			4686
$\mu^+\mu^-$	(1.93 ± 0.17) %		S=2.2	5011
e^+e^-	(1.91 ± 0.16) %			5012
$\Upsilon(1S)\pi^0$	< 4	$\times 10^{-5}$	CL=90%	531
$\Upsilon(1S)\eta$	$(2.9 \pm 0.4) \times 10^{-4}$		S=2.0	126
$J/\psi(1S)$ anything	< 6	$\times 10^{-3}$	CL=90%	4533
$J/\psi(1S)\eta_c$	< 5.4	$\times 10^{-6}$	CL=90%	3984
$J/\psi(1S)\chi_{c0}$	< 3.4	$\times 10^{-6}$	CL=90%	3808
$J/\psi(1S)\chi_{c1}$	< 1.2	$\times 10^{-6}$	CL=90%	3765
$J/\psi(1S)\chi_{c2}$	< 2.0	$\times 10^{-6}$	CL=90%	3745
$J/\psi(1S)\eta_c(2S)$	< 2.5	$\times 10^{-6}$	CL=90%	3706
$J/\psi(1S)X(3940)$	< 2.0	$\times 10^{-6}$	CL=90%	3555
$J/\psi(1S)X(4160)$	< 2.0	$\times 10^{-6}$	CL=90%	3442
χ_{c1} anything	$(2.2 \pm 0.5) \times 10^{-4}$			–
$\chi_{c1}(1P)^0 X_{tetra}$	< 3.67	$\times 10^{-5}$	CL=90%	–
χ_{c2} anything	$(2.3 \pm 0.8) \times 10^{-4}$			–
$\psi(2S)\eta_c$	< 5.1	$\times 10^{-6}$	CL=90%	3732
$\psi(2S)\chi_{c0}$	< 4.7	$\times 10^{-6}$	CL=90%	3536
$\psi(2S)\chi_{c1}$	< 2.5	$\times 10^{-6}$	CL=90%	3488
$\psi(2S)\chi_{c2}$	< 1.9	$\times 10^{-6}$	CL=90%	3464
$\psi(2S)\eta_c(2S)$	< 3.3	$\times 10^{-6}$	CL=90%	3422
$\psi(2S)X(3940)$	< 3.9	$\times 10^{-6}$	CL=90%	3250
$\psi(2S)X(4160)$	< 3.9	$\times 10^{-6}$	CL=90%	3120
$T_{c\overline{c}1}(3900)^+ T_{c\overline{c}1}(3900)^-$	< 1.0	$\times 10^{-6}$	CL=90%	–
$T_{c\overline{c}1}(4200)^+ T_{c\overline{c}1}(4200)^-$	< 1.67	$\times 10^{-5}$	CL=90%	–
$T_{c\overline{c}1}(3900)^\pm T_{c\overline{c}1}(4200)^\mp$	< 7.3	$\times 10^{-6}$	CL=90%	–
$T_{c\overline{c}}(4050)^+ T_{c\overline{c}}(4050)^-$	< 1.35	$\times 10^{-5}$	CL=90%	–
$T_{c\overline{c}}(4250)^+ T_{c\overline{c}}(4250)^-$	< 2.67	$\times 10^{-5}$	CL=90%	–
$T_{c\overline{c}}(4050)^\pm T_{c\overline{c}}(4250)^\mp$	< 2.72	$\times 10^{-5}$	CL=90%	–
$T_{c\overline{c}1}(4430)^+ T_{c\overline{c}1}(4430)^-$	< 2.03	$\times 10^{-5}$	CL=90%	–

Int. J. Mod. Phys. A 2026.41. Downloaded from www.worldscientific.com
by UNIVERSITY OF CALIFORNIA @ BERKELEY on 09/16/26. Re-use and distribution is strictly not permitted, except for Open Acce

$T_{c\overline{c}}(4055)^{\pm}\, T_{c\overline{c}}(4055)^{\mp}$	$< 1.11 \times 10^{-5}$	CL=90%	–
$T_{c\overline{c}}(4055)^{\pm}\, T_{c\overline{c}1}(4430)^{\mp}$	$< 2.11 \times 10^{-5}$	CL=90%	–
$P_{c\overline{c}s}(4459)/\overline{P}_{c\overline{c}s}(4459)$ anything	$(2.9 \pm 1.7) \times 10^{-6}$		–
$P_{c\overline{c}s}(4338)/\overline{P}_{c\overline{c}s}(4338)$ anything	$< 1.6 \times 10^{-6}$	CL=90%	–
$P_c(4457)$ anything, $P_c(4457) \to p J/\psi(1S)$	$< 4.6 \times 10^{-6}$	CL=90%	–
$P_c(4440)$ anything, $P_c(4440) \to p J/\psi(1S)$	$< 1.18 \times 10^{-5}$	CL=90%	–
$P_c(4312)$ anything, $P_c(4312) \to p J/\psi(1S)$	$< 7.2 \times 10^{-6}$	CL=90%	–
$p/\overline{p} J/\psi(1S)$ anything	$(4.3 \pm 0.6) \times 10^{-5}$		–
$J/\psi(1S)\Lambda/\overline{\Lambda}$ anything	$(2.2 \pm 0.6) \times 10^{-5}$		–
$\overline{^2H}$ anything	$(2.78^{+0.30}_{-0.26}) \times 10^{-5}$	S=1.2	–
hadrons	(94 ± 11) %		–
ggg	(58.8 ± 1.2) %		–
γgg	(1.87 ± 0.28) %		–
$\phi K^+ K^-$	$(1.6 \pm 0.4) \times 10^{-6}$		4910
$\omega \pi^+ \pi^-$	$< 2.58 \times 10^{-6}$	CL=90%	4977
$K^*(892)^0 K^- \pi^+ +$ c.c.	$(2.3 \pm 0.7) \times 10^{-6}$		4952
$\phi f_2'(1525)$	$< 1.33 \times 10^{-6}$	CL=90%	4843
$\omega f_2(1270)$	$< 5.7 \times 10^{-7}$	CL=90%	4899
$\rho(770) a_2(1320)$	$< 8.8 \times 10^{-7}$	CL=90%	4894
$K^*(892)^0 \overline{K}_2^*(1430)^0 +$ c.c.	$(1.5 \pm 0.6) \times 10^{-6}$		4869
$K_1(1270)^{\pm} K^{\mp}$	$< 3.22 \times 10^{-6}$	CL=90%	4920
$K_1(1400)^{\pm} K^{\mp}$	$< 8.3 \times 10^{-7}$	CL=90%	4901
$b_1(1235)^{\pm} \pi^{\mp}$	$< 4.0 \times 10^{-7}$	CL=90%	4935
$\rho\pi$	$< 1.16 \times 10^{-6}$	CL=90%	4981
$\pi^+ \pi^- \pi^0$	$< 8.0 \times 10^{-7}$	CL=90%	5007
$\omega \pi^0$	$< 1.63 \times 10^{-6}$	CL=90%	4980
$\pi^+ \pi^- \pi^0 \pi^0$	$(1.30 \pm 0.28) \times 10^{-5}$		5002
$K_S^0 K^+ \pi^- +$ c.c.	$(1.14 \pm 0.33) \times 10^{-6}$		4979
$K^*(892)^0 \overline{K}^0 +$ c.c.	$< 4.22 \times 10^{-6}$	CL=90%	4959
$K^*(892)^- K^+ +$ c.c.	$< 1.45 \times 10^{-6}$	CL=90%	4960
$f_1(1285)$ anything	$(2.2 \pm 1.6) \times 10^{-3}$		–
$f_1(1285) X_{tetra}$	$< 6.47 \times 10^{-5}$	CL=90%	–
$D_s^+ D_{s1}(2536)^-$, $D_{s1}^- \to K^- D^*(2007)^0$	$(1.6 \pm 0.4) \times 10^{-5}$		–
$D_s^+ D_{s1}(2536)^-$, $D_{s1}^- \to K_S^0 D^*(2010)^-$	$(8.4 \pm 2.3) \times 10^{-6}$		–
$D_s^{*+} D_{s1}(2536)^-$, $D_{s1}^- \to K^- D^*(2007)^0$	$(1.4 \pm 0.4) \times 10^{-5}$		–
$D_s^{*+} D_{s1}(2536)^-$, $D_{s1}^- \to K_S^0 D^*(2010)^-$	$(8.2 \pm 3.1) \times 10^{-6}$		–
$D_s^+ D_{s2}^*(2573)^-$, $D_{s2}^{*-} \to K^- D^0$	$(1.4 \pm 0.4) \times 10^{-5}$		–
$D_s^+ D_{s2}^*(2573)^-$, $D_{s2}^{*-} \to K_S^0 D^-$	$(6.9 \pm 3.0) \times 10^{-6}$		–
$D_s^{*+} D_{s2}^*(2573)^-$, $D_{s2}^{*-} \to K^- D^0$	$(9 \pm 5) \times 10^{-6}$		–
$D_s^{*+} D_{s2}^*(2573)^-$, $D_{s2}^{*-} \to K_S^0 D^-$	$(5 \pm 6) \times 10^{-6}$		–
Sum of 100 exclusive modes	$(2.90 \pm 0.30) \times 10^{-3}$		–

Radiative decays

$\gamma \chi_{b1}(1P)$	(6.9 ± 0.4) %		130
$\gamma \chi_{b2}(1P)$	(7.15 ± 0.35) %		111
$\gamma \chi_{b0}(1P)$	(3.8 ± 0.4) %		163
$\gamma f_0(1710)$	$< 5.9 \times 10^{-4}$	CL=90%	4864
$\gamma f_2'(1525)$	$< 5.3 \times 10^{-4}$	CL=90%	4897
$\gamma f_2(1270)$	$< 2.41 \times 10^{-4}$	CL=90%	4931
$\gamma \eta_c(1S)$	$< 2.7 \times 10^{-5}$	CL=90%	4567
$\gamma \chi_{c0}$	$< 1.0 \times 10^{-4}$	CL=90%	4430
$\gamma \chi_{c1}$	$< 3.6 \times 10^{-6}$	CL=90%	4397
$\gamma \chi_{c2}$	$< 1.5 \times 10^{-5}$	CL=90%	4381
$\gamma \chi_{c1}(3872)$	$< 1.8 \times 10^{-5}$	CL=90%	4264
$\gamma \chi_{c1}(3872)$, $\chi_{c1} \to \pi^+ \pi^- \pi^0 J/\psi$	$< 2.4 \times 10^{-6}$	CL=90%	–
$\gamma \chi_{c0}(3915) \to \omega J/\psi$	$< 2.8 \times 10^{-6}$	CL=90%	–
$\gamma \chi_{c1}(4140) \to \phi J/\psi$	$< 1.2 \times 10^{-6}$	CL=90%	–
$\gamma X(4350) \to \phi J/\psi$	$< 1.3 \times 10^{-6}$	CL=90%	–
$\gamma \eta_b(1S)$	$(5.5^{+1.1}_{-0.9}) \times 10^{-4}$	S=1.2	605
$\gamma \eta_b(1S) \to \gamma$ Sum of 26 exclusive modes	$< 3.7 \times 10^{-6}$	CL=90%	–
$\gamma X_{b\overline{b}} \to \gamma$ Sum of 26 exclusive modes	$< 4.9 \times 10^{-6}$	CL=90%	–
$\gamma X \to \gamma + \geq 4$ prongs [aabb]	$< 1.95 \times 10^{-4}$	CL=95%	–
$\gamma A^0 \to \gamma$ hadrons	$< 8 \times 10^{-5}$	CL=90%	–
$\gamma A^0 \to \gamma \mu^+ \mu^-$	$< 8.3 \times 10^{-6}$	CL=90%	–

Lepton Family number (*LF*) violating modes

$e^{\pm} \tau^{\mp}$	*LF*	$< 1.12 \times 10^{-6}$	CL=90%	4854
$\mu^{\pm} \tau^{\mp}$	*LF*	$< 2.3 \times 10^{-7}$	CL=90%	4854

$\Upsilon_2(1D)$

$I^G(J^{PC}) = 0^-(2^{--})$

was $\Upsilon(1D)$

Mass $m = 10163.7 \pm 1.4$ MeV (S = 1.7)

$\Upsilon_2(1D)$ DECAY MODES	Fraction (Γ_i/Γ)	p (MeV/c)
$\gamma\gamma \Upsilon(1S)$	seen	679
$\gamma \chi_{bJ}(1P)$	seen	300
$\eta \Upsilon(1S)$	not seen	426
$\pi^+ \pi^- \Upsilon(1S)$	$(6.6 \pm 1.6) \times 10^{-3}$	623

$\chi_{b0}(2P)$

$I^G(J^{PC}) = 0^+(0^{++})$
J needs confirmation.

Mass $m = 10232.5 \pm 0.4 \pm 0.5$ MeV

$\chi_{b0}(2P)$ DECAY MODES	Fraction (Γ_i/Γ)	Confidence level	p (MeV/c)
$\gamma \Upsilon(2S)$	(1.38 ± 0.30) %		207
$\omega \Upsilon(1S)$	$(5.5 \pm 2.0) \times 10^{-3}$		†
$\gamma \Upsilon(1S)$	$(3.8 \pm 1.7) \times 10^{-3}$		743
$D^0 X$	< 8.2 %	90%	–
$\pi^+ \pi^- K^+ K^- \pi^0$	$< 3.4 \times 10^{-5}$	90%	5064
$2\pi^+ \pi^- K^- K_S^0$	$< 5 \times 10^{-5}$	90%	5063
$2\pi^+ \pi^- K^- K_S^0 2\pi^0$	$< 2.2 \times 10^{-4}$	90%	5036
$2\pi^+ 2\pi^- 2\pi^0$	$< 2.4 \times 10^{-4}$	90%	5092
$2\pi^+ 2\pi^- K^+ K^-$	$< 1.5 \times 10^{-4}$	90%	5050
$2\pi^+ 2\pi^- K^+ K^- \pi^0$	$< 2.2 \times 10^{-4}$	90%	5035
$2\pi^+ 2\pi^- K^+ K^- 2\pi^0$	$< 1.1 \times 10^{-3}$	90%	5019
$3\pi^+ 2\pi^- K^- K_S^0 \pi^0$	$< 7 \times 10^{-4}$	90%	5018
$3\pi^+ 3\pi^-$	$< 7 \times 10^{-5}$	90%	5091
$3\pi^+ 3\pi^- 2\pi^0$	$< 1.2 \times 10^{-3}$	90%	5070
$3\pi^+ 3\pi^- K^+ K^-$	$< 1.5 \times 10^{-4}$	90%	5017
$3\pi^+ 3\pi^- K^+ K^- \pi^0$	$< 7 \times 10^{-4}$	90%	4999
$4\pi^+ 4\pi^-$	$< 1.7 \times 10^{-4}$	90%	5069
$4\pi^+ 4\pi^- 2\pi^0$	$< 6 \times 10^{-4}$	90%	5039

$\chi_{b1}(2P)$

$I^G(J^{PC}) = 0^+(1^{++})$
J needs confirmation.

Mass $m = 10255.46 \pm 0.22 \pm 0.50$ MeV
$m_{\chi_{b1}(2P)} - m_{\chi_{b0}(2P)} = 23.5 \pm 1.0$ MeV
$m_{\chi_{b1}(2P)} - m_{\Upsilon(1S)} = 793.6 \pm 0.8$ MeV

$\chi_{b1}(2P)$ DECAY MODES	Fraction (Γ_i/Γ)	Scale factor	p (MeV/c)
$\omega \Upsilon(1S)$	(2.1 ± 0.4) %	1.6	134
$\gamma \Upsilon(2S)$	(18.1 ± 1.9) %		229
$\gamma \Upsilon(1S)$	(9.9 ± 1.0) %		764
$\pi\pi \chi_{b1}(1P)$	$(9.1 \pm 1.3) \times 10^{-3}$		238
$D^0 X$	(8.8 ± 1.7) %		–
$\pi^+ \pi^- K^+ K^- \pi^0$	$(3.1 \pm 1.0) \times 10^{-4}$		5075
$2\pi^+ \pi^- K^- K_S^0$	$(1.1 \pm 0.5) \times 10^{-4}$		5075
$2\pi^+ \pi^- K^- K_S^0 2\pi^0$	$(7.7 \pm 3.2) \times 10^{-4}$		5047
$2\pi^+ 2\pi^- 2\pi^0$	$(5.9 \pm 2.0) \times 10^{-4}$		5104
$2\pi^+ 2\pi^- K^+ K^-$	$(10 \pm 4) \times 10^{-5}$		5062
$2\pi^+ 2\pi^- K^+ K^- \pi^0$	$(5.5 \pm 1.8) \times 10^{-4}$		5047
$2\pi^+ 2\pi^- K^+ K^- 2\pi^0$	$(10 \pm 4) \times 10^{-4}$		5030
$3\pi^+ 2\pi^- K^- K_S^0 \pi^0$	$(6.7 \pm 2.6) \times 10^{-4}$		5029
$3\pi^+ 3\pi^-$	$(1.2 \pm 0.4) \times 10^{-4}$		5103
$3\pi^+ 3\pi^- 2\pi^0$	$(1.2 \pm 0.4) \times 10^{-3}$		5081
$3\pi^+ 3\pi^- K^+ K^-$	$(2.0 \pm 0.8) \times 10^{-4}$		5029
$3\pi^+ 3\pi^- K^+ K^- \pi^0$	$(6.1 \pm 2.2) \times 10^{-4}$		5011
$4\pi^+ 4\pi^-$	$(1.7 \pm 0.6) \times 10^{-4}$		5080
$4\pi^+ 4\pi^- 2\pi^0$	$(1.9 \pm 0.7) \times 10^{-3}$		5051

Int. J. Mod. Phys. A 2026.41. Downloaded from www.worldscientific.com
by UNIVERSITY OF CALIFORNIA @ BERKELEY on 09/16/26. Re-use and distribution is strictly not permitted, except for Open Access articles.

$h_b(2P)$

$I^G(J^{PC}) = 0^-(1^{+-})$

Mass $m = 10259.8 \pm 1.2$ MeV

$h_b(2P)$ DECAY MODES	Fraction (Γ_i/Γ)	Confidence level	p (MeV/c)
hadrons	not seen		–
$\eta_b(1S)\gamma$	(22 ± 5) %		825
$\eta_b(2S)\gamma$	(48 ± 13) %		257
$\Upsilon(1S)\eta$	$(7.1^{+4.0}_{-3.3}) \times 10^{-3}$		559
$\Upsilon(1S)\pi^0$	$< 1.8 \times 10^{-3}$	90%	757
$\gamma\chi_{b0}(1P)$	< 27 %	90%	393
$\gamma\chi_{b1}(1P)$	$< 5.4 \times 10^{-3}$	90%	360
$\gamma\chi_{b2}(1P)$	< 1.3 %	90%	342

$\chi_{b2}(2P)$

$I^G(J^{PC}) = 0^+(2^{++})$
J needs confirmation.

Mass $m = 10268.65 \pm 0.22 \pm 0.50$ MeV
$m_{\chi_{b2}(2P)} - m_{\chi_{b1}(2P)} = 13.2 \pm 0.4$ MeV (S = 1.8)

$\chi_{b2}(2P)$ DECAY MODES	Fraction (Γ_i/Γ)	Scale factor/ Confidence level	p (MeV/c)
$\omega\Upsilon(1S)$	$(5.7\pm2.0) \times 10^{-3}$	S=1.5	194
$\gamma\Upsilon(2S)$	(8.9 ± 1.2) %		242
$\gamma\Upsilon(1S)$	(6.6 ± 0.8) %		776
$\pi\pi\chi_{b2}(1P)$	$(5.1\pm0.9) \times 10^{-3}$		229
D^0X	< 2.4 %	CL=90%	–
$\pi^+\pi^-K^+K^-\pi^0$	$< 1.1 \times 10^{-4}$	CL=90%	5082
$2\pi^+\pi^-K^-K^0_S$	$< 9 \times 10^{-5}$	CL=90%	5082
$2\pi^+\pi^-K^-K^0_S2\pi^0$	$< 7 \times 10^{-4}$	CL=90%	5054
$2\pi^+2\pi^-2\pi^0$	$(3.9\pm1.6) \times 10^{-4}$		5110
$2\pi^+2\pi^-K^+K^-$	$(9 \pm 4) \times 10^{-5}$		5068
$2\pi^+2\pi^-K^+K^-\pi^0$	$(2.4\pm1.1) \times 10^{-4}$		5054
$2\pi^+2\pi^-K^+K^-2\pi^0$	$(4.7\pm2.3) \times 10^{-4}$		5037
$3\pi^+2\pi^-K^-K^0_S\pi^0$	$< 4 \times 10^{-4}$	CL=90%	5036
$3\pi^+3\pi^-$	$(9 \pm 4) \times 10^{-5}$		5110
$3\pi^+3\pi^-2\pi^0$	$(1.2\pm0.4) \times 10^{-3}$		5088
$3\pi^+3\pi^-K^+K^-$	$(1.4\pm0.7) \times 10^{-4}$		5036
$3\pi^+3\pi^-K^+K^-\pi^0$	$(4.2\pm1.7) \times 10^{-4}$		5017
$4\pi^+4\pi^-$	$(9 \pm 5) \times 10^{-5}$		5087
$4\pi^+4\pi^-2\pi^0$	$(1.3\pm0.5) \times 10^{-3}$		5058

$\Upsilon(3S)$

$I^G(J^{PC}) = 0^-(1^{--})$

Mass $m = 10355.1 \pm 0.5$ MeV
$m_{\Upsilon(3S)} - m_{\Upsilon(2S)} = 331.82 \pm 0.08$ MeV (S = 1.9)
Full width $\Gamma = 20.32 \pm 1.85$ keV

$\Upsilon(3S)$ DECAY MODES	Fraction (Γ_i/Γ)	Scale factor/ Confidence level	p (MeV/c)
$\Upsilon(2S)$ anything	(10.6 ± 0.8) %		296
$\Upsilon(2S)\pi^+\pi^-$	(2.82 ± 0.18) %	S=1.6	176
$\Upsilon(2S)\pi^0\pi^0$	(1.85 ± 0.14) %		190
$\Upsilon(2S)\gamma\gamma$	(5.0 ± 0.7) %		326
$\Upsilon(2S)\pi^0$	$< 5.1 \times 10^{-4}$	CL=90%	298
$\Upsilon(1S)\pi^+\pi^-$	(4.37 ± 0.08) %		813
$\Upsilon(1S)\pi^0\pi^0$	(2.20 ± 0.13) %		816
$\Upsilon(1S)\eta$	$< 1 \times 10^{-4}$	CL=90%	677
$\Upsilon(1S)\pi^0$	$< 7 \times 10^{-5}$	CL=90%	846
$h_b(1P)\pi^0$	$< 1.2 \times 10^{-3}$	CL=90%	426
$h_b(1P)\pi^0 \to \gamma\eta_b(1S)\pi^0$	$(4.3 \pm 1.4) \times 10^{-4}$		–
$h_b(1P)\pi^+\pi^-$	$< 1.2 \times 10^{-4}$	CL=90%	352
$\tau^+\tau^-$	(2.29 ± 0.30) %		4863
$\mu^+\mu^-$	(2.18 ± 0.21) %	S=2.1	5176
e^+e^-	(2.18 ± 0.20) %		5178
hadrons	(93 ± 12) %		–
ggg	(35.7 ± 2.6) %		–
γgg	$(9.7 \pm 1.8) \times 10^{-3}$		–
${}^2H$ anything	$(2.33\pm 0.33) \times 10^{-5}$		–
Radiative decays			
$\gamma\chi_{b2}(2P)$	(13.1 ± 1.6) %	S=3.4	86
$\gamma\chi_{b1}(2P)$	(12.6 ± 1.2) %	S=2.4	99
$\gamma\chi_{b0}(2P)$	(5.9 ± 0.6) %	S=1.4	122
$\gamma\chi_{b2}(1P)$	$(10.0 \pm 1.0) \times 10^{-3}$	S=1.7	433
$\gamma\chi_{b1}(1P)$	$(9 \pm 5) \times 10^{-4}$	S=1.8	452
$\gamma\chi_{b0}(1P)$	$(2.7 \pm 0.4) \times 10^{-3}$		484
$\gamma\eta_b(2S)$	$< 6.2 \times 10^{-4}$	CL=90%	350
$\gamma\eta_b(1S)$	$(5.1 \pm 0.7) \times 10^{-4}$		912
$\gamma A^0 \to \gamma$ hadrons	$< 8 \times 10^{-5}$	CL=90%	–
$\gamma X \to \gamma + \geq 4$ prongs	[bbbb] $< 2.2 \times 10^{-4}$	CL=95%	–
$\gamma A^0 \to \gamma\mu^+\mu^-$	$< 5.5 \times 10^{-6}$	CL=90%	–
$\gamma A^0 \to \gamma\tau^+\tau^-$	[ccbb] $< 1.6 \times 10^{-4}$	CL=90%	–
Lepton Family number (*LF*) violating modes			
$e^\pm\tau^\mp$	*LF* $< 4.2 \times 10^{-6}$	CL=90%	5025
$e^\pm\mu^\mp$	*LF* $< 3.6 \times 10^{-7}$	CL=90%	5177
$\mu^\pm\tau^\mp$	*LF* $< 3.1 \times 10^{-6}$	CL=90%	5025

$\chi_{b1}(3P)$

$I^G(J^{PC}) = 0^+(1^{++})$
J needs confirmation.

Mass $m = 10513.4 \pm 0.7$ MeV

$\chi_{b1}(3P)$ DECAY MODES	Fraction (Γ_i/Γ)	p (MeV/c)
$\Upsilon(1S)\gamma$	seen	1000
$\Upsilon(2S)\gamma$	seen	479
$\Upsilon(3S)\gamma$	seen	157

$\chi_{b2}(3P)$

$I^G(J^{PC}) = 0^+(2^{++})$
J needs confirmation.

Mass $m = 10524.0 \pm 0.8$ MeV

$\chi_{b2}(3P)$ DECAY MODES	Fraction (Γ_i/Γ)	p (MeV/c)
$\Upsilon(3S)\gamma$	seen	168

$\Upsilon(4S)$

$I^G(J^{PC}) = 0^-(1^{--})$

also known as $\Upsilon(10580)$
Mass $m = 10579.4 \pm 1.2$ MeV
Full width $\Gamma = 20.5 \pm 2.5$ MeV

$\Upsilon(4S)$ DECAY MODES	Fraction (Γ_i/Γ)	Confidence level	p (MeV/c)
$B\overline{B}$	> 96 %	95%	326
B^+B^-	$(51.1 {}^{+0.7}_{-1.1})$ %		331
D^+_s anything + c.c.	(17.8 ± 2.6) %		–
$B^0\overline{B}^0$	(48.6 ± 0.8) %		326
$J/\psi K^0_S + (J/\psi, \eta_c)K^0_S$	$< 4 \times 10^{-7}$	90%	–
non-$B\overline{B}$	$(2.64^{+13.00}_{-0.20}) \times 10^{-3}$		–
e^+e^-	$(1.57\pm 0.08) \times 10^{-5}$		5290
$\rho^+\rho^-$	$< 5.7 \times 10^{-6}$	90%	5233
$K^*(892)^0\overline{K}^0$	$< 2.0 \times 10^{-6}$	90%	5240
$J/\psi(1S)$ anything	$< 1.9 \times 10^{-4}$	95%	–
D^{*+} anything + c.c.	< 7.4 %	90%	5099
ϕ anything	(7.1 ± 0.6) %		5240
$\phi\eta$	$< 1.8 \times 10^{-6}$	90%	5226
$\phi\eta'$	$< 4.3 \times 10^{-6}$	90%	5196
$\rho\eta$	$< 1.3 \times 10^{-6}$	90%	5247
$\rho\eta'$	$< 2.5 \times 10^{-6}$	90%	5217
$\Upsilon(1S)$ anything	$< 4 \times 10^{-3}$	90%	1053
$\Upsilon(1S)\pi^+\pi^-$	$(8.2 \pm 0.4) \times 10^{-5}$		1026
$\Upsilon(1S)\eta$	$(1.81\pm 0.18) \times 10^{-4}$		924
$\Upsilon(1S)\eta'$	$(3.4 \pm 0.9) \times 10^{-5}$		–
$\Upsilon(2S)\pi^+\pi^-$	$(8.2 \pm 0.8) \times 10^{-5}$		468
$h_b(1P)\pi^+\pi^-$	not seen		600
$h_b(1P)\eta$	$(2.18\pm 0.21) \times 10^{-3}$		390
$\eta_b(1S)\omega$	$< 1.8 \times 10^{-4}$	90%	–
${}^2H$ anything	$< 1.3 \times 10^{-5}$	90%	–
Double Radiative Decays			
$\gamma\gamma\Upsilon(D) \to \gamma\gamma\eta\Upsilon(1S)$	$< 2.3 \times 10^{-5}$	90%	–

$\Upsilon(10753)$

$I^G(J^{PC}) = ?^?(1^{--})$

Mass $m = 10756.6 \pm 2.8$ MeV
Full width $\Gamma = 29 \pm 9$ MeV

Int. J. Mod. Phys. A 2026.41. Downloaded from www.worldscientific.com
by UNIVERSITY OF CALIFORNIA @ BERKELEY on 09/16/26. Re-use and distribution is strictly not permitted, except for Open Acce

$\Upsilon(10860)$

$I^G(J^{PC}) = 0^-(1^{--})$

Mass $m = 10885.2^{+2.6}_{-1.6}$ MeV
Full width $\Gamma = 37 \pm 4$ MeV

$\Upsilon(10860)$ DECAY MODES	Fraction (Γ_i/Γ)	Confidence level	p (MeV/c)
$B\overline{B}X$	$(73.5^{+1.5}_{-2.8})$ %		–
$B\overline{B}$	(5.5 ± 1.0) %		1322
$B\overline{B}^* +$ c.c.	(13.7 ± 1.6) %		–
$B^*\overline{B}^*$	(38.1 ± 3.4) %		1127
$B\overline{B}^{(*)}\pi$	< 19.7 %	90%	1015
$B\overline{B}\pi$	(0.0 ± 1.2) %		1015
$B^*\overline{B}\pi + B\overline{B}^*\pi$	(7.3 ± 2.3) %		–
$B^*\overline{B}^*\pi$	(1.0 ± 1.4) %		739
$B\overline{B}\pi\pi$	< 8.9 %	90%	550
$B_s^{(*)}\overline{B}_s^{(*)}$	(21.3 ± 1.5) %		904
$B_s\overline{B}_s$	$(6 \pm 5) \times 10^{-3}$		904
$B_s\overline{B}_s^* +$ c.c.	(1.44 ± 0.28) %		–
$B_s^*\overline{B}_s^*$	(18.7 ± 1.3) %		543
no open-bottom	$(4.8^{+4.0}_{-0.5})$ %		–
e^+e^-	$(8.3 \pm 2.1) \times 10^{-6}$		5443
$K^*(892)^0\overline{K}^0$	$< 1.0 \times 10^{-5}$	90%	5395
$\Upsilon(1S)\pi^+\pi^-$	$(5.3 \pm 0.6) \times 10^{-3}$		1306
$\Upsilon(1S)\eta$	$(8.5 \pm 1.7) \times 10^{-4}$		1229
$\Upsilon(1S)\eta'$	$< 6.9 \times 10^{-5}$	90%	985
$\Upsilon(2S)\pi^+\pi^-$	$(7.8 \pm 1.3) \times 10^{-3}$		783
$\Upsilon(2S)\eta$	$(4.1 \pm 0.6) \times 10^{-3}$		639
$\Upsilon(3S)\pi^+\pi^-$	$(4.8^{+1.9}_{-1.7}) \times 10^{-3}$		440
$\Upsilon(1S)K^+K^-$	$(6.1 \pm 1.8) \times 10^{-4}$		959
$\eta\Upsilon_J(1D)$	$(4.8 \pm 1.1) \times 10^{-3}$		–
$h_b(1P)\pi^+\pi^-$	$(3.5^{+1.0}_{-1.3}) \times 10^{-3}$		903
$h_b(2P)\pi^+\pi^-$	$(5.7^{+1.7}_{-2.1}) \times 10^{-3}$		544
$\chi_{bJ}(1P)\pi^+\pi^-\pi^0$	$(2.5 \pm 2.3) \times 10^{-3}$		894
$\chi_{b0}(1P)\pi^+\pi^-\pi^0$	$< 6.3 \times 10^{-3}$	90%	894
$\chi_{b0}(1P)\omega$	$< 3.9 \times 10^{-3}$	90%	631
$\chi_{b0}(1P)(\pi^+\pi^-\pi^0)_{\text{non}-\omega}$	$< 4.8 \times 10^{-3}$	90%	–
$\chi_{b1}(1P)\pi^+\pi^-\pi^0$	$(1.85 \pm 0.33) \times 10^{-3}$		861
$\chi_{b1}(1P)\omega$	$(1.57 \pm 0.30) \times 10^{-3}$		582
$\chi_{b1}(1P)(\pi^+\pi^-\pi^0)_{\text{non}-\omega}$	$(5.2 \pm 1.9) \times 10^{-4}$		–
$\chi_{b2}(1P)\pi^+\pi^-\pi^0$	$(1.17 \pm 0.30) \times 10^{-3}$		841
$\chi_{b2}(1P)\omega$	$(6.0 \pm 2.7) \times 10^{-4}$		552
$\chi_{b2}(1P)(\pi^+\pi^-\pi^0)_{\text{non}-\omega}$	$(6 \pm 4) \times 10^{-4}$		–
$\gamma X_b \to \gamma\Upsilon(1S)\omega$	$< 3.8 \times 10^{-5}$	90%	–
$\eta_b(1S)\omega$	$< 1.3 \times 10^{-3}$	90%	1177
$\eta_b(2S)\omega$	$< 5.6 \times 10^{-3}$	90%	399

Inclusive Decays.

These decay modes are submodes of one or more of the decay modes above.

ϕ anything	$(13.8^{+2.4}_{-1.7})$ %		–
D^0 anything + c.c.	(112 ± 6) %		–
D_s anything + c.c.	(44.7 ± 2.6) %		–
J/ψ anything	(2.06 ± 0.21) %		–
B^0 anything + c.c.	(77 ± 8) %		–
B^+ anything + c.c.	(72 ± 6) %		–

$\Upsilon(11020)$

$I^G(J^{PC}) = 0^-(1^{--})$

Mass $m = 11000 \pm 4$ MeV
Full width $\Gamma = 24^{+8}_{-6}$ MeV

$\Upsilon(11020)$ DECAY MODES	Fraction (Γ_i/Γ)	p (MeV/c)
e^+e^-	$(5.4^{+1.9}_{-2.1}) \times 10^{-6}$	5500
$\chi_{bJ}(1P)\pi^+\pi^-\pi^0$	$(9^{+9}_{-8}) \times 10^{-3}$	1007
$\chi_{b1}(1P)\pi^+\pi^-\pi^0$	seen	975
$\chi_{b2}(1P)\pi^+\pi^-\pi^0$	seen	956

OTHER MESONS

$T_{c\overline{c}1}(3900)$

$I^G(J^{PC}) = 1^+(1^{+-})$

was $Z_c(3900)$, $X(3900)$

Mass $m = 3886.7 \pm 2.3$ MeV (S = 1.7)
Full width $\Gamma = 29.5 \pm 2.4$ MeV

$T_{c\overline{c}1}(3900)$ DECAY MODES	Fraction (Γ_i/Γ)	p (MeV/c)
$J/\psi\pi$	seen	699
$h_c\pi^\pm$	not seen	318
$\eta_c\pi^+\pi^-$	not seen	758
$\eta_c(1S)\rho(770)^\pm$	seen	–
$(D\overline{D}^*)^\pm$	seen	–
$D^0D^{*-} +$ c.c.	seen	152
$D^-D^{*0} +$ c.c.	seen	143
$\omega\pi^\pm$	not seen	1862
$J/\psi\eta$	not seen	510
$D^+D^{*-} +$ c.c	seen	–
$D^0\overline{D}^{*0} +$ c.c	seen	–

$T_{c\overline{c}}(4020)$

$I^G(J^{PC}) = 1^+(?^{?-})$

was $X(4020)$

Mass $m = 4024.1 \pm 1.9$ MeV
Full width $\Gamma = 13 \pm 5$ MeV (S = 1.7)

$T_{c\overline{c}}(4020)$ DECAY MODES	Fraction (Γ_i/Γ)	p (MeV/c)
$h_c(1P)\pi$	seen	450
$D^*\overline{D}^*$	seen	85
$D\overline{D}^* +$ c.c.	not seen	542
$\eta_c\pi^+\pi^-$	not seen	872
$\eta_c(1S)\rho(770)^\pm$	not seen	–
$J/\psi(1S)\pi^\pm$	not seen	811

$T_{c\overline{c}1}(4430)^+$

$I^G(J^{PC}) = 1^+(1^{+-})$
G, C need confirmation.

was $Z_c(4430)$, $X(4430)^\pm$

Mass $m = 4478^{+15}_{-17}$ MeV
Full width $\Gamma = 189 \pm 29$ MeV

$T_{c\overline{c}1}(4430)^+$ DECAY MODES	Fraction (Γ_i/Γ)	p (MeV/c)
$\pi^+\psi(2S)$	seen	711
π^+J/ψ	seen	1162

$T_{cc\overline{c}\overline{c}}(6900)^0$

$I^G(J^{PC}) = 0^+(2^{++})$

was $X(6900)$

Mass $m = 6898 \pm 12$ MeV (S = 1.2)
Full width $\Gamma = 161 \pm 26$ MeV

$T_{cc\overline{c}\overline{c}}(6900)^0$ DECAY MODES	Fraction (Γ_i/Γ)	p (MeV/c)
$J/\psi J/\psi$	seen	–

$T_{b\overline{b}1}(10610)$

$I^G(J^{PC}) = 1^+(1^{+-})$

was $Z_b(10610)$, $X(10610)$

Mass $m = 10607.2 \pm 2.0$ MeV
Mass $m = 10609 \pm 6$ MeV
Full width $\Gamma = 18.4 \pm 2.4$ MeV

$T_{b\overline{b}1}(10610)$ DECAY MODES	Fraction (Γ_i/Γ)	p (MeV/c)
$\Upsilon(1S)\pi^+$	$(5.4^{+1.9}_{-1.5}) \times 10^{-3}$	1077
$\Upsilon(1S)\pi^0$	not seen	1077
$\Upsilon(2S)\pi^+$	$(3.6^{+1.1}_{-0.8})$ %	551
$\Upsilon(2S)\pi^0$	seen	552

$\Upsilon(3S)\pi^+$	$(2.1^{+0.8}_{-0.6})$ %	207
$\Upsilon(3S)\pi^0$	seen	210
$h_b(1P)\pi^+$	$(3.5^{+1.2}_{-0.9})$ %	671
$h_b(2P)\pi^+$	$(4.7^{+1.7}_{-1.3})$ %	313
$B^+\overline{B}^0$	not seen	504
$B^+\overline{B}^{*0} + B^{*+}\overline{B}^0$	$(85.6^{+2.1}_{-2.9})$ %	–

$T_{b\overline{b}1}(10650)$

$I^G(J^{PC}) = 1^+(1^{+-})$
I, G, C need confirmation.

was $Z_b(10650)$, $X(10650)^\pm$

Mass $m = 10652.2 \pm 1.5$ MeV
Full width $\Gamma = 11.5 \pm 2.2$ MeV

$T_{b\overline{b}1}(10650)$ DECAY MODES	Fraction (Γ_i/Γ)	p (MeV/c)
$\Upsilon(1S)\pi^+$	$(1.7^{+0.8}_{-0.6}) \times 10^{-3}$	1117
$\Upsilon(2S)\pi^+$	$(1.4^{+0.6}_{-0.4})$ %	595
$\Upsilon(3S)\pi^+$	$(1.6^{+0.7}_{-0.5})$ %	259
$h_b(1P)\pi^+$	$(8.4^{+2.9}_{-2.4})$ %	714
$h_b(2P)\pi^+$	(15 ± 4) %	360
$B^+\overline{B}^0$	not seen	703
$B^+\overline{B}^{*0} + B^{*+}\overline{B}^0$	not seen	–
$B^{*+}\overline{B}^{*0}$	(74^{+4}_{-6}) %	120

NOTES

In this Summary Table:

When a quantity has "(S = ...)" to its right, the error on the quantity has been enlarged by the "scale factor" S, defined as $S = \sqrt{\chi^2/(N-1)}$, where N is the number of measurements used in calculating the quantity. We do this when $S > 1$, which often indicates that the measurements are inconsistent. When $S > 1.25$, we also show in the Particle Listings an ideogram of the measurements. For more about S, see the Introduction.

A decay momentum p is given for each decay mode. For a 2-body decay, p is the momentum of each decay product in the rest frame of the decaying particle. For a 3-or-more-body decay, p is the largest momentum any of the products can have in this frame.

[a] See the review on "Form Factors for Radiative Pion and Kaon Decays" for definitions and details.

[b] Measurements of $\Gamma(e^+\nu_e)/\Gamma(\mu^+\nu_\mu)$ always include decays with γ's, and measurements of $\Gamma(e^+\nu_e\gamma)$ and $\Gamma(\mu^+\nu_\mu\gamma)$ never include low-energy γ's. Therefore, since no clean separation is possible, we consider the modes with γ's to be subreactions of the modes without them, and let $[\Gamma(e^+\nu_e) + \Gamma(\mu^+\nu_\mu)]/\Gamma_{\rm total} = 100\%$.

[c] See the $\pi^\pm$ Particle Listings for the energy limits used in this measurement; low-energy γ's are not included.

[d] Derived from an analysis of neutrino-oscillation experiments.

[e] Forbidden by angular momentum conservation.

[f] C parity forbids this to occur as a single-photon process.

[g] As measured in $e^+e^- \to \rho^0$.

[h] As measured in $e^+e^- \to \pi^+\pi^-\pi^0$ and τ decays.

[i] The $\omega\rho$ interference is then due to $\omega\rho$ mixing only, and is expected to be small. If $e\mu$ universality holds, $\Gamma(\rho^0 \to \mu^+\mu^-) = \Gamma(\rho^0 \to e^+e^-) \times 0.99785$.

[j] Our estimate. See the Particle Listings for details.

[k] See the "Note on $a_1(1260)$" in the $a_1(1260)$ Particle Listings in PDG 06, Journal of Physics **G33** 1 (2006).

[l] See also the $\omega(1650)$.

[n] See also the $\omega(1420)$.

[o] See the note in the $K^\pm$ Particle Listings.

[p] Neglecting photon channels. See, *e.g.*, A. Pais and S.B. Treiman, Phys. Rev. **D12**, 2744 (1975).

[q] The definition of the slope parameters of the $K \to 3\pi$ Dalitz plot is as follows (see also "Note on Dalitz Plot Parameters for $K \to 3\pi$ Decays" in the $K^\pm$ Particle Listings):

$$|M|^2 = 1 + g(s_3 - s_0)/m^2_{\pi^+} + \cdots .$$

[r] For more details and definitions of parameters see the Particle Listings.

[s] See the $K^\pm$ Particle Listings for the energy limits used in this measurement.

[t] Most of this radiative mode, the low-momentum γ part, is also included in the parent mode listed without γ's.

[u] Structure-dependent part.

[v] Direct-emission branching fraction.

[x] Violates angular-momentum conservation.

[y] Derived from measured values of ϕ_{+-}, ϕ_{00}, $|\eta|$, $|m_{K^0_L} - m_{K^0_S}|$, and $\tau_{K^0_S}$, as described in the introduction to "Tests of Conservation Laws."

[z] The CP-violation parameters are defined as follows (see also "Note on CP Violation in $K_S \to 3\pi$" and "Note on CP Violation in K^0_L Decay" in the Particle Listings):

$$\eta_{+-} = |\eta_{+-}|e^{i\phi_{+-}} = \frac{A(K^0_L \to \pi^+\pi^-)}{A(K^0_S \to \pi^+\pi^-)} = \epsilon + \epsilon'$$

$$\eta_{00} = |\eta_{00}|e^{i\phi_{00}} = \frac{A(K^0_L \to \pi^0\pi^0)}{A(K^0_S \to \pi^0\pi^0)} = \epsilon - 2\epsilon'$$

$$\delta = \frac{\Gamma(K^0_L \to \pi^-\ell^+\nu) - \Gamma(K^0_L \to \pi^+\ell^-\nu)}{\Gamma(K^0_L \to \pi^-\ell^+\nu) + \Gamma(K^0_L \to \pi^+\ell^-\nu)} ,$$

$$\mathrm{Im}(\eta_{+-0})^2 = \frac{\Gamma(K^0_S \to \pi^+\pi^-\pi^0)^{CP\ \mathrm{viol.}}}{\Gamma(K^0_L \to \pi^+\pi^-\pi^0)} ,$$

$$\mathrm{Im}(\eta_{000})^2 = \frac{\Gamma(K^0_S \to \pi^0\pi^0\pi^0)}{\Gamma(K^0_L \to \pi^0\pi^0\pi^0)} .$$

where for the last two relations CPT is assumed valid, *i.e.*, $\mathrm{Re}(\eta_{+-0}) \simeq 0$ and $\mathrm{Re}(\eta_{000}) \simeq 0$.

[aa] See the K^0_S Particle Listings for the energy limits used in this measurement.

[bb] The value is for the sum of the charge states or particle/antiparticle states indicated.

[cc] $\mathrm{Re}(\epsilon'/\epsilon) = \epsilon'/\epsilon$ to a very good approximation provided the phases satisfy CPT invariance.

[dd] This mode includes gammas from inner bremsstrahlung but not the direct emission mode $K^0_L \to \pi^+\pi^-\gamma$(DE).

[ee] See the K^0_L Particle Listings for the energy limits used in this measurement.

[ff] Allowed by higher-order electroweak interactions.

[gg] Violates CP in leading order. Test of direct CP violation since the indirect CP-violating and CP-conserving contributions are expected to be suppressed.

[hh] See our minireview under the $K_2(1770)$ in the 2004 edition of this *Review*.

[ii] This result applies to $Z^0 \to c\overline{c}$ decays only. Here ℓ^+ is an average (not a sum) of e^+ and μ^+ decays.

[jj] See the Particle Listings for the (complicated) definition of this quantity.

[kk] The branching fraction for this mode may differ from the sum of the submodes that contribute to it, due to interference effects. See the relevant papers in the Particle Listings.

[ll] These subfractions of the $K^-2\pi^+$ mode are uncertain: see the Particle Listings.

[nn] See the listings under "$D \to K\pi\pi\pi$ partial wave analyses" and our 2008 Review (Physics Letters **B667** 1 (2008)) for measurements of submodes of this mode.

[oo] The unseen decay modes of the resonances are included.

[pp] This is *not* a test for the ΔC=1 weak neutral current, but leads to the $\pi^+\ell^+\ell^-$ final state.

[qq] This mode is not a useful test for a ΔC=1 weak neutral current because both quarks must change flavor in this decay.

[rr] In the 2010 *Review*, the values for these quantities were given using a measure of the asymmetry that was inconsistent with the usual definition.

[ss] This value is obtained by subtracting the branching fractions for 2-, 4- and 6-prongs from unity.

Int. J. Mod. Phys. A 2026.41. Downloaded from www.worldscientific.com
by UNIVERSITY OF CALIFORNIA @ BERKELEY on 09/16/26. Re-use and distribution is strictly not permitted, except for Open Access articles.

[*tt*] This is the sum of our $K^- 2\pi^+ \pi^-$, $K^- 2\pi^+ \pi^- \pi^0$, $\overline{K}^0 2\pi^+ 2\pi^-$, $K^+ 2K^- \pi^+$, $2\pi^+ 2\pi^-$, $2\pi^+ 2\pi^- \pi^0$, $K^+ K^- \pi^+ \pi^-$, and $K^+ K^- \pi^+ \pi^- \pi^0$, branching fractions.

[*uu*] This is the sum of our $K^- 3\pi^+ 2\pi^-$ and $3\pi^+ 3\pi^-$ branching fractions.

[*vv*] The branching fractions for the $K^- e^+ \nu_e$, $K^*(892)^- e^+ \nu_e$, $\pi^- e^+ \nu_e$, and $\rho^- e^+ \nu_e$ modes add up to 6.17 ± 0.17 %.

[*xx*] This is a doubly Cabibbo-suppressed mode.

[*yy*] Submodes of the $D^0 \to K^0_S \pi^+ \pi^- \pi^0$ mode with a K^* and/or ρ were studied by COFFMAN 92B, but with only 140 events. With nothing new for 18 years, we refer to our 2008 edition, Physics Letters **B667** 1 (2008), for those results.

[*zz*] This branching fraction includes all the decay modes of the resonance in the final state.

[*aaa*] This limit assumes the average of $B(D^0 \to K^- e^+ \nu_e)$ and $B(D^0 \to K^- \mu^+ \nu_\mu)$ for the $B(D^0 \to K^- \ell^+ \nu_\ell)$ value.

[*bbb*] Here γ_D stands for massless dark photon.

[*ccc*] This is the purely e^+ semileptonic branching fraction: the e^+ fraction from τ^+ decays has been subtracted off. The sum of our (non-τ) e^+ exclusive fractions — an $e^+ \nu_e$ with an η, η', ϕ, K^0, or K^{*0} — is 5.99 ± 0.31 %.

[*ddd*] This fraction includes η from η' decays.

[*eee*] The sum of our exclusive η' fractions — $\eta' e^+ \nu_e$, $\eta' \mu^+ \nu_\mu$, $\eta' \pi^+$, $\eta' \rho^+$, and $\eta' K^+$ — is 11.8 ± 1.6%.

[*fff*] This branching fraction includes all the decay modes of the final-state resonance.

[*ggg*] A test for $u\overline{u}$ or $d\overline{d}$ content in the D^+_s. Neither Cabibbo-favored nor Cabibbo-suppressed decays can contribute, and $\omega - \phi$ mixing is an unlikely explanation for any fraction above about 2×10^{-4}.

[*hhh*] We decouple the $D^+_s \to \phi\pi^+$ branching fraction obtained from mass projections (and used to get some of the other branching fractions) from the $D^+_s \to \phi\pi^+$, $\phi \to K^+ K^-$ branching fraction obtained from the Dalitz-plot analysis of $D^+_s \to K^+ K^- \pi^+$. That is, the ratio of these two branching fractions is not exactly the $\phi \to K^+ K^-$ branching fraction 0.491.

[*iii*] This is the average of a model-independent and a K-matrix parametrization of the $\pi^+ \pi^-$ S-wave and is a sum over several f_0 mesons.

[*jjj*] An ℓ indicates an e or a μ mode, not a sum over these modes.

[*kkk*] An $CP(\pm 1)$ indicates the CP=+1 and CP=−1 eigenstates of the D^0-$\overline{D}^0$ system.

[*lll*] D denotes D^0 or $\overline{D}^0$.

[*nnn*] D^0_{CP+} decays into $D^0 \pi^0$ with the D^0 reconstructed in CP-even eigenstates $K^+ K^-$ and $\pi^+ \pi^-$.

[*ooo*] $\overline{D}^{**}$ represents an excited state with mass $2.2 < M < 2.8$ GeV/c^2.

[*ppp*] $\chi_{c1}(3872)^+$ is a hypothetical charged partner of the $\chi_{c1}(3872)$.

[*qqq*] $\Theta(1710)^{++}$ is a possible narrow pentaquark state and $G(2220)$ is a possible glueball resonance.

[*rrr*] $(\overline{\Lambda}^-_c p)_s$ denotes a low-mass enhancement near 3.35 GeV/c^2.

[*sss*] Stands for the possible candidates of $K^*(1410)$, $K^*_0(1430)$ and $K^*_2(1430)$.

[*ttt*] B^0 and B^0_s contributions not separated. Limit is on weighted average of the two decay rates.

[*uuu*] This decay refers to the coherent sum of resonant and nonresonant $J^P = 0^+$ $K\pi$ components with $1.60 < m_{K\pi} < 2.15$ GeV/c^2.

[*vvv*] $X(214)$ is a hypothetical particle of mass 214 MeV/c^2 reported by the HyperCP experiment, Physical Review Letters **94** 021801 (2005)

[*xxx*] $\Theta(1540)^+$ denotes a possible narrow pentaquark state.

[*yyy*] ψ_{DS} is a GeV-scale dark sector antibaryon (mass range 1–4 GeV/c^2).

[*zzz*] Here S and P are the hypothetical scalar and pseudoscalar particles with masses of 2.5 GeV/c^2 and 214.3 MeV/c^2, respectively.

[*aaaa*] These values are model dependent.

[*bbaa*] Here "anything" means at least one particle observed.

[*ccaa*] This is a $B(B^0 \to D^{*-} \ell^+ \nu_\ell)$ value.

[*ddaa*] D^{**} stands for the sum of the $D(1\,^1P_1)$, $D(1\,^3P_0)$, $D(1\,^3P_1)$, $D(1\,^3P_2)$, $D(2\,^1S_0)$, and $D(2\,^1S_1)$ resonances.

[*eeaa*] $D^{(*)}\overline{D}^{(*)}$ stands for the sum of $D^*\overline{D}^*$, $D^*\overline{D}$, $D\overline{D}^*$, and $D\overline{D}$.

[*ffaa*] $X(3915)$ denotes a near-threshold enhancement in the $\omega J/\psi$ mass spectrum.

[*ggaa*] Inclusive branching fractions have a multiplicity definition and can be greater than 100%.

[*hhaa*] D_j represents an unresolved mixture of pseudoscalar and tensor D^{**} (P-wave) states.

[*iiaa*] Not a pure measurement. See note at head of B^0_s Decay Modes.

[*jjaa*] For $E_\gamma > 100$ MeV.

[*kkaa*] $\Theta(1540)$ is a hypothetical pentaquark state of 1.54 GeV/c^2 mass and a width of less than 25 MeV/c^2.

[*llaa*] Includes $p\overline{p}\pi^+ \pi^- \gamma$ and excludes $p\overline{p}\eta$, $p\overline{p}\omega$, $p\overline{p}\eta'$.

[*nnaa*] For a narrow state A with mass less than 960 MeV.

[*ooaa*] For a narrow scalar or pseudoscalar A^0 with mass 0.21–3.0 GeV.

[*ppaa*] For a dark photon U with mass between 100 and 2100 MeV.

[*qqaa*] For a narrow resonance in the range $2.2 < M(X) < 2.8$ GeV.

[*rraa*] J^{PC} known by production in $e^+ e^-$ via single photon annihilation. I^G is not known; interpretation of this state as a single resonance is unclear because of the expectation of substantial threshold effects in this energy region.

[*ssaa*] $2m_\tau < M(\tau^+ \tau^-) < 9.2$ GeV

[*ttaa*] 2 GeV $< m_{K^+ K^-} <$ 3 GeV

[*uuaa*] $X\overline{X}$ = vectors with $m < 3.1$ GeV

[*vvaa*] X and $\overline{X}$ = zero spin with $m < 4.5$ GeV

[*xxaa*] 1.5 GeV $< m_X <$ 5.0 GeV

[*yyaa*] 201 MeV $< M(\mu^+ \mu^-) <$ 3565 MeV

[*zzaa*] 0.5 GeV $< m_X <$ 9.0 GeV, where m_X is the invariant mass of the hadronic final state.

[*aabb*] 1.5 GeV $< m_X <$ 5.0 GeV

[*bbbb*] 1.5 GeV $< m_X <$ 5.0 GeV

[*ccbb*] For $m_{\tau^+ \tau^-}$ in the ranges 4.03–9.52 and 9.61–10.10 GeV.

Int. J. Mod. Phys. A 2026.41. Downloaded from www.worldscientific.com
by UNIVERSITY OF CALIFORNIA @ BERKELEY on 09/16/26. Re-use and distribution is strictly not permitted, except for Open Acce

See also the table of suggested $q\overline{q}$ quark-model assignments in the Quark Model section.
• Indicates particles that appear in the preceding Meson Summary Table. We do not regard the other entries as being established.

LIGHT UNFLAVORED
($S = C = B = 0$)

	$I^G(J^{PC})$
• $\pi^\pm$	$1^-(0^-)$
• π^0	$1^-(0^{-+})$
• η	$0^+(0^{-+})$
• $f_0(500)$	$0^+(0^{++})$
• $\rho(770)$	$1^+(1^{--})$
• $\omega(782)$	$0^-(1^{--})$
• $\eta'(958)$	$0^+(0^{-+})$
• $f_0(980)$	$0^+(0^{++})$
• $a_0(980)$	$1^-(0^{++})$
• $\phi(1020)$	$0^-(1^{--})$
• $h_1(1170)$	$0^-(1^{+-})$
• $b_1(1235)$	$1^+(1^{+-})$
• $a_1(1260)$	$1^-(1^{++})$
• $f_2(1270)$	$0^+(2^{++})$
• $f_1(1285)$	$0^+(1^{++})$
• $\eta(1295)$	$0^+(0^{-+})$
• $\pi(1300)$	$1^-(0^{-+})$
• $a_2(1320)$	$1^-(2^{++})$
• $f_0(1370)$	$0^+(0^{++})$
$\pi_1(1400)$	$1^-(1^{-+})$
• $\eta(1405)$	$0^+(0^{-+})$
• $h_1(1415)$	$0^-(1^{+-})$
• $f_1(1420)$	$0^+(1^{++})$
• $\omega(1420)$	$0^-(1^{--})$
$f_2(1430)$	$0^+(2^{++})$
• $a_0(1450)$	$1^-(0^{++})$
• $\rho(1450)$	$1^+(1^{--})$
• $\eta(1475)$	$0^+(0^{-+})$
• $f_0(1500)$	$0^+(0^{++})$
$f_1(1510)$	$0^+(1^{++})$
• $f'_2(1525)$	$0^+(2^{++})$
• $f_2(1565)$	$0^+(2^{++})$
$\rho(1570)$	$1^+(1^{--})$
$h_1(1595)$	$0^-(1^{+-})$
• $\pi_1(1600)$	$1^-(1^{-+})$
• $a_1(1640)$	$1^-(1^{++})$
$f_2(1640)$	$0^+(2^{++})$
• $\eta_2(1645)$	$0^+(2^{-+})$
• $\omega(1650)$	$0^-(1^{--})$
• $\omega_3(1670)$	$0^-(3^{--})$
• $\pi_2(1670)$	$1^-(2^{-+})$
• $\phi(1680)$	$0^-(1^{--})$
• $\rho_3(1690)$	$1^+(3^{--})$

	$I^G(J^{PC})$
• $\rho(1700)$	$1^+(1^{--})$
• $a_2(1700)$	$1^-(2^{++})$
$a_0(1710)$	$1^-(0^{++})$
• $f_0(1710)$	$0^+(0^{++})$
$X(1750)$	$?^-(1^{--})$
$\eta(1760)$	$0^+(0^{-+})$
• $\pi(1800)$	$1^-(0^{-+})$
$f_0(1810)$	$0^+(0^{++})$
$f_2(1810)$	$0^+(2^{++})$
$X(1835)$	$0^+(0^{-+})$
• $\phi_3(1850)$	$0^-(3^{--})$
$\eta_1(1855)$	$0^+(1^{-+})$
• $\eta_2(1870)$	$0^+(2^{-+})$
• $\pi_2(1880)$	$1^-(2^{-+})$
$\rho(1900)$	$1^+(1^{--})$
$f_2(1910)$	$0^+(2^{++})$
$a_0(1950)$	$1^-(0^{++})$
• $f_2(1950)$	$0^+(2^{++})$
• $a_4(1970)$	$1^-(4^{++})$
$\rho_3(1990)$	$1^+(3^{--})$
$\pi_2(2005)$	$1^-(2^{-+})$
• $f_2(2010)$	$0^+(2^{++})$
• $f_0(2020)$	$0^+(0^{++})$
• $f_4(2050)$	$0^+(4^{++})$
$\pi_2(2100)$	$1^-(2^{-+})$
$f_0(2100)$	$0^+(0^{++})$
• $f_2(2150)$	$0^+(2^{++})$
$\rho(2150)$	$1^+(1^{--})$
• $\phi(2170)$	$0^-(1^{--})$
$f_0(2200)$	$0^+(0^{++})$
$f_J(2220)$	$0^+(2^{++}$ or $4^{++})$
$\omega(2220)$	$0^-(1^{--})$
$\eta(2225)$	$0^+(0^{-+})$
$\rho_3(2250)$	$1^+(3^{--})$
• $f_2(2300)$	$0^+(2^{++})$
$f_4(2300)$	$0^+(4^{++})$
$f_0(2330)$	$0^+(0^{++})$
• $f_2(2340)$	$0^+(2^{++})$
$\rho_5(2350)$	$1^+(5^{--})$
$\eta(2370)$	$0^+(0^{-+})$
$f_0(2470)$	$0^+(0^{++})$
$f_6(2510)$	$0^+(6^{++})$

STRANGE
($S = \pm1$, $C = B = 0$)

	$I(J^P)$
• $K^\pm$	$1/2(0^-)$
• K^0	$1/2(0^-)$
• K^0_S	$1/2(0^-)$
• K^0_L	$1/2(0^-)$
• $K^*_0(700)$	$1/2(0^+)$
• $K^*(892)$	$1/2(1^-)$
• $K_1(1270)$	$1/2(1^+)$
• $K_1(1400)$	$1/2(1^+)$
• $K^*(1410)$	$1/2(1^-)$
• $K^*_0(1430)$	$1/2(0^+)$
• $K^*_2(1430)$	$1/2(2^+)$
• $K(1460)$	$1/2(0^-)$
$K_2(1580)$	$1/2(2^-)$
$K(1630)$	$1/2(?^?)$
• $K_1(1650)$	$1/2(1^+)$
• $K^*(1680)$	$1/2(1^-)$
• $K_2(1770)$	$1/2(2^-)$
• $K^*_3(1780)$	$1/2(3^-)$
• $K_2(1820)$	$1/2(2^-)$
$K(1830)$	$1/2(0^-)$
• $K^*_0(1950)$	$1/2(0^+)$
• $K^*_2(1980)$	$1/2(2^+)$
• $K^*_4(2045)$	$1/2(4^+)$
$K_2(2250)$	$1/2(2^-)$
$K_3(2320)$	$1/2(3^+)$
$K^*_5(2380)$	$1/2(5^-)$
$K_4(2500)$	$1/2(4^-)$
$K(3100)$	$?^?(?^{??})$

CHARMED
($C = \pm1$)

• $D^\pm$	$1/2(0^-)$
• D^0	$1/2(0^-)$
• $D^*(2007)^0$	$1/2(1^-)$
• $D^*(2010)^\pm$	$1/2(1^-)$
• $D^*_0(2300)$	$1/2(0^+)$
• $D_1(2420)$	$1/2(1^+)$
• $D_1(2430)^0$	$1/2(1^+)$
• $D^*_2(2460)$	$1/2(2^+)$
$D_0(2550)^0$	$1/2(0^-)$
$D^*_1(2600)^0$	$1/2(1^-)$
$D^*(2640)^\pm$	$1/2(?^?)$
$D_2(2740)^0$	$1/2(2^-)$
• $D^*_3(2750)$	$1/2(3^-)$
$D^*_1(2760)^0$	$1/2(1^-)$
$D^*_2(3000)^0$	$1/2(2^+)$

CHARMED, STRANGE
($C = \pm1$, $S = \pm1$)

• $D^\pm_s$	$0(0^-)$
• $D^{*\pm}_s$	$0(1^-)$
• $D^*_{s0}(2317)^\pm$	$0(0^+)$
• $D_{s1}(2460)^\pm$	$0(1^+)$
• $D_{s1}(2536)^\pm$	$0(1^+)$
• $D^*_{s2}(2573)$	$0(2^+)$

CHARMED, STRANGE
continued

	$I(J^P)$
$D_{s0}(2590)^+$	$0(0^-)$
• $D^*_{s1}(2700)^\pm$	$0(1^-)$
$D^*_{s1}(2860)^\pm$	$0(1^-)$
• $D^*_{s3}(2860)^\pm$	$0(3^-)$
$D_{sJ}(3040)^\pm$	$0(?^?)$

BOTTOM
($B = \pm1$)

• $B^\pm$	$1/2(0^-)$
• B^0	$1/2(0^-)$
• $B^\pm/B^0$ ADMIXTURE	
• $B^\pm/B^0/B^0_s/b$-baryon ADMIXTURE	
V_{cb} and V_{ub} CKM Matrix Elements	
• B^*	$1/2(1^-)$
• $B_1(5721)$	$1/2(1^+)$
$B^*_J(5732)$	$?(?^?)$
• $B^*_2(5747)$	$1/2(2^+)$
$B_J(5840)$	$1/2(?^?)$
• $B_J(5970)$	$1/2(?^?)$

BOTTOM, STRANGE
($B = \pm1$, $S = \mp1$)

• B^0_s	$0(0^-)$
• B^*_s	$0(1^-)$
• $B_{s1}(5830)^0$	$0(1^+)$
• $B^*_{s2}(5840)^0$	$0(2^+)$
$B^*_{sJ}(5850)$	$?(?^?)$
$B_{sJ}(6063)^0$	$0(?^?)$
$B_{sJ}(6114)^0$	$0(?^?)$

BOTTOM, CHARMED
($B = C = \pm1$)

• B^+_c	$0(0^-)$
$B_c(1P)^\pm$	$0(?^?)$
• $B_c(2S)^\pm$	$0(0^-)$

$c\overline{c}$

	$I^G(J^{PC})$
• $\eta_c(1S)$	$0^+(0^{-+})$
• $J/\psi(1S)$	$0^-(1^{--})$
• $\chi_{c0}(1P)$	$0^+(0^{++})$
• $\chi_{c1}(1P)$	$0^+(1^{++})$
• $h_c(1P)$	$0^-(1^{+-})$
• $\chi_{c2}(1P)$	$0^+(2^{++})$
• $\eta_c(2S)$	$0^+(0^{-+})$
• $\psi(2S)$	$0^-(1^{--})$
• $\psi(3770)$	$0^-(1^{--})$
• $\psi_2(3823)$	$0^-(2^{--})$
• $\psi_3(3842)$	$0^-(3^{--})$
$\chi_{c0}(3860)$	$0^+(0^{++})$
• $\chi_{c1}(3872)$	$0^+(1^{++})$
• $\chi_{c0}(3915)$	$0^+(0^{++})$
• $\chi_{c2}(3930)$	$0^+(2^{++})$
$X(3940)$	$?^?(?^{??})$
• $\psi(4040)$	$0^-(1^{--})$
• $\chi_{c1}(4140)$	$0^+(1^{++})$
• $\psi(4160)$	$0^-(1^{--})$

$c\overline{c}$ continued

	$I^G(J^{PC})$
$X(4160)$	$?^?(?^{??})$
• $\psi(4230)$	$0^-(1^{--})$
• $\chi_{c1}(4274)$	$0^+(1^{++})$
$X(4350)$	$0^+(?^{?+})$
• $\psi(4360)$	$0^-(1^{--})$
• $\psi(4415)$	$0^-(1^{--})$
• $\chi_{c0}(4500)$	$0^+(0^{++})$
$X(4630)$	$0^+(?^{?+})$
• $\psi(4660)$	$0^-(1^{--})$
$\chi_{c1}(4685)$	$0^+(1^{++})$
$\chi_{c0}(4700)$	$0^+(0^{++})$

$b\overline{b}$

• $\eta_b(1S)$	$0^+(0^{-+})$
• $\Upsilon(1S)$	$0^-(1^{--})$
• $\chi_{b0}(1P)$	$0^+(0^{++})$
• $\chi_{b1}(1P)$	$0^+(1^{++})$
• $h_b(1P)$	$0^-(1^{+-})$
• $\chi_{b2}(1P)$	$0^+(2^{++})$
$\eta_b(2S)$	$0^+(0^{-+})$
• $\Upsilon(2S)$	$0^-(1^{--})$
• $\Upsilon_2(1D)$	$0^-(2^{--})$
• $\chi_{b0}(2P)$	$0^+(0^{++})$
• $\chi_{b1}(2P)$	$0^+(1^{++})$
• $h_b(2P)$	$0^-(1^{+-})$
• $\chi_{b2}(2P)$	$0^+(2^{++})$
• $\Upsilon(3S)$	$0^-(1^{--})$
• $\chi_{b1}(3P)$	$0^+(1^{++})$
• $\chi_{b2}(3P)$	$0^+(2^{++})$
• $\Upsilon(4S)$	$0^-(1^{--})$
• $\Upsilon(10753)$	$?^?(1^{--})$
• $\Upsilon(10860)$	$0^-(1^{--})$
• $\Upsilon(11020)$	$0^-(1^{--})$

OTHER

$T^*_{\overline{c}s0}(2870)^0$	$?(0^+)$
$T^*_{\overline{c}s1}(2900)^0$	$?(1^-)$
$T^*_{\overline{c}s0}(2900)$	$1(0^+)$
$T_{cc}(3875)^+$	$?(?^?)$
• $T_{c\overline{c}1}(3900)$	$1^+(1^{+-})$
$T_{c\overline{c}s1}(4000)$	$1/2(1^+)$
• $T_{c\overline{c}}(4020)$	$1^+(?^{?-})$
$T_{c\overline{c}}(4050)^+$	$1^-(?^{?+})$
$T_{c\overline{c}}(4055)^+$	$1^+(?^{?-})$
$T_{c\overline{c}}(4100)^+$	$1^-(?^{?+})$
$T_{c\overline{c}1}(4200)^+$	$1^+(1^{+-})$
$T_{c\overline{c}s1}(4220)^+$	$1/2(1^+)$
$T_{c\overline{c}0}(4240)^+$	$1^+(0^{--})$
$T_{c\overline{c}}(4250)^+$	$1^-(?^{?+})$
• $T_{c\overline{c}1}(4430)^+$	$1^+(1^{+-})$
$T_{b\overline{s}}(5568)^+$	$1(?^?)$
$T_{cc\overline{c}\overline{c}}(6600)$	$0^+(2^{++})$
• $T_{cc\overline{c}\overline{c}}(6900)^0$	$0^+(2^{++})$
$T_{cc\overline{c}\overline{c}}(7100)$	$0^+(2^{++})$
• $T_{b\overline{b}1}(10610)$	$1^+(1^{+-})$
• $T_{b\overline{b}1}(10650)$	$1^+(1^{+-})$
Further States	

Int. J. Mod. Phys. A 2026.41. Downloaded from www.worldscientific.com
by UNIVERSITY OF CALIFORNIA @ BERKELEY on 09/16/26. Re-use and distribution is strictly not permitted, except for Open Access articles.

Baryon Summary Table

This short table gives the name, the quantum numbers (where known), and the status of baryons in the Review. Only the baryons with 3- or 4-star status are included in the Baryon Summary Table. Due to insufficient data or uncertain interpretation, the other entries in the table are not established baryons. The names with masses are of baryons that decay strongly. The spin-parity J^P (when known) is given with each particle. For the strongly decaying particles, the J^P values are considered to be part of the names.

p	$1/2^+$	****
n	$1/2^+$	****
$N(1440)$	$1/2^+$	****
$N(1520)$	$3/2^-$	****
$N(1535)$	$1/2^-$	****
$N(1650)$	$1/2^-$	****
$N(1675)$	$5/2^-$	****
$N(1680)$	$5/2^+$	****
$N(1700)$	$3/2^-$	***
$N(1710)$	$1/2^+$	****
$N(1720)$	$3/2^+$	****
$N(1860)$	$5/2^+$	**
$N(1875)$	$3/2^-$	***
$N(1880)$	$1/2^+$	***
$N(1895)$	$1/2^-$	****
$N(1900)$	$3/2^+$	****
$N(1990)$	$7/2^+$	**
$N(2000)$	$5/2^+$	**
$N(2040)$	$3/2^+$	*
$N(2060)$	$5/2^-$	***
$N(2100)$	$1/2^+$	***
$N(2120)$	$3/2^-$	***
$N(2190)$	$7/2^-$	****
$N(2220)$	$9/2^+$	****
$N(2250)$	$9/2^-$	****
$N(2300)$	$1/2^+$	**
$N(2570)$	$5/2^-$	**
$N(2600)$	$11/2^-$	***
$N(2700)$	$13/2^+$	**

$\Delta(1232)$	$3/2^+$	****
$\Delta(1600)$	$3/2^+$	****
$\Delta(1620)$	$1/2^-$	****
$\Delta(1700)$	$3/2^-$	****
$\Delta(1750)$	$1/2^+$	*
$\Delta(1900)$	$1/2^-$	***
$\Delta(1905)$	$5/2^+$	****
$\Delta(1910)$	$1/2^+$	****
$\Delta(1920)$	$3/2^+$	***
$\Delta(1930)$	$5/2^-$	***
$\Delta(1940)$	$3/2^-$	**
$\Delta(1950)$	$7/2^+$	****
$\Delta(2000)$	$5/2^+$	**
$\Delta(2150)$	$1/2^-$	*
$\Delta(2200)$	$7/2^-$	***
$\Delta(2300)$	$9/2^+$	**
$\Delta(2350)$	$5/2^-$	*
$\Delta(2390)$	$7/2^+$	*
$\Delta(2400)$	$9/2^-$	**
$\Delta(2420)$	$11/2^+$	****
$\Delta(2750)$	$13/2^-$	**
$\Delta(2950)$	$15/2^+$	**
Λ	$1/2^+$	****
$\Lambda(1380)$	$1/2^-$	**
$\Lambda(1405)$	$1/2^-$	****
$\Lambda(1520)$	$3/2^-$	****
$\Lambda(1600)$	$1/2^+$	****
$\Lambda(1670)$	$1/2^-$	****
$\Lambda(1690)$	$3/2^-$	****
$\Lambda(1710)$	$1/2^+$	*
$\Lambda(1800)$	$1/2^-$	***
$\Lambda(1810)$	$1/2^+$	***
$\Lambda(1820)$	$5/2^+$	****
$\Lambda(1830)$	$5/2^-$	****
$\Lambda(1890)$	$3/2^+$	****
$\Lambda(2000)$	$1/2^-$	*
$\Lambda(2050)$	$3/2^-$	*
$\Lambda(2070)$	$3/2^+$	*
$\Lambda(2080)$	$5/2^-$	*
$\Lambda(2085)$	$7/2^+$	**
$\Lambda(2100)$	$7/2^-$	****
$\Lambda(2110)$	$5/2^+$	***
$\Lambda(2325)$	$3/2^-$	*
$\Lambda(2350)$	$9/2^+$	***
$\Lambda(2585)$		*

Σ^+	$1/2^+$	****
Σ^0	$1/2^+$	****
Σ^-	$1/2^+$	****
$\Sigma(1385)$	$3/2^+$	****
$\Sigma(1580)$	$3/2^-$	*
$\Sigma(1620)$	$1/2^-$	*
$\Sigma(1660)$	$1/2^+$	***
$\Sigma(1670)$	$3/2^-$	****
$\Sigma(1750)$	$1/2^-$	***
$\Sigma(1775)$	$5/2^-$	****
$\Sigma(1780)$	$3/2^+$	*
$\Sigma(1880)$	$1/2^+$	**
$\Sigma(1900)$	$1/2^-$	**
$\Sigma(1910)$	$3/2^-$	***
$\Sigma(1915)$	$5/2^+$	****
$\Sigma(1940)$	$3/2^+$	*
$\Sigma(2010)$	$3/2^-$	*
$\Sigma(2030)$	$7/2^+$	****
$\Sigma(2070)$	$5/2^+$	*
$\Sigma(2080)$	$3/2^+$	*
$\Sigma(2100)$	$7/2^-$	*
$\Sigma(2110)$	$1/2^-$	*
$\Sigma(2230)$	$3/2^+$	*
$\Sigma(2250)$		**
$\Sigma(2455)$		*
$\Sigma(2620)$		*
$\Sigma(3000)$		*
$\Sigma(3170)$		*
Ξ^0	$1/2^+$	****
Ξ^-	$1/2^+$	****
$\Xi(1530)$	$3/2^+$	****
$\Xi(1620)$		**
$\Xi(1690)$		***
$\Xi(1820)$	$3/2^-$	***
$\Xi(1950)$		***
$\Xi(2030)$	$\geq \frac{5}{2}?$	***
$\Xi(2120)$		*
$\Xi(2250)$		**
$\Xi(2370)$		**
$\Xi(2500)$		*
Ω^-	$3/2^+$	****
$\Omega(2012)^-$	$?^-$	***
$\Omega(2109)^-$		*
$\Omega(2250)^-$		***
$\Omega(2380)^-$		**
$\Omega(2470)^-$		**

Λ_c^+	$1/2^+$	****
$\Lambda_c(2595)^+$	$1/2^-$	***
$\Lambda_c(2625)^+$	$3/2^-$	***
$\Lambda_c(2765)^+$		*
$\Lambda_c(2860)^+$	$3/2^+$	***
$\Lambda_c(2880)^+$	$5/2^+$	***
$\Lambda_c(2910)^+$		*
$\Lambda_c(2940)^+$	$3/2^-$	***
$\Sigma_c(2455)$	$1/2^+$	****
$\Sigma_c(2520)$	$3/2^+$	***
$\Sigma_c(2800)$		***
Ξ_c^+	$1/2^+$	***
Ξ_c^0	$1/2^+$	****
$\Xi_c^{\prime +}$	$1/2^+$	***
$\Xi_c^{\prime 0}$	$1/2^+$	***
$\Xi_c(2645)$	$3/2^+$	***
$\Xi_c(2790)$	$1/2^-$	***
$\Xi_c(2815)$	$3/2^-$	***
$\Xi_c(2882)$		*
$\Xi_c(2923)$		**
$\Xi_c(2930)$		**
$\Xi_c(2970)$	$1/2^+$	***
$\Xi_c(3055)$	$3/2^+$	***
$\Xi_c(3080)$		***
$\Xi_c(3123)$		*
Ω_c^0	$1/2^+$	***
$\Omega_c(2770)^0$	$3/2^+$	***
$\Omega_c(3000)^0$		***
$\Omega_c(3050)^0$		***
$\Omega_c(3065)^0$		***
$\Omega_c(3090)^0$		***
$\Omega_c(3120)^0$		***
$\Omega_c(3185)^0$		***
$\Omega_c(3327)^0$		***
Ξ_{cc}^+		*
Ξ_{cc}^{++}		***

Λ_b^0	$1/2^+$	***
$\Lambda_b(5912)^0$	$1/2^-$	***
$\Lambda_b(5920)^0$	$3/2^-$	***
$\Lambda_b(6070)^0$	$1/2^+$	***
$\Lambda_b(6146)^0$	$3/2^+$	***
$\Lambda_b(6152)^0$	$5/2^+$	***
Σ_b	$1/2^+$	***
Σ_b^*	$3/2^+$	***
$\Sigma_b(6097)^+$		***
$\Sigma_b(6097)^-$		***
Ξ_b^-	$1/2^+$	***
Ξ_b^0	$1/2^+$	***
$\Xi_b^{\prime}(5935)^-$	$1/2^+$	***
$\Xi_b(5945)^0$	$3/2^+$	***
$\Xi_b(5955)^-$	$3/2^+$	***
$\Xi_b(6087)^0$		***
$\Xi_b(6095)^0$		***
$\Xi_b(6100)^-$	$3/2^-$	***
$\Xi_b(6227)^-$		***
$\Xi_b(6227)^0$		***
$\Xi_b(6327)^0$		***
$\Xi_b(6333)^0$		***
Ω_b^-	$1/2^+$	***
$\Omega_b(6316)^-$		***
$\Omega_b(6330)^-$		***
$\Omega_b(6340)^-$		***
$\Omega_b(6350)^-$		***
$P_{c\overline{c}}(4312)^+$		*
$P_{c\overline{c}s}(4338)^0$	$1/2^-$	*
$P_{c\overline{c}}(4380)^+$		*
$P_{c\overline{c}}(4440)^+$		*
$P_{c\overline{c}}(4457)^+$		*
$P_{c\overline{c}s}(4459)^0$		*

**** Existence is certain, and properties are at least fairly well explored.

*** Existence ranges from very likely to certain, but further confirmation is desirable and/or quantum numbers, branching fractions, etc. are not well determined.

** Evidence of existence is only fair.

* Evidence of existence is poor.

Int. J. Mod. Phys. A 2026.41. Downloaded from www.worldscientific.com
by UNIVERSITY OF CALIFORNIA @ BERKELEY on 09/16/26. Re-use and distribution is strictly not permitted, except for Open Access

Int. J. Mod. Phys. A 2026.41. Downloaded from www.worldscientific.com
by UNIVERSITY OF CALIFORNIA @ BERKELEY on 09/16/26. Re-use and distribution is strictly not permitted, except for Open Access articles.

N BARYONS ($S = 0$, $I = 1/2$)

p, $N^+ = uud$; n, $N^0 = udd$

p

$I(J^P) = \frac{1}{2}(\frac{1}{2}^+)$

Mass $m = 1.0072764665789 \pm 0.0000000000083$ u
Mass $m = 938.27208943 \pm 0.00000029$ MeV [a]
$|m_p - m_{\overline{p}}|/m_p < 7 \times 10^{-10}$, CL = 90% [b]
$|\frac{q_{\overline{p}}}{m_{\overline{p}}}|/(\frac{q_p}{m_p}) = 1.000000000003 \pm 0.000000000016$
$|q_p + q_{\overline{p}}|/e < 7 \times 10^{-10}$, CL = 90% [b]
$|q_p + q_e|/e < 1 \times 10^{-21}$ [c]
Magnetic moment $\mu = 2.7928473446 \pm 0.0000000008\ \mu_N$
$(\mu_p + \mu_{\overline{p}}) / \mu_p = (0.002 \pm 0.004) \times 10^{-6}$
Electric dipole moment $d < 0.021 \times 10^{-23}$ e cm
Electric polarizability $\alpha = (11.5 \pm 0.4) \times 10^{-4}$ fm^3 (S = 1.1)
Magnetic polarizability $\beta = (2.31 \pm 0.29) \times 10^{-4}$ fm^3 (S = 1.1)
p SPIN POLARIZABILITY $\gamma_{E1E1} = (-3.0 \pm 0.7) \times 10^{-4}$ fm^4
p SPIN POLARIZABILITY $\gamma_{M1M1} = (3.7 \pm 0.5) \times 10^{-4}$ fm^4
p SPIN POLARIZABILITY $\gamma_{E1M2} = (-1.2 \pm 1.0) \times 10^{-4}$ fm^4
p SPIN POLARIZABILITY $\gamma_{M1E2} = (2.0 \pm 0.8) \times 10^{-4}$ fm^4
Charge radius, μp Lamb shift = 0.84075 ± 0.00064 fm [d]
Charge radius = 0.8407 ± 0.0006 fm [d]
Magnetic radius = 0.851 ± 0.026 fm [e]
Mean life $\tau > 9 \times 10^{29}$ years, CL = 90% ($p \to$ invisible mode)

See the "Note on Nucleon Decay" in our 1994 edition (Phys. Rev. **D50**, 1173) for a short review.

The "partial mean life" limits tabulated here are the limits on τ/B_i, where τ is the total mean life and B_i is the branching fraction for the mode in question. For N decays, p and n indicate proton and neutron partial lifetimes.

p DECAY MODES	Partial mean life (10^{30} years)	Confidence level	p (MeV/c)
Antilepton + meson			
$N \to e^+ \pi$	> 5300 (n), > 24000 (p)	90%	459
$N \to \mu^+ \pi$	> 3500 (n), > 16000 (p)	90%	453
$N \to \nu \pi$	> 1100 (n), > 390 (p)	90%	459
$p \to e^+ \eta$	> 10000	90%	309
$p \to \mu^+ \eta$	> 4700	90%	297
$n \to \nu \eta$	> 158	90%	310
$N \to e^+ \rho$	> 217 (n), > 720 (p)	90%	149
$N \to \mu^+ \rho$	> 228 (n), > 570 (p)	90%	113
$N \to \nu \rho$	> 19 (n), > 162 (p)	90%	149
$p \to e^+ \omega$	> 1600	90%	143
$p \to \mu^+ \omega$	> 2800	90%	105
$n \to \nu \omega$	> 108	90%	144
$N \to e^+ K$	> 17 (n), > 1000 (p)	90%	339
$N \to \mu^+ K$	> 26 (n), > 4500 (p)	90%	329
$N \to \nu K$	> 86 (n), > 5900 (p)	90%	339
$n \to \nu K^0_S$	> 1560	90%	338
$p \to e^+ K^*(892)^0$	> 84	90%	45
$N \to \nu K^*(892)$	> 78 (n), > 51 (p)	90%	45
Antilepton + mesons			
$p \to e^+ \pi^+ \pi^-$	> 82	90%	448
$p \to e^+ \pi^0 \pi^0$	> 147	90%	449
$n \to e^+ \pi^- \pi^0$	> 52	90%	449
$p \to \mu^+ \pi^+ \pi^-$	> 133	90%	425
$p \to \mu^+ \pi^0 \pi^0$	> 101	90%	427
$n \to \mu^+ \pi^- \pi^0$	> 74	90%	427
$n \to e^+ K^0 \pi^-$	> 18	90%	319
Lepton + meson			
$n \to e^- \pi^+$	> 65	90%	459
$n \to \mu^- \pi^+$	> 49	90%	453
$n \to e^- \rho^+$	> 62	90%	150
$n \to \mu^- \rho^+$	> 7	90%	115
$n \to e^- K^+$	> 32	90%	340
$n \to \mu^- K^+$	> 57	90%	330
Lepton + mesons			
$p \to e^- \pi^+ \pi^+$	> 30	90%	448
$n \to e^- \pi^+ \pi^0$	> 29	90%	449
$p \to \mu^- \pi^+ \pi^+$	> 17	90%	425
$n \to \mu^- \pi^+ \pi^0$	> 34	90%	427
$p \to e^- \pi^+ K^+$	> 75	90%	320
$p \to \mu^- \pi^+ K^+$	> 245	90%	279
Antilepton + photon(s)			
$p \to e^+ \gamma$	> 670	90%	469
$p \to \mu^+ \gamma$	> 478	90%	463
$n \to \nu \gamma$	> 550	90%	470
$p \to e^+ \gamma\gamma$	> 100	90%	469
$n \to \nu \gamma\gamma$	> 219	90%	470
Antilepton + single massless			
$p \to e^+ X$	> 790	90%	–
$p \to \mu^+ X$	> 410	90%	–
Three (or more) leptons			
$p \to e^+ e^+ e^-$	> 34000	90%	469
$p \to e^+ \mu^+ \mu^-$	> 9200	90%	457
$p \to e^+ \nu \nu$	> 170	90%	469
$n \to e^+ e^- \nu$	> 257	90%	470
$n \to \mu^+ e^- \nu$	> 83	90%	464
$n \to \mu^+ \mu^- \nu$	> 79	90%	458
$p \to \mu^+ e^+ e^-$	> 23000	90%	463
$p \to \mu^- e^+ e^+$	> 19000	90%	463
$p \to \mu^+ \mu^+ \mu^-$	> 10000	90%	439
$p \to \mu^+ \nu \nu$	> 220	90%	463
$p \to e^- \mu^+ \mu^+$	> 11000	90%	457
$n \to 3\nu$	$> 5 \times 10^{-4}$	90%	470
Inclusive modes			
$N \to e^+$ anything	> 0.6 (n, p)	90%	–
$N \to \mu^+$ anything	> 12 (n, p)	90%	–
$N \to e^+ \pi^0$ anything	> 0.6 (n, p)	90%	–
$\Delta B = 2$ dinucleon modes			
The following are lifetime limits per iron nucleus.			
$p p \to \pi^+ \pi^+$	> 72.2	90%	–
$p n \to \pi^+ \pi^0$	> 170	90%	–
$n n \to \pi^+ \pi^-$	> 0.7	90%	–
$n n \to \pi^0 \pi^0$	> 404	90%	–
$p p \to K^+ K^+$	> 170	90%	–
$p p \to e^+ e^+$	> 5.8	90%	–
$p p \to e^+ \mu^+$	> 3.6	90%	–
$p p \to \mu^+ \mu^+$	> 1.7	90%	–
$p n \to e^+ \overline{\nu}$	> 260	90%	–
$p n \to \mu^+ \overline{\nu}$	> 200	90%	–
$p n \to \tau^+ \overline{\nu}_\tau$	> 29	90%	–
$n n \to$ invisible	> 1.4	90%	–
$n n \to \nu_e \overline{\nu}_e$	> 1.4	90%	–
$n n \to \nu_\mu \overline{\nu}_\mu$	> 1.4	90%	–
$p n \to$ invisible	> 0.06	90%	–
$p p \to$ invisible	> 0.11	90%	–

$\overline{p}$ DECAY MODES

$\overline{p}$ DECAY MODES	Partial mean life (years)	Confidence level	p (MeV/c)
$\overline{p} \to e^- \gamma$	$> 7 \times 10^5$	90%	469
$\overline{p} \to \mu^- \gamma$	$> 5 \times 10^4$	90%	463
$\overline{p} \to e^- \pi^0$	$> 4 \times 10^5$	90%	459
$\overline{p} \to \mu^- \pi^0$	$> 5 \times 10^4$	90%	453
$\overline{p} \to e^- \eta$	$> 2 \times 10^4$	90%	309
$\overline{p} \to \mu^- \eta$	$> 8 \times 10^3$	90%	297
$\overline{p} \to e^- K^0_S$	> 900	90%	337
$\overline{p} \to \mu^- K^0_S$	$> 4 \times 10^3$	90%	326
$\overline{p} \to e^- K^0_L$	$> 9 \times 10^3$	90%	337
$\overline{p} \to \mu^- K^0_L$	$> 7 \times 10^3$	90%	326
$\overline{p} \to e^- \gamma\gamma$	$> 2 \times 10^4$	90%	469
$\overline{p} \to \mu^- \gamma\gamma$	$> 2 \times 10^4$	90%	463
$\overline{p} \to e^- \omega$	> 200	90%	143

n

$I(J^P) = \frac{1}{2}(\frac{1}{2}^+)$

Mass $m = 1.0086649161 \pm 0.0000000004$ u
Mass $m = 939.5654219 \pm 0.0000005$ MeV [a]
$(m_n - m_{\overline{n}})/ m_n = (9 \pm 5) \times 10^{-5}$
$m_n - m_p = 1.2933325 \pm 0.0000004$ MeV
$= 0.0013884495 \pm 0.0000000004$ u

Int. J. Mod. Phys. A 2026.41. Downloaded from www.worldscientific.com
by UNIVERSITY OF CALIFORNIA @ BERKELEY on 09/16/26. Re-use and distribution is strictly not permitted, except for Open Acce

Mean life $\tau = 878.3 \pm 0.4$ s (S = 1.8)
$c\tau = 2.6332 \times 10^8$ km
Magnetic moment $\mu = -1.9130428 \pm 0.0000005\ \mu_N$
Electric dipole moment $d < 0.18 \times 10^{-25}$ $e$cm, CL = 90%
Mean-square charge radius $\langle r_n^2 \rangle = -0.1155 \pm 0.0017$ fm^2
Magnetic radius $\sqrt{\langle r_M^2 \rangle} = 0.864^{+0.009}_{-0.008}$ fm
Electric polarizability $\alpha = (11.8 \pm 1.1) \times 10^{-4}$ fm^3
Magnetic polarizability $\beta = (3.7 \pm 1.2) \times 10^{-4}$ fm^3
Charge $q = (-0.2 \pm 0.8) \times 10^{-21}$ e
Mean $n\overline{n}$-oscillation time $> 8.6 \times 10^7$ s, CL = 90% (free n)
Mean $n\overline{n}$-oscillation time $> 4.7 \times 10^8$ s, CL = 90% [f] (bound n)
Mean nn'-oscillation time > 448 s, CL = 90% [g]

$pe^-\nu_e$ decay parameters [h]

$\lambda \equiv g_A / g_V = -1.2753 \pm 0.0013$ (S = 2.7)
$A = -0.11958 \pm 0.00021$ (S = 1.2)
$B = 0.9807 \pm 0.0030$
$C = -0.2377 \pm 0.0026$
$a = -0.1044 \pm 0.0007$
$\phi_{AV} = (180.017 \pm 0.026)^\circ$ [i]
$D = (-1.2 \pm 2.0) \times 10^{-4}$ [j]
$R = 0.004 \pm 0.013$ [j]
Fierz interference term $b = 0.017 \pm 0.020$

See the proton listings for many other neutron decay modes.

n DECAY MODES		Fraction (Γ_i/Γ)	Confidence level	p (MeV/c)
$pe^-\overline{\nu}_e$		100 %		1
$pe^-\overline{\nu}_e\gamma$	[k]	$(9.2\pm0.7) \times 10^{-3}$		1
hydrogen-atom $\overline{\nu}_e$		$< 2.7 \times 10^{-3}$	95%	1.19
Charge conservation (Q) violating mode				
$p\nu_e\overline{\nu}_e$	Q	$< 8 \times 10^{-27}$	68%	1

$N(1440)\ 1/2^+$

$I(J^P) = \frac{1}{2}(\frac{1}{2}^+)$

Re(pole position) = 1360 to 1380 ($\approx$ 1370) MeV
-2Im(pole position) = 180 to 205 ($\approx$ 190) MeV
Breit-Wigner mass = 1410 to 1470 ($\approx$ 1440) MeV
Breit-Wigner full width = 250 to 450 ($\approx$ 350) MeV

$N(1440)$ DECAY MODES	Fraction (Γ_i/Γ)	p (MeV/c)
$N\pi$	55–75 %	398
$N\eta$	< 1 %	†
$N\pi\pi$	17–50 %	347
$\Delta(1232)\pi$	6–27 %	147
$N\rho$	(18 ± 6) %	†
$N\rho$, S=1/2	(9 ± 4) %	†
$N\rho$, S=3/2	(9 ± 4) %	†
$N\sigma$	11–23 %	–
$p\gamma$, helicity=1/2	0.035–0.048 %	414
$n\gamma$, helicity=1/2	0.02–0.04 %	413

$N(1520)\ 3/2^-$

$I(J^P) = \frac{1}{2}(\frac{3}{2}^-)$

Re(pole position) = 1505 to 1515 ($\approx$ 1510) MeV
-2Im(pole position) = 105 to 120 ($\approx$ 110) MeV
Breit-Wigner mass = 1510 to 1520 ($\approx$ 1515) MeV
Breit-Wigner full width = 100 to 120 ($\approx$ 110) MeV

$N(1520)$ DECAY MODES	Fraction (Γ_i/Γ)	p (MeV/c)
$N\pi$	55–65 %	453
$N\eta$	0.07–0.09 %	142
$N\pi\pi$	25–35 %	410
$\Delta(1232)\pi$	22–34 %	225
$\Delta(1232)\pi$, S-wave	15–23 %	225
$\Delta(1232)\pi$, D-wave	7–11 %	225
$N\rho$	10–16 %	†
$N\rho$, S=1/2	0.2–0.4 %	†
$N\rho$, S=3/2, S-wave	10–16 %	†
$N\rho$, S=3/2, D-wave	<1 %	†
$N\sigma$	<10 %	–
$p\gamma$	0.31–0.52 %	467
$p\gamma$, helicity=1/2	0.01–0.02 %	467
$p\gamma$, helicity=3/2	0.30–0.50 %	467
$n\gamma$	0.30–0.53 %	466
$n\gamma$, helicity=1/2	0.04–0.10 %	466
$n\gamma$, helicity=3/2	0.25–0.45 %	466

$N(1535)\ 1/2^-$

$I(J^P) = \frac{1}{2}(\frac{1}{2}^-)$

Re(pole position) = 1500 to 1520 ($\approx$ 1510) MeV
-2Im(pole position) = 80 to 130 ($\approx$ 110) MeV
Breit-Wigner mass = 1515 to 1545 ($\approx$ 1530) MeV
Breit-Wigner full width = 125 to 175 ($\approx$ 150) MeV

$N(1535)$ DECAY MODES	Fraction (Γ_i/Γ)	p (MeV/c)
$N\pi$	32–52 %	464
$N\eta$	30–55 %	176
$N\pi\pi$	4–31 %	422
$\Delta(1232)\pi$	1–4 %	240
$N\rho$	2–17 %	†
$N\rho$, S=1/2	2–16 %	†
$N\rho$, S=3/2	<1 %	†
$N\sigma$	2–10 %	–
$N(1440)\pi$	5–12 %	†
$p\gamma$, helicity=1/2	0.15–0.30 %	477
$n\gamma$, helicity=1/2	0.01–0.25 %	477

$N(1650)\ 1/2^-$

$I(J^P) = \frac{1}{2}(\frac{1}{2}^-)$

Re(pole position) = 1650 to 1680 ($\approx$ 1665) MeV
-2Im(pole position) = 100 to 170 ($\approx$ 135) MeV
Breit-Wigner mass = 1635 to 1665 ($\approx$ 1650) MeV
Breit-Wigner full width = 100 to 150 ($\approx$ 125) MeV

$N(1650)$ DECAY MODES	Fraction (Γ_i/Γ)	p (MeV/c)
$N\pi$	50–70 %	547
$N\eta$	15–35 %	348
ΛK	5–15 %	169
$N\pi\pi$	20–58 %	514
$\Delta(1232)\pi$	6–18 %	345
$N\rho$	12–22 %	†
$N\rho$, S=1/2	<4 %	†
$N\rho$, S=3/2	12–18 %	†
$N\sigma$	2–18 %	–
$N(1440)\pi$	6–26 %	150
$p\gamma$, helicity=1/2	0.04–0.20 %	558
$n\gamma$, helicity=1/2	0.003–0.17 %	557

$N(1675)\ 5/2^-$

$I(J^P) = \frac{1}{2}(\frac{5}{2}^-)$

Re(pole position) = 1650 to 1660 ($\approx$ 1655) MeV
-2Im(pole position) = 120 to 150 ($\approx$ 135) MeV
Breit-Wigner mass = 1665 to 1680 ($\approx$ 1675) MeV
Breit-Wigner full width = 130 to 160 ($\approx$ 145) MeV

$N(1675)$ DECAY MODES	Fraction (Γ_i/Γ)	p (MeV/c)
$N\pi$	38–42 %	564
$N\eta$	< 1 %	376
ΛK	<0.04 %	216
$N\pi\pi$	25–45 %	532
$\Delta(1232)\pi$	(19 ± 4) %	366
$\Delta(1232)\pi$, D-wave	23–37 %	366
$N\rho$	0.1–0.9 %	†
$N\rho$, S=1/2	<0.2 %	†
$N\rho$, S=3/2, D-wave	0.1–0.7 %	†
$N\sigma$	3–7 %	–
$p\gamma$	0–0.02 %	575
$p\gamma$, helicity=1/2	0–0.01 %	575
$p\gamma$, helicity=3/2	0–0.01 %	575
$n\gamma$	0–0.15 %	574
$n\gamma$, helicity=1/2	0–0.05 %	574
$n\gamma$, helicity=3/2	0–0.10 %	574

Int. J. Mod. Phys. A 2026.41. Downloaded from www.worldscientific.com
by UNIVERSITY OF CALIFORNIA @ BERKELEY on 09/16/26. Re-use and distribution is strictly not permitted, except for Open Access articles.

$N(1680)\ 5/2^+$

$I(J^P) = \frac{1}{2}(\frac{5}{2}^+)$

Re(pole position) = 1660 to 1680 (≈ 1670) MeV
−2Im(pole position) = 110 to 135 (≈ 120) MeV
Breit-Wigner mass = 1680 to 1690 (≈ 1685) MeV
Breit-Wigner full width = 115 to 130 (≈ 120) MeV

$N(1680)$ DECAY MODES	Fraction (Γ_i/Γ)	p (MeV/c)
$N\pi$	60–70 %	571
$N\eta$	<1 %	386
$N\pi\pi$	28–53 %	539
$\Delta(1232)\pi$	11–23 %	374
$\Delta(1232)\pi$, P-wave	4–10 %	374
$\Delta(1232)\pi$, F-wave	1–13 %	374
$N\rho$	8–11 %	†
$N\rho$, S=3/2 , P-wave	6–8 %	†
$N\rho$, S=3/2 , F-wave	2–3 %	†
$N\sigma$	9–19 %	–
$p\gamma$	0.21–0.32 %	581
$p\gamma$, helicity=1/2	0.001–0.011 %	581
$p\gamma$, helicity=3/2	0.20–0.32 %	581
$n\gamma$	0.021–0.046 %	581
$n\gamma$, helicity=1/2	0.004–0.029 %	581
$n\gamma$, helicity=3/2	0.01–0.024 %	581

$N(1700)\ 3/2^-$

$I(J^P) = \frac{1}{2}(\frac{3}{2}^-)$

Re(pole position) = 1650 to 1750 (≈ 1700) MeV
−2Im(pole position) = 100 to 300 (≈ 200) MeV
Breit-Wigner mass = 1650 to 1800 (≈ 1720) MeV
Breit-Wigner full width = 100 to 300 (≈ 200) MeV

$N(1700)$ DECAY MODES	Fraction (Γ_i/Γ)	p (MeV/c)
$N\pi$	7–17 %	594
$N\eta$	1–2 %	422
$N\omega$	10–34 %	†
ΛK	1–2 %	283
$N\pi\pi$	>89 %	564
$\Delta(1232)\pi$	55–85 %	402
$\Delta(1232)\pi$, S-wave	50–80 %	402
$\Delta(1232)\pi$, D-wave	4–14 %	402
$N\rho$	(21 ±9) %	75
$N\rho$, S=1/2	(5.0±3.0) %	75
$N\rho$, S=3/2 , S-wave	32–44 %	75
$N\rho$, S=3/2 , D-wave	(16 ±8) %	75
$N\sigma$	2–14 %	–
$N(1440)\pi$	3–11 %	225
$N(1520)\pi$	<4 %	145
$N(1535)\pi$	< 1 %	126
$p\gamma$	0.01–0.05 %	604
$p\gamma$, helicity=1/2	0.0–0.024 %	604
$p\gamma$, helicity=3/2	0.002–0.026 %	604
$n\gamma$	0.01–0.13 %	603
$n\gamma$, helicity=1/2	0.0–0.09 %	603
$n\gamma$, helicity=3/2	0.01–0.05 %	603

$N(1710)\ 1/2^+$

$I(J^P) = \frac{1}{2}(\frac{1}{2}^+)$

Re(pole position) = 1650 to 1750 (≈ 1700) MeV
−2Im(pole position) = 80 to 160 (≈ 120) MeV
Breit-Wigner mass = 1680 to 1740 (≈ 1710) MeV
Breit-Wigner full width = 80 to 200 (≈ 140) MeV

$N(1710)$ DECAY MODES	Fraction (Γ_i/Γ)	p (MeV/c)
$N\pi$	5–20 %	588
$N\eta$	10–50 %	412
$N\omega$	1–5 %	†
ΛK	5–25 %	269
ΣK	seen	138
$N\pi\pi$	14–48 %	557
$\Delta(1232)\pi$	3–9 %	394
$N\rho$	(17 ± 4) %	†
$N\rho$, S=1/2	11–23 %	†
$N\rho$, S=3/2	(11.0± 3.0) %	†
$N\sigma$	<16 %	–
$N(1440)\pi$	(22 ±12) %	215
$N(1520)\pi$	< 2 %	133
$N(1535)\pi$	9–21 %	113
$p\gamma$, helicity=1/2	0.002–0.08 %	598
$n\gamma$, helicity=1/2	0.0–0.02%	597

$N(1720)\ 3/2^+$

$I(J^P) = \frac{1}{2}(\frac{3}{2}^+)$

Re(pole position) = 1660 to 1710 (≈ 1680) MeV
−2Im(pole position) = 150 to 300 (≈ 200) MeV
Breit-Wigner mass = 1680 to 1750 (≈ 1720) MeV
Breit-Wigner full width = 150 to 400 (≈ 250) MeV

$N(1720)$ DECAY MODES	Fraction (Γ_i/Γ)	p (MeV/c)
$N\pi$	8–14 %	594
$N\eta$	1–5 %	422
$N\omega$	12–40 %	†
ΛK	4–19 %	283
$N\pi\pi$	>50 %	564
$\Delta(1232)\pi$	47–89 %	402
$\Delta(1232)\pi$, P-wave	47–77 %	402
$\Delta(1232)\pi$, F-wave	<12 %	402
$N\rho$	(29 ±8) %	75
$N\rho$, S=1/2	1–2 %	75
$N\rho$, S=3/2 , P-wave	(17 ±6) %	75
$N\sigma$	2–14 %	–
$N(1440)\pi$	<2 %	225
$N(1520)\pi$, S-wave	1–5 %	145
$N(1535)\pi$	(4.0±2.0) %	126
$p\gamma$	0.05–0.25 %	604
$p\gamma$, helicity=1/2	0.05–0.15 %	604
$p\gamma$, helicity=3/2	0.002–0.16 %	604
$n\gamma$	0.0–0.016 %	603
$n\gamma$, helicity=1/2	0.0–0.01 %	603
$n\gamma$, helicity=3/2	0.0–0.015 %	603

$N(1875)\ 3/2^-$

$I(J^P) = \frac{1}{2}(\frac{3}{2}^-)$

was $N(2080)$

Re(pole position) = 1850 to 1950 (≈ 1900) MeV
−2Im(pole position) = 100 to 220 (≈ 160) MeV
Breit-Wigner mass = 1850 to 1920 (≈ 1875) MeV
Breit-Wigner full width = 120 to 250 (≈ 200) MeV

$N(1875)$ DECAY MODES	Fraction (Γ_i/Γ)	p (MeV/c)
$N\pi$	3–11 %	695
$N\eta$	3–16 %	559
$N\omega$	15–25 %	371
ΛK	1–2 %	454
ΣK	0.3–1.1 %	384
$N\pi\pi$	>56 %	670
$\Delta(1232)\pi$	4–44 %	520
$\Delta(1232)\pi$, S-wave	2–21 %	520
$\Delta(1232)\pi$, D-wave	2–23 %	520
$N\rho$, S=3/2, S-wave	36–56 %	379
$N\sigma$	16–60 %	–
$N(1440)\pi$	2–8 %	365
$N(1520)\pi$	<2 %	301
$N(1535)\pi$	(2.0±2.0) %	288
$\Lambda K^*(892)$	<0.2 %	†
$p\gamma$	0.001–0.025 %	703
$p\gamma$, helicity=1/2	0.001–0.021 %	703
$p\gamma$, helicity=3/2	<0.003 %	703
$n\gamma$	<0.040 %	702
$n\gamma$, helicity=1/2	<0.007 %	702
$n\gamma$, helicity=3/2	<0.033 %	702

$N(1880)\ 1/2^+$

$I(J^P) = \frac{1}{2}(\frac{1}{2}^+)$

Re(pole position) = 1820 to 1900 (≈ 1860) MeV
−2Im(pole position) = 180 to 280 (≈ 230) MeV
Breit-Wigner mass = 1830 to 1930 (≈ 1880) MeV
Breit-Wigner full width = 200 to 400 (≈ 300) MeV

Int. J. Mod. Phys. A 2026.41. Downloaded from www.worldscientific.com
by UNIVERSITY OF CALIFORNIA @ BERKELEY on 09/16/26. Re-use and distribution is strictly not permitted, except for Open Acce

$N(1880)$ DECAY MODES	Fraction (Γ_i/Γ)	p (MeV/c)
$N\pi$	3–31 %	698
$N\eta$	1–55 %	563
$N\omega$	12–28 %	377
ΛK	1–3 %	459
ΣK	10–24 %	389
$N\pi\pi$	>32 %	673
$\Delta(1232)\pi$	5–42 %	524
$N\rho$	(28 ±7) %	385
$N\rho$, S=1/2	19–45 %	385
$N\rho$, S=3/2	(8.0±3.0) %	385
$N\sigma$	8–40 %	539
$N(1535)\pi$	4–12 %	293
$Na_0(980)$	1–5 %	†
$\Lambda K^*(892)$	0.5–1.1 %	†
$p\gamma$, helicity=1/2	seen	706
$n\gamma$, helicity=1/2	0.002–0.63 %	705

$N(1895)\ 1/2^-$

$I(J^P) = \frac{1}{2}(\frac{1}{2}^-)$

was $N(2090)$

Re(pole position) = 1890 to 1930 (≈ 1910) MeV
−2Im(pole position) = 80 to 140 (≈ 110) MeV
Breit-Wigner mass = 1870 to 1920 (≈ 1895) MeV
Breit-Wigner full width = 80 to 200 (≈ 120) MeV

$N(1895)$ DECAY MODES	Fraction (Γ_i/Γ)	p (MeV/c)
$N\pi$	2–18 %	707
$N\eta$	15–45 %	575
$N\eta'$	10–40 %	†
$N\omega$	16–40 %	395
ΛK	3–23 %	473
ΣK	6–20 %	405
$N\pi\pi$	17–74 %	683
$\Delta(1232)\pi$	3–11 %	535
$N\rho$	14–50 %	403
$N\rho$, S=1/2	<18 %	403
$N\rho$, S=3/2	14–32 %	403
$N\sigma$	<13 %	–
$N(1440)\pi$	2–12 %	382
$\Lambda K^*(892)$	4–9 %	†
$p\gamma$, helicity=1/2	0.01–0.06 %	715
$n\gamma$, helicity=1/2	0.003–0.05 %	715

$N(1900)\ 3/2^+$

$I(J^P) = \frac{1}{2}(\frac{3}{2}^+)$

Re(pole position) = 1900 to 1940 (≈ 1920) MeV
−2Im(pole position) = 90 to 160 (≈ 130) MeV
Breit-Wigner mass = 1890 to 1950 (≈ 1920) MeV
Breit-Wigner full width = 100 to 320 (≈ 200) MeV

$N(1900)$ DECAY MODES	Fraction (Γ_i/Γ)	p (MeV/c)
$N\pi$	1–20 %	723
$N\eta$	2–14 %	595
$N\eta'$	4–8 %	151
$N\omega$	7–13 %	424
ΛK	2–20 %	495
ΣK	3–7 %	431
$N\pi\pi$	>56 %	699
$\Delta(1232)\pi$	30–70 %	553
$\Delta(1232)\pi$, P-wave	9–25 %	553
$\Delta(1232)\pi$, F-wave	21–45 %	553
$N\rho$	(46 ±13) %	432
$N\rho$, S=1/2	25–40 %	432
$N\rho$, S=3/2 , P-wave	(9.0± 3.0) %	432
$N\rho$, S=3/2 , F-wave	(30 ±12) %	432
$N\sigma$	1–7 %	–
$N(1440)\pi$	(9 ± 6) %	403
$N(1520)\pi$, S-wave	7–23 %	341
$N(1535)\pi$	4–10 %	328
$\Lambda K^*(892)$	< 0.2 %	†
$p\gamma$	0.001–0.025 %	731
$p\gamma$, helicity=1/2	0.001–0.021 %	731
$p\gamma$, helicity=3/2	<0.003 %	731
$n\gamma$	<0.040 %	730
$n\gamma$, helicity=1/2	<0.007 %	730
$n\gamma$, helicity=3/2	<0.033 %	730

$N(2060)\ 5/2^-$

$I(J^P) = \frac{1}{2}(\frac{5}{2}^-)$

was $N(2200)$

Re(pole position) = 2020 to 2130 (≈ 2070) MeV
−2Im(pole position) = 350 to 430 (≈ 400) MeV
Breit-Wigner mass = 2030 to 2200 (≈ 2100) MeV
Breit-Wigner full width = 300 to 450 (≈ 400) MeV

$N(2060)$ DECAY MODES	Fraction (Γ_i/Γ)	p (MeV/c)
$N\pi$	7–12 %	834
$N\eta$	2–38 %	729
$N\omega$	1–7 %	600
ΛK	10–20 %	644
ΣK	1–5 %	593
$N\pi\pi$	12–52 %	814
$\Delta(1232)\pi$	(12.0±3.0) %	680
$\Delta(1232)\pi$, D-wave	4–10 %	680
$N\rho$	5–33 %	605
$N\rho$, S=3/2 , D-wave	5–23 %	605
$N\sigma$	3–9 %	–
$N(1440)\pi$	4–14 %	544
$N(1520)\pi$, P-wave	9–21 %	490
$N(1680)\pi$, S-wave	8–22 %	353
$\Lambda K^*(892)$	0.3–1.3 %	306
$p\gamma$	0.03–0.19 %	840
$p\gamma$, helicity=1/2	0.02–0.08 %	840
$p\gamma$, helicity=3/2	0.01–0.10 %	840
$n\gamma$	0.003–0.07 %	840
$n\gamma$, helicity=1/2	0.001–0.02 %	840
$n\gamma$, helicity=3/2	0.002–0.05 %	840

$N(2100)\ 1/2^+$

$I(J^P) = \frac{1}{2}(\frac{1}{2}^+)$

Re(pole position) = 2050 to 2150 (≈ 2100) MeV
−2Im(pole position) = 240 to 340 (≈ 300) MeV
Breit-Wigner mass = 2050 to 2150 (≈ 2100) MeV
Breit-Wigner full width = 200 to 320 (≈ 260) MeV

$N(2100)$ DECAY MODES	Fraction (Γ_i/Γ)	p (MeV/c)
$N\pi$	8–32 %	834
$N\eta$	5–45 %	729
$N\eta'$	5–11 %	451
$N\omega$	10–25 %	600
ΛK	<1.0 %	644
$N\pi\pi$	>55 %	814
$\Delta(1232)\pi$	6–14 %	680
$N\rho$	(17 ±6) %	605
$N\rho$, S=1/2	35–70 %	605
$N\rho$, S=3/2	(5.0±3.0) %	605
$N\sigma$	14–35 %	–
$N(1535)\pi$	26–34 %	478
$N(1520)\pi$, D-wave	< 2 %	490
$\Lambda K^*(892)$	3–11 %	306
$p\gamma$, helicity=1/2	0.001–0.13 %	840
$n\gamma$, helicity=1/2	0.004–0.09 %	840

$N(2120)\ 3/2^-$

$I(J^P) = \frac{1}{2}(\frac{3}{2}^-)$

Re(pole position) = 2050 to 2150 (≈ 2100) MeV
−2Im(pole position) = 200 to 360 (≈ 280) MeV
Breit-Wigner mass = 2060 to 2160 (≈ 2120) MeV
Breit-Wigner full width = 260 to 360 (≈ 300) MeV

$N(2120)$ DECAY MODES	Fraction (Γ_i/Γ)	p (MeV/c)
$N\pi$	5–15 %	846
$N\eta$	1–5 %	743
$N\eta'$	2–6 %	474
$N\omega$	4–20 %	617

Int. J. Mod. Phys. A 2026.41. Downloaded from www.worldscientific.com
by UNIVERSITY OF CALIFORNIA @ BERKELEY on 09/16/26. Re-use and distribution is strictly not permitted, except for Open Access articles.

ΛK	6–11 %	660
$N\pi\pi$	>27 %	827
$\Delta(1232)\pi$	>23 %	693
$\Delta(1232)\pi$, S-wave	15–70 %	693
$\Delta(1232)\pi$, D-wave	8–45 %	693
$N\rho$	(28 ±6) %	622
$N\rho$, S=1/2	(4.0±2.0) %	622
$N\rho$, S=3/2 , S-wave	< 3 %	622
$N\rho$, S=3/2 , D-wave	(5.0±3.0) %	622
$N\sigma$	4–15 %	–
$N(1440)\pi$	(6 ±6) %	559
$N(1520)\pi$, P-wave	(10 ±5) %	505
$N(1535)\pi$	7–23 %	494
$\Lambda K^*(892)$	< 0.2 %	339
$p\gamma$	0.16–2.1 %	852
$p\gamma$, helicity=1/2	0.07–0.80 %	852
$p\gamma$, helicity=3/2	0.09–1.3 %	852
$n\gamma$	0.04–0.72 %	852
$n\gamma$, helicity=1/2	0.04–0.60 %	852
$n\gamma$, helicity=3/2	0.001–0.12 %	852

$N(2190)\ 7/2^-$

$I(J^P) = \frac{1}{2}(\frac{7}{2}^-)$

Re(pole position) = 1950 to 2150 (≈ 2050) MeV
−2Im(pole position) = 300 to 500 (≈ 400) MeV
Breit-Wigner mass = 2140 to 2220 (≈ 2180) MeV
Breit-Wigner full width = 300 to 500 (≈ 400) MeV

$N(2190)$ DECAY MODES	Fraction (Γ_i/Γ)	p (MeV/c)
$N\pi$	10–20 %	882
$N\eta$	1–5 %	785
$N\omega$	8–20 %	667
ΛK	0.2–0.8 %	705
$N\pi\pi$	22–51 %	864
$\Delta\pi$	(4.0±2.0) %	734
$\Delta(1232)\pi$, D-wave	19–31 %	734
$N\rho$	(8 ±7) %	672
$N\rho$, S=3/2, D-wave	<11 %	672
$N\sigma$	3–9 %	–
$\Lambda K^*(892)$	0.2–0.8 %	423
$p\gamma$	<0.08 %	888
$p\gamma$, helicity=1/2	<0.06 %	888
$p\gamma$, helicity=3/2	<0.02 %	888
$n\gamma$	<0.04 %	888
$n\gamma$, helicity=1/2	<0.01 %	888
$n\gamma$, helicity=3/2	<0.03 %	888

$N(2220)\ 9/2^+$

$I(J^P) = \frac{1}{2}(\frac{9}{2}^+)$

Re(pole position) = 2130 to 2200 (≈ 2150) MeV
−2Im(pole position) = 360 to 480 (≈ 400) MeV
Breit-Wigner mass = 2200 to 2300 (≈ 2250) MeV
Breit-Wigner full width = 350 to 500 (≈ 400) MeV

$N(2220)$ DECAY MODES	Fraction (Γ_i/Γ)	p (MeV/c)
$N\pi$	15–30 %	924
$\Delta\pi$	(15±10) %	780
$\Delta\pi$, F-wave	(15±10) %	780
$N\rho$	(10±10) %	727
$N\rho$, S=3/2 , F-wave	(10±10) %	727
$N\sigma$	(5± 5) %	–

$N(2250)\ 9/2^-$

$I(J^P) = \frac{1}{2}(\frac{9}{2}^-)$

Re(pole position) = 2100 to 2200 (≈ 2150) MeV
−2Im(pole position) = 350 to 500 (≈ 420) MeV
Breit-Wigner mass = 2250 to 2320 (≈ 2280) MeV
Breit-Wigner full width = 300 to 600 (≈ 500) MeV

$N(2250)$ DECAY MODES	Fraction (Γ_i/Γ)	p (MeV/c)
$N\pi$	5–15 %	941
$N\eta$	<5 %	852
ΛK	1–3 %	777
$\Delta\pi$	(10±7) %	800
$\Delta\pi$, G-wave	(10±7) %	800
$N\rho$	(11±7) %	750
$N\rho$, S=1/2	(5±5) %	750
$N\rho$, S=3/2 , G-wave	(6±4) %	750

$N(2600)\ 11/2^-$

$I(J^P) = \frac{1}{2}(\frac{11}{2}^-)$

Breit-Wigner mass = 2550 to 2750 (≈ 2600) MeV
Breit-Wigner full width = 500 to 800 (≈ 650) MeV

$N(2600)$ DECAY MODES	Fraction (Γ_i/Γ)	p (MeV/c)
$N\pi$	3–8 %	1126

Δ BARYONS
($S=0, I=3/2$)

$\Delta^{++} = uuu$, $\Delta^+ = uud$, $\Delta^0 = udd$, $\Delta^- = ddd$

$\Delta(1232)\ 3/2^+$

$I(J^P) = \frac{3}{2}(\frac{3}{2}^+)$

Re(pole position) = 1209 to 1211 (≈ 1210) MeV
−2Im(pole position) = 98 to 102 (≈ 100) MeV
Breit-Wigner mass (mixed charges) = 1230 to 1234 (≈ 1232) MeV
Breit-Wigner full width (mixed charges) = 114 to 120 (≈ 117) MeV

$\Delta(1232)$ DECAY MODES	Fraction (Γ_i/Γ)	p (MeV/c)
$N\pi$	99.4 %	229
$N\gamma$	0.55–0.65 %	259
$N\gamma$, helicity=1/2	0.11–0.13 %	259
$N\gamma$, helicity=3/2	0.44–0.52 %	259
pe^+e^-	$(4.2\pm0.7)\times10^{-5}$	259

$\Delta(1600)\ 3/2^+$

$I(J^P) = \frac{3}{2}(\frac{3}{2}^+)$

Re(pole position) = 1470 to 1590 (≈ 1520) MeV
−2Im(pole position) = 150 to 320 (≈ 280) MeV
Breit-Wigner mass = 1500 to 1640 (≈ 1570) MeV
Breit-Wigner full width = 200 to 300 (≈ 250) MeV

$\Delta(1600)$ DECAY MODES	Fraction (Γ_i/Γ)	p (MeV/c)
$N\pi$	8–24%	492
$N\pi\pi$	58–84 %	454
$\Delta(1232)\pi$	58–82 %	276
$\Delta(1232)\pi$, P-wave	72–82%	276
$\Delta(1232)\pi$, F-wave	<2%	276
$N\rho$	(7 ±4) %	†
$N\rho$, S=1/2	(2.0±2.0) %	†
$N\rho$, S=3/2 , P-wave	(5.0±3.0) %	†
$N(1440)\pi$	17–27%	†
$N\gamma$	0.001–0.035 %	505
$N\gamma$, helicity=1/2	0.0–0.02 %	505
$N\gamma$, helicity=3/2	0.001–0.015 %	505

$\Delta(1620)\ 1/2^-$

$I(J^P) = \frac{3}{2}(\frac{1}{2}^-)$

Re(pole position) = 1590 to 1610 (≈ 1600) MeV
−2Im(pole position) = 80 to 140 (≈ 110) MeV
Breit-Wigner mass = 1590 to 1630 (≈ 1610) MeV
Breit-Wigner full width = 110 to 150 (≈ 130) MeV

$\Delta(1620)$ DECAY MODES	Fraction (Γ_i/Γ)	p (MeV/c)
$N\pi$	25–35 %	520
$N\pi\pi$	>67 %	484
$\Delta(1232)\pi$	44–72 %	311
$N\rho$	23–32%	†
$N\rho$, S=1/2	23–32%	†
$N\rho$, S=3/2	<0.04%	†

$N(1440)\pi$	<9 %	98
$N\gamma$, helicity=1/2	0.03–0.10 %	532

$\Delta(1700)\ 3/2^-$ $\quad I(J^P) = \frac{3}{2}(\frac{3}{2}^-)$

Re(pole position) = 1640 to 1690 (≈ 1665) MeV
−2Im(pole position) = 200 to 300 (≈ 250) MeV
Breit-Wigner mass = 1690 to 1730 (≈ 1710) MeV
Breit-Wigner full width = 220 to 380 (≈ 300) MeV

$\Delta(1700)$ DECAY MODES	Fraction (Γ_i/Γ)	p (MeV/c)
$N\pi$	10–20 %	588
$N\pi\pi$	>31 %	557
$\Delta(1232)\pi$	9–70 %	394
$\Delta(1232)\pi$, S-wave	5–54 %	394
$\Delta(1232)\pi$, D-wave	4–16 %	394
$N\rho$	(15 ±4) %	†
$N\rho$, S=3/2, S-wave	22–32%	†
$N(1440)\pi$	(3.0±2.0) %	215
$N(1520)\pi$, P-wave	1–5 %	133
$N(1535)\pi$	0.5–1.5 %	113
$\Delta(1232)\eta$	3–7 %	†
$N\gamma$	0.22–0.60 %	598
$N\gamma$, helicity=1/2	0.12–0.30 %	598
$N\gamma$, helicity=3/2	0.10–0.30 %	598

$\Delta(1900)\ 1/2^-$ $\quad I(J^P) = \frac{3}{2}(\frac{1}{2}^-)$

Re(pole position) = 1830 to 1900 (≈ 1865) MeV
−2Im(pole position) = 180 to 300 (≈ 240) MeV
Breit-Wigner mass = 1840 to 1920 (≈ 1860) MeV
Breit-Wigner full width = 180 to 320 (≈ 250) MeV

$\Delta(1900)$ DECAY MODES	Fraction (Γ_i/Γ)	p (MeV/c)
$N\pi$	4–12%	685
ΣK	seen	367
$N\pi\pi$	> 52%	660
$\Delta(1232)\pi$	30–70%	509
$N\rho$	22–60 %	361
$N\rho$, S=1/2	11–35%	361
$N\rho$, S=3/2	11–25%	361
$N(1440)\pi$	3–32%	353
$N(1520)\pi$	2–10%	288
$\Delta(1232)\eta$	< 2%	251
$N\gamma$, helicity=1/2	0.06–0.43 %	693

$\Delta(1905)\ 5/2^+$ $\quad I(J^P) = \frac{3}{2}(\frac{5}{2}^+)$

Re(pole position) = 1750 to 1800 (≈ 1770) MeV
−2Im(pole position) = 260 to 340 (≈ 300) MeV
Breit-Wigner mass = 1855 to 1910 (≈ 1880) MeV
Breit-Wigner full width = 270 to 400 (≈ 330) MeV

$\Delta(1905)$ DECAY MODES	Fraction (Γ_i/Γ)	p (MeV/c)
$N\pi$	9–15%	698
$N\pi\pi$	>65%	673
$\Delta(1232)\pi$	>48%	524
$\Delta(1232)\pi$, P-wave	8–43%	524
$\Delta(1232)\pi$, F-wave	40–58%	524
$N\rho$	(25±10) %	385
$N\rho$, S=3/2, P-wave	17–35%	385
$N(1535)\pi$	< 1 %	293
$N(1680)\pi$, P-wave	5–15%	133
$\Delta(1232)\eta$	2–6%	282
$N\gamma$	0.012–0.036 %	706
$N\gamma$, helicity=1/2	0.002–0.006 %	706
$N\gamma$, helicity=3/2	0.01–0.03 %	706

$\Delta(1910)\ 1/2^+$ $\quad I(J^P) = \frac{3}{2}(\frac{1}{2}^+)$

Re(pole position) = 1800 to 1900 (≈ 1850) MeV
−2Im(pole position) = 200 to 500 (≈ 350) MeV
Breit-Wigner mass = 1850 to 1950 (≈ 1900) MeV
Breit-Wigner full width = 200 to 400 (≈ 300) MeV

$\Delta(1910)$ DECAY MODES	Fraction (Γ_i/Γ)	p (MeV/c)
$N\pi$	10–30%	710
ΣK	4–14%	410
$\Delta(1232)\pi$	34–66%	539
$N\rho$	(10 ±4) %	409
$N\rho$, S=1/2	(5.0±3.0) %	409
$N\rho$, S=3/2	(5.0±3.0) %	409
$N(1440)\pi$	3–45%	386
$N(1535)\pi$	(4.0±2.0) %	311
$\Delta(1232)\eta$	5–13%	310
$N\gamma$, helicity=1/2	0.0–0.02 %	718

$\Delta(1920)\ 3/2^+$ $\quad I(J^P) = \frac{3}{2}(\frac{3}{2}^+)$

Re(pole position) = 1850 to 1950 (≈ 1900) MeV
−2Im(pole position) = 200 to 400 (≈ 300) MeV
Breit-Wigner mass = 1870 to 1970 (≈ 1920) MeV
Breit-Wigner full width = 240 to 360 (≈ 300) MeV

$\Delta(1920)$ DECAY MODES	Fraction (Γ_i/Γ)	p (MeV/c)
$N\pi$	5–20 %	723
ΣK	2–6 %	431
$N\pi\pi$	>46 %	699
$\Delta(1232)\pi$	(38±15) %	553
$\Delta(1232)\pi$, P-wave	2–28 %	553
$\Delta(1232)\pi$, F-wave	44–72 %	553
$N\rho$	(57± 8) %	432
$N\rho$, S=1/2	(8± 4) %	432
$N\rho$, S=3/2 , P-wave	(14± 5) %	432
$N\rho$, S=3/2 , F-wave	(35± 6) %	432
$N(1440)\pi$, P-wave	4–86 %	403
$N(1520)\pi$, S-wave	< 5 %	341
$N(1535)\pi$	< 2 %	328
$N a_0(980)$	seen	41
$\Delta(1232)\eta$	5–17 %	336
$N\gamma$	0.01–0.84 %	731
$N\gamma$, helicity=1/2	0.0–0.42 %	731
$N\gamma$, helicity=3/2	0.01–0.42 %	731

$\Delta(1930)\ 5/2^-$ $\quad I(J^P) = \frac{3}{2}(\frac{5}{2}^-)$

Re(pole position) = 1820 to 1880 (≈ 1850) MeV
−2Im(pole position) = 300 to 450 (≈ 320) MeV
Breit-Wigner mass = 1900 to 2000 (≈ 1950) MeV
Breit-Wigner full width = 200 to 400 (≈ 300) MeV

$\Delta(1930)$ DECAY MODES	Fraction (Γ_i/Γ)	p (MeV/c)
$N\pi$	5–15 %	742
$\Delta(1232)\pi$	(33 ±9) %	575
$\Delta(1232)\pi$, D-wave	(28 ±7) %	575
$\Delta(1232)\pi$, G-wave	(5 ±5) %	575
$N\rho$	(33 ±8) %	464
$N\rho$, S=1/2	(3.0±2.0) %	464
$N\rho$, S=3/2 , G-wave	(30 ±8) %	464
$N\gamma$	0.0–0.01 %	749
$N\gamma$, helicity=1/2	0.0–0.005 %	749
$N\gamma$, helicity=3/2	0.0–0.004 %	749

$\Delta(1950)\ 7/2^+$ $\quad I(J^P) = \frac{3}{2}(\frac{7}{2}^+)$

Re(pole position) = 1870 to 1890 (≈ 1880) MeV
−2Im(pole position) = 220 to 260 (≈ 240) MeV
Breit-Wigner mass = 1915 to 1950 (≈ 1930) MeV
Breit-Wigner full width = 235 to 335 (≈ 285) MeV

$\Delta(1950)$ DECAY MODES	Fraction (Γ_i/Γ)	p (MeV/c)
$N\pi$	35–45 %	729
ΣK	0.3–0.5 %	441
$N\pi\pi$	37–77 %	706
$\Delta(1232)\pi$	(4.0±3.0) %	560
$\Delta(1232)\pi$, F-wave	1–9 %	560
$N\rho$	(10 ±5) %	443

Int. J. Mod. Phys. A 2026.41. Downloaded from www.worldscientific.com
by UNIVERSITY OF CALIFORNIA @ BERKELEY on 09/16/26. Re-use and distribution is strictly not permitted, except for Open Acce

Int. J. Mod. Phys. A 2026.41. Downloaded from www.worldscientific.com
by UNIVERSITY OF CALIFORNIA @ BERKELEY on 09/16/26. Re-use and distribution is strictly not permitted, except for Open Access articles.

$N\rho$, S=1/2	(10 ±5) %	443
$N(1680)\pi$, P-wave	3–9 %	191
$\Delta(1232)\eta$	< 0.6 %	349
$N\gamma$	0.06–0.14 %	737
$N\gamma$, helicity=1/2	0.03–0.05 %	737
$N\gamma$, helicity=3/2	0.04–0.09 %	737

$\Delta(2200)$ 7/2$^-$

$I(J^P) = \frac{3}{2}(\frac{7}{2}^-)$

Re(pole position) = 2050 to 2150 (≈ 2100) MeV
−2Im(pole position) = 260 to 420 (≈ 340) MeV
Breit-Wigner mass = 2150 to 2250 (≈ 2200) MeV
Breit-Wigner full width = 200 to 500 (≈ 350) MeV

$\Delta(2200)$ DECAY MODES	Fraction (Γ_i/Γ)	p (MeV/c)
$N\pi$	2–8 %	894
ΣK	1–7 %	672
$N\pi\pi$	>45 %	876
$\Delta\pi$	>45 %	747
$\Delta\pi$, D-wave	(70±30) %	747
$\Delta\pi$, G-wave	5–25 %	747
$\Delta\eta$, D-wave	seen	614

$\Delta(2420)$ 11/2$^+$

$I(J^P) = \frac{3}{2}(\frac{11}{2}^+)$

Re(pole position) = 2300 to 2500 (≈ 2400) MeV
−2Im(pole position) = 350 to 550 (≈ 450) MeV
Breit-Wigner mass = 2300 to 2600 (≈ 2450) MeV
Breit-Wigner full width = 300 to 700 (≈ 500) MeV

$\Delta(2420)$ DECAY MODES	Fraction (Γ_i/Γ)	p (MeV/c)
$N\pi$	5–10 %	1040

Λ BARYONS
($S = -1$, $I = 0$)

$\Lambda^0 = uds$

Λ

$I(J^P) = 0(\frac{1}{2}^+)$

Mass $m = 1115.683 \pm 0.006$ MeV
$(m_\Lambda - m_{\overline{\Lambda}}) / m_\Lambda = (-0.1 \pm 1.1) \times 10^{-5}$ (S = 1.6)
Mean life $\tau = (2.617 \pm 0.010) \times 10^{-10}$ s (S = 1.5)
$(\tau_\Lambda - \tau_{\overline{\Lambda}}) / \tau_\Lambda = (0.9 \pm 3.2) \times 10^{-3}$
$c\tau = 7.845$ cm
Magnetic moment $\mu = -0.613 \pm 0.004\ \mu_N$
Electric dipole moment $d < 1.5 \times 10^{-16}$ $e$cm, CL = 95%

Decay parameters

$p\pi^-$	$\alpha_- = 0.748 \pm 0.008$ (S = 2.4)
$\overline{p}\pi^+$	$\alpha_+ = -0.758 \pm 0.005$ (S = 1.2)
$\overline{n}\pi^0$	$\overline{\alpha}_0 = -0.675 \pm 0.011$ (S = 1.2)
$n\pi^0$	$\alpha_0 = 0.670 \pm 0.012$
$n\gamma$	$\alpha_\gamma = -0.16 \pm 0.11$
$p\pi^-$	$\phi_- = (-6.5 \pm 3.5)^\circ$
$p\pi^-$	$\gamma_- = 0.66 \pm 0.01$ [l]
$p\pi^-$	$\Delta_- = (5.7 \pm 3.0)^\circ$ [l]

$\overline{\alpha}_0 / \alpha_+$ in $\overline{\Lambda} \to \overline{n}\pi^0$, $\overline{\Lambda} \to \overline{p}\pi^+ = 0.876^{+0.022}_{-0.020}$ (S = 1.4)
$(\alpha_0 + \overline{\alpha}_0)/(\alpha_0 - \overline{\alpha}_0)$ in $\Lambda \to n\pi^0$, $\overline{\Lambda} \to \overline{n}\pi^0 = (0.1^{+1.0}_{-1.1}) \times 10^{-2}$
$pe^-\overline{\nu}_e$ $g_A/g_V = -0.718 \pm 0.015$ [h]

Λ DECAY MODES		Fraction (Γ_i/Γ)	Confidence level	p (MeV/c)
$p\pi^-$		(64.1 ±0.5) %		101
$n\pi^0$		(35.9 ±0.5) %		104
$n\gamma$		(8.3 ±0.7) $\times 10^{-4}$		162
$p\pi^-\gamma$	[n]	(8.5 ±1.4) $\times 10^{-4}$		101
$pe^-\overline{\nu}_e$		(8.34±0.14) $\times 10^{-4}$		163
$p\mu^-\overline{\nu}_\mu$		(1.51±0.19) $\times 10^{-4}$		131
Lepton (L) and/or Baryon (B) number violating decay modes				
π^+e^-	L,B	< 6 $\times 10^{-7}$	90%	549
$\pi^+\mu^-$	L,B	< 6 $\times 10^{-7}$	90%	544
π^-e^+	L,B	< 4 $\times 10^{-7}$	90%	549
$\pi^-\mu^+$	L,B	< 6 $\times 10^{-7}$	90%	544
K^+e^-	L,B	< 2 $\times 10^{-6}$	90%	449
$K^+\mu^-$	L,B	< 3 $\times 10^{-6}$	90%	441
K^-e^+	L,B	< 2 $\times 10^{-6}$	90%	449
$K^-\mu^+$	L,B	< 3 $\times 10^{-6}$	90%	441
$K^0_S\nu$	L,B	< 2 $\times 10^{-5}$	90%	447
$\overline{p}\pi^+$	B	< 9 $\times 10^{-7}$	90%	101
invisible		< 7.4 $\times 10^{-5}$	90%	–

$\Lambda(1405)$ 1/2$^-$

$I(J^P) = 0(\frac{1}{2}^-)$

Mass $m = 1405.1^{+1.3}_{-1.0}$ MeV
Full width $\Gamma = 50.5 \pm 2.0$ MeV
Below $\overline{K}N$ threshold

$\Lambda(1405)$ DECAY MODES	Fraction (Γ_i/Γ)	p (MeV/c)
$\Sigma\pi$	100 %	155

$\Lambda(1520)$ 3/2$^-$

$I(J^P) = 0(\frac{3}{2}^-)$

Mass $m = 1518$ to 1520 (≈ 1519) MeV [o]
Full width $\Gamma = 15$ to 17 (≈ 16) MeV [o]

$\Lambda(1520)$ DECAY MODES	Fraction (Γ_i/Γ)	p (MeV/c)
$N\overline{K}$	(45 ±1) %	242
$\Sigma\pi$	(42 ±1) %	268
$\Lambda\pi\pi$	(10 ±1) %	259
$\Sigma\pi\pi$	(0.9 ±0.1) %	168
$\Lambda\gamma$	(0.85±0.15) %	350

$\Lambda(1600)$ 1/2$^+$

$I(J^P) = 0(\frac{1}{2}^+)$

Mass $m = 1570$ to 1630 (≈ 1600) MeV
Full width $\Gamma = 150$ to 250 (≈ 200) MeV

$\Lambda(1600)$ DECAY MODES	Fraction (Γ_i/Γ)	p (MeV/c)
$N\overline{K}$	15–30 %	343
$\Sigma\pi$	10–60 %	338
$\Lambda\sigma$	(19±4) %	–
$\Sigma(1385)\pi$	(9±4) %	158

$\Lambda(1670)$ 1/2$^-$

$I(J^P) = 0(\frac{1}{2}^-)$

Mass $m = 1670$ to 1678 (≈ 1674) MeV
Full width $\Gamma = 25$ to 35 (≈ 30) MeV

$\Lambda(1670)$ DECAY MODES	Fraction (Γ_i/Γ)	p (MeV/c)
$N\overline{K}$	20–30 %	418
$\Sigma\pi$	25–55 %	398
$\Lambda\eta$	10–25 %	88
$\Sigma(1385)\pi$, D-wave	(6.0±2.0) %	235
$N\overline{K}^*(892)$, S=3/2, D-wave	(5 ±4) %	†
$\Lambda\sigma$	(20 ±8) %	–

$\Lambda(1690)$ 3/2$^-$

$I(J^P) = 0(\frac{3}{2}^-)$

Mass $m = 1685$ to 1695 (≈ 1690) MeV
Full width $\Gamma = 60$ to 80 (≈ 70) MeV

$\Lambda(1690)$ DECAY MODES	Fraction (Γ_i/Γ)	p (MeV/c)
$N\overline{K}$	20–30 %	433
$\Sigma\pi$	20–40 %	410
$\Lambda\sigma$	(5.0±2.0) %	–
$\Lambda\pi\pi$	∼ 25 %	419
$\Sigma\pi\pi$	∼ 20 %	358
$\Sigma(1385)\pi$, S-wave	(9 ±5) %	251
$\Sigma(1385)\pi$, D-wave	(3.0±2.0) %	251

Int. J. Mod. Phys. A 2026.41. Downloaded from www.worldscientific.com
by UNIVERSITY OF CALIFORNIA @ BERKELEY on 09/16/26. Re-use and distribution is strictly not permitted, except for Open Acce

$\Lambda(1800)\ 1/2^-$

$I(J^P) = 0(\frac{1}{2}^-)$

Mass m = 1750 to 1850 (≈ 1800) MeV
Full width Γ = 150 to 250 (≈ 200) MeV

$\Lambda(1800)$ DECAY MODES	Fraction (Γ_i/Γ)	p (MeV/c)
$N\overline{K}$	25–40 %	528
$\Sigma\pi$	(27 ±6) %	494
$\Lambda\sigma$	(15 ±4) %	–
$\Sigma(1385)\pi$	(9 ±4) %	349
$\Lambda\eta$	0.01 to 0.10	326
$N\overline{K}^*(892)$	seen	†

$\Lambda(1810)\ 1/2^+$

$I(J^P) = 0(\frac{1}{2}^+)$

Mass m = 1740 to 1840 (≈ 1790) MeV
Full width Γ = 50 to 170 (≈ 110) MeV

$\Lambda(1810)$ DECAY MODES	Fraction (Γ_i/Γ)	p (MeV/c)
$N\overline{K}$	0.05 to 0.35	520
$\Sigma\pi$	(16 ± 5) %	487
$\Sigma(1385)\pi$	(40 ±15) %	340
$N\overline{K}^*(892)$	30–60 %	†

$\Lambda(1820)\ 5/2^+$

$I(J^P) = 0(\frac{5}{2}^+)$

Mass m = 1815 to 1825 (≈ 1820) MeV
Full width Γ = 70 to 90 (≈ 80) MeV

$\Lambda(1820)$ DECAY MODES	Fraction (Γ_i/Γ)	p (MeV/c)
$N\overline{K}$	55–65 %	545
$\Sigma\pi$	8–14 %	509
$\Sigma(1385)\pi$	5–10 %	366
$N\overline{K}^*(892)$, S=3/2, P-wave	(3.0±1.0) %	†

$\Lambda(1830)\ 5/2^-$

$I(J^P) = 0(\frac{5}{2}^-)$

Mass m = 1820 to 1830 (≈ 1825) MeV
Full width Γ = 60 to 120 (≈ 90) MeV

$\Lambda(1830)$ DECAY MODES	Fraction (Γ_i/Γ)	Scale factor	p (MeV/c)
$N\overline{K}$	0.04 to 0.08		549
$\Sigma\pi$	35–75 %		512
$\Sigma(1385)\pi$	>15 %		370
$\Sigma(1385)\pi$, D-wave	(40 ±15) %	3.2	370

$\Lambda(1890)\ 3/2^+$

$I(J^P) = 0(\frac{3}{2}^+)$

Mass m = 1870 to 1910 (≈ 1890) MeV
Full width Γ = 80 to 160 (≈ 120) MeV

$\Lambda(1890)$ DECAY MODES	Fraction (Γ_i/Γ)	p (MeV/c)
$N\overline{K}$	0.24 to 0.36	599
$\Sigma\pi$	3–10 %	560
$\Sigma(1385)\pi$	seen	423
$\Sigma(1385)\pi$, P-wave	(6.0 ±3.0) %	423
$\Sigma(1385)\pi$, F-wave	(4.0 ±2.0) %	423
$N\overline{K}^*(892)$	seen	236

$\Lambda(2100)\ 7/2^-$

$I(J^P) = 0(\frac{7}{2}^-)$

Mass m = 2090 to 2110 (≈ 2100) MeV
Full width Γ = 100 to 250 (≈ 200) MeV

$\Lambda(2100)$ DECAY MODES	Fraction (Γ_i/Γ)	p (MeV/c)
$N\overline{K}$	25–35 %	751
$\Sigma\pi$	∼ 5 %	705
$\Lambda\eta$	<3 %	617
ΞK	<3 %	491
$\Lambda\omega$	<8 %	443
$\Sigma(1385)\pi$, G-wave	(1.0±1.0) %	584
$N\overline{K}^*(892)$	10–20 %	515
$N\overline{K}^*(892)$, S=3/2, D-wave	(4.0±2.0) %	515

$\Lambda(2110)\ 5/2^+$

$I(J^P) = 0(\frac{5}{2}^+)$

Mass m = 2050 to 2130 (≈ 2090) MeV
Full width Γ = 200 to 300 (≈ 250) MeV

$\Lambda(2110)$ DECAY MODES	Fraction (Γ_i/Γ)	p (MeV/c)
$N\overline{K}$	5–25 %	744
$\Sigma\pi$	10–40 %	698
$\Lambda\omega$	seen	432
$\Lambda\omega$, S=3/2 , P-wave	(5.0±2.0) %	432
$\Sigma(1385)\pi$	seen	576
$N\overline{K}^*(892)$	10–60 %	505

$\Lambda(2350)\ 9/2^+$

$I(J^P) = 0(\frac{9}{2}^+)$

Mass m = 2340 to 2370 (≈ 2350) MeV
Full width Γ = 100 to 250 (≈ 150) MeV

$\Lambda(2350)$ DECAY MODES	Fraction (Γ_i/Γ)	p (MeV/c)
$N\overline{K}$	∼ 12 %	915
$\Sigma\pi$	∼ 10 %	867

Σ BARYONS
($S = -1, I = 1$)

$\Sigma^+ = uus, \quad \Sigma^0 = uds, \quad \Sigma^- = dds$

Σ^+

$I(J^P) = 1(\frac{1}{2}^+)$

Mass $m = 1189.37 \pm 0.07$ MeV (S = 2.2)
Mean life $\tau = (0.8018 \pm 0.0026) \times 10^{-10}$ s
$c\tau = 2.404$ cm
$(\tau_{\Sigma^+} - \tau_{\overline{\Sigma}^-}) / \tau_{\Sigma^+} = -0.0006 \pm 0.0012$
Magnetic moment $\mu = 2.458 \pm 0.010\ \mu_N$ (S = 2.1)
$(\mu_{\Sigma^+} + \mu_{\overline{\Sigma}^-}) / \mu_{\Sigma^+} = 0.014 \pm 0.015$
$\Gamma(\Sigma^+ \to n\ell^+\nu)/\Gamma(\Sigma^- \to n\ell^-\overline{\nu}_\ell) < 0.043$

Decay parameters

$p\pi^0$ $\alpha_0 = -0.977 \pm 0.009$
$\overline{p}\pi^0$ $\overline{\alpha}_0 = 0.999 \pm 0.012$
$(\alpha_0 + \overline{\alpha}_0) / (\alpha_0 - \overline{\alpha}_0) = (-1.2 \pm 0.9) \times 10^{-2}$
$(\alpha_0 - \overline{\alpha}_0)/2 = -0.9869 \pm 0.0019$
$p\pi^0$ $\phi_0 = (36 \pm 34)^\circ$
" $\gamma_0 = 0.16$ [l]
" $\Delta_0 = (187 \pm 6)^\circ$ [l]
$n\pi^+$ $\alpha_+ = (4.88 \pm 0.26) \times 10^{-2}$
" $\phi_+ = (167 \pm 20)^\circ$ (S = 1.1)
$\overline{\alpha}_-$ FOR $\overline{\Sigma}^- \to \overline{n}\pi^- = (-5.7 \pm 0.5) \times 10^{-2}$
$\overline{\alpha}_- / \overline{\alpha}_0 = (-5.7 \pm 0.6) \times 10^{-2}$
$(\alpha_+ + \overline{\alpha}_-) / (\alpha_+ - \overline{\alpha}_-) = (-8 \pm 6) \times 10^{-2}$
" $\gamma_+ = -0.97$ [l]
" $\Delta_+ = (-73^{+133}_{-10})^\circ$ [l]
$p\gamma$ $\alpha_\gamma = -0.69 \pm 0.05$

Σ^+ DECAY MODES		Fraction (Γ_i/Γ)	Scale factor/ Confidence level	p (MeV/c)
$p\pi^0$		(51.47±0.30) %		189
$n\pi^+$		(48.43±0.30) %		185
$p\gamma$		(1.04±0.06) $\times 10^{-3}$	S=2.4	225
$n\pi^+\gamma$	[n]	(4.5 ±0.5) $\times 10^{-4}$		185
$\Lambda e^+\nu_e$		(2.3 ±0.4) $\times 10^{-5}$		71

$\Delta S = \Delta Q$ (SQ) violating modes or
$\Delta S = 1$ weak neutral current ($S1$) modes

$ne^+\nu_e$	SQ	< 5	$\times 10^{-6}$	CL=90%	224
$n\mu^+\nu_\mu$	SQ	< 3.0	$\times 10^{-5}$	CL=90%	202

Int. J. Mod. Phys. A 2026.41. Downloaded from www.worldscientific.com
by UNIVERSITY OF CALIFORNIA @ BERKELEY on 09/16/26. Re-use and distribution is strictly not permitted, except for Open Access articles.

pe^+e^-	S1	$< 7 \times 10^{-6}$			225
$p\mu^+\mu^-$	S1	$(1.09 \pm 0.17) \times 10^{-8}$			121
$p\gamma_{dark}$		$< 3.2 \times 10^{-5}$	CL=90%		–

Σ^0

$I(J^P) = 1(\frac{1}{2}^+)$

Mass $m = 1192.642 \pm 0.024$ MeV
$m_{\Sigma^-} - m_{\Sigma^0} = 4.807 \pm 0.035$ MeV (S = 1.1)
$m_{\Sigma^0} - m_{\Lambda} = 76.959 \pm 0.023$ MeV
Mean life $\tau = (7.4 \pm 0.7) \times 10^{-20}$ s
$c\tau = 2.22 \times 10^{-11}$ m
Transition magnetic moment $|\mu_{\Sigma\Lambda}| = 1.61 \pm 0.08\ \mu_N$
Magnetic moment $\mu = (-1.7 \pm 2.8) \times 10^{-3}$
Magnetic moment $\mu = (2.1 \pm 3.0) \times 10^{-3}$
Magnetic moment $\mu = (0.4 \pm 3.2) \times 10^{-3}$

Σ^0 DECAY MODES		Fraction (Γ_i/Γ)	Confidence level	p (MeV/c)
$\Lambda\gamma$		100 %		74
$\Lambda\gamma\gamma$		< 3 %	90%	74
Λe^+e^-	[p]	5×10^{-3}		74

Σ^-

$I(J^P) = 1(\frac{1}{2}^+)$

Mass $m = 1197.449 \pm 0.029$ MeV (S = 1.1)
$m_{\Sigma^-} - m_{\Sigma^+} = 8.08 \pm 0.08$ MeV (S = 1.9)
$m_{\Sigma^-} - m_{\Lambda} = 81.766 \pm 0.029$ MeV (S = 1.1)
Mean life $\tau = (1.479 \pm 0.011) \times 10^{-10}$ s (S = 1.3)
$c\tau = 4.434$ cm
Magnetic moment $\mu = -1.160 \pm 0.025\ \mu_N$ (S = 1.7)
Σ^- charge radius = 0.78 ± 0.10 fm

Decay parameters

$n\pi^-$	$\alpha_- = -0.068 \pm 0.008$
"	$\phi_- = (10 \pm 15)^\circ$
"	$\gamma_- = 0.98$ [l]
"	$\Delta_- = (249^{+12}_{-120})^\circ$ [l]
$ne^-\overline{\nu}_e$	$g_A/g_V = 0.340 \pm 0.017$ [h]
"	$f_2(0)/f_1(0) = 0.97 \pm 0.14$
"	$D = 0.11 \pm 0.10$
$\Lambda e^-\overline{\nu}_e$	$g_V/g_A = 0.01 \pm 0.10$ [h] (S = 1.5)
"	$g_{WM}/g_A = 2.4 \pm 1.7$ [h]

Σ^- DECAY MODES		Fraction (Γ_i/Γ)	Confidence level	p (MeV/c)
$n\pi^-$		(99.848 ± 0.005) %		193
$n\pi^-\gamma$	[n]	$(4.6 \pm 0.6) \times 10^{-4}$		193
$ne^-\overline{\nu}_e$		$(1.017 \pm 0.034) \times 10^{-3}$		230
$n\mu^-\overline{\nu}_\mu$		$(4.5 \pm 0.4) \times 10^{-4}$		210
$\Lambda e^-\overline{\nu}_e$		$(5.73 \pm 0.27) \times 10^{-5}$		79
$\Sigma^+ X$		$< 1.2 \times 10^{-4}$	90%	–
Lepton number (L) violating modes				
pe^-e^-	L	$< 6.7 \times 10^{-5}$	90%	231

$\Sigma(1385)\ 3/2^+$

$I(J^P) = 1(\frac{3}{2}^+)$

$\Sigma(1385)^+$ mass $m = 1382.83 \pm 0.34$ MeV (S = 1.9)
$\Sigma(1385)^0$ mass $m = 1383.8 \pm 0.9$ MeV (S = 1.3)
$\Sigma(1385)^-$ mass $m = 1387.2 \pm 0.5$ MeV (S = 2.2)
$\Sigma(1385)^+$ full width $\Gamma = 36.2 \pm 0.7$ MeV
$\Sigma(1385)^0$ full width $\Gamma = 44 \pm 8$ MeV (S = 2.0)
$\Sigma(1385)^-$ full width $\Gamma = 39.4 \pm 2.1$ MeV (S = 1.7)
Below $\overline{K}N$ threshold

$\Sigma(1385)$ DECAY MODES	Fraction (Γ_i/Γ)	Confidence level	p (MeV/c)
$\Lambda\pi$	(87.0 ± 1.5) %		208
$\Sigma\pi$	(11.7 ± 1.5) %		129
$\Lambda\gamma$	$(1.25^{+0.13}_{-0.12})$ %		241
$\Sigma^+\gamma$	$(7.0 \pm 1.7) \times 10^{-3}$		180
$\Sigma^-\gamma$	$< 2.4 \times 10^{-4}$	90%	173

$\Sigma(1660)\ 1/2^+$

$I(J^P) = 1(\frac{1}{2}^+)$

Re(pole position) = 1585 ± 20 MeV
-2Im(pole position) = 290^{+140}_{-40} MeV
Mass $m = 1640$ to 1680 (≈ 1660) MeV
Full width $\Gamma = 100$ to 300 (≈ 200) MeV

$\Sigma(1660)$ DECAY MODES	Fraction (Γ_i/Γ)	p (MeV/c)
$N\overline{K}$	0.05 to 0.15 (≈ 0.10)	405
$\Lambda\pi$	(35 ± 12) %	440
$\Sigma\pi$	(37 ± 10) %	387
$\Sigma\sigma$	(20 ± 8) %	–
$\Lambda(1405)\pi$	(4.0 ± 2.0) %	199

$\Sigma(1670)\ 3/2^-$

$I(J^P) = 1(\frac{3}{2}^-)$

Mass $m = 1665$ to 1685 (≈ 1675) MeV
Full width $\Gamma = 40$ to 100 (≈ 70) MeV

$\Sigma(1670)$ DECAY MODES	Fraction (Γ_i/Γ)	p (MeV/c)
$N\overline{K}$	0.06 to 0.12	419
$\Lambda\pi$	5–15 %	452
$\Sigma\pi$	30–60 %	398
$\Sigma\sigma$	(7.0 ± 3.0) %	–

$\Sigma(1750)\ 1/2^-$

$I(J^P) = 1(\frac{1}{2}^-)$

Mass $m = 1700$ to 1800 (≈ 1750) MeV
Full width $\Gamma = 100$ to 200 (≈ 150) MeV

$\Sigma(1750)$ DECAY MODES	Fraction (Γ_i/Γ)	p (MeV/c)
$N\overline{K}$	0.06 to 0.12	486
$\Lambda\pi$	(14 ± 5) %	507
$\Sigma\pi$	(16 ± 4) %	456
$\Sigma\eta$	15–55 %	98
$\Sigma(1385)\pi$, D-wave	< 1 %	305
$\Lambda(1520)\pi$	(2.0 ± 1.0) %	175
$N\overline{K}^*(892)$, S=1/2	(8 ± 4) %	†

$\Sigma(1775)\ 5/2^-$

$I(J^P) = 1(\frac{5}{2}^-)$

Mass $m = 1770$ to 1780 (≈ 1775) MeV
Full width $\Gamma = 105$ to 135 (≈ 120) MeV

$\Sigma(1775)$ DECAY MODES	Fraction (Γ_i/Γ)	p (MeV/c)
$N\overline{K}$	37–43%	508
$\Lambda\pi$	14–20%	525
$\Sigma\pi$	2–5%	475
$\Sigma(1385)\pi$	8–12%	327
$\Lambda(1520)\pi$, P-wave	17–23%	202

$\Sigma(1910)\ 3/2^-$

$I(J^P) = 1(\frac{3}{2}^-)$

was $\Sigma(1940)$

Mass $m = 1870$ to 1950 (≈ 1910) MeV
Full width $\Gamma = 150$ to 300 (≈ 220) MeV

$\Sigma(1910)$ DECAY MODES	Fraction (Γ_i/Γ)	p (MeV/c)
$N\overline{K}$	0.01 to 0.05 (≈ 0.02)	615
$\Lambda\pi$	(6 ± 4) %	619
$\Sigma\pi$	(86 ± 21) %	574
$\Sigma(1385)\pi$	seen	439
$\Lambda(1520)\pi$	seen	329
$\Delta(1232)\overline{K}$	(3.0 ± 1.0) %	377
$N\overline{K}^*(892)$	seen	273
$N\overline{K}^*(892)$, S=1/2, D-wave	(1.0 ± 1.0) %	273

Int. J. Mod. Phys. A 2026.41. Downloaded from www.worldscientific.com
by UNIVERSITY OF CALIFORNIA @ BERKELEY on 09/16/26. Re-use and distribution is strictly not permitted, except for Open Acce

$\Sigma(1915)\ 5/2^+$

$I(J^P) = 1(\frac{5}{2}^+)$

Mass $m = 1900$ to 1935 (≈ 1915) MeV
Full width $\Gamma = 80$ to 160 (≈ 120) MeV

$\Sigma(1915)$ DECAY MODES	Fraction (Γ_i/Γ)	p (MeV/c)
$N\overline{K}$	0.05 to 0.15	618
$\Lambda\pi$	(6.0 ±2.0) %	623
$\Sigma\pi$	(10.0 ±2.0) %	577
$\Sigma(1385)\pi$, P-wave	(2.0 ±2.0) %	443
$\Sigma(1385)\pi$, F-wave	(4.0 ±2.0) %	443
$\Lambda(1520)\pi$, D-wave	(8.0 ±2.0) %	334
$N\overline{K}^*(892)$, S=1/2, F-wave	(5.0 ±3.0) %	282
$N\overline{K}^*(892)$, S=3/2, F-wave	(5.0 ±2.0) %	282
$\Delta\overline{K}$, P-wave	(16 ±5) %	383
$\Delta\overline{K}$, F-wave	(5.0 ±3.0) %	383

$\Sigma(2030)\ 7/2^+$

$I(J^P) = 1(\frac{7}{2}^+)$

Mass $m = 2025$ to 2040 (≈ 2030) MeV
Full width $\Gamma = 150$ to 200 (≈ 180) MeV

$\Sigma(2030)$ DECAY MODES	Fraction (Γ_i/Γ)	p (MeV/c)
$N\overline{K}$	17–23 %	702
$\Lambda\pi$	17–23 %	700
$\Sigma\pi$	5–10 %	657
ΞK	<2 %	422
$\Sigma(1385)\pi$	5–15 %	532
$\Sigma(1385)\pi$, F-wave	(1.0±1.0) %	532
$\Lambda(1520)\pi$	10–20 %	431
$\Delta(1232)\overline{K}$	10–20 %	498
$\Delta(1232)\overline{K}$, F-wave	(15 ±5) %	498
$\Delta(1232)\overline{K}$, H-wave	(1.0±1.0) %	498
$N\overline{K}^*(892)$, S=3/2, F-wave	(14 ±8) %	439

Ξ BARYONS
($S = -2$, $I = 1/2$)

$\Xi^0 = uss$, $\Xi^- = dss$

Ξ^0

$I(J^P) = \frac{1}{2}(\frac{1}{2}^+)$

P is not yet measured; + is the quark model prediction.

Mass $m = 1314.86 \pm 0.20$ MeV
$m_{\Xi^-} - m_{\Xi^0} = 6.85 \pm 0.21$ MeV
Mean life $\tau = (2.90 \pm 0.09) \times 10^{-10}$ s
$c\tau = 8.71$ cm
Magnetic moment $\mu = -1.250 \pm 0.014\ \mu_N$

Decay parameters

α for $\Xi^0 \to \Lambda\pi^0 = -0.371 \pm 0.010$ (S = 3.0)
α for $\overline{\Xi}^0 \to \overline{\Lambda}\pi^0 = 0.379 \pm 0.004$
ϕ for $\Xi^0 \to \Lambda\pi^0 = (0.3 \pm 0.6)^\circ$
ϕ for $\overline{\Xi}^0 \to \overline{\Lambda}\pi^0 = (-0.3 \pm 0.6)^\circ$
$\Delta\phi_{CP}(\Xi^0) = (\phi_{\overline{\Xi}^0} + \phi_{\Xi^0})/2 = (0.0 \pm 0.4)^\circ$
A_{CP} for $\Xi^0 \to \Lambda\pi^0$, $\overline{\Xi}^0 \to \overline{\Lambda}\pi^0 = (-5 \pm 7) \times 10^{-3}$
γ for $\Xi^0 \to \Lambda\pi^0 = 0.937 \pm 0.002$ [l]
Δ for $\Xi^0 \to \Lambda\pi^0 = (0.8 \pm 1.6)^\circ$ [l]
α for $\Xi^0 \to \Lambda\gamma = -0.72 \pm 0.05$
A_{CP} for $\Xi^0 \to \Lambda\gamma$, $\overline{\Xi}^0 \to \overline{\Lambda}\gamma = -0.12 \pm 0.09$
α for $\Xi^0 \to \Lambda e^+ e^- = -0.8 \pm 0.2$
α for $\Xi^0 \to \Sigma^0\gamma = -0.69 \pm 0.06$
$g_1(0)/f_1(0)$ for $\Xi^0 \to \Sigma^+ e^- \overline{\nu}_e = 1.22 \pm 0.05$
$f_2(0)/f_1(0)$ for $\Xi^0 \to \Sigma^+ e^- \overline{\nu}_e = 2.0 \pm 0.9$

Ξ^0 DECAY MODES	Fraction (Γ_i/Γ)	Scale factor/ Confidence level	p (MeV/c)
$\Lambda\pi^0$	(99.517±0.012) %	S=1.1	135
$\Lambda\gamma$	(1.24 ±0.07) $\times 10^{-3}$	S=1.3	184
$\Lambda e^+ e^-$	(7.6 ±0.6) $\times 10^{-6}$		184
$\Sigma^0\gamma$	(3.33 ±0.10) $\times 10^{-3}$		117
$\Sigma^+ e^- \overline{\nu}_e$	(2.52 ±0.08) $\times 10^{-4}$		120
$\Sigma^+ \mu^- \overline{\nu}_\mu$	(2.3 ±0.4) $\times 10^{-6}$		64

$\Delta S = \Delta Q$ (SQ) violating modes or $\Delta S = 2$ forbidden ($S2$) modes

$\Sigma^- e^+ \nu_e$	SQ	< 1.6	$\times 10^{-4}$	CL=90%	112
$\Sigma^- \mu^+ \nu_\mu$	SQ	< 9	$\times 10^{-4}$	CL=90%	49
$p\pi^-$	$S2$	< 8	$\times 10^{-6}$	CL=90%	299
$p e^- \overline{\nu}_e$	$S2$	< 1.3	$\times 10^{-3}$		323
$p\mu^- \overline{\nu}_\mu$	$S2$	< 1.3	$\times 10^{-3}$		309

Ξ^-

$I(J^P) = \frac{1}{2}(\frac{1}{2}^+)$

P is not yet measured; + is the quark model prediction.

Mass $m = 1321.71 \pm 0.07$ MeV
$(m_{\Xi^-} - m_{\overline{\Xi}^+}) / m_{\Xi^-} = (-3 \pm 9) \times 10^{-5}$
Mean life $\tau = (1.639 \pm 0.015) \times 10^{-10}$ s
$c\tau = 4.91$ cm
$(\tau_{\Xi^-} - \tau_{\overline{\Xi}^+}) / \tau_{\Xi^-} = -0.01 \pm 0.07$
Magnetic moment $\mu = -0.6507 \pm 0.0025\ \mu_N$
$(\mu_{\Xi^-} + \mu_{\overline{\Xi}^+}) / |\mu_{\Xi^-}| = +0.01 \pm 0.05$

Decay parameters

$\Lambda\pi^-$ $\alpha = -0.385 \pm 0.008$ (S = 2.4)
$\overline{\Lambda}\pi^+$ $\overline{\alpha} = 0.374^{+0.005}_{-0.006}$
$(\alpha + \overline{\alpha}) / (\alpha - \overline{\alpha})$ for $\Xi^- \to \Lambda\pi^-$, $\overline{\Xi}^+ \to \overline{\Lambda}\pi^+ = (-9^{+11}_{-8}) \times 10^{-3}$
$[\alpha(\Xi^-)\alpha_-(\Lambda) - \overline{\alpha}\overline{\Xi}^+\alpha_+(\overline{\Lambda})] / [\text{sum}] = (0 \pm 7) \times 10^{-4}$
$\Lambda\pi^-$ $\phi_- = (-1.5 \pm 0.6)^\circ$
" $\gamma = 0.89$ [l]
" $\Delta = (175.9 \pm 1.5)^\circ$ [l]
$\overline{\Lambda}\pi^+$ $\phi_+ = (0.6^{+0.7}_{-1.0})^\circ$
$\Delta\phi_{CP} = (\phi_- + \phi_+)/2 = (-0.2^{+0.5}_{-0.6})^\circ$
$\Lambda e^- \overline{\nu}_e$ $g_A/g_V = -0.25 \pm 0.05$ [h]

Ξ^- DECAY MODES	Fraction (Γ_i/Γ)	Confidence level	p (MeV/c)
$\Lambda\pi^-$	(99.887±0.035) %		140
$\Sigma^-\gamma$	(1.27 ±0.23) $\times 10^{-4}$		118
$\Lambda e^- \overline{\nu}_e$	(5.63 ±0.31) $\times 10^{-4}$		190
$\Lambda\mu^- \overline{\nu}_\mu$	(3.5 $^{+3.5}_{-2.2}$) $\times 10^{-4}$		163
$\Sigma^0 e^- \overline{\nu}_e$	(8.7 ±1.7) $\times 10^{-5}$		123
$\Sigma^0 \mu^- \overline{\nu}_\mu$	< 8 $\times 10^{-4}$	90%	70
$\Xi^0 e^- \overline{\nu}_e$	< 2.59 $\times 10^{-4}$	90%	7

$\Delta S = 2$ forbidden ($S2$) modes

$n\pi^-$	$S2$	< 1.9	$\times 10^{-5}$	90%	304
$n e^- \overline{\nu}_e$	$S2$	< 3.2	$\times 10^{-3}$	90%	327
$n\mu^- \overline{\nu}_\mu$	$S2$	< 1.5	%	90%	314
$p\pi^-\pi^-$	$S2$	< 4	$\times 10^{-4}$	90%	223
$p\pi^- e^- \overline{\nu}_e$	$S2$	< 4	$\times 10^{-4}$	90%	305
$p\pi^-\mu^- \overline{\nu}_\mu$	$S2$	< 4	$\times 10^{-4}$	90%	251
$p\mu^-\mu^-$	L	< 4	$\times 10^{-8}$	90%	272
π^- invisible		not seen			–

$\Xi(1530)\ 3/2^+$

$I(J^P) = \frac{1}{2}(\frac{3}{2}^+)$

$\Xi(1530)^0$ mass $m = 1531.80 \pm 0.32$ MeV (S = 1.3)
$\Xi(1530)^-$ mass $m = 1535.0 \pm 0.6$ MeV
$\Xi(1530)^0$ full width $\Gamma = 9.1 \pm 0.5$ MeV
$\Xi(1530)^-$ full width $\Gamma = 9.9^{+1.7}_{-1.9}$ MeV

$\Xi(1530)$ DECAY MODES	Fraction (Γ_i/Γ)	Confidence level	p (MeV/c)
$\Xi\pi$	100 %		158
$\Xi\gamma$	<3.7 %	90%	202

$\Xi(1690)$

$I(J^P) = \frac{1}{2}(?^?)$

Mass $m = 1690 \pm 10$ MeV [o]
Full width $\Gamma = 20 \pm 15$ MeV

$\Xi(1690)$ DECAY MODES	Fraction (Γ_i/Γ)	p (MeV/c)
$\Lambda\overline{K}$	seen	240
$\Sigma\overline{K}$	seen	70
$\Xi\pi$	seen	311
$\Xi^-\pi^+\pi^-$	possibly seen	213

Int. J. Mod. Phys. A 2026.41. Downloaded from www.worldscientific.com
by UNIVERSITY OF CALIFORNIA @ BERKELEY on 09/16/26. Re-use and distribution is strictly not permitted, except for Open Access articles.

$\Xi(1820)\ 3/2^-$

$I(J^P) = \frac{1}{2}(\frac{3}{2}^-)$

Mass $m = 1823 \pm 5$ MeV [o]
Full width $\Gamma = 24^{+15}_{-10}$ MeV [o]

$\Xi(1820)$ DECAY MODES	Fraction (Γ_i/Γ)	p (MeV/c)
$\Lambda\overline{K}$	large	402
$\Sigma\overline{K}$	small	324
$\Xi\pi$	small	421
$\Xi(1530)\pi$	small	237

$\Xi(1950)$

$I(J^P) = \frac{1}{2}(?^?)$

Mass $m = 1950 \pm 15$ MeV [o]
Full width $\Gamma = 60 \pm 20$ MeV [o]

$\Xi(1950)$ DECAY MODES	Fraction (Γ_i/Γ)	p (MeV/c)
$\Lambda\overline{K}$	seen	522
$\Sigma\overline{K}$	possibly seen	460
$\Xi\pi$	seen	519

$\Xi(2030)$

$I(J^P) = \frac{1}{2}(\geq \frac{5}{2}^?)$

Mass $m = 2025 \pm 5$ MeV [o]
Full width $\Gamma = 20^{+15}_{-5}$ MeV [o]

$\Xi(2030)$ DECAY MODES	Fraction (Γ_i/Γ)	p (MeV/c)
$\Lambda\overline{K}$	~ 20 %	585
$\Sigma\overline{K}$	~ 80 %	529
$\Xi\pi$	small	574
$\Xi(1530)\pi$	small	416
$\Lambda\overline{K}\pi$	small	499
$\Sigma\overline{K}\pi$	small	428

Ω BARYONS ($S=-3, I=0$)

$\Omega^- = sss$

Ω^-

$I(J^P) = 0(\frac{3}{2}^+)$

$J^P = \frac{3}{2}^+$ is the quark-model prediction; and $J = 3/2$ is fairly well established.

Mass $m = 1672.45 \pm 0.29$ MeV
$(m_{\Omega^-} - m_{\overline{\Omega}^+}) / m_{\Omega^-} = (-1 \pm 8) \times 10^{-5}$
Mean life $\tau = (0.821 \pm 0.011) \times 10^{-10}$ s
$c\tau = 2.461$ cm
$(\tau_{\Omega^-} - \tau_{\overline{\Omega}^+}) / \tau_{\Omega^-} = 0.00 \pm 0.05$
Magnetic moment $\mu = -2.02 \pm 0.05\ \mu_N$

Decay parameters

$\alpha(\Omega^-)\ \alpha_-(\Lambda)$ FOR $\Omega^- \to \Lambda K^- = 0.0115 \pm 0.0015$
ΛK^- $\alpha = 0.0154 \pm 0.0020$
$\Lambda K^-, \overline{\Lambda} K^+$ $(\alpha + \overline{\alpha})/(\alpha - \overline{\alpha}) = -0.02 \pm 0.13$
$\Xi^0\pi^-$ $\alpha = 0.09 \pm 0.14$
$\Xi^-\pi^0$ $\alpha = 0.05 \pm 0.21$

Ω^- DECAY MODES		Fraction (Γ_i/Γ)	Scale factor/ Confidence level	p (MeV/c)
ΛK^-		(67.7 ± 0.7) %		211
$\Xi^0\pi^-$		(24.3 ± 0.7) %	S=1.5	294
$\Xi^-\pi^0$		(8.55 ± 0.33) %		289
$\Xi^-\pi^+\pi^-$		$(3.7\ ^{+0.7}_{-0.6}) \times 10^{-4}$		189
$\Xi(1530)^0\pi^-$		$< 7 \times 10^{-5}$	CL=90%	17
$\Xi^0 e^-\overline{\nu}_e$		$(5.6 \pm 2.8) \times 10^{-3}$		319
$\Xi^-\gamma$		$< 4.6 \times 10^{-4}$	CL=90%	314
$\Delta S = 2$ forbidden ($S2$) modes				
$\Lambda\pi^-$	$S2$	$< 2.9 \times 10^{-6}$	CL=90%	449
$\Sigma^0\pi^-$		$< 5.4 \times 10^{-4}$	CL=90%	393
nK^-		$< 2.4 \times 10^{-4}$	CL=90%	415

$\Omega(2012)^-$

$I(J^P) = 0(?^-)$

Mass $m = 2012.9 \pm 0.4$ MeV
Full width $\Gamma = 6.3 \pm 2.0$ MeV

$\Omega(2012)^-$ DECAY MODES	Fraction (Γ_i/Γ)	p (MeV/c)
$\Xi^0 K^-$	(34^{+17}_{-12}) %	403
$\Xi^-\overline{K}^0$	(28^{+12}_{-7}) %	393
$\Xi^-\pi^+K^-$	seen	225

$\Omega(2250)^-$

$I(J^P) = 0(?^?)$

Mass $m = 2252 \pm 9$ MeV
Full width $\Gamma = 55 \pm 18$ MeV

$\Omega(2250)^-$ DECAY MODES	Fraction (Γ_i/Γ)	p (MeV/c)
$\Xi^-\pi^+K^-$	seen	532
$\Xi(1530)^0K^-$	seen	437

CHARMED BARYONS ($C=+1$)

$\Lambda_c^+ = udc,\ \Sigma_c^{++} = uuc,\ \Sigma_c^+ = udc,\ \Sigma_c^0 = ddc,$
$\Xi_c^+ = usc,\ \Xi_c^0 = dsc,\ \Omega_c^0 = ssc$

Λ_c^+

$I(J^P) = 0(\frac{1}{2}^+)$

Mass $m = 2286.46 \pm 0.14$ MeV
Mean life $\tau = (202.6 \pm 1.0) \times 10^{-15}$ s
$c\tau = 60.75\ \mu$m

Decay asymmetry parameters

α FOR $\Lambda_c^+ \to \Lambda\pi^+ = -0.768 \pm 0.015$ (S = 3.4)
α FOR $\Lambda_c^+ \to \Lambda\rho^+ = -0.76 \pm 0.07$
α FOR $\Lambda_c^+ \to \Sigma^+\pi^0 = -0.484 \pm 0.027$
α FOR $\Lambda_c^+ \to \Sigma^+\eta = -0.99 \pm 0.06$
α FOR $\Lambda_c^+ \to \Sigma^+\eta' = -0.46 \pm 0.07$
α FOR $\Lambda_c^+ \to \Sigma^0\pi^+ = -0.466 \pm 0.018$
α FOR $\Lambda_c^+ \to \Sigma(1385)^+\pi^0 = -0.92 \pm 0.09$
α FOR $\Lambda_c^+ \to \Sigma(1385)^0\pi^+ = -0.79 \pm 0.11$
α FOR $\Lambda_c^+ \to \Lambda\ell^+\nu_\ell = -0.875 \pm 0.033$
α FOR $\Lambda_c^+ \to pK_S^0 = -0.754 \pm 0.010$
α FOR $\Lambda_c^+ \to \Lambda K^+ = -0.546 \pm 0.035$
α FOR $\Lambda_c^+ \to \Sigma^0K^+ = -0.54 \pm 0.20$
α FOR $\Lambda_c^+ \to \Lambda(1405)\pi^+ = 0.58 \pm 0.28$
α FOR $\Lambda_c^+ \to \Lambda(1520)\pi^+ = 0.93 \pm 0.09$
α FOR $\Lambda_c^+ \to \Lambda(1600)\pi^+ = 0.2 \pm 0.5$
α FOR $\Lambda_c^+ \to \Lambda(1670)\pi^+ = 0.82 \pm 0.08$
α FOR $\Lambda_c^+ \to \Lambda(1690)\pi^+ = 0.958 \pm 0.034$
α FOR $\Lambda_c^+ \to \Lambda(2000)\pi^+ = -0.57 \pm 0.19$
α FOR $\Lambda_c^+ \to \Delta(1232)^{++}K^- = 0.55 \pm 0.04$
α FOR $\Lambda_c^+ \to \Delta(1600)^{++}K^- = -0.50 \pm 0.18$
α FOR $\Lambda_c^+ \to \Delta(1700)^{++}K^- = 0.22 \pm 0.08$
α FOR $\Lambda_c^+ \to \overline{K}_0^*(700)^0p = -0.1 \pm 0.7$
α FOR $\Lambda_c^+ \to \overline{K}_0^*(1430)^0p = 0.34 \pm 0.14$
α FOR $\Lambda_c^+ \to \Xi^0K^+ = 0.01 \pm 0.16$
$(\alpha + \overline{\alpha})/(\alpha - \overline{\alpha})$ in $\Lambda_c^+ \to \Lambda\pi^+, \overline{\Lambda}_c^- \to \overline{\Lambda}\pi^- = 0.020 \pm 0.016$
$(\alpha + \overline{\alpha})/(\alpha - \overline{\alpha})$ in $\Lambda_c^+ \to \Sigma^0\pi^+, \overline{\Lambda}_c^- \to \overline{\Sigma}^0\pi^- = -0.02 \pm 0.05$
$(\alpha + \overline{\alpha})/(\alpha - \overline{\alpha})$ in $\Lambda_c^+ \to \Lambda e^+\nu_e, \overline{\Lambda}_c^- \to \overline{\Lambda}e^-\overline{\nu}_e = 0.00 \pm 0.04$
$(\alpha + \overline{\alpha})/(\alpha - \overline{\alpha})$ in $\Lambda_c^+ \to \Lambda K^+, \overline{\Lambda}_c^- \to \overline{\Lambda}K^- = -0.02 \pm 0.11$
$(\alpha + \overline{\alpha})/(\alpha - \overline{\alpha})$ in $\Lambda_c^+ \to \Sigma^0K^+, \overline{\Lambda}_c^- \to \overline{\Sigma}^0K^- = 0.1 \pm 0.4$
$A_{CP}(\Lambda X)$ in $\Lambda_c \to \Lambda X, \overline{\Lambda}_c \to \overline{\Lambda}X = (2 \pm 7)$%
$A_{CP}(\Lambda K^+)$ in $\Lambda_c \to \Lambda K^+, \overline{\Lambda}_c \to \overline{\Lambda}K^- = 0.021 \pm 0.026$
$A_{CP}(\Sigma^0K^+)$ in $\Lambda_c \to \Sigma^0K^+, \overline{\Lambda}_c \to \overline{\Sigma}^0K^- = 0.03 \pm 0.05$
$\Delta A_{CP} = A_{CP}(\Lambda_c^+ \to pK^+K^-) - A_{CP}(\Lambda_c^+ \to p\pi^+\pi^-) = (0.3 \pm 1.1)$%

Branching fractions marked with a footnote, e.g. [a], have been corrected for decay modes not observed in the experiments. For example, the submode fraction $\Lambda_c^+ \to p\overline{K}^*(892)^0$ seen in $\Lambda_c^+ \to pK^-\pi^+$ has been multiplied up to include $\overline{K}^*(892)^0 \to \overline{K}^0\pi^0$ decays.

Λ_c^+ DECAY MODES		Fraction (Γ_i/Γ)	Scale factor/ Confidence level	p (MeV/c)
Hadronic modes with a p or n: $S = -1$ final states				
pK^0_S		(1.63 ± 0.07) %	S=1.1	873
pK^0_L		(1.67 ± 0.07) %		873
$pK^-\pi^+$		(6.37 ± 0.21) %	S=1.2	823
$p\overline{K}^*_0(700)^0$		$(1.9 \pm 0.6) \times 10^{-3}$		719
$p\overline{K}^*(892)^0$	[q]	(1.42 ± 0.06) %		685
$p\overline{K}^*_0(1430)$		$(9.4 \pm 1.8) \times 10^{-3}$		†
$\Delta(1232)^{++}K^-$		(1.80 ± 0.08) %		710
$\Delta(1600)^{++}K^-$		$(2.9 \pm 1.0) \times 10^{-3}$		–
$\Delta(1700)^{++}K^-$		$(2.5 \pm 0.6) \times 10^{-3}$		–
$\Lambda(1405)^0\pi^+$		$(4.9 \pm 1.9) \times 10^{-3}$		–
$\Lambda(1520)\pi^+$	[q]	$(1.19 \pm 0.16) \times 10^{-3}$		628
$\Lambda(1600)\pi^+$		$(3.3 \pm 1.2) \times 10^{-3}$		571
$\Lambda(1670)\pi^+$		$(7.5 \pm 2.1) \times 10^{-4}$		516
$\Lambda(1690)\pi^+$		$(7.6 \pm 2.3) \times 10^{-4}$		504
$\Lambda(2000)\pi^+$		$(6.1 \pm 0.7) \times 10^{-3}$		234
$pK^-\pi^+$ nonresonant		(3.5 ± 0.4) %		823
$pK^0_S\pi^0$		(2.12 ± 0.09) %	S=1.3	823
$pK^0_L\pi^0$		(2.02 ± 0.14) %		823
$nK^0_S\pi^+$		(1.86 ± 0.09) %		821
$nK^0_SK^+$		$(3.9 {}^{+1.7}_{-1.4}) \times 10^{-4}$		612
$nK^0_S\pi^+\pi^0$		$(8.5 \pm 1.3) \times 10^{-3}$		756
$nK^-\pi^+\pi^+$		(1.90 ± 0.12) %		756
$p\overline{K}^0\eta$		$(9.0 \pm 0.6) \times 10^{-3}$	S=1.1	568
$pK^0_S\pi^+\pi^-$		(1.63 ± 0.10) %	S=1.1	754
$pK^0_L\pi^+\pi^-$		(1.69 ± 0.11) %		754
$pK^-\pi^+\pi^0$		(4.54 ± 0.27) %	S=1.6	759
$pK^*(892)^-\pi^+$	[q]	(1.4 ± 0.5) %		580
$p(K^-\pi^+)_{\text{nonresonant}}\pi^0$		(4.7 ± 0.8) %		759
$\Delta(1232)\overline{K}^*(892)$		seen		419
$pK^-2\pi^+\pi^-$		$(1.4 \pm 1.0) \times 10^{-3}$		671
$pK^-\pi^+2\pi^0$		(1.0 ± 0.5) %		678
Hadronic modes with a p or n: $S = 0$ final states				
$p\pi^0$		$(1.8 \pm 0.4) \times 10^{-4}$		945
$n\pi^+$		$(6.6 \pm 1.3) \times 10^{-4}$		944
$p\eta$		$(1.49 \pm 0.08) \times 10^{-3}$		856
$p\eta'$		$(4.9 \pm 0.9) \times 10^{-4}$		639
$p\omega(782)^0$		$(9.0 \pm 1.0) \times 10^{-4}$	S=1.2	751
$p\pi^+\pi^-$		$(4.69 \pm 0.22) \times 10^{-3}$		927
$pf_0(980)$	[q]	$(3.5 \pm 2.3) \times 10^{-3}$		614
$p\rho(770)^0$		$(1.5 \pm 0.4) \times 10^{-3}$		–
$n\pi^+\pi^0$		$(6.4 \pm 0.9) \times 10^{-3}$		927
$nK^+\pi^0$		$< 7.1 \times 10^{-4}$	CL=90%	824
$n\pi^+\pi^-\pi^+$		$(4.5 \pm 0.8) \times 10^{-3}$		895
$p2\pi^+2\pi^-$		$(2.3 \pm 1.5) \times 10^{-3}$		852
pK^+K^-		$(1.08 \pm 0.04) \times 10^{-3}$		616
$p\phi$	[q]	$(1.06 \pm 0.13) \times 10^{-3}$	S=1.1	590
pK^+K^- non-ϕ		$(5.4 \pm 1.2) \times 10^{-4}$		616
$pK^0_SK^0_S$		$(2.41 \pm 0.18) \times 10^{-4}$		610
$p\phi\pi^0$		$(10 \pm 4) \times 10^{-5}$		460
$pK^+K^-\pi^0$ nonresonant		$< 6.3 \times 10^{-5}$	CL=90%	494
Hadronic modes with a hyperon: $S = -1$ final states				
$\Lambda\pi^+$		(1.32 ± 0.05) %	S=1.1	864
$\Lambda(1670)\pi^+$, $\Lambda(1670) \to \eta\Lambda$		$(3.5 \pm 0.5) \times 10^{-3}$		–
$\Lambda\pi^+\pi^0$		(7.16 ± 0.33) %		844
$\Lambda\rho^+$		(4.1 ± 0.5) %		636
$\Sigma(1385)^+\pi^0$, $\Sigma^+ \to \Lambda\pi^+$		$(5.1 \pm 0.7) \times 10^{-3}$		–
$\Sigma(1385)^0\pi^+$, $\Sigma^0 \to \Lambda\pi^0$		$(5.7 \pm 0.8) \times 10^{-3}$		–
$\Lambda\pi^-2\pi^+$		(3.69 ± 0.26) %	S=1.5	807
$\Sigma(1385)^+\pi^+\pi^-$, $\Sigma^{*+} \to \Lambda\pi^+$		(1.0 ± 0.5) %		688
$\Sigma(1385)^-2\pi^+$, $\Sigma^{*-} \to \Lambda\pi^-$		$(7.8 \pm 1.4) \times 10^{-3}$		688
$\Lambda\pi^+\rho^0$		(1.5 ± 0.6) %		524
$\Sigma(1385)^+\rho^0$, $\Sigma^{*+} \to \Lambda\pi^+$		$(5 \pm 4) \times 10^{-3}$		363
$\Lambda\pi^-2\pi^+$ nonresonant		< 1.1 %	CL=90%	807
$\Lambda\pi^-\pi^02\pi^+$ total		(2.3 ± 0.8) %		757
$\Lambda\pi^+\omega$	[q]	(1.5 ± 0.5) %		517
$\Lambda\pi^-\pi^02\pi^+$, no η or ω		$< 8 \times 10^{-3}$	CL=90%	757
$\Lambda\pi^+\eta$	[q]	(1.92 ± 0.06) %		691
$\Sigma(1385)^+\eta$	[q]	$(6.7 \pm 0.6) \times 10^{-3}$		570
$\Lambda a_0(980)^+$, $a_0^+ \to \pi^+\eta$		(1.04 ± 0.17) %		–
$\Lambda(1670)\pi^+$, $\Lambda(1670) \to \Lambda\eta$		$(2.7 \pm 0.6) \times 10^{-3}$		–
$\Lambda K^+\overline{K}^0$		$(5.9 \pm 0.5) \times 10^{-3}$	S=1.2	443
$\Xi(1690)^0K^+$, $\Xi^{*0} \to \Lambda\overline{K}^0$		$(1.7 \pm 0.4) \times 10^{-3}$		286
$\Sigma^0\pi^+$		(1.29 ± 0.05) %	S=1.1	825
$\Sigma^0\pi^+\eta$		$(7.6 \pm 0.8) \times 10^{-3}$		635
$\Sigma^+\pi^0$		(1.27 ± 0.10) %	S=1.1	827
$\Sigma^+\eta$		$(3.4 \pm 0.4) \times 10^{-3}$		713
$\Sigma^+\eta'$		$(4.2 \pm 0.9) \times 10^{-3}$		391
$\Sigma^+\pi^+\pi^-$		(4.57 ± 0.18) %	S=1.1	804
$\Sigma^+\rho^0$		< 1.7 %	CL=95%	575
$\Sigma^-2\pi^+$		(1.87 ± 0.18) %		799
$\Sigma^0\pi^+\pi^0$		(3.6 ± 0.4) %		803
$\Sigma^+\pi^0\pi^0$		(1.57 ± 0.14) %		806
$\Sigma^0\pi^-2\pi^+$		(1.13 ± 0.31) %		763
$\Sigma^+\omega$		(1.72 ± 0.20) %		569
$\Sigma^-\pi^02\pi^+$		(2.1 ± 0.4) %		762
$\Sigma^0K^0_SK^+$		$< 1.28 \times 10^{-3}$	CL=90%	337
$\Sigma^+K^+K^-$		$(3.66 \pm 0.35) \times 10^{-3}$	S=1.1	349
$\Sigma^+\phi$	[q]	$(4.0 \pm 0.5) \times 10^{-3}$	S=1.1	295
$\Xi(1690)^0K^+$, $\Xi^{*0} \to \Sigma^+K^-$		$(1.03 \pm 0.25) \times 10^{-3}$		286
$\Sigma^+K^+K^-$ nonresonant		$< 8 \times 10^{-4}$	CL=90%	349
Ξ^0K^+		$(5.5 \pm 0.7) \times 10^{-3}$		653
$\Xi^-K^+\pi^+$		$(6.3 \pm 0.5) \times 10^{-3}$		565
$\Xi^0K^+\pi^0$		$(7.8 \pm 1.7) \times 10^{-3}$		574
$\Xi^0K^0_S\pi^+$		$(3.7 \pm 0.6) \times 10^{-3}$		569
$\Xi(1530)^0K^+$		$(4.9 \pm 0.6) \times 10^{-3}$	S=1.1	473
Hadronic modes with a hyperon: $S = 0$ final states				
ΛK^+		$(6.54 \pm 0.30) \times 10^{-4}$		781
$\Lambda K^+\pi^0$		$(1.50 \pm 0.29) \times 10^{-3}$		722
$\Lambda K^0_S\pi^+$		$(1.73 \pm 0.28) \times 10^{-3}$		718
$\Lambda K^*(892)K^{*+} \to K^0_S\pi^+$		seen		–
$\Lambda K^+\pi^+\pi^-$		$(4.2 \pm 1.6) \times 10^{-4}$		637
Σ^0K^+		$(3.76 \pm 0.31) \times 10^{-4}$		735
$\Sigma^+K^0_S$		$(4.8 \pm 1.4) \times 10^{-4}$		736
$\Sigma^0K^+\pi^+\pi^-$		$< 6.5 \times 10^{-4}$	CL=90%	574
$\Sigma^0K^+\pi^0$		$< 5.0 \times 10^{-4}$	CL=90%	670
$\Sigma^+K^+\pi^-$		$(2.05 \pm 0.26) \times 10^{-3}$		670
$\Sigma^+K^*(892)^0$	[q]	$(3.6 \pm 1.0) \times 10^{-3}$		469
$\Sigma^+K^+\pi^-\pi^0$		$< 1.1 \times 10^{-3}$	CL=90%	581
$\Sigma^-K^+\pi^+$		$(3.8 \pm 1.2) \times 10^{-4}$		664
Doubly Cabibbo-suppressed modes				
$pK^+\pi^-$		$(1.13 \pm 0.17) \times 10^{-4}$		823
Semileptonic modes				
$\Lambda e^+\nu_e$		(3.56 ± 0.13) %		871
$\Lambda\pi^+\pi^-e^+\nu_e$		$< 3.9 \times 10^{-4}$	CL=90%	843
$pK^-e^+\nu_e$		$(8.8 \pm 1.8) \times 10^{-4}$		874
$pK^0_S\pi^-e^+\nu_e$		$< 3.3 \times 10^{-4}$	CL=90%	821
$\Lambda(1520)e^+\nu_e$		$(1.0 \pm 0.5) \times 10^{-3}$		639
$\Lambda(1405)^0e^+\nu_e$, $\Lambda^0 \to pK^-$		$(4.2 \pm 1.9) \times 10^{-4}$		–
$\Lambda\mu^+\nu_\mu$		(3.48 ± 0.17) %		867
Inclusive modes				
e^+ anything		(4.06 ± 0.13) %		–
p anything		(50 ± 16) %		–
n anything		(32.6 ± 1.6) %		–
Λ anything		$(38.2 {}^{+2.9}_{-2.4})$ %		–
K^0_S anything		(10.90 ± 0.22) %		–
3prongs		(24 ± 8) %		–
$\Delta C = 1$ weak neutral current ($C1$) modes, or Lepton Family number (LF), or Lepton number (L), or Baryon number (B) violating modes				
pe^+e^-	$C1$	$< 5.5 \times 10^{-6}$	CL=90%	951
$p\mu^+\mu^-$ non-resonant	$C1$	$< 2.9 \times 10^{-8}$	CL=90%	937
$pe^+\mu^-$	LF	$< 9.9 \times 10^{-6}$	CL=90%	947
$pe^-\mu^+$	LF	$< 1.9 \times 10^{-5}$	CL=90%	947
$\overline{p}2e^+$	L,B	$< 2.7 \times 10^{-6}$	CL=90%	951
$\overline{p}2\mu^+$	L,B	$< 9.4 \times 10^{-6}$	CL=90%	937
$\overline{p}e^+\mu^+$	L,B	$< 1.6 \times 10^{-5}$	CL=90%	947
$\Sigma^-\mu^+\mu^+$	L	$< 7.0 \times 10^{-4}$	CL=90%	812

Int. J. Mod. Phys. A 2026.41. Downloaded from www.worldscientific.com
by UNIVERSITY OF CALIFORNIA @ BERKELEY on 09/16/26. Re-use and distribution is strictly not permitted, except for Open Acce

Int. J. Mod. Phys. A 2026.41. Downloaded from www.worldscientific.com
by UNIVERSITY OF CALIFORNIA @ BERKELEY on 09/16/26. Re-use and distribution is strictly not permitted, except for Open Access articles.

Radiative modes				
$\Sigma^+\gamma$	< 2.5	$\times 10^{-4}$	CL=90%	834
Exotic modes				
$p\gamma_D$	$[r] < 8.0$	$\times 10^{-5}$	CL=90%	–

$\Lambda_c(2595)^+$ $I(J^P) = 0(\frac{1}{2}^-)$

The spin-parity follows from the fact that $\Sigma_c(2455)\pi$ decays, with little available phase space, are dominant. This assumes that $J^P = 1/2^+$ for the $\Sigma_c(2455)$.

Mass $m = 2592.25 \pm 0.28$ MeV
$m - m_{\Lambda_c^+} = 305.79 \pm 0.24$ MeV
Full width $\Gamma = 2.6 \pm 0.6$ MeV

$\Lambda_c^+\pi\pi$ and its submode $\Sigma_c(2455)\pi$ — the latter just barely — are the only strong decays allowed for an excited Λ_c^+ having this mass; and the submode seems to dominate.

$\Lambda_c(2595)^+$ DECAY MODES		Fraction (Γ_i/Γ)	Confidence level	p (MeV/c)
$\Lambda_c^+\pi^+\pi^-$	[s]	(40 ± 14) %		117
$\Sigma_c(2455)^{++}\pi^-$		(15 ± 6) %		3
$\Sigma_c(2455)^0\pi^+$		(15 ± 6) %		3
$\Lambda_c^+\pi^0\pi^0$	[s]	(60 ± 14) %		135
$\Lambda_c^+\pi^0$	[t]	< 140 %	90%	258
$\Lambda_c^+\gamma$		< 40 %	90%	288

$\Lambda_c(2625)^+$ $I(J^P) = 0(\frac{3}{2}^-)$

J^P has not been measured; $\frac{3}{2}^-$ is the quark-model prediction.

Mass $m = 2628.00 \pm 0.15$ MeV
$m - m_{\Lambda_c^+} = 341.54 \pm 0.05$ MeV
Full width $\Gamma < 0.52$ MeV, CL = 90%

$\Lambda_c^+\pi\pi$ and its submode $\Sigma(2455)\pi$ are the only strong decays allowed for an excited Λ_c^+ having this mass.

$\Lambda_c(2625)^+$ DECAY MODES		Fraction (Γ_i/Γ)	Confidence level	p (MeV/c)
$\Lambda_c^+\pi^+\pi^-$	[u]	$(50\ \pm7\ )$ %		184
$\Sigma_c(2455)^{++}\pi^-$		(2.6 ± 0.4) %		103
$\Sigma_c(2455)^0\pi^+$		(2.6 ± 0.4) %		103
$\Lambda_c^+\pi^+\pi^-$ 3-body		seen		184
$\Lambda_c^+\pi^0\pi^0$	[u]	$(41\ \pm6\ )$ %		195
$\Lambda_c^+\pi^0$	[t]	< 50 %	90%	293
$\Lambda_c^+\gamma$		< 26 %	90%	319

$\Lambda_c(2860)^+$ $I(J^P) = 0(\frac{3}{2}^+)$

Mass $m = 2856.1^{+2.3}_{-6.0}$ MeV
Full width $\Gamma = 68^{+12}_{-22}$ MeV

$\Lambda_c(2860)^+$ DECAY MODES	Fraction (Γ_i/Γ)	p (MeV/c)
D^0p	seen	259

$\Lambda_c(2880)^+$ $I(J^P) = 0(\frac{5}{2}^+)$

Mass $m = 2881.63 \pm 0.24$ MeV
$m - m_{\Lambda_c^+} = 595.17 \pm 0.28$ MeV
Full width $\Gamma = 5.6^{+0.8}_{-0.6}$ MeV

$\Lambda_c(2880)^+$ DECAY MODES	Fraction (Γ_i/Γ)	p (MeV/c)
$\Lambda_c^+\pi^+\pi^-$	seen	471
$\Sigma_c(2455)^{0,++}\pi^\pm$	seen	376
$\Sigma_c(2520)^{0,++}\pi^\pm$	seen	317
pD^0	seen	316

$\Lambda_c(2940)^+$ $I(J^P) = 0(\frac{3}{2}^-)$

$J^P = 3/2^-$ is favored, but is not certain

Mass $m = 2939.6^{+1.3}_{-1.5}$ MeV
Full width $\Gamma = 20^{+6}_{-5}$ MeV

$\Lambda_c(2940)^+$ DECAY MODES	Fraction (Γ_i/Γ)	p (MeV/c)
pD^0	seen	420
$\Sigma_c(2455)^{0,++}\pi^\pm$	seen	–

$\Sigma_c(2455)$ $I(J^P) = 1(\frac{1}{2}^+)$

$\Sigma_c(2455)^{++}$ mass $m = 2453.97 \pm 0.14$ MeV
$\Sigma_c(2455)^+$ mass $m = 2452.65^{+0.22}_{-0.16}$ MeV
$\Sigma_c(2455)^0$ mass $m = 2453.75 \pm 0.14$ MeV
$m_{\Sigma_c(2455)^{++}} - m_{\Lambda_c^+} = 167.510 \pm 0.017$ MeV
$m_{\Sigma_c(2455)^+} - m_{\Lambda_c^+} = 166.19^{+0.16}_{-0.08}$ MeV
$m_{\Sigma^0_{c2455}} - m_{\Lambda_c^+} = 167.290 \pm 0.017$ MeV
$m_{\Sigma_c(2455)^{++}} - m_{\Sigma_c(2455)^0} = 0.220 \pm 0.013$ MeV
$m_{\Sigma_c(2455)^+} - m_{\Sigma_c(2455)^0} = -1.10^{+0.16}_{-0.08}$ MeV
$\Sigma_c(2455)^{++}$ full width $\Gamma = 1.89^{+0.09}_{-0.18}$ MeV (S = 1.1)
$\Sigma_c(2455)^+$ full width $\Gamma = 2.3 \pm 0.4$ MeV
$\Sigma_c(2455)^0$ full width $\Gamma = 1.83^{+0.11}_{-0.19}$ MeV (S = 1.2)

$\Lambda_c^+\pi$ is the only strong decay allowed to a Σ_c having this mass.

$\Sigma_c(2455)$ DECAY MODES	Fraction (Γ_i/Γ)	p (MeV/c)
$\Lambda_c^+\pi$	≈ 100 %	94

$\Sigma_c(2520)$ $I(J^P) = 1(\frac{3}{2}^+)$

J^P has not been measured; $\frac{3}{2}^+$ is the quark-model prediction.

$\Sigma_c(2520)^{++}$ mass $m = 2518.41 \pm 0.22$ MeV (S = 1.3)
$\Sigma_c(2520)^+$ mass $m = 2517.4^{+0.7}_{-0.5}$ MeV
$\Sigma_c(2520)^0$ mass $m = 2518.48 \pm 0.21$ MeV (S = 1.2)
$m_{\Sigma_c(2520)^{++}} - m_{\Lambda_c^+} = 231.95 \pm 0.18$ MeV (S = 1.8)
$m_{\Sigma_c(2520)^+} - m_{\Lambda_c^+} = 230.9^{+0.7}_{-0.5}$ MeV
$m_{\Sigma_c(2520)^0} - m_{\Lambda_c^+} = 232.02 \pm 0.15$ MeV (S = 1.4)
$m_{\Sigma_c(2520)^{++}} - m_{\Sigma_c(2520)^0} = 0.01 \pm 0.15$ MeV
$\Sigma_c(2520)^{++}$ full width $\Gamma = 14.78^{+0.30}_{-0.40}$ MeV
$\Sigma_c(2520)^+$ full width $\Gamma = 17.2^{+4.0}_{-2.2}$ MeV
$\Sigma_c(2520)^0$ full width $\Gamma = 15.3^{+0.4}_{-0.5}$ MeV

$\Lambda_c^+\pi$ is the only strong decay allowed to a Σ_c having this mass.

$\Sigma_c(2520)$ DECAY MODES	Fraction (Γ_i/Γ)	p (MeV/c)
$\Lambda_c^+\pi$	≈ 100 %	179

$\Sigma_c(2800)$ $I(J^P) = 1(?^?)$

$\Sigma_c(2800)^{++}$ mass $m = 2801^{+4}_{-6}$ MeV
$\Sigma_c(2800)^+$ mass $m = 2792^{+14}_{-5}$ MeV
$\Sigma_c(2800)^0$ mass $m = 2806^{+5}_{-7}$ MeV (S = 1.3)
$m_{\Sigma_c(2800)^{++}} - m_{\Lambda_c^+} = 514^{+4}_{-6}$ MeV
$m_{\Sigma_c(2800)^+} - m_{\Lambda_c^+} = 505^{+14}_{-5}$ MeV
$m_{\Sigma_c(2800)^0} - m_{\Lambda_c^+} = 519^{+5}_{-7}$ MeV (S = 1.3)
$\Sigma_c(2800)^{++}$ full width $\Gamma = 75^{+22}_{-17}$ MeV
$\Sigma_c(2800)^+$ full width $\Gamma = 60^{+60}_{-40}$ MeV
$\Sigma_c(2800)^0$ full width $\Gamma = 72^{+22}_{-15}$ MeV

$\Sigma_c(2800)$ DECAY MODES	Fraction (Γ_i/Γ)	p (MeV/c)
$\Lambda_c^+\pi$	seen	443

Int. J. Mod. Phys. A 2026.41. Downloaded from www.worldscientific.com
by UNIVERSITY OF CALIFORNIA @ BERKELEY on 09/16/26. Re-use and distribution is strictly not permitted, except for Open Acce

Ξ_c^+ $I(J^P) = \frac{1}{2}(\frac{1}{2}^+)$

J^P has not been measured; $\frac{1}{2}^+$ is the quark-model prediction.

Mass $m = 2467.79 \pm 0.15$ MeV (S = 1.1)
Mean life $\tau = (453 \pm 5) \times 10^{-15}$ s
$c\tau = 135.8\ \mu$m

Branching fractions marked with a footnote, e.g. [a], have been corrected for decay modes not observed in the experiments. For example, the submode fraction $\Xi_c^+ \to \Sigma^+ \overline{K}^*(892)^0$ seen in $\Xi_c^+ \to \Sigma^+ K^- \pi^+$ has been multiplied up to include $\overline{K}^*(892)^0 \to \overline{K}^0 \pi^0$ decays.

Ξ_c^+ DECAY MODES		Fraction (Γ_i/Γ)	Scale factor/ Confidence level	p (MeV/c)
Cabibbo-favored ($S = -2$) decays				
$p 2K_S^0$		$(2.5 \pm 1.3) \times 10^{-3}$		767
$\Lambda \overline{K}^0 \pi^+$		—		852
$\Sigma(1385)^+ \overline{K}^0$	[q]	(2.9 ± 2.0) %		746
$\Lambda K^- 2\pi^+$		$(9 \pm 4) \times 10^{-3}$		787
$\Lambda \overline{K}^*(892)^0 \pi^+$	[q]	$< 5 \times 10^{-3}$	CL=90%	608
$\Sigma(1385)^+ K^- \pi^+$	[q]	$< 6 \times 10^{-3}$	CL=90%	678
$\Sigma^+ K_S^0$		$(1.9 \pm 0.9) \times 10^{-3}$		864
$\Sigma^+ K^- \pi^+$		(2.7 ± 1.2) %		810
$\Sigma^+ \overline{K}^*(892)^0$	[q]	(2.3 ± 1.1) %		658
$\Sigma^0 K^- 2\pi^+$		$(8 \pm 5) \times 10^{-3}$		735
$\Xi^0 \pi^+$		$(7.2 \pm 3.2) \times 10^{-3}$		877
$\Xi^- 2\pi^+$		(2.9 ± 1.3) %		851
$\Xi(1530)^0 \pi^+$	[q]	$< 2.9 \times 10^{-3}$	CL=90%	750
$\Xi(1620)^0 \pi^+$		seen		–
$\Xi(1690)^0 \pi^+$		seen		644
$\Xi^0 \pi^+ \pi^0$		(6.7 ± 3.5) %		856
$\Xi^0 \pi^- 2\pi^+$		(5.0 ± 2.6) %		818
$\Xi^0 e^+ \nu_e$		(7 ± 4) %		884
$\Omega^- K^+ \pi^+$		$(2.0 \pm 1.5) \times 10^{-3}$		399
Cabibbo-suppressed decays				
$p K^- \pi^+$		$(6.2 \pm 3.0) \times 10^{-3}$	S=1.5	944
$p \overline{K}^*(892)^0$	[q]	$(3.3 \pm 1.7) \times 10^{-3}$		828
$p \overline{K}_0^*(700)^0$, $\overline{K}_0^*(700)^0 \to K^- \pi^+$		$(5 \pm 4) \times 10^{-4}$		–
$p \overline{K}^*(892)^0$, $\overline{K}^* \to K^- \pi^+$		$(1.8 \pm 0.8) \times 10^{-3}$		–
$p \overline{K}_0^*(1430)^0$, $\overline{K}_0^*(1430)^0 \to K^- \pi^+$		$(10 \pm 6) \times 10^{-4}$		–
$\Delta(1232)^{++} K^-$, $\Delta(1232)^{++} \to p\pi^+$		$(1.1 \pm 0.5) \times 10^{-3}$		–
$\Delta(1600)^{++} K^-$, $\Delta(1600)^{++} \to p\pi^+$		$(2.7 \pm 1.5) \times 10^{-4}$		–
$\Delta(1700)^{++} K^-$, $\Delta(1700)^{++} \to p\pi^+$		$(1.2 \pm 0.7) \times 10^{-4}$		–
$\Lambda(1405) \pi^+$, $\Lambda(1405) \to p K^-$		$(2.0 \pm 1.4) \times 10^{-4}$		–
$\Lambda(1520) \pi^+$, $\Lambda(1520) \to p K^-$		$(1.6 \pm 0.8) \times 10^{-4}$		–
$\Lambda(1670) \pi^+$, $\Lambda(1670) \to p K^-$		$(1.9 \pm 0.9) \times 10^{-4}$		–
$\Lambda(1820) \pi^+$, $\Lambda(1820) \to p K^-$		$(5.1 \pm 2.7) \times 10^{-5}$		–
$\Lambda(2000) \pi^+$, $\Lambda(2000) \to p K^-$		$(4.6 \pm 2.3) \times 10^{-4}$		–
$p K_S^0$		$(7.1 \pm 3.2) \times 10^{-4}$		987
$\Lambda \pi^+$		$(4.5 \pm 2.0) \times 10^{-4}$		976
$\Sigma^+ \pi^+ \pi^-$		(1.4 ± 0.8) %		922
$\Sigma^- 2\pi^+$		$(5.1 \pm 3.4) \times 10^{-3}$		918
$\Sigma^+ K^+ K^-$		$(4.3 \pm 2.5) \times 10^{-3}$		579
$\Sigma^+ \phi$	[q]	$< 3.2 \times 10^{-3}$	CL=90%	549
$\Xi(1690)^0 K^+$, $\Xi^0 \to \Sigma^+ K^-$		$< 1.3 \times 10^{-3}$	CL=90%	501
$\Sigma^0 \pi^+$		$(1.2 \pm 0.5) \times 10^{-3}$		–
$\Xi^0 K^+$		$(4.9 \pm 2.3) \times 10^{-4}$		–
$p\phi(1020)$		$(1.2 \pm 0.6) \times 10^{-4}$		751

Ξ_c^0 $I(J^P) = \frac{1}{2}(\frac{1}{2}^+)$

J^P has not been measured; $\frac{1}{2}^+$ is the quark-model prediction.

Mass $m = 2470.50 \pm 0.25$ MeV (S = 1.1)
$m_{\Xi_c^0} - m_{\Xi_c^+} = 2.72 \pm 0.23$ MeV (S = 1.1)
Mean life $\tau = (150.0 \pm 1.7) \times 10^{-15}$ s (S = 1.1)
$c\tau = 45.0\ \mu$m

Decay asymmetry parameters

$\Xi^- \pi^+$ $\alpha = -0.64 \pm 0.05$
α FOR $\overline{\Xi}_c^0 \to \overline{\Xi}^+ \pi^- = 0.61 \pm 0.05$
α FOR $\Xi_c^0 \to \Lambda \overline{K}^*(892)^0 = 0.15 \pm 0.22$
α FOR $\Xi_c^0 \to \Sigma^+ K^*(892)^- = -0.52 \pm 0.30$
α FOR $\Xi_c^0 \to \Xi^0 \pi^0 = -0.90 \pm 0.27$
τ_{mix}, $\Xi_c^0 - \overline{\Xi}_c^0$ oscillation period $> 1.3 \times 10^{-12}$ s

Ξ_c^0 DECAY MODES	Fraction (Γ_i/Γ)	Confidence level	p (MeV/c)
Cabibbo-favored decays			
$p K^- K^- \pi^+$	$(4.9 \pm 1.0) \times 10^{-3}$		676
$p K^- \overline{K}^*(892)^0$, $\overline{K}^{*0} \to K^- \pi^+$	$(2.0 \pm 0.6) \times 10^{-3}$		413
$p K^- K^- \pi^+$ (no $\overline{K}^{*0}$)	$(3.0 \pm 0.8) \times 10^{-3}$		676
ΛK_S^0	$(3.2 \pm 0.6) \times 10^{-3}$		906
$\Lambda K^- \pi^+$	(1.45 ± 0.28) %		856
$\Lambda \overline{K}^*(892)^0$	$(2.6 \pm 0.6) \times 10^{-3}$		717
$\Lambda \overline{K}^0 \pi^+ \pi^-$	seen		787
$\Lambda K^- \pi^+ \pi^+ \pi^-$	seen		703
$\Sigma^0 K_S^0$	$(5.4 \pm 1.4) \times 10^{-4}$		865
$\Sigma^+ K^-$	$(1.8 \pm 0.4) \times 10^{-3}$		868
$\Sigma^0 \overline{K}^*(892)^0$	$(9.9 \pm 1.9) \times 10^{-3}$		658
$\Sigma^+ K^*(892)^-$	$(4.9 \pm 1.3) \times 10^{-3}$		661
$\Xi^- \pi^+$	(1.43 ± 0.27) %		875
$\Xi^- \pi^+ \pi^+ \pi^-$	(4.8 ± 2.3) %		816
$\Xi^0 \pi^0$	$(6.9 \pm 1.4) \times 10^{-3}$		879
$\Xi^0 \eta$	$(1.6 \pm 0.4) \times 10^{-3}$		771
$\Xi^0 \eta'$	$(1.1 \pm 0.4) \times 10^{-3}$		479
$\Xi^0 \phi$, $\phi \to K^+ K^-$	$(5.2 \pm 1.2) \times 10^{-4}$		–
$\Xi^0 K^+ K^-$ nonresonant	$(5.6 \pm 1.2) \times 10^{-4}$		444
$\Omega^- K^+$	$(4.2 \pm 0.9) \times 10^{-3}$		522
$\Xi^- e^+ \nu_e$	(1.06 ± 0.21) %		882
$\Xi^- \mu^+ \nu_\mu$	(1.01 ± 0.21) %		878
$\Xi^0 \gamma$	$< 1.7 \times 10^{-4}$	90%	885
$\Xi^0 \mu^+ \mu^-$	$< 6 \times 10^{-5}$	90%	869
$\Xi^0 e^+ e^-$	$< 1.0 \times 10^{-4}$	90%	885
Cabibbo-suppressed decays			
$\Lambda_c^+ \pi^-$	$(5.5 \pm 1.1) \times 10^{-3}$		115
$\Xi^- K^+$	$(3.9 \pm 1.1) \times 10^{-4}$		789
$\Lambda K^+ K^-$ (no ϕ)	$(4.1 \pm 1.3) \times 10^{-4}$		648
$\Lambda \phi$	$(4.9 \pm 1.3) \times 10^{-4}$		621

$\Xi_c^{\prime +}$ $I(J^P) = \frac{1}{2}(\frac{1}{2}^+)$

J^P has not been measured; $\frac{1}{2}^+$ is the quark-model prediction.

Mass $m = 2578.3 \pm 0.4$ MeV
$m_{\Xi_c^{\prime +}} - m_{\Xi_c^+} = 110.5 \pm 0.4$ MeV
$m_{\Xi_c^{\prime +}} - m_{\Xi_c^0} = -0.5 \pm 0.6$ MeV

The $\Xi_c^{\prime +}$–Ξ_c^+ mass difference is too small for any strong decay to occur.

$\Xi_c^{\prime +}$ DECAY MODES	Fraction (Γ_i/Γ)	p (MeV/c)
$\Xi_c^+ \gamma$	seen	108

$\Xi_c^{\prime 0}$ $I(J^P) = \frac{1}{2}(\frac{1}{2}^+)$

J^P has not been measured; $\frac{1}{2}^+$ is the quark-model prediction.

Mass $m = 2578.8 \pm 0.5$ MeV
$m_{\Xi_c^{\prime 0}} - m_{\Xi_c^0} = 108.3 \pm 0.4$ MeV

Int. J. Mod. Phys. A 2026.41. Downloaded from www.worldscientific.com
by UNIVERSITY OF CALIFORNIA @ BERKELEY on 09/16/26. Re-use and distribution is strictly not permitted, except for Open Access articles.

The $\Xi_c'^0 - \Xi_c^0$ mass difference is too small for any strong decay to occur.

$\Xi_c'^0$ DECAY MODES	Fraction (Γ_i/Γ)	p (MeV/c)
$\Xi_c^0\gamma$	seen	106

$\Xi_c(2645)$

$I(J^P) = \frac{1}{2}(\frac{3}{2}^+)$

J^P has not been measured; $\frac{3}{2}^+$ is the quark-model prediction.

$\Xi_c(2645)^+$ mass $m = 2645.17 \pm 0.27$ MeV (S = 1.1)
$\Xi_c(2645)^0$ mass $m = 2646.24 \pm 0.18$ MeV (S = 1.1)
$m_{\Xi_c(2645)^+} - m_{\Xi_c^0} = 174.67 \pm 0.09$ MeV
$m_{\Xi_c(2645)^0} - m_{\Xi_c^+} = 178.45 \pm 0.10$ MeV
$m_{\Xi_c(2645)^+} - m_{\Xi_c(2645)^0} = -1.06 \pm 0.27$ MeV (S = 1.1)
$\Xi_c(2645)^+$ full width $\Gamma = 2.14 \pm 0.19$ MeV (S = 1.1)
$\Xi_c(2645)^0$ full width $\Gamma = 2.35 \pm 0.22$ MeV

$\Xi_c\pi$ is the only strong decay allowed to a Ξ_c resonance having this mass.

$\Xi_c(2645)$ DECAY MODES	Fraction (Γ_i/Γ)	p (MeV/c)
$\Xi_c^0\pi^+$	seen	102
$\Xi_c^+\pi^-$	seen	106

$\Xi_c(2790)$

$I(J^P) = \frac{1}{2}(\frac{1}{2}^-)$

J^P has not been measured; $\frac{1}{2}^-$ is the quark-model prediction.

$\Xi_c(2790)^+$ mass $= 2792.0 \pm 0.5$ MeV
$\Xi_c(2790)^0$ mass $= 2794.0 \pm 0.5$ MeV
$m_{\Xi_c(2790)^+} - m_{\Xi_c'^0} = 213.20 \pm 0.22$ MeV
$m_{\Xi_c(2790)^0} - m_{\Xi_c'^+} = 215.70 \pm 0.22$ MeV
$m_{\Xi_c(2790)^+} - m_{\Xi_c(2790)^0} = -2.0 \pm 0.7$ MeV
$\Xi_c(2790)^+$ width $= 8.9 \pm 1.0$ MeV
$\Xi_c(2790)^0$ width $= 10.0 \pm 1.1$ MeV

$\Xi_c(2790)$ DECAY MODES	Fraction (Γ_i/Γ)	p (MeV/c)
$\Xi_c'\pi$	seen	159
$\Lambda_c^+K^-$	seen	99

$\Xi_c(2815)$

$I(J^P) = \frac{1}{2}(\frac{3}{2}^-)$

J^P has not been measured; $\frac{3}{2}^-$ is the quark-model prediction.

$\Xi_c(2815)^+$ mass $m = 2816.60 \pm 0.16$ MeV
$\Xi_c(2815)^0$ mass $m = 2819.85 \pm 0.27$ MeV (S = 1.1)
$m_{\Xi_c(2815)^+} - m_{\Xi_c^+} = 348.81 \pm 0.09$ MeV
$m_{\Xi_c(2815)^0} - m_{\Xi_c^0} = 349.35 \pm 0.11$ MeV
$m_{\Xi_c(2815)^+} - m_{\Xi_c(2815)^0} = -3.26 \pm 0.27$ MeV
$\Xi_c(2815)^+$ full width $\Gamma = 2.15 \pm 0.15$ MeV (S = 1.2)
$\Xi_c(2815)^0$ full width $\Gamma = 2.54 \pm 0.25$ MeV

The $\Xi_c\pi\pi$ modes are consistent with being entirely via $\Xi_c(2645)\pi$.

$\Xi_c(2815)$ DECAY MODES	Fraction (Γ_i/Γ)	p (MeV/c)
$\Xi_c'\pi$	seen	188
$\Xi_c(2645)\pi$	seen	102
$\Xi_c^+\pi^+\pi^-$	seen	196
$\Xi_c^0\gamma$	seen	325

$\Xi_c(2970)$

$I(J^P) = \frac{1}{2}(\frac{1}{2}^+)$

was $\Xi_c(2980)$

$\Xi_c(2970)^+$ $m = 2965.2 \pm 1.0$ MeV (S = 2.9)
$\Xi_c(2970)^0$ $m = 2967.3 \pm 1.9$ MeV (S = 7.2)
$m_{\Xi_c(2970)^+} - m_{\Xi_c^+} = 497.4 \pm 1.0$ MeV (S = 2.7)
$m_{\Xi_c(2970)^0} - m_{\Xi_c^0} = 496.8 \pm 1.9$ MeV (S = 5.8)
$m_{\Xi_c(2970)^+} - m_{\Xi_c(2970)^0} = -2.1 \pm 2.0$ MeV (S = 5.4)
$\Xi_c(2970)^+$ width $\Gamma = 27.2^{+2.8}_{-3.3}$ MeV (S = 1.7)

$\Xi_c(2970)$ DECAY MODES	Fraction (Γ_i/Γ)	p (MeV/c)
$\Lambda_c^+\overline{K}\pi$	seen	225
$\Sigma_c(2455)\overline{K}$	seen	125
$\Lambda_c^+\overline{K}$	not seen	411
$\Lambda_c^+K^-$	seen	411
$\Xi_c^+\pi^+\pi^-$	seen	377
$\Xi_c 2\pi$	seen	382
$\Xi_c'\pi$	seen	–
$\Xi_c(2645)\pi$	seen	274

$\Xi_c(3055)$

$I(J^P) = ?(\frac{3}{2}^+)$

Mass $m = 3055.2 \pm 0.7$ MeV (S = 2.4)
Mass $m = 3061.0 \pm 0.8$ MeV
Full width $\Gamma = 8.0 \pm 0.8$ MeV
Full width $\Gamma = 12.4 \pm 2.3$ MeV

$\Xi_c(3055)$ DECAY MODES	Fraction (Γ_i/Γ)	p (MeV/c)
$\Sigma^{++}K^-$	seen	–
ΛD^+	seen	315
ΛD^0	seen	325

$\Xi_c(3080)$

$I(J^P) = \frac{1}{2}(?^?)$

$\Xi_c(3080)^+$ $m = 3077.2 \pm 0.4$ MeV
$\Xi_c(3080)^0$ $m = 3079.9 \pm 1.4$ MeV (S = 1.3)
$\Xi_c(3080)^+$ width $\Gamma = 3.8 \pm 0.9$ MeV (S = 1.4)
$\Xi_c(3080)^0$ width $\Gamma = 5.6 \pm 2.2$ MeV

$\Xi_c(3080)$ DECAY MODES	Fraction (Γ_i/Γ)	p (MeV/c)
$\Lambda_c^+\overline{K}\pi$	seen	415
$\Xi_c^+\pi^+\pi^-$	seen	487
$\Sigma_c(2455)\overline{K}$	seen	342
$\Sigma_c(2455)^{++}K^-$	seen	342
$\Sigma_c(2520)^{++}K^-$	seen	239
$\Sigma_c(2455)\overline{K} + \Sigma_c(2520)\overline{K}$	seen	–
$\Lambda_c^+\overline{K}$	not seen	536
$\Lambda_c^+\overline{K}\pi^+\pi^-$	not seen	144
ΛD^+	seen	362

Ω_c^0

$I(J^P) = 0(\frac{1}{2}^+)$

J^P has not been measured; $\frac{1}{2}^+$ is the quark-model prediction.

Mass $m = 2695.3 \pm 0.4$ MeV
Mean life $\tau = (274 \pm 10) \times 10^{-15}$ s
$c\tau = 82.0$ μm

No absolute branching fractions have been measured. The following are branching *ratios* relative to $\Omega^-\pi^+$.

Ω_c^0 DECAY MODES	Fraction (Γ_i/Γ)	Confidence level	p (MeV/c)
Cabibbo-favored ($S = -3$) decays — relative to $\Omega^-\pi^+$			
$\Omega^-\pi^+$	**DEFINED AS 1**		821
$\Omega^-\pi^+\pi^0$	1.80 ± 0.33		797
$\Omega^-\rho^+$	>1.3	90%	532
$\Omega^-\pi^-2\pi^+$	0.31 ± 0.05		753
$\Omega^-e^+\nu_e$	1.98 ± 0.29		829
$\Omega^-\mu^+\nu_\mu$	1.94 ± 0.21		824
$\Xi^0\overline{K}^0$	1.64 ± 0.29		950
$\Xi^0K^-\pi^+$	1.20 ± 0.18		901
$\Xi^0\overline{K}^{*0}$, $\overline{K}^{*0} \to K^-\pi^+$	0.68 ± 0.16		764
$\Omega(2012)^-\pi^+$, $\Omega(2012)^- \to \Xi^0K^-$	0.12 ± 0.05		–
$\Xi^-\overline{K}^0\pi^+$	2.12 ± 0.28		895
$\Omega(2012)^-\pi^+$, $\Omega(2012)^- \to \Xi^-\overline{K}^0$	0.12 ± 0.06		–
$\Xi^-K^-2\pi^+$	0.63 ± 0.09		830
$\Xi(1530)^0K^-\pi^+$, $\Xi^{*0} \to \Xi^-\pi^+$	0.21 ± 0.06		757
$\Xi^-\overline{K}^{*0}\pi^+$	0.34 ± 0.11		653

Int. J. Mod. Phys. A 2026.41. Downloaded from www.worldscientific.com
by UNIVERSITY OF CALIFORNIA @ BERKELEY on 09/16/26. Re-use and distribution is strictly not permitted, except for Open Acce

$pK^-K^-\pi^+$	seen		864
$\Sigma^+K^-K^-\pi^+$	<0.32	90%	689
$\Lambda\overline{K}^0\overline{K}^0$	1.72 ± 0.35		837
Singly Cabibbo-suppressed modes — relative to $\Omega^-\pi^+$			
$\Xi^-\pi^+$	0.161 ± 0.010		–
Ω^-K^+	0.061 ± 0.006		–
Doubly Cabibbo-suppressed modes — relative to $\Omega^-\pi^+$			
Ξ^-K^+	<0.07	90%	–

$\Omega_c(2770)^0$ $I(J^P) = 0(\frac{3}{2}^+)$

J^P has not been measured; $\frac{3}{2}^+$ is the quark-model prediction.

Mass $m = 2766.0^{+0.9}_{-1.0}$ MeV
$m_{\Omega_c(2770)^0} - m_{\Omega_c^0} = 70.7^{+0.8}_{-0.9}$ MeV

The $\Omega_c(2770)^0$–Ω_c^0 mass difference is too small for any strong decay to occur.

$\Omega_c(2770)^0$ DECAY MODES	Fraction (Γ_i/Γ)	p (MeV/c)
$\Omega_c^0\gamma$	presumably 100%	70

$\Omega_c(3000)^0$ $I(J^P) = ?(?^?)$

Mass $m = 3000.46 \pm 0.25$ MeV
Full width $\Gamma = 3.8^{+1.6}_{-0.4}$ MeV

$\Omega_c(3000)^0$ DECAY MODES	Fraction (Γ_i/Γ)	p (MeV/c)
$\Xi_c^+K^-$	seen	182

$\Omega_c(3050)^0$ $I(J^P) = ?(?^?)$

Mass $m = 3050.17 \pm 0.19$ MeV
Full width $\Gamma < 1.8$ MeV, CL = 95%

$\Omega_c(3050)^0$ DECAY MODES	Fraction (Γ_i/Γ)	p (MeV/c)
$\Xi_c^+K^-$	seen	278

$\Omega_c(3065)^0$ $I(J^P) = ?(?^?)$

Mass $m = 3065.58 \pm 0.21$ MeV
Full width $\Gamma = 3.4^{+0.7}_{-0.8}$ MeV (S = 1.7)

$\Omega_c(3065)^0$ DECAY MODES	Fraction (Γ_i/Γ)	p (MeV/c)
$\Xi_c^+K^-$	seen	303

$\Omega_c(3090)^0$ $I(J^P) = ?(?^?)$

Mass $m = 3090.15 \pm 0.26$ MeV
Full width $\Gamma = 8.5^{+0.8}_{-1.7}$ MeV

$\Omega_c(3090)^0$ DECAY MODES	Fraction (Γ_i/Γ)	p (MeV/c)
$\Xi_c^+K^-$	seen	339

$\Omega_c(3120)^0$ $I(J^P) = ?(?^?)$

Mass $m = 3118.98^{+0.27}_{-0.35}$ MeV
Full width $\Gamma < 2.5$ MeV, CL = 95%

$\Omega_c(3120)^0$ DECAY MODES	Fraction (Γ_i/Γ)	p (MeV/c)
$\Xi_c^+K^-$	seen	379

$\Omega_c(3185)^0$ $I(J^P) = ?(?^?)$

Mass $m = 3185^{+7.6}_{-1.9}$ MeV
Full width $\Gamma = 50^{+12}_{-21}$ MeV

$\Omega_c(3185)^0$ DECAY MODES	Fraction (Γ_i/Γ)	p (MeV/c)
$\Xi_c^+K^-$	seen	460

$\Omega_c(3327)^0$ $I(J^P) = ?(?^?)$

Mass $m = 3327.1^{+1.2}_{-1.8}$ MeV
Full width $\Gamma = 20^{+14}_{-5}$ MeV

$\Omega_c(3327)^0$ DECAY MODES	Fraction (Γ_i/Γ)	p (MeV/c)
$\Xi_c^+K^-$	seen	610

DOUBLY CHARMED BARYONS ($C = +2$)

$\Xi_{cc}^{++} = ucc$, $\Xi_{cc}^+ = dcc$, $\Omega_{cc}^+ = scc$

Ξ_{cc}^{++} $I(J^P) = ?(?^?)$

Mass $m = 3621.6 \pm 0.4$ MeV
Mean life $\tau = (256 \pm 27) \times 10^{-15}$ s

Ξ_{cc}^{++} DECAY MODES	Fraction (Γ_i/Γ)	Confidence level	p (MeV/c)
$\Lambda_c^+K^-\pi^+\pi^+$	**DEFINED AS 1**		880
$\Xi_c^+\pi^+$, $\Xi_c^+ \to pK^-\pi^+$	0.0022 ± 0.0006		–
$\Xi_c'^+\pi^+$, $\Xi_c'^+ \to \Xi_c^+\gamma$, $\Xi_c^+ \to pK^-\pi^+$	0.0031 ± 0.0010		–
$\Xi_c^0\pi^+\pi^+$, $\Xi_c^0 \to pK^-K^-\pi^+$	0.0067 ± 0.0010		–
$D^+pK^-\pi^+$	<0.017	90%	562

BOTTOM BARYONS ($B = -1$)

$\Lambda_b^0 = udb$, $\Sigma_b^0 = udb$, $\Sigma_b^+ = uub$, $\Sigma_b^- = ddb$
$\Xi_b^0 = usb$, $\Xi_b^- = dsb$, $\Omega_b^- = ssb$

Λ_b^0 $I(J^P) = 0(\frac{1}{2}^+)$

$I(J^P)$ not yet measured; $0(\frac{1}{2}^+)$ is the quark model prediction.

Mass $m = 5619.57 \pm 0.16$ MeV
$m_{\Lambda_b^0} - m_{B^0} = 339.2 \pm 1.4$ MeV
$m_{\Lambda_b^0} - m_{B^+} = 339.72 \pm 0.28$ MeV
Mean life $\tau = (1.465 \pm 0.009) \times 10^{-12}$ s
$c\tau = 439.2\ \mu$m
$A_{CP}(\Lambda_b \to p\pi^-) = (0.3 \pm 0.9) \times 10^{-2}$
$A_{CP}(\Lambda_b \to pK^-) = (-1.2 \pm 0.8) \times 10^{-2}$
$A_{CP}(\Lambda_b \to DpK^-) = 0.12 \pm 0.09$
$A_{CP}(\Lambda_b^0 \to \Lambda_c^+\pi^-) = 0.007 \pm 0.009$
$A_{CP}(\Lambda_b^0 \to \Lambda_c^+K^-) = -0.032 \pm 0.030$
$\Delta A_{CP}(pK^-/\pi^-) = 0.014 \pm 0.024$
$A_{CP}(\Lambda_b \to p\overline{K}^0\pi^-) = 0.039 \pm 0.021$
$A_{CP}(\Lambda_b \to p\overline{K}^0K^-) = 0.02 \pm 0.16$
$\Delta A_{CP}(J/\psi p\pi^-/K^-) = (5.7 \pm 2.7) \times 10^{-2}$
$A_{CP}(\Lambda_b \to \Lambda\pi^+\pi^-) = -0.01 \pm 0.06$
$A_{CP}(\Lambda_b \to \Lambda K^+\pi^-) = -0.12 \pm 0.05$
$A_{CP}(\Lambda_b \to \Lambda K^+K^-) = 0.083 \pm 0.028$
$\Delta A_{CP}(\Lambda_b^0 \to pK^-\mu^+\mu^-) = (-4 \pm 5) \times 10^{-2}$
$\Delta A_{CP}(\Lambda_b^0 \to p\pi^-\pi^+\pi^-) = (1.1 \pm 2.6) \times 10^{-2}$
$\Delta A_{CP}(\Lambda_b^0 \to (p\pi^-\pi^+\pi^-)_{LBM}) = (4 \pm 4) \times 10^{-2}$
$\Delta A_{CP}(\Lambda_b^0 \to pa_1(1260)^-) = (-1 \pm 4) \times 10^{-2}$
$\Delta A_{CP}(\Lambda_b^0 \to N(1520)^0\rho(770)^0) = (2 \pm 5) \times 10^{-2}$
$\Delta A_{CP}(\Lambda_b^0 \to \Delta(1232)^{++}\pi^-\pi^-) = (0.1 \pm 3.3) \times 10^{-2}$
$\Delta A_{CP}(\Lambda_b^0 \to pK^-\pi^+\pi^-) = (2.5 \pm 0.5) \times 10^{-2}$
$\Delta A_{CP}(\Lambda_b^0 \to (pK^-\pi^+\pi^-)_{LBM}) = (3.5 \pm 1.6) \times 10^{-2}$
$\Delta A_{CP}(\Lambda_b^0 \to N(1520)^0K^*(892)^0) = (5.5 \pm 2.5) \times 10^{-2}$

Int. J. Mod. Phys. A 2026.41. Downloaded from www.worldscientific.com
by UNIVERSITY OF CALIFORNIA @ BERKELEY on 09/16/26. Re-use and distribution is strictly not permitted, except for Open Access articles.

$\Delta A_{CP}(\Lambda_b^0 \to \Lambda(1520)\rho(770)^0) = (1 \pm 6) \times 10^{-2}$
$\Delta A_{CP}(\Lambda_b^0 \to \Delta(1232)^{++} K^- \pi^-) = (4.4 \pm 2.7) \times 10^{-2}$
$\Delta A_{CP}(\Lambda_b^0 \to p K_1(1410)^-) = (5 \pm 4) \times 10^{-2}$
$\Delta A_{CP}(\Lambda_b^0 \to p K^- K^+ \pi^-) = (-7 \pm 5) \times 10^{-2}$
$\Delta A_{CP}(\Lambda_b^0 \to p K^- K^+ K^-) = (0.2 \pm 1.9) \times 10^{-2}$
$\Delta A_{CP}(\Lambda_b^0 \to \Lambda(1520)\phi(1020)) = (4 \pm 6) \times 10^{-2}$
$\Delta A_{CP}(\Lambda_b^0 \to (p K^-)_{highmass}\, \phi(1020)) = (-0.7 \pm 3.4) \times 10^{-2}$
$\Delta A_{CP}(\Lambda_b^0 \to (p K^- K^+ K^-)_{LBM}) = (2.7 \pm 2.4) \times 10^{-2}$
$A_{FB}^{\ell}(\mu\mu)$ in $\Lambda_b \to \Lambda\mu^+\mu^- = -0.39 \pm 0.04$
$\Delta(A_{FB}^{\ell}(\mu\mu))$ in $\Lambda_b \to \Lambda\mu^+\mu^- = -0.05 \pm 0.09$
$A_{FB}^{h}(p\pi)$ in $\Lambda_b \to \Lambda(p\pi)\mu^+\mu^- = -0.30 \pm 0.05$
$A_{FB}^{\ell h}$ in $\Lambda_b \to \Lambda\mu^+\mu^- = 0.25 \pm 0.04$

The branching fractions B(b-baryon $\to \Lambda\ell^-\overline{\nu}_\ell$anything) and B($\Lambda_b^0 \to \Lambda_c^+\ell^-\overline{\nu}_\ell$anything) are not pure measurements because the underlying measured products of these with B($b \to b$-baryon) were used to determine B($b \to b$-baryon), as described in the note "Production and Decay of b-Flavored Hadrons."

For inclusive branching fractions, *e.g.*, $\Lambda_b \to \overline{\Lambda}_c$anything, the values usually are multiplicities, not branching fractions. They can be greater than one.

Λ_b^0 DECAY MODES		Fraction (Γ_i/Γ)	Scale factor/ Confidence level	p (MeV/c)
$J/\psi(1S)\Lambda$		$(3.0 \pm 0.8) \times 10^{-4}$		1740
$J/\psi(1S)\Lambda\phi$		$(1.2 \pm 0.4) \times 10^{-5}$		1010
$\psi(2S)\Lambda$		$(1.5 \pm 0.4) \times 10^{-4}$		1298
$p D^0 \pi^-$		$(6.4 \pm 0.6) \times 10^{-4}$		2370
$p D^+ \pi^- \pi^-$		$(2.8 \pm 0.4) \times 10^{-4}$		2332
$p D^*(2010)^+ \pi^- \pi^-$		$(5.3 \pm 1.0) \times 10^{-4}$		2277
$p D^0 K^-$		$(4.6 \pm 0.8) \times 10^{-5}$		2269
$p J/\psi \pi^-$		$(2.6 {}^{+0.5}_{-0.4}) \times 10^{-5}$		1755
$p\pi^- J/\psi,\ J/\psi \to \mu^+\mu^-$		$(1.6 \pm 0.8) \times 10^{-6}$		–
$p J/\psi K^-$		$(3.2 {}^{+0.6}_{-0.5}) \times 10^{-4}$		1589
$J/\psi \Xi^- K^+$		$(3.6 \pm 1.1) \times 10^{-6}$		1329
$p\eta_c(1S) K^-$		$(1.06 \pm 0.26) \times 10^{-4}$		1670
$P_{c\overline{c}}(4312)^+ K^-,\ P_{c\overline{c}}^+ \to p\eta_c(1S)$		$< 2.5 \times 10^{-5}$	CL=95%	–
$P_{c\overline{c}}(4380)^+ K^-,\ P_{c\overline{c}}^+ \to p J/\psi$	[v]	$(2.7 \pm 1.4) \times 10^{-5}$		–
$P_c(4450)^+ K^-,\ P_c \to p J/\psi$	[v]	$(1.3 \pm 0.4) \times 10^{-5}$		–
$\chi_{c1}(1P) p K^-$		$(7.7 {}^{+1.5}_{-1.3}) \times 10^{-5}$		1242
$\chi_{c1}(1P) p\pi^-$		$(5.1 {}^{+1.3}_{-1.2}) \times 10^{-6}$		1462
$\chi_{c2}(1P) p K^-$		$(8.0 {}^{+1.7}_{-1.4}) \times 10^{-5}$		1198
$\chi_{c2}(1P) p\pi^-$		$(4.8 \pm 1.9) \times 10^{-6}$		1427
$p J/\psi(1S)\pi^+\pi^- K^-$		$(6.6 {}^{+1.3}_{-1.1}) \times 10^{-5}$		1410
$p\psi(2S) K^-$		$(6.6 {}^{+1.2}_{-1.0}) \times 10^{-5}$		1063
$\chi_{c1}(3872) p K^-$		$(2.8 \pm 1.2) \times 10^{-5}$		837
$\chi_{c1}(3872)\Lambda(1520)$		$(1.6 \pm 0.8) \times 10^{-5}$		721
$\psi(2S) p\pi^-$		$(7.5 {}^{+1.6}_{-1.4}) \times 10^{-6}$		1320
$p\overline{K}^0\pi^-$		$(1.95 \pm 0.34) \times 10^{-5}$	S=1.9	2693
$p K^0 K^-$		$(1.22 \pm 0.23) \times 10^{-6}$		2639
$\Lambda_c^+\pi^-$		$(4.9 \pm 0.4) \times 10^{-3}$	S=1.2	2342
$\Lambda_c^+ K^-$		$(3.56 \pm 0.28) \times 10^{-4}$	S=1.2	2314
$\Lambda_c^+ a_1(1260)^-$		seen		2153
$\Lambda_c^+ D^-$		$(4.6 \pm 0.6) \times 10^{-4}$		1886
$\Lambda_c^+ D_s^-$		(1.10 ± 0.10) %		1833
$\Lambda_c^+ D_s^{*-}$		(1.83 ± 0.18) %		1748
$\Lambda_c^+ D_s^- K^+ K^-$		$(1.55 \pm 0.28) \times 10^{-4}$		1005
$P_{c\overline{c}s}(4459) K^+ K^-,\ P_{c\overline{c}s}(4459) \to \Lambda_c^+ D_s^-$		$< 2.6 \times 10^{-5}$	CL=90%	–
$P_{c\overline{c}s}(4338) K^+ K^-,\ P_{c\overline{c}s}(4338) \to \Lambda_c^+ D_s^-$		$< 1.6 \times 10^{-5}$	CL=90%	–
$\Lambda_c^+ \overline{D}^0 K^-$		$(2.13 \pm 0.20) \times 10^{-3}$		1581
$\Lambda_c^+ \overline{D}^{*0} K^-$		$(6.6 \pm 0.7) \times 10^{-3}$		1471
$\Lambda_c^+\pi^+\pi^-\pi^-$		$(7.6 \pm 1.1) \times 10^{-3}$	S=1.1	2323
$\Lambda_c(2595)^+\pi^-,\ \Lambda_c(2595)^+ \to \Lambda_c^+\pi^+\pi^-$		$(3.4 \pm 1.4) \times 10^{-4}$		2210
$\Lambda_c(2625)^+\pi^-,\ \Lambda_c(2625)^+ \to \Lambda_c^+\pi^+\pi^-$		$(3.3 \pm 1.3) \times 10^{-4}$		2193
$\Sigma_c(2455)^0\pi^+\pi^-,\ \Sigma_c^0 \to \Lambda_c^+\pi^-$		$(5.7 \pm 2.2) \times 10^{-4}$		2265
$\Sigma_c(2455)^{++}\pi^-\pi^-,\ \Sigma_c^{++} \to \Lambda_c^+\pi^+$		$(3.2 \pm 1.5) \times 10^{-4}$		2265
$\Sigma_c(2455)^{++} D^- K^-$		$(6.0 \pm 0.8) \times 10^{-4}$		1448
$\Sigma_c(2455)^{++} D^{*-} K^-$		$(1.36 \pm 0.23) \times 10^{-3}$		1324
$\Sigma_c(2520)^{++} D^- K^-$		$(2.8 \pm 0.5) \times 10^{-4}$		1392
$\Sigma_c(2520)^{++} D^{*-} K^-$		$(5.4 \pm 1.1) \times 10^{-4}$		1262
$\Lambda_c^+ K^+ K^-\pi^-$		$(1.02 \pm 0.11) \times 10^{-3}$		2184
$\Lambda_c^+ p\overline{p}\pi^-$		$(2.63 \pm 0.27) \times 10^{-4}$		1805
$\Sigma_c(2455)^0 p\overline{p},\ \Sigma_c^0 \to \Lambda_c^+\pi^-$		$(2.3 \pm 0.5) \times 10^{-5}$		–
$\Sigma_c(2520)^0 p\overline{p},\ \Sigma_c(2520)^0 \to \Lambda_c^+\pi^-$		$(3.1 \pm 0.7) \times 10^{-5}$		–
$\Lambda_c^+\ell^-\overline{\nu}_\ell$anything	[x]	(10.9 ± 2.2) %		–
$\Lambda_c^+\ell^-\overline{\nu}_\ell$		$(6.2 {}^{+1.4}_{-1.3})$ %		2345
$\Lambda_c^+\tau^-\overline{\nu}_\tau$		(1.9 ± 0.5) %		1933
$\Lambda_c^+\pi^+\pi^-\ell^-\overline{\nu}_\ell$		(5.6 ± 3.1) %		2335
$\Lambda_c(2595)^+\ell^-\overline{\nu}_\ell$		$(7.9 {}^{+4.0}_{-3.5}) \times 10^{-3}$		2212
$\Lambda_c(2625)^+\ell^-\overline{\nu}_\ell$		$(1.3 {}^{+0.6}_{-0.5})$ %		2195
$p h^-$	[y]	$< 2.3 \times 10^{-5}$	CL=90%	2730
$p\pi^-$		$(4.6 \pm 0.8) \times 10^{-6}$		2730
$p K^-$		$(5.5 \pm 1.0) \times 10^{-6}$		2709
$p D_s^-$		$(1.25 \pm 0.13) \times 10^{-5}$		2364
$p\mu^-\overline{\nu}_\mu$		$(4.1 \pm 1.0) \times 10^{-4}$		2730
$\Lambda\mu^+\mu^-$		$(1.08 \pm 0.28) \times 10^{-6}$		2695
$p\pi^-\mu^+\mu^-$		$(6.9 \pm 2.5) \times 10^{-8}$		2720
$p K^- e^+ e^-$		$(3.1 \pm 0.6) \times 10^{-7}$		2708
$p K^-\mu^+\mu^-$		$(2.6 {}^{+0.5}_{-0.4}) \times 10^{-7}$		2685
$\Lambda\gamma$		$(7.1 \pm 1.7) \times 10^{-6}$		2699
$\Lambda\eta$		$(9 {}^{+7}_{-5}) \times 10^{-6}$		2670
$\Lambda\eta'(958)$		$< 3.1 \times 10^{-6}$	CL=90%	2610
$\Lambda\pi^+\pi^-$		$(6.4 \pm 0.9) \times 10^{-6}$		2692
$\Lambda K^+\pi^-$		$(5.5 \pm 0.7) \times 10^{-6}$		2660
$\Lambda K^+ K^-$		$(1.29 \pm 0.12) \times 10^{-5}$		2605
$\Lambda D^+ D^-$		$(1.24 \pm 0.35) \times 10^{-4}$		1387
$\Lambda\phi$		$(9.8 \pm 2.6) \times 10^{-6}$		2599
$p\pi^-\pi^+\pi^-$		$(2.13 \pm 0.21) \times 10^{-5}$		2715
$p K^- K^+\pi^-$		$(4.1 \pm 0.6) \times 10^{-6}$		2612
$p K^-\pi^+\pi^-$		$(5.1 \pm 0.5) \times 10^{-5}$		2675
$p K^- K^+ K^-$		$(1.28 \pm 0.13) \times 10^{-5}$		2524

$\Lambda_b(5912)^0$

$J^P = \frac{1}{2}^-$

Mass $m = 5912.16 \pm 0.16$ MeV
Full width $\Gamma < 0.25$ MeV, CL = 90%

$\Lambda_b(5912)^0$ DECAY MODES	Fraction (Γ_i/Γ)	p (MeV/c)
$\Lambda_b^0\pi^+\pi^-$	seen	86

$\Lambda_b(5920)^0$

$J^P = \frac{3}{2}^-$

Mass $m = 5920.07 \pm 0.16$ MeV
Full width $\Gamma < 0.19$ MeV, CL = 90%

$\Lambda_b(5920)^0$ DECAY MODES	Fraction (Γ_i/Γ)	p (MeV/c)
$\Lambda_b^0\pi^+\pi^-$	seen	108

$\Lambda_b(6070)^0$

$J^P = \frac{1}{2}^+$

Quantum numbers based on quark model expectations.

Mass $m = 6072.3 \pm 2.9$ MeV
Full width $\Gamma = 72 \pm 11$ MeV

$\Lambda_b(6070)^0$ DECAY MODES	Fraction (Γ_i/Γ)	p (MeV/c)
$\Lambda_b^0\pi^+\pi^-$	seen	343

Int. J. Mod. Phys. A 2026.41. Downloaded from www.worldscientific.com
by UNIVERSITY OF CALIFORNIA @ BERKELEY on 09/16/26. Re-use and distribution is strictly not permitted, except for Open Acce

$\Lambda_b(6146)^0$

$J^P = \frac{3}{2}^+$

Mass $m = 6146.2 \pm 0.4$ MeV
$m_{\Lambda_b(6146)^0} - m_{\Lambda_b^0} = 526.55 \pm 0.34$ MeV
Full width $\Gamma = 2.9 \pm 1.3$ MeV

$\Lambda_b(6146)^0$ DECAY MODES	Fraction (Γ_i/Γ)	p (MeV/c)
$\Lambda_b^0 \pi^+ \pi^-$	seen	427

$\Lambda_b(6152)^0$

$J^P = \frac{5}{2}^+$

Mass $m = 6152.5 \pm 0.4$ MeV
$m_{\Lambda_b(6152)^0} - m_{\Lambda_b^0} = 532.89 \pm 0.28$ MeV
$m_{\Lambda_b(6152)^0} - m_{\Lambda_b(6146)^0} = 6.34 \pm 0.32$ MeV
Full width $\Gamma = 2.1 \pm 0.9$ MeV

$\Lambda_b(6152)^0$ DECAY MODES	Fraction (Γ_i/Γ)	p (MeV/c)
$\Lambda_b^0 \pi^+ \pi^-$	seen	434

Σ_b

$I(J^P) = 1(\frac{1}{2}^+)$
I, J, P need confirmation.

Mass $m(\Sigma_b^+) = 5810.56 \pm 0.25$ MeV
Mass $m(\Sigma_b^-) = 5815.64 \pm 0.27$ MeV
$m_{\Sigma_b^+} - m_{\Sigma_b^-} = -5.06 \pm 0.18$ MeV
$\Gamma(\Sigma_b^+) = 5.0 \pm 0.5$ MeV
$\Gamma(\Sigma_b^-) = 5.3 \pm 0.5$ MeV

Σ_b DECAY MODES	Fraction (Γ_i/Γ)	p (MeV/c)
$\Lambda_b^0 \pi$	dominant	133

Σ_b^*

$I(J^P) = 1(\frac{3}{2}^+)$
I, J, P need confirmation.

Mass $m(\Sigma_b^{*+}) = 5830.32 \pm 0.27$ MeV
Mass $m(\Sigma_b^{*-}) = 5834.74 \pm 0.30$ MeV
$m_{\Sigma_b^{*+}} - m_{\Sigma_b^{*-}} = -4.37 \pm 0.33$ MeV (S = 1.6)
$m_{\Sigma_b^{*+}} - m_{\Sigma_b^+} = 19.73 \pm 0.18$
$m_{\Sigma_b^{*-}} - m_{\Sigma_b^-} = 19.09 \pm 0.22$
$\Gamma(\Sigma_b^{*+}) = 9.4 \pm 0.5$ MeV
$\Gamma(\Sigma_b^{*-}) = 10.4 \pm 0.8$ MeV (S = 1.3)
$m_{\Sigma_b^*} - m_{\Sigma_b} = 21.2 \pm 2.0$ MeV

Σ_b^* DECAY MODES	Fraction (Γ_i/Γ)	p (MeV/c)
$\Lambda_b^0 \pi$	dominant	159

$\Sigma_b(6097)^+$

$J^P = ?^?$

Mass $m = 6095.8 \pm 1.7$ MeV
Full width $\Gamma = 31 \pm 6$ MeV

$\Sigma_b(6097)^+$ DECAY MODES	Fraction (Γ_i/Γ)	p (MeV/c)
$\Lambda_b \pi^+ \times B(b \to \Sigma_b(6097)^+)$	seen	–

$\Sigma_b(6097)^-$

$J^P = ?^?$

Mass $m = 6098.0 \pm 1.8$ MeV
Full width $\Gamma = 29 \pm 4$ MeV

$\Sigma_b(6097)^-$ DECAY MODES	Fraction (Γ_i/Γ)	p (MeV/c)
$\Lambda_b \pi^- \times B(b \to \Sigma_b(6097)^-)$	seen	–

Ξ_b^-

$I(J^P) = \frac{1}{2}(\frac{1}{2}^+)$
I, J, P need confirmation.

$m(\Xi_b^-) = 5797.0 \pm 0.4$ MeV (S = 1.4)
$m_{\Xi_b^-} - m_{\Lambda_b^0} = 177.48 \pm 0.24$ MeV (S = 1.1)
$m_{\Xi_b^-} - m_{\Xi_b^0} = 5.9 \pm 0.5$ MeV
Mean life $\tau_{\Xi_b^-} = (1.575 \pm 0.021) \times 10^{-12}$ s

Ξ_b^- DECAY MODES	Fraction (Γ_i/Γ)	Confidence level	p (MeV/c)
$J/\psi \Xi^- \times B(b \to \Xi_b^-)$	$(1.0 \pm 0.4) \times 10^{-5}$		1786
$J/\psi \Lambda K^- \times B(b \to \Xi_b^-)$	$(2.3 \pm 0.7) \times 10^{-6}$		1636
$p K^- K^- \times B(b \to \Xi_b^-)$	$(3.7 \pm 0.8) \times 10^{-8}$		2734
$p K^- K^-$	$(2.3 \pm 0.9) \times 10^{-6}$		2734
$p \pi^- \pi^-$	$< 1.3 \times 10^{-6}$	90%	2815
$p K^- \pi^-$	$(2.3 \pm 1.1) \times 10^{-6}$		2786
$\Lambda_b^0 \pi^- \times B(b \to \Xi_b^-)/B(b \to \Lambda_b^0)$	$(7.0 \pm 0.9) \times 10^{-4}$		108
$\Xi_c^0 \pi^-$	seen		2370
$\Xi_c^0 D_s^- \times B(b \to \Xi_b^-)/B(b \to \Lambda_b^0)$	$(1.9 \pm 0.5) \times 10^{-3}$		1857
$\Sigma(1385) K^-$	$(2.6 \pm 2.3) \times 10^{-7}$		2710
$\Lambda(1405) K^-$	$(1.9 \pm 1.2) \times 10^{-7}$		2705
$\Lambda(1520) K^-$	$(7.6 \pm 3.2) \times 10^{-7}$		2675
$\Lambda(1670) K^-$	$(4.5 \pm 2.3) \times 10^{-7}$		2632
$\Sigma(1775) K^-$	$(2.2 \pm 1.5) \times 10^{-7}$		2601
$\Sigma(1915) K^-$	$(2.6 \pm 2.5) \times 10^{-7}$		2556
$J/\psi \Xi^-$	seen		1786
$\psi(2S) \Xi^-$	seen		1333
$\Xi^- \gamma$	$< 1.3 \times 10^{-4}$	95%	2748

Ξ_b^0

$I(J^P) = \frac{1}{2}(\frac{1}{2}^+)$
I, J, P need confirmation.

$m(\Xi_b^0) = 5791.7 \pm 0.4$ MeV
$m_{\Xi_b^0} - m_{\Lambda_b^0} = 172.3 \pm 0.4$ MeV
Mean life $\tau_{\Xi_b^0} = (1.472 \pm 0.016) \times 10^{-12}$ s

Ξ_b^0 DECAY MODES	Fraction (Γ_i/Γ)	Confidence level	p (MeV/c)
$p D^0 K^- \times B(b \to \Xi_b^0)$	$(1.7 \pm 0.6) \times 10^{-6}$		2374
$p \overline{K}^0 \pi^- \times B(b \to \Xi_b^0)/B(\overline{b} \to B^0)$	$< 1.6 \times 10^{-6}$	90%	2783
$p \overline{K}^0 \pi^-$	$< 5.6 \times 10^{-6}$	90%	2783
$p K^0 K^- \times B(b \to \Xi_b^0)/B(\overline{b} \to B^0)$	$< 1.1 \times 10^{-6}$	90%	2730
$p \overline{K}^0 K^-$	$(7.8 \pm 3.3) \times 10^{-6}$		2730
$\Lambda \pi^+ \pi^- \times B(b \to \Xi_b^0)/B(b \to \Lambda_b^0)$	$< 1.7 \times 10^{-6}$	90%	2781
$\Lambda K^- \pi^+ \times B(b \to \Xi_b^0)/B(b \to \Lambda_b^0)$	$< 8 \times 10^{-7}$	90%	2751
$\Lambda K^+ K^- \times B(b \to \Xi_b^0)/B(b \to \Lambda_b^0)$	$< 3 \times 10^{-7}$	90%	2698
$\Lambda \pi^+ \pi^-$	$(1.3 \pm 0.6) \times 10^{-5}$		2781
$\Lambda K^- \pi^+$	$(1.3 \pm 0.5) \times 10^{-5}$		2751
$\Lambda K^+ K^-$	$< 3.4 \times 10^{-6}$	95%	2698
$J/\psi \Lambda$	seen		1867
$J/\psi \Xi^0$	seen		1785
$J/\psi \Xi^- \pi^+ \times B(b \to \Xi_b^0)$	$(1.2 \pm 0.5) \times 10^{-6}$		1714
$\Xi_c^+ D_s^- \times B(b \to \Xi_b^0)/B(b \to \Lambda_b^0)$	$(1.7 \pm 0.9) \times 10^{-3}$		1855
$\Lambda_c^+ K^- \times B(b \to \Xi_b^0)$	$(6 \pm 4) \times 10^{-7}$		2416
$p K^- \pi^+ \pi^- \times B(b \to \Xi_b^0)/B(b \to \Lambda_b^0)$	$(1.9 \pm 0.4) \times 10^{-6}$		2765
$p K^- K^- \pi^+ \times B(b \to \Xi_b^0)/B(b \to \Lambda_b^0)$	$(1.74 \pm 0.31) \times 10^{-6}$		2704
$p K^- K^+ K^- \times B(b \to \Xi_b^0)/B(b \to \Lambda_b^0)$	$(1.8 \pm 1.0) \times 10^{-7}$		2619

$\Xi_b'(5935)^-$

$J^P = \frac{1}{2}^+$

Mass $m = 5934.9 \pm 0.4$ MeV
Full width $\Gamma = 0.03 \pm 0.032$ MeV

$\Xi_b'(5935)^-$ DECAY MODES	Fraction (Γ_i/Γ)	p (MeV/c)
$\Xi_b^0 \pi^- \times B(\overline{b} \to \Xi_b'(5935)^-)/B(\overline{b} \to \Xi_b^0)$	(11.8 ± 1.8) %	32

Int. J. Mod. Phys. A 2026.41. Downloaded from www.worldscientific.com
by UNIVERSITY OF CALIFORNIA @ BERKELEY on 09/16/26. Re-use and distribution is strictly not permitted, except for Open Access articles.

$\Xi_b(5945)^0$

$J^P = \frac{3}{2}^+$

Mass $m = 5952.3 \pm 0.6$ MeV
Full width $\Gamma = 0.87 \pm 0.07$ MeV

$\Xi_b(5945)^0$ DECAY MODES	Fraction (Γ_i/Γ)	p (MeV/c)
$\Xi_b^- \pi^+$	seen	67

$\Xi_b(5955)^-$

$J^P = \frac{3}{2}^+$

Mass $m = 5955.5 \pm 0.4$ MeV
Full width $\Gamma = 1.43 \pm 0.11$ MeV

$\Xi_b(5955)^-$ DECAY MODES	Fraction (Γ_i/Γ)	p (MeV/c)
$\Xi_b^0 \pi^- \times B(\overline{b} \to \Xi_b^*(5955)^-)/B(\overline{b} \to \Xi_b^0)$	(20.7 ± 3.5) %	84

$\Xi_b(6087)^0$

$I(J^P) = \frac{1}{2}(?^?)$

Mass $m = 6087.0 \pm 0.5$ MeV
Full width $\Gamma = 2.4 \pm 0.5$ MeV

$\Xi_b(6087)^0$ DECAY MODES	Fraction (Γ_i/Γ)	p (MeV/c)
$\Xi_b^0 \pi^+ \pi^-$	seen	94

$\Xi_b(6095)^0$

$I(J^P) = \frac{1}{2}(?^?)$

Mass $m = 6095.1 \pm 0.4$ MeV
Full width $\Gamma = 0.50 \pm 0.35$ MeV

$\Xi_b(6095)^0$ DECAY MODES	Fraction (Γ_i/Γ)	p (MeV/c)
$\Xi_b^0 \pi^+ \pi^-$	seen	116

$\Xi_b(6100)^-$

$J^P = \frac{3}{2}^-$
J, P need confirmation.

Mass $m = 6099.8 \pm 0.4$ MeV
Full width $\Gamma = 0.94 \pm 0.31$ MeV

$\Xi_b(6100)^-$ DECAY MODES	Fraction (Γ_i/Γ)	p (MeV/c)
$\Xi_b^- \pi^+ \pi^-$	seen	114

$\Xi_b(6227)^-$

$J^P = ?^?$

Mass $m = 6227.9 \pm 0.9$ MeV
Full width $\Gamma = 19.9 \pm 2.6$ MeV

$\Xi_b(6227)^-$ DECAY MODES	Fraction (Γ_i/Γ)	Scale factor	p (MeV/c)
$\Lambda_b^0 K^- \times B(b \to \Xi_b(6227))/B(b \to \Lambda_b^0)$	$(3.20 \pm 0.35) \times 10^{-3}$		336
$\Xi_b^0 \pi^- \times B(b \to \Xi_b(6227))/B(b \to \Xi_b^0)$	(2.8 ± 1.1) %	1.8	398

$\Xi_b(6227)^0$

$J^P = ?^?$

Mass $m = 6226.8 \pm 1.6$ MeV
Full width $\Gamma = 19^{+5}_{-4}$ MeV

$\Xi_b(6227)^0$ DECAY MODES	Fraction (Γ_i/Γ)	p (MeV/c)
$\Xi_b^- \pi^+ \times B(b \to \Xi_b(6227)^0)/B(b \to \Xi_b^-)$	(4.5 ± 0.9) %	392

$\Xi_b(6327)^0$

$J^P = ?^?$

Mass $m = 6327.28 \pm 0.35$ MeV
Full width $\Gamma < 2.56$ MeV, CL = 95%

$\Xi_b(6327)^0$ DECAY MODES	Fraction (Γ_i/Γ)	p (MeV/c)
$\Lambda_b^0 K^- \pi^+$	seen	298

$\Xi_b(6333)^0$

$J^P = ?^?$

Mass $m = 6332.69 \pm 0.28$ MeV
Full width $\Gamma < 1.92$ MeV, CL = 95%

$\Xi_b(6333)^0$ DECAY MODES	Fraction (Γ_i/Γ)	p (MeV/c)
$\Lambda_b^0 K^- \pi^+$	seen	309

Ω_b^-

$I(J^P) = 0(\frac{1}{2}^+)$
I, J, P need confirmation.

Mass $m = 6045.8 \pm 0.8$ MeV
$m_{\Omega_b^-} - m_{\Lambda_b^0} = 426.4 \pm 2.2$ MeV
$m_{\Omega_b^-} - m_{\Xi_b^-} = 248.5 \pm 0.6$ MeV
Mean life $\tau = (1.64 \pm 0.16) \times 10^{-12}$ s
$\tau(\Omega_b^-)/\tau(\Xi_b^-)$ mean life ratio $= 1.11 \pm 0.16$

Ω_b^- DECAY MODES	Fraction (Γ_i/Γ)	Scale factor/ Confidence level	p (MeV/c)
$J/\psi\, \Omega^- \times B(b \to \Omega_b)$	$(1.5 \pm 0.5) \times 10^{-6}$	S=1.1	1805
$p K^- K^- \times B(\overline{b} \to \Omega_b)$	$< 2.3 \times 10^{-9}$	CL=90%	2865
$p \pi^- \pi^- \times B(\overline{b} \to \Omega_b)$	$< 1.5 \times 10^{-8}$	CL=90%	2943
$p K^- \pi^- \times B(\overline{b} \to \Omega_b)$	$< 7 \times 10^{-9}$	CL=90%	2915
$\Omega_c^0 \pi^-$	seen		2420
$\Omega_c^0 \pi^-$, $\Omega_c^0 \to p K^- K^- \pi^+$	seen		–
$\Xi_c^+ K^- \pi^-$	seen		2473

$\Omega_b(6316)^-$

$I(J^P) = ?(?^?)$
I, J, P need confirmation.

Mass $m = 6315.6 \pm 0.6$ MeV
Full width $\Gamma < 4.2$ MeV, CL = 95%

$\Omega_b(6316)^-$ DECAY MODES	Fraction (Γ_i/Γ)	p (MeV/c)
$\Xi_b^0 K^-$	seen	168

$\Omega_b(6330)^-$

$I(J^P) = ?(?^?)$
I, J, P need confirmation.

Mass $m = 6330.3 \pm 0.6$ MeV
Full width $\Gamma < 4.7$ MeV, CL = 95%

$\Omega_b(6330)^-$ DECAY MODES	Fraction (Γ_i/Γ)	p (MeV/c)
$\Xi_b^0 K^-$	seen	206

$\Omega_b(6340)^-$

$I(J^P) = ?(?^?)$
I, J, P need confirmation.

Mass $m = 6339.7 \pm 0.6$ MeV
Full width $\Gamma < 1.8$ MeV, CL = 95%

$\Omega_b(6340)^-$ DECAY MODES	Fraction (Γ_i/Γ)	p (MeV/c)
$\Xi_b^0 K^-$	seen	227

$\Omega_b(6350)^-$

$I(J^P) = ?(?^?)$
I, J, P need confirmation.

Mass $m = 6349.8 \pm 0.6$ MeV
Full width $\Gamma < 3.2$ MeV, CL = 95%

$\Omega_b(6350)^-$ DECAY MODES	Fraction (Γ_i/Γ)	p (MeV/c)
$\Xi_b^0 K^-$	seen	249

Int. J. Mod. Phys. A 2026.41. Downloaded from www.worldscientific.com
by UNIVERSITY OF CALIFORNIA @ BERKELEY on 09/16/26. Re-use and distribution is strictly not permitted, except for Open Acce

b-baryon ADMIXTURE (Λ_b, Ξ_b, Ω_b)

These branching fractions are actually an average over weakly decaying b-baryons weighted by their production rates at the LHC, LEP, and Tevatron, branching ratios, and detection efficiencies. They scale with the b-baryon production fraction B($b \to$ b-baryon).

The branching fractions B(b-baryon $\to \Lambda \ell^- \overline{\nu}_\ell$ anything) and B($\Lambda_b^0 \to \Lambda_c^+ \ell^- \overline{\nu}_\ell$ anything) are not pure measurements because the underlying measured products of these with B($b \to$ b-baryon) were used to determine B($b \to$ b-baryon), as described in the note "Production and Decay of b-Flavored Hadrons."

For inclusive branching fractions, *e.g.*, $B \to D^\pm$ anything, the values usually are multiplicities, not branching fractions. They can be greater than one.

b-baryon ADMIXTURE DECAY MODES (Λ_b, Ξ_b, Ω_b)	Fraction (Γ_i/Γ)	Scale factor	p (MeV/c)
$p\mu^-\overline{\nu}$ anything	$(5.8^{+2.3}_{-2.0})$ %		–
$p\ell\overline{\nu}_\ell$ anything	(5.6 ± 1.2) %		–
p anything	(70 ± 22) %		–
$\Lambda\ell^-\overline{\nu}_\ell$ anything	(3.8 ± 0.6) %		–
$\Lambda\ell^+\nu_\ell$ anything	(3.2 ± 0.8) %		–
Λ anything	(39 ± 7) %		–
$\Xi^-\ell^-\overline{\nu}_\ell$ anything	$(4.6 \pm 1.4) \times 10^{-3}$	1.2	–

EXOTIC BARYONS

$P_{c\overline{c}s}(4338)^0$

$I(J^P) = 0(\frac{1}{2}^-)$

Mass $m = 4338.2 \pm 0.8$ MeV
Full width $\Gamma = 7.0 \pm 1.8$ MeV

$P_{c\overline{c}s}(4338)^0$ DECAY MODES	Fraction (Γ_i/Γ)	p (MeV/c)
$J/\psi\Lambda$	seen	–
$\Lambda_c^+ D_s^-$	not seen	–

NOTES

This Summary Table only includes established baryons. The Particle Listings include evidence for other baryons. The masses, widths, and branching fractions for the resonances in this Table are Breit-Wigner parameters, but pole positions are also given for most of the N and Δ resonances.

For most of the resonances, the parameters come from various partial-wave analyses of more or less the same sets of data, and it is not appropriate to treat the results of the analyses as independent or to average them together. Furthermore, the systematic errors on the results are not well understood. Thus, we usually only give ranges for the parameters. We then also give a best guess for the mass (as part of the name of the resonance) and for the width. The *Note on N and Δ Resonances* and the *Note on Λ and Σ Resonances* in the Particle Listings review the partial-wave analyses.

When a quantity has "(S = ...)" to its right, the error on the quantity has been enlarged by the "scale factor" S, defined as $S = \sqrt{\chi^2/(N-1)}$, where N is the number of measurements used in calculating the quantity. We do this when $S > 1$, which often indicates that the measurements are inconsistent. When $S > 1.25$, we also show in the Particle Listings an ideogram of the measurements. For more about S, see the Introduction.

A decay momentum p is given for each decay mode. For a 2-body decay, p is the momentum of each decay product in the rest frame of the decaying particle. For a 3-or-more-body decay, p is the largest momentum any of the products can have in this frame. For any resonance, the *nominal* mass is used in calculating p. A dagger ("†") in this column indicates that the mode is forbidden when the nominal masses of resonances are used, but is in fact allowed due to the nonzero widths of the resonances.

[a] The masses of the p and n are most precisely known in u (unified atomic mass units). The conversion factor to MeV, 1 u = 931.494 103 72(29) MeV, is less well known than are the masses in u.

[b] The $|m_p - m_{\overline{p}}|/m_p$ and $|q_p + q_{\overline{p}}|/e$ are not independent, and both use the more precise measurement of $|q_{\overline{p}}/m_{\overline{p}}|/(q_p/m_p)$.

[c] The limit is from neutrality-of-matter experiments; it assumes $q_n = q_p + q_e$. See also the charge of the neutron.

[d] The μp and ep values for the charge radius are much too different to average them. The disagreement is not yet understood.

[e] There is a lot of disagreement about the value of the proton magnetic charge radius. See the Listings.

[f] There is some controversy about whether nuclear physics and model dependence complicate the analysis for bound neutrons (from which the best limit comes). The first limit here is from reactor experiments with free neutrons.

[g] Lee and Yang in 1956 proposed the existence of a mirror world in an attempt to restore global parity symmetry—thus a search for oscillations between the two worlds. Oscillations between the worlds would be maximal when the magnetic fields B and B' were equal. The limit for any B' in the range 0 to 12.5 μT is >12 s (95% CL).

[h] The parameters g_A, g_V, and g_{WM} for semileptonic modes are defined by $\overline{B}_f[\gamma_\lambda(g_V + g_A\gamma_5) + i(g_{WM}/m_{B_i})\,\sigma_{\lambda\nu}\,q^\nu]B_i$, and ϕ_{AV} is defined by $g_A/g_V = |g_A/g_V|e^{i\phi_{AV}}$. See the "Note on Baryon Decay Parameters" in the neutron Particle Listings.

[i] Time-reversal invariance requires this to be 0° or 180°.

[j] This coefficient is zero if time invariance is not violated.

[k] This limit is for γ energies between 0.4 and 782 keV.

[l] The decay parameters γ and Δ are calculated from α and ϕ using

$$\gamma = \sqrt{1-\alpha^2}\,\cos\phi\,, \qquad \tan\Delta = -\frac{1}{\alpha}\sqrt{1-\alpha^2}\,\sin\phi\,.$$

See the "Note on Baryon Decay Parameters" in the neutron Particle Listings.

[n] See the Listings for the pion momentum range used in this measurement.

[o] Our estimate. See the Particle Listings for details.

[p] A theoretical value using QED.

[q] This branching fraction includes all the decay modes of the final-state resonance.

[r] Here γ_D stands for a dark photon.

[s] See AALTONEN 11H, Fig. 8, for the calculated ratio of $\Lambda_c^+\pi^0\pi^0$ and $\Lambda_c^+\pi^+\pi^-$ partial widths as a function of the $\Lambda_c(2595)^+ - \Lambda_c^+$ mass difference. At our value of the mass difference, the predicted ratio is about 4. Using the measured value of $\Lambda_c^+\pi^0\pi^0$ branching fraction and assuming the $\Lambda_c\pi\pi$ branching fractions sum to unity, we derive the $\Lambda_c\pi^+\pi^-$ branching fraction. The derived ratio of the $\Lambda_c\pi^0\pi^0$ to $\Lambda_c\pi^+\pi^-$ partial widths is correspondingly 1.5 ± 0.2.

[t] A test that the isospin is indeed 0, so that the particle is indeed a Λ_c^+.

[u] In the isospin limit, with no other decays, the $\Lambda_c^+\pi^+\pi^-$ branching fraction would be 2/3 and the $\Lambda_c^+\pi^0\pi^0$ branching fraction would be 1/3.

[v] P_c^+ is a pentaquark-charmonium state.

[x] Not a pure measurement. See note at head of Λ_b^0 Decay Modes.

[y] Here h^- means π^- or K^-.

Int. J. Mod. Phys. A 2026.41. Downloaded from www.worldscientific.com
by UNIVERSITY OF CALIFORNIA @ BERKELEY on 09/16/26. Re-use and distribution is strictly not permitted, except for Open Access articles.

SEARCHES not in other sections

Magnetic Monopole Searches

The most sensitive experiments obtain negative results.

Best cosmic-ray supermassive monopole flux limit:

$< 1.4 \times 10^{-16}$ cm^{-2}sr^{-1}s^{-1} for $1.1 \times 10^{-4} < \beta < 0.99$

Supersymmetric Particle Searches

All supersymmetric mass bounds here are model dependent.

The limits assume:

1) $\widetilde{\chi}^0_1$ is the lightest supersymmetric particle; 2) R-parity is conserved, unless stated otherwise;

See the Particle Listings for a Note giving details of supersymmetry.

$\widetilde{\chi}^0_i$ — neutralinos (mixtures of $\widetilde{\gamma}$, $\widetilde{Z}^0$, and $\widetilde{H}^0_i$)

Mass $m_{\widetilde{\chi}^0_1} > 0$ GeV, CL = 95%
[general MSSM, non-universal gaugino masses]

Mass $m_{\widetilde{\chi}^0_1} > 46$ GeV, CL = 95%
[all tanβ, all m_0, all $m_{\widetilde{\chi}^0_2} - m_{\widetilde{\chi}^0_1}$]

Mass $m_{\widetilde{\chi}^0_2} > 62.4$ GeV, CL = 95%
[1<tanβ <40, all m_0, all $m_{\widetilde{\chi}^0_2} - m_{\widetilde{\chi}^0_1}$]

Mass $m_{\widetilde{\chi}^0_3} > 99.9$ GeV, CL = 95%
[1<tanβ <40, all m_0, all $m_{\widetilde{\chi}^0_2} - m_{\widetilde{\chi}^0_1}$]

Mass $m_{\widetilde{\chi}^0_4} > 116$ GeV, CL = 95%
[1<tanβ <40, all m_0, all $m_{\widetilde{\chi}^0_2} - m_{\widetilde{\chi}^0_1}$]

Mass $m_{\widetilde{\chi}}$ none 200–670 GeV, CL = 95% [R-Parity Violating]
[wino production, $\widetilde{\chi} \to b + \ell/\nu + t/b$ via λ'_{i33} coupling]

$\widetilde{\chi}^\pm_i$ — charginos (mixtures of $\widetilde{W}^\pm$ and $\widetilde{H}^\pm_i$)

Mass $m_{\widetilde{\chi}^\pm_1} > 1170$ GeV, CL = 95% [R-Parity Violating]
[$\chi^0_1 \to b\,t\,\tau$]

Mass $m_{\widetilde{\chi}^\pm_1} > 94$ GeV, CL = 95%
[tan$\beta < 40$, $m_{\widetilde{\chi}^\pm_1} - m_{\widetilde{\chi}^0_1} > 3$ GeV, all m_0]

Mass $m_{\widetilde{\chi}^\pm_1} > 1000$ GeV, CL = 95%
[$2\ell + \not{E}_T$, Tchi1chi1C, $m_{\widetilde{\chi}^0_1}$=0 GeV]

Mass $m_{\widetilde{\chi}^\pm_1} > 1600$ GeV, CL = 95% [R-Parity Violating]
[Tchi1n2l , $\widetilde{\chi}^0_1 \to \ell^\pm\ell^\mp\nu$, $\lambda_{12k} \neq 0$, $m_{\widetilde{\chi}^0_1} = 1200$ GeV]

$\widetilde{\chi}^\pm$ — long-lived chargino

Mass $m_{\widetilde{\chi}^\pm} > 1300$ GeV, CL = 95%
[$\widetilde{\chi}^\pm \to \widetilde{\chi}^0_1\pi^\pm$, wino LSP, stable, $\tau_{\widetilde{\chi}^\pm_1} > 100$ ns]

Mass $m_{\widetilde{\chi}^\pm} > 1050$ GeV, CL = 95%
[$\widetilde{\chi}^\pm \to \widetilde{\chi}^0_1\pi^\pm$, wino LSP,$\tau$=20 ns]

$\widetilde{\nu}$ — sneutrino

Mass $m > 41$ GeV, CL = 95% [model independent]

Mass $m > 94$ GeV, CL = 95%
[CMSSM, $1 \leq \tan\beta \leq 40$, $m_{\widetilde{e}_R} - m_{\widetilde{\chi}^0_1} > 10$ GeV]

Mass $m > 4200$ GeV, CL = 95% [R-Parity Violating]
[$1e + 1\mu$, $\nu_\tau \to e\mu$, $\lambda = \lambda' = 0.1$]

$\widetilde{e}$ — scalar electron (selectron)

Mass $m > 107$ GeV, CL = 95% [all $m_{\widetilde{e}_L} - m_{\widetilde{\chi}^0_1}$]

Mass $m > 700$ GeV, CL = 95%
[$2\ell + \not{E}_T$, $m_{\widetilde{\ell}_R} = m_{\widetilde{\ell}_L}$ and $\widetilde{\ell}$=$\widetilde{e}$, $\widetilde{\mu}$, $m_{\widetilde{\chi}^0_1}$=0 GeV]

Mass $m > 250$ GeV, CL = 95%
[$\ell^\pm\ell^\mp + \not{E}_T$, $\widetilde{e}_R$, $m_{\widetilde{\chi}^0_1} = 0$ GeV]

Mass $m > 410$ GeV, CL = 95% [R-Parity Violating]
[$\geq 4\ell^\pm$, $\widetilde{\ell} \to l\widetilde{\chi}^0_1$, $\widetilde{\chi}^0_1 \to \ell^\pm\ell^\mp\nu$]

Mass $m > 1200$ GeV, CL = 95% [R-Parity Violating]
[$\geq 4\ell$, $\lambda_{12k} \neq 0$, $m_{\widetilde{\chi}^0_1} = 900$ GeV (m-degenerate $\widetilde{\ell}_L$, $\widetilde{\nu}$)]

$\widetilde{\mu}$ — scalar muon (smuon)

Mass $m > 700$ GeV, CL = 95%
[$2\ell + \not{E}_T$, $m_{\widetilde{\ell}_R} = m_{\widetilde{\ell}_L}$ and $\widetilde{\ell}$=$\widetilde{e}$, $\widetilde{\mu}$, $m_{\widetilde{\chi}^0_1}$=0 GeV]

Mass $m > 210$, CL = 95%
[$\ell^\pm\ell^\mp + \not{E}_T$, $\widetilde{\mu}_R$, $m_{\widetilde{\chi}^0_1} = 0$ GeV]

Mass $m > 94$ GeV, CL = 95%
[CMSSM, $1 \leq \tan\beta \leq 40$, $m_{\widetilde{\mu}_R} - m_{\widetilde{\chi}^0_1} > 10$ GeV]

Mass $m > 410$ GeV, CL = 95% [R-Parity Violating]
[$\geq 4\ell^\pm$, $\widetilde{\ell} \to l\widetilde{\chi}^0_1$, $\widetilde{\chi}^0_1 \to \ell^\pm\ell^\mp\nu$]

Mass $m > 1200$ GeV, CL = 95% [R-Parity Violating]
[$\geq 4\ell$, $\lambda_{12k} \neq 0$, $m_{\widetilde{\chi}^0_1} = 900$ GeV (m-degenerate $\widetilde{\ell}_L$, $\widetilde{\nu}$)]

$\widetilde{\tau}$ — scalar tau (stau)

Mass $m > 81.9$ GeV, CL = 95%
[$m_{\widetilde{\tau}_R} - m_{\widetilde{\chi}^0_1} > 15$ GeV, all θ_τ, B($\widetilde{\tau} \to \tau\widetilde{\chi}^0_1$) = 100%]

Mass $m > 500$ GeV, CL = 95%
[2 hadronic $\tau + \not{E}_T$, $\widetilde{\tau}_{R,L} \to \tau\widetilde{\chi}^0_1$, $m_{\widetilde{\chi}^0_1} = 1$ GeV]

Mass $m > 90$ GeV, CL = 95% [R-Parity Violating]
[$\widetilde{\tau}_R$, indirect, $\Delta m > 5$ GeV]

Mass $m > 1200$, CL = 95% [R-Parity Violating]
[$\geq 4\ell$, $\lambda_{12k} \neq 0$, $m_{\widetilde{\chi}^0_1} = 900$ GeV (m-degenerate $\widetilde{\ell}_L$, $\widetilde{\nu}$)]

Mass $m > 286$ GeV, CL = 95% [long-lived $\widetilde{\tau}$]

$\widetilde{q}$ – squarks of the first two quark generations

Mass $m > 1.220 \times 10^3$ GeV, CL = 95%
[jets + $\not{E}_T$, Tsqk1, 1 non-degenerate $\widetilde{q}$, $m_{\widetilde{\chi}^0_1} = 0$ GeV]

Mass $m > 1.600 \times 10^3$ GeV, CL = 95% [R-Parity Violating]
[$\widetilde{q} \to q\widetilde{\chi}^0_1$, $\widetilde{\chi}^0_1 \to \ell\ell\nu$, λ_{121},$\lambda_{122} \neq 0$, $m_{\widetilde{g}}$=2400GeV]

Mass $m > 1000$ GeV, CL = 95% [R-Parity Violating]
[jets, $\widetilde{q} \to q\widetilde{\chi}^0_1$, $\widetilde{\chi}^0_1 \to \ell q q$, $m_{\widetilde{\chi}^0_1} = 108$ GeV and $2.5 < c\tau_{\widetilde{\chi}^0_1} < 200$ mm]

$\widetilde{q}$ — long-lived squark

Mass $m > 1340$ GeV, CL = 95% [$\widetilde{t}$ R-hadrons]

Mass $m > 1250$ GeV, CL = 95% [$\widetilde{b}$ R-hadrons]

Mass $m > 1470$ GeV, CL = 95% [$\widetilde{t}$ R-hadrons]

$\widetilde{b}$ — scalar bottom (sbottom)

Mass $m > 1.270 \times 10^3$ GeV, CL = 95%
[b-jets + $\not{E}_T$, Tsbot1, $m_{\widetilde{\chi}^0_1}$=0 GeV]

Mass $m > 307$ GeV, CL = 95% [R-Parity Violating]
[$\widetilde{b} \to t\,d$ or $t\,s$, λ''_{332} or λ''_{331} coupling]

$\widetilde{t}$ — scalar top (stop)

Mass $m > 1.310 \times 10^3$ GeV, CL = 95%
[jets + $\not{E}_T$, Tstop1, $m_{\widetilde{\chi}^0_1} < 300$ GeV]

Mass $m > 1900$ GeV, CL = 95% [R-Parity Violating]
[$\widetilde{t} \to b\,e$, prompt, Tstop2RPV]

Mass $m > 1800$ GeV, CL = 95% [R-Parity Violating]
[$\widetilde{t} \to b\,\mu$, prompt, Tstop2RPV]

Mass $m > 800$ GeV, CL = 95% [R-Parity Violating]
[$\widetilde{t} \to b\,\tau$, prompt, Tstop2RPV]

Mass $m > 460$ GeV, CL = 95%
[R-Parity Violating, long-lived $\widetilde{t}$, $\widetilde{t} \to d\overline{\ell}$, 0.01cm < $c\tau$ < 1000 cm]

$\widetilde{g}$ — gluino

Mass $m > 2.300 \times 10^3$ GeV, CL = 95%
[jets + $\not{E}_T$, Tglu1A, $m_{\widetilde{\chi}^0_1} < 200$ GeV]

Mass $m > 2.260 \times 10^3$ GeV, CL = 95% [R-Parity Violating]
[$\geq 4\ell$, $\lambda_{12k} \neq 0$, $m_{\widetilde{\chi}^0_1} > 1000$ GeV]

Technicolor

The limits for technicolor (and top-color) particles are quite varied depending on assumptions. See the Technicolor section of the full *Review* (the data listings).

Int. J. Mod. Phys. A 2026.41. Downloaded from www.worldscientific.com
by UNIVERSITY OF CALIFORNIA @ BERKELEY on 09/16/26. Re-use and distribution is strictly not permitted, except for Open Acce

Quark and Lepton Compositeness, Searches for

Scale Limits Λ for Contact Interactions (the lowest dimensional interactions with four fermions)

If the Lagrangian has the form

$$\pm \frac{g^2}{2\Lambda^2}\, \overline{\psi}_L \gamma_\mu \psi_L \overline{\psi}_L \gamma^\mu \psi_L$$

(with $g^2/4\pi$ set equal to 1), then we define $\Lambda \equiv \Lambda^{\pm}_{LL}$. For the full definitions and for other forms, see the Note in the Listings on Searches for Quark and Lepton Compositeness in the full *Review* and the original literature.

$\Lambda^{+}_{LL}(eeee)$ > 8.3 TeV, CL = 95%
$\Lambda^{-}_{LL}(eeee)$ > 10.3 TeV, CL = 95%
$\Lambda^{+}_{LL}(ee\mu\mu)$ > 8.5 TeV, CL = 95%
$\Lambda^{-}_{LL}(ee\mu\mu)$ > 9.5 TeV, CL = 95%
$\Lambda^{+}_{LL}(ee\tau\tau)$ > 7.9 TeV, CL = 95%
$\Lambda^{-}_{LL}(ee\tau\tau)$ > 7.2 TeV, CL = 95%
$\Lambda^{+}_{LL}(\ell\ell\ell\ell)$ > 9.1 TeV, CL = 95%
$\Lambda^{-}_{LL}(\ell\ell\ell\ell)$ > 10.3 TeV, CL = 95%
$\Lambda^{+}_{LL}(eeqq)$ > 24 TeV, CL = 95%
$\Lambda^{-}_{LL}(eeqq)$ > 37 TeV, CL = 95%
$\Lambda^{+}_{LL}(eeuu)$ > 23.3 TeV, CL = 95%
$\Lambda^{-}_{LL}(eeuu)$ > 12.5 TeV, CL = 95%
$\Lambda^{+}_{LL}(eedd)$ > 11.1 TeV, CL = 95%
$\Lambda^{-}_{LL}(eedd)$ > 26.4 TeV, CL = 95%
$\Lambda^{+}_{LL}(eecc)$ > 9.4 TeV, CL = 95%
$\Lambda^{-}_{LL}(eecc)$ > 5.6 TeV, CL = 95%
$\Lambda^{+}_{LL}(eebb)$ > 9.4 TeV, CL = 95%
$\Lambda^{-}_{LL}(eebb)$ > 10.2 TeV, CL = 95%
$\Lambda^{+}_{LL}(\mu\mu qq)$ > 23.3 TeV, CL = 95%
$\Lambda^{-}_{LL}(\mu\mu qq)$ > 40.0 TeV, CL = 95%
$\Lambda(\ell\nu\ell\nu)$ > 3.10 TeV, CL = 90%
$\Lambda(e\nu qq)$ > 2.81 TeV, CL = 95%
$\Lambda^{+}_{LL}(qqqq)$ > 13.1 none 17.4–29.5 TeV, CL = 95%
$\Lambda^{-}_{LL}(qqqq)$ > 21.8 TeV, CL = 95%
$\Lambda^{+}_{LL}(\nu\nu qq)$ > 5.0 TeV, CL = 95%
$\Lambda^{-}_{LL}(\nu\nu qq)$ > 5.4 TeV, CL = 95%

Excited Leptons

The limits from $\ell^{*+}\ell^{*-}$ do not depend on λ (where λ is the $\ell\ell^*$ transition coupling). The λ-dependent limits assume chiral coupling.

$e^{*\pm}$ — excited electron
Mass $m >$ 103.2 GeV, CL = 95% (from $e^* e^*$)
Mass $m >$ 5.600×10^3 GeV, CL = 95% (from $e e^*$)
Mass $m >$ 356 GeV, CL = 95% (if $\lambda_\gamma = 1$)

$\mu^{*\pm}$ — excited muon
Mass $m >$ 103.2 GeV, CL = 95% (from $\mu^* \mu^*$)
Mass $m >$ 5.700×10^3 GeV, CL = 95% (from $\mu\mu^*$)

$\tau^{*\pm}$ — excited tau
Mass $m >$ 103.2 GeV, CL = 95% (from $\tau^* \tau^*$)
Mass $m >$ 4.700×10^3 GeV, CL = 95% (from $\tau\tau^*$)

ν^* — excited neutrino
Mass $m >$ 1.600×10^3 GeV, CL = 95% (from $\nu^* \nu^*$)
Mass $m >$ 213 GeV, CL = 95% (from $\nu^* X$)

q^* — excited quark
(from $q^* q^*$)
Mass $m >$ 6700 GeV, CL = 95% (from $q^* X$)

Color Sextet and Octet Particles

Color Sextet Quarks (q_6)
Mass $m >$ 84 GeV, CL = 95% (Stable q_6)

Color Octet Charged Leptons (ℓ_8)
Mass $m >$ 86 GeV, CL = 95% (Stable ℓ_8)

Color Octet Neutrinos (ν_8)
Mass $m >$ 110 GeV, CL = 90% ($\nu_8 \to \nu g$)

Extra Dimensions

Please refer to the Extra Dimensions section of the full *Review* for a discussion of the model-dependence of these bounds, and further constraints.

Constraints on the radius of the extra dimensions, for the case of two-flat dimensions of equal radii

(direct tests of Newton's law)
$R <$ 3.8 μm, CL = 95% ($pp \to jG$)
$R <$ 0.16–916 nm (astrophysics; limits depend on technique and assumptions)

Constraints on the fundamental gravity scale

$M_{TT} >$ 9.02 TeV, CL = 95% ($pp \to$ dijet, angular distribution)
$M_c >$ 4.16 TeV, CL = 95% ($pp \to \ell\overline{\ell}$)

Constraints on the Kaluza-Klein graviton in warped extra dimensions

$M_G >$ 4.78 TeV, CL = 95% ($pp \to e^+e^-,\ \mu^+\mu^-$)

Constraints on the Kaluza-Klein gluon in warped extra dimensions

$M_{g_{KK}} >$ 3.8 TeV, CL = 95% ($g_{KK} \to t\overline{t}$)

WIMP and Dark Matter Searches

No confirmed evidence found for galactic WIMPs from the GeV to the TeV mass scales and down to 1×10^{-10} pb spin independent cross section at M = 100 GeV.

Int. J. Mod. Phys. A 2026.41. Downloaded from www.worldscientific.com by UNIVERSITY OF CALIFORNIA @ BERKELEY on 09/16/26. Re-use and distribution is strictly not permitted, except for Open Access articles.

Tests of Conservation Laws

Revised October 2025 by A. Pich (IFIC, Valencia) and M. Ramsey-Musolf (Tsung-Dao Lee Inst.; SJTU; U. Massachusetts).

In keeping with the current interest in tests of conservation laws, we collect together a Table of experimental limits on all weak and electromagnetic decays, mass differences, and moments, and on a few reactions, whose observation would violate conservation laws. The Table is given only in the full Review of Particle Physics (RPP), not in the Particle Physics Booklet, and organizes the data in two main sections: "Discrete Space-Time Symmetries", *i.e.*, C, P, T, CP and CPT; and "Number Conservation Laws", *i.e.*, lepton, baryon, flavor and charge conservation. The references for these data can be found in the Particle Listings. The following text discusses the best limits among those included in the Table and gives a brief overview of the current status. For some topics, a more extensive discussion of the framework for theoretical interpretation is provided, particularly where the analogous discussion does not appear elsewhere in the RPP. References to more extensive review articles are also included where appropriate. Unless otherwise specified, all limits quoted in this review are given at a C.L. of 90%.

DISCRETE SPACE-TIME SYMMETRIES

Charge conjugation (C), parity (P) and time reversal (T) are empirically exact symmetries of the electromagnetic (QED) and strong (QCD) interactions, but they are violated by the weak forces. Owing to the left-handed nature of the $SU(2)_L \otimes U(1)_Y$ electroweak theory, C and P are maximally violated in the fermionic couplings of the $W^\pm$ and (up to $\sin^2\theta_W$ corrections) the Z. However, their product CP is still an exact symmetry when only one or two fermion families are considered. With three generations of fermions, CP is violated through the single complex phase present in the Cabibbo-Kobayashi-Maskawa (CKM) quark mixing matrix. An analogous CP-violating (CPV) phase appears in the lepton sector when non-vanishing neutrino masses are taken into account (plus two additional phases if neutrinos are Majorana particles). The product of the three discrete symmetries, CPT, is an exact symmetry of any local and Lorentz-invariant quantum field theory with a positive-definite hermitian Hamiltonian that preserves micro-causality [1, 2]. Therefore, the breaking of CP implies a corresponding violation of T.

Violations of charge-conjugation symmetry have never been observed in electromagnetic and strong phenomena. The most stringent limits are extracted from C-violating transitions of neutral (self-conjugate) particles such as $\mathrm{Br}(\pi^0 \to 3\gamma) < 3.1 \times 10^{-8}$ [3] and $\mathrm{Br}(J/\psi \to 2\gamma) < 2.7 \times 10^{-7}$ [4]. P (and CP) conservation has been also precisely tested through forbidden decays such as $\mathrm{Br}(\eta \to 4\pi^0) < 6.9 \times 10^{-7}$ [5], but the best limits on P and T are set by the non-observation of electric dipole moments (see section 2). Obviously, the interplay of the weak interaction puts a lower bound in sensitivity for this type of tests, beyond which violations of the corresponding conservation laws should be detected.

1 Violations of CP and T

The first evidence of CP non-invariance in particle physics was the observation in 1964 of $K_L^0 \to \pi^+\pi^-$ decays [6]. For many years afterwards, the non-zero ratio

$$|\eta_{+-}| \equiv |\mathcal{M}(K_L^0 \to \pi^+\pi^-)/\mathcal{M}(K_S^0 \to \pi^+\pi^-)| = (2.233 \pm 0.012) \times 10^{-3} \tag{1}$$

could be explained as a K^0–$\overline{K}^0$ mixing effect, $\eta_{+-} = \epsilon$ (superweak CP violation), which would imply an identical ratio $\eta_{00} \equiv \mathcal{M}(K_L^0 \to \pi^0\pi^0)/\mathcal{M}(K_S^0 \to \pi^0\pi^0)$ in the neutral decay mode and successfully predicts the observed CPV semileptonic asymmetry ($A_L(e) \approx 2\,\mathrm{Re}\,\epsilon$)

$$A_L(e) \equiv \frac{\Gamma(K_L^0 \to \pi^- e^+ \nu_e) - \Gamma(K_L^0 \to \pi^+ e^- \bar{\nu}_e)}{\Gamma(K_L^0 \to \pi^- e^+ \nu_e) + \Gamma(K_L^0 \to \pi^+ e^- \bar{\nu}_e)} = (3.34 \pm 0.07) \times 10^{-3}\,. \tag{2}$$

A tiny difference between η_{+-} and η_{00} was reported for the first time in 1988 by the CERN NA31 collaboration [7], and later established at the 7.2σ level with the full data samples from the NA31 [8], E731 [9], NA48 [10] and KTeV [11] experiments:

$$\mathrm{Re}(\epsilon'/\epsilon) = \frac{1}{3}\,(1 - |\eta_{00}/\eta_{+-}|) = (1.67 \pm 0.23) \times 10^{-3}\,. \tag{3}$$

This important measurement confirmed that CP violation is associated with a $\Delta S = 1$ transition, as predicted by the CKM mechanism. The Standard Model (SM) prediction, $\mathrm{Re}(\epsilon'/\epsilon) = (1.4 \pm 0.5) \times 10^{-3}$ [12–14], is in good agreement with the measured ratio, although the theoretical uncertainty is unfortunately large.

Much larger CP asymmetries have been later measured in B meson decays, many of them involving the interference between B^0–$\overline{B}^0$ mixing and the decay amplitude. They provide many successful tests of the CKM unitarity structure, validating the SM mechanism of CP violation (see the review on CP violation in the quark sector). Prominent signals of direct CP violation in the decay amplitudes have been also clearly established in several $B^\pm$, B_d^0 and B_s^0 decays, and, more recently, in charm decays [15, 16]:

$$\Delta a_{CP}^{\mathrm{dir}} \equiv a_{CP}^{\mathrm{dir}}(D^0 \to K^+K^-) - a_{CP}^{\mathrm{dir}}(D^0 \to \pi^+\pi^-) = (-15.7 \pm 2.9) \times 10^{-4}\,. \tag{4a}$$

$$a_{CP}^{\mathrm{dir}}(D^0 \to \pi^+\pi^-) = (23.2 \pm 6.1) \times 10^{-4}\,. \tag{4b}$$

The first observation of CP violation in baryon decays has been reported recently [17]:

$$\mathcal{A}_{CP}(\Lambda_b^0 \to pK^-\pi^+\pi^-) = (2.45 \pm 0.46 \pm 0.10)\%\,. \tag{5}$$

These direct CP asymmetries necessarily involve the presence of a strong phase-shift difference between (at least) two interfering amplitudes, which makes very challenging to perform reliable SM predictions for heavy-flavored hadrons.

Global fits to neutrino oscillation data provide some hints of a non-zero mixing phase [18, 19]. Although the statistical significance is not yet compelling, they suggest that CP-violation effects in neutrino oscillations could be large (see the review on neutrino masses, mixings and oscillations). The future DUNE and Hyper-Kamiokande experiments are expected to confirm the presence of CP violation in the lepton sector or constrain the phase in the leptonic mixing matrix to be smaller than $O(10°)$.

While CP violation implies a breaking of time-reversal symmetry, direct tests of T violation are much more difficult. The CPLEAR experiment observed longtime ago a non-zero difference between the oscillation probabilities of $K^0 \to \overline{K}^0$ and $\overline{K}^0 \to K^0$ [20]. Initial neutral kaons with defined strangeness were produced from proton-antiproton annihilations at rest, $p\bar{p} \to K^-\pi^+K^0, K^+\pi^-\overline{K}^0$, and tagged by the accompanying charged kaon, while the strangeness of the final neutral kaon was identified through its semileptonic decay: $K^0 \to e^+\pi^-\nu_e$, $\overline{K}^0 \to e^-\pi^+\bar{\nu}_e$. The average asymmetry over the time interval from 1 to 20 K_S^0 lifetimes was found to be different from zero at 4σ [20]:

$$\frac{R[\overline{K}^0\,(t=0) \to e^+\pi^-\nu_e\,(t)] - R[K^0\,(t=0) \to e^-\pi^+\bar{\nu}_e\,(t)]}{R[\overline{K}^0\,(t=0) \to e^+\pi^-\nu_e\,(t)] + R[K^0\,(t=0) \to e^-\pi^+\bar{\nu}_e\,(t)]} = (6.6 \pm 1.3 \pm 1.0) \times 10^{-3}\,. \tag{6}$$

Since this asymmetry violates also CP, its interpretation as direct evidence of T violation requires a detailed analysis of the underlying K^0–$\overline{K}^0$ mixing process [21–23].

The exchange of initial and final states has been made possible in B decays, taking advantage of the entanglement of the two daughter mesons produced in the decay $\Upsilon(4S) \to B\bar{B}$ which allows for both flavor ($B^0 \to \ell^+X$, $\overline{B}^0 \to \ell^-X$) and CP ($B_+ \to J/\psi K_L^0$, $B_- \to J/\psi K_S^0$) tagging. Selecting events where one B candidate is reconstructed in a CP eigenstate and the flavor of the other B is identified, one can compare the rates of the $\overline{B}^0 \to B_\pm$ and $B^0 \to B_\pm$ transitions with their T-reversed $B_\pm \to \overline{B}^0$ and $B_\pm \to B^0$ processes, as a function of the time difference Δt between the two B decays [24–26]. Neglecting the small width difference between the two B_d^0 mass eigenstates, each

Int. J. Mod. Phys. A 2026.41. Downloaded from www.worldscientific.com
by UNIVERSITY OF CALIFORNIA @ BERKELEY on 09/16/26. Re-use and distribution is strictly not permitted, except for Open Access

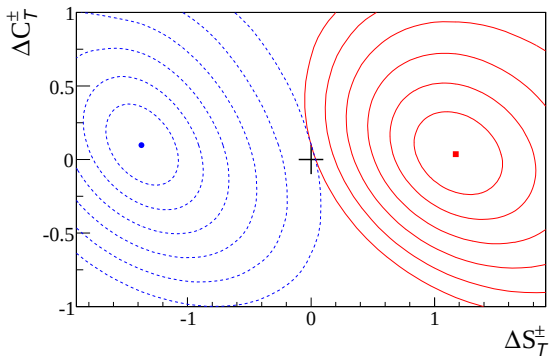

Figure 1: Measured values of ΔS_T^+, ΔC_T^+ (blue point, dashed lines) and ΔS_T^-, ΔC_T^- (red square, solid lines) [27]. The two-dimensional contours correspond to $1 - \mathrm{CL} = 0.317$, 4.55×10^{-2}, 2.70×10^{-3}, 6.33×10^{-5}, 5.73×10^{-7}, and 1.97×10^{-9}. The + sign indicates the T-invariant point.

of these eight transitions has a time-dependent decay rate of the form $\mathrm{e}^{-\Gamma_d \Delta t}\{1+S^{\pm}_{\alpha,\beta}\sin(\Delta m_d \Delta t)+C^{\pm}_{\alpha,\beta}\cos(\Delta m_d \Delta t)\}$, where Γ_d is the average decay width, Δm_d the B_d^0 mass difference, the subindices $\alpha = \ell^+, \ell^-$ and $\beta = K_S^0, K_L^0$ stand for the reconstructed final states of the two B mesons and the superindex + or − indicates whether the decay to the flavor final state α occurs before or after the decay to the CP final state β. Figure 1 shows confidence-level contours for the T-asymmetry parameters $\Delta S_T^{\pm} \equiv S^{\mp}_{\ell^-,K_L^0} - S^{\pm}_{\ell^+,K_S^0}$ and $\Delta C_T^{\pm} \equiv C^{\mp}_{\ell^-,K_L^0} - C^{\pm}_{\ell^+,K_S^0}$, reported by the BABAR experiment [27], which clearly demonstrate a violation of T in $\Delta S_T^{\pm}$, with a significance of 14σ.

2 Electric dipole moments

Among the most powerful tests of CP invariance is the search for a permanent electric dipole moment (EDM) of an elementary fermion or non-degenerate quantum system. The EDM of an elementary spin-1/2 fermion f is defined by the effective, non-renormalizable interaction

$$\mathcal{L}_{\mathrm{EDM}} = -\frac{i}{2} d_f\, \bar{f}\sigma_{\mu\nu}\gamma_5 f\, F^{\mu\nu} \tag{7}$$

where $F^{\mu\nu}$ is the QED field strength tensor. The values for d_f are conventionally expressed in units of $e\,\mathrm{cm}$. The interaction (7) is separately odd under T and P. In the non-relativistic limit, Eq. (7) reduces to

$$\mathcal{L}_{\mathrm{EDM}} \to d_f\, \chi_f^{\dagger}\vec{\sigma}\chi_f \cdot \vec{E} \tag{8}$$

where χ is a two-component Pauli spinor and $\vec{E}$ is the electric field. Note the interaction (8) is manifestly T-odd and carries no direct information on CP. The observation of a non-zero EDM of a non-relativistic (and non-degenerate) quantum system, such as the mercury atom (see below) would imply CP violation under the assumption of CPT invariance.

To date, no experimental observation of an EDM of an elementary particle or non-degenerate bound quantum system has been observed. The most stringent limits have been obtained for the EDMs of the electron, mercury atom, and neutron. A selection of the representative, most stringent limits is given in Table 1. The limits on the electron EDM are inferred from experiments involving polar molecules, paramagnetic systems with an unpaired electron spin. In contrast, the neutron and ^{199}Hg atom are diamagnetic. A variety of experimental efforts aimed at improved sensitivities are underway. For reviews of the experimental and theoretical situation, see, *e.g.* [28–31].

EDMs in the Standard Model

The SM provides two sources of d_f: the CPV phase in the CKM matrix and the P- and T-odd 'θ term' in the QCD Lagrangian. The former is characterized by the Jarlskog invariant [38]

$$\mathcal{J} = \mathrm{Im}(V_{us}V_{cs}^*V_{cb}V_{ub}^*) \sim A^2\lambda^6\eta < 10^{-4}\,, \tag{9}$$

Table 1: Most stringent limits on electric dipole moments.

EDM	Limit ($e\,\mathrm{cm}$)		Source
Electron	1.1×10^{-29}	(90% C.L.)	ThO [32]
	4.1×10^{-30}	(90% C.L.)	HfF^+ [33]
Muon	1.8×10^{-19}	(95% C.L.)	[34]
Neutron	1.8×10^{-26}	(90% C.L.)	[35]
^{199}Hg Atom	7.4×10^{-30}	(95% C.L.)	[36]
^{129}Xe Atom	1.5×10^{-27}	(95% C.L.)	[37]

while the latter is given by

$$\mathcal{L}_{\bar{\theta}} = -\frac{g_3^2}{16\pi^2}\,\bar{\theta}\,\mathrm{Tr}\left(G^{\mu\nu}\tilde{G}_{\mu\nu}\right), \tag{10}$$

where $G_{\mu\nu}$ ($\tilde{G}_{\mu\nu} = \epsilon_{\mu\nu\alpha\beta}\,G^{\alpha\beta}/2$) is the QCD field strength tensor (dual).

The CKM-induced EDMs of quarks and charged leptons arise at three- and four-loop orders, respectively [39–42]. The resulting numerical impact for the experimental observables (see below) falls well below present and prospective experimental sensitivities. The most important impact of $\mathcal{J}$ for the EDMs of the neutron and diamagnetic atoms arise via induced hadronic interactions. The resulting theoretical expectations for the electron, neutron and ^{199}Hg EDMs are

$$|d_e|_{\mathrm{CKM}} \approx 10^{-44}\ e\,\mathrm{cm}\quad [42], \tag{11a}$$

$$|d_n|_{\mathrm{CKM}} \approx (1-6)\times 10^{-32}\ e\,\mathrm{cm}\quad [43], \tag{11b}$$

$$|d_A(^{199}\mathrm{Hg})|_{\mathrm{CKM}} \lesssim 4\times 10^{-34}\ e\,\mathrm{cm}\quad [28]. \tag{11c}$$

For d_n and $d_A(^{199}\mathrm{Hg})$, the dominant CKM contributions arise from four-quark operators (generated after integrating out the electroweak gauge bosons) rather than from the EDMs of the individual quarks. The corresponding sensitivities to the QCD $\bar{\theta}$ parameter are given by

$$|d_n|_{\bar{\theta}} \approx (0.9-1.2)\times 10^{-16}\ \bar{\theta}\ e\,\mathrm{cm}\quad [43], \tag{12a}$$

$$|d_A(^{199}\mathrm{Hg})|_{\bar{\theta}} \approx (0.07-8)\times 10^{-20}\ \bar{\theta}\ e\,\mathrm{cm}\quad [28,29], \tag{12b}$$

where the ranges quoted include the impacts of hadronic, nuclear, and atomic theory uncertainties. The neutron EDM puts then a stringent limit on 'strong' CP violation: $\bar{\theta} \lesssim 2\times 10^{-10}$. The corresponding limit from $d_A(^{199}\mathrm{Hg})$ is weaker due to the large theoretical uncertainty.

EDMs Beyond the Standard Model

It is possible that the next generation of EDM searches will yield a non-zero result, arising from the $\bar{\theta}$-term interaction and/or physics beyond the SM (BSM). Most of the considered BSM scenarios involve new particles with masses well above the electroweak scale. At energies much lower than the BSM mass scale Λ, the dynamics can be described through an effective field theory (SMEFT) involving an infinite set of non-renormalizable operators $\mathcal{O}_k^{(d)}$, with dimensions $d > 4$, that are invariant under the SM gauge group:

$$\mathcal{L}_{\mathrm{SMEFT}} = \mathcal{L}_{\mathrm{SM}} + \sum_{k,d}\alpha_k^{(d)}\left(\frac{1}{\Lambda}\right)^{d-4}\mathcal{O}_k^{(d)}\,. \tag{13}$$

The operators contain only SM fields, while all short-distance information on the BSM physics is encoded in their Wilson coefficients $\alpha_k^{(d)}$. The $d = 4$ term corresponds to the SM Lagrangian.

For the systems of Table 1 and for many BSM scenarios of recent interest, it suffices to consider the leading contributions from $d = 6$ operators. Considering only the first-generation SM fermions, there exist 12 independent CPV pertinent operators. For a complete listing, see *e.g.*, Refs. [29, 44]. For a given elementary fermion f, two of these operators reduce to the EDM interaction in Eq. (7). Of the remaining, the most relevant include the chromo-electric dipole moments (cEDMs) of the quarks;

Int. J. Mod. Phys. A 2026.41. Downloaded from www.worldscientific.com
by UNIVERSITY OF CALIFORNIA @ BERKELEY on 09/16/26. Re-use and distribution is strictly not permitted, except for Open Access articles.

Table 2: Pertinent dimension-six EDM and cEDM sources (first generation fermions only).

System	$d = 6$ Source	Wilson Coefficient
Paramagnetic	Electron EDM	Im $C_{e\gamma}$
	Electron-quark	$C_{eq}^{(\pm)}$
Diamagnetic	Quark EDM	Im $C_{q\gamma}$
	Quark cEDM	Im C_{qG}
	Three gluon	$C_{\tilde{G}}$
	Four quark	Im $C_{quqd}^{(1,8)}$
	Quark-Higgs	Im $C_{\varphi ud}$
	Electron-quark tensor*	Im $C_{\ell equ}^{(3)}$

*Applicable only to atoms.

a CP-odd three gluon operator; three semileptonic, four-fermion operators; two four-quark operators; and a CPV interaction involving two Higgs fields and a right-handed quark current. For the dipole operators, it is useful to define a rescaled Wilson coefficient $\alpha_{fV_j}^{(6)} \equiv g_j\, C_{fV_j}$, where V_j $(j = 1, 2, 3)$ denote the gauge bosons for the three SM gauge groups with corresponding couplings g_j; for all other $d = 6$ operators we correspondingly identify $\alpha_k^{(6)} \equiv C_k$. In this case, one has for the EDM (d_f) and cEDM ($\tilde{d}_q$)

$$d_f = -(1.13 \times 10^{-16}\ e\ \text{cm}) \left(\frac{v}{\Lambda}\right)^2 \text{Im}\ C_{f\gamma}\,, \tag{14a}$$

$$\tilde{d}_q = -(1.13 \times 10^{-16}\ \text{cm}) \left(\frac{v}{\Lambda}\right)^2 \text{Im}\ C_{qG}\,, \tag{14b}$$

with $\text{Im}\ C_{f\gamma} = \text{Im}\ C_{fB} + 3I_3^f\, \text{Im}\ C_{fW}$. As the expressions (14a,14b) illustrate, the magnitude of the BSM contributions scales with two inverse powers of the scale Λ. A similar conclusion holds for the contributions from the other $d = 6$ operators to the EDMs of Table 1.

It is important to emphasize that if the BSM mediators are light, with masses below the weak scale, the effective field theory description of Eq. (13) does not apply. For recent studies along these lines, see, *e.g.* [45, 46].

EDM Interpretation: From Short Distances to the Atomic Scale

The EDM limits in Table 1 are obtained using composite quantum systems, wherein the relevant dynamics involve physics at the hadronic, nuclear, atomic and molecular scales. The manifestation of a given CPV source (CKM, $\bar{\theta}$ term, BSM) involves an interplay of these dynamics. In all cases, one must first evolve the Wilson coefficients from the weak scale to the hadronic scale, then match onto the relevant low-energy degrees of freedom (electrons, nucleons, pions, *etc.*). At this level, the most straightforward interpretation involves the paramagnetic systems, for which two sources dominate: the electron EDM and the electron spin-dependent semileptonic interaction $\bar{e}\gamma_5 e\, \bar{q}q$. The latter gives rise to an spin-independent Hamiltonian, for an atom with Z electrons/protons and N neutrons,

$$\hat{H}_S = \frac{iG_F}{\sqrt{2}}\, \delta(\vec{r}) \left[(Z+N)\, C_S^{(0)} + (Z-N)\, C_S^{(1)}\right] \gamma_0\gamma_5\,, \tag{15}$$

where $C_S^{(0)}$ ($C_S^{(1)}$) is proportional to $C_{eq}^{(+)}$ ($C_{eq}^{(-)}$). The computation of $C_S^{(0,1)}$ is relatively free from theoretical uncertainty since the operator $\bar{q}q$ essentially counts the number of quarks of flavor q in the nucleus. Experimental results for paramagnetic systems, thus, often quote bounds on

$$C_S \equiv C_S^{(0)} + \left(\frac{Z-N}{Z+N}\right) C_S^{(1)} \tag{16}$$

as well as on d_e, assuming only one of these two sources is non-vanishing. Combining results from ThO and HfF$^+$ (see Figure 2) allows one to obtain the global, 90% C.L. bounds

$$|d_e| < 2.1 \times 10^{-29}\ e\ \text{cm}\,, \qquad |C_S| < 1.9 \times 10^{-9}\,. \tag{17}$$

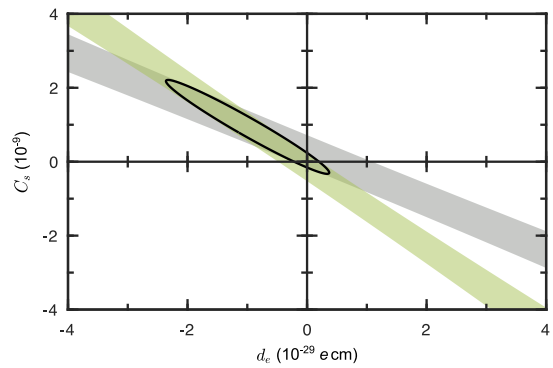

Figure 2: Constraints on d_e and C_S from EDM searches using polar molecules [33]. The green and grey bands are the 90% confidence regions from HfF+ and ThO, while the ellipse shows the 90% CL limits from the global fit. Parameters used in fits are from Ref. [47].

Note that the limits on d_e given in Table 1 have been obtained assuming $C_S = 0$.

For the diamagnetic systems, the situation is considerably more involved. For the neutron, a variety of approaches – including lattice QCD, chiral perturbation theory, QCD sum rules, and the quark model – have been employed to compute the relevant hadronic matrix elements of the CPV sources (see, *e.g.*, [29,30,48,49]). For diamagnetic atoms, the non-leptonic sources of Table 2 give rise to the EDM of the nucleus as well as other P- and T-odd nuclear moments, as allowed by the nuclear spin. However, according to a theorem by Schiff [50], the nuclear EDM generates no contribution to the neutral-atom EDM due to screening by atomic electrons. The leading contribution from these sources, instead, arises via the nuclear Schiff moment, $\vec{S}$, an r^3-weighted moment of the T- and P-odd component of the nuclear charge density. The resulting effective atomic Hamiltonian is

$$\hat{H}_{\text{Schiff}} = -4\pi\, \vec{\nabla}\rho_e(0) \cdot \vec{S}\,, \tag{18}$$

where $\vec{\nabla}\rho_e(0)$ is the gradient of the electron density at the nucleus. To date, computations of the nuclear Schiff moment have assumed that the leading contribution arises from a pion-exchange induced nuclear force, with the P- and T-odd πN interaction given by

$$\mathcal{L}_{\pi N}^{T,P} = \bar{N}\left[\bar{g}_\pi^{(0)} \vec{\tau}\cdot\vec{\pi} + \bar{g}_\pi^{(1)} \pi^0 + \bar{g}_\pi^{(2)} (3\tau_3\pi^0 - \vec{\tau}\cdot\vec{\pi})\right] N\,. \tag{19}$$

Chiral effective field theory power counting implies that in general the magnitude of $\bar{g}_\pi^{(2)}$ is suppressed with respect to the isoscalar and isovector couplings. The CPV sources then generate a diamagnetic atom EDM d_A via the sequence

$$\text{CPV source} \longrightarrow \bar{g}_\pi^{(i)} \longrightarrow \vec{S} \longrightarrow d_A\,. \tag{20}$$

The steps in this sequence involve dynamics at the hadronic, nuclear, and atomic scales, respectively. In addition, d_A may receive contributions from the nuclear spin-dependent interaction generated by the semileptonic tensor interaction listed in Table 2, with the corresponding atomic Hamiltonian

$$\hat{H}_T = \frac{2iG_F}{\sqrt{2}}\, \delta(\vec{r}) \sum_N \left[C_T^{(0)} + C_T^{(1)}\tau_3\right] \vec{\sigma}_N \cdot \vec{\gamma}\,, \tag{21}$$

where σ_N is the nucleon spin Pauli matrix and $C_T^{(0,1)} \propto \text{Im}\ C_{\ell equ}^{(3)}$.

Given the large number of CPV sources and existing diagmagnetic EDM limits, it is not possible to obtain a set of global constraints on the former. One may, however, do so for the low-energy effective parameters $\bar{g}_\pi^{(0,1)}$, $C_T^{(0,1)}$ and $\bar{d}_n^{\text{sr}}$, where the latter denotes a 'short-range' contribution to the neutron EDM [28, 51]. In this context, the dominant source of theoretical uncertainty involves computations of the nuclear Schiff moment. From the

Int. J. Mod. Phys. A 2026.41. Downloaded from www.worldscientific.com by UNIVERSITY OF CALIFORNIA @ BERKELEY on 09/16/26. Re-use and distribution is strictly not permitted, except for Open Access

bounds on the low-energy parameters, one may then derive constraints on the CPV sources by utilizing computations of the hadronic matrix elements. Reducing the degree of theoretical hadronic and nuclear physics uncertainty is an area of active effort.

3 Tests of *CPT*

CPT symmetry implies the equality of the masses and widths of a particle and its antiparticle. The most constraining limits are extracted from the neutral kaons [52, 53]:

$$\begin{aligned} 2\,\frac{|m_{K^0}-m_{\overline{K}^0}|}{(m_{K^0}+m_{\overline{K}^0})} &< 6\times 10^{-19}\,, \\ 2\,\frac{|\Gamma_{K^0}-\Gamma_{\overline{K}^0}|}{(m_{K^0}+m_{\overline{K}^0})} &= (8\pm 8)\times 10^{-18}\,. \end{aligned} \tag{22}$$

The limit on the K^0–$\overline{K}^0$ mass difference is extracted from the measured CP-violation parameters through the relation [54]

$$m_{\overline{K}^0}-m_{K^0} \approx \frac{2\left(m_{K^0_L}-m_{K^0_S}\right)}{\sin\phi_{\rm SW}}\,|\eta|\left(\frac{2}{3}\,\phi_{+-}+\frac{1}{3}\,\phi_{00}-\phi_{\rm SW}\right), \tag{23}$$

which assumes that there is no other source of CPT violation than this mass difference, where $\phi_{\rm SW}=(43.52\pm 0.05)^\circ$ is the superweak angle. An upper bound on CPT breaking in $K^0_L\to 2\pi$ has been also set through the measured phase difference of the CPV ratios η_{00} and η_{+-}, $\phi_{00}-\phi_{+-}=(0.34\pm 0.32)^\circ$, thanks to the small value of $(1-|\eta_{00}/\eta_{+-}|)$ (see the review on CP violation in K^0_L decays).

The measured masses and electric charges of the electron, the proton and their antiparticles provide also strong limits on CPT violation [55–58]:

$$\begin{aligned} &2\,\frac{|m_{e^+}-m_{e^-}|}{m_{e^+}+m_{e^-}} < 8\times 10^{-9}\,, \qquad \frac{|q_{e^+}+q_{e^-}|}{e} < 4\times 10^{-8}\,, \\ &\left|\frac{q_{\bar p}/m_{\bar p}}{q_p/m_p}\right| - 1 = (0.3\pm 1.6)\times 10^{-11}\,. \end{aligned} \tag{24}$$

Worth mentioning are also the tight constraints derived from the lepton and antilepton magnetic moments [59, 60],

$$\begin{aligned} 2\,\frac{g_{e^+}-g_{e^-}}{g_{e^+}+g_{e^-}} &= (-0.5\pm 2.1)\times 10^{-12}\,, \\ 2\,\frac{g_{\mu^+}-g_{\mu^-}}{g_{\mu^+}+g_{\mu^-}} &= (-0.11\pm 0.12)\times 10^{-8}\,, \end{aligned} \tag{25}$$

those of the proton and antiproton [61],

$$(\mu_p+\mu_{\bar p})/\mu_p = (2\pm 4)\times 10^{-9}\,, \tag{26}$$

and the measurement of the 1S-2S atomic transition in antihydrogen which agrees with the corresponding frequency spectral line in hydrogen at a relative precision of 2×10^{-12} [62].

A violation of CPT in an interacting local quantum field theory would imply that Lorentz symmetry is also violated [63]. Signatures of Lorentz-invariance violation have been searched for with atomic clocks, penning traps, matter and antimatter spectroscopy, colliders and astroparticle experiments, with so far negative results [64]. A compilation of experimental bounds is given in Ref. [65], parametrized through the coefficients of the so-called Standard Model Extension (SME) Lagrangian which contains all possible Lorentz- and CPT-violating operators preserving gauge invariance, renormalizability, locality and observer causality [66].

QUANTUM-NUMBER CONSERVATION LAWS

Conservation laws of several quantum numbers have been empirically established with a very high degree of confidence. They are usually associated with some global phase symmetry. However, while some of them are deeply rooted in basic principles such as gauge invariance (charge conservation; local symmetry implies global symmetry) or Lorentz symmetry (fermion number conservation), others appear to be accidental symmetries of the SM Lagrangian and could be broken by new physics interactions.

In fact, if one only assumes the SM gauge symmetries and particle content, the most general dynamics at energies below the BSM mass scale is described by the SMEFT Lagrangian in Eq. (13). All $d=4$ operators (*i.e.*, the SM) happen to preserve the B and L quantum numbers, but this is no-longer true for the gauge-invariant structures of higher dimensionality. There is only one operator with $d=5$ (up to hermitian conjugation and flavor assignments), and it violates lepton number by two units [67], giving rise to Majorana neutrino masses after the electroweak spontaneous symmetry breaking. With $d=6$, there are five operators that violate B and L [68, 69]. Thus, violations of these quantum numbers can be generically expected, unless there is an explicit symmetry protecting them.

4 Electric charge

The conservation of electric charges is associated with the QED gauge symmetry. The most precise tests are the non-observation of the decays $e\to\nu_e\gamma$ (lifetime larger than 6.6×10^{28} yr [70]) and $n\to p\nu_e\bar\nu_e$ (Br $<8\times 10^{-27}$, 68% C.L. [71]). The neutrality of matter can be also interpreted as a test of electric charge conservation. Worth mentioning are the experimental limits on the electric charge of the neutron, $q_n/e=(-0.2\pm 0.8)\times 10^{-21}$, and on the sum of the proton and electron charges, $|q_p+q_e|/e<1\times 10^{-21}$ [72].

The isotropy of the cosmic microwave background has been used to set stringent limits on a possible charge asymmetry of the Universe [73]. Assuming that charge asymmetries produced by different particles are not anticorrelated, this implies upper bounds on the photon ($|q_\gamma|/e<1\times 10^{-35}$) and neutrino ($|q_\nu|/e<4\times 10^{-35}$) electric charges. A much stronger upper bound on the photon charge ($|q_\gamma|/e<1\times 10^{-46}$) has been derived from the non-observation of Aharonov-Bohm phase differences in interferometric experiments with photons that have traversed cosmological distances, under the assumption that both positive and negative charged photons exist [74].

5 Lepton family numbers

In the SM with massless left-handed neutrinos there is a separate conservation number for each lepton family. However, neutrino oscillations show that neutrinos have tiny masses and there are sizable mixings among the different lepton flavors. Compelling evidence from solar, atmospheric, accelerator and reactor neutrino experiments has established a quite solid pattern of neutrino mass differences and mixing angles [18, 19]. (see the review on neutrino masses, mixings and oscillations). Nevertheless, flavor mixing among the different charged leptons has never been observed.

If neutrino masses and mixings among the three active neutrinos were the only sources of lepton-flavor violation (LFV), neutrinoless transitions from one charged lepton flavor to another would be heavily suppressed by powers of m_{ν_i} (GIM mechanism), leading to un-observably small rates; for instance [77–82],

$$\mathrm{Br}(\mu\to e\gamma)=\frac{3\alpha}{32\pi}\left|\sum_i U^*_{\mu i}U_{ei}\,\frac{m^2_{\nu_i}-m^2_{\nu_1}}{M^2_W}\right|^2 < 10^{-54}\,, \tag{27}$$

where U_{ia} are the relevant elements of the PMNS mixing matrix. This contribution is clearly too small to be observed in any realistic experiment, so any experimentally accessible effect would arise from BSM physics with sources of LFV not related to m_{ν_i}. The search for charged LFV (CLFV) remains an area of active interest, which has the potential to probe physics at scales much higher than the TeV.

Among the most sensitive probes are searches for the CLFV decays of the muon, $\mu\to e\gamma$ and $\mu\to 3e$, as well as the conversion process $\mu^-+A(N,Z)\to e^-+A(N,Z)$, where $A(N,Z)$ denotes a nucleus with N neutrons and Z protons. Searches for rare τ decays such as $\tau\to\ell\gamma$ ($\ell=e,\mu$) also provide interesting probes of CLFV. A variety of BSM scenarios predict that rates for these CLFV processes could be sufficiently large to be observed in the present or planned searches. To date, no observation has been

Int. J. Mod. Phys. A 2026.41. Downloaded from www.worldscientific.com
by UNIVERSITY OF CALIFORNIA @ BERKELEY on 09/16/26. Re-use and distribution is strictly not permitted, except for Open Access articles.

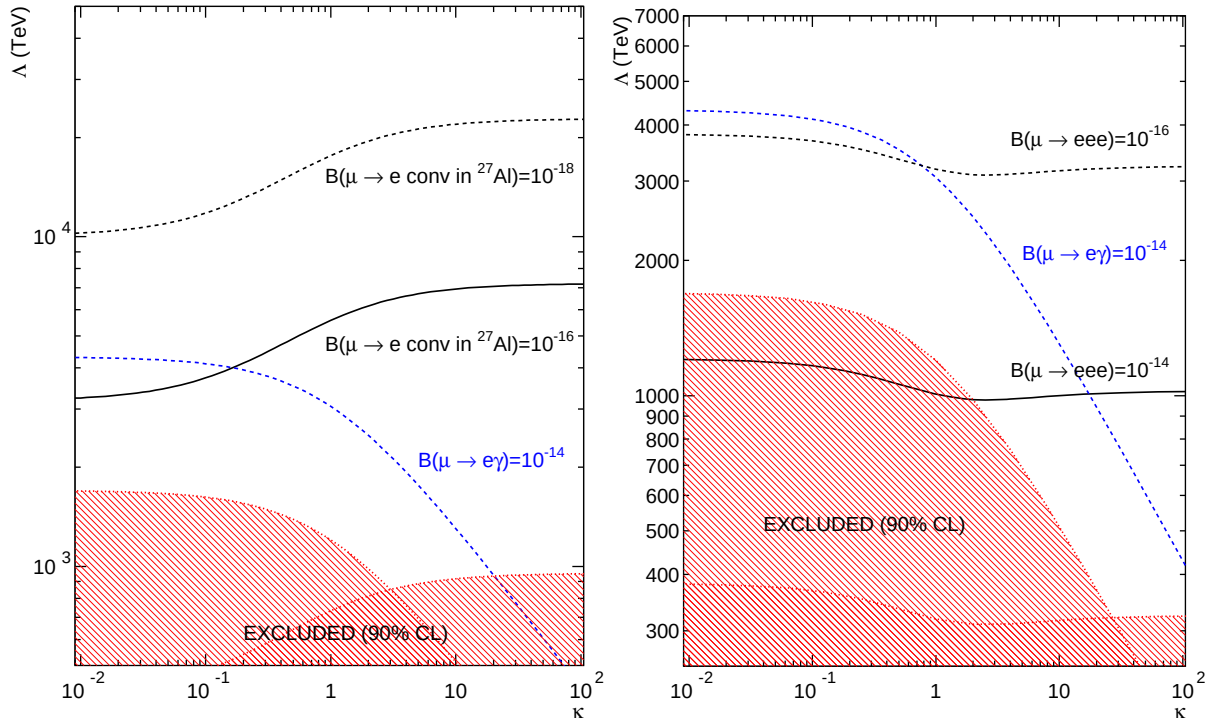

Figure 3: Model-independent CLFV sensitivities based on Eq (33). Left panel shows the comparison of present constraints with prospective future sensitivities for $\mu \to e\gamma$ and $\mu \to e$ conversion. Right panel gives analogous comparison for $\mu \to e\gamma$ and $\mu \to 3e$. Updated by [75] from Ref. [76].

reported, and the resulting null results place strong constraints on BSM scenarios. For extensive reviews of the experimental and theoretical status and prospects, see Refs. [76, 83, 84].

A detailed set of upper bounds on CLFV branching rations is given in the listings for the muon and tau leptons. Here we emphasize those with the strongest limits:

$$\begin{aligned} &\mathrm{Br}(\mu \to e\gamma) < 1.5 \times 10^{-13} \quad [85], \\ &\mathrm{Br}(\mu \to 3e) < 1.0 \times 10^{-12} \quad [86] \end{aligned} \tag{28}$$

and

$$B_{\mu\to e} \equiv \frac{\Gamma(\mu^- + A(N,Z) \to e^- + A(N,Z)}{\Gamma(\mu^- + A(N,Z) \to \nu + A(N+1, Z-1)} \tag{29}$$

with the best limit so far, $B_{\mu\to e} < 7 \times 10^{-13}$ [87], obtained with gold. Several proposed experiments aim to improve these limits by several orders of magnitude with different atoms.

One may interpret both $\mu \to e\gamma$ and $\mu \to e$ conversion in terms of the amplitudes to emit a real or virtual photon:

$$\begin{aligned} \mathcal{M}_{\mu\to e\gamma^{(*)}} = eG_\mu \varepsilon^{\alpha *} \bar{e}(p-q) \Big[\left(q^2 \gamma_\alpha - \not{q} q_\alpha\right) \left(\tilde{A}_1^R P_R + \tilde{A}_1^L P_L\right) \\ + i m_\mu \sigma_{\alpha\beta} q^\beta \left(\tilde{A}_2^R P_R + \tilde{A}_2^L P_L\right) \Big] \mu(p) \,, \end{aligned} \tag{30}$$

where it is conventional to normalize the amplitude to the Fermi constant. One then has

$$\mathrm{Br}(\mu \to e\gamma) = 48\pi^3 \alpha \left(|\tilde{A}_2^R|^2 + |\tilde{A}_2^L|^2 \right) \,. \tag{31}$$

For the conversion process, the virtual photon is absorbed by the quarks in the nucleus, yielding an effective four-fermion operator. In general, the exchange of other particles could lead to similar or alternate Lorentz structures, and it is not possible to distinguish between the exchange of a virtual photon or other particle. It is conventional to write the most general four-fermion amplitude, valid for energies below the electroweak scale as (adapted from Ref. [90])

$$\mathcal{M}_{\mu\to e} = G_\mu \sum_{n,a,q} a_{a,q}^{(n)} \, \bar{e} \Gamma^n P_a \mu \, \bar{q} \Gamma_n q \,, \tag{32}$$

where P_a $(a = L, R)$ denote the left and right-handed projectors and Γ^n denotes 1, γ_5, γ^μ, $\gamma^\mu\gamma_5$, and $\sigma_{\mu\nu}$. If any of the coefficients $a_{a,q}^{(n)}$ are generated by physics at a scale $\Lambda > v$, then their effects would be encoded in the SMEFT Lagrangian (13). For scenarios in which the leading CLFV operators occur at $d = 6$, the $a_{a,q}^{(n)}$ will scale as $(v/\Lambda)^2$. The corresponding decay and conversion rates will then scale as $(v/\Lambda)^4$. Note that the scalar and time component of the vector interactions are coherent over the nucleus, essentially counting the number of quarks. Consequently, these interactions typically yield the greatest sensitivities to high BSM mass scales.

It is sometimes convenient to compare the relative sensitivities of the decay and conversion processes using the following simplified effective Lagrangian [76]:

$$\begin{aligned} \mathcal{L}_{\mathrm{eff}}^{\mathrm{CLFV}} = &\frac{m_\mu}{(\kappa+1)\Lambda^2} \, \bar{\mu}_R \sigma_{\mu\nu} e_L \, F^{\mu\nu} \\ &+ \frac{\kappa}{(\kappa+1)\Lambda^2} \, \bar{\mu}\gamma_\mu e \sum_q \bar{q}\gamma^\mu q + \mathrm{h.c.} \,. \end{aligned} \tag{33}$$

Note that one may replace the second term in Eq. (33) by any one of the other four-fermion interactions given in Eq. (32). An analogous expression applies to the process $\mu \to 3e$ when replacing the sum over quarks by the corresponding electron bilinear. A comparison of the present and prospective sensitivities for various muon CLFV searches in this framework is shown in Figure 3.

Stringent limits have been also set on the LFV decay modes of the τ lepton [91]. As shown in Figure 4, the large τ data samples collected at the B factories have made possible to reach a 10^{-8} sensitivity for many of its leptonic ($\tau \to \ell\gamma$, $\tau \to \ell'\ell^+\ell^-$) and semileptonic ($\tau \to \ell P^0$, $\tau \to \ell V^0$, $\tau \to \ell P^0 P^0$, $\tau \to \ell P^+ P'^-$) neutrinoless LFV decays, and BELLE-II is expected to push these limits beyond the 10^{-9} level [92]. Being a third generation lepton,

Int. J. Mod. Phys. A 2026.41. Downloaded from www.worldscientific.com
by UNIVERSITY OF CALIFORNIA @ BERKELEY on 09/16/26. Re-use and distribution is strictly not permitted, except for Open Access

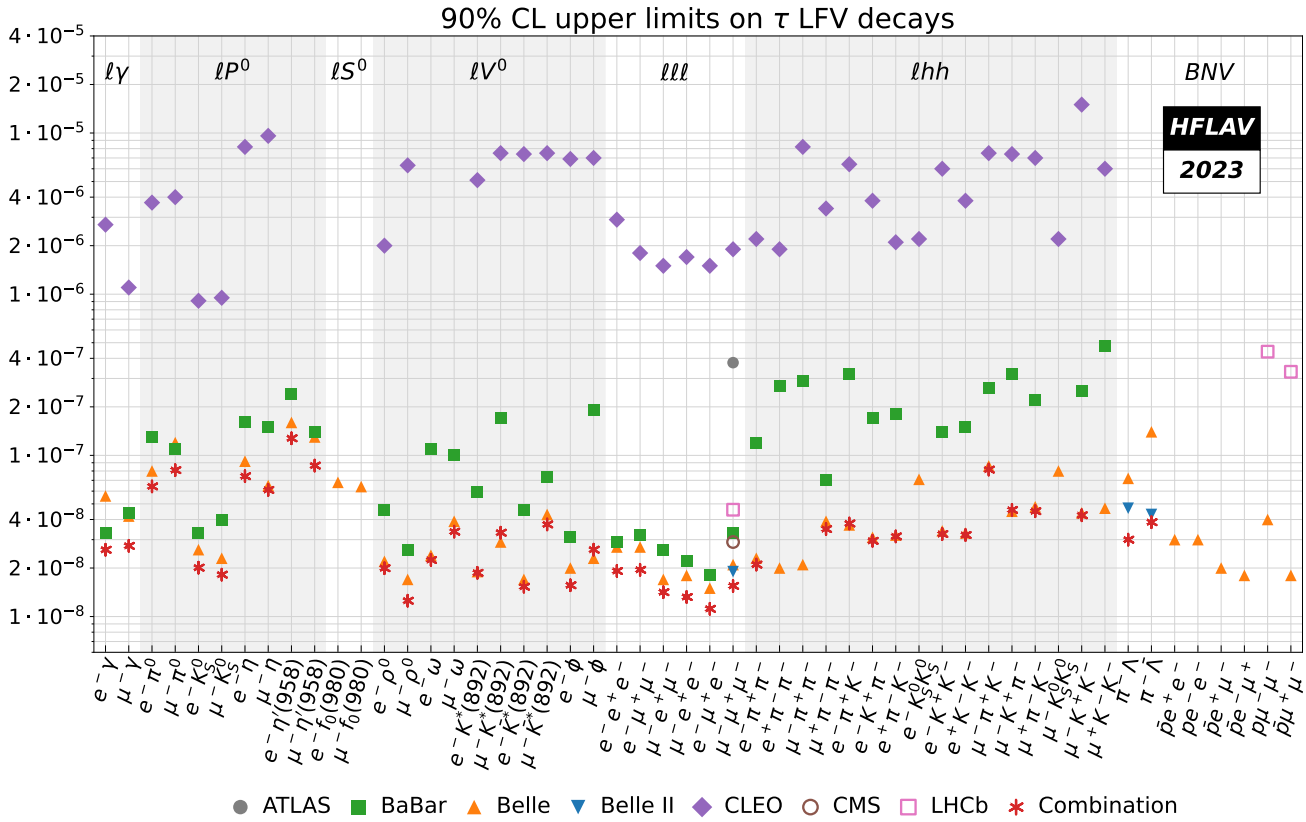

Figure 4: Current experimental limits on neutrinoless LFV τ decays [88]

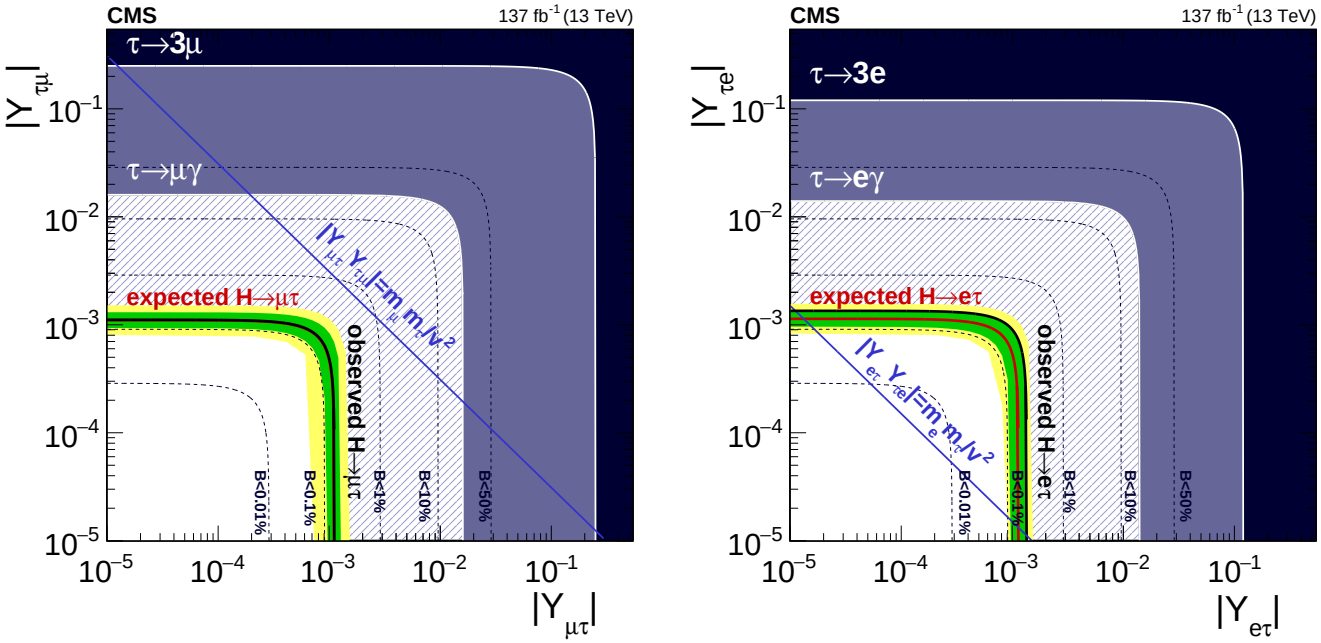

Figure 5: Current limits on the Higgs LFV τ Yukawas from direct $H^0 \to \ell^\pm\tau^\mp$ decays ($\ell = e, \mu$), and indirect constraints from τ decays [89].

the τ could be more sensitive to heavier new-physics scales, which makes his LFV decays particularly interesting. Compared to the muon, the τ decay amplitudes could be enhanced by a chirality ratio $(m_\tau/m_\mu)^2 \sim 280$ and/or by lepton-mixing factors such as $|U_{\tau 3}/U_{e3}|^2 \sim 20$, but the exact relation is model dependent. In any case, the τ LFV decays provide a rich data set that is very complementary to the μ bounds. If LFV is finally observed, the correlations between μ and τ data, and among different LFV τ decays will allow to probe the underlying mechanism of lepton flavor breaking.

Interesting limits on LFV are also obtained in meson decays. The best bounds come from kaon experiments, e.g., $\mathrm{Br}(K_L^0 \to e^\pm\mu^\mp) < 4.7 \times 10^{-12}$ [93], $\mathrm{Br}(K^+ \to \pi^+\mu^+e^-) < 1.3 \times 10^{-11}$ [94]. Quite strong limits have also been set in decays of B and D

Int. J. Mod. Phys. A 2026.41. Downloaded from www.worldscientific.com
by UNIVERSITY OF CALIFORNIA @ BERKELEY on 09/16/26. Re-use and distribution is strictly not permitted, except for Open Access articles.

mesons, the best upper bounds being $\mathrm{Br}(B^0 \to e^\pm\mu^\mp) < 1.0 \times 10^{-9}$ [95] and $\mathrm{Br}(D^0 \to e^\pm\mu^\mp) < 1.3 \times 10^{-8}$ [96].

The LFV decays of the Z boson were probed at LEP at the 10^{-5} to 10^{-6} level. Stronger (95% C.L.) limits have been set recently at the LHC by the ATLAS and CMS collaborations [97, 98]:

$$\mathrm{Br}(Z \to e^\pm\mu^\mp) < 1.9 \times 10^{-7}\,, \qquad \mathrm{Br}(Z \to e^\pm\tau^\mp) < 5.0 \times 10^{-6}\,, \qquad \mathrm{Br}(Z \to \mu^\pm\tau^\mp) < 6.5 \times 10^{-6}\,. \tag{34}$$

LHC is now testing LFV in Higgs decays, within the available statistics. From the current (95% C.L.) experimental upper bounds [89, 99–103],

$$\mathrm{Br}(H^0 \to e^\pm\mu^\mp) < 4.4 \times 10^{-5}\,, \qquad \mathrm{Br}(H^0 \to e^\pm\tau^\mp) < 0.20\%\,, \qquad \mathrm{Br}(H^0 \to \mu^\pm\tau^\mp) < 0.15\%\,, \tag{35}$$

one can derive direct limits on the LFV Yukawa couplings of the Higgs boson,

$$\mathcal{L}_Y = -H^0 \sum_{i\neq j} \left(Y_{\ell_i\ell_j}\, \bar{\ell}^i_L \ell^j_R + \mathrm{h.c.} \right)\,. \tag{36}$$

From $H^0 \to e^\pm\mu^\mp$, one obtains $\sqrt{Y^2_{\mu e} + Y^2_{e\mu}} < 1.9 \times 10^{-4}$, which is not yet competitive with the indirect limit set by $\mu \to e\gamma$ through a (one-loop) virtual Higgs exchange:

$$\sqrt{Y^2_{\mu e} + Y^2_{e\mu}} < 3.6 \times 10^{-6}\,. \tag{37}$$

However, the LHC data provide at present the strongest bounds on the LFV τ Yukawas [89, 102]:

$$\sqrt{Y^2_{e\tau} + Y^2_{\tau e}} < 1.3 \times 10^{-3}\,, \qquad \sqrt{Y^2_{\mu\tau} + Y^2_{\tau\mu}} < 1.11 \times 10^{-3}\,. \tag{38}$$

Figure 5 compares the Higgs exclusion limits on the τ Yukawas with the current indirect constraints from LFV τ decays.

6 Baryon and Lepton Number

The transitions discussed in the previous section preserve the total lepton number $L = L_e + L_\mu + L_\tau$. In the SM, conservation of $B - L$ is an accidental symmetry of the Lagrangian. At the classical level, $B + L$ is also conserved, though it is violated at the loop level by the anomaly. The latter is a topological effect that is highly suppressed at zero temperature and, moreover, does not contribute to the processes discussed in the review. Going beyond renormalizable interactions, there exists a tower of operators in the SMEFT Lagrangian (13), containing only SM fields, that break one or both of these symmetries. We briefly review these possibilities in turn.

Lepton Number

The lowest-dimension operator containing only SM fields that breaks baryon or lepton number is the $d = 5$, lepton-number-violating (LNV) 'Weinberg' neutrino-mass operator [67]:

$$\mathcal{L}^{\mathrm{LNV}} = \frac{y}{\Lambda}\, \bar{L}^C H H^T L\,. \tag{39}$$

When the neutral component of the Higgs field obtains its vacuum expectation value, this $\Delta L = 2$ interaction yields a Majorana mass for the light, active neutrinos. The most comprehensive approach for probing this effect is the search for neutrinoless double-beta decay ($0\nu\beta\beta$) of atomic nuclei, $(Z, A) \to (Z + 2, A) + e^- + e^-$ [104, 105] (see the review on neutrinoless double-β decay). The detection of a non-zero $0\nu\beta\beta$ signal could represent a spectacular evidence of Majorana neutrinos. The current best limit, $\tau_{1/2} > 3.8 \times 10^{26}$ yr, has been obtained by the KamLAND-Zen experiment with ^{136}Xe [106].

Theoretically, the interaction (39) can arise from BSM interactions in the well-known see-saw mechanism for neutrino mass (for a review, see [107]). In this context, the conventional choice for the scale Λ is of order the GUT scale, yielding light neutrino masses of order eV and below when the couplings y are of order the charged elementary fermion Yukawa couplings. BSM theories may also give rise to LNV observables in other contexts. In these scenarios, if the LNV scale is of order 1 TeV, one may observe signatures of LNV not only in $0\nu\beta\beta$ but also in collider searches for final states containing same sign dileptons. Searches for same sign dileptons plus a di-jet pair at the LHC have placed constraints on TeV-scale LNV [108, 109] that in some cases complement those obtained from $0\nu\beta\beta$.

Stringent constraints on violations of L have been also set in $\mu^- \to e^+$ conversion in muonic atoms, the best limit being $\sigma(\mu^-\mathrm{Ti} \to e^+\mathrm{Ca})/\sigma(\mu^-\mathrm{Ti} \to \mathrm{all}) < 3.6 \times 10^{-11}$ [110], and at the flavor factories through L-violating decays of the τ lepton and K, D and B mesons. Some representative examples are $\mathrm{Br}(\tau^- \to e^+\pi^-\pi^-) < 2.0 \times 10^{-8}$ [111], $\mathrm{Br}(K^+ \to \pi^-\mu^+\mu^+) < 4.2 \times 10^{-11}$ [112], $\mathrm{Br}(D^+ \to \pi^-\mu^+\mu^+) < 1.4 \times 10^{-8}$ [113] and $\mathrm{Br}(B^- \to \pi^+\mu^-\mu^-) < 4.0 \times 10^{-9}$ (95% CL) [114]. All these $|\Delta L| = 2$ processes could be mediated by a massive Majorana neutrino. They provide useful bounds on the effective Majorana neutrino mass matrix $m_{\ell\ell'} \sim \sum_i U_{\ell i} U_{\ell' i} m_{\nu_i}$ [115], although not as strong as the $0\nu\beta\beta$ constraint on m_{ee}.

Baryon Number

Grand Unified Theories (GUTs) combine leptons and quarks in the same symmetry multiplets and, therefore, predict the violation of the baryon and lepton quantum numbers. Many experiments have searched for B-violating transitions, but no positive signal has been identified so far. Proton decay would be the most relevant violation of B, as it would imply the unstability of matter. The current lower bound on the proton lifetime is 9×10^{29} yr [116]. Stronger limits have been set for particular decay modes, such as $\tau(p \to e^+\pi^0) > 2.4 \times 10^{34}$ yr [117]. For a discussion of proton decay in the context of GUTs, see the review on Grand Unified Theories.

Another spectacular signal would be neutron-antineutron oscillations. Searches have been performed for quasi-free n–$\bar{n}$ oscillations and for $n\bar{n}$ annihilation products in a nucleus. The latter would arise when the $\bar{n}$ produced through oscillations annihilates with another neutron in the nuclear medium. The corresponding best limits, expressed in terms of the free and bound oscillation times, $\tau_{n\bar{n}}$ and τ_m, respectively, are:

$$\tau_{n\bar{n}} > 0.86 \times 10^8 \text{ s} \quad [118], \tag{40a}$$

$$\tau_m > 3.6 \times 10^{32} \text{ yr} \quad [119] \tag{40b}$$

From the latter, one may infer a bound $\tau_{n\bar{n}} > 4.7 \times 10^8$ s, as discussed below. See Ref. [120] for a recent review.

The theoretical interpretation of these bounds starts with an assumed, effective Hamiltonian for the free (anti-)neutron, $\mathcal{H}_{\mathrm{eff}}$ that contains a B-violating part, yielding matrix elements

$$\langle n|\mathcal{H}_{\mathrm{eff}}|n\rangle = \langle \bar{n}|\mathcal{H}_{\mathrm{eff}}|\bar{n}\rangle = m - i\frac{\lambda}{2}\,, \tag{41a}$$

$$\langle n|\mathcal{H}_{\mathrm{eff}}|\bar{n}\rangle = \langle \bar{n}|\mathcal{H}_{\mathrm{eff}}|n\rangle \equiv \delta m\,, \tag{41b}$$

where CPT is assumed to be conserved, the neutron lifetime $\tau_n = 1/\lambda$ and $\tau_{n\bar{n}} = 1/|\delta m|$. The rate for a neutron to oscillate into an antineutron after a time t is given by

$$\mathcal{P}_{n\bar{n}}(t) = \sin^2\left(\frac{t}{\tau_{n\bar{n}}}\right) e^{-\lambda t}\,. \tag{42}$$

For $t << \tau_n << \tau_{n\bar{n}}$, one has

$$\mathcal{P}_{n\bar{n}}(t) \to (t/\tau_{n\bar{n}})^2\,. \tag{43}$$

In realistic experiments, there exist effects, such as background magnetic fields, that split the energies of the neutron and antineutron. One must ensure that the observation time is sufficiently short so that these effects do not overwhelm the small B-violating term δm and that Eq. (42) applies.

In nuclei, the interactions of neutrons and antineutrons with the surrounding medium are sufficiently distinct that one must take the corresponding matter potentials into account. In particular, the matrix elements in Eq. (41a) become

$$\langle n|\mathcal{H}_{\mathrm{eff}}|n\rangle = m + V_n\,, \qquad \langle \bar{n}|\mathcal{H}_{\mathrm{eff}}|\bar{n}\rangle = m + V_{\bar{n}}\,, \tag{44}$$

Int. J. Mod. Phys. A 2026.41. Downloaded from www.worldscientific.com by UNIVERSITY OF CALIFORNIA @ BERKELEY on 09/16/26. Re-use and distribution is strictly not permitted, except for Open Access

with V_n being essentially real ($V_n \equiv V_{nR}$) and $V_{\bar{n}} = V_{\bar{n}R} - iV_{\bar{n}I}$. The imaginary part $V_{\bar{n}I}$ characterizes the annihilation of the antineutron with bound nucleons into secondary hadrons. The rate for a bound neutron to disappear is given by

$$\Gamma_m = \frac{2(\delta m)^2 |V_{\bar{n}I}|}{(V_{nR} - V_{\bar{n}R})^2 + V_{\bar{n}I}^2} \equiv \left(R\,\tau_{n\bar{n}}^2\right)^{-1} . \tag{45}$$

For the nuclei of experimental interest, nuclear theory computations yield $R \sim 10^{23} s^{-1}$. Null results of bound n-$\bar{n}$ oscillation searches thus allow one to infer a bound on $\tau_{n\bar{n}}$ via Eq. (45).

From an elementary particle standpoint, n-$\bar{n}$ oscillations involve the conversion of three quarks into three antiquarks (and vice-versa). The lowest-dimension operators mediating such process arise at dimension nine in the SMEFT:

$$\mathcal{L}_{n\text{-}\bar{n}} = \frac{1}{\Lambda^5} \sum_j \alpha_j^{(9)}\, \mathcal{O}_j^{\rm BNV} . \tag{46}$$

Consequently, one expects

$$\delta m \sim \alpha_j^{(9)}\, \frac{\Lambda_{\rm HAD}^6}{\Lambda^5} , \tag{47}$$

where $\Lambda_{\rm HAD}$ is a hadronic scale set by the n-$\bar{n}$ matrix elements in Eq. (41b). Taking $\Lambda_{\rm HAD}$ to be of order the QCD scale and using the present bounds on $\tau_{n\bar{n}}$ yields a lower bound on the B-violating mass scale of ~ 100 TeV.

The search for B-violating decays of short-lived particles such as Z bosons, τ leptons and B mesons provides also relevant constraints. The best limits are $\mathrm{Br}(Z \to pe, p\mu) < 1.8 \times 10^{-6}$ (95% C.L.) [121], $\mathrm{Br}(\tau^- \to \bar{p}\mu^-\mu^+) < 1.8 \times 10^{-8}$ [122] and $\mathrm{Br}(B^0 \to p\mu^-) < 2.6 \times 10^{-9}$ [123]

7 Quark flavors

While strong and electromagnetic forces preserve the quark flavor, the charged-current weak interactions generate transitions among the different quark species (see the review on the CKM quark-mixing matrix). Since the SM flavor-changing mechanism is associated with the $W^\pm$ fermionic vertices, the tree-level transitions satisfy a $\Delta F = \Delta Q$ rule where ΔQ denotes the change in charge of the relevant hadrons. Remember that the flavor quantum number F is defined to be $+1$ for positively charged quarks ($F = U, C, T$) and -1 for quarks with negative charges ($F = D, S, B$). The strongest tests on this conservation law have been obtained in kaon decays such as $\mathrm{Br}(K^+ \to \pi^+\pi^+e^-\bar{\nu}_e) < 1.3 \times 10^{-8}$ [124], and $(\mathrm{Re}\,x, \mathrm{Im}\,x) = (-0.002 \pm 0.006, 0.0012 \pm 0.0021)$ [125,126] where $x \equiv \mathcal{M}(\overline{K}^0 \to \pi^-\ell^+\nu)/\mathcal{M}(K^0 \to \pi^-\ell^+\nu)$.

The $\Delta F = \Delta Q$ rule can be violated through quantum loop contributions giving rise to flavor-changing neutral-current transitions (FCNCs). Owing to the GIM mechanism, processes of this type are very suppressed in the SM, which makes them a superb tool in the search for new physics associated with the flavor dynamics. Within the SM itself, these transitions are also sensitive to the heavy-quark mass scales and have played a crucial role identifying the size of the charm (K^0–$\overline{K}^0$ mixing) and top (B^0–$\overline{B}^0$ mixing) masses before the discovery of those quarks. In addition to the well-established $\Delta F = 2$ mixings in neutral K and B mesons, $\Delta M_{K^0} \equiv M_{K_L^0} - M_{K_S^0} = (0.5293 \pm 0.0009) \times 10^{10}\ \mathrm{s}^{-1}$, $\Delta M_{B^0} \equiv M_{B_H^0} - M_{B_L^0} = (0.5068 \pm 0.0019) \times 10^{12}\ \mathrm{s}^{-1}$ and $\Delta M_{B_s^0} \equiv M_{B_{sH}^0} - M_{B_{sL}^0} = (17.766 \pm 0.006) \times 10^{12}\ \mathrm{s}^{-1}$, the mixing of the D^0 meson and its antiparticle has been recently observed with a significance of more than seven standard deviations [127], showing that there is a nonzero mass difference between the two neutral charm-meson eigenstates, of the expected size:

$$M_{D_H^0} - M_{D_L^0} = (0.997 \pm 0.116) \times 10^{10}\ \mathrm{s}^{-1}. \tag{48}$$

The SM prediction of the D_H^0–D_L^0 mass difference is dominated by long-distance physics, because it involves virtual loops with down-type light quarks, and has unfortunately quite large uncertainties [128].

The FCNC kaon decays into lepton-antilepton pairs put stringent constraints on new flavor-changing interactions. The measured $K_L^0 \to \mu^+\mu^-$ rate, $\mathrm{Br}(K_L^0 \to \mu^+\mu^-) = (6.84 \pm 0.11) \times 10^{-9}$, is completely dominated by the known 2γ absorptive contribution, leaving very little room for new-physics, and $\mathrm{Br}(K_L^0 \to e^+e^-) = (9^{+6}_{-4}) \times 10^{-12}$ [129] (the tiniest branching ratio ever measured) also agrees with the SM expectation [130]. The experimental K_S^0 upper bounds on the electron, $\mathrm{Br}(K_S^0 \to e^+e^-) < 9 \times 10^{-9}$ [131], and muon, $\mathrm{Br}(K_S^0 \to \mu^+\mu^-) < 2.1 \times 10^{-10}$ [132], modes are still five and two orders of magnitude, respectively, larger than their SM predictions [130]. Another very clean test of FCNCs is provided by the decay $K^+ \to \pi^+\nu\bar{\nu}$. The CERN NA62 experiment has already collected 51 events, with a significance above 5σ, providing the first observation of this decay [133]. This leads to $\mathrm{Br}(K^+ \to \pi^+\nu\bar{\nu}) = (1.30^{+0.33}_{-0.30}) \times 10^{-10}$, in agreement with the predicted SM branching fraction of $(7.73 \pm 0.61) \times 10^{-11}$ [134,135]. Even more interesting is the CP-violating neutral mode $K_L^0 \to \pi^0\nu\bar{\nu}$, expected at a rate of $(2.59 \pm 0.29) \times 10^{-11}$ [134,135] that is still far away from the current upper bound of 2.2×10^{-9} [136]. The KOTO experiment at KEK is expected to substantially increase the sensitivity to this mode.

The strongest bound on FCNC transitions in charm decays is $\mathrm{Br}(D^0 \to \mu^+\mu^-) < 2.1 \times 10^{-9}$ [137], while in B decays the LHC experiments have recently reached the SM sensitivity: $\mathrm{Br}(B_d^0 \to \mu^+\mu^-) < 1.5 \times 10^{-10}$ [138] and $\mathrm{Br}(B_s^0 \to \mu^+\mu^-) = (3.34 \pm 0.27) \times 10^{-9}$.

References

[1] G. Luders, Kong. Dan. Vid. Sel. Mat. Fys. Med. **28N5**, 5, 1 (1954).

[2] W. Pauli, in L. Rosenfelf and V. Weisskopf, editors, "Niels Bohr and the Development of Physics," 30–51, McGraw-Hill, New York (1955).

[3] J. McDonough *et al.*, Phys. Rev. **D38**, 2121 (1988).

[4] M. Ablikim *et al.* (BESIII), Phys. Rev. **D90**, 9, 092002 (2014), [arXiv:1409.4040].

[5] S. Prakhov *et al.* (Crystal Ball), Phys. Rev. Lett. **84**, 4802 (2000).

[6] J. H. Christenson *et al.*, Phys. Rev. Lett. **13**, 138 (1964).

[7] H. Burkhardt *et al.* (NA31), Phys. Lett. **B206**, 169 (1988).

[8] G. D. Barr *et al.* (NA31), Phys. Lett. **B317**, 233 (1993).

[9] L. K. Gibbons *et al.*, Phys. Rev. Lett. **70**, 1203 (1993).

[10] J. R. Batley *et al.* (NA48), Phys. Lett. **B544**, 97 (2002), [hep-ex/0208009].

[11] E. Abouzaid *et al.* (KTeV), Phys. Rev. **D83**, 092001 (2011), [arXiv:1011.0127].

[12] H. Gisbert and A. Pich, Rept. Prog. Phys. **81**, 7, 076201 (2018), [arXiv:1712.06147].

[13] V. Cirigliano *et al.*, JHEP **02**, 032 (2020), [arXiv:1911.01359].

[14] R. Abbott *et al.* (RBC, UKQCD), Phys. Rev. D **102**, 5, 054509 (2020), [arXiv:2004.09440].

[15] R. Aaij *et al.* (LHCb), Phys. Rev. Lett. **122**, 21, 211803 (2019), [arXiv:1903.08726].

[16] R. Aaij *et al.* (LHCb), Phys. Rev. Lett. **131**, 9, 091802 (2023), [arXiv:2209.03179].

[17] R. Aaij *et al.* (LHCb), Nature **643**, 8074, 1223 (2025), [arXiv:2503.16954].

[18] P. F. de Salas *et al.*, JHEP **02**, 071 (2021), [arXiv:2006.11237].

[19] I. Esteban *et al.*, JHEP **12**, 216 (2024), [arXiv:2410.05380].

[20] A. Angelopoulos *et al.* (CPLEAR), Phys. Lett. **B444**, 43 (1998).

[21] L. Wolfenstein, Phys. Rev. Lett. **83**, 911 (1999).

[22] L. Alvarez-Gaume *et al.*, Phys. Lett. **B458**, 347 (1999), [hep-ph/9812326].

Int. J. Mod. Phys. A 2026.41. Downloaded from www.worldscientific.com
by UNIVERSITY OF CALIFORNIA @ BERKELEY on 09/16/26. Re-use and distribution is strictly not permitted, except for Open Access articles.

[23] H. J. Gerber, Eur. Phys. J. **C35**, 195 (2004).

[24] M. C. Bañuls and J. Bernabeu, Phys. Lett. **B464**, 117 (1999), [hep-ph/9908353].

[25] M. C. Bañuls and J. Bernabeu, Nucl. Phys. **B590**, 19 (2000), [hep-ph/0005323].

[26] J. Bernabeu, F. Martinez-Vidal and P. Villanueva-Perez, JHEP **08**, 064 (2012), [arXiv:1203.0171].

[27] J. P. Lees *et al.* (BaBar), Phys. Rev. Lett. **109**, 211801 (2012), [arXiv:1207.5832].

[28] T. Chupp *et al.*, Rev. Mod. Phys. **91**, 1, 015001 (2019), [arXiv:1710.02504].

[29] J. Engel, M. J. Ramsey-Musolf and U. van Kolck, Prog. Part. Nucl. Phys. **71**, 21 (2013), [arXiv:1303.2371].

[30] M. Pospelov and A. Ritz, Annals Phys. **318**, 119 (2005), [hep-ph/0504231].

[31] J. S. M. Ginges and V. V. Flambaum, Phys. Rept. **397**, 63 (2004), [arXiv:physics/0309054].

[32] V. Andreev *et al.* (ACME), Nature **562**, 7727, 355 (2018).

[33] T. S. Roussy *et al.*, Science **381**, 6653, adg4084 (2023), [arXiv:2212.11841].

[34] G. W. Bennett *et al.* (Muon (g-2)), Phys. Rev. **D80**, 052008 (2009), [arXiv:0811.1207].

[35] C. Abel *et al.* (nEDM), Phys. Rev. Lett. **124**, 8, 081803 (2020), [arXiv:2001.11966].

[36] B. Graner *et al.*, Phys. Rev. Lett. **116**, 16, 161601 (2016), [Erratum: Phys. Rev. Lett.119,no.11,119901(2017)], [arXiv:1601.04339].

[37] F. Allmendinger *et al.*, Phys. Rev. **A100**, 2, 022505 (2019), [arXiv:1904.12295].

[38] C. Jarlskog, Phys. Rev. Lett. **55**, 1039 (1985); C. Jarlskog, Z. Phys. **C29**, 491 (1985).

[39] E. P. Shabalin, Sov. J. Nucl. Phys. **28**, 75 (1978), [Yad. Fiz.28,151(1978)].

[40] E. P. Shabalin, Sov. Phys. Usp. **26**, 297 (1983), [Usp. Fiz. Nauk139,561(1983)].

[41] W. Bernreuther and M. Suzuki, Rev. Mod. Phys. **63**, 313 (1991), [Erratum: Rev. Mod. Phys.64,633(1992)].

[42] M. Pospelov and A. Ritz, Phys. Rev. **D89**, 5, 056006 (2014), [arXiv:1311.5537].

[43] C.-Y. Seng, Phys. Rev. **C91**, 2, 025502 (2015), [arXiv:1411.1476].

[44] B. Grzadkowski *et al.*, JHEP **10**, 085 (2010), [arXiv:1008.4884].

[45] S. Mantry, M. Pitschmann and M. J. Ramsey-Musolf, Phys. Rev. **D90**, 5, 054016 (2014), [arXiv:1401.7339].

[46] B. K. Sahoo, Phys. Rev. **D95**, 1, 013002 (2017), [arXiv:1612.09371].

[47] T. Fleig and M. Jung, JHEP **07**, 012 (2018), [arXiv:1802.02171].

[48] J. Bsaisou *et al.*, Annals Phys. **359**, 317 (2015), [arXiv:1412.5471].

[49] J. de Vries *et al.*, Annals Phys. **338**, 50 (2013), [arXiv:1212.0990].

[50] L. I. Schiff, Phys. Rev. **132**, 2194 (1963).

[51] T. Chupp and M. Ramsey-Musolf, Phys. Rev. **C91**, 3, 035502 (2015), [arXiv:1407.1064].

[52] J. Beringer *et al.* (Particle Data Group), Phys. Rev. **D86**, 010001 (2012).

[53] A. Angelopoulos *et al.* (CPLEAR), Phys. Lett. **B471**, 332 (1999).

[54] R. Carosi *et al.* (NA31), Phys. Lett. B **237**, 303 (1990).

[55] M. S. Fee *et al.*, Phys. Rev. **A48**, 192 (1993).

[56] R. J. Hughes and B. I. Deutch, Phys. Rev. Lett. **69**, 578 (1992).

[57] S. Ulmer *et al.* (BASE), Nature **524**, 7564, 196 (2015).

[58] M. J. Borchert *et al.* (BASE), Nature **601**, 7891, 53 (2022).

[59] R. S. Van Dyck, P. B. Schwinberg and H. G. Dehmelt, Phys. Rev. Lett. **59**, 26 (1987).

[60] G. W. Bennett *et al.* (Muon g-2), Phys. Rev. Lett. **92**, 161802 (2004), [hep-ex/0401008].

[61] C. Smorra *et al.* (BASE), Nature **550**, 7676, 371 (2017).

[62] M. Ahmadi *et al.*, Nature **557**, 7703, 71 (2018).

[63] O. W. Greenberg, Phys. Rev. Lett. **89**, 231602 (2002), [hep-ph/0201258].

[64] S. Liberati, Class. Quant. Grav. **30**, 133001 (2013), [arXiv:1304.5795].

[65] V. A. Kostelecky and N. Russell, Rev. Mod. Phys. **83**, 11 (2011), [arXiv:0801.0287].

[66] D. Colladay and V. A. Kostelecky, Phys. Rev. **D58**, 116002 (1998), [hep-ph/9809521].

[67] S. Weinberg, Phys. Rev. Lett. **43**, 1566 (1979).

[68] F. Wilczek and A. Zee, Phys. Rev. Lett. **43**, 1571 (1979).

[69] L. F. Abbott and M. B. Wise, Phys. Rev. **D22**, 2208 (1980).

[70] M. Agostini *et al.* (Borexino), Phys. Rev. Lett. **115**, 231802 (2015), [arXiv:1509.01223].

[71] E. B. Norman, J. N. Bahcall and M. Goldhaber, Phys. Rev. **D53**, 4086 (1996).

[72] G. Bressi *et al.*, Phys. Rev. **A83**, 5, 052101 (2011), [arXiv:1102.2766].

[73] C. Caprini, S. Biller and P. G. Ferreira, JCAP **0502**, 006 (2005), [hep-ph/0310066].

[74] B. Altschul, Phys. Rev. Lett. **98**, 261801 (2007), [hep-ph/0703126].

[75] A. de Gouvea, Private Communication (2019).

[76] A. de Gouvea and P. Vogel, Prog. Part. Nucl. Phys. **71**, 75 (2013), [arXiv:1303.4097].

[77] S. T. Petcov, Sov. J. Nucl. Phys. **25**, 340 (1977), [Erratum: Yad. Fiz.25,1336(1977)].

[78] W. J. Marciano and A. I. Sanda, Phys. Lett. **67B**, 303 (1977).

[79] S. M. Bilenky, S. T. Petcov and B. Pontecorvo, Phys. Lett. **67B**, 309 (1977).

[80] T.-P. Cheng and L.-F. Li, Phys. Rev. **D16**, 1425 (1977).

[81] B. W. Lee and R. E. Shrock, Phys. Rev. **D16**, 1444 (1977).

[82] B. W. Lee *et al.*, Phys. Rev. Lett. **38**, 937 (1977), [Erratum: Phys. Rev. Lett.38,1230(1977)].

[83] R. H. Bernstein and P. S. Cooper, Phys. Rept. **532**, 27 (2013), [arXiv:1307.5787].

[84] L. Calibbi and G. Signorelli, Riv. Nuovo Cim. **41**, 2, 71 (2018), [arXiv:1709.00294].

[85] K. Afanaciev *et al.* (MEG II), Eur. Phys. J. C **85**, 10, 1177 (2025), [Erratum: Eur.Phys.J.C 85, 1317 (2025)], [arXiv:2504.15711].

[86] U. Bellgardt *et al.* (SINDRUM), Nucl. Phys. **B299**, 1 (1988).

[87] W. H. Bertl *et al.* (SINDRUM II), Eur. Phys. J. **C47**, 337 (2006).

[88] S. Banerjee *et al.* (Heavy Flavor Averaging Group (HFLAV)) (2024), [arXiv:2411.18639].

[89] A. M. Sirunyan *et al.* (CMS), Phys. Rev. D **104**, 3, 032013 (2021), [arXiv:2105.03007].

[90] R. Kitano, M. Koike and Y. Okada, Phys. Rev. **D66**, 096002 (2002), [Erratum: Phys. Rev.D76,059902(2007)], [hep-ph/0203110].

[91] A. Pich, Prog. Part. Nucl. Phys. **75**, 41 (2014), [arXiv:1310.7922].

Int. J. Mod. Phys. A 2026.41. Downloaded from www.worldscientific.com
by UNIVERSITY OF CALIFORNIA @ BERKELEY on 09/16/26. Re-use and distribution is strictly not permitted, except for Open Access

[92] W. Altmannshofer *et al.* (Belle-II), PTEP **2019**, 12, 123C01 (2019), [arXiv:1808.10567].

[93] D. Ambrose *et al.* (BNL), Phys. Rev. Lett. **81**, 5734 (1998), [hep-ex/9811038].

[94] A. Sher *et al.*, Phys. Rev. **D72**, 012005 (2005), [hep-ex/0502020].

[95] R. Aaij *et al.* (LHCb), JHEP **03**, 078 (2018), [arXiv:1710.04111].

[96] R. Aaij *et al.* (LHCb), Phys. Lett. **B754**, 167 (2016), [arXiv:1512.00322].

[97] G. Aad *et al.* (ATLAS), Nature Phys. **17**, 7, 819 (2021), [arXiv:2105.12491].

[98] A. Hayrapetyan *et al.* (CMS), Phys. Rev. D **112**, 11, 112011 (2025), [arXiv:2508.07512].

[99] G. Aad *et al.* (ATLAS), Phys. Lett. **B801**, 135148 (2020), [arXiv:1909.10235].

[100] G. Aad *et al.* (ATLAS), Phys. Lett. **B800**, 135069 (2020), [arXiv:1907.06131].

[101] A. M. Sirunyan *et al.* (CMS), JHEP **06**, 001 (2018), [arXiv:1712.07173].

[102] G. Aad *et al.* (ATLAS), JHEP **07**, 166 (2023), [arXiv:2302.05225].

[103] A. Hayrapetyan *et al.* (CMS), Phys. Rev. D **108**, 7, 072004 (2023), [arXiv:2305.18106].

[104] S. Dell'Oro *et al.*, Adv. High Energy Phys. **2016**, 2162659 (2016), [arXiv:1601.07512].

[105] J. Engel and J. Menéndez, Rept. Prog. Phys. **80**, 4, 046301 (2017), [arXiv:1610.06548].

[106] S. Abe *et al.* (KamLAND-Zen), Phys. Rev. Lett. **135**, 26, 262501 (2025), [arXiv:2406.11438].

[107] P. Fileviez Perez, Phys. Rept. **597**, 1 (2015), [arXiv:1501.01886].

[108] G. Aad *et al.* (ATLAS), Eur. Phys. J. C **83**, 12, 1164 (2023), [arXiv:2304.09553].

[109] A. Tumasyan *et al.* (CMS), JHEP **04**, 047 (2022), [arXiv:2112.03949].

[110] J. Kaulard *et al.* (SINDRUM II), Phys. Lett. **B422**, 334 (1998).

[111] Y. Miyazaki *et al.* (Belle), Phys. Lett. **B719**, 346 (2013), [arXiv:1206.5595].

[112] E. Cortina Gil *et al.* (NA62), Phys. Lett. **B797**, 134794 (2019), [arXiv:1905.07770].

[113] R. Aaij *et al.* (LHCb), JHEP **06**, 044 (2021), [arXiv:2011.00217].

[114] R. Aaij *et al.* (LHCb), Phys. Rev. Lett. **112**, 13, 131802 (2014), [arXiv:1401.5361].

[115] A. Abada *et al.*, JHEP **02**, 169 (2018), [arXiv:1712.03984].

[116] A. Allega *et al.* (SNO+), Phys. Rev. D **105**, 11, 112012 (2022), [arXiv:2205.06400].

[117] A. Takenaka *et al.* (Super-Kamiokande), Phys. Rev. D **102**, 11, 112011 (2020), [arXiv:2010.16098].

[118] M. Baldo-Ceolin *et al.*, Z. Phys. **C63**, 409 (1994).

[119] K. Abe *et al.* (Super-Kamiokande), Phys. Rev. D **103**, 1, 012008 (2021), [arXiv:2012.02607].

[120] D. G. Phillips, II *et al.*, Phys. Rept. **612**, 1 (2016), [arXiv:1410.1100].

[121] G. Abbiendi *et al.* (OPAL), Phys. Lett. **B447**, 157 (1999), [hep-ex/9901011].

[122] D. Sahoo *et al.* (Belle), Phys. Rev. D **102**, 111101 (2020), [arXiv:2010.15361].

[123] R. Aaij *et al.* (LHCb), Phys. Rev. D **108**, 1, 012021 (2023), [arXiv:2210.10412].

[124] P. Bloch *et al.* (Geneva-Saclay), Phys. Lett. **60B**, 393 (1976).

[125] A. Angelopoulos *et al.* (CPLEAR), Phys. Lett. **B444**, 38 (1998).

[126] A. Angelopoulos *et al.* (CPLEAR), Eur. Phys. J. **C22**, 55 (2001).

[127] R. Aaij *et al.* (LHCb), Phys. Rev. Lett. **127**, 11, 111801 (2021), [arXiv:2106.03744].

[128] A. A. Petrov, Int. J. Mod. Phys. **A21**, 5686 (2006), [hep-ph/0611361].

[129] D. Ambrose *et al.* (BNL E871), Phys. Rev. Lett. **81**, 4309 (1998), [hep-ex/9810007].

[130] V. Cirigliano *et al.*, Rev. Mod. Phys. **84**, 399 (2012), [arXiv:1107.6001].

[131] F. Ambrosino *et al.* (KLOE), Phys. Lett. **B672**, 203 (2009), [arXiv:0811.1007].

[132] R. Aaij *et al.* (LHCb), Phys. Rev. Lett. **125**, 23, 231801 (2020), [arXiv:2001.10354].

[133] E. Cortina Gil *et al.* (NA62), JHEP **02**, 191 (2025), [arXiv:2412.12015].

[134] J. Brod, M. Gorbahn and E. Stamou, Phys. Rev. **D83**, 034030 (2011), [arXiv:1009.0947].

[135] J. Brod, M. Gorbahn and E. Stamou, PoS **BEAUTY2020**, 056 (2021), [arXiv:2105.02868].

[136] J. K. Ahn *et al.* (KOTO), Phys. Rev. Lett. **134**, 8, 081802 (2025), [arXiv:2411.11237].

[137] V. Chekhovsky *et al.* (CMS), Phys. Rev. Lett. **135**, 15, 151803 (2025), [arXiv:2506.06152].

[138] A. Tumasyan *et al.* (CMS), Phys. Lett. B **842**, 137955 (2023), [arXiv:2212.10311].

Int. J. Mod. Phys. A 2026.41. Downloaded from www.worldscientific.com
by UNIVERSITY OF CALIFORNIA @ BERKELEY on 09/16/26. Re-use and distribution is strictly not permitted, except for Open Access articles.

TESTS OF DISCRETE SPACE-TIME SYMMETRIES

CHARGE CONJUGATION (C) INVARIANCE

$\Gamma(\pi^0 \to 3\gamma)/\Gamma_{total}$		$<3.1 \times 10^{-8}$, CL = 90%
η C-nonconserving decay parameters		
$\pi^+\pi^-\pi^0$ left-right asymmetry		$(0.09^{+0.11}_{-0.12}) \times 10^{-2}$
$\pi^+\pi^-\pi^0$ sextant asymmetry		$(0.12^{+0.10}_{-0.11}) \times 10^{-2}$
$\pi^+\pi^-\pi^0$ quadrant asymmetry		$(-0.09 \pm 0.09) \times 10^{-2}$
$\pi^+\pi^-\gamma$ left-right asymmetry		$(0.9 \pm 0.4) \times 10^{-2}$
$\pi^+\pi^-\gamma$ parameter β (D-wave)		-0.02 ± 0.07 (S = 1.3)
$\Gamma(\eta \to \pi^0\gamma)/\Gamma_{total}$	[a]	$<9 \times 10^{-5}$, CL = 90%
$\Gamma(\eta \to 2\pi^0\gamma)/\Gamma_{total}$		$<5 \times 10^{-4}$, CL = 90%
$\Gamma(\eta \to 3\pi^0\gamma)/\Gamma_{total}$		$<6 \times 10^{-5}$, CL = 90%
$\Gamma(\eta \to 3\gamma)/\Gamma_{total}$		$<1.6 \times 10^{-5}$, CL = 90%
$\Gamma(\eta \to \pi^0 e^+e^-)/\Gamma_{total}$	[b]	$<8 \times 10^{-6}$, CL = 90%
$\Gamma(\eta \to \pi^0\mu^+\mu^-)/\Gamma_{total}$	[b]	$<5 \times 10^{-6}$, CL = 90%
$\Gamma(\omega(782) \to \eta\pi^0)/\Gamma_{total}$		$<2.1 \times 10^{-4}$, CL = 90%
$\Gamma(\omega(782) \to 2\pi^0)/\Gamma_{total}$		$<2.2 \times 10^{-4}$, CL = 90%
$\Gamma(\omega(782) \to 3\pi^0)/\Gamma_{total}$		$<2.3 \times 10^{-4}$, CL = 90%
$\eta'(958) \to \pi^+\pi^-\gamma$ decay asymmetry parameter		-0.03 ± 0.04
$\Gamma(\eta'(958) \to \pi^0 e^+e^-)/\Gamma_{total}$	[b]	$<1.4 \times 10^{-3}$, CL = 90%
$\Gamma(\eta'(958) \to \pi^0\rho^0)/\Gamma_{total}$		$<4 \times 10^{-2}$, CL = 90%
$\Gamma(\eta'(958) \to \eta e^+e^-)/\Gamma_{total}$	[b]	$<2.4 \times 10^{-3}$, CL = 90%
$\Gamma(\eta'(958) \to 3\gamma)/\Gamma_{total}$		$<1.0 \times 10^{-4}$, CL = 90%
$\Gamma(\eta'(958) \to \mu^+\mu^-\pi^0)/\Gamma_{total}$	[b]	$<6.0 \times 10^{-5}$, CL = 90%
$\Gamma(\eta'(958) \to \mu^+\mu^-\eta)/\Gamma_{total}$	[b]	$<1.5 \times 10^{-5}$, CL = 90%
$\Gamma(J/\psi(1S) \to \gamma\gamma)/\Gamma_{total}$		$<2.7 \times 10^{-7}$, CL = 90%
$\Gamma(J/\psi(1S) \to \gamma\phi)/\Gamma_{total}$		$<1.4 \times 10^{-6}$, CL = 90%

PARITY (P) INVARIANCE

e electric dipole moment		$<0.041 \times 10^{-28}$ $e$cm, CL = 90%
μ electric dipole moment $\lvert d \rvert$		$<1.8 \times 10^{-19}$ $e$cm, CL = 95%
Re($d_\tau = \tau$ electric dipole moment)		-0.185 to 0.061×10^{-16} $e$cm, CL = 95%
$\Gamma(\eta \to \pi^+\pi^-)/\Gamma_{total}$		$<4.4 \times 10^{-6}$, CL = 90%
$\Gamma(\eta \to 2\pi^0)/\Gamma_{total}$		$<3.5 \times 10^{-4}$, CL = 90%
$\Gamma(\eta \to 4\pi^0)/\Gamma_{total}$		$<6.9 \times 10^{-7}$, CL = 90%
$\Gamma(\eta'(958) \to \pi^+\pi^-)/\Gamma_{total}$		$<1.8 \times 10^{-5}$, CL = 90%
$\Gamma(\eta'(958) \to \pi^0\pi^0)/\Gamma_{total}$		$<4 \times 10^{-4}$, CL = 90%
$a_P(B^0 \to p\overline{p}K^+\pi^-)$		(1.5 ± 0.9)%
$\Gamma(\eta_c(1S) \to \pi^+\pi^-)/\Gamma_{total}$		$<1.0 \times 10^{-4}$, CL = 90%
$\Gamma(\eta_c(1S) \to \pi^0\pi^0)/\Gamma_{total}$		$<3.3 \times 10^{-5}$, CL = 90%
$\Gamma(\eta_c(1S) \to K^+K^-)/\Gamma_{total}$		$<5 \times 10^{-4}$, CL = 90%
$\Gamma(\eta_c(1S) \to K^0_S K^0_S)/\Gamma_{total}$		$<2.9 \times 10^{-4}$, CL = 90%
p electric dipole moment		$<0.021 \times 10^{-23}$ $e$cm
n electric dipole moment		$<0.18 \times 10^{-25}$ $e$cm, CL = 90%
Λ electric dipole moment		$<1.5 \times 10^{-16}$ $e$cm, CL = 95%
$a_P(\Lambda^0_b \to p\pi^-\pi^+\pi^-)$		(-4.0 ± 0.7)%
$a_P(\Lambda^0_b \to pK^-\pi^+\pi^-)$		(-0.6 ± 0.9)%
$a_P(\Lambda^0_b \to pK^-K^+\pi^-)$		(4 ± 5)%
$a_P(\Lambda^0_b \to pK^-K^+K^-)$		(-1.6 ± 1.5)%
$a_P(\Lambda^0_b \to pK^-\mu^+\mu^-)$		(-5 ± 5)%
$A_P(\Xi_b)$, $\Xi^-_b - \Xi^+_b$ production asymmetry		$(-2 \pm 4) \times 10^{-2}$
$a_P(\Xi^0_b \to pK^-K^-\pi^+)$		(-3 ± 5)%

TIME REVERSAL (T) INVARIANCE

e electric dipole moment		$<0.041 \times 10^{-28}$ $e$cm, CL = 90%
μ electric dipole moment $\lvert d \rvert$		$<1.8 \times 10^{-19}$ $e$cm, CL = 95%
μ decay parameters		
transverse e^+ polarization normal to plane of μ spin, e^+ momentum		$(-2 \pm 8) \times 10^{-3}$
α'/A		$(-10 \pm 20) \times 10^{-3}$
β'/A		$(2 \pm 7) \times 10^{-3}$
Re($d_\tau = \tau$ electric dipole moment)		-0.185 to 0.061×10^{-16} $e$cm, CL = 95%
P_T in $K^+ \to \pi^0\mu^+\nu_\mu$		$(-1.7 \pm 2.5) \times 10^{-3}$
P_T in $K^+ \to \mu^+\nu_\mu\gamma$		$(-0.6 \pm 1.9) \times 10^{-2}$
Im(ξ) in $K^+ \to \pi^0\mu^+\nu_\mu$ decay (from transverse μ pol.)		-0.006 ± 0.008
asymmetry A_T in K^0-$\overline{K}^0$ mixing		$(6.6 \pm 1.6) \times 10^{-3}$
Im(ξ) in $K^0_{\mu 3}$ decay (from transverse μ pol.)		-0.007 ± 0.026
$A_T(D^\pm \to K^0_S K^\pm\pi^+\pi^-)$	[c]	$(-3 \pm 8) \times 10^{-3}$ (S = 1.1)
$A_T(D^0 \to K^+K^-\pi^+\pi^-)$	[c]	$(2.9 \pm 2.2) \times 10^{-3}$
$A_T(D^\pm_s \to K^0_S K^\pm\pi^+\pi^-)$	[c]	$(-8 \pm 6) \times 10^{-3}$
ΔS^+_T $(S^-_{\ell^-,K^0_S} - S^+_{\ell^+,K^0_S})$		-1.37 ± 0.15
ΔS^-_T $(S^+_{\ell^-,K^0_S} - S^-_{\ell^+,K^0_S})$		1.17 ± 0.21
ΔC^+_T $(C^-_{\ell^-,K^0_S} - C^+_{\ell^+,K^0_S})$		0.10 ± 0.16
ΔC^-_T $(C^+_{\ell^-,K^0_S} - C^-_{\ell^+,K^0_S})$		0.04 ± 0.16
p electric dipole moment		$<0.021 \times 10^{-23}$ $e$cm
n electric dipole moment		$<0.18 \times 10^{-25}$ $e$cm, CL = 90%
$n \to pe^-\overline{\nu}_e$ decay parameters		
ϕ_{AV}, phase of g_A relative to g_V	[d]	$(180.017 \pm 0.026)^\circ$
triple correlation coefficient D	[e]	$(-1.2 \pm 2.0) \times 10^{-4}$
triple correlation coefficient R	[e]	0.004 ± 0.013
Λ electric dipole moment		$<1.5 \times 10^{-16}$ $e$cm, CL = 95%
triple correlation coefficient D for $\Sigma^- \to ne^-\overline{\nu}_e$		0.11 ± 0.10

CP INVARIANCE

Re(d^W_τ)		$<0.50 \times 10^{-17}$ $e$cm, CL = 95%
Im(d^W_τ)		$<1.1 \times 10^{-17}$ $e$cm, CL = 95%
δ (CP violating phase in neutrino mixing)		$1.21^{+0.19}_{-0.17}$ π rad (S = 1.2)
$\eta \to \pi^+\pi^-e^+e^-$ decay-plane asymmetry		$(-1.6 \pm 2.6) \times 10^{-2}$
$\Gamma(\eta \to \pi^+\pi^-)/\Gamma_{total}$		$<4.4 \times 10^{-6}$, CL = 90%
$\Gamma(\eta \to 2\pi^0)/\Gamma_{total}$		$<3.5 \times 10^{-4}$, CL = 90%
$\Gamma(\eta \to 4\pi^0)/\Gamma_{total}$		$<6.9 \times 10^{-7}$, CL = 90%
$\Gamma(\eta'(958) \to \pi^+\pi^-)/\Gamma_{total}$		$<1.8 \times 10^{-5}$, CL = 90%
$\Gamma(\eta'(958) \to \pi^0\pi^0)/\Gamma_{total}$		$<4 \times 10^{-4}$, CL = 90%
$K^\pm \to \mu^\pm\nu_\mu$ rate difference/sum		(-0.27 ± 0.21)%
$K^\pm \to \pi^\pm\pi^0$ rate difference/sum	[f]	(0.4 ± 0.6)%
$K^\pm \to \pi^\pm e^+e^-$ rate difference/sum		$(-2.2 \pm 1.6) \times 10^{-2}$
$K^\pm \to \pi^\pm\mu^+\mu^-$ rate difference/sum		0.010 ± 0.023
$K^\pm \to \pi^\pm\pi^0\gamma$ rate difference/sum		$(0.0 \pm 1.2) \times 10^{-3}$
$K^\pm \to \pi^\pm\pi^+\pi^-$ rate difference/sum		(0.04 ± 0.06)%
$K^\pm \to \pi^\pm\pi^0\pi^0$ rate difference/sum		(-0.02 ± 0.28)%
$K^\pm \to \pi^\pm\pi^+\pi^-$ $(g_+ - g_-)$ / $(g_+ + g_-)$		$(-1.5 \pm 2.2) \times 10^{-4}$
$K^\pm \to \pi^\pm\pi^0\pi^0$ $(g_+ - g_-)$ / $(g_+ + g_-)$		$(1.8 \pm 1.8) \times 10^{-4}$
$A_S = [\,\Gamma(K^0_S \to \pi^-e^+\nu_e) - \Gamma(K^0_S \to \pi^+e^-\overline{\nu}_e)\,]$ / SUM		$(-4 \pm 6) \times 10^{-3}$
Im(η_{+-0}) = Im(A($K^0_S \to \pi^+\pi^-\pi^0$, CP-violating) / A($K^0_L \to \pi^+\pi^-\pi^0$))		-0.002 ± 0.009
Im(η_{000}) = Im($A(K^0_S \to \pi^0\pi^0\pi^0)/A(K^0_L \to \pi^0\pi^0\pi^0)$)		-0.001 ± 0.016
$\lvert\eta_{000}\rvert = \lvert A(K^0_S \to 3\pi^0)/A(K^0_L \to 3\pi^0)\rvert$		<0.0088, CL = 90%
CP asymmetry A in $K^0_S \to \pi^+\pi^-e^+e^-$		(-0.4 ± 0.8)%
$\Gamma(K^0_S \to 3\pi^0)/\Gamma_{total}$		$<2.6 \times 10^{-8}$, CL = 90%
linear coefficient j for $K^0_L \to \pi^+\pi^-\pi^0$		0.0012 ± 0.0008
quadratic coefficient f for $K^0_L \to \pi^+\pi^-\pi^0$		0.004 ± 0.006
$\lvert\epsilon'_{+-\gamma}\rvert/\epsilon$ for $K^0_L \to \pi^+\pi^-\gamma$		<0.3, CL = 90%
$\lvert g_{E1}\rvert$ for $K^0_L \to \pi^+\pi^-\gamma$		<0.21, CL = 90%
$\Gamma(K^0_L \to \pi^0\mu^+\mu^-)/\Gamma_{total}$	[g]	$<3.8 \times 10^{-10}$, CL = 90%
$\Gamma(K^0_L \to \pi^0e^+e^-)/\Gamma_{total}$	[g]	$<2.8 \times 10^{-10}$, CL = 90%
$\Gamma(K^0_L \to \pi^0\nu\overline{\nu})/\Gamma_{total}$	[h]	$<2.2 \times 10^{-9}$, CL = 90%
$A_{CP}(D^\pm \to \mu^\pm\nu)$		(8 ± 8)%
$A_{CP}(D^\pm \to K^0_L e^\pm\nu)$		(-0.6 ± 1.6)%
$A_{CP}(D^\pm \to K^0_S\pi^\pm)$		(-0.41 ± 0.09)%
$A_{CP}(D^\pm \to K^\mp 2\pi^\pm)$		(-0.18 ± 0.16)%
$A_{CP}(D^\pm \to K^\mp\pi^\pm\pi^\pm\pi^0)$		(-0.3 ± 0.7)%
$A_{CP}(D^\pm \to K^0_S\pi^\pm\pi^0)$		(-0.1 ± 0.7)%
$A_{CP}(D^\pm \to K^0_S\pi^\pm\pi^+\pi^-)$		(0.0 ± 1.2)%
$A_{CP}(D^\pm \to \pi^\pm\pi^0)$		(-0.5 ± 1.0)% (S = 1.7)
$A_{CP}(D^\pm \to \pi^\pm\eta)$		(0.3 ± 0.5)%
$A_{CP}(D^\pm \to \pi^\pm\eta'(958))$		(0.41 ± 0.23)% (S = 1.2)
$A_{CP}(D^\pm \to \overline{K}^0/K^0K^\pm)$		(0.11 ± 0.17)%

Int. J. Mod. Phys. A 2026.41. Downloaded from www.worldscientific.com
by UNIVERSITY OF CALIFORNIA @ BERKELEY on 09/16/26. Re-use and distribution is strictly not permitted, except for Open Acce

$A_{CP}(D^{\pm} \to K^0_S K^{\pm})$		$(-0.01 \pm 0.07)\%$
$A_{CP}(D^{\pm} \to K^+ K^- \pi^{\pm})$		$(0.37 \pm 0.29)\%$
$A_{CP}(D^{\pm} \to K^{\pm} K^{*0})$		$(-0.3 \pm 0.4)\%$
$A_{CP}(D^{\pm} \to \phi \pi^{\pm})$		$(0.01 \pm 0.09)\%$ (S = 1.8)
$A_{CP}(D^{\pm} \to K^{\pm} K^*_0(1430)^0)$		$(8^{+7}_{-6})\%$
$A_{CP}(D^{\pm} \to K^{\pm} K^*_2(1430)^0)$		$(43^{+20}_{-26})\%$
$A_{CP}(D^{\pm} \to K^{\pm} K^*_0(700))$		$(-12^{+18}_{-13})\%$
$A_{CP}(D^{\pm} \to a_0(1450)^0 \pi^{\pm})$		$(-19^{+14}_{-16})\%$
$A_{CP}(D^{\pm} \to \phi(1680) \pi^{\pm})$		$(-9 \pm 26)\%$
$A_{CP}(D^{\pm} \to \pi^+ \pi^- \pi^{\pm})$		$(0.5 \pm 2.0)\%$
$A_{CP}(D^{\pm} \to K^0_S K^{\pm} \pi^+ \pi^-)$		$(-4 \pm 7)\%$
$A_{CP}(D^{\pm} \to K^{\pm} \pi^0)$		$(-3 \pm 5)\%$
Local CPV in $D^{\pm} \to \pi^+ \pi^- \pi^{\pm}$		78.1%
Local CPV in $D^{\pm} \to K^+ K^- \pi^{\pm}$		31%
Local CPV in $D^{\pm} \to K^+ K^- K^{\pm}$		31.6%
$\lvert q/p \rvert$ of D^0–$\overline{D}^0$ mixing		0.995 ± 0.016
A_{Γ} of D^0–$\overline{D}^0$ mixing		$(0.89 \pm 1.13) \times 10^{-4}$
CP-even fraction in $D^0 \to \pi^+ \pi^- \pi^0$ decays		$(94.2 \pm 0.7)\%$ (S = 1.9)
CP-even fraction in $D^0 \to \pi^+ \pi^- \pi^+ \pi^-$ decays		$(74.6 \pm 0.8)\%$
CP-even fraction in $D^0 \to K^+ K^- \pi^0$ decays		$(64.1 \pm 3.0)\%$ (S = 1.7)
Where there is ambiguity, the CP test is labelled by the D^0 decay mode.		
$A_{CP}(D^0 \to K^+ K^-)$		$(4 \pm 5) \times 10^{-4}$
$A_{CP}(D^0 \to K^0_S K^0_S)$		$(-0.9 \pm 1.2)\%$ (S = 1.7)
$A_{CP}(D^0 \to \pi^+ \pi^-)$		$(0.13 \pm 0.14)\%$
$A_{CP}(D^0 \to \pi^0 \pi^0)$		$(0.1 \pm 0.5)\%$
$A_{CP}(D^0 \to \rho \gamma)$		$(6 \pm 15) \times 10^{-2}$
$A_{CP}(D^0 \to \phi \gamma)$		$(-9 \pm 7) \times 10^{-2}$
$A_{CP}(D^0 \to \overline{K}^*(892)^0 \gamma)$		$(-0.3 \pm 2.0) \times 10^{-2}$
$A_{CP}(D^0 \to \pi^+ \pi^- \pi^0)$		$(0.4 \pm 0.4)\%$
$A_{CP}(D^0 \to \rho(770)^+ \pi^- \to \pi^+ \pi^- \pi^0)$	[i]	$(1.2 \pm 0.9)\%$
$A_{CP}(D^0 \to \rho(770)^0 \pi^0 \to \pi^+ \pi^- \pi^0)$	[i]	$(-3.1 \pm 3.0)\%$
$A_{CP}(D^0 \to \rho(770)^- \pi^+ \to \pi^+ \pi^- \pi^0)$	[i]	$(-1.0 \pm 1.7)\%$
$A_{CP}(D^0 \to \rho(1450)^+ \pi^- \to \pi^+ \pi^- \pi^0)$	[i]	$(0 \pm 70)\%$
$A_{CP}(D^0 \to \rho(1450)^0 \pi^0 \to \pi^+ \pi^- \pi^0)$	[i]	$(-20 \pm 40)\%$
$A_{CP}(D^0 \to \rho(1450)^- \pi^+ \to \pi^+ \pi^- \pi^0)$	[i]	$(6 \pm 9)\%$
$A_{CP}(D^0 \to \rho(1700)^+ \pi^- \to \pi^+ \pi^- \pi^0)$	[i]	$(-5 \pm 14)\%$
$A_{CP}(D^0 \to \rho(1700)^0 \pi^0 \to \pi^+ \pi^- \pi^0)$	[i]	$(13 \pm 9)\%$
$A_{CP}(D^0 \to \rho(1700)^- \pi^+ \to \pi^+ \pi^- \pi^0)$	[i]	$(8 \pm 11)\%$
$A_{CP}(D^0 \to f_0(980) \pi^0 \to \pi^+ \pi^- \pi^0)$	[i]	$(0 \pm 35)\%$
$A_{CP}(D^0 \to f_0(1370) \pi^0 \to \pi^+ \pi^- \pi^0)$	[i]	$(25 \pm 18)\%$
$A_{CP}(D^0 \to f_0(1500) \pi^0 \to \pi^+ \pi^- \pi^0)$	[i]	$(0 \pm 18)\%$
$A_{CP}(D^0 \to f_0(1710) \pi^0 \to \pi^+ \pi^- \pi^0)$	[i]	$(0 \pm 24)\%$
$A_{CP}(D^0 \to f_2(1270) \pi^0 \to \pi^+ \pi^- \pi^0)$	[i]	$(-4 \pm 6)\%$
$A_{CP}(D^0 \to \sigma(400) \pi^0 \to \pi^+ \pi^- \pi^0)$	[i]	$(6 \pm 8)\%$
$A_{CP}(\text{nonresonant } D^0 \to \pi^+ \pi^- \pi^0)$	[i]	$(-13 \pm 23)\%$
$A_{CP}(D^0, \overline{D}^0 \to 2\pi^+ 2\pi^-)$		$(0.5 \pm 1.2)\%$
$A_{CP}(D^0 \to a_1(1260)^+ \pi^- \to 2\pi^+ 2\pi^-)$		$(5 \pm 6)\%$
$A_{CP}(D^0 \to a_1(1260)^- \pi^+ \to 2\pi^+ 2\pi^-)$		$(14 \pm 18)\%$
$A_{CP}(D^0 \to \pi(1300)^+ \pi^- \to 2\pi^+ 2\pi^-)$		$(-2 \pm 15)\%$
$A_{CP}(D^0 \to \pi(1300)^- \pi^+ \to 2\pi^+ 2\pi^-)$		$(-6 \pm 30)\%$
$A_{CP}(D^0 \to a_1(1640)^+ \pi^- \to 2\pi^+ 2\pi^-)$		$(9 \pm 26)\%$
$A_{CP}(D^0 \to \pi_2(1670)^+ \pi^- \to 2\pi^+ 2\pi^-)$		$(7 \pm 18)\%$
$A_{CP}(D^0 \to \sigma f_0(1370) \to 2\pi^+ 2\pi^-)$		$(-15 \pm 19)\%$
$A_{CP}(D^0 \to \sigma \rho(770)^0 \to 2\pi^+ 2\pi^-)$		$(3 \pm 27)\%$
$A_{CP}(D^0 \to 2\rho(770)^0 \to 2\pi^+ 2\pi^-)$		$(-6 \pm 6)\%$
$A_{CP}(D^0 \to 2f_2(1270) \to 2\pi^+ 2\pi^-)$		$(-28 \pm 24)\%$
$A_{CP}(D^0 \to K^+ K^- \pi^0)$		$(-1.0 \pm 1.7)\%$
$A_{CP}(D^0 \to K^*(892)^+ K^- \to K^+ K^- \pi^0)$	[i]	$(-0.9 \pm 1.3)\%$
$A_{CP}(D^0 \to K^*(1410)^+ K^- \to K^+ K^- \pi^0)$	[i]	$(-21 \pm 24)\%$
$A_{CP}(D^0 \to (K^+ \pi^0)_S K^- \to K^+ K^- \pi^0)$	[i]	$(7 \pm 15)\%$
$A_{CP}(D^0 \to \phi(1020) \pi^0 \to K^+ K^- \pi^0)$	[i]	$(1.1 \pm 2.2)\%$
$A_{CP}(D^0 \to f_0(980) \pi^0 \to K^+ K^- \pi^0)$	[i]	$(-3 \pm 19)\%$
$A_{CP}(D^0 \to a_0(980)^0 \pi^0 \to K^+ K^- \pi^0)$	[i]	$(-5 \pm 16)\%$
$A_{CP}(D^0 \to f'_2(1525) \pi^0 \to K^+ K^- \pi^0)$	[i]	$(0 \pm 160)\%$
$A_{CP}(D^0 \to K^*(892)^- K^+ \to K^+ K^- \pi^0)$	[i]	$(-5 \pm 4)\%$
$A_{CP}(D^0 \to K^*(1410)^- K^+ \to K^+ K^- \pi^0)$	[i]	$(-17 \pm 29)\%$
$A_{CP}(D^0 \to (K^- \pi^0)_{S-wave} K^+ \to K^+ K^- \pi^0)$	[i]	$(-10 \pm 40)\%$
$A_{CP}(D^0 \to K^0_S \pi^0)$		$(-0.20 \pm 0.17)\%$
$A_{CP}(D^0 \to K^0_S \eta)$		$(0.5 \pm 0.5)\%$
$A_{CP}(D^0 \to K^0_S \eta')$		$(1.0 \pm 0.7)\%$
$A_{CP}(D^0 \to K^0_S \phi)$		$(-3 \pm 9)\%$
$A_{CP}(D^0 \to K^- \pi^+)$		$(0.2 \pm 0.5)\%$
$A_{CP}(D^0 \to K^+ \pi^-)$		$(-0.4 \pm 0.7)\%$ (S = 1.3)
$A_{CP}(D_{CP(\pm 1)} \to K^{\mp} \pi^{\pm})$		$(13.1 \pm 1.0)\%$
$A_{CP}(D^0 \to K^- \pi^+ \pi^0)$		$(0.1 \pm 0.5)\%$
$A_{CP}(D^0 \to K^+ \pi^- \pi^0)$		$(0 \pm 5)\%$
$A_{CP}(D^0 \to K^0_S \pi^+ \pi^-)$		$(-0.1 \pm 0.8)\%$
$A_{CP}(D^0 \to K^*(892)^- \pi^+ \to K^0_S \pi^+ \pi^-)$		$(0.4 \pm 0.5)\%$
$A_{CP}(D^0 \to K^*(892)^+ \pi^- \to K^0_S \pi^+ \pi^-)$		$(1 \pm 6)\%$
$A_{CP}(D^0 \to K^0_S \rho^0 \to K^0_S \pi^+ \pi^-)$		$(-0.1 \pm 0.5)\%$
$A_{CP}(D^0 \to K^0_S \omega \to K^0_S \pi^+ \pi^-)$		$(-13 \pm 7)\%$
$A_{CP}(D^0 \to K^0_S f_0(980) \to K^0_S \pi^+ \pi^-)$		$(-0.4 \pm 2.7)\%$
$A_{CP}(D^0 \to K^0_S f_2(1270) \to K^0_S \pi^+ \pi^-)$		$(-4 \pm 5)\%$
$A_{CP}(D^0 \to K^0_S f_0(1370) \to K^0_S \pi^+ \pi^-)$		$(-1 \pm 9)\%$
$A_{CP}(D^0 \to \overline{K}^0 \rho^0(1450) \to K^0_S \pi^+ \pi^-)$		$(-4 \pm 10)\%$
$A_{CP}(D^0 \to \overline{K}^0 f_0(600) \to K^0_S \pi^+ \pi^-)$		$(-3 \pm 5)\%$
$A_{CP}(D^0 \to K^*(1410)^- \pi^+ \to K^0_S \pi^+ \pi^-)$		$(-2 \pm 9)\%$
$A_{CP}(D^0 \to K^*_0(1430)^- \pi^+ \to K^0_S \pi^+ \pi^-)$		$(4 \pm 4)\%$
$A_{CP}(D^0 \to K^*_0(1430)^- \pi^+ \to K^0_S \pi^+ \pi^-)$		$(12 \pm 15)\%$
$A_{CP}(D^0 \to K^*_2(1430)^- \pi^+ \to K^0_S \pi^+ \pi^-)$		$(3 \pm 6)\%$
$A_{CP}(D^0 \to K^*_2(1430)^+ \pi^- \to K^0_S \pi^+ \pi^-)$		$(-10 \pm 32)\%$
$A_{CP}(D^0 \to K^- \pi^+ \pi^+ \pi^-)$		$(0.2 \pm 0.5)\%$
$A_{CP}(D^0 \to K^+ \pi^- \pi^+ \pi^-)$		$(-2 \pm 4)\%$
$A_{CP}(D^0 \to K^+ K^- \pi^+ \pi^-)$		$(1.3 \pm 1.7)\%$
$A_{CP}(D^0 \to K^*_1(1270)^+ K^- \to K^+ K^- \pi^+ \pi^-)$		$(-2.3 \pm 1.7)\%$
$A_{CP}(D^0 \to K^*_1(1270)^+ K^- \to K^{*0} \pi^+ K^-)$		$(-1 \pm 10)\%$
$A_{CP}(D^0 \to K^*_1(1270)^- K^+ \to \overline{K}^{*0} \pi^- K^+)$		$(-10 \pm 32)\%$
$A_{CP}(D^0 \to K^*_1(1270)^- K^+ \to K^+ K^- \pi^+ \pi^-)$		$(1.7 \pm 3.5)\%$
$A_{CP}(D^0 \to K^*_1(1270)^+ K^- \to \rho^0 K^+ K^-)$		$(-7 \pm 17)\%$
$A_{CP}(D^0 \to K^*_1(1270)^- K^+ \to \rho^0 K^- K^+)$		$(10 \pm 13)\%$
$A_{CP}(D^0 \to K_1(1400)^+ K^- \to K^+ K^- \pi^+ \pi^-)$		$(-4.4 \pm 2.1)\%$
$A_{CP}(D^0 \to K^*(1410)^+ K^- \to K^{*0} \pi^+ K^-)$		$(-20 \pm 17)\%$
$A_{CP}(D^0 \to K^*(1410)^- K^+ \to \overline{K}^{*0} \pi^- K^+)$		$(-1 \pm 14)\%$
$A_{CP}(D^0 \to K^*(1680)^+ K^- \to K^+ K^- \pi^+ \pi^-)$		$(-17 \pm 29)\%$
$A_{CP}(K^{*0} \overline{K}^{*0})$ in $D^0, \overline{D}^0 \to K^{*0} \overline{K}^{*0}$		$(-5 \pm 14)\%$
$A_{CP}(D^0 \to K^{*0} \overline{K}^{*0}$ S-wave)		$(-3.9 \pm 2.2)\%$
$A_{CP}(\phi \rho^0)$ in $D^0, \overline{D}^0 \to \phi \rho^0$		$(1 \pm 9)\%$
$A_{CP}(D^0 \to \phi \rho^0$ S-wave)		$(-3 \pm 5)\%$
$A_{CP}(D^0 \to \phi \rho^0$ D-wave)		$(-37 \pm 19)\%$
$A_{CP}(D^0 \to \phi(\pi^+ \pi^-)_{S-wave})$		$(6 \pm 6)\%$
$A_{CP}(D^0 \to K^*(892)^0 (K^- \pi^+)_{S-wave})$		$(-10 \pm 40)\%$
$A_{CP}(D^0 \to K^+ K^- \pi^+ \pi^-$ non-resonant)		$(8 \pm 20)\%$
$A_{CP}((K^- \pi^+)_{P-wave} (K^+ \pi^-)_{S-wave})$		$(3 \pm 11)\%$
Local CPV p-value in $D^0, \overline{D}^0 \to \pi^+ \pi^- \pi^0$		10.6%
Local CPV p-value in $D^0, \overline{D}^0 \to \pi^+ \pi^- \pi^+ \pi^-$		$(0.6 \pm 0.2)\%$
Local CPV p-value in $D^0, \overline{D}^0 \to K^0_S \pi^+ \pi^-$		96%

Unless otherwise stated, limits are given at the 90% confidence level, while errors are given as ± 1 standard deviation.

Int. J. Mod. Phys. A 2026.41. Downloaded from www.worldscientific.com
by UNIVERSITY OF CALIFORNIA @ BERKELEY on 09/16/26. Re-use and distribution is strictly not permitted, except for Open Access articles.

Local *CPV* p-value in $D^0, \overline{D}^0 \to K^+K^-\pi^0$	16.6%
Local *CPV* p-value in $D^0, \overline{D}^0 \to K^+K^-\pi^+\pi^-$	9.1%
$A_{CP}(D_s^\pm \to \mu^\pm\nu)$	(-0.2 ± 2.5)%
$A_{CP}(D_s^\pm \to K^\pm K_S^0)$	(0.07 ± 0.24)%
$A_{CP}(D_s^\pm \to K^+K^-\pi^\pm)$	(0.35 ± 0.34)%
$A_{CP}(D_s^\pm \to \phi\pi^\pm)$	(-0.38 ± 0.27)%
$A_{CP}(D_s^\pm \to K^\pm K_S^0\pi^0)$	(-0.9 ± 1.9)%
$A_{CP}(D_s^\pm \to 2K_S^0\pi^\pm)$	(1.3 ± 1.6)%
$A_{CP}(D_s^\pm \to K^+K^-\pi^\pm\pi^0)$	(-0.6 ± 0.9)%
$A_{CP}(D_s^\pm \to K^\pm K_S^0\pi^+\pi^-)$	(0.7 ± 2.9)% (S = 1.3)
$A_{CP}(D_s^\pm \to K_S^0K^\mp 2\pi^\pm)$	(0.7 ± 1.8)% (S = 1.3)
$A_{CP}(D_s^\pm \to \pi^+\pi^-\pi^\pm)$	(-0.9 ± 1.1)%
$A_{CP}(D_s^\pm \to \pi^\pm\eta)$	(0.24 ± 0.29)%
$A_{CP}(D_s^\pm \to \pi^\pm\pi^+\pi^-\eta)$	(2.4 ± 3.0)%
$A_{CP}(D_s^\pm \to \pi^\pm\eta')$	(-0.08 ± 0.17)% (S = 1.2)
$A_{CP}(D_s^\pm \to \eta\pi^\pm\pi^0)$	(0.9 ± 1.5)%
$A_{CP}(D_s^\pm \to \eta'\pi^\pm\pi^0)$	(-1.5 ± 2.5)%
$A_{CP}(D_s^\pm \to K^\pm\pi^0)$	(2 ± 4)% (S = 1.2)
$A_{CP}(D_s^\pm \to \overline{K}^0/K^0\pi^\pm)$	(0.4 ± 0.5)%
$A_{CP}(D_s^\pm \to K_S^0\pi^\pm)$	(0.20 ± 0.18)%
$A_{CP}(D_s^\pm \to K^\pm\pi^+\pi^-)$	(2.2 ± 1.9)%
$A_{CP}(D_s^\pm \to K^\pm\eta)$	(1.8 ± 1.9)%
$A_{CP}(D_s^\pm \to K^\pm\eta'(958))$	(6 ± 19)%
$A_{CP}(B^+ \to J/\psi(1S)K^+)$	$(1.8 \pm 3.0) \times 10^{-3}$ (S = 1.5)
$A_{CP}(B^+ \to J/\psi(1S)\pi^+)$	$(1.5 \pm 0.5) \times 10^{-2}$
$A_{CP}(B^+ \to J/\psi\rho^+)$	-0.05 ± 0.05
$A_{CP}(B^+ \to J/\psi K^*(892)^+)$	-0.048 ± 0.033
$A_{CP}(B^+ \to \eta_c K^+)$	-0.05 ± 0.05 (S = 1.5)
$A_{CP}(B^+ \to \psi(2S)\pi^+)$	0.03 ± 0.06
$A_{CP}(B^+ \to \psi(2S)K^+)$	0.004 ± 0.020 (S = 1.5)
$A_{CP}(B^+ \to \psi(2S)K^*(892)^+)$	0.08 ± 0.21
$A_{CP}(B^+ \to \chi_{c1}(1P)\pi^+)$	0.07 ± 0.18
$A_{CP}(B^+ \to \chi_{c0}K^+)$	-0.20 ± 0.18 (S = 1.5)
$A_{CP}(B^+ \to \chi_{c1}K^+)$	-0.009 ± 0.033
$A_{CP}(B^+ \to \chi_{c1}K^*(892)^+)$	0.5 ± 0.5
$A_{CP}(B^+ \to \overline{D}^0\pi^+)$	$(-3.2 \pm 3.5) \times 10^{-3}$
$A_{CP}(B^+ \to D_{CP(+1)}\pi^+)$	-0.0088 ± 0.0024
$A_{CP}(B^+ \to D_{CP(-1)}\pi^+)$	-0.003 ± 0.012
$A_{CP}([K^\mp\pi^\pm\pi^+\pi^-]_D\pi^+)$	0.070 ± 0.020
$A_{CP}(B^+ \to [\pi^+\pi^+\pi^-\pi^-]_D K^+)$	0.061 ± 0.013
$A_{CP}(B^+ \to [\pi^+\pi^-\pi^+\pi^-]_D K^*(892)^+)$	0.02 ± 0.11
$A_{CP}(B^+ \to [K^+K^-\pi^+\pi^-]_D K^+)$	0.095 ± 0.023
$A_{CP}(B^+ \to [K^+K^-\pi^+\pi^-]_D\pi^+)$	-0.009 ± 0.006
$A_{CP}(B^+ \to \overline{D}^0K^+)$	-0.018 ± 0.004
$A_{CP}([K^\mp\pi^\pm\pi^+\pi^-]_D K^+)$	-0.32 ± 0.04
$A_{CP}(B^+ \to [\pi^+\pi^+\pi^-\pi^-]_D\pi^+)$	$(-8.2 \pm 3.2) \times 10^{-3}$
$A_{CP}(B^+ \to [K^-\pi^+]_D K^+)$	-0.58 ± 0.21
$A_{CP}(B^+ \to [K^-\pi^+\pi^0]_D K^+)$	-0.27 ± 0.27 (S = 2.4)
$A_{CP}(B^+ \to [K^+\pi^-\pi^0]_D K^+)$	-0.024 ± 0.013
$A_{CP}(B^+ \to [K^+K^-\pi^0]_D K^+)$	0.07 ± 0.07
$A_{CP}(B^+ \to [\pi^+\pi^-\pi^0]_D K^+)$	0.11 ± 0.04
$A_{CP}(B^+ \to \overline{D}^0K^*(892)^+)$	-0.007 ± 0.019
$A_{CP}(B^+ \to [K^-\pi^+\pi^-\pi^+]_{\overline{D}}K^*(892)^+)$	-0.45 ± 0.25
$A_{CP}(B^+ \to [K^-\pi^+]_D\pi^+)$	0.00 ± 0.09
$A_{CP}(B^+ \to [K^-\pi^+\pi^0]_D\pi^+)$	0.08 ± 0.09
$A_{CP}(B^+ \to [K^+K^-\pi^0]_D\pi^+)$	-0.001 ± 0.019
$A_{CP}(B^+ \to [\pi^+\pi^-\pi^0]_D\pi^+)$	0.001 ± 0.010
$A_{CP}(B^+ \to [K^-\pi^+]_{(D\pi)}\pi^+)$	-0.09 ± 0.27
$A_{CP}(B^+ \to [K^-\pi^+]_{(D\gamma)}\pi^+)$	-0.7 ± 0.6
$A_{CP}(B^+ \to [K^-\pi^+]_{(D\pi)}K^+)$	0.8 ± 0.4
$A_{CP}(B^+ \to [K^-\pi^+]_{(D\gamma)}K^+)$	0.4 ± 1.0
$A_{CP}(B^+ \to [\pi^+\pi^-\pi^0]_D K^+)$	-0.02 ± 0.15
$A_{CP}(B^+ \to [K_S^0K^+\pi^-]_D K^+)$	0.00 ± 0.09 (S = 1.4)
$A_{CP}(B^+ \to [K_S^0K^-\pi^+]_D K^+)$	0.00 ± 0.07
$A_{CP}(B^+ \to [K_S^0K^-\pi^+]_D\pi^+)$	-0.003 ± 0.014
$A_{CP}(B^+ \to [K_S^0K^+\pi^-]_D\pi^+)$	-0.016 ± 0.025 (S = 1.5)
$A_{CP}(B^+ \to [K^*(892)^-K^+]_D K^+)$	0.08 ± 0.05
$A_{CP}(B^+ \to [K^*(892)^+K^-]_D K^+)$	0.07 ± 0.09
$A_{CP}(B^+ \to [K^*(892)^+K^-]_D\pi^+)$	0.007 ± 0.016
$A_{CP}(B^+ \to [K^*(892)^-K^+]_D\pi^+)$	-0.013 ± 0.020 (S = 1.9)
$A_{ADS}(B^+ \to [D\gamma]_{D^*}K^+)$	-0.6 ± 1.3
$A_{ADS}(B^+ \to [D\pi^0]_{D^*}K^+)$	0.72 ± 0.29
$A_{ADS}(B^+ \to [D\gamma]_{D^*}\pi^+)$	0.08 ± 0.13
$A_{ADS}(B^+ \to [D\pi^0]_{D^*}\pi^+)$	-0.14 ± 0.06
$A_{ADS}(B^+ \to [K^-\pi^+]_D K^+\pi^-\pi^+)$	-0.33 ± 0.35
$A_{ADS}(B^+ \to [K^-\pi^+]_D\pi^+\pi^-\pi^+)$	-0.01 ± 0.09
$A_{CP}(B^+ \to D_{CP(-1)}K^+)$	-0.14 ± 0.05
$A_{CP}(B^+ \to [K^+K^-]_D K^+\pi^-\pi^+)$	-0.04 ± 0.06
$A_{CP}(B^+ \to [\pi^+\pi^-]_D K^+\pi^-\pi^+)$	-0.05 ± 0.10
$A_{CP}(B^+ \to [K^-\pi^+]_D K^+\pi^-\pi^+)$	0.013 ± 0.023
$A_{CP}(B^+ \to [K^+K^-]_D\pi^+\pi^-\pi^+)$	-0.019 ± 0.015
$A_{CP}(B^+ \to [\pi^+\pi^-]_D\pi^+\pi^-\pi^+)$	-0.013 ± 0.019
$A_{CP}(B^+ \to [K^-\pi^+]_D\pi^+\pi^-\pi^+)$	-0.002 ± 0.011
$A_{CP}(B^+ \to [\overline{D}^0\pi^0]_{\overline{D}^*}\pi^+)$	0.0007 ± 0.0022
$A_{CP}(B^+ \to [\overline{D}^0\pi^0]_{D^*_{CP(+1)}}\pi^+)$	0.012 ± 0.008
$A_{CP}(B^+ \to [\overline{D}^0\pi^0]_{D^*_{CP(-1)}}\pi^+)$	-0.09 ± 0.05
$A_{CP}(B^+ \to [\overline{D}^0\pi^0]_{\overline{D}^{*0}}K^+)$	0.017 ± 0.007
$A_{CP}(B^+ \to [D^0\pi^0]_{D^*_{CP(+1)}}K^+)$	-0.115 ± 0.020
$A_{CP}(B^+ \to [D^0\pi^0]_{D^*_{CP(-1)}}K^+)$	0.07 ± 0.10
$A_{CP}(B^+ \to D_{CP(+1)}K^*(892)^+)$	0.08 ± 0.06
$A_{CP}(B^+ \to D_{CP(-1)}K^*(892)^+)$	-0.23 ± 0.22
$A_{CP}(B^+ \to D_s^+\phi)$	0.0 ± 0.4
$A_{CP}(B^+ \to D_s^+\overline{D}^0)$	(0.5 ± 0.6)%
$A_{CP}(B^+ \to D_s^{*+}\overline{D}^0)$	$(-0.5 \pm 1.5) \times 10^{-2}$
$A_{CP}(B^+ \to D_s^+\overline{D}^{*0})$	$(1.1 \pm 1.1) \times 10^{-2}$
$A_{CP}(B^+ \to D^{*+}\overline{D}^{*0})$	$(1.3 \pm 2.6) \times 10^{-2}$
$A_{CP}(B^+ \to D^{*+}\overline{D}^0)$	$(3.1 \pm 1.7) \times 10^{-2}$
$A_{CP}(B^+ \to D^+\overline{D}^{*0})$	$(0.0 \pm 2.4) \times 10^{-2}$
$A_{CP}(B^+ \to D^+\overline{D}^0)$	$(2.4 \pm 1.1) \times 10^{-2}$
$A_{CP}(B^+ \to K_S^0\pi^+)$	-0.003 ± 0.015 (S = 1.1)
$A_{CP}(B^+ \to K^+\pi^0)$	0.027 ± 0.012
$A_{CP}(B^+ \to \eta' K^+)$	0.004 ± 0.011
$A_{CP}(B^+ \to \eta' K^*(892)^+)$	-0.26 ± 0.27
$A_{CP}(B^+ \to \eta' K_0^*(1430)^+)$	0.06 ± 0.20
$A_{CP}(B^+ \to \eta' K_2^*(1430)^+)$	0.15 ± 0.13
$A_{CP}(B^+ \to \eta K^*(892)^+)$	0.02 ± 0.06
$A_{CP}(B^+ \to \eta K_0^*(1430)^+)$	0.05 ± 0.13
$A_{CP}(B^+ \to \eta K_2^*(1430)^+)$	-0.45 ± 0.30
$A_{CP}(B^+ \to \omega K^+)$	-0.02 ± 0.04
$A_{CP}(B^+ \to \omega K^{*+})$	0.29 ± 0.35
$A_{CP}(B^+ \to \omega(K\pi)_0^{*+})$	-0.10 ± 0.09
$A_{CP}(B^+ \to \omega K_2^*(1430)^+)$	0.14 ± 0.15
$A_{CP}(B^+ \to K^{*0}\pi^+)$	-0.021 ± 0.032 (S = 1.5)
$A_{CP}(B^+ \to K^*(892)^+\pi^0)$	-0.39 ± 0.21 (S = 1.6)
$A_{CP}(B^+ \to K^+\pi^-\pi^+)$	0.015 ± 0.006 (S = 1.4)
$A_{CP}(B^+ \to K^+K^-K^+$ nonresonant)	0.06 ± 0.05
$A_{CP}(B^+ \to f(980)^0K^+)$	-0.08 ± 0.09
$A_{CP}(B^+ \to f_2(1270)K^+)$	$-0.68^{+0.19}_{-0.17}$
$A_{CP}(B^+ \to f_0(1500)K^+)$	0.28 ± 0.30
$A_{CP}(B^+ \to f_2'(1525)^0K^+)$	$-0.08^{+0.05}_{-0.04}$
$A_{CP}(B^+ \to K^0\pi^+\pi^0)$	0.07 ± 0.06
$A_{CP}(B^+ \to K_0^*(1430)^0\pi^+)$	0.061 ± 0.032
$A_{CP}(B^+ \to K_0^*(1430)^+\pi^0)$	$0.26^{+0.18}_{-0.14}$
$A_{CP}(B^+ \to K_2^*(1430)^0\pi^+)$	$0.05^{+0.29}_{-0.24}$
$A_{CP}(B^+ \to K^+\pi^0\pi^0)$	-0.06 ± 0.07
$A_{CP}(B^+ \to K^0\rho^+)$	-0.03 ± 0.15
$A_{CP}(B^+ \to K^{*+}\pi^+\pi^-)$	0.07 ± 0.08
$A_{CP}(B^+ \to \rho^0K^*(892)^+)$	0.31 ± 0.13
$A_{CP}(B^+ \to K^*(892)^+f_0(980))$	-0.15 ± 0.12
$A_{CP}(B^+ \to a_1^+K^0)$	0.12 ± 0.11
$A_{CP}(B^+ \to b_1^+K^0)$	-0.03 ± 0.15
$A_{CP}(B^+ \to K^*(892)^0\rho^+)$	-0.01 ± 0.16

Unless otherwise stated, limits are given at the 90% confidence level, while errors are given as ± 1 standard deviation.

Tests of Conservation Laws

$A_{CP}(B^+ \to b_1^0 K^+)$	-0.46 ± 0.20
$A_{CP}(B^+ \to K^0 K^+)$	0.04 ± 0.14
$A_{CP}(B^+ \to K_S^0 K^+)$	-0.21 ± 0.14
$A_{CP}(B^+ \to K^+ K_S^0 K_S^0)$	0.025 ± 0.031
$A_{CP}(B^+ \to K^+ K^- \pi^+$ nonresonant)	-0.11 ± 0.06
$A_{CP}(B^+ \to \pi^+ K^+ K^-, m_{K^+K^-} < 1.1$ GeV)	-0.17 ± 0.07
$A_{CP}(B^+ \to K^+ \overline{K}^*(892)^0)$	0.04 ± 0.05
$A_{CP}(B^+ \to K^+ \overline{K}_0^*(1430)^0)$	0.10 ± 0.17
$A_{CP}(B^+ \to \phi\pi^+)$	0.1 ± 0.5
$A_{CP}(B^+ \to \phi K^+)$	0.017 ± 0.017 (S = 1.8)
$A_{CP}(B^+ \to X_0(1550) K^+)$	-0.04 ± 0.07
$A_{CP}(B^+ \to K^{*+} K^+ K^-)$	0.11 ± 0.09
$A_{CP}(B^+ \to \phi K^*(892)^+)$	-0.01 ± 0.08
$A_{CP}(B^+ \to \phi(K\pi)_0^{*+})$	0.04 ± 0.16
$A_{CP}(B^+ \to \phi K_1(1270)^+)$	0.15 ± 0.20
$A_{CP}(B^+ \to \phi K_2^*(1430)^+)$	-0.23 ± 0.20
$A_{CP}(B^+ \to K^+ \phi\phi)$	-0.08 ± 0.07
$A_{CP}(B^+ \to K^+[\phi\phi]_{\eta_c})$	0.10 ± 0.08
$A_{CP}(B^+ \to K^*(892)^+\gamma)$	0.008 ± 0.015
$A_{CP}(B^+ \to X_s\gamma)$	0.028 ± 0.019
$A_{CP}(B^+ \to \eta K^+\gamma)$	-0.12 ± 0.07
$A_{CP}(B^+ \to \phi K^+\gamma)$	-0.13 ± 0.11 (S = 1.1)
$A_{CP}(B^+ \to \rho^+\gamma)$	$(-9 \pm 14) \times 10^{-2}$
$A_{CP}(B^+ \to \pi^+\pi^0)$	-0.01 ± 0.04 (S = 1.1)
$A_{CP}(B^+ \to \pi^+\pi^0\pi^0)$	$(9 \pm 7) \times 10^{-2}$
$A_{CP}(B^+ \to \rho^0\pi^+)$	0.003 ± 0.014
$A_{CP}(B^+ \to \rho^0(1450)\pi^+)$	-0.11 ± 0.05
$A_{CP}(B^+ \to \rho_3(1690)\pi^+)$	-0.80 ± 0.28
$A_{CP}(B^+ \to f_0(1370)\pi^+)$	0.72 ± 0.22
$A_{CP}(B^+ \to \pi^+\pi^-\pi^+$ nonresonant)	$-0.14^{+0.23}_{-0.16}$
$A_{CP}(B^+ \to \rho^+\pi^0)$	0.03 ± 0.10
$A_{CP}(B^+ \to X\pi^+,\ X \to \pi^0\pi^0)$	0.18 ± 0.12
$A_{CP}(B^+ \to \rho^+\rho^0)$	-0.05 ± 0.05
$A_{CP}(B^+ \to \omega\pi^+)$	-0.04 ± 0.05
$A_{CP}(B^+ \to \omega\rho^+)$	-0.20 ± 0.09
$A_{CP}(B^+ \to \eta\pi^+)$	-0.14 ± 0.07 (S = 1.4)
$A_{CP}(B^+ \to \eta\rho^+)$	0.11 ± 0.11
$A_{CP}(B^+ \to \eta'\pi^+)$	0.06 ± 0.16
$A_{CP}(B^+ \to \eta'\rho^+)$	0.26 ± 0.17
$A_{CP}(B^+ \to b_1^0\pi^+)$	0.05 ± 0.16
$A_{CP}(B^+ \to p\overline{p}\pi^+)$	0.021 ± 0.030
$A_{CP}(B^+ \to p\overline{p}K^+)$	-0.02 ± 0.04 (S = 1.9)
$A_{CP}(B^+ \to p\overline{p}K^*(892)^+)$	0.21 ± 0.16 (S = 1.4)
$A_{CP}(B^+ \to p\overline{\Lambda}\gamma)$	0.17 ± 0.17
$A_{CP}(B^+ \to p\overline{\Lambda}\pi^0)$	0.01 ± 0.17
$A_{CP}(B^+ \to \overline{\Lambda}p\overline{p}p)$	$(5 \pm 16)\%$
$A_{CP}(B^+ \to K^+\ell^+\ell^-)$	-0.02 ± 0.08
$A_{CP}(B^+ \to K^+e^+e^-)$	0.14 ± 0.14
$A_{CP}(B^+ \to K^+\mu^+\mu^-)$	0.011 ± 0.017
$A_{CP}(B^+ \to \pi^+\mu^+\mu^-)$	-0.11 ± 0.12
$A_{CP}(B^+ \to K^{*+}\ell^+\ell^-)$	-0.09 ± 0.14
$A_{CP}(B^+ \to K^*e^+e^-)$	-0.14 ± 0.23
$A_{CP}(B^+ \to K^*\mu^+\mu^-)$	-0.12 ± 0.24
$r_B(B^+ \to D^0\pi^+)$	$(17 \pm 5) \times 10^{-3}$
$r_B(B^+ \to D^0K^{*+})$	$0.101^{+0.016}_{-0.036}$
$\delta_B(B^+ \to D^0K^{*+})$	$(47^{+61}_{-16})^\circ$
$\mathrm{Re}(\epsilon_{B^0})/(1+\lvert\epsilon_{B^0}\rvert^2)$	$(-0.5 \pm 0.4) \times 10^{-3}$
$A_{T/CP}(B^0 \leftrightarrow \overline{B}^0)$	0.005 ± 0.018
$A_{CP}(B^0 \to D^*(2010)^+D^-)$	0.013 ± 0.014
$A_{CP}(B^0 \to \overline{D}^0\pi^0)$	$(0.4 \pm 2.4) \times 10^{-2}$
$A_{CP}(B^0 \to [K^+K^-]_D K^*(892)^0)$	-0.05 ± 0.06
$A_{CP}(B^0 \to [K^+\pi^-]_D K^*(892)^0)$	0.031 ± 0.023
$A_{CP}(B^0 \to [K^+\pi^-\pi^+\pi^-]_D K^*(892)^0)$	-0.012 ± 0.024
$A_{CP}(B^0 \to [K^-\pi^+]_D K^*(892)^0)$	0.19 ± 0.19
$A_{CP}(B^0 \to [K^-\pi^+\pi^+\pi^-]_D K^*(892)^0)$	-0.01 ± 0.24
$R_d^+(B^0 \to [\pi^\pm K^\mp]_D K^{*0})$	0.069 ± 0.014
$R_d^-(\overline{B}^0 \to [\pi^\mp K^\pm]_D K^{*0})$	0.093 ± 0.014
$A_{CP}(B^0 \to [\pi^+\pi^-]_D K^*(892)^0)$	-0.03 ± 0.10
$A_{CP}(B^0 \to [\pi^+\pi^-\pi^+\pi^-]_D K^*(892)^0)$	0.02 ± 0.09
$R_d^+(B^0 \to [\pi^\pm K^\mp\pi^\pm\pi^\mp]_D K^{*0})$	0.060 ± 0.015
$R_d^-(\overline{B}^0 \to [\pi^\mp K^\pm\pi^\pm\pi^\mp]_D K^{*0})$	0.038 ± 0.015
$A_{CP}(B^0 \to \eta' K^*(892)^0)$	-0.07 ± 0.18
$A_{CP}(B^0 \to \eta' K_0^*(1430)^0)$	-0.19 ± 0.17
$A_{CP}(B^0 \to \eta' K_2^*(1430)^0)$	0.14 ± 0.18
$A_{CP}(B^0 \to \eta K_0^*(1430)^0)$	0.06 ± 0.13
$A_{CP}(B^0 \to \eta K_2^*(1430)^0)$	-0.07 ± 0.19
$A_{CP}(B^0 \to b_1 K^+)$	-0.07 ± 0.12
$A_{CP}(B^0 \to \omega K^{*0})$	0.45 ± 0.25
$A_{CP}(B^0 \to \omega(K\pi)_0^{*0})$	-0.07 ± 0.09
$A_{CP}(B^0 \to \omega K_2^*(1430)^0)$	-0.37 ± 0.17
$A_{CP}(B^0 \to K^+\pi^-\pi^0)$	$(0 \pm 6) \times 10^{-2}$
$A_{CP}(B^0 \to \rho^- K^+)$	0.20 ± 0.11
$A_{CP}(B^0 \to \rho(1450)^- K^+)$	-0.10 ± 0.33
$A_{CP}(B^0 \to \rho(1700)^- K^+)$	-0.4 ± 0.6
$A_{CP}(B^0 \to K^+\pi^-\pi^0$ nonresonant)	0.10 ± 0.18
$A_{CP}(B^0 \to K^0\pi^+\pi^-)$	-0.01 ± 0.05
$A_{CP}(B^0 \to (K\pi)_0^{*+}\pi^-)$	0.02 ± 0.04
$A_{CP}(B^0 \to K_2^*(1430)^+\pi^-)$	-0.29 ± 0.24
$A_{CP}(B^0 \to K^*(1680)^+\pi^-)$	-0.07 ± 0.14
$A_{CP}(B^0 \to f_0(980) K_S^0)$	0.28 ± 0.31
$A_{CP}(B^0 \to (K\pi)_0^{*0}\pi^0)$	-0.15 ± 0.11
$A_{CP}(B^0 \to K^{*0}\pi^0)$	-0.15 ± 0.13
$A_{CP}(B^0 \to K^*(892)^0\pi^+\pi^-)$	0.07 ± 0.05
$A_{CP}(B^0 \to K^*(892)^0\rho^0)$	-0.06 ± 0.09
$A_{CP}(B^0 \to K^{*0} f_0(980))$	0.07 ± 0.10
$A_{CP}(B^0 \to K^{*+}\rho^-)$	0.21 ± 0.15
$A_{CP}(B^0 \to K^*(892)^0 K^+K^-)$	0.01 ± 0.05
$A_{CP}(B^0 \to a_1^- K^+)$	-0.16 ± 0.12
$A_{CP}(B^0 \to K^0K^0)$	-0.6 ± 0.7
$A_{CP}(B^0 \to K^*(892)^0\phi)$	0.00 ± 0.04
$A_{CP}(B^0 \to K^*(892)^0 K^-\pi^+)$	0.2 ± 0.4
$A_{CP}(B^0 \to \phi(K\pi)_0^{*0})$	0.12 ± 0.08
$A_{CP}(B^0 \to \phi K_2^*(1430)^0)$	-0.11 ± 0.10
$A_{CP}(B^0 \to K^*(892)^0\gamma)$	-0.012 ± 0.010
$A_{CP}(B^0 \to K_2^*(1430)^0\gamma)$	-0.08 ± 0.15
$A_{CP}(B^0 \to X_s\gamma)$	-0.009 ± 0.018
$A_{CP}(B^0 \to \rho^+\pi^-)$	0.13 ± 0.06 (S = 1.1)
$A_{CP}(B^0 \to \rho^-\pi^+)$	-0.08 ± 0.08
$A_{CP}(B^0 \to a_1(1260)^\pm\pi^\mp)$	-0.07 ± 0.06
$A_{CP}(B^0 \to b_1^-\pi^+)$	-0.05 ± 0.10
$A_{CP}(B^0 \to p\overline{p}K^*(892)^0)$	0.05 ± 0.12
$A_{CP}(B^0 \to p\overline{\Lambda}\pi^-)$	0.04 ± 0.07
$A_{CP}(B^0 \to K^{*0}\ell^+\ell^-)$	-0.05 ± 0.10
$A_{CP}(B^0 \to K^{*0}e^+e^-)$	-0.21 ± 0.19
$A_{CP}(B^0 \to K^{*0}\mu^+\mu^-)$	-0.034 ± 0.024
$C_{D^*(2010)^-D^+}(B^0 \to D^*(2010)^-D^+)$	-0.02 ± 0.08
$C_{D^*(2010)^+D^-}(B^0 \to D^*(2010)^+D^-)$	-0.03 ± 0.09 (S = 1.1)
$C_{D^{*+}D^{*-}}(B^0 \to D^{*+}D^{*-})$	0.01 ± 0.09 (S = 1.6)
$C_+(B^0 \to D^{*+}D^{*-})$	0.00 ± 0.10 (S = 1.6)
$C_-(B^0 \to D^{*+}D^{*-})$	0.19 ± 0.31
$S_-(B^0 \to D^{*+}D^{*-})$	-1.6 ± 0.5
$C(B^0 \to D^*(2010)^+D^*(2010)^-K_S^0)$	0.01 ± 0.29
$S(B^0 \to D^*(2010)^+D^*(2010)^-K_S^0)$	0.1 ± 0.4
$C_{D^+D^-}(B^0 \to D^+D^-)$	-0.06 ± 0.18 (S = 2.5)
$C_{J/\psi(1S)\pi^0}(B^0 \to J/\psi(1S)\pi^0)$	0.07 ± 0.09 (S = 1.1)
$C(B^0 \to J/\psi(1S)\rho^0)$	-0.06 ± 0.06
$C_{D_{CP}^{(*)}h^0}(B^0 \to D_{CP}^{(*)}h^0)$	-0.02 ± 0.08
$S_{D_{CP}^{(*)}h^0}(B^0 \to D_{CP}^{(*)}h^0)$	-0.66 ± 0.12
$C_{K^0\pi^0}(B^0 \to K^0\pi^0)$	0.00 ± 0.08
$C_{\eta'(958)K_S^0}(B^0 \to \eta'(958)K_S^0)$	-0.04 ± 0.20 (S = 2.5)
$S_{\eta'(958)K_S^0}(B^0 \to \eta'(958)K_S^0)$	0.43 ± 0.17 (S = 1.5)
$C_{\eta'K^0}(B^0 \to \eta'K^0)$	-0.08 ± 0.04 (S = 1.1)
$C_{\omega K_S^0}(B^0 \to \omega K_S^0)$	0.0 ± 0.4 (S = 3.0)
$S_{\omega K_S^0}(B^0 \to \omega K_S^0)$	0.70 ± 0.21

Unless otherwise stated, limits are given at the 90% confidence level, while errors are given as ± 1 standard deviation.

Int. J. Mod. Phys. A 2026.41. Downloaded from www.worldscientific.com
by UNIVERSITY OF CALIFORNIA @ BERKELEY on 09/16/26. Re-use and distribution is strictly not permitted, except for Open Acce

Int. J. Mod. Phys. A 2026.41. Downloaded from www.worldscientific.com
by UNIVERSITY OF CALIFORNIA @ BERKELEY on 09/16/26. Re-use and distribution is strictly not permitted, except for Open Access articles.

$C\,(B^0 \to K^0_S \pi^0 \pi^0)$	-0.21 ± 0.20
$S\,(B^0 \to K^0_S \pi^0 \pi^0)$	$0.89^{+0.27}_{-0.30}$
$C_{\rho^0 K^0_S}\,(B^0 \to \rho^0 K^0_S)$	-0.04 ± 0.20
$S_{\rho^0 K^0_S}\,(B^0 \to \rho^0 K^0_S)$	$0.50^{+0.17}_{-0.21}$
$C_{f_0(980) K^0_S}\,(B^0 \to f_0(980) K^0_S)$	0.29 ± 0.20
$S_{f_0(980) K^0_S}\,(B^0 \to f_0(980) K^0_S)$	-0.50 ± 0.16
$S_{f_2(1270) K^0_S}\,(B^0 \to f_2(1270) K^0_S)$	-0.5 ± 0.5
$C_{f_2(1270) K^0_S}\,(B^0 \to f_2(1270) K^0_S)$	0.3 ± 0.4
$S_{f_x(1300) K^0_S}\,(B^0 \to f_x(1300) K^0_S)$	-0.2 ± 0.5
$C_{f_x(1300) K^0_S}\,(B^0 \to f_x(1300) K^0_S)$	0.13 ± 0.35
$S_{K^0 \pi^+ \pi^-}\,(B^0 \to K^0 \pi^+ \pi^-$ nonresonant$)$	-0.01 ± 0.33
$C_{K^0 \pi^+ \pi^-}\,(B^0 \to K^0 \pi^+ \pi^-$ nonresonant$)$	0.01 ± 0.26
$C_{K^0_S K^0_S}\,(B^0 \to K^0_S K^0_S)$	0.0 ± 0.4 (S = 1.4)
$S_{K^0_S K^0_S}\,(B^0 \to K^0_S K^0_S)$	-0.8 ± 0.5
$C_{K^+ K^- K^0_S}\,(B^0 \to K^+ K^- K^0_S$ nonresonant$)$	0.06 ± 0.08
$C_{K^+ K^- K^0_S}\,(B^0 \to K^+ K^- K^0_S$ inclusive$)$	0.01 ± 0.09
$C_{\phi K^0_S}\,(B^0 \to \phi K^0_S)$	-0.09 ± 0.12
$S_{\phi K^0_S}\,(B^0 \to \phi K^0_S)$	0.58 ± 0.12
$C_{K_S K_S K_S}(B^0 \to K_S K_S K_S)$	-0.14 ± 0.12
$S_{K_S K_S K_S}(B^0 \to K_S K_S K_S)$	-0.82 ± 0.17
$C_{K^0_S \pi^0 \gamma}(B^0 \to K^0_S \pi^0 \gamma)$	—
$S_{K^0_S \pi^0 \gamma}(B^0 \to K^0_S \pi^0 \gamma)$	—
$C_{K^*(892)^0 \gamma}\,(B^0 \to K^*(892)^0 \gamma)$	0.03 ± 0.10
$S_{K^*(892)^0 \gamma}\,(B^0 \to K^*(892)^0 \gamma)$	-0.08 ± 0.17
$C_{\eta K^0 \gamma}\,(B^0 \to \eta K^0 \gamma)$	0.1 ± 0.4 (S = 1.4)
$S_{\eta K^0 \gamma}\,(B^0 \to \eta K^0 \gamma)$	-0.5 ± 0.5 (S = 1.2)
$C_{K^0 \phi \gamma}\,(B^0 \to K^0 \phi \gamma)$	-0.3 ± 0.6
$S_{K^0 \phi \gamma}\,(B^0 \to K^0 \phi \gamma)$	$0.7^{+0.7}_{-1.1}$
$C(B^0 \to K^0_S \rho^0 \gamma)$	-0.05 ± 0.19
$S(B^0 \to K^0_S \rho^0 \gamma)$	-0.04 ± 0.23
$C\,(B^0 \to \rho^0 \gamma)$	0.4 ± 0.5
$S\,(B^0 \to \rho^0 \gamma)$	-0.8 ± 0.7
$C_{\pi^0 \pi^0}(B^0 \to \pi^0 \pi^0)$	-0.23 ± 0.18
$C_{\rho\pi}\,(B^0 \to \rho^+ \pi^-)$	-0.03 ± 0.07 (S = 1.2)
$S_{\rho\pi}\,(B^0 \to \rho^+ \pi^-)$	0.05 ± 0.07
$\Delta S_{\rho\pi}\,(B^0 \to \rho^+ \pi^-)$	0.01 ± 0.08
$C_{\rho^0 \pi^0}\,(B^0 \to \rho^0 \pi^0)$	0.27 ± 0.24
$S_{\rho^0 \pi^0}\,(B^0 \to \rho^0 \pi^0)$	-0.23 ± 0.34
$C_{a_1 \pi}\,(B^0 \to a_1(1260)^+ \pi^-)$	-0.05 ± 0.11
$S_{a_1 \pi}\,(B^0 \to a_1(1260)^+ \pi^-)$	-0.2 ± 0.4 (S = 3.2)
$\Delta C_{a_1 \pi}\,(B^0 \to a_1(1260)^+ \pi^-)$	0.43 ± 0.14 (S = 1.3)
$\Delta S_{a_1 \pi}\,(B^0 \to a_1(1260)^+ \pi^-)$	-0.11 ± 0.12
$C\,(B^0 \to b_1^- K^+)$	-0.22 ± 0.24
$\Delta C\,(B^0 \to b_1^- \pi^+)$	-1.04 ± 0.24
$C_{\rho^0 \rho^0}\,(B^0 \to \rho^0 \rho^0)$	0.2 ± 0.9
$S_{\rho^0 \rho^0}\,(B^0 \to \rho^0 \rho^0)$	0.3 ± 0.7
$C_{\rho\rho}\,(B^0 \to \rho^+ \rho^-)$	0.00 ± 0.08
$S_{\rho\rho}\,(B^0 \to \rho^+ \rho^-)$	-0.18 ± 0.11
$\lvert\lambda\rvert\,(B^0 \to J/\psi K^*(892)^0)$	<0.25, CL = 95%
$\cos 2\beta\,(B^0 \to J/\psi K^*(892)^0)$	$1.7^{+0.7}_{-0.9}$ (S = 1.6)
$\cos 2\beta\,(B^0 \to [K^0_S \pi^+ \pi^-]_{D^{(*)}}\, h^0)$	0.91 ± 0.25
$(S_+ + S_-)/2\,(B^0 \to D^{*-} \pi^+)$	-0.039 ± 0.011
$(S_- - S_+)/2\,(B^0 \to D^{*-} \pi^+)$	-0.009 ± 0.015
$(S_+ + S_-)/2\,(B^0 \to D^- \pi^+)$	-0.046 ± 0.023
$(S_- - S_+)/2\,(B^0 \to D^- \pi^+)$	-0.022 ± 0.021
$S_+\,(B^0 \to D^- \pi^+)$	0.058 ± 0.023
$S_-\,(B^0 \to D^+ \pi^-)$	0.038 ± 0.021
$(S_+ + S_-)/2\,(B^0 \to D^- \rho^+)$	-0.024 ± 0.032
$(S_- - S_+)/2\,(B^0 \to D^- \rho^+)$	-0.10 ± 0.06
$C_{\eta_c K^0_S}\,(B^0 \to \eta_c K^0_S)$	0.08 ± 0.13
$C_{c\overline{c} K^{(*)0}}\,(B^0 \to c\overline{c} K^{(*)0})$	$(0.4 \pm 1.0) \times 10^{-2}$
$C_{J/\psi(nS) K^0}\,(B^0 \to J/\psi(nS) K^0)$	$(0.2 \pm 1.0) \times 10^{-2}$
$C_{J/\psi K^{*0}}\,(B^0 \to J/\psi K^{*0})$	0.03 ± 0.10
$S_{J/\psi K^{*0}}\,(B^0 \to J/\psi K^{*0})$	0.60 ± 0.25
$C_{\chi_{c0} K^0_S}\,(B^0 \to \chi_{c0} K^0_S)$	$-0.3^{+0.5}_{-0.4}$
$S_{\chi_{c0} K^0_S}\,(B^0 \to \chi_{c0} K^0_S)$	-0.7 ± 0.5
$C_{\chi_{c1} K^0_S}\,(B^0 \to \chi_{c1} K^0_S)$	0.06 ± 0.07
$\sin(2\beta_{\rm eff})(B^0 \to \phi K^0)$	0.22 ± 0.30
$\lvert\lambda\rvert\,(B^0 \to [K^0_S \pi^+ \pi^-]_{D^{(*)}}\, h^0)$	1.01 ± 0.08
$\lvert\sin(2\beta + \gamma)\rvert$	>0.40, CL = 90%
$2\beta + \gamma$	$(80 \pm 60)^\circ$
$x_+(B^0 \to D K^{*0})$	0.07 ± 0.08
$x_-(B^0 \to D K^{*0})$	-0.18 ± 0.08
$y_+(B^0 \to D K^{*0})$	-0.35 ± 0.10
$y_-(B^0 \to D K^{*0})$	-0.03 ± 0.13
${}^{a}{}_{CP}(B^0 \to p\overline{p} K^+ \pi^-)$	$(0.5 \pm 0.9)\%$
$A_{CP}(B \to K^*(892)\gamma)$	-0.003 ± 0.011
$A_{CP}(B \to s\gamma)$	0.015 ± 0.011
$A_{CP}(B \to (s+d)\gamma)$	0.010 ± 0.031
$A_{CP}(B \to X_s \ell^+ \ell^-)$	0.04 ± 0.11
$A_{CP}(B \to K^* e^+ e^-)$	-0.18 ± 0.15
$A_{CP}(B \to K^* \mu^+ \mu^-)$	-0.03 ± 0.13
$A_{CP}(B \to K^* \ell^+ \ell^-)$	-0.04 ± 0.07
$A_{CP}(B \to \eta$ anything$)$	$-0.13^{+0.04}_{-0.05}$
$\Delta A_{CP}(X_s\gamma) = A_{CP}(B^\pm \to X_s\gamma) - A_{CP}(B^0 \to X_s\gamma)$	0.041 ± 0.023
$\overline{A}_{CP}(B \to X_s\gamma) = (A_{CP}(B^+ \to X_s\gamma) + A_{CP}(B^0 \to X_s\gamma))/2$	0.009 ± 0.012
$\overline{A}_{CP}(B \to K^*\gamma) = (A_{CP}(B^+ \to K^{*+}\gamma) + A_{CP}(B^0 \to K^{*0}\gamma))/2$	-0.009 ± 0.011
$\mathrm{Re}(\epsilon_{B^0_s})\,/\,(1 + \lvert\epsilon_{B^0_s}\rvert^2)$	$(-0.15 \pm 0.70) \times 10^{-3}$
$S_{KK}(B^0_s \to K^+ K^-)$	0.14 ± 0.05 (S = 1.3)
$\delta_B(B^0_s \to D_s^\pm K^\mp \pi^\pm \pi^\mp)$	$(-6^{+10}_{-13})^\circ$
CP Violation phase β_s $(b \to c\overline{c}s)$	$(2.7 \pm 0.7) \times 10^{-2}$ rad
CP Violation phase β_s $(b \to s\overline{s}s)$	$(3.7 \pm 3.5) \times 10^{-2}$ rad
CP Violation phase β_s $(B^0_s \to J/\psi(1S)\phi)$	$(3.0 \pm 0.7) \times 10^{-2}$ rad
$\lvert\lambda\rvert\,(b \to c\overline{c}s)$	0.989 ± 0.008
$A^L_{CP}(B_s \to J/\psi \overline{K}^*(892)^0)$	0.021 ± 0.027
$A^{\parallel}_{CP}(B_s \to J/\psi \overline{K}^*(892)^0)$	-0.07 ± 0.06
$A^{\perp}_{CP}(B_s \to J/\psi \overline{K}^*(892)^0)$	0.06 ± 0.05
$A_{CP}(B^0_s \to [K^+ K^-]_D \overline{K}^*(892)^0)$	0.06 ± 0.04
$A_{CP}(B^0_s \to [\pi^+ K^-]_D K^*(892)^0)$	-0.009 ± 0.023
$A_{CP}(B^0_s \to [K^+ \pi^-]_D \overline{K}^*(892)^0)$	—
$A_{CP}(B^0_s \to [\pi^+ \pi^-]_D K^*(892)^0)$	0.00 ± 0.06
$A_{CP}(B^0_s \to [K^+ \pi^- \pi^+ \pi^-]_D \overline{K}^*(892)^0)$	-0.029 ± 0.024
$A_{CP}(B^0_s \to [K^- \pi^+ \pi^+ \pi^-]_D \overline{K}^*(892)^0)$	—
$A_{CP}(B^0_s \to [\pi^+ \pi^- \pi^+ \pi^-]_D \overline{K}^*(892)^0)$	0.02 ± 0.05
$R^+_s = \Gamma(B^0_s \to [\pi^- K^+]_D \overline{K}^{*0})\,/\,\Gamma(B^0_s \to [\pi^+ K^-]_D \overline{K}^{*0})$	0.004 ± 0.006
$R^-_s = \Gamma(\overline{B}^0_s \to [\pi^+ K^-]_D K^{*0})\,/\,\Gamma(\overline{B}^0_s \to [\pi^- K^+]_D K^{*0})$	0.004 ± 0.006
$R^+_s = \Gamma(B^0_s \to [\pi^- K^+ \pi^+ \pi^-]_D \overline{K}^{*0})\,/\,\Gamma(B^0_s \to [\pi^+ K^- \pi^+ \pi^-]_D \overline{K}^{*0})$	0.019 ± 0.008
$R^-_s = \Gamma(\overline{B}^0_s \to [\pi^+ K^- \pi^+ \pi^-]_D K^{*0})\,/\,\Gamma(\overline{B}^0_s \to [\pi^- K^+ \pi^+ \pi^-]_D K^{*0})$	0.015 ± 0.008
$S(B^0_s \to \phi\gamma)$	0.43 ± 0.32
$C(B^0_s \to \phi\gamma)$	0.11 ± 0.31
$A^\Delta(B^0_s \to \phi\gamma)$	-0.7 ± 0.4
$\Gamma(\eta_c(1S) \to \pi^+ \pi^-)/\Gamma_{\rm total}$	$<1.0 \times 10^{-4}$, CL = 90%
$\Gamma(\eta_c(1S) \to \pi^0 \pi^0)/\Gamma_{\rm total}$	$<3.3 \times 10^{-5}$, CL = 90%
$\Gamma(\eta_c(1S) \to K^+ K^-)/\Gamma_{\rm total}$	$<5 \times 10^{-4}$, CL = 90%
$\Gamma(\eta_c(1S) \to K^0_S K^0_S)/\Gamma_{\rm total}$	$<2.9 \times 10^{-4}$, CL = 90%
n electric dipole moment	$<0.18 \times 10^{-25}$ e cm, CL = 90%

Unless otherwise stated, limits are given at the 90% confidence level, while errors are given as ± 1 standard deviation.

Int. J. Mod. Phys. A 2026.41. Downloaded from www.worldscientific.com
by UNIVERSITY OF CALIFORNIA @ BERKELEY on 09/16/26. Re-use and distribution is strictly not permitted, except for Open Acce

$(\alpha_- + \alpha_+)/(\alpha_- - \alpha_+)$ in $\Lambda \to p\pi^-$, $\overline{\Lambda} \to \overline{p}\pi^+$	$(-0.3 \pm 0.4) \times 10^{-2}$
$\frac{[\alpha(\Xi^-)\alpha_-(\Lambda) - \overline{\alpha}\overline{\Xi}^+\alpha_+(\overline{\Lambda})]}{[\alpha(\Xi^-)\alpha_-(\Lambda) + \overline{\alpha}\overline{\Xi}^+\alpha_+(\overline{\Lambda})]}$	$(0 \pm 7) \times 10^{-4}$
$(\alpha + \overline{\alpha})/(\alpha - \overline{\alpha})$ in $\Omega^- \to \Lambda K^-$, $\overline{\Omega}^+ \to \overline{\Lambda} K^+$	-0.02 ± 0.13
$(\alpha + \overline{\alpha})/(\alpha - \overline{\alpha})$ in $\Lambda_c^+ \to \Lambda\pi^+$, $\overline{\Lambda}_c^- \to \overline{\Lambda}\pi^-$	0.020 ± 0.016
$(\alpha + \overline{\alpha})/(\alpha - \overline{\alpha})$ in $\Lambda_c^+ \to \Lambda e^+\nu_e$, $\overline{\Lambda}_c^- \to \overline{\Lambda} e^-\overline{\nu}_e$	0.00 ± 0.04
$A_{CP}(\Lambda_b \to p\pi^-)$	$(0.3 \pm 0.9) \times 10^{-2}$
$A_{CP}(\Lambda_b \to pK^-)$	$(-1.2 \pm 0.8) \times 10^{-2}$
$A_{CP}(\Lambda_b \to DpK^-)$	0.12 ± 0.09
$\Delta A_{CP}(pK^-/\pi^-)$	0.014 ± 0.024
$A_{CP}(\Lambda_b \to p\overline{K}^0\pi^-)$	0.039 ± 0.021
$A_{CP}(\Lambda_b \to p\overline{K}^0 K^-)$	0.02 ± 0.16
$\Delta A_{CP}(J/\psi p\pi^-/K^-)$	$(5.7 \pm 2.7) \times 10^{-2}$
$A_{CP}(\Lambda_b \to \Lambda\pi^+\pi^-)$	-0.01 ± 0.06
$A_{CP}(\Lambda_b \to \Lambda K^+\pi^-)$	-0.12 ± 0.05
$A_{CP}(\Lambda_b \to \Lambda K^+K^-)$	0.083 ± 0.028
$\Delta A_{CP}(\Lambda_b^0 \to pK^-\mu^+\mu^-)$	$(-4 \pm 5) \times 10^{-2}$
$\Delta A_{CP}(\Lambda_b^0 \to p\pi^-\pi^+\pi^-)$	$(1.1 \pm 2.6) \times 10^{-2}$
$\Delta A_{CP}(\Lambda_b^0 \to (p\pi^-\pi^+\pi^-)_{LBM})$	$(4 \pm 4) \times 10^{-2}$
$\Delta A_{CP}(\Lambda_b^0 \to pa_1(1260)^-)$	$(-1 \pm 4) \times 10^{-2}$
$\Delta A_{CP}(\Lambda_b^0 \to N(1520)^0\rho(770)^0)$	$(2 \pm 5) \times 10^{-2}$
$\Delta A_{CP}(\Lambda_b^0 \to \Delta(1232)^{++}\pi^-\pi^-)$	$(0.1 \pm 3.3) \times 10^{-2}$
$\Delta A_{CP}(\Lambda_b^0 \to (pK^-\pi^+\pi^-)_{LBM})$	$(3.5 \pm 1.6) \times 10^{-2}$
$\Delta A_{CP}(\Lambda_b^0 \to N(1520)^0 K^*(892)^0)$	$(5.5 \pm 2.5) \times 10^{-2}$
$\Delta A_{CP}(\Lambda_b^0 \to \Lambda(1520)\rho(770)^0)$	$(1 \pm 6) \times 10^{-2}$
$\Delta A_{CP}(\Lambda_b^0 \to \Delta(1232)^{++}K^-\pi^-)$	$(4.4 \pm 2.7) \times 10^{-2}$
$\Delta A_{CP}(\Lambda_b^0 \to pK_1(1410)^-)$	$(5 \pm 4) \times 10^{-2}$
$\Delta A_{CP}(\Lambda_b^0 \to pK^-K^+\pi^-)$	$(-7 \pm 5) \times 10^{-2}$
$\Delta A_{CP}(\Lambda_b^0 \to pK^-K^+K^-)$	$(0.2 \pm 1.9) \times 10^{-2}$
$\Delta A_{CP}(\Lambda_b^0 \to \Lambda(1520)\phi(1020))$	$(4 \pm 6) \times 10^{-2}$
$\Delta A_{CP}(\Lambda_b^0 \to (pK^-)_{highmass}\,\phi(1020))$	$(-0.7 \pm 3.4) \times 10^{-2}$
$\Delta A_{CP}(\Lambda_b^0 \to (pK^-K^+K^-)_{LBM})$	$(2.7 \pm 2.4) \times 10^{-2}$
$A_c(\Lambda)$	-0.22 ± 0.13
$A_s(\Lambda)$	0.13 ± 0.13
$A_c(\phi)$	-0.01 ± 0.12
$A_s(\phi)$	-0.07 ± 0.12
$a_{CP}(\Lambda_b^0 \to p\pi^-\pi^+\pi^-)$	$(-0.7 \pm 0.7)\%$
$a_{CP}(\Lambda_b^0 \to pK^-\pi^+\pi^-)$	$(-0.8 \pm 0.9)\%$
$a_{CP}(\Lambda_b^0 \to pK^-K^+\pi^-)$	$(-1 \pm 5)\%$
$a_{CP}(\Lambda_b^0 \to pK^-K^+K^-)$	$(1.1 \pm 1.5)\%$
$a_{CP}(\Lambda_b^0 \to pK^-\mu^+\mu^-)$	$(1 \pm 5)\%$
$A_P(\Xi_b)$, $\Xi_b^- - \Xi_b^+$ production asymmetry	$(-2 \pm 4) \times 10^{-2}$
$A_{CP}(\Xi_b^- \to \Sigma(1385)K^-)$	$(-30 \pm 80) \times 10^{-2}$
$A_{CP}(\Xi_b^- \to \Lambda(1405)K^-)$	$(0 \pm 40) \times 10^{-2}$
$A_{CP}(\Xi_b^- \to \Lambda(1520)K^-)$	$(-5 \pm 12) \times 10^{-2}$
$A_{CP}(\Xi_b^- \to \Lambda(1670)K^-)$	$(3 \pm 17) \times 10^{-2}$
$A_{CP}(\Xi_b^- \to \Sigma(1775)K^-)$	$(-47 \pm 30) \times 10^{-2}$
$A_{CP}(\Xi_b^- \to \Sigma(1915)K^-)$	$(11 \pm 34) \times 10^{-2}$
$a_P(\Xi_b^0 \to pK^-K^-\pi^+)$	$(-3 \pm 5)\%$
$a_{CP}(\Xi_b^0 \to pK^-K^-\pi^+)$	$(-4 \pm 5)\%$
$\Delta A_{CP}(\Xi_b^0 \to pK^-\pi^+\pi^-)$	$(-17 \pm 11) \times 10^{-2}$
$\Delta A_{CP}(\Xi_b^0 \to pK^-\pi^+K^-)$	$(-7 \pm 8) \times 10^{-2}$
$A_{CP}(\Xi_b^0 \to p\overline{K}^0K^-)$	0.22 ± 0.19
$A_{CP}(\Xi_b^0 \to \Lambda K^-\pi^+)$	0.27 ± 0.13

CP VIOLATION OBSERVED

$\mathrm{Re}(\epsilon)$	$(1.596 \pm 0.013) \times 10^{-3}$
charge asymmetry in $K^0_{\ell 3}$ decays	
A_L = weighted average of $A_L(\mu)$ and $A_L(e)$	$(0.332 \pm 0.006)\%$
$A_L(\mu) = [\Gamma(\pi^-\mu^+\nu_\mu) - \Gamma(\pi^+\mu^-\overline{\nu}_\mu)]/\mathrm{sum}$	$(0.304 \pm 0.025)\%$
$A_L(e) = [\Gamma(\pi^-e^+\nu_e) - \Gamma(\pi^+e^-\overline{\nu}_e)]/\mathrm{sum}$	$(0.334 \pm 0.007)\%$
parameters for $K^0_L \to 2\pi$ decay	
$\lvert\eta_{00}\rvert = \lvert A(K^0_L \to 2\pi^0)/A(K^0_S \to 2\pi^0)\rvert$	$(2.222 \pm 0.012) \times 10^{-3}$ (S = 1.7)
$\lvert\eta_{+-}\rvert = \lvert A(K^0_L \to \pi^+\pi^-)/A(K^0_S \to \pi^+\pi^-)\rvert$	$(2.233 \pm 0.012) \times 10^{-3}$ (S = 1.7)
$\lvert\epsilon\rvert = (2\lvert\eta_{+-}\rvert + \lvert\eta_{00}\rvert)/3$	$(2.229 \pm 0.012) \times 10^{-3}$ (S = 1.7)
$\lvert\eta_{00}/\eta_{+-}\rvert$ [j]	0.9950 ± 0.0007 (S = 1.6)
$\mathrm{Re}(\epsilon'/\epsilon) = (1 - \lvert\eta_{00}/\eta_{+-}\rvert)/3$ [j]	$(1.67 \pm 0.23) \times 10^{-3}$ (S = 1.6)
Assuming *CPT*	
ϕ_{+-}, phase of η_{+-}	$(43.51 \pm 0.05)^\circ$ (S = 1.2)
ϕ_{00}, phase of η_{00}	$(43.52 \pm 0.05)^\circ$ (S = 1.2)
$\phi_\epsilon = (2\phi_{+-} + \phi_{00})/3$	$(43.52 \pm 0.04)^\circ$ (S = 1.2)
Not assuming *CPT*	
ϕ_{+-}, phase of η_{+-}	$(43.4 \pm 0.5)^\circ$ (S = 1.2)
ϕ_{00}, phase of η_{00}	$(43.7 \pm 0.6)^\circ$ (S = 1.2)
$\phi_\epsilon = (2\phi_{+-} + \phi_{00})/3$	$(43.5 \pm 0.5)^\circ$ (S = 1.3)
CP asymmetry A in $K^0_L \to \pi^+\pi^-e^+e^-$	$(13.7 \pm 1.5)\%$
β_{CP} from $K^0_L \to e^+e^-e^+e^-$	-0.19 ± 0.07
γ_{CP} from $K^0_L \to e^+e^-e^+e^-$	0.01 ± 0.11 (S = 1.6)
parameters for $K^0_L \to \pi^+\pi^-\gamma$ decay	
$\lvert\eta_{+-\gamma}\rvert = \lvert A(K^0_L \to \pi^+\pi^-\gamma, CP\ \text{violating})/A(K^0_S \to \pi^+\pi^-\gamma)\rvert$	$(2.35 \pm 0.07) \times 10^{-3}$
$\phi_{+-\gamma}$ = phase of $\eta_{+-\gamma}$	$(44 \pm 4)^\circ$
$\Gamma(K^0_L \to \pi^+\pi^-)/\Gamma_{\mathrm{total}}$ [k]	$(1.967 \pm 0.010) \times 10^{-3}$ (S = 1.5)
$\Gamma(K^0_L \to \pi^0\pi^0)/\Gamma_{\mathrm{total}}$	$(8.64 \pm 0.06) \times 10^{-4}$ (S = 1.8)
$\Delta A^{D^0}_{CP} = A_{CP}(K^+K^-) - A_{CP}(\pi^+\pi^-)$	$(-0.154 \pm 0.029)\%$
$A_{CP}(B^+ \to [K^-\pi^+]_{\overline{D}}K^*(892)^+)$	-0.75 ± 0.16
$A_{CP}(B^+ \to D_{CP(+1)}K^+)$	0.132 ± 0.015 (S = 1.8)
$A_{ADS}(B^+ \to DK^+)$	-0.451 ± 0.026
$A_{ADS}(B^+ \to D\pi^+)$	0.129 ± 0.014
$A_{CP}(B^+ \to \eta K^+)$	-0.37 ± 0.08
$A_{CP}(B^+ \to K^+\pi^-\pi^+)$	0.015 ± 0.006 (S = 1.4)
$A_{CP}(B^+ \to \rho^0K^+)$	0.160 ± 0.021
$A_{CP}(B^+ \to K^+K^-\pi^+)$	-0.115 ± 0.008
$A_{CP}(B^+ \to \pi^+(K^+K^-)_{S-wave})$	-0.66 ± 0.04
$A_{CP}(B^+ \to K^+K^-K^+)$	-0.036 ± 0.004
$A_{CP}(B^+ \to \pi^+\pi^-\pi^+)$	0.076 ± 0.008 (S = 1.5)
$A_{CP}(B^+ \to f_2(1270)\pi^+)$	0.40 ± 0.06
γ	$(66.4^{+2.7}_{-2.8})^\circ$
$r_B(B^+ \to D^0K^+)$	$(9.88^{+0.22}_{-0.21}) \times 10^{-2}$
$\delta_B(B^+ \to D^0K^+)$	$(128.5^{+2.8}_{-3.0})^\circ$
$r_B(B^+ \to D^{*0}K^+)$	$0.103^{+0.010}_{-0.011}$
$\delta_B(B^+ \to D^{*0}K^+)$	$(312.2^{+6.3}_{-7.1})^\circ$
$A_{CP}(B^0 \to K^+\pi^-)$	-0.0831 ± 0.0031
$A_{CP}(B^0 \to \eta K^*(892)^0)$	0.19 ± 0.05
$A_{CP}(B^0 \to K^*(892)^+\pi^-)$	-0.27 ± 0.04
$S_{D^*(2010)^-D^+}(B^0 \to D^*(2010)^-D^+)$	-0.83 ± 0.09
$S_{D^*(2010)^+D^-}(B^0 \to D^*(2010)^+D^-)$	-0.80 ± 0.09
$S_{D^{*+}D^{*-}}(B^0 \to D^{*+}D^{*-})$	-0.59 ± 0.14 (S = 1.8)
$S_+(B^0 \to D^{*+}D^{*-})$	-0.73 ± 0.09
$S_{D^+D^-}(B^0 \to D^+D^-)$	-0.64 ± 0.09 (S = 1.3)
$S_{J/\psi(1S)\pi^0}(B^0 \to J/\psi(1S)\pi^0)$	-0.88 ± 0.17 (S = 1.6)
$S(B^0 \to J/\psi(1S)\rho^0)$	$-0.66^{+0.16}_{-0.12}$
$S_{K^0\pi^0}(B^0 \to K^0\pi^0)$	0.64 ± 0.13
$S_{\eta' K^0}(B^0 \to \eta' K^0)$	0.64 ± 0.05
$S_{K^+K^-K^0_S}(B^0 \to K^+K^-K^0_S$ nonresonant)	-0.66 ± 0.11
$S_{K^+K^-K^0_S}(B^0 \to K^+K^-K^0_S$ inclusive)	-0.65 ± 0.12
$C_{\pi\pi}(B^0 \to \pi^+\pi^-)$	-0.314 ± 0.030
$S_{\pi\pi}(B^0 \to \pi^+\pi^-)$	-0.670 ± 0.030
$\Delta C_{\rho\pi}(B^0 \to \rho^+\pi^-)$	0.27 ± 0.06
$S_{\eta_c K^0_S}(B^0 \to \eta_c K^0_S)$	0.93 ± 0.17
$\sin(2\beta)\ (B^0 \to J/\psi K^0_S)$	0.710 ± 0.011
$S_{J/\psi(nS)K^0}(B^0 \to J/\psi(nS)K^0)$	0.711 ± 0.011
$S_{\chi_{c1}K^0_S}(B^0 \to \chi_{c1}K^0_S)$	0.63 ± 0.10

Unless otherwise stated, limits are given at the 90% confidence level, while errors are given as ±1 standard deviation.

Int. J. Mod. Phys. A 2026.41. Downloaded from www.worldscientific.com
by UNIVERSITY OF CALIFORNIA @ BERKELEY on 09/16/26. Re-use and distribution is strictly not permitted, except for Open Access articles.

$\sin(2\beta_{\rm eff})(B^0 \to \phi K_0^*(1430)^0)$	$0.97^{+0.03}_{-0.52}$
$\sin(2\beta_{\rm eff})(B^0 \to K^+K^-K_S^0)$	$0.77^{+0.13}_{-0.12}$
$\sin(2\beta_{\rm eff})(B^0 \to [K_S^0\pi^+\pi^-]_{D^{(*)}}\ h^0)$	0.80 ± 0.16
α	$(84.1^{+3.7}_{-3.0})^\circ$
$r_{B^0}(B^0 \to D K^{*0})$	0.250 ± 0.022
$\delta_{B^0}(B^0 \to D K^{*0})$	$(202.8^{+10.3}_{-9.0})^\circ$
$C_{KK}(B_s^0 \to K^+K^-)$	0.162 ± 0.035
$r_B(B_s^0 \to D_s^\mp K^\pm)$	0.318 ± 0.034
$r_B(B_s^0 \to D_s^\mp K^\pm\pi^\pm\pi^\mp)$	0.47 ± 0.08
$\delta_B(B_s^0 \to D_s^\pm K^\mp)$	$(348 \pm 6)^\circ$
$A_{CP}(B_s \to \pi^+K^-)$	0.224 ± 0.012
$\Delta A_{CP}(\Lambda_b^0 \to pK^-\pi^+\pi^-)$	$(2.5 \pm 0.5) \times 10^{-2}$

CPT INVARIANCE

$(m_{W^+} - m_{W^-})\ /\ m_{\rm average}$	$(-3.7 \pm 3.5) \times 10^{-4}$
$(m_{e^+} - m_{e^-})\ /\ m_{\rm average}$	$<8 \times 10^{-9}$, CL = 90%
$\lvert q_{e^+} + q_{e^-}\rvert/e$	$<4 \times 10^{-8}$
$(g_{e^+} - g_{e^-})\ /\ g_{\rm average}$	$(-0.5 \pm 2.1) \times 10^{-12}$
$(\tau_{\mu^+} - \tau_{\mu^-})\ /\ \tau_{\rm average}$	$(2 \pm 8) \times 10^{-5}$
$(g_{\mu^+} - g_{\mu^-})\ /\ g_{\rm average}$	$(-0.11 \pm 0.12) \times 10^{-8}$
$(m_{\tau^+} - m_{\tau^-})/m_{\rm average}$	$<2.8 \times 10^{-4}$, CL = 90%
$\langle \Delta m_{21}^2 - \Delta\overline{m}_{21}^2 \rangle$ in neutrino mixing	$<1.1 \times 10^{-4}$ eV^2, CL = 99.7%
$\langle \Delta m_{32}^2 - \Delta\overline{m}_{32}^2 \rangle$ in neutrino mixing	$(-0.12 \pm 0.25) \times 10^{-3}$ eV^2
$m_t - m_{\overline{t}}$	-0.15 ± 0.20 GeV (S = 1.1)
$(m_{\pi^+} - m_{\pi^-})\ /\ m_{\rm average}$	$(2 \pm 5) \times 10^{-4}$
$(\tau_{\pi^+} - \tau_{\pi^-})\ /\ \tau_{\rm average}$	$(6 \pm 7) \times 10^{-4}$
$(m_{K^+} - m_{K^-})\ /\ m_{\rm average}$	$(-0.6 \pm 1.8) \times 10^{-4}$
$(\tau_{K^+} - \tau_{K^-})\ /\ \tau_{\rm average}$	$(0.10 \pm 0.09)\%$ (S = 1.2)
δ in $K^0 - \overline{K}^0$ mixing	
real part of δ	$(2.5 \pm 2.3) \times 10^{-4}$
imaginary part of δ	$(-1.5 \pm 1.6) \times 10^{-5}$
Re(y), K_{e3} parameter	$(0.4 \pm 2.5) \times 10^{-3}$
Re(x$_-$), K_{e3} parameter	$(-2.9 \pm 2.0) \times 10^{-3}$
$\lvert m_{K^0} - m_{\overline{K}^0}\rvert\ /\ m_{\rm average}$ [l]	$<6 \times 10^{-19}$, CL = 90%
$(\Gamma_{K^0} - \Gamma_{\overline{K}^0})/m_{\rm average}$	$(8 \pm 8) \times 10^{-18}$
phase difference $\phi_{00} - \phi_{+-}$	$(0.34 \pm 0.32)^\circ$
$\mathrm{Re}(\frac{2}{3}\eta_{+-} + \frac{1}{3}\eta_{00}) - \frac{A_L}{2}$	$(-3 \pm 35) \times 10^{-6}$
$A_{CPT}(D^0 \to K^-\pi^+)$	-1.46×10^{-4} to 6.6×10^{-5}, CL = 95%
$\Delta S^+_{CPT}\ (S^-_{\ell^+,K_S^0} - S^+_{\ell^+,K_S^0})$	0.16 ± 0.23
$\Delta S^-_{CPT}\ (S^+_{\ell^+,K_S^0} - S^-_{\ell^+,K_S^0})$	-0.03 ± 0.14
$\Delta C^+_{CPT}\ (C^-_{\ell^+,K_S^0} - C^+_{\ell^+,K_S^0})$	0.14 ± 0.17
$\Delta C^-_{CPT}\ (C^+_{\ell^+,K_S^0} - C^-_{\ell^+,K_S^0})$	0.03 ± 0.14
$\lvert m_p - m_{\overline{p}}\rvert/m_p$ [n]	$<7 \times 10^{-10}$, CL = 90%
$(\lvert\frac{q_{\overline{p}}}{m_{\overline{p}}}\rvert - \frac{q_p}{m_p})/\frac{q_p}{m_p}$	$(0.3 \pm 1.6) \times 10^{-11}$
$\lvert q_p + q_{\overline{p}}\rvert/e$ [n]	$<7 \times 10^{-10}$, CL = 90%
$(\mu_p + \mu_{\overline{p}})\ /\ \mu_p$	$(0.002 \pm 0.004) \times 10^{-6}$
$(m_n - m_{\overline{n}})\ /\ m_n$	$(9 \pm 5) \times 10^{-5}$
$(m_\Lambda - m_{\overline{\Lambda}})\ /\ m_\Lambda$	$(-0.1 \pm 1.1) \times 10^{-5}$ (S = 1.6)
$(\tau_\Lambda - \tau_{\overline{\Lambda}})\ /\ \tau_\Lambda$	$(0.9 \pm 3.2) \times 10^{-3}$
$(\tau_{\Sigma^+} - \tau_{\overline{\Sigma}^-})\ /\ \tau_{\Sigma^+}$	-0.0006 ± 0.0012
$(\mu_{\Sigma^+} + \mu_{\overline{\Sigma}^-})\ /\ \mu_{\Sigma^+}$	0.014 ± 0.015
$(m_{\Xi^-} - m_{\overline{\Xi}^+})\ /\ m_{\Xi^-}$	$(-3 \pm 9) \times 10^{-5}$
$(\tau_{\Xi^-} - \tau_{\overline{\Xi}^+})\ /\ \tau_{\Xi^-}$	-0.01 ± 0.07
$(\mu_{\Xi^-} + \mu_{\overline{\Xi}^+})\ /\ \lvert\mu_{\Xi^-}\rvert$	$+0.01 \pm 0.05$
$(m_{\Omega^-} - m_{\overline{\Omega}^+})\ /\ m_{\Omega^-}$	$(-1 \pm 8) \times 10^{-5}$
$(\tau_{\Omega^-} - \tau_{\overline{\Omega}^+})\ /\ \tau_{\Omega^-}$	0.00 ± 0.05

Unless otherwise stated, limits are given at the 90% confidence level, while errors are given as ±1 standard deviation.

TESTS OF NUMBER CONSERVATION LAWS

LEPTON FAMILY NUMBER

Lepton family number conservation means separate conservation of each of L_e, L_μ, L_τ.

$\Gamma(Z \to e^\pm\mu^\mp)/\Gamma_{\rm total}$	[o]	$<1.9 \times 10^{-7}$, CL = 95%
$\Gamma(Z \to e^\pm\tau^\mp)/\Gamma_{\rm total}$	[o]	$<5.0 \times 10^{-6}$, CL = 95%
$\Gamma(Z \to \mu^\pm\tau^\mp)/\Gamma_{\rm total}$	[o]	$<6.5 \times 10^{-6}$, CL = 95%
$\Gamma(H \to e\mu)/\Gamma_{\rm total}$		$<4.4 \times 10^{-5}$, CL = 95%
$\Gamma(H \to e\tau)/\Gamma_{\rm total}$		$<2.0 \times 10^{-3}$, CL = 95%
$\Gamma(H \to \mu\tau)/\Gamma_{\rm total}$		$<1.5 \times 10^{-3}$, CL = 95%
$\sigma(e^+e^- \to e^\pm\tau^\mp)\ /\ \sigma(e^+e^- \to \mu^+\mu^-)$		$<8.9 \times 10^{-6}$, CL = 95%
$\sigma(e^+e^- \to \mu^\pm\tau^\mp)\ /\ \sigma(e^+e^- \to \mu^+\mu^-)$		$<4.0 \times 10^{-6}$, CL = 95%
limit on $\mu^- \to e^-$ conversion		
$\sigma(\mu^-\,{}^{32}\mathrm{S} \to e^-\,{}^{32}\mathrm{S})\ /\ \sigma(\mu^-\,{}^{32}\mathrm{S} \to \nu_\mu\,{}^{32}\mathrm{P}^*)$		$<7 \times 10^{-11}$, CL = 90%
$\sigma(\mu^-\mathrm{Ti} \to e^-\mathrm{Ti})\ /\ \sigma(\mu^-\mathrm{Ti} \to \text{capture})$		$<4.3 \times 10^{-12}$, CL = 90%
$\sigma(\mu^-\mathrm{Pb} \to e^-\mathrm{Pb})\ /\ \sigma(\mu^-\mathrm{Pb} \to \text{capture})$		$<4.6 \times 10^{-11}$, CL = 90%
$\sigma(\mu^-\mathrm{Au} \to e^-\mathrm{Au})\ /\ \sigma(\mu^-\mathrm{Au} \to \text{capture})$		$<7 \times 10^{-13}$, CL = 90%
limit on muonium $\to$ antimuonium conversion $R_g = G_C\ /\ G_F$		<0.0030, CL = 90%
$\Gamma(\mu^- \to e^-\nu_e\overline{\nu}_\mu)/\Gamma_{\rm total}$	[p]	$<1.2 \times 10^{-2}$, CL = 90%
$\Gamma(\mu^- \to e^-\gamma)/\Gamma_{\rm total}$		$<1.5 \times 10^{-13}$, CL = 90%
$\Gamma(\mu^- \to e^-e^+e^-)/\Gamma_{\rm total}$		$<1.0 \times 10^{-12}$, CL = 90%
$\Gamma(\mu^- \to e^-2\gamma)/\Gamma_{\rm total}$		$<7.2 \times 10^{-11}$, CL = 90%
$\Gamma(\tau^- \to e^-\gamma)/\Gamma_{\rm total}$		$<3.3 \times 10^{-8}$, CL = 90%
$\Gamma(\tau^- \to e^-\gamma\gamma)/\Gamma_{\rm total}$		$<2.5 \times 10^{-4}$, CL = 90%
$\Gamma(\tau^- \to \mu^-\gamma)/\Gamma_{\rm total}$		$<4.2 \times 10^{-8}$, CL = 90%
$\Gamma(\tau^- \to \mu^-\gamma\gamma)/\Gamma_{\rm total}$		$<5.8 \times 10^{-4}$, CL = 90%
$\Gamma(\tau^- \to e^-\pi^0)/\Gamma_{\rm total}$		$<8.0 \times 10^{-8}$, CL = 90%
$\Gamma(\tau^- \to \mu^-\pi^0)/\Gamma_{\rm total}$		$<1.1 \times 10^{-7}$, CL = 90%
$\Gamma(\tau^- \to e^-K_S^0)/\Gamma_{\rm total}$		$<8 \times 10^{-9}$, CL = 90%
$\Gamma(\tau^- \to \mu^-K_S^0)/\Gamma_{\rm total}$		$<1.2 \times 10^{-8}$, CL = 90%
$\Gamma(\tau^- \to e^-\eta)/\Gamma_{\rm total}$		$<9.2 \times 10^{-8}$, CL = 90%
$\Gamma(\tau^- \to \mu^-\eta)/\Gamma_{\rm total}$		$<6.5 \times 10^{-8}$, CL = 90%
$\Gamma(\tau^- \to e^-\rho^0)/\Gamma_{\rm total}$		$<2.2 \times 10^{-8}$, CL = 90%
$\Gamma(\tau^- \to \mu^-\rho^0)/\Gamma_{\rm total}$		$<1.7 \times 10^{-8}$, CL = 90%
$\Gamma(\tau^- \to e^-\omega)/\Gamma_{\rm total}$		$<2.4 \times 10^{-8}$, CL = 90%
$\Gamma(\tau^- \to \mu^-\omega)/\Gamma_{\rm total}$		$<3.9 \times 10^{-8}$, CL = 90%
$\Gamma(\tau^- \to e^-K^*(892)^0)/\Gamma_{\rm total}$		$<1.9 \times 10^{-8}$, CL = 90%
$\Gamma(\tau^- \to \mu^-K^*(892)^0)/\Gamma_{\rm total}$		$<2.9 \times 10^{-8}$, CL = 90%
$\Gamma(\tau^- \to e^-\overline{K}^*(892)^0)/\Gamma_{\rm total}$		$<1.7 \times 10^{-8}$, CL = 90%
$\Gamma(\tau^- \to \mu^-\overline{K}^*(892)^0)/\Gamma_{\rm total}$		$<4.3 \times 10^{-8}$, CL = 90%
$\Gamma(\tau^- \to e^-\eta'(958))/\Gamma_{\rm total}$		$<1.6 \times 10^{-7}$, CL = 90%
$\Gamma(\tau^- \to \mu^-\eta'(958))/\Gamma_{\rm total}$		$<1.3 \times 10^{-7}$, CL = 90%
$\Gamma(\tau^- \to e^-f_0(980) \to e^-\pi^+\pi^-)/\Gamma_{\rm total}$		$<3.2 \times 10^{-8}$, CL = 90%
$\Gamma(\tau^- \to \mu^-f_0(980) \to \mu^-\pi^+\pi^-)/\Gamma_{\rm total}$		$<3.4 \times 10^{-8}$, CL = 90%
$\Gamma(\tau^- \to e^-\phi)/\Gamma_{\rm total}$		$<2.0 \times 10^{-8}$, CL = 90%
$\Gamma(\tau^- \to \mu^-\phi)/\Gamma_{\rm total}$		$<2.3 \times 10^{-8}$, CL = 90%
$\Gamma(\tau^- \to e^-e^+e^-)/\Gamma_{\rm total}$		$<2.5 \times 10^{-8}$, CL = 90%
$\Gamma(\tau^- \to e^-\mu^+\mu^-)/\Gamma_{\rm total}$		$<2.4 \times 10^{-8}$, CL = 90%
$\Gamma(\tau^- \to e^+\mu^-\mu^-)/\Gamma_{\rm total}$		$<1.3 \times 10^{-8}$, CL = 90%
$\Gamma(\tau^- \to \mu^-e^+e^-)/\Gamma_{\rm total}$		$<1.6 \times 10^{-8}$, CL = 90%
$\Gamma(\tau^- \to \mu^+e^-e^-)/\Gamma_{\rm total}$		$<1.5 \times 10^{-8}$, CL = 90%
$\Gamma(\tau^- \to \mu^-\mu^+\mu^-)/\Gamma_{\rm total}$		$<1.9 \times 10^{-8}$, CL = 90%
$\Gamma(\tau^- \to e^-\pi^+\pi^-)/\Gamma_{\rm total}$		$<2.3 \times 10^{-8}$, CL = 90%
$\Gamma(\tau^- \to \mu^-\pi^+\pi^-)/\Gamma_{\rm total}$		$<2.1 \times 10^{-8}$, CL = 90%
$\Gamma(\tau^- \to e^-\pi^+K^-)/\Gamma_{\rm total}$		$<3.7 \times 10^{-8}$, CL = 90%
$\Gamma(\tau^- \to e^-\pi^-K^+)/\Gamma_{\rm total}$		$<3.1 \times 10^{-8}$, CL = 90%
$\Gamma(\tau^- \to e^-K_S^0K_S^0)/\Gamma_{\rm total}$		$<7.1 \times 10^{-8}$, CL = 90%
$\Gamma(\tau^- \to e^-K^+K^-)/\Gamma_{\rm total}$		$<3.4 \times 10^{-8}$, CL = 90%
$\Gamma(\tau^- \to \mu^-\pi^+K^-)/\Gamma_{\rm total}$		$<8.6 \times 10^{-8}$, CL = 90%
$\Gamma(\tau^- \to \mu^-\pi^-K^+)/\Gamma_{\rm total}$		$<4.5 \times 10^{-8}$, CL = 90%

Int. J. Mod. Phys. A 2026.41. Downloaded from www.worldscientific.com
by UNIVERSITY OF CALIFORNIA @ BERKELEY on 09/16/26. Re-use and distribution is strictly not permitted, except for Open Acce

$\Gamma(\tau^- \to \mu^- K^0_S K^0_S)/\Gamma_{total}$		$<8.0 \times 10^{-8}$, CL = 90%
$\Gamma(\tau^- \to \mu^- K^+ K^-)/\Gamma_{total}$		$<4.4 \times 10^{-8}$, CL = 90%
$\Gamma(\tau^- \to e^- \pi^0 \pi^0)/\Gamma_{total}$		$<6.5 \times 10^{-6}$, CL = 90%
$\Gamma(\tau^- \to \mu^- \pi^0 \pi^0)/\Gamma_{total}$		$<1.4 \times 10^{-5}$, CL = 90%
$\Gamma(\tau^- \to e^- \eta\eta)/\Gamma_{total}$		$<3.5 \times 10^{-5}$, CL = 90%
$\Gamma(\tau^- \to \mu^- \eta\eta)/\Gamma_{total}$		$<6.0 \times 10^{-5}$, CL = 90%
$\Gamma(\tau^- \to e^- \pi^0 \eta)/\Gamma_{total}$		$<2.4 \times 10^{-5}$, CL = 90%
$\Gamma(\tau^- \to \mu^- \pi^0 \eta)/\Gamma_{total}$		$<2.2 \times 10^{-5}$, CL = 90%
$\Gamma(\tau^- \to e^-$ light boson$)/\Gamma_{total}$		$<4.5 \times 10^{-4}$, CL = 90%
$\Gamma(\tau^- \to \mu^-$ light boson$)/\Gamma_{total}$		$<2.8 \times 10^{-4}$, CL = 90%
LEPTON FAMILY NUMBER VIOLATION IN NEUTRINOS		
$\sin^2(\theta_{12})$		0.307 ± 0.012
Δm^2_{21}		$(7.60 \pm 0.17) \times 10^{-5}$ eV^2
$\sin^2(\theta_{23})$ (Inverted order)		$0.523^{+0.031}_{-0.027}$ (S = 1.3)
$\sin^2(\theta_{23})$ (Normal order)		0.533 ± 0.018
Δm^2_{32} (Inverted order)		$(-2.52 \pm 0.04) \times 10^{-3}$ eV^2 (S = 1.3)
Δm^2_{32} (Normal order)		$(2.445 \pm 0.023) \times 10^{-3}$ eV^2
$\sin^2(\theta_{13})$		$(2.17 \pm 0.07) \times 10^{-2}$ (S = 1.4)
$\Gamma(t \to e^\pm \mu^\mp c)/\Gamma_{total}$		$<2.16 \times 10^{-7}$, CL = 95%
$\Gamma(t \to e^\pm \mu^\mp u)/\Gamma_{total}$		$<1.2 \times 10^{-8}$, CL = 95%
$\Gamma(\pi^+ \to \mu^+ \nu_e)/\Gamma_{total}$	[q]	$<8.0 \times 10^{-3}$, CL = 90%
$\Gamma(\pi^+ \to \mu^- e^+ e^+ \nu)/\Gamma_{total}$		$<1.6 \times 10^{-6}$, CL = 90%
$\Gamma(\pi^0 \to \mu^+ e^-)/\Gamma_{total}$		$<3.8 \times 10^{-10}$, CL = 90%
$\Gamma(\pi^0 \to \mu^- e^+)/\Gamma_{total}$		$<3.2 \times 10^{-10}$, CL = 90%
$\Gamma(\pi^0 \to \mu^+ e^- + \mu^- e^+)/\Gamma_{total}$		$<3.6 \times 10^{-10}$, CL = 90%
$\Gamma(\eta \to \mu^+ e^- + \mu^- e^+)/\Gamma_{total}$		$<6 \times 10^{-6}$, CL = 90%
$\Gamma(\eta \to \pi^+ \pi^+ e^- e^-$ + c.c.$)/\Gamma_{total}$		$<4.6 \times 10^{-6}$, CL = 90%
$\Gamma(\eta'(958) \to e\mu)/\Gamma_{total}$		$<4.7 \times 10^{-4}$, CL = 90%
$\Gamma(\phi(1020) \to e^\pm \mu^\mp)/\Gamma_{total}$		$<2 \times 10^{-6}$, CL = 90%
$\Gamma(K^+ \to \mu^- \nu e^+ e^+)/\Gamma_{total}$		$<8.1 \times 10^{-11}$, CL = 90%
$\Gamma(K^+ \to \mu^+ \nu_e)/\Gamma_{total}$	[q]	$<4 \times 10^{-3}$, CL = 90%
$\Gamma(K^+ \to \pi^+ \mu^+ e^-)/\Gamma_{total}$		$<1.3 \times 10^{-11}$, CL = 90%
$\Gamma(K^+ \to \pi^0 \pi^+ \mu^+ e^-)/\Gamma_{total}$		$<5.0 \times 10^{-10}$, CL = 90%
$\Gamma(K^+ \to \pi^+ \mu^- e^+)/\Gamma_{total}$		$<6.6 \times 10^{-11}$, CL = 90%
$\Gamma(K^+ \to \pi^0 \pi^+ \mu^- e^+)/\Gamma_{total}$		$<3.1 \times 10^{-10}$, CL = 90%
$\Gamma(K^0_L \to e^\pm \mu^\mp)/\Gamma_{total}$	[o]	$<4.7 \times 10^{-12}$, CL = 90%
$\Gamma(K^0_L \to e^\pm e^\pm \mu^\mp \mu^\mp)/\Gamma_{total}$	[o]	$<4.12 \times 10^{-11}$, CL = 90%
$\Gamma(K^0_L \to \pi^0 \mu^\pm e^\mp)/\Gamma_{total}$	[o]	$<7.6 \times 10^{-11}$, CL = 90%
$\Gamma(K^0_L \to \pi^0 \pi^0 \mu^\pm e^\mp)/\Gamma_{total}$		$<1.7 \times 10^{-10}$, CL = 90%
$\Gamma(D^+ \to \pi^+ e^+ \mu^-)/\Gamma_{total}$		$<2.1 \times 10^{-7}$, CL = 90%
$\Gamma(D^+ \to \pi^+ e^- \mu^+)/\Gamma_{total}$		$<2.2 \times 10^{-7}$, CL = 90%
$\Gamma(D^+ \to K^+ e^+ \mu^-)/\Gamma_{total}$		$<7.5 \times 10^{-8}$, CL = 90%
$\Gamma(D^+ \to K^+ e^- \mu^+)/\Gamma_{total}$		$<1.0 \times 10^{-7}$, CL = 90%
$\Gamma(D^0 \to \mu^\pm e^\mp)/\Gamma_{total}$	[o]	$<1.3 \times 10^{-8}$, CL = 90%
$\Gamma(D^0 \to \pi^0 e^\pm \mu^\mp)/\Gamma_{total}$	[o]	$<8.0 \times 10^{-7}$, CL = 90%
$\Gamma(D^0 \to \eta e^\pm \mu^\mp)/\Gamma_{total}$	[o]	$<2.25 \times 10^{-6}$, CL = 90%
$\Gamma(D^0 \to \pi^+ \pi^- e^\pm \mu^\mp)/\Gamma_{total}$	[o]	$<1.71 \times 10^{-6}$, CL = 90%
$\Gamma(D^0 \to \rho^0 e^\pm \mu^\mp)/\Gamma_{total}$	[o]	$<5.0 \times 10^{-7}$, CL = 90%
$\Gamma(D^0 \to \omega e^\pm \mu^\mp)/\Gamma_{total}$	[o]	$<1.71 \times 10^{-6}$, CL = 90%
$\Gamma(D^0 \to K^- K^+ e^\pm \mu^\mp)/\Gamma_{total}$	[o]	$<1.00 \times 10^{-6}$, CL = 90%
$\Gamma(D^0 \to \phi e^\pm \mu^\mp)/\Gamma_{total}$	[o]	$<5.1 \times 10^{-7}$, CL = 90%
$\Gamma(D^0 \to \overline{K}^0 e^\pm \mu^\mp)/\Gamma_{total}$	[o]	$<1.74 \times 10^{-6}$, CL = 90%
$\Gamma(D^0 \to K^- \pi^+ e^\pm \mu^\mp)/\Gamma_{total}$	[o]	$<1.90 \times 10^{-6}$, CL = 90%
$\Gamma(D^0 \to \overline{K}^*(892)^0 e^\pm \mu^\mp)/\Gamma_{total}$	[o]	$<1.25 \times 10^{-6}$, CL = 90%
$\Gamma(D^+_s \to \pi^+ e^+ \mu^-)/\Gamma_{total}$		$<1.1 \times 10^{-6}$, CL = 90%
$\Gamma(D^+_s \to \pi^+ e^- \mu^+)/\Gamma_{total}$		$<9.4 \times 10^{-7}$, CL = 90%
$\Gamma(D^+_s \to K^+ e^+ \mu^-)/\Gamma_{total}$		$<7.9 \times 10^{-7}$, CL = 90%
$\Gamma(D^+_s \to K^+ e^- \mu^+)/\Gamma_{total}$		$<5.6 \times 10^{-7}$, CL = 90%
$\Gamma(B^+ \to \pi^+ e^+ \mu^-)/\Gamma_{total}$		$<6.4 \times 10^{-3}$, CL = 90%
$\Gamma(B^+ \to \pi^+ e^- \mu^+)/\Gamma_{total}$		$<6.4 \times 10^{-3}$, CL = 90%
$\Gamma(B^+ \to \pi^+ e^\pm \mu^\mp)/\Gamma_{total}$		$<1.7 \times 10^{-7}$, CL = 90%
$\Gamma(B^+ \to \pi^+ e^+ \tau^-)/\Gamma_{total}$		$<7.4 \times 10^{-5}$, CL = 90%
$\Gamma(B^+ \to \pi^+ e^- \tau^+)/\Gamma_{total}$		$<2.0 \times 10^{-5}$, CL = 90%
$\Gamma(B^+ \to \pi^+ e^\pm \tau^\mp)/\Gamma_{total}$		$<7.5 \times 10^{-5}$, CL = 90%
$\Gamma(B^+ \to \pi^+ \mu^+ \tau^-)/\Gamma_{total}$		$<6.2 \times 10^{-5}$, CL = 90%
$\Gamma(B^+ \to \pi^+ \mu^- \tau^+)/\Gamma_{total}$		$<4.5 \times 10^{-5}$, CL = 90%
$\Gamma(B^+ \to \pi^+ \mu^\pm \tau^\mp)/\Gamma_{total}$		$<7.2 \times 10^{-5}$, CL = 90%
$\Gamma(B^+ \to K^+ e^+ \mu^-)/\Gamma_{total}$		$<7.0 \times 10^{-9}$, CL = 90%
$\Gamma(B^+ \to K^+ e^- \mu^+)/\Gamma_{total}$		$<6.4 \times 10^{-9}$, CL = 90%
$\Gamma(B^+ \to K^+ e^\pm \mu^\mp)/\Gamma_{total}$		$<9.1 \times 10^{-8}$, CL = 90%
$\Gamma(B^+ \to K^+ e^+ \tau^-)/\Gamma_{total}$		$<1.53 \times 10^{-5}$, CL = 90%
$\Gamma(B^+ \to K^+ e^- \tau^+)/\Gamma_{total}$		$<1.5 \times 10^{-5}$, CL = 90%
$\Gamma(B^+ \to K^+ e^\pm \tau^\mp)/\Gamma_{total}$		$<3.0 \times 10^{-5}$, CL = 90%
$\Gamma(B^+ \to K^+ \mu^+ \tau^-)/\Gamma_{total}$		$<2.45 \times 10^{-5}$, CL = 90%
$\Gamma(B^+ \to K^+ \mu^- \tau^+)/\Gamma_{total}$		$<5.9 \times 10^{-6}$, CL = 90%
$\Gamma(B^+ \to K^+ \mu^\pm \tau^\mp)/\Gamma_{total}$		$<4.8 \times 10^{-5}$, CL = 90%
$\Gamma(B^+ \to K^*(892)^+ e^+ \mu^-)/\Gamma_{total}$		$<1.3 \times 10^{-6}$, CL = 90%
$\Gamma(B^+ \to K^*(892)^+ e^- \mu^+)/\Gamma_{total}$		$<9.9 \times 10^{-7}$, CL = 90%
$\Gamma(B^+ \to K^*(892)^+ e^\pm \mu^\mp)/\Gamma_{total}$		$<1.4 \times 10^{-6}$, CL = 90%
$\Gamma(K^0_S \tau^+ e^-)/\Gamma_{total}$		$<1.5 \times 10^{-5}$, CL = 90%
$\Gamma(K^0_S \tau^- e^+)/\Gamma_{total}$		$<8 \times 10^{-6}$, CL = 90%
$\Gamma(K^0_S \tau^+ \mu^-)/\Gamma_{total}$		$<1.1 \times 10^{-5}$, CL = 90%
$\Gamma(K^0_S \tau^- \mu^+)/\Gamma_{total}$		$<3.6 \times 10^{-5}$, CL = 90%
$\Gamma(K^*(892)^0 \tau^+ e^-)/\Gamma_{total}$		$<4.9 \times 10^{-6}$, CL = 90%
$\Gamma(K^*(892)^0 \tau^- e^+)/\Gamma_{total}$		$<5.9 \times 10^{-6}$, CL = 90%
$\Gamma(B^0 \to e^\pm \mu^\mp)/\Gamma_{total}$	[o]	$<1.0 \times 10^{-9}$, CL = 90%
$\Gamma(B^0 \to \pi^0 e^\pm \mu^\mp)/\Gamma_{total}$		$<1.4 \times 10^{-7}$, CL = 90%
$\Gamma(B^0 \to K^0 e^\pm \mu^\mp)/\Gamma_{total}$		$<3.8 \times 10^{-8}$, CL = 90%
$\Gamma(B^0 \to K^*(892)^0 e^+ \mu^-)/\Gamma_{total}$		$<6.8 \times 10^{-9}$, CL = 90%
$\Gamma(B^0 \to K^*(892)^0 e^- \mu^+)/\Gamma_{total}$		$<5.7 \times 10^{-9}$, CL = 90%
$\Gamma(B^0 \to K^*(892)^0 e^\pm \mu^\mp)/\Gamma_{total}$		$<1.01 \times 10^{-8}$, CL = 90%
$\Gamma(B^0 \to K^*(892)^0 \tau^+ \mu^-)/\Gamma_{total}$		$<1.0 \times 10^{-5}$, CL = 90%
$\Gamma(B^0 \to K^*(892)^0 \tau^- \mu^+)/\Gamma_{total}$		$<8.2 \times 10^{-6}$, CL = 90%
$\Gamma(B^0 \to e^\pm \tau^\mp)/\Gamma_{total}$	[o]	$<1.6 \times 10^{-5}$, CL = 90%
$\Gamma(B^0 \to \mu^\pm \tau^\mp)/\Gamma_{total}$	[o]	$<1.4 \times 10^{-5}$, CL = 95%
$\Gamma(B \to s e^\pm \mu^\mp)/\Gamma_{total}$	[o]	$<2.2 \times 10^{-5}$, CL = 90%
$\Gamma(B \to \pi e^\pm \mu^\mp)/\Gamma_{total}$		$<9.2 \times 10^{-8}$, CL = 90%
$\Gamma(B \to \rho e^\pm \mu^\mp)/\Gamma_{total}$		$<3.2 \times 10^{-6}$, CL = 90%
$\Gamma(B \to K e^\pm \mu^\mp)/\Gamma_{total}$		$<3.8 \times 10^{-8}$, CL = 90%
$\Gamma(B \to K^*(892) e^\pm \mu^\mp)/\Gamma_{total}$		$<5.1 \times 10^{-7}$, CL = 90%
$\Gamma(B^0_s \to e^\pm \mu^\mp)/\Gamma_{total}$	[o]	$<5.4 \times 10^{-9}$, CL = 90%
$\Gamma(B^0_s \to e^\pm \tau^\mp)/\Gamma_{total}$		$<1.4 \times 10^{-3}$, CL = 90%
$\Gamma(B^0_s \to \mu^\pm \tau^\mp)/\Gamma_{total}$		$<4.2 \times 10^{-5}$, CL = 95%
$\Gamma(B^0_s \to \phi \mu^\pm e^\mp)/\Gamma_{total}$		$<1.6 \times 10^{-8}$, CL = 90%
$\Gamma(B^0_s \to \phi \mu^\pm \tau^\mp)/\Gamma_{total}$		$<1.0 \times 10^{-5}$, CL = 90%
$\Gamma(J/\psi(1S) \to e^\pm \mu^\mp)/\Gamma_{total}$		$<1.6 \times 10^{-7}$, CL = 90%
$\Gamma(J/\psi(1S) \to e^\pm \tau^\mp)/\Gamma_{total}$		$<7.5 \times 10^{-8}$, CL = 90%
$\Gamma(J/\psi(1S) \to \mu^\pm \tau^\mp)/\Gamma_{total}$		$<2.0 \times 10^{-6}$, CL = 90%
$\Gamma(\Upsilon(1S) \to e^\pm \mu^\mp)/\Gamma_{total}$		$<3.9 \times 10^{-7}$, CL = 90%
$\Gamma(\Upsilon(1S) \to \mu^\pm \tau^\mp)/\Gamma_{total}$		$<2.7 \times 10^{-6}$, CL = 90%
$\Gamma(\Upsilon(1S) \to e^\pm \tau^\mp)/\Gamma_{total}$		$<2.7 \times 10^{-6}$, CL = 90%
$\Gamma(\Upsilon(1S) \to \gamma e^\pm \mu^\mp)/\Gamma_{total}$		$<4.2 \times 10^{-7}$, CL = 90%
$\Gamma(\Upsilon(1S) \to \gamma \mu^\pm \tau^\mp)/\Gamma_{total}$		$<6.1 \times 10^{-6}$, CL = 90%
$\Gamma(\Upsilon(1S) \to \gamma e^\pm \tau^\mp)/\Gamma_{total}$		$<6.5 \times 10^{-6}$, CL = 90%
$\Gamma(\Upsilon(2S) \to e^\pm \tau^\mp)/\Gamma_{total}$		$<1.12 \times 10^{-6}$, CL = 90%
$\Gamma(\Upsilon(2S) \to \mu^\pm \tau^\mp)/\Gamma_{total}$		$<2.3 \times 10^{-7}$, CL = 90%
$\Gamma(\Upsilon(3S) \to e^\pm \tau^\mp)/\Gamma_{total}$		$<4.2 \times 10^{-6}$, CL = 90%
$\Gamma(\Upsilon(3S) \to e^\pm \mu^\mp)/\Gamma_{total}$		$<3.6 \times 10^{-7}$, CL = 90%
$\Gamma(\Upsilon(3S) \to \mu^\pm \tau^\mp)/\Gamma_{total}$		$<3.1 \times 10^{-6}$, CL = 90%
$\Gamma(\Lambda^+_c \to p e^+ \mu^-)/\Gamma_{total}$		$<9.9 \times 10^{-6}$, CL = 90%
$\Gamma(\Lambda^+_c \to p e^- \mu^+)/\Gamma_{total}$		$<1.9 \times 10^{-5}$, CL = 90%

TOTAL LEPTON NUMBER

Violation of total lepton number conservation also implies violation of lepton family number conservation.

$\Gamma(Z \to pe)/\Gamma_{total}$	$<1.8 \times 10^{-6}$, CL = 95%
$\Gamma(Z \to p\mu)/\Gamma_{total}$	$<1.8 \times 10^{-6}$, CL = 95%
limit on $\mu^- \to e^+$ conversion	
$\sigma(\mu^- {}^{32}S \to e^+ {}^{32}Si^*)$ / $\sigma(\mu^- {}^{32}S \to \nu_\mu {}^{32}P^*)$	$<9 \times 10^{-10}$, CL = 90%
$\sigma(\mu^- {}^{127}I \to e^+ {}^{127}Sb^*)$ / $\sigma(\mu^- {}^{127}I \to$ anything$)$	$<3 \times 10^{-10}$, CL = 90%
$\sigma(\mu^- Ti \to e^+ Ca)$ / $\sigma(\mu^- Ti \to$ capture$)$	$<3.6 \times 10^{-11}$, CL = 90%
$\Gamma(\tau^- \to e^+ \pi^- \pi^-)/\Gamma_{total}$	$<2.0 \times 10^{-8}$, CL = 90%
$\Gamma(\tau^- \to \mu^+ \pi^- \pi^-)/\Gamma_{total}$	$<3.9 \times 10^{-8}$, CL = 90%
$\Gamma(\tau^- \to e^+ \pi^- K^-)/\Gamma_{total}$	$<3.2 \times 10^{-8}$, CL = 90%

Unless otherwise stated, limits are given at the 90% confidence level, while errors are given as ±1 standard deviation.

Int. J. Mod. Phys. A 2026.41. Downloaded from www.worldscientific.com
by UNIVERSITY OF CALIFORNIA @ BERKELEY on 09/16/26. Re-use and distribution is strictly not permitted, except for Open Access articles.

$\Gamma(\tau^- \to e^+ K^- K^-)/\Gamma_{total}$		$<3.3 \times 10^{-8}$, CL = 90%
$\Gamma(\tau^- \to \mu^+ \pi^- K^-)/\Gamma_{total}$		$<4.8 \times 10^{-8}$, CL = 90%
$\Gamma(\tau^- \to \mu^+ K^- K^-)/\Gamma_{total}$		$<4.7 \times 10^{-8}$, CL = 90%
$\Gamma(\tau^- \to p e^- e^-)/\Gamma_{total}$		$<3.0 \times 10^{-8}$, CL = 90%
$\Gamma(\tau^- \to \overline{p} e^+ e^-)/\Gamma_{total}$		$<3.0 \times 10^{-8}$, CL = 90%
$\Gamma(\tau^- \to \overline{p} e^+ \mu^-)/\Gamma_{total}$		$<2.0 \times 10^{-8}$, CL = 90%
$\Gamma(\tau^- \to \overline{p} e^- \mu^+)/\Gamma_{total}$		$<1.8 \times 10^{-8}$, CL = 90%
$\Gamma(\tau^- \to p \mu^- \mu^-)/\Gamma_{total}$		$<4.0 \times 10^{-8}$, CL = 90%
$\Gamma(\tau^- \to \overline{p} \mu^+ \mu^-)/\Gamma_{total}$		$<1.8 \times 10^{-8}$, CL = 90%
$\Gamma(\tau^- \to \overline{p} \gamma)/\Gamma_{total}$		$<3.5 \times 10^{-6}$, CL = 90%
$\Gamma(\tau^- \to \overline{p} \pi^0)/\Gamma_{total}$		$<1.5 \times 10^{-5}$, CL = 90%
$\Gamma(\tau^- \to \overline{p} 2\pi^0)/\Gamma_{total}$		$<3.3 \times 10^{-5}$, CL = 90%
$\Gamma(\tau^- \to \overline{p} \eta)/\Gamma_{total}$		$<8.9 \times 10^{-6}$, CL = 90%
$\Gamma(\tau^- \to \overline{p} \pi^0 \eta)/\Gamma_{total}$		$<2.7 \times 10^{-5}$, CL = 90%
$\Gamma(\tau^- \to \Lambda \pi^-)/\Gamma_{total}$		$<4.7 \times 10^{-8}$, CL = 90%
$\Gamma(\tau^- \to \overline{\Lambda} \pi^-)/\Gamma_{total}$		$<4.3 \times 10^{-8}$, CL = 90%
$t_{1/2}(\,^{76}\mathrm{Ge} \to \,^{76}\mathrm{Se} + 2\,e^-)$		$>18.0 \times 10^{25}$ yr, CL = 90%
$t_{1/2}(\,^{136}\mathrm{Xe} \to \,^{136}\mathrm{Ba} + 2\,e^-)$		$>38.0 \times 10^{25}$ yr, CL = 90%
$t_{1/2}(\,^{130}\mathrm{Te} \to \,^{130}\mathrm{Xe} + 2\,e^-)$		$>3.5 \times 10^{25}$ yr, CL = 90%
$\Gamma(\pi^+ \to \mu^+ \overline{\nu}_e)/\Gamma_{total}$	[q]	$<1.5 \times 10^{-3}$, CL = 90%
$\Gamma(\phi(1020) \to \pi^+ \pi^+ e^- e^-)/\Gamma_{total}$		$<1.3 \times 10^{-5}$, CL = 90%
$\Gamma(K^+ \to \pi^- \mu^+ e^+)/\Gamma_{total}$		$<4.2 \times 10^{-11}$, CL = 90%
$\Gamma(K^+ \to \pi^0 \pi^- \mu^+ e^+)/\Gamma_{total}$		$<2.9 \times 10^{-10}$, CL = 90%
$\Gamma(K^+ \to \pi^- e^+ e^+)/\Gamma_{total}$		$<5.3 \times 10^{-11}$, CL = 90%
$\Gamma(K^+ \to \pi^- \mu^+ \mu^+)/\Gamma_{total}$		$<4.2 \times 10^{-11}$, CL = 90%
$\Gamma(K^+ \to \pi^- \pi^0 e^+ e^+)/\Gamma_{total}$		$<8.5 \times 10^{-10}$, CL = 90%
$\Gamma(K^+ \to \mu^+ \overline{\nu}_e)/\Gamma_{total}$	[q]	$<3.3 \times 10^{-3}$, CL = 90%
$\Gamma(K^+ \to \pi^0 e^+ \overline{\nu}_e)/\Gamma_{total}$		$<3 \times 10^{-3}$, CL = 90%
$\Gamma(D^+ \to \pi^- 2e^+)/\Gamma_{total}$		$<5.3 \times 10^{-7}$, CL = 90%
$\Gamma(D^+ \to \pi^- 2\mu^+)/\Gamma_{total}$		$<1.4 \times 10^{-8}$, CL = 90%
$\Gamma(D^+ \to \pi^- e^+ \mu^+)/\Gamma_{total}$		$<1.3 \times 10^{-7}$, CL = 90%
$\Gamma(D^+ \to \rho^- 2\mu^+)/\Gamma_{total}$		$<5.6 \times 10^{-4}$, CL = 90%
$\Gamma(D^+ \to K^- 2e^+)/\Gamma_{total}$		$<9 \times 10^{-7}$, CL = 90%
$\Gamma(D^+ \to K^0_S \pi^- 2e^+)/\Gamma_{total}$		$<3.3 \times 10^{-6}$, CL = 90%
$\Gamma(D^+ \to K^- \pi^0 2e^+)/\Gamma_{total}$		$<8.5 \times 10^{-6}$, CL = 90%
$\Gamma(D^+ \to K^- 2\mu^+)/\Gamma_{total}$		$<1.0 \times 10^{-5}$, CL = 90%
$\Gamma(D^+ \to K^- e^+ \mu^+)/\Gamma_{total}$		$<1.9 \times 10^{-6}$, CL = 90%
$\Gamma(D^+ \to K^*(892)^- 2\mu^+)/\Gamma_{total}$		$<8.5 \times 10^{-4}$, CL = 90%
$\Gamma(D^+ \to \Lambda e^+)/\Gamma_{total}$		$<1.1 \times 10^{-6}$, CL = 90%
$\Gamma(D^+ \to \overline{\Lambda} e^+)/\Gamma_{total}$		$<6.5 \times 10^{-7}$, CL = 90%
$\Gamma(D^+ \to \Sigma^0 e^+)/\Gamma_{total}$		$<1.7 \times 10^{-6}$, CL = 90%
$\Gamma(D^+ \to \overline{\Sigma}^0 e^+)/\Gamma_{total}$		$<1.3 \times 10^{-6}$, CL = 90%
$\Gamma(D^0 \to 2\pi^- 2e^+)/\Gamma_{total}$		$<9.1 \times 10^{-7}$, CL = 90%
$\Gamma(D^0 \to 2\pi^- 2\mu^+)/\Gamma_{total}$		$<1.52 \times 10^{-6}$, CL = 90%
$\Gamma(D^0 \to K^- \pi^- 2e^+)/\Gamma_{total}$		$<5.0 \times 10^{-7}$, CL = 90%
$\Gamma(D^0 \to K^- \pi^- 2\mu^+)/\Gamma_{total}$		$<5.3 \times 10^{-7}$, CL = 90%
$\Gamma(D^0 \to 2K^- 2e^+)/\Gamma_{total}$		$<3.4 \times 10^{-7}$, CL = 90%
$\Gamma(D^0 \to 2K^- 2\mu^+)/\Gamma_{total}$		$<1.0 \times 10^{-7}$, CL = 90%
$\Gamma(D^0 \to \pi^- \pi^- e^+ \mu^+)/\Gamma_{total}$		$<3.06 \times 10^{-6}$, CL = 90%
$\Gamma(D^0 \to K^- \pi^- e^+ \mu^+)/\Gamma_{total}$		$<2.10 \times 10^{-6}$, CL = 90%
$\Gamma(D^0 \to 2K^- e^+ \mu^+)/\Gamma_{total}$		$<5.8 \times 10^{-7}$, CL = 90%
$\Gamma(D^0 \to p e^-)/\Gamma_{total}$		$<5.5 \times 10^{-7}$, CL = 90%
$\Gamma(D^0 \to \overline{p} e^+)/\Gamma_{total}$		$<6.9 \times 10^{-7}$, CL = 90%
$\Gamma(D^0 \to p \mu^-)/\Gamma_{total}$		$<5.1 \times 10^{-7}$, CL = 90%
$\Gamma(D^0 \to \overline{p} \mu^+)/\Gamma_{total}$		$<6.3 \times 10^{-7}$, CL = 90%
$\Gamma(D^+_s \to \pi^- 2e^+)/\Gamma_{total}$		$<1.4 \times 10^{-6}$, CL = 90%
$\Gamma(D^+_s \to \pi^- 2\mu^+)/\Gamma_{total}$		$<8.6 \times 10^{-8}$, CL = 90%
$\Gamma(D^+_s \to \pi^- e^+ \mu^+)/\Gamma_{total}$		$<6.3 \times 10^{-7}$, CL = 90%
$\Gamma(D^+_s \to K^- 2e^+)/\Gamma_{total}$		$<7.7 \times 10^{-7}$, CL = 90%
$\Gamma(D^+_s \to K^- 2\mu^+)/\Gamma_{total}$		$<2.6 \times 10^{-8}$, CL = 90%
$\Gamma(D^+_s \to K^- e^+ \mu^+)/\Gamma_{total}$		$<2.6 \times 10^{-7}$, CL = 90%
$\Gamma(D^+_s \to K^*(892)^- 2\mu^+)/\Gamma_{total}$		$<1.4 \times 10^{-3}$, CL = 90%
$\Gamma(B^+ \to \pi^- e^+ e^+)/\Gamma_{total}$		$<2.3 \times 10^{-8}$, CL = 90%
$\Gamma(B^+ \to \pi^- \mu^+ \mu^+)/\Gamma_{total}$		$<4.0 \times 10^{-9}$, CL = 95%
$\Gamma(B^+ \to \pi^- e^+ \mu^+)/\Gamma_{total}$		$<1.5 \times 10^{-7}$, CL = 90%
$\Gamma(B^+ \to \rho^- e^+ e^+)/\Gamma_{total}$		$<1.7 \times 10^{-7}$, CL = 90%
$\Gamma(B^+ \to \rho^- \mu^+ \mu^+)/\Gamma_{total}$		$<4.2 \times 10^{-7}$, CL = 90%
$\Gamma(B^+ \to \rho^- e^+ \mu^+)/\Gamma_{total}$		$<4.7 \times 10^{-7}$, CL = 90%
$\Gamma(B^+ \to K^- e^+ e^+)/\Gamma_{total}$		$<3.0 \times 10^{-8}$, CL = 90%
$\Gamma(B^+ \to K^- \mu^+ \mu^+)/\Gamma_{total}$		$<4.1 \times 10^{-8}$, CL = 90%
$\Gamma(B^+ \to K^- e^+ \mu^+)/\Gamma_{total}$		$<1.6 \times 10^{-7}$, CL = 90%
$\Gamma(B^+ \to K^*(892)^- e^+ e^+)/\Gamma_{total}$		$<4.0 \times 10^{-7}$, CL = 90%
$\Gamma(B^+ \to K^*(892)^- \mu^+ \mu^+)/\Gamma_{total}$		$<5.9 \times 10^{-7}$, CL = 90%
$\Gamma(B^+ \to K^*(892)^- e^+ \mu^+)/\Gamma_{total}$		$<3.0 \times 10^{-7}$, CL = 90%
$\Gamma(B^+ \to D^- e^+ e^+)/\Gamma_{total}$		$<2.6 \times 10^{-6}$, CL = 90%
$\Gamma(B^+ \to D^- e^+ \mu^+)/\Gamma_{total}$		$<1.8 \times 10^{-6}$, CL = 90%
$\Gamma(B^+ \to D^- \mu^+ \mu^+)/\Gamma_{total}$		$<6.9 \times 10^{-7}$, CL = 95%
$\Gamma(B^+ \to D^{*-} \mu^+ \mu^+)/\Gamma_{total}$		$<2.4 \times 10^{-6}$, CL = 95%
$\Gamma(B^+ \to D^-_s \mu^+ \mu^+)/\Gamma_{total}$		$<5.8 \times 10^{-7}$, CL = 95%
$\Gamma(B^+ \to \overline{D}^0 \pi^- \mu^+ \mu^+)/\Gamma_{total}$		$<1.5 \times 10^{-6}$, CL = 95%
$\Gamma(B^+ \to \Lambda^0 \mu^+)/\Gamma_{total}$		$<6 \times 10^{-8}$, CL = 90%
$\Gamma(B^+ \to \Lambda^0 e^+)/\Gamma_{total}$		$<3.2 \times 10^{-8}$, CL = 90%
$\Gamma(B^+ \to \overline{\Lambda}^0 \mu^+)/\Gamma_{total}$		$<6 \times 10^{-8}$, CL = 90%
$\Gamma(B^+ \to \overline{\Lambda}^0 e^+)/\Gamma_{total}$		$<8 \times 10^{-8}$, CL = 90%
$\Gamma(B^0 \to p \mu^-)/\Gamma_{total}$		$<2.6 \times 10^{-9}$, CL = 90%
$\Gamma(B^0 \to \Lambda^+_c \mu^-)/\Gamma_{total}$		$<1.4 \times 10^{-6}$, CL = 90%
$\Gamma(B^0 \to \Lambda^+_c e^-)/\Gamma_{total}$		$<4 \times 10^{-6}$, CL = 90%
$\Gamma(B^0_s \to p \mu^-)/\Gamma_{total}$		$<1.21 \times 10^{-8}$, CL = 90%
$\Gamma(J/\psi(1S) \to K^+ K^+ e^- e^-$ + c.c.$)/\Gamma_{total}$		$<2.1 \times 10^{-9}$, CL = 90%
$\Gamma(J/\psi(1S) \to p e^-$ + c.c.$)/\Gamma_{total}$		$<3.1 \times 10^{-8}$, CL = 90%
$\Gamma(\Lambda \to \pi^+ e^-)/\Gamma_{total}$		$<6 \times 10^{-7}$, CL = 90%
$\Gamma(\Lambda \to \pi^+ \mu^-)/\Gamma_{total}$		$<6 \times 10^{-7}$, CL = 90%
$\Gamma(\Lambda \to \pi^- e^+)/\Gamma_{total}$		$<4 \times 10^{-7}$, CL = 90%
$\Gamma(\Lambda \to \pi^- \mu^+)/\Gamma_{total}$		$<6 \times 10^{-7}$, CL = 90%
$\Gamma(\Lambda \to K^+ e^-)/\Gamma_{total}$		$<2 \times 10^{-6}$, CL = 90%
$\Gamma(\Lambda \to K^+ \mu^-)/\Gamma_{total}$		$<3 \times 10^{-6}$, CL = 90%
$\Gamma(\Lambda \to K^- e^+)/\Gamma_{total}$		$<2 \times 10^{-6}$, CL = 90%
$\Gamma(\Lambda \to K^- \mu^+)/\Gamma_{total}$		$<3 \times 10^{-6}$, CL = 90%
$\Gamma(\Lambda \to K^0_S \nu)/\Gamma_{total}$		$<2 \times 10^{-5}$, CL = 90%
$\Gamma(\Sigma^- \to p e^- e^-)/\Gamma_{total}$		$<6.7 \times 10^{-5}$, CL = 90%
$\Gamma(\Xi^- \to p \mu^- \mu^-)/\Gamma_{total}$		$<4 \times 10^{-8}$, CL = 90%
$\Gamma(\Lambda^+_c \to \overline{p} 2e^+)/\Gamma_{total}$		$<2.7 \times 10^{-6}$, CL = 90%
$\Gamma(\Lambda^+_c \to \overline{p} 2\mu^+)/\Gamma_{total}$		$<9.4 \times 10^{-6}$, CL = 90%
$\Gamma(\Lambda^+_c \to \overline{p} e^+ \mu^+)/\Gamma_{total}$		$<1.6 \times 10^{-5}$, CL = 90%
$\Gamma(\Lambda^+_c \to \Sigma^- \mu^+ \mu^+)/\Gamma_{total}$		$<7.0 \times 10^{-4}$, CL = 90%

BARYON NUMBER

$\Gamma(Z \to p e)/\Gamma_{total}$		$<1.8 \times 10^{-6}$, CL = 95%
$\Gamma(Z \to p \mu)/\Gamma_{total}$		$<1.8 \times 10^{-6}$, CL = 95%
$\Gamma(\tau^- \to p e^- e^-)/\Gamma_{total}$		$<3.0 \times 10^{-8}$, CL = 90%
$\Gamma(\tau^- \to \overline{p} e^+ e^-)/\Gamma_{total}$		$<3.0 \times 10^{-8}$, CL = 90%
$\Gamma(\tau^- \to \overline{p} e^+ \mu^-)/\Gamma_{total}$		$<2.0 \times 10^{-8}$, CL = 90%
$\Gamma(\tau^- \to \overline{p} e^- \mu^+)/\Gamma_{total}$		$<1.8 \times 10^{-8}$, CL = 90%
$\Gamma(\tau^- \to p \mu^- \mu^-)/\Gamma_{total}$		$<4.0 \times 10^{-8}$, CL = 90%
$\Gamma(\tau^- \to \overline{p} \mu^+ \mu^-)/\Gamma_{total}$		$<1.8 \times 10^{-8}$, CL = 90%
$\Gamma(\tau^- \to \overline{p} \gamma)/\Gamma_{total}$		$<3.5 \times 10^{-6}$, CL = 90%
$\Gamma(\tau^- \to \overline{p} \pi^0)/\Gamma_{total}$		$<1.5 \times 10^{-5}$, CL = 90%
$\Gamma(\tau^- \to \overline{p} 2\pi^0)/\Gamma_{total}$		$<3.3 \times 10^{-5}$, CL = 90%
$\Gamma(\tau^- \to \overline{p} \eta)/\Gamma_{total}$		$<8.9 \times 10^{-6}$, CL = 90%
$\Gamma(\tau^- \to \overline{p} \pi^0 \eta)/\Gamma_{total}$		$<2.7 \times 10^{-5}$, CL = 90%
$\Gamma(\tau^- \to \Lambda \pi^-)/\Gamma_{total}$		$<4.7 \times 10^{-8}$, CL = 90%
$\Gamma(\tau^- \to \overline{\Lambda} \pi^-)/\Gamma_{total}$		$<4.3 \times 10^{-8}$, CL = 90%
$\Gamma(D^+ \to \Lambda e^+)/\Gamma_{total}$		$<1.1 \times 10^{-6}$, CL = 90%
$\Gamma(D^+ \to \overline{\Lambda} e^+)/\Gamma_{total}$		$<6.5 \times 10^{-7}$, CL = 90%
$\Gamma(D^+ \to \Sigma^0 e^+)/\Gamma_{total}$		$<1.7 \times 10^{-6}$, CL = 90%
$\Gamma(D^+ \to \overline{\Sigma}^0 e^+)/\Gamma_{total}$		$<1.3 \times 10^{-6}$, CL = 90%
$\Gamma(D^0 \to p e^-)/\Gamma_{total}$		$<5.5 \times 10^{-7}$, CL = 90%
$\Gamma(D^0 \to \overline{p} e^+)/\Gamma_{total}$		$<6.9 \times 10^{-7}$, CL = 90%
$\Gamma(D^0 \to p \mu^-)/\Gamma_{total}$		$<5.1 \times 10^{-7}$, CL = 90%
$\Gamma(D^0 \to \overline{p} \mu^+)/\Gamma_{total}$		$<6.3 \times 10^{-7}$, CL = 90%
$\Gamma(B^+ \to \Lambda^0 \mu^+)/\Gamma_{total}$		$<6 \times 10^{-8}$, CL = 90%
$\Gamma(B^+ \to \Lambda^0 e^+)/\Gamma_{total}$		$<3.2 \times 10^{-8}$, CL = 90%
$\Gamma(B^+ \to \overline{\Lambda}^0 \mu^+)/\Gamma_{total}$		$<6 \times 10^{-8}$, CL = 90%
$\Gamma(B^+ \to \overline{\Lambda}^0 e^+)/\Gamma_{total}$		$<8 \times 10^{-8}$, CL = 90%
$\Gamma(B^0 \to p \mu^-)/\Gamma_{total}$		$<2.6 \times 10^{-9}$, CL = 90%
$\Gamma(B^0 \to \Lambda^+_c \mu^-)/\Gamma_{total}$		$<1.4 \times 10^{-6}$, CL = 90%
$\Gamma(B^0 \to \Lambda^+_c e^-)/\Gamma_{total}$		$<4 \times 10^{-6}$, CL = 90%
$\Gamma(B^0_s \to p \mu^-)/\Gamma_{total}$		$<1.21 \times 10^{-8}$, CL = 90%

Unless otherwise stated, limits are given at the 90% confidence level, while errors are given as ±1 standard deviation.

Int. J. Mod. Phys. A 2026.41. Downloaded from www.worldscientific.com
by UNIVERSITY OF CALIFORNIA @ BERKELEY on 09/16/26. Re-use and distribution is strictly not permitted, except for Open Acce

$\Gamma(J/\psi(1S) \to p e^- + \text{c.c.})/\Gamma_{\text{total}}$		$<3.1 \times 10^{-8}$, CL = 90%
p mean life		$>9 \times 10^{29}$ years, CL = 90%

A few examples of proton or bound neutron decay follow. For limits on many other nucleon decay channels, see the Baryon Summary Table.

$\tau(N \to e^+ \pi)$		$> 5300\ (n)$, $> 24000\ (p) \times 10^{30}$ years, CL = 90%
$\tau(N \to \mu^+ \pi)$		$> 3500\ (n)$, $> 16000\ (p) \times 10^{30}$ years, CL = 90%
$\tau(N \to e^+ K)$		$> 17\ (n)$, $> 1000\ (p) \times 10^{30}$ years, CL = 90%
$\tau(N \to \mu^+ K)$		$> 26\ (n)$, $> 4500\ (p) \times 10^{30}$ years, CL = 90%
Mean $n\overline{n}$-oscillation time (free n)		$>8.6 \times 10^7$ s, CL = 90%
Mean $n\overline{n}$-oscillation time (bound n)	[r]	$>4.7 \times 10^8$ s, CL = 90%
$\Gamma(\Lambda \to \pi^+ e^-)/\Gamma_{\text{total}}$		$<6 \times 10^{-7}$, CL = 90%
$\Gamma(\Lambda \to \pi^+ \mu^-)/\Gamma_{\text{total}}$		$<6 \times 10^{-7}$, CL = 90%
$\Gamma(\Lambda \to \pi^- e^+)/\Gamma_{\text{total}}$		$<4 \times 10^{-7}$, CL = 90%
$\Gamma(\Lambda \to \pi^- \mu^+)/\Gamma_{\text{total}}$		$<6 \times 10^{-7}$, CL = 90%
$\Gamma(\Lambda \to K^+ e^-)/\Gamma_{\text{total}}$		$<2 \times 10^{-6}$, CL = 90%
$\Gamma(\Lambda \to K^+ \mu^-)/\Gamma_{\text{total}}$		$<3 \times 10^{-6}$, CL = 90%
$\Gamma(\Lambda \to K^- e^+)/\Gamma_{\text{total}}$		$<2 \times 10^{-6}$, CL = 90%
$\Gamma(\Lambda \to K^- \mu^+)/\Gamma_{\text{total}}$		$<3 \times 10^{-6}$, CL = 90%
$\Gamma(\Lambda \to K^0_S \nu)/\Gamma_{\text{total}}$		$<2 \times 10^{-5}$, CL = 90%
$\Gamma(\Lambda \to \overline{p}\pi^+)/\Gamma_{\text{total}}$		$<9 \times 10^{-7}$, CL = 90%
$\Gamma(\Lambda_c^+ \to \overline{p} 2e^+)/\Gamma_{\text{total}}$		$<2.7 \times 10^{-6}$, CL = 90%
$\Gamma(\Lambda_c^+ \to \overline{p} 2\mu^+)/\Gamma_{\text{total}}$		$<9.4 \times 10^{-6}$, CL = 90%
$\Gamma(\Lambda_c^+ \to \overline{p} e^+ \mu^+)/\Gamma_{\text{total}}$		$<1.6 \times 10^{-5}$, CL = 90%

ELECTRIC CHARGE (Q)

γ charge (mixed)		$<1 \times 10^{-46}\ e$
γ charge (single)		$<1 \times 10^{-35}\ e$
$e \to \nu_e \gamma$ and astrophysical limits	[s]	$>6.6 \times 10^{28}$ yr, CL = 90%
ν charge		$<4 \times 10^{-35}\ e$, CL = 95%
$\lvert q_p + q_e \rvert / e$	[t]	$<1 \times 10^{-21}$
n charge		$(-0.2 \pm 0.8) \times 10^{-21}\ e$
$\Gamma(n \to p \nu_e \overline{\nu}_e)/\Gamma_{\text{total}}$		$<8 \times 10^{-27}$, CL = 68%

$\Delta S = \Delta Q$ RULE

Violations allowed in second-order weak interactions.

$\Gamma(K^+ \to \pi^+ \pi^+ e^- \overline{\nu}_e)/\Gamma_{\text{total}}$		$<1.3 \times 10^{-8}$, CL = 90%
$\Gamma(K^+ \to \pi^+ \pi^+ \mu^- \overline{\nu}_\mu)/\Gamma_{\text{total}}$		$<3.0 \times 10^{-6}$, CL = 95%
$\text{Re}(x_+)$, K_{e3} parameter		$(-0.9 \pm 3.0) \times 10^{-3}$
$x = A(\overline{K}^0 \to \pi^- \ell^+ \nu)/A(K^0 \to \pi^- \ell^+ \nu) = A(\Delta S{=}{-}\Delta Q)/A(\Delta S{=}\Delta Q)$		
real part of x		-0.002 ± 0.006
imaginary part of x		0.0012 ± 0.0021
$\Gamma(\Sigma^+ \to n \ell^+ \nu)/\Gamma(\Sigma^- \to n \ell^- \overline{\nu}_\ell)$		<0.043
$\Gamma(\Sigma^+ \to n e^+ \nu_e)/\Gamma_{\text{total}}$		$<5 \times 10^{-6}$, CL = 90%
$\Gamma(\Sigma^+ \to n \mu^+ \nu_\mu)/\Gamma_{\text{total}}$		$<3.0 \times 10^{-5}$, CL = 90%
$\Gamma(\Xi^0 \to \Sigma^- e^+ \nu_e)/\Gamma_{\text{total}}$		$<1.6 \times 10^{-4}$, CL = 90%
$\Gamma(\Xi^0 \to \Sigma^- \mu^+ \nu_\mu)/\Gamma_{\text{total}}$		$<9 \times 10^{-4}$, CL = 90%

$\Delta S = 2$ FORBIDDEN

Allowed in second-order weak interactions.

$\Gamma(\Xi^0 \to p \pi^-)/\Gamma_{\text{total}}$		$<8 \times 10^{-6}$, CL = 90%
$\Gamma(\Xi^0 \to p e^- \overline{\nu}_e)/\Gamma_{\text{total}}$		$<1.3 \times 10^{-3}$
$\Gamma(\Xi^0 \to p \mu^- \overline{\nu}_\mu)/\Gamma_{\text{total}}$		$<1.3 \times 10^{-3}$
$\Gamma(\Xi^- \to n \pi^-)/\Gamma_{\text{total}}$		$<1.9 \times 10^{-5}$, CL = 90%
$\Gamma(\Xi^- \to n e^- \overline{\nu}_e)/\Gamma_{\text{total}}$		$<3.2 \times 10^{-3}$, CL = 90%
$\Gamma(\Xi^- \to n \mu^- \overline{\nu}_\mu)/\Gamma_{\text{total}}$		$<1.5 \times 10^{-2}$, CL = 90%
$\Gamma(\Xi^- \to p \pi^- \pi^-)/\Gamma_{\text{total}}$		$<4 \times 10^{-4}$, CL = 90%
$\Gamma(\Xi^- \to p \pi^- e^- \overline{\nu}_e)/\Gamma_{\text{total}}$		$<4 \times 10^{-4}$, CL = 90%
$\Gamma(\Xi^- \to p \pi^- \mu^- \overline{\nu}_\mu)/\Gamma_{\text{total}}$		$<4 \times 10^{-4}$, CL = 90%
$\Gamma(\Omega^- \to \Lambda \pi^-)/\Gamma_{\text{total}}$		$<2.9 \times 10^{-6}$, CL = 90%

$\Delta S = 2$ VIA MIXING

Allowed in second-order weak interactions, e.g. mixing.

$m_{K^0_L} - m_{K^0_S}$	$(0.5293 \pm 0.0009) \times 10^{10}\ \hbar\ \text{s}^{-1}$ (S = 1.3)
$m_{K^0_L} - m_{K^0_S}$	$(3.484 \pm 0.006) \times 10^{-12}$ MeV

$\Delta C = 2$ VIA MIXING

Allowed in second-order weak interactions, e.g. mixing.

$\lvert m_{D^0_1} - m_{D^0_2} \rvert = x\Gamma$	$(0.997 \pm 0.116) \times 10^{10}\ \hbar\ \text{s}^{-1}$
$(\Gamma_{D^0_1} - \Gamma_{D^0_2})/\Gamma = 2y$	$(1.394 \pm 0.056) \times 10^{-2}$

$\Delta B = 2$ VIA MIXING

Allowed in second-order weak interactions, e.g. mixing.

χ_d (B^0-$\overline{B}^0$ mixing probability)	0.1849 ± 0.0010
$\Delta m_{B^0} = m_{B^0_H} - m_{B^0_L}$	$(0.5068 \pm 0.0019) \times 10^{12}\ \hbar\ \text{s}^{-1}$
$x_d = \Delta m_{B^0}/\Gamma_{B^0}$	0.7659 ± 0.0032
$\Delta m_{B^0_s} = m_{B^0_{sH}} - m_{B^0_{sL}}$	$(17.766 \pm 0.006) \times 10^{12}\ \hbar\ \text{s}^{-1}$
$x_s = \Delta m_{B^0_s}/\Gamma_{B^0_s}$	26.91 ± 0.11
χ_s (B^0_s-$\overline{B}^0_s$ mixing parameter)	0.499313 ± 0.000006

$\Delta S = 1$ WEAK NEUTRAL CURRENT FORBIDDEN

Allowed by higher-order electroweak interactions.

$\Gamma(K^+ \to \pi^+ e^+ e^-)/\Gamma_{\text{total}}$		$(3.00 \pm 0.09) \times 10^{-7}$
$\Gamma(K^+ \to \pi^+ \mu^+ \mu^-)/\Gamma_{\text{total}}$		$(9.17 \pm 0.14) \times 10^{-8}$ (S = 1.8)
$\Gamma(K^+ \to \pi^+ e^+ e^- e^+ e^-)/\Gamma_{\text{total}}$		$<1.4 \times 10^{-8}$, CL = 90%
$\Gamma(K^+ \to \pi^+ \nu\overline{\nu})/\Gamma_{\text{total}}$		$(1.33 \pm 0.30) \times 10^{-10}$
$\Gamma(K^+ \to \pi^+ \pi^0 \nu\overline{\nu})/\Gamma_{\text{total}}$		$<4.3 \times 10^{-5}$, CL = 90%
$\Gamma(K^0_S \to \mu^+ \mu^-)/\Gamma_{\text{total}}$		$<2.1 \times 10^{-10}$, CL = 90%
$\Gamma(K^0_S \to e^+ e^-)/\Gamma_{\text{total}}$		$<9 \times 10^{-9}$, CL = 90%
$\Gamma(K^0_S \to \pi^0 e^+ e^-)/\Gamma_{\text{total}}$	[u]	$(3.0^{+1.5}_{-1.2}) \times 10^{-9}$
$\Gamma(K^0_S \to \pi^0 \mu^+ \mu^-)/\Gamma_{\text{total}}$		$(2.9^{+1.5}_{-1.2}) \times 10^{-9}$
$\Gamma(K^0_L \to \mu^+ \mu^-)/\Gamma_{\text{total}}$		$(6.84 \pm 0.11) \times 10^{-9}$
$\Gamma(K^0_L \to e^+ e^-)/\Gamma_{\text{total}}$		$(9^{+6}_{-4}) \times 10^{-12}$
$\Gamma(K^0_L \to \pi^+ \pi^- e^+ e^-)/\Gamma_{\text{total}}$	[v]	$(3.11 \pm 0.19) \times 10^{-7}$
$\Gamma(K^0_L \to \pi^0 \pi^0 e^+ e^-)/\Gamma_{\text{total}}$		$<6.6 \times 10^{-9}$, CL = 90%
$\Gamma(K^0_L \to \pi^0 \pi^0 \mu^+ \mu^-)/\Gamma_{\text{total}}$		$<9.2 \times 10^{-11}$, CL = 90%
$\Gamma(K^0_L \to \mu^+ \mu^- e^+ e^-)/\Gamma_{\text{total}}$		$(2.69 \pm 0.27) \times 10^{-9}$
$\Gamma(K^0_L \to e^+ e^- e^+ e^-)/\Gamma_{\text{total}}$		$(3.56 \pm 0.21) \times 10^{-8}$
$\Gamma(K^0_L \to \pi^0 \mu^+ \mu^-)/\Gamma_{\text{total}}$		$<3.8 \times 10^{-10}$, CL = 90%
$\Gamma(K^0_L \to \pi^0 e^+ e^-)/\Gamma_{\text{total}}$		$<2.8 \times 10^{-10}$, CL = 90%
$\Gamma(K^0_L \to \pi^0 \nu\overline{\nu})/\Gamma_{\text{total}}$		$<2.2 \times 10^{-9}$, CL = 90%
$\Gamma(K^0_L \to \pi^0 \pi^0 \nu\overline{\nu})/\Gamma_{\text{total}}$		$<8.1 \times 10^{-7}$, CL = 90%
$\Gamma(\Sigma^+ \to p e^+ e^-)/\Gamma_{\text{total}}$		$<7 \times 10^{-6}$
$\Gamma(\Sigma^+ \to p \mu^+ \mu^-)/\Gamma_{\text{total}}$		$(1.09 \pm 0.17) \times 10^{-8}$

Unless otherwise stated, limits are given at the 90% confidence level, while errors are given as ± 1 standard deviation.

Int. J. Mod. Phys. A 2026.41. Downloaded from www.worldscientific.com
by UNIVERSITY OF CALIFORNIA @ BERKELEY on 09/16/26. Re-use and distribution is strictly not permitted, except for Open Access articles.

$\Delta C = 1$ WEAK NEUTRAL CURRENT FORBIDDEN

Allowed by higher-order electroweak interactions.

$\Gamma(D^+ \to \pi^+ e^+ e^-)/\Gamma_{total}$		$<1.1 \times 10^{-6}$, CL = 90%
$\Gamma(D^+ \to \pi^+ \mu^+ \mu^-)/\Gamma_{total}$		$<6.7 \times 10^{-8}$, CL = 90%
$\Gamma(D^+ \to \rho^+ \mu^+ \mu^-)/\Gamma_{total}$		$<5.6 \times 10^{-4}$, CL = 90%
$\Gamma(D^0 \to \gamma\gamma)/\Gamma_{total}$		$<8.5 \times 10^{-7}$, CL = 90%
$\Gamma(D^0 \to e^+ e^-)/\Gamma_{total}$		$<7.9 \times 10^{-8}$, CL = 90%
$\Gamma(D^0 \to \mu^+ \mu^-)/\Gamma_{total}$		$<2.1 \times 10^{-9}$, CL = 90%
$\Gamma(D^0 \to \pi^0 e^+ e^-)/\Gamma_{total}$		$<4 \times 10^{-6}$, CL = 90%
$\Gamma(D^0 \to \pi^0 \mu^+ \mu^-)/\Gamma_{total}$		$<1.8 \times 10^{-4}$, CL = 90%
$\Gamma(D^0 \to \eta e^+ e^-)/\Gamma_{total}$		$<3 \times 10^{-6}$, CL = 90%
$\Gamma(D^0 \to \eta \mu^+ \mu^-)/\Gamma_{total}$		$<5.3 \times 10^{-4}$, CL = 90%
$\Gamma(D^0 \to \pi^+ \pi^- e^+ e^-)/\Gamma_{total}$		$<7 \times 10^{-6}$, CL = 90%
$\Gamma(D^0 \to \rho^0 e^+ e^-)/\Gamma_{total}$		$<1.0 \times 10^{-4}$, CL = 90%
$\Gamma(D^0 \to \pi^+ \pi^- \mu^+ \mu^-)/\Gamma_{total}$		$(9.6 \pm 1.2) \times 10^{-7}$
$\Gamma(D^0 \to \rho^0 \mu^+ \mu^-)/\Gamma_{total}$		$<2.2 \times 10^{-5}$, CL = 90%
$\Gamma(D^0 \to \omega e^+ e^-)/\Gamma_{total}$		$<6 \times 10^{-6}$, CL = 90%
$\Gamma(D^0 \to \omega \mu^+ \mu^-)/\Gamma_{total}$		$<8.3 \times 10^{-4}$, CL = 90%
$\Gamma(D^0 \to K^- K^+ e^+ e^-)/\Gamma_{total}$		$<1.1 \times 10^{-5}$, CL = 90%
$\Gamma(D^0 \to \phi e^+ e^-)/\Gamma_{total}$		$<5.2 \times 10^{-5}$, CL = 90%
$\Gamma(D^0 \to K^- K^+ \mu^+ \mu^-)/\Gamma_{total}$		$(1.54 \pm 0.32) \times 10^{-7}$
$\Gamma(D^0 \to \phi \mu^+ \mu^-)/\Gamma_{total}$		$<3.1 \times 10^{-5}$, CL = 90%
$\Gamma(D^0 \to K^- \pi^+ \mu^+ \mu^-)/\Gamma_{total}$		$<3.59 \times 10^{-4}$, CL = 90%
$\Gamma(D^0 \to \pi^+ \pi^- \pi^0 \mu^+ \mu^-)/\Gamma_{total}$		$<8.1 \times 10^{-4}$, CL = 90%
$\Gamma(D_s^+ \to K^+ e^+ e^-)/\Gamma_{total}$		$<3.7 \times 10^{-6}$, CL = 90%
$\Gamma(D_s^+ \to K^+ \mu^+ \mu^-)/\Gamma_{total}$		$<1.4 \times 10^{-7}$, CL = 90%
$\Gamma(D_s^+ \to K^*(892)^+ \mu^+ \mu^-)/\Gamma_{total}$		$<1.4 \times 10^{-3}$, CL = 90%
$\Gamma(\Lambda_c^+ \to p e^+ e^-)/\Gamma_{total}$		$<5.5 \times 10^{-6}$, CL = 90%
$\Gamma(\Lambda_c^+ \to p \mu^+ \mu^- \text{non-resonant})/\Gamma_{total}$		$<2.9 \times 10^{-8}$, CL = 90%

$\Delta B = 1$ WEAK NEUTRAL CURRENT FORBIDDEN

Allowed by higher-order electroweak interactions.

$\Gamma(B^+ \to \pi^+ \ell^+ \ell^-)/\Gamma_{total}$	[x]	$<4.9 \times 10^{-8}$, CL = 90%
$\Gamma(B^+ \to \pi^+ e^+ e^-)/\Gamma_{total}$		$<5.4 \times 10^{-8}$, CL = 90%
$\Gamma(B^+ \to \pi^+ \mu^+ \mu^-)/\Gamma_{total}$		$(1.78 \pm 0.22) \times 10^{-8}$
$\Gamma(B^+ \to \rho(770)^+ e^+ e^-)/\Gamma_{total}$		$<4.67 \times 10^{-7}$, CL = 90%
$\Gamma(B^+ \to \rho(770)^+ \mu^+ \mu^-)/\Gamma_{total}$		$<3.81 \times 10^{-7}$, CL = 90%
$\Gamma(B^+ \to \rho(770)^+ \ell^+ \ell^-)/\Gamma_{total}$		$<1.89 \times 10^{-7}$, CL = 90%
$\Gamma(B^+ \to \pi^+ \nu\overline{\nu})/\Gamma_{total}$		$<1.4 \times 10^{-5}$, CL = 90%
$\Gamma(B^+ \to K^+ \ell^+ \ell^-)/\Gamma_{total}$	[x]	$(4.7 \pm 0.5) \times 10^{-7}$ (S = 2.3)
$\Gamma(B^+ \to K^+ e^+ e^-)/\Gamma_{total}$		$(5.6 \pm 0.6) \times 10^{-7}$
$\Gamma(B^+ \to K^+ \mu^+ \mu^-)/\Gamma_{total}$		$(4.53 \pm 0.35) \times 10^{-7}$ (S = 1.8)
$\Gamma(B^+ \to K^+ \mu^+ \mu^- \text{nonresonant})/\Gamma_{total}$		$(4.37 \pm 0.27) \times 10^{-7}$
$\Gamma(B^+ \to K^+ \tau^+ \tau^-)/\Gamma_{total}$		$<2.25 \times 10^{-3}$, CL = 90%
$\Gamma(B^+ \to K^+ \overline{\nu}\nu)/\Gamma_{total}$		$(2.3 \pm 0.7) \times 10^{-5}$
$\Gamma(B^+ \to \rho^+ \nu\overline{\nu})/\Gamma_{total}$		$<3.0 \times 10^{-5}$, CL = 90%
$\Gamma(B^+ \to K^*(892)^+ \ell^+ \ell^-)/\Gamma_{total}$	[x]	$(1.01 \pm 0.11) \times 10^{-6}$ (S = 1.1)
$\Gamma(B^+ \to K^*(892)^+ e^+ e^-)/\Gamma_{total}$		$(1.55^{+0.40}_{-0.31}) \times 10^{-6}$
$\Gamma(B^+ \to K^*(892)^+ \mu^+ \mu^-)/\Gamma_{total}$		$(9.6 \pm 1.0) \times 10^{-7}$
$\Gamma(B^+ \to K^*(892)^+ \nu\overline{\nu})/\Gamma_{total}$		$<4.0 \times 10^{-5}$, CL = 90%
$\Gamma(B^+ \to K^+ \pi^+ \pi^- \mu^+ \mu^-)/\Gamma_{total}$		$(4.3 \pm 0.4) \times 10^{-7}$
$\Gamma(B^+ \to D_s^+ \mu^+ \mu^-)/\Gamma_{total}$		$<2.4 \times 10^{-8}$, CL = 90%
$\Gamma(B^+ \to \phi K^+ \mu^+ \mu^-)/\Gamma_{total}$		$(7.9^{+2.1}_{-1.7}) \times 10^{-8}$
$\Gamma(B^+ \to \overline{\Lambda} p \nu\overline{\nu})/\Gamma_{total}$		$<3.0 \times 10^{-5}$, CL = 90%
$\Gamma(B^0 \to \gamma\gamma)/\Gamma_{total}$		$<6.4 \times 10^{-8}$, CL = 90%
$\Gamma(B^0 \to e^+ e^-)/\Gamma_{total}$		$<2.5 \times 10^{-9}$, CL = 90%
$\Gamma(B^0 \to e^+ e^- \gamma)/\Gamma_{total}$		$<1.2 \times 10^{-7}$, CL = 90%
$\Gamma(B^0 \to \mu^+ \mu^-)/\Gamma_{total}$		$<1.5 \times 10^{-10}$, CL = 90%
$\Gamma(B^0 \to \mu^+ \mu^- \mu^+ \mu^-)/\Gamma_{total}$		$<1.8 \times 10^{-10}$, CL = 95%
$\Gamma(B^0 \to SP,\ S \to \mu^+ \mu^-,\ P \to \mu^+ \mu^-)/\Gamma_{total}$	[y]	$<6.0 \times 10^{-10}$, CL = 95%
$\Gamma(B^0 \to aa,\ a \to \mu^+ \mu^-)/\Gamma_{total}$		$<2.3 \times 10^{-10}$, CL = 95%
$\Gamma(B^0 \to \tau^+ \tau^-)/\Gamma_{total}$		$<2.1 \times 10^{-3}$, CL = 95%
$\Gamma(B^0 \to \pi^0 \ell^+ \ell^-)/\Gamma_{total}$	[x]	$<3.8 \times 10^{-8}$, CL = 90%
$\Gamma(B^0 \to \pi^0 e^+ e^-)/\Gamma_{total}$		$<7.9 \times 10^{-8}$, CL = 90%
$\Gamma(B^0 \to \pi^0 \mu^+ \mu^-)/\Gamma_{total}$		$<5.9 \times 10^{-8}$, CL = 90%
$\Gamma(B^0 \to \eta \ell^+ \ell^-)/\Gamma_{total}$	[x]	$<4.8 \times 10^{-8}$, CL = 90%
$\Gamma(B^0 \to \eta e^+ e^-)/\Gamma_{total}$		$<1.05 \times 10^{-7}$, CL = 90%
$\Gamma(B^0 \to \eta \mu^+ \mu^-)/\Gamma_{total}$		$<9.4 \times 10^{-8}$, CL = 90%
$\Gamma(B^0 \to \rho(770)^0 e^+ e^-)/\Gamma_{total}$		$<4.55 \times 10^{-7}$, CL = 90%
$\Gamma(B^0 \to \omega e^+ e^-)/\Gamma_{total}$		$<3.07 \times 10^{-7}$, CL = 90%
$\Gamma(B^0 \to \omega \mu^+ \mu^-)/\Gamma_{total}$		$<2.49 \times 10^{-7}$, CL = 90%
$\Gamma(B^0 \to \omega \ell^+ \ell^-)/\Gamma_{total}$		$<2.20 \times 10^{-7}$, CL = 90%
$\Gamma(B^0 \to \pi^0 \nu\overline{\nu})/\Gamma_{total}$		$<9 \times 10^{-6}$, CL = 90%
$\Gamma(B^0 \to K^0 \ell^+ \ell^-)/\Gamma_{total}$	[x]	$(3.3 \pm 0.6) \times 10^{-7}$
$\Gamma(B^0 \to K^0 e^+ e^-)/\Gamma_{total}$		$(2.5^{+1.1}_{-0.9}) \times 10^{-7}$ (S = 1.3)
$\Gamma(B^0 \to K^0 \mu^+ \mu^-)/\Gamma_{total}$		$(3.39 \pm 0.35) \times 10^{-7}$ (S = 1.1)
$\Gamma(B^0 \to K^0 \nu\overline{\nu})/\Gamma_{total}$		$<2.6 \times 10^{-5}$, CL = 90%
$\Gamma(B^0 \to \rho^0 \nu\overline{\nu})/\Gamma_{total}$		$<4.0 \times 10^{-5}$, CL = 90%
$\Gamma(B^0 \to K^*(892)^0 \ell^+ \ell^-)/\Gamma_{total}$	[x]	$(9.9^{+1.2}_{-1.1}) \times 10^{-7}$
$\Gamma(B^0 \to K^*(892)^0 e^+ e^-)/\Gamma_{total}$		$(1.03^{+0.19}_{-0.17}) \times 10^{-6}$
$\Gamma(B^0 \to K^*(892)^0 \mu^+ \mu^-)/\Gamma_{total}$		$(9.4 \pm 0.5) \times 10^{-7}$
$\Gamma(B^0 \to K^*(892)^0 \tau^+ \tau^-)/\Gamma_{total}$		$<1.8 \times 10^{-3}$, CL = 90%
$\Gamma(B^0 \to \overline{D}^0 \mu^+ \mu^-)/\Gamma_{total}$		$<4.0 \times 10^{-8}$, CL = 90%
$\Gamma(B^0 \to \pi^+ \pi^- \mu^+ \mu^-)/\Gamma_{total}$		$(2.1 \pm 0.5) \times 10^{-8}$
$\Gamma(B^0 \to K^*(892)^0 \nu\overline{\nu})/\Gamma_{total}$		$<1.8 \times 10^{-5}$, CL = 90%
$\Gamma(B^0 \to \text{invisible})/\Gamma_{total}$		$<2.4 \times 10^{-5}$, CL = 90%
$\Gamma(B^0 \to \nu\overline{\nu}\gamma)/\Gamma_{total}$		$<1.6 \times 10^{-5}$, CL = 90%
$\Gamma(B^0 \to \phi \mu^+ \mu^-)/\Gamma_{total}$		$<3.2 \times 10^{-9}$, CL = 90%
$\Gamma(B^0 \to \phi \nu\overline{\nu})/\Gamma_{total}$		$<1.27 \times 10^{-4}$, CL = 90%
$\Gamma(B \to s e^+ e^-)/\Gamma_{total}$		$(6.7 \pm 1.7) \times 10^{-6}$ (S = 2.0)
$\Gamma(B \to s \mu^+ \mu^-)/\Gamma_{total}$		$(4.3 \pm 1.0) \times 10^{-6}$
$\Gamma(B \to s \ell^+ \ell^-)/\Gamma_{total}$	[x]	$(5.8 \pm 1.3) \times 10^{-6}$ (S = 1.8)
$\Gamma(B \to \pi \ell^+ \ell^-)/\Gamma_{total}$		$<5.9 \times 10^{-8}$, CL = 90%
$\Gamma(B \to \pi e^+ e^-)/\Gamma_{total}$		$<1.10 \times 10^{-7}$, CL = 90%
$\Gamma(B \to \pi \mu^+ \mu^-)/\Gamma_{total}$		$<5.0 \times 10^{-8}$, CL = 90%
$\Gamma(B \to K e^+ e^-)/\Gamma_{total}$		$(4.4 \pm 0.6) \times 10^{-7}$
$\Gamma(B \to K^*(892) e^+ e^-)/\Gamma_{total}$		$(1.19 \pm 0.20) \times 10^{-6}$ (S = 1.2)
$\Gamma(B \to K \mu^+ \mu^-)/\Gamma_{total}$		$(4.4 \pm 0.4) \times 10^{-7}$
$\Gamma(B \to K^*(892) \mu^+ \mu^-)/\Gamma_{total}$		$(1.06 \pm 0.09) \times 10^{-6}$
$\Gamma(B \to K \ell^+ \ell^-)/\Gamma_{total}$		$(4.8 \pm 0.4) \times 10^{-7}$
$\Gamma(B \to K^*(892) \ell^+ \ell^-)/\Gamma_{total}$		$(1.05 \pm 0.10) \times 10^{-6}$
$\Gamma(B \to K \nu\overline{\nu})/\Gamma_{total}$		$<1.6 \times 10^{-5}$, CL = 90%
$\Gamma(B \to K^* \nu\overline{\nu})/\Gamma_{total}$		$<2.7 \times 10^{-5}$, CL = 90%
$\Gamma(B \to \pi \nu\overline{\nu})/\Gamma_{total}$		$<8 \times 10^{-6}$, CL = 90%
$\Gamma(B \to \rho \nu\overline{\nu})/\Gamma_{total}$		$<2.8 \times 10^{-5}$, CL = 90%
$\Gamma(\overline{b} \to \overline{s}\overline{\nu}\nu)/\Gamma_{total}$		$<6.4 \times 10^{-4}$, CL = 90%
$\Gamma(\overline{b} \to \mu^+ \mu^- \text{anything})/\Gamma_{total}$		$<3.2 \times 10^{-4}$, CL = 90%
$\Gamma(B_s^0 \to \gamma\gamma)/\Gamma_{total}$		$<3.1 \times 10^{-6}$, CL = 90%
$\Gamma(B_s^0 \to \phi\gamma)/\Gamma_{total}$		$(3.4 \pm 0.4) \times 10^{-5}$
$\Gamma(B_s^0 \to f_2(1270)\gamma)/\Gamma_{total}$		$(9^{+4}_{-5}) \times 10^{-6}$
$\Gamma(B_s^0 \to f_2'(1525)\gamma)/\Gamma_{total}$		$(6.7^{+0.9}_{-0.8}) \times 10^{-6}$
$\Gamma(B_s^0 \to \phi(1680)\gamma,\ \phi \to K^+ K^-)/\Gamma_{total}$		$(9.3 \pm 2.4) \times 10^{-7}$
$\Gamma(B_s^0 \to \phi_3(1850)\gamma,\ \phi_3 \to K^+ K^-)/\Gamma_{total}$		$(7^{+6}_{-5}) \times 10^{-8}$
$\Gamma(B_s^0 \to f_2(2010)\gamma,\ f_2 \to K^+ K^-)/\Gamma_{total}$		$(1.0^{+0.7}_{-0.5}) \times 10^{-7}$
$\Gamma(B_s^0 \to \mu^+ \mu^-)/\Gamma_{total}$		$(3.34 \pm 0.27) \times 10^{-9}$
$\Gamma(B_s^0 \to e^+ e^-)/\Gamma_{total}$		$<9.4 \times 10^{-9}$, CL = 90%
$\Gamma(B_s^0 \to \tau^+ \tau^-)/\Gamma_{total}$		$<6.8 \times 10^{-3}$, CL = 95%
$\Gamma(B_s^0 \to \mu^+ \mu^- \gamma)/\Gamma_{total}$		$<4.2 \times 10^{-8}$, CL = 95%
$\Gamma(B_s^0 \to \mu^+ \mu^- \mu^+ \mu^-)/\Gamma_{total}$		$<8.6 \times 10^{-10}$, CL = 95%
$\Gamma(B_s^0 \to SP,\ S \to \mu^+ \mu^-,\ P \to \mu^+ \mu^-)/\Gamma_{total}$	[y]	$<2.2 \times 10^{-9}$, CL = 95%
$\Gamma(B_s^0 \to aa,\ a \to \mu^+ \mu^-)/\Gamma_{total}$		$<5.8 \times 10^{-10}$, CL = 95%
$\Gamma(B_s^0 \to \phi(1020) \mu^+ \mu^-)/\Gamma_{total}$		$(8.2 \pm 0.4) \times 10^{-7}$
$\Gamma(B_s^0 \to f_2'(1525) \mu^+ \mu^-)/\Gamma_{total}$		$(1.57 \pm 0.22) \times 10^{-7}$
$\Gamma(B_s^0 \to \overline{K}^*(892)^0 \mu^+ \mu^-)/\Gamma_{total}$		$(2.9 \pm 1.1) \times 10^{-8}$
$\Gamma(B_s^0 \to \pi^+ \pi^- \mu^+ \mu^-)/\Gamma_{total}$		$(8.4 \pm 1.7) \times 10^{-8}$
$\Gamma(B_s^0 \to \overline{D}^0 \mu^+ \mu^-)/\Gamma_{total}$		$<1.2 \times 10^{-7}$, CL = 90%
$\Gamma(B_s^0 \to \phi \nu\overline{\nu})/\Gamma_{total}$		$<5.4 \times 10^{-3}$, CL = 90%

Unless otherwise stated, limits are given at the 90% confidence level, while errors are given as ±1 standard deviation.

Int. J. Mod. Phys. A 2026.41. Downloaded from www.worldscientific.com
by UNIVERSITY OF CALIFORNIA @ BERKELEY on 09/16/26. Re-use and distribution is strictly not permitted, except for Open Acce

$\Delta T = 1$ WEAK NEUTRAL CURRENT FORBIDDEN

Allowed by higher-order electroweak interactions.

$\Gamma(t \to Zq(q{=}u,c))/\Gamma_{\text{total}}$	[z]	$<1.2 \times 10^{-4}$, CL = 95%
$\Gamma(t \to Hu)/\Gamma_{\text{total}}$		$<1.9 \times 10^{-4}$, CL = 95%
$\Gamma(t \to Hc)/\Gamma_{\text{total}}$		$<3.4 \times 10^{-4}$, CL = 95%
$\Gamma(t \to \ell^+ \overline{q}q'(q{=}d,s,b;\, q'{=}u,c))/\Gamma_{\text{total}}$		$<1.6 \times 10^{-3}$, CL = 95%

NOTES

In this Summary Table:

When a quantity has "(S = ...)" to its right, the error on the quantity has been enlarged by the "scale factor" S, defined as $S = \sqrt{\chi^2/(N-1)}$, where N is the number of measurements used in calculating the quantity. We do this when $S > 1$, which often indicates that the measurements are inconsistent. When $S > 1.25$, we also show in the Particle Listings an ideogram of the measurements. For more about S, see the Introduction.

[a] Forbidden by angular momentum conservation.

[b] C parity forbids this to occur as a single-photon process.

[c] See the Particle Listings for the (complicated) definition of this quantity.

[d] Time-reversal invariance requires this to be 0° or 180°.

[e] This coefficient is zero if time invariance is not violated.

[f] Neglecting photon channels. See, *e.g.*, A. Pais and S.B. Treiman, Phys. Rev. **D12**, 2744 (1975).

[g] Allowed by higher-order electroweak interactions.

[h] Violates CP in leading order. Test of direct CP violation since the indirect CP-violating and CP-conserving contributions are expected to be suppressed.

[i] In the 2010 *Review*, the values for these quantities were given using a measure of the asymmetry that was inconsistent with the usual definition.

[j] $\text{Re}(\epsilon'/\epsilon) = \epsilon'/\epsilon$ to a very good approximation provided the phases satisfy CPT invariance.

[k] This mode includes gammas from inner bremsstrahlung but not the direct emission mode $K^0_L \to \pi^+\pi^-\gamma(\text{DE})$.

[l] Derived from measured values of ϕ_{+-}, ϕ_{00}, $|\eta|$, $|m_{K^0_L} - m_{K^0_S}|$, and $\tau_{K^0_S}$, as described in the introduction to "Tests of Conservation Laws."

[n] The $|m_p - m_{\overline{p}}|/m_p$ and $|q_p + q_{\overline{p}}|/e$ are not independent, and both use the more precise measurement of $|q_{\overline{p}}/m_{\overline{p}}|/(q_p/m_p)$.

[o] The value is for the sum of the charge states or particle/antiparticle states indicated.

[p] A test of additive vs. multiplicative lepton family number conservation.

[q] Derived from an analysis of neutrino-oscillation experiments.

[r] There is some controversy about whether nuclear physics and model dependence complicate the analysis for bound neutrons (from which the best limit comes). The first limit here is from reactor experiments with free neutrons.

[s] This is the best limit for the mode $e^- \to \nu\gamma$.

[t] The limit is from neutrality-of-matter experiments; it assumes $q_n = q_p + q_e$. See also the charge of the neutron.

[u] See the K^0_S Particle Listings for the energy limits used in this measurement.

[v] See the K^0_L Particle Listings for the energy limits used in this measurement.

[x] An ℓ indicates an e or a μ mode, not a sum over these modes.

[y] Here S and P are the hypothetical scalar and pseudoscalar particles with masses of 2.5 GeV/c^2 and 214.3 MeV/c^2, respectively.

[z] This limit is for $\Gamma(t \to Zq)/\Gamma(t \to Wb)$.

Unless otherwise stated, limits are given at the 90% confidence level, while errors are given as ±1 standard deviation.

REVIEWS, TABLES, AND PLOTS

Constants, Units, Atomic and Nuclear Properties

1. Physical constants (rev.) 145
2. Astrophysical constants and parameters (rev.) 146
3. International system of units (SI) 148
4. Periodic table of the elements 149
5. Electronic structure of the elements 150
6. Atomic and nuclear properties of materials 152
7. Electromagnetic relations (rev.) 153
8. Naming scheme for hadrons (rev.) 155

Int. J. Mod. Phys. A 2026.41. Downloaded from www.worldscientific.com
by UNIVERSITY OF CALIFORNIA @ BERKELEY on 09/16/26. Re-use and distribution is strictly not permitted, except for Open Access articles.

Int. J. Mod. Phys. A 2026.41. Downloaded from www.worldscientific.com
by UNIVERSITY OF CALIFORNIA @ BERKELEY on 09/16/26. Re-use and distribution is strictly not permitted, [redacted]ss articles.

1. Physical Constants

Table 1.1: Revised May 2026 by D. Robinson (LBNL) and P.A. Zyla (LBNL). Mainly from "CODATA recommended values of the fundamental physical constants: 2022," P.J. Mohr, D.B. Newell, B.N. Taylor, and E. Tiesinga [1]. The electron charge magnitude e, and the Planck, Boltzmann, and Avogadro constants h, k, and N_A, now join c as having defined values; the free-space permittivity and permeability constants ϵ_0 and μ_0 are no longer exact. These changes affect practically everything else in the Table. Figures in parentheses after the values are the 1-standard-deviation uncertainties in the last digits; the fractional uncertainties in parts per 10^9 (ppb) are in the last column. The full 2022 CODATA Committee on Data for Science and Technology set of constants are found at `https://physics.nist.gov/Constants`. The last set of constants (beginning with the Fermi coupling constant) comes from the Particle Data Group. See also "The International System of Units (SI)," 9th ed. (2019) of the International Bureau of Weights and Measures (BIPM), `https://www.bipm.org/utils/common/pdf/si-brochure/SI-Brochure-9-EN.pdf`.

Quantity	Symbol, equation	Value	Uncertainty (ppb)
speed of light in vacuum	c	299 792 458 m s^{-1}	exact
Planck constant	h	6.626 070 15$\times10^{-34}$ J s (or J/Hz) §	exact
Planck constant, reduced	$\hbar \equiv h/2\pi$	1.054 571 817... $\times 10^{-34}$ J s	exact*
		= 6.582 119 569... $\times 10^{-22}$ MeV s	exact*
electron charge magnitude***	e	1.602 176 634$\times10^{-19}$ C	exact
conversion constant	$\hbar c$	197.326 980 4... MeV fm	exact*
conversion constant	$(\hbar c)^2$	0.389 379 372 1... GeV^2 mbarn	exact*
electron mass	m_e	0.510 998 950 69(16) MeV/c^2 = 9.109 383 7139(28)$\times10^{-31}$ kg	0.31
proton mass	m_p	938.272 089 43(29) MeV/c^2 = 1.672 621 925 95(52)$\times10^{-27}$ kg	0.31
		= 1.007 276 466 5789(83) u =1836.152 673 426(32) m_e	0.0083, 0.017
neutron mass	m_n	939.565 421 94(48) MeV/c^2 = 1.008 664 916 06(40) u	0.51, 0.40
deuteron mass	m_d	1875.612 945 00(58) MeV/c^2	0.31
unified atomic mass unit**	u = (mass ^{12}C atom)/12	931.494 103 72(29) MeV/c^2 = 1.660 539 068 92(52)$\times10^{-27}$ kg	0.31
permittivity of free space	$\epsilon_0 = 1/\mu_0 c^2$	8.854 187 8188(14) $\times10^{-12}$ F m^{-1}	0.16
permeability of free space	$\mu_0/(4\pi\times10^{-7})$	0.999 999 999 87(16) N A^{-2}	0.16
fine-structure constant	$\alpha = e^2/4\pi\epsilon_0\hbar c$	7.297 352 5643(11)$\times10^{-3}$=1/137.035 999 177(21) †	0.16
classical electron radius	$r_e = e^2/4\pi\epsilon_0 m_e c^2$	2.817 940 3205(13)$\times10^{-15}$ m	0.47
(e^- Compton wavelength)/2π	$\lambda\!\!\!^{-}_e = \hbar/m_e c = r_e\alpha^{-1}$	3.861 592 6744(12)$\times10^{-13}$ m	0.31
Bohr radius ($m_{\rm nucleus}=\infty$)	$a_\infty = 4\pi\epsilon_0\hbar^2/m_e e^2 = r_e\alpha^{-2}$	0.529 177 210 544(82)$\times10^{-10}$ m	0.16
wavelength of 1 eV/c particle	$hc/(1\ \text{eV})$	1.239 841 984... $\times 10^{-6}$ m	exact*
Rydberg energy	$hcR_\infty = m_e e^4/2(4\pi\epsilon_0)^2\hbar^2 = m_e c^2\alpha^2/2$	13.605 693 122 990(15) eV	1.1$\times10^{-3}$
Thomson cross section	$\sigma_T = 8\pi r_e^2/3$	0.665 245 870 51(62) barn	0.93
Bohr magneton	$\mu_B = e\hbar/2m_e$	5.788 381 7982(18)$\times10^{-11}$ MeV T^{-1}	0.31
nuclear magneton	$\mu_N = e\hbar/2m_p$	3.152 451 254 17(98)$\times10^{-14}$ MeV T^{-1}	0.31
electron cyclotron freq./field	$\omega^e_{\rm cycl}/B = e/m_e$	1.758 820 008 38(55)$\times10^{11}$ rad s^{-1} T^{-1}	0.31
proton cyclotron freq./field	$\omega^p_{\rm cycl}/B = e/m_p$	9.578 833 1430(30)$\times10^{7}$ rad s^{-1} T^{-1}	0.31
gravitational constant‡	G_N	6.674 30(15)$\times10^{-11}$ m^3 kg^{-1} s^{-2}	2.2×10^4
		= 6.708 83(15)$\times10^{-39}$ $\hbar c$ (GeV/c^2)$^{-2}$	2.2×10^4
standard gravitational accel.	g_N	9.806 65 m s^{-2}	exact
Avogadro constant	N_A	6.022 140 76$\times10^{23}$ mol^{-1}	exact
Boltzmann constant	k	1.380 649$\times10^{-23}$ J K^{-1}	exact
		= 8.617 333 262... $\times 10^{-5}$ eV K^{-1}	exact*
molar volume, ideal gas at STP	$N_A k$ (273.15 K)/(101 325 Pa)	22.413 969 54... $\times 10^{-3}$ m^3 mol^{-1}	exact*
Wien displacement law constant	$b = \lambda_{\rm max}T$	2.897 771 955... $\times 10^{-3}$ m K	exact*
Stefan-Boltzmann constant	$\sigma = \pi^2k^4/60\hbar^3c^2$	5.670 374 419... $\times 10^{-8}$ W m^{-2} K^{-4}	exact*
Fermi coupling constant‡‡	$G_F/(\hbar c)^3$	1.166 378 5(6) $\times10^{-5}$ GeV^{-2}	514
weak-mixing angle‡‡	$\sin^2\widehat{\theta}(M_Z)$ ($\overline{\rm MS}$)	0.231 22(6)††	2.6×10^5
$W^\pm$ boson mass	m_W	80.3625(77) GeV/c^2¶	9.6×10^4
Z^0 boson mass	m_Z	91.1879(20) GeV/c^2‖	2.2×10^4
strong coupling constant	$\alpha_s(m_Z)$	0.1180(9)	7.6×10^6

π = 3.141 592 653 589 793 238 ...	e = 2.718 281 828 459 045 235...	γ = 0.577 215 664 901 532 860...
1 in ≡ 0.0254 m 1 G ≡ $10^{-4}\times r_{\mu_0}$ T§§	1 eV = 1.602 176 634 $\times 10^{-19}$ J (exact)	kT at 300 K = [38.681 727 0718...]$^{-1}$eV (exact*)
1 Å ≡ 0.1 nm 1 dyne ≡ 10^{-5} N	(1 kg)c^2 = 5.609 588 603... $\times 10^{35}$ eV(exact*)	0 °C ≡ 273.15K
1 barn ≡ 10^{-28} m^2 1 erg ≡ 10^{-7} J	1 C ≡ 299 792 458 $\times$ 10 $\times$ r_{μ_0} esu§§	1 atmosphere ≡ 760 Torr ≡ 101 325Pa

§CODATA recommends that the unit be J/Hz to stress that in $h = E/\nu$ the frequency ν is in cycles/sec (Hz), not radians/sec.

*These are calculated from exact values and are exact to the number of places given (*i.e.* no rounding).

***While e is exact in SI units, in natural units $e = \sqrt{4\pi\alpha}$ is a measured quantity.

**The molar mass of ^{12}C is 12.000 000 0126(37) g.

†CODATA recommended value at $Q^2 = 0$. At $Q^2 \approx m_W^2$ the value is $\sim 1/128$. ‡‡

‡Absolute laboratory measurements of G_N have been made only on scales of about 1 cm to 1 m.

‡‡See the discussion in "Electroweak model and constraints on new physics" review.

††Derived from $\sin^2\theta$ for the effective angle $\bar{s}^2_\ell = 0.23154(6)$.

¶See the "Mass and width of the W boson" and "Electroweak model and constraints on new physics" reviews.

‖See the "Z boson" and "Electroweak model and constraints on new physics" reviews.

§§The ratio $r_{\mu_0} \equiv \sqrt{\mu_0/(4\pi\times10^{-7}\ \text{N A}^{-2})} = 0.999\ 999\ 999\ 93(8)$. Prior to the 2019 revision of the SI unit system, $\mu_0 \equiv 4\pi\times10^{-7}$ N A^{-2}.

References

[1] P. J. Mohr *et al.*, Rev. Mod. Phys. **97**, 2, 025002 (2025), [arXiv:2409.03787].

Int. J. Mod. Phys. A 2026.41. Downloaded from www.worldscientific.com
by UNIVERSITY OF CALIFORNIA @ BERKELEY on 09/16/26. Re-use and distribution is strictly not permitted, except for Open Access articles.

2. Astrophysical Constants and Parameters

Table 2.1: Revised August 2025 by D.E. Groom (LBNL) and D. Scott (U. of British Columbia). The figures in parentheses after some values give the 1-σ uncertainties in the last digit(s). Physical constants are from Ref. [1]. While every effort has been made to obtain the most accurate current values of the listed quantities, this table does not represent a critical review or adjustment of the constants, and is not intended as a primary reference. The values and uncertainties for the cosmological parameters depend on the exact data sets, priors, and basis parameters used in the fit. Many of the derived parameters reported in this table have non-Gaussian likelihoods and parameters may be highly correlated, so care must be taken in propagating errors. Unless otherwise specified, cosmological parameters are derived from a 6-parameter ΛCDM cosmology fit to *Planck* cosmic microwave background 2018 temperature (TT) + polarization (TE,EE+lowE) + lensing data [2]. For more information see Ref. [3] and the original papers.

Quantity	Symbol, equation	Value	Reference, footnote
Newtonian constant of gravitation	G_N	$6.674\,30(15) \times 10^{-11}\,\mathrm{m^3\,kg^{-1}\,s^{-2}}$	[1]
Planck mass	$M_P = \sqrt{\hbar c/G_N}$	$1.220\,890(14) \times 10^{19}\,\mathrm{GeV}/c^2 = 2.176\,434(24) \times 10^{-8}\,\mathrm{kg}$	[1]
Planck length	$l_P = \sqrt{\hbar G_N/c^3}$	$1.616\,255(18) \times 10^{-35}\,\mathrm{m}$	[1]
tropical year (equinox to equinox, 2020)	yr	$31\,556\,925.1\,\mathrm{s} = 365.242\,189\,\mathrm{days}$	[4]
sidereal year (period of Earth around Sun relative to stars)		$31\,558\,149.8\,\mathrm{s} \approx \pi \times 10^7\,\mathrm{s}$	[4]
mean sidereal day (Earth rotation period relative to stars)		$23^{\mathrm{h}}\,56^{\mathrm{m}}\,04\overset{\mathrm{s}}{.}090\,53$	[4]
astronomical unit	au	$149\,597\,870\,700\,\mathrm{m}$	exact [5]
parsec (1 au/1 arcsec)	pc	$3.085\,677\,581\,49\ldots \times 10^{16}\,\mathrm{m} = 3.261\,56\ldots\,\mathrm{ly}$	exact [6]
light year	ly	$0.306\,601\ldots\,\mathrm{pc} = 0.946\,073\ldots \times 10^{16}\,\mathrm{m}$	[7]
solid angle	deg^2	$(\pi/180)^2\,\mathrm{sr} = 3.046\,17\ldots \times 10^{-4}\,\mathrm{sr}$	[8]
Schwarzschild radius of the Sun	$2(\mathcal{G}_N\mathcal{M})_\odot/c^2$	$2.953\,250\,0\ldots\,\mathrm{km}$	exact [9, 10]
Solar mass	$M_\odot$	$1.988\,41(4) \times 10^{30}\,\mathrm{kg}$	[11]
nominal Solar equatorial radius	$\mathcal{R}_\odot$	$6.957 \times 10^8\,\mathrm{m}$	exact [10]
nominal Solar constant	$\mathcal{S}_\odot$	$1361\,\mathrm{W\,m^{-2}}$	exact [10, 12]
nominal Solar photosphere temperature	$\mathcal{T}_\odot$	$5772\,\mathrm{K}$	exact [10]
nominal Solar luminosity	$\mathcal{L}_\odot$	$3.828 \times 10^{26}\,\mathrm{W}$	exact [10, 13]
Schwarzschild radius of the Earth	$2(\mathcal{G}_N\mathcal{M})_\oplus/c^2$	$8.870\,055\ldots\,\mathrm{mm}$	exact [9, 10]
Earth mass	$M_\oplus$	$5.972\,17(13) \times 10^{24}\,\mathrm{kg}$	[11]
nominal Earth equatorial radius	$\mathcal{R}_\oplus$	$6.3781 \times 10^6\,\mathrm{m}$	exact [10]
Chandrasekhar mass	M_{Ch}	$3.097\,972\,\mu^{-2}\,M_P^3/m_H^2 = 1.433\,77(6)\,(\mu/2)^{-2}\,M_\odot$	[14, 15]
Eddington luminosity	L_{Ed}	$1.257\,065\,2\ldots \times 10^{31}\,(M/M_\odot)\,\mathrm{W}$	[16, 17]
		$= 3.283\,869\,3\ldots \times 10^4\,(M/M_\odot)\,\mathcal{L}_\odot$	
jansky (flux density)	Jy	$10^{-26}\,\mathrm{W\,m^{-2}\,Hz^{-1}}$	definition
luminosity conversion	f_0	$3.0128 \times 10^{28} \times 10^{-0.4\,M_{\mathrm{Bol}}}\,\mathrm{W}$	exact [18]
		(M_{Bol} = absolute bolometric magnitude = bolometric magnitude at 10 pc)	
flux conversion	$\mathcal{F}$	$2.518\,021\,002 \times 10^{-8} \times 10^{-0.4\,m_{\mathrm{Bol}}}\,\mathrm{W\,m^{-2}}$	exact [18]
		(m_{Bol} = apparent bolometric magnitude)	
ABsolute monochromatic magnitude	AB	$-2.5\,\log_{10} f_\nu - 56.10$ (for f_ν in $\mathrm{W\,m^{-2}\,Hz^{-1}}$)	[19]
		$= -2.5\,\log_{10} f_\nu + 8.90$ (for f_ν in Jy)	
Solar distance from Galactic center	R_0	$8.275 \pm 0.009(\mathrm{stat.}) \pm 0.033(\mathrm{sys.})\,\mathrm{kpc}$	[20]
local circular angular velocity	Θ_0/R_0	$28.2(10)\,\mathrm{km\,s^{-1}\,kpc^{-1}}$	[21]
circular velocity at R_0	v_0 or Θ_0	$233.4 \pm 0.3(\mathrm{stat.}) \pm 8.0(\mathrm{sys.})\,\mathrm{km\,s^{-1}}$	[22]
local escape velocity from the Galaxy	v_{esc}	$477\,\mathrm{km\,s^{-1}} < v_{\mathrm{esc}} < 502\,\mathrm{km\,s^{-1}}$ (68%)	[23]
local disk density	ρ_{disk}	$6.6(9) \times 10^{-24}\,\mathrm{g\,cm^{-3}} = 3.7(5)\,\mathrm{GeV}/c^2\,\mathrm{cm^{-3}}$	[24]
local dark matter density	ρ_χ	canonical value $0.3\,\mathrm{GeV}/c^2\,\mathrm{cm^{-3}}$ within factor 2–3	[25]
present-day CMB temperature	T_0	$2.7255(6)\,\mathrm{K}$	[26, 27]
present-day CMB dipole amplitude	d	$3.3621(10)\,\mathrm{mK}$	[26, 28]
Solar velocity with respect to CMB	$v_\odot$	$369.82(11)\,\mathrm{km\,s^{-1}}$ towards $(l, b) = (264.021(11)^\circ,\ 48.253(5)^\circ)$	[28]
Local Group velocity with respect to CMB	v_{LG}	$620(15)\,\mathrm{km\,s^{-1}}$ towards $(l, b) = (271.9(20)^\circ, 29.6(14)^\circ)$	[28]
number density of CMB photons	n_γ	$410.73(27)\,(T/2.7255\,\mathrm{K})^3\,\mathrm{cm^{-3}}$	[29]
density of CMB photons	ρ_γ	$4.645(4)\,(T/2.7255\,\mathrm{K})^4 \times 10^{-34}\,\mathrm{g\,cm^{-3}} \approx 0.260\,\mathrm{eV\,cm^{-3}}$	[29]
entropy density/Boltzmann constant	s/k	$2\,891.2\,(T/2.7255\,\mathrm{K})^3\,\mathrm{cm^{-3}}$	[29]
present-day Hubble expansion rate	H_0	$100\,h\,\mathrm{km\,s^{-1}\,Mpc^{-1}} = h \times (9.777\,752\,\mathrm{Gyr})^{-1}$	[30]
scaling factor for Hubble expansion rate	h	$0.674(5)$ from CMB anisotropies (*Planck*)	[2]
		or $0.730(10)$ from the distance ladder (SH0ES)	[31, 32]
Hubble length	c/H_0	$0.925\,0629 \times 10^{26}\,h^{-1}\,\mathrm{m} = 1.372(11)$ *or* $1.267(18) \times 10^{26}\,\mathrm{m}$	[2, 31]
scaling for cosmological constant	$c^2/3H_0^2$	$2.85247 \times 10^{51}\,h^{-2}\,\mathrm{m^2} = 6.29(10)$ *or* $5.35(15) \times 10^{51}\,\mathrm{m^2}$	[2, 31]
critical density of the Universe	$\rho_{\mathrm{crit}} = 3H_0^2/8\pi G_N$	$1.878\,34(4) \times 10^{-29}\,h^2\,\mathrm{g\,cm^{-3}}$	
		$= 1.053\,672(24) \times 10^{-5}\,h^2\,(\mathrm{GeV}/c^2)\,\mathrm{cm^{-3}}$	
		$= 2.77536627 \times 10^{11}\,h^2\,M_\odot\,\mathrm{Mpc^{-3}}$	
baryon-to-photon ratio (from BBN)	$\eta = n_{\mathrm{b}}/n_\gamma$	$6.04(12) \times 10^{-10}$	[33, 34]
number density of baryons	n_{b}	$2.515(17) \times 10^{-7}\,\mathrm{cm^{-3}}$ (from CMB)	[2, 35]
		$2.48(5) \times 10^{-7}\,\mathrm{cm^{-3}}$ (from BBN, $\eta \times n_\gamma$)	[3, 33]
CMB radiation density of the Universe	$\Omega_\gamma = \rho_\gamma/\rho_{\mathrm{crit}}$	$2.473 \times 10^{-5}\,(T/2.7255\,\mathrm{K})^4\,h^{-2} = 5.38(15) \times 10^{-5}$	[29]
primordial helium fraction	Y_{p}	$0.2448(33)$	[36]
- - - *Planck* 2018 6-parameter fit to flat ΛCDM cosmology - - -			
baryon density of the Universe	$\Omega_{\mathrm{b}} = \rho_{\mathrm{b}}/\rho_{\mathrm{crit}}$	$^\ddagger\,0.02237(15)\,h^{-2} = {}^\dagger\,0.0493(6)$	[2, 3, 26]
cold dark matter density of the Universe	$\Omega_{\mathrm{c}} = \rho_{\mathrm{c}}/\rho_{\mathrm{crit}}$	$^\ddagger\,0.1200(12)\,h^{-2} = {}^\dagger\,0.265(7)$	[2, 3, 26]
100 × approximation to r_*/D_{A}	$100 \times \theta_{\mathrm{MC}}$	$^\ddagger\,1.04092(31)$	[2, 3, 26]
reionization optical depth	τ	$^\ddagger\,0.054(7)$	[2, 3, 26]
ln(power prim. curv. pert.) ($k_0 = 0.05\,\mathrm{Mpc^{-1}}$)	$\ln(10^{10}\Delta^2_{\mathcal{R}})$	$^\ddagger\,3.044(14)$	[2, 3, 26]
scalar spectral index	n_{s}	$^\ddagger\,0.965(4)$	[2, 3, 26]
pressureless matter density parameter	$\Omega_{\mathrm{m}} = \Omega_{\mathrm{c}} + \Omega_{\mathrm{b}}$	$^\dagger\,0.315(7)$	[2, 3]
dark energy density parameter	Ω_Λ	$^\dagger\,0.685(7)$	[2, 3]
density of dark energy	ρ_Λ	$^\dagger\,5.83(16) \times 10^{-30}\,\mathrm{g\,cm^{-3}}$	[2]
cosmological constant	Λ	$^\dagger\,1.088(30) \times 10^{-56}\,\mathrm{cm^{-2}}$	[2]
fluctuation amplitude at $8\,h^{-1}$ Mpc scale	σ_8	$^\dagger\,0.811(6)$	[2, 3]

Int. J. Mod. Phys. A 2026.41. Downloaded from www.worldscientific.com by UNIVERSITY OF CALIFORNIA @ BERKELEY on 09/16/26. Re-use and distribution is strictly not permitted, e articles.

Quantity	Symbol, equation.	Value	Reference,footnote
amplitude of matter fluctuations	$\sigma_8\,(\Omega_{\rm m}/0.3)^{0.5}$	† 0.832(13)	[2,3]
redshift of matter-radiation equality	$z_{\rm eq}$	† 3402(26)	[2,37]
age at matter-radiation equality	$t_{\rm eq}$	† 51.7(8) kyr	[38]
redshift at which optical depth equals unity	z_*	† 1089.92(25)	[2]
comoving size of sound horizon at z_*	r_*	† 144.43(26) Mpc	[2,39]
age when optical depth equals unity	t_*	† 372.6(10) kyr	[38]
redshift at half reionization	$z_{\rm i}$	† 7.7(7)	[2,40]
age at half reionization	$t_{\rm i}$	† 630(60) Myr	[38]
redshift when acceleration was zero	z_q	† 0.642(17)	[38]
age when acceleration was zero	t_q	† 7.66(9) Gyr	[38]
age of the Universe today	t_0	† 13.797(23) Gyr	[2]
effective number of neutrinos	$N_{\rm eff}$	♯ 2.99(17) (CMB + BAO)	[2,41,42]
sum of neutrino masses	Σm_ν	♯ < 0.12 eV (95%, CMB + BAO); ≥ 0.06 eV (mixing)	[2,42–44]
neutrino density of the Universe	$\Omega_\nu = h^{-2}\Sigma m_\nu/93.14\,{\rm eV}$	♯ < 0.003 (95%, CMB + BAO); ≥ 0.0012 (mixing)	[2,43,44]
curvature	Ω_K	♯ 0.0007(19) (CMB + BAO)	[2]
running spectral index, $k_0 = 0.05\,{\rm Mpc}^{-1}$	$dn_{\rm s}/d\ln k$	♯ $-0.004(7)$	[2]
tensor-to-scalar perturbation ratio	$r_{0.05} = T/S$	< 0.036 (95%, $k_0 = 0.05\,{\rm Mpc}^{-1}$)	[2,45–48]
dark energy equation of state parameter	w	♯ $-1.028(31)$ (CMB + BAO +SNe)	[2,49]

‡ Parameter in 6-parameter ΛCDM fit; † derived parameter in 6-parameter ΛCDM fit; ♯ extended model parameter, *Planck* + BAO data [2].

References

[1] CODATA recommended 2018 values of the fundamental physical constants: `physics.nist.gov/cuu/Constants/index.html`.

[2] Planck Collab. 2018 Results VI, Astron. Astrophys. **641**, A6 (2020), [arXiv:1807.06209].

[3] O. Lahav and A. R. Liddle, "The Cosmological Parameters," Sec. 25 in this *Review*.

[4] *The Astronomical Almanac for the year 2020*.

[5] The astronomical unit of length (au) in meters is re-defined (IAU XXVIII General Assembly 2012, Resolution B2) to be a conventional unit of length in agreement with the value adopted in IAU XXVII GA 2009, Resolution B2. It is to be used with all time scales.

[6] The distance at which 1 au subtends 1 arc sec: 1 au divided by $\pi/648\,000$.

[7] This unit is rarely used by professional astrophysicists. From $c\times$(tropical year)/pc and $c\times$(tropical year), see IAU XVI GA 1976, Recommendations; T. Lederle, Astron. Gesellschaft **48**, 59 (1980).

[8] The number of square degrees on a sphere is $360^2/\pi = 41\,259.9\ldots$.

[9] Nominal mass parameters $(\mathcal{G}_N\mathcal{M})$ for the Sun and Earth are $(\mathcal{G}_N\mathcal{M})_\odot = 1.327\,124\,4\times10^{20}\,{\rm m}^3\,{\rm s}^{-2}$ and $(\mathcal{G}_N\mathcal{M})_\oplus = 3.986\,004\times10^{14}\,{\rm m}^3\,{\rm s}^{-2}$.

[10] IAU XXIX GA 2015 Resolution B3; nominal values are indicated with calligraphic symbols; A. Prša *et al.*, Astron. J. **152**, 2, 41 (2016), [arXiv:1605.09788].

[11] $(\mathcal{G}_N\mathcal{M}) \div G_N$ [1,10].

[12] See also G. Kopp and J. L. Lean, Geophys. Res. Lett. **38**, L01706 (2011), who give $(1360.8 \pm 0.6)\ {\rm W\,m^{-2}}$; see paper for caveats and other measurements.

[13] $4\pi\,(1\ {\rm au})^2 \times \mathcal{S}_\odot$, assuming isotropic irradiance.

[14] S. Chandrasekhar, Astrophys. J. **74**, 81 (1931).

[15] This value assumes an ideal Fermi gas, using a numerical constant from the Lane-Emden equation [50], and with μ the average molecular weight per electron, defined relative to the mass of the single-proton hydrogen atom.

[16] A. S. Eddington, Mon. Not. Roy. Astron. Soc. **77**, 16 (1916).

[17] The maximum luminosity assuming pure electron scattering for the outward force arising from radiation pressure in a hydrogen-only atmosphere: $4\pi G_N M m_p c/\sigma_T$.

[18] IAU XXIX GA 2015, Resolution B2; E. E. Mamajek *et al.*, arXiv:1510.06262 (2015).

[19] J. B. Oke and J. E. Gunn, Astrophys. J. **266**, 713 (1983).

[20] GRAVITY Collaboration, Astron. Astrophys. **647**, A59 (2021), [arXiv:2101.12098].

[21] A.-C. Eilers *et al.*, Astrophys. J. **871**, 1, 120 (2019), [arXiv:1810.09466]; this is representative of other published values and the systematic uncertainty here is an estimate.

[22] Product of angular velocity and R_0, derived from Ref. [21] with an estimate of the systematic uncertainty.

[23] L. Necib and T. Lin, Astrophys. J. **926**, 2, 189 (2022), [arXiv:2102.02211].

[24] C. F. McKee, A. Parravano and D. J. Hollenbach, Astrophys. J. **814**, 1, 13 (2015), [arXiv:1509.05334]; this is representative of other published estimates.

[25] J. I. Read, J. Phys. **G41**, 063101 (2014), [arXiv:1404.1938]; A. M. Green, J. Phys. **G44**, 8, 084001 (2017), [arXiv:1703.10102]; the conclusion is $\rho_{\rm DM}^{\rm local} = 0.39 \pm 0.03\,{\rm GeV\,cm^{-3}}$.

[26] D. Scott and G. F. Smoot, "Cosmic Microwave Background," Sec. 29 in this *Review*.

[27] D. J. Fixsen, Astrophys. J. **707**, 916 (2009), [arXiv:0911.1955].

[28] Planck Collab. 2018 Results I, Astron. Astrophys. **641**, A1 (2020), [arXiv:1807.06205].

[29] $n_\gamma = \frac{2\zeta(3)}{\pi^2}\left(\frac{kT}{\hbar c}\right)^3$; $\rho_\gamma = \frac{\pi^2 kT}{15\,c^2}\left(\frac{kT}{\hbar c}\right)^3$; $s/k = \frac{2\cdot43\cdot\pi^2}{11\cdot45}\left(\frac{kT}{\hbar c}\right)^3$; $kT/\hbar c = 11.90\,235(T/2.7255)/{\rm cm}$.

[30] Conversion using length of sidereal year.

[31] A. G. Riess *et al.*, Astrophys. J. Lett. **934**, 1, L7 (2022), [arXiv:2112.04510].

[32] Distance-ladder estimates of H_0 tend to give higher values than derived from the CMB; Lahav and A. R. Liddle, "The Cosmological Parameters," Sec. 25 in this *Review*.

[33] T.-H. Yeh *et al.*, J. Cosmol. Astropart. Phys. **2022**, 10, 046 (2022), [arXiv:2207.13133].

[34] B. D. Fields, P. Molaro and S. Sarkar, "Big-Bang Nucleosynthesis," Sec. 24 in this *Review*.

[35] $n_{\rm b}$ depends only upon the measured $\Omega_{\rm b}h^2$, the average baryon mass at the present epoch (G. Steigman, J. Cosmol. Astropart. Phys., **0610**, 016 (2006), [astro-ph/0606206]), and G_N: $n_{\rm b} = (\Omega_{\rm b}h^2)(h^{-2}\rho_{\rm crit})/(0.93711\,{\rm GeV}/c^2$ per baryon).

[36] E. Aver *et al.*, Mon. Not. Roy. Astron. Soc. **510**, 1, 373 (2022), [arXiv:2109.00178].

[37] Here "radiation" includes three species of light neutrinos as well as photons.

[38] L. T. Hergt and D. Scott, J. Cosmol. Astropart. Phys. **2025**, 5, 092 (2025), [arXiv:2411.07703]; times are calculated from Markov chains, but using a slightly different data combination with *Planck* Public Release 4; M. Tristram *et al.*, Astron. Astrophys. **682**, A37 (2024), [arXiv:2309.10034].

[39] D. H. Weinberg and M. White, "Dark Energy," Sec. 28 in this *Review*.

[40] Planck Collab. Interm. Results XLVI, Astron. Astrophys. **596**, A107 (2016), [arXiv:1605.02985]; the range can be extended by $\Delta z \approx 1$, depending on the reionization model.

[41] Summary Tables in this *Review* list $N_\nu = 2.984(8)$ (Standard Model fits to LEP-SLC data). Because neutrinos are not completely decoupled at $e^\pm$ annihilation, the effective number of massless neutrino species is 3.044, rather than 3.

[42] J. Lesgourgues and L. Verde, "Neutrinos in Cosmology," Sec. 26 in this *Review*.

[43] The sum is over all neutrino mass eigenstates, the lower limit following from neutrino mixing results reported in this *Review* combined with the assumptions that there are three light neutrinos and that the lightest neutrino is substantially less massive than the others.

[44] Astrophysical determinations of Σm_ν, reported in the Full Listings of this *Review* under "Sum of the neutrino masses," range from < 0.17 eV to < 2.3 eV in papers published since 2003.

[45] P. A. R. Ade *et al.* (BICEP2, Keck Array), Phys. Rev. Lett. **121**, 221301 (2018), [arXiv:1810.05216].

[46] M. Tristram *et al.*, Astron. Astrophys. **647**, A128 (2021), [arXiv:2010.01139].

[47] BICEP/Keck Collaboration, Phys. Rev. Lett. **127**, 151301 (2021), [arXiv:2110.00483].

[48] *Planck* data alone give $r < 0.056$, using all power spectra; the currently tightest constraint comes from BICEP/Keck data, using *WMAP* and *Planck* to remove foregrounds.

[49] This constraint uses BAO and SNe data, as described in Ref. [2]; see discussion in D. H. Weinberg and M. White, "Dark Energy," Sec. 28 in this *Review*.

[50] G. P. Horedt, Astrophys. Space Sci. **126**, 2, 357 (1986).

Int. J. Mod. Phys. A 2026.41. Downloaded from www.worldscientific.com by UNIVERSITY OF CALIFORNIA @ BERKELEY on 09/16/26. Re-use and distribution is strictly not permitted, except for Open Access articles.

3. International System of Units (SI)

See D.B. Newell and E. Tiesinga, ed. (2019), "The International System of Units (SI)" (National Institute of Standards and Technology, Gaithersburg, MD), NIST Special Publication **330**, 2019 edition, `https://doi.org/10.6028/NIST.SP.330-2019`; and A. Thompson and B.N. Taylor (2008), "Guide for the Use of the International System of Units (SI)" (National Institute of Standards and Technology, Gaithersburg, MD), NIST Special Publication **811**, 2008 edition, `https://doi.org/10.6028/NIST.SP.811e2008`.

SI prefixes

10^{24}	yotta	(Y)
10^{21}	zetta	(Z)
10^{18}	exa	(E)
10^{15}	peta	(P)
10^{12}	tera	(T)
10^{9}	giga	(G)
10^{6}	mega	(M)
10^{3}	kilo	(k)
10^{2}	hecto	(h)
10	deca	(da)
10^{-1}	deci	(d)
10^{-2}	centi	(c)
10^{-3}	milli	(m)
10^{-6}	micro	(μ)
10^{-9}	nano	(n)
10^{-12}	pico	(p)
10^{-15}	femto	(f)
10^{-18}	atto	(a)
10^{-21}	zepto	(z)
10^{-24}	yocto	(y)

Physical quantity	**Name of unit**	**Symbol**
Base units		
length	meter	m
mass	kilogram	kg
time	second	s
electric current	ampere	A
thermodynamic temperature	kelvin	K
amount of substance	mole	mol
luminous intensity	candela	cd
Derived units with special names		
plane angle	radian	rad
solid angle	steradian	sr
frequency	hertz	Hz
energy	joule	J
force	newton	N
pressure	pascal	Pa
power	watt	W
electric charge	coulomb	C
electric potential	volt	V
electric resistance	ohm	Ω
electric conductance	siemens	S
electric capacitance	farad	F
magnetic flux	weber	Wb
inductance	henry	H
magnetic flux density	tesla	T
luminous flux	lumen	lm
illuminance	lux	lx
celsius temperature	degree celsius	°C
activity (of a radioactive source)*	becquerel	Bq
absorbed dose (of ionizing radiation)*	gray	Gy
dose equivalent*	sievert	Sv

*See our section 37, on "Radioactivity and radiation protection."

Int. J. Mod. Phys. A 2026.41. Downloaded from www.worldscientific.com
by UNIVERSITY OF CALIFORNIA @ BERKELEY on 09/16/26. Re-use and distribution is strictly not permitted, e
s articles.

Int. J. Mod. Phys. A 2026.41. Downloaded from www.worldscientific.com
by UNIVERSITY OF CALIFORNIA @ BERKELEY on 09/16/26. Re-use and distribution is strictly not permitted, except for Open Access articles.

4. Periodic Table of the Elements

Table 4.1. Revised March 2024 by D.E. Groom (LBNL). The atomic number (top left) is the number of protons in the nucleus. The atomic masses (bottom) of stable elements are weighted by isotopic abundances in the Earth's surface. Atomic masses are relative to the mass of ^{12}C, defined to be exactly 12 unified atomic mass units (u). The exceptions are Th, Pa, and U, which have no stable isotopes but do have characteristic terrestrial compositions. Relative isotopic abundances often vary considerably, both in natural and commercial samples; this is reflected in the number of significant figures given for the mass. Masses may be found at `https://physics.nist.gov/cgi-bin/Compositions/stand_alone.pl`. If there is no stable isotope, the atomic mass of the most stable isotope known as of June 2019 is given in parentheses.

IUPAC announced verification of the discoveries of elements 113, 115, 117, and 118 in December 2015. The names were approved November 2016. The 7th period of the periodic table is now complete. Attempts to synthesize elements with $Z > 118$ are under way, but as of March 2024 no discoveries have been announced.

PERIODIC TABLE OF THE ELEMENTS

1 IA	2 IIA	3 IIIB	4 IVB	5 VB	6 VIB	7 VIIB	8 VIII	9 VIII	10 VIII	11 IB	12 IIB	13 IIIA	14 IVA	15 VA	16 VIA	17 VIIA	18 VIIIA
1 H hydrogen 1.008																	2 He helium 4.002602
3 Li lithium 6.94	4 Be beryllium 9.012182											5 B boron 10.81	6 C carbon 12.0107	7 N nitrogen 14.007	8 O oxygen 15.999	9 F fluorine 18.998403163	10 Ne neon 20.1797
11 Na sodium 22.98976928	12 Mg magnesium 24.305											13 Al aluminum 26.9815385	14 Si silicon 28.085	15 P phosphorus 30.973761998	16 S sulfur 32.06	17 Cl chlorine 35.45	18 Ar argon 39.948
19 K potassium 39.0983	20 Ca calcium 40.078	21 Sc scandium 44.955908	22 Ti titanium 47.867	23 V vanadium 50.9415	24 Cr chromium 51.9961	25 Mn manganese 54.938044	26 Fe iron 55.845	27 Co cobalt 58.933195	28 Ni nickel 58.6934	29 Cu copper 63.546	30 Zn zinc 65.38	31 Ga gallium 69.723	32 Ge germanium 72.630	33 As arsenic 74.921595	34 Se selenium 78.971	35 Br bromine 79.904	36 Kr krypton 83.798
37 Rb rubidium 85.4678	38 Sr strontium 87.62	39 Y yttrium 88.90584	40 Zr zirconium 91.224	41 Nb niobium 92.90637	42 Mo molybdenum 95.95	43 Tc technetium (97.907212)	44 Ru ruthenium 101.07	45 Rh rhodium 102.90550	46 Pd palladium 106.42	47 Ag silver 107.8682	48 Cd cadmium 112.414	49 In indium 114.818	50 Sn tin 118.710	51 Sb antimony 121.760	52 Te tellurium 127.60	53 I iodine 126.90447	54 Xe xenon 131.293
55 Cs caesium 132.90545196	56 Ba barium 137.327	57–71 LANTHA- NIDES	72 Hf hafnium 178.49	73 Ta tantalum 180.94788	74 W tungsten 183.84	75 Re rhenium 186.207	76 Os osmium 190.23	77 Ir iridium 192.217	78 Pt platinum 195.084	79 Au gold 196.966569	80 Hg mercury 200.592	81 Tl thallium 204.38	82 Pb lead 207.2	83 Bi bismuth 208.98040	84 Po polonium (208.98243)	85 At astatine (209.98715)	86 Rn radon (222.01758)
87 Fr francium (223.01974)	88 Ra radium (226.02541)	89–103 ACTINIDES	104 Rf rutherford. (267.12169)	105 Db dubnium (268.12567)	106 Sg seaborgium (269.12863)	107 Bh bohrium (270.13336)	108 Hs hassium (269.13375)	109 Mt meitnerium (278.15631)	110 Ds darmstadt. (281.16451)	111 Rg roentgen. (282.16912)	112 Cn copernicium (285.17712)	113 Nh nihonium (286.18221)	114 Fl flerovium (289.19042)	115 Mc moscovium (290.19598)	116 Lv livermorium (293.20449	117 Ts tennessine (294.21046)	118 Og oganesson (294.21392)

Lanthanide series	57 La lanthanum 138.90547	58 Ce cerium 140.116	59 Pr praseodym. 140.90766	60 Nd neodymium 144.242	61 Pm promethium (144.91276)	62 Sm samarium 150.36	63 Eu europium 151.964	64 Gd gadolinum 157.25	65 Tb terbium 158.92535	66 Dy dysprosium 162.500	67 Ho holmium 164.93033	68 Er erbium 167.259	69 Tm thulium 168.93422	70 Yb ytterbium 173.054	71 Lu lutetium 174.9668		
Actinide series	89 Ac actinium (227.02775)	90 Th thorium 232.0377	91 Pa protactinium 231.03588	92 U uranium 238.02891	93 Np neptunium (237.04817)	94 Pu plutonium (244.06420)	95 Am americium (243.06138)	96 Cm curium (247.07035)	97 Bk berkelium (247.07031)	98 Cf californium (251.07959)	99 Es einsteinium (252.08298)	100 Fm fermium (257.09511)	101 Md mendelevium (258.09844)	102 No nobelium (259.10103)	103 Lr lawrencium (262.10961)		

5. Electronic Structure of the Elements

Table 5.1: Reviewed 2022 by A. Kramida (NIST). The electronic configurations, ground state levels, and ionization energies are from A. Kramida, Yu. Ralchenko, J. Reader, and NIST ASD Team (2024), "NIST Atomic Spectra Database" (ver. 5.12), [Online], Available: `https://physics.nist.gov/asd` [2025, Aug 19]. National Institute of Standards and Technology, Gaithersburg, MD. DOI: `https://doi.org/10.18434/T4W30F`. The electron configuration for, say, iron indicates an argon electronic core (see argon) plus six $3d$ electrons and two $4s$ electrons.

		Element	Electron configuration ($3d^5$ = five $3d$ electrons, *etc.*)					Ground state $^{2S+1}L_J$	Ionization energy (eV)
1	H	Hydrogen	$1s$					$^2S_{1/2}$	13.5984
2	He	Helium	$1s^2$					$^1S_0$	24.5874
3	Li	Lithium	(He)	2s				$^2S_{1/2}$	5.3917
4	Be	Beryllium	(He)	$2s^2$				$^1S_0$	9.3227
5	B	Boron	(He)	$2s^2$	$2p$			$^2P^\circ_{1/2}$	8.2980
6	C	Carbon	(He)	$2s^2$	$2p^2$			$^3P_0$	11.2603
7	N	Nitrogen	(He)	$2s^2$	$2p^3$			$^4S^\circ_{3/2}$	14.5341
8	O	Oxygen	(He)	$2s^2$	$2p^4$			$^3P_2$	13.6181
9	F	Fluorine	(He)	$2s^2$	$2p^5$			$^2P^\circ_{3/2}$	17.4228
10	Ne	Neon	(He)	$2s^2$	$2p^6$			$^1S_0$	21.5645
11	Na	Sodium	(Ne)	3s				$^2S_{1/2}$	5.1391
12	Mg	Magnesium	(Ne)	$3s^2$				$^1S_0$	7.6462
13	Al	Aluminum	(Ne)	$3s^2$	$3p$			$^2P^\circ_{1/2}$	5.9858
14	Si	Silicon	(Ne)	$3s^2$	$3p^2$			$^3P_0$	8.1517
15	P	Phosphorus	(Ne)	$3s^2$	$3p^3$			$^4S^\circ_{3/2}$	10.4867
16	S	Sulfur	(Ne)	$3s^2$	$3p^4$			$^3P_2$	10.3600
17	Cl	Chlorine	(Ne)	$3s^2$	$3p^5$			$^2P^\circ_{3/2}$	12.9676
18	Ar	Argon	(Ne)	$3s^2$	$3p^6$			$^1S_0$	15.7596
19	K	Potassium	(Ar)		$4s$			$^2S_{1/2}$	4.3407
20	Ca	Calcium	(Ar)		$4s^2$			$^1S_0$	6.1132
21	Sc	Scandium	(Ar)	$3d$	$4s^2$		T	$^2D_{3/2}$	6.5615
22	Ti	Titanium	(Ar)	$3d^2$	$4s^2$		r e	$^3F_2$	6.8281
23	V	Vanadium	(Ar)	$3d^3$	$4s^2$		a l	$^4F_{3/2}$	6.7462
24	Cr	Chromium	(Ar)	$3d^5$	$4s$		n e	$^7S_3$	6.7665
25	Mn	Manganese	(Ar)	$3d^5$	$4s^2$		s m	$^6S_{5/2}$	7.4340
26	Fe	Iron	(Ar)	$3d^6$	$4s^2$		i e	$^5D_4$	7.9025
27	Co	Cobalt	(Ar)	$3d^7$	$4s^2$		t n	$^4F_{9/2}$	7.8810
28	Ni	Nickel	(Ar)	$3d^8$	$4s^2$		i t	$^3F_4$	7.6399
29	Cu	Copper	(Ar)	$3d^{10}$	$4s$		o s	$^2S_{1/2}$	7.7264
30	Zn	Zinc	(Ar)	$3d^{10}$	$4s^2$		n	$^1S_0$	9.3942
31	Ga	Gallium	(Ar)	$3d^{10}$	$4s^2$	$4p$		$^2P^\circ_{1/2}$	5.9993
32	Ge	Germanium	(Ar)	$3d^{10}$	$4s^2$	$4p^2$		$^3P_0$	7.8994
33	As	Arsenic	(Ar)	$3d^{10}$	$4s^2$	$4p^3$		$^4S^\circ_{3/2}$	9.7886
34	Se	Selenium	(Ar)	$3d^{10}$	$4s^2$	$4p^4$		$^3P_2$	9.7524
35	Br	Bromine	(Ar)	$3d^{10}$	$4s^2$	$4p^5$		$^2P^\circ_{3/2}$	11.8138
36	Kr	Krypton	(Ar)	$3d^{10}$	$4s^2$	$4p^6$		$^1S_0$	13.9996
37	Rb	Rubidium	(Kr)		$5s$			$^2S_{1/2}$	4.1771
38	Sr	Strontium	(Kr)		$5s^2$			$^1S_0$	5.6949
39	Y	Yttrium	(Kr)	$4d$	$5s^2$		T	$^2D_{3/2}$	6.2173
40	Zr	Zirconium	(Kr)	$4d^2$	$5s^2$		r e	$^3F_2$	6.6341
41	Nb	Niobium	(Kr)	$4d^4$	$5s$		a l	$^6D_{1/2}$	6.7589
42	Mo	Molybdenum	(Kr)	$4d^5$	$5s$		n e	$^7S_3$	7.0924
43	Tc	Technetium	(Kr)	$4d^5$	$5s^2$		s m	$^6S_{5/2}$	7.1194
44	Ru	Ruthenium	(Kr)	$4d^7$	$5s$		i e	$^5F_5$	7.3605
45	Rh	Rhodium	(Kr)	$4d^8$	$5s$		t n	$^4F_{9/2}$	7.4589
46	Pd	Palladium	(Kr)	$4d^{10}$			i t	$^1S_0$	8.3368
47	Ag	Silver	(Kr)	$4d^{10}$	$5s$		o s	$^2S_{1/2}$	7.5762
48	Cd	Cadmium	(Kr)	$4d^{10}$	$5s^2$		n	$^1S_0$	8.9938

Int. J. Mod. Phys. A 2026.41. Downloaded from www.worldscientific.com
by UNIVERSITY OF CALIFORNIA @ BERKELEY on 09/16/26. Re-use and distribution is strictly not permitted, e
s articles.

Int. J. Mod. Phys. A 2026.41. Downloaded from www.worldscientific.com
by UNIVERSITY OF CALIFORNIA @ BERKELEY on 09/16/26. Re-use and distribution is strictly not permitted, except for Open Access articles.

		Element	Electron configuration ($3d^5$ = five $3d$ electrons, *etc.*)						Ground state $^{2S+1}L_J$	Ionization energy (eV)
49	In	Indium	(Kr)	$4d^{10}$	$5s^2$	$5p$			$^2P^\circ_{1/2}$	5.7864
50	Sn	Tin	(Kr)	$4d^{10}$	$5s^2$	$5p^2$			$^3P_0$	7.3439
51	Sb	Antimony	(Kr)	$4d^{10}$	$5s^2$	$5p^3$			$^4S^\circ_{3/2}$	8.6084
52	Te	Tellurium	(Kr)	$4d^{10}$	$5s^2$	$5p^4$			$^3P_2$	9.0098
53	I	Iodine	(Kr)	$4d^{10}$	$5s^2$	$5p^5$			$^2P^\circ_{3/2}$	10.4513
54	Xe	Xenon	(Kr)	$4d^{10}$	$5s^2$	$5p^6$			$^1S_0$	12.1298
55	Cs	Cesium	(Xe)			$6s$			$^2S_{1/2}$	3.8939
56	Ba	Barium	(Xe)			$6s^2$			$^1S_0$	5.2117
57	La	Lanthanum	(Xe)		$5d$	$6s^2$			$^2D_{3/2}$	5.5769
58	Ce	Cerium	(Xe)	$4f$	$5d$	$6s^2$			$^1G^\circ_4$	5.5386
59	Pr	Praseodymium	(Xe)	$4f^3$		$6s^2$		L	$^4I^\circ_{9/2}$	5.4702
60	Nd	Neodymium	(*Xe*)	$4f^4$		$6s^2$		a	$^5I_4$	5.5248
61	Pm	Promethium	(Xe)	$4f^5$		$6s^2$		n	$^6H^\circ_{5/2}$	5.5819
62	Sm	Samarium	(Xe)	$4f^6$		$6s^2$		t	$^7F_0$	5.6437
63	Eu	Europium	(Xe)	$4f^7$		$6s^2$		a	$^8S^\circ_{7/2}$	5.6704
64	Gd	Gadolinium	(Xe)	$4f^7$	$5d$	$6s^2$		n	$^9D^\circ_2$	6.1498
65	Tb	Terbium	(Xe)	$4f^9$		$6s^2$		i	$^6H^\circ_{15/2}$	5.8638
66	Dy	Dysprosium	(Xe)	$4f^{10}$		$6s^2$		d	$^5I_8$	5.9391
67	Ho	Holmium	(Xe)	$4f^{11}$		$6s^2$		e	$^4I^\circ_{15/2}$	6.0215
68	Er	Erbium	(Xe)	$4f^{12}$		$6s^2$		s	$^3H_6$	6.1077
69	Tm	Thulium	(Xe)	$4f^{13}$		$6s^2$			$^2F^\circ_{7/2}$	6.1844
70	Yb	Ytterbium	(Xe)	$4f^{14}$		$6s^2$			$^1S_0$	6.2542
71	Lu	Lutetium	(Xe)	$4f^{14}$	$5d$	$6s^2$			$^2D_{3/2}$	5.4259
72	Hf	Hafnium	(Xe)	$4f^{14}$	$5d^2$	$6s^2$		T	$^3F_2$	6.8251
73	Ta	Tantalum	(Xe)	$4f^{14}$	$5d^3$	$6s^2$		r e	$^4F_{3/2}$	7.5496
74	W	Tungsten	(Xe)	$4f^{14}$	$5d^4$	$6s^2$		a l	$^5D_0$	7.8640
75	Re	Rhenium	(Xe)	$4f^{14}$	$5d^5$	$6s^2$		n e	$^6S_{5/2}$	7.8335
76	Os	Osmium	(Xe)	$4f^{14}$	$5d^6$	$6s^2$		s m	$^5D_4$	8.4382
77	Ir	Iridium	(Xe)	$4f^{14}$	$5d^7$	$6s^2$		i e	$^4F_{9/2}$	8.9670
78	Pt	Platinum	(Xe)	$4f^{14}$	$5d^9$	$6s$		t n	$^3D_3$	8.9588
79	Au	Gold	(Xe)	$4f^{14}$	$5d^{10}$	$6s$		i t	$^2S_{1/2}$	9.2256
80	Hg	Mercury	(Xe)	$4f^{14}$	$5d^{10}$	$6s^2$		o s	$^1S_0$	10.4375
								n		
81	Tl	Thallium	(Hg)	$6p$					$^2P^\circ_{1/2}$	6.1083
82	Pb	Lead	(Hg)	$6p^2$					$^3P_0$	7.4167
83	Bi	Bismuth	(Hg)	$6p^3$					$^4S^\circ_{3/2}$	7.2855
84	Po	Polonium	(Hg)	$6p^4$					$^3P_2$	8.4181
85	At	Astatine	(Hg)	$6p^5$					$^2P^\circ_{3/2}$	9.3175
86	Rn	Radon	(Hg)	$6p^6$					$^1S_0$	10.7485
87	Fr	Francium	(Rn)			$7s$			$^2S_{1/2}$	4.0727
88	Ra	Radium	(Rn)			$7s^2$			$^1S_0$	5.2784
89	Ac	Actinium	(Rn)		$6d$	$7s^2$			$^2D_{3/2}$	5.3802
90	Th	Thorium	(Rn)		$6d^2$	$7s^2$			$^3F_2$	6.3067
91	Pa	Protactinium	(Rn)	$5f^2$	$6d$	$7s^2$		A	$^4K_{11/2}{}^*$	5.89
92	U	Uranium	(Rn)	$5f^3$	$6d$	$7s^2$		c	$^5L^{\circ *}_6$	6.1941
93	Np	Neptunium	(Rn)	$5f^4$	$6d$	$7s^2$		t	$^6L_{11/2}{}^*$	6.2656
94	Pu	Plutonium	(Rn)	$5f^6$		$7s^2$		i	$^7F_0$	6.0258
95	Am	Americium	(Rn)	$5f^7$		$7s^2$		n	$^8S^\circ_{7/2}$	5.9738
96	Cm	Curium	(Rn)	$5f^7$	$6d$	$7s^2$		i	$^9D^\circ_2$	5.9922
97	Bk	Berkelium	(Rn)	$5f^9$		$7s^2$		d	$^6H^\circ_{15/2}$	6.1979
98	Cf	Californium	(Rn)	$5f^{10}$		$7s^2$		e	$^5I_8$	6.2819
99	Es	Einsteinium	(Rn)	$5f^{11}$		$7s^2$		s	$^4I^\circ_{15/2}$	6.3684
100	Fm	Fermium	(Rn)	$5f^{12}$		$7s^2$			$^3H_6$	6.50
101	Md	Mendelevium	(Rn)	$5f^{13}$		$7s^2$			$^2F^\circ_{7/2}$	6.58
102	No	Nobelium	(Rn)	$5f^{14}$		$7s^2$			$^1S_0$	6.6262
103	Lr	Lawrencium	(Rn)	$5f^{14}$		$7s^2$	$7p$		$^2P^\circ_{1/2}$	4.96
104	Rf	Rutherfordium	(Rn)	$5f^{14}$	$6d^2$	$7s^2$			$^3F_2$	6.02
105	Db	Dubnium	(Rn)	$5f^{14}$	$6d^3$	$7s^2$			$^4F_{3/2}$	6.8
106	Sg	Seaborgium	(Rn)	$5f^{14}$	$6d^4$	$7s^2$			$_0$	7.8
107	Bh	Bohrium	(Rn)	$5f^{14}$	$6d^5$	$7s^2$			$_{5/2}$	7.7
108	Hs	Hassium	(Rn)	$5f^{14}$	$6d^6$	$7s^2$			$_4$	7.6

* The usual LS coupling scheme does not apply for these three elements.

See the introductory note to the NIST table at `https://www.nist.gov/pml/data/ion_energy.cfm`.

6. Atomic and Nuclear Properties of Materials

Table 6.1: Abridged from `https://pdg.lbl.gov/current/AtomicNuclearProperties` by D.E. Groom (2023). See web pages for more detail about entries in this table and for several hundred others. Parentheses in the dE/dx and density columns indicate gases at 20° C and 1 atm. Boiling points are at 1 atm. Refractive indices n are evaluated at the sodium D line blend (589.2 nm); values $\gg$1 in brackets indicate $(n-1)\times 10^6$ for gases at 0° C and 1 atm.

Material	Z	A	$\langle Z/A \rangle$	Nucl.coll. length λ_T {g cm^{-2}}	Nucl.inter. length λ_I {g cm^{-2}}	Rad.len. X_0 {g cm^{-2}}	$dE/dx\|_{\rm min}$ {MeV g^{-1}cm^2}	Density {g cm^{-3}} ({g ℓ^{-1}})	Melting point (K)	Boiling point (K)	Refract. index @ Na D
H_2	1	1.008(7)	0.99212	42.8	52.0	63.05	(4.103)	0.071(0.084)	13.81	20.28	1.11[132.]
D_2	1	2.014101764(8)	0.49650	51.3	71.8	125.97	(2.053)	0.169(0.168)	18.7	23.65	1.11[138.]
He	2	4.002602(2)	0.49967	51.8	71.0	94.32	(1.937)	0.125(0.166)		4.220	1.02[35.0]
Li	3	6.94(2)	0.43221	52.2	71.3	82.78	1.639	0.534	453.6	1615.	
Be	4	9.0121831(5)	0.44384	55.3	77.8	65.19	1.595	1.848	1560.	2744.	
C diamond	6	12.0107(8)	0.49955	59.2	85.8	42.70	1.725	3.520			2.419
C graphite	6	12.0107(8)	0.49955	59.2	85.8	42.70	1.742	2.210	Sublimes at 4098. K		
N_2	7	14.007(2)	0.49976	61.1	89.7	37.99	(1.825)	0.807(1.165)	63.15	77.29	1.20[298.]
O_2	8	15.999(3)	0.50002	61.3	90.2	34.24	(1.801)	1.141(1.332)	54.36	90.20	1.22[271.]
F_2	9	18.998403163(6)	0.47372	65.0	97.4	32.93	(1.676)	1.507(1.580)	53.53	85.03	[195.]
Ne	10	20.1797(6)	0.49555	65.7	99.0	28.93	(1.724)	1.204(0.839)	24.56	27.07	1.09[67.1]
Al	13	26.9815385(7)	0.48181	69.7	107.2	24.01	1.615	2.699	933.5	2792.	
Si	14	28.0855(3)	0.49848	70.2	108.4	21.82	1.664	2.329	1687.	3538.	3.95
Cl_2	17	35.453(2)	0.47951	73.8	115.7	19.28	(1.630)	1.574(2.980)	171.6	239.1	[773.]
Ar	18	39.948(1)	0.45059	75.7	119.7	19.55	(1.519)	1.396(1.662)	83.81	87.26	1.23[281.]
Ti	22	47.867(1)	0.45961	78.8	126.2	16.16	1.477	4.540	1941.	3560.	
Fe	26	55.845(2)	0.46557	81.7	132.1	13.84	1.451	7.874	1811.	3134.	
Cu	29	63.546(3)	0.45636	84.2	137.3	12.86	1.403	8.960	1358.	2835.	
Ge	32	72.630(1)	0.44053	86.9	143.0	12.25	1.370	5.323	1211.	3106.	
Sn	50	118.710(7)	0.42119	98.2	166.7	8.82	1.263	7.310	505.1	2875.	
Xe	54	131.293(6)	0.41129	100.8	172.1	8.48	(1.255)	2.953(5.483)	161.4	165.1	1.39[701.]
W	74	183.84(1)	0.40252	110.4	191.9	6.76	1.145	19.300	3695.	5828.	
Pt	78	195.084(9)	0.39983	112.2	195.7	6.54	1.128	21.450	2042.	4098.	
Au	79	196.966569(5)	0.40108	112.5	196.3	6.46	1.134	19.320	1337.	3129.	
Pb	82	207.2(1)	0.39575	114.1	199.6	6.37	1.122	11.350	600.6	2022.	
U	92	[238.02891(3)]	0.38651	118.6	209.0	6.00	1.081	18.950	1408.	4404.	
Air (dry, 1 atm)			0.49919	61.3	90.1	36.62	(1.815)	(1.205)		78.80	[289]
Shielding concrete			0.50274	65.1	97.5	26.57	1.711	2.300			
Borosilicate glass (Pyrex)			0.49707	64.6	96.5	28.17	1.696	2.230			
Lead glass SF5			0.44522	84.0	133.4	10.07	1.406	4.080			1.6727
Standard rock			0.50000	66.8	101.3	26.54	1.688	2.650			
Methane (CH_4)			0.62334	54.0	73.8	46.47	(2.417)	(0.667)	90.68	111.7	[444.]
Ethane (C_2H_6)			0.59861	55.0	75.9	45.66	(2.304)	(1.263)	90.36	184.5	
Propane (C_3H_8)			0.58962	55.3	76.7	45.37	(2.262)	0.493(1.868)	85.52	231.0	
Butane (C_4H_{10})			0.59497	55.5	77.1	45.23	(2.278)	(2.489)	134.9	272.6	
Octane (C_8H_{18})			0.57778	55.8	77.8	45.00	2.123	0.703	214.4	398.8	
Paraffin ($CH_3(CH_2)_{n\approx 23}CH_3$)			0.57275	56.0	78.3	44.85	2.088	0.930			
Nylon (type 6, 6/6)			0.54790	57.5	81.6	41.92	1.973	1.18			
Polycarbonate (Lexan)			0.52697	58.3	83.6	41.50	1.886	1.20			
Polyethylene ($[CH_2CH_2]_n$)			0.57034	56.1	78.5	44.77	2.079	0.89			
Polyethylene terephthalate (Mylar)			0.52037	58.9	84.9	39.95	1.848	1.40			
Polyimide film (Kapton)			0.51264	59.2	85.5	40.58	1.820	1.42			
Polymethylmethacrylate (acrylic)			0.53937	58.1	82.8	40.55	1.929	1.19			1.49
Polypropylene			0.55998	56.1	78.5	44.77	2.041	0.90			
Polystyrene ($[C_6H_5CHCH_2]_n$)			0.53768	57.5	81.7	43.79	1.936	1.06			1.59
Polytetrafluoroethylene (Teflon)			0.47992	63.5	94.4	34.84	1.671	2.20			
Polyvinyltoluene			0.54141	57.3	81.3	43.90	1.956	1.03			1.58
Aluminum oxide (sapphire)			0.49038	65.5	98.4	27.94	1.647	3.970	2327.	3273.	1.77
Barium flouride (BaF_2)			0.42207	90.8	149.0	9.91	1.303	4.893	1641.	2533.	1.47
Bismuth germanate (BGO)			0.42065	96.2	159.1	7.97	1.251	7.130	1317.		2.15
Carbon dioxide gas (CO_2)			0.49989	60.7	88.9	36.20	1.819	(1.842)			[449.]
Solid carbon dioxide (dry ice)			0.49989	60.7	88.9	36.20	1.787	1.563	Sublimes at 194.7 K		
Cesium iodide (CsI)			0.41569	100.6	171.5	8.39	1.243	4.510	894.2	1553.	1.79
Lithium fluoride (LiF)			0.46262	61.0	88.7	39.26	1.614	2.635	1121.	1946.	1.39
Lithium hydride (LiH)			0.50321	50.8	68.1	79.62	1.897	0.820	965.		
Lead tungstate ($PbWO_4$)			0.41315	100.6	168.3	7.39	1.229	8.300	1403.		2.20
Silicon dioxide (SiO_2, fused quartz)			0.49930	65.2	97.8	27.05	1.699	2.200	1986.	3223.	1.46
Sodium chloride (NaCl)			0.47910	71.2	110.1	21.91	1.847	2.170	1075.	1738.	1.54
Sodium iodide (NaI)			0.42697	93.1	154.6	9.49	1.305	3.667	933.2	1577.	1.77
Water (H_2O)			0.55509	58.5	83.3	36.08	1.992	1.000	273.1	373.1	1.33
Silica aerogel			0.50093	65.0	97.3	27.25	1.740	0.200	(0.03 H_2O, 0.97 SiO_2)		
Epoxy (Epotek-301-1)			0.53409	58.1	83.0	41.22	1.925	1.190			
G10			0.51166	56.8	78.4	32.17	1.762	1.800			

Int. J. Mod. Phys. A 2026.41. Downloaded from www.worldscientific.com
by UNIVERSITY OF CALIFORNIA @ BERKELEY on 09/16/26. Re-use and distribution is strictly not permitted, e
s articles.

Int. J. Mod. Phys. A 2026.41. Downloaded from www.worldscientific.com
by UNIVERSITY OF CALIFORNIA @ BERKELEY on 09/16/26. Re-use and distribution is strictly not permitted, except for Open Access articles.

7. Electromagnetic Relations

Revised September 2005 by H.G. Spieler (LBNL).

Quantity	Gaussian CGS	SI
Conversion factors:		
Charge:	$2.997\,924\,58 \times 10^9$ esu	$= 1$ C $= 1$ A s
Potential:	(1/299.792 458) statvolt (ergs/esu)	$= 1$ V $= 1$ J C^{-1}
Magnetic field:	10^4 gauss $= 10^4$ dyne/esu	$= 1$ T $= 1$ N A^{-1}m^{-1}
	$\mathbf{F} = q\,(\mathbf{E} + \frac{\mathbf{v}}{c} \times \mathbf{B})$	$\mathbf{F} = q\,(\mathbf{E} + \mathbf{v} \times \mathbf{B})$
	$\nabla \bullet \mathbf{D} = 4\pi\rho$ $\nabla \times \mathbf{H} - \frac{1}{c}\frac{\partial \mathbf{D}}{\partial t} = \frac{4\pi}{c}\mathbf{J}$ $\nabla \bullet \mathbf{B} = 0$ $\nabla \times \mathbf{E} + \frac{1}{c}\frac{\partial \mathbf{B}}{\partial t} = 0$	$\nabla \bullet \mathbf{D} = \rho$ $\nabla \times \mathbf{H} - \frac{\partial \mathbf{D}}{\partial t} = \mathbf{J}$ $\nabla \bullet \mathbf{B} = 0$ $\nabla \times \mathbf{E} + \frac{\partial \mathbf{B}}{\partial t} = 0$
Constitutive relations:	$\mathbf{D} = \mathbf{E} + 4\pi\mathbf{P}, \quad \mathbf{H} = \mathbf{B} - 4\pi\mathbf{M}$	$\mathbf{D} = \epsilon_0\mathbf{E} + \mathbf{P}, \quad \mathbf{H} = \mathbf{B}/\mu_0 - \mathbf{M}$
Linear media:	$\mathbf{D} = \epsilon\mathbf{E}, \quad \mathbf{H} = \mathbf{B}/\mu$ 1 1	$\mathbf{D} = \epsilon\mathbf{E}, \quad \mathbf{H} = \mathbf{B}/\mu$ $\epsilon_0 = 8.854\,187\ldots \times 10^{-12}$ F m^{-1} $\mu_0/4\pi = 0.999\,999\,9\ldots \times 10^{-7}$ N A^{-2}
	$\mathbf{E} = -\nabla V - \frac{1}{c}\frac{\partial \mathbf{A}}{\partial t}$ $\mathbf{B} = \nabla \times \mathbf{A}$	$\mathbf{E} = -\nabla V - \frac{\partial \mathbf{A}}{\partial t}$ $\mathbf{B} = \nabla \times \mathbf{A}$
	$V = \sum_{\text{charges}} \frac{q_i}{r_i} = \int \frac{\rho\,(\mathbf{r}')}{\lvert\mathbf{r}-\mathbf{r}'\rvert}\, d^3x'$ $\mathbf{A} = \frac{1}{c}\oint \frac{I\,\mathbf{d}\ell}{\lvert\mathbf{r}-\mathbf{r}'\rvert} = \frac{1}{c}\int \frac{\mathbf{J}(\mathbf{r}')}{\lvert\mathbf{r}-\mathbf{r}'\rvert}\, d^3x'$	$V = \frac{1}{4\pi\epsilon_0}\sum_{\text{charges}} \frac{q_i}{r_i} = \frac{1}{4\pi\epsilon_0}\int \frac{\rho\,(\mathbf{r}')}{\lvert\mathbf{r}-\mathbf{r}'\rvert}\, d^3x'$ $\mathbf{A} = \frac{\mu_0}{4\pi}\oint \frac{I\,\mathbf{d}\ell}{\lvert\mathbf{r}-\mathbf{r}'\rvert} = \frac{\mu_0}{4\pi}\int \frac{\mathbf{J}(\mathbf{r}')}{\lvert\mathbf{r}-\mathbf{r}'\rvert}\, d^3x'$
	$\mathbf{E}'_\parallel = \mathbf{E}_\parallel$ $\mathbf{E}'_\perp = \gamma(\mathbf{E}_\perp + \frac{1}{c}\mathbf{v} \times \mathbf{B})$ $\mathbf{B}'_\parallel = \mathbf{B}_\parallel$ $\mathbf{B}'_\perp = \gamma(\mathbf{B}_\perp - \frac{1}{c}\mathbf{v} \times \mathbf{E})$	$\mathbf{E}'_\parallel = \mathbf{E}_\parallel$ $\mathbf{E}'_\perp = \gamma(\mathbf{E}_\perp + \mathbf{v} \times \mathbf{B})$ $\mathbf{B}'_\parallel = \mathbf{B}_\parallel$ $\mathbf{B}'_\perp = \gamma(\mathbf{B}_\perp - \frac{1}{c^2}\mathbf{v} \times \mathbf{E})$

$$\frac{1}{4\pi\epsilon_0} = c^2 \times 10^{-7}\ \text{N A}^{-2} = 8.987\,55\ldots \times 10^9\ \text{m F}^{-1}\ ;\quad \frac{\mu_0}{4\pi} = 10^{-7}\ \text{N A}^{-2}\ ;\quad c = \frac{1}{\sqrt{\mu_0\epsilon_0}} = 2.997\,924\,58 \times 10^8\ \text{m s}^{-1}$$

7.1 Impedances (SI units)

ρ = resistivity at room temperature in $10^{-8}\,\Omega$ m:

~ 1.7 for Cu $\quad \sim 5.5$ for W
~ 2.4 for Au $\quad \sim 73$ for SS 304
~ 2.8 for Al $\quad \sim 100$ for Nichrome
(Al alloys may have double the Al value.)

For alternating currents, instantaneous current I, voltage V, angular frequency ω:

$$V = V_0\, e^{j\omega t} = ZI\ . \tag{7.1}$$

Impedance of self-inductance L: $Z = j\omega L$.

Impedance of capacitance C: $Z = 1/j\omega C$.

Impedance of free space: $Z = \sqrt{\mu_0/\epsilon_0} = 376.7\ \Omega$.

High-frequency surface impedance of a good conductor:

$$Z = \frac{(1+j)\,\rho}{\delta}\ , \quad \text{where } \delta = \text{skin depth}\ ; \tag{7.2}$$

$$\delta = \sqrt{\frac{\rho}{\pi\nu\mu}} \approx \frac{6.6\ \text{cm}}{\sqrt{\nu\,(\text{Hz})}} \quad \text{for Cu}\ . \tag{7.3}$$

7.2 Capacitors, inductors, and transmission Lines

The capacitance between two parallel plates of area A spaced by the distance d and enclosing a medium with the dielectric constant ε is

$$C = K\varepsilon A/d\,, \tag{7.4}$$

where the correction factor K depends on the extent of the fringing field. If the dielectric fills the capacitor volume without extending beyond the electrodes. The correction factor $K \approx 0.8$ for capacitors of typical geometry.

The inductance at high frequencies of a straight wire whose length ℓ is much greater than the wire diameter d is

$$L \approx 2.0\left[\frac{\text{nH}}{\text{cm}}\right]\cdot \ell\left(\ln\left(\frac{4\ell}{d}\right) - 1\right)\ . \tag{7.5}$$

For very short wires, representative of vias in a printed circuit board, the inductance is

$$L(\text{in nH}) \approx \ell/d\,. \tag{7.6}$$

A transmission line is a pair of conductors with inductance L and capacitance C. The characteristic impedance $Z = \sqrt{L/C}$ and the phase velocity $v_p = 1/\sqrt{LC} = 1/\sqrt{\mu\varepsilon}$, which decreases with the inverse square root of the dielectric constant of the medium. Typical coaxial and ribbon cables have a propagation delay of about 5 ns/m.

Int. J. Mod. Phys. A 2026.41. Downloaded from www.worldscientific.com
by UNIVERSITY OF CALIFORNIA @ BERKELEY on 09/16/26. Re-use and distribution is strictly not permitted, except for articles.

The impedance of a coaxial cable with outer diameter D and inner diameter d is

$$Z = 60\,\Omega \cdot \frac{1}{\sqrt{\varepsilon_r}} \ln \frac{D}{d}\,, \tag{7.7}$$

where the relative dielectric constant $\varepsilon_r = \varepsilon/\varepsilon_0$. A pair of parallel wires of diameter d and spacing $a > 2.5\,d$ has the impedance

$$Z = 120\,\Omega \cdot \frac{1}{\sqrt{\varepsilon_r}} \ln \frac{2a}{d}\,. \tag{7.8}$$

This yields the impedance of a wire at a spacing h above a ground plane,

$$Z = 60\,\Omega \cdot \frac{1}{\sqrt{\varepsilon_r}} \ln \frac{4h}{d}\,. \tag{7.9}$$

A common configuration utilizes a thin rectangular conductor above a ground plane with an intermediate dielectric (microstrip). Detailed calculations for this and other transmission line configurations are given by Gunston [1].

7.3 Synchrotron radiation (CGS units)

For a particle of charge e, velocity $v = \beta c$, and energy $E = \gamma mc^2$, traveling in a circular orbit of radius R, the classical energy loss per revolution δE is

$$\delta E = \frac{4\pi}{3}\,\frac{e^2}{R}\,\beta^3\,\gamma^4\,. \tag{7.10}$$

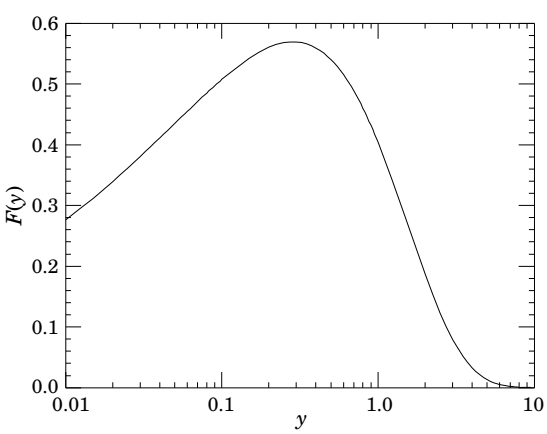

Figure 7.1: The normalized synchrotron radiation spectrum $F(y)$.

For high-energy electrons or positrons ($\beta \approx 1$), this becomes

$$\delta E\ (\text{in MeV}) \approx 0.0885\ [E(\text{in GeV})]^4/R(\text{in m})\,. \tag{7.11}$$

For $\gamma \gg 1$, the energy radiated per revolution into the photon energy interval $d(\hbar\omega)$ is

$$dI = \frac{8\pi}{9}\alpha\,\gamma\,F(\omega/\omega_c)\,d(\hbar\omega)\,, \tag{7.12}$$

where $\alpha = e^2/\hbar c$ is the fine-structure constant and

$$\omega_c = \frac{3\gamma^3 c}{2R} \tag{7.13}$$

is the critical frequency. The normalized function $F(y)$ is

$$F(y) = \frac{9}{8\pi}\sqrt{3}\,y \int_y^\infty K_{5/3}(x)\ dx\,, \tag{7.14}$$

where $K_{5/3}(x)$ is a modified Bessel function of the third kind. For electrons or positrons,

$$\hbar\omega_c\,(\text{in keV}) \approx 2.22\ [E(\text{in GeV})]^3/R(\text{in m})\,. \tag{7.15}$$

For $\gamma \gg 1$ and $\omega \ll \omega_c$,

$$\frac{dI}{d(\hbar\omega)} \approx 3.3\alpha\,(\omega R/c)^{1/3}\,, \tag{7.16}$$

whereas for

$$\gamma \gg 1 \text{ and } \omega \gtrsim 3\omega_c\,,$$

$$\frac{dI}{d(\hbar\omega)} \approx \sqrt{\frac{3\pi}{2}}\,\alpha\,\gamma\left(\frac{\omega}{\omega_c}\right)^{1/2} e^{-\omega/\omega_c}\left[1 + \frac{55}{72}\frac{\omega_c}{\omega} + \ldots\right]\,. \tag{7.17}$$

The radiation is confined to angles $\lesssim 1/\gamma$ relative to the instantaneous direction of motion. For $\gamma \gg 1$, where Eq. (7.12) applies, the mean number of photons emitted per revolution is

$$N_\gamma = \frac{5\pi}{\sqrt{3}}\alpha\gamma\,, \tag{7.18}$$

and the mean energy per photon is

$$\langle\hbar\omega\rangle = \frac{8}{15\sqrt{3}}\hbar\omega_c\,. \tag{7.19}$$

When $\langle\hbar\omega\rangle \gtrsim \mathrm{O}(E)$, quantum corrections are important [2].[1]

References

[1] M.A.R. Gunston. Microwave Transmission Line Data, Noble Publishing Corp., Atlanta (1997) ISBN 1-884932-57-6, TK6565.T73G85.

[2] J.D. Jackson, *Classical Electrodynamics*, 3rd edition (John Wiley & Sons, New York, 1998) for more formulae and details.

[1] Note that earlier editions of Ref. [2] had ω_c twice as large as Eq. (7.13).

Int. J. Mod. Phys. A 2026.41. Downloaded from www.worldscientific.com
by UNIVERSITY OF CALIFORNIA @ BERKELEY on 09/16/26. Re-use and distribution is strictly not permitted, except for Open Access articles.

8. Naming Scheme for Hadrons

Revised August 2025 by C. Amsler (Marietta Blau Inst.), E. Pianori (LBNL), D.J. Robinson (LBNL) and R.L. Workman (George Washington U.).

In the 1986 edition [1], the Particle Data Group introduced an extended and systematized naming scheme for mesons and baryons. The extensions were necessary in order to name the new particles containing c or b quarks that were then rapidly being discovered. The 1986 naming scheme has been retained in all subsequent editions, including this one. However, a number of particles were since discovered that could not be accommodated in the 1986 scheme. These include, for example the meson state originally named $Z_c(3900)^+$ (now $T_{c\bar{c}1}(3900)^+$) containing $c\bar{c}$ but with isospin $I = 1$ [2,3]. Because of such discoveries, in the 2017 edition [4] the 1986 naming scheme was extended to cover $c\bar{c}$ and $b\bar{b}$ states with $I = 1$, including the Z_c and Z_b states.

The further discovery of various exotic hadron states—including in particular tetraquarks and pentaquarks containing $qq\bar{q}\bar{q}$ and $q\bar{q}qqq$ minimal quark content, respectively—has rendered the 2017 extension insufficient. These include, for example: the meson state $T_{cc}(3875)^+$ containing two charm quarks and with unknown isospin [5]; and the baryon state originally named $P_c(4312)^+$ (now $P_{c\bar{c}}(4312)^+$) containing minimal quark content $c\bar{c}uud$ [6]. In this edition, the 2017 scheme is revised and extended to cover all experimentally known states.

The naming scheme as a whole provides a name for each hadron, driven primarily by consideration of its quantum numbers, its minimal quark content—the smallest combination of quarks required to produce a color singlet with the required isospin, parities, strangeness, and open or hidden-heavy flavor—and its mass. While much of the naming scheme has been developed within the context of the naive quark model, a hadron name does *not* designate the internal structure of a state per se: we make no attempt, for example, to distinguish meson states that are "mostly gluonium" from those that are "mostly $q\bar{q}$." (Other reviews within the RPP discuss our current understanding of the nature of various hadron states). While the naming scheme conventions aim to be comprehensive, exceptions to the scheme are occasionally made for historical reasons (e.g. J/ψ, p, or n) or in cases where the spectroscopic identity of a state is considered established (e.g. $\Upsilon(1S)$). Note also the mass label used in particle names is chosen using the best information available when a name is assigned. A more accurate value of a particle mass may become available at a later time. PDG decides on a case-by-case basis whether to revise the mass label, taking into account the updated information.

8.1 Light unflavored, $c\bar{c}$, and $b\bar{b}$ mesons

Unflavored mesons—also referred to as "neutral-flavor" mesons—have zero strangeness and all heavy-flavor quantum numbers are equal to zero. Their minimal quark content is denoted $q\bar{q}$, with the understanding that for $q = u$ or d, such states may carry unit isospin: the "light unflavored" nomenclature is understood to encompass all states furnishing an isospin-1 multiplet that contains a $q\bar{q}$ neutral meson. Mesons composed of $c\bar{c}$ or $b\bar{b}$ are said to have hidden-heavy flavor.

Within the naive quark model, a neutral $q\bar{q}$ bound state has quantum numbers $P = (-1)^{L+1}$ and $C = (-1)^{L+S}$, where $S(= 0, 1)$ and L are the spin and orbital angular momentum of the $q\bar{q}$ system, respectively. The total angular momentum J satisfies $|L-S| \leq J \leq L+S$ as usual. There is thus a selection rule between the angular-momentum state ${}^{2S+1}L_J$ and the PC configuration, such that

$$PC \quad = \quad -+, \qquad +-, \qquad --, \qquad ++, \tag{8.1}$$

corresponds to

$${}^{2S+1}L_J \quad = \quad {}^1(L\text{ even})_L\,, \qquad {}^1(L\text{ odd})_L\,, \qquad {}^3(L\text{ even})_{|L-1|\leq J\leq L+1}\,, \qquad {}^3(L\text{ odd})_{L-1,L,L+1}\,. \tag{8.2}$$

Table 8.1 describes the naming scheme for unflavored mesons. The scheme is categorized by isospin and hidden-heavy flavor (rows) and parity/charge-conjugation configurations (columns); the first few allowed J^{PC} combinations for each column are shown in the header. Note C-parity is only well-defined for neutral unflavored mesons; the states furnishing an isospin-1 multiplet instead have a well-defined G-parity$= (-1)^{L+S+I}$; see the review on the quark model. The angular momentum J is included as a subscript to the base symbol for most unflavored mesons, but is omitted for various pseudoscalar, vector, and axial vector mesons whenever disambiguation by the J subscript is deemed superfluous. The mass is added in parentheses for mesons that decay strongly. However, for some of the familiar mesons (e.g. η', ϕ, ω), we omit the mass.

For light unflavored mesons—i.e. those unflavored mesons formed from u, d, and s quarks—there can be two isospin-0 mesons: a prime is used to distinguish one from the other (e.g. η and η'), with the exception that vector mesons comprised of $u\bar{u} + d\bar{d}$ and $s\bar{s}$ (ideal mixing) are labeled ω and ϕ, respectively. As usual, we assign the spectroscopic name (e.g. $\Upsilon(1S)$) as the primary name to most of those ψ, Υ, and χ states whose spectroscopic identity is known. We use the form $\Upsilon(9460)$ as an alternative, and as the primary name when the spectroscopic identity is not known.

Determination of the quark content (where relevant) and the quantum numbers I, J, P, and C (or G) of an unflavored meson thus determine its symbol. For example, the light unflavored isospin-1 2^{--} meson would be the ρ_2. Conversely, these properties may be inferred unambiguously from the symbol. The name X is used for states with still unknown quantum numbers. In some cases names are assigned when quantum numbers have not been strictly measured but have instead been inferred from a broader context. These cases typically include an explanation in the header, such as "Quantum numbers shown are quark-model predictions." One example is the $\psi_2(3823)$, for which the $I^G(J^{PC}) = 0^-(2^{--})$ assignment needs confirmation. Since the top quark is so heavy that it decays too rapidly to form bound states, no name is assigned to structures like $t\bar{t}$.

The selection rules in Eq. (8.2) impose restrictions on the J^{PC} quantum numbers that are allowed for $q\bar{q}$ states. These do not apply to more complicated structures such as tetraquarks, hybrid mesons, or glueballs. In particular, unflavored mesons with quantum numbers $J^{PC} = 0^{--}, 0^{+-}, 1^{-+}, 2^{+-}, 3^{-+}, \ldots$ cannot

Table 8.1: Base symbols for unflavored mesons (zero strangeness and heavy-flavor quantum numbers equal to zero). Each base symbol is uniquely determined by the isospin/hidden-heavy flavor and PC configuration.

$J^{PC} =$	0^{-+}	1^{+-}	1^{--}	0^{++}
	2^{-+}	3^{+-}	2^{--}	1^{++}
	$\vdots$	$\vdots$	$\vdots$	$\vdots$
Minimal quark content				
$u\bar{d}, u\bar{u} - d\bar{d}, d\bar{u}$ $(I = 1)$	π	b	ρ	a
$d\bar{d} + u\bar{u}$, $s\bar{s}$ and/or gluons $(I = 0)$	η,η'	h,h'	ω,ϕ	f,f'
$c\bar{c}$ $(I = 0)$	η_c	h_c	ψ *	χ_c
$b\bar{b}$ $(I = 0)$	η_b	h_b	Υ	χ_b

*With the exception of the J/ψ.

Int. J. Mod. Phys. A 2026.41. Downloaded from www.worldscientific.com by UNIVERSITY OF CALIFORNIA @ BERKELEY on 09/16/26. Re-use and distribution is strictly not permitted, e articles.

be $q\bar{q}$ bound states, but might be glueballs or $q\bar{q}g$ etc. (This is distinct from light unflavored mesons with $I \geq 2$ or hidden-heavy flavor mesons with $I \geq 1$, which could be interpreted as tetraquarks). For such a "manifestly exotic" unflavored meson, the naming scheme nonetheless assigns the same base symbol as solely determined by the isospin/hidden-heavy flavor and PC in Tab. 8.1. For example, an isospin-0 light unflavored 1^{-+} meson would be denoted η_1 while an isospin-1 0^{--} light unflavored meson would be denoted ρ_0. The exotic nature of the meson can be inferred from its PC quantum numbers—given by the symbol—and the spin J—given by the subscript.

8.2 Remarks on "neutral-flavor" mesons with hidden charm or bottom not classified as $q\bar{q}$

In the heavy-quark sector, there are several states with properties – such as masses, decay patterns, and widths – that are in disagreement with predictions from the naive quark model. For example, the vector state at 4230 MeV (the $\psi(4230)$) apparently does not decay into $D\overline{D}$, although within the naive quark model its quantum numbers would call for this decay channel to be dominant. These states were originally named X, Y, or Z, with their masses added in parentheses. This nomenclature differs from the conventions outlined in the previous section, since the meson names are not related to their quantum numbers. However, these states have properties in conflict with the naive quark model and therefore deserve some special labeling.

Since their original discovery, the properties of some of these states have become better understood and it has become possible to include them in the Listings as well as Summary Tables using the name assigned according to this review. The X-, Y-, or Z-based names used at the time of the discovery are also reported in the Listings and Summary Tables from the 2018 edition onwards as a sub-header (listed are only some examples of the particles that appear in the Summary Tables),

- the state originally named $X(3872)$ appears as '$\chi_{c1}(3872)$ also known as $X(3872)$';
- the state originally named $Z_c(3900)$ appears[1] as '$T_{c\bar{c}1}(3900)$ also known as $Z_c(3900)$';
- the state originally named $Y(4260)$ appears[2] as '$\psi(4230)$ also known as $Y(4230)$';

In addition, states with quantum numbers allowed by the naive quark model but showing some peculiarities, such as an unusual decay pattern, will have the following information in the header:

> This state shows properties different from a conventional $q\bar{q}$ state. A candidate for an exotic structure. See the review on ⟨name of the proper review⟩.

8.3 Mesons with nonzero S, C and/or B

Mesons with nonzero strangeness S or heavy flavor C and/or B are not eigenstates of charge conjugation, and in each of them one of the quarks is heavier than the other (as above, states containing top quarks are not considered). The rules have been and remain:

1. The main symbol is an upper-case italic letter indicating the heavier quark as follows:

   $$s \to \overline{K} \qquad c \to D \qquad b \to \overline{B},$$

   We use the convention that *the flavor quantum number and the charge of a quark have the same sign.* Thus the strangeness of the s quark is negative, the charm of the c quark is positive, and the bottomness of the b quark is negative. The effect of this convention is as follows: *any flavor carried by a charged meson has the same sign as its charge.* Thus the K^+, D^+, and B^+ have positive strangeness, charm, and bottomness, respectively, and all have positive I_3. The D_s^+ has positive charm *and* strangeness. Furthermore, the $\Delta(\text{flavor}) = \Delta Q$ rule, best known for the strange kaons, applies to every flavor.
2. If the lighter quark is not a u or a d quark, its identity is given by a subscript. The D_s^+ is an example.
3. When the spin-parity is in the natural series, $J^P = 0^+, 1^-, 2^+, \cdots$, a superscript "$*$" is added.
4. The spin is added as a subscript except for pseudoscalar or vector mesons.

8.4 Baryons with ordinary quantum numbers

All baryons having quantum numbers consistent with a minimal quark content of three quarks are denoted by the symbols N, Δ, Λ, Σ, Ξ, and Ω introduced more than 50 years ago. These symbols are followed by J^P signifying their spin J and parity P. For those where the minimal content involves one or more heavier quarks than the light (u, d, and s) quarks, subscripts are added to their symbols, (c and b) as appropriate. The rules are:

1. Baryons with minimal content of *three* u and/or d quarks are N's (isospin 1/2) or Δ's (isospin 3/2).
2. Baryons with *two* u and/or d quarks are Λ's (isospin 0) or Σ's (isospin 1). If the third quark is a c or b quark, its identity is given by a subscript.
3. Baryons with *one* u or d quark are Ξ's (isospin 1/2). One or two subscripts are used if one or both of the remaining quarks are heavy: thus Ξ_c, Ξ_{cc}, Ξ_b, etc.[3]
4. Baryons with *no* u or d quarks are Ω's (isospin 0), and subscripts indicate any heavy-quark content.
5. A baryon that decays strongly has its mass in parentheses. Examples are the $\Delta(1232)$ $3/2^+$, $\Sigma(1385)$ $3/2^+$, $N(1440)$ $1/2^+$, $\Xi_c(2645)$ $3/2^+$.
6. If individual states of isospin multiplets are addressed, the electric charge is specified as a superscript. The electric charge is not necessary for isospin-0 states (Λ and Ω), as there is no ambiguity, but may still be included.
7. Antibaryons are labeled by an overline (bar) on the base symbol. For example, $\bar{p}$ for the antiproton, or $\bar{\Lambda}_c^-$ for the antiparticle of Λ_c^+. Alternatively, particle and antiparticle can be distinguished by including only a charge-label superscript, so long as the flavor structure of the baryon is defined solely by the base symbol (and subscripts). Thus one may also write Λ_c^- or p^- for the antiparticles of the Λ_c^+ and p^+, but the Σ^- is not the antiparticle of Σ^+, which is called $\bar{\Sigma}^-$.

In short, the minimal number of u plus d quarks together with the isospin determine the main symbol, and subscripts indicate any content of heavy quarks. A Σ always has isospin 1, an Ω always has isospin 0, etc.

8.5 Hadrons with a minimal quark content of $qq\bar{q}\bar{q}$ or $q\bar{q}qqq$

The naming scheme described above does not accommodate various $qq\bar{q}\bar{q}$ mesons and $q\bar{q}qqq$ baryons. In such cases, the 1986 naming scheme must be extended. Following discussion initiated by the proposal made by the LHCb collaboration [7], we adopt the notation

$$T^{(*)}_{\text{quarks}J}(\text{mass})^q \qquad \text{for tetraquarks,} \tag{8.3a}$$

$$P_{\text{quarks}}(\text{mass})^q\ J^P \qquad \text{for pentaquarks,} \tag{8.3b}$$

according to the following rules:

1. The basename T or P is chosen in cases where the minimal quark content of a state is $qq\bar{q}\bar{q}$ (tetraquark) or $q\bar{q}qqq$ (pentaquark), respectively.
2. The bottom, charm, and strange quark content (b, $\bar{b}$, c, $\bar{c}$, s, $\bar{s}$) is explicitly listed as a subscript, in order from the heaviest quarks and antiquarks to the lightest and listing quarks before antiquarks. The hidden-flavor $c\bar{c}$ and $b\bar{b}$ combinations

[1] The name $T_{c\bar{c}1}(3900)$ derives from the scheme outlined in a later section.

[2] This is one example where the mass label needed to be shifted given improved experimental information.

[3] See the "Charmed and Bottom Baryons" section of the "Quark Model" review.

Table 8.2: Names used from the 2024 edition onward compared to those in the 2022 edition. Whenever the C-parity of a charged tetraquark is specified in the Particle Listings, it refers to the C-parity of the prospective/observed neutral isospin partner. Only one member per isospin multiplet is shown (see the Listings for more information).

2024 Name	minimal quark content	$I^{(G)}(J^{P(C)})$	2022 Name	2024 Name	minimal quark content	$I^{(G)}(J^{P(C)})$	2022 Name
$T^*_{cs0}(2870)^0$	$cs\bar{u}\bar{d}$	$?(0^+)$	$X_0(2900)$	$T_{c\bar{c}\bar{s}1}(4000)^+$	$c\bar{c}u\bar{s}$	$1/2(1^+)$	$Z_{cs}(4000)^+$
$T^*_{cs1}(2900)^0$	$cs\bar{u}\bar{d}$	$?(1^-)$	$X_1(2900)$	$T_{c\bar{c}\bar{s}1}(4220)^+$	$c\bar{c}u\bar{s}$	$1/2(1^+)$	$Z_{cs}(4220)^+$
$T^*_{c\bar{s}0}(2900)^{++}$	$c\bar{s}u\bar{d}$	$1(0^+)$		$T_{b\bar{s}}(5568)^+$	$b\bar{s}\bar{u}d$	$1(?^?)$	$X(5568)^+$
$T_{cc}(3875)^+$	$cc\bar{u}\bar{d}$	$?(?^?)$		$T_{b\bar{b}1}(10610)^+$	$b\bar{b}u\bar{d}$	$1^+(1^{+-})$	$Z_b(10610)^+$
$T_{c\bar{c}1}(3900)^+$	$c\bar{c}u\bar{d}$	$1^+(1^{+-})$	$Z_c(3900)^+$	$T_{b\bar{b}1}(10650)^+$	$b\bar{b}u\bar{d}$	$1^+(1^{+-})$	$Z_b(10650)^+$
$T_{c\bar{c}}(4020)^+$	$c\bar{c}u\bar{d}$	$1^+(?^{?-})$	$X(4020)^+$	$T_{cc\bar{c}\bar{c}}(6900)^0$	$cc\bar{c}\bar{c}$	$0^+(?^{?+})$	$X(6900)$
$T_{c\bar{c}}(4050)^+$	$c\bar{c}u\bar{d}$	$1^-(?^{?+})$	$X(4050)^+$	$P_{c\bar{c}}(4312)^+$	$c\bar{c}uud$	$1/2(?^?)$	$P_c(4312)^+$
$T_{c\bar{c}}(4055)^+$	$c\bar{c}u\bar{d}$	$1^+(?^{?-})$	$X(4055)^+$	$P_{c\bar{c}}(4380)^+$	$c\bar{c}uud$	$1/2(?^?)$	$P_c(4380)^+$
$T_{c\bar{c}}(4100)^+$	$c\bar{c}u\bar{d}$	$1^-(?^{?+})$	$X(4100)^+$	$P_{c\bar{c}}(4440)^+$	$c\bar{c}uud$	$1/2(?^?)$	$P_c(4440)^+$
$T_{c\bar{c}1}(4200)^+$	$c\bar{c}u\bar{d}$	$1^+(1^{+-})$	$Z_c(4200)^+$	$P_{c\bar{c}}(4457)^+$	$c\bar{c}uud$	$1/2(?^?)$	$P_c(4457)^+$
$T_{c\bar{c}0}(4240)^+$	$c\bar{c}u\bar{d}$	$1^+(0^{--})$	$R_{c0}(4240)^+$	$P_{c\bar{c}s}(4459)^0$	$c\bar{c}uds$	$0(?^?)$	
$T_{c\bar{c}}(4250)^+$	$c\bar{c}u\bar{d}$	$1^-(?^{?+})$	$X(4250)^+$	$P_{c\bar{c}s}(4338)^0$	$c\bar{c}sud$	$0(1/2^-)$	
$T_{c\bar{c}1}(4430)^+$	$c\bar{c}u\bar{d}$	$1^+(1^{+-})$	$Z_c(4430)^+$				

are listed explicitly when their presence can be inferred from production or decay patterns.

3. The approximate mass of a state, in MeV/c^2, is given in parentheses.
4. The electric charge (q) can be specified as a superscript after the mass, for example when referring to a specific member of an isospin multiplet.
5. Antibaryons are marked with an overline ($\overline{P}$). The antiparticle of a meson can be specified either with an overline or by the quark content label (e.g. the charge conjugate of $T_{cc}(3875)^+$ is $\overline{T}_{cc}(3875)^-$, which is equivalent to $T_{\bar{c}\bar{c}}(3875)^-$).
6. For pentaquarks, as in the case of ordinary baryons, when known the spin-parity, J^P, of the state is included as a suffix.
7. For tetraquarks, similarly to the naming scheme for mesons, the spin J is appended as a subscript after the quark content. When the spin-parity is in the natural series, $J^P = 0^+, 1^-, 2^+, \cdots$, a superscript "*" is added.

Table 8.2 summarizes PDG name changes with respect to the 2022 edition [8]. We acknowledge that experiments might choose to add $I^{(G)}J^{P(C)}$ information to hadron names using experiment-specific conventions that differ from the one utilized by the PDG.

References

[1] M. Aguilar-Benitez *et al.* (Particle Data Group), Phys. Lett. **170B**, 1 (1986).

[2] M. Ablikim *et al.* (BESIII), Phys. Rev. Lett. **110**, 252001 (2013), [arXiv:1303.5949].

[3] Z. Q. Liu *et al.* (Belle), Phys. Rev. Lett. **110**, 252002 (2013), [Erratum: Phys.Rev.Lett. 111, 019901 (2013)], [arXiv:1304.0121].

[4] M. Tanabashi *et al.* (Particle Data Group), Phys. Rev. D **98**, 3, 030001 (2018).

[5] R. Aaij *et al.* (LHCb), Nature Phys. **18**, 7, 751 (2022), [arXiv:2109.01038].

[6] R. Aaij *et al.* (LHCb), Phys. Rev. Lett. **122**, 22, 222001 (2019), [arXiv:1904.03947].

[7] LHCb (2022), [arXiv:2206.15233].

[8] R. L. Workman and Others (Particle Data Group), PTEP **2022**, 083C01 (2022).

Int. J. Mod. Phys. A 2026.41. Downloaded from www.worldscientific.com
by UNIVERSITY OF CALIFORNIA @ BERKELEY on 09/16/26. Re-use and distribution is strictly not permitted, except for Open Access articles.

Int. J. Mod. Phys. A 2026.41. Downloaded from www.worldscientific.com
by UNIVERSITY OF CALIFORNIA @ BERKELEY on 09/16/26. Re-use and distribution is strictly not permitted, e[redacted]s articles.

Standard Model and Related Topics

9. Quantum chromodynamics (rev.) 161
10. Electroweak model and constraints on new physics (rev.) . . . 196
11. Higgs boson physics, status of (rev.) 226
12. CKM quark-mixing matrix (rev.) 273
13. CP violation in the quark sector (rev.) 283
14. Neutrino masses, mixing, and oscillations (rev.) 297
15. Quark model (rev.) 324
16. Heavy-quark & soft-collinear effective theory 343
17. Lattice quantum chromodynamics (rev.) 352
18. Structure functions (rev.) 373
19. Fragmentation functions in e^+e^-, ep and pp collisions 396
20. High Energy Soft QCD and Diffraction (rev.) 413

Int. J. Mod. Phys. A 2026.41. Downloaded from www.worldscientific.com
by UNIVERSITY OF CALIFORNIA @ BERKELEY on 09/16/26. Re-use and distribution is strictly not permitted, except for Open Access articles.

Int. J. Mod. Phys. A 2026.41. Downloaded from www.w[redacted]
by UNIVERSITY OF CALIFORNIA @ BERKELEY on 09/16/26. Re-use and distribution is [redacted] except for Open Access articles.

Int. J. Mod. Phys. A 2026.41. Downloaded from www.worldscientific.com
by UNIVERSITY OF CALIFORNIA @ BERKELEY on 09/16/26. Re-use and distribution is strictly not permitted, except for Open Access articles.

9. Quantum Chromodynamics

Revised August 2025 by J. Huston (Michigan State U.), K. Rabbertz (KIT) and G. Zanderighi (MPP, Garching; TU Munich).

9.1 Basics . . . 161
9.1.1 Running coupling . . . 161
9.1.2 Quark masses . . . 162
9.2 Structure of QCD predictions . . . 162
9.2.1 Fully inclusive cross sections . . . 162
9.2.2 Processes with initial-state hadrons . . . 163
9.2.3 Cross sections with phase-space restrictions 165
9.2.4 Accuracy of predictions . . . 170
9.3 Experimental studies of QCD . . . 170
9.3.1 Hadronic final-state observables . . . 171
9.3.2 QCD measurements at colliders . . . 172
9.4 Determinations of the strong coupling constant . 176
9.4.1 Hadronic τ decays and low Q^2 continuum: 176
9.4.2 Heavy quarkonia decays: . . . 177
9.4.3 PDF fits: . . . 177
9.4.4 Hadronic final states of e^+e^- annihilations: 178
9.4.5 Observables from hadron-induced collisions: 178
9.4.6 Electroweak precision fit: . . . 179
9.4.7 Lattice QCD: . . . 179
9.4.8 Determination of the world average value of $\alpha_s(m_Z^2)$: . . . 180

9.1 Basics

Quantum Chromodynamics (QCD), the gauge field theory that describes the strong interactions of colored quarks and gluons, is the SU(3) component of the SU(3)×SU(2)×U(1) Standard Model of Particle Physics. The Lagrangian of QCD is given by

$$\mathcal{L} = \sum_q \bar{\psi}_{q,a}(i\gamma^\mu \partial_\mu \delta_{ab} - g_s \gamma^\mu t^C_{ab} \mathcal{A}^C_\mu - m_q \delta_{ab})\psi_{q,b} - \frac{1}{4} F^A_{\mu\nu} F^{A\,\mu\nu}\,, \tag{9.1}$$

where repeated indices are summed over. The γ^μ are the Dirac γ-matrices. The $\psi_{q,a}$ are quark-field spinors for a quark of flavor q and mass m_q, with a color index a that runs from $a = 1$ to $N_c = 3$, *i.e.* quarks come in three "colors." Quarks are said to be in the fundamental representation of the SU(3) color group.

The $\mathcal{A}^C_\mu$ correspond to the gluon fields, with C running from 1 to $N_c^2 - 1 = 8$, so that there are eight kinds of gluons. Gluons transform under the adjoint representation of the SU(3) color group. The t^C_{ab} correspond to eight 3×3 matrices and are the generators of the SU(3) group (*cf.* the section on "SU(3) isoscalar factors and representation matrices" in this *Review*, with $t^C_{ab} \equiv \lambda^C_{ab}/2$), where λ^C_{ab} are the Gell-Mann matrices. They encode the fact that a gluon's interaction with a quark rotates the quark's color in SU(3) space. The quantity g_s (or $\alpha_s = \frac{g_s^2}{4\pi}$) is the QCD coupling constant. Besides quark masses, which have electroweak origin, it is the most fundamental parameter of QCD. Finally, the field tensor $F^A_{\mu\nu}$ is given by

$$\begin{aligned} F^A_{\mu\nu} &= \partial_\mu \mathcal{A}^A_\nu - \partial_\nu \mathcal{A}^A_\mu - g_s\, f_{ABC} \mathcal{A}^B_\mu \mathcal{A}^C_\nu\,, \\ [t^A, t^B] &= i f_{ABC} t^C\,, \end{aligned} \tag{9.2}$$

where the f_{ABC} are the structure constants of the SU(3) group.

Neither quarks nor gluons are observed as free particles. Hadrons are color-singlet (*i.e.* color-neutral) combinations of quarks, antiquarks, and gluons.

Ab-initio predictive methods for QCD include lattice gauge theory and perturbative expansions in the coupling. The Feynman rules of QCD involve a quark-antiquark-gluon ($q\bar{q}g$) vertex, a 3-gluon vertex (both proportional to g_s), and a 4-gluon vertex (proportional to g_s^2). A full set of Feynman rules is to be found for example in Refs. [1, 2].

Adopting a standard notation where repeated indices are summed over, useful color-algebra relations include: $t^A_{ab} t^A_{bc} = C_F \delta_{ac}$, where $C_F \equiv (N_c^2 - 1)/(2N_c) = 4/3$ is the color factor ("Casimir") associated with gluon emission from a quark; $f_{ACD} f_{BCD} = C_A \delta_{AB}$, where $C_A \equiv N_c = 3$ is the color factor associated with gluon emission from a gluon; $t^A_{ab} t^B_{ab} = T_R \delta_{AB}$, where $T_R = 1/2$ is the color factor for a gluon to split to a $q\bar{q}$ pair.

There is freedom for an additional CP-violating term to be present in the QCD Lagrangian, $\theta \frac{\alpha_s}{8\pi} F^{A\,\mu\nu} \tilde{F}^A_{\mu\nu}$, where θ is an additional free parameter, and $\tilde{F}^A_{\mu\nu}$ is the dual of the gluon field tensor, $\frac{1}{2}\epsilon_{\mu\nu\sigma\rho} F^{A\,\sigma\rho}$, with $\epsilon_{\mu\nu\sigma\rho}$ being the fully antisymmetric Levi-Civita symbol. Experimental limits on the electric dipole moment (EDM) of ultracold neutrons [3,4] and atomic mercury [5] constrain the QCD vacuum angle to satisfy $|\theta| \lesssim 10^{-10}$. For an overview of current and future experiments measuring EDMs see [6]. Further discussion is to be found in Ref. [7] and in the Axions section in the Listings of this *Review*.

This section will concentrate mainly on perturbative aspects of QCD as they relate to collider physics. Related textbooks and lecture notes include Refs. [1, 2, 8–11]. Aspects specific to Monte Carlo event generators are reviewed in the dedicated section 43. Lattice QCD is also reviewed in a section of its own, Sec. 17, with further discussion of perturbative and non-perturbative aspects to be found in the sections on "Quark Masses", "The CKM quark-mixing matrix", "Structure functions", "Fragmentation Functions", "High Energy Soft QCD and Diffraction", "Passage of Particles Through Matter" and "Heavy-Quark and Soft-Collinear Effective Theory" in this *Review*.

9.1.1 *Running coupling*

In the framework of perturbative QCD (pQCD), predictions for observables are expressed in terms of the renormalized coupling $\alpha_s(\mu_R^2)$, a function of an (unphysical) renormalization scale μ_R. When one takes μ_R close to the scale of the momentum transfer Q in a given process, then $\alpha_s(\mu_R^2 \simeq Q^2)$ is indicative of the effective strength of the strong interaction in that process.

The coupling satisfies the following renormalization group equation (RGE):

$$\mu_R^2 \frac{d\alpha_s}{d\mu_R^2} = \beta(\alpha_s) = -(b_0 \alpha_s^2 + b_1 \alpha_s^3 + b_2 \alpha_s^4 + \cdots)\,, \tag{9.3}$$

where $b_0 = (11C_A - 4n_f T_R)/(12\pi) = (33 - 2n_f)/(12\pi)$ is referred to as the 1-loop β-function coefficient, the 2-loop coefficient is $b_1 = (17C_A^2 - n_f T_R(10C_A + 6C_F))/(24\pi^2) = (153 - 19n_f)/(24\pi^2)$, and the 3-loop coefficient is $b_2 = (2857 - \frac{5033}{9} n_f + \frac{325}{27} n_f^2)/(128\pi^3)$ for the SU(3) values of C_A and C_F. Here n_f is the number of quark flavors. The 4-loop coefficient, b_3, is to be found in Refs. [12, 13], while the 5-loop coefficient, b_4, is in Refs. [14–18]. The coefficients b_2 and b_3 (and beyond) are renormalization-scheme-dependent and given here in the modified minimal subtraction scheme ($\overline{\text{MS}}$) [19], by far the most widely used scheme in QCD and the one adopted in the following.

The minus sign in Eq. (9.3) is the origin of "asymptotic freedom" [20, 21], *i.e.* the fact that the strong coupling becomes weak for processes involving large momentum transfers ("hard processes"). For momentum transfers in the 0.1–1 TeV range, $\alpha_s \sim 0.1$, while the theory is strongly interacting for scales around and below 1 GeV.

The β-function coefficients, the b_i, are given for the coupling of an *effective theory* in which n_f of the quark flavors are considered light ($m_q \ll \mu_R$), and in which the remaining heavier quark flavors decouple from the theory. One may relate the coupling for the theory with $n_f + 1$ light flavors to that with n_f flavors through an equation of the form

$$\begin{aligned} \alpha_s^{(n_f+1)}(\mu_R^2) =& \alpha_s^{(n_f)}(\mu_R^2) \times \\ & \times \left(1 + \sum_{n=1}^{\infty} \sum_{\ell=0}^{n} c_{n\ell}\, [\alpha_s^{(n_f)}(\mu_R^2)]^n \ln^\ell \frac{\mu_R^2}{m_h^2}\right), \end{aligned} \tag{9.4}$$

where m_h is the mass of the $(n_f+1)^{\text{th}}$ flavor, and the first few $c_{n\ell}$ coefficients are $c_{11} = \frac{1}{6\pi}$, $c_{10} = 0$, $c_{22} = c_{11}^2$, $c_{21} = \frac{11}{24\pi^2}$, and $c_{20} = -\frac{11}{72\pi^2}$ when m_h is the $\overline{\text{MS}}$ mass at scale m_h, while

Int. J. Mod. Phys. A 2026.41. Downloaded from www.worldscientific.com by UNIVERSITY OF CALIFORNIA @ BERKELEY on 09/16/26. Re-use and distribution is except for Open Access articles.

$c_{20} = \frac{7}{24\pi^2}$ when m_h is the pole mass (mass definitions are discussed below in Sec. (9.1.2) and in the review on "Quark Masses"). Terms up to $c_{4\ell}$ with $0 \le \ell \le 4$ are to be found in Refs. [22, 23]. Numerically, when one chooses $\mu_R = m_h$, the matching is a modest effect, owing to the zero value for the c_{10} coefficient. Relations between n_f and (n_f+2) flavors where the two heavy flavors are close in mass are given to three loops in Ref. [24].

Working in an energy range where the number of flavors is taken constant, a simple exact analytic solution exists for Eq. (9.3) only if one neglects all but the b_0 term, giving $\alpha_s(\mu_R^2) = (b_0 \ln(\mu_R^2/\Lambda^2))^{-1}$. Here Λ is a constant of integration, which corresponds to the scale where the perturbatively-defined coupling would diverge. Its value is indicative of the energy range where non-perturbative dynamics dominates. A convenient approximate analytic solution to the RGE that includes terms up to b_4 is given by solving iteratively Eq. (9.3)

$$\begin{aligned}\alpha_s(\mu_R^2) \simeq \frac{1}{b_0 t}\Bigg(1 - \frac{b_1}{b_0^2}\frac{\ell}{t} + \frac{b_1^2(\ell^2-\ell-1)+b_0 b_2}{b_0^4 t^2} + \\ + \frac{b_1^3\left(-2\ell^3+5\ell^2+4\ell-1\right) - 6b_0 b_2 b_1 \ell + b_0^2 b_3}{2b_0^6 t^3} + \\ + \frac{18 b_0 b_2 b_1^2\left(2\ell^2-\ell-1\right) + b_1^4\left(6\ell^4-26\ell^3-9\ell^2+24\ell+7\right)}{6b_0^8 t^4} \\ + \frac{-b_0^2 b_3 b_1(12\ell+1) + 2b_0^2\left(5b_2^2+b_0 b_4\right)}{6b_0^8 t^4}\Bigg), \end{aligned} \tag{9.5}$$

with $t \equiv \ln\frac{\mu_R^2}{\Lambda^2}$ and $\ell = \ln t$, again parameterized in terms of a constant Λ. Note that Eq. (9.5) is one of several possible approximate 4-loop solutions for $\alpha_s(\mu_R^2)$, and that a value for Λ only defines $\alpha_s(\mu_R^2)$ once one knows which particular approximation is being used. An alternative to the use of formulas such as Eq. (9.5) is to solve the RGE exactly, numerically (including the discontinuities, Eq. (9.4), at flavor thresholds). In such cases the quantity Λ does not directly arise (though it can be defined, *cf.* Eqs. (1–3) of Ref. [25]). For these reasons, in determinations of the coupling, it has become standard practice to quote the value of α_s at a given scale (typically the mass of the Z boson, m_Z) rather than to quote a value for Λ.

A discussion of determinations of the coupling and a graph illustrating its scale dependence ("running") are to be found in Section 9.4.

9.1.2 *Quark masses*

Free quarks have never been observed, which is understood as a result of a long-distance, confining property of the strong QCD force: up, down, strange, charm, and bottom quarks all *hadronize*, *i.e.* become part of a meson or baryon, on a timescale $\sim 1/\Lambda$; the top quark instead decays before it has time to hadronize. This means that the question of what one means by the quark mass is a complex one, which requires one to adopt a specific prescription. A perturbatively defined prescription is the pole mass, m_q, which corresponds to the position of the divergence of the quark propagator. This is close to one's physical picture of mass. However, when relating it to observable quantities, it suffers from a badly behaved perturbative series which makes it ambiguous to an amount related to Λ (see *e.g.* Ref. [26–28]). An alternative is the $\overline{\rm MS}$ mass, $\overline{m}_q(\mu_R^2)$, which depends on the renormalization scale μ_R.

Results for the masses of heavier quarks are often quoted either as the pole mass or as the $\overline{\rm MS}$ mass evaluated at a scale equal to the mass, $\overline{m}_q(\overline{m}_q^2)$; light quark masses are often quoted in the $\overline{\rm MS}$ scheme at a scale $\mu_R \sim 2\,$GeV. The pole and $\overline{\rm MS}$ masses are related by a series that starts as $m_q = \overline{m}_q(\overline{m}_q^2)(1 + \frac{4\alpha_s(\overline{m}_q^2)}{3\pi} + \mathcal{O}(\alpha_s^2))$, while the scale dependence of $\overline{\rm MS}$ masses is given at lowest order by

$$\mu_R^2 \frac{d\overline{m}_q(\mu_R^2)}{d\mu_R^2} = \left[-\frac{\alpha_s(\mu_R^2)}{\pi} + \mathcal{O}(\alpha_s^2)\right]\overline{m}_q(\mu_R^2)\,. \tag{9.6}$$

A more detailed discussion is to be found in a dedicated section of the *Review*, "Quark Masses", with detailed formulas also in Ref. [29] and references therein.

In perturbative QCD calculations of scattering processes, it is customary to employ an approximation where the masses of all quarks, whose magnitudes are much smaller than the momentum transfer involved in the process, are neglected or set to zero.

9.2 Structure of QCD predictions

9.2.1 *Fully inclusive cross sections*

The simplest observables in perturbative QCD are those that do not depend on initial-state hadrons and are fully inclusive, disregarding specific details of the final state. An example of such an observable is the total cross section for the process $e^+e^- \to$ hadrons at a center-of-mass energy Q. It can be expressed as follows:

$$\frac{\sigma(e^+e^- \to \text{hadrons}, Q)}{\sigma(e^+e^- \to \mu^+\mu^-, Q)} \equiv R(Q) = R_{\rm EW}(Q)(1+\delta_{\rm QCD}(Q))\,, \tag{9.7}$$

where $R_{\rm EW}(Q)$ is the purely electroweak prediction for the ratio and $\delta_{\rm QCD}(Q)$ is the correction due to QCD effects.

For the sake of simplicity, we can focus on energies where $Q \ll m_Z$, where the primary contribution to the process comes from photon exchange (while disregarding electroweak and finite-quark-mass corrections) denoted as $R_{\rm EW} = N_c \sum_q e_q^2$, with e_q representing the electric charges of the quarks in units of e. The QCD correction reads

$$\delta_{\rm QCD}(Q) = \sum_{n=1}^{\infty} c_n \cdot \left(\frac{\alpha_s(Q^2)}{\pi}\right)^n + \mathcal{O}\left(\frac{\Lambda^4}{Q^4}\right)\,. \tag{9.8}$$

The first four terms in the α_s series expansion are [30]

$$c_1 = 1\,, \qquad c_2 = 1.9857 - 0.1152 n_f\,, \tag{9.9a}$$

$$c_3 = -6.63694 - 1.20013 n_f - 0.00518 n_f^2 - 1.240\eta\,, \tag{9.9b}$$

$$\begin{aligned} c_4 = &-156.61 + 18.775 n_f - 0.7974 n_f^2 + 0.0215 n_f^3 \\ &- (17.828 - 0.575 n_f)\eta\,, \end{aligned} \tag{9.9c}$$

with $\eta = (\sum e_q)^2/(N_c \sum e_q^2)$ and $N_c = 3$. For corresponding expressions including also Z exchange and finite-quark-mass effects, see Refs. [31–33].

A related series holds also for the QCD corrections to the W-boson decay or to the hadronic decay width of the τ lepton. The latter essentially involves an integral of $R(Q)$ over the allowed range of invariant masses of the hadronic part of the τ decay (see *e.g.* Ref. [34]). The series expansions for QCD corrections to Higgs-boson hadronic (partial) decay widths in the limit of heavy top quark and massless light flavors up to fifth order are given in Ref. [35].

One characteristic feature of Eqs. (9.8) and (9.9) is that the coefficients of α_s^n increase order by order: calculations in perturbative QCD tend to converge more slowly than would be expected based just on the size of α_s. The situation is significantly worse near thresholds or in the presence of tight kinematic cuts. Another feature is the existence of an extra "power-correction" term $\mathcal{O}(\Lambda^4/Q^4)$ in Eq. (9.8), which accounts for contributions that are fundamentally non-perturbative. All high-energy QCD predictions involve power corrections $(\Lambda/Q)^p$, although typically the suppression of these corrections with Q is smaller than given in Eq. (9.8), where $p = 4$. The exact power p depends on the observable and, for many processes and observables, it is possible to introduce an operator product expansion and associate power-suppressed terms with specific higher-dimension (non-perturbative) operators [36].

Scale dependence. In Eq. (9.8) the renormalization scale for α_s has been chosen equal to Q. The result can also be expressed in terms of the coupling at an arbitrary renormalization scale μ_R,

$$\delta_{\rm QCD}(Q) = \sum_{n=1}^{\infty} \bar{c}_n\left(\frac{\mu_R^2}{Q^2}\right) \cdot \left(\frac{\alpha_s(\mu_R^2)}{\pi}\right)^n + \mathcal{O}\left(\frac{\Lambda^4}{Q^4}\right)\,, \tag{9.10}$$

Int. J. Mod. Phys. A 2026.41. Downloaded from www.worldscientific.com
by UNIVERSITY OF CALIFORNIA @ BERKELEY on 09/16/26. Re-use and distribution is strictly not permitted, except for Open Access articles.

where $\bar{c}_1(\mu_R^2/Q^2) \equiv c_1$, $\bar{c}_2(\mu_R^2/Q^2) = c_2 + \pi b_0 c_1 \ln(\mu_R^2/Q^2)$, $\bar{c}_3(\mu_R^2/Q^2) = c_3 + (2b_0c_2\pi + b_1c_1\pi^2) \times \ln(\mu_R^2/Q^2) + b_0^2c_1\pi^2\ln^2(\mu_R^2/Q^2)$, *etc.* Given an infinite number of terms in the α_s expansion, the μ_R dependence of the $\bar{c}_n(\mu_R^2/Q^2)$ coefficients will exactly cancel that of $\alpha_s(\mu_R^2)$, and the final result will be independent of the choice of μ_R: physical observables do not depend on unphysical scales.[1]

With just terms up to some finite $n = N$, a residual μ_R dependence will remain, which implies an uncertainty on the prediction of $R(Q)$ due to the arbitrariness of the scale choice. This uncertainty will be $\mathcal{O}(\alpha_s^{N+1})$, *i.e.* of the same order as the neglected higher-order terms. For this reason it is customary to use the scale dependence of QCD predictions as an estimate of the uncertainties due to neglected terms. One usually takes a central value for $\mu_R \sim Q$, in order to avoid the poor convergence of the perturbative series that results from the large $\ln^{n-1}(\mu_R^2/Q^2)$ terms in the $\bar{c}_n$ coefficients when $\mu_R \ll Q$ or $\mu_R \gg Q$. Uncertainties are then commonly determined by varying μ_R by a factor of two up and down around the central scale choice. This is not a rigorous prescription for determining the uncertainty, but is motivated by the requirement that there should not be large logarithms introduced into a calculation by large ratios of scales. A more detailed discussion on the accuracy of theoretical predictions and on ways to estimate the theoretical uncertainties can be found in Section 9.2.4.

9.2.2 *Processes with initial-state hadrons*

Deep-Inelastic Scattering. To illustrate the key features of QCD cross sections in processes with initial-state hadrons, let us consider deep-inelastic scattering (DIS), $e + p \to e + X$, where an electron e with four-momentum k emits a highly off-shell photon (momentum q) that interacts with the proton (momentum p). For photon virtualities $Q^2 \equiv -q^2$ far above the squared proton mass (but far below the squared Z mass), the differential cross section in terms of the kinematic variables Q^2, $x = Q^2/(2p \cdot q)$ and $y = (q \cdot p)/(k \cdot p)$ is

$$\frac{d^2\sigma}{dxdQ^2} = \frac{4\pi\alpha^2}{2xQ^4}\left[(1 + (1-y)^2)F_2(x,Q^2) - y^2F_L(x,Q^2)\right], \tag{9.11}$$

where α is the electromagnetic coupling and $F_2(x,Q^2)$ and $F_L(x,Q^2)$ are proton structure functions, which encode the interaction between the photon and the proton. In the presence of parity-violating interactions (*e.g.* νp scattering) an additional F_3 structure function is present. For an extended review, including equations for the full electroweak and polarized cases, see Sec. 18 of this *Review*.

Structure functions are not calculable in perturbative QCD, nor is any other cross section that involves QCD interactions and initial-state hadrons. To zeroth order in α_s, the structure functions are given directly in terms of non-perturbative parton (quark or gluon) distribution functions (PDFs),

$$F_2(x,Q^2) = x\sum_q e_q^2 f_{q/p}(x), \qquad F_L(x,Q^2) = 0, \tag{9.12}$$

where $f_{q/p}(x)$ is the non-perturbative PDF for quarks of type q inside the proton, *i.e.* the number density of quarks of type q inside a fast-moving proton that carry a fraction x of its longitudinal momentum.

The result in Eq. (9.12), with PDFs $f_{q/p}(x)$ that are independent of the scale Q, corresponds to the "quark-parton model" picture, in which the photon interacts with point-like free quarks, or equivalently, one has incoherent elastic scattering between the electron and individual constituents of the proton. As a consequence, in this picture also F_2 and F_L are independent of Q [37].

[1] With respect to pQCD there is an important caveat to this statement: at sufficiently high orders, perturbative series generally suffer from "renormalon" divergences $\alpha_s^n n!$ (reviewed in Ref. [26]). This phenomenon is not usually visible with the limited number of perturbative terms available today. However, it is closely connected with non-perturbative contributions and sets a limit on the possible precision of perturbative predictions. The cancellation of scale dependence will also ultimately be affected by this renormalon-induced breakdown of perturbation theory.

When including higher orders in pQCD, one has

$$F_2(x,Q^2) = x\sum_{n=0}^{\infty}\frac{\alpha_s^n(\mu_R^2)}{(2\pi)^n}\times$$
$$\times\sum_{i=q,g}\int_x^1\frac{dz}{z}C_{2,i}^{(n)}(z,Q^2,\mu_R^2,\mu_F^2)f_{i/p}\left(\frac{x}{z},\mu_F^2\right) + \mathcal{O}\left(\frac{\Lambda^2}{Q^2}\right). \tag{9.13}$$

Just as in Eq. (9.10), we have a series in powers of $\alpha_s(\mu_R^2)$, each term involving a coefficient $C_{2,i}^{(n)}$ that can be calculated using Feynman diagrams. At variance with the parton model, the PDFs in pQCD depend on an additional scale, the factorization scale μ_F, whose significance will be discussed in the following. Another important difference is the additional integral over z. The parton that comes from the proton can undergo a splitting before it enters the hard scattering. As a result, the $C_{2,i}^{(n)}$ coefficients are functions that depend on the ratio, z, of the parton's momentum before and after radiation, and one must integrate over that ratio. For the electromagnetic component of DIS with light quarks and gluons, the zeroth order coefficient functions are $C_{2,q}^{(0)} = e_q^2\delta(1-z)$ and $C_{2,g}^{(0)} = 0$. Corrections are known up to $\mathcal{O}(\alpha_s^3)$ (next-to-next-to-next-to-leading order, N^{3}LO) for both electromagnetic [38] and weak currents [39,40]. For heavy-quark production they are known to $\mathcal{O}(\alpha_s^2)$ [41,42] (next-to-leading order, NLO, insofar as the series starts at $\mathcal{O}(\alpha_s)$). The current status of the theoretical description of unpolarized and polarized DIS is summarized in Ref. [43].

The majority of the emissions that modify a parton's momentum are collinear (parallel) to that parton, and do not depend on whether the parton will interact with a photon. It is natural to view these emissions as modifying the proton's structure rather than being part of the coefficient function for the parton's interaction with the photon. Technically, one uses a procedure known as *collinear factorization* to give a well-defined meaning to this distinction, most commonly through the $\overline{\text{MS}}$ factorization scheme, defined in the context of dimensional regularization. The $\overline{\text{MS}}$ factorization scheme involves an arbitrary choice of *factorization scale*, μ_F, whose meaning can be understood roughly as follows: emissions with transverse momenta above μ_F are included in the $C_{2,q}^{(n)}(z,Q^2,\mu_R^2,\mu_F^2)$; emissions with transverse momenta below μ_F are accounted for within the PDFs, $f_{i/p}(x,\mu_F^2)$. While collinear factorization is generally believed to be valid for suitable (sufficiently inclusive) observables in processes with hard scales, Ref. [44], which reviews the factorization proofs in detail, is cautious in the statements it makes about their exhaustivity, notably for the hadron-collider processes which we shall discuss below. Interesting considerations on the current status of our understanding of factorization can be found in Refs. [45,46]. While the transverse degrees of freedom have been integrated over for collinear PDFs, it is also possible to produce transverse-momentum dependent (or unintegrated) PDFs where these degrees of freedom remain. For a recent comprehensive review of transverse-momentum dependent parton distribution functions and fragmentation functions see Ref. [47].

For collinear PDFs, the resulting dependence on μ_F is described by the Dokshitzer-Gribov-Lipatov-Altarelli-Parisi (DGLAP) equations [48], which to leading order (LO) read[2]

$$\mu_F^2\frac{\partial f_{i/p}(x,\mu_F^2)}{\partial\mu_F^2} = \sum_j\frac{\alpha_s(\mu_F^2)}{2\pi}\int_x^1\frac{dz}{z}P_{i\leftarrow j}^{(1)}(z)f_{j/p}\left(\frac{x}{z},\mu_F^2\right), \tag{9.14}$$

with, for example, $P_{q\leftarrow g}^{(1)}(z) = T_R(z^2 + (1-z)^2)$. The other LO splitting functions are listed in Sec. 18 of this *Review*, while results up to NLO, α_s^2, and NNLO, α_s^3, are given in Refs. [49] and [50] respectively. At N^{3}LO accuracy, several partial results

[2] LO is generally taken to mean the lowest order at which a quantity is non-zero.

Int. J. Mod. Phys. A 2026.41. Downloaded from www.worldscientific.com by UNIVERSITY OF CALIFORNIA @ BERKELEY on 09/16/26. Re-use and distribution is except for Open Access articles.

are currently available [51–65], some of which have been used to derive approximate N^{3}LO PDFs [66, 67].

Beyond LO, the coefficient functions are also μ_F dependent, for example $C^{(1)}_{2,i}(x, Q^2, \mu_R^2, \mu_F^2) = C^{(1)}_{2,i}(x, Q^2, \mu_R^2, Q^2) - \ln\left(\frac{\mu_F^2}{Q^2}\right) \sum_j \int_x^1 \frac{dz}{z} \times C^{(0)}_{2,j}(\frac{x}{z}) P^{(1)}_{j\leftarrow i}(z)$. Progress in higher-order QED and mixed QED-QCD corrections to the splitting functions can be found in Refs. [68, 69].

As with the renormalization scale, the choice of factorization scale is arbitrary, but if one has an infinite number of terms in the perturbative series, the μ_F-dependencies of the coefficient functions and PDFs will compensate each other fully. Given only N terms of the series, a residual $\mathcal{O}(\alpha_s^{N+1})$ uncertainty is associated with the ambiguity in the choice of μ_F. As with μ_R, varying μ_F provides an input in estimating uncertainties on predictions. In inclusive DIS predictions, the default choice for the scales is usually $\mu_R = \mu_F = Q$.

As is the case for the running coupling, in DGLAP evolution one can introduce flavor thresholds near the heavy-quark masses: below a given heavy quark's mass, that quark is not considered to be part of the proton's structure, while above it is considered to be part of the proton's structure and evolves with massless DGLAP splitting kernels. With appropriate parton distribution matching terms at threshold, such a variable flavor number scheme (VFNS), when used with massless coefficient functions, gives the full heavy-quark contributions at high Q^2 scales. For scales near the threshold, it is instead necessary to appropriately adapt the standard massive coefficient functions to account for the heavy-quark contribution already included in the PDFs [70–72]. At sufficiently small x and Q^2 in inclusive DIS, resummation of small x logarithms may be necessary [73, 74].

In situations, in which the center-of-mass energy $\sqrt{s}$ is much larger than all other momentum-transfer scales in the problem (*e.g.* Q in DIS, m_b for $b\bar{b}$ production in pp collisions, *etc.*), each power of α_s beyond LO can be accompanied by a power of $\ln(s/Q^2)$ (or $\ln(s/m_b^2)$, *etc.*). This is variously referred to as the high-energy, small-x or Balitsky-Fadin-Kuraev-Lipatov (BFKL) limit [74–76]. Currently it is possible to account for the dominant and first subdominant [77, 78] powers of such logarithms at each order of α_s, and also to estimate further subdominant contributions that are numerically large (see Refs. [79–82] and references therein). Progress towards NNLO is discussed in Ref. [83].

Physically, the summation of all orders in α_s can be understood as leading to a growth with s of the gluon density in the proton. At sufficiently high energies this implies non-linear effects (commonly referred to as parton saturation), whose treatment has been the subject of intense study (see for example Refs. [84, 85] and references thereto).

The PDFs themselves are primarily determined from data in global fits. PDF sets are available at different orders in perturbation theory (LO, NLO, NNLO and what has been termed approximate N^{3}LO) based on the order at which cross sections used in the fits are calculated. The evolution equations for the PDFs from one scale to another matches the perturbative accuracy of the cross sections. In modern global PDF fits, data are included from DIS, Drell-Yan (DY), jets and $t\bar{t}$ processes, and other LHC collider data, with the global PDF fits using 4000–5000 data points. There is a large change in the PDFs from LO to NLO, with a much smaller change from NLO to NNLO. LO PDFs can be unreliable for collider predictions, especially at low and high x. The uncertainties for the resulting PDFs are determined primarily from the experimental uncertainties of the data that serve as input to the global PDF fits. There is also a component due to the limitations of the parameterizations used, as discussed *e.g.* in Ref. [86], although this may be reduced with the use of more flexible forms. The PDF uncertainties can either be determined through a Hessian approach or through the use of Monte Carlo replicas. It is now relatively straightforward to convert results from one approach to the other. A combination (PDF4LHC21) of the CT18, MSHT20 and (an updated version of) NNPDF3.1 PDFs, each produced from a global PDF fit, serves to provide a more comprehensive view of both the central PDFs and of their uncertainties [87]. The PDF4LHC21 PDFs are often used by the experiments for Monte Carlo generation, as they represent a more realistic representation of the central values and uncertainties of the PDFs.

Theoretical uncertainties related to missing higher orders (MHO) have been included in global PDF determinations [88–91], using scale variations at the fit order as an estimate of the uncertainties at the higher order. The uncertainties are added into the experimental covariance matrix and are treated as uncorrelated with the experimental uncertainties. By tying renormalization scales for related processes, and factorization scales for all processes, together in the global fit, an estimate of the higher order uncertainties can be added to the PDF fit. Another technique, used by MSHT [92], is to create theory nuisance parameters using information from the form of corrections observed at lower orders. The global PDF fit then determines the combination of shapes and sizes of the theory nuisance parameters that allow the best fit to the data.

These two techniques have been used to determine approximate N^{3}LO PDFs [66, 67], using the available information at that order. Many of the crucial N^{3}LO cross sections, such as for dijet and top pair production, are not known and so predictions have to rely on the above two techniques, but the evolution at N^{3}LO seems to be under good control [93].

Since the original work of Ref. [94], one of the intriguing questions is whether lattice calculations can provide valuable insights for extracting PDFs. Despite initial debates surrounding the underlying methodologies [95, 96], it is now understood that lattice data in Euclidean space can be connected to light-cone PDFs through factorization theorems, once lattice observables have been renormalized and extrapolated to the continuum limit [97]. Initial determinations based on lattice data have begun to emerge [97–121], see also Refs. [122, 123] for overviews on lattice PDFs, and the comparisons with determinations based on conventional data show great promise. However, the uncertainties in lattice-based determinations are still quite large, therefore, for practical applications, PDFs are currently derived from global fits of experimental data (*cf.* Sec. 18 of this *Review* and also Refs. [124, 125]). It is likely that lattice simulations for light-cone PDFs will have an impact in the short- to medium-term, if they focus on flavor components (strange and charm) and on the kinematic regions that are poorly covered by the experimental data [126]. Similarly, lattice determinations of transverse-momentum dependent PDFs (TMDs), generalized parton distributions (GPDs) and polarized PDFs will be more relevant for phenomenology since the experimental data for these quantities are much less abundant and precise.

Hadron-hadron collisions.

The extension to processes with two initial-state hadrons can be illustrated with the example of the total (inclusive) cross section for W boson production in collisions of hadrons h_1 and h_2, which can be written as

$$\begin{aligned}\sigma(h_1 h_2 \to W + X) = &\sum_{n=0}^{\infty} \alpha_s^n(\mu_R^2) \\ &\times \sum_{i,j} \int dx_1 dx_2\, f_{i/h_1}\left(x_1, \mu_F^2\right) f_{j/h_2}\left(x_2, \mu_F^2\right) \\ &\times \hat{\sigma}^{(n)}_{ij\to W+X}\left(x_1 x_2 s, \mu_R^2, \mu_F^2\right) + \mathcal{O}\left(\frac{\Lambda^2}{m_W^4}\right),\end{aligned} \tag{9.15}$$

where s is the squared center-of-mass energy of the collision. At LO, $n = 0$, the hard (partonic) cross section $\hat{\sigma}^{(0)}_{ij\to W+X}(x_1 x_2 s, \mu_R^2, \mu_F^2)$ is simply proportional to $\delta(x_1 x_2 s - m_W^2)$, in the narrow W-boson width approximation (see Sec. 51 of this *Review* for detailed expressions for this and other hard scattering cross sections). It is non-zero only for choices of i, j that can directly give a W, such as $i = u$, $j = \bar{d}$. At higher orders, $n \geq 1$, new partonic channels contribute, such as gq, and $x_1 x_2 s \geq m_W^2$ in the narrow W-boson width approximation.

Equation (9.15) involves a collinear factorization between the

Int. J. Mod. Phys. A 2026.41. Downloaded from www.worldscientific.com by UNIVERSITY OF CALIFORNIA @ BERKELEY on 09/16/26. Re-use and distribution is strictly not permitted, except for Open Access articles.

hard cross section and the PDFs, just like Eq. (9.13). As long as the same factorization scheme is used in DIS and pp or $p\bar{p}$ (usually the $\overline{\text{MS}}$ scheme), then PDFs extracted in DIS can be directly used in pp and $p\bar{p}$ predictions [44,127] (with the antiquark distributions in an anti-proton being the same as the quark distributions in a proton).

A number of fully inclusive cross sections have been computed up to N^{3}LO, *i.e.* including corrections up to relative order α_s^3, in recent years. These include inclusive Higgs production through gluon fusion in the large m_t limit, calculated at N^{3}LO in Refs. [128, 129]. Higgs boson pair production via gluon fusion in the same approximation was computed at N^{3}LO in Ref. [130]. Calculations at this order, differential in the Higgs rapidity [131, 132] and fully differential [133] have been presented recently. Bottom-induced Higgs boson production has also been computed at N^{3}LO [134]. Vector-boson fusion single- [135] and double-pair [136] productions are also known to N^{3}LO [135] in the factorized approximation. Neutral [137,138] and charged [139] Drell-Yan processes, as well as associated Higgs production [134] have also been computed at N^{3}LO. Differential rapidity distributions are available, but not yet with fiducial cuts. A number of public codes are now available which allow for phenomenological studies at N^{3}LO [134, 135, 140–142].

The uncertainty band derived by varying the renormalization and factorization scales in the perturbative predictions is not always contained within the corresponding uncertainty band of the previous order, as might be expected from a well-behaved process. For Drell-Yan production, this has been ascribed to cancellations between channels at NNLO that lead to underestimates of the uncertainty at that order. This effect does not seem to be present in other processes, such as Higgs boson production through gluon-gluon fusion. Note that there is currently a mismatch in N^{3}LO calculations in that PDFs at the same order are not yet available. Preliminary approximate N^{3}LO PDFs [66, 67] suggest that N^{3}LO effects can be large, especially as far as heavy-quark distributions and low scales are concerned, as well as the gluon distribution in a region important for Higgs boson production through gluon-gluon fusion. These differences between approximate N^{3}LO distributions do not arise from differences in the data sets being considered in the PDF fits, and need to be studied in further detail. This may have implications for predictions of gluon-gluon fusion Higgs cross sections at the LHC. A comparison of these sets, as well as a preliminary combination, can be found in Ref. [143].

The hard cross sections for several other processes are known to NNLO, [3] for instance, Higgs-boson production in association with a vector boson [144], Higgs-pair production in the large m_t approximation [145], and with full m_t dependence [146], top-antitop production [147, 148], bottom-anti-bottom production [149] and vector-boson pair production [150–152]. For a comprehensive overview on other recent NNLO $2 \to 2$ calculations see Ref. [153, 154]. Other NNLO calculations with fiducial cuts will be discussed in Sec. 9.2.3.

At the level of precision needed/desired at the LHC, electroweak corrections need to be taken into account, both on the relevant matrix elements and on the parton distribution functions. In particular, the proton acquires a photon PDF component, whose magnitude can be precisely calculated [155, 156]. All recent photon PDFs [157–159] are based on the calculation in Ref. [155,156]. A benchmarking exercise of the photon PDFs was carried out in Ref. [160]. The photon component can contribute to new production channels, for example for VBF Higgs boson production. A secondary impact is due to the momentum taken by the photon, and the resultant reduction of the gluon and quark momentum, of the order of 0.3–0.5%. In addition, the re-fit, allowing the photon component, may result in an additional redistribution of the quark and gluon momentum. The net result is a reduction of the gluon-gluon fusion Higgs boson cross section that can vary from 0.6–1.2% [160]. It will be difficult to reduce the PDF uncertainty to the order of 1% if the uncertainty of the electroweak corrections is of that order. More recently, the PDF for leptons has also been computed [161]. The photon PDF has an elastic and an inelastic component, where the photon is generated from the intact proton or from the splitting of quarks inside the proton, respectively, while the lepton PDF is generated by photons splitting into collinear leptons.

Photoproduction.

γp (and $\gamma\gamma$) collisions are similar to pp collisions, with the subtlety that the photon can behave in two ways: there is "direct" photoproduction, in which the photon behaves as a point-like particle and takes part directly in the hard collision, with hard subprocesses such as $\gamma g \to q\bar{q}$; there is also resolved photoproduction, in which the photon behaves like a hadron, with non-perturbative partonic substructure and a corresponding PDF for its quark and gluon content, $f_{i/\gamma}(x, Q^2)$. While useful to understand the general structure of γp collisions, the distinction between direct and resolved photoproduction is not well defined beyond leading order, as discussed for example in Ref. [162].

9.2.3 *Cross sections with phase-space restrictions*

QCD final states always consist of hadrons, while perturbative QCD calculations deal with partons. Physically, an energetic parton fragments ("showers") into many further partons, which then, on later timescales, undergo a transition to hadrons ("hadronization"). Fixed-order perturbation theory captures only a small part of these dynamics. This does not matter for the fully inclusive cross sections discussed in Section 9.2.1: the showering and hadronization stages are approximately unitary, *i.e.* they do not substantially change the overall probability of hard scattering, because they occur long after it has taken place (they introduce at most a correction proportional to a power of the ratio of timescales involved, *i.e.* a power of Λ/Q, where Q is the hard scattering scale).

Less inclusive measurements, in contrast, may be affected by the extra dynamics. For those sensitive just to the main directions of energy flow (jet rates, event shapes, *cf.* Sec. 9.3.1) fixed-order perturbation theory is often still adequate, because showering and hadronization do not substantially change the overall energy flow. This means that one can make a prediction using just a small number of partons, which should correspond well to a measurement of the same observable carried out on hadrons. For observables that instead depend on distributions of individual hadrons (which, *e.g.*, are the inputs to detector simulations), it is mandatory to account for showering and hadronization. The range of predictive techniques available for QCD final states reflects this diversity of needs of different measurements.

While illustrating the different methods, we shall for simplicity mainly use expressions that hold for e^+e^- scattering. The extension to cases with initial-state partons will be mostly straightforward (space constraints unfortunately prevent us from addressing hard diffraction and exclusive hadron-production processes; extensive discussion is to be found in Sec. 20 of this *Review* and in Refs. [163, 164]).

9.2.3.1 *Soft and collinear limits*

Before examining specific predictive methods, it is useful to be aware of a general property of QCD matrix elements in the soft and collinear limits. Consider a squared tree-level matrix element $|M_n^2(p_1, \ldots, p_n)|$ for the process $e^+e^- \to n$ partons with momenta $p_1, \ldots, p_n$, and a corresponding phase-space integration measure $d\Phi_n$. If particle n is a gluon, which becomes collinear (parallel) to another particle i and additionally its momentum tends to zero (is "soft"), the matrix element simplifies as follows,

$$\lim_{\theta_{in}\to 0,\, E_n \to 0} d\Phi_n |M_n^2(p_1, \ldots, p_n)| = d\Phi_{n-1} |M_{n-1}^2(p_1, \ldots, p_{n-1})| \frac{\alpha_s C_i}{\pi} \frac{d\theta_{in}^2}{\theta_{in}^2} \frac{dE_n}{E_n}\,, \qquad (9.16)$$

where $C_i = C_F$ (C_A) if i is a quark (gluon). This formula has non-integrable divergences both for the inter-parton angle $\theta_{in} \to 0$ and for the gluon energy $E_n \to 0$, which are mirrored also in the structure of divergences in loop diagrams. These divergences are important for at least two reasons: firstly, they govern the typical structure of events (inducing many emissions either with low

[3] Processes with light jets or photons in the final state have divergent cross sections unless one places a cut on the jet or (dressed) photon momentum. Accordingly, they are discussed below in Section 9.2.3.2.

Int. J. Mod. Phys. A 2026.41. Downloaded from www.w
by UNIVERSITY OF CALIFORNIA @ BERKELEY on 09/16/26. Re-use and distribution is
except for Open Access articles.

energy or at small angle with respect to hard partons); secondly, they will determine which observables can be calculated within fixed-order perturbative QCD.

9.2.3.2 *Fixed-order predictions*

Let us consider an observable $\mathcal{O}$ that is a function $\mathcal{O}_n(p_1,\ldots,p_n)$ of the four-momenta of the n final-state particles in an event (either partons or hadrons). In what follows, we shall consider the cross section for events weighted with the value of the observable, $\sigma_{\mathcal{O}}$. As examples, if $\mathcal{O}_n \equiv 1$ for all n, then $\sigma_{\mathcal{O}}$ is just the total cross section; if $\mathcal{O}_n \equiv \hat{\tau}(p_1,\ldots,p_n)$ where $\hat{\tau}$ is the value of the thrust for that event (see Eq. (9.22) in Sec. 9.3.1.2), then the average value of the thrust is $\langle\tau\rangle = \sigma_{\mathcal{O}}/\sigma_{\rm tot}$; if $\mathcal{O}_n \equiv \delta(\tau - \hat{\tau}(p_1,\ldots,p_n))$ then one gets the differential cross section as a function of the thrust, $\sigma_{\mathcal{O}} \equiv d\sigma/d\tau$.

In the expressions below, we shall omit to write the non-perturbative power correction term, which for most common observables is proportional to a single power of Λ/Q.

Leading Order. If the observable $\mathcal{O}$ is non-zero only for events with at least n final-state particles, then the LO QCD prediction for the weighted cross section in e^+e^- annihilation is

$$\sigma_{\mathcal{O}}^{\rm LO} = \alpha_s^{n-2}(\mu_R^2)\int d\Phi_n |M_n^2(p_1,\ldots,p_n)|\,\mathcal{O}_n(p_1,\ldots,p_n)\,, \tag{9.17}$$

where the squared tree-level matrix element, $|M_n^2(p_1,\ldots,p_n)|$, including relevant symmetry factors, has been summed over all subprocesses (*e.g.* $e^+e^- \to q\bar{q}q\bar{q}$, $e^+e^- \to q\bar{q}gg$) and has had all factors of α_s extracted in front. In processes other than e^+e^- collisions, the center-of-mass energy of the LO process is generally not fixed, and so the powers of the coupling are often brought inside the integrals, with the scale μ_R chosen event by event, as a function of the event kinematics.

Other than in the simplest cases (see the review on Cross Sections in this *Review*), the matrix elements in Eq. (9.17) are usually calculated automatically with programs such as CompHEP [165], MadGraph [166], Alpgen [167], Comix/Sherpa [168], and Helac/Phegas [169]. Some of these (CompHEP, MadGraph) use formulas obtained from direct evaluations of Feynman diagrams. Others (Alpgen, Helac/Phegas and Comix/Sherpa) use methods designed to be particularly efficient at high multiplicities, such as Berends-Giele recursion [170], which builds up amplitudes for complex processes from simpler ones (see also Refs. [171–173] for other tree-level calculational methods).

The phase-space integration is usually carried out by Monte Carlo sampling or other numerical techniques, because of the high dimensionality of the integration and in order to deal with the possibly involved kinematic cuts that are used in the corresponding experimental measurements. Perturbatively calculable observables should be insensitive to the emission of soft and collinear radiation. Because of the divergences in the matrix element, Eq. (9.16), at lowest order the integral converges only if the observable vanishes for kinematic configurations in which one of the n particles is arbitrarily soft or it is collinear to another particle. As an example, the cross section for producing any configuration of n partons will lead to an infinite integral, whereas a finite result will be obtained for the cross section for producing n deposits of energy (or jets, see Sec. 9.3.1.1), each above some energy threshold and well separated from each other in angle.

At a practical level, LO calculations can be carried out for $2 \to n$ processes with $n \lesssim 6-10$. The exact upper limit depends on the process, the method used to evaluate the matrix elements and the extent to which the phase-space integration can be optimized to work around the large variations in the values of the matrix elements.

NLO. Given an observable that is non-zero starting from n final-state particles, its prediction at NLO involves supplementing the LO result, Eq. (9.17), with the $2 \to (n+1)$-particle squared tree-level matrix element ($|M_{n+1}^2|$), and the interference of a $2 \to n$ tree-level and $2 \to n$ 1-loop amplitude ($2{\rm Re}(M_n M_{n,1-{\rm loop}}^*)$),

$$\begin{aligned}\sigma_{\mathcal{O}}^{\rm NLO} = \sigma_{\mathcal{O}}^{\rm LO} &+ \alpha_s^{n-1}(\mu_R^2)\int d\Phi_{n+1}|M_{n+1}^2(p_1,\ldots,p_{n+1})| \\ &\times \mathcal{O}_{n+1}(p_1,\ldots,p_{n+1}) \;+\; \alpha_s^{n-1}(\mu_R^2) \\ &\times \int d\Phi_n\, 2{\rm Re}\,[\; M_n(p_1,\ldots,p_n)\, M_{n,1-{\rm loop}}^*(p_1,\ldots,p_n)\;] \\ &\times \mathcal{O}_n(p_1,\ldots,p_n)\;.\end{aligned} \tag{9.18}$$

Relative to LO calculations, two important issues appear in the NLO calculations. Firstly, the extra complexity of loop- relative to tree-level calculations means that automated calculations started to appear only about fifteen years ago (see below). Secondly, loop amplitudes are infinite in four dimensions, while tree-level amplitudes are finite, but their *integrals over the phase space* are infinite, due to the divergences of Eq. (9.16). These two sources of infinities have the same soft and collinear origins and cancel after the integration only if the observable $\mathcal{O}$ satisfies the property of infrared and collinear safety, which means that the observable is non-sensitive to soft emissions or to collinear splittings, *i.e.*

$$\begin{aligned}&\mathcal{O}_{n+1}(p_1,\ldots,p_s,\ldots,p_n) \quad \to \mathcal{O}_n(p_1,\ldots,p_{s-1},p_{s+1},\ldots,p_n) \\ &\qquad\qquad\qquad\qquad\qquad\qquad \text{if } p_s \to 0 \\ &\mathcal{O}_{n+1}(p_1,\ldots,p_a,p_b,\ldots,p_n) \;\to \mathcal{O}_n(p_1,\ldots,p_a+p_b,\ldots,p_n) \\ &\qquad\qquad\qquad\qquad\qquad\qquad \text{if } p_a \,||\, p_b\,.\end{aligned} \tag{9.19}$$

Examples of infrared-safe quantities include event-shape distributions and jet cross sections (with appropriate jet algorithms, see below). Unsafe quantities include the distribution of the momentum of the hardest QCD particle (which is not conserved under collinear splitting), observables that require the complete absence of radiation in some region of phase space (*e.g.* rapidity gaps or 100% isolation cuts, which are affected by soft emissions), or the particle multiplicity (affected by both soft and collinear emissions). The non-cancellation of divergences at NLO due to infrared or collinear unsafety compromises the usefulness not only of the NLO calculation, but also that of a LO calculation, since LO is only an acceptable approximation if one can prove that higher-order terms are smaller. Infrared and collinear unsafety usually also implies large non-perturbative effects.

As with LO calculations, the phase-space integrals in Eq. (9.18) are usually carried out by Monte Carlo integration, so as to facilitate the study of arbitrary observables. Various methods exist to obtain numerically efficient cancellation among the different infinities. These include notably dipole [174], FKS [175] and antenna [176] subtraction.

Thanks to new ideas like the OPP method [177], generalized [178] and D-dimensional [179] unitarity, on-shell methods [180], and on-the-fly reduction algorithms [181], the first decade of the 2000s has seen a breakthrough in the calculation of one-loop matrix elements (for reviews on unitarity based method see Ref. [182, 183]). Thanks to these innovative methods, automated tools for NLO calculations have been developed and a number of programs are available publicly: MadGraph5_aMC@NLO [166] and Helac-NLO [184] provide full frameworks for NLO calculations; GoSam [185], Njet [186], OpenLoops [187] and Recola [188] calculate just the 1-loop part and are typically interfaced with an external tool for a combination with the appropriate tree-level amplitudes. Other tools such as NLOJet++ [189], MCFM [190,191], Vnfnlo [192], the Phox family [193] or BlackHat [194] implement analytic calculations and provide full frameworks to compute NLO cross sections for selected classes of processes. These tools are regularly updated and upgraded to enable more efficient amplitude evaluations, as well as to incorporate electroweak effects and corrections due to beyond-standard-model effects modelled using operators in the Standard Model Effective Theory (SMEFT) [195–206]. Recently, a lot of attention has also been paid to the calculation of NLO electroweak corrections. Electroweak corrections are especially important for transverse

Int. J. Mod. Phys. A 2026.41. Downloaded from www.worldscientific.com by UNIVERSITY OF CALIFORNIA @ BERKELEY on 09/16/26. Re-use and distribution is strictly not permitted, except for Open Access articles.

momenta significantly above the W and Z masses, because they are enhanced by two powers of $\ln p_t/m_W$ for each power of the electroweak coupling, and close to Sudakov peaks[4], where most of the data lie and the best experimental precision can be achieved. For a review on EW corrections to collider processes see Ref. [207].

Given the progress in QCD and EW fixed-order computations, the largest unknown from fixed-order corrections is often given by the mixed QCD-electroweak corrections of $\mathcal{O}(\alpha_s\alpha)$. These mixed two-loop corrections are often available in an approximate form [208–222]. Complete computations of the mixed QCD–EW corrections to the neutral-current and charged-current Drell–Yan processes are now available [223–225].

NNLO. NNLO is considerably more complicated than NLO as it involves a further order in α_s, consisting of: the squared $(n+2)$-parton tree-level amplitude, the interference of the $(n+1)$-parton tree-level and 1-loop amplitudes, the interference of the n-parton tree-level and 2-loop amplitudes, and the squared n-parton 1-loop amplitude. Each of these elements involves large numbers of soft and collinear divergences, satisfying relations analogous to Eq. (9.16) which now involve multiple collinear or soft particles and higher loop orders (see *e.g.* Refs. [226–228]). Arranging for the cancellation of the divergences after numerical Monte Carlo integration has been one of the significant challenges of NNLO calculations, as has been the determination of the relevant 2-loop amplitudes.

After first differential calculations of $2 \to 1$ processes for hadron colliders, e.g. for vector boson [229] [230] and Higgs boson production in the large m_t limit [231] [232], a large variety of methods have been developed for the cancellation of divergences.

The most common are:

- **Antenna subtraction** [233, 234]: It is a local subtraction scheme with analytically integrated counterterms, removing angular correlations by averaging over azimuthal angles. Extensions of the original method include the generalization to identified jet flavours [235–238], photon fragmentation [239, 240], hadron fragmentation [241, 242], a streamlined antenna construction reducing spurious divergences [243–246], and a color-space formulation to enable a semi-automated computation beyond-leading-color [247,248].
- **q_T subtraction** [232]: This is a slicing method for processes with colourless final states or pairs of massive coloured particles. Extensions to top-pair production [148, 149, 249–251], beyond back-to-back Born kinematics (e.g. $t\bar{t}H$, $t\bar{t}W$) [252–254], mixed QCD–EW corrections [221, 223, 255, 256], power corrections at subleading order [257–259], treatments of fiducial cuts [258, 260–264], as well as to N^{3}LO [265–268] have been formulated recently.
- **Sector-improved residue subtraction** [269–271]: This is a fully local subtraction method combining FKS subtraction [175, 272] with sector decomposition [273–276]. Counterterms are obtained numerically, with improvements in a four-dimensional formulation [277]. Extensions to flavoured jets [278, 279] and B-hadron production [280–282] have been developed recently.
- **ColorFul subtraction** [283, 284]: This is a fully local subtraction method extending the Catani–Seymour dipole method [174] to NNLO, with analytic poles and numerical integration of finite terms. Extensions to colourless final states in hadronic collisions have been formulated [285] and implemented in the code `NNLOCAL` [286].
- **N-jettiness subtraction** [287–289]: This is a slicing method based on the resolution variable τ_N, suited for jet final states. It has been explicitly developed up to one jet at NNLO. Extensions towards N^{3}LO with known zero-jettiness ingredients is work in progress [290–302]. Subleading power corrections to improve the numerical efficiency of the method via SCET [303, 304], direct QCD [305], and for $V+j$ [306] have been computed. A treatment of fiducial and isolation cuts [258], as well as projection-to-Born correction factors to improving numerical stability [303, 307] have also been proposed.
- **Nested soft–collinear subtraction** [308–310]: This is a fully local subtraction method with analytic counterterms, formulated for hadronic initial/final states [311–313]. Extensions include the treatment of arbitrary multi-gluon final states in quark-antiquark annihilation [314], while the treatment of other partonic channels is ongoing.
- **Local analytic sector subtraction** [315–317]: This subtraction method combines FKS [175,272] and dipole subtraction [174], with analytic integration of counterterms. Extensions include the analytic pole cancellation for arbitrary multiplicity in e^+e^- [318], progress toward hadronic initial states [319] as well as first steps towards N^{3}LO [320].
- **Projection to Born** [321]: The method utilizes an inclusive NNLO calculation differential in Born kinematics, as well as a differential NLO cross section for the corresponding process with one extra jet in the final state. It is in principle generalisable to any order. It has been generalized to obtain fully differential N^{3}LO results in DIS jet production, Higgs decays, and gluon-fusion Higgs production [133, 322–324].
- **Locally finite subtraction** [325]: The method employs subtractions expressed as form-factor integrands with known integrals. The resulting subtracted amplitudes can then be evaluated efficiently through numerical integration. This approach exploits the universality of infrared singularities and requires only a relatively small set of subtraction terms.
- **Dual subtractions** [326]: This scheme constructs subtraction terms directly from loop diagrams by exploiting their dual representation, rather than from real-radiation matrix elements. It features built-in exact phase-space factorization and is applicable to both initial and final states, as well as to processes involving either massless or massive particles.

For overviews of NNLO subtraction methods see Ref [327] and Ref [328].

These methods have been applied to compute a large number of processes at NNLO, specifically:

- **Antenna subtraction** was applied to the NNLO calculations of $e^+e^- \to 3j$ [329–332], DIS jets [333–335], $pp \to$ (di-)jets [336–338], $pp \to \gamma\gamma$ [339], $pp \to \gamma + j/X$ [340], $pp \to V + j$ [341–343], $pp \to H + j$ [344], $pp \to VH(+j)$ [235, 345, 346], and Higgs in VBF [347].
- **Sector-improved residue subtraction** was applied to the NNLO calculation of top-quark processes [147, 348–352], $pp \to H + j$ [353, 354], inclusive jets [355], $pp \to 3\gamma$ [356], $pp \to 2\gamma + j$ [357], $pp \to \gamma + 2j$ [358], $pp \to W + j$ [359], $pp \to 3j$ [360] and $Wb\bar{b}$ production [361]. The finite top-mass corrections to inclusive Higgs production have also been computed [362].
- **q_T subtraction** was applied for the NNLO calculations of H [232, 363], V [230, 364], VV' [150, 151, 365–373] in MATRIX [152] or in MCFM [374–376], VH [377–379], HH [380, 381], VHH [382, 383], $t\bar{t}$ [148, 251], $b\bar{b}$ [149], three photons [384], $t\bar{t}H$ [252, 253], and $t\bar{t}W$ [254].
- **N-jettiness** was applied for the NNLO calculations of colour singlet processes [385], $V(+j)$ [288, 386–393], $H + j$ [394], colorless states [385, 395], top decay [396], and single-top s- [397] and t-channel [398, 399].
- **ColorFul subtraction** was applied to $H \to b\bar{b}$ [284] and $e^+e^- \to 3j$ [400–402].
- **Nested soft–collinear subtraction** was applied to VH [403] and VBF [404, 405].
- **Local analytic sector subtraction** was applied to $e^+e^- \to 2j$ [315].
- **Projection-to-Born** was applied to VBF [321], Higgs pair [406], single-top [398, 407], DIS jets [322, 323], and $H \to b\bar{b}$ [324].

Cross sections at the LHC are most often measured with fiducial cuts, for example on the transverse momenta and rapidities

[4]For the definition of Sudakov form factors or Sudakov peaks see e.g. Refs. [1, 2, 11].

Int. J. Mod. Phys. A 2026.41. Downloaded from www.worldscientific.com by UNIVERSITY OF CALIFORNIA @ BERKELEY on 09/16/26. Re-use and distribution is [redacted] except for Open Access articles.

of the measured objects, restricting the measurement to regions where the objects have a good efficiency to be detected and are well-reconstructed. Ideally, the theoretical predictions should also be constructed at the same fiducial level; the other possibility is to extrapolate the experimental fiducial results to the full phase space. Such an extrapolation, however, requires the extrapolation (typically using a parton shower Monte Carlo) to be accurate over the full phase space.

Comparisons of fixed-order predictions to fiducial measurements can sometimes result in the presence of large logarithms which degrade the accuracy of the prediction. Such is the case, for example, in the calculation of the Higgs rapidity distribution, in the diphoton final state. The imposition of transverse momenta and rapidity cuts on the two photons leads to an uncertainty notably greater at N^{3}LO than at NNLO, due to the presence of these logarithms. One possible solution is to change the form of the kinematic cut on the photons, to a product of the two photon transverse momenta [264], reducing the impact of the logarithms; another solution is to perform a resummation of the logarithms, restoring the expected precision [263]. The product cut is currently being implemented in both the ATLAS and CMS Higgs diphoton analyses.

The Les Houches precision wishlist compiles predictions needed to fully exploit the data that will be taken at the High Luminosity LHC [328, 408]. Most of the needed calculations require accuracy of at least NNLO QCD and NLO EW, and many require the prediction of $2 \to 3$ processes, such as, e.g., $W/Z+ \geq 2$ jets, $H+ \geq 2$ jets, and ttH to NNLO. The latter process has been computed at NNLO in Ref. [252] in the approximation where the Higgs boson in the double-virtual contribution is soft. This calculation considerably reduces the theory uncertainty on this process.

As discussed in this section, calculations at NLO can now be relatively easily generated by non-experts using the programs mentioned above. By now there are also a number of publicly available tools to compute a range of processes at NNLO accuracy in QCD, such as Eerad3 [330] (for e^+e^- collisions), [232], Dynnlo [230], Dyturbo [409], Fehip [231], Fewz [410], Hturbo [411], Matrix [152], MCFM [385], Sushi [142, 412] or Nnlojet [413]. However, in some cases NNLO calculations can be too complex and CPU-intensive to allow such an approach. In these cases, the relevant matrix element information for a specific observable can be stored by means of interpolation grids developed originally for cross sections at NLO [414–416] and recently extended to include electroweak corrections [417]. The application to NNLO has been demonstrated for $t\bar{t}$ and for DIS jet cross sections in Refs. [418, 419] and for jet production in hadron-hadron collisions in Ref. [420]. Each such interpolation grid corresponds to one fixed observable with specific selection criteria and binning, but is flexible with respect to the renormalization or factorization scale, the PDF, or the α_s evolution chosen for the cross-section computation. An even more flexible method, at the cost of requiring large amounts of storage space, saves huge numbers of partonic events in the form of ROOT n-tuples, which allow predictions to be generated on-the-fly for many observables of a particular process [421, 422]. Recent developments of both techniques for pp collisions at NNLO are described in Ref. [328].

9.2.3.3 *Resummation*

Many experimental measurements place tight constraints on emissions in the final state. For example, in e^+e^- events, that one minus the thrust should be less than some value $\tau \ll 1$, or, in $pp \to Z$, events that the Z-boson transverse momentum or the transverse momentum of the accompanying jet should be much smaller than the Z-boson mass. A further example is the production of heavy particles or jets near threshold (so that little energy is left over for real emissions) in DIS and pp collisions.

In such cases, the constraint vetoes a significant part of the integral over the soft and collinear divergence of Eq. (9.16). As a result, there is only a partial cancellation between real emission terms (subject to the constraint) and loop (virtual) contributions (not subject to the constraint), causing each order of α_s to be accompanied by a large coefficient $\sim L^2$, where *e.g.* $L = \ln \tau$ or $L = \ln(m_Z/p_t^Z)$. One ends up with a perturbative series, whose terms go as $\sim (\alpha_s L^2)^n$. It is not uncommon that $\alpha_s L^2 \gg 1$, so that the perturbative series converges very poorly if at all.[5] In such cases one may carry out a "resummation", which accounts for the dominant logarithmically enhanced terms to all orders in α_s, by making use of known properties of matrix elements for multiple soft and collinear emissions, and of the all-orders properties of the divergent parts of virtual corrections, following original works such as Refs. [423–432] and also through soft-collinear effective theory [433, 434] (*cf.* also the section on "Heavy-Quark and Soft-Collinear Effective Theory" in this *Review*, as well as Ref. [435]).

For cases with double logarithmic enhancements (two powers of logarithm per power of α_s), there are two classification schemes for resummation accuracy. Writing the cross section including the constraint as $\sigma(L)$ and the unconstrained (total) cross section as $\sigma_{\rm tot}$, the series expansion takes the form

$$\sigma(L) \simeq \sigma_{\rm tot} \sum_{n=0}^{\infty} \sum_{k=0}^{2n} R_{nk} \alpha_s^n(\mu_R^2) L^k, \qquad L \gg 1\,, \tag{9.20}$$

and leading log (LL) resummation means that one accounts for all terms with $k = 2n$, next-to-leading-log (NLL) includes additionally all terms with $k = 2n-1$, *etc.* Often $\sigma(L)$ (or its Fourier or Mellin transform) *exponentiates*,[6]

$$\sigma(L) \simeq \sigma_{\rm tot} \exp\left[\sum_{n=1}^{\infty} \sum_{k=0}^{n+1} G_{nk} \alpha_s^n(\mu_R^2) L^k\right], \qquad L \gg 1\,, \tag{9.21}$$

where one notes the different upper limit on k ($\leq n+1$) compared to Eq. (9.20). This is a more powerful form of resummation: the G_{12} term alone reproduces the full LL series in Eq. (9.20). With the form Eq. (9.21) one still uses the nomenclature LL, but this now means that all terms with $k = n+1$ are included, and NLL implies all terms with $k = n$, *etc.*

For a large number of observables, NLL resummations are available in the sense of Eq. (9.21) (see Refs. [439–441] and references therein). NNLL has been achieved for the DY and Higgs-boson p_t distributions [442–445] (also available in the CuTe [446], HRes [447] and ResBos [448] families of programs and also differentially in vector-boson decay products [262]) and related variables [449], for the p_t of vector-boson pairs [450], for the back-to-back energy-energy correlation in e^+e^- [451], the jet broadening in e^+e^- collisions [452], the jet-veto survival probability in Higgs and Z boson production in pp collisions [453–455],[7] an event-shape type observable known as the beam thrust [456], hadron-collider jet masses in specific limits [457] (see also Ref. [458]), the production of top anti-top pairs near threshold [459–461] (and references therein), and high-p_t W and Z production [462]. Automation of NNLL jet-veto resummations for different processes has been achieved in Ref. [463] (*cf.* also the NLL automation in Ref. [464]), while automation for a certain class of e^+e^- observables has been achieved in Ref. [465]. N^{3}LL resummations are available for the thrust variable, C-parameter and heavy-jet mass in e^+e^- annihilations [466–468], for p_t distribution of the Higgs boson [469, 470] and Drell-Yan [471–474, 474], also in heavy-quark annihilation [475], and weak gauge bosons [476–479], diphotons [480], for the jet-veto distribution [455, 481], for Higgs- and vector-boson production near threshold [482] and for Z-boson plus jet production using one-jettiness [483]. In order to make better contact with experimental measurements, recent years have

[5] To be precise one should be aware of two causes of the divergence of perturbative series. That which interests us here is associated with the presence of a new large parameter (*e.g.* ratio of scales). It is distinct from the renormalon-induced factorial divergences of perturbation theory discussed above.

[6] Whether or not this happens depends on the quantity being resummed. A classic example involves two-jet rate in e^+e^- collisions as a function of a jet-resolution parameter $y_{\rm cut}$. The logarithms of $1/y_{\rm cut}$ exponentiate for the k_t (Durham) jet algorithm [436], but not [437] for the JADE algorithm [438] (both are discussed below in Sec. 9.3.1.1).

[7] A veto on the jet phase space can be severe, for example by requiring exactly zero jets above a given transverse-momentum cut accompanying a Higgs boson, or relatively mild, for example by placing a transverse momentum cut of 30 GeV on the measurement of the production of a Higgs boson with one or more jets. In general, inclusive cross sections are preferable, as uncertainties on both the theoretical and experimental sides are smaller.

Int. J. Mod. Phys. A 2026.41. Downloaded from www.worldscientific.com
by UNIVERSITY OF CALIFORNIA @ BERKELEY on 09/16/26. Re-use and distribution is strictly not permitted, except for Open Access articles.

seen an increasing interest in resummations in exclusive phase-space regions and joint resummations [481, 484–492]. Finally, there has also been considerable progress in resummed calculations for jet substructure, whose observables involve more complicated definitions than is the case for standard resummations, see *e.g.* Refs. [493–497] and references therein (see also Sec. 9.3.1.3).

9.2.3.4 *Fragmentation functions*

Since the parton-hadron transition is non-perturbative, it is not possible to perturbatively calculate quantities such as the energy-spectra of specific hadrons in high-energy collisions. However, one can factorize perturbative and non-perturbative contributions via the concept of fragmentation functions. These are the final-state analogue of the parton distribution functions which are used for initial-state hadrons. Like parton distribution functions, they depend on a (fragmentation) factorization scale and satisfy a DGLAP evolution equation.

It should be added that if one ignores the non-perturbative difficulties and just calculates the energy and angular spectrum of partons in perturbative QCD with some low cutoff scale $\sim \Lambda$ (using resummation to sum large logarithms of $\sqrt{s}/\Lambda$), then this reproduces many features of the corresponding hadron spectra [498]. This is often taken to suggest that hadronization is "local", in this sense it mainly involves partons that are close both in position and in momentum.

Section 19 of this *Review* provides further information and references on these topics, including also the question of heavy-quark fragmentation.

9.2.3.5 *Parton-shower Monte Carlo event generators*

Parton-shower Monte Carlo (MC) event generators like Pythia [499–501], Herwig [502–504], and Sherpa [505][8] provide fully exclusive simulations of QCD events at the level of measurable particles, the so-called "particle level" or "hadron level". Here, "measurable" refers to color-neutral particles with mean lifetimes τ long enough to be associated with tracks or decay vertices in particle detectors. Usually, this requires mean decay lengths $c\tau$ of around 10 mm. As such, MC event generators are a crucial tool for all applications that involve simulating the response of detectors to QCD events. Here we give only a brief outline of how they work and refer the reader to Sec. 43 for a full overview.

In general, we expect parton-shower matched predictions to differ from the underlying fixed-order results in regions where (1) there is a large sensitivity to jet shapes (for instance small R jets), (2) there is a restriction in phase space such that soft gluon resummation effects become important, (3) the observable contains multiple disparate scales, (4) there are perturbative instabilities at fixed order, *e.g.* related to kinematical cuts, and (5) the observable is sensitive to higher multiplicity states than those described by the fixed-order calculation (for an explicit study of some of these effects see *e.g.* [507]).

The MC generation of an event involves several stages. It starts with the random generation of the kinematics and partonic channels of whatever *hard scattering process* the user has requested at some high scale Q_0 (for complex processes and/or higher-order processes, this may be carried out by an external program). This is followed by a *parton shower*, usually based on the successive random generation of gluon emissions (and $g \to q\bar{q}$ splittings). Leading contributions to the shower have emissions that are ordered according to some ordering variable. Common choices of scale for the ordering of emissions are virtuality, transverse momentum or angle. Each emission is generated at a scale lower than the previous emission, following a (soft and collinear resummed) perturbative QCD distribution, which depends on the momenta of all previous emissions. Parton showering stops at a scale of order 1 GeV, at which point a *hadronization model* is used to convert the resulting partons into hadrons. One widely-used model involves stretching a color "string" across quarks and gluons, and breaking it up into hadrons [508, 509]. Another breaks each gluon into a $q\bar{q}$ pair and then groups quarks and antiquarks into colorless "clusters", which then give the hadrons [502]. As both models are tuned primarily to LEP data, the cluster and string models provide similar results for most observables sensitive to hadronization [507]. For pp and γp processes, modeling is also needed to treat the collision between the two hadron remnants, which generates an *underlying event* (UE), usually implemented via additional $2 \to 2$ scatterings ("multiple parton interactions", MPI) at a scale of a few GeV, following Ref. [510]. The parameter values for the MPI models must be determined from fits to minimum-bias and/or underlying-event observables of LHC collision data. As the different MC event generators are adapted to essentially the same measurements, ideally the respective MPI implementations should lead to similar predictions for each program. One complication, however, is some non-universality of the underlying event among different physics processes.

If possible, determinations of the uncertainties encountered in parton-shower Monte Carlo programs should be divided into perturbative and non-perturbative sources, as this will lead to better possibilities for understanding/improving them. If there is a mismatch between the components, then the accuracy obtained by the matrix elements and the parton shower may be compromised (as for example if the parton shower tuning may involve an enhanced strong coupling constant different from that used in the matrix elements). Such a tuned prescription may provide a good description of a particular data set, but it is more of a fit than a prediction. It is not clear if this perturbative tuning can be transferred to other processes or kinematics.

A deficiency of the soft and collinear approximations that underlie parton showers is that they may fail to reproduce the full pattern of hard wide-angle emissions, important, for example, in many new physics searches. It is therefore common to use LO multi-parton matrix elements to generate hard high-multiplicity partonic configurations as additional starting points for the showering, supplemented with some prescription (CKKW [511], MLM [512]) for consistently merging samples with different initial multiplicities. Monte Carlo generators, as described above, compute cross sections for the requested hard process that are correct at LO.

A wide variety of processes are available in MC implementations that are accurate at NLO, using the MC@NLO [513] or Powheg [514] prescriptions, through the MadGraph5_aMC@NLO [166], Powheg-Box [515] and Sherpa [168] programs. Techniques have also been developed to combine NLO plus parton shower (PS) accuracy for different multiplicities of final-state jets [516]. While NLO+PS accurate predictions can now be implemented in the above tools rather easily and are available for a range of processes, given the advances in NNLO calculations it is natural to seek for NNLO+PS accurate Monte Carlos as well. The two main approaches today are the MiNNLO [517] and Geneva [518] ones. NNLO plus shower accuracy was achieved first for Drell-Yan and Higgs production [519–521] and is now available for several $2 \to 2$ color singlet processes [522–538], as well as for heavy-quark pair-production, also accompained by a colour singlet [539–543]. Recently NNLO+PS accuracy for Drell Yan was also obtained using matching conditions at next-to-next-to-leading order in the sectorised VINCIA parton shower [544].

It is important to understand/verify the accuracy of the parton shower predictions in the Monte Carlo programs. A general framework for assessing the logarithmic accuracy of parton-shower algorithms has been formulated, based on their ability to reproduce the singularity structure of multi-parton matrix elements, and their ability to reproduce logarithmic resummation results [545]. The dominant contributions relevant for the extension of parton showers to higher logarithmic accuracy have been computed [546–550] and included in some algorithms.

There exist ways to improve on current parton-shower algorithms [551, 552] and to demonstrate the parton shower accuracy through a comparison to analytic next-to-leading logarithmic calculations for a range of observables [552]. Considerable progress has been achieved in recent years [551–563]. References [552, 555, 556, 559, 560] introduced the first shower implementations towards NLL, but these implementations did not include spin-correlation effects and lacked full color dependence at LL level. Reference [553] incorporated full color effects at

[8] The program ARIADNE [506] has also been widely used for simulating e^+e^- and DIS collisions.

Int. J. Mod. Phys. A 2026.41. Downloaded from www.worldscientific.com by UNIVERSITY OF CALIFORNIA @ BERKELEY on 09/16/26. Re-use and distribution is except for Open Access articles.

the NLL level, while spin correlations at NLL were included in Refs. [557, 558], resulting in an NLL accurate parton shower for proton-proton collisions [561, 562]. The modifications necessary for processes such as Deep Inelastic Scattering (DIS) and Vector Boson Fusion (VBF) are addressed in [563]. The novel Alaric parton shower for hadron colliders is introduced in Ref. [564]. First steps towards NNLL parton showers for classes of observables dominantly sensitive to low-energy (soft) emissions have been presented in Ref. [565]. The first public implementation within the PanScales framework is described in Ref. [566]. Finally, a new standard for assessing the logarithmic accuracy of NNLL parton showers is proposed in Ref. [567].

9.2.4 *Accuracy of predictions*

Estimating the accuracy of perturbative QCD predictions is not an exact science. It is often said that LO calculations are accurate to within a factor of two. This is based on experience with NLO corrections in the cases where these are available. In processes involving new partonic scattering channels at NLO and/or large ratios of scales (such as jet observables in processes with vector bosons, or the production of high-p_t jets containing B-hadrons), the ratio of the NLO to LO predictions, commonly called the "K factor", can be substantially larger than two. NLO corrections tend to be large for processes for which there is a great deal of color annihilation in the interaction. In addition, NLO corrections tend to decrease as more final state legs are added.

For calculations beyond LO, one approach to estimate the perturbative uncertainty is to base it on the last known perturbative correction; this may lead to misleading results if new subprocesses are present at the next-higher order. A more widely used method is to estimate it from the change in the prediction when varying the renormalization and factorization scales around a central value Q that is taken close to the physical scale of the process. A conventional range of variation is $Q/2 < \mu_R, \mu_F < 2Q$, varying the two scales independently with the restriction $\frac{1}{2} < \mu_F/\mu_R < 2$ [568]. This constraint limits the risk of misleadingly small uncertainties due to fortuitous cancellations between the μ_F and μ_R dependence when both are varied together, while avoiding the appearance of large logarithms of μ_R^2/μ_F^2 when both are varied completely independently. Where possible, it can be instructive to examine the two-dimensional scale distributions (μ_R *vs.* μ_F) to obtain a better understanding of the interplay between μ_R and μ_F. This procedure should not be assumed to always estimate the full uncertainty from missing higher orders, but it does indicate the size of one important known source of higher-order ambiguity.[9]

As discussed before, several $2 \to 2$ processes at the LHC are now known to NNLO. This typically results in a large reduction in the uncertainty from that obtained at NLO. However, care must be taken in the estimate of the uncertainty in processes containing jets, as accidental cancellations of the scale uncertainties may result in an artificial reduction of the scale uncertainty; for some values of the jet radius R the uncertainty may even be close to zero. There are several possibilities for providing a more realistic estimate of the scale uncertainty for such processes [507], but none have been widely adopted at the LHC. A recent study [576] has carried out a NNLL resummation matched to a NNLO perturbative calculation for inclusive jet production and has found a more realistic scale uncertainty for cross sections involving small-R jets.

Calculations that involve resummations usually have an additional source of uncertainty associated with the choice of argument of the logarithms being resummed, *e.g.* $\ln(2\frac{p_t^Z}{m_Z})$ as opposed to $\ln(\frac{1}{2}\frac{p_t^Z}{m_Z})$, as well as a prescription to switch off resummation effects when the logarithm is not large. In addition to varying renormalization and factorization scales, it is common practice to vary the argument of the logarithm by a suitable factor in either direction with respect to the default argument.

The accuracy of QCD predictions is limited also by non-perturbative (or hadronization) corrections, which typically scale as a power of Λ/Q.[10] For measurements that are directly sensitive to the structure of the hadronic final state, the corrections are usually linear in Λ/Q. The non-perturbative corrections are further enhanced in processes with a significant underlying event (*i.e.* in pp and $p\bar{p}$ collisions) and the impact of non-perturbative corrections is larger in cases where the perturbative cross sections fall steeply as a function of p_t or some other kinematic variable, for example in inclusive jet p_t or dijet mass spectra.

Under high-luminosity running conditions, such as 13 TeV at the LHC, there can be about 50 minimum-bias interactions occurring at each beam-beam crossing. This additional energy needs to be subtracted, and is typically removed by means of a rapidity-dependent transverse-energy density determined on an event-by-event basis [577]. This subtraction usually also removes the underlying event, which must be added back in by means of MC event generator modelling, if one wants to restore the measured event to the particle level.

Non-perturbative corrections are commonly estimated from the difference between Monte Carlo events at the "parton level" and at particle level. Parton level refers to the stage of the parton shower, where the evolution is stopped at an energy scale of typical hadron masses of a few GeV. An issue to be aware of is that "parton level" is not a uniquely defined concept. For example, in a MC event generator such a procedure depends on an arbitrary and tunable internal cutoff scale that separates the parton showering from the hadronization. In contrast, no such cutoff scale exists in an NLO or NNLO partonic calculation. The uncertainties in these corrections are often estimated by comparing different tunes of the various MC event generators. It should be noted that such estimates are not guaranteed to fully cover the true uncertainties.

Alternative methods exist for estimating hadronization corrections that attempt to analytically deduce non-perturbative effects in one observable based on measurements of other observables (see the reviews [26, 578]). While they directly address the problem of different possible definitions of parton level, it should also be said that they are far less flexible than Monte Carlo programs and not always able to provide equally good descriptions of the data.

One of the main issues is whether the fixed-order partonic final state of a NLO or NNLO prediction can match the parton shower in its ability to describe the experimental jet shape (minus any underlying event). Calculations at NNLO provide a better match to the parton shower predictions than do NLO ones, as might be expected from the additional gluon available to describe the jet shape. The hadronization predictions appear to work for both orders, but at an unknown accuracy.

9.3 Experimental studies of QCD

Since we are not able to directly measure partons (quarks or gluons), but only hadrons and their decay products, a central issue for every experimental study of perturbative QCD is establishing a correspondence between observables obtained at the parton and the hadron level. The only theoretically sound correspondence is achieved by means of *infrared and collinear safe* quantities, which allow one to obtain finite predictions at any order of perturbative QCD.

As stated above, the simplest case of infrared- and collinear-safe observables are some inclusive cross sections or including decay widths.

More generally, when measuring fully inclusive observables, the final state is not analyzed at all regarding its (topological, kinematical) structure or its composition. Basically, the relevant information consists of the rate of a process ending up in a partonic or hadronic final state. In e^+e^- annihilation, widely used examples are the ratios of partial widths or branching ratios for the electroweak decay of particles into hadrons or leptons such as Z or τ decays (*cf.* Sec. 9.2.1). Such ratios are often favored over absolute cross sections or partial widths because of large cancellations of experimental and theoretical systematic uncertainties. The strong suppression of non-perturbative effects, $\mathcal{O}(\Lambda^4/Q^4)$, is one of the attractive features of such observables, however, at the same time, the sensitivity to radiative QCD corrections is small,

[9] Various studies have been carried out on how to estimate uncertainties from missing higher orders that go beyond scale variations [569–573], including recently the use of theory nuisance parameters [574, 575].

[10] In some circumstances, the scale in the denominator could be a smaller kinematic or physical scale that depends on the observable.

Int. J. Mod. Phys. A 2026.41. Downloaded from www.worldscientific.com
by UNIVERSITY OF CALIFORNIA @ BERKELEY on 09/16/26. Re-use and distribution is strictly not permitted, except for Open Access articles.

which for example leads to a larger statistical uncertainty when using them for the determination of the strong coupling constant. In the case of τ decays not only the hadronic branching ratio is of interest, but also moments of the spectral functions of hadronic τ decays, which sample different parts of the decay spectrum and thus provide additional information. Other examples of fully inclusive observables are structure functions (and related sum rules) in DIS. These are extensively discussed in Sec. 18 of this *Review*.

On the other hand, often the structure or composition of the final state are analyzed, and cross sections differential in one or more variables characterizing this structure are of interest. Examples are jet rates, jet substructure, event shapes or transverse-momentum distributions of jets or vector bosons in hadron collisions. The case of fragmentation functions, *i.e.* the measurement of hadron production as a function of the hadron momentum relative to some hard scattering scale, is discussed in Sec. 19 of this *Review*.

It is worth mentioning that, besides the correspondence between the parton and hadron level, also a correspondence between the hadron level and the actually measured quantities in the detector has to be established. The simplest examples are corrections for finite experimental acceptance and efficiencies. Whereas acceptance corrections essentially are of theoretical nature, since they involve extrapolations from the measurable (partial) to the full phase space, other corrections such as for efficiency, resolution and response are of experimental nature. For example, measurements of differential cross sections such as jet rates require corrections in order to relate, *e.g.*, the energy deposits in a calorimeter to the jets at the hadron level. Note that, while the underlying event energy is part of the event to be measured, particles from additional interactions from other proton-proton collisions are not, and this energy must be subtracted from the jet energy measurement [577]. Typically, detector simulations and/or data-driven methods are used in order to obtain these corrections. Care should be taken here to clearly separate between the parton-to-hadron level and hadron-to-detector level corrections. Finally, for the sake of an easy comparison to the results of other experiments and/or theoretical calculations, it is suggested to provide, whenever possible, measurements corrected for detector effects and/or all necessary information related to the detector response (*e.g.*, the detector response matrix). Any fiducial phase space for measurements should be defined as close as possible to the detector-level selection in order to minimize model-dependent extrapolations. A versatile repository for storing such information is the use of Rivet routines [579].

9.3.1 *Hadronic final-state observables*

9.3.1.1 *Jets*

In hard interactions, final-state partons and hadrons appear predominantly in collimated bunches, which are generically called *jets*. To a first approximation, a jet can be thought of as a hard parton that has undergone soft and collinear showering and then hadronization. Jets are used both for testing our understanding and predictions of high-energy QCD processes, and also for identifying the hard partonic structure of decays of massive particles such as top quarks and W, Z, and Higgs bosons.

In order to map observed hadrons onto a set of jets, one uses a *jet definition*. The mapping involves explicit choices: for example when a gluon is radiated from a quark, establishing for what range of kinematics the gluon should be part of the quark jet, or instead form a separate jet. Good jet definitions are infrared and collinear safe, simple to use in theoretical and experimental contexts, applicable to any type of inputs (parton or hadron momenta, charged particle tracks, and/or energy deposits in the detectors) and lead to jets that are not too sensitive to non-perturbative effects.

An extensive treatment of the topic of jet definitions is given in Ref. [580] (for e^+e^- collisions) and Refs. [581–583]. Here we briefly review the two main classes: cone algorithms, extensively used at hadron colliders before the LHC, and sequential recombination algorithms, more widespread in e^+e^- and ep colliders and at the LHC.

Cone algorithms typically start from a seed particle, summing the momenta of all particles within a cone of radius (R) in rapidity–azimuth space. The cone axis is iteratively updated until stable, and a jet is defined if its transverse momentum exceeds ($p_{t,\min}$). Variants differ in the seed choice and in how they resolve overlapping cones. Seeded algorithms (e.g. JetCLU, MidPoint) suffer from infrared and collinear unsafety, incompatibility with higher-order QCD, and instabilities. They were used at the Tevatron but are deprecated and not employed at the LHC. The modern alternative is the seedless SISCone algorithm [584], which is infrared safe.

Sequential recombination algorithms at hadron colliders (and in DIS) are characterized by a distance $d_{ij} = \min(k_{t,i}^{2p}, k_{t,j}^{2p})\Delta_{ij}^2/R^2$ between all pairs of particles i, j, where Δ_{ij} is their separation in the rapidity-azimuthal plane, $k_{t,i}$ is the transverse momentum w.r.t. the incoming beams, and R is a free parameter. At the LHC, R is typically in the range from 0.4 to 0.8, although analyses can also use jet sizes up to 1.0-1.2. They also involve a "beam" distance $d_{iB} = k_{t,i}^{2p}$. One identifies the smallest of all the d_{ij} and d_{iB}, and if it is a d_{ij}, then i and j are merged into a new pseudo-particle (with some prescription, a recombination scheme, for the definition of the merged four-momentum). If the smallest distance is a d_{iB}, then i is removed from the list of particles and called a jet. As with cone algorithms, one usually considers only jets above some transverse-momentum threshold $p_{t,\min}$. The parameter p determines the kind of algorithm: $p = 1$ corresponds to the (*inclusive*-)k_t algorithm [436, 585, 586], $p = 0$ defines the *Cambridge-Aachen* algorithm [587, 588], while for the *anti*-k_t algorithm $p = -1$ [589]. All these variants are infrared and collinear safe. Whereas the former two lead to irregularly shaped jet boundaries, the latter results in cone-like boundaries, except in situations where there are nearby jets. The *anti*-k_t algorithm has become the de-facto standard for the LHC experiments.

In e^+e^- annihilation the k_t algorithm [436] uses $y_{ij} = 2\min(E_i^2, E_j^2)(1-\cos\theta_{ij})/Q^2$ as distance measure between two particles/partons i and j and repeatedly merges the pair with smallest y_{ij}, until all y_{ij} distances are above some threshold $y_{\rm cut}$, the jet resolution parameter. Q is a measure of the overall hardness of the event. The (pseudo)-particles that remain at this point are called the jets. Here it is $y_{\rm cut}$ (rather than R and $p_{t,\min}$) that should be chosen according to the needs of the analysis. The two-jet rate in the k_t algorithm has the property that logarithms $\ln(1/y_{\rm cut})$ exponentiate. This is one reason why it is preferred over the earlier JADE algorithm [438], which uses the distance measure $y_{ij} = 2\,E_i\,E_j\,(1-\cos\theta_{ij})/Q^2$. Note that other variants of sequential recombination algorithms for e^+e^- annihilations, using different definitions of the resolution measure y_{ij}, exhibit much larger sensitivities to fragmentation and hadronization effects than the k_t and JADE algorithms [590]. Exclusive versions of sequential algorithms recombine objects into a predefined number of jets. Efficient implementations of all the above algorithms are available through the *FastJet* package [591].

While building infrared safe jets is generally considered a solved problem, this is not quite the case when one also wishes to assign a flavor to a jet. In fact, the general experimental definition considers a flavored-jet to be a jet that contains at least one flavor tag (such as a B or D meson) above a given transverse-momentum threshold. Because of collinear or soft wide-angle $g \to q\bar{q}$ splittings, it is easy to see that such a definition is neither collinear nor infrared safe. This problem was addressed in Ref. [592,593] in the context of heavy-flavor production at the Tevatron. However, the jet-algorithm proposed in that work was impractical to implement experimentally because it was based on the k_t-algorithm. Furthermore, it required tagging two nearby flavored hadrons and involved a rather complex beam-distance measure. Since most experimental studies at the LHC instead rely on the anti-k_t algorithm, recent investigations have focused on developing algorithms that preserve the anti-k_t kinematics of the jets while assigning jet flavors in an infrared-safe way [594–596]. It turns out that the problem is more involved than anticipated, and a formulation of infrared-safe anti-k_t-like jets could only be achieved by introducing an interleaved flavor neutralization procedure [597]. For a comparison between these algorithms see Ref. [598].

An unfolding procedure will be necessary to convert experimental measurements of flavor-jets to a form that can be precisely compared to theoretical predictions. In any experimental setting,

Int. J. Mod. Phys. A 2026.41. Downloaded from www.worldscientific.com by UNIVERSITY OF CALIFORNIA @ BERKELEY on 09/16/26. Re-use and distribution is [redacted] except for Open Access articles.

not all gluon splittings into b or c quark pairs can be identified. In addition, the gluon splitting treatment incorporated into the parton shower Monte Carlos does not agree exactly with what is measured in the data. To reach an improved level of precision in the comparison of theory to experiment, an improved understanding of gluon splitting into $b\bar{b}$ and $c\bar{c}$ pairs between data and parton shower Monte Carlos is needed.

9.3.1.2 *Event Shapes*

Event-shape variables are functions of the four momenta of the particles in the final state and characterize the topology of an event's energy flow. They are sensitive to QCD radiation (and correspondingly to the strong coupling) insofar as gluon emission changes the shape of the energy flow.

The classic example of an event shape is the *thrust* [599,600] in e^+e^- annihilations, defined as

$$\hat{\tau} = \max_{\vec{n}_\tau} \frac{\sum_i |\vec{p}_i \cdot \vec{n}_\tau|}{\sum_i |\vec{p}_i|} \,, \tag{9.22}$$

where $\vec{p}_i$ are the momenta of the particles or the jets in the final-state and the maximum is obtained for the thrust axis $\vec{n}_\tau$. In the Born limit of the production of a perfect back-to-back $q\bar{q}$ pair, the limit $\hat{\tau} \to 1$ is obtained, whereas a perfectly spherical many-particle configuration leads to $\hat{\tau} \to 1/2$. Further event shapes of similar nature have been extensively measured at LEP and at HERA, and for their definitions and reviews we refer to Refs. [1, 8, 578, 601, 602]. The energy-energy correlation function [603], namely the energy-weighted angular distribution of produced hadron pairs, and its associated asymmetry are further shape variables which have been studied in detail at e^+e^- colliders. For hadron colliders the appropriate modification consists in only taking the transverse-momentum component [604]. The event shape variable *N-jettiness* has been proposed [605] that measures the degree to which the hadrons in the final state are aligned along N jet axes or the beam direction. It vanishes in the limit of exactly N infinitely narrow jets.

Phenomenological discussions of event shapes at hadron colliders can be found in Refs. [605–609]. Measurements of hadronic event-shape distributions have been published by CDF [610], ATLAS [611–617] and CMS [618–621].

Event shapes are used for many purposes. These include measuring the strong coupling (see *e.g.* Ref. [617]), tuning the parameters of Monte Carlo programs, investigating analytical models of hadronization and distinguishing QCD events from events that might involve decays of new particles (giving event-shape values closer to the spherical limit).

9.3.1.3 *Jet substructure, quark vs. gluon jets*

Jet substructure, which can be resolved by finding subjets or by measuring jet shapes, is sensitive to the details of QCD radiation in the shower development inside a jet and has been extensively used to study differences in the properties of quark and gluon induced jets, strongly related to their different color charges. There is clear experimental evidence that gluon jets have a softer particle spectrum and are "broader" than (light-) quark jets (as expected from perturbative QCD) when looking at observables such as the jet shape $\Psi(r/R)$ (see *e.g.* Ref. [622]). This is the fraction of transverse momentum contained within a subcone of cone-size r for jets of cone-size R. It is sensitive to the relative fractions of quark and gluon jets in an inclusive jet sample and receives contributions from soft-gluon initial-state radiation and the underlying event. Therefore, it has been widely employed for validation and tuning of Monte Carlo parton-shower models. Furthermore, this quantity turns out to be sensitive to the modification of the gluon radiation pattern in heavy ion collisions (see *e.g.* Ref. [623]).

Jet shape measurements using proton-proton collision data have been presented for inclusive jet samples [624–626] and for top-quark production [627]. Further discussions, references and summaries can be found in Refs. [602,628–630] and Sec. 4 of Ref. [631].

The use of jet substructure has also been investigated in order to distinguish QCD jets from jets that originate from hadronic decays of boosted massive particles (high-p_t electroweak bosons, top quarks and hypothesized new particles). A considerable number of experimental studies have been carried out with Tevatron and LHC data, in order to investigate the performance of the proposed algorithms for resolving jet substructure and to apply them to searches for new physics, as well as to the reconstruction of boosted top quarks, vector bosons and the Higgs boson. For reviews of this rapidly growing field, see Sec. 5.3 of Ref. [581], Refs. [496, 497, 631–637] and references therein. One convenient representation for visualizing jet substructure is through the Lund plane [638]. From a theoretical perspective, the Lund plane would be constructed using quarks and gluons, but similar observables can be constructed through the use of jets, as described in detail in Ref. [639].

Neural network techniques and deep learning methods have also been applied to jet and top physics and jet substructure, see *e.g.* Refs. [640–643]. Perhaps no other subfield has benefitted as much from machine learning techniques as the study of jet substructure. As a jet can have O(100) constituents each with kinematic and other information, jet substructure analysis is naturally a highly multivariate problem. Deep learning techniques can use all of the available information to study jets in their natural high dimensionality. Such techniques have not only improved discrimination between different final states/types of jets, but have also improved our understanding of perturbative QCD. For a review see Ref. [495].

9.3.2 *QCD measurements at colliders*

There exists a wealth of data on QCD-related measurements in e^+e^-, ep, pp, and $p\bar{p}$ collisions, to which a short overview like this would not be able to do any justice. Reviews of the subject have been published in Refs. [601, 602] for e^+e^- colliders and in Ref. [644] for ep scattering, whereas for hadron colliders overviews are given in, *e.g.*, Refs. [582, 629] and Refs. [2, 11, 645–647].

Below we concentrate our discussion on measurements that are most sensitive to hard QCD processes with focus on jet production.

9.3.2.1 e^+e^- *colliders*

Analyses of jet production in e^+e^- collisions are mostly based on data from the JADE experiment at center-of-mass energies between 14 and 44 GeV, as well as on LEP collider data at the Z resonance and up to 209 GeV. The analyses cover the measurements of (differential or exclusive) jet rates (with multiplicities typically up to 4, 5 or 6 jets), the study of three-jet events and particle production between the jets, as well as four-jet production and angular correlations in four-jet events.

Event-shape distributions from e^+e^- data have been an important input to the tuning of parton shower MC models, typically matched to matrix elements for three-jet production. In general these models provide good descriptions of the available, highly precise data. Especially for the large LEP data sample at the Z peak, the statistical uncertainties are mostly negligible and the experimental systematic uncertainties are at the percent level or even below. These are usually dominated by the uncertainties related to the MC model dependence of the efficiency and acceptance corrections (often referred to as "detector corrections").

Observables measured in e^+e^- collisions have been used for determinations of the strong coupling constant (*cf.* Section 9.4 below) and for putting constraints on the QCD color factors (*cf.* Sec. 9.1 for their definitions), thus probing the non-Abelian nature of QCD. Angular correlations in four-jet events are sensitive at leading order. Some sensitivity to these color factors, although only at NLO, is also obtained from event-shape distributions. Scaling violations of fragmentation functions and the different subjet structure in quark and gluon induced jets also give access to these color factors. A compilation of results [602] quotes world average values of $C_A = 2.89 \pm 0.03\,(\text{stat}) \pm 0.21\,(\text{syst})$ and $C_F = 1.30 \pm 0.01\,(\text{stat}) \pm 0.09\,(\text{syst})$, with a correlation coefficient of 82%. These results are in perfect agreement with the expectations from SU(3) of $C_A = 3$ and $C_F = 4/3$.

9.3.2.2 *DIS and photoproduction*

Jet measurements in ep collisions, both in the DIS and photoproduction regimes, allow for tests of QCD factorization (as they involve only one initial state proton and thus one PDF function), and provide sensitivity to both the gluon PDF and to the strong

Int. J. Mod. Phys. A 2026.41. Downloaded from www.worldscientific.com by UNIVERSITY OF CALIFORNIA @ BERKELEY on 09/16/26. Re-use and distribution is strictly not permitted, except for Open Access articles.

coupling constant. Calculations are available at NNLO in both regimes [333, 334]. An N^3LO calculation using the Projection-to-Born method was also presented in Ref. [322, 323]. Experimental uncertainties of the order of 5–10% have been achieved, whereas statistical uncertainties are negligible to a large extent. For comparison to theoretical predictions, at large jet p_t the PDF uncertainty dominates the theoretical uncertainty (typically of order 5–10%, in some regions of phase space up to 20%), therefore jet observables become useful inputs for PDF fits.

In general, the data are well described by the NLO and NNLO matrix-element calculations, combined with DGLAP evolution equations, in particular at large Q^2 and central values of jet pseudo-rapidity.

In the case of photoproduction, a wealth of measurements with low p_t jets were performed in order to constrain the photon content of the proton (which is by now determined with percent accuracy thanks to the LUX approach [155, 156]). A few examples of measurements can be found in Refs. [648–652] for photoproduction and in Refs. [653–662] for DIS.

9.3.2.3 *Hadron-hadron colliders*

The spectrum of observables and the number of measurements performed at hadron colliders is enormous, probing many regions of phase space and covering a huge range of cross sections, as exemplified in Fig. 9.1 for a wide class of processes by the CMS (top) and ATLAS (bottom) experiments. In general, the theory agreement with data is excellent for a wide variety of processes, indicating the success of perturbative QCD with the PDF and the strong coupling as inputs. For the sake of brevity, in the following only certain classes of those measurements will be discussed, which permit various aspects of the QCD studies to be addressed. Most of our discussion will focus on LHC results, which are available for center-of-mass energies of 2.76, 5, 7, 8 13, and 13.6 TeV, with integrated luminosities of up to $140\,\mathrm{fb}^{-1}$ at 13 TeV, and up to $250\,\mathrm{fb}^{-1}$ at 13.6 TeV.

Generally speaking, besides representing precision tests of the Standard Model and QCD in particular, these measurements serve several purposes, such as: (i) probing pQCD and its various approximations and implementations in MC models to quantify the order of magnitude of not yet calculated contributions and to gauge their precision when used as background predictions to searches for new physics, or (ii) extracting/constraining model parameters such as the strong coupling constant or PDFs.

The final states measured at the LHC include single, double and triple gauge boson production, top production (single top, top pair and four top production), Higgs boson production, alone and in conjunction with a W or Z boson, and with a top quark pair. Many/most of these events are accompanied by additional jets. So far only limits have been placed on double Higgs production. The volume of LHC results prohibits a comprehensive description in this *Review*; hence, only a few highlights will be presented [663–667].

Among the most important cross sections measured, and the one with the largest dynamic range, is the inclusive jet spectrum as a function of the jet transverse momentum (p_t), for several rapidity regions and for p_t up to 700 GeV at the Tevatron and ~ 3.5 TeV at the LHC. It is worth noting that this latter upper limit in p_t corresponds to a distance scale of $\sim 10^{-19}$ m: no other experiment so far is able to directly probe smaller distance scales of nature than this measurement. The Tevatron inclusive jet measurements in Run 2 (Refs. [670–673]) were carried out with the MidPoint jet clustering algorithm (or its equivalent) and, in a few cases, with the k_t jet clustering algorithm. Most of the LHC measurements use the *anti-*k_t algorithm, with a variety of jet radii. The use of multiple jet radii in the same analysis allows a better understanding of the underlying QCD dynamics. For example, as discussed earlier, a study of the R-dependence of jet production at NNLO made clear that there are accidental cancellations in the scale dependence. The typical central scale choices used in the theoretical comparisons are related either to the transverse momentum of each jet (p_T^{jet}), or the sum of transverse energies in the event (H_T). Measurements by ALICE, ATLAS and CMS have been published in Refs. [674–685].

In general, we observe a good description of the data by the NLO and NNLO QCD predictions over about 11 orders of magnitude in cross section, as long as care is taken for the functional form of the central scale choice [686]. The experimental systematic uncertainties are dominated by the jet energy scale uncertainty, quoted to be in the range of a few percent (see for instance the review in Ref. [687]), leading to uncertainties of $\sim 5-30\%$ on the cross section, increasing with p_t and rapidity. The PDF uncertainties dominate the theoretical uncertainty at large p_t and rapidity. In fact, inclusive jet data are among the most important inputs to global PDF fits, in particular for constraining the high-x gluon PDF [688–690]. Constraints on the PDFs can also be obtained from ratios of inclusive cross sections at different center-of-mass energies [675, 680]. Ratios of jet cross sections are a means to (at least partially) cancel the jet energy scale uncertainties and thus provide jet observables with significantly improved precision.

Dijet events are typically analyzed in terms of their invariant mass or average dijet p_t and angular distributions, which allows for tests of NLO and NNLO QCD predictions (see *e.g.* Refs. [679, 691, 692] for recent LHC results), and for setting stringent limits on deviations from the Standard Model, such as quark compositeness or contact interactions (some examples can be found in Refs. [682, 693–699]). Furthermore, dijet azimuthal correlations between the two leading jets, normalized to the total dijet cross section, are an extremely valuable tool for studying the spectrum of gluon radiation in the event. The azimuthal separation of the two leading jets is sensitive to multi-jet production, avoiding at the same time large systematic uncertainties from the jet energy calibration. For example, results from the Tevatron [700, 701] and the LHC [616, 702–706] show that the LO (non-trivial) prediction for this observable, with at most three partons in the final state, is not able to describe the data for an azimuthal separation below $2\pi/3$, where NLO contributions (with 4 partons) restore the agreement with data. In addition, this observable can be employed to tune Monte Carlo predictions of soft gluon radiation. Further examples of dijet observables that probe special corners of phase space are those that involve forward (large rapidity) jets and where a large rapidity separation, possibly also a rapidity gap, is required between the two jets. Reviews of such measurements can be found in Ref. [629], showing that no single prediction is capable of describing the data in all phase-space regions. In particular, no conclusive evidence for BFKL effects in these observables has been established so far.

Beyond dijet final states, measurements of the production of three or more jets, including cross section ratios, have been performed (see Refs. [629, 707] for recent reviews), as a means of testing perturbative QCD predictions, determining the strong coupling constant, and probing/tuning MC models, in particular those combining multi-parton matrix elements with parton showers [617, 708]. The calculation of three-jet production to NNLO [360] will allow more precise predictions of the three-jet to two-jet ratio, and thus the extraction of $\alpha_s(m_Z^2)$ from this observable. This calculation also allows for the use of transverse energy-energy correlations (TEEC) for the determination of $\alpha_s(m_Z^2)$ [617].

W and Z production serve as benchmark cross sections at the LHC. The large boson mass stabilizes perturbative predictions, which results in better theoretical accuracy. In terms of experimental precision, measurements of inclusive vector boson (W, Z) production provide the most precisely determined observables at hadron colliders so far. This is because the experimental signatures are based on charged leptons which are measured much more accurately than jets or photons. At the LHC [709–719], the dominant uncertainty stems from the luminosity determination ($\sim 1.7\%$), while other uncertainties (*e.g.* statistical or from lepton efficiencies) are controlled at the $\sim$0.5–3% level. The uncertainty from the acceptance correction of about $\sim$1–2% can be reduced by measuring so-called fiducial cross sections, *i.e.* by applying kinematic cuts also to the particle level of the theoretical predictions. Measurements combining the electron and muon final states were able to achieve a precision a few per mille level in the dilepton final state for the normalized cross section for p_T^{ll} less than 30 GeV [720,721]. This level of precision can also be achieved by measuring cross section ratios (W/Z or W^+/W^-). On the

Int. J. Mod. Phys. A 2026.41. Downloaded from www.worldscientific.com
by UNIVERSITY OF CALIFORNIA @ BERKELEY on 09/16/26. Re-use and distribution is except for Open Access articles.

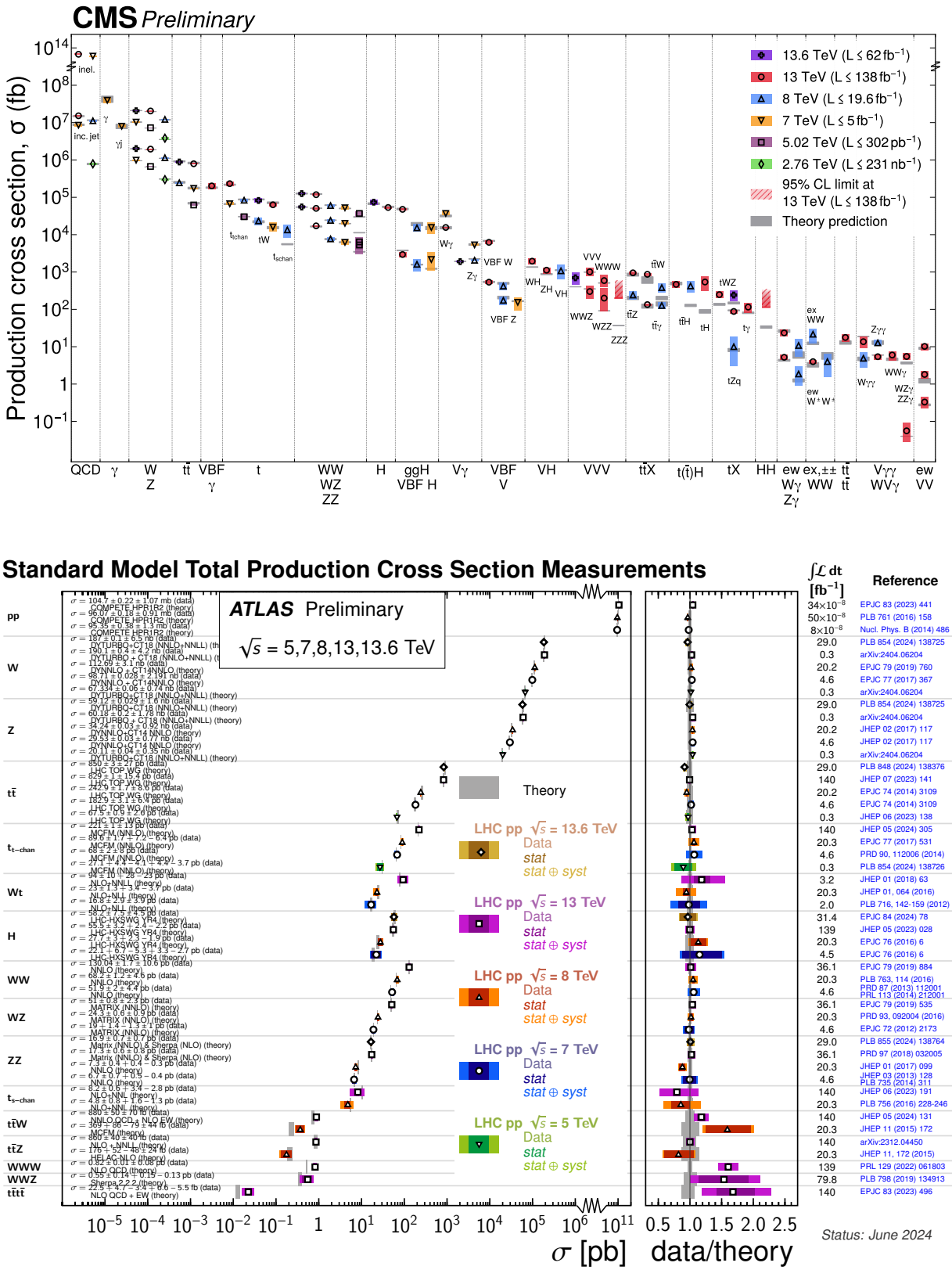

Figure 9.1: Overview of cross section measurements for a wide class of processes by the CMS [668] experiment, and by the ATLAS [669] experiment at the LHC, for center-of-mass energies of 5, 7, 8, 13, and 13.6 TeV. Also shown are the theoretical predictions and their uncertainties.

Int. J. Mod. Phys. A 2026.41. Downloaded from www.worldscientific.com by UNIVERSITY OF CALIFORNIA @ BERKELEY on 09/16/26. Re-use and distribution is strictly not permitted, except for Open Access articles.

theory side, as discussed earlier in this *Review*, the production of these color-singlet states has been calculated to N^3LO [137–139]. Since the dominant theoretical uncertainty is related to the choice of PDFs, these high-precision data provide useful handles for PDF determinations.

Further insights are obtained from measurements of differential vector boson production, as a function of the invariant dilepton mass, the boson's rapidity or its transverse momentum. For example, the dilepton invariant mass distribution has been measured [722–727] for masses between 15 and 3000 GeV, covering more than 8 orders of magnitude in cross section. NNLO QCD predictions, together with modern PDF sets and including higher-order electroweak and QED final-state radiation corrections, describe the data to within 5–10% over this large range, whereas NLO predictions show larger deviations, unless matched to a parton shower.

Similar conclusions can be drawn from the observed rapidity distribution of the dilepton system (see *e.g.* Refs. [709, 717, 723]) or, in the case of W production, from the observed charged lepton rapidity distribution and its charge asymmetry. The latter is particularly sensitive to differences among PDF sets [709, 728–730], also thanks to the high precision achieved by the ATLAS and CMS experiments for central rapidity ranges. These measurements are extended to the very forward region, up to 4.5 in lepton rapidity, by the LHCb experiment [715, 716, 731].

An overview of these kinds of measurement can be found in Ref. [629]. There one can also find a discussion of and references to LHC results from studies of the vector boson's transverse-momentum distribution, p_t^V (see also Refs. [720, 732–734]). This observable covers a wide kinematic range and probes different aspects of higher-order QCD effects. It is sensitive to jet production in association with the vector boson, without suffering from the large jet energy scale uncertainties. In the p_t^V region of several tens of GeV to over 1 TeV, the NNLO predictions for V+jet can be used to predict the high-p_t boson production cross section.[11] The NNLO predictions agree with the data to about 10%, and agree somewhat better at high transverse momentum than do the NLO predictions [735]. At transverse momenta below $\sim$20 GeV, the fixed-order predictions fail and soft-gluon resummation is needed to restore the agreement with data. The soft gluon resummation can either be performed analytically, or effectively using parton showering implemented in Monte Carlo programs. While analytic approaches reach a higher perturbative precision, they typically refer to inclusive measurements without fiducial cuts.

The addition of further jets to the final state extends the kinematic range as well as increasing the complexity of the calculation/measurements. The number of results obtained both at the Tevatron and at the LHC is extensive; summaries can be found in Refs. [629, 736], and more recent results can be found in Refs. [735, 737–741]. The measurements cover a very large phase space, *e.g.* with jet transverse momenta between 30 GeV and $\sim$ 1.5 TeV and jet rapidities up to $|y| < 4.4$ [735, 741, 742]. Jet multiplicities as high as seven jets accompanying the vector boson have already been measured at the LHC, together with a substantial number of other kinematical observables, such as angular correlations among the various jets or among the jets and the vector boson, or the sum of jet transverse momenta, H_T. Whereas the jet p_t and H_T distributions are dominated by jet energy scale uncertainties at levels similar to those discussed above for inclusive jet production, angular correlations and jet multiplicity ratios have been measured with a precision of $\sim$ 10%, see *e.g.* Refs. [619, 743].

NLO calculations for up to five jets [744] in addition to the vector boson are in good agreement with the data over that phase space, where the calculations are applicable. Predictions for V+jet at NNLO improve the description of the data for distributions involving the vector boson or the leading jet. MC models that implement parton shower matching to matrix elements (either at LO or NLO) have mixed results.

[11] For these calculations, there is a requirement of the presence of a jet, but the p_t cut is typically small (30 GeV) compared to the high p_t region being discussed here.

The challenges get even more severe in the case of vector boson plus heavy-quark (b, c) production: on the theory side because an additional scale is introduced by the heavy-quark mass, and different schemes exist for the handling of heavy quarks and their mass effects in the initial and/or final state; and on the experimental side because additional uncertainties related to the heavy-flavor tagging must be considered [745] (see also the discussion regarding flavor-jet definition in Sec. 9.3.1.1). A review of heavy-quark production at the LHC is presented in Ref. [746], where the p_t and mass spectra of the pair of b-jets are found to be well modeled within uncertainties by most generators for b-jet production with or without associated W and Z bosons. However, sizable differences between data and predictions are seen in the modeling of events with single b jets, particularly at large b-jet p_t, where gluon splitting processes become dominant, as also confirmed by studies of b-hadron and b-jet angular correlations.

The precision reached in photon measurements is in between that for lepton and jet measurements. The photon energy and angles can be measured at about the same precision as the lepton energy and angles in Drell-Yan production, but there are greater challenges encountered in photon reconstruction (for example isolation) and in purity determination. It should be noted though, that the photon purity approaches unity as the photon p_t increases. At high p_t, it becomes increasingly difficult for a jet to fragment into an isolated neutral electromagnetic cluster, which mimics the photon signature. The inclusive photon cross section can be measured [691, 747–750] as well as the production of a photon accompanied by one or more jets [750–752, 752–756]. The kinematic range for photon production is less than that for jet production because of the presence of the electromagnetic coupling, but still reaches about 2 TeV. Better agreement is obtained with NNLO predictions [238, 240] for photon production than for NLO ones [757, 758], except when the latter are matched to matrix element plus parton shower predictions [759]. Photon production in association with a heavy-flavor jet is a useful input for the determination of the b and c quark PDFs [760].

Electroweak corrections are expected to become more and more relevant in the TeV energy range being explored, and EW corrections can now also be computed automatically [198]. For a comprehensive review on electroweak corrections see Ref. [207]. For example, such corrections were found [761, 762] to be sizable (tens of percent) when studying the ratio $(d\sigma^\gamma/dp_t)/(d\sigma^Z/dp_t)$ in $\gamma\,(Z)$+jet production, p_t being the boson's transverse momentum, and might account for (some of) the differences observed in a CMS measurement [763] of this quantity.

A number of interesting developments, in terms of probing higher-order QCD effects, have occurred in the sector of diboson production, in particular for the WW and $\gamma\gamma$ cases. The statistical reach of the LHC has resulted in the discovery of triple massive gauge boson production [764–766].

In the case of diphoton production, ATLAS [767–769] and CMS [770] have provided accurate measurements, in particular for phase-space regions that are sensitive to radiative QCD corrections (multi-jet production), such as small azimuthal photon separation. While there are large deviations between data and NLO predictions in this region, a calculation [365] at NNLO accuracy manages to mostly fill this gap. This is an interesting example where scale variations can not provide a reliable estimate of missing contributions beyond NLO, since at NNLO new channels appear in the initial state (gluon fusion in this case). These missing channels can be included in a matrix element plus parton shower calculation in which two additional jets are included at NLO. The result exhibits a similar level of agreement as that obtained at NNLO. Three-photon production has also been measured [771] and is in good agreement with NNLO theory predictions [356, 384].

In terms of heaviest particle involved, top-quark production at the LHC has become an important tool for probing higher-order QCD calculations, thanks to very impressive achievements both on the experimental and theoretical side, as extensively summarized in Ref. [772]. Regarding $t\bar{t}$ production, the most precise inclusive cross section measurements are achieved using the dilepton ($e\,\mu$) final state, with a total uncertainty of 4% [773–777].

Int. J. Mod. Phys. A 2026.41. Downloaded from www.w[redacted]except for Open Access articles.
by UNIVERSITY OF CALIFORNIA @ BERKELEY on 09/16/26. Re-use and distribution is

This is of about the same size as the uncertainty on the most advanced theoretical predictions [147, 148, 251, 349], obtained at NNLO with additional soft-gluon resummation at NNLL accuracy [778]. There is excellent agreement between data and the QCD predictions.

The $t\bar{t}$ final state allows multiple observables to be measured. A large number of differential cross section measurements have been performed at 7, 8, 13 and 13.6 TeV center-of-mass energy, studying distributions such as the top-quark p_t and rapidity, the transverse momentum and invariant mass of the $t\bar{t}$ system (probing the TeV range), or the number of additional jets. These measurements have been compared to a wide range of predictions, at fixed order up to NNLO as well as using LO or NLO matrix elements matched to parton showers. Each of the observables provides information on the high x gluon, and do so in global PDF fits. However, there are tensions among the multiple observables that can lead to difficulties in PDF fits. Quadruple top production has been measured in multi-lepton final states [779] by the ATLAS and CMS collaboration, with results consistent with the standard model prediction [780].

Thanks to both the precise measurements of, and predictions for, the inclusive top-pair cross section, which is sensitive to the strong coupling constant and the top-quark mass, this observable has been used to measure the strong coupling constant at NNLO accuracy from hadron collider data [781, 782] (*cf.* Section 9.4 below), as well as to obtain a measurement of the top-quark's pole mass without employing direct reconstruction methods [781, 783, 784].

The Higgs boson provides a tool for QCD studies, especially as the dominant production mechanism is gg fusion, which is subject to very large QCD corrections. Higgs boson production has been measured in the major decay channels [785]. A measurement of the cross section in the ZZ and $\gamma\gamma$ channels is one of the first measurements at 13.6 TeV to be published [786]. The experimental cross section is now known with a precision approaching 10% [787, 788], similar to the size of the theoretical uncertainty [789], of which the PDF+α_s uncertainty is the largest component. Part of this systematic is the mismatch in orders between the PDF determination (NNLO) and the cross section evaluation (N^{3}LO), as discussed earlier. The experimental precision has allowed detailed fiducial and differential cross section measurements. For example, with the diphoton final state, the transverse momentum of the Higgs boson can be measured out to the order of 650 GeV, with constraints on the Higgs boson cross section up to 1 TeV [790–793], where top quark mass effects become important. The use of the boosted $H \to b\bar{b}$ topology allows probing Higgs boson transverse momenta of the order of 600 GeV and greater [788]. The production of a Higgs boson with up to 4 jets has been measured [788, 790]. The experimental cross sections have been compared to NNLO predictions (for $H+\geq 1$ jet), NLO for 2 and 3 jets, and NNLO+NNLL for the transverse-momentum distribution. In addition, finite top quark mass effects have been taken into account at NLO.

9.4 Determinations of the strong coupling constant

Assuming zero quark masses, the only free parameter in the QCD Lagrangian is the strong coupling constant α_s. The coupling constant in itself is not a physical observable, but rather a quantity defined in the context of perturbation theory, which enters predictions for experimentally measurable observables, such as R in Eq. (9.7). The value of the strong coupling constant must be inferred from such measurements and is subject to experimental and theoretical uncertainties. The incomplete knowledge of α_s propagates into uncertainties in numerous precision tests of the Standard Model. Here, we present an update of the 2024 PDG average value of $\alpha_s(m_Z^2)$ and its uncertainty [794].

Many experimental observables are used to determine α_s. A number of recent determinations are collected in Refs. [795, 796]. Further discussions and considerations on determinations of α_s can also be found in Refs. [797–799]. Such considerations include:

- The observable's sensitivity to α_s as compared to the experimental precision. For example, for the e^+e^- cross section to hadrons (*cf.* R in Sec. 9.2.1), QCD effects are only a small correction, since the perturbative series starts at order α_s^0; three-jet production or event shapes in e^+e^- annihilations are directly sensitive to α_s since they start at order α_s; the hadronic decay width of heavy quarkonia, $\Gamma(\Upsilon \to \text{hadrons})$, is very sensitive to α_s since its leading order term is $\propto \alpha_s^3$.
- The accuracy of the perturbative prediction, or equivalently of the relation between α_s and the value of the observable. Several observables have been known to NNLO for quite some time. These include, for instance, inclusive observables, as well as three-jet rates and event shapes in e^+e^- collisions, inclusive jet and dijet production in DIS, and inclusive jet, dijet, $t\bar{t}$, W/Z+jet and three-jet production cross sections in pp or $p\bar{p}$ collisions. The e^+e^- hadronic cross section and τ, W and Z branching fractions to hadrons are even known to N^{3}LO, if one denotes the LO as the first non-trivial term. In certain cases, fixed-order predictions are supplemented with resummation. The precise magnitude of the associated theory uncertainties usually is estimated as discussed in Sec. 9.2.4.
- The size of non-perturbative effects. Sufficiently inclusive quantities, like the e^+e^- cross section to hadrons, have small non-perturbative contributions $\sim \Lambda^4/Q^4$. Others, such as event-shape distributions, have typically larger contributions $\sim \Lambda/Q$.
- The scale at which the measurement is performed. An uncertainty δ on a measurement of $\alpha_s(Q^2)$, at a scale Q, translates to an uncertainty $\delta' = (\alpha_s^2(m_Z^2)/\alpha_s^2(Q^2)) \cdot \delta$ on $\alpha_s(m_Z^2)$. For example, this enhances the already important impact of precise low-Q measurements, such as from τ decays, in combinations performed at the m_Z scale.

The selection of results from which to determine the world average value of $\alpha_s(m_Z^2)$ is restricted to those that are

- published in a peer-reviewed journal at the time of writing this report,
- based on the most complete perturbative QCD predictions of at least NNLO accuracy,
- accompanied by reliable estimates of all experimental and theoretical uncertainties.

In order to calculate the world average value of $\alpha_s(m_Z^2)$, we apply, as in earlier editions, an intermediate step of pre-averaging results within the subfields now labeled "Hadronic τ decays and low Q^2 continuum" (τ decays and low Q^2), "Heavy quarkonia decays" ($Q\bar{Q}$ bound states), "PDF fits" (PDF fits), "Hadronic final states of e^+e^- annihilations" (e^+e^- jets & shapes), "Observables from hadron-induced collisions" (hadron colliders), and "Electroweak precision fit" (electroweak) as explained in the following sections. For each subfield, the *unweighted average* of all selected results is taken as the pre-average value of $\alpha_s(m_Z^2)$, and the *unweighted average* of the total uncertainties is assigned to be the respective overall error of this pre-average. Asymmetric total uncertainties are symmetrised beforehand by adopting the larger of the two values as the ($\pm$) uncertainty. For the "Lattice QCD" (lattice) subfield we do not perform a pre-averaging; instead, we adopt for this subfield the $\alpha_s(m_Z^2)$ estimate and uncertainty derived by the Flavour Lattice Averaging Group (FLAG) in Ref. [800].

Assuming that the six subfields (excluding lattice) are largely independent of each other, we determine a non-lattice world average value using a 'χ^2 *averaging*' method. In a last step we perform an unweighted average of the values and uncertainties of $\alpha_s(m_Z^2)$ from our non-lattice result and the lattice result presented in the FLAG 2024 report [800].

9.4.1 *Hadronic τ decays and low Q^2 continuum:*

Based on complete N^{3}LO predictions [34], analyses of the τ hadronic decay width and spectral functions have been performed, *e.g.* in Refs. [34, 801–806], and lead to precise determinations of α_s at the energy scale of m_τ^2. They are based on different approaches to treat perturbative and non-perturbative contributions, the impacts of which have been a matter of intense discussions for a long time, see *e.g.* Refs. [805–808]. In particular, in τ decays there is

Int. J. Mod. Phys. A 2026.41. Downloaded from www.worldscientific.com
by UNIVERSITY OF CALIFORNIA @ BERKELEY on 09/16/26. Re-use and distribution is strictly not permitted, except for Open Access articles.

a significant difference between results obtained using fixed-order (FOPT) or contour-improved perturbation theory (CIPT), such that analyses based on CIPT generally arrive at larger values of $\alpha_s(m_\tau^2)$ than those based on FOPT.

As detailed in the last edition of this *Review* we do not consider anymore determinations of the strong coupling constant based on CIPT, as long as a dedicated treatment of non-perturbative contributions in such derivations is missing. More details on recent developments can be found in Refs. [809–813].

We determine the pre-average value of $\alpha_s(m_Z^2)$ for this subfield only from studies that employ FOPT expansions and remove any eventual averaging with CIPT central values or increased uncertainties due to the differences in CIPT vs. FOPT. As the results from Refs. [34] and [808] are not totally independent, we pre-average these two results, $\alpha_s(m_Z^2) = 0.1183 \pm 0.0026$ and $\alpha_s(m_Z^2) = 0.1181 \pm 0.0015$, to give the first entry to this category of $\alpha_s(m_Z^2) = 0.1182 \pm 0.0021$ (summarized as BP 2008-16 FO in Fig. 9.2).

Subsequently, this is combined with $\alpha_s(m_Z^2) = 0.1158 \pm 0.0022$ [814] and $\alpha_s(m_Z^2) = 0.1159 \pm 0.0014$ [815], which replaces the previous result from Ref. [816]. We note that the uncertainty increased, even though more and more precise data, *e.g.* from the Belle experiment, are included in the updated analysis. The authors of Ref. [815] trace this back to updated particle properties as reported by the Heavy Flavor Averaging Group in Ref. [817].

We also include the result from τ decay and lifetime measurements, obtained in Sec. *Electroweak Model and constraints on New Physics* of the 2024 edition of this *Review* [794], $\alpha_s(m_Z^2) = 0.1171 \pm 0.0018$, which is unchanged as compared to the previous edition. The latter result, being a global fit of τ data, involves some correlations with the other extractions of this category. However, since we perform an unweighted average of the central value and uncertainty, the effects of the potential correlations are reduced. As before, the determination reported in Ref. [818] is added to this category: $\alpha_s(m_Z^2) = 0.1183^{+0.0009}_{-0.0012}$.

All these results are summarized in Fig. 9.2. Determining the unweighted average of the central values and their overall uncertainties, we arrive at $\alpha_s(m_Z^2) = 0.1171 \pm 0.0017$, which we will use as the first input for determining the world average value of $\alpha_s(m_Z^2)$.

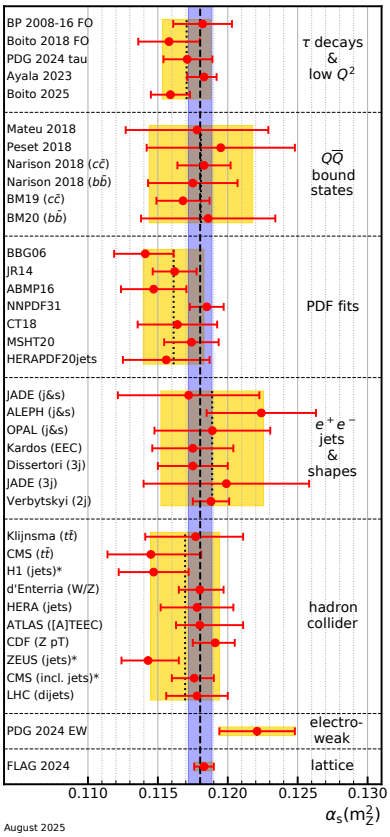

Figure 9.2: Summary of determinations of $\alpha_s(m_Z^2)$ with uncertainty in the seven subfields as discussed in the text. The yellow (light shaded) bands and dotted lines indicate the pre-average values of each subfield. The dashed line and blue (dark shaded) band represent the final world average value of $\alpha_s(m_Z^2)$. The "*" symbol within the "hadron colliders" subfield indicates a determination including a simultaneous fit of PDFs.

9.4.2 *Heavy quarkonia decays:*

Since the previous edition, a determination of $\alpha_s(m_Z^2)$ from inclusive semileptonic decay of charmed meson appeared resulting in $\alpha_s(Q = 1.37GeV) = 0.445 \pm 0.114$ [819], and has clearly an uncertainty which is not competitive to other determinations in this category. Lacking any new inputs the result of this subfield is unchanged from the previous edition.

Two determinations of $\alpha_s(m_Z^2)$ have been performed [820, 821] that are based on N^{3}LO accurate predictions. Reference [820] performs a simultaneous fit of the strong coupling and the bottom mass $\overline{m_b}$, including states with principal quantum number up to $n \leq 2$ in order to break the degeneracy between α_s and $\overline{m_b}$, finding $\alpha_s(m_Z^2) = 0.1178 \pm 0.0051$. Reference [821] instead uses as input of the fit the renormalon-free combination of masses of the meson B_c, the bottomonium η_b and the charmonium η_c, $M_{B_c} - M_{\eta_b}/2 - M_{\eta_c}/2$, which is weakly dependent on the heavy-quark masses, but shows a good dependence on α_s. Using this observable, they obtain $\alpha_s(m_Z^2) = 0.1195 \pm 0.0053$. Two further values are derived at NNLO in Ref. [822, 823] from mass splittings and sum rules giving $\alpha_s(m_Z^2) = 0.1183 \pm 0.0019$ and $\alpha_s(m_Z^2) = 0.1175 \pm 0.0032$ when evolved from the relevant charmonium respectively bottomonium mass scales to m_Z^2. Finally, by means of quarkonium sum rules, Refs. [824, 825] quote $\alpha_s(m_Z^2) = 0.1168 \pm 0.0019$ and $\alpha_s(m_Z^2) = 0.1186 \pm 0.0048$ for charmonium and bottomonium respectively. These six determinations satisfy our criteria to be included in the heavy-quarkonia category of the world average. Their unweighted combination leads to the pre-average for this category of $\alpha_s(m_Z^2) = 0.1181 \pm 0.0037$.

9.4.3 *PDF fits:*

Also in this subfield the $\alpha_s(m_Z^2)$ averaging remains for now unchanged from the previous edition. A few recent results, discussed in the following, did not yet qualify for inclusion.

Studies analyzing structure functions at NNLO QCD (and partly beyond), provide results that serve as relevant inputs for the world average of α_s. Some of these studies do *not*, however, explicitly include estimates of theoretical uncertainties when quoting fit results of α_s. In such cases we add, in quadrature, half of the difference between the results obtained in NNLO and NLO to the quoted errors.

A combined analysis of non-singlet structure functions from DIS [826], based on QCD predictions up to N^{3}LO in some of its parts, results in $\alpha_s(m_Z^2) = 0.1141 \pm 0.0022$ (BBG). Studies of singlet and non-singlet structure functions, based on NNLO predictions, result in $\alpha_s(m_Z^2) = 0.1162 \pm 0.0017$ [827] (JR14). The AMBP group [828, 829] determined a set of parton distribution functions using data from HERA, NOMAD, CHORUS, from the Tevatron and the LHC using the Drell-Yan process and the hadro-production of single-top and top-quark pairs, and determined $\alpha_s(m_Z^2) = 0.1147 \pm 0.0024$ [828]. A new analysis with the same methodology [830] compares significantly more and double-differential data on top-quark production to calculations at NNLO and quotes a value of $\alpha_s(m_Z^2) = 0.1150 \pm 0.0009$, but without estimation of a MHO uncertainty.

The MSHT group [831], also including hadron collider data, determined a set of parton distribution functions (MSHT20) together with $\alpha_s(m_Z^2) = 0.1174 \pm 0.0013$. Moreover, in Ref. [832] they present a first simultaneous fit of PDFs and $\alpha_s(m_Z^2)$ at approximate N^{3}LO (aN^{3}LO) giving $\alpha_s(m_Z^2) = 0.1170 \pm 0.0016$, where the uncertainty also comprises an estimate of the MHO uncertainty by means of theory nuisance parameters as mentioned in Section 9.2.2. This first attempt is much appreciated, however, we

Int. J. Mod. Phys. A 2026.41. Downloaded from www.w
by UNIVERSITY OF CALIFORNIA @ BERKELEY on 09/16/26. Re-use and distribution is
except for Open Access articles.

feel that, considering the number of approximations to be made, it would be somewhat premature to include this number already in the averaging or the uncertainty derivation for the value derived at NNLO in the same publication. Therefore, lacking an NLO result to estimate a MHO uncertainty, we stick with the previous MSHT result for this edition of the review.

The CT group [86] determined the CT18 PDF set together with $\alpha_s(m_Z^2) = 0.1164 \pm 0.0026$. The NNPDF group [833] presented NNPDF3.1 parton distribution functions together with $\alpha_s(m_Z^2) = 0.1185 \pm 0.0012$. They also advanced to an $\alpha_s(m_Z^2)$ extraction at aN^{3}LO employing their fit methodology to include MHO effects through scale variations as described in Ref. [834], which, at the time of writing, is not yet published in a peer-reviewed journal. The last result in this category, $\alpha_s(m_Z^2) = 0.1156 \pm 0.0031$, is reported as HERAPDF2.0Jets in Ref. [835]. In addition to DIS data from HERA, jet cross sections are considered in this fit to theory at NNLO. For criticism expressed on some of the above extractions please confer references in the previous edition of this *Review* and the recent more extensive discussions in Ref. [87].

Summarizing the results from world data on structure functions, taking the *unweighted average* of the central values and errors of all selected results, leads to a pre-average value of $\alpha_s(m_Z^2) = 0.1161 \pm 0.0022$, see also Fig. 9.2.

9.4.4 *Hadronic final states of e^+e^- annihilations:*

An analysis of JADE data [836] from e^+e^- annihilation (j&s) at center-of-mass energies between 14 and 46 GeV gives $\alpha_s(m_Z^2) = 0.1172 \pm 0.0051$, with contributions from the hadronization model and from perturbative QCD uncertainties of 0.0035 and 0.0030, respectively. Similarly, re-analyses of jets and event shapes measured around the Z peak and at LEP2 center-of-mass energies up to 209 GeV, using NNLO predictions matched to NLL resummation and Monte Carlo models to correct for hadronization effects, resulted in $\alpha_s(m_Z^2) = 0.1224 \pm 0.0039$ (ALEPH) [837], and in $\alpha_s(m_Z^2) = 0.1189 \pm 0.0043$ (OPAL) [838]. A fit of energy-energy-correlation (EEC), also based on an NNLO+NNLL calculation, together with a Monte Carlo based modeling of hadronization corrections gives $\alpha_s(m_Z^2) = 0.1175 \pm 0.0029$ [839]. Precise determinations of α_s from three-jet production alone (3j), at NNLO, resulted in $\alpha_s(m_Z^2) = 0.1175 \pm 0.0025$ [840] from ALEPH data and in $\alpha_s(m_Z^2) = 0.1199 \pm 0.0059$ [841] from JADE. A determination based on an NNLO+NNLL accurate calculation allows to fit the region of lower three-jet rate (2j) using data collected at LEP and PETRA at different energies. This fit gives $\alpha_s(m_Z^2) = 0.1188 \pm 0.0013$ [842], where the dominant uncertainty is the hadronization uncertainty, which is estimated from Monte Carlo simulations. These results are summarized in the e^+e^- sector of Fig. 9.2.

Another class of α_s determinations is based on analytic modeling of non-perturbative and hadronization effects, rather than on Monte Carlo models, using methods like power corrections, factorization of soft-collinear effective field theory, dispersive models and low scale QCD effective couplings. In these studies, data on thrust distributions, or the C-parameter distributions, are analyzed and fitted to perturbative QCD predictions at NNLO matched with resummation of leading logs up to N^{3}LL accuracy, see Sec. 9.2.3.3. Earlier determinations include $\alpha_s(m_Z^2) = 0.1135 \pm 0.0011$ [843] and $\alpha_s(m_Z^2) = 0.1134^{+0.0031}_{-0.0025}$ [844] from thrust, and $\alpha_s(m_Z^2) = 0.1123 \pm 0.0015$ [845] from C-parameter.

A long-standing question was why this latter class of determinations led systematically to rather small values of $\alpha_s(m_Z^2)$ as compared to the former one based on Monte Carlo models to correct for hadronization effects. New insights have now been gained in this regard, but the subject is still under active development. First, the leading non-perturbative contribution to the C-parameter in the three-jet symmetric limit based on an effective coupling approach was calculated and it was found to differ by a factor of two from the one in the two-jet limit [846]. Subsequently, using the same effective coupling approach, the leading $1/Q$ power correction was computed for thrust and the C-parameter in the full three-jet region under the assumption of a large (negative) n_f limit [847]. Expanding on this approach, Ref. [848] extended the calculation of non-perturbative corrections to include the heavy-jet mass, the difference of jet masses, wide broadening, and, with some caveat, the three-jet resolution variable in the Durham algorithm. The key finding in Refs. [848,849] is that non-perturbative corrections computed in the three-jet region significantly deviate from those computed in the two-jet limit, which can impact determinations of $\alpha_s(m_Z^2)$. Another important observation is that the inclusion of resummation effects introduces a relatively substantial ambiguity outside the two-jet limit. Currently there is no general agreement concerning the range of the dijet and three-jet regions. Moreover, other factors such as ambiguities related to the procedure used to evaluate the inverse Laplace transform [850, 851], or the choice of mass-scheme used to extend the definition of event shapes to massive hadrons can have significant effects. Since the seminal renormalon-based analyses [26, 852] it has been understood that hadron masses can break the universality of leading power corrections. In particular, Ref. [853] showed that they can induce logarithmically enhanced power corrections of the form $\sim \ln^{1.6} Q/Q$. More recently, Ref. [854], building on the operator-based framework of Ref. [855] and expressing the leading power correction in terms of matrix elements of a *transverse velocity* operator, demonstrated that event shapes in the dijet limit fall into different, scheme-specific universality classes that nevertheless share universal power corrections. This provides a field-theoretic confirmation of the results of Ref. [853]. Reference [856], whose main result is a remarkably simple expression for the all-order anomalous scaling of non-perturbative linear power corrections — reproducing both the Q-dependence and the event-shape dependence observed in PYTHIA — provides arguments in favor of the so-called decay scheme over alternative mass schemes. These findings merit further investigation.

The novel determinations of α_s presented in Refs. [857–859] extend and refine earlier analyses [843, 845]. Key improvements include optimized choices of renormalization scales, modifications to the renormalon subtraction scheme, an assessment of the impact of the fit range, and the incorporation of three-jet power-correction models. Despite these refinements, the extracted values of the strong coupling remain, consistent with previous results, rather small yielding for instance $\alpha_s(m_Z^2) = 0.1136 \pm 0.0012$ from thrust [858] and $\alpha_s(m_Z^2) = 0.1123 \pm 0.0015$ from the C-parameter [845]. Although the newly quoted uncertainties are more conservative than in previous determinations, they still fail to account for important sources of uncertainty associated with the choice of mass scheme, as highlighted *e.g.* in Refs. [848, 849].

Given the rapid progress currently being made in this field, we consider it premature to include any of the recent determinations based on analytic models for estimating power corrections. Determinations based on corrections for non-perturbative hadronization effects using QCD-inspired Monte Carlo generators have also faced criticism due to the differing nature of parton-level simulations compared to fixed-order calculations. However, these determinations typically exhibit a more conservative theoretical uncertainty.

Other determinations, not included in the computation of the world average but worth mentioning are a computation of the NLO corrections to 5-jet production and comparison to the measured 5-jet rates at LEP [860], giving $\alpha_s(m_Z^2) = 0.1156^{+0.0041}_{-0.0034}$, and a computation of non-perturbative and perturbative QCD contributions to the scale evolution of quark and gluon jet multiplicities, including resummation, resulting in $\alpha_s(m_Z^2) = 0.1199 \pm 0.0026$ [861].

The unweighted average of the considered determinations as shown in the e^+e^- sector of Fig. 9.2 remains unchanged from the previous edition of this *Review* and yields $\alpha_s(m_Z^2) = 0.1189 \pm 0.0037$.

9.4.5 *Observables from hadron-induced collisions:*

In the last decade, several determinations of α_s using hadron collider data in comparison to NNLO calculations have become available. Complementing $t\bar{t}$ [147, 251, 349] and Z+jet production [342, 387], inclusive jet, dijet, and three-jet production [336, 337, 355, 360, 862] have joined this subfield. In addition to NNLO, also logarithms to NNLL or N^{3}LL have been resummed for the $t\bar{t}$ and Z+jet processes, *cf.* also Section 9.2.3.3. For high-p_T collisions at the LHC, these predictions must be supplemented

Int. J. Mod. Phys. A 2026.41. Downloaded from www.worldscientific.com
by UNIVERSITY OF CALIFORNIA @ BERKELEY on 09/16/26. Re-use and distribution is strictly not permitted, except for Open Access articles.

by electroweak corrections [863–866].

Moreover, determinations of α_s from production cross sections at hadron colliders also require a knowledge of the relevant PDFs for those α_s values. Three strategies of increasing sophistication are pursued: The first two make use of input PDFs that are predetermined for a central value of $\alpha_s(m_Z^2) = 0.118$, close or equal to the world average, together with complementary PDF sets that are produced by each global PDF group for a wide range above and below 0.118 in increments of 0.001. In the simplest method, the pre-determined central PDF set is taken as it is, ignoring a potential impact of the new data on the central PDFs when they would have been combined beforehand with all the datasets entering the original PDF fit. The alternative PDF sets for the range of pre-set $\alpha_s(m_Z^2)$ values are used only to estimate an additional uncertainty. This technique has been critisized to potentially result in a bias of unknown magnitude [867]. In the second method, the impact of new data on the PDFs is examined by means of a technique known as Hessian profiling. As long as their impact is found to be limited and the new data are not in conflict with the original datasets, correlations among a determination of $\alpha_s(m_Z^2)$ and the PDFs can be accounted for, albeit at a level less accurate than obtained from method three, *i.e.* a simultaneous global $\alpha_s(m_Z^2)$ and PDF fit. In particular, the new data used in the determination of $\alpha_s(m_Z^2)$ may require PDF adaptations in a manner not taken into account by the $\alpha_s(m_Z^2)$-variation PDFs provided by the fitting collaborations. Another caveat in the use of Hessian profiling is the determination of the appropriate value of $\Delta\chi^2$ that should be assumed for a 1-sigma uncertainty on the resultant value of $\alpha_s(m_Z^2)$. Assuming a $\Delta\chi^2$ of unity does not necessarily reflect the correct level of uncertainty inherent in the PDF fit [868]. As the LHC experiments have the ability to combine a PDF fit with the $\alpha_s(m_Z^2)$ determination, for example with tools like described in Refs. [869, 870], we expect more experimental joint determinations of PDFs and of $\alpha_s(m_Z^2)$ for future iterations of this *Review*.

The first determination of α_s at NNLO accuracy in QCD has been reported by CMS from the $t\bar{t}$ production cross section at $\sqrt{s} = 7$ TeV [781]. In former *Reviews* this opened up a new subfield on its own. In the meantime, multiple datasets on $t\bar{t}$ production from Tevatron at $\sqrt{s} = 1.96$ TeV and from LHC at $\sqrt{s} = 7$, 8, and 13 TeV have been analyzed simultaneously to determine α_s [782] to $\alpha_s(m_Z^2) = 0.1177^{+0.0034}_{-0.0036}$, where the largest uncertainties are associated with missing higher orders and with PDFs, and where an additional complication arises from the top-mass dependence. Since this combined analysis contains among other things an updated measurement as compared to the dataset used by CMS, the latter is replaced in the averaging by this combined result. A second entry into this subfield is given by an analysis of $t\bar{t}$ production data at $\sqrt{s} = 13$ TeV from the CMS Collaboration [775]. From the four values derived for different PDF sets, the unweighted average is taken: $\alpha_s(m_Z^2) = 0.1145^{+0.0036}_{-0.0031}$. A second analysis by CMS using differential distributions of $t\bar{t}$ production [776] has been performed at NLO only and is not further considered.

From collisions at HERA the α_s determination at NNLO using inclusive jet and dijet measurements in addition to DIS data of the H1 Collaboration [662] has been corrected for an issue with the theory prediction reported in Ref. [334]. We choose the result $\alpha_s(m_Z^2) = 0.1147 \pm 0.0025$ that is derived from a simultaneous fit of the strong coupling constant together with proton PDFs. We note that results of this section derived from such a simultaneous fit will be marked with a "*" in the corresponding figures. A second determination [419] combines multiple datasets on inclusive jet production of the H1 and ZEUS collaborations into one fit also using interpolation grids at NNLO. The result of $\alpha_s(m_Z^2) = 0.1178 \pm 0.0026$ has been updated for the same issue reported above [334] and is included in the unweighted average, although some of the inclusive jet data have already been used in the previous analysis. This is also the case for a new result by the ZEUS Collaboration [871], where previously published jet cross sections have been combined with a new inclusive jet measurement to give $\alpha_s(m_Z^2) = 0.1143^{+0.0022}_{-0.0019}$, where the scale-variation uncertainty has been treated as fully correlated.

A first determination of $\alpha_s(m_Z^2)$ at NNLO from inclusive jet production at the LHC by the CMS Collaboration [684] giving $\alpha_s(m_Z^2) = 0.1166 \pm 0.0016$ has been superseded by $\alpha_s(m_Z^2) = 0.1176^{+0.0014}_{-0.0016}$, also from a simultaneous fit of $\alpha_s(m_Z^2)$ and the proton PDFs to the HERA DIS and CMS jet data at four center-of-mass energies [872]. Using dijet production at $\sqrt{s} = 13$ TeV instead of the inclusive jet datasets the CMS Collaboration derived a value of $\alpha_s(m_Z^2) = 0.1179 \pm 0.0019$ at NNLO in the leading-color approximation. Since in the meantime a more complete analysis at full NNLO evaluating all dijet cross sections from the ATLAS and CMS collaborations has been published in Ref. [873], we include the corresponding result of $\alpha_s(m_Z^2) = 0.1178 \pm 0.0022$ in this subfield. The ATLAS Collaboration has extracted of $\alpha_s(m_Z^2)$ at NNLO from the transverse energy-energy correlation (TEEC) and its asymmetry (ATEEC) [617]. The results of this first derivation from an event shape observable requiring three-jet predictions at NNLO are $\alpha_s(m_Z^2) = 0.1175^{+0.0035}_{-0.0018}$ for the TEEC and $\alpha_s(m_Z^2) = 0.1185^{+0.0027}_{-0.0015}$ for the ATEEC, respectively. We include the unweighted average of the two numbers $\alpha_s(m_Z^2) = 0.1180^{+0.0031}_{-0.0017}$ as a new result in this category. Also, two determinations of the strong coupling constant, albeit at NLO, have been reported by CMS based on novel observables from energy correlators inside jets and from azimuthal correlations among jets [874, 875].

Reference [876] extracts the strong coupling constant from a fit at NNLO to measurements of inclusive Z and W boson production by experiments at the LHC and Tevatron colliders. From the four values quoted for different PDF sets we include the unweighted average for the CT14 and MMHT14 PDFs $\alpha_s(m_Z^2) = 0.1180^{+0.0017}_{-0.0015}$. The other results suffer from either a bad fit quality or $\alpha_s(m_Z^2)$ values outside the range of validity for the PDF set. Furthermore, a determination using the Z boson's recoil at low p_{T} as measured by the CDF experiment is reported in Ref. [877] and gives $\alpha_s(m_Z^2) = 0.1191^{+0.0014}_{-0.0016}$. A similar result by the ATLAS experiment [878] has not been considered as it is yet unpublished. Furthermore, it has been critisized for example in Ref. [574] concerning the estimated uncertainties.

As unweighted pre-average for this subfield we now obtain $\alpha_s(m_Z^2) = 0.1170 \pm 0.0025$. If the stricter requirement of simultaneous fits with PDFs is imposed, then only the H1, ZEUS, and CMS results as well as a result from the appendix of Ref. [877] $\alpha_s(m_Z^2) = 0.1188^{+0.0014}_{-0.0017}$ are left giving $\alpha_s(m_Z^2) = 0.1155 \pm 0.0021$. In sect. 9.4.8 below, we will also report the outcome for this choice.

9.4.6 *Electroweak precision fit:*

From this category, we removed the outdated global electroweak fit of Ref. [879], which does not consider important updates on the LEP luminosity at the Z pole from beam-beam effects [880] and from the Bhabha cross section reported in Ref. [881]. In view of a new, precise measurement of the W boson mass by the CMS experiment [882] that agrees with the standard model prediction as well as with other measurements but contradicts the outlying CDF result [883], we also excluded the $\alpha_s(m_Z^2)$ value reported in Ref. [884], even though we were using the result with increased uncertainty ("conservative scenario"). The only result left in this category therefore is the electroweak fit at the Z mass pole from LEP and SLC data presented in Sec. *Electroweak Model and constraints on New Physics* of the 2024 edition of this *Review* giving $\alpha_s(m_Z^2) = 0.1221 \pm 0.0027$ [794], which is unchanged as compared to the previous one from 2022. This is higher by more than one standard deviation as compared to our world average for $\alpha_s(m_Z^2)$ reported here.

We note, however, that results from electroweak precision data strongly depend on the strict validity of Standard Model predictions and the existence of the minimal Higgs mechanism to implement electroweak symmetry breaking. Any - even small - deviation of nature from this model could strongly influence this extraction of α_s.

9.4.7 *Lattice QCD:*

Several methods exist to extract the strong coupling constant from lattice QCD, as reviewed also in Sec. *Lattice QCD* of this *Review* and in Ref. [885]. The Flavour Lattice Averaging Group maintains

Int. J. Mod. Phys. A 2026.41. Downloaded from www.worldscientific.com by UNIVERSITY OF CALIFORNIA @ BERKELEY on 09/16/26. Re-use and distribution is except for Open Access articles.

a list of the most up-to-date determinations that are considered as input for their $\alpha_s(m_Z^2)$ estimate [800, 886, 887]. From a multitude of possible input calculations only those are retained that fulfill predefined quality criteria, *cf. e.g.* Sec. 9.2.1 of Ref. [800], which so far are unchanged since the FLAG 2019 Review [886]. In summary, a determination of α_s needs to satisfy the following requirements:

- The determination of α_s should be based on a comparison of a short-distance quantity $\mathcal{Q}$ at scale μ with a well-defined continuum limit, which does not involve UV or infrared divergences, when the quantity is expressed by using an expansion in terms of a short distance definition of the strong coupling (*e.g.* in the $\overline{\text{MS}}$ scheme);
- The scale μ, at which the determination is carried out, has to be sufficiently large such that the error associated with the perturbative truncation remains small enough;
- If $\mathcal{Q}$ is defined by physical quantities in infinite volume, one needs to satisfy the constraints $L/a \gg \mu/\Lambda_{\text{QCD}}$, where L is the lattice size and a the lattice spacing;
- Only results for $n_f \geq 3$ are considered.
- As is the case for the PDG average, a calculation must be published in a peer-reviewed journal to be eligible for inclusion into the FLAG estimate.

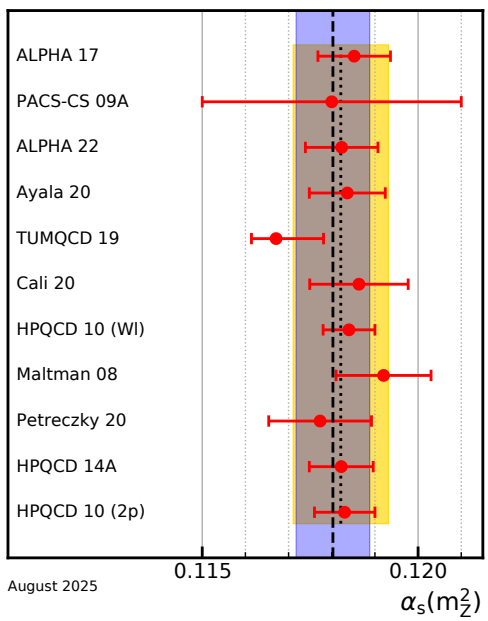

Figure 9.3: Lattice determinations that enter the FLAG 2024 estimate. The yellow (light shaded) band and dotted line indicate the *unweighted average* value for this subfield. The dashed line and blue (dark shaded) band represent our final world average value of $\alpha_s(m_Z^2)$.

Altogether, from a large number of previous results, six from the 2019 [888–892][12] and three from the 2021 edition of the FLAG review [893–895] are kept for the 2024 FLAG estimate. Moreover, two new determinations qualified for inclusion: one from heavy-quark current two-point functions [896] giving $\alpha_s(m_Z^2) = 0.1177 \pm 0.0012$, and a first one from the decoupling method [897] resulting in $\alpha_s(m_Z^2) = 0.1182 \pm 0.0008$.

These determinations, together with their uncertainties, are displayed in Fig. 9.3. The yellow (light shaded) band and dotted line indicate the *unweighted average* value for this subfield, while the dashed line and blue (dark shaded) band represent the world average (see later). The level of agreement of individual results to the world average, or to the non-lattice world average is very similar.

[12] Reference [890] contains two results.

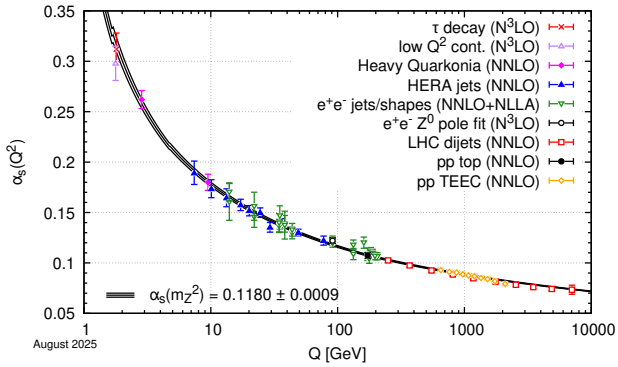

Figure 9.4: Summary of determinations of α_s as a function of the energy scale Q compared to the running of the coupling computed at five loops taking as an input the current PDG average, $\alpha_s(m_Z^2) = 0.1180 \pm 0.0009$. Compared to the previous edition, numerous points have been updated or added.

Similarly to what is done in this *Review*, the FLAG Collaboration built dedicated pre-averages of results within the various classes. The six categories that contribute to their final estimate are: step-scaling methods ($\alpha_s(m_Z^2) = 0.11848 \pm 0.00081$), for the first time the decoupling method ($\alpha_s(m_Z^2) = 0.11823 \pm 0.00084$), the potential at short distances ($\alpha_s(m_Z^2) = 0.11782 \pm 0.00165$), light quark vacuum polarization ($\alpha_s(m_Z^2) = 0.11863 \pm 0.00360$), Wilson loops ($\alpha_s(m_Z^2) = 0.11871 \pm 0.00128$), and heavy-quark current two-point functions ($\alpha_s(m_Z^2) = 0.11818 \pm 0.00119$). Other categories such as the calculation of QCD vertices, or of the eigenvalue spectrum of the Dirac operator have not yet published results that fulfill all requirements.

We note that the novel approach to non-perturbative renormalization called decoupling introduced by the ALPHA Collaboration [898] now has lead to a first result included in the 2024 FLAG estimate. This strategy shifts the perspective on results involving unphysical flavor numbers, particularly $n_f = 0$. By performing a non-perturbative matching calculation, these results can be non-perturbatively related to results with $n_f > 0$. Consequently, obtaining precise and controlled $n_f = 0$ results becomes of great importance as further discussed in the 2024 edition of the FLAG report.

The final value is obtained in two steps. First, accounting for their known correlation, a combination of the two results ALPHA 17 and ALPHA 22 is performed, which subsequently is combined with PACS-CS 09A to give a number of $\alpha_s(m_Z^2) = 0.1184 \pm 0.0007$ for the two categories of step scaling and decoupling, where the dominating uncertainty is of statistical origin. This uncertainty is also chosen to be the one of the final FLAG estimate, while the central value is derived from the weighted average together with the remaining pre-averages. The final FLAG 2024 estimate (rounded to four digits) is

$$\alpha_s(m_Z^2) = 0.1183 \pm 0.0007 \qquad \text{(FLAG 2024 estimate)}\,, \tag{9.23}$$

which is very close to the previous FLAG result of $\alpha_s(m_Z^2) = 0.1184 \pm 0.0008$.

We believe that this result expresses to a large extent the consensus of the lattice community and that the imposed criteria and the rigorous assessment of systematic uncertainties qualify for a direct inclusion of this FLAG estimate here. As in the previous review, we therefore adopt the FLAG estimate with its uncertainty as our value of α_s for the lattice category. Moreover, this lattice result will not be directly combined with any other subfield average, but with our non-lattice average to give our final world average value for α_s.

9.4.8 ***Determination of the world average value of $\alpha_s(m_Z^2)$:*** Obtaining a world average value for $\alpha_s(m_Z^2)$ is a non-trivial exercise. A certain arbitrariness and subjective component is inevitable because of the choice of measurements to be included in

Int. J. Mod. Phys. A 2026.41. Downloaded from www.worldscientific.com
by UNIVERSITY OF CALIFORNIA @ BERKELEY on 09/16/26. Re-use and distribution is strictly not permitted, except for Open Access articles.

Table 9.1: Unweighted and weighted pre-averages of $\alpha_s(m_Z^2)$ for each subfield in columns two and three. The bottom line corresponds to the combined result (without lattice gauge theory) using the χ^2 averaging method. The same χ^2 averaging is used for column four combining all unweighted averages except for the subfield of column one. See text for more details.

averages per subfield	unweighted	weighted	unweighted without subfield
τ decays & low Q^2	0.1171 ± 0.0017	0.1172 ± 0.0011	0.1181 ± 0.0012
$Q\bar{Q}$ bound states	0.1181 ± 0.0037	0.1177 ± 0.0011	0.1177 ± 0.0010
PDF fits	0.1161 ± 0.0022	0.1168 ± 0.0014	0.1182 ± 0.0011
e^+e^- jets & shapes	0.1189 ± 0.0037	0.1187 ± 0.0017	0.1177 ± 0.0011
hadron colliders	0.1170 ± 0.0025	0.1173 ± 0.0017	0.1179 ± 0.0011
electroweak	0.1221 ± 0.0027	0.1221 ± 0.0027	0.1171 ± 0.0011
PDG 2025 (without lattice)	0.1178 ± 0.0010	0.1177 ± 0.0006	n/a

the average, the treatment of (non-Gaussian) systematic uncertainties of mostly theoretical nature, as well as the treatment of correlations among the various inputs, of theoretical as well as experimental origin.

We have chosen to determine pre-averages for subfields of measurements that are considered to exhibit a maximum degree of independence among each other, considering experimental as well as theoretical issues. The six pre-averages, illustrated also in Fig. 9.2, are listed in column two of Table 9.1. We recall that these are exclusively obtained from extractions that are based on (at least) NNLO QCD predictions, and are published in peer-reviewed journals at the time of completing this *Review*. To obtain our final world average, we first combine these six pre-averages, excluding the lattice result, using a χ^2 *averaging method*. This gives

$$\alpha_s(m_Z^2) = 0.1178 \pm 0.0010 \qquad \text{(PDG 2025 without lattice)}\,. \tag{9.24}$$

This result is fully compatible with the lattice estimate Eq. (9.23) and has a slightly larger uncertainty. To avoid overestimating the precision, we combine these two numbers using an unweighted average and take as an uncertainty the average between these two uncertainties rounded to give the same number of digits as for α_s itself. This gives our final world average value

$$\alpha_s(m_Z^2) = 0.1180 \pm 0.0009 \qquad \text{(PDG 2025 average)}\,. \tag{9.25}$$

If for the subfield of hadron colliders we are more restrictive and instead only accept results from a simultaneous fit of PDFs, we arrive at $\alpha_s(m_Z^2) = 0.1164 \pm 0.0020$ for this subfield leading to 0.1176 ± 0.0010 (without lattice) and $\alpha_s(m_Z^2) = 0.1179 \pm 0.0008$ for the final average. Both the new world average value and the restricted result are compatible with each other and changed only marginally as compared to the values reported in the last edition of this *Review*.

It also stands to question whether the subfields of PDF fits and hadron colliders still are as independent as originally assumed. To test the potential impact, the fit has been repeated while grouping all $\alpha_s(m_Z^2)$ determinations of both subfields into a common one. We obtain 0.1166 ± 0.0024 for the new larger subfield and 0.1177 ± 0.0010 for the combination with all other subfields except lattice, which is well within the estimated uncertainties. Moreover, we present in column four of Table 9.1 the combined result for $\alpha_s(m_Z^2)$ when the respective subfield is omitted from the combination. The variation in values obtained for $\alpha_s(m_Z^2)$ is ± 0.0006, which is roughly half our estimated uncertainty.

Since two long-standing issues causing offsets among determinations of $\alpha_s(m_Z^2)$ in the subfields of τ decays and low Q^2 and e^+e^- jets & shapes have been better understood, it may be argued that a weighted fit among the non-lattice subfields may be warranted. We compare the outcome of weighted fits with our standard procedure in columns two and three of Table 9.1. We observe that the weighted averages are rather close to the unweighted ones. However, the uncertainties become significantly smaller. This approach may be too aggressive as it ignores the correlations among the data, methods, and theory ingredients of the various determinations. We feel that the uncertainty of ± 0.0006 is an underestimation of the true error. We also note that in the unweighted combination the estimated uncertainty for each subfield is larger than the spread of the results as given by the standard deviation. In the weighted fit this crosscheck fails in four out of five cases (not counting the electroweak subfield with only one entry).

The last several years have seen clarification of some persistent concerns and a wealth of new results at NNLO, providing not only a rather precise and reasonably stable world average value of $\alpha_s(m_Z^2)$, but also a clear signature and proof of the energy dependence of α_s in full agreement with the QCD prediction of asymptotic freedom.This is demonstrated in Fig. 9.4, where results of $\alpha_s(Q^2)$ obtained at discrete energy scales Q are summarized, which now include only those based on at least NNLO QCD. the results from the LHC, the energy scales, at which α_s is determined, now extend up to 7 TeV. [13] The points in this plot are extracted from Refs. [419,617,782,794,814,823,836–838,841,873].

In this combination, as in the past, we have considered lattice QCD calculations of α_s independently of other determinations. In the future, when the lattice continuum extrapolations are under better control, it may be useful to group lattice QCD determinations of α_s with experimental determinations of α_s that have systematics of similar origin, in a similar manner as we currently group, for example, hadron collider results together [885].

References

[1] R. K. Ellis, W. J. Stirling and B. R. Webber, Camb. Monogr. Part. Phys. Nucl. Phys. Cosmol. **8**, 1 (1996).

[2] J. Campbell, J. Huston, F. Krauss *"The Black Book of Quantum Chromodynamics, a Primer for the QCD Era,"*Oxford University Press, UK (2017).

[3] C. A. Baker *et al.*, Phys. Rev. Lett. **97**, 131801 (2006), [hep-ex/0602020].

[4] J. M. Pendlebury *et al.*, Phys. Rev. D **92**, 9, 092003 (2015), [arXiv:1509.04411].

[5] B. Graner *et al.*, Phys. Rev. Lett. **116**, 16, 161601 (2016), [Erratum: Phys. Rev. Lett.119,no.11,119901(2017)], [arXiv:1601.04339].

[6] `https://www.psi.ch/en/nedm/edms-world-wide`.

[7] J. E. Kim and G. Carosi, Rev. Mod. Phys. **82**, 557 (2010), [arXiv:0807.3125].

[8] G. Dissertori, I. G. Knowles and M. Schmelling, *High energy experiments and theory,* Oxford, UK: Clarendon (2003).

[9] R. Brock *et al.* (CTEQ), Rev. Mod. Phys. **67**, 157 (1995).

[10] K. Melnikov, CERN Yellow Rep. School Proc. **3**, 37 (2018).

[11] F. Gross *et al.*, Eur. Phys. J. C **83**, 1125 (2023), [arXiv:2212.11107].

[12] T. van Ritbergen, J. A. M. Vermaseren and S. A. Larin, Phys. Lett. B **400**, 379 (1997), [hep-ph/9701390].

[13] M. Czakon, Nucl. Phys. B **710**, 485 (2005), [hep-ph/0411261].

[13] We note, however, that the relevant energy scale of a measurement is not uniquely defined. In addition to being multiplied by factors of *e.g.* 1/2 or 2, for instance in studies of the ratio of three- to two-jet cross sections at the LHC, the relevant scale can be taken to be the average of the transverse momenta of the two leading jets [899], or alternatively might be chosen to be the transverse momentum of the 3rd jet.

Int. J. Mod. Phys. A 2026.41. Downloaded from www.worldscientific.com by UNIVERSITY OF CALIFORNIA @ BERKELEY on 09/16/26. Re-use and distribution is [redacted] except for Open Access articles.

[14] P. A. Baikov, K. G. Chetyrkin and J. H. Kühn, Phys. Rev. Lett. **118**, 8, 082002 (2017), [arXiv:1606.08659].

[15] T. Luthe *et al.*, JHEP **07**, 127 (2016), [arXiv:1606.08662].

[16] F. Herzog *et al.*, JHEP **02**, 090 (2017), [arXiv:1701.01404].

[17] T. Luthe *et al.*, JHEP **10**, 166 (2017), [arXiv:1709.07718].

[18] K. G. Chetyrkin *et al.*, JHEP **10**, 179 (2017), [Addendum: JHEP12,006(2017)], [arXiv:1709.08541].

[19] W. A. Bardeen *et al.*, Phys. Rev. D **18**, 3998 (1978).

[20] D. J. Gross and F. Wilczek, Phys. Rev. Lett. **30**, 1343 (1973), [,271(1973)].

[21] H. D. Politzer, Phys. Rev. Lett. **30**, 1346 (1973), [,274(1973)].

[22] Y. Schroder and M. Steinhauser, JHEP **01**, 051 (2006), [hep-ph/0512058].

[23] K. G. Chetyrkin, J. H. Kuhn and C. Sturm, Nucl. Phys. B **744**, 121 (2006), [hep-ph/0512060].

[24] A. G. Grozin *et al.*, JHEP **09**, 066 (2011), [arXiv:1107.5970].

[25] M. Dalla Brida *et al.* (ALPHA), Phys. Rev. Lett. **117**, 18, 182001 (2016), [arXiv:1604.06193].

[26] M. Beneke, Phys. Rept. **317**, 1 (1999), [hep-ph/9807443].

[27] M. Beneke *et al.*, Phys. Lett. B **775**, 63 (2017), [arXiv:1605.03609].

[28] A. H. Hoang, C. Lepenik and M. Preisser, JHEP **09**, 099 (2017), [arXiv:1706.08526].

[29] P. Marquard *et al.*, Phys. Rev. Lett. **114**, 14, 142002 (2015), [arXiv:1502.01030].

[30] P. A. Baikov *et al.*, Phys. Lett. B **714**, 62 (2012), [arXiv:1206.1288].

[31] K. G. Chetyrkin, J. H. Kuhn and A. Kwiatkowski, Phys. Rept. **277**, 189 (1996), [hep-ph/9503396].

[32] Y. Kiyo *et al.*, Nucl. Phys. B **823**, 269 (2009), [arXiv:0907.2120].

[33] P. A. Baikov *et al.*, Phys. Rev. Lett. **108**, 222003 (2012), [arXiv:1201.5804].

[34] P. A. Baikov, K. G. Chetyrkin and J. H. Kuhn, Phys. Rev. Lett. **101**, 012002 (2008), [arXiv:0801.1821].

[35] F. Herzog *et al.*, JHEP **08**, 113 (2017), [arXiv:1707.01044].

[36] V. A. Novikov *et al.*, Nucl. Phys. B **174**, 378 (1980).

[37] J. D. Bjorken and E. A. Paschos, Phys. Rev. **185**, 1975 (1969).

[38] J. A. M. Vermaseren, A. Vogt and S. Moch, Nucl. Phys. B **724**, 3 (2005), [hep-ph/0504242].

[39] S. Moch, J. A. M. Vermaseren and A. Vogt, Nucl. Phys. B **813**, 220 (2009), [arXiv:0812.4168].

[40] J. Davies *et al.*, PoS **DIS2016**, 059 (2016), [arXiv:1606.08907].

[41] E. Laenen *et al.*, Nucl. Phys. B **392**, 162 (1993); S. Riemersma, J. Smith and W. L. van Neerven, Phys. Lett. B **347**, 143 (1995), [hep-ph/9411431].

[42] J. Blümlein *et al.*, Nucl. Phys. B **945**, 114659 (2019), [arXiv:1903.06155].

[43] J. Blümlein, Int. J. Mod. Phys. A **39**, 09n10, 2441004 (2024), [arXiv:2306.01362].

[44] J. C. Collins, D. E. Soper and G. F. Sterman, Adv. Ser. Direct. High Energy Phys. **5**, 1 (1989), [hep-ph/0409313].

[45] J. Collins and J.-W. Qiu, Phys. Rev. D **75**, 114014 (2007), [arXiv:0705.2141].

[46] G. Sterman, in "Snowmass 2021," (2022), [arXiv:2207.06507].

[47] R. Boussarie *et al.* (2023), [arXiv:2304.03302].

[48] V. N. Gribov and L. N. Lipatov, Sov. J. Nucl. Phys. **15**, 438 (1972), [Yad. Fiz.15,781(1972)]; L. N. Lipatov, Sov. J. Nucl. Phys. **20**, 94 (1975), [Yad. Fiz.20,181(1974)]; G. Altarelli and G. Parisi, Nucl. Phys. B **126**, 298 (1977); Y. L. Dokshitzer, Sov. Phys. JETP **46**, 641 (1977), [Zh. Eksp. Teor. Fiz.73,1216(1977)].

[49] G. Curci, W. Furmanski and R. Petronzio, Nucl. Phys. B **175**, 27 (1980); W. Furmanski and R. Petronzio, Phys. Lett. B **97B**, 437 (1980).

[50] A. Vogt, S. Moch and J. A. M. Vermaseren, Nucl. Phys. B **691**, 129 (2004), [hep-ph/0404111]; S. Moch, J. A. M. Vermaseren and A. Vogt, Nucl. Phys. B **688**, 101 (2004), [hep-ph/0403192].

[51] J. Davies *et al.*, Nucl. Phys. B **915**, 335 (2017), [arXiv:1610.07477].

[52] S. Moch *et al.*, JHEP **10**, 041 (2017), [arXiv:1707.08315].

[53] A. Vogt *et al.*, PoS **RADCOR2017**, 046 (2018), [arXiv:1801.06085].

[54] A. Vogt *et al.*, PoS **LL2018**, 050 (2018), [arXiv:1808.08981].

[55] S. Moch *et al.*, Phys. Lett. B **825**, 136853 (2022), [arXiv:2111.15561].

[56] A. Basdew-Sharma *et al.*, JHEP **03**, 183 (2023), [arXiv:2211.16485].

[57] G. Falcioni *et al.*, Phys. Lett. B **848**, 138351 (2024), [arXiv:2310.01245].

[58] G. Falcioni *et al.*, Phys. Lett. B **842**, 137944 (2023), [arXiv:2302.07593].

[59] G. Falcioni *et al.*, Phys. Lett. B **846**, 138215 (2023), [arXiv:2307.04158].

[60] T. Gehrmann *et al.*, JHEP **01**, 029 (2024), [arXiv:2308.07958].

[61] T. Gehrmann *et al.*, Phys. Lett. B **849**, 138427 (2024), [arXiv:2310.12240].

[62] S. Moch *et al.*, Phys. Lett. B **849**, 138468 (2024), [arXiv:2310.05744].

[63] G. Falcioni *et al.*, Phys. Lett. B **856**, 138906 (2024), [arXiv:2404.09701].

[64] G. Falcioni *et al.*, Phys. Lett. B **860**, 139194 (2025), [arXiv:2410.08089].

[65] B. A. Kniehl *et al.*, Phys. Rev. Lett. **135**, 7, 071902 (2025), [arXiv:2505.09381].

[66] J. McGowan *et al.*, Eur. Phys. J. C **83**, 3, 185 (2023), [Erratum: Eur.Phys.J.C 83, 302 (2023)], [arXiv:2207.04739].

[67] R. D. Ball *et al.* (NNPDF), Eur. Phys. J. C **84**, 7, 659 (2024), [arXiv:2402.18635].

[68] D. de Florian, G. F. R. Sborlini and G. Rodrigo, Eur. Phys. J. C **76**, 5, 282 (2016), [arXiv:1512.00612]; D. de Florian, G. F. R. Sborlini and G. Rodrigo, JHEP **10**, 056 (2016), [arXiv:1606.02887].

[69] D. de Florian and L. P. Conte, Eur. Phys. J. C **83**, 8, 695 (2023), [arXiv:2305.14144].

[70] R. S. Thorne, Phys. Rev. D **73**, 054019 (2006), [hep-ph/0601245].

[71] S. Forte *et al.*, Nucl. Phys. B **834**, 116 (2010), [arXiv:1001.2312].

[72] M. Guzzi *et al.*, Phys. Rev. D **86**, 053005 (2012), [arXiv:1108.5112].

[73] V. S. Fadin, E. A. Kuraev and L. N. Lipatov, Phys. Lett. B **60B**, 50 (1975).

[74] I. I. Balitsky and L. N. Lipatov, Sov. J. Nucl. Phys. **28**, 822 (1978), [Yad. Fiz.28,1597(1978)].

[75] L. N. Lipatov, Sov. J. Nucl. Phys. **23**, 338 (1976), [Yad. Fiz.23,642(1976)].

[76] E. A. Kuraev, L. N. Lipatov and V. S. Fadin, Sov. Phys. JETP **45**, 199 (1977), [Zh. Eksp. Teor. Fiz.72,377(1977)].

Int. J. Mod. Phys. A 2026.41. Downloaded from www.worldscientific.com
by UNIVERSITY OF CALIFORNIA @ BERKELEY on 09/16/26. Re-use and distribution is strictly not permitted, except for Open Access articles.

[77] V. S. Fadin and L. N. Lipatov, Phys. Lett. B **429**, 127 (1998), [hep-ph/9802290].

[78] M. Ciafaloni and G. Camici, Phys. Lett. B **430**, 349 (1998), [hep-ph/9803389].

[79] G. Altarelli, R. D. Ball and S. Forte, Nucl. Phys. B **799**, 199 (2008), [arXiv:0802.0032].

[80] M. Ciafaloni *et al.*, JHEP **08**, 046 (2007), [arXiv:0707.1453].

[81] C. D. White and R. S. Thorne, Phys. Rev. D **75**, 034005 (2007), [hep-ph/0611204].

[82] E. Iancu *et al.*, Phys. Lett. B **744**, 293 (2015), [arXiv:1502.05642].

[83] N. Gromov, F. Levkovich-Maslyuk and G. Sizov, Phys. Rev. Lett. **115**, 25, 251601 (2015), [arXiv:1507.04010]; V. N. Velizhanin (2015), [arXiv:1508.02857]; S. Caron-Huot and M. Herranen, JHEP **02**, 058 (2018), [arXiv:1604.07417]; V. Fadin, *Chapter 4: BFKL — Past and Future*, 63–90 (2021), [arXiv:2012.11931].

[84] I. Balitsky, Nucl. Phys. B **463**, 99 (1996), [hep-ph/9509348].

[85] Y. V. Kovchegov, Phys. Rev. D **60**, 034008 (1999), [hep-ph/9901281].

[86] T.-J. Hou *et al.*, Phys. Rev. D **103**, 1, 014013 (2021), [arXiv:1912.10053].

[87] R. D. Ball *et al.* (PDF4LHC Working Group), J. Phys. G **49**, 8, 080501 (2022), [arXiv:2203.05506].

[88] R. Abdul Khalek *et al.* (NNPDF), Eur. Phys. J. C **79**, 838 (2019), [arXiv:1905.04311].

[89] R. Abdul Khalek *et al.* (NNPDF), Eur. Phys. J. C **79**, 11, 931 (2019), [arXiv:1906.10698].

[90] R. D. Ball and R. L. Pearson, Eur. Phys. J. C **81**, 9, 830 (2021), [arXiv:2105.05114].

[91] Z. Kassabov, M. Ubiali and C. Voisey, JHEP **03**, 148 (2023), [arXiv:2207.07616].

[92] S. Bailey *et al.*, Eur. Phys. J. C **81**, 4, 341 (2021), [arXiv:2012.04684].

[93] A. Cooper-Sarkar *et al.* (2024), [arXiv:2406.16188].

[94] X. Ji, Phys. Rev. Lett. **110**, 262002 (2013), [arXiv:1305.1539].

[95] G. C. Rossi and M. Testa, Phys. Rev. D **96**, 1, 014507 (2017), [arXiv:1706.04428].

[96] G. Rossi and M. Testa, Phys. Rev. D **98**, 5, 054028 (2018), [arXiv:1806.00808].

[97] L. Del Debbio, T. Giani and C. J. Monahan, JHEP **09**, 021 (2020), [arXiv:2007.02131].

[98] H.-W. Lin *et al.*, Phys. Rev. D **91**, 054510 (2015), [arXiv:1402.1462].

[99] C. Alexandrou *et al.*, Phys. Rev. D **92**, 014502 (2015), [arXiv:1504.07455].

[100] H.-W. Lin *et al.*, Prog. Part. Nucl. Phys. **100**, 107 (2018), [arXiv:1711.07916].

[101] C. Alexandrou *et al.*, Phys. Rev. Lett. **121**, 11, 112001 (2018), [arXiv:1803.02685].

[102] J.-W. Chen *et al.* (2018), [arXiv:1803.04393].

[103] K. Cichy, L. Del Debbio and T. Giani, JHEP **10**, 137 (2019), [arXiv:1907.06037].

[104] K. Cichy and M. Constantinou, Adv. High Energy Phys. **2019**, 3036904 (2019), [arXiv:1811.07248].

[105] M. A. Ebert, I. W. Stewart and Y. Zhao, JHEP **09**, 037 (2019), [arXiv:1901.03685].

[106] M. Constantinou, Eur. Phys. J. A **57**, 2, 77 (2021), [arXiv:2010.02445].

[107] M. Constantinou *et al.*, Prog. Part. Nucl. Phys. **121**, 103908 (2021), [arXiv:2006.08636].

[108] L. Del Debbio *et al.*, JHEP **02**, 138 (2021), [arXiv:2010.03996].

[109] Z. Fan, R. Zhang and H.-W. Lin, Int. J. Mod. Phys. A **36**, 13, 2150080 (2021), [arXiv:2007.16113].

[110] M. Bhat *et al.*, Phys. Rev. D **103**, 3, 034510 (2021), [arXiv:2005.02102].

[111] X. Ji *et al.*, Rev. Mod. Phys. **93**, 3, 035005 (2021), [arXiv:2004.03543].

[112] T. Khan *et al.* (HadStruc), Phys. Rev. D **104**, 9, 094516 (2021), [arXiv:2107.08960].

[113] C. Egerer *et al.* (HadStruc), JHEP **11**, 148 (2021), [arXiv:2107.05199].

[114] Z. Fan, W. Good and H.-W. Lin, Phys. Rev. D **108**, 1, 014508 (2023), [arXiv:2210.09985].

[115] C. Egerer *et al.* (HadStruc), Phys. Rev. D **106**, 9, 094511 (2022), [arXiv:2207.08733].

[116] M. Bhat *et al.*, Phys. Rev. D **106**, 5, 054504 (2022), [arXiv:2205.07585].

[117] X. Gao *et al.*, Phys. Rev. D **106**, 11, 114510 (2022), [arXiv:2208.02297].

[118] A. Candido *et al.*, Eur. Phys. J. C **84**, 7, 716 (2024), [arXiv:2404.07573].

[119] C. Zimmermann and A. Schäfer, Phys. Rev. D **110**, 7, 074503 (2024), [arXiv:2405.07712].

[120] J. Karpie *et al.*, Phys. Rev. Lett. **135**, 19, 191901 (2025), [arXiv:2505.22795].

[121] S. Bhattacharya *et al.*, Phys. Rev. D **112**, 11, 114504 (2025), [arXiv:2505.11288].

[122] M. Constantinou *et al.* (2022), [arXiv:2202.07193].

[123] H.-W. Lin, Prog. Part. Nucl. Phys. **144**, 104177 (2025), [arXiv:2506.05025].

[124] J. Gao, L. Harland-Lang and J. Rojo, Phys. Rept. **742**, 1 (2018), [arXiv:1709.04922].

[125] K. Kovařík, P. M. Nadolsky and D. E. Soper, Rev. Mod. Phys. **92**, 4, 045003 (2020), [arXiv:1905.06957].

[126] T.-J. Hou *et al.*, Phys. Rev. D **107**, 7, 076018 (2023), [arXiv:2211.11064].

[127] J. C. Collins, D. E. Soper and G. F. Sterman, Nucl. Phys. B **261**, 104 (1985).

[128] C. Anastasiou *et al.*, Phys. Rev. Lett. **114**, 212001 (2015), [arXiv:1503.06056]; C. Anastasiou *et al.*, JHEP **05**, 058 (2016), [arXiv:1602.00695].

[129] B. Mistlberger, JHEP **05**, 028 (2018), [arXiv:1802.00833].

[130] L.-B. Chen *et al.*, Phys. Lett. B **803**, 135292 (2020), [arXiv:1909.06808].

[131] F. Dulat, B. Mistlberger and A. Pelloni, Phys. Rev. D **99**, 3, 034004 (2019), [arXiv:1810.09462].

[132] L. Cieri *et al.*, JHEP **02**, 096 (2019), [arXiv:1807.11501].

[133] X. Chen *et al.*, Phys. Rev. Lett. **127**, 7, 072002 (2021), [arXiv:2102.07607].

[134] J. Baglio *et al.*, JHEP **12**, 066 (2022), [arXiv:2209.06138].

[135] F. A. Dreyer and A. Karlberg, Phys. Rev. Lett. **117**, 7, 072001 (2016), [arXiv:1606.00840].

[136] F. A. Dreyer and A. Karlberg, Phys. Rev. D **98**, 11, 114016 (2018), [arXiv:1811.07906].

[137] C. Duhr, F. Dulat and B. Mistlberger, Phys. Rev. Lett. **125**, 17, 172001 (2020), [arXiv:2001.07717].

[138] X. Chen *et al.*, Phys. Rev. Lett. **128**, 5, 052001 (2022), [arXiv:2107.09085].

[139] C. Duhr, F. Dulat and B. Mistlberger, JHEP **11**, 143 (2020), [arXiv:2007.13313].

[140] M. Bonvini *et al.*, JHEP **08**, 105 (2016), [arXiv:1603.08000].

[141] F. Dulat, A. Lazopoulos and B. Mistlberger, Comput. Phys. Commun. **233**, 243 (2018), [arXiv:1802.00827].

[142] R. V. Harlander, S. Liebler and H. Mantler, Comput. Phys. Commun. **212**, 239 (2017), [arXiv:1605.03190].

Int. J. Mod. Phys. A 2026.41. Downloaded from www.wo
by UNIVERSITY OF CALIFORNIA @ BERKELEY on 09/16/26. Re-use and distribution is
except for Open Access articles.

[143] T. Cridge *et al.*, J. Phys. G **52**, 6 (2025), [arXiv:2411.05373].

[144] O. Brein, A. Djouadi and R. Harlander, Phys. Lett. B **579**, 149 (2004), [hep-ph/0307206].

[145] D. de Florian and J. Mazzitelli, Phys. Rev. Lett. **111**, 201801 (2013), [arXiv:1309.6594].

[146] S. Borowka *et al.*, Phys. Rev. Lett. **117**, 1, 012001 (2016), [Erratum: Phys. Rev. Lett.117,no.7,079901(2016)], [arXiv:1604.06447].

[147] M. Czakon, P. Fiedler and A. Mitov, Phys. Rev. Lett. **110**, 252004 (2013), [arXiv:1303.6254].

[148] S. Catani *et al.*, Phys. Rev. D **99**, 5, 051501 (2019), [arXiv:1901.04005].

[149] S. Catani *et al.*, JHEP **03**, 029 (2021), [arXiv:2010.11906].

[150] T. Gehrmann *et al.*, Phys. Rev. Lett. **113**, 21, 212001 (2014), [arXiv:1408.5243].

[151] F. Cascioli *et al.*, Phys. Lett. B **735**, 311 (2014), [arXiv:1405.2219].

[152] M. Grazzini, S. Kallweit and M. Wiesemann, Eur. Phys. J. C **78**, 7, 537 (2018), [arXiv:1711.06631].

[153] G. Heinrich, Phys. Rept. **922**, 1 (2021), [arXiv:2009.00516].

[154] A. Huss *et al.*, J. Phys. G **50**, 4, 043001 (2023), [arXiv:2207.02122].

[155] A. Manohar *et al.*, Phys. Rev. Lett. **117**, 24, 242002 (2016), [arXiv:1607.04266].

[156] A. V. Manohar *et al.*, JHEP **12**, 046 (2017), [arXiv:1708.01256].

[157] K. Xie *et al.* (CTEQ-TEA), Phys. Rev. D **105**, 5, 054006 (2022), [arXiv:2106.10299].

[158] T. Cridge *et al.*, Eur. Phys. J. C **82**, 1, 90 (2022), [arXiv:2111.05357].

[159] R. D. Ball *et al.* (NNPDF), Eur. Phys. J. C **84**, 5, 540 (2024), [arXiv:2401.08749].

[160] A. M. Cooper-Sarkar *et al.* (2025), [arXiv:2508.06603].

[161] L. Buonocore *et al.*, JHEP **08**, 08, 019 (2020), [arXiv:2005.06477].

[162] M. Greco and A. Vicini, Nucl. Phys. B **415**, 386 (1994).

[163] A. Hebecker, Phys. Rept. **331**, 1 (2000), [hep-ph/9905226].

[164] A. V. Belitsky and A. V. Radyushkin, Phys. Rept. **418**, 1 (2005), [hep-ph/0504030].

[165] E. Boos *et al.* (CompHEP), Nucl. Instrum. Meth. **A534**, 250 (2004), [hep-ph/0403113].

[166] J. Alwall *et al.*, JHEP **07**, 079 (2014), [arXiv:1405.0301]; `https://launchpad.net/mg5amcnlo`.

[167] M. L. Mangano *et al.*, JHEP **07**, 001 (2003), [hep-ph/0206293]; `http://cern.ch/mlm/alpgen/`.

[168] T. Gleisberg and S. Hoeche, JHEP **12**, 039 (2008), [arXiv:0808.3674]; `https://sherpa-team.gitlab.io/`.

[169] A. Cafarella, C. G. Papadopoulos and M. Worek, Comput. Phys. Commun. **180**, 1941 (2009), [arXiv:0710.2427]; `http://cern.ch/helac-phegas/`.

[170] F. A. Berends and W. T. Giele, Nucl. Phys. B **306**, 759 (1988).

[171] L. J. Dixon, in "QCD and beyond. Proceedings, Theoretical Advanced Study Institute in Elementary Particle Physics, TASI-95, Boulder, USA, June 4-30, 1995," 539–584 (1996), [hep-ph/9601359], URL `http://www-public.slac.stanford.edu/sciDoc/docMeta.aspx?slacPubNumber=SLAC-PUB-7106`.

[172] R. Britto, F. Cachazo and B. Feng, Nucl. Phys. B **715**, 499 (2005), [hep-th/0412308].

[173] F. Cachazo, P. Svrcek and E. Witten, JHEP **09**, 006 (2004), [hep-th/0403047].

[174] S. Catani and M. H. Seymour, Nucl. Phys. B **485**, 291 (1997), [Erratum: Nucl. Phys.B510,503(1998)], [hep-ph/9605323].

[175] S. Frixione, Z. Kunszt and A. Signer, Nucl. Phys. B **467**, 399 (1996), [hep-ph/9512328].

[176] D. A. Kosower, Phys. Rev. D **57**, 5410 (1998), [hep-ph/9710213]; J. M. Campbell, M. A. Cullen and E. W. N. Glover, Eur. Phys. J. C **9**, 245 (1999), [hep-ph/9809429]; D. A. Kosower, Phys. Rev. D **71**, 045016 (2005), [hep-ph/0311272].

[177] G. Ossola, C. G. Papadopoulos and R. Pittau, Nucl. Phys. B **763**, 147 (2007), [hep-ph/0609007].

[178] R. Britto, F. Cachazo and B. Feng, Nucl. Phys. B **725**, 275 (2005), [hep-th/0412103].

[179] R. K. Ellis *et al.*, Nucl. Phys. B **822**, 270 (2009), [arXiv:0806.3467].

[180] C. F. Berger and D. Forde, Ann. Rev. Nucl. Part. Sci. **60**, 181 (2010), [arXiv:0912.3534].

[181] F. Cascioli, P. Maierhofer and S. Pozzorini, Phys. Rev. Lett. **108**, 111601 (2012), [arXiv:1111.5206].

[182] Z. Bern, L. J. Dixon and D. A. Kosower, Annals Phys. **322**, 1587 (2007), [arXiv:0704.2798].

[183] R. K. Ellis *et al.*, Phys. Rept. **518**, 141 (2012), [arXiv:1105.4319].

[184] G. Bevilacqua *et al.*, Comput. Phys. Commun. **184**, 986 (2013), [arXiv:1110.1499]; `http://cern.ch/helac-phegas/`.

[185] G. Cullen *et al.*, Eur. Phys. J. C **74**, 8, 3001 (2014), [arXiv:1404.7096]; `http://gosam.hepforge.org/`.

[186] S. Badger *et al.*, Comput. Phys. Commun. **184**, 1981 (2013), [arXiv:1209.0100]; `https://bitbucket.org/njet/wiki/Home/`.

[187] F. Buccioni, S. Pozzorini and M. Zoller, Eur. Phys. J. C **78**, 1, 70 (2018), [arXiv:1710.11452]; `https://openloops.hepforge.org/`.

[188] S. Actis *et al.*, Comput. Phys. Commun. **214**, 140 (2017), [arXiv:1605.01090].

[189] Z. Nagy, Phys. Rev. D **68**, 094002 (2003), [hep-ph/0307268]; `http://www.desy.de/~znagy/Site/NLOJet++.html`.

[190] J. M. Campbell and R. K. Ellis, Phys. Rev. D **60**, 113006 (1999), [hep-ph/9905386].

[191] J. M. Campbell and R. K. Ellis, Phys. Rev. D **62**, 114012 (2000), [hep-ph/0006304].

[192] J. Baglio *et al.* (2011), [arXiv:1107.4038]; `http://www-itp.particle.uni-karlsruhe.de/~vbfnloweb`.

[193] T. Binoth *et al.*, Eur. Phys. J. C **16**, 311 (2000), [hep-ph/9911340]; `http://lapth.in2p3.fr/PHOX_FAMILY/`.

[194] Z. Bern *et al.*, PoS **LL2012**, 018 (2012), [arXiv:1210.6684].

[195] G. Cullen, N. Greiner and G. Heinrich, Eur. Phys. J. C **73**, 4, 2388 (2013), [arXiv:1212.5154].

[196] S. Kallweit *et al.*, JHEP **04**, 012 (2015), [arXiv:1412.5157].

[197] A. Denner *et al.*, JHEP **04**, 018 (2015), [arXiv:1412.7421].

[198] M. Chiesa, N. Greiner and F. Tramontano, J. Phys. G **43**, 1, 013002 (2016), [arXiv:1507.08579].

[199] S. Frixione *et al.*, JHEP **06**, 184 (2015), [arXiv:1504.03446].

[200] B. Biedermann *et al.*, Eur. Phys. J. C **77**, 492 (2017), [arXiv:1704.05783].

[201] R. Frederix *et al.*, JHEP **07**, 185 (2018), [Erratum: JHEP 11, 085 (2021)], [arXiv:1804.10017].

[202] E. Bothmann and D. Napoletano, Eur. Phys. J. C **80**, 11, 1024 (2020), [arXiv:2006.14635].

[203] D. Pagani *et al.*, JHEP **09**, 155 (2021), [arXiv:2106.02059].

[204] D. Pagani and M. Zaro, JHEP **02**, 161 (2022), [arXiv:2110.03714].

[205] D. Pagani, T. Vitos and M. Zaro, Eur. Phys. J. C **84**, 5, 514 (2024), [arXiv:2309.00452].

[206] H.-S. Shao, *Automation of Electroweak Corrections*, Other thesis (2025), [arXiv:2501.05199].

Int. J. Mod. Phys. A 2026.41. Downloaded from www.worldscientific.com
by UNIVERSITY OF CALIFORNIA @ BERKELEY on 09/16/26. Re-use and distribution is strictly not permitted, except for Open Access articles.

[207] A. Denner and S. Dittmaier, Phys. Rept. **864**, 1 (2020), [arXiv:1912.06823].

[208] C. Anastasiou, R. Boughezal and F. Petriello, JHEP **04**, 003 (2009), [arXiv:0811.3458].

[209] S. Dittmaier, A. Huss and C. Schwinn, Nucl. Phys. B **885**, 318 (2014), [arXiv:1403.3216].

[210] S. Dittmaier, A. Huss and C. Schwinn, Nucl. Phys. B **904**, 216 (2016), [arXiv:1511.08016].

[211] D. de Florian, M. Der and I. Fabre, Phys. Rev. D **98**, 9, 094008 (2018), [arXiv:1805.12214].

[212] M. Bonetti, K. Melnikov and L. Tancredi, Phys. Rev. D **97**, 3, 034004 (2018), [arXiv:1711.11113].

[213] M. Bonetti, K. Melnikov and L. Tancredi, Phys. Rev. D **97**, 5, 056017 (2018), [Erratum: Phys. Rev.D97,no.9,099906(2018)], [arXiv:1801.10403].

[214] C. Anastasiou *et al.*, JHEP **03**, 162 (2019), [arXiv:1811.11211].

[215] V. Hirschi, S. Lionetti and A. Schweitzer, JHEP **05**, 002 (2019), [arXiv:1902.10167].

[216] M. Becchetti *et al.*, Phys. Rev. D **103**, 5, 054037 (2021), [arXiv:2010.09451].

[217] M. Bonetti *et al.*, JHEP **11**, 045 (2020), [arXiv:2007.09813].

[218] A. Behring *et al.*, Phys. Rev. D **103**, 1, 013008 (2021), [arXiv:2009.10386].

[219] S. Dittmaier, T. Schmidt and J. Schwarz, JHEP **12**, 201 (2020), [arXiv:2009.02229].

[220] F. Buccioni *et al.*, Phys. Lett. B **811**, 135969 (2020), [arXiv:2005.10221].

[221] L. Buonocore *et al.*, Phys. Rev. D **103**, 114012 (2021), [arXiv:2102.12539].

[222] S. Dittmaier, A. Huss and J. Schwarz, JHEP **05**, 170 (2024), [arXiv:2401.15682].

[223] R. Bonciani *et al.*, Phys. Rev. Lett. **128**, 1, 012002 (2022), [arXiv:2106.11953].

[224] T. Armadillo *et al.*, JHEP **05**, 072 (2022), [arXiv:2201.01754].

[225] F. Buccioni *et al.*, JHEP **06**, 022 (2022), [arXiv:2203.11237].

[226] Z. Bern *et al.*, Nucl. Phys. B **425**, 217 (1994), [hep-ph/9403226].

[227] J. M. Campbell and E. W. N. Glover, Nucl. Phys. B **527**, 264 (1998), [hep-ph/9710255].

[228] S. Catani and M. Grazzini, Phys. Lett. B **446**, 143 (1999), [hep-ph/9810389].

[229] K. Melnikov and F. Petriello, Phys. Rev. D **74**, 114017 (2006), [hep-ph/0609070]; `http://gate.hep.anl.gov/fpetriello/FEWZ.html`.

[230] S. Catani *et al.*, Phys. Rev. Lett. **103**, 082001 (2009), [arXiv:0903.2120]; `http://theory.fi.infn.it/gazzani/dy.html`.

[231] C. Anastasiou, K. Melnikov and F. Petriello, Nucl. Phys. B **724**, 197 (2005), [hep-ph/0501130]; `http://www.phys.ethz.ch/~pheno/fehipro/`.

[232] S. Catani and M. Grazzini, Phys. Rev. Lett. **98**, 222002 (2007), [hep-ph/0703012]; `http://theory.fi.infn.it/grazzini/codes.html`.

[233] A. Gehrmann-De Ridder, T. Gehrmann and E. W. N. Glover, JHEP **09**, 056 (2005), [hep-ph/0505111].

[234] J. Currie, E. W. N. Glover and S. Wells, JHEP **04**, 066 (2013), [arXiv:1301.4693].

[235] R. Gauld *et al.*, JHEP **10**, 002 (2019), [arXiv:1907.05836].

[236] R. Gauld *et al.*, Phys. Rev. Lett. **125**, 22, 222002 (2020), [arXiv:2005.03016].

[237] R. Gauld *et al.*, Eur. Phys. J. C **83**, 4, 336 (2023), [arXiv:2302.12844].

[238] A. Gehrmann-De Ridder *et al.*, Eur. Phys. J. C **84**, 4, 361 (2024), [arXiv:2311.14991].

[239] T. Gehrmann and R. Schürmann, JHEP **04**, 031 (2022), [arXiv:2201.06982].

[240] X. Chen *et al.*, JHEP **08**, 094 (2022), [arXiv:2205.01516].

[241] L. Bonino *et al.*, JHEP **08**, 073 (2024), [arXiv:2406.09925].

[242] S. Caletti *et al.*, JHEP **10**, 027 (2024), [arXiv:2405.17540].

[243] O. Braun-White, N. Glover and C. T. Preuss, JHEP **06**, 065 (2023), [arXiv:2302.12787].

[244] O. Braun-White, N. Glover and C. T. Preuss, JHEP **11**, 179 (2023), [arXiv:2307.14999].

[245] E. Fox and N. Glover, JHEP **12**, 171 (2023), [arXiv:2308.10829].

[246] E. Fox, N. Glover and M. Marcoli, JHEP **12**, 225 (2024), [arXiv:2410.12904].

[247] T. Gehrmann, E. W. N. Glover and M. Marcoli, JHEP **03**, 114 (2024), [arXiv:2310.19757].

[248] X. Chen *et al.*, JHEP **10**, 099 (2022), [arXiv:2203.13531].

[249] R. Bonciani *et al.*, Eur. Phys. J. C **75**, 12, 581 (2015), [arXiv:1508.03585].

[250] R. Angeles-Martinez, M. Czakon and S. Sapeta, JHEP **10**, 201 (2018), [arXiv:1809.01459].

[251] S. Catani *et al.*, JHEP **07**, 100 (2019), [arXiv:1906.06535].

[252] S. Catani *et al.*, Phys. Rev. Lett. **130**, 11, 111902 (2023), [arXiv:2210.07846].

[253] S. Devoto *et al.*, JHEP **03**, 189 (2025), [arXiv:2411.15340].

[254] L. Buonocore *et al.*, Phys. Rev. Lett. **131**, 23, 231901 (2023), [arXiv:2306.16311].

[255] L. Cieri *et al.*, JHEP **09**, 155 (2020), [arXiv:2005.01315].

[256] T. Armadillo *et al.*, JHEP **07**, 141 (2025), [arXiv:2412.16095].

[257] M. A. Ebert *et al.*, JHEP **04**, 123 (2019), [arXiv:1812.08189].

[258] M. A. Ebert and F. J. Tackmann, JHEP **03**, 158 (2020), [arXiv:1911.08486].

[259] G. Ferrera, W.-L. Ju and M. Schönherr, JHEP **04**, 005 (2024), [arXiv:2312.14911].

[260] S. Frixione and G. Ridolfi, Nucl. Phys. B **507**, 315 (1997), [hep-ph/9707345].

[261] S. Alekhin *et al.*, Eur. Phys. J. C **81**, 7, 573 (2021), [arXiv:2104.02400].

[262] S. Catani *et al.*, JHEP **12**, 047 (2015), [arXiv:1507.06937].

[263] M. A. Ebert *et al.*, JHEP **04**, 102 (2021), [arXiv:2006.11382].

[264] G. P. Salam and E. Slade, JHEP **11**, 220 (2021), [arXiv:2106.08329].

[265] T. Gehrmann *et al.*, JHEP **06**, 094 (2010), [arXiv:1004.3653].

[266] Y. Li and H. X. Zhu, Phys. Rev. Lett. **118**, 2, 022004 (2017), [arXiv:1604.01404].

[267] M.-x. Luo *et al.*, Phys. Rev. Lett. **124**, 9, 092001 (2020), [arXiv:1912.05778].

[268] M. A. Ebert, B. Mistlberger and G. Vita, JHEP **09**, 146 (2020), [arXiv:2006.05329].

[269] M. Czakon, Phys. Lett. B **693**, 259 (2010), [arXiv:1005.0274].

[270] M. Czakon, Nucl. Phys. B **849**, 250 (2011), [arXiv:1101.0642].

[271] R. Boughezal, K. Melnikov and F. Petriello, Phys. Rev. D **85**, 034025 (2012), [arXiv:1111.7041].

[272] R. Frederix *et al.*, JHEP **10**, 003 (2009), [arXiv:0908.4272].

[273] T. Binoth and G. Heinrich, Nucl. Phys. B **585**, 741 (2000), [hep-ph/0004013].

Int. J. Mod. Phys. A 2026.41. Downloaded from www.wo
by UNIVERSITY OF CALIFORNIA @ BERKELEY on 09/16/26. Re-use and distribution is
except for Open Access articles.

[274] G. Heinrich, Nucl. Phys. B Proc. Suppl. **116**, 368 (2003), [hep-ph/0211144].

[275] C. Anastasiou, K. Melnikov and F. Petriello, Phys. Rev. D **69**, 076010 (2004), [hep-ph/0311311].

[276] T. Binoth and G. Heinrich, Nucl. Phys. B **693**, 134 (2004), [hep-ph/0402265].

[277] M. Czakon and D. Heymes, Nucl. Phys. B **890**, 152 (2014), [arXiv:1408.2500].

[278] M. Czakon *et al.* (2020), [arXiv:2011.01011].

[279] M. Czakon *et al.*, JHEP **02**, 241 (2023), [arXiv:2212.00467].

[280] M. L. Czakon *et al.*, JHEP **10**, 216 (2021), [arXiv:2102.08267].

[281] M. Czakon *et al.*, JHEP **03**, 251 (2023), [arXiv:2210.06078].

[282] M. Czakon *et al.*, Phys. Rev. Lett. **135**, 16, 161903 (2025), [arXiv:2411.09684].

[283] G. Somogyi, Z. Trocsanyi and V. Del Duca, JHEP **01**, 070 (2007), [hep-ph/0609042].

[284] V. Del Duca *et al.*, JHEP **04**, 036 (2015), [arXiv:1501.07226].

[285] S. Van Thurenhout *et al.*, volume 18, 6–A31 (2025), [arXiv:2412.12750].

[286] V. Del Duca *et al.*, JHEP **05**, 151 (2025), [arXiv:2412.21028].

[287] R. Boughezal, X. Liu and F. Petriello, Phys. Rev. D **91**, 9, 094035 (2015), [arXiv:1504.02540].

[288] R. Boughezal *et al.*, Phys. Rev. Lett. **115**, 6, 062002 (2015), [arXiv:1504.02131].

[289] J. Gaunt *et al.*, JHEP **09**, 058 (2015), [arXiv:1505.04794].

[290] K. Melnikov *et al.*, JHEP **02**, 159 (2019), [arXiv:1809.06300].

[291] K. Melnikov *et al.*, JHEP **06**, 033 (2019), [arXiv:1904.02433].

[292] A. Behring *et al.*, Phys. Rev. D **100**, 11, 114034 (2019), [arXiv:1910.10059].

[293] G. Billis *et al.*, Eur. Phys. J. Plus **136**, 2, 214 (2021), [arXiv:1909.00811].

[294] D. Baranowski, Eur. Phys. J. C **80**, 6, 523 (2020), [arXiv:2004.03285].

[295] M. A. Ebert, B. Mistlberger and G. Vita, JHEP **09**, 143 (2020), [arXiv:2006.03056].

[296] D. Baranowski *et al.*, Phys. Rev. D **106**, 1, 014004 (2022), [arXiv:2204.09459].

[297] D. Baranowski *et al.*, JHEP **02**, 073 (2023), [arXiv:2211.05722].

[298] G. Bell *et al.*, JHEP **07**, 077 (2024), [arXiv:2312.11626].

[299] P. Agarwal, K. Melnikov and I. Pedron, JHEP **05**, 005 (2024), [arXiv:2403.03078].

[300] D. Baranowski *et al.*, JHEP **04**, 114 (2024), [arXiv:2401.05245].

[301] D. Baranowski *et al.*, Phys. Rev. Lett. **134**, 19, 191902 (2025), [arXiv:2409.11042].

[302] D. Baranowski *et al.*, JHEP **04**, 084 (2025), [arXiv:2412.14001].

[303] G. Vita, JHEP **07**, 241 (2024), [arXiv:2401.03017].

[304] M. A. Ebert *et al.*, JHEP **12**, 084 (2018), [arXiv:1807.10764].

[305] R. Boughezal, A. Isgrò and F. Petriello, Phys. Rev. D **97**, 7, 076006 (2018), [arXiv:1802.00456].

[306] R. Boughezal, A. Isgrò and F. Petriello, Phys. Rev. D **101**, 1, 016005 (2020), [arXiv:1907.12213].

[307] J. Campbell, T. Neumann and G. Vita, JHEP **05**, 172 (2025), [arXiv:2408.05265].

[308] F. Caola, K. Melnikov and R. Röntsch, Eur. Phys. J. C **77**, 4, 248 (2017), [arXiv:1702.01352].

[309] F. Caola *et al.*, Eur. Phys. J. C **78**, 8, 687 (2018), [arXiv:1807.05835].

[310] M. Delto and K. Melnikov, JHEP **05**, 148 (2019), [arXiv:1901.05213].

[311] F. Caola, K. Melnikov and R. Röntsch, Eur. Phys. J. C **79**, 5, 386 (2019), [arXiv:1902.02081].

[312] F. Caola, K. Melnikov and R. Röntsch, Eur. Phys. J. C **79**, 12, 1013 (2019), [arXiv:1907.05398].

[313] K. Asteriadis *et al.*, Eur. Phys. J. C **80**, 1, 8 (2020), [arXiv:1910.13761].

[314] F. Devoto *et al.*, JHEP **02**, 016 (2024), [arXiv:2310.17598].

[315] L. Magnea *et al.*, JHEP **12**, 107 (2018), [Erratum: JHEP 06, 013 (2019)], [arXiv:1806.09570].

[316] L. Magnea *et al.*, JHEP **12**, 062 (2018), [arXiv:1809.05444].

[317] L. Magnea *et al.*, JHEP **02**, 037 (2021), [arXiv:2010.14493].

[318] G. Bertolotti *et al.*, JHEP **07**, 140 (2023), [Erratum: JHEP 05, 019 (2024)], [arXiv:2212.11190].

[319] G. Bertolotti *et al.*, JHEP **12**, 042 (2022), [arXiv:2209.09123].

[320] L. Magnea *et al.*, JHEP **06**, 021 (2024), [arXiv:2403.11975].

[321] M. Cacciari *et al.*, Phys. Rev. Lett. **115**, 8, 082002 (2015), [Erratum: Phys. Rev. Lett.120,no.13,139901(2018)], [arXiv:1506.02660].

[322] J. Currie *et al.*, JHEP **05**, 209 (2018), [arXiv:1803.09973].

[323] T. Gehrmann *et al.*, Phys. Lett. B **792**, 182 (2019), [arXiv:1812.06104].

[324] R. Mondini, M. Schiavi and C. Williams, JHEP **06**, 079 (2019), [arXiv:1904.08960].

[325] C. Anastasiou and G. Sterman, JHEP **05**, 242 (2023), [arXiv:2212.12162].

[326] R. M. Prisco and F. Tramontano, JHEP **06**, 089 (2021), [arXiv:2012.05012].

[327] W. J. Torres Bobadilla *et al.*, Eur. Phys. J. C **81**, 3, 250 (2021), [arXiv:2012.02567].

[328] A. Huss *et al.* (2025), [arXiv:2504.06689].

[329] A. Gehrmann-De Ridder *et al.*, Phys. Rev. Lett. **99**, 132002 (2007), [arXiv:0707.1285]; A. Gehrmann-De Ridder *et al.*, JHEP **12**, 094 (2007), [arXiv:0711.4711]; A. Gehrmann-De Ridder *et al.*, Phys. Rev. Lett. **100**, 172001 (2008), [arXiv:0802.0813].

[330] A. Gehrmann-De Ridder *et al.*, Comput. Phys. Commun. **185**, 3331 (2014), [arXiv:1402.4140]; `https://eerad3.hepforge.org/`.

[331] S. Weinzierl, Phys. Rev. Lett. **101**, 162001 (2008), [arXiv:0807.3241]; S. Weinzierl, JHEP **06**, 041 (2009), [arXiv:0904.1077].

[332] T. Gehrmann *et al.*, Phys. Lett. B **775**, 185 (2017), [arXiv:1709.01097].

[333] J. Currie, T. Gehrmann and J. Niehues, Phys. Rev. Lett. **117**, 4, 042001 (2016), [arXiv:1606.03991].

[334] J. Currie *et al.*, JHEP **07**, 018 (2017), [Erratum: JHEP 12, 042 (2020)], [arXiv:1703.05977].

[335] J. Niehues and D. M. Walker, Phys. Lett. B **788**, 243 (2019), [arXiv:1807.02529].

[336] J. Currie, E. W. N. Glover and J. Pires, Phys. Rev. Lett. **118**, 7, 072002 (2017), [arXiv:1611.01460].

[337] J. Currie *et al.*, Phys. Rev. Lett. **119**, 15, 152001 (2017), [arXiv:1705.10271].

[338] X. Chen *et al.*, JHEP **09**, 025 (2022), [arXiv:2204.10173].

[339] T. Gehrmann *et al.*, JHEP **01**, 108 (2021), [arXiv:2009.11310].

[340] X. Chen *et al.*, JHEP **04**, 166 (2020), [arXiv:1904.01044].

Int. J. Mod. Phys. A 2026.41. Downloaded from www.worldscientific.com
by UNIVERSITY OF CALIFORNIA @ BERKELEY on 09/16/26. Re-use and distribution is strictly not permitted, except for Open Access articles.

[341] A. Gehrmann-De Ridder *et al.*, Phys. Rev. Lett. **117**, 2, 022001 (2016), [arXiv:1507.02850].

[342] A. Gehrmann-De Ridder *et al.*, JHEP **07**, 133 (2016), [arXiv:1605.04295].

[343] A. Gehrmann-De Ridder *et al.*, Phys. Rev. Lett. **120**, 12, 122001 (2018), [arXiv:1712.07543].

[344] X. Chen *et al.*, JHEP **10**, 066 (2016), [arXiv:1607.08817].

[345] R. Gauld *et al.*, Phys. Lett. B **817**, 136335 (2021), [arXiv:2009.14209].

[346] R. Gauld *et al.*, JHEP **03**, 008 (2022), [arXiv:2110.12992].

[347] J. Cruz-Martinez *et al.*, Phys. Lett. B **781**, 672 (2018), [arXiv:1802.02445].

[348] M. Czakon, P. Fiedler and A. Mitov, Phys. Rev. Lett. **115**, 5, 052001 (2015), [arXiv:1411.3007].

[349] M. Czakon, D. Heymes and A. Mitov, Phys. Rev. Lett. **116**, 8, 082003 (2016), [arXiv:1511.00549].

[350] M. Czakon *et al.*, JHEP **05**, 034 (2016), [arXiv:1601.05375].

[351] M. Brucherseifer, F. Caola and K. Melnikov, JHEP **04**, 059 (2013), [arXiv:1301.7133].

[352] M. Brucherseifer, F. Caola and K. Melnikov, Phys. Lett. B **736**, 58 (2014), [arXiv:1404.7116].

[353] R. Boughezal *et al.*, Phys. Rev. Lett. **115**, 8, 082003 (2015), [arXiv:1504.07922].

[354] F. Caola, K. Melnikov and M. Schulze, Phys. Rev. D **92**, 7, 074032 (2015), [arXiv:1508.02684].

[355] M. Czakon *et al.*, JHEP **10**, 262 (2019), [arXiv:1907.12911].

[356] H. A. Chawdhry *et al.*, JHEP **02**, 057 (2020), [arXiv:1911.00479].

[357] H. A. Chawdhry *et al.*, JHEP **09**, 093 (2021), [arXiv:2105.06940].

[358] S. Badger *et al.*, JHEP **10**, 071 (2023), [arXiv:2304.06682].

[359] M. Pellen *et al.*, Eur. Phys. J. C **82**, 8, 693 (2022), [arXiv:2204.12394].

[360] M. Czakon, A. Mitov and R. Poncelet, Phys. Rev. Lett. **127**, 15, 152001 (2021), [Erratum: Phys.Rev.Lett. 129, 119901 (2022)], [arXiv:2106.05331].

[361] H. B. Hartanto *et al.*, Phys. Rev. D **106**, 7, 074016 (2022), [arXiv:2205.01687].

[362] M. Czakon *et al.*, Phys. Rev. Lett. **127**, 16, 162002 (2021), [Erratum: Phys.Rev.Lett. 131, 179901 (2023)], [arXiv:2105.04436].

[363] M. Grazzini, JHEP **02**, 043 (2008), [arXiv:0801.3232].

[364] S. Catani, G. Ferrera and M. Grazzini, JHEP **05**, 006 (2010), [arXiv:1002.3115].

[365] S. Catani *et al.*, Phys. Rev. Lett. **108**, 072001 (2012), [Erratum: Phys. Rev. Lett.117,no.8,089901(2016)], [arXiv:1110.2375].

[366] M. Grazzini *et al.*, Phys. Lett. B **731**, 204 (2014), [arXiv:1309.7000].

[367] M. Grazzini, S. Kallweit and D. Rathlev, JHEP **07**, 085 (2015), [arXiv:1504.01330].

[368] M. Grazzini, S. Kallweit and D. Rathlev, Phys. Lett. B **750**, 407 (2015), [arXiv:1507.06257].

[369] M. Grazzini *et al.*, Phys. Lett. B **761**, 179 (2016), [arXiv:1604.08576].

[370] M. Grazzini *et al.*, JHEP **08**, 140 (2016), [arXiv:1605.02716].

[371] M. Grazzini *et al.*, JHEP **05**, 139 (2017), [arXiv:1703.09065].

[372] S. Catani *et al.*, JHEP **04**, 142 (2018), [arXiv:1802.02095].

[373] S. Kallweit and M. Wiesemann, Phys. Lett. B **786**, 382 (2018), [arXiv:1806.05941].

[374] J. M. Campbell *et al.*, JHEP **07**, 148 (2016), [arXiv:1603.02663].

[375] J. M. Campbell, R. K. Ellis and C. Williams, Phys. Rev. D **96**, 1, 014037 (2017), [arXiv:1703.10109].

[376] J. M. Campbell, R. K. Ellis and S. Seth, JHEP **06**, 002 (2022), [arXiv:2202.07738].

[377] G. Ferrera, M. Grazzini and F. Tramontano, Phys. Rev. Lett. **107**, 152003 (2011), [arXiv:1107.1164].

[378] G. Ferrera, M. Grazzini and F. Tramontano, JHEP **04**, 039 (2014), [arXiv:1312.1669].

[379] G. Ferrera, M. Grazzini and F. Tramontano, Phys. Lett. B **740**, 51 (2015), [arXiv:1407.4747].

[380] D. de Florian *et al.*, JHEP **09**, 151 (2016), [arXiv:1606.09519].

[381] M. Grazzini *et al.*, JHEP **05**, 059 (2018), [arXiv:1803.02463].

[382] H. T. Li and J. Wang, Phys. Lett. B **765**, 265 (2017), [arXiv:1607.06382].

[383] H. T. Li, C. S. Li and J. Wang, Phys. Rev. D **97**, 7, 074026 (2018), [arXiv:1710.02464].

[384] S. Kallweit, V. Sotnikov and M. Wiesemann, Phys. Lett. B **812**, 136013 (2021), [arXiv:2010.04681].

[385] R. Boughezal *et al.*, Eur. Phys. J. C **77**, 1, 7 (2017), [arXiv:1605.08011].

[386] R. Boughezal *et al.*, Phys. Lett. B **748**, 5 (2015), [arXiv:1505.03893].

[387] R. Boughezal *et al.*, Phys. Rev. Lett. **116**, 15, 152001 (2016), [arXiv:1512.01291].

[388] R. Boughezal, X. Liu and F. Petriello, Phys. Rev. D **94**, 7, 074015 (2016), [arXiv:1602.08140].

[389] R. Boughezal, X. Liu and F. Petriello, Phys. Lett. B **760**, 6 (2016), [arXiv:1602.05612].

[390] R. Boughezal, X. Liu and F. Petriello, Phys. Rev. D **94**, 11, 113009 (2016), [arXiv:1602.06965].

[391] J. M. Campbell, R. K. Ellis and C. Williams, JHEP **06**, 179 (2016), [arXiv:1601.00658].

[392] J. M. Campbell, R. K. Ellis and C. Williams, Phys. Rev. Lett. **118**, 22, 222001 (2017), [arXiv:1612.04333].

[393] J. M. Campbell, T. Neumann and C. Williams, JHEP **11**, 150 (2017), [arXiv:1708.02925].

[394] J. M. Campbell, R. K. Ellis and S. Seth, JHEP **10**, 136 (2019), [arXiv:1906.01020].

[395] J. Campbell and T. Neumann, JHEP **12**, 034 (2019), [arXiv:1909.09117].

[396] J. Gao, C. S. Li and H. X. Zhu, Phys. Rev. Lett. **110**, 4, 042001 (2013), [arXiv:1210.2808].

[397] Z. L. Liu and J. Gao, Phys. Rev. D **98**, 7, 071501 (2018), [arXiv:1807.03835].

[398] E. L. Berger *et al.*, Phys. Rev. D **94**, 7, 071501 (2016), [arXiv:1606.08463].

[399] E. L. Berger, J. Gao and H. X. Zhu, JHEP **11**, 158 (2017), [arXiv:1708.09405].

[400] V. Del Duca *et al.*, Phys. Rev. Lett. **117**, 15, 152004 (2016), [arXiv:1603.08927].

[401] V. Del Duca *et al.*, Phys. Rev. D **94**, 7, 074019 (2016), [arXiv:1606.03453].

[402] Z. Tulipánt, A. Kardos and G. Somogyi, Eur. Phys. J. C **77**, 11, 749 (2017), [arXiv:1708.04093].

[403] F. Caola *et al.*, Phys. Rev. D **97**, 7, 074022 (2018), [arXiv:1712.06954].

[404] K. Asteriadis *et al.*, JHEP **02**, 046 (2022), [arXiv:2110.02818].

[405] T. Liu, K. Melnikov and A. A. Penin, Phys. Rev. Lett. **123**, 12, 122002 (2019), [arXiv:1906.10899].

[406] F. A. Dreyer and A. Karlberg, Phys. Rev. D **99**, 7, 074028 (2019), [arXiv:1811.07918].

Int. J. Mod. Phys. A 2026.41. Downloaded from www.worldscientific.com by UNIVERSITY OF CALIFORNIA @ BERKELEY on 09/16/26. Re-use and distribution is except for Open Access articles.

[407] J. Campbell, T. Neumann and Z. Sullivan, JHEP **02**, 040 (2021), [arXiv:2012.01574].

[408] S. Amoroso *et al.*, in "11th Les Houches Workshop on Physics at TeV Colliders: PhysTeV Les Houches," (2020), [arXiv:2003.01700].

[409] S. Camarda *et al.*, Eur. Phys. J. C **80**, 3, 251 (2020), [Erratum: Eur.Phys.J.C 80, 440 (2020)], [arXiv:1910.07049].

[410] R. Gavin *et al.*, Comput. Phys. Commun. **182**, 2388 (2011), [arXiv:1011.3540].

[411] S. Camarda *et al.*, Eur. Phys. J. C **82**, 5, 492 (2022), [arXiv:2202.10343].

[412] R. V. Harlander, S. Liebler and H. Mantler, Comput. Phys. Commun. **184**, 1605 (2013), [arXiv:1212.3249].

[413] A. Huss *et al.* (NNLOJET) (2025), [arXiv:2503.22804].

[414] T. Carli *et al.*, Eur. Phys. J. C **66**, 503 (2010), [arXiv:0911.2985].

[415] T. Kluge, K. Rabbertz and M. Wobisch, in "14th International Workshop on Deep Inelastic Scattering (DIS 2006)," 483, Tsukuba, Japan, April 20-24 (2006), [hep-ph/0609285].

[416] D. Britzger *et al.*, in "Proceedings, XX. International Workshop on Deep-Inelastic Scattering and Related Subjects (DIS 2012)," 217, Bonn, Germany, March 26-30 (2012), [arXiv:1208.3641].

[417] S. Carrazza *et al.*, JHEP **12**, 108 (2020), [arXiv:2008.12789].

[418] M. Czakon, D. Heymes and A. Mitov (2017), [arXiv:1704.08551].

[419] D. Britzger *et al.*, Eur. Phys. J. C **79**, 10, 845 (2019), [Erratum: Eur.Phys.J.C 81, 957 (2021)], [arXiv:1906.05303].

[420] D. Britzger *et al.*, Eur. Phys. J. C **82**, 10, 930 (2022), [arXiv:2207.13735].

[421] D. Maître, J. Phys. Conf. Ser. **1525**, 1, 012014 (2020).

[422] D. Maître, G. Heinrich and M. Johnson, PoS **LL2016**, 016 (2016), [arXiv:1607.06259].

[423] Y. L. Dokshitzer, D. Diakonov and S. I. Troian, Phys. Rept. **58**, 269 (1980).

[424] G. Parisi and R. Petronzio, Nucl. Phys. B **154**, 427 (1979).

[425] G. Curci, M. Greco and Y. Srivastava, Nucl. Phys. B **159**, 451 (1979).

[426] A. Bassetto, M. Ciafaloni and G. Marchesini, Nucl. Phys. B **163**, 477 (1980).

[427] J. C. Collins and D. E. Soper, Nucl. Phys. B **193**, 381 (1981), [Erratum: Nucl. Phys.B213,545(1983)].

[428] J. C. Collins and D. E. Soper, Nucl. Phys. B **197**, 446 (1982).

[429] J. Kodaira and L. Trentadue, Phys. Lett. B **112B**, 66 (1982).

[430] J. Kodaira and L. Trentadue, Phys. Lett. B **123**, 335 (1983).

[431] J. C. Collins, D. E. Soper and G. F. Sterman, Nucl. Phys. B **250**, 199 (1985).

[432] S. Catani *et al.*, Nucl. Phys. B **407**, 3 (1993).

[433] C. W. Bauer *et al.*, Phys. Rev. D **63**, 114020 (2001), [hep-ph/0011336].

[434] C. W. Bauer, D. Pirjol and I. W. Stewart, Phys. Rev. D **65**, 054022 (2002), [hep-ph/0109045].

[435] T. Becher, A. Broggio and A. Ferroglia, Lect. Notes Phys. **896**, pp.1 (2015), [arXiv:1410.1892].

[436] S. Catani *et al.*, Phys. Lett. B **269**, 432 (1991).

[437] N. Brown and W. J. Stirling, Phys. Lett. B **252**, 657 (1990).

[438] W. Bartel *et al.* (JADE), Z. Phys. **33**, 23 (1986), [,53(1986)].

[439] N. Kidonakis, G. Oderda and G. F. Sterman, Nucl. Phys. B **531**, 365 (1998), [hep-ph/9803241].

[440] R. Bonciani *et al.*, Phys. Lett. B **575**, 268 (2003), [hep-ph/0307035].

[441] A. Banfi, G. P. Salam and G. Zanderighi, JHEP **03**, 073 (2005), [hep-ph/0407286].

[442] D. de Florian and M. Grazzini, Phys. Rev. Lett. **85**, 4678 (2000), [hep-ph/0008152].

[443] G. Bozzi *et al.*, Nucl. Phys. B **737**, 73 (2006), [hep-ph/0508068]; `http://theory.fi.infn.it/grazzini/codes.html`.

[444] G. Bozzi *et al.*, Phys. Lett. B **696**, 207 (2011), [arXiv:1007.2351].

[445] T. Becher and M. Neubert, Eur. Phys. J. C **71**, 1665 (2011), [arXiv:1007.4005].

[446] `http://cute.hepforge.org/`.

[447] D. de Florian *et al.*, JHEP **06**, 132 (2012), [arXiv:1203.6321]; `http://theory.fi.infn.it/grazzini/codes.html`.

[448] C. Balazs and C. P. Yuan, Phys. Rev. D **56**, 5558 (1997), [hep-ph/9704258].

[449] A. Banfi *et al.*, Phys. Lett. B **715**, 152 (2012), [arXiv:1205.4760].

[450] M. Grazzini *et al.*, JHEP **08**, 154 (2015), [arXiv:1507.02565].

[451] D. de Florian and M. Grazzini, Nucl. Phys. B **704**, 387 (2005), [hep-ph/0407241].

[452] T. Becher and G. Bell, JHEP **11**, 126 (2012), [arXiv:1210.0580].

[453] A. Banfi *et al.*, Phys. Rev. Lett. **109**, 202001 (2012), [arXiv:1206.4998]; T. Becher, M. Neubert and L. Rothen, JHEP **10**, 125 (2013), [arXiv:1307.0025].

[454] I. W. Stewart *et al.*, Phys. Rev. D **89**, 5, 054001 (2014), [arXiv:1307.1808].

[455] J. M. Campbell *et al.*, JHEP **04**, 106 (2023), [arXiv:2301.11768].

[456] I. W. Stewart, F. J. Tackmann and W. J. Waalewijn, Phys. Rev. Lett. **106**, 032001 (2011), [arXiv:1005.4060].

[457] Y.-T. Chien *et al.*, Phys. Rev. D **87**, 1, 014010 (2013), [arXiv:1208.0010]; T. T. Jouttenus *et al.*, Phys. Rev. D **88**, 5, 054031 (2013), [arXiv:1302.0846].

[458] M. Dasgupta *et al.*, JHEP **10**, 126 (2012), [arXiv:1207.1640].

[459] V. Ahrens *et al.*, JHEP **09**, 097 (2010), [arXiv:1003.5827].

[460] M. Aliev *et al.*, Comput. Phys. Commun. **182**, 1034 (2011), [arXiv:1007.1327].

[461] N. Kidonakis, Phys. Rev. D **82**, 114030 (2010), [arXiv:1009.4935].

[462] T. Becher, C. Lorentzen and M. D. Schwartz, Phys. Rev. Lett. **108**, 012001 (2012), [arXiv:1106.4310].

[463] T. Becher *et al.*, Eur. Phys. J. C **75**, 4, 154 (2015), [arXiv:1412.8408].

[464] E. Gerwick *et al.*, JHEP **02**, 106 (2015), [arXiv:1411.7325].

[465] A. Banfi *et al.*, JHEP **05**, 102 (2015), [arXiv:1412.2126].

[466] T. Becher and M. D. Schwartz, JHEP **07**, 034 (2008), [arXiv:0803.0342].

[467] A. H. Hoang *et al.*, Phys. Rev. D **91**, 9, 094017 (2015), [arXiv:1411.6633].

[468] Y.-T. Chien and M. D. Schwartz, JHEP **08**, 058 (2010), [arXiv:1005.1644].

[469] W. Bizon *et al.*, JHEP **02**, 108 (2018), [arXiv:1705.09127].

[470] X. Chen *et al.*, Phys. Lett. B **788**, 425 (2019), [arXiv:1805.00736].

[471] E. Re, L. Rottoli and P. Torrielli, JHEP **2109**, 108 (2021), [arXiv:2104.07509].

[472] T. Neumann and J. Campbell, Phys. Rev. D **107**, 1, L011506 (2023), [arXiv:2207.07056].

Int. J. Mod. Phys. A 2026.41. Downloaded from www.worldscientific.com
by UNIVERSITY OF CALIFORNIA @ BERKELEY on 09/16/26. Re-use and distribution is strictly not permitted, except for Open Access articles.

[473] S. Camarda, L. Cieri and G. Ferrera, Phys. Rev. D **104**, 11, L111503 (2021), [arXiv:2103.04974].

[474] G. Billis, J. K. L. Michel and F. J. Tackmann, JHEP **02**, 170 (2025), [arXiv:2411.16004].

[475] P. Cal *et al.*, Phys. Rev. D **110**, 7, 076005 (2024), [arXiv:2306.16458].

[476] W. Bizon *et al.*, Eur. Phys. J. C **79**, 10, 868 (2019), [arXiv:1905.05171].

[477] S. Kallweit *et al.*, JHEP **12**, 147 (2020), [arXiv:2004.07720].

[478] J. M. Campbell *et al.*, JHEP **03**, 080 (2023), [arXiv:2210.10724].

[479] M. Wiesemann, L. Rottoli and P. Torrielli, Phys. Lett. B **809**, 135718 (2020), [arXiv:2006.09338].

[480] T. Neumann, Eur. Phys. J. C **81**, 10, 905 (2021), [arXiv:2107.12478].

[481] A. Banfi *et al.*, JHEP **04**, 049 (2016), [arXiv:1511.02886].

[482] S. Catani *et al.*, Nucl. Phys. B **888**, 75 (2014), [arXiv:1405.4827].

[483] S. Alioli *et al.*, Phys. Rev. D **109**, 9, 094009 (2024), [arXiv:2312.06496].

[484] A. J. Larkoski and I. Moult, Phys. Rev. D **93**, 014017 (2016), [arXiv:1510.08459].

[485] G. Lustermans, W. J. Waalewijn and L. Zeune, Phys. Lett. B **762**, 447 (2016), [arXiv:1605.02740].

[486] C. Muselli, S. Forte and G. Ridolfi, JHEP **03**, 106 (2017), [arXiv:1701.01464].

[487] W. Bizoń *et al.*, JHEP **12**, 132 (2018), [arXiv:1805.05916].

[488] M. Bonvini and S. Marzani, Phys. Rev. Lett. **120**, 20, 202003 (2018), [arXiv:1802.07758].

[489] M. Procura, W. J. Waalewijn and L. Zeune, JHEP **10**, 098 (2018), [arXiv:1806.10622].

[490] G. Lustermans *et al.*, JHEP **03**, 124 (2019), [arXiv:1901.03331].

[491] P. F. Monni, L. Rottoli and P. Torrielli, Phys. Rev. Lett. **124**, 25, 252001 (2020), [arXiv:1909.04704].

[492] T. Becher and T. Neumann, JHEP **03**, 199 (2021), [arXiv:2009.11437].

[493] M. Dasgupta *et al.*, JHEP **09**, 029 (2013), [arXiv:1307.0007].

[494] A. J. Larkoski *et al.*, JHEP **05**, 146 (2014), [arXiv:1402.2657].

[495] A. J. Larkoski, I. Moult and B. Nachman, Phys. Rept. **841**, 1 (2020), [arXiv:1709.04464].

[496] S. Marzani, G. Soyez and M. Spannowsky **958** (2019), [Lect. Notes Phys.958,pp.(2019)], [arXiv:1901.10342].

[497] R. Kogler *et al.*, Rev. Mod. Phys. **91**, 4, 045003 (2019), [arXiv:1803.06991].

[498] Yu.L. Dokshitzer *et al.*, *"Basics of perturbative QCD,"* Gif-sur-Yvette, France: Éditions frontières (1991), see also `http://www.lpthe.jussieu.fr/~{}yuri/` BPQCD/-cover.html.

[499] T. Sj ostrand *et al.*, Comput. Phys. Commun. **135**, 238 (2001), [hep-ph/0010017].

[500] T. Sj ostrand, S. Mrenna and P. Z. Skands, JHEP **05**, 026 (2006), [hep-ph/0603175]; `http://projects.hepforge.org/pythia6/`.

[501] T. Sjostrand *et al.*, Comput. Phys. Commun. **191**, 159 (2015), [arXiv:1410.3012]; `http://home.thep.lu.se/~torbjorn/Pythia.html`.

[502] B. R. Webber, Nucl. Phys. B **238**, 492 (1984).

[503] G. Corcella *et al.*, JHEP **01**, 010 (2001), [hep-ph/0011363]; `http://www.hep.phy.cam.ac.uk/theory/webber/Herwig/`.

[504] M. Bahr *et al.*, Eur. Phys. J. C **58**, 639 (2008), [arXiv:0803.0883]; `http://projects.hepforge.org/herwig/`.

[505] T. Gleisberg *et al.*, JHEP **02**, 007 (2009), [arXiv:0811.4622].

[506] L. Lonnblad, Comput. Phys. Commun. **71**, 15 (1992).

[507] J. Bellm *et al.*, Eur. Phys. J. C **80**, 2, 93 (2020), [arXiv:1903.12563].

[508] B. Andersson *et al.*, Phys. Rept. **97**, 31 (1983).

[509] T. Sjostrand, Nucl. Phys. B **248**, 469 (1984).

[510] T. Sjostrand and M. van Zijl, Phys. Rev. D **36**, 2019 (1987).

[511] S. Catani *et al.*, JHEP **11**, 063 (2001), [hep-ph/0109231].

[512] J. Alwall *et al.*, Eur. Phys. J. C **53**, 473 (2008), [arXiv:0706.2569].

[513] S. Frixione and B. R. Webber, JHEP **06**, 029 (2002), [hep-ph/0204244].

[514] P. Nason, JHEP **11**, 040 (2004), [hep-ph/0409146].

[515] S. Alioli *et al.*, JHEP **06**, 043 (2010), [arXiv:1002.2581]; `http://powhegbox.mib.infn.it/`.

[516] S. Plätzer, JHEP **08**, 114 (2013), [arXiv:1211.5467]; R. Frederix and S. Frixione, JHEP **12**, 061 (2012), [arXiv:1209.6215]; K. Hamilton *et al.*, JHEP **05**, 082 (2013), [arXiv:1212.4504].

[517] P. F. Monni *et al.*, JHEP **05**, 143 (2020), [arXiv:1908.06987].

[518] S. Alioli *et al.*, JHEP **06**, 089 (2014), [arXiv:1311.0286].

[519] K. Hamilton *et al.*, JHEP **10**, 222 (2013), [arXiv:1309.0017].

[520] A. Karlberg, E. Re and G. Zanderighi, JHEP **09**, 134 (2014), [arXiv:1407.2940]; S. Höche, Y. Li and S. Prestel, Phys. Rev. D **91**, 7, 074015 (2015), [arXiv:1405.3607]; S. Höche, Y. Li and S. Prestel, Phys. Rev. D **90**, 5, 054011 (2014), [arXiv:1407.3773]; S. Alioli *et al.*, Phys. Rev. D **92**, 9, 094020 (2015), [arXiv:1508.01475]; S. Alioli *et al.*, Phys. Rev. D **104**, 9, 094020 (2021), [arXiv:2102.08390]; S. Alioli *et al.*, JHEP **05**, 128 (2023), [arXiv:2301.11875].

[521] C. Biello *et al.*, Eur. Phys. J. C **84**, 5, 479 (2024), [arXiv:2402.04025].

[522] W. Astill *et al.*, JHEP **06**, 154 (2016), [arXiv:1603.01620].

[523] W. Astill *et al.*, JHEP **11**, 157 (2018), [arXiv:1804.08141].

[524] E. Re, M. Wiesemann and G. Zanderighi, JHEP **12**, 121 (2018), [arXiv:1805.09857].

[525] S. Alioli *et al.*, Phys. Rev. D **100**, 9, 096016 (2019), [arXiv:1909.02026].

[526] D. Lombardi, M. Wiesemann and G. Zanderighi, JHEP **06**, 095 (2021), [arXiv:2010.10478].

[527] D. Lombardi, M. Wiesemann and G. Zanderighi, Phys. Lett. B **824**, 136846 (2022), [arXiv:2108.11315].

[528] S. Alioli *et al.*, JHEP **04**, 041 (2021), [arXiv:2010.10498].

[529] D. Lombardi, M. Wiesemann and G. Zanderighi, JHEP **11**, 230 (2021), [arXiv:2103.12077].

[530] S. Alioli *et al.*, Phys. Lett. B **818**, 136380 (2021), [arXiv:2103.01214].

[531] S. Alioli *et al.*, JHEP **06**, 205 (2022), [arXiv:2212.10489].

[532] J. M. Lindert *et al.*, JHEP **11**, 036 (2022), [arXiv:2208.12660].

[533] A. Gavardi, C. Oleari and E. Re, JHEP **09**, 061 (2022), [arXiv:2204.12602].

[534] L. Buonocore *et al.*, JHEP **01**, 072 (2022), [arXiv:2108.05337].

[535] U. Haisch *et al.*, JHEP **07**, 054 (2022), [arXiv:2204.00663].

[536] S. Zanoli *et al.*, JHEP **07**, 008 (2022), [arXiv:2112.04168].

[537] A. Gavardi *et al.*, JHEP **12**, 069 (2023), [arXiv:2308.11577].

[538] S. Alioli, G. Marinelli and D. Napoletano, JHEP **09**, 206 (2025), [arXiv:2507.08558].

[539] J. Mazzitelli *et al.*, Phys. Rev. Lett. **127**, 6, 062001 (2021), [arXiv:2012.14267].

[540] J. Mazzitelli *et al.*, JHEP **04**, 079 (2022), [arXiv:2112.12135].

Int. J. Mod. Phys. A 2026.41. Downloaded from www.worldscientific.com
by UNIVERSITY OF CALIFORNIA @ BERKELEY on 09/16/26. Re-use and distribution is [redacted] except for Open Access articles.

[541] J. Mazzitelli *et al.*, Phys. Lett. B **843**, 137991 (2023), [arXiv:2302.01645].

[542] C. Biello *et al.*, JHEP **04**, 088 (2025), [arXiv:2412.09510].

[543] J. Mazzitelli, V. Sotnikov and M. Wiesemann, Phys. Rev. D **112**, 5, 056031 (2025), [arXiv:2404.08598].

[544] B. K. El-Menoufi *et al.*, JHEP **11**, 045 (2025), [arXiv:2412.14242].

[545] M. Dasgupta *et al.*, JHEP **09**, 033 (2018), [Erratum: JHEP 03, 083 (2020)], [arXiv:1805.09327].

[546] L. Hartgring, E. Laenen and P. Skands, JHEP **10**, 127 (2013), [arXiv:1303.4974].

[547] H. T. Li and P. Skands, Phys. Lett. B **771**, 59 (2017), [arXiv:1611.00013].

[548] S. Höche and S. Prestel, Phys. Rev. D **96**, 7, 074017 (2017), [arXiv:1705.00742].

[549] F. Dulat, S. Höche and S. Prestel, Phys. Rev. D **98**, 7, 074013 (2018), [arXiv:1805.03757].

[550] A. Banfi, B. K. El-Menoufi and P. F. Monni, JHEP **01**, 083 (2019), [arXiv:1807.11487].

[551] G. Bewick *et al.*, JHEP **04**, 019 (2020), [arXiv:1904.11866].

[552] M. Dasgupta *et al.*, Phys. Rev. Lett. **125**, 5, 052002 (2020), [arXiv:2002.11114].

[553] K. Hamilton *et al.*, JHEP **03**, 041, 041 (2021), [arXiv:2011.10054].

[554] J. R. Forshaw, J. Holguin and S. Plätzer, JHEP **09**, 014 (2020), [arXiv:2003.06400].

[555] Z. Nagy and D. E. Soper, Phys. Rev. D **104**, 5, 054049 (2021), [arXiv:2011.04773].

[556] Z. Nagy and D. E. Soper (2020), [arXiv:2011.04777].

[557] A. Karlberg *et al.*, Eur. Phys. J. C **81**, 8, 681 (2021), [arXiv:2103.16526].

[558] K. Hamilton *et al.*, JHEP **03**, 193 (2022), [arXiv:2111.01161].

[559] F. Herren *et al.*, JHEP **10**, 091 (2023), [arXiv:2208.06057].

[560] Z. Nagy and D. E. Soper, Phys. Rev. D **106**, 1, 014024 (2022), [arXiv:2204.05631].

[561] M. van Beekveld *et al.*, JHEP **11**, 019 (2022), [arXiv:2205.02237].

[562] M. van Beekveld *et al.*, JHEP **11**, 020 (2022), [arXiv:2207.09467].

[563] M. van Beekveld and S. Ferrario Ravasio, JHEP **02**, 001 (2024), [arXiv:2305.08645].

[564] S. Höche, F. Krauss and D. Reichelt, Phys. Rev. D **111**, 9, 094032 (2025), [arXiv:2404.14360].

[565] S. Ferrario Ravasio *et al.*, Phys. Rev. Lett. **131**, 16, 161906 (2023), [arXiv:2307.11142].

[566] M. van Beekveld *et al.*, SciPost Phys. Codeb. **2024**, 31 (2024), [arXiv:2312.13275].

[567] M. van Beekveld *et al.*, Phys. Rev. Lett. **134**, 1, 011901 (2025), [arXiv:2406.02661].

[568] M. Cacciari *et al.*, JHEP **04**, 068 (2004), [hep-ph/0303085].

[569] M. Cacciari and N. Houdeau, JHEP **09**, 039 (2011), [arXiv:1105.5152].

[570] A. David and G. Passarino, Phys. Lett. B **726**, 266 (2013), [arXiv:1307.1843].

[571] E. Bagnaschi *et al.*, JHEP **02**, 133 (2015), [arXiv:1409.5036].

[572] C. Duhr *et al.*, JHEP **09**, 122 (2021), [arXiv:2106.04585].

[573] A. Ghosh *et al.*, SciPost Phys. Core **6**, 045 (2023), [arXiv:2210.15167].

[574] T. Cridge, G. Marinelli and F. J. Tackmann, JHEP **12**, 043 (2025), [arXiv:2506.13874].

[575] M. A. Lim and R. Poncelet, Phys. Rev. D **112**, 11, L111901 (2025), [arXiv:2412.14910].

[576] T. Generet *et al.*, JHEP **08**, 015 (2025), [arXiv:2503.21866].

[577] G. Soyez *et al.*, Phys. Rev. Lett. **110**, 16, 162001 (2013), [arXiv:1211.2811].

[578] M. Dasgupta and G. P. Salam, J. Phys. G **30**, R143 (2004), [hep-ph/0312283].

[579] C. Bierlich *et al.*, SciPost Phys. **8**, 026 (2020), [arXiv:1912.05451].

[580] S. Moretti, L. Lonnblad and T. Sjostrand, JHEP **08**, 001 (1998), [hep-ph/9804296].

[581] G. P. Salam, Eur. Phys. J. C **67**, 637 (2010), [arXiv:0906.1833].

[582] S. D. Ellis *et al.*, Prog. Part. Nucl. Phys. **60**, 484 (2008), [arXiv:0712.2447].

[583] M. Cacciari, Int. J. Mod. Phys. A **30**, 31, 1546001 (2015), [arXiv:1509.02272].

[584] G. P. Salam and G. Soyez, JHEP **05**, 086 (2007), [arXiv:0704.0292].

[585] S. Catani *et al.*, Nucl. Phys. B **406**, 187 (1993).

[586] S. D. Ellis and D. E. Soper, Phys. Rev. D **48**, 3160 (1993), [hep-ph/9305266].

[587] Y. L. Dokshitzer *et al.*, JHEP **08**, 001 (1997), [hep-ph/9707323].

[588] M. Wobisch and T. Wengler, in "Monte Carlo generators for HERA physics. Proceedings, Workshop, Hamburg, Germany, 1998-1999," 270–279 (1998), [hep-ph/9907280].

[589] M. Cacciari, G. P. Salam and G. Soyez, JHEP **04**, 063 (2008), [arXiv:0802.1189].

[590] S. Bethke *et al.*, Nucl. Phys. B **370**, 310 (1992), [Erratum: Nucl. Phys.B523,681(1998)].

[591] M. Cacciari and G. P. Salam, Phys. Lett. B **641**, 57 (2006), [hep-ph/0512210]; M. Cacciari, G. P. Salam and G. Soyez, Eur. Phys. J. C **72**, 1896 (2012), [arXiv:1111.6097].

[592] A. Banfi, G. P. Salam and G. Zanderighi, Eur. Phys. J. C **47**, 113 (2006), [hep-ph/0601139].

[593] A. Banfi, G. P. Salam and G. Zanderighi, JHEP **07**, 026 (2007), [arXiv:0704.2999].

[594] M. Czakon, A. Mitov and R. Poncelet, JHEP **04**, 138 (2023), [arXiv:2205.11879].

[595] R. Gauld, A. Huss and G. Stagnitto, Phys. Rev. Lett. **130**, 16, 161901 (2023), [arXiv:2208.11138].

[596] S. Caletti *et al.*, JHEP **10**, 158 (2022), [arXiv:2205.01117].

[597] F. Caola *et al.*, Phys. Rev. D **108**, 9, 094010 (2023), [arXiv:2306.07314].

[598] A. Behring *et al.*, JHEP **09**, 149 (2025), [arXiv:2506.13449].

[599] S. Brandt *et al.*, Phys. Lett. **12**, 57 (1964).

[600] E. Farhi, Phys. Rev. Lett. **39**, 1587 (1977).

[601] O. Biebel, Phys. Rept. **340**, 165 (2001).

[602] S. Kluth, Rept. Prog. Phys. **69**, 1771 (2006), [hep-ex/0603011].

[603] C. L. Basham *et al.*, Phys. Rev. Lett. **41**, 1585 (1978).

[604] A. Ali, E. Pietarinen and W. J. Stirling, Phys. Lett. B **141B**, 447 (1984).

[605] I. W. Stewart, F. J. Tackmann and W. J. Waalewijn, Phys. Rev. Lett. **105**, 092002 (2010), [arXiv:1004.2489].

[606] A. Banfi, G. P. Salam and G. Zanderighi, JHEP **08**, 062 (2004), [hep-ph/0407287].

[607] A. Banfi, G. P. Salam and G. Zanderighi, JHEP **06**, 038 (2010), [arXiv:1001.4082].

[608] T. Becher, X. Garcia i Tormo and J. Piclum, Phys. Rev. D **93**, 5, 054038 (2016), [Erratum: Phys. Rev.D93,no.7,079905(2016)], [arXiv:1512.00022].

Int. J. Mod. Phys. A 2026.41. Downloaded from www.worldscientific.com
by UNIVERSITY OF CALIFORNIA @ BERKELEY on 09/16/26. Re-use and distribution is strictly not permitted, except for Open Access articles.

[609] A. Gao *et al.*, Phys. Rev. Lett. **123**, 6, 062001 (2019), [arXiv:1901.04497].

[610] T. Aaltonen *et al.* (CDF), Phys. Rev. D **83**, 112007 (2011), [arXiv:1103.5143].

[611] G. Aad *et al.* (ATLAS), Eur. Phys. J. C **72**, 2211 (2012), [arXiv:1206.2135].

[612] G. Aad *et al.* (ATLAS), Phys. Rev. D **88**, 3, 032004 (2013), [arXiv:1207.6915].

[613] G. Aad *et al.* (ATLAS), Phys. Lett. B **750**, 427 (2015), [arXiv:1508.01579].

[614] G. Aad *et al.* (ATLAS), Eur. Phys. J. C **76**, 7, 375 (2016), [arXiv:1602.08980].

[615] M. Aaboud *et al.* (ATLAS), Eur. Phys. J. C **77**, 12, 872 (2017), [arXiv:1707.02562].

[616] M. Aaboud *et al.* (ATLAS), Phys. Rev. D **98**, 9, 092004 (2018), [arXiv:1805.04691].

[617] G. Aad *et al.* (ATLAS), JHEP **07**, 085 (2023), [arXiv:2301.09351].

[618] V. Khachatryan *et al.* (CMS), Phys. Lett. B **699**, 48 (2011), [arXiv:1102.0068].

[619] S. Chatrchyan *et al.* (CMS), Phys. Lett. B **722**, 238 (2013), [arXiv:1301.1646].

[620] V. Khachatryan *et al.* (CMS), JHEP **10**, 87 (2014), [arXiv:1407.2856].

[621] A. M. Sirunyan *et al.* (CMS), JHEP **12**, 117 (2018), [arXiv:1811.00588].

[622] A. Ali and G. Kramer, Eur. Phys. J. H **36**, 245 (2011), [arXiv:1012.2288].

[623] S. Chatrchyan *et al.* (CMS), Phys. Lett. B **730**, 243 (2014), [arXiv:1310.0878].

[624] G. Aad *et al.* (ATLAS), Phys. Rev. D **83**, 052003 (2011), [arXiv:1101.0070].

[625] S. Chatrchyan *et al.* (CMS), JHEP **06**, 160 (2012), [arXiv:1204.3170].

[626] B. B. Abelev *et al.* (ALICE), Phys. Rev. D **91**, 11, 112012 (2015), [arXiv:1411.4969].

[627] G. Aad *et al.* (ATLAS), Eur. Phys. J. C **73**, 12, 2676 (2013), [arXiv:1307.5749].

[628] C. Glasman (H1, ZEUS), Nucl. Phys. Proc. Suppl. **191**, 121 (2009), [arXiv:0812.0757].

[629] T. Carli, K. Rabbertz and S. Schumann, in T. Schörner-Sadenius, editor, "The Large Hadron Collider: Harvest of Run 1," 139–194 (2015), [arXiv:1506.03239].

[630] P. Gras *et al.*, JHEP **07**, 091 (2017), [arXiv:1704.03878].

[631] A. Abdesselam *et al.*, Eur. Phys. J. C **71**, 1661 (2011), [arXiv:1012.5412].

[632] D. Krohn, J. Thaler and L.-T. Wang, JHEP **02**, 084 (2010), [arXiv:0912.1342].

[633] A. Altheimer *et al.*, J. Phys. G **39**, 063001 (2012), [arXiv:1201.0008].

[634] A. Altheimer *et al.*, Eur. Phys. J. C **74**, 3, 2792 (2014), [arXiv:1311.2708].

[635] P. C. Stichel and W. J. Zakrzewski, Eur. Phys. J. C **75**, 1, 9 (2015), [arXiv:1409.1363].

[636] D. Adams *et al.*, Eur. Phys. J. C **75**, 9, 409 (2015), [arXiv:1504.00679].

[637] L. de Oliveira *et al.*, JHEP **07**, 069 (2016), [arXiv:1511.05190].

[638] F. A. Dreyer, G. P. Salam and G. Soyez, JHEP **12**, 064 (2018), [arXiv:1807.04758].

[639] G. Aad *et al.* (ATLAS), Phys. Rev. Lett. **124**, 22, 222002 (2020), [arXiv:2004.03540].

[640] G. Louppe *et al.*, JHEP **01**, 057 (2019), [arXiv:1702.00748].

[641] D. Guest, K. Cranmer and D. Whiteson, Ann. Rev. Nucl. Part. Sci. **68**, 161 (2018), [arXiv:1806.11484].

[642] A. Butter *et al.*, SciPost Phys. **7**, 014 (2019), [arXiv:1902.09914].

[643] P. T. Komiske, E. M. Metodiev and J. Thaler, JHEP **01**, 121 (2019), [arXiv:1810.05165].

[644] T. Schorner-Sadenius, Eur. Phys. J. C **72**, 2060 (2012), [Erratum: Eur. Phys. J.C72,2133(2012)].

[645] J. M. Campbell, J. W. Huston and W. J. Stirling, Rept. Prog. Phys. **70**, 89 (2007), [hep-ph/0611148].

[646] M. L. Mangano, Phys. Usp. **53**, 109 (2010), [Usp. Fiz. Nauk180,113(2010)].

[647] J. M. Butterworth, G. Dissertori and G. P. Salam, Ann. Rev. Nucl. Part. Sci. **62**, 387 (2012), [arXiv:1202.0583].

[648] S. Chekanov *et al.* (ZEUS), Nucl. Phys. B **792**, 1 (2008), [arXiv:0707.3749].

[649] S. Chekanov *et al.* (ZEUS), Phys. Rev. D **76**, 072011 (2007), [arXiv:0706.3809].

[650] A. Aktas *et al.* (H1), Phys. Lett. B **639**, 21 (2006), [hep-ex/0603014].

[651] H. Abramowicz *et al.* (ZEUS), Eur. Phys. J. C **71**, 1659 (2011), [arXiv:1104.5444].

[652] H. Abramowicz *et al.* (ZEUS), Nucl. Phys. B **864**, 1 (2012), [arXiv:1205.6153].

[653] F. D. Aaron *et al.* (H1), Eur. Phys. J. C **65**, 363 (2010), [arXiv:0904.3870].

[654] F. D. Aaron *et al.* (H1), Eur. Phys. J. C **54**, 389 (2008), [arXiv:0711.2606].

[655] S. Chekanov *et al.* (ZEUS), Eur. Phys. J. C **52**, 515 (2007), [arXiv:0707.3093].

[656] S. Chekanov *et al.* (ZEUS), Phys. Rev. D **78**, 032004 (2008), [arXiv:0802.3955].

[657] H. Abramowicz *et al.* (ZEUS), Eur. Phys. J. C **70**, 965 (2010), [arXiv:1010.6167].

[658] H. Abramowicz *et al.* (ZEUS), Phys. Lett. B **691**, 127 (2010), [arXiv:1003.2923].

[659] S. Chekanov *et al.* (ZEUS), Phys. Rev. D **85**, 052008 (2012), [arXiv:0808.3783].

[660] F. D. Aaron *et al.* (H1), Eur. Phys. J. C **67**, 1 (2010), [arXiv:0911.5678].

[661] V. Andreev *et al.* (H1), Eur. Phys. J. C **75**, 2, 65 (2015), [arXiv:1406.4709].

[662] V. Andreev *et al.* (H1), Eur. Phys. J. C **77**, 11, 791 (2017), [Erratum: Eur. Phys. J. **C81**, 8, 738 (2021)], [arXiv:1709.07251].

[663] G. Aad *et al.* (ATLAS), Phys. Rept. **1116**, 127 (2025), [arXiv:2404.10674].

[664] G. Aad *et al.* (ATLAS), Phys. Rept. **1116**, 57 (2025), [arXiv:2404.06829].

[665] G. Aad *et al.* (ATLAS), Phys. Rept. **1116**, 4 (2025), [arXiv:2404.05498].

[666] A. Hayrapetyan *et al.* (CMS), Phys. Rept. **1115**, 3 (2025), [arXiv:2405.18661].

[667] A. Hayrapetyan *et al.* (CMS), Phys. Rept. **1115**, 116 (2025), [arXiv:2403.01313].

[668] `http://twiki.cern.ch/twiki/bin/view/CMSPublic/PhysicsResultsCombined`.

[669] `http://atlas.web.cern.ch/Atlas/GROUPS/PHYSICS/CombinedSummaryPlots/SM`.

[670] A. Abulencia *et al.* (CDF), Phys. Rev. D **75**, 092006 (2007), [Erratum: Phys. Rev.D75,119901(2007)], [hep-ex/0701051].

[671] T. Aaltonen *et al.* (CDF), Phys. Rev. D **78**, 052006 (2008), [Erratum: Phys. Rev.D79,119902(2009)], [arXiv:0807.2204].

Int. J. Mod. Phys. A 2026.41. Downloaded from www.worldscientific.com by UNIVERSITY OF CALIFORNIA @ BERKELEY on 09/16/26. Re-use and distribution is [redacted] except for Open Access articles.

[672] V. M. Abazov *et al.* (D0), Phys. Rev. Lett. **101**, 062001 (2008), [arXiv:0802.2400].

[673] V. M. Abazov *et al.* (D0), Phys. Rev. D **85**, 052006 (2012), [arXiv:1110.3771].

[674] B. Abelev *et al.* (ALICE), Phys. Lett. B **722**, 262 (2013), [arXiv:1301.3475].

[675] G. Aad *et al.* (ATLAS), Eur. Phys. J. C **73**, 8, 2509 (2013), [arXiv:1304.4739].

[676] G. Aad *et al.* (ATLAS), JHEP **02**, 153 (2015), [Erratum: JHEP09,141(2015)], [arXiv:1410.8857].

[677] M. Aaboud *et al.* (ATLAS), JHEP **09**, 020 (2017), [arXiv:1706.03192].

[678] V. Khachatryan *et al.* (CMS), Eur. Phys. J. C **76**, 5, 265 (2016), [arXiv:1512.06212].

[679] S. Chatrchyan *et al.* (CMS), Phys. Rev. D **87**, 11, 112002 (2013), [Erratum: Phys. Rev.D87,no.11,119902(2013)], [arXiv:1212.6660].

[680] V. Khachatryan *et al.* (CMS), JHEP **03**, 156 (2017), [arXiv:1609.05331].

[681] V. Khachatryan *et al.* (CMS), Eur. Phys. J. C **76**, 8, 451 (2016), [arXiv:1605.04436].

[682] M. Aaboud *et al.* (ATLAS), JHEP **05**, 195 (2018), [arXiv:1711.02692].

[683] A. M. Sirunyan *et al.* (CMS), JHEP **12**, 082 (2020), [arXiv:2005.05159].

[684] A. Tumasyan *et al.* (CMS), JHEP **02**, 142 (2022), [Addendum: JHEP 12, 035 (2022)], [arXiv:2111.10431].

[685] A. Tumasyan *et al.* (CMS), Eur. Phys. J. C **83**, 8, 742 (2023), [arXiv:2210.13557].

[686] J. Currie *et al.*, JHEP **10**, 155 (2018), [arXiv:1807.03692].

[687] A. Schwartzman, Int. J. Mod. Phys. A **30**, 31, 1546002 (2015), [arXiv:1509.05459].

[688] T.-J. Hou *et al.* (2019), [arXiv:1908.11238].

[689] R. Abdul Khalek *et al.*, Eur. Phys. J. C **80**, 8, 797 (2020), [arXiv:2005.11327].

[690] X. Jing *et al.*, Phys. Rev. D **108**, 3, 034029 (2023), [arXiv:2306.03918].

[691] G. Aad *et al.* (ATLAS), JHEP **05**, 059 (2014), [arXiv:1312.3524].

[692] A. M. Sirunyan *et al.* (CMS), Eur. Phys. J. C **77**, 11, 746 (2017), [arXiv:1705.02628].

[693] T. Aaltonen *et al.* (CDF), Phys. Rev. D **79**, 112002 (2009), [arXiv:0812.4036].

[694] V. M. Abazov *et al.* (D0), Phys. Rev. Lett. **103**, 191803 (2009), [arXiv:0906.4819].

[695] S. Chatrchyan *et al.* (CMS), JHEP **05**, 055 (2012), [arXiv:1202.5535].

[696] V. Khachatryan *et al.* (CMS), Phys. Lett. B **746**, 79 (2015), [arXiv:1411.2646].

[697] A. M. Sirunyan *et al.* (CMS), JHEP **07**, 013 (2017), [arXiv:1703.09986].

[698] G. Aad *et al.* (ATLAS), JHEP **01**, 029 (2013), [arXiv:1210.1718].

[699] M. Aaboud *et al.* (ATLAS), Phys. Rev. D **96**, 5, 052004 (2017), [arXiv:1703.09127].

[700] V. M. Abazov *et al.* (D0), Phys. Rev. Lett. **94**, 221801 (2005), [hep-ex/0409040].

[701] V. M. Abazov *et al.* (D0), Phys. Lett. B **721**, 212 (2013), [arXiv:1212.1842].

[702] G. Aad *et al.* (ATLAS), Phys. Rev. Lett. **106**, 172002 (2011), [arXiv:1102.2696].

[703] V. Khachatryan *et al.* (CMS), Phys. Rev. Lett. **106**, 122003 (2011), [arXiv:1101.5029].

[704] V. Khachatryan *et al.* (CMS), Eur. Phys. J. C **76**, 10, 536 (2016), [arXiv:1602.04384].

[705] A. M. Sirunyan *et al.* (CMS), Eur. Phys. J. C **78**, 7, 566 (2018), [arXiv:1712.05471].

[706] A. M. Sirunyan *et al.* (CMS), Eur. Phys. J. C **79**, 9, 773 (2019), [arXiv:1902.04374].

[707] P. Kokkas, Int. J. Mod. Phys. A **30**, 31, 1546004 (2015), [arXiv:1509.02144].

[708] G. Aad *et al.* (ATLAS), JHEP **01**, 188 (2021), [Erratum: JHEP 12, 053 (2021)], [arXiv:2007.12600].

[709] M. Aaboud *et al.* (ATLAS), Eur. Phys. J. C **77**, 6, 367 (2017), [arXiv:1612.03016].

[710] G. Aad *et al.* (ATLAS), Phys. Lett. B **759**, 601 (2016), [arXiv:1603.09222].

[711] R. Aaij *et al.* (LHCb), JHEP **08**, 039 (2015), [arXiv:1505.07024].

[712] S. Chatrchyan *et al.* (CMS), JHEP **10**, 132 (2011), [arXiv:1107.4789].

[713] S. Chatrchyan *et al.* (CMS), Phys. Rev. Lett. **112**, 191802 (2014), [arXiv:1402.0923].

[714] R. Aaij *et al.* (LHCb), JHEP **06**, 058 (2012), [arXiv:1204.1620].

[715] R. Aaij *et al.* (LHCb), JHEP **01**, 155 (2016), [arXiv:1511.08039].

[716] R. Aaij *et al.* (LHCb), JHEP **09**, 136 (2016), [arXiv:1607.06495].

[717] M. Aaboud *et al.* (ATLAS), JHEP **12**, 059 (2017), [arXiv:1710.05167].

[718] A. Hayrapetyan *et al.* (CMS), JHEP **04**, 162 (2025), [arXiv:2408.03744].

[719] G. Aad *et al.* (ATLAS), Phys. Lett. B **854**, 138725 (2024), [arXiv:2403.12902].

[720] G. Aad *et al.* (ATLAS), Eur. Phys. J. C **80**, 7, 616 (2020), [arXiv:1912.02844].

[721] A. M. Sirunyan *et al.* (CMS), JHEP **12**, 061 (2019), [arXiv:1909.04133].

[722] S. Chatrchyan *et al.* (CMS), JHEP **10**, 007 (2011), [arXiv:1108.0566].

[723] V. Khachatryan *et al.* (CMS), Eur. Phys. J. C **75**, 4, 147 (2015), [arXiv:1412.1115].

[724] G. Aad *et al.* (ATLAS), Phys. Lett. B **725**, 223 (2013), [arXiv:1305.4192].

[725] G. Aad *et al.* (ATLAS), JHEP **06**, 112 (2014), [arXiv:1404.1212].

[726] G. Aad *et al.* (ATLAS), JHEP **08**, 009 (2016), [arXiv:1606.01736].

[727] A. M. Sirunyan *et al.* (CMS), JHEP **12**, 059 (2019), [arXiv:1812.10529].

[728] S. Chatrchyan *et al.* (CMS), Phys. Rev. D **90**, 3, 032004 (2014), [arXiv:1312.6283].

[729] V. Khachatryan *et al.* (CMS), Eur. Phys. J. C **76**, 8, 469 (2016), [arXiv:1603.01803].

[730] G. Aad *et al.* (ATLAS), Eur. Phys. J. C **79**, 9, 760 (2019), [arXiv:1904.05631].

[731] R. Aaij *et al.* (LHCb), JHEP **10**, 030 (2016), [arXiv:1608.01484].

[732] G. Aad *et al.* (ATLAS), Eur. Phys. J. C **76**, 5, 291 (2016), [arXiv:1512.02192].

[733] V. Khachatryan *et al.* (CMS), JHEP **02**, 096 (2017), [arXiv:1606.05864].

[734] A. M. Sirunyan *et al.* (CMS), JHEP **03**, 172 (2018), [arXiv:1710.07955].

[735] M. Aaboud *et al.* (ATLAS), JHEP **05**, 077 (2018), [arXiv:1711.03296].

Int. J. Mod. Phys. A 2026.41. Downloaded from www.worldscientific.com
by UNIVERSITY OF CALIFORNIA @ BERKELEY on 09/16/26. Re-use and distribution is strictly not permitted, except for Open Access articles.

[736] U. Blumenschein, Int. J. Mod. Phys. A **30**, 31, 1546007 (2015), [arXiv:1509.04885].

[737] G. Aad *et al.* (ATLAS), Eur. Phys. J. C **79**, 10, 847 (2019), [arXiv:1907.06728].

[738] V. Khachatryan *et al.* (CMS), Phys. Rev. D **95**, 052002 (2017), [arXiv:1610.04222].

[739] A. M. Sirunyan *et al.* (CMS), Phys. Rev. D **96**, 7, 072005 (2017), [arXiv:1707.05979].

[740] A. M. Sirunyan *et al.* (CMS), Eur. Phys. J. C **78**, 11, 965 (2018), [arXiv:1804.05252].

[741] G. Aad *et al.* (ATLAS), Eur. Phys. J. C **85**, 7, 738 (2025), [arXiv:2412.11644].

[742] G. Aad *et al.* (ATLAS), JHEP **06**, 080 (2023), [arXiv:2205.02597].

[743] G. Aad *et al.* (ATLAS), JHEP **07**, 032 (2013), [arXiv:1304.7098].

[744] Z. Bern *et al.*, Phys. Rev. D **88**, 1, 014025 (2013), [arXiv:1304.1253].

[745] G. Aad *et al.* (ATLAS), Phys. Rev. D **108**, 1, 012022 (2023), [arXiv:2204.12355].

[746] M. Voutilainen, Int. J. Mod. Phys. A **30**, 31, 1546008 (2015), [arXiv:1509.05026].

[747] G. Aad *et al.* (ATLAS), JHEP **08**, 005 (2016), [arXiv:1605.03495].

[748] G. Aad *et al.* (ATLAS), JHEP **10**, 203 (2019), [arXiv:1908.02746].

[749] S. Chatrchyan *et al.* (CMS), Phys. Rev. D **84**, 052011 (2011), [arXiv:1108.2044].

[750] S. Chatrchyan *et al.* (CMS), JHEP **06**, 009 (2014), [arXiv:1311.6141].

[751] G. Aad *et al.* (ATLAS), Phys. Rev. D **89**, 5, 052004 (2014), [arXiv:1311.1440].

[752] M. Aaboud *et al.* (ATLAS), Phys. Lett. B **780**, 578 (2018), [arXiv:1801.00112].

[753] M. Aaboud *et al.* (ATLAS), Nucl. Phys. B **918**, 257 (2017), [arXiv:1611.06586].

[754] A. M. Sirunyan *et al.* (CMS), Eur. Phys. J. C **79**, 1, 20 (2019), [arXiv:1807.00782].

[755] A. M. Sirunyan *et al.* (CMS), Eur. Phys. J. C **79**, 11, 969 (2019), [arXiv:1907.08155].

[756] G. Aad *et al.* (ATLAS), JHEP **03**, 179 (2020), [arXiv:1912.09866].

[757] D. d'Enterria and J. Rojo, Nucl. Phys. B **860**, 311 (2012), [arXiv:1202.1762].

[758] L. Carminati *et al.*, EPL **101**, 6, 61002 (2013), [arXiv:1212.5511].

[759] F. Siegert, J. Phys. G **44**, 4, 044007 (2017), [arXiv:1611.07226].

[760] M. Aaboud *et al.* (ATLAS), Phys. Lett. B **776**, 295 (2018), [arXiv:1710.09560].

[761] J. H. Kuhn *et al.*, JHEP **03**, 059 (2006), [hep-ph/0508253].

[762] J. M. Lindert *et al.*, Eur. Phys. J. C **77**, 12, 829 (2017), [arXiv:1705.04664].

[763] V. Khachatryan *et al.* (CMS), JHEP **10**, 128 (2015), [Erratum: JHEP04,010(2016)], [arXiv:1505.06520].

[764] G. Aad *et al.* (ATLAS), Phys. Lett. B **798**, 134913 (2019), [arXiv:1903.10415].

[765] G. Aad *et al.* (ATLAS), Phys. Rev. Lett. **129**, 6, 061803 (2022), [arXiv:2201.13045].

[766] A. M. Sirunyan *et al.* (CMS), Phys. Rev. Lett. **125**, 15, 151802 (2020), [arXiv:2006.11191].

[767] G. Aad *et al.* (ATLAS), JHEP **01**, 086 (2013), [arXiv:1211.1913].

[768] M. Aaboud *et al.* (ATLAS), Phys. Rev. D **95**, 11, 112005 (2017), [arXiv:1704.03839].

[769] G. Aad *et al.* (ATLAS), JHEP **11**, 169 (2021), [arXiv:2107.09330].

[770] S. Chatrchyan *et al.* (CMS), Eur. Phys. J. C **74**, 11, 3129 (2014), [arXiv:1405.7225].

[771] M. Aaboud *et al.* (ATLAS), Phys. Lett. B **781**, 55 (2018), [arXiv:1712.07291].

[772] K. Kröninger, A. B. Meyer and P. Uwer, in T. Schörner-Sadenius, editor, "The Large Hadron Collider: Harvest of Run 1," 259–300 (2015), [arXiv:1506.02800].

[773] M. Aaboud *et al.* (ATLAS), Phys. Rev. D **94**, 9, 092003 (2016), [arXiv:1607.07281].

[774] M. Aaboud *et al.* (ATLAS), Eur. Phys. J. C **77**, 5, 292 (2017), [arXiv:1612.05220].

[775] A. M. Sirunyan *et al.* (CMS), Eur. Phys. J. C **79**, 5, 368 (2019), [arXiv:1812.10505].

[776] A. M. Sirunyan *et al.* (CMS), Eur. Phys. J. C **80**, 7, 658 (2020), [arXiv:1904.05237].

[777] G. Aad *et al.* (ATLAS), JHEP **07**, 141 (2023), [arXiv:2303.15340].

[778] M. Czakon *et al.*, JHEP **05**, 149 (2018), [arXiv:1803.07623].

[779] G. Aad *et al.* (ATLAS), Eur. Phys. J. C **83**, 6, 496 (2023), [arXiv:2303.15061].

[780] G. Bevilacqua and M. Worek, JHEP **07**, 111 (2012), [arXiv:1206.3064].

[781] S. Chatrchyan *et al.* (CMS), Phys. Lett. B **728**, 496 (2014), [Erratum: Phys. Lett.B738,526(2014)], [arXiv:1307.1907].

[782] T. Klijnsma *et al.*, Eur. Phys. J. C **77**, 11, 778 (2017), [arXiv:1708.07495].

[783] G. Aad *et al.* (ATLAS), Eur. Phys. J. C **74**, 10, 3109 (2014), [Addendum: Eur.Phys.J.C 76, 642 (2016)], [arXiv:1406.5375].

[784] A. M. Sirunyan *et al.* (CMS), JHEP **09**, 051 (2017), [arXiv:1701.06228].

[785] G. Aad *et al.* (ATLAS), Phys. Rev. Lett. **135**, 23, 231802 (2025), [arXiv:2507.03595].

[786] G. Aad *et al.* (ATLAS), Eur. Phys. J. C **84**, 1, 78 (2024), [arXiv:2306.11379].

[787] M. Aaboud *et al.* (ATLAS), Phys. Lett. B **786**, 114 (2018), [arXiv:1805.10197].

[788] A. M. Sirunyan *et al.* (CMS), Phys. Lett. B **792**, 369 (2019), [arXiv:1812.06504].

[789] D. de Florian *et al.* (LHC Higgs Cross Section Working Group), CERN Yellow Rep. Monogr. **2**, 1 (2017), [arXiv:1610.07922].

[790] M. Aaboud *et al.* (ATLAS), Phys. Rev. D **98**, 052005 (2018), [arXiv:1802.04146].

[791] A. M. Sirunyan *et al.* (CMS), JHEP **01**, 183 (2019), [arXiv:1807.03825].

[792] G. Aad *et al.* (ATLAS), JHEP **08**, 027 (2022), [arXiv:2202.00487].

[793] A. Tumasyan *et al.* (CMS), JHEP **07**, 091 (2023), [arXiv:2208.12279].

[794] S. Navas *et al.* (Particle Data Group), Phys. Rev. D **110**, 3, 030001 (2024).

[795] D. d'Enterria *et al.*, in "Workshop on precision measurements of the QCD coupling constant (alphas-2019) Trento, Trentino, Italy, February 11-15, 2019," (2019), [arXiv:1907.01435].

[796] D. d'Enterria *et al.*, J. Phys. G **51**, 9, 090501 (2024), [arXiv:2203.08271].

[797] G. P. Salam, in A. Levy, S. Forte and G. Ridolfi, editors, "From My Vast Repertoire ...: Guido Altarelli's Legacy," 101–121 (2019), [arXiv:1712.05165].

Int. J. Mod. Phys. A 2026.41. Downloaded from www.worldscientific.com by UNIVERSITY OF CALIFORNIA @ BERKELEY on 09/16/26. Re-use and distribution is [redacted] except for Open Access articles.

[798] A. Pich *et al.*, in "13th Conference on Quark Confinement and the Hadron Spectrum (Confinement XIII) Maynooth, Ireland, July 31-August 6, 2018," (2018), [arXiv:1811.11801].

[799] A. Pich, Prog. Part. Nucl. Phys. **117**, 103846 (2021), [arXiv:2012.04716].

[800] Y. Aoki *et al.* (Flavour Lattice Averaging Group (FLAG)), Phys. Rev. D **113**, 1, 014508 (2026), [arXiv:2411.04268].

[801] M. Beneke and M. Jamin, JHEP **09**, 044 (2008), [arXiv:0806.3156].

[802] K. Maltman and T. Yavin, Phys. Rev. D **78**, 094020 (2008), [arXiv:0807.0650].

[803] S. Narison, Phys. Lett. B **673**, 30 (2009), [arXiv:0901.3823].

[804] I. Caprini and J. Fischer, Eur. Phys. J. C **64**, 35 (2009), [arXiv:0906.5211].

[805] A. Pich, Prog. Part. Nucl. Phys. **75**, 41 (2014), [arXiv:1310.7922].

[806] D. Boito *et al.*, Phys. Rev. D **91**, 3, 034003 (2015), [arXiv:1410.3528].

[807] G. Altarelli, PoS **Corfu2012**, 002 (2013), [arXiv:1303.6065].

[808] A. Pich and A. Rodríguez-Sánchez, Phys. Rev. D **94**, 3, 034027 (2016), [arXiv:1605.06830].

[809] A. H. Hoang and C. Regner, Phys. Rev. D **105**, 9, 096023 (2022), [arXiv:2008.00578].

[810] A. H. Hoang and C. Regner, Eur. Phys. J. ST **230**, 12-13, 2625 (2021), [arXiv:2105.11222].

[811] M. Golterman, K. Maltman and S. Peris, Phys. Rev. D **108**, 1, 014007 (2023), [arXiv:2305.10386].

[812] M. A. Benitez-Rathgeb *et al.*, JHEP **09**, 223 (2022), [arXiv:2207.01116].

[813] M. A. Benitez-Rathgeb *et al.*, JHEP **07**, 016 (2022), [arXiv:2202.10957].

[814] D. Boito *et al.*, Phys. Rev. D **98**, 7, 074030 (2018), [arXiv:1805.08176].

[815] D. Boito *et al.*, Phys. Rev. D **111**, 7, 074010 (2025), [arXiv:2502.08147].

[816] D. Boito *et al.*, Phys. Rev. D **103**, 3, 034028 (2021), [arXiv:2012.10440].

[817] Y. S. Amhis *et al.* (HFLAV), Phys. Rev. D **107**, 5, 052008 (2023), [arXiv:2206.07501].

[818] C. Ayala, G. Cvetic and D. Teca, J. Phys. G **50**, 4, 045004 (2023), [arXiv:2206.05631].

[819] J. Wu *et al.*, Chin. Phys. C **49**, 2, 023001 (2025), [arXiv:2406.16119].

[820] V. Mateu and P. G. Ortega, JHEP **01**, 122 (2018), [arXiv:1711.05755].

[821] C. Peset, A. Pineda and J. Segovia, JHEP **09**, 167 (2018), [arXiv:1806.05197].

[822] S. Narison, Int. J. Mod. Phys. A **33**, 10, 1850045 (2018), [Addendum: Int. J. Mod. Phys. A 33, 1850045 (2018)], [arXiv:1801.00592].

[823] S. Narison, Int. J. Mod. Phys. A **33**, 33, 1892004 (2018), [arXiv:1812.09360].

[824] D. Boito and V. Mateu, Phys. Lett. B **806**, 135482 (2020), [arXiv:1912.06237].

[825] D. Boito and V. Mateu, JHEP **03**, 094 (2020), [arXiv:2001.11041].

[826] J. Blümlein, H. Bottcher and A. Guffanti, Nucl. Phys. B **774**, 182 (2007), [hep-ph/0607200].

[827] P. Jimenez-Delgado and E. Reya, Phys. Rev. D **89**, 7, 074049 (2014), [arXiv:1403.1852].

[828] S. Alekhin *et al.*, Phys. Rev. D **96**, 1, 014011 (2017), [arXiv:1701.05838].

[829] S. Alekhin, J. Blümlein and S. Moch, Eur. Phys. J. C **78**, 6, 477 (2018), [arXiv:1803.07537].

[830] S. Alekhin *et al.*, Eur. Phys. J. C **85**, 2, 162 (2025), [arXiv:2407.00545].

[831] T. Cridge *et al.*, Eur. Phys. J. C **81**, 8, 744 (2021), [arXiv:2106.10289].

[832] T. Cridge, L. A. Harland-Lang and R. S. Thorne, Eur. Phys. J. C **84**, 10, 1009 (2024), [arXiv:2404.02964].

[833] R. D. Ball *et al.* (NNPDF), Eur. Phys. J. C **78**, 5, 408 (2018), [arXiv:1802.03398].

[834] R. D. Ball *et al.* (NNPDF), Eur. Phys. J. C **85**, 9, 1001 (2025), [arXiv:2506.13871].

[835] I. Abt *et al.* (H1, ZEUS), Eur. Phys. J. C **82**, 3, 243 (2022), [arXiv:2112.01120].

[836] S. Bethke *et al.* (JADE), Eur. Phys. J. C **64**, 351 (2009), [arXiv:0810.1389].

[837] G. Dissertori *et al.*, JHEP **08**, 036 (2009), [arXiv:0906.3436].

[838] G. Abbiendi *et al.* (OPAL), Eur. Phys. J. C **71**, 1733 (2011), [arXiv:1101.1470].

[839] A. Kardos *et al.*, Eur. Phys. J. C **78**, 6, 498 (2018), [arXiv:1804.09146].

[840] G. Dissertori *et al.*, Phys. Rev. Lett. **104**, 072002 (2010), [arXiv:0910.4283].

[841] J. Schieck *et al.* (JADE), Eur. Phys. J. C **73**, 3, 2332 (2013), [arXiv:1205.3714].

[842] A. Verbytskyi *et al.*, JHEP **08**, 129 (2019), [arXiv:1902.08158].

[843] R. Abbate *et al.*, Phys. Rev. D **83**, 074021 (2011), [arXiv:1006.3080].

[844] T. Gehrmann, G. Luisoni and P. F. Monni, Eur. Phys. J. C **73**, 1, 2265 (2013), [arXiv:1210.6945].

[845] A. H. Hoang *et al.*, Phys. Rev. D **91**, 9, 094018 (2015), [arXiv:1501.04111].

[846] G. Luisoni, P. F. Monni and G. P. Salam, Eur. Phys. J. C **81**, 2, 158 (2021), [arXiv:2012.00622].

[847] F. Caola *et al.*, JHEP **01**, 093 (2022), [arXiv:2108.08897]; F. Caola *et al.*, JHEP **12**, 062 (2022), [arXiv:2204.02247].

[848] P. Nason and G. Zanderighi, JHEP **06**, 058 (2023), [arXiv:2301.03607].

[849] P. Nason and G. Zanderighi, JHEP **06**, 200 (2025), [arXiv:2501.18173].

[850] L. G. Almeida *et al.*, JHEP **04**, 174 (2014), [arXiv:1401.4460].

[851] U. G. Aglietti *et al.*, Phys. Rev. Lett. **134**, 25, 251904 (2025), [arXiv:2502.01570].

[852] M. Beneke and V. M. Braun, Nucl. Phys. B **426**, 301 (1994), [hep-ph/9402364].

[853] G. P. Salam and D. Wicke, JHEP **05**, 061 (2001), [hep-ph/0102343].

[854] V. Mateu, I. W. Stewart and J. Thaler, Phys. Rev. D **87**, 1, 014025 (2013), [arXiv:1209.3781].

[855] C. Lee and G. F. Sterman, Phys. Rev. D **75**, 014022 (2007), [hep-ph/0611061].

[856] C. Farren-Colloty *et al.* (2025), [arXiv:2507.18696].

[857] M. A. Benitez *et al.*, JHEP **07**, 249 (2025), [arXiv:2412.15164].

[858] M. A. Benitez *et al.* (2025), [arXiv:2502.12253].

[859] A. H. Hoang *et al.*, JHEP **09**, 092 (2025), [arXiv:2506.09130].

[860] R. Frederix *et al.*, JHEP **11**, 050 (2010), [arXiv:1008.5313].

[861] P. Bolzoni, B. A. Kniehl and A. V. Kotikov, Nucl. Phys. B **875**, 18 (2013), [arXiv:1305.6017].

[862] M. Alvarez *et al.*, JHEP **03**, 129 (2023), [arXiv:2301.01086].

Int. J. Mod. Phys. A 2026.41. Downloaded from www.worldscientific.com
by UNIVERSITY OF CALIFORNIA @ BERKELEY on 09/16/26. Re-use and distribution is strictly not permitted, except for Open Access articles.

[863] S. Dittmaier, A. Huss and C. Speckner, JHEP **11**, 095 (2012), [arXiv:1210.0438].

[864] R. Frederix *et al.*, JHEP **04**, 076 (2017), [arXiv:1612.06548].

[865] M. Czakon *et al.*, JHEP **10**, 186 (2017), [arXiv:1705.04105].

[866] M. Reyer, M. Schönherr and S. Schumann, Eur. Phys. J. C **79**, 4, 321 (2019), [arXiv:1902.01763].

[867] S. Forte and Z. Kassabov, Eur. Phys. J. C **80**, 3, 182 (2020), [arXiv:2001.04986].

[868] C. Willis *et al.*, Phys. Rev. D **99**, 5, 054004 (2019), [arXiv:1809.09481].

[869] S. Alekhin *et al.*, Eur. Phys. J. C **75**, 304 (2015), [arXiv:1410.4412].

[870] R. D. Ball *et al.* (NNPDF), Eur. Phys. J. C **81**, 10, 958 (2021), [arXiv:2109.02671].

[871] I. Abt *et al.* (ZEUS), Eur. Phys. J. C **83**, 11, 1082 (2023), [arXiv:2309.02889].

[872] V. Chekhovsky *et al.* (CMS), Phys. Lett. B **868**, 139651 (2025), [arXiv:2412.16665].

[873] F. Ahmadova *et al.*, Phys. Rev. Lett. **135**, 3, 031903 (2025), [arXiv:2412.21165].

[874] A. Hayrapetyan *et al.* (CMS), Phys. Rev. Lett. **133**, 7, 071903 (2024), [arXiv:2402.13864].

[875] A. Hayrapetyan *et al.* (CMS), Eur. Phys. J. C **84**, 8, 842 (2024), [arXiv:2404.16082].

[876] D. d'Enterria and A. Poldaru, JHEP **06**, 016 (2020), [arXiv:1912.11733].

[877] S. Camarda, G. Ferrera and M. Schott, Eur. Phys. J. C **84**, 1, 39 (2024), [arXiv:2203.05394].

[878] G. Aad *et al.* (ATLAS) (2023), [arXiv:2309.12986].

[879] J. Haller *et al.*, Eur. Phys. J. C **78**, 8, 675 (2018), [arXiv:1803.01853].

[880] G. Voutsinas *et al.*, Phys. Lett. B **800**, 135068 (2020), [arXiv:1908.01704].

[881] P. Janot and S. Jadach, Phys. Lett. B **803**, 135319 (2020), [arXiv:1912.02067].

[882] V. Chekhovsky *et al.* (CMS) (2024), [arXiv:2412.13872].

[883] T. Aaltonen *et al.* (CDF), Science **376**, 6589, 170 (2022).

[884] J. de Blas *et al.*, Phys. Rev. Lett. **129**, 27, 271801 (2022), [Supplemental Material: Phys.Rev.Lett. 129, 271801 (2022)], [arXiv:2204.04204].

[885] L. Del Debbio and A. Ramos, Physics Reports **920**, 1 (2021), ISSN 0370-1573, [arXiv:2101.04762].

[886] S. Aoki *et al.* (Flavour Lattice Averaging Group), Eur. Phys. J. C **80**, 2, 113 (2020), [arXiv:1902.08191].

[887] Y. Aoki *et al.* (Flavour Lattice Averaging Group (FLAG)), Eur. Phys. J. C **82**, 10, 869 (2022), [arXiv:2111.09849].

[888] M. Bruno *et al.* (ALPHA), Phys. Rev. Lett. **119**, 10, 102001 (2017), [arXiv:1706.03821].

[889] S. Aoki *et al.* (PACS-CS), JHEP **10**, 053 (2009), [arXiv:0906.3906].

[890] C. McNeile *et al.*, Phys. Rev. D **82**, 034512 (2010), [arXiv:1004.4285].

[891] K. Maltman *et al.*, Phys. Rev. D **78**, 114504 (2008), [arXiv:0807.2020].

[892] B. Chakraborty *et al.*, Phys. Rev. D **91**, 5, 054508 (2015), [arXiv:1408.4169].

[893] C. Ayala, X. Lobregat and A. Pineda, JHEP **09**, 016 (2020), [arXiv:2005.12301].

[894] A. Bazavov *et al.* (TUMQCD), Phys. Rev. D **100**, 11, 114511 (2019), [arXiv:1907.11747].

[895] S. Cali *et al.*, Phys. Rev. Lett. **125**, 242002 (2020), [arXiv:2003.05781].

[896] P. Petreczky and J. H. Weber, Eur. Phys. J. C **82**, 1, 64 (2022), [arXiv:2012.06193].

[897] M. Dalla Brida *et al.* (ALPHA), Eur. Phys. J. C **82**, 12, 1092 (2022), [arXiv:2209.14204].

[898] M. Dalla Brida *et al.* (ALPHA), Phys. Lett. B **807**, 135571 (2020), [arXiv:1912.06001].

[899] S. Chatrchyan *et al.* (CMS), Eur. Phys. J. C **73**, 10, 2604 (2013), [arXiv:1304.7498].

10. Electroweak Model and Constraints on New Physics

Revised May 2026 by J. de Blas (Granada U.), S. Dittmaier (Freiburg U.) and R. Kogler (DESY, Hamburg).

10.1 Introduction . . . 196
10.2 Renormalization and radiative corrections . . . 197
10.2.1 Ultraviolet and infrared divergences and regularization . . . 197
10.2.2 Renormalization procedure and renormalization schemes . . . 197
10.2.3 Electroweak input parameter schemes . . . 198
10.2.4 Particle masses . . . 200
10.2.5 Radiative corrections to electroweak processes 201
10.3 Low-energy observables . . . 202
10.3.1 The electromagnetic coupling . . . 202
10.3.2 The Fermi constant . . . 203
10.3.3 The muon anomalous magnetic moment . . . 203
10.4 Electroweak precision physics . . . 204
10.4.1 Z- and W-boson masses and widths . . . 204
10.4.2 Higgs-boson mass and width . . . 205
10.4.3 Quark masses . . . 205
10.4.4 The strong coupling constant . . . 206
10.4.5 The weak mixing angle . . . 206
10.4.6 Z-pole physics . . . 207
10.4.7 W and Z decays . . . 210
10.5 Global fit results . . . 211
10.6 Constraints on new physics . . . 214

Int. J. Mod. Phys. A 2026.41. Downloaded from www.wo
by UNIVERSITY OF CALIFORNIA @ BERKELEY on 09/16/26. Re-use and distribution is
except for Open Access articles.

10.1 Introduction

The *Standard Model* of the electroweak interactions (SM) [1–4] is a renormalizable gauge quantum field theory based on the group SU(2) × U(1), with gauge bosons W^i_μ, $i = 1, 2, 3$, and B_μ for the SU(2) and U(1) factors, respectively, and the corresponding gauge coupling constants g and g'. The quantum numbers of the two subgroups are known as *weak isospin* and *weak hypercharge,* respectively. The left-handed lepton and quark fields of the $i^{\rm th}$ fermion family transform as doublets $\Psi_i = \begin{pmatrix}\nu_i\\ \ell_i^-\end{pmatrix}$ and $\begin{pmatrix}u_i\\ d'_i\end{pmatrix}$ under SU(2), respectively. Here we assume a flavor basis where the lepton and up-quark fields are aligned with the physical basis, whereas for the down-type quarks the interaction and mass bases are related by the Cabibbo–Kobayashi–Maskawa mixing [5,6] matrix $V^{\rm CKM}$: $d'_i \equiv \sum_j V^{\rm CKM}_{ij}\, d_j$. The right-handed fermion fields transform as SU(2) singlets. From Higgs and electroweak (EW) precision data it is known that there are precisely three sequential fermion families. Constraints on $V^{\rm CKM}$ and tests of universality are discussed in Ref. [7] and in Section 12 on the "CKM Quark-Mixing Matrix" in this *Review.* The extension of the formalism to allow for an analogous leptonic mixing matrix is discussed in Section 14 on "Neutrino Masses, Mixing, and Oscillations" in this *Review.*

A complex scalar Higgs doublet, ϕ, is added to the model for mass generation through spontaneous symmetry breaking with the Higgs potential given by

$$V(\phi) = \mu^2\phi^\dagger\phi + \frac{\lambda^2}{2}(\phi^\dagger\phi)^2\ , \qquad \phi \equiv \begin{pmatrix}\phi^+\\ \phi^0\end{pmatrix}\ . \tag{10.1}$$

For μ^2 negative, ϕ develops a vacuum expectation value, $\langle\phi\rangle = (0, v/\sqrt{2})^{\rm T}$, where $v = \sqrt{2}|\mu|/\lambda \approx 246$ GeV, breaking the EW symmetry down to the remaining $U(1)_{\rm em}$ symmetry of *Quantum Electrodynamics* (QED). After this, only one neutral Higgs scalar, H, remains in the physical particle spectrum. The three remaining degrees of freedom in the doublet ϕ correspond to *would-be Goldstone fields,* which open up longitudinal polarizations of the W/Z bosons, but do not correspond to additional particles. In the following we assume the use of the *unitary gauge*, in which the would-be Goldstone fields formally vanish and the vector fields for the W/Z bosons directly describe three physical polarizations. In non-minimal models there are additional charged and neutral scalar Higgs particles. Higgs-boson physics is reviewed in Section 11 on the "Status of Higgs Boson Physics" in this *Review.*

After symmetry breaking the Lagrangian for the fermion fields, ψ_i, is

$$\begin{aligned}\mathscr{L}_F = &\sum_i \bar\psi_i\left(i\,\partial\!\!\!/ - m_i - \frac{m_i H}{v}\right)\psi_i\\ &- \frac{g}{2\sqrt{2}}\sum_i \overline{\Psi}_i\,\gamma^\mu\,(1-\gamma^5)(T^+\,W^+_\mu + T^-\,W^-_\mu)\,\Psi_i\\ &- e\sum_i Q_i\,\bar\psi_i\,\gamma^\mu\,\psi_i\,A_\mu\\ &- \frac{g}{2\cos\theta_W}\sum_i \bar\psi_i\,\gamma^\mu(g^i_V - g^i_A\gamma^5)\,\psi_i\,Z_\mu\ .\end{aligned} \tag{10.2}$$

Here $\theta_W \equiv \tan^{-1}(g'/g)$ is the weak mixing angle and $e = g\sin\theta_W$ is the positron electric charge. Furthermore,

$$A_\mu \equiv B_\mu\cos\theta_W + W^3_\mu\sin\theta_W\ , \tag{10.3a}$$

$$Z_\mu \equiv -B_\mu\sin\theta_W + W^3_\mu\cos\theta_W\ , \tag{10.3b}$$

$$W^\pm_\mu \equiv \frac{W^1_\mu \mp iW^2_\mu}{\sqrt{2}} \tag{10.3c}$$

are the photon field (A) and the neutral (Z) and charged ($W^\pm$) weak boson fields, respectively.

The Yukawa coupling of H to ψ_i in the first term in $\mathscr{L}_F$, which is flavor diagonal in the minimal model, is $gm_i/2M_W$. From the bosonic interaction Lagrangian,

$$\begin{aligned}\mathscr{L}_{HV} = &\frac{1}{2}(v+H)^2\left[\frac{g^2}{2}W^+_\mu W^{\mu-} + \frac{g^2+g'^2}{4}Z_\mu Z^\mu\right]\\ &- V\left(\frac{v+H}{\sqrt{2}}\right)\ ,\end{aligned} \tag{10.4}$$

one obtains the EW boson masses (at tree level, *i.e.*, to lowest order in perturbation theory)

$$M_H = \sqrt{2}|\mu| = \lambda\,v\ , \tag{10.5a}$$

$$M_W = \frac{gv}{2} = \frac{ev}{2\sin\theta_W}\ , \tag{10.5b}$$

$$M_Z = \sqrt{g^2+g'^2}\,\frac{v}{2} = \frac{ev}{2\sin\theta_W\cos\theta_W}\ , \tag{10.5c}$$

$$M_\gamma = 0\ . \tag{10.5d}$$

The second term in $\mathscr{L}_F$ represents the charged-current weak interaction [8–10], where $T^\pm = (\sigma_1 \pm i\sigma_2)/2$ are the weak isospin raising and lowering operators, with σ_a denoting the Pauli matrices.

For example, the coupling of a W to an electron and a neutrino is

$$-\frac{e}{2\sqrt{2}\sin\theta_W}\left[W^-_\mu\,\bar e\,\gamma^\mu(1-\gamma^5)\nu + W^+_\mu\,\bar\nu\,\gamma^\mu\,(1-\gamma^5)e\right]\ . \tag{10.6}$$

For momenta small compared to M_W, this term gives rise to the effective four-fermion interaction with the Fermi constant given by $G_F/\sqrt{2} = 1/(2v^2) = g^2/(8M_W^2)$. CP violation is incorporated into the EW model by a single observable phase in $V^{\rm CKM}$.

The third term in $\mathscr{L}_F$ describes electromagnetic interactions [11, 12], and the last is the weak neutral-current interaction [9,10,13]. The vector and axial-vector couplings of the Z boson are

$$g^i_V \equiv T^3_i - 2Q_i\sin^2\theta_W\ , \tag{10.7a}$$

$$g^i_A \equiv T^3_i\ , \tag{10.7b}$$

where $T^3_i = \sigma_3/2$ is the third component of the weak isospin of fermion i ($+1/2$ for left-handed u_i and ν_i; $-1/2$ for left-handed d_i and e_i; zero for right-handed fields), and Q_i is the charge of ψ_i

Int. J. Mod. Phys. A 2026.41. Downloaded from www.worldscientific.com by UNIVERSITY OF CALIFORNIA @ BERKELEY on 09/16/26. Re-use and distribution is strictly not permitted, except for Open Access articles.

in units of e. The weak hypercharge Y_i is related to weak isospin and electric charge according to the *Gellman-Nishijima relation*, $Q_i = T_i^3 + Y_i/2$.

The first term in Eq. (10.2) also gives rise to Dirac fermion masses. In the SM, for the case of the neutrinos, the absence of the corresponding right-handed fields prevents the existence of such terms. Furthermore, the requirements of gauge invariance and renormalizability prevents writing Lagrangian terms with the SM fields that can give rise to Majorana neutrino masses after EW symmetry breaking. We refer to Section 14 on "Neutrino Mass, Mixing, and Oscillations" in this *Review* for a discussion on the possible origin of neutrino masses.

We recall that the full Lagrangian for EW interactions also contains gauge-boson self-interactions, encoded in its Yang–Mills part not spelled out here, which influence the predictions for the observables discussed below via EW radiative corrections.

This review is organized as follows: In Section 10.2 we cover several theoretical aspects that are fundamental for the understanding of the SM at the quantum level and the calculation of the phenomenology of the EW sector. Section 10.3 describes several low-energy observables that are key inputs for the SM description of EW interactions, such as the electromagnetic and Fermi constants. We also comment on the latest updates in the experimental status of the determination of the muon anomalous magnetic moment; however, this section has been substantially simplified with respect to previous editions of this *Review*. Section 10.4 focuses mostly on the description of the so-called EW precision observables that are used in the global EW fit, whose results are presented and discussed in Section 10.5. Finally, in Section 10.6 we move our focus to scenarios of physics beyond the SM and discuss the implications of the global EW fit from the point of view of constraining new physics.

10.2 Renormalization and radiative corrections

Before going into detail in the confrontation of the EW theory with experimental results, we clarify some notions and concepts that are essential in the perturbative evaluation of quantum field theories.

10.2.1 *Ultraviolet and infrared divergences and regularization*

Perturbative calculations in quantum field theories are typically plagued with different types of divergences. *Ultraviolet (UV)* divergences originate from the high-momentum regions in loop diagrams, while singularities resulting from finite momentum transfer are known as *infrared (IR)* divergences. Before eliminating the various divergences from predictions, it is necessary to map them to finite quantities in a mathematically consistent way, a step called *regularization*. This step embeds the whole theory into a wider class of theories parametrized by some new parameter δ, and the original theory corresponds to a specific value δ_0. Quantities that diverge in the original theory are finite for $\delta \neq \delta_0$, but diverge for $\delta \to \delta_0$, typically like $\ln(\delta - \delta_0)$ or some power of $1/(\delta - \delta_0)$. The most common regularization scheme is *dimensional regularization*, where the whole theory is formulated in D-dimensional flat space–time and both UV and IR divergences take the form of poles in the parameter $\epsilon = (4 - D)/2$, which is consistently treated as a complex parameter. Other regularization schemes are possible as well, such as the use of small mass parameters for regularizing IR singularities, but dimensional regularization has the advantage of maximal simplicity and preserving gauge and Lorentz invariance.

While the IR divergences are eliminated from physical predictions upon properly designing observables in such a way that IR singularities cancel by virtue of the Kinoshita–Lee–Nauenberg (KLN) theorem [14,15],[1] UV singularities are dealt in the context of the *renormalization* of the quantum field theory, as described in the next section.

[1]The KLN theorem states that singularities cancel in predictions for observables that are "sufficiently inclusive" with respect to the selected initial and final states, a property called *IR safety*. If IR safety cannot be achieved, IR singularities often exhibit *universal factorization properties* allowing for their absorption into non-perturbative quantities, such as *parton distribution* or *fragmentation functions* in the theory of strong interactions (see Section 9 on "Quantum Chromodynamics" in this *Review*).

Since symmetries are central in the construction of successful quantum field theories, regularization schemes should respect symmetries as much as possible. However, it might happen that a specific symmetry is necessarily broken by any regularization scheme. In this case the symmetry is *anomalous*, and the underlying theory is in danger of developing an *anomaly* in the sense that the quantized theory is less symmetric than the corresponding classical theory. Anomalies seriously jeopardize the cancellation of UV divergences, even if the cancellation existed in the presence of the considered symmetry. In this context, one of the most important symmetries is the *chiral symmetry*, which rules the relation between right- and left-handed fermions, because there is no regularization scheme that fully respects all algebraic properties of the Dirac matrix γ_5 as well as Lorentz and gauge symmetry simultaneously—a fact known as the γ_5 *problem* (see, *e.g.*, Ref. [16] for general facts and Refs. [17–20] for more recent developments and further literature). In spite of the existence of chiral couplings in the standard EW theory, the model does not develop a corresponding anomaly owing to special relations among the quantum numbers within the fermion spectrum. In practice, this means that chiral symmetry might be broken in intermediate steps of calculations, a fact that can seriously complicate higher-order calculations, but complete predictions do respect the symmetry.

10.2.2 *Renormalization procedure and renormalization schemes*

In the SM briefly outlined above, the mass parameters m_i have been identified such that the squared masses correspond to the locations of the poles of the lowest-order propagators of the corresponding fields. In the full theory, however, m_i does not have this property owing to higher-order corrections. Similarly, coupling parameters c_i appearing in the Lagrangian determine certain processes, such as decay rates, in lowest-order, but the relation between c_i and observables are modified by perturbative corrections as well. Finally, the fields encoding particle creation and annihilation are typically canonically normalized (to produce normalized states) in lowest order, but lose this property owing to corrections. The intended physical meaning of model parameters (*e.g.* masses and couplings) and the normalization of quantum fields of an underlying theory, generically denoted p and F in the following, can be restored by proper redefinitions, a step known as *renormalization*.

Marking the initial *bare* parameters and fields with subscript "0", p_0 and F_0, the *renormalized parameters and fields* p and F can be introduced by the *renormalization transformation*

$$p_0 \equiv Z_p\, p \equiv p + \delta p, \quad F_0 \equiv Z_F\, F, \tag{10.8}$$

where Z_p, δp and Z_F are parameter and field *renormalization constants,* which have to be determined by imposing appropriate *renormalization conditions* on field-theoretical quantities or physical observables. Assuming that the leading-order quantities p_0 and F_0 already fulfill the conditions, the deviations $\delta Z_i \equiv Z_i - 1$ are due to higher-order corrections. Substituting the bare quantities in favor of the renormalized quantities in the original Lagrangian $\mathcal{L}(p_0, F_0)$ according to (10.8), the leading-order parts of Z_i reproduce the original Lagrangian, $\mathcal{L}(p, F)$, but now parametrized in terms of renormalized quantities p and F, and the parts containing all δZ_i dependence form the *counterterm Lagrangian*

$$\delta\mathcal{L}(p, F, \delta Z_p, \delta Z_F) = \mathcal{L}(p_0, F_0) - \mathcal{L}(p, F) = \mathcal{L}(Z_p p, Z_F F) - \mathcal{L}(p, F), \tag{10.9}$$

which implies Feynman rules for *counterterm* contributions to Green functions. In other words, the step of renormalization just represents a reparametrization of the original theory.

The choice of renormalization conditions defines the *renormalization scheme,* which, thus, gives the model parameters their physical meaning. The details of the field renormalization, on the other hand, are merely a matter of convenience without any influence on predictions for observables. In order to avoid mixing between asymptotic states used in the calculation of scattering amplitudes, matrix-valued field renormalization constants Z_F are necessary in general. The form of the renormalization transformation (10.8) corresponds to the *multiplicative renormalization*

Int. J. Mod. Phys. A 2026.41. Downloaded from www.worldscientific.com by UNIVERSITY OF CALIFORNIA @ BERKELEY on 09/16/26. Re-use and distribution is [redacted] except for Open Access articles.

of a theory, which might not be general enough in the presence of *anomalies*, which appear if symmetries observed for a classical Lagrangian do not survive the step of quantization. On the other hand, the use of multiplicative (Z_p) or additive (δp) renormalization constants for parameters is a mere question of taste.

Theories that allow for the complete elimination of UV divergences from predictions are called *renormalizable*, otherwise they are *non-renormalizable*. Note that even UV-finite theories require the step of renormalization to define the precise meaning of input parameters, *i.e.* renormalization is more than eliminating UV divergences. In spite of the fact that predictions of non-renormalizable theories are not free of UV divergences, such theories can often still be exploited in the framework of *effective field theories* which involve a cutoff scale Λ that sets the order of the maximal energy up to which predictions can be made; for energies above Λ, effects of a more comprehensive *UV-complete theory* are expected to restore renormalizability.

Giving the model parameters their physical meaning, the renormalization scheme determines the parametrization of predictions for physical observables in terms of the renormalized input parameters p. The actual scheme choice might depend on various factors, such as the accessibility or precision to which a parameter can be determined by experiment, the perturbative stability of predictions, *i.e.* whether the size of higher-order corrections show the necessary decrease with increasing orders, or the transportability of the input parameters to predictions of observables that are connected to very different energy scales. In practice, a confrontation of a very comprehensive theory, such as the EW SM, with experimental results requires the use of different schemes adapted to different observables, so that a *conversion* of parameters and fields between different renormalization schemes is necessary. To this end, the renormalized parameters and fields in one scheme have to be expressed in terms of the ones in another scheme. For EW physics two different types of schemes are in use: (i) *on-shell (OS) renormalization* and (ii) renormalization based on *modified minimal subtraction* ($\overline{MS}$). Some schemes also mix these types of conditions, *i.e.* different parameters might employ different types of schemes. However, it is crucial that independent renormalization conditions are posed only for truly independent parameters, and that one and the same condition is consistently used for each independent input parameter within a given scheme.

In OS schemes, the renormalization conditions are imposed on S-matrix elements, *i.e.* on (at least in principle) measurable quantities. Typical examples are OS conditions for masses that tie mass parameters to the locations of the poles in full propagators, which might be experimentally reconstructed from event kinematics. On-shell conditions for coupling parameters can, *e.g.*, be tied to specific decay widths of particles or specific scattering cross sections in certain kinematic regimes. The advantage of OS schemes often lies in the accessibility of input parameters by experiment and the fact that predictions are rather safe against the introduction of artificial gauge dependences in predictions. On the other hand, $\overline{\mathrm{MS}}$ renormalization has the advantage of maximal simplicity, because $\overline{\mathrm{MS}}$ conditions reduce all renormalization constants to the UV-divergent contributions that are necessary to render all Green functions of the underlying theory UV finite in the framework of dimensional regularization. Moreover, the necessity of keeping all input parameters and fields at their canonical mass dimension introduces an arbitrary *renormalization scale* μ_{ren} in the $\overline{\mathrm{MS}}$ scheme, so that Green functions obey *renormalization group equations (RGEs)* which rule the behaviour of input parameters, fields, and Green functions under the change of μ_{ren} while keeping (all-order) predictions for physical observables fixed. The RGEs can, thus, be used to transport the input quantities from one scale to another, and the residual μ_{ren}-dependence of predictions, which occurs because the perturbative series is necessarily truncated somewhere, offers a convenient device for estimating (at least part of) the theoretical uncertainty due to missing higher-order corrections.

The concept for renormalization and explicit schemes have been worked out in the 1970s to 1990s for the EW SM in different variants. The idea of EW OS renormalization dates back to Ref. [21] and has, *e.g.*, been worked out in Refs. [22–25]. Electroweak renormalization in the $\overline{\mathrm{MS}}$ scheme is, for instance, described in Ref. [26]. A detailed review and more original references can be found in Ref. [27]. Most formulations are restricted to the one-loop level, a complete renormalization framework for the EW SM at the two-loop level is laid out in Refs. [28–30]. The renormalization of the EW SM is considerably more involved than for QED and Quantum Chromodynamics (QCD); major issues are:

- Any solution to the γ_5 problem actually goes beyond pure multiplicative renormalization. For instance, in dimensional regularization one of the defining algebraic properties of γ_5 valid in four dimensions has to be abandoned, and counterterms involving *evanescent operators* have to be fixed to restore symmetries. For more details and possible solutions, see, Ref. [16].
- Most particles of the EW SM are unstable, and experimental analyses of W/Z bosons, the Higgs boson, and the top-quark have to be based on event signatures of their decay products. Predictions for resonance processes necessarily go beyond any fixed perturbative order, since lowest-order propagators involve a pole, which diverges, instead of a proper resonance structure, which remains finite. Perturbation theory solves this problem by an infinite power series, known as *Dyson series*, of propagator corrections that shifts the pole into the complex k^2 plane for four-momentum transfer k, leading to a Breit–Wigner-like resonance structure with the total decay width of the unstable particle delivering the finite width of the resonance. Identifying the mass square of an unstable particle with the location of the propagator pole, renders the mass of an unstable particle a complex quantity, posing a challenge for the renormalization of the input mass parameter, which is a real quantity. Moreover, the Dyson summation of propagator corrections has to be done with great care, since it necessarily leads to perturbative orders that are only partially included. This jeopardizes the mathematical consistency in predictions, as further discussed at the end of Sec. 10.2.4.
- Non-vanishing vacuum expectation values (vevs) in quantum field theories lead to the appearance of *tadpole graphs,* which are subdiagrams with exactly one external field leg. It is very convenient to eliminate such diagrams by generating a corresponding tadpole counterterm in the renormalization transformation. It is a matter of choice, defining the *tadpole scheme*, to generate the tadpole counterterm in the context of parameter renormalization [24, 25, 31] or field renormalization [28, 32], or both [33]. While predictions within pure OS renormalization schemes do not depend on this choice, predictions employing $\overline{\mathrm{MS}}$-renormalized mass parameters in general do depend on the tadpole scheme. Since some tadpole schemes are prone to lead to very large higher-order corrections and others introduce gauge dependences in predictions, care is needed in applications, especially in the context of $\overline{\mathrm{MS}}$-renormalized masses, see, *e.g.*, Ref. [33].

10.2.3 *Electroweak input parameter schemes*

Starting from its original form, the Lagrangian of the EW SM contains the following free parameters: the couplings g and g' from the gauge interactions, the parameters μ^2, λ from the Higgs potential, and three complex 3×3 matrices y^ℓ, y^u, y^d from the Yukawa interactions of charged leptons and quarks to the Higgs field—there is no such interactions for neutrinos, which are massless in the SM. Owing to possible reparametrizations of the fermion fields that have no effect on observables, not all coefficients of the matrices y^f ($f = \ell, u, d$) are "physical": Only the nine fermion masses $m_{f,i}$, with $i = 1, 2, 3$ labelling the fermion generations, and four independent variables (three angles and one phase) parametrizing the unitary CKM matrix V^{CKM} describing quark mixing are "physical" and have to be taken from experiment. In total, this makes a set of 17 free parameters of the EW model, which are completed to the full SM input by the strong coupling constant α_s and possibly a non-zero parameter θ quantifying strong CP-violation.

The choice of the input parameters for the fermionic sector is widely independent from the input in the bosonic sector. The use

Int. J. Mod. Phys. A 2026.41. Downloaded from www.worldscientific.com
by UNIVERSITY OF CALIFORNIA @ BERKELEY on 09/16/26. Re-use and distribution is strictly not permitted, except for Open Access articles.

of OS-renormalized lepton masses is uncontroversial and common practice. If perturbative predictions sensitively depend on the masses of light quarks, this is a sign of significant non-perturbative effects and mostly connected to strong interactions. In such cases, an input scheme for the perturbative part of a prediction should be chosen to avoid mass-singular contributions from light quarks; if non-perturbative contributions are unavoidable (such as in the running of the electromagnetic coupling at low energies, in parton distribution, or fragmentation functions) these require dedicated additional input from experiment or non-perturbative calculations. Concerning input and renormalization schemes for heavy quarks (top, bottom, etc., in detail depending on the considered observables), the aspects relevant for EW physics are discussed in Sec. 10.4.3; more details can be found in the "Quantum chromodynamics" and "Heavy-quark and soft-collinear effective theory" sections of this *Review*. The determination and use of the CKM parameters is discussed in the section "CKM Quark-Mixing Matrix".

The original set g, g', μ^2, λ of free parameters of the bosonic sector, in practice, is replaced by an equivalent set of four parameters that are more directly accessible by experiment. Candidates for such parameters are the electromagnetic coupling $\alpha = e^2/(4\pi)$, the weak mixing angle θ_W, the weak-boson masses M_W, M_Z, M_H, and the Fermi constant G_F. The ideal choice of four input parameters, which aims at minimal uncertainty in predictions, depends on actual applications. However, it is crucial to consistently stick to one choice for the set of four parameters within a prediction for an observable, in order to guarantee the self-consistency of the result (finiteness, gauge invariance). Apart from the selection of the set of input parameters, the choice of renormalization scheme for each input parameter matters as well. Below we describe the most important choices of input sets and renormalization schemes, also known as *EW input schemes* that are used in calculations of EW precision observables and EW corrections to particle processes. All of these schemes take the (OS-renormalized) Higgs-boson mass M_H as direct input, but differ in the choice or scheme of the other three EW parameters (see, *e.g.*, Refs. [27,34,35] for more details):

- *LEP scheme* with input parameters $\alpha(0), G_F, M_Z$. The W-boson mass M_W can be calculated to high precision in this scheme, exploiting the prediction for muon lifetime τ_μ including radiative corrections, which are encoded in the quantity Δr [22]. In most applications the masses M_Z and M_W are renormalized on-shell, but $\overline{\text{MS}}$ masses can be used as well, proper scheme conversion assumed. The evaluation of Δr requires non-perturbative input in terms of the running effect of $\alpha(Q^2)$ from $Q^2 = 0$ to the EW scale, which is quantified in terms of the quantity $\Delta\alpha(Q^2)$, which in turn is obtained from the *R-ratio* in e^+e^- annihilation via dispersion relations or from lattice calculations. Since M_W, $c_W \equiv \cos\theta_W^{\text{OS}} = M_W/M_Z$, and $s_W \equiv \sin\theta_W^{\text{OS}}$ enter the prediction for τ_μ in a rather complicated way, technically M_W is obtained by solving the experimental τ_μ constraint numerically. Calculations for observables other than the W-boson mass, then best proceed in one of the following schemes employing the calculated value for M_W and dropping $\alpha(0)$ or G_F from the input set.
- $\alpha(0)$*-scheme* with input parameters $\alpha(0), M_W, M_Z$. The electromagnetic coupling is directly fixed by the fine-structure constant $\alpha(0)$, and the weak mixing angle by the OS relation $c_W \equiv \cos\theta_W^{\text{OS}} = M_W/M_Z$. Radiative corrections to most processes at and above the GeV energy range involve the running effect $\Delta\alpha(M_Z^2)$, which then has to be taken as additional non-perturbative input.
- $\alpha(M_Z^2)$*-scheme* with input parameters $\alpha(M_Z^2), M_W, M_Z$. This scheme takes the running coupling constant $\alpha(M_Z^2) \equiv \alpha(0)/[1 - \Delta\alpha(M_Z^2)]$ as input instead of $\alpha(0)$ as in the $\alpha(0)$-scheme. For many processes at and above the EW energy scale, this absorbs the non-perturbative running effects of α into the coupling constant and, thus, into lowest-order predictions, so that no additional non-perturbative input beyond the value of $\alpha(M_Z^2)$ is required in the radiative corrections.
- G_F*-scheme* with input parameters G_F, M_W, M_Z. In this scheme the electromagnetic coupling α, called α_{G_F} in the following, is derived from the lowest-order prediction for τ_μ (*i.e.* G_F) in the $\alpha(0)$ scheme. This procedure effectively absorbs the correction Δr [22] to muon decay into the electromagnetic coupling, which can be expressed by

$$\alpha_{G_F} \equiv \frac{\sqrt{2}G_F M_W^2(1 - M_W^2/M_Z^2)}{\pi} = \alpha(0)[1 + \Delta r]. \quad (10.10)$$

  Since muon decay is a charged-current process, the G_F-scheme effectively absorbs the universal corrections related to the transition from the electromagnetic to the weak charged-current interaction into the lowest-order coupling. These universal corrections are intrinsically connected to the ρ-parameter [36, 37], which relates the ratio of neutral- to charged current-current interactions to the corresponding gauge-boson mass ratio and is discussed in more detail in Sec. 10.2.5 below. Similarly, and although not completely, the G_F-scheme also absorbs into the lowest-order weak neutral-current couplings a large part of corrections to the ρ-parameter.
- EW input parameter schemes with the *leptonic effective weak mixing angle* $\sin^2\theta_{\text{eff}}^\ell$ as free parameter [38] (for the precise definition of $\sin^2\theta_{\text{eff}}^\ell$, see Sec. 10.4.5). Such schemes are motivated by an analysis of neutral-current processes, such as Drell–Yan production, to fit $\sin^2\theta_{\text{eff}}^\ell$ to experimental data and can be obtained from the $\alpha(0)$-, $\alpha(M_Z^2)$-, or G_F-schemes upon replacing M_W by $\sin^2\theta_{\text{eff}}^\ell$ in the list of input parameters. Using $\sin^2\theta_{\text{eff}}^\ell$ as input, the renormalized mass M_W is derived from $\sin^2\theta_{\text{eff}}^\ell$ and M_Z via their LO relation, and the renormalization constant δM_W^2 contains the EW corrections contained in the difference $\sin^2\theta_{\text{eff}}^\ell - (1 - M_W^2/M_Z^2)$ from the renormalization scheme change. The schemes should not be used to predict processes where M_W enters already at LO apart from its indirect appearance via gauge couplings, since the derived LO value for M_W is not in line with precision data. Although this mismatch is cured in higher orders, the scheme would be prone to large corrections, e.g., in predictions for charged-current processes.

From the above, it is clear that a judicious choice of the EW input scheme can be used to absorb the universal effects from the running of α and the ρ-parameter into lowest-order predictions, which systematically helps to minimize EW corrections and, thus, to stabilize predictions. Processes dominated by charged- or neutral-current weak interactions at the EW scale or somewhat above are best described in the G_F-scheme, while processes dominated by the electromagnetic interaction are best described by the $\alpha(0)$ or $\alpha(M_Z^2)$ schemes. Which of the two is more appropriate depends on the number of external photons involved that are truly identified as photons, *i.e.* that are distinguishable from low-virtuality photons splitting in $f\bar{f}$ pairs. True on-shell photons effectively couple with strength $\alpha(0)$, while photons that include splittings $\gamma^* \to f\bar{f}$ up to some scale Q effectively couple with strength $\alpha(Q^2)$.

Note that there are many particle processes for which none of the EW input schemes directly absorbs all universal corrections from $\Delta\alpha$ and $\Delta\rho$ (where $\rho = 1/(1 - \Delta\rho)$) because neither weak nor electromagnetic interactions are dominating all involved couplings. In many cases, however, uniformly[2] rescaling cross-section contributions that are proportinal to some power α^N according to $\alpha(0)^k\alpha(M_Z^2)^l\alpha_{G_F}^m$ with $N = k + l + m$ can help to absorb these universal corrections into lowest-order predictions. Finally, note that any change in the input value of α comes along with some additive contribution from $\Delta\alpha$ and/or Δr to the EW corrections. More details on optimal scheme choices and the necessary modifications in the renormalization procedure can be found in Ref. [27].

[2] Uniformly, in this context means that contributions of a given perturbative order are not taken apart, in order to avoid any disturbance in the cancellation of divergences or gauge dependences.

Int. J. Mod. Phys. A 2026.41. Downloaded from www.worldscientific.com by UNIVERSITY OF CALIFORNIA @ BERKELEY on 09/16/26. Re-use and distribution is [redacted] except for Open Access articles.

10.2.4 *Particle masses*

The masses of the SM particles are a cornerstone in the phenomenological input of the EW SM and its extensions. The masses of the leptons are most uncontroversial in this context: The masses of the charged leptons are measured to very high precision, and the instability of the μ and the τ leptons does not entail any problems owing to their long lifetimes (with ratios of width over mass $\sim 10^{-18}$ and $\sim 10^{-12}$, respectively). We note that, despite the knowledge from neutrino oscillations, which imply that said particles possess non-vanishing masses, neutrinos are treated to be massless in the SM. However, because of the smallness of neutrino masses compared to the energy scales in collider experiments, this approximation is valid to high precision in collider physics.

The situation with quarks is rather different and more complicated: Because of quark confinement, the masses of the quarks u, d, s, c, and b are not directly experimentally accessible; their role in EW physics is described in Sec. 10.4.3 below and more generally in Section 60 on "Quark Masses" in this *Review*. The top-quark is special, since it decays before hadronization. Its mass is directly accessible via kinematical reconstruction in collider experiments or through cross-section measurements of processes involving top-quarks; see the above-mentioned sections as well.

The masses of the EW gauge bosons Z and W play a key role in EW precision physics. Due to the large ratio of total decay width over mass, $\Gamma_V/M_V \sim 3\%$ with $V = Z, W$, and the experimental accessibility of their decay signatures, the masses M_Z and M_W can be extracted from the analysis of differential cross sections featuring resonance structures, i.e. via kinematical reconstruction. On the other hand, the significant ratio Γ_V/M_V implies theoretical subtleties in the calculation of predictions for EW observables, as discussed in the subsequent section.

Since the total decay width Γ_H is rather small ($\sim 4\,\mathrm{MeV}$ in the SM), the resonance lineshape of the Higgs boson cannot be resolved at the LHC, and Γ_H is accessible only indirectly with the caveat of model-dependent assumptions. On the other hand, the smallness of $\Gamma_H/M_H \sim 3 \times 10^{-5}$ implies that there are no subtleties in theory predictions for a SM-like Higgs boson originating from its instability.

Up to higher-order corrections, resonances of an unstable particle P are of Breit–Wigner type, *i.e.* the scattering matrix elements involve contributions enhanced by propagator factors of the form

$$P_P(p^2) = \frac{1}{p^2 - M_P^2 + iM_P\Gamma_P(p^2)}, \tag{10.11}$$

where p is the momentum transferred by the propagator. If the experimental resolution is of the order of the decay width Γ_P, cross-section predictions featuring this resonance, such as invariant-mass distributions of decay products of P, can be fitted to experimental data with fit values for the mass M_P and $\Gamma_P(M_P^2)$. In detail, the fit result depends on the assumed or predicted momentum dependence of $\Gamma_P(p^2)$. Fitting the resonance structure for a constant width, $\Gamma_P(M_P^2) \equiv \overline{\Gamma}_P$, produces the location

$$\mu_P^2 = \overline{M}_P^2 - i\overline{M}_P\overline{\Gamma}_P \tag{10.12}$$

of the propagator pole in the complex p^2-plane, and the resulting masses μ_P and $\overline{M}_P$ are called *complex* and *real pole masses* of P, respectively. Note, however, that most of the existing results on the Z- and W-boson masses M_V ($V = Z, W$) have been based on the parametrization $\Gamma_V(p^2) = p^2/M_P^2 \times \Gamma_V$ with constant Γ_V, which parametrizes the momentum dependence of propagator corrections near the resonance ($p^2 \sim M_V^2$) for the decay of $V = Z, W$ into massless particles. The corresponding mass and width values, M_V and Γ_V, are known as *LEP masses* and *LEP widths*, owing to their first use in the analysis of LEP precision data. The two sets of mass and width are related by [39]

$$\overline{M}_V = \frac{M_V}{\sqrt{1 + \Gamma_V^2/M_V^2}}, \qquad \overline{\Gamma}_V = \frac{\Gamma_V}{\sqrt{1 + \Gamma_V^2/M_V^2}}, \tag{10.13}$$

in particular implying

$$M_W - \overline{M}_W \approx 27\,\mathrm{MeV}, \qquad M_Z - \overline{M}_Z \approx 34\,\mathrm{MeV}, \tag{10.14}$$

i.e. the scheme differences are much larger than the corresponding experimental uncertainties on the W and Z masses (see next section).

To make use of the masses obtained via fitting resonances, it is necessary to identify renormalization schemes that lead to the parametrizations of the resonances employed in the fit:

- In OS renormalization schemes that identify the renormalized (squared) mass with the real part of the location μ_P^2 of the complex pole of the propagator $G^{PP^\dagger}$, the renormalized mass directly corresponds to $\overline{M}_P$. The location of the propagator pole is identical to the complex position of the zero in the (physical part) of the corresponding inverse propagator, also known as *two-point vertex function* $\Gamma^{P^\dagger P} = -i(G^{PP^\dagger})^{-1}$. Since the location of the propagator pole is an intrisinc (and measurable) property of the S-matrix, adopting $\overline{M}_P$ as independent input quantity of the theory does not induce any gauge dependences in predictions [40, 41]. The OS renormalization for $\overline{M}_Z$ and $\overline{M}_W$ is worked out in Ref. [30, 42] at the two-loop level. The complex-mass scheme [43] (see also [27, 44]), which is employed in most EW NLO calculations for resonance processes at the LHC, is an OS renormalization scheme with the complex renormalized mass μ_P based on $\overline{M}_P$ and the (measured or calculated) value of $\overline{\Gamma}_P$.
- Tying the OS renormalized mass to the real zero in $\mathrm{Re}\{\Gamma^{P^\dagger P}\}$ (which is the prescription in the real OS scheme, see *e.g.* Refs. [22, 24, 25]), instead of taking the real part of the complex zero of $\Gamma^{P^\dagger P}$, is equivalent at NLO, but not beyond. For the Z and W masses, these differences have, *e.g.*, been worked out in Refs. [27, 30, 42, 45, 46], revealing that the Z and W masses in the real OS scheme (based on the zeroes of $\mathrm{Re}\{\Gamma^{V^\dagger V}\}$, $V = Z, W$) correspond to the LEP masses M_Z and M_W introduced above that result from the fit to Breit–Wigner distributions with running widths (at least in the 't Hooft–Feynman gauge). As already pointed out in Ref. [45], using renormalized masses of this real OS scheme to parametrize predictions leads to gauge dependences starting at the two-loop level.[3] For predictions beyond NLO precision, the use of $\overline{M}_P$ is, thus, preferable over the use of M_P.
- $\overline{\mathrm{MS}}$-renormalized masses are not directly related to parameters appearing in any form of Breit–Wigner-like resonances. To extract them from data, one either has to make use of precision calculations for measured observables (such as cross sections or decay widths) with complicated mass dependences, or to convert measured OS masses into the $\overline{\mathrm{MS}}$ scheme. For the Z and W bosons this scheme conversion is carried out in Refs. [47–50].
- Extracting the top-quark mass from kinematical distributions is impeded by strong-interaction effects, limiting the concept of *long-distance top-quark masses* such as OS-renormalized masses. Perturbative predictions are more stable if a *short-distance top-quark mass* is employed, such as provided by the $\overline{\mathrm{MS}}$ scheme. More details on this subject can be found section "Top Quark" of this *Review*.

We finally emphasize that the issue of calculating higher-order corrections to processes with unstable particles goes far beyond a proper definition of mass and width of the unstable particle, and beyond parametrizing resonance patterns and identifying resonance parameters with renormalized parameters of the underlying field theory. Issues with gauge invariance, unitarity, UV and IR divergences, and the embedding of resonances into full off-shell processes concern the complete underlying matrix elements. These issues are due to the fact that the identities ruling gauge invariance *(Ward and Slavnov-Taylor identities)* and finiteness are typically working order by order in perturbation theory, but the inclusion of finite-width effects in resonance propagators originates from a Dyson summation of propagator corrections, necessarily resulting

[3] This means that all higher-order calculations beyond NLO (including the ones used to extract M_Z and M_W from data) would have to be carried out in the same gauge, or proper parameter conversions would have to be made when changing the gauge.

Int. J. Mod. Phys. A 2026.41. Downloaded from www.worldscientific.com
by UNIVERSITY OF CALIFORNIA @ BERKELEY on 09/16/26. Re-use and distribution is strictly not permitted, except for Open Access articles.

in perturbative orders that are taken into account only partially in predictions. Different solutions to these problems have been described in the literature, targeting at different kinematical situations and different levels of sophistication: If resonances need not be resolved, variants of *narrow-width approximations* based on production and decay subprocesses might be sufficient (depending on the experimental precision). The neighborhood of resonances can be described via dedicated *pole expansions* [51, 52] of matrix elements leading to *pole approximations*, as described for single resonances in Refs. [35, 53–58]. The concept of leading pole approximations has also been successfully applied to processes with multiple resonances, see, *e.g.*, Refs. [59–63]. Many modern analyses of many-particle processes even require precision in resonant and non-resonant regions of phase space, as, *e.g.*, provided by the complex-mass scheme [43, 44] at NLO. Descriptions of these concepts as well as further references can be found in Ref. [27].

10.2.5 *Radiative corrections to electroweak processes*

Radiative corrections, in particular the ones induced by the EW interactions, play an integral role in the simulation of EW processes and predictions for corresponding observables analyzed at particle colliders. For instance, for a proper analysis of data collected at the LHC [64–67], most precision calculations have reached the standard that QCD and EW corrections are known at NLO for virtually all EW key processes and even at next-to-next-to-leading order (NNLO) QCD for the $2 \to 2$ processes [68–70]. The underlying modern methods for calculating radiative corrections are very well advanced and implemented in public tools that make (semi-)automatic calculations possible, depending on their complexity (see, *e.g.*, Refs. [27,71] and references therein). Predictions for specific kinematic configurations, such as low-p_{T} production of W/Z production, might call for improvements beyond fixed perturbative orders; details and references on the corresponding QCD resummation and parton-shower techniques can be found in Section 9 on "Quantum Chromodynamics" in this *Review*. Event simulations typically require additional improvements on particle emission effects in QCD and QED via matching fixed-order predictions, as provided by dedicated precision Monte Carlo programs or MadGraph/MadEvent [72, 73], with *parton showers* and merging them with corrections for higher jet multiplicities based on matrix elements. This matching and merging is provided in different variants within the multi-purpose Monte Carlo event generators Herwig [74,75], Pythia [76], and Sherpa [77–79]. For the analysis of high-precision EW observables (see, *e.g.*, Ref. [80]) even NNLO EW corrections and the dominant effects beyond the two-loop level are relevant.

Different types of radiative corrections to particle processes have to be combined with care in order to avoid double-counting of effects, to respect gauge invariance, and to guarantee a proper cancellations of IR singularities.

- Complicated processes, such as vector-boson scattering, often receive LO contributions from different perturbative orders $\propto \alpha_s^m \alpha^n$, so that already NLO corrections lead to a tower of mixed orders formed by contributions $\propto \alpha_s^{m+1}\alpha^n$ or $\propto \alpha_s^m \alpha^{n+1}$. In such cases, a strict classification of corrections into QCD and EW contributions is not generally possible, but separating the various orders is possible and often instructive.
- Single perturbative orders $\propto \alpha_s^m \alpha^n$ can be further split into gauge-invariant subcontributions by considering contributions featuring closed fermion loops or the emission of fermion–antifermion pairs.[4] These *fermionic corrections* can be further classified according to their multiplicity factor N_f^k, where N_f is the number of light fermion flavors. Isolating such subcontributions often helps to locate dominant corrections that warrant the inclusion of higher-order corrections with similar enhancements.
- Since photonic corrections can be potentially large, their separation from the remaining EW corrections is desirable, but this is not always possible in a gauge-invariant way. For processes that feature only neutral-current interactions at LO, this separation can be achieved, however. Arguments for this gauge-invariant separation of QED effects, which can be further decomposed into photonic and fermionic parts as described in the previous item, can be based on the observation that the charged-current sector can be removed from the SM in such a way that a fully consistent "neutral-current theory" with gauge group $\mathrm{U}(1)_Z \times \mathrm{U}(1)_{\mathrm{em}}$ results [27]. The separation of photonic corrections was extremely useful in precision calculations for Z production via e^+e^- annihilation at LEP and SLC, $e^+e^- \to Z/\gamma^* \to f\bar{f}$, so that the inclusion of higher-order photonic corrections to the Z lineshape was possible without knowing the full EW corrections beyond NLO [34, 35, 54].

The analysis of the Z resonance in $e^+e^- \to Z/\gamma^* \to f\bar{f}$ is a cornerstone of EW precision physics. The separation of the large photonic corrections from the remaining weak corrections to the Z lineshape, in combination with the smallness of the irreducible (box) weak corrections near the Z resonance, is the basis of the parametrization of the cross section and its asymmetries in terms of *pseudo-observables*, such as the Z peak cross section, the total and partial Z decay widths, forward–backward (FB) as well as polarization asymmetry variables, effective Z couplings, and the *effective weak mixing angle for each fermion* f quantified by $\bar{s}_f^2 \equiv \sin^2\theta_{\mathrm{eff}}^f$, etc. (see Section 10.4 for a precise definition of these quantities). The Z-pole pseudo-observables can be predicted to high precision, independent of the full prediction of the Z-boson lineshape, and play a key role in the global SM fit to data:

- EW corrections to the Z-pole pseudo-observables comprise (flavor-dependent) $Zf\bar{f}$ vertex corrections (see, *e.g.*, Refs. [24, 81]) as well as (flavor-independent) contributions to the $\gamma\gamma$, γZ, ZZ, and WW gauge-boson self-energies (*i.e.vacuum polarization* diagrams), the latter entering via EW renormalization constants (see, *e.g.*, Refs. [24, 25]).
  While being gauge dependent in general, there are several distinct and important contributions from gauge-boson self-energies that lead to gauge-invariant corrections to EW precision observables, in particular contributions from closed fermion loops and the corresponding QCD corrections. For instance, the mixed QCD–EW contributions to gauge-boson self-energies of orders $\alpha\alpha_s m_t^2$ [82, 83], $\alpha\alpha_s^2 m_t^2$ [84, 85], and $\alpha\alpha_s^3 m_t^2$ [86–88] increase the predicted value of m_t by 6%.[5] The sub-leading $\alpha\alpha_s$ corrections [89–93] are also included in the predictions for the Z-pole pseudo-observables. Further three-loop corrections of order $\alpha\alpha_s^2$ [94, 95], $\alpha^3 m_t^6$, $\alpha^2\alpha_s m_t^4$ [96, 97], α_f^3 and $\alpha_f^2\alpha_s$ [98, 99] are rather small (here α_f denotes EW corrections with a closed fermion loop).
- Z-pole pseudo-observables are among the still very few examples for which complete NNLO EW corrections are known. The EW two-loop corrections for the relation between $\bar{s}_\ell^2$ and s_W^2 are given in Refs. [100–105], the ones to $\bar{s}_f^2$ ($f \neq$ top), the effective couplings of fermions f to the Z boson, and the partial and total Z decay widths in Refs. [58, 106–110].
- All EW observables that depend on the weak mixing angle θ_W in LO receive contributions from its renormalization, in particular significant corrections from the ρ parameter [36, 37], $\rho = 1/(1-\Delta\rho)$, as defined from the neutral-to-charged-current cross-section ratio at low energies, *i.e.*

$$\Delta\rho = \frac{\Sigma_{\mathrm{T}}^{ZZ}(0)}{M_Z^2} - \frac{\Sigma_{\mathrm{T}}^{WW}(0)}{M_W^2}, \tag{10.15}$$

  where $\Sigma_{\mathrm{T}}^{VV}(0)$ is the (transverse part of the) Z/W boson self-energy at zero momentum transfer, following the notation of

[4] This is due to the fact that adding or removing fermion generations to or from the SM respects gauge invariance. (Working in a field basis corresponding to mass eigenstates, the added/removed generations should not mix with the other generations.)

[5] This is, however, almost entirely an artifact of using the pole mass definition for m_t. The equivalent corrections when using the $\overline{\mathrm{MS}}$ definition $\widehat{m}_t(\widehat{m}_t)$ increase m_t by less than 0.5%.

Int. J. Mod. Phys. A 2026.41. Downloaded from www.worldscientific.com by UNIVERSITY OF CALIFORNIA @ BERKELEY on 09/16/26. Re-use and distribution is [redacted] except for Open Access articles.

Refs. [24, 25, 27]. The largest contribution $\Delta\rho_t$ to $\Delta\rho$,

$$\Delta\rho_t = \frac{3G_F m_t^2}{8\sqrt{2}\pi^2} = 0.00934 \times \frac{m_t^2}{(172.61\ \text{GeV})^2}\ , \qquad (10.16)$$

results from one-loop diagrams with closed fermion loops involving the top-quark. Two-loop corrections involving the top-quark modify $\Delta\rho_t$ by

$$\Delta\rho_t \to \Delta\rho_t \left[1 + R(M_H, m_t)\,\frac{\Delta\rho_t}{3}\right]\ . \qquad (10.17)$$

The function $R(M_H, m_t)$ can be described as an expansion in M_Z^2/m_t^2, for which the leading m_t^4/M_Z^4 [111, 112] and next-to-leading m_t^2/M_Z^2 [113, 114] terms are known. Beyond the two-loop level, leading top-mass-enhanced contributions to $\Delta\rho$ have been calculated to the orders $\alpha_s^2\alpha m_t^2$ [84, 85, 95], $\alpha_s\alpha^2 m_t^4$ and $\alpha^3 m_t^6$ [96, 97], and $\alpha_s^3\alpha m_t^2$ [86–88].

The extraction of the W-boson mass M_W from the measured muon decay lifetime (or Fermi constant) is another cornerstone in the fit of the SM to precision observables. In detail, M_W is obtained by solving the implicit equation (10.10) for M_W, where the Fermi constant G_F is extracted from the measured muon lifetime (see Section 10.3.2) and the quantity Δr [22] represents the radiative corrections to muon decay. At NLO, the correction Δr receives sizeable contributions from $\Delta\alpha$ and $\Delta\rho$ of $\sim +6\%$ and $\sim -3\%$, respectively, leaving only a small remainder Δr_{rem} of $\sim 1\%$,

$$\Delta r^{(1)} = \Delta\alpha - \frac{c_W^2}{s_W^2}\,\Delta\rho + \Delta r_{\text{rem}}\ . \qquad (10.18)$$

The complete two-loop calculation of Δr in the OS renormalization scheme has been performed in Refs. [42, 115–118]. The two-loop QCD correction of order $\alpha\alpha_s$ and the fermionic[6] electroweak two-loop correction of order α^2 amount to about 10% of the one-loop correction to Δr, both with the same sign, $\sim +0.4\%$ and $\sim 0.3\%$, respectively. The three-loop QCD correction, $\alpha\alpha_s^2$, amounts to $\sim 0.07\%$ while the bosonic two-loop electroweak correction is very small ($\sim 0.006\%$). Taking into account leading higher-order effects from $\Delta\rho$, the theoretical uncertainty from unknown higher-order corrections is estimated to 4 MeV for the prediction of M_W [119]. The recent calculation [120] of $\alpha^2\alpha_s$ corrections to Δr, which is not yet employed in the SM fits described below, revealed a further shift of ~ 3 MeV in M_W, confirming that the 4 MeV theory uncertainty in M_W is quite realistic and not too conservative. In an alternative approach, Ref. [121] obtained the $\overline{\text{MS}}$ quantities $\Delta\widehat{r}$ and $\widehat{\rho}$ to two-loop accuracy, confirming the prediction of M_W in the OS scheme from Refs. [42, 119] within about 4 MeV. More recently, Δr has been calculated within an alternative ("tadpole-free") version of EW $\overline{\text{MS}}$ renormalization at the two- and three-loop levels in Refs. [122, 123], respectively, the latter in the approximation of the "gauge-less limit"; the calculations within this scheme, however, have not yet been applied to predictions for the OS-renormalized W-boson mass.

Throughout this *Review* we utilize predictions for EW precision observables including the relevant EW radiative corrections from the programs `Gfitter` [124–127] and `HEPfit` [128–132]. Both `Gfitter` and `HEPfit` follow the OS renormalization scheme in their implementations of the radiative corrections for EW precision observables, in contrast to the `GAPP` package [133], used in the fits presented in previous editions of this *Review*, which works entirely in the $\overline{\text{MS}}$ scheme. Observables including corrections beyond NLO, such as the W-boson mass, the effective weak mixing angle(s), and the pseudo-observables at the Z resonance are implemented via the semi-analytical approximations provided in Refs. [105, 106, 110, 119]. The uncertainties from missing higher-order corrections on the different (pseudo-)observables are also taken into account, using the estimates given in those references, in the computation of the SM predictions. The W-boson decay width is computed at the one-loop level, using the expressions given in Refs. [55, 134, 135] (in agreement with the independent results of Ref. [136]). This observable is currently known with comparatively lower precision than those at the Z pole, but the corresponding theory uncertainty is still smaller than the experimental precision.

Several other tools are available in the literature for the calculation of EW corrections to the considered (pseudo-)observables and to perform the EW fit. The package `GRIFFIN` [58] provides a framework for the calculation of $2 \to 2$ fermion processes which, in its current version provides the full NNLO and the leading higher-order corrections for processes at the Z pole. Among the different codes for calculating EW precision observables available in the literature, `ZFITTER` has a prominent place [137, 138], due to its key role in the original studies of the LEP Electroweak Working Group [139, 140].

After this overview of the practical aspects relevant to SM calculations in the EW sector, we next discuss some of the most important observables that validate the SM description of EW interactions.

10.3 Low-energy observables

10.3.1 *The electromagnetic coupling*

As in pure QED, the coupling constant e is identified with the electromagnetic coupling strength of physical (on-shell) electrons in the limit of low-energy transfer *(Thomson limit), i.e.*, e is the electric unit charge of classical electrodynamics.[7] This OS renormalization of e in the Thomson limit ensures the property of *charge universality, i.e.* it guarantees that, in this limit, one can renormalize e via the electromagnetic interaction of any fermion (actually any charged particle), obtaining the same result as for electrons.

The *fine structure constant* $\alpha(0) \equiv e^2/(4\pi)$ can be extracted from the anomalous magnetic moment of the electron, $a_e = (1\,159\,652\,180.59 \pm 0.13) \times 10^{-12}$ [143]. Application of QED corrections up to five-loop order [144–146] produces the value $\alpha(0)^{-1} = 137.035\,999\,166(15)$. Here, the number in parentheses denotes the uncertainty in the last digits shown. This determination of $\alpha(0)^{-1}$ from a_e has recently been re-evaluated [147], updating the tenth-order QED term of a_e and the evaluation of the hadronic vacuum polarization (HVP) contribution, finding the compatible value $\alpha(0)^{-1} = 137.035\,999\,163(15)$. Another approach combines measurements of the Rydberg constant and atomic masses with interferometry of atomic recoil kinematics. Applied to ^{87}Rb [148] and ^{133}Cs [149], this method implies the results $\alpha(0)^{-1} = 137.035\,999\,206(11)$ and $\alpha(0)^{-1} = 137.035\,999\,046(27)$, respectively. These two measurements differ by 5.5 σ, where the origin of this discrepancy is currently not understood. While it is not advisable to combine measurements with such a tension, it is worth pointing out that the absolute magnitude of this discrepancy is at a level where it has no significant impact on the EW fit. We use the value quoted in Section 1 ("Physical Constants") in this *Review*,

$$\alpha(0)^{-1} = 137.035\,999\,177(21), \qquad (10.19)$$

which is a combination of the results from a_e and atomic interferometry.

As explained in Section 10.2.3, in EW higher-order calculations it can be convenient to define a running α dependent on the energy scale of the process, with $\alpha(0)^{-1} \approx 137.036$ appropriate at very low energy, *i.e.* close to the Thomson limit. The L3 [150] and OPAL [151] collaborations at LEP could also observe the running directly in small and large angle Bhabha scattering, respectively. For scales above a few GeV the low-energy hadronic contribution to the electromagnetic vacuum polarization introduces a theoretical uncertainty in α, so that it is often convenient to use the value

$$\alpha(M_Z^2) = \frac{\alpha(0)}{1 - \Delta\alpha(M_Z^2)} \qquad (10.20)$$

[6] Fermionic contributions at NNLO denote contributions from diagrams with closed fermion loops, whereas bosonic contributions are all remaining two-loop diagrams.

[7] *Thirring's QED theorem [141],* which is valid in the EW theory as well [142], makes this link between quantum field theory and classical electrodynamics very explicit, as it states that the Compton scattering cross section turns into the classical Thomson cross section in the low-energy limit, *i.e.*, the radiative corrections to Compton scattering vanish in the Thomson limit to all perturbative orders.

Int. J. Mod. Phys. A 2026.41. Downloaded from www.worldscientific.com
by UNIVERSITY OF CALIFORNIA @ BERKELEY on 09/16/26. Re-use and distribution is strictly not permitted, except for Open Access articles.

as phenomenological input, where $\Delta\alpha(M_Z^2)$ contains the running effects of $\alpha(Q^2)$ from $Q^2 = 0$ to $Q^2 = M_Z^2$. In particular, the hadronic contribution $\Delta\alpha_{\rm had}^{(5)}(M_Z^2)$, corresponding to five active quark flavors (*i.e.* without top-quark contribution) driving the running, is a non-perturbative input obtained from measurements of the R ratio in e^+e^- annihilation at low energies, and perturbative QCD predictions of R at medium and large energies. Various evaluations of $\Delta\alpha_{\rm had}^{(5)}(M_Z^2)$ are summarized in Table 10.1.

The quantity $\alpha(Q^2)$ is closely related to the running electromagnetic coupling $\widehat{\alpha}(Q^2)$ in the $\overline{\rm MS}$ scheme[8] [26] used in previous editions of this *Review*. The precise relation between $\alpha(M_Z^2)$ and $\widehat{\alpha}(M_Z^2)$ is determined by the difference in $\Delta\alpha(M_Z^2)$ (obtained using Refs. [152, 153]),[9]

$$\begin{aligned}
&\Delta\widehat{\alpha}(M_Z^2) - \Delta\alpha(M_Z^2) \\
&= \frac{\alpha}{\pi}\left[\frac{100}{27} - \frac{1}{6} - \frac{7}{4}\ln\frac{M_Z^2}{M_W^2} + \frac{\alpha_s(M_Z^2)}{\pi}\left(\frac{605}{108} - \frac{44}{9}\zeta(3)\right)\right. \\
&+ \frac{\alpha_s^2}{\pi^2}\left(\frac{976481}{23328} - \frac{253}{36}\zeta(2) - \frac{781}{18}\zeta(3) + \frac{275}{27}\zeta(5)\right) \\
&+ \frac{\alpha_s^3}{\pi^3}\left(\frac{1483517111}{3359232} - \frac{22781}{144}\zeta(2) - \frac{3972649}{7776}\zeta(3) - \frac{31}{81}\zeta(2)^2\right. \\
&\left.\left. + \frac{521255}{7776}\zeta(5) - \frac{7315}{324}\zeta(7) + \frac{5819}{54}\zeta(2)\zeta(3) + \frac{14675}{162}\zeta(3)^2\right)\right] \\
&= 0.007123(1)(5)\ , \qquad (10.21)
\end{aligned}$$

where the first part of the lowest-order term is from fermions and the other two are from $W^\pm$ loops, which are usually excluded from the OS definition. Fermion mass effects and corrections of $\mathcal{O}(\alpha^2)$ contributing to Eq. (10.21) are small, partly cancel each other and are not included here. The first error in Eq. (10.21) is parametric from α_s and the second is from the truncation of the perturbative expansion.

The most recent results of $\Delta\alpha_{\rm had}^{(5)}(M_Z^2)$ [163–166] typically assume the validity of perturbative QCD (pQCD) at scales of about 2 GeV and above for the continuum contribution and are in good agreement with each other. In regions where pQCD cannot be trusted, one can use $e^+e^- \to$ hadrons cross-section data (for a list of references see, *e.g.*, Ref. [165]) and isospin rotated information derived from τ decay spectral functions [167], where the latter derive from ALEPH [168], Belle [169], CLEO [170], and OPAL [171]. More recently, new results at low energy ($\pi^+\pi^-$) have been published from the CMD-3 experiment [172] at the e^+e^- collider VEPP-2000. There is noticeable spread in the existing results, with lattice QCD [156] and CMD-3 suggesting a stronger running than KLOE data. While VEPP-2000 and VEPP-4M scanned center-of-mass (CM) energies up to 2 GeV and between about 3 and 4 GeV, respectively, the BABAR collaboration studied multi-hadron events radiatively returned from the $\Upsilon(4S)$, reconstructing the radiated photon and normalizing to $\mu^+\mu^-\gamma$ final states. A discrepancy in the $e^+e^- \to \pi^+\pi^-$ data from BABAR and KLOE has been taken into account in Ref. [165] as an additional uncertainty. The new results from CMD-3 cannot be included in determinations of $\Delta\alpha_{\rm had}^{(5)}(M_Z^2)$ without introducing additional uncertainties to accommodate for the discrepancy with KLOE data or taking into account small p-values. We use the value $\Delta\alpha_{\rm had}^{(5)}(M_Z^2) = 0.02760 \pm 0.00010$ from Ref. [165] in our fit, which has been obtained for $\alpha_s(M_Z^2) = 0.1193 \pm 0.0028$. The dependence on $\alpha_s(M_Z^2)$ is taken into account in the fit. The uncertainty on $\Delta\alpha_{\rm had}^{(5)}(M_Z^2)$ is dominated by systematic effects in the cross-section data and the uncertainty in the pQCD prediction.

10.3.2 *The Fermi constant*

Owing to its extraordinarily high experimental precision, the Fermi constant G_F is often taken as input in the EW model, *e.g.*, replacing the electromagnetic coupling α or the W-boson mass M_W in the list of input parameters. The parameter G_F is derived from the muon lifetime $\tau_\mu = 2196981.1 \pm 2.2$ ps, obtained in the Particle Listings in this *Review*. The average is dominated by the result of the MuLan Collaboration [173, 174] at the PSI that reduced the uncertainty by an order of magnitude compared to previous results. The Fermi constant is derived from τ_μ according to[10]

$$\begin{aligned}
\frac{\hbar}{\tau_\mu} = \frac{G_F^2 m_\mu^5}{192\pi^3}\, F(\rho)\Big[1 + H_1(\rho)\frac{\widehat{\alpha}(m_\mu^2)}{\pi} + H_2(\rho)\frac{\widehat{\alpha}^2(m_\mu^2)}{\pi^2} \\
+ H_3\frac{\widehat{\alpha}^3(m_\mu^2)}{\pi^3}\Big]\ , \qquad (10.22)
\end{aligned}$$

where $\rho = m_e^2/m_\mu^2$, $\widehat{\alpha}(Q^2)$ is the electromagnetic coupling in the $\overline{\rm MS}$ scheme, and

$$F(\rho) = 1 - 8\rho + 8\rho^3 - \rho^4 - 12\rho^2\ln\rho = 0.99981295\ , \qquad (10.23a)$$

$$\begin{aligned}
H_1(\rho) = \frac{25}{8} - \frac{\pi^2}{2} - \left(9 + 4\pi^2 + 12\ln\rho\right)\rho \\
+ 16\pi^2\rho^{3/2} + \mathcal{O}(\rho^2) = -1.80793\ , \qquad (10.23b)
\end{aligned}$$

$$\begin{aligned}
H_2(\rho) = \frac{156815}{5184} - \frac{518}{81}\pi^2 - \frac{895}{36}\zeta(3) + \frac{67}{720}\pi^4 + \frac{53}{6}\pi^2\ln 2 \\
- (0.042 \pm 0.002)_{\rm had} - \frac{5}{4}\pi^2\sqrt{\rho} + \mathcal{O}(\rho) = 6.64\ , \qquad (10.23c)
\end{aligned}$$

$$\widehat{\alpha}(m_\mu^2)^{-1} = \alpha^{-1} + \frac{1}{3\pi}\ln\rho + \mathcal{O}(\alpha) = 135.901\ . \qquad (10.23d)$$

H_1, H_2, and H_3 capture the QED corrections within the Fermi model. The results for $\rho = 0$ have been obtained in Refs. [175] and [176, 177] for H_1 and H_2, respectively, where the term in parentheses is from the hadronic vacuum polarization [176]. The mass corrections to H_1 and H_2 have been calculated in [178] and [179], respectively. Notice the term linear in m_e in H_2 whose appearance was unforeseen and can be traced to the use of the muon pole mass in the prefactor [179]. The coefficient $H_3 = -15.3 \pm 2.3$ has been estimated in Refs. [180–182].

The estimation of H_3 reduces the uncertainty from missing higher orders significantly, resulting in

$$G_F = 1.1663785(6) \times 10^{-5}\ {\rm GeV}^{-2}, \qquad (10.24)$$

where the remaining uncertainty in G_F is mostly from experimental sources in the measurement of τ_μ.

10.3.3 *The muon anomalous magnetic moment*

In 2025 the Muon $g-2$ Collaboration at Fermilab has released a new measurement [183] of the muon anomalous magnetic moment $a_\mu \equiv (g_\mu - 2)/2$, based on theirs Runs 4–6, which combines with their previous result from Runs 1–3 [184, 185] to

$$a_\mu^{\rm FNAL} = (116592070.5 \pm 14.8) \times 10^{-11}\ . \qquad (10.25)$$

Combining the FNAL result with the result from the BNL E821 collaboration [186], which is compatible with all FNAL results on a_μ, leads to the world average

$$a_\mu^{\rm exp} = (116592071.5 \pm 14.5) \times 10^{-11}\ . \qquad (10.26)$$

[8] In this Section we denote quantities defined in the $\overline{\rm MS}$ scheme by a caret; the exception is the strong coupling constant, α_s, which will always correspond to the $\overline{\rm MS}$ definition and where the caret will be dropped. Furthermore, $\alpha^{(n)}$ and $\alpha_s^{(n)}$ denote the running couplings with n active quark flavors.

[9] $\widehat{\alpha}(M_Z^2)$ can be directly evaluated in the $\overline{\rm MS}$ scheme using the FORTRAN package GAPP [133], including the QED contributions of both leptons and quarks. The leptonic three-loop [154] and four-loop [155] contributions in the OS scheme are known as well.

[10] In the spirit of the Fermi theory, the small propagator correction, $3/5\ m_\mu^2/M_W^2$, is included into the correction Δr (see below). This is also the convention adopted by the MuLan collaboration [173]. While this breaks with historical consistency, the numerical difference was negligible in the past.

Int. J. Mod. Phys. A 2026.41. Downloaded from www.worldscientific.com by UNIVERSITY OF CALIFORNIA @ BERKELEY on 09/16/26. Re-use and distribution is except for Open Access articles.

Table 10.1: Evaluations of the on-shell $\Delta\alpha_{\rm had}^{(5)}(M_Z^2)$ by different groups. For better comparison we adjusted central values and errors to correspond to a common and fixed value of $\alpha_s(M_Z^2) = 0.120$, except for Ref. [156], for which α_s is not an explicit input. References quoting results without the top-quark decoupled are converted to the five flavor definition. Ref. [157] uses $\Lambda_{\rm QCD} = 380 \pm 60$ MeV; for the conversion we assumed $\alpha_s(M_Z^2) = 0.118 \pm 0.003$.

Reference	Result	Comment
Krasnikov, Rodenberg (1997) [158]	0.02737 ± 0.00039	pQCD for $\sqrt{s} > 2.3$ GeV
Kühn & Steinhauser (1998) [159]	0.02778 ± 0.00016	full $\mathcal{O}(\alpha_s^2)$ for $\sqrt{s} > 1.8$ GeV
Groote *et al.* (1998) [157]	0.02787 ± 0.00032	use of QCD sum rules
Martin *et al.* (2000) [160]	0.02741 ± 0.00019	incl. new BES data
de Troconiz, Yndurain (2001) [161]	0.02754 ± 0.00010	pQCD for $s > 2$ GeV^2
Burkhardt, Pietrzyk (2011) [162]	0.02750 ± 0.00033	pQCD for $\sqrt{s} > 12$ GeV
Erler, Ferro-Hernández (2017) [163]	0.02761 ± 0.00010	conv. from $\overline{\rm MS}$ scheme
Jegerlehner (2019) [164]	0.02755 ± 0.00013	Euclidean split technique
Davier *et al.* (2019) [165]	0.02761 ± 0.00010	pQCD for $\sqrt{s} = 1.8{-}3.7$ & > 5 GeV
Keshavarzi *et al.* (2019) [166]	0.02761 ± 0.00011	pQCD for $\sqrt{s} > 11.2$ GeV
Cè *et al.* (2022) [156]	0.02773 ± 0.00015	LQCD for Euclidian $Q^2 < 5$ GeV^2

This experimental result is in good agreement with the SM prediction released in the 2025 White Paper (WP25) [147],

$$a_\mu^{\rm SM} = (116592033 \pm 62) \times 10^{-11} \ , \qquad (10.27)$$

which contains a significant upward shift with respect to the previous SM prediction reported in the 2020 White Paper (WP20) [187], resolving a long-standing tension of $\sim 2{-}4\,\sigma$ between experiment and theory.

The by far dominating contribution to $a_\mu^{\rm SM}$ is due to QED corrections, which have been calculated to five loops [144, 146, 188–190] (fully analytic to three loops [191–195]). The SM EW contribution [196–201], reported in [147] to $a_\mu^{\rm EW} = (154.4{\pm}4.0){\times}10^{-11}$, includes two-loop [202–206] and leading three-loop [207, 208] corrections and is roughly an order of magnitude larger than the current experimental uncertainty. The major part of the theory uncertainties result from HVP effects, which were entirely taken from lattice-QCD calculations in WP25 (see references therein). The small, but non-negligible NLO and NNLO HVP contributions are taken from mixing data from $e^+e^- \to$ hadrons with perturbative QCD predictions, with the corresponding uncertainties. The switch from the previously used experimental HVP results from $e^+e^- \to$ hadrons cross sections to lattice results accounts for the significant change in $a_\mu^{\rm SM}$ from WP20 to WP25. This paradigm shift was justified in WP25 in part by the great consolidation of lattice HVP results in recent years and in part by the increasing tension among the relevant experimental $e^+e^- \to \pi^+\pi^-$ cross-section data after including recent measurements by CMD-3 [172,209]. The second largest uncertainty in $a_\mu^{\rm SM}$ is due to effects from hadronic light-by-light (HLbL) scattering. In the step from WP20 to WP25, the predictions for HLbL effects, both on the lattice and data-driven side (see WP25 for references) have increased in precision and show good mutual agreement. Further reducing the theory uncertainty in $a_\mu^{\rm SM}$ and resolving the tension between lattice and data-driven HVP determinations will be an important goal for future work. For more details and references, see Section 56 on the "Muon Anomalous Magnetic Moment" in this *Review*.

The results on a_μ have not been taken into account in the SM fit to data below, because they do not influence the fit significantly. The sensitivity of $a_\mu^{\rm SM}$ to the EW parameters is way below the remaining theory uncertainty. On the other hand, predictions for a_μ are sensitive to new physics effects, such as in supersymmetric models with large $\tan\beta$ and moderately light superparticle masses [210], or a dark Z boson [211].

10.4 Electroweak precision physics

10.4.1 *Z- and W-boson masses and widths*

The most precise measurement of the mass of the Z boson has been obtained by a combination of the ALEPH, DELPHI, L3, and OPAL data from LEP 1 [139],

$$M_Z = 91.1876 \pm 0.0021\,{\rm GeV} \ . \qquad (10.28)$$

The uncertainty in this result is dominated by the knowledge of the LEP beam energy. Recently, new results from hadron colliders have been obtained. The CDF Collaboration determined M_Z from fits to the dimuon and dielectron mass distributions [212], resulting in $M_Z = 91.1920 \pm 0.0075$ GeV and 91.1943 ± 0.0158 GeV, respectively. The LHCb Collaboration used $Z \to \mu^+\mu^-$ decays only and obtained a value of 91.1857 ± 0.0092 GeV [213]. Combined, these measurements result in the current world average

$$M_Z = 91.1879 \pm 0.0020\,{\rm GeV}, \qquad (10.29)$$

which we use in the global fit presented below. In the context of a measurement of the W-boson mass, the CMS Collaboration reports $M_Z = 91.1858 \pm 0.0048$ GeV [214], obtained from $Z \to \mu^+\mu^-$ decays. While the uncertainty in this measurement is only about two times larger than the LEP 1 combination, this measurement is only used to define the systematic uncertainty in the muon momentum scale calibration for the M_W measurement and detailed studies of systematic uncertainties are missing. Hence, we do not include this measurement in the M_Z combination.

The values above correspond to a definition based on a Breit–Wigner shape with an energy-dependent width, which differs from $\overline{M}_Z$ derived from the complex location of the propagator pole as given in Eq. (10.14).

The LEP 1 results also include a determination of the total Z-boson decay width with a precision of one per-mil [139, 215],

$$\Gamma_Z = 2.4955 \pm 0.0023\,{\rm GeV}. \qquad (10.30)$$

Among the most important LEP 2 results were the measurements of the W-boson mass, M_W [216][11]. These were dominated by measurements using the direct kinematic reconstruction of the W-boson decay products, but included a complementary determination from a WW threshold cross-section measurement. The latter determination resulted in a less precise value of M_W because of a large statistical uncertainty, but this technique offers

[11] LEP 2 [216] ran at several energies above the Z pole up to ~ 209 GeV. Measurements were made of a number of observables, including the total production cross sections of $f\bar{f}$ pairs for $f = \mu, \tau$, and q (hadrons), of four-fermion final states, of $\gamma\gamma$, ZZ, WW and $WW\gamma$. The differential cross sections for all three lepton flavors, and the leptonic and hadronic W branching ratios were also extracted, as discussed in Section 10.4.7. The measurements of single- and di-boson production were also used to set constraints on anomalous triple and quartic gauge couplings. These anomalous interactions have also been studied in hadron collisions at the Tevatron and the LHC. We refer the reader to the "Extraction of Triple Gauge Couplings (TGCs)", "Anomalous W/Z Quartic Couplings (QGCs)" notes in the W particle listing and the "Anomalous $ZZ\gamma$, $Z\gamma\gamma$, and ZZV Couplings" note in the Z particle listing for details.

Int. J. Mod. Phys. A 2026.41. Downloaded from www.worldscientific.com
by UNIVERSITY OF CALIFORNIA @ BERKELEY on 09/16/26. Re-use and distribution is strictly not permitted, except for Open Access articles.

the possibility for precise determinations at future e^+e^- colliders. The kinematic method was also employed at the Tevatron [217] and by ATLAS [218] and LHCb [219] at the LHC. A combination [220] of all M_W measurements available until 2023, using a careful calibration of simulation tools and parton distribution functions (PDFs), resulted in

$$M_W = 80.395 \pm 0.012 \text{ GeV}. \tag{10.31}$$

However, the χ^2 probability of this combination is 0.5% or less, depending on the chosen PDF set, which is mostly due to the W-mass measurement by CDF from Run II at the Tevatron [212], $M_W = 80.432 \pm 0.016$ GeV (adjusted to the common PDF set CT18 [221] in Ref. [220]). It differs by almost 4σ from the combination of the other measurements of M_W, while the latter agree well among each other, with the average [220]

$$M_W = 80.369 \pm 0.013 \text{ GeV}, \tag{10.32}$$

without CDF II. In 2024, the ATLAS result was updated by incorporating nuisance parameters encoding the effect of systematic uncertainties in the fit to data, including those from the PDFs [222]. This resulted in a downward shift of M_W by 3.5 MeV with a reduced uncertainty, $M_W = 80.3665 \pm 0.0159$ GeV. Most recently, the CMS Collaboration has presented their first determination of M_W [214]. The measurement reported in the nominal analysis, which used the CT18Z PDF set [221], is $M_W = 80.3602 \pm 0.0099$ GeV. When performing the measurement with the CT18 PDF set, the same used in the ATLAS 2024 measurement and in the 2023 M_W combination in (10.32), CMS reports $M_W = 80.3618 \pm 0.0100$ GeV. This value is in agreement with both the SM prediction and previous M_W determinations, and it further increases the tension with the latest CDF value [212].

For the global fits presented in the next section, we use an update of the M_W combination by the LHC-TeVatron M_W Working Group, released in May 2026 [223]. The combination is based on the methods developed for the previous combination [220]. It includes the M_W measurements from LEP 2 [216], DØ [224, 225], LHCb [219], ATLAS [222], and CMS [214]. All measurements are performed using the CT18 PDF set, where the DØ value has been adjusted to this PDF set and to the latest signal modelling [220]. The total fit uncertainties of profile-likelihood measurements are decomposed into elementary uncertainty components following Ref. [226], and the PDF-induced correlations are propagated coherently across all measurements. The resulting average has a very high p-value of 0.97 and is

$$M_W = 80.3625 \pm 0.0077 \text{ GeV}, \tag{10.33}$$

which we use in the global fits. Note that this average does not include the CDF M_W measurement [212], which would reduce the p-value of the combination to 0.0006.

Again, these values on M_W correspond to an energy-dependent W width in the resonance propagator and differ from $\overline{M}_W$ from the complex location of the propagator pole as given in Eq. (10.14).

The ATLAS update in Ref. [222] also included the first LHC measurement of the W-boson width, $\Gamma_W = 2.202 \pm 0.047$ GeV, the most precise single measurement of this quantity. When derived simultaneously with M_W, the two measurements show a 30% anticorrelation. Although consistent with the LEP 2 determination [216], the new and more precise ATLAS Γ_W value differs by about 2σ from the Tevatron result [227] and the SM prediction. We refer again to Section 54 on the "Mass and Width of the W Boson" in this *Review* for more details and references.

10.4.2 *Higgs-boson mass and width*

After their discovery of the Higgs boson [228, 229], the LHC experiments ATLAS and CMS have performed high precision measurements of its mass, M_H. The PDG average

$$M_H = 125.13 \pm 0.11 \text{ GeV (LHC)} \tag{10.34}$$

is a result from a combination of the LHC Run 1 average from ATLAS and CMS [230], a CMS measurement in the $H \to \gamma\gamma$ channel at 13 TeV [231], a CMS measurement in the $H \to ZZ^* \to 4\ell$ channel at 13 TeV [232], and an ATLAS combination at 13 TeV [233]. The uncertainty includes a scale factor of 1.5 because of the incompatibility of the CMS $H \to \gamma\gamma$ result [231] with the other measurements. This increased uncertainty has a negligible impact in the global fits.

Measurements of the Higgs-boson width Γ_H at the LHC are based on the comparison between off-shell and on-shell Higgs boson production rates assuming the validity of the SM. The most precise results are $\Gamma_H = 3.0^{+2.0}_{-1.5}$ MeV from CMS [232] and $\Gamma_H = 4.3^{+2.7}_{-1.9}$ MeV from ATLAS [234]. Both measurements are compatible with the SM prediction $\Gamma_H = 4.10 \pm 0.06$ MeV [235]. Owing to the smallness of $\Gamma_H/M_H \sim 3 \times 10^{-5}$, there is no significant difference between the two variants of OS masses and widths (M_H, Γ_H versus $\overline{M}_H$, $\overline{\Gamma}_H$) at the current (and most likely also future) level of precision.

For further references and more details on Higgs-boson properties, see Section 11 on the "Status of Higgs Boson Physics" in this *Review*.

10.4.3 *Quark masses*

The top-quark mass m_t, being the largest mass in the SM, plays a prominent role in the description of the EW sector, inducing some of the largest fermionic radiative corrections to EW precision observables. As in the case of the other SM parameters that can be obtained indirectly from the EW precision fit, it is important to have direct determinations of m_t to perform consistency tests of the SM. The top-quark mass has been measured in top-quark decays by directly reconstructing the decay products, also known as "direct measurements", by the Tevatron collaborations, CDF and DØ, in leptonic, hadronic, and mixed channels with the result [236],

$$m_t = 174.30 \pm 0.35_{\text{stat.}} \pm 0.54_{\text{syst.}} \text{ GeV (Tevatron)}\ . \tag{10.35}$$

Likewise, using data from CM energies $\sqrt{s} = 7$ and 8 TeV (Run 1), ATLAS and CMS (including alternative technique measurements) at the LHC obtained [237],

$$m_t = 172.52 \pm 0.14_{\text{stat.}} \pm 0.30_{\text{syst.}} \text{ GeV (LHC Run 1)}\ . \tag{10.36}$$

In addition, there are results derived from $\sqrt{s} = 13$ TeV data (Run 2). The CMS collaboration obtained $m_t = 171.77 \pm 0.37_{\text{tot.}}$ GeV [238] in the lepton+jets channel with a kinematic fit of the decay products combined with a profile likelihood method. Using the same channel, CMS measured $m_t = 173.06 \pm 0.24_{\text{stat.}} \pm 0.80_{\text{syst.}}$ GeV [239] using a template fit to the jet mass in hadronic decays of highly boosted top quarks. In addition, CMS reports $m_t = 172.33 \pm 0.14_{\text{stat.}} \pm 0.69_{\text{syst.}}$ GeV [240] in the dilepton channel, $m_t = 172.34 \pm 0.20_{\text{stat+JSE}} \pm 0.70_{\text{syst.}}$ GeV [241] in the all-jets channel, and $m_t = 172.13 \pm 0.32_{\text{stat.}} \pm 0.70_{\text{syst.}}$ GeV [242] in t-channel single top events (leptonic decays), where the uncertainty named stat+JSE denotes the combination of the statistical uncertainty and the uncertainty in the jet energy scale. A comprehensive summary of the CMS measurements of the top-quark mass is given in Ref. [243]. ATLAS measured $m_t = 174.41 \pm 0.39_{\text{stat.}} \pm 0.71_{\text{syst.}}$ GeV [244] in the lepton+jets channel by identifying soft leptons from the semileptonic decays of b-hadrons assigned to the leptonically decaying top quark, $m_t = 172.95 \pm 0.53$ GeV [245] in the lepton+jets channel with boosted hadronically decaying top quarks, and $m_t = 172.21 \pm 0.20_{\text{stat.}} \pm 0.78_{\text{syst.}}$ GeV [246] in the dilepton channel.

There is some ambiguity in relating these measurements to the top-quark pole mass [247], which we discuss below. Alternatively, the experimental collaborations have determined the top-quark mass from inclusive cross-section measurements [248–254]. While these determinations represent unambiguous measurements of the top-quark pole mass, they have larger uncertainties than the direct measurements presently. For the fits discussed later we will use the average value of direct measurements reported in the Top Quark Listings in this *Review*, which is based exclusively on fully published results. It must be noted that this combination assumes vanishing correlations between the different measurements and across experiments. We note that there exists some tension at

Int. J. Mod. Phys. A 2026.41. Downloaded from www.wo
by UNIVERSITY OF CALIFORNIA @ BERKELEY on 09/16/26. Re-use and distribution is
except for Open Access articles.

the 2σ level between the Tevatron combination and some LHC measurements, which results in a scaling of the uncertainty by a factor of 1.5. We take

$$m_t = 172.60 \pm 0.27\,\text{GeV} + \Delta m_{\text{MC}}, \tag{10.37}$$

where the term Δm_{MC} has been added to account for any difference between the top-quark pole mass, m_t, and the mass parameter implemented in the Monte Carlo event generators employed by the experimental groups. The parameter Δm_{MC} is expected to be of order $\alpha_s(Q_0)Q_0$ with a low scale $Q_0 \sim \mathcal{O}(1\text{ GeV})$ [255], but its value is unknown in hadron collider environments so that we will treat it as an uncertainty instead,[12] and choose for definiteness $Q_0 = \Gamma_t = 1.42$ GeV to arrive at $\Delta m_{\text{MC}} = 0 \pm 0.52$ GeV. We further assume that an uncertainty [258] of ± 0.32 GeV in the relation [259] between m_t and the $\overline{\text{MS}}$ definition, $\widehat{m}_t(\widehat{m}_t^2)$, entering EW radiative correction libraries, including the renormalon ambiguity [260], is already included in Δm_{MC}, as m_t merely serves as an intermediate bookkeeping device in Ref. [255]. A complementary direction to arrive at a competitive independent constraint on m_t is to analyze differential top-quark pair production cross sections at NNLO QCD [261, 262]. Extractions of m_t using fixed-order perturbative calculations can remove the Δm_{MC} uncertainty and benefit from the recently increased experimental precision of differential measurements [263–266]. We note that m_t determinations from cross sections assume the validity of the SM within the energy range accessible to the LHC. For more details and references, see Section 61 on the "Top Quark" and the Quarks Listings in this *Review*.

The charm and bottom quark masses play a minor but non-negligible role in the EW fit. We consider the running $\overline{\text{MS}}$ masses for these quarks, evaluated at a scale equal to the quark mass itself, $\widehat{m}_q(\widehat{m}_q^2)$:

$$\widehat{m}_c(\widehat{m}_c^2) = 1273.0 \pm 2.8\text{ MeV}, \quad \widehat{m}_b(\widehat{m}_b^2) = 4183 \pm 4\text{ MeV}. \tag{10.38}$$

To improve the precisions in $\widehat{m}_c(\widehat{m}_c^2)$ and $\widehat{m}_b(\widehat{m}_b^2)$ in the future it would help to remeasure the threshold regions of the heavy quarks, as well as the electronic decay widths of the narrow $c\bar{c}$ and $b\bar{b}$ resonances. It would also be important to obtain data on the R-ratio in e^+e^- annihilation for center-of-mass energies $\gtrsim 11.2$ GeV, as in this region QCD perturbation theory cannot be sufficiently relied upon for b quarks [267].

The masses of the light quarks play a subordinate role in the calculation of EW observables. Indeed, in order to minimize non-perturbative effects in the predictions of high-energy observables, these observables are typically defined to be *infrared safe*, *i.e.* insensitive to energy scales near the QCD parameter Λ_{QCD}, allowing for the neglect of the light-quark masses. In cases where these masses are relevant, they are typically defined in the $\overline{\text{MS}}$ scheme. As further explained in Section 60 on "Quark Masses" in this *Review*, a fit for the u, d, and s masses gives

$$\widehat{m}_u = 2.16 \pm 0.04\text{ MeV}, \quad \widehat{m}_d = 4.70 \pm 0.04\text{ MeV}, \quad \widehat{m}_s = 93.5 \pm 0.5\text{ MeV}, \tag{10.39}$$

where these running $\overline{\text{MS}}$ masses are evaluated at the scale $\mu = 2$ GeV.

10.4.4 *The strong coupling constant*

The strong coupling constant is one of the key parameters of the SM, setting the strength of QCD interactions. While not contributing to the EW precision observables at leading order, it enters in the EW precision fit via radiative corrections, most notably to hadronic observables at the one-loop order or to the W mass and the weak mixing angle starting at two loops. From the point of view of EW precision observables, in particular measurements of the Z-lineshape, the relevant scale is $Q^2 \sim M_Z^2$, and the SM EW precision fit provides a determination of $\alpha_s(M_Z^2)$. It is important to complement the information from the EW fit on this input with additional measurements at lower and higher energy scales. Alternative determinations, both from low- and high-energy observables are available, and reduce the dependence of the extraction of $\alpha_s(M_Z^2)$ on potential new physics effects. These determinations differ in statistical precision, experimental systematic uncertainties, and uncertainties from theoretical considerations. Considering the total uncertainty, some of these determinations are more precise than the one from the EW fit, *e.g.*, from lattice QCD, PDF fits, LHC data, or from τ decays. However, the EW fit provides a determination of $\alpha_s(M_Z^2)$ with the smallest uncertainty from missing higher orders or non-perturbative effects compared to other measurements, making it an important element in the combination with other determinations. We refer to Section 9 on Quantum Chromodynamics in this *Review* for more details on the different methods to obtain α_s and probe its energy dependence.

While measurements of the Z-lineshape have the power to determine $\alpha_s(M_Z^2)$ without further experimental input, the most precise test of the EW sector of the SM is obtained by including external information on $\alpha_s(M_Z^2)$. Following the methods reported in the *Review on Quantum Chromodynamics*, we consider the average of $\alpha_s(M_Z^2)$ excluding information from the EW fit, and before combining it with the lattice QCD results,

$$\alpha_s(M_Z^2) = 0.1171 \pm 0.0011 \quad \text{(PDG 2025 average without EW fit)}, \tag{10.40}$$

and perform an unweighted average of this value with the FLAG 2024 estimate, combining the best results from lattice QCD, $\alpha_s(M_Z^2) = 0.1183 \pm 0.0007$ [268]. This results in

$$\alpha_s(M_Z^2) = 0.1177 \pm 0.0009\ , \tag{10.41}$$

which we use as a constraint in our fits.

10.4.5 *The weak mixing angle*

The quantities $\sin^2\theta_W$ and M_W can be calculated from M_Z, $\alpha(M_Z^2)$, and G_F, when values for m_t and M_H are given, or conversely, M_H can be constrained by $\sin^2\theta_W$ and M_W. The value of $\sin^2\theta_W$ depends on the renormalization prescription. There are a number of popular schemes [9] leading to values which differ by small factors depending on m_t and M_H. The notation for these schemes is shown in Table 10.2.

(i) As proposed in Ref. [22], the OS scheme promotes the tree-level formula $\sin^2\theta_W = 1 - M_W^2/M_Z^2$ to a definition of the renormalized $\sin^2\theta_W$ to all orders in perturbation theory, *i.e.*,

$$\sin^2\theta_W \to s_W^2 \equiv 1 - \frac{M_W^2}{M_Z^2}\ , \tag{10.42a}$$

$$M_W = \frac{A_0}{s_W(1-\Delta r)^{1/2}}\ , \qquad M_Z = \frac{M_W}{c_W}\ , \tag{10.42b}$$

where $c_W \equiv \cos\theta_W$, $A_0 = (\pi\alpha(0)/\sqrt{2}G_F)^{1/2} = 37.28038(1)$ GeV, and Δr includes the radiative corrections relating $\alpha(0)$, $\alpha(M_Z^2)$, G_F, M_W, and M_Z (see Sect. 10.2.5). Other definitions are motivated by the tree-level coupling constant definition $\theta_W = \tan^{-1}(g'/g)$:

(ii) The $\overline{\text{MS}}$ scheme introduces the quantity,

$$\sin^2\widehat{\theta}_W(\mu^2) \equiv \frac{\widehat{g}'(\mu^2)^2}{\widehat{g}(\mu^2)^2 + \widehat{g}'(\mu^2)^2}\ , \tag{10.43}$$

where the couplings $\widehat{g}$ and $\widehat{g}'$ are defined by modified minimal subtraction and the scale μ is conveniently chosen to be M_Z for many EW processes. The value of $\widehat{s}_Z^2 \equiv \sin^2\widehat{\theta}_W(M_Z^2)$ is less sensitive than s_W^2 to m_t (by a factor of $\tan^2\theta_W$), and is less sensitive to most types of new physics. It is also useful for comparisons with the predictions of grand unification. There are several definitions of $\sin^2\widehat{\theta}_W(M_Z^2)$, which differ in whether and how finite $\alpha\ln(m_t/M_Z)$ terms are decoupled (i.e. subtracted from the couplings). One cannot entirely decouple these terms from all EW quantities

[12] However, see Refs. [256, 257] for proposed procedures to calibrate the Monte Carlo mass parameter at hadron colliders.

Int. J. Mod. Phys. A 2026.41. Downloaded from www.worldscientific.com
by UNIVERSITY OF CALIFORNIA @ BERKELEY on 09/16/26. Re-use and distribution is strictly not permitted, except for Open Access articles.

Table 10.2: Notations and numerical values of the weak mixing angle $\sin^2\theta_W$ discussed in the text. The effective weak mixing angle $\bar{s}^2_\ell$ is obtained using the two-loop results of Ref. [106] with the direct experimental measurements of $\alpha_s(M_Z^2)$, $\Delta\alpha^{(5)}_{\rm had}(M_Z^2)$, M_Z, m_t, and M_H as input parameters, given in Table 10.5 below. The on-shell and $\overline{\rm MS}$ quantities are derived from $\bar{s}^2_\ell$. The uncertainties induced by the imperfectly known input parameters and unknown higher orders [106] are also given.

Scheme	Notation	Value	Uncertainty
On-shell	s^2_W	0.22342	± 0.00009
Effective angle	$\bar{s}^2_\ell$	0.23154	± 0.00006
$\overline{\rm MS}$	$\widehat{s}^2_Z$	0.23122	± 0.00006
$\overline{\rm MS}$ (ND)	$\widehat{s}^2_{\rm ND}$	0.23140	± 0.00006

because $m_t \gg m_b$ breaks SU(2) symmetry. The scheme adopted in the EW fits presented in the previous editions of this *Review* decouples the $\alpha\ln(m_t/M_Z)$ terms from the γ–Z mixing [26,269], essentially eliminating any $\ln(m_t/M_Z)$ dependence in the formulae for asymmetries at the Z pole when written in terms of $\widehat{s}^2_Z$. (A similar definition was used for $\widehat{\alpha}$.) The OS and $\overline{\rm MS}$ definitions are related by

$$\widehat{s}^2_Z = c\,(m_t, M_H)s^2_W = (1.0349 \pm 0.0003)s^2_W\ . \qquad (10.44)$$

The quadratic m_t dependence is given by $c \sim 1 + \Delta\rho_t/\tan^2\theta_W$. The expressions for M_W and M_Z in the $\overline{\rm MS}$ scheme are

$$M_W = \frac{A_0}{\widehat{s}_Z(1-\Delta\widehat{r}_W)^{1/2}}\ , \quad M_Z = \frac{M_W}{\widehat{\rho}^{\,1/2}\,\widehat{c}_Z}\ , \qquad (10.45)$$

and one predicts $\Delta\widehat{r}_W = 0.06937 \pm 0.00006$. $\Delta\widehat{r}_W$ has no quadratic m_t dependence, because shifts in M_W are absorbed into the observed G_F, so that the error in $\Delta\widehat{r}_W$ is almost entirely due to $\Delta r_0 = 1-\alpha(0)/\widehat{\alpha}(M_Z^2)$. The quadratic m_t dependence has been shifted into $\widehat{\rho} \sim 1 + \Delta\rho_t$, where including bosonic loops, $\widehat{\rho} = 1.01016 \pm 0.00009$.

(iii) A variant $\overline{\rm MS}$ quantity $\widehat{s}^2_{\rm ND}$ (used in the 1992 edition of this *Review*) does not decouple the $\alpha\ln(m_t/M_Z)$ terms [270]. It is related to $\widehat{s}^2_Z$ by

$$\widehat{s}^2_Z = \frac{\widehat{s}^2_{\rm ND}}{1+\frac{\widehat{\alpha}}{\pi}d}\ ,$$
$$d = \frac{1}{3}\left(\frac{1}{\widehat{s}^2} - \frac{8}{3}\right)\left[\left(1+\frac{\alpha_s}{\pi}\right)\ln\frac{m_t}{M_Z} - \frac{15\alpha_s}{8\pi}\right]\ . \qquad (10.46)$$

Thus, $\widehat{s}^2_Z - \widehat{s}^2_{\rm ND} = -0.00018$.

(iv) Another very useful definition of the mixing angle, known as the *effective weak mixing angle* [271, 272] $\bar{s}^2_f \equiv \sin^2\theta^f_{\rm eff}$, is based on effective couplings of a fermion f to the Z boson on the Z pole, as discussed in detail in Sec. 10.4.6 below.

In previous versions of this *Review,* special attention was dedicated to EW precision observables obtained at low momentum transfers [273], *i.e.*, $|Q^2| \ll M_Z^2$, in particular those measured in neutrino and electron scattering experiments, namely ν–hadron, ν–e, as well as parity violating e–hadron and e–e neutral-current processes. Within the SM, these are sensitive to the weak mixing angle at almost vanishing momentum transfer $\widehat{s}^2_0 \equiv \sin^2\widehat{\theta}_W(0)$ [163, 274–276]. Similarly, new physics effects contributing to the EW neutral-currents interactions or new particle exchanges in the form of additional four-fermion interactions could be tested in these types of processes.

A precise determination of the OS quantity s^2_W, which depends only very weakly on m_t and M_H, is obtained from deep inelastic scattering (DIS) of neutrinos [277, 278] from (approximately) isoscalar targets. The ratio $R_\nu \equiv \sigma^{NC}_{\nu N}/\sigma^{CC}_{\nu N}$ of neutral-to-charged-current cross sections has been measured to 1% accuracy by CDHS [279] and CHARM [280] at CERN. CCFR [281] at Fermilab has obtained an even more precise result. The NuTeV collaboration found $s^2_W = 0.2277 \pm 0.0016$, which was $\sim 3\sigma$ higher than the SM prediction [282]. However, since then several groups have raised concerns about the interpretation of the NuTeV result, which could affect the extracted value of s^2_W. A detailed discussion and a list of references can be found in the 2016 edition of this *Review.* Similarly, experiments of parity violation electron scattering can probe the weak mixing angle by measuring the parity violating left–right (LR) asymmetry $A_{\rm LR} \equiv \frac{\sigma_{\rm L}-\sigma_{\rm R}}{\sigma_{\rm L}+\sigma_{\rm R}}$. This was determined by the SLAC polarized electron-deuteron DIS (eDIS) experiment [283] and improved by the Jefferson Lab Hall A collaboration [284, 285], measuring the weak mixing angle to 2% precision, $\widehat{s}^2_Z = 0.2299 \pm 0.0043$. $A_{\rm LR}$ can also be measured in fixed target polarized Møller scattering, and has been determined at low $Q^2 = 0.026$ GeV^2 in the SLAC E158 experiment [286], yielding $\widehat{s}^2(161\ {\rm MeV}) = 0.2403 \pm 0.0013$, and, as shown in Fig. 10.1, established the scale dependence of the weak mixing angle at the level of 6σ. Finally, measurement of the nuclear weak charge, $Q_W(Z,N)$, in experiments of atomic parity violation, in particular for Cesium, when interpreted in terms of the SM lead to value of the weak mixing angle $\widehat{s}^2(2.4\ {\rm MeV}) = 0.2349 \pm 0.0018$ [287–294]. We refer to the review article by M. A. and C. Bouchiat [295] and to previous editions of this *Review* for a much more in-depth description of these types of low-energy probes of the weak mixing angle.

The scale dependence of the weak mixing angle defined in the $\overline{\rm MS}$ scheme [163, 275] is shown in Fig. 10.1.

10.4.6 *Z-pole physics*

If the CM energy $\sqrt{s}$ is large compared to the fermion mass m_f, the unpolarized Born cross section for $e^+e^- \to f\bar{f}$, including γ exchange, Z-boson exchange, and γ–Z interference can be written as [297]

$$\frac{d\sigma}{d\cos\theta} = \frac{\pi\alpha^2(s)}{2s}\left[F_1(1+\cos^2\theta) + 2F_2\cos\theta\right] + B\ , \qquad (10.47a)$$

$$F_1 = Q_e^2Q_f^2 - 2\chi Q_eQ_f\bar{g}^e_V\bar{g}^f_V\cos\delta_R + \chi^2(\bar{g}^{e2}_V + \bar{g}^{e2}_A)(\bar{g}^{f2}_V + \bar{g}^{f2}_A)\ , \qquad (10.47b)$$

$$F_2 = -2\chi Q_eQ_f\bar{g}^e_A\bar{g}^f_A\cos\delta_R + 4\chi^2\bar{g}^e_V\bar{g}^e_A\bar{g}^f_V\bar{g}^f_A\ , \qquad (10.47c)$$

where

$$\tan\delta_R = \frac{\overline{M}_Z\overline{\Gamma}_Z}{\overline{M}^2_Z - s}\ , \quad \chi = \frac{G_F}{2\sqrt{2}\pi\alpha(s)}\frac{s\overline{M}^2_Z}{\left[(\overline{M}^2_Z - s)^2 + \overline{M}^2_Z\overline{\Gamma}^2_Z\right]^{1/2}}\ . \qquad (10.48)$$

Here, B accounts for box graphs involving virtual Z and W bosons, and the $\bar{g}^f_{V,A}$ are defined in Eq. (10.49) below. $\overline{M}_Z$ and $\overline{\Gamma}_Z$ correspond to mass and width definitions based on a Breit–Wigner shape with an energy-independent width (see Sec. 10.2.4 and Section 55 on the "Z Boson" in this *Review*). The differential cross section receives important corrections from QED effects in the initial and final states, and interference between the two [298]. For $q\bar{q}$ production, there are additional final-state QCD corrections, which are relatively large. Note also that the equations above are written in the CM frame of the incident e^+e^- system, which may be boosted due to the initial-state QED radiation.

Int. J. Mod. Phys. A 2026.41. Downloaded from www.worldscientific.com by UNIVERSITY OF CALIFORNIA @ BERKELEY on 09/16/26. Re-use and distribution is except for Open Access articles.

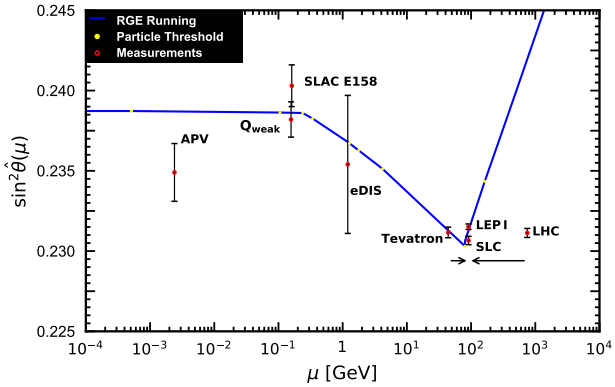

Figure 10.1: Scale dependence of the weak mixing angle defined in the $\overline{\rm MS}$ scheme [163, 275] (for the scale dependence in a mass-dependent renormalization scheme, see Ref. [274]). The minimum of the curve corresponds to $\mu = M_W$, below which an effective theory is used with the $W^\pm$ bosons integrated out, and where the β-function for $\widehat{s}^2(\mu^2)$ changes sign. At M_W and each fermion mass there are also discontinuities arising from scheme dependent matching terms, which are necessary to ensure that the various effective field theories within a given loop order describe the same physics. However, in the $\overline{\rm MS}$ scheme these are very small numerically and barely visible in the figure provided one decouples quarks at $\mu = \widehat{m}_q(\widehat{m}_q^2)$. The width of the curve exceeds the theory uncertainty from strong interaction effects which at low energies is at the level of $\pm 2\times 10^{-5}$ [163]. The Tevatron and LHC measurements are strongly dominated by invariant masses of the final-state di-lepton pair of $\mathcal{O}(M_Z)$ and can thus be considered as additional Z pole data points. For clarity, the Tevatron and LHC points are slightly shifted horizontally to the left and right, respectively. Figure taken from the previous edition of this *Review*, which we refer to for more details [296].

Some of the leading virtual EW corrections are captured by the running QED coupling $\alpha(s)$ and the Fermi constant G_F. The remaining corrections to the $Zf\bar{f}$ interactions are absorbed by replacing the tree-level couplings in Eq. (10.7) with the s-dependent *effective couplings* [139],

$$\bar{g}_V^f = \sqrt{\rho_f}\left(t_{3L}^f - 2Q_f\kappa_f \sin^2\theta_W\right) , \tag{10.49a}$$

$$\bar{g}_A^f = \sqrt{\rho_f}\, t_{3L}^f . \tag{10.49b}$$

In these equations, the effective couplings are to be taken at the scale $\sqrt{s}$, but for notational simplicity we do not show this explicitly. At tree level, $\rho_f = \kappa_f = 1$, but inclusion of EW radiative corrections leads to $\rho_f \neq 1$ and $\kappa_f \neq 1$, which depend on the fermion f and on the renormalization scheme. In the OS scheme, the quadratic m_t dependence is given by,

$$\rho_f \sim 1 + \Delta\rho_t , \qquad \kappa_f \sim 1 + \frac{\Delta\rho_t}{\tan^2\theta_W} , \tag{10.50}$$

while in $\overline{\rm MS}$, $\widehat{\rho}_f \sim \widehat{\kappa}_f \sim 1$, for $f \neq b$, and

$$\widehat{\rho}_b \sim 1 - \frac{4}{3}\Delta\rho_t , \qquad \widehat{\kappa}_b \sim 1 + \frac{2}{3}\Delta\rho_t , \tag{10.51}$$

which account for the non-flavor-universal effects arising from diagrams where a virtual top quark couples to a W boson inducing a correction to the $Zb\bar{b}$ vertex. In the $\overline{\rm MS}$ scheme the normalization is changed according to $G_F M_Z^2/2\sqrt{2}\pi \to \widehat{\alpha}/4\widehat{s}_Z^2\widehat{c}_Z^2$ in the second Eq. (10.48).

As reviewed in Sec. 10.2.5, for the high precision Z pole observables discussed below, many additional bosonic and fermionic loop effects, vertex corrections, and higher order contributions, *etc.*, must be included.

To connect to measured quantities, it is convenient to define the effective angle

$$\bar{s}_f^2 \equiv \sin^2\bar{\theta}_{Wf} \equiv \widehat{\kappa}_f\widehat{s}_Z^2 = \kappa_f s_W^2 , \tag{10.52}$$

in terms of which $\bar{g}_V^f$ and $\bar{g}_A^f$ are given by $\sqrt{\rho_f}$ times their tree-level formulae. One finds that the $\widehat{\kappa}_f$ ($f \neq b$) are almost independent of m_t and M_H, and thus one can write,

$$\bar{s}_\ell^2 = \widehat{s}_Z^2 + 0.00032 , \tag{10.53}$$

while the κ_f for the OS scheme are m_t dependent.

High-precision measurements of various Z pole ($\sqrt{s} \approx M_Z$) observables [9, 308, 309] have been performed at LEP 1 and SLC [139, 305, 306, 310, 311], as summarized in Table 10.3. These include the Z mass and total width, Γ_Z, and partial widths $\Gamma_{f\bar{f}}$ for $Z \to f\bar{f}$, where $f = e$, μ, τ, light hadrons, b, and c. It is convenient to use the variables, also called "pseudo-observables", because these need to be determined from cross-section measurements,

$$M_Z, \quad \Gamma_Z, \quad \sigma_{\rm had} \equiv \frac{12\pi\Gamma_{e^+e^-}\Gamma_{\rm had}}{M_Z^2\,\Gamma_Z^2}, \quad R_\ell \equiv \frac{\Gamma_{\rm had}}{\Gamma_{\ell^+\ell^-}}, \quad R_q \equiv \frac{\Gamma_{q\bar{q}}}{\Gamma_{\rm had}}, \tag{10.54}$$

for $\ell = e, \mu$, or τ, and $q = b$ or c, where $\Gamma_{\rm had}$ is the partial decay width into hadrons. [13] Most of these are weakly correlated experimentally. These quantities have been obtained by the LEP collaborations from fits to the measured cross sections around the Z pole in e^+e^- collisions. Initial-state radiation reduces the peak cross section by more than 25%, where $\mathcal{O}(\alpha^3)$ QED effects and the dependence on Γ_Z induce an anti-correlation of about -30% between Γ_Z and $\sigma_{\rm had}$, and correlations of about 10% between $\sigma_{\rm had}$ and R_e, R_μ, and R_τ. Newer calculations of beam-beam effects on the luminosity measurement at LEP [312] and an improved Bhabha cross section [215], which was underestimated by 0.048% when the measurements were done, result in updated values

$$\Gamma_Z = 2.4955 \pm 0.0023 \text{ GeV} \quad \text{and} \quad \sigma_{\rm had} = 41.480 \pm 0.033 \text{ nb}. \tag{10.55}$$

The anti-correlation between R_b and R_c amounts to -18% [139]. The observable R_ℓ exhibits only a mild dependence on m_t, which enters through the $Z \to b\bar{b}$ vertex in the total Z boson width, final-state corrections, and the implicit dependence through $\sin^2\theta_W$. Thus, R_ℓ is especially useful for constraining $\alpha_s(M_Z^2)$.

Very important constraints follow from measurements of various Z-pole asymmetries. These include the FB asymmetry $A_{\rm FB}$, and the polarization or LR asymmetry $A_{\rm LR}$, defined by

$$A_{\rm FB}^f = \frac{\sigma_{\rm F}^f - \sigma_{\rm B}^f}{\sigma_{\rm F}^f + \sigma_{\rm B}^f} , \qquad A_{\rm LR} = \frac{\sigma_{\rm L}^f - \sigma_{\rm R}^f}{\sigma_{\rm L}^f + \sigma_{\rm R}^f} . \tag{10.56}$$

Here, $\sigma_{\rm F(B)}^f$ are the cross sections to produce a fermion in the forward (backward) hemisphere, defined with respect to the direction of the electron beam, and $\sigma_{\rm L(R)}^f$ are the total cross sections for left-handed (right-handed) incoming electrons. The LR asymmetry was measured precisely by the SLD collaboration at the SLC [305] using a polarized electron beam, and has the advantages of being very sensitive to $\bar{s}_\ell^2$ and that systematic uncertainties largely cancel. After removing initial-state QED corrections and contributions from photon exchange, γ–Z interference, as well as the EW boxes in Eq. (10.47a), one can use the effective tree-level expressions,

$$A_{\rm LR} = A_e P_e , \qquad A_{\rm FB}^f = \frac{3}{4}A_f\,\frac{A_e + P_e}{1 + P_e A_e} , \tag{10.57}$$

where,

$$A_f \equiv \frac{2\bar{g}_V^f\bar{g}_A^f}{\bar{g}_V^{f2} + \bar{g}_A^{f2}} = \frac{1 - 4|Q_f|\bar{s}_f^2}{1 - 4|Q_f|\bar{s}_f^2 + 8Q_f^2\bar{s}_f^4} . \tag{10.58}$$

P_e is the initial e^- polarization. The Z-pole FB asymmetries at LEP 1 ($P_e = 0$) are given by $A_{\rm FB}^f = \frac{3}{4}A_e A_f$ for $f = e$, μ,

[13] In this review, we only consider Z-pole observables corrected for radiative effects, photon exchange, γ–Z interference, and EW boxes. These are denoted with a superscript '0' in the original LEP literature, *e.g.* $\sigma_{\rm had}^0$, but here we drop the '0' from the superscript.

Int. J. Mod. Phys. A 2026.41. Downloaded from www.worldscientific.com
by UNIVERSITY OF CALIFORNIA @ BERKELEY on 09/16/26. Re-use and distribution is strictly not permitted, except for Open Access articles.

Table 10.3: Principal Z-pole observables and their SM predictions. The first M_Z is from LEP 1 [139] and the second from CDF [212]. The first $\bar{s}^2_\ell$ is the effective weak mixing angle extracted from the hadronic charge asymmetry at LEP 1 [139], the second is the combined value from the Tevatron [299], and the third is from the LHC [300–304]. The values of A_e are (i) from $A_{\rm LR}$ for hadronic final states [305]; (ii) from $A_{\rm LR}$ for leptonic final states and from polarized Bhabha scattering [306]; and (iii) from the angular distribution of the τ polarization at LEP 1 [139]. The A_τ values are from SLD [306], the total τ polarization from LEP [139] and from CMS [307], respectively. The SM predictions are obtained using the values of the first five parameters listed in the second column of Table 10.5. Note that the SM errors in Γ_Z, the R_ℓ, and $\sigma_{\rm had}$ are largely dominated by the uncertainty in α_s.

Quantity		Value	Standard Model
M_Z [GeV]	(LEP 1)	91.1876 ± 0.0021	
	(CDF)	91.192 ± 0.007	
Γ_Z [GeV]		2.4955 ± 0.0023	2.4942 ± 0.0005
$\sigma_{\rm had}$ [nb]		41.4802 ± 0.0325	41.492 ± 0.008
R_e		20.804 ± 0.050	20.747 ± 0.006
R_μ		20.784 ± 0.034	20.747 ± 0.006
R_τ		20.764 ± 0.045	20.794 ± 0.006
R_b		0.21629 ± 0.00066	0.21588 ± 0.00003
R_c		0.1721 ± 0.0030	0.17220 ± 0.00003
$A^e_{\rm FB}$		0.0145 ± 0.0025	0.01618 ± 0.00006
$A^\mu_{\rm FB}$		0.0169 ± 0.0013	
$A^\tau_{\rm FB}$		0.0188 ± 0.0017	
$A^b_{\rm FB}$		0.0996 ± 0.0016	0.1030 ± 0.0003
$A^c_{\rm FB}$		0.0707 ± 0.0035	0.0736 ± 0.0002
$A^s_{\rm FB}$		0.0976 ± 0.0114	0.1027 ± 0.0002
$\bar{s}^2_\ell$	(LEP 1)	0.2324 ± 0.0012	0.23154 ± 0.00006
	(Tevatron)	0.23148 ± 0.00033	
	(LHC)	0.23148 ± 0.00027	
A_e	($A^{\rm had}_{\rm LR}$ SLD)	0.15138 ± 0.00216	0.1469 ± 0.0004
	($A^\ell_{\rm LR}$ SLD)	0.1544 ± 0.0060	
	(τ-pol. LEP 1)	0.1498 ± 0.0049	
A_μ		0.142 ± 0.015	
A_τ	(SLD)	0.136 ± 0.015	
	(τ-pol. LEP 1)	0.1439 ± 0.0043	
	(CMS)	0.144 ± 0.015	
A_b		0.923 ± 0.020	0.93474 ± 0.00003
A_c		0.670 ± 0.027	0.6678 ± 0.0002
A_s		0.895 ± 0.091	0.9357 ± 0.00004

τ, b, c, s [139], and q, and where $A^q_{\rm FB}$ refers to the hadronic charge asymmetry. Corrections for t-channel exchange and s/t-channel interference cause $A^e_{\rm FB}$ to be strongly anti-correlated with R_e with a coefficient of -37%. The m_b-dependence [313] of the $\mathcal{O}(\alpha_s^2)$ QCD correction [314], affecting the reference axis of the b-quark asymmetry [315], increased the extracted $A^b_{\rm FB}$ by about 0.2σ. The correlation between $A^b_{\rm FB}$ and $A^c_{\rm FB}$ amounts to 15%.

The six measured values of R_ℓ and $A^\ell_{\rm FB}$ are consistent with lepton universality[14] within their 68% confidence level contours, as shown in Fig. 10.2. The value of R_τ has been corrected for mass effects [110] to be comparable to R_e and R_μ. In our global SM fit, we use the combined values

$$R_\ell = 20.767 \pm 0.025 \ , \qquad A^\ell_{\rm FB} = 0.0171 \pm 0.0010 \ , \qquad (10.59)$$

obtained for massless leptons with an anti-correlation of -5.6% [139].

The SLD collaboration extracted the final-state couplings A_b, A_c [139], A_s [310], A_τ, and A_μ [306], from left–right forward–backward asymmetries, using

$$A^{\rm FB}_{\rm LR}(f) = \frac{\sigma^f_{LF} - \sigma^f_{LB} - \sigma^f_{RF} + \sigma^f_{RB}}{\sigma^f_{LF} + \sigma^f_{LB} + \sigma^f_{RF} + \sigma^f_{RB}} = \frac{3}{4} A_f \ , \qquad (10.60)$$

where, for example, σ^f_{LF} is the cross section for a left-handed incident electron to produce a fermion f traveling in the forward hemisphere. We note that $A^{\rm FB}_{\rm LR}$ is equal to $A^f_{\rm FB}$ in Eq. (10.57) for $P_e = 1$. Similarly, A_τ and A_e were measured at LEP 1 [139] (A_τ also recently by CMS [307]) through the τ polarization, $\mathcal{P}_\tau$, as a function of the scattering angle θ, which can be written as,

$$\mathcal{P}_\tau = -\frac{A_\tau(1+\cos^2\theta) + 2A_e\cos\theta}{(1+\cos^2\theta) + 2A_\tau A_e \cos\theta} \ . \qquad (10.61)$$

The average polarization, $\langle \mathcal{P}_\tau \rangle$, obtained by integrating over $\cos\theta$ in the numerator and denominator of Eq. (10.61), yields $\langle \mathcal{P}_\tau \rangle = -A_\tau$, and A_e can be extracted from the $\mathcal{P}_\tau$ angular distribution. The initial-state coupling, A_e, was also determined through the LR charge asymmetry [311] and in polarized Bhabha scattering [306] at the SLC. Because $\bar{g}^\ell_V$ is very small, not only $A_{\rm LR} = A_e$, $A^\ell_{\rm FB}$, and $\mathcal{P}_\tau$, but also $A^q_{\rm FB}$ for $q = b$, c, and s, as well as the hadronic asymmetries are mainly sensitive to $\bar{s}^2_\ell$. The leptonic results are compatible with lepton universality and can be combined into [139]

$$A_\ell({\rm SLD}) = 0.1513 \pm 0.0021 \ , \quad A_\ell({\rm LEP}) = 0.1465 \pm 0.0033 \ , \qquad (10.62)$$

[14] Tests of lepton universality of the neutral current are also available from hadron collider data. The ratio of branching fractions for Z bosons decaying into e^+e^- relative to $\mu^+\mu^-$ final states has also been measured by ATLAS [316], obtaining $R_{e/\mu} = 1.0026 \pm 0.0050$, in perfect agreement with lepton universality. Similar tests have also been performed with $Z \to \tau^+\tau^-$ decays by the LHCb collaboration, finding also good agreement with lepton universality at the few-percent level: $R_{\tau/e} = 1.02 \pm 0.06$, $R_{\tau/\mu} = 1.01 \pm 0.05$ [317].

Int. J. Mod. Phys. A 2026.41. Downloaded from www.worldscientific.com by UNIVERSITY OF CALIFORNIA @ BERKELEY on 09/16/26. Re-use and distribution is except for Open Access articles.

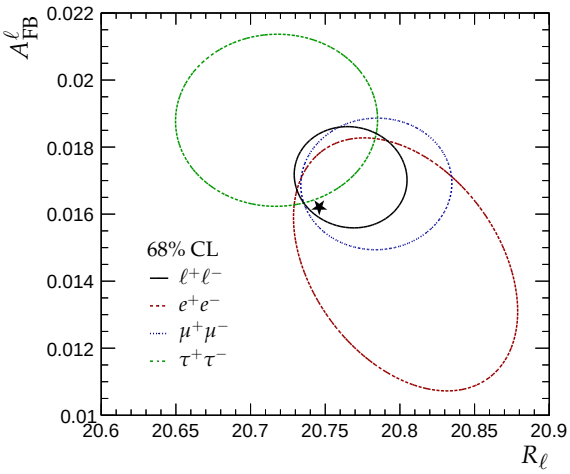

Figure 10.2: Contour lines at 68% confidence level for the LEP 1 measurements of R_ℓ and $A_{\rm FB}^\ell$ for e^+e^-, $\mu^+\mu^-$, $\tau^+\tau^-$ final states, and all leptons combined. The value of R_τ has been corrected for mass effects, shifting the measurement by -0.047. The SM prediction for massless leptons is shown as a black star.

where the first value is obtained from SLD data and the second one from LEP. The two values are statistically compatible within 1.2 standard deviations and are compatible with the CMS determination [307]

$$A_\tau(\text{CMS}) = 0.144 \pm 0.015 \ . \tag{10.63}$$

The LEP and SLD Collaborations reported a value of $\bar{s}_\ell^2 = 0.23153 \pm 0.00016$ [139] from the combination of $A_{\rm FB}^\ell$, A_ℓ(SLD), A_ℓ(LEP), $A_{\rm FB}^b$, $A_{\rm FB}^c$, and the direct measurement 0.2324 ± 0.0012 from the hadronic charge asymmetry at LEP 1 [139]. The correction of the reference axis in the b-quark asymmetry [313] leads to a reduced value of $\bar{s}_\ell^2$ when extracted from $A_{\rm FB}^b$ alone, 0.23214 ± 0.00029, which is smaller by 0.00007 than without this correction. Including this correction in the combination of all LEP and SLD asymmetries yields

$$\bar{s}_\ell^2 = 0.23150 \pm 0.00016 \ (\text{LEP + SLD}) \tag{10.64}$$

with a χ^2/d.o.f. of 10.7/5, corresponding to a p-value of 0.06.

As for hadron colliders, the FB asymmetry, $A_{\rm FB}$, for e^+e^- and $\mu^+\mu^-$ final states (with invariant masses restricted to or dominated by values around M_Z) in $p\bar{p}$ collisions has been measured by the CDF [318] and DØ [319] collaborations, and the values $\bar{s}_\ell^2 = 0.23221 \pm 0.00046$ and $\bar{s}_\ell^2 = 0.23095 \pm 0.00040$ were extracted, respectively. The combination of these measurements (which differ by more than 2 σ) yields [299],

$$\bar{s}_\ell^2 = 0.23148 \pm 0.00033 \ (\text{Tevatron}) \ . \tag{10.65}$$

By varying the invariant mass and the scattering angle (and assuming the electron couplings), information on the effective Z couplings to light quarks, $\bar{g}_{V,A}^{u,d}$, could also be obtained [320,321], but with large uncertainties, mutual correlations, and not independently of $\bar{s}_\ell^2$ above. Similar analyses have also been reported by the H1 [322] and ZEUS [323] collaborations at HERA and by the LEP collaborations [139]. This kind of measurement is harder in the pp environment due to the difficulty to assign the initial quark and antiquark in the underlying Drell–Yan process to the protons, thus requiring excellent control of uncertainties from parton distribution functions. ATLAS obtained $\bar{s}_\ell^2 = 0.2308 \pm 0.0012$ using 7 TeV data [300] and a preliminary result $\bar{s}_\ell^2 = 0.23140 \pm 0.00036$ at 8 TeV [301], while CMS measured $\bar{s}_\ell^2 = 0.23101 \pm 0.00053$ at 8 TeV [302] and $\bar{s}_\ell^2 = 0.23152 \pm 0.00031$ at 13 TeV [324]. [15] The LHCb collaboration measured $\bar{s}_\ell^2 = 0.23142 \pm 0.00106$ using 7 and 8 TeV data [304], and $\bar{s}_\ell^2 = 0.23147 \pm 0.00050$ using 13 TeV data [325], both in $\mu^+\mu^-$ final states. In all hadron-collider measurements of $\bar{s}_\ell^2$, the largest systematic uncertainty stems from uncertainties in the PDFs. The correlated part of these uncertainties is difficult to estimate without a dedicated analysis, exacerbated by a different choice of PDF set in each measurement. We assume that the PDF uncertainties are correlated between 25% and 75%, depending on the CM energy, the choice of PDF, and the fiducial region of the measurement. We take the other systematic uncertainties to be 50% correlated for measurements by the same experiment at different CM energies, and else assume no correlation. This choice leads to an uncertainty of $20 \cdot 10^{-5}$ in the hadron collider (HC) average of $\bar{s}_\ell^2$. Varying these assumptions by $\pm 25\%$ for the PDF correlations and between 0 and 100% for the correlations in the other systematic uncertainties, the central value changes by $10 \cdot 10^{-5}$, which we take as an additional systematic uncertainty. The resulting average is

$$\bar{s}_\ell^2 = 0.23149 \pm 0.00022 \ (\text{HC}). \tag{10.66}$$

Removing the Tevatron combination from this average results in the LHC value $\bar{s}_\ell^2 = 0.23148 \pm 0.00027$, where an uncertainty of $13 \cdot 10^{-5}$ from varying the correlations is included in the total uncertainty.

The combination of LEP, Tevatron, and LHC results is still mostly dominated by the lepton collider measurement and gives [16]

$$\bar{s}_\ell^2 = 0.23150 \pm 0.00013 \ (\text{collider average}). \tag{10.67}$$

Since this average includes $\bar{s}_\ell^2$ determinations from asymmetry measurements at LEP and SLD, it cannot be used in a global EW fit that already includes these measurements. Instead, we use the HC combination (10.66) as additional input in the fit.

10.4.7 *W and Z decays*

The partial widths of weak gauge boson decays into massless fermion pairs $f_1\bar{f}_2$ (the numerical values include small final-state mass effects) are given by,

$$\begin{aligned}\Gamma(W^+ \to e^+\nu_e) &= \frac{M_W^3 G_F}{6\sqrt{2}\pi} + \text{EW corrections} \\ &= 226.29 \pm 0.04\,\text{MeV} \ ,\end{aligned} \tag{10.68a}$$

$$\begin{aligned}\Gamma(W^+ \to u_i\bar{d}_j) &= \frac{M_W^3 G_F}{6\sqrt{2}\pi}\,|V_{ij}|^2 \mathcal{R}_V^q \\ &\quad + \text{EW corrections} = (705.3 \pm 0.4\,\text{MeV})|V_{ij}|^2 \ ,\end{aligned} \tag{10.68b}$$

$$\Gamma(Z \to f\bar{f}) = \frac{M_W^3 G_F}{6\sqrt{2}\pi}\left[\mathcal{R}_V^f \bar{g}_V^{f2} + \mathcal{R}_A^f \bar{g}_A^{f2}\right] \ , \tag{10.68c}$$

where the result for the latter are shown in Table 10.4. Final-state QED and QCD corrections [326] to the vector and axial-vector form factors are given by,

$$\mathcal{R}_{V,A}^f = N_C\left[1 + \frac{3}{4}\left(Q_f^2\frac{\alpha(s)}{\pi} + \frac{N_C^2-1}{2N_C}\frac{\alpha_s(s)}{\pi}\right) + \cdots\right] \ , \tag{10.69}$$

where $N_C = 3$ (1) is the color factor for quarks (leptons) and the dots indicate finite fermion mass effects proportional to m_f^2/s which are different for $\mathcal{R}_V^f$ and $\mathcal{R}_A^f$, as well as higher-order QCD corrections [327], which are known to $\mathcal{O}(\alpha_s^4)$ [328]. For the Z boson, these include singlet contributions starting from two-loop order in QCD that are large, strongly top-quark mass dependent, family universal, and flavor non-universal [329–333]. The $\mathcal{O}(\alpha^2)$

[15] The measurement of the τ polarization in Eq. (10.63) provides another determination of the weak mixing angle, $\bar{s}_\ell^2 = 0.2319 \pm 0.0019$. Due to its large uncertainty, this measurement has a negligible impact in the collider average of $\bar{s}_\ell^2$ presented below.

[16] This differs from the value presented in the Particle Listings in this *Review* due to the inclusion of the ATLAS 8 TeV measurement [301] in this combination, and the correction of the b-quark forward-backward asymmetry determination from LEP 1.

Int. J. Mod. Phys. A 2026.41. Downloaded from www.worldscientific.com
by UNIVERSITY OF CALIFORNIA @ BERKELEY on 09/16/26. Re-use and distribution is strictly not permitted, except for Open Access articles.

Table 10.4: Partial and total Z decay widths [in MeV]. The results are derived from Table 10.3 and the corresponding covariance matrices [139,215]. The results in the second column are derived without the assumption of lepton universality, while lepton universality is assumed in the third column. The SM predictions are given in the fourth column.

Quantity	Value	Value (universal)	Standard Model
$\Gamma_{e^+e^-}$	83.87 ± 0.12	83.942 ± 0.085	83.983 ± 0.018
$\Gamma_{\mu^+\mu^-}$	83.95 ± 0.18	83.941 ± 0.085	83.982 ± 0.018
$\Gamma_{\tau^+\tau^-}$	84.03 ± 0.21	83.759 ± 0.085	83.793 ± 0.018
$\Gamma_{\rm inv}$	498.9 ± 2.5	500.5 ± 1.5	501.605 ± 0.048
$\Gamma_{u\bar{u}}$	—	—	299.88 ± 0.16
$\Gamma_{c\bar{c}}$	300.3 ± 5.3	300.0 ± 5.2	299.80 ± 0.16
$\Gamma_{d\bar{d}}, \Gamma_{s\bar{s}}$	—	—	382.82 ± 0.12
$\Gamma_{b\bar{b}}$	377.4 ± 1.3	377.0 ± 1.2	375.90 ± 0.20
$\Gamma_{\rm had}$	1744.8 ± 2.6	1743.2 ± 1.9	1741.21 ± 0.65
Γ_Z	2495.5 ± 2.3	2495.5 ± 2.3	2494.56 ± 0.73

QED self-energy corrections from Ref. [334] are also taken into account.

For the W decay into quarks, Eq. (10.68b), only the universal massless part (non-singlet and $m_q = 0$) of the final-state QCD radiator function in $\mathcal{R}_V$ from Eq. (10.69) is used, and some remaining QED corrections are part of the EW corrections. Expressing the widths in terms of $G_F M_{W,Z}^3$ incorporates the largest radiative corrections from the running QED coupling. EW corrections to the Z widths are then taken into account through the effective couplings $\bar{g}^{\,i\,2}_{V,A}$. Hence, in the OS scheme the Z widths are proportional to $\rho_i \sim 1 + \Delta\rho_t$. There is additional (negative) quadratic m_t dependence in the $Z \to b\bar{b}$ vertex corrections [335, 336] which causes $\Gamma_{b\bar{b}}$ to decrease with m_t. The dominant effect is to multiply $\Gamma_{b\bar{b}}$ by the vertex correction $1 + \delta\rho_{b\bar{b}}$, where $\delta\rho_{b\bar{b}} \sim 10^{-2}(-\frac{1}{2}m_t^2/M_Z^2 + \frac{1}{5})$.

Starting at $\mathcal{O}(\alpha\alpha_s)$, the factorized form indicated in Eq. (10.68) is violated and corrections need to be included [337–339]. They add coherently, resulting in a sizable effect, and shift $\alpha_s(M_Z^2)$ when extracted from Z lineshape observables by about $+0.0007$. Similar non-factorizable corrections are also known for mixed QED-EW corrections [106, 108, 109].

For three fermion families, the total widths of the Z [53, 340–343] and W [25, 136] bosons are predicted to be

$$\Gamma_Z = 2.4944 \pm 0.0006\,\text{GeV}\ , \qquad \Gamma_W = 2.090 \pm 0.001\,\text{GeV}\ . \tag{10.70}$$

The uncertainties in these predictions are almost entirely induced by the parametric error from the strong coupling constant, $\alpha_s(M_Z^2) = 0.1177 \pm 0.0009$, from the average in Eq. (10.41). These predictions can be compared with the experimental results, $\Gamma_Z = 2.4955 \pm 0.0023$ GeV [139, 215] and the average from LEP, Tevatron and ATLAS, $\Gamma_W = 2.14 \pm 0.05$ GeV presented in the Gauge & Higgs Bosons Particle Listings in this *Review*. The different leptonic branching fractions of the W boson, $\mathcal{B}(W \to \ell\nu_\ell)$ have been measured at high precision by the LEP 2 experiments [216]. The measurements of the total and partial widths are generally in good agreement with the SM. The exceptions are Γ_W, which is 1.3σ larger than the SM prediction, and the branching fraction $W \to \tau + \nu_\tau$ from LEP 2, which is 2.6σ larger than the electron–muon average [216]. However, a measurement from ATLAS more precise than LEP 2 on the ratio of branching fractions $W \to \tau + \nu_\tau$ to $W \to \mu + \nu_\mu$, using top quark decays, shows good agreement with the SM prediction and lepton universality [344]. Additional measurements from ATLAS, CMS, and LHCb, on ratios of branching fractions for W decays into different lepton flavors are also in agreement with lepton universality [316, 344–347].

The invisible decay width, $\Gamma_{\rm inv} = \Gamma_Z - \Gamma_{e^+e^-} - \Gamma_{\mu^+\mu^-} - \Gamma_{\tau^+\tau^-} - \Gamma_{\rm had}$, can be used to determine the number of neutrino flavors, N_ν, much lighter than $M_Z/2$. The hadronic peak cross section, and therefore the extracted $\Gamma_{\rm had}$, relies on the precise knowledge of the LEP luminosity measured by each experiment using small-angle Bhabha scattering. However, the earlier prediction for the Bhabha cross section was found to be overestimated, and consequently the luminosity underestimated [215]. An updated analysis led to a significant reduction in $\sigma_{\rm had}$ and a small increase in Γ_Z, as given in Eq. (10.55). The resulting value, $N_\nu = 2.9963 \pm 0.0074$ [215], is in agreement with the observed number of three fermion generations $N_\nu = 3$.

10.5 Global fit results

In this section, we present the results of global fits, subject to the experimental data and theoretical predictions discussed in Sections 10.2−10.4. For earlier analyses and other recent global fits, see Refs. [80, 127, 131, 132, 139, 348–351] and previous editions of this *Review*. We recall that the latter have been obtained with the `GAPP` package [133], which consistently employs $\overline{\rm MS}$-renormalized quantities. For the results given here, we use the observables summarized in Table 10.5. This includes non-Z-pole observables such as the values of m_t (see Sec. 10.4.3), M_H [231,352], M_W [220,222], Γ_W [216, 222, 227], and $\mathcal{BR}(W \to \ell\nu)$ [216, 345]. We also use the values of $\alpha_s(M_Z^2)$, $\Delta\alpha_{\rm had}^{(5)}(M_Z^2)$, and the heavy-quark masses as inputs, as explained in the previous sections. The heavy-quark masses, other than m_t, have a negligible impact on the fit and are omitted in Table 10.5. The principal Z-pole observables from the LEP 1 averages of the ALEPH, DELPHI, L3, and OPAL results include the corresponding correlations [139,215]. We assume lepton universality throughout this section, as confirmed by the measurements discussed above. In the SM fit, we use as inputs the combinations of leptonic observables obtained under this assumption. The recent τ-polarization measurement from CMS [307] (10.63) is not included in the fit, because of its negligible impact due to its large uncertainty compared to the LEP and SLD measurements. The heavy-flavor results [139, 313] of LEP 1 and SLD are based on common inputs, and are thus correlated as well. For the effective weak mixing angle, we use the value extracted from the hadronic charge asymmetry at LEP 1 ($Q_{\rm FB}$) [139] and the hadron-collider (HC) average from Eq. (10.66).

Next to the experimental values in Table 10.5, we report the SM predictions from the EW fit. In the column labelled "SM fit", the result is shown from a fit with all experimental inputs included. The next column, labelled "indirect determination", shows the result of the fit where the observable in the given line is excluded from the fit. This column can be understood as the unbiased prediction for a given observable, obtained from the current best theoretical knowledge for the given observable, combined with the best experimental and theoretical knowledge of all observables relevant for the corresponding prediction. The fits presented in this *Review* have been performed using the `HEPfit` [128] and `Gfitter` [124] codes. The `HEPfit` results are derived following a Bayesian statistical analysis of the data and hypotheses, whereas `Gfitter` follows a frequentist approach with a global least-squares (χ^2) fit. Experimental uncertainties of all input observables are treated as one standard deviation of a Gaussian function. For simplicity, theoretical uncertainties estimating the size of missing higher-order contributions are also treated as Gaussian. However, we note that this assumption is not strictly fulfilled. This choice is justified by the fact that current theory uncertainties are smaller

Int. J. Mod. Phys. A 2026.41. Downloaded from www.worldscientific.com by UNIVERSITY OF CALIFORNIA @ BERKELEY on 09/16/26. Re-use and distribution is [redacted] except for Open Access articles.

Table 10.5: Electroweak precision observables included in the SM fit. The second column gives the experimental input, the third the result of the full fit, the fourth shows the value of the parameter in this line if the respective parameter is not included in the fit, and the last column gives the pull of the parameter. The pull is defined as the difference between the experimental value and the value of the indirect determination, divided by the total uncertainty, given by the quadratic sum of experimental uncertainty and uncertainty in the prediction. The first set of five parameters consists of the SM input parameters in the LEP input scheme, where G_F and $\alpha(0)$ are fixed. These five input parameters are constrained by the observables included in the fit, also encompassing their direct experimental measurements. The other three sets of parameters are measurements related to the W boson, leptonic Z-pole observables together with Γ_Z, $\sigma_{\rm had}$ and the hadron collider average of $\bar{s}^2_\ell$ from Eq. (10.66), and asymmetries of heavy quarks.

Parameter	Experimental value	SM fit	Indirect determination	Pull
$\alpha_s(M_Z^2)$	0.1177 ± 0.0009	0.1179 ± 0.0009	0.1200 ± 0.0028	-0.8
$\Delta\alpha_{\rm had}^{(5)}(M_Z^2)$ $^{(\triangle)}$	0.02758 ± 0.00010	0.02757 ± 0.00009	0.02734 ± 0.00033	$+0.7$
M_Z [GeV]	91.1879 ± 0.0020	91.1882 ± 0.0019	91.1939 ± 0.0069	-0.8
m_t [GeV]$^{(\triangledown)}$	172.60 ± 0.59	172.74 ± 0.54	173.65 ± 1.47	-0.7
M_H [GeV]	125.1 ± 0.1	125.1 ± 0.1	111^{+19}_{-17}	$+0.8$
M_W [GeV]	80.363 ± 0.008	80.359 ± 0.005	80.357 ± 0.006	$+0.6$
Γ_W [GeV]	2.140 ± 0.050	2.090 ± 0.001	2.090 ± 0.001	$+1.0$
$\mathcal{BR}(W \to \ell\bar{\nu}_\ell)$	0.1088 ± 0.0006	0.10838 ± 0.00002	0.10838 ± 0.00002	$+0.7$
$\bar{s}^2_\ell = \sin^2\theta^\ell_{\rm eff}({\rm HC})$	0.23149 ± 0.00022	0.23152 ± 0.00005	0.23152 ± 0.00006	-0.1
$\bar{s}^2_\ell = \sin^2\theta^\ell_{\rm eff}(Q_{\rm FB})$	0.2324 ± 0.0012	0.23152 ± 0.00005	0.23152 ± 0.00005	$+0.7$
A_ℓ(LEP)	0.1465 ± 0.0033	0.1470 ± 0.0004	0.1471 ± 0.0004	-0.2
A_ℓ(SLD)	0.1513 ± 0.0021	0.1470 ± 0.0004	0.1469 ± 0.0004	$+2.1$
Γ_Z [GeV]	2.4955 ± 0.0023	2.4945 ± 0.0006	2.4944 ± 0.0006	$+0.5$
$\sigma_{\rm had}$ [nb]	41.480 ± 0.033	41.490 ± 0.008	41.491 ± 0.008	-0.3
R_ℓ	20.767 ± 0.025	20.749 ± 0.006	20.748 ± 0.006	$+0.7$
$A^\ell_{\rm FB}$	0.0171 ± 0.0009	0.01622 ± 0.0001	0.01621 ± 0.0001	$+1.0$
R_b	0.21629 ± 0.00066	0.21587 ± 0.00003	0.21587 ± 0.00003	$+0.6$
R_c	0.1721 ± 0.0030	0.17220 ± 0.00003	0.17220 ± 0.00003	-0.0
$A^b_{\rm FB}$	0.0996 ± 0.0016	0.1031 ± 0.0003	0.1032 ± 0.0003	-2.2
$A^c_{\rm FB}$	0.0707 ± 0.0035	0.0737 ± 0.0002	0.0737 ± 0.0002	-0.9
A_b	0.923 ± 0.020	0.93475 ± 0.00003	0.93475 ± 0.00003	-0.6
A_c	0.670 ± 0.027	0.6679 ± 0.00019	0.6679 ± 0.00019	$+0.1$
A_s	0.895 ± 0.091	0.9357 ± 0.00003	0.9357 ± 0.00003	-0.4

$^{(\triangle)}$Rescaled due to α_s dependency. $^{(\triangledown)}$Combination of experimental (0.27 GeV) and theory uncertainty (0.52 GeV).

by more than a factor of two than the experimental uncertainties, so that the fit result is driven by the experimental uncertainties. The main uncertainties associated with missing higher-order corrections are given by [110]

$$\delta_{\rm th} M_W = 4\,{\rm MeV}\,, \quad \delta_{\rm th}\sin^2\theta^f_{\rm eff} = 4.7\cdot 10^{-5}\,, \qquad (10.71)$$
$$\delta_{\rm th}\Gamma_Z = 0.4\,{\rm MeV}\,, \quad \delta_{\rm th}\sigma_{\rm had} = 6\,{\rm pb}\,,$$
$$\delta_{\rm th} R_\ell = 0.006\,, \quad \delta_{\rm th} R_c = 0.00005\,, \quad \delta_{\rm th} R_b = 0.0001\,.$$

The reported uncertainty for each parameter is defined from the 68.3% probability range, upon profiling or marginalizing (depending on the approach) over the other parameters. These uncerainties are, in general, well approximated by the 1σ errors obtained from the values satisfying $\Delta\chi^2 = \chi^2 - \chi^2_{\rm min} = 1$. For the two-dimensional figures presented here, we show contours corresponding to the 68.3% and 95.5% confidence levels.

All results presented here have been obtained with both fit programs, `HEPfit` and `Gfitter`. We cross-checked these against each other and found excellent agreement between the numerical results from the two programs, with differences typically smaller than 10% of the quoted uncertainties in the predictions. In the Bayesian approach of `HEPfit`, the shapes of most of the posterior distributions follow Gaussian functions to a good approximation, such that the uncertainties from the two fit programs agree very well.

The agreement between the measurements and the predictions is generally very good. Despite the few discrepancies addressed in the following, the global EW fit describes the data very well, with a $\chi^2/{\rm d.o.f.} = 14.4/17$, corresponding to a p-value of 64%. The largest tensions are only at the 2σ level, which correspond to A_ℓ(SLD), $A^b_{\rm FB}$ from LEP 1, and Γ_W(ATLAS). Also, there is currently no understanding as to why the M_W value reported by the CDF collaboration [212] (not included in the fit) is significantly larger than the measurements by other experiments. We also emphasize that there are a number of discrepancies among individual measurements of certain quantities, as discussed in previous sections, but these are not reflected in the overall χ^2 of the fit as only the corresponding combinations are used as constraints.

There is still a long-standing tension in the EW fit with the combined measurement of the bottom-quark asymmetry $A^b_{\rm FB}$ that is below the SM prediction by 2.2σ, despite a slight improvement in recent years thanks to developments in related theory calculations [313]. The value of A_b can be extracted from $A^b_{\rm FB}$ when $A_e = 0.1501 \pm 0.0016$ is taken from a fit to leptonic asymmetries. The result, $A_b = 0.885 \pm 0.017$, is 2.9σ below the SM prediction[17] and also 1.4σ below $A_b = 0.923 \pm 0.020$ obtained from $A^{\rm FB}_{\rm LR}(b)$ at SLD. Thus, it seems that at least some of the tension in A_b is due to a statistical fluctuation. We note that the uncertainties in $A^b_{\rm FB}$ from LEP 1 and $A_{\rm LR}$ from SLD are dominated by the statistical component. The combined value, $A_b = 0.901 \pm 0.013$ deviates by 2.6σ from the SM prediction.

The left-right asymmetry $A_{\rm LR} = 0.15138 \pm 0.00216$ [305], obtained by counting hadronically decaying Z bosons for each electron-beam polarization at SLD, differs by 2σ from the SM fit value of 0.1470 ± 0.0004. The combined value of $A_\ell = 0.1513 \pm 0.0021$ from SLD is also 2.1σ above the SM prediction; but there is experimental agreement between this SLD value and the LEP 1 value, $A_\ell = 0.1481 \pm 0.0027$, obtained from a fit to $A^\ell_{\rm FB}$, $A_e(\mathcal{P}_\tau)$, and $A_\tau(\mathcal{P}_\tau)$.

The third and fourth columns in Table 10.5 reveal that the results from the full fit, including the Higgs-boson mass [231, 352], do not deviate from the indirect determinations by more than 1σ. Except for the input parameters, each parameter can be predicted with a precision better than the experimental precision. The indirect determinations of the input parameters M_H and m_t have uncertainties of about $^{+19}_{-17}$ GeV and ± 1.5 GeV, compared to experimental precisions of 0.1 GeV and 0.27 GeV, respectively. The logarithmic dependence of the SM predictions on M_H results

[17] Alternatively, one can use $A_\ell = 0.1481 \pm 0.0027$, which is from LEP 1 alone and in excellent agreement with the SM, and obtain $A_b = 0.897 \pm 0.022$, which is 1.7σ low.

Int. J. Mod. Phys. A 2026.41. Downloaded from www.worldscientific.com
by UNIVERSITY OF CALIFORNIA @ BERKELEY on 09/16/26. Re-use and distribution is strictly not permitted, except for Open Access articles.

in an uncertainty much larger than the experimental precision from the kinematic reconstruction of the Higgs boson. The precision of the indirect determination of m_t is strongly influenced by the uncertainty in the M_W measurement. In the full fit in column three, no input parameter is pulled from its measured value by more than 1σ, with small correlations among the input parameters. Moreover, because the SM parameters entering the predictions of the EW observables are measured with high precision, the parametric uncertainties in the predictions are currently smaller than the corresponding experimental uncertainties. This is shown in Table 10.6, indicating the contribution from the experimental measurements in each of the input parameters to the total uncertainty in a given observable.

Despite the high precision of the direct measurements of the chosen set of SM input parameters, M_Z, M_H, m_t, $\Delta\alpha^{(5)}_{\rm had}(M_Z^2)$, and $\alpha_s(M_Z^2)$, it is interesting to note that the data allow for a simultaneous determination of these parameters from the global EW fit without constraints from direct measurements. Excluding the direct measurement of the SM input parameters from the fit, the resulting values for each of these inputs and their correlations are shown in Table 10.7. Whereas M_Z and $\alpha_{\rm em}(M_Z^2)$ enter the predictions of most observables at the tree level, the dependence on M_H, m_t, and $\alpha_s(M_Z^2)$ is solely through radiative corrections. We note the consistency between the values in Table 10.7 and the actual measurements in Table 10.5.

From the EW precision observables, the strong coupling constant $\alpha_s(M_Z^2)$ is determined mainly through R_ℓ, Γ_Z, $\sigma_{\rm had}$, but Γ_W and the W branching fractions also have an impact. When including only the most sensitive observables in the fit, together with the experimental constraints on the input parameters but leaving $\alpha_s(M_Z^2)$ unconstrained, we obtain the following values:

$$R_\ell : \alpha_s(M_Z^2) = 0.1210 \pm 0.0042\,, \tag{10.72}$$

$$\Gamma_Z : \alpha_s(M_Z^2) = 0.1203 \pm 0.0049\,, \tag{10.73}$$

$$\sigma_{\rm had} : \alpha_s(M_Z^2) = 0.1202 \pm 0.0068\,, \tag{10.74}$$

$$\text{all three} : \alpha_s(M_Z^2) = 0.1206 \pm 0.0029\,. \tag{10.75}$$

The values of $\alpha_s(M_Z^2)$ are compatible with each other within the uncertainties. The corrections from beam–beam effects on the luminosity measurement at LEP [312] and the improved Bhabha cross section [215] result in an upwards shift in $\alpha_s(M_Z^2)$ from $\sigma_{\rm had}$ and as a consequence the fit with all three observables gives a very small $\chi^2/\text{d.o.f.} = 0.02/2$. The full EW fit gives

$$\alpha_s(M_Z^2) = 0.1200 \pm 0.0028\,, \tag{10.76}$$

with a central value very close to the one from the reduced fit to R_ℓ, Γ_Z, and $\sigma_{\rm had}$, and only a slightly smaller uncertainty. This value is compatible at about 1σ with the averages obtained from τ decays ($\alpha_s(M_Z^2) = 0.1171^{+0.0018}_{-0.0017}$), heavy quarkonia spectroscopy (0.1181 ± 0.0037), DIS and global PDF fits (0.1161 ± 0.0022), hadronic final states of e^+e^- annihilations (0.1189 ± 0.0037), hadron colliders (0.1168 ± 0.0027), as well as lattice QCD simulations (0.1184 ± 0.0008). For more details, other determinations, and references, see Section 9 on "Quantum Chromodynamics" in this *Review*.

The loop-level sensitivity of the EW fit to M_H and m_t comes mainly from M_W and $\bar{s}_\ell^2$. The dependence of M_W on m_t is illustrated in Fig. 10.3. The EW fit contour, including all observables except M_W and m_t, is still somewhat larger than the precision of the direct measurements. Without M_W included in the fit, the uncertainty in the predicted value of m_t is ± 4.1 GeV. Without an experimental constraint on M_H, the allowed range for m_t is significantly larger, increasing to $^{+9.8}_{-8.1}$ GeV. The measurements of A_ℓ, $\bar{s}_\ell^2$, and $A^b_{\rm FB}$ result in a determination of m_t with an uncertainty of about ± 7, ± 7.5, and ± 8 GeV, respectively. The strongest constraint on m_t comes from the measurement of M_W, resulting in $m_t = 173.6 \pm 1.5$ GeV. The slight preference for a larger value of m_t compared to the experimental measurement is correlated with the equally slightly larger observed value of M_W compared to the prediction, see Table 10.5 and Fig. 10.3. The result is, in

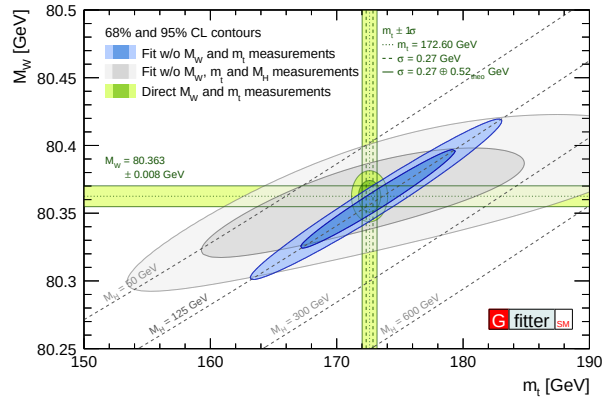

Figure 10.3: Determination of the W-boson and top-quark masses from the EW fit, compared to the experimental values. Shown are the 68% and 95% confidence level contours, together with the SM prediction of M_W as a function of m_t, where the other input parameters are given in Table 10.5. The grey contours show the EW fit without using the measured M_H as input.

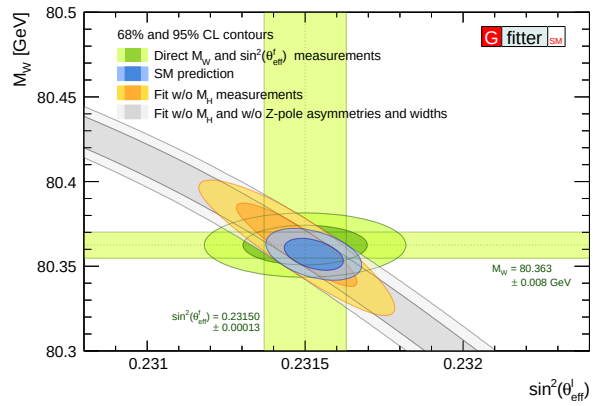

Figure 10.4: Prediction of the W-boson mass and $\bar{s}_\ell^2$ in the EW fit obtained with the input values from Table 10.5 (blue contours), compared to the world average of M_W and the collider average of $\bar{s}_\ell^2$ (10.67) (green contours). Shown are the 68% and 95% confidence level contours. The orange contours show the result of a fit that includes Z-pole data (asymmetries and partial widths), but without M_H. The grey contours show the fit result without M_H and without the Z-pole data.

any case, compatible with the direct constraint at less than 1σ, illustrating again the good agreement of the SM with data.

In Fig. 10.4, we compare the predictions of M_W and $\bar{s}_\ell^2$ with the experimental measurements. The largest uncertainties in the prediction of M_W are the parametric uncertainties in m_t and $\alpha_s(M_Z^2)$ and the theoretical uncertainties of ± 4 MeV from missing higher orders and $\Delta m_{\rm MC}$ from Eq. (10.37). In the prediction of $\bar{s}_\ell^2$, the largest uncertainties are the parametric uncertainties in $\Delta\alpha^{(5)}_{\rm had}(M_Z^2)$, m_t, and M_Z, which are of similar size as the uncertainty from missing higher orders, $4.7 \cdot 10^{-5}$. The experimental uncertainty in M_W comes from a combination of results from the LEP, Tevatron, and LHC experiments. The experimental uncertainty in $\bar{s}_\ell^2$ is still dominated by the precise asymmetry measurements from LEP 1, but hadron-collider measurements start to become relevant. In hadron-collider measurements, the uncertainty in $\bar{s}_\ell^2$ is currently dominated by PDF uncertainties, but with a prospect of reduced future uncertainties because PDFs can be simultaneously constrained with $\bar{s}_\ell^2$ using large data sets. The result of a fit including Z-pole observables, most notably the asymmetry measurements, but without the experimental value of M_H (shown in orange), has an uncertainty larger by a factor of

Int. J. Mod. Phys. A 2026.41. Downloaded from www.wo
by UNIVERSITY OF CALIFORNIA @ BERKELEY on 09/16/26. Re-use and distribution is
except for Open Access articles.

Table 10.6: Contributions to the parametric uncertainties in the SM predictions of different EW precision observables. The contribution from the uncertainty in M_H is negligible and is omitted here. The last column shows the present experimental precision in the respective observable for comparison.

	Contribution to parametric uncertainty				Total	Total
	$\alpha_s(M_Z^2)$	$\Delta\alpha_{\rm had}^{(5)}(M_Z^2)$	M_Z	m_t	param. unc.	exp. unc.
M_W [GeV]	0.0006	0.0018	0.0025	0.0036	0.0048	0.008
Γ_W [GeV]	0.00036	0.00014	0.00020	0.00028	0.00052	0.050
$\mathcal{BR}(W \to \ell\bar{\nu}_\ell)$	$2.1 \cdot 10^{-5}$	–	$2.0 \cdot 10^{-7}$	$2.2 \cdot 10^{-7}$	$2.1 \cdot 10^{-5}$	$6 \cdot 10^{-4}$
$\bar{s}_\ell^2 = \sin^2\theta_{\rm eff}^\ell$	$3.0 \cdot 10^{-6}$	$3.5 \cdot 10^{-5}$	$1.4 \cdot 10^{-5}$	$1.8 \cdot 10^{-5}$	$4.2 \cdot 10^{-5}$	$2.2 \cdot 10^{-4}$
Γ_Z [GeV]	0.00044	$9.5 \cdot 10^{-5}$	0.00020	0.00014	0.00052	0.0023
$\sigma_{\rm had}$ [nb]	± 0.0044	0.00018	0.0019	0.00041	0.0048	0.033
R_ℓ	0.0055	0.00061	0.00026	0.00026	0.0056	0.025
$A_{\rm FB}^\ell$	$5.1 \cdot 10^{-6}$	$6.1 \cdot 10^{-5}$	$2.5 \cdot 10^{-5}$	$3.1 \cdot 10^{-5}$	$7.3 \cdot 10^{-5}$	0.0010
A_ℓ	$2.3 \cdot 10^{-5}$	0.00027	0.00011	0.00014	0.00033	0.0021
R_b	$9.9 \cdot 10^{-6}$	$1.1 \cdot 10^{-6}$	$5.5 \cdot 10^{-7}$	$2.0 \cdot 10^{-5}$	$2.3 \cdot 10^{-5}$	$6.6 \cdot 10^{-4}$
R_c	$1.7 \cdot 10^{-5}$	$2.0 \cdot 10^{-6}$	$7.1 \cdot 10^{-7}$	$6.9 \cdot 10^{-6}$	$1.9 \cdot 10^{-5}$	0.0030
$A_{\rm FB}^b$	$1.6 \cdot 10^{-5}$	0.00019	$8.0 \cdot 10^{-5}$	$9.6 \cdot 10^{-5}$	0.00023	0.0016
$A_{\rm FB}^c$	$1.3 \cdot 10^{-5}$	0.00015	$6.2 \cdot 10^{-5}$	$7.8 \cdot 10^{-5}$	0.00018	0.0035
A_b	$1.6 \cdot 10^{-6}$	$2.2 \cdot 10^{-5}$	$9.1 \cdot 10^{-6}$	$4.0 \cdot 10^{-6}$	$2.5 \cdot 10^{-5}$	0.020
A_c	$1.1 \cdot 10^{-5}$	0.00012	$4.9 \cdot 10^{-5}$	$6.6 \cdot 10^{-5}$	0.00015	0.027
A_s	$1.8 \cdot 10^{-6}$	$2.2 \cdot 10^{-5}$	$9.0 \cdot 10^{-6}$	$1.2 \cdot 10^{-5}$	$2.7 \cdot 10^{-5}$	0.091

Table 10.7: Values of the SM input parameters from a simultaneous indirect determination from the SM fit to all other EW precision measurements. We also show the correlations from the fit.

M_Z [GeV]	91.189 ± 0.038	1.00				
m_t [GeV]	$170.3^{+9.6}_{-7.5}$	−0.52	1.00			
M_H [GeV]	80^{+188}_{-54}	0.49	0.45	1.00		
$\alpha_s(M_Z^2)$	0.1201 ± 0.0040	−0.73	0.45	−0.36	1.00	
$\Delta\alpha_{\rm had}^{(5)}(M_Z^2)$	0.02786 ± 0.00089	−0.43	−0.22	−0.83	0.44	1.00

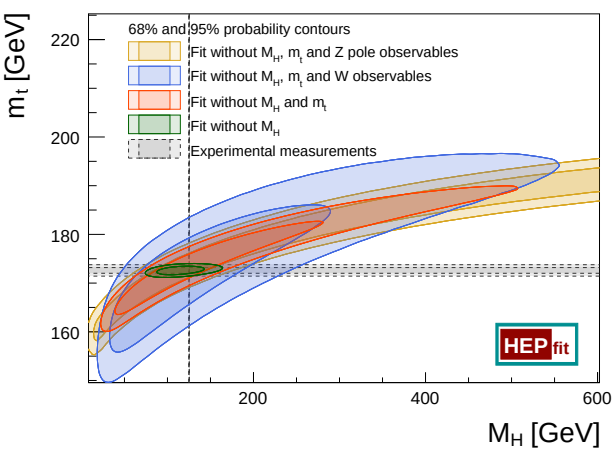

Figure 10.5: Bayesian probability contours at 68% and 95% for the Higgs-boson and top-quark masses from EW fits excluding different sets of input measurements. The grey bands indicate the experimental precision of the direct measurements of the two parameters. The width of the vertical band, corresponding to the precision in M_H, is not visible on the scale of the plot.

about 2.5 compared to the SM prediction. This fit matches the experimental precision in $\bar{s}_\ell^2$, but has an uncertainty about twice as large in M_W when compared to the world average Eq. (10.33). Without M_H and without Z-pole observables, the prediction becomes undetermined in the $\bar{s}_\ell^2$–M_W plane, as shown by the grey contours in Fig. 10.4.

The sensitivity of the EW fit to M_H is substantially increased when including the measurements of the other SM input parameters, as illustrated in Fig. 10.5. Despite the very precise determinations of these observables, the sensitivity to the actual value of M_H is diminished by the fact that the leading contributions to the predictions of EW observables is logarithmic. Removing the direct LHC measurements of M_H from the EW fit results in a loop-level determination of M_H from precision data, given in the fourth column in Table 10.5. At 95% confidence level, we obtain

$$80 \text{ GeV} < M_H < 150 \text{ GeV}\,, \tag{10.77}$$

which encloses the observed value in Eq. (10.34). The measurements of $\bar{s}_\ell^2$, M_W, A_ℓ, and $A_{\rm FB}^b$ show the highest sensitivity to M_H. Including only one of these observables at a time, the value of M_H is determined to be

$$\bar{s}_\ell^2(\text{HC}) : M_H = 114^{+69}_{-44} \text{ GeV}\,, \tag{10.78}$$

$$M_W : M_H = 112^{+21}_{-19} \text{ GeV}\,, \tag{10.79}$$

$$A_\ell(\text{SLD}) : M_H = 36.7^{+31.4}_{-18.9} \text{ GeV}\,, \tag{10.80}$$

$$A_\ell(\text{LEP}) : M_H = 140^{+190}_{-84} \text{ GeV}\,, \tag{10.81}$$

$$A_{\rm FB}^b : M_H = 487^{+398}_{-212} \text{ GeV}\,. \tag{10.82}$$

The obtained values agree well within the uncertainties, except for the values from $A_{\rm FB}^b$ and A_ℓ(SLD), which are apart by about 2.2σ. The predicted value from the full EW fit,

$$M_H = 111^{+19}_{-17} \text{ GeV}\,, \tag{10.83}$$

agrees with the individual values and the direct measurement, evidencing the excellent internal consistency of the SM and its capability of predicting observables to very high precision.

In summary, the remarkable agreement between SM predictions and experimental EW precision data, which is reached only after including radiative (meaning *quantum*) corrections, impressively confirms the model as a *quantum field theory*, while tree-level predictions (without quantum corrections) are away from data by many standard deviations.

10.6 Constraints on new physics

The precise measurements of EW observables available at different energies and their overall agreement with the SM predictions can be used to set strong limits on new physics modifying, in particular, the properties of the EW gauge bosons. Since the LEP era, the limits from EW precision measurements have

Int. J. Mod. Phys. A 2026.41. Downloaded from www.worldscientific.com
by UNIVERSITY OF CALIFORNIA @ BERKELEY on 09/16/26. Re-use and distribution is strictly not permitted, except for Open Access articles.

typically been interpreted in terms of the so-called oblique new physics, which assumes only modifications in the gauge-boson self-energies coming from new particles (*e.g.*, heavy particles with masses $\Lambda \gg M_W$), and have been traditionally parametrized in terms of the Peskin-Takeuchi S, T, and U parameters [353].[18] Denoting the contributions of new physics to the various self-energies by $\Pi_{ij}^{\rm new}$, we have

$$\alpha(M_Z^2)T \equiv \frac{\Pi_{WW}^{\rm new}(0)}{M_W^2} - \frac{\Pi_{ZZ}^{\rm new}(0)}{M_Z^2}\ , \tag{10.84a}$$

$$\frac{\alpha(M_Z^2)}{4\,s_W^2 c_W^2} S \equiv \frac{\Pi_{ZZ}^{\rm new}(M_Z^2) - \Pi_{ZZ}^{\rm new}(0)}{M_Z^2} - \frac{c_W^2 - s_W^2}{c_W s_W}\frac{\Pi_{Z\gamma}^{\rm new}(M_Z^2)}{M_Z^2} - \frac{\Pi_{\gamma\gamma}^{\rm new}(M_Z^2)}{M_Z^2}\ , \tag{10.84b}$$

$$\frac{\alpha(M_Z^2)}{4\,s_W^2}(S+U) \equiv \frac{\Pi_{WW}^{\rm new}(M_W^2) - \Pi_{WW}^{\rm new}(0)}{M_W^2} - \frac{c_W}{s_W}\frac{\Pi_{Z\gamma}^{\rm new}(M_Z^2)}{M_Z^2} - \frac{\Pi_{\gamma\gamma}^{\rm new}(M_Z^2)}{M_Z^2}\ . \tag{10.84c}$$

The S, T, and U parameters are defined with a coupling factor proportional to α, so that they are expected to be of order unity in the presence of new physics. The S parameter measures the momentum dependence of custodial-symmetric new-physics effects modifying the neutral-current interactions. On the other hand, the parameter T only receives contributions from custodial SU(2) breaking new physics, measuring the difference between contributions to neutral and charged-current processes at low energies. Finally, the momentum dependence of such contributions is probed by the U parameter. Note that the full SM contributions to S, T, and U are gauge dependent, which is the reason that the gauge-boson self-energies are restricted to their non-standard contributions $\Pi_{VV'}^{\rm new}(q^2)$, with SM parts subtracted for a given input scenario.

The *STU* formalism was also the approach taken in previous versions of this *Review*, and its results can be translated into bounds of a large class of new-physics models, as long as the leading-order effects are oblique in the previous sense, and therefore also flavor universal. The available EW precision data does, however, allow to test a larger type of new-physics effects beyond the one of oblique nature. For instance, new physics that couples directly to ordinary fermions cannot be fully parametrized in the *STU* framework. Such examples include heavy Z' bosons [358], mixing with exotic fermions [9, 359, 360], leptoquark exchange [216, 361, 362], supersymmetric models, strong EW dynamics [363], Little Higgs models [364, 365], and TeV-scale extra spatial dimensions [366–369] (for more details and references, see Section 84 on "Extra Dimensions" in this *Review*). These types of new-physics scenarios, and more, can be described within the more general framework of *Effective Field Theories* (EFTs).

Under the assumptions that new physics is heavy compared to the scale of energies explored so far, and that at those energies the symmetries and field content are those of the SM, with the Higgs field being part of an SU(2) doublet ϕ like in the SM,[19] the so-called *Standard Model Effective Field Theory (SMEFT)* [373, 374] provides a rather general description of new-physics effects, parametrized in terms of an expansion in higher-dimensional operators, suppressed by the cut-off of the EFT, $\Lambda \gg v$, where new physics is expected to complete the SM:

$$\mathcal{L} = \mathcal{L}_{\rm SM} + \sum_{d>4}\sum_i \frac{C_i}{\Lambda^{d-4}}\mathcal{O}_i\ . \tag{10.85}$$

In this $1/\Lambda$ expansion, the observable effects of each higher-dimensional operator are suppressed by increasing powers of E/Λ, with $E \ll \Lambda$ the typical energy of a physical process. For a given level of experimental precision δ, one can then truncate the EFT expansion as long as $(E/\Lambda)^{d-4} \ll \delta$ and work with a finite number of operators. In this regard, although the EFT is technically non-renormalizable in the strict sense, at each order in the EFT expansion only a finite number of counterterms is needed, and the theory remains predictive at the desired level of experimental precision. In Eq. (10.85) the specific information about the new physics is encoded in the values of the *Wilson coefficients* C_i. These can be computed in terms of the masses and couplings of the new particles in a given model by, *e.g.*, matching the EFT and model results for a representative set of amplitudes.

Assuming lepton and baryon number conservation and a SMEFT-type new physics scenario, the leading-order new-physics effects in the $1/\Lambda$ expansion are given by dimension-six operators, and we restrict the discussion to this level of approximation in the following.[20] The full set of all possible new-physics effects can be parametrized in a widely model-independent way specifying a basis for the SMEFT at each order in the $1/\Lambda$ expansion and, to dimension six, several bases have been proposed [372–375]. In particular, the so-called *Warsaw basis* [374] presented the first complete set of physically independent dimension-six interactions which, assuming individual conservation of baryon and lepton number, contains a total of 59 operator structures, and 2499 interactions for three generations of fermions. Despite this large number of operators, at the (leading) order of $1/\Lambda$ only a relatively small number of operators modify the SM predictions for the EW precision observables measuring the properties of the W and Z bosons. For instance, assuming fermion-universal new-physics effects, in the Warsaw basis only 10 operators modify the SM predictions at order $1/\Lambda^2$ and tree level. These are:[21]

$$\mathcal{O}_{\phi D} = (\phi^\dagger D_\mu \phi)^*\,(\phi^\dagger D^\mu \phi),\ \ \mathcal{O}_{\phi WB} = (\phi^\dagger \sigma_a \phi)\,(B^{\mu\nu}W^a_{\mu\nu}), \tag{10.86}$$

$$\begin{aligned}
(\mathcal{O}^{(1)}_{\phi F})_{ij} &= i(\phi^\dagger \overleftrightarrow{D}_\mu \phi)\,(\overline{F^i_L}\gamma^\mu F^j_L),\\
(\mathcal{O}^{(3)}_{\phi F})_{ij} &= i(\phi^\dagger \overleftrightarrow{D}^a_\mu \phi)\,(\overline{F^i_L}\gamma^\mu F^j_L),\\
(\mathcal{O}_{\phi f})_{ij} &= i(\phi^\dagger \overleftrightarrow{D}_\mu \phi)\,(\overline{f^i_R}\gamma^\mu f^j_R), \qquad F = l, q, \quad f = e, u, d,
\end{aligned} \tag{10.87}$$

$$(\mathcal{O}_{ll})_{1221} = (\overline{l^1_L}\gamma_\mu l^2_L)\,(\overline{l^2_L}\gamma^\mu l^1_L). \tag{10.88}$$

The effects of the operators $\mathcal{O}_{\phi WB}$ and $\mathcal{O}_{\phi D}$ can be described in terms of the oblique S and T parameters introduced above, respectively. To be more precise, the S and T parameters can be directly associated to linear combinations of these two dimension-six bosonic operators and fermion-universal contributions from the interactions $\mathcal{O}^{(1),(3)}_{\phi F}$ and $\mathcal{O}_{\phi f}$ in Eq. (10.87) [376]. These operators also describe cases where new physics couples to the different SM fermion generations in a non-universal manner. These induce modifications to the EW couplings to the Z and W bosons parameterized by:

$$(\Delta g^f_L)_{ij} = -\frac{1}{2}\left(C^{(1)}_{\phi F} \pm C^{(3)}_{\phi F}\right)_{ij}\frac{v^2}{\Lambda^2},\ (\Delta g^f_R)_{ij} = -\frac{1}{2}(C_{\phi f})_{ij}\frac{v^2}{\Lambda^2}, \tag{10.89}$$

$$(\Delta U^f_L)_{ij} = (C^{(3)}_{\phi F})_{ij}\frac{v^2}{\Lambda^2}. \tag{10.90}$$

In Eq. (10.89), Δg^f_L and Δg^f_R give the corrections to the left-handed and right-handed neutral currents, respectively, and

[18] We note that other parametrizations exist, see for example Refs. [354–357].

[19] A more general type of EFT, known as *Higgs Effective Field Theory (HEFT)* [370–372], relaxes this assumption by allowing the physical Higgs field to be a gauge singlet and including the Goldstone fields as SU(2) triplet in some non-linear field representation.

[20] From the point of view of observables measuring the W and Z boson properties, with experimental precision in some cases at the per-mil level, this truncation is justified if new physics is not present well below the TeV scale, in which case effects of dimension-eight operators are suppressed by $M_W^4/(1\,\text{TeV})^4 \sim \mathcal{O}(10^{-4})$.

[21] The hermitian covariant derivatives $\overleftrightarrow{D}$ and $\overleftrightarrow{D}^a$ appearing below are defined as $\overleftrightarrow{D}_\mu = D_\mu - \overleftarrow{D}_\mu$, $\overleftrightarrow{D}^a_\mu = \sigma_a D_\mu - \overleftarrow{D}_\mu \sigma_a$, with σ_a the Pauli matrices.

Int. J. Mod. Phys. A 2026.41. Downloaded from www.wo
by UNIVERSITY OF CALIFORNIA @ BERKELEY on 09/16/26. Re-use and distribution is
except for Open Access articles.

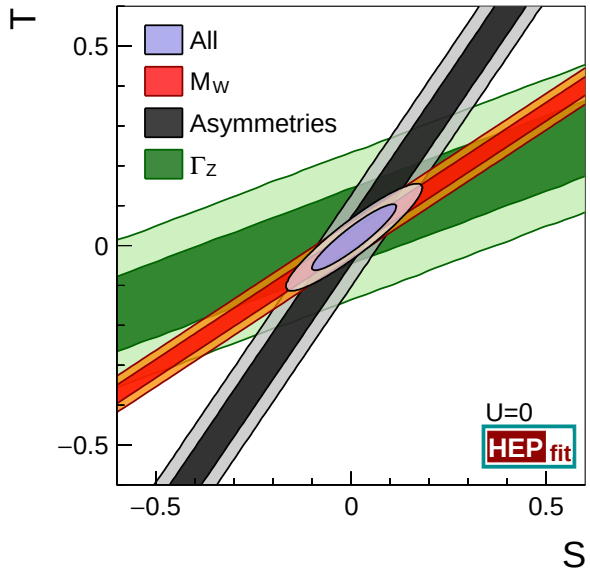

Figure 10.6: EW precision constraints on the S and T plane (assuming $U = 0$). The boundaries of the dark and light regions correspond to the 68% and 95% probability contours, respectively. We also show the constraints imposed by different sets of EW precision measurements. See text for details.

the plus (minus) sign corresponds to fermions of weak isospin $-1/2\,(+1/2)$. On the other hand, Eq. (10.90) denote the modifications of the (left-handed) charged currents. For simplicity, for the quark interactions we have ignored the CKM effects that would be introduced when rotating to the physical basis. Finally, the operator $(\mathcal{O}_{ll})_{1221}$ in Eq. (10.88) contributes to the muon decay and, therefore, the determination of the Fermi constant. In recent years, NLO calculations including the complete dimension-six effects in EW precision observables have become available [377,378], including also calculations in different input schemes [379]. More details can be found in the original references.

The EFT formalism also gives additional context to the description of EW precision observables via oblique parameters and the connection to new physics generating these effects. For instance, while the S and T parameters arise from contributions of dimension-six operators, the U parameter is a dimension-eight effect, and it is therefore expected to be parametrically suppressed with respect to S and T by a factor M_Z^2/Λ^2. Furthermore, additional oblique effects coming from the q^4 terms of the expansions of the gauge-boson self-energies also contribute to EW observables at the level of dimension-six EFT operators. Their inclusion leads to the so-called W and Y parameters [357], which, however, also generate universal four-fermion interactions whose effects are expected to be better constrained at high-energy $2 \to 2$ fermion processes.

As in previous editions of this *Review,* in this section we update the results coming from the interpretation of the EW precision measurements in terms of the STU formalism, and the implications for several types of new-physics models. These results are then extended beyond the case of fermion-universal theories with the interpretation within the SMEFT formalism, where we discuss the bounds from EW precision observables on the leading interactions in the dimension-six effective Lagrangian, keeping the discussion at a more model-independent level.

The results of the EW fit extending the SM with the S, T, and U parameters are presented in Table 10.8. We present the cases where $U = 0$, as a proxy for the case of heavy decoupling new physics where $|U| \ll |S|, |T|$, and a scenario where all three parameters are freely floating. Regardless of whether U is assumed to be zero or not, the results from the EW fit to the oblique parameters is fully consistent with the SM hypothesis.[22] The impact of the different EW observables in the S–T plane, assuming $U = 0$, is shown in Figure 10.6. The shape of these regions can be understood from the fact that, in the LEP scheme used in this figure, Γ_Z only depends on the combination

$$-10(3 - 8s_W^2)S + (63 - 126s_W^2 - 40s_W^4)T,$$

the U parameter only contributes to the W mass and width via

$$S - 2c_W^2 T - \frac{c_W^2 - s_W^2}{2s_W^2} U,$$

and the corrections to all other EW precision observables can be written in terms of

$$S - 4c_W^2 s_W^2 T.$$

From the results in Table 10.8 one can also derive individual limits on each parameter (*i.e.* assuming all the other oblique parameters are zero). We obtain the following 95% probability individual bounds,

$$T, U = 0: \quad -0.072 \le S \le 0.039; \quad S \ge -0.068 \quad (S \le 0); \tag{10.91a}$$
$$S \le 0.045 \quad (S \ge 0);$$
$$S, U = 0: \quad -0.027 \le T \le 0.058; \quad T \ge -0.034 \quad (T \le 0); \tag{10.91b}$$
$$T \le 0.054 \quad (T \ge 0);$$
$$S, T = 0: \quad -0.039 \le U \le 0.074; \quad U \ge -0.046 \quad (U \le 0); \tag{10.91c}$$
$$U \le 0.069 \quad (U \ge 0);$$

where the numbers in each row are obtained assuming the corresponding parameter can have any sign, or is restricted to be negative or positive, respectively.

As mentioned above, the STU results can be used to set constraints on a relatively large class of new-physics models inducing universal corrections to the SM predictions. For instance, the T parameter modifies the ρ parameter according to

$$\Delta\rho = \alpha(M_Z^2)T\ . \tag{10.92}$$

In this way, T can be connected to new-physics violations of custodial symmetry. These can be generated by additional sources of SU(2) breaking not induced by Higgs doublets, via

$$\rho = \frac{\sum_i [T_i(T_i+1) - T_{3i}^2]|v_i|^2}{2\sum_i T_{3i}^2 |v_i|^2}\ , \tag{10.93}$$

where v_i is the expectation value of the neutral component of a Higgs multiplet with weak isospin T_i and third component T_{3i}. Thus, the limits on T can be translated into constraints on higher-dimensional Higgs representations, such that their vacuum expectation values can only be less than a few percent of those of the doublets.

Similarly, the bounds on T can be used to set constraints on non-degenerate multiplets of heavy fermions or scalars, since these break the vector part of weak SU(2) and lead to a decrease in the value of M_Z/M_W. Each non-degenerate SU(2) doublet $\binom{f_1}{f_2}$ yields a positive contribution to ρ (and therefore T) [37,384,385] of

$$\frac{N_C\, G_F}{8\sqrt{2}\pi^2}\Delta m^2\ , \tag{10.94}$$

where

$$\Delta m^2 \equiv m_1^2 + m_2^2 - \frac{4m_1^2 m_2^2}{m_1^2 - m_2^2}\ln\frac{m_1}{m_2} \ge (m_1 - m_2)^2\ , \tag{10.95}$$

and $N_C = 1$ (3) for color singlets (triplets). The limit on the T parameter (assuming $T \ge 0$) taken together with Eq. (10.92) and

[22] For a discussion of the impact of the M_W CDF measurement [212] on the EW fit, we refer the reader to, e.g., Refs. [132, 380–383] and to the previous edition of this *Review*.

Table 10.8: Results of the global fit of the oblique parameters to EW precision observables. The left half of the table presents the results assuming $U = 0$, whereas this parameter is an independent degree of freedom in the fit in the right half of the table.

	Result	Correlation		Result	Correlation		
S	0.008 ± 0.071	1.00		0.018 ± 0.095	1.00		
T	0.021 ± 0.055	0.92	1.00	0.04 ± 0.12	0.91	1.00	
U	0	–	–	-0.013 ± 0.086	−0.66	−0.88	1.00

Int. J. Mod. Phys. A 2026.41. Downloaded from www.worldscientific.com by UNIVERSITY OF CALIFORNIA @ BERKELEY on 09/16/26. Re-use and distribution is strictly not permitted, except for Open Access articles.

Eq. (10.94) implies the following constraint on the mass splitting at the 95% probability,

$$\sum_i \frac{N_C^i}{3}\, \Delta m_i^2 \leq (37 \text{ GeV})^2 \ , \tag{10.96}$$

where the sum runs over all new-physics doublets, for example fourth-family quarks or leptons, $\binom{t'}{b'}$ or $\binom{\nu'}{\ell'-}$, vector-like fermion doublets (which contribute to the sum in Eq. (10.96) with an extra factor of 2), and scalar doublets such as $\binom{\tilde{t}}{\tilde{b}}$ in supersymmetry (in the absence of L–R mixing).

Non-degenerate multiplets usually imply $\Delta\rho > 0$ ($T > 0$). Similarly, heavy Z' bosons decrease the prediction for M_Z due to mixing and generally lead to $\Delta\rho > 0$ ($T > 0$) [358]. On the other hand, extra Higgs doublets participating in spontaneous symmetry breaking [386–388] or heavy lepton doublets involving Majorana neutrinos [389], both of which have more complicated expressions, and the v_i of higher-dimensional Higgs representations can contribute to ρ with either sign.

The effects of non-standard Higgs representations cannot be separated from heavy non-degenerate multiplets unless the new physics has other consequences, such as vertex corrections. Most of the original papers defined T to include the effects of loops only. However, the way T has been defined here includes all new sources of SU(2) breaking, including non-standard Higgs bosons.

A multiplet of heavy degenerate chiral fermions yields

$$S = \frac{N_C}{3\pi} \sum_i \left(T_{3i}^L - T_{3i}^R\right)^2 \ , \tag{10.97}$$

where $T_{3i}^{L,R}$ is the third component of weak isospin of the left-(right-)handed component of fermion i. For example, a heavy degenerate ordinary or mirror family would contribute $2/(3\pi)$ to S. Therefore, the S parameter can also be used to constrain the number of fermion families, *under the assumption* that there are no other contributions to T or U, and therefore that any new families are degenerate. Then an extra generation of SM fermions is excluded with more than 8σ confidence, corresponding to $N_F = 2.92 \pm 0.13$. Allowing T to vary as well, the constraint on a fourth family is weaker [390]. However, a heavy fourth family would increase the Higgs production cross section through gluon fusion by a factor of about nine [391, 392], which has been excluded by ATLAS and CMS at the LHC [393]. Combining the limits from EW precision data with the measured Higgs production rate and limits from direct searches for heavy quarks [394], a fourth family of chiral fermions is now excluded by more than five standard deviations [395, 396]. Similar remarks apply to a heavy mirror family [397] involving right-handed SU(2) doublets and left-handed singlets. In contrast, new doublets that receive most of their mass from a different source than the Higgs vacuum expectation value, such as vector-like fermion doublets or scalar doublets in supersymmetry, give small or no contribution to S, T, U, and the Higgs production cross section and are therefore still not excluded. Partial or complete vector-like fermion families are predicted in many Grand Unified Theories [398] (see Section 92 on "Grand Unified Theories" in this *Review*), and many other models including supersymmetric and superstring inspired ones [399–402].

In models with warped extra dimensions [403], sizeable corrections to the S parameter are generated through mixing between the SM gauge bosons and their Kaluza-Klein (KK) excitations, and one finds $S \approx 30\, v^2 M_{KK}^{-2}$ [404], where M_{KK} is the mass scale of the KK gauge bosons. Large positive values of S can also be generated in models with dynamical EW symmetry breaking, where the Higgs boson is composite. In simple composite Higgs models, the dominant contribution stems from heavy spin-1 resonances of the strong dynamics leading to $S \approx 4\pi v^2 (M_V^{-2} + M_A^{-2})$, where $M_{V,A}$ are the masses of the lightest vector and axial-vector resonances, respectively [405]. From the results in Table 10.8 one obtains $S \leq 0.15$ at 95% probability, which puts the constraint $M_{KK} \gtrsim 3.5$ TeV on the masses of KK gauge bosons in warped extra dimensions. In minimal composite Higgs models, the bound on S requires $M_V \gtrsim 4.1$ TeV, which is obtained from the one-sided 95% probability bound on $S > 0$ for $T = 0$ and using Weinberg sum rules [406]. However, this constraint can be relaxed, *e.g.*, if the fermionic sector is also allowed to be partially composite [363, 407] and in soft-wall models [408].

Negative values of S are possible, for example, in composite Higgs models with larger gauge group representations [409,410], or from loops involving scalars or Majorana particles [411–413]. The simplest origin of $S < 0$ would probably be an additional heavy Z' boson [358]. Supersymmetric extensions of the SM [414, 415] generally give very small effects. For more details and references, see Refs. [416–425] and Sections 87 and 88 on "Supersymmetry" in this *Review*. Most simple types of new physics yield $U = 0$, although there are counter-examples, such as the effects of anomalous triple gauge vertices [426].

We conclude this section by moving beyond fermion-universal extensions of the SM and presenting the results of a SMEFT fit to electroweak precision observables. In this case, we adopt the G_F-scheme (with G_F, M_Z, M_W as input), which has become the standard in SMEFT combinations of different observables with LHC measurements [427].[23] We assume all the operators in Eqs. (10.86)–(10.88) can be generated by new physics. On the lepton side we allow new-physics corrections to be non-universal. Because of this, and contrary to what was done for the SM fits, for the fits in the SMEFT formalism we use as experimental inputs for leptonic observables, such as the ratios $R_{e,\mu,\tau}$ and asymmetries $A_{e,\mu,\tau}$, the values reported in Refs. [139, 215, 216, 345] *without* assuming lepton flavor universality. For quarks, we impose a U(2) flavor symmetry on the first two families to avoid large contributions to flavor-changing neutral currents. The third family is defined in flavor space along the direction of the top-quark. The operators in Eqs. (10.86)-(10.88) are the interactions that enter in EW precision observables at leading EFT order and tree level. Although many other operators contribute at NLO, we restrict the fit to this setup, as a full global analysis taking into account the constraints on all interactions would require combining with numerous additional data sets, which is beyond the scope of this *Review*. Finally, in the calculation of new-physics effects, we work consistently with the truncation of the SMEFT Lagrangian to dimension six, *i.e.* up to $O(1/\Lambda^2)$, and keep only corrections of this order in the observables.

It is well known that in the Warsaw basis the EW fit has two blind directions [428, 429]. In Table 10.9 we present the central values and 1σ uncertainties from this EW SMEFT fit, in terms of the following combinations of Wilson coefficients at the EW

[23] One of the main reasons is practical, since including the EW gauge-boson masses reduces the SMEFT dependences in propagators, but any choice for the EW input scheme will lead to equivalent fit results within theoretical uncertainties.

Int. J. Mod. Phys. A 2026.41. Downloaded from www.worldscientific.com by UNIVERSITY OF CALIFORNIA @ BERKELEY on 09/16/26. Re-use and distribution is [redacted] except for Open Access articles.

Table 10.9: Results from the global SMEFT fit discussed in the text, in terms of the combinations of Wilson coefficients in Eq. (10.98). All the operators in those combinations as well as the SM input parameters are taken as free parameters in the fit. The coefficients $(\hat{C}^{(1),(3)}_{\phi l,\phi e})_{11,22,33}$ denote interactions with each of the three lepton generations. For quarks, interactions with the light two families are assumed to be flavour universal, denoted by $(\hat{C}^{(1),(3)}_{\phi q,\phi u,\phi d})_{aa}$, but independent of the ones with the third family. Results in units of TeV^{-2}.

$(\hat{C}^{(1)}_{\phi l})_{11}$	$(\hat{C}^{(1)}_{\phi l})_{22}$	$(\hat{C}^{(1)}_{\phi l})_{33}$	$(\hat{C}^{(3)}_{\phi l})_{11}$	$(\hat{C}^{(3)}_{\phi l})_{22}$	$(\hat{C}^{(3)}_{\phi l})_{33}$	$(\hat{C}_{\phi e})_{11}$	$(\hat{C}_{\phi e})_{22}$	$(\hat{C}_{\phi e})_{33}$
0.03 ± 0.04	0.00 ± 0.05	0.00 ± 0.06	-0.03 ± 0.04	-0.01 ± 0.04	0.00 ± 0.06	0.01 ± 0.01	0.00 ± 0.04	-0.02 ± 0.02

$(\hat{C}^{(1)}_{\phi q})_{aa}$	$(\hat{C}^{(3)}_{\phi q})_{aa}$	$(\hat{C}^{(+)}_{\phi q})_{33}$	$(\hat{C}_{\phi d})_{aa}$	$(\hat{C}_{\phi d})_{33}$	$(\hat{C}_{\phi u})_{aa}$	$(\hat{C}_{ll})_{1221}$
0.01 ± 0.13	-0.06 ± 0.07	-0.05 ± 0.03	-0.40 ± 0.81	-0.71 ± 0.27	0.10 ± 0.17	-0.03 ± 0.07

Table 10.10: Projection of the results of the global SMEFT fit discussed in the text in terms of relative modifications of the neutral-current effective EW couplings of the different SM fermions, $\delta g_{\rm eff} = \Delta g_{\rm eff}/g_{\rm SM}$. The numbers are given in percent.

$\delta g_L^{\nu_e}$	$\delta g_L^{\nu_\mu}$	$\delta g_L^{\nu_\tau}$	δg_L^{e}	δg_L^{μ}	δg_L^{τ}	δg_R^{e}	δg_R^{μ}	δg_R^{τ}
-0.32 ± 0.51	-0.03 ± 0.47	-0.01 ± 0.71	0.03 ± 0.12	-0.13 ± 0.40	-0.02 ± 0.21	-0.15 ± 0.15	0.02 ± 0.60	0.31 ± 0.29

$\delta g_L^{u=c}$	$\delta g_L^{d=s}$	δg_L^{b}	$\delta g_R^{u=c}$	$\delta g_R^{d=s}$	δg_R^{b}
-0.58 ± 0.99	-0.3 ± 1.2	-0.77 ± 0.38	2.2 ± 3.6	17 ± 34	31 ± 12

scale [428]:

$$\begin{aligned}
\hat{C}^{(1)}_{\phi f} &= \frac{C^{(1)}_{\phi f}}{\Lambda^2} - \frac{Y_f}{4}\frac{C_{\phi D}}{\Lambda^2}, \quad f = l, q, e, u, d, \\
\hat{C}^{(3)}_{\phi f} &= \frac{C^{(3)}_{\phi f}}{\Lambda^2} + \frac{c_W^2}{4 s_W^2}\frac{C_{\phi D}}{\Lambda^2} + \frac{c_W}{s_W}\frac{C_{\phi WB}}{\Lambda^2}, \quad f = l, q, \qquad (10.98) \\
\hat{C}_{ll} &= \frac{1}{2}\frac{(C_{ll})_{1221} + (C_{ll})_{2112}}{\Lambda^2} = \frac{(C_{ll})_{1221}}{\Lambda^2}.
\end{aligned}$$

For the case of left-handed quarks, we further consider the combination $(\hat{C}^{(+)}_{\phi q})_{33} = ((\hat{C}^{(1)}_{\phi q})_{33} + (\hat{C}^{(3)}_{\phi q})_{33})/2$, which modifies the $Z \to b_L \bar{b}_L$ vertex, whereas the orthogonal combination modified the corresponding top-quark coupling and does not enter in the fit at the tree level. (In the previous expressions, s_W, c_W are the tree-level values of the sine and cosine of the weak mixing angle and Y_f denotes the fermion hypercharge.) In order to resolve the blind directions of this SMEFT EW fit, one would need to add additional observables, *e.g.* Higgs observables or measurements from diboson processes [428]. These, however, introduce further dependences on operators not entering in the EW fit and, in general, extra flat directions that need to be resolved including additional data. Eventually, this leads to the study of global SMEFT analyses that are becoming more popular in the literature, both from the theory and experimental sides, and that combine many types of observables from the EW, Higgs, top, and flavor sectors, to constrain as many directions in the SMEFT parameter space as possible. Some examples of these studies, with different levels of completeness in terms of both the scope of experimental observables included and the number of new-physics interactions considered, are presented in Refs. [430–440].

The presence of flat directions in the SMEFT fit is, however, not an impediment to derive interesting conclusions about the physics in the EW sector. For instance, the results in Table 10.9 can be translated into the space allowed for the modifications of the *effective* EW couplings of the fermions to the neutral currents in the SMEFT formalism, $\Delta g_{\rm eff}$, defined such that the tree-level relations between the EW pseudo-observables and couplings are preserved in the presence of new-physics effects. The corresponding values are shown in Table 10.10.

In general, the results of the fit show again good agreement with the SM, with the data suggesting that new-physics modifications of the leptonic couplings must be below a few per-mil, whereas the bounds are significantly weaker for quarks. There is one notable exception to this good agreement with the SM predictions. As discussed in Sec. 10.5, there is a $(3.6 \pm 1.4)\%$ deviation in the asymmetry parameter A_b. This becomes manifest in the results in Table 10.10 in terms of a preference for a non-SM value of the $Z \to b_R \bar{b}_R$ vertex with right-handed b quarks (equivalently, in a non-zero value for the coefficient $(\hat{C}_{\phi d})_{33}$ in Table 10.9). Similarly, the $Z \to b_L \bar{b}_L$ vertex with left-handed b quarks also shows a tension with the SM prediction, and both corrections are highly correlated. This is due to the fact that R_b is in good agreement with the SM, and is also much better determined than A_b. Given the size of the correction to the $Zb\bar{b}$ interactions required to account for the deviation in A_b, it is difficult to attribute this solely to new physics entering through radiative corrections. Thus, if new physics is responsible, it is most likely of tree-level origin and affects preferentially the third generation. Examples include the decay of a scalar neutrino resonance [441], mixing of the b quark with heavy exotic particles [442], and a heavy Z' with family non-universal couplings [443, 444]. It is difficult, however, to simultaneously account for R_b without tuning, which has been measured on the Z peak and off-peak [445] at LEP 1. Measurements at future e^+e^- colliders will help to test different scenarios modifying the $Zb\bar{b}$ interaction [446].

Acknowledgments

References

[1] S. Glashow, Nucl. Phys. **22**, 579 (1961).

[2] S. Weinberg, Phys. Rev. Lett. **19**, 1264 (1967).

[3] A. Salam, Conf. Proc. C **680519**, 367 (1968).

[4] S. Glashow, J. Iliopoulos and L. Maiani, Phys. Rev. D **2**, 1285 (1970).

[5] N. Cabibbo, Phys. Rev. Lett. **10**, 531 (1963).

[6] M. Kobayashi and T. Maskawa, Prog. Theor. Phys. **49**, 652 (1973).

[7] S. Descotes-Genon and P. Koppenburg, Ann. Rev. Nucl. Part. Sci. **67**, 97 (2017), [arXiv:1702.08834].

[8] E. Commins and P. Bucksbaum, *Weak Interactions of Leptons and Quarks*, Cambridge Univ. Pr., Cambridge, USA (1983), ISBN 978-0-521-27370-1.

[9] P. Langacker, editor, *Precision tests of the standard electroweak model*, volume 14, WSP, Singapore (1996).

[10] P. Langacker, *The standard model and beyond*, CRC Pr., Boca Raton, USA (2010), ISBN 978-1-4200-7906-7.

[11] T. Kinoshita, editor, *Quantum electrodynamics*, volume 7, WSP, Singapore (1990).

Int. J. Mod. Phys. A 2026.41. Downloaded from www.worldscientific.com
by UNIVERSITY OF CALIFORNIA @ BERKELEY on 09/16/26. Re-use and distribution is strictly not permitted, except for Open Access articles.

[12] S. G. Karshenboim, Phys. Rept. **422**, 1 (2005), [hep-ph/0509010].

[13] J. Erler and S. Su, Prog. Part. Nucl. Phys. **71**, 119 (2013), [arXiv:1303.5522].

[14] T. Kinoshita, J. Math. Phys. **3**, 650 (1962).

[15] T. D. Lee and M. Nauenberg, Phys. Rev. **133**, B1549 (1964).

[16] F. Jegerlehner, Eur. Phys. J. C **18**, 673 (2001), [hep-th/0005255].

[17] W. B. Kilgore, Phys. Rev. D **83**, 114005 (2011), [arXiv:1102.5353].

[18] H. Bélusca-Maïto *et al.*, Symmetry **15**, 3, 622 (2023), [arXiv:2303.09120].

[19] L. Chen, JHEP **2023**, 11, 30 (2023), [arXiv:2304.13814].

[20] P. L. Ebert *et al.*, JHEP **01**, 114 (2025), [arXiv:2411.02543].

[21] D. A. Ross and J. C. Taylor, Nucl. Phys. **B51**, 125 (1973), [Erratum: Nucl. Phys. B58 (1973) 643].

[22] A. Sirlin, Phys. Rev. D **22**, 971 (1980).

[23] K.-i. Aoki *et al.*, Prog. Theor. Phys. **65**, 1001 (1981).

[24] M. Böhm, H. Spiesberger and W. Hollik, Fortsch. Phys. **34**, 687 (1986).

[25] A. Denner, Fortsch. Phys. **41**, 307 (1993), [arXiv:0709.1075].

[26] S. Fanchiotti, B. A. Kniehl and A. Sirlin, Phys. Rev. D **48**, 307 (1993), [hep-ph/9212285].

[27] A. Denner and S. Dittmaier, Phys. Rept. **864**, 1 (2020), [arXiv:1912.06823].

[28] S. Actis *et al.*, Nucl. Phys. **B777**, 1 (2007), [hep-ph/0612122].

[29] S. Actis and G. Passarino, Nucl. Phys. **B777**, 35 (2007), [hep-ph/0612123].

[30] S. Actis and G. Passarino, Nucl. Phys. **B777**, 100 (2007), [hep-ph/0612124].

[31] A. Sirlin and R. Zucchini, Nucl. Phys. B **266**, 389 (1986).

[32] J. Fleischer and F. Jegerlehner, Phys. Rev. **D23**, 2001 (1981).

[33] S. Dittmaier and H. Rzehak, JHEP **05**, 125 (2022), [arXiv:2203.07236].

[34] G. Altarelli, R. Kleiss and C. Verzegnassi, editors, *Z physics at LEP 1. Vol. 1: Standard Physics*, CERN, Geneva (1989), CERN-89-08, URL `http://www.slac.stanford.edu/spires/find/books/www?cl=QCD161:L39:1989`.

[35] D. Bardin, W. Hollik, G. Passarino, editor, *Electroweak working group report* (1995), CERN-95-03, [hep-ph/9709229], URL `http://doc.cern.ch/cernrep/1995/95-03/95-03.html`.

[36] D. A. Ross and M. J. G. Veltman, Nucl. Phys. B **95**, 135 (1975).

[37] M. Veltman, Nucl. Phys. B **123**, 89 (1977).

[38] M. Chiesa, F. Piccinini and A. Vicini, Phys. Rev. D **100**, 7, 071302 (2019), [arXiv:1906.11569].

[39] D. Y. Bardin *et al.*, Phys. Lett. B **206**, 539 (1988).

[40] P. Gambino and P. A. Grassi, Phys. Rev. D **62**, 076002 (2000), [hep-ph/9907254].

[41] P. A. Grassi, B. A. Kniehl and A. Sirlin, Phys. Rev. D **65**, 085001 (2002), [hep-ph/0109228].

[42] A. Freitas *et al.*, Nucl. Phys. B **632**, 189 (2002), [Erratum: Nucl. Phys. B 666, 305 (2003)], [hep-ph/0202131].

[43] A. Denner *et al.*, Nucl. Phys. **B724**, 247 (2005), [Erratum: Nucl. Phys. B 854 (2012) 504], [hep-ph/0505042].

[44] R. Frederix *et al.*, JHEP **07**, 185 (2018), [Erratum: JHEP 11, 085 (2021)], [arXiv:1804.10017].

[45] A. Sirlin, Phys. Rev. Lett. **67**, 2127 (1991).

[46] W. Beenakker *et al.*, Nucl. Phys. B **500**, 255 (1997), [hep-ph/9612260].

[47] F. Jegerlehner, M. Y. Kalmykov and O. Veretin, Nucl. Phys. B **641**, 285 (2002), [hep-ph/0105304].

[48] F. Jegerlehner, M. Y. Kalmykov and O. Veretin, Nucl. Phys. B **658**, 49 (2003), [hep-ph/0212319].

[49] S. P. Martin, Phys. Rev. D **91**, 11, 114003 (2015), [arXiv:1503.03782].

[50] S. P. Martin, Phys. Rev. D **92**, 1, 014026 (2015), [arXiv:1505.04833].

[51] R. G. Stuart, Phys. Lett. **B262**, 113 (1991).

[52] A. Aeppli, G. J. van Oldenborgh and D. Wyler, Nucl. Phys. **B428**, 126 (1994), [hep-ph/9312212].

[53] D. Bardin *et al.*, Z. Phys. C **44**, 493 (1989).

[54] D. Yu. Bardin, M. Grünewald and G. Passarino, "Precision calculation project report," (1999), [hep-ph/9902452].

[55] D. Y. Bardin and G. Passarino, *The standard model in the making: Precision study of the electroweak interactions* (1999).

[56] S. Dittmaier and M. Huber, JHEP **01**, 060 (2010), [arXiv:0911.2329].

[57] G. Passarino, C. Sturm and S. Uccirati, Nucl. Phys. B **834**, 77 (2010), [arXiv:1001.3360].

[58] L. Chen and A. Freitas, SciPost Phys. Codeb. **2023**, 18 (2023), [arXiv:2211.16272].

[59] S. Jadach *et al.*, Phys. Lett. B **417**, 326 (1998), [hep-ph/9705429].

[60] W. Beenakker, F. A. Berends and A. P. Chapovsky, Nucl. Phys. **B548**, 3 (1999), [hep-ph/9811481].

[61] A. Denner *et al.*, Nucl. Phys. B **587**, 67 (2000), [hep-ph/0006307].

[62] M. W. Grünewald *et al.*, in S. Jadach, G. Passarino, R. Pittau, editor, "Reports of the Working Groups on Precision Calculations for LEP2 Physics," 1–135, CERN (2000), CERN-2000-009, [hep-ph/0005309].

[63] S. Dittmaier, G. Knippen and C. Schwan, JHEP **02**, 003 (2020), [arXiv:1912.04117].

[64] G. Aad *et al.* (ATLAS), Phys. Rept. **1116**, 4 (2025), [arXiv:2404.05498].

[65] G. Aad *et al.* (ATLAS), Phys. Rept. **1116**, 57 (2025), [arXiv:2404.06829].

[66] G. Aad *et al.* (ATLAS), Phys. Rept. **1116**, 127 (2025), [arXiv:2404.10674].

[67] A. Hayrapetyan *et al.* (CMS), Phys. Rept. **1115**, 3 (2025), [arXiv:2405.18661].

[68] S. Amoroso *et al.*, in "11th Les Houches Workshop on Physics at TeV Colliders: PhysTeV Les Houches," (2020), [arXiv:2003.01700].

[69] F. Maltoni *et al.* (2022), [arXiv:2210.02591].

[70] A. Huss *et al.* (2025), [arXiv:2504.06689].

[71] G. Heinrich, Phys. Rept. **922**, 1 (2021), [arXiv:2009.00516].

[72] J. Alwall *et al.*, JHEP **06**, 128 (2011), [arXiv:1106.0522].

[73] V. Hirschi *et al.*, JHEP **1105**, 044 (2011), [arXiv:1103.0621].

[74] M. H. Seymour, Z. Phys. **C56**, 161 (1992).

[75] K. Hamilton and P. Richardson, JHEP **07**, 010 (2006), [hep-ph/0603034].

[76] T. Sjöstrand *et al.*, Comput. Phys. Commun. **191**, 159 (2015), [arXiv:1410.3012].

[77] T. Gleisberg *et al.*, JHEP **02**, 007 (2009), [arXiv:0811.4622].

[78] M. Schönherr and F. Krauss, JHEP **12**, 018 (2008), [arXiv:0810.5071].

[79] S. Höche, S. Schumann and F. Siegert, Phys. Rev. **D81**, 034026 (2010), [arXiv:0912.3501].

[80] J. Erler and M. Schott, Prog. Part. Nucl. Phys. **106**, 68 (2019), [arXiv:1902.05142].

Int. J. Mod. Phys. A 2026.41. Downloaded from www.wo
by UNIVERSITY OF CALIFORNIA @ BERKELEY on 09/16/26. Re-use and distribution is
except for Open Access articles.

[81] W. Hollik, Fortsch. Phys. **38**, 165 (1990).

[82] A. Djouadi and C. Verzegnassi, Phys. Lett. B **195**, 265 (1987).

[83] A. Djouadi, Nuovo Cim. A **100**, 357 (1988).

[84] K. Chetyrkin, J. H. Kuhn and M. Steinhauser, Phys. Lett. B **351**, 331 (1995), [hep-ph/9502291].

[85] L. Avdeev *et al.*, Phys. Lett. B **336**, 560 (1994), [Erratum: Phys. Lett. B 349, 597 (1995)], [hep-ph/9406363].

[86] Y. Schroder and M. Steinhauser, Phys. Lett. B **622**, 124 (2005), [hep-ph/0504055].

[87] K. Chetyrkin *et al.*, Phys. Rev. Lett. **97**, 102003 (2006), [hep-ph/0605201].

[88] R. Boughezal and M. Czakon, Nucl. Phys. B **755**, 221 (2006), [hep-ph/0606232].

[89] B. A. Kniehl, J. H. Kuhn and R. Stuart, Phys. Lett. B **214**, 621 (1988).

[90] B. A. Kniehl, Nucl. Phys. B **347**, 86 (1990).

[91] F. Halzen and B. A. Kniehl, Nucl. Phys. B **353**, 567 (1991).

[92] A. Djouadi and P. Gambino, Phys. Rev. D **49**, 3499 (1994), [Erratum: Phys. Rev. D 53, 4111 (1996)], [hep-ph/9309298].

[93] S. Dittmaier, T. Schmidt and J. Schwarz, JHEP **12**, 201 (2020), [arXiv:2009.02229].

[94] A. Anselm, N. Dombey and E. Leader, Phys. Lett. B **312**, 232 (1993).

[95] K. Chetyrkin, J. H. Kuhn and M. Steinhauser, Phys. Rev. Lett. **75**, 3394 (1995), [hep-ph/9504413].

[96] J. van der Bij *et al.*, Phys. Lett. B **498**, 156 (2001), [hep-ph/0011373].

[97] M. Faisst *et al.*, Nucl. Phys. B **665**, 649 (2003), [hep-ph/0302275].

[98] L. Chen and A. Freitas, JHEP **07**, 210 (2020), [arXiv:2002.05845].

[99] L. Chen and A. Freitas, JHEP **03**, 215 (2021), [arXiv:2012.08605].

[100] M. Awramik *et al.*, Phys. Rev. Lett. **93**, 201805 (2004), [hep-ph/0407317].

[101] W. Hollik, U. Meier and S. Uccirati, Nucl. Phys. B **731**, 213 (2005), [hep-ph/0507158].

[102] M. Awramik, M. Czakon and A. Freitas, Phys. Lett. B **642**, 563 (2006), [hep-ph/0605339].

[103] W. Hollik, U. Meier and S. Uccirati, Nucl. Phys. B **765**, 154 (2007), [hep-ph/0610312].

[104] M. Awramik *et al.*, Nucl. Phys. B **813**, 174 (2009), [arXiv:0811.1364].

[105] I. Dubovyk *et al.*, Phys. Lett. B **762**, 184 (2016), [arXiv:1607.08375].

[106] M. Awramik, M. Czakon and A. Freitas, JHEP **11**, 048 (2006), [hep-ph/0608099].

[107] A. Freitas, Phys. Lett. B **730**, 50 (2014), [arXiv:1310.2256].

[108] A. Freitas, JHEP **04**, 070 (2014), [arXiv:1401.2447].

[109] I. Dubovyk *et al.*, Phys. Lett. B **783**, 86 (2018), [arXiv:1804.10236].

[110] I. Dubovyk *et al.*, JHEP **08**, 113 (2019), [arXiv:1906.08815].

[111] R. Barbieri *et al.*, Nucl. Phys. B **409**, 105 (1993).

[112] J. Fleischer, O. Tarasov and F. Jegerlehner, Phys. Lett. B **319**, 249 (1993).

[113] G. Degrassi, P. Gambino and A. Vicini, Phys. Lett. B **383**, 219 (1996), [hep-ph/9603374].

[114] G. Degrassi, P. Gambino and A. Sirlin, Phys. Lett. B **394**, 188 (1997), [hep-ph/9611363].

[115] A. Freitas *et al.*, Phys. Lett. B **495**, 338 (2000), [Erratum: Phys. Lett. B 570, 265 (2003)], [hep-ph/0007091].

[116] M. Awramik and M. Czakon, Phys. Lett. B **568**, 48 (2003), [hep-ph/0305248].

[117] M. Awramik and M. Czakon, Phys. Rev. Lett. **89**, 241801 (2002), [hep-ph/0208113].

[118] A. Onishchenko and O. Veretin, Phys. Lett. B **551**, 111 (2003), [hep-ph/0209010].

[119] M. Awramik *et al.*, Phys. Rev. D **69**, 053006 (2004), [hep-ph/0311148].

[120] I. Dubovyk *et al.* (2026), [arXiv:2603.06571].

[121] G. Degrassi, P. Gambino and P. P. Giardino, JHEP **05**, 154 (2015), [arXiv:1411.7040].

[122] S. P. Martin and D. G. Robertson, Phys. Rev. D **100**, 7, 073004 (2019), [arXiv:1907.02500].

[123] S. P. Martin (2025), [arXiv:2507.15946].

[124] H. Flacher *et al.*, Eur. Phys. J. C **60**, 543 (2009), [Erratum: Eur. Phys. J.C 71, 1718 (2011)], [arXiv:0811.0009].

[125] M. Baak *et al.*, Eur. Phys. J. C **72**, 2205 (2012), [arXiv:1209.2716].

[126] M. Baak *et al.* (Gfitter Group), Eur. Phys. J. C **74**, 3046 (2014), [arXiv:1407.3792].

[127] J. Haller *et al.*, Eur. Phys. J. C **78**, 8, 675 (2018), [arXiv:1803.01853].

[128] J. de Blas *et al.*, Eur. Phys. J. C **80**, 5, 456 (2020), [arXiv:1910.14012].

[129] M. Ciuchini *et al.*, JHEP **08**, 106 (2013), [arXiv:1306.4644].

[130] J. de Blas *et al.*, JHEP **12**, 135 (2016), [arXiv:1608.01509].

[131] J. de Blas *et al.*, Phys. Rev. D **106**, 3, 033003 (2022), [arXiv:2112.07274].

[132] J. de Blas *et al.*, Phys. Rev. Lett. **129**, 27, 271801 (2022), [arXiv:2204.04204].

[133] J. Erler (1999), [hep-ph/0005084].

[134] D. Y. Bardin, P. K. Khristova and O. M. Fedorenko, Nucl. Phys. B **197**, 1 (1982).

[135] D. Y. Bardin, S. Riemann and T. Riemann, Z. Phys. C **32**, 121 (1986).

[136] A. Denner and T. Sack, Z. Phys. C **46**, 653 (1990).

[137] A. Arbuzov *et al.*, Comput. Phys. Commun. **174**, 728 (2006), [hep-ph/0507146].

[138] A. Akhundov *et al.*, Phys. Part. Nucl. **45**, 3, 529 (2014), [arXiv:1302.1395].

[139] S. Schael *et al.* (ALEPH, DELPHI, L3, OPAL, SLD, LEP Electroweak Working Group, SLD Electroweak Group, SLD Heavy Flavour Group), Phys. Rept. **427**, 257 (2006), [hep-ex/0509008].

[140] S. Schael *et al.* (ALEPH, DELPHI, L3, OPAL, LEP Electroweak), Phys. Rept. **532**, 119 (2013), [arXiv:1302.3415].

[141] W. E. Thirring, Phil. Mag. Ser. 7 **41**, 1193 (1950).

[142] S. Dittmaier, Phys. Lett. B **409**, 509 (1997), [hep-ph/9704368].

[143] X. Fan *et al.*, Phys. Rev. Lett. **130**, 7, 071801 (2023), [arXiv:2209.13084].

[144] T. Aoyama *et al.*, Phys. Rev. Lett. **109**, 111808 (2012), [arXiv:1205.5370].

[145] T. Aoyama, T. Kinoshita and M. Nio, Atoms **7**, 1, 28 (2019).

[146] S. Volkov (2024), [arXiv:2404.00649].

[147] R. Aliberti *et al.*, Phys. Rept. **1143**, 1 (2025), [arXiv:2505.21476].

[148] L. Morel *et al.*, Nature **588**, 7836, 61 (2020).

[149] R. H. Parker *et al.*, Science **360**, 191 (2018), [arXiv:1812.04130].

[150] P. Achard *et al.* (L3), Phys. Lett. B **623**, 26 (2005), [hep-ex/0507078].

Int. J. Mod. Phys. A 2026.41. Downloaded from www.worldscientific.com
by UNIVERSITY OF CALIFORNIA @ BERKELEY on 09/16/26. Re-use and distribution is strictly not permitted, except for Open Access articles.

[151] G. Abbiendi *et al.* (OPAL), Eur. Phys. J. C **45**, 1 (2006), [hep-ex/0505072].

[152] K. Chetyrkin, J. H. Kuhn and M. Steinhauser, Nucl. Phys. B **482**, 213 (1996), [hep-ph/9606230].

[153] A. V. Nesterenko, *Strong interactions in spacelike and timelike domains: dispersive approach*, Elsevier (2016), ISBN 978-0-12-803448-4.

[154] M. Steinhauser, Phys. Lett. B **429**, 158 (1998), [hep-ph/9803313].

[155] C. Sturm, Nucl. Phys. B **874**, 698 (2013), [arXiv:1305.0581].

[156] M. Cè *et al.*, JHEP **08**, 220 (2022), [arXiv:2203.08676].

[157] S. Groote *et al.*, Phys. Lett. B **440**, 375 (1998), [hep-ph/9802374].

[158] N. Krasnikov and R. Rodenberg, Nuovo Cim. A **111**, 217 (1998), [hep-ph/9711367].

[159] J. H. Kuhn and M. Steinhauser, Phys. Lett. B **437**, 425 (1998), [hep-ph/9802241].

[160] A. D. Martin, J. Outhwaite and M. Ryskin, Phys. Lett. B **492**, 69 (2000), [hep-ph/0008078].

[161] J. de Troconiz and F. Yndurain, Phys. Rev. D **65**, 093002 (2002), [hep-ph/0107318].

[162] H. Burkhardt and B. Pietrzyk, Phys. Rev. D **84**, 037502 (2011), [arXiv:1106.2991].

[163] J. Erler and R. Ferro-Hernández, JHEP **03**, 196 (2018), [arXiv:1712.09146].

[164] A. Blondel *et al.*, editors, *Theory for the FCC-ee: Report on the 11th FCC-ee Workshop Theory and Experiments*, volume 3/2020 of *CERN Yellow Reports: Monographs*, CERN, Geneva (2019), [arXiv:1905.05078].

[165] M. Davier *et al.*, Eur. Phys. J. C **80**, 3, 241 (2020), [arXiv:1908.00921].

[166] A. Keshavarzi, D. Nomura and T. Teubner, Phys. Rev. D **101**, 1, 014029 (2020), [arXiv:1911.00367].

[167] M. Davier *et al.*, Eur. Phys. J. C **71**, 1515 (2011), [Erratum: Eur. Phys. J. C 72, 1874 (2012)], [arXiv:1010.4180].

[168] S. Schael *et al.* (ALEPH), Phys. Rept. **421**, 191 (2005), [hep-ex/0506072].

[169] M. Fujikawa *et al.* (Belle), Phys. Rev. D **78**, 072006 (2008), [arXiv:0805.3773].

[170] S. Anderson *et al.* (CLEO), Phys. Rev. D **61**, 112002 (2000), [hep-ex/9910046].

[171] K. Ackerstaff *et al.* (OPAL), Eur. Phys. J. C **7**, 571 (1999), [hep-ex/9808019].

[172] F. V. Ignatov *et al.* (CMD-3), Phys. Rev. D **109**, 11, 112002 (2024), [arXiv:2302.08834].

[173] D. Webber *et al.* (MuLan), Phys. Rev. Lett. **106**, 041803 (2011), [arXiv:1010.0991].

[174] V. Tishchenko *et al.* (MuLan), Phys. Rev. D **87**, 5, 052003 (2013), [arXiv:1211.0960].

[175] T. Kinoshita and A. Sirlin, Phys. Rev. **113**, 1652 (1959).

[176] T. van Ritbergen and R. G. Stuart, Nucl. Phys. B **564**, 343 (2000), [hep-ph/9904240].

[177] M. Steinhauser and T. Seidensticker, Phys. Lett. B **467**, 271 (1999), [hep-ph/9909436].

[178] Y. Nir, Phys. Lett. B **221**, 184 (1989).

[179] A. Pak and A. Czarnecki, Phys. Rev. Lett. **100**, 241807 (2008), [arXiv:0803.0960].

[180] A. Ferroglia, G. Ossola and A. Sirlin, Nucl. Phys. B **560**, 23 (1999), [hep-ph/9905442].

[181] M. Fael, K. Schönwald and M. Steinhauser, Phys. Rev. D **104**, 1, 016003 (2021), [arXiv:2011.13654].

[182] M. Czakon, A. Czarnecki and M. Dowling, Phys. Rev. D **103**, L111301 (2021), [arXiv:2104.05804].

[183] D. P. Aguillard *et al.* (Muon g-2) (2025), [arXiv:2506.03069].

[184] B. Abi *et al.* (Muon g-2), Phys. Rev. Lett. **126**, 14, 141801 (2021), [arXiv:2104.03281].

[185] D. P. Aguillard *et al.* (Muon g-2), Phys. Rev. Lett. **131**, 16, 161802 (2023), [arXiv:2308.06230].

[186] G. Bennett *et al.* (Muon g-2), Phys. Rev. Lett. **92**, 161802 (2004), [hep-ex/0401008].

[187] T. Aoyama *et al.*, Phys. Rept. **887**, 1 (2020), [arXiv:2006.04822].

[188] T. Aoyama *et al.*, PTEP **2012**, 01A107 (2012).

[189] P. Baikov, A. Maier and P. Marquard, Nucl. Phys. B **877**, 647 (2013), [arXiv:1307.6105].

[190] S. Laporta, Phys. Lett. B **772**, 232 (2017), [arXiv:1704.06996].

[191] G. Li, R. Mendel and M. A. Samuel, Phys. Rev. D **47**, 1723 (1993).

[192] S. Laporta and E. Remiddi, Phys. Lett. B **301**, 440 (1993).

[193] S. Laporta and E. Remiddi, Phys. Lett. B **379**, 283 (1996), [hep-ph/9602417].

[194] A. Czarnecki and M. Skrzypek, Phys. Lett. B **449**, 354 (1999), [hep-ph/9812394].

[195] J. Erler and M. Luo, Phys. Rev. Lett. **87**, 071804 (2001), [hep-ph/0101010].

[196] S. J. Brodsky and J. D. Sullivan, Phys. Rev. **156**, 1644 (1967).

[197] T. Burnett and M. Levine, Phys. Lett. B **24**, 467 (1967).

[198] R. Jackiw and S. Weinberg, Phys. Rev. D **5**, 2396 (1972).

[199] I. Bars and M. Yoshimura, Phys. Rev. D **6**, 374 (1972).

[200] K. Fujikawa, B. Lee and A. Sanda, Phys. Rev. D **6**, 2923 (1972).

[201] W. A. Bardeen, R. Gastmans and B. Lautrup, Nucl. Phys. B **46**, 319 (1972).

[202] T. Kukhto *et al.*, Nucl. Phys. B **371**, 567 (1992).

[203] S. Peris, M. Perrottet and E. de Rafael, Phys. Lett. B **355**, 523 (1995), [hep-ph/9505405].

[204] A. Czarnecki, B. Krause and W. J. Marciano, Phys. Rev. D **52**, 2619 (1995), [hep-ph/9506256].

[205] A. Czarnecki, B. Krause and W. J. Marciano, Phys. Rev. Lett. **76**, 3267 (1996), [hep-ph/9512369].

[206] C. Gnendiger, D. Stöckinger and H. Stöckinger-Kim, Phys. Rev. D **88**, 053005 (2013), [arXiv:1306.5546].

[207] G. Degrassi and G. Giudice, Phys. Rev. D **58**, 053007 (1998), [hep-ph/9803384].

[208] A. Czarnecki, W. J. Marciano and A. Vainshtein, Phys. Rev. D **67**, 073006 (2003), [Erratum: Phys. Rev. D 73, 119901 (2006)], [hep-ph/0212229].

[209] F. V. Ignatov *et al.* (CMD-3), Phys. Rev. Lett. **132**, 23, 231903 (2024), [arXiv:2309.12910].

[210] J. L. Lopez, D. V. Nanopoulos and X. Wang, Phys. Rev. D **49**, 366 (1994), [hep-ph/9308336].

[211] H. Davoudiasl, H.-S. Lee and W. J. Marciano, Phys. Rev. D **86**, 095009 (2012), [arXiv:1208.2973].

[212] T. Aaltonen *et al.* (CDF), Science **376**, 6589, 170 (2022).

[213] R. Aaij *et al.* (LHCb), Phys. Rev. Lett. **135**, 16, 161802 (2025), [arXiv:2505.15582].

[214] V. Chekhovsky *et al.* (CMS) (2024), [arXiv:2412.13872].

[215] P. Janot and S. Jadach, Phys. Lett. B **803**, 135319 (2020), [arXiv:1912.02067].

[216] S. Schael *et al.* (ALEPH, DELPHI, L3, OPAL, LEP Electroweak), Phys. Rept. **532**, 119 (2013), [arXiv:1302.3415].

[217] T. A. Aaltonen *et al.* (CDF, DØ), Phys. Rev. D **88**, 5, 052018 (2013), [arXiv:1307.7627].

[218] M. Aaboud *et al.* (ATLAS), Eur. Phys. J. C **78**, 2, 110 (2018), [Erratum: Eur. Phys. J. C 78, 898 (2018)], [arXiv:1701.07240].

Int. J. Mod. Phys. A 2026.41. Downloaded from www.worldscientific.com by UNIVERSITY OF CALIFORNIA @ BERKELEY on 09/16/26. Re-use and distribution is [redacted] except for Open Access articles.

[219] R. Aaij *et al.* (LHCb), JHEP **01**, 036 (2022), [arXiv:2109.01113].

[220] S. Amoroso *et al.* (LHC-TeV MW Working Group), Eur. Phys. J. C **84**, 5, 451 (2024), [arXiv:2308.09417].

[221] T.-J. Hou *et al.*, Phys. Rev. D **103**, 1, 014013 (2021), [arXiv:1912.10053].

[222] G. Aad *et al.* (ATLAS), Eur. Phys. J. C **84**, 12, 1309 (2024), [arXiv:2403.15085].

[223] LHC-TeV MW Working Group, Technical report (2026), URL `https://twiki.cern.ch/twiki/bin/view/LHCPhysics/LHC-TEV-MWWG`.

[224] V. M. Abazov *et al.* (D0), Phys. Rev. Lett. **108**, 151804 (2012), [arXiv:1203.0293].

[225] V. M. Abazov *et al.* (D0), Phys. Rev. D **89**, 1, 012005 (2014), [arXiv:1310.8628].

[226] A. Pinto *et al.*, Eur. Phys. J. C **84**, 6, 593 (2024), [arXiv:2307.04007].

[227] Technical Report TEVEWWG/WZ 2010/01, FERMILAB, Batavia (2010), [arXiv:1003.2826], URL `https://www-d0.fnal.gov/Run2Physics/WWW/results/prelim/EW/E34`.

[228] G. Aad *et al.* (ATLAS), Phys. Lett. B **716**, 1 (2012), [arXiv:1207.7214].

[229] S. Chatrchyan *et al.* (CMS), Phys. Lett. B **716**, 30 (2012), [arXiv:1207.7235].

[230] G. Aad *et al.* (ATLAS, CMS), Phys. Rev. Lett. **114**, 191803 (2015), [arXiv:1503.07589].

[231] A. M. Sirunyan *et al.* (CMS), Phys. Lett. B **805**, 135425 (2020), [arXiv:2002.06398].

[232] A. Hayrapetyan *et al.* (CMS), Phys. Rev. D **111**, 9, 092014 (2025), [arXiv:2409.13663].

[233] G. Aad *et al.* (ATLAS), Phys. Rev. Lett. **131**, 25, 251802 (2023), [arXiv:2308.04775].

[234] G. Aad *et al.* (ATLAS), Rept. Prog. Phys. **88**, 5, 057803 (2025), [arXiv:2412.01548].

[235] D. de Florian *et al.* (LHC Higgs Cross Section Working Group) (2016), [arXiv:1610.07922].

[236] T. Aaltonen *et al.* (CDF, DØ, Tevatron Electroweak Working Group) (2016), [arXiv:1608.01881].

[237] A. Hayrapetyan *et al.* (ATLAS, CMS) (2023), [arXiv:2402.08713].

[238] A. Tumasyan *et al.* (CMS), Eur. Phys. J. C **83**, 10, 963 (2023), [arXiv:2302.01967].

[239] A. Tumasyan *et al.* (CMS), Eur. Phys. J. C **83**, 7, 560 (2023), [arXiv:2211.01456].

[240] A. M. Sirunyan *et al.* (CMS), Eur. Phys. J. C **79**, 5, 368 (2019), [arXiv:1812.10505].

[241] A. M. Sirunyan *et al.* (CMS), Eur. Phys. J. C **79**, 4, 313 (2019), [arXiv:1812.10534].

[242] A. Tumasyan *et al.* (CMS), JHEP **12**, 161 (2021), [arXiv:2108.10407].

[243] A. Hayrapetyan *et al.* (CMS), Phys. Rept. **1115**, 116 (2025), [arXiv:2403.01313].

[244] G. Aad *et al.* (ATLAS), JHEP **06**, 019 (2023), [arXiv:2209.00583].

[245] G. Aad *et al.* (ATLAS), Phys. Lett. B **867**, 139608 (2025), [arXiv:2502.18216].

[246] Technical Report ATLAS-CONF-2023-058, CERN, Geneva (2022), URL `http://cds.cern.ch/record/2826701`.

[247] A. H. Hoang, Ann. Rev. Nucl. Part. Sci. **70**, 225 (2020), [arXiv:2004.12915].

[248] G. Aad *et al.* (ATLAS), Eur. Phys. J. C **74**, 10, 3109 (2014), [Addendum: Eur. Phys. J. C 76, 642 (2016)], [arXiv:1406.5375].

[249] M. Aaboud *et al.* (ATLAS), Eur. Phys. J. C **77**, 11, 804 (2017), [arXiv:1709.09407].

[250] G. Aad *et al.* (ATLAS) (2025), [arXiv:2509.15066].

[251] S. Chatrchyan *et al.* (CMS), Phys. Lett. B **728**, 496 (2014), [Erratum: Phys. Lett. B 738, 526 (2014)], [arXiv:1307.1907].

[252] V. Khachatryan *et al.* (CMS), JHEP **08**, 029 (2016), [arXiv:1603.02303].

[253] A. M. Sirunyan *et al.* (CMS), JHEP **09**, 051 (2017), [arXiv:1701.06228].

[254] A. M. Sirunyan *et al.* (CMS), Eur. Phys. J. C **79**, 5, 368 (2019), [arXiv:1812.10505].

[255] A. H. Hoang, S. Plätzer and D. Samitz, JHEP **10**, 200 (2018), [arXiv:1807.06617].

[256] J. Kieseler, K. Lipka and S.-O. Moch, Phys. Rev. Lett. **116**, 16, 162001 (2016), [arXiv:1511.00841].

[257] B. Dehnadi *et al.*, JHEP **12**, 065 (2023), [arXiv:2309.00547].

[258] M. Beneke *et al.*, Phys. Lett. B **775**, 63 (2017), [arXiv:1605.03609].

[259] P. Marquard *et al.*, Phys. Rev. Lett. **114**, 14, 142002 (2015), [arXiv:1502.01030].

[260] M. Beneke, Phys. Rept. **317**, 1 (1999), [hep-ph/9807443].

[261] S. Catani *et al.*, JHEP **07**, 100 (2019), [arXiv:1906.06535].

[262] S. Catani *et al.*, Eur. Phys. J. C **81**, 6, 491 (2021), [arXiv:2102.03256].

[263] A. M. Sirunyan *et al.* (CMS), Eur. Phys. J. C **80**, 7, 658 (2020), [arXiv:1904.05237].

[264] G. Aad *et al.* (ATLAS), JHEP **11**, 150 (2019), [arXiv:1905.02302].

[265] A. Tumasyan *et al.* (CMS), JHEP **07**, 077 (2023), [arXiv:2207.02270].

[266] G. Aad *et al.* (ATLAS, CMS), JHEP **07**, 213 (2023), [arXiv:2205.13830].

[267] J. Erler, P. Masjuan and H. Spiesberger, Eur. Phys. J. C **82**, 11, 1023 (2022), [arXiv:2203.02348].

[268] Y. Aoki *et al.* (Flavour Lattice Averaging Group (FLAG)) (2024), [arXiv:2411.04268].

[269] W. J. Marciano and J. L. Rosner, Phys. Rev. Lett. **65**, 2963 (1990), [Erratum: Phys. Rev. Lett. 68, 898 (1992)].

[270] G. Degrassi, S. Fanchiotti and A. Sirlin, Nucl. Phys. B **351**, 49 (1991).

[271] G. Degrassi and A. Sirlin, Nucl. Phys. B **352**, 342 (1991).

[272] P. Gambino and A. Sirlin, Phys. Rev. D **49**, 1160 (1994), [hep-ph/9309326].

[273] J. Erler and M. J. Ramsey-Musolf, Prog. Part. Nucl. Phys. **54**, 351 (2005), [hep-ph/0404291].

[274] A. Czarnecki and W. J. Marciano, Int. J. Mod. Phys. A **15**, 2365 (2000), [hep-ph/0003049].

[275] J. Erler and M. J. Ramsey-Musolf, Phys. Rev. D **72**, 073003 (2005), [hep-ph/0409169].

[276] K. Kumar *et al.*, Ann. Rev. Nucl. Part. Sci. **63**, 237 (2013), [arXiv:1302.6263].

[277] J. M. Conrad, M. H. Shaevitz and T. Bolton, Rev. Mod. Phys. **70**, 1341 (1998), [hep-ex/9707015].

[278] J. Formaggio and G. Zeller, Rev. Mod. Phys. **84**, 1307 (2012), [arXiv:1305.7513].

[279] A. Blondel *et al.*, Z. Phys. C **45**, 361 (1990).

[280] J. Allaby *et al.* (CHARM), Z. Phys. C **36**, 611 (1987).

[281] K. S. McFarland *et al.* (CCFR, E744, E770), Eur. Phys. J. C **1**, 509 (1998), [hep-ex/9701010].

[282] G. Zeller *et al.* (NuTeV), Phys. Rev. Lett. **88**, 091802 (2002), [Erratum: Phys. Rev. Lett. 90, 239902 (2003)], [hep-ex/0110059].

[283] C. Prescott *et al.*, Phys. Lett. B **84**, 524 (1979).

[284] D. Wang *et al.* (PVDIS), Nature **506**, 7486, 67 (2014).

Int. J. Mod. Phys. A 2026.41. Downloaded from www.worldscientific.com
by UNIVERSITY OF CALIFORNIA @ BERKELEY on 09/16/26. Re-use and distribution is strictly not permitted, except for Open Access articles.

[285] D. Wang *et al.*, Phys. Rev. C **91**, 4, 045506 (2015), [arXiv:1411.3200].

[286] P. Anthony *et al.* (SLAC E158), Phys. Rev. Lett. **95**, 081601 (2005), [hep-ex/0504049].

[287] C. Wood *et al.*, Science **275**, 1759 (1997).

[288] J. Guena, M. Lintz and M. Bouchiat, Phys. Rev. A **71**, 042108 (2005), [arXiv:physics/0412017].

[289] A. Derevianko, Phys. Rev. Lett. **85**, 1618 (2000), [hep-ph/0005274].

[290] W. Johnson, I. Bednyakov and G. Soff, Phys. Rev. Lett. **87**, 233001 (2001), [Erratum: Phys. Rev. Lett. 88, 079903 (2002)], [hep-ph/0110262].

[291] M. Kuchiev and V. Flambaum, Phys. Rev. Lett. **89**, 283002 (2002), [hep-ph/0206124].

[292] A. Milstein, O. Sushkov and I. Terekhov, Phys. Rev. Lett. **89**, 283003 (2002), [hep-ph/0208227].

[293] S. Porsev, K. Beloy and A. Derevianko, Phys. Rev. Lett. **102**, 181601 (2009), [arXiv:0902.0335].

[294] V. Dzuba *et al.*, Phys. Rev. Lett. **109**, 203003 (2012), [arXiv:1207.5864].

[295] M.-A. Bouchiat and C. Bouchiat, Rep. Prog. Phys. **60**, 11, 1351 (1997).

[296] S. Navas *et al.* (Particle Data Group), Phys. Rev. D **110**, 3, 030001 (2024).

[297] G. Passarino and M. Veltman, Nucl. Phys. B **160**, 151 (1979).

[298] W. Hollik and G. Duckeck, Springer Tracts Mod. Phys. **162**, 1 (2000).

[299] T. A. Aaltonen *et al.* (CDF, DØ), Phys. Rev. D **97**, 11, 112007 (2018), [arXiv:1801.06283].

[300] G. Aad *et al.* (ATLAS), JHEP **09**, 049 (2015), [arXiv:1503.03709].

[301] Technical Report ATLAS-CONF-2018-037, CERN, Geneva (2018), URL `https://cds.cern.ch/record/2630340`.

[302] A. M. Sirunyan *et al.* (CMS), Eur. Phys. J. C **78**, 9, 701 (2018), [arXiv:1806.00863].

[303] Technical Report CMS-PAS-SMP-22-010, CERN, Geneva (2024), URL `http://cds.cern.ch/record/2893842`.

[304] R. Aaij *et al.* (LHCb), JHEP **11**, 190 (2015), [arXiv:1509.07645].

[305] K. Abe *et al.* (SLD), Phys. Rev. Lett. **84**, 5945 (2000), [hep-ex/0004026].

[306] K. Abe *et al.* (SLD), Phys. Rev. Lett. **86**, 1162 (2001), [hep-ex/0010015].

[307] A. Hayrapetyan *et al.* (CMS), JHEP **01**, 101 (2024), [arXiv:2309.12408].

[308] D. Kennedy *et al.*, Nucl. Phys. B **321**, 83 (1989).

[309] S. Riemann, Rept. Prog. Phys. **73**, 126201 (2010).

[310] K. Abe *et al.* (SLD), Phys. Rev. Lett. **85**, 5059 (2000), [hep-ex/0006019].

[311] K. Abe *et al.* (SLD), Phys. Rev. Lett. **78**, 17 (1997), [hep-ex/9609019].

[312] G. Voutsinas *et al.*, Phys. Lett. B **800**, 135068 (2020), [arXiv:1908.01704].

[313] W. Bernreuther *et al.*, JHEP **01**, 053 (2017), [arXiv:1611.07942].

[314] S. Catani and M. H. Seymour, JHEP **07**, 023 (1999), [hep-ph/9905424].

[315] A. Djouadi, J. H. Kuhn and P. Zerwas, Z. Phys. C **46**, 411 (1990).

[316] M. Aaboud *et al.* (ATLAS), Eur. Phys. J. C **77**, 6, 367 (2017), [arXiv:1612.03016].

[317] R. Aaij *et al.* (LHCb), JHEP **09**, 159 (2018), [arXiv:1806.05008].

[318] T. A. Aaltonen *et al.* (CDF), Phys. Rev. D **93**, 11, 112016 (2016), [Addendum: Phys.Rev.D 95, 119901 (2017)], [arXiv:1605.02719].

[319] V. M. Abazov *et al.* (DØ), Phys. Rev. Lett. **120**, 24, 241802 (2018), [arXiv:1710.03951].

[320] V. Abazov *et al.* (DØ), Phys. Rev. D **84**, 012007 (2011), [arXiv:1104.4590].

[321] D. Acosta *et al.* (CDF), Phys. Rev. D **71**, 052002 (2005), [hep-ex/0411059].

[322] V. Andreev *et al.* (H1), Eur. Phys. J. C **78**, 9, 777 (2018), [arXiv:1806.01176].

[323] H. Abramowicz *et al.* (ZEUS), Phys. Rev. D **93**, 9, 092002 (2016), [arXiv:1603.09628].

[324] A. Hayrapetyan *et al.* (CMS), Phys. Lett. B **866**, 139526 (2025), [arXiv:2408.07622].

[325] R. Aaij *et al.* (LHCb), JHEP **12**, 026 (2024), [arXiv:2410.02502].

[326] D. Albert *et al.*, Nucl. Phys. B **166**, 460 (1980).

[327] K. Chetyrkin, J. H. Kuhn and A. Kwiatkowski, Phys. Rept. **277**, 189 (1996), [hep-ph/9503396].

[328] P. Baikov, K. Chetyrkin and J. H. Kuhn, Phys. Rev. Lett. **101**, 012002 (2008), [arXiv:0801.1821].

[329] B. A. Kniehl and J. H. Kuhn, Nucl. Phys. B **329**, 547 (1990).

[330] K. Chetyrkin and A. Kwiatkowski, Phys. Lett. B **319**, 307 (1993), [hep-ph/9310229].

[331] S. Larin, T. van Ritbergen and J. Vermaseren, Phys. Lett. B **320**, 159 (1994), [hep-ph/9310378].

[332] K. Chetyrkin and O. Tarasov, Phys. Lett. B **327**, 114 (1994), [hep-ph/9312323].

[333] P. Baikov *et al.*, Phys. Rev. Lett. **108**, 222003 (2012), [arXiv:1201.5804].

[334] A. Kataev, Phys. Lett. B **287**, 209 (1992).

[335] B. W. Lynn and R. G. Stuart, Phys. Lett. B **252**, 676 (1990).

[336] J. Bernabeu, A. Pich and A. Santamaria, Nucl. Phys. B **363**, 326 (1991).

[337] A. Czarnecki and J. H. Kuhn, Phys. Rev. Lett. **77**, 3955 (1996), [hep-ph/9608366].

[338] R. Harlander, T. Seidensticker and M. Steinhauser, Phys. Lett. B **426**, 125 (1998), [hep-ph/9712228].

[339] J. Fleischer *et al.*, Phys. Lett. B **459**, 625 (1999), [hep-ph/9904256].

[340] A. Akhundov, D. Bardin and T. Riemann, Nucl. Phys. B **276**, 1 (1986).

[341] F. Jegerlehner, Z. Phys. C **32**, 425 (1986), [Erratum: Z. Phys. C 38, 519 (1988)].

[342] W. Beenakker and W. Hollik, Z. Phys. C **40**, 141 (1988).

[343] A. Borrelli *et al.*, Nucl. Phys. B **333**, 357 (1990).

[344] G. Aad *et al.* (ATLAS), Nature Phys. **17**, 7, 813 (2021), [arXiv:2007.14040].

[345] A. Tumasyan *et al.* (CMS), Phys. Rev. D **105**, 7, 072008 (2022), [arXiv:2201.07861].

[346] G. Aad *et al.* (ATLAS), Eur. Phys. J. C **84**, 10, 993 (2024), [arXiv:2403.02133].

[347] R. Aaij *et al.* (LHCb), JHEP **10**, 030 (2016), [arXiv:1608.01484].

[348] U. Amaldi *et al.*, Phys. Rev. D **36**, 1385 (1987).

[349] G. Costa *et al.*, Nucl. Phys. B **297**, 244 (1988).

[350] P. Langacker and M. Luo, Phys. Rev. D **44**, 817 (1991).

[351] J. Erler and P. Langacker, Phys. Rev. D **52**, 441 (1995), [hep-ph/9411203].

[352] M. Aaboud *et al.* (ATLAS), Phys. Lett. B **784**, 345 (2018), [arXiv:1806.00242].

[353] M. E. Peskin and T. Takeuchi, Phys. Rev. D **46**, 381 (1992).

Int. J. Mod. Phys. A 2026.41. Downloaded from www.worldscientific.com by UNIVERSITY OF CALIFORNIA @ BERKELEY on 09/16/26. Re-use and distribution is [redacted] except for Open Access articles.

[354] G. Altarelli, R. Barbieri and S. Jadach, Nucl. Phys. B **369**, 3 (1992), [Erratum: Nucl. Phys. B 376, 444 (1992)].

[355] G. Altarelli, R. Barbieri and F. Caravaglios, Nucl. Phys. B **405**, 3 (1993).

[356] G. Altarelli, R. Barbieri and F. Caravaglios, Int. J. Mod. Phys. A **13**, 1031 (1998), [hep-ph/9712368].

[357] R. Barbieri *et al.*, Nucl. Phys. B **703**, 127 (2004), [hep-ph/0405040].

[358] P. Langacker and M. Luo, Phys. Rev. D **45**, 278 (1992).

[359] P. Langacker and D. London, Phys. Rev. D **38**, 886 (1988).

[360] F. del Aguila, J. de Blas and M. Perez-Victoria, Phys. Rev. D **78**, 013010 (2008), [arXiv:0803.4008].

[361] M. Chemtob, Prog. Part. Nucl. Phys. **54**, 71 (2005), [hep-ph/0406029].

[362] R. Barbier *et al.*, Phys. Rept. **420**, 1 (2005), [hep-ph/0406039].

[363] C. T. Hill and E. H. Simmons, Phys. Rept. **381**, 235 (2003), [Erratum: Phys. Rept. 390, 553 (2004)], [hep-ph/0203079].

[364] T. Han, H. E. Logan and L.-T. Wang, JHEP **01**, 099 (2006), [hep-ph/0506313].

[365] M. Perelstein, Prog. Part. Nucl. Phys. **58**, 247 (2007), [hep-ph/0512128].

[366] I. Antoniadis, in "Supergravity, Superstrings and M-Theory," (2001), [hep-th/0102202].

[367] M. Carena *et al.*, Phys. Rev. D **68**, 035010 (2003), [hep-ph/0305188].

[368] K. Agashe *et al.*, JHEP **08**, 050 (2003), [hep-ph/0308036].

[369] I. Gogoladze and C. Macesanu, Phys. Rev. D **74**, 093012 (2006), [hep-ph/0605207].

[370] B. Grinstein and M. Trott, Phys. Rev. D **76**, 073002 (2007), [arXiv:0704.1505].

[371] R. Alonso *et al.*, Phys. Lett. B **722**, 330 (2013), [Erratum: Phys. Lett. B 726, 926 (2013)], [arXiv:1212.3305].

[372] R. Contino *et al.*, JHEP **07**, 035 (2013), [arXiv:1303.3876].

[373] W. Buchmuller and D. Wyler, Nucl. Phys. B **268**, 621 (1986).

[374] B. Grzadkowski *et al.*, JHEP **10**, 085 (2010), [arXiv:1008.4884].

[375] S. Weinberg, Phys. Rev. Lett. **43**, 1566 (1979).

[376] J. D. Wells and Z. Zhang, JHEP **01**, 123 (2016), [arXiv:1510.08462].

[377] S. Dawson and P. P. Giardino, Phys. Rev. D **101**, 1, 013001 (2020), [arXiv:1909.02000].

[378] L. Bellafronte, S. Dawson and P. P. Giardino, JHEP **05**, 208 (2023), [arXiv:2304.00029].

[379] A. Biekötter and B. D. Pecjak, JHEP **07**, 134 (2025), [arXiv:2503.07724].

[380] P. Asadi *et al.*, Phys. Rev. D **108**, 5, 055026 (2023), [arXiv:2204.05283].

[381] E. Bagnaschi *et al.*, JHEP **08**, 308 (2022), [arXiv:2204.05260].

[382] J. Gu *et al.*, Chin. Phys. C **46**, 12, 123107 (2022), [arXiv:2204.05296].

[383] A. Paul and M. Valli, Phys. Rev. D **106**, 1, 013008 (2022), [arXiv:2204.05267].

[384] M. S. Chanowitz, M. Furman and I. Hinchliffe, Phys. Lett. B **78**, 285 (1978).

[385] J. van der Bij and F. Hoogeveen, Nucl. Phys. B **283**, 477 (1987).

[386] A. Denner, R. Guth and J. H. Kuhn, Phys. Lett. B **240**, 438 (1990).

[387] W. Grimus *et al.*, J. Phys. G **35**, 075001 (2008), [arXiv:0711.4022].

[388] H. E. Haber and D. O'Neil, Phys. Rev. D **83**, 055017 (2011), [arXiv:1011.6188].

[389] S. Bertolini and A. Sirlin, Phys. Lett. B **257**, 179 (1991).

[390] J. Erler and P. Langacker, Phys. Rev. Lett. **105**, 031801 (2010), [arXiv:1003.3211].

[391] J. Gunion, D. W. McKay and H. Pois, Phys. Rev. D **53**, 1616 (1996), [hep-ph/9507323].

[392] A. Denner *et al.*, Eur. Phys. J. C **72**, 1992 (2012), [arXiv:1111.6395].

[393] A. Lenz, Adv. High Energy Phys. **2013**, 910275 (2013).

[394] S. Chatrchyan *et al.* (CMS), Phys. Rev. D **86**, 112003 (2012), [arXiv:1209.1062].

[395] A. Djouadi and A. Lenz, Phys. Lett. B **715**, 310 (2012), [arXiv:1204.1252].

[396] O. Eberhardt *et al.*, Phys. Rev. Lett. **109**, 241802 (2012), [arXiv:1209.1101].

[397] J. Maalampi and M. Roos, Phys. Rept. **186**, 53 (1990).

[398] P. Langacker, Phys. Rept. **72**, 185 (1981).

[399] J. L. Hewett and T. G. Rizzo, Phys. Rept. **183**, 193 (1989).

[400] J. Kang, P. Langacker and B. D. Nelson, Phys. Rev. D **77**, 035003 (2008), [arXiv:0708.2701].

[401] S. P. Martin, Phys. Rev. D **81**, 035004 (2010), [arXiv:0910.2732].

[402] P. W. Graham *et al.*, Phys. Rev. D **81**, 055016 (2010), [arXiv:0910.3020].

[403] L. Randall and R. Sundrum, Phys. Rev. Lett. **83**, 3370 (1999), [hep-ph/9905221].

[404] M. Carena *et al.*, Nucl. Phys. B **759**, 202 (2006), [hep-ph/0607106].

[405] R. Contino, in "Theoretical Advanced Study Institute in Elementary Particle Physics: Physics of the Large and the Small," 235–306 (2011), [arXiv:1005.4269].

[406] A. Pich, I. Rosell and J. Sanz-Cillero, JHEP **01**, 157 (2014), [arXiv:1310.3121].

[407] G. Panico and A. Wulzer, *The Composite Nambu-Goldstone Higgs*, volume 913, Springer (2016), [arXiv:1506.01961].

[408] J. A. Cabrer, G. von Gersdorff and M. Quiros, JHEP **05**, 083 (2011), [arXiv:1103.1388].

[409] D. D. Dietrich, F. Sannino and K. Tuominen, Phys. Rev. D **72**, 055001 (2005), [hep-ph/0505059].

[410] M. T. Frandsen and M. Rosenlyst, JHEP **03**, 222 (2023), [arXiv:2207.01465].

[411] E. Gates and J. Terning, Phys. Rev. Lett. **67**, 1840 (1991).

[412] H. Georgi, Nucl. Phys. B **363**, 301 (1991).

[413] M. J. Dugan and L. Randall, Phys. Lett. B **264**, 154 (1991).

[414] H. E. Haber and G. L. Kane, Phys. Rept. **117**, 75 (1985).

[415] A. Djouadi, Phys. Rept. **459**, 1 (2008), [hep-ph/0503173].

[416] R. Barbieri *et al.*, Nucl. Phys. B **341**, 309 (1990).

[417] R. Barbieri, M. Frigeni and F. Caravaglios, Phys. Lett. B **279**, 169 (1992).

[418] J. Erler and D. M. Pierce, Nucl. Phys. B **526**, 53 (1998), [hep-ph/9801238].

[419] G.-C. Cho and K. Hagiwara, Nucl. Phys. B **574**, 623 (2000), [hep-ph/9912260].

[420] G. Altarelli *et al.*, JHEP **06**, 018 (2001), [hep-ph/0106029].

[421] S. Heinemeyer, W. Hollik and G. Weiglein, Phys. Rept. **425**, 265 (2006), [hep-ph/0412214].

[422] S. P. Martin, K. Tobe and J. D. Wells, Phys. Rev. D **71**, 073014 (2005), [hep-ph/0412424].

[423] M. Ramsey-Musolf and S. Su, Phys. Rept. **456**, 1 (2008), [hep-ph/0612057].

[424] S. Heinemeyer *et al.*, JHEP **04**, 039 (2008), [arXiv:0710.2972].

[425] O. Buchmueller *et al.*, Eur. Phys. J. C **72**, 2020 (2012), [arXiv:1112.3564].

[426] G. Altarelli and R. Barbieri, Phys. Lett. B **253**, 161 (1991).

[427] I. Brivio *et al.* (2021), [arXiv:2111.12515].

[428] A. Falkowski and F. Riva, JHEP **02**, 039 (2015), [arXiv:1411.0669].

[429] I. Brivio and M. Trott, JHEP **07**, 148 (2017), [Addendum: JHEP 05, 136 (2018)], [arXiv:1701.06424].

[430] J. Ellis *et al.*, JHEP **04**, 279 (2021), [arXiv:2012.02779].

[431] J. J. Ethier *et al.* (SMEFiT), JHEP **11**, 089 (2021), [arXiv:2105.00006].

[432] F. Garosi *et al.*, JHEP **12**, 129 (2023), [arXiv:2310.00047].

[433] L. Allwicher *et al.*, JHEP **03**, 049 (2024), [arXiv:2311.00020].

[434] R. Bartocci, A. Biekötter and T. Hurth, JHEP **05**, 074 (2024), [arXiv:2311.04963].

[435] E. Celada *et al.*, JHEP **09**, 091 (2024), [arXiv:2404.12809].

[436] G. Aad *et al.* (ATLAS), JHEP **11**, 097 (2024), [arXiv:2402.05742].

[437] R. Bartocci, A. Biekötter and T. Hurth, JHEP **05**, 203 (2025), [arXiv:2412.09674].

[438] V. Chekhovsky *et al.* (CMS) (2025), [arXiv:2504.02958].

[439] J. ter Hoeve *et al.*, JHEP **06**, 125 (2025), [arXiv:2502.20453].

[440] J. de Blas *et al.* (2025), [arXiv:2507.06191].

[441] J. Erler, J. L. Feng and N. Polonsky, Phys. Rev. Lett. **78**, 3063 (1997), [hep-ph/9612397].

[442] D. Choudhury, T. M. Tait and C. Wagner, Phys. Rev. D **65**, 053002 (2002), [hep-ph/0109097].

[443] J. Erler and P. Langacker, Phys. Rev. Lett. **84**, 212 (2000), [hep-ph/9910315].

[444] P. Langacker and M. Plumacher, Phys. Rev. D **62**, 013006 (2000), [hep-ph/0001204].

[445] P. Abreu *et al.* (DELPHI), Eur. Phys. J. C **10**, 415 (1999).

[446] S. Gori, J. Gu and L.-T. Wang, JHEP **04**, 062 (2016), [arXiv:1508.07010].

Int. J. Mod. Phys. A 2026.41. Downloaded from www.worldscientific.com
by UNIVERSITY OF CALIFORNIA @ BERKELEY on 09/16/26. Re-use and distribution is strictly not permitted, except for Open Access articles.

11. Status of Higgs Boson Physics

Revised August 2025 by M. Cepeda (CIEMAT), L. Reina (Florida State U.) and P. Savard (Toronto U.; TRIUMF).

11.1 Introduction 226
11.1.1 Searches for the SM Higgs boson 226
11.1.2 Discovery of the SM Higgs boson 226
11.1.3 The SM Higgs boson as a portal to new physics 226
11.1.4 Synopsis of this review 227
11.2 The Standard Model and the mechanism of electroweak symmetry breaking 227
11.2.1 The scalar Lagrangian of the Standard Model 227
11.2.2 The Yukawa Lagrangian of the Standard Model 228
11.2.3 The Standard Model custodial symmetry . 228
11.2.4 Stability of the scalar potential of the Standard Model 229
11.2.5 Production and decay modes of the Standard-Model Higgs boson 229
11.3 Phenomenology of the 125 GeV Higgs boson . . 235
11.3.1 Higgs-Boson Decay Channels 235
11.3.2 Higgs-Boson Production Channels 236
11.3.3 Inclusive Cross Section and Branching Ratio Measurements 236
11.3.4 Differential and Template Cross Sections . . 238
11.3.5 Probing the Couplings of the Higgs Boson: $\boldsymbol{\kappa}$ framework and EFT approach 239
11.3.6 Higgs-boson Self-Couplings 245
11.3.7 Higgs-Boson Mass Measurements 246
11.3.8 Higgs-boson Width Measurements 247
11.3.9 Higgs-boson Spin and CP Properties 249
11.4 Beyond the Standard Model (BSM) Higgs boson 251
11.4.1 Weakly coupled approach to EWSB 252
11.4.2 EWSB induced by strong dynamics 257
11.4.3 Exotic Higgs-boson decays 258
11.4.4 Summary of BSM Higgs boson search results 260
11.5 Summary and Outlook 261

11.1 Introduction

Understanding how the masses of the known elementary particles are generated has been one of the fundamental endeavors in particle physics for several decades. Due to the nature of the $SU(2)_L \times U(1)_Y$ electroweak (EW) gauge symmetry that defines the Standard Model (SM) [1], mass terms for the W and Z weak gauge bosons as well as for all fermions (quarks and leptons) can only appear as emergent quantities after the spontaneous breaking of the EW symmetry. The mechanism of electroweak symmetry breaking (EWSB) [2] provides a general framework to keep untouched the structure of the SM gauge interactions at high energies and still generate all observed particle masses at the scale of EW interactions. The EWSB mechanism posits a self-interacting complex EW doublet scalar field, whose CP-even neutral component acquires a vacuum expectation value (VEV) $v \approx 246\,\text{GeV}$[1], which sets the scale of the symmetry breaking. Three massless Goldstone bosons are generated and are absorbed to give masses to the W and Z gauge bosons. The remaining component of the complex doublet becomes the Higgs boson – a new, and so far unique, fundamental scalar particle. The masses of all fermions are also a consequence of EWSB since the Higgs doublet is postulated to couple to the fermions through Yukawa interactions in a way consistent with all the gauge symmetries of the SM.

The existence of a Higgs boson as predicted by the mechanism of EWSB is crucial to the consistency of the SM at the quantum level such that its mass has been indirectly constrained by SM precision measurements well before its discovery. In fact, without the Higgs boson, SM predictions would show clear indications of new phenomena at the TeV scale. Perturbative unitarity [3] would be lost at high energies since the longitudinal W/Z boson scattering amplitudes would grow with the center-of-mass energy. In addition, the radiative corrections to the gauge boson self-energies would exhibit dangerous logarithmic divergences that would be difficult to reconcile with EW precision data.

The observation of a Higgs boson as predicted by the mechanism of EWSB of the SM has therefore been the holy grail of particle physics for the decades that led up to its discovery in 2012.

11.1.1 *Searches for the SM Higgs boson*

Prior to the observation of the Higgs boson in July of 2012, searches for the SM Higgs boson were carried out by the LEP and Tevatron experiments. The combined results of the LEP experiments [4] yielded a lower bound of $m_H > 114.4$ GeV at the 95% confidence level (CL). The Tevatron experiments [5] subsequently excluded the mass range between 156 and 177 GeV at the 95% CL. These exclusions are shown in Fig. 11.1 (left) together with those obtained by the CERN Large Hadron Collider (LHC) [6] experiments in the Summer of 2011.

Right before its discovery, the latest direct searches from the LHC experiments had excluded Higgs-boson mass hypotheses below 600 GeV at the 95% CL, except for a narrow window around $115.5 < m_H < 127$ GeV. This was also the mass range independently favored by indirect constraints from precision measurements of EW-boson masses and couplings in e^+e^- collisions, on and off the Z-boson mass peak, at SLD, LEP, and LEP2, supplemented by results at the $p\bar{p}$ Tevatron collider that also measured the top-quark mass [7–9]. The right-hand-side plot of Fig. 11.1 illustrates the indirect constraint on m_H from precision fits of the SM as of March 2012 [10], i.e. right before the Higgs-boson discovery. In the SM, m_W and m_t are correlated by their dependence on m_H through radiative corrections. The diagonal green band in Fig. 11.1 represents the region of the (m_t, m_W) plane corresponding to values of m_H between 114 GeV and 1 TeV, a large portion of which (the diagonal yellow band) was already excluded in 2012 by the aforementioned direct LHC limits. On the other hand, the blue ellipse in Fig. 11.1 defines the experimentally allowed region of (m_t, m_W) as of March 2012, greatly improved by LEP2 and Tevatron direct measurements with respect to the case in which LEP1 and SLD data only could be used (red-dashed contour). Consistency with SM measurements, corresponding to the tiny region at the intersection between the blue ellipse and the green diagonal band in Fig. 11.1, yielded a best fit Higgs-boson mass value of $m_H = 94^{+29}_{-24}$ GeV, and a 95% CL upper bound of $m_H < 154$ GeV, in agreement with the LHC exclusion limits and quite on top of where the SM Higgs boson was soon to be found. More details on pre-discovery Higgs-boson direct and indirect bounds can be found in previous PDG reviews [11].

11.1.2 *Discovery of the SM Higgs boson*

In July 2012, the ATLAS [12] and CMS [13] experiments at CERN's LHC announced the discovery of a new particle with properties consistent with the SM Higgs boson [14, 15]. Subsequent analyses of the complete 2011–2012 Run 1 proton–proton dataset provided additional evidence of its compatibility with SM predictions: measurements of its spin, CP properties and width [16–21], and combined fits [22] all agreed well with theoretical expectations.

The characterization of the Higgs boson has continued during the Run 2 (2015-2018) and Run 3 (2022-2026) data-taking periods. The results presented in this Review provide a summary of these measurements.

11.1.3 *The SM Higgs boson as a portal to new physics*

With the discovery of the Higgs boson, the SM is confirmed to be a spontaneously broken gauge theory and, as such, it could a priori be consistently extrapolated well above the masses of the W and Z bosons. Hence, formally there is no need for new physics at the EW scale. However, as the SM Higgs boson is a scalar particle, it has sensitivity to possible new physics scales. Quite generally, the Higgs-boson mass is affected by the presence of heavy particles and it receives large quantum corrections which destabilize the weak scale barring a large fine-tuning of unrelated parameters. This is known as the Higgs naturalness or hierarchy

[1] As measured in muon decay with high precision, see Sec. 11.2.1.

Int. J. Mod. Phys. A 2026.41. Downloaded from www.w
by UNIVERSITY OF CALIFORNIA @ BERKELEY on 09/16/26. Re-use and distribution is
except for Open Access articles.

Int. J. Mod. Phys. A 2026.41. Downloaded from www.worldscientific.com
by UNIVERSITY OF CALIFORNIA @ BERKELEY on 09/16/26. Re-use and distribution is strictly not permitted, except for Open Access articles.

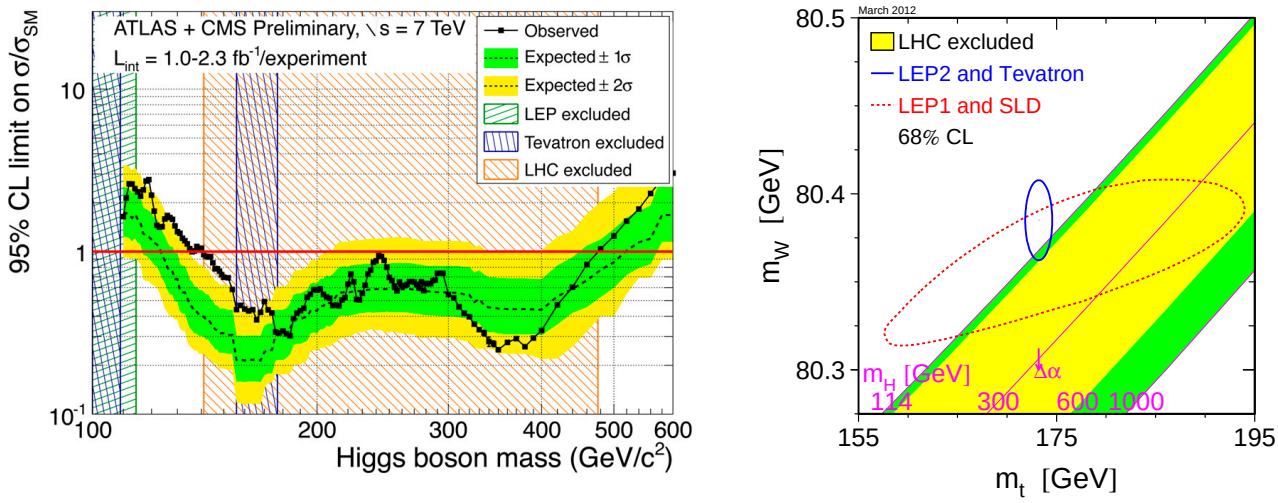

Figure 11.1: Left: Combined 95 % CL upper limits on SM Higgs-boson production prior to the discovery at the LHC in the Summer of 2011. The limits are normalized to the SM expectation, as a function of the Higgs-boson mass. Regions where the observed limit falls below unity are excluded. Right: indirect bounds on m_H from EW precision fits (March 2012).

problem [23], and it has been the prime argument for expecting new physics around and not far above the TeV scale.

To remedy this unsatisfactory feature, theoretically motivated paradigms have been explored for several decades, such as a new fermion-boson symmetry called supersymmetry (SUSY) [24] (for recent reviews, see Refs. [25, 26]), or the existence of strong interactions at a scale of the order of a TeV from which the Higgs boson would emerge as a composite state [27] (see Refs. [28, 29] for recent reviews). Alternatively, new agents stabilizing the weak scale could also be light but elusive, like in models of neutral naturalness [30, 31]. It was also recently appreciated [32, 33] that the cosmological evolution of the Universe could drive the Higgs-boson mass to a value much smaller than the cutoff of the theory, alleviating the hierarchy problem without the need for TeV scale new physics, even though there might still be interesting and spectacular signatures [32,34]. This approach spurs a change in perspective invoking our Universe as part of a multiverse that should be treated as a quantum statistical system [35].

Another puzzling aspect of the SM Higgs boson concerns the arbitrariness of its couplings to fermions. This is encoded in the SM through a series of Yukawa couplings, one per massive fermion, proportional to the corresponding fermion mass and therefore displaying a huge and unexplained scale hierarchy. Furthermore, fermion masses and fermion mass eigenstates are intrinsically related to the origin of flavor mixing and CP-violation in the SM charged gauge currents, where four more arbitrary parameters are embedded in the Cabibbo-Kobayashi-Maskawa (CKM) matrix. Hence, the scalar sector of the SM is responsible for introducing 15 of the 19 input parameters of the theory, 13 of which are related to the Yukawa interaction between the Higgs-boson and massive-fermion (9 masses, excluding neutrinos which are strictly speaking massless in the SM, and 4 CKM parameters) while the remaining two define the scalar potential). These interactions are not of gauge nature and could be messengers of new physics (NP) that will eventually explain the hierarchy of fermion masses and the flavor dynamics of the SM at a deeper level [36].

The Higgs boson offers a special portal to new physics and, in the years since its discovery, it has become a powerful tool to stress test the quantum structure of the SM and to probe the physics landscape beyond it. This has greatly influenced the discussion about future facilities which has emphasized the need for both high-luminosity lower-energy e^+e^- colliders to obtain percent-level measurements of Higgs-boson couplings and higher-energy pp or $\mu^+\mu^-$ colliders to explore NP up to about 10 TeV.

11.1.4 *Synopsis of this review*

This review is organized as follows. Section 11.2 is a theoretical introduction to the SM Higgs boson, its properties, production mechanisms and decay rates, and a concise updated review of the corresponding theoretical predictions. The state-of-the-art of experimental measurements are described in Section 11.3, including measurements of SM Higgs-boson inclusive cross sections and branching ratios, differential cross sections and simplified template cross sections, couplings to gauge bosons and fermions, self-coupling, mass, width, and spin and CP properties. Section 11.4 reviews how the discovery of the SM Higgs boson has provided a portal to NP exploration and has greatly influenced the direct search for NP at the LHC. Finally, Section 11.5 provides a short summary and a brief outlook.

11.2 The Standard Model and the mechanism of electroweak symmetry breaking

11.2.1 *The scalar Lagrangian of the Standard Model*

In the SM [1] EWSB [2] is responsible for generating a mass for the W and Z gauge bosons rendering the weak interactions short ranged. The SM $\mathrm{SU}(3)_C \times \mathrm{SU}(2)_L \times \mathrm{U}(1)_Y$ gauge symmetry is spontaneously broken to $\mathrm{SU}(3)_C \times \mathrm{U}(1)_Q$ by introducing a complex scalar field (Φ), doublet of $\mathrm{SU}(2)_L$ and with hypercharge $Y = 1$, through the gauge-invariant *Higgs Lagrangian* [2],

$$\mathcal{L}_{\mathrm{Higgs}} = (D_\mu \Phi)^\dagger (D^\mu \Phi) - V(\Phi)\,, \tag{11.1}$$

where $D_\mu \Phi = (\partial_\mu + ig\sigma^a W^a_\mu/2 + ig' Y B_\mu/2)\Phi$, g and g' are the $\mathrm{SU}(2)_L$ and $\mathrm{U}(1)_Y$ gauge couplings, respectively, σ^a $(a = 1, 2, 3)$ are the Pauli matrices, Y is the hypercharge quantum number, and the potential $V(\Phi)$ reads:

$$V(\Phi) = \mu^2 \Phi^\dagger \Phi + \lambda (\Phi^\dagger \Phi)^2\,. \tag{11.2}$$

$Q = T_{3L} + Y/2$ is the conserved electric charge quantum number, with T_{3L} the eigenvalue of the diagonal generator of $\mathrm{SU}(2)_L$ (e.g. $T_{3L} = 1/2$ for up-type quarks, etc.).

The scalar field Φ can be written as

$$\Phi = \frac{1}{\sqrt{2}} \begin{pmatrix} \sqrt{2}\phi^+ \\ \phi^0 + ia^0 \end{pmatrix}, \tag{11.3}$$

where ϕ^0 and a^0 denote the doublet's CP-even and CP-odd neutral components, and ϕ^+ its complex charged component, respectively. The covariant-derivative *kinetic* term in Eq. (11.1) contains both truly kinetic terms and the interaction terms between the

Int. J. Mod. Phys. A 2026.41. Downloaded from www.worldscientific.com by UNIVERSITY OF CALIFORNIA @ BERKELEY on 09/16/26. Re-use and distribution is [redacted] except for Open Access articles.

gauge fields and the scalar field Φ. Upon spontaneous symmetry breaking it is also responsible for the W and Z gauge-boson mass terms. $V(\Phi)$ is the most general renormalizable scalar potential invariant under $\mathrm{SU}(2)_L \times \mathrm{U}(1)_Y$. If the quadratic term is negative ($\mu^2 < 0$), the global minimum of the $V(\Phi)$ potential occurs for a non-zero vacuum expectation value (VEV) of the field Φ such that $\langle \Phi^\dagger \Phi \rangle = v^2/2 = -\mu^2/2\lambda$. Choosing a particular field configuration that satisfies this condition breaks the $\mathrm{SU}(2)_L \times \mathrm{U}(1)_Y$ gauge symmetry on the vacuum and induces the spontaneous breaking of the electroweak SM gauge symmetry $\mathrm{SU}(2)_L \times \mathrm{U}(1)_Y$ to the residual $\mathrm{U}(1)_Q$ gauge symmetry of quantum electrodynamics (QED). In particular, if one chooses the neutral component of the scalar doublet to acquire a non-zero (real) vacuum expectation value $\langle \phi^0 \rangle \equiv v = \sqrt{-\mu^2/\lambda}$, the global minimum of the theory is realized by

$$\langle \Phi \rangle = \frac{1}{\sqrt{2}} \begin{pmatrix} 0 \\ v \end{pmatrix} . \tag{11.4}$$

The global minimum of the theory defines the ground state, and spontaneous symmetry breaking occurs since the (global and/or local) symmetry of the Lagrangian is not respected by the ground state. From the four generators of the $\mathrm{SU}(2)_L \times \mathrm{U}(1)_Y$ SM gauge group, three are spontaneously broken on the vacuum, i.e. they do not leave the ground state invariant. This implies the existence of three massless (would-be) Goldstone bosons identified with three of the four degrees of freedom of the scalar field Φ. Using a gauge choice (*unitary gauge*) where three components of the scalar field Φ are reabsorbed by an $\mathrm{SU}(2)_L$ gauge transformation into the longitudinal components of the W and Z gauge fields, one can then parametrize the field Φ in terms of a single scalar (CP-even, spin $s = 0$) real component (H), the physical *Higgs field*, as

$$\Phi = \frac{1}{\sqrt{2}} \begin{pmatrix} 0 \\ H + v \end{pmatrix} . \tag{11.5}$$

This parametrization makes the physical content of the scalar Lagrangian in Eq. (11.1) completely manifest. The scalar field Φ couples to the W_μ and B_μ gauge fields associated with the $\mathrm{SU}(2)_L \times \mathrm{U}(1)_Y$ local symmetry through the covariant derivative appearing in the kinetic term of the Higgs Lagrangian in Eq. (11.1). The neutral and the two charged massless Goldstone degrees of freedom mix with the gauge fields corresponding to the broken generators of $\mathrm{SU}(2)_L \times \mathrm{U}(1)_Y$ and become, in the unitarity gauge, the longitudinal components of the Z and W physical gauge bosons, respectively. As a result, the Z and W gauge bosons acquire masses,

$$m_W^2 = \frac{g^2 v^2}{4} , \quad m_Z^2 = \frac{(g'^2 + g^2) v^2}{4} . \tag{11.6}$$

The fourth generator remains unbroken since it is the one associated with the conserved $\mathrm{U}(1)_Q$ gauge symmetry, and its corresponding gauge field, the photon, remains massless. Similarly, the eight color gauge bosons, the gluons, corresponding to the conserved $\mathrm{SU}(3)_C$ gauge symmetry with eight unbroken generators, also remain massless (though confined inside hadrons and mesons as the result of the asymptotic freedom behavior of Quantum ChromoDynamics (QCD)). Hence, from the initial four degrees of freedom of the Higgs field, two are absorbed by the $W^\pm$ gauge bosons, one by the Z gauge boson, and there is one remaining degree of freedom, H, that is the physical Higgs boson [2].

The Higgs boson couples to the $W^\pm$ and Z gauge-boson with strength proportional to their mass square as dictated by the minimal coupling induced by the covariant-derivative terms, namely:

$$\mathcal{L}^V_{\mathrm{Higgs}} = \delta_V \frac{2m_V^2}{v} V_\mu V^\mu H + \delta_V \frac{m_V^2}{v^2} V_\mu V^\mu H^2 , \tag{11.7}$$

where $V = W^\pm$ or Z and $\delta_W = 1, \delta_Z = 1/2$. On the other hand, the Higgs boson is neutral under the electromagnetic interactions and transforms as a singlet under $\mathrm{SU}(3)_C$. Hence it does not couple at tree level to photons and gluons. The Higgs boson coupling to gluons [37, 38] is induced at the lowest perturbative order by a one-loop process in which H couples to a virtual $t\bar{t}$ pair (with minor contributions from the other lighter quarks). Likewise, the Higgs boson coupling to photons is also generated via loops, although in this case the one-loop graph with a virtual W^+W^- pair provides the dominant contribution [39] and it is interfering destructively with the smaller contribution involving a virtual $t\bar{t}$ pair (as such, the Higgs coupling to photons is sensitive to the relative phase of the interactions between bosons and fermions).

Finally the $V(\Phi)$ potential once expressed in terms of the Higgs-field H through Eq. (11.5) contributes the following terms to the Higgs Lagrangian:

$$\mathcal{L}^H_{\mathrm{Higgs}} = -\frac{1}{2} m_H^2 H^2 - \frac{3m_H^2}{v} \frac{H^3}{3!} - \frac{3m_H^2}{v^2} \frac{H^4}{4!} , \tag{11.8}$$

where one can identify the first term as the Higgs-field mass term ($m_H^2 = 2\lambda v^2$) and the remaining two terms as the H-field cubic and quartic self-interaction terms. We notice that the Higgs Lagrangian depends on two parameters, μ^2 and λ, that can be traded for any other two precisely measured quantities, such as m_H and v, which are normally chosen as input parameters in precision fits of the SM. Indeed, the Higgs-boson mass is not predicted by the SM and its precise measurement (see Sec. 11.3.7) is therefore essential to test the consistency of the SM theory. We remind that $v = (\sqrt{2} G_F)^{-1/2} \simeq 246$ GeV can be determined very precisely in terms of the so-called Fermi constant (G_F) which is measured in muon decay with a precision of 0.6 ppm [40].

11.2.2 *The Yukawa Lagrangian of the Standard Model*

A separate term in the SM Lagrangian, the so-called Yukawa Lagrangian,

$$\mathcal{L}_{\mathrm{Yukawa}} = -\hat{Y}_{d_{ij}} \bar{q}_{L_i} \Phi \, d_{R_j} - \hat{Y}_{u_{ij}} \bar{q}_{L_i} \tilde{\Phi} u_{R_j} - \hat{Y}_{l_{ij}} \bar{l}_{L_i} \Phi \, e_{R_j} + h.c., \tag{11.9}$$

introduces a renormalizable gauge invariant interaction between the scalar field Φ and all the massive fermions (quarks and leptons) of the SM and, upon spontaneous symmetry breaking, generates their mass terms. In fact, Dirac-type mass terms violates the chiral gauge symmetry of the SM that assigns left-handed and right-handed fermion fields to different $\mathrm{SU}(2)_L$ representations. In the Lagrangian above, $\tilde{\Phi} = i\sigma_2 \Phi^*$ and q_L (l_L) and u_R, d_R (e_R) are the quark (lepton) $\mathrm{SU}(2)_L$ doublets and singlets, respectively, while in each term $\hat{Y}_{f_{ij}}$ is a 3×3 matrix of couplings in family space with indices ($i, j = 1, 2, 3$) referring to the three families in the up-quark, down-quark or charged lepton sectors ($f = u, d, l$). The mass term for neutrinos is omitted, but could be added in an analogous manner to the up-type quarks when right-handed neutrinos are supplementing the SM particle content. Neutrinos (having $Q = 0$) can also acquire Majorana masses via non-renormalizable dimension-5 effective interactions with the Higgs field [41]. Because of the special nature of neutrino masses and their potential origin from the interactions with new physics well above the electroweak scale, the extension of adding right-handed neutrino fields to the SM is considered in the context of models beyond the SM. Once the Higgs field acquires a VEV, and after rotation to the fermion mass-eigenstate basis that also diagonalizes the Higgs-fermion interactions, $\hat{Y}_{f_{ij}} \to y_{f_i} \delta_{ij}$, all fermions acquire a mass given by $m_{f_i} = y_{f_i} v/\sqrt{2}$ ($i = 1, 2, 3$). Rotating to the fermion mass-eigenstate basis has two major consequences: 1) it simultaneously diagonalizes the fermion mass matrices and their couplings to the Higgs boson therefore forbidding Higgs-mediated flavor changing neutral currents, and 2) since the rotations of the up-type (U_L^u) and down-type (U_L^d) left-handed quarks are independent ($U_L^u \neq U_L^d$) rotating to the mass eigenstates gives rise to the Cabibbo-Kobayashi-Maskawa (CKM) mixing matrix in the charged gauge currents, where $V_{\mathrm{CKM}} = (U_L^u)^\dagger U_L^d$, and can therefore be considered as the origin of flavor dynamics and CP-violation in the EW sector of the SM. The Yukawa Lagrangian therefore connects some of the aspects of the SM that are most likely to offer a natural portal to new physics.

11.2.3 *The Standard Model custodial symmetry*

The SM Higgs and Yukawa Lagrangians, $\mathcal{L}_{\mathrm{Higgs}} + \mathcal{L}_{\mathrm{Yukawa}}$ of Eq. (11.1) and Eq. (11.9), are, by construction, $\mathrm{SU}(2)_L \times \mathrm{U}(1)_Y$ gauge invariant, but they also have an approximate global symmetry. In the limit $g' \to 0$ and $y_f \to 0$, a global $\mathrm{SU}(2)_R$ symmetry

Int. J. Mod. Phys. A 2026.41. Downloaded from www.worldscientific.com
by UNIVERSITY OF CALIFORNIA @ BERKELEY on 09/16/26. Re-use and distribution is strictly not permitted, except for Open Access articles.

emerges. This symmetry is preserved for non-vanishing Yukawa couplings provided $\hat{Y}_u = \hat{Y}_d$. Once the Higgs field acquires a VEV, both the $\mathrm{SU}(2)_L$ and $\mathrm{SU}(2)_R$ symmetry groups are broken but the diagonal subgroup $\mathrm{SU}(2)_{L+R}$ remains unbroken and it is this subgroup that defines the so-called custodial symmetry of the SM [42].

In the limit $g' \to 0$, the $W^\pm$ and Z gauge bosons have equal mass and form a triplet of the $\mathrm{SU}(2)_{L+R}$ unbroken global symmetry. Using the expressions for the W and Z gauge boson masses in term of the gauge couplings, one obtains at tree level

$$\frac{m_W^2}{m_Z^2} = \frac{g^2}{g'^2 + g^2} \equiv \cos^2\theta_W \quad \text{i.e.} \quad \rho \equiv \frac{m_W^2}{m_Z^2 \cos^2\theta_W} = 1. \tag{11.10}$$

The custodial symmetry protects the above relation from large radiative corrections. All corrections to the ρ parameter are therefore proportional to terms that break the custodial symmetry. For instance, radiative corrections involving the Higgs boson are proportional to $\sin^2\theta_W$, $\delta\rho = -11 G_F m_Z^2 \sin^2\theta_W \log(m_H^2/m_Z^2)/(24\sqrt{2}\pi^2)$, and vanish in the limit $g' \to 0$. Since $m_t \neq m_b$, there are also relevant radiative corrections generated by massive fermions. They are proportional to $m_t^2 + m_b^2 - 2(m_t^2 m_b^2)\log(m_t^2/m_b^2)/(m_t^2 - m_b^2)$ and would indeed vanish for $m_t = m_b$ [43]. Precision measurements of electroweak observables are powerful in constraining such large radiative corrections.

Given the extreme precision with which the ρ parameter has been measured experimentally, the custodial isospin symmetry is a very powerful probe of physics beyond the SM since it imposes the same strong constraints on any large radiative corrections coming from new-physics degrees of freedom.

11.2.4 *Stability of the scalar potential of the Standard Model*

Quantum effects determine the evolution of the parameters of the SM and can therefore affect the shape of the scalar potential and the stability of the SM vacuum (for a recent review on the topic see [44]). Proving absolute stability versus metastability depends in a very sensitive way on the values of the Higgs-boson mass, the top-quark mass, and the strong coupling constant, their uncertainties, and correlations [45]. In this respect, the discovery of the Higgs boson with $m_H \approx 125$ GeV has far reaching consequences within the SM framework.

For the value of Higgs-boson mass experimentally measured, the EW vacuum of the Higgs potential is most likely metastable [45], although this is influenced by new physics that may exists below the Planck scale. The high-energy evolution of λ shows that it becomes negative at energies $\Lambda = \mathcal{O}(10^{11})$ GeV (even though λ could remain positive till higher energy, maybe all the way to the Planck scale, if the top quark mass exceeds its current measured value by 3σ). When this occurs, the SM Higgs potential develops an instability and the long term existence of the EW vacuum is challenged. This behavior may call for new physics at an intermediate scale before the instability develops, i.e., below M_{Planck}, even though new physics at M_{Planck} could influence the stability of the EW vacuum and possibly modify this conclusion [46]. The consequences of the instability of the EW vacuum on high-scale inflation have been discussed in Ref. [47]. It was also noticed that Higgs field fluctuations during inflation could seed the formation of primordial black holes, possibly making up the Dark Matter relic abundance [48] or they could produce a stochastic background of gravitational waves with characteristic structures [49], offering a probe of the EW vacuum near criticality.

The lifetime of the EW metastable vacuum is determined by the rate of quantum tunneling from this vacuum into the true vacuum of the theory (for the most recent computation of the EW vacuum lifetime within the SM, see Ref. [44, 50, 51]).

Within the SM, the running of the Higgs self coupling slows down at high energies with a cancellation of its β-function at energies just one to two orders of magnitude below the Planck scale [52]. This slow evolution of the quartic coupling is responsible for saving the EW vacuum from premature collapse. It might also help the Higgs boson to play the role of an inflaton [53] (see, however, Ref. [54] for potential issues with this Higgs-boson-as-an-inflaton idea).

11.2.5 *Production and decay modes of the Standard-Model Higgs boson*

Production and decay modes of the SM Higgs boson (H) can be calculated within the Standard Model including quantum corrections. This section briefly reviews the state-of-the-art of SM predictions for Higgs-boson production cross sections at hadron colliders and discusses the main characteristics of Higgs-boson production at lepton colliders. The most updated predictions for the SM Higgs-boson decay branching ratios and total decay width are also presented. In-depth studies of the corresponding theoretical uncertainties are available in the literature and will be referred to in the following as needed. A summary of all most recent measurements of SM Higgs-boson production and decay rates by the LHC experiments is the subject of Sec. 11.3.

11.2.5.1 *Standard-Model Higgs-boson production at hadron colliders*

The main production mechanisms of the SM Higgs boson at the Tevatron collider and the LHC are gluon fusion ($gg \to H$), vector-boson fusion ($qq \to qqH$, for both quarks and antiquarks), associated production with a gauge boson ($q\bar{q}^{(\prime)} \to ZH/WH$ and $gg \to ZH$), associated production with a $t\bar{t}$ pair ($q\bar{q}, gg \to t\bar{t}H$) or $b\bar{b}$ pair ($q\bar{q}, gg \to b\bar{b}H$), and associated production with a single top quark ($bq \to tH + q'$). [2] Examples of Feynman diagrams for each production mode are illustrated in Figures 11.2(a)–(f).

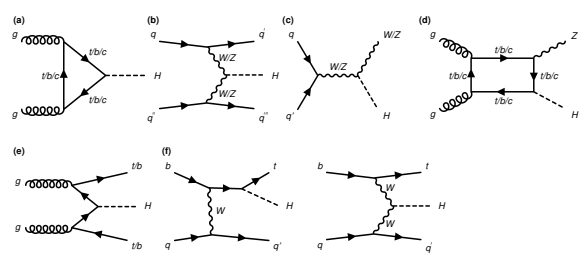

Figure 11.2: Examples of Feynman diagrams for Higgs-boson production via (a) gluon fusion, (b) vector-boson fusion, and associated production with (c)-(d) vector bosons, (e) top- or bottom-quark pairs, or (f) a single top quark.

The total cross sections for the main production processes of a SM Higgs boson with $m_H = 125$ GeV in pp collisions (LHC) as a function of $\sqrt{s}$, the center-of-mass energy, are summarized in Fig. 11.3 (left) [55].

The bands indicate the residual theoretical uncertainties based on the studies presented in Refs. [56–60] and correspond to the perturbative order of QCD and EW corrections indicated on each band. The corresponding results for $\sqrt{s} = 7$, 8, 13, 13.6, and 14 TeV are summarized in Table 11.1 which has been updated with results that will be published in Report 5 of the LHC Higgs Working Group. A detailed discussion, including uncertainties in the theoretical calculations due to missing higher-order effects and experimental uncertainties on the determination of SM parameters involved in the calculations, can be found in Refs. [56–60]. These references also contain state-of-the-art discussions on the impact of PDF uncertainties, QCD scale uncertainties, and uncertainties due to different procedures for including higher-order corrections matched to parton shower simulations, as well as uncertainties due to hadronization and parton-shower effects.

More recent improved calculations and the corresponding accuracy will be highlighted in the following discussion of individual production modes, where the status of the corresponding differential distributions is also illustrated.

[2] The order in which the SM Higgs-boson production modes have been listed here reflects their cross-section hierarchy at the LHC for $\sqrt{s} = 13$ TeV. The relative importance of various production modes is different between pp and $p\bar{p}$ colliders and depends on the center-of-mass energy.

Int. J. Mod. Phys. A 2026.41. Downloaded from www.wo
by UNIVERSITY OF CALIFORNIA @ BERKELEY on 09/16/26. Re-use and distribution is
except for Open Access articles.

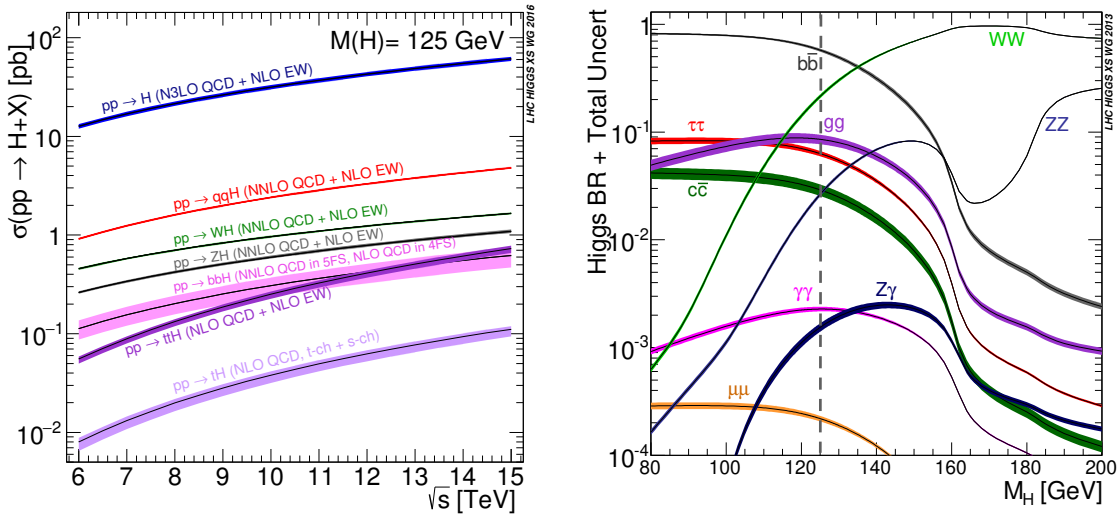

Figure 11.3: (Left) The SM Higgs boson production cross sections as a function of the center-of-mass energy, $\sqrt{s}$, for pp collisions [55]. The VBF process is indicated here as qqH. (Right) Branching ratios for the main decays of a SM-like Higgs boson in the low mass region, including near $m_H = 125\,\text{GeV}$ [56, 57]. The theoretical uncertainties are indicated as bands.

i. *Gluon fusion production mechanism*

At high-energy hadron colliders, the Higgs boson production mechanism with the largest cross section is the gluon-fusion process (ggF), $gg \to H + X$, mediated by the exchange of a virtual heavy quark (see Fig. 11.2-a), where the top quark is dominant due to its large Yukawa coupling [61]. Perturbative corrections to the gluon-fusion process are extremely important and have been studied in detail with the goal of reducing the theoretical uncertainty to a few percent, as needed to realize the HL-LHC Higgs-physics program. Including the full dependence on the quark and Higgs boson masses, the cross section has been calculated at the next-to-leading order (NLO) α_s in Refs. [62, 63]. To a very good approximation, the leading top-quark contribution can be evaluated in the limit $m_t \to \infty$ by matching the SM to an effective theory [64]. The gluon-fusion amplitude is then evaluated from an effective Lagrangian containing a local $HG^a_{\mu\nu}G^{a\,\mu\nu}$ operator [37, 38]. In this approximation, the cross section has been first calculated at next-to-next-to-leading order (NNLO) [65] and is now known at next-to-next-to-next-to-leading order in the α_s expansion (N3LO QCD) [66,67]. Recently, first building blocks towards the next-to-N3LO calculation (N4LO) have appeared in the literature [68–71]. Public tools such as `iHixs` [72] and `SusHi` [73] allow to derive state-of-the-art predictions for ggF inclusive production in the $m_t \to \infty$ approximation[3].

The validity of the effective theory with infinite m_t is greatly enhanced by rescaling the result by the exact LO result: $\sigma = (\sigma^{\text{LO}}_{m_t}/\sigma^{\text{LO}}_{m_t=\infty}) \times \sigma_{m_t=\infty}$ [57]. The large top-quark mass approximation, after this rescaling of the cross section, yields a NNLO QCD result that has been found to approximate the full NNLO total cross section to percent level accuracy [65], as confirmed by the the exact NNLO QCD calculation including full top-quark mass dependence [75]. Contributions from lighter quarks propagating in the loop are suppressed proportionally to m_q^2/m_H^2. Their leading contribution arise from the interference with top-quark induced gluon fusion, and can be enhanced by logarithms of m_q^2/m_H^2 [76–78]. Finite-mass effects from bottom-top quark interference at NNLO in QCD have been recently calculated [79] including their dependence on the light-quark renormalization and flavor scheme [80]. These studies have reduced the residual 6% theoretical uncertainty of the N3LO results by more than a third.

The LO contribution and NLO QCD corrections [64] amount to about 80% of the total N3LO QCD cross section. The NNLO QCD corrections [81] further enhance the cross section by approximately 30% of the LO plus NLO result (at $\mu_f = \mu_r = m_H/2$). At N3LO QCD, the perturbation series is rather stable with a mere enhancement of 3% with respect to the NNLO QCD total cross section, and a central value quite insensitive to threshold resummation effects with the scale choice $\mu_f = \mu_r = m_H/2$ [57,66,67,82,83]. EW radiative corrections have been computed at NLO and increase the LO cross section by about 5% for $m_H \simeq 125\,\text{GeV}$ [84]. Mixed QCD-EW corrections have been intensively investigated beyond initial studies obtained in either limit of heavy [85] or massless [86] gauge bosons, and first estimates including most relevant building blocks have been calculated, reducing the residual uncertainties from mixed QCD-EW corrections to less than 1% [87]. The residual PDF uncertainty, estimated to contribute 1-2% to the total theoretical uncertainty, relies on NNLO or approximate N3LO (aN3LO) PDF sets [88–90], and, given the shift observed when using aN3LO versus NNLO PDF, may have been underestimated. Up-to-date values of the N3LO QCD+NLO EW predictions for ggF production of a SM Higgs boson with $m_H = 125$ GeV for different LHC center-of-mass energies are collected in Table 11.1, from an update of the results reported in Ref. [57] to which we refer for a comprehensive discussion of input parameters and residual uncertainties.

Besides considering the inclusive Higgs boson production cross section at the LHC, it is crucial to study differential distributions in order to probe the properties of the Higgs boson in regions that could be particularly sensitive to new physics effects. The Higgs boson rapidity distribution has been computed in the $m_t \to \infty$ limit at the N3LO QCD order in Ref. [91] and fully differential N3LO QCD predictions for Higgs production in gluon fusion have been obtained by combining N3LO QCD predictions for the Higgs rapidity distribution with NNLO QCD predictions for H+jet [92, 93]. First results for the prediction of H+jet at N3LO have been presented in Ref. [94]. Finite quark-mass effects in the Higgs-boson p_T distribution significantly alter its shape. At NLO QCD both top-quark mass effects [95–97] and bottom-quark mass [76, 77, 98] as well as top-bottom interference effects [99] are known in an approximation based on expansions in the quark mass. Beyond NLO, the first differential calculation of NNLO QCD corrections with full top-quark mass dependence, consistently matched to parton shower has been presented in Ref. [100]. Experimental analyses often impose cuts on the kinematics of final-state products in order to improve the signal-to-background ratio. To provide a more exclusive account of Higgs-boson production, NNLO fully differential calculations have been interfaced with parton-shower event generators in various frameworks [101–103]. Using soft-collinear effective theory, large

[3] In `iHixs`, the top-quark mass dependence is exact at NLO, and only the NNLO is calculated in the $m_t \to \infty$ approximation

Int. J. Mod. Phys. A 2026.41. Downloaded from www.worldscientific.com
by UNIVERSITY OF CALIFORNIA @ BERKELEY on 09/16/26. Re-use and distribution is strictly not permitted, except for Open Access articles.

Table 11.1: The SM Higgs boson production cross sections for $m_H = 125\,\text{GeV}$: 1) at the Tevatron ($*$), corresponding to $p\bar{p}$ collisions at center-of-mass energy $\sqrt{s} = 1.96$ TeV, and 2) at the LHC, corresponding to pp collisions at center-of-mass energies $\sqrt{s} = 7, 8$ TeV (Run 1), 13 TeV (Run 2), 13.6 TeV (Run 3), and 14 TeV (Run 4). The predictions for the Tevatron energy are the ones used in Ref. [74], while the ones for the LHC energies are taken from Refs. [55–60] with updates that will be published in the Report 5 of the LHC Higgs Working Group. The uncertainties are estimated assuming no correlation between α_S and PDF uncertainties. Parametric uncertainties are combined linearly with the rest of theoretical uncertainties. A detailed discussion of the estimated uncertainties is given for each case in the references above.

$\sqrt{s}$ (TeV)	Production cross section (in pb) for $m_H = 125\,\text{GeV}$							
	ggF	VBF	WH	ZH	$t\bar{t}H$	tH	$b\bar{b}H$	total
1.96*	$0.95^{+17\%}_{-17\%}$	$0.065^{+8\%}_{-7\%}$	$0.13^{+8\%}_{-8\%}$	$0.079^{+8\%}_{-8\%}$	$0.004^{+10\%}_{-10\%}$	–	–	$1.23^{+13\%}_{-13\%}$
7	$16.7^{+6.3\%}_{-9.4\%}$	$1.25^{+3.4\%}_{-3.4\%}$	$0.582^{+3.1\%}_{-3.3\%}$	$0.342^{+4.8\%}_{-4.5\%}$	$0.09^{+5.6\%}_{-10.2\%}$	$0.013^{+8.2\%}_{-16.6\%}$	$0.171^{+17\%}_{-17\%}$	$19.2^{+5.5\%}_{-8.2\%}$
8	$21.3^{+6.4\%}_{-9.4\%}$	$1.61^{+3.3\%}_{-3.3\%}$	$0.708^{+2.9\%}_{-3.2\%}$	$0.424^{+4.8\%}_{-4.3\%}$	$0.13^{+5.9\%}_{-10.1\%}$	$0.020^{+8.1\%}_{-16.1\%}$	$0.221^{+16\%}_{-16\%}$	$24.4^{+5.6\%}_{-8.2\%}$
13	$48.4^{+6.9\%}_{-9.5\%}$	$3.81^{+3.4\%}_{-3.4\%}$	$1.38^{+2.4\%}_{-2.6\%}$	$0.893^{+5.4\%}_{-4.8\%}$	$0.531^{+5.5\%}_{-6.3\%}$	$0.076^{+8.5\%}_{-18\%}$	$0.528^{+15\%}_{-16\%}$	$55.6^{+6.0\%}_{-8.3\%}$
13.6	$52.1^{+6.9\%}_{-9.5\%}$	$4.11^{+3.3\%}_{-3.3\%}$	$1.47^{+2.4\%}_{-2.6\%}$	$0.954^{+5.6\%}_{-5.0\%}$	$0.592^{+4.3\%}_{-5.0\%}$	$0.085^{+8.5\%}_{-18\%}$	$0.569^{+12\%}_{-12\%}$	$59.9^{+6.0\%}_{-8.3\%}$
14	$54.5^{+7.0\%}_{-9.5\%}$	$4.32^{+3.3\%}_{-3.3\%}$	$1.52^{+2.3\%}_{-2.5\%}$	$0.995^{+5.6\%}_{-4.9\%}$	$0.639^{+4.3\%}_{-5.0\%}$	$0.092^{+8.0}_{-17\%}$	$0.597^{+14\%}_{-15\%}$	$62.7^{+6.1\%}_{-8.3\%}$

fiducial power corrections induced by fiducial cuts have been resummed at N3LO+N3LL′ QCD accuracy, i.e. at next-to-next-to-next-leading-log (N3LL), incorporating the complete $\mathcal{O}(\alpha_s^3)$ singular structure for $q_T \to 0$ allowing one to consistently match to N3LO QCD [83]. This allows for the direct comparison with fiducial measurements and explore different fiducial cuts to suppress fiducial effects. At the same time, resummed calculation are often less flexible and less transparent than fixed-order ones. Given the level of precision currently reached in fixed-order calculations, recent studies for $H \to \gamma\gamma$ in gluon fusion [104] motivate revisiting the choice of standard fiducial cuts and design new ones that could at the same time maximize signal significances and minimize experimental and perturbative systematics, to fully retain the power and conceptual simplicity of fixed-order calculations.

In addition progress has been made to improve the calculation of the Higgs-boson production cross section with a jet veto (the "0-jet bin" or in the presence of a veto bounding the transverse momentum of the hardest accompanying jet) [105], reaching NNLL accuracy matched to N3LO QCD. These accurate predictions for the jet-veto cross section are required, e.g., to suppress the $t\bar{t}$ background in the $H \to WW$ channel [106, 107], and to accurately quantify Higgs-boson production in specific regions of phase space.

ii. *Vector-boson fusion production mechanism*

The SM Higgs boson production mode with the second-largest cross section at the LHC is vector-boson fusion (VBF). At the Tevatron collider, VBF also occurred, but for $m_H = 125\,\text{GeV}$ had a smaller cross section than Higgs boson production in association with a W or Z boson. Higgs boson production via VBF, $qq \to qqH$, proceeds by the scattering of two (anti-)quarks, mediated by t- or u-channel exchange of a W or Z boson, with the Higgs boson radiated off the weak-boson propagator (see Fig. 11.2-b). The scattered quarks give rise to two hard jets in the forward and backward regions of the detector with a large rapidity gap [108]. Because of the color-singlet nature of the weak-gauge boson exchange, gluon radiation from the central-rapidity regions is strongly suppressed. These characteristic features of VBF processes can be exploited to distinguish them from overwhelming QCD backgrounds, including gluon-fusion induced Higgs boson + 2 jet production, and from s-channel WH or ZH production with a hadronically decaying weak gauge boson. After the application of specific selection cuts, the VBF channel provides a clean environment, not only for the Higgs boson searches originally performed, but also for the subsequent determination of Higgs boson couplings at the LHC.

The cross-section is known at N3LO QCD at the inclusive level [109] and at NNLO enforcing the VBF cuts [110–112]. Uncertainties have been estimated to be quite small (permille) at the inclusive level but can be larger (percent) at differential and fiducial level. However, this result is obtained in the DIS/factorized approximation [113] where the fusing gauge bosons are emitted from the two quark legs independently. The leading non-factorizable contributions with two forward jets have been estimated [114, 115] and the impact of non-factorizable effects have been studied in Ref. [116]. They give some corrections, also of the order of few permille, to inclusive quantities, but they are an order of magnitude larger for differential observables. Overall, the residual uncertainty is of the order of a few percent but is quite sensitive to the tagging jet cuts and jet radius modeling [117]. VBF production followed by $H \to b\bar{b}$ or $H \to W^+W^-$ with the W bosons decaying leptonically have been studied at NLO QCD in Ref. [118]. Extensive studies on VBF at fixed order and with parton shower matched computations can be found in Ref. [119], and more recently in Ref. [120]. In addition, EW corrections have been calculated and the VBF process is known at NLO QCD+EW order for some time [121, 122]. When EW corrections are considered, a separation of the $H + 2$ jets production process into VBF and HV ($V = W, Z$) contributions is no longer straightforward and recent studies [123] have implemented the NLO QCD+EW calculation of $H + 2$ jets with parton-shower including both VBF and HV topologies. A state-of-the-art review of VBF can be found in Ref. [124].

iii. *WH and ZH associated production mechanism*

The next most relevant Higgs boson production mechanisms are associated production with W and Z gauge bosons (see Fig. 11.2-c). The cross sections for the associated production processes, $pp \to VH + X$, with $V = W^\pm, Z$ receive contributions at NLO from NLO QCD corrections to the Drell–Yan cross section [125, 126] and from NLO EW corrections. The latter, unlike the QCD corrections, do not respect the factorization into Drell–

Int. J. Mod. Phys. A 2026.41. Downloaded from www.worldscientific.com by UNIVERSITY OF CALIFORNIA @ BERKELEY on 09/16/26. Re-use and distribution is [redacted] except for Open Access articles.

Yan production since there are irreducible box contributions already at one loop [121,127]. At NNLO QCD, while Drell–Yan-like contributions give the bulk of the corrections to WH production, corrections to ZH production consist of both Drell–Yan-like [128] and gluon-gluon induced contributions that do not involve a virtual Z gauge boson but are such that the Z gauge boson and H boson couple to gluons via top-quark loops (see Fig. 11.2-d) [129]. NLO QCD virtual corrections to the partonic cross section for $gg \to ZH$, in the high-energy and large top mass limits were calculated in Ref. [130], while NLO QCD corrections with full top-quark mass dependence have obtained in Ref. [131, 132], and an updated review can be found in Ref. [133]. In addition, WH and ZH production receive non Drell–Yan-like corrections in the $q\bar{q}'$ and $q\bar{q}$ initiated channels, respectively, at the NNLO level in QCD, where the Higgs boson is radiated off top-quark loops [134]. The full QCD corrections up to NNLO order, the NLO EW corrections and the NLO corrections to the gluon-gluon channel are available in `VH@NNLO` [135]. NNLO QCD corrections to $pp \to WH$+jet are important for signal modeling. NLO corrections to the cross section inclusive in the number of jets show excellent convergence while NNLO QCD corrections to exclusive single jet cross section are much more significant [136]. More recently, the inclusive cross section for associated Higgs boson production with a massive gauge boson has been determined up to N3LO QCD too [137].Recently, the inclusive cross section for associated Higgs-boson production with a massive gauge boson has been determined up to N3LO QCD [137].

As neither the Higgs boson nor the weak gauge bosons are stable particles, their decays also have to be taken into account. Providing full kinematical information for the decay products can furthermore help in the suppression of large QCD backgrounds. Differential distributions for the processes $pp \to WH \to \bar{\nu}_\ell \ell H$ and $pp \to ZH \to \ell^+\ell^- H/\nu_\ell\bar{\nu}_\ell H$, including NLO QCD and EW corrections, have been presented in Ref. [138]. The NNLO QCD corrections to differential observables for WH production at the LHC, including the leptonic decays of the W boson and the decay of the Higgs boson into a $b\bar{b}$ pair, are presented in Ref. [139]. Full NNLO QCD results for both the production and decay are available [140] and show a large impact of radiation from the final-state bottom quarks. Calculations at the same level, including also the ZH process have been performed [141]. The WH production mode has also been matched to a parton shower at NNLO QCD accuracy [142]. The WH and ZH production modes, especially in the boosted regime, provide a relatively clean environment for studying the decay of the Higgs boson into bottom quarks [143]. Bottom mass effects have been computed at NNLO [144, 145] and tend to increase the rates by 6-7%.

iv. *Higgs boson production in association with $t\bar{t}$*

Higgs boson radiation off top quarks, $pp \to t\bar{t}H$ (see Fig. 11.2-e), provides a direct probe of the top-Higgs Yukawa coupling. The LO cross section for this production process was computed in Ref. [146]. Later, the NLO QCD [147] and NLO EW corrections [148] were evaluated yielding a moderate increase in the total cross section of at most 20%, but significantly reducing the scale dependence of the inclusive cross section. The EW corrections can be enhanced by large electroweak Sudakov logarithms in particular in the boosted regime often used in the phenomenological analyses [149]. The resummation of soft and Coulomb gluon corrections is presented in Ref. [150] while the resummation of soft gluon contributions close to the partonic kinematical threshold are considered in Refs. [151] to reach a result at NLO+NNLL QCD order. Full off-shell calculations with decaying top quarks are computed at NLO QCD [152] and NLO QCD + EW [153] order, respectively. The fixed-order NLO QCD calculation has been interfaced with the standard parton shower Monte-Carlo generators in Refs. [154], allowing an accurate description of the $t\bar{t}H$ signal, from the energy scale of the hard scattering to the hadronization energy scale. These programs provide the most flexible tools to date for the computation of differential distributions, including experimental selection cuts and vetoes on the final-state particles and their decay products.

The total theoretical uncertainty has been further reduced from 10-15% to about 4% at 13 TeV center-of-mass energy by the first approximate NNLO QCD calculation [155, 156] combined with NLO EW corrections in a fully differential comprehensive study of this production mode [157]. These results do not yet include the two-loop virtual corrections, but they evaluate them using two different methods that yield consistent results within their respective uncertainties. The first method relies on a soft Higgs-boson factorization formula, while the second is based on a high-energy expansion in the small top-quark mass limit. The missing two-loop virtual contributions, which are essential to have a consistent NNLO calculation of $pp \to t\bar{t}H$, are quite challenging and at the cutting edge of current technologies due to the presence of several mass scales (m_H, m_t, plus five kinematic invariants of the $2 \to 3$ process). Partial results for well-defined gauge-invariant classes of leading-color two-loop QCD virtual amplitudes have been calculated [158–160] and progress is ongoing to complete the remaining building blocks. For a recent review of the state-of-the-art of theoretical predictions for $pp \to t\bar{t}H$ production see Ref. [161].

Also recently, the fragmentation and splitting functions for the production of a Higgs boson have been computed at order $y_t^2\alpha_s$ and they can be used in the fragmentation region to compute differential cross sections with arbitrary top-quark and Higgs-boson masses directly from the results in the massless limit [162].

Apart from the case in which $H \to \gamma\gamma$, the exploitation of the $t\bar{t}H$ channel requires a proper description of the background, in particular $t\bar{t}b\bar{b}$, which exhibits an enhancement from shower effects, see Ref. [57] for a detailed discussion. Off-shell effects in $t\bar{t}b\bar{b}$ have been studied in Ref. [163]. Besides the $H \to b\bar{b}$ decay mode, the focus has been broadened and other modes have been studied, in particular the multilepton channel (which combines $H \to \tau^+\tau^-$, $H \to WW^*$, and $H \to ZZ^*$ with subsequent decay to leptons). Other backgrounds such as $t\bar{t}W$ and $t\bar{t}Z$ have also become relevant and intensively analyzed.

v. *Other single Higgs-boson production mechanisms at the LHC*

The Higgs boson production in association with a single top quark, though subdominant, can bring valuable information on the sign of the top Yukawa coupling. This is due to an almost totally destructive interference between two large contributions, one where the Higgs boson couples to a space-like W boson and the other where it couples to the top quark (see Fig, 11.2-f). This process has been computed at NLO QCD in a five-flavor scheme [164] and amounts to about 90 fb at $\sqrt{s} = 14$ TeV (with the opposite sign of the top Yukawa coupling, the cross section increases by one order of magnitude while the cross section for associated production with a pair of top quarks is unaffected). Recently, the tHj (and tZj) process has been computed at NLO QCD+EW accuracy [165]. The NLO EW correction is found to be within the NLO QCD theory uncertainties if the 4 vs 5 flavor scheme uncertainty is taken into account. The EW corrections reduce the total cross section by 3-4%.

The inclusive Higgs boson production in association with a pair of bottom quarks ($b\bar{b}H$) has been computed at the N3LO QCD order in the 5-flavor scheme [166][4], while the production with one/two b-jets, defined by specific kinematic cuts, is known respectively at NLO QCD in the 4-flavor scheme and at NNLO QCD in the 5-flavor scheme [167, 168]. Recently, full-color two-loop amplitudes for the $pp \to b\bar{b}H$ have been computed [169], extending previous leading-color results [170]. They contribute at NNLO QCD to the production of a Higgs boson with 2 tagged b jets, and at N3LO QCD to the production with 1 tagged b jet. The first NNLO calculation of $b\bar{b}H$ production in the 4FS interfaced with parton-shower has been recently presented in Ref. [171].

The coupling of the Higgs boson to a bottom quark is suppressed in the SM by the bottom-quark mass over the Higgs VEV, m_b/v, implying that associated production of a SM Higgs boson with bottom quarks is small at the LHC. Yet, at high energy, large logarithms are present and need to be resummed, leading to

[4] The Higgs boson production in association with charm quarks at N3LO QCD can also be obtained from the same calculation modulus a change of parton densities. NNLO QCD results for the cross section as a function of m_H can be found in [57].

Int. J. Mod. Phys. A 2026.41. Downloaded from www.worldscientific.com
by UNIVERSITY OF CALIFORNIA @ BERKELEY on 09/16/26. Re-use and distribution is strictly not permitted, except for Open Access articles.

an enhancement of the inclusive cross section. At $\sqrt{s} = 14\,\text{TeV}$, the $b\bar{b}H$ cross section can be as large as 550 fb, still two orders of magnitude below the ggF production cross section. Furthermore, the overwhelming ZH and VBF backgrounds (at the inclusive but also differential levels) make it challenging to extract a genuine bottom-quark Yukawa signal in a traditional cut-based analysis [172]. Innovative machine-learning techniques are a promising avenue to obtain information complementary to the ones extracted from $gg \to h \to b\bar{b}$, in particular for what concerns the phase of the bottom-quark Yukawa coupling [173]. In a two Higgs doublet model or a SUSY model, which will be discussed in Section 11.4, this coupling is proportional to the ratio of neutral Higgs boson vacuum expectation values, $\tan\beta$, and can be significantly enhanced for large values of this ratio. Consequently, the $b\bar{b}H$ mode can even become the dominant production process for the Higgs boson, unlike in the SM.

The Higgs boson production in association with charm quarks is also known at NNLO QCD and its cross section is approximately 85 fb at $\sqrt{s} = 13\,\text{TeV}$ [57].

vi. *Double Higgs boson production at the LHC*

The main interest in the double Higgs-boson production is that it can provide invaluable information on the Higgs potential. In particular, it gives access to the Higgs-boson trilinear self coupling. The dominant production is via ggF $gg \to HH$ (slightly more than 33 fb at 13 TeV) which accounts for more than 90% of the total inclusive cross-section. The sub-leading production mechanisms are VBF $HHjj$ (around 1.7 fb at 13 TeV), HHW^+ (0.33 fb), HHW^- (0.17 fb), HHZ (0.36 fb), and $t\bar{t}HH$ (0.8 fb).[5] Examples of ggF and VBF double-Higgs production are illustrated in Fig. 11.4, where the possibility of anomalous couplings parametrized by κ_X rescaling factors have also been indicated for future reference (see Sec. 11.3.5.1).

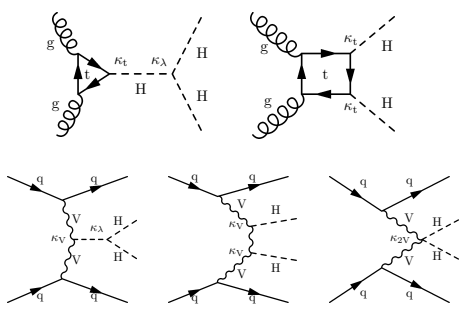

Figure 11.4: Feynman Diagrams for double-Higgs production in proton-proton collisions for ggF (top) and VBF (bottom) production. κ_X factors denote ratios of measured to SM couplings that will be introduced in the discussion of Higgs-boson couplings in Sec. 11.3.5.1.

The fixed order QCD corrections to ggF double-Higgs production, computed in the infinite top mass limit, are large, typically doubling the cross section from LO to NLO QCD [174], further enhancing it by 20% and reducing the scale uncertainty by a factor 2-3 from NLO to NNLO QCD [175], with a milder increase of order 3% at N3LO [176]. The complete NLO corrections with all top-quark mass effects has also become available numerically [177], revealing a differential K-factor much less flat than predicted in the large top-quark mass approximation. The non-trivial dependence of the results on the renormalization scheme and scale for the top-quark mass has been recognized as one of the main sources of uncertainty and progress has been made in identifying the logarithmic terms responsible for such dependence [178]. In terms of accounting for the top-quark mass dependence, the most complete results so far have been obtained in Ref. [179]. These results include the full top-quark mass dependence at NLO and in the NNLO QCD real radiation matrix elements, and and form the basis of the current recommendation of the LHC Higgs Working Group. A definite assessment of the scale uncertainty would warrant a proper NNLO computation that remains out of reach for the moment, although considerable progress towards it has been recently made [180–182]. The current state-of-the-art for Higgs-pair production via ggF is N3LO+N3LL QCD including full top-quark mass dependence at NLO QCD, with a predicted cross section at 13 TeV of

$$\sigma(gg \to HH)^{\text{N3LO}+N3LL}_{\text{ggF}} = 33.47\,^{+0.88\%}_{-0.85\%}\,\text{fb}. \tag{11.11}$$

Among the subleading production modes, double-Higgs production in VBF can be used to derive bounds on both the triple Higgs-boson coupling and the quartic HHVV coupling. Although the rate is quite small, the experiments have been performing searches including the VBF channel [183, 184]. The process is known at N3LO QCD [185] and NLO EW [186]. While the NNLO QCD [111, 187, 188] and NLO-EW corrections are quite sizable in some kinematic regions, the N3LO QCD are small. NNLO-QCD non-factorizable corrections have been calculated and shown to be small [116]. VBF di-Higgs production has also been interfaced with parton-shower at NLO QCD in multiple frameworks [189, 190].

With a small inclusive cross section and a difficult signal vs background discrimination, the double-Higgs boson production remains a challenging channel to probe and will greatly benefit from the high-luminosity run of the LHC. Nevertheless, as discussed in Section 11.3.6, by combining various decay modes, and using full Run 2 and partial Run 3 data, both ATLAS and CMS have already been able to constrain the trilinear Higgs-boson coupling via double-Higgs production beyond expectations. Continuous theoretical progress will therefore be necessary and timely.

11.2.5.2 *Standard-Model Higgs-boson production at lepton colliders*

Recently Higgs-boson production at lepton colliders has been a major component of the discussion for future colliders [191, 192]. For a more detailed discussion of Higgs boson production properties at lepton colliders see for example Refs. [193–198].

Lepton colliders, both e^+e^- and $\mu^+\mu^-$, provide alternative mechanisms of Higgs-boson production compared to hadron colliders. The leading production modes depend on the center-of-mass energy and the type of collider.

The dominant Higgs-boson production cross sections at an e^+e^- collider are from the Higgs-strahlung process [37, 199], $e^+e^- \to ZH$, and the WWfusion process [200], $e^+e^- \to \bar{\nu}_e\nu_e W^*W^* \to \bar{\nu}_e\nu_e H$. The cross-section for the Higgs-strahlung process scales as the inverse of the collision center-of-mass squared energy, s, and is predominant at lower energies, while the cross-section for the WW-fusion process scales as $\ln(s/m_H^2)$ and dominates at higher energies [201]. The ZZ-fusion mechanism, $e^+e^- \to e^+e^-Z^*Z^* \to e^+e^-H$, also contributes to the Higgs boson production, with a cross-section suppressed by an order of magnitude with respect to that of WW-fusion. The process $e^+e^- \to t\bar{t}H$ [202] becomes important for $\sqrt{s} \geq 500\,\text{GeV}$. e^+e^- lepton colliders with energies between 350 and 500 GeV can provide an absolute measurement of the $e^+e^- \to ZH$ cross section independent of the Higgs-boson detailed properties by counting events with an identified Z boson and a recoiling mass against the Z that clusters around the Higgs-boson mass. This allows for a model-independent measurement of the HZZ coupling. Combined with the measurement of the $H \to ZZ$ branching ratio, this allows for an indirect measurement of the Higgs-boson width.

All e^+e^- Higgs-production modes are known at NLO of SM interactions (QCD+EW). First results for two-loop EW corrections to $e^+e^- \to ZH$ have been calculated in Refs. [203, 204]. In order to match the experimental precision expected at potential future e^+e^- colliders all processes will have to be known at NNLO, SM input parameters will have to be known with higher precision, and matching schemes between EW corrections and QED parton shower event generators will have to be fully developed [205, 206]. In this respect, interesting progress has been made recently [207]

[5] Results for the subleading modes are from the wiki-page of WG4 of the LHC Higgs Working Group (`https://twiki.cern.ch/twiki/bin/view/LHCPhysics/LHCHWGHH`.

Int. J. Mod. Phys. A 2026.41. Downloaded from www.worldscientific.com by UNIVERSITY OF CALIFORNIA @ BERKELEY on 09/16/26. Re-use and distribution is exclusive for Open Access articles.

to accurately account for beamstrahlung and initial state radiation using the factorization approach primarily developed for hadron colliders and this method is being implemented in Monte Carlo event generators.

Muon colliders running at low-energy can scan the Higgs-boson threshold around $m_H = 125$ GeV and measure the Higgs-boson line shape through $\mu^+\mu^- \to H$ s-channel Higgs-boson production. This could give direct access to a precision absolute measurement of the Higgs-boson width and of the muon Yukawa coupling, as well as other couplings entering in the decay of the resonant Higgs boson. Most recently, the focus has shifted to multi-TeV muon collider scenarios with center-of-mass energies between 3 and 10 TeV. In this regime, the virtual electroweak gauge boson content of the muon beam becomes relevant and vector-boson, as W-boson fusion $\mu^+\mu^- \to H\nu_\mu\bar{\nu}_\mu$ and Z-boson fusion $\mu^+\mu^- \to H\mu^+\mu^-$, dominates by several orders of magnitude over off-shell production and associated production ($\mu^+\mu^- \to ZH$ or $\mu^+\mu^- \to t\bar{t}H$).

11.2.5.3 *Standard-Model Higgs-boson decays: branching ratios and total width*

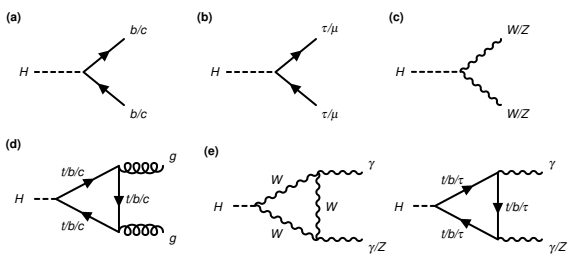

Figure 11.5: Feynman diagrams for the Higgs-boson decays into (a) a pair of quarks, (b) a pair of charged leptons, (c) a pair of vector bosons, (d) a pair of gluons, (e) a pair of photons or a Z boson and a photon.

For the understanding and interpretation of the experimental results, the computation of all relevant Higgs boson decay widths is essential, including an estimate of their uncertainties and, when appropriate, the effects of Higgs boson decays into off-shell particles with successive decays into lighter SM ones.

The most relevant decay modes of a SM Higgs boson are illustrated in Fig. 11.5(a)-(e) and the corresponding branching ratios as a function of m_H, for m_H up to 200 GeV, are shown in Fig. 11.3 (right), including the most recent theoretical uncertainties. It is interesting to notice how a Higgs boson in the low-mass region allows for the exploration of its couplings to many SM particles through a variety of available decay channels. For the SM Higgs boson with a mass of about 125 GeV the dominant decay modes are $H \to b\bar{b}$ and $H \to WW^*$, followed by $H \to gg$, $H \to \tau^+\tau^-$, $H \to c\bar{c}$ and $H \to ZZ^*$. With much smaller rates follow the Higgs boson decays into $H \to \gamma\gamma$, $H \to Z\gamma$ and $H \to \mu^+\mu^-$. Since the decays into pairs of gluons or photons, and $Z\gamma$ are loop induced, they provide indirect information on the Higgs-boson couplings to WW, ZZ and $t\bar{t}$ in different combinations. They are also sensitive to possible NP contributions running in the loop.

Theoretical results for the branching ratios of the most relevant decay modes of the SM Higgs boson with $m_H = 125$ GeV are listed in Table 11.2. The uncertainties in the branching ratios include the missing higher-order corrections in the theoretical calculations as well as the errors in the SM input parameters, in particular fermion masses and the QCD gauge coupling, involved in the decay. In the following the state-of-the-art of the theoretical calculations compiled by the LHC Higgs Working Group [55] will be discussed and the reader is referred to Refs. [56–59, 208] for more details.

The evaluation of the radiative corrections to the fermionic decays of the SM Higgs boson are implemented in HDECAY [209] at different levels of accuracy. The computations of the $H \to b\bar{b}$ and $H \to c\bar{c}$ decays include the NLO QCD corrections with full mass effects and up to N4LO QCD corrections with leading mass corrections, resulting in a corresponding scale dependence of about 0.1% [210, 211]. The top-induced QCD corrections, which are related to interference effects between $H \to gg$ and $H \to q\bar{q}$, are known at NNLO in the limit of heavy top quarks and light bottom quarks [211–213] and more recently including the full mass dependence [214–217] with first results at N3LO [218]. Both the electroweak corrections to $H \to b\bar{b}$, $c\bar{c}$ as well as $H \to \tau^+\tau^-$ are known at NLO [219] providing predictions with an overall accuracy of about 1–2% for $m_H \simeq 125$ GeV.

The loop induced decays of the SM Higgs boson are known fully at NLO and partially beyond that approximation. For $H \to gg$, the N4LO QCD corrections calculated in the limit of heavy top quarks [220] have reduced the uncertainty from scale dependence to about 0.6% from the 3% uncertainty of the N3LO prediction [63, 221]. For $H \to \gamma\gamma$, the full NLO QCD corrections are available [63, 222] and the three-loop QCD corrections have also been evaluated [223]. The NLO electroweak corrections to $H \to gg$ and $H \to \gamma\gamma$ have been computed in Ref. [224]. All these corrections are implemented in `HDECAY` [209]. For $m_H \simeq 125$ GeV, the overall impact of known QCD and EW radiative effects turns out to be well below 1%. In addition, the contribution of the $H \to \gamma e^+e^-$ decay via virtual photon conversion has been computed in Ref. [225]. The partial decay width $H \to Z\gamma$ is only implemented at LO in `HDECAY`, including the virtual W, top-, bottom-, and τ-loop contributions. The NLO QCD corrections have been calculated in Refs. [226–228] leaving a residual estimated uncertainty of about 1.7%. The theoretical uncertainty due to unknown electroweak corrections is estimated to be less than 5%, an accuracy that will be hard to achieve in the measurement of this process at the LHC.

Table 11.2: The branching ratios and the relative uncertainty for a SM Higgs boson with $m_H = 125$ GeV. The uncertainties in the branching ratios include the missing higher-order corrections in the theoretical calculations as well as the errors in the SM input parameters, in particular fermion masses and the QCD gauge coupling, involved in the decay [55–57].

Decay channel	Branching ratio	Rel. uncertainty
$H \to b\bar{b}$	5.82×10^{-1}	$\pm 1.7\%$
$H \to W^+W^-$	2.14×10^{-1}	$\pm 2.2\%$
$H \to gg$	8.18×10^{-2}	$\pm 7.2\%$
$H \to \tau^+\tau^-$	6.27×10^{-2}	$\pm 2.3\%$
$H \to c\bar{c}$	2.89×10^{-2}	$^{+6.6\%}_{-2.8\%}$
$H \to ZZ$	2.62×10^{-2}	$\pm 2.2\%$
$H \to \gamma\gamma$	2.27×10^{-3}	$\pm 2.8\%$
$H \to Z\gamma$	1.53×10^{-3}	$\pm 6.9\%$
$H \to \mu^+\mu^-$	2.18×10^{-4}	$\pm 2.4\%$

The decays $H \to WW/ZZ \to 4f$ can be simulated with the `Prophecy4f` Monte-Carlo generator [229] that includes complete NLO QCD and EW corrections for Higgs decays into any possible four-fermion final state. All calculations are consistently performed with off-shell gauge bosons, without any on-shell approximation. For the SM Higgs boson, the missing higher-order corrections are estimated to be roughly 0.5%. Such uncertainties will have to be combined with the parametric uncertainties, in particular those associated to the bottom-quark mass and the

Int. J. Mod. Phys. A 2026.41. Downloaded from www.worldscientific.com
by UNIVERSITY OF CALIFORNIA @ BERKELEY on 09/16/26. Re-use and distribution is strictly not permitted, except for Open Access articles.

strong gauge coupling, to arrive at the full theory uncertainty. A detailed treatment of the differential distributions for a Higgs boson decay into four charged leptons in the final state is discussed in Refs. [56, 230].

The total width of a 125 GeV SM Higgs boson is $\Gamma_H = 4.1$ MeV, with a relative uncertainty of $\pm 1.37\%$. As discussed in Section 11.3.8, the width of the SM Higgs-boson is too narrow to allow for a direct mass line-shape measurement at the LHC. Even the channels with the best mass resolution, namely $H \to \gamma\gamma$ and $H \to ZZ^{(*)} \to 4\ell$ ($\ell =$ leptons), can only place an upper bound on Γ_H around 50 MeV at 68% CL (330 MeV at 95% CL) [231]. On the other hand, much stricter indirect constraints on the Higgs-boson widths can be obtained using simultaneously on-shell and off-shell measurements in the $pp \to VV \to 4\ell$ ($V = Z, W$) channels [232, 233]. For a given Higgs-boson production channel i ($i =$ ggF,VBF, etc.) followed by the decay of the Higgs boson to four leptons ($pp \to H \to VV \to 4\ell$), the on-shell and off-shell cross sections are proportional to

$$\sigma_i^{\text{on-shell}} \propto \frac{g_p^2 g_d^2}{\Gamma_H} \propto \mu_i^{\text{on-shell}} \quad \text{and} \quad \sigma_i^{\text{off-shell}} \propto g_p^2 g_d^2 \propto \mu_i^{\text{off-shell}} \tag{11.12}$$

where g_p and g_d are the couplings associated with the Higgs boson production and decay, respectively, and $\mu_i^{\text{on/off-shell}} = \sigma_i^{\text{on/off-shell}} / \sigma_{i,\text{SM}}^{\text{on/off-shell}}$ are the on/off-shell signal strengths. Measuring only on-shell production cannot constrain the Higgs-boson width since, in the presence of new physics, the rescaling of the couplings and of the total width can conspire to compensate each other. On the other hand, a bound on the Higgs boson width can then be obtained at hadron colliders from the simultaneous measurements of the on-shell and off-shell signal strengths. This assumes that no new physics alters the Higgs boson couplings in the on-shell and off-shell regime differently [234, 235].

While $pp \to 4\ell$ production on the Higgs-boson peak is dominated by the Higgs-boson exchange (*signal*), off-peak other $pp \to VV \to 4\ell$ *background* processes dominate ($gg \to VV \to 4\ell$ for ggF and $qq/q\bar{q} \to VV \to 4\ell$ for EW Higgs-boson production). Nevertheless, the Higgs-mediated *signal* is still sizable due to the enhanced couplings of the Higgs boson to the longitudinal polarization of the massive vector bosons at high energy. Furthermore, the interference between signal and background processes is quite large and negative, leaving as a characteristic feature a deficit of expected events from background only. Based on the most recent theoretical prediction for both on-shell and off-shell $pp \to VV \to 4\ell$ production [232, 233, 236–238] the LHC experiments have obtained the quite constraining bounds on Γ_H presented in Section 11.3.8.

11.3 Phenomenology of the 125 GeV Higgs boson

The properties of the SM Higgs boson, discovered at CERN in 2012 with a mass near 125 GeV, have been measured with increasing precision by both the ATLAS and CMS experiments. At the LHC, Higgs-boson measurements typically focus on a specific production mechanism and decay mode, taking advantage of the fact that each production–decay combination exhibits distinctive kinematic and topological features. Analysis selections are designed to exploit these features to enhance the separation of the Higgs-boson signal from background processes, and to distinguish among different production and decay modes. To improve the analysis sensitivity, events are typically categorized into exclusive regions based on kinematic properties, such as jet multiplicity, transverse momentum, or invariant mass, as well as lepton flavor. In addition, multivariate algorithms, including boosted decision trees (BDTs) and deep neural networks (DNNs), are used to exploit correlations among observables and to improve the separation between signal and background. The combined use of categorization and multivariate techniques has led to significant improvements in the overall sensitivity of Higgs boson production and decay measurements.

The discussion in this section begins with the experimental features and challenges associated with each decay channel, followed by a treatment of the main production channels. It then reviews the latest measurements of inclusive cross sections, branching ratios, differential cross sections, and simplified template cross sections, and concludes with measurements of the Higgs-boson couplings, mass, width, spin, and CP properties.

11.3.1 *Higgs-Boson Decay Channels*

As discussed in Section 11.2.5.3, a Higgs boson with a mass of 125 GeV is predicted to decay within 10^{-21} seconds to a wide variety of final states. The identification of each decay mode relies on the distinctive experimental signatures summarized below.

- $H \to b\bar{b}$: This decay mode has by far the largest branching ratio but its measurement is particularly challenging due to a very large multi-jet background, which can be suppressed by identifying the presence of two b hadrons and also requiring the presence of additional particles associated with the WH or ZH, VBF and $t\bar{t}H$ production processes. Despite these challenges, this channel is particularly useful for Higgs boson transverse momentum measurements in the high-p_{T} regime, where the signal-to-background ratio is enhanced.
- $H \to W^+W^-$: the fully leptonic final state is targeted for this decay mode as it presents two important advantages. The first is the reduction of the multi-jet background that would dominate if one or both W bosons decayed hadronically. The second is related to the particular kinematics resulting from the decay of a scalar and the subsequent decay of the W bosons via the (V-A) interaction. This leads to the charged leptons having a smaller opening angle and a smaller invariant mass compared to the inclusive WW background. The disadvantage of this final state is the presence of neutrinos, which, because they are not detected, leads to a loss of information and prevents a full reconstruction of the final state.
- $H \to gg$: This final state has not been searched for directly since the multi-jet background would overwhelm the signal. It can be inferred indirectly as an "unobserved" decay in combinations of measurements.
- $H \to \tau\bar{\tau}$: The final states targeted for this decay process involve all the decay modes of the tau leptons. Typically, the most sensitive final state involves a combination of one tau lepton that decayed hadronically, and one that decayed leptonically. This decay mode provides sensitive measurements particularly when paired with the VBF production process and in the Higgs boson high-p_t regime when using the ggF production process.
- $H \to c\bar{c}$: Like the $b\bar{b}$ decay mode above, $c\bar{c}$ suffers from a large multi-jet background, from a smaller branching ratio than $b\bar{b}$, and from the $H \to b\bar{b}$ background. In addition, the efficiency for identifying c quarks is less than for b quarks. All of these factors make this final state very challenging to observe at a hadron collider.
- $H \to ZZ$: the decay of the Z bosons to charged leptons is targeted for most measurements, except for off-shell measurements where the decay of one Z boson to neutrinos is also considered. The four charged lepton final state has the advantage of having small backgrounds and allows for a full and precise reconstruction of the Higgs boson's kinematics, including its mass. Its main drawback is the limited event yield, which results in large statistical uncertainties.
- $H \to \gamma\gamma$: Although this final state suffers from a small branching ratio and a very large continuum $\gamma\gamma$ background, a clear resonance in the $\gamma\gamma$ spectrum can be observed thanks to the excellent electromagnetic calorimeter resolution of both experiments. Like the ZZ decay mode, this channel allows for a full reconstruction of the Higgs boson kinematics and provides a high-resolution mass peak used in mass measurements.
- $H \to Z\gamma$: The final state targeted for this decay mode involves the decay of the Z boson to charged leptons. As was the case for $\gamma\gamma$, this decay mode suffers from a very large continuum background and an even smaller branching ratio.
- $H \to \mu\bar{\mu}$: This decay mode is particularly challenging because of of the very small branching ratio predicted in the SM

Int. J. Mod. Phys. A 2026.41. Downloaded from www.worldscientific.com by UNIVERSITY OF CALIFORNIA @ BERKELEY on 09/16/26. Re-use and distribution is except for Open Access articles.

and the comparatively much larger Drell-Yan background. However, this Higgs boson final state can be fully reconstructed and features a narrow dimuon mass peak.

There are other SM Higgs boson decays often referred to as 'rare'. Examples of these are the decays to lighter quarks, to meson plus photon final states, or to an electron–positron pair. While many of these modes are searched for at the LHC, either directly or indirectly, the current experimental sensitivity is far from the SM expectation.

11.3.2 *Higgs-Boson Production Channels*

The main production processes of a SM Higgs boson were discussed in Section 11.2.5. The experimental signatures used to identify these various production modes in measurements at the LHC are summarized below:

- ggH: ggH is the process that contributes the most to Higgs production at the LHC. Unlike other production processes, it does not result in extra particles in the final states (at leading order), which turns out to be its distinguishing feature.
- VBF: This process is characterized by the presence of two forward jets that result from the emission of the two fusing W or Z bosons from the quarks that originate from the incoming protons. The final state consists of two jets that tend to be emitted in the forward and backward directions, respectively, resulting in a large rapidity difference between the jets and a large invariant mass. These kinematic features are also used to reduce the multi-jet background.
- ZH: This production process takes advantage of the leptonic decay of the Z boson, either to two charged leptons or to two neutrinos, to reduce the background.
- WH: The final state targeted by this process also involves the leptonic decay of the W boson. The final state signature of a charged lepton and missing momentum from the undetected neutrino allows for a clear identification of the production process and a reduction of the backgrounds.
- ttH: This production process results in the most complex of the final states considered in this list. The two top quarks decay to a b quark and a W boson, which in turn can decay leptonically or hadronically. The presence of two b hadrons that can be identified and the possible presence of leptons from the W decays allow for what is generally a clear identification of the production process.
- bbH: this production process corresponds to about 1% of the Higgs production cross section and no attempt has yet been made to distinguish it from ggH. It has therefore been added to the ggH process in the categorization of production modes.
- tH: The experimental considerations for this process are similar to ttH, but the production rate is smaller, and the final state has only one top quark which reduces the identification efficiency compared to ttH. Finally, ttH itself can contribute as a background.

11.3.3 *Inclusive Cross Section and Branching Ratio Measurements*

The most basic experimental results in Higgs boson physics are measurements of the product of the production cross section and the decay branching fraction, $\sigma \times \mathrm{BR}$, for a given combination of production and decay modes. These quantities correspond to the number of Higgs bosons produced through a particular process and observed in a specific decay channel, normalized to the integrated luminosity and corrected for acceptance and efficiency.

As mentioned previously, analyses are typically divided into event categories defined by final-state or kinematic properties in order to maximize the precision of these $\sigma \times \mathrm{BR}$ measurements. For example, in measurements targeting $H \to \tau^+\tau^-$ decays, separate categories may be defined according to the τ-lepton decay mode (leptonic or hadronic) and the presence of additional jets, which can indicate a specific production process such as vector boson fusion. The sensitivity in each category depends on factors such as the production cross section for the chosen mode, its decay branching fraction, the reconstructed mass resolution, the selection efficiency, and the background level in the final state. These categories form the input granularity for more advanced combinations that will be discussed later, including those aimed at measuring production cross sections, extracting branching fractions, or determining Higgs boson couplings.

The extraction of the coupling strengths of the Higgs boson with various SM particles proceeds through the simultaneous fit of many such measurements. The contributions of those input measurements in the combination depend on the relative sensitivity of each analysis, which is determined by their associated statistical or systematic uncertainties. Both ATLAS and CMS have performed comprehensive combinations of measurements that use the full Run 2 dataset collected at a center-of-mass energy of 13 TeV. The input measurements presented below were mostly performed with this dataset.

The agreement between the measurement of the signal yields and the SM predictions can be expressed in terms of the signal-strength modifiers μ: the ratio of the observed yield to that of the SM prediction. The specific definition of μ will depend on the analysis. For given initial (i) and final (f) state, the signal-strength modifiers for individual production channels, μ_i, and decay modes, μ^f, are defined as the ratio of the measured event rate to its SM prediction:

$$\mu_i = \sigma_i/(\sigma_i)_{\mathrm{SM}}, \quad \mu^f = B^f/(B^f)_{\mathrm{SM}}, \quad \text{and}$$
$$\mu_{if} = \frac{\sigma_i \times B_f}{\left(\sigma_i^{\mathrm{SM}} \times B_f^{\mathrm{SM}}\right)}\,. \tag{11.13}$$

This way of presenting the experimental results gives a global indication of their compatibility with the Standard Model. A more generic treatment of potential BSM effects will be given in Section 11.4.

The input measurements of the CMS [239] and ATLAS [240] experiments that enter some of the combinations presented below are shown in Figure 11.6. It is important to note that the theoretical uncertainty on the SM prediction is included in μ measurements through the denominator in the formula above. The p-value for the compatibility of the measurements and the SM predictions is 3% for CMS and 84% for ATLAS. Taking into account the results of both experiments, the overall agreement between the data and the SM prediction is good.

The combination of Higgs boson analysis channels, both within each experiment and across the two experiments, is performed by fitting a combined signal–plus–background model to the data. The principle underlying this combination is captured by the combination formula 11.14. As mentioned previously, the input granularity for the fits is the "category", where the category can represent, for example, particular kinematic selections or lepton flavours. Then, for each category "c" within a given channel, the measured number of signal events, n_s^c, is expressed in terms of a small set of parameters as follows:

$$n_s^c = \left(\sum_{i,f} \mu_i\, \sigma_i^{\mathrm{SM}} \times A_{if}^c \times \varepsilon_{if}^c \times \mu_f\, \mathrm{BR}_f^{\mathrm{SM}}\right) \times \mathcal{L}^c. \tag{11.14}$$

The production index is defined as $i \in \{\mathrm{ggF}, \mathrm{VBF}, ZH, WH, t\bar{t}H, tH, \ldots\}$ (including specific modes and regions of phase space) and the decay index is defined as $f \in \{\gamma\gamma, WW, ZZ, bb, \tau\tau, \mu\mu, Z\gamma\}$, while σ_i^{SM} and $\mathrm{BR}_f^{\mathrm{SM}}$ are the corresponding production cross sections and decay branching fractions, estimated as described in Section 11.2.5, assuming that the observed Higgs boson is described by the SM. A_{if}^c and ε_{if}^c are the signal acceptance and the reconstruction efficiency for the given production and decay modes in the category c. Bins are defined such that the acceptance A_i and efficiency ε_i are approximately uniform within each bin and stable under plausible BSM-induced shape variations. As a result, A_i and ε_i can be computed from SM simulation. $\mathcal{L}^c$ is the integrated luminosity used for that specific category.

In the combination formula, the parameters of interest are the signal strengths for production (μ_i) and decay (μ_f). The expression assumes factorization of the production cross section and

Int. J. Mod. Phys. A 2026.41. Downloaded from www.worldscientific.com
by UNIVERSITY OF CALIFORNIA @ BERKELEY on 09/16/26. Re-use and distribution is strictly not permitted, except for Open Access articles.

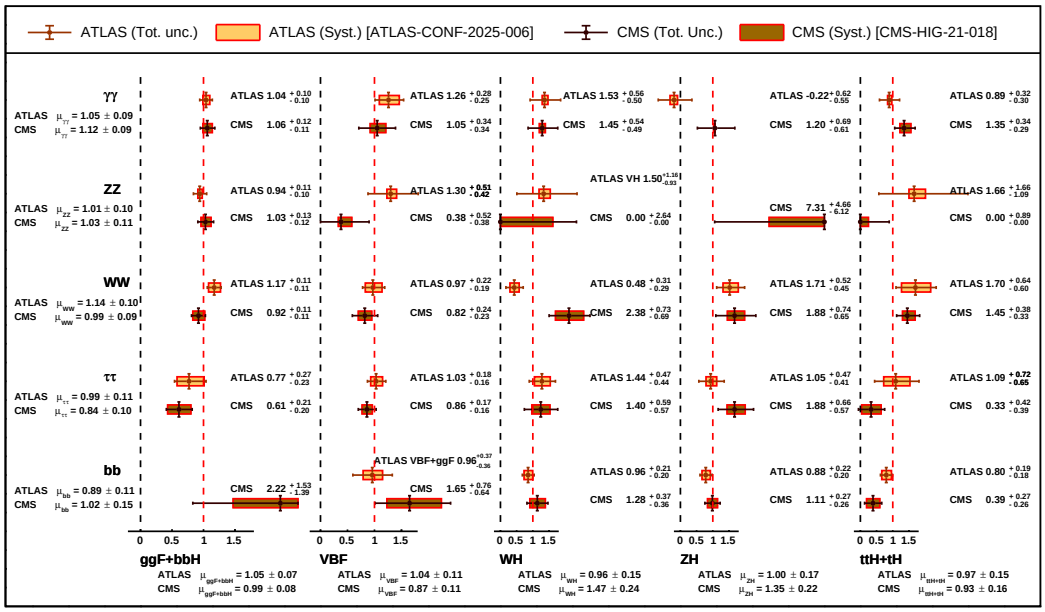

Figure 11.6: Ratio of observed rate to predicted SM event rate (μ_{if}) for different combinations of Higgs boson production and decay processes. The theoretical predictions are based on a Higgs boson mass of 125.09 GeV in the ATLAS fit [240] and 125.38 in the CMS one [239]. The original references consider similar but not identical set of measurements in the combined fit. As a result, in some cases a particular measurement is only available for one of the experiments. This is clarified in the labels with the numerical value. Both experiments also include the $\mu\mu$ and $Z\gamma$ decay modes in their fits, and, in the case of ATLAS, the VH $c\bar{c}$ process as well.

decay branching fraction, which are valid under the narrow-width approximation. The observation of a narrow resonance in high-mass-resolution channels is sufficient for the precision required here. The equation also makes it clear that μ_i and μ_f cannot be extracted independently, which implies that the total cross sections or branching fractions cannot be determined without additional assumptions.

The combination formula also highlights an important limitation in the interpretation of the signal strength parameters. If these are treated as scale factors for the production cross sections or branching fractions, then all other inputs, such as the acceptances and efficiencies, A^c_{if} and ε^c_{if}, must be assumed independent of the couplings and fixed to their Standard Model estimates. Another caveat is that, in the combined fits, only the overall normalization is varied, and the shapes of the discriminating variables for the signal are kept fixed. These assumptions are particularly relevant when using the combination to extract the Higgs boson coupling properties, as discussed in Section 11.3.5. For small deviations of the couplings from their Standard Model values, these approximations remain valid.

In an individual measurement, the quantity directly determined is the product of the production cross section and the decay branching fraction, $\sigma \cdot \mathrm{BR}$, which corresponds to $\mu_i \times \mu_f$ in the signal strength framework. These products can be treated as free parameters and, provided there is sufficient sensitivity from the chosen categories, can be measured without additional assumptions. The separate values of μ_i and μ_f can then be inferred only through a global combination of multiple measurements.

The most constrained fit in the combination allows for only one single parameter to vary, i.e., $\forall(i,f), \mu_i = \mu_f = \mu$. This global signal strength model provides the simplest probe of the compatibility of the signal with the SM Higgs boson. Indeed, it is sensitive to any deviation from the SM Higgs boson couplings provided that these deviations do not cancel overall. The ATLAS measurement of this inclusive μ yields [240]:

$$\mu = 1.023^{+0.056}_{-0.053}$$

$$= 1.023 \pm 0.028(\mathrm{stat})^{+0.026}_{-0.025}(\mathrm{exp})^{+0.039}_{-0.036}(\mathrm{sig\ theo}) \pm 0.012(\mathrm{bkg\ theo})$$

where (stat.) refers to the statistical uncertainties, (exp.) to the experimental systematic uncertainties, (sig. theo.) to theory uncertainties on the Higgs boson signal, and (bkg. theo.) to theory uncertainties on the background processes.

The equivalent result for CMS yields [239]:

$$\mu = 1.014^{+0.055}_{-0.053} = 1.014 \pm 0.028\,(\mathrm{stat})^{+0.025}_{-0.024}\,(\mathrm{exp})^{+0.040}_{-0.039}\,(\mathrm{theory})$$

The results from the two experiments are in excellent agreement with each other and with the Standard Model prediction. It is worth emphasizing that the overall theoretical uncertainty is larger than both the experimental systematic component and the statistical component, making it the dominant contribution to the total uncertainty. Reducing this theoretical component is therefore essential for fully exploiting the increasing precision of current and future measurements.

In one variant of the Higgs boson combination, the focus is placed on determining the branching fractions for various decay modes. For each mode included in the combinations performed by ATLAS and CMS, a specific production process is identified via event classification, based on the properties of particles produced in association with the Higgs boson, as described above. The branching fractions are then extracted by fixing the cross sections for all Higgs boson production processes to their Standard Model values. The resulting measurements [240] for the ATLAS experiment are shown in Figure 11.7 (left), and equivalent results from CMS can be found in [239].

In another variant of the Higgs boson combination, the emphasis is placed on the determination of the production process.

Int. J. Mod. Phys. A 2026.41. Downloaded from www.wo
by UNIVERSITY OF CALIFORNIA @ BERKELEY on 09/16/26. Re-use and distribution is
except for Open Access articles.

Where several production processes are combined, the combination assumes the relative fractions to be those from the SM within their corresponding theory uncertainties. Here, Higgs boson branching fractions are then set to their SM values, within the uncertainties specified in Ref. [57]. The results [240] are shown for the ATLAS experiment in Figure 11.7 (right). The corresponding production cross section results expressed in picobarns are provided in Table 11.3, and the equivalent results for CMS, adapted from [239] are presented in Table 11.4. It is important to note that the SM theory predictions from ATLAS and CMS differ from those presented in 11.1 because of the addition of a fiducial cut on rapidity, different mass assumptions, and different decay mode selections for associated particles (e.g. for the W and Z bosons in WH and ZH production).

Table 11.3: Measured values of Higgs boson production cross-sections by ATLAS [240] at a center-of-mass energy of 13 TeV, assuming branching ratios to match their expectations in the SM. The second column provides SM predictions with theory uncertainties based on a Higgs boson mass of 125.09 GeV, and the third column gives the ratio of the measured values to the SM predictions.

Cross-section	Measurement (pb)	SM prediction (pb)	Ratio to SM
$ggF + bbH$	$47.0^{+3.1}_{-2.7}$	44.8 ± 2.6	$1.05^{+0.07}_{-0.06}$
VBF	3.6 ± 0.4	3.50 ± 0.07	$1.04^{+0.12}_{-0.11}$
WH	1.17 ± 0.18	1.216 ± 0.024	0.96 ± 0.15
ZH	0.80 ± 0.14	0.796 ± 0.029	$1.00^{+0.18}_{-0.17}$
$ttH + tH$	$0.57^{+0.09}_{-0.08}$	0.58 ± 0.05	$0.97^{+0.15}_{-0.14}$

Table 11.4: Measured values of Higgs boson production cross-sections by CMS [239] at a center-of-mass energy of 13 TeV, assuming branching ratios to match their expectations in the SM. The second column provides SM predictions with theory uncertainties based on a Higgs boson mass of 125.38 GeV, and the third column gives the ratio of the measured values to the SM predictions.

Cross-section	Measurement (pb)	SM prediction (pb)	Ratio to SM
ggF+bbH	$44.9^{+2.7}_{-2.7}$	$44.9^{+3.4}_{-3.3}$	$1.00^{+0.06}_{-0.06}$
VBF	$2.96^{+0.39}_{-0.39}$	$3.52^{+0.08}_{-0.08}$	$0.84^{+0.11}_{-0.11}$
V(qq)H	$0.77^{+0.86}_{-0.94}$	$1.27^{+0.02}_{-0.02}$	$0.61^{+0.68}_{-0.74}$
WH	$0.58^{+0.10}_{-0.09}$	$0.39^{+0.01}_{-0.01}$	$1.49^{+0.26}_{-0.24}$
ZH	$0.33^{+0.06}_{-0.05}$	$0.24^{+0.02}_{-0.02}$	$1.38^{+0.26}_{-0.22}$
ttH	$0.38^{+0.07}_{-0.07}$	$0.50^{+0.03}_{-0.05}$	$0.76^{+0.15}_{-0.15}$
tH	$0.55^{+0.21}_{-0.20}$	$0.088^{+0.013}_{-0.007}$	$6.25^{+2.36}_{-2.22}$

The branching fractions of the $\gamma\gamma$, ZZ, $W^{\pm}W^{\mp}$, bb, and $\tau^+\tau^-$ decays, are measured with a precision of 10%. The observed signal significance for the rare $H \to \mu^+\mu^-$ decay was found to be above 3σ by CMS [241] using the Run 2 dataset, and above 3σ by ATLAS [242] using a combination of Run 2 and Run 3 datasets. The significance for the rare $H \to Z\gamma$ decay mode was found to be above 3σ when ATLAS and CMS combined their Run 2 search results [243]. All production modes are in agreement with the SM prediction. The gluon fusion process yields the most precise cross-section measurement, with a 6% uncertainty, which is of comparable size to the theoretical uncertainty on the SM prediction. In general, for both the production and decay processes, the statistical uncertainties are comparable to the systematic uncertainties.

Measuring the Higgs boson production cross section as a function of the center-of-mass energy also provides an important test of Standard Model predictions. This is illustrated in Figure 11.8, which shows the combined results from the diphoton and four-lepton decay channels at four different collision energies collected from Run 1 to Run 3 [244].

The predicted cross sections increase steadily with center-of-mass energy, more than doubling from Run 1 to Run 3. The measurements follow this trend and are, overall, consistent with Standard Model predictions.

In summary, Higgs boson measurements from both ATLAS and CMS exhibit good overall agreement with SM expectations, reinforcing the interpretation of the observed particle as a very "SM-like" Higgs boson. In some cases, the experimental uncertainties have reached a level comparable to that of theoretical uncertainties on cross sections. This highlights the critical importance of reducing theoretical uncertainties to fully exploit the precision of current and future Higgs measurements, especially in the high-luminosity LHC era.

11.3.4 *Differential and Template Cross Sections*

The characterization of Higgs boson production at the LHC goes beyond inclusive cross section measurements. The large datasets collected enable the experiments to perform detailed studies of kinematic observables that can be essential for probing the structure of the Higgs sector and identifying potential deviations from SM expectations. Differential cross section measurements as a function of key variables offer a sensitive test of higher-order corrections in perturbative theory and allow for indirect constraints on new physics. These measurements are also key for improving the modeling accuracy of Higgs boson production in Monte Carlo simulations, providing essential input for both theoretical predictions and experimental analyses. Two primary approaches are employed by the LHC experiments to characterize this information: traditional differential cross-section measurements and simplified template cross sections (STXS).

Differential distributions have been measured in the decay modes of the Higgs boson ($H \to ZZ$, $H \to \gamma\gamma$, $H \to WW$, $H \to \tau^+\tau^-$, and $H \to b\bar{b}$), mapping the kinematics of Higgs production. The size of the Run 2 dataset allows for the measurement of single- and in some cases double-differential cross sections for key observables such as the transverse momentum of the Higgs boson (p_T^H). These measurements are unfolded to particle or parton level to enable direct comparison with theoretical predictions (see the PDG review on Statistics [245] for a general discussion of unfolding techniques).

The decay channels $H \to ZZ^* \to 4\ell$ and $H \to \gamma\gamma$ provide the cleanest experimental signatures due to their fully reconstructed final states and excellent invariant mass resolution. Despite their relatively small branching ratios, these modes allow for the most precise measurements of differential cross sections, including a broad array of observables related to the Higgs boson and its decay products, the accompanying jets, and global event topology. Double-differential cross sections have also been extracted for key observables, offering a deeper view into the event structure.

Complementing these channels are the higher-branching-ratio decay modes $H \to b\bar{b}$, $H \to WW$, and $H \to \tau^+\tau^-$, which enable differential studies in regions of phase space with lower production cross sections such as events with high jet multiplicities or large Lorentz boosts of the Higgs boson. These channels are especially valuable for probing the high-p_T regime, where the sensitivity to BSM physics is enhanced. Advances in the identification of large-radius jets originating from highly boosted decays to $b\bar{b}$ or $\tau^+\tau^-$ pairs have been fundamental to enabling these measurements in the highest p_T ranges. See for instance Refs. [246–248].

While most of these measurements currently focus on the gluon-gluon fusion (ggF) production mode, subleading modes such as VBF and ttH are also now being mapped differentially with increasing precision. Individual final state measurements of the cross section have been combined in ATLAS [249] and CMS [250, 251]. Figure 11.9 shows an example of two observables.

These measurements of Higgs kinematics can be exploited to constrain Higgs boson couplings and other parameters of the theory. For instance, the shape of the Higgs p_T distribution is sensitive to loop-level effects and can be used to place bounds on the charm Yukawa coupling modifier κ_c. See 11.3.5 for further discussion on coupling constraints.

An alternative approach to characterizing Higgs boson production is the Simplified Template Cross Sections (STXS) framework [252]. In this method, fiducial cross sections are measured for each production mode in a set of predefined kinematic regions (*bins*) of phase space. These regions are defined using observ-

Int. J. Mod. Phys. A 2026.41. Downloaded from www.worldscientific.com
by UNIVERSITY OF CALIFORNIA @ BERKELEY on 09/16/26. Re-use and distribution is strictly not permitted, except for Open Access articles.

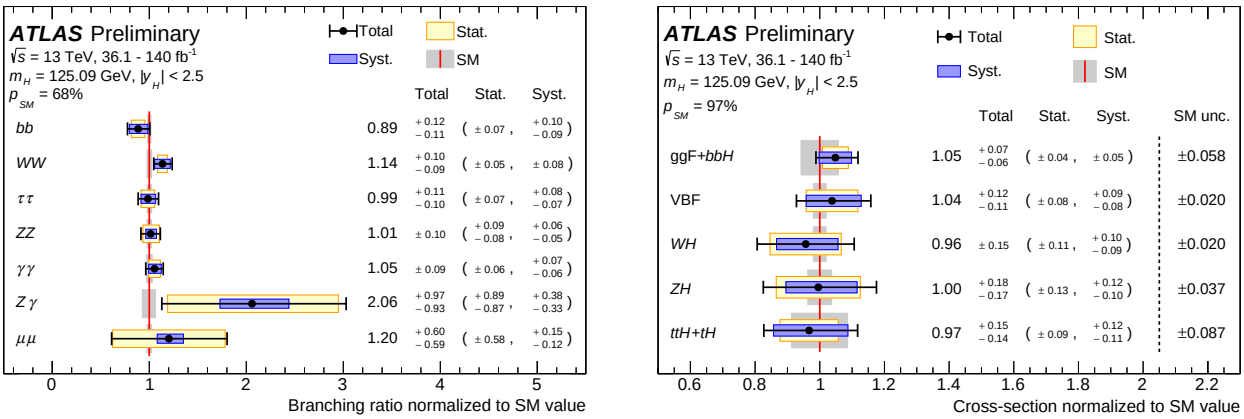

Figure 11.7: (Left) Observed and predicted branching fractions for different Higgs boson decay modes assuming SM values for the production cross sections. (Right) Observed and predicted cross sections for different Higgs boson production processes, assuming SM values for the decay branching fractions. Equivalent results from CMS can be found in Ref. [239]

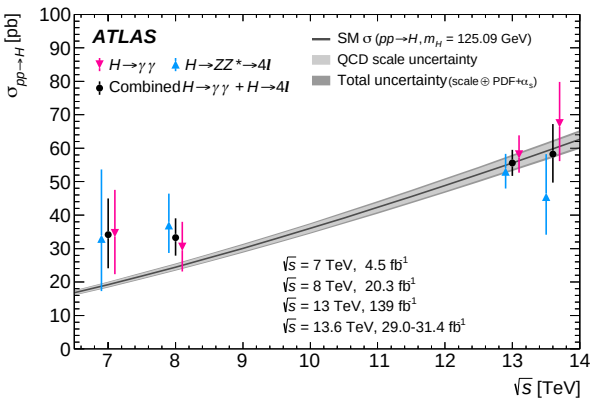

Figure 11.8: ATLAS measurements of the Higgs boson production cross section in the four-lepton and diphoton channels as a function of the proton-proton center-of-mass energy.

ables such as the transverse momentum of the Higgs boson (p_T^H), the dijet invariant mass (m_{jj}), the transverse momentum of the Higgs plus leading jets (p_T^{Hjj}), and the transverse momentum of the associated vector boson (p_T^V). The STXS bins are carefully chosen through consensus between the theoretical and experimental community to optimize sensitivity to new physics while minimizing minimal theoretical uncertainties. These regions isolate contributions from different production mechanisms and improve the stability of theoretical predictions. They are designed with the combination of measurements across decay channels and experiments in mind. The goal is to reduce the dependence on extrapolations beyond the experimentally accessible phase space, improving the fidelity of comparisons between data and theory. STXS measurements serve as well-defined benchmarks that test both Standard Model (SM) predictions and potential BSM deviations in differential distributions.

The LHC Higgs Working Group proposed this framework [57, 252] to address the challenges of combining measurements across a large number of decay channels, each affected by its own set of systematic uncertainties. To facilitate this, fiducial phase space definitions are standardized across analyses, focusing on Higgs boson production characteristics rather than specific decay signatures. The observables used correspond to the production modes $gg \to H$ (gluon fusion and $gg \to Z(\to qq)H$), EW qqH (vector boson fusion and $qq \to V(\to qq)H$), VH (associated production with vector bosons in leptonic channels, $qq + gg \to V(\to \text{leptons})H$), and top-associated production ($t\bar{t}H$), constrained to well-defined and mutually exclusive kinematic regions.

ATLAS and CMS experiment has produced STXS measurements in all the main production modes and decay channels with the Run-2 dataset. A combination of STXS across decay channels has also been carried out by ATLAS [253–255] and CMS [239], also with the full Run-2 dataset. Figure 11.10 illustrates the results obtained by ATLAS in each of the kinematic regions. These combined STXS measurements provide a powerful probe of Higgs production mechanisms and constitute an important input for interpretations in the κ formalism, in global EFT fits, or in dedicated BSM analyses.

11.3.5 *Probing the Couplings of the Higgs Boson: κ framework and EFT approach*

As discussed in Section 11.2.1 and Section 11.2.2, all the SM Higgs-boson couplings are proportional to the mass of the particle it couples to. More precisely, the SM Higgs-boson couplings to fundamental fermions are linearly proportional to the fermion masses, whereas the couplings to bosons are proportional to the square of the boson masses. The Higgs terms in the SM Lagrangian were presented in Eqns. 11.8 and 11.9. Reformulating these expressions to highlight the SM Higgs-boson couplings to gauge bosons and fermions, as well as the Higgs-boson self coupling, we find the following Lagrangian:

$$\mathcal{L} = -g_{Hf\bar{f}}\bar{f}fH - \frac{g_{3H}}{6}H^3 - \frac{g_{4H}}{24}H^4 + \delta_V V_\mu V^\mu \left(g_{HVV}H + \frac{g_{HHVV}}{2}H^2\right), \tag{11.15}$$

with

$$g_{Hf\bar{f}} = \frac{m_f}{v},\ g_{HVV} = \frac{2m_V^2}{v},\ g_{HHVV} = \frac{2m_V^2}{v^2},\quad g_{3H} = \frac{3m_H^2}{v},\ g_{4H} = \frac{3m_H^2}{v^2}, \tag{11.16}$$

where $V = W^\pm$ or Z and $\delta_W = 1, \delta_Z = 1/2$. The Higgs-boson couplings are therefore unambiguously determined once the particle masses are known. Any deviation from such pattern in the measurement of the couplings of the Higgs boson would therefore provide a clear indication of the existence of BSM physics. Later in this section (see Figure 11.11), we will present the recent results of the ATLAS and CMS constraints of these potential deviations.

Measuring the Higgs-boson couplings without relying on the SM assumption requires a general framework treating deviations from the SM coherently at the quantum level in order to provide theoretical predictions for relevant observables to be con-

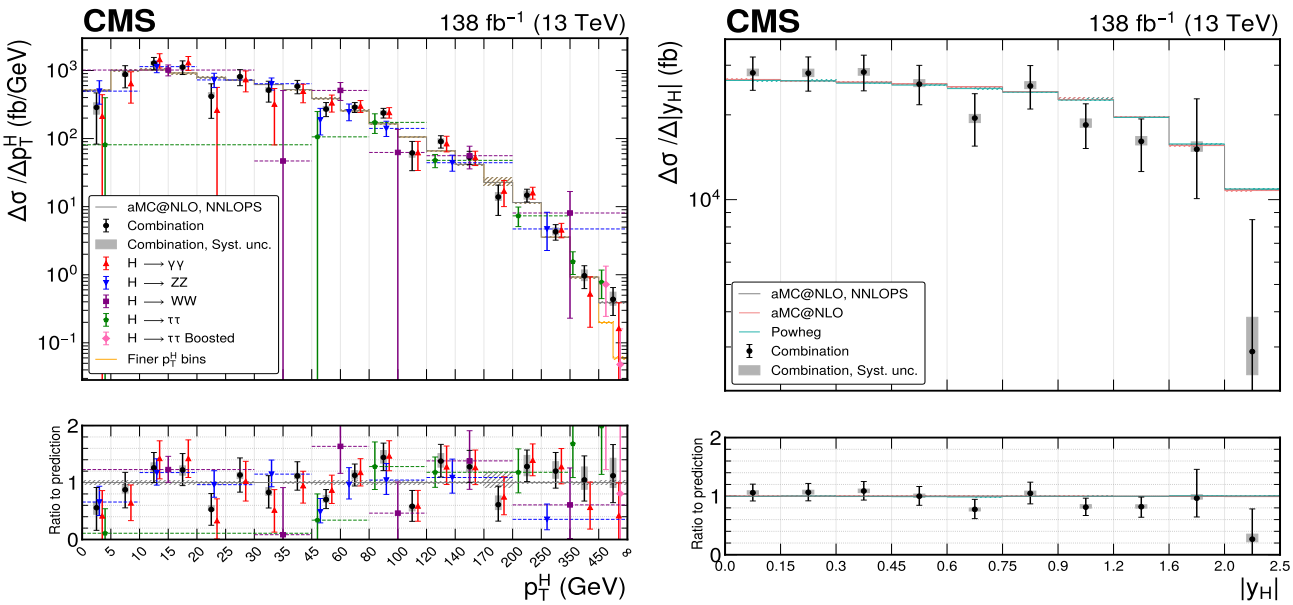

Figure 11.9: (Left) Combination of the fiducial differential cross sections in Higgs boson transverse momentum in the $H \to \gamma\gamma$, $H \to ZZ$, $H \to WW$, $H \to \tau\tau$ decay modes. (Right) Differential cross section as a function of the Higgs boson rapidity, combining the $H \to \gamma\gamma$ and $H \to ZZ$ modes, comparing to different Monte Carlo generators [251].

fronted with experimental data. Out of the different approaches to this problem, two approaches have been mainly followed by the LHC experimental collaborations in interpreting their measurements. The first is the so-called kappa (κ) formalism [256], in which Higgs-boson couplings are rescaled by arbitrary multiplicative factors (κ parameters), while preserving the Lorentz structure of the SM interactions. This approach has been extensively used by the LHC experimental collaborations due to its close connection to the measurement of the signal strengths described in Section 11.3.3. It allows for well-defined scenarios with various degrees of flexibility for incorporating BSM effects, and provides a global picture of the behavior in the Higgs sector. However, this κ formalism is limited in scope, as it does not fully account for modifications to the tensor structure of the interactions that influence both the kinematic distributions and the total rates. Also, arbitrary rescalings can destroy gauge invariance.

An alternative approach is the use of Effective Field Theories (EFTs) to parameterize BSM effects through higher-dimensional effective operators originating from the EW-scale projection of generic extensions of the SM living at a much higher ultraviolet (UV) scale. Indeed, while light new physics cannot be fully excluded, stringent direct limits on many well-motivated models makes the assumption of heavy new physics a very well-justified starting point. The EFT approach reaches beyond a purely phenomenological approach, and, as a coherent quantum-field-theory, also allows for the correlation of different effects and a systematic estimate of the residual uncertainties of its predictions. Depending on the assumptions made on the scalar field introduced in the SM to generate EWSB, two main EFT options have been considered in exploring potential deviations from SM-like Higgs-boson couplings: the so-called Standard Model Effective Field Theory (SMEFT), where the scalar field is assumed to be a doublet of $SU(2)_{\rm L}$ as in the SM, and the Higgs Effective Field theory (HEFT) where such assumption is not made. The SMEFT approach has received particular attention in recent phenomenological explorations of BSM physics. This approach includes both targeted analyses in specific final states (e.g., $H \to ZZ$, $H \to \tau^+\tau^-$), which directly probe operators through the use of dedicated discriminators that are sensitive to specific BSM-induced deformations of the Higgs-boson kinematics, and also global analyses that typically exploit cross section measurements including differential distributions, and target a full spectra of observables. The latter normally require combination with other precision measurements, such as electroweak precision observables (EWPO), top-quark, Drell-Yan, as well as flavor-physics and low-energy observables, for a complete coverage. On the other hand, the HEFT approach has been recently considered in analyses aimed at constraining the Higgs-boson self-coupling since, at the lowest order, the EFT couplings involved in this case have a straightforward relation to the κ formalism.

In the following, the κ and SMEFT approaches are discussed in more detail given their broad applications to the interpretation of experimental data.

11.3.5.1 *Kappa Framework*

The κ-formalism [256] was developed within the LHC Higgs Working Group [55]. It introduces arbitrary factors called κ parameters that rescale the SM Higgs boson couplings (e.g. $\kappa_j = g_{Hjj}/g_{Hjj}^{SM}$ for $j = f, V$ and similarly for other couplings), keeping the same Lorentz structure of the SM interactions. It followed earlier attempts [257] and initial phenomenological studies of the first hints of the existence of the Higgs boson [258]. It has been utilized to test various physics scenarios, like the existence of additional new particles contributing to the radiative Higgs-boson production and decays, or to probe various symmetries of the SM itself, as for example the custodial symmetry (see Sec. 11.2.3). It only compares the experimental measurements to their best SM predictions and does not require any new BSM computations per se. From a more theoretical perspective, its relevance arises from the fact that it fully captures the leading effects in Higgs processes of well-motivated scenarios.

The κ framework, described in detail in Refs. [56, 256], facilitates the characterization of Higgs coupling properties in terms of a series of Higgs coupling strength modifier parameters κ_i, which are defined as the ratios of the couplings of the Higgs boson to particles i and their corresponding SM values. It is the simplest parametrization directly related to experimental measurements of the Higgs boson production and decay modes, and, in some cases, it coincides with the lowest-order of the consistent EFT framework of the HEFT. The κ framework has been widely used by the community, exploiting the framework described in Section 11.3.3 to combine the very large number of exclusive categories aimed at reconstructing the main production and decay modes of the Higgs boson. The μ_i and μ_f signal strength parameters defined there can be further interpreted in terms of modifiers of the SM couplings κ_j. The list of couplings g_j included in the experimental fits has been expanded progressively since the first results. In the latest experimental combinations,

Int. J. Mod. Phys. A 2026.41. Downloaded from www.wo
by UNIVERSITY OF CALIFORNIA @ BERKELEY on 09/16/26. Re-use and distribution is
except for Open Access articles.

Int. J. Mod. Phys. A 2026.41. Downloaded from www.worldscientific.com
by UNIVERSITY OF CALIFORNIA @ BERKELEY on 09/16/26. Re-use and distribution is strictly not permitted, except for Open Access articles.

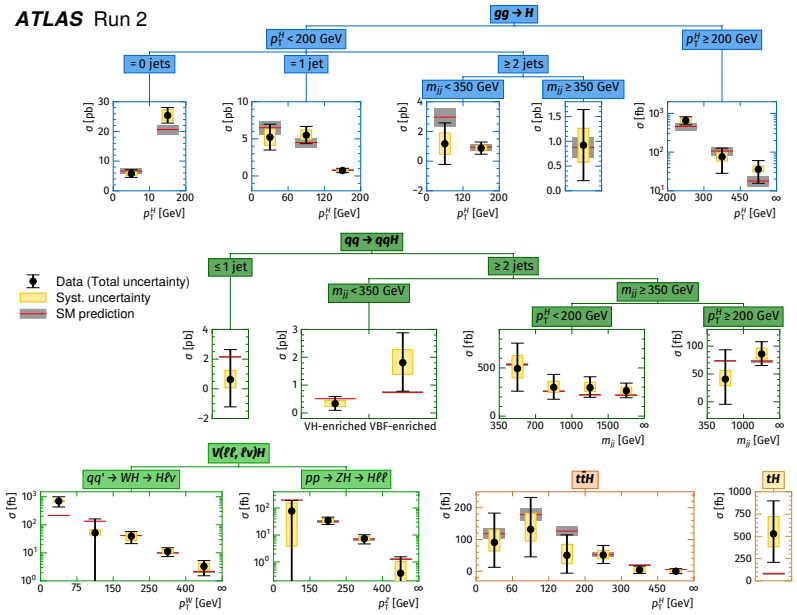

Figure 11.10: Simultaneous combined measurement of simplified template cross sections assuming SM branching fractions of the Higgs boson [255]

$j \in \{HZZ, HWW, H\tau\tau, Hbb, Htt, H\mu\mu, Hcc, Hgg, H\gamma\gamma, HZ\gamma\}$.

The κ framework assumes a single narrow resonance so that the narrow-width approximation can be used to decompose the cross section as a product of two factors characterizing the production and the decay of the Higgs boson. The κ parameters are introduced by expressing each of the these factors as their SM expectation multiplied by the square of a coupling strength modifier for the corresponding process at leading order:

$$(\sigma \cdot \mathrm{BR})(i \to \mathrm{H} \to f) = \frac{\sigma_i^{SM}\kappa_i^2 \cdot \Gamma_f^{SM}\kappa_f^2}{\Gamma_H^{SM}\kappa_H^2} \quad \to \quad \to \quad \mu_i^f \equiv \frac{\sigma \cdot \mathrm{BR}}{\sigma_{\mathrm{SM}} \cdot \mathrm{BR}_{\mathrm{SM}}} = \frac{\kappa_i^2 \cdot \kappa_f^2}{\kappa_H^2}, \tag{11.17}$$

where μ_i^f is the rate relative to the SM expectation, Γ_H is the total Higgs width, and κ_H^2 is an expression that adjusts the SM Higgs width to take into account the modifications induced by the deformed Higgs boson couplings. κ_H is a priori an independent parameter. However, when it is assumed that the Higgs boson cannot decay to new particles beyond those of the SM, κ_H can also be treated as an effective parameter and expressed in terms of the coupling modifiers to the SM field content. The κ_j modifiers scale either production cross sections or decay partial widths:

$$\kappa_i^2 = \frac{\sigma_i}{\sigma_i^{\mathrm{SM}}} \quad \text{or} \quad \kappa_j^2 = \frac{\Gamma_j}{\Gamma_j^{\mathrm{SM}}}, \tag{11.18}$$

depending on the process. Here, σ_i is the measured cross section in production mode i and Γ_j the partial Higgs width in decay mode j. σ_i^{SM} and Γ_j^{SM} are their respective theoretical predictions in the SM. When all κ_j are set to 1, the SM is reproduced.

In the simplest configuration of the kappa framework, all loops in Higgs boson production and decay diagrams are resolved, coupling modifiers are introduced for each tree-level Higgs boson coupling to another SM particle, and no BSM decay of the Higgs is considered. The parameters include therefore κ_W, κ_Z, κ_t, κ_b, κ_τ, and κ_μ. This configuration can be extended to account for loop induced processes and to better incorporate possible new physics effects. For loop-induced processes, $gg \to H$, $H \to \gamma\gamma$ and $H \to Z\gamma$, there is a choice of either resolving the coupling strength modification in its SM expectation, e.g. $\kappa_\gamma(\kappa_t, \kappa_W)$, or keeping them as an effective coupling strength parameter, determined in the fit [259].

In the absence of a measurement of the Higgs-boson width the LHC requires some hypotheses in order to extract the Higgs couplings from the measured Higgs signal strengths. In particular, one can assume either (i) that there are no BSM particles in the decay, (ii) that any BSM particles in the decay would only give rise to invisible signatures and therefore be detectable through invisible Higgs boson channels (or in other terms that there is no BSM undetected contribution), or (iii) that BSM physics would modify the κ_j according to specific patterns favored by several new physics models. An external constraint is needed when BSM decays are allowed. For instance, the requirement that $|\kappa_V| \leq 1$ ($V = W, Z$) (see for instance the ATLAS+CMS Run 1 combination [260] for a discussion of this constraint) or constraints on Γ_H from indirect measurements (eg offshell/onshell cross sections (see Section 11.3.8). The general expression of the total width of the Higgs boson can be written as follows:

$$\Gamma_H = \frac{\kappa_H^2 \Gamma_H^{\mathrm{SM}}}{1 - \mathrm{BR}_{\mathrm{BSM}}} = \frac{\kappa_H^2 \Gamma_H^{\mathrm{SM}}}{1 - (\mathrm{BR}_{\mathrm{inv}} + BR_{\mathrm{undet}})} \tag{11.19}$$

where Γ_H^{SM} is the total width of the SM Higgs boson and $\mathrm{BR}_{\mathrm{BSM}}$ is the branching fraction of the Higgs boson to new particles beyond the SM. This BSM fraction can be broken down into two contributions. The first one, $\mathrm{BR}_{\mathrm{inv}}$, corresponds to an "invisible" branching ratio of the Higgs boson that can be directly constrained through H → (invisible) searches (see Section 11.4.3) and included as an input in the coupling fits. The second, $\mathrm{BR}_{\mathrm{undet}}$, corresponds to the *undetected* or *unprobed* Higgs-boson branching ratio. This contribution is not directly measured by any search, and therefore not included as an input to the fits.

Negative values of Higgs couplings, i.e. negative κ_j, are not excluded a priori although they are not favored by the most recent measurements (see Table 11.5). With increased sensitivity to interference effects between vector (κ_V, $V = W, Z$) and fermion couplings (κ_F, $F = t, \ldots$), their relative sign could be established. The relative sign of κ_W and κ_Z has also been explored through associated production of Higgs and W bosons via vector-boson fusion (VBF) in Refs. [261, 262], which exclude opposite-sign scenarios for κ_W and κ_Z with a significance of more than 5 standard deviations. Among the five main Higgs-boson decay channels, only the $\gamma\gamma$ channel is sensitive to the sign of κ_F (or κ_V) through the interference of the W and t loops (see Ref. [259] for the parametrization). Access to the sign of the κ_F coupling can be obtained through the inclusion of analyses targeting single

Int. J. Mod. Phys. A 2026.41. Downloaded from www.worldscientific.com by UNIVERSITY OF CALIFORNIA @ BERKELEY on 09/16/26. Re-use and distribution is except for Open Access articles.

top-quark production, proposed in Ref. [263, 264], and currently part of the standard LHC combinations.

Taking into account the above discussion of the different possible scenarios that can be implemented, the ATLAS and CMS collaborations followed a common interpretation approach that yielded the first LHC combination of Higgs-boson couplings results already at the end of the first Run of the LHC [260]. A very similar configuration is used in the subsequent Run-2 results [239, 240, 255, 265].

Figure 11.11 and Table 11.5 summarize the measurements of the kappa parameters by ATLAS [240] and CMS [239], using the full LHC Run-2 dataset, with an integrated luminosity of up to 140 fb^{-1} of pp collisions at $\sqrt{s} = 13$ TeV. For the statistically dominated modes, $H \to Z\gamma$ and $H \to \mu\mu$, ATLAS has also included partial Run-3 statistics, 165 fb^{-1} of 13.6 TeV collisions. These correspond to the cross section measurements presented in Section 11.3.3. Figure 11.11 (left) shows one of the interpretations discussed above: the measured coupling modifiers in the approach where the Higgs-boson loop couplings are resolved, as a function of the mass of the probed particles. Remarkable agreement with the SM is observed over several orders of magnitude. See the original references [239, 240] for further details.

Table 11.5 presents the coupling measurements for the scenario that includes effective couplings. The Run-2 results (13 TeV, $\approx$ 140 fb^{-1}) are compared to the Run-1 ATLAS+CMS combination (7 and 8 TeV, 5+20 fb^{-1}) and the latest HL-LHC projection for the measurements, based on a combination of ATLAS and CMS for an integrated luminosity of 3000 fb^{-1} per experiment. The interpretation included in the table assumes no BSM physics in the decay of the Higgs boson.

The combinations and projections can incorporate in the fit the searches for invisible decays of the Higgs boson. These searches directly constrain $BR_{\rm inv}$ and enable the distinction between *invisible* (directly constrained) versus *undetermined* or *unprobed* (not accesses experimentally in any measurement or search) decays mentioned earlier through a modification of the combination fit. Starting from the no BSM scenario, one may relax the assumptions on the Higgs boson decay by introducing $BR_{\rm inv}$ and $BR_{\rm undet}$ as parameters, allowing for a modification of the decays but introducing an external constraint to alleviate a complete degeneracy in the Higgs boson total decay width, where each coupling modifier can be scaled up equally to account for a non-zero $BR_{\rm undet}$. An example of constraint is $\kappa_V \leq 1$, commonly used since Run-1, as shown for example in Ref. [260]. An alternative constraint uses the Higgs boson width derived from the off-shell Higgs boson production measurements. In this interpretation, the off-shell Higgs measurement constrains the visible, invisible and undetected branching fractions. The *visible* branching fractions corresponds to the measured Higgs decays to SM particles. The invisible branching fraction is constrained from the direct, *invisible* Higgs searches. The *undetected* branching fraction will be then constrained by the off-shell Higgs boson measurements. Figure 11.11 (right) shows a comparison of the kappa measurements in the three models: no BSM allowed, BSM constrained by $\kappa_V \leq 1$, and BSM constrained by the inclusion of off-shell production ($H \to 4\ell$). More details on this comparison can be found in the CMS paper [239], and a discussion of off-shell production and the measurement of the total width in Section 11.3.8.

The limits obtained at the 95%CL on the invisible and undetected branching fractions with the Higgs combination and the corresponding HL-LHC constraints are:

$$\begin{aligned} &\mathrm{BR_{inv}} < 13\% \ , \ \mathrm{BR_{undet}} < 12\% \ \text{(ATLAS [255], Run2)} \,, \\ &\mathrm{BR_{inv}} < 12\% \ , \ \mathrm{BR_{undet}} < 11\% \ \text{(CMS [239], Run2)} \,, \\ &\mathrm{BR_{inv}} < 1.9\% \ , \ \mathrm{BR_{undet}} < 4\% \ \text{(HL-LHC [194])} \,. \end{aligned} \tag{11.20}$$

A longer discussion of the different Higgs invisible searches can be found in Section 11.4.3, including updated BR_{inv} constraints not yet included in some of these combinations.

Interpretations which are less sensitive to modeling systematic uncertainties and require no constraints on the natural width of the Higgs bosons have been considered, either through the ratio of cross section and branching ratios (see Ref. [263]) or through a more generic approach to avoid the degeneracy in the measurement of the coupling modifiers, probing the coupling properties of the Higgs boson through ratios of couplings ($\lambda_{ij} = \kappa_i/\kappa_j$). In the latter model, all combination signals can be parametrized with the ratios of coupling modifiers. For example, (i) the $\lambda_{Zg} = \kappa_Z/\kappa_g$ ratio which is mainly probed by the measurements of the VBF and ZH production; (ii) the $\lambda_{tg} = \kappa_t/\kappa_g$ ratio constrained by the $t\bar{t}H$ production process; (iii) the $\lambda_{WZ} = \kappa_W/\kappa_Z$ ratio mainly probed by the WW and ZZ decay modes; (iv) the $\lambda_{\tau Z} = \kappa_\tau/\kappa_Z$ ratio constrained by the $\tau^+\tau^-$ channel; (v) the $\lambda_{bZ} = \kappa_b/\kappa_Z$ ratio probed mainly by the $VH(b\bar{b})$ channels; and (vi) the $\lambda_{\gamma Z} = \kappa_\gamma/\kappa_Z$ ratio constrained by the diphoton channel. In this parametrization, the ZZ channel plays an important normalization role, and a reference combined coupling modifier, κ_{gZ}, is introduced to represent the high-precision measurement of the $gg \to H \to ZZ$ production rate $\kappa_{gZ} = \kappa_g \times \frac{\kappa_Z}{\kappa_H}$. Current uncertainties on the ratios vary from 5 to 20% [239]. They are expected to be reduced to a few percent level at the HL-LHC [266].

It is important to note that the global fit described above does not include all possible Higgs couplings, but only those related to measurements included as inputs in the fit. A particularly important example is the coupling to charm quarks, κ_c. The significant experimental challenges in isolating Higgs decays to charm at the LHC limit the LHC sensitivity. Generally speaking, this coupling is considered a target for future Higgs factories, that will be able to measure it precisely [194]. Nevertheless, the progress in recent years has been impressive and it deserves a special mention. Dedicated analyses have been developed in ATLAS and CMS to probe this coupling both directly and indirectly. Direct searches target the decay mode $H \to c\bar{c}$, relying heavily on associated production and advanced charm-tagging algorithms. The most stringent current constraint comes from CMS using the full Run-2 dataset, which combines VH and ttH production and yields a constraint at 95% CL of $|\kappa_c| < 3.5$ (expected 2.7) [267]. ATLAS set a limit of $|\kappa_c| < 4.2$ at 95% CL [268] using the VH channel alone. These limits are significantly looser than those for third-generation fermions, illustrating the difficulty of separating charm from background in hadronic environments. Indirect constraints on κ_c have also been derived from differential distributions sensitive to loop contributions involving charm quarks [249, 251]. Searches for rare Higgs boson decays to a meson and a photon [269] as well as searches for Higgs boson production in association with a charm quark (cH) [270, 271] or a photon (γH) [272] have also been used to set constraints on $|\kappa_c|$. At present, these searches allow values of κ_c several times larger than the SM expectation. Looking ahead, the HL-LHC is expected to improve sensitivity significantly, potentially reaching observation of the decay and its first measurement. The available projections [266] propose a sensitivity to the charm Yukawa coupling of $\kappa_c < 1.5$ by the end of HL-LHC at 95%. This projection is likely conservative considering the newest results and the rate of improvement in recent years. Measuring κ_c remains one of the key challenges in precision Higgs-boson physics and a critical test of the Yukawa-type interaction assumed in the SM.

Beyond the charm quark, probing the Yukawa couplings of the first- and second-generation fermions remains an even greater challenge. Current LHC studies can only set very loose indirect constraints on the light quark Yukawa couplings. As an example, in Ref. [272] CMS excludes scenarios where first- or second-generation quarks have Yukawa couplings comparable to those of the third generation, probing $H\gamma$ production. The Yukawa coupling to the electron has also been constrained via direct searches for $H \to ee$ by ATLAS [273] and CMS [274], with limits several orders of magnitude above the SM prediction. Future lepton colliders and dedicated Higgs factories are expected to significantly improve these constraints.

A more in-depth discussion of the kappa framework formalism can be found in the LHC Higgs Working Group Reports [56, 256].

11.3.5.2 *SMEFT Formalism and Results*

The SMEFT Lagrangian has the same field content and it respects the same linearly-realized $\mathrm{SU(3)}_C \times \mathrm{SU(2)}_L \times \mathrm{U(1)}_Y$ local symmetry as the SM. The difference is the presence of operators

Int. J. Mod. Phys. A 2026.41. Downloaded from www.worldscientific.com
by UNIVERSITY OF CALIFORNIA @ BERKELEY on 09/16/26. Re-use and distribution is strictly not permitted, except for Open Access articles.

Table 11.5: Coupling modifier combined measurements assuming no new physics in the decay of the Higgs boson. No assumption is made for the loop level couplings of the Higgs boson to gluons and photons which are considered as effective. The last column gives the expected precision at the HL-LHC.

	LHC Run 1 [260]	ATLAS Run 2 [240] + Run 3 ($\mu\mu$, Zγ)	CMS Run 2 [239]	HL-LHC [266] (expected)
κ_W	$0.87^{+0.13}_{-0.09}$	1.00 ± 0.05	1.03 ± 0.06	1.6%
κ_Z	-0.98 ± 0.10	0.96 ± 0.05	1.07 ± 0.06	1.6%
κ_γ	$0.87^{+0.14}_{-0.09}$	0.97 ± 0.06	1.10 ± 0.07	1.8%
κ_g	$0.91^{+0.07}_{-0.06}$	$0.99^{+0.07}_{-0.06}$	$0.91^{+0.07}_{-0.06}$	2.4%
κ_t	$1.40^{+0.24}_{-0.21}$	0.99 ± 0.09	$0.92^{+0.09}_{-0.08}$	3.4%
κ_b	$0.49^{+0.27}_{-0.15}$	$0.89^{+0.10}_{-0.09}$	$0.98^{+0.13}_{-0.12}$	3.6%
κ_τ	$0.84^{+0.15}_{-0.11}$	0.94 ± 0.06	0.91 ± 0.07	1.9%
κ_μ	–	$1.04^{+0.23}_{-0.30}$	$1.09^{+0.20}_{-0.22}$	3.0%
$\kappa_{Z\gamma}$	–	$1.36^{+0.30}_{-0.36}$	$1.61^{+0.32}_{-0.35}$	6.8%

with canonical mass-dimension d larger than 4, built of SM fields, and representing the projection at the EW scale of generic extensions of the SM living at a UV mass scale Λ well above the EW scale. At the EW scale the heavy particles of the UV-complete theory cannot be produced as physical states and only leave their imprint as quantum effects induced by $d > 4$ effective operators that can affect SM couplings and masses but also introduce new interactions not present in the SM Lagrangian. While a modification of the SM Higgs-boson couplings as introduced by the κ-formalism discussed in Sec. 11.3.5.1 can only describe BSM effects that amount to a rescaling of production rates and branching ratios, the SMEFT formalism (similarly to the HEFT formalism) can be used to also explain anomalies arising in differential distributions since it introduces Lorentz structures not existing in the SM Lagrangian. Furthermore, the same SMEFT operators contribute not only to Higgs-boson processes but to a much larger number of observables and can therefore be constrained by a broad spectrum of measurements that could reveal underneath correlations among EFT couplings and point to classes of preferred BSM models.[6] Last but not least, the SMEFT is a full fledged quantum field theory and as such can systematically include effects induced by SM quantum corrections below the scale Λ and can also seamlessly be matched to low-energy EFT below the EW scale, e.g. the 4-fermion operator Lagrangian commonly used to describe the dynamics of flavor physics[7].

The SMEFT Lagrangian consists of the SM Lagrangian ($\mathcal{L}_{\rm SM}$) and a series of operators organized in a systematic expansion in d, where each consecutive term is suppressed by an increasingly larger power of a the high mass scale Λ such that the SMEFT Lagrangian can be written as:

$$\mathcal{L}_{\rm SMEFT} = \mathcal{L}_{\rm SM} + \sum_d \sum_i \frac{C_i^{(d)}}{\Lambda^{(d-4)}} \mathcal{O}_i^{(d)} \,. \tag{11.21}$$

The contribution of the SMEFT operators of dimension $d > 4$ to physical amplitudes is therefore suppressed by $(E/\Lambda)^{d-4}$, where E is the relevant energy scale of the process. The applicability of the SMEFT approach requires that $\Lambda \gg E$, under which assumption the expansion in d can be truncated and only a finite number of new interactions is considered. The Wilson coefficients $C_i^{(d)}$ encode the virtual effects of the heavy new physics in low-energy observables. For a given UV completion of the SM, their dependence on masses and couplings of the new particles can be obtained via matching with the UV theory at the scale Λ. More generally, and in the absence of a specific assumption on the UV theory, they can be inferred using specific power-counting rules [278, 279], or constrained by fitting to specific sets of observables. All parameters of the SMEFT Lagrangian, namely SM parameters and Wilson coefficients, are scale dependent and their scale dependence is determined by the renormalization group equations of the full SMEFT.

The SMEFT approach is clearly very general, and can be made more specific and predictive by further assumptions on the UV physics of which it is a low-energy projection. For instance, assuming baryon and lepton number conservation, the most general SMEFT Lagrangian only contains even-dimension operators. This is commonly assumed in studies of Higgs-boson and more generally collider observables which therefore start by including $d = 6$ operators, while the inclusion of $d = 8$ or higher-dimension operators is considered in assessing the validity of truncating the SMEFT expansion at $d = 6$ or for those observables that are more sensitive to $d = 8$ operators, such as e.g. certain Drell-Yan angular distributions [280–282].

The list of $d = 6$ operators was first classified in a systematic way in Ref. [283] after the works of Ref. [284]. Subsequent analyses pointed out the presence of redundant operators, and a minimal and complete list of operators was finally provided in Ref. [285][8]. For a single family of fermions, i.e. not considering flavor indices, the SMEFT Lagrangian can be expressed in terms of 59 independent operators. Considering the 3 families of fermions of the SM, flavor indices can be added to these 59 operators, and furthermore, new operator structures, that have been dismissed by means of Fierz transformations in the single family case, have to be considered, for a total of 2499 independent operators that do not violate baryon and lepton number [288].

The numbers of operators can be reduced by requiring additional symmetry properties of the UV-complete theory. For instance, requiring no additional CP-violation besides the one already introduced in the SM via the CKM matrix restricts the number of $d = 6$ operators for a single family to 53 (out of 59) and requires the Wilson coefficients to be real. At the same time, assumptions on the level of flavor-violation introduced by NP at the UV scale can drastically limit the number of flavor-structures allowed in the SMEFT operators. Requiring the UV theory to have maximal flavor symmetry, namely $U(3)^5$, and therefore assuming that the SM Yukawa couplings are the only sources of

[6] It should be pointed out that some of the processes considered in global fits of the SMEFT are backgrounds to Higgs-boson analyses and their SMEFT interpretation should be consistently considered along with the signal one in such analyses. This is true in general for all background processes, and, together with other improvements, is part of the ongoing effort to improve SMEFT global fits.

[7] For comprehensive reviews of the SMEFT see Ref. [275–277].

[8] Complete enumerations of $d = 8$ operators have been obtained [286] and some preliminary constraints on particular subsets of these operators have been derived from experimental measurements [287]. Still, in this review, the SMEFT Lagrangian will be truncated at the level of dimension-6 operators.

Int. J. Mod. Phys. A 2026.41. Downloaded from www.wo
by UNIVERSITY OF CALIFORNIA @ BERKELEY on 09/16/26. Re-use and distribution is
except for Open Access articles.

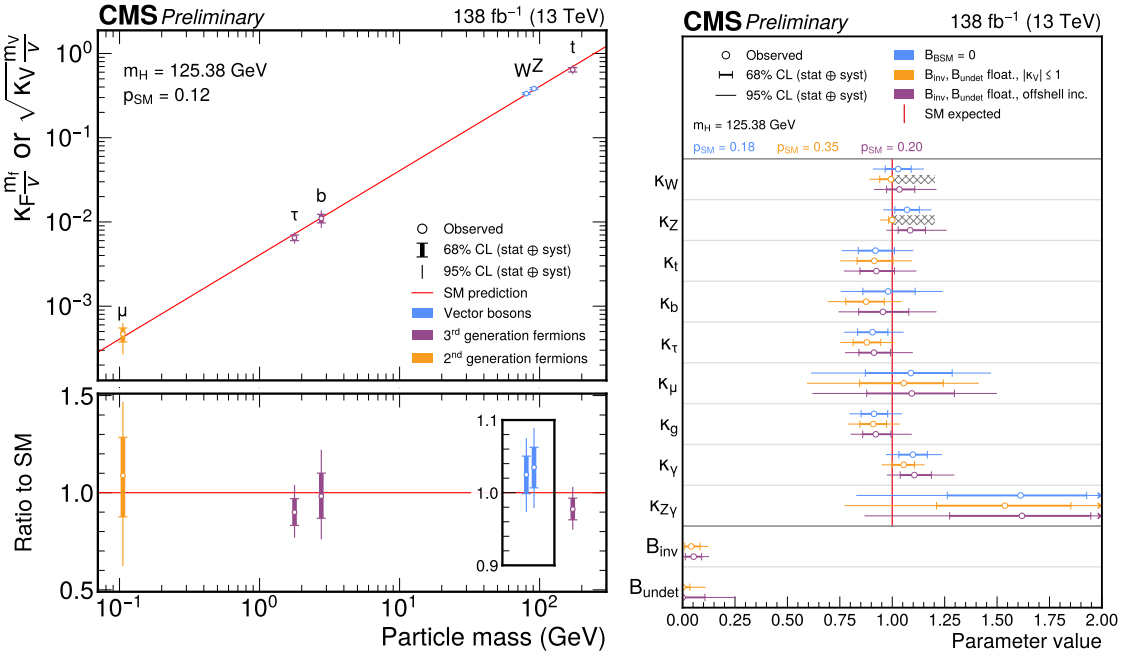

Figure 11.11: Reduced Higgs boson coupling strength modifiers and their uncertainties, CMS [239] (left). Combined measurements of coupling modifiers with various assumptions, CMS [239] (right). Equivalent plots for ATLAS can be found in Ref. [240].

$U(3)^5$ breaking (a.k.a. Minimal Flavor Violation), reduces the number of allowed SMEFT operators to 41. If NP breaks flavor by distinguishing the first two generations from the third one, the SMEFT operators only respect a $U(2)^5$ flavor symmetry, and a total of 124 SMEFT operators needs to be considered [289]. Further generalization are possible although most of the existing studies have so far considered the $U(3)^5$ and $U(2)^5$ benchmarks, or a hybrid $U(2)^3$ for quarks and $U(3)^2$ for leptons.

Given a set of $d = 6$ SMEFT operators generated at the UV scale Λ, their mixing under renormalization and the scale evolution of the corresponding Wilson coefficients is completely known at leading-order of SM interactions (QCD and EW). The tree-level matching conditions at the UV scale have been systematically calculated [290–293] and their evolution from Λ to the EW scale can be obtained via the LO anomalous dimensions of SMEFT operators [288,294,295]. A variety of tools exist that allow to automatically perform both the matching at the UV scale [292,293,296] and the LO scale evolution [297–299]. Observables at the EW scale are either computed with independent codes or obtained with automated tools such as `MadGraph5_aMC@NLO` [300] interfaced with SMEFT Feynman-rules generators such as `SMEFTsim` [301,302] or `SMEFT@NLO` [303]. They can be calculated including $d = 6$ effects at linear or quadratic order, although these last ones are technically of $O(1/\Lambda^4)$ and therefore of the same order in Λ as the effects generated by the $d = 8$ operators. Several studies have included them to quantitatively estimate their impact and test the validity of the EFT expansion.

Once the EFT formalism is in place, it can be used either *top-down* with a specific UV-completion in mind and a specific decoupling scale Λ or *bottom-up* when no or little assumptions are made on the BSM physics above a generic scale Λ. In the first case the matching to the SMEFT at the given scale Λ can be calculated at the desired perturbative order, singling out only a limited number of operators that are generated by such theory and testing how they can successfully reproduce the EW and low-energy phenomenology. Vice versa, if the UV theory is not known, the Wilson coefficients at the scale Λ are fitted, together with the SM parameters, to existing data and information on the UV theory is obtained. In this last case, the fit will identify preferred $c_i(\Lambda)/\Lambda^2$ ratios, such that from perturbativity arguments a lower bound on the scale of new physics Λ can be placed.

The Higgs-boson mass, width, branching ratios, as well as total and differential cross sections can be calculated in the SMEFT in terms of Wilson coefficients at the EW scale and the role of different SMEFT operators can be constrained by comparing to LHC experimental measurements. Individual Higgs-boson couplings can be expressed in terms of SMEFT Wilson coefficients such that their deformation can be related to effects in non-Higgs related observables. In fact, through the EFT formalism individual operators both mix by the effect of SM radiative corrections and at the same time contribute to multiple processes, not only Higgs-boson related, such that considering their broad impact can stress-test the SMEFT framework and isolate the regions of SMEFT parameters that are phenomenologically allowed. An exhaustive review of the SMEFT and its phenomenological studies, including studies limited to specific Higgs-boson observables and assuming different orders of SM effects, can be found in [277] (and references therein). Among them, several recent studies have presented individual and global fits of SMEFT Wilson coefficients that consider a broad spectrum of observables including Higgs-boson production and decay rates as well as STXS, top-quark rates and asymmetries, electroweak precision observables and diboson production, Drell-Yan observables, jet production cross sections, and flavor observables [304–312].

As an illustration, Fig. 11.12 shows the result of a global fit of SMEFT operators containing the SM scalar field ϕ, and hence directly affecting Higgs-boson observables, but also being constrained by electroweak, top-quark, Drell-Yan, and flavor observables through renormalization group evolution (RGE). The lower plot gives the 95% probability bounds obtained on the $C_i(\Lambda)/\Lambda^2$ coefficients, while the upper plot translates those bounds into a lower bound on the scale of new physics (normalized by the square root of the maximum of the 95% Highest Posterior Density Interval, or HPDI, for $|C_i|$). Both panels show results for the three cases 1)$\Lambda = 10$ TeV with RGE, 2) $\Lambda = 3$ TeV with RGE, and 3) $\Lambda = 1$ TeV with no RGE. Furthermore, the horizontal lines indicate the maximum value allowed for each Wilson coefficient in the fit, corresponding to the perturbativity limit (4π), for the different values chosen for the scale Λ. The cases in which the 95% HPDI interval touches the prior's edges are hatched with red diagonal lines, indicating that the fit is just returning what assumed in the prior and further precision in the determination of the most con-

Int. J. Mod. Phys. A 2026.41. Downloaded from www.worldscientific.com
by UNIVERSITY OF CALIFORNIA @ BERKELEY on 09/16/26. Re-use and distribution is strictly not permitted, except for Open Access articles.

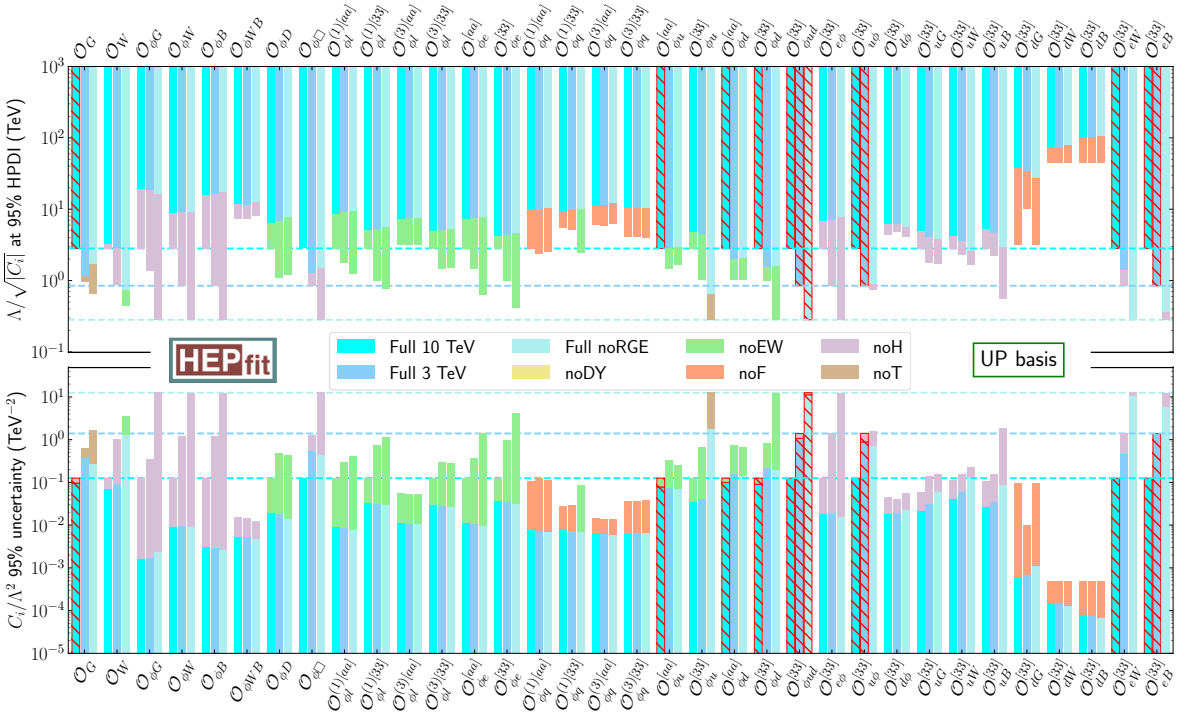

Figure 11.12: Results from a global fit in the $U(2)^5$ flavor-symmetric SMEFT (from Ref. [304]). For each coefficient C_i, the bottom panel shows the width of the 95% probability range divided by two, while the top panel shows the (normalized) scale of new physics allowed by the data at 95% probability. Each case includes results obtained for different values of Λ and removing the most constraining data set for that particular coefficient. The color code is as explained in the legend (see text for more details).

straining observables is needed. When the posterior distribution of a coefficient is completely flat, indicating that more observables need to be included in the fit, the 95% HPDI interval is hatched with diagonal white lines. The role of Higgs-boson measurements of signal strengths and STXS on several new physics interaction is manifest (see difference between blue and purple bounds). More details can be found in Ref. [304].

Overall, several operators that directly affect leading Higgs-boson production or decay modes are strongly constrained by LHC measurements, while operators whose main role is to affect e.g. high-p_T^H distributions are still marginally constrained, due to limited statistics in the experimental measurements, but their effects will be within the reach of the HL-LHC sensitivity. At the same time, several correlations have emerged with operators that are mainly constrained by non-Higgs observables, such that precision measurements of SM parameters, top-quark couplings, and Drell-Yan cross sections will provide very constraining complementary information.

In addition to the global fits prepared by theoretical groups, ATLAS and CMS have published interpretations of the Higgs boson measurements discussed in this document in terms of EFT constraints. The studies range from interpretations of differential cross sections or of STXS measurements (see for instance Refs. [239, 251, 311]) to analyses based on the construction of dedicated observables sensitive to specific operators. Several examples of the latter, related to CP properties, will be discussed in Section 11.3.9. Finally, first attempts by the collaborations to perform global fits including data from LHC Higgs boson, EW vector boson, top quark, and multi-jet measurements, and also EWPO measurements from LEP and SLC, have been reported in Refs. [312, 313].

11.3.6 *Higgs-boson Self-Couplings*

One of the most important open questions in the field is the precise mapping of the Higgs potential and the exploration of the inner workings of the EWSB mechanism. Probing the structure of the Higgs potential has deep implications in several areas of fundamental physics, including electroweak phase transitions, baryogenesis, and early universe cosmology (see Section 11.2.4).

As discussed in the introduction (see Eq. 11.8), in the SM the Higgs potential can be decomposed in a Higgs-field mass term and two self-interaction terms, one trilinear and one quadrilinear in the Higgs-boson field. In the SM they can both be expressed through the unique self-coupling $\lambda_{SM} = \frac{m_H^2}{2v^2}$, but in the presence of new physics they could be interpreted as independent effective interactions expressed through different self-coupling parameters λ_3 and λ_4. In the spirit of the κ framework described in Section 11.3.5.1, these self-couplings can be parameterized by modifiers κ_3 and κ_4, both equal to 1 in the SM:

$$\kappa_3 = \frac{\lambda_3}{\lambda_3^{\rm SM}}, \quad \kappa_4 = \frac{\lambda_4}{\lambda_4^{\rm SM}}. \tag{11.22}$$

Probing these couplings is one of the central goals of the HL-LHC program. Current datasets do not yet provide sufficient sensitivity to directly measure κ_3 or κ_4. However, κ_3 can already be constrained through studies of Higgs pair production ($pp \to HH$). See Figure 11.4 for the main Feynman diagrams for HH production at the LHC. Single Higgs production processes also provide indirect sensitivity to κ_3 through global fits. In contrast, probing κ_4 directly requires access to triple Higgs production ($pp \to HHH$), which has an extremely low cross section in the SM and is out of reach even for the HL-LHC. Nevertheless, recent analyses have begun placing first experimental constraints on κ_4.

i. *Higgs Pair Production at the LHC*

The theory of double-Higgs (HH) production is discussed in Section 11.2.5.1. This process has not been observed yet at the LHC due to its very small production cross section in the SM. We recall that the N3LO+N3LL prediction for $\sigma_{\rm ggF}^{HH}$ is $33.46^{+0.88\%}_{-0.85\%}$ fb

Int. J. Mod. Phys. A 2026.41. Downloaded from www.wo
by UNIVERSITY OF CALIFORNIA @ BERKELEY on 09/16/26. Re-use and distribution is
except for Open Access articles.

at the 13 TeV LHC (see Sec. 11.2).

Experimentally, the most sensitive final states are HH $\to \gamma\gamma b\bar{b}$, HH $\to \tau\tau b\bar{b}$, HH $\to b\bar{b}b\bar{b}$, which benefit from the larger branching fraction of $b\bar{b}$ decays and the identification of the diphoton or ditau pair. Other decay modes, such as $VVb\bar{b}$, multilepton final states, and other final states involving tau leptons, are more limited in sensitivity, though they can provide complementary information and can help to constrain specific regions of phase space in a combined HH global fit.

The study of HH production provided the best avenue to access the trilinear self-coupling κ_3 at the LHC. Variations in the value of the κ_3 affect not only the total yield of HH events produced, but also the shape of key kinematical distributions such as the mass of the HH system. These changes need to be taken into account in the analysis for an optimal sensitivity to the self-coupling. Furthermore, a precise knowledge of the top-Yukawa coupling is needed. The best measurements of the HH production and of κ_3 require different optimizations that probe different regimes in p_T^H: lower for the measurement of κ_3 and higher for the observation of HH production.

ATLAS Ref. [183] and CMS Ref. [184] have placed limits at 95% CL on HH production cross section through the combination of all available Run-2 analyses, for an integrated luminosity of up to 140 fb^{-1} at 13 TeV. The results target the dominant ggF production and the subleading qqHH production, which provides access to the VVHH vertex and enables constraints on the κ_{2V} parameter. The experiments are starting to explore also rarer production modes, like VHH [314, 315] or ttHH production modes [316].

The latest observed and expected upper limits on the HH production signal strength at 95% CL for ATLAS Ref. [183] and CMS Ref. [184] are:

$$\begin{aligned} \text{ATLAS:} \quad & \mu_{\text{HH}} < 2.9 \quad (\text{expected}: 2.4)\,, \\ \text{CMS:} \quad & \mu_{\text{HH}} < 3.5 \quad (\text{expected}: 2.5)\,. \end{aligned} \tag{11.23}$$

For the VBF production mode the upper limits are $\mu_{\text{VBFHH}} <$ 44 (47) (ATLAS) and $\mu_{\text{VBFHH}} < 79$ (91) (CMS) also at 95% CL. These HH combinations yield the following constraints on the coupling modifiers κ_3 and κ_{2V}:

$$\begin{aligned} \text{ATLAS:} \quad & -1.2 < \kappa_3 < 7.2 \quad (-1.6 < \kappa_3 < 7.2 \quad \text{expected})\,, \\ & 0.6 < \kappa_{2V} < 1.5 \quad (0.4 < \kappa_{2V} < 1.6 \text{ expected})\,. \\ \text{CMS:} \quad & -1.39 < \kappa_3 < 7.02 \quad (-1.02 < \kappa_3 < 7.19 \quad \text{expected})\,, \\ & 0.62 < \kappa_{2V} < 1.42 \quad (0.69 < \kappa_{2V} < 1.35 \quad \text{expected})\,. \end{aligned} \tag{11.24}$$

These results have been combined in a joint ATLAS and CMS study of HH production using Run-2 data [317], including the most sensitive channels from each experiment, with integrated luminosities ranging between 126 and 140 fb^{-1}. An observed 95% CL upper limit on $\mu_{HH} < 2.5$ is set, with an expected value of 1.7 (2.8) assuming the absence (presence) of the SM HH signal. The HH signal strength is measured to be $0.8^{+0.9}_{-0.7}$, for an observed significance of 1.1 standard deviations (1.3 expected for the SM HH signal). Corresponding constraints are set on the couplings, also at 95% CL: $-0.71 < \kappa_3 < 6.1$ and $0.73 < \kappa_{2V} < 1.3$.

ATLAS and CMS have extended the study of HH production to new physics scenarios using the HEFT frameworks [184,318]. The results are interpreted in terms of constraints on HEFT operators and the correlation between them. They are also presented in terms of upper limits on specific benchmarks proposed by the LHC Higgs Working Group. In Ref. [318], constraints on individual SMEFT operators are also proposed, while in Refs. [184, 318] the possibility of constraining HEFT operators whose coefficients, at the lowest order, are in direct correspondence with κ modifiers, is also explored. Overall, the results are consistent with the SM predictions. For more details, see the original references.

The Higgs pair searches can be combined with single-Higgs coupling measurements. We can exploit the complementarity between single-Higgs and di-Higgs processes to simultaneously probe multiple Higgs boson couplings, including the self-coupling and the top-quark Yukawa coupling. A joint fit enables the simultaneous constraint of key Higgs boson couplings such as κ_t, κ_V, κ_3, and κ_{2V}, and the study of their correlation. For the latest experimental $H + HH$ constraints see Refs. [319, 320].

Given the statistically limited nature of the Higgs boson pair production analyses and the ongoing advancements in experimental techniques, incorporating data from the LHC Run 3 is of particular importance. The first analysis utilizing the Run 3 dataset is presented in Ref. [321], where ATLAS presents a search for HH production in the $b\bar{b}\gamma\gamma$ final state using a combined dataset of 140 fb^{-1} at 13 TeV and 168 fb^{-1} at 13.6 TeV. This search sets a 95% CL upper limit on the signal strength of $\mu_{HH} < 3.8$, and constrains the Higgs boson self-coupling to $-1.7 < \kappa_3 < 6.6$. CMS has recently made public their first Run 3 search for this final state, for an integrated luminosity of 61.9 fb^{-1} at 13.6 TeV (2022-2023) [322]. They report a limit on the signal strength of $\mu_{HH} < 11.0$ (7.3) and a constraint on the self-coupling of $-5 < \kappa_3 < 12$ using a two-dimensional fit to the diphoton and dijet mass observables. CMS has also released a study of the $HH \to 4b$ final state using the same dataset [323]. The analysis sets observed (expected) upper limits of $\mu_{HH} < 4.4$ (4.4), as well as couplings constraints of $-3.3 < \kappa_3 < 9.7$, and $0.63 < \kappa_{2V} < 1.43$. Compared to previous LHC results in this final state, the sensitivity for an equivalent integrated luminosity shows a very significant improvement. Although these results do not yet exceed the sensitivity of the full Run 2 combinations, they clearly demonstrate the power of the Run 3 dataset and its potential to significantly improve κ_3 constraints already in the near term.

Projections for the HL-LHC, shown in Figure 11.13, indicate that each experiment can achieve a sensitivity better than 4σ by the end of the HL-LHC [266]. The combined ATLAS+CMS significance will result in an expected $> 5\sigma$ observation of the process already with 2 ab^{-1}. The uncertainty on the κ_3 parameter is projected to be better than 30% at 3ab^{-1}, with the statistical uncertainty expected to remain dominant. Ongoing improvements in analysis techniques are likely to outperform this expectation. Projections for κ_{2V} based on the performance of the ATLAS boosted VBF 4b analysis [324] search yield a precision of about 13% with 3 ab^{-1}.

ii. *The Hunt for Triple Higgs Boson Production*

Recent studies have focused on the extremely rare HHH production. Although the SM cross section for this process is far below the LHC sensitivity, its direct access to the Higgs quartic self-coupling λ_4 has motivated the first experimental attempts to constrain potential deviations from the SM prediction.

ATLAS placed a first 95% upper limit of 59 fb on the cross section for SM HHH production through the 6b final state, using the full Run-2 dataset [325] . This limit is equivalent to 760 times the SM cross section (750 expected). Assuming $\kappa_3 = 1$ then κ_4 is constrained to $-230 < \kappa_4 < 240$ at 95% CL (both for expected and observed limits). CMS has searched for HHH in the final states with four b jets and two photons [326] and six b jets [327] with the full Run-2 dataset. The observed (expected) 95% CL upper limits on the inclusive HHH production cross section are found to be 244 (152) fb and 44 (43) fb, respectively. They can be translated to constraints of $-533 < \kappa_4 < 541$ ([-397,406] expected) and $-190 < \kappa_4 < 190$ ([-190,190] expected), also at 95% CL. In these analyses simultaneous constraints of κ_3 and κ_4 are also explored. The ATLAS 4b results have been projected to the end of the HL-LHC, yielding a limit on HHH production that amounts to 86 times the SM expectation. This is a conservative estimation, since more final states will be explored in the future.

11.3.7 *Higgs-Boson Mass Measurements*

The mass of the Higgs boson is not predicted by the SM and must be determined experimentally. A precise determination of its value is therefore an essential input to all theoretical predictions of Higgs boson production cross sections and decay branching ratios. And, as discussed in Section 11.2, the Higgs boson mass not only plays a key role in Higgs phenomenology but also has fundamental consequences for the structure and long-term stability of the electroweak vacuum.

Int. J. Mod. Phys. A 2026.41. Downloaded from www.worldscientific.com
by UNIVERSITY OF CALIFORNIA @ BERKELEY on 09/16/26. Re-use and distribution is strictly not permitted, except for Open Access articles.

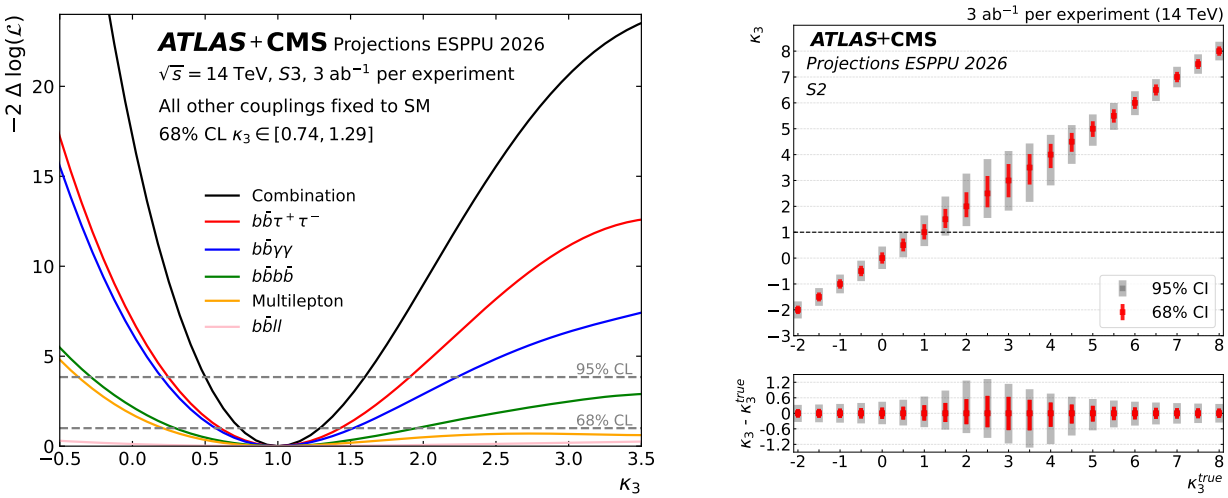

Figure 11.13: (Left) Expected ATLAS+CMS κ_3 likelihood scans for single decay channels and the combination for 3ab^{-1}, fixing $\kappa_3 = 1$ (Right) Precision on κ_3 as a function of its value [266].

The precision measurements of the Higgs boson mass at the LHC are based on two decay channels: $\gamma\gamma$ and $ZZ^*/4\ell$. These channels allow for a complete reconstruction of the decay products and provide mass resolutions that range from 1.4 GeV to 2 GeV for ATLAS and from 1.0 GeV to 2.8 GeV for CMS (see Ref. [328] and the reconstruction-performance references therein). The diphoton channel provides a larger sample of Higgs bosons but with a much larger background. The four-lepton channel has less signal events, but a much smaller background and better mass resolution. The measurements require a precise calibration of the energy and momentum scales for electrons, muons, and photons. The electron and muon calibrations are based primarily on the large $Z \to ee$ and $Z \to \mu\mu$ data samples, taking advantage of the precisely known mass of the Z boson. Since photons interact differently from electrons, an extrapolation from the electron calibration is necessary, which introduces additional systematic uncertainties.

ATLAS and CMS have published many Higgs boson mass measurements using both the Run 1 and Run 2 datasets. The most precise results from both experiments are summarized below:

- The most precise measurement of the Higgs boson mass was obtained by ATLAS using the Run 1 and Run 2 datasets by combining the diphoton and ZZ channels [329]. This yielded a mass of:

$$m_H = 125.11 \pm 0.09\,(\text{stat.}) \pm 0.06(\text{syst.})\ \text{GeV}.$$

- The most precise diphoton channel measurement was obtained by ATLAS [330], combining their Run 1 and Run 2 measurements. The mass was measured to be:

$$m_H = 125.22 \pm 0.11\,(\text{stat.}) \pm 0.09(\text{syst.})\ \text{GeV}.$$

  The systematic uncertainty of 90 MeV is worth noting, as it results from a highly challenging calibration procedure and the estimation of the material upstream of the calorimeter, which is required to extrapolate the calorimeter energy response from electrons in Z boson decays to photons. This result is promising for future precision measurements in this channel. In addition, ATLAS estimated the expected effect of the interference between the signal and the gluon fusion continuum di-photon background to be about 24 MeV (Ref. [330]).
- The most precise four-lepton channel result was obtained by CMS [231], combining the Run 1 and Run 2 measurements. This yielded a mass of :

$$m_H = 125.08 \pm 0.10\,(\text{stat.}) \pm 0.05(\text{syst.})\ \text{GeV}.$$

  It is the most precise single-channel measurement at the LHC. Since the result is dominated by the statistical uncertainty of 100 MeV, this channel will very likely continue to yield the most precise measurements in the future as the sizes of the data sets increase.

The ATLAS and CMS collaborations combined their mass measurements using the Run-1 dataset [328] yielding

$$m_H = 125.09 \pm 0.21\,(\text{stat.}) \pm 0.11(\text{syst.})\ \text{GeV}.$$

The mass combination using the full Run-2 datasets of the two collaborations will significantly improve our knowledge of the Higgs boson mass, given the doubling of the signal sample and the fact that most uncertainties are uncorrelated. It will be a useful input to future SM predictions and for the LHC combination of current and future Higgs boson measurements.

11.3.8 *Higgs-boson Width Measurements*

In the SM, the Higgs boson width is very precisely predicted once the Higgs boson mass is known. For a mass of 125 GeV, the Higgs boson has a very narrow width of 4.1 MeV [57]. It is dominated by the fermionic decays partial width at approximately 75%, while the vector boson modes are suppressed and contribute 25% only.

In proton-proton collisions such as the ones at the LHC only the cross sections times branching fractions can be measured in all production modes. As a consequence, the total width of the Higgs boson cannot be directly derived form the measurements of Higgs boson rates without additional assumptions. Direct constraints on the Higgs boson width are much larger than the expected width of the SM Higgs boson. Indirect constraints, subject to assumptions, with all the statistics of the HL-LHC will constrain the measurement only to the $\approx 20\%$ level. In contrast, a future Higgs factory would be able to constrain the width to the level of 1% through the recoil against a Z boson in $e^+e^- \to ZH$ events [194]. The different approaches at LHC and the latest experimental measurements are discussed in the following.

11.3.8.1 *Direct constraints*

Analyses of the reconstructed mass line-shape in the two channels with a good mass resolution, the $H \to \gamma\gamma$ and $H \to ZZ^{(*)} \to 4\ell$ channels, allow for a direct measurement of the width of the SM Higgs boson. The intrinsic mass resolution in these channels is much larger than the expected width of the SM Higgs boson. As a result, only upper limits on the Higgs boson width have been set by ATLAS [331] and CMS [231]. The two main challenges of direct constraints on the width through the

Int. J. Mod. Phys. A 2026.41. Downloaded from www.worldscientific.com by UNIVERSITY OF CALIFORNIA @ BERKELEY on 09/16/26. Re-use and distribution is except for Open Access articles.

measurement of the line-shape are: (i) the modeling of resolution uncertainties and (ii) the modeling of the interference between the signal and the continuum background which can be sizeable for large widths, in particular in the range where direct constraints are set. These challenges affect mostly the diphoton channel. Given that these interference effects are small with respect to the individual channels sensitivity, they are usually neglected in deriving constraints on the total width. The combined constraints, however, being more precise, could be affected by the interference. Direct lineshape measurements provide the most unambiguous access to the Higgs boson width, however constraints are still much larger than the expected SM width. The current results are fully compatible with the SM hypothesis.

CMS reported an upper limit on the total width of $\Gamma_H <$ 50 MeV at 68% CL (330 MeV at 95% CL) [231] for the $H \to ZZ^{(*)} \to 4\ell$ channel, using the 138 fb^{-1} collision dataset at 13 TeV. This is the most stringent constraint to date in this final state. Recently CMS followed this result with a new constraint in the diphoton channel [332] which considers the effect of the interference with the continuum, for the first time at the LHC. See more details in the following section.

11.3.8.2 *Constraints in the diphoton channel*

In the diphoton channel, it was noticed in Refs. [236, 333–335] that the effect of the interference between the main signal $gg \to H \to \gamma\gamma$ and the continuum irreducible background $gg \to \gamma\gamma$, taking into account detector resolution effects, is responsible for a non negligible mass shift. A similar interference effect is found between $q\gamma \to \gamma\gamma$ and $q\gamma \to H \to \gamma\gamma$. The size of the mass shift depends on the total width of the Higgs boson and it was suggested that measuring this mass shift could provide a constraint on the width [333]. It was further noticed that the mass shift has a dependence also on the diphoton transverse momentum. The total width of the Higgs boson could therefore be constrained using the diphoton channel alone.

Furthermore, Ref. [336], reported that the interference between the main signal $gg \to H \to \gamma\gamma$ amplitude and the continuum irreducible background $gg \to \gamma\gamma$ amplitude generates non-negligible change in the on-shell cross sections, as a result of the existence of a relative phase between these amplitudes. The size of this on-shell interference effect depends on the total width of the Higgs boson and it was suggested that measuring this on-shell cross section precisely could provide a constraint on the Higgs total width. This interference effect yields a reduction of around 2% for the $gg \to H \to \gamma\gamma$ cross section measurement in the SM. The current evaluation of this interference effect is performed at NLO and has a $^{+50\%}_{-30\%}$ uncertainty, due to the fact that the large relative phase is driven by the two-loop $gg \to \gamma\gamma$ background amplitude [236, 333, 336]. This on-shell interference effect has a dependence on the p_T of the diphoton system and the photon polar angle in the diphoton rest frame, which can be further exploited to improve the measurement to constrain the Higgs total width. Taking the ratios of the on-shell cross section of the Higgs boson to diphoton channel and the cross section of the Higgs boson to four-leptons channel where the interference effect is negligible could put a bound on the Higgs boson total width. This ratio is free from many dominant sources of systematic uncertainties for cross section measurements, i.e., PDF uncertainty and luminosity uncertainty, and can be further improved by the accumulation of the LHC data.

Experimental studies were performed to estimate the size of these effects [330, 337]. As discussed in Section 11.3.7, the estimation of the expected mass shift in the diphoton channel in ATLAS is 24 MeV. Very preliminary studies of the sensitivity of the mass shift method to estimate the width of the Higgs boson in the HL-LHC were made by ATLAS [338] and yielded an expected 95% CL upper limit on the total width of approximately 200 MeV from 3 ab^{-1} of 14 TeV data. Similarly, a preliminary estimation of the current limit from the cross section ratio measurement and the the interference effect set constraints of 60 MeV for 3 ab^{-1} of 14 TeV data [339].

These projections are superseded by a new Run-2 result by CMS that reports the first Higgs width constraint in the diphoton channel exploiting the effect of interference [332]. It uses the $H \to \gamma\gamma$ lineshape and studies the distortions in the mass spectrum caused by the interference between $gg \to H \to \gamma\gamma$ and the continuum $gg \to \gamma\gamma$ background. The measurement yields an upper limit of $\Gamma_H < 92$ (138) MeV at 95% CL and is the most stringent Γ_H constraint to date using measurements of on-shell Higgs boson final states.

11.3.8.3 *Indirect constraints from off-shell couplings*

The total width of the Higgs boson can also be constrained through the simultaneous analysis of on-shell and off-shell production measurements in the VV channel [232, 233]. In the off-shell regime, introduced in Section 11.2.5.3, production in the VV final state is enhanced when the invariant mass exceeds $2m_V$ and both vector bosons become on-shell. This enhancement partially offsets the decline in Higgs boson production away from its mass peak and enables the measurement described here.

The signal strength measurements for on-shell $\mu_{\text{on-shell}}$ and off-shell $\mu_{\text{off-shell}}$ for a given production mechanism j can be expressed in terms of coupling modifiers g_p and g_d for production and decay respectively. The corresponding cross-sections are given by Eq. 11.12, repeated here for completeness:

$$\begin{aligned} \sigma_j^{\text{on-shell}} &\propto \frac{g_p^2 g_d^2}{\Gamma_H} \propto \mu_j^{\text{on-shell}} \quad \text{and} \\ \sigma_j^{\text{off-shell}} &\propto g_p^2 g_d^2 \propto \mu_j^{\text{on-shell}} \Gamma_H \end{aligned} \tag{11.25}$$

Assuming that the coupling modifiers are identical in both regimes, the total Higgs boson width Γ_H can be extracted from the ratio of the measured on-shell and off-shell signal strengths. This measurement relies on the assumption that the ratio of couplings in the off-shell and on-shell regimes follows the SM prediction, that ggF is the dominant production mechanism, and that there are no significant contributions from BSM particles to the ggH loop within the mass range considered in the analysis. Another important aspect to consider is the sizable destructive interference between the Higgs boson signal and the non-resonant VV production in the off-shell region. This interference scales with $\sqrt{\mu_j^{on-shell}}$.

ATLAS and CMS have studied off-shell production in the $H \to ZZ \to 4\ell$ channel, and are able to exclude the background-only hypothesis $\mu_{\text{off-shell}} = 0$ with a significance of 3.7σ (2.4σ) observed (expected) for ATLAS [340] and 3.8σ (2.4σ expected) for CMS [231]. This corresponds to evidence for the off-shell production of a Higgs boson, through the measurement of a significant deficit in the overall $gg \to VV$ production. The measured total off-shell signal strengths $\mu_{\text{off-shell}}$, combining the 4ℓ and $2\ell 2\nu$ final states and the ggF, VBF and VH production modes, are the following:

$$\begin{aligned} &(\text{ATLAS}) \;\; \mu_{\text{off-shell}} = 1.06^{+0.62}_{-0.45}\,(\text{obs}) \;\; [1.00^{+0.83}_{-0.83}\,(\text{exp})], \\ &(\text{CMS}) \;\; \mu_{\text{off-shell}} = 0.67^{+0.42}_{-0.32}(\text{obs}) \;\; [1.00^{0.83}_{-0.84}\,(\text{exp})]. \end{aligned} \tag{11.26}$$

These off-shell production analyses exploit kinematic event characteristics to further gain in sensitivity to discriminate between the signal and background. From these measurements of the cross-section a constraint on the total width can be derived as mentioned above, following 11.25. The sensitivity to the Higgs width already reached at Run 2 is remarkable:

$$(\text{ATLAS}) \;\; \Gamma_H = 4.3^{+2.7}_{-1.9} \;\; [4.1^{+3.5}_{-3.4}\,(\text{exp})]\ \text{MeV}, \tag{11.27}$$

$$(\text{CMS}) \;\; \Gamma_H = 3.0^{+2.0}_{-1.5} \;\; [4.1 \pm 3.5\,(\text{exp})]\ \text{MeV}. \tag{11.28}$$

CMS has also derived results allowing for anomalous couplings of the Higgs boson [341], reducing the discriminating power of the kinematic variables used in the analysis but also mitigating the model dependence. Neither the results nor the sensitivities are significantly affected by allowing specific anomalous coupling parameters to float in the fits. The best fit of Γ_H in the anomalous couplings scenario ranges from $\Gamma_H = 2.7^{+2.1}_{-1.4}$ MeV to $\Gamma_H = 3.4^{+2.3}_{-1.8}$

Int. J. Mod. Phys. A 2026.41. Downloaded from www.worldscientific.com
by UNIVERSITY OF CALIFORNIA @ BERKELEY on 09/16/26. Re-use and distribution is strictly not permitted, except for Open Access articles.

MeV, depending on the coupling addressed. CMS has also investigated the impact of heavy particles in the ggH loop, through the introduction of a new heavy quark with an unconstrained coupling strength κ_Q [231]. This scenario results in less stringent limits on Γ_H, though largely consistent with the previous quoted values. The resulting Γ_H measurement in this case is $\Gamma_H = 2.7^{+2.7}_{-1.8}$ MeV (expected $4.1^{+5.5}_{-4.1}$). More details can be found in Refs. [341] and [231], respectively.

ATLAS has recently applied the "on-shell to off-shell" technique to constrain the total width of the Higgs boson in the $H \to WW \to 2\ell 2\nu$ decay mode the 140 fb^{-1} Run-2 dataset [342]. The analysis sets an observed (expected) 95% CL upper limit on the rate of off-shell Higgs boson production at 3.4 (4.4) times the SM prediction. This translates into an observed (expected) upper limit on the Higgs boson total width of 13.1 (17.3) MeV. ATLAS has applied a similar on-sell to off-shell logic to $t\bar{t}H$ production, assuming the tree-level Higgs-top Yukawa coupling is the same in the on-sell and off-sell regimes. The measurements of on-shell $t\bar{t}H$ production and four-top-quark production, which includes contributions from off-shell processes, are combined to yield an observed (expected) 95% CL upper limit of 450 MeV (75 MeV). Considering as well the constraint on the Higgs-top Yukawa coupling from loop-induced Higgs boson production and decay processes improves this result down to 160 MeV (55 MeV) [343].

Finally, ATLAS and CMS performed a study of the prospects for HL-LHC for measuring the Higgs boson width in the four lepton channel using the on-shell to off-shell method. Within assumptions similar to the ones mentioned above for the Run-2 measurements and assuming the SM central value, the width of the Higgs boson could be constrained with a $\approx 20\%$ precision with a luminosity of $3\,\mathrm{ab}^{-1}$ [344]:

$$\Gamma_H = 4.1^{+0.7}_{-0.8}\,\mathrm{MeV}. \tag{11.29}$$

11.3.9 *Higgs-boson Spin and CP Properties*

In the SM, the Higgs boson has quantum numbers $J^{PC} = 0^{++}$, meaning that it is a spin-0 particle, with even charge-parity (CP). The determination of the spin and CP quantum numbers of the observed Higgs boson is therefore an essential test of the theory. Alternative spin and parity hypotheses can be tested through measurements of the kinematic distributions of the particles produced in association with the Higgs boson or resulting from the Higgs boson's decay. The charge conjugation quantum number can be inferred by the fact that the observed particle decays to two photons: since charge conjugation is multiplicative and since photons are C-odd eigenstates, the observation of the decay to two photons implies that the observed neutral particle is C-even, if we assume C conservation.

The spin of a particle directly impacts the angular distributions and relative momenta of its decay products. For example, in the decay of a spin-0 particle, the matrix element does not depend on the production and decay angles in its rest frame, which results in isotropic distributions. In contrast, a spin-2 boson would generate characteristic angular modulations and correlations among final-state momenta.

Channels in which the Higgs boson decays can be fully or partially reconstructed provide sensitivity to spin-parity assignments, anomalous couplings, and possible CP-violating contributions. The most powerful channel in this respect is $H \to ZZ^* \to 4\ell$, where all final-state momenta are measured with high precision. The fully differential decay rate depends on seven observables: the invariant masses of the two lepton pairs, and five angles defined in the Higgs boson rest frame [345, 346]. These include the decay angles θ_1 and θ_2 (the angles between the negatively charged leptons and the directions of the Z_1 and Z_2 bosons in their respective rest frames), Φ (the angle between the decay planes of the two Z bosons), Φ_1 (the angle between the Z_1 decay plane and the production plane defined by the beam axis), and θ^* (the polar angle of the Z_1 boson relative to the beam axis). These observables, illustrated in Fig. 11.14, provide detailed information on the spin and CP structure of the Higgs boson and are used in both model-specific and effective field theory interpretations.

In this channel, both ATLAS and CMS have used matrix element-based kinematic discriminants and multivariate techniques to test alternative J^P hypotheses. The results show excellent agreement with the scalar (0^+) hypothesis and exclude a pure pseudoscalar (0^-) interpretation, as well as a wide range of spin-1 and spin-2 models, at high confidence levels [40].

Complementary information is provided by the $H \to WW^* \to \ell\nu\ell\nu$ decay channel. Although a full kinematic reconstruction is not possible due to the presence of neutrinos, spin correlations induced by the V–A structure of the W boson decay lead to distinctive patterns in the final-state leptons. In particular, for a scalar Higgs boson, the charged leptons tend to be emitted close together in the transverse plane, have a small invariant mass $m_{\ell\ell}$, and the transverse mass of the reconstructed Higgs boson candidate has a distinctive distribution. These kinematic features provide discrimination power between scalar, pseudoscalar, and higher-spin hypotheses. Both experiments have excluded spin-1 alternatives in this channel at the 95% confidence level or higher.

The $H \to \gamma\gamma$ channel contributes useful constraints on alternative spin-CP scenarios. For example, the production angle of the photons in the Collins–Soper frame is sensitive to the spin of the decaying boson. Spin-2 hypotheses predict markedly different distributions from spin-0 and have been excluded with high significance. Moreover, spin-1 hypotheses are strongly disfavored on theoretical grounds: the Landau–Yang theorem forbids the decay of a spin-1 particle into two identical massless vector bosons. While exotic models involving intermediate decays to collimated photons can evade this constraint, they are not consistent with global fits to the data and are tightly constrained by existing measurements.

In addition to information from the decay kinematics, production observables sensitive to the structure of the Higgs–vector boson and Higgs-fermion couplings have been exploited in channels such as vector boson fusion (VBF), and associated production channels (VH and ttH).

In summary, the combined data from ATLAS and CMS have excluded a pure pseudoscalar (CP-odd) Higgs boson and a range of spin-1 and spin-2 models at confidence levels that exceed 99%. These results are covered in more detail in previous reviews [40].

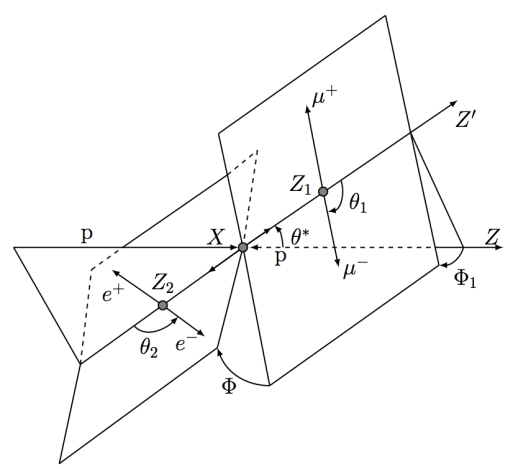

Figure 11.14: Definition of the production and decay angles defined for the $H \to ZZ^{(*)} \to 4\ell$ final state.

11.3.9.1 *CP-odd interactions and CP-mixing*

While a pure CP-odd hypothesis for the observed Higgs boson has been excluded at high confidence level, the presence of a small CP-odd admixture, which would signal CP violation in the Higgs sector, remains experimentally allowed. CP-odd interactions can be expressed in the framework of the SMEFT, formulated in various operator bases (as discussed in Section 11.3.5.2). This formalism aligns naturally with global analyses of a broader set of observables probing the Standard Model and its possible extensions. The CP properties inferred for the Higgs boson depend on the coupling being probed, since different inter-

Int. J. Mod. Phys. A 2026.41. Downloaded from www.worldscientific.com by UNIVERSITY OF CALIFORNIA @ BERKELEY on 09/16/26. Re-use and distribution is except for Open Access articles.

actions can exhibit different CP-mixing structures. In the context of Higgs boson interactions with electroweak bosons, the effective Lagrangian includes higher-dimensional operators constructed from the gauge-invariant combination $\Phi^\dagger\Phi$ and the electroweak field-strength tensors $W^I_{\mu\nu}$ and $B_{\mu\nu}$, defined prior to electroweak symmetry breaking. The CP-odd interactions are then encoded in three dimension-six operators: $\Phi^\dagger\Phi\,\tilde{W}^I_{\mu\nu}W^{I\mu\nu}$, $\Phi^\dagger\Phi\,\tilde{W}^I_{\mu\nu}B^{\mu\nu}$, and $\Phi^\dagger\Phi\,\tilde{B}_{\mu\nu}B^{\mu\nu}$, with corresponding Wilson coefficients $c_{H\tilde{W}}$, $c_{H\tilde{W}B}$, and $c_{H\tilde{B}}$, respectively.

It is important to note that CP-odd couplings of the Higgs boson to vector bosons are not allowed at tree level [347] and are therefore suppressed by Λ, the scale of new physics. However, CP-odd couplings of the Higgs boson to fermions are allowed at tree level, and these can be parametrised in a somewhat simpler way with the following Lagrangian, which accounts only for an additional pseudo-scalar term:

$$\mathcal{L}_0^{\psi_f} \supset \frac{\lambda_f}{\sqrt{2}}\left(\kappa_f H\overline{\psi}_f\psi_f + i\tilde{\kappa}_f H\overline{\psi}_f\gamma_5\psi_f\right). \tag{11.30}$$

This formulation is equivalent to the definition of the CP-mixing angle $\varphi_f = \tan\frac{\tilde{\kappa}_f}{\kappa_f}$.

It is interesting to note that CP-odd Higgs couplings to fermions can have sizable effects on low-energy observables, such as the electron electric dipole moment (EDM), which is both precisely measured and theoretically well understood [348, 349]. In particular, due to the large value of the top Yukawa coupling, CP-violating interactions involving the top quark are subject to stringent indirect limits. Current bounds on the electron EDM constrain the CP-odd top Yukawa coupling to values below $\tilde{\kappa}_t < 0.001$ [348], a level of precision that is extremely challenging to surpass with direct measurements at the LHC. It should be emphasized, however, that EDM experiments constrain the product of Yukawa couplings, in this case $\kappa_e \times \tilde{\kappa}_t$. As a result, assumptions must be made about the value of κ_e, which is itself not experimentally accessible at present.

By contrast, the constraints on the CP-odd Yukawa coupling of the tau lepton are considerably weaker. The current electron EDM bounds allow values as large as $\tilde{\kappa}_\tau < 0.3$ [348], leaving significant room for potential CP violation in the Higgs–tau sector. This makes direct searches for CP-odd or mixed CP Higgs couplings to taus particularly compelling. Such effects can be probed using kinematic observables sensitive to tau polarization in Higgs decays, as will be discussed in Sec. 11.3.9.3 of this review. For a discussion of searches for CP-odd couplings to vector bosons, we refer the reader to previous editions of this review [40].

With the full Run 2 dataset, analyses began to simultaneously exploit both the production and decay kinematics of the Higgs boson for CP measurements. This strategy is exemplified by the analysis of the $H \to ZZ^* \to 4\ell$, $H \to \gamma\gamma$, and $H \to WW^{(*)} \to \ell\nu\ell\nu$ channels, in both ATLAS and CMS, which combine information from the production and decay angles of the process with observables sensitive to VBF production [350, 351]. In addition, studies of off-shell Higgs boson production have provided complementary information on the CP structure of the Higgs–electroweak boson interaction [341].

Some of these studies make use of "optimal observables" constructed from matrix elements within the SMEFT framework. Specifically, they are defined as the ratio of the interference term between the SM and SMEFT amplitudes to the squared SM matrix element, evaluated for given values of the Wilson coefficients $c_{H\tilde{W}}$, $c_{H\tilde{W}B}$, and $c_{H\tilde{B}}$.

Tests of CP in the HVV coupling can also be probed with the VBF production process in the $H \to \tau^+\tau^-$ channel or in the WH($b\bar{b}$) channels. Some examples of such measurements performed by ATLAS [352] are shown in Fig. 11.15. All results are found to be in agreement with the SM expectations. CMS has performed an analysis using the VBF and VH production channels and has combined its results with the aforementioned ZZ^* channel using the same dataset [353].

These results emphasize the complementarity between production and decay observables and the power of a global strategy that combines all accessible experimental information to test the Higgs boson's properties.

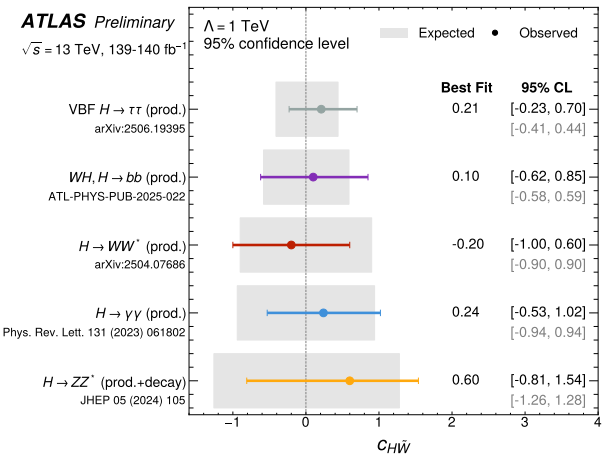

Figure 11.15: Comparison of results for the expected and observed measurements of the CP-odd Wilson coefficient $c_{H\tilde{W}}$ by ATLAS using the Run 2 dataset. The data and 95% confidence level (CL) bars show the observed values with statistical and systematic uncertainties, and the grey bands centered at zero show the expected 95% CL intervals. The test fit values and 95% CL observed (expected) limits are also explicitly listed on the rightmost side of the plot in black (gray). All couplings scale as $1/\Lambda^2$ with the assumed value of $\Lambda = 1$ TeV.

11.3.9.2 *Probing the $Hf\bar{f}$ coupling CP properties in $pp \to t\bar{t}H$ production*

As mentioned above, although EDM experiments provide stringent constraints on CP-violating effects in the top Yukawa sector, these limits are subject to model-dependent uncertainties. It is therefore important to probe such CP-violating effects through direct measurements. The associated production of a Higgs boson with a top-quark pair ($pp \to t\bar{t}H$) offers a powerful channel for this purpose. In particular, Run 2 data have provided enhanced sensitivity to the CP structure of the top Yukawa coupling, especially in final states where the Higgs boson decays to two photons. In this channel, angular and kinematic correlations between the Higgs boson and the top quarks offer sensitivity to possible CP-odd contributions.

Using the full Run 2 dataset, several Higgs boson decay channels have been studied in this context. In the $H \to \gamma\gamma$ channel, ATLAS excludes CP-mixing angles $\varphi_t > 43°$ and $\varphi_t < -43°$ at 95% confidence level [354]. More recently, constraints from the $H \to b\bar{b}$ channel have been reported, with a measured value of $\varphi_t = 11°\,^{+52°}_{-73°}$ [355].

Using the full Run 2 dataset, CMS [356] measured the CP-odd fraction of the top Yukawa coupling in the diphoton channel, defined as:

$$f_{CP} = \frac{|\tilde{\kappa}_t|^2}{|\kappa_t|^2 + |\tilde{\kappa}_t|^2} \times \text{sign}\left(\frac{\tilde{\kappa}_t}{\kappa_t}\right), \tag{11.31}$$

and obtained a value of $|f_{CP}| = 0.00 \pm 0.33$. A complementary constraint on the CP-odd fraction was also derived using the $H \to 4\ell$ channel [357]. More recently, CMS has analyzed the $t\bar{t}H$ multi-lepton channel, which is sensitive to both $H \to WW$ and $H \to \tau^+\tau^-$ decays, to further probe the CP properties of the top Yukawa interaction [358]. Combining this analysis with those from the diphoton and four-lepton channels, CMS obtained an updated constraint on the CP-odd fraction:

$$|f_{CP}| = 0.28^{+0.27}_{-0.28}. \tag{11.32}$$

In these analyses, events with both leptonic and hadronic top-quark decays were included to maximize acceptance and statistical power.

Int. J. Mod. Phys. A 2026.41. Downloaded from www.worldscientific.com
by UNIVERSITY OF CALIFORNIA @ BERKELEY on 09/16/26. Re-use and distribution is strictly not permitted, except for Open Access articles.

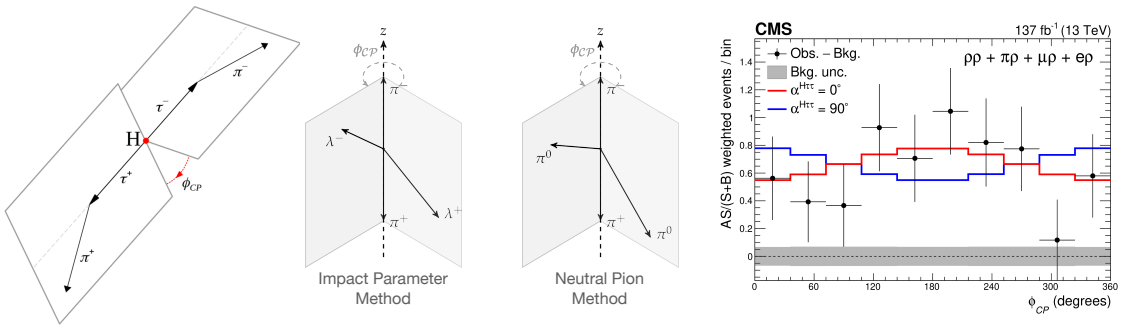

Figure 11.16: Sketch of the definition of the φ_{CP} angle for for the decays $\tau^\pm \to \pi^\pm \nu_\tau$ (left) and the definition at reconstruction level of φ_{CP} observables (center). The rightmost plot shows the distribution weighted per tau decay categories of the φ_{CP} observables, including the expected distributions for the expected pure scalar or pure pseudo scalar cases.

11.3.9.3 *Probing $Hf\bar{f}$ coupling CP properties in $H \to \tau^+\tau^-$ decays*

As discussed in Section 11.3.9.1, the decay of the Higgs boson to tau leptons provides opportunities to probe the CP properties of the $Hf\bar{f}$ coupling, thanks to the sensitivity of certain observables to tau polarization.

Using the full Run 2 dataset, CMS performed the first analysis of transverse spin correlations between the tau leptons in this final state [359]. These correlations are sensitive to the CP-mixing angle, which characterizes the relative contributions of scalar and pseudoscalar components in the Higgs–tau coupling. The transverse spin correlations manifest themselves through the angular distributions of the visible tau decay products, which are experimentally accessible.

In the case of the two-body decay of a tau lepton into a charged pion and a neutrino, the transverse momenta of the two charged pions tend to be anti-aligned for a scalar Higgs boson and aligned for a pseudoscalar. Consequently, the angle between the decay planes of the two tau leptons, as illustrated in Fig. 11.16 (left), is sensitive to the CP-mixing of the Higgs–tau coupling.

Since the tau direction cannot be reconstructed directly, the direction of the impact parameter is used as a proxy. The impact parameter is defined as the vector pointing from the interaction point to the point of closest approach of the charged pion track. In the Higgs boson rest frame, these directions are denoted by $\lambda^\pm$, as shown in Fig. 11.16 (center).

For multi-body tau decays—such as those proceeding via intermediate vector mesons like the ρ or $a_1(1260)$, the decay planes are constructed from the visible final-state particles. In the case of $\rho \to \pi^+\pi^0$, the decay plane is defined by the charged and neutral pion momenta. For $a_1 \to \pi^+\pi^0\pi^0$, the plane is typically defined using the charged pion and the combined momentum of the two neutral pions. These angular correlations provide sensitivity to the CP structure of the Higgs–tau interaction. The separation between pure scalar and pure pseudoscalar scenarios is illustrated in Fig. 11.16 (right). A similar analysis was performed by ATLAS [360]. The observed (expected) results are summarized below:

$$\begin{array}{lll} \text{ATLAS} & \varphi_\tau = 9^o \pm 16^o & (0^o \pm 28^o) \quad [359]\,, \\ \text{CMS} & \varphi_\tau = -1^o \pm 19^o & (0^o \pm 21^o) \quad [360]\,. \end{array}$$

The current experimental precision achieved by ATLAS and CMS is already comparable to the targets originally foreseen for the HL-LHC, as outlined in Ref. [361], which projected an angular resolution between $\pm 18°$ and $\pm 30°$.

11.3.9.4 *Implications of Higgs boson measurements on its CP properties*

Beyond the hypothesis testing performed in specific final states, the global consistency of measured Higgs production and decay kinematics, which assumes a spin-0, CP-even boson, provides compelling evidence for this assignment. Kinematic features, including transverse momentum spectra, jet correlations, and angular observables, have been measured with high precision across various production and decay channels. The excellent agreement with SM expectations implies that large deviations from the spin-0, CP-even scenario are highly disfavored. While small admixtures of non-SM CP-odd components in the coupling structure remain experimentally allowed, the data strongly support the conclusion that the observed particle is dominantly a spin-0 scalar with positive parity.

11.4 Beyond the Standard Model (BSM) Higgs boson

The discovery of a light scalar with couplings to gauge bosons and fermions that are consistent with SM predictions, together with the slow running of the Higgs boson self-coupling at high energies allow one to consider the SM as a valid perturbative description of nature all the way to the Planck scale. This picture is admittedly very attractive, but it posits that the Higgs boson is an elementary scalar field, whose mass has quantum sensitivity to possible new physics scales. As discussed in Section 11.1.3 this EW/Higgs naturalness problem [23] has become much more definite after the Higgs boson discovery at $m_H = 125$ GeV. Finding a more fundamental explanation of the origin of EWSB and of the EW scale is by itself a strong motivation to explore BSM theories that could induce the existence of the scalar sector of the SM as it has now been experimentally confirmed.

There are two broad classes of models addressing the naturalness problem[9], that we can in full generality classify as based on a weakly coupled or strongly coupled approach to EWSB. The first one is based on SUSY [24] (for comprehensive reviews, see Refs. [25,26]). This is a weakly coupled approach to EWSB, maintaining the perturbativity of the SM. The Higgs boson remains elementary and the corrections to its mass are screened at the scale at which SUSY is broken, generically identified with the soft SUSY breaking parameter, $M_{\rm SUSY}$. Provided $M_{\rm SUSY}$ is of order of a few TeV, the fine-tuning problem is solved, in the sense that the low energy mass parameters of the Higgs sector become insensitive to physics at the GUT or Planck scale. Another interesting feature of SUSY theories is related to the dynamical generation of EWSB [363]. While in the SM a negative Higgs-boson mass parameter μ^2 (see Eq. 11.2) needs to be inserted by hand to induce EWSB, in SUSY, even if the relevant Higgs mass parameter is positive in the ultraviolet, it may become negative and induce EWSB radiatively through the strong effect of the top quark-Higgs boson coupling in its renormalization group evolution [363]. The scalar sector of SUSY-based theories is a particular realization of a Two Higgs-Doublet Model (2HDM) that only extend the scalar sector of the SM by one extra complex $SU(2)$ doublet, under certain additional symmetry conditions. It predicts three neutral and a pair of charged Higgs particles [39]. One of the neutral Higgs bosons, most often the lightest CP-even one, has properties that can resemble those of the SM Higgs boson (at least in some regions of

[9] Another solution to the naturalness problem is to lower the fundamental scale of quantum gravity, like for instance in models with large extra-dimensions, see Ref. [362].

Int. J. Mod. Phys. A 2026.41. Downloaded from www.worldscientific.com by UNIVERSITY OF CALIFORNIA @ BERKELEY on 09/16/26. Re-use and distribution is except for Open Access articles.

the parameter space referred to as the alignment limit [364,365], which in the case of sufficiently heavy additional Higgs bosons is dubbed the decoupling limit [366,367]). Such scalar is referred to as a SM-like Higgs boson, meaning that its couplings are close to the ones predicted in the SM.

The other approach invokes the existence of strong interactions at a scale of the order of one TeV or above and these new interactions induce the breaking of the electroweak symmetry [368]. In the original incarnation, dubbed technicolor, the strong interactions themselves trigger EWSB without the need of a Higgs boson. Another possibility, compatible with the ATLAS and CMS discovery, is that the strong interactions produce four light resonances identified with the Higgs-field doublet and EWSB proceeds through vacuum misalignment [27] (see also Refs. [28, 29] for recent reviews). In that case, the Higgs boson itself has a finite size and thus never feels the UV degrees of freedom that would otherwise have dragged its mass to much higher scales. The Higgs boson could also correspond to the Goldstone boson associated with the spontaneous breaking of scale invariance, see Ref. [369] and references therein. However, this dilaton/radion scenario now requires a jumbled model-building to be consistent with the constraints from the coupling measurements. The idea that the Higgs boson itself could be a composite bound state emerging from a new strongly-coupled sector has been also reconsidered thanks to the insights gained from the AdS/CFT duality. The composite Higgs boson idea is a realization of EWSB via strong dynamics that smoothly interpolates between the standard technicolor approach and the true SM limit. To avoid the usual conflict with EW data, it is sufficient, if not necessary, that a mass gap separates the Higgs resonance from the other resonances of the strong sector. Such a mass gap can naturally follow from dynamics if the strongly-interacting sector exhibits a global symmetry, G, broken dynamically to a subgroup H at the scale f, such that, in addition to the three Nambu–Goldstone bosons of SO(4)/SO(3) that describe the longitudinal components of the massive W and Z, the coset G/H contains a fourth Nambu–Goldstone boson that can be identified with the physical Higgs boson. Modern incarnations of composite Higgs models have been recently investigated in the framework of 5D warped models where, according to the principles of the AdS/CFT correspondence, the holographic composite Higgs boson then originates from a component of a gauge field along the 5th dimension with appropriate boundary conditions. A last proposed ingredient in the construction of viable composite Higgs-boson models is the concept of partial compositeness [370], i.e., the idea that there are only linear mass mixings between elementary fields and composite states. After diagonalization of the mass matrices, the SM particles, fermions and gauge bosons, are admixtures of elementary and composite states and thus they interact with the strong sector, and in particular with the Higgs boson through their composite component. This setup has important consequences on the flavor properties, chiefly the suppression of large flavor-changing neutral currents involving light fermions. It also plays an important role in dynamically generating a potential for the would-be Goldstone bosons. Partial compositeness also links the properties of the Higgs boson to the spectrum of the fermionic resonances, i.e., the partners of the top quark. The bounds from the direct searches for the top partners, in addition to the usual constraints from EW precision data, force the minimal composite Higgs models into some unnatural corners of their parameter spaces [371].

Beyond models that directly address the problem of naturalness and the origin of the EWSB, NP explorations through the Higgs portal can be more agnostic and test the existence of exotic particles from unknown extensions of the SM. Among weakly-interactive theories derived from extended gauge symmetry groups (e.g. grand-unified theories [372]), many include extended scalar sectors, that involve scalar singlets, extra doublets, triplets, or even more complicated scalar multiplet structures. In these models, as for SUSY-inspired models, EWSB is realized in such a way to generate a physical scalar mass eigenstate with the property of the SM Higgs boson. However, the spectrum of physical scalars also includes a variety of extra heavier CP-even scalars, both neutral and charged, as well as CP-odd pseudoscalars, that can be searched for at the LHC. At the same time, many NP scenarios involve light scalar degrees of freedom, such as axion-like-particles [373].

All these BSM scenarios can have important effects on the phenomenology of the discovered Higgs boson and reveal themselves through precision measurements of its branching ratios, width, mass, and couplings. For instance, deviations from the SM Higgs-boson pattern of couplings, explored through the κ or EFT frameworks described in Section 11.3.5, could point to specific classes of BSM theories. At the same time, direct search for heavy scalar resonances decaying into SM particles or for exotic decays of the SM Higgs boson become essential to identify evidence of NP. Furthermore, in all cases, the role of the Higgs boson in the unitarization of scattering amplitudes is shared by other particles, not just scalar particles, which remain targets of experimental searches, both in the heavy and light mass regime [29, 373–375].

In the following, we will briefly recall the most relevant phenomenological implications of NP models that motivates existing BSM Higgs searches at the LHC. Because of their distinct phenomenology, they will be grouped into weakly- and strongly-coupled models, discussed in Sections 11.4.1 and 11.4.2 respectively. Constraints on exotic decays of the discovered Higgs boson will be presented in Section 11.4.3 and a comprehensive summary of existing searches for BSM scalars will be the subject of Section 11.4.4.

11.4.1 *Weakly coupled approach to EWSB*

11.4.1.1 *Higgs bosons in the Minimal Supersymmetric Standard Model (MSSM)*

The simplest realistic model of low-energy SUSY is the minimal SUSY extension of the SM (MSSM) [26, 376], that associates a SUSY partner to each gauge boson and chiral fermion of the SM, and provides a realistic model of physics at the weak scale. Of the more than 100 new parameters that are introduced in the general MSSM [26] only a subset of them impact the Higgs-boson phenomenology either directly at tree-level or through quantum effects.

The MSSM contains the particle spectrum of a 2HDM extension of the SM and the corresponding SUSY partners (see Section 11.4.1.2 for a brief overview of 2HDM). Two Higgs doublets, Φ_1 and Φ_2, with hypercharge $Y = -1$ and $Y = 1$, respectively, are required to ensure an anomaly-free SUSY extension of the SM and to generate mass for down-type quarks/charged leptons (Φ_1) and up-type quarks (Φ_2) [39]. The Higgs potential reads

$$\begin{aligned} V =& m_1^2 \Phi_1^\dagger \Phi_1 + m_2^2 \Phi_2^\dagger \Phi_2 - m_3^2 (\Phi_1^T i\sigma_2 \Phi_2 + \text{h.c.}) \\ &+ \frac{1}{2}\lambda_1 (\Phi_1^\dagger \Phi_1)^2 + \frac{1}{2}\lambda_2 (\Phi_2^\dagger \Phi_2)^2 + \lambda_3 (\Phi_1^\dagger \Phi_1)(\Phi_2^\dagger \Phi_2) \\ &+ \lambda_4 |\Phi_1^T i\sigma_2 \Phi_2|^2 + \frac{1}{2}\lambda_5 \left[(\Phi_1^T i\sigma_2 \Phi_2)^2 + \text{h.c.} \right] \\ &+ \left[[\lambda_6 (\Phi_1^\dagger \Phi_1) + \lambda_7 (\Phi_2^\dagger \Phi_2)] \Phi_1^T i\sigma_2 \Phi_2 + \text{h.c.} \right], \end{aligned} \tag{11.33}$$

where $m_i^2 = \mu^2 + m_{H_i}^2$ $(i = 1, 2)$, with μ being the supersymmetric Higgsino mass parameter and m_{H_i} the soft supersymmetric breaking mass parameters of the two Higgs doublets; $m_3^2 \equiv B\mu$ is associated to the B-term soft SUSY breaking parameter; and λ_i, for $i = 1$ to 7, are all the Higgs quartic couplings.

After the spontaneous breaking of the electroweak symmetry, five physical Higgs particles are left in the MSSM spectrum: one charged Higgs pair, $H^\pm$, one CP-odd neutral scalar, A, and two CP-even neutral states, H and h, with h being the lightest.[10] The Higgs sector at tree level depends on the electroweak gauge coupling constants and the vacuum expectation value v – or equivalently the Z gauge boson mass – and is determined by only two

[10] Observe that in the SM sections of this review, H denotes the SM Higgs boson, whereas in the sections about SUSY, or extensions of the SM with two Higgs doublets, H is used for the heaviest CP-even Higgs boson, since this is the standard notation in the literature, and the 125 GeV SM-like light Higgs boson will be denoted by h. Generically, in the MSSM, the lightest CP-even Higgs boson is indeed SM-like and thus it is naturally identified with the 125 GeV Higgs boson discovered by ATLAS and CMS, while in general 2HDM extensions, with or without SUSY, there could still be lighter scalar states below 125 GeV. To avoid confusion we will keep denoting the SM-like Higgs boson by h in the entire BSM Higgs section.

Int. J. Mod. Phys. A 2026.41. Downloaded from www.worldscientific.com by UNIVERSITY OF CALIFORNIA @ BERKELEY on 09/16/26. Re-use and distribution is strictly not permitted, except for Open Access articles.

free parameters: $\tan\beta$ - the ratio of the two Higgs doublets' vacuum expectation values v_2/v_1 - and one Higgs boson mass, conventionally chosen to be the CP-odd Higgs boson mass, m_A. The other tree-level Higgs boson masses are then given in terms of these parameters. The tree level value of m_h is maximized not only for $m_A \gg m_Z$ but also for $\tan\beta \gg 1$. For $m_A \gg m_Z$ it acquires a maximum value $m_h = m_Z \cos 2\beta$. Radiative corrections have a significant impact on the values of Higgs boson masses and couplings in the MSSM. They have been computed using a number of techniques, with a variety of approximations, see Ref. [377] for a recent review. The discovered SM-like Higgs boson, if interpreted as the lightest MSSM Higgs boson with a mass of about 125 GeV, provides information on the possible MSSM parameter space [26].

The phenomenology of the Higgs sector depends on the couplings of the Higgs bosons to gauge bosons and fermions [11]. At tree-level, the couplings of the two CP-even Higgs bosons to W and Z bosons are given in terms of the angles α, that diagonalizes the CP-even Higgs boson squared-mass matrix, and β

$$g_{hVV} = g_V m_V \sin(\beta-\alpha), \quad g_{HVV} = g_V m_V \cos(\beta-\alpha), \quad (11.34)$$

where $g_V \equiv 2m_V/v$, for $V = W$ or Z ($g_V m_V$ is the SM hVV coupling). Observe that in the limit $\cos(\beta-\alpha) \to 0$, the lightest CP-even Higgs boson h behaves as the SM Higgs boson. This situation is called alignment and is achieved in specific regions of parameter space for $m_A \geq m_Z$ [366] or in the large $m_A \gg m_Z$ limit, in which alignment is achieved through decoupling [366, 367]. There are no tree-level couplings of A or $H^\pm$ to VV. The couplings of the Z boson to two neutral Higgs bosons are given by $g_{\phi AZ}(p_\phi - p_A)$, where $\phi = H$ or h, the momenta p_ϕ and p_A point into the vertex, and

$$g_{hAZ} = g_Z \cos(\beta-\alpha)/2, \quad g_{HAZ} = -g_Z \sin(\beta-\alpha)/2\,. \quad (11.35)$$

The expressions of the couplings between a charged Higgs boson, a neutral Higgs boson and the W boson as well as the expressions of the four-point couplings of vector bosons and Higgs bosons can be found in Ref. [39].

The tree-level Higgs boson couplings to fermions obey the following property: the neutral components of one Higgs doublet, Φ_1, couple exclusively to down-type fermion pairs while the neutral components of the other doublet, Φ_2, couple exclusively to up-type fermion pairs [39]. This Higgs-fermion coupling structure corresponds to a Type-II 2HDM (see Section 11.4.1.2). In the MSSM, fermion masses are generated when both neutral Higgs components acquire a vacuum expectation value, and the relations between Yukawa couplings and fermion masses are (in third-generation notation)

$$y_{b,\tau} = \sqrt{2}\, m_{b,\tau}/(v\cos\beta), \quad y_t = \sqrt{2}\, m_t/(v\sin\beta)\,. \quad (11.36)$$

The couplings of the neutral Higgs bosons to $f\bar{f}$, relative to their SM values, $g\, m_f/(2m_W)$, are therefore given by

$$\begin{aligned} &hb\bar{b}: \ -\sin\alpha/\cos\beta, && ht\bar{t}: \cos\alpha/\sin\beta\,, \\ &Hb\bar{b}: \ \cos\alpha/\cos\beta, && Ht\bar{t}: \sin\alpha/\sin\beta\,, \\ &Ab\bar{b}: \ \gamma_5 \tan\beta, && At\bar{t}: \gamma_5 \cot\beta\,. \end{aligned} \quad (11.37)$$

In each relation above, the factor listed for $b\bar{b}$ also pertains to $\tau^+\tau^-$. The charged Higgs boson couplings to fermion pairs, normalized to $g/(\sqrt{2}m_W)$, are given by

$$\begin{aligned} &g_{H^- t\bar{b}}: m_t \cot\beta \frac{1+\gamma_5}{2} + m_b \tan\beta \frac{1-\gamma_5}{2}, \\ &g_{H^-\tau^+\nu}: m_\tau \tan\beta \frac{1-\gamma_5}{2}\,. \end{aligned} \quad (11.38)$$

The non-standard neutral Higgs bosons have significantly enhanced couplings to down-type fermions at sizable $\tan\beta$. Radiative corrections can modify significantly the values of the Higgs boson couplings to fermion pairs and to vector boson pairs, through a radiatively-corrected value for $\cos(\beta-\alpha)$ as well as from the one-loop vertex corrections to tree-level Higgs-fermion Yukawa couplings, see Ref. [26] and references therein, for a detailed discussion.

Given the outlined structure of the MSSM Higgs bosons couplings to SM fermions and gauge bosons the MSSM parameters have to be arranged such that the mass, the CP properties, as well as the decay and production properties of one of the neutral Higgs bosons agree with the LHC Higgs data. Given that present data allows only for moderate departures from the SM predictions, it implies that some degree of alignment is necessary.

The SM-like branching ratios of h can be modified if decays into SUSY particles are kinematically allowed, and, in particular, decays into a pair of the lightest SUSY particles – i.e., the lightest neutralinos, $\tilde{\chi}_1^0$, can become dominant and would be invisible if R-parity is conserved [380]. Moreover, if light superpartners exist and couple to photons and/or gluons, the h loop-induced coupling to gg and $\gamma\gamma$ could deviate sizeably from the corresponding SM predictions (see for instance the review [379]), and would be in conflict with present data (see Section 11.3.5). For the heavier Higgs states, there are two possibilities to be considered[12]:

i) Alignment triggered by decoupling, hence $m_A \geq$ several hundred GeV: the HWW and HZZ couplings are very small. The dominant H, A decay branching ratios strongly depend on $\tan\beta$. The decay modes $H, A \to b\bar{b}, \tau^+\tau^-$ dominate when $\tan\beta$ is large (this holds even away from decoupling). For small $\tan\beta$, the $t\bar{t}$ decay mode dominates above its kinematic threshold. For the charged Higgs boson, $H^+ \to t\bar{b}$ dominates.

ii) Some degree of alignment without decoupling, hence $m_A \leq$ a few hundred GeV: the main difference with the previous case is that, in the low $\tan\beta$ regime ($\tan\beta \leq 5$), additional decay channels may be allowed which involve decays into the lightest SM-like Higgs boson; $A \to Zh$, $H \to hh$ as well as $H \to WW/ZZ$ decay modes are available (they are suppressed in the strict alignment limit). When kinematically open, the decays $A/H \to t\bar{t}$ become relevant or even dominant for sufficiently small $\tan\beta$. For the charged Higgs boson, $H^+ \to \tau^+\nu_\tau$ dominates below the $t\bar{b}$ threshold, and also $H^\pm \to W^\pm h$ may be searched for.

In both cases i) and ii), the heavier Higgs states, H, A and $H^\pm$, are roughly mass degenerate (with masses $\pm$ 20 GeV or less apart). If kinematically allowed, the heavy Higgs boson decays into charginos, neutralinos and third-generation squarks and sleptons can be important [383].

At hadron colliders, the dominant neutral Higgs boson production mechanism at moderate values of $\tan\beta$ is gluon fusion, mediated by loops containing heavy top and bottom quarks and the corresponding SUSY partners. The effect of light stops that may contribute to the gluon fusion production can be partially cancelled by mixing effects. Higgs boson radiation off bottom quarks becomes important for large $\tan\beta$, where at least two of the three neutral Higgs bosons have enhanced couplings to bottom-type fermions [384, 385]. Detailed discussions of the impact of radiative corrections in these search modes are presented for instance in Ref. [386]. The vector boson fusion and Higgs-strahlung production of the CP-even Higgs bosons as well as the associated production of neutral Higgs bosons with top quark pairs have lower production cross sections by at least an order of magnitude with respect to the dominant ones, depending on the precise region of MSSM parameter space [56–59]. Higgs boson pair production of non-standard MSSM Higgs bosons has been studied in Ref. [387, 388]. For a discussion of charged Higgs boson production at LHC, see Refs. [56, 59, 389]. Strong production of a heavy neutral Higgs boson followed by its decay into top-quark pairs is a challenging channel, only most recently being searched for by ATLAS and CMS. Interference effects between the signal and the SM $t\bar{t}$ background need to be carefully taken into account [390, 391].

[11] Reviews of the properties and phenomenology of the Higgs bosons of the MSSM can be found for example in Refs. [26, 378, 379].

[12] In very special regions of the parameter space, there is still the possibility that the heavier CP-even Higgs state is identified with the 125 GeV Higgs boson discovered by ATLAS and CMS, see for instance the discussion in Ref. [381] and the benchmark M_H^{125} defined in Ref. [382].

Int. J. Mod. Phys. A 2026.41. Downloaded from www.worldscientific.com by UNIVERSITY OF CALIFORNIA @ BERKELEY on 09/16/26. Re-use and distribution is ... except for Open Access articles.

In summary, the additional Higgs bosons are sought for mainly via the following channels:

$$
\begin{aligned}
&pp \to A/H \to \tau^+\tau^- \text{ (inclusive)},\\
&b\bar{b}A/H, A/H \to \tau^+\tau^- \text{ (with } b\text{-tag)},\\
&b\bar{b}A/H, A/H \to b\bar{b} \text{ (with } b\text{-tag)},\\
&pp \to t\bar{t} \to H^\pm W^\mp b\bar{b},\ H^\pm \to \tau^+\nu_\tau(\tau^-\bar{\nu}_\tau) \text{ or } t\bar{b}\,(b\bar{t})\,,\\
&gb \to H^- t \text{ or } g\bar{b} \to H^+\bar{t},\ H^\pm \to \tau^+\nu_\tau(\tau^-\bar{\nu}_\tau) \text{ or } t\bar{b}\,(b\bar{t}).
\end{aligned}
\tag{11.39}
$$

After the Higgs boson discovery, updated MSSM benchmarks scenarios have been defined to highlight interesting conditions for the MSSM Higgs boson searches [56, 382] and are scrutinised by the LHC Higgs Working Group [392].

The compatibility between the predicted and measured Higgs boson mass sets stringent constraints on the parameter space of BSM models. As an example, Fig. 11.17 illustrates the constraints imposed on a specific scenario labeled as M_h^{125} [393] by Higgs-boson searches at the LHC. The M_h^{125} benchmark assumes that super partners are heavy, so that the phenomenology of the observed Higgs boson is not altered except in its couplings due to the existence of another doublet. Note that to use the predicted Higgs boson mass as a constraint (exclusion at nearly constant $\tan\beta$ at high M_A in the (M_A,$\tan\beta$) plane), it is important to account for the theoretical uncertainty on the prediction which is in excess of an order of magnitude larger than the experimental uncertainty on the measured mass of the Higgs boson. The theoretical uncertainty depends itself on the specific SUSY spectrum for a given MSSM parameter set. It is therefore highly model-dependent and influenced by parameters that do not affect much the phenomenology of the heavy Higgs bosons. A more generic estimate of ± 3 GeV is made and found to be a conservative choice [377]. It should also be noticed that the red region of parameter space is highly model-dependent and it depends on parameters that do not affect much the phenomenology of the heavy Higgs bosons.

The scalar sector of the MSSM can be also extended to include extra singlets. The addition of a singlet superfield to the MSSM may come along with additional symmetries imposed to the theory. Depending on such symmetries, different models with singlet extensions of the MSSM (xMSSM) have been proposed, see Ref. [395] for a general review. A singlet extended SUSY Higgs sector opens new avenues for discovery. Since the singlet pseudoscalar particle may be identified as the pseudo-Goldstone boson of a spontaneously broken Peccei–Quinn symmetry, it may become naturally light [396]. Generally, there is mixing of the singlet sector with the MSSM Higgs sector, and for a sufficiently light, singlet-dominated scalar or pseudoscalar, h_S or A_S, respectively, the SM-like Higgs boson h may decay to pairs of h_S or A_S. The light scalar and/or pseudoscalar may subsequently decay to $\tau\tau$ or $b\bar{b}$ pairs. Such cascade decays are more difficult to detect than in standard searches due to the potentially soft decay products. There is also a rich phenomenology for the decays of the heavy CP-even and CP-odd doublets, H and A into two lighter Higgs bosons such as $H \to hh_S$, hh, $h_S h_S$ or $A \to A_S h_S$, $A_S h$ as well as into a light Higgs boson and a gauge boson: $H \to A_S Z$; $A \to h_S Z$, hZ. If kinematically allowed, the heavy Higgs bosons decay into $t\bar{t}$. If the singlet-dominated scalar or pseudoscalar are somewhat heavier, the decays $h_S \to WW$ or $A_S \to h_S Z$ will be allowed.

Additional extensions of the MSSM have been considered to either avoid phenomenological constraints or address phenomena not explained in the SM. For instance, SUSY scenarios with CP-violation (CPV) phases are theoretically appealing, since additional CPV beyond that observed in the $K-$, $D-$, and B-meson systems is required to explain the observed cosmic matter-antimatter asymmetry. In the MSSM, CPV effects in the Higgs sector appear at the quantum level, while in singlet extensions of the MSSM CPV effects can already be present at tree level. In general, CPV effects in the Higgs sector have significant constraints from electric dipole moments data [397]. Major variations to the Higgs-boson phenomenology occur in the presence of explicit CPV phases. In the CPV case, vector-boson pairs couple to all three neutral Higgs-boson mass eigenstates. The discovery of a 125 GeV Higgs boson has put strong constraints on the realization of the CPV scenario within the MSSM. This is partly due to the fact that the observed Higgs-boson rates are close to the SM values, and a large CPV component would necessarily induce a large variation in the rate of the SM-like Higgs-boson decays into the weak gauge bosons $W^\pm$ and Z. The measured Higgs-boson mass imposes additional constraints on the realization of this scenario.

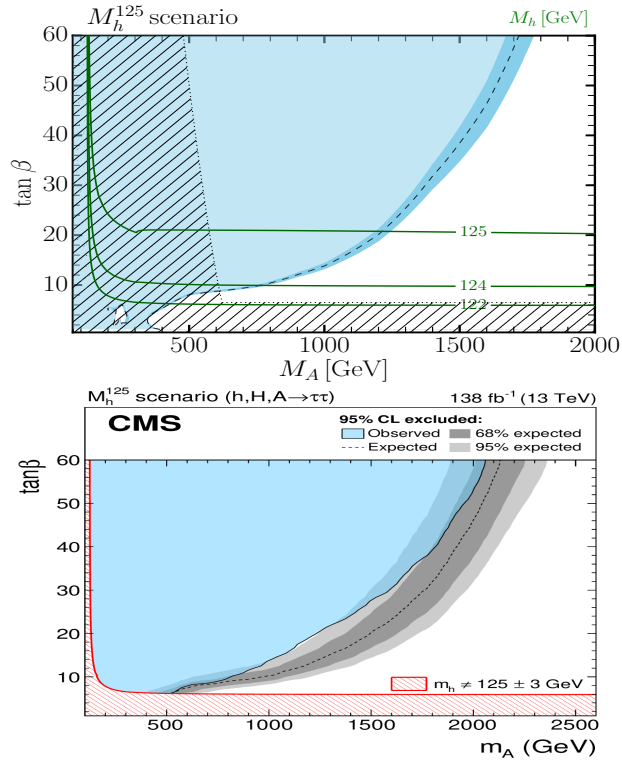

Figure 11.17: (Left) The predicted 95% CL exclusion contours in the (M_A, $\tan\beta$) parameter space for the M_h^{125} benchmark scenarios [393]. The blue area represents the bounds from searches for heavy Higgs bosons (H and A), with the darker blue band indicating the theoretical uncertainty. The green solid lines are predictions for the mass of the lighter CP-even scalar h, the hatched area is excluded by a mismatch between the properties of h and those of the observed Higgs boson. The nearly vertical dotted line illustrates the lower limit on the mass of the A boson from precision measurements of the Higgs-boson couplings and the close-to horizontal dotted line represents the limit on $\tan\beta$ from the compatibility of the measured mass of the observed Higgs boson and the prediction using radiative corrections. (Right) Expected and observed 95% CL exclusion contours. The expected median in the absence of a signal is shown as a dashed black line. The dark and bright grey bands indicate the central 68% and 95% intervals of the expected exclusion. The observed exclusion contour is indicated by the colored blue area. Those parts of the parameter space where M_h deviates by more then ± 3 GeV from the mass of $h(125)$ are indicated by a red hatched area [394].

Future precision measurements of the Higgs-boson couplings to fermions and gauge bosons together with information on heavy Higgs-boson searches will provide powerful information on the SUSY parameter space [398]. Improvements in our understanding of B-physics observables put indirect constraints on additional Higgs bosons in mass ranges that would not be accessible in direct LHC searches. In particular, BR($B_s \to \mu^+\mu^-$), BR($b \to s\gamma$), and BR($B_u \to \tau\nu$) play an important role within minimal flavour-violating (MFV) models [399], in which flavour effects proportional to the CKM matrix elements are induced as in the SM [400].

Int. J. Mod. Phys. A 2026.41. Downloaded from www.worldscientific.com
by UNIVERSITY OF CALIFORNIA @ BERKELEY on 09/16/26. Re-use and distribution is strictly not permitted, except for Open Access articles.

11.4.1.2 *Non-supersymmetric extensions of the Higgs sector*

There are many ways to extend the minimal scalar sector of the SM. In the case of SUSY models illustrated in Section 11.4.1.1, the scalar sector consists of a constrained *type-II* 2HDM (see point i. below), with restrictions on the Higgs-boson masses and couplings induced by SUSY. In the following discussion, more generic 2HDM's are presented (for some comprehensive reviews, see [401]). These models are theoretically less compelling since they do not provide an explanation for the SM Higgs naturalness problem, but on the other hand they are agnostic about the overall theoretical framework they may derive from, and can lead to different patterns of Higgs-fermion couplings, hence, to different phenomenology. It is also possible to consider models with a SM Higgs boson and one or more additional scalar SU(2) doublets that acquire no VEV and hence play no role in the EWSB mechanism. Such models are dubbed Inert Higgs Doublet Models (IHD) [402]. Without a VEV associated to it, a Higgs boson from an inert doublet has no tree-level coupling to gauge bosons and hence cannot decay into a pair of them. Moreover, imposing a Z_2 symmetry that prevents them from coupling to the fermions, it follows that, if the lightest inert Higgs boson is neutral, it becomes a good DM candidate with interesting associated collider signals. Various studies of IHD models in the light of a 125 GeV Higgs boson have been performed, see for instance Ref. [403], showing an interesting interplay between collider and direct DM detection signals.

An interesting type of 2HDMs are those in which an Abelian flavour symmetry broken at the electroweak scale creates the fermion mass hierarchies and mixing angles [404]. This idea is based on the Froggatt–Nielsen model [405], where a flavon field couples differently to the SM fermions of different flavour charges. Such flavon acquires a vacuum expectation value, breaking the flavour symmetry but leaving both the flavour breaking and the new physics scales undetermined. In Refs. [406], it was proposed to relate the flavour breaking scale to the electroweak scale by identifying the flavon with the modulus square of the Higgs field. A 2HDM, however, provides a more compelling realisation of the electroweak scale flavour breaking idea. In the most ambitious constructions of two Higgs doublet flavour models (2HDFM), the textures of the Yukawa couplings are a result of an Abelian flavour symmetry that only allows renormalisable Yukawa couplings of the top quark to the Higgs bosons. All other Yukawa couplings are generated by higher dimensional operators that produce hierarchical entries of the Yukawa matrices, explaining the observed quark masses and mixing angles. Flavour observables, LHC Higgs signal strength measurements, electroweak precision measurements, unitarity and perturbativity bounds, as well as collider searches for new scalar resonances result in precise predictions for the parameters of these 2HDFMs. In particular, correlated departures from SM Higgs boson couplings, as well as additional Higgs bosons with masses < 700 GeV must be observed at the LHC. Other incarnations of 2HDFMs can aim at only partially explaining the fermion mass hierarchies but are therefore less restrictive.

Other extensions of the Higgs sector can include multiple copies of $\mathrm{SU}(2)_L$ doublets [407], additional scalar singlets [408], triplets or more complicated combinations of scalar multiplets in the Higgs Lagrangian . It is also possible to enlarge the gauge symmetry beyond $\mathrm{SU}(2)_L\times\mathrm{U}(1)_Y$ along with the necessary Higgs-field structure to generate gauge boson and fermion masses. There are two main experimental constraints on these extensions: (i) precision measurements which constrain $\rho = m_W^2/(m_Z^2\cos^2\theta_W)$ to be very close to 1 and (ii) flavour changing neutral current (FCNC) effects. In electroweak models based on the SM gauge group, the tree-level value of ρ is determined by the Higgs multiplet structure. By suitable choices for the hypercharges, and in some cases the mass splitting between the charged and neutral Higgs sector or the vacuum expectation values of the Higgs fields, it is possible to obtain a richer combination of singlets, doublets, triplets and higher multiplets compatible with precision measurements.

In the following the case of 2HDMs and models with an additional Higgs triplet will be briefly discussed as the most common examples constrained by experiments. There is a lot of activity on the study of non-supersymmetric models with an extended Higgs sector, with an intense collaboration between theorists and experimentalists in particular inside the LHC Higgs Working Group [392].

i. *Two-Higgs-doublet models*

General two-Higgs-doublet models [401] can have a more diverse Higgs-fermion coupling structure than in SUSY, and can be viewed as a simple extension of the SM to realize the spontaneous breakdown of $\mathrm{SU}(2)_L\times\mathrm{U}(1)_Y$ to $\mathrm{U}(1)_{\mathrm{em}}$. Quite generally, if the two Higgs doublets contain opposite hypercharges, the scalar potential will contain mixing mass parameters of the kind $m_{12}^2\Phi_1^T i\sigma_2\Phi_2 + h.c.$. In the presence of such terms, both Higgs doublets will acquire vacuum expectation values, $v_1/\sqrt{2}$ and $v_2/\sqrt{2}$, respectively, and the gauge boson masses will keep their SM expressions with the Higgs VEV v replaced by $\sqrt{v_1^2+v_2^2}$. Apart from the mass terms, the most generic renormalisable and gauge invariant scalar potential for two Higgs doublets with opposite hypercharges contains seven quartic couplings, as presented in Eq. (11.33).

Just as in the MSSM case, after electroweak symmetry breaking and in the absence of CP-violation in the scalar sector, the physical spectrum contains a pair of charged Higgs bosons $H^\pm$, a CP-odd Higgs boson A and two neutral CP-even Higgs bosons, h and H. The angles α and β diagonalize the CP-even, and the CP-odd and charged Higgs sectors, respectively. The complete 2HDM is defined only after considering the interactions of the Higgs fields to fermions. Yukawa couplings of the generic form

$$-\,y_{ij}^a\bar{\Psi}_L^i H_a \Psi_R^j + h.c. \tag{11.40}$$

may be added to the renormalisable Lagrangian of the theory. Contrary to the SM, the two Higgs doublet structure does not ensure the alignment of the fermion mass terms $m_{ij} = y_{ij}^a v_a/\sqrt{2}$ with the Yukawa couplings y_{ij}^a. This implies that quite generally the neutral Higgs bosons will mediate flavour changing interactions between the different mass eigenstates of the fermion fields. Such flavour changing interactions should be suppressed in order to describe properly the Kaon, D and B meson phenomenology. Based on the Glashow–Weinberg criterion [409], according to which the tree-level FCNC's mediated by neutral Higgs bosons will be absent if all fermions of a given electric charge couple to no more than one Higgs doublet, the simplest way of avoiding such transitions is to assume the existence of a symmetry that ensures the couplings of the fermions of each given quantum number (up-type and down-type quarks, charged and neutral leptons) to only one of the two Higgs doublets. Different models may be defined depending on which of these fermion fields couple to a given Higgs boson. Conventionally, models of *type-I* are those in which all SM fermions couple to a single Higgs field, while in *type-II* models, down-type quarks and charged leptons couple to a common Higgs field, while the up-type quarks and neutral leptons couple to the other. Two other realizations of type-II models are commonly referred to as "*lepton-specific*", when quarks couple to one of the Higgs bosons while leptons couple to the other, or "*flipped*" when up-type quarks and charged leptons couple to one of the Higgs fields while down-quarks and neutral leptons couple to the other. Finally, alternative ways of suppressing tree-level scalar FCNC in a 2HDM through specific assumptions on the structure of the Yukawa mixing matrices have been proposed, the so-called *type-III* models [410, 411], and shown to be phenomenologically viable [412].

The two Higgs doublet model phenomenology depends strongly on the size of the mixing angle α and therefore on the quartic couplings. For large values of m_A, $\sin\alpha \to -\cos\beta$, $\cos\alpha \to \sin\beta$, $\cos(\beta-\alpha) \to 0$, and the lightest CP-even Higgs boson h behaves as the SM Higgs boson. The same behaviour is obtained if the quartic couplings are such that $\mathcal{M}_{12}^2\sin\beta = -(\mathcal{M}_{11}^2 - m_h^2)\cos\beta$. The latter condition represents a situation in which the couplings of h to fermions and weak gauge bosons become the same as in the SM, without decoupling the rest of the non-standard scalars and it is of particular interest due to the fact that the discovered Higgs boson has SM-like properties. This situation will be referred to as alignment, as in the MSSM case.

Int. J. Mod. Phys. A 2026.41. Downloaded from www.worldscientific.com
by UNIVERSITY OF CALIFORNIA @ BERKELEY on 09/16/26. Re-use and distribution is except for Open Access articles.

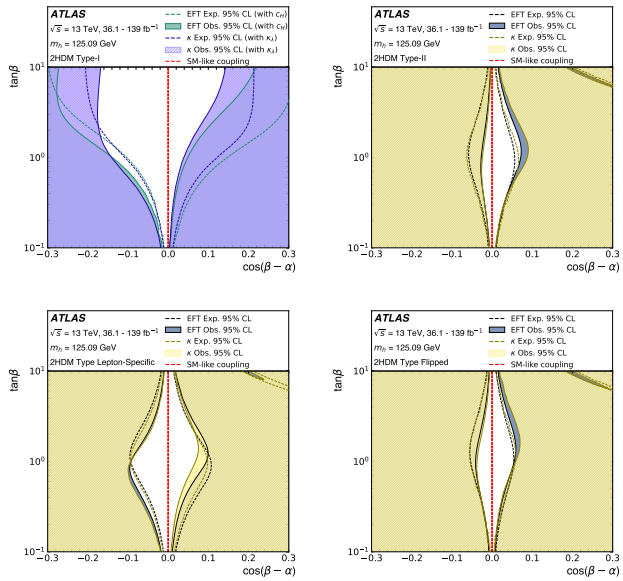

Figure 11.18: Constraints on the parameters space of 2HDM of Type I and II, based on either the κ or SMEFT approach to the parametrization of NP effects in the SM Higgs boson couplings. See Ref. [311] for more details.

In type-II 2HDM, at large values of $\tan\beta$ and moderate values of m_A, the non-standard Higgs bosons H, A and $H^\pm$ couple strongly to bottom quarks and τ leptons. Hence, the decay modes of the non-standard Higgs bosons tend to be dominated by the b-quark and τ-lepton modes, including top quarks or neutrinos in the case of the charged Higgs boson. However, for large and negative values of λ_4 (see Eq. 11.33), the charged Higgs boson mass may be sufficiently heavy to allow on-shell decays $H^\pm \to W^\pm + (H, A)$, via a trilinear coupling

$$g_{H^\pm W^\mp H,A} \simeq \frac{M_W}{v}\sin(\beta-\alpha)(p_{H^+} - p_{H,A})\,, \quad (11.41)$$

where p_{H^+} and $p_{H,A}$ are the charged and neutral scalar Higgs-boson momenta pointing into the vertex. On the other hand, for large and positive values of λ_5 (see Eq. 11.33), the above charged Higgs-boson decay into a $W^\pm$ and the CP-odd Higgs boson may be allowed, but the heavy Higgs boson H may be sufficiently heavy to decay into a CP-odd Higgs boson and an on-shell Z, $H \to Z + A$, via

$$g_{HZA} \simeq \frac{M_Z}{v}\sin(\beta-\alpha)(p_H - p_A). \quad (11.42)$$

The decay $H^\pm \to W^\pm + H$, on the other hand may be allowed only if $\lambda_4 < -\lambda_5$. The couplings controlling all the above decay modes are proportional to $\sin(\beta-\alpha)$ and therefore they are unsuppressed in the alignment limit. Moreover, these could still be the dominant decay modes at moderate values of $\tan\beta$, offering a way to evade the current bounds obtained assuming a dominant decay into b-quarks or τ-leptons. The quartic couplings are restricted by the condition of stability of the effective potential as well as by the restriction of obtaining the proper value of the lightest CP-even Higgs boson mass. LHC measurements of Higgs-boson couplings are already constraining the 2HDM parameter space, as illustrated in Fig. 11.18 for the case of models of Type I and II.

As discussed in the case of the SUSY 2HDM, additional effects of explicit CPV can be introduced by allowing some of the parameters of the Higgs potential to be complex. As for the SUSY case, the three neutral mass eigenstates mix with each other and give origin to a different phenomenology. For a comprehensive detailed discussions of 2HDM phenomenology, see for example Refs. [57, 401].

ii. *Higgs-boson triplets*

Electroweak triplet scalars are the simplest non-doublet extension of the SM that can participate in the spontaneous breakdown of $\mathrm{SU}(2)_L \times \mathrm{U}(1)_Y$ to $\mathrm{U}(1)_{\mathrm{em}}$. Two types of model have been developed in enough detail to make a meaningful comparison to LHC data: the Higgs triplet model (HTM) [413] and the Georgi–Machacek model (GM) [414].

The Higgs triplet model extends the SM by the addition of a complex $\mathrm{SU}(2)_L$ triplet scalar field Δ with hypercharge $Y = 2$, and a general gauge-invariant renormalisable potential $V(\Phi, \Delta)$ for Δ and the SM Higgs doublet Φ. The components of the triplet field can be parameterised as

$$\Delta = \frac{1}{\sqrt{2}}\begin{pmatrix} \Delta^+ & \sqrt{2}\Delta^{++} \\ v_\Delta + \delta + i\xi & -\Delta^+ \end{pmatrix}, \quad (11.43)$$

where Δ^+ is a singly-charged field, Δ^{++} is a doubly-charged field, δ is a neutral CP-even scalar, ξ is a neutral CP-odd scalar, and v_Δ is the triplet VEV. The general scalar potential mixes the doublet and triplet components. After electroweak symmetry breaking there are seven physical mass eigenstates, denoted $H^{\pm\pm}$, $H^\pm$, A, H, and h.

A distinguishing feature of the HTM is that it violates the custodial symmetry of the SM (see Sec. 11.2.3); thus the ρ parameter deviates from 1 even at tree level. Letting x denote the ratio of triplet and doublet VEVs, the tree level expression is

$$\rho = \frac{1+2x^2}{1+4x^2}\,. \quad (11.44)$$

The measured value of the ρ parameter then limits the triplet VEV to be quite small, $x \lesssim 0.03$, or $v_\Delta < 8\,\mathrm{GeV}$. This constraint severely limits the role of the triplet scalar in the EWSB mechanism.

The small VEV of the Higgs triplet in the HTM is a virtue from the point of view of generating neutrino masses without the necessity for introducing right-handed neutrino fields. The gauge invariant dimension four interaction

$$h_{\nu_{ij}}\,\ell_i^T C^{-1} i\sigma_2\,\Delta\,\ell_j\,, \quad (11.45)$$

where ℓ_i are the lepton doublets, C is the charge conjugation matrix, and $h_{\nu_{ij}}$ is a complex symmetric coupling matrix, generates a Majorana mass matrix for the neutrinos:

$$m_{\nu_{ij}} = \sqrt{2}h_{\nu_{ij}}v_\Delta\,. \quad (11.46)$$

This can be combined with the usual neutrino seesaw to produce what is known as the type-II seesaw [415].

The HTM suggests the exciting possibility of measuring parameters of the neutrino mass matrix at the LHC. If the doubly-charged Higgs boson is light enough and/or its couplings to W^+W^+ are sufficiently suppressed, then its primary decay is into same-sign lepton pairs: $H^{++} \to \ell_i^+\ell_j^+$; from Eq. (11.45) and Eq. (11.46), it is apparent that these decays are in general lepton-flavour violating with branchings proportional to elements of the neutrino mass matrix [416].

Precision electroweak data constrain the mass spectrum as well as the triplet VEV of the HTM [417]. These constraints favor a spectrum where H^{++} is the lightest of the exotic bosons, and where the mass difference between H^+ and H^{++} is a few hundred GeV. The favored triplet VEV is a few GeV, which also favors H^{++} decays into W^+W^+ over same-sign dileptons.

The GM model addresses the ρ parameter constraint directly by building in a custodial symmetry (it was however argued that large corrections to $\rho = 1$ are generated at one-loop [418], requiring some fine-tuning to preserves agreement with EW precision data). Writing the complex scalar doublet of the SM as a $(2,2)$ under $\mathrm{SU}(2)_L \times \mathrm{SU}(2)_R$, it is obvious that the next simplest construction respecting custodial symmetry is a scalar transforming like a $(3,3)$ [419]. These nine real degrees of freedom correspond to a complex electroweak triplet combined with a real triplet, with the scalar potential required to be invariant under $\mathrm{SU}(2)_R$. Under the custodial $\mathrm{SU}(2)_{L+R}$, they transform as $1 \oplus 3 \oplus 5$, with a

Int. J. Mod. Phys. A 2026.41. Downloaded from www.worldscientific.com
by UNIVERSITY OF CALIFORNIA @ BERKELEY on 09/16/26. Re-use and distribution is strictly not permitted, except for Open Access articles.

CP-even neutral scalar as the custodial singlet (thus matching the SM Higgs boson), a CP-odd neutral scalar in the custodial triplet, and another CP-even neutral scalar in the custodial 5-plet. The scalar components can be decomposed as

$$\Xi = \begin{pmatrix} \chi_3^* & \xi_1 & \chi_1 \\ -\chi_2^* & \xi_2 & \chi_2 \\ \chi_1^* & -\xi_1^* & \chi_3 \end{pmatrix}, \tag{11.47}$$

where ξ_2 is a real scalar and the others are complex scalars. Linear combinations of these scalars account for the neutral custodial singlet, a neutral and singly-charged field making up the custodial triplet, and neutral, singly-charged, and doubly-charged fields making up the custodial 5-plet.

When combined with the usual SM doublet field Φ, the electroweak scale v is now related to the doublet and triplet VEVs by

$$v^2 = v_\Phi^2 + 8v_\Xi^2 \,. \tag{11.48}$$

Note that the GM triplets by themselves are sufficient to explain electroweak symmetry breaking and the existence of a 125 GeV neutral boson along with a custodial triplet of Goldstone bosons; the complex doublet field in the GM model is required to generate fermion masses via the usual dimension four Yukawa couplings. This raises the question of whether one can rule out the possibility that the 125 GeV boson is the neutral member of a custodial 5-plet rather than a custodial singlet, without invoking decays to fermions. A conclusive answer is given by observing that the ratio of the branching fractions to W versus Z bosons is completely determined by the custodial symmetry properties of the boson. For a custodial 5-plet, the ratio of the signal strength to WW over that to ZZ is predicted to be 1/4 that of a SM Higgs boson [419], and thus already ruled out by the experimental results presented in Section 11.3.5.

Another interesting general feature of Higgs triplet models is that, after mixing, the SM-like neutral boson can have stronger couplings to WW and ZZ than predicted by the SM [420]; this is in contrast to mixing with additional doublets and singlet, which can only reduce the WW and ZZ couplings versus the SM. This emphasises that LHC Higgs data cannot extract model independent coupling strengths for the Higgs boson [256].

Because of the built-in custodial symmetry, the triplet VEV in the GM model can be large compared to the doublet VEV. The custodial singlet neutral boson from the triplets mixes with the neutral boson from the doublet. Two interesting special cases are (i) the triplet VEV is small and the 125 GeV boson is SM-like except for small deviations, and (ii) the 125 GeV boson is mostly the custodial singlet neutral boson from the electroweak triplets. The phenomenology of the doubly-charged and singly-charged bosons is similar to that of the HTM. The constraints on the GM model from precision electroweak data, LEP data, and current LHC data are summarised in Ref. [57].

11.4.2 *EWSB induced by strong dynamics*

11.4.2.1 *Little Higgs models*

The idea behind the Little Higgs boson models [421] is to identify the Higgs doublet as a (pseudo) Nambu–Goldstone boson while keeping some sizeable non-derivative interactions, in particular a larger Higgs-boson quartic interaction. By analogy with QCD where the pions $\pi^{\pm,0}$ appear as Nambu–Goldstone bosons associated to the breaking of the chiral symmetry $\mathrm{SU(2)_L} \times \mathrm{SU(2)_R}/\mathrm{SU(2)}$, switching on some interactions that break explicitly the global symmetry will generate masses for the would-be massless Nambu–Goldstone bosons of the order of $g\Lambda_{G/H}/(4\pi)$, where g is the coupling of the symmetry breaking interaction and $\Lambda_{G/H} = 4\pi f_{G/H}$ is the dynamical scale of the global symmetry breaking G/H. In the case of the Higgs boson, the top Yukawa interaction or the gauge interactions themselves will certainly break explicitly (part of) the global symmetry since they act non-linearly on the Higgs boson. Therefore, obtaining a Higgs boson mass around 125 GeV would demand a dynamical scale $\Lambda_{G/H}$ of the order of 1 TeV, which is known to lead to too large oblique corrections. Raising the strong dynamical scale by at least one order of magnitude requires an additional selection rule to ensure that a Higgs boson mass is generated at the 2-loop level only

$$m_h^2 = \frac{g^2}{16\pi^2}\Lambda_{G/H}^2 \to m_h^2 = \frac{g_1^2 g_2^2}{(16\pi^2)^2}\Lambda_{G/H}^2. \tag{11.49}$$

The way to enforce this selection rule is through a "collective breaking" of the global symmetry:

$$\mathcal{L} = \mathcal{L}_{G/H} + g_1\mathcal{L}_1 + g_2\mathcal{L}_2. \tag{11.50}$$

Each interaction $\mathcal{L}_1$ or $\mathcal{L}_2$ individually preserves a subset of the global symmetry such that the Higgs boson remains an exact Nambu–Goldstone boson whenever either g_1 or g_2 is vanishing. A mass term for the Higgs boson can be generated only by diagrams involving simultaneously both interactions. At one-loop, such diagrams are not quadratically divergent, so the Higgs boson mass is not UV sensitive. Explicitly, the cancellation of the SM quadratic divergences is achieved by a set of new particles around the Fermi scale: gauge bosons, vector-like quarks, and extra massive scalars, which are related, by the original global symmetry, to the SM particles with the same spin. Contrary to SUSY, the cancellation of the quadratic divergences is achieved by same-spin particles. These new particles, with definite couplings to SM particles as dictated by the global symmetries of the theory, are perfect goals for the LHC.

The simplest incarnation of the collective breaking idea, the so-called littlest Higgs boson model, is based on a non-linear σ-model describing the spontaneous breaking SU(5) down to SO(5). A subgroup $\mathrm{SU(2)_1} \times \mathrm{U(1)_1} \times \mathrm{SU(2)_2} \times \mathrm{U(1)_2}$ is weakly gauged. This model contains a weak doublet, that is identified with the Higgs doublet, and a complex weak triplet whose mass is not protected by collective breaking. Other popular little Higgs models are based on different coset spaces: minimal moose ($\mathrm{SU(3)}^2/\mathrm{SU(3)}$), the simplest little Higgs ($\mathrm{SU(3)}^2/\mathrm{SU(2)}^2$), the bestest little Higgs ($\mathrm{SO(6)}^2/\mathrm{SO(6)}$). For comprehensive reviews, see Ref. [422].

11.4.2.2 *Models of partial compositeness*

As in all composite-Higgs models the Higgs boson appears as a pseudo Nambu–Goldstone boson: the new strongly coupled sector is supposed to be invariant under a global symmetry G spontaneously broken to a subgroup H at the scale f (the typical mass scale of the resonances of the strong sector is $m_\rho \sim g_\rho f$ with g_ρ the characteristic coupling of the strong sector). To avoid conflict with EW precision measurements, the strong interactions themselves should better not break the EW symmetry. Hence the SM gauge symmetry itself should be contained in H. The SM (light) fermions and gauge bosons cannot be part of the strong sector itself since LEP data have already put stringent bounds on the compositeness scale of these particles far above the TeV scale. The gauge bosons couple to the strong sector by a weak gauging of a SU(2)×U(1) subgroup of the global symmetry G. The couplings of the SM fermions to the strong sector could a priori take two different forms:

(i) a bilinear coupling of two SM fermions to a composite scalar operator, $\mathcal{O}$, of the form $\mathcal{L} = y\,\bar{q}_L u_R \mathcal{O} + h.c.$, in simple analogy with the SM Yukawa interactions. This is the way fermion masses were introduced in technicolor theories and it generically comes with severe flavour problems and calls for extended model-building gymnastics [29] to circumvent them;

(ii) a linear mass mixing with fermionic vector-like operators: $\mathcal{L} = \lambda_L\,\bar{q}_L\mathcal{Q}_R + \lambda_R\bar{\mathcal{U}}_L u_R$. $\mathcal{Q}$ and $\mathcal{U}$ are two fermionic composite operators of mass M_Q and M_U.

Being part of the composite sector, the composite fermionic operators can have a direct coupling of generic order Y_* to the Higgs boson. In analogy with the photon-ρ mixing in QCD, once the linear mixings are diagonalised, the physical states are a linear combination of elementary and composite fields. Effective Yukawa couplings are generated and read for instance for the up-type quark

$$y = Y_* \sin\theta_L \sin\theta_R \tag{11.51}$$

where $\sin\theta_i = \lambda_i/\sqrt{M_{Q,U}^2 + \lambda_i^2}$, $i = L, R$, measure the amount of compositeness of the SM left- and right-handed up-type quark.

Int. J. Mod. Phys. A 2026.41. Downloaded from www.worldscientific.com by UNIVERSITY OF CALIFORNIA @ BERKELEY on 09/16/26. Re-use and distribution is [redacted] except for Open Access articles.

If the strong sector is flavour-anarchic, i.e., if the couplings of the Higgs boson to the composite fermions does not exhibit any particular flavour structure, the relation Eq. (11.51) implies that the light fermions are mostly elementary states ($\sin\theta_i \ll 1$), while the third generation quarks need to have a sizable degree of compositeness. The partial compositeness paradigm offers an appealing dynamical explanation of the hierarchies in the fermion masses. In fact, if the UV scale at which the linear mixings are generated is large, then $\mathcal{O}(1)$ differences in the anomalous dimensions can generate naturally large hierarchies in the fermion masses via renormalisation group running [423].

Another nice aspect of the partial compositeness structure is the dynamical generation of the Higgs potential that is not arbitrary like in the SM. The Higgs boson being a pseudo-Nambu–Goldstone boson, its mass does not receive any contribution from the strong sector itself but it is generated at the one-loop level via the couplings of the SM particles to the strong sector since these interactions are breaking the global symmetries under which the Higgs doublet transforms non-linearly. Obtaining $v \ll f$, as required phenomenologically, requires some degree of tuning, which scales like $\xi \equiv v^2/f^2$. A mild tuning of the order of 10% ($\xi \approx 0.1$) is typically enough to comply with electroweak precision constraints.

As in SUSY scenarios, the top sector is playing a crucial role in the dynamics of EWSB and can provide the first direct signs of new physics. The direct searches for these top partners, in particular the ones with exotic electric charges 5/3, are already exploring the natural parameter spaces of these models [424].

The main physics properties of a pseudo Nambu–Goldstone Higgs boson can be captured in a model-independent way by a small number of higher-dimensional operators. Indeed, the strong dynamics at the origin of the composite Higgs boson singles out a few operators among the complete list discussed earlier in Section 11.3.5: these are the operators that involve extra powers of the Higgs doublets, and they are therefore generically suppressed by a factor $1/f^2$ as opposed to the operators that involve extra derivatives or gauge bosons that are suppressed by a factor $1/(g_\rho^2 f^2)$. Typically, these new interactions induce deviations in the Higgs boson couplings that scale like $\mathcal{O}(v^2/f^2)$. Hence, the measurements of the Higgs boson couplings can be translated into some constraints on the compositeness scale, $4\pi f$, of the Higgs boson. The peculiarity of these composite models is that, due to the Goldstone nature of the Higgs boson, the direct couplings to photons and gluons are further suppressed and generically the coupling modifiers defined in Section 11.3.5 scale like

$$\begin{aligned} &\kappa_{W,Z,f} \sim 1 + \mathcal{O}\left(\frac{v^2}{f^2}\right), \quad \kappa_{Z\gamma} \sim \mathcal{O}\left(\frac{v^2}{f^2}\right), \\ &\kappa_{\gamma,g} \sim \mathcal{O}\left(\frac{v^2}{f^2} \times \frac{y_t^2}{g_\rho^2}\right), \end{aligned} \tag{11.52}$$

where g_ρ denotes the typical coupling strength among the states of the strongly coupled sector and y_t is the top Yukawa coupling, the largest interaction that breaks the Goldstone symmetry. The coupling modifiers also receive additional contributions from the other resonances of the strong sector, in particular the fermionic resonances of the top-quark sector that are required to be light to generate a 125 GeV Higgs-boson mass. Some indirect information on the resonance spectrum could thus be inferred by a precise measurement of the Higgs boson coupling deviations. Measurable effects of the top-quark partner have been predicted for differential distribution, like the Higgs boson p_T distribution [425]. The off-shell channel $gg \to h^* \to 4\ell$ [235] and the double Higgs boson production $gg \to hh$ [426] can also help to resolve the gluon loop and separate the top and top-partner contributions.

11.4.2.3 *Minimal composite Higgs models*

The minimal composite Higgs models (MCHM) are concrete examples of the partial compositeness paradigm. The Higgs doublet is described by the coset space SO(5)/SO(4) where a subgroup $\mathrm{SU}(2)_L \times \mathrm{U}(1)_Y$ is weakly gauged and under which the four Goldstone bosons transform as a doublet of hypercharge 1. There is some freedom on how the global symmetry is acting on the SM fermions, and the Higgs boson couplings to the fermions depend on the representation which the SM fermions are embedded into [427]. The non-linearly realised symmetry acting on the Goldstone bosons leads to general predictions of the coupling of the Higgs boson to the EW gauge bosons. For instance, it can be shown that the quadratic terms in the W and Z bosons read

$$m_W^2(h)\left(W_\mu W^\mu + \frac{1}{2\cos^2\theta_W} Z_\mu Z^\mu\right), \tag{11.53}$$

with $m_W(h) = \frac{gf}{2}\sin\frac{H}{f}$. Expanding around the EW vacuum, the expression of the weak scale is $v = f\sin(\langle H\rangle/f)$. And the values of the modified Higgs boson couplings to the W and Z become:

$$g_{hVV} = \frac{2m_V^2}{v}\sqrt{1 - v^2/f^2}, \quad g_{hhVV} = \frac{2m_V^2}{v^2}(1 - 2v^2/f^2). \tag{11.54}$$

Note that the Higgs boson couplings to gauge bosons is always suppressed compared to the SM prediction. This is a general result [428] that holds as long as the coset space is compact.

The (κ_V, κ_f) experimental fit of the Higgs boson couplings can be used to derive a lower bound on the Higgs boson compositeness scale $4\pi f \gtrsim 9$ TeV, which is less stringent than the indirect bound obtained from EW precision data, $4\pi f \gtrsim 15$ TeV [429] but more robust and less subject on assumptions [430].

11.4.2.4 *Twin Higgs models*

In all composite models presented above, the particles responsible for canceling the quadratic divergences in the Higgs boson mass are charged under the SM gauge symmetries. In particular, the top partner carries color charge, implying a reasonably large minimal production cross section at the LHC. An alternative scenario, which is experimentally quite challenging and might explain the null result in various new physics searches, is the case nowadays referred to as "neutral naturalness" [30, 31], where the particles canceling the 1-loop quadratic divergences are neutral under the SM. The canonical example for such theories is the Twin Higgs model of Ref. [30]. This is an example of a pseudo-Goldstone boson model with an approximate global SU(4) symmetry broken to SU(3). The Twin Higgs model is obtained by gauging the $\mathrm{SU}(2)_A \times \mathrm{SU}(2)_B$ subgroup of SU(4), where $\mathrm{SU}(2)_A$ is identified with the SM $\mathrm{SU}(2)_L$, while $\mathrm{SU}(2)_B$ is the twin SU(2) group. Gauging this subgroup breaks the SU(4) symmetry explicitly, but quadratically divergent corrections do not involve the Higgs boson when the gauge couplings of the two SU(2) subgroups are equal, $g_A = g_B$. The SU(4)$\to$ SU(3) breaking will also result in the breaking of the twin $\mathrm{SU}(2)_B$ group and, as a result, three of the seven Goldstone bosons will be eaten, leaving 4 Goldstone bosons corresponding to the SM Higgs doublet. In fact, imposing the Z_2 symmetry on the full model will ensure the cancellation of all 1-loop quadratic divergences to the Higgs boson mass. Logarithmically divergent terms can, however, arise for example from gauge loops, leading to a Higgs boson mass of order $g^2 f/4\pi$, which is of the order of the physical Higgs boson mass for $f \sim 1$ TeV. The quadratic divergences from the top sector can be eliminated if the Z_2 protecting the Higgs boson mass remains unbroken by the couplings that result in the top Yukawa coupling. This can be achieved by introducing top partners charged under a twin $\mathrm{SU}(3)_C$. In this case, the quadratic divergences are canceled by top partners that are neutral under the SM gauge symmetries. For more details about the composite twin Higgs models, see Refs. [432].

11.4.3 *Exotic Higgs-boson decays*

While the measured properties of the Higgs boson are roughly consistent with SM predictions, the Higgs-boson total width remains only loosely constrained as discussed in Section 11.3.8. This leaves ample room for BSM decays, often referred to as "exotic Higgs decays". These include invisible decays into dark matter candidates, non-standard signatures like lepton-flavor-violating (LFV) modes, and decays into new light scalars or pseudoscalars, which may decay promptly or be long-lived. They probe a broad spectrum of models, including for instance Higgs portal dark matter and dark photons, two-Higgs-doublet plus singlet (2HDM+S) frameworks, and axion-like particle scenarios. For a theoretical

Int. J. Mod. Phys. A 2026.41. Downloaded from www.worldscientific.com
by UNIVERSITY OF CALIFORNIA @ BERKELEY on 09/16/26. Re-use and distribution is strictly not permitted, except for Open Access articles.

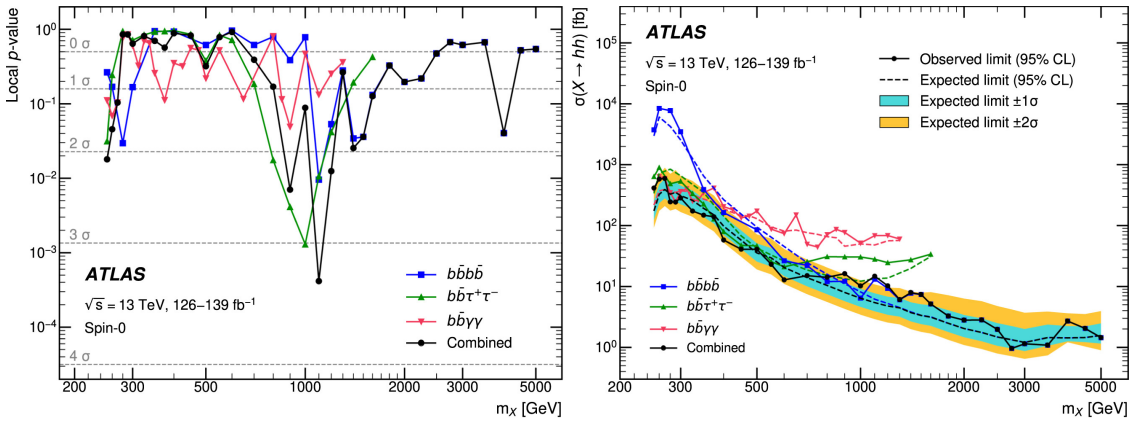

Figure 11.19: (left) Local p-value and (right) observed and expected upper limits at the 95% CL on the resonant Higgs boson pair production cross section as a function of the resonance mass m_X. The symbol h denotes a SM Higgs boson with a mass of 125 GeV. The results are taken from Ref. [431].

review of exotic signatures, see for instance Ref. [433, 434] and the documents of the LHC Higgs Working Group WG3 [392]. In the following we discuss some of these cases and their current experimental status.

11.4.3.1 *Invisible Higgs Decays*

A hypothetical coupling of the Higgs to dark matter candidates is motivated in many theoretical models [392, 436]. Higgs-boson decay modes in which the decay products escape detection are commonly named "invisible" Higgs decays, first proposed in Ref. [437]. Experimentally they are characterized by signatures dominated by a large imbalance of the transverse momentum in the detector (missing transverse energy, MET). These decays are possible in the SM through the very rare $h \to ZZ \to 4\nu$ final state (Br$\approx$ 0.1%), which is far below the reach of the LHC. An observation of a Higgs invisible decay rate would therefore signify new physics, such as a coupling of the Higgs boson to dark matter candidates.

Direct searches for invisible decays are performed in multiple Higgs production modes, including vector boson fusion (VBF), associated production with a Z or W boson (Zh, Wh), $t\bar{t}h$, and inclusive gluon fusion (jet+$E_{\mathrm{T}}^{\mathrm{miss}}$-based signatures). The VBF mode dominates the sensitivity due to its distinctive topology of forward jets which leads to reduced background contamination, and its larger production cross section when compared to VH production. Current Run 2 results yield 95% CL upper limits on the invisible branching fraction at $\mathcal{B}(h \to \mathrm{inv}) < 10.7\%$ (7.7% expected) in ATLAS [438] and $< 15\%$ (8% expected) in CMS [439]. These direct bounds are incorporated into the global Higgs coupling fits discussed in Section 11.3.5.1, Eq.(11.20).

Invisible Higgs-boson decays can also be interpreted in the context of "Higgs portal" models, where the Higgs boson mediates interactions between the SM and a dark sector. A more detailed discussion of such models and their connection to direct dark matter searches can be found in this volume's dark matter review [440].

11.4.3.2 *Flavor violating decays*

The measurement of the Yukawa couplings of the Higgs boson to quarks and leptons is an important piece in the puzzle of flavor and its connection to the mechanism of EWSB. The lepton-flavor-violating (LFV) decays $h \to e\mu$, $h \to e\tau$, and $h \to \mu\tau$ are forbidden in the SM but can arise in a variety of BSM scenarios, including 2HDM models or composite Higgs models. These LFV Higgs decays probe off-diagonal Yukawa couplings $Y_{e\mu}$, $Y_{e\tau}$, or $Y_{\mu\tau}$, which couple the Higgs boson to leptons of different flavors.

The analysis of the full 13 TeV Run 2 datasets collected by ATLAS and CMS has set stringent 95% confidence level (CL) upper limits on the branching ratios of LFV decays of the Higgs in the $h \to \mu\tau$, $h \to e\tau$, and $h \to e\mu$ channels. For $h \to \mu\tau$, the observed (expected) limits are $\mathcal{B}(h \to \mu\tau) < 0.18\%$ (0.09%) from ATLAS [441] and $< 0.15\%$ (0.15%) from CMS [442]. For $h \to e\tau$, the corresponding limits are $\mathcal{B}(h \to e\tau) < 0.20\%$ (0.12%) from ATLAS [441] and $< 0.22\%$ (0.16%) from CMS [442]. In the $h \to e\mu$ channel, the limits are $\mathcal{B}(h \to e\mu) < 6.2 \times 10^{-5}$ (5.9×10^{-5}) from ATLAS [273] and $< 4.4 \times 10^{-5}$ (4.7×10^{-5}) from CMS [443]. These numbers correspond to exotic decays of a 125 Higgs boson. The CMS search in the $e\mu$ channel was expanded to a wider mass range between 110 GeV and 160 GeV. A mild excess with a global significance of 2.8 standard deviations is observed for a mass hypothesis of approximately 146 GeV.

The presence of these off-diagonal LFV Yukawa couplings may enhance processes such as $\mu \to 3e$, $\mu \to e\gamma$, $\tau \to 3\mu$, $\tau \to \mu\gamma$ that can proceed via a virtual Higgs boson exchange. The direct limits derived by ATLAS and CMS on $Br(h \to \mu\tau)$ and $Br(h \to e\tau)$ are more than an order of magnitude stronger than limits derived from tau decays. On the other hand, the most stringent constraint on the $h \to e\mu$ branching ratio is derived indirectly from the results of searches for $\mu \to e\gamma$ [444], which yield a bound of $B(h \to e\mu) < O(10^{-8})$ [445].

Flavor-violating interactions of the Higgs boson may also involve quarks. These are studied in the context of top-quark flavor changing decays, such as $t \to hq$ ($q = u, c$), which provide complementary constraints on flavor-violating Yukawa couplings in the quark sector. ATLAS and CMS have searched for these processes with Run-1 and Run-2 data. Focusing on the Run-2 results, ATLAS has searched for FCNC top decays with subsequent decays of the Higgs boson to a pair of photons [446], yielding a 95% CL upper limit on BR($t \to hc$) $< 0.22\%$ with an expected sensitivity of 0.16%. CMS has searched for FCNC top decays with subsequent decays of the Higgs boson to a pair of b-quarks [447], yielding a 95% CL upper limit on BR($t \to hu$) $< 0.079\%$ with an expected sensitivity of 0.011% and on BR($t \to hc$) $< 0.094\%$ with an expected sensitivity of 0.086%.

11.4.3.3 *Other exotic decays: prompt and long-lived decays*

Higgs decays into pairs of light scalars or pseudoscalars ($h \to ss$ or $h \to aa$) are particularly well motivated in extended Higgs sectors such as the 2HDM+S and axion-like particle models. These provide a very rich phenomenology, with different final states favored depending on the intermediate particle and its mass (4μ, 4τ, $2\mu 2\tau$, $2b2\mu$, $2b2\tau$, $4b$, 4γ, $2\gamma 2\tau$...). They include both prompt decays of the mediator and long lived signatures. Experimental results on $h \to ss/aa$ signatures and their references can be found in the general summary of BSM Higgs searches presented in Table 11.6. An recent overview of the different decays from the point of view of ATLAS can also be found in Ref. [448]. For decays into axion-like particles, see the PDG review on the topic, Ref. [373].

Another class of models explores the connection between the Higgs boson and a "dark" sector of matter that does not interact directly with SM particles, and manifests itself only through mixing effects. A well known example is the hidden Abelian Higgs model (HAHM) [449], which introduces a dark photon, Z_D, that

Int. J. Mod. Phys. A 2026.41. Downloaded from www.worldscientific.com
by UNIVERSITY OF CALIFORNIA @ BERKELEY on 09/16/26. Re-use and distribution is except for Open Access articles.

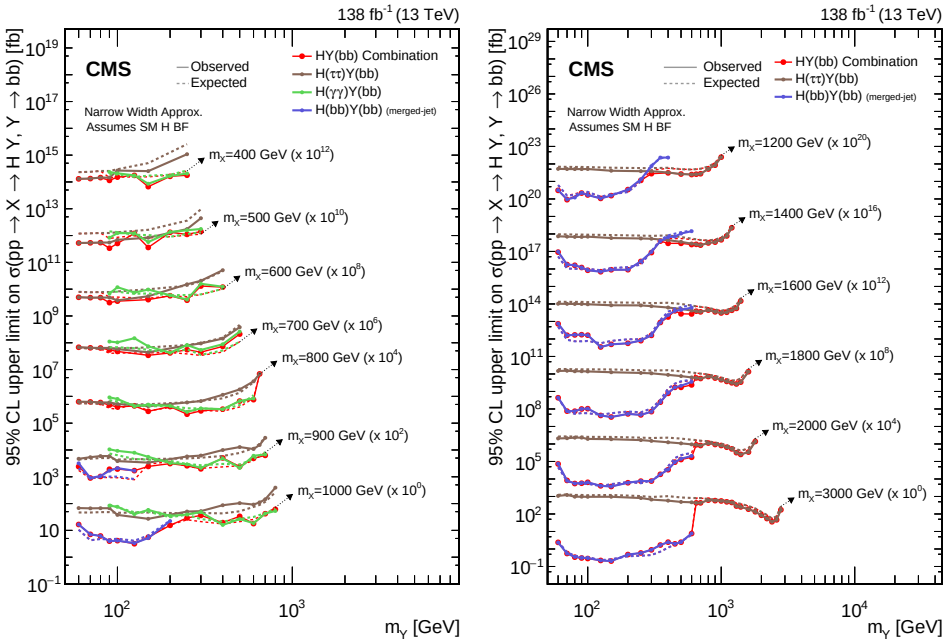

Figure 11.20: Search for $X \to YH$ where "H" is the 125 GeV Higgs boson: Observed and expected upper limits, at 95% CL, on the product of the cross section σ for the production of a resonance X via gluon–gluon fusion and the branching fraction $\mathcal{B}$ for the $X \to Y(b\bar{b})H$ decay. For the branching fractions of the $H \to \tau^+\tau^-$, $H \to \gamma\gamma$ and $H \to b\bar{b}$ decays, the SM values are assumed. The results derived from the individual analyses presented here and the result of their combined likelihood analysis are shown as functions of m_Y and m_X for $m_X \leq 1$ TeV (left), and $m_X \geq 1.2$ TeV (right). Observed limits are indicated by markers connected with solid lines, expected limits by dashed lines. For presentation purposes, the limits have been scaled in successive steps by two orders of magnitude, each. For each set of graphs, a black arrow points to the m_X-related legend. The results are taken from Ref. [435].

mediates a dark $U(1)_D$ gauge symmetry spontaneously broken by a dark Higgs mechanism. The Z_D can couple to SM particles via a hypercharge portal through kinetic mixing or via a Higgs portal through mixing with the SM Higgs. Higgs exotic decay searches in this framework have been performed by ATLAS and CMS, targeting both $h \to ZZ_D$ and $h \to Z_D Z_D$ decays [450–452], and probing both prompt and displaced signatures. Other examples of searches for dark photons in Higgs boson decays target final states with a visible photon and an undetected dark photon [453–455]. Further discussion on the dark sector comparing different search approaches can be found in Refs. [448, 456], and from a more general perspective in the dark matter PDG review [440].

Long lived signatures are an area in particularly rapid development in the current LHC Run 3 and with great room for improvement in HL-LHC. These searches involve non-standard objects that require dedicated reconstructed algorithms for displaced objects, both at trigger and at reconstruction level as shown for example in Ref. [457] from the point of view of CMS. Although no deviations from SM expectations have yet been observed, the HL-LHC will clearly expand the discovery potential, with sensitivities to exotic branching fractions as low as 10^{-5}–10^{-6} in some channels [344].

11.4.4 *Summary of BSM Higgs boson search results*

The measurements presented in Sections 11.3.3–11.3.9 have established the existence of a single scalar particle in the electroweak symmetry-breaking sector, consistent with the SM Higgs boson. However, they do not exclude the possibility of additional scalar particles. As discussed above, many classes of models beyond the SM predict extended Higgs sectors. The corresponding searches are typically designed to be as model-independent as possible[13], and can be grouped into the following categories (in the following,"h" refers to the 125 GeV scalar):

(i) Searches for an additional CP-even state, primarily in the high-mass region, decaying to vector bosons. This could correspond either to the heavy CP-even state in a generic 2HDM, with the lighter state being the 125 GeV Higgs boson, or to an additional scalar singlet.

(ii) Searches for an additional CP-even state, decaying to a pair of 125 GeV Higgs bosons ($H \to hh$), or a pair of heavier scalars ($X \to YY$). Examples of results obtained by ATLAS in the search for $X \to hh$ given in Figure 11.19.

(iii) Searches for an additional scalar state X, with cascade decays to the 125 GeV Higgs boson and another scalar ($X \to Yh$). An example of results obtained by CMS in the search for $X \to Yh$ is given in Figure 11.20.

(iv) Searches for a heavy state decaying to fermion pairs, such as the CP-odd A or the heavy CP-even H in a generic 2HDM.

(v) Searches for charged Higgs bosons, also predicted in generic 2HDMs.

(vi) Searches for a light CP-odd state a in the low-mass region, as predicted in the NMSSM (an extension of the MSSM by one singlet chiral superfield containing a scalar), in a variety of final states. These include decays with one or two a bosons to photon, muon, tau, or b-quark pairs.

(vii) Searches for doubly charged Higgs bosons, expected in Higgs sector extensions with triplet representations.

A concise overview of the most recent searches at the LHC and elsewhere is given in Table 11.6. It summarizes these searches by final state, with the corresponding references provided for further

[13] Nevertheless, most non-SUSY models are expected to include additional states and dynamics above the weak scale to stabilize the scalar sector. Such new, unknown physics may influence the searches described in this section in ways that are difficult to quantify.

Int. J. Mod. Phys. A 2026.41. Downloaded from www.worldscientific.com
by UNIVERSITY OF CALIFORNIA @ BERKELEY on 09/16/26. Re-use and distribution is strictly not permitted, except for Open Access articles.

Table 11.6: Summary of references to the searches for additional states from extended Higgs sectors. (BBr) denotes the BaBar experiment and (TeV) the Tevatron experiments. V denotes either the W or the Z boson.

	ATLAS	CMS	Other experiments
CP-even H			
$H \to \gamma\gamma$	[458, 459]	[460, 461]	—
$H \to \gamma\gamma$ (low mass)	[462]	[460, 461, 463]	—
$H \to Z\gamma$	[464, 465]	[466]	—
$H \to ZZ \to 4\ell$	[467]	[468, 469]	—
$H \to ZZ \to \ell\ell\nu\nu$	[467]	[470]	—
$H \to WZ \to \ell\ell\ell\nu$	—	[471]	—
$H \to ZZ \to \ell\ell q\bar{q}$	[472]	[473, 474]	—
$H \to ZZ \to \nu\nu q\bar{q}$	[475]	—	—
$H \to WW \to \ell\nu\ell\nu$	[476, 477]	[478]	—
$H \to WW \to \ell\nu q\bar{q}'$	[479]	[478]	—
$H \to VV \to q\bar{q}'q\bar{q}'(JJ)$	[480, 481]	[482]	—
$H \to VV$ combination	[483]	—	—
$H \to hh \to b\bar{b}\tau\tau, b\bar{b}\gamma\gamma, bbWW^*, bbZZ^*, 4b$ $\gamma\gamma WW^*, WW^*\tau\tau, WW^*WW^*, 4\tau$	[484–488]	[474, 489–491]	—
CP-odd A (and/or CP-even H)			
$H, A \to \tau^+\tau^-$	[492]	[394, 493]	[494, 495] (TeV) [496] (LHCb)
$A \to \tau^+\tau^-$ (low mass)	[497]	[498]	—
$H, A \to \mu^+\mu^-$	[499]	[500]	—
$H/h \to \mu\tau, e\tau$ LFV	[441]	[501]	—
$H/h \to e\mu$ LFV	[273]	[443]	—
$H, A \to t\bar{t}$	[481, 502–504]	[505, 506]	—
$H, A \to b\bar{b}$	[507]	[508, 509]	[510, 511] (TeV)
$A \to hZ \to b\bar{b}q\bar{q}', b\bar{b}\ell\ell, \ell\ell\tau\tau, \nu\bar{\nu}b\bar{b}, b\bar{b}b\bar{b}$	[512, 513]	[514–516]	—
$A \to ZH$	[517–519]	[520, 521]	—
$H \to ZA \to b\bar{b}\ell^+\ell^-$	[522]	[523]	—
Charged $H^\pm$			
$H^\pm \to \tau^\pm\nu$	[524–526]	[527]	—
$H^\pm \to cs$	[528, 529]	[530]	—
$H^\pm \to tb$	[531]	[532]	—
$H^\pm \to W^\pm Z$	[533, 534]	[535, 536]	—
$H^\pm \to W^\pm A$	—	[537]	—
$H^\pm \to HW^\pm$	[538]	[539]	—
$H^\pm \to cb$	[540]	[541]	—
CP-odd a			
$a \to \mu^+\mu^-, \tau^+\tau^-$	[542, 543]	[544]	—
$h \to aa \to 4\mu, 4\tau, 2\mu 2\tau, 2\gamma 2\tau, 4\gamma$	[545–549]	[532, 550–560]	[561] (LEP) [562] (TeV)
$h \to aa \to bb\mu\mu, bb\tau\tau, 4b$	[563–566]	[567–571]	—
$H \to Za$	[572, 573]	[574]	—
$\Upsilon_{1s,3s} \to a\gamma$	—	—	[575, 576] (BBr)
$X \to YY$ and $X \to hY$			
$X \to YY$	[577]	[578]	—
$X \to hY$	[579–582]	[583–588]	—
Doubly charged $H^{\pm\pm}$	[534, 589, 589, 590]	[536, 591]	—

details. Comprehensive reviews of Run-2 searches can be found in Refs. [435, 448] and references for Run-1 searches are available in Ref. [263].

11.5 Summary and Outlook

Summary– The discovery of the Higgs boson is a major milestone in the history of particle physics as well as an extraordinary achievement of the LHC machine and the ATLAS and CMS experiments. Thirteen years after the discovery, substantial progress in the field of Higgs-boson physics has been accomplished and a significant number of measurements probing the nature of this unique particle have been made. They are revealing an increasingly precise profile of the Higgs boson.

The LHC has concluded its Run 2 in 2018, delivering a dataset of 13 TeV pp collisions corresponding to an integrated luminosity of more than 150 fb^{-1} of which more than 140 fb^{-1} have been collected by ATLAS and CMS. The Run 3 started in 2022 at 13.6 TeV and has already delivered more than the total Run 2 integrated luminosity. With the substantial increase in production rates at the higher center-of-mass energy (mostly from Run 1 to Run 2) and the larger datasets, the LHC collaborations have delivered detailed studies of not only inclusive but also differential cross sections that are essential to probe the structure of the scalar sector of the SM and identify potential deviations from SM predictions.

Results of fundamental importance have been achieved with Run-2 datasets by ATLAS and CMS independently [255, 265], such as the clear and unambiguous observation of the Higgs-boson decay to τ leptons and to b quarks, as well as the clear and unambiguous observation of the production of the Higgs boson through the $t\bar{t}H$ process. These results provide direct evidence for the Yukawa coupling of the Higgs boson to fermions of the third generation: taus, bottom quarks and top quarks, at rates compatible with those expected in the SM. The most recent combination of Run 2 results has established all Higgs-boson couplings to gauge bosons and third-generation fermions with a precision between 5 and 10%. In addition, data analyzed so far have already brought evidence for the $H \to \mu^+\mu^-$ rare decay above the 3σ level for each experiment, and at the 3σ level for the $H \to Z\gamma$ rare decay when ATLAS and CMS combine their Run 2 results. The challenging study of the Higgs–charm coupling is a good example of LHC performance exceeding original expectations, with constraints on κ_c already at about 3 at 95% CL, thanks to improvements in charm tagging. New ideas have been implemented to indirectly determine the Higgs-boson width from both on-shell and off-shell measurements reaching a remarkable sensitivity of about 4 MeV. The Higgs-boson mass has been measured with per-mille-level precision. Last but not least, great progress has been made in constraining the Higgs-boson self-coupling via di-Higgs production, which will probe the SM scalar potential and the origin of EWSB. These, and all other experimental measurements, are consistent at the moment with the EWSB mechanism of the SM.

New theoretical calculations and developments in Monte-Carlo simulations pertaining to Higgs physics are occurring at a rapid pace. For example, the theoretical prediction for the dominant gluon fusion production mode now includes the latest N3LO result at the inclusive and differential levels, which is twice as precise as previous NNLO calculations. All Higgs-boson production modes are known at (a)NNLO of QCD and NLO of EW corrections at both the inclusive and differential level, as well as in several fiducial volumes that have often been explored by interfacing fixed-order calculation with parton shower event generators at NNLO in QCD. At the inclusive level VBF and VH associate production are also known at N3LO. With these improvements in the state-of-the-art theory predictions and the increase in luminosity and center-of-mass energy, Higgs physics has definitively entered a precision era. Its impact can already be seen on the latest Run-2 combined measurements of the Higgs boson couplings (see Section 11.3.5). This situation allows for new challenges to ultimately increase further the reach in precision and it also widens the possibilities of unveiling the true nature and the dynamics of the EWSB mechanism.

Many extensions of the SM at higher energies call for an enlargement of the EWSB sector. Hence, direct searches for additional scalar states can provide valuable insights on the dynamics of the EWSB mechanism. The ATLAS and CMS experiments have searched for additional Higgs bosons in the Run-2 data, and have imposed constraints in broad ranges of mass and couplings for various scenarios with an extended Higgs sector.

Outlook– The unitarization of the vector boson scattering (VBS) amplitudes, dominated at high energies by their longitudinal polarization, has been the basis of the *no lose* theorem at the LHC, and was a determining consideration in the building of the accelerator and detectors. It motivated the existence of a Higgs boson or the observability of manifestations of strong dynamics at the TeV scale. Now that a Higgs boson has been found and its couplings to gauge bosons are - within current accuracy - consistent with the SM predictions, perturbative unitarity is preserved to a large extent with the sole exchange of the Higgs boson, and without the need for any additional states. VBS remains still an important channel to further investigate in order to better understand the nature of the Higgs sector and the possible completion of the SM at the TeV scale. In association with the double Higgs boson production channel by vector boson fusion, VBS could, for instance, confirm that the Higgs boson is part of a weak doublet and also establish whether it is an elementary object or a composite state that could emerge as a pseudo-Nambu–Goldstone boson from a new underlying broken symmetry.

The fermion-Higgs boson couplings are not governed by local gauge symmetry. Thus, in addition to a new particle, the LHC has also discovered a new force, different in nature from the other fundamental interactions since it is non-universal and distinguishes between the three families of quarks and leptons. The existence of the Higgs boson embodies the problem of an unnatural cancella-

Int. J. Mod. Phys. A 2026.41. Downloaded from www.wo
by UNIVERSITY OF CALIFORNIA @ BERKELEY on 09/16/26. Re-use and distribution is
except for Open Access articles.

tion among the quantum corrections to its mass if new physics is present at scales significantly higher than the EW scale. The non-observation of additional states which could stabilise the Higgs boson mass is a challenge for natural scenarios like SUSY or models with a new strong interaction in which the Higgs boson is not a fundamental particle. This increasingly pressing paradox starts questioning the principle of naturalness and it also inspires new solutions tied to the cosmological evolution of the Universe.

The search for the Higgs boson has occupied the particle physics community for the last 50 years. Its discovery has shaped and sharpened the physics programs of the LHC and the HL-LHC and has been central to the discussion of prospective future accelerators [191, 192, 194, 195, 592, 593]. Given the exceptional performance of the LHC so far, projections for the HL-LHC promise to establish a legacy Higgs-boson precision physics program that will test the SM at an unprecedented level and will serve to deepen our understanding of fundamental physics. In particular, with respect to current data, the HL-LHC with an integrated luminosity of 3 ab^{-1} per experiment is expected to (i) determine the $H \to \mu^+\mu^-$ and $H \to Z\gamma$ couplings with 3-7% precision; (ii) measure the other main Higgs-boson couplings to SM fermions and vector bosons, including loop-induced couplings to gluons and photons, with precision ranging from 1.6% to 3.6%; (iii) reach a sensitivity to the charm Yukawa coupling of 1.5 times the SM value at 95% C.L.; (iv) observe SM di-Higgs production with a significance exceeding 7σ; (v) measure the Higgs-boson trilinear coupling with a precision better than 30%; (vi) observe longitudinally polarized vector boson $W_L W_L$ scattering and measure its cross section with precision better than 20%; and (vi) continue placing strong bounds on high-scale new physics models both through direct searches and precision measurements of EW, top-quark, and flavor-physics observables [266]. The projected experimental systematic uncertainties are similar to the statistical uncertainties, but the dominant source of uncertainty arises from theory, and this remains the case even after assuming that, by the end of the HL-LHC run, the theory uncertainties can be reduced by a factor two compared to the current uncertainties [266]. Theoretical progress is hard to predict, but given the progress witnessed in theoretical calculations during the lifetime of the LHC, as well as the wealth of new ideas that have been employed and are currently being considered, a progress in theoretical predictions by a factor of two or more appears realistic but still requires dedicated and concerted effort.

Based on these outstanding achievements, future colliders currently being considered will improve our present knowledge of Higgs-boson physics by either increasing the precision or the energy reach of the HL-LHC [191, 192, 593, 593, 594]. Proposed e^+e^- colliders, both circular and linear, with center-of-mass energies between M_Z and about 350 GeV, the so called *Higgs factories*, will be able to measure all Higgs-boson couplings at percent and sub-percent level, including the couplings to charm and strange quarks, and put first bounds on the extremely small electron Yukawa coupling. Only the measurement of the top-quark Yukawa coupling will require energies of about $550 - 600$ GeV to reach a precision higher than the HL-LHC. Such energy upgrade is part of the proposed plan for an e^+e^- linear collider. e^+e^- colliders will also deliver a largely model-independent measurements of the Higgs-boson width and, for the case of circular e^+e^- colliders, even obtain a meaningful upper bound on the Yukawa couplings of the electron, getting us closer to establishing the origin of the electron mass which lies at the core of all atomic structures. A different class of colliders referred to as *Multi-TeV* colliders, colliding either pp or $\mu^+\mu^-$ beams, will explore LHC center-of-mass energy by roughly one order of magnitude and, besides measuring all Higgs-boson properties in a new energy regime, search for evidence of NP between the EW scale and about 10 TeV as suggested by the Higgs portal.

For both hadron and lepton colliders, substantial theoretical progress is crucial to fully exploit and capitalize on the experimental data. In particular, the expected HL-LHC data together with rapid ongoing progress in theoretical calculations are defining a new era of precision Higgs boson measurements.

References

[1] S.L. Glashow, Nucl. Phys. **20**, 579 (1961); S. Weinberg, Phys. Rev. Lett. **19**, 1264 (1967); A. Salam, *Elementary Particle Theory*, eds.: Svartholm, Almquist and Wiksells, Stockholm, 1968; S. L. Glashow, J. Iliopoulos and L. Maiani, Phys. Rev. **D2**, 1285 (1970).

[2] F. Englert and R. Brout, Phys. Rev. Lett. **13**, 321 (1964), [,157(1964)]; P. W. Higgs, Phys. Lett. **12**, 132 (1964); P. W. Higgs, Phys. Rev. **145**, 1156 (1966); G. S. Guralnik, C. R. Hagen and T. W. B. Kibble, Phys. Rev. Lett. **13**, 585 (1964), [,162(1964)].

[3] J. M. Cornwall, D. N. Levin and G. Tiktopoulos, Phys. Rev. Lett. **30**, 1268 (1973), [Erratum: Phys. Rev. Lett. **31**, 572 (1973)]; J. M. Cornwall, D. N. Levin and G. Tiktopoulos, Phys. Rev. **D10**, 1145 (1974), [Erratum: Phys. Rev. **D11**, 972 (1975)]; C. H. Llewellyn Smith, Phys. Lett. **46B**, 233 (1973); B. W. Lee, C. Quigg and H. B. Thacker, Phys. Rev. **D16**, 1519 (1977).

[4] R. Barate *et al.* (LEP Working Group for Higgs boson searches, ALEPH, DELPHI, L3, OPAL), Phys. Lett. B **565**, 61 (2003), [hep-ex/0306033].

[5] CDF and D. collaborations (CDF and D0), Technical report, Fermilab (2011), [arXiv:1107.5518].

[6] L. Evans and P. Bryant, JINST **3**, S08001 (2008).

[7] S. Schael *et al.* (ALEPH, DELPHI, L3, OPAL, SLD, LEP Electroweak Working Group, SLD Electroweak Group, SLD Heavy Flavour Group), Phys. Rept. **427**, 257 (2006), [hep-ex/0509008].

[8] ALEPH, CDF, D0, DELPHI, L3, OPAL, SLD Collaborations, LEP Electroweak Working Group, Tevatron Electroweak Working Group, and SLD Electroweak and Heavy Flavour Groups, "Precision electroweak measurements and constraints on the standard model," (2010), [arXiv:1012.2367].

[9] S. Schael *et al.* (ALEPH, DELPHI, L3, OPAL, LEP Electroweak), Phys. Rept. **532**, 119 (2013), [arXiv:1302.3415].

[10] The LEP Electroweak Working Group`https://lepewwg.web.cern.ch/lepewwg/`.

[11] J. Beringer *et al.* (Particle Data Group), Phys. Rev. D **86**, 010001 (2012).

[12] ATLAS Collaboration, JINST **3**, S08003 (2008).

[13] CMS Collaboration, JINST **3**, S08004 (2008).

[14] ATLAS Collaboration, Phys. Lett. B **716**, 1 (2012), [arXiv:1207.7214].

[15] CMS Collaboration, Phys. Lett. B **716**, 30 (2012), [arXiv:1207.7235].

[16] ATLAS Collaboration, Phys. Lett. B **726**, 120 (2013), [arXiv:1307.1432].

[17] ATLAS Collaboration, Eur. Phys. J. C **75**, 476 (2015), [arXiv:1506.05669].

[18] CMS Collaboration, Phys. Rev. D **92**, 012004 (2015), [arXiv:1411.3441].

[19] CMS Collaboration, Eur. Phys. J. C **75**, 212 (2015), [arXiv:1412.8662].

[20] ATLAS Collaboration, Phys. Rev. D **90**, 052004 (2014), [arXiv:1408.0017].

[21] CMS Collaboration, Phys. Rev. D **92**, 072010 (2015), [arXiv:1507.06656].

[22] ATLAS and CMS Collaborations, JHEP **08**, 045 (2016), [arXiv:1606.02266].

[23] K. G. Wilson, Phys. Rev. **D3**, 1818 (1971); G. 't Hooft, in *Proc. of 1979 Cargèse Institute on Recent Developments in Gauge Theories,* p. 135 Press, New York 1980; For a modern discussion, see the GGI Tea Break's Seminar by G.F. Giudice and R. Rattazzi, https://is.gd/nUnjAr (2021).

[24] J. Wess and B. Zumino, Phys. Lett. **49B**, 52 (1974).

Int. J. Mod. Phys. A 2026.41. Downloaded from www.worldscientific.com
by UNIVERSITY OF CALIFORNIA @ BERKELEY on 09/16/26. Re-use and distribution is strictly not permitted, except for Open Access articles.

[25] S. P. Martin, Adv. Ser. Direct. High Energy Phys. 1–98 (1998), [hep-ph/9709356].

[26] B.C. Allanach and H.E. Haber, *Supersymmetry, Part I (Theory)*, in this volume.

[27] D. B. Kaplan and H. Georgi, Phys. Lett. **136B**, 183 (1984).

[28] B. Bellazzini, C. Csaki and J. Serra, Eur. Phys. J. **C74**, 5, 2766 (2014), [arXiv:1401.2457]; G. Panico and A. Wulzer, Lect. Notes Phys. **913**, pp.1 (2016), [arXiv:1506.01961]; C. Csaki, C. Grojean and J. Terning, Rev. Mod. Phys. **88**, 4, 045001 (2016), [arXiv:1512.00468].

[29] K.M. Black, R.S. Chivukula and M. Narain, *Dynamical Electroweak Symmetry Breaking: Implications of the H0*, in this volume.

[30] Z. Chacko, H.-S. Goh and R. Harnik, Phys. Rev. Lett. **96**, 231802 (2006), [hep-ph/0506256]; Z. Chacko, H.-S. Goh and R. Harnik, JHEP **01**, 108 (2006), [hep-ph/0512088].

[31] N. Craig *et al.*, JHEP **07**, 105 (2015), [arXiv:1501.05310]; N. Craig, S. Knapen and P. Longhi, Phys. Rev. Lett. **114**, 6, 061803 (2015), [arXiv:1410.6808].

[32] P. W. Graham, D. E. Kaplan and S. Rajendran, Phys. Rev. Lett. **115**, 22, 221801 (2015), [arXiv:1504.07551]; J. R. Espinosa *et al.*, Phys. Rev. Lett. **115**, 25, 251803 (2015), [arXiv:1506.09217]; G. Dvali (2019), [arXiv:1908.05984].

[33] C. Csaki *et al.*, Phys. Rev. Lett. **126**, 091801 (2021), [arXiv:2007.14396]; N. Arkani-Hamed, R. Tito D'agnolo and H. D. Kim (2020), [arXiv:2012.04652]; R. Tito D'Agnolo and D. Teresi (2021), [arXiv:2106.04591].

[34] T. Flacke *et al.*, JHEP **06**, 050 (2017), [arXiv:1610.02025].

[35] J. Khoury and O. Parrikar, JCAP **12**, 014 (2019), [arXiv:1907.07693]; G. F. Giudice, M. McCullough and T. You (2021), [arXiv:2105.08617].

[36] W. Altmannshofer and A. Greljo (2024), [arXiv:2412.04549].

[37] J. R. Ellis, M. K. Gaillard and D. V. Nanopoulos, Nucl. Phys. **B106**, 292 (1976).

[38] M. A. Shifman *et al.*, Sov. J. Nucl. Phys. **30**, 711 (1979), [Yad. Fiz.30,1368(1979)].

[39] J. F. Gunion *et al.*, *The Higgs Hunter's Guide*, Addison-Wesley (1990).

[40] R. L. Workman *et al.* (Particle Data Group), PTEP **2022**, 083C01 (2022).

[41] S. Weinberg, Phys. Rev. Lett. **43**, 1566 (1979).

[42] P. Sikivie *et al.*, Nucl. Phys. **B173**, 189 (1980); H. Georgi, Ann. Rev. Nucl. Part. Sci. **43**, 209 (1993).

[43] M. J. G. Veltman, Nucl. Phys. **B123**, 89 (1977).

[44] F. Devoto *et al.*, J. Phys. G **49**, 10, 103001 (2022), [arXiv:2205.03140].

[45] G. Degrassi *et al.*, JHEP **08**, 098 (2012), [arXiv:1205.6497]; S. Alekhin, A. Djouadi and S. Moch, Phys. Lett. **B716**, 214 (2012), [arXiv:1207.0980]; D. Buttazzo *et al.*, JHEP **12**, 089 (2013), [arXiv:1307.3536]; A. V. Bednyakov *et al.*, Phys. Rev. Lett. **115**, 20, 201802 (2015), [arXiv:1507.08833]; G. Hiller *et al.*, Phys. Rev. D **110**, 11, 115017 (2024), [arXiv:2401.08811].

[46] V. Branchina, E. Messina and M. Sher, Phys. Rev. **D91**, 013003 (2015), [arXiv:1408.5302].

[47] A. Hook *et al.*, JHEP **01**, 061 (2015), [arXiv:1404.5953]; J. Kearney, H. Yoo and K. M. Zurek, Phys. Rev. **D91**, 12, 123537 (2015), [arXiv:1503.05193].

[48] J. R. Espinosa, D. Racco and A. Riotto, Phys. Rev. Lett. **120**, 12, 121301 (2018), [arXiv:1710.11196].

[49] J. R. Espinosa, D. Racco and A. Riotto, JCAP **1809**, 09, 012 (2018), [arXiv:1804.07732].

[50] A. Andreassen, W. Frost and M. D. Schwartz, Phys. Rev. **D97**, 5, 056006 (2018), [arXiv:1707.08124].

[51] S. Chigusa, T. Moroi and Y. Shoji, Phys. Rev. Lett. **119**, 21, 211801 (2017), [arXiv:1707.09301].

[52] M. Shaposhnikov and C. Wetterich, Phys. Lett. **B683**, 196 (2010), [arXiv:0912.0208]; M. Holthausen, K. S. Lim and M. Lindner, JHEP **02**, 037 (2012), [arXiv:1112.2415].

[53] F. L. Bezrukov and M. Shaposhnikov, Phys. Lett. **B659**, 703 (2008), [arXiv:0710.3755]; F. L. Bezrukov, A. Magnin and M. Shaposhnikov, Phys. Lett. **B675**, 88 (2009), [arXiv:0812.4950].

[54] C. P. Burgess, H. M. Lee and M. Trott, JHEP **09**, 103 (2009), [arXiv:0902.4465]; J. L. F. Barbon and J. R. Espinosa, Phys. Rev. **D79**, 081302 (2009), [arXiv:0903.0355]; M. P. Hertzberg, JHEP **11**, 023 (2010), [arXiv:1002.2995].

[55] LHC Higgs Working Group, `https://twiki.cern.ch/twiki/bin/view/LHCPhysics/LHCHWG`.

[56] S. Heinemeyer *et al.* (LHC Higgs Cross Section Working Group), CERN Report **2013-004** (2013), [arXiv:1307.1347].

[57] D. de Florian *et al.* (LHC Higgs Cross Section Working Group), CERN Report **2017-002** (2016), [arXiv:1610.07922].

[58] S. Dittmaier *et al.* (LHC Higgs Cross Section Working Group), CERN Report **2011-002** (2011), [arXiv:1101.0593].

[59] S. Dittmaier *et al.* (LHC Higgs Cross Section Working Group), CERN Report **2012-002** (2012), [arXiv:1201.3084].

[60] A. Karlberg *et al.* (2024), [arXiv:2402.09955].

[61] H. M. Georgi *et al.*, Phys. Rev. Lett. **40**, 692 (1978).

[62] D. Graudenz, M. Spira and P. M. Zerwas, Phys. Rev. Lett. **70**, 1372 (1993).

[63] M. Spira *et al.*, Nucl. Phys. **B453**, 17 (1995), [hep-ph/9504378].

[64] S. Dawson, Nucl. Phys. **B359**, 283 (1991); A. Djouadi, M. Spira and P. M. Zerwas, Phys. Lett. **B264**, 440 (1991).

[65] R. V. Harlander and K. J. Ozeren, JHEP **11**, 088 (2009), [arXiv:0909.3420]; A. Pak, M. Rogal and M. Steinhauser, JHEP **02**, 025 (2010), [arXiv:0911.4662].

[66] C. Anastasiou *et al.*, Phys. Rev. Lett. **114**, 212001 (2015), [arXiv:1503.06056]; C. Anastasiou *et al.*, JHEP **05**, 058 (2016), [arXiv:1602.00695].

[67] B. Mistlberger, JHEP **05**, 028 (2018), [arXiv:1802.00833].

[68] G. Das, S. Moch and A. Vogt, Phys. Lett. B **807**, 135546 (2020), [arXiv:2004.00563].

[69] R. N. Lee *et al.*, Phys. Rev. D **104**, 7, 074008 (2021), [arXiv:2105.11504].

[70] R. N. Lee *et al.*, Phys. Rev. Lett. **128**, 21, 212002 (2022), [arXiv:2202.04660].

[71] B. Mistlberger and A. Suresh (2025), [arXiv:2504.10574].

[72] F. Dulat, A. Lazopoulos and B. Mistlberger, Comput. Phys. Commun. **233**, 243 (2018), [arXiv:1802.00827].

[73] R. V. Harlander, S. Liebler and H. Mantler, Comput. Phys. Commun. **212**, 239 (2017), [arXiv:1605.03190].

[74] T. Aaltonen *et al.* (CDF, D0), Phys. Rev. **D88**, 5, 052014 (2013), [arXiv:1303.6346].

[75] J. Davies *et al.*, Phys. Rev. **D100**, 3, 034017 (2019), [arXiv:1906.00982]; M. Czakon *et al.* (2021), [arXiv:2105.04436].

[76] F. Caola *et al.*, JHEP **09**, 035 (2018), [arXiv:1804.07632].

[77] K. Melnikov and A. Penin, JHEP **05**, 172 (2016), [arXiv:1602.09020].

[78] C. Anastasiou and A. Penin, JHEP **07**, 195 (2020), [Erratum: JHEP 01, 164 (2021)], [arXiv:2004.03602].

[79] M. Czakon *et al.*, Phys. Rev. Lett. **132**, 21, 211902 (2024), [arXiv:2312.09896].

Int. J. Mod. Phys. A 2026.41. Downloaded from www.wo
by UNIVERSITY OF CALIFORNIA @ BERKELEY on 09/16/26. Re-use and distribution is
except for Open Access articles.

[80] M. Czakon *et al.*, JHEP **10**, 210 (2024), [arXiv:2407.12413].

[81] R. V. Harlander and W. B. Kilgore, Phys. Rev. Lett. **88**, 201801 (2002), [hep-ph/0201206]; C. Anastasiou and K. Melnikov, Nucl. Phys. **B646**, 220 (2002), [hep-ph/0207004]; V. Ravindran, J. Smith and W. L. van Neerven, Nucl. Phys. **B665**, 325 (2003), [hep-ph/0302135].

[82] M. Bonvini *et al.*, JHEP **08**, 105 (2016), [arXiv:1603.08000].

[83] G. Billis *et al.*, Phys. Rev. Lett. **127**, 7, 072001 (2021), [arXiv:2102.08039].

[84] A. Djouadi and P. Gambino, Phys. Rev. Lett. **73**, 2528 (1994), [hep-ph/9406432]; S. Actis *et al.*, Phys. Lett. **B670**, 12 (2008), [arXiv:0809.1301]; U. Aglietti *et al.*, Phys. Lett. **B595**, 432 (2004), [hep-ph/0404071]; G. Degrassi and F. Maltoni, Phys. Lett. **B600**, 255 (2004), [hep-ph/0407249].

[85] C. Anastasiou, R. Boughezal and F. Petriello, JHEP **04**, 003 (2009), [arXiv:0811.3458].

[86] C. Anastasiou *et al.*, JHEP **03**, 162 (2019), [arXiv:1811.11211].

[87] M. Bonetti, K. Melnikov and L. Tancredi, Phys. Rev. **D97**, 5, 056017 (2018), [Erratum: Phys. Rev. **D97**, 9, 099906 (2018)], [arXiv:1801.10403]; M. Bonetti *et al.*, JHEP **11**, 045 (2020), [arXiv:2007.09813]; M. Becchetti *et al.*, Phys. Rev. D **103**, 5, 054037 (2021), [arXiv:2010.09451]; M. Becchetti, F. Moriello and A. Schweitzer, JHEP **04**, 139 (2022), [arXiv:2112.07578]; M. Bonetti, E. Panzer and L. Tancredi, JHEP **06**, 115 (2022), [arXiv:2203.17202].

[88] J. McGowan *et al.*, Eur. Phys. J. C **83**, 3, 185 (2023), [Erratum: Eur.Phys.J.C 83, 302 (2023)], [arXiv:2207.04739].

[89] R. D. Ball *et al.* (NNPDF), Eur. Phys. J. C **84**, 7, 659 (2024), [arXiv:2402.18635].

[90] T. Cridge *et al.*, J. Phys. G **52**, 6 (2025), [arXiv:2411.05373].

[91] F. Dulat, B. Mistlberger and A. Pelloni, Phys. Rev. D **99**, 3, 034004 (2019), [arXiv:1810.09462].

[92] L. Cieri *et al.*, JHEP **02**, 096 (2019), [arXiv:1807.11501].

[93] X. Chen *et al.*, Phys. Rev. Lett. **127**, 7, 072002 (2021), [arXiv:2102.07607].

[94] X. Chen, X. Guan and B. Mistlberger (2025), [arXiv:2504.06490].

[95] S. P. Jones, M. Kerner and G. Luisoni, Phys. Rev. Lett. **120**, 16, 162001 (2018), [Erratum: Phys.Rev.Lett. 128, 059901 (2022)], [arXiv:1802.00349].

[96] X. Chen *et al.*, JHEP **03**, 096 (2022), [arXiv:2110.06953].

[97] R. Bonciani *et al.*, Phys. Lett. B **843**, 137995 (2023), [arXiv:2206.10490].

[98] E. Braaten, H. Zhang and J.-W. Zhang, Phys. Rev. D **97**, 9, 096014 (2018), [arXiv:1707.09857].

[99] J. M. Lindert *et al.*, Phys. Rev. Lett. **118**, 25, 252002 (2017), [arXiv:1703.03886].

[100] M. Niggetiedt and M. Wiesemann, Phys. Lett. B **858**, 139043 (2024), [arXiv:2407.01354].

[101] K. Hamilton *et al.*, JHEP **10**, 222 (2013), [arXiv:1309.0017].

[102] S. Höche, Y. Li and S. Prestel, Phys. Rev. D **90**, 5, 054011 (2014), [arXiv:1407.3773].

[103] P. F. Monni, E. Re and M. Wiesemann, Eur. Phys. J. C **80**, 11, 1075 (2020), [arXiv:2006.04133].

[104] G. P. Salam and E. Slade, JHEP **11**, 220 (2021), [arXiv:2106.08329].

[105] A. Banfi, G. P. Salam and G. Zanderighi, JHEP **06**, 159 (2012), [arXiv:1203.5773]; T. Becher, M. Neubert and D. Wilhelm, JHEP **05**, 110 (2013), [arXiv:1212.2621]; A. Banfi *et al.*, JHEP **04**, 049 (2016), [arXiv:1511.02886]; J. K. L. Michel, P. Pietrulewicz and F. J. Tackmann, JHEP **04**, 142 (2019), [arXiv:1810.12911]; P. F. Monni, L. Rottoli and P. Torrielli, Phys. Rev. Lett. **124**, 25, 252001 (2020), [arXiv:1909.04704].

[106] I. Moult and I. W. Stewart, JHEP **09**, 129 (2014), [arXiv:1405.5534].

[107] P. Cal *et al.*, JHEP **03**, 155 (2025), [arXiv:2408.13301].

[108] V. D. Barger *et al.*, Phys. Rev. **D44**, 1426 (1991).

[109] F. A. Dreyer and A. Karlberg, Phys. Rev. Lett. **117**, 7, 072001 (2016), [arXiv:1606.00840].

[110] P. Bolzoni *et al.*, Phys. Rev. Lett. **105**, 011801 (2010), [arXiv:1003.4451].

[111] M. Cacciari *et al.*, Phys. Rev. Lett. **115**, 8, 082002 (2015), [Erratum: Phys. Rev. Lett. **120**, 13,139901 (2018)], [arXiv:1506.02660].

[112] J. Cruz-Martinez *et al.*, Phys. Lett. **B781**, 672 (2018), [arXiv:1802.02445].

[113] T. Han, G. Valencia and S. Willenbrock, Phys. Rev. Lett. **69**, 3274 (1992), [hep-ph/9206246].

[114] T. Liu, K. Melnikov and A. A. Penin, Phys. Rev. Lett. **123**, 12, 122002 (2019), [arXiv:1906.10899].

[115] C. Brønnum-Hansen, M.-M. Long and K. Melnikov, JHEP **11**, 130 (2023), [arXiv:2309.06292].

[116] F. A. Dreyer, A. Karlberg and L. Tancredi, JHEP **10**, 131 (2020), [Erratum: JHEP 04, 009 (2022)], [arXiv:2005.11334].

[117] M. Rauch and D. Zeppenfeld, Phys. Rev. **D95**, 11, 114015 (2017), [arXiv:1703.05676].

[118] K. Asteriadis *et al.*, JHEP **02**, 046 (2022), [arXiv:2110.02818].

[119] A. Buckley *et al.* (2021), [arXiv:2105.11399].

[120] A. Behring *et al.* (2025), [arXiv:2507.01448].

[121] A. Denner *et al.*, JHEP **03**, 075 (2012), [arXiv:1112.5142].

[122] A. Denner *et al.*, Comput. Phys. Commun. **195**, 161 (2015), [arXiv:1412.5390].

[123] B. Jäger and J. Scheller, JHEP **09**, 191 (2022), [arXiv:2208.00013].

[124] G. Barone *et al.* (2025), [arXiv:2507.22574].

[125] S. L. Glashow, D. V. Nanopoulos and A. Yildiz, Phys. Rev. **D18**, 1724 (1978); T. Han and S. Willenbrock, Phys. Lett. **B273**, 167 (1991); T. Han, G. Valencia, and S. Willenbrock, Phys. Rev. Lett. **69**, 3274 (1992); H. Baer, B. Bailey and J. F. Owens, Phys. Rev. **D47**, 2730 (1993); J. Ohnemus and W. J. Stirling, Phys. Rev. **D47**, 2722 (1993).

[126] A. Stange, W. J. Marciano and S. Willenbrock, Phys. Rev. **D49**, 1354 (1994), [hep-ph/9309294]; A. Stange, W. J. Marciano and S. Willenbrock, Phys. Rev. **D50**, 4491 (1994), [hep-ph/9404247].

[127] M. L. Ciccolini, S. Dittmaier and M. Krämer, Phys. Rev. **D68**, 073003 (2003), [hep-ph/0306234].

[128] R. Hamberg, W. L. van Neerven and T. Matsuura, Nucl. Phys. **B359**, 343 (1991), [Erratum: Nucl. Phys. **B644**, 403 (2002)].

[129] O. Brein, A. Djouadi and R. Harlander, Phys. Lett. **B579**, 149 (2004), [hep-ph/0307206]; L. Altenkamp *et al.*, JHEP **02**, 078 (2013), [arXiv:1211.5015].

[130] J. Davies, G. Mishima and M. Steinhauser, JHEP **03**, 034 (2021), [arXiv:2011.12314].

[131] L. Chen *et al.*, JHEP **03**, 125 (2021), [arXiv:2011.12325].

[132] L. Chen *et al.*, JHEP **08**, 056 (2022), [arXiv:2204.05225].

[133] B. Campillo Aveleira *et al.* (2025), [arXiv:2508.09905].

[134] O. Brein *et al.*, Eur. Phys. J. **C72**, 1868 (2012), [arXiv:1111.0761].

[135] O. Brein, R. V. Harlander and T. J. E. Zirke, Comput. Phys. Commun. **184**, 998 (2013), [arXiv:1210.5347]; R. V. Harlander *et al.*, JHEP **05**, 089 (2018), [arXiv:1802.04817].

[136] R. Gauld *et al.*, Phys. Lett. B **817**, 136335 (2021), [arXiv:2009.14209].

Int. J. Mod. Phys. A 2026.41. Downloaded from www.worldscientific.com
by UNIVERSITY OF CALIFORNIA @ BERKELEY on 09/16/26. Re-use and distribution is strictly not permitted, except for Open Access articles.

[137] J. Baglio *et al.*, JHEP **12**, 066 (2022), [arXiv:2209.06138].

[138] A. Denner *et al.*, JHEP **03**, 075 (2012), [arXiv:1112.5142].

[139] G. Ferrera, M. Grazzini, and F. Tramontano, Phys. Rev. Lett. **107**, 152003 (2011).

[140] F. Caola *et al.*, Phys. Rev. **D97**, 7, 074022 (2018), [arXiv:1712.06954]; G. Ferrera, G. Somogyi and F. Tramontano, Phys. Lett. B **780**, 346 (2018), [arXiv:1705.10304]; R. Gauld *et al.*, JHEP **10**, 002 (2019), [arXiv:1907.05836].

[141] G. Ferrera, M. Grazzini and F. Tramontano, Phys. Lett. **B740**, 51 (2015), [arXiv:1407.4747]; J. M. Campbell, R. K. Ellis and C. Williams, JHEP **06**, 179 (2016), [arXiv:1601.00658].

[142] W. Astill *et al.*, JHEP **06**, 154 (2016), [arXiv:1603.01620].

[143] J. M. Butterworth *et al.*, Phys. Rev. Lett. **100**, 242001 (2008), [arXiv:0802.2470].

[144] A. Behring *et al.*, Phys. Rev. D **101**, 11, 114012 (2020), [arXiv:2003.08321].

[145] W. Bizon *et al.* (2021), [arXiv:2106.06328].

[146] R. Raitio and W. W. Wada, Phys. Rev. **D19**, 941 (1979); Z. Kunszt, Nucl. Phys. **B247**, 339 (1984); J. N. Ng and P. Zakarauskas, Phys. Rev. D **29**, 876 (1984); J. F. Gunion, Phys. Lett. **B261**, 510 (1991); W. J. Marciano and F. E. Paige, Phys. Rev. Lett. **66**, 2433 (1991).

[147] W. Beenakker *et al.*, Phys. Rev. Lett. **87**, 201805 (2001), [hep-ph/0107081]; L. Reina and S. Dawson, Phys. Rev. Lett. **87**, 201804 (2001), [hep-ph/0107101]; L. Reina, S. Dawson and D. Wackeroth, Phys. Rev. D **65**, 053017 (2002), [hep-ph/0109066]; S. Dawson *et al.*, Phys. Rev. **D67**, 071503 (2003), [hep-ph/0211438]; W. Beenakker *et al.*, Nucl. Phys. **B653**, 151 (2003), [hep-ph/0211352]; S. Dawson *et al.*, Phys. Rev. **D68**, 034022 (2003), [hep-ph/0305087].

[148] Y. Zhang *et al.*, Phys. Lett. **B738**, 1 (2014), [arXiv:1407.1110]; S. Frixione *et al.*, JHEP **09**, 065 (2014), [arXiv:1407.0823]; S. Frixione *et al.*, JHEP **06**, 184 (2015), [arXiv:1504.03446].

[149] T. Plehn, G. P. Salam and M. Spannowsky, Phys. Rev. Lett. **104**, 111801 (2010), [arXiv:0910.5472].

[150] W.-L. Ju and L. L. Yang, JHEP **06**, 050 (2019), [arXiv:1904.08744].

[151] A. Kulesza *et al.*, JHEP **03**, 065 (2016), [arXiv:1509.02780]; A. Broggio *et al.*, JHEP **03**, 124 (2016), [arXiv:1510.01914]; A. Broggio *et al.*, JHEP **02**, 126 (2017), [arXiv:1611.00049]; A. Kulesza *et al.*, Phys. Rev. D **97**, 11, 114007 (2018), [arXiv:1704.03363]; A. Broggio *et al.*, JHEP **08**, 039 (2019), [arXiv:1907.04343]; A. Kulesza *et al.*, Eur. Phys. J. C **80**, 5, 428 (2020), [arXiv:2001.03031].

[152] A. Denner and R. Feger, JHEP **11**, 209 (2015), [arXiv:1506.07448].

[153] A. Denner *et al.*, JHEP **02**, 053 (2017), [arXiv:1612.07138].

[154] R. Frederix *et al.*, Phys. Lett. **B701**, 427 (2011), [arXiv:1104.5613]; H. B. Hartanto *et al.*, Phys. Rev. D **91**, 9, 094003 (2015), [arXiv:1501.04498].

[155] S. Catani *et al.*, Eur. Phys. J. C **81**, 6, 491 (2021), [arXiv:2102.03256].

[156] S. Catani *et al.*, Phys. Rev. Lett. **130**, 11, 111902 (2023), [arXiv:2210.07846].

[157] S. Devoto *et al.*, JHEP **03**, 189 (2025), [arXiv:2411.15340].

[158] F. Febres Cordero *et al.*, JHEP **07**, 084 (2024), [arXiv:2312.08131].

[159] G. Wang *et al.*, JHEP **07**, 121 (2024), [arXiv:2402.00431].

[160] B. Agarwal *et al.*, JHEP **05**, 013 (2024), [Erratum: JHEP 06, 142 (2024)], [arXiv:2402.03301].

[161] R. Balsach *et al.* (2025), [arXiv:2503.15043].

[162] C. Brancaccio *et al.*, JHEP **08**, 145 (2021), [arXiv:2106.06516].

[163] G. Bevilacqua *et al.*, Phys. Rev. D **107**, 1, 014028 (2023), [arXiv:2202.11186].

[164] F. Demartin *et al.*, Eur. Phys. J. **C75**, 6, 267 (2015), [arXiv:1504.00611].

[165] D. Pagani, I. Tsinikos and E. Vryonidou, JHEP **08**, 082 (2020), [arXiv:2006.10086].

[166] C. Duhr *et al.*, JHEP **08**, 08, 017 (2020), [arXiv:2004.04752].

[167] K.A. Assamagan *et al.*, [Higgs Working Group, "Physics at TeV Colliders" workshop, Les Houches, 2003], `arXiv:hep-ph/0406152` (2004).

[168] R. V. Harlander and W. B. Kilgore, Phys. Rev. **D68**, 013001 (2003), [hep-ph/0304035]; J. M. Campbell *et al.*, Phys. Rev. **D67**, 095002 (2003), [hep-ph/0204093]; S. Dawson *et al.*, Phys. Rev. Lett. **94**, 031802 (2005), [hep-ph/0408077]; S. Dittmaier, M. Krämer and M. Spira, Phys. Rev. **D70**, 074010 (2004), [hep-ph/0309204]; S. Dawson *et al.*, Phys. Rev. **D69**, 074027 (2004), [hep-ph/0311067].

[169] S. Badger *et al.*, JHEP **03**, 066 (2025), [arXiv:2412.06519].

[170] S. Badger *et al.*, JHEP **11**, 012 (2021), [arXiv:2107.14733].

[171] C. Biello *et al.*, JHEP **04**, 088 (2025), [arXiv:2412.09510].

[172] D. Pagani, H.-S. Shao and M. Zaro, JHEP **11**, 036 (2020), [arXiv:2005.10277].

[173] C. Grojean, A. Paul and Z. Qian, JHEP **04**, 139 (2021), [arXiv:2011.13945].

[174] S. Dawson, S. Dittmaier and M. Spira, Phys. Rev. **D58**, 115012 (1998), [hep-ph/9805244].

[175] D. de Florian and J. Mazzitelli, Phys. Rev. Lett. **111**, 201801 (2013), [arXiv:1309.6594].

[176] L.-B. Chen *et al.*, Phys. Lett. B **803**, 135292 (2020), [arXiv:1909.06808].

[177] S. Borowka *et al.*, Phys. Rev. Lett. **117**, 1, 012001 (2016), [Erratum: Phys. Rev. Lett. **117**, 7, 079901 (2016)], [arXiv:1604.06447]; J. Baglio *et al.*, Eur. Phys. J. **C79**, 6, 459 (2019), [arXiv:1811.05692]; J. Davies *et al.*, JHEP **11**, 024 (2019), [arXiv:1907.06408].

[178] S. Jaskiewicz *et al.*, JHEP **09**, 015 (2025), [arXiv:2501.00587].

[179] M. Grazzini *et al.*, JHEP **05**, 059 (2018), [arXiv:1803.02463].

[180] J. Davies, K. Schönwald and M. Steinhauser, Phys. Lett. B **845**, 138146 (2023), [arXiv:2307.04796].

[181] J. Davies *et al.*, JHEP **08**, 096 (2024), [arXiv:2405.20372].

[182] J. Davies, K. Schönwald and M. Steinhauser, JHEP **08**, 192 (2025), [arXiv:2503.17449].

[183] G. Aad *et al.* (ATLAS), Phys. Rev. Lett. **133**, 10, 101801 (2024), [arXiv:2406.09971].

[184] CMS Collaboration, CMS-HIG-20-011 (2025), [arXiv:2510.07527].

[185] F. A. Dreyer and A. Karlberg, Phys. Rev. D **98**, 11, 114016 (2018), [arXiv:1811.07906].

[186] F. A. Dreyer *et al.*, Eur. Phys. J. C **80**, 11, 1037 (2020), [arXiv:2005.13341].

[187] L.-S. Ling *et al.*, Phys. Rev. D **89**, 7, 073001 (2014), [arXiv:1401.7754].

[188] F. A. Dreyer and A. Karlberg, Phys. Rev. D **99**, 7, 074028 (2019), [arXiv:1811.07918].

[189] R. Frederix *et al.*, Phys. Lett. B **732**, 142 (2014), [arXiv:1401.7340].

[190] B. Jäger, A. Karlberg and S. Reinhardt, JHEP **06**, 022 (2025), [arXiv:2502.09112].

[191] R. K. Ellis *et al.* (2019), [arXiv:1910.11775].

[192] M. Narain *et al.* (2022), [arXiv:2211.11084].

[193] A. Arbey *et al.*, Eur. Phys. J. **C75**, 8, 371 (2015), [arXiv:1504.01726]; A. Freitas *et al.* (2019), [arXiv:1906.05379].

Int. J. Mod. Phys. A 2026.41. Downloaded from www.worldscientific.com by UNIVERSITY OF CALIFORNIA @ BERKELEY on 09/16/26. Re-use and distribution is [redacted] except for Open Access articles.

[194] J. de Blas *et al.*, JHEP **01**, 139 (2020), [arXiv:1905.03764].

[195] S. Dawson *et al.*, in "Snowmass 2021," (2022), [arXiv:2209.07510].

[196] H. Al Ali *et al.*, Rept. Prog. Phys. **85**, 8, 084201 (2022), [arXiv:2103.14043].

[197] J. de Blas, J. Gu and Z. Liu, Phys. Rev. D **106**, 7, 073007 (2022), [arXiv:2203.04324].

[198] J. de Blas *et al.* (Muon Collider) (2022), [arXiv:2203.07261].

[199] B.L. Ioffe and V.A. Khoze, Sov. J. Nucl. Phys. **9**, 50 (1978).

[200] D. R. T. Jones and S. T. Petcov, Phys. Lett. **84B**, 440 (1979); R. N. Cahn and S. Dawson, Phys. Lett. **136B**, 196 (1984), [Erratum: Phys. Lett. **138B**, 464 (1984)]; G. L. Kane, W. W. Repko and W. B. Rolnick, Phys. Lett. **148B**, 367 (1984); G. Altarelli, B. Mele and F. Pitolli, Nucl. Phys. **B287**, 205 (1987); W. Kilian, M. Krämer and P. M. Zerwas, Phys. Lett. **B373**, 135 (1996), [hep-ph/9512355].

[201] B. A. Kniehl, Z. Phys. **C55**, 605 (1992); J. Fleischer and F. Jegerlehner, Nucl. Phys. **B216**, 469 (1983); A. Denner *et al.*, Z. Phys. **C56**, 261 (1992); B. A. Kniehl, Int. J. Mod. Phys. **A17**, 1457 (2002), [hep-ph/0112023].

[202] K. J. F. Gaemers and G. J. Gounaris, Phys. Lett. **77B**, 379 (1978); A. Djouadi, J. Kalinowski and P. M. Zerwas, Z. Phys. **C54**, 255 (1992); B. A. Kniehl, F. Madricardo and M. Steinhauser, Phys. Rev. **D66**, 054016 (2002), [hep-ph/0205312]; S. Dittmaier *et al.*, Phys. Lett. **B441**, 383 (1998), [hep-ph/9808433]; S. Dittmaier *et al.*, Phys. Lett. **B478**, 247 (2000), [hep-ph/0002035]; S. Dawson and L. Reina, Phys. Rev. **D59**, 054012 (1999), [hep-ph/9808443].

[203] X. Chen *et al.* (2022), [arXiv:2209.14953].

[204] A. Freitas and Q. Song, Phys. Rev. Lett. **130**, 3, 031801 (2023), [arXiv:2209.07612].

[205] S. Heinemeyer, S. Jadach and J. Reuter, Eur. Phys. J. Plus **136**, 9, 911 (2021), [arXiv:2106.11802].

[206] A. Belloni *et al.* (2022), [arXiv:2209.08078].

[207] S. Frixione *et al.* (2021), [arXiv:2108.10261].

[208] A. Denner *et al.*, Eur. Phys. J. **C71**, 1753 (2011), [arXiv:1107.5909].

[209] A. Djouadi, J. Kalinowski, and M. Spira, Comp. Phys. Comm. **108**, 56 (1998); A. Djouadi *et al.*, `arXiv:1003.1643 [hep-ph]` (2010).

[210] S. G. Gorishnii *et al.*, Mod. Phys. Lett. **A5**, 2703 (1990); S. G. Gorishnii *et al.*, Phys. Rev. **D43**, 1633 (1991); A. L. Kataev and V. T. Kim, Mod. Phys. Lett. **A9**, 1309 (1994); L. R. Surguladze, Phys. Lett. **B341**, 60 (1994), [hep-ph/9405325].

[211] S. A. Larin, T. van Ritbergen and J. A. M. Vermaseren, Phys. Lett. **B362**, 134 (1995), [hep-ph/9506465]; K. G. Chetyrkin, Phys. Lett. **B390**, 309 (1997), [hep-ph/9608318]; P. A. Baikov, K. G. Chetyrkin and J. H. Kuhn, Phys. Rev. Lett. **96**, 012003 (2006), [hep-ph/0511063].

[212] K. G. Chetyrkin and A. Kwiatkowski, Nucl. Phys. **B461**, 3 (1996), [hep-ph/9505358].

[213] A. Primo *et al.*, Phys. Rev. D **99**, 5, 054013 (2019), [arXiv:1812.07811].

[214] W. Bernreuther, L. Chen and Z.-G. Si, JHEP **07**, 159 (2018), [arXiv:1805.06658].

[215] A. Behring and W. Bizoń, JHEP **01**, 189 (2020), [arXiv:1911.11524].

[216] G. Somogyi and F. Tramontano, JHEP **11**, 142 (2020), [arXiv:2007.15015].

[217] J. Wang, Y. Wang and D.-J. Zhang, JHEP **03**, 068 (2024), [arXiv:2310.20514].

[218] J. Wang, X. Wang and Y. Wang, JHEP **03**, 163 (2025), [arXiv:2411.07493].

[219] J. Fleischer and F. Jegerlehner, Phys. Rev. **D23**, 2001 (1981); D. Yu. Bardin, B. M. Vilensky and P. K. Khristova, Sov. J. Nucl. Phys. **53**, 152 (1991), [Yad. Fiz.53,240(1991)]; A. Dabelstein and W. Hollik, Z. Phys. **C53**, 507 (1992); B. A. Kniehl, Nucl. Phys. **B376**, 3 (1992); A. Djouadi *et al.*, in "In *Munich/Annecy/Hamburg 1991, Proceedings, e+ e- collisions at 500 GeV, pt. A* 11-30," (1991).

[220] F. Herzog *et al.*, JHEP **08**, 113 (2017), [arXiv:1707.01044].

[221] T. Inami, T. Kubota and Y. Okada, Z. Phys. **C18**, 69 (1983); K. G. Chetyrkin, B. A. Kniehl and M. Steinhauser, Phys. Rev. Lett. **79**, 353 (1997), [hep-ph/9705240]; P. A. Baikov and K. G. Chetyrkin, Phys. Rev. Lett. **97**, 061803 (2006), [hep-ph/0604194].

[222] H.-Q. Zheng and D.-D. Wu, Phys. Rev. **D42**, 3760 (1990); A. Djouadi *et al.*, Phys. Lett. **B257**, 187 (1991); S. Dawson and R. P. Kauffman, Phys. Rev. **D47**, 1264 (1993); A. Djouadi, M. Spira and P. M. Zerwas, Phys. Lett. **B311**, 255 (1993), [hep-ph/9305335]; K. Melnikov and O. I. Yakovlev, Phys. Lett. **B312**, 179 (1993), [hep-ph/9302281]; M. Inoue *et al.*, Mod. Phys. Lett. **A9**, 1189 (1994).

[223] P. Maierhöfer and P. Marquard, Phys. Lett. **B721**, 131 (2013), [arXiv:1212.6233].

[224] U. Aglietti *et al.*, Phys. Lett. **B595**, 432 (2004), [hep-ph/0404071]; G. Degrassi and F. Maltoni, Phys. Lett. **B600**, 255 (2004), [hep-ph/0407249]; S. Actis *et al.*, Phys. Lett. **B670**, 12 (2008), [arXiv:0809.1301]; U. Aglietti *et al.*, Phys. Lett. **B600**, 57 (2004), [hep-ph/0407162]; G. Degrassi and F. Maltoni, Nucl. Phys. **B724**, 183 (2005), [hep-ph/0504137]; U. Aglietti *et al.*, FERMILAB-CONF (2006), [hep-ph/0612172].

[225] A. Abbasabadi *et al.*, Phys. Rev. **D55**, 5647 (1997), [hep-ph/9611209]; A. Abbasabadi and W. W. Repko, Phys. Rev. **D71**, 017304 (2005), [hep-ph/0411152]; A. Abbasabadi and W. W. Repko, JHEP **08**, 048 (2006), [hep-ph/0602087]; D. A. Dicus and W. W. Repko, Phys. Rev. **D87**, 7, 077301 (2013), [arXiv:1302.2159]; L.-B. Chen, C.-F. Qiao and R.-L. Zhu, Phys. Lett. **B726**, 306 (2013), [arXiv:1211.6058]; Y. Sun, H.-R. Chang and D.-N. Gao, JHEP **05**, 061 (2013), [arXiv:1303.2230]; G. Passarino, Phys. Lett. **B727**, 424 (2013), [arXiv:1308.0422].

[226] M. Spira, A. Djouadi and P. M. Zerwas, Phys. Lett. **B276**, 350 (1992).

[227] R. Bonciani *et al.*, JHEP **08**, 108 (2015), [arXiv:1505.00567].

[228] T. Gehrmann, S. Guns and D. Kara, JHEP **09**, 038 (2015), [arXiv:1505.00561].

[229] A. Bredenstein *et al.*, Phys. Rev. **D74**, 013004 (2006), [hep-ph/0604011]; A. Bredenstein *et al.*, JHEP **02**, 080 (2007), [hep-ph/0611234]; A. Bredenstein *et al.*, `Prophecy4f`: A Monte Carlo generator for a proper description of the Higgs decay into 4 fermions, `http://omnibus.uni-freiburg.de/~sd565/programs/prophecy4f/prophecy4f.html`.

[230] A. Ghinculov, Phys. Lett. **B337**, 137 (1994), [Erratum: Phys. Lett. **B346**, 426 (1995)], [hep-ph/9405394]; L. Durand, B. A. Kniehl and K. Riesselmann, Phys. Rev. **D51**, 5007 (1995), [hep-ph/9412311]; L. Durand, K. Riesselmann and B. A. Kniehl, Phys. Rev. Lett. **72**, 2534 (1994), [Erratum: Phys. Rev. Lett. **74**, 1699 (1995)].

[231] A. Hayrapetyan *et al.* (CMS), Phys. Rev. D **111**, 9, 092014 (2025), [arXiv:2409.13663].

[232] N. Kauer and G. Passarino, JHEP **08**, 116 (2012), [arXiv:1206.4803].

[233] F. Caola and K. Melnikov, Phys. Rev. **D88**, 054024 (2013), [arXiv:1307.4935]; J. M. Campbell, R. K. Ellis and C. Williams, JHEP **04**, 060 (2014), [arXiv:1311.3589]; J. M. Campbell, R. K. Ellis and C. Williams, Phys. Rev. **D89**, 5, 053011 (2014), [arXiv:1312.1628].

[234] C. Englert and M. Spannowsky, Phys. Rev. **D90**, 053003 (2014), [arXiv:1405.0285].

Int. J. Mod. Phys. A 2026.41. Downloaded from www.worldscientific.com
by UNIVERSITY OF CALIFORNIA @ BERKELEY on 09/16/26. Re-use and distribution is strictly not permitted, except for Open Access articles.

[235] A. Azatov *et al.*, Zh. Eksp. Teor. Fiz. **147**, 410 (2015), [J. Exp. Theor. Phys.120,354(2015)], [arXiv:1406.6338]; A. Azatov *et al.*, JHEP **09**, 123 (2016), [arXiv:1608.00977].

[236] P. Bargiela *et al.*, Eur. Phys. J. C **83**, 2, 174 (2023), [arXiv:2212.06287].

[237] B. Agarwal *et al.*, Phys. Rev. Lett. **134**, 3, 031901 (2025), [arXiv:2404.05684].

[238] R. C. L. de Sá *et al.* (2025), [arXiv:2506.17022].

[239] A. Hayrapetyan *et al.* (CMS), CMS-HIG-21-018 (2026), [arXiv:2602.18611].

[240] ATLAS Collaboration, ATLAS-CONF-2025-006 (2025).

[241] A. M. Sirunyan *et al.* (CMS), JHEP **01**, 148 (2021), [arXiv:2009.04363].

[242] G. Aad *et al.* (ATLAS), Phys. Rev. Lett. **135**, 23, 231802 (2025), [arXiv:2507.03595].

[243] G. Aad *et al.* (ATLAS, CMS), Phys. Rev. Lett. **132**, 2, 021803 (2024), [arXiv:2309.03501].

[244] G. Aad *et al.* (ATLAS), Eur. Phys. J. C **84**, 1, 78 (2024), [arXiv:2306.11379].

[245] G. Cowan, *Statistics*, in this volume.

[246] G. Aad *et al.* (ATLAS), Phys. Lett. B **816**, 136204 (2021), [arXiv:2008.02508].

[247] A. Hayrapetyan *et al.* (CMS), JHEP **12**, 035 (2024), [arXiv:2407.08012].

[248] A. Hayrapetyan *et al.* (CMS), Phys. Lett. B **857**, 138964 (2024), [arXiv:2403.20201].

[249] G. Aad *et al.* (ATLAS), JHEP **05**, 028 (2023), [arXiv:2207.08615].

[250] A. M. Sirunyan *et al.* (CMS), Phys. Lett. **B792**, 369 (2019), [arXiv:1812.06504].

[251] V. Chekhovsky *et al.* (CMS), CMS-HIG-23-013 (2025), [arXiv:2504.13081].

[252] N. Berger *et al.* (2019), [arXiv:1906.02754].

[253] ATLAS Collaboration, ATLAS-CONF-2020-027 (2020).

[254] ATLAS Collaboration, ATLAS-CONF-2020-053 (2020).

[255] G. Aad *et al.* (ATLAS), Nature **607**, 7917, 52 (2022), [Erratum: Nature 612, E24 (2022)], [arXiv:2207.00092].

[256] A. David *et al.* (LHC Higgs Cross Section Working Group), LHC HXSWG interim recommendations to explore the coupling structure of a Higgs-like particle (2012), [arXiv:1209.0040].

[257] M. Dührssen, Prospects for the measurement of Higgs boson coupling parameters in the mass range from 110–190 GeV (2003); M. Duhrssen *et al.*, Phys. Rev. **D70**, 113009 (2004), [hep-ph/0406323]; R. Lafaye *et al.*, JHEP **08**, 009 (2009), [arXiv:0904.3866].

[258] J. R. Espinosa *et al.*, JHEP **05**, 097 (2012), [arXiv:1202.3697]; A. Azatov, R. Contino and J. Galloway, JHEP **04**, 127 (2012), [Erratum: JHEP **04**, 140 (2013)], [arXiv:1202.3415]; D. Carmi *et al.*, JHEP **07**, 136 (2012), [arXiv:1202.3144]; J. R. Espinosa *et al.*, JHEP **12**, 045 (2012), [arXiv:1207.1717].

[259] LHC Higgs Cross Section Working Group, `https://twiki.cern.ch/twiki/bin/view/LHCPhysics/LHCHWG2KAPPA`.

[260] G. Aad *et al.* (ATLAS, CMS), JHEP **08**, 045 (2016), [arXiv:1606.02266].

[261] A. Hayrapetyan *et al.* (CMS), Phys. Lett. B **860**, 139202 (2025), [arXiv:2405.16566].

[262] G. Aad *et al.* (ATLAS), Phys. Rev. Lett. **133**, 14, 141801 (2024), [arXiv:2402.00426].

[263] M. Tanabashi *et al.* (Particle Data Group), Phys. Rev. **D98**, 3, 030001 (2018).

[264] M. Farina *et al.*, JHEP **05**, 022 (2013), [arXiv:1211.3736].

[265] A. Tumasyan *et al.* (CMS), Nature **607**, 7917, 60 (2022), [arXiv:2207.00043].

[266] ATLAS and CMS Collaborations, CDS (2025), [arXiv:2504.00672], URL `https://cds.cern.ch/record/2928907`.

[267] A. Hayrapetyan *et al.* (CMS), Phys. Rev. Lett. **136**, 1, 011801 (2026), [arXiv:2509.22535].

[268] G. Aad *et al.* (ATLAS), JHEP **04**, 075 (2025), [arXiv:2410.19611].

[269] A. Hayrapetyan *et al.* (CMS), Phys. Lett. B **865**, 139462 (2025), [arXiv:2411.15000].

[270] A. Hayrapetyan *et al.* (CMS) (2025), [arXiv:2508.14988].

[271] V. Chekhovsky *et al.* (CMS), JHEP **11**, 060 (2025), [arXiv:2503.08797].

[272] V. Chekhovsky *et al.* (CMS), Phys. Rev. D **112**, 11, 112001 (2025), [arXiv:2502.05665].

[273] G. Aad *et al.* (ATLAS), Phys. Lett. B **801**, 135148 (2020), [arXiv:1909.10235].

[274] A. Tumasyan *et al.* (CMS), Phys. Lett. B **846**, 137783 (2023), [arXiv:2208.00265].

[275] I. Brivio and M. Trott, Phys. Rept. **793**, 1 (2019), [arXiv:1706.08945].

[276] G. Isidori, F. Wilsch and D. Wyler, Rev. Mod. Phys. **96**, 1, 015006 (2024), [arXiv:2303.16922].

[277] J. Aebischer, A. J. Buras and J. Kumar (2025), [arXiv:2507.05926].

[278] A. Manohar and H. Georgi, Nucl. Phys. **B234**, 189 (1984); M. A. Luty, Phys. Rev. **D57**, 1531 (1998), [hep-ph/9706235]; D. Liu *et al.*, JHEP **11**, 141 (2016), [arXiv:1603.03064].

[279] G. F. Giudice *et al.*, JHEP **06**, 045 (2007), [hep-ph/0703164].

[280] S. Alioli *et al.*, Phys. Lett. B **809**, 135703 (2020), [arXiv:2003.11615].

[281] R. Boughezal, Y. Huang and F. Petriello, Phys. Rev. D **106**, 3, 036020 (2022), [arXiv:2207.01703].

[282] S. Alioli *et al.*, in "Snowmass 2021," (2022), [arXiv:2203.06771].

[283] W. Buchmuller and D. Wyler, Nucl. Phys. **B268**, 621 (1986).

[284] C. J. C. Burges and H. J. Schnitzer, Nucl. Phys. **B228**, 464 (1983); C. N. Leung, S. T. Love and S. Rao, Z. Phys. **C31**, 433 (1986).

[285] B. Grzadkowski *et al.*, JHEP **10**, 085 (2010), [arXiv:1008.4884].

[286] L. Lehman and A. Martin, JHEP **02**, 081 (2016), [arXiv:1510.00372]; B. Henning *et al.*, JHEP **08**, 016 (2017), [arXiv:1512.03433].

[287] C. Hays *et al.*, JHEP **02**, 123 (2019), [arXiv:1808.00442].

[288] R. Alonso *et al.*, JHEP **04**, 159 (2014), [arXiv:1312.2014].

[289] D. A. Faroughy *et al.*, JHEP **08**, 166 (2020), [arXiv:2005.05366].

[290] J. de Blas *et al.*, JHEP **03**, 109 (2018), [arXiv:1711.10391].

[291] I. Brivio *et al.*, SciPost Phys. **12**, 1, 036 (2022), [arXiv:2108.01094].

[292] A. Carmona *et al.*, SciPost Phys. **12**, 6, 198 (2022), [arXiv:2112.10787].

[293] J. Fuentes-Martín *et al.*, Eur. Phys. J. C **83**, 7, 662 (2023), [arXiv:2212.04510].

[294] E. E. Jenkins, A. V. Manohar and M. Trott, JHEP **10**, 087 (2013), [arXiv:1308.2627].

[295] E. E. Jenkins, A. V. Manohar and M. Trott, JHEP **01**, 035 (2014), [arXiv:1310.4838].

[296] J. C. Criado, Comput. Phys. Commun. **227**, 42 (2018), [arXiv:1710.06445].

Int. J. Mod. Phys. A 2026.41. Downloaded from www.worldscientific.com by UNIVERSITY OF CALIFORNIA @ BERKELEY on 09/16/26. Re-use and distribution is except for Open Access articles.

[297] A. Celis *et al.*, Eur. Phys. J. C **77**, 6, 405 (2017), [arXiv:1704.04504].

[298] J. Aebischer, J. Kumar and D. M. Straub, Eur. Phys. J. C **78**, 12, 1026 (2018), [arXiv:1804.05033].

[299] S. Di Noi and L. Silvestrini, Eur. Phys. J. C **83**, 3, 200 (2023), [arXiv:2210.06838].

[300] J. Alwall *et al.*, JHEP **07**, 079 (2014), [arXiv:1405.0301].

[301] I. Brivio, Y. Jiang and M. Trott, JHEP **12**, 070 (2017), [arXiv:1709.06492].

[302] I. Brivio, JHEP **04**, 073 (2021), [arXiv:2012.11343].

[303] C. Degrande *et al.*, Phys. Rev. D **103**, 9, 096024 (2021), [arXiv:2008.11743].

[304] J. de Blas *et al.* (2025), [arXiv:2507.06191].

[305] J. Ellis *et al.*, JHEP **04**, 279 (2021), [arXiv:2012.02779].

[306] J. J. Ethier *et al.* (SMEFiT), JHEP **11**, 089 (2021), [arXiv:2105.00006].

[307] L. Allwicher *et al.* (2023), [arXiv:2311.00020].

[308] R. Bartocci, A. Biekötter and T. Hurth, JHEP **05**, 074 (2024), [arXiv:2311.04963].

[309] R. Bartocci, A. Biekötter and T. Hurth, JHEP **05**, 203 (2025), [arXiv:2412.09674].

[310] E. Celada *et al.*, JHEP **09**, 091 (2024), [arXiv:2404.12809].

[311] G. Aad *et al.* (ATLAS), JHEP **11**, 097 (2024), [arXiv:2402.05742].

[312] V. Chekhovsky *et al.* (CMS), CMS-SMP-24-003 (2025), [arXiv:2504.02958].

[313] ATLAS Collaboration, ATL-PHYS-PUB-2022-037 (2022).

[314] A. Hayrapetyan *et al.* (CMS), JHEP **10**, 061 (2024), [arXiv:2404.08462].

[315] G. Aad *et al.* (ATLAS), Eur. Phys. J. C **83**, 6, 519 (2023), [arXiv:2210.05415].

[316] CMS Collaboration, CMS-PAS-HIG-23-004 (2025).

[317] ATLAS and CMS Collaborations, CMS-PAS-HIG-25-014, ATLAS-CONF-2025-012 (2025).

[318] ATLAS Collaboration, ATL-PHYS-PUB-2025-034 (2025).

[319] A. Hayrapetyan *et al.* (CMS), Phys. Lett. B **861**, 139210 (2025), [arXiv:2407.13554].

[320] G. Aad *et al.* (ATLAS), Phys. Lett. B **843**, 137745 (2023), [arXiv:2211.01216].

[321] G. Aad *et al.* (ATLAS) (2025), [arXiv:2507.03495].

[322] CMS Collaboration, CMS-PAS-HIG-25-007 (2025).

[323] CMS Collaboration, CMS-PAS-HIG-24-010 (2025).

[324] ATLAS Collaboration, ATL-PHYS-PUB-2025-005 (2025).

[325] G. Aad *et al.* (ATLAS), Phys. Rev. D **111**, 3, 032006 (2025), [arXiv:2411.02040].

[326] CMS Collaboration, CMS-PAS-HIG-24-015 (2025).

[327] CMS Collaboration, CMS-PAS-HIG-24-012 (2025).

[328] G. Aad *et al.* (ATLAS, CMS), Phys. Rev. Lett. **114**, 191803 (2015), [arXiv:1503.07589].

[329] G. Aad *et al.* (ATLAS), Phys. Rev. Lett. **131**, 25, 251802 (2023), [arXiv:2308.04775].

[330] G. Aad *et al.* (ATLAS), Phys. Lett. B **847**, 138315 (2023), [arXiv:2308.07216].

[331] G. Aad *et al.* (ATLAS), Phys. Rev. **D90**, 5, 052004 (2014), [arXiv:1406.3827].

[332] CMS Collaboration, CMS-PAS-HIG-25-004 (2025).

[333] L. J. Dixon and M. S. Siu, Phys. Rev. Lett. **90**, 252001 (2003), [hep-ph/0302233].

[334] S. P. Martin, Phys. Rev. **D86**, 073016 (2012), [arXiv:1208.1533].

[335] L. J. Dixon and Y. Li, Phys. Rev. Lett. **111**, 111802 (2013), [arXiv:1305.3854].

[336] J. Campbell *et al.*, Phys. Rev. Lett. **119**, 18, 181801 (2017), [Addendum: Phys. Rev. Lett.119,19,199901(2017)], [arXiv:1704.08259].

[337] ATLAS Collaboration, ATL-PHYS-PUB-2016-009 (2016).

[338] ATLAS Collaboration, ATL-PHYS-PUB-2013-014 (2013).

[339] ATLAS Collaboration, ATL-PHYS-PUB-2014-016 (2014).

[340] G. Aad *et al.* (ATLAS), Rept. Prog. Phys. **88**, 5, 057803 (2025), [arXiv:2412.01548].

[341] A. Tumasyan *et al.* (CMS), Nature Phys. **18**, 11, 1329 (2022), [arXiv:2202.06923].

[342] G. Aad *et al.* (ATLAS), Phys. Lett. B **870**, 139898 (2025), [arXiv:2504.07710].

[343] G. Aad *et al.* (ATLAS), Phys. Lett. B **861**, 139277 (2025), [arXiv:2407.10631].

[344] M. Cepeda *et al.* (HL/HE-LHC WG2 group) (2019), [arXiv:1902.00134].

[345] Y. Gao *et al.*, Phys. Rev. D **81**, 075022 (2010), [arXiv:1001.3396].

[346] S. Bolognesi *et al.*, Phys. Rev. **D86**, 095031 (2012), [arXiv:1208.4018].

[347] J. F. Gunion *et al.*, *The Higgs Hunter's Guide*, volume 80 (2000), ISBN 978-0-429-49644-8.

[348] J. Brod, U. Haisch and J. Zupan, JHEP **11**, 180 (2013), [arXiv:1310.1385].

[349] S. Degenkolb *et al.* (2024), [arXiv:2403.02052].

[350] G. Aad *et al.* (ATLAS) (2023), [arXiv:2304.09612].

[351] CMS Collaboration, CMS-PAS-HIG-24-006 (2025).

[352] ATLAS Collaboration, ATL-PHYS-PUB-2025-031 (2025).

[353] A. M. Sirunyan *et al.* (CMS), Phys. Rev. D **100**, 11, 112002 (2019), [arXiv:1903.06973].

[354] G. Aad *et al.* (ATLAS), Phys. Rev. Lett. **125**, 6, 061802 (2020), [arXiv:2004.04545].

[355] (2023), [arXiv:2303.05974].

[356] A. M. Sirunyan *et al.* (CMS), Phys. Rev. Lett. **125**, 6, 061801 (2020), [arXiv:2003.10866].

[357] A. M. Sirunyan *et al.* (CMS), Phys. Rev. D **104**, 5, 052004 (2021), [arXiv:2104.12152].

[358] A. Tumasyan *et al.* (CMS), JHEP **07**, 092 (2023), [arXiv:2208.02686].

[359] A. Tumasyan *et al.* (CMS), JHEP **06**, 012 (2022), [arXiv:2110.04836].

[360] G. Aad *et al.* (ATLAS), Eur. Phys. J. C **83**, 7, 563 (2023), [arXiv:2212.05833].

[361] ATLAS Collaboration, ATL-PHYS-PUB-2019-008 (2019).

[362] Y. Gershtein, and A. Pomarol, *Extra Dimensions*, in this volume.

[363] L. E. Ibanez and G. G. Ross, Phys. Lett. **110B**, 215 (1982); L. E. Ibanez, Phys. Lett. **118B**, 73 (1982); J. R. Ellis, D. V. Nanopoulos and K. Tamvakis, Phys. Lett. **121B**, 123 (1983); L. Alvarez-Gaume, J. Polchinski and M. B. Wise, Nucl. Phys. **B221**, 495 (1983).

[364] M. Carena *et al.*, Phys. Rev. **D91**, 3, 035003 (2015), [arXiv:1410.4969].

[365] M. Carena *et al.*, Phys. Rev. **D93**, 3, 035013 (2016), [arXiv:1510.09137].

[366] J. F. Gunion and H. E. Haber, Phys. Rev. **D67**, 075019 (2003), [hep-ph/0207010].

[367] H. E. Haber and Y. Nir, Nucl. Phys. **B335**, 363 (1990).

[368] S. Weinberg, Phys. Rev. **D13**, 974 (1976), [Addendum: Phys. Rev.D19,1277(1979)]; L. Susskind, Phys. Rev. **D20**, 2619 (1979); For a review, see C. T. Hill and E. H. Simmons, Phys. Reports **381**, 235 (2003) [Erratum: 390, 553 (2004)], [arXiv:hep-ph/0203079].

Int. J. Mod. Phys. A 2026.41. Downloaded from www.worldscientific.com
by UNIVERSITY OF CALIFORNIA @ BERKELEY on 09/16/26. Re-use and distribution is strictly not permitted, except for Open Access articles.

[369] Z. Chacko, R. Franceschini and R. K. Mishra, JHEP **04**, 015 (2013), [arXiv:1209.3259].

[370] D. B. Kaplan, Nucl. Phys. **B365**, 259 (1991).

[371] G. Panico *et al.*, JHEP **03**, 051 (2013), [arXiv:1210.7114].

[372] A. Hebecker, J. Hisano, and N. Nagata, *Grand Unified Theories*, in this volume.

[373] L.J. Rosenberg, G. Rybka, and B. Safdi, *Axions and Other Similar Particles*, in this volume.

[374] M. D'Onofrio and F. Moortgat, *Supersymmetry, Part II (Experiment)*, in this volume.

[375] K. Hikasa, and M. Tanabashi, K. Terashi, N. Varelas *Searches for Quark and Lepton Compositeness*, in this volume.

[376] H. E. Haber and G. L. Kane, Phys. Rept. **117**, 75 (1985).

[377] P. Slavich *et al.*, Eur. Phys. J. C **81**, 5, 450 (2021), [arXiv:2012.15629].

[378] M. Carena and H. E. Haber, Prog. Part. Nucl. Phys. **50**, 63 (2003), [hep-ph/0208209].

[379] A. Djouadi, Phys. Rept. **459**, 1 (2008), [hep-ph/0503173].

[380] E. L. Berger *et al.*, Phys. Rev. **D66**, 095001 (2002), [hep-ph/0205342].

[381] P. Bechtle *et al.*, Eur. Phys. J. **C77**, 2, 67 (2017), [arXiv:1608.00638].

[382] E. Bagnaschi *et al.*, Eur. Phys. J. **C79**, 7, 617 (2019), [arXiv:1808.07542].

[383] A. Djouadi, J. Kalinowski and P. M. Zerwas, Z. Phys. **C57**, 569 (1993).

[384] G. Lee and C. E. M. Wagner, Phys. Rev. **D92**, 7, 075032 (2015), [arXiv:1508.00576].

[385] D. Dicus *et al.*, Phys. Rev. **D59**, 094016 (1999), [hep-ph/9811492].

[386] M. Carena *et al.*, JHEP **07**, 091 (2012), [arXiv:1203.1041].

[387] A. A. Barrientos Bendezu and B. A. Kniehl, Phys. Rev. **D64**, 035006 (2001), [hep-ph/0103018].

[388] J. Alison *et al.*, Rev. Phys. **5**, 100045 (2020), [arXiv:1910.00012].

[389] LHC Higgs Working Group, `https://twiki.cern.ch/twiki/bin/view/LHCPhysics/LHCHWGMSSMCharged`.

[390] D. Dicus, A. Stange and S. Willenbrock, Phys. Lett. B **333**, 126 (1994), [hep-ph/9404359]; N. Craig *et al.*, JHEP **06**, 137 (2015), [arXiv:1504.04630]; S. Gori *et al.*, Phys. Rev. D **93**, 7, 075038 (2016), [arXiv:1602.02782].

[391] A. Djouadi, J. Ellis and J. Quevillon, JHEP **07**, 105 (2016), [arXiv:1605.00542]; M. Carena and Z. Liu, JHEP **11**, 159 (2016), [arXiv:1608.07282].

[392] LHC Higgs Working Group for BSM Higgs, `https://twiki.cern.ch/twiki/bin/view/LHCPhysics/LHCHWG3`.

[393] E. Bagnaschi *et al.*, Eur. Phys. J. C **79**, 7, 617 (2019), [arXiv:1808.07542].

[394] A. Tumasyan *et al.* (CMS), JHEP **07**, 073 (2023), [arXiv:2208.02717].

[395] U. Ellwanger, C. Hugonie and A. M. Teixeira, Phys. Rept. **496**, 1 (2010), [arXiv:0910.1785].

[396] B. A. Dobrescu, G. L. Landsberg and K. T. Matchev, Phys. Rev. **D63**, 075003 (2001), [hep-ph/0005308]; R. Dermisek and J. F. Gunion, Phys. Rev. Lett. **95**, 041801 (2005), [hep-ph/0502105].

[397] J. Engel, M. J. Ramsey-Musolf and U. van Kolck, Prog. Part. Nucl. Phys. **71**, 21 (2013), [arXiv:1303.2371].

[398] H. Bahl *et al.*, Eur. Phys. J. C **80**, 10, 916 (2020), [arXiv:2005.14536].

[399] R. S. Chivukula and H. Georgi, Phys. Lett. **B188**, 99 (1987); L. J. Hall and L. Randall, Phys. Rev. Lett. **65**, 2939 (1990); A. J. Buras *et al.*, Phys. Lett. **B500**, 161 (2001), [hep-ph/0007085]; G. D'Ambrosio *et al.*, Nucl. Phys. **B645**, 155 (2002), [hep-ph/0207036].

[400] M. Misiak and M. Steinhauser, Eur. Phys. J. C **77**, 3, 201 (2017), [arXiv:1702.04571].

[401] J. F. Gunion and H. E. Haber, Phys. Rev. **D67**, 075019 (2003), [hep-ph/0207010]; G. C. Branco *et al.*, Phys. Rept. **516**, 1 (2012), [arXiv:1106.0034].

[402] N. G. Deshpande and E. Ma, Phys. Rev. **D18**, 2574 (1978).

[403] A. Goudelis, B. Herrmann and S. O., JHEP **09**, 106 (2013), [arXiv:1303.3010].

[404] M. Bauer, M. Carena and K. Gemmler, JHEP **11**, 016 (2015), [arXiv:1506.01719]; M. Bauer, M. Carena and K. Gemmler, Phys. Rev. **D94**, 11, 115030 (2016), [arXiv:1512.03458].

[405] C. D. Froggatt and H. B. Nielsen, Nucl. Phys. **B147**, 277 (1979).

[406] K. S. Babu and S. Nandi, Phys. Rev. **D62**, 033002 (2000), [hep-ph/9907213]; G. F. Giudice and O. Lebedev, Phys. Lett. **B665**, 79 (2008), [arXiv:0804.1753].

[407] E. Accomando *et al.*, CERN Report **2006-009** (2006), [hep-ph/0608079].

[408] T. Robens and T. Stefaniak, Eur. Phys. J. **C75**, 104 (2015), [arXiv:1501.02234].

[409] S. L. Glashow and S. Weinberg, Phys. Rev. **D15**, 1958 (1977); E. A. Paschos, Phys. Rev. **D15**, 1966 (1977).

[410] G. C. Branco, W. Grimus and L. Lavoura, Phys. Lett. **B380**, 119 (1996), [hep-ph/9601383]; F. J. Botella, G. C. Branco and M. N. Rebelo, Phys. Lett. **B687**, 194 (2010), [arXiv:0911.1753].

[411] T. P. Cheng and M. Sher, Phys. Rev. D **35**, 3484 (1987).

[412] D. Atwood, L. Reina and A. Soni, Phys. Rev. D **55**, 3156 (1997), [hep-ph/9609279].

[413] J. Schechter and J. W. F. Valle, Phys. Rev. **D22**, 2227 (1980); T. P. Cheng and L.-F. Li, Phys. Rev. **D22**, 2860 (1980).

[414] H. Georgi and M. Machacek, Nucl. Phys. **B262**, 463 (1985); M. S. Chanowitz and M. Golden, Phys. Lett. **165B**, 105 (1985); J. F. Gunion, R. Vega and J. Wudka, Phys. Rev. **D42**, 1673 (1990).

[415] P. Nath *et al.*, Nucl. Phys. Proc. Suppl. **200-202**, 185 (2010), [arXiv:1001.2693].

[416] J. Garayoa and T. Schwetz, JHEP **03**, 009 (2008), [arXiv:0712.1453].

[417] H. E. Haber and H. E. Logan, Phys. Rev. **D62**, 015011 (2000), [hep-ph/9909335]; S. Kanemura and K. Yagyu, Phys. Rev. **D85**, 115009 (2012), [arXiv:1201.6287].

[418] J. F. Gunion, R. Vega and J. Wudka, Phys. Rev. **D43**, 2322 (1991).

[419] I. Low and J. Lykken, JHEP **10**, 053 (2010), [arXiv:1005.0872]; I. Low, J. Lykken and G. Shaughnessy, Phys. Rev. **D86**, 093012 (2012), [arXiv:1207.1093].

[420] H. E. Logan and M.-A. Roy, Phys. Rev. **D82**, 115011 (2010), [arXiv:1008.4869]; A. Falkowski, S. Rychkov and A. Urbano, JHEP **04**, 073 (2012), [arXiv:1202.1532].

[421] N. Arkani-Hamed *et al.*, JHEP **07**, 034 (2002), [hep-ph/0206021]; N. Arkani-Hamed, A. G. Cohen and H. Georgi, Phys. Lett. **B513**, 232 (2001), [hep-ph/0105239].

[422] M. Perelstein, Prog. Part. Nucl. Phys. **58**, 247 (2007), [hep-ph/0512128]; M. Schmaltz and D. Tucker-Smith, Ann. Rev. Nucl. Part. Sci. **55**, 229 (2005), [hep-ph/0502182].

[423] H. Georgi, A. E. Nelson and A. Manohar, Phys. Lett. **126B**, 169 (1983); A. E. Nelson and M. J. Strassler, JHEP **09**, 030 (2000), [hep-ph/0006251]; S. Davidson, G. Isidori and S. Uhlig, Phys. Lett. **B663**, 73 (2008), [arXiv:0711.3376].

[424] R. Contino and G. Servant, JHEP **06**, 026 (2008), [arXiv:0801.1679]; J. Mrazek and A. Wulzer, Phys. Rev. **D81**, 075006 (2010), [arXiv:0909.3977]; A. De Simone *et al.*, JHEP **04**, 004 (2013), [arXiv:1211.5663]; A. Azatov *et al.*, Phys. Rev. **D89**, 7, 075001 (2014), [arXiv:1308.6601].

Int. J. Mod. Phys. A 2026.41. Downloaded from www.worldscientific.com by UNIVERSITY OF CALIFORNIA @ BERKELEY on 09/16/26. Re-use and distribution is [redacted] except for Open Access articles.

[425] A. Banfi, A. Martin and V. Sanz, JHEP **08**, 053 (2014), [arXiv:1308.4771]; A. Azatov and A. Paul, JHEP **01**, 014 (2014), [arXiv:1309.5273]; C. Grojean *et al.*, JHEP **05**, 022 (2014), [arXiv:1312.3317].

[426] A. Azatov *et al.*, Phys. Rev. **D92**, 3, 035001 (2015), [arXiv:1502.00539].

[427] K. Agashe, R. Contino and A. Pomarol, Nucl. Phys. **B719**, 165 (2005), [hep-ph/0412089]; R. Contino, L. Da Rold and A. Pomarol, Phys. Rev. **D75**, 055014 (2007), [hep-ph/0612048]; D. Pappadopulo, A. Thamm and R. Torre, JHEP **07**, 058 (2013), [arXiv:1303.3062]; M. Montull *et al.*, Phys. Rev. **D88**, 095006 (2013), [arXiv:1308.0559].

[428] I. Low, R. Rattazzi and A. Vichi, JHEP **04**, 126 (2010), [arXiv:0907.5413].

[429] M. Ciuchini *et al.*, JHEP **08**, 106 (2013), [arXiv:1306.4644].

[430] C. Grojean, O. Matsedonskyi and G. Panico, JHEP **10**, 160 (2013), [arXiv:1306.4655].

[431] G. Aad *et al.* (ATLAS), Phys. Rev. Lett. **132**, 23, 231801 (2024), [arXiv:2311.15956].

[432] P. Batra and Z. Chacko, Phys. Rev. **D79**, 095012 (2009), [arXiv:0811.0394]; R. Barbieri *et al.*, JHEP **08**, 161 (2015), [arXiv:1501.07803]; M. Low, A. Tesi and L.-T. Wang, Phys. Rev. **D91**, 095012 (2015), [arXiv:1501.07890].

[433] D. Curtin *et al.*, Phys. Rev. D **90**, 7, 075004 (2014), [arXiv:1312.4992].

[434] M. Cepeda *et al.*, Annual Review of Nuclear and Particle Science **72** (2022), [arXiv:2111.12751].

[435] A. Hayrapetyan *et al.* (CMS), Phys. Rept. **1115**, 368 (2025), [arXiv:2403.16926].

[436] G. Arcadi, A. Djouadi and M. Raidal, Phys. Rept. **842**, 1 (2020), [arXiv:1903.03616].

[437] R. E. Shrock and M. Suzuki, Phys. Lett. B **110**, 250 (1982).

[438] G. Aad *et al.* (ATLAS), Phys. Lett. B **842**, 137963 (2023), [arXiv:2301.10731].

[439] A. Tumasyan *et al.* (CMS), Eur. Phys. J. C **83**, 10, 933 (2023), [arXiv:2303.01214].

[440] B L. Baudis and S. Profumo, *Dark Matter*, in this volume.

[441] G. Aad *et al.* (ATLAS), JHEP **07**, 166 (2023), [arXiv:2302.05225].

[442] A. M. Sirunyan *et al.* (CMS), Phys. Rev. D **104**, 3, 032013 (2021), [arXiv:2105.03007].

[443] A. Hayrapetyan *et al.* (CMS) (2023), [arXiv:2305.18106].

[444] J. Adam *et al.* (MEG), Phys. Rev. Lett. **110**, 201801 (2013), [arXiv:1303.0754].

[445] R. Harnik, J. Kopp and J. Zupan, JHEP **03**, 026 (2013), [arXiv:1209.1397].

[446] ATLAS Collaboration, JHEP **129**, 010 (2017).

[447] A. Tumasyan *et al.* (CMS), JHEP **02**, 169 (2022), [arXiv:2112.09734].

[448] G. Aad *et al.* (ATLAS), Phys. Rept. **1116**, 184 (2025), [arXiv:2405.04914].

[449] D. Curtin *et al.*, JHEP **02**, 157 (2015), [arXiv:1412.0018].

[450] A. Hayrapetyan *et al.* (CMS), JHEP **05**, 047 (2024), [arXiv:2402.14491].

[451] A. Tumasyan *et al.* (CMS), Eur. Phys. J. C **82**, 4, 290 (2022), [arXiv:2111.01299].

[452] G. Aad *et al.* (ATLAS), JHEP **03**, 041 (2022), [arXiv:2110.13673].

[453] G. Aad *et al.* (ATLAS), JHEP **08**, 153 (2024), [arXiv:2406.01656].

[454] A. M. Sirunyan *et al.* (CMS), JHEP **03**, 011 (2021), [arXiv:2009.14009].

[455] A. M. Sirunyan *et al.* (CMS), JHEP **10**, 139 (2019), [arXiv:1908.02699].

[456] A. Hayrapetyan *et al.* (CMS), Phys. Rept. **1115**, 448 (2025), [arXiv:2405.13778].

[457] A. Hayrapetyan *et al.* (CMS), Phys. Rept. **1115**, 678 (2025), [arXiv:2403.16134].

[458] G. Aad *et al.* (ATLAS), JHEP **07**, 155 (2023), [arXiv:2211.04172].

[459] G. Aad *et al.* (ATLAS), JHEP **01**, 053 (2025), [arXiv:2407.07546].

[460] A. Hayrapetyan *et al.* (CMS), Phys. Lett. B **860**, 139067 (2025), [arXiv:2405.18149].

[461] A. M. Sirunyan *et al.* (CMS), Phys. Lett. B **793**, 320 (2019), [arXiv:1811.08459].

[462] M. Aaboud *et al.* (ATLAS), Phys. Lett. **B775**, 105 (2017), [arXiv:1707.04147].

[463] CMS Collaboration, CMS-PAS-HIG-24-014 (2025).

[464] G. Aad *et al.* (ATLAS), Phys. Lett. B **848**, 138394 (2024), [arXiv:2309.04364].

[465] M. Aaboud *et al.* (ATLAS), JHEP **10**, 112 (2017), [arXiv:1708.00212].

[466] CMS Collaboration, CMS-PAS-HIG-16-014 (2016).

[467] G. Aad *et al.* (ATLAS), Eur. Phys. J. C **81**, 4, 332 (2021), [arXiv:2009.14791].

[468] CMS Collaboration, CMS-PAS-HIG-16-033 (2016).

[469] CMS Collaboration, CMS-PAS-HIG-24-002 (2024).

[470] CMS Collaboration, CMS-PAS-HIG-16-023 (2016).

[471] G. Aad *et al.* (ATLAS), Eur. Phys. J. C **83**, 7, 633 (2023), [arXiv:2207.03925].

[472] G. Aad *et al.* (ATLAS), Eur. Phys. J. C **80**, 12, 1165 (2020), [arXiv:2004.14636].

[473] CMS Collaboration, CMS-PAS-HIG-16-034 (2017).

[474] A. M. Sirunyan *et al.* (CMS), Phys. Rev. D **102**, 3, 032003 (2020), [arXiv:2006.06391].

[475] M. Aaboud *et al.* (ATLAS), JHEP **03**, 009 (2018), [arXiv:1708.09638].

[476] G. Aad *et al.* (ATLAS), JHEP **01**, 032 (2016), [arXiv:1509.00389].

[477] ATLAS Collaboration, ATLAS-CONF-2022-066 (2022).

[478] A. M. Sirunyan *et al.* (CMS), JHEP **03**, 034 (2020), [arXiv:1912.01594].

[479] G. Aad *et al.* (ATLAS), Phys. Lett. B **718**, 391 (2012), [arXiv:1206.6074].

[480] M. Aaboud *et al.* (ATLAS), Phys. Lett. **B777**, 91 (2018), [arXiv:1708.04445].

[481] G. Aad *et al.* (ATLAS), JHEP **09**, 091 (2019), [arXiv:1906.08589].

[482] CMS Collaboration, CMS-PAS-B2G-23-007 (2025).

[483] M. Aaboud *et al.* (ATLAS), Phys. Rev. **D98**, 5, 052008 (2018), [arXiv:1808.02380].

[484] G. Aad *et al.* (ATLAS), Phys. Rev. D **105**, 9, 092002 (2022), [arXiv:2202.07288].

[485] G. Aad *et al.* (ATLAS), Phys. Lett. B **858**, 139007 (2024), [arXiv:2404.17193].

[486] G. Aad *et al.* (ATLAS), Phys. Rev. D **106**, 5, 052001 (2022), [arXiv:2112.11876].

[487] ATLAS Collaboration (2016); M. Aaboud *et al.* (ATLAS), JHEP **05**, 124 (2019), [arXiv:1811.11028]; M. Aaboud *et al.* (ATLAS), Eur. Phys. J. **C78**, 12, 1007 (2018), [arXiv:1807.08567].

[488] G. Aad *et al.* (ATLAS), JHEP **07**, 108 (2020), [Erratum: JHEP 01, 145 (2021), Erratum: JHEP 05, 207 (2021)], [arXiv:2001.05178]; M. Aaboud *et al.* (ATLAS), Phys. Rev. Lett. **121**, 19, 191801 (2018), [Erratum: Phys. Rev. Lett. **122**, 089901 (2019)], [arXiv:1808.00336]; G. Aad *et al.* (ATLAS) (2019), [arXiv:1908.06765].

Int. J. Mod. Phys. A 2026.41. Downloaded from www.worldscientific.com
by UNIVERSITY OF CALIFORNIA @ BERKELEY on 09/16/26. Re-use and distribution is strictly not permitted, except for Open Access articles.

[489] A. M. Sirunyan *et al.* (CMS), Phys. Lett. B **788**, 7 (2019), [arXiv:1806.00408].

[490] V. Khachatryan *et al.* (CMS), Phys. Lett. **B755**, 217 (2016), [arXiv:1510.01181].

[491] A. Tumasyan *et al.* (CMS), JHEP **07**, 095 (2023), [arXiv:2206.10268].

[492] G. Aad *et al.* (ATLAS), Phys. Rev. Lett. **125**, 5, 051801 (2020), [arXiv:2002.12223].

[493] A. M. Sirunyan *et al.* (CMS), JHEP **09**, 007 (2018), [arXiv:1803.06553].

[494] V. M. Abazov *et al.* (D0), Phys. Rev. Lett. **104**, 151801 (2010), [arXiv:0912.0968].

[495] D0 Collaboration, D0Note 5974-CONF (2011).

[496] R. Aaij *et al.* (LHCb), JHEP **05**, 132 (2013), [arXiv:1304.2591].

[497] G. Aad *et al.* (ATLAS), JHEP **12**, 126 (2024), [arXiv:2409.20381].

[498] A. M. Sirunyan *et al.* (CMS), JHEP **05**, 210 (2019), [arXiv:1903.10228].

[499] M. Aaboud *et al.* (ATLAS), JHEP **07**, 117 (2019), [arXiv:1901.08144].

[500] A. M. Sirunyan *et al.* (CMS) (2019), [arXiv:1907.03152].

[501] A. M. Sirunyan *et al.* (CMS), JHEP **03**, 103 (2020), [arXiv:1911.10267].

[502] G. Aad *et al.* (ATLAS), JHEP **08**, 148 (2015), [arXiv:1505.07018].

[503] G. Aad *et al.* (ATLAS), JHEP **08**, 013 (2024), [arXiv:2404.18986].

[504] G. Aad *et al.* (ATLAS), JHEP **07**, 203 (2023), [arXiv:2211.01136].

[505] A. M. Sirunyan *et al.* (CMS), JHEP **04**, 171 (2020), [arXiv:1908.01115].

[506] A. Hayrapetyan *et al.* (CMS), CMS-HIG-22-013 (2025), [arXiv:2507.05119].

[507] G. Aad *et al.* (ATLAS), Phys. Rev. D **102**, 3, 032004 (2020), [arXiv:1907.02749].

[508] V. Chekhovsky *et al.* (CMS), JHEP **06**, 144 (2025), [arXiv:2502.06568].

[509] S. Chatrchyan *et al.* (CMS), Phys. Lett. **B722**, 207 (2013), [arXiv:1302.2892]; A. M. Sirunyan *et al.* (CMS), JHEP **08**, 113 (2018), [arXiv:1805.12191].

[510] V. M. Abazov *et al.* (D0), Phys. Lett. **B698**, 97 (2011), [arXiv:1011.1931].

[511] T. Aaltonen *et al.* (CDF), Phys. Rev. **D85**, 032005 (2012), [arXiv:1106.4782].

[512] M. Aaboud *et al.* (ATLAS), JHEP **03**, 174 (2018), [Erratum: JHEP 11, 051 (2018)], [arXiv:1712.06518].

[513] G. Aad *et al.* (ATLAS), Phys. Rev. D **102**, 11, 112008 (2020), [arXiv:2007.05293]; G. Aad *et al.* (ATLAS), Phys. Lett. **B744**, 163 (2015), [arXiv:1502.04478].

[514] A. M. Sirunyan *et al.* (CMS), JHEP **03**, 065 (2020), [arXiv:1910.11634].

[515] A. M. Sirunyan *et al.* (CMS), Eur. Phys. J. **C79**, 7, 564 (2019), [arXiv:1903.00941].

[516] V. Chekhovsky *et al.* (CMS) (2025), [arXiv:2501.14825].

[517] M. Aaboud *et al.* (ATLAS), Phys. Lett. B **783**, 392 (2018), [arXiv:1804.01126].

[518] G. Aad *et al.* (ATLAS), JHEP **10**, 130 (2024), [arXiv:2401.04742].

[519] G. Aad *et al.* (ATLAS), JHEP **02**, 197 (2024), [arXiv:2311.04033].

[520] V. Khachatryan *et al.* (CMS), Phys. Lett. B **759**, 369 (2016), [arXiv:1603.02991].

[521] A. Hayrapetyan *et al.* (CMS), Phys. Lett. B **866**, 139568 (2025), [arXiv:2412.00570].

[522] G. Aad *et al.* (ATLAS), Phys. Rev. Lett. **125**, 22, 221802 (2020), [arXiv:2004.01678].

[523] A. M. Sirunyan *et al.* (CMS), JHEP **03**, 055 (2020), [arXiv:1911.03781].

[524] M. Aaboud *et al.* (ATLAS), Phys. Lett. **B759**, 555 (2016), [arXiv:1603.09203].

[525] M. Aaboud *et al.* (ATLAS), JHEP **09**, 139 (2018), [arXiv:1807.07915].

[526] G. Aad *et al.* (ATLAS), Phys. Rev. D **111**, 7, 072006 (2025), [arXiv:2412.17584].

[527] CMS Collaboration, CMS-PAS-HIG-16-031 (2016); A. M. Sirunyan *et al.* (CMS), JHEP **07**, 142 (2019), [arXiv:1903.04560].

[528] ATLAS Collaboration, ATLAS-CONF-2012-010 (2012).

[529] G. Aad *et al.* (ATLAS), Eur. Phys. J. C **85**, 2, 153 (2025), [arXiv:2407.10096].

[530] A. M. Sirunyan *et al.* (CMS), Phys. Rev. D **102**, 7, 072001 (2020), [arXiv:2005.08900].

[531] G. Aad *et al.* (ATLAS), JHEP **06**, 145 (2021), [arXiv:2102.10076].

[532] A. M. Sirunyan *et al.* (CMS), JHEP **07**, 126 (2020), [arXiv:2001.07763]; V. Khachatryan *et al.* (CMS), JHEP **11**, 018 (2015), [arXiv:1508.07774]; A. M. Sirunyan *et al.* (CMS) (2019), [arXiv:1908.09206].

[533] G. Aad *et al.* (ATLAS), Phys. Rev. Lett. **114**, 23, 231801 (2015), [arXiv:1503.04233].

[534] G. Aad *et al.* (ATLAS), Phys. Lett. B **860**, 139137 (2025), [arXiv:2407.10798].

[535] A. M. Sirunyan *et al.* (CMS), Phys. Rev. Lett. **119**, 14, 141802 (2017), [arXiv:1705.02942].

[536] A. M. Sirunyan *et al.* (CMS), Eur. Phys. J. C **81**, 8, 723 (2021), [arXiv:2104.04762].

[537] A. M. Sirunyan *et al.* (CMS), Phys. Rev. Lett. **123**, 13, 131802 (2019), [arXiv:1905.07453].

[538] G. Aad *et al.* (ATLAS), JHEP **02**, 143 (2025), [arXiv:2411.03969].

[539] A. Tumasyan *et al.* (CMS), JHEP **09**, 032 (2023), [arXiv:2207.01046].

[540] G. Aad *et al.* (ATLAS), JHEP **09**, 004 (2023), [arXiv:2302.11739].

[541] A. M. Sirunyan *et al.* (CMS), JHEP **11**, 115 (2018), [arXiv:1808.06575].

[542] ATLAS Collaboration, ATLAS-CONF-2011-020 (2011).

[543] G. Aad *et al.* (ATLAS), Phys. Rev. D **108**, 9, 092007 (2023), [arXiv:2304.14247].

[544] A. M. Sirunyan *et al.* (CMS), JHEP **11**, 010 (2017), [arXiv:1707.07283].

[545] G. Aad *et al.* (ATLAS), Phys. Rev. **D92**, 5, 052002 (2015), [arXiv:1505.01609].

[546] ATLAS Collaboration, ATLAS-CONF-2012-079 (2012).

[547] G. Aad *et al.* (ATLAS) (2025), [arXiv:2503.05463].

[548] G. Aad *et al.* (ATLAS), JHEP **03**, 190 (2025), [arXiv:2412.14046].

[549] G. Aad *et al.* (ATLAS), Eur. Phys. J. C **84**, 7, 742 (2024), [arXiv:2312.03306].

[550] CMS Collaboration, CMS-PAS-EXO-24-025 (2025).

[551] A. Tumasyan *et al.* (CMS), JHEP **07**, 148 (2023), [arXiv:2208.01469].

[552] A. Tumasyan *et al.* (CMS), Phys. Rev. Lett. **131**, 101801 (2023), [arXiv:2209.06197].

[553] A. M. Sirunyan *et al.* (CMS), JHEP **08**, 139 (2020), [arXiv:2005.08694].

Int. J. Mod. Phys. A 2026.41. Downloaded from www.worldscientific.com
by UNIVERSITY OF CALIFORNIA @ BERKELEY on 09/16/26. Re-use and distribution is [redacted] except for Open Access articles.

[554] V. Khachatryan *et al.* (CMS), JHEP **10**, 076 (2017), [arXiv:1701.02032].

[555] A. M. Sirunyan *et al.* (CMS), Phys. Lett. **B795**, 398 (2019), [arXiv:1812.06359].

[556] A. M. Sirunyan *et al.* (CMS), Phys. Lett. **B796**, 131 (2019), [arXiv:1812.00380].

[557] A. M. Sirunyan *et al.* (CMS) (2019), [arXiv:1907.07235].

[558] A. M. Sirunyan *et al.* (CMS), Phys. Lett. **B785**, 462 (2018), [arXiv:1805.10191].

[559] A. M. Sirunyan *et al.* (CMS), JHEP **11**, 018 (2018), [arXiv:1805.04865].

[560] V. Chekhovsky *et al.* (CMS) (2025), [arXiv:2508.06947].

[561] S. Schael *et al.* (ALEPH), JHEP **05**, 049 (2010), [arXiv:1003.0705].

[562] V. M. Abazov *et al.* (D0), Phys. Rev. Lett. **103**, 061801 (2009), [arXiv:0905.3381].

[563] G. Aad *et al.* (ATLAS), Phys. Rev. D **105**, 1, 012006 (2022), [arXiv:2110.00313].

[564] M. Aaboud *et al.* (ATLAS), JHEP **10**, 031 (2018), [arXiv:1806.07355].

[565] G. Aad *et al.* (ATLAS) (2025), [arXiv:2507.01165].

[566] G. Aad *et al.* (ATLAS), Phys. Rev. D **110**, 5, 052013 (2024), [arXiv:2407.01335].

[567] A. M. Sirunyan *et al.* (CMS), Phys. Lett. B **795**, 398 (2019), [arXiv:1812.06359].

[568] A. M. Sirunyan *et al.* (CMS), Phys. Lett. B **785**, 462 (2018), [arXiv:1805.10191].

[569] CMS Collaboration, CMS-PAS-HIG-21-021 (2022).

[570] A. Hayrapetyan *et al.* (CMS), JHEP **06**, 097 (2024), [arXiv:2403.10341].

[571] A. Hayrapetyan *et al.* (CMS), Eur. Phys. J. C **84**, 5, 493 (2024), [arXiv:2402.13358].

[572] G. Aad *et al.* (ATLAS), Phys. Lett. B **868**, 139671 (2025), [arXiv:2411.16361].

[573] G. Aad *et al.* (ATLAS), Phys. Lett. B **850**, 138536 (2024), [arXiv:2312.01942].

[574] A. Hayrapetyan *et al.* (CMS), Phys. Lett. B **852**, 138582 (2024), [arXiv:2311.00130].

[575] B. Aubert *et al.* (BaBar), Phys. Rev. Lett. **103**, 081803 (2009), [arXiv:0905.4539].

[576] B. Aubert *et al.* (BaBar), Phys. Rev. Lett. **103**, 181801 (2009), [arXiv:0906.2219].

[577] M. Aaboud *et al.* (ATLAS), JHEP **05**, 124 (2019), [arXiv:1811.11028].

[578] A. Tumasyan *et al.* (CMS), Phys. Lett. B **835**, 137566 (2022), [arXiv:2203.00480].

[579] G. Aad *et al.* (ATLAS), JHEP **10**, 009 (2023), [arXiv:2307.11120].

[580] G. Aad *et al.* (ATLAS), JHEP **11**, 047 (2024), [arXiv:2404.12915].

[581] G. Aad *et al.* (ATLAS), JHEP **10**, 104 (2024), [arXiv:2405.20926].

[582] G. Aad *et al.* (ATLAS) (2025), [arXiv:2510.02857].

[583] CMS Collaboration, CMS-PAS-HIG-20-012 (2024).

[584] A. Tumasyan *et al.* (CMS), Phys. Lett. B **842**, 137392 (2023), [arXiv:2204.12413].

[585] A. Tumasyan *et al.* (CMS), JHEP **11**, 057 (2021), [arXiv:2106.10361].

[586] A. Hayrapetyan *et al.* (CMS) (2025), [arXiv:2508.11494].

[587] A. Hayrapetyan *et al.* (CMS) (2025), [arXiv:2506.23012].

[588] CMS Collaboration, CMS-PAS-B2G-23-007 (2025).

[589] M. Aaboud *et al.* (ATLAS), Eur. Phys. J. C **78**, 3, 199 (2018), [arXiv:1710.09748].

[590] M. Aaboud *et al.* (ATLAS), Eur. Phys. J. **C79**, 1, 58 (2019), [arXiv:1808.01899].

[591] CMS Collaboration, CMS-PAS-HIG-16-036 (2017).

[592] J. de Blas *et al.*, in "Snowmass 2021," (2022), [arXiv:2206.08326].

[593] J. de Blas *et al.*, Briefing Book CERN-ESU-2025-001 (2025), URL `https://cds.cern.ch/record/2944678`.

[594] J. Altmann *et al.*, *ECFA Higgs, electroweak, and top Factory Study*, volume 5/2025 of *CERN Yellow Reports: Monographs* (2025), ISBN 978-92-9083-700-8, 978-92-9083-701-5, [arXiv:2506.15390].

Int. J. Mod. Phys. A 2026.41. Downloaded from www.worldscientific.com
by UNIVERSITY OF CALIFORNIA @ BERKELEY on 09/16/26. Re-use and distribution is strictly not permitted, except for Open Access articles.

12. CKM Quark-Mixing Matrix

Revised March 2026 by A. Ceccucci (CERN), Z. Ligeti (LBNL) and Y. Sakai (KEK).

12.1 Introduction

The masses and mixings of quarks have a common origin in the Standard Model (SM). They arise from the Yukawa interactions with the Higgs condensate,

$$\mathcal{L}_Y = -Y^d_{ij}\,\overline{Q^I_{Li}}\,\phi\,d^I_{Rj} - Y^u_{ij}\,\overline{Q^I_{Li}}\,\epsilon\,\phi^*\,u^I_{Rj} + \text{h.c.}, \tag{12.1}$$

where $Y^{u,d}$ are 3×3 complex matrices, ϕ is the Higgs field, i,j are generation labels, and ϵ is the 2×2 antisymmetric tensor. Q^I_L are left-handed quark doublets, and d^I_R and u^I_R are right-handed down- and up-type quark singlets, respectively, in the weak-eigenstate basis. When ϕ acquires a vacuum expectation value, $\langle\phi\rangle = (0, v/\sqrt{2})$, Eq. (12.1) yields mass terms for the quarks. The physical states are obtained by diagonalizing $Y^{u,d}$ by four unitary matrices, $V^{u,d}_{L,R}$, as $M^f_{\text{diag}} = V^f_L\,Y^f\,V^{f\dagger}_R(v/\sqrt{2})$, $f = u, d$. As a result, the charged-current $W^\pm$ interactions couple to the physical u_{Lj} and d_{Lk} quarks with couplings given by

$$\frac{-g}{\sqrt{2}}(\overline{u_L},\,\overline{c_L},\,\overline{t_L})\gamma^\mu\,W^+_\mu\,V_{\text{CKM}}\begin{pmatrix} d_L\\ s_L\\ b_L\end{pmatrix} + \text{h.c.},$$
$$V_{\text{CKM}} \equiv V^u_L V^{d\dagger}_L = \begin{pmatrix} V_{ud} & V_{us} & V_{ub}\\ V_{cd} & V_{cs} & V_{cb}\\ V_{td} & V_{ts} & V_{tb}\end{pmatrix}. \tag{12.2}$$

This Cabibbo-Kobayashi-Maskawa (CKM) matrix [1,2] is a 3×3 unitary matrix. It can be parameterized by three mixing angles and the CP-violating KM phase [2]. Of the many possible conventions, a standard choice has become [3]

$$\begin{aligned} V_{\text{CKM}} &= \begin{pmatrix} 1 & 0 & 0\\ 0 & c_{23} & s_{23}\\ 0 & -s_{23} & c_{23}\end{pmatrix}\begin{pmatrix} c_{13} & 0 & s_{13}e^{-i\delta}\\ 0 & 1 & 0\\ -s_{13}e^{i\delta} & 0 & c_{13}\end{pmatrix}\begin{pmatrix} c_{12} & s_{12} & 0\\ -s_{12} & c_{12} & 0\\ 0 & 0 & 1\end{pmatrix}\\ &= \begin{pmatrix} c_{12}c_{13} & s_{12}c_{13} & s_{13}e^{-i\delta}\\ -s_{12}c_{23} - c_{12}s_{23}s_{13}e^{i\delta} & c_{12}c_{23} - s_{12}s_{23}s_{13}e^{i\delta} & s_{23}c_{13}\\ s_{12}s_{23} - c_{12}c_{23}s_{13}e^{i\delta} & -c_{12}s_{23} - s_{12}c_{23}s_{13}e^{i\delta} & c_{23}c_{13}\end{pmatrix}, \end{aligned} \tag{12.3}$$

where $s_{ij} = \sin\theta_{ij}$, $c_{ij} = \cos\theta_{ij}$, and δ is the phase responsible for all CP-violating phenomena in flavor-changing processes in the SM. The angles θ_{ij} can be chosen to lie in the first quadrant, so $s_{ij}, c_{ij} \geq 0$.

It is known experimentally that $s_{13} \ll s_{23} \ll s_{12} \ll 1$, and it is convenient to exhibit this hierarchy using the Wolfenstein parameterization. We define [4–6]

$$s_{12} = \lambda = \frac{|V_{us}|}{\sqrt{|V_{ud}|^2 + |V_{us}|^2}}\,, \qquad s_{23} = A\lambda^2 = \lambda\left|\frac{V_{cb}}{V_{us}}\right|,$$
$$s_{13}e^{i\delta} = V^*_{ub} = A\lambda^3(\rho + i\eta) = \frac{A\lambda^3(\bar\rho + i\bar\eta)\sqrt{1 - A^2\lambda^4}}{\sqrt{1-\lambda^2}\,[1 - A^2\lambda^4(\bar\rho + i\bar\eta)]}\,. \tag{12.4}$$

These relations ensure that $\bar\rho + i\bar\eta = -(V_{ud}V^*_{ub})/(V_{cd}V^*_{cb})$ is phase convention independent, and the CKM matrix written in terms of λ, A, $\bar\rho$, and $\bar\eta$ is unitary to all orders in λ. The definitions of $\bar\rho$, $\bar\eta$ reproduce all approximate results in the literature; *i.e.*, $\bar\rho = \rho(1-\lambda^2/2+\ldots)$ and $\bar\eta = \eta(1-\lambda^2/2+\ldots)$, and one can write V_{CKM} to $\mathcal{O}(\lambda^4)$ either in terms of $\bar\rho, \bar\eta$ or, traditionally,

$$V_{\text{CKM}} = \begin{pmatrix} 1-\lambda^2/2 & \lambda & A\lambda^3(\rho - i\eta)\\ -\lambda & 1-\lambda^2/2 & A\lambda^2\\ A\lambda^3(1-\rho-i\eta) & -A\lambda^2 & 1\end{pmatrix} + \mathcal{O}(\lambda^4)\,. \tag{12.5}$$

The CKM matrix elements are fundamental parameters of the SM, so their precise determination is important. The unitarity of the CKM matrix imposes $\sum_i V_{ij}V^*_{ik} = \delta_{jk}$ and $\sum_j V_{ij}V^*_{kj} = \delta_{ik}$. The six vanishing combinations can be represented as triangles in a complex plane, of which those obtained by taking scalar products of neighboring rows or columns are nearly degenerate. The areas of all triangles are the same, half of the Jarlskog invariant, J [7], which is a phase-convention-independent measure of CP violation, defined by $\text{Im}\left[V_{ij}V_{kl}V^*_{il}V^*_{kj}\right] = J\sum_{m,n}\varepsilon_{ikm}\varepsilon_{jln}$.

The most commonly used unitarity triangle arises from

$$V_{ud}\,V^*_{ub} + V_{cd}\,V^*_{cb} + V_{td}\,V^*_{tb} = 0\,, \tag{12.6}$$

by dividing each side by $V_{cd}V^*_{cb}$ (see Fig. 12.1). Its vertices are exactly $(0,0)$, $(1,0)$, and, due to the definition in Eq. (12.4), $(\bar\rho, \bar\eta)$. An important goal of flavor physics is to overconstrain the CKM elements, and many measurements can be conveniently displayed and compared in the $\bar\rho, \bar\eta$ plane. While the Lagrangian in Eq. (12.1) is renormalized, and the CKM matrix has a well-known scale dependence above the weak scale [8], below $\mu = m_W$ the CKM elements can be treated as constants, with all μ-dependence contained in the running of quark masses and higher-dimension operators.

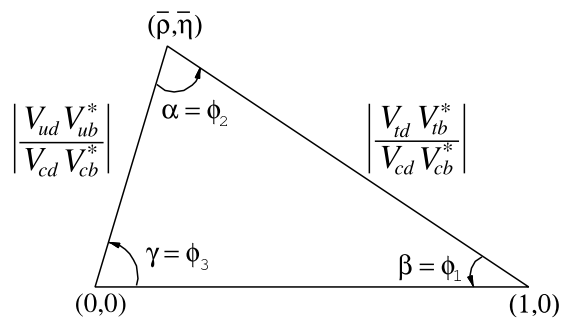

Figure 12.1: Sketch of the unitarity triangle.

Unless explicitly stated otherwise, we describe all measurements assuming the SM, to extract magnitudes and phases of CKM elements in Sec. 12.2 and 12.3. Processes dominated by loop-level contributions in the SM are particularly sensitive to new physics beyond the SM (BSM). We give the global fit results for the CKM elements in Sec. 12.4, and discuss some implications for beyond standard model physics in Sec. 12.5.

12.2 Magnitudes of CKM elements

12.2.1 $|V_{ud}|$

The most precise determination of $|V_{ud}|$ comes from the study of superallowed $0^+ \to 0^+$ nuclear beta decays, which are pure vector transitions. Taking the average of the fifteen most precise determinations [9] yields [10]

$$|V_{ud}| = 0.97367 \pm 0.00032\,. \tag{12.7}$$

This uncertainty is slightly more than twice as large as that in the 2020 edition, due to a more conservative estimate of the nuclear structure uncertainties. A less precise determination of $|V_{ud}|$ can be obtained from the measurement of the neutron lifetime. The theoretical uncertainties are very small, but the determination is limited by the knowledge of the ratio of the axial-vector and vector couplings, $g_A = G_A/G_V$ [10]. The PIBETA experiment [11] has improved the measurement of the $\pi^+ \to \pi^0 e^+\nu$ branching ratio to 0.6%, and Ref. [12] quotes $|V_{ud}| = 0.9739 \pm 0.0027$, in

Int. J. Mod. Phys. A 2026.41. Downloaded from www.worldscientific.com by UNIVERSITY OF CALIFORNIA @ BERKELEY on 09/16/26. Re-use and distribution is except for Open Access articles.

agreement with the more precise result listed above. The interest in this measurement is that the determination of $|V_{ud}|$ is very clean theoretically, because it is a pure vector transition and is free from nuclear-structure uncertainties.

12.2.2 $|V_{us}|$

The product of $|V_{us}|$ and the form factor at $q^2 = 0$, $|V_{us}|\, f_+(0)$, has been extracted traditionally from $K_L^0 \to \pi e\nu$ decays in order to avoid isospin-breaking corrections ($\pi^0 - \eta$ mixing) that affect $K^\pm$ semileptonic decay, and the complications induced by a second (scalar) form factor present in the muonic decays. The last round of measurements has led to enough experimental constraints to justify the comparison between different decay modes. Systematic errors related to the experimental quantities, *e.g.*, the lifetime of neutral or charged kaons, and the form factor determinations for electron and muonic decays, differ among decay modes, and the consistency between different determinations enhances the confidence in the final result. For this reason, we follow the prescription [13] to average $K_L^0 \to \pi e\nu$, $K_L^0 \to \pi\mu\nu$, $K^\pm \to \pi^0 e^\pm\nu$, $K^\pm \to \pi^0\mu^\pm\nu$ and $K_S^0 \to \pi e\nu$. The average of these five decay modes yields $|V_{us}|\, f_+(0) = 0.21656 \pm 0.00035$. Results obtained from each decay mode, and exhaustive references to the experimental data, are listed for instance in Ref. [10]. The form factor average $f_+(0) = 0.9698 \pm 0.0017$ [14] from $N_f = 2+1+1$ lattice QCD calculations gives $|V_{us}| = 0.2233 \pm 0.0005$ [10].[1] The broadly used classic calculation of $f_+(0)$ [16] is in good agreement with this value, while other calculations [18] differ by as much as 2%.

The calculation of the ratio of the kaon and pion decay constants enables one to extract $|V_{us}/V_{ud}|$ from $K \to \mu\nu(\gamma)$ and $\pi \to \mu\nu(\gamma)$, where (γ) indicates that radiative decays are included [19]. The value of $\Gamma(K \to \mu\nu(\gamma))$ [10] derived from the KLOE measurement of the corresponding branching ratio [20], combined with the lattice QCD result, $f_K/f_\pi = 1.1978 \pm 0.0022$ [10], leads to $|V_{us}| = 0.2250 \pm 0.0004$, where the accuracy is limited by the knowledge of the ratio of the decay constants. The average of these two determinations, with the error scaled according to the PDG prescription [21] by $\sqrt{\chi^2} = 2.5$, is quoted as [10]

$$|V_{us}| = 0.22431 \pm 0.00085\,. \tag{12.8}$$

It is important to include both QED and QCD sources of isospin violations in the lattice QCD calculations.

The latest determination from hyperon decays can be found in Ref. [22]. The authors focus on the analysis of the vector form factor, protected from first order flavor $SU(3)$ breaking effects by the Ademollo-Gatto theorem [23], and treat the ratio between the axial and vector form factors g_1/f_1 as experimental input, thus avoiding first order $SU(3)$ breaking effects in the axial-vector contribution. They find $|V_{us}| = 0.2250 \pm 0.0027$, although this does not include an estimate of the theoretical uncertainty due to second-order $SU(3)$ breaking, contrary to Eq. (12.8). Concerning hadronic τ decays to strange particles, averaging the inclusive decay and the exclusive $\tau \to h\nu$ ($h = \pi$, K) measurements yields $|V_{us}| = 0.2208 \pm 0.0014$ [24].

12.2.3 $|V_{cd}|$

The magnitude of V_{cd} can be extracted from semileptonic charm decays, using theoretical knowledge of the form factors. In semileptonic D decays, lattice QCD calculations have predicted the normalization of the $D \to \pi\ell\nu$ and $D \to K\ell\nu$ form factors [14]. The dependence on the invariant mass of the lepton pair, q^2, is determined from lattice QCD and theoretical constraints from analyticity [15]. Using $N_f = 2+1+1$ lattice QCD calculations for $D \to \pi\ell\nu$, $f_+^{D\pi}(0) = 0.6296 \pm 0.0050$ [14], and the average [24] of the measurements of $D \to \pi\ell\nu$ decays by *BaBar* [25], BESIII [26], CLEO-c [27], and Belle [28], one obtains $|V_{cd}| = 0.2265 \pm 0.0029 \pm 0.0018$, where the first uncertainty is experimental, and the second is from the theoretical uncertainty of the form factor.

[1] For lattice QCD inputs, we use the averages from Ref. [14], unless the minireviews [10,15] choose different values. We only use unquenched results, and if both $N_f = 2+1+1$ and $2+1$ calculations are available, we use the former.

The determination of $|V_{cd}|$ is also possible from the leptonic decay $D^+ \to \mu^+\nu$ and $\tau^+\nu$. The experimental uncertainties decreased significantly recently [29]. We take the average [30] (which includes the Sirlin factor, the universal short-distance electromagnetic correction), the BESIII [29] and earlier CLEO [31] measurements for $\mu^+\nu$ and BESIII [32] for $\tau^+\nu$, and use the $N_f = 2+1+1$ lattice QCD result, $f_D = 212.0 \pm 0.7$ MeV [14], to obtain $|V_{cd}| = 0.2330 \pm 0.0028 \pm 0.0007$.[2]

Earlier determinations of $|V_{cd}|$ came from neutrino scattering data. The difference of the ratio of double-muon to single-muon production by neutrino and antineutrino beams is proportional to the charm cross section off valence d quarks, and therefore to $|V_{cd}|^2$ times the average semileptonic branching ratio of charm mesons, $\mathcal{B}_\mu$. The method was used first by CDHS [33] and then by CCFR [34] and CHARM II [35]. Averaging these results is complicated, because it requires assumptions about the scale of the QCD corrections, and because $\mathcal{B}_\mu$ is an effective quantity, which depends on the specific neutrino beam characteristics. With no recent experimental input available, we quote the average from a past review, $\mathcal{B}_\mu |V_{cd}|^2 = (0.463 \pm 0.034) \times 10^{-2}$ [36]. Analysis cuts make these experiments insensitive to neutrino energies smaller than 30 GeV. Thus, $\mathcal{B}_\mu$ should be computed using only neutrino interactions with visible energy larger than 30 GeV. An appraisal [37] based on charm-production fractions measured in neutrino interactions [38] gives $\mathcal{B}_\mu = 0.088 \pm 0.006$. Data from the CHORUS experiment [39] are sufficiently precise to extract $\mathcal{B}_\mu$ directly, by comparing the number of charm decays with a muon to the total number of charmed hadrons found in the nuclear emulsions. Requiring the visible energy to be larger than 30 GeV, CHORUS found $\mathcal{B}_\mu = 0.085 \pm 0.009 \pm 0.006$. We use the average of these two determinations, $\mathcal{B}_\mu = 0.087 \pm 0.005$, and obtain $|V_{cd}| = 0.230 \pm 0.011$. Averaging the three determinations above, we find

$$|V_{cd}| = 0.2247 \pm 0.0022\,. \tag{12.9}$$

12.2.4 $|V_{cs}|$

The direct determination of $|V_{cs}|$ is possible from semileptonic D or leptonic D_s decays, using lattice QCD calculations of the semileptonic D form factor or the D_s decay constant. For muonic decays, the average of Belle [40], CLEO-c [41], *BaBar* [42], and BESIII [43,44] is $\mathcal{B}(D_s^+ \to \mu^+\nu) = (5.34 \pm 0.12) \times 10^{-3}$ [30]. For decays to τ leptons, the average of CLEO-c [41,45], *BaBar* [42], Belle [40], and BESIII [44,46] gives $\mathcal{B}(D_s^+ \to \tau^+\nu) = (5.388 \pm 0.093) \times 10^{-2}$ [30]. From each of these values, determinations of $|V_{cs}|$ can be obtained using the PDG values for the mass and lifetime of the D_s, the masses of the leptons, and $f_{D_s} = (249.9 \pm 0.5)$ MeV [14]. The average of these determinations gives $|V_{cs}| = 0.976 \pm 0.010$, where the error is dominated by the experimental uncertainty.

In semileptonic D decays, lattice QCD calculations of the $D \to K\ell\nu$ form factor are available [14]. Using $f_+^{DK}(0) = 0.7430 \pm 0.0027$ and the average [24] of CLEO-c [27], Belle [28], *BaBar* [47], and recent BESIII [26,48] measurements of $D \to K\ell\nu$ decays, one obtains $|V_{cs}| = 0.966 \pm 0.006$, where the dominant uncertainty is from the theoretical calculation of the form factor. Averaging the determinations from leptonic and semileptonic decays, we find

$$|V_{cs}| = 0.969 \pm 0.005\,. \tag{12.10}$$

Measurements of on-shell $W^\pm$ decays sensitive to $|V_{cs}|$ were made at LEP-2 and the LHC. The W branching ratios depend on the six CKM elements involving only the quarks lighter than m_W. The W branching ratio to each lepton flavor is $1/\mathcal{B}(W \to \ell\bar{\nu}_\ell) = 3\left[1 + \sum_{u,c,d,s,b} |V_{ij}|^2 \left(1 + \alpha_s(m_W)/\pi\right) + \ldots\right]$. Assuming lepton universality, and averaging the LEP [49] and CMS [50] measurements, we find $\mathcal{B}(W \to \ell\bar{\nu}_\ell) = (10.88 \pm 0.06)\%$, which implies $\sum_{u,c,d,s,b} |V_{ij}|^2 = 1.988 \pm 0.017$. This is a precise test of unitarity of the 1st and 2nd raw of the CKM matrix. However, only flavor-tagged W-decays determine $|V_{cs}|$ directly, such as DELPHI's tagged $W^+ \to c\bar{s}$ analysis, yielding $|V_{cs}| = 0.94^{+0.32}_{-0.26} \pm 0.13$ [51].

[2] Hereafter the first error is statistical and the second is systematic, unless mentioned otherwise.

Int. J. Mod. Phys. A 2026.41. Downloaded from www.worldscientific.com
by UNIVERSITY OF CALIFORNIA @ BERKELEY on 09/16/26. Re-use and distribution is strictly not permitted, except for Open Access articles.

12.2.5 $|V_{cb}|$

This matrix element can be determined from exclusive and inclusive semileptonic decays of B mesons to charm. The inclusive determinations use the semileptonic decay rate measurement, together with (certain moments of) the lepton energy and the hadronic invariant-mass spectra. The theoretical basis is the operator product expansion [52, 53], which allows calculation of the decay rate and various spectra as expansions in α_s and inverse powers of the heavy-quark mass. The dependence on m_b, m_c, and the parameters that occur at subleading order is different for different moments. The measurements of many moments overconstrain these parameters, and also test the consistency of their determination. The precise extraction of $|V_{cb}|$ requires using a "threshold" quark mass definition [54, 55]. Inclusive measurements have been performed using B mesons from Z^0 decays at LEP, and at e^+e^- colliders operated at the $\Upsilon(4S)$. At LEP, the large boost of B mesons from the Z^0 decay allows the determination of the moments throughout phase space, which is not possible otherwise, but the large statistics available at the B factories lead to more precise determinations. An average of the measurements and a compilation of the references are provided in Ref. [15]: $|V_{cb}| = (42.0 \pm 0.5) \times 10^{-3}$.

Complementary determinations are based on exclusive semileptonic B decays to D and D^*. In the $m_{b,c} \gg \Lambda_{\rm QCD}$ limit, all form factors are given by a single Isgur-Wise function [56], which depends on the product of the four-velocities of the B and $D^{(*)}$ mesons, $w = v \cdot v'$. Heavy-quark symmetry determines the rate (in the symmetry limit) at $w = 1$, the point in phase space at which the invariant mass of the $\ell\bar{\nu}$ pair is maximal; $|V_{cb}|$ is obtained from extrapolating a fit to the spectrum to $w = 1$. The current update of the V_{cb} and V_{ub} minireview quotes from exclusive decays $|V_{cb}| = (39.5 \pm 0.5) \times 10^{-3}$ [15], based on the only unfolded measurement of $B \to D^*$ semileptonic decay distributions [57], and using a more general fit [58] than in earlier B factory measurements. With the uncertainty scaled by $\sqrt{\chi^2} = 3.7$, this yields the combination [15],

$$|V_{cb}| = (40.7 \pm 1.3) \times 10^{-3} \,. \tag{12.11}$$

Determinations of $|V_{cb}|$ that are currently less precise and not included in this average, can be obtained from the measurement of $B_s \to D_s^{(*)}\mu\bar{\nu}$ decays [59]. In addition, semileptonic decays to τ leptons measured in $B \to D^{(*)}\tau\bar{\nu}$ and related modes are also sensitive to $|V_{cb}|$. The most precise data involving τ leptons are the $|V_{cb}|$-independent ratios, $\mathcal{B}(B \to D^{(*)}\tau\bar{\nu})/\mathcal{B}(B \to D^{(*)}\ell\bar{\nu})$ measured by BaBar, Belle, and LHCb. If the current, approximately $3.8\,\sigma$ [24] hint of lepton non-universality prevails, the determination of $|V_{cb}|$ becomes more complicated.

12.2.6 $|V_{ub}|$

The determination of $|V_{ub}|$ from inclusive $B \to X_u\ell\bar{\nu}$ decay is complicated due to large $B \to X_c\ell\bar{\nu}$ backgrounds. In most regions of phase space where the charm background is kinematically forbidden, the hadronic physics enters via unknown nonperturbative functions, so-called shape functions. (By contrast, the nonperturbative physics for $|V_{cb}|$ is encoded in a few parameters.) At leading order in $\Lambda_{\rm QCD}/m_b$, there is only one shape function, which can be extracted from the photon energy spectrum in $B \to X_s\gamma$ [60, 61], and applied to several spectra in $B \to X_u\ell\bar{\nu}$. The subleading shape functions are modeled in the current determinations. Phase space cuts for which the rate has only subleading dependence on the shape function are also possible [62]. The measurements of both the hadronic and the leptonic systems are important for an optimal choice of phase space. A different approach is to make the measurements more inclusive by extending them deeper into the $B \to X_c\ell\bar{\nu}$ region, and thus reduce the theoretical uncertainties. Analyses of the electron-energy endpoint from CLEO [63], BABAR [64], and Belle [65] quote $B \to X_u e\bar{\nu}$ partial rates for $|\vec{p}_e| \geq 2.0\,$GeV and $1.9\,$GeV, which are well below the charm endpoint. The large and pure $B\overline{B}$ samples at the B factories permit the selection of $B \to X_u\ell\bar{\nu}$ decays in events where the other B is fully reconstructed [66]. With this full-reconstruction tag method, the four-momenta of both the leptonic and the hadronic final states can be measured. It also gives access to a wider kinematic region, because of improved signal purity. Ref. [15] quotes the inclusive average, $|V_{ub}| = (4.06 \pm 0.11 \pm 0.13 \pm 0.18) \times 10^{-3}$, where the first error is experimental, the second arises from the model dependence quoted by the individual measurements, and the third is an additional one estimated in Ref. [15].

To extract $|V_{ub}|$ from exclusive decays, the form factors have to be known. Experimentally, better signal-to-background ratios are offset by smaller yields. The $B \to \pi\ell\bar{\nu}$ branching ratio is now known to 5%. Lattice QCD calculations of the $B \to \pi\ell\bar{\nu}$ form factor are available [67] for the high q^2 region ($q^2 > 16$ or $18\,{\rm GeV}^2$). A fit to the experimental partial rates and lattice QCD results versus q^2 yields $|V_{ub}| = (3.75 \pm 0.06 \pm 0.19) \times 10^{-3}$ [24].

The uncertainties in extracting $|V_{ub}|$ from inclusive and exclusive decays are different to a large extent. An average of these determinations, with the uncertainty scaled by $\sqrt{\chi^2} = 1.1$, is [15]

$$|V_{ub}| = (3.89 \pm 0.16) \times 10^{-3} \,. \tag{12.12}$$

A determination of $|V_{ub}|$ not included in this average can be obtained from $\mathcal{B}(B \to \tau\bar{\nu}) = (1.12 \pm 0.19) \times 10^{-4}$ [24]. Using $f_B = (190.0 \pm 1.3)\,$MeV [14] and $\tau_{B^\pm} = (1.638 \pm 0.004)\,$ps [68], we find the remarkably consistent result, $|V_{ub}| = (4.16 \pm 0.35) \times 10^{-3}$. This decay is sensitive, for example, to tree-level charged Higgs contributions, and the measured rate is consistent with the SM expectation. The LHCb measurements of $|V_{ub}/V_{cb}|$ from the ratios of $\Lambda_b \to p^+\mu^-\bar{\nu}$ and $\Lambda_b \to \Lambda_c^+\mu^-\bar{\nu}$ [69] and $B_s^0 \to K^-\mu^+\nu$ and $B_s^0 \to D_s^-\mu^+\nu$ [70] in different regions of q^2, provides another complementary determination.

12.2.7 $|V_{td}|$ *and* $|V_{ts}|$

The CKM elements $|V_{td}|$ and $|V_{ts}|$ are not likely to be precisely measurable in tree-level processes involving top quarks, so one has to rely on determinations from $B^0 - \overline{B}^0$ mixing, dominated by box diagrams with top quarks, or loop-mediated rare K and B decays. Theoretical uncertainties in hadronic effects limit the accuracy of the current determinations. These can be reduced by taking ratios of processes that are equal in the flavor $SU(3)$ limit to determine $|V_{td}/V_{ts}|$.

The phenomenon of $B^0 - \overline{B}^0$ mixing was discovered by ARGUS [71], and the mass difference is now precisely measured as $\Delta m_d = (0.5068 \pm 0.0019)\,{\rm ps}^{-1}$ [72]. In the B_s^0 system, Δm_s was first measured significantly by CDF [73] and the world average, dominated by an LHCb measurement [74], is $\Delta m_s = (17.765 \pm 0.006)\,{\rm ps}^{-1}$ [72]. Neglecting corrections suppressed by $|V_{tb}| - 1$, and using the lattice QCD results $f_{B_d}\sqrt{\widehat{B}_{B_d}} = (210.6 \pm 5.5)\,$MeV and $f_{B_s}\sqrt{\widehat{B}_{B_s}} = (256.1 \pm 5.7)\,$MeV [14],

$$|V_{td}| = (8.6 \pm 0.2) \times 10^{-3} \,, \qquad |V_{ts}| = (41.5 \pm 0.9) \times 10^{-3} \,. \tag{12.13}$$

The uncertainties are dominated by lattice QCD. Several uncertainties are reduced in the calculation of the ratio $\xi = \left(f_{B_s}\sqrt{\widehat{B}_{B_s}}\right)/\left(f_{B_d}\sqrt{\widehat{B}_{B_d}}\right) = 1.216 \pm 0.016$ [14] and therefore the constraint on $|V_{td}/V_{ts}|$ from $\Delta m_d/\Delta m_s$ is more reliable theoretically. These provide a theoretically clean and significantly improved determination,

$$\left|V_{td}/V_{ts}\right| = 0.207 \pm 0.001 \pm 0.003 \,. \tag{12.14}$$

The inclusive branching ratio $\mathcal{B}(B \to X_s\gamma) = (3.49 \pm 0.19) \times 10^{-4}$ extrapolated to $E_\gamma > E_0 = 1.6\,$GeV [24] is also sensitive to $|V_{tb}V_{ts}|$. In addition to t-quark penguins, a substantial part of the rate comes from charm contributions proportional to $V_{cb}V_{cs}^*$ via the application of 3×3 CKM unitarity (which is used here). With the NNLO calculation of $\mathcal{B}(B \to X_s\gamma)_{E_\gamma > E_0}/\mathcal{B}(B \to X_c e\bar{\nu})$ [75], we obtain $|V_{ts}/V_{cb}| = 1.00 \pm 0.04$. The $B_s \to \mu^+\mu^-$ rate is also proportional to $|V_{tb}V_{ts}|^2$ in the SM, and the world average, $\mathcal{B}(B_s \to \mu^+\mu^-) = (3.34 \pm 0.27) \times 10^{-9}$ [68], is consistent with the SM, with sizable uncertainties.

A complementary determination of $|V_{td}/V_{ts}|$ is possible from the ratio of $B \to \rho\gamma$ and $K^*\gamma$ rates. The ratio of the neutral modes is theoretically cleaner than that of the charged ones, because the poorly known spectator-interaction contribution is expected to be

Int. J. Mod. Phys. A 2026.41. Downloaded from www.worldscientific.com by UNIVERSITY OF CALIFORNIA @ BERKELEY on 09/16/26. Re-use and distribution is except for Open Access articles.

smaller (W-exchange vs. weak annihilation). For now, because of low statistics, we average the charged and neutral rates assuming the isospin symmetry and heavy-quark limit motivated relation, $|V_{td}/V_{ts}|^2/\xi_\gamma^2 = [\Gamma(B^+ \to \rho^+\gamma) + 2\Gamma(B^0 \to \rho^0\gamma)]/[\Gamma(B^+ \to K^{*+}\gamma) + \Gamma(B^0 \to K^{*0}\gamma)] = (3.63 \pm 0.41)\%$ [24, 76]. Here ξ_γ contains the poorly known hadronic physics. Using $\xi_\gamma = 1.2 \pm 0.2$ [77] gives $|V_{td}/V_{ts}| = 0.228 \pm 0.013 \pm 0.038$, where the first uncertainty is experimental and the second is theoretical.

A theoretically clean determination of $|V_{td}V_{ts}^*|$ is possible from $K^+ \to \pi^+\nu\bar{\nu}$ decay [78]. Experimentally, the decay has been observed by NA62 [79] and the branching fraction is consistent with the SM within uncertainties. Much more data are needed for a precision measurement.

12.2.8 $|V_{tb}|$

The determination of $|V_{tb}|$ from top decays uses the ratio of branching fractions $R = \mathcal{B}(t \to Wb)/\mathcal{B}(t \to Wq) = |V_{tb}|^2/(\sum_q |V_{tq}|^2) = |V_{tb}|^2$, where $q = b, s, d$. The CDF and DØ measurements performed on data collected during Run II of the Tevatron give $|V_{tb}| > 0.85$ [80] and $0.99 > |V_{tb}| > 0.90$ [81], respectively, at 95% CL. CMS measured the same quantity at 8 TeV and obtained $|V_{tb}| > 0.975$ [82] at 95% CL.

The direct determination of $|V_{tb}|$, without assuming unitarity, is possible from the single top quark production cross section. The $(3.30^{+0.52}_{-0.40})$ pb combined cross section [83] of DØ and CDF measurements implies $|V_{tb}| = 1.02^{+0.06}_{-0.05}$. The LHC experiments, ATLAS and CMS, have measured single top quark production cross sections (and extracted $|V_{tb}|$) in t-channel, Wt-channel, and s-channel at 7 TeV, 8 TeV, and 13 TeV [84]. The average of these $|V_{tb}|$ values is calculated to be $|V_{tb}| = 0.998 \pm 0.026$, where all systematic errors and theoretical errors are treated to be fully correlated. The average of Tevatron and LHC values gives

$$|V_{tb}| = 1.002 \pm 0.024\,. \tag{12.15}$$

The experimental systematic uncertainties dominate, and a dedicated combination would be welcome.

A weak constraint on $|V_{tb}|$ can be obtained from precision electroweak data, where top quarks enter in loops. The sensitivity is best in $\Gamma(Z \to b\bar{b})$ and yields $|V_{tb}| = 0.77^{+0.18}_{-0.24}$ [85].

12.3 Phases of CKM elements

As can be seen from Fig. 12.1, the angles of the unitarity triangle are

$$\begin{aligned}
\beta = \phi_1 &= \arg\Big(-\frac{V_{cd}V_{cb}^*}{V_{td}V_{tb}^*}\Big),\\
\alpha = \phi_2 &= \arg\Big(-\frac{V_{td}V_{tb}^*}{V_{ud}V_{ub}^*}\Big),\\
\gamma = \phi_3 &= \arg\Big(-\frac{V_{ud}V_{ub}^*}{V_{cd}V_{cb}^*}\Big).
\end{aligned} \tag{12.16}$$

Since CP violation involves phases of CKM elements, many measurements of CP-violating observables can be used to constrain these angles and the $\bar{\rho}, \bar{\eta}$ parameters.

12.3.1 ϵ *and* ϵ'

The measurement of CP violation in K^0–$\overline{K}^0$ mixing, $|\epsilon| = (2.228 \pm 0.011) \times 10^{-3}$ [86], provides important information about the CKM matrix. The phase of ϵ is determined by long-distance physics, $\epsilon = \frac{1}{2}\, e^{i\phi_\epsilon} \sin\phi_\epsilon \arg(-M_{12}/\Gamma_{12})$, where $\phi_\epsilon = \arctan|2\Delta m_K/\Delta\Gamma_K| \simeq 43.5°$. The SM prediction can be written as

$$\begin{aligned}
\epsilon = \kappa_\epsilon\, e^{i\phi_\epsilon} \frac{G_F^2 m_W^2 m_K}{12\sqrt{2}\,\pi^2 \Delta m_K} f_K^2 \widehat{B}_K \Big\{ &\eta_{tt} S(x_t)\, \mathrm{Im}[(V_{ts}V_{td}^*)^2]\\
&+ 2\eta_{ct} S(x_c, x_t)\, \mathrm{Im}(V_{cs}V_{cd}^* V_{ts}V_{td}^*) + \eta_{cc}\, x_c\, \mathrm{Im}[(V_{cs}V_{cd}^*)^2] \Big\},
\end{aligned} \tag{12.17}$$

where $\kappa_\epsilon \simeq 0.94 \pm 0.02$ [87] includes the effects of strangeness changing $\Delta s = 1$ operators and additional dependence on $\phi_\epsilon \neq \pi/4$ (see also Ref. [88]). The displayed terms are the short-distance $\Delta s = 2$ contribution to $\mathrm{Im}M_{12}$ in the usual phase convention, S is an Inami-Lim function [89], $x_q = m_q^2/m_W^2$, and η_{ij} are perturbative QCD corrections. The constraint from ϵ in the $\bar{\rho}, \bar{\eta}$ plane is bounded by approximate hyperbolas. Lattice QCD determined the bag parameter $\widehat{B}_K = 0.717 \pm 0.024$ [14] and the main uncertainties are from $(V_{ts}V_{td}^*)^2$ (approximately given by that of $|V_{cb}|^4$ or A^4), the η_{ij} coefficients, and estimates of κ_ϵ.

The measurement of $6\,\mathrm{Re}(\epsilon'/\epsilon) = 1 - |\eta_{00}/\eta_{+-}|^2$, where each $\eta_{ij} = \langle\pi^i\pi^j|\mathcal{H}|K_L\rangle/\langle\pi^i\pi^j|\mathcal{H}|K_S\rangle$ violates CP, provides a qualitative test of the CKM mechanism, and strong constraints on many BSM scenarios. Its nonzero value, $\mathrm{Re}(\epsilon'/\epsilon) = (1.67 \pm 0.23) \times 10^{-3}$ [86], demonstrated the existence of direct CP violation, a prediction of the KM ansatz. While $\mathrm{Re}(\epsilon'/\epsilon) \propto \mathrm{Im}(V_{td}V_{ts}^*)$, this quantity cannot easily be used to extract CKM parameters, because cancellations between the electromagnetic and gluonic penguin contributions for large m_t [90] enhance the hadronic uncertainties. Most SM estimates [91] agree with the observed value, indicating that $\bar{\eta}$ is positive. Progress in lattice QCD [92] may yield a precise SM prediction in the future, and trigger new work on assessing the consistency of the SM with the measured value [93, 94].

12.3.2 β / ϕ_1

12.3.2.1 *Charmonium modes*

CP-violation measurements in B-meson decays provide direct information on the angles of the unitarity triangle, shown in Fig. 12.1. These overconstraining measurements serve to improve the determination of the CKM elements, and to reveal possible effects beyond the SM.

The time-dependent CP asymmetry of neutral B decays to a final state f common to B^0 and $\overline{B}^0$ is given by [95–97]

$$\begin{aligned}
\mathcal{A}_f &= \frac{\Gamma(\overline{B}^0(t) \to f) - \Gamma(B^0(t) \to f)}{\Gamma(\overline{B}^0(t) \to f) + \Gamma(B^0(t) \to f)}\,,\\
&= S_f \sin(\Delta m_d\, t) - C_f \cos(\Delta m_d\, t)\,,
\end{aligned} \tag{12.18}$$

where

$$S_f = \frac{2\,\mathrm{Im}\lambda_f}{1 + |\lambda_f|^2}\,, \qquad C_f = \frac{1 - |\lambda_f|^2}{1 + |\lambda_f|^2}\,, \qquad \lambda_f = \frac{q}{p}\frac{\bar{A}_f}{A_f}\,. \tag{12.19}$$

Here, q/p describes B^0–$\overline{B}^0$ mixing and, to a good approximation in the SM, $q/p = V_{tb}^* V_{td}/V_{tb}V_{td}^* = e^{-2i\beta + \mathcal{O}(\lambda^4)}$ in the usual phase convention. A_f ($\bar{A}_f$) is the amplitude of the $B^0 \to f$ ($\overline{B}^0 \to f$) decay. If f is a CP eigenstate, and amplitudes with one CKM phase dominate the decay, then $|A_f| = |\bar{A}_f|$, $C_f = 0$, and $S_f = \sin(\arg\lambda_f) = \eta_f \sin 2\phi$, where η_f is the CP eigenvalue of f and 2ϕ is the phase difference between the $B^0 \to f$ and $B^0 \to \overline{B}^0 \to f$ decay paths. A contribution of another amplitude to the decay with a different CKM phase makes the value of S_f sensitive to relative strong-interaction phases between the decay amplitudes (it also makes $C_f \neq 0$ possible).

The $b \to c\bar{c}s$ decays to CP eigenstates ($B^0 \to$ charmonium $K^0_{S,L}$) give currently the most precise measurements of $S_f = -\eta_f \sin 2\beta$. The $b \to s$ penguin amplitudes have dominantly the same weak phase as the $b \to c\bar{c}s$ tree amplitude. Since only λ^2-suppressed penguin amplitudes introduce a different CP-violating phase, amplitudes with a single weak phase dominate, and we expect $\Big||\bar{A}_{\psi K}/A_{\psi K}| - 1\Big| < 0.01$. The e^+e^- asymmetric-energy B-factory experiments, *BABAR* [98] and Belle [99], and LHCb [100] provided precise measurements. The world average, including some other measurements, is [24, 97, 101]

$$\sin 2\beta = 0.710 \pm 0.011\,. \tag{12.20}$$

This measurement has a four-fold ambiguity in β, which can be resolved by a global fit as mentioned in Sec. 12.4. Experimentally, the two-fold ambiguity $\beta \to \pi/2 - \beta$ (but not $\beta \to \pi + \beta$) can be resolved by a time-dependent angular analysis of $B^0 \to J/\psi K^{*0}$ [102, 103], or a time-dependent Dalitz plot analysis of $B^0 \to \overline{D}^0 h^0$. The time-dependent Dalitz plot analysis of $B^0 \to \overline{D}^0 h^0$ ($h^0 = \pi^0, \eta, \omega$) with $\overline{D}^0 \to K^0_S\pi^+\pi^-$, jointly performed by Belle and *BABAR*, excludes the $\pi/2 - \beta$ solution with

Int. J. Mod. Phys. A 2026.41. Downloaded from www.worldscientific.com by UNIVERSITY OF CALIFORNIA @ BERKELEY on 09/16/26. Re-use and distribution is strictly not permitted, except for Open Access articles.

7.3σ confidence level [104]. These results exclude the negative $\cos 2\beta$ solutions, in agreement with the global CKM fit, which is no longer shown in Fig. 12.2.

The $b \to c\bar{c}d$ mediated transitions, such as $B^0 \to J/\psi\pi^0$ and $B^0 \to D^{(*)+}D^{(*)-}$, also measure approximately $\sin 2\beta$. However, the dominant component of the $b \to d$ penguin amplitude has a different CKM phase ($V_{tb}^*V_{td}$) than the tree amplitude ($V_{cb}^*V_{cd}$), and their magnitudes are of the same order in λ. Therefore, the effect of penguins could be large, resulting in $S_f \neq -\eta_f \sin 2\beta$ and $C_f \neq 0$. Such decay modes have been measured by *BABAR*, Belle, and LHCb. The world averages [24], $S_{J/\psi\pi^0} = -0.87 \pm 0.11$, $S_{J/\psi\rho^0} = -0.66^{+0.16}_{-0.12}$, $S_{D^+D^-} = -0.69 \pm 0.07$, and $S_{D^{*+}D^{*-}} = -0.71 \pm 0.09$ (where $\eta_f = +1$ for the $J/\psi\pi^0$ and D^+D^- modes, while $J/\psi\rho^0$ and $D^{*+}D^{*-}$ are mixtures of CP even and odd states), are consistent with $\sin 2\beta$ obtained from $B^0 \to$ charmonium K^0 decays, and the C_f's are consistent with zero, although the uncertainties are sizable.

The $b \to c\bar{u}d$ decays $B^0 \to \overline{D}^{0(*)}h^0$, with $\overline{D}^0 \to CP$ eigenstates and $\overline{D}^0 \to K_S^0\pi^+\pi^-$ with Dalitz plot analysis, have no penguin contributions, and provide theoretically clean $\sin 2\beta$ measurements. The average of joint analyses of *BABAR* and Belle data [104, 105] give $\sin 2\beta = 0.71 \pm 0.09$ [24].

12.3.2.2 *Penguin-dominated modes*

The $b \to s\bar{q}q$ penguin-dominated decays have the same CKM phase as the $b \to c\bar{c}s$ tree level decays, up to corrections suppressed by λ^2, since $V_{tb}^*V_{ts} = -V_{cb}^*V_{cs}[1 + \mathcal{O}(\lambda^2)]$. Therefore, decays such as $B^0 \to \phi K^0$ and $\eta' K^0$ provide $\sin 2\beta$ measurements in the SM. Any BSM contribution to the amplitude with a different weak phase would give rise to $S_f \neq -\eta_f \sin 2\beta$, and possibly $C_f \neq 0$. Therefore, the main interest in these modes is not simply to measure $\sin 2\beta$, but to search for new physics. Measurements of many other decay modes in this category, such as $B \to \pi^0 K_S^0$, $K_S^0 K_S^0 K_S^0$, *etc.*, have also been performed by *BABAR* and Belle. The results and their uncertainties are summarized in Fig. 13.3 and Table 13.1 of Ref. [96]. The comparison of CP violation measurements between tree-dominated and penguin-dominated modes in B_s^0 decays provides similar sensitivity to new physics.

12.3.3 α / ϕ_2

Since α is the phase between $V_{tb}^*V_{td}$ and $V_{ub}^*V_{ud}$, only time-dependent CP asymmetries in decay modes dominated by $b \to u\bar{u}d$ transitions can directly measure $\sin 2\alpha$, in contrast to $\sin 2\beta$, where several different quark-level transitions can be used. Since $b \to d$ penguin amplitudes have a different CKM phase than $b \to u\bar{u}d$ tree amplitudes, and their magnitudes are of the same order in λ, the penguin contribution can be sizable, which makes the determination of α complicated. To date, α has been measured in $B \to \pi\pi$, $\rho\pi$ and $\rho\rho$ decay modes.

12.3.3.1 $B \to \pi\pi$

It is well-established from the data that there is a sizable contribution of $b \to d$ penguin amplitudes in $B \to \pi\pi$ decays. Thus, $S_{\pi^+\pi^-}$ in the time-dependent $B^0 \to \pi^+\pi^-$ analysis does not measure $\sin 2\alpha$, but

$$S_{\pi^+\pi^-} = \sqrt{1 - C^2_{\pi^+\pi^-}}\,\sin(2\alpha + 2\Delta\alpha)\,, \tag{12.21}$$

where $2\Delta\alpha$ is the phase difference between $e^{2i\gamma}\bar{A}_{\pi^+\pi^-}$ and $A_{\pi^+\pi^-}$. The value of $\Delta\alpha$, and hence α, can be extracted using the isospin relation among the amplitudes of $B^0 \to \pi^+\pi^-$, $B^0 \to \pi^0\pi^0$, and $B^+ \to \pi^+\pi^0$ decays [106],

$$\frac{1}{\sqrt{2}}\,A_{\pi^+\pi^-} + A_{\pi^0\pi^0} - A_{\pi^+\pi^0} = 0\,, \tag{12.22}$$

and a similar expression for the $\bar{A}_{\pi\pi}$'s. This method utilizes the fact that a pair of pions from $B \to \pi\pi$ decay must be in a zero angular momentum state, and, because of Bose statistics, they must have even isospin. Consequently, $\pi^\pm\pi^0$ is in a pure isospin-2 state, while the penguin amplitudes only contribute to the isospin-0 final state. The latter does not hold for the electroweak penguin amplitudes, but their effect is expected to be small. The isospin analysis uses the world averages of *BABAR*, Belle, and LHCb measurements, $S_{\pi^+\pi^-} = -0.666 \pm 0.029$, $C_{\pi^+\pi^-} = -0.311 \pm 0.030$, the decay widths of all three modes, and the direct CP asymmetry $C_{\pi^0\pi^0} = -0.23 \pm 0.18$ [24]. This analysis leads to 16 mirror solutions for $0 \leq \alpha < 2\pi$. Because of this, and due to the experimental uncertainties, some of these solutions are not well separated [97].

12.3.3.2 $B \to \rho\rho$

The decay $B^0 \to \rho^+\rho^-$ contains two vector mesons in the final state, and so in general is a mixture of CP-even and CP-odd components. At the current level of precision, it simplifies the analysis that the longitudinal polarization fractions in $B^+ \to \rho^+\rho^0$ and $B^0 \to \rho^+\rho^-$ decays were measured to be close to unity [107], which implies that the final states are almost purely CP-even. Furthermore, $\mathcal{B}(B^0 \to \rho^0\rho^0) = (0.95 \pm 0.15) \times 10^{-6}$ is much smaller than $\mathcal{B}(B^0 \to \rho^+\rho^-) = (28.0 \pm 1.7) \times 10^{-6}$ and $\mathcal{B}(B^+ \to \rho^+\rho^0) = (24,0 \pm 1.9) \times 10^{-6}$ [24], which implies that the effect of the penguin contributions is small. The isospin analysis using the world averages, $S_{\rho^+\rho^-} = -0.18 \pm 0.11$ and $C_{\rho^+\rho^-} = -0.01 \pm 0.08$ [24], together with the time-dependent CP asymmetry, $S_{\rho^0\rho^0} = 0.3 \pm 0.7$ and $C_{\rho^0\rho^0} = 0.2 \pm 0.9$ [108], and the above mentioned branching fractions and longitudinal polarization fractions, gives two solutions (with mirror solutions at $3\pi/2 - \alpha$) [97]. A possible small violation of Eq. (12.22) due to the finite width of the ρ [109] is so far neglected.

12.3.3.3 $B \to \rho\pi$

The final state in $B^0 \to \rho^+\pi^-$ decay is not a CP eigenstate, but this decay proceeds via the same quark-level diagrams as $B^0 \to \pi^+\pi^-$, and both B^0 and $\overline{B}^0$ can decay to $\rho^+\pi^-$, while the final state in $B^0 \to \rho^0\pi^0$ is a CP eigenstate. Consequently, mixing-induced CP violation can occur in B^0 and $\overline{B}^0$ decays to $\rho^\pm\pi^\mp$ and $\rho^0\pi^0$. The time-dependent Dalitz plot analysis of $B^0 \to \pi^+\pi^-\pi^0$ decays permits the extraction of α with a single discrete ambiguity, $\alpha \to \alpha + \pi$, since one knows the variation of the strong phases in the interference regions of the $\rho^+\pi^-$, $\rho^-\pi^+$, and $\rho^0\pi^0$ amplitudes in the Dalitz plot [110]. The combination of Belle [111] and *BABAR* [112] measurements gives only moderate constraints [97].

Combining the $B \to \pi\pi$, $\rho\pi$, and $\rho\rho$ decay modes [24, 97, 101], α is constrained as

$$\alpha = \left(84.1^{+3.7}_{-3.0}\right)^\circ\,. \tag{12.23}$$

Similar results can be found in Refs. [113, 114].

12.3.4 γ / ϕ_3

By virtue of Eq. (12.16), γ does not depend on CKM elements involving the top quark, so it can be measured in tree-level B decays. This is an important distinction from the measurements of α and β, and implies that measurements of γ are unlikely to be affected by physics beyond the SM.

12.3.4.1 $B_{(s)} \to D_{(s)}K^{(*)}$

The interference of $B^- \to D^0K^-$ ($b \to c\bar{u}s$) and $B^- \to \overline{D}^0K^-$ ($b \to u\bar{c}s$) transitions can be studied in final states accessible in both D^0 and $\overline{D}^0$ decays [95]. In principle, it is possible to extract the B and D decay amplitudes, the relative strong phases, and the weak phase γ from the data [97].

A practical complication is that the precision depends sensitively on the ratio of the interfering amplitudes

$$r_B = \left|A(B^- \to \overline{D}^0K^-)\big/A(B^- \to D^0K^-)\right|, \tag{12.24}$$

which is around 0.1. The original GLW method [115, 116] considers D decays to CP eigenstates, such as $B^\pm \to D^{(*)}_{CP}(\to \pi^+\pi^-)K^{(*)\pm}$. To alleviate the smallness of r_B and make the interfering amplitudes (which are products of the B and D decay amplitudes) comparable in magnitude, the ADS method [117] considers final states where Cabibbo-allowed $\overline{D}^0$ and doubly-Cabibbo-suppressed D^0 decays interfere. Measurements have been made by the B factories, CDF, and LHCb, using both methods [24]. The GLW method currently gives only a loose constraint on γ, while the ADS method provides a moderate constraint.

The BPGGSZ method [118, 119] utilizes the fact that both D^0 and $\overline{D}^0$ can have large branching fractions to CP self-conjugate

Int. J. Mod. Phys. A 2026.41. Downloaded from www.worldscientific.com by UNIVERSITY OF CALIFORNIA @ BERKELEY on 09/16/26. Re-use and distribution is except for Open Access articles.

three- and four-body final states, such as $K_S^0\pi^+\pi^-$, and the analysis can be optimized by studying the Dalitz plot dependence of the interferences. The best present determination of γ comes from this method, dominated by 3-body D decay modes. Combining results in 3-body decay modes from Belle [120], *BABAR* [121], and the most precise LHCb [122] one, $\gamma = (68 \pm 4)^\circ$ is obtained [97]. The uncertainty is sensitive to the central value of the amplitude ratio r_B (and r_B^* for the D^*K mode), for which Belle found somewhat larger central values than *BABAR* and LHCb. The same values of $r_B^{(*)}$ enter the ADS analyses, and the data (including 4-body D decays [123]) can be combined to fit for $r_B^{(*)}$ and γ. The effect of $D^0-\overline{D}^0$ mixing on γ is either below the present experimental accuracy or can be taken into account in the analysis [124] (even if $D^0-\overline{D}^0$ mixing is due to CP-violating new physics [125]).

The amplitude ratio is much larger in the analogous $B_s^0 \to D_s^\pm K^\mp$ decays, which allows a model-independent extraction of $\gamma - 2\beta_s$ [126] (here $\beta_s = \arg(-V_{ts}V_{tb}^*/V_{cs}V_{cb}^*)$ is related to the phase of B_s mixing). Measurements by LHCb with $B_s^0 \to D_s^\pm K^\mp$ [127] and $B_s^0 \to D_s^\pm K^\mp\pi^+\pi^-$ [128] give $\gamma = (76 \pm 10)^\circ$ using a constraint on $2\beta_s$ (see Sec. 12.5).

Combining all the above measurements [24, 97, 101], γ is constrained as

$$\gamma = \left(66.4^{+2.7}_{-2.8}\right)^\circ . \tag{12.25}$$

Similar results can be found in Refs. [113, 114].

12.3.4.2 $B^0 \to D^{(*)\pm}\pi^\mp$

The interference of $b \to u$ and $b \to c$ transitions can be studied in $\overline{B}^0 \to D^{(*)+}\pi^-$ ($b \to c\bar{u}d$) and $\overline{B}^0 \to B^0 \to D^{(*)+}\pi^-$ ($\bar{b} \to \bar{u}c\bar{d}$) decays and their CP conjugates, since both B^0 and $\overline{B}^0$ decay to $D^{(*)\pm}\pi^\mp$ (or $D^\pm\rho^\mp$, *etc.*). Since there are only tree and no penguin contributions to these decays, in principle, it is possible to extract from the four time-dependent rates the magnitudes of the two hadronic amplitudes, their relative strong phase, and the weak phase between the two decay paths, which is $2\beta + \gamma$.

A complication is that the ratio of the interfering amplitudes is very small, $r_{D\pi} = A(B^0 \to D^+\pi^-)/A(\overline{B}^0 \to D^+\pi^-) = \mathcal{O}(0.01)$ (and similarly for $r_{D^*\pi}$ and $r_{D\rho}$), and therefore it has not been possible to measure it. To obtain $2\beta + \gamma$, $SU(3)$ flavor symmetry and dynamical assumptions have been used to relate $A(\overline{B}^0 \to D^-\pi^+)$ to $A(\overline{B}^0 \to D_s^-\pi^+)$, so this measurement is not model independent at present. Combining the $D^\pm\pi^\mp$, $D^{*\pm}\pi^\mp$ and $D^\pm\rho^\mp$ measurements [129] gives $\sin(2\beta+\gamma) > 0.68$ at 68% CL [113], consistent with the previously discussed results for β and γ.

12.4 Global fit in the Standard Model

Using the independently measured CKM elements mentioned in the previous sections, the unitarity of the CKM matrix can be checked. We obtain $|V_{ud}|^2 + |V_{us}|^2 + |V_{ub}|^2 = 0.9984 \pm 0.0007$ (1st row), $|V_{cd}|^2 + |V_{cs}|^2 + |V_{cb}|^2 = 0.991 \pm 0.010$ (2nd row), $|V_{ud}|^2 + |V_{cd}|^2 + |V_{td}|^2 = 0.9986 \pm 0.0011$ (1st column), and $|V_{us}|^2 + |V_{cs}|^2 + |V_{ts}|^2 = 0.991 \pm 0.010$ (2nd column), respectively. There is currently a $2.3\,\sigma$ tension with unitarity in the 1st row. The uncertainties in the second row and column are dominated by that of $|V_{cs}|$. (Less precise tests of 1st and 2nd row unitarity can be obtained from the measurement of $\sum_{u,c,d,s,b} |V_{ij}|^2$ in Sec. 12.2.4, combined with either the LEP–LHC average of $\mathcal{B}(W \to cq)/\mathcal{B}(W \to qq') = 0.490 \pm 0.018$ [130] or with the 1st row unitarity check above.) These provide strong tests of the unitarity of the CKM matrix. With the significantly improved direct determination of $|V_{tb}|$, the unitarity checks for the third row and column have also become fairly precise, leaving decreasing room for mixing with other states. The sum of the three angles of the unitarity triangle, $\alpha + \beta + \gamma = \left(173^{+5}_{-4}\right)^\circ$, is also consistent with the SM expectation.

The CKM matrix elements can be most precisely determined using a global fit to all available measurements and imposing the SM constraints (*i.e.*, three generation unitarity). The fit must also use theory predictions for hadronic matrix elements, which sometimes have significant uncertainties. There are several approaches to combining the experimental data. CKMfitter [6, 113] and Ref. [131] (which develops [132, 133] further) use frequentist

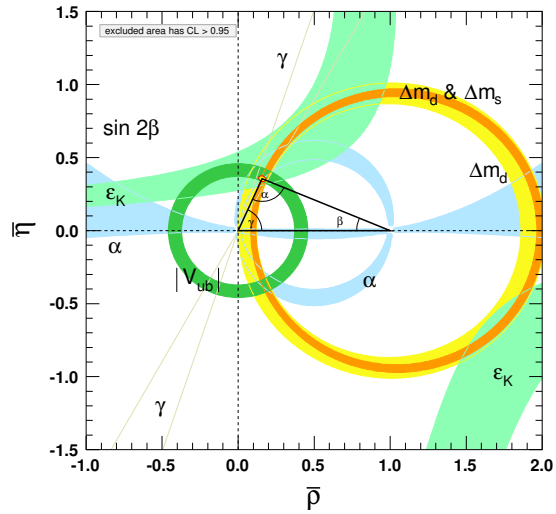

Figure 12.2: Constraints on the $\bar{\rho}, \bar{\eta}$ plane. The shaded areas have 95% CL.

statistics, while UTfit [114, 134] uses a Bayesian approach. These approaches provide similar results.

The constraints implied by the unitarity of the three generation CKM matrix significantly reduce the allowed range of some of the CKM elements. The fit for the Wolfenstein parameters defined in Eq. (12.4) gives

$$\lambda = 0.22517 \pm 0.00068\,, \qquad A = 0.826^{+0.017}_{-0.015}\,,$$
$$\bar{\rho} = 0.1576^{+0.0092}_{-0.0091}\,, \qquad \bar{\eta} = 0.3556^{+0.0071}_{-0.0069}\,. \tag{12.26}$$

These values are obtained using the method of Refs. [6, 113]. The prescription of Refs. [114, 134] gives $\lambda = 0.22519 \pm 0.00068$, $A = 0.820 \pm 0.011$, $\bar{\rho} = 0.1561 \pm 0.0088$, and $\bar{\eta} = 0.3587 \pm 0.0069$ [135]; these results are very close to one another. The fit results for the magnitudes of all nine CKM elements are

$$\left|V_{\rm CKM}\right| = \begin{pmatrix} 0.97431 \pm 0.00016 & 0.22517 \pm 0.00068 & 0.003763^{+0.000088}_{-0.000083} \\ 0.22503 \pm 0.00068 & 0.97345 \pm 0.00016 & 0.04189^{+0.00081}_{-0.00069} \\ 0.00863^{+0.00019}_{-0.00017} & 0.04117^{+0.00079}_{-0.00068} & 0.999115^{+0.000029}_{-0.000034} \end{pmatrix}, \tag{12.27}$$

and the Jarlskog invariant is $J = \left(3.16^{+0.13}_{-0.11}\right) \times 10^{-5}$. The parameters in Eq. (12.3) are

$$\sin\theta_{12} = 0.22517 \pm 0.00068\,, \quad \sin\theta_{13} = 0.003763^{+0.000088}_{-0.000083}\,,$$
$$\sin\theta_{23} = 0.04189^{+0.00081}_{-0.00069}\,, \qquad \delta = 1.154 \pm 0.025\,. \tag{12.28}$$

Fig. 12.2 illustrates the constraints on the $\bar{\rho}, \bar{\eta}$ plane from various measurements, and the global fit result. The shaded 95% CL regions all overlap consistently around the global fit region.

If one uses only tree-level inputs (magnitudes of CKM elements not coupling to the top quark and the angle γ), the resulting fit is almost identical for λ in Eq. (12.26), while the other parameters' central values can change by about a sigma and their uncertainties double, yielding $\lambda = 0.22528 \pm 0.00069$, $A = 0.802 \pm 0.026$, $\bar{\rho} = 0.166^{+0.021}_{-0.020}$, and $\bar{\eta} = 0.379^{+0.022}_{-0.021}$. This illustrates how the constraints can be less tight in the presence of BSM physics.

12.5 Implications beyond the SM

The effects in B, B_s, K, and D decays and mixings due to high-scale physics (W, Z, t, H in the SM, and unknown heavier particles) can be parameterized by operators composed of SM fields, obeying the $SU(3)\times SU(2)\times U(1)$ gauge symmetry. Flavor-changing neutral currents, suppressed in the SM, are especially sensitive to beyond SM contributions. Processes studied in great

Int. J. Mod. Phys. A 2026.41. Downloaded from www.worldscientific.com
by UNIVERSITY OF CALIFORNIA @ BERKELEY on 09/16/26. Re-use and distribution is strictly not permitted, except for Open Access articles.

detail, both experimentally and theoretically, include neutral meson mixings, $B_{(s)} \to X\gamma$, $X\ell^+\ell^-$, $\ell^+\ell^-$, $K \to \pi\nu\bar{\nu}$, etc. The BSM contributions to these operators are suppressed by powers of the scale at which they are generated. Already at lowest order, there are many dimension-6 operators, and the observable effects of BSM interactions are encoded in their coefficients. In the SM, these coefficients are determined by just the four CKM parameters, and the W, Z, and quark masses. For example, Δm_d, $\Gamma(B \to \rho\gamma)$, $\Gamma(B \to \pi\ell^+\ell^-)$, and $\Gamma(B \to \ell^+\ell^-)$ are all proportional to $|V_{td}V_{tb}|^2$ in the SM, however, they may receive unrelated BSM contributions. These BSM contributions may or may not obey the SM relations. (For example, the flavor sector of the MSSM contains 69 CP-conserving parameters and 41 CP-violating phases, *i.e.*, 40 new ones [136]). Thus, similar to the measurements of $\sin 2\beta$ in tree- and loop-dominated decay modes, overconstraining measurements of the magnitudes and phases of flavor-changing neutral-current amplitudes gives good sensitivity to BSM.

To illustrate the level of suppression required for BSM contributions, consider a class of models in which the unitarity of the CKM matrix is maintained, and the dominant BSM effects modify the neutral meson mixing amplitudes [137] by $(z_{ij}/\Lambda^2)(\bar{q}_i\gamma^\mu P_L q_j)^2$, where z_{ij} is an unknown coefficient and Λ is the scale suppressing this BSM contribution (see, [138, 139]). It is only known since the first measurements of γ and α that the SM gives the leading contribution to $B^0-\overline{B}^0$ mixing [6,140]. Nevertheless, new physics with a generic weak phase may still contribute to neutral meson mixings at a significant fraction of the SM [134, 141, 142]. The existing data imply that $\Lambda/|z_{ij}|^{1/2}$ has to exceed about 10^4 TeV for $K^0-\overline{K}^0$ mixing, 10^3 TeV for $D^0-\overline{D}^0$ mixing, 500 TeV for $B^0-\overline{B}^0$ mixing, and 100 TeV for $B_s^0-\overline{B}_s^0$ mixing [134, 139]. (Some other operators are even better constrained [134].) The constraints are the strongest in the kaon sector, because the CKM suppression is the most severe. Thus, if there is new physics at the TeV scale, $|z_{ij}| \ll 1$ is required. Even if $|z_{ij}|$ are suppressed by a loop factor and $|V_{ti}^*V_{tj}|^2$ (in the down quark sector), similar to the SM, one expects percent-level effects, which may be observable in forthcoming flavor physics experiments. To constrain such extensions of the SM, many measurements irrelevant for the SM-CKM fit, such as the CP asymmetry in semileptonic $B_{d,s}^0$ decays, $A_{\rm SL}^{d,s}$, are important [143]. The current world averages [24] are consistent with the SM, with experimental uncertainties far greater than those of the theory predictions.

There are many key measurements sensitive to BSM physics, which do not constrain the unitarity triangle in Fig. 12.1. For example, a key quantity in the B_s system is $\beta_s = \arg(-V_{ts}V_{tb}^*/V_{cs}V_{cb}^*)$, which is the small, λ^2-suppressed, angle of a "squashed" unitarity triangle, obtained by taking the scalar product of the second and third columns of the CKM matrix. This angle can be measured via time-dependent CP violation in $B_s^0 \to J/\psi\,\phi$, similar to β in $B^0 \to J/\psi K^0$. Since the $J/\psi\,\phi$ final state is not a CP eigenstate, an angular analysis of the decay products is needed to separate the CP-even and CP-odd components, which give opposite asymmetries. In the SM, the asymmetry for the CP-even part is $2\beta_s$, when one neglects subdominant amplitudes with a weak phase V_{ub}. (Sometimes the notation $\phi_s = -2\beta_s$ plus a possible BSM contribution to the B_s mixing phase is used.) Testing if the data agree with the SM prediction, $2\beta_s = 0.03768^{+0.00076}_{-0.00075}$ [113], is another sensitive probe of the SM. The current world average, dominated by LHC measurements including the $B_s \to J/\psi\,K^+K^-$ and $J/\psi\,\pi^+\pi^-$ decay modes, is $2\beta_s = 0.053 \pm 0.013$ [72]. Since the uncertainty is much larger than that in the SM, a lot will be learned from more precise future measurements. Searches for CP violation in the charm sector, in particular in $D^0-\overline{D}^0$ mixing, provide complementary sensitivity to BSM.

In the kaon sector, the CP-violating observables, ϵ and ϵ', are tiny, so models in which all sources of CP violation are small were viable before the B-factory measurements. Since the measurement of $\sin 2\beta$, we know that CP violation can be an $\mathcal{O}(1)$ effect, and only flavor mixing is suppressed between the three quark generations. Thus, many models with spontaneous CP violation were excluded. In the kaon sector, clean tests of the SM can come from measurements of $K^+ \to \pi^+\nu\bar{\nu}$ [79] and $K_L^0 \to \pi^0\nu\bar{\nu}$ [144] These loop-induced rare decays are sensitive to BSM, and will allow precise tests [145] of the CKM paradigm, independent of B decays.

The CKM elements are fundamental parameters, so they should be measured as precisely as possible. The overconstraining measurements of CP asymmetries, mixing, semileptonic, and rare decays severely constrain the magnitudes and phases of possible BSM contributions to flavor-changing interactions. If new particles are observed at the LHC, it will be important to explore their flavor parameters as precisely as possible to understand the underlying physics.

References

[1] N. Cabibbo, Phys. Rev. Lett. **10**, 531 (1963).

[2] M. Kobayashi and T. Maskawa, Prog. Theor. Phys. **49**, 652 (1973).

[3] L.-L. Chau and W.-Y. Keung, Phys. Rev. Lett. **53**, 1802 (1984).

[4] L. Wolfenstein, Phys. Rev. Lett. **51**, 1945 (1983).

[5] A. J. Buras, M. E. Lautenbacher and G. Ostermaier, Phys. Rev. **D50**, 3433 (1994), [hep-ph/9403384].

[6] J. Charles *et al.* (CKMfitter Group), Eur. Phys. J. **C41**, 1, 1 (2005), [hep-ph/0406184].

[7] C. Jarlskog, Phys. Rev. Lett. **55**, 1039 (1985).

[8] W. J. Marciano and A. Sirlin, Nucl. Phys. **B93**, 303 (1975); K. S. Babu, Z. Phys. **C35**, 69 (1987).

[9] J. C. Hardy and I. S. Towner, Phys. Rev. C **102**, 4, 045501 (2020).

[10] E. Blucher, G. D'Ambrosio, and W.J. Marciano, "V_{ud}, V_{us}, the Cabibbo Angle and CKM Unitarity," in this *Review*.

[11] D. Pocanic *et al.*, Phys. Rev. Lett. **93**, 181803 (2004), [hep-ex/0312030].

[12] A. Czarnecki, W. J. Marciano and A. Sirlin, Phys. Rev. D **101**, 9, 091301 (2020), [arXiv:1911.04685].

[13] M. Antonelli *et al.* (FlaviaNet Working Group on Kaon Decays), Eur. Phys. J. **C69**, 399 (2010), [arXiv:1005.2323]; see also `http://www.lnf.infn.it/wg/vus`.

[14] Y. Aoki *et al.* (Flavour Lattice Averaging Group (FLAG)), Phys. Rev. D **113**, 1, 014508 (2026), the original papers that led to the quoted averages are cited in this reference or on the web page `https://flag.itp.unibe.ch/`, [arXiv:2411.04268].

[15] A.X. El-Khadra and P. Urquijo, "Semileptonic b-Hadron Decays, Determination of V_{cb} and V_{ub}," in this *Review*.

[16] H. Leutwyler and M. Roos, Z. Phys. **C25**, 91 (1984); For earlier fits for $|V_{ud}|$ and $|V_{us}|$ in the 3-generation SM, see Ref. [17].

[17] R. E. Shrock and L.-L. Wang, Phys. Rev. Lett. **41**, 1692 (1978).

[18] J. Bijnens and P. Talavera, Nucl. Phys. **B669**, 341 (2003), [hep-ph/0303103]; M. Jamin, J. A. Oller and A. Pich, JHEP **02**, 047 (2004), [hep-ph/0401080]; V. Cirigliano *et al.*, JHEP **04**, 006 (2005), [hep-ph/0503108]; C. Dawson *et al.*, PoS **LAT2005**, 337 (2006), [hep-lat/0510018]; N. Tsutsui *et al.* (JLQCD), PoS **LAT2005**, 357 (2006), [hep-lat/0510068]; M. Okamoto (Fermilab Lattice, MILC, HPQCD), in "3rd Conference on Flavor Physics and CP Violation (FPCP 2004) Daegu, Korea, October 4-9, 2004," (2004), [hep-lat/0412044].

[19] W. J. Marciano, Phys. Rev. Lett. **93**, 231803 (2004), [hep-ph/0402299].

[20] F. Ambrosino *et al.* (KLOE), Phys. Lett. **B632**, 76 (2006), [hep-ex/0509045].

[21] See Sec. 5.2, "Averages and fits," in the Introduction to this *Review*, `https://pdg.lbl.gov/2023/reviews/rpp2023-rev-rpp-intro.pdf`.

Int. J. Mod. Phys. A 2026.41. Downloaded from www.wo
by UNIVERSITY OF CALIFORNIA @ BERKELEY on 09/16/26. Re-use and distribution is
except for Open Access articles.

[22] N. Cabibbo, E. C. Swallow and R. Winston, Ann. Rev. Nucl. Part. Sci. **53**, 39 (2003), [hep-ph/0307298]; N. Cabibbo, E. C. Swallow and R. Winston, Phys. Rev. Lett. **92**, 251803 (2004), [hep-ph/0307214].

[23] M. Ademollo and R. Gatto, Phys. Rev. Lett. **13**, 264 (1964).

[24] S. Banerjee *et al.* (HFLAV), Phys. Rev. D **113**, 1, 012008 (2026), [arXiv:2411.18639]; and updates at `https://hflav.web.cern.ch/`.

[25] J. P. Lees *et al.* (BaBar), Phys. Rev. **D91**, 5, 052022 (2015), [arXiv:1412.5502].

[26] M. Ablikim *et al.* (BESIII), Phys. Rev. **D92**, 7, 072012 (2015), [arXiv:1508.07560]; M. Ablikim *et al.* (BESIII), Phys. Rev. **D96**, 1, 012002 (2017), [arXiv:1703.09084].

[27] D. Besson *et al.* (CLEO), Phys. Rev. **D80**, 032005 (2009), [arXiv:0906.2983].

[28] L. Widhalm *et al.* (Belle), Phys. Rev. Lett. **97**, 061804 (2006), [hep-ex/0604049].

[29] M. Ablikim *et al.* (BESIII), Phys. Rev. Lett. **135**, 061801 (2025), [arXiv:2410.07626].

[30] R.A. Briere, J.L. Rosner, S.L. Stone and R. Van de Water, "Leptonic Decays of Charged Pseudoscalar Mesons," in this *Review*.

[31] B. I. Eisenstein *et al.* (CLEO), Phys. Rev. **D78**, 052003 (2008), [arXiv:0806.2112].

[32] M. Ablikim *et al.* (BESIII), JHEP **01**, 089 (2025), [arXiv:2410.20063].

[33] H. Abramowicz *et al.*, Z. Phys. **C15**, 19 (1982).

[34] S. A. Rabinowitz *et al.*, Phys. Rev. Lett. **70**, 134 (1993); A. O. Bazarko *et al.* (CCFR), Z. Phys. **C65**, 189 (1995), [hep-ex/9406007].

[35] P. Vilain *et al.* (CHARM II), Eur. Phys. J. **C11**, 19 (1999).

[36] F. J. Gilman, K. Kleinknecht and B. Renk (2004).

[37] G. De Lellis, P. Migliozzi and P. Santorelli, Phys. Rept. **399**, 227 (2004), [Erratum: Phys. Rept.411,323(2005)].

[38] N. Ushida *et al.* (Fermilab E531), Phys. Lett. **B206**, 380 (1988); T. Bolton (1997), [hep-ex/9708014].

[39] A. Kayis-Topaksu *et al.* (CHORUS), Phys. Lett. **B626**, 24 (2005).

[40] A. Zupanc *et al.* (Belle), JHEP **09**, 139 (2013), [arXiv:1307.6240].

[41] J. P. Alexander *et al.* (CLEO), Phys. Rev. **D79**, 052001 (2009), [arXiv:0901.1216].

[42] P. del Amo Sanchez *et al.* (BaBar), Phys. Rev. **D82**, 091103 (2010), [Erratum: Phys. Rev.D91,no.1,019901(2015)], [arXiv:1008.4080].

[43] M. Ablikim *et al.* (BESIII), Phys. Rev. D **108**, 11, 112001 (2023), [arXiv:2307.14585].

[44] M. Ablikim *et al.* (BESIII), Phys. Rev. **D94**, 7, 072004 (2016), [arXiv:1608.06732]; M. Ablikim *et al.* (BESIII), Phys. Rev. D **110**, 5, 052002 (2024), [arXiv:2407.11727].

[45] P. U. E. Onyisi *et al.* (CLEO), Phys. Rev. **D79**, 052002 (2009), [arXiv:0901.1147]; P. Naik *et al.* (CLEO), Phys. Rev. **D80**, 112004 (2009), [arXiv:0910.3602].

[46] M. Ablikim *et al.* (BESIII), Phys. Rev. D **104**, 3, 032001 (2021), [arXiv:2105.07178]; M. Ablikim *et al.* (BESIII), Phys. Rev. Lett. **127**, 17, 171801 (2021), [arXiv:2106.02218]; M. Ablikim *et al.* (BESIII), Phys. Rev. D **108**, 9, 092014 (2023), [arXiv:2303.12600]; M. Ablikim *et al.* (BESIII), JHEP **09**, 124 (2023), [arXiv:2303.12468].

[47] B. Aubert *et al.* (BaBar), Phys. Rev. **D76**, 052005 (2007), [arXiv:0704.0020].

[48] M. Ablikim *et al.* (BESIII), Phys. Rev. Lett. **122**, 1, 011804 (2019), [arXiv:1810.03127].

[49] S. Schael *et al.* (ALEPH, DELPHI, L3, OPAL, LEP Electroweak), Phys. Rept. **532**, 119 (2013), [arXiv:1302.3415].

[50] A. Tumasyan *et al.* (CMS), Phys. Rev. D **105**, 7, 072008 (2022), [arXiv:2201.07861].

[51] P. Abreu *et al.* (DELPHI), Phys. Lett. **B439**, 209 (1998).

[52] I. I. Y. Bigi *et al.*, Phys. Rev. Lett. **71**, 496 (1993), [hep-ph/9304225].

[53] A. V. Manohar and M. B. Wise, Phys. Rev. **D49**, 1310 (1994), [hep-ph/9308246].

[54] I. I. Y. Bigi *et al.*, Phys. Rev. **D56**, 4017 (1997), [hep-ph/9704245].

[55] A. H. Hoang, Z. Ligeti and A. V. Manohar, Phys. Rev. **D59**, 074017 (1999), [hep-ph/9811239]; A. H. Hoang, Z. Ligeti and A. V. Manohar, Phys. Rev. Lett. **82**, 277 (1999), [hep-ph/9809423]; A. H. Hoang and T. Teubner, Phys. Rev. **D60**, 114027 (1999), [hep-ph/9904468].

[56] N. Isgur and M. B. Wise, Phys. Lett. **B237**, 527 (1990); N. Isgur and M. B. Wise, Phys. Lett. **B232**, 113 (1989).

[57] A. Abdesselam *et al.* (Belle) (2017), [arXiv:1702.01521].

[58] C. G. Boyd, B. Grinstein and R. F. Lebed, Phys. Rev. **D56**, 6895 (1997), [hep-ph/9705252]; C. G. Boyd, B. Grinstein and R. F. Lebed, Nucl. Phys. **B461**, 493 (1996), [hep-ph/9508211].

[59] R. Aaij *et al.* (LHCb), Phys. Rev. D **101**, 7, 072004 (2020), [arXiv:2001.03225].

[60] M. Neubert, Phys. Rev. **D49**, 3392 (1994), [hep-ph/9311325]; M. Neubert, Phys. Rev. **D49**, 4623 (1994), [hep-ph/9312311].

[61] I. I. Y. Bigi *et al.*, Int. J. Mod. Phys. **A9**, 2467 (1994), [hep-ph/9312359].

[62] C. W. Bauer, Z. Ligeti and M. E. Luke, Phys. Lett. **B479**, 395 (2000), [hep-ph/0002161]; C. W. Bauer, Z. Ligeti and M. E. Luke, Phys. Rev. **D64**, 113004 (2001), [hep-ph/0107074].

[63] A. Bornheim *et al.* (CLEO), Phys. Rev. Lett. **88**, 231803 (2002), [hep-ex/0202019].

[64] B. Aubert *et al.* (BaBar), Phys. Rev. **D73**, 012006 (2006), [hep-ex/0509040].

[65] A. Limosani *et al.* (Belle), Phys. Lett. **B621**, 28 (2005), [hep-ex/0504046].

[66] P. Urquijo *et al.* (Belle), Phys. Rev. Lett. **104**, 021801 (2010), [arXiv:0907.0379]; J. P. Lees *et al.* (BaBar), Phys. Rev. **D86**, 032004 (2012), [arXiv:1112.0702].

[67] J. A. Bailey *et al.* (Fermilab Lattice, MILC), Phys. Rev. **D92**, 1, 014024 (2015), [arXiv:1503.07839]; J. M. Flynn *et al.*, Phys. Rev. **D91**, 7, 074510 (2015), [arXiv:1501.05373]; B. Colquhoun *et al.*, Phys. Rev. **D93**, 3, 034502 (2016), [arXiv:1510.07446].

[68] Particle listing, in this *Review*.

[69] R. Aaij *et al.* (LHCb), Nature Phys. **11**, 743 (2015), [arXiv:1504.01568].

[70] R. Aaij *et al.* (LHCb), Phys. Rev. Lett. **126**, 8, 081804 (2021), [arXiv:2012.05143].

[71] H. Albrecht *et al.* (ARGUS), Phys. Lett. **B192**, 245 (1987).

[72] O. Schneider, "B^0–$\overline{B}^0$ mixing," in this *Review*.

[73] A. Abulencia *et al.* (CDF), Phys. Rev. Lett. **97**, 242003 (2006), [hep-ex/0609040].

[74] R. Aaij *et al.* (LHCb), Nature Phys. **18**, 1, 1 (2022), [arXiv:2104.04421].

[75] M. Misiak *et al.*, Phys. Rev. Lett. **114**, 22, 221801 (2015), [arXiv:1503.01789]; M. Czakon *et al.*, JHEP **04**, 168 (2015), [arXiv:1503.01791].

[76] Heavy Flavor Averaging Group [24] CP Asymmetries in Charmless B Decay, End of April 2023, `https://hflav-eos.web.cern.ch/hflav-eos/rare/Apr2023/html/index.html`.

Int. J. Mod. Phys. A 2026.41. Downloaded from www.worldscientific.com
by UNIVERSITY OF CALIFORNIA @ BERKELEY on 09/16/26. Re-use and distribution is strictly not permitted, except for Open Access articles.

[77] B. Grinstein and D. Pirjol, Phys. Rev. **D62**, 093002 (2000), [hep-ph/0002216]; A. Ali, E. Lunghi and A. Ya. Parkhomenko, Phys. Lett. **B595**, 323 (2004), [hep-ph/0405075]; M. Beneke, T. Feldmann and D. Seidel, Nucl. Phys. **B612**, 25 (2001), [hep-ph/0106067]; S. W. Bosch and G. Buchalla, Nucl. Phys. **B621**, 459 (2002), [hep-ph/0106081]; Z. Ligeti and M. B. Wise, Phys. Rev. **D60**, 117506 (1999), [hep-ph/9905277]; D. Becirevic *et al.*, JHEP **05**, 007 (2003), [hep-lat/0301020]; P. Ball, G. W. Jones and R. Zwicky, Phys. Rev. **D75**, 054004 (2007), [hep-ph/0612081]; W. Wang, R.-H. Li and C.-D. Lu (2007), [arXiv:0711.0432]; C.-D. Lu, W. Wang and Z.-T. Wei, Phys. Rev. **D76**, 014013 (2007), [hep-ph/0701265].

[78] A. J. Buras *et al.*, Phys. Rev. Lett. **95**, 261805 (2005), [hep-ph/0508165].

[79] E. Cortina Gil *et al.* (NA62), JHEP **02**, 191 (2025), [arXiv:2412.12015].

[80] T. A. Aaltonen *et al.* (CDF), Phys. Rev. Lett. **112**, 22, 221801 (2014), [arXiv:1404.3392].

[81] V. M. Abazov *et al.* (D0), Phys. Rev. Lett. **107**, 121802 (2011), [arXiv:1106.5436].

[82] V. Khachatryan *et al.* (CMS), Phys. Lett. **B736**, 33 (2014), [arXiv:1404.2292].

[83] T. A. Aaltonen *et al.* (CDF, D0), Phys. Rev. Lett. **115**, 15, 152003 (2015), [arXiv:1503.05027].

[84] LHC Top Working Group summary plots, single top quark production, May 2025, `https://twiki.cern.ch/twiki/bin/view/LHCPhysics/LHCTopWGSummaryPlots`.

[85] J. Swain and L. Taylor, Phys. Rev. **D58**, 093006 (1998), [hep-ph/9712420].

[86] "K_L^0 meson" particle listing, in this *Review*.

[87] A. J. Buras, D. Guadagnoli and G. Isidori, Phys. Lett. **B688**, 309 (2010), [arXiv:1002.3612]; For earlier discussions, see Ref. [88].

[88] E. A. Andriyash, G. G. Ovanesyan and M. I. Vysotsky, Phys. Lett. **B599**, 253 (2004), [hep-ph/0310314]; K. Anikeev *et al.*, in "Workshop on B Physics at the Tevatron: Run II and Beyond Batavia, Illinois, September 23-25, 1999," (2001), [hep-ph/0201071]; A. J. Buras and D. Guadagnoli, Phys. Rev. **D78**, 033005 (2008), [arXiv:0805.3887].

[89] T. Inami and C. S. Lim, Prog. Theor. Phys. **65**, 297 (1981), [Erratum: Prog. Theor. Phys.65,1772(1981)].

[90] J. M. Flynn and L. Randall, Phys. Lett. **B224**, 221 (1989), [Erratum: Phys. Lett.B235,412(1990)]; G. Buchalla, A. J. Buras and M. K. Harlander, Nucl. Phys. **B337**, 313 (1990).

[91] M. Ciuchini *et al.*, Phys. Lett. **B301**, 263 (1993), [hep-ph/9212203]; A. J. Buras, M. Jamin and M. E. Lautenbacher, Nucl. Phys. **B408**, 209 (1993), [hep-ph/9303284]; T. Hambye *et al.*, Nucl. Phys. **B564**, 391 (2000), [hep-ph/9906434]; S. Bertolini, J. O. Eeg and M. Fabbrichesi, Phys. Rev. **D63**, 056009 (2001), [hep-ph/0002234]; V. Cirigliano *et al.*, Phys. Rev. Lett. **91**, 162001 (2003), [hep-ph/0307030].

[92] R. Abbott *et al.* (RBC, UKQCD), Phys. Rev. D **102**, 5, 054509 (2020), [arXiv:2004.09440].

[93] A. J. Buras *et al.*, JHEP **11**, 202 (2015), [arXiv:1507.06345].

[94] V. Cirigliano *et al.*, JHEP **02**, 032 (2020), [arXiv:1911.01359].

[95] A. B. Carter and A. I. Sanda, Phys. Rev. Lett. **45**, 952 (1980); A. B. Carter and A. I. Sanda, Phys. Rev. **D23**, 1567 (1981).

[96] A more detailed discussion and references can be found in: T. Gershon and Y. Nir, "CP violation in meson decays," in this *Review*.

[97] T. Gershon, M. Kenzie and K. Trabelsi, "Determination of CKM angles from B hadrons," in this *Review*.

[98] B. Aubert *et al.* (BaBar), Phys. Rev. **D79**, 072009 (2009), [arXiv:0902.1708].

[99] I. Adachi *et al.* (Belle), Phys. Rev. Lett. **108**, 171802 (2012), [arXiv:1201.4643].

[100] R. Aaij *et al.* (LHCb), Phys. Rev. Lett. **132**, 2, 021801 (2024), [arXiv:2309.09728].

[101] Heavy Flavor Averaging Group [24], Results on Time-Dependent CP Violation and Measurements Related to the Angles of the Unitarity Triangle: Winter conferences (Moriond, etc.) 2024: `https://hflav-eos.web.cern.ch/hflav-eos/triangle/moriond2024/`.

[102] B. Aubert *et al.* (BaBar), Phys. Rev. **D71**, 032005 (2005), [hep-ex/0411016].

[103] R. Itoh *et al.* (Belle), Phys. Rev. Lett. **95**, 091601 (2005), [hep-ex/0504030].

[104] I. Adachi *et al.* (BaBar, Belle), Phys. Rev. Lett. **121**, 26, 261801 (2018), [arXiv:1804.06152]; I. Adachi *et al.* (BaBar, Belle), Phys. Rev. **D98**, 11, 112012 (2018), [arXiv:1804.06153].

[105] A. Abdesselam *et al.* (BaBar, Belle), Phys. Rev. Lett. **115**, 12, 121604 (2015), [arXiv:1505.04147].

[106] M. Gronau and D. London, Phys. Rev. Lett. **65**, 3381 (1990).

[107] J. Zhang *et al.* (Belle), Phys. Rev. Lett. **91**, 221801 (2003), [hep-ex/0306007]; A. Somov *et al.* (Belle), Phys. Rev. Lett. **96**, 171801 (2006), [hep-ex/0601024]; B. Aubert *et al.* (BaBar), Phys. Rev. Lett. **97**, 261801 (2006), [hep-ex/0607092]; B. Aubert *et al.* (BaBar), Phys. Rev. **D76**, 052007 (2007), [arXiv:0705.2157].

[108] B. Aubert *et al.* (BaBar), Phys. Rev. **D78**, 071104 (2008), [arXiv:0807.4977].

[109] A. F. Falk *et al.*, Phys. Rev. **D69**, 011502 (2004), [hep-ph/0310242].

[110] A. E. Snyder and H. R. Quinn, Phys. Rev. **D48**, 2139 (1993).

[111] A. Kusaka *et al.* (Belle), Phys. Rev. Lett. **98**, 221602 (2007), [hep-ex/0701015].

[112] J. P. Lees *et al.* (BaBar), Phys. Rev. **D88**, 1, 012003 (2013), [arXiv:1304.3503].

[113] A. Hocker *et al.*, Eur. Phys. J. **C21**, 225 (2001), [hep-ph/0104062]; and updates at `http://ckmfitter.in2p3.fr/`.

[114] M. Bona *et al.* (UTfit), JHEP **07**, 028 (2005), [hep-ph/0501199]; and updates at `http://www.utfit.org`.

[115] M. Gronau and D. London, Phys. Lett. **B253**, 483 (1991).

[116] M. Gronau and D. Wyler, Phys. Lett. **B265**, 172 (1991).

[117] D. Atwood, I. Dunietz and A. Soni, Phys. Rev. Lett. **78**, 3257 (1997), [hep-ph/9612433]; D. Atwood, I. Dunietz and A. Soni, Phys. Rev. **D63**, 036005 (2001), [hep-ph/0008090].

[118] A. Bondar, talk at the Belle analysis workshop, Novosibirsk, September 2002; A. Poluektov *et al.* (Belle), Phys. Rev. **D70**, 072003 (2004), [hep-ex/0406067].

[119] A. Giri *et al.*, Phys. Rev. **D68**, 054018 (2003), [hep-ph/0303187].

[120] A. Poluektov *et al.* (Belle), Phys. Rev. **D81**, 112002 (2010), [arXiv:1003.3360].

[121] P. del Amo Sanchez *et al.* (BaBar), Phys. Rev. Lett. **105**, 121801 (2010), [arXiv:1005.1096].

[122] R. Aaij *et al.* (LHCb), JHEP **02**, 169 (2021), [arXiv:2010.08483].

[123] R. Aaij *et al.* (LHCb), JHEP **07**, 138 (2023), [arXiv:2209.03692]; R. Aaij *et al.* (LHCb), Eur. Phys. J. C **83**, 6, 547 (2023), [Erratum: Eur.Phys.J.C 83, 672 (2023)], [arXiv:2301.10328].

[124] Y. Grossman, A. Soffer and J. Zupan, Phys. Rev. **D72**, 031501 (2005), [hep-ph/0505270]; M. Rama, Phys. Rev. D **89**, 1, 014021 (2014), [arXiv:1307.4384].

[125] A. Amorim, M. G. Santos and J. P. Silva, Phys. Rev. **D59**, 056001 (1999), [hep-ph/9807364].

[126] R. Aleksan, I. Dunietz and B. Kayser, Z. Phys. **C54**, 653 (1992).

[127] R. Aaij *et al.* (LHCb), JHEP **03**, 059 (2018), [arXiv:1712.07428].

[128] R. Aaij *et al.* (LHCb), JHEP **03**, 137 (2021), [arXiv:2011.12041].

[129] B. Aubert *et al.* (BaBar), Phys. Rev. **D71**, 112003 (2005), [hep-ex/0504035]; B. Aubert *et al.* (BaBar), Phys. Rev. **D73**, 111101 (2006), [hep-ex/0602049]; F. J. Ronga *et al.* (Belle), Phys. Rev. **D73**, 092003 (2006), [hep-ex/0604013]; S. Bahinipati *et al.* (Belle), Phys. Rev. **D84**, 021101 (2011), [arXiv:1102.0888]; R. Aaij *et al.* (LHCb), JHEP **06**, 084 (2018), [arXiv:1805.03448].

[130] R. Barate *et al.* (ALEPH), Phys. Lett. B **465**, 349 (1999); G. Abbiendi *et al.* (OPAL), Phys. Lett. B **490**, 71 (2000), [hep-ex/0009020]; A. Hayrapetyan *et al.* (CMS), Phys. Lett. B **868**, 139754 (2025), [arXiv:2412.16296].

[131] G. P. Dubois-Felsmann *et al.*, *Sensitivity of CKM fits to theoretical uncertainties and their representation* (2003), [hep-ph/0308262]; G. Eigen *et al.*, Phys. Rev. **D89**, 3, 033004 (2014), [arXiv:1301.5867].

[132] D. Boutigny *et al.* (BaBar), in "Workshop on Physics at an Asymmetric B Factory (BaBar Collaboration Meeting) Pasadena, California, September 22-24, 1997," (1998), URL `http://www-public.slac.stanford.edu/sciDoc/docMeta.aspx?slacPubNumber=SLAC-R-504`.

[133] S. Plaszczynski and M.-H. Schune hf8/019 (1999), [PoShf8,019(1999)], [hep-ph/9911280].

[134] M. Bona *et al.* (UTfit), JHEP **03**, 049 (2008), [arXiv:0707.0636].

[135] We thank the CKMfitter and UTfit groups for performing fits and preparing plots using input values from this *Review*.

[136] H. E. Haber, Nucl. Phys. Proc. Suppl. **62**, 469 (1998), [hep-ph/9709450]; Y. Nir, *CP violation: A New era* (2001), [hep-ph/0109090].

[137] J. M. Soares and L. Wolfenstein, Phys. Rev. **D47**, 1021 (1993); T. Goto *et al.*, Phys. Rev. **D53**, 6662 (1996), [hep-ph/9506311]; J. P. Silva and L. Wolfenstein, Phys. Rev. **D55**, 5331 (1997), [hep-ph/9610208].

[138] Y. Grossman, Z. Ligeti and Y. Nir, Prog. Theor. Phys. **122**, 125 (2009), [arXiv:0904.4262].

[139] G. Isidori, Y. Nir and G. Perez, Ann. Rev. Nucl. Part. Sci. **60**, 355 (2010), [arXiv:1002.0900]; G. Isidori, in "Proceedings, 2012 European School of High-Energy Physics (ESHEP 2012): La Pommeraye, Anjou, France, June 06-19, 2012," 69–105 (2014), [arXiv:1302.0661].

[140] Z. Ligeti, Int. J. Mod. Phys. **A20**, 5105 (2005), [hep-ph/0408267].

[141] J. Charles *et al.*, Phys. Rev. **D89**, 3, 033016 (2014), [arXiv:1309.2293].

[142] K. Agashe *et al.* (2005), [hep-ph/0509117].

[143] S. Laplace *et al.*, Phys. Rev. **D65**, 094040 (2002), [hep-ph/0202010].

[144] J. K. Ahn *et al.* (KOTO), Phys. Rev. Lett. **134**, 8, 081802 (2025), [arXiv:2411.11237].

[145] A. J. Buras *et al.*, JHEP **11**, 033 (2015), [arXiv:1503.02693].

Int. J. Mod. Phys. A 2026.41. Downloaded from www.wo
by UNIVERSITY OF CALIFORNIA @ BERKELEY on 09/16/26. Re-use and distribution is
except for Open Access articles.

Int. J. Mod. Phys. A 2026.41. Downloaded from www.worldscientific.com
by UNIVERSITY OF CALIFORNIA @ BERKELEY on 09/16/26. Re-use and distribution is strictly not permitted, except for Open Access articles.

13. *CP* Violation in the Quark Sector

Revised August 2025 by T. Gershon (Warwick U.) and Y. Nir (Weizmann Inst.).

The *CP* transformation combines charge conjugation C with parity P. Under C, particles and antiparticles are interchanged, by conjugating all internal quantum numbers, *e.g.*, $Q \to -Q$ for electromagnetic charge. Under P, the handedness of space is reversed, $\vec{x} \to -\vec{x}$. Thus, for example, a left-handed electron e^-_L is transformed under *CP* into a right-handed positron, e^+_R.

If *CP* were an exact symmetry, the laws of nature would be the same for matter and for antimatter. We observe that most phenomena are C- and P-symmetric, and therefore, also *CP*-symmetric. In particular, these symmetries are respected by the electromagnetic and strong interactions. The weak interactions, on the other hand, violate C and P in the strongest possible way. For example, the W bosons couple to left-handed electrons, e^-_L, and to their *CP*-conjugate right-handed positrons, e^+_R, but to neither their C-conjugate left-handed positrons, e^+_L, nor their P-conjugate right-handed electrons, e^-_R. While weak interactions violate C and P separately, *CP* is still preserved in most weak interaction processes. The *CP* symmetry is, however, violated in certain processes involving interference effects, as discovered in neutral K decays in 1964 [1], and established later in B (2001) and D (2019) decays. For example, as discovered in 1967, a K_L meson decays more often to $\pi^- e^+ \nu_e$ than to $\pi^+ e^- \overline{\nu}_e$, thus allowing electrons and positrons to be unambiguously distinguished, but the decay-rate asymmetry is only at the 0.003 level. The *CP*-violating effects observed in the B system are larger: the parameter describing the *CP* asymmetry in the decay time distribution of $B^0/\overline{B}^0$ meson transitions to *CP* eigenstates like $J/\psi K_S$ is about 0.7 [2,3]. These effects are related to K^0–$\overline{K}^0$ and B^0–$\overline{B}^0$ mixing, but *CP* violation arising solely from decay amplitudes has also been observed, first in $K \to \pi\pi$ decays [4–6], and subsequently in B^0 [7,8], B^+ [9–11], B^0_s [12] and Λ^0_b [13] decays. *CP* violation arising solely from decay amplitudes has also been observed in charm decays [14]. All of these observed *CP* asymmetries are within the range of Standard Model predictions. Given that neutrino masses and lepton mixing have been established, it is expected that *CP* is violated also in the lepton sector [15]. Discovering *CP* violation in the lepton sector is one of the main goals of current and near-future experiments. *CP* violation has not yet been observed in processes involving the top quark, nor in flavor-conserving processes such as electric dipole moments; for these, any significant observation would be a clear indication of physics beyond the Standard Model.

In addition to parity and to continuous Lorentz transformations, there is one other spacetime operation that could be a symmetry of the interactions: time reversal T, $t \to -t$. Violations of T symmetry have been observed in neutral K decays [16]. More recently, T violation has been observed between states that are not *CP*-conjugate [17], exploiting the fact that for neutral B mesons both flavor tagging and *CP* tagging can be used [18]. Moreover, T violation is expected as a corollary of *CP* violation if the combined *CPT* transformation is a fundamental symmetry of nature [19]. All observations indicate that *CPT* is indeed a symmetry of nature [16]. Furthermore, one cannot build a locally Lorentz-invariant quantum field theory with a Hermitian Hamiltonian that violates *CPT*. (At several points in our discussion, we avoid assumptions about *CPT*, in order to identify cases where evidence for *CP* violation relies on assumptions about *CPT*.)

Within the Standard Model, *CP* symmetry is broken by complex phases in the Yukawa couplings (that is, the couplings of the Higgs scalar to quarks). When all transformations to remove unphysical phases in this model are exhausted, a single *CP*-violating parameter remains [20]. In the basis of mass eigenstates, this single phase appears in the 3×3 unitary matrix that gives the W-boson couplings to an up-type antiquark and a down-type quark. (If the Standard Model is supplemented with Majorana mass terms for the neutrinos, the analogous mixing matrix for leptons has three *CP*-violating phases.) The beautifully consistent and economical Standard-Model description of *CP* violation in terms of Yukawa couplings, known as the Kobayashi-Maskawa (KM) mechanism [20], agrees with all measurements to date. Furthermore, one can fit the data allowing contributions from beyond the Standard Model (referred to subsequently as new physics) to loop processes to compete with, or even dominate over, the Standard Model amplitudes [21,22]. Such an analysis provides model-independent proof that the KM phase is different from zero, and that the matrix of three-generation quark mixing is the dominant source of *CP* violation in the quark sector.

The current level of experimental accuracy and the theoretical uncertainties involved in the interpretation of the various observations leave room, however, for additional subdominant sources of *CP* violation from new physics. Indeed, almost all extensions of the Standard Model imply that there are such additional sources. Moreover, *CP* violation is a necessary condition for baryogenesis, the process of dynamically generating the matter-antimatter asymmetry of the Universe [23]. Despite the phenomenological success of the KM mechanism, it fails (by several orders of magnitude) to accommodate the observed asymmetry [24]. This discrepancy strongly suggests that nature provides additional sources of *CP* violation beyond the KM mechanism. The evidence for neutrino masses implies that *CP* can be violated also in the lepton sector. This situation makes leptogenesis [25,26], a scenario where *CP*-violating phases in the Yukawa couplings of the neutrinos play a crucial role in the generation of the baryon asymmetry, a very attractive possibility. The expectation of new sources motivates the large ongoing experimental effort to find deviations from the predictions of the KM mechanism.

CP violation can be experimentally searched for in a variety of processes, such as hadron decays, electric dipole moments of neutrons, electrons and nuclei, and neutrino oscillations. Hadron decays via the weak interaction probe flavor-changing *CP* violation. The search for electric dipole moments may find (or constrain) sources of *CP* violation that, unlike the KM phase, are not related to flavor-changing couplings. Following the discovery of the Higgs boson [27,28], searches for *CP* violation in the Higgs sector are becoming feasible. Future searches for *CP* violation in neutrino oscillations might provide further input on leptogenesis.

The present measurements of *CP* asymmetries provide some of the strongest constraints on the weak couplings of quarks. Future measurements of *CP* violation in K, D, B, and B^0_s meson decays will provide additional constraints on the flavor parameters of the Standard Model, and can probe new physics. In this review, we give the formalism and basic physics motivations that are relevant to present and near future measurements of *CP* violation in the quark sector.

13.1 Formalism

The phenomenology of *CP* violation for neutral flavored mesons is particularly interesting, since many of the observables can be cleanly interpreted. Although the phenomenology is superficially different for K^0, D^0, B^0, and B^0_s decays, this is primarily because each of these systems is governed by a different balance between decay rates, oscillations, and lifetime splitting. However, the general considerations presented in this section are identical for all flavored neutral pseudoscalar mesons. The phenomenology of *CP* violation for neutral mesons that do not carry flavor quantum numbers (such as the $\eta^{(\prime)}$ state) is quite different: such states are their own antiparticles and have definite *CP* eigenvalues, so the signature of *CP* violation is simply the decay to a final state with the opposite *CP*. Such decays are mediated by the electromagnetic or (OZI-suppressed [29–31]) strong interaction, where *CP* violation is not expected and has not yet been observed. In the remainder of this review, we restrict ourselves to considerations of weakly decaying hadrons.

In this section, we present a general formalism for, and classification of, *CP* violation in the decay of a weakly decaying hadron, denoted M. We pay particular attention to the case that M is a K^0, D^0, B^0, or B^0_s meson. Subsequent sections describe the *CP*-violating phenomenology, approximations, and alternative formalisms that are specific to each system.

13.1.1 *Charged- and neutral-hadron decays*

We define decay amplitudes of M (which could be charged or neutral) and its *CP* conjugate $\overline{M}$ to a multi-particle final state f

Int. J. Mod. Phys. A 2026.41. Downloaded from www.wo
by UNIVERSITY OF CALIFORNIA @ BERKELEY on 09/16/26. Re-use and distribution is
except for Open Access articles.

and its CP conjugate $\overline{f}$ as

$$A_f = \langle f\,|\mathcal{H}|\,M\rangle\ , \quad \overline{A}_f = \langle f\,|\mathcal{H}|\,\overline{M}\rangle\ , \tag{13.1a}$$

$$A_{\overline{f}} = \langle \overline{f}\,|\mathcal{H}|\,M\rangle\ , \quad \overline{A}_{\overline{f}} = \langle \overline{f}\,|\mathcal{H}|\,\overline{M}\rangle\ , \tag{13.1b}$$

where $\mathcal{H}$ is the Hamiltonian governing weak interactions. The action of CP on these states introduces phases ξ_M and ξ_f that depend on their flavor content, according to

$$CP|M\rangle = e^{+i\xi_M}\,|\overline{M}\rangle\ , \quad CP|f\rangle = e^{+i\xi_f}\,|\overline{f}\rangle\ , \tag{13.2a}$$

$$CP|\overline{M}\rangle = e^{-i\xi_M}\,|M\rangle\ , \quad CP|\overline{f}\rangle = e^{-i\xi_f}\,|f\rangle\ , \tag{13.2b}$$

so that $(CP)^2 = 1$. The phases ξ_M and ξ_f are arbitrary and unobservable because of the flavor symmetry of the strong interaction. If CP is conserved by the dynamics, $[CP, \mathcal{H}] = 0$, then A_f and $\overline{A}_{\overline{f}}$ have the same magnitude and an arbitrary unphysical relative phase

$$\overline{A}_{\overline{f}} = e^{i(\xi_f - \xi_M)}\,A_f\ . \tag{13.3}$$

13.1.2 *Neutral-meson mixing*

A state that is initially a superposition of M^0 and $\overline{M}^0$, say

$$|\psi(0)\rangle = a(0)|M^0\rangle + b(0)|\overline{M}^0\rangle\ , \tag{13.4}$$

will evolve in time acquiring components that describe all possible decay final states $\{f_1, f_2, \ldots\}$, that is,

$$|\psi(t)\rangle = a(t)|M^0\rangle + b(t)|\overline{M}^0\rangle + c_1(t)|f_1\rangle + c_2(t)|f_2\rangle + \cdots\ . \tag{13.5}$$

If we are interested in computing only the values of $a(t)$ and $b(t)$ (and not the values of all $c_i(t)$), and if the times t under study are much larger than the typical strong interaction scale, then we can use a much simplified formalism [32]. The simplified time evolution is determined by a 2×2 effective Hamiltonian $\mathbf{H}$ that is not Hermitian, since otherwise the mesons would only oscillate and not decay. Any complex matrix, such as $\mathbf{H}$, can be written in terms of Hermitian matrices $\mathbf{M}$ and $\mathbf{\Gamma}$ as

$$\mathbf{H} = \mathbf{M} - \frac{i}{2}\,\mathbf{\Gamma}\ . \tag{13.6}$$

$\mathbf{M}$ and $\mathbf{\Gamma}$ are associated with $(M^0, \overline{M}^0) \leftrightarrow (M^0, \overline{M}^0)$ transitions via off-shell (dispersive), and on-shell (absorptive) intermediate states, respectively. Diagonal elements of $\mathbf{M}$ and $\mathbf{\Gamma}$ are associated with the flavor-conserving transitions $M^0 \to M^0$ and $\overline{M}^0 \to \overline{M}^0$, while off-diagonal elements are associated with flavor-changing transitions $M^0 \leftrightarrow \overline{M}^0$.

The eigenvectors of $\mathbf{H}$ have well-defined masses and decay widths. To specify the components of the strong interaction eigenstates, M^0 and $\overline{M}^0$, in the light (M_L) and heavy (M_H) mass eigenstates, we introduce three complex parameters: p, q, and, for the case that both CP and CPT are violated in mixing, z. Then

$$|M_L\rangle \propto p\sqrt{1-z}\,|M^0\rangle + q\sqrt{1+z}\,|\overline{M}^0\rangle\ , \tag{13.7a}$$

$$|M_H\rangle \propto p\sqrt{1+z}\,|M^0\rangle - q\sqrt{1-z}\,|\overline{M}^0\rangle\ , \tag{13.7b}$$

with the normalization $|q|^2 + |p|^2 = 1$ when $z = 0$. (Another possible choice of labeling, which is in standard usage for K mesons, defines the mass eigenstates according to their lifetimes: K_S for the short-lived and K_L for the long-lived state. The K_L is experimentally found to be the heavier state. Yet another choice is often used for the D mesons [33]: the eigenstates are labeled according to their dominant CP content.)

The real and imaginary parts of the eigenvalues $\omega_{L,H}$ corresponding to $|M_{L,H}\rangle$ represent their masses and decay widths, respectively. The mass and width splittings are

$$\Delta m \equiv m_H - m_L = \mathcal{R}e(\omega_H - \omega_L)\ , \tag{13.8a}$$

$$\Delta\Gamma \equiv \Gamma_H - \Gamma_L = -2\,\mathcal{I}m(\omega_H - \omega_L)\ . \tag{13.8b}$$

Note that here Δm is positive by definition, while the sign of $\Delta\Gamma$ must be experimentally determined. The sign of $\Delta\Gamma$ has not yet been established for B^0 mesons, while $\Delta\Gamma < 0$ is established for K and B^0_s mesons. The Standard Model predicts $\Gamma_L > \Gamma_H$ for $B^0_{(s)}$ mesons; for this reason, $\Delta\Gamma = \Gamma_L - \Gamma_H$, which is still a signed quantity, is often used in the $B^0_{(s)}$ literature and is the convention used in the PDG experimental summaries.

Solving the eigenvalue problem for $\mathbf{H}$ yields

$$\left(\frac{q}{p}\right)^2 = \frac{\mathbf{M}^*_{12} - (i/2)\mathbf{\Gamma}^*_{12}}{\mathbf{M}_{12} - (i/2)\mathbf{\Gamma}_{12}} \tag{13.9}$$

and

$$z \equiv \frac{\delta m - (i/2)\delta\Gamma}{\Delta m - (i/2)\Delta\Gamma}\ , \tag{13.10}$$

where

$$\delta m \equiv \mathbf{M}_{11} - \mathbf{M}_{22}\ , \quad \delta\Gamma \equiv \mathbf{\Gamma}_{11} - \mathbf{\Gamma}_{22} \tag{13.11}$$

are the differences in effective mass and decay-rate expectation values for the strong interaction states M^0 and $\overline{M}^0$.

If either CP or CPT is a symmetry of $\mathbf{H}$ (independently of whether T is conserved or violated), then the values of δm and $\delta\Gamma$ are both zero, and hence $z = 0$. We also find that

$$\omega_H - \omega_L = 2\sqrt{\left(\mathbf{M}_{12} - \frac{i}{2}\mathbf{\Gamma}_{12}\right)\left(\mathbf{M}^*_{12} - \frac{i}{2}\mathbf{\Gamma}^*_{12}\right)}\ . \tag{13.12}$$

If either CP or T is a symmetry of $\mathbf{H}$ (independently of whether CPT is conserved or violated), then $\mathbf{\Gamma}_{12}/\mathbf{M}_{12}$ is real, leading to

$$\left(\frac{q}{p}\right)^2 = e^{2i\xi_M} \quad \Rightarrow \quad \left|\frac{q}{p}\right| = 1\ , \tag{13.13}$$

where ξ_M is the arbitrary unphysical phase introduced in Eq. (13.2). If, and only if, CP is a symmetry of $\mathbf{H}$ (independently of CPT and T), then both of the above conditions hold, with the result that the mass eigenstates are orthogonal

$$\langle M_H|M_L\rangle = |p|^2 - |q|^2 = 0\ . \tag{13.14}$$

13.1.3 *CP-violating observables*

All CP-violating observables in M and $\overline{M}$ decays to final states f and $\overline{f}$ can be expressed in terms of phase-convention-independent combinations of A_f, $\overline{A}_f$, $A_{\overline{f}}$, and $\overline{A}_{\overline{f}}$, together with, for neutral meson decays only, q/p. CP violation in charged meson and all baryon decays depends only on the combination $|\overline{A}_{\overline{f}}/A_f|$, while CP violation in flavored neutral meson decays is enriched by $M^0 \leftrightarrow \overline{M}^0$ oscillations, and depends, additionally, on $|q/p|$ and on $\lambda_f \equiv (q/p)(\overline{A}_f/A_f)$.

The decay rates of the two neutral kaon mass eigenstates, K_S and K_L, are different enough ($\Gamma_S/\Gamma_L \sim 500$) that one can, in most cases, actually study their decays independently. For D^0, B^0, and B^0_s mesons, however, values of $\Delta\Gamma/\Gamma$ (where $\Gamma \equiv (\Gamma_H + \Gamma_L)/2$) are relatively small, and so both mass eigenstates must be considered in their evolution. We denote the state of an initially pure $|M^0\rangle$ or $|\overline{M}^0\rangle$ after an elapsed proper time t as $|M^0_{\rm phys}(t)\rangle$ or $|\overline{M}^0_{\rm phys}(t)\rangle$, respectively. Using the effective Hamiltonian approximation, but not assuming CPT to be a good symmetry, we obtain

$$|M^0_{\rm phys}(t)\rangle = (g_+(t) + z\,g_-(t))\,|M^0\rangle - \sqrt{1-z^2}\,\frac{q}{p}\,g_-(t)|\overline{M}^0\rangle\ , \tag{13.15a}$$

$$|\overline{M}^0_{\rm phys}(t)\rangle = (g_+(t) - z\,g_-(t))\,|\overline{M}^0\rangle - \sqrt{1-z^2}\,\frac{p}{q}\,g_-(t)|M^0\rangle\ , \tag{13.15b}$$

where

$$g_\pm(t) \equiv \frac{1}{2}\left[\exp\left(-im_H t - \frac{1}{2}\Gamma_H t\right) \pm \exp\left(-im_L t - \frac{1}{2}\Gamma_L t\right)\right] \tag{13.16}$$

and $z = 0$ if either CPT or CP is conserved.

Int. J. Mod. Phys. A 2026.41. Downloaded from www.worldscientific.com
by UNIVERSITY OF CALIFORNIA @ BERKELEY on 09/16/26. Re-use and distribution is strictly not permitted, except for Open Access articles.

Defining $x \equiv \Delta m/\Gamma$ and $y \equiv \Delta\Gamma/(2\Gamma)$, and assuming $z = 0$, one obtains the following time-dependent decay rates:

$$\begin{aligned}\frac{d\Gamma\left[M^0_{\rm phys}(t) \to f\right]/dt}{e^{-\Gamma t}\mathcal{N}_f} &= \left(|A_f|^2 + |(q/p)\overline{A}_f|^2\right)\cosh(y\Gamma t) \\ &+ \left(|A_f|^2 - |(q/p)\overline{A}_f|^2\right)\cos(x\Gamma t) \\ &+ 2\,\mathcal{R}e((q/p)A_f^*\overline{A}_f)\sinh(y\Gamma t) \\ &- 2\,\mathcal{I}m((q/p)A_f^*\overline{A}_f)\sin(x\Gamma t)\ ,\end{aligned} \tag{13.17a}$$

$$\begin{aligned}\frac{d\Gamma\left[\overline{M}^0_{\rm phys}(t) \to f\right]/dt}{e^{-\Gamma t}\mathcal{N}_f} &= \left(|(p/q)A_f|^2 + |\overline{A}_f|^2\right)\cosh(y\Gamma t) \\ &- \left(|(p/q)A_f|^2 - |\overline{A}_f|^2\right)\cos(x\Gamma t) \\ &+ 2\,\mathcal{R}e((p/q)A_f\overline{A}_f^*)\sinh(y\Gamma t) \\ &- 2\,\mathcal{I}m((p/q)A_f\overline{A}_f^*)\sin(x\Gamma t)\ ,\end{aligned} \tag{13.17b}$$

where $\mathcal{N}_f$ is a common, time-independent, normalization factor that can be determined bearing in mind that the range of t is $0 < t < \infty$. Decay rates to the *CP*-conjugate final state $\overline{f}$ are obtained analogously, with $\mathcal{N}_f = \mathcal{N}_{\overline{f}}$ and the substitutions $A_f \to A_{\overline{f}}$ and $\overline{A}_f \to \overline{A}_{\overline{f}}$ in Eqs. (13.17a) and (13.17b). Terms proportional to $|A_f|^2$ or $|\overline{A}_f|^2$ are associated with decays that occur without any net $M^0 \leftrightarrow \overline{M}^0$ oscillation, while terms proportional to $|(q/p)\overline{A}_f|^2$ or $|(p/q)A_f|^2$ are associated with decays following a net oscillation. The $\sinh(y\Gamma t)$ and $\sin(x\Gamma t)$ terms of Eqs. (13.17a) and (13.17b) are associated with the interference between these two cases. Note that, in multi-body decays such as $D^0 \to K_S\pi^+\pi^-$ or $B^0 \to \pi^+\pi^-\pi^+\pi^-$, amplitudes are functions of variables that describe the phase-space of the final state. Interference may be present in some regions but not others, and is strongly influenced by resonant substructure.

When neutral pseudoscalar mesons are produced coherently in pairs from the decay of a vector resonance, $V \to M^0\overline{M}^0$ (for example, $\Upsilon(4S) \to B^0\overline{B}^0$, $\psi(3770) \to D^0\overline{D}^0$ or $\phi \to K^0\overline{K}^0$), the time-dependence of their subsequent decays to final states f_1 and f_2 has a similar form to Eqs. (13.17a) and (13.17b):

$$\begin{aligned}\frac{d\Gamma\left[V_{\rm phys}(t_1,t_2) \to f_1 f_2\right]/d(\Delta t)}{e^{-\Gamma|\Delta t|}\mathcal{N}_{f_1 f_2}} &= \left(|a_+|^2 + |a_-|^2\right)\cosh(y\Gamma\Delta t) \\ &+ \left(|a_+|^2 - |a_-|^2\right)\cos(x\Gamma\Delta t) \\ &- 2\,\mathcal{R}e(a_+^* a_-)\sinh(y\Gamma\Delta t) \\ &+ 2\,\mathcal{I}m(a_+^* a_-)\sin(x\Gamma\Delta t)\ ,\end{aligned} \tag{13.18}$$

where $\Delta t \equiv t_2 - t_1$ is the difference in the production times, t_1 and t_2, of f_1 and f_2, respectively, and the dependence on the average decay time and on decay angles has been integrated out. The normalization factor $\mathcal{N}_{f_1 f_2}$ can be evaluated, noting that the range of Δt is $-\infty < \Delta t < \infty$. The coefficients in Eq. (13.18) are determined by the amplitudes for no net oscillation from $t_1 \to t_2$, $\overline{A}_{f_1}A_{f_2}$, and $A_{f_1}\overline{A}_{f_2}$, and for a net oscillation, $(q/p)\overline{A}_{f_1}\overline{A}_{f_2}$ and $(p/q)A_{f_1}A_{f_2}$, via

$$a_+ \equiv \overline{A}_{f_1}A_{f_2} - A_{f_1}\overline{A}_{f_2}\ , \tag{13.19a}$$

$$\begin{aligned}a_- \equiv &-\sqrt{1-z^2}\left(\frac{q}{p}\overline{A}_{f_1}\overline{A}_{f_2} - \frac{p}{q}A_{f_1}A_{f_2}\right) \\ &+ z\left(\overline{A}_{f_1}A_{f_2} + A_{f_1}\overline{A}_{f_2}\right)\ .\end{aligned} \tag{13.19b}$$

Assuming *CPT* conservation, $z = 0$, and identifying $\Delta t \to t$ and $f_2 \to f$, we find that Eqs. (13.18) and (13.19) reduce to Eq. (13.17a) with $A_{f_1} = 0$, $\overline{A}_{f_1} = 1$, or to Eq. (13.17b) with $\overline{A}_{f_1} = 0$, $A_{f_1} = 1$. Indeed, this plays an important role in experiments that exploit the coherence of $V \to M^0\overline{M}^0$ production. Final states f_1 with $A_{f_1} = 0$ or $\overline{A}_{f_1} = 0$ are called tagging states, because they identify the decaying pseudoscalar meson as, respectively, $\overline{M}^0$ or M^0. Before one of M^0 or $\overline{M}^0$ decays, they evolve in phase, so that there is always one M^0 and one $\overline{M}^0$ present. A tagging decay of one meson sets the clock for the time evolution of the other: it starts at t_1 as purely M^0 or $\overline{M}^0$, with time evolution that depends only on $t_2 - t_1$.

When f_1 is a state that both M^0 and $\overline{M}^0$ can decay into, then Eq. (13.18) contains interference terms proportional to $A_{f_1}\overline{A}_{f_1} \neq 0$ that are not present in Eqs. (13.17a) and (13.17b). Even when f_1 is dominantly produced by M^0 decays rather than $\overline{M}^0$ decays, or vice versa, $A_{f_1}\overline{A}_{f_1}$ can be non-zero owing to doubly-CKM-suppressed decays (with amplitudes suppressed by at least two powers of λ relative to the dominant amplitude, in the language of Section 13.3), and these terms should be considered for precision studies of *CP* violation in coherent $V \to M^0\overline{M}^0$ decays [34]. The correlations in $V \to M^0\overline{M}^0$ decays can also be exploited to determine phase differences between favored and suppressed decay amplitudes [35, 36].

13.1.4 *Classification of CP-violating effects*

We distinguish three types of *CP*-violating effects that can occur in the quark sector:

I. *CP* violation in decay is defined by

$$|\overline{A}_{\overline{f}}/A_f| \neq 1\ . \tag{13.20}$$

In charged meson (and all baryon) decays, where mixing effects are absent, this is the only possible source of *CP* asymmetries:

$$\mathcal{A}_{f^\pm} \equiv \frac{\Gamma(M^- \to f^-) - \Gamma(M^+ \to f^+)}{\Gamma(M^- \to f^-) + \Gamma(M^+ \to f^+)} = \frac{|\overline{A}_{f^-}/A_{f^+}|^2 - 1}{|\overline{A}_{f^-}/A_{f^+}|^2 + 1}\ . \tag{13.21}$$

Note that the usual sign convention for *CP* asymmetries of hadrons is for the difference between the rate involving the particle that contains a heavy quark and that which contains an antiquark. Hence, Eq. (13.21) corresponds to the definition for $B^\pm$ mesons, but the opposite sign is used for $D^\pm_{(s)}$ decays.

II. *CP* (and *T*) violation in mixing is defined by

$$|q/p| \neq 1\ . \tag{13.22}$$

In charged-current semileptonic neutral meson decays $M, \overline{M} \to \ell^\pm X^\mp$ (taking $|A_{\ell^+X^-}| = |\overline{A}_{\ell^-X^+}|$ and $A_{\ell^-X^+} = \overline{A}_{\ell^+X^-} = 0$, as is the case in the Standard Model, to lowest order in G_F, and in most of its extensions), this is the only source of *CP* violation, and can be measured via the asymmetry of "wrong-sign" decays induced by oscillations:

$$\begin{aligned}&\mathcal{A}_{\rm SL}(t) \\ &\equiv \frac{d\Gamma/dt\left[\overline{M}^0_{\rm phys}(t) \to \ell^+X^-\right] - d\Gamma/dt\left[M^0_{\rm phys}(t) \to \ell^-X^+\right]}{d\Gamma/dt\left[\overline{M}^0_{\rm phys}(t) \to \ell^+X^-\right] + d\Gamma/dt\left[M^0_{\rm phys}(t) \to \ell^-X^+\right]}\ ,\end{aligned} \tag{13.23a}$$

$$= \frac{1 - |q/p|^4}{1 + |q/p|^4}\ . \tag{13.23b}$$

Note that this asymmetry of time-dependent decay rates is actually time-independent.

III. *CP* violation in interference between a decay without mixing, $M^0 \to f$, and a decay with mixing, $M^0 \to \overline{M}^0 \to f$ (such an effect occurs only in decays to final states that are common to M^0 and $\overline{M}^0$, including all *CP* eigenstates), is defined by

$$\arg(\lambda_f) + \arg(\lambda_{\bar{f}}) \neq 0\ , \qquad \text{with} \qquad \lambda_f \equiv \frac{q}{p}\frac{\overline{A}_f}{A_f}\ . \tag{13.24}$$

For final *CP* eigenstates, f_{CP}, the condition Eq. (13.24) simplifies to

$$\mathcal{I}m(\lambda_{f_{CP}}) \neq 0\ , \tag{13.25}$$

Int. J. Mod. Phys. A 2026.41. Downloaded from www.worldscientific.com by UNIVERSITY OF CALIFORNIA @ BERKELEY on 09/16/26. Re-use and distribution is except for Open Access articles.

This form of *CP* violation can be observed, for example, using the asymmetry of neutral meson decay rates into *CP* eigenstates

$$\mathcal{A}_{f_{CP}}(t) \equiv \\ \equiv \frac{d\Gamma/dt\left[\overline{M}^0_{\rm phys}(t) \to f_{CP}\right] - d\Gamma/dt\left[M^0_{\rm phys}(t) \to f_{CP}\right]}{d\Gamma/dt\left[\overline{M}^0_{\rm phys}(t) \to f_{CP}\right] + d\Gamma/dt\left[M^0_{\rm phys}(t) \to f_{CP}\right]} \,. \tag{13.26}$$

If $\Delta\Gamma = 0$, as expected to a good approximation for B^0 mesons but not for K^0 and B^0_s mesons, and $|q/p| = 1$, then $\mathcal{A}_{f_{CP}}$ has a particularly simple form (see Eq. (13.75), below). If, in addition, the decay amplitudes fulfill $|\overline{A}_{f_{CP}}| = |A_{f_{CP}}|$, the interference between decays with and without mixing is the only source of asymmetry and $\mathcal{A}_{f_{CP}}(t) = \mathcal{I}m(\lambda_{f_{CP}})\sin(x\Gamma t)$.

Examples of these three types of *CP* violation will be given in Sections 13.4, 13.5, and 13.6.

13.2 Theoretical Interpretation: General Considerations

Consider the $M \to f$ decay amplitude A_f, and the *CP* conjugate process, $\overline{M} \to \overline{f}$, with decay amplitude $\overline{A}_{\overline{f}}$. There are two types of phases that may appear in these decay amplitudes. Complex parameters in any Lagrangian term that contributes to the amplitude will appear in complex conjugate form in the *CP*-conjugate amplitude. Thus, their phases appear in A_f and $\overline{A}_{\overline{f}}$ with opposite signs. In the Standard Model, these phases occur only in the couplings of the $W^\pm$ bosons, and hence, are often called "weak phases." The weak phase of any single term is convention-dependent. However, the difference between the weak phases in two different terms in A_f is convention-independent. A second type of phase can appear in scattering or decay amplitudes, even when the Lagrangian is real. This phase originates from the possible contribution from intermediate on-shell states in the decay process. Since such phases are generated by *CP*-invariant interactions, they are the same in A_f and $\overline{A}_{\overline{f}}$. Usually the dominant rescattering is due to strong interactions; hence the designation "strong phases" for the phase shifts so induced. Again, only the relative strong phases between different terms in the amplitude are physically meaningful.

The "weak" and "strong" phases discussed here appear in addition to the spurious *CP*-transformation phases of Eq. (13.3). Those spurious phases are due to an arbitrary choice of phase convention, and do not originate from any dynamics or induce any *CP* violation. For simplicity, we set them to zero from here on.

It is useful to write each contribution a_i to A_f in three parts: its magnitude $|a_i|$, its weak phase ϕ_i, and its strong phase δ_i. If, for example, there are two such contributions, $A_f = a_1 + a_2$, we have

$$A_f = |a_1|e^{i(\delta_1+\phi_1)} + |a_2|e^{i(\delta_2+\phi_2)} \,, \tag{13.27a}$$

$$\overline{A}_{\overline{f}} = |a_1|e^{i(\delta_1-\phi_1)} + |a_2|e^{i(\delta_2-\phi_2)} \,. \tag{13.27b}$$

Similarly, for neutral mesons, it is useful to write

$$\mathbf{M}_{12} = |\mathbf{M}_{12}|e^{i\phi_M} \,, \quad \mathbf{\Gamma}_{12} = |\mathbf{\Gamma}_{12}|e^{i\phi_\Gamma} \,. \tag{13.28}$$

Each of the phases appearing in Eqs. (13.27) and (13.28) is convention-dependent, but combinations such as $\delta_1 - \delta_2$, $\phi_1 - \phi_2$, $\phi_M - \phi_\Gamma$, and $\phi_M + \phi_1 - \overline{\phi}_1$ (where $\overline{\phi}_1$ is a weak phase contributing to $\overline{A}_f$) are physical.

It is now straightforward to evaluate the various asymmetries in terms of the theoretical parameters introduced here. We will do so with approximations that are often relevant to the most interesting measured asymmetries.

1. The *CP* asymmetry in charged meson and all baryon decays [Eq. (13.21)] is given by

$$\mathcal{A}_f = -\frac{2|a_1a_2|\sin(\delta_2-\delta_1)\sin(\phi_2-\phi_1)}{|a_1|^2+|a_2|^2+2|a_1a_2|\cos(\delta_2-\delta_1)\cos(\phi_2-\phi_1)} \,. \tag{13.29}$$

Ideally, this relation would be used to determine the weak phase difference $\phi_2 - \phi_1$, enabling comparison with theoretical predictions for this quantity. This is only possible, however, if the amplitude ratio $|a_2/a_1|$ and the strong phase difference $\delta_2 - \delta_1$ are known. Both quantities depend on non-perturbative hadronic parameters that are difficult to calculate, but in some cases can be obtained from experiment.

2. In the approximation that $|\mathbf{\Gamma}_{12}/\mathbf{M}_{12}| \ll 1$ (valid for B^0 and B^0_s mesons), the *CP* asymmetry in semileptonic neutral-meson decays [Eq. (13.23)] is given by

$$\mathcal{A}_{\rm SL} = -\left|\frac{\mathbf{\Gamma}_{12}}{\mathbf{M}_{12}}\right| \sin(\phi_M - \phi_\Gamma) \,. \tag{13.30}$$

The quantity of most interest to theory is the weak phase $\phi_M - \phi_\Gamma$. Its extraction from the asymmetry requires, however, that $|\mathbf{\Gamma}_{12}/\mathbf{M}_{12}|$ is known. State of the art calculations of this quantity for the B^0 and B^0_s mesons have uncertainties of around 10% [37].

3. In the approximations that only a single weak phase contributes to decay, $A_f = |a_f|e^{i(\delta_f+\phi_f)}$, and that $|\mathbf{\Gamma}_{12}/\mathbf{M}_{12}| = 0$, we obtain $|\lambda_f| = 1$, and the *CP* asymmetries in decays to a final *CP* eigenstate f [Eq. (13.26)] with eigenvalue $\eta_f = \pm 1$ are given by

$$\mathcal{A}_{f_{CP}}(t) = \mathcal{I}m(\lambda_f)\ \sin(\Delta m t) \ \text{ with } \ \mathcal{I}m(\lambda_f) = \eta_f \sin(\phi_M + 2\phi_f) \,. \tag{13.31}$$

Note that the phase measured is purely a weak phase, and no hadronic parameters are involved in the extraction of its value from $\mathcal{I}m(\lambda_f)$.

The discussion above allows us to introduce another classification of *CP*-violating effects:

1. *Indirect CP violation* is consistent with taking $\phi_M \neq 0$ and setting all other *CP* violating phases to zero. *CP* violation in mixing (type II) belongs to this class.
2. *Direct CP violation* cannot be accounted for by just $\phi_M \neq 0$. *CP* violation in decay (type I) belongs to this class.

The historical significance of this classification is related to theory. In superweak models [38], *CP* violation appears only in diagrams that contribute to $\mathbf{M}_{12}$, hence predicting no direct *CP* violation. In most models and, in particular, in the Standard Model, *CP* violation is both direct and indirect. As concerns type III *CP* violation, a single observation of such an effect would be consistent with indirect *CP* violation, but observing $\eta_{f_1}\mathcal{I}m(\lambda_{f_1}) \neq \eta_{f_2}\mathcal{I}m(\lambda_{f_2})$ (for the same decaying meson and two different final *CP* eigenstates f_1 and f_2) would establish direct *CP* violation. The experimental observation of $\epsilon' \neq 0$, which was achieved by establishing that $\mathcal{I}m(\lambda_{\pi^+\pi^-}) \neq \mathcal{I}m(\lambda_{\pi^0\pi^0})$ (see Section 13.4), excluded the superweak scenario.

13.3 Theoretical Interpretation: The KM Mechanism

Of all the Standard Model quark parameters, only the Kobayashi-Maskawa (KM) phase is *CP*-violating. Having a single source of *CP* violation, the Standard Model is very predictive for *CP* asymmetries: some vanish, and those that do not are correlated.

To be precise, *CP* could be violated also by strong interactions. The experimental upper bound on the electric-dipole moment of the neutron [39] implies, however, that $\theta_{\rm QCD}$, the non-perturbative parameter that determines the strength of this type of *CP* violation, is tiny, if not zero [40]. The smallness of $\theta_{\rm QCD}$ constitutes a theoretical puzzle, known as "the strong *CP* problem." This, however, is irrelevant to our discussion of hadron decays.

The charged current interactions (that is, the $W^\pm$ interactions) for quarks are given by

$$-\mathcal{L}_{W^\pm} = \frac{g}{\sqrt{2}}\ \overline{u_{Li}}\ \gamma^\mu\ (V_{\rm CKM})_{ij}\ d_{Lj}\ W^+_\mu + \text{h.c.} \tag{13.32}$$

Int. J. Mod. Phys. A 2026.41. Downloaded from www.worldscientific.com by UNIVERSITY OF CALIFORNIA @ BERKELEY on 09/16/26. Re-use and distribution is strictly not permitted, except for Open Access articles.

Here $i, j = 1, 2, 3$ are generation numbers. The Cabibbo-Kobayashi-Maskawa (CKM) mixing matrix for quarks is a 3×3 unitary matrix [41]. Ordering the quarks by their masses, *i.e.*, $(u_1, u_2, u_3) \to (u, c, t)$ and $(d_1, d_2, d_3) \to (d, s, b)$, the elements of $V_{\rm CKM}$ are written as follows:

$$V_{\rm CKM} = \begin{pmatrix} V_{ud} & V_{us} & V_{ub} \\ V_{cd} & V_{cs} & V_{cb} \\ V_{td} & V_{ts} & V_{tb} \end{pmatrix} . \tag{13.33}$$

While a general 3×3 unitary matrix depends on three real angles and six phases, the freedom to redefine the phases of the quark mass eigenstates can be used to remove five of the phases, leaving a single physical phase, the Kobayashi-Maskawa phase, that is responsible for all *CP* violation in the Standard Model.

The fact that one can parameterize $V_{\rm CKM}$ by three real and only one imaginary physical parameters can be made manifest by choosing an explicit parametrization. The Wolfenstein parametrization [42, 43] is particularly useful:

$$V_{\rm CKM} = \begin{pmatrix} 1 - \frac{1}{2}\lambda^2 - \frac{1}{8}\lambda^4 & \lambda & A\lambda^3(\rho - i\eta) \\ -\lambda + \frac{1}{2}A^2\lambda^5[1 - 2(\rho + i\eta)] & 1 - \frac{1}{2}\lambda^2 - \frac{1}{8}\lambda^4(1 + 4A^2) & A\lambda^2 \\ A\lambda^3[1 - (1 - \frac{1}{2}\lambda^2)(\rho + i\eta)] & -A\lambda^2 + \frac{1}{2}A\lambda^4[1 - 2(\rho + i\eta)] & 1 - \frac{1}{2}A^2\lambda^4 \end{pmatrix} . \tag{13.34}$$

Here $\lambda \approx 0.23$ (not to be confused with λ_f), the sine of the Cabibbo angle, plays the role of an expansion parameter, and η represents the *CP*-violating phase. Terms of $\mathcal{O}(\lambda^6)$ have been neglected.

The unitarity of the CKM matrix, $(VV^\dagger)_{ij} = (V^\dagger V)_{ij} = \delta_{ij}$, leads to twelve distinct complex relations among the matrix elements. The six relations with $i \neq j$ can be represented geometrically as triangles in the complex plane. Two of these,

$$V_{ud}V_{ub}^* + V_{cd}V_{cb}^* + V_{td}V_{tb}^* = 0 , \tag{13.35a}$$

$$V_{td}V_{ud}^* + V_{ts}V_{us}^* + V_{tb}V_{ub}^* = 0 , \tag{13.35b}$$

have terms of equal order, $\mathcal{O}(A\lambda^3)$, and so have corresponding triangles whose interior angles are all $\mathcal{O}(1)$ physical quantities that can be independently measured. The angles of the first triangle (see Fig. 13.1) are given by

$$\alpha \equiv \varphi_2 \equiv \arg\left(-\frac{V_{td}V_{tb}^*}{V_{ud}V_{ub}^*}\right) \simeq \arg\left(-\frac{1 - \rho - i\eta}{\rho + i\eta}\right) , \tag{13.36a}$$

$$\beta \equiv \varphi_1 \equiv \arg\left(-\frac{V_{cd}V_{cb}^*}{V_{td}V_{tb}^*}\right) \simeq \arg\left(\frac{1}{1 - \rho - i\eta}\right) , \tag{13.36b}$$

$$\gamma \equiv \varphi_3 \equiv \arg\left(-\frac{V_{ud}V_{ub}^*}{V_{cd}V_{cb}^*}\right) \simeq \arg(\rho + i\eta) . \tag{13.36c}$$

The angles of the second triangle are equal to (α, β, γ) up to corrections of $\mathcal{O}(\lambda^2)$. The notations (α, β, γ) and $(\varphi_1, \varphi_2, \varphi_3)$ are both in common usage but, for convenience, we only use the first convention in the following.

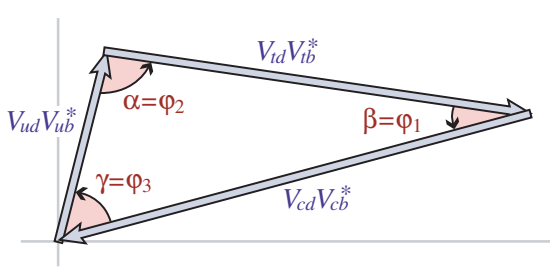

Figure 13.1: Graphical representation of the unitarity constraint $V_{ud}V_{ub}^* + V_{cd}V_{cb}^* + V_{td}V_{tb}^* = 0$ as a triangle in the complex plane.

Another relation that can be represented as a triangle,

$$V_{us}V_{ub}^* + V_{cs}V_{cb}^* + V_{ts}V_{tb}^* = 0 , \tag{13.37}$$

and, in particular, its small angle, of $\mathcal{O}(\lambda^2)$,

$$\beta_s \equiv \arg\left(-\frac{V_{ts}V_{tb}^*}{V_{cs}V_{cb}^*}\right) , \tag{13.38}$$

is convenient for analyzing *CP* violation in the B_s^0 sector.

All unitarity triangles have the same area, commonly denoted by $J/2$ [44]. If *CP* is violated, J is different from zero and can be taken as the single *CP*-violating parameter. In the Wolfenstein parametrization of Eq. (13.34), $J \simeq \lambda^6 A^2 \eta$.

13.4 Kaons

CP violation was discovered in $K \to \pi\pi$ decays in 1964 [1]. The same mode provided the first observation of direct *CP* violation [4–6].

The decay amplitudes actually measured in neutral K decays refer to the mass eigenstates K_L and K_S, rather than to the K and $\overline{K}$ states referred to in Eq. (13.1). The final $\pi^+\pi^-$ and $\pi^0\pi^0$ states are *CP*-even. In the *CP* conservation limit, K_S (K_L) would be *CP*-even (odd), and therefore would (would not) decay to two pions. We define *CP*-violating amplitude ratios for two-pion final states,

$$\eta_{00} \equiv \frac{\langle \pi^0\pi^0|\mathcal{H}|K_L\rangle}{\langle \pi^0\pi^0|\mathcal{H}|K_S\rangle} , \quad \eta_{+-} \equiv \frac{\langle \pi^+\pi^-|\mathcal{H}|K_L\rangle}{\langle \pi^+\pi^-|\mathcal{H}|K_S\rangle} . \tag{13.39}$$

Another important observable is the asymmetry of time-integrated semileptonic decay rates:

$$A_L \equiv \frac{\Gamma(K_L \to \ell^+\nu_\ell\pi^-) - \Gamma(K_L \to \ell^-\overline{\nu}_\ell\pi^+)}{\Gamma(K_L \to \ell^+\nu_\ell\pi^-) + \Gamma(K_L \to \ell^-\overline{\nu}_\ell\pi^+)} . \tag{13.40}$$

CP violation has been observed as an appearance of K_L decays to two-pion final states [45],

$$|\eta_{00}| = (2.220 \pm 0.011) \times 10^{-3} , \tag{13.41a}$$

$$|\eta_{+-}| = (2.232 \pm 0.011) \times 10^{-3} , \tag{13.41b}$$

$$|\eta_{00}/\eta_{+-}| = 0.9950 \pm 0.0007 , \tag{13.41c}$$

where the *CP*-conserving phases ϕ_{ij} of the amplitude ratios η_{ij} have been determined both assuming *CPT* invariance:

$$\phi_{00} = (43.52 \pm 0.05)^\circ , \qquad \phi_{+-} = (43.51 \pm 0.05)^\circ , \tag{13.42}$$

and without assuming *CPT* invariance:

$$\phi_{00} = (43.7 \pm 0.6)^\circ , \qquad \phi_{+-} = (43.4 \pm 0.5)^\circ . \tag{13.43}$$

CP violation has also been observed in semileptonic K_L decays [45]

$$A_L = (3.32 \pm 0.06) \times 10^{-3} , \tag{13.44}$$

where A_L is a weighted average of muon and electron measurements, as well as in K_L decays to $\pi^+\pi^-\gamma$ and $\pi^+\pi^-e^+e^-$ [45]. *CP* violation in $K \to 3\pi$ decays has not yet been observed [45, 46].

Historically, *CP* violation in neutral K decays has been described in terms of the complex parameters ϵ and ϵ'. The observables η_{00}, η_{+-}, and A_L are related to these parameters, and to

Int. J. Mod. Phys. A 2026.41. Downloaded from www.worldscientific.com by UNIVERSITY OF CALIFORNIA @ BERKELEY on 09/16/26. Re-use and distribution is [redacted] except for Open Access articles.

those of Section 13.1, by

$$\eta_{00} = \frac{1-\lambda_{\pi^0\pi^0}}{1+\lambda_{\pi^0\pi^0}} = \epsilon - 2\epsilon' , \tag{13.45a}$$

$$\eta_{+-} = \frac{1-\lambda_{\pi^+\pi^-}}{1+\lambda_{\pi^+\pi^-}} = \epsilon + \epsilon' , \tag{13.45b}$$

$$A_L = \frac{1-|q/p|^2}{1+|q/p|^2} = \frac{2\mathcal{R}e(\epsilon)}{1+|\epsilon|^2} , \tag{13.45c}$$

where, in the last line, we have assumed that $\left|A_{\ell^+\nu_\ell\pi^-}\right| = \left|\overline{A}_{\ell^-\overline{\nu}_\ell\pi^+}\right|$ and $\left|A_{\ell^-\overline{\nu}_\ell\pi^+}\right| = \left|\overline{A}_{\ell^+\nu_\ell\pi^-}\right| = 0$. (The convention-dependent parameter $\tilde{\epsilon} \equiv (1-q/p)/(1+q/p)$, sometimes used in the literature, is, in general, different from ϵ but yields a similar expression, $A_L = 2\mathcal{R}e(\tilde{\epsilon})/(1+|\tilde{\epsilon}|^2)$. Further alternative definitions of ϵ and ϵ' can be found in the literature, as discussed in detail in Ref. [47].) A fit to the $K \to \pi\pi$ data yields [45]

$$|\epsilon| = (2.228 \pm 0.011) \times 10^{-3} , \tag{13.46a}$$

$$\mathcal{R}e(\epsilon'/\epsilon) = (1.66 \pm 0.23) \times 10^{-3} . \tag{13.46b}$$

In discussing two-pion final states, it is useful to express the amplitudes $A_{\pi^0\pi^0}$ and $A_{\pi^+\pi^-}$ in terms of their isospin components via

$$A_{\pi^0\pi^0} = \sqrt{\frac{1}{3}}\,|A_0|\,e^{i(\delta_0+\phi_0)} - \sqrt{\frac{2}{3}}\,|A_2|\,e^{i(\delta_2+\phi_2)} , \tag{13.47a}$$

$$A_{\pi^+\pi^-} = \sqrt{\frac{2}{3}}\,|A_0|\,e^{i(\delta_0+\phi_0)} + \sqrt{\frac{1}{3}}\,|A_2|\,e^{i(\delta_2+\phi_2)} , \tag{13.47b}$$

where we parameterize the amplitude $A_I(\overline{A}_I)$ for $K^0(\overline{K}^0)$ decay into two pions with total isospin $I = 0$ or 2 as

$$A_I \equiv \langle(\pi\pi)_I\,|\mathcal{H}|\,K^0\rangle = |A_I|\,e^{i(\delta_I+\phi_I)} , \tag{13.48a}$$

$$\overline{A}_I \equiv \langle(\pi\pi)_I\,|\mathcal{H}|\,\overline{K}^0\rangle = |A_I|\,e^{i(\delta_I-\phi_I)} . \tag{13.48b}$$

The smallness of $|\eta_{00}|$ and $|\eta_{+-}|$ allows us to approximate

$$\epsilon \simeq \frac{1}{2}(1-\lambda_{(\pi\pi)_{I=0}}) , \qquad \epsilon' \simeq \frac{1}{6}\left(\lambda_{\pi^0\pi^0} - \lambda_{\pi^+\pi^-}\right) . \tag{13.49}$$

The parameter ϵ represents indirect *CP* violation, while ϵ' parameterizes direct *CP* violation: $\mathcal{R}e(\epsilon')$ measures *CP* violation in decay (type I), $\mathcal{R}e(\epsilon)$ measures *CP* violation in mixing (type II), and $\mathcal{I}m(\epsilon)$ and $\mathcal{I}m(\epsilon')$ measure the interference between decays with and without mixing (type III).

The following expressions for ϵ and ϵ' are useful for theoretical evaluations:

$$\epsilon \simeq \frac{e^{i\pi/4}}{\sqrt{2}}\frac{\mathcal{I}m(\mathbf{M}_{12})}{\Delta m} , \qquad \epsilon' = \frac{i}{\sqrt{2}}\left|\frac{A_2}{A_0}\right| e^{i(\delta_2-\delta_0)}\sin(\phi_2-\phi_0) . \tag{13.50}$$

The expression for ϵ is only valid in a phase convention where $\phi_2 = 0$, corresponding to a real $V_{ud}V_{us}^*$, and in the approximation that also $\phi_0 = 0$. The phase of ϵ, $\arg(\epsilon) \approx \arctan(-2\Delta m/\Delta\Gamma)$, is determined by non-perturbative QCD dynamics and is experimentally determined to be about $\pi/4$. The calculation of ϵ benefits from the fact that $\mathcal{I}m(\mathbf{M}_{12})$ is dominated by short distance physics. Consequently, the main sources of uncertainty in theoretical interpretations of ϵ are the values of matrix elements, such as $\langle K^0\,|(\overline{s}d)_{V-A}(\overline{s}d)_{V-A}|\,\overline{K}^0\rangle$. The expression for ϵ' is valid to first order in $|A_2/A_0| \sim 1/20$. The phase of ϵ' is experimentally determined, $\pi/2+\delta_2-\delta_0 \approx \pi/4$, and is independent of the model of electroweak interactions. Note that, accidentally, ϵ'/ϵ is real to a good approximation. Determination of weak phase information from the measurement of $\mathcal{R}e(\epsilon'/\epsilon)$ given in Eq. (13.46) has until now been precluded by uncertainties in the hadronic parameters, but recent advances in lattice QCD calculations and other theoretical approaches [48–50] suggest that it may become possible.

A future measurement of much interest is that of *CP* violation in the rare $K \to \pi\nu\overline{\nu}$ decays. The signal for *CP* violation is simply observing the $K_L \to \pi^0\nu\overline{\nu}$ decay. The effect here is that of interference between decays with and without mixing (type III) [51]:

$$\frac{\Gamma(K_L \to \pi^0\nu\overline{\nu})}{\Gamma(K^+ \to \pi^+\nu\overline{\nu})} = \frac{1}{2}\left[1 + |\lambda_{\pi\nu\overline{\nu}}|^2 - 2\,\mathcal{R}e(\lambda_{\pi\nu\overline{\nu}})\right] \simeq 1 - \mathcal{R}e(\lambda_{\pi\nu\overline{\nu}}) , \tag{13.51}$$

where in the last equation we neglect *CP* violation in decay and in mixing (expected, model-independently, to be of order 10^{-5} and 10^{-3}, respectively). Such a measurement is experimentally very challenging but would be theoretically very rewarding [52]. Similar to the *CP* asymmetry in $B^0 \to J/\psi K_S$, the *CP* violation in $K \to \pi\nu\overline{\nu}$ decay is predicted to be large (that is, the ratio in Eq. (13.51) is neither CKM- nor loop-suppressed) and can be very cleanly interpreted. In particular, the independent determinations of the CKM parameters via B-meson and K-meson decays and mixing will over-constrain the unitarity triangle and provide a stringent text of the KM mechanism.

Within the Standard Model, the $K_L \to \pi^0\nu\overline{\nu}$ decay is dominated by an intermediate top quark contribution and, consequently, can be interpreted in terms of CKM parameters [53]. (For the charged mode, $K^+ \to \pi^+\nu\overline{\nu}$, the contribution from an intermediate charm quark is not negligible, and constitutes a source of hadronic uncertainty.) In particular, $\mathcal{B}(K_L \to \pi^0\nu\overline{\nu})$ provides a theoretically clean way to determine the Wolfenstein parameter η [54]:

$$\mathcal{B}(K_L \to \pi^0\nu\overline{\nu}) = \kappa_L[X(m_t^2/m_W^2)]^2 A^4\eta^2 , \tag{13.52}$$

where the hadronic parameter $\kappa_L \sim 2\times10^{-10}$ incorporates the value of the four-fermion matrix element which is deduced, using isospin relations, from $\mathcal{B}(K^+ \to \pi^0 e^+\nu_e)$, and $X(m_t^2/m_W^2)$ is a known function of the top mass. An explicit calculation gives $\mathcal{B}(K_L \to \pi^0\nu\overline{\nu}) = (3.00 \pm 0.30) \times 10^{-11}$ [55].

Currently the most stringent experimental limit is $\mathcal{B}(K_L \to \pi^0\nu\overline{\nu}) < 2.2\times10^{-9}$ [56] which does not yet reach the bound that can be derived from Eq. (13.51), $\mathcal{B}(K_L \to \pi^0\nu\overline{\nu}) < 4.4\times\mathcal{B}(K^+ \to \pi^+\nu\overline{\nu})$ [51], with the most precise result for the charged kaon decay being $\mathcal{B}(K^+ \to \pi^+\nu\overline{\nu}) = \left(13.0^{+3.3}_{-3.0}\right) \times 10^{-11}$ [57]. Significant further progress is anticipated from experiments searching for $K \to \pi\nu\overline{\nu}$ decays in the next few years.

13.5 Charm

The existence of D^0–$\overline{D}^0$ mixing is well established [58–62], with the latest experimental constraints giving [63, 64] $x \equiv \Delta m/\Gamma = (0.407 \pm 0.044) \times 10^{-2}$ and $y \equiv \Delta\Gamma/(2\Gamma) = (0.645^{+0.024}_{-0.023}) \times 10^{-2}$. Long-distance contributions make it difficult to calculate Standard Model predictions for the D^0–$\overline{D}^0$ mixing parameters. Therefore, the goal of the search for D^0–$\overline{D}^0$ mixing is not to constrain the CKM parameters, but rather to probe new physics. Here *CP* violation plays an important role. Within the Standard Model, the *CP*-violating effects are predicted to be small, since the mixing and the relevant decays are described, to an excellent approximation, by the physics of the first two generations only. The expectation is that the Standard Model size of *CP* violation in D decays is $\mathcal{O}(10^{-3})$ or less. At present, the most sensitive searches involve the $D^0 \to K^+K^-$, $D^0 \to \pi^+\pi^-$ and $D^0 \to K^\pm\pi^\mp$ modes.

The neutral D mesons decay via a singly-Cabibbo-suppressed transition to the *CP* eigenstates K^+K^- and $\pi^+\pi^-$. These decays are dominated by Standard-Model tree diagrams. Thus, we can write, for $f = K^+K^-$ or $\pi^+\pi^-$,

$$A_f = A_f^T e^{+i\phi_f^T}\left[1 + r_f e^{i(\delta_f+\phi_f)}\right] , \tag{13.53a}$$

$$\bar{A}_f = A_f^T e^{-i\phi_f^T}\left[1 + r_f e^{i(\delta_f-\phi_f)}\right] , \tag{13.53b}$$

where $A_f^T e^{\pm i\phi_f^T}$ is the Standard Model tree-level contribution, ϕ_f^T and ϕ_f are weak, *CP* violating phases, δ_f is a strong phase difference, and r_f is the ratio between a subleading ($r_f \ll 1$) contribution with a weak phase different from ϕ_f^T and the Standard

Int. J. Mod. Phys. A 2026.41. Downloaded from www.worldscientific.com
by UNIVERSITY OF CALIFORNIA @ BERKELEY on 09/16/26. Re-use and distribution is strictly not permitted, except for Open Access articles.

Model tree-level contribution. Neglecting r_f, λ_f is universal, and we can define an observable phase ϕ_D via

$$\lambda_f \equiv -|q/p|e^{i\phi_D} \,. \tag{13.54}$$

(In the limit of CP conservation, choosing $\phi_D = 0$ is equivalent to defining the mass eigenstates by their CP eigenvalue: $|D_\mp\rangle = p|D^0\rangle \pm q|\overline{D}^0\rangle$, with D_- (D_+) being the CP-odd (CP-even) state; that is, the state that does not (does) decay into K^+K^-.)

We define the time integrated CP asymmetry for a final CP eigenstate f as follows:

$$a_f \equiv \frac{\int_0^\infty \Gamma(D^0_{\rm phys}(t)\to f)dt - \int_0^\infty \Gamma(\overline{D}^0_{\rm phys}(t)\to f)dt}{\int_0^\infty \Gamma(D^0_{\rm phys}(t)\to f)dt + \int_0^\infty \Gamma(\overline{D}^0_{\rm phys}(t)\to f)dt} \,. \tag{13.55}$$

(This expression corresponds to the D meson being tagged at production, hence the integration goes from 0 to $+\infty$; measurements are also possible with $\psi(3770)\to D^0\overline{D}^0$, in which case the integration goes from $-\infty$ to $+\infty$ giving slightly different results; see the discussion in Section 13.1.3.) We take $x, y, r_f \ll 1$ and expand to leading order in these parameters. We can then separate the contribution to a_f into three parts [65],

$$a_f = a_f^d + a_f^m + a_f^i \,, \tag{13.56}$$

with the following underlying mechanisms:

1. a_f^d signals CP violation in decay (similar to Eq. (13.21)):

$$a_f^d = 2r_f \sin\phi_f \sin\delta_f \,. \tag{13.57}$$

2. a_f^m signals CP violation in mixing (similar to Eq. (13.30)). With our approximations, it is universal:

$$a^m = -\frac{y}{2}\left(\left|\frac{q}{p}\right| - \left|\frac{p}{q}\right|\right)\cos\phi_D \,. \tag{13.58}$$

3. a_f^i signals CP violation in the interference of mixing and decay (similar to Eq. (13.31)). With our approximations, it is universal:

$$a^i = \frac{x}{2}\left(\left|\frac{q}{p}\right| + \left|\frac{p}{q}\right|\right)\sin\phi_D \,. \tag{13.59}$$

In the SM, both a^m and a^i are $\mathcal{O}(10^{-5})$ or less, while a^d could be up to two orders of magnitude larger.

One can isolate the effects of direct CP violation by taking the difference between the CP asymmetries in the K^+K^- and $\pi^+\pi^-$ modes:

$$\Delta a_{CP} \equiv a_{K^+K^-} - a_{\pi^+\pi^-} = a^d_{K^+K^-} - a^d_{\pi^+\pi^-} \,, \tag{13.60}$$

where we neglected a residual, experiment-dependent, contribution from indirect CP violation due to the fact that there may be a decay time-dependent acceptance function that can be different for the K^+K^- and $\pi^+\pi^-$ channels. The current average gives [14, 63]:

$$a^d_{K^+K^-} - a^d_{\pi^+\pi^-} = (-0.159 \pm 0.029)\times 10^{-2} \,, \tag{13.61}$$

demonstrating CP violation in charm decay. While the asymmetry is somewhat larger than the theoretical predictions that preceded the measurement, it can in principle be explained by non-perturbative QCD effects.

One can also isolate the effects of indirect CP violation in the following way. Consider the time-dependent decay rates in Eq. (13.17a) and Eq. (13.17b). The mixing processes modify the time dependence from a pure exponential. However, given the small values of x and y, the time dependences can be recast, to a good approximation, into purely exponential form, but with modified decay-rate parameters [66,67] (given here for the K^+K^- final state):

$$\Gamma_{D^0\to K^+K^-} = \Gamma \times [1 + |q/p|\,(y\cos\phi_D - x\sin\phi_D)] \,, \tag{13.62a}$$

$$\Gamma_{\overline{D}^0\to K^+K^-} = \Gamma \times [1 + |p/q|\,(y\cos\phi_D + x\sin\phi_D)] \,. \tag{13.62b}$$

One can define CP-conserving and CP-violating combinations of these two observables (normalized to the true width Γ):

$$\begin{aligned} y_{CP} &\equiv \frac{\Gamma_{\overline{D}^0\to K^+K^-} + \Gamma_{D^0\to K^+K^-}}{2\Gamma} - 1 \\ &= (y/2)\,(|q/p| + |p/q|)\cos\phi_D - (x/2)\,(|q/p| - |p/q|)\sin\phi_D \,, \end{aligned} \tag{13.63a}$$

$$\begin{aligned} A_\Gamma &\equiv \frac{\Gamma_{D^0\to K^+K^-} - \Gamma_{\overline{D}^0\to K^+K^-}}{2\Gamma} \\ &= -(a^m + a^i) \,. \end{aligned} \tag{13.63b}$$

In the limit of CP conservation (and, in particular, within the Standard Model), $y_{CP} = (\Gamma_+ - \Gamma_-)/2\Gamma = y$ (where $\Gamma_+(\Gamma_-)$ is the decay width of the CP-even (-odd) mass eigenstate) and $A_\Gamma = 0$. Indeed, present measurements imply that CP violation is small [63],

$$y_{CP} - y_{CP}(K\pi) = (+0.697 \pm 0.028)\times 10^{-2} \,, \tag{13.64a}$$

$$A_\Gamma = (0.009 \pm 0.011)\times 10^{-2} \,, \tag{13.64b}$$

where the correction $y_{CP}(K\pi)$ is necessary at high precision since experimentally the denominator of the relative widths in Eq. (13.63a) is measured with the $D^0 \to K^-\pi^+$ mode [68, 69].

The $K^\pm\pi^\mp$ states are not CP eigenstates, but they are still common final states for D^0 and $\overline{D}^0$ decays. Since $D^0(\overline{D}^0) \to K^-\pi^+$ is a Cabibbo-favored (doubly-Cabibbo-suppressed) process, these processes are particularly sensitive to x and/or $y = \mathcal{O}(\lambda^2)$. Taking into account that $|\lambda_{K^-\pi^+}|, \left|\lambda^{-1}_{K^+\pi^-}\right| \ll 1$ and $x, y \ll 1$, assuming that there is no direct CP violation (these are Standard Model tree-level decays dominated by a single weak phase, and there is no contribution from penguin-like and chromomagnetic operators), and expanding the time-dependent rates for $xt, yt \lesssim \Gamma^{-1}$, one obtains

$$\begin{aligned} &\Gamma[D^0_{\rm phys}(t)\to K^+\pi^-] = e^{-\Gamma t}|\overline{A}_{K^-\pi^+}|^2 \\ &\times\left[r_d^2 + r_d\left|\frac{q}{p}\right|(y'\cos\phi_D - x'\sin\phi_D)\Gamma t + \left|\frac{q}{p}\right|^2\frac{y^2+x^2}{4}(\Gamma t)^2\right] \,, \end{aligned} \tag{13.65a}$$

$$\begin{aligned} &\Gamma[\overline{D}^0_{\rm phys}(t)\to K^-\pi^+] = e^{-\Gamma t}|\overline{A}_{K^-\pi^+}|^2 \\ &\times\left[r_d^2 + r_d\left|\frac{p}{q}\right|(y'\cos\phi_D + x'\sin\phi_D)\Gamma t + \left|\frac{p}{q}\right|^2\frac{y^2+x^2}{4}(\Gamma t)^2\right] \,, \end{aligned} \tag{13.65b}$$

where

$$y' \equiv y\cos\delta - x\sin\delta \quad \text{and} \quad x' \equiv x\cos\delta + y\sin\delta \,. \tag{13.66}$$

The weak phase ϕ_D is the same as that of Eq. (13.54) (a consequence of neglecting direct CP violation) and $r_d = \mathcal{O}(\tan^2\theta_c)$ is the amplitude ratio, $r_d = \left|\overline{A}_{K^-\pi^+}/A_{K^-\pi^+}\right| = \left|A_{K^+\pi^-}/\overline{A}_{K^+\pi^-}\right|$, that is, $\lambda_{K^-\pi^+} = r_d|q/p|e^{-i(\delta-\phi_D)}$ and $\lambda^{-1}_{K^+\pi^-} = r_d|p/q|e^{-i(\delta+\phi_D)}$. The parameter δ is a strong-phase difference for these processes, that can be obtained from measurements of quantum correlated $\psi(3770)\to D^0\overline{D}^0$ decays [70,71]. By fitting to the six coefficients of the various time-dependences, one can determine r_d, $|q/p|$, (x^2+y^2), $y'\cos\phi_D$, and $x'\sin\phi_D$. In particular, finding CP violation ($|q/p| \neq 1$ and/or $\sin\phi_D \neq 0$) at a level much higher than 10^{-3} would constitute evidence for new physics. The most stringent constraints to date on CP violation in charm mixing have been obtained with this method [72] and from the A_Γ measurement [73].

A fit to all data [63], including also results from time-dependent analyses of $D^0 \to K_S\pi^+\pi^-$ decays, from which x, y, $|q/p|$ and ϕ_D can be determined directly, yields no evidence for indirect CP violation:

$$1 - |q/p| = +0.006\,^{+0.015}_{-0.016} \,, \tag{13.67a}$$

$$\phi_D = \left(-2.6\,^{+1.1}_{-1.2}\right)^\circ \,. \tag{13.67b}$$

Int. J. Mod. Phys. A 2026.41. Downloaded from www.worldscientific.com by UNIVERSITY OF CALIFORNIA @ BERKELEY on 09/16/26. Re-use and distribution is exclusive for Open Access articles.

With the additional assumption of no direct *CP* violation in doubly-Cabibbo-suppressed D decays [74–76], more stringent constraints are obtained:

$$1 - |q/p| = -0.005 \pm 0.007\,, \tag{13.68a}$$

$$\phi_D = (-0.19 \pm 0.26)^\circ\,. \tag{13.68b}$$

More details on various theoretical and experimental aspects of D^0–$\overline{D}^0$ mixing can be found in Ref. [33].

Searches for *CP* violation in charged $D_{(s)}$ decays have been performed in many modes. Searches in decays mediated by Cabibbo-suppressed amplitudes are particularly interesting, since in other channels effects are likely to be too small to be observable in current experiments. Examples of relevant two-body modes are $D^+ \to \pi^+\pi^0$, $K_S K^+$, $\phi\pi^+$ and $D_s^+ \to K^+\pi^0$, $K_S\pi^+$, ϕK^+. The most precise results are $\mathcal{A}_{D^+\to K_S K^+} = +0.0011 \pm 0.0017$ and $\mathcal{A}_{D_s^+\to K_S\pi^+} = +0.0038 \pm 0.0048$ [63]. The precision of experiments is now sufficient that the effect from *CP* violation in the neutral kaon system can be seen in $D^+ \to K_S\pi^+$ decays [77,78].

Three- and four-body final states provide additional possibilities to search for *CP* violation, since effects may vary over the phase-space [79]. A number of methods have been proposed to exploit this feature and search for *CP* violation in ways that do not require modelling of the decay distribution [80–83]. Such methods are useful for analysis of charm decays since they are less sensitive to biases from production asymmetries, and are well suited to address the issue of whether or not *CP* violation effects are present. They can also be applied to tagged neutral D mesons as well as to charged $D_{(s)}$ decays (flavor tagging is typically achieved from the charge of the pion produced in $D^{*+} \to D^0\pi^+$ decays). The results of all searches to date are consistent with the absence of *CP* violation, with the most significant hint at the level of 2.7σ [84].

13.6 Beauty

13.6.1 *CP violation in mixing of* B^0 *and* B_s^0 *mesons*

The upper bound on the *CP* asymmetry in semileptonic B decays [85] implies that *CP* violation in B^0–$\overline{B}^0$ mixing is a small effect (we use $\mathcal{A}_{\rm SL}/2 \approx 1 - |q/p|$, see Eq. (13.23)):

$$\mathcal{A}^d_{\rm SL} = (-2.1 \pm 1.7) \times 10^{-3} \quad\Longrightarrow\quad |q/p| = 1.0010 \pm 0.0008\,. \tag{13.69}$$

The Standard Model prediction is

$$\mathcal{A}^d_{\rm SL} = \mathcal{O}\left[(m_c^2/m_t^2)\sin\beta\right] \lesssim 0.001\,. \tag{13.70}$$

An explicit calculation gives $(-4.73 \pm 0.42) \times 10^{-4}$ [37].

The experimental constraint on *CP* violation in B_s^0–$\overline{B}_s^0$ mixing is somewhat weaker than that in the B^0–$\overline{B}^0$ system [85]

$$\mathcal{A}^s_{\rm SL} = (-0.6 \pm 2.8) \times 10^{-3} \quad\Longrightarrow\quad |q/p| = 1.0003 \pm 0.0014\,. \tag{13.71}$$

The Standard Model prediction is $\mathcal{A}^s_{\rm SL} = \mathcal{O}\left[(m_c^2/m_t^2)\sin\beta_s\right] \lesssim 10^{-4}$, with an explicit calculation giving $(2.06 \pm 0.18) \times 10^{-5}$ [37].

The fit to experimental data that results in the averages quoted above has a χ^2 probability of 4.5% indicating some tension between the different measurements [63]. This originates in part from a result from the D0 collaboration for the inclusive same-sign dimuon asymmetry that deviates from the Standard Model prediction by 3.6σ [86]. As yet, this has not been confirmed by independent studies.

In models where $\mathbf{\Gamma}_{12}/\mathbf{M}_{12}$ is approximately real, such as the Standard Model, an upper bound on $\Delta\Gamma/\Delta m \approx \mathcal{R}e(\mathbf{\Gamma}_{12}/\mathbf{M}_{12})$ provides yet another upper bound on the deviation of $|q/p|$ from one. This constraint does not hold if $\mathbf{\Gamma}_{12}/\mathbf{M}_{12}$ is approximately imaginary. (An alternative parameterization uses $q/p = (1 - \tilde{\epsilon}_B)/(1 + \tilde{\epsilon}_B)$, leading to $\mathcal{A}_{\rm SL} \simeq 4\mathcal{R}e(\tilde{\epsilon}_B)$.)

13.6.2 *CP violation in interference of* B^0 *decays with and without mixing*

The small deviation (less than one percent) of $|q/p|$ from 1 implies that, at the present level of experimental precision, *CP* violation in B^0 mixing is a negligible effect. Thus, for the purpose of analyzing *CP* asymmetries in hadronic B^0 decays, we can use

$$\lambda_f = e^{-i\phi_{M(B^0)}}(\overline{A}_f/A_f)\,, \tag{13.72}$$

where $\phi_{M(B^0)}$ refers to the phase of $\mathbf{M}_{12}$ appearing in Eq. (13.28) that is appropriate for B^0–$\overline{B}^0$ oscillations. Within the Standard Model, the corresponding phase factor is given by

$$e^{-i\phi_{M(B^0)}} = (V_{tb}^* V_{td})/(V_{tb} V_{td}^*)\,. \tag{13.73}$$

The class of *CP* violation effects in interference between mixing and decay is studied with final states that are common to B^0 and $\overline{B}^0$ decays [87–89]. It is convenient to rewrite Eq. (13.26) for B^0 decays as [90–92]

$$\mathcal{A}_f(t) = S_f \sin(\Delta m t) - C_f \cos(\Delta m t)\,, \tag{13.74}$$

$$S_f \equiv \frac{2\,\mathcal{I}m(\lambda_f)}{1 + \left|\lambda_f\right|^2}\,, \quad C_f \equiv \frac{1 - \left|\lambda_f\right|^2}{1 + \left|\lambda_f\right|^2}\,, \tag{13.75}$$

where we assume that $\Delta\Gamma = 0$ and $|q/p| = 1$. An alternative notation in use is $A_f \equiv -C_f$ – this A_f should not be confused with the A_f of Eq. (13.1), but is equivalent with the $\mathcal{A}_f$ of Eq. (13.21) in the limit that $|q/p| = 1$.

A large class of interesting processes proceed via quark transitions of the form $\overline{b} \to \overline{q}q\overline{q}'$ with $q' = s$ or d. For $q = c$ or u, there are contributions from both tree (t) and penguin (p^{q_u}, where $q_u = u, c, t$ is the quark in the loop) diagrams (see Fig. 13.2) which carry different weak phases:

$$A_f = \left(V_{qb}^* V_{qq'}\right) t_f + \sum_{q_u=u,c,t} \left(V_{q_u b}^* V_{q_u q'}\right) p_f^{q_u}\,. \tag{13.76}$$

(The distinction between tree and penguin contributions is a heuristic one; the separation by the operator that enters is more precise. A more detailed discussion of the operator product expansion approach, which also includes higher order QCD corrections, can be found in Ref. [93,94] for example.) Using CKM unitarity, the various decay amplitudes can always be written in terms of just two CKM combinations. For example, for $f = \pi\pi$, which proceeds via a $\overline{b} \to \overline{u}u\overline{d}$ transition, we can write

$$A_{\pi\pi} = \left(V_{ub}^* V_{ud}\right) T_{\pi\pi} + \left(V_{tb}^* V_{td}\right) P_{\pi\pi}^t\,, \tag{13.77}$$

where $T_{\pi\pi} = t_{\pi\pi} + p_{\pi\pi}^u - p_{\pi\pi}^c$ and $P_{\pi\pi}^t = p_{\pi\pi}^t - p_{\pi\pi}^c$. *CP*-violating phases in Eq. (13.77) appear only in the CKM elements, so that

$$\frac{\overline{A}_{\pi\pi}}{A_{\pi\pi}} = \frac{\left(V_{ub} V_{ud}^*\right) T_{\pi\pi} + \left(V_{tb} V_{td}^*\right) P_{\pi\pi}^t}{\left(V_{ub}^* V_{ud}\right) T_{\pi\pi} + \left(V_{tb}^* V_{td}\right) P_{\pi\pi}^t}\,. \tag{13.78}$$

For $f = J/\psi K$, which proceeds via a $\overline{b} \to \overline{c}c\overline{s}$ transition, we can write

$$A_{\psi K} = \left(V_{cb}^* V_{cs}\right) T_{\psi K} + \left(V_{ub}^* V_{us}\right) P_{\psi K}^u\,, \tag{13.79}$$

where $T_{\psi K} = t_{\psi K} + p_{\psi K}^c - p_{\psi K}^t$ and $P_{\psi K}^u = p_{\psi K}^u - p_{\psi K}^t$. A subtlety arises in this decay that is related to the fact that B^0 decays into a final $J/\psi K^0$ state while $\overline{B}^0$ decays into a final $J/\psi\overline{K}^0$ state. A common final state, *e.g.*, $J/\psi K_S$, is reached only via K^0–$\overline{K}^0$ mixing. Consequently, the phase factor (defined in Eq. (13.28)) corresponding to neutral K mixing, $e^{-i\phi_{M(K)}} = (V_{cd}^* V_{cs})/(V_{cd} V_{cs}^*)$, plays a role:

$$\frac{\overline{A}_{\psi K_S}}{A_{\psi K_S}} = -\frac{\left(V_{cb} V_{cs}^*\right) T_{\psi K} + \left(V_{ub} V_{us}^*\right) P_{\psi K}^u}{\left(V_{cb}^* V_{cs}\right) T_{\psi K} + \left(V_{ub}^* V_{us}\right) P_{\psi K}^u} \times \frac{V_{cd}^* V_{cs}}{V_{cd} V_{cs}^*}\,. \tag{13.80}$$

For $q = s$ or d, there are only penguin contributions to A_f, that is, $t_f = 0$ in Eq. (13.76). (The tree $\overline{b} \to \overline{u}u\overline{q}'$ transition followed by $\overline{u}u \to \overline{q}q$ rescattering is included below in the P^u terms.) Again, CKM unitarity allows us to write A_f in terms of two CKM combinations. For example, for $f = \phi K_S$, which proceeds via a $\overline{b} \to \overline{s}s\overline{s}$ transition, we can write

$$\frac{\overline{A}_{\phi K_S}}{A_{\phi K_S}} = -\frac{\left(V_{cb} V_{cs}^*\right) P_{\phi K}^c + \left(V_{ub} V_{us}^*\right) P_{\phi K}^u}{\left(V_{cb}^* V_{cs}\right) P_{\phi K}^c + \left(V_{ub}^* V_{us}\right) P_{\phi K}^u} \times \frac{V_{cd}^* V_{cs}}{V_{cd} V_{cs}^*}\,, \tag{13.81}$$

Int. J. Mod. Phys. A 2026.41. Downloaded from www.worldscientific.com
by UNIVERSITY OF CALIFORNIA @ BERKELEY on 09/16/26. Re-use and distribution is strictly not permitted, except for Open Access articles.

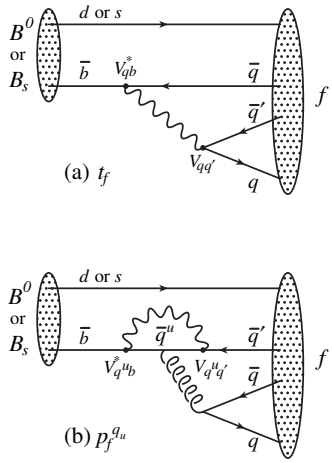

Figure 13.2: Feynman diagrams for (a) tree and (b) penguin amplitudes contributing to $B^0 \to f$ or $B_s^0 \to f$ via a $\bar{b} \to \bar{q}q\bar{q}'$ quark-level process.

where $P^c_{\phi K} = p^c_{\phi K} - p^t_{\phi K}$ and $P^u_{\phi K} = p^u_{\phi K} - p^t_{\phi K}$.

Since in general the amplitude A_f involves two different weak phases, the corresponding decays can exhibit both *CP* violation in the interference of decays with and without mixing, $S_f \neq 0$, and *CP* violation in decay, $C_f \neq 0$. (At the present level of experimental precision, the contribution to C_f from *CP* violation in mixing is negligible, see Eq. (13.69).) If the contribution from a second weak phase is suppressed, then the interpretation of S_f in terms of Lagrangian *CP*-violating parameters is clean, while C_f is small. If such a second contribution is not suppressed, S_f depends on hadronic parameters and, if the relevant strong phase difference is large, C_f is large.

A summary of $\bar{b} \to \bar{q}q\bar{q}'$ modes with $q' = s$ or d is given in Table 13.1. The $\bar{b} \to \bar{d}d\bar{q}$ transitions lead to final states that are similar to those from $\bar{b} \to \bar{u}u\bar{q}$ transitions and have similar phase dependence. Final states that consist of two vector mesons ($\psi\phi$ and $\phi\phi$) are not *CP* eigenstates, and angular analysis is needed to separate the *CP*-even from the *CP*-odd contributions.

The cleanliness of the theoretical interpretation of S_f can be assessed from the information in the last column of Table 13.1. In case of small uncertainties, the expression for S_f in terms of CKM phases can be deduced from the fourth column of Table 13.1 in combination with Eq. (13.73) (and, for $b \to q\bar{q}s$ decays, the example in Eq. (13.80)). Here we consider several interesting examples.

For $B^0 \to J/\psi K_S$ and other $\bar{b} \to \bar{c}c\bar{s}$ processes, we can neglect the P^u contribution to A_f, in the Standard Model, to an approximation that is better than one percent, giving

$$\lambda_{\psi K_S} = -e^{-2i\beta} \;\Rightarrow\; S_{\psi K_S} = \sin(2\beta)\,, \quad C_{\psi K_S} = 0\,. \qquad (13.82)$$

It is important to verify experimentally the level of suppression of the penguin contribution. Methods based on flavor symmetries [95–98] allow limits to be obtained. All are currently consistent with the P^u term being negligible. Explicit calculations [98–101] also support this conclusion.

In the presence of new physics, A_f is still likely to be dominated by the T term, but the mixing amplitude might be modified. Thus, model-independently, $C_f \approx 0$ while S_f cleanly determines the mixing phase ($\phi_M - 2\arg(V_{cb}V^*_{cd})$). The experimental measurement gave the first precision test of the Kobayashi-Maskawa mechanism. The latest world average [63] is

$$S_{\psi K^0} = +0.710 \pm 0.011\,. \qquad (13.83)$$

(We use K^0 throughout to denote results that combine K_S and K_L modes, but use the sign appropriate to K_S.) The consistency of this measurement with the predictions for $\sin 2\beta$ makes it very likely that this mechanism is indeed the dominant source of *CP* violation in the quark sector.

For $B^0 \to \phi K_S$ and other $\bar{b} \to \bar{s}s\bar{s}$ processes (as well as some $\bar{b} \to \bar{u}u\bar{s}$ processes), we can neglect the subdominant contributions, in the Standard Model, to an approximation that is good to the order of a few percent:

$$\lambda_{\phi K_S} = -e^{-2i\beta} \;\Rightarrow\; S_{\phi K_S} = \sin 2\beta\,, \quad C_{\phi K_S} = 0\,. \qquad (13.84)$$

A review of explicit calculations of the effects of subleading amplitudes can be found in Ref. [102]. In the presence of new physics, both A_f and $\mathbf{M}_{12}$ can have contributions that are comparable in size to those of the Standard Model and carry new weak phases. Such a situation gives several interesting consequences for penguin-dominated $\bar{b} \to \bar{q}q\bar{s}$ decays ($q = u, d, s$) to a final state f:

1. The value of $-\eta_f S_f$ may be different from $S_{\psi K_S}$ by more than a few percent, where η_f is the *CP* eigenvalue of the final state.
2. The values of $\eta_f S_f$ for different final states f may be different from each other by more than a few percent (for example, $S_{\phi K_S} \neq S_{\eta' K_S}$).
3. The value of C_f may be different from zero by more than a few percent.

While a clear interpretation of such signals in terms of Lagrangian parameters will be difficult because, under these circumstances, hadronic parameters play a role, any of the above three options will clearly signal new physics. In addition, flavor symmetry relations, such as those that relate observables in $B \to K\pi$ decays [103,104] can be used to provide further tests of the Standard Model. Fig. 13.3 summarizes the present experimental results: none of the possible signatures listed above is unambiguously established, but there is definitely still room for new physics.

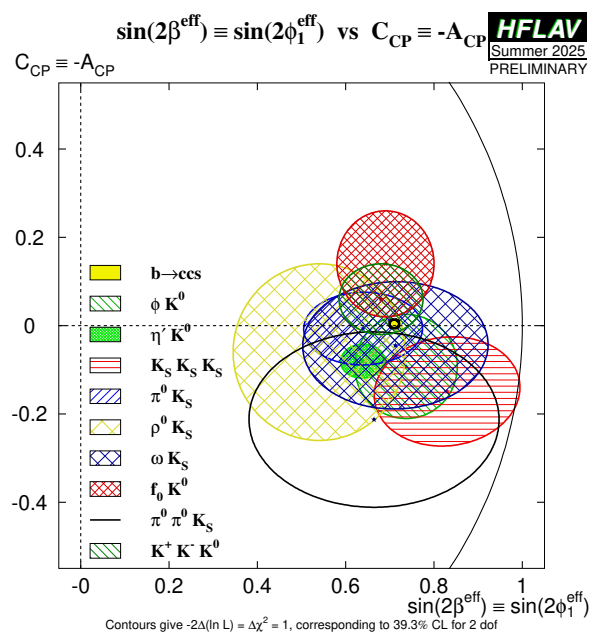

Figure 13.3: Summary of the results [63] of time-dependent analyses of $b \to q\bar{q}s$ decays, which are potentially sensitive to new physics.

For the $\bar{b} \to \bar{u}u\bar{d}$ process $B \to \pi\pi$ and other related channels, the penguin-to-tree ratio can be estimated using SU(3) relations and experimental data on related $B \to K\pi$ decays. The result (for $\pi\pi$) is that the suppression is at the level of $0.2 - 0.3$ and so cannot be neglected. The expressions for $S_{\pi\pi}$ and $C_{\pi\pi}$ to leading order in $R_{PT} \equiv (|V_{tb}V_{td}|\, P^t_{\pi\pi})/(|V_{ub}V_{ud}|\, T_{\pi\pi})$ are:

$$\lambda_{\pi\pi} = e^{2i\alpha}\left[(1 - R_{PT}e^{-i\alpha})/(1 - R_{PT}e^{+i\alpha})\right] \;\Rightarrow \qquad (13.85)$$

$$S_{\pi\pi} \approx \sin 2\alpha + 2\,\mathcal{R}e(R_{PT})\cos 2\alpha \sin\alpha\,, \quad C_{\pi\pi} \approx 2\,\mathcal{I}m(R_{PT})\sin\alpha\,. \qquad (13.86)$$

Int. J. Mod. Phys. A 2026.41. Downloaded from www.worldscientific.com by UNIVERSITY OF CALIFORNIA @ BERKELEY on 09/16/26. Re-use and distribution is except for Open Access articles.

Table 13.1: Summary of $\bar{b} \to \bar{q}q\bar{q}'$ modes with $q' = s$ or d. The second and third columns give examples of hadronic final states (usually those which are experimentally most convenient to study). The fourth column gives the CKM dependence of the amplitude A_f, using the notation of Eqs. ((13.77), (13.79), (13.81)), with the dominant term first and the subdominant second. The suppression factor of the second term compared to the first is given in the last column. "Loop" refers to a penguin versus tree-suppression factor (it is mode-dependent and roughly $\mathcal{O}(0.2-0.3)$) and $\lambda \simeq 0.23$ is the expansion parameter of Eq. (13.34).

$\bar{b} \to \bar{q}q\bar{q}'$	$B^0 \to f$	$B_s^0 \to f$	CKM dependence of A_f	Suppression
$\bar{b} \to \bar{c}c\bar{s}$	ψK_S	$\psi\phi$	$(V_{cb}^* V_{cs})T + (V_{ub}^* V_{us})P^u$	loop $\times \lambda^2$
$\bar{b} \to \bar{s}s\bar{s}$	ϕK_S	$\phi\phi$	$(V_{cb}^* V_{cs})P^c + (V_{ub}^* V_{us})P^u$	λ^2
$\bar{b} \to \bar{u}u\bar{s}$	$\pi^0 K_S$	K^+K^-	$(V_{cb}^* V_{cs})P^c + (V_{ub}^* V_{us})T$	λ^2/loop
$\bar{b} \to \bar{c}c\bar{d}$	D^+D^-	ψK_S	$(V_{cb}^* V_{cd})T + (V_{tb}^* V_{td})P^t$	loop
$\bar{b} \to \bar{s}s\bar{d}$	$K_S K_S$	ϕK_S	$(V_{tb}^* V_{td})P^t + (V_{cb}^* V_{cd})P^c$	$\lesssim 1$
$\bar{b} \to \bar{u}u\bar{d}$	$\pi^+\pi^-$	$\rho^0 K_S$	$(V_{ub}^* V_{ud})T + (V_{tb}^* V_{td})P^t$	loop
$\bar{b} \to \bar{c}u\bar{d}$	$D_{CP}\pi^0$	$D_{CP}K_S$	$(V_{cb}^* V_{ud})T + (V_{ub}^* V_{cd})T'$	λ^2
$\bar{b} \to \bar{c}u\bar{s}$	$D_{CP}K_S$	$D_{CP}\phi$	$(V_{cb}^* V_{us})T + (V_{ub}^* V_{cs})T'$	$\lesssim 1$

Note that R_{PT} is mode-dependent and, in particular, could be different for $\pi^+\pi^-$ and $\pi^0\pi^0$. If strong phases can be neglected, then R_{PT} is real, resulting in $C_{\pi\pi} = 0$. The size of $C_{\pi\pi}$ is an indicator of how large the strong phase is. The present experimental average is $C_{\pi^+\pi^-} = -0.311 \pm 0.030$ [63]. As concerns $S_{\pi\pi}$, it is clear from Eq. (13.86) that the relative size or strong phase of the penguin contribution must be known to extract α. The theoretical uncertainty stemming from $|R_{PT}| \not\ll 1$ is referred to in the literature as penguin pollution.

The cleanest solution involves isospin relations among the $B \to \pi\pi$ amplitudes [105]:

$$\frac{1}{\sqrt{2}} A_{\pi^+\pi^-} + A_{\pi^0\pi^0} = A_{\pi^+\pi^0} \ . \tag{13.87}$$

The method exploits the fact that the penguin contribution to $P_{\pi\pi}^t$ is pure $\Delta I = 1/2$ (this is not true for the electroweak penguins which, however, are expected to be small), while the tree contribution to $T_{\pi\pi}$ contains amplitudes that are both $\Delta I = 1/2$ and $\Delta I = 3/2$. A simple geometric construction then allows one to find R_{PT} and extract α cleanly from $S_{\pi^+\pi^-}$. The key experimental difficulty is that one must measure accurately the separate rates for B^0 and $\overline{B}^0 \to \pi^0\pi^0$.

CP asymmetries in $B \to \rho\pi$ and $B \to \rho\rho$ can also be used to determine α. In particular, the $B \to \rho\rho$ measurements are presently very significant in constraining α. The extraction proceeds via isospin analysis similar to that of $B \to \pi\pi$. There are, however, several important differences. First, due to the finite width of the ρ mesons, a final $(\rho\rho)_{I=1}$ state is possible [106]. The effect is, however, of the order of $(\Gamma_\rho/m_\rho)^2 \sim 0.04$. Second, due to the presence of three helicity states for the two vector mesons, angular analysis is needed to separate the *CP*-even and *CP*-odd components. The theoretical expectation is that the *CP*-odd component is small. This is supported by experiments which find that the $\rho^+\rho^-$ and $\rho^\pm\rho^0$ modes are dominantly longitudinally polarized. Third, an important advantage of the $\rho\rho$ modes is that the penguin contribution is expected to be small due to different hadronic dynamics. This expectation is confirmed by the smallness of $\mathcal{B}(B^0 \to \rho^0\rho^0) = (0.96 \pm 0.15) \times 10^{-6}$ compared to $\mathcal{B}(B^0 \to \rho^+\rho^-) = (27.7 \pm 1.9) \times 10^{-6}$ [63]. Thus, $S_{\rho^+\rho^-}$ is not far from $\sin 2\alpha$. Finally, both $S_{\rho^0\rho^0}$ and $C_{\rho^0\rho^0}$ are experimentally accessible, which may allow a precise determination of α. However, a full isospin analysis should allow that the fractions of longitudinal polarization in B and $\overline{B}$ decays may differ, which has not yet been done by the experiments.

Detailed discussion of the determination of α with these methods can be found in Refs. [107, 108]. The latest world average is

$$\alpha = \left(84.1\,^{+3.7}_{-3.0}\right)^\circ \ . \tag{13.88}$$

The consistency between the range of α determined by the $B \to \pi\pi$, $\rho\pi$ and $\rho\rho$ measurements and the range allowed by CKM fits (excluding these direct determinations) provides further support to the Kobayashi-Maskawa mechanism.

All modes discussed in this Section so far have possible contributions from penguin amplitudes. As shown in Table 13.1, *CP* violation can also be studied with final states, typically containing charmed mesons, where no such contribution is possible. The neutral charmed meson must be reconstructed in a final state, such as a *CP* eigenstate, common to D^0 and $\overline{D}^0$ so that the amplitudes for the B and $\overline{B}$ meson decays interfere. Although there is a second tree amplitude with a different weak phase, the contributions of the different diagrams can in many cases be separated experimentally (for example by exploiting different decays of the neutral D mesons) making these channels very clean theoretically. A determination of $\sin(2\beta)$, with significance of *CP* violation over 5σ, with this method has been reported [109]. Moreover, the interference between the two tree diagrams gives sensitivity to γ, as will be discussed in Section 13.6.4.

13.6.3 *CP violation in interference of B_s^0 decays with and without mixing*

Similarly to the B^0 case, the value of $|q/p|$ in the B_s^0 system reported in Eq. (13.71) is consistent with unity with sufficient precision that *CP* violation in B_s^0 mixing can be considered negligible. We therefore use

$$\lambda_f = e^{-i\phi_M(B_s^0)}(\overline{A}_f/A_f) \ . \tag{13.89}$$

Within the Standard Model,

$$e^{-i\phi_M(B_s^0)} = (V_{tb}^* V_{ts})/(V_{tb} V_{ts}^*) \ . \tag{13.90}$$

Note that in the B_s^0 system, and with the sign convention of Eq. (13.8b), $\Delta\Gamma/\Gamma = -0.126 \pm 0.007$ [63] and therefore y should not be put to zero in Eqs. (13.17a) and (13.17b). However, $|q/p| = 1$ is expected to hold to an even better approximation than for B^0 mesons. One therefore obtains

$$\mathcal{A}_f(t) = \frac{S_f \sin(\Delta m t) - C_f \cos(\Delta m t)}{\cosh(\Delta\Gamma t/2) - A_f^{\Delta\Gamma} \sinh(\Delta\Gamma t/2)} \ , \tag{13.91}$$

$$\text{where} \quad A_f^{\Delta\Gamma} \equiv \frac{-2\,\mathcal{R}e(\lambda_f)}{1 + \left|\lambda_f\right|^2} \ . \tag{13.92}$$

The presence of the $A_f^{\Delta\Gamma}$ term implies that information on λ_f can be obtained from analyses that do not use tagging of the initial flavor, through so-called effective lifetime measurements [110].

The $B_s^0 \to J/\psi\phi$ decay proceeds via the $\bar{b} \to \bar{c}c\bar{s}$ transition. The *CP* asymmetry in this mode thus determines $\sin 2\beta_s$, where β_s is defined in Eq. (13.38) [111]. Angular analysis is needed to disentangle the *CP*-even and *CP*-odd components of the final state, and the interference between these components also allows $\cos 2\beta_s$ to be determined. The $B_s^0 \to J/\psi\pi^+\pi^-$ decay, which has a large contribution from $J/\psi f_0(980)$ and is assumed to also proceed dominantly via the $\bar{b} \to \bar{c}c\bar{s}$ transition, has also been used to determine $\sin 2\beta_s$. In this case no angular analysis is necessary, since the final state has been shown to be dominated by the *CP*-odd component [112]. The combination of measurements yields [63]

$$2\beta_s = 0.052 \pm 0.013 \ , \tag{13.93}$$

Int. J. Mod. Phys. A 2026.41. Downloaded from www.worldscientific.com by UNIVERSITY OF CALIFORNIA @ BERKELEY on 09/16/26. Re-use and distribution is strictly not permitted, except for Open Access articles.

consistent with the Standard Model prediction, assuming negligible penguin contributions, $\beta_s = 0.01882\,^{+0.00026}_{-0.00028}$ [21].

A time-dependent CP asymmetry was established in $B_s^0 \to K^+K^-$ decay, which proceeds via the $\bar{b} \to \bar{u}u\bar{s}$ transition [113]:

$$C_{KK} = +0.172 \pm 0.031\,, \quad S_{KK} = +0.139 \pm 0.032\,. \tag{13.94}$$

For both C_{KK} and S_{KK}, the hadronic ratio (T/P^c) plays an important role (see Table 13.1), making a clean theoretical interpretation challenging. Results on time-dependent CP violation in the $\bar{b} \to \bar{q}q\bar{s}$ decays $B_s^0 \to \phi\phi$ and $K^{*0}\overline{K}^{*0}$ have also been reported. These are penguin-dominated $\bar{b} \to \bar{q}q\bar{s}$ decays, in which the CP violation effects are expected to be very small in the Standard Model; measurements to date are consistent with these predictions. Parameters of CP violation have also been determined from the decay-time distributions of $B_s^0 \to D_s^{\mp}K^{\pm}$ and $D_s^{\mp}K^{\pm}\pi^+\pi^-$ decays, involving interference between $\bar{b} \to \bar{c}u\bar{s}$ and $\bar{b} \to \bar{u}c\bar{s}$ tree amplitudes. The latest results in $B_s^0 \to D_s^{\mp}K^{\pm}$ decays [114] provide observation of CP violation in the interference between mixing and decay, through $\arg(\lambda_f) + \arg(\lambda_{\bar{f}}) \neq 0$ (see Eq. (13.24)).

13.6.4 *Direct CP violation in the B system*

An interesting class of decay modes is that of the tree-level decays $B^{\pm} \to D^{(*)}K^{\pm}$, which allow a theoretically pristine determination of the angle γ [115–120]. The method uses the decays $B^+ \to D^0K^+$, which proceeds via the quark transition $\bar{b} \to \bar{u}c\bar{s}$, and $B^+ \to \overline{D}^0K^+$, which proceeds via the quark transition $\bar{b} \to \bar{c}u\bar{s}$, with the D^0 and $\overline{D}^0$ decaying into a common final state. The decays into common final states, such $(\pi^0K_S)_DK^+$, involve interference effects between the two amplitudes, with sensitivity to the relative phase, $\delta + \gamma$ (δ is the relevant strong phase difference). The CP-conjugate processes are sensitive to $\delta - \gamma$. Measurements of branching ratios and CP asymmetries allow the determination of γ and δ from amplitude triangle relations. The method suffers from discrete ambiguities but, since all hadronic parameters can be determined from the data, has negligible theoretical uncertainty [121].

Unfortunately, the smallness of the CKM-suppressed $b \to u$ transitions makes it difficult to use the simplest methods alone [115–117] to determine γ. These difficulties are overcome (and the discrete ambiguities are removed) by performing a Dalitz plot analysis for multi-body D decays [118–120]. Detailed discussion of the determination of γ with these methods can be found in Ref. [108].

Constraints on γ from combinations of results on various $B \to D^{(*)}K^{(*)}$ processes have been obtained by experiments [122,123]. The latest world average is [63,108]

$$\gamma = \left(66.3\,^{+2.7}_{-2.8}\right)^{\circ}\,. \tag{13.95}$$

The consistency between the range of γ determined by the $B \to DK$ measurements and the range allowed by CKM fits (excluding these direct determinations) provides further support to the Kobayashi-Maskawa mechanism. As more data become available, determinations of γ from $B_s^0 \to D_s^{\mp}K^{\pm}$ [124, 125] and $B^0 \to DK^{*0}$ [126–130] are expected to also give competitive measurements.

Decays to the final state $K^{\mp}\pi^{\pm}$ provided the first observations of direct CP violation in both B^0 and B_s^0 systems. The asymmetry arises due to interference between tree and penguin diagrams [131], similar to the effect discussed in Section 13.6.2. In principle, measurements of $\mathcal{A}_{B^0\to K^+\pi^-}$ and $\mathcal{A}_{B_s^0\to K^-\pi^+}$ could be used to determine the weak phase difference γ, but lack of knowledge of the relative magnitude and strong phase of the contributing amplitudes limits the achievable precision. The uncertainties on these hadronic parameters can be reduced by exploiting flavor symmetries, which predict a number of relations between asymmetries in different modes. One such relation is that the partial rate differences for B^0 and B_s^0 decays to $K^{\mp}\pi^{\pm}$ are expected to be approximately equal and opposite [132], which is consistent with current data. It is also expected that the partial rate asymmetries for $B^0 \to K^+\pi^-$ and $B^+ \to K^+\pi^0$ should be approximately equal; however, the experimental results currently show a significant discrepancy [63]:

$$\mathcal{A}_{B^0\to K^+\pi^-} = -0.0831 \pm 0.0031\,, \quad \mathcal{A}_{B^+\to K^+\pi^0} = +0.027 \pm 0.012\,. \tag{13.96}$$

It is therefore of great interest to understand whether this originates from Standard Model QCD corrections, or whether it is a signature of new dynamics. Improved tests of a more precise relation between the partial rate differences of all four $K\pi$ final states [133–136], currently limited by knowledge of the CP asymmetry in $\overline{B}^0 \to K_S\pi^0$ decays, may help to resolve the situation.

It is also of interest to investigate whether similar patterns appear among the CP violating asymmetries in B meson decays to final states containing one pseudoscalar and one vector meson. Since the vector resonance decays to two particles, such channels can be studied through Dalitz plot analysis of the three-body final state. Model-independent analyses of $B^+ \to K^+K^-K^+$, $\pi^+\pi^-K^+$, $\pi^+\pi^-\pi^+$ and $K^+K^-\pi^+$ decays have revealed large CP violation effects in certain regions of phase space [137]. For the $B^+ \to K^+K^-\pi^+$ decay, an amplitude analysis has established a large CP violation effect associated with $\pi\pi \leftrightarrow KK$ S-wave rescattering [138]. In $B^+ \to \pi^+\pi^-\pi^+$ decays, amplitude analysis has established CP violation effects in the decay amplitude involving the $f_2(1270)$ resonance, in the $\pi^+\pi^-$ S-wave at low invariant mass, and in the interference between the $\pi^+\pi^-$ S-wave and the P-wave $B^+ \to \rho(770)^0\pi^+$ amplitude [139, 140]. For the other channels it remains to be seen whether the CP violation effects are associated to particular resonances or to interference effects, which will be necessary to understand the underlying dynamics.

13.7 Summary and Outlook

CP violation has been experimentally established in K, D and B meson decays. In Section 13.1.4 we introduced three types of CP-violating effects. Examples of these three types include the following:

1. All three types of CP violation have been observed in $K \to \pi\pi$ decays:

$$\begin{aligned}
\mathcal{R}e(\epsilon') &= \frac{1}{6}\left(\left|\frac{\overline{A}_{\pi^0\pi^0}}{A_{\pi^0\pi^0}}\right| - \left|\frac{\overline{A}_{\pi^+\pi^-}}{A_{\pi^+\pi^-}}\right|\right) \\
&= (2.5 \pm 0.4) \times 10^{-6}\,, \qquad \text{(I)} \qquad (13.97a)\\
\mathcal{R}e(\epsilon) &= \frac{1}{2}\left(1 - \left|\frac{q}{p}\right|\right) \\
&= (1.66 \pm 0.02) \times 10^{-3}\,, \qquad \text{(II)} \qquad (13.97b)\\
\mathcal{I}m(\epsilon) &= -\frac{1}{2}\mathcal{I}m(\lambda_{(\pi\pi)_{I=0}}) \\
&= (1.57 \pm 0.02) \times 10^{-3}\,. \qquad \text{(III)} \qquad (13.97c)
\end{aligned}$$

2. For D mesons, CP violation in decay has been established in the difference of asymmetries for $D^0 \to K^+K^-$ and $D^0 \to \pi^+\pi^-$ decays.

$$\begin{aligned}
\Delta a_{CP} &= \frac{|\overline{A}_{K^+K^-}/A_{K^+K^-}|^2 - 1}{|\overline{A}_{K^+K^-}/A_{K^+K^-}|^2 + 1} - \frac{|\overline{A}_{\pi^+\pi^-}/A_{\pi^+\pi^-}|^2 - 1}{|\overline{A}_{\pi^+\pi^-}/A_{\pi^+\pi^-}|^2 + 1} \\
&= (-0.159 \pm 0.029) \times 10^{-2}\,. \quad \text{(I)}
\end{aligned} \tag{13.98}$$

3. In the B meson system, CP violation in decay has been observed in, for example, $B^0 \to K^+\pi^-$ transitions, while CP violation in interference of decays with and without mixing has been observed in, for example, the $B^0 \to J/\psi K_S$ channel:

$$\begin{aligned}
\mathcal{A}_{K^+\pi^-} &= \frac{|\overline{A}_{K^-\pi^+}/A_{K^+\pi^-}|^2 - 1}{|\overline{A}_{K^-\pi^+}/A_{K^+\pi^-}|^2 + 1} \\
&= -0.0831 \pm 0.0031\,, \qquad \text{(I)} \qquad (13.99a)\\
S_{\psi K^0} &= \mathcal{I}m(\lambda_{\psi K^0}) \\
&= +0.710 \pm 0.011\,. \qquad \text{(III)} \qquad (13.99b)
\end{aligned}$$

Int. J. Mod. Phys. A 2026.41. Downloaded from www.worldscientific.com by UNIVERSITY OF CALIFORNIA @ BERKELEY on 09/16/26. Re-use and distribution is [redacted] except for Open Access articles.

Based on Standard Model predictions, further observations of *CP* violation in b hadron decays seem likely in the near future, at both LHCb and its upgrades [141–143] as well as the Belle II experiment [144]. Further improvements in the sensitivity to *CP* violation effects in the charm sector can also be anticipated, though uncertainty in the Standard Model predictions makes it difficult to forecast whether or not additional discoveries will be forthcoming. Further progress on rare kaon decays is also anticipated. Observables that are subject to clean theoretical interpretation, such as β from $S_{\psi K_S}$, β_s from $B_s^0 \to J/\psi\phi$, $\mathcal{B}(K_L \to \pi^0\nu\overline{\nu})$ and γ from *CP* violation in $B \to DK$ decays, are of particular value for constraining the values of the CKM parameters and probing the flavor sector of extensions to the Standard Model. Progress in lattice QCD calculations is also needed to complement the anticipated experimental results. Other probes of *CP* violation now being pursued experimentally include the electric dipole moments of the neutron and electron, and the decays of tau leptons. Additional processes that are likely to play an important role in future *CP* studies include top-quark production and decay, Higgs boson decays and neutrino oscillations.

All measurements of *CP* violation to date are consistent with the predictions of the Kobayashi-Maskawa mechanism of the Standard Model. In fact, it is now established that the KM mechanism plays a dominant role in the *CP* violation measured in the quark sector. However, a dynamically-generated matter-antimatter asymmetry of the universe requires additional sources of *CP* violation, and such sources are naturally generated by extensions to the Standard Model. New sources might eventually reveal themselves as small deviations from the predictions of the KM mechanism, or else might not be observable in quark flavor-changing processes at all, but rather with future probes such as neutrino oscillations or electric dipole moments. The fundamental nature of *CP* violation demands a vigorous search.

A number of excellent reviews of *CP* violation are available [145–152], where the interested reader may find a detailed discussion of the various topics that are briefly reviewed here.

We thank David Kirkby for significant contributions to earlier versions of this review.

References

[1] J. H. Christenson *et al.*, Phys. Rev. Lett. **13**, 138 (1964).

[2] B. Aubert *et al.* (BaBar), Phys. Rev. Lett. **87**, 091801 (2001), [hep-ex/0107013].

[3] K. Abe *et al.* (Belle), Phys. Rev. Lett. **87**, 091802 (2001), [hep-ex/0107061].

[4] H. Burkhardt *et al.* (NA31), Phys. Lett. **B206**, 169 (1988).

[5] V. Fanti *et al.* (NA48), Phys. Lett. **B465**, 335 (1999), [hep-ex/9909022].

[6] A. Alavi-Harati *et al.* (KTeV), Phys. Rev. Lett. **83**, 22 (1999), [hep-ex/9905060].

[7] B. Aubert *et al.* (BaBar), Phys. Rev. Lett. **93**, 131801 (2004), [hep-ex/0407057].

[8] Y. Chao *et al.* (Belle), Phys. Rev. Lett. **93**, 191802 (2004), [hep-ex/0408100].

[9] A. Poluektov *et al.* (Belle), Phys. Rev. **D81**, 112002 (2010), [arXiv:1003.3360].

[10] P. del Amo Sanchez *et al.* (BaBar), Phys. Rev. **D82**, 072004 (2010), [arXiv:1007.0504].

[11] R. Aaij *et al.* (LHCb), Phys. Lett. **B712**, 203 (2012), [Erratum-ibid. **B713**, 351 (2012)], [arXiv:1203.3662].

[12] R. Aaij *et al.* (LHCb), Phys. Rev. Lett. **110**, 221601 (2013), [arXiv:1304.6173].

[13] R. Aaij *et al.* (LHCb), Nature **643**, 1223 (2025), [arXiv:2503.16954].

[14] R. Aaij *et al.* (LHCb), Phys. Rev. Lett. **122**, 211803 (2019), [arXiv:1903.08726].

[15] See the review on "Neutrino Masses, Mixing, and Oscillations," in this *Review*.

[16] See the review on "Tests of Conservation Laws," in this *Review*.

[17] J. P. Lees *et al.* (BaBar), Phys. Rev. Lett. **109**, 211801 (2012), [arXiv:1207.5832].

[18] J. Bernabeu, F. Martinez-Vidal and P. Villanueva-Perez, JHEP **08**, 064 (2012), [arXiv:1203.0171].

[19] See, for example, R. F. Streater and A. S. Wightman, *CPT, Spin and Statistics, and All That,* reprinted by Addison-Wesley, New York (1989).

[20] M. Kobayashi and T. Maskawa, Prog. Theor. Phys. **49**, 652 (1973).

[21] J. Charles *et al.* (CKMfitter Group), Eur. Phys. J. **C41**, 1 (2005), updated results and plots available at: `http://ckmfitter.in2p3.fr`, [hep-ph/0406184].

[22] M. Bona *et al.* (UTfit), JHEP **10**, 081 (2006), updated results and plots available at: `http://www.utfit.org/UTfit`, [hep-ph/0606167].

[23] A. D. Sakharov, Pisma Zh. Eksp. Teor. Fiz. **5**, 32 (1967), [Usp. Fiz. Nauk161,no.5,61(1991)].

[24] A. Riotto, in "Proceedings, Summer School in High-energy physics and cosmology: Trieste, Italy, June 29-July 17, 1998," 326–436 (1998), [hep-ph/9807454].

[25] M. Fukugita and T. Yanagida, Phys. Lett. **B174**, 45 (1986).

[26] S. Davidson, E. Nardi and Y. Nir, Phys. Rept. **466**, 105 (2008), [arXiv:0802.2962].

[27] G. Aad *et al.* (ATLAS), Phys. Lett. **B716**, 1 (2012), [arXiv:1207.7214].

[28] S. Chatrchyan *et al.* (CMS), Phys. Lett. **B716**, 30 (2012), [arXiv:1207.7235].

[29] S. Okubo, Phys. Lett. **5**, 165 (1963).

[30] G. Zweig (1964), *An SU_3 model for strong interaction symmetry and its breaking; Version 2*, CERN-TH-412.

[31] J. Iizuka, Prog. Theor. Phys. Suppl. **37**, 21 (1966).

[32] V. Weisskopf and E. P. Wigner, Z. Phys. **63**, 54 (1930).

[33] See the review on "D^0–$\overline{D}^0$ Mixing" in this *Review*.

[34] O. Long *et al.*, Phys. Rev. **D68**, 034010 (2003), [hep-ex/0303030].

[35] M. Gronau, Y. Grossman and J. L. Rosner, Phys. Lett. **B508**, 37 (2001), [hep-ph/0103110].

[36] D. Atwood and A. Soni, Phys. Rev. **D68**, 033003 (2003), [hep-ph/0304085].

[37] A. Lenz and G. Tetlalmatzi-Xolocotzi, JHEP **07**, 177 (2020), [arXiv:1912.07621].

[38] L. Wolfenstein, Phys. Rev. Lett. **13**, 562 (1964).

[39] C. Abel *et al.* (nEDM), Phys. Rev. Lett. **124**, 081803 (2020), [arXiv:2001.11966].

[40] R. J. Crewther *et al.*, Phys. Lett. **B88**, 123 (1979), [Erratum-ibid. **B91**, 487 (1980)].

[41] See the review on "Cabibbo-Kobayashi-Maskawa Mixing Matrix," in this *Review*.

[42] L. Wolfenstein, Phys. Rev. Lett. **51**, 1945 (1983).

[43] A. J. Buras, M. E. Lautenbacher and G. Ostermaier, Phys. Rev. **D50**, 3433 (1994), [hep-ph/9403384].

[44] C. Jarlskog, Phys. Rev. Lett. **55**, 1039 (1985).

[45] See the K-meson Listings in this *Review*.

[46] See the review on "*CP* violation in $K_S \to 3\pi$," in this *Review*.

[47] M. S. Sozzi, Eur. Phys. J. **C36**, 37 (2004), [hep-ph/0401176].

[48] R. Abbott *et al.* (RBC, UKQCD), Phys. Rev. **D102**, 5, 054509 (2020), [arXiv:2004.09440].

[49] V. Cirigliano *et al.*, JHEP **02**, 032 (2020), [arXiv:1911.01359].

[50] A. J. Buras, Acta Phys. Polon. **B52**, 1, 7 (2021), [arXiv:2101.00020].

Int. J. Mod. Phys. A 2026.41. Downloaded from www.worldscientific.com
by UNIVERSITY OF CALIFORNIA @ BERKELEY on 09/16/26. Re-use and distribution is strictly not permitted, except for Open Access articles.

[51] Y. Grossman and Y. Nir, Phys. Lett. **B398**, 163 (1997), [hep-ph/9701313].

[52] L. S. Littenberg, Phys. Rev. **D39**, 3322 (1989).

[53] A. J. Buras, Phys. Lett. **B333**, 476 (1994), [hep-ph/9405368].

[54] G. Buchalla and A. J. Buras, Nucl. Phys. **B400**, 225 (1993).

[55] A. J. Buras *et al.*, JHEP **11**, 033 (2015), [arXiv:1503.02693].

[56] J. K. Ahn *et al.* (KOTO), Phys. Rev. Lett. **134**, 8, 081802 (2025), [arXiv:2411.11237].

[57] E. Cortina Gil *et al.* (NA62), JHEP **02**, 191 (2025), [arXiv:2412.12015].

[58] B. Aubert *et al.* (BaBar), Phys. Rev. Lett. **98**, 211802 (2007), [hep-ex/0703020].

[59] M. Staric *et al.* (Belle), Phys. Rev. Lett. **98**, 211803 (2007), [hep-ex/0703036].

[60] T. Aaltonen *et al.* (CDF), Phys. Rev. Lett. **100**, 121802 (2008), [arXiv:0712.1567].

[61] R. Aaij *et al.* (LHCb), Phys. Rev. Lett. **110**, 101802 (2013), [arXiv:1211.1230].

[62] R. Aaij *et al.* (LHCb), Phys. Rev. Lett. **127**, 11, 111801 (2021), [arXiv:2106.03744].

[63] Y. S. Amhis *et al.* (HFLAV), Eur. Phys. J. **C81**, 226 (2021), updated results and plots available at `https://hflav.web.cern.ch/`, [arXiv:1909.12524].

[64] See the D-meson Listings in this *Review*.

[65] Y. Grossman, A. L. Kagan and Y. Nir, Phys. Rev. **D75**, 036008 (2007), [hep-ph/0609178].

[66] S. Bergmann *et al.*, Phys. Lett. **B486**, 418 (2000), [hep-ph/0005181].

[67] M. Gersabeck *et al.*, J. Phys. **G39**, 045005 (2012), [arXiv:1111.6515].

[68] T. Pajero and M. J. Morello, JHEP **03**, 162 (2022), [arXiv:2106.02014].

[69] R. Aaij *et al.* (LHCb), Phys. Rev. **D105**, 9, 092013 (2022), [arXiv:2202.09106].

[70] D. M. Asner *et al.* (CLEO), Phys. Rev. **D78**, 012001 (2008), [arXiv:0802.2268].

[71] M. Ablikim *et al.* (BESIII), Phys. Lett. **B734**, 227 (2014), [arXiv:1404.4691].

[72] R. Aaij *et al.* (LHCb), Phys. Rev. **D111**, 1, 012001 (2025), [arXiv:2407.18001].

[73] R. Aaij *et al.* (LHCb), Phys. Rev. **D104**, 7, 072010 (2021), [arXiv:2105.09889].

[74] M. Ciuchini *et al.*, Phys. Lett. **B655**, 162 (2007), [hep-ph/0703204].

[75] Y. Grossman, Y. Nir and G. Perez, Phys. Rev. Lett. **103**, 071602 (2009), [arXiv:0904.0305].

[76] A. L. Kagan and M. D. Sokoloff, Phys. Rev. **D80**, 076008 (2009), [arXiv:0907.3917].

[77] Y. Grossman and Y. Nir, JHEP **04**, 002 (2012), [arXiv:1110.3790].

[78] B. R. Ko *et al.* (Belle), Phys. Rev. Lett. **109**, 021601 (2012), [Erratum-ibid. **109**, 119903 (2012)], [arXiv:1203.6409].

[79] See the "Review of Multibody Charm Analyses" in this *Review*.

[80] B. Aubert *et al.* (BaBar), Phys. Rev. **D78**, 051102 (2008), [arXiv:0802.4035].

[81] I. Bediaga *et al.*, Phys. Rev. **D80**, 096006 (2009), [arXiv:0905.4233].

[82] I. Bediaga *et al.*, Phys. Rev. **D86**, 036005 (2012), [arXiv:1205.3036].

[83] M. Williams, Phys. Rev. **D84**, 054015 (2011), [arXiv:1105.5338].

[84] R. Aaij *et al.* (LHCb), Phys. Lett. **B769**, 345 (2017), [arXiv:1612.03207].

[85] See the B-meson Listings in this *Review*.

[86] V. M. Abazov *et al.* (D0), Phys. Rev. **D82**, 032001 (2010), [arXiv:1005.2757].

[87] A. B. Carter and A. I. Sanda, Phys. Rev. Lett. **45**, 952 (1980).

[88] A. B. Carter and A. I. Sanda, Phys. Rev. **D23**, 1567 (1981).

[89] I. I. Y. Bigi and A. I. Sanda, Nucl. Phys. **B193**, 85 (1981).

[90] I. Dunietz and J. L. Rosner, Phys. Rev. **D34**, 1404 (1986).

[91] Y. I. Azimov, N. G. Uraltsev and V. A. Khoze, Sov. J. Nucl. Phys. **45**, 878 (1987), [Yad. Fiz. **45**, 1412 (1987)].

[92] I. I. Y. Bigi and A. I. Sanda, Nucl. Phys. **B281**, 41 (1987).

[93] G. Buchalla, A. J. Buras and M. E. Lautenbacher, Rev. Mod. Phys. **68**, 1125 (1996), [hep-ph/9512380].

[94] A. J. Buras and L. Silvestrini, Nucl. Phys. **B569**, 3 (2000), [hep-ph/9812392].

[95] R. Fleischer, Eur. Phys. J. **C10**, 299 (1999), [hep-ph/9903455].

[96] M. Ciuchini, M. Pierini and L. Silvestrini, Phys. Rev. Lett. **95**, 221804 (2005), [hep-ph/0507290].

[97] S. Faller *et al.*, Phys. Rev. **D79**, 014030 (2009), [arXiv:0809.0842].

[98] M. Jung, Phys. Rev. **D86**, 053008 (2012), [arXiv:1206.2050].

[99] H.-n. Li and S. Mishima, JHEP **03**, 009 (2007), [hep-ph/0610120].

[100] K. De Bruyn and R. Fleischer, JHEP **03**, 145 (2015), [arXiv:1412.6834].

[101] P. Frings, U. Nierste and M. Wiebusch, Phys. Rev. Lett. **115**, 061802 (2015), [arXiv:1503.00859].

[102] L. Silvestrini, Ann. Rev. Nucl. Part. Sci. **57**, 405 (2007), [arXiv:0705.1624].

[103] R. Fleischer *et al.*, Phys. Rev. **D78**, 111501 (2008), [arXiv:0806.2900].

[104] R. Fleischer *et al.*, Eur. Phys. J. **C78**, 943 (2018), [arXiv:1806.08783].

[105] M. Gronau and D. London, Phys. Rev. Lett. **65**, 3381 (1990).

[106] A. F. Falk *et al.*, Phys. Rev. **D69**, 011502 (2004), [hep-ph/0310242].

[107] J. Charles *et al.*, Eur. Phys. J. **C77**, 574 (2017), [arXiv:1705.02981].

[108] See the review on "Determination of CKM Angles from B hadrons," in this *Review*.

[109] A. Abdesselam *et al.* (BaBar, Belle), Phys. Rev. Lett. **115**, 121604 (2015), [arXiv:1505.04147].

[110] R. Fleischer and R. Knegjens, Eur. Phys. J. **C71**, 1789 (2011), [arXiv:1109.5115].

[111] A. S. Dighe, I. Dunietz and R. Fleischer, Eur. Phys. J. **C6**, 647 (1999), [hep-ph/9804253].

[112] R. Aaij *et al.* (LHCb), Phys. Rev. **D89**, 092006 (2014), [arXiv:1402.6248].

[113] R. Aaij *et al.* (LHCb), JHEP **03**, 075 (2021), [arXiv:2012.05319].

[114] R. Aaij *et al.* (LHCb), JHEP **03**, 139 (2025), [arXiv:2412.14074].

[115] M. Gronau and D. London, Phys. Lett. **B253**, 483 (1991).

[116] M. Gronau and D. Wyler, Phys. Lett. **B265**, 172 (1991).

[117] D. Atwood, I. Dunietz and A. Soni, Phys. Rev. Lett. **78**, 3257 (1997), [hep-ph/9612433].

[118] D. Atwood, I. Dunietz and A. Soni, Phys. Rev. **D63**, 036005 (2001), [hep-ph/0008090].

[119] A. Giri *et al.*, Phys. Rev. **D68**, 054018 (2003), [hep-ph/0303187].

[120] A. Bondar, *Proceedings of BINP special analysis meeting on Dalitz analysis*, 24-26 Sep. 2002, unpublished.

[121] J. Brod and J. Zupan, JHEP **01**, 051 (2014), [arXiv:1308.5663].

[122] J. P. Lees *et al.* (BaBar), Phys. Rev. **D87**, 052015 (2013), [arXiv:1301.1029].

[123] R. Aaij *et al.* (LHCb), JHEP **12**, 087 (2016), [arXiv:1611.03076].

[124] R. Aleksan, I. Dunietz and B. Kayser, Z. Phys. **C54**, 653 (1992).

[125] R. Fleischer, Nucl. Phys. **B671**, 459 (2003), [hep-ph/0304027].

[126] I. Dunietz, Phys. Lett. **B270**, 75 (1991).

[127] M. Gronau, Phys. Lett. **B557**, 198 (2003), [hep-ph/0211282].

[128] T. Gershon, Phys. Rev. **D79**, 051301 (2009), [arXiv:0810.2706].

[129] T. Gershon and M. Williams, Phys. Rev. **D80**, 092002 (2009), [arXiv:0909.1495].

[130] T. Gershon and A. Poluektov, Phys. Rev. **D81**, 014025 (2010), [arXiv:0910.5437].

[131] M. Bander, D. Silverman and A. Soni, Phys. Rev. Lett. **43**, 242 (1979).

[132] X.-G. He, Eur. Phys. J. **C9**, 443 (1999), [hep-ph/9810397].

[133] D. Atwood and A. Soni, Phys. Rev. **D58**, 036005 (1998), [hep-ph/9712287].

[134] M. Gronau and J. L. Rosner, Phys. Rev. **D59**, 113002 (1999), [hep-ph/9809384].

[135] H. J. Lipkin, Phys. Lett. **B445**, 403 (1999), [hep-ph/9810351].

[136] M. Gronau, Phys. Lett. **B627**, 82 (2005), [hep-ph/0508047].

[137] R. Aaij *et al.* (LHCb), Phys. Rev. **D90**, 112004 (2014), [arXiv:1408.5373].

[138] R. Aaij *et al.* (LHCb), Phys. Rev. Lett. **123**, 231802 (2019), [arXiv:1905.09244].

[139] R. Aaij *et al.* (LHCb), Phys. Rev. Lett. **124**, 031801 (2020), [arXiv:1909.05211].

[140] R. Aaij *et al.* (LHCb), Phys. Rev. **D101**, 012006 (2020), [arXiv:1909.05212].

[141] A. A. Alves, Jr. *et al.* (LHCb), JINST **3**, S08005 (2008).

[142] I. Bediaga *et al.* (LHCb) (2012), CERN-LHCC-2012-007.

[143] R. Aaij *et al.* (LHCb) (2017), CERN-LHCC-2017-003.

[144] W. Altmannshofer *et al.* (Belle-II), PTEP **2019**, 123C01 (2019), [Erratum-ibid. **2020**, 029201 (2020)], [arXiv:1808.10567].

[145] G. C. Branco, L. Lavoura and J. P. Silva, Int. Ser. Monogr. Phys. **103**, 1 (1999).

[146] I. I. Bigi and A. I. Sanda (2000), [Camb. Monogr. Part. Phys. Nucl. Phys. Cosmol.9,1(2009)].

[147] A. J. Bevan *et al.* (BaBar, Belle), Eur. Phys. J. **C74**, 3026 (2014), [arXiv:1406.6311].

[148] H.R. Quinn and Y. Nir, *"The Mystery of the Missing Antimatter,"* Princeton University Press, Princeton (2008).

[149] T. E. Browder *et al.*, Rev. Mod. Phys. **81**, 1887 (2009), [arXiv:0802.3201].

[150] M. Ciuchini and A. Stocchi, Ann. Rev. Nucl. Part. Sci. **61**, 491 (2011), [arXiv:1110.3920].

[151] R. Aaij *et al.* (LHCb), Eur. Phys. J. **C73**, 2373 (2013), [arXiv:1208.3355].

[152] T. Gershon and V. V. Gligorov, Rept. Prog. Phys. **80**, 046201 (2017), [arXiv:1607.06746].

Int. J. Mod. Phys. A 2026.41. Downloaded from www.wo
by UNIVERSITY OF CALIFORNIA @ BERKELEY on 09/16/26. Re-use and distribution is
except for Open Access articles.

Int. J. Mod. Phys. A 2026.41. Downloaded from www.worldscientific.com
by UNIVERSITY OF CALIFORNIA @ BERKELEY on 09/16/26. Re-use and distribution is strictly not permitted, except for Open Access articles.

14. Neutrino Masses, Mixing, and Oscillations

Revised March 2026 by M.C. Gonzalez-Garcia (YITP, Stony Brook; ICREA, Barcelona; ICC, U. of Barcelona) and R. Wendell (Kyoto U.).

14.1 Neutrinos in the Standard Model: Massless Neutrinos . . . 297
14.2 Extending the Standard Model to Introduce Massive Neutrinos . . . 298
14.2.1 Dirac Neutrinos . . . 298
14.2.2 The See-saw Mechanism . . . 298
14.2.3 Light Sterile Neutrinos . . . 299
14.2.4 Neutrino Masses from Generic New Physics 299
14.3 Lepton Mixing . . . 299
14.4 Mass-Induced Flavour Oscillations in Vacuum . 300
14.5 Propagation of Massive Neutrinos in Matter . . 301
14.5.1 The Mikheyev-Smirnov-Wolfenstein Effect for Solar Neutrinos . . . 303
14.6 Experimental Study of Neutrino Oscillations . . 303
14.6.1 Solar Neutrinos . . . 304
14.6.2 Atmospheric Neutrinos . . . 305
14.6.3 Accelerator Neutrinos . . . 306
14.6.4 Reactor Antineutrinos . . . 310
14.7 Combined Analysis of Experimental Results: The 3ν Paradigm . . . 312
14.7.1 3ν Oscillation Probabilities . . . 313
14.7.2 3ν Oscillation Analysis . . . 314
14.7.3 Convention-independent Measures of Leptonic CP Violation in 3ν Mixing . . . 315
14.8 Beyond 3ν: Additional Neutrinos at the eV Scale 316
14.9 Laboratory Probes of ν Mass Scale and its Nature317
14.9.1 Constraints from Kinematics of Weak Decays317
14.9.2 Dirac vs. Majorana: Neutrinoless Double-beta Decay . . . 319
14.9.3 Experimental Search for Neutrinoless Double-beta Decay . . . 319

14.1 Neutrinos in the Standard Model: Massless Neutrinos

The gauge symmetry principle is one of the pillars of the great success of modern particle physics as it establishes an unambiguous connection between local (gauge) symmetries and forces mediated by spin-1 particles. In the Standard Model (SM) of particle physics the strong, weak, and electromagnetic interactions are connected to gauge symmetry under $SU(3)_{\rm C} \times SU(2)_L \times U(1)_Y$ where C stands for colour, L for left-handedness, and Y for hypercharge. The SM gauge symmetry is spontaneously broken to $SU(3)_{\rm C} \times U(1)_{\rm EM}$ where $U(1)_{\rm EM}$ couples to the electromagnetic charge $Q_{\rm EM} = T_{L3} + Y$ (T_{L3} is the third generator of the weak isospin $SU(2)_L$). The model explains all the interactions of the known fermions once they are assigned to a well defined representation of the gauge group. The construction and tests of the Standard Model as a gauge theory are covered in Chapter 9 "Quantum chromodynamics" and Chapter 10 "Electroweak model and constraints on new physics" of this *Review*. Here we emphasize that the gauge invariance principle requires that all terms in the Lagrangian, including the mass terms, respect the local symmetry. This has important implications for the neutrino and in particular for the question of the neutrino mass [1].

In the SM, neutrinos are fermions that do not have strong nor electromagnetic interactions. Consequently, they are singlets of the subgroup $SU(3)_C \times U(1)_{\rm EM}$. They are part of the lepton doublets $L_{L\ell} = \begin{pmatrix} \nu_\ell \\ \ell \end{pmatrix}_L$ where f_L is the left-handed component of the fermion f, $f_L = P_L f \equiv \frac{1-\gamma_5}{2} f$. In what follows we will refer as *active* neutrinos to neutrinos that are part of these lepton doublets. In the SM there is one active neutrino for each charged leptons, $\ell = e, \mu, \tau$. $SU(2)_L$ gauge invariance dictates the form of weak charged current (CC) interactions between the neutrinos and their corresponding charged leptons and neutral current (NC) among themselves to be:

$$-\mathcal{L}_{\rm CC} = \frac{g}{\sqrt{2}} \sum_\ell \bar{\nu}_{L\ell} \gamma^\mu \ell_L^- W_\mu^\dagger + \text{h.c.}\,, \tag{14.1}$$

$$-\mathcal{L}_{\rm NC} = \frac{g}{2\cos\theta_W} \sum_\ell \bar{\nu}_{L\ell} \gamma^\mu \nu_{L\ell} Z_\mu^0\,. \tag{14.2}$$

In the above equations, g is the coupling constant associated with $SU(2)$ and θ_W is the Weinberg angle. Equations (14.1) and (14.2) describe all the neutrino interactions in the SM. In particular, Eq. (14.2) determines the decay width of the Z boson into light ($m_\nu \leq m_Z/2$) left-handed neutrinos states. Thus from the measurement of the total decay width of the Z one can infer the number of such states. At present the measurement implies $N_\nu = 2.984 \pm 0.008$ (see Particle Listing). As a result any extension of the SM should contain three, and only three, light active neutrinos.

Sterile neutrinos are defined as having no SM gauge interactions, that is, they are singlets of the complete SM gauge group. Thus the SM, as the gauge theory able to describe all known particle interactions, contains no sterile neutrinos.

The SM with its gauge symmetry and the particle content required for the gauge interactions, that is, in the absence of SM singlets, respects an accidental global symmetry that is not imposed but appears as a consequence of the gauge symmetry and the representation of the matter fields:

$$G_{\rm SM}^{\rm global} = U(1)_B \times U(1)_{L_e} \times U(1)_{L_\mu} \times U(1)_{L_\tau}\,, \tag{14.3}$$

where $U(1)_B$ is the baryon number symmetry, and $U(1)_{L_e,L_\mu,L_\tau}$ are the three lepton flavour symmetries. The total lepton number, $L_e + L_\mu + L_\tau$, is then also an accidental symmetry since it is a subgroup of $G_{\rm SM}^{\rm global}$. This fact has consequences that are relevant to the question of the neutrino mass as we argue next.

In the SM, the masses of the fermions are generated via a Yukawa coupling of the scalar Higgs doublet ϕ with a fermion right-handed and left-handed component. The former is an $SU(2)_L$ singlet, the latter is part of a doublet. For leptons, we can build such a term coupling the left-handed lepton doublets L_L with the right-handed charged lepton fields E_R:

$$-\mathcal{L}_{\rm Yukawa,lep} = Y_{ij}^\ell \bar{L}_{Li} \phi E_{Rj} + \text{h.c.}\,. \tag{14.4}$$

After spontaneous symmetry breaking these terms lead to charged lepton masses

$$m_{ij}^\ell = Y_{ij}^\ell \frac{v}{\sqrt{2}}\,, \tag{14.5}$$

where v is the vacuum expectation value of the Higgs field. However, since the model does not contain right-handed neutrinos, no such Yukawa interaction can be built for the neutrinos, which are consequently massless at the Lagrangian level.

In principle, a neutrino mass term could be generated at loop level. With the particle content of the SM the only possible neutrino mass term that could be constructed is the bilinear $\bar{L}_L L_L^c$, where L_L^c is the charge conjugated field, $L_L^c = C\bar{L_L}^T$ and C is the charge conjugation matrix. However this term is forbidden in the SM because it violates the total lepton symmetry by two units and therefore it cannot be induced by loop corrections because it breaks the accidental symmetry of the model. Also, because $U(1)_{B-L}$ is a non-anomalous subgroup of $G_{\rm SM}^{\rm global}$, the bilinear $\bar{L}_L L_L^c$, cannot be induced by nonperturbative corrections either since it breaks $B - L$.

We conclude that within the SM neutrinos are precisely massless. Consequently one must go beyond the SM in order to add a mass to the neutrino.

[1] The physics of massive neutrinos has been the subject of excellent books such as [1–5] and multiple review articles. The contents of the present review is built upon the structure and the contents of the review articles [6, 7].

Int. J. Mod. Phys. A 2026.41. Downloaded from www.worldscientific.com by UNIVERSITY OF CALIFORNIA @ BERKELEY on 09/16/26. Re-use and distribution is [redacted] except for Open Access articles.

14.2 Extending the Standard Model to Introduce Massive Neutrinos

From the above discussion, we conclude that it is not possible to construct a renormalizable mass term for the neutrinos with the fermionic content and gauge symmetry of the SM. The obvious consequence is that in order to introduce a neutrino mass in the theory one must extend the particle content of the model, depart from gauge invariance and/or renormalizability, or do both.

As a matter of fact, neutrino mass terms can be constructed in different ways. In the following we shall assume that the gauge symmetry is mantained and explore the different possibilities to introduce a neutrino mass term adding to the SM an arbitrary number of sterile neutrinos ν_{si} $(i = 1, \dots m)$.

In the SM extended with the addition of m number of sterile neutrinos one can construct two gauge invariant renormalizable operators leading to two types of mass terms

$$-\mathcal{L}_{M_\nu} = M_{D\,ij}\bar{\nu}_{si}\nu_{Lj} + \frac{1}{2}M_{N\,ij}\bar{\nu}_{si}\nu^c_{sj} + \text{h.c.}\,, \tag{14.6}$$

where ν^c is the neutrino charge conjugated field (defined in section 14.1). M_D is a complex matrix of dimension $m \times 3$ and M_N is a symmetric $m \times m$ matrix.

The first term is generated after spontaneous electroweak symmetry breaking from Yukawa interactions,

$$Y^\nu_{ij}\bar{\nu}_{si}\tilde{\phi}^\dagger L_{Lj} \Rightarrow M_{D\,ij} = Y^\nu_{ij}\frac{v}{\sqrt{2}}\,, \tag{14.7}$$

in a similar way to Eqs.(14.4) and (14.5) for the charged fermion masses. It is correspondingly called a Dirac mass term. It conserves total lepton number but it can break the lepton flavour number symmetries.

The second term in Eq. (14.6) is a Majorana mass term and it differs from the Dirac mass terms in several relevant aspects. First, it is a singlet of the SM gauge group and, as such, it can appear as a bare mass term in the Lagrangian. Second, since it involves two neutrino fields (right-handed in this case), it breaks lepton number by two units. In general, such a term is not allowed if the neutrinos carry any additive conserved charge.

It is possible to rewrite Eq. (14.6) as:

$$-\mathcal{L}_{M_\nu} = \frac{1}{2}(\overline{\vec{\nu}^c_L}, \overline{\vec{\nu}_s})\begin{pmatrix} 0 & M_D^T \\ M_D & M_N \end{pmatrix}\begin{pmatrix} \vec{\nu}_L \\ \vec{\nu}^c_s \end{pmatrix} + \text{h.c.} \equiv \overline{\vec{\nu}^c}M_\nu\vec{\nu} + \text{h.c.}\,, \tag{14.8}$$

where $\vec{\nu} = (\vec{\nu}_L,\, \vec{\nu}^c_s)^T$ is a $(3+m)$-dimensional vector. The matrix M_ν is complex and symmetric[2]. Thus it can be diagonalized by a unitary matrix V^ν of dimension$(3+m)$, so

$$(V^\nu)^T M_\nu V^\nu = \text{diag}(m_1, m_2, \dots, m_{3+m})\,. \tag{14.9}$$

One can express the original weak eigenstates in terms of the resulting $3+m$ mass eigenstates

$$\vec{\nu}_{\text{mass}} = (V^\nu)^\dagger\vec{\nu}\,, \tag{14.10}$$

and in terms of the mass eigenstates, Eq. (14.8) takes the form:

$$\begin{aligned} -\mathcal{L}_{M_\nu} &= \frac{1}{2}\sum_{k=1}^{3+m} m_k\left(\bar{\nu}^c_{\text{mass},k}\nu_{\text{mass},k} + \bar{\nu}_{\text{mass},k}\nu^c_{\text{mass},k}\right) \\ &= \frac{1}{2}\sum_{k=1}^{3+m} m_k\bar{\nu}_{Mk}\nu_{Mk}\,, \end{aligned} \tag{14.11}$$

where

$$\nu_{Mk} = \nu_{\text{mass},k} + \nu^c_{\text{mass},k} = (V^{\nu\dagger}\vec{\nu})_k + (V^{\nu\dagger}\vec{\nu})^c_k\,. \tag{14.12}$$

So these states obey the Majorana condition

$$\nu_M = \nu^c_M\,, \tag{14.13}$$

and are referred to as Majorana neutrinos. The Majorana condition implies that only one field describes both neutrino and antineutrino states, unlike the case of a charged fermion for which particles and antiparticles are described by two different fields. So a Majorana neutrino can be described by a two-component spinor unlike the charged fermions, which are Dirac particles, and are represented by four-component spinors.

Inverting Eq. (14.12) we can write the weak-doublet components of the neutrino fields as:

$$\nu_{Li} = P_L\sum_{j=1}^{3+m} V^\nu_{ij}\nu_{Mj} \quad i = 1, 2, 3\,, \tag{14.14}$$

where P_L is the left projector.

In the following, we will discuss some interesting particular cases of this general framework: light Dirac neutrinos in Sec. 14.2.1, and light Majorana neutrinos and the see-saw mechanism in Sec. 14.2.2. A special case of the second example is the possibility of light-sterile neutrinos discussed in Sec. 14.2.3. In Sec. 14.2.4 we shall discuss the effective generation of neutrino masses from non-renormalizable operators (of which the see-saw mechanism is a particular realization).

14.2.1 *Dirac Neutrinos*

Imposing $M_N = 0$ is equivalent to imposing lepton number symmetry on the model. In doing this only the first term in Eq. (14.6), the Dirac mass term, is allowed. If there are only three sterile neutrinos($m = 3$), we can identify them with the right-handed component of a four-spinor neutrino field. In this case the Dirac mass term can be diagonalized with two 3×3 unitary matrices, V^ν and V^ν_R as:

$$V^{\nu\dagger}_R M_D V^\nu = \text{diag}(m_1, m_2, m_3)\,. \tag{14.15}$$

The neutrino mass term can be written as:

$$-\mathcal{L}_{M_\nu} = \sum_{k=1}^{3} m_k\bar{\nu}_{Dk}\nu_{Dk}\,, \tag{14.16}$$

where

$$\nu_{D\,k} = (V^{\nu\dagger}\vec{\nu}_L)_k + (V^{\nu\dagger}_R\vec{\nu}_s)_k\,, \tag{14.17}$$

so the weak-doublet components of the neutrino fields are

$$\nu_{Li} = P_L\sum_{j=1}^{3} V^\nu_{ij}\nu_{Dj}\,. \qquad i = 1, 2, 3\,. \tag{14.18}$$

Let us stress that in this case both the low-energy matter content and the assumed symmetries are different from those of the SM. Consequently, the SM is not even a good low-energy effective theory. Furthermore, this scenario does not explain the fact that neutrinos are much lighter than the corresponding charged fermions, because all of them acquire their mass via the same mechanism.

14.2.2 *The See-saw Mechanism*

If the mass eigenvalues of M_N are much higher than the scale of electroweak symmetry breaking v, the diagonalization of M_ν leads to three light neutrinos, ν_l, and m heavy neutrinos, N:

$$-\mathcal{L}_{M_\nu} = \frac{1}{2}\bar{\nu}_l M^l\nu_l + \frac{1}{2}\bar{N}M^h N\,, \tag{14.19}$$

with

$$M^l \simeq -V_l^T M_D^T M_N^{-1} M_D V_l, \qquad M^h \simeq V_h^T M_N V_h\,, \tag{14.20}$$

and

$$V^\nu \simeq \begin{bmatrix} \left(1 - \frac{1}{2}M_D^\dagger M_N^{*\,-1} 1 M_N^{-1} M_D\right) V_l & M_D^\dagger M_N^{*\,-1} V_h \\ -M_N^{-1} M_D V_l & \left(1 - \frac{1}{2}M_N{}^{-1} M_D M_D^\dagger M_N^{*\,-1}\right) V_h \end{bmatrix}, \tag{14.21}$$

[2]Notice that Eq. (14.8) corresponds to the tree-level neutrino mass matrix. Corrections are induced at the loop level, which in particular lead to non-vanishing $\bar{\nu}^c_L\nu_L$ entry [8].

Int. J. Mod. Phys. A 2026.41. Downloaded from www.worldscientific.com
by UNIVERSITY OF CALIFORNIA @ BERKELEY on 09/16/26. Re-use and distribution is strictly not permitted, except for Open Access articles.

where V_l and V_h are 3×3 and $m\times m$ unitary matrices respectively. From Eq. (14.20) we see that the masses of the heavier states are proportional to M_N while those of the lighter ones to M_N^{-1}, hence the name *see-saw mechanism* [9–13]. Also, as seen from Eq. (14.21), the heavy states are mostly right-handed while the light ones are mostly left-handed. Both the light and the heavy neutrinos are Majorana particles. Two well-known examples of extensions of the SM leading to a see-saw mechanism for neutrino masses are SO(10) Grand Unified Theories [10, 11] and left-right symmetric models [13].

In this case, the SM is a good effective low energy theory. Indeed the see-saw mechanism is a particular example of a full theory whose low energy effective realization is the SM with three light Majorana neutrinos which we describe in Sec. 14.2.4.

14.2.3 *Light Sterile Neutrinos*

If the scale of some $n_s \leq m$ eigenvalues of M_N are not higher than the electroweak scale, the low energy spectrum contains n_s additional light states with a large admixture of sterile component. As in the case with Dirac Neutrinos, the SM is not a good low energy effective theory: there are more than three $(3+n_s)$ light neutrinos, and they are admixtures of doublet and singlet fields. As in the general case, both light and heavy neutrinos are Majorana particles.

14.2.4 *Neutrino Masses from Generic New Physics*

Under the generic hypothesis that new physics (NP) beyond the SM only manifests itself directly above some scale $\Lambda_{\rm NP}$, we can consider that the SM is an effective low energy theory which is valid to describe the physical world at energies well below $\Lambda_{\rm NP}$ with the same gauge group, fermionic spectrum, and the pattern of spontaneous symmetry breaking of the SM. However, this is an effective theory, holding only till energy below $\Lambda_{\rm NP}$, and consequently does not need to be renormalizable. In this case, the low energy Lagrangian can contain non-renormalizable higher dimensional terms whose effect will be suppressed by powers $1/\Lambda_{\rm NP}^{\rm dim-4}$.

In this approach, the least suppressed NP effects at low energy are expected to come from dim= 5 operators. With the SM fields and gauge symmetry one can only construct the following set of dimension-five terms

$$\mathcal{O}_5 = \frac{Z^\nu_{ij}}{\Lambda_{\rm NP}}\left(\bar{L}_{Li}\tilde{\phi}\right)\left(\tilde{\phi}^T L^C_{Lj}\right) + \text{h.c.}\,. \tag{14.22}$$

This set violates (14.3), which poses no problem since, in general, there is no reason for the NP to respect the accidental symmetries of the SM. In particular, it violates the total lepton number by two units, and after spontaneous symmetry breaking it generates a bilinear neutrino field term:

$$-\mathcal{L}_{M_\nu} = \frac{Z^\nu_{ij}}{2}\frac{v^2}{\Lambda_{\rm NP}}\bar{\nu}_{Li}\nu^c_{Lj} + \text{h.c.}\,. \tag{14.23}$$

This is a Majorana mass term (see Eq. (14.8)). It is built with the left-handed neutrino fields and with mass matrix:

$$(M_\nu)_{ij} = Z^\nu_{ij}\frac{v^2}{\Lambda_{\rm NP}}\,. \tag{14.24}$$

We conclude that Eq. (14.24) would arise in a generic extension of the SM and that neutrino masses are very likely to appear if there is NP. Comparing Eq. (14.24) and Eq. (14.5), we also find that the scale of neutrino masses is suppressed by $v/\Lambda_{\rm NP}$ when compared to the scale of charged fermion masses, which provides an explanation for their smallness. Furthermore, both total lepton number and the lepton flavour symmetry $U(1)_e\times U(1)_\mu\times U(1)_\tau$ are broken by Eq. (14.24), which means that, generically, in the absence of additional symmetries on the coefficients Z_{ij}, we can expect lepton flavour mixing and CP violation as we discuss in the next section.

Finally, we notice that, as mentioned in Sec. 14.2.2, a theory where the NP is composed of m heavy sterile neutrinos, provides an specific example of a theory which at low energy contains three light mass eigenstates with an effective dim-5 interaction of the form (14.22) with $\Lambda_{\rm NP} = M_N$. In this case, the NP scale is the characteristic mass scale of the heavy sterile neutrinos.

14.3 Lepton Mixing

Let us start by considering $n = 3+m$ massive neutrino states and denote the neutrino mass eigenstates by $(\nu_1,\nu_2,\nu_3,\ldots,\nu_n)$. The neutrino interaction eigenstates are denoted by $\vec{\nu} = (\nu_{Le},\nu_{L\mu},\nu_{L\tau},\nu_{s1},\ldots,\nu_{sm})$. We label the corresponding mass and interaction eigenstates for the charged leptons as (e,μ,τ) and (e^I,μ^I,τ^I), respectively. The Lagrangian for the leptonic charged current interactions in the mass basis takes the form:

$$-\mathcal{L}_{\rm CC} = \frac{g}{\sqrt{2}}(\bar{e}_L,\,\bar{\mu}_L,\,\bar{\tau}_L)\gamma^\mu U\begin{pmatrix}\nu_1\\ \nu_2\\ \nu_3\\ \vdots\\ \nu_n\end{pmatrix}W_\mu + \text{h.c.}\,, \tag{14.25}$$

where U is a $3\times n$ matrix [14–16]. It satisfies the unitary condition

$$UU^\dagger = I_{3\times3}\,. \tag{14.26}$$

However, in general $U^\dagger U \neq I_{n\times n}$.

In the interaction basis, the mass terms for the leptons are:

$$-\mathcal{L}_M = [(\bar{e}^I_L,\,\bar{\mu}^I_L,\,\bar{\tau}^I_L)M_\ell\begin{pmatrix}e^I_R\\ \mu^I_R\\ \tau^I_R\end{pmatrix} + \text{h.c.}] - \mathcal{L}_{M_\nu}\,, \tag{14.27}$$

with $\mathcal{L}_{M_\nu}$ given in Eq. (14.8). M_ℓ can be diagonalized with two 3×3 unitary matrices V^ℓ and V^ℓ_R which satisfy

$$V^{\ell\dagger}M_\ell V^\ell_R = \text{diag}(m_e,m_\mu,m_\tau)\,. \tag{14.28}$$

Then for the charged leptons we have

$$-\mathcal{L}_{M_\ell} = \sum_{k=1}^{3} m_{\ell_k}\bar{\ell}_k\ell_k\,, \tag{14.29}$$

with

$$\ell_k = (V^{\ell\dagger}\ell^I_L)_k + (V^{\ell\dagger}_R\ell^I_R)_k\,. \tag{14.30}$$

Inverting the equation above we find that the weak-doublet components of the charged lepton fields are

$$\ell^I_{Li} = P_L\sum_{j=1}^{3}V^\ell_{ij}\ell_j\,. \qquad i=1,2,3 \tag{14.31}$$

From Eqs.(14.14), (14.18) and (14.31) we find that the mixing matrix U can be expressed as:

$$U_{ij} = \mathcal{P}_{\ell,ii}\,V^{\ell\,\dagger}_{ik}\,V^\nu_{kj}\,(\mathcal{P}_{\nu,jj}). \tag{14.32}$$

The matrix $V^{\ell\dagger}\,V^\nu$ contains a number of phases that are not physical. Three of them are eliminated by the diagonal 3×3 phase matrix $\mathcal{P}_\ell$ that absorbs them in the charged lepton mass eigenstates. If neutrinos are Dirac states, further $n-1$ are similarly eliminated by absorbing them in the neutrino mass eigenstates with the diagonal $n\times n$ phase matrix $\mathcal{P}_\nu$. For Majorana neutrinos, $\mathcal{P}_\nu = I_{n\times n}$ because one cannot rotate by an arbitrary phase a Majorana field without physical effects. If one rotates a Majorana neutrino by a phase, this phase will appear in its mass term, which will no longer be real. Consequently, the number of phases that can be absorbed by redefining the mass eigenstates depends on whether the neutrinos are Dirac or Majorana particles. Altogether for $n\geq3$ Majorana [Dirac] neutrinos, the U matrix contains a total of $6(n-2)$ $[5n-11]$ real parameters, of which $3(n-2)$ are angles, and $3(n-2)$ $[2n-5]$ can be interpreted as physical phases.

The possibility of arbitrary mixing between massive neutrino states was first discussed in the context of two neutrinos in Ref. [17] (the possibility of two mixed massless flavour neutrino states had been previously considered in the literature [18], and the possibility of mixing between neutrino and antineutrino states even earlier, in the seminal paper of Pontecorvo [19]). For the case

Int. J. Mod. Phys. A 2026.41. Downloaded from www.wo[redacted]except for Open Access articles.
by UNIVERSITY OF CALIFORNIA @ BERKELEY on 09/16/26. Re-use and distribution is

where only mixing between two generations is considered with $n = 2$ distinct neutrino masses, the U matrix is 2×2 and contains one mixing angle if the neutrinos are Dirac and an additional physical phase if they are Majorana.

If there are only $n = 3$ Majorana neutrinos, U is a 3×3 matrix analogous to the CKM matrix for the quarks [20, 21], but due to the Majorana nature of the neutrinos it depends on six independent parameters: three mixing angles and three phases. In this case the mixing matrix can be conveniently parameterized as:

$$U = \begin{pmatrix} 1 & 0 & 0 \\ 0 & c_{23} & s_{23} \\ 0 & -s_{23} & c_{23} \end{pmatrix} \cdot \begin{pmatrix} c_{13} & 0 & s_{13}e^{-i\delta_{\rm CP}} \\ 0 & 1 & 0 \\ -s_{13}e^{i\delta_{\rm CP}} & 0 & c_{13} \end{pmatrix} \cdot \begin{pmatrix} c_{12} & s_{12} & 0 \\ -s_{12} & c_{12} & 0 \\ 0 & 0 & 1 \end{pmatrix} \cdot \begin{pmatrix} e^{i\eta_1} & 0 & 0 \\ 0 & e^{i\eta_2} & 0 \\ 0 & 0 & 1 \end{pmatrix} , \tag{14.33}$$

where $c_{ij} \equiv \cos\theta_{ij}$ and $s_{ij} \equiv \sin\theta_{ij}$. The angles θ_{ij} can be taken without loss of generality to lie in the first quadrant, $\theta_{ij} \in [0, \pi/2]$ and the phases $\delta_{\rm CP}$, $\eta_i \in [0, 2\pi]$. This is to be compared to the case of three Dirac neutrinos. In this case, the Majorana phases, η_1 and η_2, can be absorbed in the neutrino states so the number of physical phases is one (similar to the CKM matrix). Thus we can write U as:

$$U = \begin{pmatrix} c_{12}\, c_{13} & s_{12}\, c_{13} & s_{13}\, e^{-i\delta_{\rm CP}} \\ -s_{12}\, c_{23} - c_{12}\, s_{13}\, s_{23}\, e^{i\delta_{\rm CP}} & c_{12}\, c_{23} - s_{12}\, s_{13}\, s_{23}\, e^{i\delta_{\rm CP}} & c_{13}\, s_{23} \\ s_{12}\, s_{23} - c_{12}\, s_{13}\, c_{23}\, e^{i\delta_{\rm CP}} & -c_{12}\, s_{23} - s_{12}\, s_{13}\, c_{23}\, e^{i\delta_{\rm CP}} & c_{13}\, c_{23} \end{pmatrix} . \tag{14.34}$$

The matrices in Eqs. (14.33) and (14.34) are often called the Pontecorvo-Maki-Nakagawa-Sakata (PMNS) mixing matrix.

Notice that when the charged leptons have no other interactions than the SM ones, one can identify their interaction eigenstates with the corresponding mass eigenstates up to phase redefinition. This implies that, in this case, U is just a $3 \times n$ sub-matrix of the unitary neutrino mass diagonalizing matrix V^ν.

Finally, let us point out that for the case of 3 light Dirac neutrinos, the procedure above leads to a unitary U matrix for the light states. But for three light Majorana neutrinos, this is not the case since the full spectrum contains states which are heavy and are not in the low energy spectrum as seen, for example, in Eq. (14.21). This implies that, strictly speaking, the parametrization in Eq. (14.33) is not valid to describe the flavour mixing of the three light Majorana neutrinos in the see-saw mechanism. The violation of unitarity, however, is rather small, of the order $\mathcal{O}(M_D/M_N)$ as seen in Eq. (14.21). It is also severely constrained experimentally [22, 23]. For all these reasons, for all practical purposes, we will consider the U matrix for the 3ν mixing case to be unitary independently of whether neutrinos are Dirac or Majorana particles.

14.4 Mass-Induced Flavour Oscillations in Vacuum

If neutrinos have masses and lepton flavours are mixed in the weak CC interactions, lepton flavour is not conserved in neutrino propagation [19, 24]. This phenomenon is usually referred to as *neutrino oscillations*. In brief, a weak eigenstates, ν_α, which by default is the state produced in the weak CC interaction of a charged lepton ℓ_α, is the linear combination determined by the mixing matrix U

$$|\nu_\alpha\rangle = \sum_{i=1}^{n} U^*_{\alpha i} |\nu_i\rangle , \tag{14.35}$$

where ν_i are the mass eigenstates, and here n is the number of light neutrino species (implicit in our definition of the state $|\nu\rangle$ is its energy-momentum and space-time dependence). After traveling a distance L ($L \simeq ct$ for relativistic neutrinos), that state evolves as:

$$|\nu_\alpha(t)\rangle = \sum_{i=1}^{n} U^*_{\alpha i} |\nu_i(t)\rangle . \tag{14.36}$$

This neutrino can then undergo a charged-current (CC) interaction producing a charge lepton ℓ_β, $\nu_\alpha(t)N' \to \ell_\beta N$, with a probability

$$P_{\alpha\beta} = |\langle\nu_\beta|\nu_\alpha(t)\rangle|^2 = |\sum_{i=1}^{n}\sum_{j=1}^{n} U^*_{\alpha i} U_{\beta j} \langle\nu_j|\nu_i(t)\rangle|^2 . \tag{14.37}$$

Assuming that $|\nu\rangle$ is a plane wave, $|\nu_i(t)\rangle = e^{-i\,E_i t}|\nu_i(0)\rangle$, [3] with $E_i = \sqrt{p_i^2 + m_i^2}$ and m_i being, respectively, the energy and the mass of the neutrino mass eigenstate ν_i. In all practical cases neutrinos are very relativistic ,so $p_i \simeq p_j \equiv p \simeq E$. We can then write

$$E_i = \sqrt{p_i^2 + m_i^2} \simeq p + \frac{m_i^2}{2E} , \tag{14.38}$$

and use the orthogonality of the mass eigenstates, $\langle\nu_j|\nu_i\rangle = \delta_{ij}$, to arrive to the following form for $P_{\alpha\beta}$:

$$P_{\alpha\beta} = \delta_{\alpha\beta} - 4\sum_{i<j}^{n} {\rm Re}[U_{\alpha i}U^*_{\beta i}U^*_{\alpha j}U_{\beta j}] \sin^2 X_{ij} + 2\sum_{i<j}^{n} {\rm Im}[U_{\alpha i}U^*_{\beta i}U^*_{\alpha j}U_{\beta j}] \sin 2X_{ij} , \tag{14.39}$$

where

$$X_{ij} = \frac{(m_i^2 - m_j^2)L}{4E} = 1.267\, \frac{\Delta m^2_{ij}}{{\rm eV}^2}\, \frac{L/E}{{\rm m/MeV}} . \tag{14.40}$$

If we had made the same derivation for antineutrino states, we would have ended with a similar expression but with the exchange $U \to U^*$. Consequently, we conclude that the first term in the right-hand-side of Eq. (14.39) is CP conserving since it is the same for neutrinos and antineutrinos, while the last one is CP violating because it has opposite signs for neutrinos and antineutrinos.

Equation (14.39) is oscillatory in distance with oscillation lengths

$$L^{\rm osc}_{0,ij} = \frac{4\pi E}{|\Delta m^2_{ij}|} , \tag{14.41}$$

and with amplitudes proportional to products of elements in the mixing matrix. Thus, neutrinos must have different masses ($\Delta m^2_{ij} \neq 0$) and they must have not vanishing mixing ($U_{\alpha_i}U_{\beta i} \neq 0$) in order to undergo flavour oscillations. Also, from Eq. (14.39) we see that the Majorana phases cancel out in the oscillation probability. This is expected because flavour oscillation is a total lepton number conserving process.

Ideally, a neutrino oscillation experiment would like to measure an oscillation probability over a distance L between the source and the detector, for neutrinos of a definite energy E. In practice, neutrino beams, both from natural or artificial sources, are

[3] For a pedagogical discussion of the quantum mechanical description of flavour oscillations in the wave packet approach see for example Ref. [3]. A recent review of the quantum mechanical aspects and subtleties on neutrino oscillations can be found in in Ref. [25].

Int. J. Mod. Phys. A 2026.41. Downloaded from www.worldscientific.com
by UNIVERSITY OF CALIFORNIA @ BERKELEY on 09/16/26. Re-use and distribution is strictly not permitted, except for Open Access articles.

Table 14.1: Characteristic values of L and E for experiments performed using various neutrino sources and the corresponding ranges of $|\Delta m^2|$ to which they can be most sensitive to flavour oscillations in vacuum. SBL stands for Short Baseline, VSBL stands for Very Short Baseline , MBL stands for Medium Baseline, and LBL for Long Baseline.

Experiment		L (m)	E (MeV)	$\lvert\Delta m^2\rvert$ (eV^2)
Solar		10^{10}	1	10^{-10}
Atmospheric		$10^4 - 10^7$	10^2–10^5	$10^{-1} - 10^{-4}$
Reactor	VSBL–SBL–MBL	$10 - 10^3$	1	$1 - 10^{-3}$
	LBL	$10^4 - 10^5$		$10^{-4} - 10^{-5}$
Accelerator	SBL	10^2	10^3–10^4	> 0.1
	LBL	$10^5 - 10^6$	$10^3 - 10^4$	$10^{-2} - 10^{-3}$

never monoenergetic but have an energy spectrum $\Phi(E)$. In addition, each detector has a finite energy resolution. Under these circumstances what is measured is an average probability

$$\begin{aligned}\langle P_{\alpha\beta}\rangle &= \frac{\int dE \frac{d\Phi}{dE}\sigma_{CC}(E)P_{\alpha\beta}(E)\epsilon(E)}{\int dE \frac{d\Phi}{dE}\sigma_{CC}(E)\epsilon(E)} \\ &= \delta_{\alpha\beta} - 4\sum_{i<j}^{n} \mathrm{Re}[U_{\alpha i}U^*_{\beta i}U^*_{\alpha j}U_{\beta j}]\langle \sin^2 X_{ij}\rangle \\ &\quad + 2\sum_{i<j}^{n} \mathrm{Im}[U_{\alpha i}U^*_{\beta i}U^*_{\alpha j}U_{\beta j}]\langle \sin 2X_{ij}\rangle\,.\end{aligned} \tag{14.42}$$

σ is the cross-section for the process in which the neutrino flavour is detected, and $\epsilon(E)$ is the detection efficiency. The minimal range of the energy integral is determined by the energy resolution of the experiment.

It is clear from the above expression that if $(E/L) \gg |\Delta m^2_{ij}|$ ($L \ll L^{\rm osc}_{0,ij}$) so $\sin^2 X_{ij} \ll 1$, the oscillation phase does not give any appreciable effect. Conversely, if $L \gg L^{\rm osc}_{0,ij}$, many oscillation cycles occur between production and detection, so the oscillating term is averaged to $\langle \sin^2 X_{ij}\rangle = 1/2$. We summarize in Table 14.1 the typical values of L/E for different types of neutrino sources and experiments and the corresponding ranges of Δm^2 to which they can be most sensitive.

Historically, the results of neutrino oscillation experiments were interpreted assuming two-neutrino states so there is only one oscillating phase; the mixing matrix depends on a single mixing angle θ, and no CP violation effect in oscillations is possible. At present, as we will discuss in Sec. 14.7, we need at least the mixing among three-neutrino states to fully describe the bulk of experimental results. However, in many cases, the observed results can be understood in terms of oscillations dominantly driven by one Δm^2. In this limit $P_{\alpha\beta}$ of Eq. (14.39) takes the form [24]

$$P_{\alpha\beta} = \delta_{\alpha\beta} - (2\delta_{\alpha\beta} - 1)\sin^2 2\theta \sin^2 X\,. \tag{14.43}$$

In this effective $2-\nu$ limit, changing the sign of the mass difference, $\Delta m^2 \to -\Delta m^2$, and changing the octant of the mixing angle, $\theta \to \frac{\pi}{2} - \theta$, is just redefining the mass eigenstates, $\nu_1 \leftrightarrow \nu_2$: $P_{\alpha\beta}$ must be invariant under such transformation. So the physical parameter space can be covered with either $\Delta m^2 \geq 0$ with $0 \leq \theta \leq \frac{\pi}{2}$, or, alternatively, $0 \leq \theta \leq \frac{\pi}{4}$ with either sign for Δm^2.

However, from Eq. (14.43) we see that $P_{\alpha\beta}$ is actually invariant under the change of sign of the mass splitting *and* the change of octant of the mixing angle separately. This implies that there is a two-fold discrete ambiguity since the two different sets of physical parameters, $(\Delta m^2, \theta)$ and $(\Delta m^2, \frac{\pi}{2} - \theta)$, give the same transition probability in vacuum. In other words, one could not tell from a measurement of, say, $P_{e\mu}$ in vacuum whether the larger component of ν_e resides in the heavier or in the lighter neutrino mass eigenstate. This symmetry is broken when one considers mixing of three or more neutrinos in the flavour evolution and or when the neutrinos traverse regions of dense matter as we describe in Sec. 14.7.1 and Sec. 14.5, respectively.

14.5 Propagation of Massive Neutrinos in Matter

Neutrinos propagating in a dense medium can interact with the particles in the medium. The probability of an incoherent inelastic scattering is very small. For example the characteristic cross section for ν-proton scattering is of the order

$$\sigma \sim \frac{G_F^2 s}{\pi} \sim 10^{-43}\ \mathrm{cm}^2 \left(\frac{E}{\mathrm{MeV}}\right)^2, \tag{14.44}$$

where G_F is the Fermi constant and s is the square of the center of mass energy of the collision.

But when neutrinos propagate in dense matter, they can also interact coherently with the particles in the medium. By definition, in coherent interactions, the medium remains unchanged so it is possible to have interference of the forward scattered and the unscattered neutrino waves which enhances the effect of matter in the neutrino propagation. In this case, the effect of the medium is not on the intensity of the propagating neutrino beam, which remains unchanged, but on the phase velocity of the neutrino wave, and for this reason the effect is proportional to G_F, instead of the G_F^2 dependence of the incoherent scattering. Coherence also allows decoupling the evolution equation of the neutrinos from those of the medium. In this limit, the effect of the medium is introduced in the evolution equation for the neutrinos in the form of an effective potential which depends on the density and composition of the matter [26].

As an example, let us consider the evolution of ν_e in a medium with electrons, protons, and neutrons with corresponding n_e, n_p, and n_n number densities. The effective low-energy Hamiltonian describing the relevant neutrino interactions at point x is given by

$$H_W = \frac{G_F}{\sqrt{2}}\left[J^{(+)\alpha}(x)J^{(-)}_\alpha(x) + \frac{1}{4}J^{(N)\alpha}(x)J^{(N)}_\alpha(x)\right], \tag{14.45}$$

where the J_α's are the standard fermionic currents

$$J^{(+)}_\alpha(x) = \bar\nu_e(x)\gamma_\alpha(1-\gamma_5)e(x)\,, \tag{14.46}$$

$$J^{(-)}_\alpha(x) = \bar e(x)\gamma_\alpha(1-\gamma_5)\nu_e(x)\,, \tag{14.47}$$

$$\begin{aligned}J^{(N)}_\alpha(x) &= \bar\nu_e(x)\gamma_\alpha(1-\gamma_5)\nu_e(x) \\ &\quad - \bar e(x)[\gamma_\alpha(1-\gamma_5) - 4\sin^2\theta_W\gamma_\alpha]e(x) \\ &\quad + \bar p(x)[\gamma_\alpha(1-g^{(p)}_A\gamma_5) - 4\sin^2\theta_W\gamma_\alpha]p(x) \\ &\quad - \bar n(x)\gamma_\alpha(1-g^{(n)}_A\gamma_5)n(x)\,,\end{aligned} \tag{14.48}$$

and $g^{(n,p)}_A$ are the axial couplings for neutrons and protons, respectively.

Let us focus first on the effect of the charged current interactions. The effective CC Hamiltonian due to electrons in the medium is

$$H_C^{(e)} = \frac{G_F}{\sqrt{2}} \int d^3p_e f(E_e,T) \times \Big\langle \langle e(s,p_e)\,|\,\bar{e}(x)\gamma^\alpha(1-\gamma_5)\nu_e(x)\bar{\nu}_e(x)\gamma_\alpha(1-\gamma_5)e(x)\,|\,e(s,p_e)\rangle \Big\rangle$$
$$= \frac{G_F}{\sqrt{2}}\bar{\nu}_e(x)\gamma_\alpha(1-\gamma_5)\nu_e(x) \int d^3p_e f(E_e,T)\Big\langle \langle e(s,p_e)\,|\,\bar{e}(x)\gamma_\alpha(1-\gamma_5)e(x)\,|\,e(s,p_e)\rangle \Big\rangle\,. \tag{14.49}$$

In the above equation, we denote by s the electron spin, and by p_e its momentum, and $f(E_e,T)$ is the energy distribution function of the electrons in the medium which is assumed to be homogeneous and isotropic and is normalized as

$$\int d^3p_e f(E_e,T) = 1\,. \tag{14.50}$$

We denote by $\Big\langle \ldots \Big\rangle$ the averaging over electron spinors and summing over all electrons in the medium. Coherence dictates that s, p_e are the same for initial and final electrons. The axial current reduces to the spin in the non-relativistic limit and therefore averages to zero for a background of non-relativistic electrons. The spatial components of the vector current cancel because of isotropy. Therefore, the only non-trivial average is

$$\int d^3p_e f(E_e,T)\Big\langle \langle e(s,p_e)\,|\,\bar{e}(x)\gamma_0 e(x)\,|\,e(s,p_e)\rangle \Big\rangle = n_e(x)\,, \tag{14.51}$$

which gives a contribution to the effective Hamiltonian

$$H_C^{(e)} = \sqrt{2}G_F n_e \bar{\nu}_{eL}(x)\gamma_0\nu_{eL}(x)\,. \tag{14.52}$$

This can be interpreted as a contribution to the ν_{eL} potential energy

$$V_C = \sqrt{2}G_F n_e\,. \tag{14.53}$$

Should we have considered antineutrino states, we would have ended up with $V_C = -\sqrt{2}G_F n_e$ For a more detailed derivation of the matter potentials see, for example, Ref. [3].

With an equivalent derivation, we find that for ν_μ and ν_τ, the potential due to its CC interactions is zero for most media since neither μ's nor $\tau's$ are present, while the effective potential for any active neutrino due to the neutral current interactions is found to be

$$V_{NC} = \frac{\sqrt{2}}{2}G_F\left[-n_e(1-4\sin^2\theta_w) + n_p(1-4\sin^2\theta_w) - n_n\right]\,. \tag{14.54}$$

In neutral matter, $n_e = n_p$ and the contribution from electrons and protons cancel each other. So we are left only with the neutron contribution

$$V_{NC} = -1/\sqrt{2}G_F n_n\,. \tag{14.55}$$

After including these effects, the evolution equation for n ultrarelativistic neutrinos propagating in matter written in the mass basis is (see for instance Ref. [27–29] for the derivation):

$$i\frac{d\vec{\nu}}{dx} = H\,\vec{\nu}, \qquad H = H_m + U^{\nu\,\dagger}\,V\,U^\nu\,. \tag{14.56}$$

Here $\vec{\nu} \equiv (\nu_1,\,\nu_2,\,\ldots,\,\nu_n)^T$, H_m is the the kinetic Hamiltonian,

$$H_m = \frac{1}{2E}\,\mathrm{diag}(m_1^2,\,m_2^2,\,\ldots,\,m_n^2), \tag{14.57}$$

and V is the effective neutrino potential in the interaction basis. U^ν is the $n\times n$ submatrix of the unitary V^ν matrix corresponding to the n ultrarelativistic neutrino states. For the three SM active neutrinos with purely SM interactions crossing a neutral medium with electrons, protons and neutrons, the evolution equation takes the form (14.56) with $U^\nu \equiv U$, and the effective potential:

$$V = \mathrm{diag}\left(\pm\sqrt{2}G_F n_e(x),\,0,\,0\right) \equiv \mathrm{diag}\,(V_e,\,0,\,0)\,. \tag{14.58}$$

The sign + (−) in Eq. (14.58) applies to neutrinos (antineutrinos), and $n_e(x)$ is the electron number density in the medium, which in general is not constant along the neutrino trajectory so the potential is not constant. The characteristic value of the potential at the Earth core is $V_e \sim 10^{-13}$ eV, while at the solar core $V_e \sim 10^{-12}$ eV. Since the neutral current potential Eq. (14.55) is flavour diagonal, it can be eliminated from the evolution equation as it only contributes to an overall unobservable phase.

The instantaneous mass eigenstates in matter, ν_i^m, are the eigenstates of the Hamiltonian H in (14.56) for a fixed value of x, and they are related to the interaction basis by

$$\vec{\nu} = \tilde{U}(x)\nu^{\vec{m}}\,. \tag{14.59}$$

The corresponding instantaneous eigenvalues of H are $\mu_i(x)^2/(2E)$ with $\mu_i(x)$ being the instantaneous effective neutrino masses.

Let us take for simplicity a neutrino state which is an admixture of only two neutrino species $|\nu_\alpha\rangle$ and $|\nu_\beta\rangle$, so the two instantaneous mass eigenstates in matter ν_1^m and ν_2^m have instantaneous effective neutrino masses

$$\mu_{1,2}^2(x) = \frac{m_1^2+m_2^2}{2} + E[V_\alpha + V_\beta]$$
$$\mp\frac{1}{2}\sqrt{[\Delta m^2\cos 2\theta - A]^2 + [\Delta m^2\sin 2\theta]^2}\,, \tag{14.60}$$

and $\tilde{U}(x)$ is a 2x2 rotation matrix with the instantaneous mixing angle in matter given by

$$\tan 2\theta_m = \frac{\Delta m^2\sin 2\theta}{\Delta m^2\cos 2\theta - A}\,. \tag{14.61}$$

In the Eqs.(14.60) and (14.61) A is

$$A \equiv 2E(V_\alpha - V_\beta)\,, \tag{14.62}$$

and its sign depends on the composition of the medium and on the flavour composition of the neutrino state considered. From the expressions above, we see that for a given sign of A the mixing angle in matter is larger(smaller) than in vacuum if this last one is in the first (second) octant. We see that the symmetry about $\theta = 45°$ which exists in vacuum oscillations between two neutrino states is broken by the matter potential in propagation in a medium. The expressions above show that signficant effects are present when A, is close to $\Delta m^2\cos 2\theta$. In particular, as seen in Eq. (14.61), the tangent of the mixing angle changes sign if, along its path, the neutrino passes by some matter density region satisfying, for its energy, the *resonance condition*

$$A_R = \Delta m^2\cos 2\theta\,. \tag{14.63}$$

This implies that if the neutrino is created in a region where the relevant potential satisfies $A_0 > A_R$ (A_0 here is the value of the relevant potential at the production point), then the effective mixing angle in matter at the production point is such that $\mathrm{sgn}(\cos 2\theta_{m,0}) = -\mathrm{sgn}(\cos 2\theta)$. So the flavour component of the mass eigenstates is inverted as compared to their composition in vacuum. In particular, if at the production point we have $A_0 = 2A_R$, then $\theta_{m,0} = \frac{\pi}{2} - \theta$. Asymptotically, for $A_0 \gg A_R$, $\theta_{m,0} \to \frac{\pi}{2}$. In other words, if in vacuum the lightest (heaviest) mass eigenstate has a larger projection on the flavour α (β), inside a matter with density and composition such that $A > A_R$, the opposite holds. So if the neutrino system is traveling across a monotonically varying matter potential, the dominant flavour

Int. J. Mod. Phys. A 2026.41. Downloaded from www.wo[redacted]xcept for Open Access articles.
by UNIVERSITY OF CALIFORNIA @ BERKELEY on 09/16/26. Re-use and distribution is

Int. J. Mod. Phys. A 2026.41. Downloaded from www.worldscientific.com by UNIVERSITY OF CALIFORNIA @ BERKELEY on 09/16/26. Re-use and distribution is strictly not permitted, except for Open Access articles.

component of a given mass eigenstate changes when crossing the region with $A = A_R$. This phenomenon is known as *level crossing*.

Taking the derivative of Eq. (14.59) with respect to x and using Eq. (14.56), we find that in the instantaneous mass basis the evolution equation reads:

$$i\frac{d\vec{\nu}^m}{dx} = \\ = \left[\frac{1}{2E}\,\mathrm{diag}\left(\mu_1^2(x),\,\mu_2^2(x),\,\ldots,\,\mu_n^2(x)\right) - i\,\tilde{U}^\dagger(x)\,\frac{d\tilde{U}(x)}{dx}\right]\vec{\nu}^m\,. \tag{14.64}$$

The presence of the last term, Eq. (14.64) implies that this is a system of coupled equations. So, in general, the instantaneous mass eigenstates, ν_i^m are not energy eigenstates. For constant or slowly enough varying matter potential this last term can be neglected and the instantaneous mass eigenstates, ν_i^m, behave approximately as energy eigenstates, and they do not mix in the evolution. This is the *adiabatic* transition approximation. On the contrary, when the last term in Eq. (14.64) cannot be neglected, the instantaneous mass eigenstates mix along the neutrino path. This implies there can be *level-jumping* [30–33], and the evolution is *non-adiabatic*.

For adiabatic evolution in matter, the oscillation probability take a form very similar to the vacuum oscillation expression, Eq. (14.39). For example, neglecting CP violation:

$$P_{\alpha\beta} = \left|\sum_i \tilde{U}_{\alpha i}(0)\tilde{U}_{\beta i}(L)\exp\left(-\frac{i}{2E}\int_0^L \mu_i^2(x')dx'\right)\right|^2\,. \tag{14.65}$$

To compute $P_{\alpha\beta}$ in a varying potential, one can always solve the evolution equation numerically. Also, several analytic approximations for specific profiles of the matter potential can be found in the literature [34].

14.5.1 *The Mikheyev-Smirnov-Wolfenstein Effect for Solar Neutrinos*

The matter effects discussed in the previous section are of special relevance for solar neutrinos. As the Sun produces ν_e's in its core, we consider the propagation of a $\nu_e - \nu_X$ neutrino system (X is some superposition of μ and τ, which is arbitrary because ν_μ and ν_τ have only and equal neutral current interactions) in the matter density of the Sun.

The density of solar matter is a monotonically decreasing function of the distance R from the center of the Sun, and it can be approximated by an exponential for $R < 0.9R_\odot$

$$n_e(R) = n_e(0)\exp\left(-R/r_0\right)\,, \tag{14.66}$$

with $r_0 = R_\odot/10.54 = 6.6\times10^7$ m $= 3.3\times10^{14}$ eV^{-1}.

As mentioned above, the nuclear reactions in the Sun produce electron neutrinos. After crossing the Sun, the composition of the neutrino state exiting the Sun will depend on the relative size of $\Delta m^2\cos2\theta$ versus $A_0 = 2\,E\,G_F\,n_{e,0}$ (where 0 refers to the neutrino production point, which is near but not exactly at the center of the Sun, $R = 0$).

If the relevant matter potential at production is well below the resonant value, $A_R = \Delta m^2\cos2\theta \gg A_0$, matter effects are negligible. With the characteristic matter density and energy of the solar neutrinos, this condition is fulfilled for values of Δm^2 such that $\Delta m^2/E \gg L_{\mathrm{Sun-Earth}}$. So the propagation occurs as in vacuum with the oscillating phase averaged to 1/2 and the survival probability at the exposed surface of the Earth is

$$P_{ee}(\Delta m^2\cos2\theta \gg A_0) = 1 - \frac{1}{2}\sin^2 2\theta > \frac{1}{2}\,. \tag{14.67}$$

If the relevant matter potential at production is only slightly below the resonant value, $A_R = \Delta m^2\cos2\theta \gtrsim A_0$, the neutrino does not cross a region with resonant density, but matter effects are sizable enough to modify the mixing. The oscillating phase is averaged in the propagation between the Sun and the Earth. This regime is well described by an adiabatic propagation, Eq. (14.65). Using that $\tilde{U}(0)$ is a 2x2 rotation of angle $\theta_{m,0}$ – the mixing angle in matter at the neutrino production point–, and $\tilde{U}(L)$ is the corresponding rotation with vacuum mixing angle θ, we get

$$P_{ee}(\Delta m^2\cos2\theta \geq A_0) = \cos^2\theta_{m,0}\cos^2\theta + \sin^2\theta_{m,0}\sin^2\theta \\ = \frac{1}{2}\left[1+\cos2\theta_{m,0}\cos2\theta\right]\,. \tag{14.68}$$

This expression reflects that an electron neutrino produced at A_0 is an admixture of ν_1 with fraction $P_{e1,0} = \cos^2\theta_{m,0}$ and ν_2 with fraction $P_{e2,0} = \sin^2\theta_{m,0}$. On exiting the Sun, ν_1 consists of ν_e with fraction $P_{1e} = \cos^2\theta$, and ν_2 consists of ν_e with fraction $P_{2e} = \sin^2\theta$ so $P_{ee} = P_{e1,0}P_{1e} + P_{e2,0}P_{2e} = \cos^2\theta_{m,0}\cos^2\theta + \sin^2\theta_{m,0}\sin^2\theta$ [35–37], exactly as given in Eq. (14.68). Since $A_0 < A_R$ the resonance is not crossed so $\cos2\theta_{m,0}$ has the same sign as $\cos2\theta$ and still $P_{ee} \geq 1/2$.

Finally, in the case that $A_R = \Delta m^2\cos2\theta < A_0$, the neutrino can cross the resonance on its way out. In the convention of $\Delta m^2 > 0$ this occurs if $\cos2\theta > 0$ ($\theta < \pi/4$). which means that in vacuum ν_e is a combination of ν_1 and ν_2 with a larger ν_1 component, while at the production point ν_e is a combination of ν_1^m and ν_2^m with larger ν_2^m component. In particular, if the density at the production point is much higher than the resonant density, $\Delta m^2\cos2\theta \ll A_0$,

$$\theta_{m,0} = \frac{\pi}{2} \quad\Rightarrow\quad \cos2\theta_{m,0} = -1\,, \tag{14.69}$$

and the produced ν_e is purely ν_2^m.

In this regime, the evolution of the neutrino ensemble can be adiabatic or non-adiabatic depending on the particular values of Δm^2 and the mixing angle. The oscillation parameters (see Secs.14.6.1 and 14.7) happen to be such that the transition is adiabatic in all ranges of solar neutrino energies. Thus the survival probability at the exposed surface of the Earth is given by Eq. (14.68) but now with mixing angle (14.69) so

$$P_{ee}(\Delta m^2\cos2\theta < A_0) = \frac{1}{2}\left[1+\cos2\theta_{m,0}\cos2\theta\right] = \sin^2\theta\,. \tag{14.70}$$

So, in this case, P_{ee} can be much smaller than 1/2 because $\cos2\theta_{m,0}$ and $\cos2\theta$ have opposite signs. This is referred to as the Mihheev-Smirnov-Wolfenstein (MSW) effect [26, 38], which plays a fundamental role in the interpretation of the solar neutrino data.

The resulting energy dependence of the survival probability of solar neutrinos is shown in Fig.14.3 (together with a compilation of data from solar experiments). The plotted curve corresponds to $\Delta m^2 \sim 7.5\times10^{-5}$ eV^2 and $\sin^2\theta \sim 0.3$ (the so-called large mixing angle, LMA, solution). The figure illustrates the regimes described above. For these values of the oscillation parameters, neutrinos with $E \ll 1$ MeV are in the regime with $\Delta m^2\cos2\theta \gg A_0$ so the curve represents the value of vacuum averaged survival probability, Eq. (14.67), and therefore $P_{ee} > 0.5$. For $E > 10$ MeV, on the contrary, $\Delta m^2\cos2\theta \ll A_0$ and the survival probability is given by Eq. (14.70), so $P_{ee} = \sin^2\theta \sim 0.3$. In between, the survival probability is given by Eq. (14.68) with θ_0 changing rapidly from its vacuum value to the asymptotic matter value (14.69), 90°.

14.6 Experimental Study of Neutrino Oscillations

Neutrino flavor transitions, or neutrino oscillations, have been experimentally studied using various neutrino sources and detection techniques for several decades. For these studies intense sources and large detectors are mandatory because large distances are required for observable oscillation effects and neutrino interaction cross sections are small. Another critical ingredient is knowledge of the neutrino flux before oscillations at a level of precision sufficient to make a definitive measurement of the oscillation effect. This is particularly true for so-called "disappearance" searches, where part of the primary flux oscillates into unseen flavors, as well as for "appearance" measurements, where oscillations induce transitions into a neutrino flavor that is not present, or

Int. J. Mod. Phys. A 2026.41. Downloaded from www.wo
by UNIVERSITY OF CALIFORNIA @ BERKELEY on 09/16/26. Re-use and distribution is
except for Open Access articles.

present in only small quantities, in the primary flux. The following reviews the experimental status of neutrino oscillations organized by different neutrino sources: the Sun, Earth's atmosphere, accelerators, and nuclear reactors. The terminology "disappearance" is often used to describe oscillation measurements where the initial neutrino flavor is observed to decrease, whereas "appearance" is used when another flavor, not present in the original source, is observed.

14.6.1 *Solar Neutrinos*

14.6.1.1 *Solar neutrino flux*

Electron neutrinos are produced in the Sun in thermonuclear reactions that generate solar energy. These reactions occur via two main chains, the *pp* chain and the CNO cycle. The *pp* chain includes the reactions $p+p \to d+e^+ + \nu$ (*pp*), $p+e^- + p \to d+\nu$ (*pep*), $^3\mathrm{He}+p \to {}^4\mathrm{He}+e^+ + \nu$ (*hep*), $^7\mathrm{Be}+e^- \to {}^7\mathrm{Li}+\nu(+\gamma)$ (^{7}Be), and $^8\mathrm{B} \to {}^8\mathrm{Be}^* + e^+ + \nu$ (^{8}B). These reactions result in the overall fusion of four protons into a ^{4}He nucleus, $4p \to {}^4\mathrm{He} + 2e^+ + 2\nu_e$, where the energy released in the reaction, $Q = 4m_p - m_{^4\mathrm{He}} - 2m_e \sim 26$ MeV, is mostly radiated by photons and only a small fraction is carried by the neutrinos, $\langle E_{2\nu_e}\rangle = 0.59$ MeV. Neutrinos from the CNO cycle are produced via the $^{13}\mathrm{N} \to {}^{13}\mathrm{C}+e^+ + \nu$ (^{13}N), $^{15}\mathrm{O} \to {}^{15}\mathrm{N}+e^+ + \nu$ (^{15}O), and $^{17}\mathrm{F} \to {}^{17}\mathrm{O}+e^+ + \nu$ (^{17}F) reactions. Further, electron capture on ^{13}N, ^{15}O, and ^{17}F produces line spectra of neutrinos called ecCNO neutrinos. Dividing the solar luminosity by the energy released per neutrino production, allows the total neutrino flux to be estimated. In the absence of oscillations, the *pp* solar neutrino flux arriving at Earth is about 6×10^{10} cm^{-2}s^{-1}.

The solar neutrino flux has been calculated based on the Standard Solar Model (SSM). The SSM describes the structure and evolution of the Sun based on a variety of inputs such as its mass, luminosity, radius, surface temperature, age, and surface elemental abundances. To completely describe the flux, knowledge of the absolute nuclear reaction cross sections for the relevant fusion reactions as well radiative opacities are necessary. Bahcall and collaborators continuously updated the SSM calculations over several decades [39, 40]. Figure 14.1 shows the solar neutrino fluxes predicted by the SSM calculation in [41] and ecCNO neutrinos in [42].

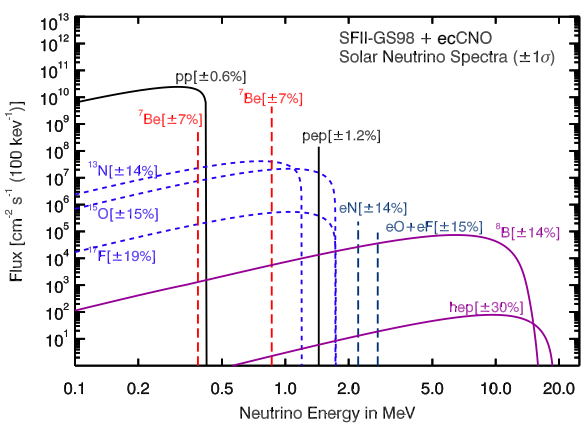

Figure 14.1: Spectrum of solar neutrino fluxes predicted by SSM calculation in [41]. In addition to standard fluxes, ecCNO neutrinos have been added based on [42]. Electron capture fluxes are given in cm^{-2}s^{-1}. Taken from [43].

14.6.1.2 *Detection of solar neutrinos and the solar neutrino problem*

Experiments that observe solar neutrinos are summarized in Table 14.2. Starting in the late 1960's, R. Davis and collaborators carried out a pioneering solar neutrino experiment in the Homestake mine [44], utilizing the reaction $\nu_e + {}^{37}\mathrm{Cl} \to e^- + {}^{37}\mathrm{Ar}$. Since this process has an energy threshold of 814 keV, the fluxes of the ^{7}Be and ^{8}B are the most relevant. The detector contained ~ 615 t of C_2Cl_4. The produced ^{37}Ar, with a half-life of 34.8 days, was chemically extracted and introduced into a low-background proportional chamber every few months. Auger electrons from ^{37}Ar electron capture were counted to determine the neutrino-^{37}Cl reaction rate.

From the beginning of the experiment the observed number of neutrinos was nearly one-third of the SSM prediction. Since this discrepancy could not be traced to deficiencies in either the experiment or theoretical framework it became known as the "solar neutrino problem." The final result from the Homestake experiment was $2.56 \pm 0.16 \pm 0.16$ SNU [45], where SNU (solar neutrino unit) is a unit of event rate with 1 SNU $= 10^{-36}$ captures per second per atom. This can be compared with the SSM prediction of $8.46^{+0.87}_{-0.88}$ SNU [46].

Detecting neutrinos from other production processes was recognized as important to investigate the origin of the solar neutrino problem. The *pp* neutrinos are particularly useful for this purpose as they are the most abundant and have the smallest flux uncertainty. They can be observed using a radiochemical reaction with gallium, $\nu_e + {}^{71}\mathrm{Ga} \to e^- + {}^{71}\mathrm{Ge}$, which has an energy threshold of 233 keV. According to the SSM, more than half of the events on ^{71}Ga are due to *pp* neutrinos, with the second most dominant contribution coming from ^{7}Be neutrinos. Generated ^{71}Ge nuclei decay via electron capture with a half-life of 11.4 days and can be chemically extracted. The SAGE experiment in Baksan [47] used about 50 t of liquid metallic gallium as a target, whereas the GALLEX experiment at LNGS [48] used 101 t of $GaCl_3$, containing 30.3 t of gallium. Both experiments used natural gallium, 39.9% of which is the ^{71}Ga isotope. GALLEX was followed by its successor, the GNO experiment. The measured capture rates were $69.3 \pm 4.1 \pm 3.6$ SNU for GALLEX+GNO [49] and $65.4^{+3.1+2.6}_{-3.0-2.8}$ SNU for SAGE [50], which are well below the SSM prediction of $127.9^{+8.1}_{-8.2}$ SNU [46].

While radiochemical detectors measure the reaction rate integrated between extractions, the first real-time measurement of solar neutrinos was realized by the Kamiokande experiment [51] and later by its successor, Super-Kamiokande. The Kamiokande detector was an upright cylindrical 3,000-t water Cherenkov detector in the Kamioka mine that operated throughout the 1980's. Super-Kamiokande started operations in 1996, employing a similar, but much larger design containing 50 kt of ultrapure water [4]. An inner detector volume corresponding to a 32 kt water mass is viewed by more than 11,000 inward-facing 50 cm diameter photomultiplier tubes (PMTs). Kamiokande and Super-Kamiokande observe solar neutrinos using ν-e elastic scattering (ES), $\nu_x + e^- \to \nu_x + e^-$. This reaction occurs via both charged and neutral current (NC) pathways and is therefore sensitive to all active neutrino flavors. However, the cross-section for ν_e, which is the only flavor to interact via the charged current, is about six times larger than that for ν_μ or ν_τ. Since the energy threshold was 6.5 MeV in Kamiokande and is 3.5 MeV[5] for the present Super-Kamiokande these experiments are primarily sensitive to ^{8}B neutrinos.

The results from both Kamiokande [52] and Super-Kamiokande [53] show significantly smaller solar neutrino rates compared to predictions. Super-Kamiokande's most recent solar neutrino flux measurement is $(2.345 \pm 0.014 \pm 0.036) \times 10^6$ cm^{-2}s^{-1} [54], while the prediction based on the SSM is $(5.46 \pm 0.66) \times 10^6$ cm^{-2}s^{-1} [55]. No significant zenith angle variation or spectral distortions were observed in the initial phase of Super-Kamiokande, which placed strong constraints on the solution of the solar neutrino problem [56].

14.6.1.3 *Solution of the solar neutrino problem*

The SNO experiment in Canada used 1,000 t of heavy water (D_2O) contained in a spherical acrylic vessel which was surrounded by a water (H_2O) shield. An array of PMTs installed on a stainless steel structure detected Cherenkov radiation produced in both the D_2O and H_2O. SNO observed ^{8}B neutrinos using the ES channel as well as two other interactions specific to its D_2O target, the CC $\nu_e + d \to e^- + p + p$ and the NC

[4] Recently, gadolinium (0.01% by weight in 2020, 0.03% in 2022) has been loaded to the water to enhance the detector's neutron tagging capabilities.

[5] Based on the recoil electron's kinetic energy

Int. J. Mod. Phys. A 2026.41. Downloaded from www.worldscientific.com
by UNIVERSITY OF CALIFORNIA @ BERKELEY on 09/16/26. Re-use and distribution is strictly not permitted, except for Open Access articles.

Table 14.2: List of solar neutrino experiments

Name	Target material	Energy threshold (MeV)	Mass (ton)	Years
Homestake	C_2Cl_4	0.814	615	1970–1994
SAGE	Ga	0.233	50	1989–
GALLEX	$GaCl_3$	0.233	100 [30.3 for Ga]	1991–1997
GNO	$GaCl_3$	0.233	100 [30.3 for Ga]	1998–2003
Kamiokande	H_2O	6.5	3,000	1987–1995
Super-Kamiokande	H_2O	3.5	50,000	1996–
SNO	D_2O	3.5	1,000	1999–2006
KamLAND	Liquid scintillator	0.5/5.5	1,000	2001–
Borexino	Liquid scintillator	0.19	300	2007–2021

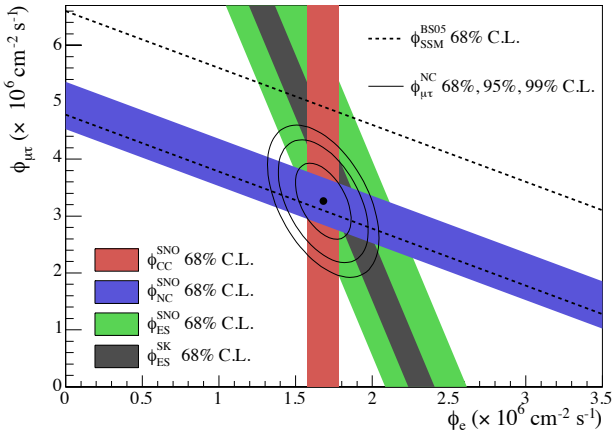

Figure 14.2: Fluxes of ^{8}B solar neutrinos, $\phi(\nu_e)$, and $\phi(\nu_{\mu,\tau})$, deduced from the SNO's CC, ES, and NC results [58]. The Super-Kamiokande ES flux is from [59]. The BS05(OP) standard solar model prediction [40] is also shown. The bands represent the 1σ error. The contours show the 68%, 95%, and 99% joint probability for $\phi(\nu_e)$ and $\phi(\nu_{\mu,\tau})$. The figure is from [58].

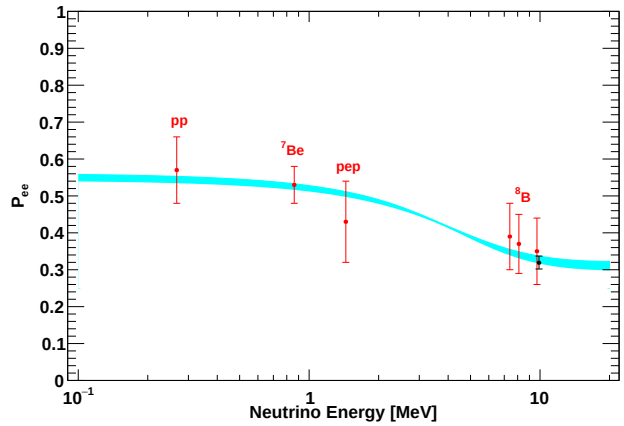

Figure 14.3: Electron neutrino survival probability as a function of neutrino energy. The points represent, from left to right, the Borexino pp, ^{7}Be, pep, and ^{8}B data (red points) and the SNO+SK ^{8}B data (black point). The three Borexino ^{8}B data points correspond, from left to right, to the low-energy (LE) range, LE+HE range, and the high-energy (HE) range. The electron neutrino survival probabilities from experimental points are determined using a high metallicity SSM from [55]. The error bars represent the $\pm1\sigma$ experimental + theoretical uncertainties. The curve corresponds to the $\pm1\sigma$ prediction of the MSW-LMA solution using the parameter values given in [64]. This figure is provided by A. Ianni.

$\nu_x + d \to \nu_x + p + n$ interactions. Importantly, the CC interaction is sensitive to only ν_e, while the NC interaction is sensitive to all active flavors of neutrinos with equal cross-sections for all. By comparing measurements of these different interactions, SNO provides a model-independent test of neutrino flavor change [57].

In 2001 SNO reported its initial CC measurement [60], which when combined with the high statistics measurement of ν-e elastic scattering from Super-Kamiokande [61], provided direct evidence for the existence of a non-ν_e component in solar neutrino flux. SNO's subsequent NC result in 2002 [62] established the existence of this component with 5.3σ significance. Figure 14.2 shows SNO's measured electron neutrino ($\phi(\nu_e)$) and combined muon and tau neutrino fluxes ($\phi(\nu_{\mu,\tau})$) at various confidence levels together with prediction from the SSM. These results together with measurements from the reactor neutrino experiment KamLAND (see Sec. 14.6.4), finally proved that the so-called large mixing angle (LMA) solution, which describes MSW-driven adiabatic flavor transitions in the solar matter, was the resolution of the solar neutrino problem. From a combined result of three phases of SNO data [63], the total flux of ^{8}B solar neutrino is found to be $(5.25 \pm 0.16^{+0.11}_{-0.13})$ cm^{-2}s^{-1}, consistent with the SSM prediction. This consistency is one of the major accomplishments of SSM.

In order to understand the SSM as well as to study the MSW effect on solar neutrinos, it is important to measure fluxes other than the ^{8}B. The Borexino experiment at Gran Sasso detected solar neutrino via ν-e scattering using 300 t of ultra-pure liquid scintillator. It achieved a 0.19 MeV energy threshold with 5% energy resolution at 1 MeV, enabling Borexino to make the first real-time detection of ^{7}Be solar neutrinos [65]. Further, the experiment also measured the *pep* [66], *pp* [67], and CNO [68] neutrino fluxes for the first time. Together with its ^{8}B [69] neutrino flux, Borexino provides both high- and low-energy measurements to probe the solar MSW effect. Figure 14.3 shows the survival probability of solar ν_e as a function of neutrino energy with data from Borexino [70, 71] and SNO+SK ^{8}B measurements overlaid with the theoretical curve from the MSW-LMA solution. The data are consistent with the prediction. Though not included in the figure, the KamLAND experiment has also measured ^{8}B [72] and ^{7}Be [73] solar neutrinos.

Matter effects within the Earth are also expected to affect the propagation of solar neutrinos when they are detected during the night. Comparison of the measured event rates during daytime and nighttime therefore provides a clean and direct test of those matter effects on neutrino oscillations. Super-Kamiokande reported an indication of a day-night asymmetry in the ^{8}B solar neutrino flux [54]. This asymmetry, defined as the difference of the average interaction rate during the day and the average at night divided by the average of the two, is $(-3.3\pm1.0(\text{stat.})\pm0.5(\text{syst.}))\%$, corresponding to a statistical significance of 2.9σ.

14.6.2 *Atmospheric Neutrinos*

14.6.2.1 *Atmospheric neutrino flux*

Atmospheric neutrinos are produced by the decays of hadrons, pions and kaons at low energies, generated in the interactions of cosmic rays and nucleons in the Earth's atmosphere. They have energies ranging from ∼0.1 GeV to TeV and beyond. Since the cosmic ray flux impinges on the atmosphere from all directions,

Int. J. Mod. Phys. A 2026.41. Downloaded from www.worldscientific.com by UNIVERSITY OF CALIFORNIA @ BERKELEY on 09/16/26. Re-use and distribution is except for Open Access articles.

atmospheric neutrinos can travel between ∼10 and ∼ 10^4 km before detection. This combination of energies and pathlengths make them a broad probe of the L/E nature of oscillations (c.f. Equation 14.39). Importantly for oscillation studies, the atmospheric neutrino flux below 100 GeV is composed of electron and muon neutrinos as well as their antineutrinos, where as the tau flavors do not populate the flux appreciably until higher energies.

Based on the dominant atmospheric neutrino production modes, it is possible to understand the ratios of the different flavors' fluxes without detailed calculations. From the decay chain of the charged pion $\pi^+ \to \mu^+\nu_\mu$ and the subsequent muon decay $\mu^+ \to e^+\nu_e\bar{\nu}_\mu$ (and the charge conjugate decays for the π^- chain), the flux ratio $(\nu_\mu+\bar{\nu}_\mu)/(\nu_e+\bar{\nu}_e)$ is expected to be around 2 at low energies (∼ 1 GeV), where most muons decay in the atmosphere. At higher energies some muons will reach the Earth before decaying, increasing this ratio. Further, at O(10) GeV and above, the isotropy of the primary cosmic ray flux implies the neutrino fluxes are up-down symmetric above O(1) GeV. At lower energies the cosmic rays are deflected in the geomagnetic field, inducing up-down asymmetries in the neutrino flux.

Atmospheric neutrino fluxes are calculated in detail using the primary cosmic ray spectrum and particle composition as well as hadronic interaction cross sections to simulate interactions in the atmosphere. Generated particles are tracked through the atmosphere accounting for additional interactions with air nuclei before decaying to produce neutrinos. Effects from solar activity and the propagation in the geomagnetic field are taken into account. Several groups have produced flux estimates for terrestrial detectors [74–77]. Typically the absolute flux is uncertain to 10–20%, depending upon the energy range, while the flux ratios are more precisely constrained, varying by less than 5%.

14.6.2.2 *Observation of atmospheric neutrino oscillations*

The first detection of atmospheric neutrinos was reported in the 1960's by the underground experiments in the Kolar Gold Field in India [78] and in South Africa [79]. In the 1980's, experiments searching for nucleon decays started operations with detectors large enough to observe their dominant background source, atmospheric neutrinos. Among the early experiments were the water Cherenkov experiments, Kamiokande [80] and IMB [81], and the iron tracking calorimeters, Frejus [82] and NUSEX [83]. These detectors identify the incident atmospheric neutrino flavor via its charged current interactions with nuclei, which produce the corresponding flavor of charged lepton.

Early atmospheric neutrino measurements focused on the flux ratio, $\nu_\mu/\nu_e \equiv (\nu_\mu + \bar{\nu}_\mu)/(\nu_e + \bar{\nu}_e)$, as well as the double ratio of this quantity with its expected value, $(\nu_\mu/\nu_e)_{\rm obs}/(\nu_\mu/\nu_e)_{\rm exp}$, in order to reduce the impact of flux uncertainties. The Kamiokande experiment reported an indication of a deficit of the $(\nu_\mu + \bar{\nu}_\mu)$ flux [80], which IMB also observed [81]. However, observations from the iron calorimeters, Frejus [82] and NUSEX [83], were consistent with predictions. This discrepancy became known as the atmospheric neutrino anomaly. Kamiokande later reported studies with a larger sub-GeV (< 1.33 GeV) [84] data as well as with multi-GeV (> 1.33 GeV) [85] samples that strengthened the muon flavor deficit observation. The latter reported an analysis of zenith angle distributions, which showed an indication that the muon disappearance probability is dependent on the zenith angle and hence the travel length of neutrinos. However, the statistical significance was not sufficient to provide a conclusive interpretation.

The resolution of the atmospheric neutrino anomaly was achieved by Super-Kamiokande, which reported compelling evidence for atmospheric neutrino oscillations in 1998 [86]. Zenith angle (θ_z, with $\theta_z = 0$ for vertically downward-going) data showed a clear deficit of upward-going muon-like neutrino events, while no significant asymmetry was observed for electron-like events. Defining the up-down asymmetry as $A = (U-D)/(U+D)$, where U is the number of upward-going ($-1 < \cos\theta_z < -0.2$) events and D is the number of downward-going ($0.2 < \cos\theta_z < 1.0$) events, the Super-Kamiokande multi-GeV muon-like data alone had $A = -0.296 \pm 0.048 \pm 0.001$, a 6σ deviation from zero. Other data samples, including the sub-GeV (< 1.33 GeV) muon-like, upward through going, and upward stopping μ samples, which together a span several decades in neutrino energy showed similar distortions of varying degrees. Super-Kamiokande's results were later confirmed by other atmospheric neutrino observations from MACRO [87] and Soudan2 [88].

Although the energy and zenith-angle-dependent muon neutrino disappearance observed with atmospheric neutrinos could be consistently explained by neutrino oscillations predominantly between ν_μ and ν_τ, other exotic explanations such as neutrino decay [89] and decoherence [90] could not be ruled out initially. Using a selected sample from Super-Kamiokande's atmospheric data with good measured L/E resolution, the L/E dependence of the survival probability was measured [91]. The observed dip in the L/E distribution was consistent with the expectation from neutrino oscillation, strongly disfavoring alternative models.

The strongest experimental proof of ν_μ-ν_τ oscillations in atmospheric neutrino experiments is observation of the appearance of oscillation-induced ν_τ. However, the high production threshold of the τ in CC ν_τ interactions, 3.5 GeV, coupled with its short lifetime (0.3 ps) and decays into several particles, makes identifying ν_τ appearance events experimentally challenging. Nonetheless, Super-Kamiokande has reported evidence of tau neutrino appearance using atmospheric neutrino data with 4.6σ significance [92]. Recently, IceCube has also reported evidence (3.2σ) of ν_τ appearance [93] using atmospheric neutrinos. Definitive observation of ν_τ appearance, however, was made by the long-baseline experiment, OPERA (See Sec. 14.6.3.3).

14.6.2.3 *Neutrino oscillation measurements using atmospheric neutrinos*

Figure 14.4 shows the zenith angle distributions of atmospheric neutrino data from Super-Kamiokande. For a wide range of neutrino energies and path lengths, the observed distributions are consistent with the expectation from neutrino oscillation. Upward-going atmospheric neutrinos with energies from a few to ∼10 GeV provide information for the determination of the neutrino mass ordering [94].

Neutrino telescopes primarily built for high-energy neutrino astronomy, such as ANTARES and IceCube, also measure neutrino oscillations with atmospheric neutrinos. ANTARES consists of a sparse array of PMTs deployed under the Mediterranean Sea at a depth of about 2.5 km that instruments a 10^5 m^3 volume. Similarly, the IceCube detector is located in the Antarctic ice near the South Pole with PMTs deployed depths between 1.45 and 2.45 km. The bottom center of the detector houses DeepCore, a low energy extension to the experiment instrumenting a ∼ 10^7 m^3 volume with a denser PMT array. Both ANTARES [95], with a 20 GeV threshold, and IceCube [96], with events reconstructed above about 5 GeV, have observed atmospheric ν_μ disappearance. Despite the larger threshold, the latter's oscillation constraints have similar precision to those from long-baseline accelerator experiments.

There are several projects for atmospheric neutrino observations either proposed or under preparation. The atmospheric neutrino observation program is included in the plans for future neutrino telescopes such as the IceCube Upgrade [97] and the ORCA detector of KM3NeT project [98]. Indeed, with only 5% of the detector installed and instrumenting a 4×10^5 m^3 volume, the ORCA6 detector has observed atmospheric neutrino oscillations [99]. In India a 50 kt magnetized iron tracking calorimeter ICAL is planned at the INO [100]. Future large underground detectors, Hyper-Kamiokande in Japan [101] and DUNE in US [102] will also study the atmospheric neutrinos.

14.6.3 *Accelerator Neutrinos*

14.6.3.1 *Accelerator neutrino beams*

Conventional neutrino beams are produced with accelerators by colliding high-energy protons onto a target, producing π and K, which are then allowed to decay in a low-density volume, producing neutrinos. Undecayed mesons and muons are stopped in beam dumps or soil downstream of this volume. Since pions are the most abundant product of the proton-target collisions, a conventional neutrino beams are predominantly composed of muon-type neutrinos (or antineutrinos). A comprehensive description of accelerator neutrino beams is found in [103].

Int. J. Mod. Phys. A 2026.41. Downloaded from www.worldscientific.com
by UNIVERSITY OF CALIFORNIA @ BERKELEY on 09/16/26. Re-use and distribution is strictly not permitted, except for Open Access articles.

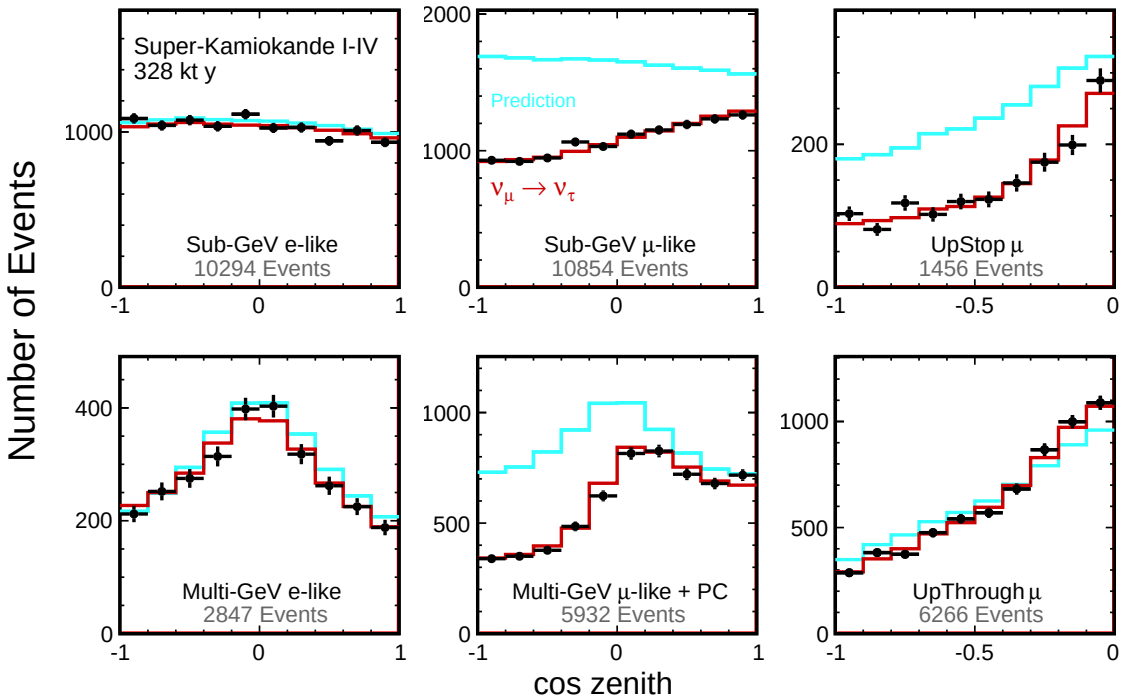

Figure 14.4: Zenith angle distributions of Super-Kamiokande atmospheric neutrino events corresponding to a 328 kton-year exposure of the detector. Fully contained 1-ring e-like and μ-like events with visible energy < 1.33 GeV (sub-GeV) and > 1.33 GeV (multi-GeV), as well as upward stopping and upward through going μ samples are shown. Partially contained (PC) events are combined with multi-GeV μ-like events. Blue histograms show the non-oscillated Monte Carlo prediction and red histograms show the best-fit expectation for neutrino oscillations. (Figure is provided by the Super-Kamiokande Collaboration)

Focusing devices called magnetic horns are used to concentrate the neutrino beam flux in the desired direction [104]. A magnetic horn is a pulsed electromagnet with toroidal magnetic fields that focus (or defocus) the charged particles that are neutrino parents. One can therefore enrich the beam in either neutrinos or antineutrinos by selecting the direction of the horn's current, and hence the magnetic field direction, to focus positive or negative particles, respectively. Even with this focusing, there are still neutrinos from the opposite charge-sign particle decays, so-called *wrong sign* neutrinos, contaminating the beam. There is also a small amount of ν_e and $\bar{\nu}_e$ contamination coming primarily from kaon and muon decays.

To maximize the sensitivity of an experiment, the ratio of the baseline and neutrino energy (L/E) is chosen to match the oscillation effects to be studied. Maximizing the flux of neutrinos with the desired energy, while suppressing other energies, is important for precise oscillation studies. The energy of neutrinos from pion decays is given by

$$E_\nu = \frac{[1-(m_\mu/m_\pi)^2]E_\pi}{1+\gamma^2\theta^2}, \tag{14.71}$$

where E_ν and E_π are the energy of neutrino and pion, respectively, θ is the angle between the pion and neutrino directions, and $\gamma = E_\pi/m_\pi$. For $\theta = 0$, representing so-called *on-axis* neutrinos, the neutrino energy is linearly proportional to the pion energy. In this scenario a narrow band neutrino beam can be made by selecting pions with a desired momentum. Both the MINOS [105] and K2K [106] experiments were operated on-axis. On the other hand, for other angles, the neutrino energy is not strongly dependent on the parent pion energy for a wide range energies, but is instead dependent on the *off-axis* angle θ. Using this relation a narrow band neutrino beam centered around the energy determined by θ can be produced. This off-axis beam method was first introduced in the BNL E889 proposal [107] and adopted in T2K [108] and NOvA [109] experiments. For a list of neutrino beamlines, see also Chapter 33 of this *Review*, "Neutrino Beam Lines at High-Energy Proton Synchrotrons."

The so-called atmospheric mass splitting observed by atmospheric neutrino oscillation experiments, $\Delta m^2 \sim 2.5 \times 10^{-3}$ eV^2, gives rise to a first maximum in the oscillation probability when $L/E \sim 500$ km/GeV. As indicated in Table 14.1, accelerator experiments studying oscillations around this mass splitting have baselines with a ~ 1 GeV neutrino beam require a baseline of a few hundred to a thousand km. For this reason such experiments are termed "long-baseline" experiments. On the other hand, for neutrino oscillations at the $\Delta m^2 \sim 1$ eV^2 scale, as has been reported in some experiments, a ~ 1 km baseline is needed for the same neutrino energies. Accordingly, these experiments are often called "short-baseline" experiments.

Determining the flux of a neutrino beam is done using Monte Carlo simulation of the beamline constrained by in-situ measurements of the primary proton beam as well as beamline components. An important ingredient to the neutrino flux prediction is the hadron production and interaction cross-sections, not only for modeling the initial particle generation in the target, but also to track their subsequent interactions with materials in the beamline, such as the magnetic focusing horns and shielding materials. Data from dedicated hadron production experiments [110–113] are used to tune the beam simulation and to constrain flux uncertainties. The uncertainty on the predicted neutrino flux for the most relevant energy region is 5–10% based on the latest hadron production data [114–116].

14.6.3.2 *Near detectors and neutrino interaction cross sections*

Many long-baseline experiments use two detectors to reduce systematic uncertainties arising from neutrino flux and neutrino-nucleus interactions. Near detectors, situated close enough to the neutrino production target that oscillation effects are small, follow two generic design schemes. They either use the same detection technology as the far detector, itself situated at baseline long enough to observe significant oscillation effects, or they consist of sub-detectors with complementary functions to obtain detailed information of the neutrino beam and neutrino-nucleus interactions. The near detectors provide in-situ measurements of the neutrino

Int. J. Mod. Phys. A 2026.41. Downloaded from www.wo[redacted]except for Open Access articles.
by UNIVERSITY OF CALIFORNIA @ BERKELEY on 09/16/26. Re-use and distribution is

Table 14.3: List of long-baseline neutrino oscillation experiments

Name	Beamline	Far Detector	L (km)	E_ν (GeV)	Year	Orientation
K2K	KEK-PS	Water Cherenkov	250	1.3	1999–2004	On-axis
MINOS	NuMI	Iron-scintillator	735	3	2005–2013	On-axis
MINOS+	NuMI	Iron-scintillator	735	7	2013–2016	On-axis
OPERA	CNGS	Emulsion hybrid	730	17	2008–2012	On-axis
ICARUS	CNGS	Liquid argon TPC	730	17	2010–2012	On-axis
T2K	J-PARC	Water Cherenkov	295	0.6	2010–	Off-axis
NOvA	NuMI	Liquid scint. tracking calorimeter	810	2	2014–	Off-axis
DUNE	LBNF	Liquid argon TPC	1300	2–3	On-axis	
Hyper-Kamiokande	J-PARC	Water Cherenkov	295	0.6	Off-axis	

flux, energy spectrum, and interaction cross-sections, which are then used as inputs to predict the event rate at the far detector. However, even with a two-detector configuration, the neutrino flux and energy spectrum is inevitably different between the near and the far detectors, due to distortions from the oscillation effect. Further, while near detectors observe the neutrino beam as line source, the same beam appears as point source at the far detector.

As modern experiments use heavy nuclei as the neutrino interaction target, primary interactions on correlated nucleons as well as the particles produced in subsequent interactions within the nuclear environment can alter the observed final state, potentially biasing oscillation measurements. In order to make precise oscillation measurements at long-baseline experiments, a detailed understanding of neutrino-nucleus interactions is therefore crucial, particularly for experiments where final-state hadronic activity is not observable. The current status of neutrino cross-sections is summarized in Chapter 52 of this *Review*, "Neutrino Cross Section Measurements."

14.6.3.3 *Long-baseline experiments*

Table 14.3 summarizes long-baseline neutrino oscillation experiments. K2K was the first long-baseline experiment and used a neutrino beam directed towards Super-Kamiokande with a 250 km baseline. Neutrinos were generated with the KEK 12 GeV proton synchrotron and had an average energy of 1.3 GeV. The experiment used a set of fine-grained detectors and a 1 kt water Cherenkov detector located 300 m downstream of the neutrino production target for its near detectors. K2K confirmed the muon neutrino disappearance originally reported by Super-Kamiokande's atmospheric neutrino observation [117].

The MINOS experiment used a beam from Fermilab and a detector located 735 km away in the Soudan mine. Neutrinos were produced in the NuMI beamline using 120 GeV protons from the Main Injector. Both the near and far detectors were iron-scintillator tracking calorimeters, 0.98 kt and 5.4 kt, respectively, with toroidal magnetic fields to enable charge-sign selection of muons. By varying the relative positions of the neutrino target and focusing horns, the energy spectrum of neutrinos from NuMI could be changed. Most of the MINOS data were taken in the "low energy" configuration, which produced a peak energy of around 3 GeV. For a three-year period starting in 2013 the experiment was operated as MINOS+ with NuMI in the "medium energy" configuration which produced a peak neutrino energy of around 7 GeV. MINOS and MINOS+ combined accelerator and atmospheric neutrino data in both disappearance and appearance modes to measure oscillation parameters [118, 119].

In Europe, the CNGS neutrino beamline provided a neutrino beam with a mean energy of 17 GeV along a 750 km baseline from CERN to LNGS. The beam energy was chosen so that oscillation-induced ν_τ had enough energy to undergo CC interactions and therefore provide confirmation of ν_τ appearance. Since there are no ν_τ in the beam before oscillations, no near detector was needed. The OPERA experiment's single detector used consisted of an emulsion-lead target with about 1.25 kt total mass, complemented by electronic detectors. The excellent spatial resolution of the emulsion enabled the event-by-event identification of τ leptons. Ultimately, OPERA observed ten ν_τ CC candidate events with an expected background of 2.0±0.4 [120], observing $\nu_\mu \to \nu_\tau$ appearance with a significance of 6.1σ. Another neutrino experiment, ICARUS [121], which used 600 t liquid argon time projection chambers (TPCs), was operated at Gran Sasso from 2010 to 2012.

This first generation of long-baseline experiments confirmed the existence of neutrino oscillations in the $\nu_\mu \to \nu_\tau$ channel dominated by the atmospheric mixing parameters. Oscillations from ν_μ to ν_e, induced by non-zero θ_{13} (see Eq. 14.33), became the focus of second-generation experiments, which are still running today. This appearance channel opens the possibility of studying several still-open problems in neutrino mixing, including neutrino CP violation, determination of the neutrino mass ordering, and determination of the θ_{23} octant.

The T2K experiment started in 2010 using a newly constructed high-intensity proton synchrotron at J-PARC and Super-Kamiokande as its far detector, located 295 km away. It employs a set of near detectors at about 280 m from the production target with several nuclear targets, including water. T2K is the first long-baseline experiment to employ the off-axis technique, directing its beam 2.5° away from Super-Kamiokande. At this angle the neutrino energy spectrum peaks at 0.6 GeV, which corresponds to first oscillation maximum for the atmospheric mass splitting, $\Delta m^2 \sim 2.5 \times 10^{-3}$ eV^2.

In 2011, T2K reported the first indication of $\nu_\mu \to \nu_e$ oscillations with a statistical significance of 2.5σ [122]. Later T2K established oscillation into this appearance channel with more than 7σ 2014 [123]. Figure 14.5 shows T2K's muon neutrino and electron neutrino candidates' kinematic distributions from both its neutrino and antineutrino beam data. Using a combined analysis of all of its data, T2K reported a hint of CP violation at the 2σ level [124].

The NOvA experiment uses the upgraded NuMI beamline in an off-axis configuration, with functionally equivalent near and far detectors. Its 14 kt far detector is located near Ash River, Minnesota, 810 km away from the neutrino source. The near detector is around 1 km downstream of the production target and has a total active mass of 290 t. Both detectors are tracking calorimeters consisting of planes of polyvinyl chloride cells filled with liquid scintillator and alternately arrayed vertical and horizontal orientations. At 14.6 mrad off-axis of the NuMI beam, the neutrino energy at the far detector peaks at around 2 GeV.

NOvA's physics run started in 2014 and quickly confirmed oscillations from ν_μ to ν_e [125], The experiment started operating its antineutrino beam in 2016 and has reported an observation of $\bar{\nu}_e$ appearance in its $\bar{\nu}_\mu$ beam with 4.4σ significance [126]. Figure 14.6 shows reconstructed neutrino energy distributions from NOvA [127]. The data do not show a strong asymmetry in the rates of ν_e and $\bar{\nu}_e$ appearance, excluding $\delta_{\rm CP} = 90°$ for the inverted mass ordering ($m_3 < m_1 < m_2$, see Sec. 14.7 for definitions) at more than 3σ and disfavoring $\delta_{\rm CP} = 270°$ assuming the normal mass ordering ($m_1 < m_2 < m_3$, see Sec. 14.7 for definitions) at more than 2σ.

Two large-scale next-generation long-baseline experiments are currently under construction. DUNE [102] sends neutrinos from Fermilab to the Sanford Underground Research Facility in South Dakota, a 1,300 km-long baseline. The DUNE far detector will consist of four liquid argon time projection modules, each with at least a 10 kt fiducial mass. When operations start DUNE will use

Int. J. Mod. Phys. A 2026.41. Downloaded from www.worldscientific.com
by UNIVERSITY OF CALIFORNIA @ BERKELEY on 09/16/26. Re-use and distribution is strictly not permitted, except for Open Access articles.

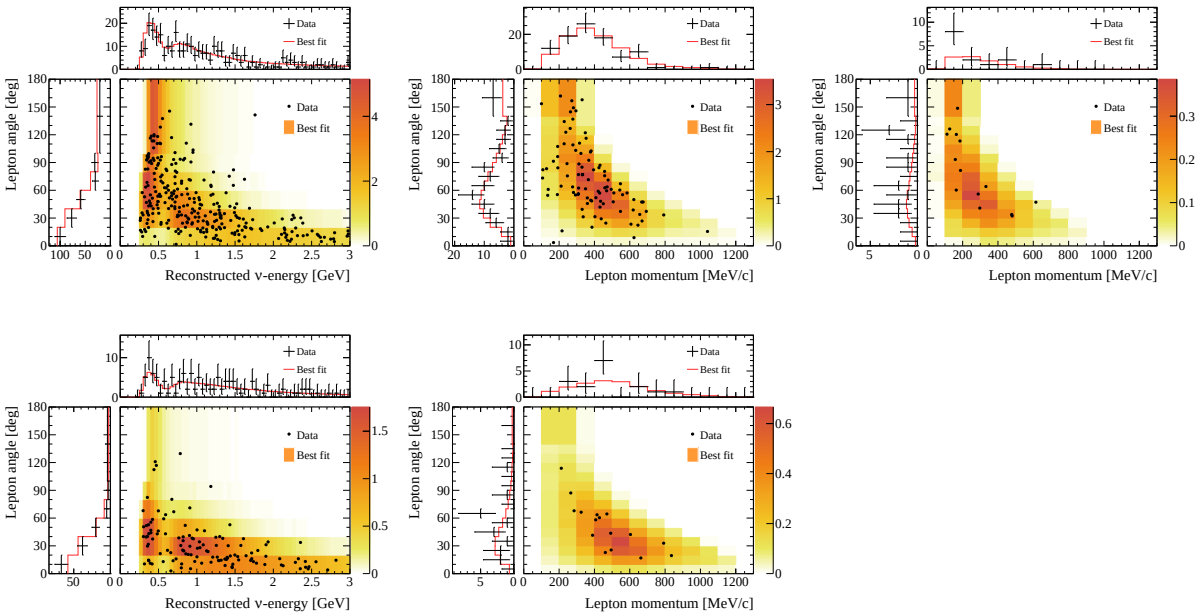

Figure 14.5: Observed kinematic distributions from T2K compared to the expectations with the best-fit parameters [124]. Top and bottom panels correspond to data from neutrino and antineutrino beam mode, respectively. Left, middle, and right panels show distributions for single ring μ-like events, single ring e-like events with no associated decay electron, and single ring e-like events with one associated decay electron (only for neutrino beam mode data), respectively.

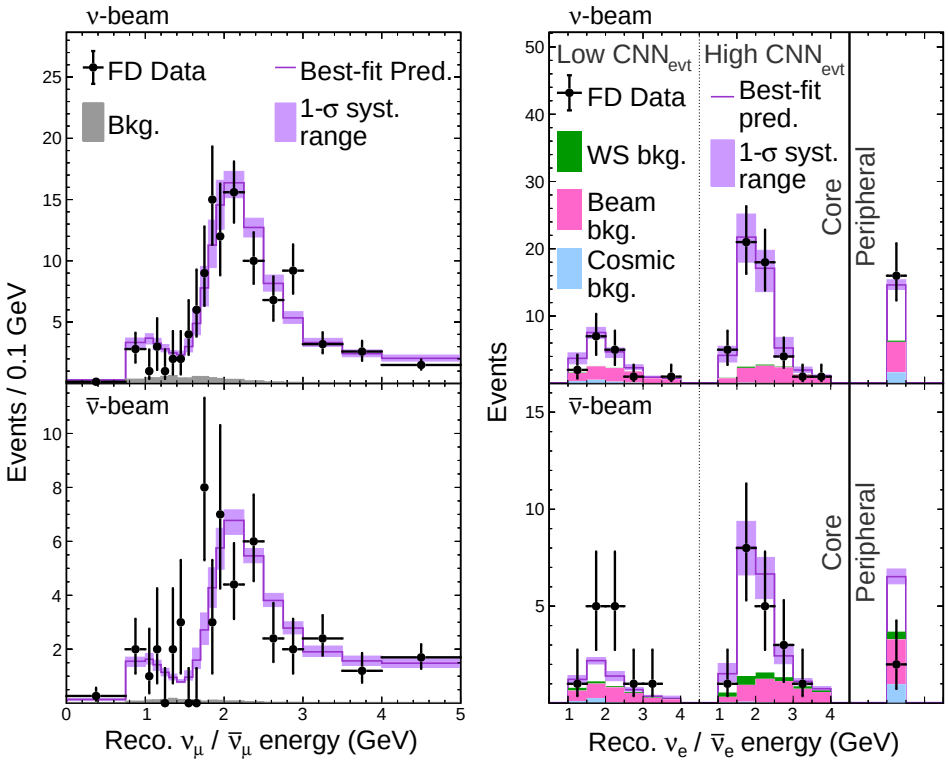

Figure 14.6: Reconstructed neutrino energy distributions from the NOvA far detector [127]. Top plots are for neutrino beam mode, and bottom plots are for antineutrino beam mode. Left: muon-type candidates. Right: electron-type candidates, split into a low and high purity sample as well as the event counts in the peripheral sample, which occurred near the edge of the detector.

Int. J. Mod. Phys. A 2026.41. Downloaded from www.worldscientific.com by UNIVERSITY OF CALIFORNIA @ BERKELEY on 09/16/26. Re-use and distribution is except for Open Access articles.

a 1.2 MW beam that can later be upgraded to 2.4 MW.

In Japan the Hyper-Kamiokande experiment [101] is being built to succeed Super-Kamiokande and T2K as the next-generation large water Cherenkov experiment. Its far detector will have a total water mass of 260 kt. Hyper-Kamiokande will use the T2K near detectors and receive a 1.3 MW beam from an upgraded J-PARC neutrino accelerator and beamline. Both DUNE and Hyper-Kamiokande will have rich physics programs including long-baseline neutrino oscillation studies, searches for nucleon decays, and observations of supernova neutrinos.

14.6.3.4 *Short-baseline experiments*

The LSND experiment searched for neutrino oscillation using neutrinos from stopped pions at Los Alamos. An 800 MeV linac was used to produce pions that stopped in the target. Most of the generated π^-s were absorbed by the nuclei within the target, while π^+s and daughter μ^+s decay to produce neutrinos. Accordingly, ν_μ, $\bar{\nu}_\mu$, and ν_e dominate the resulting flux, with minimal contamination from $\bar{\nu}_e$. The LSND detector was a tank filled with 167 t of diluted liquid scintillator, located about 30 m from the neutrino source. LSND searched for $\bar{\nu}_\mu \to \bar{\nu}_e$ appearance using the inverse beta decay process, $\bar{\nu}_e + p \to e^+ + n$, and found an excess of $87.9 \pm 22.4 \pm 6.0$ events over the expected background [128]. Interpreting this excess as a two-flavor oscillation yields a mass squared splitting of O(1) eV^2.

The KARMEN experiment was performed at the ISIS neutron spallation facility at Rutherford Appleton Laboratory and also used neutrinos from stopped pions. Using the KARMEN 2 detector, a segmented liquid scintillation calorimeter with a total volume of 65 m^3 located at a mean distance of 17.7 m from the ISIS target, the experiment searched for $\bar{\nu}_\mu \to \bar{\nu}_e$ oscillations. No excess of signal was seen above the background expectation, which excluded a large region of the oscillation parameter space favored by LSND [129].

To further test the LSND result, the MiniBooNE experiment at Fermilab was performed with the same average L/E, but with a larger energy and longer baseline. It used the booster neutrino beam (BNB) beam produced by the 8 GeV protons of the Fermilab booster impinging on a beryllium target surrounded by single magnetic horn. Neutrino and antineutrino beams with peak energies of 600 and 400 MeV, respectively, were directed towards the MiniBoonNE detector, 12.2 m diameter sphere filled with 818 t of mineral oil located 541 m from the target. MiniBooNE reported excesses of both ν_e (neutrino beam) and $\bar{\nu}_e$ (antineutrino beam) events. The combined ν_e and $\bar{\nu}_e$ excess was $638.0 \pm 52.1 \pm 122.2$ over backgrounds, which corresponds to 4.8σ significance [130]. When interpreted as an oscillation signal, the MiniBooNE allowed region is consistent with both the LSND and KARMEN results in parts of the oscillation parameter space.

The short-baseline neutrino (SBN) program at Fermilab BNB [131] is designed to further investigate the reported excess. Whereas both LSND and MiniBooNE were single-detector experiments, the SBN program comprises three liquid argon time projection chambers at different baselines viewing the same neutrino beamline. The 85 t MicroBooNE detector was operated at 470 m from the target, the 112 t Short-Baseline Near Detector is operated at 110 m, and the 476 t ICARUS is located at 600 m downstream. The latter was transplanted to Fermilab after refurbishment at CERN and serves as the SBN far detector. As of this writing, MicroBooNE is the only experiment that has published results from SBN, observing no excess of ν_e events [132] and no evidence of light sterile neutrino oscillations [133]. ICARUS (SBND) has been taking data since 2022 (2024).

The JSNS^2 experiment at J-PARC has started a search for neutrino oscillations with $\Delta m^2 \sim 1$ eV^2 [134]. It observes neutrinos from muon decay at rest produced by the 1 MW proton beam from the 3 GeV J-PARC Rapid Cycling Synchrotron. With a 17 t fiducial mass detector filled with gadolinium-loaded liquid scintillator of located 24 m from the production target, JSNS^2 aims to provide a direct test of the LSND anomaly. The second phase of the experiment, which will add a second detector at 48 m, is now in preparation.

14.6.4 *Reactor Antineutrinos*

14.6.4.1 *Reactor antineutrino flux*

Nuclear reactors are intense sources of MeV-scale $\bar{\nu}_e$ which are generated in the nuclear fission of heavy isotopes, mainly ^{235}U, ^{238}U, ^{239}Pu, and ^{241}Pu. The $\bar{\nu}_e$ flux can be estimated based on the thermal power output and fuel composition of the reactor as a function of time. On average, about six $\bar{\nu}_e$ are emitted with about 200 MeV of energy per fission. Therefore, a 1 GW$_{\rm th}$ (thermal power) reactor produces about 2×10^{20} $\bar{\nu}_e$ per second.

Detailed estimates of the $\bar{\nu}_e$ flux and energy spectrum can be obtained by either summing up the spectra of the various decays from each fission fragment using available nuclear data, or by using measurements of the cumulative electron spectra associated with the beta decays of those fission fragments. Since the fission of the four main fuel isotopes involves thousands of beta-decay branches, a complete *ab initio* flux calculation is challenging. Cumulative electron spectra for ^{235}U, ^{239}Pu, and ^{241}Pu were measured at the Institut Laue-Langevin (ILL) reactor in Grenoble, France in the 1980s [135–137]. Predictions of the $\bar{\nu}_e$ flux from ^{238}U often use a summation calculation from [138] together with the ILL results.

A 2011 calculation of the reactor $\bar{\nu}_e$ flux [139] uses an improved *ab initio* approach for ^{238}U as well as combined information from nuclear databases and electron spectra measured at ILL for ^{235}U, ^{239}Pu, and ^{241}Pu. Another calculation [140] is provided for ^{235}U, ^{239}Pu, and ^{241}Pu based on the ILL measurement of electron spectra, taking into account higher-order corrections and minimizing the use of nuclear databases. Both calculations predict a few percent higher normalization for the energy-averaged antineutrino fluxes of ^{235}U, ^{239}Pu, and ^{241}Pu compared to the original analyses of ILL data. However, the reactor antineutrino flux measurement at Daya Bay [141–144] are consistent with a lower flux. Reactor flux calculations have recently been updated [145–147] and are now in better agreement with the Daya Bay data. Despite this improvement, a $\bar{\nu}_e$ excesses relative to predictions, both old and new, at around 5 MeV has been observed by recent reactor experiments [144, 148–150].

14.6.4.2 *Reactor antineutrino oscillation experiments*

Charged current interactions are not possible at reactor neutrino energies if the produced $\bar{\nu}_e$ oscillate into $\bar{\nu}_\mu$ or $\bar{\nu}_\tau$. For this reason, $\bar{\nu}_e$ disappearance is the only channel available to study neutrino flavor change at reactor experiments. Inverse beta decay $\bar{\nu}_e + p \to e^+ + n$ provides a clean way to detect $\bar{\nu}_e$ in this energy region. A delayed-coincidence measurement of the prompt e^+ and delayed γ rays emitted when the n thermalizes and captures on a nucleus allows for efficient background suppression. Further, energy from the prompt e^+, E_p, can be used to form a simple, but robust estimator for the neutrino energy, $E_{\bar{\nu}} \sim E_p + 0.8$ MeV. Liquid scintillator is often used to realize large detectors since they have high light yield and offer many hydrogen nuclei that serve as both the inverse beta decay target and neutron capture nucleus. To increase the neutron detection efficiency, the scintillator may be loaded with gadolinium because of its large neutron capture cross-section. Additionally, gadolinium neutron captures liberate γ rays whose total energy is about 8 MeV, making it easier to detect than the 2.2 MeV produced by capture on hydrogen.

Table 14.4 shows a list of reactor antineutrino experiments measuring neutrino oscillations. As was also shown in Table 14.1, experiments are designed with different baselines because of the different scale of mass splittings found by solar and atmospheric neutrino experiments. Experiments with O(100) km baseline are sensitive to Δm^2 of 10^{-4}–10^{-5} eV^2, while ~ 1 km baseline results in a sensitivity in the range of 10^{-2}–10^{-3} eV^2.

The KamLAND detector consists of 1,000 t of ultra-pure liquid scintillator contained in a 13-m diameter spherical balloon [151]. It is located in the original Kamiokande cavern, where the $\bar{\nu}_e$ flux is dominated by a few reactors, whose average distance from the detector is $\sim$180 km. KamLAND reported first results in 2002 showing that the ratio of the observed number of $\bar{\nu}_e$ events and unoscillated expectations is $0.611 \pm 0.085 \pm 0.041$, which was evidence for reactor $\bar{\nu}_e$ disappearance at the 99.95% confidence level [151]. This result confirmed the large value of the mixing angle corresponding to the LMA solution reported by solar neutrino

Int. J. Mod. Phys. A 2026.41. Downloaded from www.worldscientific.com
by UNIVERSITY OF CALIFORNIA @ BERKELEY on 09/16/26. Re-use and distribution is strictly not permitted, except for Open Access articles.

Table 14.4: List of reactor antineutrino oscillation experiments

Name	Reactor power (GW_{th})	Baseline (km)	Detector mass (t)	Year
KamLAND	various	180 (ave.)	1,000	2001–
Double Chooz	4.25×2	1.05	8.3	2011–2018
Daya Bay	2.9×6	1.65	20×4	2011–2020
RENO	2.8×6	1.38	16	2011–2023
JUNO	26.6 (total)	53	20,000	2025–

experiments. KamLAND also showed evidence of $\bar{\nu}_e$ spectrum distortion consistent with the expectation from neutrino oscillations [152]. Figure 14.7 shows KamLAND's ratio of the observed $\bar{\nu}_e$ spectrum to the expectation without oscillations as a function of L_0/E, $L_0 = 180$ km. A clear oscillatory signature can be seen.

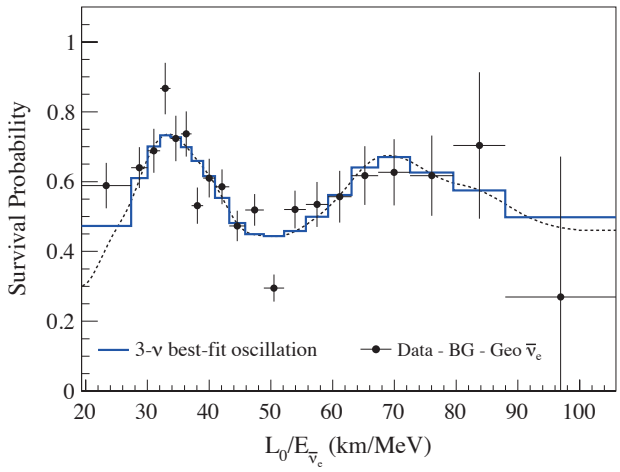

Figure 14.7: Ratio of the observed $\bar{\nu}_e$ spectrum to the expectation for no-oscillation versus L_0/E for the KamLAND data. $L_0 = 180$ km is the flux-weighted average reactor baseline. The 3-ν histogram is the best-fit survival probability curve from the three-flavor unbinned maximum-likelihood analysis using only the KamLAND data. This figure is taken from [153].

Following the establishment of neutrino oscillations with atmospheric, solar, accelerator, and reactor experiments, measurement of the remaining mixing angle, θ_{13}, was recognized as the next major milestone. A reactor neutrino experiment with a ∼1 km baseline can make an almost pure measurement of $\sin^2 2\theta_{13}$ from the disappearance of $\bar{\nu}_e$. In order to be sensitive to a small value of of this angle, experiments with multiple detectors, emulating the near- and far-detector strategy of accelerator experiments, were proposed. Three experiments were realized: Double Chooz in France, Daya Bay in China, and RENO in Korea.

These three experiments employ a similar detector design optimized for the precise measurement of reactor antineutrinos. Each detector consists of a cylindrical stainless steel vessel that houses two nested acrylic cylindrical vessels. A gadolinium-doped liquid scintillator in the innermost vessel is used as the primary antineutrino target. It is surrounded by an undoped liquid scintillator layer that fills the larger acrylic vessel to contain γ rays emitted from the target volume. Light from the liquid scintillator is detected by an array of PMTs mounted on the stainless steel vessel. Finally, mineral oil fills the region between the stainless steel vessel and acrylic volumes to shield them from radioactivity in the detector PMTs and surrounding rock. The region outside of the stainless steel vessel is instrumented as a veto detector filled with either liquid scintillator (Double Chooz) or with water (Daya Bay and RENO) detector.

The Double Chooz detector concept used a gadolinium-doped liquid scintillator with a mass of 8.3 t. Its far detector was located at a baseline of ∼1050 m from two 4.25 GW_{th} reactors and started physics data taking in 2011. The near detector, located at ∼400 m from the reactors, was completed in the end of 2014. Double Chooz finished data taking in early 2018.

Daya Bay has two near detector sites with flux-weighted baselines of 470 m and 576 m, respectively, and one far site located underground and 1648 m from six reactors each with 2.9 GW_{th}. Daya Bay operated from 2011 until 2020 and used eight antineutrino detectors in total: two detectors in each of the near detector halls and four detectors in the far detector hall. Each detector contains 20 t of gadolinium-loaded liquid scintillator.

RENO has two identical detectors located at 294 m and 1383 m from the center of an array of six 2.8 GW_{th} reactors. The mass of the gadolinium-loaded liquid scintillator is 16 t per detector. RENO took data with both near and far detectors from 2011 until 2023.

All three reactor neutrino experiments published their first results in 2012. Double Chooz reported results first, announcing an indication of reactor electron antineutrino disappearance with a ratio of observed to expected events of $R = 0.944 \pm 0.016 \pm 0.04$, which ruled out the no-oscillation hypothesis at 94.6% CL [154]. Shortly thereafter, Daya Bay observed $R = 0.940 \pm 0.011 \pm 0.004$, corresponding to 5.2σ significance of non-zero value of θ_{13} [155]. RENO also reported $R = 0.920 \pm 0.009 \pm 0.014$, indicating a non-zero value of θ_{13} with a significance of 4.9σ [156].

Both Daya Bay [157] and RENO [148, 158] report results constraining the mass-squared difference as well as the mixing angle using both relative near-far $\bar{\nu}_e$ rate and energy spectra information. Double Chooz has reported an analysis based on both far and near detectors [149] for the mixing angle, using neutron capture on any element (primarily gadolinium and hydrogen) to increase the effective target mass.

Figure 14.8 shows the energy spectra of the prompt signals observed in the far detectors of the three experiments. In all three experiments, an excess of $\bar{\nu}_e$ events over the expected energy spectrum has been observed around 5 MeV, as mentioned earlier. This excess is observed in both near and far detectors and scales with the reactor power. Due to cancellation between the near and far detectors, their neutrino oscillation measurements are not affected by this anomaly.

At a baseline of ∼50 km and with excellent energy measurement, reactor antineutrino experiments have significant sensitivity to the mass ordering by observing the precise distortion of the $\bar{\nu}_e$ spectrum over several oscillations in the detector. The JUNO experiment started taking data in August 2025 and is designed for this goal. It consists of a 20 kt liquid scintillator that is located 53 km from two nuclear power plants in China [159, 160]. In addition to the mass ordering, JUNO can make precision measurements of other oscillation parameters, including the solar parameters, and is large enough to host a broad program of non-oscillation physics.

14.6.4.3 *Reactor experiments sensitive to O(1) eV^2 oscillations*

Possible hints of neutrino oscillations at a scale of $\Delta m^2 \sim 1$ eV^2 (see Sec. 14.8) have motivated reactor experiments at a distance of ∼10 m from the core. Recent experiments searching for ∼1 eV^2 oscillation at reactors are summarized in Table 14.5. Some use commercial reactors as the antineutrino flux which can provide a large flux and therefore provide high statistical precision. Others use research reactors, which despite the orders-of-magnitude smaller flux, often have other advantages, such as easier access to short baselines, simpler fuel composition and smaller core sizes.

For these studies detectors typically use organic scintillators, either liquid scintillator (LS) or solid plastic scintillator (PS), which

Int. J. Mod. Phys. A 2026.41. Downloaded from www.wo
by UNIVERSITY OF CALIFORNIA @ BERKELEY on 09/16/26. Re-use and distribution is
except for Open Access articles.

Table 14.5: List of reactor antineutrino experiments for O(eV^2) oscillations

Name	Reactor power (MW_{th})	Baseline (m)	Detector mass (t)	Detector technology	σ_E/E @1 MeV(%)	S/B
NEOS	2,800	24	1	Gd-LS	5	22
DANSS	3,100	10–13	0.9	Gd-PS	34	∼30
STEREO	57	9–11	1.7	Gd-LS	10	0.9
PROSPECT	85	7–9	4	^{6}Li-LS	4.5	1.3
NEUTRINO-4	100	6–12	1.5	Gd-LS	16	0.5
SoLid	80	6–9	1.6	^{6}Li-PS	14	

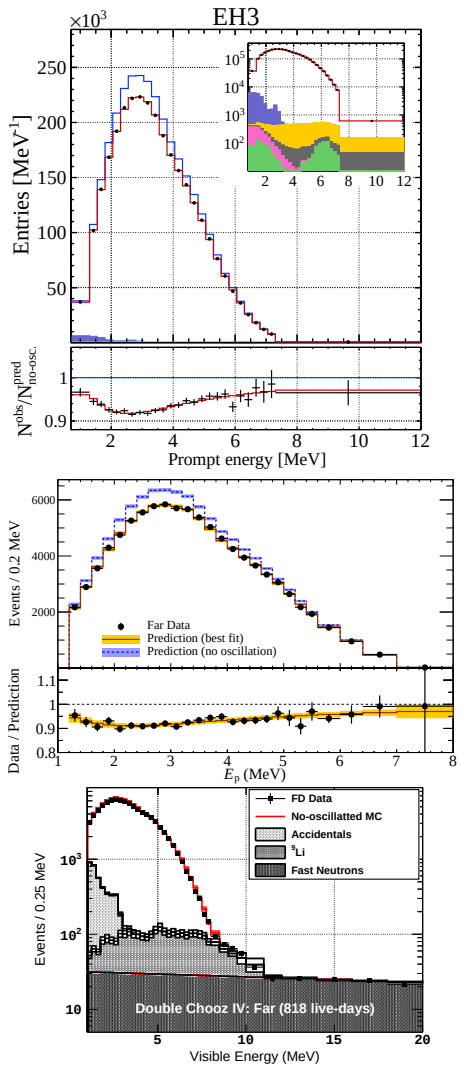

Figure 14.8: Energy spectra for prompt events at the far detectors for Daya Bay [157], RENO [148], and Double Chooz [149].

have hydrogen for the inverse beta decay target. To identify the signal delayed-coincidence with neutron capture on either gadolinium (Gd), as discussed above, or ^{6}Li is used. Following neutron capture on ^{6}Li, the excited nuclei decays into a triton and an α. The effect of neutrino oscillation appears as a distortion of energy spectrum. In order to reduce reactor neutrino spectrum uncertainties, some experiments compare spectra at different baselines either by using a segmented detector or by moving the detector.

NEOS [150, 161] uses about 1 t of gadolinium-loaded liquid scintillator in an unsegmented detector. It is located at 23.7 m from the center of a commercial reactor and is covered by an overburden of about 20 meters of water equivalent. Using 180 days of data, NEOS and RENO have ruled out oscillations with $0.1 < |\Delta m^2| < 7\text{eV}^2$ [161].

DANSS [162] is another experiment using a commercial reactor. The detector is highly segmented, consisting of 2,500 plastic scintillator strips, each with size $1 \times 4 \times 100$ cm^3 and coated with a thin gadolinium-loaded reflective layer. The detector is placed on a movable platform below the reactor core, which enables the distance to the core to vary from 10.7 to 12.7 m. DANSS did not observe oscillations with a mass splitting of O(1) eV^2 [162].

The STEREO detector [163, 164] has six identical target cells each 37 cm in length, a $\sim$ 2m^3 total volume, filled with gadolinium-loaded liquid scintillator. They are placed at distances ranging from 9.4 to 11.1 m from the compact (80 cm high, 40 cm diameter) core of the ILL research reactor. Using a data sample with more than 100,000 detected antineutrinos, STEREO has rejected neutrino mixing with Δm^2 between 0.1 and 10 eV^2 over a variety of mixing angles [164].

The PROSPECT detector [165] consists of a segmented 4 t ^{6}Li-doped liquid scintillator detector. It covers a baseline range of 7–9 m from the highly enriched ^{235}U reactor core of the High Flux Isotope Reactor (HFIR) at Oak Ridge National Laboratory. Thin reflecting panels divide the LS volume into an 11 × 14 two-dimensional array of 154 optically isolated rectangular segments ($14.5 \times 14.5 \times 117.6$ cm^3). PROSPECT found no significant indication of oscillations in the range $0.1 < |\Delta m^2| < 15$ eV^2 [165].

NEUTRINO-4 [166, 167] uses a gadolinium-loaded liquid scintillator detector segmented in 10×5 sections with a total volume of 1.8 m^3. The detector is installed on a movable platform and can be moved to baselines spanning 6–12 m from the SM-3 reactor core in Russia. Using data collected between 2014 and 2021, NEUTRINO-4 observed an indication of oscillations consistent with $\Delta m^2 = 7.3 \pm 0.13(\text{stat.}) \pm 1.16(\text{syst.})$ and a mixing angle $\sin^2 2\theta = 0.36 \pm 0.12(\text{stat.})$ at 2.9σ significance.

The SoLid detector [168] is a finely segmented detector made of $5 \times 5 \times 5$ cm^3 plastic scintillator cubes and ^{6}LiF:ZnS sheets. Using the difference of scintillation time constants between the ZnS and plastic scintillator, n-γ separation is achieved. A detector with 1.6 t of active volume is installed at a distance of 6–9 m from the research reactor core at the BR2 reactor in Belgium.

14.7 Combined Analysis of Experimental Results: The 3ν Paradigm

From the experimental situation described in Sec. 14.6 we conclude that

- Atmospheric ν_μ and $\bar{\nu}_\mu$ disappear most likely converting to ν_τ and $\bar{\nu}_\tau$. The results show an energy and distance dependence perfectly described by mass-induced oscillations.
- Accelerator ν_μ and $\bar{\nu}_\mu$ disappear over distances of $\sim$ 200 to 800 km. The energy spectrum of the results show a clear oscillatory behavior also in accordance with mass-induced oscillations with a wavelength in agreement with the effect observed in atmospheric neutrinos.
- Accelerator ν_μ and $\bar{\nu}_\mu$ appear as ν_e and $\bar{\nu}_e$ at distances $\sim$ 200 to 800 km.
- Solar ν_e convert to ν_μ and/or ν_τ. The observed energy dependence of the effect is well described by massive neutrino conversion in the Sun matter according to the MSW effect
- Reactor $\bar{\nu}_e$ disappear over distances of $\sim$ 200 km and $\sim$ 1.5 km with different probabilities. The observed energy spectra

Int. J. Mod. Phys. A 2026.41. Downloaded from www.worldscientific.com
by UNIVERSITY OF CALIFORNIA @ BERKELEY on 09/16/26. Re-use and distribution is strictly not permitted, except for Open Access articles.

show two different mass-induced oscillation wavelengths: at short distances in agreement with the one observed in accelerator ν_μ disappearance, and a long distance compatible with the required parameters for MSW conversion in the Sun.

The minimum scenario to describe these results requires the mixing between the three flavour neutrinos of the standard model in three distinct mass eigenstates. In this case U in Eq. (14.32) is a 3×3 matrix analogous to the CKM matrix for the quarks [21], but due to the possible Majorana nature of the neutrinos it can depend on six independent parameters: three mixing angles and three phases. There are several possible conventions for the ranges of the angles and ordering of the states. The community finally agreed to a parametrization of the leptonic mixing matrix as in Eq. (14.33). The angles θ_{ij} can be taken without loss of generality to lie in the first quadrant, $\theta_{ij} \in [0, \pi/2]$, and the phase $\delta_{\rm CP} \in [0, 2\pi]$. Values of $\delta_{\rm CP}$ different from 0 and π imply CP violation in neutrino oscillations in vacuum [169–171]. The Majorana phases η_1 and η_2 play no role in neutrino oscillations [170, 172]. Hence for the study of neutrino oscillations in the 3ν mixing scenario one can use the parametrization in Eq. (14.34) irrespective of whether neutrinos are Dirac or Majorana particles. Indeed, Majorana phases are very hard to measure since they are only physical if neutrino mass is non-zero, and therefore, the amplitude of any process involving them is suppressed by a factor m_ν/E to some power where E is the energy involved in the process, which is typically much larger than the neutrino mass. The most sensitive experimental probe of Majorana phases is the rate of neutrinoless $\beta\beta$ decay discussed in Secs. 14.9.3 and 14.9.2.

In this convention there are two non-equivalent orderings for the spectrum of neutrino masses:

– Spectrum with Normal Ordering (NO) with $m_1 < m_2 < m_3$
– Spectrum Inverted ordering (IO) with $m_3 < m_1 < m_2$.

Furthermore, the data show a hierarchy between the mass splittings, $\Delta m^2_{21} \ll |\Delta m^2_{31}| \simeq |\Delta m^2_{32}|$ with $\Delta m^2_{ij} \equiv m_i^2 - m_j^2$.

In this section, we follow the convention used in the listing section of the PDG and discuss the results for both, NO and IO, using Δm^2_{21}, which is always the smallest mass splitting, and Δm^2_{32}, which up to a sign, is the largest mass splitting for IO, while for NO the largest mass splitting is $\Delta m^2_{31} = \Delta m^2_{32} + \Delta m^2_{21}$.

With what we know of the mass differences (see table 14.7) and the neutrino mass scale (see Sec. 14.9), depending on the value of the lightest neutrino mass, the neutrino mass spectrum can be further classified in:

– Normal Hierarchical Spectrum (NH): $m_1 \ll m_2 < m_3$, $\Rightarrow m_2 \simeq \sqrt{\Delta m^2_{21}} \sim 8.6{\times}10^{-3}$eV, $m_3 \simeq \sqrt{\Delta m^2_{32} + \Delta m^2_{21}} \sim$ 0.05eV,

– Inverted Hierarchical Spectrum (IH): $m_3 \ll m_1 < m_2$, $\Rightarrow m_1 \simeq \sqrt{|\Delta m^2_{32} + \Delta m^2_{21}|} \sim 0.0492$eV, $m_2 \simeq \sqrt{|\Delta m^2_{32}|} \sim$ 0.05eV,

– Quasidegenerate Spectrum (QD): $m_1 \simeq m_2 \simeq m_3 \gg \sqrt{|\Delta m^2_{32}|}$.

Sometimes in the literature the determination of the neutrino mass spectrum is referred to as determination of the neutrino hierarchy. However, as described above, with what we know so far of the neutrino mass scale, the neutrino spectrum may or may not be hierarchical. Therefore determination of neutrino mass ordering is a more precise expression, and it is the one used in this review.

In total, the 3-ν oscillation analysis of the existing data involves six parameters: 2 mass differences (one of which can be positive or negative), 3 mixing angles, and the CP phase. The different experiments described in Sec. 14.6 provide information on different subsets of these parameters. The precise statistical analysis of the data requires the numerical evaluation of the corresponding oscillation probabilities by solving the evolution equation of the neutrino ensemble from their source to the experiment. Nevertheless, the dominant effects in the different experiments can be qualitatively understood in terms of approximate expressions for the oscillation probabilities which, for convenience, we briefly summarize here.

14.7.1 *3ν Oscillation Probabilities*

The relevant survival probabilities for solar and KamLAND experiments in the framework of three neutrino oscillations can be written as:

$$P^{3\nu}_{ee} = \sin^4\theta_{13} + \cos^4\theta_{13} P^{2\nu}_{ee}(\Delta m^2_{21}, \theta_{12})\,, \tag{14.72}$$

where we have used the fact that $L^{\rm osc}_{0,32} = 4\pi E_\nu/\Delta m^2_{32}$ is much shorter than the distance traveled by both solar and KamLAND neutrinos, so that the oscillations related to $L^{\rm osc}_{0,32}$ are averaged. In the presence of matter effects $P^{2\nu}_{ee}(\Delta m^2_{21}, \theta_{12})$ should be calculated, taking into account the evolution in an effective matter density $n_e^{\rm eff} = n_e \cos^2\theta_{13}$. For $10^{-5} \lesssim \Delta m^2/{\rm eV}^2 \lesssim 10^{-4}$, $P^{2\nu}_{ee}(\Delta m^2_{21}, \theta_{12})$ presents the following asymptotic behaviors [173]:

$$P^{2\nu,{\rm sun}}_{ee} \simeq 1 - \frac{1}{2}\sin^2(2\theta_{12}) \qquad \text{for } E_\nu \lesssim \text{few} \times 100 \text{ keV}\,, \tag{14.73}$$

$$P^{2\nu,{\rm sun}}_{ee} \simeq \sin^2(\theta_{12}) \qquad \text{for } E_\nu \gtrsim \text{few} \times 1 \text{ MeV}\,, \tag{14.74}$$

$$P^{2\nu,{\rm kam}}_{ee} = 1 - \sin^2(2\theta_{12})\sin^2\frac{\Delta m^2_{21} L}{4E_\nu}. \tag{14.75}$$

At present most of the precision of the solar analysis is provided by SNO and SK, for which the relevant MSW survival probability provides a direct measurement of $\sin^2\theta_{12}$, as seen in Eq. (14.74). In the MSW regime, the determination of Δm^2_{21} in solar experiments comes dominantly from the ratio between the solar potential and the Δm^2_{21} term required to simultaneously describe the CC/NC data at SNO and the undistorted spectra of ^{8}B neutrinos as measured in both SK and SNO. Conversely, KamLAND $\bar\nu_e$ survival probability proceeds dominantly as vacuum oscillations and provides a most precise determination of Δm^2_{21} via the strong effect of the oscillating phase in the distortion of the reactor energy spectrum. On the contrary, it yields a weaker constraint on θ_{12} as the vacuum oscillation probability depends on the double-valued and "flatter" function $\sin^2(2\theta_{12})$.

In what respects the interpretation of ν_μ disappearance data, at LBL experiments, the ν_μ survival probability can be expanded in the small parameters $\sin\theta_{13}$ and $\alpha \equiv \Delta m^2_{21}/\Delta m^2_{31}$ to good accuracy as [174, 175]

$$\begin{aligned} P_{\nu_\mu\to\nu_\mu} &\approx 1 - \sin^2 2\theta_{\mu\mu}\sin^2\frac{\Delta m^2_{\mu\mu} L}{4E_\nu} \\ &\approx 1 - \cos^2\theta_{13}\sin^2(2\theta_{23})\sin^2\frac{\Delta m^2_{32} L}{4E_\nu} + \mathcal{O}(\alpha, s^2_{13})\,, \end{aligned} \tag{14.76}$$

with

$$\begin{aligned} \sin^2\theta_{\mu\mu} &= \cos^2\theta_{13}\sin^2\theta_{23}\,, \\ \Delta m^2_{\mu\mu} &= \sin^2\theta_{12}\Delta m^2_{31} + \cos^2\theta_{12}\Delta m^2_{32} \\ &\quad + \cos\delta_{\rm CP}\sin\theta_{13}\sin 2\theta_{12}\tan\theta_{23}\Delta m^2_{21}. \end{aligned}$$

At present ν_μ disappearance results at LBL provide the best determination of $|\Delta m^2_{32}|$ and θ_{23}, but as seen above, the probability is symmetric with respect to the octant of $\theta_{\mu\mu}$, which implies symmetry around $s^2_{23} = 0.5/c^2_{13}$.

The relevant oscillation probability for ν_e appearance at LBL experiments can be expanded at the second order in the small parameters $\sin\theta_{13}$ and α, and assuming a constant matter density

Int. J. Mod. Phys. A 2026.41. Downloaded from www.worldscientific.com by UNIVERSITY OF CALIFORNIA @ BERKELEY on 09/16/26. Re-use and distribution is [redacted] except for Open Access articles.

it takes the form [176–178]:

$$P_{\nu_\mu\to\nu_e,(\bar\nu_\mu\to\bar\nu_e)} \approx 4\,\sin^2\theta_{13}\,\sin^2\theta_{23}\frac{\sin^2\Delta(1-A)}{(1-A)^2} + \alpha^2\sin^2 2\theta_{12}\,\cos^2\theta_{23}\frac{\sin^2 A\Delta}{A^2} + 8\,\alpha\,J_{\rm CP}^{\rm max}\cos(\Delta\pm\delta_{\rm CP})\,\frac{\sin\Delta A}{A}\,\frac{\sin\Delta(1-A)}{1-A}\,, \tag{14.77}$$

with

$$J_{\rm CP}^{\rm max} = \cos\theta_{12}\sin\theta_{12}\cos\theta_{23}\sin\theta_{23}\cos^2\theta_{13}\sin\theta_{13}\,, \tag{14.78}$$

and

$$\Delta \equiv \frac{\Delta m^2_{31}L}{4E_\nu}\,,\quad A\equiv\frac{2E_\nu V}{\Delta m^2_{31}}\,, \tag{14.79}$$

where V is the effective matter potential in the Earth's crust. Results on ν_e appearance at LBL provide us with the dominant information on leptonic CP violation. Furthermore, α, Δ, and A are sensitive to the sign of Δm^2_{32} (*i.e.*, the type of the neutrino mass ordering). The plus (minus) sign in Eq. (14.77) applies for neutrinos (antineutrinos), and for antineutrinos $V\to -V$, which implies $A\to -A$. Numerically one finds for a typical Earth crust matter density of 3 g/cm^3 that at T2K with $E\sim 0.7$ GeV, matter effects cause $\sim\pm 10\%$ differences in the rates, whereas in NOvA with $E\sim 2$ GeV, we can have $|A|\sim 0.2$. Also, $\alpha^2\approx 10^{-3}$, which implies that the second term in the first line of Eq. (14.77) gives a very small contribution compared to the other terms. Also, the first term in Eq. (14.77) (which dominates for large θ_{13}) depends on $\sin^2\theta_{23}$ and therefore is sensitive to the octant.

The ν_e survival probability relevant for reactor experiments with medium baseline (MBL), $L\sim 1$ km, can be approximated as [175, 179]:

$$P_{\nu_e\to\nu_e} = 1-\sin^2 2\theta_{13}\sin^2\frac{\Delta m^2_{ee}L}{4E_\nu} + \mathcal{O}(\alpha^2)\,, \tag{14.80}$$

where

$$\Delta m^2_{ee} = \cos^2\theta_{12}\Delta m^2_{31} + \sin^2\theta_{12}\Delta m^2_{32}\,. \tag{14.81}$$

These MBL reactor experiments provide the most precise determination of θ_{13}. Furthermore there is an additional effect sensitive to the mass ordering when comparing the disappearance of ν_μ at LBL experiments – which is symmetric with respect to the sign of $\Delta m^2_{\mu\mu}$ given in Eq. (14.7.1) – with that of ν_e disappearance at MBL reactors which is symmetric with respect to the slightly different effective mass-squared difference Δm^2_{ee} given in Eq. (14.81).

Finally, for atmospheric neutrinos, the fluxes contain ν_e, ν_μ, $\bar\nu_e$, and $\bar\nu_\mu$, and for a good fraction of the events, neutrinos travel through the Earth's matter. In the context of 3ν mixing, the dominant oscillation channel of atmospheric neutrinos is $\nu_\mu\to\nu_\tau$ driven by $|\Delta m^2_{32}|$ with an amplitude controlled by θ_{23} with subleading oscillation modes, triggered by Δm^2_{21} and/or θ_{13}, which depend on the octant of θ_{23}, on the mass ordering, and on $\delta_{\rm CP}$. In that respect, an interesting observable is the deviation of e-like events relative to the no-oscillation prediction N_e^0, since in the two-flavour limit one expects $N_e = N_e^0$. Such deviation can be written in the following way (see, *e.g.*, [180]):

$$\frac{N_e}{N_e^0} - 1 \approx (r\sin^2\theta_{23}-1)P_{2\nu}(\Delta m^2_{32},\theta_{13}) + (r\cos^2\theta_{23}-1)P_{2\nu}(\Delta m^2_{21},\theta_{12}) - \sin\theta_{13}\sin 2\theta_{23}\,r\,\Re(A^*_{ee}A_{\mu e})\,. \tag{14.82}$$

Here $r\equiv\Phi_\mu/\Phi_e$ is the flux ratio with $r\approx 2$ in the sub-GeV range and $r\approx 2.6\to 4.5$ in the multi-GeV range. $P_{2\nu}(\Delta m^2,\theta)$ is an effective two-flavour oscillation probability, and $A_{ee}, A_{\mu e}$ are elements of a transition amplitude matrix. The three terms appearing in Eq. (14.82) have a well-defined physical interpretation. The first term is important in the multi-GeV range and is controlled by the mixing angle θ_{13} in $P_{2\nu}(\Delta m^2_{32},\theta_{13})$. This probability can be strongly affected by resonant matter effects [181–186]. Depending on the mass ordering, the resonance will occur either for neutrinos or antineutrinos. The second term is important for sub-GeV events, and it takes into account the effect of oscillations due to Δm^2_{21} and θ_{12} [187–190]. Via the pre-factor containing the flux ratio r, both the first and second terms in Eq. (14.82) depend on the octant of θ_{23}, though in opposite directions: the multi-GeV (sub-GeV) excess is suppressed (enhanced) for $\theta_{23}<45^\circ$. Finally, the last term in Eq. (14.82) is an interference term between θ_{13} and Δm^2_{21} amplitudes and this term shows also dependence on the CP phase $\delta_{\rm CP}$ [180, 190].

Subdominant three neutrino effects can also affect μ-like events. For example, for multi-GeV muon events one can write the excess in μ-like events as [191, 192]

$$\frac{N_\mu}{N_\mu^0} - 1 \approx \sin^2\theta_{23}\left(\frac{1}{r}-\sin^2\theta_{23}\right)P_{2\nu}(\Delta m^2_{32},\theta_{13}) - \frac{1}{2}\sin^2 2\theta_{23}\,[1-\Re(A_{33})]\,. \tag{14.83}$$

The first term is controlled by θ_{13} and is subject to resonant matter effects, similar to the first term in Eq. (14.82), though with a different dependence on θ_{23} and the flux ratio. In the second term, A_{33} is a probability amplitude satisfying $P_{2\nu}(\Delta m^2_{32},\theta_{13}) = 1-|A_{33}|^2$. In the limit $\theta_{13}=0$ we have $\Re(A_{33})=\cos(\Delta m^2_{32}L/2E)$, such that the second term in Eq. (14.83) just describes two-flavour $\nu_\mu\to\nu_\mu$ vacuum oscillations.

14.7.2 *3ν Oscillation Analysis*

We summarize in Table 14.6 the different experiments which dominantly contribute to the present determination of the different parameters in the chosen convention.

The table illustrates that the determination of the leptonic parameters requires global analyses of the data from the different experiments. Over the years, these analyses have been in the hands of a few phenomenological groups. We show in Table 14.7 the results from the latest analyses in Refs. [193–196]. For the sake of comparison, all results are presented in the convention of the listing section as described above.

The table displays the dependence of the present determination of the parameters on variations of the statistical analysis performed by the different groups and on the data samples included. In that last respect, the main difference resides in the latest results from Super-Kamiokande [197, 199] and IceCube/DeepCore [198, 200] atmospheric data which, at present, can only be included in these analysis by directly adding the tabulated χ^2 map provided by the experiments [197, 198].

Altogether the different analyses find consistent results, in particular on the better-known parameters, θ_{12}, θ_{13} and Δm^2_{21} and $|\Delta m^2_{32}|$. The issues which still require clarification are the mass ordering discrimination, the determination of θ_{23} and the leptonic CP phase $\delta_{\rm CP}$:

- The analysis without including the atmospheric χ^2 tables from Refs. [197, 198] show no statistically significant preference for any ordering. Including them, the best fit is for the normal mass ordering with inverted ordering disfavoured with a $\Delta\chi^2$ slightly above 2σ. The result emerges from opposite trends in the long-baseline accelerator appearance data from T2K and NOvA on the one hand, and in the combination of the disappearance channels from accelerator and reactor experiments on the other hand. In the former case, at the time of this review, the tension between T2K and NOvA for NO has reached $\sim 2\sigma$ with the latest NOvA update, whereas they are perfectly consistent for IO. There are ongoing efforts for a joint T2K+NOvA analysis by the collaborations (their preliminary joint analysis [201] performed with previous data samples fully agrees with the results from the analysis of the phenomenological groups). Conversely, the determination of $|\Delta m^2_{3\ell}|$ from ν_μ and ν_e disappearance agrees better for NO than for IO.
- There is no statistically significant preference for the octact of θ_{23} in any of the analysis.

Int. J. Mod. Phys. A 2026.41. Downloaded from www.worldscientific.com
by UNIVERSITY OF CALIFORNIA @ BERKELEY on 09/16/26. Re-use and distribution is strictly not permitted, except for Open Access articles.

Table 14.6: Experiments contributing to the present determination of the oscillation parameters.

Experiment	Dominant	Important
Solar Experiments	θ_{12}	Δm^2_{21}, θ_{13}
Reactor LBL (KamLAND)	Δm^2_{21}	θ_{12}, θ_{13}
Reactor MBL (Daya-Bay, Reno, D-Chooz)	θ_{13}, $\lvert\Delta m^2_{31,32}\rvert$	
Atmospheric Experiments (IC-DC,SK)	θ_{23}, $\lvert\Delta m^2_{31,32}\rvert$, sign$(\Delta m^2_{31,32})$	θ_{13}, $\delta_{\rm CP}$
Accel LBL ν_μ,$\bar\nu_\mu$, Disapp (T2K, NOνA, MINOS, K2K)	$\lvert\Delta m^2_{31,32}\rvert$, θ_{23}	
Accel LBL ν_e,$\bar\nu_e$ App (T2K, NOνA, MINOS)	$\delta_{\rm CP}$, θ_{23}, sign$(\Delta m^2_{31,32})$	θ_{13}

Table 14.7: 3ν oscillation parameters obtained from different global analyses of neutrino data. In all cases, the numbers labeled as NO (IO) are obtained assuming NO (IO), *i.e.*, relative to the respective local minimum. SK-ATM and IC24 makes reference to the tabulated χ^2 maps from Super-Kamiokande [197] and IceCube/DeepCore [198] atmospheric data.

	Ref. [193] w/o SK-ATM & IC24		Ref. [193] w SK-ATM & IC24		Ref. [194] w SK-ATM & IC24		Ref. [195] w SK-ATM*	
NO	$\Delta\chi^2 = 0.6$		Best Fit Ordering		Best Fit Ordering		Best Fit Ordering	
Param	bfp $\pm1\sigma$	3σ range	bfp $\pm1\sigma$	3σ range	bfp $\pm1\sigma$	3σ range	bfp $\pm1\sigma$	3σ range
$\frac{\sin^2\theta_{12}}{10^{-1}}$	$3.07^{+0.12}_{-0.11}$	$2.75 \to 3.45$	$3.08^{+0.12}_{-0.11}$	$2.75 \to 3.45$	$3.03^{+0.14}_{-0.12}$	$2.64 \to 3.45$	$3.04^{+0.16}_{-0.16}$	$2.57 \to 3.55$
$\theta_{12}/^\circ$	$33.68^{+0.73}_{-0.70}$	$31.63 \to 35.95$	$33.68^{+0.73}_{-0.70}$	$31.63 \to 35.95$	$33.40^{+0.87}_{-0.75}$	$30.92 \to 35.97$	$33.46^{+0.99}_{-1.1}$	$30.46 \to 36.57$
$\frac{\sin^2\theta_{23}}{10^{-1}}$	$5.61^{+0.12}_{-0.15}$	$4.30 \to 5.96$	$4.70^{+0.17}_{-0.13}$	$4.35 \to 5.85$	$4.73^{+0.23}_{-0.13}$	$4.37 \to 5.81$	$5.60^{+0.13}_{-0.22}$	$4.32 \to 5.96$
$\theta_{23}/^\circ$	$48.5^{+0.7}_{-0.9}$	$41.0 \to 50.4$	$43.3^{+1.0}_{-0.9}$	$41.3 \to 49.9$	$43.4^{+1.3}_{-0.8}$	$41.4 \to 49.7$	$48.4^{+0.7}_{-1.2}$	$41.2 \to 50.5$
$\frac{\sin^2\theta_{13}}{10^{-2}}$	$2.195^{+0.054}_{-0.058}$	$2.023 \to 2.376$	$2.215^{+0.056}_{-0.058}$	$2.030 \to 2.388$	$2.23^{+0.04}_{-0.06}$	$2.06 \to 2.38$	$2.20^{+0.07}_{-0.04}$	$2.05 \to 2.38$
$\theta_{13}/^\circ$	$8.52^{+0.11}_{-0.11}$	$8.18 \to 8.87$	$8.56^{+0.11}_{-0.11}$	$8.19 \to 8.89$	$8.59^{+0.08}_{-0.12}$	$8.25 \to 8.87$	$8.53^{+0.14}_{-0.08}$	$8.23 \to 8.87$
$\delta_{\rm CP}/^\circ$	177^{+19}_{-20}	$96 \to 422$	212^{+26}_{-41}	$124 \to 364$	216^{+31}_{-23}	$131 \to 365$	202^{+29}_{-22}	$137 \to 360$
$\frac{\Delta m^2_{21}}{10^{-5}\ \mathrm{eV}^2}$	$7.49^{+0.19}_{-0.20}$	$6.92 \to 8.05$	$7.49^{+0.19}_{-0.20}$	$6.92 \to 8.05$	$7.37^{+0.15}_{-0.16}$	$6.93 \to 7.93$	$7.55^{+0.22}_{-0.20}$	$6.98 \to 8.19$
$\frac{\Delta m^2_{32}}{10^{-3}\ \mathrm{eV}^2}$	$2.459^{+0.025}_{-0.023}$	$2.388 \to 2.531$	$2.438^{+0.021}_{-0.019}$	$2.376 \to 2.503$	$2.458^{+0.020}_{-0.020}$	$2.396 \to 2.521$	$2.42^{+0.02}_{-0.02}$	$2.35 \to 2.49$
IO	Best Fit Ordering		$\Delta\chi^2 = 6.1$		$\Delta\chi^2 = 5.0$		$\Delta\chi^2 = 7.7$	
$\frac{\sin^2\theta_{12}}{10^{-1}}$	$3.08^{+0.12}_{-0.11}$	$2.75 \to 3.45$	$3.08^{+0.12}_{-0.11}$	$2.75 \to 3.45$	$3.03^{+0.14}_{-0.12}$	$2.64 \to 3.45$	$3.04^{+0.16}_{-0.16}$	$2.57 \to 3.55$
$\theta_{12}/^\circ$	$33.68^{+0.73}_{-0.70}$	$31.63 \to 35.95$	$33.68^{+0.73}_{-0.70}$	$31.63 \to 35.95$	$33.40^{+0.87}_{-0.75}$	$30.92 \to 35.97$	$33.46^{+0.99}_{-1.1}$	$30.46 \to 36.57$
$\frac{\sin^2\theta_{23}}{10^{-1}}$	$5.62^{+0.12}_{-0.15}$	$4.37 \to 5.97$	$5.50^{+0.12}_{-0.15}$	$4.40 \to 5.84$	$5.45^{+0.15}_{-0.17}$	$4.43 \to 5.83$	$5.57^{+0.14}_{-0.20}$	$4.34 \to 5.93$
$\theta_{23}/^\circ$	$48.6^{+0.7}_{-0.9}$	$41.4 \to 50.6$	$47.9^{+0.7}_{-0.9}$	$41.5 \to 49.8$	$47.6^{+0.9}_{-1.0}$	$41.7 \to 50.0$	$48.3^{+0.8}_{-1.1}$	$41.2 \to 50.3$
$\frac{\sin^2\theta_{13}}{10^{-2}}$	$2.224^{+0.056}_{-0.057}$	$2.053 \to 2.397$	$2.221^{+0.056}_{-0.056}$	$2.060 \to 2.409$	$2.23^{+0.07}_{-0.04}$	$2.08 \to 2.41$	$2.23^{+0.05}_{-0.06}$	$2.06 \to 2.39$
$\theta_{13}/^\circ$	$8.58^{+0.11}_{-0.11}$	$8.24 \to 8.91$	$8.59^{+0.11}_{-0.11}$	$8.25 \to 8.93$	$8.59^{+0.13}_{-0.08}$	$8.29 \to 8.93$	$8.58^{+0.10}_{-0.12}$	$8.25 \to 8.89$
$\delta_{\rm CP}/^\circ$	285^{+25}_{-28}	$201 \to 348$	274^{+22}_{-25}	$201 \to 335$	274^{+25}_{-27}	$193 \to 329$	270^{+23}_{-25}	$200 \to 355$
$\frac{\Delta m^2_{21}}{10^{-5}\ \mathrm{eV}^2}$	$7.49^{+0.19}_{-0.19}$	$6.92 \to 8.05$	$7.49^{+0.19}_{-0.19}$	$6.92 \to 8.05$	$7.37^{+0.15}_{-0.16}$	$6.93 \to 7.93$	$7.55^{+0.22}_{-0.20}$	$6.98 \to 8.19$
$\frac{\Delta m^2_{32}}{10^{-3}\ \mathrm{eV}^2}$	$-2.510^{+0.024}_{-0.025}$	$-2.584 \to -2.438$	$-2.484^{+0.020}_{-0.020}$	$-2.547 \to -2.421$	$-2.502^{+0.021}_{-0.020}$	$-2.564 \to -2.440$	$-2.48\pm^{+0.02}_{-0.02}$	$-2.53 \to -2.40$

*This analysis does not include the latest results of T2K and NOvA presented in the Intern. Conference Neutrino 2024.

- The determination of the leptonic CP phase strongly depends on the mass ordering. For normal ordering the best-fit point is very close to the CP-conserving value of 180° (with $\Delta\chi^2 < 1$) while for inverted ordering, the best fit points for both data variants are close to maximal CP violation $\delta_{\rm CP} = 270^\circ$ (within 1σ).

14.7.3 *Convention-independent Measures of Leptonic CP Violation in 3ν Mixing*

In the framework of 3ν mixing leptonic CP violation can also be quantified in terms of the leptonic Jarlskog invariant [202], defined by:

$$\Im\left[U_{\alpha i}U^*_{\alpha j}U^*_{\beta i}U_{\beta j}\right] \equiv \sum_{\gamma=e,\mu,\tau}\sum_{k=1,2,3} J_{\rm CP}\,\epsilon_{\alpha\beta\gamma}\,\epsilon_{ijk} \equiv J^{\rm max}_{\rm CP}\,\sin\delta_{\rm CP}\,. \tag{14.84}$$

With the convention in Eq. (14.33) $J^{\rm max}_{\rm CP}$ is the combination of mixing angles in Eq. (14.78). For example, from the analysis in Ref. [193]

$$J^{\rm max}_{\rm CP} = 0.0333 \pm 0.0007\,(\pm 0.0017)\,, \tag{14.85}$$

at 1σ (3σ) for both orderings, while the the dependence of the prefered value of $\delta_{\rm CP}$ on the octant implies a a value $J^{\rm best}_{\rm CP} = 0.0015$ (-0.032) in normal (inverted) ordering.

The status of the determination of leptonic CP violation can also be graphically displayed by projecting the results of the global analysis in terms of leptonic unitarity triangles [203–205]. Since in the analysis U is unitary by construction, any given pair of rows or columns can be used to define a triangle in the complex plane. There are a total of six possible triangles corresponding to the unitary conditions

$$\sum_{i=1,2,3} U_{\alpha i}U^*_{\beta i} = 0 \text{ with } \alpha \neq \beta\,, \qquad \sum_{\alpha=e,\mu,\tau} U_{\alpha i}U^*_{\alpha j} = 0 \text{ with } i \neq j\,. \tag{14.86}$$

As an illustration we show in Fig. 14.9 the recasting of the allowed regions of the analysis in Ref. [193] in terms of one leptonic unitarity triangle. We show the triangle corresponding to the unitarity conditions on the first and third columns (after the shown rescaling), which is the equivalent to the one usually shown for the quark sector. In this figure, the absence of CP violation would imply a flat triangle, *i.e.*, $\Im(z) = 0$. So the CL at which leptonic

Int. J. Mod. Phys. A 2026.41. Downloaded from www.worldscientific.com by UNIVERSITY OF CALIFORNIA @ BERKELEY on 09/16/26. Re-use and distribution is except for Open Access articles.

CP violation is being observed would be given by the CL at which the region crosses the horizontal axis. Notice however, that this representation is made *under the assumption of a unitary U matrix* and therefore does not provide any test of unitarity in the leptonic sector.

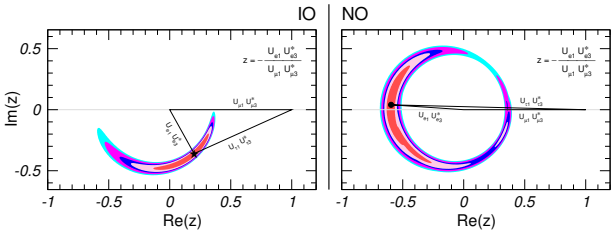

Figure 14.9: Leptonic unitarity triangle for the first and third columns of the mixing matrix. After scaling and rotating the triangle so that two of its vertices always coincide with $(0,0)$ and $(1,0)$ the figure shows the 1σ, 90%, 2σ, 99%, 3σ CL (2 dof) allowed regions of the third vertex for the IO (left) and NO (right) from the analysis in Ref. [193].

14.8 Beyond 3ν: Additional Neutrinos at the eV Scale

As mentioned in Sec. 14.1, whatever the extension of the SM we want to consider, it must contain only three light active neutrinos. Therefore if we need more than three light massive neutrinos, we must add sterile neutrinos to the particle content of the model.

Historically, models with extended light neutrino sectors were invoked to explain a set of anomalies observed at short baselines and which could not be explained within the 3ν framework but could be interpreted as hints for the existence of additional neutrino states with masses at the eV scale. These anomalies have been under study by the experimental community with a set of follow-up measurements performed at SBL both at reactors and accelerators (see the corresponding subsections in Sec. 14.6.4 and Sec. 14.6.3). In brief:

- the LSND experiment [128] reported evidence for $\bar{\nu}_\mu \to \bar{\nu}_e$ transitions with $E/L \sim 1$ eV^2, where E and L are the neutrino energy and the distance between source and detector, respectively (see *Short Baseline Experiments* subsection of Sec.14.6.3).
- this effect was further explored by the MiniBooNE experiment [206], which reported a yet unexplained event excess in the low-energy region of the electron neutrino and antineutrino event spectra. No significant excess is found at higher neutrino energies. Interpreting the data in terms of oscillations, parameter values consistent with the ones from LSND were obtained. The MicroBooNE experiment [207] was designed to identify the nature of the low-energy MiniBooNE excess and was able to exclude that it was composed enterely of ν_e at 99%CL [208] and rule out part of the sterile neutrino oscillation parameter space [133].
- the calculations of the neutrino flux emitted by nuclear reactors in Refs. [139,140] predicted a neutrino rate that was a few percent higher than observed in short-baseline ($L \lesssim 100$ m) reactor experiments at the time. This "reactor anomaly" could be explained by assuming $\bar{\nu}_e$ disappearance due to averaged oscillations with $\Delta m^2 \sim 1$ eV^2 [209]. Over the years the flux predictions from [139,140] have not been supported by the reactor antineutrino flux measurement at Daya Bay [141, 142] pointing to a lower flux from ^{235}U, in particular. In addition, several reactor experiments NEOS, STEREO, PROSPECT, DANSS, SOLID and Neutrino4 have searched, and, all except the last one, have excluded a L/E variation compatible with $\Delta m^2 \sim 1$ eV^2 oscillations. In the last years the reactor flux calculations have been revisited [145–147] and in most cases lower fluxes are predicted, in agreement with the flux measurement at Daya Bay [144]. These new fluxes, correspondingly eliminate the significance of the anomaly [210].
- radioactive source experiments at the Gallium solar neutrino experiments both in SAGE and GALLEX/GNO obtained an event rate lower than expected. This result was confirmed by the BEST experiment [211]. If not due to uncertainties in the interaction cross-section, this effect by itself can be explained by the hypothesis of ν_e disappearance due to oscillations with $\Delta m^2 \gtrsim 1$ eV^2 ("Gallium anomaly") [212–214]. This intepretation, however is in tension with the analysis of solar neutrino experiments [215], and most recently has been excluded with high significance by KATRIN [216] (see left panel in Fig. 14.10, taken from Ref. [217]).

As mentioned above, historically, these anomalies opened the question of whether they could all be consistently described in combination with the rest of the neutrino data – in particular with the negative results on the disappearance of ν_μ at short distances – by extending the neutrino mass and mixing framework to account for some additional sterile states.

Quantitatively one can start by adding a fourth massive neutrino state to the spectrum and perform a global data analysis to answer this question. In this case there are six possible four-neutrino schemes that can, in principle, accommodate the results of solar+KamLAND and atmospheric+LBL neutrino experiments as well as the SBL result. They can be divided into two classes: (2+2) and (3+1). In (2+2) schemes, there are two pairs of close masses (one pair responsible for solar results and the other for atmospheric [218]) separated by the $\mathcal{O}(\,\text{eV})$ gap. In this case the transition into the sterile neutrino is a solution of either the solar or the atmospheric neutrino problem, or the sterile neutrino takes part in both. Consequently, a (2+2)-spectrum is easier to test because the required mixing of sterile neutrinos in either solar and/or atmospheric oscillations would modify their effective matter potential in the Sun and in the Earth, giving distinctive effects in the solar and/or atmospheric neutrino observables. Those distinctive effects were not observed so oscillations into sterile neutrinos did not describe well either solar or atmospheric data. Consequently, as soon as the early 2000's 2+2 spectra could be ruled out already beyond 3-4 σ.

On the contrary, for a (3+1)-spectrum (and more generally for a $3+N$-spectrum with an arbitrary N number of sterile states), the sterile neutrino(s) could be only slightly mixed with the active ones and mainly provide a description of the SBL results. In this case, the oscillation probabilities for experiments working at $E/L \sim 1$ eV^2 take a simple form:

$$P_{\alpha\alpha} = 1 - \sin^2 2\theta_{\alpha\alpha} \sin^2 \Delta\,, \qquad P_{\mu e} = \sin^2 2\theta_{\mu e} \sin^2 \Delta\,, \quad (14.87)$$

where $\Delta \equiv \Delta m^2_{41} L/4E$ and one can define effective mixing angles

$$\sin^2 2\theta_{\alpha\alpha} \equiv 4|U_{\alpha 4}|^2(1-|U_{\alpha 4}|^2)\,, \qquad \sin^2 2\theta_{\mu e} \equiv 4|U_{\mu 4}|^2|U_{e4}|^2\,. \quad (14.88)$$

In here $\alpha = e, \mu$ and $U_{\alpha 4}$ are the elements of the lepton mixing matrix describing the mixing of the 4th neutrino mass state with the electron and muon flavour. In this scenario, there is no sensitivity to CP violation in the the Δ driven oscillations, so the relations above are valid for both neutrinos and antineutrinos. At linear order in the mixing elements one can derive a relation between the amplitudes of appearance and disappearance probabilities:

$$4\sin^2 2\theta_{\mu e} \approx \sin^2 2\theta_{ee} \sin^2 2\theta_{\mu\mu}\,. \quad (14.89)$$

This relation implies a constraint between the possible results in disappearance and appearance experiments which jeopardizes a consistent description of all of the SBL anomalies. Over the years, different groups have performed a variety of such global analyses leading to different quantitative conclusions on the statistical quality of the global fit (see for example [219–224]).

But, generically, the results of all global analysis show that there is significant tension between groups of different data sets – in particular between appearance and disappearance results – and Eq. (14.89) makes it difficult to obtain a good global fit as illustrated in the right panel of Fig. 14.10 taken from Ref. [224] which

Int. J. Mod. Phys. A 2026.41. Downloaded from www.worldscientific.com
by UNIVERSITY OF CALIFORNIA @ BERKELEY on 09/16/26. Re-use and distribution is strictly not permitted, except for Open Access articles.

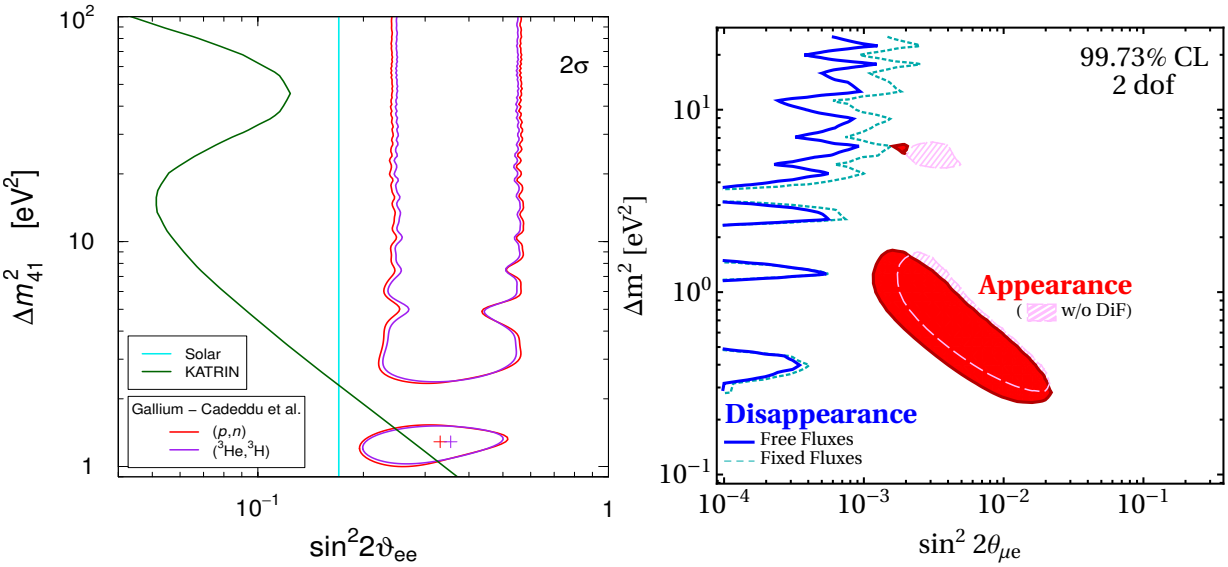

Figure 14.10: *Left*: Status of the intepretation of the Gallium anomaly in 3+1 scenarios from Ref. [217]. The contours *Right*: Preferred region of short-baseline appearance experiments (red region), compared to the region excluded by disappearance experiments (blue line) from Ref. [224].

concluded that 3+1 scenario is excluded at 4.7σ level pointing to the need of some additional form of new physics or to a combination of BSM and SM effects to account for all the anomalies. See Ref. [225] for a recent review on the subject. Cosmological observations can provide complementary information on the number of relativistic neutrino states in thermal equilibrium in the early Universe and on the sum of their masses, which sets further constraints on light sterile neutrino scenarios (see Chapter 26 of this *Review*, "Neutrinos in cosmology").

14.9 Laboratory Probes of ν Mass Scale and its Nature

As described in Secs.14.4 and 14.5, neutrino flavour oscillations in vacuum and flavour transitions in matter only depend on the differences between the neutrino masses-squared, Δm^2_{ij}, and on the mixing matrix elements, U_{ij}. However, they are insensitive to the absolute mass scale for the neutrinos, m_i. They also give us no information on whether they are Dirac or Majorana particles.

Clearly, the observation of flavour oscillations implies a lower bound on the mass of the heavier neutrino in Δm^2_{ij}, $|m_i| \geq \sqrt{\Delta m^2_{ij}}$ for $\Delta m^2_{ij} > 0$. However, there is no upper bound on m_i. In particular, oscillation results allow the neutrino spectrum to be approximately degenerate at a mass scale that is much higher than the $\sqrt{\Delta m^2_{ij}}$ that they determine. Information of the mass scale of the neutrino is provided by other types of experiments. Here we briefly summarize the most sensitive laboratory probes of the neutrino mass scale and on whether they are Dirac or Majorana particles. Cosmological observations provide, albeit indirectly, complementary information on the neutrino mass scale as it is reviewed in Chapter 26 of this *Review*, "Neutrinos in cosmology".

14.9.1 *Constraints from Kinematics of Weak Decays*

The only model-independent information on the neutrino masses, rather than mass differences, can be extracted from the energy-momentum conservation relation in reactions in which a neutrino or an antineutrino is involved.

Historically these bounds were labeled as limits on the mass of the flavour neutrino states corresponding to the charged flavour involved in the decay. Fermi proposed in 1933 such a kinematic search for the ν_e neutrino mass (which we will label here as $m^{\rm eff}_{\nu_e}$) in the end part of the beta spectra in ^{3}H beta decay $^3\text{H} \to {}^3\text{He} + e^- + \bar{\nu}_e$.

Because ^{3}H beta decay is a superallowed transition, the nuclear matrix elements are energy independent, so the electron spectrum is determined exclusively by the phase space

$$\begin{aligned} \frac{dN}{dE} &= C\,p\,E\,(Q-T)\sqrt{(Q-T)^2-(m^{\rm eff}_{\nu_e})^2}\,F(E) \\ &\equiv R(E)\,\sqrt{(E_0-E)^2-(m^{\rm eff}_{\nu_e})^2}\,. \end{aligned} \tag{14.90}$$

E_0 is the mass difference between the inital and final nucleus, $E = T + m_e$ is the total electron energy, p its momentum, $Q \equiv E_0 - m_e$ is the maximum kinetic energy of the electron and final state Coulomb interactions are contained in the Fermi function $F(E)$. $R(E)$ in the second equality contains all the m_ν-independent factors.

The Kurie function is defined as $K(T) \equiv \sqrt{\frac{dN}{dE}\,\frac{1}{pEF(E)}}$. From Eq. (14.90), we see that if $m^{\rm eff}_{\nu_e}$=0 $K(T)$ would depend linearly on T. A non-vanishing neutrino mass then provokes a distortion from the straight-line T-dependence at the endpoint, So for $m^{\rm eff}_{\nu_e} = 0$, $T_{\rm max} = Q$, while for $m^{\rm eff}_{\nu_e} \neq 0$, $T_{\rm max} = Q - m^{\rm eff}_{\nu_e}$. In ^{3}H beta decay $Q = 18.6$ KeV is very small and therefore, this decay is more sensitive to this $m^{\rm eff}_{\nu_e}$-induced distortion.

The most recent result on the kinematic search for neutrino mass in tritium decay is from KATRIN [226], an experiment which has found so far no indication of $m^{\rm eff}_{\nu_e} \neq 0$ and sets an upper limit

$$m^{\rm eff}_{\nu_e} < 0.45 \text{ eV}\,, \tag{14.91}$$

at 90% CL improving over the previous bound from the Mainz [227] and Troitsk [228] experiments which constrained $m^{\rm eff}_{\nu_e} < 2.2$ eV at 95% CL. KATRIN continues running and should soon reach its target sensitivity limit of $m^{\rm eff}_{\nu_e} \sim 0.3$ eV. Future experimental efforts on tritium beta decay include KATRIN++, PTOLEMY, and Project-8. In particular, Project 8 is exploring a new technique for β-spectrometry based on cyclotron radiation [229].

An alternative isotope to Tritium is ^{163}Ho [230] which presents the advantage of a smaller $Q = 2.8$ KeV. It decays via electron capture to ^{163}Dy. Currently, there are two experiments exploring this decay to probe the neutrino mass: ECHo [231], and HOLMES [232]. These experiments are complementary to tritium-based searches from a technical point of view. Also, the decay of ^{163}Ho determines the effective electron neutrino mass as opposed to antineutrino in Tritium.

For the other flavours the present limits compiled in the listing

Int. J. Mod. Phys. A 2026.41. Downloaded from www.wo
by UNIVERSITY OF CALIFORNIA @ BERKELEY on 09/16/26. Re-use and distribution is
except for Open Access articles.

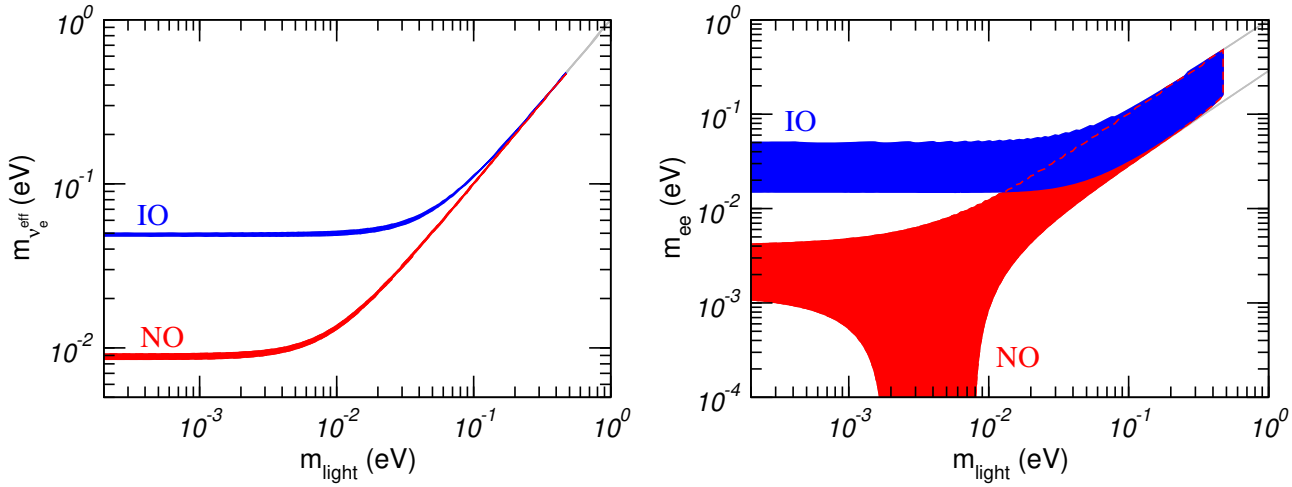

Figure 14.11: Allowed 95% CL ranges (1 dof) for the neutrino mass observable determined in ^{3}H beta decay (left panel) and in $0\nu\beta\beta$ (right panel) in the framework of 3ν mixing as a function of the lightest neutrino mass. The ranges are obtained by projecting the results of the global analysis of oscillation data (w/o SK-atm) in Ref. [193]. The region for each ordering is defined with respect to its local minimum.

section of the PDG read

$$m_{\nu_\mu}^{\rm eff} < 190 \text{ keV (90\% CL)} \qquad \text{from} \qquad \pi^- \to \mu^- + \bar\nu_\mu\,, \quad (14.92)$$

$$m_{\nu_\tau}^{\rm eff} < 18.2 \text{ MeV (95\% CL)} \qquad \text{from} \qquad \tau^- \to n\pi + \nu_\tau\,. \quad (14.93)$$

In the presence of mixing and for neutrinos with small mass differences, the distortion of the beta spectrum is given by the sum of the individual spectra generated incoherently by each neutrino massive state weighted with the relevant mixing matrix element squared [233]:

$$\frac{dN}{dE} = R(E)\sum_i |U_{ei}|^2 \sqrt{(E_0-E)^2 - m_i^2}\,\Theta(E_0-E-m_i)\,. \quad (14.94)$$

The step function $\Theta(E_0 - E - m_i)$ arises because a neutrino with a given mass m_i can only be produced if the available energy is larger than its mass. Equation (14.94) shows the two main effects of the neutrino masses and mixings on the electron energy spectrum: First, kinks appear at the electron energies $E_e^{(i)} = E \sim E_0 - m_i$ with sizes that are determined by $|U_{ei}|^2$. Second, the endpoint shifts to $E_{\rm ep} = E_0 - m_0$, where m_0 is the lightest neutrino mass. Corrections are induced once the energy resolution of the experiment is considered. [234, 235]

In the 3-ν mixing scenario, the distortion of the spectrum can still be effectively described by a single parameter – which we denote as $m_{\nu_e}^{\rm eff}$ – if for all neutrino states $E_0 - E = Q - T \gg m_i$. In this case, one can expand Eq. (14.94) as:

$$\frac{dN}{dE} \simeq R(E)\sum_i |U_{ei}|^2 \sqrt{(E_0-E)^2 - (m_{\nu_e}^{\rm eff})^2}\,, \quad (14.95)$$

with

$$(m_{\nu_e}^{\rm eff})^2 = \frac{\sum_i m_i^2 |U_{ei}|^2}{\sum_i |U_{ei}|^2} = \sum_i m_i^2 |U_{ei}|^2\,, \quad (14.96)$$

where unitarity is assumed in the second equality. In this approximation, the distortion of the endpoint of the spectrum is described by a single parameter, and with the present results from KATRIN, it is bounded to be

$$0.45 \text{ eV} \geq m_{\nu_e}^{\rm eff} = \sqrt{\sum_i m_i^2 |U_{ei}|^2}$$
$$= \begin{cases} \sqrt{m_0^2 + \Delta m_{21}^2(1 - c_{13}^2 c_{12}^2) + \Delta m_{32}^2 s_{13}^2} & \text{in NO}\,, \\ \sqrt{m_0^2 - \Delta m_{21}^2 c_{13}^2 c_{12}^2 - \Delta m_{32}^2 c_{13}^2} & \text{in IO}\,, \end{cases} \quad (14.97)$$

where $m_0 = m_1\,(m_3)$ is the lightest neutrino mass in the NO (IO) spectrum. Correspondingly the bounds in Eqs.(14.92) and (14.93) apply to the combinations $\sum_i m_i^2 |U_{\alpha i}|^2$ for $\alpha = \mu$ and τ respectively. So with the values known of the mixing matrix elements, the strongest constraint on the absolute value of the neutrino mass comes from Tritium beta decay.

From Eq. (14.97) we see that, given the present knowledge of the neutrino mass differences and their mixing from oscillation experiments, it is possible to translate the experimental information of $m_{\nu_e}^{\rm eff}$ on a corresponding range for the lightest neutrino mass and that such relation depends on the ordering of the states. We plot in Fig. 14.11 the recasting of the allowed regions of the analysis in Ref. [193] in terms of the allowed range $m_{\nu_e}^{\rm eff}$ as a function of $m_{\rm light} \equiv m_0$. In particular, one finds that the results of oscillation experiments imply a lower bound on $m_{\nu_e}^{\rm eff} > 0.048$ (0.0085) eV for IO (NO) at 95% CL.

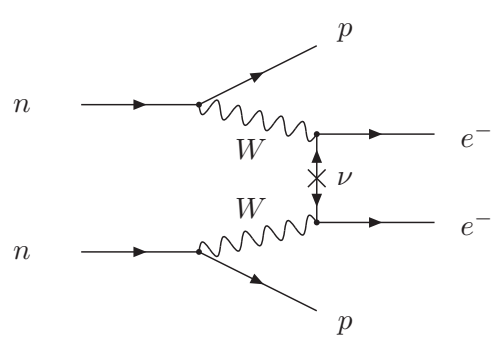

Figure 14.12: Feynman diagram for neutrinoless double-beta decay.

Int. J. Mod. Phys. A 2026.41. Downloaded from www.worldscientific.com
by UNIVERSITY OF CALIFORNIA @ BERKELEY on 09/16/26. Re-use and distribution is strictly not permitted, except for Open Access articles.

14.9.2 *Dirac vs. Majorana: Neutrinoless Double-beta Decay*

The most sensitive probe to whether neutrinos are Dirac or Majorana states is the neutrinoless double beta decay ($0\nu\beta\beta$):

$$(A, Z) \to (A, Z+2) + e^- + e^- . \tag{14.98}$$

In the presence of neutrino masses and mixing, the process in Eq. (14.98) can be generated at lower order in perturbation theory by the term represented in Fig. 14.12. The corresponding amplitude is proportional to the product of the two leptonic currents

$$\begin{aligned} M_{\alpha\beta} &\propto \left[\bar{e}\gamma_\alpha(1-\gamma_5)\nu_e\right]\left[\bar{e}\gamma_\beta(1-\gamma_5)\nu_e\right] \\ &\propto \sum_i (U_{ei})^2 \left[\bar{e}\gamma_\alpha(1-\gamma_5)\nu_i\right]\left[\bar{e}\gamma_\beta(1-\gamma_5)\nu_i\right] . \end{aligned} \tag{14.99}$$

The neutrino propagator in Fig. 14.12 can only arise from the contraction $\langle 0 \,|\, \nu_i(x)\nu_i(y)^T \,|\, 0\rangle$. However, if the neutrino is a Dirac particle ν_i field annihilates a neutrino state and creates an antineutrino state, and neutrino and antineutrino states are different, so the contraction $\langle 0 \,|\, \nu_i(x)\nu_i(y)^T \,|\, 0\rangle = 0$ and $M_{\alpha\beta} = 0$. On the other hand, if ν_i is a Majorana particle, neutrino and antineutrino are described by the same field and $\langle 0 \,|\, \nu_i(x)\nu_i(y)^T \,|\, 0\rangle \neq 0$.

The conclusion is that in order to induce the $0\nu\beta\beta$ decay, neutrinos must be Majorana particles. This is consistent with the fact that the process (14.98) violates the total lepton number by two units. Conversely, if $0\nu\beta\beta$ decay is observed, massive neutrinos cannot be Dirac states [236].

It is important to stress that neutrinoless double-beta decay could be dominantly induced by other new physics effects beyond that of Majorana neutrino masses. Consequently, the connection between the observation or limitation of the neutrinoless double beta decay and the neutrino mass can only be made under some assumption about the source of total lepton number violation in the model.

The observable determined by the experiments is the half-life of the decay. Under the assumption that the Majorana neutrino mass is the only source of lepton number violation at low energies, the decay half-life is given by:

$$(T^{0\nu}_{1/2})^{-1} = G^{0\nu} \left|M^{0\nu}\right|^2 \left(\frac{m_{ee}}{m_e}\right)^2 , \tag{14.100}$$

where $G^{0\nu}$ is the phase space integral taking into account the final atomic state, $|M^{0\nu}\ |$ is the nuclear matrix element of the transition, and m_{ee} is the *effective Majorana mass of* ν_e,

$$\begin{aligned} m_{ee} &= \left|\sum_i m_i U_{ei}^2\right| \\ &= \begin{cases} \left|m_0 c_{12}^2 c_{13}^2 + \sqrt{\Delta m_{21}^2 + m_0^2}\, s_{12}^2 c_{13}^2 e^{2i(\eta_2-\eta_1)} + \sqrt{\Delta m_{32}^2 + \Delta m_{21}^2 + m_0^2}\, s_{13}^2 e^{-2i(\delta_{\rm CP}+\eta_1)}\right| & \text{in NO} , \\ \left|m_0 s_{13}^2 + \sqrt{m_0^2 - \Delta m_{32}^2}\, s_{12}^2 c_{13}^2 e^{2i(\eta_2+\delta_{\rm CP})} + \sqrt{m_0^2 - \Delta m_{32}^2 - \Delta m_{21}^2}\, c_{12}^2 c_{13}^2 e^{2i(\eta_1+\delta_{\rm CP})}\right| & \text{in IO} , \end{cases} \end{aligned} \tag{14.101}$$

which, in addition to the masses and mixing parameters that affect the tritium beta decay spectrum, also depends on the leptonic CP-violating phases. We plot in Fig. 14.11 the recasting of the allowed regions of the analysis in Ref. [193] in terms of the allowed range m_{ee} as a function of $m_{\rm light} \equiv m_0$ for the two orderings. As a consequence of the dependence on the unknown Majorana phases, the allowed range of m_{ee} for a given value of $m_{\rm light}$ and ordering is substantially broader than that of $m^{\rm eff}_{\nu_e}$. Nevertheless, the results of oscillation experiments imply a lower bound on the effective Majorana mass for the IO, which at 95%CL reads $m_{ee} > 0.016$ eV.

From Eq. (14.100) we see that nuclear structure details enter the relation between the decay rate (or lifetime) and the effective Majorana mass. As a consequence, uncertainties in the nuclear structure calculations result in a spread of m_{ee} values for a given $T^{0\nu}_{1/2}$ by a factor of 2–3 [237].

We present in Sec. 14.9.3 a brief description of the experimental searches for neutrinoless double-beta decay. At the time of writing of this review, the strongest bound on $0\nu\beta\beta$ decay lifetimes came for Xenon and Germanium from the KamLAND-Zen [238] and GERDA [239] experiments, respectively. They have set a bound on the corresponding half-lives of $T^{0\nu}_{1/2} > 3.8 \times 10^{26}$ yr, and $T^{0\nu}_{1/2} > 1.8 \times 10^{26}$ yr, at 90% CL. Using a variety of nuclear matrix element calculations, the corresponding upper bounds on the effective Majorana mass are

$$m_{ee} < 28 - 122 \text{ meV} \tag{14.102}$$

$$m_{ee} < 79 - 180 \text{ meV} . \tag{14.103}$$

14.9.3 *Experimental Search for Neutrinoless Double-beta Decay*

There are 35 candidate nuclei for double-beta decay. Currently, experiments using ^{136}Xe and ^{76}Ge have reported the most sensitive searches for $0\nu\beta\beta$. In order to optimize the ability to observe this process it is important to pursue searches with as many isotopes as possible. Indeed, different isotopes require different, complementary detection technologies, offer different uncertainties from nuclear matrix elements, different backgrounds, and further enable investigation of the mechanism behind the $0\nu\beta\beta$.

The $0\nu\beta\beta$ signature has two electrons whose energies sum to the Q-value of the nuclear transition. Their energies can be measured with ionization, scintillation, or through phonons, depending upon the detector technology. In some experiments, a combination of two techniques is used to enhance sensitivity. Assuming a background-free measurement, the sensitivity to the half-life is proportional to the product of the signal detection efficiency ε, the source mass M, and the measurement time t. If instead there are backgrounds, it is proportional to $\varepsilon\sqrt{\frac{Mt}{b\Delta E}}$, where b is the background rate, and ΔE is the energy resolution.

Among experiments using ionization detection, ultra-high-purity germanium detectors provides the best sensitivity due to their high energy resolution and low background. GERDA has achieved a background level of $(5.2^{+1.6}_{-1.3}) \times 10^{-4}$ counts/(keV·kg·year) [239], which enabled a background-free search. The final result from GERDA on the $0\nu\beta\beta$ half-life of ^{76}Ge limits it to $T_{1/2} > 1.8 \times 10^{26}$ years at 90% CL. The Majorana Demonstrator achieved energy resolution of 2.5 keV FWHM (full width at half maximum) at the Q-value (2.039 MeV) [240] and set a half-life limit of $T_{1/2} > 8.3 \times 10^{25}$ years at 90% CL. The GERDA and Majorana collaborations have united and formed, together with new groups, the LEGEND collaboration. LEGEND has adopted a phased approach toward the deployment of a tonne of enriched Ge detectors [241]. The first phase of LEGEND based on approximately 200 kg of enriched Ge uses the GERDA infrastructure at LNGS and has sharted taking it's first data. The second phase of LEGEND has been approved as a one ton experiment in a new cryostat reaching a discovery sensitivity of half-lifes beyond 10^{28} years. In China, CDEX-300ν will use 225 kg of enriched Ge is under preparation [242] in the existing CEDX-DM infrastructure at the China Jinping Underground Laboratory.

Liquid scintillator detectors have a simple structure that can be used in existing large detectors with low background environments. By adding an inner balloon to contain xenon-loaded liquid scintillator to the KamLAND detector, KamLAND-Zen uses

Int. J. Mod. Phys. A 2026.41. Downloaded from www.worldscientific.com by UNIVERSITY OF CALIFORNIA @ BERKELEY on 09/16/26. Re-use and distribution is [redacted] except for Open Access articles.

745 kg of xenon that is 90.9% enriched in ^{136}Xe. KamLAND-Zen reported a half-life limit of $> 3.8 \times 10^{26}$ years at 90% CL [238]. The SNO detector has also been upgraded to hold liquid scintillator for the SNO+ experiment [243]. SNO+ will be loaded with 0.5% natural tellurium, corresponding to approximately 1.3 t of ^{130}Te in order to search for $0\nu\beta\beta$.

With a time projection chamber, one can utilize both ionization and scintillation signals. EXO-200 used a liquid xenon time projection chamber with enriched Xe and reported a half-life limit of $T_{1/2} > 3.5 \times 10^{25}$ years at 90% CL [244] for ^{136}Xe. Based on the technology validated by EXO-200, nEXO plans to use about 5,000 kg of enriched xenon [245]. NEXT has been developing a high-pressure xenon gas time projection chamber with electroluminescent amplification and optical readouts. An energy resolution of 1% FWHM at the Q-value of ^{136}Xe $0\nu\beta\beta$ has demonstrated with NEXT-White detector [246].

CUORE uses a cryogenic bolometer to measure the recoil electron energies in a calorimetric way. The detector is composed of 988 TeO_2 bolometers with a total mass of 742 kg, corresponding to 206 kg of ^{130}Te, and was operated at 10 mK. CUORE set a half-life limit of $T_{1/2} > 3.5 \times 10^{25}$ years at 90% CL for ^{130}Te [247]. In order to further reduce backgrounds for future searches based on the CUORE technology, CUPID proposes to simultaneously measure the calorimetric signal and the scintillation light with a tonne-scale bolometric detector. A prototype has been used to demonstrate the technology and also to search for $0\nu\beta\beta$ with ^{82}Se [248] and ^{100}Mo [249].

AMoRE also uses the simultaneous detection of heat and scintillation. Using ^{100}Mo-enriched and ^{48}Ca-depleted $CaMoO_4$ crystals with a total mass of 6.2 kg (AMoRE-I) were operated in Yangyang underground laboratory located in South Korea, searching for $0\nu\beta\beta$ with ^{100}Mo [250]. The AMoRE-I experiment has established a half-life limit of $T_{1/2} > 2.9 \times 10^{24}$ with this isotope [251].

A tracker-calorimeter technique is employed in NEMO. Source isotopes are hosted in thin foils surrounded by a tracking detector, which in turn is surrounded by a calorimeter. Full topological event reconstruction with this configuration enables background rejection and which can provide additional event information in the event of a discovery. The NEMO-3 experiment used seven isotopes, the largest of which was 7 kg of ^{100}Mo. No evidence of a signal was found in a 34.3 kg-yr exposure of this isotope, resulting in a lower limit of $T_{1/2} > 1.1 \times 10^{24}$ [252].

References

[1] J. N. Bahcall, *NEUTRINO ASTROPHYSICS* (1989), ISBN 9780521379755.

[2] R. N. Mohapatra and P. B. Pal, World Sci. Lect. Notes Phys. **60**, 1 (1998), [World Sci. Lect. Notes Phys.72,1(2004)].

[3] C. W. Kim and A. Pevsner, Contemp. Concepts Phys. **8**, 1 (1993).

[4] B. Kayser, F. Gibrat-Debu and F. Perrier, World Sci. Lect. Notes Phys. **25**, 1 (1989).

[5] C. Giunti and C. W. Kim, *Fundamentals of Neutrino Physics and Astrophysics* (2007), ISBN 9780198508717.

[6] M. C. Gonzalez-Garcia and Y. Nir, Rev. Mod. Phys. **75**, 345 (2003), [hep-ph/0202058].

[7] M. C. Gonzalez-Garcia and M. Maltoni, Phys. Rept. **460**, 1 (2008), [arXiv:0704.1800].

[8] A. Pilaftsis, Z. Phys. **C55**, 275 (1992), [hep-ph/9901206].

[9] P. Minkowski, Phys. Lett. **67B**, 421 (1977).

[10] P. Ramond, in "International Symposium on Fundamentals of Quantum Theory and Quantum Field Theory," (1979), [hep-ph/9809459].

[11] M. Gell-Mann, P. Ramond and R. Slansky, Conf. Proc. **C790927**, 315 (1979), [arXiv:1306.4669].

[12] T. Yanagida, Conf. Proc. C **7902131**, 95 (1979).

[13] R. N. Mohapatra and G. Senjanovic, Phys. Rev. Lett. **44**, 912 (1980).

[14] J. Schechter and J. W. F. Valle, Phys. Rev. **D21**, 309 (1980).

[15] J. Schechter and J. W. F. Valle, Phys. Rev. **D22**, 2227 (1980).

[16] J. Schechter and J. W. F. Valle, Phys. Rev. **D24**, 1883 (1981), [Erratum: Phys. Rev.D25,283(1982)].

[17] Z. Maki, M. Nakagawa and S. Sakata, Prog. Theor. Phys. **28**, 870 (1962).

[18] Y. Katayama *et al.*, Prog. Theor. Phys. **28**, 675 (1962).

[19] B. Pontecorvo, Zh. Eksp. Teor. Fiz. **53**, 1717 (1967).

[20] N. Cabibbo, Phys. Rev. Lett. **10**, 531 (1963).

[21] M. Kobayashi and T. Maskawa, Prog. Theor. Phys. **49**, 652 (1973).

[22] S. Antusch *et al.*, JHEP **10**, 084 (2006), [hep-ph/0607020].

[23] S. Antusch and O. Fischer, JHEP **10**, 094 (2014), [arXiv:1407.6607].

[24] V. N. Gribov and B. Pontecorvo, Phys. Lett. **28B**, 493 (1969).

[25] E. Akhmedov, in "International Conference on History of the Neutrino: 1930-2018 Paris, France, September 5-7, 2018," (2019), [arXiv:1901.05232].

[26] L. Wolfenstein, Phys. Rev. D **17**, 2369 (1978).

[27] A. Halprin, Phys. Rev. **D34**, 3462 (1986).

[28] A. J. Baltz and J. Weneser, Phys. Rev. **D37**, 3364 (1988).

[29] P. D. Mannheim, Phys. Rev. **D37**, 1935 (1988).

[30] L. Landau, Phys. Z. Sov. **2**, 46 (1932).

[31] C. Zener, Proc. Roy. Soc. Lond. **A137**, 696 (1932).

[32] E. Majorana, Nuovo Cim. **9**, 43 (1932).

[33] E. C. G. Stueckelberg, Helv. Phys. Acta **5**, 369 (1932).

[34] T.-K. Kuo and J. T. Pantaleone, Rev. Mod. Phys. **61**, 937 (1989).

[35] S. J. Parke, Phys. Rev. Lett. **57**, 1275 (1986).

[36] W. C. Haxton, Phys. Rev. Lett. **57**, 1271 (1986).

[37] S. T. Petcov, Phys. Lett. B **191**, 299 (1987).

[38] S. P. Mikheyev and A. Y. Smirnov, Sov. J. Nucl. Phys. **42**, 913 (1985).

[39] J. N. Bahcall *et al.*, Rev. Mod. Phys. **54**, 767 (1982).

[40] J. N. Bahcall, A. M. Serenelli and S. Basu, Astrophys. J. **621**, L85 (2005), [arXiv:astro-ph/0412440].

[41] A. M. Serenelli, W. C. Haxton and C. Pena-Garay, Astrophys. J. **743**, 24 (2011), [arXiv:1104.1639].

[42] F. L. Villante, Phys. Lett. **B742**, 279 (2015), [arXiv:1410.2796].

[43] A. Serenelli, Eur. Phys. J. **A52**, 4, 78 (2016), [arXiv:1601.07179].

[44] R. Davis, Jr., D. S. Harmer and K. C. Hoffman, Phys. Rev. Lett. **20**, 1205 (1968).

[45] B. T. Cleveland *et al.*, Astrophys. J. **496**, 505 (1998).

[46] C. Pena-Garay and A. Serenelli (2008), [arXiv:0811.2424].

[47] J. N. Abdurashitov *et al.* (SAGE), J. Exp. Theor. Phys. **95**, 181 (2002), [Zh. Eksp. Teor. Fiz.122,211(2002)], [arXiv:astro-ph/0204245].

[48] W. Hampel *et al.* (GALLEX), Phys. Lett. **B447**, 127 (1999).

[49] M. Altmann *et al.* (GNO), Phys. Lett. **B616**, 174 (2005), [hep-ex/0504037].

[50] J. N. Abdurashitov *et al.* (SAGE), Phys. Rev. **C80**, 015807 (2009), [arXiv:0901.2200].

[51] K. S. Hirata *et al.* (Kamiokande-II), Phys. Rev. Lett. **63**, 16 (1989).

[52] Y. Fukuda *et al.* (Kamiokande), Phys. Rev. Lett. **77**, 1683 (1996).

[53] Y. Fukuda *et al.* (Super-Kamiokande), Phys. Rev. Lett. **81**, 1158 (1998), [Erratum: Phys.Rev.Lett. 81, 4279 (1998)], [hep-ex/9805021].

Int. J. Mod. Phys. A 2026.41. Downloaded from www.worldscientific.com
by UNIVERSITY OF CALIFORNIA @ BERKELEY on 09/16/26. Re-use and distribution is strictly not permitted, except for Open Access articles.

[54] K. Abe *et al.* (Super-Kamiokande), Phys. Rev. D **94**, 5, 052010 (2016), [arXiv:1606.07538].

[55] N. Vinyoles *et al.*, Astrophys. J. **835**, 2, 202 (2017), [arXiv:1611.09867].

[56] S. Fukuda *et al.* (Super-Kamiokande), Phys. Rev. Lett. **86**, 5656 (2001), [hep-ex/0103033].

[57] H. H. Chen, Phys. Rev. Lett. **55**, 1534 (1985).

[58] B. Aharmim *et al.* (SNO), Phys. Rev. **C72**, 055502 (2005), [arXiv:nucl-ex/0502021].

[59] S. Fukuda *et al.* (Super-Kamiokande), Phys. Lett. **B539**, 179 (2002), [hep-ex/0205075].

[60] Q. R. Ahmad *et al.* (SNO), Phys. Rev. Lett. **87**, 071301 (2001), [arXiv:nucl-ex/0106015].

[61] S. Fukuda *et al.* (Super-Kamiokande), Phys. Rev. Lett. **86**, 5651 (2001), [hep-ex/0103032].

[62] Q. R. Ahmad *et al.* (SNO), Phys. Rev. Lett. **89**, 011301 (2002), [arXiv:nucl-ex/0204008].

[63] B. Aharmim *et al.* (SNO), Phys. Rev. **C88**, 025501 (2013), [arXiv:1109.0763].

[64] J. Bergstrom *et al.*, JHEP **03**, 132 (2016), [arXiv:1601.00972].

[65] C. Arpesella *et al.* (Borexino), Phys. Lett. B **658**, 101 (2008), [arXiv:0708.2251].

[66] G. Bellini *et al.* (Borexino), Phys. Rev. Lett. **108**, 051302 (2012), [arXiv:1110.3230].

[67] M. Agostini *et al.* (BOREXINO), Nature **562**, 7728, 505 (2018).

[68] M. Agostini *et al.* (BOREXINO), Nature **587**, 577 (2020), [arXiv:2006.15115].

[69] G. Bellini *et al.* (Borexino), Phys. Rev. D **82**, 033006 (2010), [arXiv:0808.2868].

[70] M. Agostini *et al.* (Borexino), Phys. Rev. D **100**, 8, 082004 (2019), [arXiv:1707.09279].

[71] M. Agostini *et al.* (Borexino), Phys. Rev. D **101**, 6, 062001 (2020), [arXiv:1709.00756].

[72] S. Abe *et al.* (KamLAND), Phys. Rev. **C84**, 035804 (2011), [arXiv:1106.0861].

[73] A. Gando *et al.* (KamLAND), Phys. Rev. **C92**, 5, 055808 (2015), [arXiv:1405.6190].

[74] M. Honda *et al.*, Phys. Rev. **D92**, 2, 023004 (2015), [arXiv:1502.03916].

[75] G. D. Barr *et al.*, Phys. Rev. **D74**, 094009 (2006), [arXiv:astro-ph/0611266].

[76] G. Battistoni *et al.*, Astropart. Phys. **19**, 269 (2003), [Erratum: Astropart. Phys.19,291(2003)], [hep-ph/0207035].

[77] J. Evans *et al.*, Phys. Rev. **D95**, 2, 023012 (2017), [arXiv:1612.03219].

[78] C. V. Achar *et al.*, Phys. Lett. **18**, 196 (1965).

[79] F. Reines *et al.*, Phys. Rev. Lett. **15**, 429 (1965).

[80] K. S. Hirata *et al.* (Kamiokande-II), Phys. Lett. B **205**, 416 (1988).

[81] D. Casper *et al.*, Phys. Rev. Lett. **66**, 2561 (1991).

[82] K. Daum *et al.* (Frejus), Z. Phys. **C66**, 417 (1995).

[83] M. Aglietta *et al.* (NUSEX), Europhys. Lett. **8**, 611 (1989).

[84] K. S. Hirata *et al.* (Kamiokande-II), Phys. Lett. **B280**, 146 (1992).

[85] Y. Fukuda *et al.* (Kamiokande), Phys. Lett. **B335**, 237 (1994).

[86] Y. Fukuda *et al.* (Super-Kamiokande), Phys. Rev. Lett. **81**, 1562 (1998), [hep-ex/9807003].

[87] M. Ambrosio *et al.* (MACRO), Phys. Lett. **B517**, 59 (2001), [hep-ex/0106049].

[88] M. C. Sanchez *et al.* (Soudan 2), Phys. Rev. **D68**, 113004 (2003), [hep-ex/0307069].

[89] V. D. Barger *et al.*, Phys. Rev. Lett. **82**, 2640 (1999), [arXiv:astro-ph/9810121].

[90] E. Lisi, A. Marrone and D. Montanino, Phys. Rev. Lett. **85**, 1166 (2000), [hep-ph/0002053].

[91] Y. Ashie *et al.* (Super-Kamiokande), Phys. Rev. Lett. **93**, 101801 (2004), [hep-ex/0404034].

[92] Z. Li *et al.* (Super-Kamiokande), Phys. Rev. **D98**, 5, 052006 (2018), [arXiv:1711.09436].

[93] M. G. Aartsen *et al.* (IceCube), Phys. Rev. **D99**, 3, 032007 (2019), [arXiv:1901.05366].

[94] K. Abe *et al.* (Super-Kamiokande), Phys. Rev. **D97**, 7, 072001 (2018), [arXiv:1710.09126].

[95] A. Albert *et al.* (ANTARES), JHEP **06**, 113 (2019), [arXiv:1812.08650].

[96] R. Abbasi *et al.* ((IceCube Collaboration)‖, IceCube), Phys. Rev. Lett. **134**, 9, 091801 (2025), [arXiv:2405.02163].

[97] M. G. Aartsen *et al.* (IceCube-Gen2), J. Phys. G **48**, 6, 060501 (2021), [arXiv:2008.04323].

[98] S. Adrian-Martinez *et al.* (KM3Net), J. Phys. **G43**, 8, 084001 (2016), [arXiv:1601.07459].

[99] S. Aiello *et al.* (KM3NeT), JHEP **10**, 206 (2024), [arXiv:2408.07015].

[100] S. Ahmed *et al.* (ICAL), Pramana **88**, 5, 79 (2017), [arXiv:1505.07380].

[101] K. Abe *et al.* (Hyper-Kamiokande) (2018), [arXiv:1805.04163].

[102] B. Abi *et al.* (DUNE), JINST **15**, 08, T08008 (2020), [arXiv:2002.02967].

[103] S. E. Kopp, Phys. Rept. **439**, 101 (2007), [arXiv:physics/0609129].

[104] S. van der Meer (1961), CERN-61-07.

[105] D. G. Michael *et al.* (MINOS), Nucl. Instrum. Meth. A **596**, 190 (2008), [arXiv:0805.3170].

[106] S. H. Ahn *et al.* (K2K), Phys. Lett. B **511**, 178 (2001), [hep-ex/0103001].

[107] D. Beavis *et al.* (E899) (1995), BNL-52459.

[108] K. Abe *et al.* (T2K), Nucl. Instrum. Meth. A **659**, 106 (2011), [arXiv:1106.1238].

[109] D. S. Ayres *et al.* (NOvA) (2007).

[110] M. G. Catanesi *et al.* (HARP), Nucl. Instrum. Meth. **A571**, 527 (2007).

[111] J. M. Paley *et al.* (MIPP), Phys. Rev. **D90**, 3, 032001 (2014), [arXiv:1404.5882].

[112] N. Abgrall *et al.* (NA61), JINST **9**, P06005 (2014), [arXiv:1401.4699].

[113] M. Pavin *et al.* (EMPHATIC), Phys. Rev. D **106**, 11, 112008 (2022), [arXiv:2106.15723].

[114] N. Abgrall *et al.* (NA61/SHINE), Eur. Phys. J. C **76**, 2, 84 (2016), [arXiv:1510.02703].

[115] N. Abgrall *et al.* (NA61/SHINE), Eur. Phys. J. C **79**, 2, 100 (2019), [arXiv:1808.04927].

[116] H. Adhikary *et al.* (NA61/SHINE) (2023), [arXiv:2306.02961].

[117] M. H. Ahn *et al.* (K2K), Phys. Rev. **D74**, 072003 (2006), [hep-ex/0606032].

[118] P. Adamson *et al.* (MINOS), Phys. Rev. Lett. **112**, 191801 (2014), [arXiv:1403.0867].

[119] P. Adamson *et al.* (MINOS+), Phys. Rev. Lett. **125**, 13, 131802 (2020), [arXiv:2006.15208].

[120] N. Agafonova *et al.* (OPERA), Phys. Rev. Lett. **120**, 21, 211801 (2018), [Erratum: Phys. Rev. Lett.121,no.13,139901(2018)], [arXiv:1804.04912].

Int. J. Mod. Phys. A 2026.41. Downloaded from www.wo
by UNIVERSITY OF CALIFORNIA @ BERKELEY on 09/16/26. Re-use and distribution is
except for Open Access articles.

[121] C. Rubbia *et al.*, JINST **6**, P07011 (2011), [arXiv:1106.0975].

[122] K. Abe *et al.* (T2K), Phys. Rev. Lett. **107**, 041801 (2011), [arXiv:1106.2822].

[123] K. Abe *et al.* (T2K), Phys. Rev. Lett. **112**, 061802 (2014), [arXiv:1311.4750].

[124] K. Abe *et al.* (T2K), Eur. Phys. J. C **83**, 9, 782 (2023), [arXiv:2303.03222].

[125] P. Adamson *et al.* (NOvA), Phys. Rev. Lett. **118**, 23, 231801 (2017), [arXiv:1703.03328].

[126] M. A. Acero *et al.* (NOvA), Phys. Rev. Lett. **123**, 15, 151803 (2019), [arXiv:1906.04907].

[127] M. A. Acero *et al.* (NOvA), Phys. Rev. D **106**, 3, 032004 (2022), [arXiv:2108.08219].

[128] A. Aguilar-Arevalo *et al.* (LSND), Phys. Rev. **D64**, 112007 (2001), [hep-ex/0104049].

[129] B. Armbruster *et al.* (KARMEN), Phys. Rev. **D65**, 112001 (2002), [hep-ex/0203021].

[130] A. A. Aguilar-Arevalo *et al.* (MiniBooNE), Phys. Rev. D **103**, 5, 052002 (2021), [arXiv:2006.16883].

[131] M. Antonello *et al.* (MicroBooNE, LAr1-ND, ICARUS-WA104) (2015), [arXiv:1503.01520].

[132] P. Abratenko *et al.* (MicroBooNE), Phys. Rev. Lett. **128**, 24, 241801 (2022), [arXiv:2110.14054].

[133] P. Abratenko *et al.* (MicroBooNE), Phys. Rev. Lett. **130**, 1, 011801 (2023), [arXiv:2210.10216].

[134] S. Ajimura *et al.* (JSNS2), Nucl. Instrum. Meth. A **1014**, 165742 (2021), [arXiv:2104.13169].

[135] F. Von Feilitzsch, A. A. Hahn and K. Schreckenbach, Phys. Lett. **118B**, 162 (1982).

[136] K. Schreckenbach *et al.*, Phys. Lett. **160B**, 325 (1985).

[137] A. A. Hahn *et al.*, Phys. Lett. **B218**, 365 (1989).

[138] P. Vogel *et al.*, Phys. Rev. **C24**, 1543 (1981).

[139] T. A. Mueller *et al.*, Phys. Rev. **C83**, 054615 (2011), [arXiv:1101.2663].

[140] P. Huber, Phys. Rev. **C84**, 024617 (2011), [Erratum: Phys. Rev.C85,029901(2012)], [arXiv:1106.0687].

[141] F. P. An *et al.* (Daya Bay), Phys. Rev. Lett. **116**, 6, 061801 (2016), [Erratum: Phys. Rev. Lett.118,no.9,099902(2017)], [arXiv:1508.04233].

[142] F. P. An *et al.* (Daya Bay), Phys. Rev. Lett. **118**, 25, 251801 (2017), [arXiv:1704.01082].

[143] D. Adey *et al.* (Daya Bay), Phys. Rev. D **100**, 5, 052004 (2019), [arXiv:1808.10836].

[144] F. P. An *et al.* (Daya Bay), Phys. Rev. Lett. **134**, 20, 201802 (2025), [arXiv:2501.00746].

[145] V. Kopeikin, M. Skorokhvatov and O. Titov, Phys. Rev. D **104**, 7, L071301 (2021), [arXiv:2103.01684].

[146] M. Estienne *et al.*, Phys. Rev. Lett. **123**, 2, 022502 (2019), [arXiv:1904.09358].

[147] L. Hayen *et al.*, Phys. Rev. C **100**, 5, 054323 (2019), [arXiv:1908.08302].

[148] G. Bak *et al.* (RENO), Phys. Rev. Lett. **121**, 20, 201801 (2018), [arXiv:1806.00248].

[149] H. de Kerret *et al.* (Double Chooz), Nature Phys. **16**, 5, 558 (2020), [arXiv:1901.09445].

[150] Y. J. Ko *et al.* (NEOS), Phys. Rev. Lett. **118**, 12, 121802 (2017), [arXiv:1610.05134].

[151] K. Eguchi *et al.* (KamLAND), Phys. Rev. Lett. **90**, 021802 (2003), [hep-ex/0212021].

[152] T. Araki *et al.* (KamLAND), Phys. Rev. Lett. **94**, 081801 (2005), [hep-ex/0406035].

[153] A. Gando *et al.* (KamLAND), Phys. Rev. **D88**, 3, 033001 (2013), [arXiv:1303.4667].

[154] Y. Abe *et al.* (Double Chooz), Phys. Rev. Lett. **108**, 131801 (2012), [arXiv:1112.6353].

[155] F. P. An *et al.* (Daya Bay), Phys. Rev. Lett. **108**, 171803 (2012), [arXiv:1203.1669].

[156] J. K. Ahn *et al.* (RENO), Phys. Rev. Lett. **108**, 191802 (2012), [arXiv:1204.0626].

[157] F. P. An *et al.* (Daya Bay), Phys. Rev. Lett. **130**, 16, 161802 (2023), [arXiv:2211.14988].

[158] S. Jeon *et al.* (RENO), Phys. Rev. D **111**, 11, 112006 (2025).

[159] A. Abusleme *et al.* (JUNO), Prog. Part. Nucl. Phys. **123**, 103927 (2022), [arXiv:2104.02565].

[160] A. Abusleme *et al.* (JUNO), Chin. Phys. C **46**, 12, 123001 (2022), [arXiv:2204.13249].

[161] Z. Atif *et al.* (RENO, NEOS), Phys. Rev. D **105**, 11, L111101 (2022), [arXiv:2011.00896].

[162] I. Alekseev *et al.* (DANSS), Phys. Lett. **B787**, 56 (2018), [arXiv:1804.04046].

[163] H. Almazán *et al.* (STEREO), Phys. Rev. D **102**, 5, 052002 (2020), [arXiv:1912.06582].

[164] H. Almazán *et al.* (STEREO), Nature **613**, 7943, 257 (2023), [arXiv:2210.07664].

[165] M. Andriamirado *et al.* (PROSPECT), Phys. Rev. D **103**, 3, 032001 (2021), [arXiv:2006.11210].

[166] A. P. Serebrov *et al.* (NEUTRINO-4), Pisma Zh. Eksp. Teor. Fiz. **109**, 4, 209 (2019), [JETP Lett.109,no.4,213(2019)], [arXiv:1809.10561].

[167] A. P. Serebrov *et al.*, Phys. Rev. D **104**, 3, 032003 (2021), [arXiv:2005.05301].

[168] Y. Abreu *et al.* (SoLid), JINST **16**, 02, P02025 (2021), [arXiv:2002.05914].

[169] N. Cabibbo, Phys. Lett. **72B**, 333 (1978).

[170] S. M. Bilenky, J. Hosek and S. T. Petcov, Phys. Lett. **94B**, 495 (1980).

[171] V. D. Barger, K. Whisnant and R. J. N. Phillips, Phys. Rev. Lett. **45**, 2084 (1980).

[172] P. Langacker *et al.*, Nucl. Phys. **B282**, 589 (1987).

[173] S. Goswami and A. Yu. Smirnov, Phys. Rev. **D72**, 053011 (2005), [hep-ph/0411359].

[174] N. Okamura, Prog. Theor. Phys. **114**, 1045 (2006), [hep-ph/0411388].

[175] H. Nunokawa, S. J. Parke and R. Zukanovich Funchal, Phys. Rev. **D72**, 013009 (2005), [hep-ph/0503283].

[176] A. Cervera *et al.*, Nucl. Phys. **B579**, 17 (2000), [Erratum: Nucl. Phys.B593,731(2001)], [hep-ph/0002108].

[177] M. Freund, Phys. Rev. **D64**, 053003 (2001), [hep-ph/0103300].

[178] E. K. Akhmedov *et al.*, JHEP **04**, 078 (2004), [hep-ph/0402175].

[179] H. Minakata *et al.*, Phys. Rev. **D74**, 053008 (2006), [hep-ph/0607284].

[180] O. L. G. Peres and A. Yu. Smirnov, Nucl. Phys. **B680**, 479 (2004), [hep-ph/0309312].

[181] S. Petcov, Phys.Lett. **B434**, 321 (1998), [hep-ph/9805262].

[182] E. K. Akhmedov *et al.*, Nucl.Phys. **B542**, 3 (1999), [hep-ph/9808270].

[183] E. K. Akhmedov, Nucl.Phys. **B538**, 25 (1999), [hep-ph/9805272].

[184] M. Chizhov, M. Maris and S. Petcov (1998), SISSA-53-98-EP, [hep-ph/9810501].

[185] M. Chizhov and S. Petcov, Phys.Rev.Lett. **83**, 1096 (1999), [hep-ph/9903399].

[186] E. K. Akhmedov, M. Maltoni and A. Y. Smirnov, JHEP **0705**, 077 (2007), [hep-ph/0612285].

Int. J. Mod. Phys. A 2026.41. Downloaded from www.worldscientific.com
by UNIVERSITY OF CALIFORNIA @ BERKELEY on 09/16/26. Re-use and distribution is strictly not permitted, except for Open Access articles.

[187] C. Kim and U. Lee, Phys.Lett. **B444**, 204 (1998), [hep-ph/9809491].

[188] O. Peres and A. Y. Smirnov, Phys.Lett. **B456**, 204 (1999), [hep-ph/9902312].

[189] M. Gonzalez-Garcia, M. Maltoni and A. Y. Smirnov, Phys.Rev. **D70**, 093005 (2004), [hep-ph/0408170].

[190] E. K. Akhmedov, M. Maltoni and A. Y. Smirnov, JHEP **0806**, 072 (2008), [arXiv:0804.1466].

[191] J. Bernabeu, S. Palomares Ruiz and S. Petcov, Nucl.Phys. **B669**, 255 (2003), [hep-ph/0305152].

[192] S. Petcov and T. Schwetz, Nucl.Phys. **B740**, 1 (2006), [hep-ph/0511277].

[193] I. Esteban *et al.*, JHEP **12**, 216 (2024), [arXiv:2410.05380].

[194] F. Capozzi *et al.*, Phys. Rev. D **111**, 9, 093006 (2025), [arXiv:2503.07752].

[195] M. Tortola, Neutrinos global fit (2024), Talk at XV Latin American Symposium on High Energy Physics, URL `https://indico.nucleares.unam.mx/event/2125/contribution/40`.

[196] P. F. de Salas *et al.*, JHEP **02**, 071 (2021), [arXiv:2006.11237].

[197] Atmospheric neutrino oscillation analysis with neutron tagging and an expanded fiducial volume in Super-Kamiokande I-V (2024), ZENODO.

[198] Data release for neutrino oscillation parameters using convolutional neural networks with 9.3 years of data in IceCube DeepCore (2024), .

[199] T. Wester *et al.* (Super-Kamiokande) (2023), [arXiv:2311.05105].

[200] R. Abbasi *et al.* (IceCube) (2024), [arXiv:2405.02163].

[201] J. Wolcott (NOvA) FERMILAB-SLIDES-24-0130-PPD (2024).

[202] C. Jarlskog, Phys. Rev. Lett. **55**, 1039 (1985).

[203] M. C. Gonzalez-Garcia, M. Maltoni and T. Schwetz, JHEP **11**, 052 (2014), [arXiv:1409.5439].

[204] Y. Farzan and A. Yu. Smirnov, Phys. Rev. **D65**, 113001 (2002), [hep-ph/0201105].

[205] A. Dueck, S. Petcov and W. Rodejohann, Phys. Rev. **D82**, 013005 (2010), [arXiv:1006.0227].

[206] A. Aguilar-Arevalo *et al.* (MiniBooNE) (2012), [arXiv:1207.4809].

[207] R. Acciarri *et al.* (MicroBooNE), JINST **12**, 02, P02017 (2017), [arXiv:1612.05824].

[208] P. Abratenko *et al.* ((MicroBooNE Collaboration)*, MicroBooNE), Phys. Rev. Lett. **135**, 8, 081802 (2025), [arXiv:2412.14407].

[209] G. Mention *et al.*, Phys. Rev. **D83**, 073006 (2011), [arXiv:1101.2755].

[210] C. Giunti *et al.*, Phys. Lett. B **829**, 137054 (2022), [arXiv:2110.06820].

[211] V. V. Barinov *et al.*, Phys. Rev. Lett. **128**, 23, 232501 (2022), [arXiv:2109.11482].

[212] M. A. Acero, C. Giunti and M. Laveder, Phys. Rev. **D78**, 073009 (2008), [arXiv:0711.4222].

[213] C. Giunti and M. Laveder, Phys. Rev. **C83**, 065504 (2011), [arXiv:1006.3244].

[214] C. Giunti *et al.*, JHEP **10**, 164 (2022), [arXiv:2209.00916].

[215] M. C. Gonzalez-Garcia, M. Maltoni and J. P. Pinheiro, Phys. Lett. B **862**, 139297 (2025), [arXiv:2411.16840].

[216] H. Acharya *et al.* (KATRIN) (2025), [arXiv:2503.18667].

[217] M. Cadeddu *et al.* (2025), [arXiv:2507.13103].

[218] J. J. Gomez-Cadenas and M. C. Gonzalez-Garcia, Z. Phys. **C71**, 443 (1996), [hep-ph/9504246].

[219] C. Giunti and M. Laveder, Phys. Rev. **D84**, 093006 (2011), [arXiv:1109.4033].

[220] J. M. Conrad *et al.*, Adv. High Energy Phys. **2013**, 163897 (2013), [arXiv:1207.4765].

[221] J. Kopp *et al.*, JHEP **05**, 050 (2013), [arXiv:1303.3011].

[222] G. H. Collin *et al.*, Phys. Rev. Lett. **117**, 22, 221801 (2016), [arXiv:1607.00011].

[223] S. Gariazzo *et al.*, JHEP **06**, 135 (2017), [arXiv:1703.00860].

[224] M. Dentler *et al.*, JHEP **08**, 010 (2018), [arXiv:1803.10661].

[225] M. A. Acero *et al.*, J. Phys. G **51**, 12, 120501 (2024), [arXiv:2203.07323].

[226] M. Aker *et al.* (KATRIN), Science **388**, 6743, adq9592 (2025), [arXiv:2406.13516].

[227] J. Bonn *et al.*, Nucl. Phys. B Proc. Suppl. **91**, 273 (2001).

[228] V. M. Lobashev *et al.*, Nucl. Phys. B Proc. Suppl. **91**, 280 (2001).

[229] A. Ashtari Esfahani *et al.* (Project 8), Phys. Rev. Lett. **131**, 10, 102502 (2023), [arXiv:2212.05048].

[230] A. De Rujula and M. Lusignoli, Phys. Lett. **118B**, 429 (1982).

[231] L. Gastaldo *et al.*, J. Low Temp. Phys. **176**, 5-6, 876 (2014), [arXiv:1309.5214].

[232] B. Alpert *et al.*, Eur. Phys. J. **C75**, 3, 112 (2015), [arXiv:1412.5060].

[233] R. E. Shrock, Phys. Lett. **96B**, 159 (1980).

[234] F. Vissani, Nucl. Phys. B Proc. Suppl. **100**, 273 (2001), [hep-ph/0012018].

[235] Y. Farzan, O. L. G. Peres and A. Yu. Smirnov, Nucl. Phys. **B612**, 59 (2001), [hep-ph/0105105].

[236] J. Schechter and J. W. F. Valle, Phys. Rev. D **25**, 2951 (1982).

[237] J. Engel and J. Menendez, Rept. Prog. Phys. **80**, 4, 046301 (2017), [arXiv:1610.06548].

[238] S. Abe *et al.* (KamLAND-Zen) (2024), [arXiv:2406.11438].

[239] M. Agostini *et al.* (GERDA), Phys. Rev. Lett. **125**, 25, 252502 (2020), [arXiv:2009.06079].

[240] I. J. Arnquist *et al.* (Majorana), Phys. Rev. Lett. **130**, 6, 062501 (2023), [arXiv:2207.07638].

[241] N. Abgrall *et al.* (LEGEND) (2021), [arXiv:2107.11462].

[242] W. H. Dai *et al.* (CDEX), Phys. Rev. D **106**, 3, 032012 (2022), [arXiv:2205.10718].

[243] V. Albanese *et al.* (SNO+), JINST **16**, 08, P08059 (2021), [arXiv:2104.11687].

[244] G. Anton *et al.* (EXO-200), Phys. Rev. Lett. **123**, 16, 161802 (2019), [arXiv:1906.02723].

[245] G. Adhikari *et al.* (nEXO), J. Phys. G **49**, 1, 015104 (2022), [arXiv:2106.16243].

[246] J. Renner *et al.* (NEXT), JINST **13**, 10, P10020 (2018), [arXiv:1808.01804].

[247] D. Q. Adams *et al.* (CUORE), Science **390**, 6777, 1029 (2025), [arXiv:2404.04453].

[248] O. Azzolini *et al.* (CUPID), Phys. Rev. Lett. **129**, 11, 111801 (2022), [arXiv:2206.05130].

[249] C. Augier *et al.* (CUPID), Eur. Phys. J. C **82**, 11, 1033 (2022), [arXiv:2202.08716].

[250] V. Alenkov *et al.* (AMoRE), Eur. Phys. J. **C79**, 9, 791 (2019), [arXiv:1903.09483].

[251] A. Agrawal *et al.* (AMoRE), Phys. Rev. Lett. **134**, 8, 082501 (2025), [arXiv:2407.05618].

[252] R. Arnold *et al.* (NEMO-3), Phys. Rev. **D92**, 7, 072011 (2015), [arXiv:1506.05825].

15. Quark Model

Revised August 2025 by C. Amsler (Marietta Blau Inst.), V. Crede (Florida State U.) and T. DeGrand (Colorado U., Boulder).

15.1 Introduction . . . 324
15.2 Quantum numbers of the quarks . . . 324
15.3 Mesons . . . 325
15.4 Exotic mesons . . . 328
15.4.1 Tetraquarks . . . 328
15.4.2 Glueballs . . . 328
15.4.3 Hybrids . . . 329
15.5 Baryons: qqq states . . . 329
15.5.1 Light baryons . . . 329
15.5.2 Charmed and bottom baryons . . . 332
15.6 Magnetic moments . . . 334
15.7 Dynamics . . . 335
15.8 Lattice Calculations of Hadronic Spectroscopy . 336
15.8.1 Spectroscopy of low-lying states . . . 336
15.8.2 Excited state spectroscopy . . . 336
15.8.3 Electromagnetic effects . . . 339

Int. J. Mod. Phys. A 2026.41. Downloaded from www.wo[redacted]except for Open Access articles.
by UNIVERSITY OF CALIFORNIA @ BERKELEY on 09/16/26. Re-use and distribution is

15.1 Introduction

Quantum chromodynamics (QCD) is the theory of strong interactions. QCD is a quantum field theory with an $SU(N_c)$ local "color" gauge symmetry with $N_c = 3$ colors and a collection of N_f "flavors" of colored fermions, the quarks. It involves a set of $N_c^2 - 1 = 8$ non-Abelian gauge fields, the gluons. QCD is believed to confine, that is, its physical states are color singlets with internal quark and gluon degrees of freedom. This review is concerned with the description of the properties (masses and matrix elements for couplings to electromagnetism and the weak intractions) of the low lying bound states of QCD. The shorthand expression for describing this physics is called the "quark model".

The spectrum of strongly interacting particles consists of a tower of many states, which can be either bosons (labelled as "mesons") or fermions (labelled as "baryons"). The spectrum of baryons and mesons exhibits a high degree of regularity. The organizational principle which best categorizes this regularity is encoded in the quark model. All descriptions of strongly interacting states use the language of the quark model. At the same time, the language is not precise. The quark model exists on many levels: at the simplest level, it is an almost dynamics-free picture of strongly interacting particles as bound states of quarks and antiquarks. As one refines the description, the quark model can become a framework with more detailed descriptions of dynamics. At its most fundamental level, it might be a description of QCD. In effective field theories of QCD at low energies the hadron spectrum is not simply given by a series of states but is the manifestation of a complex dynamics involving various types of states [1].

At its heart, the quark model assumes that mesons are bound states of quark - antiquark pairs, and baryons are bound states of three quarks. These are the minimal particle content states which can be color singlets in an $SU(3)$ gauge theory. This approach cannot be justified directly from QCD; however, there is indirect evidence that this description has some fundamental validity from the version of QCD where the number of colors N_c is taken to infinity [2–4]. In that limit, mesons are dominantly narrow (width proportional to $1/N_c$) bound states of a quark - antiquark pair, and baryons have a mass which scales as N_c.

A better justification is that this approach works. Indeed, the quark model is much older than QCD as a theory of the strong interactions (1973-1974, see the article on "50 Years of Quantum Chromodynamics" [5]). In fact, the principal issue (circa 1963-64) in strong interaction physics before QCD was to justify the success of the quark model in systemizing the properties of mesons and baryons in terms of some more fundamental dynamics (QCD).

Today one knows that this is not the whole story. There are experimentally observed states which either cannot be described, or have an uncomfortable description, as minimal quark number states. Some of them have "exotic" (non-$\bar{q}q$ or qqq) quantum numbers. Given the successes of the quark model, these are classified as "tetraquarks" ($qq\bar{q}\bar{q}$), "pentaquarks" ($qqqq\bar{q}$) or "glueballs", bound states of gluons, the gluonic degrees of freedom in QCD. Of course, such labels are imprecise: bound states with the same overall quantum numbers can mix, regardless of their internal degrees of freedom.

This review has several parts. We start by describing the properties of strongly interacting particles in terms of the properties of states made of a minimal number of quark fields which can be coupled into a color singlet – two fields (a quark and an antiquark) for the mesons, and three quarks, for a baryon. Quarks come in six flavors. We describe the properties of mesons as $\bar{q}q$ systems and baryons as qqq systems. Along the way we discuss hadronic bound states which do not fit into this classification.

Finally, at the end of this review, we present results from lattice simulations of QCD, a direct approach to the solution of QCD from its Lagrangian, without reference to models. Lattice simulations interact with the quark model in (at least) two ways: first, the interpolating fields which are used in lattice simulations are usually directly based on quark model constructions. That is the simplest way to create states with the desired quantum numbers, which can then be processed by the lattice calculation. The second way that lattice calculations interact with the quark model comes when one wishes to put the lattice calculations into some context: without the quark model, there are simply the results from the lattice calculations, and the results from experiment, and no way to understand why they are similar or different. The quark model is the framework which is almost universally used to generate that context. Of course, that statement is equally valid when one tries to systemize actual experimental data: the context is always some variation of a quark model.

15.2 Quantum numbers of the quarks

As gluons carry no intrinsic quantum numbers beyond color charge, and because color is believed to be permanently confined, the quantum numbers of strongly interacting particles are given by the quantum numbers of their constituent quarks and antiquarks.

Quarks are strongly interacting fermions with spin 1/2 and, by convention, positive parity. Antiquarks have negative parity. Quarks have the additive baryon number 1/3, antiquarks −1/3. Table 15.1 gives the other additive quantum numbers (flavors) for the three generations of quarks. They are related to the charge Q (in units of the elementary charge e) through the generalized Gell-Mann-Nishijima formula

$$\mathsf{Q} = \mathsf{I}_z + \frac{\mathcal{B} + \mathsf{S} + \mathsf{C} + \mathsf{B} + \mathsf{T}}{2} , \qquad (15.1)$$

where $\mathcal{B}$ is the baryon number. The convention is that the quark *flavor* (I_z, S, C, B, or T) has the same sign as its *charge* Q. Antiquarks have the opposite flavor signs. With this convention, any flavor carried by a charged meson has the same sign as its charge, *e.g.*, the strangeness of the K^+ ($u\bar{s}$) is +1, the bottomness of the B^+ ($u\bar{b}$) is +1, and the charm and strangeness of the D_s^- ($s\bar{c}$) are each −1.

Table 15.1: Quark quantum numbers.

	d	u	s	c	b	t
Q – electric charge	$-\frac{1}{3}$	$+\frac{2}{3}$	$-\frac{1}{3}$	$+\frac{2}{3}$	$-\frac{1}{3}$	$+\frac{2}{3}$
I – isospin	$\frac{1}{2}$	$\frac{1}{2}$	0	0	0	0
I_z – isospin z-component	$-\frac{1}{2}$	$+\frac{1}{2}$	0	0	0	0
S – strangeness	0	0	−1	0	0	0
C – charm	0	0	0	+1	0	0
B – bottomness	0	0	0	0	−1	0
T – topness	0	0	0	0	0	+1

The hypercharge is defined as

$$\mathsf{Y} = \mathcal{B} + \mathsf{S} - \frac{\mathsf{C} - \mathsf{B} + \mathsf{T}}{3} . \qquad (15.2)$$

Thus Y is equal to $\frac{1}{3}$ for the u and d quarks, $-\frac{2}{3}$ for the s quark, and 0 for all other quarks. More details and derivations on

Int. J. Mod. Phys. A 2026.41. Downloaded from www.worldscientific.com
by UNIVERSITY OF CALIFORNIA @ BERKELEY on 09/16/26. Re-use and distribution is strictly not permitted, except for Open Access articles.

the quark structure of mesons and baryons can be found *e.g.* in Ref. [6].

The naming scheme for hadrons has been updated by the Particle Data Group in 2023, to include the heavy "exotic" states discovered recently, the tetraquark ($qq\bar{q}\bar{q}$) and pentaquark ($qqqq\bar{q}$) candidates (see "Naming Scheme for Hadrons" in this *Review*).

15.3 Mesons

Mesons have baryon number $\mathcal{B} = 0$. In the quark model, they are $q\bar{q}'$ bound states of quarks q and antiquarks $\bar{q}'$ (the flavors of q and q' may be different).

If the orbital angular momentum of the $q\bar{q}'$ state is ℓ, then the parity P is $(-1)^{\ell+1}$. The meson spin J is given by the usual relation $|\ell - s| \leq J \leq |\ell + s|$, where $s = 0$ (antiparallel quark spins) or $s = 1$ (parallel quark spins). The charge conjugation, or C-parity $C = (-1)^{\ell+s}$, is defined only for states made of quarks and their own antiquarks. The C-parity can be generalized to the G-parity $G = (-1)^{I+\ell+s}$ for mesons made of quarks and their own antiquarks (isospin $\mathsf{I}_z = 0$), and for the charged $u\bar{d}$ and $d\bar{u}$ states (isospin $\mathsf{I} = 1$).

The mesons are classified in J^{PC} multiplets. The $\ell = 0$ states are the pseudoscalars (0^{-+}) and the vectors (1^{--}). The orbital excitations $\ell = 1$ are the scalars (0^{++}), the axial vectors (1^{++}) and (1^{+-}) *aka* pseudovectors, and the tensors (2^{++}). Assignments for many of the known mesons are given in Tables 15.2, 15.3 and 15.4. Radial excitations are denoted by the principal quantum number n. The very short lifetime of the t quark ($\to W^+b$) makes it likely that bound-state hadrons containing t quarks and/or antiquarks do not exist.

States in the natural spin-parity series $P = (-1)^J$ must, according to the above, have $s = 1$ and hence, $CP = +1$. Thus, mesons with natural spin-parity and $CP = -1$ (0^{+-}, 1^{-+}, 2^{+-}, 3^{-+}, *etc.*) are forbidden in the $q\bar{q}'$ model. The $J^{PC} = 0^{--}$ state is forbidden as well. Mesons with such *exotic* quantum numbers may exist, but would lie outside the $q\bar{q}'$ model (see section 15.4 below on exotic mesons).

Following SU(3), the nine possible $q\bar{q}'$ combinations containing the light u, d, and s quarks are grouped into an octet and a singlet of light quark mesons:

$$\mathbf{3} \otimes \overline{\mathbf{3}} = \mathbf{8} \oplus \mathbf{1} \ . \tag{15.3}$$

A fourth quark such as charm c can be included by extending SU(3) to SU(4). However, SU(4) is badly broken owing to the much heavier c quark. Nevertheless, in an SU(4) classification, the sixteen mesons are grouped into a 15-plet and a singlet:

$$\mathbf{4} \otimes \overline{\mathbf{4}} = \mathbf{15} \oplus \mathbf{1} \ . \tag{15.4}$$

The *weight diagrams* for the ground-state pseudoscalar (0^{-+}) and vector (1^{--}) mesons are depicted in Fig. 15.1. The light quark mesons are members of nonets building the middle plane in Fig. 15.1(a) and (b).

Isoscalar states with the same J^{PC} mix, but mixing between the two light quark isoscalar mesons, and the much heavier charmonium and bottomonium states, are generally assumed to be negligible. In the following, we shall use the generic names a for the $\mathsf{I} = 1$, K for the $\mathsf{I} = 1/2$, f and f' for the $\mathsf{I} = 0$ members of the light quark nonets. Thus, the physical isoscalars are mixtures of the SU(3) wave function ψ_8 and ψ_1:

$$f' = \psi_8 \cos\theta - \psi_1 \sin\theta \ , \tag{15.5}$$

$$f = \psi_8 \sin\theta + \psi_1 \cos\theta \ , \tag{15.6}$$

where θ is the nonet mixing angle and

$$\psi_8 = \frac{1}{\sqrt{6}}(u\bar{u} + d\bar{d} - 2s\bar{s}) \ , \tag{15.7}$$

$$\psi_1 = \frac{1}{\sqrt{3}}(u\bar{u} + d\bar{d} + s\bar{s}) \ . \tag{15.8}$$

The mixing relations are often rewritten to exhibit the $u\bar{u} + d\bar{d}$ and $s\bar{s}$ components which decouple for the "ideal" mixing angle

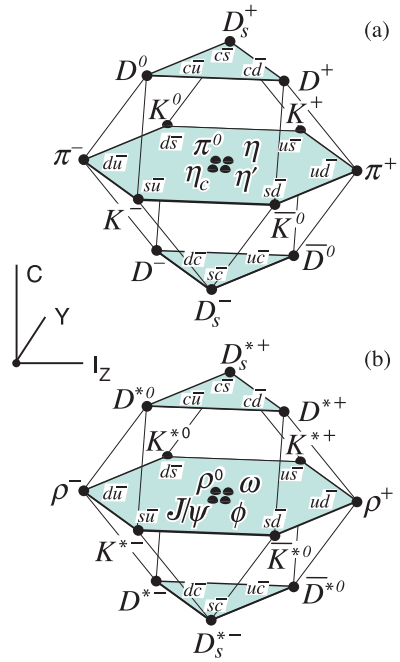

Figure 15.1: SU(4) weight diagram showing the 16-plets for the pseudoscalar (a) and vector mesons (b) made of the u, d, s, and c quarks as a function of isospin I_z, charm C, and hypercharge $\mathsf{Y} = \mathcal{B} + \mathsf{S} - \frac{\mathsf{C}}{3}$. The nonets of light mesons occupy the central planes to which the $c\bar{c}$ states have been added.

θ_i, such that $\tan\theta_i = 1/\sqrt{2}$ (or $\theta_i = 35.3°$). Defining $\alpha = \theta + 54.7°$, one obtains the physical isoscalar state in the flavor basis

$$f' = \frac{1}{\sqrt{2}}(u\bar{u} + d\bar{d})\cos\alpha - s\bar{s}\ \sin\alpha \ , \tag{15.9}$$

and its orthogonal partner f (replace α by α –90°). Thus for ideal mixing ($\alpha_i = 90°$), the f' becomes pure $s\bar{s}$ and the f pure $u\bar{u} + d\bar{d}$. The mixing angle θ can be derived by diagonalizing the mass matrix

$$\begin{pmatrix} m_8 & m_{81} \\ m_{18} & m_1 \end{pmatrix} . \tag{15.10}$$

The mass eigenvalues are $m_{f'}$ and m_f. The mixing angle is given by

$$\tan\theta = \frac{m_8 - m_{f'}}{m_{81}} \ . \tag{15.11}$$

Calculating m_8 and m_{81} from the wave functions Eq. (15.7) and Eq. (15.8), and expressing the quark masses as a function of the $\mathsf{I} = 1/2$ and $\mathsf{I} = 1$ meson masses, one obtains

$$\tan\theta = \frac{4m_K - m_a - 3m_{f'}}{2\sqrt{2}(m_a - m_K)} \ , \tag{15.12}$$

which also determines the sign of θ. Alternatively, one can express the mixing angle as a function of all nonet masses. The octet mass is given by

$$m_8 = m_{f'}\cos^2\theta + m_f \sin^2\theta \tag{15.13}$$

whence

$$\tan^2\theta = \frac{4m_K - m_a - 3m_{f'}}{-4m_K + m_a + 3m_f} \ . \tag{15.14}$$

Eliminating θ from Eq. (15.12) and Eq. (15.14) leads to the sum rule [14]

$$(m_f + m_{f'})(4m_K - m_a) - 3m_f m_{f'} = 8m_K^2 - 8m_K m_a + 3m_a^2. \tag{15.15}$$

This relation is verified for the ground-state vector mesons. We identify the $\phi(1020)$ with the f' and the $\omega(783)$ with the f. Thus

$$\phi(1020) = \psi_8 \cos\theta_V - \psi_1 \sin\theta_V \ , \tag{15.16}$$

$$\omega(782) = \psi_8 \sin\theta_V + \psi_1 \cos\theta_V \ , \tag{15.17}$$

Int. J. Mod. Phys. A 2026.41. Downloaded from www.worldscientific.com by UNIVERSITY OF CALIFORNIA @ BERKELEY on 09/16/26. Re-use and distribution is [redacted] except for Open Access articles.

Table 15.2: Suggested $q\bar{q}$ quark-model assignments for the lightest mesons made of u, d and s quarks. Mesons in boldface are included in the Summary Table. The wave functions f and f' are given in the text (Eq. (15.9)) and the singlet-octet mixing angles in Table 15.5 below for the well established nonets. The classification of the 0^{++} mesons is controversial: (i) the scalars $a_0(980)$, $K_0^*(700)$, $f_0(980)$ and $f_0(500)$, omitted from the table, are often considered to be four-quark states, but are also proposed for the ground state scalar nonet (see the chapter "Scalar Mesons below 1 GeV" in this *Review*); (ii) there are three isoscalar 0^{++} mesons, $f_0(1370)$, $f_0(1500)$ and $f_0(1710)$, both $f_0(1500)$ and $f_0(1710)$ being proposed as glueballs. The three states are expected to mix. The isoscalar assignments in the 2^1S_0 (0^{-+}) nonet are also tentative. Details and alternative schemes can be found in "Spectroscopy of Light Meson Resonances" in this *Review*.
[a] The $1^{+\pm}$ and $2^{-\pm}$ isospin $\frac{1}{2}$ states mix. In particular, the K_{1A} and K_{1B} are nearly equal mixtures of the $K_1(1270)$ and $K_1(1400)$ [7]. The $2^{-\pm}$ mixed partner of the $K_2(1770)$ is the established $K_2(1820)$.
[b] The physical vector mesons are mixtures of 1^3D_1 and 2^3S_1 (for a discussion see [8]).
[c] This state has also been proposed as a tetraquark state [9].
[d] The $\eta(1475)$ and $\eta(1405)$ (not shown) may be manifestations of a single state [10].
[e] This state has also been proposed as the ground state tensor glueball [11,12].

$n^{2s+1}\ell_J$	J^{PC}	I = 1	I = $\frac{1}{2}$	I = 0	I = 0
		$u\bar{d}$, $\bar{u}d$, $\frac{1}{\sqrt{2}}(d\bar{d}-u\bar{u})$	$u\bar{s}$, $d\bar{s}$; $\bar{d}s$, $\bar{u}s$	f'	f
1^1S_0	0^{-+}	$\boldsymbol{\pi}$	$\boldsymbol{K}$	$\boldsymbol{\eta}$	$\boldsymbol{\eta'}(958)$
1^3S_1	1^{--}	$\boldsymbol{\rho(770)}$	$\boldsymbol{K^*(892)}$	$\boldsymbol{\phi(1020)}$	$\boldsymbol{\omega(782)}$
1^3P_0	0^{++}	$\boldsymbol{a_0(1450)}$	$\boldsymbol{K_0^*(1430)}$	$\boldsymbol{f_0(1370,1500,1710)}$	
1^1P_1	1^{+-}	$\boldsymbol{b_1(1235)}$	$\boldsymbol{K_{1B}}$[a]	$\boldsymbol{h_1(1415)}$	$\boldsymbol{h_1(1170)}$
1^3P_1	1^{++}	$\boldsymbol{a_1(1260)}$	$\boldsymbol{K_{1A}}$[a]	$\boldsymbol{f_1(1420)}$	$\boldsymbol{f_1(1285)}$
1^3P_2	2^{++}	$\boldsymbol{a_2(1320)}$	$\boldsymbol{K_2^*(1430)}$	$\boldsymbol{f_2'(1525)}$	$\boldsymbol{f_2(1270)}$
1^3D_1	1^{--}	$\boldsymbol{\rho(1700)}$	$\boldsymbol{K^*(1680)}$[b]	$\boldsymbol{\phi(2170)}$[c]	$\boldsymbol{\omega(1650)}$
1^1D_2	2^{-+}	$\boldsymbol{\pi_2(1670)}$	$\boldsymbol{K_2(1770)}$[a]	$\boldsymbol{\eta_2(1870)}$	$\boldsymbol{\eta_2(1645)}$
1^3D_3	3^{--}	$\boldsymbol{\rho_3(1690)}$	$\boldsymbol{K_3^*(1780)}$	$\boldsymbol{\phi_3(1850)}$	$\boldsymbol{\omega_3(1670)}$
1^3F_4	4^{++}	$\boldsymbol{a_4(1970)}$	$\boldsymbol{K_4^*(2045)}$	$f_4(2300)$	$\boldsymbol{f_4(2050)}$
1^3G_5	5^{--}	$\rho_5(2350)$	$K_5^*(2380)$		
2^1S_0	0^{-+}	$\boldsymbol{\pi(1300)}$	$\boldsymbol{K(1460)}$	$\boldsymbol{\eta(1475)}$[d]	$\boldsymbol{\eta(1295)}$
2^3S_1	1^{--}	$\boldsymbol{\rho(1450)}$	$\boldsymbol{K^*(1410)}$[b]	$\boldsymbol{\phi(1680)}$	$\boldsymbol{\omega(1420)}$
2^3P_1	1^{++}	$\boldsymbol{a_1(1640)}$	$\boldsymbol{K_1(1650)}$		
2^3P_2	2^{++}	$\boldsymbol{a_2(1700)}$	$\boldsymbol{K_2^*(1980)}$	$\boldsymbol{f_2(1950)}$[e]	$f_2(1640)$
2^1D_2	2^{-+}	$\boldsymbol{\pi_2(1880)}$			
3^1S_0	0^{-+}	$\boldsymbol{\pi(1800)}$	$K(1830)$		$\eta(1760)$

Table 15.3: $c\bar{c}$ quark-model assignments for the charmonium mesons with established J^{PC} and their corresponding open charm mesons. Mesons in boldface are included in the Meson Summary Table. The open flavor states in the 1^{+-} and 1^{++} rows are mixtures of the $1^{+\pm}$ states.
[a] In unitarized chiral perturbation theory this meson splits into two states at 2105 and 2451 MeV [1,13].
[b] The masses are considerably smaller than most theoretical predictions. They have also been considered as tetraquark or $D^{(*)}K$ molecular states.
[c] This meson splits into two states at 2247 and 2555 MeV [1].
[d] Mixtures of the $1\,^3D_1$ and $2\,^3S_1$ states.
[e] The interpretation of this state as a single resonance is unclear due to substantial threshold effects in this energy region.

$n^{2s+1}\ell_J$	J^{PC}	I = 0	I = $\frac{1}{2}$	I = 0
		$c\bar{c}$	$c\bar{u}$, $c\bar{d}$; $\bar{c}u$, $\bar{c}d$	$c\bar{s}$; $\bar{c}s$
$1\,^1S_0$	0^{-+}	$\boldsymbol{\eta_c(1S)}$	$\boldsymbol{D}$	$\boldsymbol{D_s^{\pm}}$
$1\,^3S_1$	1^{--}	$\boldsymbol{J/\psi(1S)}$	$\boldsymbol{D^*}$	$\boldsymbol{D_s^{*\pm}}$
$1\,^3P_0$	0^{++}	$\boldsymbol{\chi_{c0}(1P)}$	$\boldsymbol{D_0^*(2300)}$[a]	$\boldsymbol{D_{s0}^*(2317)^{\pm}}$[b]
$1\,^3P_1$	1^{++}	$\boldsymbol{\chi_{c1}(1P)}$	$\boldsymbol{D_1(2430)}$[c]	$\boldsymbol{D_{s1}(2460)^{\pm}}$[b]
$1\,^1P_1$	1^{+-}	$\boldsymbol{h_c(1P)}$	$\boldsymbol{D_1(2420)}$	$\boldsymbol{D_{s1}(2536)^{\pm}}$
$1\,^3P_2$	2^{++}	$\boldsymbol{\chi_{c2}(1P)}$	$\boldsymbol{D_2^*(2460)}$	$\boldsymbol{D_{s2}^*(2573)^{\pm}}$
$2\,^1S_0$	0^{-+}	$\boldsymbol{\eta_c(2S)}$	$D_0(2550)^0$	$D_{s0}(2590)^+$
$2\,^3S_1$	1^{--}	$\boldsymbol{\psi(2S)}$	$D_1^*(2600)^0$	$\boldsymbol{D_{s1}^*(2700)^{\pm}}$[d]
$1\,^3D_1$	1^{--}	$\boldsymbol{\psi(3770)}$	$D_1^*(2760)^0$	$D_{s1}^*(2860)^{\pm}$[d]
$1\,^3D_2$	2^{--}	$\boldsymbol{\psi_2(3823)}$	$D_2(2740)^0$	
$2\,^3P_J$	0^{++}	$\chi_{c0}(3860)$		
	2^{++}	$\boldsymbol{\chi_{c2}(3930)}$	$D_2^*(3000)^0$	
$3\,^3S_1$	1^{--}	$\boldsymbol{\psi(4040)}$		
$2\,^3D_1$	1^{--}	$\boldsymbol{\psi(4160)}$[e]		
$4\,^3S_1$	1^{--}	$\boldsymbol{\psi(4415)}$		
$1\,^3D_3$	3^{--}	$\boldsymbol{\psi_3(3842)}$	$\boldsymbol{D_3^*(2750)}$	$\boldsymbol{D_{s3}^*(2860)^{\pm}}$

Int. J. Mod. Phys. A 2026.41. Downloaded from www.worldscientific.com
by UNIVERSITY OF CALIFORNIA @ BERKELEY on 09/16/26. Re-use and distribution is strictly not permitted, except for Open Access articles.

Table 15.4: $b\bar{b}$ quark-model assignments for the bottomonium mesons with established J^{PC} and their corresponding open bottom mesons.

$n^{2s+1}\ell_J$	J^{PC}	I = 0	I = $\frac{1}{2}$	I = 0	I = 0
		$b\bar{b}$	$b\bar{u}$, $b\bar{d}$; $\bar{b}u$, $\bar{b}d$	$b\bar{s}$; $\bar{b}s$	$b\bar{c}$; $\bar{b}c$
$1\,^1S_0$	0^{-+}	$\boldsymbol{\eta_b(1S)}$	$\boldsymbol{B}$	$\boldsymbol{B_s^0}$	$\boldsymbol{B_c^\pm}$
$1\,^3S_1$	1^{--}	$\boldsymbol{\Upsilon(1S)}$	$\boldsymbol{B^*}$	$\boldsymbol{B_s^*}$	
$1\,^3P_0$	0^{++}	$\boldsymbol{\chi_{b0}(1P)}$			
$1\,^3P_1$	1^{++}	$\boldsymbol{\chi_{b1}(1P)}$			
$1\,^1P_1$	1^{+-}	$\boldsymbol{h_b(1P)}$	$\boldsymbol{B_1(5721)}$	$\boldsymbol{B_{s1}(5830)^0}$	
$1\,^3P_2$	2^{++}	$\boldsymbol{\chi_{b2}(1P)}$	$\boldsymbol{B_2^*(5747)}$	$\boldsymbol{B_{s2}^*(5840)^0}$	
$2\,^1S_0$	0^{-+}	$\eta_b(2S)$			$\boldsymbol{B_c(2S)^\pm}$
$2\,^3S_1$	1^{--}	$\boldsymbol{\Upsilon(2S)}$			
$1\,^3D_2$	2^{--}	$\boldsymbol{\Upsilon_2(1D)}$			
$2\,^3P_J$	$0,1,2^{++}$	$\boldsymbol{\chi_{b0,1,2}(2P)}$			
$2\,^1P_1$	1^{+-}	$\boldsymbol{h_b(2P)}$			
$3\,^3S_1$	1^{--}	$\boldsymbol{\Upsilon(3S)}$			
$3\,^3P_J$	$0,1,2^{++}$	$\boldsymbol{\chi_{b1,2}(3P)}$			
$4\,^3S_1$	1^{--}	$\boldsymbol{\Upsilon(4S)}$			

with the vector mixing angle $\theta_V = 36.5°$ from Eq. (15.14), very close to ideal mixing. Thus $\phi(1020)$ is nearly pure $s\bar{s}$. For ideal mixing, Eq. (15.12) and Eq. (15.14) lead to the relations

$$m_K = \frac{m_f + m_{f'}}{2} \ , \quad m_a = m_f \ , \tag{15.18}$$

which are satisfied for the vector mesons.

The situation for the pseudoscalar and scalar mesons is not so clear cut, either theoretically or experimentally. For the pseudoscalars, the mixing angle is small. This can be understood qualitatively via gluon-line counting of the mixing process. The size of the mixing process between the nonstrange and strange mass bases scales as α_s^2, not α_s^3, because of two rather than three gluon exchange as it does for the vector mesons. It may also be that the lightest isoscalar pseudoscalars mix more strongly with excited states or with states of substantial non-$\bar{q}q$ content, as will be discussed below.

In fact a large mixing from hadronic loops is expected for scalar mesons, no matter what model is assumed for $q\bar{q}$ pair production [15]. A variety of analysis methods lead to similar results: First, for these states, Eq. (15.15) is satisfied only approximately. Then Eq. (15.12) and Eq. (15.14) lead to somewhat different values for the mixing angle. Identifying the η with the f' one gets

$$\eta = \psi_8 \ \cos\theta_P - \psi_1 \ \sin\theta_P \ , \tag{15.19}$$

$$\eta' = \psi_8 \ \sin\theta_P + \psi_1 \ \cos\theta_P \ . \tag{15.20}$$

Following chiral perturbation theory, the meson masses in the mass formulae (Eq. (15.12) and Eq. (15.14)) might be replaced by their squares. Table 15.5 lists the mixing angle $\theta_{\rm lin}$ from Eq. (15.14) (using the neutral members of the nonets) and the corresponding $\theta_{\rm quad}$ obtained by replacing the meson masses by their squares throughout. The mixing angles in the 1^{--}, 2^{++} and 3^{--} nonets are not far from ideal, while larger $s\bar{s}$-$(u\bar{u} + d\bar{d})$ mixing is predicted from hadronic loops in the 0^{++}, 0^{-+} and $1^{+\pm}$ nonets [15].

The pseudoscalar mixing angle θ_P can also be measured by comparing the partial widths for radiative J/ψ decay into a vector and a pseudoscalar [16], radiative $\phi(1020)$ decay into η and η' [17], radiative decays between pseudoscalar and vector mesons [18], or $\bar{p}p$ annihilation at rest into a pair of vector and pseudoscalar or into two pseudoscalars [19, 20]. One obtains a mixing angle between –10° and –20°. More recently, a lattice QCD simulation, Ref. [21], has successfully reproduced the masses of the η and η', and as a byproduct find a mixing angle $\theta_{lin} = -14.1(2.8)°$. We return to this point in Sec. 15.8.

The nonet mixing angles can be measured in $\gamma\gamma$ collisions, *e.g.*, for the 0^{-+}, 0^{++}, and 2^{++} nonets. In the quark model, the amplitude for the coupling of neutral mesons to two photons is proportional to $\sum_i Q_i^2$, where Q_i is the charge of the i-th quark.

Table 15.5: Singlet-octet mixing angles for the well established nonets from the linear mass formula Eq. (15.14) and its quadratic version in which the masses are squared. The 1^{++} and 1^{+-} nonet mixing angles depend on the mixing angle θ_{K_1} between K_{1A} and K_{1B}. The recommended values are ∼23° and ∼28° for 1^{++} and 1^{+-}, respectively, with θ_{K_1}∼35° [7].

$n^{2s+1}\ell_J$	J^{PC}	$\theta_{\rm quad}$ [°]	$\theta_{\rm lin}$ [°]
1^1S_0	0^{-+}	−11.3	−24.5
1^3S_1	1^{--}	39.2	36.5
1^3P_2	2^{++}	29.6	28.0
1^3D_3	3^{--}	31.8	30.8

The 2γ partial width of an isoscalar meson with mass m is then given in terms of the mixing angle α by

$$\Gamma_{2\gamma} = C(5\cos\alpha - \sqrt{2}\sin\alpha)^2 m^3 \ , \tag{15.21}$$

for f' and f ($\alpha \to \alpha - 90°$). The coupling C may depend on the meson mass. It is often assumed to be a constant in the nonet. For the isovector a, one finds $\Gamma_{2\gamma} = 9\,C\,m^3$. Thus the members of an ideally mixed nonet couple to 2γ with partial widths in the ratios $f : f' : a = 25 : 2 : 9$. For tensor mesons, one finds from the ratios of the measured 2γ partial widths for the $f_2(1270)$ and $f_2'(1525)$ mesons a mixing angle α_T of $(81\pm 1)°$, or $\theta_T = (27 \pm 1)°$, in accord with the linear mass formula. For the pseudoscalars, one finds from the ratios of partial widths $\Gamma(\eta' \to 2\gamma)/\Gamma(\eta \to 2\gamma)$ a mixing angle $\theta_P = (-18 \pm 2)°$, while the ratio $\Gamma(\eta' \to 2\gamma)/\Gamma(\pi^0 \to 2\gamma)$ leads to ∼ –24 °. SU(3) breaking effects for pseudoscalars are discussed in [22].

The partial width Γ for the decay of a scalar or a tensor meson into a pair of pseudoscalar mesons is model-dependent. Following Ref. [23],

$$\Gamma = C \times \gamma^2 \times |F(q)|^2 \times q \ , \tag{15.22}$$

where C is a nonet constant, q the momentum of the decay products, $F(q)$ a form factor, and γ^2 the SU(3) coupling. Details and explicit expressions for γ^2 and $F(q)$ are given in "Spectroscopy of Light Meson Resonances". The decay of a $q\bar{q}$ meson into a pair of mesons involves the creation of a $q\bar{q}$ pair, and SU(3) symmetry assumes that the matrix elements for the creation of $s\bar{s}$, $u\bar{u}$, and $d\bar{d}$ pairs are equal. An excellent fit to the tensor meson decay widths is obtained assuming SU(3) symmetry and a pseudoscalar mixing angle $\theta_P \simeq -17$ ° [23].

The analysis of resonances is complicated by the presence of thresholds such as $K\bar{K}$ in $a_0(980) \to \eta\pi$ or $f_0(980) \to \pi\pi$, which

Int. J. Mod. Phys. A 2026.41. Downloaded from www.worldscientific.com by UNIVERSITY OF CALIFORNIA @ BERKELEY on 09/16/26. Re-use and distribution is [redacted] except for Open Access articles.

affect the resonance masses and widths. A particularly nasty kinematic effect is the triangle singularity in which one of the primary decay daughters in turn decays and is emitted backwards, catching up and scattering with the second primary product. This mechanism generates fake peaks in the final state and has been proposed as alternative explanation for several meson (and baryon) signals. Prominent examples are the $\eta(1475) \to K^*(\to K\pi)\bar{K}$ and $\eta(1410) \to a_0(980)(\to \eta\pi)\pi$ signals which could be due to one single state [10] (as shown in Table 15.2).

Furthermore, to parametrize resonances, many data analyses resort to Breit-Wigner amplitudes which are not suitable to describe broad interfering mesons with the same quantum numbers, as they violate unitarity. This is in particular the case in the mass range above 1500 MeV where radial and orbital excitations, e.g. of broad scalar and tensor mesons, start to accumulate. A better approach is to determine the T-matrix poles in the complex plane, where resonances are usually located on the second Riemann sheet.

15.4 Exotic mesons

There are two classes of colorless exotic mesons allowed in QCD: multiquark states (section 15.4.1) and mesons with active gluons, bound states of gluons (the glueballs, section 15.4.2) and $q\bar{q}$ states with "valence" gluons (the hybrids, section 15.4.3). The first class contains the simplest system consisting of two quarks and two antiquarks (tetraquarks). Compact tetraquarks (also called "diquonium" in the older literature) are made of diquarks and antidiquarks. Hadroquarkonia consist of a pair of heavy quark and antiquark in a compact core surrounded by a light-quark cloud. In hadronic "molecules" the building blocks are color-neutral hadrons bound by meson exchanges.

15.4.1 *Tetraquarks*

The existence of a light nonet composed of four quarks (tetraquarks) with masses below 1 GeV was suggested a long time ago [24,25]. Coupling two triplets of light quarks u, d, and s, one obtains nine states, of which the six symmetric (uu, dd, ss, $ud+du$, $us+su$, $ds+sd$) form the six dimensional representation $\mathbf{6}$, while the three antisymmetric ($ud-du$, $us-su$, $ds-sd$) form the three dimensional representation $\bar{\mathbf{3}}$ of SU(3):

$$\mathbf{3} \otimes \mathbf{3} = \mathbf{6} \oplus \bar{\mathbf{3}} \ . \tag{15.23}$$

Hence for tetraquarks one gets the reduction

$$\begin{aligned} &\mathbf{3} \otimes \mathbf{3} \otimes \bar{\mathbf{3}} \otimes \bar{\mathbf{3}} \\ &= \mathbf{6} \oplus \bar{\mathbf{3}} \otimes \bar{\mathbf{6}} \otimes \mathbf{3} \\ &= \bar{\mathbf{3}} \otimes \mathbf{3} \oplus \mathbf{6} \otimes \bar{\mathbf{6}} \oplus \mathbf{6} \otimes \mathbf{3} \oplus \bar{\mathbf{3}} \otimes \bar{\mathbf{6}} \\ &= \mathbf{9} \oplus \mathbf{36} \oplus \mathbf{18} \oplus \overline{\mathbf{18}}. \end{aligned} \tag{15.24}$$

Combining with spin and color and requiring antisymmetry for diquarks and antidiquarks, one finds for ground states (zero angular momenta) that the most deeply bound tetraquarks (and hence the lightest ones) form a nonet and are scalar mesons (see also [6]). The masses are estimated to be below 900 MeV. The strange quark determines the mass splittings and one obtains a mass inverted spectrum with a light isosinglet ($f_0(500)$), a medium heavy isodoublet ($K_0^*(700)$) and a heavy isotriplet ($a_0(980)$) + isosinglet ($f_0(980)$). In alternative schemes these states build the lightest $q\bar{q}$ scalar nonet (for details see "Scalar mesons below 1 GeV" in this *Review*).

A plethora of new heavy multiquark candidates have been reported in the charmonium spectrum (Fig. 15.2). Details and references can be found in the review "Heavy non-$q\bar{q}$ Mesons", see also Refs. [26–29].

The most prominent one is the $\chi_{c1}(3872)$ (was $X(3872)$), first observed by BELLE in 2003 in B-decays in the final state $J/\psi\,\pi^+\pi^-$ [30] and firmly established by many experiments (Babar, BESIII, CDF, D0, LHCb) in several production modes (e^+e^-, Λ_b decay, $\bar{p}p$, pp). This narrow state ($<$ 1 MeV) decays mainly into $D^0\bar{D}^{0*}$ and is right at the $D^0\bar{D}^{0*}$ threshold. Its composition is believed to be mostly molecular, bound by pion exchange. Its existence was already predicted in 1991 [31]. Many non-$c\bar{c}$ candidates have been reported since then above the open

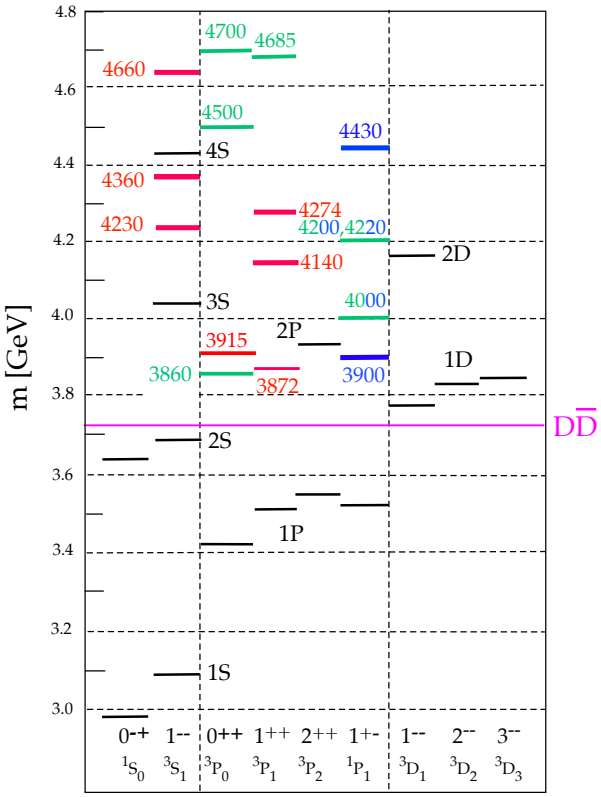

Figure 15.2: Mass spectrum with known $I^G(J^{PC})$ observed in the charmonium region. The $D\bar{D}$ line shows the open charm threshold. The well-known $c\bar{c}$ mesons are shown in black. (The 1^1D_2 η_{c2}, expected around 3800 MeV, has not been seen yet.) The established additional observed states are shown in red, and the states needing confirmation (i.e. omitted from the Summary Tables) are labeled in green. The blue color denotes exotic isovectors.

charm threshold, with quantum numbers compatible with $c\bar{c}$, but which are not expected in the pure charmonium spectrum. In addition, one observes isovector (charged) mesons decaying into $c\bar{c}$ states plus a charged pion or kaon. (They are listed in this *Review* under "Other mesons".) For example, the 1^{+-} $T_{c\bar{c}1}(3900)^+$ (was $Z_c(3900)^+$) and $T_{c\bar{c}s1}(4000)^+$ (was $Z_{cs}(4000)^-$) cannot be pure charmonia, but are compatible with $c\bar{c}u\bar{d}$ and $c\bar{c}s\bar{u}$, respectively. They could belong to the same nonet, hence identifying the other multiplet members might shed light on the structure of such states.

Even more remarkable are the observations by LHCb of a doubly charmed state $T_{cc}(3875)^+$ ($cc\bar{u}\bar{d}$)) [32] at the $D_0D_0^*$ threshold and of a $T_{cc\bar{c}\bar{c}}(6900)$ [33] decaying into a pair of $J/\psi(1S)$. Similar states begin to emerge also in the bottomonium spectrum, such as the 1^{+-} $T_{b\bar{b}1}(10610)^+$ (was $Z_b(10610)^+$) and $T_{b\bar{b}1}(10650)^+$ (was $Z_b(10650)^+$), both $b\bar{b}u\bar{d}$. Many of these states may be hadronic modules made of charge conjugated pairs of mesons such as $D^{(*)}, D_s^{(*)}$ or their excitations, and their B and B^* counterparts. They could also be mimicked by kinematical effects such as triangle singularities.

15.4.2 *Glueballs*

QCD predicts the existence of extra isoscalar mesons which cannot be addressed by the quark model. In the pure gauge theory they contain only gluons. The ground state glueball is predicted by lattice gauge theories to be 0^{++}, the first excited state 2^{++}. Errors on the mass predictions are large. From Ref. [34] one obtains 1750 (50) (80) MeV for the mass of the lightest 0^{++} glueball from quenched QCD. As an example for the glueball mass spectrum, we show in Fig. 15.3 a calculation from [35]. A mass of 1710 MeV is predicted for the ground state, also with an error of

Int. J. Mod. Phys. A 2026.41. Downloaded from www.worldscientific.com
by UNIVERSITY OF CALIFORNIA @ BERKELEY on 09/16/26. Re-use and distribution is strictly not permitted, except for Open Access articles.

about 100 MeV. Earlier work by other groups produced masses at 1650 MeV [36] and 1550 MeV [37] (see also [38].

These calculations are made in the so-called "quenched approximation" which neglects $q\bar{q}$ loops. However, both glue and $q\bar{q}$ states couple to singlet scalar mesons. Therefore glueballs will mix with nearby $q\bar{q}$ states of the same quantum numbers. The first results from lattice calculations, which include these effects, indicate that the mass shifts are small. We return to a discussion of this point in Sec. 15.8, see also Fig. 15.15. The most recent prediction [39] quotes the more precise masses 1653 ± 26, 2376 ± 32 and 2561 ± 40 MeV for the 0^{++}, 2^{++} and 0^{-+} respectively. Heavier glueballs with quantum numbers 0^{-+}, 2^{-+}, 1^{+-}, etc. are predicted above 2500 MeV and the lowest exotic ones (with exotic quantum numbers such as 0^{+-} and 2^{+-}) are expected above 4000 MeV (Fig. 15.3). In holographic QCD the 0^{-+} is predicted to be very broad [40] and the 1^{+-} is at least as broad as its mass [41]. Calculations of the three lowest scalar and pseudoscalar glueballs masses in pure Yang-Mills theory are in quantitative agreement with lattice results [42].

The existence of three singlet scalar mesons around 1.5 GeV suggests additional degrees of freedom such as glue, since only two mesons are predicted in this mass range (as indicated in Table 15.2). The $f_0(1500)$ [23, 43] or, alternatively, the $f_0(1710)$ [36], have been proposed as candidates for the scalar glueball, both states having considerable mixing also with the $f_0(1370)$. Following Ref. [44] the glue is distributed among the 0^{++} isoscalars $q\bar{q}$ mesons around 2 GeV. Other mixing schemes, in particular with the $f_0(500)$ and the $f_0(980)$, have also been proposed [45]. According to a holographic model of low-energy QCD scalar glueballs decay strongly into kaons and η mesons, in good agreement with data on the $f_0(1710)$ [46]. Details can be found in the review "Spectroscopy of Light Meson Resonances" and in Ref. [47]. See also the review "Scalar Mesons below 1 GeV" in this *Review*.

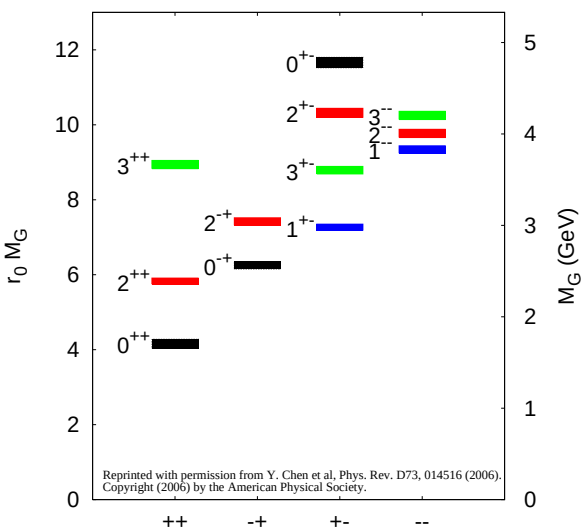

Figure 15.3: Predicted glueball spectrum from the lattice in quenched approximation (from [35]).

15.4.3 *Hybrids*

Mesons made of $q\bar{q}$ pairs bound by excited gluons ($q\bar{q}g$) are also predicted. Early model estimates placed them in the 1.9 GeV mass region, according to gluon flux tube models [48]. In the bag model there are four nonets, among them an exotic 1^{-+}, around or above 1.4 GeV [49, 50].

Lattice QCD calculations show that the lightest hybrid is an exotic 1^{-+} state, at a mass around 2 GeV [51–53]. Fig. 15.13 will show an example of the spectroscopy from one group's [53] simulation.

There are so far two candidates for exotic states with quantum numbers 1^{-+}, the $\pi_1(1400)$ and $\pi_1(1600)$, which could be hybrids or four-quark states. However, a recent combined re-analysis of π_1 production in diffractive $\pi^- p$ interaction and low energy $\bar{p}p$ annihilation leads to a single pole at ∼1560 MeV with a width of ∼390 MeV, although a two-pole scenario cannot be excluded [54]. Recently BESIII has reported evidence for the existence of a 1^{-+} $\eta_1(1855) \to \eta\eta'$ [55] which could be one of the isoscalar partners of the $\pi_1(1600)$ in the 1^{-+} hybrid nonet [56]. (For details and references, see the review "Spectroscopy of Light Meson Resonances" in this *Review*.)

15.5 Baryons: qqq states

Baryons are fermions with baryon number $\mathcal{B} = 1$, *i.e.*, in the most general case, they are composed of three quarks plus any number of quark - antiquark pairs. Until recently, all established baryons were consistent with 3-quark (qqq) configurations, which we mainly discuss in this section. However, in 2015 the LHCb collaboration published first evidence for charmed 'pentaquark' states of minimal quark content $c\bar{c}uud$ at invariant masses close to 4.4 GeV [57]. More refined LHCb [58] and D0 [59] experiments have revealed evidence for six such states called $P_{c\bar{c}}(4312)^+$, $P_{c\bar{c}s}(4338)^0$, $P_{c\bar{c}}(4380)^+$, $P_{c\bar{c}}(4440)^+$, $P_{c\bar{c}}(4457)^+$, and $P_{c\bar{c}}(4459)^0$. These states are located close to the thresholds of the production of ordinary baryon-meson pairs like $\Sigma_c^+ \bar{D}^0$ and $\Sigma_c^+ \bar{D}^{\star 0}$ and are consistent with the predictions in terms of molecular-like states [60, 61]. A nice overview on the discussion of pentaquark and tetraquark states is given in Ref. [62]. See also the article on "Pentaquarks" in this *Review*.

The color part of the baryon wave function is an SU(3) singlet, a completely antisymmetric state of the three colors. Since the quarks are fermions, the wave function must be antisymmetric under interchange of any two equal-mass quarks (up and down quarks in the limit of isospin symmetry). Thus, it can be written as

$$|\, qqq \,\rangle_A = |\, \text{color} \,\rangle_A \times |\, \text{space, spin, flavor} \,\rangle_S, \tag{15.25}$$

where the subscripts S and A indicate symmetry or antisymmetry under interchange of any two equal-mass quarks. Note the contrast with the state function for the three nucleons in ^{3}H or ^{3}He:

$$|\, NNN \,\rangle_A = |\, \text{space, spin, isospin} \,\rangle_A. \tag{15.26}$$

This difference has major implications for the internal structure, magnetic moments, *etc.* (For a nice discussion, see [63].)

15.5.1 *Light baryons*

The "ordinary" light-flavor baryons are made up of u, d, and s quarks. The three flavors imply an approximate SU(3) flavor symmetry, which requires that baryons made of these quarks belong to the multiplets on the right side of

$$\mathbf{3} \otimes \mathbf{3} \otimes \mathbf{3} = \mathbf{10}_S \oplus \mathbf{8}_M \oplus \mathbf{8}_M \oplus \mathbf{1}_A \tag{15.27}$$

(see the section on "SU(n) Multiplets and Young Diagrams" in this *Review*). Here the subscripts indicate symmetric, mixed-symmetry, or antisymmetric states under interchange of any two quarks. The $\mathbf{1}$ is a $|uds\rangle$ singlet state (Λ_1), and the octet contains a similar state (Λ_8). If these have the same spin and parity, they can mix. The mechanism is the same as for the mesons (see above). In the ground state multiplet, the SU(3) flavor singlet Λ_1 is forbidden by Fermi statistics. The section on "SU(3) Isoscalar Factors and Representation Matrices," shows how relative decay rates in, say, $\mathbf{10} \to \mathbf{8} \otimes \mathbf{8}$ decays may be calculated.

For the light-flavor baryons (no c or b quark), flavor and spin may be combined in an approximate flavor-spin SU(6), in which the six basic states are $d\uparrow$, $d\downarrow$, $\cdots$, $s\downarrow$ ($\uparrow, \downarrow$ = spin up, down). Then the baryons belong to the multiplets on the right side of

$$\mathbf{6} \otimes \mathbf{6} \otimes \mathbf{6} = \mathbf{56}_S \oplus \mathbf{70}_M \oplus \mathbf{70}_M \oplus \mathbf{20}_A. \tag{15.28}$$

These SU(6) multiplets decompose into flavor SU(3) multiplets as follows:

$$\mathbf{56} = {}^4\mathbf{10} \oplus {}^2\mathbf{8} \tag{15.29a}$$

$$\mathbf{70} = {}^2\mathbf{10} \oplus {}^4\mathbf{8} \oplus {}^2\mathbf{8} \oplus {}^2\mathbf{1} \tag{15.29b}$$

$$\mathbf{20} = {}^2\mathbf{8} \oplus {}^4\mathbf{1}, \tag{15.29c}$$

where the superscript $(2S{+}1)$ gives the net spin S of the quarks for each particle in the SU(3) multiplet. The $J^P = 1/2^+$ octet containing the nucleon and the $J^P = 3/2^+$ decuplet containing the

Int. J. Mod. Phys. A 2026.41. Downloaded from www.wo
by UNIVERSITY OF CALIFORNIA @ BERKELEY on 09/16/26. Re-use and distribution is
except for Open Access articles.

$\Delta(1232)$ together make up the "ground-state" 56-plet, in which the orbital angular momenta between the quark pairs are zero (so that the spatial part of the state function is trivially symmetric). The **70** and **20** require some excitation of the spatial part of the wave function in order to make the overall wave function symmetric. States with nonzero orbital angular momenta are classified in SU(6)⊗O(3) supermultiplets.

It is useful to classify the baryons into bands that have the same number N of quanta of excitation. Each band consists of a number of supermultiplets, specified by (D, L^P_N), where D is the dimensionality of the SU(6) representation, L is the total quark orbital angular momentum, and P is the total parity. Supermultiplets contained in bands up to N = 12 are given in [64]. The N = 0 band (with positive parity), which contains the nucleon and $\Delta(1232)$, consists only of the $(56,0^+_0)$ supermultiplet. The N = 1 band (with negative parity) consists only of the $(70,1^-_1)$ multiplet and contains the negative-parity baryons with masses below about 1.9 GeV. The N = 2 band (with positive parity) contains five supermultiplets: $(56,0^+_2)$, $(70,0^+_2)$, $(56,2^+_2)$, $(70,2^+_2)$, and $(20,1^+_2)$, where the $(56,0^+_0)$ represents the multiplet that contains the first radial excitations having the same quantum numbers as the ground state.

The wave functions of the non-strange baryons in the harmonic oscillator basis are often labeled by $|X^{2S+1}L_\pi J^P\rangle$, where S, L, J, P are as above, $X = N$ or Δ, and $\pi = S, M$ or A denotes the symmetry of the spatial wave function. The possible model states for the bands with N=0,1,2 are given in Table 15.7. The assignment of experimentally observed states is only complete and well established up to the N=1 band. Some more tentative assignments for higher multiplets are suggested in [65].

In Table 15.6, quark-model assignments are given for many of the established baryons whose SU(6)⊗O(3) compositions are relatively unmixed. Apart from the mixing of the Λ singlet and octet states, one must, however, keep in mind that states with same J^P but different L, S combinations can also mix. In the quark model with one-gluon exchange motivated interactions, the size of the mixing is determined by the relative strength of the tensor term with respect to the contact term (see below). The mixing is more important for the decay patterns of the states than for their positions. An example are the lowest lying $(70, 1^-_1)$ states with J^P=1/2$^-$ and 3/2$^-$. The physical states are

$$|\,N(1535)1/2^-\rangle = \cos(\Theta_S)|N^2P_M1/2^-\rangle - \sin(\Theta_S)|N^4P_M1/2^-\rangle \tag{15.30}$$

$$|\,N(1520)3/2^-\rangle = \cos(\Theta_D)|N^2P_M3/2^-\rangle - \sin(\Theta)_D|N^4P_M3/2^-\rangle \tag{15.31}$$

and the orthogonal combinations for $N(1650)1/2^-$ and $N(1700)3/2^-$. The mixing is large for the J^P=1/2$^-$ states ($\Theta_S \approx$ -32°), but small for the J^P=3/2$^-$ states ($\Theta_D \approx +6^o$) [67–69].

All baryons of the ground state multiplets are known. Many of their properties, in particular their masses, are in good agreement with even the most basic versions of the quark model, including harmonic (or linear) confinement and a spin-spin interaction, which is responsible for the octet - decuplet mass shifts. A consistent description of the ground-state electroweak properties, however, requires refined relativistic constituent quark models.

The situation for the excited states is much less clear. The assignment of some experimentally observed states with strange quarks to model configurations is only tentative and in many cases candidates are completely missing. Melde, Plessas and Sengl [66] have calculated baryon properties in relativistic constituent quark models, using one-gluon exchange and Goldstone-boson exchange for the modeling of the hyperfine interactions (see Sec. 15.7 on Dynamics). Both types of models give qualitatively comparable results and in geneeral, underestimate experimentally observed decay widths. Nevertheless, in particular on the basis of the observed decay patterns, the authors have assigned some additional states with strangeness to the SU(3) multiplets and suggest reassignments for a few others. Among the new assignments are states with weak experimental evidence (two or three star ratings) and partly without firm spin/parity assignments, so that further experimental efforts are necessary before final conclusions can be drawn. We have added their suggestions in Table 15.6.

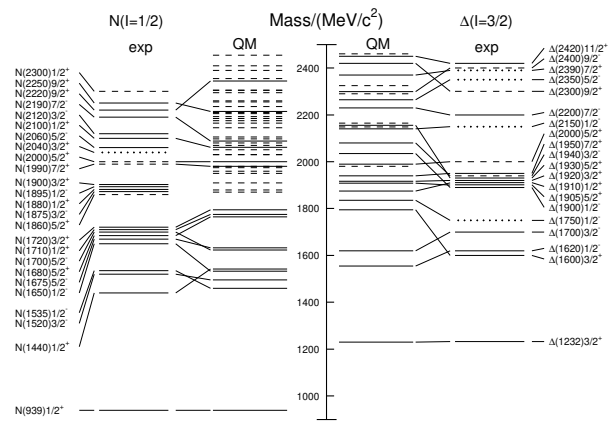

Figure 15.4: Excitation spectrum of the nucleon. Compared are the positions of the excited states identified in experiment, to those predicted by a relativized quark model calculation. Left hand side: isospin $I = 1/2$ N-states, right hand side: isospin $I = 3/2$ Δ-states. Experimental: (columns labeled 'exp'), three- and four-star states are indicated by full lines (two-star dashed lines, one-star dotted lines). At the very left and right of the figure, the spectroscopic notation of these states is given. Quark model [70, 71]: (columns labeled 'QM'), all states for the N=1,2 bands, low-lying states for the N=3,4,5 bands. Full lines: at least tentative assignment to observed states, dashed lines: so far no observed counterparts. Many of the assignments between predicted and observed states are highly tentative.

In the non-strange sector there are two main problems which are illustrated in Fig. 15.4, where the experimentally observed excitation spectrum of the nucleon (N and Δ resonances) is compared to the results of a typical quark model calculation [70]. The lowest states from the N=2 band, the $N(1440)1/2^+$, and the $\Delta(1600)3/2^+$, appear lower than the negative parity states from the N=1 band (see Table 15.7) and much lower than predicted by most models. Also negative parity Δ states from the N=3 band ($\Delta(1900)1/2^-$, $\Delta(1940)3/2^-$, and $\Delta(1930)5/2-$) are too low in energy. The low lying states show a clustering in groups of levels around 1700 MeV and 1900 MeV for $N^\star$ states and around 1900 MeV for Δ states which is not reflected in models.

Furthermore, many more states are predicted than observed. This has been known for a long time as the 'missing resonance' problem [67]. Up to an excitation energy of 2.4 GeV, about 45 N states are predicted, but only 20 are established (four- or three-star; see Note on N and Δ Resonances for the rating of the status of resonances) and 5 are tentative (two- or one-star). However, there is some recent progress. For the N=2 band, candidates have been identified for almost all predicted states with the exception of the $(20,1^+_2)$. Noteworthy is the recent addition of the new $N(1880)\,1/2^+$ state since the four states, $N(1880)\,1/2^+$, $N(1900)\,3/2^+$, $N(2000)\,5/2^+$, $N(1990)\,7/2^+$, are considered to form a quartet of nucleon states with spin 3/2 and to be members of the $(70,2^+_2)$ supermultiplet. The total number of states has perhaps not significantly changed but the number of states with four- or three-star rating has increased from 14 to 20 compared to the 2018 PDG particle listings. Most of this progress is due to the programs concentrating on the study of meson photoproduction reactions, while the most recent partial wave analysis of elastic pion scattering and charge exchange data by Arndt and collaborators [72] found no evidence for almost half of the states listed in this review (and included in Fig. 15.4). Such analyses are of course biased against resonances which couple only weakly to the $N\pi$ channel. Quark model predictions for the couplings to other hadronic channels and to photons are given in Ref. [70]. The large experimental effort ongoing at several electron accelerators to study the baryon resonance spectrum with real and virtual photon-induced meson production reactions includes the search for as-yet-unobserved states, as well as detailed studies of

Int. J. Mod. Phys. A 2026.41. Downloaded from www.worldscientific.com
by UNIVERSITY OF CALIFORNIA @ BERKELEY on 09/16/26. Re-use and distribution is strictly not permitted, except for Open Access articles.

Table 15.6: Quark-model assignments for some of the known baryons in terms of a flavor-spin SU(6) basis. Only the dominant representation is listed. Assignments for several states, especially for the $\Lambda(1810)$, $\Lambda(2350)$, $\Xi(1620)$, $\Xi(1690)$, $\Xi(1820)$, and $\Xi(2030)$, are merely educated guesses.
† suggestions for assignments and re-assignments from Ref. [66].

J^P	(D, L^P_N)	S	Octet members				Singlets
$1/2^+$	$(56,0^+_0)$	1/2	$N(939)$	$\Lambda(1116)$	$\Sigma(1193)$	$\Xi(1318)$	
$1/2^+$	$(56,0^+_2)$	1/2	$N(1440)$	$\Lambda(1600)$	$\Sigma(1660)$		
$1/2^-$	$(70,1^-_1)$	1/2	$N(1535)$	$\Lambda(1670)$	$\Sigma(1620)$ $\Sigma(1560)^\dagger$	$\Xi(1620)$	$\Lambda(1405)$
$3/2^-$	$(70,1^-_1)$	1/2	$N(1520)$	$\Lambda(1690)$	$\Sigma(1670)$	$\Xi(1820)$	$\Lambda(1520)$
$1/2^-$	$(70,1^-_1)$	3/2	$N(1650)$	$\Lambda(1800)$	$\Sigma(1750)$ $\Sigma(1620)^\dagger$	$\Xi(1690)$	
$3/2^-$	$(70,1^-_1)$	3/2	$N(1700)$	$\Lambda(?)$	$\Sigma(1940)^\dagger$	$\Xi(?)$	
$5/2^-$	$(70,1^-_1)$	3/2	$N(1675)$	$\Lambda(1830)$	$\Sigma(1775)$	$\Xi(1950)^\dagger$	
$1/2^+$	$(70,0^+_2)$	1/2	$N(1710)$	$\Lambda(1810)$	$\Sigma(1880)$	$\Xi(?)$	$\Lambda(1810)^\dagger$
$3/2^+$	$(56,2^+_2)$	1/2	$N(1720)$	$\Lambda(1890)$	$\Sigma(?)$	$\Xi(?)$	
$5/2^+$	$(56,2^+_2)$	1/2	$N(1680)$	$\Lambda(1820)$	$\Sigma(1915)$	$\Xi(2030)$	
$7/2^-$	$(70,3^-_3)$	1/2	$N(2190)$	$\Lambda(?)$	$\Sigma(?)$	$\Xi(?)$	$\Lambda(2100)$
$9/2^-$	$(70,3^-_3)$	3/2	$N(2250)$	$\Lambda(?)$	$\Sigma(?)$	$\Xi(?)$	
$9/2^+$	$(56,4^+_4)$	1/2	$N(2220)$	$\Lambda(2350)$	$\Sigma(?)$	$\Xi(?)$	
			Decuplet members				
$3/2^+$	$(56,0^+_0)$	3/2	$\Delta(1232)$	$\Sigma(1385)$	$\Xi(1530)$	$\Omega(1672)$	
$3/2^+$	$(56,0^+_2)$	3/2	$\Delta(1600)$	$\Sigma(1690)^\dagger$	$\Xi(?)$	$\Omega(?)$	
$1/2^-$	$(70,1^-_1)$	1/2	$\Delta(1620)$	$\Sigma(1750)^\dagger$	$\Xi(?)$	$\Omega(?)$	
$3/2^-$	$(70,1^-_1)$	1/2	$\Delta(1700)$	$\Sigma(?)$	$\Xi(?)$	$\Omega(2012)$	
$5/2^+$	$(56,2^+_2)$	3/2	$\Delta(1905)$	$\Sigma(?)$	$\Xi(?)$	$\Omega(?)$	
$7/2^+$	$(56,2^+_2)$	3/2	$\Delta(1950)$	$\Sigma(2030)$	$\Xi(?)$	$\Omega(?)$	
$11/2^+$	$(56,4^+_4)$	3/2	$\Delta(2420)$	$\Sigma(?)$	$\Xi(?)$	$\Omega(?)$	

Table 15.7: N and Δ states in the N=0,1,2 harmonic oscillator bands. L^P denotes angular momentum and parity, S the three-quark spin and 'sym'=A,S,M the symmetry of the spatial wave function. Listed are all possible spin/parity combinations and assignments of experimentally observed states. Only dominant components are indicated. Assignments in the N=2 band are partly tentative.

N	sym	L^P	S	$N(I=1/2)$			
2	A	1^+	1/2	$1/2^+$	$3/2^+$	-	-
2	M	2^+	3/2	$1/2^+$	$3/2^+$	$5/2^+$	$7/2^+$
2	M	2^+	1/2	-	$3/2^+$	$5/2^+$	-
2	M	0^+	3/2	-	$3/2^+$	-	-
2	M	0^+	1/2	$1/2^+$ $N(1710)$	-	-	-
2	S	2^+	3/2	-	-	-	-
2	S	2^+	1/2	-	$3/2^+$ $N(1720)$	$5/2^+$ $N(1680)$	-
2	S	0^+	3/2	-	-	-	-
2	S	0^+	1/2	$1/2^+$ $N(1440)$	-	-	-
1	M	1^-	3/2	$1/2^-$ $N(1650)$	$3/2^-$ $N(1700)$	$5/2^-$ $N(1675)$	-
1	M	1^-	1/2	$1/2^-$ $N(1535)$	$3/2^-$ $N(1520)$	-	-
0	S	0^+	3/2	-	-	-	-
0	S	0^+	1/2	$1/2^+$ $N(938)$	-	-	-
N	sym	L^P	S	$\Delta(I=3/2)$			
2	A	1^+	1/2	-	-	-	-
2	M	2^+	3/2	-	-	-	-
2	M	2^+	1/2	-	$3/2^+$	$5/2^+$	-
2	M	0^+	3/2	-	-	-	-
2	M	0^+	1/2	$1/2^+$ $\Delta(1750)$	-	-	-
2	S	2^+	3/2	$1/2^+$ $\Delta(1910)$	$3/2^+$ $\Delta(1920)$	$5/2^+$ $\Delta(1905)$	$7/2^+$ $\Delta(1950)$
2	S	2^+	1/2	-	-	-	-
2	S	0^+	3/2	-	$3/2^+$ $\Delta(1600)$	-	-
2	S	0^+	1/2	-	-	-	-
1	M	1^-	3/2	-	-	-	-
1	M	1^-	1/2	$1/2^-$ $\Delta(1620)$	$3/2^-$ $\Delta(1700)$	-	-
0	S	0^+	3/2	-	$3/2^+$ $\Delta(1232)$	-	
0	S	0^+	1/2	-	-	-	-

Int. J. Mod. Phys. A 2026.41. Downloaded from www.wo
by UNIVERSITY OF CALIFORNIA @ BERKELEY on 09/16/26. Re-use and distribution is
except for Open Access articles.

the properties of the low lying states (decay patterns, electromagnetic couplings, magnetic moments, *etc.*) (see Ref. [73] for reviews). There are two major new aspects of this program. The investigation of single and double polarization observables allows, via the study of interference terms, access to small partial waves that do not leave a footprint in unpolarized cross sections. An example for the impact of such data is given by a comparison of results from different multipole analyses of pion photoproduction [74]. It shows clearly that with the inclusion of polarization observables the reaction model results start to converge. This will in the near future much improve the database for excited baryons in the light quark sector.

The other aspect is the study of final states with meson pairs, in particular $\pi\pi$ and $\pi\eta$ pairs, which has made much progress during the last few years. This is important for higher lying states, which in the quark model may have both possible oscillations excited. Such states can be expected to decay in sequential processes de-exciting the two oscillations step-by-step so that they couple strongly to multiple-meson final states but not to single-meson production. Detailed analyses of such data are for example given in [75,76] and had already significant impact on partial wave analyses.

The excitation spectrum of hyperons containing s-quarks is even less well explored. Many experimental results date back to before 2000, although parameters listed in the review are in many cases updated by more modern partial wave analyses. A recent review on the quark model interpretation of the Λ and Σ states is given in Ref. [77]. Significant progress on excited multi-strange Ξ and Ω states has been reported in recent years from the high-energy experiments, where these strange baryons are copiously produced in the decays of heavy baryons containing a charm or bottom quark, or in the decay of heavy-flavor mesons. A new Ω^- state was reported in the ΞK mass spectrum with high significance from the Belle experiment [78]. This $\Omega(2012)^-$ resonance is fairly narrow and, therefore, has a likely $J^P = \frac{3}{2}^-$ classification since the decay into ΞK would proceed via D-wave. A state with $J^P = \frac{1}{2}^-$ would decay via S-wave and thus be wider. The latest addition to the Ω family, $\Omega(2109)$, was announced by the BES III Collaboration based on the reaction $e^+e^- \to \Omega(2109)^-\bar{\Omega}^+$ [79]. It is interesting to note that the first radial excitation of the Ω ground state is expected close to 2100 MeV.

In the doubly-strange sector, Belle reported on the most significant evidence so far for the $\Xi(1620)$ in the $\Xi\pi$ mass spectrum [80], which has warranted a recent upgrade of this resonance from one star to two stars. Most recently, the LHCb Collaboration has reported on the first observation of $\Xi(1690)$ and $\Xi(1820)$ in the decay of Ξ_b^- into $J/\psi\,\Lambda K^-$ [81]. Masses and widths have been determined with improved precision in an amplitude analysis of the $K^-\Lambda$ mass distribution. Evidence for these two states has also been reported by several other collaborations.

A recent review of strange Ξ and Ω baryons is given in Ref. [82]. In the near future, significant progress on hyperon spectroscopy is expected from JLab using the K_L facility in conjunction with the GlueX exprimental setup, J-PARC using the K^- beam at the extended hadron facility, and the PANDA experiment at FAIR [83,84].

In quark models, the number of excited states is determined by the effective degrees of freedom, while their ordering and decay properties are related to the residual quark - quark interaction. An overview of quark models for baryons is given in [85], recent discussions of baryon spectroscopy are given in [65, 86]. The effective degrees of freedom in the standard nonrelativistic quark model are three equivalent valence quarks with one-gluon exchange-motivated, flavor-independent color-magnetic interactions. The QCD aspect of gluon-gluon interactions is emphasized by the hypercentral quark model [87,88], which includes in a natural way three-body forces between the quarks. A different class of models uses interactions which give rise to a quark - diquark clustering of the baryons: for a review see [89]. If there is a tightly bound diquark, only two degrees of freedom are available at low energies, and thus *fewer* states are predicted. Furthermore, selection rules in the decay pattern may arise from the quantum numbers of the diquark. However, we note that the recent identification of new N^* resonances seriously questions the older static diquark-quark model since these resonances are likely members of the $(70,2_2^+)$, which requires both oscillators in the baryon to be excited. *More* states are predicted by collective models of the baryon like the algebraic approach in [90]. In this approach, the quantum numbers of the valence quarks are distributed over a Y-shaped string-like configuration, and additional states arise *e.g.*, from vibrations of the strings. *More* states are also predicted in the framework of flux-tube models, see [91], which are motivated by lattice QCD. In addition to the quark degrees of freedom, flux-tubes responsible for the confinement of the quarks are considered as degrees of freedom. These models include hybrid baryons containing explicit excitations of the gluon fields. However, since all half integral J^P quantum numbers are possible for ordinary baryons, such 'exotics' will be very hard to identify, and probably always mix with ordinary states. So far, the experimentally observed number of states is still far lower even than predicted by the quark–diquark models.

The influence of chiral symmetry on the excitation spectrum of the nucleon has been debated from a somewhat different perspective. Chiral symmetry, the fundamental symmetry of QCD, is strongly broken for the low lying states, resulting in large mass differences of parity partners like the $J^P{=}1/2^+$ $N(938)1/2^+$ ground state and the $J^P{=}1/2^-$ $N(1535)1/2^-$ excitation. However, at higher excitation energies there is some evidence for parity doublets and even some very tentative suggestions for full chiral multiplets of $N^\star$ and Δ resonances. An effective restoration of chiral symmetry at high excitation energies due to a decoupling from the quark condensate of the vacuum has been discussed (see [92] for recent reviews) as a possible cause. In this case, the mass generating mechanisms for low and high lying states would be essentially different. As a further consequence, the parity doublets would decouple from pions, so that experimental bias would be worse. However, parity doublets might also arise from the spin-orbital dynamics of the 3-quark system. Presently, the status of the data does not allow final conclusions.

The most recent developments on the theory side include progress in understanding the physics of baryons [93, 94] by using the Dyson-Schwinger equations of QCD and Bethe-Salpeter equations [95, 96]. In this approach, baryons are relativistic bound states of three quarks, and the treatment of their interactions arising from QCD is non-perturbative, incorporating aspects of confinement and dynamical symmetry breaking. Two paths to solving the three-body problem are taken: direct solution of the three-body Faddeev equation, and decomposition of baryons into quark-diquark systems, with all quark pairs able to constitute the diquark. Therefore, these descriptions are different from the older static diquark-quark pictures of the baryon. Moreover, the first unquenched lattice-QCD calculations for the excitation spectrum have been presented and are discussed in Sec. 15.8. The results are basically consistent with the level counting of SU(6)⊗O(3) in the standard non-relativistic quark model and show no indication for quark-diquark structures or parity doubling. Consequently, there is as yet no indication from lattice that the mis-match between the excitation spectrum predicted by the standard quark model and experimental observations is due to inappropriate degrees of freedom in the quark model.

15.5.2 *Charmed and bottom baryons*

The naming scheme for baryons with c or b quarks follows that of the light baryons (see the *Review* on the "Naming Scheme for Hadrons"): the Λ is an isosinglet and the Σ an isotriplet with one heavy (s, c or b) quark. The Ξ is an isodoublet which contains two heavy quarks, and the Ω an isosinglet with three heavy quarks. The number of c or b quarks is indicated by the subscripts c or b. Hyperons are baryons with at least one s quark. The antiparticle of the Λ_c^+ (cud) is denoted $\overline{\Lambda}_c^-$ (or simply Λ_c^-), the antiparticle of the Σ_c^+ is the $\overline{\Sigma}_c^-$.

For charmed baryons the addition of the c quark to the light quarks extends the flavor symmetry to $\mathrm{SU}(4)_f$. Due to the large mass of the c quark, this symmetry is much more strongly broken than the $\mathrm{SU}(3)_f$ of the three light quarks. Nevertheless, the

Int. J. Mod. Phys. A 2026.41. Downloaded from www.worldscientific.com
by UNIVERSITY OF CALIFORNIA @ BERKELEY on 09/16/26. Re-use and distribution is strictly not permitted, except for Open Access articles.

$SU(4)_f$ representation is still useful for bookkeeping purposes. With the additive charm quantum number C the baryons are classified in a 3-dimensional representation with the three coordinates (I_z, Y , C). Figure 15.5 shows the $SU(4)_f$ weight diagrams.

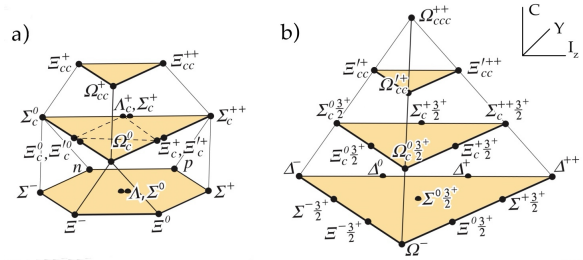

Figure 15.5: $SU(4)_f$ multiplets of ground state baryons made of u, d, s, and c quarks. (a) The spin $\frac{1}{2}$ 20-plet extends the charmless $SU(3)_f$ octet to $\mathsf{C} = 1, 2$; (b) the spin $\frac{3}{2}$ 20-plet extends the $SU(3)_f$ decuplet to $\mathsf{C} = 1, 2, 3$.

With four quarks the 64 possible configurations decompose into

$$\mathbf{4} \otimes \mathbf{4} \otimes \mathbf{4} = \bar{\mathbf{4}}_A \oplus \mathbf{20}_S \oplus \mathbf{20}_{MS} \oplus \mathbf{20}_{MA}, \tag{15.32}$$

(for a review on $SU(N)$ symmetries see *e.g.* [97]). The subscripts S and A refer to the symmetry and antisymmetry properties of the flavor wave functions. The flavor symmetric 20_S multiplet, associated with spin-$\frac{3}{2}$ baryons, contains the charmless $SU(3)_f$ decuplet at the bottom level. The 20_{MS} and 20_{MA} multiplets correspond to the mixed symmetric and mixed antisymmetric parts of the flavour wave functions of the spin-$\frac{1}{2}$ baryons, with the charmless octet baryons at the bottom level. There are two *dsc* and two *usc* spin-$\frac{1}{2}$ states, labeled Ξ_c^0, $\Xi_c'^{\,0}$ and Ξ_c^+, $\Xi_c'^{+}$. This is because one of the qq pairs can have spin 1 (symmetric) or spin 0 (antisymmetric), giving both the total spin $j = \frac{1}{2}$ with the third quark (see also Fig. 15.6 below).

For $\mathsf{C} = 1$ baryons the flavor decomposition of the diquark, made of u, d, or s quarks, is

$$\mathbf{3} \otimes \mathbf{3} = \bar{\mathbf{3}}_A \oplus \mathbf{6}_S. \tag{15.33}$$

For ground-state baryons, the overall antisymmetry of baryon wave function (including color) requires the light diquark to be symmetric under the exchange of spin and flavor, hence both symmetric or both antisymmetric, that is spin 1 for the $\mathbf{6}_S$ and spin 0 for the $\bar{\mathbf{3}}_A$. The $\bar{\mathbf{3}}$ then combines with the c quark to form the $J^P = 1/2^+$ states, while the $\mathbf{6}$ combines to form $J^P = 1/2^+$ or $J^P = 3/2^+$. The weight diagrams of the $\bar{\mathbf{3}}$ and $\mathbf{6}$ ground-state representations are shown in Fig. 15.6. Within each multiplet the $\mathsf{C} = 1$ baryons obey isospin and $SU(3)_f$ mass relations at the expected orders.

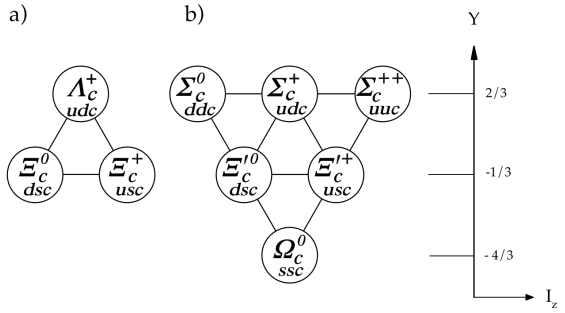

Figure 15.6: The $SU(3)_f$ $\bar{\mathbf{3}}$ (a) and $\mathbf{6}$ (b) ground state $J^P = 1/2^+$ representations. The structure of the $\mathbf{6}$ ground state with $J^P = 3/2^+$ is identical to the one in (b).

The antisymmetric quadruplet in (15.32) does not exist in the ground state but is realized for the first orbital excitations ($L = 1$). Figure 15.7 shows the weight diagram with the experimentally observed states. In the quark model the quadruplet consists of four baryon excitations with $J^P = \frac{1}{2}^-$ and four excitations with $\frac{3}{2}^-$. The charmed ones are the partners of the $\Lambda(1405)$ and $\Lambda(1520)$ singlets of $SU(3)_f$.

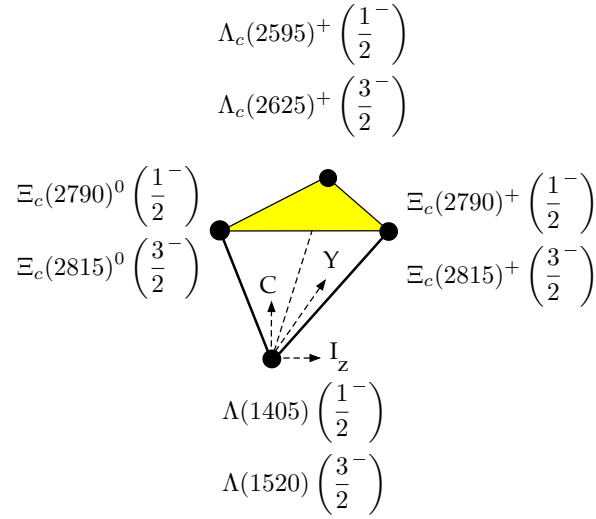

Figure 15.7: Weight diagram of the $\bar{\mathbf{4}}$ $SU(4)_f$ multiplet with the experimentally observed negative parity baryons.

For a detailed review on charmed baryons see Ref. [82]. Quark model predictions for baryons with two heavy quarks are given in Ref. [98] and lattice results for doubly and triply charmed states are discussed in Sec. 15.8 of this *Review*.

The $\mathsf{C} = 1$ ground state baryons have all been observed. Due to their relatively narrow widths the states are much easier to isolate than the light quark baryon resonances which require intricate partial wave analyses. The production cross sections are small, but the recent measurements at the e^+e^- B-factories, at the $p\bar{p}$ Tevatron collider, and at LHCb have boosted the field. The spin and parity of most charmed and bottom baryons has not been measured, they are from quark model predictions. The spin $\frac{1}{2}$ of the Λ_c^+ has been established by BES3 [99].

The LHCb collaboration has published evidence for seven new narrow Ω_c^0 states (*css*) [100,101] in proton-proton collisions. Four of these states have been confirmed by the Belle experiment in e^+e^- collisions [102]. Their quantum numbers are still unknown, but they could correspond to the $L = 1$ *ssc* orbital excitations. Constituent quark models, lattice QCD, quark-diquark models, molecular models, and pentaquark states, have been discussed to describe their structure (see e.g. [103] for references). In the meantime, also four Ω_b^- states of the *bss* type have been reported from LHCb [103]. They lie in a narrow range between 6316 - 6350 MeV, but since their intrinsic widths are on the order of just a few MeV, they are well separated in the invariant mass spectra. Spectroscopy and theory in this field is rapidly evolving.

LHCb has observed a doubly charmed Ξ_{cc}^{++} (*ccu*) baryon decaying to $\Lambda_c^+ K^- \pi^+ \pi^+$ [104], $\Xi_c^+ \pi^+$ [105] and $\Xi_c'^{+} \pi^+$ [106]. The quantum numbers of this state are not known yet. Doubly charmed baryons have a very different structure from light baryons, more resembling heavy 'double-star' systems with attached light 'planets', which opens a new window for QCD properties. The first candidate for a doubly charmed baryon Ξ_{cc}^+ (*ccd*) had been reported earlier by the SELEX experiment [107, 108], but searches by other experiments have not confirmed it so far (see *e.g.* [109] and Refs. therein) and it is therefore not included in the Summary Table. The SELEX and LHCb masses lie in the predicted 3500 – 3700 MeV mass range (see *e.g.* [98]), but the LHCb Ξ_{cc}^{++} state lies about 100 MeV above the SELEX one, with a mass splitting far too large for *ucc* and *dcc* isospin partners. However, it has also been discussed that due to the different production mechanisms this is not necessarily a contradiction [110].

Int. J. Mod. Phys. A 2026.41. Downloaded from www.wo[redacted]except for Open Access articles.
by UNIVERSITY OF CALIFORNIA @ BERKELEY on 09/16/26. Re-use and distribution is

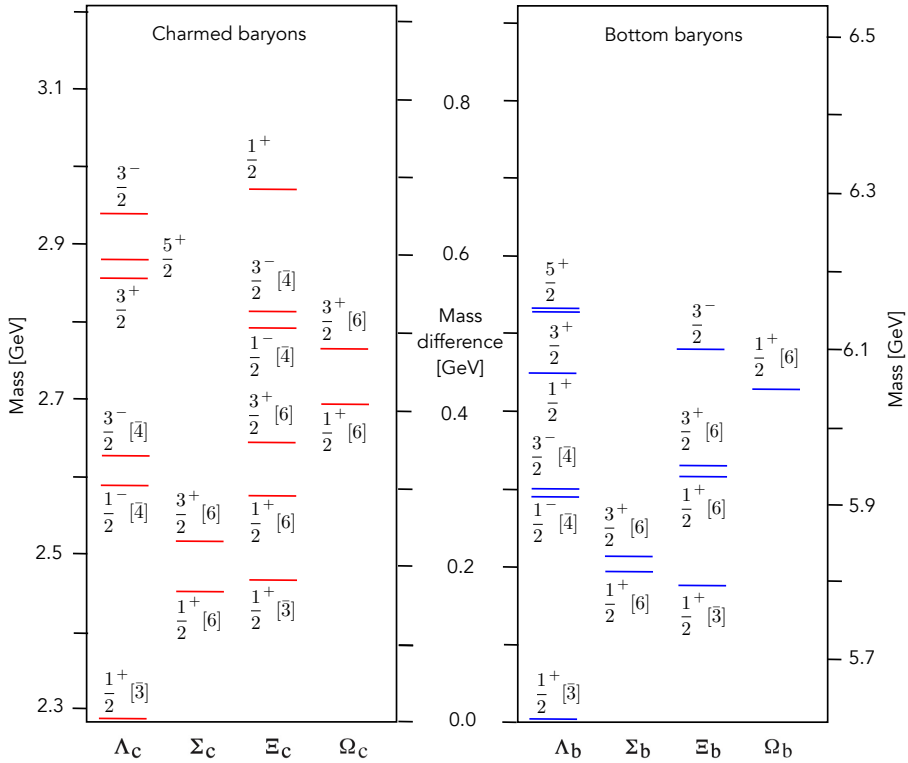

Figure 15.8: Mass spectrum of the established C = 1 charmed and B = –1 bottom baryons with known J^P, or assumed from the quark model. The flavor symmetry assignments (see 15.32) and (15.33) are given by the square brackets. According to their isospins the $\Sigma_{c,b}$ ($\Xi_{c,b}$) consist of three (two) charged or neutral states that are nearly degenerate.

Figure 15.8 shows the spectrum of the established singly-charmed baryons with known or assumed quantum numbers from the quark model. The parity of the Λ_c^+ is that of the c quark, defined as positive. Spin and parity have not been determined experimentally for most of the states. They follow the ordering and expectation from the quark model. Candidates for $L = 2$ orbital excitations of the Λ_c (with $J^P = \frac{3}{2}^+$ and $J^P = \frac{5}{2}^+$) have already been observed, as well as a $\frac{3}{2}^-$ state at 2940 MeV, possibly a radial $L = 1$ excitation [111].

The same $\mathrm{SU}(4)_f$ multiplets can be constructed for the bottom baryons by replacing the c quark by a b quark. Fig.15.8 shows the bottom baryons with known or assumed quantum numbers from the quark model. The quadruplet $\bar{\mathbf{4}}$ contains the two negative parity candidates $\Lambda_b(5912)^0$ and $\Lambda_b(5920)^0$. It appears that the confining potential is only weakly flavour dependent. For example, the mass difference between the Ξ_b and the Λ_b is roughly the same as that between the Ξ_c and the Λ_c, the mass splitting between the spin-$\frac{1}{2}$ Ω_b and the Λ_b close to that between the spin-$\frac{1}{2}$ Ω_c and the Λ_c. The spin-$\frac{3}{2}$ states are also heavier than the spin-$\frac{1}{2}$ ones, in agreement with expectations from the spin-spin force. There are three Ξ_b excitations around 6100 MeV from LHCb and CMS [112,113]. Best established is the $\Xi_b(6100)^-$, an $L = 1$ state with $J^P = \frac{3}{2}^-$ according to the quark model.

The bottom hadrons can also be embedded in a larger $\mathrm{SU}(5)_f$ group that accounts for all baryons constructed from the five quark flavors. (The existence of baryons with t-quarks is very unlikely due to the short lifetime of the t-quark.) One predicts the decomposition

$$\mathbf{5} \otimes \mathbf{5} \otimes \mathbf{5} = \overline{\mathbf{10}}_A \oplus \mathbf{40}_{MS} \oplus \mathbf{40}_{MA} \oplus \mathbf{35}_S. \tag{15.34}$$

The decuplet is not realized in the ground state. The two 40-plets have mixed symmetry ($\frac{1}{2}$-spin) and the 35-plet is symmetric ($\frac{3}{2}$-spin). The $\mathrm{SU}(4)_f$ spin-$\frac{1}{2}$ multiplet in Fig. 15.5 contains 20 spin-$\frac{1}{2}$ baryons and the corresponding one with bottom quarks an additional 12, giving together 32 states. Similarly there are 30 spin-$\frac{3}{2}$ baryons. One expects 75 ground state mesons from (15.34). Thus 13 ground state baryons containing both b and c quarks are predicted (8 spin-$\frac{1}{2}$ [$4\Omega + 4\Xi$] and 5 spin-$\frac{3}{2}$ [$3\Omega + 2\Xi$]).

15.6 Magnetic moments

The magnetic dipole moment of a baryon is conventionally written relative to the mass of the proton:

$$\vec{\mu}_B = g_B \mu_N \vec{s}, \tag{15.35}$$

where $\mu_N = \frac{e}{2m_p}$ is the nuclear magneton (in natural units). The factor g_B is calculated by adding the quark contributions. The magnetic moment of quark i with charge $q_i e$ and constituent mass m_i is $\vec{\mu}_i = 2(\frac{q_i e}{2m_i})\vec{s}$, hence for the three light quarks,

$$\mu_u = \frac{2}{3}\kappa_u, \;\; \mu_d = -\frac{1}{3}\kappa_d, \;\; \mu_s = -\frac{1}{3}\kappa_s, \;\; \text{with } \kappa_i \equiv \frac{e}{2m_i}. \tag{15.36}$$

The magnetic dipole moment of a baryon is then given by

$$\mu_B = \sum_{i=1}^{3} \langle B\uparrow|\mu_i \sigma_{zi}|B\uparrow\rangle, \tag{15.37}$$

where $|B\uparrow\rangle$ is the wavefunction for a baryon with its spin along the z-axis and $\vec{\sigma} = 2\vec{s}$. Since the quark model uses the totally *symmetric* SU(6) wavefunctions (flavor SU(3) × spin SU(2)) one predicts for the proton:

$$\mu_p = \frac{4}{3}\mu_u - \frac{1}{3}\mu_d = \frac{e}{2m} \equiv \kappa, \tag{15.38}$$

assuming $m_u = m_d \simeq m$ (for the detailed derivation see *e.g.* Ref. [6]). For the magnetic moment of the neutron one obtains likewise

$$\mu_n = -\frac{1}{3}\mu_u + \frac{4}{3}\mu_d = -\frac{2}{3}\kappa, \tag{15.39}$$

which leads to the simple prediction $\mu_n/\mu_p = g_n/g_p = -2/3$.

Int. J. Mod. Phys. A 2026.41. Downloaded from www.worldscientific.com
by UNIVERSITY OF CALIFORNIA @ BERKELEY on 09/16/26. Re-use and distribution is strictly not permitted, except for Open Access articles.

The famous Frisch and Stern experiment showed for the first time that $g_p \sim 5.58 \gg 2$. Modern measurements are performed in electromagnetic traps, see the *Listings*, while the magnetic moment of the neutron is measured with cold neutron beams. The experimental ratio $\mu_n/\mu_p = -0.6849793 \pm 0.0000003$ is impressively close to the prediction of the quark model (note that using instead the *antisymmetric* SU(6) wavefunctions would lead to $\mu_n/\mu_p = -2$ [6]). The constituent mass m of the u and d quarks can be estimated from (15.35) and (15.38): $m = 2m_p/g_p \simeq 336$ MeV.

The magnetic moment of the Λ is easy to predict: the diquark ud has isospin $i = 0$, since $i(s) = 0$ and $i(\Lambda) = 0$, and is therefore an antisymmetric isospin state. The symmetric quark model then also requires the spin to be zero, so that the magnetic moment of the Λ stems from the s quark:

$$\mu_\Lambda = \mu_s = -\frac{1}{3}\kappa_s. \tag{15.40}$$

The magnetic moment of the Λ is obtained from the Larmor precession frequency of the polarization vector in an homogeneous magnetic field. The latter is derived from the asymmetric distribution of the proton in $\Lambda \to \pi^- p$ [114]. The experimental result (Table 15.8) leads to the s quark constituent mass $m_s = -m\mu_p/3\mu_\Lambda = 509$ MeV.

Table 15.8: Quark model predictions and measured magnetic dipole moments of the ground state baryons in units of μ_N; $\kappa \equiv \frac{e}{2m} = 2.793$ μ_N and $\kappa_s \equiv \frac{e}{2m_s} = -3\mu_\Lambda = 1.84\ \mu_N$. † $\Sigma^0 \to \Lambda$ transition magnetic moment; ‡ see also Ref. [115].

Baryon	Quark model			Experimental value		
p	κ		input	2.793		
n	$-\frac{2}{3}\kappa$	=	–1.86	–1.913		
Λ	$-\frac{1}{3}\kappa_s$		input	–0.6138	±	0.0047
Σ^+	$\frac{8}{9}\kappa + \frac{1}{9}\kappa_s$	=	2.68	2.458	±	0.010
Σ^0	$\frac{2}{9}\kappa + \frac{1}{9}\kappa_s$	=	0.82			
$\Sigma^{0\dagger}$	$-\frac{1}{\sqrt{3}}\kappa$	=	–1.61	–1.61	±	0.08
Σ^-	$-\frac{4}{9}\kappa + \frac{1}{9}\kappa_s$	=	–1.04	–1.160	±	0.025
Ξ^0	$-\frac{2}{9}\kappa - \frac{4}{9}\kappa_s$	=	–1.44	–1.250	±	0.014
Ξ^-	$\frac{1}{9}\kappa - \frac{4}{9}\kappa_s$	=	–0.51	–0.6507	±	0.0025
Ω^-	$-\kappa_s$	=	–1.84	–2.024	±	0.056
Δ^{++}	2κ	=	5.58	4.52	±	0.67 ‡
Δ^+	κ	=	2.79	2.3	-	4.5

The magnetic moments of the other baryons (Table 15.8) are predicted from κ and κ_s. The magnetic moment of the Σ^+ is obtained by replacing the d quark in (15.38) by an s quark, and for the Σ^- the u quark by an s quark in (15.39). The magnetic moment of the Σ^+ has also been measured with the precession method using its decay into $p\pi^0$ [116], that of the $\Sigma^- \to n\pi^-$ likewise, or by detecting the X-rays emitted by cascading Σ^- captured in the Coulomb shells of target atoms. The magnetic moment is then derived from the fine-structure splitting [117].

The magnetic moments of the Ξ^0, Ξ^- and Ω^- are obtained from the polarization of the Λ in the decays $\Lambda\pi^0$, $\Lambda\pi^-$ and ΛK^-, respectively. The SU(6) wavefunction of the (spin 3/2) Ω^- is the product of the two symmetric SU(3) flavor and SU(2) spin wavefunctions. Summing over the three s quarks one gets

$$\mu_{\Omega^-} = \sum_{i=1}^{3} \langle \Omega^- \uparrow | \mu_i \sigma_{zi} | \Omega^- \uparrow \rangle = 3\mu_s = 3\mu_\Lambda. \tag{15.41}$$

The magnetic moment of the Ω^- is hard to measure, because the Ω^- is unpolarized at high energies, in contrast to the other hyperons. Polarized Ω^- hyperons have been obtained from polarized Λ and Ξ^0 impinging on a nuclear target [118].

In quark models with full isospin symmetry the magnetic moments of the Δ-resonances are simply related to the magnetic moment of the proton by $\mu_\Delta = Q_\Delta \cdot \mu_N$, ($Q_\Delta$ = charge) i.e. the moment of the Δ^+ should equal the proton moment and the moment of the Δ^{++} should be twice as large (sum of the three u-quarks). Magnetic moments of the decuplet baryons (with the exception of the Ω^-) are very difficult to measure because their lifetimes are so short that spin precession techniques cannot be used. For the Δ one can profit from an electromagnetic spin-reorientation transition inside the large width of the state. This leads to the emission of a magnetic dipole photon in reactions like $\pi^+ p \to \pi^+ p\gamma$ or $\gamma p \to \pi^0 p\gamma'$ which is related to the magnetic moment of the resonance. The first reaction has been used to study the magnetic moment of the Δ^{++} by measuring the left-right asymmetry with polarized protons [119]. The second one was used for the Δ^+ state [120, 121]. Taking all experimental and systematic uncertainties into account the result spans the range from (2.3 - 4.5)μ_N, covering the quark model prediction of $\approx 2.8\mu_N$, but is not very precise.

Table 15.8 lists the current experimental values for the magnetic moments of the ground state baryons, together with the predictions from the quark model. There are significant discrepancies, but given its crudeness, the quark model performs surprisingly well.

15.7 Dynamics

Quantum chromodynamics (QCD) is well-established as the theory for the strong interactions. As such, one of the goals of QCD is to predict the spectrum of strongly-interacting particles. To date, the only first-principles calculations of spectroscopy from QCD use lattice methods. These are the subject of Sec. 15.8. These calculations are difficult and unwieldy, and many interesting questions do not have a good lattice-based method of solution. Therefore, it is natural to build models, whose ingredients are abstracted from QCD, or from the low-energy limit of QCD (such as chiral Lagrangians) or from the data itself.

Phenomenological models for light quark systems typically include

1. A confining interaction, which is generally spin-independent (*e.g.*, harmonic oscillator or linear confinement);
2. A strange quark mass somewhat larger than the up and down quark masses, in order to split the SU(3) multiplets;
3. Different types of spin-dependent interactions:

   a) commonly used is a color-magnetic flavor-independent interaction modeled after the effects of gluon exchange in QCD (see *e.g.*, Ref. [122]). For example, in the S-wave states, there is a spin-spin hyperfine interaction of the form

   $$H_{HF} = -\alpha_S M \sum_{i>j} (\vec{\sigma}\lambda_a)_i (\vec{\sigma}\lambda_a)_j, \tag{15.42}$$

   where M is a constant with units of energy, λ_a ($a = 1, \cdots, 8,$) is the set of SU(3) unitary spin matrices, defined in the review "SU(3) Isoscalar Factors and Representation Matrices," and the sum runs over constituent quarks or antiquarks. Spin-orbit interactions, although allowed, seem to be small in general, but a tensor term is responsible for the mixing of states with the same J^P but different L, S combinations.

   b) other approaches include flavor-dependent short-range quark forces from instanton effects (see *e.g.*, [123,124]). This interaction acts only on scalar, isoscalar pairs of quarks in a relative S-wave state:

   $$\langle q^2; S, L, T | W | q^2; S, L, T \rangle = -4g\delta_{S,0}\delta_{L,0}\delta_{I,0}\mathcal{W} \tag{15.43}$$

   where $\mathcal{W}$ is the radial matrix element of the contact interaction.

   c) a rather different and somewhat controversial approach is based on flavor-dependent spin-spin forces arising from one-boson exchange. The interaction term is of the form:

   $$H_{HF} \propto \sum_{i<j} V(\vec{r}_{ij}) \lambda_i^F \cdot \lambda_j^F \vec{\sigma}_i \cdot \vec{\sigma}_j \tag{15.44}$$

Int. J. Mod. Phys. A 2026.41. Downloaded from www.wo[redacted]except for Open Access articles.
by UNIVERSITY OF CALIFORNIA @ BERKELEY on 09/16/26. Re-use and distribution is

where the λ_i^F are in flavor space (see *e.g.*, [125]).

4. In the case of spin-spin interactions, a flavor-symmetric interaction for mixing $q\bar{q}$ configurations of different flavors (*e.g.*, $u\bar{u} \leftrightarrow d\bar{d} \leftrightarrow s\bar{s}$), in isoscalar channels, so as to reproduce *e.g.*, the η - η' and ω - ϕ mesons.

Systems with heavy quarks have their own approaches. Besides potential models to deal with $Q\bar{Q}$ spectroscopy (which are similar to what we have just described for light quarks) there are a variety of effective field theories built on QCD. Nonrelativistic QCD or NRQCD is a nonrelativistic reduction of the QCD Lagrangian, written as an expansion in powers of the heavy quarks' velocities. Its expressions are often used in lattice calculations. Terms in the Lagrangian have obvious quark model analogs, but are derived directly from QCD. For example, the heavy quark potential is a derived quantity, extracted from simulations.

There are also many versions of heavy quark effective theory (HQET), an expansion in the inverse mass of the heavy constituent. The physics input is one of decoupling of scales: the interactions of the heavy quarks take place at short distance while the light degrees of freedom involve long distance dynamics, so to some degree they decouple. The form of terms in the expansion is fixed (often by symmetry) but the coefficients are not. These approaches allow one to interpolate from the charm sector to the bottom one, or from masses of mesons to baryons. For example, a Hamiltonian for one or more heavy quarks bound to light degrees of freedom could be written as

$$H_l^Q = m_Q + e_l + \frac{\kappa_l}{2m_Q} + \frac{s_l}{2m_Q}\vec{S}\cdot\vec{j}_l + \ldots \tag{15.45}$$

where m_Q is the mass of the heavy quark (or heavy quarks where the heavy quarks are treated as a single dynamical object) and $\vec{S}$ is the angular momentum carried by the heavy degrees of freedom. e_l, κ_l and $\vec{j}_l$ involve the light degrees of freedom. We will see an example of the use of this formula in the next section.

15.8 Lattice Calculations of Hadronic Spectroscopy

Lattice calculations are a major source of information about QCD masses and matrix elements. The necessary theoretical background is given in Sec. 17 of this *Review*. Here we confine ourselves to some general comments and illustrations of lattice calculations for spectroscopy.

It might seem a bit out of place to have a section about lattice calculations in a review of the quark model, since to many readers, the quark model is just a model while QCD could be thought of as a construct which is something deeper than a model. But this review is, despite its title, actually an introduction to the spectroscopy and related quantities of the strong interactions. From that perspective, a presentation of lattice results is entirely appropriate.

The input to lattice calculations is a discretized version of the QCD Lagrangian. Lattice calculations measure correlation functions via Monte Carlo simulation and physical observables are determined through fits of the lattice data to theoretical expectations. It is fair to say that all lattice calculations make extensive use of quark model ideas – for example, the operators used to create and annihilate hadrons are almost always based on the quark model.

There is only a sporadic literature connecting lattice results to the quark model (one recent example is [126]) but of course the qualitative understanding of lattice results depends as heavily on quark model ideas as does the qualitative understanding of experimental data.

In general, the cleanest lattice results come from computations of processes in which there is only one particle in the simulation volume. These quantities include masses of hadrons, simple decay constants, like pseudoscalar meson decay constants, and semileptonic form factors (such as the ones appropriate to $B \to Dl\nu$, $Kl\nu$, $\pi l\nu$). The cleanest predictions for masses are for states which are far below any thresholds to open channels, since the effects of final state interactions are not yet under complete control on the lattice. As a simple corollary, the lightest state in a channel is easier to study than the heavier ones.

Good-quality modern lattice calculations will present multipart error budgets with their predictions. Part of the uncertainty is statistical, from sample size. Typically, the quoted statistical uncertainty includes uncertainty from a fit: it is rare that a simulation computes one global quantity which is the desired observable. Simulations which include virtual quark-antiquark pairs (also known as "dynamical quarks" or "sea quarks") are often done at up and down quark mass values heavier than the experimental ones, and it is then necessary to extrapolate in these quark masses. Simulations can be carried out at the physical values of the heavier quarks' masses. They are always done at nonzero lattice spacing, and so it is necessary to extrapolate to zero lattice spacing. Some theoretical input is needed to do this. Much of the uncertainty in these extrapolations is systematic, from the choice of fitting function. Other systematics include the effect of finite simulation volume, the number of flavors of dynamical quarks actually simulated, and technical issues with how these dynamical quarks are included. The particular choice of a fiducial mass (to normalize other predictions) is not standardized; there are many possible choices, each with its own set of strengths and weaknesses, and determining it usually requires a second lattice simulation from that used to calculate the quantity under consideration.

A systematic error of major historical interest is the "quenched approximation," in which dynamical quarks are simply left out of the simulation. This was done because the addition of these virtual pairs presented an expensive computational problem. No generally-accepted methodology has ever allowed one to correct for quenching effects, short of redoing all calculations with dynamical quarks. (All light degrees of freedom must be included in any realistic simulation of a quantum field theory.) Advances in algorithms and computer hardware have rendered it obsolete.

With these brief remarks, we turn to examples. The field of lattice QCD simulations is vast, and so it is not possible to give a comprehensive review of them in a small space. The history of lattice QCD simulations is a story of thirty years of incremental improvements in physical understanding, algorithm development, and ever faster computers, which have combined to bring the field to a present state where it is possible to carry out very high quality calculations. We present a few representative illustrations, to show the current state of the art.

15.8.1 *Spectroscopy of low-lying states*

One of the first goals of large scale lattice simulations was to compute masses of the lightest states in all of the "conventional" $q\bar{q}$ and qqq channels. We illustrate results from many groups in Fig. 15.9, a comprehensive summary from 2012 provided by A. Kronfeld (private communication; see also [140]).

Mesons with a valence structure of identical quark - antiquark pairs such as the eta or eta-prime, $|\eta\rangle \sim \alpha|\bar{u}u + \bar{d}d\rangle + \beta|\bar{s}s\rangle$, present more of a challenge, because one must include the effects of "annihilation graphs" for the valence q and $\bar{q}$. Many groups, among them Refs. [21, 134, 141, 142], have reported calculations of the η and η' mesons. The most recent calculation is that of Ref. [142], which finds masses of 554.7 ± 9.2 and 930 ± 21 MeV for the η and η'.

The spectroscopy of mesons containing heavy quarks is truly a high-precision endeavor. These simulations typically use NRQCD for $Q\bar{Q}$ bound states. Figs. 15.10 and 15.11 show the low lying mass spectrum for charmonium and bottomonium states from several different groups [138, 143–146]. Most, but not all, of the results are for the lightest state with a given value of quantum numbers. We return to this point below.

Fig. 15.12 shows a compilation of lattice results for doubly and triply charmed baryons, provided by S. Meinel [154]. The position of the observed Ξ_{cc}^+ [104] is also shown. Note that the lattice calculations for the mass of this state were predictions, not postdictions.

15.8.2 *Excited state spectroscopy*

A close look at Fig. 15.9 reveals an issue: while many of the states shown in it are stable under the strong interactions, some of them (the vector mesons, the Delta) are not. They are resonances. And so are all the excited states of hadrons listed in the PDG be they "ordinary'," or "exotic." How do lattice calculations deal

Int. J. Mod. Phys. A 2026.41. Downloaded from www.worldscientific.com
by UNIVERSITY OF CALIFORNIA @ BERKELEY on 09/16/26. Re-use and distribution is strictly not permitted, except for Open Access articles.

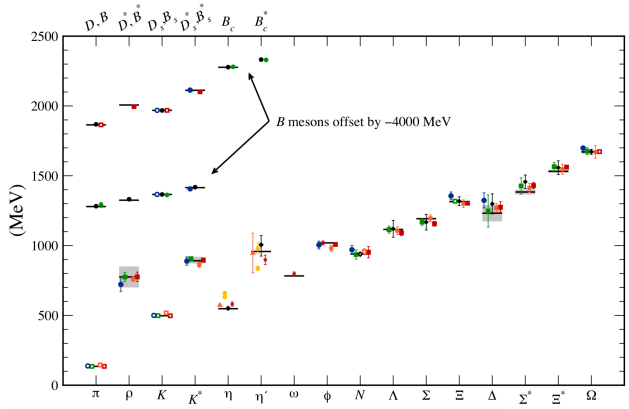

Figure 15.9: Hadron spectrum from lattice QCD. Comprehensive results for mesons and baryons are from MILC [127, 128], PACS-CS [129], BMW [130], QCDSF [131], and ETM [132]. Results for η and η' are from RBC & UKQCD [21], Hadron Spectrum [133] (also the only ω mass), UKQCD [134], and Michael, Ottnad, and Urbach [135]. Results for heavy-light hadrons from Fermilab-MILC [136], HPQCD [137, 138], and Mohler and Woloshyn [139]. Circles, squares, diamonds, and triangles stand for staggered, Wilson, twisted-mass Wilson, and chiral sea quarks, respectively. Asterisks represent anisotropic lattices. Open symbols denote the masses used to fix parameters. Filled symbols (and asterisks) denote results. Red, orange, yellow, green, and blue stand for increasing numbers of ensembles (i.e., lattice spacing and sea quark mass) Black symbols stand for results with 2+1+1 flavors of sea quarks. Horizontal bars (gray boxes) denote experimentally measured masses (widths). b-flavored meson masses are offset by -4000 MeV.

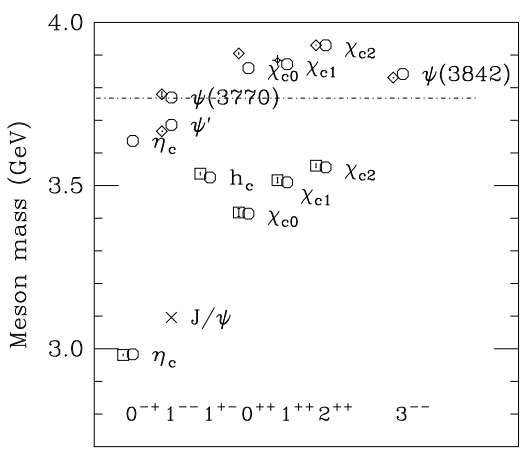

Figure 15.10: Selected spectroscopy of the $\bar{c}c$ spectrum, compared to lattice data from Ref. [143] in squares, from Refs. [144, 145] in diamonds, and from Ref. [146] as a fancy diamond. Particles whose masses are used to fix lattice parameters by Ref. [143] are shown with crosses; octagons label experimental values. The upper χ_{c1} state is also known as $X(3872)$. The dotted line shows the threshold value for two charmed mesons.

with such states? This is actually a complicated business, which is an active area of research.

There are two issues involving excited state spectroscopy, which are entangled in any lattice calculation:

1. There are many states with the same quantum numbers, all of which contribute to lattice observables
2. In finite volume, states do not decay, they only mix.

To explain what is going on, we have to describe how a lattice calculation determines a mass. This is done by measuring an observable which involves the creation of a set of quark and gluon

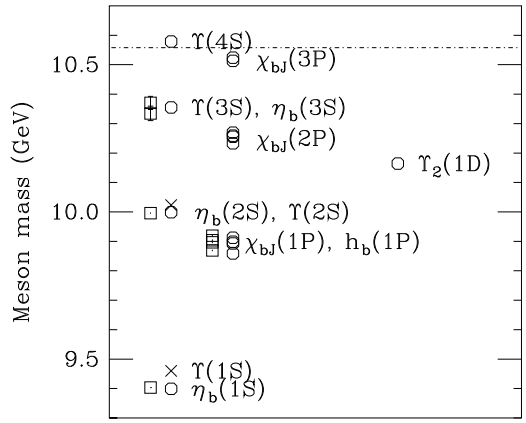

Figure 15.11: Spectroscopy of the $\bar{b}b$ system, adapted from Ref. [138]. Particles whose masses are used to fix lattice parameters are shown with crosses; octagons label experimental values, and lattice results are shown as squares. The dotted line shows the threshold value for two bottom mesons.

fields at some point on the lattice and their annihilation at other points on the lattice. To find the energies of zero momentum states, the operators are averaged over position and the observable is

$$C_{ij}(t) = \sum_x \langle O_i(x,t) O_j(0,0)\rangle \propto \sum_n \langle 0|O_i|n\rangle \langle n|O_j|0\rangle \exp(-E_n t). \tag{15.46}$$

E_n is the energy of the nth hadronic state with the quantum numbers of the source or sink. The reader can see that by taking t large, the correlator is dominated by the contribution from the lightest state, decaying with t as $\exp(-E_{min}t)$. This is a positive thing if one is interested in the ground state, but the contribution of excited states is exponentially suppressed at large t. The size of a given state's contribution, $\langle 0|O_i|n\rangle$, can provide information about the content of the state.

As we move away from hadrons which can be created by the simplest quark model operators (appropriate to the lightest meson and baryon multiplets) we encounter a host of new problems: either no good interpolating fields, or too many possible interpolating fields, and many states with the same quantum numbers. Techniques for dealing with these interrelated problems vary from collaboration to collaboration, but all share common features: typically, correlation functions from many different interpolating fields are used, and the signal is extracted in what amounts to a variational calculation using the chosen operator basis. In addition to mass spectra, wave function information can be garnered from the form of the best variational wave function.

These calculations give towers of excited states, but the states are not resonances. Lattice calculations do not see decays directly because they are done in boxes of some finite size. Generally, the energies of the single particle states do not depend strongly on the box size. Multiple particle states, such as two particle states with equal and opposite momenta, are different, though. The finite box size quantizes the allowed values of momentum and the spectrum of states, which would be a continuum in infinite volume, is just a discrete tower. As the box size is varied, some of these states can approach the energies of single particle states, and the nearby states will mix and split, participating in a quantum mechanical avoided level crossing. The mixing and splitting of single and multiparticle states is the finite volume data which is used to infer how states in the continuum interact.

As a simple example, two positive energy but interacting particles in a one dimensional box have a spatial wave function which looks like $\cos(k|z| + \delta)$ where δ is the phase shift due to their interaction. Periodic boundary conditions in a finite box of length L give a quantization condition to the allowed momentum of the state ($kL + 2\delta(E) = 0 \bmod 2\pi$, for example) which involves the phase shift. Simulations with many values of L and operators for

Int. J. Mod. Phys. A 2026.41. Downloaded from www.wo
by UNIVERSITY OF CALIFORNIA @ BERKELEY on 09/16/26. Re-use and distribution is
except for Open Access articles.

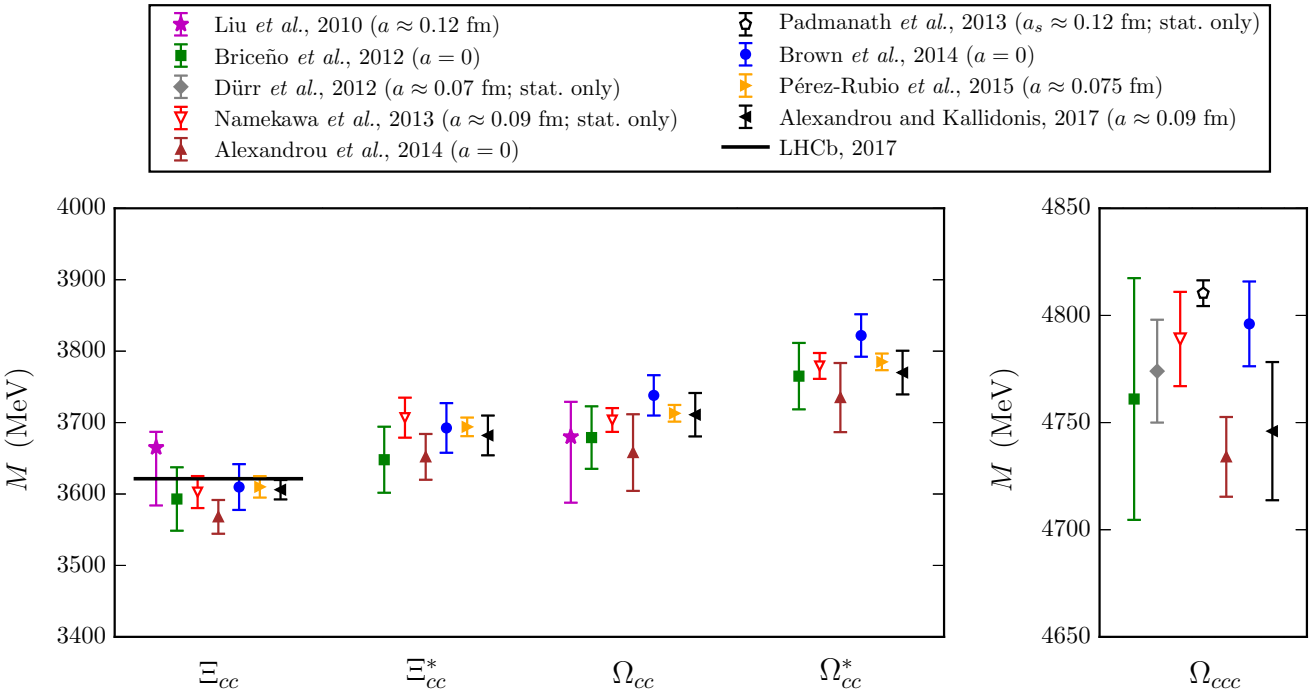

Figure 15.12: Comparison of lattice QCD results for the doubly and triply charmed baryon masses. Labels are Liu, *et al.*, [147]; Briceno, *et al.*, [148]; Namekawa, *et al.*, [149]; Padmanath, *et al.*, [150]; Alexandrou, *et al.*, [132]; Brown, *et al.*, [151]; Perez-Rubio *et al.*, [152]; Alexandrou and Kallidonis 2017, [153]. Only calculations with dynamical light quarks are included; for the doubly charmed baryons, only calculations were performed at or extrapolated to the physical pion mass are shown. Results without estimates of systematic uncertainties are labeled "stat. only". The lattice spacing values used in the calculations are also given; $a = 0$ indicates that the results have been extrapolated to the continuum limit. In the plot of the doubly charmed baryons, the position of the experimentally observed Ξ_{cc}^{+} state [104] is shown with a horizontal line.

states carrying many values of momentum can be combined into information about phase shifts, and then to statements about the location(s) of singularities in the complex energy plane.

The techniques for studying excited states of mesons and baryons, glueballs, and exotics are similar. They all use a large basis of trial states: the progression with time started with minimum quark content states, then added more complicated states (pairs of mesons or tetraquark states), then carried out simulations with multiple volumes with the goal of extracting resonance properties. The older single volume studies typically presented results for many quantum numbers, which give a broad (though incomplete) view of the QCD spectrum.

An example of meson spectroscopy where this is done, by [53], is shown in Fig. 15.13. The quark masses are still heavier than their physical values, so the pion is at 392 MeV. The authors can assign a relative composition of nonstrange and strange quark content to their states, observing, for example, a nonstrange ω and a strange ϕ. Some states also have a substantial component of gluonic excitation. Note especially the three exotic channels $J^{PC} = 1^{-+}$, 0^{+-}, and 2^{+-}, with states around 2 GeV. These calculations will become more realistic as the quark masses are carried lower and resonance effects are included.

The interesting physics questions of excited baryon spectroscopy to be addressed are precisely those enumerated in the last section. An example of a calculation involving only single particle states in a single volume, due to Ref. [155], is shown in Fig. 15.14. Notice that the pion is not yet at its physical value. The lightest positive parity state is the nucleon, and the Roper resonance has not yet appeared as a light state.

Glueballs present similar issues. In Fig. 15.3 we showed a figure from [35] presenting a lattice prediction for the glueball mass spectrum in quenched approximation. A true QCD prediction of the glueball spectrum requires dynamical light quarks, some way to deal with the mixing of glue states and quark-antiquark (and beyond) states and (because glueball operators are intrinsically noisy) high statistics. Early studies which include the 0^{++} channel are Refs. [156, 157]. Fig. 15.15 shows results from [156], done with dynamical u, d and s quarks at two lattice spacings, 0.123 and 0.092 fm, with pion masses at 280 and 360 MeV respectively, along with comparisons to the quenched lattice calculation of [34] and to experimental isosinglet mesons. This study shows that the effects of quenching seem to be small at its relatively heavy pion masses. A recent review [158] concludes "no scalar state below 2 GeV can be considered to be predominantly a glueball state."

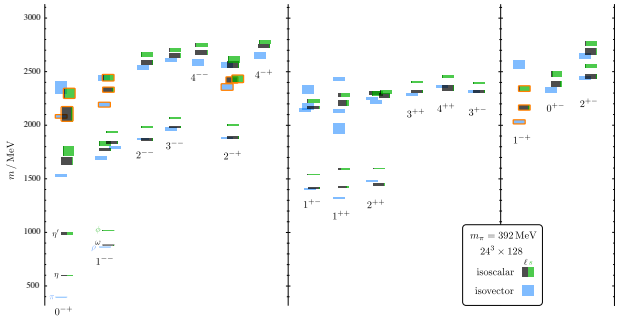

Figure 15.13: Isoscalar (green and black) and isovector (blue) spectrum from Ref. [53]. States are labeled J^{PC}. The quark mass is heavier than its physical value; $m_\pi = 392$ MeV. The vertical height of each box indicates the statistical uncertainty in the mass. Black and green indicate relative nonstrange and strange composition. Orange outlines show states with a large chromomagnetic component to their wave function, which the authors argue are hybrid states. Note the exotic states in the three rightmost columns.

Calculations of resonance properties are more recent. Two body decays with a single open channel, such as the rho coupled to two pions, have a large literature. An example of a calculation of the rho meson decay width is [159]. (See also [160].) The mass and

Int. J. Mod. Phys. A 2026.41. Downloaded from www.worldscientific.com
by UNIVERSITY OF CALIFORNIA @ BERKELEY on 09/16/26. Re-use and distribution is strictly not permitted, except for Open Access articles.

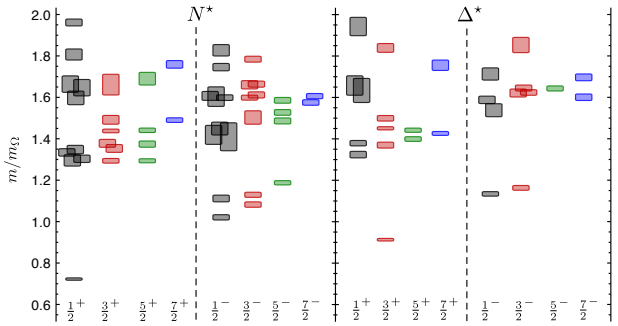

Figure 15.14: Spin-identified spectrum of nucleons and deltas, from lattices where $m_\pi = 396$ MeV, in units of the calculated Ω mass, from Ref. [155]. The colors just correspond to the different J assignments: grey for $J = 1/2$, red for $J = 3/2$, green for $5/2$, blue for $J = 7/2$.

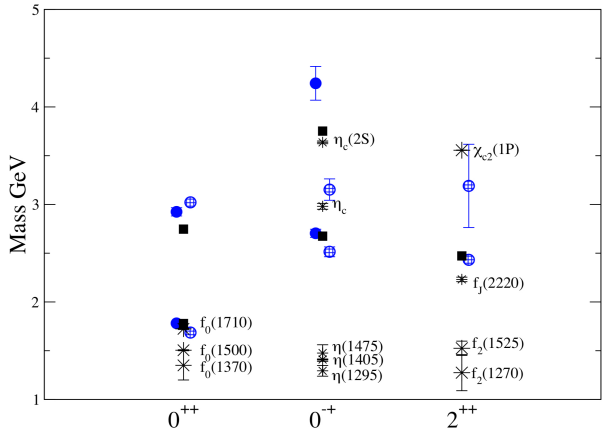

Figure 15.15: Lattice QCD predictions for glueball masses. The open and closed circles are the larger and smaller lattice spacing data of the full QCD calculation of glueball masses of Ref. [156], at pion masses of 280 and 360 MeV. Squares are the quenched data for glueball masses of Ref. [34]. The bursts labeled by particle names are experimental states with the appropriate quantum numbers.

decay width of the $f_0(500)$ have recently been computed in [161] and [162] and those of other mesons in [163]. Ref. [164] studies the decay width of the $\Delta(1238)$. A recent review [165] summarizes the lattice (and non-lattice) situation as of 2023.

Studies which observe a large basis of states across many volumes can probe excited state spectroscopy as resonances. These calculations are just beginning and the ones we know about are still performed at unphysically heavy quark masses. Examples include the decays of an exotic $J^{PC} = 1^{-+}$ resonance [166] and the spectroscopy of J^{--} resonances [167]. The results of Refs. [144, 145] in Fig. 15.10 come from similar analyses. We expect to see considerable progress in this area over the next few years.

Some excited states are better thought of as bound states of hadrons. One example is the Lambda(1405), which is the subject of its own mini-review. Calculations with unitarized chiral perturbation theory (see, for example, Ref. [168] reveal a two-pole structure for the state. This structure has been confirmed starting directly from QCD by lattice simulations [169, 170].

We conclude this section with some remarks about unusual states containing heavy quarks. Lattice calculations relevant to the extra states observed in the charmonium and bottomonium spectrum (Sec. 15.4) are difficult, because the states sit high in the spectrum of most channels, because of the number of nearby multiparticle states, and because it is necessary to have the technology to study heavy and light quarks together.

Some lattice calculations are used as input for phenomenological studies of hybrids. The theoretical motivation is that one can imagine states made of a heavy $Q\bar{Q}$ pair along with excitations of light degrees of freedom, viewed as an excited states of the string connecting them. The analogy is to an excited state of a diatomic molecule. The heavy quark potential, the potential from orbitally excited gluon configurations, and the "string breaking" potential (from the interaction between static sources and static-light mesons) are used as inputs in Born - Oppenheimer and coupled channel calculations for systems whose constituents include heavy quarks and antiquarks. Examples of such calculations include Refs. [171–173].

The system with the largest lattice literature is a bound state of two heavy quarks and two light antiquarks, for example $bb\bar{u}\bar{d}$. The story begins with the spectroscopy of doubly and triply charmed baryons in Fig. 15.12; the lattice calculations in that figure were performed in 2010 - 2017. In 2017 two groups of authors [174,175] realized that one could extrapolate from the masses of $Q\bar{q}$, Qqq, and QQq states (Q for a heavy quark, $\bar{q}$ for a light antiquark) to predict the mass of a $QQ\bar{q}\bar{q}$ tetraquark. The $QQ\bar{q}\bar{q}$ state would be stable if the mass of the Q were heavy enough. (This basically arises because the QQ diquark is in an attractive color-triplet state and the effective binding energy scales as $\alpha_s^2 m_Q$.) The $J^P = 1^+$ $bb\bar{u}\bar{d}$ state was expected to be stable. Simultaneously, a lattice calculation [176] of the mass of a $bb\bar{u}\bar{d}$ state showed that it was below threshold to fall apart into a pair of B mesons. The $I(J^P) = 0(1^+)$ state is predicted to be stable by about 128(26) MeV [177] or 189(10) MeV [176]. (These authors put the $bb\bar{s}\bar{d}$ state at 98 MeV below threshold.) These numbers are in reasonable agreement with phenomenological estimates from Refs. [174, 175].

These states are easier for the lattice theorist to study than other exotics because they are the lightest single particle states in their channels. They are difficult because they are just barely bound, and the usual approximation for a lattice calculation of unphysically heavy light quarks tends to raise their mass. The calculations have to include multiple trial states: the tetraquark itself plus pairs of mesons.

The situation with regard to the recently discovered $T_{cc}(3875)^+$ [178] is still unsettled. Both lattice calculations and HQET estimates put a $cc\bar{u}\bar{d}$ state right at threshold, which is a difficult place to explore on the lattice (or by any other method, for that matter). The $T_{cc}(3875)^+$ is seen in $D^0D^0\pi^+$ and researchers studying three body decays on the lattice (an open problem, at present) mark it as an obvious research target. One representative group describes their approach to the problem in Ref. [179].

15.8.3 *Electromagnetic effects*

As a final part of spectroscopy we mention electromagnetic mass splittings (such as the neutron - proton mass difference). They are interesting but difficult. These calculations are important for determining the values of the quark masses (for a discussion see Sec. 60 in this Review). Knowing that the neutron is heavier than the proton tells us that these splittings have a complicated origin. One part of the shift is because the up and down quarks have slightly different masses. The second is that the quarks have (different) charges. Phenomenologists (compare Ref. [180]) combine Coulomb forces and spin-dependent electromagnetic hyperfine interactions to model their charge effects. In order to compute hadronic mass differences on the lattice, electromagnetic interactions must be included in the simulations. This creates a host of technical issues. An important one is that electromagnetic interactions are long range, but lattice simulations are done in finite volumes. The theoretical situation is summarized in the recent Flavour Lattice Averaging Group (FLAG) review [181]. A 2014 calculation, Ref. [182], presented the first results for electromagnetic mass splittings in the baryon octet, with good agreement with observation. Refs. [183–185] have performed calculations for meson splittings.

There is a small lattice literature associated with magnetic moments of baryons. The calculations are done by including a static magnetic field in the simulation and computing the energy difference between baryons in different spin states. We are aware of no calculations at physical quark masses. A recent calculation [186] used 800 and 450 MeV pions. When expressed in units

of the nucleon magneton at the simulation point ($e/(2M_N(m_\pi))$) the moments are in reasonable agreement with experiment and with quark model expectations.

References

[1] M.-L. Du *et al.*, Phys. Rev. D **98**, 094018 (2018), [arXiv:1712.07957].

[2] G. 't Hooft, Nucl. Phys. B **72**, 461 (1974).

[3] G. 't Hooft, Nucl. Phys. B **75**, 461 (1974).

[4] E. Witten, Nucl. Phys. B **160**, 57 (1979).

[5] F. Gross *et al.*, Eur. Phys. J. C **83**, 1125 (2023), [arXiv:2212.11107].

[6] C. Amsler in the Quark Structure of Hadrons, Lecture Notes in Physics **949** (2018), ed. Springer.

[7] H.-Y. Cheng, Physics Letters B **707**, 116 (2012), [arXiv:1110.2249].

[8] J.-C. Feng *et al.*, Phys. Rev. D **104**, 054027 (2021), [arXiv:2104.01339].

[9] H.-W. Ke and X.-Q. Li, Phys. Rev. D **99**, 036014 (2019), [arXiv:1810.07912].

[10] M.-C. Du and Q. Zhao, Phys. Rev. D **100**, 036005 (2019), [arXiv:1905.04207].

[11] A. A. Godizov, Eur. Phys. J. C **76**, 361 (2016), [arXiv:1604.01689].

[12] S. Donnachie *et al.*, *Pomeron Physics and QCD*, Cambridge Monographs on Particle Physics, Nuclear Physics and Cosmology, Cambridge University Press, p. 85 (2002).

[13] M.-L. Du *et al.*, Phys. Rev. Lett. **126**, 192001 (2021), [arXiv:2012.04599].

[14] J. Schwinger, Phys. Rev. **135**, B816 (1964).

[15] H. J. Lipkin and B.-s. Zou, Phys. Rev. D **53**, 6693 (1996).

[16] A. Bramon, R. Escribano and M. D. Scadron, Phys. Lett. **B403**, 339 (1997), [hep-ph/9703313].

[17] A. Aloisio *et al.* (KLOE), Phys. Lett. **B541**, 45 (2002), [hep-ex/0206010].

[18] F. Ambrosino *et al.*, JHEP **07**, 105 (2009), [arXiv:0906.3819].

[19] C. Amsler *et al.* (Crystal Barrel), Phys. Lett. **B294**, 451 (1992).

[20] C. Amsler, Rev. Mod. Phys. **70**, 1293 (1998), [hep-ex/9708025].

[21] N. H. Christ *et al.*, Phys. Rev. Lett. **105**, 241601 (2010), [arXiv:1002.2999].

[22] T. Feldmann, Int. J. Mod. Phys. **A915**, 159 (2000).

[23] C. Amsler and F. E. Close, Phys. Rev. **D53**, 295 (1996), [hep-ph/9507326].

[24] R. L. Jaffe, Phys. Rev. **D15**, 267 (1977).

[25] R. L. Jaffe, Phys. Rev. **D15**, 281 (1977).

[26] S.L. Olsen, Front. Phys. **10**, 121 (2015), [arXiv:1411.7738].

[27] S. L. Olsen, T. Skwarnicki and D. Zieminska, Rev. Mod. Phys. **90**, 015003 (2018), [arXiv:1708.04012].

[28] N. Brambilla *et al.*, Physics Reports **873**, 1 (2020), [arXiv:1907.07583].

[29] N. Hüsken, E. Norella and I. Polyakov, Modern Physics Letters A **40**, 17n18, 2530002 (2025), [arXiv:2410.06923].

[30] S. K. Choi *et al.*, Physical Review Letters **91**, 262001 (2003), [hep-ex/0309032].

[31] N. A. Törnqvist, Physical Review Letters **67**, 556 (1991).

[32] R. Aaij *et al.*, Nature Physics **18**, 751 (2022), [arXiv:2109.01038].

[33] R. Aaij *et al.*, Science Bulletin **65**, 1983 (2020), [arXiv:2006.16957].

[34] C. J. Morningstar and M. J. Peardon, Phys. Rev. **D60**, 034509 (1999), [hep-lat/9901004].

[35] Y. Chen *et al.*, Phys. Rev. **D73**, 014516 (2006), [hep-lat/0510074].

[36] W.-J. Lee and D. Weingarten, Phys. Rev. **D61**, 014015 (2000), [hep-lat/9910008].

[37] G. S. Bali *et al.* (UKQCD), Phys. Lett. **B309**, 378 (1993), [hep-lat/9304012].

[38] C. Michael, AIP Conf. Proc. **432**, 657 (1998), [hep-ph/9710502].

[39] A. Athenodorou and M. Teper, Journal of High Energy Physics **2020**, 11, 172 (2020), [arXiV:2007.06422].

[40] J. Leutgeb and A. Rebhan, Phys. Rev. D **101**, 014006 (2020), [arXiv:1909.12352].

[41] F. Brünner, J. Leutgeb and A. Rebhan, Physics Letters B **788**, 431 (2019), [arXiv:1807.10164].

[42] M. Huber, C. S. Fischer and H. Sanchis-Alepuz, The European Physical Journal C **80**, 11, 1077 (2020), [arXiv:2004.00415].

[43] F. E. Close and A. Kirk, Eur. Phys. J. **C21**, 531 (2001), [hep-ph/0103173].

[44] A. V. Sarantsev *et al.*, Physics Letters B **816**, 136227 (2021), [arXiv:2103.09680].

[45] W. Ochs, J. Phys. **G40**, 043001 (2013), [arXiv:1301.5183].

[46] F. Brünner and A. Rebhan, Phys. Rev. Lett. **115**, 131601 (2015), [arXiv:1504.05815].

[47] C. Amsler and N. A. Tornqvist, Phys. Rept. **389**, 61 (2004).

[48] N. Isgur and J. E. Paton, Phys. Rev. **D31**, 2910 (1985).

[49] M. S. Chanowitz and S. R. Sharpe, Nucl. Phys. **B222**, 211 (1983), [Erratum: Nucl. Phys.B228,588(1983)].

[50] T. Barnes *et al.*, Nucl. Phys. **B224**, 241 (1983).

[51] P. Lacock *et al.* (UKQCD), Phys. Lett. **B401**, 308 (1997), [hep-lat/9611011].

[52] J. J. Dudek, Phys. Rev. D **84**, 074023 (2011), [arXiv:1106.5515].

[53] J. J. Dudek *et al.* (Hadron Spectrum), Phys. Rev. **D88**, 094505 (2013), [arXiv:1309.2608].

[54] B. Kopf *et al.*, The European Physical Journal C **81**, 1056 (2021), [arXiv:2008.11566].

[55] M. Ablikim *et al.* (BESIII), Phys. Rev. Lett. **129**, 192002 (2022), [Erratum: Phys.Rev.Lett. 130, 159901 (2023)], [arXiv:2202.00621].

[56] E. S. Swanson, Physical Review D **107**, 074028 (2023), [arXiv:2302.01372].

[57] R. Aaij *et al.* (LHCb), Phys. Rev. Lett. **115**, 072001 (2015), [arXiv:1507.03414].

[58] R. Aaij *et al.* (LHCb), Phys. Rev. Lett. **122**, 222001 (2019), [arXiv:1904.03947].

[59] A. V. Popov *et al.*, Physics of Atomic Nuclei **83**, 9, 1383 (2020).

[60] J.-J. Wu *et al.*, Phys. Rev. Lett. **105**, 232001 (2010), [arXiv:1007.0573].

[61] J.-J. Wu, T.-S. H. Lee and B. S. Zou, Phys. Rev. C **85**, 044002 (2012), [arXiv:1202.1036].

[62] Y.-R. Liu *et al.*, Prog. Part. Nucl. Phys. **107**, 237 (2019), [arXiv:1903.11976].

[63] F.E. Close, in *Quarks and Nuclear Forces* (Springer-Verlag, 1982), p. 56.

[64] R.H. Dalitz and L.J. Reinders, in "Hadron Structure as Known from Electromagnetic and Strong Interactions," *Proceedings of the Hadron '77 Conference* (Veda, 1979), p. 11.

[65] E. Klempt and J.-M. Richard, Rev. Mod. Phys. **82**, 1095 (2010), [arXiv:0901.2055].

[66] T. Melde, W. Plessas and B. Sengl, Phys. Rev. **D77**, 114002 (2008), [arXiv:0806.1454].

Int. J. Mod. Phys. A 2026.41. Downloaded from www.wo
by UNIVERSITY OF CALIFORNIA @ BERKELEY on 09/16/26. Re-use and distribution is
except for Open Access articles.

Int. J. Mod. Phys. A 2026.41. Downloaded from www.worldscientific.com
by UNIVERSITY OF CALIFORNIA @ BERKELEY on 09/16/26. Re-use and distribution is strictly not permitted, except for Open Access articles.

[67] N. Isgur and G. Karl, Phys. Rev. **D18**, 4187 (1978).

[68] N. Isgur and G. Karl, Phys. Rev. **D19**, 2653 (1979), [Erratum: Phys. Rev.D23,817(1981)].

[69] S. Capstick and W. Roberts, Prog. Part. Nucl. Phys. **45**, S241 (2000), [arXiv:nucl-th/0008028].

[70] S. Capstick and W. Roberts, Phys. Rev. **D58**, 074011 (1998), [arXiv:nucl-th/9804070].

[71] S. Capstick, Phys. Rev. **D46**, 2864 (1992).

[72] R. A. Arndt *et al.*, Phys. Rev. **C74**, 045205 (2006), [arXiv:nucl-th/0605082].

[73] B. Krusche and S. Schadmand, Prog. Part. Nucl. Phys. **51**, 399 (2003), [arXiv:nucl-ex/0306023].

[74] A. V. Anisovich *et al.*, Eur. Phys. J. **A52**, 284 (2016), [arXiv:1604.05704].

[75] E. Gutz *et al.* (CBELSA/TAPS), Eur. Phys. J. **A50**, 74 (2014), [arXiv:1402.4125].

[76] V. Sokhoyan *et al.* (CBELSA/TAPS), Eur. Phys. J. **A51**, 95 (2015), [Erratum: Eur. Phys. J.A51,no.12,187(2015)], [arXiv:1507.02488].

[77] E. Klempt *et al.*, Eur. Phys. J. **A56**, 261 (2020), [arXiv:2007.04232].

[78] J. Yelton *et al.* (Belle), Phys. Rev. Lett. **121**, 5, 052003 (2018), [arXiv:1805.09384].

[79] M. Ablikim *et al.* (BESIII), Phys. Rev. Lett. **134**, 13, 131903 (2025), [arXiv:2411.11648].

[80] M. Sumihama *et al.* (Belle Collaboration), Phys. Rev. Lett. **122**, 072501 (2019), [arXiv:1810.06181].

[81] R. Aaij *et al.* (LHCb), Sci. Bull. **66**, 1278 (2021), [arXiv:2012.10380].

[82] V. Crede and J. Yelton, Rept. Prog. Phys. **87**, 10, 106301 (2024), [arXiv:2502.08815].

[83] G. Barucca *et al.*, Eur. Phys. J. **A57**, 149 (2021).

[84] G. Barucca *et al.*, Eur. Phys. J. **A57**, 154 (2021).

[85] S. Capstick and W. Roberts, Prog. in Part. Nucl. Phys. **45**, 241 (2000), [arXiv:nucl-th/0008028].

[86] V. Crede and W. Roberts, Rept. on Prog. in Phys. **76**, 076301 (2013), [arXiv:1302.7299].

[87] M. Ferraris *et al.*, Phys. Lett. **B364**, 231 (1995).

[88] M. M. Giannini and E. Santopinto, Chin. J. Phys. **53**, 020301 (2015), [arXiv:1501.03722].

[89] M. Anselmino *et al.*, Rev. Mod. Phys. **65**, 1199 (1993).

[90] R. Bijker, F. Iachello and A. Leviatan, Annals Phys. **236**, 69 (1994), [arXiv:nucl-th/9402012].

[91] S. Capstick and P. R. Page, Phys. Rev. **C66**, 065204 (2002), [arXiv:nucl-th/0207027].

[92] R. L. Jaffe, D. Pirjol and A. Scardicchio, Phys. Rept. **435**, 157 (2006), [hep-ph/0602010].

[93] G. Eichmann *et al.*, Prog. Part. Nucl. Phys. **91**, 1 (2016), [arXiv:1606.09602].

[94] G. Eichmann and C. S. Fischer, Few Body Syst. **60**, 2 (2019).

[95] A. Bashir *et al.*, Commun. Theor. Phys. **58**, 79 (2012), [arXiv:1201.3366].

[96] C. D. Roberts, IRMA Lect. Math. Theor. Phys. **21**, 355 (2015).

[97] R. Slansky, Phys. Rept. **79**, 1 (1981).

[98] M. Karliner and J. L. Rosner, Phys. Rev. **D90**, 094007 (2014), [arXiv:1408.5877].

[99] M. Ablikim *et al.* (BESIII), Phys. Rev. D **103**, 9, L091101 (2021), [arXiv:2011.00396].

[100] R. Aaij *et al.* (LHCb), Phys. Rev. Lett. **118**, 182001 (2017), [arXiv:1703.04639].

[101] R. Aaij *et al.* (LHCb), Phys. Rev. Lett. **131**, 13, 131902 (2023), [arXiv:2302.04733].

[102] Y. Yelton *et al.*, Phys. Rev. **D97**, 051102(R) (2018).

[103] R. Aaij *et al.*, Phys. Rev. Lett **124**, 082002 (2020).

[104] R. Aaij *et al.* (LHCb), Phys. Rev. Lett. **119**, 112001 (2017), [arXiv:1707.01621].

[105] R. Aaij *et al.* (LHCb), Phys. Rev. Lett. **121**, 16, 162002 (2018), [arXiv:1807.01919].

[106] R. Aaij *et al.* (LHCb), JHEP **05**, 038 (2022), [arXiv:2202.05648].

[107] M. Mattson *et al.* (SELEX), Phys. Rev. Lett. **89**, 112001 (2002), [hep-ex/0208014].

[108] A. Ocherashvili *et al.* (SELEX), Phys. Lett. **B628**, 18 (2005), [hep-ex/0406033].

[109] R. Aaij *et al.* (LHCb), Sci. China Phys. Mech. Astron. **63**, 221062 (2020), [arXiv:1909.12273].

[110] S. Brodsky, S. Groote and S. Koshkarev, Eur. Phys. J. **C78**, 483 (2018).

[111] R. Aaij *et al.* (LHCb), JHEP **05**, 030 (2017), [arXiv:1701.07873].

[112] R. Aaij *et al.* (LHCb), Phys. Rev. Lett. **131**, 17, 171901 (2023), [arXiv:2307.13399].

[113] A. M. Sirunyan *et al.* (CMS), Phys. Rev. Lett. **126**, 25, 252003 (2021), [arXiv:2102.04524].

[114] L. Schachinger *et al.*, Phys. Rev. Lett. **41**, 1348 (1978).

[115] G. Lopez Castro and A. Mariano, Physics Letters B **517**, 3, 339 (2001), [arXiv:nucl-th/0006031].

[116] A. Morelos Pineda *et al.* (E761), Phys. Rev. Lett. **71**, 3417 (1993).

[117] D. W. Hertzog *et al.*, Phys. Rev. D **37**, 1142 (1988).

[118] N. B. Wallace *et al.*, Phys. Rev. Lett. **74**, 3732 (1995).

[119] A. Bosshard *et al.*, Phys. Rev. D **44**, 1962 (1991).

[120] M. Kotulla *et al.*, Phys. Rev. Lett **27**, 272001 (2002).

[121] S. Schumann *et al.*, The European Physical Journal A **43**, 269 (2010).

[122] A. De Rujula, H. Georgi and S. L. Glashow, Phys. Rev. **D12**, 147 (1975).

[123] W. H. Blask *et al.*, Z. Phys. **A337**, 327 (1990).

[124] U. Loring *et al.*, Eur. Phys. J. **A10**, 309 (2001), [hep-ph/0103287].

[125] L. Ya. Glozman and D. O. Riska, Phys. Rept. **268**, 263 (1996), [hep-ph/9505422].

[126] T. DeGrand and E. T. Neil, Phys. Rev. D **101**, 034504 (2020), [arXiv:1910.08561].

[127] C. Aubin *et al.*, Phys. Rev. **D70**, 094505 (2004), [hep-lat/0402030].

[128] A. Bazavov *et al.* (MILC), Rev. Mod. Phys. **82**, 1349 (2010), [arXiv:0903.3598].

[129] S. Aoki *et al.* (PACS-CS), Phys. Rev. **D79**, 034503 (2009), [arXiv:0807.1661].

[130] S. Durr *et al.*, Science **322**, 1224 (2008), [arXiv:0906.3599].

[131] W. Bietenholz *et al.*, Phys. Rev. **D84**, 054509 (2011), [arXiv:1102.5300].

[132] C. Alexandrou *et al.*, Phys. Rev. **D90**, 074501 (2014), [arXiv:1406.4310].

[133] J. J. Dudek *et al.*, Phys. Rev. **D83**, 111502 (2011), [arXiv:1102.4299].

[134] E. B. Gregory *et al.* (UKQCD), Phys. Rev. **D86**, 014504 (2012), [arXiv:1112.4384].

[135] C. Michael, K. Ottnad and C. Urbach (ETM), Phys. Rev. Lett. **111**, 181602 (2013), [arXiv:1310.1207].

[136] C. Bernard *et al.* (Fermilab Lattice, MILC), Phys. Rev. **D83**, 034503 (2011), [arXiv:1003.1937].

Int. J. Mod. Phys. A 2026.41. Downloaded from www.worldscientific.com by UNIVERSITY OF CALIFORNIA @ BERKELEY on 09/16/26. Re-use and distribution is [redacted] except for Open Access articles.

[137] E. B. Gregory *et al.*, Phys. Rev. **D83**, 014506 (2011), [arXiv:1010.3848].

[138] R. J. Dowdall *et al.*, Phys. Rev. **D86**, 094510 (2012), [arXiv:1207.5149].

[139] D. Mohler and R. M. Woloshyn, Phys. Rev. **D84**, 054505 (2011), [arXiv:1103.5506].

[140] A. S. Kronfeld, Ann. Rev. Nucl. Part. Sci. **62**, 265 (2012), [arXiv:1203.1204].

[141] K. Ottnad, C. Urbach and F. Zimmermann (OTM), Nucl. Phys. **B896**, 470 (2015), [arXiv:1501.02645].

[142] G. S. Bali *et al.* (RQCD), JHEP **08**, 137 (2021), [arXiv:2106.05398].

[143] C. DeTar *et al.* (Fermilab Lattice, MILC), Phys. Rev. D **99**, 034509 (2019), [arXiv:1810.09983].

[144] S. Piemonte *et al.*, Phys. Rev. D **100**, 074505 (2019), [arXiv:1905.03506].

[145] S. Prelovsek *et al.*, JHEP **06**, 035 (2021), [arXiv:2011.02542].

[146] M. Padmanath, C. B. Lang and S. Prelovsek, Phys. Rev. D **92**, 034501 (2015), [arXiv:1503.03257].

[147] L. Liu *et al.*, Phys. Rev. **D81**, 094505 (2010), [arXiv:0909.3294].

[148] R. A. Briceno, H.-W. Lin and D. R. Bolton, Phys. Rev. **D86**, 094504 (2012), [arXiv:1207.3536].

[149] Y. Namekawa *et al.* (PACS-CS), Phys. Rev. **D87**, 094512 (2013), [arXiv:1301.4743].

[150] M. Padmanath *et al.*, Phys. Rev. **D90**, 074504 (2014), [arXiv:1307.7022].

[151] Z. S. Brown *et al.*, Phys. Rev. **D90**, 094507 (2014), [arXiv:1409.0497].

[152] P. Pérez-Rubio, S. Collins and G. S. Bali, Phys. Rev. **D92**, 034504 (2015), [arXiv:1503.08440].

[153] C. Alexandrou and C. Kallidonis, Phys. Rev. **D96**, 034511 (2017), [arXiv:1704.02647].

[154] S. Meinel, private comunication.

[155] R. G. Edwards *et al.*, Phys. Rev. **D84**, 074508 (2011), [arXiv:1104.5152].

[156] C. M. Richards *et al.* (UKQCD), Phys. Rev. **D82**, 034501 (2010), [arXiv:1005.2473].

[157] E. Gregory *et al.*, JHEP **10**, 170 (2012), [arXiv:1208.1858].

[158] C. Morningstar, PoS **LATTICE2024**, 004 (2024), [arXiv:2502.02547].

[159] J. Bulava *et al.*, Nucl. Phys. **B910**, 842 (2016), [arXiv:1604.05593].

[160] A. Rodas, J. J. Dudek and R. G. Edwards (Hadron Spectrum), Phys. Rev. D **108**, 3, 034513 (2023), [arXiv:2303.10701].

[161] R. A. Briceno *et al.*, Phys. Rev. Lett. **118**, 022002 (2017), [arXiv:1607.05900].

[162] D. Guo *et al.*, Phys. Rev. D **98**, 014507 (2018), [arXiv:1803.02897].

[163] R. A. Briceno *et al.*, Phys. Rev. D **97**, 5, 054513 (2018), [arXiv:1708.06667].

[164] J. Bulava *et al.*, Nucl. Phys. B **987**, 116105 (2023), [arXiv:2208.03867].

[165] M. Mai, U.-G. Meißner and C. Urbach, Phys. Rept. **1001**, 1 (2023), [arXiv:2206.01477].

[166] A. J. Woss *et al.* (Hadron Spectrum), Phys. Rev. D **103**, 054502 (2021), [arXiv:2009.10034].

[167] C. T. Johnson and J. J. Dudek (Hadron Spectrum), Phys. Rev. D **103**, 074502 (2021), [arXiv:2012.00518].

[168] J. A. Oller and U. G. Meissner, Phys. Lett. B **500**, 263 (2001), [hep-ph/0011146].

[169] J. Bulava *et al.* (Baryon Scattering (BaSc)), Phys. Rev. Lett. **132**, 5, 051901 (2024), [arXiv:2307.10413].

[170] J. Bulava *et al.* (Baryon Scattering (BaSc)), Phys. Rev. D **109**, 1, 014511 (2024), [arXiv:2307.13471].

[171] R. Bruschini and P. González, Phys. Rev. D **102**, 074002 (2020), [arXiv:2007.07693].

[172] R. Bruschini and P. González, Phys. Rev. D **103**, 074009 (2021), [arXiv:2101.04636].

[173] R. F. Lebed, R. E. Mitchell and E. S. Swanson, Prog. Part. Nucl. Phys. **93**, 143 (2017), [arXiv:1610.04528].

[174] E. J. Eichten and C. Quigg, Phys. Rev. Lett. **119**, 202002 (2017), [arXiv:1707.09575].

[175] M. Karliner and J. L. Rosner, Phys. Rev. Lett. **119**, 202001 (2017), [arXiv:1707.07666].

[176] A. Francis *et al.*, Phys. Rev. Lett. **118**, 142001 (2017), [arXiv:1607.05214].

[177] L. Leskovec *et al.*, Phys. Rev. D **100**, 014503 (2019), [arXiv:1904.04197].

[178] R. Aaij *et al.* (LHCb), Nature Phys. **18**, 751 (2022), [arXiv:2109.01038].

[179] S. M. Dawid, F. Romero-López and S. R. Sharpe, JHEP **01**, 060 (2025), [arXiv:2409.17059].

[180] M. Karliner and J. L. Rosner **100**, 073006 (2019), [arXiv:1906.07799].

[181] Y. Aoki *et al.* (Flavour Lattice Averaging Group (FLAG)), Eur. Phys. J. C **82**, 869 (2022), [arXiv:2111.09849].

[182] S. Borsanyi *et al.*, Science **347**, 1452 (2015), [arXiv:1406.4088].

[183] G. M. de Divitiis *et al.* (RM123), Phys. Rev. D **87**, 114505 (2013), [arXiv:1303.4896].

[184] D. Giusti *et al.*, Phys. Rev. **D95**, 114504 (2017), [arXiv:1704.06561].

[185] S. Basak *et al.* (MILC), Phys. Rev. D **99**, 034503 (2019), [arXiv:1807.05556].

[186] A. Parreno *et al.*, Phys. Rev. D **95**, 114513 (2017), [arXiv:1609.03985].

Int. J. Mod. Phys. A 2026.41. Downloaded from www.worldscientific.com
by UNIVERSITY OF CALIFORNIA @ BERKELEY on 09/16/26. Re-use and distribution is strictly not permitted, except for Open Access articles.

16. Heavy-Quark and Soft-Collinear Effective Theory

Revised August 2023 by C.W. Bauer (LBNL) and M. Neubert (PRISMA, Mainz Inst. for Theor. Physics, JG U.).

16.1 Effective Field Theories

Quantum field theories provide the most precise computational tools for describing physics at the highest energies. One of their characteristic features is that they almost inevitably involve multiple length scales. When trying to determine the value of an observable, quantum field theory demands that all possible virtual states and hence all particles be included in the calculation. Since these particles have widely different masses, the final prediction is sensitive to many scales. This fact represents a formidable challenge from a practical point of view. No realistic quantum field theories can be solved exactly, so that one needs to resort to approximation schemes; these, however, are typically most straightforward when only a single scale is involved at a time.

Effective field theories (EFTs) provide a general theoretical framework to deal with the multi-scale problems of realistic quantum field theories. This framework aims at reducing such problems to a combination of separate and simpler single-scale problems; simultaneously, however, it provides an organization scheme whereby the other scales are not omitted but allowed to play their role in a separate step of the computation. The philosophy and basic principles of this approach are very generic, and correspondingly EFTs represent a widely used method in many different areas of high-energy physics, from the low-energy scales of atomic and nuclear physics to the high-energy scales of (partly yet unknown) elementary-particle physics, see [1–3] for some early references. EFTs can play a role both within analytic perturbative computations and in the context of non-perturbative numerical simulations. One of the simplest applications of EFTs to particle physics concerns the description of an underlying theory that is only probed at energy scales $E < \Lambda$. Any particle with mass $m > \Lambda$ cannot be produced as a real state and therefore only leads to short-distance virtual effects. Thus, one can construct an effective theory in which the quantum fluctuations of such heavy particles are "integrated out" from the generating functional for Green functions. This results in a simpler theory containing only those degrees of freedom that are relevant to the energy scales under consideration. In fact, the standard model of particle physics itself is widely viewed as an EFT of some yet unknown, more fundamental theory [4, 5].

The development of any effective theory starts by identifying the degrees of freedom that are relevant to describe the physics at a given energy (or length) scale and constructing the Lagrangian describing the interactions among these fields. Short-distance quantum fluctuations associated with much smaller length scales are absorbed into the coefficients of the various operators in the effective theory. These coefficients are determined in a matching procedure, by requiring that the EFT reproduces the matrix elements of the full theory up to power corrections. In many cases the effective Lagrangian exhibits enhanced symmetries compared with the fundamental theory, giving non-trivial relations between different observables.

16.2 Heavy-Quark Effective Theory

Heavy-quark systems provide prime examples for applications of the EFT technology, because the hierarchy $m_Q \gg \Lambda_{\rm QCD}$ (with $Q = b, c$) provides a natural separation of scales. Physics at the scale m_Q is of a short-distance nature and can be treated perturbatively, while for heavy-quark systems there is always also some hadronic physics governed by the confinement scale $\Lambda_{\rm QCD}$ of the strong interaction. Being able to separate the short-distance and long-distance effects associated with these two scales is crucial for any quantitative description. For instance, if the long-distance hadronic matrix elements are obtained from lattice QCD, then it is necessary to analytically compute the effects of short-wavelength modes that do not fit on the lattice. In many other instances, the long-distance physics can be encoded in a small number of hadronic parameters.

16.2.1 *General idea and derivation of the effective Lagrangian*

The simplest effective theory for heavy-quark systems is the heavy-quark effective theory (HQET) [6–9] (see [10, 11] for detailed discussions). It provides a simplified description of the soft interactions of a single heavy quark with light partons. This includes the interactions that bind the heavy quark with other light partons inside heavy mesons and baryons.

A softly interacting heavy quark is nearly on-shell. Its momentum may be decomposed as $p_Q = m_Q v + k$, where v is the 4-velocity of the hadron containing the heavy quark. The "residual momentum" k results from the soft interactions of the heavy quark with its environment and satisfies $v \cdot k \sim \Lambda_{\rm QCD}$ and $k^2 \sim \Lambda^2_{\rm QCD}$, which in the rest frame of the heavy hadron reduces to $k^\mu \sim \Lambda_{\rm QCD}$. In the limit $m_Q \gg \Lambda_{\rm QCD}$, the soft interactions do not change the 4-velocity of the heavy quark, which is therefore a conserved quantum number that is often used as a label on the effective heavy-quark fields.

A nearly on-shell Dirac spinor has two large and two small components. We define

$$Q(x) = e^{-im_Q v\cdot x}\,[h_v(x) + H_v(x)]\,, \tag{16.1}$$

where

$$h_v(x) = e^{im_Q v\cdot x}\,\frac{1+\not v}{2}\,Q(x)\,, \qquad H_v(x) = e^{im_Q v\cdot x}\,\frac{1-\not v}{2}\,Q(x) \tag{16.2}$$

are the large ("upper") and small ("lower") components of the spinor field, respectively. The extraction of the phase factor in (16.1) implies that the fields h_v and H_v carry the residual momentum k. The field H_v is $1/m_Q$ suppressed relative to h_v and describes quantum fluctuations far off the mass shell. Integrating it out using its equations of motion yields the HQET Lagrangian

$$\begin{aligned}\mathcal{L}_{\rm HQET} &= \bar h_v\, iv\cdot D_s\, h_v \\ &\quad + \frac{1}{2m_Q}\left[\bar h_v (iD_s)^2 h_v + C_{\rm mag}(\mu)\,\frac{g}{2}\,\bar h_v\,\sigma_{\mu\nu}\,G_s^{\mu\nu} h_v\right] + \dots\,.\end{aligned} \tag{16.3}$$

The covariant derivative $iD_s^\mu = i\partial^\mu + gA_s^\mu$ and the field strength $G_s^{\mu\nu}$ contain only the soft gluon field. Hard gluons have been integrated out, and their effects are contained in the Wilson coefficients of the operators in the effective Lagrangian. From the leading operator one derives the Feynman rules of HQET. The new operators entering at subleading order are referred to as the "kinetic energy" and "chromo-magnetic interaction". The kinetic-energy operator corresponds to the first correction term in the Taylor expansion of the relativistic energy $E = m_Q + \vec p^{\,2}/2m_Q + \dots$. Lorentz invariance, which is encoded as a reparametrization invariance of the effective Lagrangian [12], ensures that its Wilson coefficient is not renormalized ($C_{\rm kin} \equiv 1$). The coefficient $C_{\rm mag}$ of the chromo-magnetic operator receives corrections starting at one-loop order [6].

16.2.2 *Spin-flavor symmetry*

The leading term in the HQET Lagrangian exhibits a global spin-flavor symmetry. Its physical meaning is that, in the infinite mass limit, the properties of hadronic systems containing a single heavy quark are insensitive to the spin and flavor of the heavy quark [13, 14]. The spin symmetry results from the fact that there are no Dirac matrices in the leading term of the effective Lagrangian in (16.3), implying that the interactions of the heavy quark with soft gluons leave its spin unchanged. The flavor symmetry arises since the mass of the heavy quark does not appear at leading order. For n_Q heavy quarks moving at the same velocity, one can simply extend (16.3) by summing over n_Q identical terms for heavy-quark fields h_v^i. The result is invariant under rotations in flavor space. When combined with the spin symmetry, the symmetry group becomes promoted to $SU(2n_Q)$. These symmetries are broken by the operators at subleading power in the $1/m_Q$ expansion.

The spin-flavor symmetry leads to many interesting relations between the properties of hadrons containing a heavy quark. The

Int. J. Mod. Phys. A 2026.41. Downloaded from www.worldscientific.com by UNIVERSITY OF CALIFORNIA @ BERKELEY on 09/16/26. Re-use and distribution is [redacted] except for Open Access articles.

most direct consequences concern the spectroscopy of such states [15]. In the heavy-quark limit, the spin of the heavy quark and the total angular momentum j of the light degrees of freedom are separately conserved by the strong interactions. Because of heavy-quark symmetry, the dynamics is independent of the spin and mass of the heavy quark. Hadronic states can thus be classified by the quantum numbers (flavor, spin, parity, etc.) of the light degrees of freedom. The spin symmetry predicts that, for fixed $j \neq 0$, there is a doublet of degenerate states with total spin $J = j \pm \frac{1}{2}$. The flavor symmetry relates the properties of states with different heavy-quark flavor.

16.2.3 *Weak decay form factors*

Of particular interest are the relations between the weak decay form factors of heavy mesons, which parametrize hadronic matrix elements of currents between two mesons containing a heavy quark. These relations have been derived by Isgur and Wise [14], generalizing ideas developed by Nussinov and Wetzel [16] and Voloshin and Shifman [17]. For the purpose of this discussion, it is convenient to work with a mass-independent normalization of meson states and use velocity rather than momentum variables.

Consider the elastic scattering of a pseudoscalar meson, $P(v) \to P(v')$, induced by an external vector current coupled to the heavy quark contained in P, which acts as a color source moving with the meson's velocity v. The action of the current is to replace instantaneously the color source by one moving at velocity v'. Soft gluons need to be exchanged in order to rearrange the light degrees of freedom and build up the final state meson moving at velocity v'. This rearrangement leads to a form-factor suppression. The important observation is that, in the $m_Q \to \infty$ limit, the form factor can only depend on the Lorentz boost $\gamma = v \cdot v'$ connecting the rest frames of the initial and final-state mesons (as long as $\gamma = \mathcal{O}(1)$). In the effective theory the hadronic matrix element describing the scattering process can therefore be written as

$$\langle P(v')|\, \bar{h}_{v'} \gamma^\mu h_v \,|P(v)\rangle = \xi(v \cdot v')(v + v')^\mu, \tag{16.4}$$

with a form factor $\xi(v \cdot v')$ that is real and independent of m_Q. By flavor symmetry, the form factor remains identical when one replaces the heavy quark Q in one of the meson states by a heavy quark Q' of a different flavor, thereby turning P into another pseudoscalar meson P'. At the same time, the current becomes a flavor-changing vector current. This universal form factor is called the Isgur-Wise function [14]. For equal velocities the vector current $J^\mu = \bar{h}_v \gamma^\mu h_v$ is conserved in the effective theory, irrespective of the flavor of the heavy quarks. The corresponding conserved charges are the generators of the flavor symmetry. It follows that the Isgur-Wise function is normalized at the point of equal velocities: $\xi(1) = 1$. Since the recoil energy of the daughter meson P' in the rest frame of the parent meson P is $E_{\rm recoil} = m_{P'}\,(v \cdot v' - 1)$, the point $v \cdot v' = 1$ is referred to as the zero-recoil limit. The heavy-quark spin symmetry leads to additional relations among weak decay form factors. It can be used to relate matrix elements involving vector mesons to those involving pseudoscalar mesons, which once again can be described completely in terms of the universal Isgur-Wise function.

The form factor relations imposed by heavy-quark symmetry describe the semileptonic decay processes $\bar{B} \to D\,\ell\,\bar{\nu}$ and $\bar{B} \to D^*\ell\,\bar{\nu}$ in the limit of infinite heavy-quark masses. They are model-independent consequences of QCD. The known normalization of the Isgur-Wise function at zero recoil can be used to obtain a model-independent measurement of the element $|V_{cb}|$ of the Cabibbo-Kobayashi-Maskawa (CKM) matrix. The semileptonic decay $\bar{B} \to D^*\ell\,\bar{\nu}$ is particularly well suited for this purpose [18]. Experimentally this is a very clean mode, since the reconstruction of the D^* meson mass provides a powerful rejection against background. From the theoretical point of view, it is ideal since the decay rate at zero recoil is protected by Luke's theorem against first-order power corrections in $1/m_Q$ [19]. This is described in more detail in Section 12. Corrections to the heavy-quark symmetry relations for the $\bar{B} \to D^{(*)}$ form factors near zero recoil can also be constrained using sum rules derived in the small-velocity limit [20, 21].

16.2.4 *Decoupling transformation*

At leading order in $1/m_Q$, the couplings of soft gluons to heavy quarks in the effective Lagrangian (16.3) can be removed by the field redefinition $h_v(x) = Y_v(x)\, h_v^{(0)}(x)$, where $Y_v(x)$ is a soft Wilson line along the direction of v, extending from minus infinity to the point x. In terms of the new fields the leading-order HQET Lagrangian becomes $\mathcal{L}_{\rm HQET} = \bar{h}_v^{(0)} iv \cdot \partial\, h_v^{(0)}$. It describes a free theory as far as the strong interactions of heavy quarks are concerned. However, the theory is nevertheless non-trivial in the presence of external sources. Consider, e.g., the case of a weak-interaction heavy-quark current

$$\bar{h}_{v'} \gamma^\mu (1 - \gamma_5) h_v = \bar{h}_{v'}^{(0)} \gamma^\mu (1 - \gamma_5)\, Y_{v'}^\dagger Y_v\, h_v^{(0)}, \tag{16.5}$$

where v and v' are the velocities of the heavy mesons containing the heavy quarks. Unless the two velocities are equal, corresponding to the zero-recoil limit discussed above, the object $Y_{v'}^\dagger Y_v$ is non-trivial, and hence the soft gluons do not decouple from the heavy quarks inside the current operator. One may interpret $Y_{v'}^\dagger Y_v$ as a Wilson loop with a cusp at the point x, where the two paths parallel to the different velocity vectors intersect. The presence of the cusp leads to non-trivial ultra-violet behavior (for $v \neq v'$), which is described by a cusp anomalous dimension $\Gamma_{\rm cusp}(v \cdot v')$ that was calculated at two-loop order in [22]. It coincides with the velocity-dependent anomalous dimension of heavy-quark currents, which was introduced in the context of HQET in [23]. The interpretation of heavy quarks as Wilson lines is a useful tool, which was put forward in one of the very first papers on the subject [6]. This technology will be useful in the study of the interactions of heavy quarks with collinear degrees of freedom discussed later in this review.

16.2.5 *Heavy-quark expansion for inclusive decays*

The theoretical description of inclusive decays of hadrons containing a heavy quark exploits two observations [24–28]: bound-state effects related to the initial state can be calculated using the heavy-quark expansion, and the fact that the final state consists of a sum over many hadronic channels eliminates the sensitivity to the properties of individual final-state hadrons. The second feature rests on the hypothesis of quark-hadron duality, i.e. the assumption that decay rates are calculable in QCD after a smearing procedure has been applied [29]. In semileptonic decays, the integration over the lepton spectrum provides a smearing over the invariant hadronic mass of the final state (global duality). For nonleptonic decays, where the total hadronic mass is fixed, the summation over many hadronic final states provides an averaging (local duality). Since global duality is a much weaker assumption, the theoretical control of inclusive semileptonic decays is on firmer footing.

Using the optical theorem, the inclusive decay width of a hadron H_b containing a b quark can be written in the form

$$\Gamma(H_b) = \frac{1}{M_{H_b}}\, {\rm Im}\, \langle H_b|\, i \int {\rm d}^4x\, T\,\{\mathcal{H}_{\rm eff}(x), \mathcal{H}_{\rm eff}(0)\}\, |H_b\rangle\,. \tag{16.6}$$

The effective weak Hamiltonian for b-quark decays consists of dimension-6 four-fermion operators and dipole operators [30]. Because of the large mass of the b quark, it follows that the separation of fields in the time-ordered product in (16.6) is small, of order $x \sim 1/m_b$. It is thus possible to construct an operator-product expansion (OPE) for the time-ordered product, in which it is represented as a series of local operators in HQET. The leading operator $\bar{h}_v h_v$ has a trivial matrix element. The next contributions arise at $\mathcal{O}(1/m_b^2)$ and give rise to two parameters $\mu_\pi^2(H_b)$ and $\mu_G^2(H_b)$, which are defined as the matrix elements of the heavy-quark kinetic energy and chromo-magnetic interaction inside the hadron H_b, respectively [31]. For the ground-state heavy mesons and baryons, one has $\mu_G^2(B) = 3(m_{B^*}^2 - m_B^2)/4 \simeq 0.36\,{\rm GeV}^2$ and $\mu_G^2(\Lambda_b) = 0$. Thus, the total inclusive decay rate of a hadron H_b

Int. J. Mod. Phys. A 2026.41. Downloaded from www.worldscientific.com
by UNIVERSITY OF CALIFORNIA @ BERKELEY on 09/16/26. Re-use and distribution is strictly not permitted, except for Open Access articles.

can be written as [25, 26]

$$\Gamma(H_b) = \frac{G_F^2 m_b^5 |V_{cb}|^2}{192\pi^3} \left[c_1 + c_2 \frac{\mu_\pi^2(H_b)}{2m_b^2} + c_3 \frac{\mu_G^2(H_b)}{2m_b^2} + \mathcal{O}\left(\frac{1}{m_b^3}\right) + \dots \right], \tag{16.7}$$

where the prefactor arises from the loop integrations and is proportional to the fifth power of the b-quark mass. The coefficient functions c_i are calculable order by order in perturbation theory. While c_1 corresponds to the decay rate of a free heavy quark, the higher-order coefficients systematically account for bound-state effects. The coefficients of the subleading operators and of the leading operator at third order in $1/m_b$ have been calculated at NLO [32–36]. At tree level the heavy-quark expansion has been performed up to fifth order in $1/m_b$ [37].

From the fully inclusive width in (16.7) one can obtain the lifetime of a heavy hadron via $\tau(H_b) = 1/\Gamma(H_b)$. Due to the universality of the leading term in the heavy-quark expansion, lifetime ratios such as $\tau(B^-)/\tau(\bar{B}^0)$, $\tau(\bar{B}_s^0)/\tau(\bar{B}^0)$ and $\tau(\Lambda_b)/\tau(\bar{B}^0)$ are particularly sensitive to the hadronic parameters determining the power corrections in the expansion. In order to understand these ratios theoretically, it is necessary to include phase-space enhanced power corrections of order $(\Lambda_{\rm QCD}/m_b)^3$ [38, 39] as well as short-distance perturbative effects [40] in the calculation (see [41] for a discussion of the corresponding calculations).

A formula analogous to (16.7) can be derived for differential distributions in specific inclusive decay processes, assuming that these distributions are integrated over a sufficiently large region of phase space to ensure quark-hadron duality. Important examples are the distributions in the lepton energy and the lepton invariant mass, as well as moments of the invariant hadronic mass distribution in the semileptonic processes $\bar{B} \to X_u\, \ell\, \bar{\nu}$ and $\bar{B} \to X_c\, \ell\, \bar{\nu}$. A global fit of semileptonic decay distributions can be used to determine the CKM matrix elements $|V_{ub}|$ and $|V_{cb}|$ along with heavy-quark parameters such as the masses m_b, m_c and the hadronic parameters $\mu_\pi^2(B)$, $\mu_G^2(B)$. These determinations provide some of the most accurate values for these parameters (see e.g. [42–45]).

16.2.6 *Shape functions and non-local power corrections*

In certain regions of phase space, in which the hadronic final state in an inclusive heavy-hadron decay is made up of light energetic partons, the local OPE for inclusive decays must be replaced by a more complicated expansion involving hadronic matrix elements of non-local light-ray operators [46, 47]. Prominent examples are the radiative decay $\bar{B} \to X_s\gamma$ for large photon energy E_γ near $m_B/2$, and the semileptonic decay $\bar{B} \to X_u\, \ell\, \bar{\nu}$ at large lepton energy or small hadronic invariant mass. In these cases, the differential decay rates at leading order in the heavy-quark expansion can be written in the factorized form $d\Gamma = H\, J \otimes S$ [48], where the hard function H and the jet function J are calculable in perturbation theory. The characteristic scales for these functions are set by m_b and $(m_b\Lambda_{\rm QCD})^{1/2}$, respectively. The soft function

$$S(\omega) = \int \frac{dt}{4\pi}\, e^{-i\omega t}\, \langle \bar{B}(v)|\, \bar{h}_v(tn) Y_n(tn) Y_n^\dagger(0) h_v(0) |\bar{B}(v)\rangle \tag{16.8}$$

is a non-perturbative object called the shape function [46, 47]. Here Y_n are soft Wilson lines along a light-like direction n aligned with the momentum of the hadronic final-state jet. The jet function and the shape function share a common variable $\omega \sim \Lambda_{\rm QCD}$, and the symbol $\otimes$ denotes a convolution in this variable.

While the hard functions are different for the decays $\bar{B} \to X_s\gamma$ and $\bar{B} \to X_u\, \ell\bar{\nu}$, the jet and soft functions are identical at leading order in $\Lambda_{\rm QCD}/m_Q$. This is particularly important for the shape function, which introduces non-perturbative physics into the theoretical predictions for the decay rates in the regions of experimental interest. The fact that both processes depend on the same non-perturbative function makes it possible to use the measured shape of the $\bar{B} \to X_s\gamma$ photon spectrum to reduce the theoretical uncertainties in the determination of the CKM element $|V_{ub}|$ from semileptonic decays. In higher orders of the heavy-quark expansion, an increasing number of subleading jet and soft functions are required to describe the decay distributions [49]. These have been analyzed in detail at order $1/m_b$ [50–52]. In the case of $\bar{B} \to X_s\gamma$ (and also in the related case of $\bar{B} \to X_s\ell\bar{\ell}$), some of these non-local effects survive in the total decay rate and give rise to irreducible hadronic uncertainties [53]. The technology for deriving the corresponding factorization theorems relies on the soft-collinear effective theory, to which we now turn.

16.3 Soft-Collinear Effective Theory

As discussed in the previous section, soft gluons that bind a heavy quark inside a heavy meson cannot change the virtuality of that heavy quark by a significant amount. The ratio $\Lambda_{\rm QCD}/m_Q$ provides the expansion parameter in HQET, which is a small parameter since $m_Q \gg \Lambda_{\rm QCD}$. This obviously does not work when considering light quarks. However, if the energy Q (not to be confused with the flavor of a heavy quark) of the quarks is large, the ratio $\Lambda_{\rm QCD}/Q$ provides a small parameter, which can be used to construct an effective theory. One major difference to HQET is that light energetic quarks cannot only emit soft gluons, but they can also emit collinear gluons (an energetic gluon in the same direction as the original quark), without parametrically changing their virtuality. Thus, to fully reproduce the long-distance physics of energetic quarks requires that one includes their interactions with both soft and collinear particles. The resulting effective theory is therefore called soft-collinear effective theory (SCET) [54–57] (see [58] for a review).

A single energetic particle can always be boosted to a frame where all momentum components have similar size, in which case there is no small expansion parameter. Thus, the presence of energetic particles must refer to a reference frame defined by external kinematics. SCET has a wide range of applications; some examples are the production of energetic, light states in the decay of a heavy particle in its rest frame, the production of energetic jets in collider environments, and the scattering of energetic particles off a target at rest. In this brief review we will outline the main features of this effective theory and mention a few selected applications.

16.3.1 *General idea of the expansion*

Consider a quark with virtuality much less than its energy Q, moving along the direction $\vec{n}$. It is convenient to parameterize the momentum p_n of this particle in terms of its light-cone components, defined by $(p_n^-, p_n^+, p_n^\perp) = (\bar{n}\cdot p_n, n\cdot p_n, p_n^\perp)$, where $n^\mu = (1, \vec{n})$ and $\bar{n}^\mu = (1, -\vec{n})$ are light-like reference vectors, and $n\cdot p_n^\perp = \bar{n}\cdot p_n^\perp = 0$. The subscript n on the momentum indicates the direction of the collinear particle. In terms of these light-cone components, the virtuality satisfies $p_n^2 = p_n^+ p_n^- + p_n^{\perp 2}$. The individual components of the momentum obey

$$(p_n^-, p_n^+, p_n^\perp) \sim Q(1, \lambda^2, \lambda)\,, \tag{16.9}$$

where $\lambda^2 = p^2/Q^2$ is the expansion parameter of SCET. The virtuality of such an energetic particle remains parametrically unchanged if it interacts with energetic particles in the same direction n, or with soft particles with momentum scaling as

$$(p_s^-, p_s^+, p_s^\perp) \sim Q(\lambda^2, \lambda^2, \lambda^2)\,. \tag{16.10}$$

SCET is constructed in such a way as to reproduce the long-distance dynamics arising from the interactions of collinear and soft degrees of freedom.

In the above power counting the transverse momenta of soft degrees of freedom scale as $p_s^\perp \sim Q\lambda^2$, which is much smaller than the transverse momenta $p_c^\perp \sim Q\lambda$ of collinear fields. This theory is usually called SCET_I. If the external kinematics require that the transverse momenta of both soft and collinear fields are of the same size, $p_c^\perp \sim p_s^\perp$, then the appropriate degrees of freedom have the scaling $p_c \sim Q(1, \lambda^2, \lambda)$ and $p_s \sim Q(\lambda, \lambda, \lambda)$. This theory is usually called SCET_II and is required, e.g., for exclusive hadronic decays such as $\bar{B} \to D\pi$, where the virtuality of both collinear and soft degrees of freedom are set by $\Lambda_{\rm QCD}$, or for the description of transverse-momentum distributions at colliders. SCET_I power counting is assumed in the following sections, while SCET_II is discussed in more detail in 16.3.6.

Int. J. Mod. Phys. A 2026.41. Downloaded from www.worldscientific.com by UNIVERSITY OF CALIFORNIA @ BERKELEY on 09/16/26. Re-use and distribution is except for Open Access articles.

16.3.2 *Leading-order Lagrangian*

The derivation of the SCET Lagrangian follows similar steps as described for HQET in Section 16.2.1. One begins by deriving the Lagrangian for a theory containing only a single collinear sector. Similar to HQET, one separates the full QCD field into two components, $q_n(x) = \psi_n(x) + \eta_n(x)$, where (with $n \cdot \bar{n} = 2$)

$$\psi_n(x) = \frac{\not{n}\not{\bar{n}}}{4}\, q_n(x)\,, \qquad \eta_n(x) = \frac{\not{\bar{n}}\not{n}}{4}\, q_n(x)\,. \tag{16.11}$$

The degrees of freedom described by the field η_n are far off shell and can therefore be eliminated using its equation of motion. This gives

$$\mathcal{L}_n = \bar{\psi}_n(x) \left[in \cdot D + i\not{D}^\perp \frac{1}{i\bar{n}\cdot D}\, i\not{D}^\perp \right] \frac{\not{\bar{n}}}{2}\, \psi_n(x)\,. \tag{16.12}$$

As a next step, one separates the large and small momentum components by decomposing the collinear momentum into a "label" and a residual momentum, $p^\mu = P^\mu + k^\mu$ with $n \cdot P = 0$. One then performs a phase redefinition on the collinear fields, such that $\psi_n(x) = e^{-iP\cdot x}\, \xi_n(x)$. Derivatives acting on the fields $\xi_n(x)$ now only pick out the residual momentum. Since unlike in HQET the label momentum in SCET is not conserved, one defines a label operator $\mathcal{P}^\mu$ acting as $\mathcal{P}^\mu \xi_n(x) = P^\mu \xi_n(x)$ [56], as well as a corresponding covariant label operator $i\mathcal{D}_n^\mu = \mathcal{P}^\mu + gA_n^\mu(x)$. Note that at leading order in power counting $i\mathcal{D}_n^\mu$ does not contain the soft gluon field. This leads to the final SCET Lagrangian [56,57,59,60]

$$\mathcal{L}_n = \bar{\xi}_n(x) \left[in \cdot D_n + gn \cdot A_s + i\not{\mathcal{D}}_n^\perp \frac{1}{i\bar{n}\cdot \mathcal{D}_n}\, i\not{\mathcal{D}}_n^\perp \right] \frac{\not{\bar{n}}}{2}\, \xi_n(x) + \ldots\,, \tag{16.13}$$

where we have split $in \cdot D$ into a collinear piece $in \cdot D_n = in \cdot \partial + gn \cdot A_n$ and a soft piece $gn \cdot A_s$. This latter term gives rise to the only interaction between a collinear quark and soft gluons at leading power in λ. The ellipses represent higher-order interactions between soft and collinear particles.

The Lagrangian describing collinear fields in different light-like directions is simply given by the sum of the Lagrangians for each direction n, i.e. $\mathcal{L} = \sum_n \mathcal{L}_n$. The soft gluons are the same in each individual Lagrangian. An alternative way to understand the separation between large and small momentum components is to derive the Lagrangian of SCET in position space [60]. In this case no label operators are required, but the collinear field operators are separated by a light-like distance. An important difference between SCET and HQET is that the SCET Lagrangian is not corrected by short distance fluctuations. The physical reason is that in the construction described above no high-momentum modes have been integrated out [60]. Such hard modes arise when different collinear sectors are coupled via some external current (e.g. in jet production at e^+e^- or hadron colliders), or when collinear particles are produced in the rest frame of a decaying heavy object (such as in B decays). Short-distance effects are then incorporated in the Wilson coefficients of the external source operators.

16.3.3 *Collinear gauge invariance and Wilson lines*

An important aspect of SCET concerns the implementation of local gauge invariance. Because the effective field operators describe modes with certain momentum scalings, the effective Lagrangian respects only residual gauge symmetries. One of them satisfies the collinear scaling

$$(\bar{n}\cdot\partial, n\cdot\partial, \partial^\perp)\, U_n(x) \sim Q(1, \lambda^2, \lambda)\, U_n(x)\,, \tag{16.14}$$

and one the soft scaling

$$(\bar{n}\cdot\partial, n\cdot\partial, \partial^\perp)\, U_s(x) \sim Q(\lambda^2, \lambda^2, \lambda^2)\, U_s(x)\,. \tag{16.15}$$

While the soft gauge transformation is common for all fields, collinear fields in different directions each transform under their own collinear gauge transformation. In other words, each collinear sector has to be separately gauge invariant under its collinear gauge transformation. This requires the introduction of collinear Wilson lines [56]

$$W_n(x) = \mathrm{P}\exp\left[-ig \int_{-\infty}^0 ds\, \bar{n}\cdot A_n(s\bar{n} + x) \right], \tag{16.16}$$

which transform under collinear gauge transformations according to $W_n \to U_n W_n$. Thus, the combination $\chi_n \equiv W_n^\dagger\, \psi_n$ is gauge invariant. In a similar manner, one can define the gauge-invariant gluon field $B_n^\mu = g^{-1} W_n^\dagger\, iD_n^\mu\, W_n$ [61, 62]. Collinear operators in SCET are typically constructed from such collinearly gauge-invariant building blocks.

16.3.4 *Derivation of factorization theorems*

One of the important applications of SCET is to understand how to factorize cross sections or decay rates involving energetic particles moving in different directions into simpler quantities that can either be calculated perturbatively or determined from data. For the purpose of this discussion, we focus on factorization in the context of collider physics. Note that factorization theorems have been around for much longer than SCET (see [63] for a review). However, the effective theory allows for a conceptually simpler understanding of certain classes of factorization theorems [61], since most simplifications happen already at the level of the Lagrangian. The discussion in this section is valid to leading order in the power counting of the effective theory.

As discussed in the previous section, the Lagrangian of SCET does not involve any direct couplings between collinear particles moving in different directions. A process involving highly energetic initial- and/or final-state particles moving along different directions n_i is therefore described in SCET by operators involving gauge-invariant collinear building blocks for each direction, which only interact amongst each other via soft gluon exchange. At leading power, soft gluons couple to collinear quarks only through the term $\bar{\xi}_n\, gn \cdot A_s\, (\not{\bar{n}}/2)\, \xi_n$ in the effective Lagrangian in (16.13), which is similar to the coupling of soft gluons to heavy quarks in HQET, see Section 16.2.4. This coupling, and the corresponding coupling to collinear gluons can be removed by means of the field redefinitions [57]

$$\psi_n(x) = Y_n(x)\, \psi_n^{(0)}(x)\,, \qquad A_n^a(x) = Y_n^{ab}(x)\, A_n^{b(0)}(x)\,, \tag{16.17}$$

where the soft Wilson lines Y_n and Y_n^{ab} live in the fundamental and adjoint representations of $SU(3)$, respectively. Each collinear building block gives rise to a soft Wilson line. After this decoupling, the different collinear sectors no longer interact with each other and the soft interactions are entirely encoded in the product of soft Wilson lines. This is the basis of factorization proofs in SCET.

The simplest applications of this formalism concern inclusive processes, such as the Drell-Yan production of electroweak bosons in the threshold region, $pp \to Z/H + X_s$, where X_s is a final state containing only soft particles, and event shape distributions in e^+e^- collisions in the two-jet limit. For Drell-Yan the factorization formula is given by [61, 64]

$$\begin{aligned} \sigma(pp \to ZX_s) &= \sum_q H_q(\mu) \left[f_{q/p}(\mu)\, f_{\bar{q}/p}(\mu) \right] \otimes S_F(\mu)\,, \\ \sigma(pp \to HX_s) &= H_g(\mu) \left[f_{g/p}(\mu)\, f_{g/p}(\mu) \right] \otimes S_A(\mu)\,, \end{aligned} \tag{16.18}$$

where the collinear matrix elements give rise to the parton distributions $f_{a/p}(\mu)$, the soft function are vacuum matrix element of the soft Wilson lines in the fundamental or adjoint representation, and the hard functions are the squares of the Wilson coefficients of the relevant SCET operators. The convolution symbol indicates a convolution over the longitudinal momentum fractions of the colliding partons. The objects in the factorization theorem depend on the renormalization scale μ, whereas the cross sections are scale independent. Solving the renormalization group equations (RGE) allows to resum large logarithms in the cross section (see below).

For event shapes such as thrust T, no initial-state partons are present, and the factorization formula takes the form (with $\tau = 1 - T$) [65, 66]

$$\begin{aligned} \frac{d\sigma}{d\tau} = H(\mu) &\left[J_n(\mu) J_{\bar{n}}(\mu) \right] \\ &\otimes S_{n\bar{n}}(\mu)\,, \end{aligned} \tag{16.19}$$

Int. J. Mod. Phys. A 2026.41. Downloaded from www.worldscientific.com by UNIVERSITY OF CALIFORNIA @ BERKELEY on 09/16/26. Re-use and distribution is strictly not permitted, except for Open Access articles.

where the the jet functions are vacuum matrix elements of the outgoing collinear quark fields, which are convoluted with the soft function $S_{n\bar{n}}$ defined as another vacuum matrix element of the soft Wilson lines.

For a more general high-energy scattering process such as $pp \to N$ jets, where the incoming protons move along directions $n_{a,b}$ and the jets define directions $n_1, \ldots, n_N$, the factorization theorem for the differential cross section can be written as

$$d\sigma \sim \sum_{ab} H_{ab\ldots N}(\mu) \left[B_{a/p}(\mu)\, B_{b/p}(\mu)\right] \otimes \left[J_1(\mu)\ldots J_N(\mu)\right] \otimes S_{ab\ldots N}(\mu)\,. \tag{16.20}$$

where the beam functions are generalized parton distributions [67] and the jet functions depend on the algorithm used to define the jets. It should be mentioned that the most difficult part of traditional factorization proofs involves showing that so-called Glauber gluons do not spoil the above factorization theorem [68]. The description of Glauber effects within SCET [69] has been developed in [70], where a closed form for the effective Lagrangian describing these interactions was derived. The formalism has been extended to Glauber quarks in [71]. In this context, a proof of factorization requires demonstrating that this Lagrangian has no impact on a particular cross section. If an observable is non-global, in the sense that energetic radiation is restricted to certain regions in phase space, the above factorization theorem needs to be generalized [72–74].

16.3.5 *Resummation of large logarithms*

Many processes of interest depend on multiple scales which can be widely separated. The perturbative series of such processes depends logarithmically on large scale ratios. For high-energy processes involving soft and collinear particles, there can be up to two powers of large logarithms for each power of the coupling constant. These double logarithms are referred to as Sudakov logarithms and can spoil the perturbative expansion.

SCET can be used to sum large logarithms L using renormalization-group equations. This reorganizes the perturbative series in such a way that the product $\alpha_s L$ is treated as an $\mathcal{O}(1)$ parameter. In many cases, one can write a perturbative series for the logarithm of a cross section, such that

$$\sigma \sim \exp\left[L\, g_0(\alpha_s L) + g_1(\alpha_s L) + \alpha_s\, g_2(\alpha_s L) + \ldots\right]\,, \tag{16.21}$$

with functions $g_n(x)$ that need to be determined. Note that each term in this series in the exponent is one power of α_s suppressed relative to the previous term.

The important ingredient in achieving this resummation is the fact that SCET factorizes a given cross section into simpler pieces, each of which depends on a single physical scale. The only dependence on that scale can arise through logarithms of its ratio with the renormalization scale μ. Thus, for each of the components in the factorization theorem one can choose a renormalization scale μ for which the large logarithmic terms are absent. Of course, the factorization formula requires a common renormalization scale μ in all its components, and one therefore has to use the renormalization group (RG) to evolve the various component functions from their preferred scale to the common scale μ. A novel feature of RG equations in SCET, as opposed to other EFTs, is that the anomalous dimensions entering the evolution equations of the hard, beam, jet and soft functions in a factorization formula such as (16.20) contain a single power of the logarithm of the relevant energy scale. For example, the anomalous dimension γ_H of the hard function has the form

$$\gamma_H(\mu) = c_H\, \Gamma_{\rm cusp}(\alpha_s)\, \ln\frac{Q^2}{\mu^2} + \gamma(\alpha_s)\,, \tag{16.22}$$

where c_H is a process-dependent coefficient and $\Gamma_{\rm cusp}$ denotes the so-called cusp anomalous dimension [22, 75]. Collinear and soft functions have similar anomalous dimensions, which also involve a cusp and a non-cusp part. The non-cusp part γ of the anomalous dimensions is process (and observable) dependent. The presence of a logarithm in the anomalous dimension is characteristic of Sudakov problems and arises since the perturbative series contains double logarithms of scale ratios.

Solving the RG equations one can systematically resum all large logarithms of scale ratios in the factorized cross section and express the functions $g_n(\alpha_s L)$ introduced above in terms of ratios of running coupling constants. In order to compute the first two terms $L\, g_0(\alpha_s L) + g_1(\alpha_s L)$ in $\ln\sigma$, corresponding to the next-to-leading logarithmic (NLL) approximation, one needs two-loop expressions for the cusp anomalous dimension and β function, one-loop expressions for the non-cusp pieces in the anomalous dimensions, and tree-level matching conditions for all component functions at their characteristic scales. To calculate the next term $\alpha_s g_2(\alpha_s L)$ in the expansion, corresponding to NNLL order, one needs to go one order higher in the loop expansion, and so on.

16.3.6 *Factorization and resummation in* $\mathbf{SCET_{II}}$

The effective theory $\mathrm{SCET_{II}}$ contains collinear and soft particles with momenta scaling as $(p_n^-, p_n^+, p_n^\perp) \sim Q(1, \lambda^2, \lambda)$ and $(p_s^-, p_s^+, p_s^\perp) \sim Q(\lambda, \lambda, \lambda)$. They have the same small virtuality ($p_n^2 \sim p_s^2 \sim Q^2\lambda^2$) but differ in their rapidities. An important class of observables, for which this scaling is relevant, contains cross sections for processes in which the transverse momenta of particles are constrained by external kinematics. The prime example are the transverse-momentum distributions of electroweak gauge bosons or Higgs bosons produced at hadron colliders. The parton transverse momenta are constrained by the fact that their vector sum must be equal and opposite to the transverse momentum q_T of the boson. Standard RG evolution in the effective theory controls the logarithms arising from the fact that the virtualities of the collinear and soft modes are much smaller than the hard scale Q in the process (the boson mass). However, additional large logarithms arise since the rapidities of collinear and soft modes are parametrically different, such that $e^{|y_c - y_s|} \sim 1/\lambda$. These logarithms can be traced to a new source of divergences and an unusual failure of dimensional regularization. They need to be factorized in the cross section and resummed by other means.

Two approaches exist for how to deal with the additional rapidity logarithms in SCET. In the approach of [76], they are interpreted as a consequence of a "collinear anomaly" of the effective theory $\mathrm{SCET_{II}}$, resulting from the fact that a classical rescaling symmetry of the effective Lagrangian is broken by quantum effects. The extra large logarithms can be resummed by means of simple differential equations, which typically state that, to all orders in perturbation theory (and in an appropriate space), the logarithm of the cross section contains only a single extra logarithm of $\lambda \sim q_T/Q$ not contained in the hard function. Another approach to resum the rapidity logarithms uses the "rapidity renormalization group" [77], in which the relevant differential equations are obtained by considering a new type of scale variation in a parameter ν, which separates the phase space for collinear and soft particles along a hyperbola in the (p_-, p_+) plane. In contrast to the standard RG, there is no running coupling involved in the ν evolution, since the different contributions live at the same virtuality.

As an important application, consider the Higgs-boson production cross section in gluon fusion at the LHC, defined with a jet veto stating that no jet in the final state has transverse momentum above a threshold $p_T^{\rm veto}$, which can be factorized in the form [78,79]

$$\sigma(p_T^{\rm veto}) = H(m_H,\mu)\left(\frac{\nu_B}{\nu_S}\right)^{-2F_{gg}(R,p_T^{\rm veto},\mu)} S_{gg}(R, p_T^{\rm veto}, \mu, \frac{\nu_S}{p_T^{\rm veto}}) \times \int_\tau^1 \frac{dz}{z}\, B_{g/P}\left(z, R, p_T^{\rm veto}, \mu, \frac{\nu_B}{m_H}\right) B_{g/P}\left(\frac{\tau}{z}, R, p_T^{\rm veto}, \mu, \frac{\nu_B}{m_H}\right), \tag{16.23}$$

where $\tau = m_H^2/s$, and $\mu \sim p_T^{\rm veto}$ is a common factorization scale. The beam functions $B_{g/P}$, the soft function S_{gg} and the exponent F_{gg} all depend on the jet radius R as well as the jet clustering algorithm. The scale dependence of the hard function H is controlled by standard RG evolution in SCET. The beam func-

Int. J. Mod. Phys. A 2026.41. Downloaded from www.worldscientific.com by UNIVERSITY OF CALIFORNIA @ BERKELEY on 09/16/26. Re-use and distribution is except for Open Access articles.

tions can be factorized further into calculable collinear kernels convoluted with parton distribution functions. In addition to the renormalization scale μ, the beam and soft functions depend on two rapidity scales $\nu_B \sim m_H$ and $\nu_S \sim p_T^{\rm veto}$, respectively. In [78] the default values $\nu_B = m_H$ and $\nu_S = p_T^{\rm veto}$ are used for these scales, and the soft function S_{gg} is absorbed into the beam functions. In [79] the exponent F_{gg} is called $-\gamma_\nu^g/2$. The second factor on the right-hand side of the factorization formula (16.23), which resums large rapidity logarithms, implies that the logarithm of the jet-veto cross section contains a single large logarithm $\ln\sigma = -2F_{gg}(R, p_T^{\rm veto}, \mu)\,\ln(m_H/p_T^{\rm veto}) + \ldots$ not contained in the hard function. Its coefficient can be calculated in fixed-order perturbation theory.

$\mathrm{SCET_{II}}$ also plays an important role in the study of factorization for a variety of exclusive B meson decays, such as $\bar{B} \to \pi\ell\bar{\nu}$, $\bar{B} \to K^*\gamma$ and $\bar{B} \to \pi\pi$, for which the virtualities of energetic (collinear) final-state particles are of order $\Lambda_{\rm QCD}$, which is also the scale for the soft light degrees of freedom contained in the initial-state B meson.

16.3.7 *Applications*

Most of the applications of SCET are either in flavor physics, where the decay of a heavy B meson can give rise to energetic light partons, or in collider physics, where the presence of jets naturally leads to collimated sets of energetic particles. For some of these applications alternative approaches existed before the invention of SCET, but the effective theory has opened up alternative ways to understand the physics of these processes. For many examples, however, SCET has allowed new insights and new applications.

The investigation of heavy-to-light form factors has been instrumental for understanding factorization in exclusive semileptonic B decays [80]. SCET has also provided a field-theoretic basis for the QCD factorization approach to exclusive, non-leptonic decays of B mesons [81]. Using SCET methods, proofs of factorization were derived for the color-allowed decay $\bar{B}^0 \to D^+\pi^-$ [82], the color-suppressed decay $\bar{B}^0 \to D^0\pi^0$ [83], and the radiative decay $\bar{B} \to K^*\gamma$ [84]. In recent years, the factorization approach has been extended to include QED effects [85, 86]. Further examples are factorization theorems and the resummation of endpoint logarithms for quarkonia production [87], the resummation of large logarithmic terms for the thrust [88] and jet broadening [89] distributions in e^+e^- annihilation beyond NLL order, the development of new factorizable observables to veto extra jets [67,90], all-order factorization theorems for processes containing electroweak Sudakov logarithms [91], and the resummation of threshold (soft gluon) logarithms in momentum space for several important processes at hadron colliders [64, 92, 93]. There has also been a lot of activity describing p_T-based resummation at hadron colliders. Prominent examples are the transverse-momentum distributions of electroweak bosons [76, 77, 94], which give access to the p_T-dependent parton distribution functions. Higher-order resummations of event shape distributions [88], combined with two-loop fixed-order expressions [95, 96] and including nonperturbative effects by means of a shape function, have been used for an accurate determination of the strong coupling constant α_s [97, 98]. A method based on N-jettiness ($\mathcal{T}_N$) slicing [99, 100] has provided a new way of performing the IR subtractions needed for precise fixed-order calculations, using the fact that the singular dependence on $\mathcal{T}_N$ can be calculated using SCET at NNLO. This has been used to compute various processes with final states containing up to one hard, colored particle [101–105]. Calculations of the leading power corrections in $\mathcal{T}_0/Q$ [106, 107] have helped to improved the numerical stability of the method. The N-jettiness slicing method has also been used in the combination of higher-order resummation with parton showers [108–110]. Finally, SCET has given new insights into the jet substructure methods (see [111] for a review).

A novel type of SCET factorization theorem is needed to describe non-global observables, in which energetic radiation is limited to certain regions of phase space, e.g. inside jets. Jet events play a prominent role in collider physics, because they closely mirror the underlying short-distance dynamics. In the theoretical description of such observables one encounters so-called "non-global" logarithms (NGLs) [112, 113], whose resummation cannot be performed using standard techniques. Using SCET, this problem has been reduced to the solution of a RG evolution equation derived from a novel type of factorization theorem, in which the hard and soft functions are operators in color space and in the (infinite) space of parton multiplicities [72, 74] (see also [73, 114]). In e^+e^- collisions, solving the RGE in the large-N_c limit using parton-shower techniques [115] gives a result that agrees with the solution of the BSM integral equation for the NGLs [116]. The first application of this formalism was to the light jet mass distribution [117], and the extension of the resummation to NLL accuracy has been accomplished in [118, 119]. Non-global observables at hadron colliders are yet more intricate, since Glauber-gluon exchange between the colliding partons lead to a new type of double logarithmic corrections in high orders of perturbation theory, the so-called superleading logarithms (SLLs) [120, 121]. Based on the corresponding SCET factorization theorem, the all-order resummation of SLLs has been accomplished for arbitrary $pp \to n$ jet processes [122].

Recent years have seen a strong effort to push the applications of SCET factorization and resummation techniques to next-to-leading power (NLP) in the expansion in λ. The subleading SCET Lagrangian [60, 123, 124] and current operators arising in B-meson decays and their anomalous dimensions [59, 60, 125–127] have been studied a long time ago. For important collider processes, such as Drell-Yan or Higgs production, the general sets of operators have been identified [128–130], and several of their anomalous dimensions have been calculated [130, 131]. Resummed results at subleading power have been presented for event shapes [132] and the Drell-Yan process [133]. More applications of SCET can be found in Section 6.4 of the review article [134].

16.4 Open issues and perspectives

HQET has successfully passed many experimental tests, and there are not many open questions that still need to be addressed. One concept that has not been derived from first principles is the notion of quark-hadron duality, which underlies the application of HQET to the description of inclusive decays of B mesons. The validity of global duality (at energies even lower than those relevant in B decays) has been tested experimentally using high-precision data on semileptonic B decays and on hadronic τ decays. However, assigning a theoretical uncertainty due to possible duality violations remains a difficult task. Another known issue is that the measured values of the CKM elements $|V_{ub}|$ and $|V_{cb}|$ extracted from exclusive or inclusive decays of B mesons differ from each other by several standard deviations (see Section 75). This measurement relies on the heavy-quark limit, and the uncertainty quoted includes a theoretical estimate of the effect of power corrections arising from the finite b-quark mass. It remains an open question whether the discrepancy is due to underestimated theoretical or experimental uncertainties.

SCET, on the other hand, is still an active field of research, and new results are being obtained regularly. In particular, it has been realized that at NLP SCET factorization theorems generically suffer from endpoint-divergent convolution integrals [135–140]. To remove these divergences, one uses exact D-dimensional refactorization conditions, which relate different terms in the NLP factorization theorem in the singular limits, to rearrange these terms in such a way that the endpoint divergences are systematically removed. Successful applications of this technique include the NLP factorization theorem for the b-quark induced contribution to the diphoton decay amplitude of the Higgs boson [139, 141] and the $gg \to H$ production amplitude [142], the "off-diagonal gluon thrust" in e^+e^- collisions [143], and the NLP factorization theorems for some exclusive [144, 145] and inclusive [146] B-meson decays. On the other hand, for some other processes, such as electron-muon backward scattering [147], the factorization of endpoint singularities is still a subject of ongoing research.

Another active field concerns the further study and applications of Glauber gluons and quarks in SCET and their relation to the BFKL equation familiar from small-x physics [114, 148]. The theoretical formalism developed in [70, 71] sets the basis for a solid understanding of the impact of Glauber exchanges on factorization theorems. Moreover, using the rapidity renormalization group one can derive the BFKL equation in the presence of

Int. J. Mod. Phys. A 2026.41. Downloaded from www.worldscientific.com
by UNIVERSITY OF CALIFORNIA @ BERKELEY on 09/16/26. Re-use and distribution is strictly not permitted, except for Open Access articles.

a single Glauber exchange describing forward scattering [70, 148] and for small x resummation in deep inelastic scattering [149]. Glauber gluons play an important role in SCET-based analysis of jet propagation in dense QCD media [150–152], which gives rise to the jet-quenching phenomenon in heavy-ion collisions. They are also a crucial ingredient in studies of violations of collinear factorization at hadron colliders [69, 153–157].

We close this short review by mentioning a particularly nice application combining the methods of heavy-particle EFTs such as HQET and non-relativistic QCD with SCET in the context of describing the interactions of heavy dark matter (with mass $M \gg v$) with SM particles. In [158] it was realized that the interactions of heavy, weakly interacting massive particles (WIMPs) with nuclear targets can be described in a model-independent way using heavy-particle EFTs. The WIMPs are charged under $SU(2)_L$ and can interact with electroweak gauge bosons and the Higgs boson. The WIMP EFT was later extended by describing the produced, highly energetic electroweak gauge bosons in terms of soft or collinear fields in SCET [159–161]. This allows one to systematically separate all relevant mass scales, resum electroweak Sudakov logarithms and disentangle the so-called Sommerfeld enhancement from the short-distance hard annihilation process.

References

[1] E. Witten, Nucl. Phys. **B122**, 109 (1977).

[2] S. Weinberg, Phys. Lett. **91B**, 51 (1980).

[3] L. J. Hall, Nucl. Phys. **B178**, 75 (1981).

[4] W. Buchmuller and D. Wyler, Nucl. Phys. B **268**, 621 (1986).

[5] B. Grzadkowski *et al.*, JHEP **10**, 085 (2010), [arXiv:1008.4884].

[6] E. Eichten and B. R. Hill, Phys. Lett. B **234**, 511 (1990).

[7] H. Georgi, Phys. Lett. **B240**, 447 (1990).

[8] B. Grinstein, Nucl. Phys. **B339**, 253 (1990).

[9] T. Mannel, W. Roberts and Z. Ryzak, Nucl. Phys. **B368**, 204 (1992).

[10] M. Neubert, Phys. Rept. **245**, 259 (1994), [hep-ph/9306320].

[11] A. V. Manohar and M. B. Wise, Camb. Monogr. Part. Phys. Nucl. Phys. Cosmol. **10**, 1 (2000).

[12] M. E. Luke and A. V. Manohar, Phys. Lett. **B286**, 348 (1992), [hep-ph/9205228].

[13] E. V. Shuryak, Phys. Lett. **93B**, 134 (1980).

[14] N. Isgur and M. B. Wise, Phys. Lett. **B232**, 113 (1989).

[15] N. Isgur and M. B. Wise, Phys. Rev. Lett. **66**, 1130 (1991).

[16] S. Nussinov and W. Wetzel, Phys. Rev. **D36**, 130 (1987).

[17] M. A. Shifman and M. B. Voloshin, Sov. J. Nucl. Phys. **45**, 292 (1987), [Yad. Fiz.45,463(1987)].

[18] M. Neubert, Phys. Lett. **B264**, 455 (1991).

[19] M. E. Luke, Phys. Lett. **B252**, 447 (1990).

[20] I. I. Y. Bigi *et al.*, Phys. Rev. **D52**, 196 (1995), [hep-ph/9405410].

[21] N. Uraltsev, Phys. Lett. **B501**, 86 (2001), [,195(2000)], [hep-ph/0011124].

[22] G. P. Korchemsky and A. V. Radyushkin, Nucl. Phys. **B283**, 342 (1987).

[23] A. F. Falk *et al.*, Nucl. Phys. **B343**, 1 (1990).

[24] J. Chay, H. Georgi and B. Grinstein, Phys. Lett. **B247**, 399 (1990).

[25] I. I. Y. Bigi, N. G. Uraltsev and A. I. Vainshtein, Phys. Lett. **B293**, 430 (1992), [Erratum: Phys. Lett.B297,477(1992)], [hep-ph/9207214].

[26] A. V. Manohar and M. B. Wise, Phys. Rev. **D49**, 1310 (1994), [hep-ph/9308246].

[27] T. Mannel, Nucl. Phys. **B413**, 396 (1994), [hep-ph/9308262].

[28] A. F. Falk, M. E. Luke and M. J. Savage, Phys. Rev. **D49**, 3367 (1994), [hep-ph/9308288].

[29] E. C. Poggio, H. R. Quinn and S. Weinberg, Phys. Rev. **D13**, 1958 (1976).

[30] G. Buchalla, A. J. Buras and M. E. Lautenbacher, Rev. Mod. Phys. **68**, 1125 (1996), [hep-ph/9512380].

[31] A. F. Falk and M. Neubert, Phys. Rev. **D47**, 2965 (1993), [hep-ph/9209268].

[32] T. Becher, H. Boos and E. Lunghi, JHEP **12**, 062 (2007), [arXiv:0708.0855].

[33] A. Alberti, P. Gambino and S. Nandi, JHEP **01**, 147 (2014), [arXiv:1311.7381].

[34] T. Mannel, A. A. Pivovarov and D. Rosenthal, Phys. Lett. **B741**, 290 (2015), [arXiv:1405.5072].

[35] T. Mannel, A. A. Pivovarov and D. Rosenthal, Phys. Rev. **D92**, 5, 054025 (2015), [arXiv:1506.08167].

[36] T. Mannel and A. A. Pivovarov, Phys. Rev. **D100**, 9, 093001 (2019), [arXiv:1907.09187].

[37] T. Mannel, S. Turczyk and N. Uraltsev, JHEP **11**, 109 (2010), [arXiv:1009.4622].

[38] M. Neubert and C. T. Sachrajda, Nucl. Phys. **B483**, 339 (1997), [hep-ph/9603202].

[39] M. Beneke, G. Buchalla and I. Dunietz, Phys. Rev. **D54**, 4419 (1996), [Erratum: Phys. Rev.D83,119902(2011)], [hep-ph/9605259].

[40] M. Beneke *et al.*, Phys. Lett. **B459**, 631 (1999), [hep-ph/9808385].

[41] M. Kirk, A. Lenz and T. Rauh, JHEP **12**, 068 (2017), [arXiv:1711.02100].

[42] C. W. Bauer *et al.*, Phys. Rev. D **70**, 094017 (2004), [hep-ph/0408002].

[43] P. Gambino and C. Schwanda, Phys. Rev. **D89**, 1, 014022 (2014), [arXiv:1307.4551].

[44] F. U. Bernlochner *et al.* (SIMBA), Phys. Rev. Lett. **127**, 10, 102001 (2021), [arXiv:2007.04320].

[45] Y. S. Amhis *et al.* (HFLAV), Phys. Rev. D **107**, 052008 (2023), [arXiv:2206.07501].

[46] M. Neubert, Phys. Rev. **D49**, 3392 (1994), [hep-ph/9311325].

[47] I. I. Y. Bigi *et al.*, Int. J. Mod. Phys. **A9**, 2467 (1994), [hep-ph/9312359].

[48] G. P. Korchemsky and G. F. Sterman, Phys. Lett. **B340**, 96 (1994), [hep-ph/9407344].

[49] C. W. Bauer, M. E. Luke and T. Mannel, Phys. Rev. **D68**, 094001 (2003), [hep-ph/0102089].

[50] K. S. M. Lee and I. W. Stewart, Nucl. Phys. **B721**, 325 (2005), [hep-ph/0409045].

[51] S. W. Bosch, M. Neubert and G. Paz, JHEP **11**, 073 (2004), [hep-ph/0409115].

[52] M. Beneke *et al.*, JHEP **06**, 071 (2005), [hep-ph/0411395].

[53] M. Benzke *et al.*, JHEP **08**, 099 (2010), [arXiv:1003.5012].

[54] C. W. Bauer, S. Fleming and M. E. Luke, Phys. Rev. **D63**, 014006 (2000), [hep-ph/0005275].

[55] C. W. Bauer *et al.*, Phys. Rev. **D63**, 114020 (2001), [hep-ph/0011336].

[56] C. W. Bauer and I. W. Stewart, Phys. Lett. **B516**, 134 (2001), [hep-ph/0107001].

[57] C. W. Bauer, D. Pirjol and I. W. Stewart, Phys. Rev. **D65**, 054022 (2002), [hep-ph/0109045].

[58] T. Becher, A. Broggio and A. Ferroglia, Lect. Notes Phys. **896**, pp.1 (2015), [arXiv:1410.1892].

[59] J. Chay and C. Kim, Phys. Rev. **D65**, 114016 (2002), [hep-ph/0201197].

Int. J. Mod. Phys. A 2026.41. Downloaded from www.wo
by UNIVERSITY OF CALIFORNIA @ BERKELEY on 09/16/26. Re-use and distribution is
except for Open Access articles.

[60] M. Beneke *et al.*, Nucl. Phys. **B643**, 431 (2002), [hep-ph/0206152].

[61] C. W. Bauer *et al.*, Phys. Rev. **D66**, 014017 (2002), [hep-ph/0202088].

[62] R. J. Hill and M. Neubert, Nucl. Phys. **B657**, 229 (2003), [hep-ph/0211018].

[63] J. C. Collins, D. E. Soper and G. F. Sterman, Adv. Ser. Direct. High Energy Phys. **5**, 1 (1989), [hep-ph/0409313].

[64] T. Becher, M. Neubert and G. Xu, JHEP **07**, 030 (2008), [arXiv:0710.0680].

[65] S. Fleming *et al.*, Phys. Rev. D **77**, 074010 (2008), [hep-ph/0703207].

[66] M. D. Schwartz, Phys. Rev. D **77**, 014026 (2008), [arXiv:0709.2709].

[67] I. W. Stewart, F. J. Tackmann and W. J. Waalewijn, Phys. Rev. D **81**, 094035 (2010), [arXiv:0910.0467].

[68] J. C. Collins, D. E. Soper and G. F. Sterman, Nucl. Phys. **B261**, 104 (1985).

[69] C. W. Bauer, B. O. Lange and G. Ovanesyan, JHEP **07**, 077 (2011), [arXiv:1010.1027].

[70] I. Z. Rothstein and I. W. Stewart, JHEP **08**, 025 (2016), [arXiv:1601.04695].

[71] I. Moult *et al.*, JHEP **02**, 134 (2018), [arXiv:1709.09174].

[72] T. Becher *et al.*, Phys. Rev. Lett. **116**, 19, 192001 (2016), [arXiv:1508.06645].

[73] A. J. Larkoski, I. Moult and D. Neill, JHEP **09**, 143 (2015), [arXiv:1501.04596].

[74] T. Becher *et al.*, JHEP **11**, 019 (2016), [Erratum: JHEP05,154(2017)], [arXiv:1605.02737].

[75] I. A. Korchemskaya and G. P. Korchemsky, Phys. Lett. **B287**, 169 (1992).

[76] T. Becher and M. Neubert, Eur. Phys. J. **C71**, 1665 (2011), [arXiv:1007.4005].

[77] J.-Y. Chiu *et al.*, JHEP **05**, 084 (2012), [arXiv:1202.0814].

[78] T. Becher and M. Neubert, JHEP **07**, 108 (2012), [arXiv:1205.3806].

[79] I. W. Stewart *et al.*, Phys. Rev. **D89**, 5, 054001 (2014), [arXiv:1307.1808].

[80] M. Beneke and T. Feldmann, Nucl. Phys. **B685**, 249 (2004), [hep-ph/0311335].

[81] M. Beneke *et al.*, Phys. Rev. Lett. **83**, 1914 (1999), [hep-ph/9905312].

[82] C. W. Bauer, D. Pirjol and I. W. Stewart, Phys. Rev. Lett. **87**, 201806 (2001), [hep-ph/0107002].

[83] S. Mantry, D. Pirjol and I. W. Stewart, Phys. Rev. **D68**, 114009 (2003), [hep-ph/0306254].

[84] T. Becher, R. J. Hill and M. Neubert, Phys. Rev. **D72**, 094017 (2005), [hep-ph/0503263].

[85] M. Beneke, C. Bobeth and R. Szafron, JHEP **10**, 232 (2019), [Erratum: JHEP 11, 099 (2022)], [arXiv:1908.07011].

[86] M. Beneke *et al.*, JHEP **10**, 223 (2021), [arXiv:2107.03819].

[87] S. Fleming, A. K. Leibovich and T. Mehen, Phys. Rev. **D68**, 094011 (2003), [hep-ph/0306139].

[88] T. Becher and M. D. Schwartz, JHEP **07**, 034 (2008), [arXiv:0803.0342].

[89] T. Becher and G. Bell, JHEP **11**, 126 (2012), [arXiv:1210.0580].

[90] I. W. Stewart, F. J. Tackmann and W. J. Waalewijn, Phys. Rev. Lett. **105**, 092002 (2010), [arXiv:1004.2489].

[91] J.-y. Chiu, R. Kelley and A. V. Manohar, Phys. Rev. **D78**, 073006 (2008), [arXiv:0806.1240].

[92] V. Ahrens *et al.*, Eur. Phys. J. **C62**, 333 (2009), [arXiv:0809.4283].

[93] X. Liu, S. Mantry and F. Petriello, Phys. Rev. **D86**, 074004 (2012), [arXiv:1205.4465].

[94] M. G. Echevarria, A. Idilbi and I. Scimemi, JHEP **07**, 002 (2012), [arXiv:1111.4996].

[95] A. Gehrmann-De Ridder *et al.*, Phys. Rev. Lett. **99**, 132002 (2007), [arXiv:0707.1285].

[96] S. Weinzierl, Phys. Rev. Lett. **101**, 162001 (2008), [arXiv:0807.3241].

[97] R. Abbate *et al.*, Phys. Rev. **D83**, 074021 (2011), [arXiv:1006.3080].

[98] A. H. Hoang *et al.*, Phys. Rev. **D91**, 9, 094018 (2015), [arXiv:1501.04111].

[99] R. Boughezal, X. Liu and F. Petriello, Phys. Rev. **D91**, 9, 094035 (2015), [arXiv:1504.02540].

[100] J. Gaunt *et al.*, JHEP **09**, 058 (2015), [arXiv:1505.04794].

[101] R. Boughezal *et al.*, Phys. Lett. **B748**, 5 (2015), [arXiv:1505.03893].

[102] R. Boughezal *et al.*, Phys. Rev. Lett. **116**, 15, 152001 (2016), [arXiv:1512.01291].

[103] J. M. Campbell, R. K. Ellis and C. Williams, JHEP **06**, 179 (2016), [arXiv:1601.00658].

[104] J. M. Campbell *et al.*, JHEP **07**, 148 (2016), [arXiv:1603.02663].

[105] G. Heinrich *et al.*, JHEP **03**, 142 (2018), [arXiv:1710.06294].

[106] I. Moult *et al.*, Phys. Rev. **D95**, 7, 074023 (2017), [arXiv:1612.00450].

[107] R. Boughezal, X. Liu and F. Petriello, JHEP **03**, 160 (2017), [arXiv:1612.02911].

[108] S. Alioli *et al.*, JHEP **09**, 120 (2013), [arXiv:1211.7049].

[109] S. Alioli *et al.*, Phys. Rev. **D92**, 9, 094020 (2015), [arXiv:1508.01475].

[110] S. Alioli *et al.*, Phys. Rev. D **104**, 9, 094020 (2021), [arXiv:2102.08390].

[111] A. J. Larkoski, I. Moult and B. Nachman (2017), [arXiv:1709.04464].

[112] M. Dasgupta and G. P. Salam, Phys. Lett. **B512**, 323 (2001), [hep-ph/0104277].

[113] R. B. Appleby and M. H. Seymour, JHEP **12**, 063 (2002), [hep-ph/0211426].

[114] S. Caron-Huot, JHEP **03**, 036 (2018), [arXiv:1501.03754].

[115] M. Balsiger, T. Becher and D. Y. Shao, JHEP **08**, 104 (2018), [arXiv:1803.07045].

[116] A. Banfi, G. Marchesini and G. Smye, JHEP **08**, 006 (2002), [hep-ph/0206076].

[117] T. Becher, B. D. Pecjak and D. Y. Shao, JHEP **12**, 018 (2016), [arXiv:1610.01608].

[118] M. Balsiger, T. Becher and D. Y. Shao, JHEP **04**, 020 (2019), [arXiv:1901.09038].

[119] T. Becher, T. Rauh and X. Xu, JHEP **08**, 134 (2022), [arXiv:2112.02108].

[120] J. R. Forshaw, A. Kyrieleis and M. H. Seymour, JHEP **08**, 059 (2006), [hep-ph/0604094].

[121] J. R. Forshaw, A. Kyrieleis and M. H. Seymour, JHEP **09**, 128 (2008), [arXiv:0808.1269].

[122] T. Becher, M. Neubert and D. Y. Shao, Phys. Rev. Lett. **127**, 21, 212002 (2021), [arXiv:2107.01212].

[123] M. Beneke and T. Feldmann, Phys. Lett. B **553**, 267 (2003), [hep-ph/0211358].

[124] C. W. Bauer, D. Pirjol and I. W. Stewart, Phys. Rev. **D68**, 034021 (2003), [hep-ph/0303156].

[125] D. Pirjol and I. W. Stewart, Phys. Rev. **D67**, 094005 (2003), [Erratum: Phys. Rev.D69,019903(2004)], [hep-ph/0211251].

[126] R. J. Hill *et al.*, JHEP **07**, 081 (2004), [hep-ph/0404217].

Int. J. Mod. Phys. A 2026.41. Downloaded from www.worldscientific.com
by UNIVERSITY OF CALIFORNIA @ BERKELEY on 09/16/26. Re-use and distribution is strictly not permitted, except for Open Access articles.

[127] M. Beneke and D. Yang, Nucl. Phys. **B736**, 34 (2006), [hep-ph/0508250].

[128] I. Moult, I. W. Stewart and G. Vita, JHEP **07**, 067 (2017), [arXiv:1703.03408].

[129] I. Feige *et al.*, JHEP **11**, 142 (2017), [arXiv:1703.03411].

[130] M. Beneke *et al.*, JHEP **03**, 001 (2018), [arXiv:1712.04416].

[131] S. Alte, M. König and M. Neubert, JHEP **08**, 095 (2018), [arXiv:1806.01278].

[132] I. Moult *et al.*, JHEP **08**, 013 (2018), [arXiv:1804.04665].

[133] M. Beneke *et al.*, JHEP **03**, 043 (2019), [arXiv:1809.10631].

[134] F. Gross *et al.* (2022), [arXiv:2212.11107].

[135] I. Moult, I. W. Stewart and G. Vita, JHEP **11**, 153 (2019), [arXiv:1905.07411].

[136] M. Beneke *et al.*, JHEP **09**, 101 (2019), [arXiv:1907.05463].

[137] I. Moult *et al.*, JHEP **05**, 089 (2020), [arXiv:1910.14038].

[138] M. Beneke *et al.*, JHEP **07**, 078 (2020), [arXiv:1912.01585].

[139] Z. L. Liu and M. Neubert, JHEP **04**, 033 (2020), [arXiv:1912.08818].

[140] M. Beneke *et al.*, JHEP **10**, 196 (2020), [arXiv:2008.04943].

[141] Z. L. Liu *et al.*, JHEP **01**, 077 (2021), [arXiv:2009.06779].

[142] Z. L. Liu *et al.*, JHEP **06**, 183 (2023), [arXiv:2212.10447].

[143] M. Beneke *et al.*, JHEP **07**, 144 (2022), [arXiv:2205.04479].

[144] T. Feldmann *et al.*, Phys. Rev. D **107**, 1, 013007 (2023), [arXiv:2211.04209].

[145] C. Cornella, M. König and M. Neubert, Phys. Rev. D **108**, 3, L031502 (2023), [arXiv:2212.14430].

[146] T. Hurth and R. Szafron, Nucl. Phys. B **991**, 116200 (2023), [arXiv:2301.01739].

[147] G. Bell, P. Böer and T. Feldmann, JHEP **09**, 183 (2022), [arXiv:2205.06021].

[148] S. Fleming, Phys. Lett. **B735**, 266 (2014), [arXiv:1404.5672].

[149] D. Neill, A. Pathak and I. W. Stewart, JHEP **09**, 089 (2023), [arXiv:2303.13710].

[150] A. Idilbi and A. Majumder, Phys. Rev. **D80**, 054022 (2009), [arXiv:0808.1087].

[151] G. Ovanesyan and I. Vitev, JHEP **06**, 080 (2011), [arXiv:1103.1074].

[152] V. Vaidya, JHEP **11**, 064 (2021), [arXiv:2010.00028].

[153] S. Catani, D. de Florian and G. Rodrigo, JHEP **07**, 026 (2012), [arXiv:1112.4405].

[154] J. R. Forshaw, M. H. Seymour and A. Siodmok, JHEP **11**, 066 (2012), [arXiv:1206.6363].

[155] J. R. Gaunt, JHEP **07**, 110 (2014), [arXiv:1405.2080].

[156] M. Zeng, JHEP **10**, 189 (2015), [arXiv:1507.01652].

[157] M. D. Schwartz, K. Yan and H. X. Zhu, Phys. Rev. D **96**, 5, 056005 (2017), [arXiv:1703.08572].

[158] R. J. Hill and M. P. Solon, Phys. Lett. **B707**, 539 (2012), [arXiv:1111.0016].

[159] M. Bauer *et al.*, JHEP **01**, 099 (2015), [arXiv:1409.7392].

[160] M. Baumgart, I. Z. Rothstein and V. Vaidya, Phys. Rev. Lett. **114**, 211301 (2015), [arXiv:1409.4415].

[161] G. Ovanesyan, T. R. Slatyer and I. W. Stewart, Phys. Rev. Lett. **114**, 21, 211302 (2015), [arXiv:1409.8294].

17. Lattice Quantum Chromodynamics

Revised August 2025 by C. Davies (U. Glasgow), S. Hashimoto (KEK), S. Meinel (U. Arizona), and S.R. Sharpe (U. Washington); originally written September 2011 by S. Hashimoto, J. Laiho (Syracuse U.), and S.R. Sharpe

17.1 Lattice regularization of QCD . . . 352
17.1.1 Gauge invariance, gluon fields and the gluon action . . . 352
17.1.2 Lattice fermions . . . 353
17.1.3 Heavy quarks on the lattice . . . 354
17.1.4 QED on the lattice . . . 355
17.1.5 Basic inputs for lattice calculations . . . 355
17.1.6 Sources of systematic error . . . 356
17.2 Methods and status . . . 357
17.2.1 Monte-Carlo method . . . 357
17.2.2 Two-point functions . . . 358
17.2.3 Three-point functions . . . 359
17.2.4 Scattering amplitudes and resonances . . . 359
17.2.5 Status of LQCD simulations . . . 360
17.3 Physics applications . . . 360
17.3.1 Spectrum . . . 361
17.3.2 Decay constants and bag parameters . . . 361
17.3.3 Semileptonic form factors . . . 361
17.3.4 Long-distance contributions to weak-interaction processes . . . 362
17.3.5 Strong gauge coupling . . . 362
17.3.6 Quark masses . . . 363
17.3.7 The anomalous magnetic moment of the muon 363
17.3.8 Nucleon structure . . . 364
17.3.9 Other applications of lattice QCD . . . 365
17.4 Outlook . . . 365
17.5 Acknowledgments . . . 366

Many physical processes considered in the Review of Particle Properties (RPP) involve hadrons. The properties of hadrons—which are composed of quarks and gluons—are governed primarily by Quantum Chromodynamics (QCD) (with small corrections from Quantum Electrodynamics [QED]). Theoretical calculations of these properties require non-perturbative methods, and Lattice Quantum Chromodynamics (LQCD) is a tool to carry out such calculations. It has been successfully applied to many properties of hadrons. Most important for the RPP are the calculation of electroweak decay constants and form factors, which are needed to extract Cabbibo-Kobayashi-Maskawa (CKM) matrix elements when combined with the corresponding experimental measurements. LQCD has also been used to determine other fundamental parameters of the standard model, in particular the strong gauge coupling and quark masses, as well as to predict hadronic contributions to the anomalous magnetic moment of the muon, $g-2$.

This review describes the theoretical foundations of LQCD and sketches the methods used to calculate the quantities relevant for the RPP. It also describes the various sources of error that must be controlled in a LQCD calculation. Results for hadronic quantities are found in the corresponding dedicated reviews.

17.1 Lattice regularization of QCD

Gauge theories form the building blocks of the Standard Model. While the SU(2) and U(1) parts have weak couplings and can be studied accurately with perturbative methods, the SU(3) component—QCD—is only amenable to a perturbative treatment at high energies. The growth of the gauge coupling in the infrared—the flip-side of asymptotic freedom—requires the use of non-perturbative methods to determine the low energy properties of QCD. Lattice gauge theory, proposed by K. Wilson in 1974 [1], provides such a method, for it gives a non-perturbative definition of vector-like gauge field theories such as QCD. In lattice regularized QCD—commonly called lattice QCD or LQCD—Euclidean space-time is discretized, usually on a hypercubic lattice with lattice spacing a, with quark fields placed on sites and gauge fields on the links between sites. The lattice spacing plays the role of the ultraviolet regulator, rendering the quantum field theory finite. The continuum theory is recovered by taking the limit of vanishing lattice spacing, which can be reached by tuning the bare gauge coupling to zero according to the renormalization group.

Unlike dimensional regularization, which is commonly used in continuum QCD calculations, the definition of LQCD does not rely on the perturbative expansion. Indeed, LQCD allows non-perturbative calculations by numerical evaluation of the path integral that defines the theory.

Practical LQCD calculations are limited by the availability of computational resources and the efficiency of algorithms. Because of this, LQCD results come with both statistical and systematic errors, the former arising from the use of Monte-Carlo integration, the latter, for example, from the use of non-zero values of a. There are also different ways in which the QCD action can be discretized, and all must give consistent results in the continuum limit, $a \to 0$. It is the purpose of this review to provide an outline of the methods of LQCD, with particular focus on applications to particle physics, and an overview of the various sources of error. This should allow the reader to better understand the LQCD results that are presented in other reviews, primarily those on "Quark Masses," "Quark Model," "Quantum Chromodynamics," "CKM quark-mixing matrix," "V_{ud}, V_{us}, Cabibbo angle and CKM Unitarity," "Leptonic Decays of Charged Pseudoscalar Mesons," "B^0-$\bar{B}^0$ Mixing," and "Semileptonic b-Hadron Decays, Determination of V_{cb} and V_{ub}." For more extensive explanations the reader should consult the available textbooks or lecture notes, the most up-to-date of which are Refs. [2–4].

17.1.1 *Gauge invariance, gluon fields and the gluon action*

A key feature of the lattice formulation of QCD is that it preserves gauge invariance. This is in contrast to perturbative calculations, where gauge fixing is an essential step. The preservation of gauge invariance leads to considerable simplifications, e.g., restricting the form of operators that can mix under renormalization.

The gauge transformations of lattice quark fields are just as in the continuum: $q(x) \longrightarrow V(x)q(x)$ and $\bar{q}(x) \longrightarrow \bar{q}(x)V^\dagger(x)$, with $V(x)$ an arbitrary element of SU(3). The only difference is that the Euclidean space-time positions x are restricted to lie on the sites of the lattice, i.e. $x = a(n_1, n_2, n_3, n_4)$ for a hypercubic lattice, with the n_j being integers. Quark bilinears involving different lattice points can be made gauge invariant by introducing the gluon field $U_\mu(x)$. For example, for adjacent points the bilinear is $\bar{q}(x)U_\mu(x)q(x+a\hat{\mu})$, with $\hat{\mu}$ the unit vector in the μ'th direction. (This form is used in the construction of the lattice covariant derivative.) This is illustrated in Fig. 17.1. The gluon field (or "gauge link") is an element of the group, SU(3), in contrast to the continuum field A_μ which takes values in the Lie algebra. The bilinear is invariant if U_μ transforms as $U_\mu(x) \to V(x)U_\mu(x)V^\dagger(x+a\hat{\mu})$. The lattice gluon field is naturally associated with the link joining x and $x+a\hat{\mu}$, and corresponds in the continuum to a Wilson line connecting these two points, $\mathrm{P}\exp(i\int_x^{x+a\hat{\mu}} dx_\mu A_\mu^{\mathrm{cont}}(x))$ (where P indicates a path-ordered integral, and the superscript on A_μ indicates that it is a continuum field). The trace of a product of the $U_\mu(x)$ around any closed loop is easily seen to be gauge invariant and is the lattice version of a Wilson loop.

The simplest possible gauge action, usually called the Wilson gauge action, is given by the product of gauge links around elementary plaquettes:

$$S_g = \beta \sum_{x,\mu<\nu} [1 - \frac{1}{3}\mathrm{ReTr}[U_\mu(x)U_\nu(x+a\hat{\mu})U_\mu^\dagger(x+a\hat{\nu})U_\nu^\dagger(x)]] \,. \tag{17.1}$$

This is illustrated in Fig. 17.1. For small a, assuming that the fields are slowly varying, one can expand the action in powers of a using $U_\mu(x) = \exp(iaA_\mu(x))$. Keeping only the leading non-vanishing term, and replacing the sum with an integral, one finds

Int. J. Mod. Phys. A 2026.41. Downloaded from www.wo
by UNIVERSITY OF CALIFORNIA @ BERKELEY on 09/16/26. Re-use and distribution is
except for Open Access articles.

Int. J. Mod. Phys. A 2026.41. Downloaded from www.worldscientific.com
by UNIVERSITY OF CALIFORNIA @ BERKELEY on 09/16/26. Re-use and distribution is strictly not permitted, except for Open Access articles.

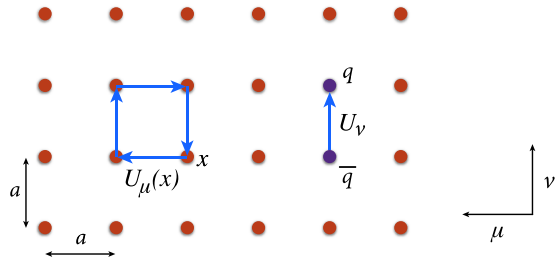

Figure 17.1: Sketch of a two-dimensional slice through the $\mu-\nu$ plane of a lattice, showing gluon fields lying on links and forming either the plaquette product appearing in the gauge action or a component of the covariant derivative connecting quark and antiquark fields.

the continuum form,

$$S_g \longrightarrow \int d^4x \frac{1}{4g_{\rm lat}^2} \mathrm{Tr}[F_{\mu\nu}^2(x)]\,, \qquad (F_{\mu\nu} = \partial_\mu A_\nu - \partial_\nu A_\mu + i[A_\mu, A_\nu]) \tag{17.2}$$

as long as one chooses $\beta = 6/g_{\rm lat}^2$ for the lattice coupling. In this expression, $g_{\rm lat}$ is the bare gauge coupling in the lattice scheme, which can be related (by combining continuum and lattice perturbation theory) to a more conventional gauge coupling such as that in the $\overline{\rm MS}$ scheme (see Sec. 17.3.5 below).

In practice, the lattice spacing a is non-zero, leading to discretization errors. In particular, the lattice breaks Euclidean rotational invariance (which is the Euclidean version of Lorentz invariance) down to a discrete hypercubic subgroup. One wants to reduce discretization errors as much as possible. A very useful tool for understanding and then reducing discretization errors is the Symanzik effective action: the interactions of quarks and gluons with momenta low compared to the lattice cutoff ($|p| \ll 1/a$) are described by a continuum action consisting of the standard continuum terms (e.g., the gauge action given in Eq. (17.2)) augmented by higher dimensional operators suppressed by powers of a [5]. For the Wilson lattice gauge action, the leading corrections to the continuum terms come in at $\mathcal{O}(a^2)$. They take the form $\sum_j a^2 c_j O_6^{(j)}$, with the sum running over all dimension-six operators $O_6^{(j)}$ allowed by the *lattice* symmetries, and c_j unknown coefficients. Some of these operators violate Euclidean rotational invariance, and all of them lead to discretization errors of the form $a^2\Lambda^2$ (up to $\log(a)$ corrections that will be discussed below), where Λ is a typical momentum scale for the quantity being calculated. These errors can, however, be reduced by adding corresponding operators to the lattice action and tuning their coefficients to eliminate the dimension-six operators in the effective action to a given order in perturbation theory or even non-perturbatively. This is the idea of the Symanzik improvement program [5]. In the case of the gauge action, one adds Wilson loops involving six gauge links (as opposed to the four links needed for the original plaquette action, Eq. (17.1)) to define the $\mathcal{O}(a^2)$ improved (or "Symanzik") action [6]. In practical implementations, the improvement is either at tree-level (so that residual errors are proportional to $\alpha_s a^2$, where the coupling is evaluated at a scale $\sim 1/a$ giving the $\log(a)$ dependence mentioned above)), or at one-loop order (errors proportional to $\alpha_s^2 a^2$). Another popular choice is motivated by studies of renormalization group (RG) flow. It has the same terms as the $\mathcal{O}(a^2)$ improved action but with different coefficients, and is called the RG-improved or "Iwasaki" action [7].

17.1.2 *Lattice fermions*

Discretizing the fermion action turns out to involve subtle issues, and the range of actions being used is more extensive than for gauge fields. Recall that the continuum fermion action is $S_f = \int d^4x\, \bar{q}[D_\mu\gamma_\mu + m_q]q$, where $D_\mu = \partial_\mu + iA_\mu$ is the gauge-covariant derivative. The simplest discretization replaces the derivative with a symmetric difference:

$$D_\mu q(x) \longrightarrow \frac{1}{2a}[U_\mu(x)q(x+a\hat{\mu}) - U_\mu(x-a\hat{\mu})^\dagger q(x-a\hat{\mu})]\,. \tag{17.3}$$

The factors of U_μ ensure that $D_\mu q(x)$ transforms under gauge transformations in the same way as $q(x)$, so that the discretized version of $\bar{q}(x)\gamma_\mu D_\mu q(x)$ is gauge invariant. The choice in Eq. (17.3) leads to the so-called naive fermion action. This, however, suffers from the fermion doubling problem—in d dimensions it describes 2^d equivalent fermion fields in the continuum limit. The appearance of the extra "doubler" fermions is related to the deeper theoretical problem of formulating chirally symmetric fermions on the lattice. This is encapsulated by the Nielsen-Ninomiya theorem [8]: one cannot define lattice fermions having exact chiral symmetry of the standard form $\delta q = \epsilon\gamma_5 q$, $\delta\bar{q} = \epsilon\bar{q}\gamma_5$ (ϵ is infinitesimal) without producing doublers. Naive lattice fermions do have chiral symmetry but at the cost of introducing 15 unwanted doublers (for $d = 4$).

There are a number of different strategies for dealing with the doubling problem, each with their own theoretical and computational advantages and disadvantages. Wilson fermions [1] add a term proportional to $a\bar{q}\Delta q$ to the fermion action (the "Wilson term"—in which Δ is a covariant lattice Laplacian). This gives a mass of $\mathcal{O}(1/a)$ to the doublers, so that they decouple in the continuum limit. The Wilson term, however, violates chiral symmetry at non-zero lattice spacing, and introduces discretization errors linear in a. A commonly used variant that eliminates the $\mathcal{O}(a)$ discretization error is the $\mathcal{O}(a)$-improved Wilson (or "clover") action [9]. In this application of Symanzik improvement, methods have been developed to remove $\mathcal{O}(a)$ terms non-perturbatively using auxiliary simulations to tune parameters [10]. Such "non-perturbative improvement" is of great practical importance as it brings the discretization error from the fermion action down to the same level as that from the Wilson gauge action.

The advantages of Wilson fermions are their theoretical simplicity and relatively low computational cost. Their main disadvantage is the lack of chiral symmetry, which makes them difficult to use in cases where mixing with wrong chirality operators can occur, particularly if this involves divergences proportional to powers of $1/a$. A related problem is the presence of potential numerical instabilities due to spurious near-zero modes of the lattice Dirac operator. There are, however, studies that successfully ameliorate the problems due to the lack of chiral symmetry and increase the range of quantities for which Wilson fermions can be used (see, e.g., Refs. [11–13]).

Twisted-mass fermions [14] are a variant of Wilson fermions in which two flavors are treated together with an isospin-breaking mass term (the "twisted mass" term). The main advantage of this approach is that all errors linear in a are automatically removed (without the need for tuning of parameters) by a clever choice of twisted mass and operators [15]. A disadvantage is the presence of isospin breaking effects (such as a splitting between charged and neutral pion masses even when up and down quarks are degenerate), which, however, vanish as $a^2\Lambda^2$ in the continuum limit. Strange and charm quarks can be added as a second pair, with a term added to split their masses [16, 17].

Staggered fermions are a reduced version of naive fermions in which there is only a single fermion Dirac component on each lattice site, with the full Dirac structure built up from neighboring sites [18]. They have the advantages of being faster to simulate than Wilson-like fermions, of preserving some chiral symmetry, and of having discretization errors of $\mathcal{O}(a^2)$. Their disadvantage is that they retain some of the doublers (3 for $d = 4$). The action thus describes four degenerate fermions in the continuum limit. These are usually called "tastes", to distinguish them from physical flavors, and the corresponding SU(4) symmetry is referred to as the "taste symmetry". The preserved chiral symmetry in this formulation has non-singlet taste. Practical applications usually introduce one staggered fermion for each physical flavor, and remove contributions from the unwanted tastes by taking the fourth-root of the fermion determinant appearing in the path integral. The validity of this "rooting" procedure is not obvious because taste symmetry is violated for non-zero lattice spacing. Theoreti-

Int. J. Mod. Phys. A 2026.41. Downloaded from www.worldscientific.com by UNIVERSITY OF CALIFORNIA @ BERKELEY on 09/16/26. Re-use and distribution is except for Open Access articles.

cal arguments, supported by numerical evidence, suggest that the procedure is valid as long as one takes the continuum limit before approaching the light quark mass region [19]. Additional issues arise for the valence quarks (those appearing in quark propagators, as described in Sec. 17.2 below), where rooting is not possible, and one must ignore the extra tastes, or account for them by including appropriate factors [20], which can be nontrivial in applications involving baryons [21].

Just as for Wilson fermions, the staggered action can be improved, so as to reduce discretization errors. The Asqtad (a-squared tadpole improved) action [22] was used until recently in many large scale simulations [23]. More recent calculations use the HISQ (highly improved staggered quark) action, introduced in Ref. [24]. At tree-level it removes both $\mathcal{O}(a^2)$ errors and, to lowest order in the quark speed v/c, $\mathcal{O}([am]^4)$ errors. It also substantially reduces effects caused by taste-symmetry breaking. This makes it attractive not only for light quarks, but means that it is also quite accurate for heavy quarks because it suppresses $(am)^n$ errors. It is being used to directly simulate charm quarks and to approach direct simulations of bottom quarks (for early studies, see, e.g., [25–27]).

There is an important class of lattice fermions, "Ginsparg-Wilson fermions," that possess a continuum-like chiral symmetry without introducing unwanted doublers. The lattice Dirac operator D for these fermions satisfies the Ginsparg-Wilson relation $D\gamma_5 + \gamma_5 D = aD\gamma_5 D$ [28]. In the continuum, the right-hand-side vanishes, leading to chiral symmetry. On the lattice, it is non-vanishing, but with a particular form (with two factors of D) that restricts the violations of chiral symmetry in Ward-Takahashi identities to short-distance terms that do not contribute to physical matrix elements [29]. In fact, one can define a modified chiral transformation on the lattice (by including dependence on the gauge fields) such that Ginsparg-Wilson fermions have an exact chiral symmetry for on-shell quantities [30]. The net result is that such fermions essentially have the same properties under chiral transformations as do continuum fermions, including the index theorem [29]. Their leading discretization errors are of $\mathcal{O}(a^2)$.

Two types of Ginsparg-Wilson fermions are currently being used in large-scale numerical simulations. The first is Domain-wall fermions (DWF). These are defined on a five-dimensional space, in which the fifth dimension is fictitious [31]. The action is chosen so that the low-lying modes are chiral, with left- and right-handed modes localized on opposite four-dimensional surfaces. For an infinite fifth dimension, these fermions satisfy the Ginsparg-Wilson relation. In practice, the fifth dimension is kept finite, and there remains a small, controllable violation of chiral symmetry. The second type is Overlap fermions. These appeared from a completely different context and have an explicit form that exactly satisfies the Ginsparg-Wilson relation [32]. Their numerical implementation requires an approximation of the matrix sign function of a Wilson-like fermion operator, and various approaches are being used. In fact, it is possible to rewrite these approximations in terms of a five-dimensional formulation, showing that the DWF and Overlap approaches are essentially equivalent [33, 34]. Numerically, the five-dimensional approach appears to be more computationally efficient.

The various lattice fermion formulations are often combined with the technique of link smearing. Here one couples the fermions to a smoother gauge link, defined by averaging with adjacent links in a gauge invariant manner. Several closely related implementations are being used. All reduce the coupling of fermions to the short-distance fluctuations in the gauge field, leading to an improvement in the numerical stability and speed of algorithms. One cannot perform this smearing too aggressively, however, since the smearing may distort short distance physics and enhance discretization errors.

As noted above, each fermion formulation has its own advantages and disadvantages. For instance, domain-wall and overlap fermions are theoretically preferred as they have chiral symmetry without doublers, but their computational cost is greater than for other choices. If the physics application of interest and the target precision do not require near-exact chiral symmetry, there is no strong motivation to use these expensive formulations. On the other hand, there is a class of applications (including the calculation of the $\Delta I = 1/2$ amplitude for $K \to \pi\pi$ decays [35–37] and the S-parameter [38]) where chiral symmetry plays an essential role and for which the use of Ginsparg-Wilson fermions is strongly favored.

17.1.3 *Heavy quarks on the lattice*

The fermion formulations described in the previous subsection can be used straightforwardly only for quarks whose masses are small compared to the lattice cutoff, $m_q \lesssim 1/a$. This is because there are discretization errors proportional to powers of am_q, and if $am_q \gtrsim 1$ these errors can become large and uncontrolled. Present LQCD simulations typically have cutoffs in the range of $1/a = 2$–5 GeV (corresponding to $a \approx 0.1$–0.04 fm). Thus, while for the up, down and strange quarks one has $am_q \ll 1$, for bottom quarks (with $m_b \approx 4.5$ GeV) one must use alternative approaches on all but the finest lattices. Charm quarks ($m_c \approx 1.5$ GeV) are an intermediate case, allowing simulations with either direct or alternative approaches, although increasingly the direct approach is being used.

For the charm quark, the straightforward approach is to simultaneously reduce the lattice spacing and to improve the fermion action so as to reduce the size of errors proportional to powers of am_c. This approach has been followed successfully using the HISQ, twisted-mass and domain-wall actions [24, 25, 27, 39–41]. It is important to note, however, that reducing a increases the computational cost because an increased number of lattice points are needed for the same physical volume. One cannot reduce the spatial size below 2–3 fm without introducing significant finite volume errors. Present lattices have typical sizes of $\sim 64^3 \times 128$ (with the long direction being Euclidean time), and thus allow a lattice cutoff up to $1/a \sim 4$–6 GeV.

This approach can, to some extent, be extended to the bottom quark, by the use of simulations with small lattice spacings [26, 42]. This has been pursued with the HISQ action [43], using lattices of size up to $144^3 \times 288$ and lattice spacings down to $a \approx 0.03$ fm ($1/a \approx 6.6$ GeV). Extrapolation in m_b is still needed [44], however, and this makes use of the mass dependence predicted by Heavy Quark Effective Theory (HQET) when heavy-light hadrons are being studied. Small lattice spacings are also helpful for the simulations of quarkonium for which a different heavy-quark mass scaling is expected. See Ref. [45] for a recent study.

Alternative approaches for discretizing heavy quarks are motivated by effective field theories. For a bottom quark in heavy-light hadrons, one can use HQET to expand about the infinite quark-mass limit. In this limit, the bottom quark is a static color source, and one can straightforwardly write the corresponding lattice action [46]. Corrections, proportional to powers of $1/m_b$, can be introduced as operator insertions, with coefficients that can be determined non-perturbatively using existing techniques [47]. This method allows the continuum limit to be taken systematically including the $1/m_b$ corrections.

Another way of introducing the $1/m_b$ corrections is to include the relevant terms in the effective action. This leads to a non-relativistic QCD (NRQCD) action, in which the heavy quark is described by a two-component spinor [48]. This approach has the advantage over HQET that it can also be used for heavy-heavy systems, such as the Υ states. Moreover, the bottom quark can be treated without any extrapolation in m_b. A disadvantage is that some of the parameters in this effective theory are determined perturbatively (at tree-level or at one-loop [49]), which limits the precision of the final results. Although discretization effects can be controlled with good numerical precision for a range of lattice spacings, these artifacts cannot be extrapolated away by taking the lattice spacing to zero. This is because NRQCD is a non-relativistic effective field theory and so ceases to work when the cutoff π/a becomes much larger than the heavy-quark mass. In practice these effects are accounted for in the error budget.

This problem can be avoided if one uses HQET power counting to analyze and reduce discretization effects for heavy quarks while using conventional fermion actions [50]. For instance, one can tune the parameters of an improved Wilson quark action so that the leading HQET corrections to the static quark limit are correctly accounted for. As the lattice spacing becomes finer, the

Int. J. Mod. Phys. A 2026.41. Downloaded from www.worldscientific.com
by UNIVERSITY OF CALIFORNIA @ BERKELEY on 09/16/26. Re-use and distribution is strictly not permitted, except for Open Access articles.

action smoothly goes over to that of a light Wilson quark action, where the continuum limit can be taken as usual. In principle, one can improve the action in the heavy quark regime up to arbitrarily high orders using HQET, but so far large-scale simulations have typically used clover improved Wilson quarks, where tuning the parameters of the action corresponds to including all corrections through next-to-leading order in HQET. Three different methods for tuning the parameters of the clover action are being used: the Fermilab [50], Tsukuba [51] and Columbia [52] approaches. An advantage of this HQET approach is that the c and b quarks can be treated on the same footing. Parameter tuning has been done perturbatively, as in NRQCD, or using non-perturbative tuning of some of the parameters [53, 54]. One can improve the effective theory including the terms beyond the next-to-leading order. The Oktay-Kronfeld action that includes dimension-six and -seven operators has been constructed [55] and used in large-scale numerical calculations [56].

Another approach is the "ratio method" introduced in Ref. [57]. Here one uses quarks with masses lying at, or slightly above, the charm mass m_c, which can be simulated with a relativistic action, and extrapolates to m_b incorporating the behavior predicted by HQET. The particular implementation relies on the use of ratios. As an example, consider the B meson decay constant f_B. According to HQET, this scales as $1/\sqrt{m_B}$ for $m_B \gg \Lambda_{\rm QCD}$, up to a logarithmic dependence that is calculable in perturbative QCD (but will be suppressed in the following). Here m_B is the B meson mass, which differs from m_b by $\sim \Lambda_{\rm QCD}$. One considers the ratio $y(\lambda, m_{b'}) \equiv f_{B''}\sqrt{m_{B''}}/f_{B'}\sqrt{m_{B'}}$ for fictitious B mesons containing b quarks with unphysical masses $m_{b'}$ and $m_{b''} = \lambda m_{b'}$. HQET implies that $y(\lambda, m_{b'})$ approaches unity for large $m_{b'}$ and any fixed $\lambda > 1$. The ratios are evaluated on the lattice for the sequence of masses $m_{b'} = m_c$, λm_c, $\lambda^2 m_c$, all well below the physical m_b, and for each the continuum limit is taken. The form of the ratio for larger values of $m_{b'}$ is obtained by fitting, incorporating the constraints implied by HQET. The result for $f_B\sqrt{m_B}$ is then obtained as a product of y's with $f_D\sqrt{m_D}$ [58].

17.1.4 *QED on the lattice*

Quarks in nature are electrically charged, and the resultant coupling to photons leads to shifts in the properties of hadrons that are generically of $\mathcal{O}(\alpha_{\rm EM})$. Thus, for example, the proton mass is increased by ~ 1 MeV relative to that of the neutron due to its overall charge although this effect is more than compensated for by the ~ 2.5 MeV relative decrease due to the up quark being lighter than the down quark [59]. This example shows that once pure QCD, isospin-symmetric lattice calculations reach percent-level accuracy, further improvement requires the inclusion of effects due to both electromagnetism and the up-down mass difference. This level of accuracy has in fact been obtained for various quantities, e.g., light hadron masses and decay constants (see Ref. [60]), and simulations including isospin-breaking and QED effects are becoming more common.

One approach for including QED is to treat electromagnetic gauge fields in a similar fashion to those of QCD. This extension is straightforward, although some new subtleties arise. The essential change is that the quark must now propagate through a background field containing both gluons and photons. The gauge field U_μ that appears in the covariant derivative of Eq. (17.3) is extended from an SU(3) matrix to one living in U(3): $U_\mu \to U_\mu e^{iaqeA_\mu^{\rm EM}}$. Here $A_\mu^{\rm EM}$ is the photon field, e the electromagnetic coupling, and q the charge of the quark, e.g., $q = 2/3$ for up and $-1/3$ for down and strange quarks. The lattice action for the photon that is typically used is a discretized version of the continuum action Eq. (17.2), rather than the form used for the gluons, Eq. (17.1). This "non-compact" action has the advantage that it is quadratic in $A_\mu^{\rm EM}$, which simplifies the QED part of the generation of configurations.

One subtlety that arises is that Gauss' law forbids a charged particle in a box with periodic boundary conditions. This can be overcome by including a uniform background charge, which can be shown to be equivalent to removing the zero-momentum mode from the photon field, an approach denoted QED$_L$ [61]. However, this modification leads to enhanced finite-volume dependence for physical quantities, scaling as $1/L^n$ with $n = 1, 2, \cdots$. This should be compared to the $\exp(-m_\pi L)$ dependence expected for many quantities (as discussed in Sec. 17.1.6.2 below). Methods to remove the leading few powers of $1/L$ have been developed [62, 63], and there is a promising alternative approach in which QED effects are calculated analytically in infinite volume [64]. Finally we note that there is an alternative approach using so-called C^* boundary conditions that avoids the Gauss' law issue altogether, although the numerical application is still at an early stage [65,66].

Substantial progress on including QED and isospin-breaking effects has been made over the last few years. The direct approach of using different up and down-quark masses and simulating QED has been successfully carried out for a range of quark masses approaching the physical values [59, 67–69]. Alternative approaches have also been used: reweighting the QCD fields *a posteriori* [70], using a massive photon [71], and keeping only the linear term in an expansion in $\alpha_{\rm EM}$ about the QCD only case [72, 73], with the latter approach by now the most popular. Most calculations to date have included QED effects for the valence quarks but not the sea quarks (the "electro-quenched approximation"). [41, 74–77].

The QED corrections to processes including leptons, such as the leptonic and semileptonic decays of hadrons, involve additional diagrams in which a photon propagator bridges between a hadron and a lepton. Such diagrams induce infrared divergences that cancel against soft photon radiation (Bloch-Nordsieck theorem [78]). Methods have been developed to implement this cancellation in lattice calculations, treating the soft photon analytically [62], and results have been reported for leptonic pion and kaon decays [79–81]. An application to semi-leptonic decays has been developed [64, 82].

17.1.5 *Basic inputs for lattice calculations*

Since LQCD is nothing but a regularization of QCD, the renormalizability of QCD implies that the number of input parameters in LQCD is the same as for continuum QCD—the strong gauge coupling $\alpha_s = g^2/(4\pi)$, the quark masses for each flavor, and the CP violating phase $\theta_{\rm QCD}$. The $\theta_{\rm QCD}$ parameter is usually assumed to be zero, while the other parameters must be determined using experimental inputs.

17.1.5.1 *Lattice spacing*

In QCD, the gauge coupling is a function of scale. With lattice regularization, this scale is the inverse lattice spacing $1/a$, and choosing the bare gauge coupling is equivalent to fixing the lattice spacing.

In principle, a can be determined using any dimensionful quantity measured accurately by experiments. For example, using the mass of hadron H one has $a = (am_H)^{\rm lat}/m_H^{\rm exp}$. One chooses quantities that can be calculated accurately on the lattice, and that are only weakly dependent on the quark masses. The latter property minimizes errors from extrapolating or interpolating to the physical light quark masses or from mistuning of other quark masses.

Commonly used choices are the spin-averaged 1S-1P or 1S-2S splittings in the Υ system, the masses of the Ξ and Ω^- baryons, and the pion decay constant f_π. Ultimately, all choices must give consistent results for physical quantities in the continuum limit, and that this is the case provides a highly non-trivial check of both the calculational method and of QCD.

Many recent lattice calculations use intermediate length scales in place of a direct determination of the lattice spacing. These length scales, which we denote $\mathcal{R}$, have the advantage that they can be precisely, and relatively cheaply, computed numerically. Examples are r_0, derived from the heavy quark potential [83], and t_0 and w_0, determined from the gradient flow of the gauge field [84]. These scales are used in the following manner, explained here in the context of calculating a quantity Q with mass dimension d (e.g. a decay constant for which $d = 1$). In the first step, one calculates the dimensionless quantities a^dQ and $\mathcal{R}/a$ in a given lattice calculation, and forms the product $(a^dQ)\times(\mathcal{R}/a)^d = Q\mathcal{R}^d$. In a second step, one uses results available from previous dedicated lattice calculations that have determined $\mathcal{R}$ in physical units (i.e. fm) by relating it to a physical quantity as discussed above. Then one obtains $Q = (Q\mathcal{R}^d)/\mathcal{R}^d$. The use of intermediate quantities

Int. J. Mod. Phys. A 2026.41. Downloaded from www.wo
by UNIVERSITY OF CALIFORNIA @ BERKELEY on 09/16/26. Re-use and distribution is
except for Open Access articles.

is reviewed in the latest edition of the Flavor Lattice Averaging Group (FLAG) report [85].

17.1.5.2 *Light quark masses*

In LQCD simulations, the up, down and strange quarks are usually referred to as the light quarks, in the sense that $m_q < \Lambda_{\rm QCD}$. (The standard definition of $\Lambda_{\rm QCD}$ is given in the "Quantum Chromodynamics" review; in this review we are using it only to indicate the approximate non-perturbative scale of QCD.) This condition is stronger than that used above to distinguish quarks with small discretization errors, $m_q < 1/a$. Loop effects from light quarks must be included in the simulations to accurately represent QCD. At present, most simulations are done in the isospin symmetric limit $m_u = m_d \equiv m_\ell < m_s$, with charm-quark loops either excluded (referred to as "$N_f = 2+1$" simulations) or included (denoted "$N_f = 2+1+1$" simulations). As noted above, precision is now reaching the point where isospin breaking effects must be included. To do so without approximation requires simulating with non-degenerate up and down quarks (leading to $N_f = 1+1+1$ or $1+1+1+1$ simulations) as well as including electromagnetism (as described above).

We now describe the tuning of m_ℓ, m_s and m_c to their physical values. (For brevity, we ignore isospin violation in the following discussion.) The most commonly used quantities for these tunings are, respectively, m_π, m_K and m_{η_c} or m_{D_s}. If the scale is being set by m_Ω, then one adjusts the lattice quark masses until the ratios m_π/m_Ω, m_K/m_Ω and m_{η_c}/m_Ω take their physical values. In the past, most calculations needed to extrapolate to the physical value of m_ℓ (typically using forms based on chiral perturbation theory [ChPT]), while simulating directly at or near to the physical values of m_s and m_c. Present calculations are increasingly done with physical or near physical values of m_ℓ, requiring at most only a short extrapolation or interpolation.

17.1.5.3 *Heavy quark masses*

The b quark is usually treated only as a valence quark, with no loop effects included. The errors introduced by this approximation can be estimated to be $\sim \alpha_s(m_b)\Lambda^2_{\rm QCD}/m_b^2$ and are likely to be very small. In the past, the same approximation has been made for the c quark, leading to errors $\sim \alpha_s(m_c)\Lambda^2_{\rm QCD}/m_c^2$. (See Ref. [86] for a quantitative estimate of the effects of including the charm quark on some low energy physical quantities, and Ref. [87] for similar estimates for B-meson matrix elements.) For high precision, however, dynamical charm quarks are necessary, and many of the most recent simulations now include them.

The b quark mass can be tuned by setting heavy-heavy (Υ) or heavy-light (B or B_s) meson masses to their experimental values. Consistency between these two determinations provides an important check that the determination of parameters in the heavy quark lattice formulations is being done correctly (see, e.g., Ref. [26, 88, 89]). For instance, the b quark masses obtained from heavy-light [44] and heavy-heavy [77] mesons are in excellent agreement within the precision of 0.5%.

17.1.6 *Sources of systematic error*

Lattice results have statistical and systematic errors that must be quantified for any calculation in order for the result to be a useful input to phenomenology. The statistical error is due to the use of Monte Carlo importance sampling to evaluate the path integral (a method discussed below). There are, in addition, a number of systematic errors that are always present to some degree in lattice calculations, although the size of any given error depends on the particular quantity under consideration and the parameters of the ensembles being used. The most common lattice errors are reviewed below.

Although not strictly a systematic error, it is important to note that the presence of long auto-correlations in the sequence of lattice configurations generated by the Monte Carlo method can lead to underestimates of statistical errors [90]. It is known that the global topological charge of the gauge fields decorrelates very slowly with certain algorithms, especially when the lattice spacing is small [90, 91]. The effect of poorly sampling topological charge is expected to be most significant for the pion mass and related quantities [92–94]. This issue becomes more relevant as the precision of the final results improves. The problem of slow decorrelation of topology can be mitigated using open boundary conditions, for which the global topological charge is not quantized [95].

17.1.6.1 *Continuum limit*

Physical results are obtained in the limit that the lattice spacing a goes to zero. Symanzik effective theory determines the scaling of lattice artefacts with a. Most lattice calculations use improved actions with leading discretization errors of $\mathcal{O}(\alpha_s a\Lambda)$, $\mathcal{O}(a^2\Lambda^2)$, or $\mathcal{O}(\alpha_s a^2\Lambda^2)$, where Λ is a typical momentum scale in the system. Knowledge of the scaling of the leading discretization errors allows controlled extrapolation to $a = 0$ when multiple lattice spacings are available, as in current state-of-the-art calculations. Terms that allow for higher powers of a are usually included in the fit form for the continuum extrapolation, with either loosely constrained or unconstrained coefficients, to be determined by the fit. There is also sub-leading a dependence with pre-factors containing powers of $\log a$. This can, in principle, be understood using the Symanzik effective theory, and first studies of this have been undertaken [96–98].

For many quantities, the typical momentum scale in the system is $\Lambda_{\rm QCD} \approx 300$ MeV. Discretization errors are expected to be larger for quantities involving larger scales, for example form factors or decays involving particles with momenta or masses larger than $\Lambda_{\rm QCD}$.

17.1.6.2 *Infinite volume limit*

LQCD calculations are necessarily carried out in finite spacetime boxes, leading to departures of physical quantities (masses, decay constants, etc.) from their measured, infinite volume values. These finite-volume shifts are an important systematic that must be estimated and minimized.

Typical lattices are asymmetric, with N_s points in the three spatial directions and N_t in the (Euclidean) temporal direction. The spatial and temporal sizes in physical units are thus $L_s = aN_s$ and $L_t = aN_t$, respectively. (Anisotropic lattice spacings are also sometimes used, as discussed below in Sec. 17.2.2.) Typically, $L_t \geq 2L_s$, a longer temporal direction being used to allow excited-state contributions to correlators to decay. This means that the dominant impact of using finite volume is from the presence of a finite spatial box.

The highest-precision LQCD calculations are of quantities involving no more than a single strongly-interacting particle in initial and final states. For such quantities, once the spatial size exceeds about 2 fm (so that the particle is not "squeezed"), the dominant finite-volume effect comes from virtual pions wrapping around the lattice in the spatial directions. This effect is exponentially suppressed as the volume becomes large, roughly as $\sim \exp(-m_\pi L_s)$, and has been estimated using ChPT [99] or other methods [100]. These estimates suggest that finite volume shifts are sub-percent effects when $m_\pi L_s \gtrsim 4$, and most large-scale simulations use lattices satisfying this condition. (See also Sec. 2.1.1 of the FLAG report [85] for more detailed discussion concerning the conditions required to control finite-volume effects.) This becomes challenging as one approaches the physical pion mass, for which $L_s \gtrsim 5$ fm is required.

Finite-volume errors are usually determined by repeating the simulations on two or more different volumes (with other parameters fixed). If different volumes are not available, the ChPT estimate can be used, often inflated to account for the fact that the ChPT calculation is truncated at some order.

LQCD calculations involving more than a single hadron are becoming increasingly precise. Examples include the calculation of resonance parameters and the $K \to \pi\pi$ amplitudes. Finite-volume effects are much larger in these cases, with power-law terms (e.g., $1/L_s^3$) in addition to exponential dependence. Indeed, as will be discussed in Sec. 17.2.4, one can use the volume dependence to indirectly extract infinite-volume quantities such as scattering lengths. Doing so, however, requires a set of lattice volumes satisfying $m_\pi L_s \gtrsim 4$ and is thus more challenging than for single-particle quantities.

Int. J. Mod. Phys. A 2026.41. Downloaded from www.worldscientific.com
by UNIVERSITY OF CALIFORNIA @ BERKELEY on 09/16/26. Re-use and distribution is strictly not permitted, except for Open Access articles.

17.1.6.3 *Chiral extrapolation*

Until recently, an important source of systematic error in LQCD calculations was the need to extrapolate in m_u and m_d (or, equivalently, in m_π). This extrapolation was usually done using functional forms based on ChPT, or with analytic functions, with the difference between different fits used as an estimate of the systematic error, which was often substantial. Increasingly, however, calculations work directly at, or very close to, the physical quark masses. This either removes entirely, or greatly reduces, the uncertainties in the extrapolation, such that this error is subdominant.

17.1.6.4 *Operator matching*

Many of the quantities that LQCD can precisely calculate involve hadronic matrix elements of operators from the electroweak Hamiltonian. Examples include the pion and kaon decay constants, semileptonic form factors and the kaon mixing parameter B_K (the latter defined in Eq. (17.13)). The operators in the lattice matrix elements are defined in the lattice regularization scheme. To be used in tests of the Standard Model, however, they must be matched to the continuum regularization scheme in which the corresponding Wilson coefficients have been calculated. The only case in which such matching is not needed is if the operator is a conserved or partially conserved current. Similar matching is also needed for the conversion of lattice bare quark masses to those in the continuum $\overline{\text{MS}}$ scheme.

Several methods are used to calculate the matching factors: perturbation theory (usually to one- or two-loop order), non-perturbative renormalization (NPR) using Landau-gauge quark and gluon external states [101], NPR based on the Schrödinger functional [102], NPR using short-distance hadron correlators [103], and NPR using heavy-heavy correlators [27, 104]. The NPR methods replace truncation errors from perturbation theory (which can only be estimated approximately) by statistical and systematic errors that can be determined reliably and systematically reduced.

An issue that arises in some of such calculations (e.g., for quark masses and B_K) is that, using NPR with Landau-gauge quark and gluon external states, one ends up with operators regularized in a MOM-like scheme (or a Schrödinger-functional scheme), rather than the $\overline{\text{MS}}$ scheme mostly used for calculating the Wilson coefficients. To make contact with this scheme requires a purely continuum perturbative matching calculation supplemented by the operator product expansion (OPE). (The importance of power corrections is emphasized in [105].) The resultant truncation error of perturbative expansion and OPE can be minimized by pushing up the momentum scale at which the matching is done using step-scaling techniques as part of the NPR calculation [106].

It should also be noted that this final step in the conversion to the $\overline{\text{MS}}$ scheme could be avoided if continuum calculations used a MOM-like scheme or if one imposes a renormalization condition for quantities that are calculable both in the $\overline{\text{MS}}$ scheme and in LQCD, such as the hadron correlators at short distances (see, e.g., Ref. [107]).

17.2 Methods and status

Once the lattice action is chosen, it is straightforward to define the quantum theory using the path integral formulation. The Euclidean-space partition function is

$$Z = \int [dU] \prod_f [dq_f][d\bar{q}_f] e^{-S_g[U] - \sum_f \bar{q}_f (D[U]+m_f) q_f}\,, \quad (17.4)$$

where link variables are integrated over the SU(3) manifold, q_f and $\bar{q}_f$ are Grassmann (anti-commuting) quark and antiquark fields of flavor f, and $D[U]$ is the chosen lattice Dirac operator with m_f the quark mass in lattice units. Integrating out the quark and antiquark fields, one arrives at a form suitable for simulation:

$$Z = \int [dU] e^{-S_g[U]} \prod_f \det(D[U]+m_f)\,. \quad (17.5)$$

The building blocks for calculations are expectation values of multi-local gauge-invariant operators, also known as "correlation functions",

$$\langle \mathcal{O}(U,q,\bar{q})\rangle = (1/Z)\int [dU] \prod_f [dq_f][d\bar{q}_f] \mathcal{O}(U,q,\bar{q}) e^{-S_g[U] - \sum_f \bar{q}_f (D[U]+m_f) q_f}\,. \quad (17.6)$$

If the operators depend on the (anti-)quark fields q_f and $\bar{q}_f$, then integrating these fields out leads not only to the fermion determinant but also, through Wick's theorem, to a series of quark "propagators", $(D[U]+m_f)^{-1}$, connecting the positions of the fields.

This set-up allows one to choose, by hand, the masses of the quarks in the determinant (the sea quarks) differently from those in the propagators (valence quarks). This is called "partial quenching", and is used by some calculations as a way of obtaining more data points from which to extrapolate both sea and valence quarks to their physical values.

17.2.1 *Monte-Carlo method*

Since the number of integration variables U is huge ($N_s^3 \times N_t \times 4 \times 8$), direct numerical integration is impractical and one has to use Monte-Carlo techniques. In this method, one generates a Markov chain of gauge configurations (a "configuration" being the set of U's on all links) distributed according to the probability measure $[dU]e^{-S_g[U]}\prod_f \det(D[U]+m_f)$. Once the configurations are generated, expectation values $\langle O(U,q,\bar{q})\rangle$ are calculated by averaging over those configurations. In this way the configurations can be used for many different calculations, and there are several large collections of ensembles of configurations (with a range of values of a, lattice sizes and quark masses) that are publicly available through the International Lattice Data Grid (ILDG) [108].

The most challenging part of the generation of gauge configurations is the need to include the fermion determinant. Direct evaluation of the determinant is not feasible, as it requires $\mathcal{O}((N_s^3 \times N_t)^3)$ computations. Instead, one rewrites it in terms of "pseudo-fermion" fields ϕ (auxiliary fermion fields with bosonic statistics). For example, for two degenerate quarks one has

$$\det(D[U]+m_f)^2 = \int [d\phi] e^{-\phi^\dagger ((D[U]+m_f)(D[U]+m_f)^\dagger)^{-1}\phi}\,. \quad (17.7)$$

By treating the pseudo-fermions as additional integration variables in the path integral, one obtains a totally bosonic representation. The price one pays is that the pseudo-fermion effective action is highly non-local since it includes the inverse Dirac operator $(D[U]+m_f)^{-1}$. Thus, the large sparse matrix $(D[U]+m)$ has to be inverted every time one needs an evaluation of the effective action.

Present simulations generate gauge configurations using the Hybrid Monte Carlo (HMC) algorithm [109], or variants thereof. This algorithm combines molecular dynamics (MD) evolution [110–112] in a fictitious time (which is also discretized) with a Metropolis "accept-reject" step [113]. It makes a global update of the configuration, and is made exact by the Metropolis step. In its original form it can be used only for two degenerate flavors, but extensions (particularly the rational HMC [114]) are available for single flavors. Considerable speed-up of the algorithms has been achieved over the last two decades using a variety of techniques.

All these algorithms spend the bulk of their computational time on the repeated inversion of $(D[U]+m)$ acting on a source (which is required at every step of the MD evolution). Inversions are done using a variety of iterative algorithms, e.g., the conjugate gradient algorithm. In this class of algorithms, computational cost is determined by the condition number of the matrix, which is the ratio of maximum and minimum eigenvalues. For $(D[U]+m)$ the smallest eigenvalue is $\approx m$, and the cost is inversely proportional to the quark mass. This is a major reason why simulations at the physical light quark masses are challenging.

Algorithmic improvements have significantly reduced this problem. The main idea is to separate different length scales [115,116].

Int. J. Mod. Phys. A 2026.41. Downloaded from www.worldscientific.com by UNIVERSITY OF CALIFORNIA @ BERKELEY on 09/16/26. Re-use and distribution is [redacted] except for Open Access articles.

Since the low eigenvalues of $(D[U]+m)$ are associated with long wavelength quark modes, one may project the problem onto that of a coarse-grained lattice by averaging the field within a block of sublattices and carrying out the inversion on this coarse lattice. The result is then fed back to the original lattice as an efficient *preconditioner* for the iterative solver, and the whole procedure may be nested multiple times. Variants of such methods have been implemented, specifically domain-decomposition [117, 118], deflation [119–122] and multigrid [123,124]. They are increasingly used in large-scale lattice simulations.

A practical concern is the inevitable presence of correlations between configurations in the Markov chain. These are characterized by an auto-correlation length in the fictitious MD time. One aims to use configurations separated in MD time by greater than this auto-correlation length. Then, as the number of decorrelated configurations, N, is increased, the statistical error decreases as $1/\sqrt{N}$. In practice, it is difficult to measure this length accurately, see, for example, [125]. This, as well as the possibility of insufficient equilibration leads to some uncertainty in the resulting statistical errors.

The computational cost of gauge generation grows with the lattice volume, $V_{\rm lat} = N_s^3 N_t$, as $V_{\rm lat}^{1+\delta}$. Here $\delta = 1/4$ for the HMC algorithm [126] and can be reduced slightly using modern variants. Such growth with $V_{\rm lat}$ provides a (time-dependent) limit on the largest lattice volumes that can be simulated. At present, the largest lattices being used have $N_s = 144$ and $N_t = 288$ or $N_s = N_T = 160$. Typically, one aims to create an ensemble of $\sim 10^3$ statistically independent configurations at each choice of parameters (a, m_q and $V_{\rm lat}$). For most physical quantities of interest, this is sufficient to make the resulting statistical errors smaller than or comparable to the systematic errors. Recently, the master-field approach is being investigated [13, 127, 128]. It aims to create a large-volume ensemble and repeat the calculation of physical quantities in different small patches of the entire lattice. Translational invariance guarantees that the correct average is obtained with fewer configurations than in the traditional approach, with the advantage of reduced finite-volume effects [129].

In the past, the cost of generating gauge configurations was larger than that of performing "measurements" on those configurations. However, as the number of quantities being calculated and their complexity has increased, the balance has shifted to the point that the total cost of measurements exceeds that of generation. Sharing the configurations, e.g. through the ILDG, has become more common, and a number of groups are utilizing them to compute a wide variety of quantities, as partly covered by the following sections.

17.2.2 *Two-point functions*

One can extract properties of stable hadrons from two-point correlation functions, $\langle O_X(x) O_Y^\dagger(0)\rangle$. Here $O_{X,Y}(x)$ are operators that have non-zero overlaps with the hadronic state of interest $|H\rangle$, *i.e.* $\langle 0|O_{X,Y}(x)|H\rangle \neq 0$. On the lattice, the two-point correlation function can be constructed, using Wick's theorem, from the quark propagators $(D[U]+m_f)^{-1}_{x0}$ from the insertion point of the source operator $O_Y(0)$ to the sink operator $O_X(x)$ (see Fig. 17.2). An average over gauge configurations yields the estimate of $\langle O_X(x) O_Y^\dagger(0)\rangle$ for all x on the lattice.

One usually Fourier transforms in the spatial directions and considers correlators as a function of Euclidean time:

$$C_{XY}(t;\boldsymbol{p}) = \sum_{\boldsymbol{x}} \langle O_X(t,\boldsymbol{x}) O_Y^\dagger(0)\rangle e^{-i\boldsymbol{p}\cdot\boldsymbol{x}}. \tag{17.8}$$

(Here and throughout this section all quantities are expressed in dimensionless lattice units, so that, for example, $\boldsymbol{p} = a\boldsymbol{p}_{\rm phys}$.) By inserting a complete set of states having spatial momentum $\boldsymbol{p}$, the two-point function can be written as

$$C_{XY}(t;\boldsymbol{p}) = \sum_{i=0}^{\infty} \frac{1}{2E_i(\boldsymbol{p})} \langle 0|O_X(0)|H_i(\boldsymbol{p})\rangle\langle H_i(\boldsymbol{p})|O_Y^\dagger(0)|0\rangle e^{-E_i(\boldsymbol{p})t}, \tag{17.9}$$

where the energy of the i-th state $E_i(\boldsymbol{p})$ appears in the eigenvalue of the Euclidean time evolution operator e^{-Ht}, $e^{-E_i(\boldsymbol{p})t}$. The factor of $1/[2E_i(\boldsymbol{p})]$ is due to the relativistic normalization used for the states. For large enough t, the dominant contribution is that of the lowest energy state $|H_0(\boldsymbol{p})\rangle$:

$$C_{XY}(t;\boldsymbol{p}) \overset{t\to\infty}{\longrightarrow} \frac{1}{2E_0(\boldsymbol{p})} \langle 0|O_X(0)|H_0(\boldsymbol{p})\rangle\langle H_0(\boldsymbol{p})|O_Y^\dagger(0)|0\rangle e^{-E_0(\boldsymbol{p})t}. \tag{17.10}$$

One can thus obtain the energy $E_0(\boldsymbol{p})$, which equals the hadron mass m_H when $\boldsymbol{p} = 0$, and the product of matrix elements $\langle 0|O_X(0)|H_i(\boldsymbol{p})\rangle\langle H_i(\boldsymbol{p})|O_Y^\dagger(0)|0\rangle$.

This method can be used to determine the masses of all the stable (in QCD) mesons and baryons by making appropriate choices of operators. For example, if one uses the axial current, $O_X = O_Y = A_\mu = \bar{d}\gamma_\mu\gamma_5 u$, then one can determine m_{π^+} from the rate of exponential fall-off, and in addition the decay constant f_π from the coefficient of the exponential since $\langle 0|A_\mu|\pi\rangle = f_\pi p_\mu$.

Because of its dominance at large times, the lowest energy ground-state is the one most accurately characterized from the lattice analysis of the correlator $C_{XY}(t;\boldsymbol{p})$. How accurately the ground-state parameters can be determined depends on the quantum numbers and quark content of H_0, however. This is because the statistical variance in $C_{XY} \sim \langle O_X O_Y^\dagger\rangle$ is controlled by $\langle (O_X O_Y^\dagger)^2\rangle$, itself a correlation function containing a set of states in a similar way to Eq. (17.9) [130, 131]. In the best-case scenario the ground-state of $\langle (O_X O_Y^\dagger)^2\rangle$ is two H_0 mesons with energy close to $2E_0$. Then the signal/noise ratio in C_{XY} is approximately independent of t and the accurate long-time tail of C_{XY} is useful in obtaining high statistical precision on E_0 and the ground-state amplitude. This is the situation for flavour-diagonal pseudoscalar mesons. For unequal valence quark masses, the signal/noise ratio falls exponentially in time t with an exponent given by $m_{Q\bar{q}} - (m_{Q\bar{Q}} + m_{q\bar{q}})/2$, where $m_{Q\bar{q}}$ denotes the pseudoscalar meson mass composed of flavor Q and q and so on. This has a small impact for the kaon, but it is a bigger problem for the B mesons, increasing the statistical uncertainty in the ground-state parameters. The signal/noise issue is also significant for light vector mesons and baryons; for ρ meson correlators, the signal/noise falls exponentially with exponent $m_\rho - m_\pi$ and for the nucleon, $m_N - 3m_\pi/2$. This limits the range of useful t values in the correlator fits. The same issue is responsible for growing statistical noise in $C_{XY}(t;\boldsymbol{p})$ as $|\boldsymbol{p}|$ is increased. Mitigation strategies include using efficient methods for calculating quark propagators, such as all-mode-averaging [132], which allows one to increase the number of samples, as well as using multi-level Monte-Carlo methods that can reduce the growth of the uncertainty with distance [133].

The expression given in (17.9) for the correlator $C_{XY}(t;\boldsymbol{p})$ shows how, in principle, one can determine the energies of the excited hadron states having the same quantum numbers as the

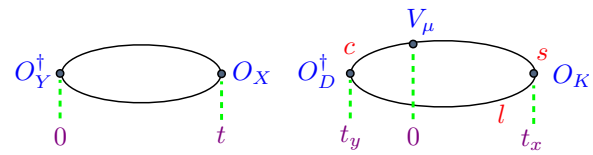

Figure 17.2: Schematic diagrams of a two-point correlation function (left) and three-point correlation function (right). Solid lines represent quark or antiquark propagators obtained by solving the Dirac equation with a source. For the two-point correlation function the quark and antiquark propagators from the source point $t = 0$ are multiplied together at each t value with appropriate γ matrices in between, corresponding to the operators $O_Y^\dagger$ and O_X. Traces are performed over spin and color and, usually, a sum over spatial positions at the sink t (see Eq. (17.8)). The three-point correlation function corresponds to that of Eq. (17.11), with the flavors of the quark propagators marked ($l = u/d$). Typically this calculation would be done by using the l propagator from t_x at timeslice t_y, after multiplication by appropriate γ matrices for O_D, as a source for the c propagator. The c and s propagators are then tied together at $t = 0$ after inserting γ_μ.

Int. J. Mod. Phys. A 2026.41. Downloaded from www.worldscientific.com by UNIVERSITY OF CALIFORNIA @ BERKELEY on 09/16/26. Re-use and distribution is strictly not permitted, except for Open Access articles.

operators $O_{X,Y}$, by fitting the correlation function to a sum of exponentials, including both ground-state and excited-state contributions. It is important to do this in order to obtain accurate results for the ground-state parameters. To reliably identify excited-state parameters in practice, one often needs to use a large basis of operators with a variety of overlaps, $\langle 0|O_X|H_i\rangle$ with the different states, and to adopt a variational approach, such as that of [134]. The use of anisotropic lattices in which a_t, the lattice spacing in the time direction, is smaller than its spatial counterpart, a_s, allows for more temporal samples of the correlation function at small times where there is a signal for excited states. Using these and and other technical improvements, extensive excited-state spectra have been obtained [135–140].

A complication arises for states with high spins ($j \geq 4$ for bosons) because the spatial rotation group on the lattice is a discrete subgroup of the continuum group SO(3). This implies that lattice operators, even when chosen to lie in irreducible representations of the lattice rotation group, have overlap with states that have a number of values of j in the continuum limit [141]. For example $j = 0$ operators can also create mesons with $j = 4$. Methods to overcome this problem in practice are available [135, 142] and have been used successfully.

The two-point function (17.8) contains, in principle, information on all possible states having the quantum numbers of the operator O. Thus, if O is chosen to be a vector current, it can be used to estimate the hadronic vacuum polarization function contribution to the muon anomalous magnetic moment, as discussed in Sec. 17.3.7.

17.2.3 *Three-point functions*

Hadronic matrix elements needed to calculate semileptonic form factors and neutral meson mixing amplitudes can be computed from three-point correlation functions. We discuss here, as a representative example, the $D \to K$ amplitude (see Fig. 17.2). As in the case of two-point correlation functions one constructs operators O_D and O_K having overlap, respectively, with the D and K mesons. We are interested in calculating the matrix element $\langle K|V_\mu|D\rangle$, with $V_\mu = \bar{c}\gamma_\mu s$ the flavor-changing vector current.

To obtain this, we use the three-point correlator constructed from three quark propagators

$$C_{KV_\mu D}(t_x, t_y; \boldsymbol{p}) = \sum_{\boldsymbol{x},\boldsymbol{y}} \langle O_K(t_x, \boldsymbol{x}) V_\mu(0) O_D^\dagger(t_y, \boldsymbol{y})\rangle e^{-i\boldsymbol{p}\cdot\boldsymbol{x}}\,, \tag{17.11}$$

and focus on the limit $t_x \to \infty$, $t_y \to -\infty$. In this example we set the D-meson at rest while the kaon carries three-momentum $\boldsymbol{p}$. Momentum conservation then implies that the weak operator V_μ inserts three-momentum $-\boldsymbol{p}$. Inserting a complete set of states between each pair of operators, we find

$$C_{KV_\mu D}(t_x, t_y; \boldsymbol{p}) = \sum_{i,j} \frac{1}{2m_{D_i} 2E_{K_j}(\boldsymbol{p})} e^{-m_{D_i} t_x - E_{K_j}(\boldsymbol{p})|t_y|} \times \langle 0|O_K(0)|K_j(\boldsymbol{p})\rangle\langle K_j(\boldsymbol{p})|V_\mu(0)|D_i(\boldsymbol{0})\rangle\langle D_i(\boldsymbol{0})|O_D^\dagger(0)|0\rangle. \tag{17.12}$$

The matrix element $\langle K_i(\boldsymbol{p})|V_\mu(0)|D_j(\boldsymbol{0})\rangle$ can then be extracted, since all other quantities in this expression can be obtained from two-point correlation functions. Typically, one is interested in the weak matrix elements of ground states, such as the lightest pseudo-scalar mesons. In the limit of large separation between the three operators in Euclidean time, the three-point correlation function yields the weak matrix element of the transition between ground states. Reliable determination of the ground-state matrix element requires the calculation of $C_{KV_\mu D}$ for multiple large values of $t_x - t_y$ so that simultaneous multi-exponential fits to three-point and two-point correlation functions can be done. This is harder for cases such as baryon matrix elements with a significant signal/noise problem (see Sec. 17.2.2). Complications may also arise in cases where a significant contribution is expected from states with an extra pion. An example relevant to $B \to \pi\ell\nu$ decay is discussed in Ref. [143].

From (17.12) the matrix element $\langle K_i(\boldsymbol{p})|V_\mu(0)|D_j(\boldsymbol{0})\rangle$ is obtained at several discretized values of momentum $\boldsymbol{p}$, given by a multiple of $2\pi/L$ in each spatial direction. Each momentum corresponds to a certain value of the momentum transfer $q^2 = (m_D - E_K(\boldsymbol{p}))^2 - \boldsymbol{p}^2$. The restriction on the available momentum can be relaxed by introducing twisted boundary conditions [144–146], which are a generalization of (anti-)periodic boundary conditions in the spatial directions that allows a general $U(1)$ phase upon translation by distance L. The choice of phase leads to a quark momentum that does not have to be a multiple of $2\pi/L$. The method has been applied in a number of lattice calculations.

To interpolate in q^2, the so-called z parametrization [147–150] is often employed. It takes account of the analytic structure of the form factor in the complex q^2 plane, and a polynomial expansion in z is justified.

17.2.4 *Scattering amplitudes and resonances*

The methods described thus far yield matrix elements involving single, stable particles (where by stable we mean here absolutely stable to strong interaction decays). Most of the particles listed in the Review of Particle Properties are, however, unstable—they are resonances decaying into final states consisting of multiple strongly interacting particles. LQCD simulations cannot directly calculate resonance properties, but methods have been developed to do so indirectly for resonances coupled to two- and three-particle final states in the elastic regime, starting from the seminal work of Lüscher [155].

The difficulty faced by LQCD calculations is that, to obtain resonance properties, one must calculate multi-particle scattering amplitudes in momentum space and put the external particles on their mass-shells. This requires analytically continuing from Euclidean to Minkowski momenta. Although it is straightforward in LQCD to generalize the methods described above to calculate four- and higher-point correlation functions, one necessarily obtains them at a discrete and finite set of Euclidean momenta. Analytic continuation to $p_E^2 = -m^2$ is then an ill-posed and numerically challenging problem. The same problem arises for single-particle states, but can be largely overcome by picking out the exponential fall-off of the Euclidean correlator, as described above. With a multi-particle state there is no corresponding trick, except for two particles at threshold [156], although recent ideas using smeared correlators and advanced spectral-reconstruction methods have made significant progress [157–160].

What LQCD can calculate are the energies of the eigenstates of the QCD Hamiltonian in a finite box. The energies of states containing stable particles, e.g., two or three pions, clearly depend on the interactions between the particles. It is possible to invert this dependence and, with plausible assumptions, determine the scattering amplitudes in a limited kinematical range. This is most straightforward in the case of two particles in the elastic regime with a single dominant partial wave, in which case one can obtain the scattering phase-shifts at a discrete set of momenta from a calculation of the two-particle energy levels for a variety of spatial volumes [155]. Determinations of two-meson and meson-nucleon interactions using generalizations of this methodology to multiple channels [161], and particles with spin [162], are now standard, albeit largely with heavier-than-physical quark masses. There is also an alternative approach using a lattice calculation of the Bethe-Salpeter amplitude to determine two-particle interaction potentials [163]. Channels studied include $\pi\pi$, $\bar{K}K$, $K\pi$, $\pi\omega$, $\pi\phi$, KD, DD^*, D^*D^*, $B\pi$, $N\pi$, $\Sigma\pi$, and NK. For results using physical quark masses see [164, 165]; recent comprehensive reviews are [166]. Extensions to two-nucleon interactions are being actively studied [167]; recent reviews are [168]. The formalism has been generalized to three particles (both identical and non-degenerate, and including spin and multiple channels) [169], and has been applied in lattice calculations of $3\pi^+$, $2\pi^+ + K^+$, $\pi^+ + 2K^+$, and $3K^*$ systems [165, 170], to the $I = 1$ and 0 three-pion channels [171], and to the $DD\pi$ system [172]. For recent reviews, see [173].

It is also possible to extend the methodology to calculate electroweak decay amplitudes to two particles below the inelastic threshold, e.g., $A(K \to \pi\pi)$ [174]. Results for both the $\Delta I = 3/2$ and 1/2 amplitudes with physical quark masses have been obtained [35–37, 175], the former now including a controlled contin-

Int. J. Mod. Phys. A 2026.41. Downloaded from www.worldscientific.com by UNIVERSITY OF CALIFORNIA @ BERKELEY on 09/16/26. Re-use and distribution is [redacted] except for Open Access articles.

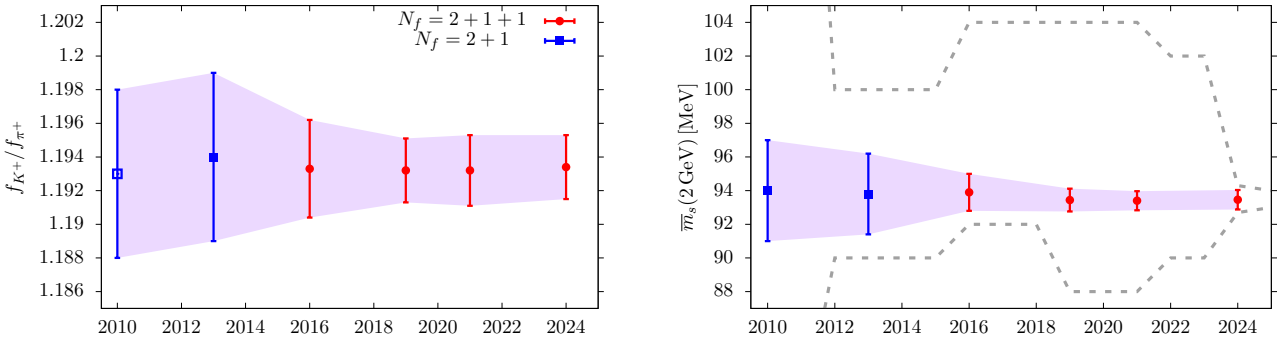

Figure 17.3: History of the FLAG averages of LQCD results for the ratio of kaon and pion decay constants f_{K^+}/f_{π^+} and the strange-quark mass $\bar{m}_s(2\text{ GeV})$ (defined in the $\overline{\text{MS}}$ scheme, μ =2 GeV) [60, 85, 151–154]. In both cases we see a large improvement in the uncertainty over the 14-year timespan—by a factor of 2.5 for f_K^+/f_π^+ (the 2010 result is for the isospin-symmetric f_K/f_π) and a factor of 5 for m_s—as ensemble sizes have grown for improved statistical errors and lattice spacings have become finer and light quark masses closer to the physical point for improved systematic errors. There has also been a shift from $n_f = 2+1$ to $n_f = 2+1+1$ simulations over time. The grey dashed lines for $\bar{m}_s$ indicate the $\pm 1\sigma$ band given in the PDG particle listings (pdglive for 2025). The PDG's evaluation of $\bar{m}_s$ is now in good agreement with the average of the lattice QCD results.

uum limit [176]. First results for the CP-violating quantity ϵ' have been obtained [35, 36].

Partial extensions of the formalism above the elastic threshold have been worked out, in particular for the case of multiple two-particle channels [161]. Another theoretical extension is to allow the calculation of form factors between a stable particle and a resonance [177], and between two resonances [178]. The former has been used to calculate the $\gamma\pi \to \rho$ amplitude, albeit for unphysically large quark masses [179, 180], as well as $\gamma K \to K^*$ [181] and $B \to \rho\ell\nu$ [182]. Finally, the formalism for using LQCD to calculate electroweak decays or transitions to three particles, e.g $\gamma^* \to 3\pi$ and $K \to 3\pi$, has recently been worked out [183, 184].

While a systematic extension to decays with many multi-particle channels, e.g., hadronic B decays, has yet to be formulated, a new direction based on smeared spectral functions is being explored [157, 185, 186]. Correlation functions computed on a Euclidean lattice contain contributions from all states allowed by the symmetry of the inserted operators. Their relative weight depends on their energy E and the time separation t between the operators, and is proportional to e^{-Et}. Correlation functions with different time separations can be combined so as to obtain various desired relative weights between the states [158, 187], leading to results for smeared spectral functions, such as the smeared R-ratio [159, 188], inclusive hadronic τ decay rates [160, 189], inclusive hadron decay rates [190–194], or cross sections [195]. The weight (or the energy-integral kernel) function has to be smooth in order that the construction using correlators with different time separations gives a good approximation. The kernel function required to obtain the inclusive decay rate, for example, does not satisfy this smoothness condition, and one has to introduce some smearing, which has then to be eliminated by taking an appropriate limit. This new source of systematic effect is currently under active investigation [193, 194].

17.2.5 *Status of LQCD simulations*

Until the 1990s, most large-scale lattice simulations were limited to the "quenched" approximation, wherein the fermion determinant is omitted from the path integral. While much of the basic methodology was developed in this era, the results obtained had uncontrolled systematic errors and were not suitable for use in placing precision constraints on the Standard Model. During the 1990s, more extensive simulations including the fermion determinant (also known as simulations with "dynamical" or "sea" quarks) were begun, but with unphysically heavy quark masses ($m_\ell \sim 50 - 100$ MeV), such that the extrapolation to the physical light quark masses was a source of large systematic errors [196]. During the 2000s, advances in both algorithms and computers allowed simulations to reach much smaller quark masses ($m_\ell \sim 10 - 20$ MeV) such that LQCD calculations of selected quantities with all sources of error controlled and small became available. Their results played an important role in constraints on the CKM matrix and other phenomenological analyses. In the last decade, simulations directly at the physical isospin-symmetric light quark masses for a range of lattice spacings have become standard, removing the need for a chiral extrapolation and thus significantly reducing the overall error. This has made many lattice QCD results critical for tests of the Standard Model and searches for new physics. Figure 17.3 shows as an example the recent history of improvement in the uncertainty of lattice QCD results for and f_{K^+}/f_{π^+} and $\bar{m}_s(2\text{ GeV})$.

A summary of lattice QCD ensembles produced by some of the international collaborations as of 2024 can be found in Ref. [197]. The present frontier for u/d quarks, as noted above, is the inclusion of isospin breaking. This will be needed to push the accuracy of calculations down to the few tenths of a percent level. For b-quark physics, realistic sea quark content on very fine lattices is needed to push uncertainties down.

On a more qualitative level, analytic and numerical results from LQCD have demonstrated that QCD confines color and spontaneously breaks chiral symmetry. Confinement can be seen as a linearly rising potential between heavy quark and anti-quark in the absence of quark loops. Analytically, this can be shown in the strong coupling limit $g_{\text{lat}} \to \infty$ [1]. At weaker couplings there are precise numerical calculations of the potential that clearly show that this behavior persists in the continuum limit [198–200].

Chiral symmetry breaking was also demonstrated in the strong coupling limit on the lattice [18, 201], and there have been a number of numerical studies showing that this holds also in the continuum limit. The accumulation of low-lying modes of the Dirac operator, which is the analog of Cooper pair condensation in superconductors, has been observed, yielding a determination of the chiral condensate [202–208]. Many relations among physical quantities that can be derived under the assumption of broken chiral symmetry have been confirmed by a number of lattice groups [153].

17.3 Physics applications

In this section we describe the main applications of LQCD that are both computationally mature and relevant for the determination of particle properties.

A general feature to keep in mind is that, since there are many different choices for lattice actions, all of which lead to the same continuum theory, a crucial test is that results for any given quantity are consistent. In many cases, different lattice calculations are completely independent and often have very different systematic errors. Thus, final agreement, if found, is a highly non-trivial check, just as it is for different experimental measurements. Indeed the process of 'blinding' results during analysis, standard in

Int. J. Mod. Phys. A 2026.41. Downloaded from www.worldscientific.com by UNIVERSITY OF CALIFORNIA @ BERKELEY on 09/16/26. Re-use and distribution is strictly not permitted, except for Open Access articles.

experiment, is being increasingly adopted in lattice calculations to eliminate comparison bias.

The number, variety and precision of the calculations has progressed to the point that an international collaboration, FLAG, has been formed, which aims to collect all lattice results of relevance for a variety of phenomenologically interesting quantities and provide averages of those results that pass appropriate quality criteria. The FLAG averages attempt to account for possible correlations between results (which can arise, for example, if they use common gauge configurations). The most recent FLAG review is from 2024 [85] (see also older editions, Refs. [60, 153, 154, 154]). Our discussion in this section provides summaries for the quantities considered by FLAG, as well as for two topics not discussed by FLAG: the hadron spectrum and the anomalous magnetics moment of the muon. The interested reader can consult the FLAG review for very extensive discussions of the details of the calculations and of the sources of systematic errors.

We stress that the results we quote below are those obtained using the physical complement of light quarks (i.e. $N_f = 2+1$ or $2+1+1$ simulations).

17.3.1 *Spectrum*

The most basic prediction of LQCD is of the hadron spectrum. Once the input parameters are fixed as described in Sec. 17.1.5, the masses or resonance parameters of all other states can be predicted. This includes hadrons composed of light (u, d and s) quarks, as well as heavy-light and heavy-heavy hadrons. It also includes quark-model exotics (e.g., $J^{PC} = 1^{-+}$ mesons) and glueballs. Thus, in principle, LQCD calculations should be able to reproduce many of the experimental results compiled in the Review of Particle Properties. Doing so would test both that the error budgets of LQCD calculations are accurate and that QCD indeed describes the strong interactions in the low-energy domain. The importance of the latter test can hardly be overstated.

What is the status of this fundamental test? As discussed in Sec. 1.2, LQCD calculations are most straightforward for stable, low-lying hadrons. Calculations of the properties of resonances that can decay into two particles are more challenging, but are becoming standard in the meson sector, with the frontier being decays involving baryons. As noted above, the formalism for resonances decaying to three particles exists, but has yet to be applied to resonant channels other than in pioneering calculations. It is also more technically challenging to calculate masses of flavor singlet states (which can annihilate into purely gluonic intermediate states) than those of flavor non-singlets, although again algorithmic and computational advances have begun to make such calculations accessible, including first calculations that reach physical quark masses [209].

The present status for light hadrons is that fully controlled results are available for the masses of the octet light baryons, while results with less than complete control are available for the decuplet baryon resonances, the vector meson resonances and the η and η'. This is discussed in the "Quark Model" review—see, in particular, Fig. 15.9. In addition, it has been possible to calculate the isospin splitting in light mesons and baryons (due to the up-down mass difference and the incorporation of QED). There are also extensive accurate results for heavy-light (D and B systems) and heavy-heavy (ψ, Υ as well as B_c systems). All present results, which are discussed in the "Quark Model" review, are consistent with experimental values, and several predictions have been made. We refer the reader to that review for references to the relevant work.

17.3.2 *Decay constants and bag parameters*

The pseudoscalar meson decay constants can be determined from two-point correlation functions involving the axial-vector current, as discussed in Sec. 17.2.2. The decay constant f_P of a meson P is extracted from the weak matrix element involving the axial-vector current $A_\mu(x)$ using the definition $\langle 0|A_\mu(x)|P(\boldsymbol{p})\rangle = f_P p_\mu \exp(-ip\cdot x)$, where p_μ is the momentum of P and $A_\mu(x)$ is the axial-vector current. (In practice, results with the smallest errors are obtained using the pseudoscalar density operator $P(x) = \bar{q}(x)\gamma_5 q(x)$ instead of $A_\mu(x)$.) Since they are among the simplest quantities to calculate, decay constants provide good benchmarks for lattice methods, in addition to being critical inputs for the flavor physics phenomenology of leptonic decay rates. Results from several lattice groups for the pion and kaon decay constants now have sub-percent errors. The decay constants in the charm and bottom sectors, $f_{D_{(s)}}$ and $f_{B_{(s)}}$, have also been calculated using the various heavy-quark formulations on the lattice outlined in Sec. 17.1.3. The precision has now reached the sub-percent level for both charmed and bottom mesons, meaning that phenomenological analysis of these leptonic decay rates is limited by the larger experimental uncertainties. Lattice results for all of these decay constants are discussed in detail in the review "Leptonic Decays of Charged Pseudoscalar Mesons." The lattice uncertainty on vector meson decay constants $f_{J/\psi}$ and f_Υ, has also reached $\sim$1% and the results agree well with the accurate experimental results for the leptonic decay rates of $J/\psi \to \ell^+\ell^-$ and $\Upsilon \to \ell^+\ell^-$ [41, 45].

Another important lattice quantity is the kaon bag parameter, B_K, which is needed to turn the precise measurement of CP-violation in kaon mixing into a constraint on the Standard Model. It is defined by

$$\frac{8}{3} m_K^2 f_K^2 B_K(\mu) = \langle \overline{K}^0 | Q_{\Delta S=2}(\mu) | K^0 \rangle, \tag{17.13}$$

where m_K is the kaon mass, f_K is the kaon decay constant, $Q_{\Delta S=2} = \bar{s}\gamma_\mu(1-\gamma_5)d\bar{s}\gamma_\mu(1-\gamma_5)d$ is the four-quark operator of the effective electroweak Hamiltonian and μ is the renormalization scale. The short distance contribution to the electroweak Hamiltonian can be calculated perturbatively, but the hadronic matrix element parameterized by B_K must be computed using non-perturbative methods. In order to be of use to phenomenology, the renormalization factor of the four-quark operator must be matched to a continuum renormalization scheme, e.g., to $\overline{\text{MS}}$, as described in Sec. 17.1.6.4. Determinations with percent-level precision using different fermion actions and $N_f = 2+1$ light sea quarks are now available using DWF [210, 211], staggered fermions [212], DWF valence on staggered sea quarks [213], and Wilson fermions [11]. The results are all consistent, and the present FLAG average is $\hat{B}_K = 0.7533(91)$ [85] for its renormalization group invariant definition (for original papers, see [11, 211, 213–215]).

The bag parameters for B and B_s meson mixing are defined analogously to that for kaon mixing. The B and B_s mesons contain a valence b-quark so that calculations of these quantities must use one of the methods for heavy quarks described above. Calculations have been done using NRQCD [216, 217], the Fermilab formalism [87], and static heavy quarks [218]. All results are consistent. The FLAG averages for the quantities relevant for B_s and B mixing with $N_f = 2+1$, which are based on results from Refs. [87, 216, 218], are $f_{B_s}\sqrt{\hat{B}_{B_s}} = 274(8)$ MeV and $f_B\sqrt{\hat{B}_B} = 225(9)$ MeV, with their ratio (which is somewhat better determined) being $\xi = 1.206(17)$. There is a single $N_f = 2+1 = 1$ calculation [217] and this gives $f_{B_s}\sqrt{\hat{B}_{B_s}} = 256(6)$ MeV $f_B\sqrt{\hat{B}_B} = 211(6)$ MeV, and $\xi = 1.216(16)$. These are consistent with the $N_f = 2+1$ results at the 2σ level. Errors for quantities involving b quarks are typically larger than those for quantities involving only light quarks, although the difference has steadily decreased in recent years.

For the K, D and B systems, one can also consider the matrix elements of four-fermion operators that arise in beyond-the-standard-model (BSM) theories, which can have a different chiral structure. Knowledge of these matrix elements allows one to constrain the parameters of the BSM theories, and is complementary to direct searches at the LHC. Reliable results are now available from lattice calculations, and are reviewed by FLAG in the case of kaon mixing [85]. Complete results for D and B mixing are presented in Ref. [219, 220] and Ref. [87, 217], respectively.

The results for mixing matrix elements are used in the reviews "The CKM Quark-Mixing Matrix," and "$B^0 - \bar{B}^0$ Mixing."

17.3.3 *Semileptonic form factors*

Semileptonic decay rates can be used to extract CKM matrix elements once the semileptonic form factors are known from lattice

Int. J. Mod. Phys. A 2026.41. Downloaded from www.worldscientific.com by UNIVERSITY OF CALIFORNIA @ BERKELEY on 09/16/26. Re-use and distribution is [redacted] except for Open Access articles.

calculations.

For example, the matrix element of a pseudoscalar meson P undergoing semileptonic decay to another pseudoscalar meson P' is mediated by the vector current, and can be written in terms of form factors as

$$\langle P'(p')|V_\mu|P(p)\rangle = f_+(q^2)(p+p'-\Delta)_\mu + f_0(q^2)\Delta_\mu\,, \quad (17.14)$$

where $q = p - p'$, $\Delta_\mu = (m_P^2 - m_{P'}^2)q_\mu/q^2$, and V_μ is the quark vector current. Typically, $f_+(q^2)$ dominates the decay rate, since the contribution from $f_0(q^2)$ is suppressed when the final state lepton is light.

For some decays, the shapes of the differential decay rates are well determined by experiment, and, in principle, the values of the form factors are needed from lattice QCD only at some reference value of q^2 in order to extract CKM matrix elements. In these cases, lattice calculations of the form factor shapes may provide further consistency checks or can further improve the precision.

The form factor $f_+(0)$ for $K \to \pi\ell\nu$ decays is highly constrained by the Ademollo-Gatto theorem [221] and chiral symmetry. Old estimates using chiral perturbation theory combined with quark models quote sub-percent precision [222], though they suffer from some model dependence. Utilizing the constraint from the vector current conservation that $f_+(0)$ is normalized to unity in the limit of degenerate up and strange quark masses, the lattice calculation can be made very precise and has now matched the precision of the phenomenological estimates [223–232]. The present FLAG average (from $N_f = 2+1+1$ simulations) is $f_+(0) = 0.9698(17)$ [85], based on Refs. [230, 231].

Charmed meson semileptonic decays have been calculated by different groups using methods similar to those used for charm decay constants, and results are steadily improving in precision [233–238]. Charmed baryon decays have also been computed using a similar method [239, 240].

For semileptonic decays involving a bottom quark, one can use HQET or NRQCD to control the discretization errors from the bottom quark mass at the cost of systematic errors from current renormalisation. Increasingly, calculations are being done with relativistic lattice quark actions and nonperturbative current normalisation. HQET is then used to constrain the extrapolation of the lattice results to the b mass from a range of lower values.

The form factors for the semileptonic decay $B \to \pi\ell\nu$ (and the similar decay $B_s \to K\ell\nu$) have been calculated by a number of groups [241–250]. These B semileptonic form factors are difficult to calculate at low q^2, *i.e.* when the mass of the B-meson must be balanced by a large pion momentum, in order to transfer a large momentum to the lepton pair. The low q^2 region has large discretization errors and very large statistical errors (see signal/noise discussion in Sec. 17.2.2), while the high q^2 region is much more accessible to the lattice. For experiment, the opposite is true. To combine lattice and experimental results it has proved helpful to use the z-parameter expansion [147–150]. This provides a theoretically constrained parameterization of the entire q^2 range, and allows one to obtain $|V_{ub}|$ without model dependence [251]. Analyticity and unitarity can be used to obtain further constraints, including extra information on susceptibilities relevant to the form factors in the time-like region [150, 252–258]. Now that LQCD results for heavy-to-light form factors are available from multiple groups, it has become evident that the results are not always compatible within the quoted errors, suggesting that systematic uncertainties have been underestimated in some cases. Recent fits performed by FLAG to average the form-factor results from different groups have χ^2/d.o.f. substantially larger than 1 and require scale factors [85]. All of the current calculations still involve an extrapolation in the light-quark mass, which is one possible source of underestimated uncertainties. This includes choices made for the form-factor bases used for the extrapolation and the inclusion of poles in the fit functions [250]. Another challenge is excited-state contamination [143].

The semileptonic decays $B \to D\ell\nu$ and $B \to D^*\ell\nu$ (and the similar decays $B_s \to D_s\ell\nu$ and $B_s \to D_s^*\ell\nu$) can be used to extract $|V_{cb}|$ once the corresponding form factors are known. The lattice calculation is most precise at zero recoil since the bulk of the systematic error cancels for appropriate ratios between $B \to D^{(*)}$ and $B \to B$ or $D^{(*)} \to D^{(*)}$ [259]. Calculations of the $B \to D^{(*)}\ell\nu$ and $B_s \to D_s^{(*)}\ell\nu$ form factors at zero recoil have been performed with various formulations for the heavy quark [260]. Calculations at non-zero recoil momenta have also been performed to constrain the functional form of the form factor, which can be used to extrapolate the experimental data to the zero-recoil point or to determine $|V_{cb}|$ directly at the non-zero recoil points [42, 261–266]. The range of q^2 that can be handled for B-meson decays in lattice QCD is growing as more accurate results become available on finer lattices. Comparison of the shape of the form factors between lattice calculations and experiments provides non-trivial cross-checks.

Semileptonic decays of the Λ_b baryon can also be used to constrain $|V_{cb}|$ and $|V_{ub}|$ using lattice calculations of the relevant form factors [267]. Another process sensitive to $|V_{ub}|$ is $B \to \rho\ell\nu$, which is more challenging for lattice QCD due to the unstable nature of the ρ resonance. A first calculation of the $B \to \pi\pi\ell\nu$ P-wave form factors and the resulting $B \to \rho\ell\nu$ resonance form factors, using the finite-volume formalism for $\pi\pi$ scattering as discussed in Sec. 17.2.4 has recently been completed, but so far only at a heavier-than-physical pion mass [182].

Rare decays such as $B \to K\ell^+\ell^-$ involve local matrix elements similar to those needed for charged-current semileptonic decays, Eq. (17.14), as well as nonlocal matrix elements, which, for example, involve the decay chain $b \to sc\bar{c} \to s\ell^+\ell^-$. Except for rare kaon and hyperon decays [268–270], only the local matrix elements have been calculated on the lattice (see, however, Ref. [271] for a possible strategy and exploratory steps to compute $b \to sc\bar{c} \to s\ell^+\ell^-$ on the lattice). In the phenomenology of $b \to s\ell^+\ell^-$ decays, the nonlocal matrix elements are currently treated using continuum methods such as operator product expansions and light-cone sum rules, and the intermediate q^2 region where $c\bar{c}$ resonances are present must be avoided. Recent lattice calculations for $b \to s\ell^+\ell^-$ decays [245, 272, 273] suggest some tension with the experimentally observed decay rates, but systematic errors, including those from the approximations used for the nonlocal matrix elements, need to be carefully studied before drawing any definite conclusions. A similar study for the baryonic decay mode $\Lambda_b \to \Lambda\ell^+\ell^-$ can be found in Ref. [274].

The results discussed in this section are used in the reviews "The CKM Quark-Mixing Matrix," "V_{ud}, V_{us}, the Cabibbo Angle and CKM Unitarity," and "Semileptonic b-hadron decays, determination of V_{cb}, V_{ub}."

17.3.4 *Long-distance contributions to weak-interaction processes*

There are other hadronic processes, for which long-distance contributions are important, where lattice calculations can significantly improve our quantitative understanding.

One example is the long-distance contribution to the neutral kaon mass splitting, ΔM_K. This requires the evaluation of a four-point function, constructed from the two-point functions described in Sec. 17.2.2 by the insertion of two electroweak Hamiltonians [275, 276]. Another example is the long-distance contribution to ϵ_K, which provides a correction to the contribution of the mixing parameter B_K [277]. Rare kaon decays $K \to \pi\ell^+\ell^-$ and $K \to \pi\nu\bar{\nu}$ also include long-distance contributions, and their lattice calculations are discussed in [268, 269]. Related processes $\pi^0 \to e^+e^-$ [278] and $K_L \to \mu^+\mu^-$ [279] have also been studied.

Radiative leptonic decays $\pi \to \ell\nu\gamma^{(*)}$, $K \to \ell\nu\gamma^{(*)}$, and $D \to \ell\nu\gamma^{(*)}$ also include two operator insertions, i.e. an electroweak Hamiltonian and an electromagnetic current, and similar techniques developed for the rare decays above can be applied [64, 280].

We note that similar lattice methods allow the calculation of the γW box contribution to the radiative corrections to semileptonic decays of pions and kaons [281]. The extension to neutron β decay is an important next step, as this promises to reduce the theoretical uncertainty in the extraction of $|V_{ud}|$ from neutron decays [282].

17.3.5 *Strong gauge coupling*

As explained in Sec. 17.1.5.1, for a given lattice action, the choice of bare lattice gauge coupling, $g_{\rm lat}$, determines the lattice

Int. J. Mod. Phys. A 2026.41. Downloaded from www.worldscientific.com
by UNIVERSITY OF CALIFORNIA @ BERKELEY on 09/16/26. Re-use and distribution is strictly not permitted, except for Open Access articles.

spacing a. If one then calculates a as described in Sec. 17.1.5.1, one knows the strong gauge coupling in the bare lattice scheme at the scale $1/a$, $\alpha_{\rm lat} = g^2_{\rm lat}/(4\pi)$. This is, however, not useful for comparing to results for α_s obtained from other inputs, such as deep inelastic scattering or jet shape variables, because the latter results give α_s in the $\overline{\rm MS}$ scheme, which is commonly used in such analyses, and the conversion factor between the lattice and $\overline{\rm MS}$ schemes is known to converge poorly in perturbation theory [283]. Instead, one must use a method that directly determines α_s on the lattice in a scheme closer to $\overline{\rm MS}$.

Several such methods have been used, all following a similar strategy. One calculates a short-distance quantity K both perturbatively ($K^{\rm PT}$) and non-perturbatively ($K^{\rm NP}$) on the lattice, and requires equality: $K^{\rm NP} = K^{\rm PT} = \sum_{i=0}^{n} c_i \alpha_s^i$. Solving this equation one obtains α_s at a scale related to the quantity being used. Often, α_s thus obtained is not defined in the conventional $\overline{\rm MS}$ scheme, and one has to convert among the different schemes using perturbation theory. Unlike for the bare lattice scheme, the required conversion factors are reasonably convergent. As a final step, one uses the renormalization group to run the resulting coupling to a canonical scale (such as M_Z). In each step described above a key systematic error comes from the truncation of the perturbative expansion. This error must be estimated carefully, for example using data-driven methods.

In the work of the HPQCD collaboration [284, 285], the short-distance quantities are Wilson loops of several sizes and their ratios. These quantities are perturbatively calculated through $\mathcal{O}(\alpha_s^3)$ using the V-scheme defined through the heavy quark potential. The coefficients of even higher orders are estimated using the data at various values of a. In addition, this work obtains a result for α_s by matching with $\alpha_{\rm lat}$ in a tadpole-improved scheme that improves convergence.

Another choice of short-distance quantities is to use current-current correlators. Appropriate moments of these correlators are ultraviolet finite, and by matching lattice results to the *continuum* perturbative predictions, one can directly extract the $\overline{\rm MS}$ coupling [286]. The method can be applied for light meson correlators [287–290] as well as heavy meson correlators [40, 285, 291–294]. Yet another choice of short-distance quantity is the static-quark potential, where the lattice result for the potential is compared to perturbative calculations; this method was used to compute α_s within 2+1 flavor QCD [295–300]. There is also a determination of α_s from a comparison of lattice data for the ghost-gluon coupling with that of perturbation theory [301, 302].

With a definition of α_s given using the Schrödinger functional, one can non-perturbatively control the evolution of α_s to high-energy scales, such as 100 GeV, where the perturbative expansion converges very well and essentially no truncation error remains in the matching to the $\overline{\rm MS}$ scheme. This step-scaling method developed by the ALPHA collaboration [106] has been applied to 2+1-flavor QCD in [303–305]. We also note that the gradient-flow coupling [306] is employed at low-energies in [84,305] to avoid large statistical errors associated with the Schrödinger functional coupling. An alternative path to determine the QCD Λ parameter for three flavors, $\Lambda^{(3)}$, from that of the quenched theory, $\Lambda^{(0)}$, has also been developed [307]. This approach aims to benefit from the fact that quenched theories are much faster to simulate. The matching between different flavors can be performed accurately at sufficiently high energy scales.

The various lattice methods for calculating α_s have significantly different sources of systematic error. The FLAG review [85] reports an estimate $\alpha^{(5)}_{\overline{\rm MS}}(M_Z) = 0.1183(7)$, based on Refs. [285, 290, 292, 300, 303, 305, 308–311]. A comparison to other phenomenological determinations can be found in the "Quantum Chromodynamics" review, where it is clear that the uncertainty in the LQCD average is smaller than that from other approaches. Since $\sigma_{\alpha_s} < \mathcal{O}(\alpha_s^3)$, high-order perturbative series are needed to take advantage of further improvements in uncertainty.

17.3.6 *Quark masses*

The quark mass parameters in the lattice QCD action are well-defined running masses, but they need to be converted into masses in a conventional scheme at a canonical scale, such as $\overline{\rm MS}$ at 2 or 3 GeV, to be useful in continuum phenomenology such as the prediction of Higgs decay rates. This conversion requires multiplication by a finite renormalisation constant, which depends on the quark action. Older calculations determined the renormalisation constant using low-order lattice perturbation theory. Most recent calculations use instead an intermediate NPR method (e.g., RI/MOM or RI/SMOM, see Sec. 17.1.6.4) which can be applied by numerical calculation on the lattice and which is then converted to the $\overline{\rm MS}$ scheme using three-loop continuum perturbation theory (see, e.g., [41, 210, 312–315]). Alternatively, using a definition based on the Schrödinger functional, the quark mass can be evolved to a high scale non-perturbatively [316,317], before applying perturbative matching to the $\overline{\rm MS}$ scheme; this minimises the perturbative matching uncertainties. Further approaches are available for heavy quarks. These include matching current-current correlators at short distances calculated on the lattice to those obtained in continuum perturbation theory in the $\overline{\rm MS}$ scheme [40, 104, 285, 291, 292, 294], or using HQET mass relations matched to $\overline{\rm MS}$ either via a ratio method [318] or using the intermediate minimal renormalon-subtracted scheme [319, 320].

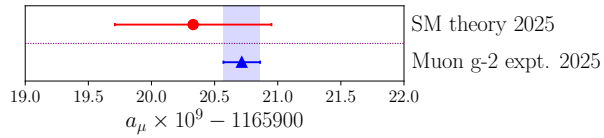

Figure 17.4: The current status of a_μ, comparing the experimental world average [322] with SM theory using lattice QCD for the largest, LOHVP, QCD contribution combined with QED, electroweak and other QCD contributions [323].

The accuracy of lattice QCD determinations of quark masses—uncertainties range from 2–4% for u quark (at a scale of 2 GeV) down to 0.3% for the b quark (at a scale equal to its mass) [85]—mean that they dominate the values given in the Particle Listings, particularly for u, d and s quarks (see right-hand plot of Fig. 17.3). As discussed in Secs. 17.1.5.2 and 17.1.5.3, the tuning of lattice quark masses uses meson masses that are known to sub-MeV precision experimentally and have no signal/noise issues in lattice QCD (see Sec. 17.2.2). Uncertainties coming from the value of the lattice spacing that might otherwise limit precision are also suppressed for heavy quarks because of the relationship between quark and meson masses [292]. A further key point is that ratios of lattice masses using the same quark action are equal in the continuum limit to the ratio of $\overline{\rm MS}$ masses at a given scale, since renormalisation constants cancel in QCD. The ratio m_c/m_s has been calculated to 0.2% [44] and m_b/m_c to 0.3% [44, 77] and these ratios can be used to "cascade" the accuracy of heavy quark masses down to light quark masses [44, 292]. When the effect of the quark's electric charge is included, mass ratios between up-type and down-type quarks are no longer scale-invariant and must be determined at a specific scale [73, 75, 77, 321]. Lattice QCD calculations are now accurate enough to discern QED effects. The ratio m_b/m_c needed for the calculation of $\Gamma(H \to b\bar{b})/\Gamma(H \to c\bar{c})$ runs from 4.586(12) at a scale of 3 GeV [77] to 4.607(12) at m_H, nearly 2σ higher, for example.

Results are summarized in the review of "Quark Masses."

17.3.7 *The anomalous magnetic moment of the muon*

A notable success for LQCD has been the determination of the QCD contributions to the anomalous magnetic moment of the muon, a_μ, in the Standard Model [323], for comparison to recent experimental results from the Muon $g-2$ experiment [322]. This comparison (see Fig. 17.4) now yields $a_\mu^{\rm expt.} - a_\mu^{\rm SM} = 39(64) \times 10^{-11}$, showing agreement between experiment and the SM at the level of 550 ppb. The uncertainty is dominated by that from theory (the experimental uncertainty is 124 ppb), and in particular by that from the largest QCD contribution known as the leading-order hadronic vacuum polarization (LO-HVP). Here we describe briefly how the lattice QCD calculations for $a_\mu^{\rm SM}$ are

Int. J. Mod. Phys. A 2026.41. Downloaded from www.wo
by UNIVERSITY OF CALIFORNIA @ BERKELEY on 09/16/26. Re-use and distribution is
except for Open Access articles.

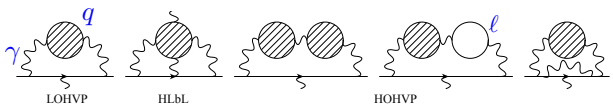

Figure 17.5: QCD contributions to a_μ. From left to right: the leading-order hadronic vacuum polarisation (LOHVP), hadronic light-by-light (HLbL), higher-order HVP (HOHVP). The horizontal lines represent the μ and wiggly lines are photons, with the vertical photon the B field probing the muon magnetic moment. Hatched loops are strongly-interacting and formed from $\gamma^* \to q\bar{q} \to \gamma^*$; open loops are lepton loops. Figure from [324].

done, giving a little more detail than on other topics covered in this review to reflect the size of the community effort involved and the timeliness of the results. For a recent review see [325].

The anomalous magnetic moment $a_\mu = (g-2)/2$ quantifies the 0.1% impact on the muon magnetic moment from the fact that the muon is embedded in a quantum field theory and can therefore interact directly and indirectly with all the SM particles (and BSM particles, if they exist). In the SM the muon can, for example, emit a virtual photon that generates for an instant a quark-antiquark pair before they are re-absorbed as a photon (see Fig. 17.5). The quark-antiquark "bubble" produced here is strongly-interacting. Because the relevant energy scale is a low one, set by the muon mass, determining the effect of the bubble on a_μ requires a fully nonperturbative QCD calculation. This LO-HVP contribution is straightforward to calculate in lattice QCD. It requires the same two-point correlation function $C_{XY}(t, \boldsymbol{p}=0) = \sum_{\boldsymbol{x}} \langle O_X(t,\boldsymbol{x}) O_Y^\dagger(0)\rangle$ (see Sec. 17.2.2) used to determine the spectrum of flavor-diagonal vector mesons (because O here is the QED current that couples to the photon). Instead of fitting $C_{XY}(t)$ as a function of time separation, t, between O_X and O_Y to isolate specific states, here $C_{XY}(t)$ is multiplied by a kernel function, $K(t)$, and summed over all t (and therefore all states) to obtain the LO-HVP contribution [326, 327]. The challenge in doing this comes from the need to achieve very high accuracy. Vector-vector correlation functions suffer from exponentially falling signal/noise as t increases (see Sec. 17.2.2) and this is particularly problematic for the correlation functions constructed from u and d quark fields that yield 90% of the LO-HVP. In the u/d case the LO-HVP time-sum has a more significant contribution from large t than for heavier quarks and the signal/noise problem is worse, making it harder to achieve good statistical accuracy. A further issue is that of the finite-volume of the lattice. Although the u/d correlation function is dominated by the ρ meson, the lowest-energy ground-state, which starts to be significant at large t values, is made of two pions. These light long-wavelength particles can 'see' the lattice boundary, generating finite-volume effects that must be corrected using ChPT or other methods.

As well as calculating the LO-HVP contribution in the continuum and chiral limits from the vector-vector correlation for each quark flavor as described above, additional small corrections must be determined from quark-line disconnected correlation functions, from QED and from $m_u \neq m_d$ effects. The first complete LQCD calculation of the LO-HVP contribution appeared in 2020 from the BMW collaboration with sub-percent uncertainty [328]. Since then multiple LQCD collaborations have obtained accurate results for different pieces of the LO-HVP allowing stringent comparisons between them and enabling a strong consensus to be obtained on the result. A particularly useful approach has been to determine the LO-HVP in a "time-window" on the lattice [327,329]. By summing over a time range that cuts out large t values, both the statistical and systematic uncertainties can be improved. Eight different groups using six different quark actions have each achieved between 0.2% and 1% precision for u/d quarks with $m_u = m_d$ in a time window from 0.4 to 1.0 fm (with rounded edges of width 0.15 fm) [328, 330–337]. The striking agreement between the results (most of which were 'blinded' during analysis) represents one of the best tests of LQCD that has been done.

The 2025 White Paper from the Muon $g-2$ Theory Initiative [323] quotes an average value for the LO-HVP from lattice QCD of $713.2(6.1) \times 10^{-11}$ [328–334, 336–345]. It is this value, added to the other contributions to $a_\mu^{\rm SM}$, that yields the SM theory result in agreement with experiment quoted above and shown in Fig. 17.4 (and dominates its uncertainty). Note that the 2025 LO-HVP value is larger than that in the 2020 White Paper [346] by 2.8σ. The earlier value was obtained using a 'data-driven' approach in which experimental data for the cross-section for $e^+e^- \to$ hadrons as a function of the centre-of-mass energy, $\sqrt{s}$, are converted using analyticity and the optical theorem into values for the hadronic vacuum polarisation function. The first hints of tension between LQCD and the data-driven value came in 2020 [328] and this has become more significant with the LQCD focusing on time-windows, since a disagreement in any time-window is sufficient to demonstrate a disagreement in the underlying hadronic vacuum polarisation function. The lattice LO-HVP value from the 0.4–1.0 fm window [323] now disagrees with that from the data-driven approach using pre-2020 experimental data [347] by 5σ. The channel which contributes most to the data-driven LO-HVP is $e^+e^- \to \pi^+\pi^-$ at low values of $\sqrt{s} < 1$ GeV^2. New values for this cross-section from the CMD3 collaboration in 2023 [348] are higher than previous results and in tension with them so that a combination has not proved possible. LQCD favors the CMD3 results.

A quantity linked to the LO-HVP is the hadronic contribution to the running of the QED coupling since both depend on the hadronic vacuum polarization function. In tandem with LO-HVP calculations, some lattice groups have calculated $\Delta\alpha_{\rm had}$ for a range of spacelike momenta, $Q^2 < 10$ GeV^2. Again, tension is seen at these Q^2 values with the pre-2020 data-driven results but the tension is much diminished on translating the results to the scale M_Z so that both agree with global EW fit values for $\Delta\alpha_{\rm had}(M_Z^2)$ [328, 349].

Along with the resolution of the issues in the experimental e^+e^- data, future progress on the LO-HVP will require reduced uncertainty from lattice QCD; an uncertainty on the SM a_μ comparable to that of the experiment will require the LO-HVP to be determined to 0.2%. This may need a combination of lattice QCD and data-driven approaches in complementary time-windows [337, 350].

The LO-HVP contribution to $a_\mu^{\rm SM}$ appears at $\mathcal{O}(\alpha^2)$. QCD contributions at $\mathcal{O}(\alpha^3)$ are about 70 times smaller and include higher-order HVP pieces as well as a diagram in which a quark bubble is connected to four photons. This is known as the hadronic light-by-light (HLbL) contribution (see Fig. 17.5). Although small, it must be determined to 10% accuracy to reach the uncertainty aim for $a_\mu^{\rm SM}$. Three LQCD groups employing different quark actions have performed direct calculations of the HLbL contribution, using a number of ingenious methods to handle the four-point correlation functions needed [351–355]. Good agreement is found and the 2025 White paper averages them to give $122.5(9.0) \times 10^{-11}$ as the HLbL contribution to a_μ. LQCD calculations are also being done to provide hadronic input to the phenomenological framework for determining the HLbL contribution. The most important of these are the transition form factors, $F_{P\gamma^*\gamma^*}(q_1^2, q_2^2)$ for pseudoscalar (π^0, η, η' etc.) meson exchange. The form factor calculation requires three-point correlation functions with a weighted sum over the time separation of the two photons to fix the (spacelike) photon virtualities. At $q_1^2 = q_2^2 = 0$ the π^0 form factor yields $\Gamma(\pi^0 \to \gamma\gamma)$ and the π^0 lifetime, for comparison to experiment. Four lattice groups using four different quark actions have calculated the π^0 pole contribution to the HLbL with good agreement [356–359]. Overall the phenomenological approach to the HLbL gives a total result in agreement with the direct lattice QCD value within 2σ, allowing a reliable combination with an uncertainty of 8.5% [323], nearly a factor of 2 improvement over that in 2020 [346] and now at the level needed.

17.3.8 *Nucleon structure*

Another topic under active investigation is nucleon structure. Matrix elements of local currents, $\langle N(P',s')|J|N(P,s)\rangle$, can be computed on the lattice using techniques similar to those used for

Int. J. Mod. Phys. A 2026.41. Downloaded from www.worldscientific.com by UNIVERSITY OF CALIFORNIA @ BERKELEY on 09/16/26. Re-use and distribution is strictly not permitted, except for Open Access articles.

meson semileptonic decays. Some of the challenges involved are the rapid degradation of the signal-to-noise ratio of correlation functions, behaving like $e^{-(E_N-3m_\pi/2)t}$ as a function of the Euclidean time separation [131] (this generalizes the result given in Sec.17.2.2 to moving nucleons with energy $E_N(P)$), excited-state contamination at finite t, such as those from nearby nucleon-pion states [360], and additional sources of statistical noise for quark-disconnected contractions and gluonic currents. In matrix elements of isovector quark currents, the disconnected contributions cancel for $m_u = m_d$. The isovector axial charge, which corresponds to a zero-momentum matrix element of the axial current, has been calculated on the lattice with 1%-level precision [361]. The latest results for the axial, scalar, and tensor charges of the nucleon—both isovector and flavor-diagonal—are reviewed by FLAG [85]. Introducing a nonzero momentum transfer, one can extract form factors in much the same way. Lattice calculations of the electromagnetic form factors are approaching the precision needed to compare with the experimental data on ep scattering; see, e.g., Refs. [362, 363]. The axial form factors play a crucial role in the estimate of the expected event rate in the current and future neutrino experiments, such as T2K and DUNE, and lattice calculations are also reaching the required precision, as reviewed in Ref. [364].

Moving beyond matrix elements of local currents, of particular interest for collider physics are parton structure functions and parton distribution functions. Their experimental determination is discussed in the "Structure Functions" section of the Review of Particle Properties. Lattice calculations increasingly contribute to the knowledge of these quantities, using methods described in the following; see [365] for a recent review. Here we provide a brief summary.

The partonic structure functions of nucleon are defined through the hadronic tensor $W_{\mu\nu}(q,\nu) = \frac{1}{4\pi}\int d^4z\, e^{iqz}\langle N(P)|[J^\dagger_\mu(z), J_\nu(0)]|N(P)\rangle$ for a nucleon state $|N(P)\rangle$ with four-momentum P. It becomes a function of $x = Q^2/2M\nu$ ($Q^2 \equiv -q^2$ and $\nu = q\cdot P/M$ with M the nucleon mass) in the limit of Q^2 and $\nu \to \infty$ (Bjorken scaling). In this kinematical limit, the two inserted currents $J^\dagger_\mu(z)$ and $J_\nu(0)$ are separated nearly on the light-cone, and its direct computation on the Euclidean lattice is ill-defined. Instead, one can use OPE to represent the current product in terms of local operators, for which the lattice calculation becomes possible at least for the lowest orders of the OPE, which corresponds to an expansion in $1/Q^2$ (or in terms of twist, strictly speaking). For example, the lowest-order moment $\langle x\rangle$ is a matrix element of operators of the form $\bar{q}\gamma_\mu D_\nu q$, and it provides an x-moment of the structure function. (There are different quantities depending on flavour and spin compositions.) Currently available results are summarized in the FLAG review [85]. Lattice calculations of higher moments are complicated by power divergences; methods to avoid this issue have been proposed in, e.g., Refs. [366–368] and are being implemented.

There are also methods that attempt to directly obtain the x-dependence of the Parton Distribution Functions (PDF) rather than their x-moments. One possibility is to compute the temporal Fourier transformation of $W_{\mu\nu}(q,\nu)$, which is a function of spatial momenta $\boldsymbol{P}$, $\boldsymbol{q}$ and the time separation τ between the currents [369]. It contains contributions from all possible states generated between the currents with a factor $e^{-q^0\tau}$, and the ν dependence (or q^0 dependence in the rest frame of the N) can be reproduced if one can invert the Laplace transform using techniques like the Backus-Gilbert method [157] and its variant [158] or the Maximum Entropy Method [370, 371]. This reconstruction is, however, an example of the infamous inverse problem and no general solution is known. The methods being studied are closely related to those being developed for calculating inclusive decay rates; see Sec. 17.2.4. The problem may be circumvented if one is interested in the hadronic tensor in a different kinematical setup, e.g. the Compton amplitude, for which q^0 is too small to produce any real hadronic states between the two currents [367]. The Compton amplitude can be written using a Cauchy integral of the hadronic tensor with physical kinematics, so that some constraints can be obtained for the structure functions.

The approach proposed by Ji [372] treats a matrix element of the form $\langle N(P)|\bar{q}(z)\gamma_\mu W(0,z)q(0)|N(P)\rangle$ with a Wilson line $W(0,z) \equiv \exp[ig\int_0^z dz' A_z(z')]$ connecting the quark fields separated in spatial z-direction on the lattice. The result can be related to PDF in the limit of large $\boldsymbol{P}$. The method is under active theoretical study including the renormalization of the non-local operator as well as the necessity of large momentum. The large momentum limit can be approached with the help of the Large Momentum Effective Theory [373]. See [365], for more details.

The signal-to-noise problem mentioned earlier becomes even more severe for large-momentum nucleon states. Several techniques have been introduced to improve the signal by modifying the interpolating operator to produce the nucleon state, including momentum-smearing [374] and the use of kinematically enhanced gamma structures [375].

More details of nucleon structure can be probed by determining Generalized Parton Distributions (GPDs), through which one can obtain the angular momentum distributions of partons. Another way to study the three-dimensional structure of the nucleon is to determine Transverse Momentum-dependent Distributions (TMDs). Developing methods to calculate these quantities is an active research area; for a recent review, see [376–378], for example. Two key ingredients in determinations of TMDs are the so-called soft function and the Collins-Soper kernel; both can be computed on the lattice [379].

Finally, we note that there are ongoing lattice calculations of the nucleon electric dipole moments caused by a nonzero value of $\theta_{\rm QCD}$ or by BSM physics; see, for example, Ref. [380] for a recent review.

17.3.9 *Other applications of lattice QCD*

In this review we have concentrated on applications of LQCD that are relevant to the quantities discussed in the Review of Particle Properties. We have not considered at all several other applications that are being actively pursued by simulations. Here we list the major such applications. The reader can consult the aforementioned texts [2–4] for further details, as well as the proceedings of recent lattice conferences [381], and several recent white papers [382, 383]

LQCD can be used, in principle, to simulate QCD at non-zero temperature and density, and in particular to study how confinement and chiral-symmetry breaking are lost as T and μ (the chemical potential) are increased. It is found that, for the physical values of the quark masses, the deconfinement and chiral-symmetry-restoration transitions are smooth crossovers, rather than phase transitions, and that they occur together. This is of relevance to heavy-ion collisions, the early Universe and neutron-star structure. In practice, finite-temperature simulations are computationally tractable and relatively mature, while simulations at finite μ suffer from a "sign problem" and are at a less developed stage.

Finally, we note that there is much recent interest in studying QCD-like theories with more fermions, possibly in other representations of the gauge group (see, e.g., [383,384]). The main interest is to find nearly-conformal theories which might be candidates for "walking technicolor" models.

17.4 Outlook

While LQCD calculations have made major strides in the last decade, and are now playing a key role in constraining the Standard Model, there are many calculations that could be done in principle but are not yet mature due to limitations in computational resources. As we move to exascale resources (10^{18} floating point operations per second), the list of mature calculations will grow. In the longer term, LQCD may be able to harness the power of quantum computers, including their potential for new types of calculation. How to do this is an active area of study, see, for example [385].

Examples of calculations that we expect to mature in the next few years are results for B meson and Λ_b baryon form factors covering the full range of q^2 (see Sec.17.3.3); results for excited hadrons, including quark-model exotics, at close to physical light-quark masses; results for structure functions and related parton distribution functions (see Sec.17.3.8); results for a variety of nucleon matrix elements; $\pi \to \gamma\gamma$ and related amplitudes; long-

Int. J. Mod. Phys. A 2026.41. Downloaded from www.worldscientific.com by UNIVERSITY OF CALIFORNIA @ BERKELEY on 09/16/26. Re-use and distribution is [redacted] except for Open Access articles.

distance contributions to $\overline{K} \leftrightarrow K$ mixing and rare kaon decays such as $K \to \pi\nu\bar{\nu}$; and results for inclusive decay rates (see Sec.17.2.4). There will also be steady improvement in the precision attained for the mature quantities discussed in previous sections. For example, an improvement of a factor of 2 in the uncertainty of QCD contributions to a_μ is required for better alignment with the experimental uncertainty (see Sec. 17.3.7). The detailed error budgets that accompany many lattice QCD calculations make it possible to see what area needs improvement for future precision gains and to judge what gains may be possible.

17.5 Acknowledgments

We are grateful to David Lin and Alejandro Vaquero for comments and suggestions.

References

[1] K. G. Wilson, Phys. Rev. **D10**, 2445 (1974).

[2] T. Degrand & C. DeTar, "Lattice Methods for Quantum Chromodynamics," World Scientific (2006).

[3] C. Gattringer & C.B. Lang, "Quantum Chromodynamics on the Lattice: An Introductory Presentation," Springer (2009).

[4] "Modern Pespectives in Lattice QCD: quantum field theory and high performance computing" (Lecture notes of the Les Houches Summer School, Vol. 93) eds. L. Lellouch *et al.*, Oxford Univ. Press. (Aug. 2011).

[5] W. Zimmermann, in "Lectures on Elementary Particles and Quantum Field Theory", ed. S. Deser et al., MIT Press, Cambridge, MA (1971); K. Symanzik, Nucl. Phys. **B226**, 187 (1983); K. Symanzik, Nucl. Phys. **B226**, 205 (1983).

[6] M. Lüscher and P. Weisz, Commun. Math. Phys. **97**, 59 (1985), [Erratum: Commun. Math. Phys. 98, 433(1985)].

[7] Y. Iwasaki (1983), UT-HEP-118, [arXiv:1111.7054].

[8] H. B. Nielsen and M. Ninomiya, Phys. Lett. **105B**, 219 (1981).

[9] B. Sheikholeslami and R. Wohlert, Nucl. Phys. **B259**, 572 (1985).

[10] K. Jansen *et al.*, Phys. Lett. **B372**, 275 (1996), [hep-lat/9512009].

[11] S. Dürr *et al.*, Phys. Lett. B **705**, 477 (2011), [arXiv:1106.3230].

[12] N. Ishizuka *et al.*, Phys. Rev. **D92**, 7, 074503 (2015), [arXiv:1505.05289].

[13] A. Francis *et al.*, Comput. Phys. Commun. **255**, 107355 (2020), [arXiv:1911.04533].

[14] R. Frezzotti *et al.* (Alpha), JHEP **08**, 058 (2001), [hep-lat/0101001].

[15] R. Frezzotti and G. C. Rossi, JHEP **08**, 007 (2004), [hep-lat/0306014].

[16] R. Frezzotti and G. C. Rossi, Nucl. Phys. Proc. Suppl. **128**, 193 (2004), [hep-lat/0311008].

[17] R. Frezzotti and G. C. Rossi, JHEP **10**, 070 (2004), [hep-lat/0407002].

[18] L. Susskind, Phys. Rev. **D16**, 3031 (1977); N. Kawamoto and J. Smit, Nucl. Phys. B **192**, 100 (1981); H. S. Sharatchandra, H. J. Thun and P. Weisz, Nucl. Phys. B **192**, 205 (1981).

[19] M. Golterman, PoS **CONFINEMENT8**, 014 (2008), [arXiv:0812.3110].

[20] C. Bernard, Phys. Rev. **D73**, 114503 (2006), [hep-lat/0603011]; S. R. Sharpe, PoS **LAT2006**, 022 (2006), [hep-lat/0610094].

[21] J. A. Bailey, Phys. Rev. D **75**, 114505 (2007), [hep-lat/0611023]; Y. Lin *et al.*, Phys. Rev. D **103**, 5, 054510 (2021), [arXiv:2010.10455].

[22] G. P. Lepage, Phys. Rev. **D59**, 074502 (1999), [hep-lat/9809157].

[23] A. Bazavov *et al.* (MILC), Rev. Mod. Phys. **82**, 1349 (2010), [arXiv:0903.3598].

[24] E. Follana *et al.* (HPQCD, UKQCD), Phys. Rev. **D75**, 054502 (2007), [hep-lat/0610092].

[25] C. T. H. Davies *et al.*, Phys. Rev. **D82**, 114504 (2010), [arXiv:1008.4018].

[26] C. McNeile *et al.*, Phys. Rev. **D85**, 031503 (2012), [arXiv:1110.4510].

[27] G. C. Donald *et al.*, Phys. Rev. **D86**, 094501 (2012), [arXiv:1208.2855].

[28] P. H. Ginsparg and K. G. Wilson, Phys. Rev. **D25**, 2649 (1982).

[29] P. Hasenfratz, V. Laliena and F. Niedermayer, Phys. Lett. **B427**, 125 (1998), [hep-lat/9801021].

[30] M. Lüscher, Phys. Lett. **B428**, 342 (1998), [hep-lat/9802011].

[31] D. B. Kaplan, Phys. Lett. **B288**, 342 (1992), [hep-lat/9206013]; Y. Shamir, Nucl. Phys. **B406**, 90 (1993), [hep-lat/9303005]; Y. Shamir, Nucl. Phys. **B417**, 167 (1994), [hep-lat/9310006].

[32] H. Neuberger, Phys. Lett. **B417**, 141 (1998), [hep-lat/9707022]; H. Neuberger, Phys. Lett. **B427**, 353 (1998), [hep-lat/9801031].

[33] A. Borici, NATO Sci. Ser. C **553**, 41 (2000), [hep-lat/9912040].

[34] A. D. Kennedy (2006), [hep-lat/0607038].

[35] Z. Bai *et al.* (RBC, UKQCD), Phys. Rev. Lett. **115**, 21, 212001 (2015), [arXiv:1505.07863].

[36] R. Abbott *et al.* (RBC, UKQCD), Phys. Rev. D **102**, 5, 054509 (2020), [arXiv:2004.09440].

[37] T. Blum *et al.* (2023), [arXiv:2306.06781].

[38] E. Shintani *et al.* (JLQCD), Phys. Rev. Lett. **101**, 242001 (2008), [arXiv:0806.4222].

[39] P. A. Boyle *et al.*, JHEP **12**, 008 (2017), [arXiv:1701.02644].

[40] K. Nakayama, B. Fahy and S. Hashimoto, Phys. Rev. **D94**, 5, 054507 (2016), [arXiv:1606.01002].

[41] D. Hatton *et al.* (HPQCD), Phys. Rev. D **102**, 5, 054511 (2020), [arXiv:2005.01845].

[42] J. Harrison and C. T. H. Davies (HPQCD), Phys. Rev. D **105**, 9, 094506 (2022), [arXiv:2105.11433].

[43] A. Bazavov *et al.*, Phys. Rev. **D98**, 7, 074512 (2018), [arXiv:1712.09262].

[44] A. Bazavov *et al.* (Fermilab Lattice, MILC, TUMQCD), Phys. Rev. **D98**, 5, 054517 (2018), [arXiv:1802.04248].

[45] D. Hatton *et al.*, Phys. Rev. D **103**, 5, 054512 (2021), [arXiv:2101.08103].

[46] E. Eichten and B. R. Hill, Phys. Lett. **B234**, 511 (1990).

[47] J. Heitger and R. Sommer (ALPHA), JHEP **02**, 022 (2004), [hep-lat/0310035]; B. Blossier *et al.* (ALPHA), JHEP **12**, 039 (2010), [arXiv:1006.5816].

[48] B. A. Thacker and G. P. Lepage, Phys. Rev. **D43**, 196 (1991); G. P. Lepage *et al.*, Phys. Rev. **D46**, 4052 (1992), [hep-lat/9205007].

[49] R. J. Dowdall *et al.* (HPQCD), Phys. Rev. **D85**, 054509 (2012), [arXiv:1110.6887].

[50] A. X. El-Khadra, A. S. Kronfeld and P. B. Mackenzie, Phys. Rev. **D55**, 3933 (1997), [hep-lat/9604004].

[51] S. Aoki, Y. Kuramashi and S.-i. Tominaga, Prog. Theor. Phys. **109**, 383 (2003), [hep-lat/0107009].

[52] N. H. Christ, M. Li and H.-W. Lin, Phys. Rev. **D76**, 074505 (2007), [hep-lat/0608006].

[53] Y. Aoki *et al.* (RBC, UKQCD), Phys. Rev. **D86**, 116003 (2012), [arXiv:1206.2554].

Int. J. Mod. Phys. A 2026.41. Downloaded from www.worldscientific.com
by UNIVERSITY OF CALIFORNIA @ BERKELEY on 09/16/26. Re-use and distribution is strictly not permitted, except for Open Access articles.

[54] N. H. Christ *et al.*, Phys. Rev. **D91**, 5, 054502 (2015), [arXiv:1404.4670].

[55] M. B. Oktay and A. S. Kronfeld, Phys. Rev. **D78**, 014504 (2008), [arXiv:0803.0523].

[56] J. A. Bailey *et al.*, Eur. Phys. J. **C77**, 11, 768 (2017), [arXiv:1701.00345].

[57] B. Blossier *et al.* (ETM), JHEP **04**, 049 (2010), [arXiv:0909.3187].

[58] A. Bussone *et al.* (ETM), Phys. Rev. D **93**, 11, 114505 (2016), [arXiv:1603.04306].

[59] S. Borsanyi *et al.*, Science **347**, 1452 (2015), [arXiv:1406.4088].

[60] S. Aoki *et al.* (Flavour Lattice Averaging Group), Eur. Phys. J. C **80**, 2, 113 (2020), [arXiv:1902.08191].

[61] M. Hayakawa and S. Uno, Prog. Theor. Phys. **120**, 413 (2008), [arXiv:0804.2044].

[62] N. Carrasco *et al.*, Phys. Rev. **D91**, 7, 074506 (2015), [arXiv:1502.00257].

[63] M. Di Carlo *et al.*, Phys. Rev. D **105**, 7, 074509 (2022), [arXiv:2109.05002].

[64] N. H. Christ *et al.*, Phys. Rev. D **108**, 1, 014501 (2023), [arXiv:2304.08026].

[65] B. Lucini *et al.*, JHEP **02**, 076 (2016), [arXiv:1509.01636].

[66] L. Bushnaq *et al.* (RCstar), JHEP **03**, 012 (2023), [arXiv:2209.13183].

[67] R. Horsley *et al.*, J. Phys. G **43**, 10, 10LT02 (2016), [arXiv:1508.06401].

[68] R. Horsley *et al.* (CSSM, QCDSF, UKQCD), J. Phys. G **46**, 115004 (2019), [arXiv:1904.02304].

[69] Z. R. Kordov *et al.* (CSSM/QCDSF/UKQCD), Phys. Rev. D **101**, 3, 034517 (2020), [arXiv:1911.02186].

[70] T. Ishikawa *et al.*, Phys. Rev. Lett. **109**, 072002 (2012), [arXiv:1202.6018].

[71] M. G. Endres *et al.*, Phys. Rev. Lett. **117**, 7, 072002 (2016), [arXiv:1507.08916].

[72] G. M. de Divitiis *et al.* (RM123), Phys. Rev. **D87**, 11, 114505 (2013), [arXiv:1303.4896].

[73] D. Giusti *et al.*, Phys. Rev. **D95**, 11, 114504 (2017), [arXiv:1704.06561].

[74] P. Boyle *et al.*, JHEP **09**, 153 (2017), [arXiv:1706.05293].

[75] S. Basak *et al.* (MILC), Phys. Rev. D **99**, 3, 034503 (2019), [arXiv:1807.05556].

[76] D. Hatton, C. T. H. Davies and G. P. Lepage, Phys. Rev. D **102**, 9, 094514 (2020), [arXiv:2009.07667].

[77] D. Hatton *et al.*, Phys. Rev. D **103**, 11, 114508 (2021), [arXiv:2102.09609].

[78] F. Bloch and A. Nordsieck, Phys. Rev. **52**, 54 (1937).

[79] D. Giusti *et al.*, Phys. Rev. Lett. **120**, 7, 072001 (2018), [arXiv:1711.06537].

[80] M. Di Carlo *et al.*, Phys. Rev. D **100**, 3, 034514 (2019), [arXiv:1904.08731].

[81] P. Boyle *et al.*, JHEP **02**, 242 (2023), [arXiv:2211.12865].

[82] C. T. Sachrajda *et al.*, PoS **LATTICE2019**, 162 (2019), [arXiv:1910.07342]; C.-Y. Seng *et al.*, JHEP **10**, 179 (2020), [arXiv:2009.00459].

[83] R. Sommer, Nucl. Phys. B **411**, 839 (1994), [hep-lat/9310022].

[84] M. Lüscher, JHEP **08**, 071 (2010), [Erratum: JHEP 03, 092 (2014)], [arXiv:1006.4518].

[85] Y. Aoki *et al.* (Flavour Lattice Averaging Group (FLAG)) (2024), [arXiv:2411.04268].

[86] M. Bruno *et al.* (ALPHA), Phys. Rev. Lett. **114**, 10, 102001 (2015), [arXiv:1410.8374].

[87] A. Bazavov *et al.* (Fermilab Lattice, MILC), Phys. Rev. **D93**, 11, 113016 (2016), [arXiv:1602.03560].

[88] R. J. Dowdall *et al.*, Phys. Rev. **D86**, 094510 (2012), [arXiv:1207.5149].

[89] C. McNeile *et al.*, Phys. Rev. **D86**, 074503 (2012), [arXiv:1207.0994].

[90] S. Schaefer, R. Sommer and F. Virotta (ALPHA), Nucl. Phys. **B845**, 93 (2011), [arXiv:1009.5228].

[91] M. Lüscher, PoS **LATTICE2010**, 015 (2010), [arXiv:1009.5877].

[92] R. Brower *et al.*, Phys. Lett. **B560**, 64 (2003), [hep-lat/0302005].

[93] S. Aoki *et al.*, Phys. Rev. **D76**, 054508 (2007), [arXiv:0707.0396].

[94] C. Bernard and D. Toussaint (MILC), Phys. Rev. D **97**, 7, 074502 (2018), [arXiv:1707.05430].

[95] M. Luscher and S. Schaefer, JHEP **07**, 036 (2011), [arXiv:1105.4749].

[96] N. Husung, P. Marquard and R. Sommer, Eur. Phys. J. C **80**, 3, 200 (2020), [arXiv:1912.08498].

[97] N. Husung, P. Marquard and R. Sommer, Phys. Lett. B **829**, 137069 (2022), [arXiv:2111.02347].

[98] N. Husung, Eur. Phys. J. C **83**, 2, 142 (2023), [arXiv:2206.03536].

[99] G. Colangelo, S. Dürr and C. Haefeli, Nucl. Phys. **B721**, 136 (2005), [hep-lat/0503014].

[100] M. Lüscher, Commun. Math. Phys. **104**, 177 (1986).

[101] G. Martinelli *et al.*, Nucl. Phys. **B445**, 81 (1995), [hep-lat/9411010].

[102] M. Lüscher *et al.*, Nucl. Phys. **B384**, 168 (1992), [hep-lat/9207009].

[103] G. Martinelli *et al.*, Phys. Lett. **B411**, 141 (1997), [hep-lat/9705018].

[104] B. Colquhoun *et al.*, Phys. Rev. **D91**, 7, 074514 (2015), [arXiv:1408.5768].

[105] D. Hatton *et al.* (HPQCD), Phys. Rev. D **100**, 11, 114513 (2019), [arXiv:1909.00756].

[106] M. Lüscher *et al.*, Nucl. Phys. **B413**, 481 (1994), [hep-lat/9309005]; M. Della Morte *et al.* (ALPHA), Nucl. Phys. **B713**, 378 (2005), [hep-lat/0411025].

[107] M. Tomii *et al.* (JLQCD), Phys. Rev. **D94**, 5, 054504 (2016), [arXiv:1604.08702].

[108] F. Karsch, H. Simma and T. Yoshie, PoS **LATTICE2022**, 244 (2023), [arXiv:2212.08392].

[109] S. Duane *et al.*, Phys. Lett. **B195**, 216 (1987).

[110] D. J. E. Callaway and A. Rahman, Phys. Rev. Lett. **49**, 613 (1982).

[111] D. J. E. Callaway and A. Rahman, Phys. Rev. D **28**, 1506 (1983).

[112] J. Polonyi and H. W. Wyld, Phys. Rev. Lett. **51**, 2257 (1983), [Erratum: Phys.Rev.Lett. 52, 401 (1984)].

[113] N. Metropolis *et al.*, J. Chem. Phys. **21**, 1087 (1953).

[114] M. A. Clark and A. D. Kennedy, Phys. Rev. Lett. **98**, 051601 (2007), [hep-lat/0608015].

[115] J. C. Sexton and D. H. Weingarten, Nucl. Phys. B **380**, 665 (1992).

[116] M. Hasenbusch, Phys. Lett. **B519**, 177 (2001), [hep-lat/0107019].

[117] M. Lüscher, JHEP **05**, 052 (2003), [hep-lat/0304007].

[118] M. Lüscher, Comput. Phys. Commun. **156**, 209 (2004), [hep-lat/0310048].

[119] M. Lüscher, JHEP **07**, 081 (2007), [arXiv:0706.2298].

[120] M. Lüscher, JHEP **12**, 011 (2007), [arXiv:0710.5417].

Int. J. Mod. Phys. A 2026.41. Downloaded from www.worldscientific.com by UNIVERSITY OF CALIFORNIA @ BERKELEY on 09/16/26. Re-use and distribution is [redacted] except for Open Access articles.

[121] A. Stathopoulos and K. Orginos, SIAM J. Sci. Comput. **32**, 439 (2010), [arXiv:0707.0131].

[122] P. A. Boyle (2014), [arXiv:1402.2585].

[123] R. Babich *et al.*, Phys. Rev. Lett. **105**, 201602 (2010), [arXiv:1005.3043].

[124] A. Frommer *et al.*, SIAM J. Sci. Comput. **36**, A1581 (2014), [arXiv:1303.1377].

[125] M. Bruno, S. Schaefer and R. Sommer (ALPHA), JHEP **08**, 150 (2014), [arXiv:1406.5363].

[126] M. Creutz, Phys. Rev. **D38**, 1228 (1988); R. Gupta, G. W. Kilcup and S. R. Sharpe, Phys. Rev. **D38**, 1278 (1988).

[127] P. Fritzsch *et al.*, PoS **LATTICE2021**, 465 (2022), [arXiv:2111.11544].

[128] M. Cè *et al.*, PoS **LATTICE2021**, 383 (2022), [arXiv:2110.15375].

[129] M. Lüscher, EPJ Web Conf. **175**, 01002 (2018), [arXiv:1707.09758].

[130] G. Parisi, Phys. Rept. **103**, 203 (1984).

[131] G. P. Lepage, in "Theoretical Advanced Study Institute in Elementary Particle Physics," (1989).

[132] E. Shintani *et al.*, Phys. Rev. D **91**, 11, 114511 (2015), [arXiv:1402.0244].

[133] M. Luscher and P. Weisz, JHEP **09**, 010 (2001), [hep-lat/0108014]; H. B. Meyer, JHEP **01**, 048 (2003), [hep-lat/0209145]; H. B. Meyer, JHEP **01**, 030 (2004), [hep-lat/0312034]; M. Cè, L. Giusti and S. Schaefer, Phys. Rev. D **93**, 9, 094507 (2016), [arXiv:1601.04587]; M. Dalla Brida *et al.*, Phys. Lett. B **816**, 136191 (2021), [arXiv:2007.02973]; L. Barca *et al.*, Phys. Rev. D **110**, 5, 054515 (2024), [arXiv:2406.12656].

[134] M. Lüscher and U. Wolff, Nucl. Phys. **B339**, 222 (1990).

[135] J. J. Dudek *et al.*, Phys. Rev. **D82**, 034508 (2010), [arXiv:1004.4930]; J. J. Dudek *et al.*, Phys. Rev. **D83**, 111502 (2011), [arXiv:1102.4299]; R. G. Edwards *et al.*, Phys. Rev. **D84**, 074508 (2011), [arXiv:1104.5152].

[136] G. P. Engel *et al.* (BGR [Bern-Graz-Regensburg]), Phys. Rev. **D82**, 034505 (2010), [arXiv:1005.1748]; D. Mohler *et al.*, Phys. Rev. Lett. **111**, 22, 222001 (2013), [arXiv:1308.3175].

[137] M. S. Mahbub *et al.*, Annals Phys. **342**, 270 (2014), [arXiv:1310.6803].

[138] J. Bulava *et al.*, Nucl. Phys. **B910**, 842 (2016), [arXiv:1604.05593].

[139] R. Brett *et al.*, Nucl. Phys. **B932**, 29 (2018), [arXiv:1802.03100].

[140] B. Hörz and A. Hanlon, Phys. Rev. Lett. **123**, 14, 142002 (2019), [arXiv:1905.04277].

[141] J. E. Mandula, G. Zweig and J. Govaerts, Nucl. Phys. **B228**, 91 (1983); J. E. Mandula and E. Shpiz, Nucl. Phys. **B232**, 180 (1984).

[142] H. B. Meyer and M. J. Teper, Nucl. Phys. **B658**, 113 (2003), [hep-lat/0212026].

[143] O. Bar, A. Broll and R. Sommer, Eur. Phys. J. C **83**, 8, 757 (2023), [arXiv:2306.02703].

[144] P. F. Bedaque, Phys. Lett. B **593**, 82 (2004), [arXiv:nucl-th/0402051].

[145] P. F. Bedaque and J.-W. Chen, Phys. Lett. B **616**, 208 (2005), [hep-lat/0412023].

[146] G. M. de Divitiis, R. Petronzio and N. Tantalo, Phys. Lett. B **595**, 408 (2004), [hep-lat/0405002].

[147] C. Bourrely, B. Machet and E. de Rafael, Nucl. Phys. **B189**, 157 (1981).

[148] C. G. Boyd, B. Grinstein and R. F. Lebed, Phys. Rev. Lett. **74**, 4603 (1995), [hep-ph/9412324].

[149] T. Becher and R. J. Hill, Phys. Lett. **B633**, 61 (2006), [hep-ph/0509090].

[150] C. Bourrely, I. Caprini and L. Lellouch, Phys. Rev. **D79**, 013008 (2009), [Erratum: Phys. Rev. D82, 099902(2010)], [arXiv:0807.2722].

[151] G. Colangelo *et al.*, Eur. Phys. J. C **71**, 1695 (2011), [arXiv:1011.4408].

[152] S. Aoki *et al.*, Eur. Phys. J. C **74**, 2890 (2014), [arXiv:1310.8555].

[153] S. Aoki *et al.*, Eur. Phys. J. **C77**, 2, 112 (2017), [arXiv:1607.00299].

[154] Y. Aoki *et al.* (Flavour Lattice Averaging Group (FLAG)), Eur. Phys. J. C **82**, 10, 869 (2022), [arXiv:2111.09849].

[155] M. Lüscher, Commun. Math. Phys. **105**, 153 (1986); M. Lüscher, Nucl. Phys. **B364**, 237 (1991).

[156] L. Maiani and M. Testa, Phys. Lett. **B245**, 585 (1990).

[157] M. T. Hansen, H. B. Meyer and D. Robaina, Phys. Rev. **D96**, 9, 094513 (2017), [arXiv:1704.08993].

[158] M. Hansen, A. Lupo and N. Tantalo, Phys. Rev. **D99**, 9, 094508 (2019), [arXiv:1903.06476]; J. Bulava and M. T. Hansen, Phys. Rev. D **100**, 3, 034521 (2019), [arXiv:1903.11735]; M. Bruno and M. T. Hansen, JHEP **06**, 043 (2021), [arXiv:2012.11488].

[159] J. Bulava *et al.*, JHEP **07**, 034 (2022), [arXiv:2111.12774]; T. Bergamaschi, W. I. Jay and P. R. Oare, Phys. Rev. D **108**, 7, 074516 (2023), [arXiv:2305.16190]; L. Del Debbio *et al.*, Eur. Phys. J. C **85**, 2, 185 (2025), [arXiv:2409.04413]; A. Patella and N. Tantalo, JHEP **01**, 091 (2025), [arXiv:2407.02069]; M. Bruno, L. Giusti and M. Saccardi, Phys. Rev. D **111**, 9, 094515 (2025), [arXiv:2407.04141].

[160] A. Evangelista *et al.* (Extended Twisted Mass), Phys. Rev. D **108**, 7, 074513 (2023), [arXiv:2308.03125].

[161] V. Bernard *et al.*, JHEP **01**, 019 (2011), [arXiv:1010.6018]; M. Doring *et al.*, Eur. Phys. J. **A47**, 139 (2011), [arXiv:1107.3988]; R. A. Briceño and Z. Davoudi, Phys. Rev. **D88**, 9, 094507 (2013), [arXiv:1204.1110]; M. T. Hansen and S. R. Sharpe, Phys. Rev. **D86**, 016007 (2012), [arXiv:1204.0826].

[162] R. A. Briceno, Phys. Rev. D **89**, 7, 074507 (2014), [arXiv:1401.3312].

[163] N. Ishii, S. Aoki and T. Hatsuda, Phys. Rev. Lett. **99**, 022001 (2007), [arXiv:nucl-th/0611096]; N. Ishii *et al.* (HAL QCD), Phys. Lett. B **712**, 437 (2012), [arXiv:1203.3642].

[164] M. Fischer *et al.* (Extended Twisted Mass, ETM), Phys. Lett. B **819**, 136449 (2021), [arXiv:2006.13805]; Y. Lyu *et al.*, Phys. Rev. Lett. **131**, 16, 161901 (2023), [arXiv:2302.04505]; P. Boyle *et al.*, Phys. Rev. Lett. **134**, 11, 111901 (2025), [arXiv:2406.19194]; Z. Wang *et al.* (2025), [arXiv:2502.03700].

[165] S. M. Dawid *et al.* (2025), [arXiv:2502.14348]; S. M. Dawid *et al.* (2025), [arXiv:2502.17976].

[166] F. Romero-López, PoS **LATTICE2022**, 235 (2023), [arXiv:2212.13793]; L. Liu, PoS **LATTICE2022**, 234 (2023); A. D. Hanlon, PoS **LATTICE2023**, 106 (2024), [arXiv:2402.05185]; J. T. Tsang, in "41st International Symposium on Lattice Field Theory," (2025), [arXiv:2503.05554].

[167] T. Inoue *et al.* (HAL QCD), Phys. Rev. **C91**, 1, 011001 (2015), [arXiv:1408.4892]; J. R. Green *et al.*, Phys. Rev. Lett. **127**, 24, 242003 (2021), [arXiv:2103.01054]; W. Detmold *et al.* (NPLQCD), Phys. Rev. D **111**, 11, 114501 (2025), [arXiv:2404.12039]; J. Bulava *et al.* (BaSc) (2025), [arXiv:2505.05547].

[168] J. R. Green, in "11th International Workshop on Chiral Dynamics," (2025), [arXiv:2502.15546]; C. Morningstar, in "11th International Workshop on Chiral Dynamics," (2025), [arXiv:2504.01950].

Int. J. Mod. Phys. A 2026.41. Downloaded from www.worldscientific.com
by UNIVERSITY OF CALIFORNIA @ BERKELEY on 09/16/26. Re-use and distribution is strictly not permitted, except for Open Access articles.

[169] K. Polejaeva and A. Rusetsky, Eur. Phys. J. **A48**, 67 (2012), [arXiv:1203.1241]; R. A. Briceno and Z. Davoudi, Phys. Rev. **D87**, 9, 094507 (2013), [arXiv:1212.3398]; M. T. Hansen and S. R. Sharpe, Phys. Rev. **D90**, 11, 116003 (2014), [arXiv:1408.5933]; M. T. Hansen and S. R. Sharpe, Phys. Rev. **D92**, 11, 114509 (2015), [arXiv:1504.04248]; R. Briceño, M. T. Hansen and S. R. Sharpe, Phys. Rev. **D95**, 7, 074510 (2017), [arXiv:1701.07465]; H. W. Hammer, J. Y. Pang and A. Rusetsky, JHEP **10**, 115 (2017), [arXiv:1707.02176]; R. A. Briceno, M. T. Hansen and S. R. Sharpe, Phys. Rev. **D99**, 1, 014516 (2019), [arXiv:1810.01429]; M. Mai and M. Döring, Eur. Phys. J. **A53**, 12, 240 (2017), [arXiv:1709.08222]; M. T. Hansen, F. Romero-López and S. R. Sharpe, JHEP **07**, 047 (2020), [Erratum: JHEP 02, 014 (2021)], [arXiv:2003.10974]; T. D. Blanton and S. R. Sharpe, Phys. Rev. D **103**, 5, 054503 (2021), [arXiv:2011.05520]; T. D. Blanton and S. R. Sharpe, Phys. Rev. D **104**, 3, 034509 (2021), [arXiv:2105.12094]; Z. T. Draper *et al.*, JHEP **07**, 226 (2023), [arXiv:2303.10219]; Z. T. Draper and S. R. Sharpe, JHEP **07**, 083 (2024), [arXiv:2403.20064].

[170] T. D. Blanton, F. Romero-López and S. R. Sharpe, Phys. Rev. Lett. **124**, 3, 032001 (2020), [arXiv:1909.02973]; C. Culver *et al.*, Phys. Rev. D **101**, 11, 114507 (2020), [arXiv:1911.09047]; A. Alexandru *et al.*, Phys. Rev. D **102**, 11, 114523 (2020), [arXiv:2009.12358]; R. Brett *et al.*, Phys. Rev. D **104**, 1, 014501 (2021), [arXiv:2101.06144]; Z. T. Draper *et al.*, JHEP **05**, 137 (2023), [arXiv:2302.13587].

[171] M. Mai *et al.* (GWQCD), Phys. Rev. Lett. **127**, 22, 222001 (2021), [arXiv:2107.03973]; H. Yan *et al.*, Phys. Rev. Lett. **133**, 21, 211906 (2024), [arXiv:2407.16659].

[172] M. T. Hansen, F. Romero-López and S. R. Sharpe, JHEP **06**, 051 (2024), [arXiv:2401.06609]; S. M. Dawid, F. Romero-López and S. R. Sharpe, JHEP **01**, 060 (2025), [arXiv:2409.17059].

[173] M. T. Hansen and S. R. Sharpe, Ann. Rev. Nucl. Part. Sci. **69**, 65 (2019), [arXiv:1901.00483]; M. Mai, M. Döring and A. Rusetsky, Eur. Phys. J. ST **230**, 6, 1623 (2021), [arXiv:2103.00577]; F. Romero-López, in "11th International Workshop on Chiral Dynamics," (2025), [arXiv:2504.00586].

[174] L. Lellouch and M. Lüscher, Commun. Math. Phys. **219**, 31 (2001), [hep-lat/0003023].

[175] T. Blum *et al.*, Phys. Rev. Lett. **108**, 141601 (2012), [arXiv:1111.1699]; T. Blum *et al.*, Phys. Rev. **D86**, 074513 (2012), [arXiv:1206.5142].

[176] T. Blum *et al.*, Phys. Rev. **D91**, 7, 074502 (2015), [arXiv:1502.00263].

[177] R. Briceño, M. T. Hansen and A. Walker-Loud, Phys. Rev. **D91**, 3, 034501 (2015), [arXiv:1406.5965].

[178] R. Briceño and M. T. Hansen, Phys. Rev. **D94**, 1, 013008 (2016), [arXiv:1509.08507].

[179] R. Briceño *et al.*, Phys. Rev. **D93**, 11, 114508 (2016), [arXiv:1604.03530].

[180] C. Alexandrou *et al.*, Phys. Rev. D **98**, 7, 074502 (2018), [Erratum: Phys.Rev.D 105, 019902 (2022)], [arXiv:1807.08357].

[181] A. Radhakrishnan, J. J. Dudek and R. G. Edwards (Hadron Spectrum), Phys. Rev. D **106**, 11, 114513 (2022), [arXiv:2208.13755].

[182] L. Leskovec *et al.*, Phys. Rev. Lett. **134**, 16, 161901 (2025), [arXiv:2501.00903].

[183] F. Müller and A. Rusetsky, JHEP **03**, 152 (2021), [arXiv:2012.13957].

[184] M. T. Hansen, F. Romero-López and S. R. Sharpe, JHEP **04**, 113 (2021), [arXiv:2101.10246].

[185] D. Agadjanov *et al.*, JHEP **06**, 043 (2016), [arXiv:1603.07205].

[186] S. Hashimoto, PTEP **2017**, 5, 053B03 (2017), [arXiv:1703.01881].

[187] G. Bailas, S. Hashimoto and T. Ishikawa, PTEP **2020**, 4, 043B07 (2020), [arXiv:2001.11779].

[188] C. Alexandrou *et al.* (Extended Twisted Mass Collaboration (ETMC)), Phys. Rev. Lett. **130**, 24, 241901 (2023), [arXiv:2212.08467].

[189] C. Alexandrou *et al.* (Extended Twisted Mass), Phys. Rev. Lett. **132**, 26, 261901 (2024), [arXiv:2403.05404].

[190] P. Gambino and S. Hashimoto, Phys. Rev. Lett. **125**, 3, 032001 (2020), [arXiv:2005.13730].

[191] P. Gambino *et al.*, JHEP **07**, 083 (2022), [arXiv:2203.11762].

[192] A. Barone *et al.*, JHEP **07**, 145 (2023), [arXiv:2305.14092].

[193] R. Kellermann *et al.* (2025), [arXiv:2504.03358].

[194] A. De Santis *et al.* (2025), [arXiv:2504.06063].

[195] H. Fukaya *et al.*, Phys. Rev. D **102**, 11, 114516 (2020), [arXiv:2010.01253].

[196] C. Bernard *et al.*, Nucl. Phys. Proc. Suppl. **119**, 170 (2003), [hep-lat/0209086].

[197] Y. Aoki *et al.*, PoS **LATTICE2024**, 412 (2025), [arXiv:2502.08303].

[198] S. Perantonis and C. Michael, Nucl. Phys. **B347**, 854 (1990).

[199] G. S. Bali and K. Schilling, Phys. Rev. **D46**, 2636 (1992).

[200] S. Necco and R. Sommer, Nucl. Phys. **B622**, 328 (2002), [hep-lat/0108008].

[201] J. M. Blairon *et al.*, Nucl. Phys. **B180**, 439 (1981).

[202] H. Fukaya *et al.* (JLQCD), Phys. Rev. Lett. **104**, 122002 (2010), [Erratum: Phys. Rev. Lett.105,159901(2010)], [arXiv:0911.5555].

[203] H. Fukaya *et al.* (JLQCD, TWQCD), Phys. Rev. **D83**, 074501 (2011), [arXiv:1012.4052].

[204] L. Giusti and M. Lüscher, JHEP **03**, 013 (2009), [arXiv:0812.3638].

[205] K. Cichy, E. Garcia-Ramos and K. Jansen, JHEP **10**, 175 (2013), [arXiv:1303.1954].

[206] G. P. Engel *et al.*, Phys. Rev. Lett. **114**, 11, 112001 (2015), [arXiv:1406.4987].

[207] G. P. Engel *et al.*, Phys. Rev. **D91**, 5, 054505 (2015), [arXiv:1411.6386].

[208] G. Cossu *et al.*, PTEP **2016**, 9, 093B06 (2016), [arXiv:1607.01099].

[209] G. S. Bali *et al.* (RQCD), JHEP **08**, 137 (2021), [arXiv:2106.05398].

[210] T. Blum *et al.* (RBC, UKQCD), Phys. Rev. **D93**, 7, 074505 (2016), [arXiv:1411.7017].

[211] P. A. Boyle *et al.* (RBC, UKQCD), Phys. Rev. D **110**, 3, 034501 (2024), [arXiv:2404.02297].

[212] B. J. Choi *et al.* (SWME), Phys. Rev. **D93**, 1, 014511 (2016), [arXiv:1509.00592].

[213] J. Laiho and R. S. Van de Water, PoS **LATTICE2011**, 293 (2011), [arXiv:1112.4861].

[214] T. Blum *et al.* (RBC, UKQCD), Phys. Rev. D **93**, 7, 074505 (2016), [arXiv:1411.7017].

[215] B. J. Choi *et al.* (SWME), Phys. Rev. D **93**, 1, 014511 (2016), [arXiv:1509.00592].

[216] E. Gamiz *et al.* (HPQCD), Phys. Rev. **D80**, 014503 (2009), [arXiv:0902.1815].

[217] R. J. Dowdall *et al.*, Phys. Rev. D **100**, 9, 094508 (2019), [arXiv:1907.01025].

[218] Y. Aoki *et al.*, Phys. Rev. **D91**, 11, 114505 (2015), [arXiv:1406.6192].

Int. J. Mod. Phys. A 2026.41. Downloaded from www.worldscientific.com by UNIVERSITY OF CALIFORNIA @ BERKELEY on 09/16/26. Re-use and distribution is [redacted] except for Open Access articles.

[219] N. Carrasco *et al.* (ETM), Phys. Rev. D **92**, 3, 034516 (2015), [arXiv:1505.06639].

[220] A. Bazavov *et al.*, Phys. Rev. **D97**, 3, 034513 (2018), [arXiv:1706.04622].

[221] M. Ademollo and R. Gatto, Phys. Rev. Lett. **13**, 264 (1964).

[222] H. Leutwyler and M. Roos, Z. Phys. **C25**, 91 (1984).

[223] P. A. Boyle *et al.*, Phys. Rev. Lett. **100**, 141601 (2008), [arXiv:0710.5136].

[224] V. Lubicz *et al.* (ETM), Phys. Rev. **D80**, 111502 (2009), [arXiv:0906.4728]; V. Lubicz *et al.* (ETM), PoS **LATTICE2010**, 316 (2010), [arXiv:1012.3573].

[225] P. A. Boyle *et al.* (RBC-UKQCD), Eur. Phys. J. **C69**, 159 (2010), [arXiv:1004.0886].

[226] A. Bazavov *et al.*, Phys. Rev. **D87**, 073012 (2013), [arXiv:1212.4993].

[227] T. Kaneko *et al.* (JLQCD), PoS **LATTICE2012**, 111 (2012), [arXiv:1211.6180].

[228] P. A. Boyle *et al.*, JHEP **08**, 132 (2013), [arXiv:1305.7217].

[229] P. A. Boyle *et al.* (RBC/UKQCD), JHEP **06**, 164 (2015), [arXiv:1504.01692].

[230] N. Carrasco *et al.*, Phys. Rev. **D93**, 11, 114512 (2016), [arXiv:1602.04113].

[231] A. Bazavov *et al.* (Fermilab Lattice, MILC), Phys. Rev. D **99**, 11, 114509 (2019), [arXiv:1809.02827].

[232] K.-i. Ishikawa *et al.* (PACS), Phys. Rev. D **106**, 9, 094501 (2022), [arXiv:2206.08654].

[233] H. Na *et al.*, Phys. Rev. **D82**, 114506 (2010), [arXiv:1008.4562].

[234] H. Na *et al.*, Phys. Rev. **D84**, 114505 (2011), [arXiv:1109.1501].

[235] V. Lubicz *et al.* (ETM), Phys. Rev. **D96**, 5, 054514 (2017), [Erratum: Phys. Rev. D99, 099902(2019)], [arXiv:1706.03017].

[236] T. Kaneko *et al.* (JLQCD), EPJ Web Conf. **175**, 13007 (2018), [arXiv:1711.11235].

[237] B. Chakraborty *et al.* ((HPQCD Collaboration)§, HPQCD), Phys. Rev. D **104**, 3, 034505 (2021), [arXiv:2104.09883].

[238] A. Bazavov *et al.* (Fermilab Lattice, MILC), Phys. Rev. D **107**, 9, 094516 (2023), [arXiv:2212.12648].

[239] S. Meinel, Phys. Rev. Lett. **118**, 8, 082001 (2017), [arXiv:1611.09696].

[240] S. Meinel, Phys. Rev. D **97**, 3, 034511 (2018), [arXiv:1712.05783].

[241] E. Dalgic *et al.*, Phys. Rev. **D73**, 074502 (2006), [Erratum: Phys. Rev. D75,119906(2007)], [hep-lat/0601021].

[242] J. M. Flynn *et al.*, Phys. Rev. **D91**, 7, 074510 (2015), [arXiv:1501.05373].

[243] J. A. Bailey *et al.* (Fermilab Lattice, MILC), Phys. Rev. **D92**, 1, 014024 (2015), [arXiv:1503.07839].

[244] B. Colquhoun *et al.*, Phys. Rev. **D93**, 3, 034502 (2016), [arXiv:1510.07446].

[245] Z. Gelzer *et al.*, EPJ Web Conf. **175**, 13024 (2018), [arXiv:1710.09442].

[246] B. Colquhoun *et al.* (JLQCD), Phys. Rev. D **106**, 5, 054502 (2022), [arXiv:2203.04938].

[247] C. M. Bouchard *et al.*, Phys. Rev. D **90**, 054506 (2014), [arXiv:1406.2279].

[248] C. J. Monahan *et al.*, Phys. Rev. D **98**, 11, 114509 (2018), [arXiv:1808.09285].

[249] A. Bazavov *et al.* (Fermilab Lattice, MILC), Phys. Rev. D **100**, 3, 034501 (2019), [arXiv:1901.02561].

[250] J. M. Flynn *et al.* (RBC/UKQCD), Phys. Rev. D **107**, 11, 114512 (2023), [arXiv:2303.11280].

[251] M. C. Arnesen *et al.*, Phys. Rev. Lett. **95**, 071802 (2005), [hep-ph/0504209]; J. A. Bailey *et al.*, Phys. Rev. **D79**, 054507 (2009), [arXiv:0811.3640].

[252] L. Lellouch, Nucl. Phys. B **479**, 353 (1996), [hep-ph/9509358].

[253] M. Di Carlo *et al.*, Phys. Rev. D **104**, 5, 054502 (2021), [arXiv:2105.02497].

[254] G. Martinelli, S. Simula and L. Vittorio, JHEP **08**, 022 (2022), [arXiv:2202.10285].

[255] J. M. Flynn, A. Jüttner and J. T. Tsang (2023), [arXiv:2303.11285].

[256] T. Blake *et al.*, Phys. Rev. D **108**, 9, 094509 (2023), [arXiv:2205.06041].

[257] J. Harrison, Phys. Rev. D **110**, 5, 054506 (2024), [arXiv:2405.01390].

[258] A. Gopal and N. Gubernari, Phys. Rev. D **111**, 3, L031501 (2025), [arXiv:2412.04388].

[259] S. Hashimoto *et al.*, Phys. Rev. **D61**, 014502 (1999), [hep-ph/9906376]; S. Hashimoto *et al.*, Phys. Rev. **D66**, 014503 (2002), [hep-ph/0110253].

[260] C. Bernard *et al.*, Phys. Rev. **D79**, 014506 (2009), [arXiv:0808.2519]; J. A. Bailey *et al.* (Fermilab Lattice, MILC), Phys. Rev. **D89**, 11, 114504 (2014), [arXiv:1403.0635]; J. Harrison, C. Davies and M. Wingate (HPQCD), Phys. Rev. **D97**, 5, 054502 (2018), [arXiv:1711.11013]; E. McLean *et al.*, Phys. Rev. **D99**, 11, 114512 (2019), [arXiv:1904.02046]; T. Bhattacharya *et al.* (LANL/SWME), PoS **LATTICE2018**, 283 (2018).

[261] J. A. Bailey *et al.* (MILC), Phys. Rev. **D92**, 3, 034506 (2015), [arXiv:1503.07237].

[262] H. Na *et al.* (HPQCD), Phys. Rev. **D92**, 5, 054510 (2015), [Erratum: Phys. Rev. D93, 19906(2016)], [arXiv:1505.03925].

[263] E. McLean *et al.*, Phys. Rev. D **101**, 7, 074513 (2020), [arXiv:1906.00701].

[264] A. Bazavov *et al.* (Fermilab Lattice, MILC, Fermilab Lattice, MILC), Eur. Phys. J. C **82**, 12, 1141 (2022), [Erratum: Eur.Phys.J.C 83, 21 (2023)], [arXiv:2105.14019].

[265] J. Harrison and C. T. H. Davies (HPQCD, (HPQCD Collaboration)‡), Phys. Rev. D **109**, 9, 094515 (2024), [arXiv:2304.03137].

[266] Y. Aoki *et al.* (JLQCD), Phys. Rev. D **109**, 7, 074503 (2024), [arXiv:2306.05657].

[267] W. Detmold, C. Lehner and S. Meinel, Phys. Rev. **D92**, 3, 034503 (2015), [arXiv:1503.01421].

[268] N. H. Christ *et al.* (RBC, UKQCD), Phys. Rev. **D92**, 9, 094512 (2015), [arXiv:1507.03094]; N. H. Christ *et al.* (RBC, UKQCD), Phys. Rev. **D93**, 11, 114517 (2016), [arXiv:1605.04442]; N. H. Christ *et al.*, Phys. Rev. **D94**, 11, 114516 (2016), [arXiv:1608.07585]; Z. Bai *et al.*, Phys. Rev. Lett. **118**, 25, 252001 (2017), [arXiv:1701.02858]; Z. Bai *et al.*, Phys. Rev. **D98**, 7, 074509 (2018), [arXiv:1806.11520]; N. H. Christ *et al.* (RBC, UKQCD), Phys. Rev. D **100**, 11, 114506 (2019), [arXiv:1910.10644].

[269] P. A. Boyle *et al.* (RBC, UKQCD), Phys. Rev. D **107**, 1, L011503 (2023), [arXiv:2202.08795].

[270] F. Erben *et al.* (2025), [arXiv:2504.07727].

[271] R. Frezzotti *et al.* (2025), [arXiv:2508.03655].

[272] R. R. Horgan *et al.*, Phys. Rev. **D89**, 9, 094501 (2014), [arXiv:1310.3722]; J. A. Bailey *et al.*, Phys. Rev. **D93**, 2, 025026 (2016), [arXiv:1509.06235]; D. Du *et al.*, Phys. Rev. **D93**, 3, 034005 (2016), [arXiv:1510.02349].

[273] W. G. Parrott, C. Bouchard and C. T. H. Davies ((HPQCD collaboration)§, HPQCD), Phys. Rev. D **107**, 1, 014510 (2023), [arXiv:2207.12468].

[274] W. Detmold and S. Meinel, Phys. Rev. **D93**, 7, 074501 (2016), [arXiv:1602.01399].

Int. J. Mod. Phys. A 2026.41. Downloaded from www.worldscientific.com
by UNIVERSITY OF CALIFORNIA @ BERKELEY on 09/16/26. Re-use and distribution is strictly not permitted, except for Open Access articles.

[275] Z. Bai *et al.*, Phys. Rev. Lett. **113**, 112003 (2014), [arXiv:1406.0916].

[276] N. H. Christ *et al.*, Phys. Rev. D **91**, 11, 114510 (2015), [arXiv:1504.01170].

[277] Z. Bai *et al.*, Phys. Rev. D **109**, 5, 054501 (2024), [arXiv:2309.01193].

[278] N. Christ *et al.*, Phys. Rev. Lett. **130**, 19, 191901 (2023), [arXiv:2208.03834].

[279] E.-H. Chao and N. Christ, Phys. Rev. D **110**, 5, 054514 (2024), [arXiv:2406.07447].

[280] A. Desiderio *et al.*, Phys. Rev. D **103**, 1, 014502 (2021), [arXiv:2006.05358]; G. Gagliardi *et al.*, Phys. Rev. D **105**, 11, 114507 (2022), [arXiv:2202.03833]; D. Giusti *et al.*, Phys. Rev. D **107**, 7, 074507 (2023), [arXiv:2302.01298]; R. Frezzotti *et al.*, Phys. Rev. D **108**, 7, 074505 (2023), [arXiv:2306.05904]; R. Frezzotti *et al.*, Phys. Rev. D **109**, 11, 114506 (2024), [arXiv:2402.03262]; R. Di Palma *et al.*, Phys. Rev. D **111**, 11, 114523 (2025), [arXiv:2504.08680]; D. Giusti *et al.* (2025), [arXiv:2505.11757].

[281] P.-X. Ma *et al.*, Phys. Rev. D **103**, 114503 (2021), [arXiv:2102.12048]; J.-S. Yoo *et al.*, Phys. Rev. D **108**, 3, 034508 (2023), [arXiv:2305.03198].

[282] P.-X. Ma *et al.* (2023), [arXiv:2308.16755].

[283] G. P. Lepage and P. B. Mackenzie, Phys. Rev. D **48**, 2250 (1993), [hep-lat/9209022].

[284] C. T. H. Davies *et al.* (HPQCD), Phys. Rev. **D78**, 114507 (2008), [arXiv:0807.1687].

[285] C. McNeile *et al.*, Phys. Rev. **D82**, 034512 (2010), [arXiv:1004.4285].

[286] A. Bochkarev and P. de Forcrand, Nucl. Phys. B **477**, 489 (1996), [hep-lat/9505025].

[287] E. Shintani *et al.*, Phys. Rev. **D82**, 7, 074505 (2010), [Erratum: Phys. Rev. D89, 099903(2014)], [arXiv:1002.0371].

[288] R. J. Hudspith *et al.*, Mod. Phys. Lett. **A31**, 32, 1630037 (2016).

[289] R. J. Hudspith *et al.* (2018), [arXiv:1804.10286].

[290] S. Cali *et al.*, Phys. Rev. Lett. **125**, 242002 (2020), [arXiv:2003.05781].

[291] I. Allison *et al.* (HPQCD), Phys. Rev. **D78**, 054513 (2008), [arXiv:0805.2999].

[292] B. Chakraborty *et al.*, Phys. Rev. **D91**, 5, 054508 (2015), [arXiv:1408.4169].

[293] Y. Maezawa and P. Petreczky, Phys. Rev. **D94**, 3, 034507 (2016), [arXiv:1606.08798].

[294] P. Petreczky and J. H. Weber, Phys. Rev. D **100**, 3, 034519 (2019), [arXiv:1901.06424].

[295] Q. Mason *et al.* (HPQCD, UKQCD), Phys. Rev. Lett. **95**, 052002 (2005), [hep-lat/0503005].

[296] A. Bazavov *et al.*, Phys. Rev. **D86**, 114031 (2012), [arXiv:1205.6155].

[297] A. Bazavov *et al.*, Phys. Rev. **D90**, 7, 074038 (2014), [arXiv:1407.8437].

[298] F. Karbstein, M. Wagner and M. Weber, Phys. Rev. **D98**, 11, 114506 (2018), [arXiv:1804.10909].

[299] H. Takaura *et al.*, JHEP **04**, 155 (2019), [arXiv:1808.01643].

[300] A. Bazavov *et al.* (TUMQCD), Phys. Rev. D **100**, 11, 114511 (2019), [arXiv:1907.11747].

[301] B. Blossier *et al.*, Phys. Rev. **D85**, 034503 (2012), [arXiv:1110.5829]; B. Blossier *et al.*, Phys. Rev. Lett. **108**, 262002 (2012), [arXiv:1201.5770].

[302] S. Zafeiropoulos *et al.*, Phys. Rev. Lett. **122**, 16, 162002 (2019), [arXiv:1902.08148].

[303] S. Aoki *et al.* (PACS-CS), JHEP **10**, 053 (2009), [arXiv:0906.3906].

[304] P. Fritzsch *et al.*, PoS **LATTICE2014**, 291 (2014), [arXiv:1411.7648].

[305] M. Bruno *et al.* (ALPHA), Phys. Rev. Lett. **119**, 10, 102001 (2017), [arXiv:1706.03821].

[306] M. Dalla Brida *et al.* (ALPHA), Phys. Rev. D **95**, 1, 014507 (2017), [arXiv:1607.06423].

[307] M. Dalla Brida *et al.* (ALPHA), Phys. Lett. B **807**, 135571 (2020), [arXiv:1912.06001].

[308] M. Dalla Brida *et al.* (ALPHA), Eur. Phys. J. C **82**, 12, 1092 (2022), [arXiv:2209.14204].

[309] C. Ayala, X. Lobregat and A. Pineda, JHEP **09**, 016 (2020), [arXiv:2005.12301].

[310] K. Maltman *et al.*, Phys. Rev. D **78**, 114504 (2008), [arXiv:0807.2020].

[311] P. Petreczky and J. H. Weber, Eur. Phys. J. C **82**, 1, 64 (2022), [arXiv:2012.06193].

[312] S. Dürr *et al.*, Phys. Lett. **B701**, 265 (2011), [arXiv:1011.2403].

[313] S. Dürr *et al.*, JHEP **08**, 148 (2011), [arXiv:1011.2711].

[314] A. T. Lytle *et al.* (HPQCD), Phys. Rev. D **98**, 1, 014513 (2018), [arXiv:1805.06225].

[315] C. Alexandrou *et al.* (Extended Twisted Mass), Phys. Rev. D **104**, 7, 074515 (2021), [arXiv:2104.13408].

[316] S. Capitani *et al.*, Nucl. Phys. **B544**, 669 (1999), [Erratum: Nucl. Phys. B582, 762(2000)], [hep-lat/9810063].

[317] M. Bruno *et al.* (ALPHA), PoS **LATTICE2018**, 220 (2019), [arXiv:1903.04094].

[318] A. Bussone *et al.* (ETM), Phys. Rev. **D93**, 11, 114505 (2016), [arXiv:1603.04306].

[319] J. Komijani, JHEP **08**, 062 (2017), [arXiv:1701.00347]; N. Brambilla *et al.* (TUMQCD), Phys. Rev. D **97**, 3, 034503 (2018), [arXiv:1712.04983].

[320] A. Bazavov *et al.* (Fermilab Lattice, MILC, TUMQCD), Phys. Rev. D **98**, 5, 054517 (2018), [arXiv:1802.04248].

[321] Z. Fodor *et al.*, Phys. Rev. Lett. **117**, 8, 082001 (2016), [arXiv:1604.07112].

[322] D. P. Aguillard *et al.* (Muon g-2) (2025), [arXiv:2506.03069].

[323] R. Aliberti *et al.* (2025), [arXiv:2505.21476].

[324] T. Blum, M. Hayakawa and T. Izubuchi, PoS **LATTICE2012**, 022 (2012), [arXiv:1301.2607].

[325] C. Davies, PoS **LATTICE2024**, 019 (2025), [arXiv:2503.03364].

[326] T. Blum, Phys. Rev. Lett. **91**, 052001 (2003), [hep-lat/0212018].

[327] D. Bernecker and H. B. Meyer, Eur. Phys. J. A **47**, 148 (2011), [arXiv:1107.4388].

[328] S. Borsanyi *et al.*, Nature **593**, 7857, 51 (2021), [arXiv:2002.12347].

[329] T. Blum *et al.* (RBC, UKQCD), Phys. Rev. Lett. **121**, 2, 022003 (2018), [arXiv:1801.07224].

[330] C. Lehner and A. S. Meyer, Phys. Rev. D **101**, 074515 (2020), [arXiv:2003.04177].

[331] G. Wang *et al.* (chiQCD), Phys. Rev. D **107**, 3, 034513 (2023), [arXiv:2204.01280].

[332] C. Aubin *et al.*, Phys. Rev. D **106**, 5, 054503 (2022), [arXiv:2204.12256].

[333] M. Cè *et al.*, Phys. Rev. D **106**, 11, 114502 (2022), [arXiv:2206.06582].

[334] C. Alexandrou *et al.* (Extended Twisted Mass), Phys. Rev. D **107**, 7, 074506 (2023), [arXiv:2206.15084].

[335] A. Bazavov *et al.* (Fermilab Lattice, HPQCD,, MILC), Phys. Rev. D **107**, 11, 114514 (2023), [arXiv:2301.08274].

[336] T. Blum *et al.* (RBC, UKQCD), Phys. Rev. D **108**, 5, 054507 (2023), [arXiv:2301.08696].

Int. J. Mod. Phys. A 2026.41. Downloaded from www.worldscientific.com
by UNIVERSITY OF CALIFORNIA @ BERKELEY on 09/16/26. Re-use and distribution is except for Open Access articles.

[337] A. Boccaletti *et al.* (2024), [arXiv:2407.10913].

[338] D. Giusti *et al.*, Phys. Rev. D **99**, 11, 114502 (2019), [arXiv:1901.10462].

[339] S. Kuberski *et al.*, JHEP **03**, 172 (2024), [arXiv:2401.11895].

[340] S. Spiegel and C. Lehner, Phys. Rev. D **111**, 11, 114517 (2025), [arXiv:2410.17053].

[341] T. Blum *et al.* (RBC, UKQCD), Phys. Rev. Lett. **134**, 20, 201901 (2025), [arXiv:2410.20590].

[342] D. Djukanovic *et al.*, JHEP **04**, 098 (2025), [arXiv:2411.07969].

[343] C. Alexandrou *et al.* (Extended Twisted Mass), Phys. Rev. D **111**, 5, 054502 (2025), [arXiv:2411.08852].

[344] A. Bazavov *et al.* (MILC, Fermilab Lattice, HPQCD), Phys. Rev. D **111**, 9, 094508 (2025), [arXiv:2411.09656].

[345] A. Bazavov *et al.* (Fermilab Lattice, HPQCD,, MILC), Phys. Rev. Lett. **135**, 1, 011901 (2025), [arXiv:2412.18491].

[346] T. Aoyama *et al.*, Phys. Rept. **887**, 1 (2020), [arXiv:2006.04822].

[347] G. Colangelo *et al.*, Phys. Lett. B **833**, 137313 (2022), [arXiv:2205.12963].

[348] F. V. Ignatov *et al.* (CMD-3), Phys. Rev. Lett. **132**, 23, 231903 (2024), [arXiv:2309.12910].

[349] M. Cè *et al.*, JHEP **08**, 220 (2022), [arXiv:2203.08676].

[350] C. T. H. Davies *et al.*, Phys. Rev. D **111**, 1, 014513 (2025), [arXiv:2410.23832].

[351] T. Blum *et al.*, Phys. Rev. Lett. **124**, 13, 132002 (2020), [arXiv:1911.08123].

[352] E.-H. Chao *et al.*, Eur. Phys. J. C **81**, 7, 651 (2021), [arXiv:2104.02632].

[353] E.-H. Chao *et al.*, Eur. Phys. J. C **82**, 8, 664 (2022), [arXiv:2204.08844].

[354] T. Blum *et al.* (2023), [arXiv:2304.04423].

[355] Z. Fodor *et al.*, Phys. Rev. D **111**, 11, 114509 (2025), [arXiv:2411.11719].

[356] A. Gérardin, H. B. Meyer and A. Nyffeler, Phys. Rev. D **100**, 3, 034520 (2019), [arXiv:1903.09471].

[357] A. Gérardin *et al.*, Phys. Rev. D **111**, 5, 054511 (2025), [arXiv:2305.04570].

[358] C. Alexandrou *et al.* (Extended Twisted Mass), Phys. Rev. D **108**, 9, 094514 (2023), [arXiv:2308.12458].

[359] T. Lin *et al.*, Rept. Prog. Phys. **88**, 8, 080501 (2025), [arXiv:2411.06349].

[360] O. Bar, Phys. Rev. D **99**, 5, 054506 (2019), [arXiv:1812.09191].

[361] C. C. Chang *et al.*, Nature **558**, 7708, 91 (2018), [arXiv:1805.12130].

[362] D. Djukanovic *et al.*, Phys. Rev. Lett. **132**, 21, 211901 (2024), [arXiv:2309.07491].

[363] D. Djukanovic *et al.*, Phys. Rev. D **110**, 1, L011503 (2024), [arXiv:2309.17232].

[364] A. S. Meyer, A. Walker-Loud and C. Wilkinson, Ann. Rev. Nucl. Part. Sci. **72**, 205 (2022), [arXiv:2201.01839].

[365] M. Constantinou *et al.* (2022), [arXiv:2202.07193].

[366] W. Detmold and C. J. D. Lin, Phys. Rev. D **73**, 014501 (2006), [hep-lat/0507007].

[367] A. J. Chambers *et al.*, Phys. Rev. Lett. **118**, 24, 242001 (2017), [arXiv:1703.01153].

[368] A. Shindler, Phys. Rev. D **110**, 5, L051503 (2024), [arXiv:2311.18704].

[369] J. Liang *et al.* (XQCD), Phys. Rev. D **101**, 11, 114503 (2020), [arXiv:1906.05312].

[370] M. Asakawa, T. Hatsuda and Y. Nakahara, Prog. Part. Nucl. Phys. **46**, 459 (2001), [hep-lat/0011040].

[371] A. Rothkopf, J. Comput. Phys. **238**, 106 (2013), [arXiv:1110.6285].

[372] X. Ji, Phys. Rev. Lett. **110**, 262002 (2013), [arXiv:1305.1539].

[373] X. Ji, Sci. China Phys. Mech. Astron. **57**, 1407 (2014), [arXiv:1404.6680].

[374] G. S. Bali *et al.*, Phys. Rev. D **93**, 9, 094515 (2016), [arXiv:1602.05525].

[375] R. Zhang *et al.* (2025), [arXiv:2501.00729].

[376] Y. Zhao, PoS **SPIN2023**, 035 (2024).

[377] S. Bhattacharya, PoS **LATTICE2024**, 013 (2025), [arXiv:2502.00481].

[378] H.-W. Lin, Prog. Part. Nucl. Phys. **144**, 104177 (2025), [arXiv:2506.05025].

[379] Q.-A. Zhang *et al.* (Lattice Parton), Phys. Rev. Lett. **125**, 19, 192001 (2020), [arXiv:2005.14572]; Y. Li *et al.*, Phys. Rev. Lett. **128**, 6, 062002 (2022), [arXiv:2106.13027]; P. Shanahan, M. Wagman and Y. Zhao, Phys. Rev. D **104**, 11, 114502 (2021), [arXiv:2107.11930]; M.-H. Chu *et al.* (Lattice Parton (LPC)), Phys. Rev. D **106**, 3, 034509 (2022), [arXiv:2204.00200]; A. Avkhadiev *et al.*, Phys. Rev. Lett. **132**, 23, 231901 (2024), [arXiv:2402.06725]; D. Bollweg *et al.*, Phys. Lett. B **852**, 138617 (2024), [arXiv:2403.00664].

[380] A. Shindler, PoS **EuroPLEx2023**, 024 (2024).

[381] *Proceedings, 41st International Symposium on Lattice Field Theory*, volume PoS **LATTICE2024** (2024), URL `https://pos.sissa.it/466/`.

[382] A. S. Kronfeld *et al.* (USQCD) (2022), [arXiv:2207.07641]; P. Boyle *et al.*, in "Snowmass 2021," (2022), [arXiv:2204.00039]; D. Boyda *et al.*, in "Snowmass 2021," (2022), [arXiv:2202.05838].

[383] Z. Davoudi *et al.*, in "Snowmass 2021," (2022), [arXiv:2209.10758].

[384] R. C. Brower *et al.* (USQCD), Eur. Phys. J. A **55**, 11, 198 (2019), [arXiv:1904.09964].

[385] C. W. Bauer *et al.*, Nature Rev. Phys. **5**, 7, 420 (2023), [arXiv:2404.06298].

18. Structure Functions

Revised August 2025 by E.C. Aschenauer (BNL), R.S. Thorne (UCL) and R. Yoshida (ANL).

18.1 Deep inelastic scattering

High-energy lepton-nucleon scattering plays a key role in determining the partonic structure of the proton. The process $\ell N \to \ell' X$ is illustrated in Fig. 18.1. The filled circle in this figure represents the internal structure of the proton which can be expressed in terms of structure functions.

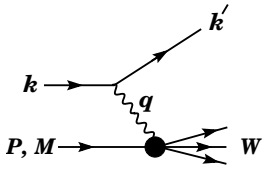

Figure 18.1: Kinematic quantities for the description of deep inelastic scattering. The quantities k and k' are the four-momenta of the incoming and outgoing leptons, P is the four-momentum of a nucleon with mass M, and W is the mass of the recoiling system X. The exchanged particle is a γ, $W^{\pm}$, or Z; it transfers four-momentum $q = k - k'$ to the nucleon.

Invariant quantities:

$\nu = \frac{q\cdot P}{M} = E - E'$ is the lepton's energy loss in the nucleon rest frame (in earlier literature sometimes $\nu = q \cdot P$). Here, E and E' are the initial and final lepton energies in the nucleon rest frame.

$Q^2 = -q^2 = 2(EE' - \vec{k} \cdot \vec{k}') - m_\ell^2 - m_{\ell'}^2$ where $m_\ell(m_{\ell'})$ is the initial (final) lepton mass. If $EE' \sin^2(\theta/2) \gg m_\ell^2, m_{\ell'}^2$, then

$\approx 4EE' \sin^2(\theta/2)$, where θ is the lepton's scattering angle with respect to the lepton beam direction.

$x = \frac{Q^2}{2M\nu}$ where, in the parton model, x is the fraction of the nucleon's momentum carried by the struck quark. Beyond leading order the equation remains the definition of x, but this is no longer identical to nucleon momentum fraction.

$y = \frac{q\cdot P}{k\cdot P} = \frac{\nu}{E}$ is the fraction of the lepton's energy lost in the nucleon rest frame.

$W^2 = (P+q)^2 = M^2 + 2M\nu - Q^2$ is the mass squared of the system X recoiling against the scattered lepton.

$s = (k+P)^2 = \frac{Q^2}{xy} + M^2 + m_\ell^2$ is the center-of-mass energy squared of the lepton-nucleon system.

The process in Fig. 18.1 is called deep ($Q^2 \gg M^2$) inelastic ($W^2 \gg M^2$) scattering (DIS). In what follows, the masses of the initial and scattered leptons, m_ℓ and $m_{\ell'}$, are neglected.

18.1.1 *DIS cross sections*

The double-differential cross section for deep inelastic scattering can be expressed in terms of kinematic variables in several ways.

$$\frac{d^2\sigma}{dx\,dy} = x\,(s - M^2)\,\frac{d^2\sigma}{dx\,dQ^2} = \frac{2\pi\,M\nu}{E'}\,\frac{d^2\sigma}{d\Omega_{\rm Nrest}\,dE'}\ . \qquad (18.1)$$

In lowest-order perturbation theory, the cross section for the scattering of polarized leptons on polarized nucleons can be expressed in terms of the products of leptonic and hadronic tensors associated with the coupling of the exchanged bosons at the upper and lower vertices in Fig. 18.1 (see Refs. [1–4])

$$\frac{d^2\sigma}{dxdy} = \frac{2\pi y\alpha^2}{Q^4}\sum_j \eta_j\, L_j^{\mu\nu}\, W_{\mu\nu}^j\ . \qquad (18.2)$$

For neutral-current processes, the summation is over $j = \gamma, Z$ and γZ representing photon and Z exchange and the interference between them, whereas for charged-current interactions there is only W exchange, $j = W$. (For transverse nucleon polarization, there is a dependence on the azimuthal angle of the scattered lepton.) The lepton tensor $L_{\mu\nu}$ is associated with the coupling of the exchange boson to the leptons. For incoming leptons of charge $e = \pm 1$ and helicity $\lambda = \pm 1$,

$$\begin{aligned} L_{\mu\nu}^{\gamma} &= 2\left(k_\mu k'_\nu + k'_\mu k_\nu - (k\cdot k' - m_\ell^2) g_{\mu\nu} - i\lambda\varepsilon_{\mu\nu\alpha\beta} k^\alpha k'^\beta\right), \\ L_{\mu\nu}^{\gamma Z} &= (g_V^e + e\lambda g_A^e)\, L_{\mu\nu}^{\gamma}, \quad L_{\mu\nu}^{Z} = (g_V^e + e\lambda g_A^e)^2\, L_{\mu\nu}^{\gamma}, \\ L_{\mu\nu}^{W} &= (1 + e\lambda)^2\, L_{\mu\nu}^{\gamma}, \end{aligned} \qquad (18.3)$$

where $g_V^e = -\frac{1}{2} + 2\sin^2\theta_W, \qquad g_A^e = -\frac{1}{2}$.

Although here the helicity basis is adopted, an alternative approach is to express the tensors in Eq. (18.3) in terms of the polarization of the lepton.

The factors η_j in Eq. (18.2) denote the ratios of the corresponding propagators and couplings to the photon propagator and coupling squared

$$\begin{aligned} \eta_\gamma &= 1\ ;\ \eta_{\gamma Z} = \left(\frac{G_F M_Z^2}{2\sqrt{2}\pi\alpha}\right)\left(\frac{Q^2}{Q^2 + M_Z^2}\right); \\ \eta_Z &= \eta_{\gamma Z}^2\ ;\ \eta_W = \frac{1}{2}\left(\frac{G_F M_W^2}{4\pi\alpha}\,\frac{Q^2}{Q^2 + M_W^2}\right)^2. \end{aligned} \qquad (18.4)$$

The hadronic tensor, which describes the interaction of the appropriate electroweak currents with the target nucleon, is given by

$$W_{\mu\nu} = \frac{1}{4\pi}\int d^4z\, e^{iq\cdot z}\, \left\langle P,S \left| \left[J_\mu^\dagger(z), J_\nu(0)\right] \right| P,S \right\rangle, \qquad (18.5)$$

where J_α is the hadronic contribution to the electromagnetic, or weak current and S denotes the nucleon-spin 4-vector, with $S^2 = -M^2$ and $S\cdot P = 0$.

18.2 Structure functions of the proton

The structure functions are defined in terms of the hadronic tensor (see Refs. [1–3])

$$\begin{aligned} W_{\mu\nu} &= \left(-g_{\mu\nu} + \frac{q_\mu q_\nu}{q^2}\right) F_1(x,Q^2) + \frac{\hat{P}_\mu \hat{P}_\nu}{P\cdot q}\, F_2(x,Q^2) \\ &- i\varepsilon_{\mu\nu\alpha\beta}\,\frac{q^\alpha P^\beta}{2P\cdot q}\, F_3(x,Q^2) \\ &+ i\varepsilon_{\mu\nu\alpha\beta}\,\frac{q^\alpha}{P\cdot q}\left[S^\beta g_1(x,Q^2) + \left(S^\beta - \frac{S\cdot q}{P\cdot q}\,P^\beta\right) g_2(x,Q^2)\right] \\ &+ \frac{1}{P\cdot q}\left[\frac{1}{2}\left(\hat{P}_\mu \hat{S}_\nu + \hat{S}_\mu \hat{P}_\nu\right) - \frac{S\cdot q}{P\cdot q}\,\hat{P}_\mu \hat{P}_\nu\right] g_3(x,Q^2) \\ &+ \frac{S\cdot q}{P\cdot q}\left[\frac{\hat{P}_\mu \hat{P}_\nu}{P\cdot q}\, g_4(x,Q^2) + \left(-g_{\mu\nu} + \frac{q_\mu q_\nu}{q^2}\right) g_5(x,Q^2)\right] \end{aligned} \qquad (18.6)$$

where

$$\hat{P}_\mu = P_\mu - \frac{P\cdot q}{q^2}\, q_\mu, \qquad \hat{S}_\mu = S_\mu - \frac{S\cdot q}{q^2}\, q_\mu\ . \qquad (18.7)$$

In [2],the definition of $W_{\mu\nu}$ with $\mu \leftrightarrow \nu$ is adopted, which changes the sign of the $\varepsilon_{\mu\nu\alpha\beta}$ terms in Eq. (18.6), although the formulae given below are unchanged. Ref. [1] tabulates the relation between the structure functions defined in Eq. (18.6) and other choices available in the literature.

The cross sections for neutral- and charged-current deep inelastic scattering on unpolarized nucleons can be written in terms of

Int. J. Mod. Phys. A 2026.41. Downloaded from www.worldscientific.com by UNIVERSITY OF CALIFORNIA @ BERKELEY on 09/16/26. Re-use and distribution is strictly not permitted, except for Open Access articles.

Int. J. Mod. Phys. A 2026.41. Downloaded from www.wo[redacted]except for Open Access articles.
by UNIVERSITY OF CALIFORNIA @ BERKELEY on 09/16/26. Re-use and distribution is

the structure functions in the generic form

$$\frac{d^2\sigma^i}{dxdy} = \frac{4\pi\alpha^2}{xyQ^2}\,\eta^i\left\{\left(1 - y - \frac{x^2y^2M^2}{Q^2}\right)F_2^i + y^2xF_1^i \mp \left(y - \frac{y^2}{2}\right)xF_3^i\right\}, \tag{18.8}$$

where $i =$ NC, CC corresponds to neutral-current ($eN \to eX$) or charged-current ($eN \to \nu X$ or $\nu N \to eX$) processes, respectively. For incoming neutrinos, $L^W_{\mu\nu}$ of Eq. (18.3) is still true, but with e, λ corresponding to the outgoing charged lepton. In the last term of Eq. (18.8), the $-$ sign is taken for an incoming e^+ or $\overline{\nu}$ and the $+$ sign for an incoming e^- or ν. The factor $\eta^{\rm NC} = 1$ for unpolarized $e^\pm$ beams, whereas

$$\eta^{\rm CC} = (1 \pm \lambda)^2\eta_W \tag{18.9}$$

with $\pm$ for $\ell^\pm$; and where λ is the helicity of the incoming lepton and η_W is defined in Eq. (18.4); for incoming neutrinos $\eta^{\rm CC} = 4\eta_W$. The CC structure functions, which derive exclusively from W exchange, are

$$F_1^{\rm CC} = F_1^W,\ F_2^{\rm CC} = F_2^W,\ xF_3^{\rm CC} = xF_3^W. \tag{18.10}$$

The NC structure functions $F_2^\gamma, F_2^{\gamma Z}, F_2^Z$ are, for $e^\pm N \to e^\pm X$, given by [5],

$$F_2^{\rm NC} = F_2^\gamma - (g_V^e \pm \lambda g_A^e)\eta_{\gamma Z}F_2^{\gamma Z} + ({g_V^e}^2 + {g_A^e}^2 \pm 2\lambda g_V^e g_A^e)\,\eta_Z F_2^Z \tag{18.11}$$

and similarly for $F_1^{\rm NC}$, whereas

$$xF_3^{\rm NC} = -(g_A^e \pm \lambda g_V^e)\eta_{\gamma Z}xF_3^{\gamma Z} + [2g_V^e g_A^e \pm \lambda({g_V^e}^2 + {g_A^e}^2)]\eta_Z xF_3^Z\,. \tag{18.12}$$

The polarized cross-section difference

$$\Delta\sigma = \sigma(\lambda_n = -1, \lambda_\ell) - \sigma(\lambda_n = 1, \lambda_\ell)\,, \tag{18.13}$$

where λ_ℓ, λ_n are the helicities (± 1) of the incoming lepton and nucleon, respectively, may be expressed in terms of the five structure functions $g_{1,\ldots 5}(x, Q^2)$ of Eq. (18.6). Explicitly,

$$\frac{d^2\Delta\sigma^i}{dxdy} = \frac{8\pi\alpha^2}{xyQ^2}\,\eta^i\left\{-\lambda_\ell y\left(2 - y - 2x^2y^2\frac{M^2}{Q^2}\right)xg_1^i + \lambda_\ell 4x^3y^2\frac{M^2}{Q^2}\,g_2^i + 2x^2y\frac{M^2}{Q^2}\left(1 - y - x^2y^2\frac{M^2}{Q^2}\right)g_3^i - \left(1 + 2x^2y\frac{M^2}{Q^2}\right)\left[\left(1 - y - x^2y^2\frac{M^2}{Q^2}\right)g_4^i + xy^2g_5^i\right]\right\} \tag{18.14}$$

with $i =$ NC or CC as before. The Eq. (18.13) corresponds to the difference of antiparallel minus parallel spins of the incoming particles for e^- or ν initiated reactions, but the difference of parallel minus antiparallel for e^+ or $\overline{\nu}$ initiated processes. For longitudinal nucleon polarization, the contributions of g_2 and g_3 are suppressed by powers of M^2/Q^2. These structure functions give an unsuppressed contribution to the cross section for transverse polarization [1], but in this case the cross-section difference vanishes as $M/Q \to 0$.

Because the same tensor structure occurs in the spin-dependent and spin-independent parts of the hadronic tensor of Eq. (18.6) in the $M^2/Q^2 \to 0$ limit, the differential cross-section difference of Eq. (18.14) may be obtained from the differential cross section Eq. (18.8) by replacing

$$F_1 \to -g_5\,,\quad F_2 \to -g_4\,,\quad F_3 \to 2g_1\,, \tag{18.15}$$

and multiplying by two, since the total cross section is the average over the initial-state polarizations. In this limit, Eq. (18.8) and Eq. (18.14) may be written in the form

$$\frac{d^2\sigma^i}{dxdy} = \frac{2\pi\alpha^2}{xyQ^2}\,\eta^i\left[Y_+F_2^i \mp Y_-xF_3^i - y^2F_L^i\right],$$

$$\frac{d^2\Delta\sigma^i}{dxdy} = \frac{4\pi\alpha^2}{xyQ^2}\,\eta^i\left[-Y_+g_4^i \mp Y_-2xg_1^i + y^2g_L^i\right], \tag{18.16}$$

with $i =$ NC or CC, where $Y_\pm = 1 \pm (1-y)^2$ and

$$F_L^i = F_2^i - 2xF_1^i\,,\qquad g_L^i = g_4^i - 2xg_5^i\,. \tag{18.17}$$

In the naive quark-parton model, the analogy with the Callan-Gross relations [6]$F_L^i = 0$, are the Dicus relations [7] $g_L^i = 0$. Therefore, there are only two independent polarized structure functions: g_1 (parity conserving) and g_5 (parity violating), in analogy with the unpolarized structure functions F_1 and F_3.

18.2.1 *Structure functions in the quark parton model*

In the naive quark-parton model [8, 9], contributions to the structure functions F^i and g^i can be expressed in terms of the quark distribution functions $q(x, Q^2)$ of the proton, where $q = u, \overline{u}, d, \overline{d}$ etc. The quantity $q(x, Q^2)dx$ is the number of quarks (or antiquarks) of designated flavor that carry a momentum fraction between x and $x + dx$ of the proton's momentum in a frame in which the proton momentum is large. One of the most striking predictions of the quark-parton model is that the structure functions F_i, g_i *scale*, i.e., $F_i(x, Q^2) \to F_i(x)$ in the Bjorken limit that Q^2 and $\nu \to \infty$ with x fixed [10]. This property is related to the assumption that the transverse momentum of the partons in the infinite-momentum frame of the proton is small.

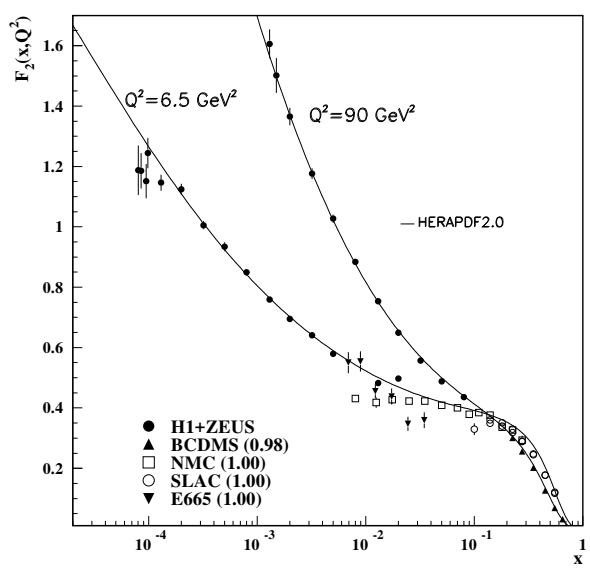

Figure 18.2: The proton structure function F_2^p given at two Q^2 values (6.5 GeV^2 and 90 GeV^2), which exhibit scaling at the 'pivot' point $x \sim 0.14$. See the captions in Fig. 18.10 and Fig. 18.12 for the references of the data. The various data sets have been renormalized by the factors shown in brackets in the key to the plot, which were globally determined in a previous HERAPDF analysis [11]. The curves were obtained using the PDFs from the HERAPDF analysis [12]. In practice, data for the reduced cross section, $F_2(x, Q^2) - (y^2/Y_+)F_L(x, Q^2)$, were fitted, rather than F_2 and F_L separately. The agreement between data and theory at low Q^2 and x can be improved by a positive higher-twist correction to $F_L(x, Q^2)$ [13, 14] (see Fig. 8 of Ref. [14]), or small-x resummation [15, 16].

Int. J. Mod. Phys. A 2026.41. Downloaded from www.worldscientific.com
by UNIVERSITY OF CALIFORNIA @ BERKELEY on 09/16/26. Re-use and distribution is strictly not permitted, except for Open Access articles.

For the neutral-current processes $ep \to eX$,

$$\begin{aligned}
\left[F_2^\gamma,\, F_2^{\gamma Z},\, F_2^Z\right] &= x\sum_q \left[e_q^2,\, 2e_q g_V^q,\, {g_V^q}^2 + {g_A^q}^2\right]\ (q+\overline{q})\ ,\\
\left[F_3^\gamma,\, F_3^{\gamma Z},\, F_3^Z\right] &= \sum_q \left[0,\, 2e_q g_A^q,\, 2g_V^q g_A^q\right]\ (q-\overline{q})\ ,\\
\left[g_1^\gamma,\, g_1^{\gamma Z},\, g_1^Z\right] &= \tfrac{1}{2}\sum_q \left[e_q^2,\, 2e_q g_V^q,\, {g_V^q}^2 + {g_A^q}^2\right]\ (\Delta q + \Delta\overline{q})\ ,\\
\left[g_5^\gamma,\, g_5^{\gamma Z},\, g_5^Z\right] &= \sum_q \left[0,\, e_q g_A^q,\, g_V^q g_A^q\right]\ (\Delta\overline{q} - \Delta q)\ ,
\end{aligned} \tag{18.18}$$

where $g_V^q = \pm\frac{1}{2} - 2e_q \sin^2\theta_W$ and $g_A^q = \pm\frac{1}{2}$, with $\pm$ according to whether q is a $u-$ or $d-$type quark respectively. The quantity Δq is the difference $q\uparrow - q\downarrow$ of the distributions with the quark spin parallel and antiparallel to the proton spin.

For the charged-current processes $e^-p \to \nu X$ and $\overline{\nu}p \to e^+X$, the structure functions are:

$$\begin{aligned}
F_2^{W^-} &= 2x(u + \overline{d} + \overline{s} + c\ldots)\ ,\\
F_3^{W^-} &= 2(u - \overline{d} - \overline{s} + c\ldots)\ ,\\
g_1^{W^-} &= (\Delta u + \Delta\overline{d} + \Delta\overline{s} + \Delta c\ldots)\ ,\\
g_5^{W^-} &= (-\Delta u + \Delta\overline{d} + \Delta\overline{s} - \Delta c\ldots)\ ,
\end{aligned} \tag{18.19}$$

where only the active flavors have been kept and where CKM mixing has been neglected. For $e^+p \to \overline{\nu}X$ and $\nu p \to e^-X$, the structure functions F^{W^+}, g^{W^+} are obtained by the flavor interchanges $d \leftrightarrow u, s \leftrightarrow c$ in the expressions for F^{W^-}, g^{W^-}. The structure functions for scattering on a neutron are obtained from those of the proton by the interchange $u \leftrightarrow d$. For both the neutral- and charged-current processes, the quark-parton model predicts $2xF_1^i = F_2^i$ and $g_4^i = 2xg_5^i$.

Neglecting masses, the structure functions g_2 and g_3 contribute only to scattering from transversely polarized nucleons, and have no simple interpretation in terms of the quark-parton model. They arise from off-diagonal matrix elements $\langle P,\lambda'|[J_\mu^\dagger(z), J_\nu(0)]|P,\lambda\rangle$, where the proton helicities satisfy $\lambda' \neq \lambda$. In fact, the leading-twist contributions to both g_2 and g_3 are both twist-2 and twist-3, which contribute at the same order of Q^2. The Wandzura-Wilczek relation [17] expresses the twist-2 part of g_2 in terms of g_1 as

$$g_2^i(x) \;=\; -g_1^i(x) \;+\; \int_x^1 \frac{dy}{y}\, g_1^i(y)\ . \tag{18.20}$$

However, the twist-3 component of g_2 is unknown. Similarly, there is a relation expressing the twist-2 part of g_3 in terms of g_4. A complete set of relations, including M^2/Q^2 effects, can be found in [18].

18.2.2 *Structure functions and QCD*

In QCD, there are perturbative corrections to the partonic cross sections defining structure functions. Also, the radiation of hard gluons from the quarks violates the assumption that the transverse momentum of the partons is small, leading to logarithmic scaling violations, which are particularly large at small x, see Fig. 18.2. The radiation of gluons produces the evolution of the partons and structure functions. As Q^2 increases, more and more gluons are radiated, which in turn split into $q\overline{q}$ pairs. This process leads both to the softening of the initial quark momentum distributions and to the growth of the gluon density and the $q\overline{q}$ sea as x decreases.

For $Q^2 \gg M^2$, the structure functions satisfy the factorization theorem [19],

$$F_i = \sum_a C_i^a \otimes f_a + \mathcal{O}(M^2/Q^2), \tag{18.21}$$

where $\otimes$ denotes the convolution integral

$$C \;\otimes\; f \;=\; \int_x^1 \frac{dy}{y}\, C(y)\, f\left(\frac{x}{y}\right)\ , \tag{18.22}$$

and where the coefficient functions C_i^a, where $a = g$ or q, are given as a power series in α_s. The scale-dependent parton distribution $f_a(x,\mu^2)$ corresponds, at a given x, to the density of parton a in the proton integrated over transverse momentum k_t up to the factorization scale μ. Typically, μ is the scale of the probe Q. For parton distributions x always refers to the nucleon momentum fraction of the parton, whereas for structure functions it retains the definition in Sec. 18.1. The parton evolution in μ is described in QCD by a DGLAP equation (see Refs. [20–23]) which has the schematic form

$$\frac{\partial f_a}{\partial \ln\mu^2} \sim \frac{\alpha_s(\mu^2)}{2\pi}\sum_b (P_{ab} \otimes f_b)\ , \tag{18.23}$$

where the P_{ab}, which describe the parton splitting $b \to a$, are also given as a power series in α_s. Although perturbative QCD can predict, via Eq. (18.23), the evolution of the parton distribution functions from a particular scale, μ_0, these DGLAP equations cannot predict them *a priori* at any particular μ_0. Thus they must be measured at a starting point μ_0 before the predictions of QCD can be compared to the data at other scales, μ. In general, all observables involving a hard hadronic interaction (such as structure functions) can be expressed as a convolution of calculable, process-dependent coefficient functions and these universal parton distributions, e.g. Eq. (18.21).

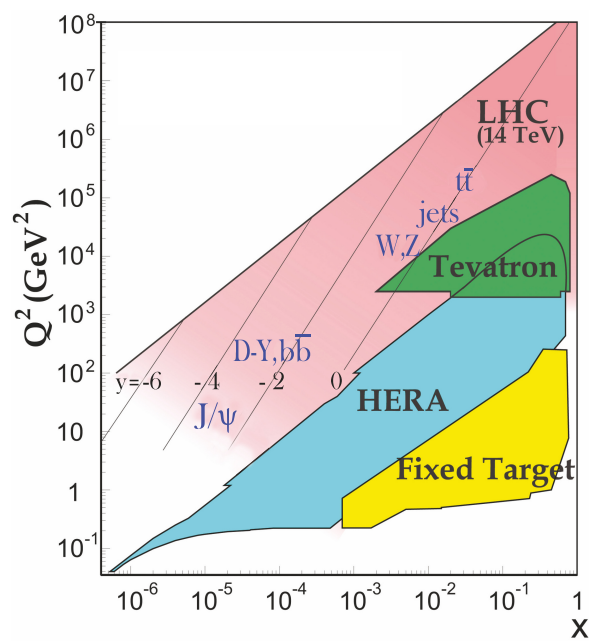

Figure 18.3: Kinematic domains in x and Q^2 probed by fixed-target and collider experiments, where here Q^2 can refer either the literal Q^2 for deep inelastic scattering, or the hard scale of the process in hadron-hadron collisions, e.g. invariant mass or transverse momentum p_T^2. Some of the final states accessible at the LHC are indicated in the appropriate regions, where y is the rapidity. The incoming partons have $x_{1,2} = (Q/14\ \text{TeV})e^{\pm y}$ where Q is the hard scale of the process shown in blue in the figure. For example, open charm production [24] and exclusive J/ψ and Υ production [25] at high $|y|$ at the LHC may probe the gluon PDF down to $x \sim 10^{-5}$.

It is often convenient to write the evolution equations in terms of the gluon, non-singlet (q^{NS}) and singlet (q^S) quark distribu-

Int. J. Mod. Phys. A 2026.41. Downloaded from www.wo
by UNIVERSITY OF CALIFORNIA @ BERKELEY on 09/16/26. Re-use and distribution is
except for Open Access articles.

Table 18.1: The main processes relevant to global PDF analyses, ordered in three groups: fixed-target experiments, HERA and the $p\bar{p}$ Tevatron / pp LHC. For each process we give an indication of their dominant partonic subprocesses, the primary partons which are probed and the approximate range of x constrained by the data. This list expands as more processes are measured and calculated with sufficient precision.

Process	Subprocess	Partons	x range
$\ell^\pm \{p,n\} \to \ell^\pm X$	$\gamma^* q \to q$	$q, \bar{q}, g$	$x \gtrsim 0.01$
$\ell^\pm n/p \to \ell^\pm X$	$\gamma^* d/u \to d/u$	d/u	$x \gtrsim 0.01$
$pp \to \mu^+\mu^- X$	$u\bar{u}, d\bar{d} \to \gamma^*$	$\bar{q}$	$0.015 \lesssim x \lesssim 0.35$
$pn/pp \to \mu^+\mu^- X$	$(u\bar{d})/(u\bar{u}) \to \gamma^*$	$\bar{d}/\bar{u}$	$0.015 \lesssim x \lesssim 0.35$
$\nu(\bar{\nu})\, N \to \mu^-(\mu^+)\, X$	$W^* q \to q'$	$q, \bar{q}$	$0.01 \lesssim x \lesssim 0.5$
$\nu\, N \to \mu^-\mu^+\, X$	$W^* s \to c$	s	$0.01 \lesssim x \lesssim 0.2$
$\bar{\nu}\, N \to \mu^+\mu^-\, X$	$W^* \bar{s} \to \bar{c}$	$\bar{s}$	$0.01 \lesssim x \lesssim 0.2$
$e^\pm p \to e^\pm X$	$\gamma^* q \to q$	$g, q, \bar{q}$	$10^{-4} \lesssim x \lesssim 0.1$
$e^+ p \to \bar{\nu} X$	$W^+ \{d,s\} \to \{u,c\}$	d, s	$x \gtrsim 0.01$
$e^\pm p \to e^\pm\, c\bar{c} X, e^\pm\, b\bar{b} X$	$\gamma^* c \to c,\ \gamma^* g \to c\bar{c}$	c, b, g	$10^{-4} \lesssim x \lesssim 0.01$
$e^\pm p \to$ jet$+X$	$\gamma^* g \to q\bar{q}$	g	$0.01 \lesssim x \lesssim 0.1$
$p\bar{p}, pp \to$ jet(dijet)$+X$	$gg, qg, qq \to 2j$	g, q	$0.00005 \lesssim x \lesssim 0.5$
$p\bar{p} \to (W^\pm \to \ell^\pm\nu)\, X$	$ud \to W^+, \bar{u}\bar{d} \to W^-$	$u, d, s, \bar{u}, \bar{d}, \bar{s}$	$x \gtrsim 0.05$
$pp \to (W^\pm \to \ell^\pm\nu)\, X$	$u\bar{d} \to W^+, d\bar{u} \to W^-$	$u, d, s, \bar{u}, \bar{d}, \bar{s}, g$	$x \gtrsim 0.001$
$p\bar{p}(pp) \to (Z \to \ell^+\ell^-) X$	$uu, dd, ..(u\bar{u}, ..) \to Z$	$u, d, s, ..(g)$	$x \gtrsim 0.001$
$pp \to W^- c,\ W^+\bar{c}$	$gs \to W^- c$	$s, \bar{s}$	$x \sim 0.01$
$pp \to (\gamma^* \to \ell^+\ell^-) X$	$u\bar{u}, d\bar{d}, .. \to \gamma^*$	$\bar{q}, g$	$x \gtrsim 10^{-5}$
$pp \to (\gamma^* \to \ell^+\ell^-) X$	$u\gamma, d\gamma, .. \to \gamma^*$	γ	$x \gtrsim 10^{-2}$
$pp \to b\bar{b}\, X,\ \ t\bar{t} X$	$gg \to b\bar{b},\ \ t\bar{t}$	g	$x \gtrsim 10^{-5}, 10^{-2}$
$pp \to t(\bar{t})\, X,$	$bu(\bar{b}d) \to td(\bar{t}u)$	$b, d/u$	$x \gtrsim 10^{-2}$
$pp \to$ exclusive $J/\psi, \Upsilon$	$\gamma^*(gg) \to J/\psi, \Upsilon$	g	$x \gtrsim 10^{-5}, 10^{-4}$
$pp \to \gamma\, X$	$gq \to \gamma q,\ g\bar{q} \to \gamma\bar{q}$	g	$x \gtrsim 0.005$

tions, such that

$$q^{NS} \;=\; q_i - \bar{q}_i \quad (\text{or } q_i - q_j), \qquad q^S \;=\; \sum_i (q_i + \bar{q}_i)\ . \quad (18.24)$$

The non-singlet distributions have non-zero values of flavor quantum numbers, such as isospin and baryon number. The DGLAP evolution equations then take the form

$$\frac{\partial q^{NS}}{\partial \ln \mu^2} = \frac{\alpha_s(\mu^2)}{2\pi}\, P_{qq} \otimes q^{NS}\ ,$$

$$\frac{\partial}{\partial \ln \mu^2} \begin{pmatrix} q^S \\ g \end{pmatrix} = \frac{\alpha_s(\mu^2)}{2\pi} \begin{pmatrix} P_{qq} & 2n_f\, P_{qg} \\ P_{gq} & P_{gg} \end{pmatrix} \otimes \begin{pmatrix} q^S \\ g \end{pmatrix}, \quad (18.25)$$

where P are splitting functions that describe the probability of a given parton splitting into two others, and n_f is the number of (active) quark flavors. The leading-order Altarelli-Parisi [22] splitting functions are

$$P_{qq} = \frac{4}{3}\left[\frac{1+x^2}{(1-x)}\right]_+ = \frac{4}{3}\left[\frac{1+x^2}{(1-x)_+}\right] + 2\delta(1-x)\ , \quad (18.26)$$

$$P_{qg} = \frac{1}{2}\left[x^2 + (1-x)^2\right]\ ,\ P_{gq} = \frac{4}{3}\left[\frac{1+(1-x)^2}{x}\right]\ , \quad (18.27)$$

$$P_{gg} = 6\left[\frac{1-x}{x} + x(1-x) + \frac{x}{(1-x)_+}\right] + \left[\frac{11}{2} - \frac{n_f}{3}\right]\delta(1-x), \quad (18.28)$$

where the notation $[F(x)]_+$ defines a distribution such that for

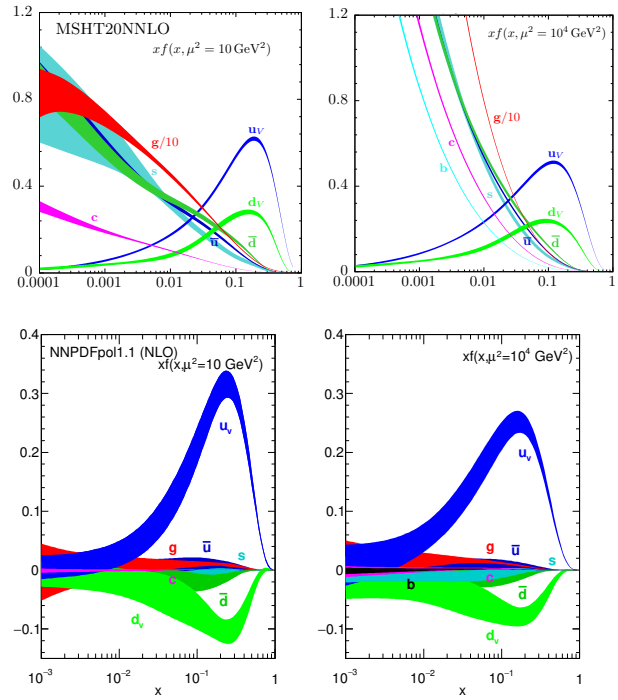

Figure 18.4: The bands are x times the unpolarized parton distributions $f(x)$ (where $f = u_v, d_v, \bar{u}, \bar{d}, s \simeq \bar{s}, c = \bar{c}, b = \bar{b}, g$) obtained in the NNLO MSHT20 global analysis [26] (top) at scales $\mu^2 = 10$ GeV^2 (left) and $\mu^2 = 10^4$ GeV^2 (right), with $\alpha_s(M_Z^2) = 0.118$. The polarized parton distributions $f(x)$ obtained in the NLO NNPDFpol1.1 fit [27] (bottom).

any sufficiently regular test function, $f(x)$,

$$\int_0^1 dx f(x)[F(x)]_+ = \int_0^1 dx\ (f(x) - f(1))F(x)\ . \quad (18.29)$$

In general, the splitting functions can be expressed as a power series in α_s. The series contains both terms proportional to $\ln \mu^2$ and to $\ln(1/x)$ and $\ln(1-x)$. The leading-order DGLAP evolution sums up the $(\alpha_s \ln \mu^2)^n$ contributions, while at next-to-leading order (NLO) the sum over the $\alpha_s(\alpha_s \ln \mu^2)^{n-1}$ terms is included [28, 29]. The NNLO contributions to the splitting functions and the DIS coefficient functions are also all known [30–32], as are the N^{3}LO corrections to the coefficient functions [33]. Some Mellin moments of the N^{3}LO splitting functions are also known [34–37], together with some other pieces of specific information.

In the kinematic region of very small x, one may also sum leading terms in $\ln(1/x)$, independent of the value of $\ln \mu^2$. At leading order, LLx, this is done by the BFKL equation for the unintegrated distributions (see Refs. [38, 39].) The leading-order $(\alpha_s \ln(1/x))^n$ terms result in a power-like growth, $x^{-\omega}$ with $\omega = (12\alpha_s \ln 2)/\pi$, at asymptotic values of $\ln 1/x$. The next-to-leading $\ln 1/x$ (NLLx) contributions are also available [40, 41]. They are so large (and negative) that the results initially appeared to be perturbatively unstable. Methods, based on a combination of collinear and small-x resummations, have been developed which reorganize the perturbative series into a more stable hierarchy [42–45], and this has been used as the basis for a framework for including the corrections in phenomenological studies [46, 47]. There are some limited indications that small-x resummations become necessary for sufficient precision for $x \lesssim 10^{-3}$ at low scales [15, 16]. At sufficiently small x it is expected that evolution should also be affected by non-linear/saturation effects due to a high density of partons, i.e. the gluon density would be so high that gluon-gluon recombination effects would become significant, see [48–50] for reviews. However, there is not yet any very convincing indication for a non-linear regime for $Q^2 \gtrsim 2$ GeV^2 in hadron DIS. Better evidence for saturation may be found in more exclu-

Int. J. Mod. Phys. A 2026.41. Downloaded from www.worldscientific.com by UNIVERSITY OF CALIFORNIA @ BERKELEY on 09/16/26. Re-use and distribution is strictly not permitted, except for Open Access articles.

sive final states such as dihadron correlations in proton-nucleus collisions, e.g. [51, 52].

The precision of the experimental data demands that at least NLO, and preferably NNLO, DGLAP evolution be used in comparisons between QCD theory and experiment. Beyond the leading order, it is necessary to specify, and to use consistently, both a renormalization and a factorization scheme. The renormalization scheme used almost universally is the modified minimal subtraction ($\overline{\text{MS}}$) scheme [53, 54]. The most popular choices for the factorization scheme is also $\overline{\text{MS}}$ [55]. Historically, sometimes the DIS [56] scheme was adopted, in which there are no higher-order corrections to the F_2 structure function. The two schemes differ in how the non-divergent pieces are assimilated in the parton distribution functions.

The discussion above relates to the Q^2 behavior of leading-twist (twist-2) contributions to the structure functions. Higher-twist terms, which involve their own non-perturbative input, exist. These die off as powers of Q; specifically twist-n terms are damped by $1/Q^{n-2}$. Provided a cut, say $W^2 > 15$ GeV^2 is imposed, the higher-twist terms appear to be numerically unimportant for Q^2 above a few GeV^2, except possibly for very small x and more definitely for x close to 1 [57–59], though it is important to note that they are likely to be larger in $xF_3(x, Q^2)$ than in $F_2(x, Q^2)$ (see e.g. [60]) due to a lack of a constraining sum rule for $xF_3(x, Q^2)$.

18.3 Determination of parton distributions

The parton distribution functions (PDFs) can be determined from an analysis of data for deep inelastic lepton-nucleon scattering and for related hard-scattering processes initiated by nucleons; see Refs. [61–67] for reviews. Table 18.1 highlights some of the processes and their primary sensitivity to PDFs. LHC data are playing an increasing role [68], and new processes are continually being added to the list. Fixed-target and collider experiments have complementary kinematic reach (as is shown in Fig. 18.3), which enables the determination of PDFs over a wide range in x and μ^2. As more precise LHC data for $W^\pm$, Z, γ, jet, $b\bar{b}$ and $t\bar{t}$ production become available, tighter constraints on the PDFs are expected in a wider kinematic range. At present about half the constraint on PDFs comes from LHC data [26], but much of the constraint still comes from structure functions.

Recent determinations and releases of the unpolarized PDFs up to NNLO have been made by five groups: MSHT [26], NNPDF [69], CT [70], ATLAS [71] and ABMP [72]. The CJ group produce PDFs at NLO and concentrate on the high x, low Q^2 regime, including data with lower kinematic cuts [73]. All groups start evolution at $Q_0^2 = 1-4$ GeV^2. Most groups use input PDFs of the form $xf = x^a(...)(1-x)^b$ with 14-32 free parameters in total. In these cases the PDF uncertainties are made available using the "Hessian" formulation. The free parameters are expanded around their best fit values, and orthogonal eigenvector sets of PDFs depending on linear combinations of the parameter variations are obtained. The uncertainty is then the quadratic sum of the uncertainties arising from each eigenvector. The NNPDF group combines a Monte Carlo representation of the probability measure in the space of PDFs with the use of neural networks. Fits are performed to a very large number of "replica" data sets obtained by allowing individual data points to fluctuate randomly by amounts determined by the size of the data uncertainties. This results in a set of replicas of unbiased PDF sets. In this case the best prediction is the average obtained using all PDF replicas and the uncertainty is the standard deviation over all replicas. It is possible to convert the eigenvectors of Hessian-based PDFs to Monte Carlo replicas [74] and *vice versa* [75]. Accumulated information on N^{3}LO calculation has been used by MSHT in order to produce a first set of approximate N^{3}LO (aN^{3}LO) global PDFs [76] together with theoretical uncertainties. An alternative approach to theoretical uncertainty has been made in [77] and a NNPDF aN^{3}LO PDF set made available [78].

In these analyses, the u, d and s quarks are taken to be massless, but the treatment of the heavy c and b quark masses, m_Q, differs, and has a long history, which may be traced from Refs. [79–90]. The MSHT, CT, NNPDF and ATLASPDF analyses use different variants of the General-Mass Variable-Flavour-Number Scheme (GM-VFNS). This combines fixed-order contributions to the coefficient functions (or partonic cross sections) calculated with the full m_Q dependence, with the all-order resummation of contributions via DGLAP evolution in which the heavy quarks are treated as massless after starting evolution at some transition point. Transition matrix elements are computed, following [82] at $\mathcal{O}(\alpha_S^2)$ or [91–95] at $\mathcal{O}(\alpha_S^3)$, which provide the boundary conditions between n_f and n_f+1 PDFs. The ABMP analysis uses for structure function calculations a FFNS where only the three light (massless) quarks enter the evolution, while the heavy quarks enter the partonic cross sections with their full m_Q dependence. The GM-VFNS and FFNS approaches yield different results: in particular $\alpha_s(M_Z^2)$ and the large-x gluon PDF at large Q^2 are both significantly smaller in the FFNS. It has been argued [58, 59, 89] that the difference is due to the slow convergence of the $\ln^n(Q^2/m_Q^2)$ terms in certain regions in a FFNS. The final HERA combination of heavy flavour structure function data has been published [96], and the evolution of these measurements and their interpretation may be traced in [97].

The recent determinations of the groups fitting a variety of data and using a GM-VFNS (MSHT, NNPDF and CT) have converged, so that now a good agreement has been achieved between the resulting PDFs. Indeed, the recent global fit PDF sets, CT18 [70], MSHT2018 [26], and NNPDF3.1 [98], have been combined [99] using the Monte Carlo approach [74] mentioned above. The single combined set of PDFs is discussed in detail in Ref. [100].

For illustration, we show in Fig. 18.4 the PDFs obtained in the NNLO MSHT analysis [26] at scales $\mu^2 = 10$ and 10^4 GeV^2 (and an equivalent plot for polarized PDFs from NNPDF [27]). The values of α_s found by MSHT [101] may be taken as representative of those resulting from the GM-VFNS analyses

$$\text{NLO} : \alpha_s(M_Z^2) = 0.1203 \pm 0.0015,$$

$$\text{NNLO} : \alpha_s(M_Z^2) = 0.1174 \pm 0.0013,$$

where the error (at 68% C.L.) corresponds to the uncertainties resulting from the data fitted (the uncertainty that might be expected from the neglect of higher orders is at least as large). A similar results is found by the NNPDF group [102], who find $\alpha_s(M_Z^2) = 0.1185 \pm 0.0012$ at NNLO and the CT group [70], who obtain $\alpha_s(M_Z^2) = 0.1164 \pm 0.0026$. The ABMP analysis [72],which uses a FFNS, finds $\alpha_s(M_Z^2) = 0.1150 \pm 0.0009$ at NNLO.

As a first step towards the inclusion of higher order electroweak corrections a recent development has been a vastly increased understanding of the photon content of the proton. Sets of PDFs with a photon contribution were considered in Refs. [103–105]. However, due to weak data constraints, the uncertainty was extremely large. Subsequently, there has been a much improved understanding of the separation into elastic and inelastic contributions [106–108]. This gives much more theoretical precision, since the elastic contribution, arising from coherent emission of a photon from the proton, can be directly related to the well-known proton electric and magnetic form factors; the model dependence of the inelastic (incoherent) contribution, related to the quark PDFs, is at the level of tens of percent. A final and decisive development directly relating the entire photon contribution to the proton structure function [109] resulted in a determination of the photon content of the proton as precise as that of the light quarks. The framework is applied within global fits to PDFs via an iterative procedure in [110] and to provide the low-scale input photon PDF in [111, 112]. A further development is the calculation of photon-initiated collider processes directly from structure functions [113].

There are also some calculations of PDFs using lattice QCD, see [114–116] for a review. There has been significant recent progress in the development of efficient algorithms for generating ensembles of gauge field configurations and in tools for extracting the required information from correlation functions. However, there remain a number of sources of systematic uncertainty; discretization effects, pion mass dependence, finite volume effects, excited state contamination and renormalization, which need to be determined and ideally minimised. Moreover, PDFs cannot be

Int. J. Mod. Phys. A 2026.41. Downloaded from www.wo
by UNIVERSITY OF CALIFORNIA @ BERKELEY on 09/16/26. Re-use and distribution is
except for Open Access articles.

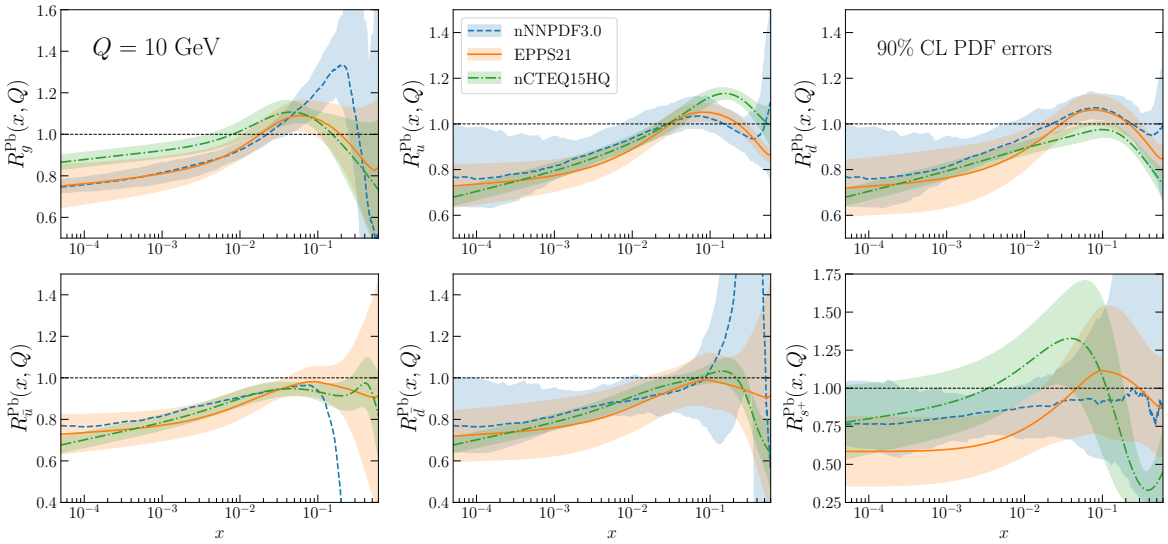

Figure 18.5: Comparison of the nNNPDF3.0, nCTEQ15HQ and EPPS21 nuclear PDFs. The curves shown are ratios to the result in the limit of no nuclear corrections. Plot from NNPDF collaboration (Juan Rojo – private communication).

determined directly in Euclidean lattice QCD because they depend on quantum fields at light-like separations. Traditionally the lattice has been used to determine matrix elements of twist two operators which can be related to integer moments of PDFs. Until recently these did not always agree well with determinations using global fit PDFs [114]. However, there have been recent improvements [117–120], though uncertainties are still relatively large. An alternative approach [121] suggested the computation of the matrix elements of frame-dependent, equal-time correlators in the large momentum limit. This leads to so-called Quasi-PDFs, which in the infinite momentum frame can be related to light-cone PDFs via a matching procedure, and there is the closely related pseudo PDF approach [122]. Recent results using physical values of the light quark masses are in [123–130].

Comprehensive sets of PDFs are available from the LHAPDF library [131], which can be linked directly into a user's programme to provide access to recent PDFs in a standard format. This also includes many nuclear and polarized PDFs.

Nuclear PDFs: The study of the parton distributions for nucleons within nuclei, so-called nuclear parton distribution functions (nPDFs), is now reaching a level of maturity and sophistication similar to nucleon PDFs (and some nuclear target data is often included in determinations of nucleon PDFs), though they are still typically performed at NLO in perturbative QCD. A review may be found in [132]. The PDFs are a function of the nucleon number of the nucleus, A. The nPDFs are obtained via fits to deep inelastic scattering data and dilepton (Drell-Yan) and pion production from proton-nucleus, and most recently also from jet and heavy flavour production data. There are a number of recent examples of NLO analyses, TUJU21 [133], nCTEQ15HQ(HiX) [134, 135], EPPS21 [136],nNNPDF3.0 [137], while NNLO analyses with a smaller selection of data types now also exist [133,138,139]. A comparison of the nuclear modification factors for nCTEQ15HQ [134], EPPS21 [136] and nNNPDF3.0 [137] is shown in Fig. 18.5 where, for example, for the up quark $R_u^{\rm Pb} = (Z_{Pb}u_{Pb} + (A_{Pb} - Z_{Pb})d_{Pb})/(Z_{Pb}u_p + (A_{Pb} - Z_{Pb})d_p)$ i.e. it involves "physical" nuclear PDFs and is normalised such that $R_u^{\rm Pb} = 1$ corresponds to no nuclear effects.

Much of the heavy-nucleus data included are in the form of ratios to proton or deuteron measurements. Initially most nuclear PDFs were related to a particular proton PDF via a nuclear modification factor, i.e.

$$f_i^{p/A}(x, Q^2) = R_i^A(x, Q^2) f_i^p(x, Q^2). \tag{18.30}$$

However, it is now common to parameterise the nuclear PDFs directly but so that they become equal to proton PDFs in the limit $A = 1$, and this approach has been adopted in [133–135, 137]. There is some variation in whether charged current neutrino DIS data is used as well as neutral current DIS data since there is no clear compatibility in the modification factors obtained [140,141]. Recently, LHC data from vector boson production [142–145] in proton-lead collisions has been used along with DIS data in most fits, though the most recent data [146] shows some tendency to require NNLO corrections. LHC jet data [147] has been included in some fits [136,137] giving extra constraint on the gluon within nuclei. Further information at smaller x values is also obtained from heavy meson production at LHCb [148]. Single inclusive hadron production e.g. [149, 150], is already sometimes used. There are also potential constraints from jet production in ultra-peripheral nucleus-nucleus collisions [151]. All the PDF extractions above are based on the Hessian formulation, except for the NNPDF studies which use Monte Carlo replicas. Agreement between the different nuclear PDFs is generally good, though uncertainty is still large compared to proton PDFs. As well as improved constraints from further LHC data, nPDFs would be very significantly improved by data from a potential high-energy Electron-Ion Collider [152–154].

Double Parton Distributions Double parton scattering (DPS) occurs when two pairs of partons initiate two distinct hard scattering processes in a single collision. It becomes more prevalent at higher collider energies as the parton flux increases. Hence, it is becoming relevant at the LHC, and even more so for planning of higher energy colliders. It has a long theoretical history [155–159], and in recent years experimental studies have started. DPS is often suppressed, but this is less the case in certain kinematic regions, e.g. when the total transverse momentum of the two hard-scattering processes is small [160–163], when they have a large rapidity separation [164, 165], or when single particle production is suppressed by coupling constants, e.g. like-sign W production [166]. There have been results with some evidence for DPS found from both the Tevatron [167, 168] involving final states with multi-jets and photons, and at the LHC [169–171] in states with multiple vector bosons or mesons. Recent developments have been involved in putting the theoretical foundations of DPS on a much more rigorous footing and describing it in terms of well-defined double partons distributions (DPDs) which extend the concept of parton distribution functions (PDFs) to the case of two partons [160–163,172–174]. The current knowledge of DPDs is still limited, though there are a number of attempts to impose theoretical constrains as a limit on the forms [175–177]. The DPDs can be calculated quite accurately when the transverse

Int. J. Mod. Phys. A 2026.41. Downloaded from www.worldscientific.com
by UNIVERSITY OF CALIFORNIA @ BERKELEY on 09/16/26. Re-use and distribution is strictly not permitted, except for Open Access articles.

separation of the two partons is small, since in this limit the observed partons are produced by a splitting from a single parton. This limit is complicated by potential double counting [163], and an approach to deal with this has been devised [174]. The full splitting functions for DPS have been calculated at LO [163], and there is progress at NLO, e.g. [178, 179].

Polarized PDFs: For spin-dependent structure functions, data exists for a more restricted range of Q^2 and has lower precision, so that the scaling violations are not seen so clearly. However, spin-dependent (or polarized) parton distributions have been extracted by comparison to data using NLO global analyses which include measurements of the g_1 structure function in inclusive polarized DIS, 'flavour-tagged' semi-inclusive DIS data, open–charm production in DIS and results from polarized pp scattering at RHIC. There are recent results on DIS from JLAB [180] (for g_1^n/F_1^n), COMPASS [181, 182] and CLAS [183]. NLO analyses are given in Refs. [184–187] and more recent extractions [188, 189]. Recently PDF fits have been performed at NNLO with inclusive DIS data [190], also with semi-inclusive DIS data [191] and with these plus hadron collider data [192]. Parton-to-hadron fragmentation functions, needed to describe the semi-inclusive DIS (SIDIS) data, can be found in Refs. [193–196]. The DSSV collaboration includes in their NLO analysis to extract polarized PDFs all the world data, inclusive and semi-inclusive DIS, double spin asymmetries

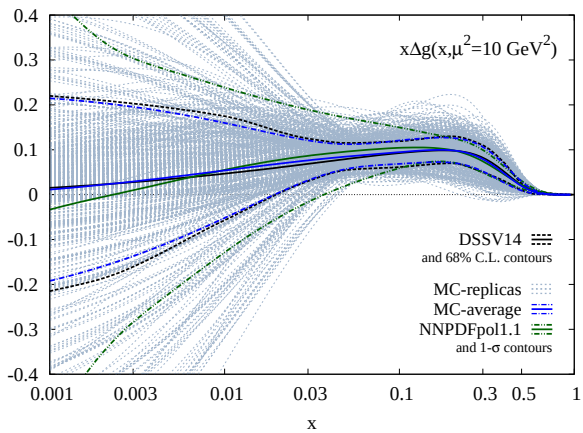

Figure 18.6: Ensemble of replicas (dotted blue lines) for the NLO gluon helicity density $\Delta g(x, Q^2)$ at $Q^2 = 10$ GeV^2 shown along with its statistical average (solid blue line) and variance (dot-dashed blue lines). The corresponding results from the DSSV14 fit (black lines) [188] and the NNPDFpol1.1 analysis (green lines) [27] are shown for comparison. Figure taken from Ref. [197].

in jet [198], dijet [199] and inclusive π^0-production [200], but not yet the single spin asymmetries in $W^\pm, Z^0$ production [201, 202]. A determination [203], using the NNPDF methodology, concentrates just on the inclusive polarized DIS data, and finds the uncertainties on the polarized gluon PDF have been underestimated in the earlier analyses. An update to this [27], where jet and $W^\pm$ data from pp collisions and open–charm DIS data have been included via reweighting, reduces the uncertainty and suggests a positive polarized gluon PDF. The evidence for a positive gluon polarization is strengthened by the most recent jet [204–206] and inclusive π^0 [207] data. The DSSV group has implemented a Monte Carlo sampling strategy to extract helicity parton densities and their uncertainties from a reference set of longitudinally polarized scattering data [197]. A simultaneous extraction of spin-dependent parton distributions and fragmentation functions has recently also been performed [208]. Calculations of polarised PDFs on the lattice are frequently produced by the same studies as for unpolarised PDFs. These are usually in better agreement with the corresponding moments obtained from global fits, than the unpolarised PDFs, and also tend to have much more competitive uncertainties, see [114, 115] for a review and e.g. [118, 209] for more recent results.

A comparison of the polarized gluon PDFs obtained in the NLO analyses of NNPDF [27] and DSSV [197] is shown in Fig. 18.6 at scale $\mu^2 = 10$ GeV^2. The world data of the inclusive structure function g_1 for proton and deuterium included in these analysis are shown in Fig. 18.16 and Fig. 18.17.

18.4 The hadronic structure of the photon

Besides the *direct* interactions of the photon, it is possible for it to fluctuate into a hadronic state via the process $\gamma \to q\bar{q}$. While in this state, the partonic content of the photon may be *resolved*, for example, through the process $e^+e^- \to e^+e^-\gamma^\star\gamma \to e^+e^-X$, where the virtual photon emitted by the DIS lepton probes the hadronic structure of the quasi-real photon emitted by the other lepton. The perturbative LO QED contributions to this process with $\gamma \to q\bar{q}$ in conjunction with $\gamma^\star q(\bar{q}) \to q(\bar{q})$, are subject to QCD corrections due to the radiation of gluons from these quarks.

Often the equivalent-photon approximation is used to express the differential cross section for deep inelastic electron–photon scattering in terms of the structure functions of the transverse quasi-real photon times a flux factor N_γ^T (for these incoming quasi-real photons of transverse polarization)

$$\frac{d^2\sigma}{dxdQ^2} = N_\gamma^T \frac{2\pi\alpha^2}{xQ^4} \left[\left(1 + (1-y)^2\right) F_2^\gamma(x, Q^2) - y^2 F_L^\gamma(x, Q^2)\right], \tag{18.31}$$

where we have used $F_2^\gamma = 2xF_T^\gamma + F_L^\gamma$ (where F_T is the transverse structure function), not to be confused with F_2^γ of Sec. 18.2. Complete formulae are given, for example, in the comprehensive review of [210].

The hadronic photon structure function, F_2^γ, evolves with increasing Q^2 from the 'hadron-like' behavior, calculable via the vector-meson-dominance model, to the dominating 'point-like' behaviour, calculable in perturbative QCD. Due to the point-like coupling, the logarithmic evolution of F_2^γ with Q^2 has a *positive* slope for all values of x, see Fig. 18.18. The 'loss' of quarks at large x due to gluon radiation is over-compensated by the 'creation' of quarks via the point-like $\gamma \to q\bar{q}$ coupling. The logarithmic evolution was first predicted in the quark–parton model ($\gamma^\star\gamma \to q\bar{q}$) [211, 212], and then an improved expression was obtained using QCD corrections in the limit of large Q^2 [213]. The evolution is now known to NLO [214–216]. The NLO data analyses to determine the parton densities of the photon can be found in Refs. [217–219]. The necessity for updates to these analyses for physics at the EIC is stressed in [220].

18.5 Diffractive DIS (DDIS)

Some 10% of DIS events are diffractive, $\gamma^* p \to X + p$, in which the slightly deflected proton and the cluster X of outgoing hadrons are well-separated in rapidity [221]. Besides x and Q^2, two extra variables are needed to describe a DDIS event: the fraction $x_{I\!P}$ of the proton's momentum transferred across the rapidity gap and t, the square of the 4-momentum transfer of the proton. The DDIS data [226, 227] are usually analysed using two levels of factorization. First, the diffractive structure function $F_2^{\rm D}$ satisfies *collinear factorization*, and can be expressed as the convolution [228]

$$F_2^{\rm D} = \sum_{a=q,g} C_2^a \otimes f_{a/p}^{\rm D}, \tag{18.32}$$

with the same coefficient functions as in DIS (see Eq. (18.21)), and where the diffractive parton distributions $f_{a/p}^{\rm D}$ $(a = q, g)$ satisfy DGLAP evolution. Second, *Regge factorization* is assumed [229],

$$f_{a/p}^{\rm D}(x_{I\!P}, t, z, \mu^2) = f_{I\!P/p}(x_{I\!P}, t)\, f_{a/I\!P}(z, \mu^2), \tag{18.33}$$

where $f_{a/I\!P}$ are the parton densities of the Pomeron, which itself is treated like a hadron, and $z \in [x/x_{I\!P}, 1]$ is the fraction of the Pomeron's momentum carried by the parton entering the hard subprocess. The Pomeron flux factor $f_{I\!P/p}(x_{I\!P}, t)$ is taken from Regge phenomenology. There are also secondary Reggeon contributions to Eq. (18.33). A sample of the t-integrated diffractive parton densities, obtained in this way, is shown in Fig. 18.7. A more recent extraction of the parton densities may be found in [230].

Int. J. Mod. Phys. A 2026.41. Downloaded from www.wo
by UNIVERSITY OF CALIFORNIA @ BERKELEY on 09/16/26. Re-use and distribution is
except for Open Access articles.

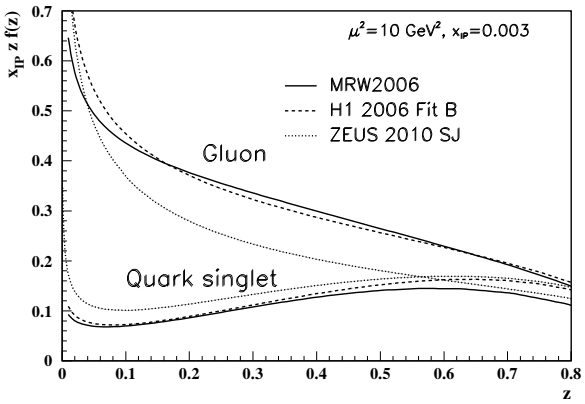

Figure 18.7: Diffractive parton distributions, $x_{I\!P}\, z f^{\rm D}_{a/p}$, obtained from fitting to the ZEUS data with $Q^2 > 5$ GeV^2 [222],H1 data with $Q^2 > 8.5$ GeV^2 assuming Regge factorization [223], and from MRW2006 [224] using a more perturbative QCD approach [224]. Only the Pomeron contributions are shown and not the secondary Reggeon contributions, which are negligible at the value of $x_{I\!P} = 0.003$ chosen here. The H1 2007 Jets distribution [225] is similar to H1 2006 Fit B.

Although collinear factorization holds as $\mu^2 \to \infty$, there are non-negligible corrections for finite μ^2 and small $x_{I\!P}$. Besides the *resolved* interactions of the Pomeron, the perturbative QCD Pomeron may also interact *directly* with the hard subprocess, giving rise to an inhomogeneous evolution equation for the diffractive parton densities analogous to the photon case. The results of the MRW analysis [224],which includes these contributions, are also shown in Fig. 18.7.

Unlike the inclusive case, the diffractive parton densities cannot be directly used to calculate diffractive hadron-hadron cross sections, since account must first be taken of "soft" rescattering effects.

18.6 Three-dimensional structure of hadrons

Generalized parton distributions (GPDs) and their compliment, transverse momentum dependent distributions (TMDs) describe the three-dimensional structure of hadrons. While GPDs encode the transverse position of a parton in a nucleon, TMDs, encompassing both the parton distributions (TMD PDF) and fragmentation functions (TMD FF), encode their transverse momenta and lead to observable transverse momenta in the final state. Both TMDs and GPDs derive, via integration over the appropriate variable, from Wigner distributions [231–233] that depend on the average transverse momentum and position of partons.

18.6.1 *Generalized parton distributions*

The parton distributions of the proton of Sec. 18.3 are given by the diagonal matrix elements $\langle P,\lambda|\hat{O}|P,\lambda\rangle$, where P and λ are the 4-momentum and helicity of the proton, and $\hat{O}$ is a twist-2 quark or gluon operator. However, there is new information in the so-called generalised parton distributions (GPDs) defined in terms of the off-diagonal matrix elements $\langle P',\lambda'|\hat{O}|P,\lambda\rangle$; see Refs. [234–239] for reviews. Unlike the diagonal PDFs, the GPDs cannot be regarded as parton densities, but are to be interpreted as probability amplitudes.

The physical significance of GPDs is best seen using light-cone coordinates, $z^\pm = (z^0 \pm z^3)/\sqrt{2}$, and in the light-cone gauge, $A^+ = 0$. It is conventional to define the generalised quark distributions in terms of quark operators at light-like separation

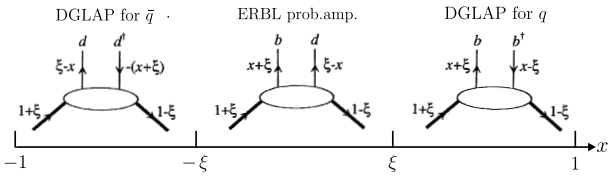

Figure 18.8: Schematic diagrams of the three distinct kinematic regions of the imaginary part of H_q. The proton and quark momentum fractions refer to $\bar{P}^+$, and x covers the interval (-1,1). In the ERBL domain the GPDs are generalisations of distribution amplitudes which occur in processes such as $p\bar{p} \to J/\psi$.

$$F_q(x,\xi,t) = \frac{1}{2}\int \frac{dz^-}{2\pi} e^{ix\bar{P}^+z^-} \langle P'|\bar{\psi}(-z/2)\gamma^+\psi(z/2)|P\rangle \Big|_{z^+=z^1=z^2=0} = \frac{1}{2\bar{P}^+} \times \left(H_q(x,\xi,t)\ \bar{u}(P')\gamma^+u(P) + E_q(x,\xi,t)\ \bar{u}(P')\frac{i\sigma^{+\alpha}\Delta_\alpha}{2m}u(P)\right) \tag{18.34}$$

with $\bar{P} = (P+P')/2$ and $\Delta = P' - P$, and where we have suppressed the helicity labels of the protons and spinors. We now have two extra kinematic variables:

$$t = \Delta^2, \qquad \xi = -\Delta^+/(P+P')^+. \tag{18.35}$$

We see that $-1 \le \xi \le 1$. Similarly, we may define GPDs $\tilde{H}_q$ and $\tilde{E}_q$ with an additional γ_5 between the quark operators in Eq. (18.34); and also an analogous set of gluon GPDs, H_g, E_g, $\tilde{H}_g$ and $\tilde{E}_g$. After a Fourier transform with respect to the transverse components of Δ, we are able to describe the spatial distribution of partons in the impact parameter plane in terms of GPDs [240, 241].

For $P' = P$, $\lambda' = \lambda$ the matrix elements reduce to the ordinary PDFs of Sec. 18.2.1

$$H_q(x,0,0) = q(x), \quad H_q(-x,0,0) = -\bar{q}(x), \quad H_g(x,0,0) = xg(x), \tag{18.36}$$

$$\tilde{H}_q(x,0,0) = \Delta q(x),\ \tilde{H}_q(-x,0,0) = \Delta\bar{q}(x),\ \tilde{H}_g(x,0,0) = x\Delta g(x), \tag{18.37}$$

where $\Delta q = q\uparrow - q\downarrow$ as in Eq. (18.18). No corresponding relations exist for E, $\tilde{E}$ as they decouple in the forward limit, $\Delta = 0$.

The functions H_g, E_g are even in x, and $\tilde{H}_g, \tilde{E}_g$ are odd functions of x. We can introduce valence and 'singlet' quark distributions which are even and odd functions of x respectively. For example

$$H_q^V(x,\xi,t) \equiv H_q(x,\xi,t) + H_q(-x,\xi,t) = H_q^V(-x,\xi,t), \tag{18.38}$$

$$H_q^S(x,\xi,t) \equiv H_q(x,\xi,t) - H_q(-x,\xi,t) = -H_q^S(-x,\xi,t). \tag{18.39}$$

All the GPDs satisfy relations of the form

$$H(x,-\xi,t) = H(x,\xi,t) \qquad \text{and} \qquad H(x,-\xi,t)^* = H(x,\xi,t), \tag{18.40}$$

and so are real-valued functions. Moreover, the moments of GPDs, that is the x integrals of $x^n H_q$ etc., are *polynomials* in ξ of order $n+1$. Another important property of GPDs are Ji's sum rule [234, 242]

$$\frac{1}{2}\int_{-1}^{1} dx\ x\,(H_q(x,\xi,t) + E_q(x,\xi,t)) = J_q(t), \tag{18.41}$$

where $J_q(0)$ is the total angular momentum carried by quarks and antiquarks of flavour q, with a similar relation for gluons.

Int. J. Mod. Phys. A 2026.41. Downloaded from www.worldscientific.com
by UNIVERSITY OF CALIFORNIA @ BERKELEY on 09/16/26. Re-use and distribution is strictly not permitted, except for Open Access articles.

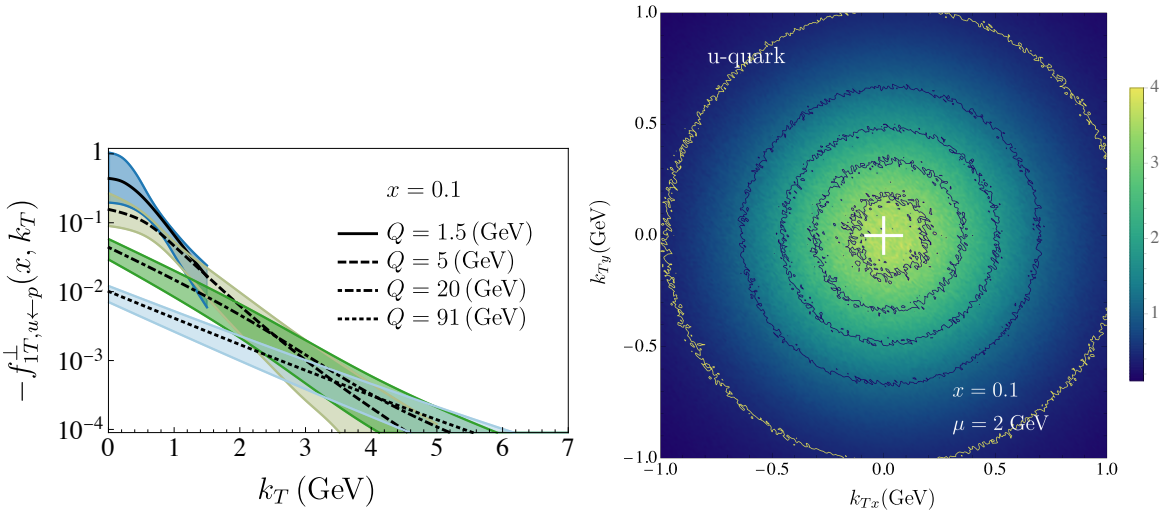

Figure 18.9: (Left) Sivers function in the momentum space for u quark [243] at $x = 0.1$ as a function of transverse momentum k_T for different values of Q. The bands are 68%CI. (Right) Momentum space density function as defined in [243] for the unpolarized u quark in a proton totally polarized in the y direction. The white cross indicates the origin with respect to which a shift of the distribution along the x-direction due to the Sivers function can be seen. The width of the patterns in the plot roughly indicates the uncertainty of the extraction.

To visualize the physical content of H_q, we Fourier expand ψ and $\bar{\psi}$ in terms of quark, antiquark creation (b, d) and annihilation $(b^\dagger, d^\dagger)$ operators, and sketch the result in Fig. 18.8. There are two types of domain: (i) the time-like or 'annihilation' domain, with $|x| < |\xi|$, where the GPDs describe the wave functions of a t-channel $q\bar{q}$ (or gluon) pair and evolve according to modified ERBL equations [244, 245]; (ii) the space-like or 'scattering' domain, with $|x| > |\xi|$, where the GPDs generalise the familiar $\bar{q}$, q (and gluon) PDFs and describe processes such as 'deeply virtual Compton scattering' ($\gamma^* p \to \gamma p$), $\gamma p \to J/\psi p$, etc., and evolve according to modified DGLAP equations. The splitting functions for the evolution of GPDs are known to NLO [246–248]. The Mellin moments of GPDs may also be related to the energy momentum tensor form factors [242], which, via Fourier transform, may be interpreted as spatial distributions of energy, momentum and stress in the hadron [249,250]. First experimental results may be found in [251].

GPDs describe new aspects of proton structure and must be determined from experiment. We can parametrise them in terms of 'double distributions' [252,253], which reduce to diagonal PDFs as $\xi \to 0$. Alternatively, flexible $SO(3)$-based parametrisations have been used to determine GPDs from DVCS data [254, 255]; summaries may be found in Ref. [256–258]. Some recent fits can be found in [259,260], and some recent results on the lattice in [261].

18.6.2 *Transverse momentum dependent distributions*

For a proton, there are eight independent transverse dependent distribution (TMD) PDFs, at leading twist, three of which correspond to the usual unpolarized, longitudinally polarized and transversely polarized quark parton distributions [262, 263]. The novel TMD PDFs have physical interpretations. For example, the Sivers function [264] represents the distribution of unpolarized partons inside a transversely polarized hadron. For (pseudo)scalar particles, such as kaon and pions, there are two independent leading-twist TMD FFs, one being the ordinary unpolarized fragmentation function and the other the Collins FF [265] which is related to the probability of a polarized quark fragmenting into an unpolarized hadron.

Factorization of TMDs has been shown for semi-inclusive DIS, for the Drell-Yan process as well as for electron-position annihilation into dihadrons [266–271]. Recently TMD global fits have become available [272–278], although there are potential problems with consistent descriptions which are highlighted in [279–281]. The results of a recent extraction of Sivers function from a global fit to polarized Semi-Inclusive DIS, polarized pion-induced Drell-Yan and W+-/Z boson production data is shown in Fig. 18.9 [243].

Because TMD PDFs encode nonperturbative information about transverse momentum and polarization degrees of freedom, they are important for descriptions of multi-scale, non-inclusive collider observables, for example, production of electroweak gauge bosons at LHC [282] and can have an effect on determination of the W boson mass [283]. The combination of TMD PDFs and FFs can give consistent global description of spin and azimuthal asymmetries and provide predictions. Some lattice results can also now be found, e.g. [284]. Some recent reviews of this rapidly developing field are given here [257, 282, 285–287].

References

[1] J. Blumlein and N. Kochelev, Nucl. Phys. **B498**, 285 (1997), [hep-ph/9612318].

[2] S. Forte, M. L. Mangano and G. Ridolfi, Nucl. Phys. **B602**, 585 (2001), [hep-ph/0101192].

[3] M. Anselmino, P. Gambino and J. Kalinowski, Z. Phys. **C64**, 267 (1994), [hep-ph/9401264].

[4] M. Anselmino, A. Efremov and E. Leader, Phys. Rept. **261**, 1 (1995), [Erratum: Phys. Rept.281,399(1997)], [hep-ph/9501369].

[5] M. Klein and T. Riemann, Z. Phys. **C24**, 151 (1984).

[6] C. G. Callan, Jr. and D. J. Gross, Phys. Rev. Lett. **22**, 156 (1969).

[7] D. A. Dicus, Phys. Rev. **D5**, 1367 (1972).

[8] J. D. Bjorken and E. A. Paschos, Phys. Rev. **185**, 1975 (1969).

[9] R.P. Feynman, Photon Hadron Interactions (Benjamin, New York, 1972).

[10] J. D. Bjorken, Phys. Rev. **179**, 1547 (1969).

[11] A.M. Cooper-Sarkar, private communication.

[12] H. Abramowicz *et al.* (H1, ZEUS), Eur. Phys. J. **C75**, 12, 580 (2015), [arXiv:1506.06042].

[13] L. A. Harland-Lang *et al.*, Eur. Phys. J. **C76**, 4, 186 (2016), [arXiv:1601.03413].

[14] I. Abt *et al.*, Phys. Rev. **D94**, 3, 034032 (2016), [arXiv:1604.02299].

[15] R. D. Ball *et al.*, Eur. Phys. J. **C78**, 4, 321 (2018), [arXiv:1710.05935].

[16] H. Abdolmaleki *et al.* (xFitter Developers' Team), Eur. Phys. J. **C78**, 8, 621 (2018), [arXiv:1802.00064].

Int. J. Mod. Phys. A 2026.41. Downloaded from www.worldscientific.com by UNIVERSITY OF CALIFORNIA @ BERKELEY on 09/16/26. Re-use and distribution is [redacted] except for Open Access articles.

[17] S. Wandzura and F. Wilczek, Phys. Lett. **72B**, 195 (1977).

[18] J. Blumlein and A. Tkabladze, Nucl. Phys. **B553**, 427 (1999), [hep-ph/9812478].

[19] J. C. Collins, D. E. Soper and G. F. Sterman, Adv. Ser. Direct. High Energy Phys. **5**, 1 (1989), [hep-ph/0409313].

[20] V. N. Gribov and L. N. Lipatov, Sov. J. Nucl. Phys. **15**, 438 (1972), [Yad. Fiz.15,781(1972)].

[21] L.N. Lipatov, Sov. J. Nucl. Phys. **20**, 95 (1975).

[22] G. Altarelli and G. Parisi, Nucl. Phys. **B126**, 298 (1977).

[23] Y. L. Dokshitzer, Sov. Phys. JETP **46**, 641 (1977), [Zh. Eksp. Teor. Fiz.73,1216(1977)].

[24] V. Bertone, R. Gauld and J. Rojo, JHEP **01**, 217 (2019), [arXiv:1808.02034].

[25] R. Aaij *et al.* (LHCb), JHEP **10**, 167 (2018), [arXiv:1806.04079].

[26] S. Bailey *et al.*, Eur. Phys. J. C **81**, 4, 341 (2021), [arXiv:2012.04684].

[27] E. R. Nocera *et al.* (NNPDF), Nucl. Phys. **B887**, 276 (2014), [arXiv:1406.5539].

[28] G. Curci, W. Furmanski and R. Petronzio, Nucl. Phys. **B175**, 27 (1980); W. Furmanski and R. Petronzio, Phys. Lett. **97B**, 437 (1980).

[29] R.K. Ellis *et al.*, QCD and Collider Physics (Cambridge UP, 1996).

[30] W. L. van Neerven and E. B. Zijlstra, Phys. Lett. **B272**, 127 (1991); E. B. Zijlstra and W. L. van Neerven, Phys. Lett. **B273**, 476 (1991); E. B. Zijlstra and W. L. van Neerven, Phys. Lett. **B297**, 377 (1992); E. B. Zijlstra and W. L. van Neerven, Nucl. Phys. **B383**, 525 (1992).

[31] S. Moch and J. A. M. Vermaseren, Nucl. Phys. **B573**, 853 (2000), [hep-ph/9912355].

[32] S. Moch, J. A. M. Vermaseren and A. Vogt, Nucl. Phys. **B688**, 101 (2004), [hep-ph/0403192]; A. Vogt, S. Moch and J. A. M. Vermaseren, Nucl. Phys. **B691**, 129 (2004), [hep-ph/0404111]; S. Moch, J. A. M. Vermaseren and A. Vogt, Phys. Lett. **B606**, 123 (2005), [hep-ph/0411112].

[33] J. A. M. Vermaseren, A. Vogt and S. Moch, Nucl. Phys. **B724**, 3 (2005), [hep-ph/0504242].

[34] S. Moch *et al.*, Phys. Lett. B **825**, 136853 (2022), [arXiv:2111.15561]; G. Falcioni *et al.*, Phys. Lett. B **842**, 137944 (2023), [arXiv:2302.07593].

[35] G. Falcioni *et al.*, Phys. Lett. B **846**, 138215 (2023), [arXiv:2307.04158].

[36] G. Falcioni *et al.*, Phys. Lett. B **856**, 138906 (2024), [arXiv:2404.09701].

[37] G. Falcioni *et al.*, Phys. Lett. B **860**, 139194 (2025), [arXiv:2410.08089].

[38] V. S. Fadin, E. A. Kuraev and L. N. Lipatov, Phys. Lett. **60B**, 50 (1975); E. A. Kuraev, L. N. Lipatov and V. S. Fadin, Sov. Phys. JETP **44**, 443 (1976), [Zh. Eksp. Teor. Fiz.71,840(1976)]; E. A. Kuraev, L. N. Lipatov and V. S. Fadin, Sov. Phys. JETP **45**, 199 (1977), [Zh. Eksp. Teor. Fiz.72,377(1977)].

[39] I. I. Balitsky and L. N. Lipatov, Sov. J. Nucl. Phys. **28**, 822 (1978), [Yad. Fiz.28,1597(1978)].

[40] V. S. Fadin and L. N. Lipatov, Phys. Lett. **B429**, 127 (1998), [hep-ph/9802290].

[41] G. Camici and M. Ciafaloni, Phys. Lett. **B412**, 396 (1997), [Erratum: Phys. Lett.B417,390(1998)], [hep-ph/9707390]; M. Ciafaloni and G. Camici, Phys. Lett. **B430**, 349 (1998), [hep-ph/9803389].

[42] M. Ciafaloni, D. Colferai and G. P. Salam, Phys. Rev. **D60**, 114036 (1999), [hep-ph/9905566]; M. Ciafaloni, D. Colferai and G. P. Salam, JHEP **07**, 054 (2000), [hep-ph/0007240].

[43] M. Ciafaloni *et al.*, Phys. Lett. **B576**, 143 (2003), [hep-ph/0305254]; M. Ciafaloni *et al.*, Phys. Rev. **D68**, 114003 (2003), [hep-ph/0307188].

[44] G. Altarelli, R. D. Ball and S. Forte, Nucl. Phys. **B742**, 1 (2006), [hep-ph/0512237]; G. Altarelli, R. D. Ball and S. Forte, Nucl. Phys. **B799**, 199 (2008), [arXiv:0802.0032].

[45] C. D. White and R. S. Thorne, Phys. Rev. **D75**, 034005 (2007), [hep-ph/0611204].

[46] M. Bonvini, S. Marzani and T. Peraro, Eur. Phys. J. **C76**, 11, 597 (2016), [arXiv:1607.02153].

[47] M. Bonvini, S. Marzani and C. Muselli, JHEP **12**, 117 (2017), [arXiv:1708.07510].

[48] Y. V. Kovchegov and E. Levin, *Quantum chromodynamics at high energy*, volume 33, Cambridge University Press (2012), ISBN 978-0-521-11257-4, 978-1-139-55768-9.

[49] J. L. Albacete and C. Marquet, Prog. Part. Nucl. Phys. **76**, 1 (2014), [arXiv:1401.4866].

[50] A. Morreale and F. Salazar, Universe **7**, 8, 312 (2021), [arXiv:2108.08254].

[51] G. Giacalone and C. Marquet, Nucl. Phys. A **982**, 291 (2019), [arXiv:1807.06388].

[52] X. Chu (STAR), in "28th International Workshop on Deep Inelastic Scattering and Related Subjects," (2021), [arXiv:2110.03731].

[53] G. 't Hooft and M. J. G. Veltman, Nucl. Phys. **B44**, 189 (1972).

[54] G. 't Hooft, Nucl. Phys. **B61**, 455 (1973).

[55] W. A. Bardeen *et al.*, Phys. Rev. **D18**, 3998 (1978).

[56] G. Altarelli, R. K. Ellis and G. Martinelli, Nucl. Phys. **B143**, 521 (1978), [Erratum: Nucl. Phys.B146,544(1978)].

[57] A. D. Martin *et al.*, Eur. Phys. J. **C35**, 325 (2004), [hep-ph/0308087].

[58] R. D. Ball *et al.* (NNPDF), Phys. Lett. **B723**, 330 (2013), [arXiv:1303.1189].

[59] R. S. Thorne, Eur. Phys. J. **C74**, 7, 2958 (2014), [arXiv:1402.3536].

[60] M. Dasgupta and B. R. Webber, Phys. Lett. **B382**, 273 (1996), [hep-ph/9604388].

[61] A. De Roeck and R. S. Thorne, Prog. Part. Nucl. Phys. **66**, 727 (2011), [arXiv:1103.0555].

[62] S. Forte and G. Watt, Ann. Rev. Nucl. Part. Sci. **63**, 291 (2013), [arXiv:1301.6754].

[63] J. Blumlein, Prog. Part. Nucl. Phys. **69**, 28 (2013), [arXiv:1208.6087].

[64] E. Perez and E. Rizvi, Rept. Prog. Phys. **76**, 046201 (2013), [arXiv:1208.1178].

[65] R. D. Ball *et al.*, JHEP **04**, 125 (2013), [arXiv:1211.5142].

[66] J. Gao, L. Harland-Lang and J. Rojo, Phys. Rept. **742**, 1 (2018), [arXiv:1709.04922].

[67] J. J. Ethier and E. R. Nocera, Ann. Rev. Nucl. Part. Sci. **70**, 43 (2020), [arXiv:2001.07722].

[68] J. Rojo *et al.*, J. Phys. **G42**, 103103 (2015), [arXiv:1507.00556].

[69] R. D. Ball *et al.* (NNPDF), Eur. Phys. J. C **82**, 5, 428 (2022), [arXiv:2109.02653].

[70] T.-J. Hou *et al.*, Phys. Rev. D **103**, 1, 014013 (2021), [arXiv:1912.10053].

[71] G. Aad *et al.* (ATLAS), Eur. Phys. J. C **82**, 5, 438 (2022), [arXiv:2112.11266].

[72] S. Alekhin *et al.*, Eur. Phys. J. C **85**, 2, 162 (2025), [arXiv:2407.00545].

[73] A. Accardi *et al.*, Phys. Rev. D **93**, 11, 114017 (2016), [arXiv:1602.03154].

Int. J. Mod. Phys. A 2026.41. Downloaded from www.worldscientific.com
by UNIVERSITY OF CALIFORNIA @ BERKELEY on 09/16/26. Re-use and distribution is strictly not permitted, except for Open Access articles.

[74] G. Watt and R. S. Thorne, JHEP **08**, 052 (2012), [arXiv:1205.4024].

[75] S. Carrazza *et al.*, Eur. Phys. J. **C75**, 8, 369 (2015), [arXiv:1505.06736].

[76] J. McGowan *et al.*, Eur. Phys. J. C **83**, 3, 185 (2023), [Erratum: Eur.Phys.J.C 83, 302 (2023)], [arXiv:2207.04739].

[77] R. Abdul Khalek *et al.* (NNPDF), Eur. Phys. J. C **79**, 11, 931 (2019), [arXiv:1906.10698].

[78] R. D. Ball *et al.* (NNPDF), Eur. Phys. J. C **84**, 7, 659 (2024), [arXiv:2402.18635].

[79] J. C. Collins, F. Wilczek and A. Zee, Phys. Rev. **D18**, 242 (1978).

[80] E. Laenen *et al.*, Nucl. Phys. **B392**, 162 (1993).

[81] M. A. G. Aivazis *et al.*, Phys. Rev. **D50**, 3102 (1994), [hep-ph/9312319].

[82] M. Buza *et al.*, Eur. Phys. J. **C1**, 301 (1998), [hep-ph/9612398].

[83] J. C. Collins, Phys. Rev. **D58**, 094002 (1998), [hep-ph/9806259].

[84] A. Chuvakin, J. Smith and W. L. van Neerven, Phys. Rev. **D61**, 096004 (2000), [hep-ph/9910250].

[85] R. S. Thorne, Phys. Rev. **D73**, 054019 (2006), [hep-ph/0601245].

[86] R. S. Thorne and W. K. Tung, in "Proceedings, HERA and the LHC Workshop Series on the implications of HERA for LHC physics: 2006-2008," 332–351 (2008), [,2(2008)], [arXiv:0809.0714].

[87] S. Alekhin and S. Moch, Phys. Lett. **B699**, 345 (2011), [arXiv:1011.5790].

[88] S. Forte *et al.*, Nucl. Phys. **B834**, 116 (2010), [arXiv:1001.2312].

[89] R. S. Thorne, Phys. Rev. **D86**, 074017 (2012), [arXiv:1201.6180].

[90] E. G. de Oliveira *et al.*, Eur. Phys. J. **C73**, 10, 2616 (2013), [arXiv:1307.3508].

[91] J. Ablinger *et al.*, Nucl. Phys. B **886**, 733 (2014), [arXiv:1406.4654].

[92] J. Ablinger *et al.*, Nucl. Phys. B **890**, 48 (2014), [arXiv:1409.1135].

[93] J. Ablinger *et al.*, Nucl. Phys. B **882**, 263 (2014), [arXiv:1402.0359].

[94] J. Ablinger *et al.*, JHEP **12**, 134 (2022), [arXiv:2211.05462].

[95] J. Ablinger *et al.*, Phys. Lett. B **854**, 138713 (2024), [arXiv:2403.00513].

[96] H. Abramowicz *et al.* (H1, ZEUS), Eur. Phys. J. **C78**, 6, 473 (2018), [arXiv:1804.01019].

[97] O. Behnke, A. Geiser and M. Lisovyi, Prog. Part. Nucl. Phys. **84**, 1 (2015), [arXiv:1506.07519].

[98] R. D. Ball *et al.* (NNPDF), Eur. Phys. J. C **77**, 10, 663 (2017), [arXiv:1706.00428].

[99] J. Butterworth *et al.*, J. Phys. **G43**, 023001 (2016), [arXiv:1510.03865].

[100] R. D. Ball *et al.* (PDF4LHC Working Group), J. Phys. G **49**, 8, 080501 (2022), [arXiv:2203.05506].

[101] T. Cridge *et al.*, Eur. Phys. J. C **81**, 744 (2021), [arXiv:2106.10289].

[102] R. D. Ball *et al.* (NNPDF), Eur. Phys. J. **C78**, 5, 408 (2018), [arXiv:1802.03398].

[103] A. D. Martin *et al.*, Eur. Phys. J. **C39**, 155 (2005), [hep-ph/0411040].

[104] R. D. Ball *et al.* (NNPDF), Nucl. Phys. **B877**, 290 (2013), [arXiv:1308.0598].

[105] C. Schmidt *et al.*, Phys. Rev. **D93**, 11, 114015 (2016), [arXiv:1509.02905].

[106] M. Gluck, C. Pisano and E. Reya, Phys. Lett. **B540**, 75 (2002), [hep-ph/0206126].

[107] A. D. Martin and M. G. Ryskin, Eur. Phys. J. **C74**, 3040 (2014), [arXiv:1406.2118].

[108] L. A. Harland-Lang, V. A. Khoze and M. G. Ryskin, Phys. Rev. **D94**, 7, 074008 (2016), [arXiv:1607.04635].

[109] A. Manohar *et al.*, Phys. Rev. Lett. **117**, 24, 242002 (2016), [arXiv:1607.04266].

[110] R. D. Ball *et al.* (NNPDF), Eur. Phys. J. C **84**, 5, 540 (2024), [arXiv:2401.08749].

[111] T. Cridge *et al.*, Eur. Phys. J. C **82**, 1, 90 (2022), [arXiv:2111.05357].

[112] K. Xie *et al.* (CTEQ-TEA), Phys. Rev. D **105**, 5, 054006 (2022), [arXiv:2106.10299].

[113] L. A. Harland-Lang, JHEP **03**, 128 (2020), [arXiv:1910.10178].

[114] H.-W. Lin *et al.*, Prog. Part. Nucl. Phys. **100**, 107 (2018), [arXiv:1711.07916].

[115] M. Constantinou *et al.*, Prog. Part. Nucl. Phys. **121**, 103908 (2021), [arXiv:2006.08636].

[116] H.-W. Lin, Few Body Syst. **64**, 3, 58 (2023).

[117] Y.-B. Yang *et al.*, Phys. Rev. Lett. **121**, 21, 212001 (2018), [arXiv:1808.08677].

[118] C. Alexandrou *et al.*, Phys. Rev. D **101**, 9, 094513 (2020), [arXiv:2003.08486].

[119] Z. Fan, H.-W. Lin and M. Zeilbeck, Phys. Rev. D **107**, 3, 034505 (2023), [arXiv:2208.00980].

[120] D. Djukanovic *et al.*, Phys. Rev. D **109**, 7, 074507 (2024), [arXiv:2402.03024].

[121] X. Ji, Phys. Rev. Lett. **110**, 262002 (2013), [arXiv:1305.1539].

[122] A. V. Radyushkin, Phys. Rev. D **96**, 3, 034025 (2017), [arXiv:1705.01488].

[123] C. Alexandrou *et al.*, Phys. Rev. Lett. **121**, 11, 112001 (2018), [arXiv:1803.02685].

[124] R. Zhang, H.-W. Lin and B. Yoon, Phys. Rev. D **104**, 9, 094511 (2021), [arXiv:2005.01124].

[125] Z. Fan, W. Good and H.-W. Lin, Phys. Rev. D **108**, 1, 014508 (2023), [arXiv:2210.09985].

[126] M. Bhat *et al.*, Phys. Rev. D **103**, 3, 034510 (2021), [arXiv:2005.02102].

[127] B. Joó *et al.*, Phys. Rev. Lett. **125**, 23, 232003 (2020), [arXiv:2004.01687].

[128] X. Gao *et al.*, Phys. Rev. D **107**, 7, 074509 (2023), [arXiv:2212.12569].

[129] R. Zhang *et al.*, Phys. Lett. B **844**, 138081 (2023), [arXiv:2305.05212].

[130] J. Delmar *et al.*, Phys. Rev. D **108**, 9, 094515 (2023), [arXiv:2310.01389].

[131] A. Buckley *et al.*, Eur. Phys. J. **C75**, 132 (2015), [arXiv:1412.7420].

[132] M. Klasen and H. Paukkunen, Ann. Rev. Nucl. Part. Sci. **74**, 49 (2024), [arXiv:2311.00450].

[133] I. Helenius, M. Walt and W. Vogelsang, Phys. Rev. D **105**, 9, 094031 (2022), [arXiv:2112.11904].

[134] P. Duwentäster *et al.*, Phys. Rev. D **105**, 11, 114043 (2022), [arXiv:2204.09982].

[135] E. P. Segarra *et al.*, Phys. Rev. D **103**, 11, 114015 (2021), [arXiv:2012.11566].

[136] K. J. Eskola *et al.*, Eur. Phys. J. C **82**, 5, 413 (2022), [arXiv:2112.12462].

[137] R. Abdul Khalek *et al.*, Eur. Phys. J. C **82**, 6, 507 (2022), [arXiv:2201.12363].

Int. J. Mod. Phys. A 2026.41. Downloaded from www.worldscientific.com by UNIVERSITY OF CALIFORNIA @ BERKELEY on 09/16/26. Re-use and distribution is [redacted] except for Open Access articles.

[138] R. Abdul Khalek, J. J. Ethier and J. Rojo (NNPDF), Eur. Phys. J. C **79**, 6, 471 (2019), [arXiv:1904.00018].

[139] H. Khanpour *et al.*, Phys. Rev. D **104**, 3, 034010 (2021), [arXiv:2010.00555].

[140] K. Kovarik *et al.*, Phys. Rev. Lett. **106**, 122301 (2011), [arXiv:1012.0286].

[141] H. Paukkunen and C. A. Salgado, Phys. Rev. Lett. **110**, 21, 212301 (2013), [arXiv:1302.2001].

[142] G. Aad *et al.* (ATLAS), Phys. Rev. **C92**, 4, 044915 (2015), [arXiv:1507.06232].

[143] V. Khachatryan *et al.* (CMS), Phys. Lett. **B750**, 565 (2015), [arXiv:1503.05825].

[144] V. Khachatryan *et al.* (CMS), Phys. Lett. B **759**, 36 (2016), [arXiv:1512.06461].

[145] A. M. Sirunyan *et al.* (CMS), Phys. Lett. B **800**, 135048 (2020), [arXiv:1905.01486].

[146] A. M. Sirunyan *et al.* (CMS), JHEP **05**, 182 (2021), [arXiv:2102.13648].

[147] A. M. Sirunyan *et al.* (CMS), Phys. Rev. Lett. **121**, 6, 062002 (2018), [arXiv:1805.04736].

[148] R. Aaij *et al.* (LHCb), JHEP **10**, 090 (2017), [arXiv:1707.02750].

[149] S. Acharya *et al.* (ALICE), Eur. Phys. J. **C78**, 8, 624 (2018), [arXiv:1801.07051].

[150] S. S. Adler *et al.* (PHENIX), Phys. Rev. Lett. **98**, 172302 (2007), [arXiv:nucl-ex/0610036].

[151] G. Aad *et al.* (ATLAS), Phys. Rev. D **111**, 5, 052006 (2025), [arXiv:2409.11060].

[152] E. C. Aschenauer *et al.*, Phys. Rev. **D96**, 11, 114005 (2017), [arXiv:1708.05654].

[153] R. Abdul Khalek *et al.*, Nucl. Phys. A **1026**, 122447 (2022), [arXiv:2103.05419].

[154] R. A. Khalek *et al.*, Phys. Rev. D **103**, 9, 096005 (2021), [arXiv:2102.00018].

[155] P. V. Landshoff and J. C. Polkinghorne, Phys. Rev. D **18**, 3344 (1978).

[156] R. Kirschner, Phys. Lett. B **84**, 266 (1979).

[157] N. Paver and D. Treleani, Nuovo Cim. A **70**, 215 (1982).

[158] V. P. Shelest, A. M. Snigirev and G. M. Zinovev, Phys. Lett. B **113**, 325 (1982).

[159] M. Mekhfi, Phys. Rev. D **32**, 2371 (1985).

[160] B. Blok *et al.*, Phys. Rev. D **83**, 071501 (2011), [arXiv:1009.2714].

[161] M. Diehl and A. Schafer, Phys. Lett. B **698**, 389 (2011), [arXiv:1102.3081].

[162] B. Blok *et al.*, Eur. Phys. J. C **72**, 1963 (2012), [arXiv:1106.5533].

[163] M. Diehl, D. Ostermeier and A. Schafer, JHEP **03**, 089 (2012), [Erratum: JHEP 03, 001 (2016)], [arXiv:1111.0910].

[164] C. H. Kom, A. Kulesza and W. J. Stirling, Phys. Rev. Lett. **107**, 082002 (2011), [arXiv:1105.4186].

[165] C. H. Kom, A. Kulesza and W. J. Stirling, Eur. Phys. J. C **71**, 1802 (2011), [arXiv:1109.0309].

[166] J. R. Gaunt *et al.*, Eur. Phys. J. C **69**, 53 (2010), [arXiv:1003.3953].

[167] F. Abe *et al.* (CDF), Phys. Rev. D **56**, 3811 (1997).

[168] V. M. Abazov *et al.* (D0), Phys. Rev. D **93**, 5, 052008 (2016), [arXiv:1512.05291].

[169] R. Aaij *et al.* (LHCb), JHEP **06**, 047 (2017), [Erratum: JHEP 10, 068 (2017)], [arXiv:1612.07451].

[170] M. Aaboud *et al.* (ATLAS), Phys. Lett. B **790**, 595 (2019), [arXiv:1811.11094].

[171] A. M. Sirunyan *et al.* (CMS), Eur. Phys. J. C **80**, 1, 41 (2020), [arXiv:1909.06265].

[172] A. V. Manohar and W. J. Waalewijn, Phys. Rev. D **85**, 114009 (2012), [arXiv:1202.3794].

[173] B. Blok *et al.*, Eur. Phys. J. C **74**, 2926 (2014), [arXiv:1306.3763].

[174] M. Diehl, J. R. Gaunt and K. Schönwald, JHEP **06**, 083 (2017), [arXiv:1702.06486].

[175] J. R. Gaunt and W. J. Stirling, JHEP **03**, 005 (2010), [arXiv:0910.4347].

[176] K. Golec-Biernat *et al.*, Phys. Lett. B **750**, 559 (2015), [arXiv:1507.08583].

[177] M. Diehl *et al.*, Eur. Phys. J. C **80**, 5, 468 (2020), [arXiv:2001.10428].

[178] M. Diehl, J. R. Gaunt and P. Ploessl, JHEP **08**, 040 (2021), [arXiv:2105.08425].

[179] M. Diehl, F. Fabry and A. Vladimirov, JHEP **05**, 067 (2023), [arXiv:2212.11843].

[180] D. Flay *et al.* (Jefferson Lab Hall A), Phys. Rev. **D94**, 5, 052003 (2016), [arXiv:1603.03612].

[181] C. Adolph *et al.* (COMPASS), Phys. Lett. **B753**, 18 (2016), [arXiv:1503.08935].

[182] C. Adolph *et al.* (COMPASS), Phys. Lett. **B769**, 34 (2017), [arXiv:1612.00620].

[183] R. Fersch *et al.* (CLAS), Phys. Rev. **C96**, 6, 065208 (2017), [arXiv:1706.10289].

[184] M. Hirai and S. Kumano (Asymmetry Analysis), Nucl. Phys. **B813**, 106 (2009), [arXiv:0808.0413].

[185] D. de Florian *et al.*, Phys. Rev. Lett. **101**, 072001 (2008), [arXiv:0804.0422]; D. de Florian *et al.*, Phys. Rev. **D80**, 034030 (2009), [arXiv:0904.3821].

[186] E. Leader, A. V. Sidorov and D. B. Stamenov, Phys. Rev. **D82**, 114018 (2010), [arXiv:1010.0574].

[187] J. Blumlein and H. Bottcher, Nucl. Phys. **B841**, 205 (2010), [arXiv:1005.3113].

[188] D. de Florian *et al.*, Phys. Rev. Lett. **113**, 1, 012001 (2014), [arXiv:1404.4293].

[189] N. Sato *et al.* (Jefferson Lab Angular Momentum), Phys. Rev. **D93**, 7, 074005 (2016), [arXiv:1601.07782].

[190] F. Taghavi-Shahri *et al.*, Phys. Rev. D **93**, 11, 114024 (2016), [arXiv:1603.03157].

[191] V. Bertone, A. Chiefa and E. R. Nocera (MAP (Multi-dimensional Analyses of Partonic distributions)), Phys. Lett. B **865**, 139497 (2025), [arXiv:2404.04712].

[192] I. Borsa *et al.*, Phys. Rev. Lett. **133**, 15, 151901 (2024), [arXiv:2407.11635].

[193] D. de Florian *et al.*, Phys. Rev. **D91**, 1, 014035 (2015), [arXiv:1410.6027].

[194] D. de Florian *et al.*, Phys. Rev. **D95**, 9, 094019 (2017), [arXiv:1702.06353].

[195] V. Bertone *et al.* (NNPDF), Eur. Phys. J. **C77**, 8, 516 (2017), [arXiv:1706.07049].

[196] V. Bertone *et al.* (NNPDF), Eur. Phys. J. **C78**, 8, 651 (2018), [arXiv:1807.03310].

[197] D. De Florian *et al.*, Phys. Rev. D **100**, 11, 114027 (2019), [arXiv:1902.10548].

[198] L. Adamczyk *et al.* (STAR), Phys. Rev. Lett. **115**, 9, 092002 (2015), [arXiv:1405.5134].

[199] L. Adamczyk *et al.* (STAR), Phys. Rev. D **95**, 7, 071103 (2017), [arXiv:1610.06616].

[200] A. Adare *et al.* (PHENIX), Phys. Rev. D **90**, 1, 012007 (2014), [arXiv:1402.6296].

[201] J. Adam *et al.* (STAR), Phys. Rev. D **99**, 5, 051102 (2019), [arXiv:1812.04817].

[202] A. Adare *et al.* (PHENIX), Phys. Rev. D **98**, 3, 032007 (2018), [arXiv:1804.04181].

Int. J. Mod. Phys. A 2026.41. Downloaded from www.worldscientific.com
by UNIVERSITY OF CALIFORNIA @ BERKELEY on 09/16/26. Re-use and distribution is strictly not permitted, except for Open Access articles.

[203] R. D. Ball *et al.* (NNPDF), Nucl. Phys. **B874**, 36 (2013), [arXiv:1303.7236].

[204] J. Adam *et al.* (STAR), Phys. Rev. D **100**, 5, 052005 (2019), [arXiv:1906.02740].

[205] M. Abdallah *et al.* (STAR), Phys. Rev. D **103**, 9, L091103 (2021), [arXiv:2103.05571].

[206] M. S. Abdallah *et al.* (STAR), Phys. Rev. D **105**, 9, 092011 (2022), [arXiv:2110.11020].

[207] A. Adare *et al.* (PHENIX), Phys. Rev. D **93**, 1, 011501 (2016), [arXiv:1510.02317].

[208] C. Cocuzza *et al.* (Jefferson Lab Angular Momentum (JAM)), Phys. Rev. D **106**, 3, L031502 (2022), [arXiv:2202.03372].

[209] J. Liang *et al.*, Phys. Rev. D **98**, 7, 074505 (2018), [arXiv:1806.08366].

[210] R. Nisius, Phys. Rept. **332**, 165 (2000), [hep-ex/9912049].

[211] T. F. Walsh and P. M. Zerwas, Phys. Lett. **44B**, 195 (1973).

[212] R. L. Kingsley, Nucl. Phys. **B60**, 45 (1973).

[213] E. Witten, Nucl. Phys. **B120**, 189 (1977).

[214] W. A. Bardeen and A. J. Buras, Phys. Rev. **D20**, 166 (1979), [Erratum: Phys. Rev.D21,2041(1980)].

[215] M. Fontannaz and E. Pilon, Phys. Rev. **D45**, 382 (1992).

[216] M. Gluck, E. Reya and A. Vogt, Phys. Rev. **D45**, 3986 (1992).

[217] F. Cornet, P. Jankowski and M. Krawczyk, Phys. Rev. **D70**, 093004 (2004), [hep-ph/0404063].

[218] P. Aurenche, M. Fontannaz and J. P. Guillet, Eur. Phys. J. **C44**, 395 (2005), [hep-ph/0503259].

[219] W. Slominski, H. Abramowicz and A. Levy, Eur. Phys. J. **C45**, 633 (2006), [hep-ph/0504003].

[220] S. Hoeche, F. Krauss and P. Meinzinger, Eur. Phys. J. C **84**, 2, 178 (2024), [arXiv:2310.18674].

[221] H. Abramowicz and A. Caldwell, Rev. Mod. Phys. **71**, 1275 (1999), [hep-ex/9903037].

[222] S. Chekanov *et al.* (ZEUS), Nucl. Phys. **B831**, 1 (2010), [arXiv:0911.4119].

[223] A. Aktas *et al.* (H1), Eur. Phys. J. **C48**, 715 (2006), [hep-ex/0606004].

[224] A. D. Martin, M. G. Ryskin and G. Watt, Phys. Lett. **B644**, 131 (2007), [hep-ph/0609273].

[225] A. Aktas *et al.* (H1), JHEP **10**, 042 (2007), [arXiv:0708.3217].

[226] F. D. Aaron *et al.* (H1, ZEUS), Eur. Phys. J. **C72**, 2175 (2012), [arXiv:1207.4864].

[227] F. D. Aaron *et al.* (H1), Eur. Phys. J. **C72**, 2074 (2012), [arXiv:1203.4495].

[228] J. C. Collins, Phys. Rev. **D57**, 3051 (1998), [Erratum: Phys. Rev.D61,019902(2000)], [hep-ph/9709499].

[229] G. Ingelman and P. E. Schlein, Phys. Lett. **152B**, 256 (1985).

[230] M. Goharipour, H. Khanpour and V. Guzey, Eur. Phys. J. **C78**, 4, 309 (2018), [arXiv:1802.01363].

[231] X. Ji, Phys. Rev. Lett. **91**, 062001 (2003), [hep-ph/0304037].

[232] A. V. Belitsky, X. Ji and F. Yuan, Phys. Rev. **D69**, 074014 (2004), [hep-ph/0307383].

[233] C. Lorce, B. Pasquini and M. Vanderhaeghen, JHEP **05**, 041 (2011), [arXiv:1102.4704].

[234] X.-D. Ji, J. Phys. **G24**, 1181 (1998), [hep-ph/9807358].

[235] K. Goeke, M. V. Polyakov and M. Vanderhaeghen, Prog. Part. Nucl. Phys. **47**, 401 (2001), [hep-ph/0106012].

[236] M. Diehl, Phys. Rept. **388**, 41 (2003), [hep-ph/0307382].

[237] A. V. Belitsky and A. V. Radyushkin, Phys. Rept. **418**, 1 (2005), [hep-ph/0504030].

[238] S. Boffi and B. Pasquini, Riv. Nuovo Cim. **30**, 387 (2007), [arXiv:0711.2625].

[239] K. Kumericki, S. Liuti and H. Moutarde, Eur. Phys. J. **A52**, 6, 157 (2016), [arXiv:1602.02763].

[240] M. Burkardt, Int. J. Mod. Phys. **A18**, 173 (2003), [hep-ph/0207047].

[241] M. Diehl, Eur. Phys. J. **C25**, 223 (2002), [Erratum: Eur. Phys. J.C31,277(2003)], [hep-ph/0205208].

[242] X.-D. Ji, Phys. Rev. Lett. **78**, 610 (1997), [hep-ph/9603249].

[243] M. Bury, A. Prokudin and A. Vladimirov, JHEP **05**, 151 (2021), [arXiv:2103.03270].

[244] A. V. Efremov and A. V. Radyushkin, Phys. Lett. **94B**, 245 (1980).

[245] G. P. Lepage and S. J. Brodsky, Phys. Rev. **D22**, 2157 (1980).

[246] A. V. Belitsky, A. Freund and D. Mueller, Phys. Lett. **B493**, 341 (2000), [hep-ph/0008005].

[247] A. V. Belitsky, A. Freund and D. Mueller, Nucl. Phys. **B574**, 347 (2000), [hep-ph/9912379].

[248] V. M. Braun *et al.*, JHEP **06**, 037 (2017), [arXiv:1703.09532].

[249] M. V. Polyakov, Phys. Lett. B **555**, 57 (2003), [hep-ph/0210165].

[250] M. V. Polyakov and P. Schweitzer, Int. J. Mod. Phys. A **33**, 26, 1830025 (2018), [arXiv:1805.06596].

[251] B. Duran *et al.*, Nature **615**, 7954, 813 (2023), [arXiv:2207.05212].

[252] A. V. Radyushkin, Phys. Rev. **D59**, 014030 (1999), [hep-ph/9805342].

[253] A. V. Radyushkin, Phys. Lett. **B449**, 81 (1999), [hep-ph/9810466].

[254] K. Kumerički and D. Mueller, Nucl. Phys. **B841**, 1 (2010), [arXiv:0904.0458].

[255] N. d'Hose, S. Niccolai and A. Rostomyan, Eur. Phys. J. **A52**, 6, 151 (2016).

[256] M. Guidal, H. Moutarde and M. Vanderhaeghen, Rept. Prog. Phys. **76**, 066202 (2013), [arXiv:1303.6600].

[257] M. Diehl, Eur. Phys. J. A **52**, 6, 149 (2016), [arXiv:1512.01328].

[258] S. Diehl, Prog. Part. Nucl. Phys. **133**, 104069 (2023).

[259] M. Čuić, K. Kumerički and A. Schäfer, Phys. Rev. Lett. **125**, 23, 232005 (2020), [arXiv:2007.00029].

[260] H. Moutarde, P. Sznajder and J. Wagner, Eur. Phys. J. C **79**, 7, 614 (2019), [arXiv:1905.02089].

[261] S. Bhattacharya *et al.*, Phys. Rev. D **106**, 11, 114512 (2022), [arXiv:2209.05373].

[262] P. J. Mulders and R. D. Tangerman, Nucl. Phys. **B461**, 197 (1996), [Erratum: Nucl. Phys.B484,538(1997)], [hep-ph/9510301].

[263] D. Boer and P. J. Mulders, Phys. Rev. **D57**, 5780 (1998), [hep-ph/9711485].

[264] D. W. Sivers, Phys. Rev. **D41**, 83 (1990).

[265] J. C. Collins, Nucl. Phys. **B396**, 161 (1993), [hep-ph/9208213].

[266] X. Ji, J. Ma and F. Yuan, Phys. Rev. **D71**, 034005 (2005), [hep-ph/0404183].

[267] J. Collins, Foundations of perturbative QCD Camb. Monogr. Part. Phys. Nucl. Phys. Cosmol. 32 (2011) 1-624 and references therein.

[268] S. M. Aybat and T. C. Rogers, Phys. Rev. **D83**, 114042 (2011), [arXiv:1101.5057].

[269] M. G. Echevarria, A. Idilbi and I. Scimemi, JHEP **07**, 002 (2012), [arXiv:1111.4996].

[270] M. G. A. Buffing, A. Mukherjee and P. J. Mulders, Phys. Rev. **D88**, 054027 (2013), [arXiv:1306.5897].

[271] T. C. Rogers and P. J. Mulders, Phys. Rev. **D81**, 094006 (2010), [arXiv:1001.2977].

[272] A. Signori *et al.*, JHEP **11**, 194 (2013), [arXiv:1309.3507].

[273] M. Anselmino *et al.*, JHEP **04**, 005 (2014), [arXiv:1312.6261].

[274] U. D'Alesio *et al.*, JHEP **11**, 098 (2014), [arXiv:1407.3311].

[275] I. Scimemi and A. Vladimirov, JHEP **06**, 137 (2020), [arXiv:1912.06532].

[276] M. G. Echevarria, Z.-B. Kang and J. Terry, JHEP **01**, 126 (2021), [arXiv:2009.10710].

[277] A. Bacchetta *et al.* (MAP (Multi-dimensional Analyses of Partonic distributions)), JHEP **10**, 127 (2022), [arXiv:2206.07598].

[278] A. Bacchetta *et al.* (MAP (Multi-dimensional Analyses of Partonic distributions)), Phys. Rev. Lett. **135**, 2, 021904 (2025), [arXiv:2502.04166].

[279] J. O. Gonzalez-Hernandez *et al.*, Phys. Rev. **D98**, 11, 114005 (2018), [arXiv:1808.04396].

[280] A. Bacchetta *et al.*, Phys. Rev. **D100**, 1, 014018 (2019), [arXiv:1901.06916].

[281] M. Bury *et al.*, JHEP **10**, 118 (2022), [arXiv:2201.07114].

[282] R. Angeles-Martinez *et al.*, Acta Phys. Polon. **B46**, 12, 2501 (2015), [arXiv:1507.05267].

[283] A. Bacchetta *et al.*, Phys. Lett. **B788**, 542 (2019), [arXiv:1807.02101].

[284] X. Gao *et al.*, Phys. Rev. D **109**, 5, 054506 (2024), [arXiv:2310.19047].

[285] A. Bacchetta, Eur. Phys. J. **A52**, 6, 163 (2016).

[286] I. Scimemi, Adv. High Energy Phys. **2019**, 3142510 (2019), [arXiv:1901.08398].

[287] R. Boussarie *et al.* (2023), [arXiv:2304.03302].

Int. J. Mod. Phys. A 2026.41. Downloaded from www.wo
by UNIVERSITY OF CALIFORNIA @ BERKELEY on 09/16/26. Re-use and distribution is
except for Open Access articles.

Int. J. Mod. Phys. A 2026.41. Downloaded from www.worldscientific.com
by UNIVERSITY OF CALIFORNIA @ BERKELEY on 09/16/26. Re-use and distribution is strictly not permitted, except for Open Access articles.

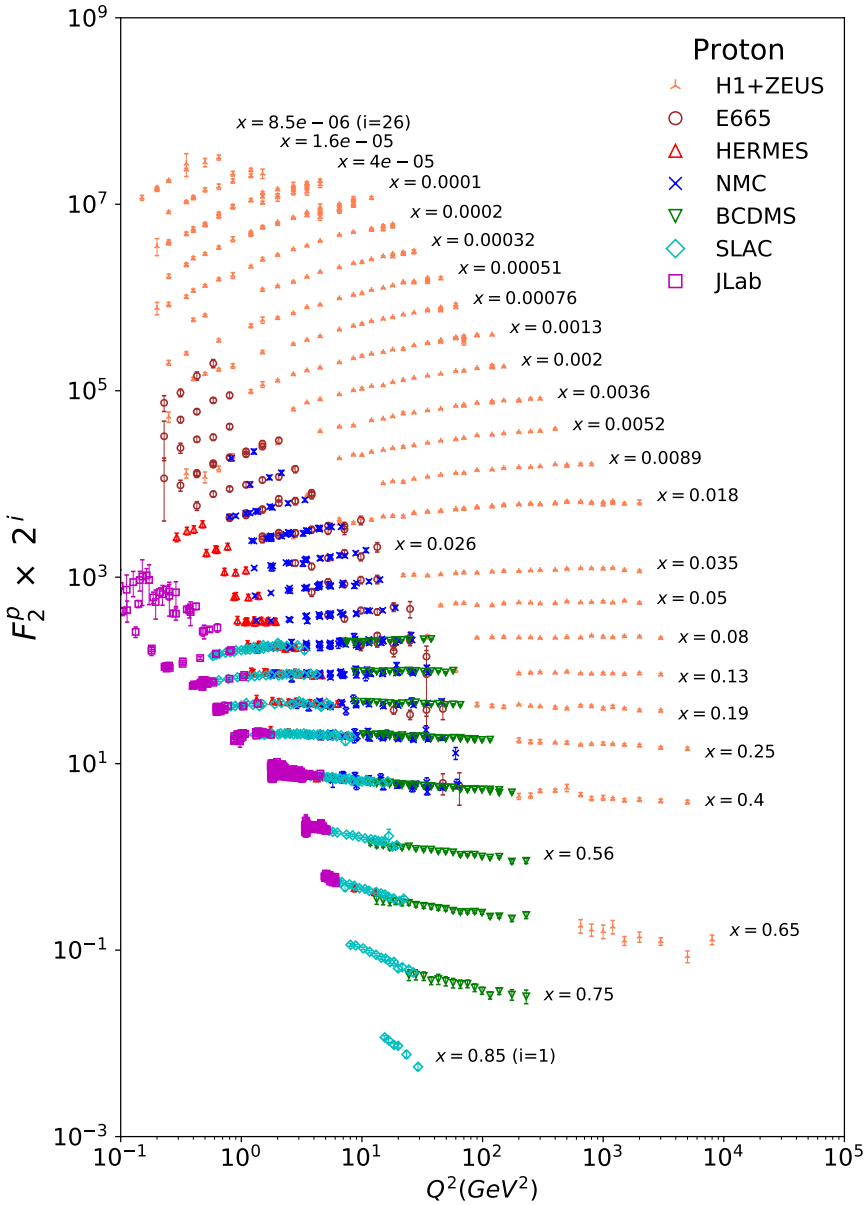

Figure 18.10: The proton structure function F_2^p measured in electromagnetic scattering of electrons and positrons on protons, and for electrons/positrons (SLAC,HERMES,JLAB) and muons (BCDMS, E665, NMC) on a fixed target. Statistical and systematic errors added in quadrature are shown. The H1+ZEUS combined values are obtained from the measured reduced cross section and converted to F_2^p with a HERAPDF NLO fit, for all measured points where the predicted ratio of F_2^p to reduced cross-section was within 10% of unity. The data are plotted as a function of Q^2 in bins of fixed x. Some points have been slightly offset in Q^2 for clarity. The H1+ZEUS combined binning in x is used in this plot; all other data are rebinned to the x values of these data. For the purpose of plotting, F_2^p has been multiplied by 2^{i_x}, where i_x is the number of the x bin, ranging from $i_x = 1$ ($x = 0.85$) to $i_x = 26$ ($x = 0.0000085$). Only data with $W^2 > 3.5$ GeV^2 is included. Plot from CJ collaboration (Shujie Li – private communication).
References: **H1 and ZEUS**—H. Abramowicz *et al.*, Eur. Phys. J. **C75**, 580 (2015) (for both data and HERAPDF parameterization); **BCDMS**—A.C. Benvenuti *et al.*, Phys. Lett. **B223**, 485 (1989) ;**E665**—M.R. Adams *et al.*, Phys. Rev. **D54**, 3006 (1996); **NMC**—M. Arneodo *et al.*, Nucl. Phys. **B483**, 3 (1997); **SLAC**—L.W. Whitlow *et al.*, Phys. Lett. **B282**, 475 (1992); **HERMES**—A. Airapetian *et al.*, JHEP **1105**, 126 (2011);**JLAB**—Y. Liang *et al.*, Jefferson Lab Hall C E94-110 collaboration, nucl-ex/0410027, M.E. Christy *et al.*, Jefferson Lab Hall C E94-110 Collaboration, Phys. Rev. **C70**, 015206 (2004), S. Malace *et al.*, Jefferson Lab Hall C E00-116 Collaboration, Phys. Rev. **C80**, 035207 (2009), V. Tvaskis *et al.*, Jefferson Lab Hall C E99-118 Collaboration, Phys. Rev. **C81**, 055207 (2010), M. Osipenko *et al.*, Jefferson Lab Hall B CLAS6 Collaboration, Phys. Rev. **D67**, 092001 (2003).

Int. J. Mod. Phys. A 2026.41. Downloaded from www.wo
by UNIVERSITY OF CALIFORNIA @ BERKELEY on 09/16/26. Re-use and distribution is
except for Open Access articles.

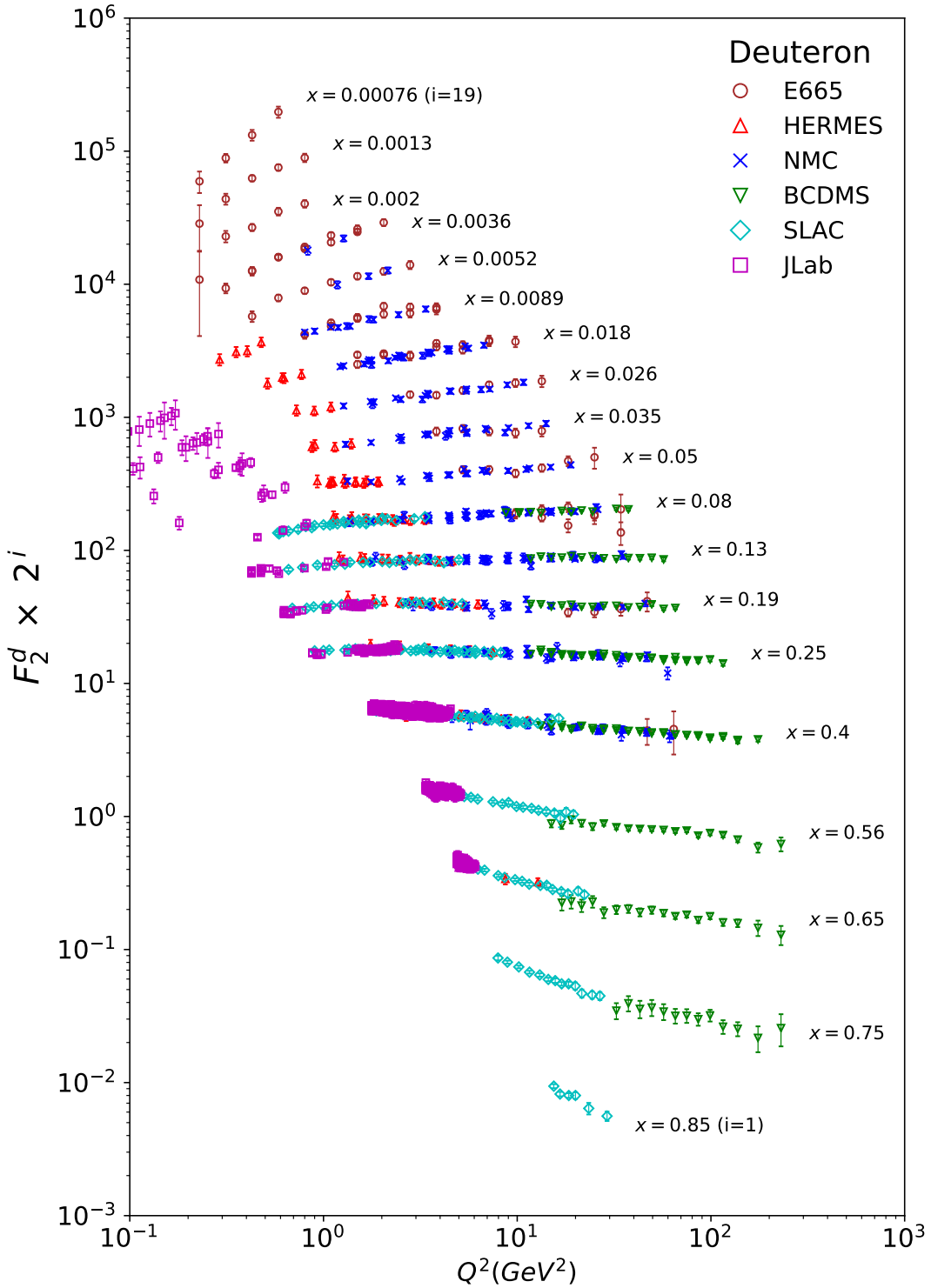

Figure 18.11: The deuteron structure function F_2^d measured in electromagnetic scattering of electrons/positrons (SLAC,HERMES,JLAB) and muons (BCDMS, E665, NMC) on a fixed target, shown as a function of Q^2 for bins of fixed x. Statistical and systematic errors added in quadrature are shown. For the purpose of plotting, F_2^d has been multiplied by 2^{i_x}, where i_x is the number of the x bin, ranging from 1 ($x = 0.85$) to 29 ($x = 0.00076$). Only data with $W^2 > 3.5$ GeV^2 is included. Plot from CJ collaboration (Shujie Li – private communication) References: **BCDMS**—A.C. Benvenuti *et al.*, Phys. Lett. **B237**, 592 (1990). **E665, NMC, SLAC,HERMES**—same references as Fig. 18.10; **JLAB**—S. Malace *et al.*, Jefferson Lab Hall C E00-116 Collaboration, Phys. Rev. **C80**, 035207 (2009), V. Tvaskis *et al.*, Jefferson Lab Hall C E99-118 Collaboration, Phys. Rev. **C81**, 055207 (2010), J. Seely (MIT, LNS) *et al.*, Jefferson Lab Hall C E03-103 Collaboration, Phys. Rev. Lett. **103**, 202301 (2009), M. Osipenko *et al.*, Jefferson Lab Hall B CLAS6 Collaboration, Phys. Rev. **C73**, 045205 (2006).

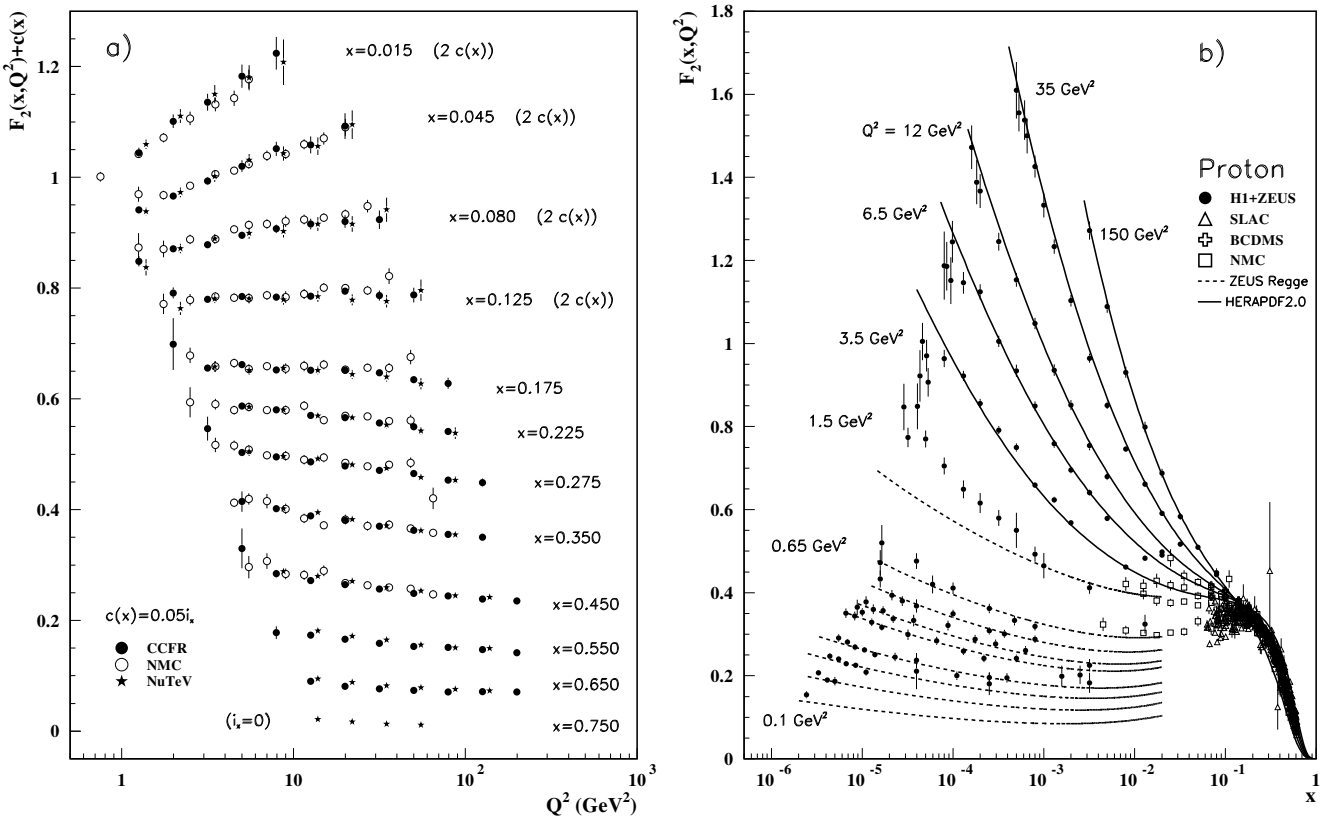

Figure 18.12: a) The deuteron structure function F_2 measured in deep inelastic scattering of muons on a fixed target (NMC) is compared to the structure function F_2 from neutrino-iron scattering (CCFR and NuTeV) using $F_2^{\mu} = (5/18)F_2^{\nu} - x(s+\overline{s})/6$, where heavy-target effects have been taken into account. The data are shown versus Q^2, for bins of fixed x. The NMC data have been rebinned to CCFR and NuTeV x values. For the purpose of plotting, a constant $c(x) = 0.05i_x$ is added to F_2, where i_x is the number of the x bin, ranging from 0 ($x = 0.75$) to 7 ($x = 0.175$). For $i_x = 8$ ($x = 0.125$) to 11 ($x = 0.015$), $2c(x)$ has been added. References: **NMC**—M. Arneodo *et al.*, Nucl. Phys. **B483**, 3 (1997); **CCFR/NuTeV**—U.K. Yang *et al.*, Phys. Rev. Lett. **86**, 2741 (2001); **NuTeV**—M. Tzanov *et al.*, Phys. Rev. **D74**, 012008 (2006).
b) The proton structure function F_2^p mostly at small x and Q^2, measured in electromagnetic scattering of electrons and positrons (H1, ZEUS), electrons (SLAC), and muons (BCDMS, NMC) on protons. Lines are ZEUS Regge and HERAPDF parameterizations for lower and higher Q^2, respectively. The width of the bins can be up to 10% of the stated Q^2. Some points have been slightly offset in x for clarity. The H1+ZEUS combined values for $Q^2 \geq 3.5$ GeV^2 are obtained from the measured reduced cross section and converted to F_2^p with a HERAPDF NLO fit, for all measured points where the predicted ratio of F_2^p to reduced cross-section was within 10% of unity. A turn-over is visible in the low-x points at medium Q^2 (3.5 GeV^2 and 6 GeV^2) for the H1+ZEUS combined values. In order to obtain F_2^p from the measured reduced cross-section, F_L must be estimated; for the points shown, this estimate is obtained from HERAPDF2.0. No F_L value consistent with the HERA data can eliminate the turn-over. This may indicate that at low x and Q^2 there are contributions to the structure functions that cannot be described in standard DGLAP evolution.
References: **H1 and ZEUS**—F.D. Aaron *et al.*, JHEP **1001**, 109 (2010) (data for $Q^2 < 3.5$ GeV^2), H. Abramowicz *et al.*, Eur. Phys. J. **C75**, 580 (2015) (data for $Q^2 \geq 3.5$ GeV^2 and HERAPDF parameterization); **ZEUS**—J. Breitweg *et al.*, Phys. Lett. **B487**, 53 (2000) (ZEUS Regge parameterization); **BCDMS, NMC, SLAC**—same references as Fig. 18.10.
Statistical and systematic errors added in quadrature are shown for both plots.

Int. J. Mod. Phys. A 2026.41. Downloaded from www.worldscientific.com
by UNIVERSITY OF CALIFORNIA @ BERKELEY on 09/16/26. Re-use and distribution is strictly not permitted, except for Open Access articles.

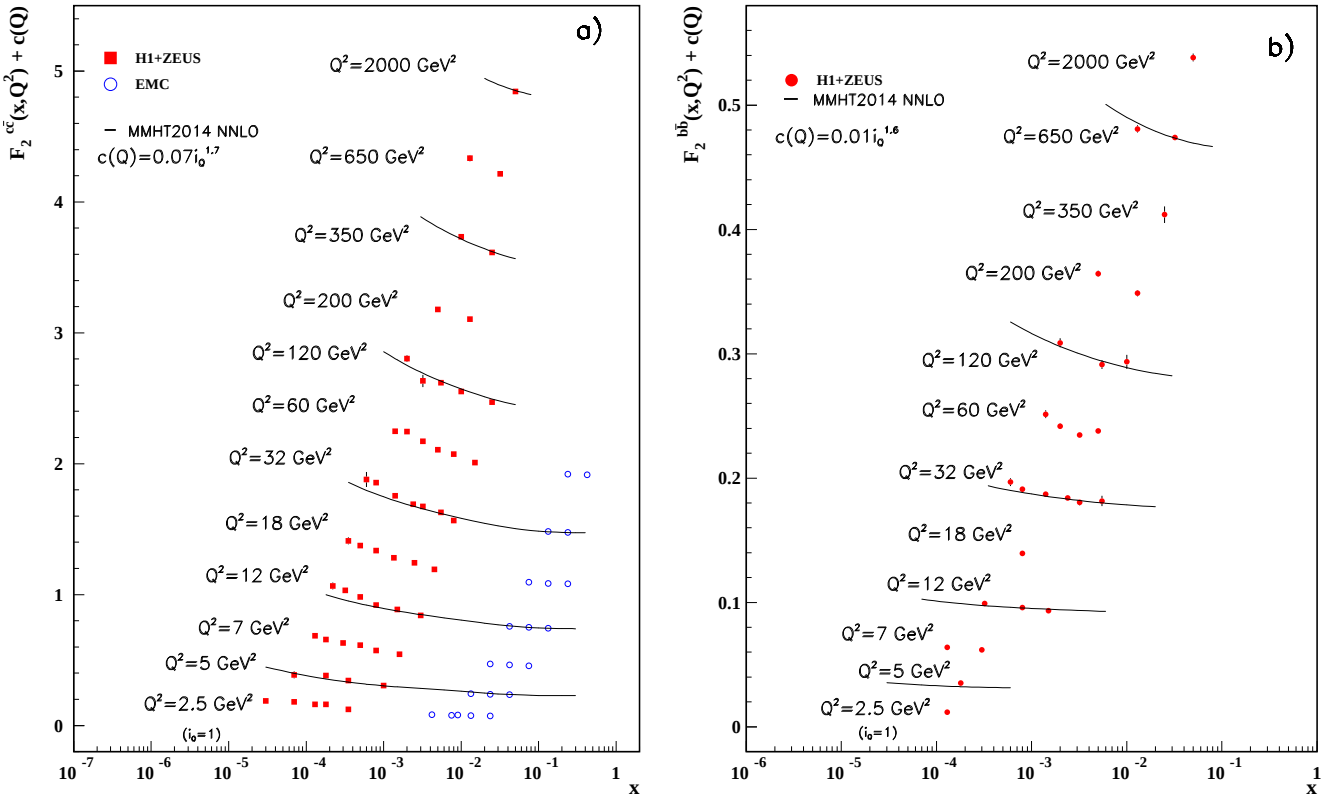

Figure 18.13: a) The charm-quark structure function $F_2^{c\bar{c}}(x)$, i.e. that part of the inclusive structure function F_2^p arising from the production of charm quarks, measured in electromagnetic scattering of positrons on protons (H1, ZEUS) (the values are obtained from the measured reduced cross section and converted to $F_2^{c\bar{c}}$ using the PDFs from the MMHT NNLO fit) and muons on iron (EMC). For the purpose of plotting, a constant $c(Q) = 0.07 i_Q{}^{1.7}$ is added to $F_2^{c\bar{c}}$ where i_Q is the number of the Q^2 bin, ranging from 1 ($Q^2 = 2.5$ GeV^2) to 12 ($Q^2 = 2000$ GeV^2). References: **H1 and ZEUS run I +II combination**—H. Abramowicz *et al.*, Eur. Phys. J. **C78**, 473 (2018); **EMC**—J.J. Aubert *et al.*, Nucl. Phys. **B213**, 31 (1983).

b) The bottom-quark structure function $F_2^{b\bar{b}}(x)$. For the purpose of plotting, a constant $c(Q) = 0.01 i_Q^{1.6}$ is added to $F_2^{b\bar{b}}$ where i_Q is the number of the Q^2 bin, ranging from 1 ($Q^2 = 2.5$ GeV^2) to 12 ($Q^2 = 2000$ GeV^2). References: **H1 and ZEUS run I combination**—H. Abramowicz *et al.*, Eur. Phys. J. **C78**, 473 (2018).

For both plots, statistical and systematic errors added in quadrature are shown. The data are given as a function of x in bins of Q^2. Points may have been slightly offset in x for clarity. Some data have been rebinned to common Q^2 values. Also shown is the MMHT2014 parameterization given at several Q^2 values (L. A. Harland-Lang *et al.*, Eur. Phys. J. **C75**, 204 (2015)).

Int. J. Mod. Phys. A 2026.41. Downloaded from www.wo
by UNIVERSITY OF CALIFORNIA @ BERKELEY on 09/16/26. Re-use and distribution is
except for Open Access articles.

Int. J. Mod. Phys. A 2026.41. Downloaded from www.worldscientific.com
by UNIVERSITY OF CALIFORNIA @ BERKELEY on 09/16/26. Re-use and distribution is strictly not permitted, except for Open Access articles.

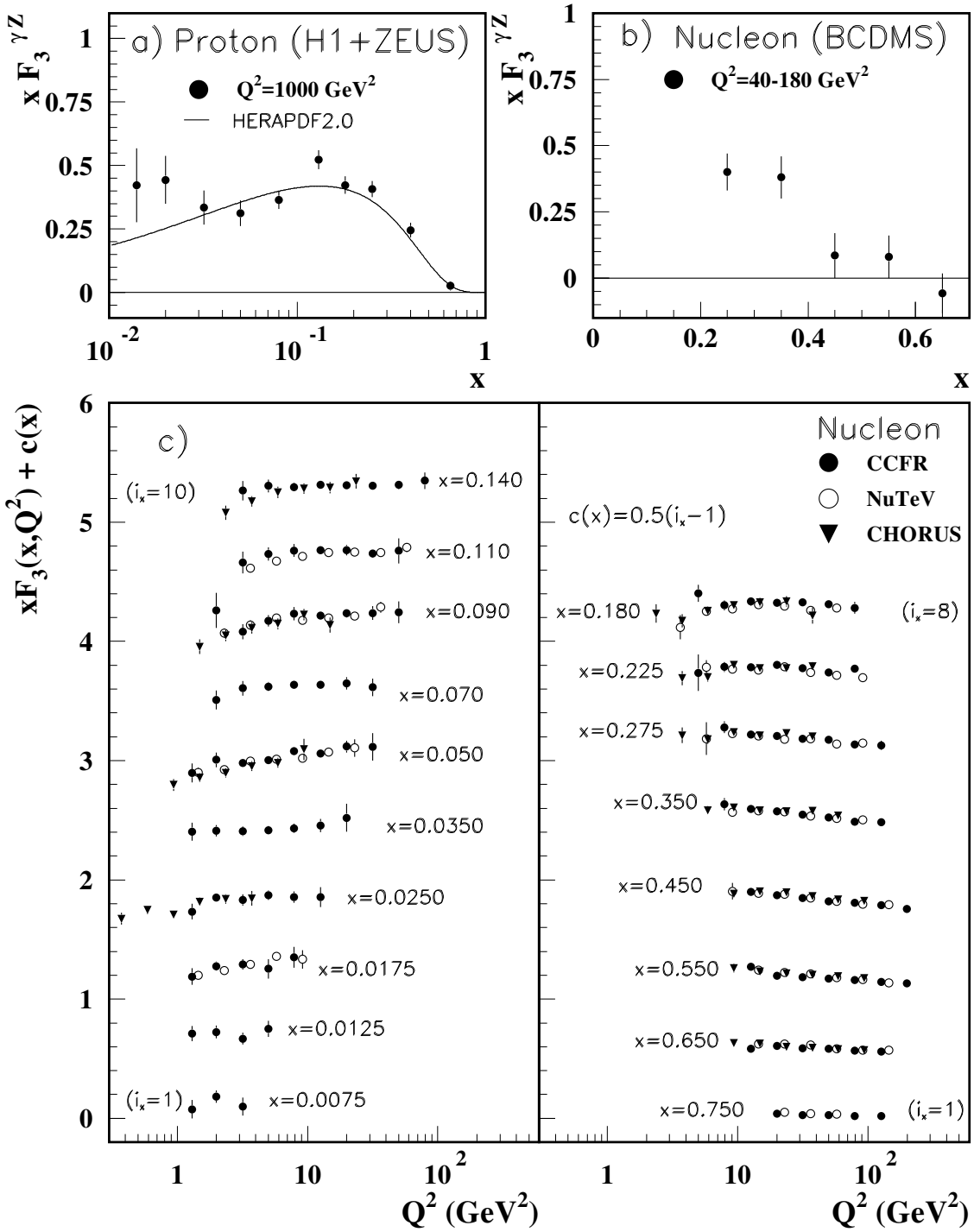

Figure 18.14: The structure function $xF_3^{\gamma Z}$ measured in electroweak scattering of **a)** electrons on protons (H1 and ZEUS) and **b)** muons on carbon (BCDMS). The line in **a)** is the HERAPDF parameterization. References: **H1 and ZEUS**—H. Abramowicz *et al.*, Eur. Phys. J. **C75**, 580 (2015) (for both data and HERAPDF parameterization); **BCDMS**—A. Argento *et al.*, Phys. Lett. **B140**, 142 (1984).
c) The structure function xF_3 of the nucleon measured in ν-Fe scattering. The data are plotted as a function of Q^2 in bins of fixed x. For the purpose of plotting, a constant $c(x) = 0.5(i_x - 1)$ is added to xF_3, where i_x is the number of the x bin as shown in the plot. The NuTeV and CHORUS points have been shifted to the nearest corresponding x bin as given in the plot and slightly offset in Q^2 for clarity. References: **CCFR**—W.G. Seligman *et al.*, Phys. Rev. Lett. **79**, 1213 (1997); **NuTeV**—M. Tzanov *et al.*, Phys. Rev. **D74**, 012008 (2006); **CHORUS**—G. Önengüt *et al.*, Phys. Lett. **B632**, 65 (2006).

Statistical and systematic errors added in quadrature are shown for all plots.

Int. J. Mod. Phys. A 2026.41. Downloaded from www.wo
by UNIVERSITY OF CALIFORNIA @ BERKELEY on 09/16/26. Re-use and distribution is
except for Open Access articles.

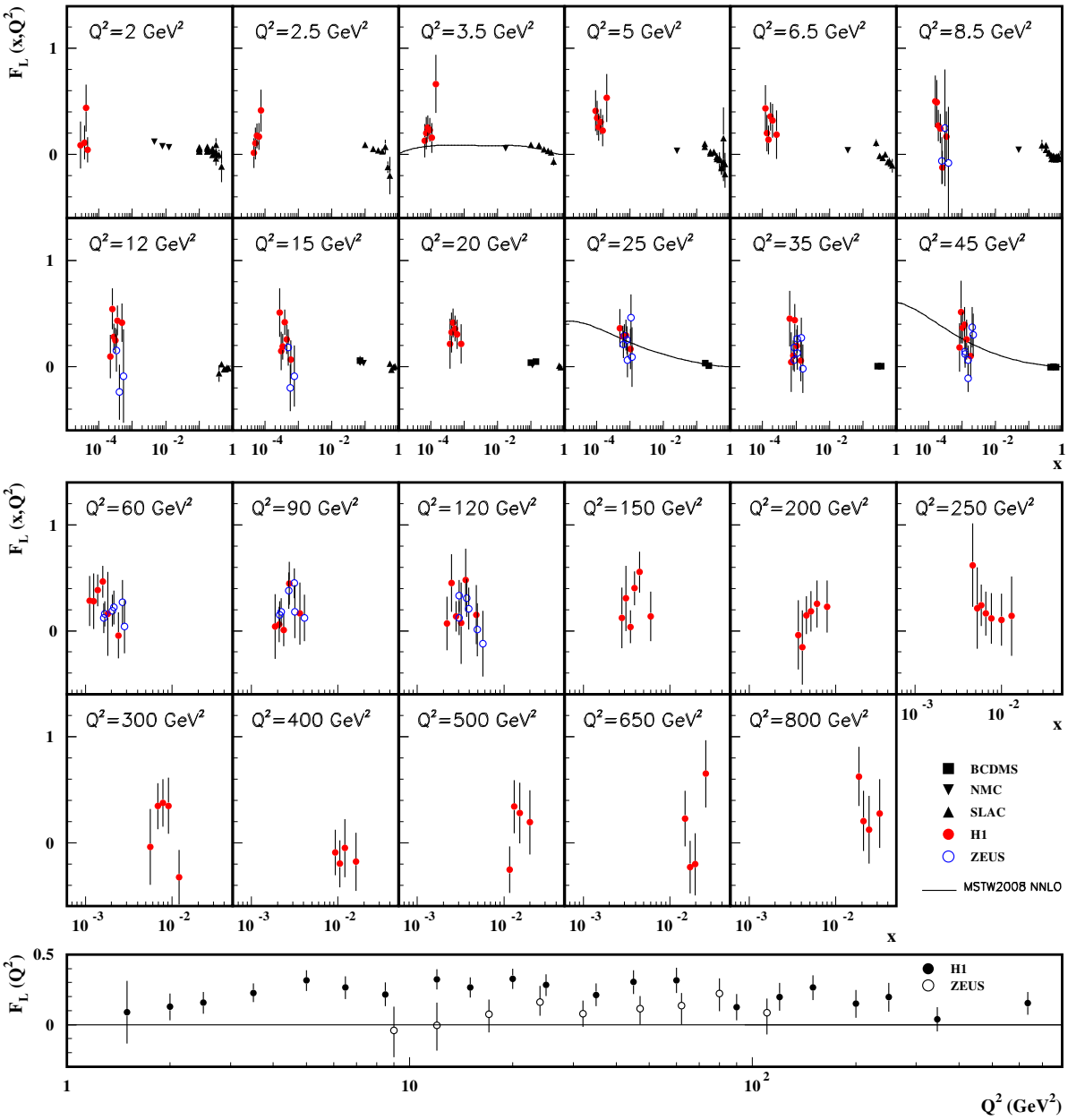

Figure 18.15: Top panels: The longitudinal structure function F_L as a function of x in bins of fixed Q^2 measured on the proton (except for the SLAC data which also contain deuterium data). BCDMS, NMC, and SLAC results are from measurements of R (the ratio of longitudinal to transverse photon absorption cross sections) which are converted to F_L by using the BDCMS parameterization of F_2 (A.C. Benvenuti *et al.*, Phys. Lett. **B223**, 485 (1989)). It is assumed that the Q^2 dependence of the fixed-target data is small within a given Q^2 bin. Some of the other data may have been rebinned to common Q^2 values. Some points have been slightly offset in x for clarity. Also shown is the MSTW2008 parameterization given at three Q^2 values (A.D. Martin *et al.*, Eur. Phys. J. **C63**, 189 (2009)). References: **H1**—V. Andreev *et al.*, Eur. Phys. J. **C74**, 2814 (2014); **ZEUS**—S. Chekanov *et al.*, Phys. Lett. **B682**, 8 (2009); H. Abramowicz et al., Phys. Rev. **D90**, 072002 (2014); **BCDMS**—A. Benvenuti *et al.*, Phys. Lett. **B223**, 485 (1989); **NMC**—M. Arneodo *et al.*, Nucl. Phys. **B483**, 3 (1997); **SLAC**—L.W. Whitlow *et al.*, Phys. Lett. **B250**, 193 (1990) and numerical values from the thesis of L.W. Whitlow (SLAC-357).
Bottom panel: The longitudinal structure function F_L as a function of Q^2. Some points have been slightly offset in Q^2 for clarity. References: **H1**—V. Andreev *et al.*, Eur. Phys. J. **C74**, 2814 (2014); **ZEUS**—H. Abramowicz et al., Phys. Rev. **D90**, 072002 (2014).
The results shown in the bottom plot require the assumption of the validity of the QCD form for the F_2 structure function in order to extract F_L. Statistical and systematic errors added in quadrature are shown for both plots.

Int. J. Mod. Phys. A 2026.41. Downloaded from www.worldscientific.com
by UNIVERSITY OF CALIFORNIA @ BERKELEY on 09/16/26. Re-use and distribution is strictly not permitted, except for Open Access articles.

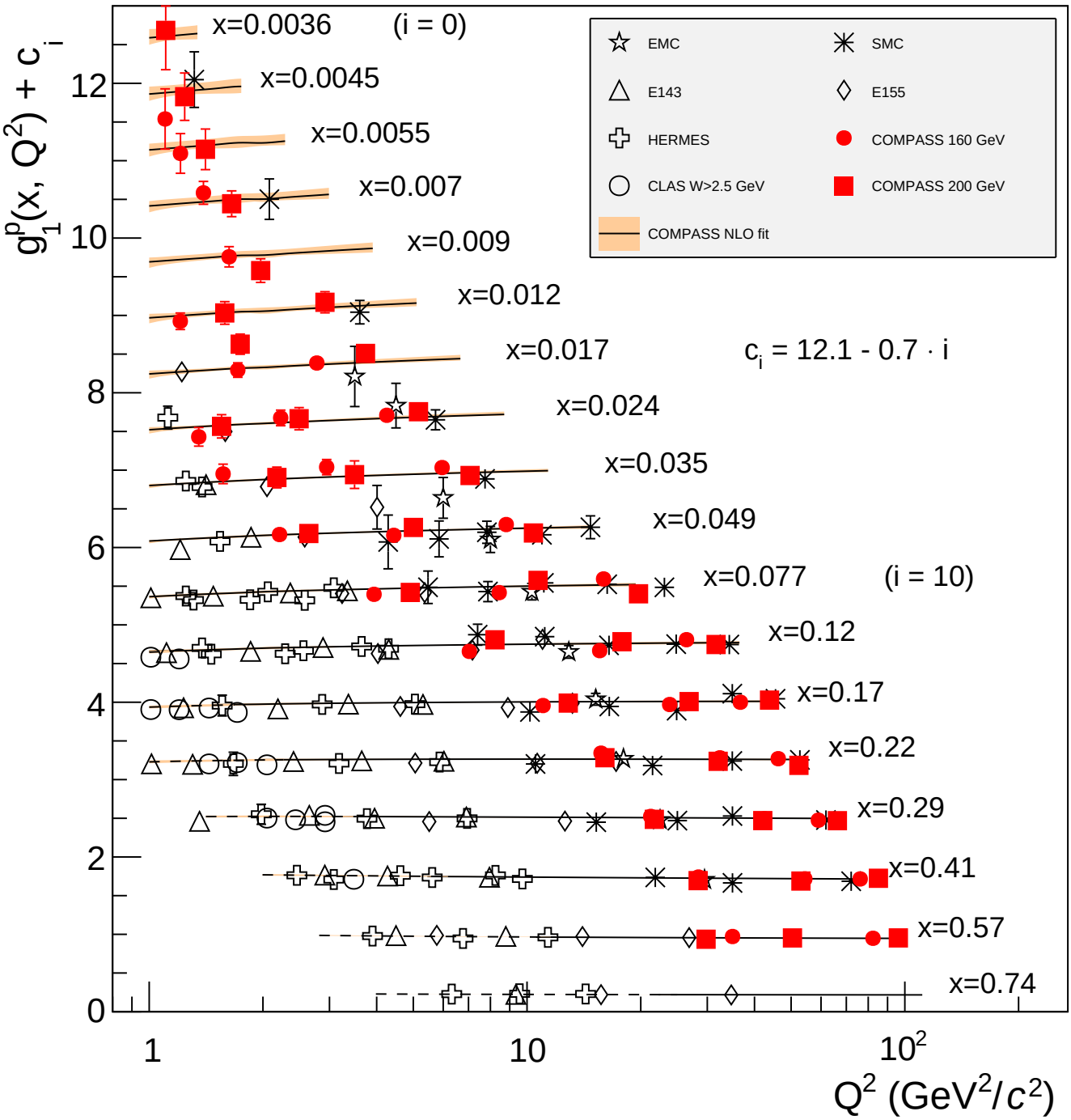

Figure 18.16: World data on the spin-dependent structure function g_1^p as a function of Q^2 for various values of x The lines represent the Q^2 dependence for each value of x, as determined from a NLO QCD fit. The dashed ranges represent the region with $W^2 < 10$ (GeV/c^2)^2. References: **EMC**—J. Ashman *et al.*, Phys. Lett. **B206**, 363 (1988); Nucl. Phys. **B328**, 1 (1989); **E143**—K. Abe *et al.*, Phys. Rev. **D58**, 112003 (1998); **SMC**—B. Adeva *et al.*, Phys. Rev. **D58**, 112001 (1998); **HERMES**—A. Airapetian *et al.*, Phys. Rev. **D75**, 012007 (2007); **E155**—P.L. Anthony *et al.*, Phys. Lett. **B493**, 19 (2000); **COMPASS**—M.G. Alekseev *et al.*, Phys. Lett. **B690**, 466 (2010), C. Adolph, *et al.*, Phys. Lett. **B753**, 18 (2016); **CLAS**—K.V. Dharmawardane *et al.*, Phys. Lett. **B641**, 11 (2006) (which also includes resonance region data not shown on this plot — there is also low W^2 CLAS data in Y. Prok *et al.*, Phys. Rev. **C90**, 025212 (2014) and N. Guler *et al.*, Phys. Rev. **C92**, 055201 (2015)).

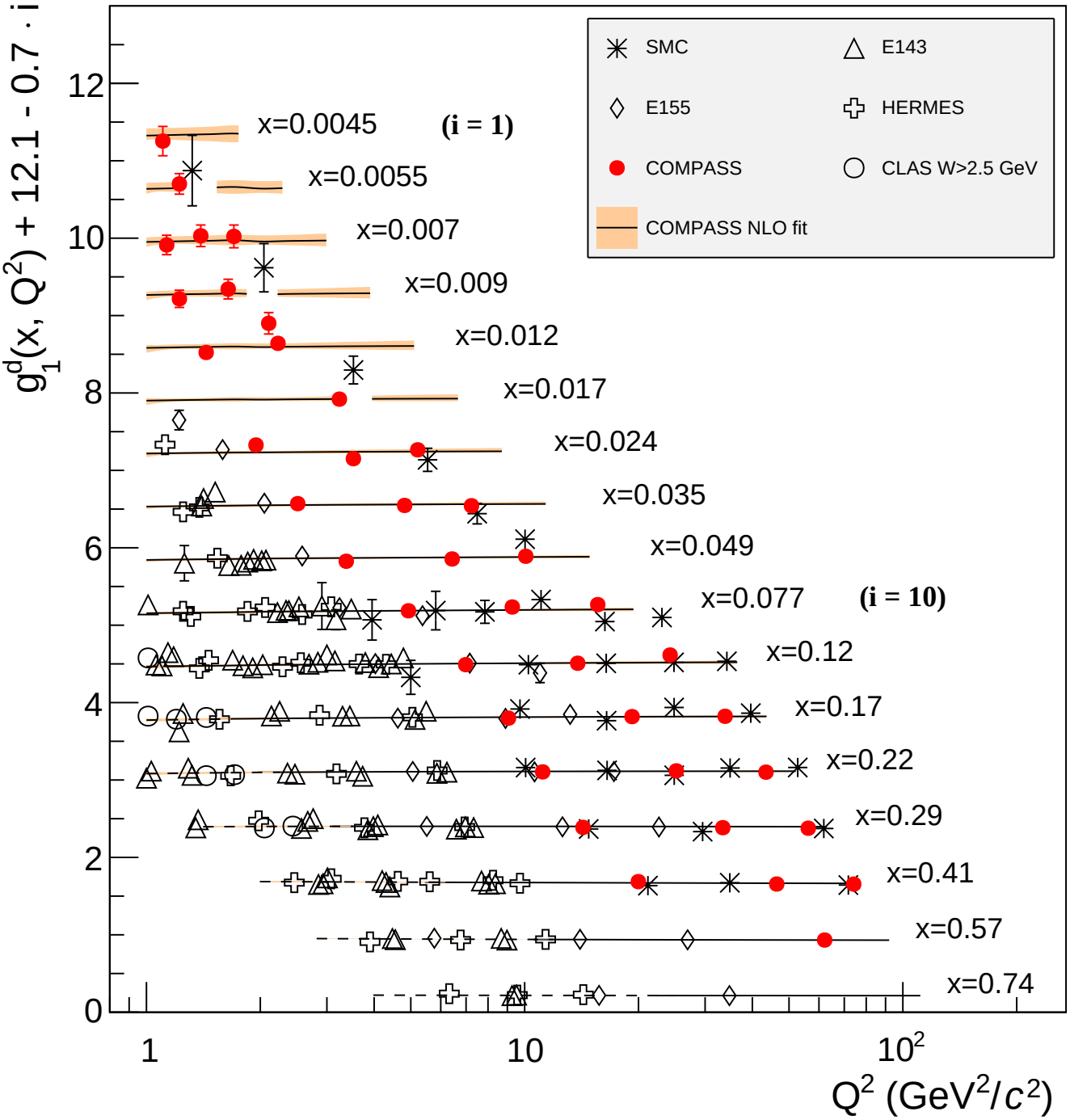

Figure 18.17: World data on the spin-dependent structure function g_1^d as a function of Q^2 for various values of x The lines represent the Q^2 dependence for each value of x, as determined from a NLO QCD fit. The dashed ranges represent the region with $W^2 < 10$ (GeV/c^2)^2. **CLAS**—K.V. Dharmawardane *et al.*, Phys. Lett. **B641**, 11 (2006) **HERMES**—A. Airapetian *et al.*, Phys. Rev. **D75**, 012007 (2007); **SMC**—B. Adeva *et al.*, Phys. Rev. **D58**, 112001 (1998); **E155**—P.L. Anthony *et al.*, Phys. Lett. **B463**, 339 (1999); **E143**—K. Abe *et al.*, Phys. Rev. **D58**, 112003 (1998); **COMPASS**—C. Adolph, *et al.*, Phys. Lett. **B769**, 34 (2017);

Int. J. Mod. Phys. A 2026.41. Downloaded from www.wo
by UNIVERSITY OF CALIFORNIA @ BERKELEY on 09/16/26. Re-use and distribution is
except for Open Access articles.

Int. J. Mod. Phys. A 2026.41. Downloaded from www.worldscientific.com
by UNIVERSITY OF CALIFORNIA @ BERKELEY on 09/16/26. Re-use and distribution is strictly not permitted, except for Open Access articles.

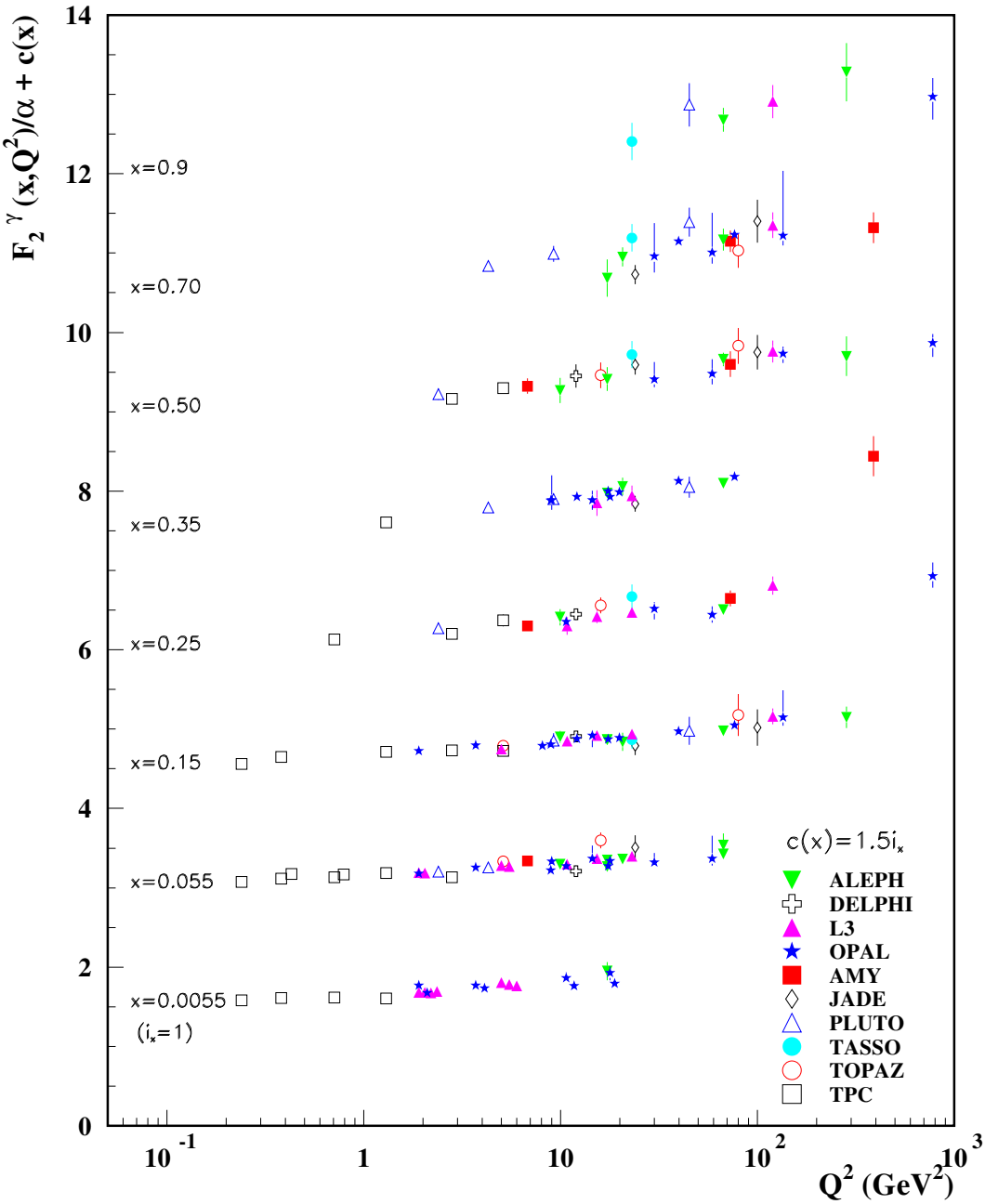

Figure 18.18: The hadronic structure function of the photon F_2^γ divided by the fine structure constant α measured in e^+e^- scattering, shown as a function of Q^2 for bins of x. Data points have been shifted to the nearest corresponding x bin as given in the plot. Some points have been offset in Q^2 for clarity. Statistical and systematic errors added in quadrature are shown. For the purpose of plotting, a constant $c(x) = 1.5i_x$ is added to F_2^γ/α where i_x is the number of the x bin, ranging from 1 ($x = 0.0055$) to 8 ($x = 0.9$). References: **ALEPH**–R. Barate *et al.*, Phys. Lett. **B458**, 152 (1999); A. Heister *et al.*, Eur. Phys. J. **C30**, 145 (2003);**DELPHI**–P. Abreu *et al.*, Z. Phys. **C69**, 223 (1995); **L3**–M. Acciarri *et al.*, Phys. Lett. **B436**, 403 (1998); M. Acciarri *et al.*, Phys. Lett. **B447**, 147 (1999); M. Acciarri *et al.*, Phys. Lett. **B483**, 373 (2000); **OPAL**–A. Ackerstaff *et al.*, Phys. Lett. **B411**, 387 (1997); A. Ackerstaff *et al.*, Z. Phys. **C74**, 33 (1997); G. Abbiendi *et al.*, Eur. Phys. J. **C18**, 15 (2000); G. Abbiendi *et al.*, Phys. Lett. **B533**, 207 (2002) (note that there is overlap of the data samples in these last two papers); **AMY**–S.K. Sahu *et al.*, Phys. Lett. **B346**, 208 (1995); T. Kojima *et al.*, Phys. Lett. **B400**, 395 (1997); **JADE**–W. Bartel *et al.*, Z. Phys. **C24**, 231 (1984); **PLUTO**–C. Berger *et al.*, Phys. Lett. **142B**, 111 (1984); C. Berger *et al.*, Nucl. Phys. **B281**, 365 (1987); **TASSO**–M. Althoff *et al.*, Z. Phys. **C31**, 527 (1986); **TOPAZ**–K. Muramatsu *et al.*, Phys. Lett. **B332**, 477 (1994); **TPC/Two Gamma**–H. Aihara *et al.*, Z. Phys. **C34**, 1 (1987).

Int. J. Mod. Phys. A 2026.41. Downloaded from www.worldscientific.com by UNIVERSITY OF CALIFORNIA @ BERKELEY on 09/16/26. Re-use and distribution is except for Open Access articles.

19. Fragmentation Functions in e^+e^-, ep, and pp Collisions

Revised August 2023 by O. Biebel (Ludwig-Maximilians U.), D. de Florian (ICAS and ICIFI, UNSAM), D. Milstead (Stockholm U.) and W. Vogelsang (Tübingen U.).

19.1 Introduction to fragmentation

Quarks and gluons produced in hard-scattering reactions will ultimately give rise to the colorless hadronic bound states that may be observed in the detector. The associated hadronization process is described by fragmentation functions $D_i^h(x,\mu^2)$ $(i = q, \bar{q}, g)$ which are universal functions representing, in the simplest picture, a measure of the probability density that an outgoing parton produces a hadron h. Here, x is the fraction of the parton's momentum transferred to the hadron, and μ is a 'resolution' scale known as factorization scale. The $D_i^h(x,\mu^2)$ may be viewed as the final-state analogs of the initial-state parton distribution functions (PDFs) addressed in Section 18 of this *Review*. They are also sometimes referred to as *timelike* distributions since they are primarily accessed in e^+e^- annihilation via a timelike intermediate boson. (See Refs. [1,2] for introductory reviews, and Refs. [3–5] for summaries of experimental and theoretical research in this field).

The cleanest laboratory for the study of fragmentation functions is provided by semi-inclusive electron-positron annihilation, $e^+e^- \to \gamma/Z \to h+X$. The cross section for this reaction may be expressed in terms of 'fragmentation structure functions' $F_{T,L,A}$ that are directly related to the fragmentation functions. At center-of-mass (CM) energy $\sqrt{s} = q^2$ we have

$$\frac{1}{\sigma_0}\frac{d^2\sigma^h}{dx\,d\cos\theta} = \frac{3}{8}(1+\cos^2\theta)F_T^h(x,q^2) + \frac{3}{4}\sin^2\theta\,F_L^h(x,q^2) + \frac{3}{4}\cos\theta\,F_A^h(x,q^2)\,. \tag{19.1}$$

Here, q is the four-momentum of the intermediate photon or Z-boson, with $q^2 > 0$, and $x = 2P_h \cdot q/q^2$ with the hadron's four-momentum P_h is the fragmentation counterpart of the familiar DIS Bjorken variable. (Note that $x = 2E_h/\sqrt{s} \le 1$ in terms of the energy E_h of the produced hadron in the CM frame of the electron positron pair.) Furthermore, in the same frame, θ is the hadron's angle relative to the electron beam direction. Eq. (19.1) is the most general form for unpolarized inclusive single-particle production via vector bosons [6]. The fragmentation structure functions F_T and F_L represent the contributions from γ/Z polarizations transverse or longitudinal with respect to the direction of motion of the hadron. The parity-violating term with the asymmetric fragmentation function F_A arises from the interference between vector and axial-vector contributions. Various normalization factors σ_0 are used in the literature, ranging from the total cross section $\sigma_{\rm tot}$ for $e^+e^- \to$ hadrons, including all weak and QCD contributions, to $\sigma_0 = 4\pi\alpha^2 N_c/3s$ with $N_c = 3$, the lowest-order QED cross section for $e^+e^- \to \mu^+\mu^-$ times the number of colors N_c. LEP1 measurements of the three fragmentation structure functions are shown in Fig. 19.1.

Integration of Eq. (19.1) over all θ yields the total fragmentation structure function $F^h = F_T^h + F_L^h$:

$$\frac{1}{\sigma_0}\frac{d\sigma^h}{dx} = F^h(x,q^2) = \sum_i \int_x^1 \frac{dz}{z}\,C_i\left(z,\alpha_s(\mu),\frac{q^2}{\mu^2}\right) D_i^h\left(\frac{x}{z},\mu^2\right)\,. \tag{19.2}$$

On the right we have written the factorized expression for the structure function in terms of a sum over convolutions of the fragmentation functions D_i^h for partons $i = u, \bar{u}, d, \bar{d}, \ldots, g$ with perturbative coefficient functions C_i. Since photons and Z bosons do not distinguish between quarks and antiquarks, e^+e^- annihilation primarily constrains the combinations $D_q^h + D_{\bar{q}}^h$. Gluon fragmentation contributes only at higher order in perturbation theory or by scaling violations. Corrections to the factorized expression in Eq. (19.2) are suppressed by inverse powers of q^2. They arise from quark and hadron mass terms and from non-perturbative effects.

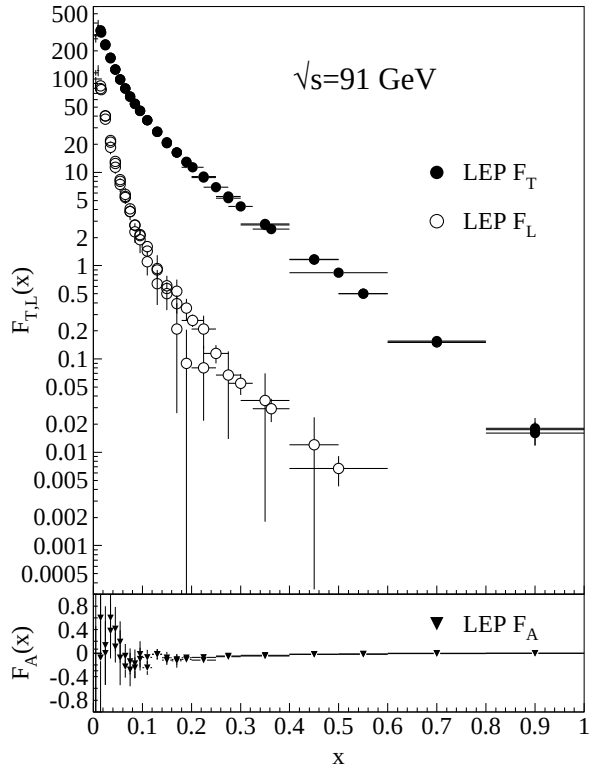

Figure 19.1: LEP1 measurements of total transverse (F_T), longitudinal (F_L), and asymmetric (F_A) fragmentation structure functions [7]. Data points with relative errors greater than 100% are omitted.

Analogous factorized expressions as in Eq. (19.2) may be written for each of the structure functions $F_{T,L,A}$ individually.

The fragmentation functions obey the momentum sum rule constraint

$$\sum_h \int_0^1 dx\,x\,D_i^h(x,\mu^2) = 1\,, \tag{19.3}$$

separately for each flavor i. Note that the sum rule involves a sum over all possible produced hadrons. The dependence of the functions D_i^h on the factorization scale μ^2 will be discussed in the next section.

Measurements of hadron production in deeply-inelastic lepton-proton scattering and hadron-hadron scattering are complementary to those in e^+e^- annihilation. The former process, $\ell p \to \ell' + h + X$, is known as *semi-inclusive deep-inelastic scattering (SIDIS)*. Here, in analogy with Eq. (19.2), the high virtuality of the photon in DIS also permits factorization of the cross section in terms of fragmentation functions, PDFs for the incoming proton, and perturbative hard-scattering cross sections. Likewise, factorization also occurs for $pp \to h + X$ at large transverse momentum of the produced hadron, and for $pp \to \text{jet}(h) + X$, where the hadron is part of a fully reconstructed jet. The fragmentation functions contributing to $e^+e^- \to h + X$, $\ell p \to \ell' + h + X$, and $pp \to h + X$, $pp \to \text{jet}(h) + X$ are universal in the sense that the same functions appear in the factorized expressions for the three reactions. Modern QCD analyses of fragmentation functions "globally" take into account experimental data sets for all three types of processes in order to obtain optimal sets of fragmentation functions.

Electron-positron annihilation has the advantage that there is no hadronic initial state and hence no beam remnant. This is in contrast to $\ell p \to \ell' + h + X$ or $pp \to h + X$, which are affected by hadron remnant contributions associated with the partons of the initial-state hadron(s) which are collaterally involved in the hard lepton-parton or parton-parton collision. On the other hand,

Int. J. Mod. Phys. A 2026.41. Downloaded from www.worldscientific.com
by UNIVERSITY OF CALIFORNIA @ BERKELEY on 09/16/26. Re-use and distribution is strictly not permitted, except for Open Access articles.

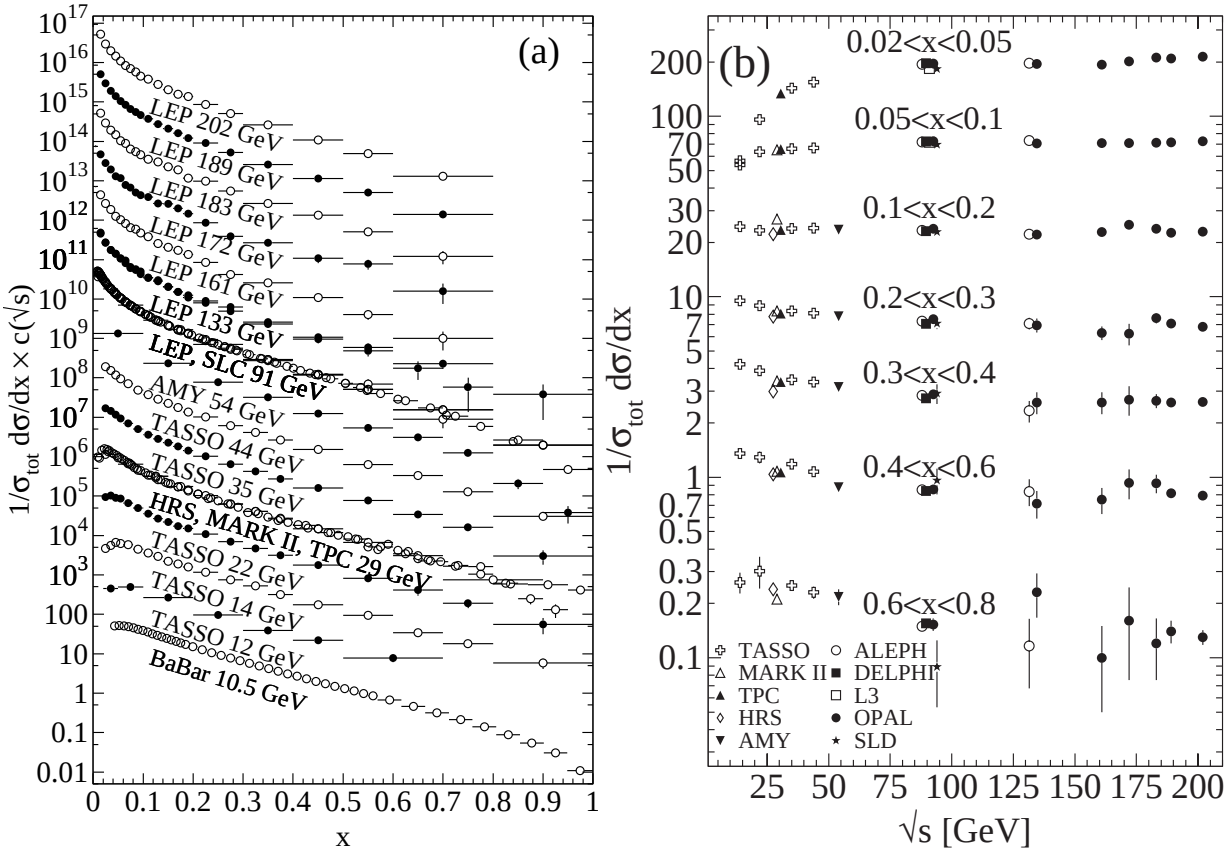

Figure 19.2: Cross section for $e^+e^- \to h + X$ for all charged hadrons [8–26], (a) for different CM energies $\sqrt{s}$ versus x, and (b) for various ranges of x versus $\sqrt{s}$. For (a) the distributions have been scaled by $c(\sqrt{s}) = 10^i$ with i ranging from $i = 0$ ($\sqrt{s} = 12$ GeV) to $i = 13$ ($\sqrt{s} = 202$ GeV).

$e^+e^- \to h + X$ has little sensitivity to D_g^h and is insensitive to the charge asymmetries $D_q^h - D_{\bar{q}}^h$. These quantities are best constrained in proton–(anti-)proton and electron-proton scattering, respectively. Especially the latter provides an environment that allows the study of the influence of initial-state QCD radiation on the fragmentation process, of the partonic and spin structure of the hadron target, and of the target remnant system. (See Ref. [27] for a comprehensive review of the measurements and models of fragmentation in lepton-hadron scattering).

Moreover, unlike e^+e^- annihilation where $q^2 = s$ is fixed by the collider energy, lepton-hadron scattering has two independent scales, $Q^2 = -q^2$ and the invariant mass squared, $W^2 \approx Q^2(1-x)/x$, of the hadronic final state, which both can vary by several orders of magnitudes for a given CM energy, thus allowing the study of fragmentation in different environments by a single experiment. For example, in photoproduction the exchanged photon is quasi-real ($Q^2 \approx 0$), leading to processes akin to hadron-hadron scattering. In DIS ($Q^2 \gg 1$ GeV^2), using factorization, the hadronic fragments of the struck quark can be directly compared with quark fragmentation in e^+e^- in a suitable frame. Results from lepton-hadron experiments quoted in this report primarily concern fragmentation in the DIS regime. Studies performed by lepton-hadron experiments of fragmentation with photoproduction data containing high transverse momentum jets or particles are also reported, when these are directly comparable to DIS and e^+e^- results.

Fragmentation studies in lepton-hadron collisions are usually performed in one of two frames in which the target hadron and the exchanged boson are collinear. The hadronic center-of-mass frame (HCMS) is defined as the rest system of the exchanged boson and incoming hadron, with the z^*-axis defined along the direction of the exchanged boson. The positive z^* direction defines the so-called current fragmentation region. Fragmentation measurements performed in the HCMS often use the Feynman-x variable $x_F = 2p_z^*/W$, where p_z^* is the longitudinal momentum of the particle in this frame. As W is the invariant mass of the hadronic final state, x_F ranges between -1 and 1.

The Breit system [28, 29] is related to the HCMS by a longitudinal boost such that the time component of q vanishes, i.e, $q = (0, 0, 0, -Q)$. In the parton model, the struck parton then has the longitudinal momentum $Q/2$ which becomes $-Q/2$ after the collision. As compared with the HCMS, the current fragmentation region of the Breit frame is more closely matched to the partonic scattering process, and is thus appropriate for direct comparisons of fragmentation functions in DIS with those from e^+e^- annihilation. The variable $x_p = 2p^*/Q$, where p^* is the particle's momentum in the current region of the Breit frame, is used at HERA for measurements in the Breit frame, enabling rather direct comparisons of DIS and e^+e^- results.

19.2 Scaling violations and QCD corrections

As mentioned, the coefficient functions for the fragmentation structure functions in $e^+e^- \to h + X$ are amenable to QCD perturbation theory. For each of the structure functions $F_{T,L,A}(x, q^2)$ in Eq. (19.1) (and hence for the total structure function F^h in Eq. (19.2)) the coefficient function has an expansion of the form

$$C_{a,i}\left(z, \alpha_s(\mu), \frac{q^2}{\mu^2}\right) = (1-\delta_{aL})\,\delta_{iq}\,\delta(1-z) + \frac{\alpha_s(\mu)}{2\pi}\, c_{a,i}^{(1)}\left(z, \frac{q^2}{\mu^2}\right) + \left(\frac{\alpha_s(\mu)}{2\pi}\right)^2 c_{a,i}^{(2)}\left(z, \frac{q^2}{\mu^2}\right) + . \quad (19,4)$$

where $a = T, L, A$. At the zeroth order in the strong coupling α_s the coefficient functions C_g for gluons vanish, while for (anti-) quarks $C_i = g_i(s)\,\delta(1-z)$ (except for F_L for which the leading contribution is of order α_s, as indicated in Eq. (19.4)). Here $g_i(s)$ is the appropriate electroweak coupling. In particular, $g_i(s)$ is pro-

Int. J. Mod. Phys. A 2026.41. Downloaded from www.wo
by UNIVERSITY OF CALIFORNIA @ BERKELEY on 09/16/26. Re-use and distribution is
except for Open Access articles.

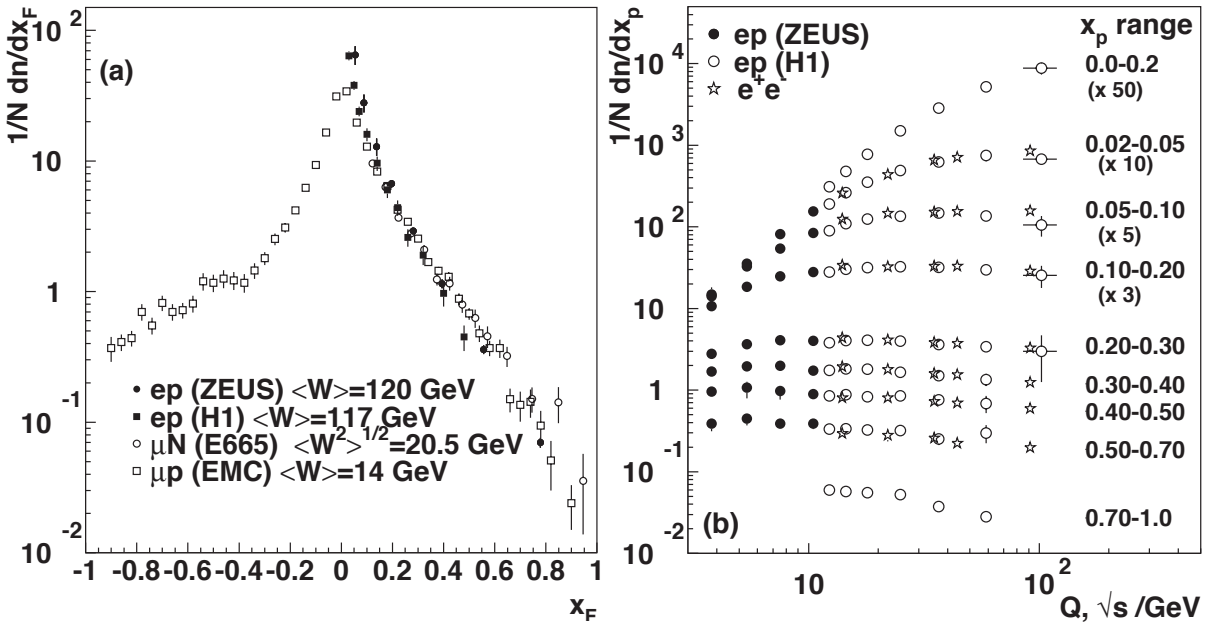

Figure 19.3: (a) The distribution $1/N \cdot dN/dx_F$ for all charged particles in DIS lepton-hadron experiments at different values of W, measured in the HCMS [30–33]. (b) Scaling violations of the fragmentation structure function for all charged particles in the current region of the Breit frame of DIS [34, 35] and in e^+e^- interactions [19, 36]. The data are shown as a function of $\sqrt{s}$ for e^+e^- results, and as a function of Q for the DIS results, each within the same indicated intervals of the scaled momentum x_p. The data for the four lowest intervals of x_p are multiplied by factors 50, 10, 5, and 3, respectively for better visibility.

portional to the squared charge of the quark i at $s \ll M_Z^2$, when weak effects can be neglected. The full electroweak prefactors $g_i(s)$ can be found in Ref. [6]. The first-order QCD corrections to the coefficient functions have been calculated in Refs. [37,38], and the second-order terms in [39–41]. Thus, the coefficient functions are known to NNLO, except for F_L. We note that beyond the leading order the coefficient functions, and hence the fragmentation functions, start to depend on the choice of factorization scheme. The standard choice in the literature is the $\overline{\text{MS}}$ scheme.

The simplest parton-model approach would predict scale-independent ('scaling') x-distributions for both the structure function F^h and the parton fragmentation functions D_i^h. Perturbative QCD corrections lead to logarithmic scaling violations via the evolution equations [42]

$$\frac{\partial}{\partial \ln \mu^2} D_i^h(x,\mu^2) \;=\; \sum_j \int_x^1 \frac{dz}{z}\, P_{ji}\big(z, \alpha_s(\mu^2)\big) D_j^h\left(\frac{x}{z}, \mu^2\right) , \tag{19.5}$$

where the functions $P_{ij}(z, \alpha_s(\mu^2))$ describe the splitting process $i \to j + X$, where parton j carries the longitudinal momentum fraction z of parton i. Note that for fragmentation the relevant splitting functions are P_{ji} (rather than P_{ij} as for the PDFs) since D_j^h represents the fragmentation of the final parton. Usually the system of evolution equations is decomposed into a 2×2 flavor-singlet sector comprising the gluon and the sum of all quark and antiquark fragmentation functions, and scalar ('non-singlet') equations for quark-antiquark and flavor differences.

The splitting functions in Eq. (19.5) have the perturbative expansion

$$P_{ji}(z, \alpha_s) \;=\; \frac{\alpha_s}{2\pi} P_{ji}^{(0)}(z) + \left(\frac{\alpha_s}{2\pi}\right)^2 P_{ji}^{(1)}(z) + \left(\frac{\alpha_s}{2\pi}\right)^3 P_{ji}^{(2)}(z) + \ldots , \tag{19.6}$$

where the leading-order (LO) functions $P^{(0)}(z)$ [42, 43] are the same as those for the initial-state parton distributions. The next-to-leading order (NLO) corrections $P^{(1)}(z)$ have been calculated in Refs. [44–48] (there are well-known misprints in the journal version of Ref. [45]). Ref. [48] also includes the spin-dependent case. The timelike functions are different from, but related to, their spacelike counterparts, see also Ref. [49]. The connections between the two sets of functions has facilitated recent calculations of the next-to-next-to-leading order (NNLO) quantities $P_{qq}^{(2)}(z)$ and $P_{gg}^{(2)}(z)$ in Eq. (19.6) [40,50]. In the same way, the corresponding off-diagonal quantities $P_{qg}^{(2)}$ and $P_{gq}^{(2)}$ were recently obtained in Ref. [51] with the help of constraints from the momentum sum rule Eq. (19.3) [50] and of the limit of $C_A = C_F = n_f$ for which QCD becomes supersymmetric. An uncertainty still remains for the $P_{qg}^{(2)}$ kernel, which however does not affect the logarithmic behavior at small and large momentum fractions. With the exception of Ref. [47], all these higher-order results refer to the standard $\overline{\text{MS}}$ scheme with a fixed number n_f of light flavors. When the threshold for the production of a heavier quark flavor is crossed in the course of the scale evolution, fragmentation functions change. The NLO treatment of these flavor thresholds in the evolution has been addressed in Ref. [52].

The phenomenological effect of scale evolution is similar in the timelike and spacelike cases: As the scale increases, one observes a scaling violation in which the x-distribution is shifted towards lower values. This can be seen from Fig. 19.2 where a set of measurements of the total fragmentation structure function in e^+e^- annihilation are shown. In particular, the figure on the right exhibits the dependence on $\sqrt{q^2} = \sqrt{s}$ at fixed values of x. QCD analyses of these data are discussed in Section 19.5 below.

The NLO coefficient functions for SIDIS, $ep \to e + h + X$, have been presented in Refs. [37, 38] Corresponding results have also been obtained for the case that a non-vanishing hadron transverse momentum is required in the HCMS frame [53, 54].

Scaling violations in DIS are shown in Fig. 19.3 for both the HCMS and the Breit frames. In Fig. 1.3(a) the distribution in terms of $x_F = 2p_z^*/W$ shows a steeper slope in ep data than for the lower-energy μp data for $x_F > 0.15$, indicating the scaling violations. At smaller values of x_F in the current jet region, the multiplicity of particles substantially increases with W, owing to the increased phase space available for the fragmentation process. The EMC data access both the current region and the region of the fragmenting target remnant system. At higher values of $|x_F|$, due to the extended nature of the remnant, the multiplicity in the target region far exceeds that in the current region. For acceptance reasons the remnant hemisphere of the HCMS is only accessible by the lower-energy fixed-target experiments.

Using hadrons from the current hemisphere in the Breit frame,

Int. J. Mod. Phys. A 2026.41. Downloaded from www.worldscientific.com
by UNIVERSITY OF CALIFORNIA @ BERKELEY on 09/16/26. Re-use and distribution is strictly not permitted, except for Open Access articles.

measurements of fragmentation functions and the production properties of particles in *ep* scattering have been reported in Refs. [34, 35, 55–58]. Fig. 19.3(b) compares results from *ep* scattering and e^+e^- experiments; the latter results have been divided by two as they cover both event hemispheres. The agreement between the DIS and e^+e^- results is fairly good. However, processes in DIS which are not present in e^+e^- annihilation, such as boson-gluon fusion and initial-state QCD radiation, can depopulate the current region. These effects become most prominent at low values of Q and x_p. Hence, when compared with e^+e^- annihilation data at $\sqrt{s} = 5.2$, 6.5 GeV [59] not shown here, the DIS particle rates tend to lie below those observed in e^+e^- annihilation. A ZEUS study [60] finds that the direct comparability of the *ep* data to e^+e^- results at low scales is improved if twice the energy in the current hemisphere of the Breit frame, $2E_B^{\rm cr}$, is used instead of $Q/2$ as the fragmentation scale. Choosing $2E_B^{\rm cr}$ for the fragmentation scale approximates QCD radiation effects relevant at low scales, as detailed in Ref. [29].

19.3 Fragmentation functions for small particle momenta

The higher-order timelike splitting functions in Eq. (19.6) are singular at small values of x. They show a double-logarithmic enhancement, with leading terms of the form $\alpha_{\rm s}^k\left(\ln^{2k-2}x\right)/x$ at the kth order of perturbation theory, corresponding to poles $\alpha_{\rm s}^k\,(N-1)^{1-2k}$ for the Mellin moments

$$P^{(k)}(N) \;=\; \int_0^1 dx\, x^{N-1}\; P^{(k)}(x)\;. \tag{19.7}$$

Despite large cancellations between leading and non-leading logarithms at non-asymptotic values of x, the resulting small-x rise in the timelike splitting functions dwarfs that of their spacelike counterparts for the evolution of the parton distributions in Section 18 of this *Review*, see Fig. 1 of Ref. [50]. Consequently, in fragmentation the fixed-order approximation to the evolution breaks down orders of magnitude earlier in x than in DIS.

The pattern of the known coefficients and other considerations suggest that the double-logarithmic terms sum to all-order expressions without any pole at $N = 1$, such as [61, 62]

$$P_{gg}^{\rm LL}(N) \;=\; -\frac{1}{4}\left(N-1-\sqrt{(N-1)^2\cdot 24\,\alpha_{\rm s}/\pi}\right) \tag{19.8}$$

for the gluon-to-gluon splitting function at leading logarithmic order. Keeping the first three terms in the resulting expansion of Eq. (19.5) around $N = 1$ and taking the Mellin inverse yields a Gaussian in the variable $\xi = \ln(1/x)$ for the small-x fragmentation functions,

$$xD(x, q^2 = s) \;\propto\; \exp\left[-\frac{1}{2\sigma^2}(\xi-\xi_p)^2\right]\;, \tag{19.9}$$

with the peak position and width varying with the energy as [63] (see also Ref. [2])

$$\xi_p \;\simeq\; \frac{1}{4}\ln\left(\frac{s}{\Lambda^2}\right)\;,\quad \sigma \;\propto\; \left[\ln\left(\frac{s}{\Lambda^2}\right)\right]^{3/4}\;. \tag{19.10}$$

Next-to-leading logarithmic corrections to the above predictions have been calculated [64]. In the method of Ref. [65], see also Refs. [66, 67], the corrections are included in an analytical form known as the 'modified leading logarithmic approximation' (MLLA). Alternatively they can be used to compute higher-moment corrections to the shape in Eq. (19.9) [68]. The small-x resummation of the coefficient functions for semi-inclusive e^+e^- annihilation and of the timelike spitting functions in the standard $\overline{\rm MS}$ scheme was extended in Refs. [69–73] and has reached full next-to-next-to-leading logarithmic accuracy. Applications of these results to gluon and quark jet multiplicities have been presented in Refs. [74].

Fig. 19.4 shows the ξ distribution for charged particles produced in the current region of the Breit frame in DIS and in e^+e^- annihilation. Consistently with Eq. (19.9) (the 'hump backed plateau') and Eq. (19.10) the distributions have a Gaussian shape, with the peak position and area increasing with CM energy (e^+e^-) and Q^2 (DIS).

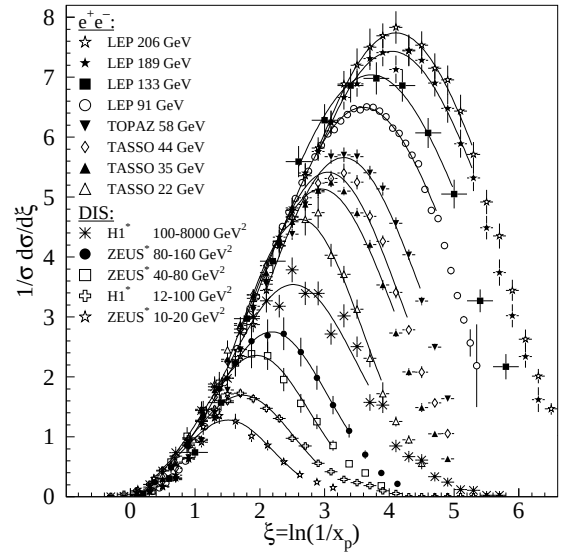

Figure 19.4: Distribution of the normalized fragmentation cross sections in $\xi = \ln(1/x_p)$ at several CM energies (e^+e^-) [10,11,16–19,57,58,75–78] and for intervals of Q^2 (DIS). At each energy only one representative measurement is displayed. For clarity some measurements at intermediate CM energies (e^+e^-) or Q^2 ranges (DIS) are not shown. The DIS measurements ($*$) have been scaled by a factor of 2 for direct comparability with the e^+e^- results. Fits of simple Gaussian functions are overlaid for illustration.

The predicted energy dependence of the peak in the ξ distribution (see Eq. (19.10)) is explained by soft gluon coherence (angular ordering), *i.e.*, the destructive interference of the color wavefunction of low energy gluon radiation, which correctly predicts the suppression of hadron production at small x. Of course, a decrease at very small x is expected on purely kinematical grounds, but this would occur at particle energies proportional to their masses, *i.e.*, at $x \propto m/\sqrt{s}$ and hence $\xi \sim \frac{1}{2}\ln s$. Thus, if the suppression were purely kinematic, the peak position ξ_p would vary twice as rapidly with the energy, which is ruled out by the data in Fig. 19.5. The e^+e^- and DIS data agree well with each other, demonstrating the universality of hadronization and the MLLA prediction. Measurements of the higher moments of the ξ distribution in e^+e^- [19,78–80] and DIS [58] have also been performed and show consistency with each other.

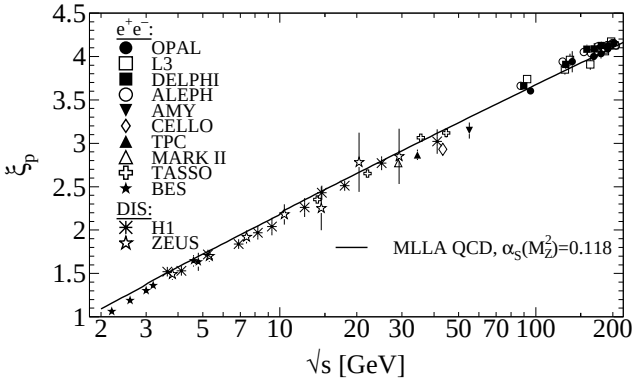

Figure 19.5: Evolution of the peak position, ξ_p, of the ξ distribution with the CM energy $\sqrt{s}$. The MLLA QCD prediction using $\alpha_{\rm s}(s = M_Z^2) = 0.118$ is superimposed to the data of Refs. [10, 12, 15, 19, 56, 57, 76, 77, 80–88].

The average charged-particle multiplicity is another observable

Int. J. Mod. Phys. A 2026.41. Downloaded from www.wo
by UNIVERSITY OF CALIFORNIA @ BERKELEY on 09/16/26. Re-use and distribution is
except for Open Access articles.

sensitive to fragmentation functions for small particle momenta. Perturbative predictions using both NLO [89] and MLLA [90, 91] have been obtained by solving Eq. (19.5) yielding

$$\left\langle n_G(Q^2)\right\rangle \propto \alpha_s^b(Q^2)\cdot\exp\left[\frac{c}{4\pi b_0\sqrt{\alpha_s(Q^2)}}\cdot\left(1+6a_2\frac{\alpha_s(Q^2)}{\pi}\right)\right], \tag{19.11}$$

where $b = \frac{1}{4} + \frac{10}{27}\frac{n_f}{4\pi b_0}$, $c = \sqrt{96\pi}$, with $b_0 = (33 - 2n_f)/(12\pi)$, cf. Section 9 of this *Review*, for n_f contributing quark flavors. Higher-order corrections to Eq. (19.11) are known up to next-to-next-to-next-to-leading order (N^3LO), for details and references see [92]. The term proportional to $a_2 \approx -0.502 + 0.0421\,n_f - 0.00036\,n_f^2$ in Eq. (19.11) is the contribution due to NNLO corrections [93]. The quantity $\langle n_G(Q^2)\rangle$ refers to the average number of gluons, while for $\langle n_q(Q^2)\rangle$ for quarks a correction factor $1/r$ is required due to the different color factors in quark and gluon couplings, so that $\langle n_q(Q^2)\rangle = \langle n_G(Q^2)\rangle/r$. The correction factor depends only weakly on Q^2; higher-order corrections up to N^3LO on the asymptotic value $r = C_A/C_F = 9/4$ [94] are quoted in [92].

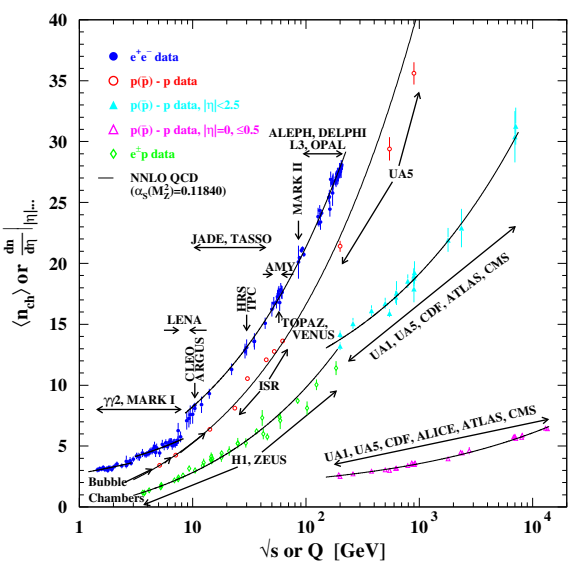

Figure 19.6: Average charged-particle multiplicity $\langle n_{\rm ch}\rangle$ as a function of $\sqrt{s}$ or Q for e^+e^- and $p\overline{p}$ annihilations, and pp and ep collisions. The indicated errors are statistical and systematic uncertainties added in quadrature, except when no systematic uncertainties are given. All NNLO QCD curves are from Eq. (19.11) with fitted normalization, $K_{\rm LHPD}$, and offset, n_0, using a fixed $\alpha_s(M_Z^2) = 0.1184$ [95] and for e^+e^- annihilation data $n_f = 3$, 4, or 5 depending on $\sqrt{s}$, else $n_f = 3$. $\mathbf{e^+e^-}$: Contributions from K_S^0 and Λ decays included. Data compiled from Refs. [8,10,16,16,22,77,83,96–106]; $\mathbf{e^\pm p}$: Multiplicities have been measured in the current fragmentation region of the Breit frame. Data compiled from Refs. [35, 57, 58, 60, 107]; $\mathbf{p^{(}\overline{p}^{)}}$: Measured values above 20 GeV refer to non-single diffractive (NSD) processes. Central pseudorapidity multiplicities $(dn/d\eta)|_{|\eta|\ldots}$ refer to either $|\eta| < 2.5$ (CMS: $|\eta| < 2.4$) or $|\eta| = 0$ (UA5, CMS, ALICE: $|\eta| < 0.5$). Data compiled from Refs. [108–123].

Employing the hypothesis of 'Local Parton-Hadron Duality' (LPHD) [90], *i.e.*, that the color charge of partons is balanced locally in phase space and, hence, their hadronization occurs locally such that (Mellin transformed) parton and hadron inclusive distributions directly correspond, Eq. (19.11) can be applied to describe average charged particle multiplicities obtained in e^+e^- annihilation. The equation can also be applied to $e^\pm p$ scattering if the current fragmentation region of the Breit frame is considered for measuring the average charged-particle multiplicity. Fig. 19.6 shows corresponding data and fits of Eq. (19.11) where apart from an LPHD normalization factor a constant offset has been allowed for, so that $\langle n_{\rm ch}(Q)\rangle = K_{\rm LHPD}\cdot\langle n_G(Q)\rangle/r + n_0$.

In hadron-hadron collisions beam remnants, e.g. from single-diffractive (SD) scattering where one colliding proton is negligibly deflected while hadrons related with the other colliding proton are well-separated in rapidity from the former proton, contribute to the measurement of the hadron multiplicity from a hard parton-parton scattering, making interpretation of the data more model dependent. Experimental results are usually given for inelastic processes or for non-single diffractive processes (NSD). Due to the large beam particle momenta at Tevatron and LHC, not all final state particles can be detected within the limited detector acceptance. Therefore, experiments at Tevatron and LHC quote particle multiplicities for limited ranges of pseudo-rapidity $\eta = -\ln\tan(\vartheta/2)$ or at central rapidity, i.e. $\eta = 0$, as shown in Fig. 19.6.

A universality of the average particle multiplicities in e^+e^- and $p^{(}\overline{p}^{)}$ processes has been reported in Ref. [124] when considering an effective collision energy $Q_{\rm eff} = \sqrt{s}/k$ in $p^{(}\overline{p}^{)}$ reduced by a factor of $k \approx 3$, plus a constant offset of $n_0 \approx 2$. A more detailed review is available in Ref. [125]. According to the investigations presented in Ref. [126] the universality of the energy dependence of average particle multiplicities also applies to hadron-hadron and nucleus-nucleus collisions for both full and central rapidity multiplicities. Evidence for this universality is given by the good agreement for the energy dependence of Eq. (19.11) when fit to the $p^{(}\overline{p}^{)}$ data as shown in Fig. 19.6.

19.4 Fragmentation models

Although the scaling violations can be calculated perturbatively, the actual form of the parton fragmentation functions is non-perturbative. Perturbative evolution gives rise to a shower of quarks and gluons (partons). Multi-parton final states from leading and higher order matrix element calculations are linked to these parton showers using factorization prescriptions, also called matching schemes, see Ref. [127] for an overview.

Phenomenological schemes are then used to model the carry-over of parton momenta and flavor to the hadrons. Implemented in Monte Carlo event generators (see Section 43 of this *Review*), these schemes have been tuned using e^+e^- data and provide good description of hadron collisions as well, thus providing evidence of the universality of fragmentation. However, e^+e^- mainly fix the quark jet fragmentation while it provides less constraints for modelling the gluon jet fragmentation.

19.5 Phenomenology of quark and gluon fragmentation functions

The fragmentation functions are solutions to the evolution equations Eq. (19.5), but need to be specified at some initial scale μ_0^2 (usually around 1 GeV^2 for light quarks and gluons, and at m_Q^2 for heavy quarks). A typical parameterization for a given light hadron is [128, 131–139]

$$D_i^h(x,\mu_0^2) = N_i\,x^{\alpha_i}(1-x)^{\beta_i}\left(1+\gamma_i(1-x)^{\delta_i}\right), \tag{19.12}$$

where as indicated the normalization N_i, and the parameters α_i, β_i, γ_i and δ_i depend on the type i of the fragmenting parton. Heavy flavor fragmentation into heavy mesons is discussed in Sec. 19.8 below. The parameters of Eq. (19.12) are obtained by performing global fits to data on various hadron types for different combinations of partons and hadrons in e^+e^-, lepton-hadron and hadron-hadron collisions. We note that the choice of parameterization of the fragmentation functions at the initial scale necessarily introduces a bias since it imposes a certain form of the functions. This bias is largely avoided in neural network approaches which offer a wide flexibility of the initial functions and have recently been applied to fragmentation functions as well [130]. Sets of fragmentation functions are now available for pions, kaons, protons, neutrons, η mesons, Λ baryons, and charged hadrons [129, 130, 132–144]. They are all at NLO level, except for Refs. [130, 141, 144] which have been performed at NNLO level. The latter sets are restricted to the analysis of e^+e^- annihilation data. Recently, data from hadron-hadron collisions have been added in the framework of the neural network approach at NLO

Int. J. Mod. Phys. A 2026.41. Downloaded from www.worldscientific.com
by UNIVERSITY OF CALIFORNIA @ BERKELEY on 09/16/26. Re-use and distribution is strictly not permitted, except for Open Access articles.

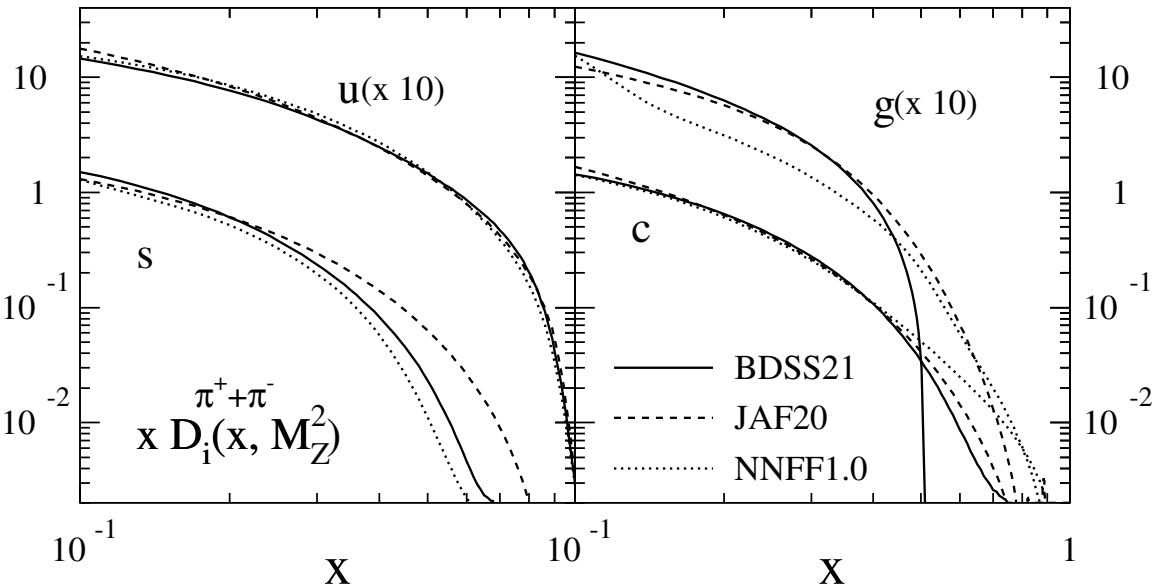

Figure 19.7: Comparison of up, strange, charm and gluon NLO fragmentation functions for $\pi^+ + \pi^-$ at the mass of the Z. The different lines correspond to the results of the analyses performed in Refs. [128–130].

accuracy for charged hadrons [145]. It is noteworthy that the NNLO effects lead to an improvement in the theoretical description of the data in e^+e^- annihilation.

Data from e^+e^- annihilation present the cleanest experimental source for the measurement of fragmentation functions, but cannot be used to disentangle quark from antiquark fragmentation. Since the bulk of the e^+e^- annihilation data is obtained at the mass of the Z-boson, where the electroweak couplings are roughly the same for the different partons, it provides the most precise determination of the flavor-singlet combination of quark and antiquark fragmentation functions. Flavor-tagged results [146], distinguishing between the light quark, charm and bottom contributions are of particular value for flavor decomposition, even though those measurements cannot be unambiguously interpreted in perturbative QCD.

The most relevant source for quark-antiquark (and also flavor) separation is provided by SIDIS data. Semi-inclusive measurements are usually performed at much lower scales than for e^+e^- annihilation. The inclusion of SIDIS data in global fits allows for a wider coverage in the evolution of the fragmentation functions, resulting at the same time in a stringent test of the universality of the distributions. Charged-hadron production data in hadronic collisions also have sensitivity to (anti-)quark fragmentation functions. A recent analysis [129] performs a simultaneous extraction of parton distributions and fragmentation functions based on SIDIS data.

The gluon fragmentation function $D_g^h(x)$ can be extracted, in principle, from the longitudinal fragmentation structure function F_L in Eq. (19.2), as the coefficient functions $C_{L,i}$ for quarks and gluons are comparable at order α_s. However at NLO, *i.e.*, including the $\mathcal{O}(\alpha_s^2)$ coefficient functions $C_{L,i}^{(2)}$ [39], quark fragmentation is dominant in F_L over a large part of the kinematic range, reducing the sensitivity to D_g^h. This distribution could be determined also by analyzing the scale evolution of the fragmentation functions. This possibility is limited by the lack of sufficiently precise data at energy scales away from the Z-resonance and the dominance of the quark contributions at medium and large values of x. In e^+e^- annihilation, D_g^h can also be deduced from the study of three-jet events in which the gluon jet is identified, for example, by tagging the other two jets with heavy quark decays. To leading order, the measured distributions of $x = E_{\rm had}/E_{\rm jet}$ for particles in gluon jets can be identified directly with the gluon fragmentation function $D_g^h(x)$.

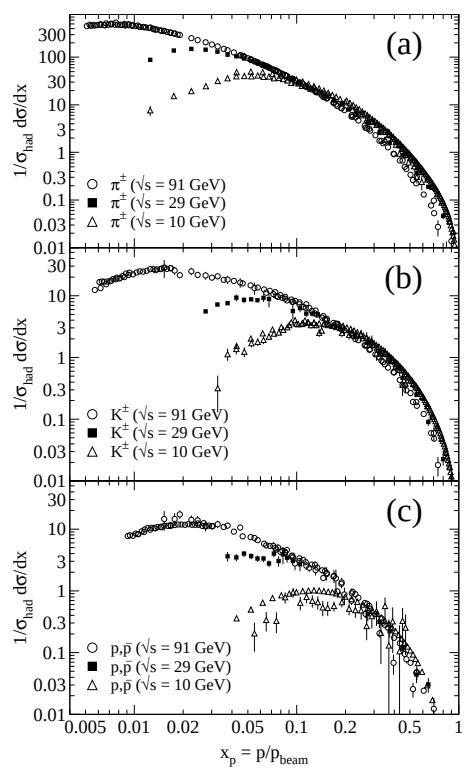

Figure 19.8: Scaled momentum spectra of (a) $\pi^\pm$, (b) $K^\pm$, and (c) $p, \overline{p}$ at $\sqrt{s} = 10$, 29, and 91 GeV [24, 26, 85, 147, 148].

Data for $p^{(}\overline{p}^{)} \to h + X$ provide much more direct constraint on D_g^h. At variance with e^+e^- annihilation and SIDIS, here gluon fragmentation contributes already at the lowest order in the coupling constant. At large $x \gtrsim 0.5$, where information from e^+e^- is sparse, data from hadronic colliders significantly improve extractions of D_g^h [131, 132, 138, 140]. Recent LHC data has been included in the NLO analyses [128, 138, 139] of pion-fragmentation

Int. J. Mod. Phys. A 2026.41. Downloaded from www.worldscientific.com
by UNIVERSITY OF CALIFORNIA @ BERKELEY on 09/16/26. Re-use and distribution is [redacted] except for Open Access articles.

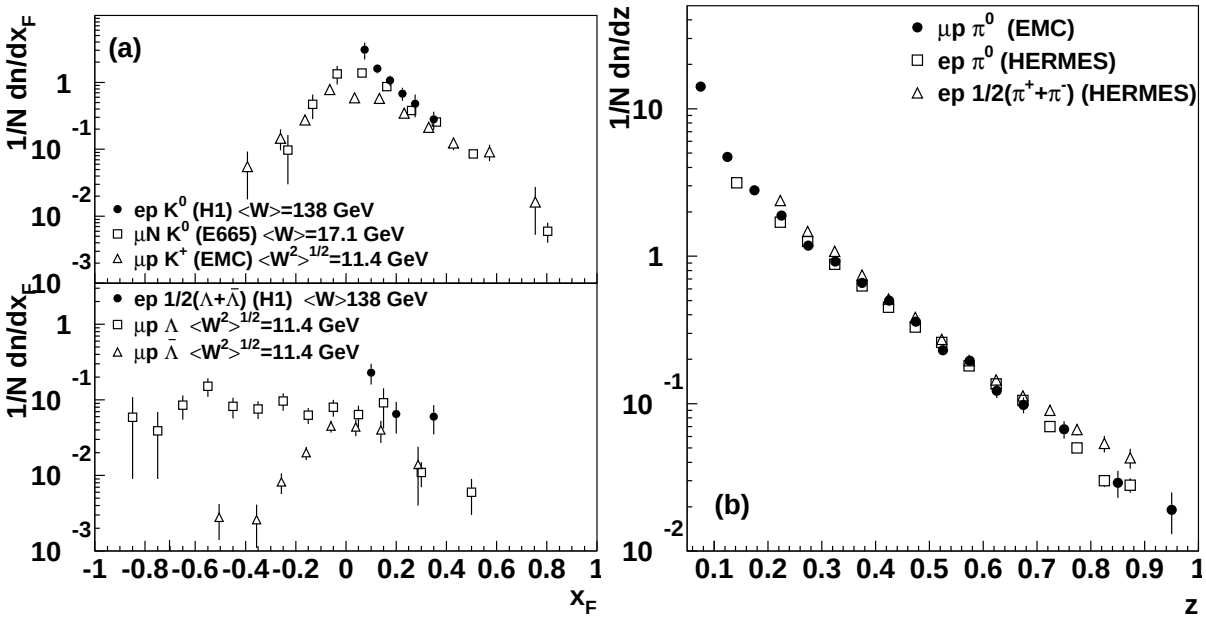

Figure 19.9: (a) $1/N \cdot dn/dx_F$ for identified strange particles in DIS at various values of W [149–151]. (b) $1/N \cdot dn/dz$ for measurements of pions in fixed-target DIS experiments [152–154].

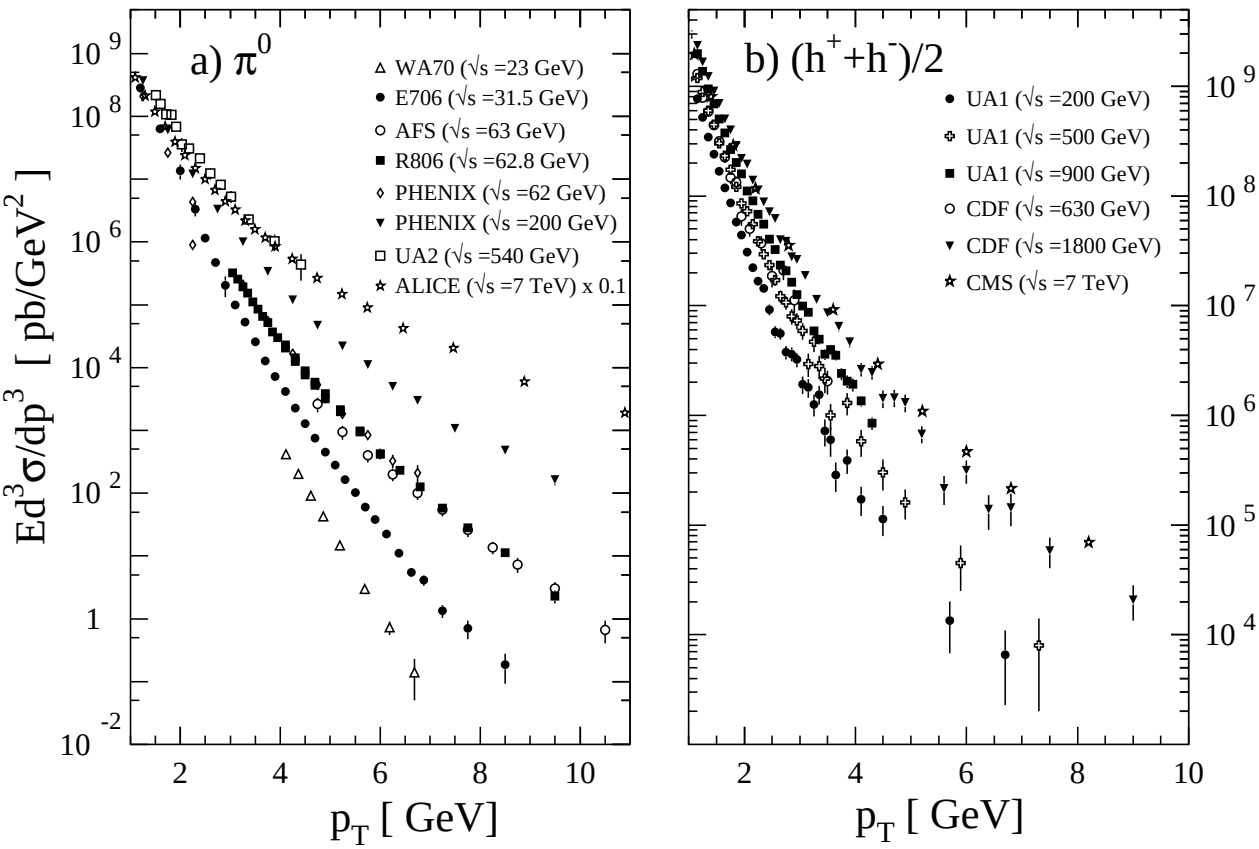

Figure 19.10: Selection of inclusive (a) π^0 and (b) charged-hadron production data from pp [118, 155–160] and $p\bar{p}$ [114, 161, 162] collisions.

functions; see Sec.(17.7) for more details. Note that these analyses are currently the only ones that 'globally' incorporate available data from all sources, $e^+e^- \to h + X$, $ep \to e'h + X$ and $pp \to h + X$.

We note that recently a 'hybrid' type of high-p_T jet/hadron observable has also been considered both theoretically [163–169] and experimentally [170–177]. It is defined by an identified specific hadron found inside a fully reconstructed jet. This gives rise to a *same-side* hadron-jet momentum correlation that may be addressed using perturbative methods. One of several relevant kinematical variables (see [168] for an overview) is $z_h \equiv (\vec{p}_T^{\,h} \cdot \vec{p}_T^{\,\rm jet})/(p_T^{\rm jet})^2$, where $\vec{p}_T^{\,h}$ and $\vec{p}_T^{\,\rm jet}$ are the transverse momenta of the hadron and the jet, respectively. The observable provides an alternative window on fragmentation functions in a

Int. J. Mod. Phys. A 2026.41. Downloaded from www.worldscientific.com
by UNIVERSITY OF CALIFORNIA @ BERKELEY on 09/16/26. Re-use and distribution is strictly not permitted, except for Open Access articles.

Table 19.1: Classification of spin- and transverse-momentum dependent quark fragmentation functions. For simplicity we have left out the ubiquitous label for flavor i of the fragmenting quark and for hadron species h. Each of the functions carries the argument $(x, x^2k_T^2)$ (plus dependence on a factorization scale), where $xk_T = p_T^h$ is the hadron's transverse momentum. λ and Λ are the quark's and hadron's helicities, respectively, and $\vec{s}_T$ and $\vec{S}_T$ are their transverse spin vectors. We have defined $\left[\vec{a} \times \vec{b}\right] \equiv a^1b^2 - a^2b^1$. Finally, m_h is the mass of the produced hadron.

	quark polarization		
hadron pol.	unpolarized	long. polarized	transv. polarized
unpol.	D	–	$\frac{\left[\vec{k}_T \times \vec{s}_T\right]}{m_h} H^\perp$
long. pol.	–	$\lambda \Lambda G_L$	$\frac{\vec{k}_T \cdot \vec{s}_T}{m_h} \Lambda H_L^\perp$
transv. pol.	$\frac{\left[\vec{k}_T \times \vec{S}_T\right]}{m_h} D_T^\perp$	$\frac{\vec{k}_T \cdot \vec{S}_T}{m_h} \lambda G_T^\perp$	$(\vec{s}_T \cdot \vec{S}_T) H_T + \frac{\vec{k}_T \cdot \vec{S}_T}{m_h} \frac{\vec{k}_T \cdot \vec{s}_T}{m_h} H_T^\perp$

more exclusive setting, enabling novel tests of the universality of fragmentation functions. Varying z_h and/or the hadron species, one can map out the fragmentation functions 'locally' as functions of x. This is in contrast to the single-inclusive observable $pp \to h + X$, which inevitably samples over a broad range of x. Although hadron-in-jet data are not yet routinely included in analyse of fragmentation functions, a 'proof-of-principle' analysis does exist [178] that shows the potential of the observable in providing constraint on fragmentation functions.

A comparison of recent NLO fits of fragmentation functions for $\pi^+ + \pi^-$ obtained by the updated version of BDSS21 [128], JAF20 [129] and NNPDF1.0 [130] is shown in Fig. 19.7. Differences among the functions for these sets are visible, especially for the gluon fragmentation function over the full range of x and for the quark functions at large momentum fractions. The differences are even larger for other species of hadrons like kaons and protons [131, 132, 136, 140]. Recent analyses [128–130, 136, 138, 139, 179–184] estimate the uncertainties involved in the extraction of fragmentation functions.

Photonic fragmentation functions play a relevant role in the theoretical understanding of inclusive photon production in (leptonic and hadronic) high energy processes. In the sprit of the analogy between parton fragmentation functions and parton distribution functions, also photonic fragmentation functions are analogous to the photon structure function F_2^γ and to the proton's photonic parton distributions (see review on structure functions in Section 18 of this *Review*). Since photons have a pointlike coupling to quarks [185], the corresponding fragmentation functions obey inhomogeneous evolution equations and are generally decomposed into a perturbative and a non-perturbative component [135, 186, 187]. The hadronic part, sometimes approximated by the Vector Meson Dominance Model, can in principle be obtained by performing a global analysis to the available prompt photon production data [7,12,15,19–21,85,147,188,189], although in practice this has not been done. We note that also the cross section for photons produced in fully reconstructed jets has been proposed [190] as a new tool for obtaining access to photon fragmentation functions, in analogy to the hadron-in-jet cross section discussed above.

19.6 Identified particles in e^+e^- and semi-inclusive DIS

There is a great wealth of measurements of e^+e^- fragmentation into identified particles. A collection of references for data on fragmentation into identified particles is provided in Table 53.1 of this *Review*. As a representative example, Figure 19.8 shows differential charged-hadron spectra as functions of the scaled hadron momentum at several CM energies.

Quantitative results of studies of scaling violations in e^+e^- fragmentation have been reported in [7,21,191,192]. Scaling violations may be used to extract a value of α_s; the values obtained are consistent with the world average (see review on QCD in Section 9 of this *Review*).

Many studies have been made of production of identified particles in lepton-hadron scattering, although fewer particle species have been measured than in e^+e^- collisions. References [149, 150, 152–154, 193–195] and [151, 196–201] are representative of the data from fixed target and ep collider experiments, respectively. QCD calculations performed at NLO provide an overall good description of the HERA data [33, 34, 58, 201–203], both for SIDIS [204] and for the hadron transverse momentum distribution [53, 205] in the kinematic regions in which the calculations are predictive. Threshold corrections to SIDIS have been computed at NNLO [206] and even at N3LO [207] and N4LO [208]. Very recently, the full set of NNLO QCD corrections to the corresponding unpolarized and polarized coefficient functions were obtained in [209–211]

Fig. 19.9(a) compares lower-energy fixed-target and HERA data on strangeness production, showing that the HERA spectra have substantially increased multiplicities, albeit with statistical precision that is insufficient to study scaling violations. The fixed-target data show that the Λ rate substantially exceeds the $\overline{\Lambda}$ rate in the remnant region, owing to the conserved baryon number from the baryon target. Fig. 19.9(b) shows $1/N \cdot dn/dz$ for neutral and charged pion production, where z is defined as the ratio of the pion energy to that of the exchanged boson, both measured in the laboratory frame. Results are shown from the HERMES and the EMC experiments, where the HERMES data have been evolved to $\langle Q^2 \rangle = 25$ GeV^2 at NLO QCD, in order to be comparable with the EMC data. Each of the experiments uses various kinematic cuts to ensure that the measured particles lie in the region that is expected to be associated with the struck quark. In the DIS kinematic regime accessed at these experiments, and over the range in z shown in Fig. 19.9, the z and x_F variables have similar values [30]. The precision data on identified particles can be used in the study of the quark flavor content of the proton [179, 227, 228].

Data on identified particle production can aid the investigation of the universality of jet fragmentation in e^+e^- and DIS. The strangeness suppression factor γ_s, as derived principally from tuning the Lund string model [229] within JETSET [230], is typically found to be around 0.3 in e^+e^- experiments [75], although values closer to 0.2 [231] have also been obtained. A number of measurements of so-called V^0-particles (K^0, Λ^0) and the relative rates of V^0's and inclusively produced charged particles have been performed at HERA [151,196,232] and fixed target experiments [149]. These typically favour a stronger suppression ($\gamma_s \approx 0.2$) than usually obtained from e^+e^- data, although values close to 0.3 have also been obtained [233, 234].

However, when comparing the description of QCD-based models for lepton-hadron interactions and e^+e^- collisions, it is important to note that the overall description by event generators of inclusively produced hadronic final states is more accurate in e^+e^- collisions than in lepton-hadron interactions [235]. Predictions of particle rates in lepton-hadron scattering are affected by uncertainties in the modelling of the parton composition of the

Int. J. Mod. Phys. A 2026.41. Downloaded from www.wo
by UNIVERSITY OF CALIFORNIA @ BERKELEY on 09/16/26. Re-use and distribution is
except for Open Access articles.

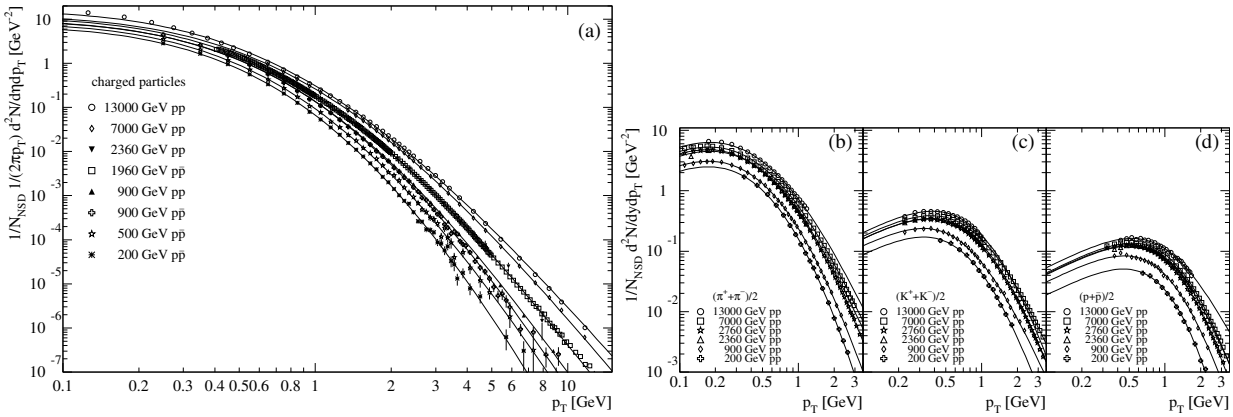

Figure 19.11: (a) Selection of inclusive charged-particle transverse momentum spectra [114,117,119,121,161,212,213], normalized to the non-single diffractive cross section (NSD). (b)-(d) Selection of identified charged-particle transverse momentum spectra [214–219] normalized to the NSD cross section. All spectra are scaled to the NSD cross-section using measurements of total, inelastic, elastic, single, or non-single diffractive cross sections from [220–224,224–226]. The overall normalization uncertainty of about 3% is not shown. Superimposed are fits of the Tsallis distribution in Eq. (19.13).

proton and photon, the extended target remnant, and initial and final-state QCD radiation. Furthermore, the tuning of event generators for e^+e^- collisions is typically based on a larger set of parameters and uses more observables [75] than are used when optimizing models for lepton-hadron data [236].

19.7 Fragmentation in hadron-hadron collisions

An extensive set on high-transverse momentum (p_T) single-inclusive hadron data has been collected in $h_1h_2 \to hX$ scattering processes, both at high energy colliders and fixed-target experiments [155–162,189,237–259]. Fig. 19.10 shows the invariant cross sections $E\mathrm{d}^3\sigma/dp^3$ for a compilation of neutral-pion and charged-hadron production data for energies in the range $\sqrt{s} \approx 23$ - 7000 GeV.

The differential cross section for high-transverse momentum hadron production has been computed to NLO accuracy in perturbative QCD [260]. The NLO corrections are typically large and can even double the prediction for the cross section at fixed-target energies. Nevertheless, the NLO calculations significantly under-predict the cross-section for several fixed-target energy data sets [255, 261, 262]. Different strategies have been developed to ameliorate the theoretical description at fixed-target energies. A possible phenomenological approach involves the introduction of a non-perturbative intrinsic partonic transverse momentum [160, 255, 263, 264]. Furthermore, the resummation of the dominant higher order corrections at threshold produces an enhancement of the theoretical calculation that significantly improves the description of the data [265, 266]. Very recently, the NNLO corrections were presented in [267].

Data collected at high energy colliders are either included in global fit analyses or used as a test for the universality of fragmentation functions. A certain tension has been observed between data sets from RHIC and the LHC [268]. The tension can be largely resolved [128] by taking properly into account the theoretical scale dependence in the global analysis, allowing factorization and renormalization scales to variate according to the kinematics of each experiment within a conventional range.

Transverse momentum distributions can usually be fit by power laws [269]. An approach to describe the low p_T particle spectra is the Tsallis distribution [270–272], which is based on a non-extensive generalization of the Boltzmann-Gibbs statistics. The functional form [273]

$$\frac{\mathrm{d}^2N}{\mathrm{d}p_T\mathrm{d}y} = p_T\frac{\mathrm{d}N}{\mathrm{d}y}\frac{(n-1)(n-2)}{nT(nT+m_0(n-2))}\left[1+\frac{m_T-m_0}{nT}\right]^{-n} \tag{19.13}$$

is frequently used to fit the transverse momentum spectra, where $\mathrm{d}N/\mathrm{d}y$ is the particle's multiplicity, T and n are fit parameters of the Tsallis distribution, m_0 is the either the mass of the most abundant particle, i.e. the pion for inclusive spectra, or the mass of an identified particle, and $m_T = \sqrt{p_T^2 + m_0^2}$. The parameter n is related to the non-extensive parameter $q = n/(n-1)$ of the original Tsallis formula [274], and T is connected to the temperature in the Boltzmann-Gibbs statistics. The Tsallis distribution has been very successfully fit to measured transverse momentum distributions of both inclusive charged particles and identified particle spectra for hadron-hadron collisions, see for example [275–277], for collisions of heavy nuclei, see for example [278], and also for e^+e^- collisions, see for example [279]. The energy dependence of the fitted Tsallis parameters has also been investigated in detail, see [273, 280]. Fig. 19.11 shows examples of hadron production data in pp and $p\bar{p}$ collisions compared to Tsallis distributions.

Hadron production provides a critical observable for probing the high energy-density matter produced in heavy-ion collisions. Measurements at colliders show a suppression of inclusive hadron yields at high transverse momentum for AA collisions compared to pp scattering, indicating the formation of a dense medium opaque to quark and gluons, see e.g. [281].

19.8 Heavy quark fragmentation

It was recognized very early [282] that a heavy flavored meson should retain a large fraction of the momentum of the primordial heavy quark, and therefore its fragmentation function should be much harder than that of a light hadron. In the limit of a very heavy quark, one expects the fragmentation function for a heavy quark to go into any heavy hadron to be peaked near $x = 1$.

When the heavy quark is produced at a momentum much larger than its mass, one expects important perturbative effects, enhanced by powers of the logarithm of the transverse momentum over the heavy quark mass, to intervene and modify the shape of the fragmentation function. In leading logarithmic order (*i.e.*, including all powers of $\alpha_s \log(m_Q/p_T)$), the total (*i.e.*, summed over all hadron types) perturbative fragmentation function is simply obtained by solving the leading evolution equation for fragmentation functions, Eq. (19.5), with the initial condition due to the finite mass of the heavy quark given by $D_Q(x,\mu^2)\big|_{\mu^2=m_Q^2} = \delta(1-x)$ and $D_i(x,\mu^2)\big|_{\mu^2=m_Q^2} = 0$ for $i \neq Q$ (here $D_i(x,\mu^2)$, stands for the probability to produce a heavy quark Q from parton i with a fraction x of the parton momentum).

Several extensions of the leading logarithmic result have appeared in the literature. Next-to-leading-log (NLL) order results for the perturbative heavy quark fragmentation function have been obtained in [286]. The resummation of the dominant logarithmic contributions at large x was performed in [287] to next-to-leading-log accuracy. Fixed-order calculations of the fragmentation function at order α_s^2 in e^+e^- annihilation have appeared in [288] while the initial condition for the perturbative heavy quark fragmentation function has been extended to NNLO

Int. J. Mod. Phys. A 2026.41. Downloaded from www.worldscientific.com
by UNIVERSITY OF CALIFORNIA @ BERKELEY on 09/16/26. Re-use and distribution is strictly not permitted, except for Open Access articles.

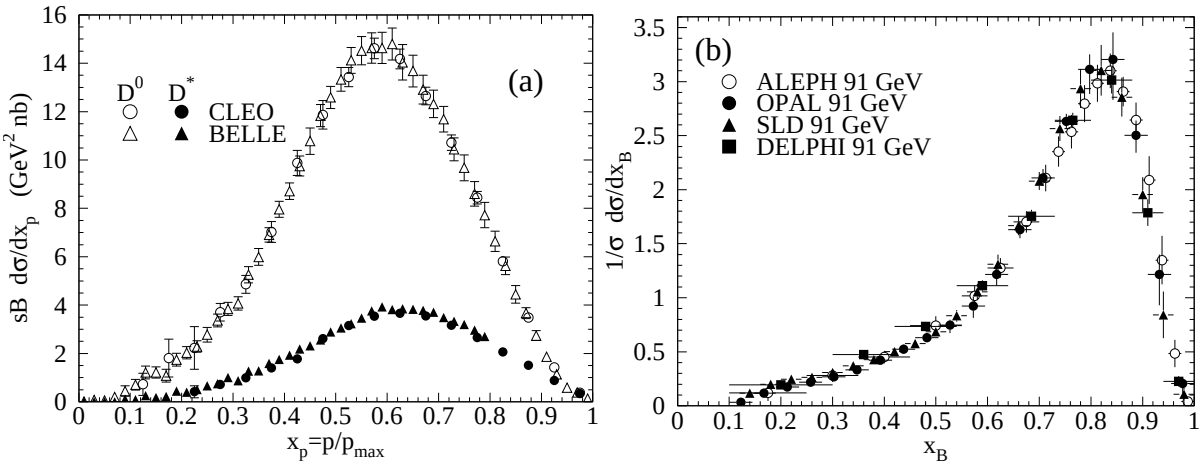

Figure 19.12: (a) Efficiency-corrected inclusive cross-section measurements for the production of D^0 and D^{*+} in e^+e^- measurements at $\sqrt{s} \approx 10.6$ GeV, excluding B decay products [283] [284]. (b) Measured e^+e^- fragmentation function of b quarks into B hadrons at $\sqrt{s} \approx 91$ GeV [285].

in [289].

Inclusion of non-perturbative effects in the calculation of the heavy-quark fragmentation function is done by convoluting the perturbative result with a phenomenological non-perturbative form. This form follows from the simple kinematical consideration that the formation of a hadron by attaching light quarks/antiquarks to the heavy quark will slightly decelerate the heavy quark. Thus, its shape will show a peak that becomes increasingly centered next to $x = 1$ the higher the quark mass. Among the most popular parameterizations we have the following:

$$\text{Peterson } et\ al.\ [290]: \quad D_{\rm np}(x) \propto \frac{1}{x}\left(1 - \frac{1}{x} - \frac{\epsilon}{1-x}\right)^{-2}, \tag{19.14}$$

$$\text{Kartvelishvili } et\ al.\ [291]: \quad D_{\rm np}(x) \propto x^{\alpha}(1-x), \tag{19.15}$$

$$\text{Collins \& Spiller } [292]: \quad D_{\rm np}(x) \propto \left(\frac{1-x}{x} + \frac{(2-x)\epsilon_C}{1-x}\right) \times (1+x^2) \times \left(1 - \frac{1}{x} - \frac{\epsilon_C}{1-x}\right)^{-2} \tag{19.16}$$

$$\text{Colangelo \& Nason } [293]: \quad D_{\rm np}(x) \propto (1-x)^{\alpha} x^{\beta} \tag{19.17}$$

$$\text{Bowler } [294]: \quad D_{\rm np}(x) \propto x^{-(1+bm^2_{h,\perp})} \times (1-x)^a \exp\left(-\frac{bm^2_{h,\perp}}{x}\right) \tag{19.18}$$

$$\text{Braaten } et\ al.\ [295]: \quad (\text{see Eqs. } (31), (32) \text{ in } [295]) \tag{19.19}$$

where ϵ, ϵ_C, a, $bm^2_{h,\perp}$, α, and β are non-perturbative parameters that depend on the heavy hadron considered. The parameters entering the non-perturbative forms are fitted together with some model of hard radiation, which can be either a shower Monte Carlo, a leading-log or NLL calculation (which may or may not include Sudakov resummation), or a fixed order calculation. In [288], for example, the Peterson *et al.* [290] ϵ parameter for charm and bottom production is fitted from the measured distributions of Refs. [296, 297] for charm, and of [298] for bottom. If the leading-logarithmic approximation (LLA) is used for the perturbative part, one finds $\epsilon_c \approx 0.05$ and $\epsilon_b \approx 0.006$; if a second order calculation is used one finds $\epsilon_c \approx 0.035$ and $\epsilon_b \approx 0.0033$; if a NLL improved fixed order $\mathcal{O}(\alpha_s^2)$ calculation is used instead of NLO $\mathcal{O}(\alpha_s)$ one finds $\epsilon_c \approx 0.022$ and $\epsilon_b \approx 0.0023$. The larger values found in the LL approximation are consistent with what is obtained in the context of parton shower models [299], as expected. The ϵ parameter for charm and bottom scales roughly with the inverse square of the heavy flavor mass. This behavior can be justified by several arguments [282, 300, 301]. It can be used to relate the non-perturbative parts of the fragmentation functions of charm and bottom quarks [288, 293, 302].

A more conventional approach [303] involves the introduction of a unique set of heavy quark fragmentation functions of non-perturbative nature that obey the usual massless evolution equations in Eq. (19.5). Finite mass terms of the form $(m_{\rm Q}/p_T)^n$ are kept in the corresponding short distance coefficient function for each scattering process. Within this approach, the initial condition for the perturbative fragmentation function provides the term needed to define the correct subtraction scheme to match the massless limit for the coefficient function (see e.g. [304]). Such an implementation is in line with the variable flavor number scheme introduced for parton distributions functions, as described in Section 18 of this *Review*.

High statistics data for charmed-meson production near the Υ resonance (excluding decay products of B mesons) have been published [283, 284]. They include results for D and D^*, D_s (see also [305, 306]) and Λ_c. Shown in Fig. 19.12(a) are the CLEO and BELLE inclusive cross-sections times branching ratio $\mathcal{B}$, $s\mathcal{B}d\sigma/dx_p$, for the production of D^0 and D^{*+}. The variable x_p approximates the light-cone momentum fraction x, but is not identical to it. The two measurements are consistent with each other.

The branching ratio $\mathcal{B}$ represents $D^0 \to K^-\pi^+$ for the D^0 results and for the D^{*+} the product of the branching fractions for $D^{*+} \to D^0\pi^+$ and $D^0 \to K^-\pi^+$. Given the high precision of CLEO's and BELLE's data, a superposition of different parametric forms for the non-perturbative contribution is needed to obtain a good fit [52]. Older studies are reported in Refs. [297, 307, 308]. Charmed meson spectra on the Z peak have been published by OPAL and ALEPH [309, 310].

Charm quark production has also been extensively studied at HERA by the H1 and ZEUS collaborations. Measurements have been made of $D^{*\pm}$, $D^{\pm}$, and $D_s^{\pm}$ mesons and the Λ_c baryon. See, for example, Refs. [311, 312].

Experimental studies of the fragmentation function for b quarks, shown in Fig. 19.12(b), have been performed at LEP and SLD [285, 298, 313]. Commonly used methods identify the B meson through its semileptonic decay or based upon tracks emerging from the B secondary vertex. Heavy flavor contributions from gluon splitting are usually explicitly removed before fitting for the fragmentation functions. The studies in [285] fit the B spectrum using a Monte Carlo shower model supplemented with non-perturbative fragmentation functions yielding consistent results.

The experiments measure primarily the spectrum of B mesons. This defines a fragmentation function that includes the effect of the decay of higher mass excitations, like the B^* and B^{**}. In the

Int. J. Mod. Phys. A 2026.41. Downloaded from www.worldscientific.com by UNIVERSITY OF CALIFORNIA @ BERKELEY on 09/16/26. Re-use and distribution is [redacted] except for Open Access articles.

literature (cf. details in Ref. [314]), there is sometimes ambiguity in what is defined to be the bottom fragmentation function. Instead of using what is directly measured (*i.e.*, the B meson spectrum), in some cases corrections are applied to account for B^* or B^{**} production.

Heavy-flavor production in e^+e^- collisions is the primary source of information for the role of fragmentation effects in heavy-flavor production in hadron-hadron and lepton-hadron collisions. The QCD calculations tend to underestimate the data in certain regions of phase space. Some experimental results from LHC summarized in [315] show such deviations e.g. at high transverse jet momentum and also at low di-jet separation angles, see [316] for details, and were already theoretically investigated in [317].

Both bottomed- and charmed-meson spectra have been measured at the Tevatron with unprecedented accuracy [318]. The measured spectra are in good agreement with QCD calculations (including non-perturbative fragmentation effects inferred from e^+e^- data [319]).

The HERA collaborations have produced a number of measurements of beauty production; see, for example, Refs. [311,320–323]. As for the Tevatron data, the HERA results are described well by QCD-based calculations using fragmentation models optimized with e^+e^- data.

Besides degrading the fragmentation function by gluon radiation, QCD evolution can also generate soft heavy quarks, increasing in the small x region as $\sqrt{s}$ increases. Several theoretical studies are available on the issue of how often $b\bar{b}$ or $c\bar{c}$ pairs are produced indirectly via a gluon splitting mechanism [324–326]. Experimental results from studies on charm and bottom production via gluon splitting, given in [310, 327–331], yield weighted averages of $\overline{n}_{g\to c\bar{c}} = 3.05 \pm 0.45\%$ and $\overline{n}_{g\to b\bar{b}} = 0.277 \pm 0.072\%$, respectively. The production of bottom-antibottom quark pairs via gluon splitting has also been investigated at hadron colliders, see for example [332–334].

19.9 Spin-dependent and transverse-momentum dependent fragmentation functions

The fragmentation functions we have considered so far apply to the spin-averaged case in which the polarization of the produced hadron is not observed, or the hadron has spin-0. We have also only considered 'collinear' fragmentation functions $D_i^h(x,\mu^2)$ which carry only one kinematical variable, the momentum fraction x. New insights into fragmentation and hadronization become available when also the dependence of fragmentation functions on the spin of the produced hadron and/or its relative transverse momentum with respect to the fragmenting parton are considered. In the latter case, one refers to the fragmentation functions as 'transverse-momentum dependent (TMD)' fragmentation functions.

Staying first with collinear fragmentation functions, two types of spin-dependent fragmentation functions to spin-1/2 hadrons can be considered. The helicity-dependent fragmentation function measures the transfer of longitudinal spin from the fragmenting parton to the hadron [38, 335–338]. It is given by

$$\Delta D_i^h(x,\mu^2) \equiv D_{i+}^{h^+}(x,\mu^2) - D_{i+}^{h^-}(x,\mu^2)\,, \tag{19.20}$$

where the superscripts $\pm$ refer to the helicities of the parton and hadron. Λ hyperons are ideally suited for measurements of the ΔD_i^h, thanks to their self-analyzing weak decay $\Lambda \to \pi p$. Measurements of the longitudinal spin transfer to Lambda hyperons have been presented in e^+e^- (on the Z resonance), ℓp, and pp scattering in Refs. [339–345]. One may readily extend Eq. (19.20) to the case of transverse polarization of hadrons and quarks [346], where the corresponding fragmentation functions are known as 'transversity' fragmentation functions. There are also measurements constraining these fragmentation functions [340, 347, 348]. A recent phenomenological analysis was presented in [349].

If the transverse-momentum (k_T) dependence of fragmentation functions is considered, there are eight types of leading-twist functions, defined by the correlations among the hadronic and partonic spin vectors and transverse-momentum vectors they represent. (For review, see [5]). We note that the eight fragmentation functions given in the table below exist separately for each quark and antiquark flavor, and a similar set may be introduced for gluons. Upon integration over the transverse momentum k_T the collinear unpolarized, helicity, and transversity fragmentation functions are reproduced.

The various fragmentation functions may be obtained from spin asymmetries and angular distributions in hadron production processes. There is a large body of precision data by now on transverse-momentum distributions in e^+e^- annihilation [350] and SIDIS [194, 351] that provide constraints on the unpolarized TMD fragmentation functions D_i^h, which have been analyzed theoretically, partly also including TMD evolution effects and high orders of perturbation theory [352–359].

Besides the unpolarized functions D most of the attention in experiment and theory has been on the function $H^\perp$ which describes the production of unpolarized (or spin-0) hadrons by transversely polarized quarks. This function is known as the 'Collins function' [360]. Its importance also derives from the fact that it may be used to probe the quark transversity PDF of the nucleon [361] which gives the probability of finding a transversely polarized quark with its spin aligned or anti-aligned with the spin of a transversely polarized nucleon. The transversity function is chiral-odd, and therefore not accessible through measurements of inclusive lepton-hadron scattering. The Collins effect in semi-inclusive DIS, on the other hand, provides an avenue for accessing transversity. The Collins fragmentation function is chiral-odd and T-odd, leading to a characteristic single-spin asymmetry in the azimuthal angular distribution of the produced hadron in the hadron scattering plane. A number of SIDIS [362–373] and e^+e^- experiments [374–378] have performed measurements of the Collins effect, for charged pions and kaons. These have been analyzed theoretically [379, 380], leading to an extraction of the nucleon's transversity distributions [380]. The Collins effect has also been studied in pp scattering, where one considers azimuthal transverse single-spin asymmetries for distributions of hadrons inside jets [177, 381, 382].

In the context of extractions of transversity PDFs also fragmentation functions for same-side pairs of hadrons with small invariant mass, *dihadrons*, have been introduced and studied [383–391]. Compared to the Collins effect, dihadron fragmentation functions have the advantage that they may be defined purely in collinear factorization. The relevant spin-dependent dihadron fragmentation function exploits a correlation between the transverse polarization of the fragmenting quark and the relative momentum of the two hadrons. In SIDIS with a transversely polarized hadron beam, the dihadron cross section then contains a specific modulation in the azimuthal orientation of the plane containing the momenta of the two hadrons. The coefficient of this modulation is a product of the spin-dependent dihadron fragmentation function and the target's transversity PDF. The dihadron fragmentation functions may be separately extracted from measurements in e^+e^- annihilation, and the Belle experiment has presented data [392] that have been analyzed theoretically [393, 394]. In lepton scattering, HERMES [395] and COMPASS [396, 397] have reported data sensitive to the spin-dependent dihadron fragmentation functions, and recently the STAR experiment at RHIC has presented data in the azimuthal distribution of $\pi^+\pi^-$ pairs produced in pp scattering with one transversely polarized proton [398]. The results have been successfully used for the extraction of transversity PDFs [394, 399–401].

References

[1] G. Altarelli, Phys. Rept. **81**, 1 (1982).

[2] R.K. Ellis *et al.*, *QCD and Collider Physics*, Cambridge University Press (1996).

[3] S. Albino *et al.* (2008), [arXiv:0804.2021].

[4] F. Arleo, Eur. Phys. J. **C61**, 603 (2009), [arXiv:0810.1193].

[5] A. Metz and A. Vossen, Prog. Part. Nucl. Phys. **91**, 136 (2016), [arXiv:1607.02521].

[6] P. Nason and B. R. Webber, Nucl. Phys. **B421**, 473 (1994), [Erratum: Nucl. Phys.B480,755(1996)].

[7] D. Buskulic *et al.* (ALEPH), Phys. Lett. **B357**, 487 (1995), [Erratum: Phys. Lett.B364,247(1995)].

Int. J. Mod. Phys. A 2026.41. Downloaded from www.worldscientific.com
by UNIVERSITY OF CALIFORNIA @ BERKELEY on 09/16/26. Re-use and distribution is strictly not permitted, except for Open Access articles.

[8] P. Abreu *et al.* (DELPHI), Eur. Phys. J. **C6**, 19 (1999).

[9] R. Barate *et al.* (ALEPH), Phys. Rept. **294**, 1 (1998).

[10] D. Buskulic *et al.* (ALEPH), Z. Phys. **C73**, 409 (1997).

[11] B. Adeva *et al.* (L3), Phys. Lett. **B259**, 199 (1991).

[12] Y. K. Li *et al.* (AMY), Phys. Rev. **D41**, 2675 (1990).

[13] D. Bender *et al.*, Phys. Rev. **D31**, 1 (1985).

[14] G. S. Abrams *et al.*, Phys. Rev. Lett. **64**, 1334 (1990).

[15] A. Petersen *et al.*, Phys. Rev. **D37**, 1 (1988).

[16] G. Alexander *et al.* (OPAL), Z. Phys. **C72**, 191 (1996).

[17] K. Ackerstaff *et al.* (OPAL), Z. Phys. **C75**, 193 (1997).

[18] G. Abbiendi *et al.* (OPAL), Eur. Phys. J. **C16**, 185 (2000), [hep-ex/0002012].

[19] W. Braunschweig *et al.* (TASSO), Z. Phys. **C47**, 187 (1990).

[20] K. Ackerstaff *et al.* (OPAL), Eur. Phys. J. **C7**, 369 (1999), [hep-ex/9807004].

[21] P. Abreu *et al.* (DELPHI), Phys. Lett. **B398**, 194 (1997).

[22] G. Abbiendi *et al.* (OPAL), Eur. Phys. J. **C37**, 1, 25 (2004), [hep-ex/0404026].

[23] R. Brandelik *et al.* (TASSO), Phys. Lett. **114B**, 65 (1982).

[24] K. Abe *et al.* (SLD), Phys. Rev. **D69**, 072003 (2004), [hep-ex/0310017].

[25] H. Aihara *et al.* (TPC/Two Gamma), Phys. Rev. Lett. **61**, 1263 (1988).

[26] M. Leitgab *et al.* (Belle), Phys. Rev. Lett. **111**, 062002 (2013), [arXiv:1301.6183].

[27] W. Kittel and E.A. De Wolf, *Soft Multihadron Dynamics*, World Scientific (2005).

[28] H.F. Jones, Nuovo Cimento **40A**, 1018 (1965).

[29] K. H. Streng, T. F. Walsh and P. M. Zerwas, Z. Phys. **C2**, 237 (1979).

[30] M. R. Adams *et al.* (E-665), Phys. Lett. **B272**, 163 (1991).

[31] M. Arneodo *et al.* (European Muon), Z. Phys. **C35**, 417 (1987).

[32] I. Abt *et al.* (H1), Z. Phys. **C63**, 377 (1994).

[33] M. Derrick *et al.* (ZEUS), Z. Phys. **C70**, 1 (1996), [hep-ex/9511010].

[34] J. Breitweg *et al.* (ZEUS), Phys. Lett. **B414**, 428 (1997), [hep-ex/9710011].

[35] F. D. Aaron *et al.* (H1), Phys. Lett. **B654**, 148 (2007), [arXiv:0706.2456].

[36] P. Abreu *et al.* (DELPHI), Phys. Lett. **B311**, 408 (1993).

[37] G. Altarelli *et al.*, Nucl. Phys. **B160**, 301 (1979); R. Baier and K. Fey, Z. Phys. **C2**, 339 (1979).

[38] D. de Florian, M. Stratmann and W. Vogelsang, Phys. Rev. **D57**, 5811 (1998), [hep-ph/9711387].

[39] P. J. Rijken and W. L. van Neerven, Phys. Lett. **B386**, 422 (1996), [hep-ph/9604436]; P. J. Rijken and W. L. van Neerven, Phys. Lett. **B392**, 207 (1997), [hep-ph/9609379]; P. J. Rijken and W. L. van Neerven, Nucl. Phys. **B487**, 233 (1997), [hep-ph/9609377].

[40] A. Mitov, S. Moch and A. Vogt, Phys. Lett. **B638**, 61 (2006), [hep-ph/0604053].

[41] A. Mitov and S.-O. Moch, Nucl. Phys. **B751**, 18 (2006), [hep-ph/0604160].

[42] V. N. Gribov and L. N. Lipatov, Sov. J. Nucl. Phys. **15**, 438 (1972), [Yad. Fiz.15,781(1972)]; V. N. Gribov and L. N. Lipatov, Sov. J. Nucl. Phys. **15**, 675 (1972), [Yad. Fiz.15,1218(1972)]; L.N. Lipatov, Sov. J. Nucl. Phys. **20**, 95 (1975); Yu.L. Dokshitzer, Sov. Phys. JETP Lett. **46**, 641 (1977); G. Altarelli and G. Parisi, Nucl. Phys. **B126**, 298 (1977).

[43] H. Georgi and H. D. Politzer, Nucl. Phys. **B136**, 445 (1978); J. F. Owens, Phys. Lett. **76B**, 85 (1978); T. Uematsu, Phys. Lett. **79B**, 97 (1978).

[44] G. Curci, W. Furmanski and R. Petronzio, Nucl. Phys. **B175**, 27 (1980).

[45] W. Furmanski and R. Petronzio, Phys. Lett. **97B**, 437 (1980).

[46] E. G. Floratos, C. Kounnas and R. Lacaze, Nucl. Phys. **B192**, 417 (1981).

[47] J. Kalinowski, K. Konishi and T. R. Taylor, Nucl. Phys. **B181**, 221 (1981).

[48] M. Stratmann and W. Vogelsang, Nucl. Phys. **B496**, 41 (1997), [hep-ph/9612250].

[49] Yu. L. Dokshitzer, G. Marchesini and G. P. Salam, Phys. Lett. **B634**, 504 (2006), [hep-ph/0511302].

[50] S. Moch and A. Vogt, Phys. Lett. **B659**, 290 (2008), [arXiv:0709.3899].

[51] A. A. Almasy, S. Moch and A. Vogt, Nucl. Phys. **B854**, 133 (2012), [arXiv:1107.2263].

[52] M. Cacciari, P. Nason and C. Oleari, JHEP **04**, 006 (2006), [hep-ph/0510032]; M. Cacciari, P. Nason and C. Oleari, JHEP **10**, 034 (2005), [hep-ph/0504192].

[53] P. Aurenche *et al.*, Eur. Phys. J. **C34**, 277 (2004), [hep-ph/0312359]; A. Daleo, D. de Florian and R. Sassot, Phys. Rev. **D71**, 034013 (2005), [hep-ph/0411212]; B. A. Kniehl, G. Kramer and M. Maniatis, Nucl. Phys. **B711**, 345 (2005), [Erratum: Nucl. Phys.B720,231(2005)], [hep-ph/0411300].

[54] B. Wang *et al.*, Phys. Rev. **D99**, 9, 094029 (2019), [arXiv:1903.01529].

[55] S. Aid *et al.* (H1), Nucl. Phys. **B445**, 3 (1995), [hep-ex/9505003].

[56] M. Derrick *et al.* (ZEUS), Z. Phys. **C67**, 93 (1995), [hep-ex/9501012].

[57] C. Adloff *et al.* (H1), Nucl. Phys. **B504**, 3 (1997), [hep-ex/9707005].

[58] J. Breitweg *et al.* (ZEUS), Eur. Phys. J. **C11**, 251 (1999), [hep-ex/9903056].

[59] J. F. Patrick *et al.*, Phys. Rev. Lett. **49**, 1232 (1982).

[60] S. Chekanov *et al.* (ZEUS), JHEP **06**, 061 (2008), [arXiv:0803.3878].

[61] A. H. Mueller, Phys. Lett. **104B**, 161 (1981).

[62] A. Bassetto *et al.*, Nucl. Phys. **B207**, 189 (1982).

[63] Yu.L. Dokshitzer *et al.*, Z. Phys. **C15**, 324 (1982).

[64] A. H. Mueller, Nucl. Phys. **B213**, 85 (1983); A. H. Mueller, Nucl. Phys. **B241**, 141 (1984).

[65] Y. L. Dokshitzer, V. A. Khoze and S. I. Troian, Int. J. Mod. Phys. **A7**, 1875 (1992).

[66] Yu.L. Dokshitzer *et al.*, *Basics of Perturbative QCD*, Editions Frontières (1991).

[67] V. A. Khoze and W. Ochs, Int. J. Mod. Phys. **A12**, 2949 (1997), [hep-ph/9701421].

[68] C. P. Fong and B. R. Webber, Nucl. Phys. **B355**, 54 (1991).

[69] S. Albino *et al.*, Phys. Rev. Lett. **95**, 232002 (2005), [hep-ph/0503170].

[70] S. Albino *et al.*, Phys. Rev. **D73**, 054020 (2006), [hep-ph/0510319].

[71] S. Albino *et al.*, Nucl. Phys. **B851**, 86 (2011), [arXiv:1104.3018]; S. Albino *et al.*, Nucl. Phys. **B855**, 801 (2012), [arXiv:1108.3948].

[72] A. Vogt, JHEP **10**, 025 (2011), [arXiv:1108.2993]; C. H. Kom, A. Vogt and K. Yeats, JHEP **10**, 033 (2012), [arXiv:1207.5631].

[73] D. P. Anderle *et al.*, Phys. Rev. **D95**, 5, 054003 (2017), [arXiv:1611.03371].

Int. J. Mod. Phys. A 2026.41. Downloaded from www.worldscientific.com by UNIVERSITY OF CALIFORNIA @ BERKELEY on 09/16/26. Re-use and distribution is [redacted] except for Open Access articles.

[74] P. Bolzoni, B. A. Kniehl and A. V. Kotikov, Phys. Rev. Lett. **109**, 242002 (2012), [arXiv:1209.5914]; P. Bolzoni, B. A. Kniehl and A. V. Kotikov, Nucl. Phys. **B875**, 18 (2013), [arXiv:1305.6017].

[75] P. Abreu *et al.* (DELPHI), Z. Phys. **C73**, 11 (1996).

[76] P. Abreu *et al.* (DELPHI), Z. Phys. **C73**, 229 (1997).

[77] P. Achard *et al.* (L3), Phys. Rept. **399**, 71 (2004), [hep-ex/0406049].

[78] R. Itoh *et al.* (TOPAZ), Phys. Lett. **B345**, 335 (1995), [hep-ex/9412015].

[79] M. Althoff *et al.* (TASSO), Z. Phys. **C22**, 307 (1984).

[80] M. Z. Akrawy *et al.* (OPAL), Phys. Lett. **B247**, 617 (1990).

[81] W. Dunwoodie *et al.* (BES), Phys. Rev. **D69**, 072002 (2004), [hep-ex/0306055].

[82] D. Buskulic *et al.* (ALEPH), Z. Phys. **C55**, 209 (1992).

[83] A. Heister *et al.* (ALEPH), Eur. Phys. J. **C35**, 457 (2004).

[84] P. Abreu *et al.* (DELPHI), Phys. Lett. **B275**, 231 (1992).

[85] P. Abreu *et al.* (DELPHI), Eur. Phys. J. **C5**, 585 (1998).

[86] P. Abreu *et al.* (DELPHI), Phys. Lett. **B459**, 397 (1999).

[87] M. Acciarri *et al.* (L3), Phys. Lett. **B444**, 569 (1998).

[88] TPC/TWO-GAMMA Collab.: H. Aihara *et al.*, LBL 23737.

[89] B. R. Webber, Phys. Lett. **143B**, 501 (1984).

[90] Y. I. Azimov *et al.*, Z. Phys. **C27**, 65 (1985).

[91] Y. I. Azimov *et al.*, Z. Phys. **C31**, 213 (1986).

[92] I. M. Dremin and J. W. Gary, Phys. Rept. **349**, 301 (2001), [hep-ph/0004215].

[93] I. M. Dremin and V. A. Nechitailo, Mod. Phys. Lett. **A9**, 1471 (1994), [hep-ex/9406002].

[94] S. J. Brodsky and J. F. Gunion, Phys. Rev. Lett. **37**, 402 (1976).

[95] J. Beringer *et al.* (Particle Data Group), Phys. Rev. **D86**, 010001 (2012).

[96] R. Akers *et al.* (OPAL), Z. Phys. **C68**, 203 (1995).

[97] P. D. Acton *et al.* (OPAL), Z. Phys. **C53**, 539 (1992).

[98] D. Buskulic *et al.* (ALEPH), Z. Phys. **C69**, 15 (1995).

[99] P. Abreu *et al.* (DELPHI), Phys. Lett. **B372**, 172 (1996).

[100] P. Abreu *et al.* (DELPHI), Phys. Lett. **B416**, 233 (1998).

[101] P. Abreu *et al.* (DELPHI), Eur. Phys. J. **C18**, 203 (2000), [Erratum: Eur. Phys. J.C25,493(2002)], [hep-ex/0103031].

[102] M. Acciarri *et al.* (L3), Phys. Lett. **B371**, 137 (1996).

[103] M. Acciarri *et al.* (L3), Phys. Lett. **B404**, 390 (1997).

[104] K. Nakabayashi *et al.* (TOPAZ), Phys. Lett. **B413**, 447 (1997).

[105] K. Okabe *et al.* (VENUS), Phys. Lett. **B423**, 407 (1998).

[106] H. Albrecht *et al.* (ARGUS), Z. Phys. **C54**, 13 (1992).

[107] S. Chekanov *et al.* (ZEUS), Phys. Lett. **B510**, 36 (2001), [hep-ex/0104036].

[108] J. Benecke *et al.* (Bonn-Hamburg-Munich), Nucl. Phys. **B76**, 29 (1974).

[109] W. M. Morse *et al.*, Phys. Rev. **D15**, 66 (1977).

[110] W. Thome *et al.* (Aachen-CERN-Heidelberg-Munich), Nucl. Phys. **B129**, 365 (1977).

[111] A. Breakstone *et al.* (Ames-Bologna-CERN-Dortmund-Heidelberg-Warsaw), Phys. Rev. **D30**, 528 (1984).

[112] G. J. Alner *et al.* (UA5), Phys. Rept. **154**, 247 (1987).

[113] R. E. Ansorge *et al.* (UA5), Z. Phys. **C43**, 357 (1989).

[114] C. Albajar *et al.* (UA1), Nucl. Phys. **B335**, 261 (1990).

[115] F. Abe *et al.* (CDF), Phys. Rev. **D41**, 2330 (1990), [,119(1989)].

[116] K. Aamodt *et al.* (ALICE), Eur. Phys. J. **C68**, 89 (2010), [arXiv:1004.3034].

[117] V. Khachatryan *et al.* (CMS), JHEP **02**, 041 (2010), [arXiv:1002.0621].

[118] V. Khachatryan *et al.* (CMS), JHEP **01**, 079 (2011), [arXiv:1011.5531].

[119] V. Khachatryan *et al.* (CMS), Phys. Rev. Lett. **105**, 022002 (2010), [arXiv:1005.3299].

[120] G. Aad *et al.* (ATLAS), Eur. Phys. J. **C76**, 7, 403 (2016), [arXiv:1603.02439].

[121] M. Aaboud *et al.* (ATLAS), Eur. Phys. J. **C76**, 9, 502 (2016), [arXiv:1606.01133].

[122] J. Adam *et al.* (ALICE), Phys. Lett. **B753**, 319 (2016), [arXiv:1509.08734].

[123] J. Adam *et al.* (ALICE), Eur. Phys. J. **C77**, 1, 33 (2017), [arXiv:1509.07541].

[124] P. V. Chliapnikov and V. A. Uvarov, Phys. Lett. **B251**, 192 (1990).

[125] J. F. Grosse-Oetringhaus and K. Reygers, J. Phys. **G37**, 083001 (2010), [arXiv:0912.0023].

[126] E. K. G. Sarkisyan and A. S. Sakharov (2004), [hep-ph/0410324]; E. K. G. Sarkisyan and A. S. Sakharov, AIP Conf. Proc. **828**, 1, 35 (2006), [hep-ph/0510191]; E. K. G. Sarkisyan and A. S. Sakharov, Eur. Phys. J. **C70**, 533 (2010), [arXiv:1004.4390].

[127] S. Hoeche *et al.*, in "HERA and the LHC: A Workshop on the implications of HERA for LHC physics: Proceedings Part A," 288–289 (2005), [hep-ph/0602031]; S. Mrenna and P. Richardson, JHEP **05**, 040 (2004), [hep-ph/0312274]; J. Alwall *et al.*, Eur. Phys. J. **C53**, 473 (2008), [arXiv:0706.2569].

[128] I. Borsa *et al.*, Phys. Rev. D **105**, 3, L031502 (2022), [arXiv:2110.14015].

[129] E. Moffat *et al.* (Jefferson Lab Angular Momentum (JAM)), Phys. Rev. D **104**, 1, 016015 (2021), [arXiv:2101.04664].

[130] V. Bertone *et al.* (NNPDF), Eur. Phys. J. **C77**, 8, 516 (2017), [arXiv:1706.07049].

[131] D. de Florian, R. Sassot and M. Stratmann, Phys. Rev. **D76**, 074033 (2007), [arXiv:0707.1506].

[132] S. Albino, B. A. Kniehl and G. Kramer, Nucl. Phys. **B803**, 42 (2008), [arXiv:0803.2768].

[133] S. Kretzer, E. Leader and E. Christova, Eur. Phys. J. **C22**, 269 (2001), [hep-ph/0108055].

[134] S. Kretzer, Phys. Rev. **D62**, 054001 (2000), [hep-ph/0003177].

[135] L. Bourhis *et al.*, Eur. Phys. J. **C19**, 89 (2001), [hep-ph/0009101].

[136] M. Hirai *et al.*, Phys. Rev. **D75**, 094009 (2007), [hep-ph/0702250].

[137] C. A. Aidala *et al.*, Phys. Rev. **D83**, 034002 (2011), [arXiv:1009.6145].

[138] D. de Florian *et al.*, Phys. Rev. **D91**, 1, 014035 (2015), [arXiv:1410.6027].

[139] D. de Florian *et al.*, Phys. Rev. **D95**, 9, 094019 (2017), [arXiv:1702.06353].

[140] D. de Florian, R. Sassot and M. Stratmann, Phys. Rev. **D75**, 114010 (2007), [hep-ph/0703242].

[141] D. P. Anderle, F. Ringer and M. Stratmann, Phys. Rev. **D92**, 11, 114017 (2015), [arXiv:1510.05845].

[142] E. Leader, A. V. Sidorov and D. B. Stamenov, Phys. Rev. **D93**, 7, 074026 (2016), [arXiv:1506.06381].

[143] R. A. Khalek, V. Bertone and E. R. Nocera (MAP (Multidimensional Analyses of Partonic distributions)), Phys. Rev. D **104**, 3, 034007 (2021), [arXiv:2105.08725].

[144] H. Abdolmaleki *et al.* (xfitter Developers' Team), Phys. Rev. D **104**, 5, 056019 (2021), [arXiv:2105.11306].

Int. J. Mod. Phys. A 2026.41. Downloaded from www.worldscientific.com
by UNIVERSITY OF CALIFORNIA @ BERKELEY on 09/16/26. Re-use and distribution is strictly not permitted, except for Open Access articles.

[145] V. Bertone *et al.* (NNPDF), Eur. Phys. J. **C78**, 8, 651 (2018), [arXiv:1807.03310].

[146] R. Barate *et al.* (ALEPH), Eur. Phys. J. **C17**, 1 (2000); R. Akers *et al.* (OPAL), Z. Phys. **C68**, 179 (1995); G. Abbiendi *et al.* (OPAL), Eur. Phys. J. **C11**, 217 (1999), [hep-ex/9903027].

[147] K. Abe *et al.* (SLD), Phys. Rev. **D59**, 052001 (1999), [hep-ex/9805029].

[148] D. Buskulic *et al.* (ALEPH), Z. Phys. **C66**, 355 (1995); H. Albrecht *et al.* (ARGUS), Z. Phys. **C44**, 547 (1989); R. Akers *et al.* (OPAL), Z. Phys. **C63**, 181 (1994).

[149] M. R. Adams *et al.* (E665), Z. Phys. **C61**, 539 (1994).

[150] M. Arneodo *et al.* (European Muon), Z. Phys. **C34**, 283 (1987).

[151] S. Aid *et al.* (H1), Nucl. Phys. **B480**, 3 (1996), [hep-ex/9607010].

[152] J. J. Aubert *et al.* (European Muon), Z. Phys. **C18**, 189 (1983).

[153] A. Airapetian *et al.* (HERMES), Eur. Phys. J. **C21**, 599 (2001), [hep-ex/0104004].

[154] T. P. McPharlin *et al.*, Phys. Lett. **90B**, 479 (1980).

[155] S. S. Adler *et al.* (PHENIX), Phys. Rev. Lett. **91**, 241803 (2003), [hep-ex/0304038].

[156] B. Abelev *et al.* (ALICE), Phys. Lett. **B717**, 162 (2012), [arXiv:1205.5724].

[157] M. Bonesini *et al.* (WA70), Z. Phys. **C38**, 371 (1988).

[158] T. Akesson *et al.* (Axial Field Spectrometer), Sov. J. Nucl. Phys. **51**, 836 (1990), [Yad. Fiz.51,1314(1990)].

[159] C. Kourkoumelis *et al.*, Z. Phys. **C5**, 95 (1980).

[160] L. Apanasevich *et al.* (Fermilab E706), Phys. Rev. **D68**, 052001 (2003), [hep-ex/0204031].

[161] F. Abe *et al.* (CDF), Phys. Rev. Lett. **61**, 1819 (1988).

[162] M. Banner *et al.* (UA2), Phys. Lett. **115B**, 59 (1982).

[163] M. Procura and I. W. Stewart, Phys. Rev. **D81**, 074009 (2010), [Erratum: Phys. Rev.D83,039902(2011)], [arXiv:0911.4980].

[164] A. Jain, M. Procura and W. J. Waalewijn, JHEP **05**, 035 (2011), [arXiv:1101.4953].

[165] M. Procura and W. J. Waalewijn, Phys. Rev. **D85**, 114041 (2012), [arXiv:1111.6605].

[166] F. Arleo *et al.*, JHEP **04**, 147 (2014), [arXiv:1311.7356].

[167] M. Ritzmann and W. J. Waalewijn, Phys. Rev. **D90**, 5, 054029 (2014), [arXiv:1407.3272].

[168] T. Kaufmann, A. Mukherjee and W. Vogelsang, Phys. Rev. **D92**, 5, 054015 (2015), [arXiv:1506.01415].

[169] Y.-T. Chien *et al.*, JHEP **05**, 125 (2016), [arXiv:1512.06851].

[170] F. Abe *et al.* (CDF), Phys. Rev. Lett. **65**, 968 (1990).

[171] T. A. collaboration (ATLAS) (2015).

[172] S. Chatrchyan *et al.* (CMS), JHEP **10**, 087 (2012), [arXiv:1205.5872].

[173] X. Lu (ALICE), Nucl. Phys. **A931**, 428 (2014), [arXiv:1407.8385].

[174] C. Bianchin (ALICE), J. Phys. Conf. Ser. **612**, 1, 012020 (2015).

[175] F. Krizek (ALICE), J. Phys. Conf. Ser. **668**, 1, 012018 (2016), [arXiv:1509.02024].

[176] M. Aaboud *et al.* (ATLAS), Nucl. Phys. **A978**, 65 (2018), [arXiv:1706.02859].

[177] L. Adamczyk *et al.* (STAR), Phys. Rev. **D97**, 3, 032004 (2018), [arXiv:1708.07080].

[178] D. P. Anderle *et al.*, Phys. Rev. **D96**, 3, 034028 (2017), [arXiv:1706.09857].

[179] N. Sato *et al.* (JAM) (2019), [arXiv:1905.03788].

[180] M. Epele *et al.*, Phys. Rev. **D86**, 074028 (2012), [arXiv:1209.3240].

[181] J. Gao *et al.* (2025), [arXiv:2502.17837].

[182] J. Gao *et al.*, Phys. Rev. D **110**, 11, 114019 (2024), [arXiv:2407.04422].

[183] R. Abdul Khalek *et al.* (MAP (Multi-dimensional Analyses of Partonic distributions)), Phys. Lett. B **834**, 137456 (2022), [arXiv:2204.10331].

[184] I. Borsa *et al.*, Phys. Rev. D **109**, 5, 052004 (2024), [arXiv:2311.17768].

[185] E. Witten, Nucl. Phys. **210**, 189 (1977).

[186] L. Bourhis, M. Fontannaz and J. P. Guillet, Eur. Phys. J. **C2**, 529 (1998), [hep-ph/9704447].

[187] M. Gluck, E. Reya and A. Vogt, Phys. Rev. **D48**, 116 (1993), [Erratum: Phys. Rev.D51,1427(1995)]; Erratum *ibid.* **D51**, 1427 (1995).

[188] G. Abbiendi *et al.* (OPAL), Eur. Phys. J. **C27**, 467 (2003), [hep-ex/0209048].

[189] G. Bocquet *et al.*, Phys. Lett. **B366**, 434 (1996).

[190] T. Kaufmann, A. Mukherjee and W. Vogelsang, Phys. Rev. **D93**, 11, 114021 (2016), [arXiv:1604.07175].

[191] P. Abreu *et al.* (DELPHI), Eur. Phys. J. **C13**, 573 (2000).

[192] B. A. Kniehl, G. Kramer and B. Potter, Phys. Rev. Lett. **85**, 5288 (2000), [hep-ph/0003297].

[193] M. Arneodo *et al.* (European Muon), Z. Phys. **C33**, 167 (1986).

[194] A. Airapetian *et al.* (HERMES), Phys. Rev. **D87**, 074029 (2013), [arXiv:1212.5407].

[195] C. Adolph *et al.* (COMPASS), Phys. Lett. **B764**, 1 (2017), [arXiv:1604.02695].

[196] F. D. Aaron *et al.* (H1), Phys. Lett. **B673**, 119 (2009), [arXiv:0901.0477].

[197] M. Derrick *et al.* (ZEUS), Z. Phys. **C68**, 29 (1995), [hep-ex/9505011].

[198] S. Chekanov *et al.* (ZEUS), Phys. Lett. **B553**, 141 (2003), [hep-ex/0211025].

[199] S. Chekanov *et al.* (ZEUS), Nucl. Phys. **B786**, 181 (2007), [arXiv:0705.3770].

[200] F. D. Aaron *et al.* (H1), Eur. Phys. J. **C61**, 185 (2009), [arXiv:0810.4036].

[201] A. Aktas *et al.* (H1), Eur. Phys. J. **C36**, 413 (2004), [hep-ex/0403056].

[202] P. Dixon, D. Kant and G. Thompson, J. Phys. **G25**, 1453 (1999).

[203] C. Adloff *et al.* (H1), Phys. Lett. **B462**, 440 (1999), [hep-ex/9907030].

[204] D. Graudenz, Fortsch. Phys. **45**, 629 (1997), [hep-ph/9701334].

[205] P. M. Nadolsky, D. R. Stump and C. P. Yuan, Phys. Rev. **D61**, 014003 (2000), [Erratum: Phys. Rev.D64,059903(2001)], [hep-ph/9906280].

[206] M. Abele, D. de Florian and W. Vogelsang, Phys. Rev. D **104**, 9, 094046 (2021), [arXiv:2109.00847].

[207] M. Abele, D. de Florian and W. Vogelsang, Phys. Rev. D **106**, 1, 014015 (2022), [arXiv:2203.07928].

[208] S. Goyal *et al.* (2025), [arXiv:2506.24078].

[209] S. Goyal *et al.*, Phys. Rev. D **111**, 9, 094007 (2025), [arXiv:2412.19309].

[210] L. Bonino *et al.*, Phys. Rev. Lett. **133**, 21, 211904 (2024), [arXiv:2404.08597].

[211] L. Bonino, T. Gehrmann and G. Stagnitto, Phys. Rev. Lett. **132**, 25, 251901 (2024), [arXiv:2401.16281].

Int. J. Mod. Phys. A 2026.41. Downloaded from www.worldscientific.com by UNIVERSITY OF CALIFORNIA @ BERKELEY on 09/16/26. Re-use and distribution is except for Open Access articles.

[212] T. Aaltonen *et al.* (CDF), Phys. Rev. **D79**, 112005 (2009), [Erratum: Phys. Rev.D82,119903(2010)], [arXiv:0904.1098].

[213] G. Aad *et al.* (ATLAS), New J. Phys. **13**, 053033 (2011), [arXiv:1012.5104].

[214] B. I. Abelev *et al.* (STAR), Phys. Rev. **C75**, 064901 (2007), [arXiv:nucl-ex/0607033].

[215] K. Aamodt *et al.* (ALICE), Eur. Phys. J. **C71**, 1655 (2011), [arXiv:1101.4110].

[216] B. B. Abelev *et al.* (ALICE), Phys. Lett. **B736**, 196 (2014), [arXiv:1401.1250].

[217] J. Adam *et al.* (ALICE), Eur. Phys. J. **C75**, 5, 226 (2015), [arXiv:1504.00024].

[218] S. Chatrchyan *et al.* (CMS), Eur. Phys. J. **C72**, 2164 (2012), [arXiv:1207.4724].

[219] A. M. Sirunyan *et al.* (CMS), Phys. Rev. **D96**, 11, 112003 (2017), [arXiv:1706.10194].

[220] G. J. Alner *et al.* (UA5), Z. Phys. **C32**, 153 (1986).

[221] B. Abelev *et al.* (ALICE), Eur. Phys. J. **C73**, 6, 2456 (2013), [arXiv:1208.4968].

[222] G. Antchev *et al.* (TOTEM), EPL **101**, 2, 21004 (2013).

[223] A. M. Sirunyan *et al.* (CMS), JHEP **07**, 161 (2018), [arXiv:1802.02613].

[224] F. Abe *et al.* (CDF), Phys. Rev. **D50**, 5550 (1994).

[225] F. Abe *et al.* (CDF), Phys. Rev. **D50**, 5518 (1994).

[226] S. S. Adler *et al.* (PHENIX), Phys. Rev. **C74**, 024904 (2006), [arXiv:nucl-ex/0603010].

[227] S. Albino *et al.*, Phys. Rev. **D75**, 034018 (2007), [hep-ph/0611029].

[228] I. Borsa, R. Sassot and M. Stratmann, Phys. Rev. **D96**, 9, 094020 (2017), [arXiv:1708.01630].

[229] B. Andersson *et al.*, Phys. Rept. **97**, 31 (1983).

[230] T. Sjostrand and M. Bengtsson, Comput. Phys. Commun. **43**, 367 (1987); T. Sjostrand, Comput. Phys. Commun. **82**, 74 (1994).

[231] P. D. Acton *et al.* (OPAL), Phys. Lett. **B305**, 407 (1993).

[232] J. Breitweg *et al.* (ZEUS), Eur. Phys. J. **C2**, 77 (1998), [hep-ex/9711018].

[233] D. DeProspo *et al.* (E632), Phys. Rev. **D50**, 6691 (1994).

[234] S. Chekanov *et al.* (ZEUS), Eur. Phys. J. **C51**, 1 (2007), [hep-ex/0612023].

[235] G. Grindhammer *et al.*, in: *Proceedings of the Workshop on Monte Carlo Generators for HERA Physics*, Hamburg, Germany, 1998/1999.

[236] N. Brook *et al.*, in: *Proceedings of the Workshop for Future HERA Physics at HERA*, Hamburg, Germany, 1996.

[237] D. Acosta *et al.* (CDF), Phys. Rev. **D72**, 052001 (2005), [hep-ex/0504048].

[238] G. Arnison *et al.* (UA1), Phys. Lett. **118B**, 167 (1982).

[239] M. Banner *et al.* (UA2), Phys. Lett. **122B**, 322 (1983).

[240] M. Banner *et al.* (UA2, Bern-CERN-Copenhagen-Orsay-Pavia-Saclay), Z. Phys. **C27**, 329 (1985).

[241] A. Adare *et al.* (PHENIX), Phys. Rev. **D76**, 051106 (2007), [arXiv:0704.3599].

[242] A. Adare *et al.* (PHENIX), Phys. Rev. **D83**, 032001 (2011), [arXiv:1009.6224].

[243] A. Adare *et al.* (PHENIX), Phys. Rev. **D86**, 092006 (2012), [arXiv:1202.4020].

[244] A. Adare *et al.* (PHENIX), Phys. Rev. **D88**, 3, 032006 (2013), [arXiv:1209.3283].

[245] A. Adare *et al.* (PHENIX), Phys. Rev. **D91**, 3, 032001 (2015), [arXiv:1409.1907].

[246] A. Adare *et al.* (PHENIX), Phys. Rev. **D90**, 7, 072008 (2014), [arXiv:1406.3541].

[247] A. Adare *et al.* (PHENIX), Phys. Rev. **D93**, 1, 011501 (2016), [arXiv:1510.02317].

[248] I. Arsene *et al.* (BRAHMS), Phys. Rev. Lett. **98**, 252001 (2007), [hep-ex/0701041].

[249] J. Adams *et al.* (STAR), Phys. Rev. Lett. **97**, 152302 (2006), [arXiv:nucl-ex/0602011].

[250] J. Adams *et al.* (STAR), Phys. Lett. **B637**, 161 (2006), [arXiv:nucl-ex/0601033].

[251] B. I. Abelev *et al.* (STAR), Phys. Rev. **D80**, 111108 (2009), [arXiv:0911.2773].

[252] G. Agakishiev *et al.* (STAR), Phys. Rev. Lett. **108**, 072302 (2012), [arXiv:1110.0579].

[253] L. Adamczyk *et al.* (STAR), Phys. Rev. **D89**, 1, 012001 (2014), [arXiv:1309.1800].

[254] B. B. Abelev *et al.* (ALICE), Eur. Phys. J. **C73**, 12, 2662 (2013), [arXiv:1307.1093].

[255] L. Apanasevich *et al.* (Fermilab E706), Phys. Rev. Lett. **81**, 2642 (1998), [hep-ex/9711017].

[256] G. Ballocchi *et al.* (UA6), Phys. Lett. **B436**, 222 (1998).

[257] K. Aamodt *et al.* (ALICE), Eur. Phys. J. **C71**, 1594 (2011), [arXiv:1012.3257].

[258] R. Aaij *et al.* (LHCb), Phys. Lett. **B703**, 267 (2011), [arXiv:1107.3935].

[259] G. Aad *et al.* (ATLAS), Phys. Lett. **B758**, 67 (2016), [arXiv:1602.01633].

[260] F. Aversa *et al.*, Nucl. Phys. **B327**, 105 (1989); D. de Florian, Phys. Rev. **D67**, 054004 (2003), [hep-ph/0210442]; B. Jager *et al.*, Phys. Rev. **D67**, 054005 (2003), [hep-ph/0211007].

[261] U. Baur *et al.*, in "QCD and weak boson physics in Run II. Proceedings, Batavia, USA, March 4-6, June 3-4, November 4-6, 1999," 115–164 (2000), [,115(2000)], [hep-ph/0005226], URL `http://lss.fnal.gov/archive/preprint/fermilab-conf-00-411-ae.shtml`.

[262] P. Aurenche *et al.*, Eur. Phys. J. **C13**, 347 (2000), [hep-ph/9910252].

[263] L. Apanasevich *et al.*, Phys. Rev. **D59**, 074007 (1999), [hep-ph/9808467].

[264] U. D'Alesio and F. Murgia, Phys. Rev. **D70**, 074009 (2004), [hep-ph/0408092].

[265] D. de Florian and W. Vogelsang, Phys. Rev. **D71**, 114004 (2005), [hep-ph/0501258].

[266] P. Hinderer *et al.*, Phys. Rev. **D99**, 5, 054019 (2019), [arXiv:1812.00915].

[267] M. Czakon *et al.* (2025), [arXiv:2503.11489].

[268] D. d'Enterria *et al.*, Nucl. Phys. **B883**, 615 (2014), [arXiv:1311.1415].

[269] G. Wilk and Z. Wlodarczyk, Eur. Phys. J. **A40**, 299 (2009), [arXiv:0810.2939].

[270] C. Tsallis, J. Statist. Phys. **52**, 479 (1988).

[271] C. Tsallis, Braz. J. Phys. **29**, 1 (1999).

[272] C. Tsallis, Eur. Phys. J. **A40**, 257 (2009), [arXiv:0812.4370].

[273] M. D. Azmi and J. Cleymans, J. Phys. **G41**, 065001 (2014), [arXiv:1401.4835].

[274] G. Wilk and Z. Wlodarczyk, Phys. Rev. Lett. **84**, 2770 (2000), [hep-ph/9908459].

[275] T. Bhattacharyya *et al.*, J. Phys. **G45**, 5, 055001 (2018), [arXiv:1709.07376].

[276] S. Grigoryan, Phys. Rev. **D95**, 5, 056021 (2017), [arXiv:1702.04110].

[277] T. Wibig, Int. J. Mod. Phys. **A29**, 1450021 (2014).

[278] K. Saraswat, P. Shukla and V. Singh, J. Phys. Comm. **2**, 3, 035003 (2018), [arXiv:1706.04860].

Int. J. Mod. Phys. A 2026.41. Downloaded from www.worldscientific.com
by UNIVERSITY OF CALIFORNIA @ BERKELEY on 09/16/26. Re-use and distribution is strictly not permitted, except for Open Access articles.

[279] K. Urmossy, G. G. Barnafoldi and T. S. Biro, Phys. Lett. **B701**, 111 (2011), [arXiv:1101.3023].

[280] A. S. Parvan, O. V. Teryaev and J. Cleymans, Eur. Phys. J. **A53**, 5, 102 (2017), [arXiv:1607.01956].

[281] K. Adcox *et al.* (PHENIX), Phys. Rev. Lett. **88**, 022301 (2002), [arXiv:nucl-ex/0109003]; C. Adler *et al.* (STAR), Phys. Rev. Lett. **90**, 082302 (2003), [arXiv:nucl-ex/0210033].

[282] V.A. Khoze *et al.*, *Proceedings, Conference on High-Energy Physics, Tbilisi 1976*; J. D. Bjorken, Phys. Rev. **D17**, 171 (1978).

[283] M. Artuso *et al.* (CLEO), Phys. Rev. **D70**, 112001 (2004), [hep-ex/0402040].

[284] R. Seuster *et al.* (Belle), Phys. Rev. **D73**, 032002 (2006), [hep-ex/0506068].

[285] A. Heister *et al.* (ALEPH), Phys. Lett. **B512**, 30 (2001), [hep-ex/0106051]; J. Abdallah *et al.* (DELPHI), Eur. Phys. J. **C71**, 1557 (2011), [arXiv:1102.4748]; G. Abbiendi *et al.* (OPAL), Eur. Phys. J. **C29**, 463 (2003), [hep-ex/0210031]; K. Abe *et al.* (SLD), Phys. Rev. **D65**, 092006 (2002), [Erratum: Phys. Rev.D66,079905(2002)], [hep-ex/0202031].

[286] B. Mele and P. Nason, Phys. Lett. **B245**, 635 (1990); B. Mele and P. Nason, Nucl. Phys. **B361**, 626 (1991), [Erratum: Nucl. Phys.B921,841(2017)].

[287] M. Cacciari and S. Catani, Nucl. Phys. **B617**, 253 (2001), [hep-ph/0107138].

[288] P. Nason and C. Oleari, Phys. Lett. **B418**, 199 (1998), [hep-ph/9709358]; P. Nason and C. Oleari, Phys. Lett. **B447**, 327 (1999), [hep-ph/9811206]; P. Nason and C. Oleari, Nucl. Phys. **B565**, 245 (2000), [hep-ph/9903541].

[289] K. Melnikov and A. Mitov, Phys. Rev. **D70**, 034027 (2004), [hep-ph/0404143].

[290] C. Peterson *et al.*, Phys. Rev. **D27**, 105 (1983).

[291] V. G. Kartvelishvili, A. K. Likhoded and V. A. Petrov, Phys. Lett. **78B**, 615 (1978).

[292] P. D. B. Collins and T. P. Spiller, J. Phys. **G11**, 1289 (1985).

[293] G. Colangelo and P. Nason, Phys. Lett. **B285**, 167 (1992).

[294] M. G. Bowler, Z. Phys. **C11**, 169 (1981).

[295] E. Braaten *et al.*, Phys. Rev. **D51**, 4819 (1995), [hep-ph/9409316].

[296] R. Akers *et al.* (OPAL), Z. Phys. **C67**, 27 (1995).

[297] H. Albrecht *et al.* (ARGUS), Z. Phys. **C52**, 353 (1991).

[298] D. Buskulic *et al.* (ALEPH), Phys. Lett. **B357**, 699 (1995).

[299] J. Chrin, Z. Phys. **C36**, 163 (1987).

[300] R. L. Jaffe and L. Randall, Nucl. Phys. **B412**, 79 (1994), [hep-ph/9306201].

[301] M. Cacciari and E. Gardi, Nucl. Phys. **B664**, 299 (2003), [hep-ph/0301047].

[302] L. Randall and N. Rius, Nucl. Phys. **B441**, 167 (1995), [hep-ph/9405217].

[303] J. C. Collins, Phys. Rev. **D58**, 094002 (1998), [hep-ph/9806259].

[304] B. A. Kniehl *et al.*, Eur. Phys. J. **C41**, 199 (2005), [hep-ph/0502194].

[305] S. Ahmed *et al.* (CLEO), Phys. Rev. **D62**, 112003 (2000), [hep-ex/0008015].

[306] B. Aubert *et al.* (BaBar), Phys. Rev. **D65**, 091104 (2002), [hep-ex/0201041].

[307] D. Bortoletto *et al.* (CLEO), Phys. Rev. **D37**, 1719 (1988), [Erratum: Phys. Rev.D39,1471(1989)].

[308] H. Albrecht *et al.* (ARGUS), Z. Phys. **C54**, 1 (1992).

[309] G. Alexander *et al.* (OPAL), Z. Phys. **C69**, 543 (1996).

[310] A. Heister *et al.* (ALEPH), Phys. Lett. **B561**, 213 (2003), [hep-ex/0302003].

[311] F. D. Aaron *et al.* (H1), Eur. Phys. J. **C65**, 89 (2010), [arXiv:0907.2643].

[312] S. Chekanov *et al.* (ZEUS), JHEP **07**, 074 (2007), [arXiv:0704.3562]; ZEUS Collab: H. Abramowicz *et al.*, JHEP , 1309 (2013); A. Aktas *et al.* (H1), Eur. Phys. J. **C51**, 271 (2007), [hep-ex/0701023]; F. D. Aaron *et al.* (H1), Eur. Phys. J. **C59**, 589 (2009), [arXiv:0808.1003].

[313] B. Adeva *et al.* (L3), Phys. Lett. **B261**, 177 (1991).

[314] O. Biebel, P. Nason and B. R. Webber (2001), [hep-ph/0109282].

[315] H. Evans (ALICE, ATLAS, CMS, LHCb), in "Proceedings, 14th International Conference on Hadron spectroscopy (Hadron 2011): Munich, Germany, June 13-17, 2011," (2011), [arXiv:1110.5294]; E. Aguilo, in "Proceedings, 47th Rencontres de Moriond on QCD and High Energy Interactions: La Thuile, France, March 10-17, 2012," 115–120 (2012), [arXiv:1205.5678]; F. Simonetto, Journal of Physics: Conference Series **347**, 012014 (2012).

[316] V. Khachatryan *et al.* (CMS), JHEP **03**, 136 (2011), [arXiv:1102.3194]; G. Aad *et al.* (ATLAS), Eur. Phys. J. **C71**, 1846 (2011), [arXiv:1109.6833]; S. Chatrchyan *et al.* (CMS), JHEP **04**, 084 (2012), [arXiv:1202.4617]; G. Aad *et al.* (ATLAS), Eur. Phys. J. **C73**, 2, 2301 (2013), [arXiv:1210.0441].

[317] H. Jung *et al.*, Phys. Rev. **D85**, 034035 (2012), [arXiv:1111.1942].

[318] D. Acosta *et al.* (CDF), Phys. Rev. Lett. **91**, 241804 (2003), [hep-ex/0307080]; D. Acosta *et al.* (CDF), Phys. Rev. **D71**, 032001 (2005), [hep-ex/0412071].

[319] M. Cacciari and P. Nason, JHEP **09**, 006 (2003), [hep-ph/0306212]; M. Cacciari *et al.*, JHEP **07**, 033 (2004), [hep-ph/0312132]; B. A. Kniehl *et al.*, Phys. Rev. Lett. **96**, 012001 (2006), [hep-ph/0508129].

[320] H. Abramowicz *et al.* (ZEUS), Eur. Phys. J. **C71**, 1573 (2011), [arXiv:1101.3692].

[321] S. Chekanov *et al.* (ZEUS), Phys. Rev. **D78**, 072001 (2008), [arXiv:0805.4390].

[322] S. Chekanov *et al.* (ZEUS), JHEP **02**, 032 (2009), [arXiv:0811.0894].

[323] F. D. Aaron *et al.* (H1), Eur. Phys. J. **C72**, 2148 (2012), [arXiv:1206.4346].

[324] M. L. Mangano and P. Nason, Phys. Lett. **B285**, 160 (1992).

[325] M. H. Seymour, Nucl. Phys. **B436**, 163 (1995).

[326] D. J. Miller and M. H. Seymour, Phys. Lett. **B435**, 213 (1998), [hep-ph/9805414].

[327] R. Barate *et al.* (ALEPH), Phys. Lett. **B434**, 437 (1998).

[328] P. Abreu *et al.* (DELPHI), Phys. Lett. **B405**, 202 (1997).

[329] M. Acciarri *et al.* (L3), Phys. Lett. **B476**, 243 (2000), [hep-ex/9911016].

[330] G. Abbiendi *et al.* (OPAL), Eur. Phys. J. **C13**, 1 (2000), [hep-ex/9908001].

[331] K. Abe *et al.* (SLD) (1999), [hep-ex/9908028], URL `http://www-public.slac.stanford.edu/sciDoc/docMeta.aspx?slacPubNumber=SLAC-PUB-8157`.

[332] C. Albajar *et al.* (UA1 Collaboration), Z. Phys. C **61**, 41 (1993), URL `http://cds.cern.ch/record/253028`.

[333] R. Aaij *et al.* (LHCb), JHEP **11**, 030 (2017), [arXiv:1708.05994].

[334] M. Aaboud *et al.* (ATLAS), Phys. Rev. **D99**, 5, 052004 (2019), [arXiv:1812.09283].

[335] M. Burkardt and R. L. Jaffe, Phys. Rev. Lett. **70**, 2537 (1993), [hep-ph/9302232].

[336] P. J. Mulders and R. D. Tangerman, Nucl. Phys. **B461**, 197 (1996), [Erratum: Nucl. Phys.B484,538(1997)], [hep-ph/9510301].

[337] R. Jakob, Nucl. Phys. **A711**, 35 (2002), [hep-ph/0206271].

Int. J. Mod. Phys. A 2026.41. Downloaded from www.worldscientific.com by UNIVERSITY OF CALIFORNIA @ BERKELEY on 09/16/26. Re-use and distribution is [redacted] except for Open Access articles.

[338] D. de Florian, M. Stratmann and W. Vogelsang, Phys. Rev. Lett. **81**, 530 (1998), [hep-ph/9802432].

[339] D. Buskulic *et al.* (ALEPH), Phys. Lett. **B374**, 319 (1996).

[340] K. Ackerstaff *et al.* (OPAL), Eur. Phys. J. **C2**, 49 (1998), [hep-ex/9708027].

[341] G. Abbiendi *et al.* (OPAL), Phys. Lett. **B444**, 539 (1998), [hep-ex/9808006].

[342] M. Alekseev *et al.* (COMPASS), Eur. Phys. J. **C64**, 171 (2009), [arXiv:0907.0388].

[343] A. Airapetian *et al.* (HERMES), Phys. Rev. **D74**, 072004 (2006), [hep-ex/0607004].

[344] G. Karyan (HERMES), Int. J. Mod. Phys. Conf. Ser. **40**, 1660067 (2016).

[345] J. Adam *et al.* (STAR), Phys. Rev. **D98**, 11, 112009 (2018), [arXiv:1808.07634].

[346] R. L. Jaffe, Phys. Rev. **D54**, 11, R6581 (1996), [hep-ph/9605456].

[347] A. Airapetian *et al.* (HERMES), Phys. Rev. **D76**, 092008 (2007), [arXiv:0704.3133].

[348] A. Moretti (COMPASS), PoS **SPIN2018**, 138 (2018), [arXiv:1901.01735].

[349] L. Gamberg *et al.*, Phys. Lett. B **818**, 136371 (2021), [arXiv:2102.05553].

[350] R. Seidl *et al.* (Belle), Phys. Rev. **D99**, 11, 112006 (2019), [arXiv:1902.01552].

[351] C. Adolph *et al.* (COMPASS), Eur. Phys. J. **C73**, 8, 2531 (2013), [Erratum: Eur. Phys. J.C75,no.2,94(2015)], [arXiv:1305.7317].

[352] A. Signori *et al.*, JHEP **11**, 194 (2013), [arXiv:1309.3507].

[353] M. Anselmino *et al.*, JHEP **04**, 005 (2014), [arXiv:1312.6261].

[354] M. G. Echevarria *et al.*, Phys. Rev. **D89**, 074013 (2014), [arXiv:1401.5078].

[355] M. G. Echevarria, I. Scimemi and A. Vladimirov, Phys. Rev. **D93**, 1, 011502 (2016), [Erratum: Phys. Rev.D94,no.9,099904(2016)], [arXiv:1509.06392].

[356] M. G. Echevarria, I. Scimemi and A. Vladimirov, JHEP **09**, 004 (2016), [arXiv:1604.07869].

[357] A. Bacchetta *et al.*, JHEP **06**, 081 (2017), [Erratum: JHEP06,051(2019)], [arXiv:1703.10157].

[358] M. A. Ebert, B. Mistlberger and G. Vita, JHEP **07**, 121 (2021), [arXiv:2012.07853].

[359] M.-x. Luo *et al.*, JHEP **06**, 115 (2021), [arXiv:2012.03256].

[360] J. C. Collins, Nucl. Phys. **B396**, 161 (1993), [hep-ph/9208213].

[361] J. P. Ralston and D. E. Soper, Nucl. Phys. **B152**, 109 (1979).

[362] H. Avakian *et al.* (CLAS), Phys. Rev. **D69**, 112004 (2004), [hep-ex/0301005].

[363] A. Airapetian *et al.* (HERMES), Phys. Rev. Lett. **84**, 4047 (2000), [hep-ex/9910062].

[364] A. Airapetian *et al.* (HERMES), Phys. Rev. **D64**, 097101 (2001), [hep-ex/0104005].

[365] A. Airapetian *et al.* (HERMES), Phys. Rev. Lett. **94**, 012002 (2005), [hep-ex/0408013].

[366] A. Airapetian *et al.* (HERMES), Phys. Lett. **B693**, 11 (2010), [arXiv:1006.4221].

[367] V. Yu. Alexakhin *et al.* (COMPASS), Phys. Rev. Lett. **94**, 202002 (2005), [hep-ex/0503002].

[368] E. S. Ageev *et al.* (COMPASS), Nucl. Phys. **B765**, 31 (2007), [hep-ex/0610068].

[369] M. Alekseev *et al.* (COMPASS), Phys. Lett. **B673**, 127 (2009), [arXiv:0802.2160].

[370] M. G. Alekseev *et al.* (COMPASS), Phys. Lett. **B692**, 240 (2010), [arXiv:1005.5609].

[371] M. G. Alekseev *et al.* (COMPASS), Eur. Phys. J. **C70**, 39 (2010), [arXiv:1007.1562].

[372] C. Adolph *et al.* (COMPASS), Phys. Lett. **B717**, 376 (2012), [arXiv:1205.5121].

[373] C. Adolph *et al.* (COMPASS), Phys. Lett. **B744**, 250 (2015), [arXiv:1408.4405].

[374] K. Abe *et al.* (Belle), Phys. Rev. Lett. **96**, 232002 (2006), [hep-ex/0507063].

[375] R. Seidl *et al.* (Belle), Phys. Rev. **D78**, 032011 (2008), [Erratum: Phys. Rev.D86,039905(2012)], [arXiv:0805.2975].

[376] J. P. Lees *et al.* (BaBar), Phys. Rev. **D90**, 5, 052003 (2014), [arXiv:1309.5278].

[377] J. P. Lees *et al.* (BaBar), Phys. Rev. **D92**, 11, 111101 (2015), [arXiv:1506.05864].

[378] M. Ablikim *et al.* (BESIII), Phys. Rev. Lett. **116**, 4, 042001 (2016), [arXiv:1507.06824].

[379] M. Anselmino *et al.*, Phys. Rev. **D92**, 11, 114023 (2015), [arXiv:1510.05389].

[380] Z.-B. Kang *et al.*, Phys. Rev. **D93**, 1, 014009 (2016), [arXiv:1505.05589].

[381] F. Yuan, Phys. Rev. Lett. **100**, 032003 (2008), [arXiv:0709.3272].

[382] Z.-B. Kang *et al.*, JHEP **11**, 068 (2017), [arXiv:1705.08443].

[383] K. Konishi, A. Ukawa and G. Veneziano, Phys. Lett. **78B**, 243 (1978).

[384] I. Vendramin, Nuovo Cim. **A66**, 339 (1981).

[385] J. C. Collins, S. F. Heppelmann and G. A. Ladinsky, Nucl. Phys. **B420**, 565 (1994), [hep-ph/9305309].

[386] R. L. Jaffe, X.-m. Jin and J. Tang, Phys. Rev. Lett. **80**, 1166 (1998), [hep-ph/9709322].

[387] R. L. Jaffe, X.-m. Jin and J.-a. Tang, Phys. Rev. **D57**, 5920 (1998), [hep-ph/9710561].

[388] A. Bianconi *et al.*, Phys. Rev. **D62**, 034008 (2000), [hep-ph/9907475].

[389] M. Radici, R. Jakob and A. Bianconi, Phys. Rev. **D65**, 074031 (2002), [hep-ph/0110252].

[390] D. de Florian and L. Vanni, Phys. Lett. **B578**, 139 (2004), [hep-ph/0310196].

[391] A. Bacchetta and M. Radici, Phys. Rev. **D67**, 094002 (2003), [hep-ph/0212300].

[392] A. Vossen *et al.* (Belle), Phys. Rev. Lett. **107**, 072004 (2011), [arXiv:1104.2425].

[393] A. Courtoy *et al.*, Phys. Rev. **D85**, 114023 (2012), [arXiv:1202.0323].

[394] M. Radici *et al.*, JHEP **05**, 123 (2015), [arXiv:1503.03495].

[395] A. Airapetian *et al.* (HERMES), JHEP **06**, 017 (2008), [arXiv:0803.2367].

[396] C. Adolph *et al.* (COMPASS), Phys. Lett. **B713**, 10 (2012), [arXiv:1202.6150].

[397] C. Adolph *et al.* (COMPASS), Phys. Lett. **B736**, 124 (2014), [arXiv:1401.7873].

[398] L. Adamczyk *et al.* (STAR), Phys. Rev. Lett. **115**, 242501 (2015), [arXiv:1504.00415].

[399] A. Bacchetta, A. Courtoy and M. Radici, Phys. Rev. Lett. **107**, 012001 (2011), [arXiv:1104.3855].

[400] A. Bacchetta, A. Courtoy and M. Radici, JHEP **03**, 119 (2013), [arXiv:1212.3568].

[401] M. Radici and A. Bacchetta, Phys. Rev. Lett. **120**, 19, 192001 (2018), [arXiv:1802.05212].

Int. J. Mod. Phys. A 2026.41. Downloaded from www.worldscientific.com by UNIVERSITY OF CALIFORNIA @ BERKELEY on 09/16/26. Re-use and distribution is strictly not permitted, except for Open Access articles.

20. High Energy Soft QCD and Diffraction

Revised August 2025 by V.A. Khoze (Durham U.), M.G. Ryskin (Petersburg Nuclear Phys. Inst.) and M. Taševský (Prague, Inst. Phys.).

20.1 Introduction

Despite the enormous successes of Quantum Chromodynamics (QCD) (see Section 9 in [1] and [2]) there remain a number of deep questions to be answered in the domain of strong interaction physics. These concern first of all small momentum transfer processes which are generically called soft interactions.

One of the most challenging problems is the high-energy behaviour of hadronic scattering processes. At high collision energies, $\sqrt{s}$, soft interactions play a dominant role. Unfortunately, soft interactions cannot be described in terms of perturbative QCD. These are non-perturbative phenomena related to confinement which are generally considered in the context of the analytic S-matrix, based on *first principles*, such as analyticity, crossing symmetry and unitarity of partial waves, see e.g. [3, 4]. At high energies the most self-consistent way to perform the calculations and to describe the data is the Regge approach (see for example [5–7]), which will be considered below. As discussed in Section 20.5, this formalism could be smoothly matched with perturbative QCD calculations at larger transverse momenta. Therefore, here we will concentrate on the properties of high energy soft interactions that can be expected from the extension of the perturbative QCD domain.

The main aim of this review is to present the well-established theoretical framework, based on Regge theory and QCD, used for describing high-energy collisions. A limited number of some new experimental results, mainly from the LHC, are shown in order to demonstrate that the gross features of the data are in agreement with this approach. We are not focussing on any particular phenomenological or Monte Carlo model, which are covered in the dedicated reviews and books, see e.g. Section 43 in [1], [2, 8–14] and Chapter 2 in [15].

Typically, in multiparticle production, the secondaries[1] fill the whole available rapidity interval.[2] However, there exists an important class of events in which a large interval of rapidity (typically at least 4 units) is devoid of any hadronic activity. Such an interval is called a Large Rapidity Gap (LRG). The most frequent case with a LRG is elastic scattering. There are also events in which one of the incoming protons (or both) is transformed (dissociates) into a set of two or more final state particles with the mass $M \ll \sqrt{s}$ and proton quantum number. All these events have properties similar to those of the well-known from optics pattern of diffraction of a beam of light on an obstacle. By analogy, in high-energy physics, the corresponding processes are usually called diffractive. The classic example is the elastic scattering of hadrons on nuclei (see e.g. [16]), which manifests an angular distribution with a series of minima and maxima, analogous to the diffraction of light on a black disk. At LHC energies diffractive processes constitute up to 40% of the total (pp) cross section, $\sigma_{\rm tot}$. Therefore, we will pay special attention to the description of the elastic scattering amplitude and proton diffractive dissociation. Diffraction dissociation can be considered as a quantum mechanical process caused by the fact that different components of the incoming hadron wave function have different probabilities for interaction with a target [17]. This feature allows us to probe the transverse size of the interaction region.

Note that besides being of a fundamental interest in their own right for understanding the high energy behaviour of the QCD amplitude, there are several reasons why it is important to study soft and diffractive processes. Firstly, soft interactions unavoidably give an underlying component to rare 'hard' events, from which we hope to extract signals for New Physics. Secondly, we should be able to estimate the probability that rapidity gaps, which occur in 'hard' diffractive events, survive rescattering effects, that is, survive the population of the gaps by the secondary particles from the underlying event. Thirdly, an understanding of diffractive processes is very important for evaluation of pile-up backgrounds in high-luminosity pp collisions, which have a direct impact on various experimental measurements. Pile-up corresponds to soft independent interactions in the same bunch crossing whose number rises with increasing instantaneous luminosity. And, finally, studies of diffractive processes should help in the understanding of the structure of high-energy cosmic ray cascades, which requires a very detailed knowledge of the spectra of particles carrying a large fraction x of the incoming momentum in proton-air and nucleus-air interactions, see for instance [18].

Experimentally, diffractive processes are selected using two distinct features:

1. large regions (typically at least $\Delta\eta > 4$) in the detector are devoid of hadronic activity (LRG) and/or
2. one or both incoming particles stay intact after collision and are registered by the dedicated forward detectors placed a few hundred meters from the interaction point. The momentum loss of the initial particle, $\xi = 1 - x$, is typically smaller than 0.15.

Thus, in the case of proton-proton collisions, diffractive events correspond to elastic $pp \to pp$ scattering and to $pp \to p + X$ (Single Dissociation, SD) and $pp \to X + Y$ (Double Dissociation, DD) processes, where the + sign denotes a large rapidity gap. Note that strictly speaking in high energy physics it is impossible to define (and select) rigorously purely diffractive events. We can always have some admixture of events of different origin. As a rule we call 'diffractive' the events with sufficiently large gap (with say $\Delta y > 4$, see above) and the vacuum quantum numbers transferred across the gap. Typically at the LHC the integrated cross sections of diffractive dissociation, $\sigma_{\rm SD}$, $\sigma_{\rm DD}$, are of the order of 5–10 mb depending on the gap size. Schematic diagrams of all discussed processes are shown in Fig. 20.1.

20.2 Regge pole approach

In pre-QCD times, in order to describe the behaviour of scattering amplitudes at high energy, $\sqrt{s}$, and small momentum-transfer squared, $-t$, Regge theory was developed and successfully applied in a wide range of energies. The Regge approach [5–7] is based on the singularities of amplitudes in the complex angular momentum, j, plane.

For instance, the measured $\pi^- p \to \pi^0 n$ amplitude behaves as

$$T_{\pi p}(s,t) \propto s^{\alpha_\rho(t)}, \tag{20.1}$$

where the process is described by the exchange of the ρ-trajectory, $j = \alpha_\rho(t) \simeq 0.5 + 0.9t$ (with $t = (p_{\pi^-} - p_{\pi^0})^2$ in GeV^2). This trajectory passes through the spin-1 ρ-meson resonance in the 'crossed' t-channel $\pi^-\pi^0 \to \bar{p}n$; that is, $\alpha_\rho(t = m_\rho^2) = 1$. The corresponding cross section decreases with increasing s.

On the other hand, high-energy total and elastic pp cross sections are observed to grow slowly with energy (see e.g. Section 53 in [1]) and in terms of Regge theory are dominated by the exchange of a trajectory with vacuum quantum numbers, $\sigma_{\rm tot} \propto s^{j-1}$. The simplest possibility is to assume that the rightmost singularity in the j-plane, which drives the high-energy behaviour of the cross section, is the leading (at $t \le 0$) Regge pole at $j = \alpha(t)$. Then the pp elastic amplitude reads

$$T_{\rm el}(s,t) \propto s^{\alpha_{\mathbb{P}}(t)} \ . \tag{20.2}$$

The total cross section can then be conveniently expressed using the so called optical theorem which states that

$$s\sigma_{\rm tot} = {\rm Im}T_{\rm el}(s, t = 0), \tag{20.3}$$

as illustrated in the upper part of Fig. 20.2, and thus

$$\sigma_{\rm tot} \propto s^{\alpha_{\mathbb{P}}(0)-1}. \tag{20.4}$$

[1] Here and in what follows, we call secondaries the new particles produced in the course of the interaction.

[2] For definition of particle rapidity (pseudorapidity), see Section 49.5.2 in [1]; $y = \frac{1}{2}\ln\frac{E+p_z}{E-p_z}$ ($\eta = -\ln(\tan(\theta/2))$; the correct variable is the rapidity y, however, experimentally it is simpler to use the pseudorapidity η which does not require identifying the particles, setting $m = 0$. For $p_T \gg m$, $\eta \simeq y$.

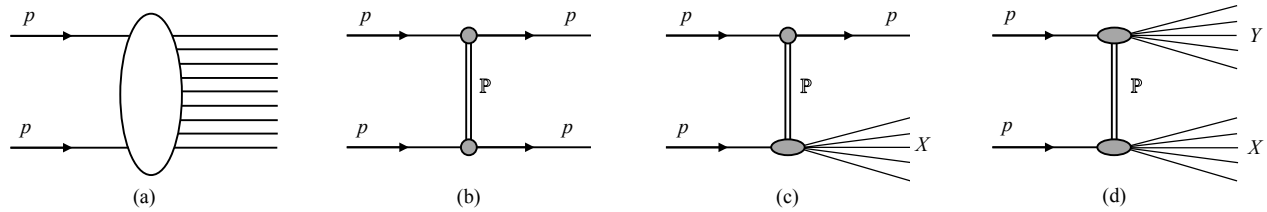

Figure 20.1: Schematic diagrams of soft pp processes. (a) non-diffractive processes, (b) elastic scattering, (c) single dissociation and (d) double dissociation. The double line corresponds to the Pomeron exchange.

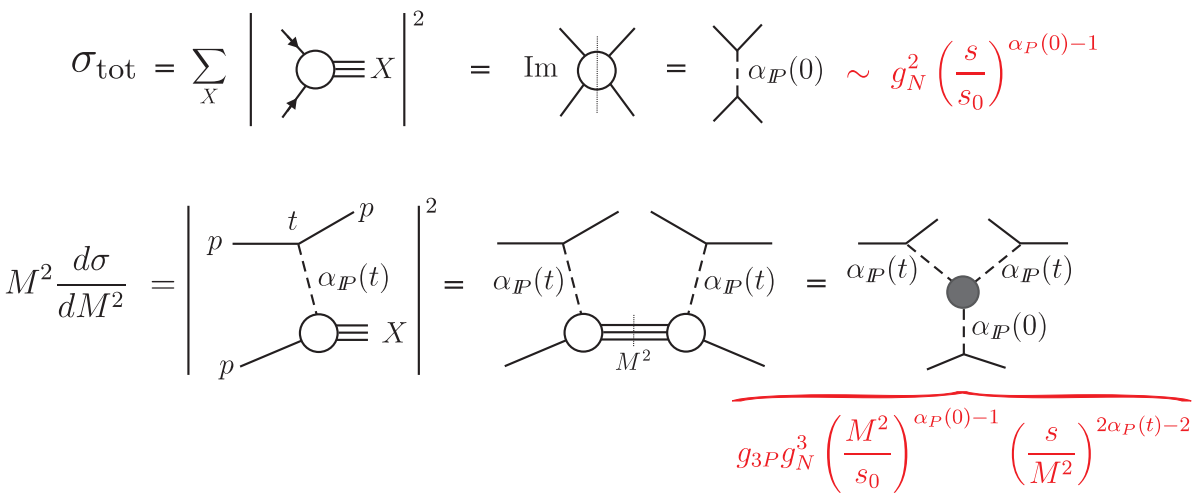

Figure 20.2: Illustration of the optical theorem for the total cross section and for high-mass diffractive dissociation in the absence of absorptive corrections.

The pole with the largest intercept, originally assumed to be $\alpha_{\mathbb{P}}(0) = 1$ since high-energy total cross sections were thought to have a constant asymptotic behaviour, is called the *Pomeron*[3]

Prior to the LHC, the energy behaviour of $pp, p\bar{p}, \pi p, Kp$ cross sections was satisfactorily reproduced by the sum of the Pomeron and secondary Reggeons (the poles at lower values of j, typically with $\alpha_\rho(0) \simeq 0.5$, see [22, 23] and Section 51 in [24]). However, above Tevatron energies the secondary Reggeon contributions (which all have intercepts $\alpha(0) \simeq 0.5$) are highly suppressed, which enables us to study the properties of the Pomeron only.

A popular parameterization of the elastic pp-scattering amplitude by Donnachie-Landshoff (DL) is the Regge form [25]

$$T_{\rm el}(s,t) = \eta_P \sigma_0 F_1^2(t) s^{\alpha_{\mathbb{P}}(t)}, \tag{20.5}$$

where $\sigma_0 = 21.7$ mb [26] and η_P is the signature factor

$$\eta_P = \frac{1 + \exp(-i\pi\alpha_{\mathbb{P}}(t))}{\sin(-\pi\alpha_{\mathbb{P}}(t))}, \tag{20.6}$$

F_1 is the Dirac electromagnetic form factor of the proton and the *effective* Pomeron trajectory

$$\alpha_{\mathbb{P}}(t) = 1 + \Delta + \alpha' t \;\simeq\; 1 + 0.0808 + 0.25t, \tag{20.7}$$

with t given in GeV^2. The intercept $\alpha_{\mathbb{P}}(0)$ just above 1 reproduces the observed slow growth of the total hadron-hadron cross sections at high energies.

However, this simple parameterization is becoming increasingly deficient at higher energies. This is because due to unitarity we have to take into account not only Regge poles, but also the cuts in the j-plane [27, 28], which correspond to the multiple exchange of Regge poles in the t-channel, see for instance [29–31]. A powerful technique to evaluate Reggeon diagrams was developed by Gribov [7, 32] (Reggeon calculus or Reggeon Field Theory (RFT)), which allows us to calculate the multi-Pomeron contributions.

[3]Pomeron pole was named after I. Y. Pomeranchuk. The history of the Pomeron is discussed in [19–21].

20.3 Theoretical description of high-energy diffraction

Diffractive processes (see e.g. reviews [33–37]) represent a rich testing ground for the dynamics of soft interactions as well as Monte Carlo models for soft hadron-hadron physics (see for reviews e.g. [8], Section 43 in [1] and Chapter 2 in [15]).

There is no universally agreed definition of diffractive processes. Theoretically, diffraction is the effect caused by the absorption of the incoming plane-wave in some region of impact parameter, b. After a decomposition of the distorted plane-wave over the outgoing momentum, q, due to absorption we arrive at some set of plane-waves with non-zero transverse momentum, $q_t \neq 0$. Experimentally, we call diffractive the events with large rapidity gaps (LRG) in the distribution of the final state particles. However, this definition is appropriate only for the events with very large gap sizes ($\Delta\eta > 4 - 5$); otherwise gaps can also be caused by fluctuations in the hadronization process [38].

In the case of proton-proton collisions, diffraction corresponds to elastic $pp \to pp$ scattering and to the $pp \to p + X$ and $pp \to X_1 + X_2$ processes where one or both protons are allowed to dissociate into a system X with the quantum numbers of the proton. The $p \to X$ dissociation is caused by the fact that the individual components of the incoming proton wave function interact differently with the target (see Section 20.3.1).

Theoretically, high-energy diffraction may be studied from either the s-channel or the t-channel viewpoint.

20.3.1 *Diffraction from the s-channel viewpoint*

Unitarity plays a central role in diffractive processes. To discuss unitarity effects it is convenient to work in terms of impact parameter, b. The total cross section is closely related to the elastic scattering amplitude and the scattering into inelastic final states via the s-channel unitarity of the S-matrix (see Sections 50 and 53 in [1]), $SS^\dagger = I$, or

$$disc\ T \equiv T - T^\dagger = iT^\dagger T \tag{20.8}$$

Int. J. Mod. Phys. A 2026.41. Downloaded from www.worldscientific.com by UNIVERSITY OF CALIFORNIA @ BERKELEY on 09/16/26. Re-use and distribution is [redacted] except for Open Access articles.

Int. J. Mod. Phys. A 2026.41. Downloaded from www.worldscientific.com
by UNIVERSITY OF CALIFORNIA @ BERKELEY on 09/16/26. Re-use and distribution is strictly not permitted, except for Open Access articles.

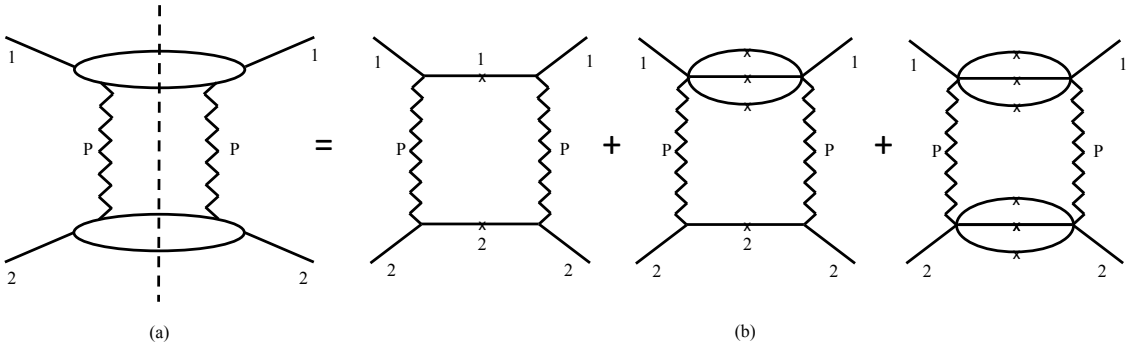

Figure 20.3: Two-Pomeron exchange in the t channel expressed as a sum over all diffractive intermediate states in the s-channel. The crosses indicate that the particles are on the mass shell.

with $S = I + iT$. If we were to focus, for example, on the unitarity for elastic and quasielastic processes, then *disc* T would simply denote a cut in s-channel between incoming and outgoing particles as visualized by crosses in Fig. 20.3.

At high energies, the s-channel unitarity relation is diagonal in the b basis such that

$$2\mathrm{Im}\, T_{\mathrm{el}}(s,b) = |T_{\mathrm{el}}(s,b)|^2 + G_{\mathrm{inel}}(s,b) \tag{20.9}$$

with

$$\sigma_{\mathrm{tot}} = 2\int d^2b\, \mathrm{Im}\, T_{\mathrm{el}}(s,b) \tag{20.10}$$

$$\sigma_{\mathrm{el}} = \int d^2b\, |T_{\mathrm{el}}(s,b)|^2 \tag{20.11}$$

$$\sigma_{\mathrm{inel}} = \int d^2b\, \left[2\mathrm{Im}\, T_{\mathrm{el}}(s,b) - |T_{\mathrm{el}}(s,b)|^2\right]. \tag{20.12}$$

The general solution of Eq. (20.9) is

$$T_{\mathrm{el}}(b) \;=\; i(1 - e^{-\Omega(b)/2}) \tag{20.13}$$

and

$$G_{\mathrm{inel}}(s,b) = 1 - \mathrm{e}^{-\mathrm{Re}\Omega(b)} = 1 - P_{\mathrm{nointer}}(s,b), \tag{20.14}$$

where G_{inel} is the sum over all inelastic intermediate states and P_{nointer} is a probability to have no inelastic interactions. $G_{\mathrm{inel}}(s,b)$ describes the b-profile of inelastic particle collisions. It satisfies the condition $0 \le G_{\mathrm{inel}} \le 1$ and determines how absorptive the interaction region is at a given impact parameter (with $G_{\mathrm{inel}}= 1$ for full absorption and $G_{\mathrm{inel}}= 0$ for the complete dominance of elastic scattering). As seen from Eq. (20.14), $\exp(-\mathrm{Re}\Omega(s,b))$ is the probability that no inelastic interactions occur at impact parameter b. Ω ($\mathrm{Re}\Omega \ge 0$) is called the opacity (optical density) or eikonal. The quantity

$$S^2(b) \equiv e^{-\mathrm{Re}\Omega(b)} \;=\; P_{\mathrm{nointer}}(b) \tag{20.15}$$

is the so-called survival factor, which enables us to calculate the probability that the LRG survives soft rescattering.

In terms of the opacity the elastic cross section takes the form

$$\frac{\mathrm{d}\sigma_{\mathrm{el}}}{\mathrm{d}t} = \frac{1}{16\pi s^2}\,|T_{\mathrm{el}}(s,t)|^2 = \frac{1}{4\pi}\left|\int \mathrm{d}^2b\; e^{i\vec{q}_t\cdot\vec{b}}(1 - e^{-\Omega(b)/2})\right|^2$$
$$= \pi\left|\int b\mathrm{d}b\; J_0(q_t b)(1 - e^{-\Omega(b)/2})\right|^2, \tag{20.16}$$

where $q_t = \sqrt{|t|}$ and J_0 is the zeroth-order Bessel function.

To describe the elastic scattering at one fixed energy we can always find an appropriate parameterization for the opacity $\Omega(b)$ and tune the parameters to reproduce the observed $\mathrm{d}\sigma_{\mathrm{el}}/\mathrm{d}t$ cross section. Moreover, we can fix the form of the parameterization, but choose, at each particular energy, the corresponding values of parameters; see, e.g. [39]. Alternatively, we may simply take the Fourier-Bessel transform from the experimental data [33, 40, 41]

$$\mathrm{Im}T_{\mathrm{el}}(b) \;=\; \int \frac{q_t \mathrm{d}q_t}{4\pi}\sqrt{\frac{\mathrm{d}\sigma_{\mathrm{el}}}{\mathrm{d}t}\,\frac{16\pi}{1+\rho^2}}\; J_0(q_t b), \tag{20.17}$$

where the square root represents $\mathrm{Im}T_{\mathrm{el}}(q_t)$, with $\rho \equiv \mathrm{Re}T_{\mathrm{el}}/\mathrm{Im}T_{\mathrm{el}}$. In this way, we first determine T_{el} from the data for $\mathrm{d}\sigma_{\mathrm{el}}/\mathrm{d}t$, and then calculate $\Omega(b)$ using Eq. (20.13), assuming in accordance with data that ρ is small (or $\rho(t) =$ constant).

At high energies $\rho^2 \ll 1$, which is usually well justified except in the diffractive dip region (see Section 20.3.3.1 for discussion of the dip region).

The value of ρ can be derived via the dispersion relation, see [3]:

$$\frac{1}{s}\mathrm{Re}T_{\mathrm{el}}(s) \;=\; \frac{1}{\pi}\int_{-\infty}^{+\infty}\frac{\mathrm{d}s'}{s'-s}\sigma_{\mathrm{tot}}(|s'|) \;=\; \frac{1}{\pi}\int_0^{\infty}\sigma_{\mathrm{tot}}(s')\frac{2s\mathrm{d}s'}{s'^2 - s^2}. \tag{20.18}$$

Since we consider just the charge-parity C-even amplitude, here for negative s' we put $\sigma_{p\bar{p}} = \sigma_{pp}$. That is, for negative s', which corresponds to the interaction with an *anti*particle, we use the same $\sigma_{pp}(|s'|)$. The major contribution comes from $s' \simeq s$. Thus, with a good accuracy we can evaluate $\rho(t = 0)$ as

$$\rho \;\simeq\; \frac{\pi}{2}\,\frac{\partial \ln \sigma_{\mathrm{tot}}(s)}{\partial \ln s}. \tag{20.19}$$

20.3.2 *Diffractive dissociation*

The elastic cross section probes the optical density of the proton. The well known example of scattering on a black disk, with $G_{\mathrm{inel}} = 1$ for $b < R$, gives $\sigma_{\mathrm{el}} = \sigma_{\mathrm{inel}} = \pi R^2$ and $\sigma_{\mathrm{tot}} = 2\pi R^2$. In general, the absorption of the initial wave (due to inelastic channels) leads, via s-channel unitarity, to elastic scattering.

Inelastic diffraction (i.e. proton dissociation) is a consequence of the *internal structure* of hadrons. This can be conveniently described at high energies, where the lifetimes of each particular Fock component of the incoming hadron/proton wave function (the hadronic fluctuations) are large, $\tau \sim E/m^2$, and during these time intervals the corresponding Fock states can be considered as 'frozen'. Each hadronic constituent can undergo a scattering with its own probability and thus destroys coherence of the fluctuations[4]. As a result, the outgoing superposition of states will be different from the incident particle, and will most likely contain multiparticle states, so we will have *inelastic*, as well as elastic scattering.

To calculate diffractive dissociation we can enlarge the set of intermediate states (p, N_a^*), from just the single elastic channel, and introduce a multichannel eikonal. However, it is more convenient

[4] At high energies the configurations with different transverse separation, r, between the quarks (valence partons) can serve as an example of such Fock states. An interaction with the QCD Pomeron does not change the value of r, while the cross section $\sigma \propto \alpha_s^2 \cdot r^2$ (see Section 20.4.2 and [42–44]).

Int. J. Mod. Phys. A 2026.41. Downloaded from www.wo
by UNIVERSITY OF CALIFORNIA @ BERKELEY on 09/16/26. Re-use and distribution is
except for Open Access articles.

to follow Good and Walker [45], and to introduce states ϕ_k diagonalising the T matrix (which e.g. in the proton case describes different $p \to N^*$, $N_a^* \to N_b^*$ transitions). Such eigenstates only undergo elastic scattering. Since there are no off-diagonal transitions,

$$\langle \phi_i | T | \phi_k \rangle = 0 \qquad \text{for } i \neq k, \tag{20.20}$$

a state k cannot diffractively dissociate into a state $j \neq k$. Working in terms of the Good-Walker eigenstates ϕ_i, we have a simple one-channel eikonal for each state. We denote the orthogonal matrix which diagonalizes T by a, so that

$$T \;=\; aFa^T \qquad \text{with} \qquad \langle \phi_i | F | \phi_k \rangle \;=\; F_k\, \delta_{ik}, \tag{20.21}$$

where F_k is the probability amplitude of the hadronic process proceeding via the diffractive eigenstate ϕ_k.

Now consider the diffractive dissociation of an incoming state $|h\rangle$. We can write

$$|h\rangle \;=\; \sum_k a_{hk}\, |\phi_k\rangle. \tag{20.22}$$

The elastic scattering amplitude satisfies

$$\langle h | T | h \rangle \;=\; \sum_k |a_{hk}|^2\, F_k \;=\; \langle F \rangle, \tag{20.23}$$

where $F_k \equiv \langle \phi_k | F | \phi_k \rangle$ and where the brackets of $\langle F \rangle$ mean that we take the average of F over the initial probability distribution of diffractive eigenstates. After the diffractive scattering described by T_{fh}, the final state $|f\rangle$ will, in general, be a different superposition of eigenstates from that of $|h\rangle$, which was shown in Eq. (20.22). Neglecting the real parts, for the cross sections at a given impact parameter b, we have

$$\begin{aligned}
\frac{\mathrm{d}\sigma_{\mathrm{tot}}}{\mathrm{d}^2 b} &= 2\,\mathrm{Im}\langle h|T|h\rangle \;=\; 2\sum_k |a_{hk}|^2\, \mathrm{Im} F_k \;=\; 2\langle \mathrm{Im} F\rangle \\
\frac{\mathrm{d}\sigma_{\mathrm{el}}}{\mathrm{d}^2 b} &= |\langle h|T|h\rangle|^2 \;=\; \left| \sum_k |a_{hk}|^2\, F_k \right|^2 \;=\; \langle |F| \rangle^2 \\
\frac{\mathrm{d}\sigma_{\mathrm{el\,+\,SD}}}{\mathrm{d}^2 b} &= \sum_k |\langle \phi_k|T|h\rangle|^2 \;=\; \sum_k |a_{hk}|^2\, |F_k^2| \;=\; \langle |F^2| \rangle.
\end{aligned} \tag{20.24}$$

It follows that the cross section for the single diffractive dissociation of a proton,

$$\frac{\mathrm{d}\sigma_{\mathrm{SD}}}{\mathrm{d}^2 b} \;=\; \langle |F^2| \rangle \;-\; \langle |F| \rangle^2, \tag{20.25}$$

is given by the statistical dispersion in the absorption probabilities of the diffractive eigenstates. Here the average is taken over the components k of the incoming proton which dissociates. If the averages are taken over the components of both of the incoming particles, then Eq. (20.25) is the sum of the cross sections for single and double dissociation, see Fig. 20.3.

Note that if all the components ϕ_k of the incoming proton $|h\rangle$ were absorbed equally, then the diffracted superposition would be proportional to the incident one and the probability of the inelastic diffraction would be zero. Thus if, at very high energies, the amplitudes F_k at small impact parameters are equal to the black disk limit, $F_k = i$, then diffractive production will be equal to zero in this impact parameter domain, and so will only occur in the peripheral b region where the edge of the disk becomes not completely black. Hence the impact parameter structure of diffractive dissociation and elastic scattering is drastically different in the presence of absorptive s-channel unitarity effects (see the G_{inel} term in Eq. (20.9)). Under the assumption that amplitudes F_k at high energies cannot exceed the black disk limit, $\mathrm{Im}\, F_k \leq 1$, equations 20.24 lead to the following bound

$$\frac{\mathrm{d}\sigma_{\mathrm{el\,+\,SD_1+SD_2+DD}}}{\mathrm{d}^2 b} \leq \frac{1}{2}\frac{\mathrm{d}\sigma_{\mathrm{tot}}}{\mathrm{d}^2 b}\,. \tag{20.26}$$

known as the Pumplin bound [46] [5].

20.3.3 *Diffraction from the t-channel viewpoint*

The t-channel approach is based on the Regge model (see Section 20.2), where high-energy diffractive processes are mediated by the exchange of a Pomeron ($\mathbb{P}$). In the case of the elastic pp-scattering amplitude in the eikonal model (see Eq. (20.13)), the opacity corresponding to the exchange of one Pomeron is

$$\Omega(s,b) = \int \frac{\mathrm{d}^2 q_t}{4\pi^2}\; \Omega(s,q_t)\; e^{i\vec{q}_t\cdot\vec{b}} \tag{20.27}$$

with

$$\Omega(s,q_t) = \frac{1}{s} T'_{\mathrm{el}} = -i\eta_P(t) g_N(t) g_N(t) \left(\frac{s}{s_0}\right)^{\alpha_{\mathbb{P}}(t)-1}, \tag{20.28}$$

where T'_{el} is the two-particle s-channel irreducible elastic amplitude, cf. Eq. (20.5), and $g_N(t)$ is the proton-Pomeron coupling.

If we assume an exponential t-dependence of the coupling, $g_N(t) = g_N(0)\exp(B_0 t)$, and neglect the Pomeron phase, then the opacity is

$$\Omega(s,q_t) = g_N(0) g_N(0) \left(\frac{s}{s_0}\right)^{\alpha_{\mathbb{P}}(0)-1} e^{Bt}, \tag{20.29}$$

with the t-slope given by

$$B \;=\; 2B_0 + \alpha'_{\mathbb{P}} \ln\left(\frac{s}{s_0}\right). \tag{20.30}$$

At high energies the opacity has a Gaussian form in the b-space:

$$\Omega(s,b) = \frac{g_N^2(0)}{4\pi B} \left(\frac{s}{s_0}\right)^{\alpha_{\mathbb{P}}(0)-1} e^{-b^2/4B}\,. \tag{20.31}$$

In terms of opacity the effective radius of interaction increases at high energies as $\sqrt{\alpha'_{\mathbb{P}} \ln(s/s_0)}$. This means that with energy increasing the differential cross section becomes steeper (the so called *shrinkage* of the diffractive peak).

If we were to take for the Pomeron the DL parametrisation [25, 26], that is to keep just the first, $T(b) = \Omega(b)/2$, term in the elastic amplitude (Eq. (20.13)) then, at LHC energies, the Gaussian would exceed the black disk limit at small b. However, the eikonal unitarization reduces the power growth of the one-Pomeron exchange cross section. Thus, in Eq. (20.31) $\Omega(s,b) \propto (s/s_0)^{\alpha_{\mathbb{P}}-1}$ gives an amplitude $\mathrm{Im}\; T_{\mathrm{el}}(s,b) = 1 - e^{-\Omega/2} < 1$. Hence the total cross section is limited by the size of the effective interaction area $\sigma_{\mathrm{tot}} < 2\pi R^2$, where the interaction radius R can be estimated from Eq. (20.31) as the value of b where $\mathrm{Re}\Omega(b)$ becomes ~ 1.

For the parameterization of Eq. (20.31) the corresponding radius grows at very large energies as

$$b^2 = R^2 = 4B \ln\left[\frac{g_N^2(0)}{4\pi B}\left(\frac{s}{s_0}\right)^{\alpha_{\mathbb{P}}(0)-1}\right] \simeq 4\Delta\alpha'_{\mathbb{P}} \ln^2(s/s_0)\,. \tag{20.32}$$

That is for $\Delta = 0.1$ and $\alpha'_{\mathbb{P}}$=0.25 GeV^{-2} we may expect that the cross section increases as

$$\sigma_{\mathrm{tot}} = 2\pi R^2 \simeq c \cdot \ln^2 s\,, \tag{20.33}$$

with $c = 8\pi\Delta\alpha'_{\mathbb{P}} = 0.24$ mb. This value is close to that obtained by the COMPETE parameterization ($c = 0.27$ mb [22, 24]) but much smaller than the Froissart-Lukaszuk-Martin (FLM) bound [47–49]. With $c^{\mathrm{FLM}} = \pi/m_\pi^2 \simeq 60$ mb, see Section 20.7,

$$\sigma_{\mathrm{tot}} \leq \frac{\pi}{m_\pi^2} \ln^2\left(\frac{s}{s_0}\right). \tag{20.34}$$

[5] Strictly speaking the proof of the Pumplin bound is justified only for low mass dissociation. When the masses $M_{1,2}$ become so large (say, $M_i^2 > \sqrt{ss_0}$) that the Good-Walker states $|\phi_i\rangle$, corresponding to two incoming protons overlap, we may face double counting. Therefore, the high mass dissociation will be considered in the next Section, in terms of the multi-Pomeron diagram. Here and in what follows s_0 is a constant which should be defined for a particular theoretical model or fitted from experiment.

Int. J. Mod. Phys. A 2026.41. Downloaded from www.worldscientific.com
by UNIVERSITY OF CALIFORNIA @ BERKELEY on 09/16/26. Re-use and distribution is strictly not permitted, except for Open Access articles.

The fact that c =(0.24–0.27) mb $\ll c^{\rm FLM} = 60$ mb demonstrates that even at the LHC we are very far from true high-energy asymptotics [6], and the observed growth of the cross section is driven by the interactions at relatively large transverse momenta $k_t \gg m_\pi$ rather than the smallest hadron mass m_π in the denominator of Eq. (20.34).

20.3.3.1 *The t-slope and dip in the elastic cross section*

We first start with a relatively small one-Pomeron amplitude and consider the two-Pomeron contribution corresponding to the Ω^2 term in the expansion of the eikonal $1-\exp(-\Omega/2)$. In this term the momentum transferred, $q_t = \sqrt{|t|}$, is divided between the two Pomerons so that each Pomeron carries about a momentum $q_t/2$. Correspondingly, the t dependence of the whole 'two-Pomeron' amplitude will be $\exp(2B(t/4)) = \exp(Bt/2)$ [7].

Since the two-Pomeron contribution has an opposite sign in comparison with the one-Pomeron exchange, their interference will result in the appearance of the first diffractive minimum which moves to smaller $|t|$ with energy increasing. Such interference effects are largely responsible for the zero in the imaginary part of the amplitude (with the minimum filled by the real part).

It is worth mentioning that the one-channel eikonal discussed so far is a rather oversimplified approximation. It provides some indications about the behaviour we may expect for the elastic cross section, but clearly it does not give the whole story. Moreover, even within the framework of the one-channel eikonal, the expectation for the elastic slope t-dependence could be masked by other effects. Firstly, there is no reason why the t-dependence of the proton-Pomeron coupling $g_N(t)$ has to be a pure exponent. Next, there exists a two-pion singularity at $t = 4m_\pi^2$ (close to the physical region) in the Pomeron trajectory which generates some curvature in the behaviour of $\mathrm{d}\sigma_{\rm el}/\mathrm{d}t$ [50–52]. So there may be some compensation between the effects caused by the eikonal (arising from the interference between the different multi-Pomeron contributions), and the curvatures coming from the form of the proton-Pomeron coupling and the two-pion singularity of the Pomeron trajectory. However, an exact compensation looks quite non-trivial and a *pure* exponential behaviour of $\mathrm{d}\sigma_{\rm el}/\mathrm{d}t$ looks highly unlikely.

Indeed, the measurements by the TOTEM collaboration at 8 TeV [53] and at 13 TeV [54] clearly demonstrate that the local slope of the elastic pp cross section,

$$B = \mathrm{d}[\ln(\mathrm{d}\sigma_{\rm el}/\mathrm{d}t)]/\mathrm{d}t, \tag{20.35}$$

at $-t \lesssim 0.3$ GeV^2 varies with t.

20.3.3.2 *High mass dissociation*

Let us turn to inelastic diffractive processes that is, to single and double proton dissociations, $pp \to X+p$ and $pp \to X_1+X_2$, where the + sign denotes the presence of a LRG in the distribution of final state particles. For example, for the diffractive dissociation of a proton into a system of mass M, the rapidity gap between the incoming proton and the remaining hadrons is

$$\Delta y = \ln\left(\frac{s}{M^2}\right) = \ln\left(\frac{1}{\xi}\right), \tag{20.36}$$

where $\xi = 1-x$ and x is the initial momentum fraction (Feynman variable) carried by the outgoing proton. The masses, M, of the diffractively excited states, produced in high $\sqrt{s}$ collisions, can be large. To separate dissociation from the common inelastic process, usually the condition $M^2 \ll s$ is imposed.

The simplest multi-Pomeron diagram used to describe the diffractive dissociation is the so-called triple-Pomeron graph, shown at the end of Fig. 20.2.

In the Regge pole model, the cross section for the inclusive single diffractive (SD) dissociation process [55–57] can be written in the form (see Fig. 20.2)

$$\frac{\xi \mathrm{d}\sigma_{\rm SD}}{\mathrm{d}t\mathrm{d}\xi} = \frac{M^2 \mathrm{d}\sigma_{\rm SD}}{\mathrm{d}t\mathrm{d}M^2} = \frac{g_{3\mathbb{P}}(t) g_N(0) g_N^2(t)}{16\pi^2} \left(\frac{s}{M^2}\right)^{2\alpha_{\mathbb{P}}(t)-2} \left(\frac{M^2}{s_0}\right)^{\alpha_{\mathbb{P}}(0)-1}, \tag{20.37}$$

where $g_{3\mathbb{P}}(t)$ is the triple-Pomeron coupling. The value of the coupling $g_{3\mathbb{P}}$ is usually obtained from a triple-Regge analysis of lower energy data (see e.g. [34]) .

In an analogous way the cross section for double dissociation reads

$$\frac{\xi_1\xi_2 \mathrm{d}\sigma_{\rm DD}}{\mathrm{d}t\mathrm{d}\xi_1\xi_2} = \frac{M_1^2 M_2^2 \mathrm{d}\sigma_{\rm DD}}{\mathrm{d}t\mathrm{d}M_1^2\mathrm{d}M_2^2} = \frac{g_{3\mathbb{P}}^2(t) g_N^2(0)}{16\pi^3} \left(\frac{s s_0}{M_1^2 M_2^2}\right)^{2\alpha_{\mathbb{P}}(t)-2} \left(\frac{M_1^2 M_2^2}{s_0^2}\right)^{\alpha_{\mathbb{P}}(0)-1}, \tag{20.38}$$

where t is the momentum squared transferred through the LRG. As discussed in Section 20.5, from a microscopic point of view the

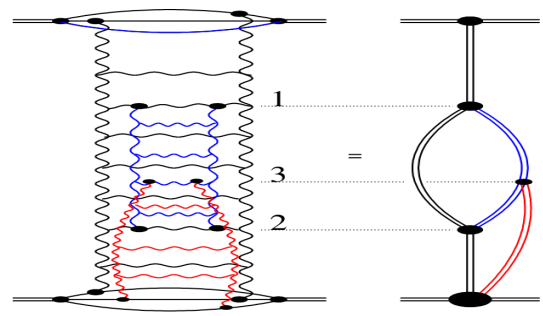

Figure 20.4: Pomeron exchange with schematic diagrams for the enhanced and semi-enhanced exchanges.

Pomeron exchange is described by a set of ladder-type diagrams (see [58–60]), which can lead to a rescattering of the intermediate partons (produced inside this ladder during the evolution), see Fig. 20.4. The left plot shows the Pomeron exchange complemented with the rescattering of partons 1 and 2 and the scattering of a parton 3 on the target. In terms of multi-Pomeron exchanges this corresponds to the diagram on the right hand side, where the Pomeron exchange is shown by the double line of a corresponding colour. The blue one is called "enhanced" (its contribution is integrated over the rapidities of both upper and lower vertices, i.e. of partons 1 and 2). The loop formed by the Pomerons shown in red is called "semi-enhanced" (it is integrated over the rapidity of one intermediate parton).

While the rescattering of the incoming hadron (proton) is already embedded in the eikonal formula (Eq. (20.13)), the rescattering of the intermediate partons in RFT is accounted for by the so-called enhanced diagrams [8] with multi-Pomeron vertices, g_m^n, which couple m to n Pomerons. It is quite a challenging task to resum all the enhanced diagrams, however this was successfully performed within the framework of the QGSJET Monte Carlo [61]. An elegant approach to sum up all enhanced diagrams in the case when each extra effective Pomeron contribution is very large was proposed in [62], assuming the analyticity of the g_m^n vertices in n and m in the right half of the complex n- and m-planes. The resulting amplitude becomes a black disk.

The simplest triple-Pomeron vertex $g_2^1 = g_{3\mathbb{P}}$ produces the first multi-Pomeron graph considered above (see the end of Fig. 20.2). However, numerically the multi-Pomeron vertices are relatively small. Note also that the value of $g_{3\mathbb{P}}$, determined from the fit to

[6] As usual, we assume s_0= 1 GeV^2, but the qualitative conclusion does not depend on any realistic choice of s_0.

[7] The two-Pomeron contribution has a factor of two smaller t-slope, and in terms of the impact parameter, the $\Omega^2(b)$ term is concentrated in the domain of a smaller radius. In such a simplified picture, the impact parameters corresponding to an exchange of n Pomerons will rapidly decrease with n increasing.

[8] This contribution is *enhanced* due to the large parton multiplicity.

Int. J. Mod. Phys. A 2026.41. Downloaded from www.wo
by UNIVERSITY OF CALIFORNIA @ BERKELEY on 09/16/26. Re-use and distribution is
except for Open Access articles.

experimental data (e.g. [63]), is actually an effective vertex with coupling

$$g_{\rm eff} \;=\; g_{3\mathbb{P}}\,\langle S^2\rangle, \tag{20.39}$$

which already includes the survival factor $S^2(b)$, see Eq. (20.15).

Since the opacity Ω increases with energy, at large Ω the number of multiple interactions grows as $N \propto \Omega$, leading to a smaller S^2. An explicit analysis [64] accounting for the survival effects gives a coupling $g_{3\mathbb{P}}$ about a factor of 3 larger than $g_{\rm eff}$, namely $g_{3\mathbb{P}} \simeq 0.2 g_N$.

Recall that the Pomeron exchange simultaneously describes both the elastic scattering amplitude, $T_{\rm el}$, and the multiparticle production cross section, $G_{\rm inel}$. The discontinuity (*disc* $T_{\rm el}$) of the ladder diagram corresponds to the production of secondary particles, practically homogeneously distributed over the whole available rapidity interval covered by the Pomeron, as illustrated by the right-hand diagram in Fig. 20.5.

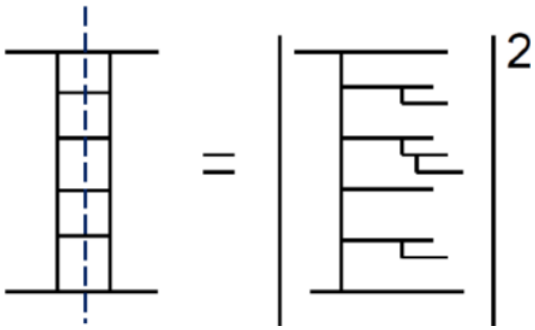

Figure 20.5: Cut Pomeron contribution to the inelastic cross section.

For the one-Pomeron case this discontinuity is called the "cut Pomeron". Correspondingly each multi-Pomeron diagram describes a series of different processes. Cutting k Pomerons in the diagram with n Pomerons we get the inelastic interaction with the multiplicity (density of secondaries) k times larger than that, N_0, produced by one cut Pomeron, $\mathrm{d}N/\mathrm{d}y = k \cdot N_0$. The remaining $n-k$ (elastic) Pomerons account for the absorptive corrections to the subprocess with k cut Pomerons. Indeed, the contribution of the diagram with n Pomerons includes also the processes with larger, $(k+i)\cdot N_0$ multiplicities (cut Pomerons), where $(i = 1, 2, ..., n-k)$. Absorptive corrections, described by the remaining elastic Pomerons, play a role of the survival factor S^2 for the process with the fixed particle density $k \cdot N_0$. They ensure probability conservation (the sum of the probabilities of all possible different channels is equal to one) and restore unitarity. Note that the multi-Pomeron diagrams represent all possible interactions between partons from the protons and partons from the Pomerons. In the case of Monte Carlo generators, the non-enhanced multi-Pomeron contributions are included in terms of the multiple parton interaction (MPI) option, see [13,65] and Section 7.2 in [2]. However, as a rule, this option accounts mainly for the multiple interactions between the partons from the protons (incoming hadrons). The energy-momentum sharing between the various inelastic rescattering processes (including the cut and uncut Pomerons) was performed at the amplitude level within the EPOS Monte Carlo [66].

20.3.3.3 *AGK cutting rules*

The relation between the cross sections of subprocesses with a different number of cut Pomerons within a given diagram with n Pomerons) is given by the AGK (Abramovsky-Gribov-Kancheli [67]) cutting rules. These rules include also the cut *between* the Pomerons with $k = 0$ which corresponds to the contribution of the particular diagram to the elastic cross section. By applying these rules, it is possible to show the self-consistency of the approach, which was lacking in the pure Regge-pole model.

Consider a diagram where the elastic scattering amplitude is mediated by an exchange of n Pomerons. The AGK cutting rules specify the coefficients c_n^k arising when k of these Pomerons are cut. Recall that the Pomeron cut discontinuities give the corresponding inelastic contributions to $\sigma_{\rm tot}$. The terms with $k = 0$ correspond to the diffractive cutting of the diagram (that is, the cut is between the Pomeron exchanges, and not through the Pomerons themselves), while the terms with $k = 1, 2, ...$ describe the processes with k cut Pomerons. The coefficients $c_n^k = \sigma_n^k / |\sigma_{\rm tot}^{(n)}|$ are [9]

$$c_n^{k=0} = (-1)^n (2^{n-1} - 1), \qquad c_n^{k\neq 0} \;=\; (-2)^{n-1}\,\frac{(-1)^{k-1} n!}{k!(n-k)!} \tag{20.40}$$

where $\sigma_{\rm tot}^{(n)}$ denotes the contribution of the n-Pomeron diagram to the total cross section. Note the alternating sign of $\sigma_{\rm tot}^{(n)}$ expressed as $(-1)^{n-1}$.

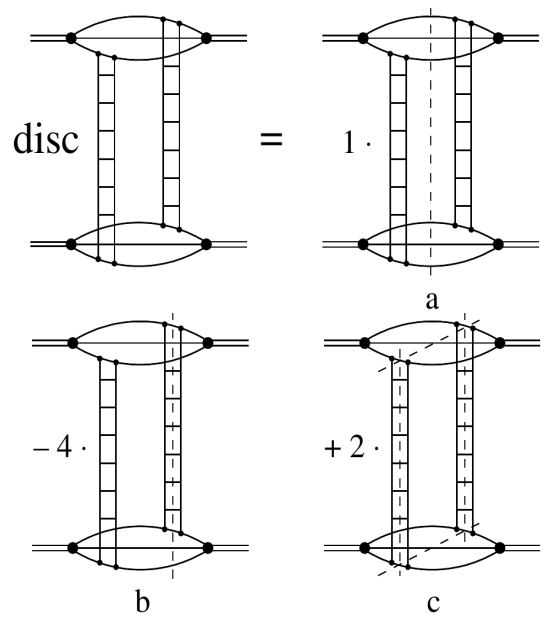

Figure 20.6: Two-Pomeron exchange diagram as a sum of different AGK cuts shown by the dashed lines.

For the two-Pomeron exchange, $n = 2$, the coefficients are $+1$, -4, or $+2$ according to whether $k = 0$, 1 or 2 Pomerons are cut, respectively. As shown in Fig. 20.6, the amplitude of the two-Pomeron exchange corresponds to a sum of three processes: i) inelastic interaction with particle density twice that caused by one Pomeron (see Fig. 20.6(c)) which enters with the coefficient '2', ii) shadowing (absorptive) correction to the one-Pomeron exchange contribution, which corresponds to events with a single Pomeron density (only one Pomeron is cut), see Fig. 20.6 (b), which enters with a factor '-4', and iii) diffractive elastic scattering or proton dissociation (when different components of the proton wave function correspond to different interaction cross sections), caused by the distortion of the incoming plane wave, see Fig. 20.6(a).

Note that the inclusive cross section is not affected by the multi-Pomeron contribution: $2 \times (2) + 1 \times (-4) = 0$. This is a general property of the AGK rules valid for any number of Pomerons n. Thus in order to calculate the inclusive single-particle cross section, it is sufficient to consider just the *one*-Pomeron exchange diagram.

Let us emphasize that the AGK rules provide a framework to consistently work with multi-Pomeron diagrams, that is, with the Regge cuts, accounting for their contributions to different processes (elastic scattering and diffractive dissociation, inelastic events with different densities, $\mathrm{d}N/\mathrm{d}y$, of secondaries, etc.).

Measurements of diffractive dissociation cross sections have been made in a wide range of pre-LHC energies, see e.g. [68–73]. At the LHC, cross sections of events with a LRG were measured by the ATLAS, CMS and ALICE collaborations at 7 and 8 TeV,

[9] In their complete form the AGK cutting rules were implemented in the QGSJET Monte Carlo [61].

Int. J. Mod. Phys. A 2026.41. Downloaded from www.worldscientific.com by UNIVERSITY OF CALIFORNIA @ BERKELEY on 09/16/26. Re-use and distribution is strictly not permitted, except for Open Access articles.

see [74–77]. ATLAS [78] and CMS and TOTEM [79] presented first measurements of SD cross sections at 8 TeV with a tagged forward proton. While ATLAS measured inclusive SD cross section, CMS and TOTEM studied SD dijet production. Note that in [78] the measured slope $B = 7.65 \pm 0.34$ GeV^{-2} of the inclusive SD cross section as well as the differential distributions $\frac{\xi \mathrm{d}\sigma_{\mathrm{SD}}}{\mathrm{d}t\mathrm{d}\xi}$ for $0.0001 \leq \xi \leq 0.025$ are (within the experimental uncertainties) in a good agreement with the theoretical expectations [29,80]. Moreover a relatively small (in comparison with the $\mathrm{d}\sigma_{\mathrm{el}}/\mathrm{d}t$) slope B indicates that the size of the triple-Pomeron vertex is much smaller than the proton size.

20.3.4 *Central Diffractive processes*

Processes $pp \to p + X + p$, where an object X, produced in the central rapidity region, is separated from the outgoing protons by a LRG on each side, are called Central Exclusive Production (CEP). They are described by the double Pomeron exchange (DPE) diagrams. When the mass of the central system, M_X, is large and the interaction in the M_X region can be described by Pomeron exchange, the corresponding cross section reads

$$\frac{\xi_1\xi_2 \mathrm{d}\sigma^{\mathrm{CEP}}}{\mathrm{d}\xi_1 \mathrm{d}t_1 \mathrm{d}\xi_2 \mathrm{d}t_2} = \frac{g_N^2(t_1) g_N^2(t_2)}{(16\pi^2)^2} \left(\frac{1}{\xi_1}\right)^{2\alpha_{\mathbb{P}}(t_1)-2} \left(\frac{1}{\xi_2}\right)^{2\alpha_{\mathbb{P}}(t_2)-2} \times g_{3\mathbb{P}}^2(0) \left(\frac{M_X^2}{s_0}\right)^{\alpha_{\mathbb{P}}(0)-1} . \tag{20.41}$$

If the mass M_X is not too large or for the cases (such as exclusive Higgs boson or dijet production) where the mass M_X is comparable with the corresponding hard scale, the last factor $g_{3\mathbb{P}}^2(0)(M_X^2/s_0)^{\alpha_{\mathbb{P}}(0)-1}$ should be replaced by the corresponding 'Pomeron-Pomeron cross section', see for instance [81,82].

Note that equations (20.37), (20.38) and (20.41) are written in a simplified way without accounting for absorptive corrections. That is, the cross sections in equations (20.37) (20.38) and (20.41) should be multiplied by the gap survival factor S^2 (see Eq. (20.15)).

Since the QCD Pomeron is built mainly from gluons it is natural to search for glueballs in double Pomeron exchange processes, and in particular, in CEP.

Resonance production in the Pomeron-Pomeron fusion was extensively studied at the CERN ISR at $\sqrt{s}$ from 22 GeV to 63 GeV (see for reviews [82–84]) and, after the ISR closure in 1983, in fixed target experiments at the CERN SPS [85] and E690 at the Tevatron [86, 87]. Glueballs were actively searched for and the properties of the f_0 and f_2 production studied in detail using multiparticle spectrometers, such as the Omega facility at the CERN SPS experiments (WA76, WA91 and WA102), see for a review [85].

An important property of CEP processes, which can be expected from matching with the perturbative QCD LO (leading order) calculation, is the $J_z = 0$ dominance. Perturbatively, for the CEP of a heavy object, the leading contribution comes from a configuration with the projection of this object spin onto the beam axis $J_z = 0$ [81]. Note that the CEP cross section is suppressed at large M_X by a strong bremsstrahlung off the incoming gluons (from the Pomeron) which would violate the 'exclusivity'. The small probability of not having such radiation is described by the Sudakov suppression factor, T_{Sud}, [88], see [81] for details.

20.3.5 *Diffractive parton distributions*

Selecting in Deep Inelastic Scattering (DIS) events with a LRG (see e.g. [89,90]) or detecting the leading proton (see Section V.C. in the review [91]) we can study the parton (quark and gluon) distributions of the Pomeron [10]. In other words, such events can be treated as DIS on the Pomeron target with the incoming Pomeron flux given by

$$f_{\mathbb{P}}(x_{\mathbb{P}}) = \int \mathrm{d}t \frac{g_N^2(t)}{16\pi^2} x_{\mathbb{P}}^{2(1-\alpha_{\mathbb{P}}(t))} , \tag{20.42}$$

[10] see also Section 18.5 in [1]

where the proton momentum fraction transferred through the Pomeron $x_{\mathbb{P}} = \xi = M^2/s$.

These Pomeron PDFs were extracted from the HERA measurements of ep scattering with leading protons or a LRG and can be used to describe the inclusive production of high E_T dijets or another hard process based on the collinear factorization theorem in the same way as that in non-diffractive collisions (see [91]). The inclusive measurements of these PDFs are described in [92–94], with the combined H1 and ZEUS data using tagged protons analyzed in [95]. The impact of diffractive jet measurements is addressed e.g. in [96] and the measured charm contribution is presented in [97, 98]. As far as the parton distributions are known, we can calculate the corresponding inelastic cross section of the Pomeron-proton interaction using one of the 'general purpose' Monte Carlo generators (see e.g. [13]), multiply it by the Pomeron flux and compare the obtained result with the Regge formula in Eq. (20.37). This approach provides another way to evaluate the triple-Pomeron vertex $g_{3\mathbb{P}}$. The corresponding analysis was performed in [99] and leads to practically the same (within the error bars) value of $g_{3\mathbb{P}} = 0.2 g_N(0)$.

It is worth mentioning that in DIS at large Q^2 we are dealing with small-size objects and the rescattering effects are small. Therefore, the survival factor $S^2 \simeq 1$ and does not affect the results.

20.4 Experimental data on diffraction at high energies

20.4.1 *Total and elastic cross sections*

The elastic scattering of protons is a process with a special and rather simple experimental signature: the central detector is empty while the incoming protons after the collisions are detected in the dedicated forward proton detectors (FPD) placed far from the interaction point (IP). Elastic scattering data are taken in special runs in order to be able to reach different ranges of t-values and thanks to the very large value of the cross section the data can be collected with a relatively low instantaneous luminosity and hence a negligible pile-up.[11]

These special runs usually have very few proton bunches and differ in the t range covered, which is governed roughly by the relation $t_{\min} \propto d^2/\beta^*$. Here d is the distance, expressed in multiples of the beam size at the detector, from the centre of the LHC beam and β^* is defined as the distance from the IP to the point where the transverse area of the beam is twice as wide as that at the IP (see Section 31 in [1]). Note that if we work at large β^*, the incoming protons have very small angular divergence leading to small average transverse momentum, which allows us to measure very small $|t|$ values. The lowest $|t|$ values measured so far at the LHC are 2.5×10^{-4} GeV^2 (ALFA) and 6×10^{-4} GeV^2 (TOTEM) reached with the 13 TeV LHC beam configured with β^*=2.5 km optics and with the 8 TeV LHC beam configured with the β^*=1.0 km optics, respectively. The largest t values of about 4 GeV^2 were measured by TOTEM at 8 and 13 TeV with $\beta^* = 90$ m thanks to special triggers. Other β^* values used in special runs are 3.5 m, and 11 m.

There are four ways to determine the σ_{tot} value:

1. **Elastic and Inelastic.** This method does not require the optical theorem and hence no extrapolation of $\mathrm{d}\sigma_{\mathrm{el}}/\mathrm{d}t$ to $t = 0$ and no ρ (defined below Eq. (20.17)) but rather the luminosity and measuring rates N_{el} (elastic) and N_{inel} (inelastic). The total cross section is then simply:

$$\sigma_{\mathrm{tot}} = \frac{1}{\mathcal{L}}(N_{\mathrm{el}} + N_{\mathrm{inel}}). \tag{20.43}$$

   Of course, both N_{el} and N_{inel} should be corrected for the detector acceptance and efficiency. This is especially important for N_{inel} since the detectors never cover the whole rapidity region (i.e. the whole 4π).

2. **Elastic only.** This approach necessitates measuring $\mathrm{d}\sigma_{\mathrm{el}}/\mathrm{d}t$ and using the optical theorem with a known value of ρ. As

[11] The pile-up is formed by additional pp collisions which typically produce low-p_T particles. These may affect the signal sample and worsen various reconstruction and identification efficiencies.

Int. J. Mod. Phys. A 2026.41. Downloaded from www.wo
by UNIVERSITY OF CALIFORNIA @ BERKELEY on 09/16/26. Re-use and distribution is
except for Open Access articles.

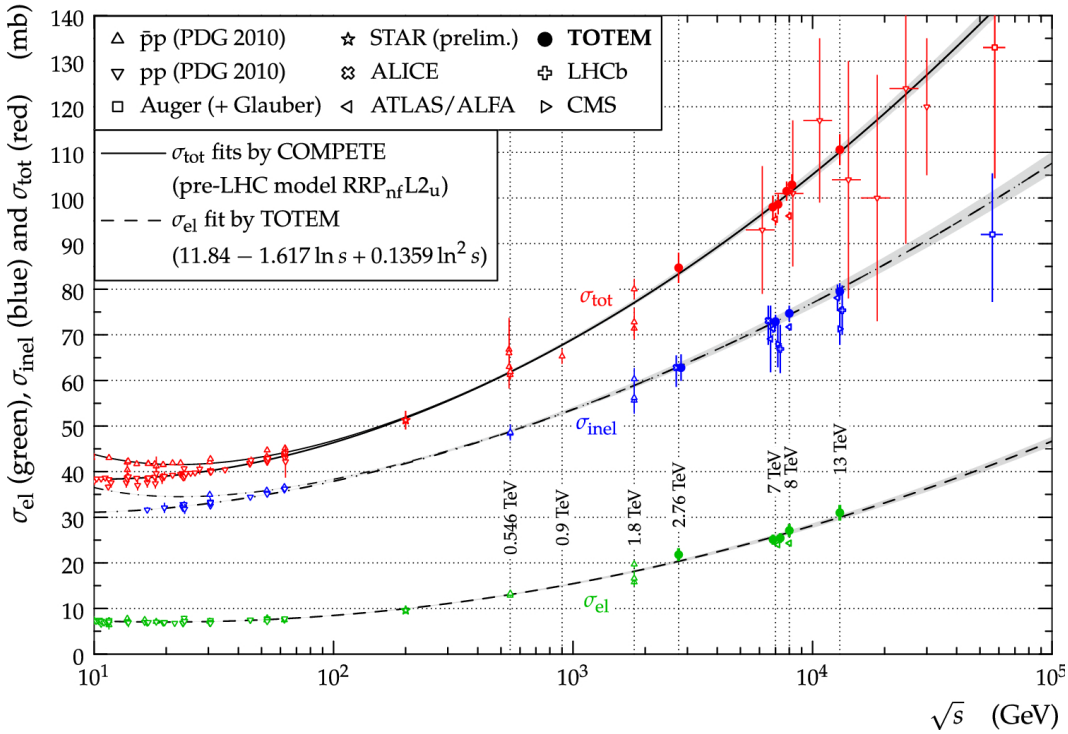

Figure 20.7: Overview of elastic ($\sigma_{\rm el}$), inelastic ($\sigma_{\rm inel}$) and total ($\sigma_{\rm tot}$) cross section data for pp and $p\bar{p}$ collisions as a function of $\sqrt{s}$. The continuous black lines (lower for pp, upper for $p\bar{p}$) represent the best fits of the total cross section data by the COMPETE collaboration [22]. The dashed line is a fit of the elastic cross section data. The dashed-dotted lines refer to the inelastic cross section and are obtained from the difference between the continuous and dashed lines. Figure from Ref. [100].

explained in Section 20.2, the optical theorem states that $\sigma_{\rm tot} \propto {\rm Im}[T_{\rm el}(t \to 0)]$, see Eq. (20.3). Since in practice it is not possible to measure down to $t = 0$, we need to extrapolate. To minimize the model dependence when extrapolating, it is vital to measure down to as low $|t|$ values as possible (i.e. high β^*). This method requires an independent luminosity measurement. Once the luminosity is known, ${\rm d}\sigma_{\rm el}/{\rm d}t$ can be normalized and used to extract $\sigma_{\rm tot}$ using the formula:

$$\sigma_{\rm tot}^2 = \frac{16\pi}{1+\rho^2} \left.\frac{{\rm d}\sigma_{\rm el}}{{\rm d}t}\right|_{t\to 0}. \qquad (20.44)$$

3. **Coulomb normalization.** Similarly to the previous method, this approach relies on the elastic observables only and requires a measurement of the elastic cross section at very low values of $|t|$, where it is sensitive to the theoretically well known Coulomb QED contribution $4\pi\alpha_{\rm QED}^2/t^2$. The normalization of ${\rm d}\sigma_{\rm el}/{\rm d}t$ is then determined by fitting the experimental data at very low $|t|$ using a formula including the Coulomb amplitude and its interference with the strongly interacting (the so-called nuclear) term. This method has been successfully used by UA4/2 [101] and TOTEM [102].
4. **Luminosity-independent.** This method does not rely on the knowledge of luminosity but rather on the knowledge of $N_{\rm el}$ and $N_{\rm inel}$ and on the optical theorem:
combining equations (20.43) and (20.44) with $\frac{{\rm d}\sigma_{\rm el}}{{\rm d}t} = \frac{1}{\mathcal{L}}\frac{{\rm d}N_{\rm el}}{{\rm d}t}$ we get

$$\sigma_{\rm tot} = \frac{16\pi}{1+\rho^2} \frac{{\rm d}N_{\rm el}/{\rm d}t\big|_{t=0}}{N_{\rm el}+N_{\rm inel}}, \qquad (20.45)$$

where ${\rm d}N_{\rm el}/{\rm d}t\big|_{t=0}$ corresponds to the extrapolation to $t = 0$ of the nuclear term only. By independently and simultaneously measuring $N_{\rm el}$ and $N_{\rm inel}$, and applying the optical theorem, we can also determine the luminosity.

The TOTEM [100, 103–105] and ATLAS [106–108] collaborations at CERN have covered an energy range from $\sqrt{s}$=2.76 TeV to 13 TeV. A compilation of high energy total pp and $p\bar{p}$ cross section measurements is shown in Fig. 20.7 (for discussion of the pre-LHC elastic scattering data see review [109]).

Despite some tension between the Tevatron CDF [110] and E811 [111] data [12] and to a lesser extent between the TOTEM [102, 104, 105] and ATLAS [106–108] measurements, the data clearly indicate that in the Tevatron – LHC energy interval the total cross section starts to grow *faster* than the power-law parametrization [26] describing the data below the Tevatron energy. In particular, while the DL fit [26] predicts $\sigma_{\rm tot} = 90.7$ mb at $\sqrt{s} = 7$ TeV, the TOTEM experiment observes 98.6±2.2 mb [104].

A compilation of the high-energy data on the elastic slope is shown in Fig. 20.8. It is clearly seen that in the TeV energy range the slope increases with $\sqrt{s}$ more rapidly than the logarithmic behaviour expected in the case of one-Pomeron exchange, see Eq. (20.30), as illustrated by comparing the dashed blue curve with the solid red and blue curves in Fig. 20.8. Such an acceleration of the t-slope derivative, ${\rm d}B/{\rm d}\ln s$, is a clear manifestation of the increasing role of the multi-Pomeron exchanges, where asymptotically the slope should rise as $\ln^2 s$, see [116]. Finally, Fig. 20.9 illustrates the energy dependence of the differential elastic pp cross section. As expected (see Section 20.3.3.1), the diffractive dip moves to smaller $|t|$ with increasing energy.

20.4.2 *Diffractive vector meson production*

The exclusive production of vector mesons was studied in detail at HERA (see for a review [91]). It is well described within the 'dipole model' (see for review and references [119]), where the incoming photon first fluctuates into a quark-antiquark, which then interacts with the target proton and, finally, with the probability given by the overlap integral between the vector meson wave function and the outgoing $q\bar{q}$-pair, the vector meson is produced. The crucial quantity is the value of cross section, $\sigma(q\bar{q} - p)$, of elastic scattering of the $q\bar{q}$-pair on the proton. The energy behaviour of $\sigma(q\bar{q} - p)$ is driven by the intercept, $\alpha_{\rm eff}(0)$, of the

[12] The CDF 1.8 TeV point [110] is 2.8 σ higher than the corresponding E811 result [111].

Int. J. Mod. Phys. A 2026.41. Downloaded from www.worldscientific.com
by UNIVERSITY OF CALIFORNIA @ BERKELEY on 09/16/26. Re-use and distribution is strictly not permitted, except for Open Access articles.

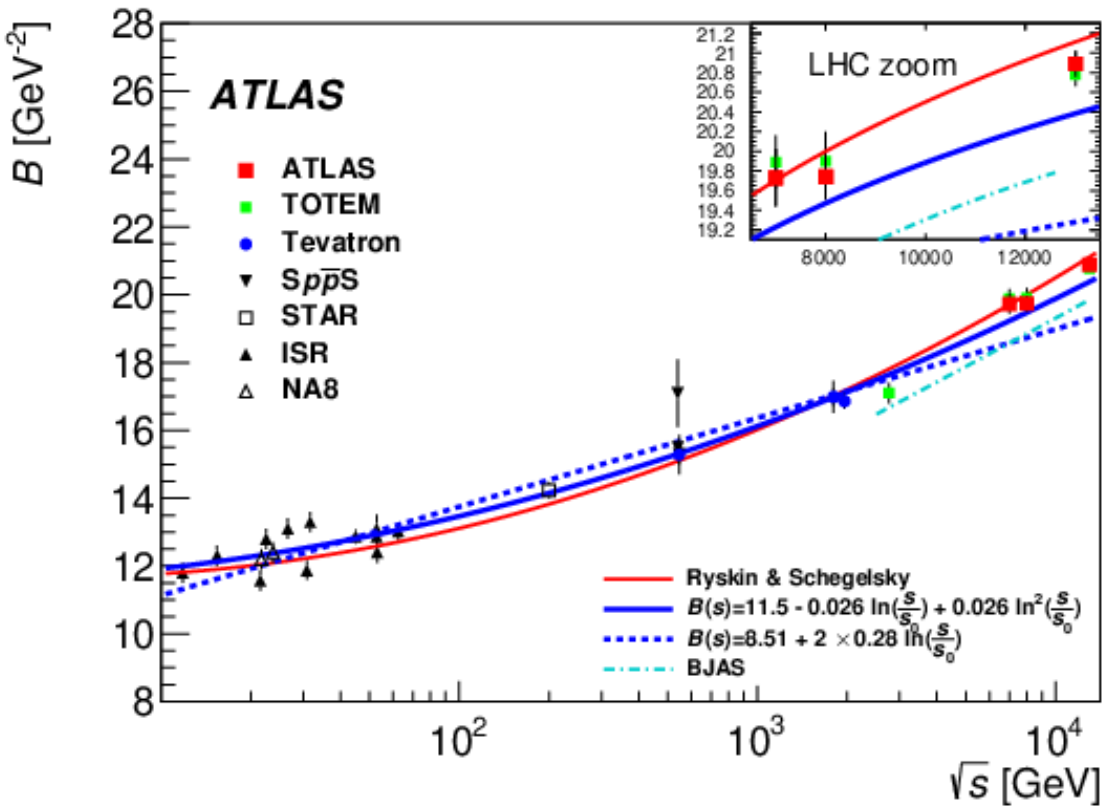

Figure 20.8: The diffractive slope B for pp and $p\bar{p}$ elastic scattering as a function of $\sqrt{s}$. For references to data points, see plots of cross sections in Refs. [108, 112]. Theory predictions are explained in Ref. [108]. Figure from Ref. [108].

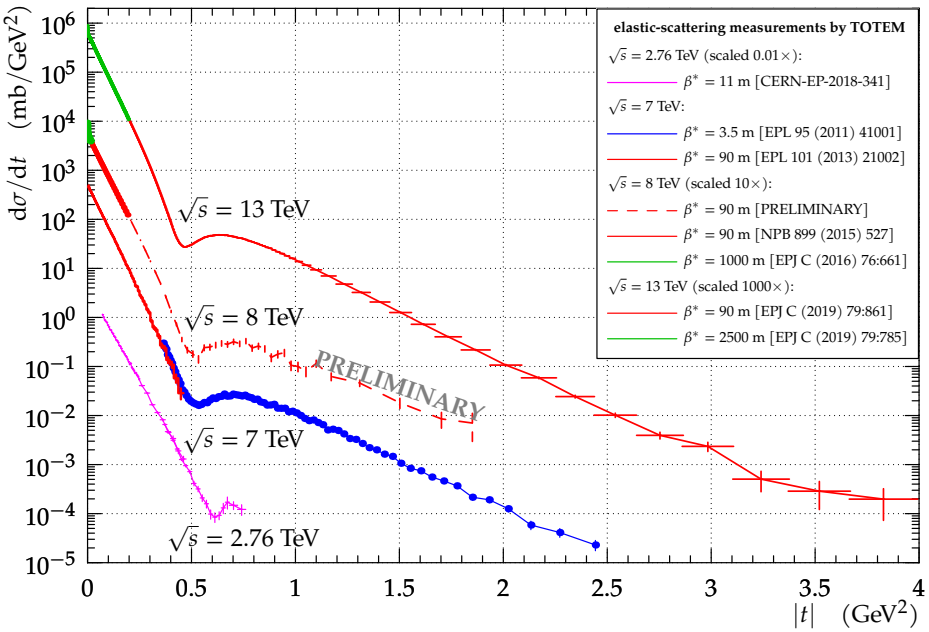

Figure 20.9: The t-dependence of the pp elastic cross section for collision energies $\sqrt{s}$ = 2.76 TeV [103], 7 TeV [104, 113], 8 TeV [53,114,115] and 13 TeV [54,102]. The experimental uncertainties represent the quadratic sum of statistical and systematic uncertainties. Figure from Ref. [115].

effective Pomeron [13] (rightmost singularity in the j-plane), while the value of the cross section depends on the quark separation, r, in the transverse plane, $\sigma(q\bar{q}-p) \propto \alpha_s^2 \langle r^2 \rangle$ [43, 44]. Thus different processes with the same $\langle r^2 \rangle$ are driven by the same $\sigma(q\bar{q}-p)$ cross section.

In the DIS case this separation in turn is controlled by the photon virtuality, Q^2, and the quark mass, m_q: $\langle r^2 \rangle \simeq 1/(z(1-$

[13] Effective Pomeron means that this is not an original pole in the j-plane, but it includes the corrections (renormalizations) caused by the enhanced diagrams (see e.g. [120]).

Int. J. Mod. Phys. A 2026.41. Downloaded from www.wo
by UNIVERSITY OF CALIFORNIA @ BERKELEY on 09/16/26. Re-use and distribution is
except for Open Access articles.

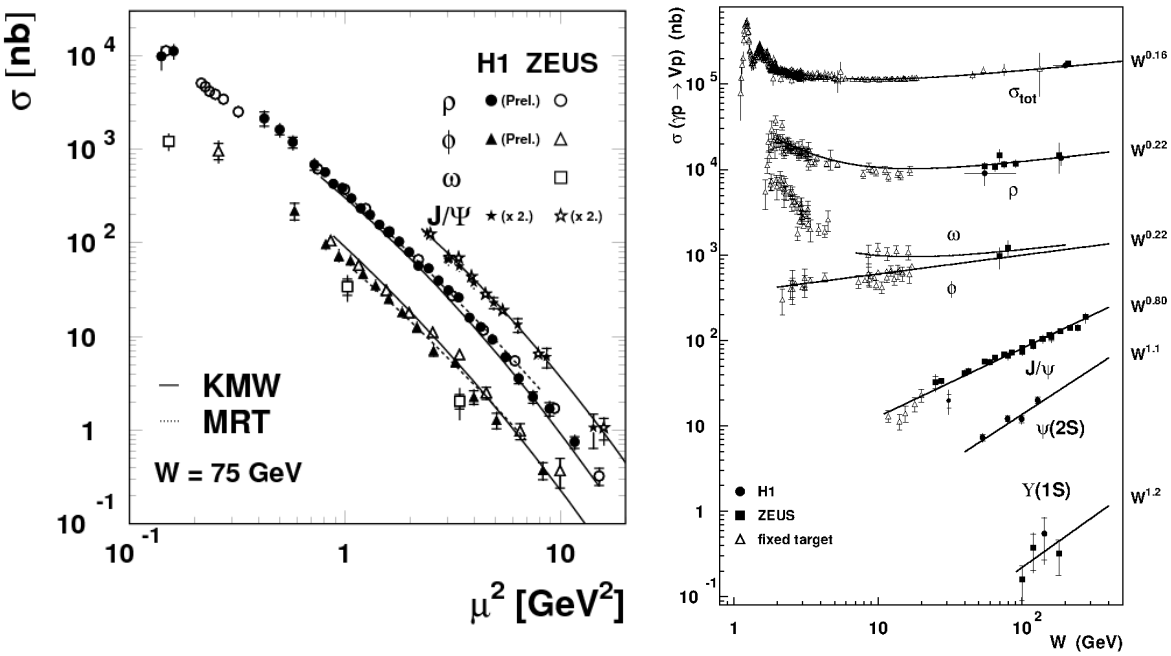

Figure 20.10: (Left) The ρ, ω, ϕ and J/ψ elastic production cross sections as a function of the scale $\mu^2 = (Q^2 + M_V^2)/4$. For readability of the figure, the J/ψ cross sections are multiplied by a factor 2. Figure from Ref. [117]. (Right) Compilation of photoproduction cross section measurements as a function of the γp centre-of-mass energy, W. The total cross section and various vector meson production cross sections are included, with the approximate power law dependences $\sigma \propto W^\delta$ indicated for each process. Figure from Ref. [118].

$z)Q^2 + m_q^2$) (z is the photon momentum fraction carried by the quark). Indeed, the cross section of the ρ meson diffractive production in DIS at $Q^2 = M_{J/\psi}^2$ is close (up to the difference in the quark electric charges) to that for the J/ψ photoproduction, see Fig. 20.10 (Left).

The production cross section depends non-trivially on W, the energy of the $\gamma^* p$ center of mass system. It increases with W as W^n, where $n = 0.2$ for ρ, ω and ϕ (light quark)-mesons but $n = 0.8$ for J/ψ. Note that in the J/ψ case the energy dependence is close to that of the BFKL (Balitsky-Fadin-Kuraev-Lipatov) Pomeron [59,121,122], that is, the singularity calculated within the leading (and next-to-leading) approximation in perturbative QCD. But at lower scales the absorptive (multi-Pomeron) corrections tame the growth which leads to smaller values of n ([123–126]), see Fig. 20.10 (Right).

A similar situation reveals in the dependence of $\alpha_{\rm eff}$ on Q^2, as can be seen in Fig. 47 of [91]. At a large scale $\mu^2 = (Q^2 + M_V^2)/4$ the value of $\alpha_{\rm eff} \simeq 1.3$ is close to the prediction for the QCD Pomeron, while for a smaller scale, the absorptive corrections described by the multi-Pomeron diagrams start to reduce the cross section, and $\alpha_{\rm eff}$ decreases.

20.5 Pomeron in QCD

All features described in the previous Sections were based on *first principles*, such as analyticity (based on causality), unitarity, crossing symmetry, etc. Since QCD theory satisfies all these principles it should reveal a corresponding "Regge" behaviour. Indeed, within perturbative QCD there is a Pomeron: an even-signature singularity in the j-plane with vacuum quantum numbers. While in the old Regge theory the Regge trajectories and their couplings were phenomenological numbers fitted from experiment, perturbative QCD allows one to calculate the positions of the singularities and the corresponding couplings with $O(\alpha_s)$ and even with $O(\alpha_s^2)$ accuracy [59,121,122,127–130].

In terms of Feynman diagrams, the QCD Pomeron may be viewed as a sum of multi-particle ladders built by the exchange of two t-channel (reggeized [14]) gluons, see the left-hand side of Fig. 20.5.

The sum of ladder diagrams of the type of Fig. 20.5 is the simplest multiparticle structure which reproduces the power-like s^α behaviour of the Pomeron pole. In other words it corresponds to a sum of completely inelastic $2 \to n$ processes, that is, to the last term $G_{\rm inel} = 1 - \exp(-\Omega)$ in the unitarity equation (20.9). This set of diagrams was resummed in the limit of a small QCD coupling, $\alpha_s \ll 1$, but large energy, such that $\alpha_s \ln(s/s_0) \sim O(1)$ [59]. The summation results in the rightmost singularity at $j = 1 + \omega_0 > 1$. After accounting for the next-to-leading logarithmic (NLL) corrections, the position of the singularity (Pomeron intercept) corresponds to $\omega_0 = 0.25$–0.3 depending only weakly on the scale [121,122,131–135], whose value is characterized by the transverse momentum, k_t, of gluons in the ladder.

It was demonstrated (see e.g. [136]) that the resummation of the $(\alpha_s \ln(1/x))^n$ terms based on the QCD Pomeron results essentially improves the description of low-x inclusive HERA data within the framework of the NNLO DGLAP evolution.

At this stage the singularity is the cut in the j-plane. However we have to account for the boundary conditions at relatively small k_t. Imposing a reasonable boundary, we arrive at a series of Regge poles in the interval from $j = 1$ to $j = 1 + \omega_0$ instead of the cut [133]. Note that the first (corresponding to the rightmost pole in the j-plane, i.e. to the pole with the largest Re j) eigenfunction consists of gluons with relatively small k_t, while for the next poles the k_t increases. DIS inclusive $\gamma^* p$ cross sections were fitted in [134] using the QCD based approach in which Pomeron is represented by series of Regge poles obtained within the perturbative QCD BFKL approach. It was concluded that the first pole has a small coupling to the proton. It is possible that this small value of the coupling to the proton is related to the fact that the enhanced multi-Pomeron diagrams (i.e. the rescattering

[14] That is, the virtual loop corrections to the one-gluon exchanges are included. These corrections are important in order to provide infrared stability of the results.

Int. J. Mod. Phys. A 2026.41. Downloaded from www.worldscientific.com
by UNIVERSITY OF CALIFORNIA @ BERKELEY on 09/16/26. Re-use and distribution is strictly not permitted, except for Open Access articles.

of intermediate partons) were neglected in the fit. The main effect of this enhanced contribution is the "renormalization" of the intercept which diminishes the effective value of ω_0. Besides this, the enhanced diagrams provide a saturation by reducing the rise of the parton densities in the $(b,\ k_t,\ y)$-space (see e.g. [137, 138]).

Note that perturbative QCD allows us to understand why the values of the phenomenological multi-Pomeron vertices and the shift, ω_0, of the intercept, are small (due to $\alpha_s \ll 1$ and some numerical factors such as N_c and π). Indeed, at the lowest α_s orders we get for the ω_0 value and the simplest multi-Pomeron vertices (see e.g. [59, 138, 139]):

$$\omega_0 \propto \frac{N_c\alpha_s}{\pi}, \quad g_{3\mathbb{P}} \propto \frac{N_c\alpha_s^2}{(N_c^2-1)\pi^2} \quad \text{and} \quad g_2^2 \propto \frac{N_c\alpha_s}{(N_c^2-1)^2}\ , \tag{20.46}$$

where g_2^2 is the coupling corresponding to the transition of 2 into 2 Pomerons.

20.5.1 *BFKL evolution in the 'dipole' representation*

It was shown in [140–143] that the LO BFKL Pomeron equation [59] can be written in terms of the evolution of the dipole density, $N(x_d, y_d; y)$, in rapidity y (here x_d and y_d are the transverse coordinates of two t-channel gluons which form the colour singlet dipole). Indeed, after the emission of a new gluon at point z_d, the initial colour dipole with coordinates (x_d, y_d) turns into a pair of dipoles (x_d, z_d) and (z_d, y_d). This can be considered as a development of a 'dipole cascade'. Moreover in this formalism it is easy to include the non-linear absorptive corrections (last term in the square brackets in Eq. (20.47)), which accounts for the rescattering of the intermediate partons (gluons) on the target proton. The corresponding contribution is described by the so-called "fan" diagrams and these are the most important corrections to the linear DGLAP (Dokshitzer-Gribov-Lipatov-Altarelli-Parisi) evolution [144] in the case of DIS at not large scales but at very small momentum fraction [138].

The resulting non-linear evolution (Balitsky-Kovchegov equation [145–147]) reads

$$\begin{aligned}\frac{\mathrm{d}}{\mathrm{d}y}N(x_d, y_d; y) =& \frac{\alpha_s N_c}{2\pi^2}\int \mathrm{d}^2 z_d \frac{(x_d-y_d)^2}{(x_d-z_d)^2(y_d-z_d)^2} \\ &\times [N(x_d, z_d; y) + N(y_d, z_d; y) - N(x_d, y_d; y) \\ &- N(x_d, z_d; y)N(y_d, z_d; y)]\ .\end{aligned} \tag{20.47}$$

For a small density N the last term in the square brackets can be neglected, and the first three terms in Eq. (20.47) reproduce the conventional BFKL equation in the coordinate representation. However, for large $N \to 1$ the right-hand side of Eq. (20.47) vanishes and we reach the saturation $N = 1$. It is worth mentioning that, as shown in [148], in terms of 'dipole' formalism, with the triple-Pomeron vertex generated by the 'one dipole to two dipoles' transition, it is possible to relate the Good-Walker approach to high mass diffraction with the triple-Pomeron diagram.

20.5.2 *Distribution of secondaries: theory versus experiment*

As already discussed, in terms of Feynman diagrams the cut Pomeron can be viewed as a set of ladder diagrams corresponding to a sum of completely inelastic $2 \to n$ processes, that is, to the last term $G_{\rm inel} = 1 - \exp(-\Omega)$ in the unitarity equation (20.9). Here $n > 2$ means the production of additional $(n-2)$ gluons which, after hadronization, form minijets. [15] Therefore, in the final state driven by one Pomeron, we expect to observe gluon minijets with a flat rapidity distribution in the central (plateau) rapidity region. This would correspond to a flat pseudorapidity distribution of produced particles if they were massless. A typical pseudorapidity distribution of charged particles in inclusive events (up to $|\eta| = 7$) is shown in Fig. 20.11 (left) [149] (see also Fig. 53.1 in [1]). The central part ($|\eta| < 2.5$) was measured by CMS, while the forward region was covered by TOTEM. The dip observed at $\eta = 0$ is explained by the presence of massive particles (the Jacobian $J(p_T, m, \eta) = p_T/E \to p_T/\sqrt{p_T^2 + m^2}$ at $\eta = 0$). A photon energy spectrum is shown in Fig. 20.11 (right) [150], measured by LHCf inclusively and in events with a diffraction topology, i.e. no charged particles with $p_T > 100$ MeV and $|\eta| < 2.5$ observed by ATLAS. As expected in diffractive events the energy flow decreases with E_γ more slowly than that in the inclusive case.

The energy dependence of the particle density $\mathrm{d}N_{\rm ch}/\mathrm{d}\eta$ at $\eta = 0$ is shown in Fig. 20.12 (left). Neglecting absorptive corrections given by the enhanced diagrams (which mainly change ('renormalize') the effective Pomeron intercept $\alpha_{\rm eff}(0) = 1 + \Delta$ [120]), we conclude that according to the AGK rules the plateau height $\mathrm{d}\sigma/\mathrm{d}\eta \propto s^{\Delta}$ is driven just by the one-Pomeron exchange with effective $\Delta \sim 0.2$ (see Section 20.3.3.3). That is, the density of secondaries observed in the inclusive process increases with increasing energy faster than the total cross section, whose growth is tamed by the multi-Pomeron diagrams. Indeed, as is seen from Fig. 20.12 (left), in the interval of collider energies $\mathrm{d}N_{\rm ch}/\mathrm{d}\eta = (1/\sigma_{\rm inel})\mathrm{d}\sigma/\mathrm{d}\eta \propto s^{0.115}$ (i.e. $\mathrm{d}\sigma/\mathrm{d}\eta \propto s^{0.215}$), while $\sigma_{\rm inel} \propto s^{0.1}$.

Contrary to the 'old' Regge theory where it was *assumed* (based on the experimental data existing in the 1950s and 1960s) that all transverse momenta are limited, in QCD the k_t distributions of jets (charged particles) have a long k_t tail ($\mathrm{d}\sigma/\mathrm{d}k_t^2 \propto \alpha_s^2(k_t^2)/k_t^4$ at large k_t and very large energy $s \gg k_t^2$). An example of the p_T distribution of charged secondaries is shown in Fig. 20.12 (right).

Note that the mean transverse momentum of secondaries, produced via jet fragmentation, slowly increases with collision energy, see Fig. 20.13 (right). This is caused by the stronger absorption (at larger $\sqrt{s}$) of the gluons with a smaller k_t ($\sigma^{\rm abs} \propto 1/k_t^2$). The growth of $\langle p_T\rangle$ with multiplicity (see Fig. 20.13 (left)) can be explained by the fact that events with larger $N_{\rm ch}$ correspond to a smaller impact parameter, b, where the absorption of a low k_t component is stronger and, next, larger multiplicity can be originated by the events with jets/minijets with higher p_T. Since the mean p_T of secondaries grows with $\sqrt{s}$, the increase with $\sqrt{s}$ of transverse energy flow is a bit faster than that of particle density.

The model [161] based on a modification of the classic RFT allows one to trace the smooth transition from the pure perturbative, large k_t, region into the *soft* domain. A strong absorption of the low k_t partons plays a crucial role here since it produces an effective infrared cutoff, $k_{\rm sat}$, and provides the possibility of extending the parton approach, used for 'hard' processes, to also describe high-energy soft and semihard interactions. This approach combines a description of soft physics and diffraction with jet physics in a coherent self-consistent way.

Another way is to include the soft and hard components independently [37, 66, 162, 163]. In this approach the soft part is described in terms of RFT with the phenomenological "soft" Pomeron pole while the hard part is calculated in terms of the parton model for minijet production with the energy dependent cutoff $k_t > k_0(s)$. A combined description of soft and hard processes in hadronic collisions is reached within the QGSJET Monte Carlo model (e.g. [61]) in the framework of the so-called "semihard Pomeron" approach (see e.g. [164]).

In [165] a model was constructed, which incorporated the attractive features of the two successful theoretical approaches to high energy QCD: BFKL Pomeron calculus [59,60] and the Colour Glass Condensate/saturation [166].

20.5.2.1 *Correlations*

All LHC experiments routinely measure tracks with $p_T > p_{\rm min}$, where $p_{\rm min}$ can vary in different studies. Typically, $p_{\rm min} =$ 200 MeV, where tracking reconstruction efficiencies are larger than 70%. In order to identify particle species, each experiment has sophisticated identification procedures usually based on the ionization energy loss, $\mathrm{d}E/\mathrm{d}x$, or other techniques, with different regions of applicability for different particle species. Thanks to usually relatively large cross sections of soft QCD processes, most of the results below come from event samples with very low or negligible pile-up.

Following the notation in [167], symmetrized inclusive particle

[15] Minijets result from hadronization of partons emitted from the cut QCD Pomeron. Typically these are groups of hadrons with comparatively low overall $E_T \lesssim$ 5–10 GeV.

Int. J. Mod. Phys. A 2026.41. Downloaded from www.wo
by UNIVERSITY OF CALIFORNIA @ BERKELEY on 09/16/26. Re-use and distribution is
except for Open Access articles.

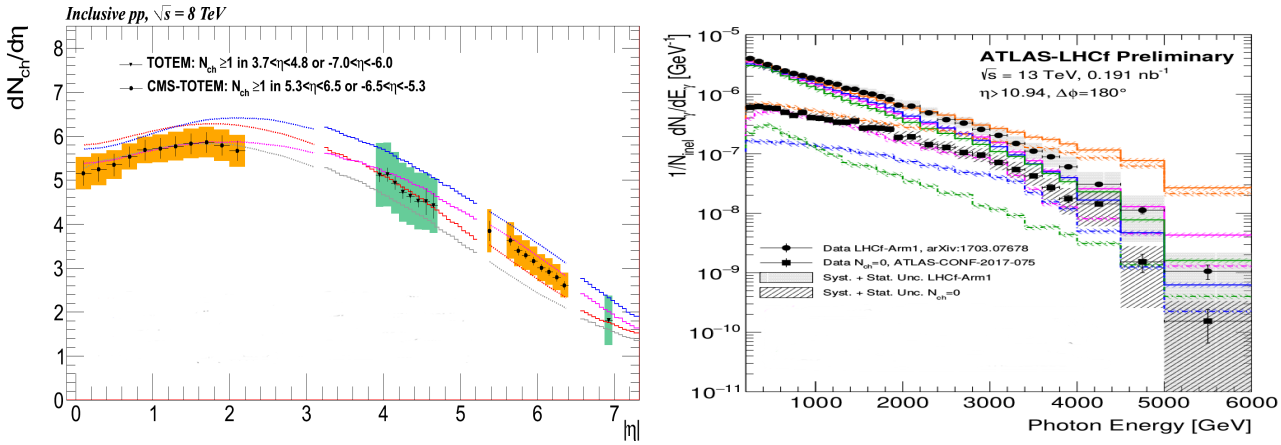

Figure 20.11: (Left) Charged-particle pseudorapidity distribution for inclusive events measured by CMS and TOTEM [149]. The error bars represent the statistical and uncorrelated systematic uncertainties between neighboring bins, while the shaded areas denote the combined statistical and full systematic uncertainties. The coloured lines indicate model predictions. (Right) Photon energy spectrum measured by LHCf at $|\eta|$ >10.94. The filled circles show the inclusive photon spectrum measured by LHCf [151] and filled squares the spectrum for $N_{\rm ch} = 0$ events where no charged particles with $p_T > 100$ MeV and $|\eta|$ <2.5 are observed by ATLAS [152]. The coloured lines indicate model predictions. The error bars correspond to the statistical uncertainties and the shaded areas denote the combined statistical and systematic uncertainties. Figure from Ref. [150].

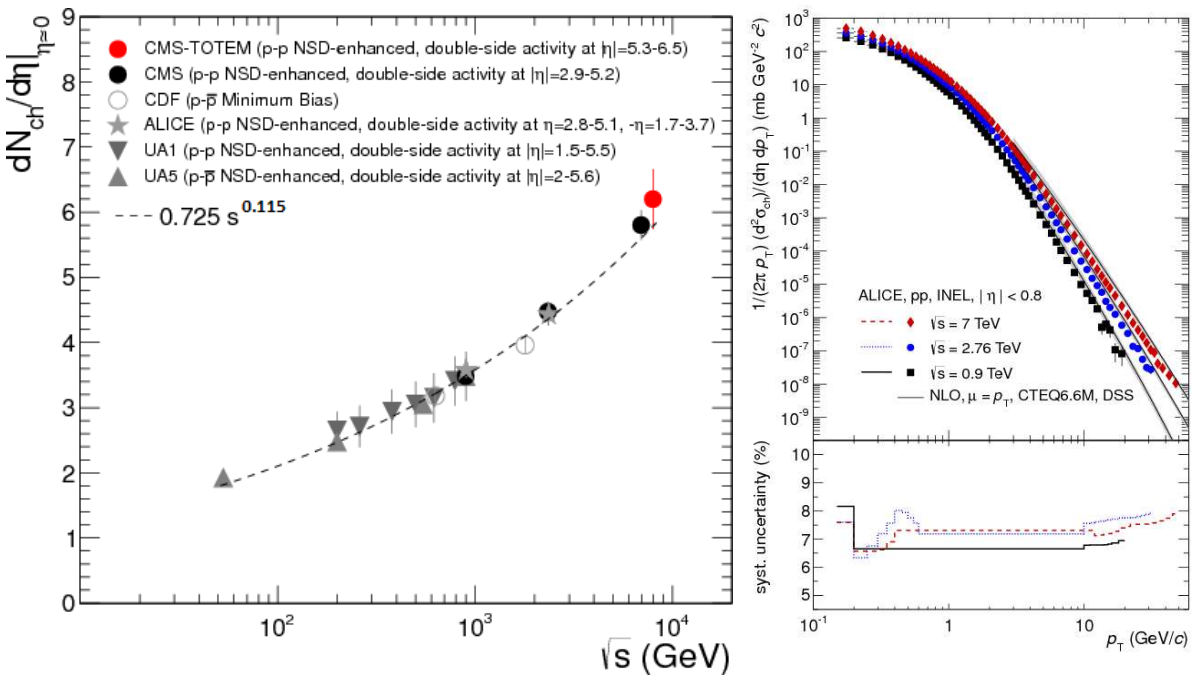

Figure 20.12: (Left) Energy dependence of the charged particle density $\mathrm{d}N_{\rm ch}/\mathrm{d}\eta$ at $\eta \approx 0$ for pp and $p\bar{p}$ collisions. Shown are measurements performed with different Non-SD event selections from UA1 [153], UA5 [154], CDF [155,156], ALICE [157] and CMS [158]. The dashed line is a power-law fit to the data. Figure from Ref. [149]. (Right) Differential cross section of charged particles with $|\eta| < 0.8$ in inelastic pp collisions at $\sqrt{s} = 0.9, 2.76$ and 7 TeV as a function of p_T. Only statistical uncertainties are shown. Figure from Ref. [159].

number densities for q points at $y_1, ..., y_q$ (where y_i represents the 4-momentum of the ith particle), $\rho_q(y_1, ..., y_q)$, are related to the inclusive differential cross section by

$$\frac{1}{\sigma_{\rm inel}}\mathrm{d}\sigma = \rho_1(y)\mathrm{d}y, \quad \frac{1}{\sigma_{\rm inel}}\mathrm{d}^2\sigma = \rho_2(y_1, y_2)\mathrm{d}y_1\mathrm{d}y_2 \quad \text{etc.} \tag{20.48}$$

By integrating we get

$$\int \rho_1(y)\mathrm{d}y = \langle n\rangle, \quad \int\int \rho_2(y_1, y_2)\mathrm{d}y_1\mathrm{d}y_2 = \langle n(n-1)\rangle \quad \text{etc.}, \tag{20.49}$$

where the angular brackets denote averaging over the event sample and n is the particle multiplicity.

Since the inclusive q-particle densities in general contain trivial contributions from lower-order densities, it is convenient to consider quantities C_q which vanish when one of their arguments becomes statistically independent of (uncorrelated with) the others. These quantities C_q, called correlation functions (or cumulant functions), are defined as:

$$C_2(1,2) = \rho_2(1,2) - \rho_1(1)\rho_1(2), \quad C_3(1,2,3) = \rho_3(1,2,3) - \sum_{(3)} \rho_1(1)\rho_2(2,3) + 2\rho_1(1)\rho_1(2)\rho_1(3), \tag{20.50}$$

Int. J. Mod. Phys. A 2026.41. Downloaded from www.worldscientific.com
by UNIVERSITY OF CALIFORNIA @ BERKELEY on 09/16/26. Re-use and distribution is strictly not permitted, except for Open Access articles.

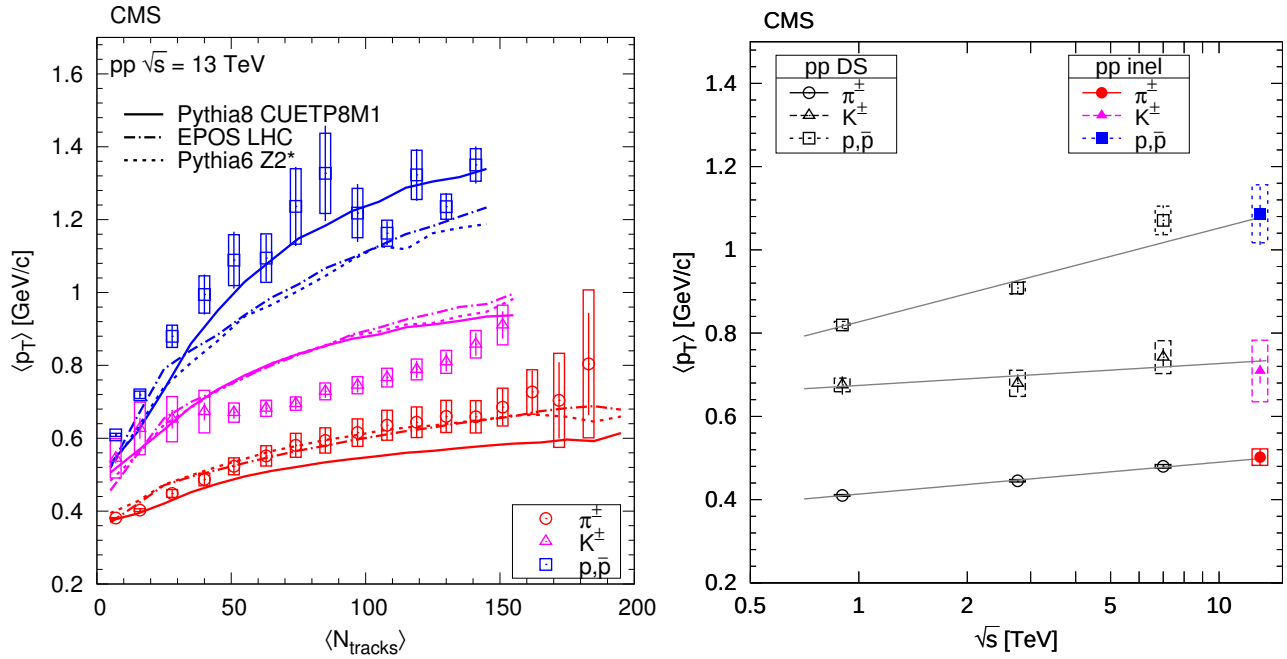

Figure 20.13: Average p_T of pions, kaons and protons in the range $|\eta| < 1.0$ as a function of (left) track multiplicity at $|\eta| < 2.4$ and (right) of center-of-mass energy where the curves show linear fits using $\ln s$. The error bars indicate the uncorrelated combined uncertainties, while the boxes show the uncorrelated systematic uncertainties. Figures from Ref. [160].

$$C_4(1,2,3,4) = \rho_4(1,2,3,4) - \sum_{(4)} \rho_1(1)\rho_3(1,2,3) - \sum_{(3)} \rho_2(1,2)\rho_2(3,4) + 2\sum_{(6)} \rho_1(1)\rho_1(2)\rho_2(3,4) - 6\rho_1(1)\rho_1(2)\rho_1(3)\rho_1(4). \tag{20.51}$$

The 2D two-particle correlation function is defined as

$$C(\Delta\eta, \Delta\phi) = \frac{\rho_2(\Delta\eta, \Delta\phi)}{\rho_1(\eta_a, \phi_a)\rho_1(\eta_b, \phi_b)}. \tag{20.52}$$

The distribution $\rho_2(\Delta\eta, \Delta\phi)$ is usually interpreted as a conditional probability to observe a particle a at the phase-space point (η_a, ϕ_a) if a particle b at (η_b, ϕ_b) is observed as well, and $\Delta\eta = \eta_a - \eta_b$ and $\Delta\phi = \phi_a - \phi_b$. The distributions $\rho_1(\eta_a, \phi_a)$ and $\rho_1(\eta_b, \phi_b)$ are probabilities to observe a single particle at (η_a, ϕ_a) and (η_b, ϕ_b), respectively. The denominator of Eq. (20.52) is constructed as a product of two single-particle distributions using an event mixing technique, where each particle in the pair comes from a different event. Experimentally, each reconstructed track is weighted by the inverse of an efficiency factor which accounts for the detector acceptance, the reconstruction and particle identification efficiencies, the contamination by secondary particles and the fraction of misreconstructed tracks.

An example of two-particle correlation functions measured in pp collisions at 7 TeV is shown in Fig. 20.14 for identical-particle pairs (right panel) and for particle–anti-particle pairs (left panel) [168].

We observe two distinct features which can be explained by short-range (in rapidity) correlations: 1) a near-side peak at $\Delta\phi \approx 0$ and 2) an away-side peak or rather a ridge at $\Delta\phi \approx \pi$. The near-side peak is considered to be caused by at least three effects:

- *fragmentation of partons scattered at a hard scale.* These relatively high p_T partons produce showers which after the hadronization form the mini-jets which create a broad structure extending over at least one unit in $\Delta\eta$ and $\Delta\phi$.
- *resonance decays.* The decay of resonances contributes to the near-side peak at $\Delta\eta \sim 0$ and extended in $\Delta\phi$ [169–171], depending on the released kinetic energy of the given resonance. This effect is mostly visible for unlike-sign particle pairs.
- *femtoscopic correlations.* The term "femtoscopic" refers to a length scale of the order of 10^{-15} m. These correlations are present at low relative momenta of the particles in a pair (representing a very small phase-space corner, so they are practically invisible in terms of $(\Delta\eta, \Delta\phi)$) and give rise to an enhancement of the correlation function (due to Bose-Einstein quantum statistics for identical bosons) or its suppression (due to Fermi-Dirac quantum statistics for identical fermions). Besides this, at low relative momenta there are correlations caused by Coulomb and/or other final state interactions. The shape of all these effects in $(\Delta\eta, \Delta\phi)$ space depend strongly on the mass of the particle type as well as on the size of the particle-emitting system. The latter is traditionally measured in Bose-Einstein correlation (BEC) analyses and is not part of this review.

The away-side peak originates from energy-momentum conservation which manifests itself by the quark and the anti-quark going back-to-back in ϕ. In this case the rapidity width of the away-side peak is much larger than the near-side peak since in the original matrix element the quark and the antiquark can be separated by some $\Delta\eta$ interval.

As discussed in Sections 20.3.3.2 and 20.3.3.3, there may be several cut Pomerons in the same event, each giving rise to particle sets which are, in general, independent of each other (except for small Bose-Einstein correlations). This leads to long-range (in rapidity) correlations. Since the density of secondaries, $\mathrm{d}N/\mathrm{d}y$, is proportional to the number of cut Pomerons, k, the probability to observe at least one particle is proportional to $\langle k\rangle$, while the probability to observe simultaneously two particles separated by some (rather large) rapidity interval is proportional to $\langle k^2\rangle$. Thus the long-range correlations are pedicted to be $C_2 = \langle k^2\rangle/\langle k\rangle^2 - 1 > 0$ which depends weakly on the separation $\Delta\eta$ between the two particles [172, 173]. In the case of the pure eikonal approach, neglecting the enhanced diagrams and the conservation law effects in the proton fragmentation region, we expect that these long-range correlations,

$$C_2(\Delta y) = \frac{\sigma_{\mathrm{inel}} \mathrm{d}^2\sigma/\mathrm{d}y_1\mathrm{d}y_2}{\mathrm{d}\sigma/\mathrm{d}y_1\ \mathrm{d}\sigma/\mathrm{d}y_2} - 1 \sim \mathrm{const}, \tag{20.53}$$

do not depend on the rapidity separation, $\Delta y = |y_1 - y_2|$, between the two particles. The contribution of the processes with

Int. J. Mod. Phys. A 2026.41. Downloaded from www.wo
by UNIVERSITY OF CALIFORNIA @ BERKELEY on 09/16/26. Re-use and distribution is
except for Open Access articles.

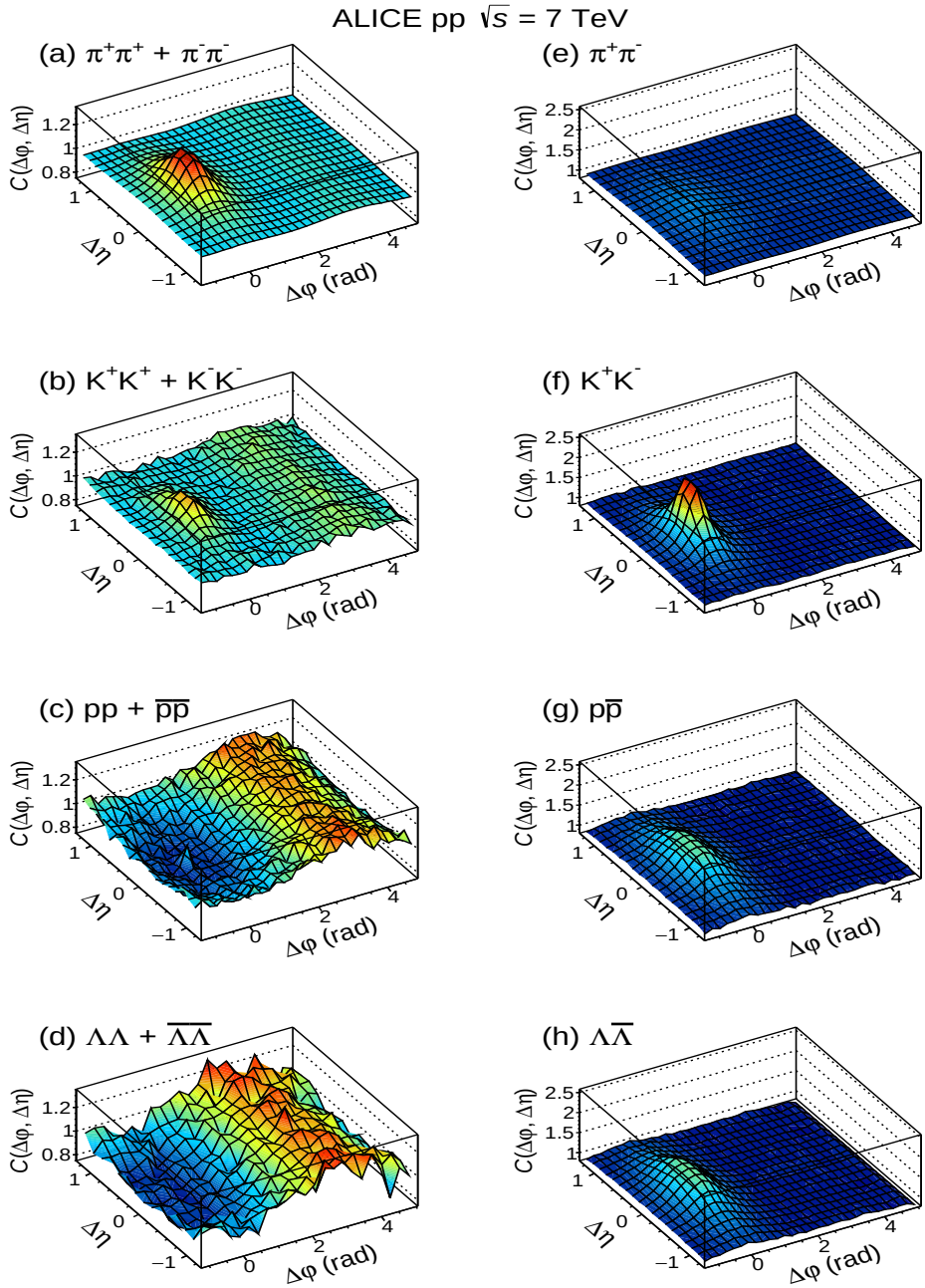

Figure 20.14: Two-particle correlation functions for identical-particle pairs: $\pi^+\pi^+ + \pi^-\pi^-$, $K^+K^+ + K^-K^-$, $pp + \bar{p}\bar{p}$, and $\Lambda\Lambda + \bar{\Lambda}\bar{\Lambda}$ (left panel) and particle–anti-particle pairs: $\pi^+\pi^-$, K^+K^-, $p\bar{p}$ and $\Lambda\bar{\Lambda}$ (right panel). Figure from Ref. [168].

more cut Pomerons also results in a much wider multiplicity distribution and in a larger density of soft particles coming from the 'underlying event'.

20.5.2.2 *Color reconnection*

In this context, we have to mention also the so-called 'colour reconnection' phenomenon. This is a pure 'soft QCD' effect. The point is that after a number of coloured secondary partons are produced, there are different possibilities to form the colour flow between these partons and to group the partons into colourless clusters. In the process of reconnection, one rearranges the colour flow in such a way as to minimize the size of the clusters. This is especially important when dealing with MPI contributions. The reconnection between the different cut Pomerons diminishes the final multiplicity and can change the form of the $N_{\rm ch}$ distributions (see e.g. Section 43.3.2 of [1] and [2, 13, 176, 177]).

20.5.2.3 *Double parton scattering*

The probability of MPI depends on the spatial distribution of partons in the incoming protons. The effects of MPI are suppressed if the density of partons is low and the partons from the incoming beam particles are separated from each other by a large interval in transverse coordinate space $\vec{x}_t$. Events in which two hard subprocesses, caused by interactions of two different parton pairs (say, (a_1b_1) and (a_2b_2)), take place simultaneously, are called Double Parton Scattering (DPS). The DPS cross section is driven by the 'double parton distributions', $D(y_{a_1}, y_{a_2}, ...)$, where y_{a_1} and y_{a_2} are momentum fractions carried by the partons from the proton a and the dots denote all other coordinates. As a rule, experiments study DPS processes at relatively small momentum fractions y_i. Here, correlations due to momentum conservation (like $y_{a_1} + y_{a_2} < 1$) are not so important, and with a reasonable accuracy we can assume a factorization

$$D(y_{a_1}, y_{a_2}, ...) \propto F(y_{a_1}) \cdot F(y_{a_2}) \ , \qquad (20.54)$$

Int. J. Mod. Phys. A 2026.41. Downloaded from www.worldscientific.com
by UNIVERSITY OF CALIFORNIA @ BERKELEY on 09/16/26. Re-use and distribution is strictly not permitted, except for Open Access articles.

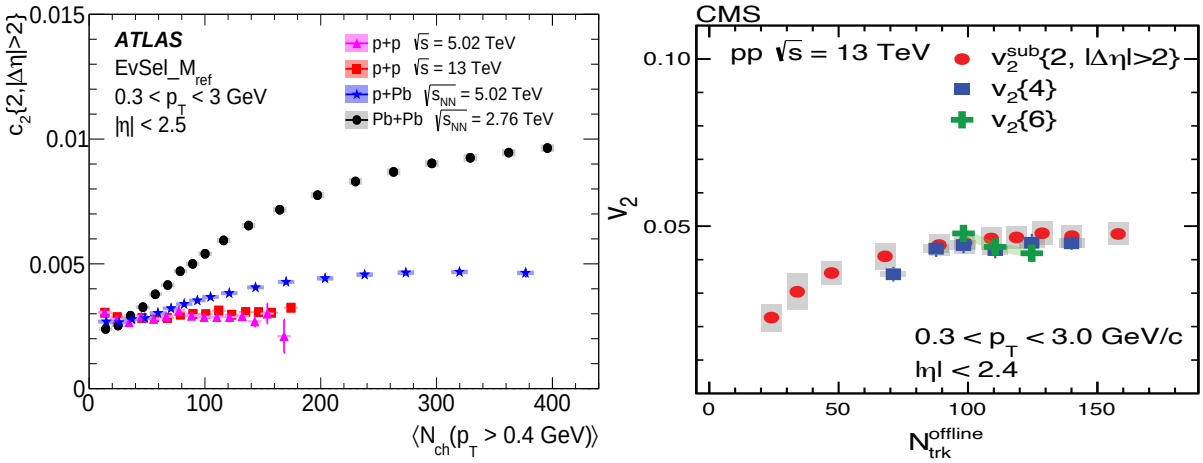

Figure 20.15: (Left) The two-particle cumulant, $c_2\{2, |\Delta\eta| > 2\}$, as a function of $\langle N_{\rm ch}(p_T > 0.4\ {\rm GeV})\rangle$ for pp collisions at $\sqrt{s} = 5.02$ and 13 TeV, pPb collisions at $\sqrt{s_{NN}} = 5.02$ TeV and low-multiplicity $PbPb$ collisions at $\sqrt{s_{NN}} = 2.76$ TeV. The data are constructed from particles with $0.3 < p_T < 3.0$ GeV. Figure from Ref. [174]. (Right) The $v_2\{2, |\Delta\eta| > 2\}$, $v_2\{4\}$ and $v_2\{6\}$ values as a function of number of charged particles, averaged over $0.3 < p_T < 3.0$ GeV and $|\eta| < 2.4$, in pp collisions at $\sqrt{s} = 13$ TeV. Figure from Ref. [175]. The error bars correspond to the statistical uncertainties, while the shaded areas denote the systematic uncertainties.

where $F(y_{a_i})$ are the single parton distributions. In such a case the DPS cross section takes the form

$$\sigma^{\rm DPS} \;=\; c\cdot\frac{\sigma_{a_1b_1}\sigma_{a_2b_2}}{\sigma_{\rm eff}}\;, \qquad (20.55)$$

where $\sigma_{a_1b_1}$ and $\sigma_{a_2b_2}$ are cross sections for the two *independent* hard processes, while $\sigma_{\rm eff}$ characterizes the mean area occupied by the partons a_1 and b_1; the constant factor $c = 1/2$ if both hard processes (a_1b_1) and (a_2b_2) are identical, otherwise $c = 1$. Thus the DPS cross section is sensitive to the spatial separations between partons in the proton (see Section 7.2.3 in [2] and [178, 179] for more explanations and reviews).

One problem is that within this approach we *assume* that the partons a_1 and a_2 are produced by two independent parton showers (and similarly for the other incoming proton). On the other hand, there is a probability that from the beginning we start with the evolution of a single shower which further splits into two different branches. In this case the separation between the two partons (two shower branches) becomes very small – of the order of the inverse scale ($\sim 1/\sqrt{q^2}$) at which the splitting occurs. The exact value of this 'splitting' scale q^2 depends on the particular kinematics of the DPS process. So, different experiments (with different kinematical conditions) can give somewhat different values of $\sigma_{\rm eff}$. In general, the value of $\sigma_{\rm eff}$ depends on the following features: a) on the measured process since the spatial (b_t) distributions of different incoming partons (light quarks, heavy quarks, gluons) can be different; b) on the splitting scale, $\sqrt{q^2}$, of one parton cascade into two branches. The typically high value of the splitting scale then explains the fact that the experimentally measured values of $\sigma_{\rm eff} \sim 7$–25 mb (see Fig. 4 of [180]) are smaller than $\sigma_{\rm tot}$ or mostly even lower than the proton area $\pi R_p^2 \sim 22$–24 mb (see e.g. [181]); c) on the p_T balance, k_T, in the individual hard process (e.g. for two dijet productions $k_T = |\overrightarrow{p_{T1}} + \overrightarrow{p_{T2}}|$ where p_{T1} and p_{T2} are jet p_T's of the first hard process (similarly for the second hard process). A small value of k_T indicates that there were no splittings or the splitting scale $\sqrt{q^2}$ was small and, therefore, we expect larger $\sigma_{\rm eff}$; d) on the contribution of single parton scatterings misidentified as DPS. For a lower scale of the hard process this contribution is larger (see [182] for more detailed discussion).

20.5.2.4 *Final state interactions*

The formalism of the RFT does not include 'final state interactions' [16]. Therefore, besides the correlations considered in the previous Section 20.5.2.1 we have to expect the correlation caused by partons and hadrons rescattering in the final state. These effects are not crucial at lower energies, but become more important at high LHC energies, in particular in heavy-ion collisions where the particle density is large. For example, the final state interactions (FSI) lead to the formation of the collective flow of secondaries (see e.g. [184] for a review), especially in high-multiplicity events. To study the collective flow experimentally, one has to subtract correlations coming from few-particle sources such as resonance decays, mini-jets, multi-jets and BEC (so called "non-flow"). The non-flow can efficiently be suppressed using the sub-event method, that is by studying the azimuthal correlations between particles separated in η [185], or subtracted using the multi-particle correlation (or cumulant) techniques.

The cumulant method is based on calculating $2k$-particle azimuthal correlations, ${\rm corr}_n\{2k\}$, and cumulants $c_n\{2k\}$ (where $k = 1, 2, ...$), for nth Fourier harmonics. The ${\rm corr}_n\{2k\}$ are defined as [186, 187]:

$$\langle\langle{\rm corr}_n\{2\}\rangle\rangle = \langle\langle e^{in(\phi_1-\phi_2)}\rangle\rangle, \quad \langle\langle{\rm corr}_n\{4\}\rangle\rangle = \langle\langle e^{in(\phi_1+\phi_2-\phi_3-\phi_4)}\rangle\rangle,$$
$$\langle\langle{\rm corr}_n\{6\}\rangle\rangle = \langle\langle e^{in(\phi_1+\phi_2+\phi_3-\phi_4-\phi_5-\phi_6}\rangle\rangle$$

and similarly for higher numbers of correlated particles. The double-brackets $\langle\langle\rangle\rangle$ denote averaging first over particles in an event and then over events within a given event class. For every event, the average is taken over all possible combinations of azimuthal angles ϕ_l $(l = 1, ..., 2k)$ of the $2k$ particles. The cumulants are then obtained from multi-particle azimuthal correlations after subtracting correlations between $2(k-1)$ particles according to the following formulae [186, 187]:

$$c_n\{2\} = \langle\langle{\rm corr}_n\{2\}\rangle\rangle,\ c_n\{4\} = \langle\langle{\rm corr}_n\{4\}\rangle\rangle - 2\langle\langle{\rm corr}_n\{2\}\rangle\rangle^2,$$
$$c_n\{6\} = \langle\langle{\rm corr}_n\{6\}\rangle\rangle - 9\langle\langle{\rm corr}_n\{2\}\rangle\rangle \times \langle\langle{\rm corr}_n\{4\}\rangle\rangle + 12\langle\langle{\rm corr}_n\{2\}\rangle\rangle^3.$$

The cumulants for higher particle multiplicities are calculated in [186, 187]. The cumulants then serve to estimate the Fourier harmonics v_n as follows [186]:

$$v_n\{2\} = \sqrt{c_n\{2\}},\ v_n\{4\} = \sqrt[4]{-c_n\{4\}},\ v_n\{6\} = \sqrt[6]{c_n\{6\}/4}.$$

Some of the long-range correlation ($|\Delta\eta| > 2$) results obtained on a sample of charged particles with $0.3 < p_T < 3.0$ GeV and $|\eta| < 2.4$ are summarized in Fig. 20.15. The left plot shows the cumulant c_2 measured for pp, pPb and $PbPb$ collisions [174], while the right plot shows the elliptical harmonics v_2 measured for pp collisions [175], both as functions of multiplicities of charged particles. The two-particle correlations are observed to be strongest

[16] In general, final state interactions can be included into the detailed structure of the multi-Pomeron vertices. However these vertices are phenomenological objects which are not well known experimentally.

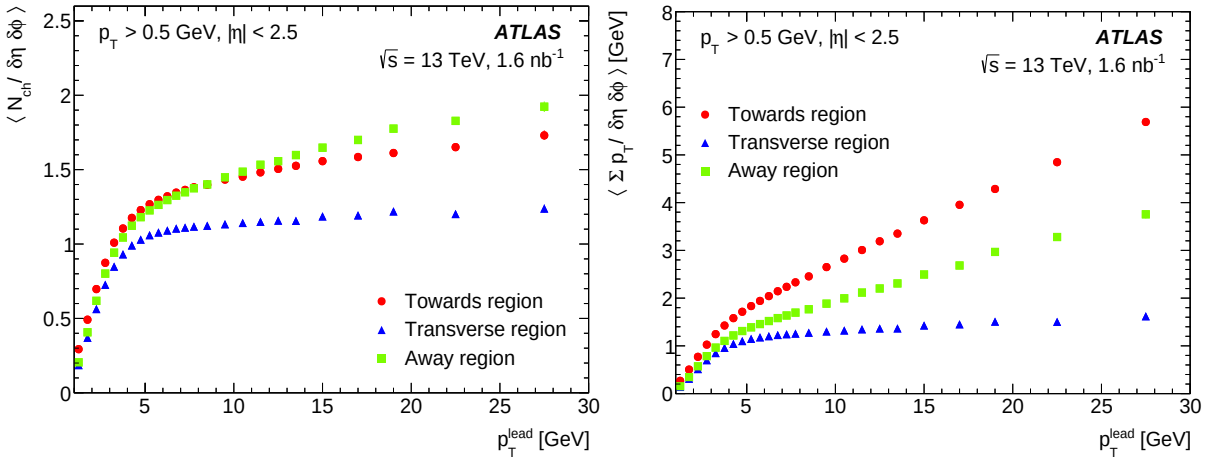

Figure 20.16: Mean charged particle density (left) and the sum of transverse momenta of secondaries (right) in events with the 'leading' high p_T particle as a function of $p_T^{\rm lead}$ in the transverse, towards and away azimuthal regions. Secondaries with $p_T > 0.5$ GeV and $|\eta| < 2.5$ are registered. The error bars (mostly hidden by the data markers) represent combined statistical and systematic uncertainties. Figures from [183].

and rising with $N_{\rm ch}$ for $PbPb$ collisions, and weakest and rather flat for pp collisions. The elliptical-flow harmonics for 4- and 6-particle correlations show again a rather flat multiplicity dependence (at least for large multiplicities). Within experimental uncertainties, the values of $v_2\{2\}, v_2\{4\}$ and $v_2\{6\}$ measured in pp collisions at 13 TeV are consistent with each other. The similarity between $v_2\{4\}$ and $v_2\{6\}$ suggests that some collective effects are occurring in pp collisions at high multiplicity and the observations are similar to those in $PbPb$ collisions, where the $v_2\{4\}$ values were measured to be close to $v_2\{6\}$ but they are both lower than $v_2\{2\}$ (not shown here)).

Another example of long-range correlations is the so-called "ridge effect". Here not only the 'back-to-back' jet correlations are registered, but also an excess of particles going in the same (in the azimuthal plane) direction as the leading (relatively high p_T) hadron. Moreover, this excess is seen at the rapidities separated from the leading hadron by a rather large interval (see e.g. [188] for a review).

It is popular to describe such FSI effects within the hydrodynamic model [189], which operates with collective (thermodynamic) variables. In terms of microscopic interactions, the collective flow can be caused by the geometry of a particular collision (the absorption is smaller for the secondaries flying in the direction orthogonal to the impact parameter vector $\vec{b}$ [190, 191]), or by the colour reconnection at the hadronization stage [192], or accounting for the rescattering of secondaries directly, as was done, for example, in the AMPT model [193].

20.5.3 *The underlying event*

Except for the exclusive case, any 'hard' subprocess is accompanied by soft secondaries coming from initial state radiation (ISR), final state radiation (FSR) and multiple parton interaction (MPI), see Subsection 7.2.2 in [2]. These extra particles distort the signal we are looking for. In particular, they affect the isolation criteria applied to photons and charged leptons and the vertex reconstruction efficiency. In general, also the effects of colour reconnection (discussed in Section 20.5.2.2) contribute to the underlying event.

The usual procedure of estimating the amount of underlying event (UE) is to spatially divide tracks in each event according to their azimuthal angle into the Toward region (where the highest p_T jet points), the Away region (opposite to the Toward region) and to two Transverse regions. The standard observables are the average track multiplicity per unit area and the average scalar sum of track p_T per unit area. Figure 20.16 shows the particle density and the sum of p_T for the UE in ATLAS events containing at least one charged particle with $p_T > 0.5$ GeV and $|\eta| < 2.5$ [183].

Note that by construction the largest values of $\langle p_T \rangle$ are observed in the 'Toward' region, while in the 'Away' region we observe a slightly larger density than in the Toward region. These are results of the 'leading' and 'backward' jet fragmentation. In the transverse region, mostly filled by particles from the UE, the particle density and sum of p_T per unit $(\Delta\eta, \Delta\phi)$ area practically do not depend on the $p_T^{\rm lead}$ since these secondaries come from the other cut Pomeron(s), that is, from other 'multiple interactions'. For low $p_T^{\rm lead} < 2$ GeV the distributions in all three regions are close to each other. These events actually do not contain a 'hard' subprocess. Moreover, for a very small $p_T^{\rm lead} \to 1$ GeV we start to select soft events with abnormally low $p_T < p_T^{\rm lead}$ particles. Since only particles with $p_T > 0.5$ GeV are registered, the signal drops fast for $p_T^{\rm lead} \to 1$ GeV. As a function of collision energy $\sqrt{s}$, the energy flow in the transverse region increases as $\sum p_T \sim s^{0.2}$ (as follows from Fig. 7 (right) in [183]) due to the larger number of MPI collisions and larger $\langle p_T \rangle$ in each collision [17]. As follows from this and other UE-dedicated LHC studies [194], from the comparisons of the data to the models with and without MPI, the necessity of MPI is convincingly demonstrated.

20.6 The Odderon

Apart from the even-signature singularity (Pomeron), in QCD with $N_c = 3$ there exists its counterpart, the odd-signature singularity placed at $j \simeq 1$ and formed by three t-channel reggeized gluons connected in colour space by the symmetric d^{abc} tensor of the colour $SU(3)$ group [199, 200]. This object is called the Odderon. The Odderon exchange amplitude has opposite sign for pp and $p\bar{p}$ scatterings. Its intercept is predicted to be very close to $j = 1$ [201–203], while according to perturbative estimates the coupling to the nucleon is rather small [204,205]. The corresponding amplitude is mainly real and is about 100 times smaller than the imaginary part of the Pomeron exchange amplitude. Calculating the elastic amplitude via the eikonal formula (20.13) we have to replace the opacity $\Omega(b)$ by the sum $\Omega = \Omega_{\rm even} + \Omega_{\rm odd}$, where $\Omega_{\rm even}$ is mainly real and $\Omega_{\rm odd}$ is imaginary. Note that at $t = 0$ this QCD Odderon does not couple to mesons, and the t-slope of the Odderon amplitude is expected to be smaller than that for the Pomeron; instead of the singularity at $t = 4m_\pi^2$ in the Pomeron case, the nearest singularity in the Odderon channel is at $t = 9m_\pi^2$, see for instance [203]. Thus, in the impact parameter b space the QCD Odderon occupies an area of a smaller radius, see e.g. [206].

Experimentally an indication in favour of a manifestation of the high energy C-odd amplitude was observed by comparing the elastic pp and $p\bar{p}$ cross sections in the dip region (where the contribution from the C-even amplitude has a minimum) at the CERN-ISR [196], see Fig. 20.17 (left) [18].

[17] Recall the stronger absorption of the low k_t partons.

[18] Note that a qualitatively similar behaviour to the $p\bar{p}$ ISR data, namely a filling in of the dip in the t-distribution, was observed by the UA4 collabo-

Int. J. Mod. Phys. A 2026.41. Downloaded from www.wo
by UNIVERSITY OF CALIFORNIA @ BERKELEY on 09/16/26. Re-use and distribution is
except for Open Access articles.

Int. J. Mod. Phys. A 2026.41. Downloaded from www.worldscientific.com
by UNIVERSITY OF CALIFORNIA @ BERKELEY on 09/16/26. Re-use and distribution is strictly not permitted, except for Open Access articles.

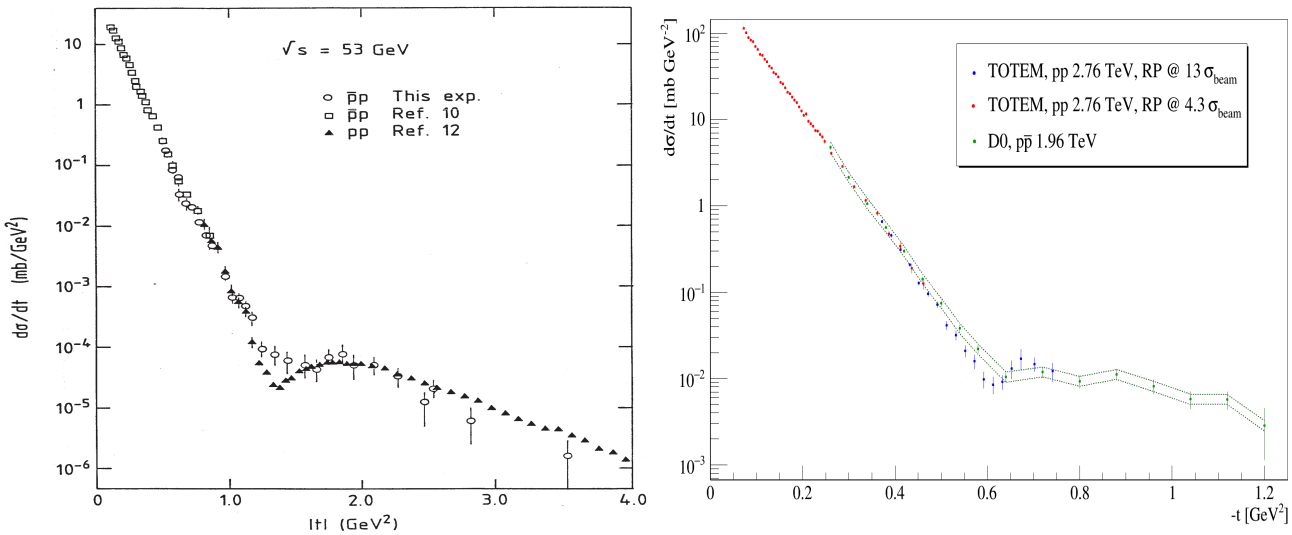

Figure 20.17: Comparison of the t-dependence of the elastic cross sections from pp and $p\bar{p}$ collisions. (Left) Data from the ISR energy of 53 GeV are shown by closed triangles [195] for pp collisions and by open circles [196] and open squares [197] for $p\bar{p}$ collisions. Only t-dependent uncertainties are shown and the systematic scale uncertainty is estimated to be ±30%. Figure from Ref. [196]. (Right) Data from the D0 experiment at 1.96 TeV [198] are compared with data from the TOTEM experiment [103]. The green dashed line indicates the normalization uncertainty of the D0 measurement. Figure from Ref. [103].

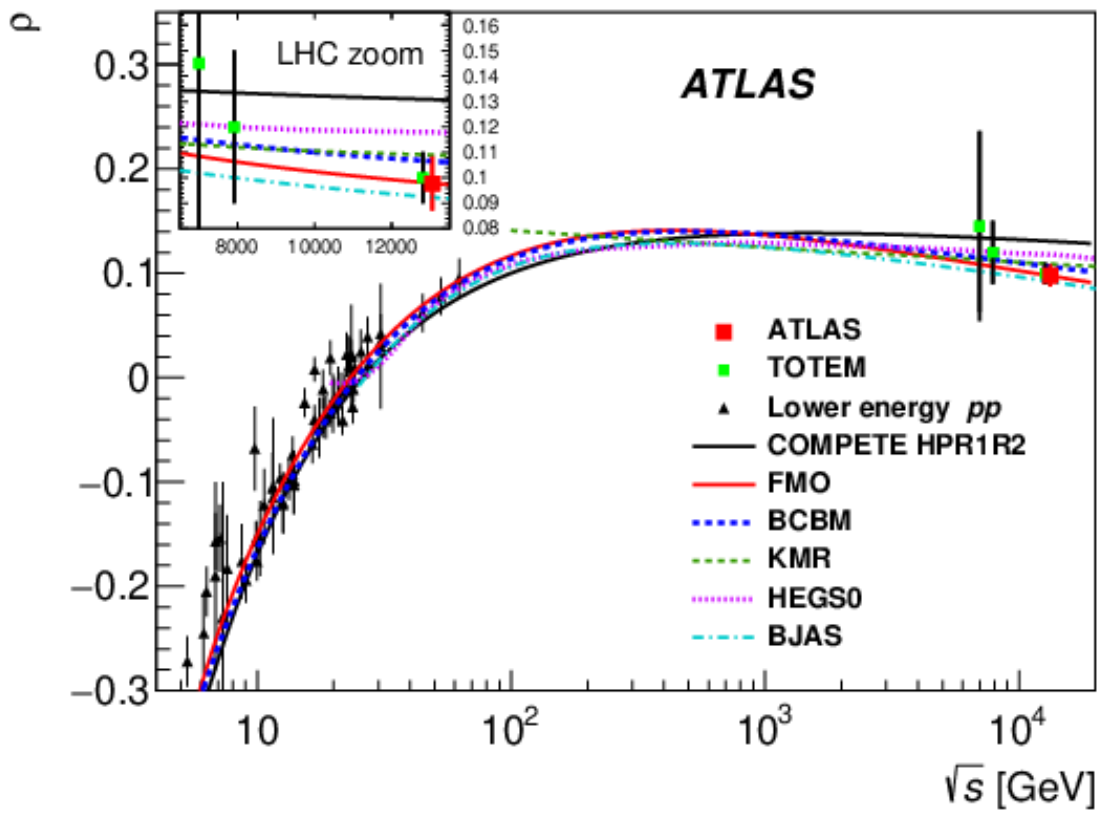

Figure 20.18: The dependence of the ρ parameter on the pp collision energy. For references to data points, see plots of cross sections in Refs. [108, 112]. Theory predictions are explained in Ref. [108]. Figure from Ref. [108].

The major constraint on the C-odd amplitude is that both the particle and antiparticle cross sections are positive (which in this case means that Im $A > 0$, according to the optical theorem $\sigma_{\rm tot}$ = Im A/s), while the C-odd amplitude changes sign from particle to antiparticle. This condition must be fulfilled at any energy and impact parameter, b, that is, at any partial wave $l = b\sqrt{s}/2$, see for a recent review [209].

This gives for the intercept of the Odderon trajectory and the

ration at the CERN S$p\bar{p}$S collider at $\sqrt{s}$=546 and 630 GeV(see [207,208] and in particular Fig. 2 in [208]) and by the $D0$ collaboration at the Tevatron at 1.96 TeV [198].

Int. J. Mod. Phys. A 2026.41. Downloaded from www.worldscientific.com by UNIVERSITY OF CALIFORNIA @ BERKELEY on 09/16/26. Re-use and distribution is [redacted] except for Open Access articles.

slope of the Odderon amplitude

$$\alpha_{odd}(0) < \alpha_{even}(0), \quad B_{odd} < B_{even} \ . \tag{20.56}$$

The perturbative QCD satisfies these conditions. For the lowest α_s order, three-gluon diagram, we get (at the leading $\ln s$ order [202]) $\alpha_{odd}(0) = 1$, while the Pomeron intercept $\alpha_{Pom}(0) > 1$.

TOTEM collaboration measured the pp cross section in the diffractive dip region at $\sqrt{s} = 2.76$ GeV [103]. A clear 'dip-bump' structure was observed while at the relatively close Tevatron energy $\sqrt{s} = 1.96$ TeV, the t- dependence of the $p\bar{p}$ cross section is more or less flat [210], see Fig. 20.17 (right).

Such an observation looks quite intriguing because in the TeV energy range the ω- and ρ-trajectory, and ωP- and ρP-cut exchange contributions, which could be responsible for the difference between the pp and $p\bar{p}$ cross sections in the dip region at the ISR energies are practically negligible. This TOTEM result was interpreted as the presence of the real part of the C-odd amplitude, which diminishes the absolute value of the real part of the pp amplitude but enlarges it, filling the dip, in the $p\bar{p}$ case [19]

Since in QCD the Odderon exchange amplitude is expected to be small and mainly real, in pp scattering the Odderon should be better observed either in the diffractive dip region where the imaginary part of the amplitude vanishes, or in the Coulomb-Nuclear Interference (CNI) region via the interference with the pure QED one-photon exchange. Note that due to dispersion relations, the real part of high-energy C-even amplitude is relatively small (Re $A_{even} \ll$ Im A_{even}). Because the one-photon exchange Coulomb amplitude contribution is sizeable only at very small momentum transferred $|t|$, this way we can study the Odderon at or near $t = 0$.

In 2018–2020 TOTEM collaboration reported the Odderon discovery based on two results. Besides the 'dip-bump' structure observed at 2.76 TeV in the dip region [103], TOTEM measured the elastic pp scattering at low $|t|$ down to $-t = 8 \cdot 10^{-4}$ GeV^2 and determined the real to imaginary part ratio ρ = Re/Im $= 0.09 \pm 0.01$ and 0.10 ± 0.01 (depending on different physics assumptions and mathematical modelling) [102]. Both values turned out to be noticeably smaller than the value 0.13–0.14 expected from dispersion relations for the case of the pure C-even interactions, see Fig. 20.18. however, it may be useful to take into account model dependences of the normalization procedure used by TOTEM [211] when trying to understand the differences. We also note that due to dispersion relations (see Eq.(20.19)), the value of ρ is strongly correlated with the energy behaviour of the total cross section.

Note that the values of σ_{tot} measured by ATLAS-ALFA proton spectrometer at 7, 8, and 13 TeV are found to be systematically lower than the TOTEM numbers. In particular, at 13 TeV, ATLAS found the same ρ value as TOTEM, $\rho = 0.10 \pm 0.01$, but the value of the total cross-section is $\sigma_{tot} = 104.68 \pm 1.09$ mb [108], which is approximately 5% lower than the weighted average of values determined by TOTEM, $\sigma_{tot} = 110.5 \pm 2.4$ mb [102] indicating that a smaller value of the real part of the C-even amplitude should be expected from the dispersion relations.

The relatively small value of ρ could indicate either that the rise of the total cross section at energies above those at LHC slows down[20] or can be explained by the admixture of the C-odd amplitude, which survives at high LHC energies.

The available low $|t|$ ($|t| < 0.1$ GeV^2) data in the range 50 GeV $< \sqrt{s} <$ 13 TeV were analyzed in the recent paper [212], including both the TOTEM and ATLAS-ALFA results with the corresponding (free) normalisation factors. The two-channel eikonal model was used, which naturally accounts for the screening of the Odderon amplitude by C-even (Pomeron) exchanges. A quite satisfactory fit was obtained with $\chi^2 = 560$ for 504 degrees of freedom, ν; $\chi^2/\nu = 1.11$. Neglecting the Odderon would lead to a much larger $\chi^2 = 726$. The main conclusions drawn from the study in [212] are:

- The description of the data with the addition of the Odderon improves the fit (significantly lowers the χ^2 value).
- The sign of the Odderon amplitude needed to describe the very low $|t|$ data is opposite to that predicted by the perturbative QCD three-gluon exchange contribution, see [213–215] [21]
- The Odderon-proton coupling, β_O, is smaller than that for the Pomeron. Moreover, after accounting for the screening of the seed Odderon (i.e. Odderon prior to inclusion of the Pomeron cuts) by the Pomeron cuts, the final C-odd contribution to ρ at 13 TeV becomes quite small, $\delta\rho = (\rho^{\bar{p}p} - \rho^{pp})/2 \leq 0.004$, i.e. 10 times less than $\delta\rho = 0.04$, originally claimed by TOTEM. Such a low value of $\delta\rho$ is expected in the quark-diquark model of the nucleon, see e.g. [205,216].

The TOTEM results [102,103] prompted a renewal of interest in the establishment of the high-energy C-odd (Odderon) contribution. Though the existence of the Odderon is a firm prediction of QCD, to additionally experimentally confirm its presence and to accurately measure its coupling to the proton, further experimental efforts are certainly needed.

In the literature, different approaches were suggested to reveal the Odderon signal. It was proposed to search for the Odderon in exclusive C-even meson ($\pi^0, \eta, f_2, \eta_c, ...$) photoproduction (see e.g. [217, 218]). However, the expected cross sections are small (e.g. for η_c), and in each channel, there is a large background caused either by Pomeron-Pomeron fusion (such as CEP for the f_2 meson production in pp or pPb collisions) or due to the vector meson radiative decay (such as $\omega \to \pi^0\gamma$ for the case of pion) [219]. Such a background can be suppressed in the future Electron Ion Collider if the energy of the outgoing electron is measured, and the incoming photon energy is compared with the C-even meson energy. Up to now, no definitive Odderon signal in the C-even meson production has been observed. At the moment, there exist only upper limits on the photoproduction cross sections obtained in the measurements at HERA at $\sqrt{s} \simeq 200$ GeV [220–222].

The possibility of searching for the Odderon in the exclusive C-even meson production in ultraperipheral proton–ion collisions was discussed in [219] and in the central exclusive processes in proton-ion and ion-ion collisions in [223].

Another interesting process, where the Odderon contribution could be important, is the $K_L^0 \to K_S^0$ regeneration in the interactions of the high-energy K_L^0 mesons with nucleons in pp collisions at LHC [224–226].

To conclude, let us emphasise that the existence of the C-odd singularity with intercept $\alpha_{odd}(0) \simeq 1$ is a firm prediction of QCD. At least in the high k_t region, there is a well-established C-odd three-gluon contribution to the scattering amplitude. However, the expected coupling of such an Odderon singularity is numerically very small. Therefore, it is quite a challenging task to observe its manifestation experimentally.

20.7 Asymptotics

The high-energy behaviour of total hadronic cross sections has been one of the oldest problems of strong interactions over many decades, beginning from Heisenberg [227]. The most important bound obtained based on general analytical properties of scattering amplitudes is the FLM bound [47–49]. It states that the growth of the total hadronic cross section with energy does not exceed $\ln^2 s$, see Eq. (20.34).

Recall that we neglected the photon contribution as well as the whole electro-weak sector, and that the parameter in Eq. (20.34) s_0 is an *a priori* unknown scale. However, if we were to assume a reasonable hadronic scale, $s_0 \simeq 1\,\text{GeV}^2$, we would find that

[19] To get a better understanding it would be instructive to have the $d\sigma_{el}/dt$ data for both pp and $p\bar{p}$ reactions at the same but high energy ~ 1 TeV (better in the same apparatus) and, in the ideal case, to study the energy dependence.

[20] Recall that analyzing the whole ensemble of high energy elastic pp ($p\bar{p}$) low $|t|$ data, a reasonable description can be obtained using the even-signature amplitude only, that is, without the Odderon.

[21] The problem can be overcome assuming that the Odderon coupling β_O vanishes (or strongly decreases) at $t = 0$. In this case, the dominant C-odd contribution at $t = 0$ comes from the Pomeron-Odderon cut [216] and has an opposite sign.

Int. J. Mod. Phys. A 2026.41. Downloaded from www.worldscientific.com
by UNIVERSITY OF CALIFORNIA @ BERKELEY on 09/16/26. Re-use and distribution is strictly not permitted, except for Open Access articles.

Eq. (20.34) implies an unrealistically high upper bound in comparison with the cross sections observed at present collider energies. Nevertheless there is a common trend in the literature (see for instance, reviews [228, 229] and references therein) to fit phenomenologically the total cross section with $\ln^2 s$, keeping in mind the saturation of the FLM bound. Such an asymptotic behaviour is assumed also by the COMPETE collaboration [22], which achieved a comprehensive description of all soft pre-LHC data measured at $\sqrt{s} \geq 4$ GeV as well as total pp cross sections from the LHC available in the first half of 2015 (see Section 51 in [24]).

It is interesting that the Froissart-type $\ln^2 s$ asymptotics of the pp total cross section are also supported by numerical results in lattice QCD [230]. Such a behaviour is also observed in the approach [231] based on Colour Glass Condensate saturation.

Finally, it is worth mentioning that the possibility that *asymptotically* the Pomeron intercept becomes smaller than 1, $\alpha_{\mathbb{P}}(0) < 1$, and at very high energies the total cross section starts to decrease with energy, though highly unlikely, is not yet completely rejected. For instance, such a behaviour is expected in a theory with only the triple-Pomeron coupling, $g_{3\mathbb{P}}$, and which neglects the more complicated multi-Pomeron vertices g^n_m, such as the $2 \to 2$ Pomeron coupling [232, 233].

It was also argued that in the case of an increasing (with energy) cross section the only regime consistent asymptotically with both the s- and the t-channel unitarities is that of a *black* disc whose radius increases as $R = c \cdot \ln s$ [234] (i.e. $R \propto (\ln s)^\gamma$, with $\gamma = 1$ exactly).

20.8 Acknowledgements

It is a pleasure to thank Michael Albrow, Robert Cahn, Robert Ciesielski, Per Grafstrom, Frank Krauss, Paul Newman, Sergey Ostapchenko and Edward Sarkisyan-Grinbaum for discussions, suggestions and comments on this review. Special thanks to Graeme Watt who read the article through and helped to improve the presentation. MT is supported by MEYS of the Czech Republic within project LTT17018. VAK thanks the Institute of Physics of the Czech Academy of Sciences in Prague for hospitality.

References

[1] M. Tanabashi *et al.* (Particle Data Group), Phys. Rev. **D98**, 3, 030001 (2018).

[2] J. Campbell, J. Huston and F. Krauss, *The Black Book of Quantum Chromodynamics*, Oxford University Press (2017), ISBN 9780199652747, URL `https://global.oup.com/academic/product/the-black-book-of-quantum-chromodynamics-9780199652747`.

[3] R. J. Eden *et al.*, *The analytic S-matrix*, Cambridge Univ. Press, Cambridge (1966).

[4] A. Martin, Lect. Notes Phys. **3**, 1 (1969).

[5] P. D. B. Collins, *An Introduction to Regge Theory and High-Energy Physics*, Cambridge Monographs on Mathematical Physics, Cambridge Univ. Press, Cambridge, UK (2009), ISBN 9780521110358, URL `http://www-spires.fnal.gov/spires/find/books/www?cl=QC793.3.R4C695`.

[6] S. Donnachie *et al.*, Camb. Monogr. Part. Phys. Nucl. Phys. Cosmol. **19**, 1 (2002).

[7] V. N. Gribov, *The theory of complex angular momenta: Gribov lectures on theoretical physics*, Cambridge Monographs on Mathematical Physics, Cambridge University Press (2007), ISBN 9780521037037, 9780521818346, 9780511055041, URL `http://www.cambridge.org/uk/catalogue/catalogue.asp?isbn=0521307848`.

[8] S. Ostapchenko, in "25th European Cosmic Ray Symposium (ECRS 2016) Turin, Italy, September 04-09, 2016," (2016), [arXiv:1612.09461].

[9] T. Sjostrand, Int. J. Mod. Phys. **A3**, 751 (1988).

[10] B. Andersson, Camb. Monogr. Part. Phys. Nucl. Phys. Cosmol. **7**, 1 (1997).

[11] W. Kittel and E. A. De Wolf, *Soft multihadron dynamics* (2005), ISBN 9789812562951.

[12] I. M. Dremin and A. B. Kaidalov, Phys. Usp. **49**, 263 (2006), [Usp. Fiz. Nauk176,275(2006)].

[13] A. Buckley *et al.*, Phys. Rept. **504**, 145 (2011), [arXiv:1101.2599].

[14] R. Ciesielski and K. Goulianos, PoS **ICHEP2012**, 301 (2013), [arXiv:1205.1446].

[15] K. Akiba *et al.* (LHC Forward Physics Working Group), J. Phys. **G43**, 110201 (2016), [arXiv:1611.05079].

[16] G. D. Alkhazov, S. L. Belostotsky and A. A. Vorobev, Phys. Rept. **42**, 89 (1978).

[17] E. L. Feinberg and I. Y. Pomeranchuk, Doklady Akad. Nauk SSSR **93**, 439 (1953); E. L. Feinberg and I. Y. Pomeranchuk, Suppl. Nuovo Cimento **III**, serie X, 652 (1956).

[18] R. Engel, D. Heck and T. Pierog, Ann. Rev. Nucl. Part. Sci. **61**, 467 (2011).

[19] M. Gell-Mann, in "High-energy physics. Proceedings, 11th International Conference, ICHEP'62, Geneva, Switzerland, Jul 4-11, 1962," 533–542 (1962).

[20] S. Frautschi, M. Gell-Mann and F. Zachariasen, Phys. Rev. **126**, 6, 2204 (1962).

[21] K. G. Boreskov, A. B. Kaidalov and O. V. Kancheli, Phys. Atom. Nucl. **69**, 1765 (2006), [Yad. Fiz.69,1802(2006)].

[22] J. R. Cudell *et al.* (COMPETE), Phys. Rev. Lett. **89**, 201801 (2002), [hep-ph/0206172].

[23] C. Bourrely, J. Soffer and T. T. Wu, Eur. Phys. J. **C28**, 97 (2003), [hep-ph/0210264].

[24] C. Patrignani *et al.* (Particle Data Group), Chin. Phys. **C40**, 10, 100001 (2016).

[25] A. Donnachie and P. V. Landshoff, Nucl. Phys. **B231**, 189 (1984).

[26] A. Donnachie and P. V. Landshoff, Phys. Lett. **B296**, 227 (1992), [hep-ph/9209205].

[27] S. Mandelstam, Nuovo Cim. **30**, 1148 (1963).

[28] V. N. Gribov, I. Ya. Pomeranchuk and K. A. Ter-Martirosian, Phys. Lett. **9**, 269 (1964).

[29] V. A. Khoze, A. D. Martin and M. G. Ryskin, Int. J. Mod. Phys. **A30**, 08, 1542004 (2015), [arXiv:1402.2778].

[30] E. Gotsman, E. Levin and U. Maor, Int. J. Mod. Phys. **A30**, 08, 1542005 (2015), [arXiv:1403.4531].

[31] S. Ostapchenko, Phys. Rev. **D81**, 114028 (2010), [arXiv:1003.0196].

[32] V. N. Gribov, Sov. Phys. JETP **26**, 414 (1968), [Zh. Eksp. Teor. Fiz.53,654(1967)].

[33] U. Amaldi, M. Jacob and G. Matthiae, Ann. Rev. Nucl. Part. Sci. **26**, 385 (1976).

[34] A. B. Kaidalov, Phys. Rept. **50**, 157 (1979).

[35] V. Barone and E. Predazzi, *High-Energy Particle Diffraction*, volume v.565 of *Texts and Monographs in Physics*, Springer-Verlag, Berlin Heidelberg (2002), ISBN 3540421076, URL `http://www-spires.fnal.gov/spires/find/books/www?cl=QC794.6.C6B37::2002`.

[36] A. B. Kaidalov *et al.*, Acta Phys. Polon. **B34**, 3163 (2003), [hep-ph/0303111].

[37] L. Frankfurt and M. Strikman, in E. M. Henley and S. D. Ellis, editors, "100 Years of Subatomic Physics," 363–423 (2013), [arXiv:1304.4308].

[38] V. A. Khoze *et al.*, Eur. Phys. J. **C69**, 85 (2010), [arXiv:1005.4839].

[39] D. A. Fagundes *et al.*, Phys. Rev. **D88**, 9, 094019 (2013), [arXiv:1306.0452].

[40] R. Fiore *et al.*, Int. J. Mod. Phys. **A24**, 2551 (2009), [arXiv:0810.2902].

[41] I. M. Dremin, Phys. Usp. **56**, 3 (2013), [Usp. Fiz. Nauk 183, 3 (2013)], [arXiv:1206.5474].

Int. J. Mod. Phys. A 2026.41. Downloaded from www.worldscientific.com by UNIVERSITY OF CALIFORNIA @ BERKELEY on 09/16/26. Re-use and distribution is [redacted] except for Open Access articles.

[42] L. Frankfurt *et al.*, Phys. Rev. Lett. **101**, 202003 (2008), [arXiv:0808.0182].

[43] G. Bertsch *et al.*, Phys. Rev. Lett. **47**, 297 (1981).

[44] B. Z. Kopeliovich, L. I. Lapidus and A. B. Zamolodchikov, JETP Lett. **33**, 595 (1981), [Pisma Zh. Eksp. Teor. Fiz. 33, 612 (1981)].

[45] M. L. Good and W. D. Walker, Phys. Rev. **120**, 1855 (1960).

[46] J. Pumplin, Phys. Rev. **D8**, 2899 (1973).

[47] M. Froissart, Phys. Rev. **123**, 1053 (1961).

[48] A. Martin, Nuovo Cim. **A42**, 930 (1965).

[49] L. Lukaszuk and A. Martin, Nuovo Cim. **A52**, 122 (1967).

[50] A. A. Anselm and V. N. Gribov, Phys. Lett. **40B**, 487 (1972).

[51] G. Cohen-Tannoudji, V. V. Ilyin and L. L. Jenkovszky, Lett. Nuovo Cim. **5S2**, 957 (1972), [Lett. Nuovo Cim.5,957(1972)].

[52] V. A. Khoze, A. D. Martin and M. G. Ryskin, Eur. Phys. J. **C18**, 167 (2000), [hep-ph/0007359].

[53] G. Antchev *et al.* (TOTEM), Nucl. Phys. **B899**, 527 (2015), [arXiv:1503.08111].

[54] G. Antchev *et al.* (TOTEM), Eur. Phys. J. **C79**, 10, 861 (2019), [arXiv:1812.08283].

[55] L. Caneschi and A. Pignotti, Phys. Rev. Lett. **22**, 1219 (1969).

[56] O. V. Kancheli, JETP Lett. **11**, 267 (1970), [Pisma Zh. Eksp. Teor. Fiz. 11, 397 (1970)].

[57] A. H. Mueller, Phys. Rev. **D4**, 150 (1971).

[58] D. Amati, A. Stanghellini and S. Fubini, Nuovo Cim. **26**, 896 (1962).

[59] V. S. Fadin, E. A. Kuraev and L. N. Lipatov, Phys. Lett. **60B**, 50 (1975); E. A. Kuraev, L. N. Lipatov and V. S. Fadin, Sov. Phys. JETP **44**, 443 (1976), [Zh. Eksp. Teor. Fiz.71,840(1976)]; E. A. Kuraev, L. N. Lipatov and V. S. Fadin, Sov. Phys. JETP **45**, 199 (1977), [Zh. Eksp. Teor. Fiz.72,377(1977)]; I. I. Balitsky and L. N. Lipatov, Sov. J. Nucl. Phys. **28**, 822 (1978), [Yad. Fiz.28,1597(1978)].

[60] B. L. Ioffe, V. S. Fadin and L. N. Lipatov, *Quantum chromodynamics: Perturbative and nonperturbative aspects*, volume 30, Cambridge Univ. Press (2010), ISBN 9781107424753, 9780521631488, 9780511717444, URL `http://www.cambridge.org/de/knowledge/isbn/item2710695`.

[61] S. Ostapchenko, Phys. Rev. **D83**, 014018 (2011), [arXiv:1010.1869].

[62] J. L. Cardy, Nucl. Phys. **B75**, 413 (1974).

[63] A. B. Kaidalov *et al.*, Phys. Lett. **45B**, 493 (1973).

[64] E. G. S. Luna *et al.*, Eur. Phys. J. **C59**, 1 (2009), [arXiv:0807.4115].

[65] T. Sjöstrand, Adv. Ser. Direct. High Energy Phys. **29**, 191 (2018), [arXiv:1706.02166].

[66] K. Werner, F.-M. Liu and T. Pierog, Phys. Rev. **C74**, 044902 (2006), [hep-ph/0506232].

[67] V. A. Abramovsky, V. N. Gribov and O. V. Kancheli, Yad. Fiz. **18**, 595 (1973), [Sov. J. Nucl. Phys. 18, 308 (1974)].

[68] G. Alberi and G. Goggi, Phys. Rept. **74**, 1 (1981).

[69] K. A. Goulianos, Phys. Rept. **101**, 169 (1983).

[70] D. Bernard *et al.* (UA4), Phys. Lett. **B186**, 227 (1987).

[71] R. E. Ansorge *et al.* (UA5), Z. Phys. **C33**, 175 (1986).

[72] N. A. Amos *et al.* (E710), Phys. Lett. **B301**, 313 (1993).

[73] F. Abe *et al.* (CDF), Phys. Rev. **D50**, 5535 (1994).

[74] G. Aad *et al.* (ATLAS), Eur. Phys. J. **C72**, 1926 (2012), [arXiv:1201.2808].

[75] V. Khachatryan *et al.* (CMS), Phys. Rev. **D92**, 1, 012003 (2015), [arXiv:1503.08689].

[76] B. Abelev *et al.* (ALICE), Eur. Phys. J. **C73**, 6, 2456 (2013), [arXiv:1208.4968].

[77] G. Aad *et al.* (ATLAS), Phys. Lett. **B754**, 214 (2016), [arXiv:1511.00502].

[78] G. Aad *et al.* (ATLAS), JHEP **02**, 042 (2020), [arXiv:1911.00453].

[79] A. M. Sirunyan *et al.* (CMS and TOTEM) (2020), [arXiv:2002.12146].

[80] V. A. Khoze, A. D. Martin and M. G. Ryskin, Eur. Phys. J. **C73**, 2503 (2013), [arXiv:1306.2149].

[81] V. A. Khoze, A. D. Martin and M. G. Ryskin, Eur. Phys. J. **C23**, 311 (2002), [hep-ph/0111078].

[82] M. G. Albrow, T. D. Coughlin and J. R. Forshaw, Prog. Part. Nucl. Phys. **65**, 149 (2010), [arXiv:1006.1289].

[83] M. Albrow, Int. J. Mod. Phys. **A29**, 1402006 (2014).

[84] H. G. Fischer, W. Geist and M. Makariev, Int. J. Mod. Phys. **A29**, 28, 1446005 (2014).

[85] A. Kirk, Int. J. Mod. Phys. **A29**, 28, 1446001 (2014), [arXiv:1408.1196].

[86] M. A. Reyes *et al.* (E690), Phys. Rev. Lett. **81**, 4079 (1998).

[87] G. Gutierrez and M. A. Reyes, Int. J. Mod. Phys. **A29**, 28, 1446008 (2014), [arXiv:1409.8243].

[88] Y. L. Dokshitzer, D. Diakonov and S. I. Troian, Phys. Rept. **58**, 269 (1980).

[89] M. Derrick *et al.* (ZEUS), Phys. Lett. **B315**, 481 (1993).

[90] T. Ahmed *et al.* (H1), Nucl. Phys. **B429**, 477 (1994).

[91] P. Newman and M. Wing, Rev. Mod. Phys. **86**, 3, 1037 (2014), [arXiv:1308.3368].

[92] A. Aktas *et al.* (H1), Eur. Phys. J. **C48**, 715 (2006), [hep-ex/0606004].

[93] S. Chekanov *et al.* (ZEUS), Nucl. Phys. **B816**, 1 (2009), [arXiv:0812.2003].

[94] F. D. Aaron *et al.* (H1), Eur. Phys. J. **C72**, 2074 (2012), [arXiv:1203.4495].

[95] F. D. Aaron *et al.* (H1, ZEUS), Eur. Phys. J. **C72**, 2175 (2012), [arXiv:1207.4864].

[96] A. Aktas *et al.* (H1), JHEP **10**, 042 (2007), [arXiv:0708.3217].

[97] A. Aktas *et al.* (H1), Eur. Phys. J. **C50**, 1 (2007), [hep-ex/0610076].

[98] S. Chekanov *et al.* (ZEUS), Nucl. Phys. **B672**, 3 (2003), [hep-ex/0307068].

[99] E. G. de Oliveira, A. D. Martin and M. G. Ryskin, Phys. Lett. **B695**, 162 (2011), [arXiv:1010.1366].

[100] G. Antchev *et al.* (TOTEM), Eur. Phys. J. **C79**, 2, 103 (2019), [arXiv:1712.06153].

[101] C. Augier *et al.* (UA4/2), Phys. Lett. **B316**, 448 (1993).

[102] G. Antchev *et al.* (TOTEM), Eur. Phys. J. **C79**, 9, 785 (2019), [arXiv:1812.04732].

[103] G. Antchev *et al.* (TOTEM), Eur. Phys. J. **C80**, 2, 91 (2020), [arXiv:1812.08610].

[104] G. Antchev *et al.* (TOTEM), EPL **101**, 2, 21002 (2013).

[105] G. Antchev *et al.* (TOTEM), Phys. Rev. Lett. **111**, 1, 012001 (2013).

[106] G. Aad *et al.* (ATLAS), Nucl. Phys. **B889**, 486 (2014), [arXiv:1408.5778].

[107] M. Aaboud *et al.* (ATLAS), Phys. Lett. **B761**, 158 (2016), [arXiv:1607.06605].

[108] G. Aad *et al.* (ATLAS), Eur. Phys. J. C **83**, 5, 441 (2023), [arXiv:2207.12246].

[109] M. M. Block and R. N. Cahn, Rev. Mod. Phys. **57**, 563 (1985).

[110] F. Abe *et al.* (CDF), Phys. Rev. **D50**, 5550 (1994).

Int. J. Mod. Phys. A 2026.41. Downloaded from www.worldscientific.com
by UNIVERSITY OF CALIFORNIA @ BERKELEY on 09/16/26. Re-use and distribution is strictly not permitted, except for Open Access articles.

[111] C. Avila *et al.* (E811), Phys. Lett. **B445**, 419 (1999).

[112] P. A. Zyla *et al.* (Particle Data Group), PTEP **2020**, 8, 083C01 (2020).

[113] G. Antchev *et al.* (TOTEM), EPL **95**, 4, 41001 (2011), [arXiv:1110.1385].

[114] G. Antchev *et al.* (TOTEM), Eur. Phys. J. **C76**, 12, 661 (2016), [arXiv:1610.00603].

[115] J. Kaspar, Invited talk at the meeting of the LHC Working Group on Forward Physics and Diffraction, CERN, Switzerland, December 16-17th, 2019.

[116] V. A. Schegelsky and M. G. Ryskin, Phys. Rev. **D85**, 094024 (2012), [arXiv:1112.3243].

[117] A. Bruni, X. Janssen and P. Marage, in "Proceedings, HERA and the LHC Workshop Series on the implications of HERA for LHC physics: 2006-2008," 427–439 (2008), [arXiv:0812.0539].

[118] A. Levy, in "Proceedings, 17th International Workshop on Deep-Inelastic Scattering and Related Subjects (DIS 2009): Madrid, Spain, April 26-30, 2009," 177 (2009), [arXiv:0907.2178].

[119] J. R. Forshaw, R. Sandapen and G. Shaw, JHEP **11**, 025 (2006), [hep-ph/0608161].

[120] A. Capella *et al.*, Nucl. Phys. **B593**, 336 (2001), [hep-ph/0005049].

[121] V. S. Fadin and L. N. Lipatov, Phys. Lett. **B429**, 127 (1998), [hep-ph/9802290].

[122] M. Ciafaloni and G. Camici, Phys. Lett. **B430**, 349 (1998), [hep-ph/9803389].

[123] F. D. Aaron *et al.* (H1), JHEP **05**, 032 (2010), [arXiv:0910.5831].

[124] C. Adloff *et al.* (H1), Eur. Phys. J. **C13**, 371 (2000), [hep-ex/9902019].

[125] J. Breitweg *et al.* (ZEUS), Eur. Phys. J. **C6**, 603 (1999), [hep-ex/9808020].

[126] S. Chekanov *et al.* (ZEUS), PMC Phys. **A1**, 6 (2007), [arXiv:0708.1478].

[127] M. Ciafaloni, Nucl. Phys. **B296**, 49 (1988).

[128] S. Catani, F. Fiorani and G. Marchesini, Phys. Lett. **B234**, 339 (1990).

[129] S. Catani, F. Fiorani and G. Marchesini, Nucl. Phys. **B336**, 18 (1990).

[130] G. Marchesini, Nucl. Phys. **B445**, 49 (1995), [hep-ph/9412327].

[131] G. P. Salam, JHEP **07**, 019 (1998), [hep-ph/9806482].

[132] M. Ciafaloni and D. Colferai, Phys. Lett. **B452**, 372 (1999), [hep-ph/9812366].

[133] H. Kowalski, L. N. Lipatov and D. A. Ross, Eur. Phys. J. **C76**, 1, 23 (2016), [arXiv:1508.05744].

[134] H. Kowalski *et al.*, Eur. Phys. J. **C77**, 11, 777 (2017), [arXiv:1707.01460].

[135] S. J. Brodsky *et al.*, JETP Lett. **70**, 155 (1999), [hep-ph/9901229].

[136] R. D. Ball *et al.*, Eur. Phys. J. **C78**, 4, 321 (2018), [arXiv:1710.05935].

[137] E. M. Levin and M. G. Ryskin, Phys. Rept. **189**, 267 (1990).

[138] L. V. Gribov, E. M. Levin and M. G. Ryskin, Phys. Rept. **100**, 1 (1983).

[139] E. M. Levin, M. G. Ryskin and A. G. Shuvaev, Nucl. Phys. **B387**, 589 (1992).

[140] A. H. Mueller, Phys. Rept. **73**, 237 (1981).

[141] A. H. Mueller, Nucl. Phys. **B415**, 373 (1994).

[142] A. H. Mueller and B. Patel, Nucl. Phys. **B425**, 471 (1994), [hep-ph/9403256].

[143] N. N. Nikolaev, B. G. Zakharov and V. R. Zoller, JETP Lett. **59**, 6 (1994), [hep-ph/9312268].

[144] V. N. Gribov and L. N. Lipatov, Sov. J. Nucl. Phys. **15**, 438 (1972), [Yad. Fiz.15,781(1972)]; G. Altarelli and G. Parisi, Nucl. Phys. **B126**, 298 (1977); Y. L. Dokshitzer, Sov. Phys. JETP **46**, 641 (1977), [Zh. Eksp. Teor. Fiz. 73, 1216 (1977)].

[145] I. Balitsky, Nucl. Phys. **B463**, 99 (1996), [hep-ph/9509348].

[146] I. Balitsky, Phys. Rev. **D60**, 014020 (1999), [hep-ph/9812311].

[147] Y. V. Kovchegov, Phys. Rev. **D60**, 034008 (1999), [hep-ph/9901281].

[148] G. Gustafson, Phys. Lett. **B718**, 1054 (2013), [arXiv:1206.1733].

[149] S. Chatrchyan *et al.* (CMS, TOTEM), Eur. Phys. J. **C74**, 10, 3053 (2014), [arXiv:1405.0722].

[150] Q.-D. Zhou (LHCF, ATLAS), EPJ Web Conf. **208**, 05008 (2019).

[151] O. Adriani *et al.* (LHCf), Phys. Lett. **B780**, 233 (2018), [arXiv:1703.07678].

[152] M. Aaboud *et al.* (ATLAS) , ATLAS-CONF-2017-075.

[153] C. Albajar *et al.* (UA1), Nucl. Phys. **B335**, 261 (1990).

[154] G. J. Alner *et al.* (UA5), Z. Phys. **C33**, 1 (1986).

[155] T. Aaltonen *et al.* (CDF), Phys. Rev. **D79**, 112005 (2009), [Erratum: Phys. Rev.D82,119903(2010)], [arXiv:0904.1098].

[156] F. Abe *et al.* (CDF), Phys. Rev. **D41**, 2330 (1990), [,119(1989)].

[157] K. Aamodt *et al.* (ALICE), Eur. Phys. J. **C68**, 89 (2010), [arXiv:1004.3034].

[158] V. Khachatryan *et al.* (CMS), Phys. Rev. Lett. **105**, 022002 (2010), [arXiv:1005.3299].

[159] B. B. Abelev *et al.* (ALICE), Eur. Phys. J. **C73**, 12, 2662 (2013), [arXiv:1307.1093].

[160] A. M. Sirunyan *et al.* (CMS), Phys. Rev. **D96**, 11, 112003 (2017), [arXiv:1706.10194].

[161] M. G. Ryskin, A. D. Martin and V. A. Khoze, Eur. Phys. J. **C71**, 1617 (2011), [arXiv:1102.2844].

[162] X.-N. Wang, Phys. Rept. **280**, 287 (1997), [hep-ph/9605214].

[163] S. Ostapchenko and M. Bleicher, Universe **5**, 5, 106 (2019).

[164] F. M. Liu *et al.*, J. Phys. **G28**, 2597 (2002), [hep-ph/0109104].

[165] E. Gotsman, E. Levin and U. Maor, Acta Phys. Polon. Supp. **8**, 777 (2015).

[166] Y. V. Kovchegov and E. Levin, Camb. Monogr. Part. Phys. Nucl. Phys. Cosmol. **33**, 1 (2012).

[167] E. A. De Wolf, I. M. Dremin and W. Kittel, Phys. Rept. **270**, 1 (1996), [hep-ph/9508325].

[168] J. Adam *et al.* (ALICE), Eur. Phys. J. **C77**, 8, 569 (2017), [arXiv:1612.08975].

[169] V. Khachatryan *et al.* (CMS), JHEP **09**, 091 (2010), [arXiv:1009.4122].

[170] K. Eggert *et al.*, Nucl. Phys. **B86**, 201 (1975).

[171] B. Alver *et al.* (PHOBOS), Phys. Rev. **C75**, 054913 (2007), [arXiv:0704.0966].

[172] E. M. Levin and M. G. Ryskin, Sov. J. Nucl. Phys. **20**, 280 (1975), [Yad. Fiz.20,519(1974)].

[173] A. Capella and A. Krzywicki, Phys. Rev. **D18**, 4120 (1978).

[174] M. Aaboud *et al.* (ATLAS), Eur. Phys. J. **C77**, 6, 428 (2017), [arXiv:1705.04176].

[175] V. Khachatryan *et al.* (CMS), Phys. Lett. **B765**, 193 (2017), [arXiv:1606.06198].

[176] S. Gieseke, Invited talk at the Workshop on Multiple Partonic Interactions at the LHC, Prague, Czech Republic, November 18th–26th, 2019.

Int. J. Mod. Phys. A 2026.41. Downloaded from www.worldscientific.com by UNIVERSITY OF CALIFORNIA @ BERKELEY on 09/16/26. Re-use and distribution is [redacted] except for Open Access articles.

[177] S. Kundu, B. Mohanty and D. Mallick (2019), [arXiv:1912.05176].

[178] M. Diehl, D. Ostermeier and A. Schafer, JHEP **03**, 089 (2012), [Erratum: JHEP03,001(2016)], [arXiv:1111.0910].

[179] T. Sjostrand and P. Z. Skands, JHEP **03**, 053 (2004), [hep-ph/0402078].

[180] M. Aaboud *et al.* (ATLAS), Phys. Lett. **B790**, 595 (2019), [Phys. Lett.790,595(2019)], [arXiv:1811.11094].

[181] M. G. Ryskin and A. M. Snigirev, Phys. Rev. **D83**, 114047 (2011), [arXiv:1103.3495].

[182] B. Blok *et al.*, Eur. Phys. J. **C74**, 2926 (2014), [arXiv:1306.3763].

[183] M. Aaboud *et al.* (ATLAS), JHEP **03**, 157 (2017), [arXiv:1701.05390].

[184] R. Snellings, New J. Phys. **13**, 055008 (2011), [arXiv:1102.3010].

[185] M. Aaboud *et al.* (ATLAS), Phys. Rev. **C97**, 2, 024904 (2018), [arXiv:1708.03559].

[186] N. Borghini, P. M. Dinh and J.-Y. Ollitrault, Phys. Rev. **C63**, 054906 (2001), [arXiv:nucl-th/0007063].

[187] A. Bilandzic, R. Snellings and S. Voloshin, Phys. Rev. **C83**, 044913 (2011), [arXiv:1010.0233].

[188] W. Li, Mod. Phys. Lett. **A27**, 1230018 (2012), [arXiv:1206.0148].

[189] B. Schenke, J. Phys. **G38**, 124009 (2011), [arXiv:1106.6012].

[190] K. G. Boreskov, A. B. Kaidalov and O. V. Kancheli, Eur. Phys. J. **C58**, 445 (2008), [arXiv:0809.0625].

[191] K. G. Boreskov, A. B. Kaidalov and O. V. Kancheli, Phys. Atom. Nucl. **72**, 361 (2009), [Yad. Fiz.72,390(2009)].

[192] C. Bierlich and J. R. Christiansen, Phys. Rev. **D92**, 9, 094010 (2015), [arXiv:1507.02091].

[193] Z.-W. Lin *et al.*, Phys. Rev. **C72**, 064901 (2005), [arXiv:nucl-th/0411110].

[194] V. Khachatryan *et al.* (CMS) , CMS-PAS-FSQ-16-008.

[195] E. Nagy *et al.*, Nucl. Phys. **B150**, 221 (1979).

[196] A. Breakstone *et al.*, Phys. Rev. Lett. **54**, 2180 (1985).

[197] A. Breakstone *et al.* (AMES-BOLOGNA-CERN-DORTMUND-HEIDELBERG-WARSAW), Nucl. Phys. **B248**, 253 (1984).

[198] V. M. Abazov *et al.* (D0), Phys. Rev. **D86**, 012009 (2012), [arXiv:1206.0687].

[199] J. Bartels, Nucl. Phys. **B175**, 365 (1980).

[200] J. Kwiecinski and M. Praszalowicz, Phys. Lett. **94B**, 413 (1980).

[201] M. A. Braun (1998), [hep-ph/9805394].

[202] J. Bartels, L. N. Lipatov and G. P. Vacca, Phys. Lett. **B477**, 178 (2000), [hep-ph/9912423].

[203] C. Ewerz (2003), [hep-ph/0306137].

[204] M. Fukugita and J. Kwiecinski, Phys. Lett. **83B**, 119 (1979), [,625(1979)].

[205] M. G. Ryskin, Sov. J. Nucl. Phys. **46**, 337 (1987), [Yad. Fiz.46,611(1987)].

[206] J. Bartels, C. Contreras and G. P. Vacca, JHEP **04**, 183 (2020), [arXiv:1910.04588].

[207] M. Bozzo *et al.* (UA4), Phys. Lett. **155B**, 197 (1985).

[208] D. Bernard *et al.* (UA4), Phys. Lett. **B171**, 142 (1986).

[209] M. G. Ryskin, Phys. Part. Nucl. Lett. **22**, 1, 187 (2025), [arXiv:2408.01990].

[210] V. M. Abazov *et al.* (D0, TOTEM), Phys. Rev. Lett. **127**, 6, 062003 (2021), [arXiv:2012.03981].

[211] P. Grafström and R. Staszewski (2025), [arXiv:2502.13618].

[212] E. G. S. Luna, M. G. Ryskin and V. A. Khoze, Phys. Rev. D **110**, 1, 014002 (2024), [arXiv:2405.09385].

[213] M. Fukugita and J. Kwiecinski, Phys. Lett. B **83**, 119 (1979).

[214] A. Donnachie and P. V. Landshoff, Phys. Lett. **123B**, 345 (1983).

[215] A. Donnachie and P. V. Landshoff, Phys. Lett. **B798**, 135008 (2019), [arXiv:1904.11218].

[216] B. G. Zakharov, Sov. J. Nucl. Phys. **49**, 860 (1989).

[217] W. Kilian and O. Nachtmann, Eur. Phys. J. **C5**, 317 (1998), [hep-ph/9712371].

[218] J. Bartels *et al.*, Eur. Phys. J. **C20**, 323 (2001), [hep-ph/0102221].

[219] L. A. Harland-Lang *et al.*, Phys. Rev. **D99**, 3, 034011 (2019), [arXiv:1811.12705].

[220] J. Olsson (H1), in "New trends in high-energy physics: Experiment, phenomenology, theory. Proceedings, International Conference, Yalta, Crimea, Ukraine, September 22-29, 2001," 79–87 (2001), [hep-ex/0112012].

[221] C. Adloff *et al.* (H1), Phys. Lett. B **544**, 35 (2002), [hep-ex/0206073].

[222] T. Berndt (H1), Acta Phys. Polon. **B33**, 3499 (2002), [,182(2002)].

[223] R. McNulty *et al.*, Eur. Phys. J. C **80**, 3, 288 (2020), [arXiv:2002.05031].

[224] A. N. Shelkovenko and B. V. Struminsky, Sov. J. Nucl. Phys. **53**, 493 (1991).

[225] B. G. Zakharov, Sov. J. Nucl. Phys. **50**, 771 (1989).

[226] P. Filip, M. Tasevsky and R. Pasechnik, PoS **ICHEP2024**, 573 (2025).

[227] W. Heisenberg, Z. Phys. **133**, 65 (1952).

[228] G. Pancheri and Y. N. Srivastava, Eur. Phys. J. **C77**, 3, 150 (2017), [arXiv:1610.10038].

[229] M. M. Block, Phys. Rept. **436**, 71 (2006), [hep-ph/0606215].

[230] M. Giordano, E. Meggiolaro and N. Moretti, JHEP **09**, 031 (2012), [arXiv:1203.0961].

[231] E. Ferreiro *et al.*, Nucl. Phys. **A710**, 373 (2002), [hep-ph/0206241].

[232] P. Grassberger and K. Sundermeyer, Phys. Lett. **77B**, 220 (1978).

[233] K. G. Boreskov, in M. Olshanetsky and A. Vainshtein, editors, "Multiple facets of quantization and supersymmetry," 322–351 (2001), [hep-ph/0112325].

[234] V. A. Khoze, A. D. Martin and M. G. Ryskin, Phys. Lett. **B787**, 167 (2018), [arXiv:1809.10406].

Astrophysics and Cosmology

21. Experimental tests of gravitational theory (rev.) 437
22. Big-Bang cosmology (rev.) 450
23. Inflation (rev.) 463
24. Big-Bang nucleosynthesis (rev.) 480
25. Cosmological parameters (rev.) 488
26. Neutrinos in cosmology (rev.) 497
27. Dark matter (rev.) 505
28. Dark energy (rev.) 523
29. Cosmic microwave background (rev.) 531
30. Cosmic rays (rev.) 542

Int. J. Mod. Phys. A 2026.41. Downloaded from www.worldscientific.com
by UNIVERSITY OF CALIFORNIA @ BERKELEY on 09/16/26. Re-use and distribution is strictly not permitted, except for Open Access articles.

Int. J. Mod. Phys. A 2026.41. Dov[redacted]orldscientific.com
by UNIVERSITY OF CALIFORNIA @ BERKELEY on 09/16/26. Re[redacted] strictly not permitted, except for Open Access articles.

Int. J. Mod. Phys. A 2026.41. Downloaded from www.worldscientific.com
by UNIVERSITY OF CALIFORNIA @ BERKELEY on 09/16/26. Re-use and distribution is strictly not permitted, except for Open Access articles.

21. Experimental Tests of Gravitational Theory

Revised August 2025 by T. Damour (IHES, Bures-sur-Yvette).

21.1 General Relativity

Einstein's theory of General Relativity (GR), the current "standard" theory of gravitation, describes gravity as a universal deformation of the Minkowski metric:

$$g_{\mu\nu}(x^\lambda) = \eta_{\mu\nu} + h_{\mu\nu}(x^\lambda)\ , \text{ where } \eta_{\mu\nu} = \mathrm{diag}(-1,+1,+1,+1)\ . \tag{21.1}$$

GR is classically defined by two postulates, embodied in the total action defining the theory:

$$S_{\rm tot}[g_{\mu\nu},\psi,A_\mu,H] = c^{-1}\int d^4x(\mathcal{L}_{\rm Ein}+\mathcal{L}_{\rm SM})\,. \tag{21.2}$$

The first postulate states that the Lagrangian density describing the propagation and self-interaction of the gravitational field is

$$\mathcal{L}_{\rm Ein}[g_{\alpha\beta}] = \frac{c^4}{16\pi G}\sqrt{g}g^{\mu\nu}R_{\mu\nu}(g_{\alpha\beta})\ , \tag{21.3}$$

where G denotes Newton's constant, $g=-\det(g_{\mu\nu})$, $g^{\mu\nu}$ is the matrix inverse of $g_{\mu\nu}$, and where the Ricci tensor $R_{\mu\nu}\equiv R^\alpha{}_{\mu\alpha\nu}$ is the only independent trace of the curvature tensor

$$R^\alpha{}_{\mu\beta\nu} = \partial_\beta\Gamma^\alpha_{\mu\nu} - \partial_\nu\Gamma^\alpha_{\mu\beta} + \Gamma^\alpha_{\sigma\beta}\Gamma^\sigma_{\mu\nu} - \Gamma^\alpha_{\sigma\nu}\Gamma^\sigma_{\mu\beta}\ , \tag{21.4}$$

$$\Gamma^\lambda_{\mu\nu} = \frac{1}{2}g^{\lambda\sigma}(\partial_\mu g_{\nu\sigma}+\partial_\nu g_{\mu\sigma}-\partial_\sigma g_{\mu\nu})\,. \tag{21.5}$$

The second postulate states that $g_{\mu\nu}$ (and its associated connection) couples universally, and minimally, to all the bosonic (respectively fermionic) fields of the Standard Model by replacing everywhere the Minkowski metric $\eta_{\mu\nu}$ (respectively the flat Minkowski connection). Schematically (suppressing matrix indices and labels for the various gauge fields and fermions and for the Higgs doublet),

$$\begin{aligned}&\mathcal{L}_{\rm SM}[\psi,A_\mu,H,g_{\mu\nu}] = \\ &-\frac{1}{4}\sum\sqrt{g}g^{\mu\alpha}g^{\nu\beta}F^a_{\mu\nu}F^a_{\alpha\beta} - \sum\sqrt{g}\,\overline{\psi}\,\gamma^\mu(D_\mu+\frac{1}{4}\omega_{ij\mu}\gamma^{ij})\psi \\ &-\tfrac{1}{2}\sqrt{g}g^{\mu\nu}\overline{D_\mu H}D_\nu H - \sqrt{g}\,V(H) - \sum\lambda\sqrt{g}\,\overline{\psi}\,H\psi\ .\end{aligned} \tag{21.6}$$

Here $F^a_{\mu\nu} = \partial_\mu A^a_\nu - \partial_\nu A^a_\mu + g_A f^a{}_{bc}A^b_\mu A^c_\nu$ and the (representation-dependent) gauge-field covariant derivative $D_\mu = \partial_\mu + g_A A^a_\mu T^{\rm rep}_a$ are defined as in Special Relativity, while the derivative of spin-$\frac{1}{2}$ fermions also includes a coupling to the gravitational "spin-connection" $\omega_{ij\mu} = -\omega_{ji\mu}$, via its contraction with $\gamma^{ij} = \frac{1}{2}(\gamma^i\gamma^j - \gamma^j\gamma^i)$, where $i,j=0,1,2,3$ and $\gamma^i = e^i{}_\mu\gamma^\mu$ are usual (numerical) Dirac matrices satisfying $\gamma^i\gamma^j+\gamma^j\gamma^i = 2\eta^{ij}$. The connection components $\omega_{ij\mu}$ are defined in terms of the local orthonormal frame (vierbein) $e^i{}_\mu$ (such that $g_{\mu\nu} = \eta_{ij}e^i{}_\mu e^j{}_\nu$) used to describe the components of the various fermions ψ, and of its inverse $e_i{}^\mu$ (such that $e_i{}^\mu e^j{}_\mu = \delta^j_i$), by $\omega_{ij\mu} = \frac{1}{2}\left(C_{i[jk]}+C_{j[ki]}-C_{k[ij]}\right)e^k_\mu$ where $C_{i[jk]} = \eta_{is}C^s{}_{[jk]}$, with $C^i{}_{[jk]} \equiv \left(\partial_\mu e^i{}_\nu - \partial_\nu e^i{}_\mu\right)e_j{}^\mu e_k{}^\nu$. From the total action follow Einstein's field equations,

$$R_{\mu\nu} - \tfrac{1}{2}Rg_{\mu\nu} = \frac{8\pi G}{c^4}T_{\mu\nu}\ . \tag{21.7}$$

Here $R = g^{\mu\nu}R_{\mu\nu}$ is the scalar curvature, and $T_{\mu\nu}\equiv g_{\mu\alpha}g_{\nu\beta}T^{\alpha\beta}$ where $T^{\mu\nu} = (2/\sqrt{g})\delta\mathcal{L}_{\rm SM}/\delta g_{\mu\nu}$ is the (symmetric) energy-momentum tensor of the Standard Model matter. The theory is invariant under arbitrary coordinate transformations: $x'^\mu = f^\mu(x^\nu)$ (as well as under arbitrary local SO(3,1) rotations of the vierbein, $e'^i{}_\mu = \Lambda^i{}_j(x)e'^j{}_\mu$). To solve the field equations Eq. (21.7), one needs to fix the coordinate gauge freedom, *e.g.*, the "harmonic gauge" (which is the analogue of the Lorenz gauge, $\partial_\mu A^\mu = 0$, in electromagnetism) corresponds to imposing the condition $\partial_\nu(\sqrt{g}g^{\mu\nu}) = 0$.

In this *Review*, we only consider the classical limit of gravitation (*i.e.* classical matter and classical gravity). Quantum gravitational effects are expected (when considered at low energy) to correct the classical action Eq. (21.2) by additional terms involving quadratic and higher powers of the curvature tensor. This suggests that the validity of classical gravity extends (at most) down to length scales of order the Planck length $L_P = \sqrt{\hbar G/c^3} \simeq 1.62\times10^{-33}$ cm, *i.e.*, up to energy scales of order the Planck energy $E_P = \sqrt{\hbar c^5/G} \simeq 1.22\times10^{19}$ GeV. Considering quantum matter in a classical gravitational background also poses interesting challenges, notably the possibility that the zero-point fluctuations of the matter fields generate a nonvanishing vacuum energy density $\rho_{\rm vac}$, corresponding to a term $-\sqrt{g}\ \rho_{\rm vac}$ in $\mathcal{L}_{\rm SM}$ [1]. This is equivalent to adding a "cosmological constant" term $+\Lambda\, g_{\mu\nu}$ on the left-hand side of Einstein's equations, Eq. (21.7), with $\Lambda = 8\pi G\,\rho_{\rm vac}/c^4$. Recent cosmological observations (see the following *Reviews*) suggest a positive value of Λ corresponding to $\rho_{\rm vac}\approx(2.3\times10^{-3}{\rm eV})^4$. Such a small value has a negligible effect on the non-cosmological tests discussed below.

21.2 Key features and predictions of GR

The definition of GR recalled above makes predictions both about the coupling of gravity to matter, and about the structure of the gravitational field beyond its previously known Newtonian aspects.

21.2.1 *Equivalence Principle*

First, the universal nature of the coupling between $g_{\mu\nu}$ and the Standard Model matter postulated in Eq. (21.6) entails many observable consequences that go under the generic name of "Equivalence Principle".

A first aspect of the Equivalence Principle is that the outcome of a local non-gravitational experiment, referred to local standards, should not depend on where, when, and in which locally inertial frame, the experiment is performed. This means, for instance, that local experiments should neither feel the cosmological evolution of the Universe (constancy of the "constants"), nor exhibit preferred directions in spacetime (isotropy of space, local Lorentz invariance).

A second aspect of the Equivalence Principle is that the kinetic terms, $g^{\mu\nu}\partial_\mu\phi\partial_\nu\phi$ or $\overline{\psi}\gamma^i e_i{}^\mu\partial_\mu\psi$, of all the fields of Nature (including the gravitational field itself) are universally coupled to the same curved spacetime metric $g_{\mu\nu}(x) = \eta_{ij}e^i{}_\mu e^j{}_\nu$. This implies in particular that all massless fields should propagate with the same speed.

A third aspect of the Equivalence Principle is that two (electrically neutral) test bodies dropped at the same location and with the same velocity in an external gravitational field should fall in the same way, independently of their masses and compositions ("universality of free fall" or "Weak Equivalence Principle"). In addition, the study (using the nonlinear structure of GR) of the motion, in an external gravitational field, of bodies having a non-negligible, or even strong, self-gravity (such as planets, neutron stars, or black holes) has shown that the latter property of free-fall universality holds equally well for self-gravitating bodies ("Strong Equivalence Principle").

A last aspect of the Equivalence Principle concerns various universality features of the gravitational redshift of clock rates. GR predicts that, when intercomparing them by means of electromagnetic signals, two (non gravity-based) clocks located along two different spacetime worldlines should exhibit a universal difference in clock rate that depends on their worldlines, but that is independent of their nature and constitution. For instance, two clocks located at two different positions in a static external Newtonian potential $U(\boldsymbol{x}) = \sum Gm/r$ should exhibit, when intercompared by electromagnetic signals, the difference in clock rate, $\tau_1/\tau_2 = \nu_2/\nu_1 = 1 + [U(\boldsymbol{x}_1)-U(\boldsymbol{x}_2)]/c^2 + O(1/c^4)$, ("universal gravitational redshift of clock rates"). Similarly, the comparison of atomic-transition frequencies when observing on Earth a transition that took place on a far-away galaxy should involve (at lowest order in cosmological perturbations) the universal cosmological redshift factor $1+z = a(t_{\rm reception})/a(t_{\rm emission})$ between the Friedmann scale factors $a(t)$ (see below).

Int. J. Mod. Phys. A 2026.41. Downloaded from www.worldscientific.com by UNIVERSITY OF CALIFORNIA @ BERKELEY on 09/16/26. Re-strictly not permitted, except for Open Access articles.

21.2.2 *Quasi-stationary, weak-field (post-Newtonian) gravity*

When applied to quasi-stationary, weak-field gravitational fields, Einstein equations, Eq. (21.7), entail a spacetime structure which predicts deviations from Newtonian gravity of the first post-Newtonian (1PN) order, *i.e.*, fractionally smaller than Newtonian effects by a factor $O(v^2/c^2) \sim O(GM/(c^2 r))$. The 1PN-accurate solution of Eq. (21.7) reads (in harmonic gauge)

$$\begin{aligned} g_{00} &= -1 + \frac{2}{c^2}V - \frac{2}{c^4}V^2 + O\left(\frac{1}{c^6}\right) , \\ g_{0i} &= -\frac{4}{c^3}V_i + O\left(\frac{1}{c^5}\right) , \\ g_{ij} &= \delta_{ij}\left[1 + \frac{2}{c^2}V\right] + O\left(\frac{1}{c^4}\right) , \end{aligned} \tag{21.8}$$

where $x^0 = ct$, $i, j = 1, 2, 3$, and where the scalar, V, and vector, V_i, (retarded) potentials are defined in terms of the sources $\sigma = \frac{T^{00}+T^{ii}}{c^2}$, $\sigma_i = \frac{T^{0i}}{c}$ by

$$V = \Box^{-1}_{\rm ret}\left[-4\pi G\sigma\right] \; ; \; V_i = \Box^{-1}_{\rm ret}\left[-4\pi G\sigma_i\right] . \tag{21.9}$$

In GR the gravitational interaction of N moving point masses (labeled by $A = 1, \ldots, N$) is described by a reduced (classical) action that admits a diagrammatic expansion:

$$S_{\rm reduced} = S^{\rm free} + S^{\rm tree-level} + S^{\rm one-loop} + \cdots \tag{21.10}$$

where the free (special-relativistic) action reads

$$\begin{aligned} S^{\rm free} &= -\sum_A \int m_A c\sqrt{-\eta_{\mu\nu}dx^\mu_A dx^\nu_A} \\ &= -\sum_A \int dt\, m_A c^2 \sqrt{1 - \mathbf{v}_A^2/c^2} , \end{aligned} \tag{21.11}$$

while the tree-level (one-graviton-exchange) interaction term reads

$$S^{\rm tree-level} = -\frac{8\pi G}{c^4}\int d^4x\, T^{\mu\nu}\Box^{-1}(T_{\mu\nu} - \tfrac{1}{2}T\eta_{\mu\nu}) \equiv \int dt L^{(2)} . \tag{21.12}$$

Corresponding to the 1PN-accurate metric of Eq. (21.8), the 1PN-accurate expansion of the latter tree-level, two-body interaction Lagrangian $L^{(2)}$ reads (with $r_{AB} \equiv |\mathbf{x}_A - \mathbf{x}_B|$, $\mathbf{n}_{AB} \equiv (\mathbf{x}_A - \mathbf{x}_B)/r_{AB}$)

$$\begin{aligned} L^{(2)} = &\tfrac{1}{2}\sum_{A\neq B}\frac{G\, m_A\, m_B}{r_{AB}}\Big[1 + \frac{3}{2c^2}(\boldsymbol{v}_A^2 + \boldsymbol{v}_B^2) - \frac{7}{2c^2}(\boldsymbol{v}_A\cdot\boldsymbol{v}_B) \\ &- \frac{1}{2c^2}(\boldsymbol{n}_{AB}\cdot\boldsymbol{v}_A)(\boldsymbol{n}_{AB}\cdot\boldsymbol{v}_B) + O\left(\frac{1}{c^4}\right)\Big] \end{aligned} \tag{21.13}$$

The two-body interactions, Eq. (21.13), exhibit v^2/c^2 corrections to Newton's $1/r$ potential induced by spin-2 exchange ("gravitomagnetism"). Consistency at the 1PN level, $v^2/c^2 \sim G\,m/rc^2$, requires that one also considers the three-body interactions contained in the one-loop contribution $S^{\rm one-loop}$, corresponding to terms induced by some of the three-graviton vertices and other non-linearities (terms $O(h^2)$ and $O(hT)$ in Eq. (21.15) below), *i.e.*, to the $O(V^2)$ term in Eq. (21.8):

$$L^{(3)} = -\frac{1}{2}\sum_{B\neq A\neq C}\frac{G^2\, m_A\, m_B\, m_C}{r_{AB}\, r_{AC}\, c^2} + O\left(\frac{1}{c^4}\right) . \tag{21.14}$$

21.2.3 *Gravitational Waves in GR*

The linearized approximation to Einstein's field equations, Eq. (21.7), in harmonic gauge $\partial^\nu(h_{\mu\nu} - \frac{1}{2}h\eta_{\mu\nu}) = 0$ (with $h \equiv \eta^{\mu\nu}h_{\mu\nu}$), reads

$$\Box h_{\mu\nu} = -\frac{16\pi G}{c^4}(T_{\mu\nu} - \tfrac{1}{2}T\eta_{\mu\nu}) + O(h^2) + O(hT) . \tag{21.15}$$

Outside of any source (*i.e.*, when $T_{\mu\nu} = 0$), this yields $\Box h_{\mu\nu} = 0$, with $\partial^\nu(h_{\mu\nu} - \frac{1}{2}h\eta_{\mu\nu}) = 0$. The generic linearized solution (modulo the diffeomorphism freedom) of the latter vacuum Einstein equations can be written as (with $k^2 = k\cdot k = \eta_{\mu\nu}k^\mu k^\nu$, $k\cdot x = k_\mu x^\mu$)

$$h_{\mu\nu}(x) = \int d^4k\, \delta(k^2)\epsilon_{\mu\nu}(k)e^{ik\cdot x} , \tag{21.16}$$

where the polarization tensor $\epsilon_{\mu\nu}(k)$ must be transverse ($\epsilon_{\mu\nu}k^\nu = 0$) and traceless ($\eta^{\mu\nu}\epsilon_{\mu\nu} = 0$). In addition, $\epsilon_{\mu\nu}(k)$ can be freely submitted to the gauge freedom $\epsilon'_{\mu\nu} = \epsilon_{\mu\nu} + \xi_\mu k_\nu + \xi_\nu k_\mu$. This implies that gravitational waves (GW) propagate with the speed of light, and (like electromagnetic waves) have only two independent polarizations. In a frame where, say, $k^\mu = (ck, 0, 0, k)$, the two independent linear polarization tensors can be taken to have components only in the transverse 1-2 plane, of the following form: $\epsilon^+_{11} = -\epsilon^+_{22} = \epsilon^+$, with $\epsilon^+_{12} = \epsilon^+_{21} = 0$; or $\epsilon^\times_{12} = +\epsilon^\times_{21} = \epsilon^\times$, with $\epsilon^\times_{11} = \epsilon^\times_{22} = 0$. Under a little-group rotation of angle θ in the 1-2 plane, the two circular polarization amplitudes $\epsilon^{(\pm)} = \epsilon^+ \mp i\,\epsilon^\times$ vary as $\epsilon'^{(\pm)} = e^{\pm 2i\theta}\epsilon^{(\pm)}$, thereby characterizing the helicity-2 nature of GWs.

When solving the inhomogeneous equation Eq. (21.15), taking into account the nonlinear contributions $O(h^2)+O(hT)$, one finds that, to lowest order, the GW amplitude emitted at large distances by a matter distribution is given by the following "quadrupole formula"

$$h^{\rm TT}_{ij}(T, \mathbf{X}) \approx \frac{2G}{c^4}P^{\rm TT}_{ijab}(\mathbf{N})\frac{\ddot{Q}_{ab}(T - R/c)}{R} , \tag{21.17}$$

where $Q_{ij}(t) = \int d^3x\sigma(t, \mathbf{x})(x^i x^j - \frac{1}{3}\delta_{ij}\mathbf{x^2})$ $(a, b, i, j = 1, 2, 3)$ is the quadrupole moment of the source, $R = |\mathbf{X}|$ the distance to the source, $\mathbf{N} = \mathbf{X}/R$ the unit direction from the source to the observer, and $P^{\rm TT}_{ijab}(\mathbf{N}) = (\delta_{ia} - N_iN_a)(\delta_{jb} - N_jN_b) - \frac{1}{2}(\delta_{ij} - N_iN_j)(\delta_{ab} - N_aN_b)$ the transverse-traceless projector onto the 2-plane orthogonal to $\mathbf{N}$.

21.2.4 *Strong gravitational fields: neutron stars and black holes*

The nonlinear structure of Einstein's equations implies many predictions for strong gravitational fields that distinguish GR from Newtonian gravity. For instance, in Newtonian gravity, there is no upper limit to the dimensionless gravitational potential U/c^2, with U satisfying Poisson's equation $\Delta U = -4\pi G\rho$, where ρ denotes the Newtonian mass density. By contrast, in GR, the dimensionless surface gravitational potential $GM/(c^2R)$ of a spherically symmetric (perfect fluid) body cannot exceed $\frac{4}{9}$ [2].

Given an equation of state $p = f(\rho)$ modeling the interior of a (cold) spherically symmetric body (say a non-rotating neutron star), Einstein equations, Eq. (21.7), with $T^{\mu\nu} = (\rho + p)u^\mu u^\nu + pg^{\mu\nu}$, and

$$g_{\mu\nu}dx^\mu dx^\nu = -e^{2\Phi(r)}c^2dt^2 + \frac{dr^2}{1 - \frac{2GM(r)}{c^2r}} + r^2\left(d\theta^2 + \sin^2\theta d\phi^2\right) , \tag{21.18}$$

yield the following Tolman-Oppenheimer-Volkoff radial equations:

$$p'(r) = -\frac{G(\rho + p/c^2)(M(r) + 4\pi r^3p/c^2)}{r^2(1 - 2GM(r)/(c^2r))} ; \tag{21.19}$$

$$M'(r) = 4\pi r^2\rho ; \tag{21.20}$$

$$\Phi'(r) = \frac{G(M(r) + 4\pi r^3p/c^2)}{r^2(1 - 2GM(r)/(c^2r))} . \tag{21.21}$$

In the exterior of the star $(r \geq R)$, the metric takes the Schwarzschild form

$$\begin{aligned} g_{\mu\nu}dx^\mu dx^\nu = &-\left(1 - \frac{2GM}{c^2r}\right)c^2dt^2 + \frac{dr^2}{1 - \frac{2GM}{c^2r}} \\ &+ r^2\left(d\theta^2 + \sin^2\theta d\phi^2\right) , \end{aligned} \tag{21.22}$$

where $M \equiv M(R)$ is the total gravitational mass of the star. GR predicts, for any given $p = f(\rho)$, several (in principle) observable

Int. J. Mod. Phys. A 2026.41. Downloaded from www.worldscientific.com
by UNIVERSITY OF CALIFORNIA @ BERKELEY on 09/16/26. Re-use and distribution is strictly not permitted, except for Open Access articles.

features of neutron stars, such as: (i) the maximum mass of a neutron star; (ii) the relation between the radius R and the total mass M; (iii) the dimensionless surface gravitational potential $GM/(c^2R)$ (linked to the surface redshift $\sqrt{-g_{00}} = \sqrt{1-\frac{2GM}{c^2R}}$ measured by an observer at infinity); (iv) the moment of inertia; and (v) the Love number (tidal polarizability). The current uncertainty on the equation of state of a neutron star yields the GR-predicted approximate range for the maximum mass of non-rotating neutron stars $1.5\,M_\odot \lesssim M_{\max} \lesssim 2.5\,M_\odot$, and the absolute upper bound $M_{\max} < 3\,M_\odot$ [3]. The surface gravitational potential of a typical neutron star is $GM/c^2R_{\rm NS} \simeq 0.17$, which is a factor $\sim 10^8$ higher than the surface potential of the Earth, and a mere factor 3 below the black hole limit $GM/c^2R_{\rm BH} = \frac{1}{2}$ to be discussed next.

The existence of a maximum mass for a neutron star led Oppenheimer and Snyder [4] to predict that the end point of stellar evolution for sufficiently heavy stars, after exhaustion of all thermonuclear sources of energy, will be what are now called "black holes." The latter are solutions of Einstein's equations whose past structure involves a gravitationally collapsing star, but whose presently observable structure is essentially described (for non-rotating black holes) by the vacuum Schwarzschild solution Eq. (21.22). It took many years for theoretical (and mathematical) physicists to understand that the apparent singularity of the Schwarzschild solution at $r = \frac{2GM}{c^2}$ was a coordinate singularity and that the Schwarzschild spacetime was regular at the "black hole horizon", $R_{\rm BH} \equiv \frac{2GM}{c^2}$. The rotating analog of the Schwarzschild spacetime is the Kerr black hole [5].

Black holes are outstanding consequences of GR which enjoy many remarkable properties, notably: (i) presence of a one-way surface (the horizon) for all waves and particles; (ii) absence of "hair" (*i.e.*, barring a possible electric charge, their structure is fully described by only two parameters, total mass, M, and total angular momentum, $J \leq GM^2/c$); (iii) existence of a spectrum of damped quasi-normal vibrational modes; and (iv) a behavior under external perturbations similar to ordinary physical objects satisfying the laws of (dissipative) thermodynamics. Moreover, though no classical waves or particles can get out of the horizon, black holes are predicted to slowly evaporate via quantum particle creation.

21.2.5 *Cosmology*

To complete our short tour of the main predictions of GR, let us mention that GR offers the current standard framework for describing the large-scale structure of the Cosmos, from the nearly homogeneous Big Bang (and its plausible inflationary beginning) to the current inhomogeneous Universe undergoing an accelerated expansion. The spacetime structure on large (temporal and spatial) scales is well described by a solution of Einstein's equations of the form

$$\begin{aligned} ds^2 = &-(1+2\Phi(t,\mathbf{x}))\,c^2dt^2 + 2W_i(t,\mathbf{x})dtdx^i \\ &+ a^2(t)\left[(1-2\Psi(t,\mathbf{x}))\,\delta_{ij} + h_{ij}(t,\mathbf{x})\right]dx^idx^j, \end{aligned} \tag{21.23}$$

where, after a suitable gauge-fixing [6], $W_i(t,\mathbf{x})$ is transverse, while $h_{ij}(t,\mathbf{x})$ is transverse and traceless. The source $T^{\mu\nu}$ must involve a certain number of postulated ingredients: an inflaton field; the matter of the Standard Model; a dark matter component; and a cosmological constant contribution $T^{\mu\nu}_\Lambda = -\rho_{\rm vac}g^{\mu\nu}$, with $\rho_{\rm vac} \equiv c^4\Lambda/(8\pi G)$. The scale factor $a(t)$ of the Friedmann background metric $ds_0^2 = -c^2dt^2 + a^2(t)\delta_{ij}dx^idx^j$ satisfies the GR-predicted Friedmann equations (with vanishing spatial curvature $k=0$),

$$H^2 \equiv \left(\frac{\dot a}{a}\right)^2 = \frac{8\pi G}{3}\rho_{\rm tot}\,, \tag{21.24}$$

$$\frac{\ddot a}{a} = -\frac{4\pi G}{3}\left(\rho_{\rm tot} + \frac{3}{c^2}p_{\rm tot}\right), \tag{21.25}$$

while the scalar $(\Phi(t,\mathbf{x}),\Psi(t,\mathbf{x}))$, vector $(W_i(t,\mathbf{x}))$, and tensor $(h_{ij}(t,\mathbf{x}))$ inhomogeneous perturbations satisfy some GR-predicted propagation equations (coupled to matter perturbations); see [6] and the following *Reviews*. When the cosmic fluid is well approximated by a perfect fluid, Einstein's equations predict the following link between the scalar perturbations

$$\Phi(t,\mathbf{x}) = \Psi(t,\mathbf{x})\,. \tag{21.26}$$

21.3 A roadmap of parametrizations of deviations from GR, and of modified gravity

As will be discussed below, all currently performed gravitational experiments are compatible with GR. However, similarly to what is done in discussions of precision electroweak experiments, it is useful to quantify the significance of precision gravitational experiments by parameterizing possible deviations from GR. One can distinguish two main approaches to considering, and parameterizing, deviations from GR: (i) theory-agnostic phenomenological approaches; or, (ii) the study of the predictions of specific classes of alternative theories of gravity. Both types have led to useful ways of discussing tests of gravity. Both types also have their limitations. Considering them together leads to cross-fertilization.

21.3.1 *Theory-agnostic phenomenological approaches to parameterizing deviations from GR*

The theory-agnostic phenomenological approach is the oldest, and, arguably, the most robust one. It essentially consists in starting from specific observable predictions within the considered standard theory, and of deforming them by introducing some free parameters measuring either deviations from effects already present within the standard theory, or new effects absent from the standard theory. A classic example is the periastron advance of Mercury (and the other planets). When working within Newtonian gravity as a standard theory of gravity, the rate of periastron advance of Mercury, $\dot\omega$, is (when neglecting the quadrupole moment of the Sun) a calculable function of the masses and semi-major axes of the other planets of the solar system, say $\dot\omega^{\rm Newton}(m_i,a_i)$. However, $\dot\omega$ is also a directly observable quantity, so that one can parameterize the periastron advance of Mercury by writing

$$\dot\omega^{\rm obs} = \dot\omega^{\rm Newton}(m_i,a_i) + \Delta\dot\omega\,. \tag{21.27}$$

Using other observable data to determine some "observed" values of the m_i's and a_i's, one can then measure the anomalous periastron precession $\Delta\dot\omega$ and see whether it is compatible with zero, or not. As is well-known, Leverrier used such a methodology and, in 1859, measured an anomalous periastron precession of about $\Delta\dot\omega \simeq 38$ arcsec/century (later re-estimated at 43 arcsec/century), which was explained in 1915 as a GR prediction. Let us discuss further examples of the use of such theory-agnostic approaches for discussing deviations from GR.

21.3.2 *Parameterized post-Newtonian (PPN) formalism.*

When considering the weak-field slow-motion limit appropriate to describing gravitational experiments in the solar system, it has been traditional to parameterize possible (long-range) deviations from the GR-predicted 1PN metric by introducing extra dimensionless coefficients in the various terms of the metric of Eq. (21.8). The minimal version of the parameterized post-Newtonian (PPN) formalism (essentially due to Eddington) involves only two parameters β and γ, namely

$$g_{00} = -1 + \frac{2}{c^2}V - \frac{2\beta}{c^4}V^2 + O\left(\frac{1}{c^6}\right), \tag{21.28}$$

$$g_{0i} = -\frac{2(\gamma+1)}{c^3}V_i + O\left(\frac{1}{c^5}\right), \tag{21.29}$$

$$g_{ij} = \delta_{ij}\left[1 + \frac{2\gamma}{c^2}V\right] + O\left(\frac{1}{c^4}\right), \tag{21.30}$$

with V and V_i defined by Eq. (21.9), with the same vectorial source $\sigma_i = \frac{T^{0i}}{c}$, but a modified scalar source

$$\sigma^{\rm PPN} = \frac{1}{c^2}\left(\left[1 + (3\gamma - 2\beta - 1)\frac{V}{c^2}\right]T^{00} + \gamma\,T^{ii}\right). \tag{21.31}$$

In GR, $\beta^{\rm GR} = 1$ and $\gamma^{\rm GR} = 1$, so that deviations from GR are parameterized by $\overline\beta \equiv \beta - 1$ and $\overline\gamma \equiv \gamma - 1$. Richer versions of the

Int. J. Mod. Phys. A 2026.41. Downloaded from www.worldscientific.com by UNIVERSITY OF CALIFORNIA @ BERKELEY on 09/16/26. Re- strictly not permitted, except for Open Access articles.

PPN formalism (involving up to ten parameters) were developed in interaction with the study of classes of alternative theories of gravity [7, 8]. This led to parameterizing new types of contributions to the 1PN metric that are absent in the GR framework.

When deriving the 1PN-accurate dynamics of N point masses predicted by the PPN-modified metric, Eq. (21.28), one finds that the free Lagrangian is not modified (because we are considering here a Lorentz-invariant subclass of PPN metrics), while there are modifications of both the two-body Lagrangian, $L^{(2)}$, Eq. (21.13), and the three-body one, $L^{(3)}$, Eq. (21.14). More precisely, denoting $\eta \equiv 4\overline{\beta} - \overline{\gamma}$, the Newtonian interaction energy term in Eq. (21.13) is modified into $G_{AB} m_A m_B / r_{AB}$, with a body-dependent gravitational "constant"

$$G_{AB} = G[1+\eta(E_A^{\rm grav}/m_A c^2 + E_B^{\rm grav}/m_B c^2) + O(1/c^4)] \,, \quad (21.32)$$

where $E_A^{\rm grav}$ denotes the gravitational binding energy of body A. In addition, there is the additional contribution $+\overline{\gamma}(\boldsymbol{v}_A - \boldsymbol{v}_B)^2/c^2$ in the brackets on the right-hand side of $L^{(2)}$, Eq. (21.13). As for the three-body interaction term $L^{(3)}$, Eq. (21.14), it is modified by the overall factor $1 + 2\overline{\beta}$.

These results show how the introduction of the two minimal PPN deviation parameters $\overline{\beta} \equiv \beta - 1$ and $\overline{\gamma} \equiv \gamma - 1$ suffices to introduce many different observable effects. Some of them (the ones linked with $\overline{\gamma}$) concern deviations at the linearized (one-graviton-exchange) level (and affect, for instance, light deflection and time-delay effects), while the deviation parameter $\overline{\beta}$ parameterizes effects linked to the cubic vertex of Einstein's gravity (and affects, for instance, periastron precession). Of particular interest is the fact that Eq. (21.32) shows that the combination $\eta \equiv 4\overline{\beta} - \overline{\gamma}$ parameterizes a violation of the Strong Equivalence Principle, because the gravitational interaction between self-gravitating bodies is seen to be influenced by the gravitational binding energy of each body [9]. As stated above, this effect is absent in GR (where $\eta^{\rm GR} = 0$). This is an example where the fact of contrasting GR with some deviations from it gives physical significance to a null effect in GR (namely the universality of free fall of self-gravitating bodies).

Finally, one can extend the PPN formalism by allowing for a slow, phenomenological time variation of Newton's constant:

$$G(t) = G_0 \left[1 + \frac{\dot{G}_0}{G_0}(t - t_0) \right] . \quad (21.33)$$

Here, one assumes that there exist units in which the masses, m_i, of elementary particles stay constant, and that G is measured in such units. A possible time variation of G then corresponds to a possible common variation of the dimensionless couplings $G m_i^2/(\hbar c)$.

21.3.3 *Parameterized post-Keplerian (PPK) formalism.*

The discovery of pulsars (*i.e.*, rotating neutron stars emitting a beam of radio noise) in gravitationally bound orbits [10, 11] has given us our first experimental handle on a regime of relativistic gravity going significantly beyond the uniformly weak-field, and quasi-stationary regime of solar-system gravity. Binary pulsars allow us to probe some radiative effects, and also some strong-gravitational-field effects. In these systems, the finite speed of propagation of the gravitational interaction between the pulsar and its companion generates damping-like terms at order $(v/c)^5$ in the equations of motion [12]. These damping forces are the local counterparts of the gravitational radiation emitted at infinity by the system ("gravitational radiation reaction"). They cause the binary orbit to shrink and its orbital period P_b to decrease. The remarkable stability of pulsar clocks has allowed one to measure the corresponding very small orbital period decay $\dot{P}_b \equiv dP_b/dt \sim -(v/c)^5 \sim -10^{-12}$–$10^{-14}$ in several binary systems, thereby giving us a direct experimental handle on the propagation properties of the gravitational field. In addition, the large surface gravitational potential of a neutron star allows one to probe the quasi-static strong-gravitational-field regime, as is discussed below.

It is possible to extract phenomenological (theory-independent) tests of gravity from binary pulsar data by using the parameterized post-Keplerian (PPK) formalism [13]. The basis of this formalism is the fact that, after correcting for the Earth's motion around the Sun and for the dispersion due to propagation in the interstellar plasma, the time of arrival of the Nth pulse t_N can be described by a generic, parameterized "timing formula" [13, 14], whose functional form is common to the whole class of tensor-scalar gravitation theories:

$$t_N - t_0 = F[T_N(\nu_p, \dot{\nu}_p, \ddot{\nu}_p) \,;\, \{p^K\} \,;\, \{p^{PK}\}] \,. \quad (21.34)$$

Here, T_N is the pulsar proper time corresponding to the Nth turn given by $N/2\pi = \nu_p T_N + \frac{1}{2}\dot{\nu}_p T_N^2 + \frac{1}{6}\ddot{\nu}_p T_N^3$ (with $\nu_p \equiv 1/P_p$ the spin frequency of the pulsar, *etc.*), $\{p^K\} = \{P_b, T_0, e, \omega_0, x\}$ is the set of "Keplerian" parameters (notably, orbital period P_b, eccentricity e, periastron longitude ω_0 and projected semi-major axis $x = a \sin i/c$), and $\{p^{PK}\} = \{k, \gamma_{\rm timing}, \dot{P}_b, r, s, \delta_\theta, \dot{e}, \dot{x}\}$ denotes the set of (separately measurable) "post-Keplerian" parameters. Most important among these are: the fractional periastron advance per orbit $k \equiv \dot{\omega} P_b/2\pi$; a dimensionful time-dilation parameter $\gamma_{\rm timing}$; the orbital period derivative $\dot{P}_b$; and the "range" and "shape" parameters of the gravitational time delay caused by the companion, r and s. In addition, by monitoring over several years the evolution of the pulsar pulse profile it is possible to measure in some binary pulsars another post-Keplerian parameter: the precession rate Ω_p of the pulsar spin axis. In GR such an effect follows from the gravitational spin-orbit coupling (a.k.a. geodetic precession) [15, 16].

Without assuming any specific theory of gravity, one can phenomenologically analyze the data from any binary pulsar by least-squares fitting the observed sequence of pulse arrival times to the timing formula of Eq. (21.34). This fit yields the "measured" values of the parameters $\{\nu_p, \dot{\nu}_p, \ddot{\nu}_p\}$, $\{p^K\}$, $\{p^{PK}\}$. Now, each specific relativistic theory of gravity predicts that, for instance, k, $\gamma_{\rm timing}$, $\dot{P}_b$, r, and s (to quote parameters that have been successfully measured from some binary pulsar data) are some theory-dependent functions of the Keplerian parameters and of the (unknown) masses m_1, m_2 of the pulsar and its companion. For instance, in GR, one finds (with $M \equiv m_1 + m_2$, $n \equiv 2\pi/P_b$),

$$\begin{aligned}
k^{\rm GR}(m_1, m_2) =& 3(1-e^2)^{-1}(GMn/c^3)^{2/3} \,, \\
\gamma_{\rm timing}^{\rm GR}(m_1, m_2) =& e n^{-1}(GMn/c^3)^{2/3} m_2(m_1 + 2m_2)/M^2 \,, \\
\dot{P}_b^{\rm GR}(m_1, m_2) =& -(192\pi/5)(1-e^2)^{-7/2}\left(1 + \tfrac{73}{24}e^2 + \tfrac{37}{96}e^4\right) \\
& \times (GMn/c^3)^{5/3} m_1 m_2/M^2 \,, \\
r^{\rm GR}(m_1, m_2) =& G m_2/c^3 \,, \\
s^{\rm GR}(m_1, m_2) =& n x (GMn/c^3)^{-1/3} M/m_2 \,, \\
\Omega_p^{\rm GR}(m_1, m_2) =& n(GMn/c^3)^{2/3}(1-e^2)^{-1} \\
& \times m_2(4m_1 + 3m_2)/(2M^2) \,. \qquad (21.35)
\end{aligned}$$

In alternative gravity theories each of the functions $k^{\rm theory}(m_1, m_2)$, $\gamma_{\rm timing}^{\rm theory}(m_1, m_2)$, $\dot{P}_b^{\rm theory}(m_1, m_2)$, *etc.*, is modified by quasi-static strong field effects (associated with the self-gravities of the pulsar and its companion), while the particular function $\dot{P}_b^{\rm theory}(m_1, m_2)$ is further modified by radiative effects [17–20]. If one measures $N > 2$ PPK parameters from the data of a specific binary pulsar, these N measurements determine, for each given theory, N curves (defined by the N equations $k_i^{\rm theory}(m_1, m_2) = k_i^{\rm obs}$) in the two-dimensional mass plane (m_1, m_2). This yields $N - 2$ tests of the specified theory, according to whether the N curves (or strips) have one point in common, as they should.

21.3.4 *Parameterized-post-Friedmannian (PPF) formalisms.*

We have recalled above that, in GR, the two functions, $\Phi(t, \mathbf{x})$, and $\Psi(t, \mathbf{x})$, parameterizing (in the "longitudinal gauge") the scalar perturbations of the background Friedmann metric are related (in absence of anisotropic stresses) by Eq. (21.26). Several authors [21–30] have defined various types of parameterized-post-Friedmannian (PPF) formalisms involving (generally space and

Int. J. Mod. Phys. A 2026.41. Downloaded from www.worldscientific.com
by UNIVERSITY OF CALIFORNIA @ BERKELEY on 09/16/26. Re-use and distribution is strictly not permitted, except for Open Access articles.

time dependent) phenomenological parameters. The simplest versions of these formalisms involve two phenomenological parameters measuring: (i) the ratio between $\Phi(t,\mathbf{x})$, and $\Psi(t,\mathbf{x})$, say (using a parametrization which parallels the usual PPN parametrization)

$$\Psi(t,\mathbf{x}) = \gamma_{\rm cosmo}(t,\mathbf{x})\Phi(t,\mathbf{x})\,; \tag{21.36}$$

and (ii) the effective gravitational constant entering the Poisson equation for $\Phi(t,\mathbf{x})$, say

$$\Delta\Phi(t,\mathbf{x}) = 4\pi G_\Phi(t,\mathbf{x})\delta\rho(t,\mathbf{x})\,. \tag{21.37}$$

However, the peculiarities of cosmological observables limit the domain of applicability of such phenomenological approaches [28] (notably because the strong dependence of cosmological probes on epochs and scales obliges one to rely on specific parameterizations of the functions $\gamma_{\rm cosmo}(t,\mathbf{x})$ and $G_\Phi(t,\mathbf{x})$, *e.g.*, [27, 30]). Approaches based on specific classes of modified-gravity theories allow for a more complete treatment involving, in principle, all existing cosmological observables: Big Bang nucleosynthesis, cosmic microwave background, large-scale structure, Hubble diagram, weak lensing, etc. Discussing the current cosmological tests using either such PPF formalisms, or comparisons with the predictions of modified-gravity theories, is beyond the scope of this review. See [31] for a comprehensive recent discussion. The bottom line is that all present cosmological data have been found to be compatible with GR (within the Friedmann-Lemaître-based ΛCDM model). Beyond the quantitative limits on various parameterized theoretical models [31], one should remember the striking (strong-field-type) qualitative verification of GR embodied in the fact that relativistic cosmological models give an accurate picture of the Universe over a period during which the spatial metric has been blown up by a gigantic factor, say $(1+z)^2 \sim 10^{19}$ between Big Bang nucleosynthesis and now.

21.3.5 *Various phenomenological tests of GR from gravitational wave (GW) data*

The observations of gravitational-wave (GW) signals [32] by the US-based Laser Interferometer Gravitational-wave Observatory (LIGO), later joined by the Europe-based Virgo detector, and more recently by the Japan-based KAGRA detector, have opened up a novel testing ground for relativistic gravity. The first four observing runs (O1, O2, O3 and O4) of the LIGO-Virgo-KAGRA (LVK) collaboration have led to the detection of about 300 GW signals, most of which come from binary black-hole coalescences. For online access to the LVK observations see the Gravitational Wave Open Science Center (https://gwosc.org).

Several approaches have been used to either test consistency with GR, or to look for special types of possible deviations. Making accurate predictions for GW signals from coalescing black holes within GR took years of both analytical [33,34] and numerical [35] work. Some works have started to derive (both analytically and numerically) the corresponding predictions within some modified-gravity theories (see [36] for a review). Phenomenological approaches are very useful for parameterizing general, conceivable deviations from GR when analyzing the GW signals emitted by coalescing black holes or neutron stars.

Various phenomenological tests of the consistency with GR of the observed GW signals emitted by coalescing compact binaries have been suggested. One general idea [37–43] (dubbed "parameterized post-Einsteinian formalism" in [39]) is to modify the GR-predicted Fourier-domain value $\psi^{\rm GR}(f,m_1,m_2,S_1,S_2)$ of the phase of black-hole coalescence GW signals $h(f) = A(f)e^{i\psi(f)}$ by introducing dimensionless GR-deviation parameters, say

$$\psi(f) = \psi^{\rm GR}(f,m_1,m_2,S_1,S_2) + \delta\psi(f,m_1,m_2,\delta\hat{p}_i)\,, \tag{21.38}$$

where the GR phase $\psi^{\rm GR}(f,m_1,m_2,S_1,S_2)$ is generally obtained by combining analytical and numerical information (e.g., [44,45]), and where

$$\delta\psi(f,m_1,m_2,\delta\hat{p}_i) = \left[\sum_i \delta\hat{p}_i\, p_i^{\rm GR,NS}(m_1,m_2)u_i(f)\right]^{\rm tapered}. \tag{21.39}$$

Here, the superscript NS refers to the nonspinning contribution, and the $u_i(f)$'s define a basis of functions of the GW frequency f.

This phenomenological approach has been particularly applied to possible non-GR modifications of the *inspiral* signal, whose leading low-frequency contributions are described by post-Newtonian perturbation theory. For instance, the leading-order (LO), quadrupolar term in the GR phase evolution during the early inspiral corresponds to $u_0(f) = f^{-5/3}$ and $p_0^{\rm GR} = \frac{3(m_1+m_2)^2}{128 m_1 m_2}(\pi G(m_1+m_2)/c^3)^{-5/3}$, while the next-to-leading-order (NLO) term is a $O(v^2/c^2)$ correction $p_2^{\rm GR}u_2(f)$ with $u_2(f) = f^{-1}$. The superscript "tapered" in Eq. (21.39) indicates that the effect of the phase deviation $\delta\psi(f,m_1,m_2,\delta\hat{p}_i)$ is shut-off beyond some conventional end of the inspiral.

Each dimensionless parameter $\delta\hat{p}_i$ introduces a fractional deviation from the corresponding individual phasing GR effect having the frequency dependence $u_i(f)$, and can, in principle, be extracted by fitting the inspiral part of the observed waveform to the deformed template of Eq. (21.38). However, one must also use this deformed template for simultaneously extracting the values of m_1, m_2, S_1, and S_2. Together with signal-to-noise ratio (SNR) considerations, and parameter-correlation issues, this presently limits the applicability of such a test to introducing only one deformation parameter $\delta\hat{p}_i$ at a time (though a principal component analysis allows to test the correlated effect of several deformation parameters [46]). A particularly meaningful test [37] is to vary only the third coefficient p_3 parameterizing the NNLO, "GW tail"-related, $O(v^3/c^3)$ correction, with $u_3(f) = f^{-2/3}$, leaving undeformed the LO and NLO terms $p_0^{\rm GR}u_0(f) + p_2^{\rm GR}u_2(f)$, as well as all the higher-order GR contributions . Another well-motivated test [39] is to introduce a new coefficient $\delta\hat{p}_{-2}$, which is absent in GR, and which parameterizes an $O((\frac{v}{c})^{-2})$ fractional correction to the LO, quadrupolar term, thereby allowing for a possible dipolar GW flux (indeed, dipolar GW radiation generally exists in theories containing scalar excitations). As $p_{-2}^{\rm GR}$ vanishes, $\delta\hat{p}_{-2}$ is added as an absolute deviation, scaled by the LO term $p_0^{\rm GR}$.

The coalescence of two black holes, or of a black hole and a neutron star (or of two heavy-enough neutron stars) leads to the formation of a black hole that is initially formed in a perturbed state. The relaxation of the latter perturbed black hole into its stationary, equilibrium state leads to the emission of characteristic (rapidly decaying) ringing GW modes (a.k.a. quasi-normal modes) [47–49], whose frequencies and decay times are functions of the mass (M_f) and spin ($S_f \equiv GM_f^2 a_f/c$) of the final black hole, say

$$\omega_{lmn} = (c^3/GM_f)[2\pi\hat{f}_{lmn}^{\rm QNM}(a_f) - i/\hat{\tau}_{lmn}^{\rm QNM}(a_f)]\,. \tag{21.40}$$

Here lmn (where $n = 0,1,2,\cdots$ is the overtone number) labels the various multipolar ringing modes, starting, for each multipole, from the least-damped fundamental tone, $n = 0$. When the SNR is large enough, one can directly test, in a phenomenological way, for the presence of one or several of these modes in the post-merger ("ring-down") signal, and measure both $f_{lmn} \equiv {\rm Re}(\omega_{lmn})/(2\pi)$ and $\tau_{lmn} \equiv -({\rm Im}(\omega_{lmn}))^{-1}$ in a theory-agnostic way. Working in the time-domain and with the complex waveform $h_c(t) = h_+(t) - ih_\times(t)$, one can indeed fit the observed ring-down signal to a sum of damped oscillations, say

$$h_c(t) = \sum_{lmn}\left(A^{\rm R}e^{-i\omega_{lmn}t} + A^{\rm L}e^{+i\omega_{lmn}t}\right). \tag{21.41}$$

The ring-down analogs of the inspiral GR-dimensionless deviation parameters $\delta\hat{p}_i$, entering (21.39), would then be $\delta\hat{f}_{lmn}$ and $\delta\hat{\tau}_{lmn}$ such that $f_{lmn} = f_{lmn}^{\rm GR}(M_f,a_f)(1+\delta\hat{f}_{lmn})$, and $\tau_{lmn} = \tau_{lmn}^{\rm GR}(M_f,a_f)(1+\delta\hat{\tau}_{lmn})$. This program was initiated in [49] and is called "Black Hole spectroscopy" [50].

As recalled above, GR predicts that GWs propagate (in vacuum) at exactly the same speed as light (*i.e.*, they have the same dispersion law $g^{\mu\nu}k_\mu k_\nu = 0$ in curved spacetime). Deviations from such a universal, scale-free dispersion law can be phenomenologically parameterized in several ways. If one phenomenologically

Int. J. Mod. Phys. A 2026.41. Downloaded from www.worldscientific.com by UNIVERSITY OF CALIFORNIA @ BERKELEY on 09/16/26. Re-[redacted] strictly not permitted, except for Open Access articles.

assumes that the graviton dispersion law includes a mass term, say $g^{\mu\nu}k_\mu k_\nu + m_g^2/\hbar^2 = 0$, or some more general type of frequency-dependent modification, such changes affect the phasing of the inspiral GW signal and can be directly tested [51]. When one observes *both* GWs and electromagnetic waves emitted by the same system, one can also directly test whether both types of waves propagate in the same way.

Let us now present some examples of theory-dependent discussions of experimental tests based on considering specific classes of alternative theories. The most conservative deviations from Einstein's pure spin-2 theory are defined by adding new, bosonic, light or massless, macroscopically coupled fields.

21.3.6 *Gravity tests within classes of tensor-scalar theories of gravity*

The possible existence of new gravitational-strength couplings leading to deviations from Einsteinian (and Newtonian) gravity has been suggested by many natural extensions of GR, starting with the classic Kaluza-Klein idea, and continuing up to now with the study of extended supergravity theories, and of (super-)string theory. In particular, a recurrent suggestion of such theories (which dates back to pioneering work by Jordan, and by Fierz [52]) is the existence of a scalar field φ coupled both to the scalar curvature R and to the various ${F^a_{\mu\nu}}^2$ gauge-field actions. Such fields ("dilaton" or "moduli") generically appear in string theory and are massless at the tree-level, but could acquire a self-interaction potential $V(\varphi)$ beyond the tree-level.

The exchange of such a dilaton-like field leads to several types of observational deviations from GR. For experimental limits on the gravitational inverse-square-law (down to the micrometer range) see Refs. [53–58]. If the potential $V(\varphi)$ is zero or negligible for the considered range, the coupling of φ to ${F^a_{\mu\nu}}^2$ leads to apparent violations of the weak equivalence principle, with rather specific composition-dependence [59]. Next, when neglecting the fractionally small composition-dependent effects, such a field approximately couples to the trace of the energy-momentum tensor $T = g_{\mu\nu}T^{\mu\nu}$. The most general such theory contains (after suitable field redefinitions) two arbitrary functions of the scalar field, namely the self-interaction potential $V(\varphi)$, and a matter-coupling function $a(\varphi)$:

$$\begin{aligned}\mathcal{L}_{\rm tot}[g_{\mu\nu},\varphi,\psi,A_\mu,H] =& \frac{c^4}{16\pi G_*}\sqrt{g}(R(g_{\mu\nu}) - 2g^{\mu\nu}\partial_\mu\varphi\partial_\nu\varphi)\\ &-\sqrt{g}V(\varphi) + \mathcal{L}_{\rm SM}[\psi,A_\mu,H,\widetilde{g}_{\mu\nu}]\,.\end{aligned} \tag{21.42}$$

Here G_* is a "bare" Newton constant, and the Standard Model matter is coupled not to the "Einstein" (pure spin-2) metric $g_{\mu\nu}$, but to the conformally related ("Jordan-Fierz") metric

$$\widetilde{g}_{\mu\nu} = \exp(2a(\varphi))g_{\mu\nu}. \tag{21.43}$$

The scalar field equation

$$\Box_g\varphi = \frac{4\pi G}{c^4}\left(-\alpha(\varphi)T + \frac{\partial V(\varphi)}{\partial\varphi}\right)\,, \tag{21.44}$$

features

$$\alpha(\varphi) \equiv \partial a(\varphi)/\partial\varphi\,, \tag{21.45}$$

as the basic (field-dependent) coupling between φ and matter [17, 60]. The best-known, special case of these theories is the one-parameter (ω) Jordan-Fierz-Brans-Dicke theory [61], with $V(\varphi) = 0$ and $a(\varphi) = \alpha_0\varphi$, leading to a field-independent coupling $\alpha(\varphi) = \alpha_0$ (with ${\alpha_0}^2 = 1/(2\omega+3)$). More generally, if we consider the massless theories ($V(\varphi) = 0$) with arbitrary (non-linear) coupling function $a(\varphi)$, they modify Einstein's predictions in the weak-field slow-motion limit appropriate to describing gravitational experiments in the solar system (1PN approximation) only through the appearance of exactly the same two "post-Einstein" dimensionless parameters $\overline{\gamma} = \gamma - 1$ and $\overline{\beta} = \beta - 1$ that entered the minimal (Eddington) PPN formalism presented above. However, we now have the following theoretical expressions relating the latter phenomenological parameters to the coupling functions entering the tensor-scalar action Eq. (21.42):

$$\overline{\gamma} = -2\frac{\alpha_0^2}{1+\alpha_0^2}\,; \tag{21.46}$$

$$\overline{\beta} = +\tfrac{1}{2}\frac{\beta_0\alpha_0^2}{(1+\alpha_0^2)^2}\,. \tag{21.47}$$

Here $\alpha_0 \equiv \alpha(\varphi_0)$, and $\beta_0 \equiv \partial\alpha(\varphi_0)/\partial\varphi_0$, with φ_0 denoting the vacuum expectation value (VEV) of φ around the solar system. In addition, the observable value $G^{\rm obs}$ of the gravitational constant is found to be field-dependent and given (at a place where $\varphi = \varphi_0$) by

$$G^{\rm obs} = G(\varphi_0) \equiv G_*\exp[2a(\varphi_0)](1+\alpha_0^2)\,. \tag{21.48}$$

This makes it clear that the parameter $\overline{\gamma}$ is the basic post-Einstein parameter, which measures the admixture of an additional field (here a spin-0 field) to the pure spin-2 GR. One also sees how the parameter $\overline{\beta}$ is linked to non-linear effects (here coupling terms $\beta_0(\varphi-\varphi_0)^2T$ in the action), and how the Nordtvedt parameter $\eta \equiv 4\overline{\beta} - \overline{\gamma}$ is related to the field-dependence of $G^{\rm obs}$ ($\eta = (\alpha_0/(1+\alpha_0^2))\partial\ln G(\varphi_0)/\partial\varphi_0$).

The advantage of a theory-dependent approach, such as Eq. (21.42), over the phenomenological minimal PPN approach of Eq. (21.28), is that it allows one to consistently predict the observational deviations from GR in all possible gravity regimes: the quasi-stationary weak-field regime; the wavelike weak-field regime; the strong-field regime; the cosmological regime, etc. All such observational deviations can be consistently worked out once one chooses specific forms of the coupling function $a(\varphi)$, and of $V(\varphi)$. The simple choice of a two-parameter quadratic coupling function, say $a(\varphi) = \alpha_0(\varphi-\varphi_0) + \frac{1}{2}\beta_0(\varphi-\varphi_0)^2$, has been found useful for describing many possible observable deviations from GR.

The observable consequences for binary pulsar observations of the strong-field and radiative effects linked to the coupling to φ have been explicitly worked out in Refs. [17, 62] in the case where φ is massless (see Ref. [63] for the case where φ is massive). In particular, the strong-field nature of the pulsar tests is demonstrated by the fact that some tensor-scalar theories can be as close as desired to GR in the weak-field regime of the solar-system (*i.e.*, $\overline{\gamma}$ and $\overline{\beta}$ can be as small as desired, or even exactly zero), while developing (via a "spontaneous scalarization" mechanism) differences of order unity with GR in binary pulsar experiments [19, 20].

21.3.7 *Attractor and screening mechanisms in modified gravity*

As will follow from the discussion of experimental data below, the comparison between the predictions of general massless tensor-scalar theories and current data shows that the basic coupling parameter α_0 must be tuned to a small value (especially when allowing for composition-dependent effects). This raises the issue of the naturalness of such small coupling parameters. It has been shown in this respect that, in many tensor-scalar theories, there is an *attractor mechanism* by which the cosmological evolution naturally drives the VEV $\varphi_0(t)$ towards a value for which the coupling parameter $\alpha_0 = \alpha(\varphi_0)$ vanishes, thereby making it natural to expect only small deviations from GR (at least for the weak-field regime) at our current cosmological epoch [64, 65].

There are other theoretical mechanisms (generically called "screening mechanisms") that could explain why a theory of gravity whose theoretical content significantly differs from that of GR could naturally pass all the stringent, GR-compatible experimental limits that will be discussed below. In particular, when considering a self-interacting scalar field ($V(\varphi) \neq 0$), the interplay between the two terms on the right-hand side of Eq. (21.44) tends to drive the local VEV φ_0 of φ to a density-dependent value. In turn, this leads to a corresponding density-dependent effective mass $m_0(\varphi_0) = \sqrt{4\pi G\partial^2V(\varphi_0)/\partial\varphi_0^2}$ of the φ field, and to density-dependent matter couplings [66]. Various choices of the functions $V(\varphi)$ and $a(\varphi)$ can then reduce the φ-induced deviations from GR in dense environments while still allowing for significant deviations in different (*e.g.*, cosmological) regimes [67–71].

Int. J. Mod. Phys. A 2026.41. Downloaded from www.worldscientific.com
by UNIVERSITY OF CALIFORNIA @ BERKELEY on 09/16/26. Re-use and distribution is strictly not permitted, except for Open Access articles.

Other screening mechanisms have been invoked, based on an environment dependence mediated by (first or second) derivatives of a scalar degree of freedom. Roughly speaking, such mechanisms involve a (possibly effective) scalar degree of freedom φ that satisfies a field equation that is more general than Eq. (21.44) in that the left-hand side, $\Box_g\varphi$, is replaced by a non-linear function of φ, $\partial\varphi$ and $\partial^2\varphi$. The presence of non-linear derivative self-interactions of φ can weaken the effective coupling of φ to matter. A simple toy-model showing this weakening would be to replace Eq. (21.44) by an equation of the form

$$Z(\varphi,\partial\varphi,\partial^2\varphi)\Box_g\varphi = \frac{4\pi G}{c^4}\left(-\alpha(\varphi)T + \frac{\partial V(\varphi)}{\partial\varphi}\right). \qquad (21.49)$$

Such an equation is equivalent, at a first level of approximation, to replacing the gravitational constant G entering Eq. (21.44) by $G_{\rm eff}(\varphi_0,\partial\varphi_0,\partial^2\varphi_0) \equiv G/Z_0$, where $Z_0 \equiv Z(\varphi_0,\partial\varphi_0,\partial^2\varphi_0)$. This has a screening effect if $Z_0 \gg 1$. Indeed, the replacement $G \to G_{\rm eff}$ diminishes the strength of the interaction potential due to φ exchange by a factor of $1/Z_0$. In addition, the range of this interaction is also affected: $m_0(\varphi_0) = \sqrt{4\pi G\partial^2 V(\varphi_0)/\partial\varphi_0^2} \to m_{0\rm eff}(\varphi_0,\partial\varphi_0,\partial^2\varphi_0) = \sqrt{4\pi G_{\rm eff}\partial^2 V(\varphi_0)/\partial\varphi_0^2} = Z_0^{-1/2}m_0$.

Screening mechanisms based on such non-linear derivative self-interactions are often referred to as being "Vainshtein-like" because a similar mechanism was first invoked in Ref. [72] as a conjectural way to ensure that the extra degrees of freedom associated with a massive (rather than massless) graviton become effectively weakly coupled to matter within a large domain around gravitational sources. Here, one is considering massive deformations of the massless spin-2 metric field of GR by a very small mass, possibly of cosmological scale: $m_g \sim \hbar H_0 \sim 10^{-33}$ eV. The construction of ghost-free potential terms for a spin-2 field has turned out to be a delicate matter [73]. The phenomenology of a very-low-mass graviton is still partly uncontrolled, both because of the unknown extent to which the Vainshtein screening is really active, and because of subtle constraints linked to an eventual UV completion of the theory beyond the unusually low energy scale where it becomes strongly coupled:

$$\Lambda_{\rm strong\ coupling} \sim (M_{\rm Planck}m_0^2)^{1/3} \sim 10^{-13}\left(\frac{m_0}{\hbar H_0}\right)^{2/3}\ {\rm eV}\,. \qquad (21.50)$$

The search for modified gravity theories incorporating an extra scalar degree of freedom potentially able to yield a Vainshtein-like screening led to writing down the following general class of tensor-scalar Lagrangian [74, 75]:

$$\begin{aligned} L_{\rm tot}[g_{\mu\nu},\varphi,\psi] =& G_2(\varphi,X) - G_3(\varphi,X)\Box_g\varphi + G_4(\varphi,X)R \\ &+G_{4X}(\varphi,X)[(\Box_g\varphi)^2 - \varphi^{\mu\nu}\varphi_{\mu\nu}] \\ &+G_5(\varphi,X)G^{\mu\nu}\varphi_{\mu\nu} - \frac{1}{6}G_{5X}(\varphi,X)[(\Box_g\varphi)^3 \\ &-3\Box_g\varphi\varphi^{\mu\nu} + 2\varphi_{\mu\nu}\varphi^{\mu\lambda}\varphi_\lambda^\nu] + L_{\rm matter}[g_{\mu\nu},\psi]\,. \end{aligned} \qquad (21.51)$$

Here $g_{\mu\nu}$ denotes the matter-coupled metric, $X \equiv -\frac{1}{2}g^{\mu\nu}\partial_\mu\varphi\partial_\nu\varphi$, $\varphi_{\mu\nu} \equiv \nabla_\mu\nabla_\nu\varphi$, $G^{\mu\nu} \equiv R^{\mu\nu} - \frac{1}{2}Rg^{\mu\nu}$, and the various coefficients $G_n(\varphi,X)$ are arbitrary functions of two variables (with $G_{nX} \equiv \partial G_n/\partial X$). The field equations derived from the Lagrangian of Eq. (21.51) are only of second order in derivatives in spite of the non-linear structure of $L_{\rm tot}$. This implies that the tensor-scalar theories defined by Eq. (21.51) feature three degrees of freedom, corresponding to a massless spin-2 excitation (GW) and a spin-0 excitation. Contrary to the simpler tensor-scalar theories of Eq. (21.42), it is found that the speed of propagation of GWs implied by Eq. (21.51) is generically different from the speed of light:

$$\frac{c_{\rm GW}^2}{c^2} = \frac{G_4 - X(\ddot\varphi G_{5X} + G_{5\varphi})}{G_4 - 2XG_{4X} - X(H\dot\varphi G_{5X} - G_{5\varphi})}\,. \qquad (21.52)$$

More general modified gravity models have been proposed (see, *e.g.* Refs. [76, 77]). Apart from the simplest of them, most of these models have a rather artificial flavor, and do not lead to convincing alternative explanations either of dark matter or of dark energy. In addition, many of them do not lead (contrary to GR) to mathematically "well-posed" evolution problems [78–80]. This entails a serious challenge to deriving strong-field predictions for such models. It has been argued that many of these (dark-energy motivated) models should be viewed as effective field theory (EFT) approximations that need some sort of UV completion at an unusually low frequency scale [81]. In spite of these shortcomings, such models are conceptually interesting because they give examples of deviations for various predictions of GR, existing independently from each other, in various regimes. For instance, some special tensor-scalar models lead to black hole solutions modified by scalar-hair [82–84]. For other types of black holes with scalar-hair, see Ref. [85]. This shows the interest of phenomenologically testing, in a democratic and agnostic way, all conceivable deviations from GR.

Let us now turn to briefly presenting current experimental results of various phenomenological tests of the main GR predictions recalled in Section 21.2 above.

21.4 Experimental tests of the Equivalence Principle (*i.e.*, of the matter-gravity coupling)

21.4.1 *Tests of the constancy of constants*

Stringent limits on a possible time variation of the basic coupling constants have been obtained by analyzing a natural fission reactor phenomenon that took place at Oklo, Gabon, two billion years ago [86–91]. These limits are at the 1×10^{-8} level for the fractional variation of the fine-structure constant $\alpha_{\rm em}$, and at the 4×10^{-9} level for the fractional variation of the ratio $m_q/\Lambda_{\rm QCD}$ between the light quark masses and $\Lambda_{\rm QCD}$. The determination of the lifetime of Rhenium 187 from isotopic measurements of some meteorites dating back to the formation of the solar system (about 4.6 Gyr ago) yields comparably strong limits [92]. Measurements of absorption lines in astronomical spectra also give stringent limits on the variability of both $\alpha_{\rm em}$ and $\mu = m_p/m_e$ at cosmological redshifts, *e.g.*,

$$\Delta\alpha_{\rm em}/\alpha_{\rm em} = (1.2 \pm 1.7_{\rm stat} \pm 0.9_{\rm sys})\times10^{-6}\,, \qquad (21.53)$$

at redshifts $z = 1.0$–2.4 [93], and

$$|\Delta\mu/\mu| < 4\times10^{-7}(95\%\ {\rm C.L.})\,, \qquad (21.54)$$

at a redshift $z = 0.88582$ [94]. There are also significant limits on the variation of $\alpha_{\rm em}$ and $\mu = m_p/m_e$ at redshift $z \sim 10^3$ from cosmic microwave background data, *e.g.*, $\Delta\alpha_{\rm em}/\alpha_{\rm em} = (3.6 \pm 3.7)\times10^{-3}$ [95]. Direct laboratory limits (based on monitoring the frequency ratio of several different atomic clocks) on the present time variation of $\alpha_{\rm em}$, and $\mu = m_p/m_e$ have reached the levels [96, 97]

$$\begin{aligned} d\ln(\alpha_{\rm em})/dt &= (1.8\pm2.5)\times10^{-19}{\rm yr}^{-1}, \\ d\ln(\mu)/dt &= (-8\pm36)\times10^{-18}{\rm yr}^{-1}. \end{aligned} \qquad (21.55)$$

There are also experimental limits on a possible dependence of coupling constants on the gravitational potential [96, 97].

Experimental limits on the present time variation of the gravitational constant, Eq. (21.33), have been derived from planetary ephemerides [98], lunar laser ranging [99], and binary-pulsar data [100]. The most stringent limits come from lunar-laser-ranging data [99]:

$$\frac{\dot G_0}{G_0} = (-5.0\pm9.6)\times10^{-15}\ {\rm yr}^{-1}\,. \qquad (21.56)$$

See [101] for more details and references about the "constancy of constants".

21.4.2 *Tests of the isotropy of space and of Local Lorentz invariance*

The highest precision tests of the isotropy of space have been performed by looking for possible quadrupolar shifts of nuclear

Int. J. Mod. Phys. A 2026.41. Downloaded from www.worldscientific.com by UNIVERSITY OF CALIFORNIA @ BERKELEY on 09/16/26. Re- strictly not permitted, except for Open Access articles.

energy levels [102]. The (null) results can be interpreted as testing the fact that the various pieces in the matter Lagrangian, Eq. (21.6), are indeed coupled to the same external metric $g_{\mu\nu}$ to the 10^{-29} level.

Stringent tests of possible violations of local Lorentz invariance in gravitational interactions have been obtained both from solar-system data [8] and pulsar data [103, 104]. For astrophysical constraints on possible Planck-scale violations of Lorentz invariance, see Ref. [105].

21.4.3 *Tests of the universality of free fall (weak, and strong equivalence principles)*

The universality of the acceleration of free fall has been verified, for laboratory bodies, both on the ground [106, 107] (at the 10^{-13} level), and in space [108, 109] (at the 10^{-15} level):

$$\begin{aligned}(\Delta a/a)_{\rm BeTi} &= (0.3 \pm 1.8) \times 10^{-13}\,;\\ (\Delta a/a)_{\rm BeAl} &= (-0.7 \pm 1.3) \times 10^{-13}\,;\\ (\Delta a/a)_{\rm TiPt} &= (-1.5 \pm 2.3({\rm stat}) \pm 1.5({\rm syst})) \times 10^{-15}\,. \end{aligned} \tag{21.57}$$

The universality of free fall has also been verified when comparing the fall of classical and quantum objects (at the 6×10^{-9} level [110]), or of two quantum objects (at the $(0.3 \pm 5.4) \times 10^{-7}$ [111], and $(1 \pm 1.4) \times 10^{-9}$, levels [112]).

The universality of free fall of self-gravitating bodies (strong equivalence principle) has been verified in both the weak-gravity, and the strong-gravity regimes. The gravitational accelerations of the Earth and the Moon toward the Sun have been checked to agree at the 10^{-14} level [99]

$$(\Delta a/a)_{\rm EarthMoon} = (-2.1 \pm 2.4) \times 10^{-14}. \tag{21.58}$$

The latter result constrains the Nordtvedt PPN parameter [9] $\eta \equiv 4\overline{\beta} - \overline{\gamma}$ to the 10^{-4} level:

$$\eta = (0.47 \pm 0.55) \times 10^{-4}\,. \tag{21.59}$$

See below for strong-field tests of the strong equivalence principle.

Finally, the universality of the gravitational redshift of clock rates has been verified at the 10^{-4} level by comparing a hydrogen-maser clock flying on a rocket up to an altitude of about 10,000 km to a similar clock on the ground [113]. The redshift due to a height change of 33 cm has been detected by comparing two optical clocks based on $^{27}{\rm Al}^+$ ions [114], and a linear frequency gradient consistent with the gravitational redshift within a single millimeter scale sample of ultracold strontium has been measured [115]. The gravitational redshift has also been detected in the orbit of a star near the supermassive black hole at the center of our Galaxy [116, 117], and its universality has been verified at the 5% level [118].

21.5 Tests of quasi-stationary, weak-field gravity

All currently performed gravitational experiments in the solar system, including perihelion advances of planetary orbits, the bending and delay of electromagnetic signals passing near the Sun, and very accurate ranging data to the Moon obtained by laser echoes, are compatible with the post-Newtonian results of Eq. (21.15), Eq. (21.13), and Eq. (21.14). The "gravito-magnetic" interactions $\propto v_A v_B$ contained in Eq. (21.13) are involved in many of these experimental tests. They have been particularly tested in lunar-laser-ranging data [119], in the combined LAGEOS-LARES satellite data [120, 121], and in the dedicated Gravity Probe B mission [122].

To assess in a quantitative manner the results of the various solar-system tests of gravity it is convenient to express them in terms of the PPN parameters defined above. The best current limit on the post-Einstein parameter $\overline{\gamma} \equiv \gamma - 1$ is

$$\overline{\gamma} = (2.1 \pm 2.3) \times 10^{-5}\,, \tag{21.60}$$

as deduced from the additional Doppler shift experienced by radio-wave beams connecting the Earth to the Cassini spacecraft when they passed near the Sun [123].

The (cubic-vertex-related) post-Einstein parameter $\overline{\beta} \equiv \beta - 1$ is constrained at the 10^{-4} level both from a study of the global sensitivity of planetary ephemerides to post-Einstein parameters [98, 124],

$$|\overline{\beta}| < 7 \times 10^{-5}\,, \tag{21.61}$$

and from lunar-laser-ranging data [99]

$$\overline{\beta} = (6.2 \pm 7.2) \times 10^{-5}\,. \tag{21.62}$$

The periastron advance of the star S2 around the Galactic center massive black hole has been observed to agree with GR within 20% [125]. More stringent limits on $\overline{\gamma}$ (*i.e.* the coupling of φ to matter) are obtained in dilaton-like models where scalar couplings violate the Equivalence Principle [126].

21.6 Tests of strong-field gravity (neutron stars and black holes)

Experimental tests of strong-field gravity have been obtained in various physical systems, notably binary pulsars and coalescing binary black holes.

It is convenient to quantitatively express binary-pulsar tests of strong-field gravity by using the PPK formalism defined above. We recall that the measurement of N phenomenological PPK parameters leads to $N-2$ tests of strong-field gravity. In all, *twenty* tests of strong-field and/or radiative gravity have been obtained in the six different (double neutron-star) binary pulsar systems PSR B1913+16, PSR J0737−3039 A,B, PSR B1534+12, PSR J1906+0746, PSR J1757−1854, and PSR J1913+1102. Specifically, these consist of $N-2 = 5-2 = 3$ tests from PSR B1913+16 ; $7-2 = 5$ tests from PSR J0737−3039; $6-2 = 4$ tests from PSR B1534+12; $6-2 = 4$ tests from PSR J1906+0746; $5-2 = 3$ tests from PSR J1757−1854; and $3-2 = 1$ test from PSR J1913+1102.

Among these tests, six of them (those involving the measurement of the PPK parameter $\dot{P}_b$) probe radiative effects, and will be discussed in the following section. The other fourteen tests probe quasi-static, strong-field gravity. GR passes all these tests within the measurement accuracy. Let us only highlight here some of the most accurate strong-field tests. For a more complete discussion (with references) of all the binary pulsar tests see [100].

In the binary pulsar PSR B1534+12 [127] one has measured *six* post-Keplerian parameters [128–130]: k, $\gamma_{\rm timing}$, r, s, $\dot{P}_b$ and (with less accuracy) Ω_p. This yields *four* tests of relativistic gravity. Among these tests, the two involving the measurements of k, $\gamma_{\rm timing}$, r, and s accurately probe strong field gravity, without mixing of radiative effects [128]. The most precise (10^{-3} level) of these pure strong-field tests is the one obtained by combining the measurements of k, $\gamma_{\rm timing}$, and s; namely, [129],

$$\left[\frac{s^{\rm obs}}{s^{\rm GR}[k^{\rm obs}, \gamma^{\rm obs}_{\rm timing}]}\right]_{1534+12} = 1.002 \pm 0.002\,. \tag{21.63}$$

The discovery of the remarkable *double* binary pulsar PSR J0737−3039 A and B [131, 132] has led to the measurement of *seven* independent parameters [133–136]: five of them are the post-Keplerian parameters k, $\gamma_{\rm timing}$, r, s, and $\dot{P}_b$ entering the relativistic timing formula of the fast-spinning pulsar PSR J0737−3039 A; a sixth is the ratio $R = x_B/x_A$ between the projected semi-major axis of the more slowly spinning companion pulsar PSR J0737−3039 B, and that of PSR J0737−3039 A (the theoretical prediction for the ratio $R = x_B/x_A$, considered as a function of the (inertial) masses $m_1 = m_A$ and $m_2 = m_B$, is $R^{\rm theory} = m_1/m_2 + O((v/c)^4)$ [13, 14], independently of the gravitational theory considered). Finally, the seventh parameter $\Omega_{p,\rm B}$ is the angular rate of (spin-orbit) precession of PSR J0737−3039 B around the total angular momentum vector [134, 135]. These seven measurements give us *five* tests of relativistic gravity, four of which are quasi-static, strong-field tests. GR passes all those tests with flying colors [136]. The most accurate is at the 2×10^{-4} level:

$$\left[\frac{s^{\rm obs}}{s^{\rm GR}[k^{\rm obs}, \gamma^{\rm obs}_{\rm timing}]}\right]_{0737-3039} = 1.00009 \pm 0.00018\,. \tag{21.64}$$

Int. J. Mod. Phys. A 2026.41. Downloaded from www.worldscientific.com by UNIVERSITY OF CALIFORNIA @ BERKELEY on 09/16/26. Re-use and distribution is strictly not permitted, except for Open Access articles.

Binary pulsar data on other types of pulsar systems can be used to test strong-field aspects of the "strong equivalence principle," namely the GR prediction that strong-self-gravity objects (such as neutron stars) should fall with the same acceleration as weak-self-gravity objects (such as white-dwarfs) in the (external) gravitational field created by other objects (such as the Galaxy, or another white dwarf). The first binary-pulsar tests of this property have been obtained in nearly circular binary systems (made of a neutron star and a white dwarf) falling in the field of the Galaxy, and have led to strong-field confirmations (at the 2×10^{-3} level) of the strong equivalence principle [137–140]. The remarkable discovery of the pulsar PSR J0337+1715 in a hierarchical triple system [141] has allowed one to derive a much more accurate test of the strong equivalence principle because the inner binary (comprising a pulsar and a close white-dwarf companion) falls toward the outer white-dwarf companion with an acceleration that is 10^8 times larger than the Galactic acceleration. This leads to a 95% confidence level limit on a possible fractional difference in free-fall acceleration of the pulsar and its close companion of [142, 143]

$$|\Delta a/a| < 2.05 \times 10^{-6} \text{ (95\% C.L.)}\,. \tag{21.65}$$

This limit yields strong constraints on tensor-scalar gravity models.

Starting in September 2015, the ultimate strong-field regime of black holes has started to be quantitatively probed via GW observations by the LIGO-Virgo(-Kagra) collaboration. Besides testing the radiative structure of gravity (see next section), the many detected GW signals have been found to be in excellent qualitative and quantitative agreement with the structure and dynamics of black-hole horizons in GR, and, in particular, with the basic black hole uniqueness theorem asserting that an (uncharged) isolated black hole is described by the Kerr solution [5]. Because of the mixing of strong-field effects with radiative effects during the coalescence of two black holes, and because of the lack of detailed alternative-theory predictions for this process (see, however, Refs. [144–149]), it is not easy to set accurate *quantitative* limits on possible strong-field deviations from GR, independently of radiative effects. Direct tests of the existence and structure of black-hole horizons are still scarce. Let us, however, mention: (i) the lack of any statistical evidence for GW echoes (see Sec. VIIIB of [150]); and (ii) the confirmations obtained with GW250114 of the GR-predicted features of black holes (Kerr structure, and Hawking's area increase law [151]). The signal GW250114 was observed (on January 14, 2025) by the two advanced LIGO detectors with an unprecedented (network) matched-filter SNR of 80. This remarkably high SNR allowed one to test some predictions of GR and black holes with more precision than the full set of GW signals in the upcoming 4th Gravitational-Wave Transient Catalog (GWTC-4). By contrasting the properties of the merger remnant to the initial inspiraling black holes, the GR-predicted area-increase theorem was verified at the 4.5 σ level [152]. In addition, GW250114 confirmed the predictions from the Kerr geometry through a comprehensive suite of tests using the GR predictions for the full inspiral–merger–ringdown signal. See next Section.

Concerning experimental tests of the structure of black holes, let us also mention that the Event Horizon Telescope collaboration has obtained event-horizon-scale images of the supermassive black hole candidates in the center of the giant elliptical galaxy M87, and in the center of our Galaxy. These images are consistent with GR models of accreting Kerr black holes [153, 154] and provide complementary evidence for the validity of the GR predictions for black holes. For discussions of the corresponding constraints on the black hole geometry in the vicinity of the light ring see Refs. [155–158].

21.7 Tests of radiative gravity (both in binary-pulsar data and in GW data)

Experimental confirmations of the GR predictions for the radiative structure of gravity have been obtained both in binary-pulsar data and in the observation of GW signals from coalescing compact binaries (binary black holes and binary neutron stars).

Binary-pulsar observations involving the measurement of the orbital period derivative $\dot{P}_b$ give *direct* experimental tests of the reality of gravitational radiation, and, in particular, an experimental confirmation that the speed of propagation of gravity c_g is equal to the speed of light c (indeed, as recalled above, $\dot{P}_b$ is a consequence of the propagation of the gravitational interaction between the two neutron stars [12]). Even in the presence of screening mechanisms within the binary system, the value of $\dot{P}_b$ yields a measurement of the speed of propagation of GWs at the 10^{-2} level [159]. The currently most accurate binary-pulsar tests of the radiative properties of gravity come from the binary neutron-star systems PSR B1913+16 and PSR J0737−3039 A,B, as well as from several neutron-star-white-dwarf systems, notably PSR J1738+0333.

After subtracting a small ($\sim 10^{-14}$ level in $\dot{P}_b^{\rm obs} = (-2.423 \pm 0.001) \times 10^{-12}$), but significant, "Galactic" perturbing effect (linked to Galactic accelerations and to the pulsar proper motion) [160], one finds that the phenomenological test obtained by combining the measurements of the three PPK parameters $(k - \gamma_{\rm timing} - \dot{P}_b)_{1913+16}$ is passed by GR with success [161, 162]:

$$\left[\frac{\dot{P}_b^{\rm obs} - \dot{P}_b^{\rm gal}}{\dot{P}_b^{\rm GR}[k^{\rm obs}, \gamma_{\rm timing}^{\rm obs}]}\right]_{1913+16} = 1.005^{+0.001}_{-0.003}\,. \tag{21.66}$$

Here $\dot{P}_b^{\rm GR}[k^{\rm obs}, \gamma_{\rm timing}^{\rm obs}]$ is the result of inserting in $\dot{P}_b^{\rm GR}(m_1, m_2)$ the values of the masses predicted by the two equations $k^{\rm obs} = k^{\rm GR}(m_1, m_2)$, and $\gamma_{\rm timing}^{\rm obs} = \gamma_{\rm timing}^{\rm GR}(m_1, m_2)$. This yields experimental evidence for the reality of gravitational radiation damping forces at the 5×10^{-3} level.

An even better experimental test of the radiative structure of gravity (6×10^{-5} level) has been recently obtained from the combined measurement in PSR J0737−3039 A,B of the three parameters k, s, and $\dot{P}_b$ [136]:

$$\left[\frac{\dot{P}_b^{\rm obs} - \dot{P}_b^{\rm gal}}{\dot{P}_b^{\rm GR}[k^{\rm obs}, s^{\rm obs}]}\right]_{0737-3039} = 0.999963 \pm 0.000063\,. \tag{21.67}$$

In addition to the above tests, further very stringent tests of radiative gravity follow from the measurement of the orbital period decay $\dot{P}_b$ of low-eccentricity pulsar-white dwarf systems. Notably, the system PSR J1738+0333 yields an intrinsic orbital decay of [100, 163]

$$\left[\dot{P}_b^{\rm obs} - \dot{P}_b^{\rm gal}\right]_{1738+0333} = (-26.1 \pm 3.1) \times 10^{-15}\,, \tag{21.68}$$

to be compared to

$$\left[\dot{P}_b^{\rm GR}\right]_{1738+0333} = (-27.7^{+1.5}_{-1.9}) \times 10^{-15}\,. \tag{21.69}$$

The fractional agreement between the (corrected) observed period decay and the GR-predicted one seems to be quantitatively less impressive than the double-neutron-star results cited above, but the crucial point is that asymmetric binary systems (such as neutron-star-white-dwarf ones) are strong emitters of dipolar gravitational radiation in tensor-scalar theories, with $\dot{P}_b$ scaling (modulo matter-scalar couplings) like $m_1 m_2/(m_1 + m_2)^2 (v/c)^3$, instead of the parametrically smaller GR-predicted quadrupolar radiation $\dot{P}_b \sim (v/c)^5$ [7, 17]. In view of the very small absolute value of $\dot{P}_b$, this makes such systems (and notably PSR J1738+0333) very sensitive probes of tensor-scalar gravity [100, 163–168]. It is then useful to turn to a theory-dependent analysis of pulsar data. Such an analysis (see, *e.g.*, [19,100,128,163,167,168]) leads to excluding a large portion of the parameter space of tensor-scalar gravity allowed by solar-system tests. As a result, the basic matter-scalar coupling α_0^2 is more strongly constrained, over most of the parameter space, than the best current solar-system limits of Eq. (21.60) (namely below the 10^{-5} level) [100, 163, 167].

We now turn to the tests of radiative gravity that can be deduced from the GW data gathered from the first four observing runs of the LIGO-Virgo-Kagra collaboration. All currently detected GW signals are consistent with GR predictions. Several approaches were used either to test consistency with GR,

Int. J. Mod. Phys. A 2026.41. Downloaded by UNIVERSITY OF CALIFORNIA @ BERKELEY on 09/16/26. Re-
[redacted]
orldscientific.com
strictly not permitted, except for Open Access articles.

or to set limits on possible phenomenological deviations from GR [42, 150, 152, 169, 170].

A quantitative way of checking the consistency with GR of the observed GW signals used by the LVK collaboration [150,169,170] is to divide each signal into two parts: (i) the lower-frequency signal emitted during the *inspiral* phase (considered up to some conventionally chosen end); and (ii) the remaining higher-frequency *post-inspiral* signal. Separately fitting each of these partial signals to GR-based templates then yields separate estimates of the binary's parameters, with corresponding separate estimates of the mass M_f and dimensionless spin parameter $a_f = J_f/(GM_f^2)$ of the final black hole that would be formed (in GR) by the coalescence of the two initial black holes. The consistency with GR then consists in testing whether the two estimates $(M_f, a_f)_{\rm insp}$ and $(M_f, a_f)_{\rm postinsp}$ are compatible with each other. They were found to be compatible for all events whose corresponding separate SNRs made such an analysis meaningful (see Figs. 3 and 4 in [170] and Fig. 3 in [150]). [These analyses used as dividing frequency an estimate of the GW frequency at the innermost stable circular orbit. This choice implies that the post-inspiral phase contains the late-inspiral, the merger and the ringdown.] Quantitatively, the (population-marginalized) fractional differences

$$\frac{\Delta M_f}{\bar{M}_f} = 2\frac{M_f^{\rm insp} - M_f^{\rm postinsp}}{M_f^{\rm insp} + M_f^{\rm postinsp}}, \qquad \frac{\Delta a_f}{\bar{a}_f} = 2\frac{a_f^{\rm insp} - a_f^{\rm postinsp}}{a_f^{\rm insp} + a_f^{\rm postinsp}}, \tag{21.70}$$

between the two estimates were found to be consistent with zero (*i.e.* with GR) [150]

$$\frac{\Delta M_f}{\bar{M}_f} = -0.02^{+0.07}_{-0.06}, \qquad \frac{\Delta a_f}{\bar{a}_f} = -0.06^{+0.10}_{-0.07}. \tag{21.71}$$

The exceptionally loud GW250114 signal (with SNR= 80) allowed one to get, by itself, consistency tests for M_f and a_f as good as Eq. (21.71), see Fig. 6 of [171]. It also allowed one to perform more informative variants of such inspiral versus post-inspiral analyses. One variant consists in dividing the GW signal into three parts: (i) the inspiral; (ii) the late-inspiral, merger and early ringdown; and (iii) the later ringdown. A GR-consistency check is then obtained by comparing the values of M_f and a_f obtained by fitting the ringdown to a sum of damped oscillations, Eq. (21.41), having the GR-predicted QNM frequencies, Eq. (21.40), to those derived from the measurement of m_1, m_2, S_1, S_2 obtained by fitting the inspiral. The results of several variants of this consistency test are displayed in Fig. 2 of [171]. The quantitative level of the latter consistency is only at the $\sim$ 20% level, but it is qualitatively important because it gives a clear confirmation of the existence of several QNM modes, notably the first overtone $l = 2, m = 2, n = 1$ above the fundamental quadrupolar mode $l = 2, m = 2, n = 0$.

A variant of the inspiral-postinspiral consistency test leading to quantitatively more precise results consists in using a parametrized version [172] of a numerical-relativity-informed effective-one-body model in which some of the GR-predicted QNM frequencies, $f_{lmn}^{\rm GR}$, and decay times, $\tau_{lmn}^{\rm GR}$, are flexed by hand into new phenomenological parameters (to be fitted together with the usual binary parameters): $f_{lmn}^{\rm GR} \to f_{lmn}$, $\tau_{lmn}^{\rm GR} \to \tau_{lmn}$. This phenomenological procedure allows one to make use of the full GW signal to constrain possible deviations from GR. Applying this approach to the GW250114 signal leads (when flexing only the 220 and 440 QNM's) to an observational confirmation of the QNM spectrum of a Kerr black hole at the few percent level, namely [171]

$$\frac{f_{220}^{\rm obs}}{f_{220}^{\rm GR}} = 1.02^{+0.02}_{-0.02} \text{ (90\% C.L.)}. \tag{21.72}$$

The parametrization of Eq. (21.39) for possible deviations in the frequency dependence of the Fourier-domain phase $\psi(f)$ of the black hole coalescence GW signal was used to measure best-fit values for each fractional deviation parameter $\delta\hat{p}_i$, considered separately (the other ones being set to zero). In all cases, the posterior distribution for each $\delta\hat{p}_i$ is consistent with the GR value, *i.e.*, $\delta\hat{p}_i^{\rm GR} = 0$ (see Fig. 6 in [150]). The current limits on $\delta\hat{p}_i$ are (roughly) of order unity, except for the two parameters highlighted above: $\delta\hat{p}_3$ (parameterizing the NNLO, fractionally $O((\frac{v}{c})^3)$, correction to the LO, quadrupolar term); and $\delta\hat{p}_{-2}$ (parameterizing a possible dipolar-radiation-related $O((\frac{v}{c})^{-2})$ fractional correction to the LO, quadrupolar term). One of the best LVK constraints on dipolar radiation comes from the double neutron-star signal GW170817, namely (reading from Fig. 1 in [43])

$$-4 \times 10^{-6} < \delta\hat{p}_{-2} < 2 \times 10^{-5} \text{ (90\% C.L.)}. \tag{21.73}$$

The (shorter) binary black hole coalescence events yield less stringent constraints (e.g., Ref. [150] gives a 90%-credible upper bound for a possible dipolar term of $|\delta\hat{p}_{-2}| \leq 7.3 \times 10^{-4}$). For comparison, the binary-pulsar constraints on dipolar radiation mentioned above would be $O(10 - 100)$ more stringent than Eq. (21.73).

Concerning GW constraints on the NNLO phasing parameter $\delta\hat{p}_3$, one of the best limits comes from GW250114 and reads [171]

$$\delta\hat{p}_3 = -0.02 \pm 0.03 \text{ (90\% C.L.)}. \tag{21.74}$$

As recalled above, GR predicts that the polarization content of GWs is pure helicity-2, *i.e.* described by the two independent components of a traceless tensor transverse to the propagation direction. A (massless) scalar excitation would add a pure-trace "breathing mode" in the plane transverse to the propagation direction. A phenomenological approach to generic metric theories of gravity would allow for up to six polarizations for a GW [173], namely two tensor, two vector and two scalar modes. The LVK collaboration tested possible polarization deviations from GR in various ways [150, 169, 174]. Though pure-scalar, pure-vector and vector-scalar hypotheses are significantly disfavored, any mixed hypothesis involving tensor modes (i.e., tensor-scalar, tensor-vector, and tensor-vector-scalar) cannot yet be ruled out conclusively.

GR also predicts that GWs are non dispersive, and propagate at the same speed as light. One can phenomenologically modify the GR-predicted GW phase evolution by adding the putative effect of an anomalous dispersion relation of the form $E^2 = p^2c^2 + Ap^\alpha c^\alpha$. GW data have been used to set bounds on the anomalous coefficient A for various values of the exponent α. The case $\alpha = 0$ is equivalent to assuming that gravitons disperse as a massive particle [51]. The current (90%-credibility) phenomenological GW limit on the graviton mass is $m_g \leq 1.27 \times 10^{-23}{\rm eV}/c^2$ [150]. For comparison, a Bayesian analysis of planetary epheremides has given the bound $m_g \leq 1.01 \times 10^{-24}{\rm eV}/c^2$ at 99.7 % C.L. [175].

Finally, a very constraining bound on the speed of propagation of gravity $c_{\rm GW}$ was derived from the observed time delay of 1.7 s between GW170817 and the associated γ-ray burst. Namely, the fractional difference between $c_{\rm GW}$ and $c_{\rm light} \equiv c$ is constrained to be [176]

$$-3 \times 10^{-15} < \frac{c_{\rm GW} - c}{c} < +7 \times 10^{-16}. \tag{21.75}$$

When comparing the latter bound to the prediction Eq. (21.52) from general second-order tensor-scalar theories, Eq. (21.51), one is led to conclude that the coupling function $G_5(\varphi, X)$ has to be ignored and that the coupling function $G_4(\varphi, X)$ has to be restricted to depend only on φ. This drastically reduces the viable tensor-scalar modified-gravity models [177–180].

Finally, multiple pulsar timing array collaborations [181–185] have reported evidence, with varying levels of significance ($\sim$ 2σ-4σ), for a stochastic gravitational wave background in the nanohertz frequency range. While the signal interpretation remains under refinement, the current evidence supports the existence of a background consistent with cosmological expectations, primarily sourced by a population of inspiraling supermassive black hole binaries.

Int. J. Mod. Phys. A 2026.41. Downloaded from www.worldscientific.com
by UNIVERSITY OF CALIFORNIA @ BERKELEY on 09/16/26. Re-use and distribution is strictly not permitted, except for Open Access articles.

21.8 Conclusions

All present experimental tests are compatible with the predictions of the current "standard" theory of gravitation, Einstein's General Relativity. Let us recap the main tests. The universality of the coupling between matter and gravity (Equivalence Principle) has been verified at the 10^{-15} level. Solar system experiments have tested the weak-field predictions of Einstein's theory at the few times 10^{-5} level. The propagation properties (in the near zone) of relativistic gravity, as well as several of its static strong-field aspects, have been verified at the 10^{-4} level (or better) in several binary pulsar experiments. Interferometric detectors of gravitational radiation have given direct observational proofs of the existence, and properties, of gravitational waves (in the wave zone), and of the existence, and Kerr structure, of coalescing black holes, and they have already set significant limits on possible deviations, notably the $O(10^{-15})$ bound, Eq. (21.75), on the speed of gravity. In addition, laboratory experiments have set strong constraints on sub-millimeter modifications of Newtonian gravity, while many different cosmological data sets have been used to set limits on possible GR deviations on cosmological scales [31]. In spite of the uneasiness of having to assume the existence of dark matter, and the presence of an unnaturally small cosmological constant (as dark energy), General Relativity stands out as a uniquely successful description of gravity on all the scales that have been explored so far. There are no modified-gravity models that naturally pass all existing experimental tests while explaining away the need for dark matter or for dark energy.

References

[1] S. Weinberg, Rev. Mod. Phys. **61**, 1 (1989).

[2] H. A. Buchdahl, Phys. Rev. **116**, 1027 (1959).

[3] N. Chamel *et al.*, Int. J. Mod. Phys. **E22**, 1330018 (2013), [arXiv:1307.3995].

[4] J. R. Oppenheimer and H. Snyder, Phys. Rev. **56**, 455 (1939).

[5] R. P. Kerr, Phys. Rev. Lett. **11**, 237 (1963).

[6] V. F. Mukhanov, H. A. Feldman and R. H. Brandenberger, Phys. Rept. **215**, 203 (1992).

[7] C. M. Will, *Theory and Experiment in Gravitational Physics*, Cambridge University Press (2018).

[8] C. M. Will, Living Rev. Rel. **17**, 4 (2014), [arXiv:1403.7377].

[9] K. Nordtvedt, Phys. Rev. **170**, 1186 (1968).

[10] R. A. Hulse, Rev. Mod. Phys. **66**, 699 (1994).

[11] J. H. Taylor, Rev. Mod. Phys. **66**, 711 (1994).

[12] T. Damour and N. Deruelle, Phys. Lett. **A87**, 81 (1981); T. Damour, C.R. Acad. Sci. Paris **294**, 1335 (1982).

[13] T. Damour and J. H. Taylor, Phys. Rev. **D45**, 1840 (1992).

[14] T. Damour and N. Deruelle, Ann. Inst. H. Poincare A, **44**, 263 (1986).

[15] T. Damour and R. Ruffini, C. R. Acad. Sc. Paris **279**, série A, 971 (1974).

[16] B. M. Barker and R. F. O'Connell, Phys. Rev. **D12**, 329 (1975).

[17] T. Damour and G. Esposito-Farese, Class. Quant. Grav. **9**, 2093 (1992).

[18] C. M. Will and H. W. Zaglauer, Astrophys. J. **346**, 366 (1989).

[19] T. Damour and G. Esposito-Farese, Phys. Rev. **D54**, 1474 (1996), [arXiv:gr-qc/9602056].

[20] T. Damour and G. Esposito-Farese, Phys. Rev. **D58**, 042001 (1998), [arXiv:gr-qc/9803031].

[21] J.-P. Uzan, Gen. Rel. Grav. **39**, 307 (2007), [arXiv:astro-ph/0605313].

[22] R. Caldwell, A. Cooray and A. Melchiorri, Phys. Rev. **D76**, 023507 (2007), [arXiv:astro-ph/0703375].

[23] P. Zhang *et al.*, Phys. Rev. Lett. **99**, 141302 (2007), [arXiv:0704.1932].

[24] L. Amendola, M. Kunz and D. Sapone, JCAP **0804**, 013 (2008), [arXiv:0704.2421].

[25] W. Hu and I. Sawicki, Phys. Rev. **D76**, 104043 (2007), [arXiv:0708.1190].

[26] S. F. Daniel *et al.*, Phys. Rev. **D77**, 103513 (2008), [arXiv:0802.1068].

[27] G.-B. Zhao *et al.*, Phys. Rev. **D79**, 083513 (2009), [arXiv:0809.3791].

[28] J.-P. Uzan, Gen. Rel. Grav. **42**, 2219 (2010), [arXiv:0908.2243].

[29] E. Bertschinger, Phil. Trans. Roy. Soc. Lond. **A369**, 4947 (2011), [arXiv:1111.4659].

[30] T. Baker, P. G. Ferreira and C. Skordis, Phys. Rev. **D87**, 2, 024015 (2013), [arXiv:1209.2117].

[31] M. Ishak, Living Rev. Rel. **22**, 1, 1 (2019), [arXiv:1806.10122].

[32] B. P. Abbott *et al.* (LIGO Scientific, Virgo), Phys. Rev. Lett. **116**, 6, 061102 (2016), [arXiv:1602.03837].

[33] A. Buonanno and T. Damour, Phys. Rev. **D62**, 064015 (2000), [arXiv:gr-qc/0001013].

[34] L. Blanchet, Living Rev. Rel. **17**, 2 (2014), [arXiv:1310.1528].

[35] F. Pretorius, Phys. Rev. Lett. **95**, 121101 (2005), [arXiv:gr-qc/0507014]; M. Campanelli *et al.*, Phys. Rev. Lett. **96**, 111101 (2006), [arXiv:gr-qc/0511048]; J. G. Baker *et al.*, Phys. Rev. Lett. **96**, 111102 (2006), [arXiv:gr-qc/0511103].

[36] N. Yunes, X. Siemens and K. Yagi, Living Rev. Rel. **28**, 1, 3 (2025).

[37] L. Blanchet and B. S. Sathyaprakash, Phys. Rev. Lett. **74**, 1067 (1995).

[38] K. G. Arun *et al.*, Phys. Rev. **D74**, 024006 (2006), [arXiv:gr-qc/0604067].

[39] N. Yunes and F. Pretorius, Phys. Rev. **D80**, 122003 (2009), [arXiv:0909.3328].

[40] C. K. Mishra *et al.*, Phys. Rev. D **82**, 064010 (2010), [arXiv:1005.0304].

[41] T. G. F. Li *et al.*, Phys. Rev. D **85**, 082003 (2012), [arXiv:1110.0530].

[42] B. P. Abbott *et al.* (LIGO Scientific, Virgo), Phys. Rev. Lett. **116**, 22, 221101 (2016), [Erratum: Phys. Rev. Lett.121,no.12,129902(2018)], [arXiv:1602.03841].

[43] B. P. Abbott *et al.* (LIGO Scientific, Virgo), Phys. Rev. Lett. **123**, 1, 011102 (2019), [arXiv:1811.00364].

[44] S. Khan *et al.*, Phys. Rev. **D93**, 4, 044007 (2016), [arXiv:1508.07253].

[45] A. Bohé *et al.*, Phys. Rev. D **95**, 4, 044028 (2017), [arXiv:1611.03703].

[46] M. Saleem *et al.*, Phys. Rev. D **105**, 8, 084062 (2022), [arXiv:2110.10147].

[47] C. V. Vishveshwara, Nature **227**, 936 (1970).

[48] W. H. Press, Astrophys. J. Lett. **170**, L105 (1971).

[49] S. L. Detweiler, Astrophys. J. **239**, 292 (1980).

[50] E. Berti, V. Cardoso and C. M. Will, Phys. Rev. D **73**, 064030 (2006), [arXiv:gr-qc/0512160].

[51] C. M. Will, Phys. Rev. **D57**, 2061 (1998), [arXiv:gr-qc/9709011].

[52] M. Fierz, Helv. Phys. Acta **29**, 128 (1956).

[53] E. G. Adelberger, B. R. Heckel and A. E. Nelson, Ann. Rev. Nucl. Part. Sci. **53**, 77 (2003), [hep-ph/0307284].

[54] D. J. Kapner *et al.*, Phys. Rev. Lett. **98**, 021101 (2007), [hep-ph/0611184].

[55] A. O. Sushkov *et al.*, Phys. Rev. Lett. **107**, 171101 (2011), [arXiv:1108.2547].

Int. J. Mod. Phys. A 2026.41. Downloaded from www.worldscientific.com by UNIVERSITY OF CALIFORNIA @ BERKELEY on 09/16/26. Re-[redacted]strictly not permitted, except for Open Access articles.

[56] J. G. Lee *et al.*, Phys. Rev. Lett. **124**, 10, 101101 (2020), [arXiv:2002.11761].

[57] W.-H. Tan *et al.*, Phys. Rev. Lett. **124**, 5, 051301 (2020).

[58] L. Bernus *et al.*, Phys. Rev. D **102**, 2, 021501 (2020), [arXiv:2006.12304].

[59] T. Damour and J. F. Donoghue, Phys. Rev. **D82**, 084033 (2010), [arXiv:1007.2792].

[60] R. V. Wagoner, Phys. Rev. **D1**, 3209 (1970).

[61] C. Brans and R. H. Dicke, Phys. Rev. **124**, 925 (1961), [,142(1961)].

[62] L. Bernard, Phys. Rev. **D98**, 4, 044004 (2018), [arXiv:1802.10201].

[63] J. Alsing *et al.*, Phys. Rev. **D85**, 064041 (2012), [arXiv:1112.4903].

[64] T. Damour and K. Nordtvedt, Phys. Rev. Lett. **70**, 2217 (1993).

[65] T. Damour and A. M. Polyakov, Nucl. Phys. **B423**, 532 (1994), [hep-th/9401069].

[66] K. A. Olive and M. Pospelov, Phys. Rev. **D77**, 043524 (2008), [arXiv:0709.3825].

[67] J. Khoury and A. Weltman, Phys. Rev. Lett. **93**, 171104 (2004), [arXiv:astro-ph/0309300].

[68] K. Hinterbichler and J. Khoury, Phys. Rev. Lett. **104**, 231301 (2010), [arXiv:1001.4525].

[69] P. Brax *et al.*, Phys. Rev. **D82**, 063519 (2010), [arXiv:1005.3735].

[70] A. Joyce *et al.*, Phys. Rept. **568**, 1 (2015), [arXiv:1407.0059].

[71] C. Burrage and J. Sakstein, Living Rev. Rel. **21**, 1, 1 (2018), [arXiv:1709.09071].

[72] A. I. Vainshtein, Phys. Lett. **39B**, 393 (1972).

[73] C. de Rham, Living Rev. Rel. **17**, 7 (2014), [arXiv:1401.4173].

[74] G. W. Horndeski, Int. J. Theor. Phys. **10**, 363 (1974).

[75] C. Deffayet *et al.*, Phys. Rev. **D84**, 064039 (2011), [arXiv:1103.3260].

[76] L. Heisenberg, Phys. Rept. **796**, 1 (2019), [arXiv:1807.01725].

[77] T. Kobayashi, Rept. Prog. Phys. **82**, 8, 086901 (2019), [arXiv:1901.07183].

[78] G. Papallo and H. S. Reall, Phys. Rev. **D96**, 4, 044019 (2017), [arXiv:1705.04370].

[79] L. Bernard, L. Lehner and R. Luna, Phys. Rev. **D100**, 2, 024011 (2019), [arXiv:1904.12866].

[80] A. D. Kovács, Phys. Rev. **D100**, 2, 024005 (2019), [arXiv:1904.00963].

[81] C. de Rham and S. Melville, Phys. Rev. Lett. **121**, 22, 221101 (2018), [arXiv:1806.09417].

[82] D. D. Doneva and S. S. Yazadjiev, Phys. Rev. Lett. **120**, 13, 131103 (2018), [arXiv:1711.01187].

[83] H. O. Silva *et al.*, Phys. Rev. Lett. **120**, 13, 131104 (2018), [arXiv:1711.02080].

[84] G. Antoniou *et al.*, Phys. Rev. D **104**, 4, 044002 (2021), [arXiv:2105.04479].

[85] C. A. R. Herdeiro and E. Radu, Int. J. Mod. Phys. **D24**, 09, 1542014 (2015), [arXiv:1504.08209].

[86] A.I. Shlyakhter, Nature **264**, 340 (1976).

[87] T. Damour and F. Dyson, Nucl. Phys. **B480**, 37 (1996), [hep-ph/9606486].

[88] C. R. Gould, E. I. Sharapov and S. K. Lamoreaux, Phys. Rev. **C74**, 024607 (2006), [arXiv:nucl-ex/0701019].

[89] E. D. Davis and L. Hamdan, Phys. Rev. **C92**, 1, 014319 (2015), [arXiv:1503.06011].

[90] Yu. V. Petrov *et al.*, Phys. Rev. **C74**, 064610 (2006), [hep-ph/0506186].

[91] V. V. Flambaum and R. B. Wiringa, Phys. Rev. **C79**, 034302 (2009), [arXiv:0807.4943].

[92] K. A. Olive *et al.*, Phys. Rev. **D69**, 027701 (2004), [arXiv:astro-ph/0309252].

[93] M. T. Murphy, A. L. Malec and J. X. Prochaska, Mon. Not. Roy. Astron. Soc. **461**, 3, 2461 (2016), [arXiv:1606.06293].

[94] N. Kanekar *et al.*, Mon. Not. Roy. Astron. Soc. **448**, 1, L104 (2015), [arXiv:1412.7757].

[95] P. A. R. Ade *et al.* (Planck), Astron. Astrophys. **580**, A22 (2015), [arXiv:1406.7482].

[96] R. Lange *et al.*, Phys. Rev. Lett. **126**, 1, 011102 (2021), [arXiv:2010.06620].

[97] M. Filzinger *et al.*, Phys. Rev. Lett. **130**, 25, 253001 (2023), [arXiv:2301.03433].

[98] A. Fienga and O. Minazzoli, Living Rev. Rel. **27**, 1, 1 (2024), [arXiv:2303.01821].

[99] L. Biskupek, J. Müller and J.-M. Torre, Universe **7**, 2, 34 (2021), [arXiv:2012.12032].

[100] P. C. C. Freire and N. Wex, Living Rev. Rel. **27**, 1, 5 (2024), [arXiv:2407.16540].

[101] J.-P. Uzan (2024), [arXiv:2410.07281].

[102] M. Smiciklas *et al.*, Phys. Rev. Lett. **107**, 171604 (2011), [arXiv:1106.0738].

[103] J. F. Bell and T. Damour, Class. Quant. Grav. **13**, 3121 (1996), [arXiv:gr-qc/9606062].

[104] L. Shao and N. Wex, Class. Quant. Grav. **29**, 215018 (2012), [arXiv:1209.4503].

[105] S. Liberati, J. Phys. Conf. Ser. **631**, 1, 012011 (2015).

[106] S. Schlamminger *et al.*, Phys. Rev. Lett. **100**, 041101 (2008), [arXiv:0712.0607].

[107] T. A. Wagner *et al.*, Class. Quant. Grav. **29**, 184002 (2012), [arXiv:1207.2442].

[108] P. Touboul *et al.* (MICROSCOPE), Phys. Rev. Lett. **129**, 12, 121102 (2022), [arXiv:2209.15487].

[109] P. Touboul *et al.*, Class. Quant. Grav. **39**, 20, 204009 (2022), [arXiv:2209.15488].

[110] S. Merlet *et al.*, Metrologia, **47**, L9-L11 (2010).

[111] D. Schlippert *et al.*, Phys. Rev. Lett. **112**, 203002 (2014), [arXiv:1406.4979].

[112] G. Rosi *et al.*, Nature Commun. **8**, 5529 (2017), [arXiv:1704.02296].

[113] R.F.C. Vessot and M.W. Levine, Gen. Rel. Grav. **10**, 181 (1978); R. F. C. Vessot *et al.*, Phys. Rev. Lett. **45**, 2081 (1980).

[114] C. W. Chou *et al.*, Science **329**, 1630 (2010).

[115] T. Bothwell *et al.*, Nature **602**, 420 (2022), [arXiv:2109.12238].

[116] R. Abuter *et al.* (GRAVITY), Astron. Astrophys. **615**, L15 (2018), [arXiv:1807.09409].

[117] T. Do *et al.*, Science **365**, 6454, 664 (2019), [arXiv:1907.10731].

[118] A. Amorim *et al.* (GRAVITY), Phys. Rev. Lett. **122**, 10, 101102 (2019), [arXiv:1902.04193].

[119] J. G. Williams, S. G. Turyshev and D. Boggs, Class. Quant. Grav. **29**, 184004 (2012), [arXiv:1203.2150].

[120] I. Ciufolini and E. C. Pavlis, Nature **431**, 958 (2004).

[121] I. Ciufolini *et al.*, Eur. Phys. J. Plus **138**, 11, 1054 (2023), [arXiv:2311.13268].

[122] C. W. F. Everitt *et al.*, Class. Quant. Grav. **32**, 22, 224001 (2015).

[123] B. Bertotti, L. Iess and P. Tortora, Nature **425**, 374 (2003).

Int. J. Mod. Phys. A 2026.41. Downloaded from www.worldscientific.com
by UNIVERSITY OF CALIFORNIA @ BERKELEY on 09/16/26. Re-use and distribution is strictly not permitted, except for Open Access articles.

[124] A. Fienga *et al.*, Cel. Mech. Dyn. Astr. **123**, Issue 2, 1 (2015).

[125] R. Abuter *et al.* (GRAVITY), Astron. Astrophys. **636**, L5 (2020), [arXiv:2004.07187].

[126] J. Bergé *et al.*, Phys. Rev. Lett. **120**, 14, 141101 (2018), [arXiv:1712.00483].

[127] A. Wolszczan, Nature **350**, 688 (1991).

[128] J. N. Taylor, A. Wolszczan and T. Damour, Nature **355**, 132 (1993).

[129] E. Fonseca, I. H. Stairs and S. E. Thorsett, Astrophys. J. **787**, 82 (2014), [arXiv:1402.4836].

[130] H. Ding *et al.*, Astrophys. J. Lett. **921**, 1, L19 (2021), [arXiv:2110.10590].

[131] M. Burgay *et al.*, Nature **426**, 531 (2003), [arXiv:astro-ph/0312071].

[132] A. G. Lyne *et al.*, Science **303**, 1153 (2004), [arXiv:astro-ph/0401086].

[133] M. Kramer *et al.*, Science **314**, 97 (2006), [arXiv:astro-ph/0609417].

[134] R. P. Breton *et al.*, Science **321**, 104 (2008), [arXiv:0807.2644].

[135] B. Perera *et al.*, Astrophys. J. **721**, 1193 (2010), [arXiv:1008.1097].

[136] M. Kramer *et al.*, Phys. Rev. X **11**, 4, 041050 (2021), [arXiv:2112.06795].

[137] T. Damour and G. Schaefer, Phys. Rev. Lett. **66**, 2549 (1991).

[138] M. E. Gonzalez *et al.*, Astrophys. J. **743**, 102 (2011), [arXiv:1109.5638].

[139] P. C. C. Freire, M. Kramer and N. Wex, Class. Quant. Grav. **29**, 184007 (2012), [arXiv:1205.3751].

[140] W. W. Zhu *et al.*, Mon. Not. Roy. Astron. Soc. **482**, 3, 3249 (2019), [arXiv:1802.09206].

[141] S. M. Ransom *et al.*, Nature **505**, 520 (2014), [arXiv:1401.0535].

[142] A. M. Archibald *et al.*, Nature **559**, 7712, 73 (2018), [arXiv:1807.02059].

[143] G. Voisin *et al.*, Astron. Astrophys. **638**, A24 (2020), [arXiv:2005.01388].

[144] M. Okounkova *et al.*, Phys. Rev. **D96**, 4, 044020 (2017), [arXiv:1705.07924].

[145] H. Witek *et al.*, Phys. Rev. **D99**, 6, 064035 (2019), [arXiv:1810.05177].

[146] M. Okounkova *et al.* (2019), [arXiv:1906.08789].

[147] T. Evstafyeva *et al.*, Class. Quant. Grav. **40**, 8, 085009 (2023), [arXiv:2212.08023].

[148] M. Corman, J. L. Ripley and W. E. East, Phys. Rev. D **107**, 2, 024014 (2023), [arXiv:2210.09235].

[149] R. Cayuso *et al.*, Phys. Rev. Lett. **131**, 11, 111403 (2023), [arXiv:2303.07246].

[150] R. Abbott *et al.* (LIGO Scientific, VIRGO, KAGRA) (2021), [arXiv:2112.06861].

[151] S. W. Hawking, Phys. Rev. Lett. **26**, 1344 (1971).

[152] A. G. Abac *et al.* (LIGO Scientific, VIRGO, KAGRA) (2025), [arXiv:??].

[153] K. Akiyama *et al.* (Event Horizon Telescope), Astrophys. J. **875**, 1, L1 (2019), [arXiv:1906.11238].

[154] K. Akiyama *et al.* (Event Horizon Telescope), Astrophys. J. Lett. **930**, 2, L12 (2022).

[155] K. Akiyama *et al.* (Event Horizon Telescope), Astrophys. J. Lett. **875**, 1, L6 (2019), [arXiv:1906.11243].

[156] D. Psaltis *et al.* (Event Horizon Telescope), Phys. Rev. Lett. **125**, 14, 141104 (2020), [arXiv:2010.01055].

[157] S. H. Völkel *et al.* (2020), [arXiv:2011.06812].

[158] K. Akiyama *et al.* (Event Horizon Telescope), Astrophys. J. Lett. **930**, 2, L17 (2022).

[159] J. Beltran Jimenez, F. Piazza and H. Velten, Phys. Rev. Lett. **116**, 6, 061101 (2016), [arXiv:1507.05047].

[160] T. Damour and J. H. Taylor, Astrophys. J. **366**, 501 (1991).

[161] J. M. Weisberg and Y. Huang, Astrophys. J. **829**, 1, 55 (2016), [arXiv:1606.02744].

[162] A. T. Deller *et al.*, Astrophys. J. **862**, 2, 139 (2018), [arXiv:1806.10265].

[163] P. C. C. Freire *et al.*, Mon. Not. Roy. Astron. Soc. **423**, 3328 (2012), [arXiv:1205.1450].

[164] K. Lazaridis *et al.*, Mon. Not. R. Astron. Soc. **400**, 805 (2009), [arXiv:0908.0285].

[165] J. Antoniadis *et al.*, Science **340**, 6131 (2013), [arXiv:1304.6875].

[166] W. W. Zhu *et al.*, Astrophys. J. **809**, 1, 41 (2015), [arXiv:1504.00662].

[167] L. Shao *et al.*, Phys. Rev. **X7**, 4, 041025 (2017), [arXiv:1704.07561].

[168] N. Wex and M. Kramer, Universe **6**, 9, 156 (2020).

[169] B. P. Abbott *et al.* (LIGO Scientific, Virgo), Phys. Rev. D **100**, 10, 104036 (2019), [arXiv:1903.04467].

[170] R. Abbott *et al.* (LIGO Scientific, Virgo), Phys. Rev. D **103**, 12, 122002 (2021), [arXiv:2010.14529].

[171] A. G. Abac *et al.* (LIGO Scientific, Virgo, KAGRA), Phys. Rev. Lett. **136**, 4, 041403 (2026), [arXiv:2509.08099].

[172] R. Brito, A. Buonanno and V. Raymond, Phys. Rev. D **98**, 8, 084038 (2018), [arXiv:1805.00293].

[173] D. M. Eardley, D. L. Lee and A. P. Lightman, Phys. Rev. **D8**, 3308 (1973).

[174] B. P. Abbott *et al.* (LIGO Scientific, Virgo), Phys. Rev. Lett. **119**, 14, 141101 (2017), [arXiv:1709.09660].

[175] V. Mariani *et al.*, Phys. Rev. D **108**, 2, 024047 (2023), [arXiv:2306.07069].

[176] B. P. Abbott *et al.* (LIGO Scientific, Virgo, Fermi-GBM, INTEGRAL), Astrophys. J. **848**, 2, L13 (2017), [arXiv:1710.05834].

[177] T. Baker *et al.*, Phys. Rev. Lett. **119**, 25, 251301 (2017), [arXiv:1710.06394].

[178] P. Creminelli and F. Vernizzi, Phys. Rev. Lett. **119**, 25, 251302 (2017), [arXiv:1710.05877].

[179] J. Sakstein and B. Jain, Phys. Rev. Lett. **119**, 25, 251303 (2017), [arXiv:1710.05893].

[180] J. M. Ezquiaga and M. Zumalacárregui, Phys. Rev. Lett. **119**, 25, 251304 (2017), [arXiv:1710.05901].

[181] G. Agazie *et al.* (NANOGrav), Astrophys. J. Lett. **951**, 1, L8 (2023), [arXiv:2306.16213].

[182] J. Antoniadis *et al.* (EPTA, InPTA:), Astron. Astrophys. **678**, A50 (2023), [arXiv:2306.16214].

[183] D. J. Reardon *et al.*, Astrophys. J. Lett. **951**, 1, L6 (2023), [arXiv:2306.16215].

[184] H. Xu *et al.*, Res. Astron. Astrophys. **23**, 7, 075024 (2023), [arXiv:2306.16216].

[185] M. T. Miles *et al.*, Mon. Not. Roy. Astron. Soc. **536**, 2, 1489 (2024), [arXiv:2412.01153].

22. Big-Bang Cosmology

Revised August 2025 by K.A. Olive (Minnesota U.) and J.A. Peacock (Edinburgh U.).

22.1 Introduction to the standard Big-Bang model

The observed expansion of the Universe [1–3] is a natural (almost inevitable) result of any homogeneous and isotropic cosmological model based on general relativity. However, by itself, the Hubble expansion does not provide sufficient evidence for what we generally refer to as the Big-Bang model of cosmology. While general relativity is in principle capable of describing the cosmology of any given distribution of matter, it is extremely fortunate that our Universe appears to be homogeneous and isotropic on large scales. Together, homogeneity and isotropy allow us to extend the Copernican Principle to the Cosmological Principle, stating that all spatial positions in the Universe are essentially equivalent.

The formulation of the Big-Bang model began in the 1940s with the work of George Gamow and his collaborators, Ralph Alpher and Robert Herman. In order to account for the possibility that the abundances of the elements had a cosmological origin, they proposed that the early Universe was once very hot and dense (enough so as to allow for the nucleosynthetic processing of hydrogen), and has subsequently expanded and cooled to its present state [4, 5]. In 1948, Alpher and Herman predicted that a direct consequence of this model is the presence of a relic background radiation with a temperature between 1 and 5 kelvin [6, 7]. Of course this radiation was observed 16 years later as the cosmic microwave background (CMB) [8]. Indeed, it was the observation of this radiation that singled out the Big-Bang model as the prime candidate to describe our Universe. Subsequent work on Big-Bang nucleosynthesis (BBN) further confirmed the necessity of our hot and dense past. See Sec. 22.3.7 for a brief discussion of BBN, and Sec. 24 of this *Review* for a detailed discussion of BBN. These relativistic cosmological models face severe problems with their initial conditions, to which the best modern solution is inflationary cosmology, discussed in Sec. 22.3.5 and in – Sec. 23 of this *Review*. If correct, these ideas would strictly render the term 'Big Bang' redundant, since it was first coined by Hoyle to represent a criticism of the lack of understanding of the initial conditions.

22.1.1 *The Robertson-Walker Universe*

The observed homogeneity and isotropy enable us to describe the overall geometry and evolution of the Universe in terms of two cosmological parameters accounting for the spatial curvature and the overall expansion (or contraction) of the Universe. These two quantities appear in the most general expression for a space-time metric that has a (3D) maximally symmetric subspace of a 4D space-time, known as the Robertson-Walker metric:

$$ds^2 = dt^2 - R^2(t)\left[\frac{dr^2}{1-kr^2} + r^2\left(d\theta^2 + \sin^2\theta\, d\phi^2\right)\right]. \qquad (22.1)$$

Note that we adopt $c = 1$ throughout. By rescaling the radial coordinate, we can choose the curvature constant k to take only the discrete values $+1$, -1, or 0 corresponding to closed, open, or spatially flat geometries. In this case, it is often more convenient to re-express the metric as

$$ds^2 = dt^2 - R^2(t)\left[d\chi^2 + S_k^2(\chi)\left(d\theta^2 + \sin^2\theta\, d\phi^2\right)\right], \qquad (22.2)$$

where the function $S_k(\chi)$ is $(\sin\chi, \chi, \sinh\chi)$ for $k = (+1, 0, -1)$. The coordinate r [in Eq. (22.1)] and the 'angle' χ [in Eq. (22.2)] are both dimensionless; the dimensions are carried by the cosmological scale factor, $R(t)$. This is the characteristic scale of spatial curvature, and it determines proper distances in terms of the comoving coordinates. A common alternative is to define a dimensionless scale factor, $a(t) = R(t)/R_0$, where $R_0 \equiv R(t_0)$ is R at the present epoch. It is also sometimes convenient to define a dimensionless or conformal time coordinate, η, by $d\eta = dt/R(t)$. Along constant spatial sections, the proper time is defined by the time coordinate, t. Similarly, for $dt = d\theta = d\phi = 0$, the proper distance is given by $R(t)\chi$. For standard texts on cosmological models see *e.g.*, Refs. [9–17].

22.1.2 *The redshift*

The cosmological redshift is a direct consequence of the Hubble expansion, determined by $R(t)$. A local observer detecting light from a distant emitter sees a redshift in frequency. We can define the redshift as

$$z \equiv \frac{\nu_1 - \nu_2}{\nu_2} \simeq v_{12}, \qquad (22.3)$$

where ν_1 is the frequency of the emitted light, ν_2 is the observed frequency, and v_{12} is the relative velocity between the emitter and the observer. While the definition, $z = (\nu_1 - \nu_2)/\nu_2$ is valid in general, relating the redshift to a simple relative velocity is only correct on small scales (*i.e.*, less than cosmological scales) such that the expansion velocity is non-relativistic. For light signals, we can use the metric given by Eq. (22.1) and $ds^2 = 0$ to write

$$v_{12} = \dot{R}\,\delta r = \frac{\dot{R}}{R}\,\delta t = \frac{\delta R}{R} = \frac{R_2 - R_1}{R_1}, \qquad (22.4)$$

where $\delta r(\delta t)$ is the radial coordinate (temporal) separation between the emitter and observer. Noting that physical distance, D, is $R\delta r$ or δt, Eq. (22.4) gives us Hubble's law, $v = HD$. In addition, we obtain a simple relation between the redshift and the scale factor:

$$1 + z = \frac{\nu_1}{\nu_2} = \frac{R_2}{R_1}. \qquad (22.5)$$

This result does not depend on the non-relativistic approximation.

22.1.3 *The Friedmann equations of motion*

The cosmological equations of motion are derived from Einstein's equations:

$$\mathcal{R}_{\mu\nu} - \tfrac{1}{2} g_{\mu\nu}\mathcal{R} = 8\pi G_{\rm N} T_{\mu\nu} + \Lambda g_{\mu\nu}\,. \qquad (22.6)$$

Gliner [18] and Zeldovich [19] pioneered the modern view, in which the Λ term is set on the rhs and interpreted as an effective energy-momentum tensor $T_{\mu\nu}$ for the vacuum of $\Lambda g_{\mu\nu}/8\pi G_{\rm N}$. It is common to assume that the matter content of the Universe is a perfect fluid, for which

$$T_{\mu\nu} = -p g_{\mu\nu} + (p + \rho)\, u_\mu u_\nu, \qquad (22.7)$$

where $g_{\mu\nu}$ is the space-time metric described by Eq. (22.1), p is the isotropic pressure, ρ is the energy density and $u = (1, 0, 0, 0)$ is the velocity vector for the isotropic fluid in co-moving coordinates. With the perfect fluid source, Einstein's equations lead to the Friedmann equations:

$$H^2 \equiv \left(\frac{\dot{R}}{R}\right)^2 = \frac{8\pi\, G_{\rm N}\, \rho}{3} - \frac{k}{R^2} + \frac{\Lambda}{3}, \qquad (22.8)$$

and

$$\frac{\ddot{R}}{R} = \frac{\Lambda}{3} - \frac{4\pi G_{\rm N}}{3}\,(\rho + 3p), \qquad (22.9)$$

where $H(t)$ is the Hubble parameter and Λ is the cosmological constant. The first of these is sometimes called *the* Friedmann equation. Energy conservation via $T^{\mu\nu}_{;\mu} = 0$, leads to a third useful equation [which can also be derived from Eq. (22.8) and Eq. (22.9)]:

$$\dot{\rho} = -3H\,(\rho + p)\,. \qquad (22.10)$$

Equation (22.10) can also be simply derived as a consequence of the first law of thermodynamics.

Equation (22.8) has a simple classical mechanical analog if we neglect (for the moment) the cosmological term Λ. By interpreting $-k/R^2$ Newtonianly as a 'total energy', then we see that the evolution of the Universe is governed by a competition between the potential energy, $8\pi G_{\rm N}\rho/3$, and the kinetic term $(\dot{R}/R)^2$. For $\Lambda = 0$, it is clear that the Universe must be expanding or contracting (except at the turning point prior to collapse in a closed Universe). The ultimate fate of the Universe is determined by the curvature constant k. For $k = +1$, the Universe will recollapse in a finite time, whereas for $k = 0, -1$, the Universe will expand indefinitely. These simple conclusions can be altered when $\Lambda \neq 0$ or more generally with some component having $(\rho + 3p) < 0$.

Int. J. Mod. Phys. A 2026.41. Downloaded from www.worldscientific.com by UNIVERSITY OF CALIFORNIA @ BERKELEY on 09/16/26. Re-[redacted] strictly not permitted, except for Open Access articles.

Int. J. Mod. Phys. A 2026.41. Downloaded from www.worldscientific.com by UNIVERSITY OF CALIFORNIA @ BERKELEY on 09/16/26. Re-use and distribution is strictly not permitted, except for Open Access articles.

22.1.4 *Definition of cosmological parameters*

In addition to the Hubble parameter, it is useful to define several other measurable cosmological parameters. The Friedmann equation can be used to define a critical density such that $k = 0$ when $\Lambda = 0$:

$$\rho_c \equiv \frac{3H^2}{8\pi G_N} = 1.88 \times 10^{-26}\, h^2 \text{ kg m}^{-3} = 1.05 \times 10^{-5}\, h^2 \text{ GeV cm}^{-3}, \tag{22.11}$$

where the scaled Hubble parameter, h, is defined by

$$H \equiv 100\, h \text{ km s}^{-1} \text{ Mpc}^{-1} \Rightarrow H^{-1} = 9.778\, h^{-1} \text{ Gyr} = 2998\, h^{-1} \text{ Mpc}. \tag{22.12}$$

The cosmological density parameter $\Omega_{\rm tot}$ is defined as the energy density relative to the critical density:

$$\Omega_{\rm tot} = \rho/\rho_c. \tag{22.13}$$

Note that one can now rewrite the Friedmann equation as

$$k/R^2 = H^2(\Omega_{\rm tot} - 1)\ . \tag{22.14}$$

From Eq. (22.14), one can see that when $\Omega_{\rm tot} > 1$, $k = +1$ and the Universe is closed, when $\Omega_{\rm tot} < 1$, $k = -1$ and the Universe is open, and when $\Omega_{\rm tot} = 1$, $k = 0$, and the Universe is spatially flat.

It is often necessary to distinguish different contributions to the density. It is therefore convenient to define present-day density parameters for pressureless matter ($\Omega_{\rm m}$) and relativistic particles ($\Omega_{\rm r}$), plus the quantity $\Omega_\Lambda = \Lambda/3H^2$. In more general models, we may wish to drop the assumption that the vacuum energy density is constant, and we therefore denote the present-day density parameter of the vacuum by $\Omega_{\rm v}$. The Friedmann equation then becomes

$$k/R_0^2 = H_0^2(\Omega_{\rm m} + \Omega_{\rm r} + \Omega_{\rm v} - 1), \tag{22.15}$$

where the subscript 0 indicates present-day values. Thus, it is the sum of the densities in matter, relativistic particles, and vacuum that determines the overall sign of the curvature. Note that the quantity $-k/R_0^2H_0^2$ is sometimes referred to as Ω_K. This usage is unfortunate: it encourages one to think of curvature as a contribution to the energy density of the Universe, which is not correct.

22.1.5 *Friedmann model solutions*

Much of the history of the Universe in the standard Big-Bang model can be easily described by assuming that either matter or radiation dominates the total energy density. During inflation and again today the expansion rate for the Universe is accelerating, and we should allow for domination by a component with a negative pressure: the cosmological constant or dark energy discussed below. In the following, we shall delineate the solutions to the Friedmann equation when a single component dominates the energy density. Each component is distinguished by an equation of state parameter $w = p/\rho$. We concentrate on solutions that expand at early times, although the Friedmann equation also permits a time-reversed contracting solution.

22.1.5.1 *Solutions for a general equation of state*

Let us first assume a general equation of state parameter for a single component, w, which is constant. In this case, Eq. (22.10) can be written as $\dot\rho = -3(1+w)\rho\dot R/R$ and is easily integrated to yield

$$\rho \propto R^{-3(1+w)}. \tag{22.16}$$

Note that at early times when R is small, the less singular curvature term k/R^2 in the Friedmann equation can be neglected so long as $w > -1/3$. Curvature domination occurs at rather late times (if a cosmological constant term does not dominate sooner). For $w \neq -1$, one can insert this result into the Friedmann equation Eq. (22.8), and if one neglects the curvature and cosmological constant terms, it is easy to integrate the equation to obtain

$$R(t) \propto t^{2/[3(1+w)]}. \tag{22.17}$$

22.1.5.2 *A Radiation-dominated Universe*

In the early hot and dense Universe, it is appropriate to assume an equation of state corresponding to a gas of radiation (or relativistic particles) for which $w = 1/3$. In this case, Eq. (22.16) becomes $\rho \propto R^{-4}$. The 'extra' factor of $1/R$ is due to the cosmological redshift; not only is the number density of particles in the radiation background decreasing as R^{-3} since volume scales as R^3, but in addition each particle's energy is decreasing as $E \propto \nu \propto R^{-1}$. Similarly, one can substitute $w = 1/3$ into Eq. (22.17) to obtain

$$R(t) \propto t^{1/2}; \qquad H = 1/2t. \tag{22.18}$$

22.1.5.3 *A Matter-dominated Universe*

At relatively late times, non-relativistic matter eventually dominates the energy density over radiation [see Eq. (22.3.8)]. A pressureless gas ($w = 0$) leads to the expected dependence $\rho \propto R^{-3}$ from Eq. (22.16) and, if $k = 0$, we obtain

$$R(t) \propto t^{2/3}; \qquad H = 2/3t. \tag{22.19}$$

22.1.5.4 *A Universe dominated by vacuum energy*

If there is a dominant source of vacuum energy, V_0, it would act as a cosmological constant with $\Lambda = 8\pi G_N V_0$ and equation of state $w = -1$. In this case, the solution to the Friedmann equation when curvature is neglected is particularly simple and leads to an exponential expansion of the Universe:

$$R(t) \propto e^{\sqrt{\Lambda/3}\, t}. \tag{22.20}$$

More generally we could write

$$a(t) = \sinh^{2/3}(\sqrt{3\Lambda}t/2), \tag{22.21}$$

which describes a flat Universe containing both matter and vacuum energy, with $a(t)$ being the scale factor normalized to unity when both components are equal.

A key parameter is the equation of state of the vacuum, $w \equiv p/\rho$; this need not be the $w = -1$ of Λ, and may not even be constant [20–22]. There is much interest in the more general possibility of a dynamically evolving vacuum energy, for which the name 'dark energy' has become commonly used. A variety of techniques exist whereby the vacuum density as a function of time may be measured, usually expressed as the value of w as a function of epoch [23, 24]. It is common to expand $w(a)$ about its present value, $w(a) \simeq w_0 + w_a(a-1) + \cdots$, thus introducing a second potential observable (w_a) in addition to w_0. The best current measurement for the equation of state (assumed constant, but without assuming zero curvature) is $w = -1.028 \pm 0.031$ [25]. Unless stated otherwise, we will assume that the vacuum energy is a cosmological constant with $w = -1$ exactly.

The presence of vacuum energy can dramatically alter the fate of the Universe. For example, if $\Lambda < 0$, the Universe will eventually recollapse independent of the sign of k. For large values of $\Lambda > 0$ (larger than the Einstein static value needed to halt any cosmological expansion or contraction), even a closed Universe will expand forever. One way to quantify this is the deceleration parameter, q_0, defined as

$$q_0 = -\left.\frac{R\ddot R}{\dot R^2}\right|_0 = \frac{1}{2}\Omega_{\rm m} + \Omega_{\rm r} + \frac{(1+3w)}{2}\Omega_{\rm v}. \tag{22.22}$$

This equation shows us that $w < -1/3$ for the vacuum may lead to an accelerating expansion. To the continuing astonishment of cosmologists, such an effect has been observed: one piece of direct evidence is the supernova Hubble diagram [26–30] (see Fig. 22.1 below). Current data indicate that vacuum energy is indeed the largest contributor to the cosmological density budget, with $\Omega_{\rm v} = 0.685 \pm 0.007$ and $\Omega_{\rm m} = 0.315 \pm 0.007$ if $k = 0$ is assumed [25].

The existence of this constituent is without doubt the greatest puzzle raised by the current cosmological model; the final section of this review discusses some of the ways in which the vacuum-energy problem is being addressed. For more details, see Dark Energy – Sec. 28 of this *Review*.

Int. J. Mod. Phys. A 2026.41. Downloaded from www.worldscientific.com
by UNIVERSITY OF CALIFORNIA @ BERKELEY on 09/16/26. Re-
strictly not permitted, except for Open Access articles.

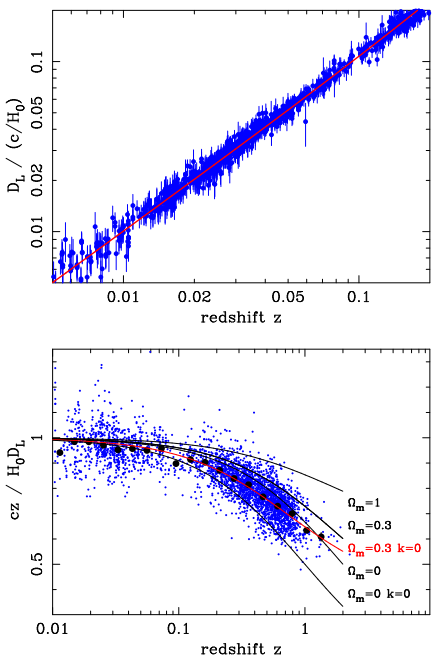

Figure 22.1: The type Ia supernova Hubble diagram, based on 3447 publicly available supernova distance estimates [29, 30]. The first panel shows that for $z \ll 1$ the large-scale Hubble flow is indeed almost perfectly linear and uniform; the second panel shows an expanded scale, with the linear trend divided out, and with the redshift range extended to show how the Hubble law becomes nonlinear. Larger points with errors show median values in redshift bins. Comparison with the prediction of Friedmann models favors a vacuum-dominated Universe.

22.2 Introduction to observational cosmology

22.2.1 *Fluxes, luminosities, and distances*

The key quantities for observational cosmology can be deduced quite directly from the metric.

(1) The *proper* transverse size of an object seen by us to subtend an angle $d\psi$ is its comoving size $d\psi\, S_k(\chi)$ times the scale factor at the time of emission:

$$d\ell = d\psi\; R_0 S_k(\chi)/(1+z). \tag{22.23}$$

(2) The apparent flux density of an object is deduced by allowing its photons to flow through a sphere of current radius $R_0 S_k(\chi)$; but photon energies and arrival rates are redshifted, and the bandwidth $d\nu$ is reduced. The observed photons at frequency ν_0 were emitted at frequency $\nu_0(1+z)$, so the flux density is the luminosity at this frequency, divided by the total area, divided by $1+z$:

$$S_\nu(\nu_0) = \frac{L_\nu([1+z]\nu_0)}{4\pi R_0^2 S_k^2(\chi)(1+z)}. \tag{22.24}$$

These relations lead to the following common definitions:

$$\begin{aligned} \text{angular-diameter distance} \quad & D_{\rm A} = (1+z)^{-1} R_0 S_k(\chi); \\ \text{luminosity distance} \quad & D_{\rm L} = (1+z)\; R_0 S_k(\chi)\;. \end{aligned} \tag{22.25}$$

These distance-redshift relations are expressed in terms of observables by using the equation of a null radial geodesic ($R(t)d\chi = dt$) plus the Friedmann equation:

$$\begin{aligned} R_0\, d\chi = \frac{1}{H(z)}\, dz = \frac{1}{H_0}\, \big[& (1-\Omega_{\rm m}-\Omega_{\rm v}-\Omega_{\rm r})(1+z)^2 \\ & + \Omega_{\rm v}(1+z)^{3+3w} + \Omega_{\rm m}(1+z)^3 \\ & + \Omega_{\rm r}(1+z)^4\big]^{-1/2}\; dz. \end{aligned} \tag{22.26}$$

The main scale for the distance here is the Hubble length, $1/H_0$. The flux density is the product of the specific intensity I_ν and the solid angle $d\Omega$ subtended by the source: $S_\nu = I_\nu\; d\Omega$. Combining the angular size and flux-density relations thus gives the relativistic version of surface-brightness conservation:

$$I_\nu(\nu_0) = \frac{B_\nu([1+z]\nu_0)}{(1+z)^3}, \tag{22.27}$$

where B_ν is surface brightness (luminosity emitted into unit solid angle per unit area of source). We can integrate over ν_0 to obtain the corresponding total or bolometric formula:

$$I_{\rm tot} = \frac{B_{\rm tot}}{(1+z)^4}. \tag{22.28}$$

This cosmology-independent form expresses Liouville's theorem: photon phase-space density is conserved along rays.

22.2.2 *Distance data and geometrical tests of cosmology*

In order to confront these theoretical predictions with data, we have to bridge the divide between two extremes. Nearby objects may have their distances measured quite easily, but their radial velocities are dominated by deviations from the ideal Hubble flow, which typically have a magnitude of several hundred $\mathrm{km\,s^{-1}}$. On the other hand, objects at redshifts $z \gtrsim 0.01$ will have observed recessional velocities that differ from their ideal values by $\lesssim 10\%$, but absolute distances are much harder to supply in this case. The traditional solution to this problem is the construction of the distance ladder: an interlocking set of methods for obtaining relative distances between various classes of object, which begins with absolute distances at the 10 to 100 pc level, and terminates with galaxies at significant redshifts. This is discussed in the article on Cosmological Parameters – Sec. 25 of this *Review*.

One of the key developments in this area has been the use of type Ia supernovae (SNe), which now allow measurement of relative distances with 5% precision. In combination with improved Cepheid data from the *HST* plus improved measurements of the distance to the Large Magellanic Cloud (or alternatively a direct geometrical distance to the 'maser galaxy' NGC4258), SNe results extend the distance ladder to the point where deviations from uniform expansion are negligible, leading to the best existing Cepheid-based value for H_0: $(73.0 \pm 1.0)\,\mathrm{km\,s^{-1}Mpc^{-1}}$ [31]. Better still, the analysis of high-z SNe has allowed a simple and direct test of cosmological geometry to be carried out: as shown in Figs. 22.1 and 22.2, supernova data and measurements of CMB anisotropies strongly favor a $k = 0$ model dominated by vacuum energy. It is worth noting that there is some tension (4.2σ) between the Cepheid and CMB determinations of H_0 (the latter is $(67.4 \pm 0.5)\,\mathrm{km\,s^{-1}Mpc^{-1}}$ [25]). While it is remarkable that the two very different methods give such similar results, the formal disagreement shows that either there are unidentified systematic errors or that some new post-CDM physics is required; there is no current consensus in the community on these options. We do note an interesting alternative direct probe of H_0, again using the SNe $D(z)$ relation but now calibrated using either (1) tip of the red giant branch (TRGB) stars; or (2) J-region asymptotic giant branch (JAGB) stars [32]. This yields figures intermediate between CMB and Cepheid-based estimates: $(68.8 \pm 1.8\,(\text{stat.}) \pm 1.3\,(\text{sys.}))\,\mathrm{km\,s^{-1}Mpc^{-1}}$ for TRGB and $(67.8 \pm 2.2\,(\text{stat.}) \pm 1.6\,(\text{sys.}))\,\mathrm{km\,s^{-1}Mpc^{-1}}$ for JAGB. See Cosmological Parameters – Sec. 25 of this *Review* for a more comprehensive review of Hubble parameter determinations.

22.2.3 *Age of the Universe*

Perhaps the most striking conclusion of relativistic cosmology is that the Universe has not existed forever. The dynamical result for the age of the Universe may be written as

$$\begin{aligned} H_0 t_0 &= \int_0^\infty \frac{dz}{(1+z)H(z)} \\ &= \int_0^\infty \frac{dz}{(1+z)\;[(1+z)^2(1+\Omega_{\rm m}z) - z(2+z)\Omega_{\rm v}]^{1/2}}, \end{aligned} \tag{22.29}$$

Int. J. Mod. Phys. A 2026.41. Downloaded from www.worldscientific.com
by UNIVERSITY OF CALIFORNIA @ BERKELEY on 09/16/26. Re-use and distribution is strictly not permitted, except for Open Access articles.

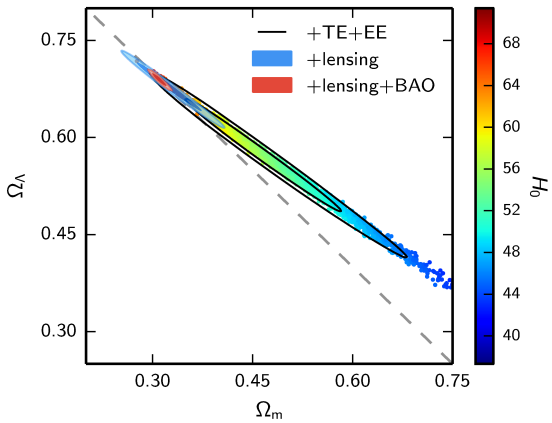

Figure 22.2: Likelihood-based probability densities over the plane Ω_Λ (*i.e.*, Ω_v assuming $w = -1$) versus Ω_m. The colored locus derives from *Planck* [33] and shows that the CMB alone requires a flat Universe $\Omega_v + \Omega_m \simeq 1$ if the Hubble constant is not too high. The SNe Ia results [34] very nearly constrain the orthogonal combination $\Omega_v - \Omega_m$, and the intersection of these constraints directly favors a flat model with $\Omega_m \simeq 0.3$, as does the measurement of the baryon acoustic oscillation lengthscale (for which a joint constraint is shown on this plot). The CMB alone is capable of breaking the degeneracy with H_0 by using the measurements of gravitational lensing that can be made with modern high-resolution CMB data.

where we have neglected Ω_r and chosen $w = -1$. Over the range of interest ($0.1 \lesssim \Omega_m \lesssim 1$, $|\Omega_v| \lesssim 1$), this exact answer may be approximated to a few per cent accuracy by

$$H_0 t_0 \simeq \tfrac{2}{3}\,(0.7\Omega_m + 0.3 - 0.3\Omega_v)^{-0.3}. \tag{22.30}$$

For the special case that $\Omega_m + \Omega_v = 1$, the integral in Eq. (22.29) can be expressed analytically as

$$H_0 t_0 = \frac{2}{3\sqrt{\Omega_v}}\,\ln\frac{1+\sqrt{\Omega_v}}{\sqrt{1-\Omega_v}} \quad (\Omega_m < 1). \tag{22.31}$$

The most accurate means of obtaining ages for astronomical objects is based on the natural clocks provided by radioactive decay. The use of these clocks is complicated by a lack of knowledge of the initial conditions of the decay. In the Solar System, chemical fractionation of different elements helps pin down a precise age for the pre-Solar nebula of 4.6 Gyr, but for stars it is necessary to attempt an a priori calculation of the relative abundances of nuclei that result from supernova explosions. In this way, a lower limit for the age of stars in the local part of the Milky Way of about 11 Gyr is obtained [35, 36].

The other major means of obtaining cosmological age estimates is based on the theory of stellar evolution. In principle, the main-sequence turnoff point in the color-magnitude diagram of a globular cluster should yield a reliable age. But these have been controversial, owing to theoretical uncertainties in the evolution model – as well as observational uncertainties in the distance, dust extinction, and metallicity of clusters. The present consensus favors ages for the oldest clusters of about 13 Gyr [37].

These methods are all consistent with the age deduced from studies of structure formation, using the microwave background and large-scale structure: $t_0 = (13.80 \pm 0.02)$ Gyr [25], where the extra accuracy comes at the price of assuming the simple 6-parameter ΛCDM model to be true.

22.2.4 *Horizon, isotropy, flatness problems*

For photons, the radial equation of motion is just $c\,dt = R\,d\chi$. How far can a photon get in a given time? The answer is clearly

$$\Delta\chi = \int_{t_1}^{t_2} \frac{dt}{R(t)} \equiv \Delta\eta, \tag{22.32}$$

i.e., just the interval of conformal time. We can replace dt by $dR/\dot{R}$, which the Friedmann equation says is $\propto dR/\sqrt{\rho R^2}$ at early times. Thus, this integral converges if $\rho R^2 \to \infty$ as $t_1 \to 0$, otherwise it diverges. Provided the equation of state is such that ρ changes faster than R^{-2}, light signals can only propagate a finite distance between the Big Bang and the present; there is then said to be a particle horizon. Such a horizon therefore exists in conventional Big-Bang models, which are dominated by radiation ($\rho \propto R^{-4}$) at early times.

At late times, the integral for the horizon is largely determined by the matter-dominated phase, for which

$$D_H = R_0\,\chi_H \equiv R_0 \int_0^{t(z)} \frac{dt}{R(t)} \simeq \frac{6000}{\sqrt{\Omega_m z}}\,h^{-1}\,\mathrm{Mpc} \quad (z \gg 1). \tag{22.33}$$

The horizon at the time of formation of the microwave background ('last scattering': $z \simeq 1100$) was thus of order 100 Mpc in size, subtending an angle of about 1°. Why then are the large number of causally disconnected regions we see on the microwave sky all at the same temperature? The Universe is very nearly isotropic and homogeneous, even though the initial conditions appear not to permit such a state to be constructed.

A related problem is that the $\Omega = 1$ Universe is unstable:

$$\Omega(a) - 1 = \frac{\Omega - 1}{1 - \Omega + \Omega_v a^2 + \Omega_m a^{-1} + \Omega_r a^{-2}}\,, \tag{22.34}$$

where Ω with no subscript is the total density parameter, and $a(t) = R(t)/R_0$. This requires $\Omega(t)$ to be unity to arbitrary precision as the initial time tends to zero; a Universe of non-zero curvature today requires very finely tuned initial conditions.

22.3 The hot thermal Universe

22.3.1 *Thermodynamics of the early Universe*

As alluded to above, we expect that much of the early Universe can be described by a radiation-dominated equation of state. In addition, through much of the radiation-dominated period, thermal equilibrium is established by the rapid rate of particle interactions relative to the expansion rate of the Universe (see Sec. 22.3.3 below). In equilibrium, it is straightforward to compute the thermodynamic quantities, ρ, p, and the entropy density, s. In general, the energy density for a given particle type i can be written as

$$\rho_i = \int E_i\,dn_{q_i}, \tag{22.35}$$

with the density of states given by

$$dn_{q_i} = \frac{g_i}{2\pi^2}\,(\exp[(E_{q_i} - \mu_i)/T_i] \pm 1)^{-1}\;q_i^2\,dq_i, \tag{22.36}$$

where g_i counts the number of degrees of freedom for particle type i, $E_{q_i}^2 = m_i^2 + q_i^2$, μ_i is the chemical potential, and the $\pm$ corresponds to either Fermi or Bose statistics. Similarly, we can define the pressure of a perfect gas as

$$p_i = \frac{1}{3}\int \frac{q_i^2}{E_i}\,dn_{q_i}. \tag{22.37}$$

The number density of species i is simply

$$n_i = \int dn_{q_i}, \tag{22.38}$$

and the entropy density is

$$s_i = \frac{\rho_i + p_i - \mu_i n_i}{T_i}\,. \tag{22.39}$$

In the standard ΛCDM model, a chemical potential is often associated with baryon number, and since the net baryon density relative to the photon density is known to be very small (of order 10^{-9}), we can neglect any such chemical potential when computing total thermodynamic quantities.

Int. J. Mod. Phys. A 2026.41. Downloaded by UNIVERSITY OF CALIFORNIA @ BERKELEY on 09/16/26. Re-
worldscientific.com
strictly not permitted, except for Open Access articles.

For photons, we can compute all of the thermodynamic quantities rather easily. Taking $g_i = 2$ for the 2 photon polarization states, we have (in units where $\hbar = k_{\rm B} = 1$)

$$\rho_\gamma = \frac{\pi^2}{15}T^4, \quad p_\gamma = \frac{1}{3}\rho_\gamma, \quad s_\gamma = \frac{4\rho_\gamma}{3T}, \quad n_\gamma = \frac{2\zeta(3)}{\pi^2}T^3, \tag{22.40}$$

with $2\zeta(3)/\pi^2 \simeq 0.2436$. Note that Eq. (22.10) can be converted into an equation for entropy conservation. Recognizing that $\dot{p} = s\dot{T}$, Eq. (22.10) becomes

$$d(sR^3)/dt = 0. \tag{22.41}$$

For radiation, this corresponds to the relationship between expansion and cooling, $T \propto R^{-1}$ in an adiabatically expanding Universe. Note also that both s and n_γ scale as T^3.

22.3.2 *Radiation content of the early Universe*

At the very high temperatures associated with the early Universe, massive particles are pair produced, and are part of the thermal bath. If for a given particle species i we have $T \gg m_i$, then we can neglect the mass in Eqs. (22.35) to (22.39), and the thermodynamic quantities are easily computed as in Eq. (22.40). In general, we can approximate the energy density (at high temperatures) by including only those particles with $m_i \ll T$. In this case, we have

$$\rho = \left(\sum_{\rm B} g_{\rm B} + \frac{7}{8}\sum_{\rm F} g_{\rm F}\right)\frac{\pi^2}{30}T^4 \equiv \frac{\pi^2}{30}\,N(T)\,T^4, \tag{22.42}$$

where $g_{\rm B(F)}$ is the number of degrees of freedom of each boson (fermion) and the sum runs over all boson and fermion states with $m \ll T$. The factor of 7/8 is due to the difference between the Fermi and Bose integrals. Eq. (22.42) defines the effective number of degrees of freedom, $N(T)$, by taking into account new particle degrees of freedom as the temperature is raised. This quantity, calculated from high temperature lattice QCD, is plotted in Fig. 22.3 [38]. Near the QCD transition, there is a slight difference between the coefficient of T^4 for ρ and the coefficient of T^3 for the entropy density $s = (2\pi^2/45)N_s(T)T^3$ [39], as seen in the figure.

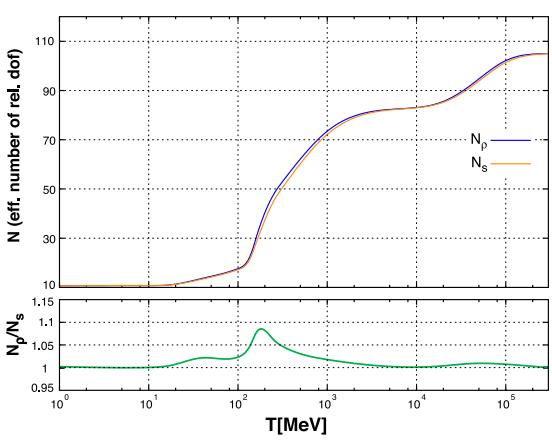

Figure 22.3: The effective numbers of relativistic degrees of freedom as a function of temperature. The sharp drop corresponds to the quark-hadron transition. The bottom panel shows the relative ratio between the number of degrees of freedom characterizing the energy density and the entropy.

The value of $N(T)$ at any given temperature depends on the particle physics model. In the standard SU(3) × SU(2) × U(1) model, we can specify $N(T)$ up to temperatures of $O(100)$ GeV. The change in N (ignoring mass effects) can be seen in the table below.

Temperature	New Particles	$4N(T)$
$T < m_e$	γ's + ν's	29
$m_e < T < m_\mu$	$e^\pm$	43
$m_\mu < T < m_\pi$	$\mu^\pm$	57
$m_\pi < T < T_{\rm c}$ †	π's	69
$T_{\rm c} < T < m_{\rm strange}$	π's + $u, \bar{u}, d, \bar{d}$ + gluons	205
$m_s < T < m_{\rm charm}$	$s, \bar{s}$	247
$m_c < T < m_\tau$	$c, \bar{c}$	289
$m_\tau < T < m_{\rm bottom}$	$\tau^\pm$	303
$m_b < T < m_{W,Z}$	$b, \bar{b}$	345
$m_{W,Z} < T < m_{\rm Higgs}$	$W^\pm, Z$	381
$m_H < T < m_{\rm top}$	H^0	385
$m_t < T$	$t, \bar{t}$	427

† $T_{\rm c}$ corresponds to the confinement-deconfinement transition between quarks and hadrons.

At higher temperatures, $N(T)$ will be model dependent. For example, in the minimal SU(5) model, one needs to add 24 states to $N(T)$ for the charged and colored X and Y gauge bosons, another 24 from the adjoint Higgs, and another six scalar degrees of freedom (in addition to the four associated with the complex Higgs doublet already counted in the longitudinal components of $W^\pm$ and Z, and in H) from the $\bar{5}$ of Higgs. Hence for $T > m_X$ in minimal SU(5), $N(T) = 160.75$. In a supersymmetric model this would at least double.

In the radiation-dominated epoch, Eq. (22.10) can be integrated (neglecting the T-dependence of N), giving us a relationship between the age of the Universe and its temperature:

$$t = \left(\frac{90}{32\pi^3 G_{\rm N} N(T)}\right)^{1/2} T^{-2}\,. \tag{22.43}$$

This can be expressed more conveniently in the form

$$t\,T_{\rm MeV}^2 = 2.4[N(T)]^{-1/2}, \tag{22.44}$$

where t is measured in seconds and $T_{\rm MeV}$ in units of MeV.

22.3.3 *Neutrinos and equilibrium*

Due to the expansion of the Universe, certain rates may be too slow to either establish or maintain equilibrium. Quantitatively, for each particle i, a minimal condition for equilibrium requires that the interaction rate Γ_i involving that type of particle should be larger than the expansion rate of the Universe:

$$\Gamma_i > H. \tag{22.45}$$

Recalling that the age of the Universe is determined by H^{-1}, this condition is equivalent to requiring that on average, approximately one or more interactions have occurred over the lifetime of the Universe.

A good example for a process that goes in and out of equilibrium is the weak interaction of neutrinos. On dimensional grounds, one can estimate the thermally averaged scattering cross-section:

$$\langle\sigma v\rangle \sim O(10^{-2})T^2/m_W^4 \tag{22.46}$$

for $T \lesssim m_W$. Recalling that the number density of leptons is $n \propto T^3$, we can compare the weak interaction rate, $\Gamma_{\rm wk} \sim n\langle\sigma v\rangle$, with the expansion rate and so obtain

$$\begin{aligned} H = \left(\frac{8\pi G_{\rm N}\rho}{3}\right)^{1/2} &= \left(\frac{8\pi^3}{90}N(T)\right)^{1/2} T^2/M_{\rm P} \\ &\simeq 1.66N(T)^{1/2}T^2/M_{\rm P}, \end{aligned} \tag{22.47}$$

where the Planck mass $M_{\rm P} = G_{\rm N}^{-1/2} = 1.22 \times 10^{19}$ GeV.

Neutrinos will be in equilibrium when $\Gamma_{\rm wk} > H$ or

$$T > (500\,m_W^4/M_{\rm P})^{1/3} \sim 1\,{\rm MeV}. \tag{22.48}$$

However, this condition assumes $T \ll m_W$; for higher temperatures, we should write $\langle\sigma v\rangle \sim O(10^{-2})/T^2$, so that $\Gamma \sim 10^{-2}T$. Thus, in the very early stages of expansion, at temperatures $T \gtrsim 10^{-2}M_{\rm P}/\sqrt{N}$, equilibrium will not have been established.

Int. J. Mod. Phys. A 2026.41. Downloaded from www.worldscientific.com by UNIVERSITY OF CALIFORNIA @ BERKELEY on 09/16/26. Re-use and distribution is strictly not permitted, except for Open Access articles.

Having attained a quasi-equilibrium stage, the Universe then cools further, to the point where the interaction and expansion timescales match once again. The temperature at which these rates are equal is commonly referred to as the neutrino decoupling or freeze-out temperature and is defined by $\Gamma_{\rm wk}(T_{\rm d}) = H(T_{\rm d})$. For $T < T_{\rm d}$, neutrinos drop out of equilibrium. The Universe becomes transparent to neutrinos and their momenta simply redshift with the cosmic expansion. The effective neutrino temperature will simply fall with $T \propto 1/R$.

Soon after decoupling, $e^{\pm}$ pairs in the thermal background begin to annihilate (when $T \lesssim m_e$). Because the neutrinos are decoupled, the energy released due to annihilation heats up the photon background relative to the neutrinos. The change in the photon temperature can be easily computed from entropy conservation. The neutrino entropy must be conserved separately from the entropy of interacting particles. A straightforward computation yields

$$T_\nu = (4/11)^{1/3}\, T_\gamma \simeq 1.9\,\mathrm{K}. \tag{22.49}$$

The total entropy density is therefore given by the contribution from photons and three flavors of neutrinos:

$$s = \frac{4}{3}\frac{\pi^2}{30}\left(2 + \frac{21}{4}(T_\nu/T_\gamma)^3\right) T_\gamma^3 = \frac{4}{3}\frac{\pi^2}{30}\left(2 + \frac{21}{11}\right) T_\gamma^3 = 7.04\, n_\gamma. \tag{22.50}$$

Similarly, the total relativistic energy density is given by

$$\rho_r = \frac{\pi^2}{30}\left[2 + \frac{21}{4}(T_\nu/T_\gamma)^4\right] T_\gamma^4 \simeq 1.68\rho_\gamma. \tag{22.51}$$

In practice, a small correction is needed to this, since neutrinos are not totally decoupled at $e^{\pm}$ annihilation: the effective number of massless neutrino species is $N_{\rm eff} = 3.044$, rather than 3 [40,41]. See Neutrinos in Cosmology – Sec. 26 of this *Review* for more on $N_{\rm eff}$.

This expression ignores neutrino rest masses, but current oscillation data require at least one neutrino eigenstate to have a mass exceeding 0.06 eV. In this minimal case, $\Omega_\nu h^2 = 6 \times 10^{-4}$, so the neutrino contribution to the matter budget would be negligibly small (which is our normal assumption). However, a nearly degenerate pattern of mass eigenstates could allow larger densities, since oscillation experiments only measure differences in m^2 values. Note that a 0.06-eV neutrino has $T_\nu = m_\nu$ at $z \simeq 357$, so the above expression for the total present relativistic density is really only an extrapolation. However, neutrinos are almost certainly relativistic at all epochs where the radiation content of the Universe is dynamically significant. Combining *Planck*, ACT, and SPT CMB data (including CMB lensing) yields an upper limit to the sum of neutrino masses, $\Sigma m_\nu < 0.17\,\mathrm{eV}$ [42]. Adding the further constraints of DESI BAO measurements and Lyman-α spectra from eBOSS [43] yields a more restrictive limit of $\Sigma m_\nu < 0.053\,\mathrm{eV}$ – but this figure may be problematic as it lies below the minimum allowed by the differences of neutrino mass^2 from oscillation data. It is presently unclear whether this situation reflects problems with the ΛCDM model or if it indicates data systematics. This issue will need to be resolved in order to have a cosmological proof that neutrino masses are non-zero. See Neutrinos in Cosmology – Sec. 26 of this *Review* for a detailed discussion of neutrinos in cosmology.

22.3.4 *Field theory and phase transitions*

It is very likely that the Universe has undergone one or more phase transitions during the course of its evolution [44–47]. Our current vacuum state is described by $\mathrm{SU}(3)_c\times\ \mathrm{U}(1)_{\rm em}$, which in the Standard Model is a remnant of an unbroken $\mathrm{SU}(3)_c\times\ \mathrm{SU}(2)_L\times\ \mathrm{U}(1)_Y$ gauge symmetry. Symmetry breaking occurs when a non-singlet gauge field (the Higgs field in the Standard Model) picks up a non-vanishing vacuum expectation value, determined by a scalar potential. For example, a simple (non-gauged) potential describing symmetry breaking is $V(\phi) = \frac{1}{4}\lambda\phi^4 - \frac{1}{2}\mu^2\phi^2 + V(0)$. The resulting expectation value is simply $\langle\phi\rangle = \mu/\sqrt{\lambda}$.

In the early Universe, finite temperature radiative corrections typically add terms to the potential of the form $\phi^2 T^2$. Thus, at very high temperatures, the symmetry is restored and $\langle\phi\rangle = 0$. As the Universe cools, depending on the details of the potential, symmetry breaking will occur via a first-order phase transition in which the field tunnels through a potential barrier, or via a second-order transition in which the field evolves smoothly from one state to another (as would be the case for the above example potential).

The evolution of scalar fields can have a profound impact on the early Universe. The equation of motion for a scalar field ϕ can be derived from the energy-momentum tensor:

$$T_{\mu\nu} = \partial_\mu\phi\partial_\nu\phi - \frac{1}{2}g_{\mu\nu}\partial_\rho\phi\partial^\rho\phi - g_{\mu\nu}V(\phi). \tag{22.52}$$

By associating $\rho = T_{00}$ and $p = R^{-2}(t)T_{ii}$ we have

$$\begin{aligned} \rho &= \frac{1}{2}\dot\phi^2 + \frac{1}{2}R^{-2}(t)(\nabla\phi)^2 + V(\phi)\,; \\ p &= \frac{1}{2}\dot\phi^2 - \frac{1}{6}R^{-2}(t)(\nabla\phi)^2 - V(\phi)\ , \end{aligned} \tag{22.53}$$

and from Eq. (22.10) we can write the equation of motion as follows (by considering a homogeneous region, we can ignore the gradient terms):

$$\ddot\phi + 3H\dot\phi = -\partial V/\partial\phi. \tag{22.54}$$

22.3.5 *Inflation*

In Sec. 22.2.4, we discussed some of the problems associated with the standard Big-Bang model. However, during a phase transition, our assumptions of an adiabatically expanding Universe are generally not valid. If, for example, a phase transition occurred in the early Universe such that the field evolved slowly from the symmetric state to the global minimum, the Universe may have been dominated by the vacuum energy density associated with the potential near $\phi \simeq 0$. During this period of slow evolution, the energy density due to radiation will fall below the vacuum energy density, $\rho \ll V(0)$. When this happens, the expansion rate will be dominated by the constant V(0), and we obtain the exponentially expanding solution given in Eq. (22.20). When the field evolves towards the global minimum it will begin to oscillate about that minimum, energy will be released during its decay, and a hot thermal Universe will be restored. If released fast enough, it will produce radiation at a temperature $NT_{\rm R}{}^4 \lesssim V(0)$. In this reheating process, entropy has been created and the final value of RT is greater than the initial value of RT. Thus, we see that, during a phase transition, the relation $RT \sim$ constant need not hold true. This is the basis of the inflationary Universe scenario [48–50].

If, during the phase transition, the value of RT changed by a factor of $O(10^{29})$, the cosmological problems discussed above would be solved. The observed isotropy would be generated by the immense expansion; one small causal region could get blown up, and thus our entire visible Universe would have been in thermal contact some time in the past. In addition, the density parameter Ω would have been driven to 1 (with exponential precision). Density perturbations will be stretched by the expansion, $\lambda \propto R(t)$. Thus it will appear that $\lambda \gg H^{-1}$ or that the perturbations have left the horizon, where in fact the size of the causally connected region is now no longer simply H^{-1}. However, not only does inflation offer an explanation for large scale homogeneity, it also offers a source for the small fluctuations about this state, which arise through quantum fluctuations.

Problems with early models of inflation based on either a first-order [51] or second-order [52,53] phase transition of a Grand Unified Theory led to models invoking a completely new scalar field: the inflaton, ϕ. The potential of this field, $V(\phi)$, needs to have a very low gradient and curvature in order to match observed metric fluctuations. For a more thorough discussion of the problems of early models and a host of current models being studied see the review on inflation – Sec. 23 of this *Review*. In most current inflation models, reheated bubbles typically do not percolate, so inflation is 'eternal' and continues with exponential expansion in the region outside the bubbles. These causally disconnected bubble Universes constitute a 'multiverse', where low-energy physics can potentially vary between different bubbles. This has led to a controversial 'anthropic' approach to cosmology [54–56], where observer selection within the multiverse can be introduced as a

Int. J. Mod. Phys. A 2026.41. Downloaded by UNIVERSITY OF CALIFORNIA @ BERKELEY on 09/16/26. Re-
orldscientific.com
strictly not permitted, except for Open Access articles.

means of understanding *e.g.* why the observed level of vacuum energy is so low (because larger values suppress growth of structure). This argument explains why the effective vacuum density must be far below the naive estimate based on a cutoff at the Planck scale, but the reduction of structure formation only becomes severe once Λ is increased by a factor 100 or more [57], so the observed value remains puzzlingly small.

22.3.6 *Baryogenesis*

The Universe appears to be populated exclusively with matter rather than antimatter [58, 59]. Indeed antimatter is only detected in accelerators or in cosmic rays. However, the presence of antimatter in the latter is understood to be the result of collisions of primary particles in the interstellar medium. There is in fact strong evidence against primary forms of antimatter in the Universe. Furthermore, the density of baryons compared to the density of photons is extremely small, $\eta \equiv n_{\rm b}/n_\gamma \sim 10^{-9}$.

The production of a net baryon asymmetry requires baryon number violating interactions, C and CP violation, and a departure from thermal equilibrium [60]. The first two of these ingredients are expected to be contained in Grand Unified Theories (GUTs) as well as in the non-perturbative sector of the Standard Model; the third can be realized in an expanding Universe where, as we have seen, interactions come in and out of equilibrium.

There are several interesting and viable mechanisms for the production of the baryon asymmetry. While we cannot review any of them here in any detail, we mention some of the important scenarios. In all cases, all three ingredients listed above are incorporated. One of the first mechanisms was based on the out of equilibrium decay of a massive particle such as a superheavy GUT gauge or Higgs boson [61, 62]. A novel mechanism involving the decay of flat directions in supersymmetric models is known as the Affleck-Dine scenario [63]. There is also the possibility of generating the baryon asymmetry at the electroweak scale using the non-perturbative interactions of sphalerons [64]. Because these interactions conserve the sum of baryon and lepton number, $B+L$, it is possible to first generate a lepton asymmetry (*e.g.*, by the out-of-equilibrium decay of a superheavy right-handed neutrino), which is converted to a baryon asymmetry at the electroweak scale [65]. This mechanism is known as lepto-baryogenesis, or simply leptogenesis. Distinguishing between these possibilities will be difficult and would require some experimental detection of physics beyond the Standard Model such as proton decay, neutrinoless double beta decay, or neutron-antineutron oscillations.

22.3.7 *Nucleosynthesis*

An essential element of the standard cosmological model is Big-Bang nucleosynthesis (BBN), the theory that predicts the abundances of the light element isotopes D, ^{3}He, ^{4}He, and ^{7}Li. Nucleosynthesis takes place at a temperature scale of order 1 MeV. The nuclear processes lead primarily to ^{4}He, with a primordial mass fraction of about 25%. Lesser amounts of the other light elements are produced: about 10^{-5} of D and ^{3}He and about 10^{-10} of ^{7}Li by number relative to H. The abundances of the light elements depend almost solely on one key parameter, the baryon-to-photon ratio, η. The nucleosynthesis predictions can be compared with observational determinations of the abundances of the light elements. Consistency between theory and observations, driven primarily by recent D/H measurements [66, 67], leads to a range of [68]

$$5.8 \times 10^{-10} < \eta < 6.3 \times 10^{-10}. \tag{22.55}$$

The value of η is related to the baryon density as follows:

$$\Omega_{\rm b} = 3.66 \times 10^7 \eta\, h^{-2}, \tag{22.56}$$

or $10^{10}\eta = 274\,\Omega_{\rm b}h^2$. The *Planck* result [25] for $\Omega_{\rm b}h^2$ of 0.0224 $\pm$ 0.0002 translates into a value of $\eta = (6.12 \pm 0.04) \times 10^{-10}$. This result can be used to 'predict' the light element abundances, which can in turn be compared with observation [69]. The resulting D/H abundance is in excellent agreement with that found in quasar absorption systems. It is in reasonable agreement with the helium abundance observed in extragalactic regions of ionized hydrogen gas (once systematic uncertainties are accounted for). The BBN predicted Li abundance is systematically higher than the Li abundance observed in the atmospheres of halo dwarf stars [70], but there is mounting evidence that effects of stellar depletion cannot be ignored so that the stellar abundances of Li may not correspond to the primordial abundance [71]. See BBN – Sec. 24 of this *Review* for a detailed discussion of BBN, in addition to Refs. [68, 72–76].

22.3.8 *The transition to a matter-dominated Universe*

In the standard ΛCDM model, the temperature (or redshift) at which the Universe undergoes a transition from a radiation-dominated to a matter-dominated Universe is determined by the amount of dark matter. Assuming three nearly massless neutrinos, the energy density in radiation at temperatures $T \ll 1\,$MeV, is given by

$$\rho_{\rm r} = \frac{\pi^2}{30}\left[2 + \frac{21}{4}\left(\frac{4}{11}\right)^{4/3}\right] T^4. \tag{22.57}$$

In the absence of non-baryonic dark matter, the matter density can be written as

$$\rho_{\rm m} = m_{\rm N}\eta\, n_\gamma, \tag{22.58}$$

where $m_{\rm N}$ is the nucleon mass. Recalling that $n_\gamma \propto T^3$ [*cf.* Eq. (22.40)], we can solve for the temperature or redshift at the matter-radiation equality when $\rho_{\rm r} = \rho_{\rm m}$:

$$T_{\rm eq} = 0.22\, m_{\rm N}\,\eta \qquad \text{or} \qquad (1 + z_{\rm eq}) = 0.22\,\eta\frac{m_{\rm N}}{T_0}, \tag{22.59}$$

where T_0 is the present temperature of the microwave background. For $\eta = 6.1 \times 10^{-10}$, this corresponds to a temperature $T_{\rm eq} \simeq 0.13$ eV or $(1+z_{\rm eq}) \simeq 550$. A transition this late would be problematic for structure formation (see Sec. 22.4.5).

The redshift of matter domination can be pushed back significantly if non-baryonic dark matter is present. If instead of Eq. (22.58), we write

$$\rho_{\rm m} = \Omega_{\rm m}\rho_{\rm c}\left(\frac{T}{T_0}\right)^3, \tag{22.60}$$

we find that

$$T_{\rm eq} = 0.9\frac{\Omega_{\rm m}\rho_{\rm c}}{T_0^3} \qquad \text{or} \qquad (1 + z_{\rm eq}) = 2.4 \times 10^4\Omega_{\rm m}h^2. \tag{22.61}$$

22.4 The Universe at late times

22.4.1 *The CMB*

One form of the infamous Olbers' paradox says that, in Euclidean space, surface brightness is independent of distance. Every line of sight will terminate on matter that is hot enough to be ionized and so scatter photons: $T \gtrsim 10^3$ K, and the sky should therefore shine as brightly as the surface of the Sun. The reason the night sky is dark is entirely due to the expansion, which cools the radiation temperature to 2.73 K. This gives a Planck function peaking at around 1 mm to produce the CMB.

The CMB spectrum is a very accurate match to a Planck function [77]; see also CMB – Sec. 29 of this *Review*. The COBE estimate of the temperature is [78]

$$T = (2.7255 \pm 0.0006)\,\text{K}. \tag{22.62}$$

The lack of any distortion of the Planck spectrum is a strong physical constraint. It is very difficult to account for in any expanding Universe other than one that passes through a hot stage. Alternative schemes for generating the radiation, such as thermalization of starlight by dust grains, inevitably generate a superposition of temperatures. What is required in addition to thermal equilibrium is that $T \propto 1/R$, so that radiation from different parts of space arrive at an observer with the same apparent temperature.

Although it is common to speak of the CMB as originating at 'recombination', a more accurate terminology is the era of 'last scattering'. In practice, this takes place at $z \simeq 1100$, almost independently of the main cosmological parameters, at which time the fractional ionization remains significant (~ 0.1). This event occurred when the age of the Universe was about 370,000 years. But the CMB photons themselves were not generated at this point, and were the result of thermalization at $z \sim 10^7$. See CMB – Sec. 29 of this *Review* for a full discussion of the CMB.

Int. J. Mod. Phys. A 2026.41. Downloaded from www.worldscientific.com by UNIVERSITY OF CALIFORNIA @ BERKELEY on 09/16/26. Re-use and distribution is strictly not permitted, except for Open Access articles.

22.4.2 *Matter in the Universe*

One of the main tasks of cosmology is to measure the density of the Universe, and to determine how this is divided between dark matter and baryons. The baryons consist partly of stars, with $0.002 \lesssim \Omega_* \lesssim 0.003$ [79] but mainly inhabit the intergalactic medium (IGM). One powerful way in which this can be studied is via the absorption of light from distant luminous objects such as quasars. Even very small amounts of neutral hydrogen can absorb rest-frame UV photons (the Gunn-Peterson effect), and should suppress the continuum by a factor $\exp(-\tau)$, where

$$\tau \simeq 10^{4.62} h^{-1} \left[\frac{n_{\rm HI}(z)/{\rm m}^{-3}}{(1+z)\sqrt{1+\Omega_{\rm m} z}} \right] , \tag{22.63}$$

and this expression applies while the Universe is matter dominated ($z \gtrsim 1$ in the $\Omega_{\rm m} = 0.3$ $\Omega_{\rm v} = 0.7$ model). At $z < 6$, the dominant effect on quasar spectra is a 'forest' of narrow absorption lines, which produce a mean $\tau = 1$ in the Lyα forest at about $z = 3$, and so we have $\Omega_{\rm HI} \simeq 10^{-6.7} h^{-1}$. This is such a small number that the IGM must be very highly ionized at these redshifts, apart from a few high-density clumps. But at $z > 6$ there is good evidence for a 'reionization' era at which the general IGM is not so strongly ionized [80]. As discussed below, this ionized IGM at low z is also detectable via the secondary Compton scattering of CMB photons.

The Lyα forest is of great importance in pinning down the abundance of deuterium. Because electrons in deuterium differ in reduced mass by about 1 part in 4000 compared to hydrogen, each absorption system in the Lyα forest is accompanied by an offset deuterium line. By careful selection of systems with an optimal hydrogen column density, a measurement of the D/H ratio can be made. This has now been done with high accuracy in 12 quasars, with consistent results [81, 82]. Combining these determinations with the theory of primordial nucleosynthesis yields a baryon density of $\Omega_{\rm b} h^2 = 0.021$–$0.023$ (95% confidence) in excellent agreement with the *Planck* result. For more details, see BBN – Sec. 24 of this *Review*.

The ionized IGM can also be detected in emission when it is densely clumped, via bremsstrahlung radiation. This generates the spectacular X-ray emission from rich clusters of galaxies. Studies of this phenomenon allow us to achieve an accounting of the total baryonic material in clusters. Within the central $\simeq 1$ Mpc, the masses in stars, X-ray emitting gas, and total dark matter can be determined with reasonable accuracy (perhaps 20% rms), and this allows a minimum baryon fraction to be determined [83, 84]:

$$\frac{M_{\rm baryons}}{M_{\rm total}} \gtrsim 0.009 + (0.066 \pm 0.003)\, h^{-3/2}. \tag{22.64}$$

Because clusters are the largest collapsed structures, it is reasonable to take this as applying to the Universe as a whole. This equation implies a minimum baryon fraction of perhaps 12% (for reasonable h), which is too high for $\Omega_{\rm m} = 1$ if we take $\Omega_{\rm b} h^2 \simeq 0.02$ from nucleosynthesis. This is therefore one of the more robust arguments in favor of $\Omega_{\rm m} \simeq 0.3$; for more details, see Cosmological Parameters – Sec. 25 of this *Review*. This argument is also consistent with the inference on $\Omega_{\rm m}$ that can be made from Fig. 22.2.

This method is much more robust than the older classical technique for weighing the Universe: '$L \times M/L$'. The overall light density of the Universe is reasonably well determined from redshift surveys of galaxies, so that a good determination of mass M and luminosity L for a single object suffices to determine $\Omega_{\rm m}$ – but only *if* the mass-to-light ratio were universal.

22.4.3 *Gravitational lensing*

A robust method for determining masses in cosmology is to use gravitational light deflection. Most systems can be treated as a geometrically thin gravitational lens, where the light bending is assumed to take place only at a single distance. Simple geometry then determines a mapping between the coordinates in the intrinsic source plane (S) and the observed image plane (I):

$$\alpha(D_{\rm L}\theta_{\rm I}) = \frac{D_{\rm S}}{D_{\rm LS}}(\theta_{\rm I} - \theta_{\rm S}), \tag{22.65}$$

where the angles $\theta_{\rm I}, \theta_{\rm S}$, and α are in general two-dimensional vectors on the sky. The distances $D_{\rm LS}$ *etc.* are given by an extension of the usual distance-redshift formula:

$$D_{\rm LS} = \frac{R_0 S_k(\chi_{\rm S} - \chi_{\rm L})}{1 + z_{\rm S}}. \tag{22.66}$$

This is the angular-diameter distance for objects on the source plane as perceived by an observer on the lens.

Solutions of this equation divide into weak lensing, where the mapping between source plane and image plane is one-to-one, and strong lensing, in which multiple imaging is possible. For circularly-symmetric lenses, an on-axis source is multiply imaged into a 'caustic' ring, whose radius is the Einstein radius:

$$\begin{aligned} \theta_{\rm E} &= \left(4GM\, \frac{D_{\rm LS}}{D_{\rm L} D_{\rm S}}\right)^{1/2} \\ &= \left(\frac{M}{10^{11.09}{\rm M}_\odot}\right)^{1/2} \left(\frac{D_{\rm L} D_{\rm S}/D_{\rm LS}}{\rm Gpc}\right)^{-1/2} \quad \text{arcsec} . \end{aligned} \tag{22.67}$$

The observation of 'arcs' (segments of near-perfect Einstein rings) in rich clusters of galaxies has thus given very accurate masses for the central parts of clusters – generally in good agreement with other indicators, such as analysis of X-ray emission from the cluster IGM [85, 86].

Gravitational lensing has also developed into a powerful independent probe of cosmological structure on 10-Mpc to 100-Mpc scales. Weak image distortions manifest themselves as an additional ellipticity of galaxy images ('shear'), which can be observed by averaging many images together (the corresponding flux amplification is less readily detected). The result is a 'cosmic shear' field of order 1% ellipticity, coherent over scales of around 30 arcmin, which is directly related to the cosmic mass field. For this reason, weak lensing is seen as potentially the cleanest probe of matter fluctuations, next to the CMB. Impressive results have been obtained in measuring cosmological parameters, based on survey data from $\sim 10^3\,{\rm deg}^2$ [87, 88]. A particular strength of lensing is its ability to measure the amplitude of mass fluctuations; this can be deduced from the amplitude of CMB fluctuations, but only with low precision on account of the poorly-known optical depth due to Compton scattering after reionization. However, the effect of weak lensing on the CMB map itself can be detected via the induced non-Gaussian signal, and this gives the CMB greater internal power [89]. The main difficulty of principle with lensing is that part of the signal is generated by small-scale density fluctuations; thus a model is required for nonlinear evolution, including astrophysical effects that separate baryons and dark matter. In this respect, the CMB is a cleaner probe of the primordial fluctuations.

22.4.4 *Density fluctuations*

The overall properties of the Universe are very close to being homogeneous; and yet telescopes reveal a wealth of detail on scales varying from single galaxies to large-scale structures of size exceeding 100 Mpc. The existence of these structures must be telling us something important about the initial conditions of the Big Bang, and about the physical processes that have operated subsequently. This motivates the study of the density perturbation field, defined as

$$\delta(\mathbf{x}) \equiv \frac{\rho(\mathbf{x}) - \langle\rho\rangle}{\langle\rho\rangle}. \tag{22.68}$$

A critical feature of the δ field is that it inhabits a Universe that is isotropic and homogeneous in its large-scale properties. This suggests that the statistical properties of δ should also be statistically homogeneous – *i.e.*, it is a stationary random process.

It is often convenient to describe δ as a Fourier superposition:

$$\delta(\mathbf{x}) = \sum \delta_{\mathbf{k}} e^{-i\mathbf{k}\cdot\mathbf{x}}. \tag{22.69}$$

We avoid difficulties with an infinite Universe by applying periodic boundary conditions in a cube of some large volume V. The cross-terms vanish when we compute the variance in the field, which is

Int. J. Mod. Phys. A 2026.41. Downloaded from www.worldscientific.com by UNIVERSITY OF CALIFORNIA @ BERKELEY on 09/16/26. Re-strictly not permitted, except for Open Access articles.

just a sum over modes of the power spectrum:

$$\langle \delta^2 \rangle = \sum |\delta_{\mathbf{k}}|^2 \equiv \sum P(k). \tag{22.70}$$

Note that the statistical nature of the fluctuations must be isotropic, so we write $P(k)$ rather than $P(\mathbf{k})$. The $\langle \ldots \rangle$ average here is a volume average. Cosmological density fields are an example of an ergodic process, in which the average over a large volume tends to the same answer as the average over a statistical ensemble.

The statistical properties of discrete objects sampled from the density field are often described in terms of N-point correlation functions, which represent the excess probability over random for finding one particle in each of N boxes in a given configuration. For the 2-point case, the correlation function is readily shown to be identical to the autocorrelation function of the δ field: $\xi(r) = \langle \delta(x)\delta(x+r) \rangle$.

The power spectrum and correlation function are Fourier conjugates, and thus are equivalent descriptions of the density field (similarly, k-space equivalents exist for the higher-order correlations). It is convenient to take the limit $V \to \infty$ and use k-space integrals, defining a dimensionless power spectrum, which measures the contribution to the fractional variance in density per unit logarithmic range of scale, as $\Delta^2(k) = d\langle \delta^2 \rangle / d\ln k = V k^3 P(k)/2\pi^2$:

$$\xi(r) = \int \Delta^2(k) \, \frac{\sin kr}{kr} \, d\ln k; \quad \Delta^2(k) = \frac{2}{\pi} k^3 \int_0^\infty \xi(r) \, \frac{\sin kr}{kr} \, r^2 \, dr. \tag{22.71}$$

For many years, an adequate approximation to observational data on galaxies was $\xi = (r/r_0)^{-\gamma}$, with $\gamma \simeq 1.8$ and $r_0 \simeq 5\,h^{-1}$ Mpc. Modern surveys are now able to probe into the large-scale linear regime where unaltered traces of the curved post-recombination spectrum can be detected [90–92].

22.4.5 *Formation of cosmological structure*

The simplest model for the generation of cosmological structure is gravitational instability acting on some low-amplitude initial fluctuations (for the origin of which a theory such as inflation is required). If the perturbations are adiabatic (*i.e.*, fractionally perturb number densities of photons and matter equally), the linear growth law for matter fluctuations is simple:

$$\delta \propto \begin{cases} a^2(t) & \text{(radiation domination; } \Omega_{\rm r} = 1); \\ a(t) & \text{(matter domination; } \Omega_{\rm m} = 1)\ . \end{cases} \tag{22.72}$$

For low-density Universes, the growth is slower:

$$d\ln\delta / d\ln a \simeq \Omega_{\rm m}^{\gamma}(a), \tag{22.73}$$

where the parameter γ is close to 0.55 independent of the vacuum density [93, 94].

The alternative perturbation mode is isocurvature: only the equation of state changes, and the total density is initially unperturbed. These modes perturb the total entropy density, and thus induce additional large-scale CMB anisotropies [95]. Although the character of perturbations in the simplest inflationary theories are purely adiabatic, correlated adiabatic and isocurvature modes are predicted in many models; the simplest example is the curvaton, which is a scalar field that decays to yield a perturbed radiation density. If the matter content already exists at this time, the overall perturbation field will have a significant isocurvature component. Such a prediction is inconsistent with current CMB data [96], and most analyses of CMB and large-scale structure (LSS) data assume the adiabatic case to hold exactly.

Linear evolution preserves the shape of the power spectrum. However, a variety of processes mean that growth actually depends on the matter content.

1. Pressure opposes gravity effectively for wavelengths below the horizon length while the Universe is radiation dominated. The *comoving* horizon size at $z_{\rm eq}$ is therefore an important scale:

$$D_{\rm H}(z_{\rm eq}) = \frac{2(\sqrt{2}-1)}{(\Omega_{\rm m} z_{\rm eq})^{1/2} H_0} = \frac{16.0}{\Omega_{\rm m} h^2} \text{ Mpc}\ . \tag{22.74}$$

2. At early times, dark matter particles will undergo free streaming at the speed of light, and so erase all scales up to the horizon – a process that only ceases when the particles go nonrelativistic. For light massive neutrinos, this happens at $z_{\rm eq}$; all structure up to the horizon-scale power-spectrum break is in fact erased. Hot(cold) dark matter models are thus sometimes dubbed large(small)-scale damping models.
3. A further important scale arises where photon diffusion can erase perturbations in the matter – radiation fluid; this process is named Silk damping.

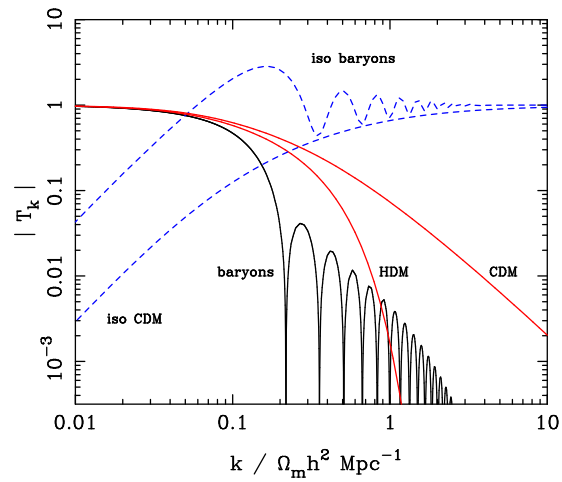

Figure 22.4: A plot of transfer functions for various models. For adiabatic models, $T_k \to 1$ at small k, whereas the opposite is true for isocurvature models. For dark-matter models, the characteristic wavenumber scales proportional to $\Omega_{\rm m} h^2$. The scaling for baryonic models does not obey this exactly; the plotted cases correspond to $\Omega_{\rm m} = 1$, $h = 0.5$.

The overall effect is encapsulated in the transfer function, which gives the ratio of the late-time amplitude of a mode to its initial value (see Fig. 22.4). The overall power spectrum is thus the primordial scalar-mode power law, times the square of the transfer function:

$$P(k) \propto k^{n_{\rm s}} \, T_k^2. \tag{22.75}$$

The most generic power-law index is $n_{\rm s} = 1$: the 'Zeldovich' or 'scale-invariant' spectrum. Inflationary models tend to predict a small 'tilt:' $|n_{\rm s} - 1| \lesssim 0.05$ [11, 12]. On the assumption that the dark matter is cold, the power spectrum then depends on five parameters: $n_{\rm s}$, h, $\Omega_{\rm b}$, $\Omega_{\rm c}$ ($\equiv \Omega_{\rm m} - \Omega_{\rm b}$), and an overall amplitude. The latter is often specified as σ_8, the linear-theory fractional rms in density when a spherical filter of radius $8\,h^{-1}$ Mpc is applied in linear theory. This scale can be probed directly via weak gravitational lensing, and also via its effect on the abundance of rich galaxy clusters. The normalization derived from samples of X-ray clusters has been given variously as [97, 98]

$$\sigma_8 = [0.746 \pm 0.012(\text{stat.}) \pm 0.022(\text{sys.})](\Omega_{\rm m}/0.3)^{-0.47}; \tag{22.76}$$

$$\sigma_8 = [0.81 \pm 0.03](\Omega_{\rm m}/0.3)^{-0.17}. \tag{22.77}$$

The higher figure is well consistent with *Planck*, whereas the lower is rather similar to the normalization inferred from weak galaxy lensing [99]:

$$S_8 \equiv \sigma_8 (\Omega_{\rm m}/0.3)^{0.5} \simeq [0.790^{+0.018}_{-0.014}]. \tag{22.78}$$

This figure is in 1.9σ tension with the *Planck* values of $(\sigma_8, \Omega_{\rm m}) = (0.811 \pm 0.006, 0.315 \pm 0.007)$. If real, such a discrepancy could indicate interesting new physics; but the current evidence is not strong enough to make such a claim. However, it is worth noting that the CMB requires an almost perfect degeneracy, $\Omega_{\rm m} h^3 =$ constant for flat models, so that raising h as far as allowed by the CMB would require a lower density, which would reduce the tension with the amplitude of the lensing measurements.

Int. J. Mod. Phys. A 2026.41. Downloaded from www.worldscientific.com
by UNIVERSITY OF CALIFORNIA @ BERKELEY on 09/16/26. Re-use and distribution is strictly not permitted, except for Open Access articles.

A direct measure of mass inhomogeneity is valuable, since the galaxies inevitably are biased with respect to the mass. This means that the fractional fluctuations in galaxy number, $\delta n/n$, may differ from the mass fluctuations, $\delta\rho/\rho$. It is commonly assumed that the two fields obey some proportionality on large scales where the fluctuations are small, $\delta n/n = b\delta\rho/\rho$, but even this is not guaranteed [100].

The main feature of the transfer function is a break around the horizon scale at $z_{\rm eq}$, which depends primarily on $\Omega_{\rm m}h$ when wavenumbers are measured in observable units ($h\,{\rm Mpc}^{-1}$). For reasonable baryon content, weak oscillations in the transfer function are also expected, and these BAOs (baryon acoustic oscillations) have been clearly detected [101, 102]. As well as directly measuring the baryon fraction, the scale of the oscillations directly measures the acoustic horizon at decoupling, $r_{\rm d}$, which can be approximated as follows [103]:

$$r_{\rm d} \simeq 147.0\,(\Omega_{\rm m}h^2/0.1424)^{-0.253}(\Omega_{\rm b}h^2/0.0224)^{-0.128}\ {\rm Mpc}. \tag{22.79}$$

This length can be used as a standard ruler for cosmological tests, and the BAO signature has thus become one of the most important applications of large galaxy surveys. Overall, current power-spectrum data [90–92] favor $\Omega_{\rm m}h \simeq 0.20$ and a baryon fraction of about 0.15 for $n_{\rm s} \simeq 1$ (see Fig. 22.5).

In principle, accurate data over a wide range of k could determine both $\Omega_{\rm m}h$ and $n_{\rm s}$, but in practice there is a strong degeneracy between these. In order to constrain $n_{\rm s}$ itself, it is necessary to examine data on anisotropies in the CMB.

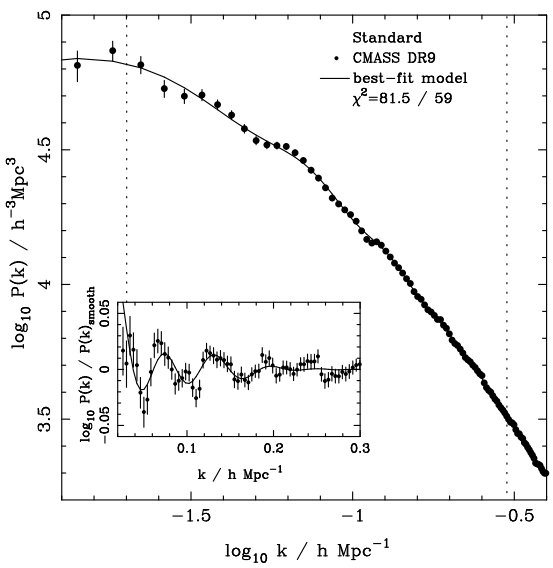

Figure 22.5: The galaxy power spectrum from the SDSS BOSS survey [92]. The solid points with error bars show the power estimate. The solid line shows a standard ΛCDM model with $\Omega_{\rm b}h^2 \simeq 0.02$ and $\Omega_{\rm m}h \simeq 0.2$. The inset amplifies the region where BAO features are visible. The fact that these perturb the power by $\sim 20\%$ rather than order unity is direct evidence that the matter content of the Universe is dominated by collisionless dark matter.

22.4.6 *CMB anisotropies*

The CMB has a clear dipole anisotropy, of magnitude 1.23×10^{-3}. This is interpreted as being due to the Earth's motion, which is equivalent to a peculiar velocity for the Milky Way of

$$v_{\rm MW} \simeq 600\,{\rm km\,s^{-1}} \quad \text{towards} \quad (\ell, b) \simeq (270^\circ, 30^\circ). \tag{22.80}$$

A continuing challenge in cosmology is to demonstrate that this dipole is indeed kinematic, as opposed to representing a violation of large-scale isotropy. Galaxy surveys have attempted to identify the accelerating superclusters responsible for the motion [104], but there are also claims that the observed matter distribution contains an intrinsic dipole, which would be incompatible with the standard interpretation [105], but see also Ref. [106, 107].

All higher-order multipole moments of the CMB are however much smaller than the dipole (of order 10^{-5}), and interpreted as signatures of density fluctuations at last scattering ($\simeq 1100$). To analyze these, the sky is expanded in spherical harmonics as explained in the review on the CMB – Sec. 29 of this *Review*. The dimensionless power per ln k or 'bandpower' for the CMB is defined as

$$\mathcal{T}^2(\ell) = \frac{\ell(\ell+1)}{2\pi}\,C_\ell. \tag{22.81}$$

This function encodes information from the three distinct mechanisms that cause CMB anisotropies:

- (1) Gravitational (Sachs – Wolfe) perturbations. Photons from high-density regions at last scattering have to climb out of potential wells, and are thus redshifted.
- (2) Intrinsic (adiabatic) perturbations. In high-density regions, the coupling of matter and radiation can compress the radiation also, giving a higher temperature.
- (3) Velocity (Doppler) perturbations. The plasma has a non-zero velocity at recombination, which leads to Doppler shifts in frequency and hence shifts in brightness temperature.

Because the potential fluctuations obey Poisson's equation, $\nabla^2\Phi/a^2 = 4\pi G\bar\rho\delta$, and the comoving velocity field satisfies the continuity equation $\nabla\cdot\mathbf{u} = -\dot\delta$, the resulting different powers of k ensure that the Sachs-Wolfe effect dominates on large scales and adiabatic effects on small scales.

The relation between angle and comoving distance on the last-scattering sphere requires the comoving angular-diameter distance to the last-scattering sphere; because of its high redshift, this is effectively identical to the horizon size at the present epoch, $D_{\rm H}$:

$$\begin{aligned} D_{\rm H} &= \frac{2}{\Omega_{\rm m}H_0} \quad (\Omega_{\rm v} = 0); \\ D_{\rm H} &\simeq \frac{2}{\Omega_{\rm m}^{0.4}H_0} \quad (\text{flat}: \Omega_{\rm m} + \Omega_{\rm v} = 1)\ . \end{aligned} \tag{22.82}$$

These relations show how the CMB is strongly sensitive to curvature: the horizon length at last scattering is $\propto 1/\sqrt{\Omega_{\rm m}}$, so that this subtends an angle that is virtually independent of $\Omega_{\rm m}$ for a flat model. Observations of a peak in the CMB power spectrum at relatively large scales ($\ell \simeq 221$) are thus strongly inconsistent with zero-Λ models with low density: current CMB + BAO + lensing data require $\Omega_{\rm m} + \Omega_{\rm v} = 0.999 \pm 0.004$ (95%) [25]. (See *e.g.*, Fig. 22.2).

In addition to curvature, the CMB encodes information about several other key cosmological parameters. Within the compass of simple adiabatic CDM models, there are nine of these:

$$\omega_{\rm c},\ \omega_{\rm b},\ \Omega_{\rm tot},\ h,\ A_s,\ n_{\rm s},\ r,\ n_{\rm t},\ \tau. \tag{22.83}$$

The symbol ω denotes the physical density, Ωh^2: the transfer function depends only on the densities of CDM ($\omega_{\rm c}$) and baryons ($\omega_{\rm b}$). The amplitude and spectral index of scalar fluctuations are specified by $A_{\rm s}$ and $n_{\rm s}$, with r and $n_{\rm t}$ playing the same role for tensor modes. See Cosmological Parameters – Sec. 25 of this *Review* for a technical definition of the r parameter. Although not a fundamental parameter, the optical depth to last-scattering from low-redshift reionization, τ, plays an important role in determining the empirical CMB signal. Transcribing the power spectrum at last scattering into an angular power spectrum brings in the total density parameter ($\Omega_{\rm tot} \equiv \Omega_{\rm m} + \Omega_{\rm v} = \Omega_{\rm c} + \Omega_{\rm b} + \Omega_{\rm v}$) and h: there is a near-exact geometrical degeneracy [108] between these parameters that keeps the angular-diameter distance to last scattering invariant, so that models with substantial spatial curvature and large vacuum energy cannot be ruled out without prior knowledge of the Hubble parameter. Even if we assume zero curvature, a degeneracy remains: we observe the angle subtended by the acoustic horizon at last scattering (a length about 2% smaller than the BAO horizon, $r_{\rm d}$). Fixing this angle, θ_*, yields the precise geometrical degeneracy $\Omega_{\rm m}h^3 = 0.09633 \pm 0.00029$ [25]. The

Int. J. Mod. Phys. A 2026.41. Downloaded from www.worldscientific.com by UNIVERSITY OF CALIFORNIA @ BERKELEY on 09/16/26. Re-use strictly not permitted, except for Open Access articles.

CMB alone therefore cannot measure the Hubble parameter without taking into account additional data, such as the line-of-sight information from CMB lensing.

A further possible degeneracy involves the tensor contribution to the CMB anisotropies. These are important at large scales (up to the horizon scales); for smaller scales, only scalar fluctuations (density perturbations) are important. Adding a large tensor contribution reduces the contrast between low ℓ and the peak at $\ell \simeq 221$ (because the tensor spectrum has no acoustic component). The previous relative height of the peak can be recovered by increasing $n_{\rm s}$ to increase the small-scale power in the scalar component; this in turn over-predicts the power at $\ell \sim 1000$, but this effect can be counteracted by raising the baryon density [109]. This approximate 3-way degeneracy is broken as we increase the range of multipoles sampled.

The reason the tensor component is introduced, and why it is so important, is that it is the only non-generic prediction of inflation. Slow-roll models of inflation involve two dimensionless parameters:

$$\epsilon \equiv \frac{M_{\rm P}^2}{16\pi}\left(\frac{V'}{V}\right)^2; \qquad \eta \equiv \frac{M_{\rm P}^2}{8\pi}\left(\frac{V''}{V}\right), \tag{22.84}$$

where V is the inflaton potential, and dashes denote derivatives with respect to the inflaton field. In terms of these, the tensor-to-scalar ratio is $r \simeq 16\epsilon$, and the spectral indices are $n_{\rm s} = 1-6\epsilon+2\eta$ and $n_{\rm t} = -2\epsilon$. The scalar amplitude can be expressed in terms of ϵ as

$$A_{[\rm s]} = \frac{8ß^2 \rm V}{3ffM_{\rm P}^4}\,. \tag{22.85}$$

This quantity is the power per $\ln k$ of the curvature invariant (variously written as ζ or $\mathcal{R}$), which is 5/3 times the Newtonian potential on superhorizon scales in the matter era.

The natural expectation of inflation is that the quasi-exponential phase ends once the magnitudes of the slow-roll parameters become of order unity, so that both $n_{\rm s} \neq 1$ and a significant tensor component are expected. These predictions can be avoided in some models, but it is undeniable that observation of such features would be a great triumph for inflation. Cosmology therefore stands at a fascinating point, given that the most recent CMB data reject the zero-tensor $n_{\rm s} = 1$ model at more than 8σ: $n_{\rm s} = 0.965 \pm 0.004$ [25]. This rejection is strong enough that it is also able to break the tensor degeneracy, so that no model with $n_{\rm s} = 1$ is acceptable, whatever the value of r.

The current limit on r is < 0.036 at 95% confidence [110, 111]. In conjunction with the measured value of $n_{\rm s}$, this upper limit sits close to the prediction of a linear potential (*i.e.* $|\eta| \ll |\epsilon|$). Any further reduction in the limit on r will force η to be negative – *i.e.* a convex potential at the point where LSS scales were generated (sometimes called a 'hilltop'), in contrast to simple early models such as $V(\phi) = m^2\phi^2$ or $\lambda\phi^4$, which are now excluded. Examples of models that are currently in excellent agreement with the *Planck* results are the Starobinsky model of $\mathcal{R} + \mathcal{R}^2$ gravity [112], or the Higgs-inflation model where the Higgs field is non-minimally coupled [113]. Assuming 55 e-foldings of inflation, these models predict $n_{\rm s} = 0.965$ and $r = 0.0035$. Assuming that no systematic error in the CMB data can be identified, cosmology has thus passed a critical hurdle in rejecting scale-invariant fluctuations. The years ahead will be devoted to the task of searching for the tensor fluctuations – for which the main tool will be the polarization of the CMB [114].

22.4.6.1 *CMB foregrounds*

As the quality of CMB data improves, there is a growing interest in effects that arise along the line of sight. The CMB temperature is perturbed by dark-matter structures and by Compton scattering from ionized gas. In the former case, we have the integrated Sachs-Wolfe effect, which is sensitive to the time derivative of the gravitational potential. In the linear regime, this is damped when the Universe becomes Λ-dominated, and this is an independent way of detecting Λ [115]. The potential also causes gravitational lensing of the CMB: structures at $z \simeq 1$–2 displace features on the CMB sky by about 2 arcmin over coherent degree-scale patches. Detection of these distortions allows a map to be made of over-density projected from $z = 0$ to 1100 [89]. This is a powerful alternative to direct studies of gravitational lensing using galaxies, and has some advantages: in particular, it is independent of astrophysical affects on galaxy shape distortions. CMB lensing information allows the breaking of parameter degeneracies that would be present when only fitting the CMB temperature fluctuations. Finally, Comptonization affects the CMB in two ways: the thermal Sunyaev-Zeldovich effect measures the blurring of photon energies by hot gas; and the kinetic Sunyaev-Zeldovich effect is sensitive to the bulk velocity of the gas. Both these effects start to dominate over the intrinsic CMB fluctuations at multipoles $\ell \gtrsim 2000$ [116].

22.4.7 *Probing dark energy and the nature of gravity*

The most radical element of our current cosmological model is the dark energy that accelerates the expansion. The energy density of this component is approximately $(2.2\,{\rm meV})^4$ (for $w = -1$, $\Omega_v = 0.68$, $h = 0.67$), or roughly $10^{-123} M_{\rm P}^4$, and such an unnaturally small number is hard to understand. Various quantum effects (most simply, zero-point energy) should make contributions to the vacuum energy density. These may be truncated by new physics at high energy, but this presumably occurs at $> 1\,{\rm TeV}$ scales, not meV; thus the apparent energy scale of the vacuum is at least 10^{15} times smaller than its natural value. A classic review of this situation is given by Weinberg [54], which lists extreme escape routes – especially the multiverse viewpoint, according to which low values of Λ are rare, but high values suppress the formation of structure and observers. It is certainly impressive that Weinberg used such reasoning to predict the value of Λ before any data strongly indicated a non-zero value.

But it may be that the phenomenon of dark energy is entirely illusory. The necessity for this constituent arises from using the Friedmann equation to describe the evolution of the cosmic expansion; if this equation is incorrect, it would require the replacement of Einstein's relativistic theory of gravity with some new alternative. A frontier of current cosmological research is to distinguish these possibilities [117, 118]. We also note that it has been suggested that dark energy might be an illusion even within general relativity, owing to an incorrect treatment of averaging in an inhomogeneous Universe [119, 120]. Most would argue that a standard Newtonian treatment of such issues should be adequate inside the cosmological horizon, but debate on this issue continues.

Dark energy can differ from a classical cosmological constant in being a dynamical phenomenon [121, 122], *e.g.*, a rolling scalar field (sometimes dubbed 'quintessence'). Empirically, this means that it is endowed with two thermodynamic properties that astronomers can try to measure: the bulk equation of state, and the sound speed. If the sound speed is close to the speed of light, the effect of this property is confined to very large scales, and mainly manifests itself in the large-angle multipoles of the CMB anisotropies [123]. The equation of state parameter governs the rate of change of the vacuum density: $d\ln\rho_v/d\ln a = -3(1+w)$, so it can be accessed via the evolving expansion rate, $H(a)$. This can be measured most cleanly by using the inbuilt natural ruler of large-scale structure: the BAO horizon scale discussed above. $H(a)$ is measured by radial clustering, since $dr/dz = c/H$; clustering in the plane of the sky measures the integral of this. The expansion rate is also measured by the growth of density fluctuations, where the pressure-free growth equation for the density perturbation is $\ddot\delta + 2H(a)\dot\delta = 4\pi G\rho_0\,\delta$.

Thus, both the scale and amplitude of density fluctuations are sensitive to $w(a)$ – but only weakly. These observables typically change by only 0.2% for a 1% change in w. Current constraints [25] place a constant w to within 5–10% of -1, depending on the data combination chosen. In fact, it has been claimed by Ref. [124] that a cosmological constant can be rejected, and that the dark-energy density changes by $\sim 10\%$ at $z < 2$. This conclusion rests on a combination of CMB, BAO, and SNe data, and requires careful investigation of possible systematics in order to be compelling. This presents a challenge for the field, since any substantial improvement in the current precision will require us to limit systematics in data or theory to a few parts in 1000.

Testing whether theories of gravity require revision can also

Int. J. Mod. Phys. A 2026.41. Downloaded from www.worldscientific.com
by UNIVERSITY OF CALIFORNIA @ BERKELEY on 09/16/26. Re-use and distribution is strictly not permitted, except for Open Access articles.

be done using data on cosmological inhomogeneities. Two separate issues arise, concerning the metric perturbation potentials Ψ and Φ, which affect respectively the time and space parts of the metric. In Einstein gravity, these potentials are both equal to the Newtonian gravitational potential, which satisfies Poisson's equation: $\nabla^2\Phi/a^2 = 4\pi G\bar{\rho}\delta$. Empirically, modifications of gravity require us to explore a change with scale and with time of the 'slip' (Ψ/Φ) and the effective G on the rhs of the Poisson equation. The former aspect can only be probed via gravitational lensing, whereas the latter can be addressed on 10–100 Mpc scales via the growth of clustering. Various schemes for parameterizing modified gravity exist, but a practical approach is to assume that the growth rate can be tied to the density parameter: $d\ln\delta/d\ln a = \Omega_{\rm m}^{\gamma}(a)$ [93,94]. The parameter γ is close to 0.55 for standard relativistic gravity, but can differ by around 0.1 from this value in many non-standard models. Clearly this parameterization is incomplete, since it explicitly rejects the possibility of early dark energy ($\Omega_{\rm m}(a) \to 1$ as $a \to 0$), but it is a convenient way of capturing the power of various experiments. Current data are consistent with standard ΛCDM [125], and exclude variations in slip or effective G of larger than a few times 10%.

Current planning envisages a set of satellite probes that, a decade hence, will have pursued these fundamental tests via gravitational lensing measurements over thousands of square degrees, $> 10^8$ redshifts, and photometry of > 1000 supernovae (*Euclid* in Europe, *Roman* in the USA) [23, 24]. These experiments will measure both w and the perturbation growth rate to an accuracy of around 1%. The outcome will be either a validation of the standard relativistic vacuum-dominated Big-Bang cosmology at a level of precision far beyond anything attempted to date, or the opening of entirely new directions in cosmological models. For a more complete discussion of dark energy and future probes see Dark Energy – Sec. 28 of this *Review*.

References

[1] V.M. Slipher, Pop. Astr. **23**, 21 (1915).

[2] K. Lundmark, Mon. Not. R. Astron. Soc **84**, 747 (1924).

[3] E. Hubble and M. L. Humason, Astrophys. J. **74**, 43 (1931).

[4] G. Gamow, Phys. Rev. **70**, 572 (1946).

[5] R. A. Alpher, H. Bethe and G. Gamow, Phys. Rev. **73**, 803 (1948).

[6] R.A. Alpher and R.C. Herman, Phys. Rev. **74**, 1737 (1948).

[7] R.A. Alpher and R.C. Herman, Phys. Rev. **75**, 1089 (1949).

[8] A. A. Penzias and R. W. Wilson, Astrophys. J. **142**, 419 (1965).

[9] P.J.E. Peebles, *Principles of Physical Cosmology*, Princeton University Press (1993) .

[10] E.W. Kolb and M.S. Turner, *The Early Universe*, Addison-Wesley (1990).

[11] J.A. Peacock, *Cosmological Physics*, Cambridge Univ. Press (1999).

[12] A.R. Liddle and D. Lyth, *Cosmological Inflation and Large-Scale Structure*, Cambridge University Press (2000).

[13] V. Mukhanov, *Physical Foundations of Cosmology*, Cambridge University Press (2005).

[14] S. Weinberg, *Cosmology*, Oxford Press (2008).

[15] P. Peter and J.-P. Uzan, *Primordial Cosmology*, Oxford Graduate Texts, Oxford University Press (2013), ISBN 978-0-19-966515-0, 978-0-19-920991-0.

[16] S. Dodelson and F. Schmidt, *Modern Cosmology*, Academic Press (2020).

[17] D. Baumann, *Cosmology*, Cambridge University Press (2022), ISBN 978-1-108-93709-2, 978-1-108-83807-8.

[18] E.B. Gliner, Sov. Phys. JETP **22**, 378 (1966).

[19] Ya. B. Zeldovich, Sov. Phys. Usp. **11**, 381 (1968), [Usp. Fiz. Nauk95,209(1968)].

[20] P.M. Garnavich *et al.*, Astrophys. J. **507**, 74 (1998), [arXiv:astro-ph/9806396].

[21] S. Perlmutter, M. S. Turner and M. J. White, Phys. Rev. Lett. **83**, 670 (1999), [arXiv:astro-ph/9901052].

[22] I. Maor *et al.*, Phys. Rev. **D65**, 123003 (2002), [arXiv:astro-ph/0112526].

[23] A. Albrecht *et al.* (2006), [arXiv:astro-ph/0609591].

[24] J. A. Peacock *et al.* (2006), [arXiv:astro-ph/0610906].

[25] N. Aghanim *et al.* (Planck), Astron. Astrophys. **641**, A6 (2020), [arXiv:1807.06209].

[26] A.G. Riess *et al.*, Astrophys. J. **116**, 1009 (1998), [arXiv:astro-ph/9805201].

[27] S. Perlmutter *et al.* (Supernova Cosmology Project), Astrophys. J. **517**, 565 (1999), [arXiv:astro-ph/9812133].

[28] A. G. Riess, Publ. Astron. Soc. Pac. **112**, 1284 (2000), [arXiv:astro-ph/0005229].

[29] D. Scolnic *et al.*, Astrophys. J. **938**, 2, 113 (2022), [arXiv:2112.03863].

[30] M. Vincenzi *et al.*, Astrophys. J. **975**, 1, 86 (2024), [arXiv:2401.02945].

[31] A. G. Riess *et al.*, Astrophys. J. Lett. **934**, 1, L7 (2022), [arXiv:2112.04510].

[32] W. L. Freedman *et al.*, "Astrophys. J." **985**, 2, 203 (2025), [arXiv:2408.06153].

[33] Planck Collab. 2015 Results XIII, Astron. & Astrophys. **594**, A13 (2016), [arXiv:1502.10589].

[34] P. Astier *et al.*, Astron. & Astrophys. **447**, 31 (2006), [arXiv:astro-ph/0510447].

[35] J. A. Johnson and M. Bolte, Astrophys. J. **554**, 888 (2001), [arXiv:astro-ph/0103299].

[36] R. Cayrel *et al.*, Nature **409**, 691 (2001), [arXiv:astro-ph/0104357].

[37] D. A. Vandenberg *et al.*, Astrophys. J. **775**, 134 (2013), [arXiv:1308.2257].

[38] S. Borsanyi *et al.*, Nature **539**, 7627, 69 (2016), [arXiv:1606.07494].

[39] M. Srednicki, R. Watkins and K. A. Olive, Nucl. Phys. B **310**, 693 (1988).

[40] J. J. Bennett *et al.*, JCAP **04**, 073 (2021), [arXiv:2012.02726].

[41] M. Drewes *et al.*, JCAP **06**, 032 (2024), [arXiv:2402.18481].

[42] E. Camphuis *et al.* (SPT-3G) (2025), [arXiv:2506.20707].

[43] D. Chebat *et al.*, JCAP **01**, 041 (2026), [arXiv:2507.12401].

[44] A. D. Linde, Phys. Rev. **D14**, 3345 (1976).

[45] A. Linde, Rept. on Prog. in Phys. **42**, 389 (1979).

[46] C.E. Vayonakis, Surv. High Energy Physics **5**, 87 (1986).

[47] S.A. Bonometto and A. Masiero, Nuovo Cimento **9N5**, 1 (1986).

[48] A. Linde, *Particle Physics And Inflationary Cosmology*, Harwood (1990).

[49] K. A. Olive, Phys. Rept. **190**, 307 (1990).

[50] D. H. Lyth and A. Riotto, Phys. Rept. **314**, 1 (1999), [hep-ph/9807278].

[51] A. H. Guth, Phys. Rev. **D23**, 347 (1981), [Adv. Ser. Astrophys. Cosmol.3,139(1987)].

[52] A. D. Linde, Phys. Lett. **108B**, 389 (1982), [Adv. Ser. Astrophys. Cosmol.3,149(1987)].

[53] A. Albrecht and P. J. Steinhardt, Phys. Rev. Lett. **48**, 1220 (1982), [Adv. Ser. Astrophys. Cosmol.3,158(1987)].

[54] S. Weinberg, Rev. Mod. Phys. **61**, 1 (1989).

[55] L. Susskind 247–266 (2003), [hep-th/0302219].

[56] B. Carr, *Universe or multiverse?* C.U.P. (2007).

[57] D. Sorini, J. A. Peacock and L. Lombriser, Mon. Not. Roy. Astron. Soc. **535**, 2, 1449 (2024), [arXiv:2411.07301].

Int. J. Mod. Phys. A 2026.41. Downloaded from www.worldscientific.com by UNIVERSITY OF CALIFORNIA @ BERKELEY on 09/16/26. Re-[redacted] strictly not permitted, except for Open Access articles.

[58] G. Steigman, Ann. Rev. Astron. Astrophys. **14**, 339 (1976).

[59] A. G. Cohen, A. De Rujula and S. L. Glashow, Astrophys. J. **495**, 539 (1998), [arXiv:astro-ph/9707087].

[60] A. D. Sakharov, Pisma Zh. Eksp. Teor. Fiz. **5**, 32 (1967), [Usp. Fiz. Nauk161,no.5,61(1991)].

[61] S. Weinberg, Phys. Rev. Lett. **42**, 850 (1979).

[62] D. Toussaint *et al.*, Phys. Rev. **D19**, 1036 (1979).

[63] I. Affleck and M. Dine, Nucl. Phys. **B249**, 361 (1985).

[64] V. A. Kuzmin, V. A. Rubakov and M. E. Shaposhnikov, Phys. Lett. **155B**, 36 (1985).

[65] M. Fukugita and T. Yanagida, Phys. Lett. **B174**, 45 (1986).

[66] S. Riemer-Sorensen and S. Jenssen, Universe **3**, 44 (2017), [arXiv:1502.10589].

[67] R. J. Cooke, M. Pettini and C. C. Steidel, Astrophys. J. **855**, 2, 102 (2018), [arXiv:1710.11129].

[68] T.-H. Yeh *et al.*, JCAP **10**, 046 (2022), [arXiv:2207.13133].

[69] R. H. Cyburt, B. D. Fields and K. A. Olive, Phys. Lett. **B567**, 227 (2003), [arXiv:astro-ph/0302431].

[70] R. H. Cyburt, B. D. Fields and K. A. Olive, JCAP **0811**, 012 (2008), [arXiv:0808.2818].

[71] B. D. Fields and K. A. Olive, JCAP **10**, 078 (2022), [arXiv:2204.03167].

[72] K. A. Olive, G. Steigman and T. P. Walker, Phys. Rept. **333**, 389 (2000), [arXiv:astro-ph/9905320].

[73] F. Iocco *et al.*, Phys. Rept. **472**, 1 (2009), [arXiv:0809.0631].

[74] R. H. Cyburt *et al.*, Rev. Mod. Phys. **88**, 015004 (2016), [arXiv:1505.01076].

[75] C. Pitrou *et al.*, Phys. Rept. **754**, 1 (2018), [arXiv:1801.08023].

[76] B. D. Fields *et al.*, JCAP **03**, 010 (2020), [Erratum: JCAP 11, E02 (2020)], [arXiv:1912.01132].

[77] D. J. Fixsen *et al.*, Astrophys. J. **473**, 576 (1996), [arXiv:astro-ph/9605054].

[78] J. C. Mather *et al.*, Astrophys. J. **512**, 511 (1999), [arXiv:astro-ph/9810373].

[79] S. Cole *et al.* (2dFGRS), Mon. Not. Roy. Astron. Soc. **326**, 255 (2001), [arXiv:astro-ph/0012429].

[80] J. Schroeder, A. Mesinger and Z. Haiman, Mon. Not. R. Astron. Soc **428**, 3058 (2013), [arXiv:1204.2838].

[81] P. A. Kislitsyn *et al.*, Mon. Not. Roy. Astron. Soc. **528**, 3, 4068 (2024), [arXiv:2401.12797].

[82] F. Guarneri *et al.*, Mon. Not. Roy. Astron. Soc. **529**, 2, 839 (2024), [arXiv:2402.05586].

[83] S. D. M. White *et al.*, Nature **366**, 429 (1993).

[84] S. W. Allen, R. W. Schmidt and A. C. Fabian, Mon. Not. Roy. Astron. Soc. **334**, L11 (2002), [arXiv:astro-ph/0205007].

[85] S. W. Allen, Mon. Not. Roy. Astron. Soc. **296**, 392 (1998), [arXiv:astro-ph/9710217].

[86] G. P. Smith *et al.*, Mon. Not. Roy. Astron. Soc. **456**, 1, L74 (2016), [arXiv:1511.01919].

[87] H. Hildebrandt *et al.*, Astron. Astrophys. **633**, A69 (2020), [arXiv:1812.06076].

[88] A. Amon *et al.* (DES), Phys. Rev. D **105**, 2, 023514 (2022), [arXiv:2105.13543].

[89] Planck Collab. 2015 Results XV, Astron. & Astrophys. **594**, A15 (2016), [arXiv:1502.01591].

[90] S. Cole *et al.* (2dFGRS), Mon. Not. Roy. Astron. Soc. **362**, 505 (2005), [arXiv:astro-ph/0501174].

[91] W. J. Percival *et al.*, Astrophys. J. **657**, 645 (2007), [arXiv:astro-ph/0608636].

[92] L. Anderson *et al.*, Mon. Not. Roy. Astron. Soc. **427**, 4, 3435 (2013), [arXiv:1203.6594].

[93] E. Linder, Phys. Rev. **D72**, 43529 (2005), [arXiv:astro-ph/0507263].

[94] D. Polarski and R. Gannouji, Phys. Lett. **B660**, 439 (2008), [arXiv:0710.1510].

[95] G. Efstathiou and J. R. Bond, Mon. Not. Roy. Astron. Soc. **218**, 1, 103 (1986).

[96] C. Gordon and A. Lewis, Phys. Rev. **D67**, 123513 (2003), [arXiv:astro-ph/0212248].

[97] A. Vikhlinin *et al.*, Astrophys. J. **692**, 1060 (2009), [arXiv:0812.2720].

[98] A. Mantz *et al.*, Mon. Not. Roy. Astron. Soc. **446**, 2205 (2015), [arXiv:1407.4516].

[99] T. M. C. Abbott *et al.* (Kilo-Degree Survey, DES), Open J. Astrophys. **6**, 2305.17173 (2023), [arXiv:2305.17173].

[100] A. Dekel and O. Lahav, Astrophys. J. **520**, 24 (1999), [arXiv:astro-ph/9806193].

[101] W. J. Percival *et al.*, Mon. Not. Roy. Astron. Soc. **381**, 1053 (2007), [arXiv:0705.3323].

[102] W. J. Percival *et al.* (SDSS), Mon. Not. Roy. Astron. Soc. **401**, 2148 (2010), [arXiv:0907.1660].

[103] É. Aubourg *et al.*, Phys. Rev. **D92**, 123516 (2015), [arXiv:1411.1074].

[104] G. Lavaux *et al.*, Astrophys. J. **709**, 483 (2010), [arXiv:0810.3658].

[105] N. J. Secrest *et al.*, Astrophys. J. **908**, L51 (2021), [arXiv:2009.14826].

[106] J. Darling, Astrophys. J. Lett. **931**, 2, L14 (2022), [arXiv:2205.06880].

[107] A. Abghari *et al.*, JCAP **11**, 067 (2024), [arXiv:2405.09762].

[108] G. Efstathiou and J. R. Bond, Mon. Not. Roy. Astron. Soc. **304**, 75 (1999), [arXiv:astro-ph/9807103].

[109] G. Efstathiou *et al.* (2dFGRS), Mon. Not. Roy. Astron. Soc. **330**, L29 (2002), [arXiv:astro-ph/0109152].

[110] M. Tristram *et al.*, Astron. Astrophys. **647**, A128 (2021), [arXiv:2010.01139].

[111] P. A. R. Ade *et al.* (BICEP/Keck), Phys. Rev. Lett. **127**, 15, 151301 (2021), [arXiv:2110.00483].

[112] A. A. Starobinsky, Phys. Lett. **B91**, 99 (1980), [,771(1980)].

[113] F. Bezrukov and M. Shaposhnikov, JHEP **07**, 089 (2009), [arXiv:0904.1537].

[114] S. Dodelson, *Modern Cosmology*, Academic Press (2003).

[115] Planck Collab. 2015 Results XXI, Astron. & Astrophys. **594**, A21 (2016), [arXiv:1502.01595].

[116] Planck Collab. 2015 Results XXII, Astron. & Astrophys. **594**, A22 (2016), [arXiv:1502.01596].

[117] W. Hu and I. Sawicki, Phys. Rev. **D76**, 4043 (2007), [arXiv:0708.1190].

[118] B. Jain and P. Zhang, Phys. Rev. **D78**, 3503 (2008), [arXiv:0709.2375].

[119] D. L. Wiltshire, Phys. Rev. Lett. **99**, 251101 (2007), [arXiv:0709.0732].

[120] T. Buchert, Gen. Rel. Grav. **40**, 467 (2008), [arXiv:0707.2153].

[121] I. Zlatev, L.-M. Wang and P. J. Steinhardt, Phys. Rev. Lett. **82**, 896 (1999), [arXiv:astro-ph/9807002].

[122] C. Armendariz-Picon, V. Mukhanov, and P.J. Steinhardt, Phys. Rev. **D63**, 3510 (2001), [arXiv:astro-ph/0006373].

[123] S. DeDeo, R.R. Caldwell, and P.J. Steinhardt, Phys. Rev. **D67**, 3509 (2003), [arXiv:astro-ph/0301284].

[124] M. Abdul Karim *et al.* (DESI), Phys. Rev. D **112**, 8, 083515 (2025), [arXiv:2503.14738].

[125] Planck Collaboration *et al.*, Astronomy & Astrophysics **594**, A14 (2016), [arXiv:1502.01590].

Int. J. Mod. Phys. A 2026.41. Downloaded from www.worldscientific.com
by UNIVERSITY OF CALIFORNIA @ BERKELEY on 09/16/26. Re-use and distribution is strictly not permitted, except for Open Access articles.

23. Inflation

Revised August 2025 by J. Ellis (King's Coll. London; CERN), V. Vennin (LPENS; CNRS) and D. Wands (Portsmouth U.).

23.1 Motivation and Introduction

The standard Big-Bang model of cosmology provides a successful framework in which to understand the thermal history of our Universe and the growth of cosmic structure, but it is essentially incomplete. As described in Sec. 22.2.4, Big-Bang cosmology requires very specific initial conditions. It postulates a uniform cosmological background, described by a spatially-flat, homogeneous and isotropic Robertson-Walker (RW) metric (Eq. (22.1) in "Big-Bang Cosmology" review), with scale factor $R(t)$. Within this setting, it also requires an initial almost scale-invariant distribution of primordial density perturbations as seen, for example, in the cosmic microwave background (CMB) radiation (described in Chap. 29, "Cosmic Microwave Background" review), on scales far larger than the causal horizon at the time the CMB photons last scattered.

The Hubble expansion rate, $H \equiv \dot{R}/R$, in an RW cosmology is given by the Friedmann constraint equation (Eq. (22.8) in "Big-Bang Cosmology" review)

$$H^2 = \frac{8\pi\rho}{3M_{\rm P}^2} + \frac{\Lambda}{3} - \frac{k}{R^2}\,, \tag{23.1}$$

where k/R^2 is the intrinsic spatial curvature. We use natural units such that the speed of light $c = 1$ and hence we have the Planck mass[1] $M_{\rm P} = G_{\rm N}^{-1/2} \simeq 10^{19}$ GeV (see "Astrophysical Constants and Parameters"). A cosmological constant, Λ, of the magnitude required to accelerate the Universe today (see Chap. 28, "Dark Energy" review) would have been completely negligible in the early Universe where the energy density $\rho \gg M_{\rm P}^2\Lambda \sim 10^{-12}({\rm eV})^4$. The standard early Universe cosmology, described in Sec. 22.1.5 in "Big-Bang Cosmology" review, is thus dominated by non-relativistic matter ($p_{\rm m} \ll \rho_{\rm m}$) or radiation ($p_{\rm r} = \rho_{\rm r}/3$ for an isotropic distribution). This leads to a decelerating expansion with $\ddot{R} < 0$.

The hypothesis of inflation [5, 6] postulates a period of accelerated expansion, $\ddot{R} > 0$, in the very early Universe, preceding the standard radiation-dominated era, which offers a physical model for the origin of these initial conditions, as reviewed in Refs. [1–4, 7–9]. Such a period of accelerated expansion (i) drives a curved Robertson-Walker spacetime (with spherical or hyperbolic spatial geometry) towards spatial flatness, and (ii) it also expands the causal horizon beyond the present Hubble length, so as to encompass all the scales relevant to describe the large-scale structure observed in our Universe today, via the following two mechanisms.

1. A spatially-flat Universe with vanishing spatial curvature, $k = 0$, has the dimensionless density parameter $\Omega_{\rm tot} = 1$, where we define (Eq. (22.13) in "Big-Bang Cosmology" review; see Chap. 25, "Cosmological Parameters" review for more complete definitions)

$$\Omega_{\rm tot} \equiv \frac{8\pi\rho_{\rm tot}}{3M_{\rm P}^2 H^2}\,, \tag{23.2}$$

with $\rho_{\rm tot} \equiv \rho + \Lambda M_{\rm P}^2/8\pi$. If we re-write the Friedmann constraint (Eq. (23.1)) in terms of $\Omega_{\rm tot}$ we have

$$1 - \Omega_{\rm tot} = -\frac{k}{\dot{R}^2}\,. \tag{23.3}$$

Observations require $|1 - \Omega_{\rm tot,0}| < 0.005$ today [10], where the subscript "0" denotes the present-day value. Taking the time derivative of Eq. (23.3) we obtain

$$\frac{d}{dt}\left(1 - \Omega_{\rm tot}\right) = -2\frac{\ddot{R}}{\dot{R}}\left(1 - \Omega_{\rm tot}\right)\,. \tag{23.4}$$

Thus in a decelerating expansion, $\dot{R} > 0$ and $\ddot{R} < 0$, any small initial deviation from spatial flatness grows, $(d/dt)|1-\Omega_{\rm tot}| > 0$. A small value such as $|1-\Omega_{\rm tot,0}| < 0.005$ today requires an even smaller value at earlier times, *e.g.*, $|1 - \Omega_{\rm tot}| < 10^{-5}$ at the last scattering of the CMB, which appears unlikely, unless for some reason space is exactly flat. However, an extended period of accelerated expansion in the very early Universe, with $\dot{R} > 0$ and $\ddot{R} > 0$ and hence $(d/dt)|1 - \Omega_{\rm tot}| < 0$, can drive $\Omega_{\rm tot}$ sufficiently close to unity, so that $|1 - \Omega_{\rm tot,0}|$ remains unobservably small today, even after the radiation- and matter-dominated eras, for a wide range of initial values of $\Omega_{\rm tot}$.

2. The comoving distance (the present-day proper distance) traversed by light between cosmic time t_1 and t_2 in an expanding Universe can be written, (see Eq. (22.32) in "Big-Bang Cosmology" review), as

$$D_0(t_1, t_2) = R_0 \int_{t_1}^{t_2} \frac{dt}{R(t)} = R_0 \int_{\ln R_1}^{\ln R_2} \frac{d(\ln R)}{\dot{R}}\,. \tag{23.5}$$

In standard decelerated (radiation- or matter-dominated) cosmology the integrand, $1/\dot{R}$, decreases towards the past, and there is a finite comoving distance traversed by light (a particle horizon) since the Big Bang ($R_1 \to 0$). For example, the comoving size of the particle horizon at the CMB last-scattering surface ($R_2 = R_{\rm lss}$) corresponds to $D_0 \simeq 100\,{\rm Mpc}$, or approximately 1° on the CMB sky today (see Sec. 22.2.4 in "Big-Bang Cosmology" review). However, during a period of inflation, $1/\dot{R}$ increases towards the past, and hence the integral (Eq. (23.5)) diverges as $R_1 \to 0$, allowing an arbitrarily large causal horizon, dependent only upon the duration of the accelerated expansion. Assuming that the Universe inflates with a finite Hubble rate H_* at $t_1 = t_*$, ending with $H_{\rm end} < H_*$ at $t_2 = t_{\rm end}$, we have

$$D_0(t_*, t_{\rm end}) > \left(\frac{R_0}{R_{\rm end}}\right) H_*^{-1}\left(e^{N_*} - 1\right)\,, \tag{23.6}$$

where $N_* \equiv \ln(R_{\rm end}/R_*)$ describes the duration of inflation, measured in terms of the logarithmic expansion (or "e-folds") from $t_1 = t_*$ up to the end of inflation at $t_2 = t_{\rm end}$, and $R_0/R_{\rm end}$ is the subsequent expansion from the end of inflation to the present day. If inflation occurs above the TeV scale, the comoving Hubble scale at the end of inflation, $(R_0/R_{\rm end})H_{\rm end}^{-1}$, is less than one astronomical unit ($\sim 10^{11}$ m), and a causally-connected patch can encompass our entire observable Universe today, which has a size $D_0 > 30$ Gpc, if there were more than 40 e-folds of inflation ($N_* > 40$). If inflation occurs at the GUT scale (10^{15} GeV) then we require more than 60 e-folds.

Producing an accelerated expansion in general relativity requires an energy-momentum tensor with negative pressure, $p < -\rho/3$ (see Eq. (22.9) in "Big-Bang Cosmology" review and Chap. 28, "Dark Energy" review), quite different from the hot dense plasma of relativistic particles in the hot Big Bang. However a positive vacuum energy $V > 0$ does exert a negative pressure, $p_V = -\rho_V$. The work done by the cosmological expansion must be negative in this case so that the local vacuum energy density remains constant in an expanding Universe, $\dot{\rho}_V = -3H(\rho_V + p_V) = 0$. Therefore, a false vacuum state can drive an exponential expansion, corresponding to a de Sitter spacetime with a constant Hubble rate $H^2 = 8\pi\rho_V/3M_{\rm P}^2$ on spatially-flat hypersurfaces.

A constant vacuum energy V, equivalent to a cosmological constant Λ in the Friedmann equation Eq. (23.1), cannot provide a complete description of inflation in the early Universe, since inflation must necessarily have come to an end in order for the standard Big-Bang cosmology to follow. A phase transition to the present true vacuum is required to release the false vacuum energy into the energetic plasma of the hot Big Bang and produce the large total entropy of our observed Universe today. Thus, we must necessarily study dynamical models of inflation, where the time-invariance of the false vacuum state is broken by a time-dependent

[1] We note that another commonly used convention in the literature (*e.g.*, Refs. [1–4] is to work in terms of the reduced Planck mass, $(8\pi G_{\rm N})^{-1/2} \simeq 2 \times 10^{18}$ GeV.

Int. J. Mod. Phys. A 2026.41. Downloaded from www.worldscientific.com by UNIVERSITY OF CALIFORNIA @ BERKELEY on 09/16/26. Re-
strictly not permitted, except for Open Access articles.

field. A first-order phase transition would produce a very inhomogeneous Universe [11], unless a time-dependent scalar field leads to a rapidly changing percolation rate [12–14]. However, a second-order phase transition [15, 16], controlled by a slowly-rolling scalar field, can lead to a smooth classical exit from the vacuum-dominated phase.

As a spectacular bonus, quantum fluctuations in that scalar field could provide a source of almost scale-invariant density fluctuations [17, 18], as detected in the CMB (see Chap. 29), which are thought to be the origin of the structures seen in the Universe today.

Accelerated expansion and primordial perturbations can also be produced in some modified gravity theories (*e.g.*, [5, 19]), which introduce additional non-minimally coupled degrees of freedom. Such inflation models can often be conveniently studied by transforming variables to an 'Einstein frame' in which Einstein's equations apply with minimally coupled scalar fields [20–22].

In the following we will review scalar field cosmology in general relativity and the spectra of primordial fluctuations produced during inflation, before studying selected inflation models.

23.2 Scalar Field Cosmology

The energy-momentum tensor for a canonical scalar field ϕ with self-interaction potential $V(\phi)$ is given in Eq. (22.52) in the "Big-Bang Cosmology" review. In a homogeneous background this corresponds to a perfect fluid with density

$$\rho = \frac{1}{2}\dot{\phi}^2 + V(\phi)\,, \tag{23.7}$$

and isotropic pressure

$$p = \frac{1}{2}\dot{\phi}^2 - V(\phi)\,, \tag{23.8}$$

while the 4-velocity is proportional to the gradient of the field, $u^\mu \propto \nabla^\mu \phi$.

A field with vanishing potential energy acts like a stiff fluid with $p = \rho = \dot{\phi}^2/2$, whereas if the time-dependence vanishes we have $p = -\rho = -V$ and the scalar field is uniform in time and space. Thus a classical, potential-dominated scalar-field cosmology, with $p \simeq -\rho$, can naturally drive a quasi-de Sitter expansion; the slow time-evolution of the energy density weakly breaks the exact $O(1,3)$ symmetry of four-dimensional de Sitter spacetime down to a Robertson-Walker (RW) spacetime, where the scalar field plays the role of the cosmic time coordinate.

In a scalar-field RW cosmology the Friedmann constraint equation (Eq. (23.1)) reduces to

$$H^2 = \frac{8\pi}{3M_{\rm P}^2}\left(\frac{1}{2}\dot{\phi}^2 + V\right) - \frac{k}{R^2}\,, \tag{23.9}$$

while energy conservation (Eq. (22.10) in "Big-Bang Cosmology" review) for a homogeneous scalar field reduces to the Klein-Gordon equation of motion (Eq. (22.54) in "Big-Bang Cosmology" review)

$$\ddot{\phi} = -3H\dot{\phi} - V'(\phi)\,. \tag{23.10}$$

The evolution of the scalar field is thus driven by the potential gradient $V' = dV/d\phi$, subject to damping by the Hubble expansion $3H\dot{\phi}$.

If we define the Hubble slow-roll parameter

$$\epsilon_H \equiv -\frac{\dot{H}}{H^2}\,, \tag{23.11}$$

then we see that inflation ($\ddot{R} > 0$ and hence $\dot{H} > -H^2$) requires $\epsilon_H < 1$. In this case the spatial curvature decreases relative to the scalar field energy density as the Universe expands. Hence, in the following we drop the spatial curvature and consider a spatially-flat RW cosmology, assuming that inflation has lasted sufficiently long that our observable Universe is very close to spatial flatness. However, we note that bubble nucleation, leading to a first-order phase transition during inflation, can lead to homogeneous hypersurfaces with a hyperbolic ('open') geometry, effectively resetting the spatial curvature inside the bubble [23]. This is the basis of so-called open inflation models [24–26], where inflation inside the bubble has a finite duration, leaving a finite negative spatial curvature.

In a scalar field-dominated cosmology, Eq. (23.11) gives

$$\epsilon_H = \frac{3\dot{\phi}^2}{2V + \dot{\phi}^2}\,, \tag{23.12}$$

in which case we see that inflation requires a potential-dominated expansion, $\dot{\phi}^2 < V$.

23.2.1 *Slow-Roll Inflation*

It is commonly assumed that the field acceleration term, $\ddot{\phi}$, in Eq. (23.10) can be neglected, in which case one can give an approximate solution for the inflationary attractor [27]. This slow-roll approximation reduces the second-order Klein-Gordon equation (23.10) to a first-order system, which is over-damped, with the potential gradient being approximately balanced against the Hubble damping:

$$3H\dot{\phi} \simeq -V'\,, \tag{23.13}$$

and at the same time the Hubble expansion (Eq. (23.9)) is dominated by the potential energy

$$H^2 \simeq \frac{8\pi}{3M_{\rm P}^2}V(\phi)\,, \tag{23.14}$$

corresponding to $\epsilon_H \ll 1$.

A necessary condition for the validity of the slow-roll approximation is that the potential slow-roll parameters

$$\epsilon \equiv \frac{M_{\rm P}^2}{16\pi}\left(\frac{V'}{V}\right)^2\,, \quad \eta \equiv \frac{M_{\rm P}^2}{8\pi}\left(\frac{V''}{V}\right)\,, \tag{23.15}$$

are small, *i.e.*, $\epsilon \ll 1$ and $|\eta| \ll 1$, requiring the potential to be correspondingly flat. If we identify V'' with the effective mass of the field, we see that the slow-roll approximation requires that the mass of the scalar field must be small compared with the Hubble scale. We note that the Hubble slow-roll parameter (Eq. (23.11)) coincides with the potential slow-roll parameter, $\epsilon_H \simeq \epsilon$, to leading order in the slow-roll approximation.

The slow-roll approximation allows one to determine the Hubble expansion rate as a function of the scalar field value, and vice versa. In particular, we can express, in terms of the scalar field value during inflation, the total logarithmic expansion, or number of "e-folds":

$$\begin{aligned} N_* &\equiv \ln\left(\frac{R_{\rm end}}{R_*}\right) \\ &= \int_{t_*}^{t_{\rm end}} H dt \simeq -\int_{\phi_*}^{\phi_{\rm end}} \sqrt{\frac{4\pi}{\epsilon}}\,\frac{d\phi}{M_{\rm P}} \text{ for } V' > 0\,. \end{aligned} \tag{23.16}$$

Given that the slow-roll parameters are approximately constant during slow-roll inflation, $d\epsilon/dN \simeq 2\epsilon(\eta - 2\epsilon) = \mathcal{O}(\epsilon^2)$, we have

$$N_* \simeq \frac{4}{\sqrt{\epsilon}}\frac{\Delta\phi}{M_{\rm P}}\,. \tag{23.17}$$

Since we require $N > 40$ to solve the flatness, horizon, and entropy problems of the standard Big-Bang cosmology, we require either very slow roll, $\epsilon < 0.01$, or a large change in the value of the scalar field relative to the Planck scale, $\Delta\phi > M_{\rm P}$.

23.2.2 *Reheating*

Slow-roll inflation can lead to an exponentially large Universe, close to spatial flatness and homogeneity, but the energy density is locked in the potential energy of the scalar field, and needs to be converted to particles and thermalised to recover a hot Big-Bang cosmology at the end of inflation [28, 29]. This process is usually referred to as reheating, although there was not necessarily any preceding thermal era. Reheating can occur when the scalar field evolves towards the minimum of its potential, converting the potential energy first to kinetic energy. This can occur either through the breakdown of the slow-roll condition in single-field

Int. J. Mod. Phys. A 2026.41. Downloaded from www.worldscientific.com by UNIVERSITY OF CALIFORNIA @ BERKELEY on 09/16/26. Re-use and distribution is strictly not permitted, except for Open Access articles.

models, or due to an instability triggered by the inflaton reaching a critical value, in multi-field models known as hybrid inflation [30].

Close to a simple minimum, the scalar field potential can be described by a quadratic function, $V = m^2\phi^2/2$, where m is the mass of the field. We can obtain slow-roll inflation in such a potential at large field values, $\phi \gg M_{\rm P}$. However, for $\phi \ll M_{\rm P}$ the field approaches an oscillatory solution:

$$\phi(t) \simeq \frac{M_{\rm P}}{\sqrt{3\pi}} \frac{\sin(mt)}{mt} \,. \tag{23.18}$$

For $|\phi| < M_{\rm P}$ the Hubble rate drops below the inflaton mass, $H < m$, and the field oscillates many times over a Hubble time. Averaging over several oscillations, $\Delta t \gg m^{-1}$, we find $\langle \dot\phi^2/2\rangle_{\Delta t} \simeq \langle m^2\phi^2/2\rangle_{\Delta t}$ and hence

$$\langle \rho\rangle_{\Delta t} \simeq \frac{M_{\rm P}^2}{6\pi t^2} \,, \quad \langle p\rangle_{\Delta t} \simeq 0 \,. \tag{23.19}$$

This coherent oscillating field corresponds to a condensate of non-relativistic massive inflaton particles, driving a matter-dominated era at the end of inflation, with scale factor $R \propto t^{2/3}$.

The inflaton condensate can lose energy through perturbative decays due to terms in the interaction Lagrangian, such as

$$\mathcal{L}_{\rm int} \subset -\lambda_i \sigma\phi\chi_i^2 - \lambda_j \phi\bar\psi_j\psi_j \tag{23.20}$$

that couple the inflation to scalar fields χ_i or fermions ψ_j, where σ has dimensions of mass and the λ_i are dimensionless couplings. When the mass of the inflaton is much larger than the decay products, the decay rate is given by [31]

$$\Gamma_i = \frac{\lambda_i^2\sigma^2}{8\pi m} \,, \quad \Gamma_j = \frac{\lambda_j^2 m}{8\pi} \,. \tag{23.21}$$

These decay products must in turn thermalise with Standard Model particles before we recover conventional hot Big-Bang cosmology. An upper limit on the reheating temperature after inflation is given by [29]

$$T_{\rm rh} = 0.2 \left(\frac{100}{g_*}\right)^{1/4} \sqrt{M_{\rm P}\Gamma_{\rm tot}} \,, \tag{23.22}$$

where g_* is the effective number of degrees of freedom and $\Gamma_{\rm tot}$ is the total decay rate for the inflaton, which is required to be less than m for perturbative decay.

The baryon asymmetry of the Universe must be generated after the main release of entropy during inflation, which is an important constraint on possible models. Also, the fact that the inflaton mass is much larger than the mass scale of the Standard Model opens up the possibility that it may decay into massive stable or metastable particles that could be connected with dark matter, constraining possible models. For example, in the context of supergravity models the reheat temperature is constrained by the requirement that gravitinos are not overproduced, potentially destroying the successes of Big-Bang nucleosynthesis. For a range of gravitino masses one must require $T_{\rm rh} < 10^9$ GeV [32, 33].

The process of inflaton decay and reheating can be significantly altered by interactions leading to space-time dependences in the effective masses of the fields. In particular, parametric resonance can lead to explosive, non-perturbative decay of the inflaton in some cases, a process often referred to as preheating [28, 34]. For example, an interaction term of the form

$$\mathcal{L}_{\rm int} \subset -\lambda^2\phi^2\chi^2 \,, \tag{23.23}$$

leads to a time-dependent effective mass for the χ field as the inflaton ϕ oscillates. This can lead to non-adiabatic particle production if the bare mass of the χ field is small for large couplings or for rapid changes of the inflaton field. The process of preheating is highly model-dependent, but it highlights the possible role of non-thermal particle production after and even during inflation.

23.3 Primordial Perturbations from Inflation

Although inflation was originally discussed as a solution to the problem of initial conditions required for homogeneous and isotropic hot Big-Bang cosmology, it was soon realised that inflation also offered a mechanism to generate the inhomogeneous initial conditions required for the formation of large-scale structure [17–19, 35].

23.3.1 *Metric Perturbations*

In a homogeneous classical inflationary cosmology driven by a scalar field, the inflaton field is uniform on constant-time hypersurfaces, $\phi = \phi_0(t)$. However, quantum fluctuations inevitably break the spatial symmetry leading to an inhomogeneous field:

$$\phi(t, x^i) = \phi_0(t) + \delta\phi(t, x^i) \,. \tag{23.24}$$

At the same time, one should consider inhomogeneous perturbations of the RW spacetime metric (see, *e.g.*, Refs. [36–38]):

$$\begin{aligned} ds^2 = (1+2A)dt^2 - 2RB_i dt dx^i \\ - R^2\left[(1+2C)\delta_{ij} + \partial_i\partial_j E + h_{ij}\right] dx^i dx^j \,, \end{aligned} \tag{23.25}$$

where A, B, C and E are scalar perturbations while h_{ij} represents transverse and tracefree, tensor metric perturbations. Vector metric perturbations can be eliminated using Einstein constraint equations in a scalar field cosmology.

The tensor perturbations remain invariant under a temporal gauge transformation $t \to t + \delta t(t, x^i)$, but both the scalar field and the scalar metric perturbations transform. For example, we have

$$\delta\phi \to \delta\phi - \dot\phi_0 \delta t \,, \quad C \to C - H\delta t \,. \tag{23.26}$$

However, there are gauge invariant combinations, such as [39]

$$Q = \delta\phi - \frac{\dot\phi_0}{H} C \,, \tag{23.27}$$

which describes the scalar field perturbations on spatially-flat ($C = 0$) hypersurfaces. This is simply related to the curvature perturbation on uniform-field ($\delta\phi = 0$) hypersurfaces:

$$\mathcal{R} = C - \frac{H}{\dot\phi_0}\delta\phi = -\frac{H}{\dot\phi_0} Q \,, \tag{23.28}$$

which coincides in slow-roll inflation, $\rho \simeq \rho(\phi)$, with the curvature perturbation on uniform-density hypersurfaces [18]

$$\zeta = C - \frac{H}{\dot\rho_0}\delta\rho \,. \tag{23.29}$$

Thus scalar field and scalar metric perturbations are coupled by the evolution of the inflaton field.

23.3.2 *Gravitational waves from inflation*

The tensor metric perturbation, h_{ij} in Eq. (23.25), is gauge-invariant and decoupled from the scalar perturbations at first order. This represents the free excitations of the spacetime, *i.e.*, gravitational waves, which are the simplest metric perturbations to study at linear order.

Each tensor mode, with wavevector $\vec k$, has two linearly-independent transverse and trace-free polarization states:

$$h_{ij}(\vec k) = h_{\vec k} q_{ij} + \bar h_{\vec k} \bar q_{ij} \,. \tag{23.30}$$

The linearised Einstein equations then yield the same evolution equation for the amplitude as that for a massless field in RW spacetime:

$$\ddot h_{\vec k} + 3H\dot h_{\vec k} + \frac{k^2}{R^2} h_{\vec k} = 0 \,, \tag{23.31}$$

(and similarly for $\bar h_{\vec k}$). This can be re-written in terms of the conformal time, $\eta = \int dt/R$, and the conformally rescaled field:

$$u_{\vec k} = \frac{M_{\rm P} R h_{\vec k}}{\sqrt{32\pi}} \,. \tag{23.32}$$

Int. J. Mod. Phys. A 2026.41. Downloaded from www.worldscientific.com by UNIVERSITY OF CALIFORNIA @ BERKELEY on 09/16/26. Re- strictly not permitted, except for Open Access articles.

This conformal field then obeys the wave equation for a canonical scalar field in Minkowski spacetime with a time-dependent mass:

$$u''_{\vec{k}} + \left(k^2 - \frac{R''}{R}\right) u_{\vec{k}} = 0\,. \tag{23.33}$$

During slow roll

$$\frac{R''}{R} \simeq (2-\epsilon)R^2H^2\,. \tag{23.34}$$

This makes it possible to quantise the linearised metric fluctuations, $u_{\vec{k}} \to \hat{u}_{\vec{k}}$, on sub-Hubble scales, $k^2/R^2 \gg H^2$, where the background expansion can be neglected.

Crucially, in an inflationary expansion, where $\ddot{R} > 0$, the comoving Hubble length $H^{-1}/R = 1/\dot{R}$ decreases with time. Thus, all modes start inside the Hubble horizon and it is possible to take the initial field fluctuations to be in a vacuum state at early times or on small scales:

$$\langle u_{\vec{k}_1} u_{\vec{k}_2}\rangle = \frac{i}{2}(2\pi)^3\delta^{(3)}\left(\vec{k}_1+\vec{k}_2\right)\,. \tag{23.35}$$

In terms of the amplitude of the tensor metric perturbations, this corresponds to

$$\langle h_{\vec{k}_1} h_{\vec{k}_2}\rangle = \frac{1}{2}\frac{\mathcal{P}_{\rm t}(k_1)}{4\pi k_1^3}(2\pi)^3\delta^{(3)}\left(\vec{k}_1+\vec{k}_2\right)\,, \tag{23.36}$$

where the factor 1/2 appears due to the two polarization states that contribute to the total tensor power spectrum:

$$\mathcal{P}_{\rm t}(k) = \frac{64\pi}{M_{\rm P}^2}\left(\frac{k}{2\pi R}\right)^2\,. \tag{23.37}$$

On super-Hubble scales, $k^2/R^2 \ll H^2$, we have the growing mode solution to Eq. (23.33), $u_{\vec{k}} \propto R$, corresponding to $h_{\vec{k}} \to$ constant, *i.e.*, tensor modes are frozen-in on super-Hubble scales, both during and after inflation. Thus, connecting the initial vacuum fluctuations on sub-Hubble scales to the late-time power spectrum for tensor modes at Hubble exit during inflation, $k = R_*H_*$, we obtain

$$\mathcal{P}_{\rm t}(k) \simeq \frac{64\pi}{M_{\rm P}^2}\left(\frac{H_*}{2\pi}\right)^2\,. \tag{23.38}$$

In the de Sitter limit, $\epsilon \to 0$, the Hubble rate becomes time-independent and the tensor spectrum on super-Hubble scales becomes scale-invariant [41]. However slow-roll evolution leads to weak time dependence of H_* and thus a scale-dependent spectrum on large scales, with a spectral tilt

$$n_{\rm t} \equiv \frac{d\ln\mathcal{P}_{\rm t}}{d\ln k} \simeq -2\epsilon_*\,. \tag{23.39}$$

23.3.3 *Density Perturbations from single-field inflation*

The inflaton field fluctuations on spatially-flat hypersurfaces are coupled to scalar metric perturbations at first order, but these can be eliminated using the Einstein constraint equations to yield an evolution equation

$$\ddot{Q}_{\vec{k}} + 3H\dot{Q}_{\vec{k}} + \left[\frac{k^2}{R^2} + V'' - \frac{8\pi}{M_{\rm P}^2R^3}\frac{d}{dt}\left(\frac{R^3\dot{\phi}^2}{H}\right)\right]Q_{\vec{k}} = 0\,. \tag{23.40}$$

Terms proportional to $M_{\rm P}^{-2}$ represent the effect on the field fluctuations of gravity at first order. As can be seen, this vanishes in the limit of a constant background field, and hence is suppressed in the slow-roll limit, but it is of the same order as the effective mass, $V'' = 3\eta H^2$, so must be included if we wish to model deviations from exact de Sitter symmetry.

This wave equation can also be written in the canonical form for a free field in Minkowski spacetime if we define [39]

$$v_{\vec{k}} \equiv RQ_{\vec{k}}\,, \tag{23.41}$$

to yield

$$v''_{\vec{k}} + \left(k^2 - \frac{z''}{z}\right)v_{\vec{k}} = 0\,, \tag{23.42}$$

where we further define

$$z \equiv \frac{R\dot{\phi}}{H}\,, \qquad \frac{z''}{z} \simeq (2+5\epsilon-3\eta)R^2H^2\,, \tag{23.43}$$

with the last approximate equality holding to leading order in the slow-roll approximation.

As previously done for gravitational waves, we quantise the linearised field fluctuations $v_{\vec{k}} \to \hat{v}_{\vec{k}}$ on sub-Hubble scales, $k^2/R^2 \gg H^2$, where the background expansion can be neglected. Thus, we impose

$$\langle v_{\vec{k}_1} v'_{\vec{k}_2}\rangle = \frac{i}{2}\delta^{(3)}\left(\vec{k}_1+\vec{k}_2\right)\,. \tag{23.44}$$

In terms of the field perturbations, this corresponds to

$$\langle Q_{\vec{k}_1} Q_{\vec{k}_2}\rangle = \frac{\mathcal{P}_Q(k_1)}{4\pi k_1^3}(2\pi)^3\delta^{(3)}\left(\vec{k}_1+\vec{k}_2\right)\,, \tag{23.45}$$

where the power spectrum for vacuum field fluctuations on sub-Hubble scales, $k^2/R^2 \gg H^2$, is simply

$$\mathcal{P}_Q(k) = \left(\frac{k}{2\pi R}\right)^2\,, \tag{23.46}$$

yielding the classic result for the vacuum fluctuations for a massless field in de Sitter at Hubble exit, $k = R_*H_*$:

$$\mathcal{P}_Q(k) \simeq \left(\frac{H}{2\pi}\right)^2_*\,. \tag{23.47}$$

In practice there are slow-roll corrections due to the small but finite mass (η) and field evolution (ϵ) [42].

Slow-roll corrections to the field fluctuations are small on sub-Hubble scales, but can become significant as the field and its perturbations evolve over time on super-Hubble scales. This is why it is helpful to work instead with the curvature perturbation, ζ defined in Eq. (23.29), which remains constant on super-Hubble scales for adiabatic density perturbations both during and after inflation [18, 43]. Thus we have an expression for the primordial curvature perturbation on super-Hubble scales produced by single-field slow-roll inflation:

$$\mathcal{P}_\zeta(k) = \left[\left(\frac{H}{\dot{\phi}}\right)^2\mathcal{P}_Q(k)\right]_* \simeq \frac{4\pi}{M_{\rm P}^2}\left[\frac{1}{\epsilon}\left(\frac{H}{2\pi}\right)^2\right]_*\,. \tag{23.48}$$

Comparing this with the primordial gravitational wave power spectrum (Eq. (23.38)) we obtain the tensor-to-scalar ratio

$$r \equiv \frac{\mathcal{P}_{\rm t}}{\mathcal{P}_\zeta} \simeq 16\epsilon_*\,. \tag{23.49}$$

Note that the scalar amplitude is boosted by a factor $1/\epsilon_*$ during slow-roll inflation, because small scalar field fluctuations can lead to relatively large curvature perturbations on hypersurfaces defined with respect to the density if the potential energy is only weakly dependent on the scalar field, as in slow roll. Indeed, the de Sitter limit is singular, since the potential energy becomes independent of the scalar field at first order, $\epsilon \to 0$, and the curvature perturbation on uniform-density hypersurfaces becomes ill-defined.

We note that in single-field inflation the tensor-to-scalar ratio and the tensor tilt (Eq. (23.39)) at the same scale are both determined by the first slow-roll parameter at Hubble exit, ϵ_*, giving rise to an important consistency test for single-field slow-roll inflation:

$$n_{\rm t} \simeq -\frac{r}{8}\,. \tag{23.50}$$

This may be hard to verify if r is small, making any tensor tilt $n_{\rm t}$ difficult to measure. On the other hand, it does offer a way to rule out single-field slow-roll inflation if either r or $n_{\rm t}$ is large.

Given the relatively large scalar power spectrum, it has proved easier to measure the scalar tilt, conventionally defined as $n_{\rm s} - 1$.

Int. J. Mod. Phys. A 2026.41. Downloaded from www.worldscientific.com
by UNIVERSITY OF CALIFORNIA @ BERKELEY on 09/16/26. Re-use and distribution is strictly not permitted, except for Open Access articles.

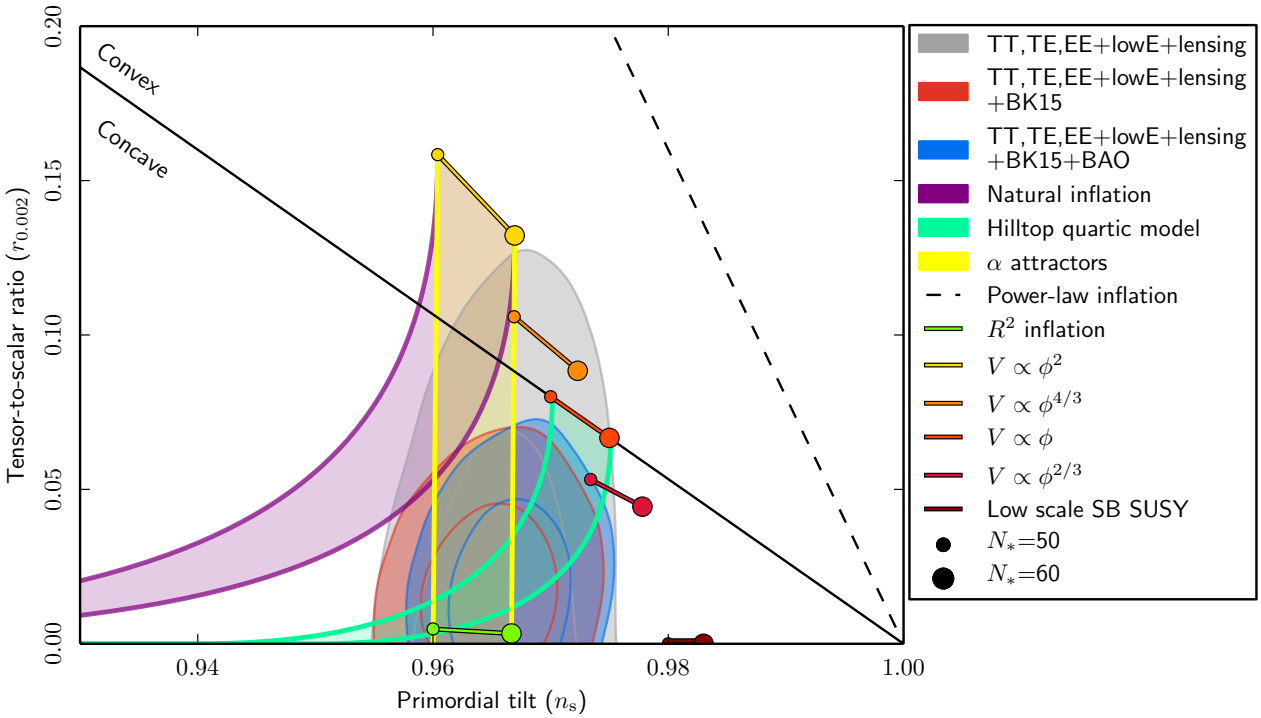

Figure 23.1: The marginalized joint 68 and 95% CL regions for the tilt in the scalar perturbation spectrum, n_s, and the relative magnitude of the tensor perturbations, r, obtained from the *Planck* 2018 and lensing data alone, and their combinations with BICEP2/Keck Array (BK15) and (optionally) BAO data, confronted with the predictions of some of the inflationary models discussed in this review. This figure is taken from Ref. [40].

Slow-roll corrections lead to slow time-dependence of both H_* and ϵ_*, giving a weak scale-dependence of the scalar power spectrum:

$$n_s - 1 \equiv \frac{d\ln \mathcal{P}_\zeta}{d\ln k} \simeq -6\epsilon_* + 2\eta_* \,, \tag{23.51}$$

and a running of this tilt at second-order in slow roll:

$$\frac{dn_s}{d\ln k} \simeq -8\epsilon_*(3\epsilon_* - 2\eta_*) - 2\xi_*^2 \,, \tag{23.52}$$

where the running introduces a new slow-roll parameter at second order:

$$\xi^2 = \frac{M_P^4}{64\pi^2}\frac{V'V'''}{V^2} \,. \tag{23.53}$$

23.3.4 *Observational Bounds*

The observed scale-dependence of the power spectrum makes it necessary to specify the comoving scale, k, at which quantities are constrained and hence the Hubble-exit time, $k = a_* H_*$, when the corresponding theoretical quantities are calculated during inflation. This is usually expressed in terms of the number of e-folds from the end of inflation [44]:

$$N_*(k) \simeq 67 - \ln\left(\frac{k}{a_0 H_0}\right) + \frac{1}{4}\ln\left(\frac{V_*^2}{M_P^4 \rho_{\rm end}}\right) + \frac{1}{12}\ln\left(\frac{\rho_{\rm rh}}{\rho_{\rm end}}\right) - \frac{1}{12}\ln(g_*), \tag{23.54}$$

where H_0^{-1}/a_0 is the present comoving Hubble length. Different models of reheating and thus different reheat temperatures and densities, $\rho_{\rm rh}$ in Eq. (23.54), lead to a range of possible values for N_* corresponding to a fixed physical scale, and hence we have a range of observational predictions for a given inflation model; this is illustrated by allowing a fixed range of values for N_* in Fig. 23.1.

The *Planck* 2018 temperature and polarization data (see Chap. 29, "Cosmic Microwave Background" review) are consistent with a smooth featureless power spectrum over a range of comoving wavenumbers, $0.008\ h^{-1}\ \mathrm{Mpc}^{-1} \le k \le 0.1\ h\ \mathrm{Mpc}^{-1}$. In the absence of running, the *Planck* data measure the spectral index to be [40]

$$n_s = 0.9649 \pm 0.0042 \,, \tag{23.55}$$

corresponding to a deviation from scale-invariance exceeding the 7σ level. Recent results from the Atacama Cosmology Telescope (ACT) [45] on small angular scales in combination with *Planck* data on larger scales, lensing measurements and DESI DR2 data [46] suggest a somewhat higher value, $n_s = 0.975 \pm 0.003$, although this is not yet a full joint analysis. There are also recent results from the South Pole Telescope [47] that are quite consistent with *Planck*. If running of the spectral tilt is included in the model, this is constrained to be [40]

$$\frac{dn_s}{d\ln k} = -0.0045 \pm 0.0067 \tag{23.56}$$

at the 95% CL, assuming no running of the running. The most recent analysis [48] of the BICEP, Keck Array and *Planck* data places an upper bound on the tensor-to-scalar ratio

$$r < 0.036 \,, \tag{23.57}$$

at the 95% CL.

These observational bounds can be converted into bounds on the slow-roll parameters and hence the potential during slow-roll inflation. Setting higher-order slow-roll parameters (beyond second-order in horizon-flow parameters [49]) to zero, the *Planck* collaboration obtain the following 95% CL bounds when lensing and BK15 data are included [40]

$$\epsilon < 0.0044 \,, \tag{23.58}$$

$$\eta = -0.015 \pm 0.006 \,, \tag{23.59}$$

$$\xi^2 = 0.0029^{+0.0073}_{-0.0069} \,, \tag{23.60}$$

which can be used to constrain models, as discussed in the next section.

Figure 23.1, which is taken from Ref. [40], compares observational CMB constraints on the tilt, n_s, in the spectrum of scalar

Int. J. Mod. Phys. A 2026.41. Downloaded from www.worldscientific.com
by UNIVERSITY OF CALIFORNIA @ BERKELEY on 09/16/26. Re-
strictly not permitted, except for Open Access articles.

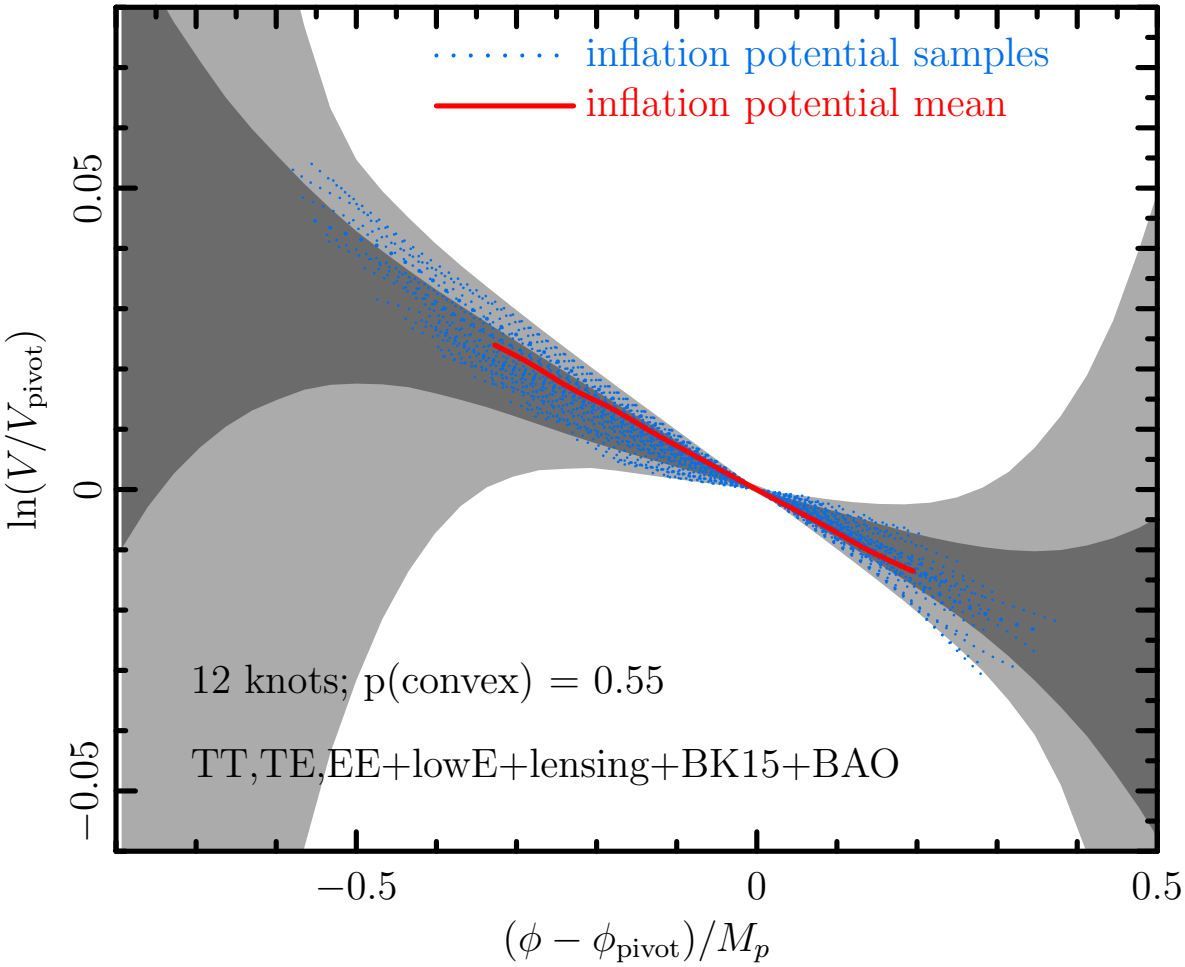

Figure 23.2: The result of reconstructing a single-field inflaton potential using a cubic-spline power-spectrum mode expansion and the full *Planck*, lensing, BK15 and BAO data set. This figure is taken from Refs. [40].

perturbations and the ratio, r, between the magnitudes of tensor and scalar perturbations. Important rôles are played by data from the *Planck* satellite and on lensing, the BICEP2/Keck Array (BK15) and measurements of baryon acoustic oscillations (BAO). The reader is referred to Ref. [40] for technical details. These experimental constraints are compared with the predictions of some of the inflationary models discussed in this review. Generally speaking, models with a concave potential are favored over those with a convex potential, and models with power-law inflation are now excluded, as opposed to models with de Sitter-like (quasi-)exponential expansion.

There is no significant evidence for local features within the range of inflaton field values probed by the data [40]. However, the data may be used to partially reconstruct the effective inflationary potential over a range of inflaton field values, assuming that it is suitably smooth. The result of one such exercise by the *Planck* collaboration [40] in the framework of a generic single-field inflaton potential is shown in Fig. 23.2. This reconstruction assumes a cubic-spline power-spectrum mode expansion and employs the full *Planck*, lensing, BK15 and BAO data set. The reader is again referred to [40] for technical details. We see that the effective inflaton potential is relatively well reconstructed over field values ϕ within ± 0.5 of the chosen pivot value, but the potential is only very weakly constrained for larger values of $|\phi - \phi_{\rm pivot}|$, providing wide scope for inflationary model-builders.

23.4 Models

23.4.1 *Pioneering Models*

The paradigm of the inflationary Universe was proposed in Ref. [6], where it was pointed out that an early period of (near-)exponential expansion, in addition to resolving the horizon and flatness problems of conventional Big-Bang cosmology as discussed above, would also dilute the prior abundance of any unseen heavy, (meta-)stable particles, as exemplified by monopoles in grand unified theories (GUTs; see Chap. 92, "Grand Unified Theories" review). The possibility of a de Sitter phase in the early history of the Universe was also proposed in the non-minimal gravity model of Ref. [5], with the motivation of avoiding an initial singularity. The original proposal in Ref. [6] was that this inflationary expansion took place while the Universe was in a metastable state (a similar suggestion was made in Refs. [50, 51], where in Ref. [50] it was also pointed out that such a mechanism could address the horizon problem) and was terminated by a first-order transition due to tunneling though a potential barrier. However, it was recognized already in Ref. [6] that this 'old inflation' scenario would need modification if the transition to the post-inflationary Universe were to be completed smoothly without generating unacceptable inhomogeneities.

This 'graceful exit' problem was addressed in the 'new inflation' model of Ref. [15] (see also Ref. [16] and footnote [39] of Ref. [6]), which studied models based on an SU(5) GUT with an effective potential of the Coleman-Weinberg type (*i.e.*, dominated by radiative corrections), in which inflation could occur during the roll-down from the local maximum of the potential towards a global minimum. However, it was realized that the Universe would evolve to a different minimum from the Standard Model [52], and it was also recognized that density fluctuations would necessarily be too large [17], since they are related to the GUT coupling strength.

These early models of inflation assumed initial conditions enforced by thermal equilibrium in the early Universe. However,

Int. J. Mod. Phys. A 2026.41. Downloaded from www.worldscientific.com by UNIVERSITY OF CALIFORNIA @ BERKELEY on 09/16/26. Re-use and distribution is strictly not permitted, except for Open Access articles.

this assumption was questionable: indeed, it was not made in the model of Ref. [5], in which a higher-order gravitational curvature term was assumed to arise from quantum corrections, and the assumption of initial thermal equilibrium was jettisoned in the 'chaotic' inflationary model of Ref. [53]. These have been the inspirations for much recent inflationary model building, so we now discuss them in more detail, before reviewing contemporary models.

In this section we will work in natural units where we set the reduced Planck mass to unity, *i.e.*, $8\pi/M_{\rm P}^2 = 1$. All masses are thus relative to the reduced Planck scale.

23.4.2 R^2 *Inflation*

The first-order Einstein-Hilbert action, $(1/2)\int d^4x\sqrt{-g}\mathrm{R}$, where R is the Ricci scalar curvature, is the minimal possible theory consistent with general coordinate invariance. However, it is possible that there might be non-minimal corrections to this action, and the unique second-order possibility is

$$S = \frac{1}{2}\int d^4x\sqrt{-g}\left(\mathrm{R} + \frac{\mathrm{R}^2}{6M^2}\right) . \tag{23.61}$$

It was pointed out in Ref. [5] that an R^2 term could be generated by quantum effects, and that Eq. (23.61) could lead to de Sitter-like expansion of the Universe. Scalar density perturbations in this model were calculated in Ref. [19]. Because the initial phase was (almost) de Sitter, these perturbations were (approximately) scale-invariant, with magnitude $\propto M$. It was also pointed out in Ref. [19] that requiring the scalar density perturbations to lie in the range 10^{-3} to 10^{-5}, consistent with upper limits at that time, would require $M \sim 10^{-3}$ to 10^{-5} in Planck units, and it was further suggested that these perturbations could lead to the observed large-scale structure of the Universe, including the formation of galaxies.

Although the action (23.61) does not contain an explicit scalar field, Ref. [19] reduced the calculation of density perturbations to that of fluctuations in the scalar curvature R, which could be identified (up to a factor) with a scalar field of mass M. The formal equivalence of R^2 gravity (23.61) to a theory of gravity with a massive scalar ϕ had been shown in Ref. [20] (see also Ref. [21]). The effective scalar potential for what we would nowadays call the 'inflaton' [54] takes the form

$$S = \frac{1}{2}\int d^4x\sqrt{-g}\left[\mathrm{R} + (\partial_\mu\phi)^2 - \frac{3}{2}M^2(1-e^{-\sqrt{2/3}\phi})^2\right] \tag{23.62}$$

when the action is written in the Einstein frame, and the potential is shown as the solid black line in Fig. 23.3. Using Eq. (23.48), one finds that the amplitude of the scalar density perturbations in this model is given by

$$\Delta_{\mathcal{R}} = \frac{3M^2}{8\pi^2}\sinh^4\left(\frac{\phi}{\sqrt{6}}\right) , \tag{23.63}$$

The measured magnitude of the density fluctuations in the CMB requires $M \simeq 1.3\times 10^{-5}$ in Planck units (assuming $N_* \simeq 55$), so one of the open questions in this model is why M is so small. Obtaining $N_* \simeq 55$ also requires an initial value of $\phi \simeq 5.5$, *i.e.*, a super-Planckian initial condition, and another issue for this and many other models is how the form of the effective potential is protected and remains valid at such large field values. Using Eq. (23.51) one finds that $n_{\rm s} \simeq 0.965$ for $N_* \simeq 55$ and using (Eq. (23.49)) one finds that $r \simeq 0.0035$. These predictions are consistent with the present data from *Planck* and other experiments, as seen in Fig. 23.1.

23.4.3 *Chaotic Models with Power-Law Potentials*

As has already been mentioned, a key innovation in inflationary model-building was the suggestion to abandon the questionable assumption of a thermal initial state, and consider 'chaotic' initial conditions with very general forms of potential [53]. (Indeed, the R^2 model discussed above can be regarded as a prototype of this approach.) The chaotic approach was first proposed in the context of a simple power-law potential of the form $\mu^{4-\alpha}\phi^\alpha$, and the specific example of $\lambda\phi^4$ was studied in Ref. [53]. Such models make the following predictions for the slow-roll parameters ϵ and η:

$$\epsilon \;=\; \frac{1}{2}\left(\frac{\alpha}{\phi}\right)^2 , \;\; \eta \;=\; \frac{\alpha(\alpha-1)}{\phi^2} , \tag{23.64}$$

leading to the predictions

$$r \;\approx\; \frac{4\alpha}{N_*} , \qquad n_{\rm s} - 1 \;\approx\; -\frac{\alpha+2}{2N_*} , \tag{23.65}$$

which are shown in Fig. 23.1 for some illustrative values of α. We note that the prediction of the original ϕ^4 model lies out of the frame, with values of r that are too large and values of $n_{\rm s}$ that are too small. The ϕ^3 model has similar problems, and would in any case require modification in order to have a well-defined minimum. The simplest possibility is ϕ^2, but this is now also disfavored by the data, at the 95% CL if only the *Planck* data are considered, and more strongly if other data are included, as seen in Fig. 23.1. (For non-minimal models of quadratic inflation that avoid this problem, see, *e.g.*, Ref. [56].) Indeed, as can be seen in Fig. 23.1, all single-field models with a convex potential (*i.e.*, one curving upwards) are disfavored compared to models with a concave potential.

23.4.4 *Hilltop Models*

This preference for a concave potential motivates interest in 'hilltop' models [57], whose starting-point is a potential of the form

$$V(\phi) \;=\; M^4\left[1 - \left(\frac{\phi}{\mu}\right)^p + \ldots\right] , \tag{23.66}$$

where the ... represent extra terms that yield a positive semi-definite potential. To first order in the slow-roll parameters, when $x \equiv \phi/\mu$ is small, one has

$$n_{\rm s} \;\simeq\; 1 - p(p-1)\mu^{-2}\frac{x^{p-2}}{(1-x^p)} - \frac{3}{8}r , \qquad r \;\simeq\; 8p^2\mu^{-2}\frac{x^{2p-2}}{(1-x^p)^2} . \tag{23.67}$$

As seen in Fig. 23.1, a hilltop model with $p = 4$ can be compatible with the *Planck* and other measurements, if $\mu \gg M_{\rm P}$.

23.4.5 *D-Brane Inflation*

Many scenarios for inflation involving extra dimensions have been proposed, *e.g.*, the possibility that observable physics resides on a three-dimensional brane, and that there is an inflationary potential that depends on the distance between our brane and an antibrane, with a potential of the form [58]

$$V(\phi) \;=\; M^4\left[1 - \left(\frac{\mu}{\phi}\right)^p + \ldots\right] . \tag{23.68}$$

In this scenario the effective potential vanishes in the limit $\phi \to \infty$, corresponding to complete separation between our brane and the antibrane. The predictions for $n_{\rm s}$ and r in this model can be obtained from Eq. (23.67) by exchanging $p \leftrightarrow -p$, and are also consistent with the *Planck* and other data.

23.4.6 *Natural Inflation*

Also seen in Fig. 23.1 are the predictions of 'natural inflation' [59], in which one postulates a non-perturbative shift symmetry that suppresses quantum corrections, so that a hierarchically small scale of inflation, $H \ll M_{\rm P}$, is technically natural. In the simplest models, there is a periodic potential of the form

$$V(\phi) \;=\; M^4\left[1 + \cos\left(\frac{\phi}{f}\right)\right] , \tag{23.69}$$

where f is a dimensional parameter reminiscent of an axion decay constant (see the next subsection) [60], which must have a value $> M_{\rm P}$. Natural inflation can yield predictions similar to quadratic inflation (which are no longer favored, as already discussed), but can also yield an effective convex potential. Thus, it may lead to values of r that are acceptably small, but for values of $n_{\rm s}$ that are in tension with the data, as seen in Fig. 23.1.

Int. J. Mod. Phys. A 2026.41. Downloaded from www.worldscientific.com
by UNIVERSITY OF CALIFORNIA @ BERKELEY on 09/16/26. Reproduction strictly not permitted, except for Open Access articles.

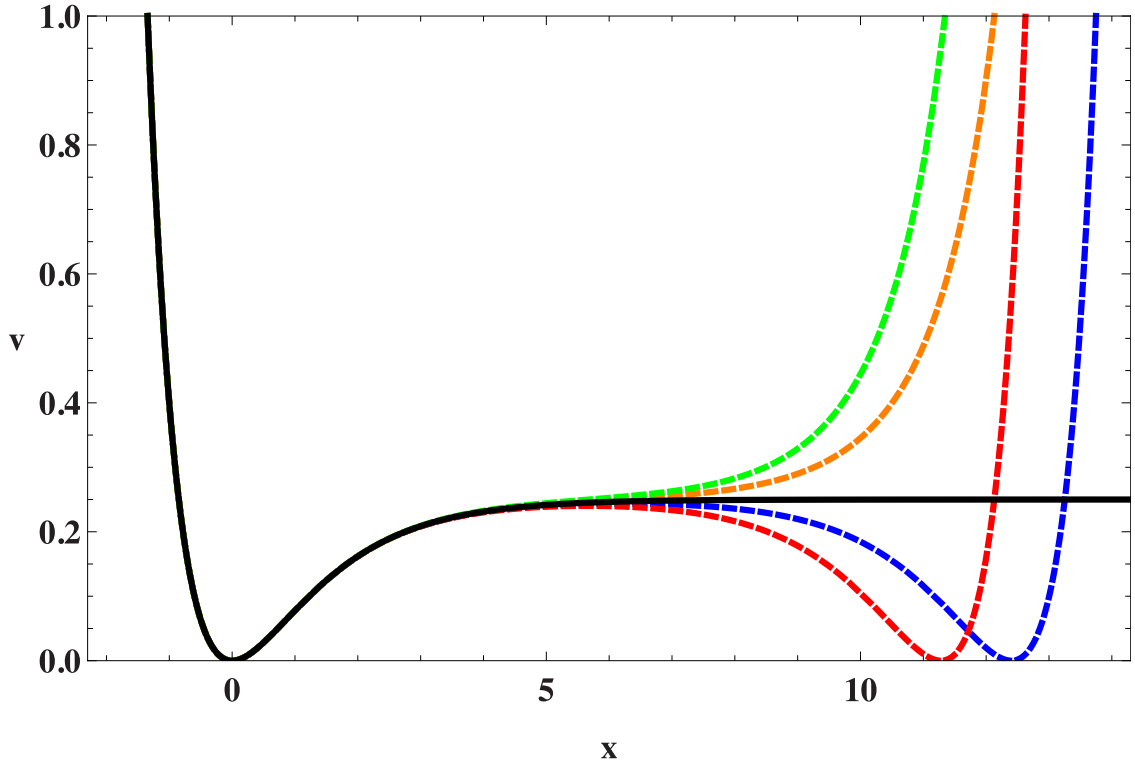

Figure 23.3: Inflationary potential V in the R^2 model (solid black line) compared with its form in various no-scale models discussed in detail in Ref. [55] (dashed coloured lines).

23.4.7 *Axion Monodromy Models*

The effective potentials in stringy models [61,62] motivated by axion monodromy may be of the form

$$V(\phi) \;=\; \mu^{4-\alpha}\phi^{\alpha} + M^4 e^{-C\left(\frac{\phi}{\phi_0}\right)^{p_M}} \cos\left[\gamma + \frac{\phi}{f}\left(\frac{\phi}{\phi_0}\right)^{p_f+1}\right], \tag{23.70}$$

where μ, M, f and ϕ_0 are parameters with the dimension of mass, and $C,\ p,\ p_M,\ p_f$ and γ are dimensionless constants, generalizing the potential [59] in the simplest models of natural inflation. The oscillations in Eq. (23.70) are associated with the axion field, and powers $p_M, p_f \neq 0$ may arise from ϕ-dependent evolutions of string moduli. Since the exponential prefactor in Eq. (23.70) is due to non-perturbative effects that may be strongly suppressed, the oscillations may be unobservably small. Specific string models having ϕ^{α} with $\alpha = 4/3, 1$ or $2/3$ have been constructed in Refs. [61,62], providing some motivation for the low-power models mentioned above.

As seen in Fig. 23.1, the simple axion monodromy models with the power $\alpha = 4/3$ or 1 are no longer compatible with the current CMB data at the 95% CL, while $\alpha = 2/3$ is only marginally compatible at 95% CL. The *Planck* Collaboration has also searched for characteristic effects associated with the second term in Eq. (23.70), such as a possible drift in the modulation amplitude (setting $p_M = C = 0$), and a possible drifting frequency generated by $p_f \neq 0$, without finding any compelling evidence [40].

23.4.8 *Higgs Inflation*

Since the energy scale during inflation is commonly expected to lie between the Planck and TeV scales, it may serve as a useful bridge with contacts both to string theory or some other quantum theory of gravity, on the one side, and particle physics on the other side. However, as the above discussion shows, much of the activity in building models of inflation has been independent of specific connections with these subjects, though some examples of string-motivated models of inflation were mentioned above.

The most economical scenario for inflation might be to use as the inflaton the only established scalar field, namely the Higgs field (see Chap.11, "Status of Higgs boson physics" review). A specific model assuming a non-minimal coupling of the Higgs field h to gravity was constructed in Ref. [63]. Its starting point is the action

$$S \;=\; \int d^4x\sqrt{-g}\left[\frac{M^2+\xi h^2}{2}\mathrm{R} + \frac{1}{2}\partial_\mu h\partial^\mu h - \frac{\lambda}{4}(h^2-v^2)^2\right], \tag{23.71}$$

where v is the Higgs vacuum expectation value. The model requires $\xi \gg 1$, in which case it can be rewritten in the Einstein frame as

$$S \;=\; \int d^4x\sqrt{-g}\left[\frac{1}{2}\mathrm{R} + \frac{1}{2}\partial_\mu\chi\partial^\mu\chi - U(\chi)\right], \tag{23.72}$$

where the effective potential for the canonically-normalized inflaton field χ has the form

$$U(\chi) \;=\; \frac{\lambda}{4\xi^2}\left[1+\exp\left(-\frac{2\chi}{\sqrt{6}M_{\mathrm{P}}}\right)\right]^{-2}, \tag{23.73}$$

which is similar to the effective potential of the R^2 model at large field values. As such, the model inflates successfully if $\xi \simeq 5\times 10^4\ m_h/(\sqrt{2}v)$, where m_h is the Higgs mass, with predictions for n_{s} and r that are indistinguishable from the predictions of the R^2 model shown in Fig. 23.1. [2]

This model is appealing because of its connection to particle physics, but must confront several issues. One is to understand the value of ξ, and another is the possibility of unitarity violation. However, a more fundamental issue is whether the effective quartic Higgs coupling is positive at the scale of the Higgs field during inflation. Extrapolations of the effective potential in the Standard Model using the measured values of the masses of the Higgs boson and the top quark indicate that probably $\lambda < 0$ at this scale [64],

[2] Although Higgs and R^2 inflation share the same inflaton potential, they may reheat the Universe through different mechanisms, resulting in different reheating temperatures and hence different values of N_* that would lead to slightly different predictions; see the discussion around Eq. (23.54).

Int. J. Mod. Phys. A 2026.41. Downloaded from www.worldscientific.com
by UNIVERSITY OF CALIFORNIA @ BERKELEY on 09/16/26. Re-use and distribution is strictly not permitted, except for Open Access articles.

though there are still significant uncertainties associated with the appropriate input value of the top mass and the extrapolation to high renormalization scales.

23.4.9 *Supersymmetric Models of Inflation*

Supersymmetry [65] is widely considered to be a well-motivated possible extension of the Standard Model that might become apparent at the TeV scale. It is therefore natural to consider supersymmetric models of inflation. These were originally proposed because of the problems of the new inflationary theory [15, 16] based on the one-loop (Coleman-Weinberg) potential for breaking SU(5). Several of these problems are related to the magnitude of the effective potential parameters: in any model of inflation based on an elementary scalar field, some parameter in the effective potential must be small in natural units, *e.g.*, the quartic coupling λ in a chaotic model with a quartic potential, or the mass parameter μ in a model of chaotic quadratic inflation. These parameters are renormalized multiplicatively in a supersymmetric theory, so that the quantum corrections to small values would be under control. Hence, it was suggested that inflation cries out for supersymmetry [66], though non-supersymmetric resolutions of the problems of Coleman-Weinberg inflation are also possible: see, *e.g.*, Ref. [67].

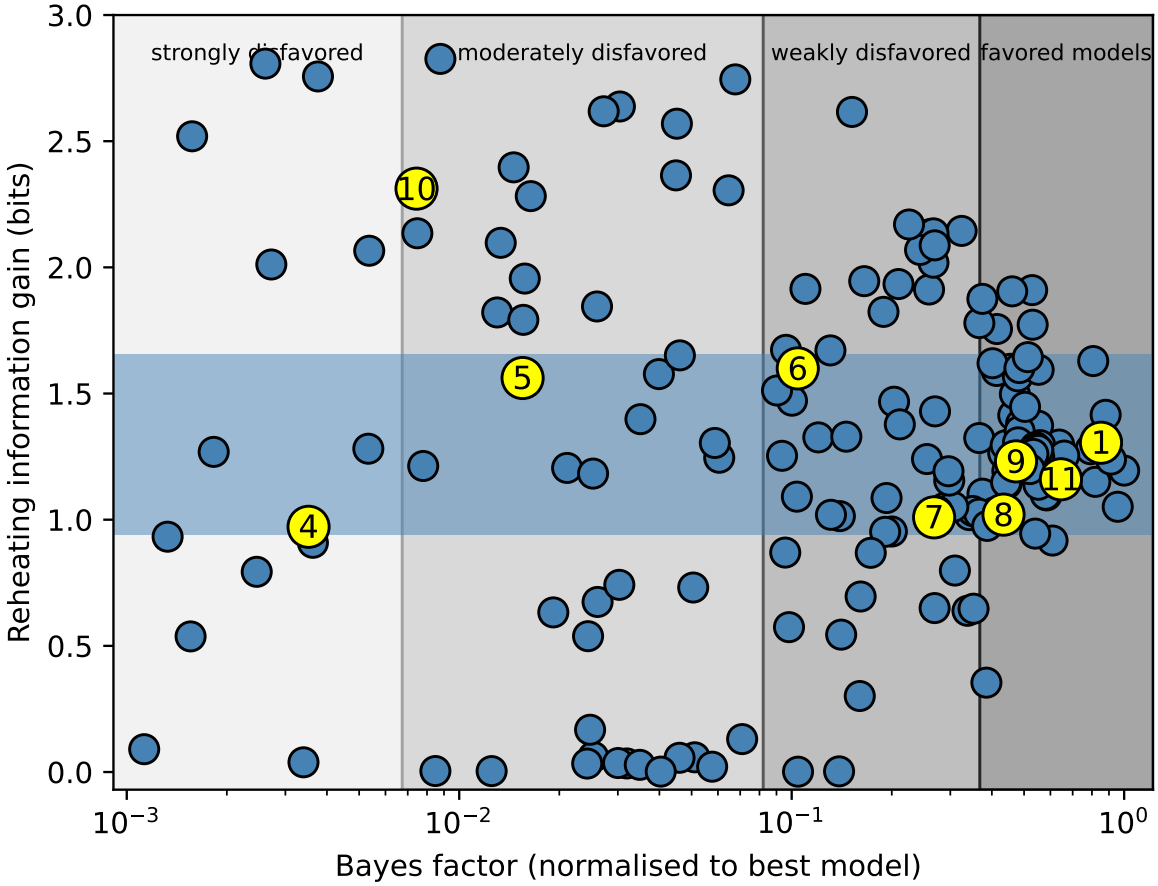

Figure 23.4: Bayes factors calculated in Refs. [68,69] for 287 single-field inflationary models using *Planck* 2018 data [70] in combination with other CMB and BAO measurements. Those highlighted in yellow are featured in this review, according to the numbers listed in the text (the models labeled "2" and "3" lie outside the plot frame because of their low Bayesian evidence). On the vertical axis, the information gain on the reheating parameter, *i.e.* the k-independent terms in the right-hand side of Eq. (23.54), is displayed in units of bits for the Kullback-Leibler divergence between its prior and posterior distributions [68].

In the Standard Model there is only one scalar field that could be a candidate for the inflaton, namely the Higgs field discussed above, but even the minimal supersymmetric extension of the Standard Model (MSSM) contains many scalar fields. However, none of these is a promising candidate for the inflaton. The minimal extension of the MSSM that may contain a suitable candidate is the supersymmetric version of the minimal seesaw model of neutrino masses, which contains the three supersymmetric partners of the heavy singlet (right-handed) neutrinos. One of these singlet sneutrinos $\tilde{\nu}$ could be the inflaton [71]: it would have a quadratic potential, the mass coefficient required would be $\sim 10^{13}$ GeV, very much in the expected ball-park for singlet (right-handed) neutrino masses, and sneutrino inflaton decays could also give rise to the cosmological baryon asymmetry via leptogenesis. However, as seen in Fig. 23.1 and already discussed, a purely quadratic inflationary potential is no longer favored by the data. This difficulty could in principle be resolved in models with multiple sneutrinos [72], or by postulating a trilinear sneutrino coupling and hence a superpotential of Wess-Zumino type [73], which can yield successful inflation with predictions intermediate between those of natural inflation and hilltop inflation in Fig. 23.1. Finally, we note that it is also possible to obtain inflation via supersymmetry breaking, as in the model of Ref. [74], whose predictions are illustrated in Fig. 23.1.

23.4.10 *Supergravity Models*

Any model of early-Universe cosmology, and specifically inflation, must necessarily incorporate gravity. In the context of supersymmetry this requires an embedding in some supergravity theory [75, 76]. An $\mathcal{N} = 1$ supergravity theory is specified by

Int. J. Mod. Phys. A 2026.41. Downloaded from www.worldscientific.com by UNIVERSITY OF CALIFORNIA @ BERKELEY on 09/16/26. Re-[redacted] strictly not permitted, except for Open Access articles.

three functions: a Hermitian function of the matter scalar fields ϕ^i, called the Kähler potential K, that describes its geometry, a holomorphic function of the superfields, called the superpotential W, which describes their interactions, and another holomorphic function $f_{\alpha\beta}$, which describes their couplings to gauge fields V_α [77].

The simplest possibility is that the Kähler metric is flat:

$$K = \phi^i \phi_i^* \,, \tag{23.74}$$

where the sum is over all scalar fields in the theory, and the simplest inflationary model in minimal supergravity has the superpotential [78]

$$W = m^2(1-\phi)^2 \,, \tag{23.75}$$

where ϕ is the inflaton. However, this model predicts a tilted scalar perturbation spectrum, $n_\mathrm{s} = 0.933$, which is now in serious disagreement with the data from *Planck* and other experiments shown in Fig. 23.1.

Moreover, there is a general problem that arises in any supergravity theory coupled to matter, namely that, since its effective scalar potential contains a factor of e^K, scalars typically receive squared masses $\propto H^2 \sim V$, where H is the Hubble parameter [79], an issue called the 'η problem'. The theory given by Eq. (23.75) avoids this η problem, but a generic supergravity inflationary model encounters this problem of a large inflaton mass. Moreover, there are additional challenges for supergravity inflation associated with the spontaneous breaking of local supersymmetry [80–82].

Various approaches to the η problem in supergravity have been proposed, including the possibility of a shift symmetry [83], and one possibility that has attracted renewed attention recently is no-scale supergravity [84, 85]. This is a form of supergravity with a Kähler potential that can be written in the form [86]

$$K \;=\; -3\ln\left(T + T^* - \frac{\sum_i |\phi^i|^2}{3}\right) \,, \tag{23.76}$$

which has the special property that it naturally has a flat potential, at the classical level and before specifying a non-trivial superpotential. As such, no-scale supergravity is well-suited for constructing models of inflation. Adding to its attraction is the feature that compactifications of string theory to supersymmetric four-dimensional models yield effective supergravity theories of the no-scale type [87]. There are many examples of superpotentials that yield effective inflationary potentials for either the T field (which is akin to a modulus field in some string compactification) or a ϕ field (generically representing matter) that are of the same form as the effective potential of the R^2 model Eq. (23.62) when the magnitude of the inflaton field is far above the Planck scale, as required to obtain sufficiently many e-folds of inflation, N_* [88, 89]. This framework also offers the possibility of using a suitable superpotential to construct models with effective potentials that are similar, but not identical, to the R^2 model, as shown by the dashed coloured lines in Fig. 23.3.

23.4.11 *Other Exponential Potential Models*

This framework also offers the possibility [88] of constructing models in which the asymptotic constant value of the potential at large inflaton field values is approached via a different exponentially-suppressed term:

$$V(\phi) \;=\; A\left[1 - \delta e^{-B\phi} + \mathcal{O}(e^{-2B\phi})\right] \,, \tag{23.77}$$

where the magnitude of the scalar density perturbations fixes A, but δ and B are regarded as free parameters. In the case of R^2 inflation, in Eq. (23.62), $\delta = 2$ and $B = \sqrt{2/3}$. In a general model such as Eq. (23.77), one finds at leading order in the small quantity $e^{-B\phi}$ that

$$\begin{aligned} n_\mathrm{s} &= 1 - 2B^2\delta e^{-B\phi} \,, \\ r &= 8B^2\delta^2 e^{-2B\phi} \,, \\ N_* &= \frac{1}{B^2\delta} e^{+B\phi} \,. \end{aligned} \tag{23.78}$$

yielding the relations

$$n_\mathrm{s} \;=\; 1 - \frac{2}{N_*} \,, \quad r \;=\; \frac{8}{B^2 N_*^2} \,. \tag{23.79}$$

These relations correspond to the class of models labeled as 'α attractors' [90] in Fig. 23.1. The spectral index in such models is determined by N_*, the number of e-folds Eq. (23.16) when modes exited the Hubble scale before the end of inflation. For example, *Planck* constraints Eq. (23.55) are consistent with $51 < N_* < 65$, placing bounds on the reheating temperature through Eq. (23.54). If the shift of n_s towards higher values suggested by the combination with recent ACT data [45] were to be confirmed, requiring values of $N_* > 60$ at 2σ, the simplest realisations of α-attractor models with conventional reheating would be ruled out [91].

Meanwhile CMB bounds on the tensor-to-scalar ratio translate into an upper bound on the parameter $\alpha = 2/3B^2$, which determines the curvature of the Kähler manifold in supergravity models [92]. There are generalizations of the simplest no-scale model (23.76) with prefactors before the logarithmic factor that are 1 or 2, leading to larger values of $B = \sqrt{2}$ or 1, respectively, and hence smaller values of r than in the R^2 model. CMB constraints on the scalar spectral index can also place a lower bound on the magnitude of α [93], due to the implicit dependence of N_* in Eq. (23.79) upon α [94].

23.5 Model Comparison

Given a particular inflationary model, one can obtain constraints on the model parameters, informed by the likelihood, corresponding to the probability of the data given a particular choice of parameters (see Sec. 40, "Statistics" review). In the light of the detailed constraints on the statistical distribution of primordial perturbations now inferred from high-precision observations of the CMB, it is also possible to make quantitative comparison of the statistical evidence for or against different inflationary models. This can be done either by comparing the logarithm of the maximum likelihood that can be obtained for the data using each model, *i.e.*, the minimum χ^2 (with some correction for the number of free parameters in each model), or by a Bayesian model comparison [95] (see also Sec. 40.3.4 in "Statistics" review).

In such a Bayesian model comparison one computes [4, 8, 9] the evidence, $\mathcal{E}(\mathcal{D}|\mathcal{M}_A)$ for a model, $\mathcal{M}_A$, given the data $\mathcal{D}$. This corresponds to the likelihood, $\mathcal{L}(\theta_{Aj}) = p(\mathcal{D}|\theta_{Aj}, \mathcal{M}_A)$, integrated over the assumed prior distribution, $\pi(\theta_{Aj}|\mathcal{M}_A)$, for all the model parameters θ_{Aj}:

$$\mathcal{E}(\mathcal{D}|\mathcal{M}_A) = \int \mathcal{L}(\theta_{Aj})\pi(\theta_{Aj}|\mathcal{M}_A) d\theta_{Aj} \,. \tag{23.80}$$

The posterior probability of the model given the data follows from Bayes' theorem

$$p(\mathcal{M}_A|\mathcal{D}) = \frac{\mathcal{E}(\mathcal{D}|\mathcal{M}_A)\pi(\mathcal{M}_A)}{p(\mathcal{D})} \,, \tag{23.81}$$

where the prior probability of the model is given by $\pi(\mathcal{M}_A)$. Assuming that all models are equally likely a priori, $\pi(\mathcal{M}_A) = \pi(\mathcal{M}_B)$, the relative probability of model A relative to a reference model, in the light of the data, is thus given by the Bayes factor

$$B_{A,\mathrm{ref}} = \frac{\mathcal{E}(\mathcal{D}|\mathcal{M}_A)}{\mathcal{E}(\mathcal{D}|\mathcal{M}_\mathrm{ref})} \,. \tag{23.82}$$

Computation of the multi-dimensional integral (Eq. (23.80)) is a challenging numerical task. Even using an efficient sampling algorithm requires hundreds of thousands of likelihood computations for each model, though slow-roll approximations can be used to rapidly calculate the primordial power spectrum using the APSIC numerical library [96] for a large number of single-field, slow-roll inflation models.

The change in χ^2 for selected slow-roll models relative to the Starobinsky R^2 inflationary model, used as a reference, is given in Table 23.1 (values taken from [69]). Table 23.1 also shows the Bayesian evidence as displayed in Fig. 23.4 for all single-field models (see Refs [4, 8, 69] for more complete descriptions of the

Int. J. Mod. Phys. A 2026.41. Downloaded from www.worldscientific.com by UNIVERSITY OF CALIFORNIA @ BERKELEY on 09/16/26. Re-use and distribution is strictly not permitted, except for Open Access articles.

models and their priors). The Jeffrey's scale distinguishes favored, weakly disfavored, moderately disfavored and strongly disfavored models, based on their Bayesian evidence. Disfavored models are those that either produce too large tensor modes, or scalar fluctuations with a spectral tilt that differs from the value preferred by the data, or that require an extreme fine tuning of their parameters. We note that although α-attractor models can provide a good fit to the data, they are slightly disfavored relative to the Starobinsky model due to their larger prior volume. There is now strong evidence ($|\ln B_{A,\mathrm{ref}}| > 5$) against large-field models such as chaotic inflation with a quadratic or a quartic potential. Indeed, over 40% of the slow-roll inflation models considered in Ref. [4, 8, 9, 69] are strongly disfavored by the *Planck* data.

Table 23.1: Observational evidence for and against selected inflation models: $\Delta\chi^2$ and the Bayes factors are calculated relative to the Starobinsky R^2 inflationary model, which is treated as a reference. Results taken from Ref. [69].

Label in Fig. 23.4	Model	$\Delta\chi^2$	$\ln B_{A,\mathrm{ref}}$
1	R^2 inflation	0	0
2	Power-law potential ϕ^2	+20.76	−7.36
3	Power-law potential ϕ^4	+20.81	−7.34
4	Power-law potential $\phi^{2/3}$	+10.82	−5.49
5	Power-law potential ϕ^p	−0.579	−4.01
6	Hilltop potential $1-\phi^2$	−1.30	−2.10
7	Hilltop potential $1-\phi^4$	−1.27	−1.16
8	Hilltop potential $1-\phi^p$	−1.30	−0.67
9	Brane inflation	−1.25	−0.59
10	Natural inflation	+0.55	−4.74
11	α attractor	−1.26	−0.28

Models discussed in this review are highlighted in yellow in Fig. 23.4, and numbered as follows: (1) R^2 inflation (Sec. 23.4.2) and models with similar predictions, such as Higgs inflation (Sec. 23.4.8) and no-scale supergravity inflation (Sec. 23.4.10); chaotic inflation models (2) with a ϕ^2 potential; (3) with a ϕ^4 potential; (4) with a $\phi^{2/3}$ potential, and (5) with a ϕ^p potential marginalising over $p \in [0.2, 6]$ (Sec. 23.4.3); hilltop inflation models (6) with $p = 2$; (7) with $p = 4$ and (8) marginalising over p (Sec. 23.4.4); (9) brane inflation Sec. 23.4.5); (10) natural inflation (Sec. 23.4.6); and (11) exponential potential models such as α-attractors (Sec. 23.4.11).

In Fig. 23.4, the information gain on reheating is also displayed. It corresponds to the Kullback-Leibler divergence (in units of bits) between the prior and posterior distributions of the so-called reheating parameter, formed by the right-hand side of Eq. (23.54). With recent CMB measurements the best inflationary models have crossed the one-bit threshold [68, 97], which opens up the possibility to constrain the physical processes at play during reheating. This is what is discussed in the next Section.

23.6 Constraints on Reheating

One connection between inflation and particle physics is provided by inflaton decay, whose products are expected to have thermalized subsequently. As seen in Eq. (23.54), the number of e-folds required during inflation depends on details of this reheating process, including the matter density upon reheating, denoted by ρ_{th}, which depends in turn on the inflaton decay rate Γ_ϕ. We see in Fig. 23.1 that, within any specific inflationary model, both n_{s} and r are sensitive to the value of N_*. In particular, the uncertainty in the experimental measurement of n_{s} is comparable to the variation in many model predictions for $N_* \in [50, 60]$. This implies that the data start to constrain scenarios for inflaton decay in many models. For example, it is clear from Fig. 23.1 that $N_* = 60$ would be preferred over $N_* = 50$ in a chaotic inflationary model with a quadratic potential.

As a specific example, let us consider α-attractor models that predict small values of r. As seen in Fig. 23.1, within these models the combination of *Planck*, BICEP2/Keck Array and BAO data would require a limited range of n_{s}, corresponding to a limited range of N_*, as seen by comparing the left and right vertical axes in Fig. 23.5:

$$N_* \gtrsim 52 \quad (68\%\ \mathrm{CL}), \quad N_* \gtrsim 44 \quad (95\%\ \mathrm{CL})\,. \tag{23.83}$$

Within any specific model for inflaton decay, these bounds can be translated into constraints on the effective decay coupling. For example, if one postulates a two-body inflaton decay (Eq. (23.21)), the bounds (Eq. (23.83)) can be translated into bounds on $y^2 \equiv 8\pi\Gamma/m$. This is illustrated in Fig. 23.5 [92], where any value of $N_{0.05}$ (the number of e-folds for a scale 0.05 Mpc^{-1}, on the left vertical axis), corresponding to the scalar tilt n_{s} shown on the right vertical axis, when projected onto the diagonal line representing one of the three illustrated choices of α-attractor models, corresponds to a specific value of y (lower horizontal axis) and T_{reh} (upper horizontal axis). For example, for $\alpha = 1$ one has

$$y \gtrsim 10^{-10} \quad (68\%\ \mathrm{CL}), \quad y \gtrsim 10^{-17} \quad (95\%\ \mathrm{CL})\,. \tag{23.84}$$

These bounds are not very constraining, but they can be expected to improve significantly in the coming years and thereby provide significant information on the connections between inflation and particle physics.

23.7 Beyond Single-Field Slow-Roll Inflation

There are numerous possible scenarios beyond the simplest single-field models of slow-roll inflation. These include models with features in the potential leading to deviations from slow roll, as well as theories in which non-canonical fields are considered, such as k-inflation [98] or DBI inflation [99], and multiple-field models, such as the curvaton scenario [100–102]. As well as altering the single-field slow-roll predictions for the primordial curvature power spectrum (Eq. (23.48)) and the tensor-scalar ratio (Eq. (23.49)), they may introduce new quantities that vanish in single-field slow-roll models, such as isocurvature matter perturbations, corresponding to entropy fluctuations in the photon-to-matter ratio, at first order:

$$S_{\mathrm{m}} = \frac{\delta n_{\mathrm{m}}}{n_{\mathrm{m}}} - \frac{\delta n_\gamma}{n_\gamma} = \frac{\delta\rho_{\mathrm{m}}}{\rho_{\mathrm{m}}} - \frac{3}{4}\frac{\delta\rho_\gamma}{\rho_\gamma}\,. \tag{23.85}$$

Another possibility is non-Gaussianity in the distribution of the primordial curvature perturbation (see Chap. 29, "Cosmic Microwave Background" review), encoded in higher-order correlators such as the primordial bispectrum [103]

$$\langle\zeta(\mathbf{k})\zeta(\mathbf{k}')\zeta(\mathbf{k}'')\rangle \equiv (2\pi)^3\delta(\mathbf{k}+\mathbf{k}'+\mathbf{k}'')B_\zeta(k,k',k'')\,, \tag{23.86}$$

which is often expressed in terms of a dimensionless non-linearity parameter

$$f_{\mathrm{NL}} \propto B_\zeta(k,k',k'')/P_\zeta(k)P_\zeta(k').$$

The three-point function (Eq. (23.86)) can be thought of as defined on a triangle whose sides are $\mathbf{k}, \mathbf{k}', \mathbf{k}''$, of which only two are independent, since they sum to zero. Further assuming statistical isotropy ensures that the bispectrum depends only on the magnitudes of the three vectors, k, k' and k''. The search for f_{NL} and other non-Gaussian effects was a prime objective of the *Planck* data analysis [104, 105].

23.7.1 *Enhanced perturbations on small scales*

Although the observed primordial power spectrum on CMB scales is constrained to be almost scale invariant, consistent with the simplest slow-roll inflation models, the form of the power spectrum is largely unconstrained on much smaller scales, corresponding to scales that would have left the horizon closer to the end of inflation. Although free-streaming and other damping of perturbations in the primordial plasma are expected to have washed out small-scale fluctuations in the matter sector [106], gravitational relics such as primordial black holes [107, 108] or induced gravitational waves [109–112] produced by sufficiently large primordial density perturbations could have survived and might be detectable in the present day. Rapid growth of the power spectrum on small scales requires violation of slow roll in single-field

Int. J. Mod. Phys. A 2026.41. Downloaded from www.worldscientific.com by UNIVERSITY OF CALIFORNIA @ BERKELEY on 09/16/26. Re-[redacted]strictly not permitted, except for Open Access articles.

models [113]. This could arise from features in the scalar field potential, such as an inflection point [114], leading to a transient phase of ultra-slow-roll evolution [115, 116] which can give a k^4-rise in the scalar power spectrum on small scales [117, 118].

The LIGO-Virgo-KAGRA collaboration has placed an upper limit on such a stochastic gravitational wave background (SGWB), conventionally expressed in terms of the effective density of gravitational waves per logarithmic frequency interval, of $\Omega_{\rm GW} \leq 5.8 \times 10^{-9}$ for a scale-invariant spectrum in the frequency range $20 - 77$ Hz [119]. On the other hand, pulsar timing arrays have found growing evidence for a low-frequency SGWB at nano-Hertz frequencies [120–123]. While this could be associated with an astrophysical background due to supermassive black hole binary systems, the NANOGrav collaboration report that a cosmological background provides a better fit to their 15-year dataset [124]. This could be generated by large primordial density fluctuations on the corresponding comoving scales, $k \sim 10^6$ Mpc^{-1}, but these are constrained by the production of primordial black holes of approximately solar mass [125] and possible one-loop or higher-order corrections to the primordial power spectrum on CMB scales.

23.7.2 *Effective Field Theory of Inflation*

Since slow-roll inflation is a phase of accelerated expansion with an almost constant Hubble parameter, one may think of inflation in terms of an effective theory where the de Sitter spacetime symmetry is spontaneously broken down to RW symmetry by the time-evolution of the Hubble rate, $\dot{H} \neq 0$. There is then a Goldstone boson, π, associated with the spontaneous breaking of time-translation invariance, which can be used to study model-independent properties of inflation. The Goldstone boson describes a spacetime-dependent shift of the time coordinate, corresponding to an adiabatic perturbation of the matter fields:

$$\delta\phi_i(t, \vec{x}) = \phi_i(t + \pi(t, \vec{x})) - \phi_i(t)\,. \tag{23.87}$$

Thus adiabatic field fluctuations can be absorbed into the spatial metric perturbation, $\mathcal{R}$ in Eq. (23.28) at first order, in the comoving gauge:

$$\mathcal{R} = -H\pi\,, \tag{23.88}$$

where we define π on spatially-flat hypersurfaces. In terms of inflaton field fluctuations, we can identify $\pi \equiv \delta\phi/\dot{\phi}$, but in principle this analysis is not restricted to inflation driven by scalar fields.

The low-energy effective action for π can be obtained by writing down the most general Lorentz-invariant action and expanding in terms of π. The second-order effective action for the free-field wave modes, π_k, to leading order in slow roll, is then

$$S_\pi^{(2)} = -\int d^4x\sqrt{-g}\frac{M_{\rm P}^2\dot{H}}{c_{\rm s}^2}\left[\dot{\pi}_k^2 - \frac{c_{\rm s}^2}{R^2}(\nabla\pi)^2\right]\,, \tag{23.89}$$

where ϵ_H is the Hubble slow-roll parameter (Eq. (23.11)). We identify $c_{\rm s}^2$ with an effective sound speed, generalising canonical slow-roll inflation, which is recovered in the limit $c_{\rm s}^2 \to 1$.

The scalar power spectrum on super-Hubble scales (Eq. (23.48)) is enhanced for a reduced sound speed, leading to a reduced tensor-scalar ratio (Eq. (23.49))

$$\mathcal{P}_\zeta(k) \simeq \frac{4\pi}{M_{\rm P}^2}\frac{1}{c_{\rm s}^2\epsilon}\left(\frac{H}{2\pi}\right)_*^2\,, \qquad r \simeq 16(c_{\rm s}^2\epsilon)_*\,. \tag{23.90}$$

At third perturbative order and to lowest order in derivatives, one obtains [126]

$$S_\pi^{(3)} = \int d^4x\sqrt{-g}\frac{M_{\rm P}^2(1-c_{\rm s}^2)\dot{H}}{c_{\rm s}^2}\left[\frac{\dot{\pi}(\nabla\pi)^2}{R^2} - \left(1 + \frac{2}{3}\frac{\tilde{c}_3}{c_{\rm s}^2}\right)\dot{\pi}^3\right]\,. \tag{23.91}$$

Note that this expression vanishes for canonical fields with $c_{\rm s}^2 = 1$. For $c_{\rm s}^2 \neq 1$ the cubic action is determined by the sound speed and an additional parameter $\tilde{c}_3$. Both terms in the cubic action give rise to primordial bispectra that are well approximated by equilateral bispectra. However, the shapes are not identical, so one can find a linear combination for which the equilateral bispectra of each term cancel, giving rise to a distinctive orthogonal-type bispectrum [126].

Analysis based on *Planck* 2018 temperature and polarization data has placed bounds on several bispectrum shapes including equilateral and orthogonal shapes [105]:

$$f_{\rm NL}^{\rm equil} = -26 \pm 47\,, \qquad f_{\rm NL}^{\rm orthog} = -38 \pm 24 \quad (68\%\ {\rm CL})\,. \tag{23.92}$$

For the simplest case of a constant sound speed, and marginalising over $\tilde{c}_3$, this provides a bound on the inflaton sound speed [105]

$$c_{\rm s} \geq 0.021 \quad (95\%\ {\rm CL})\,. \tag{23.93}$$

For a specific model such as DBI inflation [99], corresponding to $\tilde{c}_3 = 3(1 - c_{\rm s}^2)/2$, one obtains a tighter bound [105]:

$$c_{\rm s}^{\rm DBI} \geq 0.086 \quad (95\%\ {\rm CL})\,. \tag{23.94}$$

The *Planck* team analysed a wide range of non-Gaussian templates from different inflation models, including tests for deviations from an initial Bunch-Davies vacuum state, direction-dependent non-Gaussianity, and feature models with oscillatory bispectra [105]. No individual feature or resonance is above the 3σ significance level after accounting for the look-elsewhere effect. These results are consistent with the simplest canonical, slow-roll inflation models, but do not rule out most alternative models; rather, bounds on primordial non-Gaussianity place important constraints on the parameter space for non-canonical models.

23.7.3 *Multi-Field Fluctuations*

There is a very large literature on two- and multi-field models of inflation, most of which lies beyond the scope of this review [127, 128]. However, two important general topics merit being mentioned here, namely residual isocurvature perturbations and the possibility of non-Gaussian effects in the primordial perturbations.

One might expect that other scalar fields besides the inflaton might have non-negligible values that evolve and fluctuate in parallel with the inflaton, without necessarily making the dominant contribution to the energy density during the inflationary epoch. However, the energy density in such a field might persist beyond the end of inflation before decaying, at which point it might come to dominate (or at least make a non-negligible contribution to) the total energy density. In such a case, its fluctuations could end up generating the density perturbations detected in the CMB. This could occur due to a late-decaying scalar field [100–102] or a field fluctuation that modulates the end of inflation [129] or the inflaton decay [130].

23.7.3.1 *Isocurvature Perturbations*

Primordial perturbations arising in single-field slow-roll inflation are necessarily adiabatic, *i.e.*, they affect the overall density without changing the ratios of different contributions, such as the photon-matter ratio, $\delta(n_\gamma/n_{\rm m})/(n_\gamma/n_{\rm m})$. This is because inflaton perturbations represent a local shift of the time, as described in section Sec. 23.7.2:

$$\pi = \frac{\delta n_\gamma}{\dot{n}_\gamma} = \frac{\delta n_{\rm m}}{\dot{n}_{\rm m}}\,. \tag{23.95}$$

However, any light scalar field (*i.e.*, one with effective mass less than the Hubble scale) acquires a spectrum of nearly scale-invariant perturbations during inflation. Fluctuations orthogonal to the inflaton in field space are decoupled from the inflaton at Hubble exit, but can affect the subsequent evolution of the density perturbation. In particular, they can give rise to local variations in the equation of state (non-adabatic pressure perturbations) that can alter the primordial curvature perturbation ζ on super-Hubble scales. Since these fluctuations are statistically independent of the inflaton perturbations at leading order in slow roll [128], non-adiabatic field fluctuations can only increase the scalar power spectrum with respect to adiabatic perturbations at Hubble exit, while leaving the tensor modes unaffected at first perturbative order. Thus, the single-field result for the tensor-scalar ratio (Eq. (23.49)) becomes an inequality [131]

$$r \leq 16\epsilon_*\,. \tag{23.96}$$

Int. J. Mod. Phys. A 2026.41. Downloaded from www.worldscientific.com
by UNIVERSITY OF CALIFORNIA @ BERKELEY on 09/16/26. Re-use and distribution is strictly not permitted, except for Open Access articles.

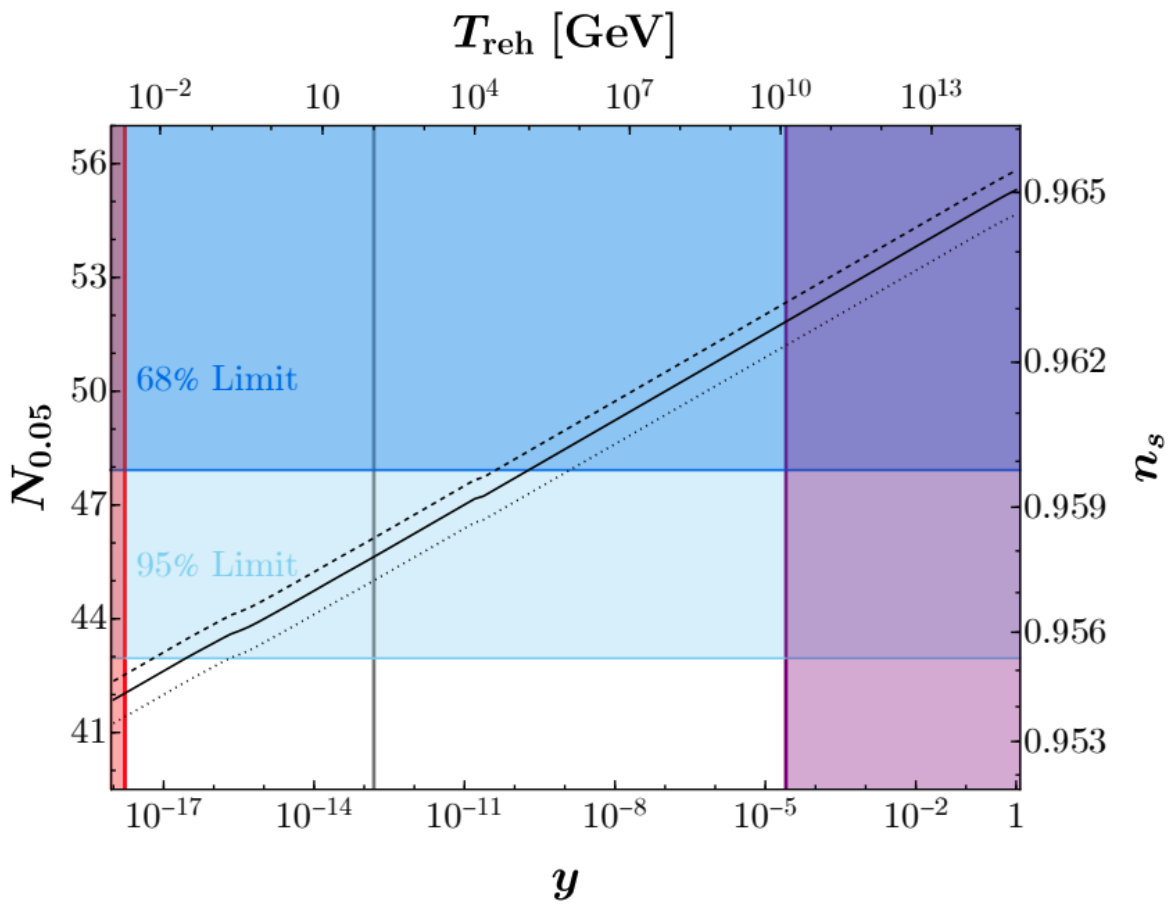

Figure 23.5: Illustration of the impact of the BICEP/Keck [48] and other constraints on the inflaton decay coupling, y, and the number of e-folds at a scale 0.05 Mpc^{-1}, $N_{0.05}$, in α-attractor models of inflation. The horizontal blue lines are 68% and 95% C.L. lower limits on $n_{\rm s}$. The left and right axes show the relation between $N_{0.05}$ and $n_{\rm s}$ and the top and bottom scales show the relation between the inflaton coupling, y, and the reheating temperature, $T_{\rm reh}$. The diagonal dashed, solid and dotted black lines illustrate the correlations between these quantities for α-attractor models with $\alpha = 0.1$, 1, and 5. We also include the lower limit on y from Big-Bang nucleosynthesis (red line), the constraint that $T_{\rm reh}$ be no smaller than the electroweak scale (gray line), and a constraint from gravitino production (purple line) for $\alpha = 1$, which strengthens for smaller α. Plot taken from Ref. [92].

Hence, an observational upper bound on the tensor-to-scalar ratio does not bound the slow-roll parameter ϵ in multi-field models.

If all the scalar fields present during inflation eventually decay completely into fully thermalized radiation, these field fluctuations are converted fully into adiabatic perturbations in the primordial plasma [132]. On the other hand, non-adiabatic field fluctuations can also leave behind primordial isocurvature perturbations (Eq. (23.85)) after inflation. In multi-field inflation models it is thus possible for non-adiabatic field fluctuations to generate both curvature and isocurvature perturbations leading to correlated primordial perturbations [133].

The amplitudes of any primordial isocurvature perturbations (Eq. (23.85)) are strongly constrained by the current CMB data, especially on large angular scales. Using temperature and low-ℓ polarization data yields the following bound on the amplitude of cold dark matter isocurvature perturbations at scale $k = 0.002h^{-1}\mathrm{Mpc}^{-1}$ (marginalising over the correlation angle and in the absence of primordial tensor perturbations) [40]:

$$\frac{\mathcal{P}_{S_{\rm m}}}{\mathcal{P}_\zeta + \mathcal{P}_{S_{\rm m}}} < 0.025 \ (95\% \ \mathrm{CL})\,. \tag{23.97}$$

For fully (anti-)correlated isocurvature perturbations, corresponding to a single isocurvature field providing a source for both the curvature and residual isocurvature perturbations, the bounds become significantly tighter [40]:

$$\frac{\mathcal{P}_{S_{\rm m}}}{\mathcal{P}_\zeta + \mathcal{P}_{S_{\rm m}}} < 0.0002 \ (95\% \ \mathrm{CL}), \ \text{correlated}\,, \tag{23.98}$$

$$\frac{\mathcal{P}_{S_{\rm m}}}{\mathcal{P}_\zeta + \mathcal{P}_{S_{\rm m}}} < 0.003 \ (95\% \ \mathrm{CL}), \ \text{anti-correlated} \tag{23.99}$$

23.7.3.2 *Local-Type Non-Gaussianity*

Since non-adiabatic field fluctuations in multi-field inflation may lead the to evolution of the primordial curvature perturbation at all orders, it becomes possible to generate significant non-Gaussianity in the primordial curvature perturbation. Non-linear evolution on super-Hubble scales leads to local-type non-Gaussianity, where the local integrated expansion is a non-linear function of the local field values during inflation, $N(\phi_i)$. While the field fluctuations at Hubble exit, $\delta\phi_{i*}$, are Gaussian in the slow-roll limit, the curvature perturbation, $\zeta = \delta N$, becomes a non-Gaussian distribution [134]:

$$\zeta = \sum_i \frac{\partial N}{\partial \phi_i}\delta\phi_i + \frac{1}{2}\sum_{i,j}\frac{\partial^2 N}{\partial\phi_i\partial\phi_j}\delta\phi_i\delta\phi_j + \ldots \tag{23.100}$$

with non-vanishing bispectrum in the squeezed limit ($k_1 \approx k_2 \gg k_3$):

$$B_\zeta(k_1,k_2,k_3) \approx \frac{12}{5} f_{\rm NL}^{\rm local}\frac{\mathcal{P}_\zeta(k_1)}{4\pi k_1^3}\frac{\mathcal{P}_\zeta(k_3)}{4\pi k_3^3}\,, \tag{23.101}$$

Int. J. Mod. Phys. A 2026.41. Downloaded by UNIVERSITY OF CALIFORNIA @ BERKELEY on 09/16/26. Re-
[redacted]
orldscientific.com
strictly not permitted, except for Open Access articles.

where

$$\frac{6}{5} f_{\rm NL}^{\rm local} = \frac{\sum_{i,j} \frac{\partial^2 N}{\partial\phi_i \partial\phi_j}}{\left(\sum_i \frac{\partial N}{\partial\phi_i}\right)^2} \,. \tag{23.102}$$

Both equilateral and orthogonal bispectra, discussed above in the context of generalised single-field inflation, vanish in the squeezed limit, enabling the three types of non-Gaussianity to be distinguished by observations, in principle.

Non-Gaussianity during multi-field inflation is highly model dependent, although $f_{\rm NL}^{\rm local}$ can often be smaller than unity in multi-field slow-roll inflation [135]. Scenarios where a second light field plays a role during or after inflation can make distinctive predictions for $f_{\rm NL}^{\rm local}$, such as $f_{\rm NL}^{\rm local} = -5/4$ in some curvaton scenarios [134, 136] or $f_{\rm NL}^{\rm local} = 5$ in simple modulated reheating scenarios [130, 137]. By contrast the constancy of ζ on super-Hubble scales in single-field slow-roll inflation leads to a very small non-Gaussianity [138, 139], and in the squeezed limit we have the simple result $f_{\rm NL}^{\rm local} = 5(1-n_{\rm s})/12$ [140, 141].

A combined analysis of the *Planck* 2018 temperature and polarization data [105] yields the following range for $f_{\rm NL}^{\rm local}$ defined in (Eq. (23.102)):

$$f_{\rm NL}^{\rm local} \;=\; -1 \pm 5 \quad (68\%\ {\rm CL})\,. \tag{23.103}$$

This sensitivity is sufficient to rule out parameter regimes giving rise to relatively large non-Gaussianity, but insufficient to probe $f_{\rm NL}^{\rm local} = \mathcal{O}(\epsilon)$, as expected in single-field models, or the range $f_{\rm NL}^{\rm local} = \mathcal{O}(1)$ found in the simplest two-field models.

Local-type primordial non-Gaussianity can also give rise to a striking scale-dependent bias in the distribution of collapsed dark matter halos and thus the galaxy distribution [142, 143]. Bounds from high-redshift galaxy surveys are not currently competitive with the best CMB constraints. An analysis based on the clustering of quasars in the final data release (DR16) of the extended Baryon acoustic Oscillation Spectroscopic Survey (eBOSS) [144] yields

$$f_{\rm NL}^{\rm local} \;=\; -12 \pm 21 \quad (68\%\ {\rm CL})\,, \tag{23.104}$$

while a recent analysis based on the clustering of luminous red galaxies in imaging surveys from the Dark Energy Spectroscopic Instrument (DESI) [145] finds $-10 < f_{\rm NL}^{\rm local} < 58$ at 68% CL.

23.8 Initial Conditions and Fine-tuning

This review is based on the assumption that the inflationary paradigm is valid. However, it remains the object of many criticisms (see, *e.g.*, Ref. [146]), many of them related to the perceived unnaturalness of the required initial conditions.

Most work on inflation is done in the context of RW cosmology, which assumes a high degree of symmetry, or small inhomogeneous perturbations (usually first order) about an RW cosmology. The isotropic RW space-time is an attractor for many homogeneous but anisotropic cosmologies in the presence of a false vacuum energy density [147], or a scalar field with suitable self-interaction potential energy [148, 149]. However it is much harder to establish the range of highly inhomogeneous initial conditions that yield a successful RW Universe, at least in limited studies initially (see, *e.g.*, Refs [150, 151]). A related open question is the general nature of the pre-inflationary state of the inflaton and other fields that could have provided initial conditions suitable for inflation [146]. They would need to have satisfied non-trivial homogeneity and isotropy conditions, and one may ask how these could have arisen, whether they are plausible, and whether there may be some observable signature of the pre-inflationary state. These and other criticisms of inflation were addressed in Ref. [152], which presented studies of the sensitivity of inflation to the initial conditions. Complementing these studies, there have been numerical relativity investigations of highly inhomogeneous initial conditions [153–155]. The general conclusion is that inflation is rather robust with respect to inhomogeneities in the initial conditions in both the scalar field profile and the extrinsic curvature, including large tensor perturbations.

To quantify the fine-tuning of initial conditions requires a measure in the space of possible cosmologies [156]; however, it has been argued that some of the measures historically used to frame this problem are formally invalid [157]. It is sometimes also objected that inflationary models predict the existence of a multiverse, and potentially a loss of predictive power [158], if it undergoes the process termed eternal inflation [159–161]. However, whether this is actually a bug or a feature remains a topic of debate [162, 163]. The existence of the multiverse is a purely philosophical problem, unless it has observable consequences, *e.g.*, in the CMB.

One might expect signatures of any pre-inflationary state to appear at large angular scales, *i.e.*, low multipoles ℓ. Indeed, various anomalies have been noted in the large-scale CMB anisotropies, as also discussed in Chap. 29, the "Cosmic Microwave Background" review, including a possible suppression of the quadrupole and other very large-scale anisotropies, an apparent feature in the range $\ell \approx 20$ to 30, and a possible hemispheric asymmetry. However, none of these are highly significant statistically, in view of the limitations due to cosmic variance [164]. They cannot yet be regarded as signatures of initial conditions, the multiverse or some pre-inflationary dynamics, such as might emerge from string theory.

A different kind of initial condition problem, called the trans-Planckian problem [165], is that the perturbations now seen in the CMB would have had wavelengths shorter than the Planck length at the onset of inflation. However, under quite general and conservative assumptions the usual inflationary predictions are quite robust [166], although with the possibility of $\mathcal{O}((H/m_{\rm P})^n)$ corrections that might have interesting signatures in the CMB [167].

When inflation was first proposed [5, 6] there was no evidence for the existence of scalar fields or the accelerated expansion of the Universe. The situation has changed dramatically in recent years with the observational evidence that the cosmic expansion is currently accelerating and with the discovery of a scalar particle, namely the Higgs boson (see Chap. 11, "Status of Higgs boson physics" review). Combined with the lack of any widely accepted alternative model for the origin of cosmic structure, these discoveries have lent support to the idea of a primordial accelerated expansion driven by a scalar field, *i.e.*, cosmological inflation. In parallel, successive CMB experiments have been consistent with generic predictions of inflationary models, although without yet providing irrefutable evidence. It was concluded in Ref. [152] that the inflationary paradigm is not currently in trouble. However, we note that inflation via a formally elementary scalar inflaton should probably only be regarded as an effective field theory valid at energy densities hierarchically smaller than the Planck scale. It should eventually be embedded in a suitable ultraviolet completion, on which inflationary dynamics may be our clearest window.

23.9 Future Probes of Inflation

Prospective future CMB experiments, both ground- and space-based are reviewed in the separate PDG "Cosmic Microwave Background" review, Chap. 29. The main emphasis in CMB experiments in the coming years will be on ground-based experiments providing improved measurements of B-mode polarization and greater sensitivity to the tensor-to-scalar ratio r, and more precise measurements at higher ℓ that will constrain $n_{\rm s}$ better. As is apparent from Fig. 23.1 and the discussion of models such as R^2 inflation, there is a strong incentive to reach a 5-σ sensitivity to $r \sim 3$ to 4×10^{-3}. This could be achieved with a moderately-sized space mission with large sky coverage [168], along with improvements in de-lensing and foreground measurements. The discussion in Sec. 23.3 (see also Fig. 23.5), also brought out the importance of reducing the uncertainty in $n_{\rm s}$, as a way to constrain post-inflationary reheating and the connection to particle physics. CMB temperature anisotropies probe primordial density perturbations down to comoving scales of order 50 Mpc, beyond which scale secondary sources of anisotropy dominate. CMB spectral distortions could potentially constrain the amplitude and shape of primordial density perturbations on comoving scales from kpc to Mpc due to distortions caused by the Silk damping of pressure waves in the radiation dominated era, before the last scattering of the CMB photons but after the plasma can be fully thermalised [106].

Improved sensitivity to non-Gaussianities is also a priority. In addition to CMB measurements, future large-scale structure sur-

Int. J. Mod. Phys. A 2026.41. Downloaded from www.worldscientific.com by UNIVERSITY OF CALIFORNIA @ BERKELEY on 09/16/26. Re-use and distribution is strictly not permitted, except for Open Access articles.

veys will also have roles to play as probes into models of inflation, for which there are excellent prospects. Current surveys such as DESI may reach $\Delta f_{\rm NL} \sim 4$ [169] comparable with the *Planck* sensitivity. In the future, radio surveys such as SKA will measure large-scale structure out to redshift $z \sim 3$ [170], initially through mapping the intensity of the neutral hydrogen 21-cm line, and eventually through radio galaxy surveys that will probe local-type non-Gaussianity to $f_{\rm NL} \sim 1$.

Galaxy clustering using DESI and *Euclid* satellite data could also constrain the running of the scalar tilt to a precision of $\Delta\alpha_{\rm s} \approx 0.0028$, a factor of 2 improvement on *Planck* constraints, or a precision of 0.0016 using Rubin-LSST data [169]. This might allow us to confirm, or refute, the prediction from the simplest inflationary models that running should be negative [171].

The satellite mission *SPHEREx* [172] will use measurements of the galaxy power spectrum to target an estimate of the running of the scalar spectral index with a sensitivity $\Delta\alpha_{\rm s} \sim 10^{-3}$ and local-type primordial non-Gaussianity, $\Delta f_{\rm NL} \sim 1$. Including information from the galaxy bispectrum one might reduce the measurement error on non-Gaussianity to $\Delta f_{\rm NL} \sim 0.2$, making it possible to distinguish between single-field slow-roll models and alternatives such as the curvaton scenario for the origin of structure, which generate $f_{\rm NL} \sim 1$.

Finally we note that future gravitational wave experiments such as the Laser Interferometer Space Antenna (LISA) will be sensitive to a stochastic gravitational wave background, including tensor perturbations produced during inflation or induced by large primordial density perturbations on small scales after inflation [173], which could provide constraints on inflationary perturbations on smaller scales.

Acknowledgements

The work of J.E. was supported in part by the UK STFC research grant ST/T000759/1. The work of D.W. was supported in part by the UK STFC research grant ST/W001225/1.

References

[1] D. H. Lyth and A. Riotto, Phys. Rept. **314**, 1 (1999), [hep-ph/9807278].

[2] A.R. Liddle and D.H. Lyth, *Cosmological inflation and large-scale structure* (Cambridge University Press, 2000).

[3] D. Baumann, in "Physics of the large and the small, TASI 09, proceedings of the Theoretical Advanced Study Institute in Elementary Particle Physics, Boulder, Colorado, USA, 1-26 June 2009," 523–686 (2011), [arXiv:0907.5424].

[4] J. Martin, C. Ringeval and V. Vennin, Phys. Dark Univ. **5-6**, 75 (2014), [arXiv:1303.3787].

[5] A. A. Starobinsky, Phys. Lett. **B91**, 99 (1980), [Adv. Ser. Astrophys. Cosmol.3,130(1987)].

[6] A. H. Guth, Phys. Rev. **D23**, 347 (1981), [Adv. Ser. Astrophys. Cosmol.3,139(1987)].

[7] K. A. Olive, Phys. Rept. **190**, 307 (1990).

[8] J. Martin *et al.*, JCAP **1403**, 039 (2014), [arXiv:1312.3529].

[9] J. Martin, Astrophys. Space Sci. Proc. **45**, 41 (2016), [arXiv:1502.05733].

[10] P. A. R. Ade *et al.* (Planck), Astron. Astrophys. **594**, A13 (2016), [arXiv:1502.01589].

[11] A. H. Guth and E. J. Weinberg, Nucl. Phys. **B212**, 321 (1983).

[12] D. La and P. J. Steinhardt, Phys. Rev. Lett. **62**, 376 (1989), [Erratum: Phys. Rev. Lett.62,1066(1989)].

[13] A. D. Linde, Phys. Lett. **B249**, 18 (1990).

[14] F. C. Adams and K. Freese, Phys. Rev. **D43**, 353 (1991), [hep-ph/0504135].

[15] A. D. Linde, Phys. Lett. **108B**, 389 (1982), [Adv. Ser. Astrophys. Cosmol.3,149(1987)].

[16] A. Albrecht and P. J. Steinhardt, Phys. Rev. Lett. **48**, 1220 (1982), [Adv. Ser. Astrophys. Cosmol.3,158(1987)].

[17] W. H. Press, Phys. Scripta **21**, 702 (1980); S. W. Hawking, Phys. Lett. **115B**, 295 (1982); A. A. Starobinsky, Phys. Lett. **117B**, 175 (1982); A. H. Guth and S. Y. Pi, Phys. Rev. Lett. **49**, 1110 (1982).

[18] J. M. Bardeen, P. J. Steinhardt and M. S. Turner, Phys. Rev. **D28**, 679 (1983).

[19] V. F. Mukhanov and G. V. Chibisov, JETP Lett. **33**, 532 (1981), [Pisma Zh. Eksp. Teor. Fiz.33,549(1981)].

[20] K. S. Stelle, Gen. Rel. Grav. **9**, 353 (1978).

[21] B. Whitt, Phys. Lett. **145B**, 176 (1984).

[22] D. Wands, Class. Quant. Grav. **11**, 269 (1994), [arXiv:gr-qc/9307034].

[23] S. R. Coleman and F. De Luccia, Phys. Rev. **D21**, 3305 (1980).

[24] M. Sasaki *et al.*, Phys. Lett. **B317**, 510 (1993).

[25] M. Bucher, A. S. Goldhaber and N. Turok, Phys. Rev. **D52**, 3314 (1995), [hep-ph/9411206].

[26] A. D. Linde and A. Mezhlumian, Phys. Rev. **D52**, 6789 (1995), [arXiv:astro-ph/9506017].

[27] A. R. Liddle, P. Parsons and J. D. Barrow, Phys. Rev. **D50**, 7222 (1994), [arXiv:astro-ph/9408015].

[28] L. Kofman, A. D. Linde and A. A. Starobinsky, Phys. Rev. **D56**, 3258 (1997), [hep-ph/9704452].

[29] B. A. Bassett, S. Tsujikawa and D. Wands, Rev. Mod. Phys. **78**, 537 (2006), [arXiv:astro-ph/0507632].

[30] A. D. Linde, Phys. Rev. **D49**, 748 (1994), [arXiv:astro-ph/9307002].

[31] A. D. Dolgov and A. D. Linde, Phys. Lett. **116B**, 329 (1982).

[32] J. R. Ellis *et al.*, Nucl. Phys. **B238**, 453 (1984), [,223(1983)].

[33] M. Kawasaki and T. Moroi, Prog. Theor. Phys. **93**, 879 (1995), [hep-ph/9403364].

[34] J. H. Traschen and R. H. Brandenberger, Phys. Rev. **D42**, 2491 (1990).

[35] G. V. Chibisov and V. F. Mukhanov, Mon. Not. Roy. Astron. Soc. **200**, 535 (1982).

[36] H. Kodama and M. Sasaki, Prog. Theor. Phys. Suppl. **78**, 1 (1984).

[37] V.F. Mukhanov, H.A. Feldman and R.H. Brandenberger, Phys. Rept. **215**, 203 (1992).

[38] K. A. Malik and D. Wands, Phys. Rept. **475**, 1 (2009), [arXiv:0809.4944].

[39] V. F. Mukhanov, Sov. Phys. JETP **67**, 1297 (1988), [Zh. Eksp. Teor. Fiz.94N7,1(1988)].

[40] Y. Akrami *et al.* (Planck), Astron. Astrophys. **641**, A10 (2020), [arXiv:1807.06211].

[41] A. A. Starobinsky, JETP Lett. **30**, 682 (1979), [,767(1979)].

[42] E. D. Stewart and D. H. Lyth, Phys. Lett. **B302**, 171 (1993), [arXiv:gr-qc/9302019].

[43] D. Wands *et al.*, Phys. Rev. **D62**, 043527 (2000), [arXiv:astro-ph/0003278].

[44] A. R. Liddle and S. M. Leach, Phys. Rev. **D68**, 103503 (2003), [arXiv:astro-ph/0305263].

[45] T. Louis *et al.* (ACT) (2025), [arXiv:2503.14452].

[46] M. Abdul Karim *et al.* (DESI), Phys. Rev. D **112**, 8, 083515 (2025), [arXiv:2503.14738].

[47] E. Camphuis *et al.* (SPT-3G) (2025), [arXiv:2506.20707].

[48] P. A. R. Ade *et al.* (BICEP/Keck), Phys. Rev. Lett. **127**, 15, 151301 (2021), [arXiv:2110.00483].

[49] S.M. Leach, A.R. Liddle, J. Martin, and D.J. Schwarz, Phys. Rev. **D66**, 23515 (2002).

[50] D. Kazanas, Astrophys. J. **241**, L59 (1980).

[51] K. Sato, Mon. Not. Roy. Astron. Soc. **195**, 467 (1981).

Int. J. Mod. Phys. A 2026.41. Downloaded from www.worldscientific.com by UNIVERSITY OF CALIFORNIA @ BERKELEY on 09/16/26. Re-[redacted]strictly not permitted, except for Open Access articles.

[52] A. Billoire and K. Tamvakis, Nucl. Phys. **B200**, 329 (1982); J. D. Breit, S. Gupta and A. Zaks, Phys. Rev. Lett. **51**, 1007 (1983).

[53] A. D. Linde, Phys. Lett. **129B**, 177 (1983).

[54] D. V. Nanopoulos, K. A. Olive and M. Srednicki, Phys. Lett. **127B**, 30 (1983).

[55] J. Ellis, D. V. Nanopoulos and K. A. Olive, Phys. Rev. Lett. **111**, 111301 (2013), [Erratum: Phys. Rev. Lett.111,no.12,129902(2013)], [arXiv:1305.1247].

[56] T. S. Koivisto and F. R. Urban, JCAP **1503**, 03, 003 (2015), [arXiv:1407.3445].

[57] L. Boubekeur and D. H. Lyth, JCAP **0507**, 010 (2005), [hep-ph/0502047].

[58] G. R. Dvali, Q. Shafi and S. Solganik, in "4th European Meeting From the Planck Scale to the Electroweak Scale (Planck 2001) La Londe les Maures, Toulon, France, May 11-16, 2001," (2001), [hep-th/0105203]; J. Garcia-Bellido, R. Rabadan and F. Zamora, JHEP **01**, 036 (2002), [hep-th/0112147]; S. Kachru *et al.*, JCAP **0310**, 013 (2003), [hep-th/0308055].

[59] F. C. Adams *et al.*, Phys. Rev. **D47**, 426 (1993), [hep-ph/9207245].

[60] E. Pajer and M. Peloso, Class. Quant. Grav. **30**, 214002 (2013), [arXiv:1305.3557].

[61] E. Silverstein and A. Westphal, Phys. Rev. **D78**, 106003 (2008), [arXiv:0803.3085].

[62] L. McAllister, E. Silverstein and A. Westphal, Phys. Rev. **D82**, 046003 (2010), [arXiv:0808.0706].

[63] F. L. Bezrukov and M. Shaposhnikov, Phys. Lett. **B659**, 703 (2008), [arXiv:0710.3755].

[64] D. Buttazzo *et al.*, JHEP **12**, 089 (2013), [arXiv:1307.3536].

[65] H. P. Nilles, Phys. Rept. **110**, 1 (1984); H. E. Haber and G. L. Kane, Phys. Rept. **117**, 75 (1985).

[66] J.R. Ellis *et al.*, Phys. Lett. **118B**, 335 (1982).

[67] N. Okada and Q. Shafi (2013), [arXiv:1311.0921].

[68] J. Martin, C. Ringeval and V. Vennin, Phys. Rev. **D93**, 10, 103532 (2016), [arXiv:1603.02606].

[69] J. Martin, C. Ringeval and V. Vennin, JCAP **07**, 087 (2024), [arXiv:2404.10647].

[70] Y. Akrami *et al.* (Planck), Astron. Astrophys. **641**, A10 (2020), [arXiv:1807.06211].

[71] H. Murayama *et al.*, Phys. Rev. Lett. **70**, 1912 (1993).

[72] J. Ellis, M. Fairbairn and M. Sueiro, JCAP **1402**, 044 (2014), [arXiv:1312.1353].

[73] D. Croon, J. Ellis and N. E. Mavromatos, Phys. Lett. **B724**, 165 (2013), [arXiv:1303.6253].

[74] G. R. Dvali, Q. Shafi and R. K. Schaefer, Phys. Rev. Lett. **73**, 1886 (1994), [hep-ph/9406319].

[75] D. V. Nanopoulos *et al.*, Phys. Lett. **123B**, 41 (1983).

[76] A. B. Goncharov and A. D. Linde, Phys. Lett. **139B**, 27 (1984).

[77] E. Cremmer *et al.*, Nucl. Phys. **B212**, 413 (1983), [,413(1982)].

[78] R. Holman, P. Ramond and G. G. Ross, Phys. Lett. **137B**, 343 (1984).

[79] E. J. Copeland *et al.*, Phys. Rev. **D49**, 6410 (1994), [arXiv:astro-ph/9401011]; E. D. Stewart, Phys. Rev. **D51**, 6847 (1995), [hep-ph/9405389].

[80] G. D. Coughlan *et al.*, Phys. Lett. **131B**, 59 (1983); A. S. Goncharov, A. D. Linde and M. I. Vysotsky, Phys. Lett. **147B**, 279 (1984); T. Banks, D. B. Kaplan and A. E. Nelson, Phys. Rev. **D49**, 779 (1994), [hep-ph/9308292]; B. de Carlos *et al.*, Phys. Lett. **B318**, 447 (1993), [hep-ph/9308325]; M. Kawasaki, T. Moroi and T. Yanagida, Phys. Lett. **B370**, 52 (1996), [hep-ph/9509399].

[81] J. R. Ellis, D. V. Nanopoulos and M. Quiros, Phys. Lett. **B174**, 176 (1986).

[82] T. Moroi, M. Yamaguchi and T. Yanagida, Phys. Lett. **B342**, 105 (1995), [hep-ph/9409367].

[83] M. Kawasaki, M. Yamaguchi and T. Yanagida, Phys. Rev. Lett. **85**, 3572 (2000), [hep-ph/0004243]; K. Nakayama, F. Takahashi and T. T. Yanagida, JCAP **1308**, 038 (2013), [arXiv:1305.5099].

[84] E. Cremmer *et al.*, Phys. Lett. **133B**, 61 (1983).

[85] A. S. Goncharov and A. D. Linde, Class. Quant. Grav. **1**, L75 (1984); C. Kounnas and M. Quiros, Phys. Lett. **151B**, 189 (1985).

[86] J. R. Ellis, C. Kounnas and D. V. Nanopoulos, Nucl. Phys. **B247**, 373 (1984).

[87] E. Witten, Phys. Lett. **155B**, 151 (1985).

[88] J. Ellis, D. V. Nanopoulos and K. A. Olive, JCAP **1310**, 009 (2013), [arXiv:1307.3537].

[89] J. Ellis *et al.*, Class. Quant. Grav. **33**, 9, 094001 (2016), [arXiv:1507.02308].

[90] R. Kallosh, A. Linde and D. Roest, JHEP **11**, 198 (2013), [arXiv:1311.0472].

[91] M. Drees and Y. Xu, Phys. Lett. B **867**, 139612 (2025), [arXiv:2504.20757].

[92] J. Ellis *et al.*, Phys. Rev. D **105**, 4, 043504 (2022), [arXiv:2112.04466].

[93] L. Iacconi *et al.*, JCAP **10**, 015 (2023), [arXiv:2306.00918].

[94] J. Ellis *et al.*, JCAP **1507**, 07, 050 (2015), [arXiv:1505.06986].

[95] A. R. Liddle, Mon. Not. Roy. Astron. Soc. **377**, L74 (2007), [arXiv:astro-ph/0701113].

[96] J. Martin, C. Ringeval and V. Vennin, ASPIC: Accurate Slow-roll Predictions for Inflationary CosmologyAstrophysics Source Code Library, record ascl:1806.031, `https://github.com/cosmicinflation/aspic` (2018).

[97] J. Martin, C. Ringeval and V. Vennin, Phys. Rev. Lett. **114**, 8, 081303 (2015), [arXiv:1410.7958].

[98] C. Armendariz-Picon, T. Damour and V. F. Mukhanov, Phys. Lett. **B458**, 209 (1999), [hep-th/9904075].

[99] M. Alishahiha, E. Silverstein and D. Tong, Phys. Rev. **D70**, 123505 (2004), [hep-th/0404084].

[100] K. Enqvist and M. S. Sloth, Nucl. Phys. **B626**, 395 (2002), [hep-ph/0109214].

[101] D. H. Lyth and D. Wands, Phys. Lett. **B524**, 5 (2002), [hep-ph/0110002].

[102] T. Moroi and T. Takahashi, Phys. Lett. **B522**, 215 (2001), [Erratum: Phys. Lett.B539,303(2002)], [hep-ph/0110096].

[103] N. Bartolo *et al.*, Phys. Rept. **402**, 103 (2004), [arXiv:astro-ph/0406398].

[104] P. A. R. Ade *et al.* (Planck), Astron. Astrophys. **594**, A17 (2016), [arXiv:1502.01592].

[105] Y. Akrami *et al.* (Planck), Astron. Astrophys. **641**, A9 (2020), [arXiv:1905.05697].

[106] J. Chluba, J. Hamann and S. P. Patil, Int. J. Mod. Phys. **D24**, 10, 1530023 (2015), [arXiv:1505.01834].

[107] Y. B. Zel'dovich and I. D. Novikov, Soviet Astron. AJ (Engl. Transl.), **10**, 602 (1967).

[108] S. W. Hawking, Nature **248**, 30 (1974).

[109] S. Matarrese, O. Pantano and D. Saez, Phys. Rev. Lett. **72**, 320 (1994), [arXiv:astro-ph/9310036].

[110] S. Matarrese, S. Mollerach and M. Bruni, Phys. Rev. D **58**, 043504 (1998), [arXiv:astro-ph/9707278].

[111] K. N. Ananda, C. Clarkson and D. Wands, Phys. Rev. D **75**, 123518 (2007), [arXiv:gr-qc/0612013].

Int. J. Mod. Phys. A 2026.41. Downloaded from www.worldscientific.com
by UNIVERSITY OF CALIFORNIA @ BERKELEY on 09/16/26. Re-use and distribution is strictly not permitted, except for Open Access articles.

[112] D. Baumann *et al.*, Phys. Rev. D **76**, 084019 (2007), [hep-th/0703290].

[113] H. Motohashi and W. Hu, Phys. Rev. D **96**, 6, 063503 (2017), [arXiv:1706.06784].

[114] J. Garcia-Bellido and E. Ruiz Morales, Phys. Dark Univ. **18**, 47 (2017), [arXiv:1702.03901].

[115] S. Inoue and J. Yokoyama, Phys. Lett. B **524**, 15 (2002), [hep-ph/0104083].

[116] W. H. Kinney, Phys. Rev. D **72**, 023515 (2005), [arXiv:gr-qc/0503017].

[117] S. M. Leach *et al.*, Phys. Rev. D **64**, 023512 (2001), [arXiv:astro-ph/0101406].

[118] C. T. Byrnes, P. S. Cole and S. P. Patil, JCAP **06**, 028 (2019), [arXiv:1811.11158].

[119] R. Abbott *et al.* (KAGRA, Virgo, LIGO Scientific), Phys. Rev. D **104**, 2, 022004 (2021), [arXiv:2101.12130].

[120] G. Agazie *et al.* (NANOGrav), Astrophys. J. Lett. **951**, 1, L8 (2023), [arXiv:2306.16213].

[121] J. Antoniadis *et al.* (EPTA) (2023), [arXiv:2306.16214].

[122] D. J. Reardon *et al.*, Astrophys. J. Lett. **951**, 1, L6 (2023), [arXiv:2306.16215].

[123] H. Xu *et al.*, Res. Astron. Astrophys. **23**, 7, 075024 (2023), [arXiv:2306.16216].

[124] A. Afzal *et al.* (NANOGrav), Astrophys. J. Lett. **951**, 1, L11 (2023), [arXiv:2306.16219].

[125] B. Carr *et al.*, Rept. Prog. Phys. **84**, 11, 116902 (2021), [arXiv:2002.12778].

[126] L. Senatore, K. M. Smith and M. Zaldarriaga, JCAP **1001**, 028 (2010), [arXiv:0905.3746].

[127] C. Gordon *et al.*, Phys. Rev. **D63**, 023506 (2001), [arXiv:astro-ph/0009131]; R. Easther *et al.*, Phys. Rev. Lett. **112**, 161302 (2014), [arXiv:1312.4035]; J. Ellis *et al.*, JCAP **1501**, 010 (2015), [arXiv:1409.8197]; S. Renaux-Petel and K. Turzynski, JCAP **1506**, 06, 010 (2015), [arXiv:1405.6195].

[128] C. T. Byrnes and D. Wands, Phys. Rev. **D74**, 043529 (2006), [arXiv:astro-ph/0605679].

[129] D. H. Lyth, JCAP **0511**, 006 (2005), [arXiv:astro-ph/0510443].

[130] G. Dvali, A. Gruzinov and M. Zaldarriaga, Phys. Rev. **D69**, 023505 (2004), [arXiv:astro-ph/0303591].

[131] D. Wands *et al.*, Phys. Rev. **D66**, 043520 (2002), [arXiv:astro-ph/0205253].

[132] S. Weinberg, Phys. Rev. **D67**, 123504 (2003), [arXiv:astro-ph/0302326].

[133] D. Langlois, Phys. Rev. **D59**, 123512 (1999), [arXiv:astro-ph/9906080].

[134] D. H. Lyth and Y. Rodriguez, Phys. Rev. Lett. **95**, 121302 (2005), [arXiv:astro-ph/0504045].

[135] F. Vernizzi and D. Wands, JCAP **0605**, 019 (2006), [arXiv:astro-ph/0603799].

[136] M. Sasaki, J. Valiviita and D. Wands, Phys. Rev. **D74**, 103003 (2006), [arXiv:astro-ph/0607627].

[137] G. Dvali, A. Gruzinov and M. Zaldarriaga, Phys. Rev. **D69**, 083505 (2004), [arXiv:astro-ph/0305548].

[138] D. S. Salopek and J. R. Bond, Phys. Rev. **D43**, 1005 (1991).

[139] A. Gangui *et al.*, Astrophys. J. **430**, 447 (1994), [arXiv:astro-ph/9312033].

[140] J. M. Maldacena, JHEP **05**, 013 (2003), [arXiv:astro-ph/0210603].

[141] V. Acquaviva *et al.*, Nucl. Phys. **B667**, 119 (2003), [arXiv:astro-ph/0209156].

[142] N. Dalal *et al.*, Phys. Rev. **D77**, 123514 (2008), [arXiv:0710.4560].

[143] S. Matarrese and L. Verde, Astrophys. J. **677**, L77 (2008), [arXiv:0801.4826].

[144] E.-M. Mueller *et al.* (eBOSS), Mon. Not. Roy. Astron. Soc. **514**, 3, 3396 (2022), [arXiv:2106.13725].

[145] M. Rezaie *et al.*, Mon. Not. Roy. Astron. Soc. **532**, 2, 1902 (2024), [arXiv:2307.01753].

[146] A. Ijjas, P. J. Steinhardt and A. Loeb, Phys. Lett. **B723**, 261 (2013), [arXiv:1304.2785].

[147] R. M. Wald, Phys. Rev. **D28**, 2118 (1983).

[148] M. Heusler, Phys. Lett. **B253**, 33 (1991).

[149] Y. Kitada and K.-i. Maeda, Phys. Rev. **D45**, 1416 (1992).

[150] D. S. Goldwirth and T. Piran, Phys. Rept. **214**, 223 (1992).

[151] T. Vachaspati and M. Trodden, Phys. Rev. **D61**, 023502 (1999), [arXiv:gr-qc/9811037].

[152] D. Chowdhury *et al.*, Phys. Rev. D **100**, 8, 083537 (2019), [arXiv:1902.03951].

[153] W. E. East *et al.*, JCAP **1609**, 09, 010 (2016), [arXiv:1511.05143].

[154] K. Clough *et al.*, JCAP **1709**, 09, 025 (2017), [arXiv:1608.04408].

[155] K. Clough, R. Flauger and E. A. Lim, JCAP **1805**, 05, 065 (2018), [arXiv:1712.07352].

[156] G. W. Gibbons, S. W. Hawking and J. M. Stewart, Nucl. Phys. **B281**, 736 (1987).

[157] J. S. Schiffrin and R. M. Wald, Phys. Rev. **D86**, 023521 (2012), [arXiv:1202.1818].

[158] A. Ijjas, P. J. Steinhardt and A. Loeb, Phys. Lett. **B736**, 142 (2014), [arXiv:1402.6980].

[159] A. Vilenkin, Phys. Rev. **D27**, 2848 (1983).

[160] A. D. Linde, Phys. Lett. **B175**, 395 (1986).

[161] A. S. Goncharov, A. D. Linde and V. F. Mukhanov, Int. J. Mod. Phys. **A2**, 561 (1987).

[162] A. H. Guth, D. I. Kaiser and Y. Nomura, Phys. Lett. **B733**, 112 (2014), [arXiv:1312.7619].

[163] A. Linde, in "Proceedings, 100th Les Houches Summer School: Post-Planck Cosmology: Les Houches, France, July 8 - August 2, 2013," 231–316 (2015), [arXiv:1402.0526].

[164] P. A. R. Ade *et al.* (Planck), Astron. Astrophys. **594**, A20 (2016), [arXiv:1502.02114].

[165] J. Martin and R. H. Brandenberger, Phys. Rev. **D63**, 123501 (2001), [hep-th/0005209].

[166] R. H. Brandenberger and J. Martin, Mod. Phys. Lett. **A16**, 999 (2001), [arXiv:astro-ph/0005432].

[167] J. Martin and R. H. Brandenberger, in "Recent developments in theoretical and experimental general relativity, gravitation and relativistic field theories. Proceedings, 9th Marcel Grossmann Meeting, MG'9, Rome, Italy, July 2-8, 2000. Pts. A-C," 2001–2002 (2000), [arXiv:astro-ph/0012031].

[168] A. Kogut *et al.*, JCAP **1107**, 025 (2011), [arXiv:1105.2044].

[169] A. Font-Ribera *et al.*, JCAP **1405**, 023 (2014), [arXiv:1308.4164].

[170] R. Maartens *et al.* (SKA Cosmology SWG), PoS **AASKA14**, 016 (2015), [arXiv:1501.04076].

[171] J. Martin, C. Ringeval and V. Vennin, EPL **148**, 2, 29002 (2024), [arXiv:2404.15089].

[172] O. Doré *et al.* (2014), [arXiv:1412.4872].

[173] P. Auclair *et al.* (LISA Cosmology Working Group), Living Rev. Rel. **26**, 1, 5 (2023), [arXiv:2204.05434].

24. Big Bang Nucleosynthesis

Revised August 2025 by B.D. Fields (Astronomy, Illinois U.; Physics, Illinois U.), P. Molaro (INAF-OATS Trieste; IFPU) and S. Sarkar (Rudolf Peierls, Oxford U.).

24.1 Abstract

Big-Bang nucleosynthesis (BBN) offers the deepest reliable probe of the early Universe, being based on well-understood Standard Model physics [1]. Predictions of the abundances of the light elements, D, ^{3}He, ^{4}He, and ^{7}Li, synthesized at the end of the *first three minutes*, are in good overall agreement with the primordial abundances inferred from observational data, thus validating the standard hot Big-Bang cosmology (see [2–5] for reviews). This is particularly impressive given that these abundances span nine orders of magnitude – from ^{4}He/H~ 0.08 down to ^{7}Li/H$\sim 10^{-10}$ (ratios by number). Thus BBN provides powerful constraints on possible deviations from the standard cosmology, and on new physics beyond the Standard Model [6–9].

24.2 Theory

The synthesis of the light elements is sensitive to physical conditions in the early radiation-dominated era at a temperature $T \sim 1$ MeV, corresponding to an age $t \sim 1$ s. At higher temperatures, weak interactions were in thermal equilibrium, thus fixing the ratio of the neutron and proton number densities to be $n/p = \mathrm{e}^{-Q/T}$, where $Q = 1.293$ MeV is the neutron-proton mass difference. As the temperature dropped, the neutron-proton inter-conversion rate per nucleon, $\Gamma_{n\leftrightarrow p} \sim G_{\rm F}^2 T^5$, fell faster than the Hubble expansion rate, $H \sim \sqrt{g_* G_{\rm N}}\, T^2$, where g_* counts the number of relativistic particle species determining the energy density in radiation (see 'Big Bang Cosmology' — Sec. 22 of this *Review*). This resulted in departure from chemical equilibrium (*freeze-out*) at $T_{\rm fr} \sim (g_* G_{\rm N}/G_{\rm F}^4)^{1/6} \simeq 1$ MeV. The neutron fraction at this time, $n/p = \mathrm{e}^{-Q/T_{\rm fr}} \simeq 1/6$, is thus sensitive to every known physical interaction, since Q is determined by both strong and electromagnetic interactions while $T_{\rm fr}$ depends on the weak as well as gravitational interactions. Moreover, the sensitivity to the Hubble expansion rate affords a probe of, *e.g.,* the number of relativistic neutrino species [10]. After freeze-out, the neutrons were free to β-decay, so the neutron fraction dropped to $n/p \simeq 1/7$ by the time nuclear reactions began. A simplified analytic model of freeze-out yields the n/p ratio to an accuracy of $\sim 1\%$ [11,12].

The rates of these reactions depend on the density of baryons (strictly speaking, nucleons), which is usually expressed normalized to the relic blackbody photon density as $\eta \equiv n_b/n_\gamma$. As we shall see, all the light-element abundances can be explained with $\eta_{10} \equiv \eta \times 10^{10}$ in the range 6.040 ± 0.118. With n_γ fixed by the present CMB temperature 2.7255 K (see 'Cosmic Microwave Background' — Sec. 29 of this *Review*), this can be stated as the allowed range for the baryon mass density today, $\rho_{\rm b} = (4.2\pm0.1)\times10^{-31}\,{\rm g\,cm^{-3}}$, or as the baryonic fraction of the critical density, $\Omega_{\rm b} = \rho_b/\rho_{\rm crit} \simeq \eta_{10} h^{-2}/274 = (0.02205 \pm 0.00043)h^{-2}$, where $h \equiv H_0/100\ {\rm km\,s^{-1}\,Mpc^{-1}} \simeq 0.7$ is the present Hubble parameter (see 'The Cosmological Parameters' — Sec. 25 of this *Review*).

The nucleosynthesis chain begins with the formation of deuterium in the process $p(n,\gamma)$D. However, photo-dissociation by the high number density of photons delays production of deuterium (and other complex nuclei) until well after T drops below the binding energy of deuterium, $\Delta_{\rm D} = 2.23$ MeV. The quantity $\eta^{-1}\mathrm{e}^{-\Delta_{\rm D}/T}$, *i.e.,* the number of photons per baryon above the deuterium photo-dissociation threshold, falls below unity at $T \simeq 0.1$ MeV; nuclei can then begin to form without being immediately photo-dissociated again. Only 2-body reactions, such as D$(p,\gamma)^3$He and ^{3}He(D$,p)^4$He are important because the density by this time has become rather low – comparable to that of air!

Nearly all neutrons end up bound in the most stable light element ^{4}He. Heavier nuclei do not form in any significant quantity both because of the absence of stable nuclei with mass number 5 or 8 (which impedes nucleosynthesis via n^4He, p^4He or ^{4}He^{4}He reactions), and the large Coulomb barriers for reactions such as ^{3}He(^{4}He$,\gamma)^7$Li and ^{3}He(^{4}He$,\gamma)^7$Be. Hence the primordial mass fraction of ^{4}He, $Y_{\rm p} \equiv \rho(^4{\rm He})/\rho_{\rm b}$, can be estimated by the simple counting argument

$$Y_{\rm p} = \frac{2(n/p)}{1+n/p} \simeq 0.25\,, \tag{24.1}$$

where strictly speaking this gives the baryon fraction in ^{4}He, which is what we will quote throughout. This differs slightly from the mass fraction due to small binding energy corrections.

There is little sensitivity here to the actual nuclear reaction rates for the production of ^{4}He. Nuclear rates are, however, critically important in determining the other 'left-over' abundances: D and ^{3}He at the level of a few times 10^{-5} by number relative to H, and ^{7}Li/H at the level of about 10^{-10} (when η_{10} is in the range 1–10). These values can be understood in terms of approximate analytic arguments [12,13].

The elemental abundances shown in Fig. 24.1 as a function of η_{10} were calculated using an updated version [14] of the Wagoner code [1]; other versions [15–18] too are publicly available. The ^{4}He curve includes small corrections due to radiative processes at zero and finite temperatures [19], non-equilibrium neutrino heating during $e^\pm$ annihilation [20], and finite nucleon mass effects [21]; the range primarily reflects the 2σ uncertainty in the neutron lifetime. The spread in the curves for D, ^{3}He, and ^{7}Li corresponds to the 2σ uncertainties in nuclear cross sections, as estimated by Monte Carlo methods [22–25]. The input nuclear data have been carefully reassessed [2,14,22–32], leading to improved precision for the abundance predictions. In particular, the uncertainty in ^{7}Li/H at interesting values of η has been reduced recently by a factor ~ 2, a consequence of a similar reduction in the error budget [33] for the dominant mass-7 production channel ^{3}He(^{4}He$,\gamma)^7$Be. Polynomial fits to the predicted abundances and the error correlation matrix have been given in refs. [24,34]. The boxes in Fig 24.1 show the observationally inferred primordial abundances with their associated uncertainties, as discussed below.

The nuclear reaction cross sections important for BBN have all been measured at the relevant energies. Recently however there have been substantial advances in the precision of light element observations (e.g., D/H) and in the determination of cosmological parameters (e.g., from *Planck*). This motivates corresponding improvement in BBN predictions and thus in the key reaction cross sections. Recent measurements of D$(p,\gamma)^3$He by the LUNA collaboration have significantly improved the precision of D/H predictions [35]. Even so, the nuclear uncertainties still leave D/H prediction errors larger than those of the observations [14,31,32]. The D$(\mathrm{D},n)^3$He and D$(\mathrm{D},p)^3H$ reactions now not only dominate the uncertainty budget, but they can give significantly different D/H predictions depending on whether one uses just the empirical determination of the cross sections, or also uses theory to guide the functional form. Clearly, more experimental data is needed.

An additional experimental parameter important in determining the light element abundances is the neutron lifetime, τ_n, which normalizes (the inverse of) $\Gamma_{n\leftrightarrow p}$. Its value has been revised downwards to $\tau_n = 878.4 \pm 0.5$ s (see *N* Baryons Listing).

24.3 Observations: the Light Element Abundances

BBN theory predicts the universal abundances of D, ^{3}He, ^{4}He, and ^{7}Li, which are essentially fixed by $t \sim 180$ s. However, these abundances are *inferred* from observations made at much later epochs, after stellar nucleosynthesis has begun. Stars produce heavier elements such as C, N, O, and Fe (collectively referred to as "metals"), and the ejecta from stellar processes can alter the light element abundances from their primordial values. To obtain measurements that more closely reflect the primordial composition, one must identify astrophysical environments with low metallicity, where stellar processing has been minimal.

BBN is the only significant source of deuterium, which is entirely destroyed when cycled through stars [36]. Thus, any detection of D provides a lower limit to the primordial abundance D/H|p, and correspondingly, an upper limit on the baryon-to-photon ratio η_{10}. The best proxy for the primordial D abundance is its measurement in distant, chemically unprocessed environ-

Int. J. Mod. Phys. A 2026.41. Downloaded from www.worldscientific.com by UNIVERSITY OF CALIFORNIA @ BERKELEY on 09/16/26. Re- strictly not permitted, except for Open Access articles.

Int. J. Mod. Phys. A 2026.41. Downloaded from www.worldscientific.com
by UNIVERSITY OF CALIFORNIA @ BERKELEY on 09/16/26. Re-use and distribution is strictly not permitted, except for Open Access articles.

ments, where stellar processing (astration) is minimal [36, 37]. These measurements have become possible with the advent of large-aperture telescopes; yet, despite nearly three decades of observational effort, only 12 high-precision determinations are currently available, as listed in Table 24.1 [38–44].

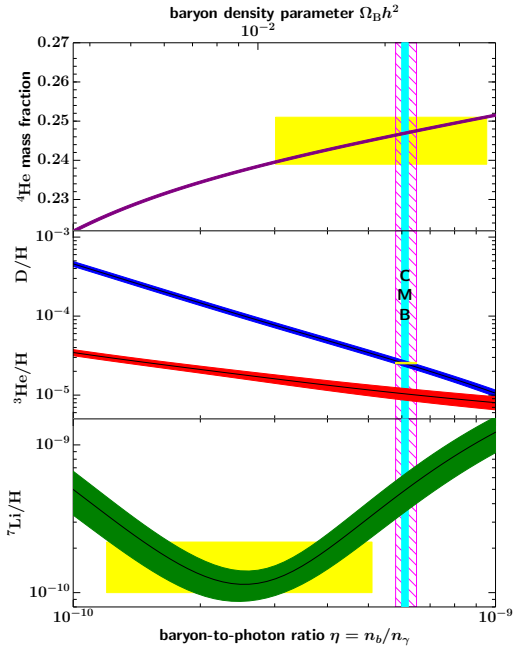

Figure 24.1: The primordial abundances of ^{4}He, D, ^{3}He, and ^{7}Li as predicted by the standard model of Big-Bang nucleosynthesis — the bands show the 95% CL range [45]. Boxes indicate the observed light element abundances. The narrow vertical band indicates the CMB measure of the cosmic baryon density, while the wider band indicates the BBN D+^{4}He concordance range (both at 95% CL).

High-resolution spectra reveal the presence of deuterium in high-redshift, low-metallicity quasar absorption systems through its isotope-shifted Lyman-α absorption lines. However, these features are often partially obscured or contaminated by intervening hydrogen in the Lyman-α forest. In a few damped Lyman-α (DLA) systems, deuterium absorption has been resolved in higher-order transitions of the Lyman series. Recent determinations [39, 41] and re-analyses [42–44] have significantly improved the precision of deuterium abundance measurements compared to earlier studies. The observed D/H ratio exhibits no correlation with metallicity, redshift, or the neutral hydrogen column density $N(\mathrm{HI})$ $(= \int_{\mathrm{los}} n_{\mathrm{HI}}\, ds)$ integrated along the line of sight through the absorber. The metallicities of these absorption systems range from $(0.001 - 0.03)\times$ the Solar value, and the level of deuterium astration is estimated to be between 0.1% and 1% [37]. In contrast, within the Milky Way, DI/HI measurements show an anti-correlation with metal abundance, suggesting that a fraction of interstellar deuterium is depleted onto dust grains [46].

However, in the absorbers where deuterium is measured, the dust content is small, as implied by Solar proportions of the abundances of refractory and non-refractory elements. Thus, the neutral atomic ratio DI/HI $\equiv$ D/H should match the underlying isotope ratio, and be truly representative of the primordial value D/H|p. The weighted mean of the 12 most precise and recent measurements in Table 24.1 is $\mathrm{D/H}|_{\mathrm{p}} \times 10^6 = (25.08 \pm 0.27)$. It is worth noting that earlier determinations by [47–51] are also consistent with this mean value. However, the ones listed in Table 24.1 yield $\chi^2/(N-1) = 1.160$, indicating that some uncertainties may be underestimated. We therefore increase the uncertainty by a factor $S = \sqrt{\chi^2/(N-1)} = 1.08$, and the recommended value for the abundance of primordial deuterium is:

$$\mathrm{D/H}|_{\mathrm{p}} \times 10^6 = 25.08\ (\pm 0.27 \times S) = 25.08\ (\pm 0.29). \qquad (24.2)$$

The primordial ^{4}He abundance is best determined through recombination emission lines of He and H in the most metal-poor extragalactic HII (ionized) regions, *viz.* blue compact galaxies, generally found at low redshift. There is now a large body of data on ^{4}He and CNO in these galaxies, with over 1000 such systems in the Sloan Digital Sky Survey alone [54]. These data confirm that the stellar contribution to the helium abundance is positively correlated with metal production, so extrapolation to zero metallicity gives the primordial ^{4}He abundance Y_{p}. However, HII regions are complex systems and several physical parameters enter in the He/H determination, notably the electron density and temperature, as well as reddening. Thus, systematic effects dominate the uncertainties in the abundance determination [55, 56]. A major step forward has been the inclusion of the He λ10830 infrared emission line which shows a strong dependence on the electron density and is thus useful to break the degeneracy with the temperature, allowing for a more robust helium abundance determination. In recent works the underlying ^{4}He stellar absorption, and/or the newly derived values of the HeI-recombination and H-excitation-collisional coefficients are adressed and the ^{4}He abundances have increased significantly. Some recent results are reported in Table 24.2.

There is a reassuring convergence towards the value of $Y_{\mathrm{p}} = 0.245$ between detailed analyses of specific extragalactic HII regions with other (statistically more significant) analyses of many systems. Thus our recommended ^{4}He abundance is:

$$Y_{\mathrm{p}} = 0.245 \pm 0.003. \qquad (24.3)$$

The central value is close to the mean/weighted average of the values in Table 24.2, however we caution that combining these partially overlapping data sets is not straightforward. The uncertainty reflects the combined statistical and systematic errors, with the latter, estimated to be ± 0.002 [62], being dominant.

The best-suited objects for determining the primordial abundance of ^{7}Li are metal-poor stars in the Galactic halo, which exhibit metallicities as low as 10^{-6} of the Solar value [64]. Observations have long shown that ^{7}Li does not vary significantly among halo dwarfs with metallicities $\lesssim 1/30$ of Solar — the *Spite plateau* [65–69]. However, more recent observations show an increase in Li depletion in metal-poor stars [70–72]. The reason for this increased scatter at low metallicity remains unknown and prevents a reliable derivation of the primordial ^{7}Li abundance by extrapolation to zero metallicity [71, 72].

To estimate the primordial ^{7}Li abundance, we restrict the analysis to stars with metallicities in the range $-3.5 < [\mathrm{Fe/H}] < -1.5$ [69, 72], where no scatter beyond the observational uncertainties is observed. Lower metallicity stars show a strong contamination of Carbon enriched stars [73]. This yields:

$$\mathrm{Li/H}|_{\mathrm{p}} = (1.45 \pm 0.25) \times 10^{-10}. \qquad (24.4)$$

Strictly speaking, the inferred primordial ^{7}Li abundance should be regarded as a *lower bound* rather than a direct measurement. This is because ^{7}Li in Population II stars may have been partially destroyed through mixing of the outer stellar layers with the hotter interior [74]. Such processes are constrained by the lack of significant scatter in ^{7}Li as a function of T_{eff}, yet a significant depletion may still have occurred [75]. Stellar determinations of Li abundances typically sum the contributions from both ^{6}Li and ^{7}Li isotopes. However, high-precision measurements indicate that ^{6}Li / ^{7}Li < 0.05 , confirming that ^{7}Li overwhelmingly dominates [76].

The primordial abundance of ^{3}He has the poorest observational determination of all of the light nuclides. The only data available come from the Solar system and from solar-metallicity HII regions in the Galaxy [77]. Therefore, inferring the primordial ^{3}He abundance is problematic, compounded by the fact that stellar nucleosynthesis models for ^{3}He are in conflict with observations. Consequently, we consider it inappropriate to use ^{3}He (and also D+^{3}He) as a cosmological probe.

Int. J. Mod. Phys. A 2026.41. Downloaded from www.worldscientific.com
by UNIVERSITY OF CALIFORNIA @ BERKELEY on 09/16/26. Reproduction strictly not permitted, except for Open Access articles.

Table 24.1: D/H measurements. For systems with multiple measurements we used the most recent one which is generally more precise.

QSO	$z_{\rm em}$	$z_{\rm abs}$	$\log N((\mathrm{HI}))$	[X/H]	$(\mathrm{D/H}) \times 10^6$	Ref
SDSS J1419+0829	3.03	3.049	20.392±0.003	-1.92[O/H]	25.06 ± 0.52	[38]
HS 0105+1619	2.65	2.536	19.426±0.006	-1.77[O/H]	25.76 ± 1.54	[38]
QSO B0913+0715	2.78	2.618	20.312±0.008	-2.40[O/H]	25.29 ± 1.05	[38]
SDSS J1358+0349	2.89	2.853	20.524±0.006	-2.80[O/H]	26.18 ± 0.72	[39]
SDSS J1358+6522	3.17	3.067	20.495±0.008	-2.33[O/H]	25.82 ± 0.71	[38]
SDSS J1558−0031	2.82	2.702	20.75±0.03	-1.55[O/H]	24.04 ± 1.44	[38]
PKS 1937−1009	3.78	3.256	18.09±0.03	-1.87[O/H]	24.49 ± 2.80	[40]
QSO J1444+2919	2.66	2.437	19.983±0.010	-2.04[O/H]	$19.68\ ^{+3.3}_{-2.8}$	[41]
PKS 1937−1009	3.78	3.572	17.925±0.006	-2.52[O/H]	26.08 ± 1.02	[52]
QSO 1009+2956	2.63	2.504	17.362±0.005	-2.50[Si/H]	$24.77\ ^{+4.1}_{-3.5}$	[43]
QSO 1243+307	2.55	2.525	19.761±0.026	-2.77[O/H]	23.88 ± 0.82	[44]
QSO J1332+0052	3.51	3.42	19.304±0.004	-1.71[O/H]	23.88 ± 0.77	[53]
Weighted mean, with $S = 1.08$					25.08 ± 0.29	

Table 24.2: Recent primordial ^{4}He measurements in extragalactic HII regions.

$Y_{\rm p}(^4\mathrm{He})$	$\pm 1\sigma_{\rm stat}$	$\pm 1\sigma_{\rm sys}$	$\pm 1\sigma_{\rm tot}$	# systems	Ref
0.2453	0.0034			16	[57]
0.2451	0.0019	0.0018	0.0026	1	[58]
0.243	0.005			16	[59]
0.2462	0.0022			120	[60]
0.2436	0.0040			54	[61]
0.2448	0.0027	0.0018	0.0033	7	[62]
0.2448			0.0033	17	[63]

24.4 Concordance, Dark Matter, and the CMB

We now use the observed light element abundances to test the theory. We first consider standard BBN, which is based on Standard Model physics alone, so $N_\nu = 3$ and the only free parameter is the baryon-to-photon ratio η. (The implications of BBN for physics beyond the Standard Model will be considered below). Thus, any abundance measurement determines η, and additional measurements overconstrain the theory and thereby provide a consistency check.

While the η ranges spanned by the boxes in Fig 24.1 do not all overlap, they are all within a factor ~ 2 of each other. In particular, the lithium abundance corresponds to η values that are inconsistent with that of the (now very precise) D/H abundance as well as the less-constraining ^{4}He abundance. This discrepancy marks the *lithium problem*. The problem could simply reflect difficulty in determining the primordial lithium abundance, or could hint at a more fundamental omission in the theory. The possibility that lithium reveals new physics is addressed in detail in the next section. If however we exclude the lithium constraint because its inferred abundance suffers from systematic uncertainties, then D/H and ^{4}He are in agreement. The concordant η range is essentially determined by D/H, and yields [78]

$$(\eta_{10})_{\rm SBBN} = 6.040 \pm 0.118 \ , \tag{24.5}$$

where the errors are 1σ. Despite the lithium problem, the overall concordance remains remarkable: using only well-established microphysics we can extrapolate back to $t \sim 1$ s to predict light element abundances spanning nine orders of magnitude, in approximate agreement with observation. This is a major success for the standard cosmology, and inspires confidence in extrapolation back to such early times.

This concordance provides a measure of the baryon content:

$$(\Omega_{\rm b} {\rm h}^2)_{\rm SBBN} = 0.02205 \pm 0.00043 \ , \tag{24.6}$$

where again errors are 1σ, a result that plays a key role in our understanding of the matter budget of the Universe. First of all $\Omega_{\rm b} \ll 1$, *i.e.*, baryons cannot close the Universe [79]. Furthermore, the cosmic density of (optically) luminous matter is $\Omega_{\rm lum} \simeq 0.0024{\rm h}^{-1}$ [80], so that $\Omega_{\rm b} \gg \Omega_{\rm lum}$: most baryons are optically dark, probably in the form of a diffuse intergalactic medium [81]. Finally, given that $\Omega_{\rm m} \sim 0.3$ (see the 'Dark Matter' and 'Cosmological Parameters' reviews), we infer that most matter in the Universe is not only dark, but also takes some non-baryonic (more precisely, non-nucleonic) form.

The BBN prediction for the cosmic baryon density can be tested through precision measurements of CMB temperature fluctuations (see the 'Cosmic Microwave Background' review). One can determine η from the amplitudes of the acoustic peaks in the CMB angular power spectrum [82], making it possible to compare two measures of η using very different physics, at two widely separated epochs. In the standard cosmology, there is no change in η between BBN and CMB decoupling, thus, a comparison of $\eta_{\rm BBN}$ and $\eta_{\rm CMB}$ is a key test. Agreement would endorse the standard picture, while disagreement could point to new physics during/-between the BBN and CMB epochs.

The analysis described in the Cosmic Microwave Background review (Sec.29), based on *Planck* TT, TE, EE + lowE data and lensing, yields [83]:

$$(\Omega_{\rm b} {\rm h}^2)_{\rm CMB} = 0.02237 \pm 0.00015; \tag{24.7}$$

which corresponds to [84]

$$(\eta_{10})_{\rm CMB} = 6.12 \pm 0.04 \ . \tag{24.8}$$

This result depends weakly on the primordial helium abundance, and the fiducial *Planck* analysis uses BBN theory to fix $Y_{\rm p}(\eta)$. Without BBN theory, the *Planck* TT, TE, EE + lowE data plus lensing give $\Omega_{\rm b}{\rm h}^2 = 0.02230 \pm 0.00021$, corresponding to $\eta_{10} = 6.104 \pm 0.058$. As shown in Fig. 24.1, this CMB estimate of the baryon density (narrow vertical band) is consistent with the BBN range, *i.e.*, in good agreement with the value inferred from high-redshift D/H measurements and local ^{4}He determinations; together these observations span diverse environments from redshifts $z \sim 1000$ to the present. Combining the CMB and BBN sharpens the baryon measures to $\eta_{10} = 6.115 \pm 0.038$ and $\Omega_{\rm b} h^2 = 0.02233 \pm 0.00014$ [78].

Int. J. Mod. Phys. A 2026.41. Downloaded from www.worldscientific.com
by UNIVERSITY OF CALIFORNIA @ BERKELEY on 09/16/26. Re-use and distribution is strictly not permitted, except for Open Access articles.

The ^{4}He abundance is proportional to the n/p ratio when the weak-interaction rate falls behind the Hubble expansion rate at $T_{\rm fr} \sim 1$ MeV. The presence of additional neutrino flavors (or of any other relativistic species) at this time increases g_*, hence the expansion rate, leading to a larger value of $T_{\rm fr}$, n/p, and therefore $Y_{\rm p}$ [10, 85]. In the Standard Model at $T = 1$ MeV, $g_* = 5.5 + \frac{7}{4}N_\nu$, where N_ν is the *effective* number of (nearly) massless neutrino flavors. The helium curves in 24.1 were computed taking $N_\nu = 3$; small corrections for non-equilibrium neutrino heating [20] are included in the thermal evolution and lead to an effective $N_\nu = 3.044$ compared to assuming instantaneous neutrino freezeout (see 'Big Bang Cosmology' — Sec. 22 of this *Review*). The computed ^{4}He abundance scales as $\Delta Y_{\rm p} \simeq 0.013\Delta N_\nu$ [11]. Clearly the central value for N_ν from BBN will depend on η, which is independently determined (with weaker sensitivity to N_ν) by the adopted D or ^{7}Li abundance. For example, if the best value for the observed primordial ^{4}He abundance is 0.249, then, for $\eta_{10} \sim 6$, the central value for N_ν is very close to 3. A maximum likelihood analysis on η and N_ν based on ^{4}He and D abundances nearly identical to those above finds the (correlated) 68% CL ranges to be $\eta_{10} = 6.088 \pm 0.054$ and [45, 78, 86]

$$N_\nu = 2.898 \pm 0.141 \tag{24.9}$$

which is consistent with the Standard Model. Identical results are obtained using a simpler method to extract such bounds based on χ^2 statistics, given a set of input abundances [87]. Very recently, the *Atacama Cosmology Telescope* and *South Pole Telescope* have each released new cosmological parameters arising from their most recent data, reporting $N_{\rm eff} = 2.86\pm0.13$ [88] and $N_{\rm eff} = 2.83\pm0.13$ [89], respectively. We look forward to joint analyses of these data with *Planck* that will sharpen the BBN/CMB interplay.

The CMB damping tail is sensitive to the primordial ^{4}He abundance independently of both BBN and local ^{4}He measurements [90]. The *Planck* analysis using TT, TE, EE+lowE and lensing but not the BBN $Y_{\rm p}(\eta)$ relation gives a ^{4}He mass fraction $0.239^{+0.024}_{-0.025}$, and nucleon fraction $Y_{\rm p} = 0.240^{+0.24}_{-0.25}$, both at 95% CL [83]. This is consistent with the HII region helium abundance determination. Moreover, this value is consistent with the Standard ($N_\nu = 3$) BBN prediction for $Y_{\rm p}$ with the *Planck*-determined baryon density. This concordance represents a successful CMB-only test of BBN.

The precision determination of the baryon density using the CMB motivates using this as an input to BBN calculations. Within the context of the Standard Model, BBN then becomes a zero-parameter theory, and the light element abundances are completely determined to within the uncertainties in $\eta_{\rm CMB}$ and the BBN theoretical errors. Comparison with the observed abundances then can be used to test the astrophysics of post-BBN light element evolution [91]. Alternatively, one can consider possible physics beyond the Standard Model (*e.g.*, which might change the expansion rate during BBN) and then use all of the abundances to test such models; this is discussed in 24.6 below.

24.5 The Lithium Problem and its Possible Resolution

As shown in Fig. 24.1, stellar Li/H measurements are inconsistent with the D/H (and CMB) constraints, given the quoted error budgets. For example, the primordial value from [45]

$$\mathrm{Li/H}|_{\rm p} = (4.72 \pm 0.7) \times 10^{-10} \tag{24.10}$$

exceeds the prediction of eq. 24.4 by a factor of 3.3, corresponding to a 4.4σ discrepancy. The universality of this problem is underscored by the fact that stars accreted into the Milky Way billions of years ago from external galaxies exhibit the same Li abundances as native stars [92–94]. The question then becomes pressing as to whether this mismatch comes from systematic errors in the observed abundances, and/or uncertainties in stellar astrophysics or nuclear inputs, or whether there might be new physics at work [9]. Nuclear inputs (cross sections) for BBN reactions are constrained by extensive laboratory measurements; to increase ^{7}Be destruction requires enhancement of otherwise subdominant processes that can be attained by missed resonances in a few reactions such as ^{7}Be$(d,p)2\alpha$ if the compound nuclear state properties are particularly favorable [30, 95–97]. However, experimental searches have now closed off these possibilities [98–100], making a *nuclear fix* increasingly unlikely.

Alternatively, lithium may be destroyed *in situ* within stars over their lifetimes. Depletion mechanisms include diffusion, rotational mixing, and pre-main-sequence burning. While these effects are real, reducing Li to the required levels generally demands some degree of fine-tuned stellar parameters or *ad hoc* mechanisms [101–104]. Diffusive models, for instance, predict both a dispersion in Li abundances and a downturn at the hot end of the Spite plateau. Additional turbulence must then be invoked to suppress diffusion and restore the observed uniformity [103].

Large surveys provide new insight. The GALAH project, which measured Li abundances for over 100,000 field stars, finds that warm stars with $-1.0 \leq$ [Fe/H] ≤ -0.5 form a plateau consistent with BBN predictions. This suggests that more metal-poor stars—now evolved beyond observability—may once have had higher Li abundances as well [105]. Pre-main-sequence depletion has also been proposed as a viable mechanism [102, 106].

Recent ^{6}Li measurements have added an important dimension. Because BBN produces negligible ^{6}Li [107], this isotope arises from later cosmic-ray interactions—fusion reactions such as $^4\mathrm{He} + {}^4\mathrm{He} \to {}^{6,7}\mathrm{Li} + \cdots$ and spallation on CNO nuclei, e.g. $p_{\rm cr} + {}^{16}\mathrm{O} \to {}^{6,7}\mathrm{Li}, {}^9\mathrm{Be}, {}^{10,11}\mathrm{B} + \cdots$. Thus ^{6}Li is co-produced with Be and B, both observed in metal-poor stars, implying that ^{6}Li must have been present at their birth. Early reports of ^{6}Li detections [108–110] suggested limited ^{7}Li depletion, since ^{6}Li is more fragile. However, recent work places strong upper limits on ^{6}Li/H in key plateau stars [111], removing the ^{6}Li-based objection for the absence of stellar depletion. Indeed, cosmic-ray production models can quantify the expected ^{6}Li levels, and the observed absence of ^{6}Li today implies significant depletion—enough that ^{7}Li destruction may also be sufficient to reconcile observations with BBN predictions [112]. This strengthens the case for stellar depletion as the leading resolution to the lithium problem [101–104, 113]. Future ^{6}Li detections or limits, together with refined models, will be critical for testing this scenario.

Finally, interstellar lithium measurements in low-metallicity systems provide a stellar depletion-free probe. In the Small Magellanic Cloud, interstellar Li/H has been measured at levels consistent with Galactic halo stars [114, 115]. Additional such measurements in other metal-poor environments would be highly valuable in disentangling primordial and stellar contributions.

It remains possible that the lithium problem points to new physics. Nucleosynthesis models in which the baryon-to-photon ratio is inhomogeneous can alter abundances for a given $\eta_{\rm BBN}$, but will overproduce ^{7}Li [116]. Entropy generation by some non-standard process could have decreased η between the BBN era and CMB decoupling, however the lack of spectral distortions in the CMB rules out any significant energy injection up to a redshift $z \sim 10^7$ [117]. The most intriguing resolution of the lithium problem thus involves new physics during BBN [7–9]

We summarize the general features of such solutions here, and later consider examples in the context of specific particle physics models. Many proposed solutions introduce perturbations to light-element formation during BBN; while all element abundances may suffer perturbations, the interplay of ^{7}Li and D is often the most important *i.e.* observations of D often provide the strongest constraints on the allowed perturbations to ^{7}Li. In this connection it is important to note that the new, very precise determination of D/H will significantly constrain the ability of such models to ameliorate or solve the lithium problem.

A well studied class of models invokes the injection of suprathermal hadronic or electromagnetic particles due to decays of dark matter particles. The effects are complex and depend on the nature of the decaying particles and their branchings and spectra. However, the models that most successfully solve the lithium problem generally feature non-thermal nucleons, which dissociate all light elements. Dissociation of even a small fraction of ^{4}He introduces a large abundance of free neutrons, which quickly thermalize. The thermal neutrons drive the ^{7}Be$(n,p)^7$Li conversion of ^{7}Be. The resulting ^{7}Li has a lower Coulomb barrier relative

Int. J. Mod. Phys. A 2026.41. Downloaded from www.worldscientific.com by UNIVERSITY OF CALIFORNIA @ BERKELEY on 09/16/26. Re- strictly not permitted, except for Open Access articles.

to ^{7}Be and is readily destroyed via $^7\mathrm{Li}(p,\alpha)^4\mathrm{He}$ [118, 119]]. But ^{4}He dissociation also produces D directly as well as via nonthermal neutron $n(p,\gamma)d$ reactions. This introduces a tension between Li/H reduction and D/H enhancement that becomes increasingly restrictive with the increasing precision of deuterium observations. Indeed, this now forces particle injection scenarios to make very small ^{7}Li perturbations — far short of the level needed. An exception is a recent model wherein MeV-scale decays by construction avoid ^{4}He dissociation and associated D/H overproduction, instead *borrowing* neutrons by dissociating only deuterons [120].

Another important class of models retains the standard cosmic particle content, but changes their interactions via time variations in the fundamental constants [121–127]. Here too, the details are model-dependent, but scenarios that solve or alleviate the lithium problem often feature perturbations to the deuteron binding energy. A weaker D binding leads to the D bottleneck being overcome later, so that element formation commences at a lower temperature and lower density. This leads in turn to slower nuclear rates that freeze out earlier. The net result is a *higher* final D/H, due to less efficient processing into ^{4}He, but also *lower* Li, due to suppressed production via $^3\mathrm{He}(\alpha,\gamma)^7\mathrm{Be}$.

The *cosmological lithium problem* remains an unresolved issue in BBN. Nevertheless, the remarkable concordance between the CMB and the D (as well as ^{4}He) abundance, is a non-trivial success, and provides important constraints on the early Universe.

24.6 Beyond the Standard Model

Given the simple physics underlying BBN, it is remarkable that it still provides the most effective test for the cosmological viability of ideas concerning physics beyond the Standard Model. Although baryogenesis and inflation must have occurred at higher temperatures in the early Universe, we do not as yet have 'standard models' for these, so BBN still marks the boundary between the established and the speculative in Big Bang cosmology. It might appear possible to push the boundary back to the quark-hadron transition at $T \sim \Lambda_{\mathrm{QCD}}$, or electroweak symmetry breaking at $T \sim 1/\sqrt{G_{\mathrm{F}}}$; however, so far no observable relics of these epochs have been identified, either theoretically or observationally. Thus, although the Standard Model provides a precise description of physics up to the Fermi scale, cosmology cannot be traced in detail before the BBN era.

The CMB power spectrum in the damping tail is independently sensitive to N_ν (*e.g.* [128]). The CMB value N_ν^{CMB} probes the cosmic radiation content at (re)combination, so a discrepancy would imply new physics or astrophysics. Indeed, observations by the South Pole Telescope implied $N_\nu^{\mathrm{CMB}} = 3.85 \pm 0.62$ [129], prompting discussion of *dark radiation* such as sterile neutrinos [130]. However, *Planck* 2018 results give $N_\nu^{\mathrm{CMB}} = 2.92^{+0.36}_{+0.37}$, 95% CL, when using Planck TT, TE, EE+lowE, a result quite consistent with 3 Standard Model neutrinos [83] (and adjusting for the CMB's measurement of $N_{\mathrm{eff}} = 3.044$ due to neutrino heading effects [131–133]). Indeed, the BBN and CMB constraints on N_ν are independent and of similar precision, so that it is now possible to limit any *change* in this parameter (and/or the baryon-to-photon ratio) between nucleosynthesis and recombination [78]. This can, for example, constrain models with late particle decays, or with early dark energy.

Just as one can use the measured helium abundance to place limits on g_* [85, 122, 134–136], any changes in the strong, weak, electromagnetic, or gravitational coupling constants, arising *e.g.*, from the dynamics of new dimensions, can be similarly constrained [137], as can any speed-up of the expansion rate in, *e.g.*, scalar-tensor theories of gravity [138].

The limits on N_ν can be translated into limits on other types of particles or particle masses that would affect the expansion rate of the Universe during nucleosynthesis. For example, consider *sterile* neutrinos with only right-handed interactions of strength $G_{\mathrm{R}} < G_{\mathrm{F}}$. Such particles would decouple at higher temperature than (left-handed) neutrinos, so their number density ($\propto T^3$) relative to neutrinos would be reduced by any subsequent entropy release, *e.g.*, due to annihilations of massive particles that become non-relativistic between the two decoupling temperatures. Thus, (relativistic) particles with less than full strength weak interactions contribute less to the energy density than particles that remain in equilibrium up to the time of nucleosynthesis [139]. If we impose $N_\nu < 4$ as an illustrative constraint, then the three right-handed neutrinos must have a temperature $3(T_{\nu_{\mathrm{R}}}/T_{\nu_{\mathrm{L}}})^4 < 1$. Since the temperature of the decoupled ν_{R} is determined by entropy conservation (see 'Big Bang Cosmology' — Sec. 22 of this *Review*), $T_{\nu_{\mathrm{R}}}/T_{\nu_{\mathrm{L}}} = [(43/4)/g_*(T_{\mathrm{d}})]^{1/3} < 0.76$, where T_{d} is the decoupling temperature of the ν_{R}. This requires $g_*(T_{\mathrm{d}}) > 24$, so decoupling must have occurred at $T_{\mathrm{d}} > 140$ MeV. The decoupling temperature is related to G_{R} through $(G_{\mathrm{R}}/G_{\mathrm{F}})^2 \sim (T_{\mathrm{d}}/3\,\mathrm{MeV})^{-3}$, where 3 MeV is the decoupling temperature for ν_{L}s. This yields a limit $G_{\mathrm{R}} \lesssim 10^{-2} G_{\mathrm{F}}$. The above argument sets lower limits on the masses of new Z' gauge bosons to which right-handed neutrinos would be coupled in models of superstrings [140], or extended technicolour [141]. Similarly a Dirac magnetic moment for neutrinos, which would allow the right-handed states to be produced through scattering and thus increase g_*, can be significantly constrained [142], as can any new interactions for neutrinos that have a similar effect [143–145]. Right-handed states can be populated directly by helicity-flip scattering if the neutrino mass is large enough, and this property has been used to infer a bound of $m_{\nu_\tau} \lesssim 1$ MeV (taking $N_\nu < 4$) [146]. If there is mixing between active and sterile neutrinos then the effect on BBN is more complicated [147, 148].

BBN limits on the cosmic expansion rate constrain supersymmetric scenarios in which the neutralino or gravitino are very light, so that they contribute to g_* [149]. A gravitino in the mass range $\sim 10^{-4} - 10$ eV will affect the expansion rate of the Universe similarly to a light neutralino (which is however now probably ruled out by collider data, especially the decays of the Higgs-like boson). The net contribution to N_ν then ranges between 0.74 and 1.69, depending on the gravitino and slepton masses [150].

The limit on the expansion rate during BBN can also be translated into bounds on the mass/lifetime of non-relativistic particles that decay during BBN. This results in an even faster speed-up rate, and typically also changes the entropy [151–153]. If the decays include Standard Model particles, the resulting electromagnetic [154] [91, 140, 155] and/or hadronic [156, 157] cascades can strongly perturb the light elements, which leads to even stronger constraints. Such arguments have been applied to rule out an MeV mass for ν_τ, which decays during nucleosynthesis [158].

Decaying-particle arguments have proved very effective in probing supersymmetry. Light-element abundances generally are complementary to accelerator data in constraining SUSY parameter space, with BBN reaching to values kinematically inaccessible to the LHC. Much recent interest has focused on the case in which the next-to-lightest supersymmetric particle is metastable and decays during or after BBN. The constraints on unstable particles discussed above imply stringent bounds on the allowed abundance of such particles [118]; if the metastable particle is charged (*e.g.*, the stau), then it is possible for it to form atom-like electromagnetic bound states with nuclei, and the resulting impact on light elements can be quite complex [8, 95, 159]. Moreover, SUSY decays can destroy ^{7}Li and/or produce ^{6}Li, leading to a possible supersymmetric solution to the lithium problems noted above [160] (see [7] for a review).

These arguments impose powerful constraints on supersymmetric inflationary cosmology [91, 140, 155–157], particularly thermal leptogenesis [161]. These limits can be evaded only if the gravitino is massive enough to decay before BBN, i.e., $m_{3/2} \gtrsim 50$ TeV [162] (which would be unnatural), or if it is in fact the lightest supersymmetric particle and thus stable [140, 155, 163, 164]. Similar constraints apply to moduli – very weakly coupled fields in string theory that obtain an electroweak-scale mass from supersymmetry breaking [165].

Finally, we mention that BBN places powerful constraints on the possibility that there are new large dimensions in nature, perhaps enabling the scale of quantum gravity to be as low as the electroweak scale [166]. Thus, Standard Model fields may be localized on a *brane*, while gravity alone propagates in the *bulk*. It has been further noted that the new dimensions may be non-compact, even infinite [167], and the cosmology of such models has attracted considerable attention. The expansion rate in the early Universe can be significantly modified, so BBN is able to set

Int. J. Mod. Phys. A 2026.41. Downloaded from www.worldscientific.com
by UNIVERSITY OF CALIFORNIA @ BERKELEY on 09/16/26. Re-use and distribution is strictly not permitted, except for Open Access articles.

interesting constraints on such possibilities [168, 169].

References

[1] R. V. Wagoner, W. A. Fowler and F. Hoyle, Astrophys. J. **148**, 3 (1967).

[2] D. N. Schramm and M. S. Turner, Rev. Mod. Phys. **70**, 303 (1998), [arXiv:astro-ph/9706069].

[3] G. Steigman, Ann. Rev. Nucl. Part. Sci. **57**, 463 (2007), [arXiv:0712.1100].

[4] F. Iocco *et al.*, Phys. Rept. **472**, 1 (2009), [arXiv:0809.0631].

[5] R. H. Cyburt *et al.*, Rev. Mod. Phys. **88**, 015004 (2016), [arXiv:1505.01076].

[6] S. Sarkar, Rept. on Prog. in Phys. **59**, 1493 (1996).

[7] K. Jedamzik and M. Pospelov, New J. Phys. **11**, 105028 (2009), [arXiv:0906.2087].

[8] M. Pospelov and J. Pradler, Ann. Rev. Nucl. Part. Sci. **60**, 539 (2010), [arXiv:1011.1054].

[9] B. D. Fields, Ann. Rev. Nucl. Part. Sci. **61**, 47 (2011), [arXiv:1203.3551].

[10] P.J.E. Peebles, Phys. Rev. Lett. **16**, 411 (1966).

[11] J. Bernstein, L. S. Brown and G. Feinberg, Rev. Mod. Phys. **61**, 25 (1989).

[12] S. Mukhanov, Int. J. Theor. Phys. **143**, 669 (2004).

[13] R. Esmailzadeh, G. D. Starkman and S. Dimopoulos, Astrophys. J. **378**, 504 (1991).

[14] T.-H. Yeh, K. A. Olive and B. D. Fields, JCAP **03**, 046 (2021), [arXiv:2011.13874].

[15] L. Kawano, Technical report (1992), URL `https://ui.adsabs.harvard.edu/abs/1992STIN...9225163K`.

[16] A. Arbey *et al.*, Comput. Phys. Commun. **248**, 106982 (2020), [arXiv:1806.11095].

[17] R. Consiglio *et al.*, Computer Physics Communications **233**, 237 (2018), [arXiv:1712.04378].

[18] A.-K. Burns, T. M. P. Tait and M. Valli, Eur. Phys. J. C **84**, 1, 86 (2024), [arXiv:2307.07061].

[19] S. Esposito *et al.*, Nucl. Phys. **B568**, 421 (2000), [arXiv:astro-ph/9906232].

[20] S. Dodelson and M. S. Turner, Phys. Rev. **D46**, 3372 (1992).

[21] D. Seckel (1993), [hep-ph/9305311].

[22] R. H. Cyburt, B. D. Fields and K. A. Olive, New Astron. **6**, 215 (2001), [arXiv:astro-ph/0102179].

[23] M. S. Smith, L. H. Kawano and R. A. Malaney, Astrophys. J. Suppl. **85**, 219 (1993).

[24] G. Fiorentini *et al.*, Phys. Rev. **D58**, 063506 (1998), [arXiv:astro-ph/9803177].

[25] A. Coc *et al.*, Astrophys. J. **744**, 158 (2012), [arXiv:1107.1117].

[26] R. H. Cyburt, B. D. Fields and K. A. Olive, JCAP **0811**, 012 (2008), [arXiv:0808.2818].

[27] K. M. Nollett and S. Burles, Phys. Rev. **D61**, 123505 (2000), [arXiv:astro-ph/0001440].

[28] R. H. Cyburt, Phys. Rev. **D70**, 023505 (2004), [arXiv:astro-ph/0401091].

[29] P. D. Serpico *et al.*, JCAP **0412**, 010 (2004), [arXiv:astro-ph/0408076].

[30] R. N. Boyd *et al.*, Phys. Rev. **D82**, 105005 (2010), [arXiv:1008.0848].

[31] C. Pitrou *et al.*, Mon. Not. Roy. Astron. Soc. **502**, 2, 2474 (2021), [arXiv:2011.11320].

[32] O. Pisanti *et al.*, JCAP **04**, 020 (2021), [arXiv:2011.11537].

[33] R.H. Cyburt and B. Davids, Phys. Rev. **C78**, 012 (2008).

[34] S. Burles, K. M. Nollett and M. S. Turner, Astrophys. J. **552**, L1 (2001), [arXiv:astro-ph/0010171].

[35] V. Mossa *et al.*, Nature **587**, 7833, 210 (2020).

[36] R. I. Epstein, J. M. Lattimer and D. N. Schramm, Nature **263**, 198 (1976).

[37] F. van de Voort *et al.*, Mon. Not. Roy. Astron. Soc. **477**, 1, 80 (2018), [arXiv:1704.08254].

[38] R. Cooke *et al.*, Astrophys. J. **781**, 1, 31 (2014), [arXiv:1308.3240].

[39] R. J. Cooke *et al.*, Astrophys. J. **830**, 2, 148 (2016), [arXiv:1607.03900].

[40] S. Riemer-Sørensen *et al.*, Mon. Not. Roy. Astron. Soc. **447**, 3, 2925 (2015), [arXiv:1412.4043].

[41] S. A. Balashev *et al.*, Mon. Not. Roy. Astron. Soc. **458**, 2, 2188 (2016), [arXiv:1511.01797].

[42] S. Riemer-Sørensen *et al.*, Mon. Not. Roy. Astron. Soc. **468**, 3, 3239 (2017), [arXiv:1703.06656].

[43] E. O. Zavarygin *et al.*, Mon. Not. Roy. Astron. Soc. **477**, 4, 5536 (2018), [arXiv:1706.09512].

[44] R. J. Cooke, M. Pettini and C. C. Steidel, Astrophys. J. **855**, 2, 102 (2018), [arXiv:1710.11129].

[45] B. D. Fields *et al.*, JCAP **2020**, 3, 010 (2020), [arXiv:1912.01132].

[46] J. L. Linsky *et al.*, Astrophys. J. **647**, 1106 (2006), [arXiv:astro-ph/0608308].

[47] M. Pettini and D. V. Bowen, Astrophys. J. **560**, 41 (2001), [arXiv:astro-ph/0104474].

[48] S. D'Odorico, M. Dessauges-Zavadsky and P. Molaro, Astron. Astrophys. **368**, L21 (2001), [arXiv:astro-ph/0102162].

[49] M. Fumagalli, J. M. O'Meara and J. X. Prochaska, Science **334**, 1245 (2011), [arXiv:1111.2334].

[50] P. Noterdaeme *et al.*, Astron. Astrophys. **542**, L33 (2012), [arXiv:1205.3777].

[51] R. Srianand *et al.*, Mon. Not. Roy. Astron. Soc. **405**, 3, 1888 (2010), [arXiv:1002.4620].

[52] F. Guarneri *et al.*, Mon. Not. Roy. Astron. Soc. **529**, 2, 839 (2024), [arXiv:2402.05586].

[53] P. A. Kislitsyn *et al.*, Mon. Not. Roy. Astron. Soc. **528**, 3, 4068 (2024), [arXiv:2401.12797].

[54] Y. I. Izotov, T. X. Thuan and N. G. Guseva, Mon. Not. Roy. Astron. Soc. **445**, 1, 778 (2014), [arXiv:1408.6953].

[55] Y. I. Izotov *et al.*, Astrophys. J. **527**, 757 (1999), [arXiv:astro-ph/9907228].

[56] K. A. Olive and E. D. Skillman, Astrophys. J. **617**, 29 (2004), [arXiv:astro-ph/0405588].

[57] E. Aver *et al.*, JCAP **2021**, 3, 027 (2021), [arXiv:2010.04180].

[58] M. Valerdi *et al.*, Astrophys. J. **876**, 2, 98 (2019), [arXiv:1904.01594].

[59] V. Fernández *et al.*, Mon. Not. Roy. Astron. Soc. **487**, 3, 3221 (2019), [arXiv:1905.09215].

[60] O. A. Kurichin *et al.*, Mon. Not. Roy. Astron. Soc. **502**, 2, 3045 (2021), [arXiv:2101.09127].

[61] T. Hsyu *et al.*, Astrophys. J. **896**, 1, 77 (2020), [arXiv:2005.12290].

[62] M. Valerdi, A. Peimbert and M. Peimbert, Mon. Not. Roy. Astr. Soc. **505**, 3, 3624 (2021), [arXiv:2105.12260].

[63] E. Aver *et al.*, Mon. Not. Roy. Astr. Soc. **510**, 1, 373 (2022), [arXiv:2109.00178].

[64] D. S. Aguado *et al.*, Astrophys. J. Lett. **874**, 2, L21 (2019), [arXiv:1904.04892].

[65] M. Spite and F. Spite, Nature **297**, 483 (1982).

[66] E. Vangioni-Flam *et al.*, New Astron. **4**, 245 (1999), [arXiv:astro-ph/9811327].

[67] S. G. Ryan *et al.*, Astrophys. J. **530**, L57 (2000), [arXiv:astro-ph/9905211].

Int. J. Mod. Phys. A 2026.41. Downloaded from www.worldscientific.com by UNIVERSITY OF CALIFORNIA @ BERKELEY on 09/16/26. Re-use strictly not permitted, except for Open Access articles.

[68] P. Bonifacio and P. Molaro, Mon. Not. Roy. Astron. Soc. **285**, 847 (1997), [arXiv:astro-ph/9611043].

[69] A. M. Matas Pinto *et al.*, Astron. Astrophys. **654**, A170 (2021), [arXiv:2110.00243].

[70] P. Bonifacio *et al.*, Astron. Astrophys. **462**, 851 (2007), [arXiv:astro-ph/0610245].

[71] W. Aoki *et al.*, Astrophys. J. **698**, 1803 (2009), [arXiv:0904.1448].

[72] L. Sbordone *et al.*, Astron. Astrophys. **522**, A26 (2010), [arXiv:1003.4510].

[73] P. Bonifacio *et al.*, Astron. & Astrophys. Rev. **33**, 1, 2 (2025), [arXiv:2504.06335].

[74] M. H. Pinsonneault *et al.*, Astrophys. J. **574**, 398 (2002), [arXiv:astro-ph/0105439].

[75] S. Borisov, N. Prantzos and C. Charbonnel, Astron. Astrophys. **691**, A142 (2024), [arXiv:2410.01880].

[76] R. Cayrel *et al.*, Astron. Astrophys. **473**, L37 (2007), [arXiv:0708.3819].

[77] D. S. Balser and T. M. Bania, Astrophys. J. **156**, 6, 280 (2018), [arXiv:1810.09422].

[78] T.-H. Yeh *et al.*, JCAP **10**, 046 (2022), [arXiv:2207.13133].

[79] H. Reeves *et al.*, Astrophys. J. **179**, 909 (1973).

[80] M. Fukugita and P. J. E. Peebles, Astrophys. J. **616**, 643 (2004), [arXiv:astro-ph/0406095].

[81] R. Cen and J. P. Ostriker, Astrophys. J. **514**, 1 (1999), [arXiv:astro-ph/9806281].

[82] G. Jungman *et al.*, Phys. Rev. **D54**, 1332 (1996), [arXiv:astro-ph/9512139].

[83] Planck Collaboration *et al.*, Astron. & Astrophys. **641**, A6 (2020), [arXiv:1807.06209].

[84] P. A. R. Ade *et al.* (Planck), Astron. Astrophys. **594**, A13 (2016), [arXiv:1502.01589].

[85] G. Steigman, D. N. Schramm and J. E. Gunn, Phys. Lett. **B66**, 202 (1977), [,159(1977)].

[86] B. D. Fields *et al.*, JCAP **2020**, 11, E02 (2020).

[87] E. Lisi, S. Sarkar and F. L. Villante, Phys. Rev. **D59**, 123520 (1999), [hep-ph/9901404].

[88] E. Calabrese *et al.*, arXiv e-prints arXiv:2503.14454 (2025), [arXiv:2503.14454].

[89] F. Ge *et al.* (SPT-3G), Phys. Rev. D **111**, 8, 083534 (2025), [arXiv:2411.06000].

[90] R. Trotta and S. H. Hansen, Phys. Rev. **D69**, 023509 (2004), [arXiv:astro-ph/0306588].

[91] R. H. Cyburt, B. D. Fields and K. A. Olive, Phys. Lett. **B567**, 227 (2003), [arXiv:astro-ph/0302431].

[92] P. Molaro, G. Cescutti and X. Fu, Mon. Not. Roy. Astron. Soc. **496**, 3, 2902 (2020), [arXiv:2006.00787].

[93] J. D. Simpson *et al.*, Mon. Not. Roy. Astron. Soc. (2021).

[94] D. S. Aguado *et al.*, Mon. Not. Roy. Astron. Soc. **500**, 1, 889 (2021), [arXiv:2007.11003].

[95] R. H. Cyburt *et al.*, JCAP **1305**, 014 (2013), [arXiv:1303.0574].

[96] N. Chakraborty, B. D. Fields and K. A. Olive, Phys. Rev. **D83**, 063006 (2011), [arXiv:1011.0722].

[97] C. Broggini *et al.*, JCAP **1206**, 030 (2012), [arXiv:1202.5232].

[98] P. D. O'Malley *et al.*, Phys. Rev. **C84**, 042801 (2011).

[99] F. Hammache *et al.*, Phys. Rev. **C88**, 6, 062802 (2013), [arXiv:1312.0894].

[100] M. W. Paris *et al.*, Nucl. Data Sheets **120**, 184 (2014), [arXiv:1304.3153].

[101] P. Molaro *et al.*, Memorie della Soc. Astronomica Italiana Supp. **22**, 233 (2012).

[102] X. Fu *et al.*, Mon. Not. Roy. Astron. Soc. **452**, 3, 3256 (2015), [arXiv:1506.05993].

[103] O. Richard, G. Michaud and J. Richer, Astrophys. J. **619**, 538 (2005), [arXiv:astro-ph/0409672].

[104] A. J. Korn *et al.*, Nature **442**, 657 (2006), [arXiv:astro-ph/0608201].

[105] X. Gao *et al.*, Mon. Not. Roy. Astron. Soc. **497**, 1, L30 (2020), [arXiv:2006.05173].

[106] C. T. Nguyen *et al.*, Astron. Astrophys. **696**, A136 (2025), [arXiv:2408.05039].

[107] D. Thomas *et al.*, Astrophys. J. **406**, 569 (1993), [arXiv:astro-ph/9206002].

[108] V. V. Smith, D. L. Lambert and P. E. Nissen, Astrophys. J. **408**, 262 (1993).

[109] L. M. Hobbs and J. A. Thorburn, Astrophys. J. Lett. **428**, L25 (1994).

[110] R. Cayrel *et al.*, Astron. Astrophys. **343**, 923 (1999), [arXiv:astro-ph/9901205].

[111] E. X. Wang *et al.*, Mon. Not. Roy. Astron. Soc. **509**, 1, 1521 (2021), [arXiv:2110.03822].

[112] B. D. Fields and K. A. Olive, JCAP **10**, 078 (2022), [arXiv:2204.03167].

[113] S. Borisov *et al.*, Astron. Astrophys. **690**, A245 (2024), [arXiv:2403.15534].

[114] J. C. Howk *et al.*, Nature **489**, 7414, 121 (2012), [arXiv:1207.3081].

[115] P. Molaro *et al.*, Astron. Astrophys. **690**, A38 (2024), [arXiv:2407.10818].

[116] K. Jedamzik and J. B. Rehm, Phys. Rev. **D64**, 023510 (2001), [arXiv:astro-ph/0101292].

[117] D. J. Fixsen *et al.*, Astrophys. J. **473**, 576 (1996), [arXiv:astro-ph/9605054].

[118] M. Kawasaki, K. Kohri and T. Moroi, Phys. Rev. **D71**, 083502 (2005), [arXiv:astro-ph/0408426].

[119] K. Jedamzik, Phys. Rev. **D70**, 063524 (2004), [arXiv:astro-ph/0402344].

[120] A. Goudelis, M. Pospelov and J. Pradler, Phys. Rev. Lett. **116**, 21, 211303 (2016), [arXiv:1510.08858].

[121] J. D. Barrow, Phys. Rev. **D35**, 1805 (1987).

[122] B. A. Campbell and K. A. Olive, Phys. Lett. **B345**, 429 (1995), [hep-ph/9411272].

[123] L. Bergstrom, S. Iguri and H. Rubinstein, Phys. Rev. **D60**, 045005 (1999), [arXiv:astro-ph/9902157].

[124] V. V. Flambaum and E. V. Shuryak, Phys. Rev. **D65**, 103503 (2002), [hep-ph/0201303].

[125] A. Coc *et al.*, Phys. Rev. **D76**, 023511 (2007), [arXiv:astro-ph/0610733].

[126] J. C. Berengut *et al.*, Phys. Rev. **D87**, 8, 085018 (2013), [arXiv:1301.1738].

[127] C. J. A. P. Martins, Astron. Astrophys. **646**, A47 (2021), [arXiv:2012.10505].

[128] Z. Hou *et al.*, Phys. Rev. **D87**, 083008 (2013), [arXiv:1104.2333].

[129] R. Keisler *et al.*, Astrophys. J. **743**, 28 (2011), [arXiv:1105.3182].

[130] J. Hamann *et al.*, Phys. Rev. Lett. **105**, 181301 (2010), [arXiv:1006.5276].

[131] K. Akita and M. Yamaguchi, JCAP **2020**, 8, 012 (2020), [arXiv:2005.07047].

[132] J. Froustey, C. Pitrou and M. C. Volpe, JCAP **2020**, 12, 015 (2020), [arXiv:2008.01074].

[133] J. J. Bennett *et al.*, JCAP **04**, 073 (2021), [arXiv:2012.02726].

Int. J. Mod. Phys. A 2026.41. Downloaded from www.worldscientific.com
by UNIVERSITY OF CALIFORNIA @ BERKELEY on 09/16/26. Re-use and distribution is strictly not permitted, except for Open Access articles.

[134] F. S. Accetta, L. M. Krauss and P. Romanelli, Phys. Lett. **B248**, 146 (1990).

[135] K. M. Nollett and R. E. Lopez, Phys. Rev. **D66**, 063507 (2002), [arXiv:astro-ph/0204325].

[136] C. Bambi, M. Giannotti and F. L. Villante, Phys. Rev. **D71**, 123524 (2005), [arXiv:astro-ph/0503502].

[137] E. W. Kolb, M. J. Perry and T. P. Walker, Phys. Rev. **D33**, 869 (1986).

[138] A. Coc *et al.*, Phys. Rev. **D73**, 083525 (2006), [arXiv:astro-ph/0601299].

[139] K. A. Olive, D. N. Schramm and G. Steigman, Nucl. Phys. **B180**, 497 (1981).

[140] J. R. Ellis *et al.*, Phys. Lett. **167B**, 457 (1986).

[141] L. M. Krauss, J. Terning and T. Appelquist, Phys. Rev. Lett. **71**, 823 (1993), [hep-ph/9305265].

[142] J. A. Morgan, Phys. Lett. **102B**, 247 (1981).

[143] E. W. Kolb, M. S. Turner and T. P. Walker, Phys. Rev. **D34**, 2197 (1986).

[144] J. A. Grifols and E. Masso, Mod. Phys. Lett. **A2**, 205 (1987).

[145] K. S. Babu, R. N. Mohapatra and I. Z. Rothstein, Phys. Rev. Lett. **67**, 545 (1991).

[146] A. D. Dolgov, S. H. Hansen and D. V. Semikoz, Nucl. Phys. **B524**, 621 (1998), [hep-ph/9712284].

[147] K. Enqvist, K. Kainulainen and M. J. Thomson, Nucl. Phys. **B373**, 498 (1992).

[148] A. D. Dolgov, Phys. Rept. **370**, 333 (2002), [hep-ph/0202122].

[149] J. A. Grifols, R. N. Mohapatra and A. Riotto, Phys. Lett. **B400**, 124 (1997), [hep-ph/9612253].

[150] H. K. Dreiner *et al.*, Phys. Rev. **D85**, 065027 (2012), [arXiv:1111.5715].

[151] K. Sato and M. Kobayashi, Prog. Theor. Phys. **58**, 1775 (1977).

[152] D. A. Dicus *et al.*, Phys. Rev. **D17**, 1529 (1978).

[153] R. J. Scherrer and M. S. Turner, Astrophys. J. **331**, 19 (1988), [Astrophys. J.331,33(1988)].

[154] D. Lindley, Mon. Not. Roy. Astron. Soc. **188**, 15P (1979).

[155] J. R. Ellis *et al.*, Nucl. Phys. **B373**, 399 (1992).

[156] M. H. Reno and D. Seckel, Phys. Rev. **D37**, 3441 (1988).

[157] S. Dimopoulos *et al.*, Nucl. Phys. **B311**, 699 (1989).

[158] S. Sarkar and A. M. Cooper-Sarkar, Phys. Lett. **148B**, 347 (1984).

[159] M. Kawasaki, K. Kohri and T. Moroi, Phys. Lett. **B649**, 436 (2007), [hep-ph/0703122].

[160] K. Jedamzik *et al.*, JCAP **0607**, 007 (2006), [hep-ph/0512044].

[161] S. Davidson *et al.*, Phys. Rev. **466**, 105 (2008).

[162] S. Weinberg, Phys. Rev. Lett. **48**, 1303 (1982).

[163] R. H. Cyburt *et al.*, Phys. Rev. **D67**, 103521 (2003), [arXiv:astro-ph/0211258].

[164] M. Bolz, A. Brandenburg and W. Buchmuller, Nucl. Phys. **B606**, 518 (2001), [Erratum: Nucl. Phys.B790,336(2008)], [hep-ph/0012052].

[165] G. D. Coughlan *et al.*, Physics Letters B **131**, 1-3, 59 (1983).

[166] N. Arkani-Hamed, S. Dimopoulos and G. R. Dvali, Phys. Rev. **D59**, 086004 (1999), [hep-ph/9807344].

[167] L. Randall and R. Sundrum, Phys. Rev. Lett. **83**, 3370 (1999), [hep-ph/9905221].

[168] J. M. Cline, C. Grojean and G. Servant, Phys. Rev. Lett. **83**, 4245 (1999), [hep-ph/9906523].

[169] P. Binetruy *et al.*, Phys. Lett. **B477**, 285 (2000), [hep-th/9910219].

25. Cosmological Parameters

Revised October 2025 by M. Cortês (ULisboa), O. Lahav (UCL) and A.R. Liddle (ULisboa).

25.1 Parameterizing the Universe

Rapid advances in observational cosmology have led to the establishment of a precision cosmological model, with many of the key cosmological parameters determined to one or two significant figure accuracy. Particularly prominent are measurements of cosmic microwave background (CMB) anisotropies, with the highest precision observations being those of the *Planck* Satellite [1, 2] (which superseded the landmark *WMAP* results [3, 4]), and at higher angular resolution measurements by the Atacama Cosmology Telescope (ACT) [5] and the South Pole Telescope (SPT) [6]. However the most accurate model of the Universe requires consideration of a range of observations, with complementary probes providing consistency checks, lifting parameter degeneracies, and enabling the strongest constraints to be placed.

The term 'cosmological parameters' now has a wide scope, and may include the parameterization of some functions as well as simple numbers describing properties of the Universe. The original usage referred to the parameters describing the global dynamics of the Universe, such as its expansion rate and curvature. Now we wish to know how the matter budget of the Universe is built up from its constituents: baryons, photons, neutrinos, dark matter, and dark energy. We also need to describe the nature of perturbations in the Universe, through global statistical descriptors such as the matter and radiation power spectra. There may be additional parameters describing the physical state of the Universe, such as the ionization fraction as a function of time during the era since recombination. Typical comparisons of cosmological models with observational data now feature between five and ten parameters.

25.1.1 *The global description of the Universe*

Ordinarily, the Universe is taken to be a perturbed Robertson–Walker space-time, with dynamics governed by Einstein's equations. This is described in detail in Big-Bang Cosmology—Sec. 22 of this *Review*. Using the density parameters Ω_i for the various matter species and Ω_Λ for the cosmological constant, the Friedmann equation can be written

$$\sum_i \Omega_i + \Omega_\Lambda - 1 = \frac{k}{R^2 H^2}\,, \tag{25.1}$$

where the sum is over all the different species of material in the Universe. This equation applies at any epoch, but later in this article we will use the symbols Ω_i and Ω_Λ to refer specifically to the present-epoch values.

The complete present-epoch state of the homogeneous Universe can be described by giving the current-epoch values of all the density parameters and the Hubble constant h (the present-day Hubble parameter being written $H_0 = 100h\,\mathrm{km\,s^{-1}\,Mpc^{-1}}$). A typical collection would be baryons Ω_b, photons Ω_γ, neutrinos Ω_ν, and cold dark matter Ω_c (given charge neutrality, the electron density is guaranteed to be too small to be worth considering separately and is effectively included with the baryons). The spatial curvature can then be determined from the other parameters using Eq. (25.1). The total present matter density $\Omega_\mathrm{m} = \Omega_\mathrm{c} + \Omega_\mathrm{b}$ may be used in place of the cold dark matter density Ω_c.

These parameters also allow us to track the history of the Universe, at least back until an epoch where interactions allow interchanges between the densities of the different species; this is believed to have last happened at neutrino decoupling, shortly before Big-Bang Nucleosynthesis (BBN). To probe further back into the Universe's history requires assumptions about particle interactions, and perhaps about the nature of physical laws themselves.

The standard neutrino sector has three flavors. For neutrinos of mass in the range $5\times10^{-4}\,\mathrm{eV}$ to $1\,\mathrm{MeV}$, the density parameter in neutrinos is predicted to be

$$\Omega_\nu h^2 = \frac{\sum m_\nu}{93.12\,\mathrm{eV}}\,, \tag{25.2}$$

where the sum is over all families with mass in that range (higher masses need a more sophisticated calculation). We use units with $c = 1$ throughout. Results on atmospheric and Solar neutrino oscillations [7] imply non-zero mass-squared differences between the three neutrino flavors. These oscillation experiments cannot tell us the absolute neutrino masses, but within the normal assumption of a mass hierarchy suggest a lower limit of approximately 0.06 eV for the sum of the neutrino masses (see Neutrinos—Sec. 14 of this *Review*).

Even a mass this small has a potentially observable effect on the formation of structure, as neutrino free-streaming damps the growth of perturbations. Analyses commonly now either assume a neutrino mass sum fixed at this lower limit, or allow the neutrino mass sum to be a variable parameter. To date there is no decisive evidence of any effects from either neutrino masses or an otherwise non-standard neutrino sector, and observations impose quite stringent limits (see Neutrinos in Cosmology—Sec. 26 of this *Review*). However, we note that the inclusion of the neutrino mass sum as a free parameter can affect the derived values of other cosmological parameters.

25.1.2 *Inflation and perturbations*

A complete model of the Universe must include a description of deviations from homogeneity, at least statistically. Indeed, the most powerful probes of the parameters described above come from the evolution of perturbations, so their study is naturally intertwined with the determination of cosmological parameters.

There are many different notations used to describe the perturbations, both in terms of the quantity used and the definition of the statistical measure. We use the dimensionless power spectrum Δ^2 as defined in Big-Bang Cosmology (Sec. 22 of this *Review*), which is also denoted $\mathcal{P}$ in some of the literature. If the perturbations obey Gaussian statistics, the power spectrum provides a complete description of their properties.

From a theoretical perspective, a useful quantity to describe the perturbations is the curvature perturbation $\mathcal{R}$, which measures the spatial curvature of a comoving slicing of the space-time. A simple case is the Harrison–Zeldovich spectrum, which corresponds to a constant $\Delta^2_\mathcal{R}$. More generally, one can approximate the spectrum by a power law, writing

$$\Delta^2_\mathcal{R}(k) = \Delta^2_\mathcal{R}(k_*)\left[\frac{k}{k_*}\right]^{n_\mathrm{s}-1}\,, \tag{25.3}$$

where n_s is known as the spectral index, always defined so that $n_\mathrm{s} = 1$ for the Harrison–Zeldovich spectrum, and k_* is an arbitrarily chosen scale. The initial spectrum, defined at some early epoch of the Universe's history, is usually taken to have a simple form such as this power law, and we will see that observations require n_s close to one. Subsequent evolution will modify the spectrum from its initial form.

The simplest mechanism for generating the observed perturbations is the inflationary cosmology, which posits a period of accelerated expansion in the Universe's early stages [8, 9]. It is a useful working hypothesis that this is the sole mechanism for generating perturbations, and it may further be assumed to be the simplest class of inflationary model, where the dynamics are equivalent to that of a single scalar field ϕ with canonical kinetic energy slowly rolling on a potential $V(\phi)$. One may seek to verify that this simple picture can match observations and to determine the properties of $V(\phi)$ from the observational data. Alternatively, more complicated models, perhaps motivated by contemporary fundamental physics ideas, may be tested on a model-by-model basis (see Inflation—Sec. 23 of this *Review*).

Inflation generates perturbations through the amplification of quantum fluctuations, which are stretched to astrophysical scales by the rapid expansion. The simplest models generate two types, density perturbations that come from fluctuations in the scalar field and its corresponding scalar metric perturbation, and gravitational waves that are tensor metric fluctuations. The former experience gravitational instability and lead to structure formation, while both generate CMB anisotropies. Defining slow-roll parameters (with primes indicating derivatives with respect to

Int. J. Mod. Phys. A 2026.41. Downloaded from www.worldscientific.com by UNIVERSITY OF CALIFORNIA @ BERKELEY on 09/16/26. Re-[redacted] strictly not permitted, except for Open Access articles.

Int. J. Mod. Phys. A 2026.41. Downloaded from www.worldscientific.com
by UNIVERSITY OF CALIFORNIA @ BERKELEY on 09/16/26. Re-use and distribution is strictly not permitted, except for Open Access articles.

the scalar field, and $m_{\rm Pl} \equiv \sqrt{\hbar c/G}$ the Planck mass) as

$$\epsilon = \frac{m_{\rm Pl}^2}{16\pi}\left(\frac{V'}{V}\right)^2 \quad , \quad \eta = \frac{m_{\rm Pl}^2}{8\pi}\frac{V''}{V}\,, \tag{25.4}$$

which should satisfy $\epsilon, |\eta| \ll 1$, the spectra can be computed using the slow-roll approximation as

$$\Delta^2_{\mathcal{R}}(k) \simeq \frac{8}{3m_{\rm Pl}^4}\,\frac{V}{\epsilon}\bigg|_{k=aH} \quad , \quad \Delta^2_{\rm t}(k) \simeq \frac{128}{3m_{\rm Pl}^4}\,V\bigg|_{k=aH} \,. \tag{25.5}$$

In each case, the expressions on the right-hand side are to be evaluated when the scale k is equal to the Hubble radius during inflation. The symbol '$\simeq$' here indicates use of the slow-roll approximation, which is expected to be accurate to a few percent or better.

From these expressions, we can compute the spectral indices [10]:

$$n_{\rm s} \simeq 1 - 6\epsilon + 2\eta \quad ; \quad n_{\rm t} \simeq -2\epsilon\,. \tag{25.6}$$

Another useful quantity is the ratio of the two spectra, defined by

$$r \equiv \frac{\Delta^2_{\rm t}(k_*)}{\Delta^2_{\mathcal{R}}(k_*)}\,. \tag{25.7}$$

We have

$$r \simeq 16\epsilon \simeq -8n_{\rm t}\,, \tag{25.8}$$

which is known as the consistency equation.

One could consider corrections to the power-law approximation, which we discuss later. However, for now we make the working assumption that the spectra can be approximated by such power laws. The consistency equation shows that r and $n_{\rm t}$ are not independent parameters, and so the simplest inflation models give initial conditions described by three parameters, usually taken as $\Delta^2_{\mathcal{R}}$, $n_{\rm s}$, and r, all to be evaluated at some scale k_*, usually the 'statistical center' of the range explored by the data. Alternatively, one could use the parameterization V, ϵ, and η, all evaluated at a point on the putative inflationary potential.

After the perturbations are created in the early Universe, they undergo a complex evolution up until the time they are observed in the present Universe. When the perturbations are small, this can be accurately followed using a linear theory numerical code such as `CAMB` or `CLASS` [11]. This works right up to the present for the CMB, but for density perturbations on small scales nonlinear evolution is important and can be addressed by a variety of semi-analytical and numerical techniques. However the analysis is made, the outcome of the evolution is in principle determined by the cosmological model and by the parameters describing the initial perturbations, and hence can be used to determine those.

Of particular interest are CMB anisotropies. Both the total intensity and two independent polarization modes are predicted to have anisotropies. These can be described by the radiation angular power spectra C_ℓ as defined in Cosmic Microwave Background (Sec. 29 of this *Review*), and again provide a complete description if the density perturbations are Gaussian.

25.1.3 *The standard cosmological model*

We now have most of the ingredients in place to describe the cosmological model. Beyond those of the previous subsections, we need a measure of the ionization state of the Universe. The Universe is known to be highly ionized at redshifts below 5 or so (otherwise radiation from distant quasars would be heavily absorbed in the ultra-violet), and the ionized electrons can scatter microwave photons, altering the pattern of observed anisotropies. The most convenient parameter to describe this is the optical depth to scattering τ (*i.e.*, the probability that a given photon scatters once); in the approximation of instantaneous and complete reionization, this could equivalently be described by the redshift of reionization $z_{\rm i}$.

As described in Sec. 25.4, models based on these parameters are able to give a good fit to the complete set of high-quality data available at present, and indeed some simplification is possible. Observations are consistent with spatial flatness, and the inflation models so far described automatically generate negligible spatial curvature, so we can set $k = 0$; the density parameters then must sum to unity, and so one of them can be eliminated. The neutrino energy density is often not taken as an independent parameter; provided that the neutrino sector has the standard interactions, the neutrino energy density, while relativistic, can be related to the photon density using thermal physics arguments, and a minimal assumption takes the neutrino mass sum to be that of the lowest mass solution to the neutrino-oscillation constraints, namely 0.06 eV. In addition, there is no observational evidence for the existence of tensor perturbations (with the upper limits now starting to become constraining on models), and so r could be set to zero. This leaves seven parameters, which is the smallest set that can usefully be compared to the present cosmological data. This model is referred to by various names, including ΛCDM, the concordance cosmology, and the standard cosmological model.

Of these parameters, only Ω_γ is accurately measured directly. The radiation density is dominated by the energy in the CMB, and the *COBE* satellite FIRAS experiment determined its temperature to be $T_\gamma = (2.7255 \pm 0.0006)$ K [12],[1] corresponding to $\Omega_\gamma = 2.47 \times 10^{-5} h^{-2}$. It typically can be taken as fixed when fitting other data. Hence the minimum number of cosmological parameters varied in fits to data is six, though as described below there may additionally be many 'nuisance' parameters necessary to describe astrophysical processes influencing the data.

In addition to this minimal set, there is a range of other parameters that might prove important in future as the datasets further improve, but for which there is so far no direct evidence, allowing them to be set to specific values for now. We discuss various speculative options in the next section. For completeness at this point, we mention one other interesting quantity, the helium fraction, which is a non-zero parameter that can affect the CMB anisotropies at a subtle level. It is usually fixed in microwave anisotropy studies, but the data are approaching a level where allowing its variation may become mandatory.

In conventional parameter estimation, a set of parameters is chosen by hand and the aim is to constrain their values. The higher-level inference problem of model selection instead compares different choices of parameter sets, as is necessary to assess whether observations are pointing towards inclusion of new physical effects. Bayesian inference offers an attractive framework for cosmological model selection, setting a tension between model predictiveness and ability to fit the data [13], and its use is becoming widespread.

25.1.4 *Derived parameters*

The parameter list of the previous subsection is sufficient to give a complete description of cosmological models that agrees with observational data. However, it is not a unique parameterization, and one could instead use parameters derived from that basic set. Parameters that can be obtained from the set given above include the age of the Universe, the present horizon distance, the present neutrino background temperature, the epoch of matter–radiation equality, the epochs of recombination and decoupling, the epoch of transition to an accelerating Universe, the baryon-to-photon ratio, and the baryon-to-dark-matter density ratio. In addition, the physical densities of the matter components, $\Omega_i h^2$, are often more useful than the density parameters. The density perturbation amplitude can be specified in many different ways other than the large-scale primordial amplitude, for instance, in terms of its effect on the CMB, or by specifying a short-scale quantity, a common choice being the present linear-theory mass dispersion in a radius of $8\,h^{-1}$Mpc, known as σ_8.

Different types of observation are sensitive to different subsets of the full cosmological parameter set, and some are more naturally interpreted in terms of some of the derived parameters of this subsection than on the original base parameter set. In particular, most types of observation feature degeneracies whereby they are unable to separate the effects of simultaneously varying specific combinations of several of the base parameters.

[1] All quoted uncertainties in this article are 1σ/68% confidence and all upper limits are 95% confidence. Cosmological parameters sometimes have significantly non-Gaussian uncertainties. Values from original sources have when appropriate been rounded according to the conventions of this volume.

Int. J. Mod. Phys. A 2026.41. Downloaded from www.worldscientific.com by UNIVERSITY OF CALIFORNIA @ BERKELEY on 09/16/26. Re-use strictly not permitted, except for Open Access articles.

25.2 Extensions to the standard model

At present, there is no secure positive evidence in favor of extensions of the standard model. But, as we will discuss later, there are some hints of possible deviations, currently under intense investigation.

25.2.1 *More general perturbations*

The standard cosmology assumes adiabatic, Gaussian perturbations. Adiabaticity means that all types of material in the Universe share a common perturbation, so that if the space-time is foliated by constant-density hypersurfaces, then all fluids and fields are homogeneous on those slices, with the perturbations completely described by the variation of the spatial curvature of the slices. Gaussianity means that the initial perturbations obey Gaussian statistics, with the amplitudes of waves of different wavenumbers being randomly drawn from a Gaussian distribution of width given by the power spectrum. Note that gravitational instability generates non-Gaussianity; in this context, Gaussianity refers to a property of the initial perturbations, before they evolve.

The simplest inflation models, based on one dynamical field, predict adiabatic perturbations and a level of non-Gaussianity that is too small to be detected by any experiment so far conceived. For present data, the primordial spectra are usually assumed to be power laws.

25.2.1.1 *Non-power-law spectra*

For typical inflation models, it is an approximation, albeit usually a good one, to take the spectra as power laws. As data quality improves, one might expect this approximation to come under pressure, requiring a more accurate description of the initial spectra, particularly for the density perturbations. In general, one can expand $\ln \Delta^2_{\mathcal{R}}$ as

$$\ln \Delta^2_{\mathcal{R}}(k) = \ln \Delta^2_{\mathcal{R}}(k_*) + (n_{\mathrm{s},*} - 1) \ln \frac{k}{k_*} + \frac{1}{2} \left. \frac{dn_{\mathrm{s}}}{d \ln k} \right|_* \ln^2 \frac{k}{k_*} + \cdots , \tag{25.9}$$

where the coefficients are all evaluated at some scale k_*. The term $dn_{\mathrm{s}}/d \ln k|_*$ is often called the running of the spectral index [14]. Once non-power-law spectra are allowed, it is necessary to specify the scale k_* at which the spectral index is defined.

25.2.1.2 *Isocurvature perturbations*

An isocurvature perturbation is one that leaves the total density unperturbed, while perturbing the relative amounts of different materials. If the Universe contains N fluids, there is one growing adiabatic mode and $N-1$ growing isocurvature modes (for reviews see Ref. [9, 15]). These can be excited, for example, in inflationary models where there are two or more fields that acquire dynamically-important perturbations. If one field decays to form normal matter, while the second survives to become the dark matter, this will generate a cold dark matter isocurvature perturbation.

In general, there are also correlations between the different modes, and so the full set of perturbations is described by a matrix giving the spectra and their correlations. Constraining such a general construct is challenging, though constraints on individual modes are beginning to become meaningful, with no evidence that any other than the adiabatic mode must be non-zero.

25.2.1.3 *Seeded perturbations*

An alternative to laying down perturbations at very early epochs is that they are seeded throughout cosmic history, for instance by topological defects such as cosmic strings. It has long been excluded that these are the sole original of structure, but they could contribute part of the perturbation signal, current limits being just a few percent [16]. In particular, cosmic defects formed in a phase transition ending inflation is a plausible scenario for such a contribution.

25.2.1.4 *Non-Gaussianity*

Multi-field inflation models can also generate primordial non-Gaussianity (reviewed, *e.g.*, in Ref. [9]). The extra fields can either be in the same sector of the underlying theory as the inflaton, or completely separate, an interesting example of the latter being the curvaton model [17]. Current upper limits on non-Gaussianity are becoming stringent, but there remains strong motivation to push down those limits and perhaps reveal trace non-Gaussianity in the data. If non-Gaussianity is observed, its nature may favor an inflationary origin, or a different one such as topological defects.

25.2.2 *Dark matter properties*

Dark matter properties are discussed in Dark Matter—Sec. 27 of this *Review*. The simplest assumption concerning the dark matter is that it has no significant interactions with other matter, and that its particles have a negligible velocity as far as structure formation is concerned. Such dark matter is described as 'cold,' and candidates include the lightest supersymmetric particle, the axion, and primordial black holes. As far as astrophysicists are concerned, a complete specification of the relevant cold dark matter properties is given by the density parameter Ω_{c}, though those seeking to detect it directly need also to know its interaction properties.

Cold dark matter is the standard assumption and gives an excellent fit to observations, except possibly on the shortest scales where there remains some controversy concerning the structure of dwarf galaxies and possible substructure in galaxy halos. It has long been excluded for all the dark matter to have a large velocity dispersion, so-called 'hot' dark matter, as it does not permit galaxies to form; for thermal relics the mass must be above about 1 keV to satisfy this constraint, though relics produced non-thermally, such as the axion, need not obey this limit. However, in future further parameters might need to be introduced to describe dark matter properties relevant to astrophysical observations. Suggestions that have been made include a modest velocity dispersion (warm dark matter) and dark matter self-interactions. There remains the possibility that the dark matter is comprised of two separate components, *e.g.*, a cold one and a hot one, an example being if massive neutrinos have a non-negligible effect.

25.2.3 *Relativistic species*

The number of relativistic species in the young Universe (omitting photons) is denoted N_{eff}. In the standard cosmological model only the three neutrino species contribute, and its baseline value is assumed fixed at 3.044 (the small shift from 3 is because of a slight predicted deviation from a thermal distribution [18]). However other species could contribute, for example an extra neutrino, possibly of sterile type, or massless Goldstone bosons or other scalars. It is hence interesting to study the effect of allowing this parameter to vary, and indeed although 3.044 is consistent with the data, most analyses currently suggest a somewhat higher value (*e.g.*, Ref. [19]).

25.2.4 *Dark energy and modified gravity*

While the standard cosmological model given above features a cosmological constant, in order to explain observations indicating that the Universe is presently accelerating, further possibilities exist under the general headings of 'dark energy' and 'modified gravity'. These topics are described in detail in Dark Energy—Sec. 28 of this *Review*). Here we focus on the case of the cosmological constant, since this simple model is a good match to existing data, but we also comment briefly on new results that consider both constant equation of state $w \neq -1$, and a time-varying equation of state [20, 21]

$$w(a) = w_0 + w_a(1-a) \tag{25.10}$$

where $a = 1/(1+z)$ is the scale factor, and w_0, w_a are free parameters. These are labeled wCDM and $w_0 w_a$CDM respectively.

If there is a redshift z_* where observations are tightest and yield w consistent with -1 (as is presently the case with observations best constraining w at $z_* \simeq 0.3$), that would advise against a wCDM analysis. This then implies that beyond ΛCDM the next $w(z)$ candidate is a parameterisation with two extra parameters, such as $w_0 w_a$CDM. Such a parameterisation can also be misleading in many ways that are well-documented in the literature.

25.2.5 *Complex ionization history*

The full ionization history of the Universe is given by the ionization fraction as a function of redshift z. The simplest scenario takes the ionization to have the small residual value left after recombination up to some redshift z_{i}, at which point the Universe instantaneously reionizes completely. Then there is a one-to-one

Int. J. Mod. Phys. A 2026.41. Downloaded from www.worldscientific.com
by UNIVERSITY OF CALIFORNIA @ BERKELEY on 09/16/26. Re-use and distribution is strictly not permitted, except for Open Access articles.

correspondence between τ and $z_{\rm i}$ (that relation, however, also depending on other cosmological parameters). An accurate treatment of this process will track separate histories for hydrogen and helium. While currently rapid ionization appears to be a good approximation, as data improve a more complex ionization history may need to be considered.

25.2.6 *Varying 'constants'*

Variation of the fundamental constants of Nature over cosmological times is another possible enhancement of the standard cosmology. There is a long history of study of variation of the gravitational constant $G_{\rm N}$, and more recently attention has been drawn to the possibility of small fractional variations in the fine-structure constant. There is presently no observational evidence for the former, which is tightly constrained by a variety of measurements. Evidence for the latter has been claimed from studies of spectral line shifts in quasar spectra at redshift $z \simeq 2$ [22], but this is presently controversial and in need of further observational study.

25.2.7 *Cosmic topology*

The usual hypothesis is that the Universe has the simplest topology consistent with its geometry, for example that a flat Universe extends forever. Observations cannot tell us whether that is true, but they can test the possibility of a non-trivial topology on scales up to roughly the present Hubble scale. Extra parameters would be needed to specify both the type and scale of the topology; for example, a cuboidal topology would need specification of the three principal axis lengths and orientation. At present, there is no evidence for non-trivial cosmic topology [23].

25.3 Cosmological Probes

The goal of the observational cosmologist is to utilize astronomical information to derive cosmological parameters. The transformation from the observables to the parameters usually involves many assumptions about the nature of the data, as well as of the dark sector. Below we outline the physical processes involved in each of the major probes, and the main recent results. The first two subsections concern probes of the homogeneous Universe, while the remainder consider constraints from perturbations.

In addition to statistical uncertainties we note three sources of systematic uncertainties that will apply to the cosmological parameters of interest: (i) due to the assumptions on the cosmological model and its priors (*i.e.*, the number of assumed cosmological parameters and their allowed range); (ii) due to the uncertainty in the astrophysics of the objects (*e.g.*, light-curve fitting for supernovae or the mass–temperature relation of galaxy clusters); and (iii) due to instrumental and observational limitations (*e.g.*, the effect of 'seeing' on weak gravitational lensing measurements, or beam shape on CMB anisotropy measurements).

These systematics, the last two of which appear as 'nuisance parameters', pose a challenging problem to the statistical analysis. We are attempting a statistical fit to the whole Universe with 6 to 12 parameters, but we might need to include hundreds of nuisance parameters, some of them highly correlated with the cosmological parameters of interest (for example time-dependent galaxy biasing could mimic the growth of mass fluctuations). Fortunately, there is some astrophysical prior knowledge on these effects, and a small number of physically-motivated free parameters would ideally be preferred in the cosmological parameter analysis.

25.3.1 *Measures of the Hubble constant*

In 1929, Edwin Hubble discovered the law governing the expansion of the Universe by measuring distances and velocities of nearby galaxies, confirming the expanding Universe proposal of Alexander Friedmann and Georges Lemaître. The slope of the relation between the distance and recession velocity is defined to be the present-epoch Hubble constant, H_0. Astronomers argued for decades about the systematic uncertainties in various methods and derived values over the wide range $40\,{\rm km\,s^{-1}\,Mpc^{-1}} \lesssim H_0 \lesssim 100\,{\rm km\,s^{-1}\,Mpc^{-1}}$.

One of the most reliable results on the Hubble constant came from the Hubble Space Telescope *(HST)* Key Project [24]. This study used the empirical period–luminosity relation for Cepheid variable stars, and calibrated a number of secondary distance indicators: Type Ia Supernovae (SNe Ia); the Tully–Fisher relation; surface-brightness fluctuations; and Type II Supernovae. Various systematics are under investigation, for example *JWST* is helping to understand the effect of field crowding [25]. This approach has been further extended, *e.g.*, using *HST* observations of Cepheids in the hosts of 42 SNe Ia and exploiting *Gaia* EDR3 parallaxes, the SH0ES team derived $H_0 = (73.0 \pm 1.0)\,{\rm km\,s^{-1}\,Mpc^{-1}}$ [26].

Three other methods have been used recently. One is a calibration of the tip of the red-giant branch (TRGB) applied to Type Ia supernovae, the Carnegie–Chicago Hubble Programme (CCHP) finding $H_0 = (68.8 \pm 1.8\,({\rm stat.}) \pm 1.3\,({\rm sys.}))\,{\rm km\,s^{-1}\,Mpc^{-1}}$ [27]. The second uses the method of time delay in gravitationally-lensed quasars, the TDCOSMO collaboration finding $H_0 = 71.6^{+3.9}_{-3.3}\,{\rm km\,s^{-1}\,Mpc^{-1}}$ from a sample of eight lenses [28]. A third method that came to fruition recently is based on gravitational waves; the 'bright standard siren' method applied to the binary neutron star GW170817 yields $H_0 = 70^{+12}_{-8}\,{\rm km\,s^{-1}\,Mpc^{-1}}$ [29]. Adding two 'dark standard siren' systems shifts this to $H_0 = 73^{+11}_{-8}\,{\rm km\,s^{-1}\,Mpc^{-1}}$ [30], still dominated by the single bright siren system. The 47 sources in the third Gravitational-Wave Transient Catalog (GWTC-3), again combined with the bright siren, yield the similar result $H_0 = 68^{+12}_{-8}\,{\rm km\,s^{-1}\,Mpc^{-1}}$ [31]. When many more gravitational-wave events have been acquired, the future uncertainties on H_0 from standard sirens will get smaller.

The determination of H_0 by the *Planck* Collaboration [2] gives a lower value than the above methods, $H_0 = (67.4 \pm 0.5)\,{\rm km\,s^{-1}\,Mpc^{-1}}$. As they discuss, there is a strong degeneracy of H_0 with other parameters, particularly $\Omega_{\rm m}$ and the neutrino mass. It is worth noting that using the 'inverse distance ladder' method gives a result $H_0 = (67.8 \pm 1.3)\,{\rm km\,s^{-1}\,Mpc^{-1}}$ [32], close to the *Planck* result. The inverse distance ladder relies on absolute-distance measurements from baryon acoustic oscillations (BAOs) to calibrate the intrinsic magnitude of the SNe Ia (rather than nearby Cepheids and parallax). This measurement was derived from 207 spectroscopically-confirmed Type Ia supernovae from the Dark Energy Survey (DES), an additional 122 low-redshift SNe Ia, and measurements of BAOs. A combination of DES Year 3 (Y3) clustering and weak lensing with BAO and BBN (assuming ΛCDM) gives $H_0 = (67.6 \pm 0.9)\,{\rm km\,s^{-1}\,Mpc^{-1}}$ [33]. The completed Extended Baryon Oscillation Spectroscopic Survey (eBOSS) [34] inverse distance ladder result, within an assumed extended cosmological model, is $H_0 = (68.2 \pm 0.8)\,{\rm km\,s^{-1}\,Mpc^{-1}}$, again close to the *Planck* value.

The above results indicate a possible tension between the H_0 values measured by *Planck* and SH0ES. This discrepancy is quoted to be at about the 5σ level by Ref. [26]. The other measures discussed above have larger uncertainties, with the TRGB, strong lensing, and gravitational wave approaches all being reasonably consistent with either the *Planck* or SH0ES value. Future improvements shall enable these to decisively enter the debate. In the meantime, the Hubble tension remains under investigation as to whether it is a signature of new physics, or due to underestimation of systematics in at least one of the anchoring probes: see Refs. [35, 36] for reviews.

25.3.2 *Supernovae as cosmological probes*

Empirically, the peak luminosity of SNe Ia can be used as an efficient distance indicator (*e.g.*, Ref. [37]), thus allowing cosmology to be constrained via the distance–redshift relation. The favorite theoretical explanation for SNe Ia is the thermonuclear disruption of carbon–oxygen white dwarfs. Although not perfect 'standard candles', it has been demonstrated that by correcting for a relation between the light-curve shape, color, and luminosity at maximum brightness, the dispersion of the measured luminosities can be greatly reduced. There are several possible systematic effects that may affect the accuracy of the use of SNe Ia as distance indicators, *e.g.*, evolution with redshift and interstellar extinction in the host galaxy and in the Milky Way.

In the late 1990s two major studies, the Supernova Cosmology Project and the High-z Supernova Search Team, found evidence for an accelerating Universe [38], interpreted as due to a cosmological constant or a dark energy component. When combined with

Int. J. Mod. Phys. A 2026.41. Downloaded from www.worldscientific.com by UNIVERSITY OF CALIFORNIA @ BERKELEY on 09/16/26. Reproduction strictly not permitted, except for Open Access articles.

the CMB data (which indicate near flatness, *i.e.*, $\Omega_{\rm m} + \Omega_\Lambda \simeq 1$), the best-fit values were $\Omega_{\rm m} \simeq 0.3$ and $\Omega_\Lambda \simeq 0.7$. Most results in the literature are consistent with the $w = -1$ cosmological constant case. A leading sample currently is the UNION3 compilation [39]. This set of over 2000 spectroscopically-confirmed SNe Ia gives $\Omega_{\rm m} = 0.356^{+0.028}_{-0.026}$ (stat+sym) for an assumed flat ΛCDM model, while in combination with the CMB, for a flat wCDM model these data give $w = -0.92 \pm 0.04$.

The DES full 5-year dataset [40] contains about 1500 photometrically-selected SNe classified by their light curves, in the redshift range $0.10 < z < 1.13$. Supplementing this with 194 low-redshift ($0.025 < z < 0.10$) SNe from other surveys they find $\Omega_{\rm m} = 0.352 \pm 0.017$ in flat-ΛCDM. For flat-wCDM $(\Omega_{\rm m}, w) = \left(0.26^{+0.07}_{-0.10}, -0.80^{+0.14}_{-0.16}\right)$, and for flat-$w_0 w_a$CDM they find

$$(\Omega_{\rm m}, w_0, w_a) = \left(0.50^{+0.03}_{-0.04}, -0.36^{+0.36}_{-0.30}, -8.8^{+3.7}_{-4.5}\right), \quad (25.11)$$

with highly non-Gaussian uncertainties. This DES SNe sample, when combined with DESI (Dark Energy Spectroscopic Instrument) BAO and *Planck* CMB data, yields the largest deviation from ΛCDM, hinting that dark energy may evolve with time (Ref. [41] and further discussion below). For debates on possible systematics in SNe see *e.g.* Ref. [42–44]. Future surveys (in particular large SNe datasets from Rubin-LSST and improved low-redshift anchoring samples) are expected to significantly refine constraints on the cosmic equation of state $w(z)$.

25.3.3 *Cosmic microwave background*

The physics of the CMB is described in detail in Cosmic Microwave Background—Sec. 29 of this *Review*. Before recombination, the baryons and photons are tightly coupled, and the perturbations oscillate in the potential wells generated primarily by the dark matter perturbations. After decoupling, the baryons are free to collapse into those potential wells. The CMB carries a record of conditions at the time of last scattering, often called primary anisotropies. In addition, it is affected by various processes as it propagates towards us, including the effect of a time-varying gravitational potential (the integrated Sachs–Wolfe effect), gravitational lensing, and scattering from ionized gas at low redshift.

The primary anisotropies, the integrated Sachs–Wolfe effect, and the scattering from a homogeneous distribution of ionized gas, can all be calculated using linear perturbation theory. Available codes include `CAMB` and `CLASS` [11], the former widely used embedded within the analysis package `CosmoMC` [45] and in higher-level analysis packages such as `CosmoSIS` [46], `CosmoLike` [47], and `Cobaya` [48]. Gravitational lensing is also calculated in these codes. Secondary effects, such as inhomogeneities in the reionization process, and scattering from gravitationally-collapsed gas (the Sunyaev–Zeldovich or SZ effect), require more complicated, and more uncertain, calculations.

The upshot is that the detailed pattern of anisotropies depends on all of the cosmological parameters. In a typical cosmology, the anisotropy power spectrum [usually plotted as $\ell(\ell+1)C_\ell/2\pi$] features a flat plateau at large angular scales (small ℓ), followed by a series of oscillatory features at higher angular scales, the first and most prominent being at around one degree ($\ell \simeq 200$). These features, known as acoustic peaks, represent the oscillations of the photon–baryon fluid around the time of decoupling. Some features can be closely related to specific parameters—for instance, the location in multipole space of the set of peaks probes the spatial geometry, while the relative heights of the peaks probe the baryon density—but many other parameters combine to determine the overall shape.

The 2018 data release from the *Planck* satellite [1] gives the most powerful results to date on the spectrum of CMB temperature anisotropies, with a precision determination of the temperature power spectrum to beyond $\ell = 2000$. ACT and SPT extend these results to higher angular resolution, though without full-sky coverage [5,6]. *Planck* and the polarization-sensitive versions of ACT and SPT give the current state of the art in measuring the spectrum of E-polarization anisotropies and the correlation spectrum between temperature and polarization. These are consistent with models based on the parameters we have described, and provide accurate determinations of many of those parameters [2]. Primordial B-mode polarization has not been detected (although the gravitational lensing effect on B modes has been measured).

The data provide an exquisite measurement of the location of the set of acoustic peaks, determining the angular-diameter distance of the last-scattering surface. In combination with other data this strongly constrains the spatial geometry, in a manner consistent with spatial flatness and excluding significantly-curved Universes. CMB data give a precision measurement of the age of the Universe. The CMB also gives a baryon density consistent with, and at higher precision than, that coming from BBN. It affirms the need for both dark matter and dark energy. It shows no evidence for dynamics of the dark energy, being consistent with a pure cosmological constant ($w = -1$). The density perturbations are consistent with a power-law primordial spectrum, and there is no indication yet of tensor perturbations. The current best-fit for the reionization optical depth from CMB data, $\tau = 0.054$, is in line with models of how early structure formation induces reionization.

Planck also made the first all-sky map of the CMB lensing field, which probes the entire matter distribution in the Universe and adds some additional constraining power to the CMB-only datasets. The recent ACT [49] and SPT [6] results demonstrate very well the reconstruction of the mass power spectrum at intermediate redshifts from CMB gravitational lensing. These measurements are consistent with *Planck*, supporting ΛCDM (see more in Cosmic Microwave Background—Sec. 29 in this *Review*).

25.3.4 *Galaxy clustering*

The power spectrum of density perturbations is affected by the nature of the dark matter. Within the ΛCDM model, the power spectrum shape depends primarily on the primordial power spectrum and on the combination $\Omega_{\rm m} h$, which determines the horizon scale at matter–radiation equality, with a subdominant dependence on the baryon density. The matter distribution is most easily probed by observing the galaxy distribution, but this must be done with care since the galaxies do not perfectly trace the dark matter distribution. Rather, they are a 'biased' tracer of the dark matter [50]. The need to allow for such bias is emphasized by the observation that different types of galaxies show bias with respect to each other. In particular, scale-dependent and stochastic biasing may introduce a systematic effect on the determination of cosmological parameters from redshift surveys [51]. Prior knowledge from simulations of galaxy formation or from gravitational lensing data could help to quantify biasing. Furthermore, the observed 3D galaxy distribution is in redshift space, *i.e.*, the observed redshift is the sum of the Hubble expansion and the line-of-sight peculiar velocity, leading to linear and non-linear dynamical effects that also depend on the cosmological parameters. On the largest length scales, the galaxies are expected to trace the location of the dark matter, except for a constant multiplier b to the power spectrum, known as the linear bias parameter. On scales smaller than 20 Mpc or so, the clustering pattern is 'squashed' in the radial direction due to coherent infall, which depends approximately on the parameter $\beta \equiv \Omega_{\rm m}^{0.6}/b$ (on these shorter scales, more complicated forms of biasing are not excluded by the data). On scales of a few Mpc, there is an effect of elongation along the line of sight (colloquially known as the 'finger of God' effect) that depends on the galaxy velocity dispersion.

25.3.4.1 *Baryon acoustic oscillations*

The power spectra of the 2-degree Field (2dF) Galaxy Redshift Survey and the Sloan Digital Sky Survey (SDSS) are well fit by a ΛCDM model and both surveys showed first evidence for baryon acoustic oscillations (BAOs) [52,53]. A big step forward for BAO science is due to DESI, whose first results in 2024 [54] have now been enhanced by a second data release, DESI-DR2 [41]. These BAO measurements are based on more than 14 million galaxies and quasars across a wide range of redshifts. From DESI data alone, they find $w = -0.916 \pm 0.078$ in a wCDM cosmology (see table V in their paper), consistent with ΛCDM.

Int. J. Mod. Phys. A 2026.41. Downloaded from www.worldscientific.com by UNIVERSITY OF CALIFORNIA @ BERKELEY on 09/16/26. Re-use and distribution is strictly not permitted, except for Open Access articles.

25.3.4.2 *Redshift distortion*

There is continuing interest in Kaiser's 'redshift distortion' effect [55]. This distortion depends on cosmological parameters via the perturbation growth rate in linear theory $f(z) = d\ln\delta/d\ln a \simeq \Omega_{\rm m}^{\gamma}(z)$, where $\gamma \simeq 0.55$ for the ΛCDM model and may be different for modified gravity models. By measuring $f(z)$ it is feasible to constrain γ and rule out certain modified gravity models [56, 57]. We note the degeneracy of the redshift-distortion pattern and the geometric distortion (the so-called Alcock–Paczynski effect [58]), *e.g.*, as illustrated by the WiggleZ survey [59] and eBOSS [34]. New results on redshift-distortion are presented in the DESI full-shape analysis of the galaxies and quasars [60]. This yields, from DESI(FS+BAO) with CMB and BBN and a spectral index prior, $\Omega_{\rm m} = 0.306 \pm 0.005$ and $\sigma_8 = 0.812 \pm 0.005$ in a flat-ΛCDM model, and consistency with $w_0 w_a$CDM derived from DESI BAO and other probes.

25.3.4.3 *Limits on neutrino mass from galaxy surveys and other probes*

Large-scale structure data place constraints on Ω_ν due to the neutrino free-streaming effect [61]. Presently there is no clear detection, and upper limits on neutrino mass are commonly estimated by comparing the observed galaxy power spectrum with a four-component model of baryons, cold dark matter, a cosmological constant, and massive neutrinos. Such analyses also assume that the primordial power spectrum is adiabatic, scale-invariant, and Gaussian. Potential systematic effects include biasing of the galaxy distribution and non-linearities of the power spectrum. An upper limit can also be derived from CMB anisotropies alone, while combination with additional cosmological datasets can improve the results.

The most recent results on neutrino mass upper limits and other neutrino properties are summarized in Neutrinos in Cosmology—Sec. 26 of this *Review*. The results depend on the combination of datasets, the complexity of the assumed model and its parameters, and the priors on the parameters. For example, one may impose a prior on the sum of the three masses to be positive, adopt the 0.06 eV lower bound from oscillation experiments, or allow complete freedom on the neutrino mass, allowing it even (unphysically) to be negative. Recent results come from combined analyses of DESI BAO and full-shape power spectrum, ACT and SPT-3G CMB and SNe. For instance, CMB alone (*Planck*+ACT+SPT) gives, for ΛCDM and a positive mass prior, the bound $\sum m_\nu < 0.17\,\text{eV}$ [6], while *Planck*+ACT+DESI-DR1 (BAO and Full Shape) give a tighter constraint, $\sum m_\nu < 0.071\,\text{eV}$ [60]. Intriguingly, if the prior on the neutrino mass is left unconstrained, the formal posterior distribution favors a "negative neutrino mass". This is likely to be due to data systematics and/or degeneracy with other parameters. For example, expanding the model to $w_0 w_a$CDM yields $\sum m_\nu < 0.186$ eV from *Planck*, ACT, and DESI-DR2, compared with $\sum m_\nu < 0.077\,\text{eV}$ if the assumed model is ΛCDM [62].

Although a neutrino mass detection remains elusive, we note that the upper limits have improved by more than a factor of 20 over the past two decades or so. Current cosmological datasets are also in good agreement with the standard value for the effective number of neutrino species $N_{\rm eff} = 3.044$ (see Neutrinos in Cosmology—Sec. 26 of this *Review*—and Ref. [63] for further discussion).

25.3.5 *Clustering in the inter-galactic medium*

It is commonly assumed, based on hydrodynamic simulations, that the neutral hydrogen in the inter-galactic medium (IGM) can be related to the underlying mass distribution. It is then possible to estimate the matter power spectrum from the absorption observed in quasar spectra, the so-called Lyman-α forest. The usual procedure is to measure the power spectrum of the transmitted flux, and then to infer the mass power spectrum. Photoionization heating by the ultraviolet background radiation and adiabatic cooling by the expansion of the Universe combine to give a simple power-law relation between the gas temperature and the baryon density. It also follows that there is a power-law relation between the optical depth τ and $\rho_{\rm b}$. Therefore, the observed flux $F = \exp(-\tau)$ is strongly correlated with $\rho_{\rm b}$, which itself traces the mass density. The matter and flux power spectra can be related by a biasing function that is calibrated from simulations. There are two variants of Lyman-alpha analyses: 1-dimensional power spectra from individual lines-of-sight that probe small (∼Mpc) scales; and 3-dimensional Lyman-alpha BAO analyses that measure large-scale correlations (over ∼100 Mpc scales) using neighboring quasar lines-of-sight.

DESI has the most up-to-date and detailed measurements of the BAO scale both in Lyman-α absorption and in its cross-correlation with quasars at an effective redshift $z = 2.33$ [64]. The Lyman-α flux power spectrum has also been used to constrain the nature of dark matter, for example limiting the amount of warm dark matter [65].

25.3.6 *Weak gravitational lensing*

Images of background galaxies are distorted by the gravitational effect of mass variations along the line of sight. Deep gravitational potential wells, such as galaxy clusters, generate 'strong lensing' leading to arcs, arclets, and multiple images, while more moderate perturbations give rise to 'weak lensing.' Weak lensing is now widely used to measure the mass power spectrum in selected regions of the sky (see Ref. [66] for reviews). Since the signal is weak, the image of deformed galaxy shapes (the 'shear map') must be analyzed statistically to measure the power spectrum, higher moments, and cosmological parameters. There are various systematic effects in the interpretation of weak lensing, *e.g.*, due to atmospheric distortions during observations, the redshift distribution of the background galaxies (usually depending on the accuracy of photometric redshifts), the intrinsic correlation of galaxy shapes, and non-linear modeling uncertainties.

Weak-lensing measurements from the Kilo-Degree Survey (KiDS) [67], the Subaru Hyper-Suprime-Cam (HSC) [68], and from DES [69] have constrained the clumpiness parameter defined as $S_8 \equiv \sigma_8(\Omega_{\rm m}/0.3)^{0.5}$. While early results suggested that the S_8 value from this technique might be significantly lower than that inferred from *Planck*, this discrepancy has essentially disappeared in the most recent measurements from KiDS [70].

25.3.7 *Other probes*

Other probes that have been used to constrain cosmological parameters, but that are not presently competitive in terms of accuracy, are the integrated Sachs-Wolfe effect [71,72], the number density or composition of galaxy clusters [73], and galaxy peculiar velocities that probe the mass fluctuations in the local Universe [74].

25.4 Bringing probes together

Although it contains two ingredients—dark matter and dark energy—which have not yet been verified by laboratory experiments, the ΛCDM model is almost universally accepted by cosmologists as an excellent general description of the present data. Existing indications against it, such as the Hubble tension and hints of evolving dark energy, are not securely established, nor have they led to specific consensus proposals for alternative cosmological models (Ref. [36] provides an extensive review of current tensions and possible explanations). Accordingly we quote parameter values assuming the validity of ΛCDM, while noting that these values might shift and/or have weakened constraints should a different paradigm take over in future.

The approximate values of some of the key parameters are $\Omega_{\rm b} \simeq 0.05$, $\Omega_{\rm c} \simeq 0.25$, $\Omega_\Lambda \simeq 0.70$, and a Hubble constant $h \simeq 0.70$. The spatial geometry is very close to flat (and usually assumed to be precisely flat), and the initial perturbations Gaussian, adiabatic, and nearly scale-invariant.

The most powerful data source is the CMB, which on its own supports all these main tenets. Values for some parameters, as given in Ref. [2,5], are reproduced in Table 25.1. These particular results presume a flat Universe. The constraints are somewhat strengthened by adding additional datasets, BAO being shown in the Table as an example, though most of the constraining power resides in the CMB data.

If the assumption of spatial flatness is lifted, it turns out that the primary CMB on its own constrains the spatial curvature fairly weakly, due to a parameter degeneracy in the angular-diameter distance. However, inclusion of other data readily re-

Int. J. Mod. Phys. A 2026.41. Downloaded by UNIVERSITY OF CALIFORNIA @ BERKELEY on 09/16/26. Reproduction strictly not permitted, except for Open Access articles. worldscientific.com

Table 25.1: Parameter constraints assuming the ΛCDM model. The first column uses *Planck* primary CMB data plus the *Planck* measurement of CMB lensing, giving our present recommended values. The second column adds CMB data from ACT and DESI-DR2 BAO data (though it also truncates the *Planck* data at $\ell = 1600$), and indicates how additional data can alter the constraints. The constraints are reproduced from Ref. [2] (Table 2, column 5) and Ref. [5] (Table 5, column 6), with some additional rounding. Both columns assume the ΛCDM cosmology with a power-law initial spectrum, no tensors, spatial flatness, a cosmological constant as dark energy, and the sum of neutrino masses fixed to 0.06 eV. Above the line are the six parameter combinations actually fit to the data ($\theta_{\rm MC}$ is a measure of the sound horizon at last scattering); those below the line are derived from these. The perturbation amplitude $\Delta^2_{\mathcal{R}}$ (denoted $A_{\rm s}$ in the original paper) is specified at the scale $0.05\,{\rm Mpc}^{-1}$. Uncertainties are shown at 68% confidence.

	Planck TT,TE,ing EE+lowE+lens	P-ACT-LB2
$\Omega_{\rm b}h^2$	0.02237 ± 0.00015	0.02258 ± 0.00010
$\Omega_{\rm c}h^2$	0.1200 ± 0.0012	0.1174 ± 0.0006
$100\,\theta_{\rm MC}$	1.0409 ± 0.0003	1.0409 ± 0.0002
$n_{\rm s}$	0.965 ± 0.004	0.975 ± 0.003
τ	0.054 ± 0.007	$0.064^{+0.006}_{-0.007}$
$\ln(10^{10}\Delta^2_{\mathcal{R}})$	3.044 ± 0.014	$3.062^{+0.010}_{-0.012}$
h	0.674 ± 0.005	0.684 ± 0.003
σ_8	0.811 ± 0.006	$0.812^{+0.004}_{-0.005}$
$\Omega_{\rm m}$	0.315 ± 0.007	0.300 ± 0.004
Ω_Λ	0.685 ± 0.007	0.700 ± 0.004

moves this degeneracy. Simply adding the *Planck* lensing measurement, and with the assumption that the dark energy is a cosmological constant, yields a 68% confidence constraint on $\Omega_{\rm tot} \equiv \sum \Omega_i + \Omega_\Lambda = 1.011 \pm 0.006$ and further adding BAO makes it 0.9993 ± 0.0019 [2]. Results of this type are normally taken as justifying the restriction to flat cosmologies.

One derived parameter that is very robust is the age of the Universe, since there is a useful coincidence that for a flat Universe the position of the first CMB acoustic peak is strongly correlated with the age. The CMB data give 13.797 ± 0.023 Gyr (assuming flatness). This is in good agreement with the ages of the oldest globular clusters and with radioactive dating.

The baryon density $\Omega_{\rm b}$ is now measured with high accuracy from CMB data alone, and is consistent with and more precise than the determination from BBN. The value quoted in Big-Bang Nucleosynthesis—Sec. 24 of this *Review*—is $\Omega_{\rm b}h^2 = 0.0220 \pm 0.0004$.

Various data provide strong support for the main predictions of the simplest inflation models: spatial flatness and adiabatic, Gaussian, nearly scale-invariant density perturbations. But it is disappointing that there is no sign of primordial gravitational waves; combining *Planck* and *WMAP* with BICEP2/Keck Array BK18 data (plus BAO data to help constrain $n_{\rm s}$) gives a 95% confidence upper limit of $r < 0.036$ at the scale $0.05\,{\rm Mpc}^{-1}$ [75]. The density perturbation spectral index is clearly required to be less than one by current data, though the strength of that conclusion can weaken if additional parameters are included in the model fits.

Tests have been made for various types of non-Gaussianity, a particular example being a parameter $f_{\rm NL}$ that measures a quadratic contribution to the perturbations. Various non-Gaussian shapes are possible (see Ref. [76] for details), and current constraints on the popular 'local', 'equilateral', and 'orthogonal' types (combining CMB temperature and polarization data) are $f_{\rm NL}^{\rm local} = -1 \pm 5$, $f_{\rm NL}^{\rm equil} = -26 \pm 47$, and $f_{\rm NL}^{\rm ortho} = -38 \pm 24$, respectively (these may appear weak, but prominent non-Gaussianity requires the product $f_{\rm NL}\Delta_{\mathcal{R}}$ to be large, and $\Delta_{\mathcal{R}}$ is of order 10^{-5}). Clearly none of these give any indication of primordial non-Gaussianity.

The above results come from the CMB alone, which is sufficient to constrain all the ΛCDM parameters well. But to go beyond that model, further data are usually necessary. Concerning dark energy, when the CMB is combined with DESI BAO and with SNe samples, and analysed using the $w_0 w_a$CDM model, there is a 'tantalizing suggestion' [54] for an evolving dark energy. Basically ΛCDM does not fit all three datasets well. Table V of the DESI-DR2 BAO key paper [41] provides a wide range of combinations of data sets and model assumptions. For example, DESI-BAO + CMB + DES-Y5 SNe give

$$(w_0, w_a) = (-0.75 \pm 0.06, -0.86^{+0.23}_{-0.20})\,. \tag{25.12}$$

This result lies 4.2σ away from ΛCDM ($w_0 = -1, w_a = 0$). However, fits substituting alternative SNe samples, Pantheon+ and Union3, give smaller discrepancies of 2.8σ and 3.8σ respectively. Ignoring SNe data entirely, the outcome for DESI-BAO + CMB is only 3.1σ away from ΛCDM. For fits to other parameterizations of $w(a)$, see Ref. [77]. The preferred dark energy models from this analysis switch from an early-time phantom regime ($w < -1$) to a non-phantom one at $z_* \simeq 0.3$. It is surprising that the transition happens at the redshift where observations are strongest, indicating the deviation from ΛCDM is entirely in the w_a parameter (consistent with no detections of deviations from ΛCDM in wCDM models, see Sec. 25.2.4). Compelling theoretical interpretations of such behaviors are presently lacking. Analyses of the final DESI data and new SNe data from Rubin-LSST will test whether the deviation from ΛCDM holds or is due to systematics. For further discussion see Dark Energy—Sec. 28 of this *Review*.

25.5 Outlook for the future

In its broad form (a model featuring dark matter and dark energy seeded by inflationary perturbations), the standard cosmological model, ΛCDM, remains a remarkable success, giving an excellent fit to thousands of high-precision datapoints. Its continuing viability depends on the ultimate resolution of the current hints and tensions discussed above. Presently dominant amongst those are the hints of evolving dark energy and the Hubble tension between *Planck* and SH0ES. However, neither of those has generated any compelling alternative cosmological model, despite considerable effort, and such explanations as do exist feature substantial tunings (for instance to mimic ΛCDM to the level the data require). To specify preferred values of cosmological parameters, as is our task here, the ΛCDM assumption remains the only reasonable option, caveats about tensions notwithstanding.

We can expect future developments to take one of two directions. Either the existing parameter set will continue to prove sufficient to explain the data, with the tensions diminishing and the parameters subject to ever-tightening constraints, or it will become necessary to deploy new parameters. The latter outcome would be very much the more interesting, offering a route towards understanding new physical processes relevant to cosmological evolution. There are many possibilities on offer for striking discoveries, for example:

- the cosmological effects of a neutrino mass may be unambiguously detected, shedding light on fundamental neutrino properties;
- detection of primordial non-Gaussianities would indicate that non-linear processes influence the perturbation generation mechanism;
- secure detection of variation in the dark energy density would provide much-needed experimental input into its nature.

These supply more than enough motivation for continued efforts to test the cosmological model and improve its accuracy. Over the coming years, there are a wide range of new observations that will bring further precision to cosmological studies. Indeed, there

Int. J. Mod. Phys. A 2026.41. Downloaded from www.worldscientific.com
by UNIVERSITY OF CALIFORNIA @ BERKELEY on 09/16/26. Re-use and distribution is strictly not permitted, except for Open Access articles.

are far too many to mention them all here, and so we highlight just a few areas.

The CMB observations will improve in several directions. A current frontier is the study of polarization, for which power spectrum measurements have now been made by several experiments. Detection of primordial B-mode anisotropies is the next major goal and a variety of projects are targeting this, though theory gives little guidance as to the likely signal level. Future CMB projects include the already-operating Simons Observatory and the planned *LiteBIRD* mission, though unfortunately it currently appears that the CMB Stage 4 experiment will not go ahead.

An impressive array of cosmology surveys are already operational, under construction, or proposed. Operating projects include the ground-based Suprime Camera and Rubin-LSST imaging surveys, spectroscopic surveys with DESI and the Prime Focus Spectrograph (PFS) on the Subaru telescope, and space missions *Euclid* (already generating science results though not yet cosmological ones) and *SPHEREx*. In the further future, the *Roman* Space Telescope is under construction and future plans include DESI-2, the 4-metre Multi-Object Spectroscopic Telescope (4MOST), the Spectroscopic Stage 5 experiment (Spec-S5), the Wide-Field Spectroscopic Telescope (WST), and the Multi-Object Spectroscopic Telescope (MUST).

An exciting area for the future is radio surveys of the redshifted 21-cm line of hydrogen. Because of the intrinsic narrowness of this line, by tuning the bandpass the emission from narrow redshift slices of the Universe will be measured to extremely high redshift, probing the details of the reionization process at redshifts up to perhaps 20, as well as measuring large-scale features such as the BAOs. LOFAR and CHIME were the first instruments able to do this. In the longer term, the Square Kilometre Array (SKA) will take these studies to higher levels of sophistication.

While the ΛCDM model will be challenged if the discrepancy between measurements of H_0 survives the rigorous scrutiny of systematics that may still lie unaccounted for, it is worth noting that the current accrual of momentum around the Hubble tension discussion (e.g. Ref. [36]) may be drawing attention away from awareness of the full set of assumptions underlying the analyses. When all factors are taken into account, we might be better advised maintaining a conservative stance, awaiting a longer-term perspective.

The establishment of the current precision standard cosmological model was a major achievement. However, it is important not to lose sight of the motivation for developing such a model, which is to understand the underlying physical processes at work governing the Universe's evolution. From that perspective, progress has been much less dramatic. For instance, there are many proposals for the nature of the dark matter, but no consensus as to which is correct. The nature of the dark energy remains a mystery. Even the baryon density, now measured to an accuracy of a percent, lacks an underlying theory able to predict it within orders of magnitude. Precision cosmology may have arrived, but at present many key questions remain, to motivate and challenge the cosmology and wider physics communities.

References

[1] Planck Collab. 2018 Results I, Astron. Astrophys. **641**, A1 (2020), [arXiv:1807.06205].

[2] Planck Collab. 2018 Results VI, Astron. Astrophys. **641**, A6 (2020), [arXiv:1807.06209].

[3] C. L. Bennett *et al.* (WMAP), Astrophys. J. Suppl. **208**, 20 (2013), [arXiv:1212.5225].

[4] G. Hinshaw *et al.* (WMAP), Astrophys. J. Suppl. **208**, 19 (2013), [arXiv:1212.5226].

[5] T. Louis *et al.* (ACT) (2025), [arXiv:2503.14452].

[6] E. Camphuis *et al.* (SPT-3G) (2025), [arXiv:2506.20707].

[7] S. Fukuda *et al.* (Super-Kamiokande), Phys. Rev. Lett. **85**, 3999 (2000), [hep-ex/0009001]; Q. R. Ahmad *et al.* (SNO), Phys. Rev. Lett. **87**, 071301 (2001), [arXiv:nucl-ex/0106015].

[8] E.W. Kolb and M.S. Turner, *The Early Universe*, Addison–Wesley (Redwood City, 1990).

[9] D.H. Lyth and A.R. Liddle, *The Primordial Density Perturbation*, Cambridge University Press (2009).

[10] A. R. Liddle and D. H. Lyth, Phys. Lett. **B291**, 391 (1992), [arXiv:astro-ph/9208007].

[11] A. Lewis, A. Challinor and A. Lasenby, Astrophys. J. **538**, 473 (2000), [arXiv:astro-ph/9911177]; D. Blas, J. Lesgourgues and T. Tram, JCAP **1107**, 034 (2011), [arXiv:1104.2933].

[12] D. J. Fixsen, Astrophys. J. **707**, 916 (2009), [arXiv:0911.1955].

[13] M. Hobson et al. (eds). *Bayesian Methods in Cosmology*, Cambridge University Press (2009).

[14] A. Kosowsky and M. S. Turner, Phys. Rev. **D52**, R1739 (1995), [arXiv:astro-ph/9504071].

[15] K. A. Malik and D. Wands, Phys. Rept. **475**, 1 (2009), [arXiv:0809.4944].

[16] Planck Collab. 2013 Results XXV, Astron. Astrophys. **571**, A25 (2014), [arXiv:1303.5085].

[17] D. H. Lyth and D. Wands, Phys. Lett. **B524**, 5 (2002), [hep-ph/0110002]; K. Enqvist and M. S. Sloth, Nucl. Phys. **B626**, 395 (2002), [hep-ph/0109214]; T. Moroi and T. Takahashi, Phys. Lett. **B522**, 215 (2001), [Erratum: Phys. Lett.B539,303(2002)], [hep-ph/0110096].

[18] J. J. Bennett *et al.*, JCAP **04**, 073 (2021), [arXiv:2012.02726].

[19] S. Riemer-Sorensen, D. Parkinson and T. M. Davis, Publ. Astron. Soc. Austral. **30**, e029 (2013), [arXiv:1301.7102].

[20] M. Chevallier and D. Polarski, Int. J. Mod. Phys. D **10**, 213 (2001), [arXiv:gr-qc/0009008].

[21] E. V. Linder, Phys. Rev. Lett. **90**, 091301 (2003), [arXiv:astro-ph/0208512].

[22] J. K. Webb *et al.*, Phys. Rev. Lett. **107**, 191101 (2011), [arXiv:1008.3907]; J. A. King *et al.*, Mon. Not. Roy. Astron. Soc. **422**, 3370 (2012), [arXiv:1202.4758]; P. Molaro *et al.*, Astron. & Astrophys. **555**, 68 (2013).

[23] Planck Collab. 2015 Results XVIII, Astron. Astrophys. **594**, A18 (2016), [arXiv:1502.01593].

[24] W. L. Freedman *et al.* (HST), Astrophys. J. **553**, 47 (2001), [arXiv:astro-ph/0012376].

[25] A. G. Riess *et al.*, Astrophys. J. Lett. **962**, 1, L17 (2024), [arXiv:2401.04773].

[26] A. G. Riess *et al.*, Astrophys. J. Lett. **934**, 1, L7 (2022), [arXiv:2112.04510].

[27] W. L. Freedman *et al.*, Astrophys. J. **985**, 2, 203 (2025), [arXiv:2408.06153].

[28] S. Birrer *et al.* (TDCOSMO), in "3rd General Meeting of CosmoVerse: Addressing observational tensions in cosmology with systematics and fundamental physics," (2025), [arXiv:2506.03023].

[29] B. P. Abbott *et al.* (LIGO Scientific, Virgo, 1M2H, Dark Energy Camera GW-E, DES, DLT40, Las Cumbres Observatory, VINROUGE, MASTER), Nature **551**, 7678, 85 (2017), [arXiv:1710.05835].

[30] A. Palmese *et al.*, Astrophys. J. **943**, 1, 56 (2023), [arXiv:2111.06445].

[31] R. Abbott *et al.* (LIGO Scientific, Virgo,, KAGRA, VIRGO), Astrophys. J. **949**, 2, 76 (2023), [arXiv:2111.03604].

[32] E. Macaulay *et al.* (DES), Mon. Not. Roy. Astron. Soc. **486**, 2, 2184 (2019), [arXiv:1811.02376].

[33] T. M. C. Abbott *et al.* (DES), Phys. Rev. D **105**, 2, 023520 (2022), [arXiv:2105.13549].

[34] S. Alam *et al.* (eBOSS), Phys. Rev. D **103**, 8, 083533 (2021), [arXiv:2007.08991].

[35] P. Shah, P. Lemos and O. Lahav, Astron. Astrophys. Rev. **29**, 1, 9 (2021), [arXiv:2109.01161].

[36] E. Di Valentino *et al.* (CosmoVerse Network), Phys. Dark Univ. **49**, 101965 (2025), [arXiv:2504.01669].

[37] B. Leibundgut, Ann. Rev. Astron. Astrophys. **39**, 67 (2001).

[38] A. G. Riess *et al.* (Supernova Search Team), Astron. J. **116**, 1009 (1998), [arXiv:astro-ph/9805201]; P. M. Garnavich *et al.* (Supernova Search Team), Astrophys. J. **509**, 74 (1998), [arXiv:astro-ph/9806396]; S. Perlmutter *et al.* (Supernova Cosmology Project), Astrophys. J. **517**, 565 (1999), [arXiv:astro-ph/9812133].

[39] D. Rubin *et al.* (2023), [arXiv:2311.12098].

[40] T. M. C. Abbott *et al.* (DES), Astrophys. J. Lett. **973**, 1, L14 (2024), [arXiv:2401.02929].

[41] M. Abdul Karim *et al.* (DESI) (2025), [arXiv:2503.14738].

[42] G. Efstathiou, Mon. Not. Roy. Astron. Soc. **538**, 2, 875 (2025), [arXiv:2408.07175].

[43] M. Vincenzi *et al.* (DES), Mon. Not. Roy. Astron. Soc. **541**, 3, 2585 (2025), [arXiv:2501.06664].

[44] M. Cortês and A. R. Liddle (2025), [arXiv:2504.15336].

[45] A. Lewis and S. Bridle, Phys. Rev. **D66**, 103511 (2002), [arXiv:astro-ph/0205436].

[46] J. Zuntz *et al.*, Astron. Comput. **12**, 45 (2015), [arXiv:1409.3409].

[47] E. Krause and T. Eifler, Mon. Not. Roy. Astron. Soc. **470**, 2, 2100 (2017), [arXiv:1601.05779].

[48] J. Torrado and A. Lewis, JCAP **05**, 057 (2021), [arXiv:2005.05290].

[49] L. Wenzl *et al.* (ACT), Phys. Rev. D **111**, 4, 043535 (2025), [arXiv:2405.12795].

[50] N. Kaiser, Astrophys. J. **284**, L9 (1984).

[51] A. Dekel and O. Lahav, Astrophys. J. **520**, 24 (1999), [arXiv:astro-ph/9806193].

[52] D. J. Eisenstein *et al.* (SDSS), Astrophys. J. **633**, 560 (2005), [arXiv:astro-ph/0501171].

[53] S. Cole *et al.* (2dFGRS), Mon. Not. Roy. Astron. Soc. **362**, 505 (2005), [arXiv:astro-ph/0501174].

[54] A. G. Adame *et al.* (DESI), JCAP **02**, 021 (2025), [arXiv:2404.03002].

[55] N. Kaiser, Mon. Not. Roy. Astron. Soc. **227**, 1 (1987).

[56] L. Guzzo *et al.*, Nature **451**, 541 (2008), [arXiv:0802.1944].

[57] A. Nusser and M. Davis, Astrophys. J. **736**, 93 (2011), [arXiv:1101.1650].

[58] C. Alcock and B. Paczynski, Nature **281**, 358 (1979).

[59] C. Blake *et al.*, Mon. Not. Roy. Astron. Soc. **425**, 405 (2012), [arXiv:1204.3674].

[60] A. G. Adame *et al.* (DESI), JCAP **07**, 028 (2025), [arXiv:2411.12022].

[61] J. Lesgourgues and S. Pastor, Phys. Rept. **429**, 307 (2006), [arXiv:astro-ph/0603494].

[62] C. Garcia-Quintero *et al.* (DESI) (2025), [arXiv:2504.18464].

[63] W. Elbers *et al.* (DESI) (2025), [arXiv:2503.14744].

[64] M. Abdul Karim *et al.* (DESI) (2025), [arXiv:2503.14739].

[65] M. Viel *et al.*, Phys. Rev. **D88**, 043502 (2013), [arXiv:1306.2314].

[66] A. Refregier, Ann. Rev. Astron. Astrophys. **41**, 645 (2003), [arXiv:astro-ph/0307212]; R. Massey *et al.*, Nature **445**, 286 (2007), [arXiv:astro-ph/0701594]; H. Hoekstra and B. Jain, Ann. Rev. Nucl. Part. Sci. **58**, 99 (2008), [arXiv:0805.0139].

[67] M. Asgari *et al.* (KiDS), Astron. Astrophys. **645**, A104 (2021), [arXiv:2007.15633].

[68] C. Hikage *et al.* (HSC), Publ. Astron. Soc. Jap. **71**, 2, 43 (2019), [arXiv:1809.09148].

[69] L. F. Secco *et al.* (DES), Phys. Rev. D **105**, 2, 023515 (2022), [arXiv:2105.13544].

[70] A. H. Wright *et al.* (2025), [arXiv:2503.19441].

[71] R. G. Crittenden and N. Turok, Phys. Rev. Lett. **75**, 2642 (1995), [arXiv:astro-ph/9505120].

[72] Planck Collab. 2015 Results XXI, Astron. Astrophys. **594**, A21 (2016), [arXiv:1502.01595].

[73] Planck Collab. 2015 Results XXIV, Astron. Astrophys. **594**, A24 (2016), [arXiv:1502.01597].

[74] A. Dekel, Ann. Rev. Astron. Astrophys. **32**, 371 (1994), [arXiv:astro-ph/9401022].

[75] P. A. R. Ade *et al.* (BICEP/Keck), Phys. Rev. Lett. **127**, 15, 151301 (2021), [arXiv:2110.00483].

[76] Planck Collab. 2018 Results IX, Astron. Astrophys. **641**, A9 (2020), [arXiv:1905.05697].

[77] K. Lodha *et al.* (DESI) (2025), [arXiv:2503.14743].

Int. J. Mod. Phys. A 2026.41. Downloaded
by UNIVERSITY OF CALIFORNIA @ BERKELEY on 09/16/26. Re-
orldscientific.com
strictly not permitted, except for Open Access articles.

Int. J. Mod. Phys. A 2026.41. Downloaded from www.worldscientific.com
by UNIVERSITY OF CALIFORNIA @ BERKELEY on 09/16/26. Re-use and distribution is strictly not permitted, except for Open Access articles.

26. Neutrinos in Cosmology

Revised August 2025 by J. Lesgourgues (RWTH Aachen U.) and L. Verde (ICC, U. of Barcelona; ICREA, Barcelona).

26.1 Standard neutrino cosmology

Neutrinos leave detectable imprints on cosmological observations that can then be used to constrain neutrino properties. This is a great example of the remarkable interconnection and interplay between nuclear physics, particle physics, astrophysics, and cosmology (for general reviews see *e.g.*, [1–4]). Present cosmological data are already providing constraints on neutrino properties that are not only complementary but also competitive with terrestrial experiments; for instance, upper bounds on the total neutrino mass have shrunk by about an order of magnitude in the past two decades. Forthcoming cosmological data may soon provide key information, not obtainable in other ways like *e.g.*, a measurement of the absolute neutrino mass scale.

A relic neutrino background pervading the Universe (the Cosmic Neutrino background, CνB) is a generic prediction of the standard hot Big Bang model (see Big Bang Nucleosynthesis – Chap. 24 of this *Review*). While it has not yet been detected directly, it has been indirectly confirmed by the accurate agreement of predictions and observations of: *a*) the primordial abundance of light elements (see Big Bang Nucleosynthesis – Chap. 24) of this *Review*; *b*) the power spectrum of Cosmic Microwave Background (CMB) anisotropies (see Cosmic Microwave Background – Chap. 29 of this *Review*); and *c*) the large-scale clustering of cosmological structures. Within the hot Big Bang model such good agreement would fail dramatically without a CνB with properties matching closely those predicted by the standard neutrino decoupling process (*i.e.*, involving only weak interactions).

We will illustrate below that cosmology is sensitive to the following neutrino properties: their density, related to the number of active (*i.e.*, left-handed, see Neutrino Mass, Mixing, and Oscillations – Chap. 14 of this *Review*) neutrino species, and their masses. At first order, cosmology is sensitive to the total neutrino mass, but is blind to the mixing angles and CP violation phase as discussed in Neutrino Mass, Mixing, and Oscillations (Chap. 14 of this *Review*). This makes cosmological constraints nicely complementary to measurements from terrestrial neutrino experiments.

The minimal cosmological model, ΛCDM, currently providing a good fit to most cosmological data sets (with the exception of some data in tension, discussed in The Cosmological Parameters Chap. 25 of this *Review*), assumes that the only massless or light (sub-keV) relic particles since the Big Bang Nucleosynthesis (BBN) epoch are photons and active neutrinos. Extended models with light sterile neutrinos, light thermal axions or other light relics –sometimes referred to as "dark radiation"– would produce effects similar to, and potentially degenerate with, those of active neutrinos. Thus neutrino bounds are often discussed together with limits on such scenarios. In the case of observational evidence for an unexpected density of radiation, it might not be obvious to discriminate between interpretation in terms of active neutrinos with non-standard decoupling, additional production mechanisms, non-standard interactions, *etc.*, or in terms of some additional light particles. Such extensions have been explored as a possible way to resolve the H_0 tension between late and early Universe determinations [5–8], but are not widely favoured [9–13].

Neutrino density and mass bounds can be derived under the assumption of no additional massless or light relic particles, and the neutrino density measured in that way provides a test of standard (*i.e.*, involving only weak interactions) neutrino decoupling.

In that model, the three active neutrino types thermalize in the early Universe, with a negligible leptonic asymmetry. Then they can be viewed as three propagating mass eigenstates sharing the same temperature and identical Fermi-Dirac distributions, thus with no visible effects of flavour oscillations. Neutrinos decouple gradually from the thermal plasma at temperatures $T \sim 2\,\mathrm{MeV}$. In the instantaneous neutrino decoupling limit, *i.e.*, assuming that neutrinos were fully decoupled at the time when electron-positrons annihilate and release entropy in the thermal bath, the neutrino-to-photon density ratio between the time of electron-positron annihilation and the non-relativistic transition of neutrinos would be given by

$$\frac{\rho_\nu}{\rho_\gamma} = \frac{7}{8} N_{\rm eff} \left(\frac{4}{11}\right)^{4/3} , \tag{26.1}$$

with $N_{\rm eff} = 3$, and the last factor comes from the fourth power of the temperature ratio $T_\nu/T_\gamma = (4/11)^{1/3}$ (see Big Bang Cosmology – Chap. 22 in this *Review*). In the above formula, $N_{\rm eff}$ is called the effective number of neutrino species because it can be viewed as a convenient parameterization of the relativistic energy density of the Universe beyond that of photons, in units of one neutrino in the instantaneous decoupling limit. Precise simulations of neutrino decoupling and electron-positron annihilation, taking into account flavor oscillations, provide accurate predictions for the actual phase-space distribution of relic neutrinos [14–22]. These distributions differ from the instantaneous decoupling approximation through a combination of a small shift in the photon temperature and small flavor-dependent non-thermal distortions, all at the percent level. The final result for the density ratio ρ_ν/ρ_γ in the relativistic regime can always be expressed as in Eq. (26.1), but with a different value of $N_{\rm eff}$. The most recent analyses, which include the effect of neutrino oscillations with the present values of the mixing parameters, an improved calculation of the collision terms, and the most recent results on plasma thermodynamics QED corrections, give $N_{\rm eff} = 3.044$ [18, 19, 21, 22]. The precise number density ratio n_ν/n_γ can also be derived from such studies, and is important for computing $\Omega_\nu h^2/\sum_i m_i$ (ratio of the physical density of neutrinos in units of the critical density to the sum of neutrino masses) in the non-relativistic regime. Once neutrinos are decoupled, their momentum redshifts like $p \propto 1/a$ but, due to the absence of interactions, their phase-space distributions remain constant when expressed in terms of the comoving momentum $q = pa$, even when they become non-relativistic.

The neutrino temperature today, $T_\nu^0 \simeq 1.7 \times 10^{-4}\,\mathrm{eV} \simeq 1.9\,\mathrm{K}$, is smaller than at least two of the neutrino masses, since the two squared-mass differences are $|\Delta m^2_{31}|^{1/2} > |\Delta m^2_{21}|^{1/2} > T_\nu^0$ (see Neutrino mass, Mixing, and oscillations – Chap. 14 of this *Review*). Thus at least two neutrino mass eigenstates are non-relativistic today and behave as a small "hot" fraction of the total dark matter (they cannot be all the dark matter, as explained in Chap. 27 of this *Review*). This fraction of hot dark matter can be probed by cosmological experiments, for two related reasons, as we now describe.

First, neutrinos are the only known particles behaving as radiation at early times (during the CMB acoustic oscillation era) and dark matter at late times (during structure formation), which has consequences on the background evolution. Neutrinos become non-relativistic when their mass is equal to their average momentum, given for any Fermi-Dirac-distributed particle by $\langle p \rangle = 3.15\,T$. Thus the redshift of the non-relativistic transition is given by $z_i^{\rm nr} = m_i/(3.15\,T_\nu^0) - 1 = m_i/[0.53\,\mathrm{meV}] - 1$ for each eigenstate of mass m_i, giving for instance $z_i^{\rm nr} = 110$ for $m_i = 60\,\mathrm{meV}$, corresponding to a time deep inside the matter-dominated regime. Second, until the non-relativistic transition, neutrinos travel at the speed of light, and later on they move at a typical velocity $\langle v_i/c \rangle = 3.15\,T_\nu(z)/m_i = 0.53(1+z)\,\mathrm{meV}/m_i$, which is several orders of magnitude larger than that of the dominant cold (or even of possibly warm) dark matter component(s). This brings their characteristic diffusion scale, called the "free-streaming length", to cosmological relevant values, with consequences for gravitational clustering and the growth of structure.

Once neutrinos are non-relativistic, their energy density is given by $\rho_\nu \simeq \sum m_i n_i$. Since the number densities n_i are equal to each other (up to negligible corrections coming from flavor effects in the decoupling phase), the total mass $\sum m_\nu = m_1 + m_2 + m_3$ can be factored out. It is possible that the lightest neutrino is still relativistic today, in which case this relation is slightly incorrect, but given that the total density is always strongly dominated by that of non-relativistic neutrinos, the error made is completely negligible. Using the expression for n_i/n_γ obtained from precise neutrino decoupling studies [18, 19], and knowing n_γ from the measurement of the CMB temperature, one can compute ρ_ν^0, the

Int. J. Mod. Phys. A 2026.41. Downloaded from www.worldscientific.com
by UNIVERSITY OF CALIFORNIA @ BERKELEY on 09/16/26. Re-[redacted] strictly not permitted, except for Open Access articles.

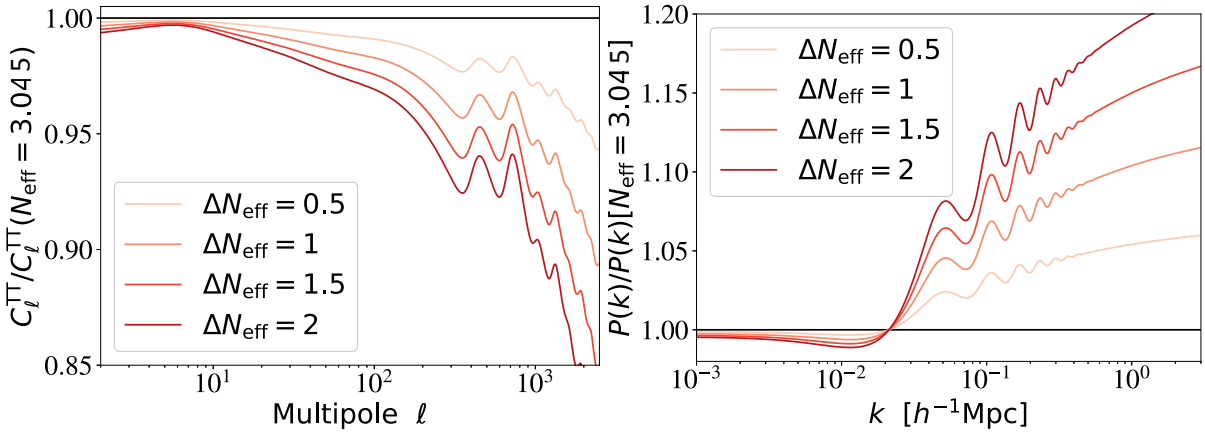

Figure 26.1: Ratio of the CMB C_ℓ^{TT} (left, including lensing effects) and matter power spectrum $P(k)$ (right, computed for each model in units of $(h^{-1}\mathrm{Mpc})^3$) for different values of $\Delta N_{\rm eff} \equiv N_{\rm eff} - 3.044$ over those of a reference model with $\Delta N_{\rm eff} = 0$. In order to minimize and better characterize the effect of $N_{\rm eff}$ on the CMB, the parameters that are kept fixed are $\{z_{\rm eq},\, z_\Lambda,\, \omega_{\rm b},\, \tau\}$ and the primordial spectrum parameters. Fixing $\{z_{\rm eq},\, z_\Lambda\}$ is equivalent to fixing the fractional density of total radiation, of total matter, and of cosmological constant $\{\Omega_{\rm r}, \Omega_{\rm m}, \Omega_\Lambda\}$, while increasing the Hubble parameter as a function of $N_{\rm eff}$. The statistical errors on the C_ℓ are about 1% for a band power of $\Delta\ell = 30$ at $\ell \sim 1000$. The error on $P(k)$ is estimated to be of the order of 5%.

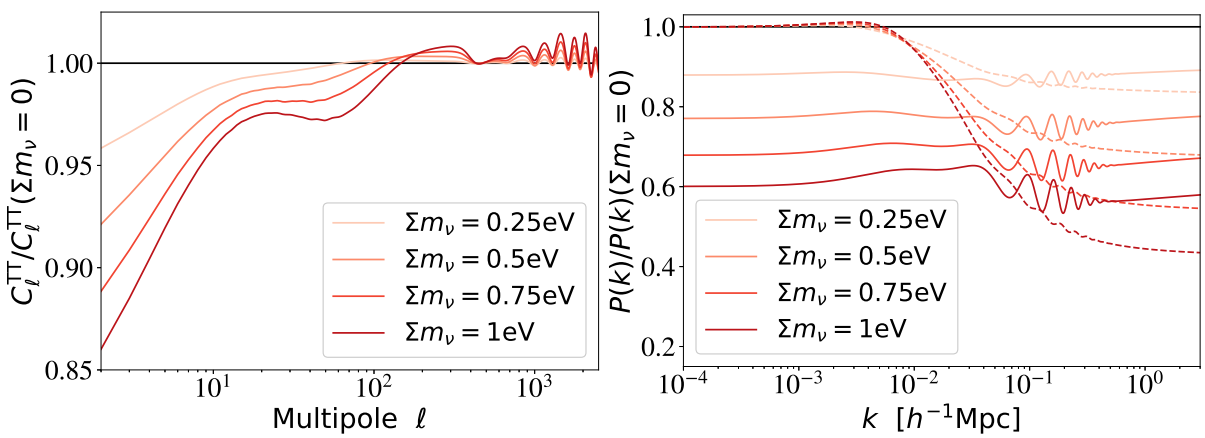

Figure 26.2: Ratio of the CMB C_ℓ^{TT} and matter power spectrum $P(k)$ (computed for each model in units of $(h^{-1}\mathrm{Mpc})^3$) for different values of $\sum m_\nu$ over those of a reference model with massless neutrinos. In order to minimize and better characterise the effect of $\sum m_\nu$ on the CMB, the parameters that are kept fixed are $\omega_{\rm b}$, $\omega_{\rm c}$, τ, the angular scale of the sound horizon $\theta_{\rm s}$ and the primordial spectrum parameters (solid lines). This implies that we are increasing the Hubble parameter h as a function of $\sum m_\nu$. For the matter power spectrum, in order to single out the effect of neutrino free-streaming on $P(k)$, the dashed lines show the spectrum ratio when $\{\omega_{\rm m}, \omega_{\rm b}, \Omega_\Lambda\}$ are kept fixed. For comparison, the error on $P(k)$ is of the order of 5% with current observations, and the fractional C_ℓ errors are of the order of $1/\sqrt{\ell}$ at low ℓ.

total neutrino density today,[1] in units of the critical density $\rho^0_{\rm crit}$:

$$\Omega_\nu = \frac{\rho^0_\nu}{\rho^0_{\rm crit}} = \frac{\sum m_\nu}{93.12 h^2\,\mathrm{eV}}\,, \tag{26.2}$$

and the total neutrino average number density today: $n^0_\nu = 339.5\ \mathrm{cm}^{-3}$ [23]. Here h is the Hubble constant in units of 100 km s^{-1} Mpc^{-1}.

26.2 Effects of neutrino properties on cosmological observables

As long as they are relativistic, *i.e.*, until some time deep inside the matter-dominated regime for neutrinos with a mass $m_i \ll 3.15\, T^{\rm eq}_\nu \simeq 1.5\,\mathrm{eV}$ (see Big Bang Cosmology, Chap. 22 in this *Review*), neutrinos enhance the density of radiation: this effect is parameterized by $N_{\rm eff}$ and can be discussed separately from the effect of the mass that will be described later in this section. Increasing $N_{\rm eff}$ impacts the observable spectra of CMB anisotropies and matter fluctuations through background and perturbation effects.

26.2.1 *Effect of* $\mathrm{N}_{\rm eff}$ *on the CMB*

The background effects depend on what is kept fixed when increasing $N_{\rm eff}$. If the densities of other species are kept fixed, a higher $N_{\rm eff}$ implies a smaller redshift of radiation-to-matter equality, with very strong effects on the CMB spectrum: when the amount of expansion between radiation-to-matter equality and photon decoupling is larger, the CMB acoustic peaks are suppressed. This effect is not truly characteristic of the neutrino density, since it can be produced by varying several other parameters. Hence, to characterize the effect of $N_{\rm eff}$, it is more useful and illuminating to enhance the density of total radiation, of total matter, and of Λ by exactly the same amount, in order to keep the redshift of radiation-to-matter equality $z_{\rm eq}$ and matter-to-Λ equality z_Λ fixed [24–27]. The primordial spectrum parameters, the baryon density $\omega_{\rm b} \equiv \Omega_{\rm b} h^2$ and the optical depth to reionization τ can be kept fixed at the same time, since we can simply vary

[1] The value 93.12 eV applies to the limit of large masses, in which $\rho^0_\nu = \sum m_i n^0_i$ and neutrinos are degenerate in mass [23]. This number would be larger by about 0.1% in the limit of minimal normal hierarchy (or smaller by about 0.06% for minimal inverted hierarchy), due the lightest mass state(s) being still relativistic today and to flavor-dependent non-thermal distortions in the neutrino phase-space distributions.

Int. J. Mod. Phys. A 2026.41. Downloaded from www.worldscientific.com
by UNIVERSITY OF CALIFORNIA @ BERKELEY on 09/16/26. Re-use and distribution is strictly not permitted, except for Open Access articles.

$N_{\rm eff}$ together with the Hubble parameter h with fixed $\{\omega_{\rm b}, \Omega_{\rm c}, \Omega_\Lambda\}$. The impact of such a transformation is shown in Fig. 26.1 for the CMB temperature spectrum C_ℓ^{TT} (defined in Chap. 29 in this *Review*) and for the matter power spectrum $P(k)$ (defined in Chap. 22 in this *Review*) for several representative values of $N_{\rm eff}$. These effects are within the reach of cosmological observations given current uncertainties, as discussed in Section 26.3.1 (for instance, with the *Planck* satellite data, the statistical error on the C_ℓs is of the order of one per cent for a band power of $\Delta\ell = 30$ at $\ell \sim 1000$).

With this transformation, the main background effect of $N_{\rm eff}$ is an increase in the diffusion scale (or Silk damping scale, see Cosmic Microwave Background – Chap. 29 in this *Review*) at the time of decoupling, responsible for the decrease in C_ℓ^{TT} at high ℓ, plus smaller effects coming from a slight increase in the redshift of photon decoupling [24–27]. At the level of perturbations, a higher $N_{\rm eff}$ implies that photons feel gravitational forces from a denser neutrino component; this tends to decrease the acoustic peaks (because neutrinos are distributed in a smoother way than photons) and to shift them to larger scales, *i.e.,* smaller multipoles (because photon perturbations traveling at the speed of sound in the photon-baryon fluid feel some dragging effect from neutrino perturbations travelling at the speed of light) [24,26–28]. The effect of increasing $N_{\rm eff}$ on the polarization spectrum features are the same as on the temperature spectrum: an increased Silk damping, and a shift in the acoustic peak amplitude and location – the latter effect is even more clear in the polarization spectrum, in which the location of acoustic peaks does not get further influenced by a Doppler effect like for temperature. The combination of these effects is truly characteristic of the radiation density parameter $N_{\rm eff}$ and cannot be mimicked by other parameters; thus $N_{\rm eff}$ can be accurately measured from the CMB alone. However, there are correlations between $N_{\rm eff}$ and other parameters. In particular, we have seen (Fig. 26.1) that in order to minimize the effect of $N_{\rm eff}$ on the CMB spectrum, one should vary h at the same time, hence there is a correlation between $N_{\rm eff}$ and h, which implies that independent measurements reducing the error bar on h also reduce that on $N_{\rm eff}$. Note that this correlation is not a perfect degeneracy, so both parameters can be constrained with CMB data alone.

26.2.2 *Effect of $N_{\rm eff}$ on the matter spectrum*

We have discussed the effect of increasing $N_{\rm eff}$ while keeping $z_{\rm eq}$ and $\omega_{\rm b}$ fixed, because the latter two quantities are very accurately constrained by CMB data. This implies that $\omega_{\rm c}$ increases with $N_{\rm eff}$, and that the ratio $\omega_{\rm b}/\omega_{\rm c} = \Omega_{\rm b}/\Omega_{\rm c}$ decreases. However, the ratio of baryonic-to-dark matter has a strong impact on the shape of the matter power spectrum, because until the time of decoupling of the baryons from the photons, CDM experiences gravitational collapse, while baryons are kept smoothly distributed by photon pressure and affected by acoustic oscillations. The decrease of $\Omega_{\rm b}/\Omega_{\rm c}$ following from the increase of $N_{\rm eff}$ gives more weight to the most clustered of the two components, namely the dark matter, and produces an enhancement of the small-scale matter power spectrum and a damping of the amplitude of baryon acoustic oscillations (BAOs), clearly visible in Fig. 26.1 (right plot). The scale of BAOs is also slightly shifted by the same neutrino dragging effect as for CMB peaks [24, 29].

The increase in the small-scale matter power spectrum is also responsible for a last effect on the CMB power spectra: the CMB last-scattering surface is slightly more affected by weak lensing from large-scale structures. This tends to smooth the maxima, the minima, and the damping scale of the CMB spectra [30].

26.2.3 *Effect of neutrino masses on the CMB*

Neutrino eigenstates with a mass $m_i \ll 0.6\,$eV become non-relativistic after photon decoupling. They contribute to the non-relativistic matter budget today, but not at the time of equality or recombination. If we increase the neutrino mass while keeping fixed the density of baryons and dark matter ($\omega_{\rm b}$ and $\omega_{\rm c}$), the early cosmological evolution remains fixed and independent of the neutrino mass, until the time of the non-relativistic transition. Thus one might expect that the CMB temperature and polarization power spectra are left invariant. This is not true for four reasons [26, 31, 32]

First, the neutrino density enhances the total non-relativistic density at late times, $\omega_{\rm m} = \omega_{\rm b} + \omega_{\rm c} + \omega_\nu$, where $\omega_\nu \equiv \Omega_\nu h^2$ is given as a function of the total mass $\sum m_\nu$ by Eq. (26.2). The late background evolution impacts the CMB spectrum through the relation between scales on the last-scattering surface and angles on the sky, and through the late ISW effect (see Cosmic Microwave Background – Chap. 29 of this *Review*). These two effects depend, respectively, on the angular diameter distance to recombination, $d_{\rm A}(z_{\rm rec})$, and on the redshift of matter-to-Λ equality. Increasing $\sum m_\nu$ tends to modify these two quantities. By playing with h and Ω_Λ, it is possible to keep one of them fixed, but not both at the same time. Since the CMB measures the angular scale of acoustic oscillations with exquisite precision, and is only loosely sensitive to the late ISW effect due to cosmic variance, we choose in Fig. 26.2 to vary the Hubble parameter in order to maintain a fixed scale $d_{\rm A}(z_{\rm rec})$. With such a choice, an increase in neutrino mass comes together with a decrease in the late ISW effect explaining the depletion of the CMB spectrum for $\ell \leq 20$. The fact that both $\sum m_\nu$ and h enter the expression of $d_A(z_{\rm rec})$ implies that measurements of the neutrino mass from CMB data are strongly correlated with h. Second, the non-relativistic transition of neutrinos affects the total pressure-to-density ratio of the Universe, and causes a small variation of the metric fluctuations. If this transition takes place not too long after photon decoupling, the variation is observable through the early ISW effect [26,31,33]. It is responsible for the dip seen in Fig. 26.2 for $20 \leq \ell \leq 200$. Third, when the neutrino mass is higher, the CMB spectrum is less affected by the weak lensing effect induced by the large-scale structure at small redshifts. This is due to a decrease in the matter power spectrum described in the next paragraphs. This reduced lensing effect is responsible for most of the oscillatory patterns visible in Fig. 26.2 (left plot) for $\ell \geq 200$. Fourth, the neutrinos with the smallest momenta start to become non-relativistic earlier than the average ones. The photon perturbations feel this through their gravitational coupling with neutrinos. This leads to a small enhancement of C_l^{TT} for $\ell \geq 500$, which is hardly visible on Fig. 26.2 because it is balanced by the lensing effect.

26.2.4 *Effect of neutrino masses on the matter spectrum*

The physical effect of neutrinos on the matter power spectrum is related to their velocity dispersion. Neutrinos free-stream over large distances without falling into small potential wells. The free-streaming scale is roughly defined as the distance traveled by neutrinos over a Hubble time scale $t_{\rm H} = (a/\dot{a})$, and approximates the scale below which neutrinos remain very smooth. On larger scales, they cluster in the same way as cold dark matter. The power spectrum of total matter fluctuations, related to the squared fluctuation $\delta_{\rm m}^2$ with $\delta_{\rm m} \equiv \delta_{\rm b} + \delta_{\rm c} + \delta_\nu$, gets a negligible contribution from the neutrino component on small scales, and is reduced by a factor $(1 - 2f_\nu)$, where $f_\nu = \omega_\nu/\omega_{\rm m}$. Additionally, on scales below the free-streaming scale, the growth of ordinary cold dark matter and baryon fluctuations is modified by the fact that neutrinos contribute to the background density, but not to the density fluctuations. This changes the balance between the gravitational forces responsible for clustering, and the Hubble friction term slowing it down. Thus the growth rate of CDM and baryon fluctuations is reduced [34]. This results today in an additional suppression of the small-scale linear matter power spectrum by approximately $(1 - 6f_\nu)$. These two effects sum up to a factor $(1 - 8f_\nu)$ [35] (more precise approximations can be found in Refs. [2, 26]). The non-linear spectrum is even more suppressed on mildly non-linear scales [3, 36–40].

This effect is often illustrated by plots of the matter power spectrum ratio with fixed parameters $\{\omega_{\rm m}, \omega_{\rm b}, \Omega_\Lambda\}$ and varying f_ν, *i.e.*, with the CDM density adjusted to get a fixed total dark matter density [2, 26, 35] (see Fig. 26.2, right plot, dashed lines). This transformation does not leave the redshift of equality $z_{\rm eq}$ invariant, and has very large effects on the CMB spectra. If one follows the logic of minimizing CMB variations and fixing $z_{\rm eq}$ like in the previous paragraphs, the increase in $\sum m_\nu$ must take place together with an increase of h, which tends to suppress the large-scale power spectrum, by approximately the same amount as the neutrino free-streaming effect [41]. In that case, the impact of neu-

Int. J. Mod. Phys. A 2026.41. Downloaded by UNIVERSITY OF CALIFORNIA @ BERKELEY on 09/16/26. Reproduced from www.worldscientific.com strictly not permitted, except for Open Access articles.

trino masses on the matter power spectrum appears as an overall amplitude suppression, which can be seen in Fig. 26.2 (right plot, solid lines). The oscillations on intermediate wavenumbers come from a small shift in the BAO scale [41]. This global effect is not degenerate with a variation of the primordial spectrum amplitude $A_{\rm s}$, because it only affects the matter power spectrum, and not the CMB spectra. However, the amplitude of the CMB temperature and polarization spectrum is given by the combination $A_{\rm s}e^{-2\tau}$. Hence a measurement of τ is necessary in order to fix $A_{\rm s}$ from CMB data, and avoid a parameter degeneracy between $\sum m_\nu$ and $A_{\rm s}$ [41–43].

A few of the neutrino mass effects described above – free-streaming scale, early ISW – depend on individual masses m_i, but most of them depend only on the total mass through f_ν – suppression of the matter power spectrum, CMB lensing, and shift in angular diameter distance. Because the latter effects are easier to measure, cosmology is primarily sensitive to the total mass $\sum m_\nu$ [44, 45]. The possibility that future data sets might be able to measure individual masses or the mass hierarchy, despite systematic errors and parameter degeneracies, is still an active subject of investigation [46–52].

26.3 Cosmological constraints on neutrino properties

In this chapter we focus on cosmological constraints on the abundance and mass of ordinary active neutrinos. Several stringent but model dependent constraints on non-standard neutrinos (*e.g.*, sterile neutrinos, active neutrinos with interactions beyond the weak force, unstable neutrinos with invisible decay, *etc.*) can also be found in the literature.

We highlight that cosmological constraints on neutrino properties are always obtained within the framework of a ΛCDM model or simple and popular extensions of this model, as spelled out in the following subsections. In light of the emergence of cosmological tensions – especially the so-called Hubble tension (see Chap. 25 of this *Review*), as well as hints of a possible tension on the late expansion history (see Chap. 28 of this *Review*) – it is important to bear in mind the following considerations. Inconsistent measurements should not be combined: bounds obtained from combination of discrepant data sets should be considered with extreme caution. Additionally, the constraints reported below assume that the solution of the H_0 tension – whatever that may be – leaves the interpretation of the adopted probes unaffected.

26.3.1 *Neutrino abundance*

Table 26.1 shows a list of constraints on $N_{\rm eff}$ obtained with several combinations of data sets. 'Pl18' denotes the *Planck* 2018 data [53], 'ACT' the Data Release 6 (DR6) of the Atacama Cosmology Telescope [54], and 'SPT-3G' the Data 1 (D1) release of the South Pole Telescope [55]. These data sets are composed of temperature and polarization likelihoods (T&E) and CMB lensing likelihoods (lensing) based on lensing extraction from quadratic estimators.[2] 'DESI-DR1' and 'DESI-DR2' refer to measurements of the BAO scale (and hence of the angular diameter distance) from the Data Release 1 or 2 of the Dark Energy Spectroscopic Instrument (DESI) [57].

Within the framework of a 7-parameter cosmological model (ΛCDM+$N_{\rm eff}$), the constraint on $N_{\rm eff}$ from the *Planck* 2018 data release [TT,TE,EE+lowE] is $N_{\rm eff} = 2.92^{+0.36}_{-0.37}$ (95%CL). This number is perfectly compatible with the prediction of the standard neutrino decoupling model, $N_{\rm eff} = 3.044$, and also with bounds on $N_{\rm eff}$ from Big Bang Nucleosynthesis and primordial element abundances (see Chapter 24 of this Review). This can be viewed as a proof of self-consistency of the cosmological model.

The bounds can be tightened by adding information from ground-based CMB experiments probing higher ℓ, CMB lensing (second and third line in the table), and complementary information on the low-redshift background expansion from BAOs (lower section of the table). While the exact central values and error-bars might depend slightly on the choice of CMB likelihood, all combinations of *Planck* 2018 data with additional CMB and/or BAO data reported in Table 26.1 return measurements consistent with the standard expectation at the 95% confidence level. The only marginal exception is the SPT-3G+BAO bound, which suggests that when large-scale CMB information from *Planck* is not included,[3] the data struggle to break parameter degeneracies [55].

One may also add to CMB and BAO data another probe of the late background expansion in the form of measurements of the distance to uncalibrated type Ia supernovae (SNIa). However, this does not change much the constraining power on $N_{\rm eff}$, as shown for instance in Ref. [56]. Finally, one may also add information from large-scale structure (LSS), *i.e.*, on the growth rate and clustering amplitude of matter as a function of scale, although the DESI DR1 analysis [58] shows that LSS data are not very constraining for the $N_{\rm eff}$ parameter.

The situation is different with the inclusion of low-redshift measurements of H_0 with distance ladders (DLs) [59–61], reaching up to 5.7σ tension with *Planck* in the ΛCDM framework. As explained in Section 26.2, the positive correlation between $N_{\rm eff}$ and h means that inclusion of the H_0 measurement would tend to push $N_{\rm eff}$ to higher values. However, the high values of $N_{\rm eff}$ needed to accommodate $H_0 \sim 73$ km/s/Mpc, as well as the sound horizon scale as seen in the CMB and BAO, are excluded by the measurement of the damping tail of the CMB temperature spectrum by *Planck*, ACT and/or SPT-3G.

Thus, the $N_{\rm eff}$ extension to the ΛCDM model does not reduce the tension significantly, and the combination of *Planck* and DL data does not return any meaningful constraint on $N_{\rm eff}$ in this context. It is currently unclear whether a resolution of the Hubble tension would require a departure from the ΛCDM (or ΛCDM+$N_{\rm eff}$) model [11–13, 62–66].

As long as DL data are not included, the error bars on $N_{\rm eff}$ degrade mildly when the data are analysed in the context of more extended cosmological scenarios. Adding only the total neutrino mass as an 8th free parameter has a negligible impact on the bounds [56]. The authors of Ref. [67] take a more extreme point of view and fit a 12-parameter model to Pl18[TT,TE,EE+lowE+lensing] data; they obtain $N_{\rm eff} = 2.95 \pm 0.24$ (68% CL), showing that it is very difficult with current cosmological data to accommodate shifts of more than 0.5 from the standard $N_{\rm eff}$ value, and to obtain good fits with, for instance, a fourth (sterile) thermalized neutrino. This is interesting, since the anomalies in some oscillation data could be interpreted as evidence for at least one sterile neutrino with a large mixing angle, which would need to be thermalised unless non-standard interactions come into play [5]. In other words, cosmology disfavours the explanation of the oscillations anomalies in terms of extra neutrinos if they are thermalized.

However, if a resolution to current tensions among cosmological data sets requires a departure from the ΛCDM model or its most simple extensions, the situation is more open. In the presence of new physical ingredients (such as non-standard interactions, exotic dark matter candidates, non-minimal dark energy properties, or modified gravity), it is in principle conceivable that $N_{\rm eff}$ reaches larger values. Still, within the w_0w_aCDM model (a dynamical dark energy extension to the ΛCDM model favored by some data set combinations, see Chap. 28 of this *Review*), the $N_{\rm eff}$ constraints do not change appreciably, as illustrated by the last bound quoted in Table 26.1.

26.3.2 *Are they really neutrinos, as expected?*

While a value of $N_{\rm eff}$ significantly different from zero (at more than 15σ) and consistent with the expected number 3.044 yields a powerful indirect confirmation of the CνB, departures from standard $N_{\rm eff}$ could be caused by any ingredient affecting the early-time expansion rate of the Universe. Extra relativistic particles (either decoupled, self-interacting, or interacting with a dark sector), a background of gravitational waves, an oscillating scalar field with quartic potential, departures from Einstein gravity, or large extra dimensions are some of the possibilities for such ingredients. In principle one could even assume that the CνB never

[2] The CMB lensing likelihoods used in Refs. [54–56] are based on different combinations of *Planck*, ACT, and SPT-3G data.

[3] The SPT-3G+DESI data set uses no information on CMB multipoles $\ell < 400$ but includes a prior on the optical depth to reionization infered from low-ℓ *Planck* data [55].

Int. J. Mod. Phys. A 2026.41. Downloaded from www.worldscientific.com
by UNIVERSITY OF CALIFORNIA @ BERKELEY on 09/16/26. Re-use and distribution is strictly not permitted, except for Open Access articles.

Table 26.1: Summary of $N_{\rm eff}$ constraints.

	Model	$N_{\rm eff}$	Ref.
CMB alone			
Pl18[T&E]	ΛCDM+$N_{\rm eff}$	2.92 ± 0.18 (68%CL)	[53]
Pl18[T&E]+ACT[T&E]	ΛCDM+$N_{\rm eff}$	2.73 ± 0.14 (68%CL)	[54]
Pl18[T&E]+ACT[T&E]+SPT-3G[T&E,lensing]	ΛCDM+$N_{\rm eff}$	2.81 ± 0.12 (68%CL)	[55]
CMB + BAO			
SPT-3G[T&E,lensing]+DESI-DR2	ΛCDM+$N_{\rm eff}$	3.52 ± 0.23 (68% CL)	[55]
Pl18[T&E]+ACT[T&E,lensing]+DESI-DR1	ΛCDM+$N_{\rm eff}$	2.86 ± 0.13 (68% CL)	[54]
Pl18[T&E]+ACT[lensing]+DESI-DR2	w_0w_aCDM+$N_{\rm eff}$	2.96 ± 0.18 (68% CL)	[56]

existed or has decayed (like in the "neutrinoless Universe" model of Ref. [68]), while another dark radiation component is responsible for $N_{\rm eff}$. At least, cosmological data allow to narrow the range of possible interpretations of $N_{\rm eff} \simeq 3$ to the presence of decoupled relativistic relics like standard neutrinos. Indeed, free-streaming particles leave specific signatures in the CMB and LSS spectra, because their density and pressure perturbations, bulk velocities, and anisotropic stress also source the metric perturbations. These signatures can be tested in several ways.

A first approach consists of introducing a self-interaction term in the neutrino equations [6, 7]. Reference [8] finds that current CMB and BAO data are compatible with no self-interactions. The upper limit to the effective coupling constant $G_{\rm eff}$ for a Fermi-like four-fermions interaction at 95% confidence is $\log_{10}(G_{\rm eff}{\rm MeV}^2) < -1.47$ for Pl18+BAO [11]. Note, however, that neutrino self-interactions as strong as $\log_{10}(G_{\rm eff}{\rm MeV}^2) \simeq -1.4$ could reconcile CMB temperature and BAO data with the direct H_0 measurement of Ref. [69], but such interactions seem to be incompatible with BBN, laboratory constraints [10], and CMB polarization [9, 11].

A second approach consists of introducing two phenomenological parameters, $c_{\rm eff}$ and $c_{\rm vis}$ (see *e.g.*, Ref. [70–72]): $c^2_{\rm eff}$ generalizes the linear relation between isotropic pressure perturbations and density perturbations; and $c^2_{\rm vis}$ modifies the neutrino anisotropic stress equation. While relativistic free-streaming species have $(c^2_{\rm eff}, c^2_{\rm vis}) = (1/3, 1/3)$, a perfect relativistic fluid would have $(c^2_{\rm eff}, c^2_{\rm vis}) = (1/3, 0)$. Other values do not necessarily refer to a concrete model, but make it possible to interpolate between these limits. *Planck* data, alone or in combination with galaxy clustering, strongly suggests $(c^2_{\rm eff}, c^2_{\rm vis}) = (1/3, 1/3)$ [73–75].

Finally, Ref. [28] (Ref. [29]) shows that current data are precise enough to detect the "neutrino drag" effect mentioned in Sec. 26.2 through the measurement of the CMB peak (BAO) scale. These findings show that current cosmological data are able to detect not just the average density of some relativistic relics, but also their anisotropies.

26.3.3 *Neutrino masses*

Table 26.2 shows a list of constraints on $\sum m_\nu$ obtained with several combinations of data sets. 'WMAP' denotes the Wilkinson Microwave Anisotropy Probe. The acronyms 'Pl18', 'ACT', 'SPT-3G', 'DESI-DR1' and 'DESI-DR2' have been described in the previous subsection. 'PR4' refers to *Planck* Release 4 data analysed with the 'CamSpec' likelihood [79]. 'DESI-DR1[BAO-FS]' denotes the combined measurement of the BAO scale and full-shape matter power spectrum from DESI DR1 data [58], and 'Lyman-α' the one-dimensional flux power spectrum of eBOSS quasars analyzed with a new inference pipeline called 'Lyssa' in Ref. [78].

Given that most determinations of $N_{\rm eff}$ are compatible with the standard prediction, $N_{\rm eff} = 3.044$, it is reasonable to adopt this value as a theoretical prior and to investigate neutrino mass constraints in the context of a minimal 7-parameter model, ΛCDM+$\sum m_\nu$.

Firstly, an extremely robust bound comes from WMAP data (or Planck data limited to large angular scales), which constrain neutrino masses mainly through the non-detection of the very specific neutrino-induced early ISW effect mentioned in Sec. 26.2.3, and set $\sum m_\nu < 1.3\,$eV (95%CL) [76]. Assuming a minimal 7-parameter model, the next most conservative constraint arises from *Planck* 2018 temperature and polarization data alone: $\sum m_\nu < 0.26\,$eV (95%CL) [53]. Among the four effects of neutrino masses on the CMB spectra described before, *Planck* (and post-*Planck*) bounds are dominated by the first and the third effects (modified late background evolution, and distortions of the temperature and polarization spectra through weak lensing) – as discussed, e.g., in Refs. [32, 80, 81]. It is worth noticing that the actual *Planck* bound depends on the version of the *Planck* data release and likelihood that one adopts (see, e.g., Ref. [81]). As a matter of fact, different versions suggest a slightly different amplitude for the distortions induced in the high-ℓ temperature spectrum by weak lensing. However, all versions of *Planck* and of other CMB high-ℓ likelihoods agree on the fact that there is a high level of such distortions. These are compatible with a large amplitude of the matter power spectrum and a negligible impact of neutrino free-streaming. This feature tightens any neutrino mass bound based on high-ℓ temperature data. Complementing *Planck* data with recent measurements of high-ℓ temperature and polarization from ACT and SPT-3G further tightens the bounds. On the other hand, adding independent information on the CMB lensing potential inferred from CMB lensing extraction has a moderate impact. The CMB-only bound from combined *Planck* 2018, ACT, and SPT-3G data (including CMB lensing) is as strong as $\sum m_\nu < 0.17$ eV (95%CL) [55].

Adding measurements of the BAO scale is crucial, since the comparison between the angular diameter distance $d_{\rm A}(z)$ to small and large redshifts makes it possible to break parameter degeneracies, for instance between $\sum m_\nu$ and H_0. However, neutrino mass bounds from BAOs are very model dependent, since the impact of massive neutrinos on the angular distance is not specific and could be confused, for instance, with dynamical dark energy. The combination of *Planck* and ACT with BAO measurements from DESI DR2 provides a strong bound, $\sum m_\nu < 0.077$ eV (95%CL) [77]. In this case, *Planck* high-ℓ data are no longer playing a crucial role: one gets essentially the same result when keeping only the low-ℓ polarization information from *Planck* [77]. The bound narrows down to $\sum m_\nu < 0.048$ eV (95%CL) when also adding recent SPT-3G data [55], which may appear like a tension with the minimal value of the summed mass allowed by oscillation experiments (when assuming ΛCDM).[4] The reason is that current CMB temperature and BAO data are better fit by models with slightly more CMB lensing and a slightly different expansion rate than in the ΛCDM model with massless neutrinos. Increasing the neutrino mass tends to worsen the fit to both data sets. Recently, some authors (see, e.g., [80]) discussed models with an unphysical "negative neutrino mass". This should be interpreted as follows: if the current trends in the data get confirmed, and the minimal ΛCDM model needs to be extended with a new ingredient, this ingredient should have an effect on CMB lensing and on the expansion rate opposite to that of neutrino masses. Dynamical dark energy is an example of such extension. The model dependence of the CMB+BAO mass bounds becomes clear when considering for instance that, in the w_0w_aCDM model, the combined *Planck*, ACT, SPT-3G, and DESI-DR2 bound relaxes to $\sum m_\nu < 0.186\,$eV (95%CL) [77].

In addition to CMB+BAO data, one could add further information on the late background expansion from uncalibrated SNIa

[4] All the bounds reported here are obtained under the agnostic prior $\sum m_\nu > 0$.

Int. J. Mod. Phys. A 2026.41. Downloaded from www.worldscientific.com
by UNIVERSITY OF CALIFORNIA @ BERKELEY on 09/16/26. Reproduction strictly not permitted, except for Open Access articles.

Table 26.2: Summary of $\sum m_\nu$ constraints (95%CL).

	Model	(eV)	Ref.
CMB alone			
WMAP[T&E]	ΛCDM+$\sum m_\nu$	< 1.3	[76]
Pl18[T&E]	ΛCDM+$\sum m_\nu$	< 0.26	[53]
Pl18[T&E+lensing]	ΛCDM+$\sum m_\nu$	< 0.24	[53]
Pl18[T&E]+ACT[T&E]+SPT-3G[T&E,lensing]	ΛCDM+$\sum m_\nu$	< 0.17	[55]
CMB + BAO			
Pl18[T&E]+ACT[T&E,lensing]+DESI-DR2	ΛCDM+$\sum m_\nu$	< 0.077	[77]
Pl18[T&E]+ACT[T&E]+SPT-3G[T&E,lensing]+DESI-DR2	ΛCDM+$\sum m_\nu$	< 0.048	[55]
Pl18[T&E]+ACT[T&E,lensing]+DESI-DR2	w_0w_aCDM+$\sum m_\nu$	< 0.186	[77]
CMB + BAO + LSS			
Pl18[T&E]+ACT[lensing]+DESI-DR1[BAO,FS]	ΛCDM+$\sum m_\nu$	< 0.071	[58]
PR4[T&E]+ACT[lensing]+DESI-DR1[BAO] + Lyman-α	ΛCDM+$\sum m_\nu$	< 0.053	[78]

luminosity. Here, we refrain from quoting such bounds due to the moderate tension between current CMB, BAO, and SNIa data in the minimal 7-parameter model [58]. Similarly, because the parameter correlation between $\sum m_\nu$ and H_0 is negative, the inclusion of DL data would tend to provide stronger bounds on neutrino masses. However, like for $N_{\rm eff}$, such bounds would not be meaningful, since they would arise from a combination of discrepant data sets.

To mitigate the model dependence of CMB+BAO bounds, it would in principle be crucial to include LSS data sets, directly sensitive to the small-scale suppression of the matter power spectrum due to neutrino free-streaming. Current mass bounds are still dominated by information on the expansion history and CMB lensing, but LSS data are increasingly constraining. Adding the full-shape information on the matter power spectrum measured by DESI-DR1 shrinks the *Planck*+ACT+BAO 95%CL bound from 0.082 eV to 0.071 eV [58]. Combining the same CMB+BAO data set with eBOSS Lyman-α data brings the bound down to 0.053 eV [78]. However, these bounds relax considerably when BAO information is omitted, and are thus still very model dependent. Finally, one may add information on the amplitude of the matter power spectrum coming from weak lensing surveys. The most recent measurements from DES [82] or KiDS [83] are in good agreement with the massless ΛCDM model inferred from CMB data, and as such, do not have a strong impact on neutrino mass bounds compared to CMB+BAO.

One should stress again that if the explanation of DL measurements (or of recent BAO and SNIa data) requires a cosmological scenario with new – and yet unknown – physical ingredients, the current neutrino mass bounds may in principle be shifted or relaxed. We have quoted a few weaker bounds assuming a particular parameterization of dynamical dark energy. However, in the absence of working scenarios that convincingly explain the Hubble tension without raising other tensions, we do not at the moment have any framework for quoting alternative mass bounds compatible with all current data sets.

26.4 Future prospects and outlook

The cosmic neutrino background has been detected indirectly at very high statistical significance. Direct detection experiments are now being planned, *e.g.*, at the Princeton Tritium Observatory for Light, Early Universe, Massive-neutrino Yield (PTOLEMY) [84]. The detection prospects crucially depend on the exact value of neutrino masses and on the enhancement of their density at the location of the Earth through gravitational clustering in the Milky Way and its sub-halos – an effect, however, that is expected to be small [85–88].

Over the past few years the upper limit on the sum of neutrino masses has become increasingly stringent, first indicating that the mass ordering is hierarchical, then putting the inverted hierarchy under pressure, and now even possibly starting to question the normal hierarchy. However, these bounds rely on the ΛCDM model, and thus, on the assumption that a resolution of the Hubble tension with DL measurements (or of a possible tension on the late expansion history with BAO and SNIa measurements) does not affect the modeling and interpretation of the data sets adopted here. If this is not the case, a shift of paradigm might be required, potentially leading to weaker neutrino density and mass bounds.

Neutrino mass and number of species bounds are expected to keep improving significantly over the next years, thanks to new LSS experiments like *Euclid* [89], *Roman* [90], SPHEREx [91] and SKA [92], in combinations with new CMB experiments like Simons Observatory [93] or LiteBird [94]. If the ΛCDM model is confirmed, and if neutrinos have standard properties, the total neutrino mass should be detected at the level of at least 3–4σ even at the minimum level allowed by oscillations. This is the conclusion reached by several independent studies, using different data set combinations (see *e.g.*, [43, 95–100]). One should note that at the minimum level allowed by oscillations $\sum m_\nu \simeq 0.06\,$eV, neutrinos constitute about 0.5% of the Universe matter density, and their effects on the matter power spectrum are only at the 5% level, implying that exquisite control of systematic errors will be crucial to achieve the required accuracy. At this level, the information coming from the power spectrum shape will be more powerful than that coming from geometrical measurements (e.g., BAO). But exploiting the shape information, especially on small, mildly non-linear or non-linear scales, requires improved understanding of the non-linear regime, and of galaxy bias for galaxy surveys. The fact that different surveys, different probes, and different data set combinations have enough statistical power to reach this level, offers a much needed redundancy and the possibility to perform consistency checks, which in turns helps immensely with the control of systematic errors and in making the measurement robust. Using the entire Universe as a particle detector, the on-going and future observational efforts hold the exciting prospect of providing a measurement of the sum of neutrino masses and possibly an indication of their mass hierarchy.

References

[1] A. D. Dolgov, Phys. Rept. **370**, 333 (2002), [hep-ph/0202122].

[2] J. Lesgourgues and S. Pastor, Phys. Rept. **429**, 307 (2006), [arXiv:astro-ph/0603494].

[3] S. Hannestad, Prog. Part. Nucl. Phys. **65**, 185 (2010), [arXiv:1007.0658].

[4] J. Lesgourgues *et al.*, *Neutrino Cosmology*, Cambridge University Press (2013), ISBN 978-1-108-70501-1, 978-1-139-60341-6.

[5] M. Archidiacono *et al.*, JCAP **1608**, 08, 067 (2016), [arXiv:1606.07673].

[6] L. Lancaster *et al.*, JCAP **1707**, 07, 033 (2017), [arXiv:1704.06657].

[7] I. M. Oldengott *et al.*, JCAP **1711**, 11, 027 (2017), [arXiv:1706.02123].

[8] M. Park *et al.*, Phys. Rev. D **100**, 6, 063524 (2019), [arXiv:1904.02625].

[9] C. D. Kreisch, F.-Y. Cyr-Racine and O. Doré, Phys. Rev. D **101**, 12, 123505 (2020), [arXiv:1902.00534].

Int. J. Mod. Phys. A 2026.41. Downloaded from www.worldscientific.com
by UNIVERSITY OF CALIFORNIA @ BERKELEY on 09/16/26. Re-use and distribution is strictly not permitted, except for Open Access articles.

[10] N. Blinov *et al.*, Phys. Rev. Lett. **123**, 19, 191102 (2019), [arXiv:1905.02727].

[11] N. Schöneberg *et al.*, Phys. Rept. **984**, 1 (2022), [arXiv:2107.10291].

[12] A. R. Khalife *et al.*, JCAP **04**, 059 (2024), [arXiv:2312.09814].

[13] E. Di Valentino *et al.* (CosmoVerse Network), Phys. Dark Univ. **49**, 101965 (2025), [arXiv:2504.01669].

[14] J. Birrell, C.-T. Yang and J. Rafelski, Nucl. Phys. **B890**, 481 (2014), [arXiv:1406.1759].

[15] G. Mangano *et al.*, Nucl. Phys. **B729**, 221 (2005), [hep-ph/0506164].

[16] E. Grohs *et al.*, Phys. Rev. **D93**, 8, 083522 (2016), [arXiv:1512.02205].

[17] P. F. de Salas and S. Pastor, JCAP **1607**, 07, 051 (2016), [arXiv:1606.06986].

[18] J. Froustey, C. Pitrou and M. C. Volpe, JCAP **12**, 015 (2020), [arXiv:2008.01074].

[19] J. J. Bennett *et al.*, JCAP **04**, 073 (2021), [arXiv:2012.02726].

[20] M. Cielo *et al.*, Phys. Rev. D **108**, 12, L121301 (2023), [arXiv:2306.05460].

[21] K. Akita and M. Yamaguchi, JCAP **08**, 012 (2020), [arXiv:2005.07047].

[22] T. Binder *et al.*, JCAP **2025**, 10, 069 (2025), [arXiv:2411.14091].

[23] J. Froustey, *The Universe at the MeV era : neutrino evolution and cosmological observables*, Ph.D. thesis, Institut d'Astrophysique de Paris, France, Paris, Inst. Astrophys. (2022), [arXiv:2209.06672].

[24] S. Bashinsky and U. Seljak, Phys. Rev. **D69**, 083002 (2004), [arXiv:astro-ph/0310198].

[25] Z. Hou *et al.*, Phys. Rev. **D87**, 083008 (2013), [arXiv:1104.2333].

[26] J. Lesgourgues *et al.*, *Neutrino cosmology* (Cambridge University Press, 2013).

[27] M. M. Saravanan *et al.*, JCAP **08**, 040 (2025), [arXiv:2503.04671].

[28] B. Follin *et al.*, Phys. Rev. Lett. **115**, 9, 091301 (2015), [arXiv:1503.07863].

[29] D. Baumann *et al.*, Nature Phys. **15**, 465 (2019), [arXiv:1803.10741].

[30] A. Lewis and A. Challinor, Phys. Rept. **429**, 1 (2006), [arXiv:astro-ph/0601594].

[31] Z. Hou *et al.*, Astrophys. J. **782**, 74 (2014), [arXiv:1212.6267].

[32] M. Loverde and Z. J. Weiner, JCAP **12**, 048 (2024), [arXiv:2410.00090].

[33] J. Lesgourgues and S. Pastor, Adv. High Energy Phys. **2012**, 608515 (2012), [arXiv:1212.6154].

[34] J. R. Bond, G. Efstathiou and J. Silk, Phys. Rev. Lett. **45**, 1980 (1980), [,61(1980)].

[35] W. Hu, D. J. Eisenstein and M. Tegmark, Phys. Rev. Lett. **80**, 5255 (1998), [arXiv:astro-ph/9712057].

[36] S. Bird, M. Viel and M. G. Haehnelt, Mon. Not. Roy. Astron. Soc. **420**, 2551 (2012), [arXiv:1109.4416].

[37] C. Wagner, L. Verde and R. Jimenez, Astrophys. J. **752**, L31 (2012), [arXiv:1203.5342].

[38] C. J. Todero Peixoto, V. de Souza and P. L. Biermann, JCAP **1507**, 07, 042 (2015), [arXiv:1502.00305].

[39] J. Brandbyge and S. Hannestad, JCAP **1710**, 10, 015 (2017), [arXiv:1706.00025].

[40] J. Adamek, R. Durrer and M. Kunz, JCAP **1711**, 11, 004 (2017), [arXiv:1707.06938].

[41] M. Archidiacono *et al.*, JCAP **1702**, 02, 052 (2017), [arXiv:1610.09852].

[42] A. Liu *et al.*, Phys. Rev. **D93**, 4, 043013 (2016), [arXiv:1509.08463].

[43] R. Allison *et al.*, Phys. Rev. **D92**, 12, 123535 (2015), [arXiv:1509.07471].

[44] J. Lesgourgues, S. Pastor and L. Perotto, Phys. Rev. **D70**, 045016 (2004), [hep-ph/0403296].

[45] A. Slosar, Phys. Rev. **D73**, 123501 (2006), [arXiv:astro-ph/0602133].

[46] R. Jimenez *et al.*, JCAP **1005**, 035 (2010), [arXiv:1003.5918].

[47] R. Jimenez, C. P. Garay and L. Verde, Phys. Dark Univ. **15**, 31 (2017), [arXiv:1602.08430].

[48] A. F. Heavens and E. Sellentin, JCAP **04**, 047 (2018), [arXiv:1802.09450].

[49] M. Archidiacono, S. Hannestad and J. Lesgourgues, JCAP **09**, 021 (2020), [arXiv:2003.03354].

[50] F. Capozzi *et al.*, Phys. Rev. D **104**, 8, 083031 (2021), [arXiv:2107.00532].

[51] R. Jimenez *et al.*, JCAP **09**, 006 (2022), [arXiv:2203.14247].

[52] S. Gariazzo, O. Mena and T. Schwetz, Phys. Dark Univ. **40**, 101226 (2023), [arXiv:2302.14159].

[53] N. Aghanim *et al.* (Planck), Astron. Astrophys. **641**, A6 (2020), [Erratum: Astron.Astrophys. 652, C4 (2021)], [arXiv:1807.06209].

[54] E. Calabrese *et al.* (Atacama Cosmology Telescope), JCAP **11**, 063 (2025), [arXiv:2503.14454].

[55] E. Camphuis *et al.* (SPT-3G) (2025), [arXiv:2506.20707].

[56] W. Elbers *et al.* (DESI), Phys. Rev. D **112**, 8, 083513 (2025), [arXiv:2503.14744].

[57] M. Abdul Karim *et al.* (DESI), Phys. Rev. D **112**, 8, 083515 (2025), [arXiv:2503.14738].

[58] A. G. Adame *et al.* (DESI), JCAP **07**, 028 (2025), [arXiv:2411.12022].

[59] A. G. Riess *et al.*, Astrophys. J. Lett. **934**, 1, L7 (2022), [arXiv:2112.04510].

[60] Y. S. Murakami *et al.*, JCAP **11**, 046 (2023), [arXiv:2306.00070].

[61] W. L. Freedman *et al.*, Astrophys. J. **985**, 2, 203 (2025), [arXiv:2408.06153].

[62] J. L. Bernal, L. Verde and A. G. Riess, JCAP **1610**, 10, 019 (2016), [arXiv:1607.05617].

[63] L. Verde, T. Treu and A. G. Riess, Nature Astron. **3**, 891 (2019), [arXiv:1907.10625].

[64] J. L. Bernal *et al.*, Phys. Rev. D **103**, 10, 103533 (2021), [arXiv:2102.05066].

[65] E. Di Valentino *et al.*, Class. Quant. Grav. **38**, 15, 153001 (2021), [arXiv:2103.01183].

[66] E. Abdalla *et al.*, JHEAp **34**, 49 (2022), [arXiv:2203.06142].

[67] E. Di Valentino, A. Melchiorri and J. Silk, JCAP **01**, 013 (2020), [arXiv:1908.01391].

[68] J. F. Beacom, N. F. Bell and S. Dodelson, Phys. Rev. Lett. **93**, 121302 (2004), [arXiv:astro-ph/0404585].

[69] A. G. Riess *et al.*, Astrophys. J. Lett. **908**, 1, L6 (2021), [arXiv:2012.08534].

[70] W. Hu, Astrophys. J. **506**, 485 (1998), [arXiv:astro-ph/9801234].

[71] W. Hu *et al.*, Phys. Rev. **D59**, 023512 (1999), [arXiv:astro-ph/9806362].

[72] M. Gerbino, E. Di Valentino and N. Said, Phys. Rev. **D88**, 6, 063538 (2013), [arXiv:1304.7400].

[73] B. Audren *et al.*, JCAP **1503**, 036 (2015), [arXiv:1412.5948].

[74] P. A. R. Ade *et al.* (Planck), Astron. Astrophys. **594**, A13 (2016), [arXiv:1502.01589].

[75] S. Kumar, R. C. Nunes and P. Yadav, JCAP **09**, 060 (2022), [arXiv:2205.04292].

[76] G. Hinshaw *et al.* (WMAP), Astrophys. J. Suppl. **208**, 19 (2013), [arXiv:1212.5226].

[77] C. Garcia-Quintero *et al.* (DESI), Phys. Rev. D **112**, 8, 083529 (2025), [arXiv:2504.18464].

[78] D. Chebat *et al.*, JCAP **01**, 041 (2026), [arXiv:2507.12401].

[79] E. Rosenberg, S. Gratton and G. Efstathiou, Mon. Not. Roy. Astron. Soc. **517**, 3, 4620 (2022), [arXiv:2205.10869].

[80] W. Elbers *et al.*, Phys. Rev. D **111**, 6, 063534 (2025), [arXiv:2407.10965].

[81] D. Naredo-Tuero *et al.*, Phys. Rev. D **110**, 12, 123537 (2024), [arXiv:2407.13831].

[82] T. M. C. Abbott *et al.* (DES), Phys. Rev. D **105**, 2, 023520 (2022), [arXiv:2105.13549].

[83] A. H. Wright *et al.* (2025), [arXiv:2503.19441].

[84] S. Betts *et al.*, in "Proceedings, 2013 Community Summer Study on the Future of U.S. Particle Physics: Snowmass on the Mississippi (CSS2013): Minneapolis, MN, USA, July 29-August 6, 2013," (2013), [arXiv:1307.4738], URL `http://www.slac.stanford.edu/econf/C1307292/docs/submittedArxivFiles/1307.4738.pdf`.

[85] A. Ringwald and Y. Y. Y. Wong, JCAP **0412**, 005 (2004), [hep-ph/0408241].

[86] F. Villaescusa-Navarro *et al.*, JCAP **1303**, 019 (2013), [arXiv:1212.4855].

[87] P. F. de Salas *et al.*, JCAP **1709**, 09, 034 (2017), [arXiv:1706.09850].

[88] M. Bauer and J. D. Shergold, JCAP **01**, 003 (2023), [arXiv:2207.12413].

[89] R. Laureijs *et al.* (EUCLID) (2011), [arXiv:1110.3193].

[90] Paul A. Abell *et al.*, LSST Science and LSST Project Collaborations, `http://lss.fnal.gov/archive/test-tm/2000/fermilab-tm-2495-a.pdf` (2009) `arXiv:0912.0201`.

[91] J. Bock and SPHEREx Science Team, in "American Astronomical Society Meeting Abstracts #231," volume 231 of *American Astronomical Society Meeting Abstracts*, 354.21 (2018).

[92] `http://www.skatelescope.org`.

[93] P. Ade *et al.* (Simons Observatory), JCAP **02**, 056 (2019), [arXiv:1808.07445].

[94] M. Hazumi *et al.*, J. Low Temp. Phys. **194**, 5-6, 443 (2019).

[95] C. Carbone *et al.*, JCAP **1103**, 030 (2011), [arXiv:1012.2868].

[96] J. Hamann, S. Hannestad and Y. Y. Y. Wong, JCAP **1211**, 052 (2012), [arXiv:1209.1043].

[97] B. Audren *et al.*, JCAP **1301**, 026 (2013), [arXiv:1210.2194].

[98] R. Pearson and O. Zahn, Phys. Rev. **D89**, 4, 043516 (2014), [arXiv:1311.0905].

[99] F. Villaescusa-Navarro, P. Bull and M. Viel, Astrophys. J. **814**, 2, 146 (2015), [arXiv:1507.05102].

[100] T. Brinckmann *et al.*, JCAP **1901**, 059 (2019), [arXiv:1808.05955].

Int. J. Mod. Phys. A 2026.41. Downloaded from www.worldscientific.com
by UNIVERSITY OF CALIFORNIA @ BERKELEY on 09/16/26. Re-use and distribution strictly not permitted, except for Open Access articles.

27. Dark Matter

Revised August 2025 by L. Baudis (Zurich U.) and S. Profumo (UC Santa Cruz).

27.1 The case for dark matter

Modern cosmological models invariably include an electromagnetically close-to-neutral, non-baryonic matter species with negligible velocity from the standpoint of structure formation, generically referred to as "cold dark matter" (CDM; see The Big-Bang Cosmology—Sec. 22 of this *Review*). For the benchmark ΛCDM cosmology adopted in the Cosmological Parameters—Sec. 25 of this *Review*, the DM accounts for 26.4% of the critical density in the universe, or 84.4% of the total matter density. The nature of only a small fraction, between at least 0.5% (given neutrino oscillations) and at most 1.6% (from combined cosmological constraints), of the non-baryonic matter content of the universe is known: the three Standard Model neutrinos (see the Neutrino Masses, Mixing, and Oscillations—Sec. 14 of this *Review*)). The fundamental makeup of the large majority of the DM is, as of yet, unknown.

Assuming the validity of General Relativity, DM is observed to be ubiquitous in gravitationally collapsed structures of size ranging from the smallest known galaxies [1] to galaxies of size comparable to the Milky Way [2], to groups and clusters of galaxies [3]. The mass-to-light ratio is observed to saturate at the largest collapsed scales to a value indicative, and close to, what inferred from other cosmological observations for the universe as a whole [4]. In such collapsed structures, the existence of DM is inferred directly using tracers of mass enclosed within a certain radius such as stellar velocity dispersion, rotation curves in axisymmetric systems, the virial theorem, gravitational lensing, and measures of the amount of non-dark, i.e. baryonic, mass such as stellar number counts and tracers of gas density such as X-ray emission [5]. The global DM abundance as determined from cosmological probes is discussed in Sec. 22.

The picture of structure formation in modern cosmology heavily relies on, and can be considered an independent and exceptionally strong motivation for, DM. Baryonic density fluctuations at CMB decoupling are observed to be at most on the order of $\delta\rho_b/\rho_b|_{\rm rec} \approx 10^{-5}$; since density perturbations grow linearly with the scale factor in the linear regime, absent any other matter fluid, one would predict that

$$\delta\rho_b/\rho_b|_{\rm today} \approx \frac{\delta\rho_b/\rho_b|_{\rm rec}}{a_{\rm rec}} \approx 10^{-2}, \qquad (27.1)$$

at odds with the observed highly non-linear structures in the universe, $\delta\rho_b/\rho_b|_{\rm obs} \gg 1$. The presence of a dominant non-relativistic ("cold") pressure-less matter component decoupled from the thermal bath well before recombination allows instead for the prediction of a matter power spectrum in remarkable agreement with observations [6].

Assuming deviations of gravitational interactions on large scales from general relativity or from its Newtonian limit, certain effects, attributed in the standard scenario to DM, can be explained by modified gravity [7]. Usually such theories mimic the effects otherwise attributed to DM on a limited range of scales, but fail globally, and especially at the largest scales. Key issues that at present appear highly problematic in the framework of theories of modified gravity without DM include (i) predicting the correct spectrum of density perturbations, (ii) predicting the observed anisotropy power spectrum of the CMB, and (iii) explaining weak lensing and X-ray observations of merging clusters such as 1E 0657-558 (the "Bullet" cluster) [8]. The inferred relative speed of gravitational and electromagnetic radiation in GW170817 additionally excludes a significant swath of modified theories of gravity where the two speeds (of gravitational and electromagnetic waves) differ [9].

27.2 Properties of dark matter candidates

Electric charge: The "darkness" of DM can be quantified based on constraints from the CMB and large-scale structure: if the DM is charged, or "milli-charged" (for instance via a kinetic mixing with a dark photon field, producing an effective suppressed coupling to the visible photon field), it might impact the baryon-photon plasma during recombination; in turn, DM density fluctuations can be suppressed by radiation pressure and photon diffusion, additionally altering the baryon acoustic peak structure. [10] finds that the most stringent constraints stem from the requirement that the DM be completely decoupled from the baryon-photon plasma at recombination, yielding a maximal "milli-electric" charge, in units of the electron charge, of $3.5\times10^{-7}(m_{\rm DM}/1\ {\rm GeV})^{0.58}$ for $m_{\rm DM} > 1$ GeV, and of $4.0\times10^{-7}(m_{\rm DM}/1\ {\rm GeV})^{0.35}$ for $m_{\rm DM} < 1$ GeV. Limits also exist from structure formation on how optically dark and dissapationaless the DM should be.

Self-interactions: Observations of merging clusters [8] and of the ellipticity of certain galaxies as inferred from X-rays [11] constrain the level of DM-DM self interactions. The figure of merit is the ratio of the DM-DM cross section and the DM mass [12] (see Ref. [13] for a review), $\sigma_{\rm DM-DM}/m_{\rm DM} < 0.47\ {\rm cm}^2/{\rm g} \simeq 0.84$ barn/GeV at 95% C.L.. Assuming a velocity dependence in $\sigma_{\rm DM-DM}$, "self-interacting DM" has been advocated as a possible solution to certain possible small-scale structure issues in the standard non-collisional ($\sigma_{\rm DM-DM} \simeq 0$) setup [13, 14] (see Sec. 27.4).

Mass: Lower Limits: Model-independent lower limits for very small DM masses are due to quantum effects: for fermionic DM particles, the phase-space density $f(\vec{x},\vec{p})$ is bounded from above due to Pauli's exclusion principle, $f < gh^{-3}$, with g the number of internal degrees of freedom and h Planck's constant; observations of the velocity dispersion (or, equivalently, measures of the enclosed mass) and physical density in dwarf galaxies, lead to a lower limit on fermionic DM masses, sometimes known as the Tremaine-Gunn limit [15]. Using the Fornax dwarf, Ref. [16] finds $m_F > 70$ eV. More stringent limits can be drawn from Lyman-α observations, although such limits depend on the thermal history of the DM. In the case of bosonic DM, the Compton wavelength of an ultra-light species might erase small-scale structure, in conflict with CMB and large-scale structure [17], Lyman-α observations [18,19], and measurements of high-redshift galaxy luminosity functions and the Milky Way satellite luminosity function [20–22]: these observations indicate that $m_B \gtrsim 10^{-22}$ eV.

Mass: Upper Limits: General upper limits exist on the mass of the DM constituent from the stability against tidal disruption of structures immersed in DM halos, such as galactic disks and globular clusters, and of individual small galaxies. The most stringent limits can be derived using wide halo binaries [23] and the stability of the star cluster within Eridanus II [24]. Such limits constrain an individual, point-like DM constituent, assuming it makes up 100% of the DM, to be lighter than around 5 $M_\odot$. (Notice that the mass limits discussed here do not assume any specific production mechanism, and do not depend on the observed cosmological DM density).

Stability: The DM lifetime must be long compared to cosmological timescales [25].

27.3 Genesis of dark matter

The generation of DM in the early universe can proceed via thermal or non-thermal production, or both, or it may result from a particle-antiparticle asymmetry.

Freeze-out: The process of chemical decoupling from the high-temperature, high-density thermal bath (freeze-out) as a paradigm for particle production in the early universe is both a predictive and a successful one. The possibility that just like light elements, neutrinos, and CMB photons, particle DM also originated from a thermal decoupling process has thus garnered significant attention.

A particle species *chemically* decouples when the rate Γ for the species' number-changing processes drops below the Hubble rate H. Rough estimates for the abundance of relics can be obtained by (i) calculating the freeze-out (i.e. "decoupling") temperature $T_{\rm f.o.}$, corresponding to $H(T_{\rm f.o.}) \sim \Gamma(T_{\rm f.o.})$, (ii) equating the comoving number density at freeze-out and today, eventually (iii) obtaining the physical density of relic particles today. This procedure assumes that entropy is conserved between $T_{\rm f.o.}$ and today, an assumption that could well be violated, especially for

Int. J. Mod. Phys. A 2026.41. Downloaded from www.worldscientific.com by UNIVERSITY OF CALIFORNIA @ BERKELEY on 09/16/26. Re-use and distribution is strictly not permitted, except for Open Access articles.

Int. J. Mod. Phys. A 2026.41. Downloaded from www.worldscientific.com by UNIVERSITY OF CALIFORNIA @ BERKELEY on 09/16/26. Re-
strictly not permitted, except for Open Access articles.

heavy relics that decouple early, for instance by entropy injection episodes [26]. Notice also that the freeze-out calculation strongly depends on the assumed background cosmology, and changes e.g. if the early universe is not radiation-dominated around DM decoupling.

The calculation of the freeze-out relic abundance hinges on a Boltzmann equation relating the Liouville operator to the collision operator acting on the phase space density. Under a variety of simplifying assumptions including homogeneity and isotropy, it is possible to reduce the relevant equation for the number density n of a single species pair-annihilating with particles in the thermal bath via 2-to-2 processes to

$$\frac{dn}{dt} - 3Hn = -\langle \sigma v \rangle \left(n^2 - n_{\rm eq}^2 \right), \tag{27.2}$$

where $\langle \sigma v \rangle$ is the thermally-averaged pair-annihilation cross section times relative velocity (see Ref. [27]), and $n_{\rm eq}$ is the equilibrium number density. Relics for which the freeze-out temperature is much larger than the particle mass (and thus that freeze-out as ultra-reltivistic) are called *hot* relics; if the opposite is true, the relic is instead considered *cold*.

A straightforward calculation shows that to leading order the frozen-out density of *hot* relics is *linearly proportional to the relic particle mass*. The comoving number density $Y = n/s$, where s is the entropy density, for a hot relic is approximately given by its equilibrium value,

$$Y_{\rm f.o.} \simeq Y_{\rm eq} \simeq 0.278 \frac{g_{\rm eff}}{g_{*s}}, \tag{27.3}$$

where $g_{\rm eff}$ is the relic's effective number of degrees of freedom, and g_{*s} is the number of entropic relativistic degrees of freedom, both calculated at $T_{\rm f.o.}$. The resulting relic abundance, assuming an iso-entropic expansion, is

$$\Omega_{\rm hot} h^2 = \frac{m Y_{\rm f.o.} s_0 h^2}{\rho_c} \simeq \frac{m}{93 \text{ eV}}, \tag{27.4}$$

with s_0 the entropy density today, and with the latter equality holding for the case of SM neutrinos, with a freeze-out temperature around 1 MeV (which enters in the final relic abundance through the degrees of freedom dependence on the right-hand-side of Eq. (27.3)).

For *cold* relics, the leading-order dependence of the relic abundance on the DM particle properties is an *inverse proportionality relation to the pair-annihilation cross section*,

$$\Omega_{\rm cold} h^2 \simeq 0.1 \left(\frac{x_{\rm f.o.}}{20} \right) \left(\frac{10^{-8} \text{ GeV}^{-2}}{\sigma_{\rm DM+DM \leftrightarrow anything}} \right), \tag{27.5}$$

where $x \equiv m_{\rm DM}/T$. In turn, the freeze-out temperature is approximately given by the solution to the equation

$$\sqrt{x} \cdot e^{-x} = \left(m_{\rm DM} \cdot M_P \cdot \sigma_{\rm DM+DM \leftrightarrow anything} \right)^{-1}, \tag{27.6}$$

where $M_P \simeq 2.435 \times 10^{18}$ GeV is the reduced Planck mass. As a result, $T_{\rm f.o.} \simeq m_{\rm DM}/x_{\rm f.o.}$, with $x_{\rm f.o.}$ a number between 10 and 50, depending on the cross section, with only a logarithmic dependence on the DM mass. Since for electroweak-scale cross sections and masses $\sigma_{\rm DM+DM} \simeq 10^{-8}$ GeV^{-2}, "weakly-interacting massive particles", or WIMPs have gained exceptional popularity. Notice that Eq. (27.5) bears, however, no connection to the weak scale [28], despite the relation being known as "WIMP miracle".

Numerous scenarios exist, including notably supersymmetry [29,30] and models with universal extra dimensions [31,32] where the relic abundance of the DM is controlled by processes involving a slightly heavier, unstable, co-annihilating species [33]. In this case the calculation of the abundance of the stable species proceeds similarly to what outlined above, with an effective pair-annihilation cross section that captures the effects of co-annihilation replacing the pair-annihilation cross section [30].

Freeze-in: Collisional processes can lead to the production of out-of-equilibrium particles that progressively accumulate over cosmic time, a process sometimes called *freeze-in*. The abundance of the frozen-in particles produced at a given redshift depends on the product of the production rate times the Hubble time at that redshift. Freeze-in generally implies that the lightest observable-sector particles decay to the DM with relatively long lifetimes, giving peculiar signals at colliders (see e.g. [34]). Gravitinos are an example of DM candidates possibly produced via a freeze-in type scenario, albeit the portal coupling is in that case via a higher dimensional, Planck-suppressed operator [35].

Cannibalization and other dark-sector number-changing processes: Thermal processes can drive the abundance of the DM beyond simple 2-to-2 number-changing interactions. For instance, DM can "cannibalize" [36, 37] itself if $n \to 2$ processes exist. In this case, a critical aspect is whether or not the DM sector is in thermal contact with the Standard Model thermal bath. If it is, $n \to 2$ processes can drive the relic abundance, e.g. in the Strongly Interacting Massive Particles (SIMP) scenario [38]. Models exist where the *kinetic decoupling* (i.e. the decoupling from the *thermal equilibrium velocity distribution*) of the two sectors drives the abundance of the DM (elastically decoupling relics, or ELDERs [39]). When the two sectors are not in thermal contact, $n \to 2$ processes heat the DM sector dramatically, rapidly affecting the temperature ratio between the visible and dark sectors [36, 38]. If the relevant cross sections are large enough, and the DM mass light enough, significant effects can arise in structure formation [36].

Non-thermal production: DM production can proceed via processes out of thermal equilibrium ("non-thermal" production). These include DM production via the decay of a "mother" particle [40,41] (or of topological defects [42], moduli [43] etc.) to the DM, or production via gravitational effects.

Asymmetric DM: An enticing alternative possibility for DM production is that of *asymmetric* DM [44,45]: the relic DM abundance arises from an asymmetry between anti-DM and DM. This asymmetry may or may not be related to the baryon-antibaryon asymmetry. If it is, then depending on the model and its thermal history, a relation exists between the mass of the DM and the proton mass. A variety of proposals have been put forward where alternately baryogenesis is explained from a DM sector asymmetry, or vice-versa (see e.g. Ref. [46] for a review).

Primordial Black Holes production: A qualitatively stand-alone class of DM candidates, primordial black holes (PBHs), arises from entirely different mechanisms from what reviewed above. PBHs are thought to originate from gravitational collapse of large density fluctuations in the early universe [47, 48]. The over-densities could be produced in a variety of ways, such as topological defects like cosmic strings, necklaces or domain walls, curvature fluctuations from a period of ultra-slow-roll, a sound speed "resonance" , an early phase of matter domination, or sub-horizon phenomena including a phase transition and preheating.Albeit the calculation depends on the details of gravitational collapse, the formation time is connected to the PBH mass via $M = \gamma M_{PBH} \simeq 2 \times 10^5 \gamma \left(\frac{t}{1 \text{ s}} \right) M_\odot$, with $\gamma \simeq (1/\sqrt{3})^3$ during radiation domination [49].

27.4 Density and velocity distribution of dark matter

27.4.1 *Local density and velocity distribution*

The density and distribution of DM in the Milky Way encipher relevant dynamical information about our Galaxy, and are particularly important for direct and indirect detection experiments. The *local density* (ρ_0) is an average over a volume of a few hundred parsecs in the Solar neighbourhood.

To determine the local density from observations, two classes of methods are used [50]. So-called *local measures* rely on the vertical motion of tracer stars in the vicinity of the Sun, while *global measures* extrapolate ρ_0 from the measured rotation curve, with additional assumptions about the Galactic halo shape. Conversely, by comparing the extrapolated local density with the one obtained from local measures, one can constrain the local shape of the Milky Way halo. A major source of uncertainty on ρ_0 is the contribution of baryons (stars, gas, stellar remnants) to the local dynamical mass. For instance, the motion of tracer stars used in local measures is dictated by the total potential generated by

Int. J. Mod. Phys. A 2026.41. Downloaded from www.worldscientific.com
by UNIVERSITY OF CALIFORNIA @ BERKELEY on 09/16/26. Re-use and distribution is strictly not permitted, except for Open Access articles.

baryons and DM, and a robust baryonic census must be available to infer the additional contribution from DM. Recent determinations from global methods lie in the range $(0.2 - 0.6)\,\mathrm{GeV/cm^3}$, while new studies of the local DM density from *Gaia* satellite data yield $(0.3 - 1.5)\,\mathrm{GeV/cm^3}$, depending on the type of stars used in the study. A novel approach to measuring the local dark matter density ρ_0 was recently presented in Ref. [51], which employed normalizing flows—a class of unsupervised machine learning models—to learn the full six-dimensional phase-space distribution of stars in the solar neighborhood using *Gaia* DR3 data. By directly solving the collisionless Boltzmann equation in a model-independent, unbinned fashion and subtracting a detailed baryonic mass model, the study obtained $\rho_0 = (0.47 \pm 0.05)\,\mathrm{GeV/cm^3}$, in excellent agreement with earlier determinations based on Jeans analyses and rotation curve modeling. The method allows for minimal symmetry assumptions and provides spatially resolved estimates of the gravitational acceleration field, offering a powerful complement to traditional techniques. While current precision is limited by stellar sample size and astrometric uncertainties, future *Gaia* data releases are expected to significantly reduce these limitations and enable more detailed studies of possible disequilibrium features in the Galactic disk.

Other observational quantities that enter in the phase space distribution of DM, and provide constraints on mass models of the Milky Way are the local circular speed v_c and the escape velocity v_{esc}. The local circular speed is measured by various methods, roughly divided into measurements of the Sun's velocity with respect to an object assumed to be at rest with respect to the Galactic centre or direct measurements of the local radial force. These methods yield values of $v_c = (218 - 246)\,\mathrm{km/s}$. A recent estimate of the escape velocity, defined as the speed above which objects are not gravitationally bound to our galaxy, is v_{esc}=533^{+54}_{-41} km/s [52] (see also the more recent estimate in [53] of v_{esc}=$484.6^{+17.8}_{-7.4}$ km/s, which is not in tension with the value we use).

The local velocity distribution of DM particles can not be measured directly at present, and is mostly derived from simulations. In general, experiments use the simplest, so-called *Standard Halo Model (SHM)* for their data analysis. It assumes an isotropic, isothermal sphere of DM particles with a density profile of $\rho(r) \propto r^{-2}$, for which the velocity distribution is Maxwellian, with a velocity dispersion $\sigma_v = v_c/\sqrt{2}$. This distribution, which formally extends to infinity, is truncated at v_{esc} [54]. Earlier high resolution, dark-matter-only simulations found velocity distributions that markedly deviated from a Maxwell-Boltzmann distribution and in addition revealed components above the dominant smooth distribution, including narrow spikes due to tidal streams. Recent hydrodynamical simulations of Milky Way-like galaxies including baryons, which have a non-negligible effect on the DM distribution in the Solar neighbourhood, find velocity distributions that are indeed close to Maxwellian, arguing that the SHM is a good approximation.

Ultimately the goal is to determine the velocity distribution from observations (for example by studying the motion of stars that share the same kinematics as the DM), and the *Gaia* satellite data offers a unique opportunity to study the various stellar populations. Recently it was revealed that the local stellar halo has two components: a quasi-spherical, weakly rotating structure with metal-poor stars, and a flattened, radially anisotropic structure of metal-rich stars, which arose due to accretion of a large $(10^{11-12}\,\mathrm{M_\odot})$ dwarf galaxy around (8-10)$\times 10^9$ y ago [55]. The expectation is that the local DM halo shows a similar bimodal structure, and first velocity distributions of the two components - using the stellar populations as tracers - were inferred in [56]. In Ref. [57], an updated halo model is introduced: it includes the anisotropic structure seen in the *Gaia* data and provides an analytic expression for the velocity distribution. The value of the local DM density is updated to $(0.55 \pm 0.17)\,\mathrm{GeV/cm^3}$, where the 30% error accounts for the systematics. The circular rotation and the escape speeds are updated to $v_c = (233 \pm 3)\,\mathrm{km/s}$ and v_{esc}=528^{+24}_{-25} km/s. The former is in agreement with a new Bayesian estimation of the circular velocity using Gaia DR3, of $v_c = (233 \pm 7)\,\mathrm{km/s}$ [58]. With Gaia DR3, new stellar streams are being discovered, some of these likely originating from the disruption and merger of dwarf galaxies. The study of the velocities of such streams will allow for increasingly improved constraints on both the DM subhalo density profiles and the velocity distributions.

27.4.2 *Small-scale challenges*

The ΛCDM framework is tremendously successful at explaining the observed large-scale structures of the Universe (corresponding to distances $\geq$1 Mpc, the typical inter-galactic distance), as well as the main properties of galaxies that form within DM haloes, see the comprehensive review in Ref. [59]. The observed large-scale structure is consistent with point-like, cold DM particles that interact purely via the gravitational force. However, in the past decades, observations at scales below $\sim$1 Mpc, where structure formation becomes strongly nonlinear, turned out more problematic to be described within the ΛCDM model. The main *small-scale challenges* are known as: the missing satellites problem, the cusp-core problem and the too-big-to-fail problem. Initially these issues, which are not all independent of one another, arose by comparing theoretical predictions from dark-matter-only simulations to observation. While their most likely solutions are in dissipative, baryonic physics (such gas cooling, star formation, supernovae feedback), see the recent reviews in Ref. [60, 61], the small-scale problems could in addition call for a modification or an extension of the ΛCDM paradigm. Most importantly, the ever increasing amount of data on the satellites of the MW and M31 are used to constrain alternative DM models.

The missing satellites problem: High-resolution cosmological simulations of DM haloes the size of the MW predict hundreds or thousands of subhaloes with masses that are in principle large enough to allow for galaxy formation ($> 10^7\,\mathrm{M_\odot}$). Yet less than $\sim$100 satellite galaxies with masses down to $\sim$300 $\mathrm{M_\odot}$ are known to orbit our galaxy within 300 kpc. Galaxies in the field show a similar under-abundance. One solution could be that galaxy formation becomes increasingly inefficient as the halo mass drops, and thus the smallest DM haloes have naturally failed to form galaxies. Progress in both observations and theoretical modeling of observable properties of dwarf galaxies show that there is very scant evidence for a "missing satellite problem" [61]. Nonetheless, additional, related strong tensions remain, including the *diversity of observed rotation curves* [62] and the *unexpected alignment of satellite planes*, the latter issue possibly solved by high-precision simulations tracking inflow along filaments of the cosmic web [63].

The cusp-core problem: The mass density profiles of DM haloes in ΛCDM simulations rise steeply at small radii, $\rho(r) \propto r^{-\gamma}$, with $\gamma \simeq 0.8 - 1.4$. This is in contrast to the observed density profiles of many low-mass galaxies (albeit not all), the rotation curves of which are best fit with constant-density cores, $\gamma \simeq 0 - 0.5$. A related issue is that simulations predict more DM than measured in the central regions of galaxies (also known as the central density problem). A likely solution is that baryonic feedback modifies the structure of DM haloes. Hydrodynamic simulations which include the effects of baryons on galaxy formation have shown that baryonic feedback (e.g., supernova-driven blowouts) can erase the central cusps and produce core-like density profiles. Surveys of satellites of hundreds of galaxies similar to the Milky Way, such as SAGA [64], will likely provide important observational information.

The too-big-to-fail problem: This problem is related to the fact that the dark matter halos of the largest observed Milky Way satellites are typically much smaller than those of the most massive subhalos of simulated Milky Way-like halos. DM haloes of such masses are thought to be too massive to have failed to form stars (hence the name of the problem), especially if lower-mass subhaloes are capable of doing so. A similar issue is present in Andromeda and in field galaxies outside the Local Group. Possible solutions include lowering the mass assumed for the Milky Way host halo, or baryonic effects including tidal stripping and larger-than-expected inner cores [61]. Other issues relate to the origin of ultra-faint galaxies, and the opposite problem of dwarf galaxies with very little dark matter given their stellar mass; there exist proposed solutions to both challenges, including the "bullet dwarf" scenario of Ref. [65].

Int. J. Mod. Phys. A 2026.41. Downloaded from www.worldscientific.com by UNIVERSITY OF CALIFORNIA @ BERKELEY on 09/16/26. Re-strictly not permitted, except for Open Access articles.

The solutions that were briefly mentioned above do not require modifications to the ΛCDM framework. Other solutions involve either modifications of linear theory predictions (via the nature of the DM particle, e.g., Warm DM - WDM) or modifications of nonlinear predictions (via DM models that involve a self-interaction of DM particles - SIDM). WDM models postulate particles with masses at the keV-scale, and the observed number of dark-matter-dominated satellites is used to set a lower limit on the number of subhaloes in the MW and thus a lower limit on the particle's mass [60]. Current constraints are in the range $m_{WDM} > (1.6 - 2.3)$ keV. Cosmological simulations with SIDM find that $\sigma/m_{SIDM} \simeq$(0.5-10) cm^2/g can alleviate the cusp-core and too-big-to-fail problems, giving rise to DM cores in dwarf galaxies with sizes of (0.3-1.5) kpc [13]. Galaxy clusters provide important constraints, and their large central DM densities prefer models with $\sigma/m_{\rm DM} \lesssim 0.1\,{\rm cm}^2/{\rm g}$ [66]. Thus, if SIDM is to solve the small-scale CDM problems and obey the constraints observed on the scales of clusters, σ must depend on the velocity of the particle: it must increase as the rms speed of the particle decreases from the scale of clusters ($v \sim 10^3$ km/s) to the scale of dwarf galaxies ($v \sim 10$ km/s).

27.5 Dark matter models

Particle DM model building is deeply intertwined with the question of the nature of physics beyond the Standard Model (BSM) of particle physics[1]. Directions in this area have followed a few strategies, including, but not limited to

(1) pursuing DM candidates embedded in frameworks that include solutions to other open issues in particle physics, for example WIMPs in connection with electroweak-scale new physics that addresses the hierarchy problem, such as supersymmetry (see the Supersymmetry reviews Sec. 87 and 87); axions in connection with frameworks that address the strong CP problem (see Axions and Other Similar Particles—Sec. 89); sterile neutrinos in connection with the problem of neutrino masses and mixing (see the Neutrino Masses, Mixing, and Oscillations—Sec. 14); or (2) *ad hoc*, or *bottom-up* models built with the intent of addressing or explaining a putative experimental (e.g. particle physical anomalies) or observational (e.g. astronomical) signal.

WIMPs: The WIMP paradigm has been a preferred framework chiefly because it often arises in beyond the Standard Model scenarios that address the hierarchy problem whilst also providing a simple mechanism to explain the observed relic abundance via the "WIMP miracle" described above. Perhaps the most notable example of a framework containing a paradigmatic WIMP is the minimal supersymmetric extension to the Standard Model, if the lightest supersymmetric particle is a neutralino (the mass eigenstate resulting from the mixing of the supersymmetric partners to the Higgses and to the SU(2) and hypercharge gauge bosons, and, possibly, of additional singlet scalars); purely SU(2) sneutrinos have long been ruled out by direct detection, but with suitable mixing with "inert" (gauge-singlet) sneutrinos they can also play the role of WIMP candidates. For more details see the the Supersymmetry—Sec. 87 and 88 in this *Review*. Other non-superysmmetric WIMP models include models with a Higgs or Z (or Z') portal, universal extra dimensions [32], and other models with extra (warped or flat) dimensions, little Higgs theories, technicolor and composite Higgs theories, among others (see e.g. the review in [67]).

Wino- and Higgsino-like Models: Among minimal electroweak multiplet dark matter candidates, pure wino and higgsino states stand out as particularly motivated scenarios, with predictive thermal relic abundances and simple gauge interactions. These candidates appear naturally in supersymmetric models, but are equally compelling in non-supersymmetric extensions, motivating a "SUSY or not" approach [68,69] (see also the experimental SUSY review). The thermal wino, with $m_\chi \simeq 2.8 - 3.1$ TeV [70, 71], features a large annihilation cross section enhanced by Sommerfeld effects, making it a prime target for indirect detection. However, recent reinterpretations of H.E.S.S. Galactic Center observations [69] suggest that previous exclusions may have overstated sensitivity due to effective-area misestimates [68]. Even so, thermal winos remain in tension with updated gamma-ray bounds, and will be further tested by next-generation telescopes. Pure higgsinos, with thermal mass near 1.1 TeV, have lower annihilation rates and produce softer gamma-ray spectra, but are still within the reach of CTAO, particularly CTAO-North, which is expected to probe the thermal parameter space within this decade [72].

Direct detection prospects for both candidates are limited [73, 74]. The pure higgsino's spin-independent scattering cross section is loop-suppressed and typically lies below the neutrino floor [75], while the wino may marginally exceed this floor due to electroweak loop contributions [76]. Inelastic transitions to heavier electroweak states are kinematically forbidden at galactic velocities, further suppressing detection rates. Nonetheless, future xenon-based experiments may begin to probe parts of the wino parameter space, especially in mixed scenarios [77]. At colliders, both candidates can lead to disappearing charged tracks due to small mass splittings: $\Delta m \sim 160$ MeV for winos and ~ 350 MeV for higgsinos. While LHC constraints currently probe sub-TeV masses, dedicated searches at future colliders may extend sensitivity further. Overall, wino and higgsino models remain well-motivated and complementary in terms of detection strategies, with indirect searches offering the most immediate discovery potential.

Axions and axion-like particles: Axions are an especially compelling example of a broad category of DM candidates encompassing very light scalar or pseudoscalar fields. The QCD axion provides a solution to the strong CP problem, and is at present a viable DM candidate (see Sec. 89 for details on motivations, production mechanisms, and detection prospects for the QCD axion). Ultra-light, bosonic DM generally implies the imprint of quantum effects on macroscopic scales (hence the name of *wave* or *fuzzy* DM). Specifically, some of the small-scale issues mentioned in sec. 27.4 can be addressed if the de Broglie wavelength of the DM, of mass m_a and velocity v_a,

$$\frac{\lambda}{2\pi} = \frac{\hbar}{m_a v_a} \simeq 1.9 \text{ kpc} \left(\frac{10^{-22} \text{ eV}}{m_a}\right) \left(\frac{10 \text{ km/s}}{v_a}\right) \tag{27.7}$$

is comparable to the size of the smallest observed gravitationally collapsed structures, roughly, for a self-gravitating system of mass M, a scale $r \simeq GM/v^2$. The typical expectation is the formation of a soliton-like core in the DM density profile of size λ, thus inversely proportional to the DM mass, with an upper limit on the central density of around

$$\rho_s \lesssim 7\ M_\odot/\text{pc}^3 \left(\frac{m_a}{10^{-22} \text{ eV}}\right)^6 \left(\frac{M}{10^9\ M_\odot}\right) \tag{27.8}$$

for a halo of virial mass M. Additionally, wave DM predicts that halos lighter than around $10^7 (m_a/10^{-22}\text{ eV})^{-3/2} M_\odot$ should not exist [78], and that the number of halos in the local universe with a mass at or less $10^9 (m_a/10^{-22}\text{ eV})^{-4/3} M_\odot$ [79] be significantly depleted, addressing in part the too big to fail and missing satellite problems (see Sec. 27.4 above). Light bosonic DM is necessarily produced non-thermally [80], and the connection with the visible sector need not, but might, exist.

Dark photons: Light *vector* bosons such as a "dark photon" V with a mass below $m_V < 2m_e$, can be cosmologically stable (depending upon its kinetic mixing coupling with the visible photon) and be a viable DM candidate. Light dark photons can be produced in the early universe through scattering or annihilation via processes such as $\gamma e^\pm \to V e^\pm$ or $e^+e^- \to V\gamma$, or via resonant photon-dark photon conversion, or from a condensate seeded by inflationary perturbations [81], or from a misalignment mechanism similar to the one commonly invoked for axion production; constraints on the parameter space stem from a combination of direct detection experiments, where the dark photon is absorbed and leads to a large ionization signal, from stellar cooling constraints from the Sun, horizontal branch stars, and red giants, and from CMB and the diffuse radiation from the $V \to 3\gamma$ decay mode. More broadly, light dark (pseudo-)scalars and vec-

[1] Notice that this includes the case of PBHs, as successful formation of the correct number density of PBHs involves new ingredients beyond standard cosmology and particle physics

Int. J. Mod. Phys. A 2026.41. Downloaded from www.worldscientific.com
by UNIVERSITY OF CALIFORNIA @ BERKELEY on 09/16/26. Re-use and distribution is strictly not permitted, except for Open Access articles.

tors can be best constrained with experiments that rely on their wave-like behaviour and/or on their possible "portal" with the visible sector. A broad assortment of experiments is sensitive to the range of masses between 10^{-22} eV and 10^{-2} eV. Among these experimental efforts, the lowest masses are probed by torsion balance experiments [82, 83], atom interferometry [84], comagnetometers [85, 86], and even gravitational wave detectors [87]; at increasing masses, if the light bosons couple electromagnetically, they can generate effective currents which are detectable with different apparata depending on the relevant, mass-dependent target frequency. The experimental portfolio includes the broadband axion search ABRACADABRA [88,89], the LC resonator DM Radio [90], lumped-element LC resonators [91], and cavity resonators such as HAYSTAC [92] and ADMX [93] .

Sterile Neutrinos: Sterile (gauge-singlet) neutrinos, assumed to share a Dirac mass term with ordinary, $\mathrm{SU}(2)_L$-active neutrinos, have long been considered viable DM candidates [94]. The mostly-sterile mass eigenstate participates in $\mathrm{SU}(2)_L$ interactions via a mixing parameter $\theta \ll 1$ that controls much of the particle's phenomenology. In particular, the sterile neutrino possesses an inverse-lifetime on the order of $\tau^{-1} \sim G_F^2 m_\nu^5 \theta^2$, requiring

$$\theta < 3.3 \times 10^{-4} \left(\frac{10 \text{ keV}}{m_\nu} \right)^5 \tag{27.9}$$

for the lifetime to exceed the age of the Universe. While the dominant decay channel is to three active neutrinos, observationally the radiative decay mode to one neutrino plus a photon is most relevant, yielding a quasi-monochromatic photon line at energy $E_\gamma \simeq m_\nu/2$. A tentative signal at 3.5 keV was reported in stacked galaxy cluster spectra and the Galactic center [95–97], but not in blank-sky or dwarf galaxy fields [98–100], casting doubt on a dark matter interpretation. Recent high-resolution observations with *XRISM* [101] and *NuSTAR* [102] have placed stringent constraints on the sterile neutrino interpretation of the 3.5 keV feature, excluding a decay origin for mixing angles $\sin^2(2\theta) \gtrsim 10^{-11}$ at $m_\nu \sim 7$ keV. Simultaneously, Lyman-α forest data and structure formation constraints now robustly disfavor most of the Dodelson-Widrow production mechanism for sterile neutrino dark matter [103], although resonant production in the presence of a lepton asymmetry remains viable [104]. Future missions like *Athena* and improved cosmological simulations may further test this scenario.

Models with rich dark sectors: The absence of any conclusive signals from DM as a particle thus far motivates the hypothesis that the DM be charged under some new "hidden" dark-sector force, an idea that dates back many decades [105], including in the guise of "mirror DM" (more recently in the context of "neutral naturalness"). Top-down motivation for hidden-sector DM comes from string theory [106], although TeV-scale BSM framework such as supersymmetry and composite Higgs models can also naturally accommodate hidden sectors [107]. Although no coupling of the visible sector to the hidden sector need exist in principle, there are a few reasons to expect it [108].The mass scale for hidden-sector DM is broader than, but overlapping with, that for WIMPs (this latter being limited to roughly between a few GeV and a few TeV). In particular, while some motivation exists for electroweak-scale hidden sectors, light, sub-GeV hidden sectors have a strong theoretical underpinning, and offer novel detection avenues and opportunities. The phenomenology of hidden-sector DM depends primarily on the nature of the force and its force carrier. The most-widely considered cases are (pseudo-)scalar and (axial-)vector mediators. Among the structures for the mediators' coupling to the visible sector, renormalizable "portals" include the $H^\dagger H$ operator, through Lagrangian terms of the type $(\mu\phi + \lambda\phi^2)H^\dagger H$, coupling to the hypercharge field strength $B^{\mu\nu}$ via kinetic mixing, $\epsilon' B_{\mu\nu} F'^{\mu\nu}$, and the "neutrino" portal, $y_n L H N$, where L is the lepton doublet of any generation, N is a right-handed neutrino, H is the SM Higgs doublet, and y_n the Yukawa coupling. Other possibilities are for instance a vector mediator directly coupled to SM fermions charged under its corresponding symmetry [109], or a Z' associated to $\mathrm{U}(1)_{B-L}$.Additional possibilities, arising for instance from vector couplings to anomalous global symmetries of the SM like baryon or lepton number, also exist [108]. The accelerator program necessary to probe hidden-sector DM often involves small-scale colliders and fixed-target experiments, with experiments utilizing missing energy and momentum offering the best sensitivity. Beam-dump experiments can test large ranges of DM-mediator couplings as long as mediators decay or scatter inside the detector (see e.g. the recent review [110]). Such experiments can also probe dark sectors with light vectors coupled to visible matter besides gauge kinetic mixing: an instance are neutrino trident scattering used to place bounds on e.g. $L_\mu - L_\tau$ Z' gauge bosons. Being virtually unconstrained, the phenomenology of dark sectors can be arbitrarily rich, with possibilities ranging from dark non-Abelian gauge interactions creating non-trivial self-interacting and/or particle number-changing dynamics, to models of "dynamical" DM, with multi-component, unstable DM candidates and a time-variable effective total DM abundance and equation of state [111].

27.6 Laboratory detection of dark matter

Laboratory searches for DM particles can be roughly classified in direct detection experiments, axion searches (see Axions and Other Similar Particles—Sec. 89), and searches at accelerators and colliders.

27.6.1 *Searches at Accelerators and Colliders*

Various searches for dark matter have been carried out by the CMS and ATLAS collaborations at the LHC in *pp* collisions [112–116]. In general, these assume that dark matter particles escape the detector without interacting, leading to significant amounts of missing energy and momentum.

Searches for DM with the LHC and other colliders have targeted DM models that interact with the SM via Higgs or Z boson exchange, effective field theories with heavy mediators, UV-complete models such as supersymmetry, models with long-lived particles, and models with rich dark sectors. The experimental program correspondingly includes searches for invisible-particle production mediated by a SM boson, generic searches for invisible particles produced via new particle mediators, and specific searches for complete models.

There are a variety of types of signals for DM, as noted by Ref. [112]:

(a) the imbalance in the transverse momentum in an event due to the presence of DM particles, produced together with one Standard Model particle,

(b) a bump in the di-jet or di-lepton invariant mass distributions, or

(c) an excess of events in the di-jet angular distribution, produced by a dark matter mediator. No signal for DM has been observed in the LHC experiments so far. Instead, limits are set on masses, couplings, and cross-sections. The latter can be compared, generally in a model-dependent way, with direct detection experiments.

Searches strategies are designed to optimize signal-to-noise by selecting search-specific cuts: a model-independent instance is initial-state electromagnetic or strong-interaction radiation plus missing transverse energy. Collider searches for DM inform, and are informed, by DM searches through direct or indirect detection (see below), and, if possible, by the inferred thermal relic DM abundance. The collider searches alone cannot prove that a discovery is of dark matter.

New fixed-target experiments are increasingly probing lighter, sub-GeV dark sectors; thermal, or quasi-thermal relics (such as asymmetric, SIMP, ELDER DM models) provide sharp, largely model-independent experimental targets in the case of direct annihilation to Standard Model particles; even "secluded" annihilation to dark-sector particles can be probed with fixed-target experiments, albeit with some model-dependent caveats. Accelerator searches provide unique ways to test light DM models in that they present a lower dependence on the DM particle nature, that could e.g. drive suppressed velocity-dependent direct detection cross sections, and on kinematic thresholds that can similarly suppress rates with other search strategies; additionally, accelerator searches offer opportunities to explore dark sectors in greater detail than other search strategies [108].

Experimental approaches to explore scenarios with a light DM χ and mediator A' include (i) searches for missing mass in exclu-

Int. J. Mod. Phys. A 2026.41. Downloaded by UNIVERSITY OF CALIFORNIA @ BERKELEY on 09/16/26. Re- worldscientific.com strictly not permitted, except for Open Access articles.

sive reactions such as $e^+e^- \to \gamma(A'\chi\bar{\chi})$ or $e^-p \to e^-p(A'\chi\bar{\chi})$, (ii) missing momentum/energy, e.g. in fixed-target reactions such as $eZ \to eZ(A'\chi\bar{\chi})$, (iii) electron and proton beam dump, where the DM particle is detected from scattering in a downstream detector after being produced in the beam dump, (iv) direct dark photon searches, when the mediator cannot decay to the dark matter, $m_{A'} < 2m_\chi$. Current facilities actively probing the methods listed above include APEX and HPS and JLab, MiniBooNE at Fermilab, NA64 at CERN, and TREK at J-PARC. Future experiments that will eventually contribute to covering the mentioned thermal targets include Belle-II at KEK, MAGIX at MESA, PADME at LNF, SHIP at CERN, VEPP3 at BINP, BDX at JLab, COHERENT at ORNL, DarkLight at JLab, LDMX at SLAC or JLab, MMAPS at Cornell, SBN at Fermilab, and SeaQuest [108].

27.6.2 *Direct detection formalism*

Direct detection experiments mostly aim to observe elastic or inelastic scatters of Galactic DM particles with atomic nuclei, or with electrons in the detector material. Predicted event rates assume a certain mass and scattering cross section, as well as a set of astrophysical parameters: the local density ρ_0, the velocity distribution $f(\vec{v})$, and the escape velocity v_{esc} (see Sec. 27.4).

Interactions with atomic nuclei: For DM scattering off nuclei, the differential scattering rate R as a function of nuclear recoil energy E_R is

$$\frac{dR(E_R,t)}{dE_R} = N_T \frac{\rho_0}{m_{\rm DM}} \int_{v>v_{min}} v f(\vec{v}+\vec{v}_E(t)) \frac{d\sigma(E_R,v)}{dE_R} d^3v, \tag{27.10}$$

where N_T is the number of target nuclei, $m_{\rm DM}$ is the mass of the DM particles, $v = |\vec{v}|$ is the speed of the particle in the experiment's rest frame, $f(\vec{v}+\vec{v}_E(t))$ is the velocity distribution in the Earth's frame, v_{min} is the minimum speed of the DM particles that can cause a recoil energy E_R and σ is the scattering cross section on the nucleus [29, 134]. For elastic scattering, the minimum velocity is $v_{min} = (m_N E_R/2m_r^2)^{1/2}$, with m_N being the mass of the nucleus, and $m_r = (m_N m_{\rm DM})/(m_N + m_{\rm DM})$ the reduced mass of the nucleus-DM system. In case of inelastic scattering, the minimum speed becomes $v_{min} = (m_N E_R/2m_r^2)^{1/2} + E^*/(2m_N E_R)^{1/2}$, with the nuclear excitation energy E^*, for part of the kinetic energy of the incoming particle will be spent on exciting the nucleus. The prompt de-excitation energy, if observed in addition to the nuclear recoil energy, will boost the region-of-interest to higher energies [135].

If one assumes the standard, leading order spin-independent (SI) and spin-dependent (SD) interactions, which couple to the charge/mass and spin of the nucleus, respectively, the differential cross-section is proportional to the inverse squared speed of the DM particle, $d\sigma/dE_R \propto v^{-2}$, and the dependence on the velocity distribution can be expressed as:

$$g(v_{min},t) = \int_{v>v_{min}} \frac{f(\vec{v}+\vec{v}_E(t))}{v} d^3v. \tag{27.11}$$

This functions allows for the comparison of various experimental results independently of the underlying velocity distribution [136], for a given DM mass. The time-integrated differential cross section is the sum of the SI and SD contributions:

$$\frac{d\sigma(E_R,v)}{dE_R} = \frac{m_N}{2m_r^2 v^2}\left(\sigma_0^{SI} F_{SI}^2(E_R) + \sigma_0^{SD} F_{SD}^2(E_R)\right), \tag{27.12}$$

where $F^2(E_R)$ are the nuclear form factors and σ_0 the cross-sections in the limit of zero momentum transfer. Since the incoming particle velocity is $v/c \sim 10^{-3}$, the nuclear recoil energy is at most tens of keV (much smaller than typical nuclear binding energies per nucleon), and the momentum transfer $q = (2m_N E_R)^{1/2} \sim \mathcal{O}(10-100)$ MeV. This implies that $1/q$ can be of the same order as nuclear radii $R \sim A^{1/3}$ fm, and that nuclei are not point-like from the perspective of a DM particle. The cross sections will thus involve nuclear form factors. These were calculated in [137] and [138] for the SI and SD case, respectively, for specific target nuclei, while the cross sections are often expressed in terms of single-nucleon cross sections and effective couplings of the DM particle to protons and neutrons. In the SI case, all the nucleons in the nucleus contribute coherently to the cross-section (under the assumption of isospin independence in the DM couplings). Dominant sources of uncertainty are the nucleon sigma terms, especially for Higgs-dominated interactions, where the couplings are proportional to the quark masses. An overview is presented in Ref. [139]. For SD scattering, the nuclear spin contents due to the protons and neutrons must be considered.

The interactions of DM particles with nuclei can be treated in a non-relativistic effective field theory (NR-EFT) approach, which considers more general DM scenarios based on the lowest-order, four-field operators that describe the couplings to nucleons. These operators, which correspond to different types of interactions between the DM and quark fields, can be momentum- and velocity-dependent, and might be leading when momentum-independent interactions are suppressed, or even vanish in the limit of zero momentum [140, 141]. In Ref. [141, 142] all 15 operators (arising from 20 possible bilinear combinations between the DM and nucleon fields) which obey Galilean-invariance, T-symmetry and are Hermitian are written out up to quadratic order in q, and the nuclear response functions evaluated in shell-model calculations for DM targets made of F, Na, Ge, I and Xe isotopes. The connection to particle physics within the context of *simplified DM models* is made in Ref. [143, 144], where the simplified models assume a single DM particle with one mediator which couples it to quarks. More recently the DM-nucleus scattering was also analysed in the framework of chiral effective field theory (Ch-EFT), a low-energy effective theory of QCD, which allows for a consistent derivation of the nuclear responses beyond the leading-order expressions [145, 146]. Ch-EFT preserves the QCD symmetries, and predicts DM couplings to two nucleons (e.g., when the hypothetical particle couples to a virtual pion exchanged between the nucleons). It also provides a power counting that suggests a hierarchy of the various NR-EFT operators, which is however approximate given that the couplings between the DM and the Standard Model fields are not known. The generalized SI structure factors for spin-1/2 and spin-0 DM particles and various isotopes of F, Si, Ar, Ge and Xe employed in direct detection experiments are provided in Ref. [146].

Scattering off bound electrons and absorption: For DM particle masses below the GeV-scale, most searches for DM-nucleus scattering rapidly lose sensitivity, due to energy thresholds around a few 100 eV - few keV. As an example, a light DM particle with a mass of 100 MeV and $v \propto 10^{-3}c$ will induce a nuclear recoil energy of about 0.5 eV in a target made of argon. Another strategy is to search for DM scattering off bound electrons, allowing for all of the kinetic energy (50 eV in the above case) to be transferred to the material [147]. The leading possibilities are ionisation, excitation, and molecular dissociation processes, which typically require energies of (1-10) eV, and thus allow to probe scattering of DM particles with masses down to the $\mathcal{O}$(MeV) range.

For a bound electron with binding energy E_B DM particle masses of $m_{\rm DM} \geq 250\,{\rm keV} \times {\rm E_B}/1$ eV can in principle be probed. The signal depends on the material, and can consist of one or more electrons (in semiconductors, noble liquids, graphene), one or more photons (in scintillators) or phonons (in superconductors and superfluids) and quasiparticles (in superconductors). As an example, the differential event rate for ionization in atoms is given by:

$$\frac{dR_{ion}}{d\ln E_R} = N_T \frac{\rho_0}{m_{\rm DM}} \frac{d\langle\sigma_{ion} v\rangle}{d\ln E_R}, \tag{27.13}$$

where E_R is the recoil energy transferred to the electron, $\langle\sigma_{ion} v\rangle$ is the thermally averaged ionization cross section and N_T is the number of target atoms per unit mass. The cross-section is related to the non relativistic DM-electron elastic scattering cross-section (σ_e):

Int. J. Mod. Phys. A 2026.41. Downloaded from www.worldscientific.com
by UNIVERSITY OF CALIFORNIA @ BERKELEY on 09/16/26. Re-use and distribution is strictly not permitted, except for Open Access articles.

Table 27.1: Best constraints from direct detection experiments on the SI (at high >5 GeV and low < 5 GeV masses) and SD DM-nucleon couplings.

Experiment	Target	Fiducial mass [kg]	Cross section [cm^2]	DM mass [GeV]	Ref.
Spin independent high mass (>5 GeV)					
LUX-ZEPLIN	Xe	5500	2.2×10^{-48}	40	[117]
PandaX-4T	Xe	2480	1.6×10^{-47}	40	[118]
XENONnT	Xe	4000	1.7×10^{-47}	30	[119]
SuperCDMS	Ge	12	1.0×10^{-44}	46	[120]
DarkSide-50	Ar	20	1.9×10^{-43}	10	[121]
DEAP-3600	Ar	2000	3.9×10^{-45}	100	[122]
Spin independent low mass (<5 GeV)					
DarkSide-50 (ionisation only)	Ar	20	1.4×10^{-42}	2	[121]
PandaX-4T (ionisation only)	Xe	3100	1.3×10^{-43}	3.5	[123]
PandaX-4T	Xe	3100	1.6×10^{-42}	3	[124]
XENONnT	Xe	4000	3.2×10^{-42}	3	[125]
SuperCDMS (CDMSlite)	Ge	0.6	2×10^{-40}	2	[126]
CRESST	$CaWO_4$ - O	0.024	1×10^{-39}	2	[127]
CRESST	Si	0.0035	4.5×10^{-32}	0.15	[128]
CRESST	Al_2O_3	0.0006	1.0×10^{-32}	0.1	[129]
DAMIC	Si	0.3	1×10^{-40}	4	[130]
NEWS-G	Ne	0.3	1×10^{-38}	2	[131]
Spin dependent proton					
NEWS-G	CH_4	0.114	3.1×10^{-35}	0.76	[132]
PICO60	C_3F_8 - F	49	3.2×10^{-41}	25	[133]
PandaX-4T	Xe	2480	7.7×10^{-41}	40	[118]
LUX-ZEPLIN	Xe	5500	9.8×10^{-42}	40	[117]
XENONnT	Xe	4000	8.5×10^{-41}	25	[119]
Spin dependent neutron					
PandaX-4T	Xe	2480	2.7×10^{-42}	40	[118]
LUX-ZEPLIN	Xe	5500	3.7×10^{-43}	46	[117]
XENONnT	Xe	4000	2.8×10^{-42}	25	[119]

$$\frac{dR_{ion}}{d\ln E_R} = \frac{6.2}{A}\left(\frac{\rho_0}{0.4\,\mathrm{GeV\,cm^{-3}}}\right)\left(\frac{\sigma_e}{10^{-40}\mathrm{cm}^2}\right)\left(\frac{10\,\mathrm{MeV}}{m_{\mathrm{DM}}}\right) \times \frac{d\langle\sigma_{ion}v\rangle/d\ln E_R}{10^{-3}\sigma_e}\,\frac{\mathrm{events}}{\mathrm{kg\,d}} \tag{27.14}$$

Predicted differential rates in various materials (He, Ar, Ge, Xe) and for different particle masses are shown in [147], together with cross section sensitivities as a function of mass and expected background rates from neutrinos. More recently, rates of electronic transitions induced by DM-electron scattering on Xe, Si and Ge for spin 0, spin 1/2, and spin 1 DM models were calculated in [148]. The code `EXCEED-DM` (extended calculation of electronic excitations for direct detection of dark matter) can compute DM-electron interaction rates with inputs from a variety of *ab initio* electronic structure calculations [149].

Two classes of DM candidates, axion-like-particles (ALPs) and dark (or hidden) photons (see Sec. 27.5), can be absorbed in a target material by interactions with bound electrons via the axioelectric effect, which is analogous to the photoelectric effect: a boson is absorbed by a bound electron, which is then ejected from the atom [81,150,151]. The dark photon arises in extensions of the SM by a new massive or massless U(1)' field, coupled to the SM $U(1)_Y$ via a kinetic mixing term κ, see Sec. 27.5. The absorption cross-section of a massive, NR particle m_V with coupling $e' = e\kappa$ to electrons is (in natural units, and for energies $E_V \ll m_e$)

$$\sigma_{abs} = \frac{\alpha'}{\alpha}\left(\frac{E_V}{2m_e}\right)^2 \sigma_{pe}, \tag{27.15}$$

where σ_{pe} is the photoelectric cross-section, and an analogue to the electromagnetic fine structure constant α is introduced, $\alpha' = (e\kappa)^2/4\pi$. The rate per atom is

$$R \simeq \frac{\rho_0}{m_V} \times \kappa^2 \sigma_{pe}. \tag{27.16}$$

Since the kinetic energy of the dark photon is negligible compared to its rest energy, a mono-energetic peak at its mass is expected in the spectrum of a direct detection experiment. Dark photons with a thermally generated abundance are excluded by direct detection experiments [81], however non-thermal mechanisms (e.g., via perturbations during inflation) could create the relic abundance, see Section 27.3.

Similarly to axions, ALPs arise in the spontaneous breaking of a global symmetry, and are phenomenologically described by a mass m_a and a decay constant f_a. Unlike for QCD axions, however, there is no strict relation between m_a and f_a. The coupling strength to electrons with mass m_e is parameterised by $g_{ae} = 2m_e/f_a$, and the absorption cross section of a particle with incoming velocity v_a is related to the cross-section for the photoelectric effect as

$$\sigma_{abs} v_a \simeq \frac{3E_a^2}{4\pi\alpha f_a^2}\sigma_{pe} = \frac{3g_{ae}^2}{4\pi\alpha}\left(\frac{E_a}{2m_e}\right)^2 \sigma_{pe}. \tag{27.17}$$

As in the case of the dark photon, the signature is a mono-energetic peak at the mass of the particle, broadened by the energy resolution of the detector. Constraints on the couplings of ALPs and dark photons to electrons from direct detection experiments in m_a and m_V mass ranges from $\sim (1 - 10^4)$ eV were derived in Ref. [73, 152], and compared to indirect limits from anomalous energy losses in the Sun, in red-giant and horizontal-branch stars. For a detailed discussion of axion and ALP searches, we refer to the *Axion* review.

27.6.3 *Current and future direct detection technologies*

Direct detection experiments aim to observe the small (keV-scale and below) and rare (fewer than ∼1 event/(kg y) at low masses and <1 event/(t y) at high masses) signals which are induced by DM particle scatters in a detector, mostly in the form of ionisation, scintillation or lattice vibrations. A majority of experiments detects more than one signal, which allows to distinguish between scattering off of electrons (electronic recoils, ER) and off of atomic nuclei (nuclear recoils, NR). A 3D position resolution

Int. J. Mod. Phys. A 2026.41. Downloaded from www.worldscientific.com by UNIVERSITY OF CALIFORNIA @ BERKELEY on 09/16/26. Reproduction strictly not permitted, except for Open Access articles.

is required to define central detector regions (or fiducial volumes) with low background rates from surrounding materials, and the distinction between single- versus multiple-scatters rejects a significant fraction of backgrounds, given that DM will scatter at most once. We refer to [153, 154] for reviews of the field.

Specific signatures: For NRs, the shape of the differential recoil spectrum is exponentially falling with recoil energy, and depends on the mass of the particle and on the nuclear mass. Unless $m_{\rm DM} \gg m_N$, $m_{\rm DM}$ can in principle be determined from the measured recoil spectrum, where multiple targets will provide tighter constraints [155]. The Earth's motion through the MW induces a seasonal variation of the total event rate and a forward-backward asymmetry in a directional signal [156, 157]. The annual modulation is due to the Earth's motion in the Galactic rest frame, which is a superposition of the Earth's rotation around the Sun and the Sun's rotation around the Galactic center. Since the Earth's orbital speed is much smaller than the Sun's speed, the expected amplitude of the modulation is $\simeq 5\%$. In the SHM, the period is one year, and the phase is 150 d (June 2), when both speeds add up maximally. This expectation is modified for different DM distributions, e.g. in the case of sub-structures such as clumps and streams [158, 159] and a DM disc [160]. In addition, the modulation changes phase at a specific recoil energy (known as crossing-energy) [161], which depends on the DM and nuclear mass, allowing to in principle determine $m_{\rm DM}$ if low energy thresholds can be achieved. A powerful signature is provided by the ability to detect the axis and direction of the recoiling nucleus. Since the DM flux in the laboratory frame is peaked in the direction of motion of the Sun towards the constellation Cygnus, the recoil spectrum is peaked in the opposite direction. The observation of such a dipole feature would provide a 'smoking-gun' evidence for DM, where the forward-backward rates can differ by a factor of $\sim$10, depending on the energy threshold. Ref. [162] provides a review of the theoretical framework and of the discovery reach of directional detectors.

Backgrounds, including neutrinos: Early direct detection experiments employing low-background Ge spectrometers featured background levels around 2 events/(kg d keV), while the latest generation of liquid Xe experiments reduced this noise by almost five orders of magnitude, to 4×10^{-5} events/(kg d keV). In liquid xenon detectors, the measured ER spectra at low energies are for the first time dominated by solar *pp* neutrino interactions, second-order weak decays, as well as ^{214}Pb β-decays from radon mixed with the xenon. Other backgrounds are due to the radioactivity of detector components, followed by cosmic muons and their secondaries such as fast neutrons. The cosmic and environmental radiation are suppressed by going deep underground and surrounding the experiments with appropriate shielding structures (mainly large water Cherenkov detectors for the current and next-generation detectors). Activation of materials via cosmic-ray interactions produce long-lived radio-nuclides (e.g., ^{39}Ar, ^{60}Co, ^{68}Ge, ^{32}Si, etc), while long-lived, human-made isotopes (^{85}Kr, ^{137}Cs, etc) can mix with detector materials or generate surface backgrounds. For details, we refer to *Section 36.6* of this *Review*.

The final backgrounds are due to the irreducible neutrino flux from the Sun, the atmosphere and the diffuse supernovae background [163]. Solar pp-neutrinos start dominating the electronic recoil background due to elastic neutrino-electron scatters, at a level of $\sim (10-25)$ events/(t y) below energies of $\sim$100 keV, while coherent elastic neutrino-nucleus scatters (CEνNS) from ^{8}B solar neutrinos will induce up to $\sim 10^3$ events/(t y) for high-A targets, at nuclear recoil energies below $\sim$few keV. Recently, the large LXe detectors PandaX-4T and XENONnT observed the ^{8}B flux for the first time, via CEνNS [125,164]. Nuclear recoils from atmospheric neutrinos and the diffuse supernovae neutrino background will yield event rates in the range $(1-5)$ events/(100 t y), depending on the detector material. In general, ^{8}B and atmospheric neutrinos will impact light (≤ 6 GeV) and heavy (100 GeV and above) DM searches for cross sections on nucleons below $\sim 10^{-45}$ cm^2 and $\sim 10^{-49}$ cm^2, respectively. The precise cross-sections where neutrinos constitute a dominant background strongly depend on the systematic uncertainties on the neutrino flux normalisation for each source [165]. For very low energy thresholds to nuclear recoils, e.g. 10-30 eV in Ge and Si detectors, CEνNS due to the ^{7}Be neutrino flux become relevant for exposures of $\sim$50 kg y [166]. For DM searches with electron recoils via DM-electron scattering and dark photon or ALP absorption, solar neutrinos will also limit the sensitivity to DM masses in the range $\sim$(1-10^3) MeV and $\sim$(1-10^3) eV, respectively, for large exposures around 1 t y, as shown in Ref. [167].

Solid-state cryogenic detectors: Current experiments using the bolometric technique (see *Section 36.5* of this *Review*), together with either charge or light readout, are SuperCDMS (Si, Ge), in construction at SNOLAB, EDELWEISS/CRYOSEL (Ge) at the Laboratoire Souterrain de Modane (LSM) and CRESST ($CaWO_4$, Al_2O_3, Si, $LiAlO_2$) at the Laboratori Nazionali del Gran Sasso (LNGS). These experiments are optimised for low-mass DM searches, and can probe WIMP masses down to $\sim$0.03 GeV. CRESST operated a 0.35-g thin wafer Si detector and reached a 10-eV energy threshold, probing DM masses in the range (115–500) MeV, improving existing limits by up to a factor 20 for masses below 160 MeV. CDMSlite operated detectors at higher bias voltages to amplify the phonon signals produced by drifting charges and thus have access to light DM around 1.5 GeV. The goal of SuperCDMS at SNOLAB is to probe the (0.05–5) GeV region down to cross sections of $\sim 10^{-44}$ cm^2. Much smaller, gram-scale versions of cryogenic detectors can have single-charge resolution and thus probe low-mass DM via inelastic electron recoils. A SuperCDMS single-charge sensitive Si detector placed upper limits on DM interacting with electrons for masses between (0.5–10^4) MeV, as well as on dark photon kinetic mixing for dark photon masses in the range (1.5–40) eV. With Ge crystals operated at Soudan, SuperCDMS constrained dark photons and ALPs in the mass range 40 eV to 500 keV.

Germanium ionisation detectors operated at 77 K can reach sub-keV energy thresholds and low backgrounds, but lack the ability to distinguish electronic from nuclear recoils. The CDEX-10 experiment at the China Jinping Underground Laboratory (CJPL) uses p-type, point-contact Ge detectors operated in liquid nitrogen to probe DM masses down to 3 GeV. It also reported constraints on the kinetic mixing of dark photons in the mass range (0.1–4.0) keV. The $0\nu\beta\beta$-decay experiments Majorana Demonstrator and GERDA have obtained constraints on the couplings of ALPs and dark photons to electrons, with masses between (6-100) keV and (60-1000) keV, respectively. The Majorana Demonstrator improved laboratory constraints on solar axion masses between (1.2–100) eV, setting limits on the axion-photons coupling of $g_{a\gamma} < 1.45 \times 10^{-9}$ GeV^{-1}(95% CL).

Noble liquids: Liquid argon (LAr) and liquid xenon (LXe) are employed as DM targets, while R&D on liquid helium is ongoing. We refer to Ref. [168] for a review of the liquid noble gas detector technology in low-energy physics, as well to *Section 36.4* of this *Review*. At present the best constraints on DM-nucleus interactions come from multi-tonne experiments using LXe: the LZ experiment at SURF, PandaX-4T at CJPL and XENONnT at LNGS. These experiments probe particle masses down to $\sim$3 GeV (when using both light and charge signals) and the SI DM-nucleon cross section down to 2.2×10^{-48} cm^2 (at 40 GeV). LAr experiments employ pulse shape discrimination (PSD) that allows for distinguishing between ER and NR events, at the expense of higher energy thresholds than in LXe. The DarkSide-50 TPC at LNGS (until 2019) sets a minimum upper limit on the SI, DM-nucleon cross-section of 6×10^{-43} cm^2 at 10 GeV, while the single-phase experiment DEAP-3600 at SNOLAB constrains the SI cross-section to values below 3.9×10^{-45} cm^2 at 100 GeV.

In noble liquids, sub-GeV DM particles can be searched for by using the amplified, charge signal only, at the expense of giving up discrimination between ERs and NRs. XENON1T probed particle masses down to 60 MeV, while DarkSide-50 published constraints on WIMP masses as low as 40 MeV. DM masses at the MeV-scale can also be probed by exploiting the scattering off electrons. PandaX-4T presented light DM searches with ionisation signals, with NR and ER energy thresholds of 0.77 keV and 0.07 keV, obtaining leading constraints in the mass range 40 MeV–100 GeV and 100 MeV–10 GeV for a heavy and light mediator, respectively [123]. DarkSide-50 set limits in the mass range

Int. J. Mod. Phys. A 2026.41. Downloaded from www.worldscientific.com
by UNIVERSITY OF CALIFORNIA @ BERKELEY on 09/16/26. Re-use and distribution is strictly not permitted, except for Open Access articles.

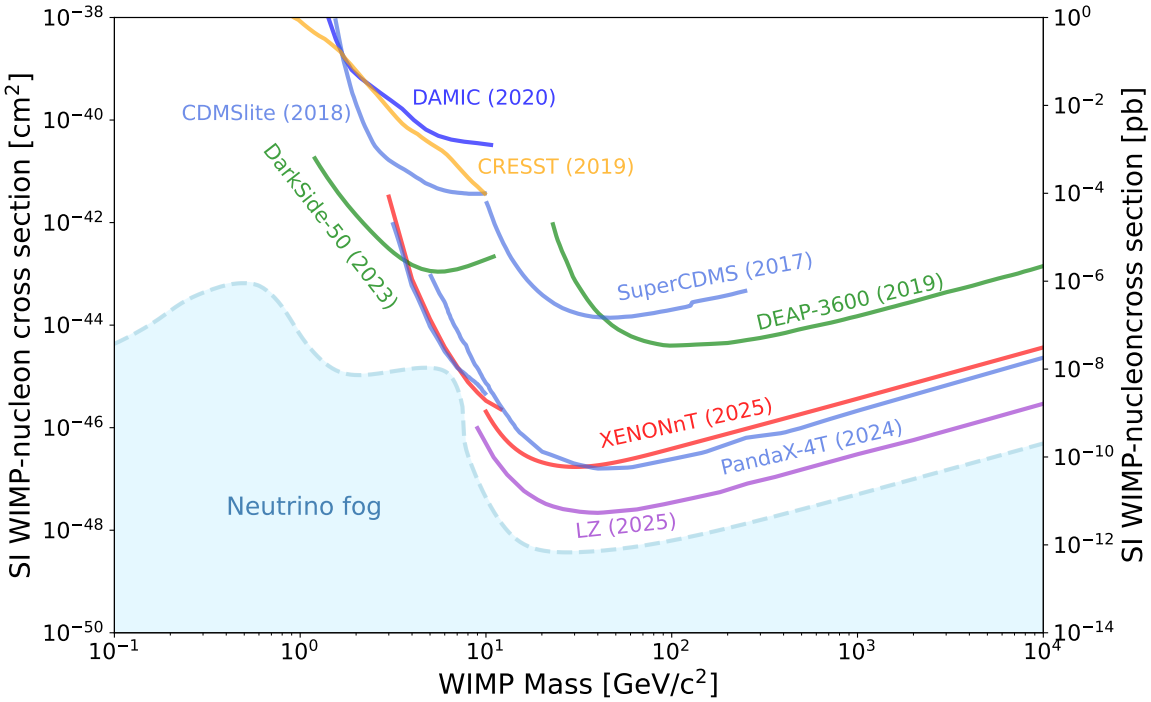

Figure 27.1: Upper limits on the SI DM-nucleon cross section as a function of DM mass.

$(16-56)$ MeV and above 80 MeV for a heavy and light mediator, respectively [169], while XENONnT set limits in the mass range 5 MeV–1 GeV [170]. Noble liquids TPCs also search for solar axions, galactic ALPs and dark photons. XENONnT set upper limits on the axion-electron coupling of 2×10^{-12} in the mass range $(10^{-6}$–$1)$ eV for solar axions, and probes couplings between $(1-2)\times10^{-14}$ in the mass range (1–10) keV for galactic ALPs [171]. DarkSide-50 probes ALP masses down to 0.03 keV with couplings in the range $10^{-13}-10^{-14}$ [169].

The next generation of liquefied noble gas detectors are in construction (DarkSide-20k) or at the design stage (Argo, PandaX-xT, XLZD). These will increase the sensitivity to various DM candidates by 1-2 orders of magnitude, with the ultimate goal of exploring the parameter space until the backgrounds from astrophysical neutrinos will start dominating the event rates.

Room temperature scintillators: Several large DM experiments using high-purity NaI(Tl) crystals are acquiring data in various underground laboratories. Of these, DAMA/LIBRA at LNGS had the highest mass, 250 kg, and the largest exposure: 1.33 t y with an energy threshold of 1 keV and 2.46 t y with an energy threshold of 2 keV. It is the only experiment in the field that reported an annually modulated event rate with a statistical significance of 12.9 σ C.L. (20 annual cycles), with a modulation amplitude around 0.02 events/(kg d keV) in the energy region (1-4) keV. These findings were interpreted as due to DM interactions via nuclear or electronic recoils. The ANAIS experiment at Canfranc operates 112.5 kg of NaI(Tl) scintillators with an energy threshold of 1 keV. An analysis of 6 years of data with an exposure of 625.75 kg y is incompatible with the DAMA/LIBRA modulation signal at 4 σ C.L. [172]. The COSINE-100 experiment, located at the Yangyang Underground Laboratory in Korea (until 2023), operated 106 kg of NaI(Tl) crystals in a liquid scintillator, with an energy threshold of 0.7 keV. A new analysis disfavors the DAMA/LIBRA signal as originating from WIMP interactions, fully excluding the 3 σ allowed regions [173]. An upgrade, COSINE-100U, with a mass of 99.1 kg, was recolated to Yemilab. With higher light collection efficiency and reduced background levels, the experiment's ability to probe low-mass DM will be improved. COSINE-200, to be constructed at Yemilab, will be a larger experiment with reduced backgrounds. The SABRE experiment plans to operate a total of 50 kg of NaI(Tl) crystals, focussing on reaching a background level of 0.1 events/(kg d keV), an order of magnitude below DAMA/LIBRA. Detectors are installed both at LNGS and at the Stawell Underground Physics Laboratory in the Southern hemisphere. While a DM-induced signal is expected to have the same phase in both hemispheres, seasonal or site-related effects would show different amplitudes and phases in the twin detectors. The COSINUS experiment, under commissioning at LNGS, uses NaI crystals operated as cryogenic scintillating calorimeters to differentiate between nuclear and electronic recoils based on the observation of phonon and light signals. The first phase aims for an exposure of 100 kg d, while the second phase aims to achieve, with 1000 kg d, a fully model-independent cross-check of a NR origin of the DAMA/LIBRA signal.

Room temperature ionisation detectors: Silicon charged-coupled devices (CCDs) are employed for low-mass DM searches, as well as for hidden photon searches in the eV-mass range. Ionisation events induced in bulk silicon of high-resistivity, fully depleted CCDs are observed with charge resolutions around 1-2 e^- and extremely low leakage currents, at the level of few $e^-\,mm^{-2}d^{-1}$. The position of an energy deposit is reconstructed in 3 dimensions and the particle type (electron, neutron, muon, α-particles, etc) is reconstructed based on the recorded track pattern.

The DAMIC experiment at SNOLAB yielded constraints on DM-electron scattering, and on the hidden-photon kinetic mixing parameter in the mass range (1-30) eV with an exposure of 7.6 kg d and on low-mass WIMPs with an exposure of 11 kg d. The SENSEI projects employs the skipper technology to achieve single-electron sensitivity. A run with a 2 g detector in the MINOS cavern at Fermilab yielded world-leading constraints on DM-electron scattering for a large range of sub-GeV dark matter masses. Currently, the experiment takes data at SNOLAB and plans for a 40 kgęxposure. An excess of events above the expected background was observed in DAMIC at SNOLAB, with both conventional and skipper CCDs. While the topology of events is consistent with ionisation events, its origin is unclear [174]. The skipper technology is also employed in by DAMIC-M at LSM, which plans for a kg-size Si mass with improved radioactive backgrounds. The goal is to achieve thresholds of 2-3 electrons and to probe the DM-nucleon cross-section down to few$\times10^{-43}$cm^2 around 2-3 GeV and the DM-electron cross section down to 2×10^{-41}cm^2 at 10 MeV

Int. J. Mod. Phys. A 2026.41. Downloaded from www.worldscientific.com by UNIVERSITY OF CALIFORNIA @ BERKELEY on 09/16/26. Re-[redacted] strictly not permitted, except for Open Access articles.

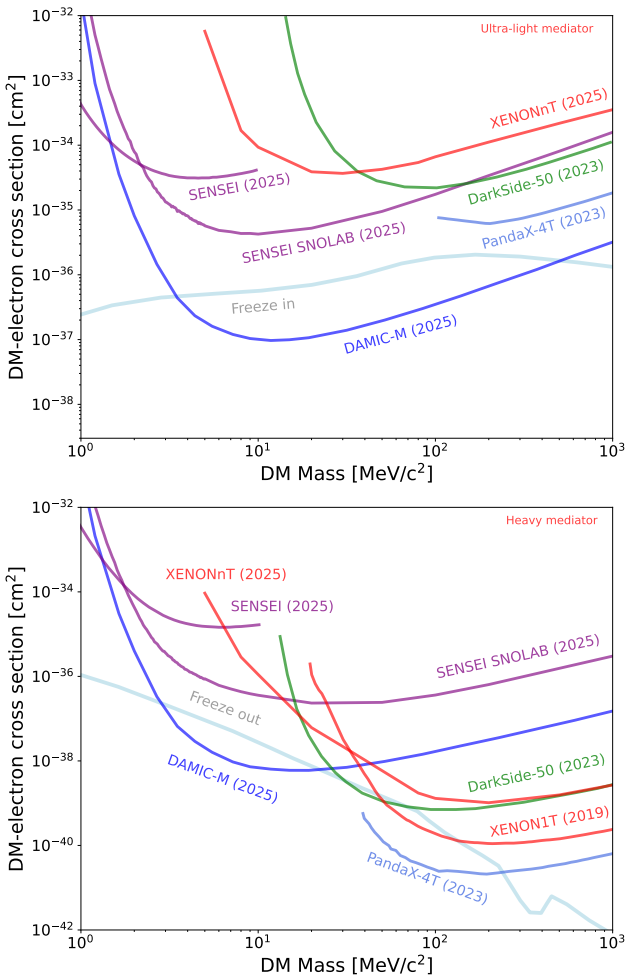

Figure 27.2: Upper limits on the DM-electron cross section as a function of DM mass for ultra-light mediators (left) and heavy mediators (right).

mass. DAMIC-M has operated first CCDs at LSM and achieved constraints on sub-GeV DM particles interacting with electrons in the mass range (1-1000) MeV, for an exposure of 1.3 kg d, probing cosmological benchmark scenarios.

The NEWS-G collaboration operates spherical proportional counters filled with light gas targets (H, He, Ne). Advantages of this technology are the low intrinsic electronic noise and a high amplification gain, allowing for low energy thresholds down to single-electron detection, and the possibility to use different targets. A 135 cm diameter chamber was operated at LSM in 2019 for 10 days with 114 g of methane target. New, leading SD constraints to proton couplings were set in the mass range (0.17-1.2) GeV, with an upper limit of 30.9 pb at 0.76 GeV, for an exposure of 0.12 kg d [132]. This detector, made of very low radioactivity copper (few μBq/kg of ^{238}U and ^{232}Th) has been installed at SNOLAB in 2021. The experiment is acquiring physics data, with a predicted background level of (5 ± 2) events/(kg keV d) for sub-keV events.

Superheated liquid detectors: Investigation of the spin-dependent interaction channel calls for target nuclei with uneven total angular momentum. A particularly favourable candidate is ^{19}F, the spin of which is carried mostly by the unpaired proton, yielding a cross-section which is almost a factor of ten higher than of other employed nuclei with spin (e.g., ^{23}Na, ^{73}Ge, ^{127}I, ^{129}Xe, ^{131}Xe). Fluorine is part of the target of experiments using superheated liquids, such as the ones operated by the PICO collaboration. A search in the PICO-60 C_3F_6 bubble chamber at SNOLAB with an exposure of 1404 kg d and an energy threshold of 2.45 keV, yielded the most stringent constraint on the DM-proton SD cross-section at 2.5×10^{-41}cm^2 for a 25 GeV particle mass. Recently, an analysis of PICO-60 data set leading constraints on SI and SD absorption via neutral current processes ($\chi + N \to \nu + N$) for DM particle masses below 23 MeV [175]. In construction at SNOLAB's Cube Hall is PICO-500, a detector with 250 l of superheated freon (C_3F_8) contained between two quartz jars inside a pressure vessel filled with mineral oil, itself inside a tank of ultra-pure water. PICO-500 will start a first run in 2026. To demonstrate the background reduction and technology improvements for PICO-500, PICO-40L was constructed and is currently in commissioning phase. With one-year background-free exposure, the goal is to improve upon PICO-60 by a factor of five.

Directional detectors: Detectors capable of measuring the direction of the recoiling nucleus would unequivocally confirm the Galactic origin of a signal and could probe the region below the neutrino floor [162]. Because nuclear recoils have a range which is about 10 times smaller than the one of Compton recoils of the same energy, gaseous detectors have an excellent intrinsic background rejection if they can measure the range of events precisely. Several directional detectors are presently in operation, where a 1 m^3 detector has a typical mass of a few 100 g and can measure the sense of an incoming nuclear recoil above a few tens of keV. Cygnus is a proto-collaboration which coordinates the R&D efforts for gas based TPCs with 1 keV threshold. One of these is CYGNO, an experiment that aims to build a 1-m drift length gaseous TPC filled with a He:CF_4 60:40 gas mixture at atmospheric pressure and room temperature at LNGS. Several prototypes were constructed and are currently being operated in preparation for CYGNO 1 m^3. A new technique is based on fine-grained nuclear emulsions (solid-state detectors with silver halide crystals uniformly dispersed in a gelatine film, where each crystal works as a sensor for charged particles), as proposed by the NEWSdm collaboration. These act as target and nanometric tracking device, and the expected NR tracks are sub-μm in size. Due to the small crystal size and larger number density, a superior spatial resolution compared to gaseous detectors is obtained. Simulations show that to reach the neutrino floor, exposures of 10 t y and 100 t y are required if a 30 nm and 50 nm threshold for detecting the track length is reached. This requires further R&D, since current emulsions allow for 100 nm tracking and target masses are around 1 kg, with 10 kg y exposures planned. A proposed approach for the directional detection of sub-GeV DM is to use quantum sensors, e.g., two-dimensional materials such as monolayer graphene [176], from which the DM particle can eject electrons. Their energy and direction, correlated with the direction of the incoming DM, can be measured for instance with the proposed PTOLEMY experiment. Another approach is to exploit the anisotropic material response function of condensed matter systems, allowing in principle for a broad range of target materials.

New techniques: To probe light (sub-GeV) DM particles, either via scatters off electrons or via couplings to phonons, new techniques beyond the ones discussed above are proposed. The DM particle mass that can be accessed in DM-electron scattering in noble liquids and semiconductors is limited by the minimum ionisation/excitation energy and the size of the band gap, respectively (at the ∼eV-scale). To reach lower energy thresholds, materials with smaller band gaps for electron excitations (∼meV), such as superconductors and superfluids, as well as Dirac materials were proposed [177]. These would in principle allow for the detection of keV-scale DM. Other ideas to detect keV-MeV scale DM are to observe NRs in superfluid He, via collective excitation modes in the fluid [178], as realised in HeRALD and DELight, or based on the breaking of chemical bonds between atoms [179].

Even lighter DM, with masses in the meV-eV range, could be detected via absorption on a conduction electron in a superconductor, followed by the emission of an athermal phonon [180]. Another proposed target for light DM are polar materials (for example GaAs, sapphire), which are especially sensitive for scattering through an ultralight dark photon, via excitation of single optical phonons [181]. If an anisotropic crystal such as sapphire is employed, a daily modulation interaction rate could be established [182]. A new class of detectors for bosonic DM, based on

Int. J. Mod. Phys. A 2026.41. Downloaded from www.worldscientific.com
by UNIVERSITY OF CALIFORNIA @ BERKELEY on 09/16/26. Re-use and distribution is strictly not permitted, except for Open Access articles.

resonant absorption onto a gas of small polyatomic molecules, is proposed in [183]. The DM would effectively act as a laser that resonantly excites transitions in molecules when its mass closely matches the transition energy. While DM with SI couplings can efficiently excite phonons, it has been shown in [184] that if DM couples to the electron spin, magnon excitations (quanta of collective spin wave excitations) in materials with magnetic dipole order may also offer a promising detection avenue. Yet another approach for sub-GeV DM is to employ superconducting nanowire single-photon detectors (SNSPD) as both target and sensor. Recent bounds on DM-electron and DM-nucleus interactions were placed by the QROCODILE experiment [185], with a WSi microwire-based SNSPD, sensitive to energy deposits (DM masses) as low as 0.11 eV (30 keV).

The detection of light DM via collective excitations in condensed matter systems and other methods is a rapidly evolving field, and a growing area of research at the interface of DM physics, condensed matter and materials science. We refer to Ref. [186] for discussions of some of these new directions and models. Critical challenges are to detect these very small energy depositions, and to reliably asses the background noise.

Table 27.1 summarizes the most stringent constraints on the DM-nucleon SI and SD cross-sections, and Figures 27.1 and 27.2 show the best constraints for DM-nucleon SI and DM-electron couplings in the cross-section versus DM mass parameter space.

27.7 Astrophysical detection of dark matter

DM as a microscopic constituent can have measurable, macroscopic effects on astrophysical systems. Indirect DM detection refers to the search for the annihilation or decay debris from DM particles, resulting in detectable species, including especially gamma rays, neutrinos, and antimatter particles. The production rate of such particles depends on (i) the annihilation (or decay) rate (ii) the density of pairs (respectively, of individual particles) in the region of interest, and (iii) the number of final-state particles produced in one annihilation (decay) event. In formulae, the rate for production of a final state particle f per unit volume from DM annihilation can be cast as

$$\Gamma_f^A = c\frac{\rho_{\rm DM}^2}{m_{\rm DM}^2}\langle\sigma v\rangle N_f^A, \tag{27.18}$$

where $\langle\sigma v\rangle$ indicates the thermally-averaged cross section for DM annihilation times relative velocity [27], calculated at the appropriate temperature, $\rho_{\rm DM}$ is the physical density of DM, and N_f^A is the number of final state particles f produced in one individual annihilation event. The constant c depends on whether the DM is its on antiparticle, in which case $c = 1/2$, or if there is a mixture of DM particles and antiparticles (in case there is no asymmetry, $c = 1/4$). The analog for decay is

$$\Gamma_f^D = \frac{\rho_{\rm DM}}{m_{\rm DM}}\frac{1}{\tau_{\rm DM}}N_f^D, \tag{27.19}$$

with the same conventions for the symbols, and where $\tau_{\rm DM}$ is the DM's lifetime.

Gamma Rays: DM annihilation to virtually any final state produces gamma rays: emission processes include the dominant two-photon decay mode of neutral pions resulting from the hadronization of strongly-interacting final states; final state radiation; and internal bremsstrahlung, the latter two including, possibly, the emission of massive gauge or Higgs bosons subsequently producing photons via their decay products. Similarly, neutrinos are produced from charged pion decay and from radiative processes. The flux of gamma rays and neutrinos is calculated integrating the rate Γ_f per steradian (simply meaning, for isotropic emission, $\Gamma_f/(4\pi)$) along the line of sight within the appropriate angular region (the *differential* flux is obtained in the same way by simply replacing N_f with the differential flux at production, at the appropriate redshift in the case of cosmologically distant sources),

$$\phi_f = \int_{\Delta\Omega} d\Omega \int_{\rm l.o.s.} dl\,\frac{\Gamma_f}{4\pi}. \tag{27.20}$$

It is customary to factor out, in the expression for the rate, a *particle physics* factor, depending upon the DM particle mass and its annihilation or decay rate, and an *astrophysical* factor, which only depends on the observational target. The latter is sometimes denoted with $J_{\Delta\Omega}(\psi)$ with ψ indicating the direction of the line of sight. Although different conventions are in use, a common choice is to define

$$J_{\Delta\Omega}(\psi) = \int_{\Delta\Omega}\int_{\rm l.o.s.(\psi)} \rho_{\rm DM}^2(l,\Omega)\; dl d\Omega. \tag{27.21}$$

For a target with uniform density ρ and radius r at a distance $d \gg r$, such that the target is entirely within the solid angle $\Delta\Omega$,

$$J \simeq \frac{4\pi r^3 \bar{\rho}_{\rm DM}^2}{3d^2}. \tag{27.22}$$

Searches for gamma-ray emission from DM annihilation have focused on targets chosen based on a variety of considerations, primarily intended to maximize signal to noise. Nearby dwarf spheroidal galaxies contain very small amounts of gas, and do not host any significant astrophysical background at gamma-ray or X-ray frequencies, and are thus an optimal target choice for DM searches. An accurate determination of the DM density profile in these objects results in somewhat large systematics when deriving constraints from the non-observation of emission from DM; future optical surveys will help pinpoint with greater accuracy stellar kinematics and thus reduce such uncertainty; a second target is the inner region of the Milky Way: while nearby and potentially hosting a large density of DM, the Galactic center region is however very bright at almost any wavelength, making the extraction of a signal highly problematic; nearby clusters of galaxies are also known to host significant astrophysical emission, but are potentially ideally suited to constrain DM decay. Finally, putative nearby DM clumps are also a possible source of a bright DM signal (albeit from an unknown direction), as is the annihilation of DM in all halos at all redshifts.

DM annihilation and decay can lead to striking spectral features. Since the process happens typically at very low particle velocities, if the DM pair-annihilates e.g. to two photons or two neutrinos, the final-state particles will be nearly monoenergetic, with an energy close to the DM particle mass and a width proportional to the DM velocity in units of c (if a $\gamma\gamma$ line is present electroweak symmetry also implies a $Z\gamma$ line, if kinematically allowed). No astrophysical processes are known to produce lines at gamma-ray or neutrino energies in the GeV and above (with, perhaps, the possible exception of cold pulsar winds [187]) making this channel virtually background-free. At lower energy, lines are expected from radiative decay modes of candidates such as sterile neutrinos (see Sec. 27.5).DM annihilation or decay can lead to additional spectral features besides lines. These include (one or more) "boxes" [188], produced by boosted final states decaying to monochromatic photons (such as e.g. neutral pions), or combinations thereof. Processes occurring at higher redshift can distort these spectral features by smearing them to lower energies. Neglecting gamma-ray attenuation, the flux of gamma rays from all redshift can be cast as

$$\frac{dN_\gamma}{dE_\gamma}(E_\gamma) = \frac{c}{8\pi}\int \frac{\langle\sigma v\rangle\rho_{\rm DM}(z)dz}{H(z)(1+z)^3 m_{\rm DM}^2}\left(\frac{dN_\gamma}{dE'}\right)_{E'=E_\gamma(1+z)}. \tag{27.23}$$

While the calculation of the differential spectrum of gamma rays from a given final state f, dN_γ^f/dE_γ, is carried out using numerical tools, such as PYTHIA [189] that reproduce hadronization and particle decay for masses well above a few GeV, in the sub-GeV range gamma-ray production follows primarily from meson decay and radiative processes well outside the range of applicability of the Altarelli-Parisi splitting function. The MeV gamma-ray range will soon be probed with forthcoming satellites [190]. Recently a code that provides the expected gamma-ray spectrum for sub-GeV DM, `Hazma`, has become available [191].

Observations with the Fermi Large Area Telescope (LAT) and with ground-based facilities such as HESS, VERITAS, MAGIC, and HAWC have provided an unprecedented picture of the

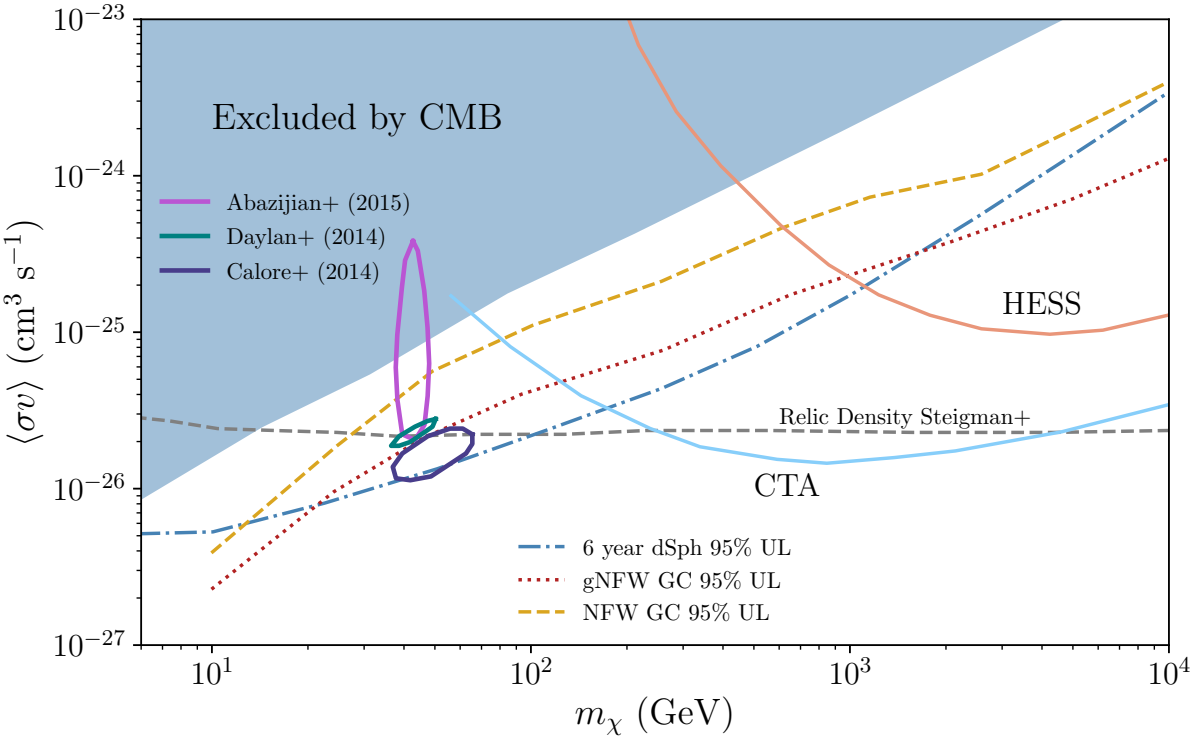

Figure 27.3: Upper limits and projected sensitivity from CTA on the pair-annihilation rate versus the DM mass from gamma-ray and CMB observations (figure courtesy of Logan Morrison).

Int. J. Mod. Phys. A 2026.41. Downloaded by UNIVERSITY OF CALIFORNIA @ BERKELEY on 09/16/26. Re-
orldscientific.com
strictly not permitted, except for Open Access articles.

gamma-ray sky ideally suited to look for a signal from DM annihilation or decay for DM particles from a few GeV mass up to several TeV. The LAT has provided some of the most stringent constraints to-date on DM pair-annihilation for a variety of annihilation final states, chiefly from stacked observations of nearby satellite dwarf spheroidal galaxies [192]. Excesses of gamma rays over the expected diffuse and point-source background have been claimed, most importantly from the direction of the inner Galaxy, where a signal from DM annihilation might be especially bright [193,194]. The nature of this excess is quite controversial: while the morphology and spectrum fall within what expected for a standard WIMP with a mass of a few tens of GeV [195], unresolved point sources, including especially an (expected) population of millisecond pulsars (MSPs) have been advocated as a possible plausible counterpart [196]. Statistical methods to discriminate between DM and MSPs have been utilized [197,198], but recent studies indicate that such results might not be conclusive [199]. Large uncertainties in the Galactic diffuse background emission model are additionally known to exist, and possible plague the morphological and spectral information [200, 201].Other notable potential gamma-ray excesses include a diffuse emission from the Andromeda galaxy (M31) [202–204], possibly in excess of what expected from cosmic-ray models [205]; and a diffuse emission at 511 keV energy in the inner Galaxy from Integral-SPI observations [206]; such emission has known astrophysical counterparts [207], as well as several proposed DM explanations (e.g. [208]).

While DM annihilation and decay typically occurs at low velocities, the possibility of "boosted" DM has also been considered [209]. In this case, the DM particle might dominantly pair-annihilate to a lighter dark species, which does interact with Standard Model particle, and could be detected with neutrino telescopes or direct detection experiments. Future facilities that promise to widen the reach of gamma-ray searches for DM include especially the Cherenkov Telescope Array (CTA), see fig. 27.3.

Neutrinos: DM can be captured in celestial bodies in significant amounts, depending on the DM scattering cross section off of nucleons, the DM mass, and the DM flux incident on the celestial body of interest. For DM masses at or around the GeV scale, evaporation from the celestial body plays an important role [210]. If enough DM accumulates, DM annihilation inside the celestial body can then lead to the production of Standard Model particles. Such particles can heat up the body, if they lose most of their energy before escaping. Utilizing models for heat production in planets, or stellar interior models in the case of stars, constraints can be put on DM particle properties. Of note are constraints from anomalous warming of cold planets such as Uranus [211], alterations to the stellar structure or the Sun's seismic activity [212], and anomalous Earth heat flow [213]. Alternately, DM annihilation in celestial bodies can result in the production of particles that can escape the body. Within the Standard Model, the only such instance is annihilation to neutrinos, but, similarly to the boosted DM case the DM can annihilate to a (stable or unstable) dark-sector particles, whose decay or interactions can be detected on Earth [214,215]. For direct annihilation to neutrinos, given the lower limit on the DM mass from evaporation, the typical neutrino energies usually exceed the energy of neutrinos from the Sun, the best target for this type of searches, making this a virtually background-free DM search. Significant neutrino fluxes can only be achieved, however, if near-equilibration is reached between the capture and annihilation rates. In turn, this requires large-enough DM-nucleon scattering cross sections, to-date very close to the limits from direct detection (see sec. 27.6). Only spin-dependent cross section, and capture in the Sun usually provide large-enough neutrino fluxes. IceCube and ANTARES searches for an anomalous flux of high-energy neutrinos from the Sun yielded null results, which can be interpreted as constraints on spin-dependent nucleon-DM interactions under the assumption of equilibration and of specific annihilation final states [216,217]. Lower-threshold detectors, including DeepCore [218] and PINGU [219], can produce interesting limits on lower-mass DM candidates above the evaporation threshold.

Cosmic-ray Antimatter: Stable charged particles produced by decays of products of, or directly from DM annihilation or decay, populate the cosmic radiation and are a prime target for indirect DM searches. To maximize signal to noise, searches focus on relatively rare particle species, such as positrons, antiprotons, and antinuclei. While in certain models the production of particles and antiparticles is not symmetric [220], generally DM anni-

Int. J. Mod. Phys. A 2026.41. Downloaded from www.worldscientific.com
by UNIVERSITY OF CALIFORNIA @ BERKELEY on 09/16/26. Re-use and distribution is strictly not permitted, except for Open Access articles.

hilation or decay produces as many particles as antiparticles in the final state. Charged particles produced by DM propagate and lose energy prior to reaching detectors. The transport of charged particles is customarily carried out in the context of diffusion models such as the Galactic "leaky box" setup, see e.g. [221]. While progress in constraining the uncertain propagation and energy-loss processes has been steady with improved data from new detectors such as PAMELA [222] and AMS-02 [223], the calculation of the particle flux at Earth from that at production suffers from significant uncertainties [221].

An excess of high-energy positrons over the standard secondary production from inelastic cosmic-ray interactions has been firmly established by several experiments, most recently and with the highest statistics by AMS-02 [224]. The excess has been ascribed to DM annihilation, although strong constraints from the non-observation of corresponding anomalies in other channels, such as antiprotons and gamma rays, and the peculiar spectral shape, force DM models to be quite convoluted (see e.g. [225]). Alternately, excess *primary* positrons can be produced in the magnetosphere of nearby pulsars [226, 227]. This latter explanation was questioned in [228] in connection with the detection of a TeV halo around two candidate pulsars, leading to the determination of a highly suppressed diffusion coefficient within the pulsar nebula; with such low diffusion coefficient, positrons from the pulsars would not contribute significantly to the flux at Earth; Ref. [229], however, showed that likely the diffusion coefficient is not constant, and that if it increases outside the nebula, as expected from other cosmic-ray measurements, pulsars can still be considered as the counterpart to the positron excess. Other explanations for the excess, albeit somewhat controversial, and increasingly constrained by data, also exist [230, 231].

The antiproton spectrum in the cosmic radiation as measured by AMS-02 [223] also exhibits features that might be considered as excess flux between 10 and 20 GeV, and energies above 100 GeV [232], which have been interpreted as possible signal of DM annihilation; more realistically, however, systematic uncertainties in the antiproton production cross section, in cosmic-ray transport, reacceleration at high energy and, at low energy, solar modulation make it extremely difficult to assess the robustness of the excesses [233, 234].

Antinuclei such as anti-deuterium and anti-helium could also form as a result of DM annihilation or decay. While baryon number conservation forces the typical kinetic energy of antinuclei produced in inelastic cosmic-ray processes to large values, antinuclei arising from hadronization of DM-initiated jets have low energy, offering optimal signal-to-noise when a low-energy cut on the antinucleus kinetic energy is used [235–239]. Specific detector designs have been developed to single out low-energy cosmic-ray antinuclei (e.g. $E < 0.25$ GeV/nucleon in the case of the General Antiparticle Spectrometer, or GAPS [240]). The detection of even a single antinucleus would have considerable importance as a possible sign of new physics [241].

Multi-wavelength studies: Electrons and positrons from DM lose energy quite efficiently, radiating at a variety of wavelengths. This *secondary* radiative emission presents spectral and morphological features that might provide an important additional indirect detection channel. The most efficient energy loss mechanisms for high-energy electrons and positrons are inverse Compton (IC) up-scattering of background photons, and synchrotron radiation in the presence of magnetic fields. Depending on the DM mass, the emitted light from synchrotron peaks at MHz-GHz frequencies, while the IC emission at X-ray to gamma-ray frequencies, depending on the energy of the background radiation, typically ranging from CMB photons up to starlight photons [242–244]. The calculation of the secondary emission from DM entails both solving the transport of the electrons and positrons from DM, and for the radiative emission; codes exist that perform these calculations for certain astrophysical environments [245–247], with diffusion playing an increasingly critical role in smaller and smaller structures such as dwarf galaxies [243]. It has been demonstrated that for large magnetic fields and for certain final states, the synchrotron emission is more constraining than the gamma-ray emission [248].

Stellar Physics: Microscopic properties of the DM can meaningfully alter, and thus be constrained by, several astrophysical environments, from planets and stars, up to the universe as a whole. DM particles light enough to be produced in collisional processes inside stars, with typically temperatures in the keV, or supernovae, with energy scales in the MeV, lead to an additional energy-loss mechanism, if capable of escaping the system. If this is the case, the increased needed energy output would also result in an increased neutrino flux, leading to constraints on the masses and couplings of the DM, see e.g. [249] for a comprehensive review. DM annihilation can even have fueled early stages of stellar evolution, perhaps with measurable consequences [250]. DM capture in neutron stars could lead to the collapse of the star into black holes; the existence of neutron stars in DM-rich environments can thus be used to constrain the mass and interaction cross section of DM with nucleons [251] and even relatively light, but stable, primordial black holes [252].

Cosmology: Energy injection from DM processes in the early universe, as well as the contribution of DM to the effective relativistic degrees of freedom, are severely constrained from data on Big Bang Nucleosynthesis (see Sec. 24 in this *Review*) and on the energy and anisotropy power spectrum of the CMB (see Sec. 29). Codes exist that perform the calculation of the constraints on particle DM models [191, 253].

Primordial Black Holes (PBHs): Primordial black holes are hypothetical black holes formed from the collapse of large density fluctuations, phase transitions, or other non-standard cosmological phenomena [254]. Unlike astrophysical black holes, PBHs could span a broad mass range—from as light as the Planck scale up to thousands of solar masses—and are considered compelling macroscopic dark matter candidates [255]. Their abundance and mass distribution are tightly constrained by a combination of astrophysical, cosmological, and gravitational-wave observations, but viable mass windows remain under active investigation.

Macroscopic DM candidates such as PBHs can gravitationally perturb astrophysical systems, potentially compromising the stability of globular clusters such as Eridanus II [24], and/or disrupting wide stellar binaries [256]. These effects constrain the maximal mass of compact dark matter candidates to not much more than a few solar masses [24, 256]. Strong constraints on PBHs also arise from their accretion of baryonic matter around and after recombination, which can affect the ionization history and thermal state of the intergalactic medium, imprinting signatures on CMB anisotropies and spectral distortions [257–259]. However, uncertainties in the accretion physics at high redshift and possible feedback effects continue to fuel debate about the precise bounds, especially for solar-mass PBHs [260, 261].

Additional constraints on PBHs come from gravitational microlensing surveys of stars in the Magellanic Clouds and M31 [262–264], as well as from quasar microlensing [265], although these limits have recently been revised to account for finite-source size and wave diffraction effects, which weaken previous exclusions in the mass range $\sim 10^{-10} - 10^{-7} M_\odot$ [266, 267]. Femtolensing of gamma-ray bursts also provides limits on sublunar mass PBHs, with ongoing refinements to modeling wave optics effects [268, 269].

A robust window for PBHs to constitute all of the dark matter persists roughly in the mass range $10^{17} \lesssim M_{\rm BH}/{\rm g} \lesssim 10^{21}$, corresponding to asteroid- to lunar-mass scales, where current constraints from microlensing, evaporation, and dynamical effects are comparatively weak [255]. Below $M_{\rm BH} \sim 10^{17}$ g, PBHs are severely constrained by the non-observation of Hawking radiation products in the gamma-ray background [270,271]. Upcoming MeV gamma-ray observatories such as AMEGO and e-ASTROGAM are expected to significantly tighten these bounds and potentially detect signals from PBH evaporation [272].

If evaporation halts near the Planck scale due to quantum gravity effects, relic PBHs with masses near the Planck mass could persist today, potentially carrying electric charge and manifesting as novel dark matter candidates detectable via direct detection experiments, neutrino observatories, or paleo-detectors [273, 274]. Meanwhile, gravitational wave observations from LIGO/Virgo/KAGRA and pulsar timing arrays have opened new avenues to

Int. J. Mod. Phys. A 2026.41. Downloaded from www.worldscientific.com by UNIVERSITY OF CALIFORNIA @ BERKELEY on 09/16/26. Re-[redacted] strictly not permitted, except for Open Access articles.

probe PBHs in the stellar to intermediate mass regime, with current data placing stringent limits on PBH dark matter fractions above a few solar masses [275, 276].

Overall, the parameter space for PBHs as a dominant DM component remains tightly constrained but not conclusively excluded, motivating ongoing efforts across multiple observational frontiers.

References

[1] J. D. Simon, arXiv e-prints arXiv:1901.05465 (2019), [arXiv:1901.05465].

[2] P. Salucci, Astron. Astrophys. Rev. **27**, 1, 2 (2019), [arXiv:1811.08843].

[3] S. W. Allen, A. E. Evrard and A. B. Mantz, Ann. Rev. Astron. Astrophys. **49**, 409 (2011), [arXiv:1103.4829].

[4] N. A. Bahcall *et al.*, ApJ **541**, 1 (2000).

[5] S. D. M. White, G. Efstathiou and C. S. Frenk, Mon. Not. Roy. Astron. Soc. **262**, 1023 (1993).

[6] A. J. S. Hamilton and M. Tegmark, Mon. Not. Roy. Astron. Soc. **330**, 506 (2002), [arXiv:astro-ph/0008392].

[7] B. Famaey and S. McGaugh, Living Rev. Rel. **15**, 10 (2012), [arXiv:1112.3960].

[8] S. W. Randall *et al.*, Astrophys. J. **679**, 1173 (2008), [arXiv:0704.0261].

[9] R. H. Sanders, Int. J. Mod. Phys. **D27**, 14, 14 (2018), [arXiv:1805.06804].

[10] S. D. McDermott, H.-B. Yu and K. M. Zurek, Phys. Rev. **D83**, 063509 (2011), [arXiv:1011.2907].

[11] D. A. Buote *et al.*, Astrophys. J. **577**, 183 (2002), [arXiv:astro-ph/0205469].

[12] D. Harvey *et al.*, Science **347**, 1462 (2015), [arXiv:1503.07675].

[13] S. Tulin and H.-B. Yu, Phys. Rept. **730**, 1 (2018), [arXiv:1705.02358].

[14] D. N. Spergel and P. J. Steinhardt, Phys. Rev. Lett. **84**, 3760 (2000), [arXiv:astro-ph/9909386].

[15] S. Tremaine and J. E. Gunn, Phys. Rev. Lett. **42**, 407 (1979), [,66(1979)].

[16] L. Randall, J. Scholtz and J. Unwin, Mon. Not. Roy. Astron. Soc. **467**, 2, 1515 (2017), [arXiv:1611.04590].

[17] R. Hlozek *et al.*, Phys. Rev. **D91**, 10, 103512 (2015), [arXiv:1410.2896].

[18] E. Armengaud *et al.*, Mon. Not. Roy. Astron. Soc. **471**, 4, 4606 (2017), [arXiv:1703.09126].

[19] M. Nori *et al.*, Mon. Not. Roy. Astron. Soc. **482**, 3, 3227 (2019), [arXiv:1809.09619].

[20] B. Bozek *et al.*, Mon. Not. Roy. Astron. Soc. **450**, 1, 209 (2015), [arXiv:1409.3544].

[21] H.-Y. Schive *et al.*, Astrophys. J. **818**, 1, 89 (2016), [arXiv:1508.04621].

[22] E. O. Nadler *et al.*, Astrophys. J. **878**, 2, L32 (2019), [Astrophys. J. Lett.878,32(2019)], [arXiv:1904.10000].

[23] M. A. Monroy-Rodríguez and C. Allen, ApJ **790**, 2, 159 (2014), [arXiv:1406.5169].

[24] T. D. Brandt, Astrophys. J. **824**, 2, L31 (2016), [arXiv:1605.03665].

[25] B. Audren *et al.*, JCAP **1412**, 12, 028 (2014), [arXiv:1407.2418].

[26] M. Dutra *et al.*, JCAP **1803**, 037 (2018), [arXiv:1801.05447].

[27] P. Gondolo and G. Gelmini, Nucl. Phys. **B360**, 145 (1991).

[28] J. L. Feng and J. Kumar, Phys. Rev. Lett. **101**, 231301 (2008), [arXiv:0803.4196].

[29] G. Jungman, M. Kamionkowski and K. Griest, Phys. Rept. **267**, 195 (1996), [hep-ph/9506380].

[30] J. Edsjo *et al.*, JCAP **0304**, 001 (2003), [hep-ph/0301106].

[31] G. Servant and T. M. P. Tait, Nucl. Phys. **B650**, 391 (2003), [hep-ph/0206071].

[32] D. Hooper and S. Profumo, Phys. Rept. **453**, 29 (2007), [hep-ph/0701197].

[33] K. Griest and D. Seckel, Phys. Rev. **D43**, 3191 (1991).

[34] R. T. Co *et al.*, JCAP **1512**, 12, 024 (2015), [arXiv:1506.07532].

[35] V. S. Rychkov and A. Strumia, Phys. Rev. **D75**, 075011 (2007), [hep-ph/0701104].

[36] E. D. Carlson, M. E. Machacek and L. J. Hall, Astrophys. J. **398**, 43 (1992).

[37] D. Pappadopulo, J. T. Ruderman and G. Trevisan, Phys. Rev. **D94**, 3, 035005 (2016), [arXiv:1602.04219].

[38] Y. Hochberg *et al.*, Phys. Rev. Lett. **113**, 171301 (2014), [arXiv:1402.5143].

[39] E. Kuflik *et al.*, Phys. Rev. Lett. **116**, 22, 221302 (2016), [arXiv:1512.04545].

[40] W. B. Lin *et al.*, Phys. Rev. Lett. **86**, 954 (2001), [arXiv:astro-ph/0009003].

[41] G. B. Gelmini and P. Gondolo, Phys. Rev. **D74**, 023510 (2006), [hep-ph/0602230].

[42] M. Hindmarsh, R. Kirk and S. M. West, JCAP **1403**, 037 (2014), [arXiv:1311.1637].

[43] T. Moroi and L. Randall, Nucl. Phys. **B570**, 455 (2000), [hep-ph/9906527].

[44] P. Hut and K. A. Olive, Phys. Lett. **87B**, 144 (1979).

[45] S. Nussinov, Phys. Lett. **165B**, 55 (1985).

[46] K. M. Zurek, Phys. Rept. **537**, 91 (2014), [arXiv:1308.0338].

[47] Y. B. Zel'dovich and I. D. Novikov, Soviet Ast. **10**, 602 (1967).

[48] S. Hawking, Mon. Not. Roy. Astron. Soc. **152**, 75 (1971).

[49] B. J. Carr, ApJ **201**, 1 (1975).

[50] J. I. Read, J. Phys. **G41**, 063101 (2014), [arXiv:1404.1938].

[51] S. H. Lim *et al.*, JCAP **01**, 021 (2025), received Jun 6 2024; revised Oct 17 2024; accepted Nov 16 2024; published Jan 08 2025, [arXiv:2305.13358].

[52] T. Piffl *et al.*, Astron. Astrophys. **562**, A91 (2014), [arXiv:1309.4293].

[53] L. Necib and T. Lin, Astrophys. J. **926**, 2, 189 (2022), [arXiv:2102.02211].

[54] A. M. Green, J. Phys. **G44**, 8, 084001 (2017), [arXiv:1703.10102].

[55] A. Helmi *et al.*, Nature **7729**, 985 (2018).

[56] L. Necib, M. Lisanti and V. Belokurov (2018), [arXiv:1807.02519].

[57] N. W. Evans, C. A. J. O'Hare and C. McCabe, Phys. Rev. **D99**, 2, 023012 (2019), [arXiv:1810.11468].

[58] S. Põder *et al.*, A&A **676**, A134 (2023).

[59] J. S. Bullock and M. Boylan-Kolchin, Ann. Rev. Astron. Astrophys. **55**, 343 (2017), [arXiv:1707.04256].

[60] J. Zavala and C. S. Frenk (2019), [arXiv:1907.11775].

[61] L. V. Sales, A. Wetzel and A. Fattahi, Nature Astron. **6**, 8, 897 (2022), [arXiv:2206.05295].

[62] I. M. E. Santos-Santos *et al.*, Mon. Not. Roy. Astron. Soc. **495**, 1, 58 (2020), [arXiv:1911.09116].

[63] J. Madhani *et al.*, in "American Astronomical Society Meeting Abstracts," volume 54 of *American Astronomical Society Meeting Abstracts*, 209.08 (2022).

[64] M. Geha *et al.*, Astrophys. J. **847**, 1, 4 (2017), [arXiv:1705.06743].

[65] P. van Dokkum *et al.*, Nature **605**, 7910, 435 (2022), [arXiv:2205.08552].

[66] K. E. Andrade *et al.* (2019), [arXiv:1901.00507].

Int. J. Mod. Phys. A 2026.41. Downloaded from www.worldscientific.com
by UNIVERSITY OF CALIFORNIA @ BERKELEY on 09/16/26. Re-use and distribution is strictly not permitted, except for Open Access articles.

[67] G. Servant, in "Particle dark matter," 164–189 (2010).

[68] A. Rinchiuso *et al.*, JCAP **10**, 013 (2020).

[69] N. L. Rodd, B. R. Safdi and W. L. Xu, Phys. Rev. D **110**, 4, 043003 (2024).

[70] E. Bagnaschi *et al.*, Eur. Phys. J. C **77**, 4, 268 (2017), [arXiv:1612.05210].

[71] M. Beneke, R. Szafron and K. Urban, JHEP **02**, 020 (2021), [arXiv:2009.00640].

[72] S. Abe, T. Inada and E. M. et al., arXiv preprint (2025).

[73] I. M. Bloch *et al.*, JHEP **06**, 087 (2017), [arXiv:1608.02123].

[74] S. Bottaro *et al.*, Eur. Phys. J. C **82**, 11, 992 (2022), [arXiv:2205.04486].

[75] H. Ramani, in "Perimeter Institute seminar (May 23, 2025)," (2025).

[76] J. Ellis *et al.*, Eur. Phys. J. C **84**, 4, 4 (2024).

[77] J. Bramante, P. J. Fox and J. Shelton, Phys. Rev. D **106**, 11, 115026 (2022).

[78] L. Hui *et al.*, Phys. Rev. **D95**, 4, 043541 (2017), [arXiv:1610.08297].

[79] A. Fattahi *et al.* (2016), [arXiv:1607.06479].

[80] D. J. E. Marsh, Phys. Rept. **643**, 1 (2016), [arXiv:1510.07633].

[81] H. An *et al.*, Phys. Lett. **B747**, 331 (2015), [arXiv:1412.8378].

[82] P. W. Graham and S. Rajendran, Phys. Rev. **D88**, 035023 (2013), [arXiv:1306.6088].

[83] P. W. Graham *et al.*, Phys. Rev. **D93**, 7, 075029 (2016), [arXiv:1512.06165].

[84] A. Arvanitaki *et al.*, Phys. Rev. **D97**, 7, 075020 (2018), [arXiv:1606.04541].

[85] P. W. Graham *et al.*, Phys. Rev. **D97**, 5, 055006 (2018), [arXiv:1709.07852].

[86] I. M. Bloch *et al.* (2019), [arXiv:1907.03767].

[87] A. Pierce, K. Riles and Y. Zhao, Phys. Rev. Lett. **121**, 6, 061102 (2018), [arXiv:1801.10161].

[88] Y. Kahn, B. R. Safdi and J. Thaler, Phys. Rev. Lett. **117**, 14, 141801 (2016), [arXiv:1602.01086].

[89] R. Henning *et al.* (ABRACADABRA), in "Proceedings, 13th Patras Workshop on Axions, WIMPs and WISPs, (PATRAS 2017): Thessaloniki, Greece, 15 May 2017 - 19, 2017," 28–31 (2018).

[90] S. Chaudhuri *et al.*, Phys. Rev. **D92**, 7, 075012 (2015), [arXiv:1411.7382].

[91] P. Sikivie, N. Sullivan and D. B. Tanner, Phys. Rev. Lett. **112**, 13, 131301 (2014), [arXiv:1310.8545].

[92] B. M. Brubaker *et al.*, Phys. Rev. **D96**, 12, 123008 (2017), [arXiv:1706.08388].

[93] G. Rybka (ADMX), Phys. Dark Univ. **4**, 14 (2014).

[94] S. Dodelson and L. M. Widrow, Phys. Rev. Lett. **72**, 17 (1994), [hep-ph/9303287].

[95] E. Bulbul *et al.*, Astrophys. J. **789**, 13 (2014), [arXiv:1402.2301].

[96] A. Boyarsky *et al.*, Phys. Rev. Lett. **113**, 251301 (2014), [arXiv:1402.4119].

[97] T. E. Jeltema and S. Profumo, Mon. Not. Roy. Astron. Soc. **450**, 2, 2143 (2015), [arXiv:1408.1699].

[98] M. E. Anderson, E. Churazov and J. N. Bregman, Mon. Not. Roy. Astron. Soc. **452**, 4, 3905 (2015), [arXiv:1408.4115].

[99] D. Malyshev, A. Neronov and D. Eckert, Phys. Rev. **D90**, 103506 (2014), [arXiv:1408.3531].

[100] T. E. Jeltema and S. Profumo, Mon. Not. Roy. Astron. Soc. **458**, 4, 3592 (2016), [arXiv:1512.01239].

[101] X. Collaboration (2024), [arXiv:2404.11234].

[102] B. M. Roach *et al.*, Phys. Rev. D **106**, 6, 063026 (2022), [arXiv:2207.06431].

[103] A. Decant *et al.*, JCAP **11**, 015 (2022), [arXiv:2205.07938].

[104] K. N. Abazajian, Phys. Rept. **711-712**, 1 (2020), [arXiv:1705.01837].

[105] I. Yu. Kobzarev, L. B. Okun and I. Ya. Pomeranchuk, Sov. J. Nucl. Phys. **3**, 6, 837 (1966), [Yad. Fiz.3,1154(1966)].

[106] M. J. Strassler and K. M. Zurek, Phys. Lett. **B651**, 374 (2007), [hep-ph/0604261].

[107] M. J. Strassler (2006), [hep-ph/0607160].

[108] M. Battaglieri *et al.*, in "U.S. Cosmic Visions: New Ideas in Dark Matter," (2017), [arXiv:1707.04591].

[109] Y. Kahn *et al.*, JHEP **05**, 002 (2017), [arXiv:1609.09072].

[110] J. Alexander *et al.* (2016), [arXiv:1608.08632], URL `http://lss.fnal.gov/archive/2016/conf/fermilab-conf-16-421.pdf`.

[111] K. R. Dienes and B. Thomas, Phys. Rev. **D85**, 083523 (2012), [arXiv:1106.4546].

[112] N. Trevisani (ATLAS, CMS), Universe **4**, 11, 131 (2018).

[113] E. Tolley (ATLAS), PoS **ICHEP2018**, 171 (2019).

[114] W. C. Kalderon (ATLAS), PoS **DIS2018**, 085 (2018).

[115] D. Vannerom (CMS), PoS **DIS2019**, 111 (2019).

[116] G. Gómez-Ceballos (CMS), PoS **EDSU2018**, 014 (2018).

[117] J. Aalbers *et al.* (LZ), Phys. Rev. Lett. **135**, 1, 011802 (2025), [arXiv:2410.17036].

[118] Z. Bo *et al.* (PandaX), Phys. Rev. Lett. **134**, 1, 011805 (2025), [arXiv:2408.00664].

[119] E. Aprile *et al.* (XENON) (2025), [arXiv:2502.18005].

[120] R. Agnese *et al.* (SuperCDMS), Phys. Rev. Lett. **120**, 6, 061802 (2018), [arXiv:1708.08869].

[121] P. Agnes *et al.* (DarkSide-50), Phys. Rev. D **107**, 6, 063001 (2023), [arXiv:2207.11966].

[122] R. Ajaj *et al.* (DEAP), Phys. Rev. **D100**, 022004 (2019), [arXiv:1902.04048].

[123] S. Li *et al.* (PandaX), Phys. Rev. Lett. **130**, 26, 261001 (2023), [arXiv:2212.10067].

[124] W. Ma *et al.* (PandaX), Phys. Rev. Lett. **130**, 2, 021802 (2023), [arXiv:2207.04883].

[125] E. Aprile *et al.* (XENON), Phys. Rev. Lett. **134**, 11, 111802 (2025), [arXiv:2409.17868].

[126] R. Agnese *et al.* (SuperCDMS), Phys. Rev. **D99**, 6, 062001 (2019), [arXiv:1808.09098].

[127] A. H. Abdelhameed *et al.* (CRESST) (2019), [arXiv:1904.00498].

[128] G. Angloher *et al.* (CRESST), Phys. Rev. D **107**, 12, 122003 (2023), [arXiv:2212.12513].

[129] G. Angloher *et al.* (CRESST), Phys. Rev. D **110**, 8, 083038 (2024), [arXiv:2405.06527].

[130] A. Aguilar-Arevalo *et al.* (DAMIC), Phys. Rev. Lett. **125**, 241803 (2020), [arXiv:2007.15622].

[131] Q. Arnaud *et al.* (NEWS-G), Astropart. Phys. **97**, 54 (2018), [arXiv:1706.04934].

[132] M. M. Arora *et al.* (NEWS-G), Phys. Rev. Lett. **134**, 14, 141002 (2025), [arXiv:2407.12769].

[133] C. Amole *et al.* (PICO), Phys. Rev. **D100**, 2, 022001 (2019), [arXiv:1902.04031].

[134] J. D. Lewin and P. F. Smith, Astropart. Phys. **6**, 87 (1996).

[135] J. R. Ellis, R. A. Flores and J. D. Lewin, Phys. Lett. **B212**, 375 (1988).

[136] P. J. Fox, J. Liu and N. Weiner, Phys. Rev. **D83**, 103514 (2011), [arXiv:1011.1915].

[137] L. Vietze *et al.*, Phys. Rev. **D91**, 4, 043520 (2015), [arXiv:1412.6091].

Int. J. Mod. Phys. A 2026.41. Downloaded by UNIVERSITY OF CALIFORNIA @ BERKELEY on 09/16/26. Re-
orldscientific.com
strictly not permitted, except for Open Access articles.

[138] B. S. Hu *et al.*, Phys. Rev. Lett. **128**, 7, 072502 (2022), [arXiv:2109.00193].

[139] J. Ellis, N. Nagata and K. A. Olive, Eur. Phys. J. **C78**, 7, 569 (2018), [arXiv:1805.09795].

[140] J. Fan, M. Reece and L.-T. Wang, JCAP **1011**, 042 (2010), [arXiv:1008.1591].

[141] A. L. Fitzpatrick *et al.*, JCAP **1302**, 004 (2013), [arXiv:1203.3542].

[142] N. Anand, A. L. Fitzpatrick and W. C. Haxton, Phys. Rev. **C89**, 6, 065501 (2014), [arXiv:1308.6288].

[143] M. I. Gresham and K. M. Zurek, Phys. Rev. **D89**, 12, 123521 (2014), [arXiv:1401.3739].

[144] J. B. Dent *et al.*, Phys. Rev. **D92**, 6, 063515 (2015), [arXiv:1505.03117].

[145] D. Gazda, R. Catena and C. Forssén, Phys. Rev. **D95**, 10, 103011 (2017), [arXiv:1612.09165].

[146] M. Hoferichter *et al.*, Phys. Rev. **D99**, 5, 055031 (2019), [arXiv:1812.05617].

[147] R. Essig, J. Mardon and T. Volansky, Phys. Rev. **D85**, 076007 (2012), [arXiv:1108.5383].

[148] R. Catena *et al.*, JCAP **03**, 052 (2023), [arXiv:2210.07305].

[149] T. Trickle, Phys. Rev. D **107**, 3, 035035 (2023), [arXiv:2210.14917].

[150] F. T. Avignone, III *et al.*, Phys. Rev. **D35**, 2752 (1987).

[151] M. Pospelov, A. Ritz and M. B. Voloshin, Phys. Rev. **D78**, 115012 (2008), [arXiv:0807.3279].

[152] Y. Hochberg, T. Lin and K. M. Zurek, Phys. Rev. **D95**, 2, 023013 (2017), [arXiv:1608.01994].

[153] M. Schumann, J. Phys. G **46**, 10, 103003 (2019), [arXiv:1903.03026].

[154] J. Billard *et al.*, Rept. Prog. Phys. **85**, 5, 056201 (2022), [arXiv:2104.07634].

[155] M. Pato *et al.*, Phys. Rev. **D83**, 083505 (2011), [arXiv:1012.3458].

[156] A. K. Drukier, K. Freese and D. N. Spergel, Phys. Rev. **D33**, 3495 (1986).

[157] D. N. Spergel, Phys. Rev. **D37**, 1353 (1988).

[158] D. Stiff, L. M. Widrow and J. Frieman, Phys. Rev. **D64**, 083516 (2001), [arXiv:astro-ph/0106048].

[159] K. Freese *et al.*, Phys. Rev. Lett. **92**, 111301 (2004), [arXiv:astro-ph/0310334].

[160] T. Bruch *et al.*, Astrophys. J. **696**, 920 (2009), [arXiv:0804.2896].

[161] M. J. Lewis and K. Freese, Phys. Rev. **D70**, 043501 (2004), [arXiv:astro-ph/0307190].

[162] F. Mayet *et al.*, Phys. Rept. **627**, 1 (2016), [arXiv:1602.03781].

[163] L. E. Strigari, New J. Phys. **11**, 105011 (2009), [arXiv:0903.3630].

[164] Z. Bo *et al.* (PandaX), Phys. Rev. Lett. **133**, 19, 191001 (2024), [arXiv:2407.10892].

[165] C. A. J. O'Hare, Phys. Rev. Lett. **127**, 25, 251802 (2021), [arXiv:2109.03116].

[166] L. E. Strigari, Phys. Rev. **D93**, 10, 103534 (2016), [arXiv:1604.00729].

[167] R. Essig, M. Sholapurkar and T.-T. Yu, Phys. Rev. **D97**, 9, 095029 (2018), [arXiv:1801.10159].

[168] V. Chepel and H. Araujo, JINST **8**, R04001 (2013), [arXiv:1207.2292].

[169] P. Agnes *et al.* (DarkSide), Phys. Rev. Lett. **130**, 10, 101002 (2023), [arXiv:2207.11968].

[170] E. Aprile *et al.* (XENON, (XENON Collaboration)**), Phys. Rev. Lett. **134**, 16, 161004 (2025), [arXiv:2411.15289].

[171] E. Aprile *et al.* (XENON), Phys. Rev. Lett. **129**, 16, 161805 (2022), [arXiv:2207.11330].

[172] J. Amaré *et al.*, Phys. Rev. Lett. **135**, 5, 051001 (2025), [arXiv:2502.01542].

[173] G. H. Yu *et al.* (COSINE-100) (2025), [arXiv:2501.13665].

[174] A. Aguilar-Arevalo *et al.* (SENSEI, DAMIC-M, DAMIC), Phys. Rev. D **109**, 6, 062007 (2024), [arXiv:2306.01717].

[175] E. Adams *et al.* (PICO), Phys. Rev. Lett. **135**, 1, 011001 (2025), [arXiv:2504.13089].

[176] Y. Hochberg *et al.*, Phys. Lett. **B772**, 239 (2017), [arXiv:1606.08849].

[177] Y. Hochberg *et al.*, Phys. Rev. **D97**, 1, 015004 (2018), [arXiv:1708.08929].

[178] S. Knapen, T. Lin and K. M. Zurek, Phys. Rev. **D95**, 5, 056019 (2017), [arXiv:1611.06228].

[179] R. Essig *et al.*, Phys. Rev. **D95**, 5, 056011 (2017), [arXiv:1608.02940].

[180] Y. Hochberg, T. Lin and K. M. Zurek, Phys. Rev. **D94**, 1, 015019 (2016), [arXiv:1604.06800].

[181] S. Knapen *et al.*, Phys. Lett. **B785**, 386 (2018), [arXiv:1712.06598].

[182] S. Griffin *et al.*, Phys. Rev. **D98**, 11, 115034 (2018), [arXiv:1807.10291].

[183] A. Arvanitaki, S. Dimopoulos and K. Van Tilburg, Phys. Rev. **X8**, 4, 041001 (2018), [arXiv:1709.05354].

[184] T. Trickle, Z. Zhang and K. M. Zurek (2019), [arXiv:1905.13744].

[185] L. Baudis *et al.* (QROCODILE), Phys. Rev. Lett. (2025), [arXiv:2412.16279].

[186] R. Essig *et al.*, in "Snowmass 2021," (2022), [arXiv:2203.08297].

[187] F. Aharonian, D. Khangulyan and D. Malyshev, Astron. Astrophys. **547**, A114 (2012), [arXiv:1207.0458].

[188] K. K. Boddy *et al.*, Phys. Rev. **D94**, 9, 095027 (2016), [arXiv:1606.07440].

[189] T. Sjöstrand (2019), [arXiv:1907.09874].

[190] M. Tavani *et al.* (e-ASTROGAM), JHEAp **19**, 1 (2018), [arXiv:1711.01265].

[191] A. Coogan, L. Morrison and S. Profumo (2019), [arXiv:1907.11846].

[192] M. Ackermann *et al.* (Fermi-LAT), Phys. Rev. Lett. **115**, 23, 231301 (2015), [arXiv:1503.02641].

[193] D. Hooper and L. Goodenough, Phys. Lett. **B697**, 412 (2011), [arXiv:1010.2752].

[194] M. Ackermann *et al.* (Fermi-LAT), Astrophys. J. **840**, 1, 43 (2017), [arXiv:1704.03910].

[195] F. Calore, I. Cholis and C. Weniger, JCAP **1503**, 038 (2015), [arXiv:1409.0042].

[196] K. N. Abazajian and M. Kaplinghat, Phys. Rev. **D86**, 083511 (2012), [Erratum: Phys. Rev. **D87**, 129902 (2013)], [arXiv:1207.6047].

[197] S. K. Lee, M. Lisanti and B. R. Safdi, JCAP **1505**, 05, 056 (2015), [arXiv:1412.6099].

[198] T. Daylan *et al.*, Phys. Dark Univ. **12**, 1 (2016), [arXiv:1402.6703].

[199] R. K. Leane and T. R. Slatyer (2019), [arXiv:1904.08430].

[200] E. Carlson, T. Linden and S. Profumo, Phys. Rev. Lett. **117**, 11, 111101 (2016), [arXiv:1510.04698].

[201] M. Ajello *et al.* (Fermi-LAT), Astrophys. J. **819**, 1, 44 (2016), [arXiv:1511.02938].

[202] M. Ackermann *et al.* (Fermi-LAT), Astrophys. J. **836**, 2, 208 (2017), [arXiv:1702.08602].

[203] A. McDaniel, T. Jeltema and S. Profumo, Phys. Rev. **D97**, 10, 103021 (2018), [arXiv:1802.05258].

Int. J. Mod. Phys. A 2026.41. Downloaded from www.worldscientific.com
by UNIVERSITY OF CALIFORNIA @ BERKELEY on 09/16/26. Re-use and distribution is strictly not permitted, except for Open Access articles.

[204] C. Karwin *et al.* (2019), [arXiv:1903.10533].

[205] A. McDaniel, T. Jeltema and S. Profumo, Phys. Rev. **D100**, 2, 023014 (2019), [arXiv:1903.06833].

[206] R. L. Kinzer *et al.*, Astrophys. J. **559**, 282 (2001).

[207] R. M. Bandyopadhyay *et al.*, Mon. Not. Roy. Astron. Soc. **392**, 1115 (2009), [arXiv:0810.3674].

[208] D. P. Finkbeiner and N. Weiner, Phys. Rev. **D76**, 083519 (2007), [arXiv:astro-ph/0702587].

[209] K. Agashe *et al.*, JCAP **1410**, 10, 062 (2014), [arXiv:1405.7370].

[210] T. Damour and L. M. Krauss, Phys. Rev. Lett. **81**, 5726 (1998), [arXiv:astro-ph/9806165].

[211] S. L. Adler, Phys. Lett. **B671**, 203 (2009), [arXiv:0808.2823].

[212] J. Casanellas and I. Lopes, Astrophys. J. **765**, L21 (2013), [arXiv:1212.2985].

[213] G. D. Mack, J. F. Beacom and G. Bertone, Phys. Rev. **D76**, 043523 (2007), [arXiv:0705.4298].

[214] J. Smolinsky and P. Tanedo, Phys. Rev. **D95**, 7, 075015 (2017), [Erratum: Phys. Rev.D96,no.9,099902(2017)], [arXiv:1701.03168].

[215] C. Niblaeus, A. Beniwal and J. Edsjo (2019), [arXiv:1903.11363].

[216] M. G. Aartsen *et al.* (IceCube), JCAP **1604**, 04, 022 (2016), [arXiv:1601.00653].

[217] S. Adrian-Martinez *et al.* (ANTARES), Phys. Lett. **B759**, 69 (2016), [arXiv:1603.02228].

[218] C. R. Das *et al.*, Phys. Lett. **B725**, 297 (2013), [arXiv:1110.5095].

[219] M. G. Aartsen *et al.* (IceCube), J. Phys. **G44**, 5, 054006 (2017), [arXiv:1607.02671].

[220] Y. Zhao and K. M. Zurek, JHEP **07**, 017 (2014), [arXiv:1401.7664].

[221] A. W. Strong, I. V. Moskalenko and V. S. Ptuskin, Ann. Rev. Nucl. Part. Sci. **57**, 285 (2007), [arXiv:astro-ph/0701517].

[222] O. Adriani *et al.* (PAMELA), Phys. Rev. Lett. **111**, 081102 (2013), [arXiv:1308.0133].

[223] M. Aguilar *et al.* (AMS), Phys. Rev. Lett. **117**, 9, 091103 (2016).

[224] M. Aguilar *et al.* (AMS), Phys. Rev. Lett. **110**, 141102 (2013).

[225] S. Profumo, F. Queiroz and C. Siqueira (2019), [arXiv:1903.07638].

[226] D. Hooper, P. Blasi and P. D. Serpico, JCAP **0901**, 025 (2009), [arXiv:0810.1527].

[227] S. Profumo, Central Eur. J. Phys. **10**, 1 (2011), [arXiv:0812.4457].

[228] A. U. Abeysekara *et al.* (HAWC), Science **358**, 6365, 911 (2017), [arXiv:1711.06223].

[229] S. Profumo *et al.*, Phys. Rev. **D97**, 12, 123008 (2018), [arXiv:1803.09731].

[230] R. Cowsik, B. Burch and T. Madziwa-Nussinov, Astrophys. J. **786**, 124 (2014), [arXiv:1305.1242].

[231] K. Blum, B. Katz and E. Waxman, Phys. Rev. Lett. **111**, 21, 211101 (2013), [arXiv:1305.1324].

[232] M.-Y. Cui *et al.*, Phys. Rev. Lett. **118**, 19, 191101 (2017), [arXiv:1610.03840].

[233] A. Reinert and M. W. Winkler, JCAP **1801**, 01, 055 (2018), [arXiv:1712.00002].

[234] M. W. Winkler, JCAP **1702**, 02, 048 (2017), [arXiv:1701.04866].

[235] F. Donato, N. Fornengo and P. Salati, Phys. Rev. **D62**, 043003 (2000), [hep-ph/9904481].

[236] K. Mori *et al.*, Astrophys. J. **566**, 604 (2002), [arXiv:astro-ph/0109463].

[237] H. Baer and S. Profumo, JCAP **0512**, 008 (2005), [arXiv:astro-ph/0510722].

[238] E. Carlson *et al.*, Phys. Rev. **D89**, 7, 076005 (2014), [arXiv:1401.2461].

[239] M. Cirelli *et al.*, JHEP **08**, 009 (2014), [arXiv:1401.4017].

[240] R. Bird *et al.*, in "36th International Cosmic Ray Conference (ICRC 2019) Madison, Wisconsin, USA, July 24-August 1, 2019," (2019), [arXiv:1908.03154].

[241] A. Coogan and S. Profumo, Phys. Rev. **D96**, 8, 083020 (2017), [arXiv:1705.09664].

[242] S. Colafrancesco, S. Profumo and P. Ullio, Astron. Astrophys. **455**, 21 (2006), [arXiv:astro-ph/0507575].

[243] S. Colafrancesco, S. Profumo and P. Ullio, Phys. Rev. **D75**, 023513 (2007), [arXiv:astro-ph/0607073].

[244] S. Profumo and P. Ullio (2010), [arXiv:1001.4086].

[245] T. E. Jeltema and S. Profumo, JCAP **0811**, 003 (2008), [arXiv:0808.2641].

[246] M. Cirelli *et al.*, JCAP **1103**, 051 (2011), [Erratum: JCAP1210,E01(2012)], [arXiv:1012.4515].

[247] A. McDaniel *et al.*, JCAP **1709**, 09, 027 (2017), [arXiv:1705.09384].

[248] E. Storm *et al.*, Astrophys. J. **768**, 106 (2013), [arXiv:1210.0872].

[249] G. G. Raffelt, *Stars as laboratories for fundamental physics* (1996), ISBN 9780226702728, URL `http://wwwth.mpp.mpg.de/members/raffelt/mypapers/199613.pdf`.

[250] D. Spolyar, K. Freese and P. Gondolo, Phys. Rev. Lett. **100**, 051101 (2008), [arXiv:0705.0521].

[251] S. Dimopoulos, J. Preskill and F. Wilczek, Phys. Lett. **119B**, 320 (1982).

[252] P. Pani and A. Loeb, JCAP **1406**, 026 (2014), [arXiv:1401.3025].

[253] H. Liu, G. W. Ridgway and T. R. Slatyer (2019), [arXiv:1904.09296].

[254] B. J. Carr and S. W. Hawking, Mon. Not. Roy. Astron. Soc. **168**, 399 (1974).

[255] B. Carr, F. Kuhnel and M. Sandstad, Ann. Rev. Nucl. Part. Sci. **70**, 355 (2020), [arXiv:2006.02838].

[256] M. A. Monroy-Rodríguez and C. Allen, Astrophys. J. **790**, 2, 159 (2014), [arXiv:1406.5169].

[257] M. Ricotti, J. P. Ostriker and K. J. Mack, Astrophys. J. **680**, 829 (2008), [arXiv:0709.0524].

[258] Y. Ali-Haïmoud and M. Kamionkowski, Phys. Rev. D **95**, 4, 043534 (2017), [arXiv:1612.05644].

[259] V. Poulin *et al.*, Phys. Rev. **D96**, 8, 083524 (2017), [arXiv:1707.04206].

[260] S. Bird *et al.*, Phys. Rev. Lett. **116**, 20, 201301 (2016), [arXiv:1603.00464].

[261] A. M. Green and B. J. Kavanagh, J. Phys. G **48**, 4, 043001 (2021), [arXiv:2007.10722].

[262] P. Tisserand *et al.* (EROS-2), Astron. Astrophys. **469**, 387 (2007), [arXiv:astro-ph/0607207].

[263] H. Niikura *et al.*, Nat. Astron. **3**, 6, 524 (2019), [arXiv:1701.02151].

[264] S. Kim, H. Lee and J.-C. Lee, Phys. Rev. D **103**, 10, 103531 (2021), [arXiv:2012.03595].

[265] E. Mediavilla *et al.*, Astrophys. J. **706**, 1451 (2009), [arXiv:0910.3645].

[266] A. Katz *et al.*, JCAP **1812**, 005 (2018), [arXiv:1807.11495].

[267] N. Smyth *et al.* (2019), [arXiv:1910.01285].

[268] A. Barnacka, J. F. Glicenstein and R. Moderski, Phys. Rev. **D86**, 043001 (2012), [arXiv:1204.2056].

[269] J. Kaur, P. K. Suresh and T. Venumadhav, Phys. Rev. D **102**, 10, 103509 (2020), [arXiv:2005.04222].

[270] B. J. Carr *et al.*, Phys. Rev. **D81**, 104019 (2010), [arXiv:0912.5297].

[271] A. Coogan, L. Morrison and S. Profumo, Phys. Rev. Lett. **126**, 17, 171101 (2021), [arXiv:2010.04797].

[272] T. Aramaki *et al.*, Astrophys. J. **933**, 2, 122 (2022), [arXiv:2206.02617].

[273] B. V. Lehmann *et al.*, JCAP **10**, 046 (2019), [arXiv:1906.06348].

[274] M. Baryakhtar, R. Lasenby and M. Teo, Phys. Rev. D **96**, 3, 035019 (2017), [arXiv:1704.05081].

[275] V. C. LIGO Scientific, Phys. Rev. Lett. **121**, 231103 (2018), [arXiv:1808.04771].

[276] NANOGrav Collaboration, Astrophys. J. Lett. **945**, 2, L34 (2023), [arXiv:2306.16213].

Int. J. Mod. Phys. A 2026.41. Downloaded
by UNIVERSITY OF CALIFORNIA @ BERKELEY on 09/16/26. Re-
orldscientific.com
strictly not permitted, except for Open Access articles.

28. Dark Energy

Revised August 2025 by D.H. Weinberg (Ohio State U.) and M. White (UC Berkeley; LBNL).

28.1 Repulsive Gravity and Cosmic Acceleration

In the first modern cosmological model, Einstein [1] modified his field equation of General Relativity (GR), introducing a "cosmological term" that enabled a solution with time-independent, spatially homogeneous matter density $\rho_{\rm m}$ and constant positive space curvature. Although Einstein did not frame it this way, one can view the "cosmological constant" Λ as representing a constant energy density of the vacuum [2], whose repulsive gravitational effect balances the attractive gravity of matter and thereby allows a static solution. After the development of dynamic cosmological models [3,4] and the discovery of cosmic expansion [5], the cosmological term appeared unnecessary, and Einstein and de Sitter [6] advocated adopting an expanding, homogeneous and isotropic, spatially flat, matter-dominated Universe as the default cosmology until observations dictated otherwise. Such a model has matter density equal to the critical density, $\Omega_{\rm m} \equiv \rho_{\rm m}/\rho_{\rm c} = 1$, and negligible contribution from other energy components [7].

By the mid-1990s, the Einstein-de Sitter model was showing numerous cracks, under the combined onslaught of data from the cosmic microwave background (CMB), large-scale galaxy clustering, and estimates of the matter density, the expansion rate (H_0), and the age of the Universe. As noted in a number of papers from this time, introducing a cosmological constant offered a potential resolution of many of these tensions, yielding the most empirically successful version of the inflationary cold dark matter scenario. In the late 1990s, supernova surveys by two independent teams provided direct evidence for accelerating cosmic expansion [8,9], establishing the cosmological constant model (with $\Omega_{\rm m} \simeq 0.3$, $\Omega_\Lambda \simeq 0.7$) as the preferred alternative to the $\Omega_{\rm m} = 1$ scenario. Shortly thereafter, CMB evidence for a spatially flat Universe [10,11], and thus for $\Omega_{\rm tot} \simeq 1$, cemented the case for cosmic acceleration by firmly eliminating the free-expansion alternative with $\Omega_{\rm m} \ll 1$ and $\Omega_\Lambda = 0$. Today, the accelerating Universe is well established by multiple lines of independent evidence from a tight web of precise cosmological measurements.

As discussed in the Big Bang Cosmology article of this *Review* (Sec. 22), the scale factor $R(t)$ of a homogeneous and isotropic Universe governed by GR grows at an accelerating rate if the pressure $p < -\frac{1}{3}\rho$ (in $c = 1$ units). A cosmological constant has $\rho_\Lambda =$ constant and pressure $p_\Lambda = -\rho_\Lambda$ (see Eq. 22.10), so it will drive acceleration if it dominates the total energy density. However, acceleration could arise from a more general form of "dark energy" that has negative pressure, typically specified in terms of the equation-of-state-parameter $w = p/\rho$ ($= -1$ for a cosmological constant). Furthermore, the conclusion that acceleration requires a new energy component beyond matter and radiation relies on the assumption that GR is the correct description of gravity on cosmological scales. The title of this article follows the common but inexact usage of "dark energy" as a catch-all term for the origin of cosmic acceleration, regardless of whether it arises from a new form of energy or a modification of GR. Our discussion in Secs. 28.2 and 28.3 draws on the extensive review of cosmic acceleration in Ref. [12], which provides further background explanation and references.

Below we will use the abbreviation ΛCDM to refer to a model with cold dark matter, a cosmological constant, inflationary initial conditions, standard radiation and neutrino content, and a flat Universe with $\Omega_{\rm tot} = 1$.

28.2 Theories of Cosmic Acceleration

28.2.1 *Dark Energy or Modified Gravity?*

A cosmological constant is the mathematically simplest, and perhaps the physically simplest, theoretical explanation for the accelerating Universe. The problem is explaining its unnaturally small magnitude, as discussed in Sec. 22.4.7 of this *Review*. An alternative (which still requires finding a way to make the cosmological constant zero or at least negligibly small) is that the accelerating cosmic expansion is driven by a new form of energy, such as a scalar field $\phi(\mathbf{x})$ with potential $V(\phi)$ [13]. The energy density and pressure of a canonical scalar field take the same forms as for inflationary scalar fields, given in Eq. (22.52) of the Big Bang Cosmology article. In the limit that $\frac{1}{2}\dot\phi^2 \ll |V(\phi)|$, the scalar field acts like a cosmological constant, with $p_\phi \simeq -\rho_\phi$. In this scenario, today's cosmic acceleration is closely akin to the epoch of inflation, but with radically different energy and timescale.

More generally, the value of $w = p_\phi/\rho_\phi$ in scalar field models evolves with time in a way that depends on $V(\phi)$ and on the initial conditions $(\phi_i, \dot\phi_i)$; some forms of $V(\phi)$ have attractor solutions in which the late-time behavior is insensitive to initial values. Many forms of time evolution are possible, including ones where w is approximately constant and broad classes where w "freezes" towards or "thaws" away from $w = -1$, with the transition occurring when the field comes to dominate the total energy budget. If ρ_ϕ is even approximately constant, then it becomes dynamically insignificant at high redshift, because the matter density scales as $\rho_{\rm m} \propto (1+z)^3$. "Early dark energy" models are ones in which ρ_ϕ is a small but not negligible fraction (*e.g.*, a few percent) of the total energy during the pre-recombination era, eventually evolving to become the dominant component at low redshift.

Instead of introducing a new energy component, one can attempt to modify gravity in a way that leads to accelerated expansion [14]. One option is to replace the Ricci scalar $\mathcal{R}$ with a function $\mathcal{R} + f(\mathcal{R})$ in the gravitational action [15]. Other changes can be more radical, such as introducing extra dimensions and allowing gravitons to "leak" off the brane that represents the observable Universe (the "DGP" model [16]). The DGP example has inspired a more general class of "galileon" and massive gravity models. Constructing viable modified gravity models is challenging, in part because it is easy to introduce theoretical inconsistencies (such as "ghost" fields with negative kinetic energy), but above all because GR is a theory with many high-precision empirical successes on solar system scales [17]. Modified gravity models typically invoke screening mechanisms that force model predictions to approach those of GR in regions of high density or strong gravitational potential. Screening offers potentially distinctive signatures, since the strength of gravity (*i.e.*, the effective value of $G_{\rm N}$) can vary by order unity in environments with different gravitational potentials.

More generally, one can search for signatures of modified gravity by comparing the history of cosmic structure growth to the history of cosmic expansion. Within GR, these two are linked by a consistency relation, as described below (Eq. (28.2)). Modifying gravity can change the predicted rate of structure growth, and it can make the growth rate dependent on scale or environment. In some circumstances, modifying gravity alters the combinations of potentials responsible for gravitational lensing and the dynamics of non-relativistic tracers (such as galaxies or stars) in different ways (see Sec. 22.4.7 in this *Review*), leading to order unity mismatches between the masses of objects inferred from lensing and those inferred from dynamics in unscreened environments.

At present there are no fully realized and empirically viable modified gravity theories that explain the observed level of cosmic acceleration. The constraints on $f(\mathcal{R})$ models now force them so close to GR that they cannot produce acceleration without introducing a separate dark energy component [18]. The DGP model is empirically ruled out by several tests, including the expansion history, the integrated Sachs-Wolfe effect, and redshift-space distortion measurements of the structure growth rate [19]. The near-simultaneous arrival of gravitational waves and electromagnetic signals from the neutron star merger event GW170817, which shows that gravitational waves travel at almost exactly the speed of light, is a further strong constraint on modified gravity theories [20]. The elimination of models should be considered an important success of the program to empirically test theories of cosmic acceleration. However, it is worth recalling that there was no fully realized gravitational explanation for the precession of Mercury's orbit prior to the completion of GR in 1915, and the fact that no complete and viable modified gravity theory exists today does not mean that one will not arise in the future. In the meantime, we can continue empirical investigations that can tighten restrictions on such theories or perhaps point towards the gravitational sector as the origin of accelerating expansion.

Int. J. Mod. Phys. A 2026.41. Downloaded from www.worldscientific.com by UNIVERSITY OF CALIFORNIA @ BERKELEY on 09/16/26. Re-use and distribution is strictly not permitted, except for Open Access articles.

Int. J. Mod. Phys. A 2026.41. Downloaded from www.worldscientific.com by UNIVERSITY OF CALIFORNIA @ BERKELEY on 09/16/26. Re-strictly not permitted, except for Open Access articles.

28.2.2 *Expansion History and Growth of Structure*

The main line of empirical attack on dark energy is to measure the history of cosmic expansion and the history of matter clustering with the greatest achievable precision over a wide range of redshift. Within GR, the expansion rate $H(z)$ is governed by the Friedmann equation (see the articles on Big Bang Cosmology and Cosmological Parameters—Secs. 22 and 25 in this *Review*). For dark energy with an equation of state $w(z)$, the cosmological constant contribution to the expansion, Ω_Λ, is replaced by a redshift-dependent contribution. The evolution of the dark energy density follows from Eq. (22.10),

$$\Omega_{\rm de}\frac{\rho_{\rm de}(z)}{\rho_{\rm de}(z=0)} = \Omega_{\rm de}\exp\left[3\int_0^z [1+w(z')]\frac{dz'}{1+z'}\right] = \Omega_{\rm de}(1+z)^{3(1+w)}, \tag{28.1}$$

where the second equality holds for constant w. If $\Omega_{\rm m}$, $\Omega_{\rm r}$, and the present value of $\Omega_{\rm tot}$ are known, then measuring $H(z)$ pins down $w(z)$. (Note that $\Omega_{\rm de}$ is the same quantity denoted $\Omega_{\rm v}$ in Sec. 22, but we have adopted the 'de' subscript to avoid implying that dark energy is necessarily a vacuum effect.) The evolution of $\rho_{\rm de}$ can be more complicated than Eq. (28.1) in scenarios with non-gravitational coupling between dark energy and other components, *e.g.*, "decay" into dark matter or radiation.

While some observations can probe $H(z)$ directly, others measure the distance-redshift relation. The basic relations between angular diameter distance or luminosity distance and $H(z)$ are given in Ch. 22 —and these are generally unaltered in time-dependent dark energy or modified gravity models. We will often refer to the comoving angular diameter distance, $D_{\rm M}(z) = (1+z)D_{\rm A}(z)$, which relates comoving transverse size to angular size. The subscript M is conventional notation because this distance is also the one that relates transverse velocity to proper motion.

In GR-based linear perturbation theory, the density contrast $\delta(\mathbf{x},t) \equiv \rho(\mathbf{x},t)/\bar\rho(t) - 1$ of pressureless matter grows in proportion to the linear growth function $G(t)$ (not to be confused with the gravitational constant $G_{\rm N}$), which follows the differential equation

$$\ddot G + 2H(z)\dot G - \frac{3}{2}\Omega_{\rm m}H_0^2(1+z)^3 G = 0\ . \tag{28.2}$$

To a good approximation, the logarithmic derivative of $G(z)$ is

$$f(z) \equiv -\frac{d\ln G}{d\ln(1+z)} \simeq \left[\Omega_{\rm m}(1+z)^3\frac{H_0^2}{H^2(z)}\right]^\gamma\ , \tag{28.3}$$

where $\gamma \simeq 0.55$ for relevant values of cosmological parameters [21]. In an $\Omega_{\rm m} = 1$ Universe, $G(z) \propto (1+z)^{-1}$, but growth slows when $\Omega_{\rm m}$ drops significantly below unity. One can integrate Eq. (28.3) to get an approximate integral relation between $G(z)$ and $H(z)$, but the full (numerical) solution to Eq. (28.2) should be used for precision calculations. Even in the non-linear regime, the amplitude of clustering is determined mainly by $G(z)$, so observations of non-linear structure can be used to infer the linear $G(z)$, provided one has good theoretical modeling to relate the two.

In modified gravity models the growth rate of gravitational clustering may differ from the GR prediction. A general strategy to test modified gravity, therefore, is to measure both the expansion history and the growth history to see whether they yield consistent results for $H(z)$ or $w(z)$.

28.2.3 *Parameters*

Constraining a general history of $w(z)$ is nearly impossible, because the dark energy density, which affects $H(z)$, is given by an integral over $w(z)$, and distances and the growth factor involve a further integration over functions of $H(z)$. Oscillations in $w(z)$ over a range $\Delta z/(1+z) \ll 1$ are therefore extremely difficult to constrain. It has become conventional to phrase constraints or projected constraints on $w(z)$ in terms of a linear evolution model,

$$w(a) = w_0 + w_{\rm a}(1-a) = w_{\rm p} + w_{\rm a}(a_{\rm p} - a), \tag{28.4}$$

where $a \equiv (1+z)^{-1}$, w_0 is the value of w at $z = 0$, and $w_{\rm p}$ is the value of w at a "pivot" redshift $z_{\rm p} \equiv a_{\rm p}^{-1} - 1$, where it is best constrained by a given set of experiments. For typical data combinations, $z_{\rm p} \simeq 0.5$. This simple parameterization can provide a good approximation to the predictions of many physically motivated models for observables measured with percent-level precision. A widely used "Figure of Merit" (FoM) for dark energy experiments [22] is the projected combination of errors $[\sigma(w_{\rm p})\sigma(w_{\rm a})]^{-1}$. Ambitious experiments with 0.1–0.3% precision on observables can constrain richer descriptions of $w(z)$, which can be characterized, *e.g.*, by principal components.

There has been less convergence on a standard parameterization for describing modified gravity theories. Deviations from the GR-predicted growth rate can be described by a deviation $\Delta\gamma$ in the index of Eq. (28.3), together with an overall multiplicative offset relative to the $G(z)$ expected from extrapolating the CMB-measured fluctuation amplitude to low redshift. However, these two parameters may not accurately capture the growth predictions of all physically interesting models. Another important parameter to constrain is the ratio of the gravitational potentials governing space curvature and the acceleration of non-relativistic test particles. The possible phenomenology of modified gravity models is rich [23], which enables many consistency tests but complicates the task of constructing parameterized descriptions.

The more general set of cosmological parameters is discussed elsewhere in this *Review* (Sec. 25), but here we highlight a few that are particularly important to the dark energy discussion.

- The dimensionless Hubble parameter $h \equiv H_0/100\ {\rm km\,s^{-1}\,Mpc^{-1}}$ determines the present day value of the critical density and the overall scaling of distances inferred from redshifts.
- $\Omega_{\rm m}$ and $\Omega_{\rm tot}$ affect the expansion history and the distance-redshift relation.
- The sound horizon $r_{\rm s} = \int_0^{t_{\rm rec}} c_{\rm s}(t)dt/a(t)$, the comoving distance that pressure waves can propagate between $t = 0$ and recombination, determines the physical scale of the acoustic peaks in the CMB and the baryon acoustic oscillation (BAO) feature in low-redshift matter clustering [24].
- The amplitude of matter fluctuations, conventionally represented by the quantity $\sigma_8(z)$, scales the overall amplitude of growth measures such as weak lensing or redshift-space distortions (discussed in the next section).

Specifically, $\sigma_8(z)$ refers to the rms fluctuation of the matter overdensity $\rho/\bar\rho$ in spheres of radius $8\,h^{-1}$Mpc, computed from the linear theory matter power spectrum at redshift z, and σ_8 on its own refers to the value at $z = 0$ (just like our convention for $\Omega_{\rm m}$).

While discussions of dark energy are frequently phrased in terms of values and errors on quantities like $w_{\rm p}$, $w_{\rm a}$, $\Delta\gamma$, and $\Omega_{\rm tot}$, parameter precision is the means to an end, not an end in itself. The underlying goal of empirical studies of cosmic acceleration is to address two physically profound questions:

- 1. Does acceleration arise from a breakdown of GR on cosmological scales or from a new energy component that exerts repulsive gravity within GR?
- 2. If acceleration is caused by a new energy component, is its energy density constant in space and time, as expected for a fundamental vacuum energy, or does it show variations that indicate a dynamical field?

Substantial progress towards answering these questions, in particular any definitive rejection of the cosmological constant "null hypothesis," would be a major breakthrough in cosmology and fundamental physics.

28.3 Observational Probes

We briefly summarize the observational probes that play the greatest role in current constraints on dark energy. Further discussion can be found in other articles of this *Review*, in particular Secs. 25 (Cosmological Parameters) and 29 (The Cosmic Microwave Background), and in Ref. [12], which provides extensive references to background literature. Recent observational results from these methods are discussed in Sec. 28.4.

Int. J. Mod. Phys. A 2026.41. Downloaded from www.worldscientific.com
by UNIVERSITY OF CALIFORNIA @ BERKELEY on 09/16/26. Re-use and distribution is strictly not permitted, except for Open Access articles.

28.3.1 *Methods, Sensitivity, Systematics*

Cosmic Microwave Background Anisotropies: Although CMB anisotropies provide limited information about dark energy on their own, CMB constraints on the geometry, matter content, and radiation content of the Universe play a critical role in dark energy studies when combined with low-redshift probes. In particular, CMB data supply measurements of $\theta_{\rm s} = r_{\rm s}/D_{\rm M}(z_{\rm rec})$, the angular size of the sound horizon at recombination, from the angular location of the acoustic peaks, measurements of $\Omega_{\rm m}h^2$ and $\Omega_{\rm b}h^2$ from the heights of the peaks, and normalization of the amplitude of matter fluctuations at $z_{\rm rec}$ from the amplitude of the CMB fluctuations themselves. The comparison of the acoustic scale to the diffusion damping scale helps to constrain the expansion rate near recombination. *Planck* data yield a 0.18% determination of $r_{\rm s}$, which scales as $(\Omega_{\rm m}h^2)^{-0.25}$ for cosmologies with standard matter and radiation content. The uncertainty in the matter fluctuation amplitude at the epoch of recombination is 0.5%. Secondary anisotropies, including the integrated Sachs-Wolfe effect, the Sunyaev-Zeldovich (SZ, [25]) effect, and weak lensing of primary anisostropies, provide additional information about dark energy by constraining low-redshift structure growth.

Type Ia Supernovae (SN): Type Ia supernovae, produced by the thermonuclear explosions of white dwarfs, exhibit 10–15% scatter in peak luminosity after correction for light-curve duration (the time to rise and fall) and color (which is a diagnostic of dust extinction). Since the peak luminosity is not known *a priori*, supernova surveys constrain ratios of luminosity distances $D_{\rm L}(z)$ at different redshifts. If one is comparing a high-redshift sample to a local calibrator sample measured with much higher precision (and distances inferred from Hubble's law), then one essentially measures the luminosity distance in h^{-1}Mpc, constraining the combination $hD_{\rm L}(z)$. With distance uncertainties of 5–8% per well observed supernova, a sample of around 100 SNe is sufficient to achieve sub-percent statistical precision. The percent-level systematic uncertainties in current samples are dominated by uncertainties associated with photometric calibration, dust extinction corrections, and modeling the correlations among supernova luminosity, color, light-curve shape, and host galaxy properties. Another potential systematic is redshift evolution of the supernova population itself, which can be tested by analyzing subsamples grouped by spectral properties or host galaxy properties to confirm that they yield consistent results. Recent analyses of large supernova compilations calibrate these systematic uncertainties internally in parallel with cosmological constraints, with an overall error budget that has similar contributions from systematic and statistical uncertainties (*e.g.*, [26]).

Baryon Acoustic Oscillations (BAO): Pressure waves that propagate in the pre-recombination photon-baryon fluid imprint a characteristic scale in the clustering of matter and galaxies, which appears in the galaxy correlation function as a localized peak at the sound horizon scale $r_{\rm s}$, or in the power spectrum as a series of oscillations. Since observed galaxy coordinates consist of angles and redshifts, measuring this "standard ruler" scale in a galaxy redshift survey determines the angular diameter distance $D_{\rm A}(z)$ and the expansion rate $H(z)$, which convert coordinate separations to comoving distances. Errors on the two quantities are correlated, and in existing galaxy surveys the best determined combination is approximately $D_{\rm V}(z) = [czD_{\rm M}^2(z)/H(z)]^{1/3}$. As a useful rule of thumb, a survey that densely maps structure at redshift z over a comoving volume V, and is therefore limited by sample variance rather than shot noise, measures $D_{\rm M}(z)$ with a fractional error of $0.005(V/10\,{\rm Gpc}^3)^{-1/2}$ and $H(z)$ with a fractional error 1.6–1.8 times higher. Large galaxy and quasar redshift surveys now provide precise BAO measurements out to $z \simeq 1.5$. At redshifts $z > 2$, BAO can also be measured in the Lyman-α forest of intergalactic hydrogen absorption towards background quasars, where the fluctuating absorption pattern provides tens or hundreds of samples of the density field along each quasar sightline. For Lyman-α forest BAO, the best measured parameter combination is more heavily weighted towards $H(z)$ because of strong redshift-space distortions, which enhance clustering in the line-of-sight direction. Cross-correlation between the Lyman-α forest and quasars sharpens the constraints on $D_{\rm M}(z)$. Photometric redshifts in optical imaging surveys can be used to measure BAO in the angular direction, though the typical distance precision is a factor of 3–4 lower compared to a well sampled spectroscopic survey of the same area, and angular BAO measurements do not directly constrain $H(z)$. BAO distance measurements complement SN distance measurements by providing absolute rather than relative distances (with precise calibration of $r_{\rm s}$ from the CMB) and by having greater achievable precision at high redshift thanks to the increasing comoving volume available. Theoretical modeling suggests that BAO measurements from even the largest feasible redshift surveys will be limited by statistical rather than systematic uncertainties [27].

Weak Gravitational Lensing: Gravitational light bending by a clustered distribution of matter shears the shapes of higher redshift background galaxies in a spatially coherent manner, producing a correlated pattern of apparent ellipticities. By studying the weak lensing signal for source galaxies binned by photometric redshift (estimated from broad-band colors), one can probe the history of structure growth. "Cosmic shear" weak lensing uses the correlation of source ellipticities to deduce the clustering of intervening matter. "Galaxy-galaxy lensing" (GGL) uses the correlation between a shear map and a foreground galaxy sample to measure the galaxy-mass cross-correlation function, which can be combined with galaxy clustering to constrain total matter clustering. For a specified expansion history, the predicted signals scale approximately as $\sigma_8\Omega_{\rm m}^{\alpha}$, with $\alpha = 0.3$–0.5. The predicted signals also depend on the distance-redshift relation, so weak lensing becomes a sharper probe of matter clustering when combined with SN or BAO measurements that pin down $D_{\rm M}(z)$. Conversely, with CMB lensing and redshift space distortions now giving competitive constraints on matter clustering (see below), weak lensing is becoming a valuable test of the expansion history.

The most challenging systematics in weak lensing are shape measurement biases, biases in the distribution of photometric redshifts, and intrinsic alignments of galaxy orientations that could contaminate the lensing-induced signal. Weak lensing of CMB anisotropies is an increasingly powerful tool, in part because it circumvents many of these observational and astrophysical systematics. Predicting the large-scale weak lensing signal is straightforward in principle, but the number of independent modes on large scales is small, and the inferences are therefore dominated by sample variance. Exploiting small-scale measurements, for tighter constraints, requires modeling the effects of complex physical processes such as star formation and feedback on the matter power spectrum. Strong gravitational lensing can also provide constraints on dark energy, either through time-delay measurements that probe the absolute distance scale, or through measurements of multiple-redshift lenses that constrain distance ratios. The primary uncertainty for strong lensing constraints is modeling the mass distribution of the lens systems.

Clusters of Galaxies: Like weak lensing, the abundance of massive dark-matter halos probes structure growth by constraining $\sigma_8\Omega_{\rm m}^{\alpha}$, where $\alpha \simeq 0.3$–0.5. These halos can be identified as dense concentrations of galaxies or through the signatures of hot (10^7–10^8 K) gas in X-ray emission or SZ distortion of the CMB. The critical challenge in cluster cosmology is calibrating the relation between the halo mass as predicted from theory and the observable mass proxy used for cluster identification, with percent-level accuracy needed for clusters to remain competitive with other growth probes. The most promising approach uses stacked weak lensing to measure projected cluster-mass cross-correlations, making cluster cosmology analogous to GGL but with clusters rather than galaxies chosen as reference points. Sample selection effects and the influence of baryonic physics on halo mass profiles remain serious challenges for cluster cosmology.

Redshift-Space Distortions (RSD) and the Alcock-Paczynski (AP) Effect: Redshift-space distortions of galaxy clustering, induced by peculiar motions, probe structure growth by constraining the parameter combination $f(z)\sigma_8(z)$, where $f(z)$ is the growth rate defined by Eq. (28.3). The most secure constraints come from large scales (comoving separations $r \gtrsim 10\,h^{-1}$Mpc or wavenumbers $k \lesssim 0.2h\,{\rm Mpc}^{-1}$), which are adequately described by perturbation theory. Taking advantage of the higher measurement

Int. J. Mod. Phys. A 2026.41. Downloaded from www.worldscientific.com by UNIVERSITY OF CALIFORNIA @ BERKELEY on 09/16/26. Re-use strictly not permitted, except for Open Access articles.

precision on smaller scales requires accurate models of non-linear gravitational evolution and the non-linear bias between galaxy and matter distributions. A second source of anisotropy arises if one adopts the wrong cosmological metric to convert angles and redshifts into comoving separations, a phenomenon known as the Alcock-Paczynski effect [28]. Demanding isotropy of clustering at redshift z constrains the parameter combination $H(z)D_{\rm M}(z)$. The main challenge for the AP method is correcting for the anisotropy induced by peculiar velocity RSD.

Low Redshift Measurement of H_0: The value of H_0 sets the current value of the critical density $\rho_{\rm c} = 3H_0^2/8\pi G_{\rm N}$, and combination with CMB measurements provides a long lever arm for constraining the evolution of dark energy. The challenge in conventional H_0 measurements is establishing distances to galaxies that are "in the Hubble flow," *i.e.*, far enough away that their peculiar velocities are small compared to the expansion velocity $v = H_0 d$. This can be done by building a ladder of distance indicators tied to stellar parallax on its lowest rung, or by using gravitational-lens time delays or geometrical measurements of maser data to circumvent this ladder.

28.3.2 *Dark Energy Experiments*

Most observational applications of the above methods now take place in the context of large cosmological surveys, for which constraining dark energy and modified gravity theories is a central objective. We are now at an exciting phase in which most of the "Stage III" experiments (in the parlance of Ref. [29]) have completed observations and in some cases final analysis, and the more powerful "Stage IV" experiments are underway or beginning operations in the near future.

Beginning with the main Stage III imaging surveys, all designed with weak lensing as a primary goal, the Kilo Degree Survey (KiDS) imaged 1350 deg^2, the Dark Energy Survey (DES) imaged 5000 deg^2, and the Subaru Hyper-Suprime Camera (HSC) imaged about 1200 deg^2. The statistical power and systematics control of a weak lensing survey depend on area, depth, and image quality, and on filter coverage and spectroscopic calibration for photometric redshifts. All three surveys have contributed to the current understanding of matter clustering evolution and its implications for dark energy. Recent cosmological analyses from these survey teams include Refs. [30] (KiDS, based on the final data set), [31] (DES, based on the 3-year data set), and [32] (HSC, based on the 3-year data set).

Supernova cosmology has advanced largely through unified analyses of compilation data sets obtained from multiple telescopes, with Pantheon+ [33] and Union3 [34] being two state-of-the-art compilations. The largest single-telescope supernova survey comes from DES, and its final sample includes about 1500 SNe Ia observed by DES with $0.1 < z < 1.1$ and 194 local SNe Ia observed by a variety of telescopes [35]. Although these three analyses have many supernovae in common, different calibration and modeling choices can lead to significant differences in their cosmological implications, as discussed in Section 28.4. The local sample plays an important role in calibrating the supernova luminosity scale, and matching these local supernovae to their higher redshift counterparts has emerged as an important challenge.

The Stage III Baryon Oscillation Spectroscopic Survey (BOSS) and its successor eBOSS used fiber-fed optical spectrographs to map the redshift-space distributions of about two million galaxies and quasars and Lyman-α forest spectra of about 200,000 high-redshift quasars. These 3-dimensional maps enabled BAO and RSD measurements over the redshift range $0.1 < z < 2.5$, including percent-level determinations of $D_{\rm M}(z)$ and $H(z)$ at multiple redshifts [36]. The combination of CMB and BAO measurements has allowed strong constraints on dark energy and cosmological parameters from probes that have relatively simple physics, mostly described by linear perturbation theory.

Stage IV experiments seek a roughly order-of-magnitude gain in data volume relative to Stage III experiments, as well as the improvements in data quality and systematics control needed to exploit their greater statistical power. First out of the gate is the Dark Energy Spectroscopic Instrument (DESI), which follows a strategy similar to BOSS/eBOSS but on a much grander scale, using a larger telescope (4-m versus 2.5-m) and a much higher fiber multiplex (5000 versus 1000). DESI began full operations in May 2021, and its three-year data set includes over 30 million galaxies and quasars and 0.8-million Lyman-α forest spectra [37]. The BAO measurements from this data set play a central role in our discussion of current dark energy constraints below.

The *Euclid* space mission, launched in July 2023, will image 14,000 deg^2 through a wide optical filter for measurements of weak lensing and photometric galaxy clustering, and it will conduct a slitless spectroscopic survey over the same area at NIR wavelengths to enable BAO and RSD measurements at $0.9 < z < 2$. *Euclid* presented early science results in mid-2024 (*e.g.*, [38]), and the consortium is now working towards its first cosmological results. Vera Rubin Observatory will obtain deep multi-band optical imaging of about 18,000 deg^2 for weak lensing and photometric galaxy clustering, with high-cadence time-domain monitoring of smaller fields to identify and measure light curves for many thousands of Type Ia supernovae. First-light images from Rubin were presented in summer 2025, and the decade-long Legacy Survey of Space and Time (LSST, [39]) will begin regular operations in autumn 2025.

The *Nancy Grace Roman Space Telescope*, scheduled for launch in October 2026, will devote 1.4 years of its 5-year prime mission to a high-latitude, wide area survey, covering 2400 deg^2 in three NIR imaging bands and slitless spectroscopy (galaxy redshifts $0.7 < z < 3$), plus an additional 2700 deg^2 of single filter imaging. A further 0.5 years of observing time will be devoted to a time-domain survey expected to measure light curves for more than 10,000 supernovae extending to $z > 2$. Both surveys are described in Ref. [40]. DESI, *Euclid*, Rubin, and *Roman* each have distinctive strengths as cosmological survey experiments, and the history of Stage III analyses suggests that comparisons and cross-calibrations among them will play a crucial role in extracting their cosmological lessons.

The next generation of CMB experiments, in particular the Simons Observatory and Advanced Simons Observatory, will provide tighter constraints on cosmological parameters from primary anisotropies *and* much higher precision CMB lensing maps. These maps will be powerful probes of matter clustering evolution on their own and in concert with galaxy surveys.

28.4 Current Constraints on Expansion, Growth, and Dark Energy

The last decade has seen dramatic progress in measurements of the cosmic expansion history and structure growth, leading to much tighter constraints on the parameters of dark energy models. Much of this progress has come from the intermediate or final results of the Stage III dark energy experiments described in the preceding Section, along with early results from DESI. Exquisitely precise maps of CMB temperature and polarization anisotropies, from *WMAP* and *Planck* and higher resolution ground-based experiments, provide tight constraints on the matter and baryon density and the distance to the last-scattering surface, as well as sharp limits on non-standard energy components in the pre-recombination Universe (see Section 29). CMB lensing maps provide increasingly powerful measurements of low redshift matter clustering, on their own and through cross-correlation with galaxy and cluster distributions. Cepheid-based distance-ladder measurements of H_0 have reached statistical precision of around 1%, though independent analyses using different distance indicators vary at the few percent level. For all of these experiments, the high statistical precision of current measurements demands stringent control of systematic uncertainties, and much of the community's effort has gone into assessing and mitigating systematics using both empirical and theoretical methods.

As a pedagogical illustration of current measurements of the cosmic expansion history, Figure 28.1 compares distance-redshift measurements from DESI BAO data and DES SN data to the predictions for a flat Universe with a cosmological constant. Transverse BAO measurements determine the comoving angular diameter distance $D_{\rm M}(z)$, and line-of-sight BAO measurements determine the expansion rate $H(z) = c/D_{\rm H}(z)$, and thus the local slope of the distance-redshift relation. DESI uses a variety of galaxy and quasar tracers to measure BAO distances in multiple redshift bins

Int. J. Mod. Phys. A 2026.41. Downloaded from www.worldscientific.com
by UNIVERSITY OF CALIFORNIA @ BERKELEY on 09/16/26. Re-use and distribution is strictly not permitted, except for Open Access articles.

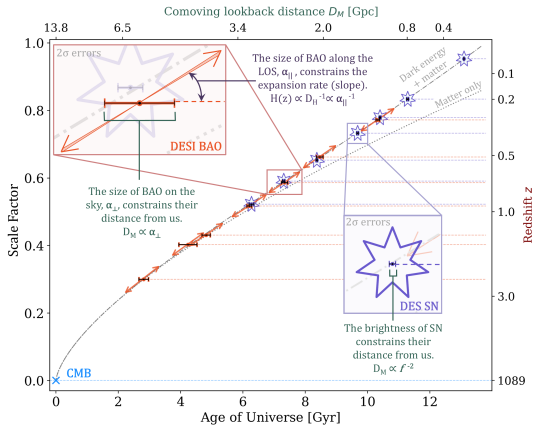

Figure 28.1: Expansion history of the Universe as measured by BAO and Type Ia SNe, adapted (by C. Lamman) from Ref. [37]. Black points with horizontal 2σ error bars show transverse BAO measurements from DESI galaxy or Lyman-α forest samples at different redshifts (right axis), plotted against the inferred comoving angular diameter distance $D_{\rm M}$ (top axis). Orange arrows show the expansion rate — the slope of the age-distance relation — inferred at these redshifts from the line-of-sight BAO measurements. Blue stars surrounding blue horizontal error bars show binned measurements of $D_{\rm M}$ from DES SNe; these measurements of relative distance have been normalized to match the absolute scale of the BAO. The dashed curve shows the predicted distance-redshift relation of a flat ΛCDM model with $\Omega_{\rm m} = 0.315$ and $h = 0.674$, the best-fit parameters inferred from *Planck* CMB data [41]. The dotted curve shows the prediction of a flat model with $\Omega_{\rm m} = 1$ and $h = 0.674$. The age of the Universe on the bottom axis corresponds to the ΛCDM model and would be slightly different for the $\Omega_{\rm m} = 1$ model. Predictions for an open universe with $\Omega_\Lambda = 0$ would be intermediate between the two models plotted, but still strongly inconsistent with the BAO and SN data and also with the angular scale of CMB anisotropies.

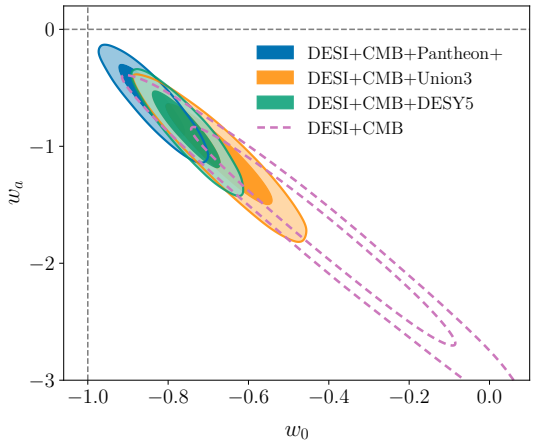

Figure 28.2: Constraints on parameters of the $\mathtt{w_0w_aCDM}$ dark energy model from combinations of CMB, BAO, and supernova (SN) data, taken from Ref. [37]. Dashed contours show 68% and 95% confidence intervals on w_0 and $w_{\rm a}$ inferred from DESI DR2 BAO measurements and *Planck* 2018 CMB anisotropy data. Filled contours show the impact of adding SN data from the DES Y5 compilation (green), the Pantheon+ compilation (blue), or the Union3 compilation (orange). Dashed gray lines mark the ΛCDM values of $w_0 = -1$, $w_{\rm a} = 0$.

from $z = 0.3$ to $z = 1.5$, and the Lyman-α forest to provide measurements in a seventh bin at $z = 2.3$. After standardizing the peak SN luminosity using light-curve shape and color, SN data determine $D_{\rm M}(z)$ from the apparent flux. For visualization, the roughly 1700 SNe of the DES sample have here been averaged into seven redshift bins from $z = 0.005$ to $z = 0.9$. At the level that is visually discernible on this plot, the BAO and SN measurements show excellent agreement with each other and with the predictions of a flat ΛCDM model, given parameter values determined independently from *Planck* CMB data.

28.4.1 *Evolving dark energy?*

In detail, the CMB, BAO, and SN data sets can each be fit well individually by a ΛCDM model, but the preferred parameter values (specifically H_0 and $\Omega_{\rm m} = 1 - \Omega_\Lambda$) are different. This tension of parameter values could be a sign that the underlying model is incorrect. Within ΛCDM, the DESI Collaboration reports a tension of about 2σ between BAO and CMB alone, with the exact value depending on the details of the CMB data set. They find that allowing non-zero curvature or a constant $w \neq -1$ does little to alleviate the tension between the CMB and BAO data, and they instead focus on $\mathtt{w_0w_aCDM}$, a flat Universe with cold dark matter and a dark energy equation-of-state described by Eq. (28.4). Figure 28.2 shows their 68% and 95% constraints in the $w_0 - w_{\rm a}$ plane inferred from DESI+*Planck* alone (pink dashed contour) or from DESI+*Planck* combined with SN data from the DES, Union3, or Pantheon+ compilations (filled contours, as labeled). In all cases, the ΛCDM values ($w_0 = -1$, $w_{\rm a} = 0$) lie outside the 95% contour, but the significance of the discrepancy depends on the chosen data combination. For DESI+CMB, Ref. [37] finds a $\Delta\chi^2_{\rm MAP} = -12.5$ between the most probable $\mathtt{w_0w_aCDM}$ model and the most probable ΛCDM model. Accounting for the two extra parameters of $\mathtt{w_0w_aCDM}$, this difference corresponds to a frequentist significance of 3.1σ assuming Gaussian error distributions. Adding DES SN raises the significance to 4.2σ, but using the Pantheon+ SNe instead of DES reduces the significance to 2.8σ.

Figure 28.3 shows the features of the data that lead to these model constraints, with all distances divided by the predictions of the fiducial *Planck* ΛCDM model so that the percent-level error bars can be clearly discerned. Several of the DESI data points in the upper panels, especially the $D_{\rm H}$ points at $z = 0.5$ and $z = 0.7$, lie outside the 1σ band of *Planck*-based ΛCDM predictions. While a joint fit (purple curve) comes closer to the DESI points, as expected, this compromise ΛCDM model does not give good agreement with either *Planck* or DESI. The red-dashed curve shows a $\mathtt{w_0w_aCDM}$ model with $w_0 = -0.752$ and $w_{\rm a} = -0.86$, the best-fit values from the DESI+*Planck*+DES SN combination. This model gives noticeably better agreement with the DESI data and (while it cannot be seen from this plot) with the CMB data. The DES SN data (lower left panel) show a sharp preference for this $\mathtt{w_0w_aCDM}$ model over the DESI+CMB ΛCDM model, with the critical distinction being a 2% difference in the local distance scale measured by the $z = 0.005$ SNe relative to those at $z = 0.3$-0.7. However, the Pantheon+ SN measurements (lower right panel) are equally consistent with the $\mathtt{w_0w_aCDM}$ and ΛCDM models, with the key difference from DES being the $z = 0.005$ data point.

Figure 28.4 shows the evolution of the dark energy density $\rho_{\rm de}$ predicted by the $\mathtt{w_0w_aCDM}$ model compared to the constant $\rho_{\rm de}$ of ΛCDM. In the $\mathtt{w_0w_aCDM}$ model, $\rho_{\rm de}/\rho_{\rm de,0}$ climbs to a maximum of about 1.1 at $z \simeq 0.5$, then falls back to 1.0 at $z \simeq 1$ and declines slowly towards zero at higher redshift. The bump in the total energy density ($\rho_{\rm tot} = \rho_{\rm de} + \rho_{\rm m}$) produces a minimum in $D_{\rm H}(z) \propto \rho_{\rm tot}^{-1/2}$ and a smoother minimum in $D_{\rm M}(z)$, as seen in the red-dashed curves of Figure 28.3. The decline in $\rho_{\rm de}$ at high redshift is required so that the model reproduces the precisely measured angular scale of CMB anisotropies, which depends on the ratio $r_{\rm s}/D_{\rm M}(z_{\rm rec})$.

This preferred model is physically surprising in at least two respects. First, the value of $w_{\rm a}$ implies rapid evolution of the equation of state, with an order-unity change of w over a $\Delta z \sim 1$ redshift interval. Second, w evolves from $w < -1$ at high redshift to $w > -1$ at low redshift, a "phantom crossing" behavior that cannot arise in dark energy models with a single scalar field [42]. This unusual behavior is not just an artifact of the $w_0 - w_{\rm a}$ parameterization, as analyses of the DESI data with more flexible $w(z)$ models still show a significant preference for phantom cross-

Int. J. Mod. Phys. A 2026.41. Downloaded from www.worldscientific.com
by UNIVERSITY OF CALIFORNIA @ BERKELEY on 09/16/26. Re-
strictly not permitted, except for Open Access articles.

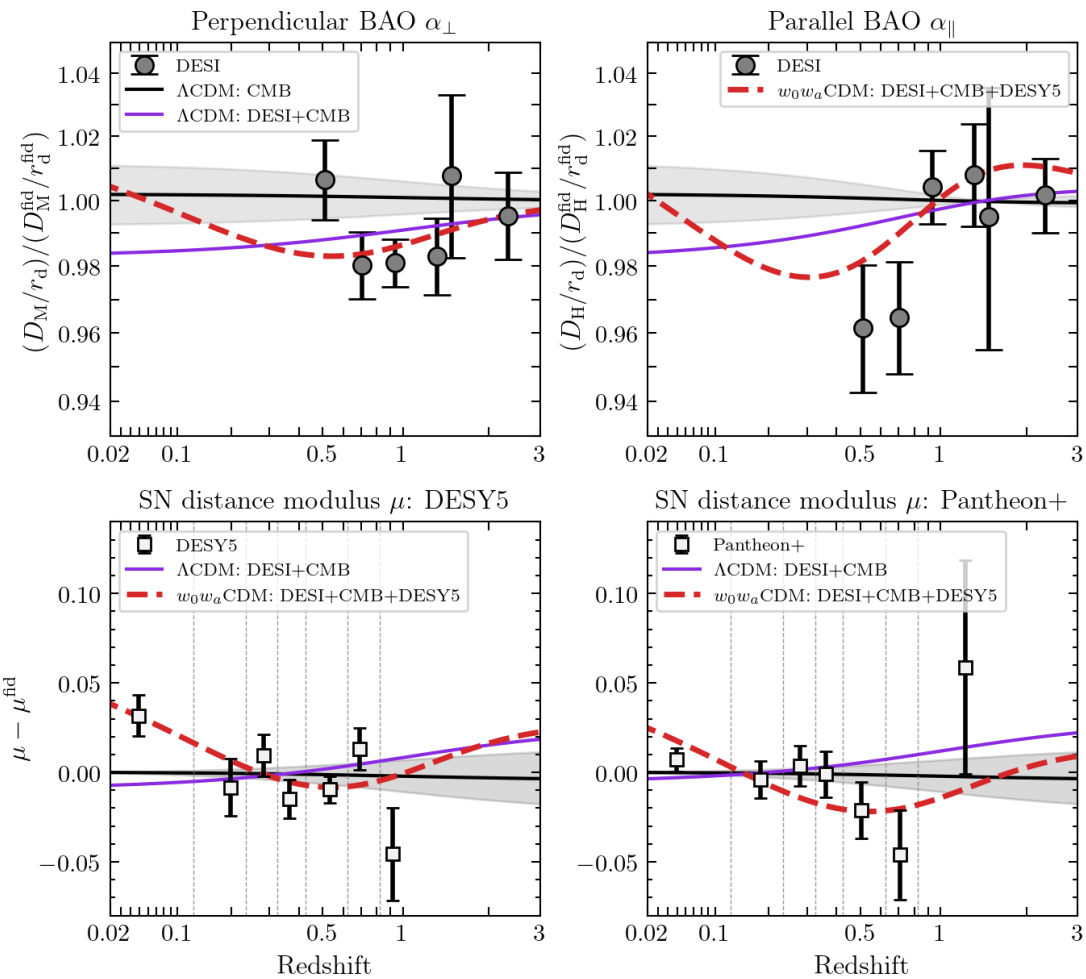

Figure 28.3: Distance-redshift measurements ("Hubble diagram") from BAO and SN, scaled by predictions of the fiducial *Planck* ΛCDM model to highlight subtle deviations, adapted (by Q. Li) from Ref. [37]. Upper panels show BAO measurements transverse (left) and parallel (right) to the line of sight, with gray circles representing the DESI DR2 measurements. Lower panels show binned measurements of the distance modulus (squares) inferred from DES Y5 (left) or Pantheon+ (right). In all panels, the gray band shows the $\pm 1\sigma$ range of the *Planck* predictions assuming ΛCDM, and purple curves show predictions of the ΛCDM model that is the best joint fit to the DESI BAO and *Planck* CMB measurements. Red dashed curves show predictions of a $\mathtt{w_0w_a CDM}$ model with $w_0 = -0.752$, $w_a = -0.86$, the best-fit parameters for the DESI+CMB+DESY5 combination. Because the fiducial SN absolute magnitude is not known *a priori*, data points in the lower panels are free to move up or down by a constant shift in μ; here they have been normalized to give an error-weighted mean of $\mu - \mu_{fid} = 0$, and each model curve is pinned to the average of the SN data. The lowest redshift DES data point disagrees by 0.04 mag (2% in distance) with the prediction of the DESI+CMB ΛCDM model.

ing, and models that are forced to maintain $w \geq -1$ fit the data less well.

Any surprising result merits healthy skepticism, and the DESI findings are no exception. While the statistical significance is only moderate, it comes from measurement methods whose systematic uncertainties are thought to be small and well understood, and are quantified in the analysis. It is possible that either the BAO or CMB systematics have been underestimated, enough to reduce the preference for evolving dark energy to the level of a plausible statistical excursion. Notably, removing CMB lensing from the data vector reduces the reported statistical significance from 3.1σ to 2.7σ. Independent of DESI, the DES Collaboration reports a 3.2σ preference for $\mathtt{w_0w_a CDM}$ over ΛCDM using *Planck* CMB, DES SN, and the DES photometric BAO measurement [43]. There is a moderate "look elsewhere" effect in interpreting these numbers, as these studies could have found other forms of interesting departure from ΛCDM. However, the $w_0 - w_a$ parameterization has been a standard component of dark energy analyses for many years, and the DESI and DES collaborations chose to consider this model before examining their data.

As shown in Figure 28.3, the distance ratio $D_M(z \simeq 0.5)/D_M(z \simeq 0.005)$ is a sharp discriminant between the ΛCDM and $\mathtt{w_0w_a CDM}$ models. Supernovae are the most statistically powerful tool for measuring this ratio. Comparison of the DES and Pantheon+ results highlights the importance of calibrating local SNe relative to those at higher redshift. Here "calibration" encompasses not just the relative flux measurements, which are already challenging because of the large dynamic range, different observing facilities, and redshift-dependent mapping between observed and rest-frame wavelengths, but also the modeling of light-curve shape, intrinsic color variation, dust extinction, and sample biases (see, *e.g.*, [44]). Substantial efforts are underway to improve the calibration and the local SN samples (*e.g.*, [45, 46]). These studies may clarify whether SNe do or do not provide supporting evidence for evolving dark energy, and the samples of well observed SNe at $z > 0.1$ will grow dramatically with the advent of Rubin and *Roman*. Independent of SNe, the statistical precision of the DESI BAO measurements will improve by the end of the survey, and the AP effect at $z \simeq 2$ is another good discriminant between ΛCDM and $\mathtt{w_0w_a CDM}$. Ground-based CMB experiments are now providing independent tests of *Planck* results and somewhat greater statistical leverage on dark energy models. Stage

Int. J. Mod. Phys. A 2026.41. Downloaded from www.worldscientific.com
by UNIVERSITY OF CALIFORNIA @ BERKELEY on 09/16/26. Re-use and distribution is strictly not permitted, except for Open Access articles.

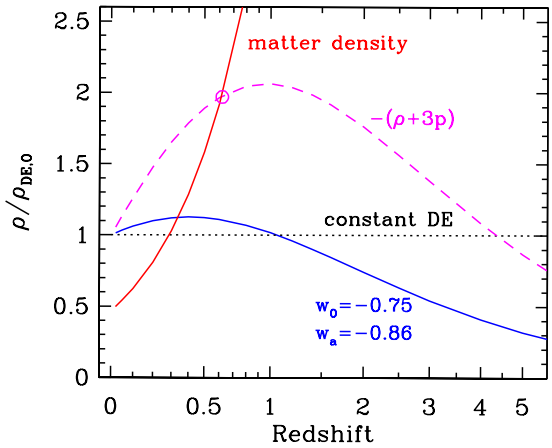

Figure 28.4: Evolution of dark energy in a model with $w_0 = -0.75$, $w_a = -0.86$, the best-fit values from DESI+CMB+DES SN (red-dashed curve of Figure 28.3). The blue solid curve shows the evolution of the dark energy density $\rho_{\rm de}(z)$, while the pink dashed curve shows the combination $-(\rho + 3p)$ that enters the acceleration equation. Cosmic acceleration begins when this curve goes above the matter density (red solid curve), which follows $\rho_{\rm m} \propto (1+z)^3$; this intersection occurs at $z \simeq 0.62$ (pink circle). The dashed horizontal line shows the constant $\rho_{\rm de}$ of the ΛCDM model, which has $-(\rho + 3p)/\rho_{\rm de,0} = 2$ at all times. The redshift axis is scaled as $\ln(1+z)$ to help show low and high redshift behavior simultaneously.

IV weak lensing surveys should also reach the statistical precision needed to discriminate ΛCDM from the $\mathtt{w_0w_a CDM}$ model favored by DESI. Thus, if this model is correct, the statistical evidence for it should grow noticeably, and perhaps dramatically, over the next several years.

28.4.2 *The amplitude of matter clustering*

KiDS, DES, and HSC measure low redshift matter clustering (roughly $z < 1$) through cosmic shear and through "3×2 pt" analyses that combine cosmic shear with galaxy-shear and galaxy-galaxy correlation functions. These measurements provide constraints in the $(\sigma_8, \Omega_{\rm m})$ plane, often summarized in the parameter combination $S_8 \equiv \sigma_8(\Omega_{\rm m}/0.3)^{0.5}$. These analyses can be extended to include constraints from optical, X-ray, or SZ clusters, with mass profiles inferred from cluster-shear correlations. The growing precision and area of CMB lensing maps has made them a competitive tool for measuring galaxy-mass correlations without reliance on optical weak lensing data.

The amplitude of CMB anisotropies is proportional to the amplitude of density fluctuations present at recombination, and by assuming GR and a specified dark energy model one can extrapolate the growth of structure forward to the present day to predict σ_8. Many analyses find $(\sigma_8, \Omega_{\rm m})$ constraints that are consistent with *Planck*-normalized ΛCDM at the 1-2σ level, but most weak lensing measurements are at least somewhat below this prediction, some of them significantly so. For example, in the 2023 edition of this *Review*, we found that an average of weak lensing estimates of S_8 from different experiments gave a value 9.3% below the *Planck* prediction, with a significance of about 3σ if the statistical error was estimated from the dispersion among these six measurements.

The evidence for a discrepancy in S_8 looks weaker than it did two years ago, for several reasons. First, there has been an upward revision in the estimate of S_8 from cosmic shear in the final KiDS data set relative to earlier analyses [30], removing the previous tension with the *Planck*-normalized prediction. Reference [30] attributes this change primarily to improved calibration of photometric redshifts, though several factors may contribute. Second, there is increasing recognition that baryonic feedback effects might be large enough to suppress cosmic shear and galaxy-mass correlations out to scales included in current analyses. Third, the parameterization of intrinsic alignments adopted in many lensing analyses may be overly restrictive, leading to error estimates that are artificially small and correlated across experiments. The range of $(\sigma_8, \Omega_{\rm m})$ constraints from different experiments and analyses remains large, so it is premature to claim good agreement between CMB-normalized predictions and low-redshift measurements. However, there are promising routes for progress in the near future, including final results from DES and HSC, steadily improving measurements from CMB lensing, and RSD measurements from DESI, which should soon be statistically competitive with weak lensing measurements. If GR is correct, then lensing-based measurements and RSD measurements should give consistent answers for σ_8 and $\Omega_{\rm m}$; in modified gravity models, the two measurements could give discrepant results because they respond to different combinations of gravitational potentials.

28.4.3 *The Hubble constant*

A flat ΛCDM model fit to *Planck* CMB data alone predicts $H_0 = (67.4 \pm 0.5)\ {\rm km\,s^{-1}\,Mpc^{-1}}$ (see Sec. 29 of this *Review*). This prediction and its error bar are sensitive to the assumptions of constant dark energy and a flat Universe. However, by adding BAO and supernova data one can construct an "inverse distance ladder" to measure H_0 precisely, even with a general dark energy model and free curvature [47]. Reference [36] applies this approach to obtain $H_0 = (68.2 \pm 0.81)\ {\rm km\,s^{-1}\,Mpc^{-1}}$, and other analyses combining CMB, BAO, and SN data give similar results. As discussed in Sec. 25.3.1 of this *Review*, some of the recent H_0 measurements from low-redshift data yield higher values. For example, Ref. [48] uses a distance ladder based on Cepheid calibration of Type Ia supernova luminosities to find $H_0 = (73.0 \pm 1.0)\ {\rm km\,s^{-1}\,Mpc^{-1}}$, in clear tension with cosmologically inferred values. New observations with the *James Webb Space Telescope* (*JWST*) allow Cepheid-based distance measurements with higher angular resolution and flux sensitivity, and their consistency with distances from *Hubble Space Telescope* is an important check on the robustness of these measurements [49]. However, some analyses based on tip-of-the-red-giant-branch (TRGB) or J-region asymptotic giant branch (JAGB) distance indicators give lower H_0 estimates consistent with the cosmological values [50].

The experimental situation with H_0 remains uncertain, though there are prospects for improvement with further *JWST* studies and *Gaia*-based parallaxes to more Galactic Cepheids. If the resolution lies in new physics rather than measurement errors, then this is probably physics that operates in the *pre-recombination* Universe, rescaling the BAO standard ruler in a way that shifts the ΛCDM and inverse-distance-ladder values upward. "Early dark energy" models can achieve this effect by increasing the early expansion rate, but these models must be finely tuned to satisfy constraints from the damping tail of CMB anisotropies and the shape of the galaxy power spectrum.

28.5 Summary and Outlook

The discovery of cosmic acceleration three decades ago came from a handful of expansion history and clustering measurements with roughly 10% precision, soon augmented by a more precise geometrical constraint from the CMB acoustic peak. Today's dark energy experiments have achieved $\sim 1\%$ measurements of the distance scale and expansion rate over a wide range of redshift ($0 \le z < 2.5$) and 2–5% measurements of matter clustering at $z < 1$. Contemporary CMB experiments also provide much more stringent constraints on the matter and baryon densities, the pre-recombination expansion history, and the amplitude and shape of the primordial power spectrum. At this higher level of precision and detail, the ΛCDM model is showing cracks. It is not clear which if any of those cracks are signs of new physics and which are signs of unrecognized or underestimated systematics.

Stage IV experiments hold the prospect of an order-of-magnitude gain in statistical power, and analyses that better exploit non-linear scales can sharpen constraints from existing and future data sets. Realizing these statistical gains requires comparable improvements in control of experimental and theoretical systematics. This is a challenging task, but large data sets allow new approaches to identifying and mitigating systematics, *e.g.*, by dividing source, lens, or supernova populations into subsets and testing for consistency, or by marginalizing over more flexible models of systematic effects. Stage IV surveys also offer substan-

Int. J. Mod. Phys. A 2026.41. Downloaded from www.worldscientific.com by UNIVERSITY OF CALIFORNIA @ BERKELEY on 09/16/26. Re-[redacted]strictly not permitted, except for Open Access articles.

tial improvements in data quality, as well as data quantity.

If any of the currently suggested deviations from ΛCDM are real — 1–2% in the expansion rate at $z \simeq 0.5$, 5–10% in H_0 or S_8 — then Stage IV experiments should be able to map these deviations in detail. For cosmological models that assume GR and minimally coupled dark energy, the observable effects are almost entirely captured by the expansion history $H(z)$, and different observational probes should yield consistent results for this governing function. However, the phenomenology could be much richer in models with modified gravity, or extensions to particle physics such as decaying dark matter or coupling between dark energy and other components. With a tightly constrained $H(z)$ from BAO+SN+CMB, weak lensing and RSD measurements can map the redshift, scale, and environment dependence of matter clustering, which could either reveal this rich phenomenology or set tight limits on departures from minimal GR-based models.

Of course, the tensions described in Section 28.4 may dissipate as the data and analysis methods improve. If so, the next generation of experiments could still reveal deviations from ΛCDM that are within the uncertainties of current data, though the detail with which these smaller deviations can be characterized will be more limited. Alternatively, ΛCDM could be the correct cosmological model, or so close that it is observationally indistinguishable, which would leave us with a relatively simple but frustratingly incomplete picture of dark energy and cosmic acceleration. We do not yet know which of these possibilities describes the Universe that we live in. We can hope that our experiments will reveal the cosmological equivalent of the anomalous precession of Mercury, and that discrepancies with our theoretical predictions will guide us to a new understanding of energy, or gravity, or the spacetime structure of the cosmos.

References

[1] A. Einstein, Sitzungsber. Preuss. Akad. Wiss. Berlin (Math. Phys.), 142 (1917).

[2] Ya. B. Zel'dovich, A. Krasinski and Ya. B. Zeldovich, Sov. Phys. Usp. **11**, 381 (1968), [Gen. Rel. Grav.40,1557(2008); Usp. Fiz. Nauk95,209(1968)].

[3] A. Friedman, Z. Phys. **10**, 377 (1922), [Gen. Rel. Grav.31,1991(1999)].

[4] G. Lemaître, Annales de la Societe Scietifique de Bruxelles **47**, 49 (1927).

[5] E. Hubble, Proc. Nat. Acad. Sci. **15**, 168 (1929).

[6] A. Einstein and W. de Sitter, Proc. Nat. Acad. Sci. **18**, 213 (1932).

[7] For background and definitions, see Big-Bang Cosmology – Sec. 22 of this *Review*.

[8] A. G. Riess *et al.* (Supernova Search Team), Astron. J. **116**, 1009 (1998), [arXiv:astro-ph/9805201].

[9] S. Perlmutter *et al.* (Supernova Cosmology Project), Astrophys. J. **517**, 565 (1999), [arXiv:astro-ph/9812133].

[10] P. de Bernardis *et al.* (Boomerang), Nature **404**, 955 (2000), [arXiv:astro-ph/0004404].

[11] S. Hanany *et al.*, Astrophys. J. **545**, L5 (2000), [arXiv:astro-ph/0005123].

[12] D. H. Weinberg *et al.*, Phys. Rept. **530**, 87 (2013), [arXiv:1201.2434].

[13] C. Wetterich, Nucl. Phys. **B302**, 668 (1988), [arXiv:1711.03844].

[14] A. Joyce *et al.*, Phys. Rept. **568**, 1 (2015), [arXiv:1407.0059].

[15] S. M. Carroll *et al.*, Phys. Rev. **D70**, 043528 (2004), [arXiv:astro-ph/0306438].

[16] G. R. Dvali, G. Gabadadze and M. Porrati, Phys. Lett. **B485**, 208 (2000), [hep-th/0005016].

[17] C.M. Will, Living Reviews in Relativity, **9**, 3 (2006). See also the chapter on Experimental Tests of Gravitational Theory — in this *Review*.

[18] J. Wang, L. Hui and J. Khoury, Phys. Rev. Lett. **109**, 241301 (2012), [arXiv:1208.4612].

[19] M. Fairbairn and A. Goobar, Phys. Lett. **B642**, 432 (2006), [arXiv:astro-ph/0511029]; Y.-S. Song, I. Sawicki and W. Hu, Phys. Rev. **D75**, 064003 (2007), [arXiv:astro-ph/0606286]; C. Blake *et al.*, Mon. Not. Roy. Astron. Soc. **415**, 2876 (2011), [arXiv:1104.2948].

[20] T. Baker *et al.*, Phys. Rev. Lett. **119**, 25, 251301 (2017), [arXiv:1710.06394].

[21] E. V. Linder, Phys. Rev. **D72**, 043529 (2005), [arXiv:astro-ph/0507263].

[22] This is essentially the FoM proposed in the Dark Energy Task Force (DETF) report, A. Albrecht *et al.*, `astro-ph/0609591`, though they based their FoM on the area of the 95% confidence contour in the $w_0 - w_a$ plane.

[23] T. Baker *et al.*, Rev. Mod. Phys. **93**, 1, 015003 (2021), [arXiv:1908.03430].

[24] For high accuracy, the impact of acoustic oscillations must be computed with a full Boltzmann code, but the simple integral for r_s captures the essential physics and the scaling with cosmological parameters.

[25] R. A. Sunyaev and Ya. B. Zeldovich, Astrophys. Space Sci. **7**, 3 (1970).

[26] D. Brout *et al.*, Astrophys. J. **938**, 2, 110 (2022), [arXiv:2202.04077].

[27] S.-F. Chen *et al.*, Mon. Not. Roy. Astron. Soc. **534**, 1, 544 (2024), [arXiv:2402.14070].

[28] C. Alcock and B. Paczynski, Nature **281**, 358 (1979).

[29] A. Albrecht *et al.* (2006), [arXiv:astro-ph/0609591].

[30] A. H. Wright *et al.* (2025), [arXiv:2503.19441].

[31] T. M. C. Abbott *et al.* (DES), Phys. Rev. D **105**, 2, 023520 (2022), [arXiv:2105.13549].

[32] R. Dalal *et al.*, Phys. Rev. D **108**, 12, 123519 (2023), [arXiv:2304.00701].

[33] D. Scolnic *et al.*, Astrophys. J. **938**, 2, 113 (2022), [arXiv:2112.03863].

[34] D. Rubin *et al.*, Astrophys. J. **986**, 2, 231 (2025), [arXiv:2311.12098].

[35] T. M. C. Abbott *et al.* (DES), Astrophys. J. Lett. **973**, 1, L14 (2024), [arXiv:2401.02929].

[36] S. Alam *et al.* (eBOSS), Phys. Rev. D **103**, 8, 083533 (2021), [arXiv:2007.08991].

[37] M. Abdul Karim *et al.* (DESI) (2025), [arXiv:2503.14738].

[38] J. C. Cuillandre *et al.* (Euclid), Astron. Astrophys. **697**, A6 (2025), [arXiv:2405.13496].

[39] Ž. Ivezić *et al.* (LSST), Astrophys. J. **873**, 2, 111 (2019), [arXiv:0805.2366].

[40] G. Zasowski *et al.* (2025), [arXiv:2505.10574].

[41] N. Aghanim *et al.* (Planck) (2018), [arXiv:1807.06209].

[42] W. Hu, Phys. Rev. D **71**, 047301 (2005), [arXiv:astro-ph/0410680].

[43] T. M. C. Abbott *et al.* (DES) (2025), [arXiv:2503.06712].

[44] M. Vincenzi *et al.* (DES) (2025), [arXiv:2501.06664].

[45] B. Popovic *et al.* (2025), [arXiv:2506.05471].

[46] M. Acevedo *et al.* (2025), [arXiv:2508.10877].

[47] E. Aubourg *et al.*, Phys. Rev. **D92**, 12, 123516 (2015), [arXiv:1411.1074].

[48] A. G. Riess *et al.*, Astrophys. J. Lett. **934**, 1, L7 (2022), [arXiv:2112.04510].

[49] A. G. Riess *et al.*, Astrophys. J. Lett. **962**, 1, L17 (2024), [arXiv:2401.04773].

[50] W. L. Freedman *et al.*, Astrophys. J. **985**, 2, 203 (2025), [arXiv:2408.06153].

Int. J. Mod. Phys. A 2026.41. Downloaded from www.worldscientific.com
by UNIVERSITY OF CALIFORNIA @ BERKELEY on 09/16/26. Re-use and distribution is strictly not permitted, except for Open Access articles.

29. Cosmic Microwave Background

Revised August 2025 by D. Scott (U. of British Columbia) and G.F. Smoot (HKUST; UC Berkeley; LBNL; DIPC; Paris U.).

29.1 Introduction

The photon number and energy content in the electromagnetic radiation from beyond our Galaxy are dominated by the cosmic microwave background (CMB), discovered in 1965 [1]. Its spectral distribution is well described by a blackbody function with $T = 2.7255\,\mathrm{K}$, which is a principal pillar of the hot Big Bang model for the Universe, with the lack of any observed deviations from a Planckian spectrum constraining physical processes over cosmic history at redshifts $z \lesssim 10^7$ (see earlier versions of this review).

The key information in the CMB sky is extracted from the observed angular variation of its temperature (or intensity) correlations, and to a growing extent polarization [2]. After the first detection of CMB anisotropies by the Cosmic Background Explorer (*COBE*) satellite in 1992 [3], there has been intense activity to map the sky at increasing levels of sensitivity and angular resolution by ground-based and balloon-borne measurements. In 2003 the first results were obtained from NASA's Wilkinson Microwave Anisotropy Probe (*WMAP*) [4], which were improved upon by analyses of data added every 2 years, culminating in the 9-year results [5]. 2013 saw the first results [6] from the third generation CMB satellite, ESA's *Planck* mission [7], which were enhanced by results from the 2015 *Planck* data release [8, 9], and then the final 2018 *Planck* data release [10, 11]. Additionally, CMB anisotropies have been extended to smaller angular scales by ground-based experiments, particularly the Atacama Cosmology Telescope (ACT) [12] and the South Pole Telescope (SPT) [13]. Together these observations have led to a stunning confirmation of the 'Standard Model of Cosmology.' In combination with other astrophysical data, the CMB anisotropy measurements place quite precise constraints on a number of cosmological parameters, and have launched us into an era of precision cosmology. After more than half a century, the program to map temperature anisotropies is effectively wrapping up, and attention is increasingly focusing on polarization measurements, which promise further tests of fundamental physics.

29.2 CMB Spectrum

The spectrum of the microwave background is very precisely that of blackbody radiation, whose temperature evolves with redshift as $T(z) = T_0(1+z)$ in an expanding Universe. As a direct confirmation of its cosmological origin, this relationship has been tested by measuring the strengths of emission and absorption lines in high-redshift systems (*e.g.*, Ref. [14]).

Measurements of the spectrum are consistent with a blackbody distribution over more than three decades in frequency (there is a claim by ARCADE [15] of a possible unexpected extragalactic emission signal at low frequency, but the interpretation is debated [16]). All viable cosmological models predict a very nearly Planckian spectrum to within the current observational limits. Because of this, measurements of deviations from a blackbody spectrum have received little attention in recent years, with only a few exceptions. However, that situation will eventually change if proposed experiments [17] are built that have the potential to dramatically improve early Universe energy release constraints. It now seems feasible to probe spectral distortion mechanisms that are *required* in the standard picture, such as those arising from the damping and dissipation of relatively small-scale primordial perturbations, or the average effect of inverse Compton scattering. A more ambitious goal would be to reach the precision needed to detect the residual lines from the cosmological recombination of hydrogen and helium and hence to test whether conditions at $z \gtrsim 1000$ accurately follow those in the standard picture [18].

29.3 Description of CMB Anisotropies

Observations show that the CMB contains temperature anisotropies at the 10^{-5} level and polarization anisotropies at the 10^{-6} (and lower) level, over a wide range of angular scales. These anisotropies are usually expressed using a spherical harmonic expansion of the CMB sky:

$$T(\theta,\phi) = \sum_{\ell m} a_{\ell m} Y_{\ell m}(\theta,\phi) \tag{29.1}$$

(with the linear polarization pattern written in a similar way using the so-called spin-2 spherical harmonics). Increasing angular resolution requires that the expansion goes to higher multipoles. Because only very weak phase correlations are observed in the CMB sky and no preferred direction is seen, the vast majority of the cosmological information is found in the temperature 2-point function, *i.e.*, the variance as a function only of angular separation. Equivalently, the anisotropy power per unit $\ln \ell$ is $\ell \sum_m |a_{\ell m}|^2/4\pi$.

29.3.1 *The Monopole*

The CMB has a mean temperature of $T_\gamma = 2.7255 \pm 0.0006\,\mathrm{K}$ (1σ) [19], which can be considered as the monopole component of CMB maps, a_{00}. Because all mapping experiments involve difference measurements, they are insensitive to this average level; monopole measurements can only be made with absolute temperature devices, such as the FIRAS instrument on the *COBE* satellite [20]. The measured kT_γ is equivalent to $0.234\,\mathrm{meV}$ or $4.60 \times 10^{-10}\, m_e c^2$. A blackbody of the measured temperature has a number density $n_\gamma = (2\zeta(3)/\pi^2)\, T_\gamma^3 \simeq 411\,\mathrm{cm}^{-3}$, energy density $\rho_\gamma = (\pi^2/15)\, T_\gamma^4 \simeq 4.64 \times 10^{-34}\,\mathrm{g\,cm}^{-3} \simeq 0.260\,\mathrm{eV\,cm}^{-3}$, and a fraction of the critical density $\Omega_\gamma \simeq 5.38 \times 10^{-5}$.

29.3.2 *The Dipole*

The largest anisotropy is in the $\ell = 1$ (dipole) first spherical harmonic, with amplitude $3.3621 \pm 0.0010\,\mathrm{mK}$ [10]. The dipole is interpreted to be the result of the Doppler boosting of the monopole caused by the Solar System motion relative to the nearly isotropic blackbody field, as broadly confirmed by measurements of the radial velocities of local galaxies (*e.g.*, Ref. [21]); the intrinsic (non-Doppler) part of the signal is expected to be 2 orders of magnitude smaller (and fundamentally difficult to distinguish). The motion of an observer with velocity $\beta \equiv v/c$ relative to an isotropic Planckian radiation field of temperature T_0 produces a Lorentz-boosted temperature pattern

$$\begin{aligned} T(\theta) &= T_0(1-\beta^2)^{1/2}/(1-\beta\cos\theta) \\ &\simeq T_0\, \left[1 + \beta\cos\theta + \left(\beta^2/2\right)\cos 2\theta + \mathrm{O}\left(\beta^3\right)\right]. \end{aligned} \tag{29.2}$$

At every point in the sky, one observes a blackbody spectrum, with temperature $T(\theta)$. The spectrum of the dipole has been confirmed to be the differential of a blackbody spectrum [22]. At higher order there are additional effects arising from aberration and from modulation of the anisotropy pattern, which have also been observed [23].

The implied velocity for the Solar System barycenter is $v = 369.82 \pm 0.11\,\mathrm{km\,s}^{-1}$, assuming a value $T_0 = T_\gamma$, towards Galactic coordinates $(l, b) = (264.021^\circ \pm 0.011^\circ, 48.253^\circ \pm 0.005^\circ)$ [10]. This Solar System motion implies a velocity for the Galaxy and the Local Group of galaxies relative to the CMB of $v_{\mathrm{LG}} = 620 \pm 15\,\mathrm{km\,s}^{-1}$ towards $(l, b) = (271.9^\circ \pm 2.0^\circ, 29.6^\circ \pm 1.4^\circ)$ [10]; most of the error comes from uncertainty in the velocity of the Solar System relative to the Local Group.

The dipole is a frame-dependent quantity, and one can thus determine the 'CMB frame' (in some sense this is a special frame) as that in which the CMB dipole would be zero. Any velocity of the receiver relative to the Earth and the Earth around the Sun is removed for the purposes of CMB anisotropy studies, while our velocity relative to the Local Group of galaxies and the Local Group's motion relative to the CMB frame are normally removed for cosmological studies. The dipole is now routinely used as a primary calibrator for mapping experiments, either via the time-varying orbital motion of the Earth, or through the cosmological dipole measured by satellite experiments.

29.3.3 *Higher-Order Multipoles*

The variations in the CMB temperature at higher multipoles ($\ell \geq 2$) are interpreted as being mostly the result of density perturbations in the early Universe, manifesting themselves at the

Int. J. Mod. Phys. A 2026.41. Downloaded from www.worldscientific.com by UNIVERSITY OF CALIFORNIA @ BERKELEY on 09/16/26. Re-use strictly not permitted, except for Open Access articles.

epoch of the last scattering of the CMB photons. In the hot Big Bang picture, the expansion of the Universe cools the plasma so that by a redshift $z \simeq 1100$ (with little dependence on the details of the model), the hydrogen and helium nuclei can bind electrons into neutral atoms, a process usually referred to as 'recombination' [24]. Before this epoch, the CMB photons were tightly coupled to electrons through Compton scattering (and the electrons were coupled by Coulomb interactions with the charged baryons), while afterwards they could freely stream towards us. By measuring the $a_{\ell m}$s we are thus learning directly about physical conditions in the early Universe.

A statistically-isotropic sky means that all ms are equivalent, *i.e.*, there is no preferred axis, so that the temperature correlation function between two positions on the sky depends only on angular separation and not orientation. Together with the assumption of Gaussian statistics (*i.e.*, no correlations between the modes), the 2-point function of the temperature field (or equivalently the power spectrum in ℓ) then fully characterizes the anisotropies. The power summed over all ms at each ℓ is $(2\ell+1)C_\ell/(4\pi)$, where $C_\ell \equiv \left\langle |a_{\ell m}|^2 \right\rangle$. Thus, averages of $a_{\ell m}$s over m can be used as estimators of the C_ℓs to constrain their expectation values, which are the quantities predicted by a theoretical model. For an idealized full-sky observation, the variance of each measured C_ℓ (*i.e.*, the variance of the variance) is $[2/(2\ell+1)]C_\ell^2$. This sampling uncertainty (known as 'cosmic variance') comes about because each C_ℓ is χ^2 distributed with $(2\ell+1)$ degrees of freedom for our observable volume of the Universe. For fractional sky coverage, $f_{\rm sky}$, this variance is increased by $1/f_{\rm sky}$ and the modes become partially correlated.

It is important to understand that theories predict the expectation value of the power spectrum, whereas our sky is a *single* realization. Hence, the cosmic variance is an unavoidable source of uncertainty when constraining models; it dominates the scatter at lower ℓs, while the effects of instrumental noise and resolution dominate at higher ℓs [25].

Theoretical models generally predict that the $a_{\ell m}$ modes are Gaussian random fields to high precision, matching the empirical tests, *e.g.*, standard slow-roll inflation's non-Gaussian contribution is expected to be at least an order of magnitude below current observational limits [26]. Although non-Gaussianity of various forms is possible in early Universe models, tests show that Gaussianity is an extremely good simplifying approximation [27]. The only current indications of any non-Gaussianity or statistical anisotropy are some relatively weak signatures at large scales, seen in both *WMAP* [28] and *Planck* data [29], but not of high enough significance to reject the simplifying assumption. Nevertheless, models that deviate from the inflationary slow-roll conditions can have measurable non-Gaussian signatures. So while the current observational limits make the power spectrum the dominant probe of cosmology, it is worth noting that higher-order correlations are tools for constraining otherwise viable theories.

29.3.4 *Angular Resolution and Binning*

There is no one-to-one conversion between multipole ℓ and the angle subtended by a particular spatial scale projected onto the sky. However, crudely speaking, a single spherical harmonic $Y_{\ell m}$ corresponds to angular variations of $\theta \sim \pi/\ell$. CMB maps contain anisotropy information from the size of the map (or in practice some fraction of that size) down to the beam-size of the instrument, σ (the standard deviation of the beam, in radians). One can think of the effect of a Gaussian beam as rolling off the power spectrum with the function $\mathrm{e}^{-\ell(\ell+1)\sigma^2}$.

For less than full sky coverage, the ℓ modes become correlated. Hence, experimental results are usually quoted as a series of 'band powers,' defined as estimators of $\ell(\ell+1)C_\ell/2\pi$ over different ranges of ℓ. Because of the strong foreground signals in the Galactic plane, even 'all-sky' surveys, such as *WMAP* and *Planck*, involve a cut sky. The amount of binning required to obtain uncorrelated estimates of power also depends on the map size.

29.4 Cosmological Parameters

The current 'Standard Model' of cosmology contains around 10 free parameters, only six of which are required to have non-null values (see The Cosmological Parameters—Sec. 25 of this *Review*). The basic framework is the Friedmann-Robertson-Walker (FRW) metric (*i.e.*, a Universe that is homogeneous and isotropic on large scales), perturbed with density variations laid down at early times and evolving into today's structures (see Big-Bang cosmology—Sec. 22 of this *Review*). The most general possible set of density variations is a linear combination of an adiabatic density perturbation and some isocurvature perturbations. Adiabatic means that there is no change to the entropy per particle for each species, *i.e.*, $\delta\rho/\rho$ for matter is $(3/4)\delta\rho/\rho$ for radiation. Isocurvature means that the set of individual density perturbations adds to zero, for example, matter perturbations compensate radiation perturbations so that the total energy density remains unperturbed, *i.e.*, $\delta\rho$ for matter is $-\delta\rho$ for radiation. These different modes give rise to distinct (temporal) phases during growth, with those of the adiabatic scenario being fully consistent with the data. Models that generate mainly isocurvature type perturbations (such as most topological defect scenarios) are not viable. However, an admixture of the adiabatic mode with up to 1.7% isocurvature contribution (depending on details of the mode) is still allowed [30].

29.4.1 *Initial Condition Parameters*

Within the adiabatic family of models, there is, in principle, a free function describing the variation of comoving curvature perturbations, $\mathcal{R}(\mathbf{x}, t)$. The great virtue of $\mathcal{R}$ is that it is constant in time on super-horizon scales for a purely adiabatic perturbation. There are physical reasons to anticipate that the variance of these perturbations will be described well by a power law in scale, *i.e.*, in Fourier space $\left\langle |\mathcal{R}|_k^2 \right\rangle \propto k^{n_{\rm s}-4}$, where k is wavenumber and $n_{\rm s}$ is the spectral index as usually defined. So-called 'scale-invariant' initial conditions (meaning gravitational potential fluctuations that are independent of k) correspond to $n_{\rm s} = 1$. In inflationary models [31] (see Inflation—Sec. 23 of this *Review*), perturbations are generated by quantum fluctuations, which are set by the energy scale of inflation together with the slope and higher derivatives of the inflationary potential. One generally expects that the Taylor series expansion of $\ln \mathcal{R}_k(\ln k)$ has terms of steadily decreasing size. For the simplest models, there are thus two parameters describing the initial conditions for density perturbations, namely the amplitude and slope of the power spectrum. These can be explicitly defined, for example, through

$$\mathcal{P}_{\mathcal{R}}^2 \equiv k^3 \left\langle |\mathcal{R}|_k^2 \right\rangle / 2\pi^2 \simeq A_{\rm s}\, (k/k_0)^{n_{\rm s}-1}\,, \qquad (29.3)$$

with $A_{\rm s} \equiv \mathcal{P}_{\mathcal{R}}^2(k_0)$ and $k_0 = 0.05\,\mathrm{Mpc}^{-1}$, say. There are other equally valid definitions of the amplitude parameter (see also Secs. 22, 23, and 25 of this *Review*), and we caution that the relationships between some of them can be cosmology-dependent. In slow-roll inflationary models, this normalization is proportional to the combination $V^3/(V')^2$, for the inflationary potential $V(\phi)$. The slope $n_{\rm s}$ also involves V'', and so the combination of $A_{\rm s}$ and $n_{\rm s}$ can constrain potentials.

Inflation generates tensor (gravitational wave) modes, as well as scalar (density perturbation) modes. This property introduces another parameter, measuring the amplitude of a possible tensor component, or equivalently the ratio of the tensor to scalar contributions. The tensor amplitude is $A_{\rm t} \propto V$, and thus one expects a larger gravitational wave contribution in models where inflation happens at higher energies. The tensor power spectrum also has a slope, often denoted $n_{\rm t}$, but since this seems unlikely to be measured in the near future (and there is also a consistency relation with tensor amplitude), it is sufficient for now to focus only on the amplitude of the gravitational wave component. It is most common to define the tensor contribution through r, the ratio of tensor to scalar perturbation spectra at some fixed value of k (*e.g.*, $k = 0.002\,\mathrm{Mpc}^{-1}$ or $k = 0.05\,\mathrm{Mpc}^{-1}$, although it was historically defined in terms of the ratio of contributions at $\ell = 2$). Different inflationary potentials will lead to different predictions, *e.g.*, for 50 e-folds, $\lambda\phi^4$ inflation gives $r = 0.32$ and $m^2\phi^2$ inflation gives $r = 0.16$ (both now strongly disfavored by the data), while other models can have arbitrarily small values of r. In any case, whatever the specific definition, and whether they come from inflation or something else, the 'initial conditions' give

Int. J. Mod. Phys. A 2026.41. Downloaded from www.worldscientific.com
by UNIVERSITY OF CALIFORNIA @ BERKELEY on 09/16/26. Re-use and distribution is strictly not permitted, except for Open Access articles.

rise to a minimum of three parameters, A_s, n_s, and r.

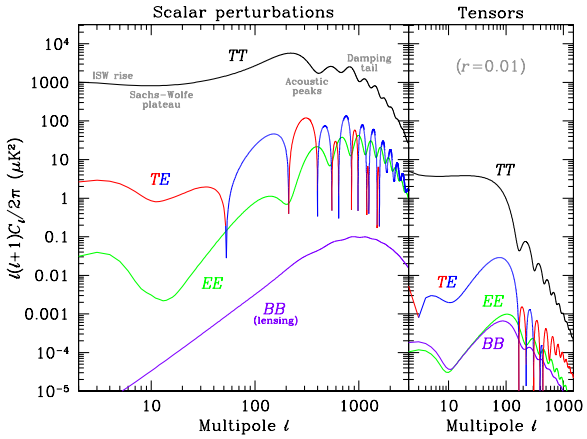

Figure 29.1: Theoretical CMB anisotropy power spectra, using the best-fitting ΛCDM model from *Planck*, calculated using `CAMB`. The panel on the left shows the theoretical expectation for scalar perturbations, while the panel on the right is for tensor perturbations, with an amplitude set to $r = 0.01$ for illustration. Note that the horizontal axis is logarithmic here. For the well-measured scalar TT spectrum, four regions, each covering roughly a decade in ℓ, are labeled as in the text: the ISW rise; Sachs-Wolfe plateau; acoustic peaks; and damping tail. The TE cross-correlation power spectrum changes sign, indicated here by plotting the absolute value, but switching color for the negative parts.

29.4.2 *Background Cosmology Parameters*

The FRW cosmology requires an expansion parameter (the Hubble constant, H_0, often represented through $H_0 = 100\,h\,\mathrm{km\,s^{-1}Mpc^{-1}}$) and several parameters to describe the matter and energy content of the Universe. These are usually given in terms of the critical density, *i.e.*, for species 'x,' $\Omega_x \equiv \rho_x/\rho_{\rm crit}$, where $\rho_{\rm crit} \equiv 3H_0^2/8\pi G$. Since physical densities $\rho_x \propto \Omega_x h^2 \equiv \omega_x$ are what govern the physics of the CMB anisotropies, it is these ωs that are best constrained by CMB data. In particular, CMB observations constrain $\Omega_b h^2$ for baryons and $\Omega_c h^2$ for cold dark matter (with $\rho_m = \rho_c + \rho_b$ for the matter sum).

The contribution of a cosmological constant Λ (or other form of dark energy, see Dark Energy—Sec. 28) is usually included, together with a parameter that quantifies the curvature, $\Omega_K \equiv 1 - \Omega_{\rm tot}$, where $\Omega_{\rm tot} = \Omega_m + \Omega_\Lambda$. The radiation content, while in principle a free parameter, is precisely enough determined by the measurement of T_γ that it can be considered fixed, making a $< 10^{-4}$ contribution to $\Omega_{\rm tot}$ today.

Astrophysical processes at relatively low redshift can also affect the C_ℓs, with a particularly significant influence during reionization. The Universe became reionized at some redshift z_i, long after recombination, affecting the CMB when it passed through the integrated Thomson-scattering optical depth:

$$\tau = \int_0^{z_i} \sigma_T n_e(z) \frac{dt}{dz} dz, \tag{29.4}$$

where σ_T is the Thomson cross-section, $n_e(z)$ is the number density of free electrons (which depends on astrophysics), and dt/dz is fixed by the background cosmology. In principle, τ could be determined from the small-scale matter power spectrum, together with the physics of structure formation and radiative feedback processes; however, because this is a sufficiently intractable calculation, in practice τ needs to be considered as a free parameter.

Thus, we have eight basic cosmological parameters, namely A_s, n_s, r, h, $\Omega_b h^2$, $\Omega_c h^2$, $\Omega_{\rm tot}$, and τ. One can add additional parameters to this list, particularly when using the CMB in combination with other data sets. The next most relevant ones might be: $\Omega_\nu h^2$, the massive neutrino contribution; w ($\equiv p/\rho$), the equation of state parameter for the dark energy; and $dn_s/d\ln k$, measuring deviations from a constant spectral index. To these 11 one could of course add further parameters describing additional physics, such as details of the reionization process, features in the initial power spectrum, a sub-dominant contribution of isocurvature modes, *etc.*

As well as these underlying parameters, there are other (dependent) quantities that can be obtained from them. Such derived parameters include the actual Ωs of the various components (*e.g.*, Ω_m), the variance of density perturbations at particular scales (*e.g.*, σ_8), the angular scale of the sound horizon (θ_*), the age of the Universe today (t_0), the age of the Universe at recombination, reionization, *etc.* (see The Cosmological Parameters—Sec. 25).

29.5 Physics of Anisotropies

The cosmological parameters affect the anisotropies through the well understood physics of the evolution of linear perturbations within a background FRW cosmology. There are very effective, fast, and publicly-available software codes for computing the CMB temperature, polarization, and matter power spectra, *e.g.*, `CMBFAST` [32], `CAMB` [33], and `CLASS` [34]. These have been tested over a wide range of cosmologies and are considered to be accurate to much better than the 1% level [35], so that numerical errors are less than 10% of the parameter uncertainties for *Planck* [6].

For pedagogical purposes, it is easiest to focus on the temperature anisotropies, before moving to the polarization power spectra. A description of the physics underlying the C_ℓ^{TT}s can be separated into four main regions (the first two combined below), as shown in the top left part of Fig. 29.1.

29.5.1 *The ISW Rise, $\ell \lesssim 10$, and Sachs-Wolfe Plateau, $10 \lesssim \ell \lesssim 100$*

The horizon scale (or more precisely, the angle subtended by the Hubble radius) at last scattering corresponds to $\ell \simeq 100$. Anisotropies at larger scales have not evolved significantly, and hence directly reflect the 'initial conditions.' Temperature variations are $\delta T/T = -(1/5)\mathcal{R}(\mathbf{x}_{\rm LSS}) \simeq (1/3)\delta\phi/c^2$, where $\delta\phi$ is the perturbation to the gravitational potential, evaluated on the last-scattering surface (LSS). This is a result of the combination of gravitational redshift and intrinsic temperature fluctuations, and is usually referred to as the Sachs-Wolfe effect [36].

Assuming that a nearly scale-invariant spectrum of curvature (and corresponding density) perturbations was laid down at early times (*i.e.*, $n_s \simeq 1$, meaning equal power per decade in k), then $\ell(\ell+1)C_\ell \simeq$ constant at low ℓs. This predicted near-flatness is hard to see unless the multipole axis is plotted logarithmically (as in Fig. 29.1, and part of Fig. 29.2).

Time variation of the potentials (*i.e.*, time-dependent metric perturbations) at late times leads to an upturn in the C_ℓs in the lowest several multipoles; any deviation from a total equation of state $w = 0$ has such an effect. So the dominance of the dark energy at low redshift (see Dark Energy—Sec. 28) makes the lowest ℓs rise above the plateau. This is usually called the integrated Sachs-Wolfe effect (or ISW rise), since it comes from the line integral of $\dot\phi$; it has been confirmed through correlations between the large-angle anisotropies and large-scale structure [37]. Specific models can also give additional contributions at low ℓ (*e.g.*, perturbations in the dark-energy component itself [38]), but typically these are buried in the cosmic variance.

In principle, the mechanism that produces primordial perturbations could generate scalar, vector, and tensor modes. However, the vector (vorticity) modes decay with the expansion of the Universe. The tensors (transverse trace-free perturbations to the metric) generate temperature anisotropies through the integrated effect of the locally-anisotropic expansion of space. Since the tensor modes also redshift away after they enter the horizon, they contribute only to angular scales above about 1° (see Fig. 29.1). Hence, some fraction of the low-ℓ signal could be due to a gravitational wave contribution, although small amounts of tensors are essentially impossible to discriminate from other effects that might raise the level of the plateau. Nevertheless, the tensors *can* be distinguished using polarization information (see Sec. 29.7).

Int. J. Mod. Phys. A 2026.41. Downloaded from www.worldscientific.com
by UNIVERSITY OF CALIFORNIA @ BERKELEY on 09/16/26. Re- strictly not permitted, except for Open Access articles.

29.5.2 *The Acoustic Peaks,* $100 \lesssim \ell \lesssim 1000$

On sub-degree scales, the rich structure in the anisotropy spectrum is the consequence of gravity-driven acoustic oscillations occurring before the atoms in the Universe became neutral [39]. Perturbations inside the horizon at last scattering were able to evolve causally and produce anisotropy at the last-scattering epoch, which reflects this evolution. The frozen-in phases of these sound waves imprint a dependence on the cosmological parameters, which gives CMB anisotropies their great constraining power.

The underlying physics can be understood as follows. Before the Universe became neutral, the proton-electron plasma was tightly coupled to the photons, and these components behaved as a single 'photon-baryon fluid.' Perturbations in the gravitational potential, dominated by the dark-matter component, were steadily evolving. They drove oscillations in the photon-baryon fluid, with photon pressure providing most of the restoring force and baryons giving some additional inertia. The perturbations were quite small in amplitude, $\mathcal{O}(10^{-5})$, and so evolved linearly. That means each Fourier mode developed independently, and hence can be described as a driven harmonic oscillator, with frequency determined by the sound speed in the fluid. Thus, the fluid density underwent oscillations, giving time variations in temperature. These combine with a velocity effect, which is $\pi/2$ out of phase and has its amplitude reduced by the sound speed.

After the Universe recombined, the radiation decoupled from the baryons and could travel freely towards us. At that point, the (temporal) phases of the oscillations were frozen-in, and became projected on the sky as a harmonic series of peaks and troughs in power. The main peak is the mode that went through 1/4 of a period, reaching maximal compression. The even peaks are maximal *under*-densities, which are generally of smaller amplitude because the rebound has to fight against the baryon inertia. The troughs, which do not extend to zero power, are partially filled by the Doppler effect because they are at the velocity maxima.

The physical length scale associated with the peaks is the sound horizon at last scattering, which can be straightforwardly calculated. This length is projected onto the sky, leading to an angular scale that depends on the geometry of space, as well as the distance to last scattering. Hence, the angular position of the peaks is a sensitive probe of a particular combination of cosmological parameters. In fact, this characteristic angular scale, θ_*, is the most precisely measured observable, and hence is usually treated as an element of the cosmological parameter set.

One additional effect arises from reionization at redshift $z_{\rm i}$. A fraction of photons (τ) will be isotropically scattered at $z < z_{\rm i}$, partially erasing the anisotropies at angular scales smaller than those subtended by the Hubble radius at $z_{\rm i}$. This corresponds typically to ℓs above about 10, depending on the specific reionization model. The acoustic peaks are therefore reduced by a factor $e^{-2\tau}$ relative to the plateau.

These acoustic peaks were a clear theoretical prediction going back to about 1970 [40]. One can think of them as a snapshot of stochastic standing waves. Since the physics governing them is simple and their structure rich, one can see how they encode extractable information about the cosmological parameters. Their empirical existence started to become clear around 1994 [41], and the emergence, over the following decade, of a coherent series of acoustic peaks and troughs is a triumph of modern cosmology. This picture has received further confirmation with the detection in the power spectrum of galaxies (at redshifts $z \lesssim 1$) of the imprint of these same acoustic oscillations in the baryon component [42], as well as through detection of the expected oscillations in CMB polarization power spectra (see Sec. 29.7).

29.5.3 *The Damping Tail,* $\ell \gtrsim 1000$

The recombination process is not instantaneous, with a width in redshift $\Delta z \simeq 90$. This extent leads to a diminution of the anisotropies at the highest ℓs, corresponding to scales smaller than that subtended by this thickness. Effectively the photon-baryon fluid had imperfect coupling, so that there is diffusion between the two components, and hence the amplitudes of the oscillations decrease with time. These effects lead to a damping of the C_ℓs, sometimes called 'Silk damping' [43], which cuts off the anisotropies at multipoles above about 2000. So, although in principle it is possible to measure to ever smaller scales, this becomes increasingly difficult in practice.

29.5.4 *Gravitational Lensing Effects*

CMB gravitational lensing along the line of sight from the LSS is caused from spatial curvature by structures at lower redshift. Photon paths are deflected by the lensing potential ϕ, such that $T(\hat{n}) \rightarrow T(\hat{n} + \nabla\phi)$. Typical deflections are around 2 arcmin, but coherent over degree scales. Lensing preserves surface brightness, which means that a uniform temperature field would be unaffected; however, since there are primordial anisotropies, several distinct effects can be identified. The C_ℓs are convolved with a smoothing function in a calculable way, partially flattening the peaks and troughs, generating a power-law tail at the highest multipoles, and complicating the polarization signal [44] (see Sec. 29.7.3). Additionally, the effect of lensing on the CMB can be detected through the 4-point function, which correlates temperature gradients and small-scale anisotropies, enabling a map of the lensing potential to be constructed [45],

Lensing is important because it gives an independent estimate of $A_{\rm s}$, breaking the parameter combination $A_{\rm s}{\rm e}^{-2\tau}$ that is largely degenerate in the temperature anisotropy power spectra. Lensing is an example of a 'secondary effect,' *i.e.*, the processing of anisotropies due to relatively nearby structures (see Sec. 29.9.2). Galaxies and clusters of galaxies give several such effects; all are estimated to be of low amplitude, but are increasingly important at the highest ℓs. Such effects carry additional cosmological information (about evolving gravitational potentials in the low-redshift Universe) and are receiving more attention as experiments push to higher sensitivity and angular resolution. The lensing power spectrum (see Sec. 29.8) can potentially constrain dark-energy evolution, while future measurements at high ℓ are a particularly sensitive probe of the sum of the neutrino masses [46].

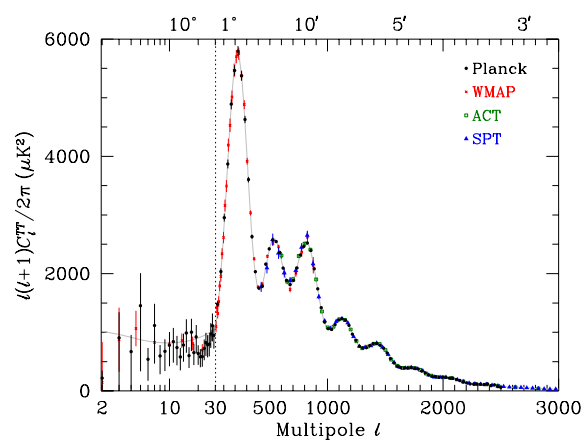

Figure 29.2: CMB temperature anisotropy band-power estimates from the *Planck*, *WMAP*, ACT, and SPT experiments. Note that the widths of the multipole bands vary between experiments and have not been plotted. This figure represents only a selection of the most recent available experimental results, and some points with large error bars have been omitted. At the higher multipoles these band-powers involve subtraction of particular foreground models, and so proper analysis requires simultaneous fitting of CMB and foregrounds over multiple frequencies. The horizontal axis here is logarithmic for the lowest multipoles, to show the Sachs-Wolfe plateau, and linear for the other multipoles. The acoustic peaks and damping region are very clearly observed, with no need for a theoretical line to guide the eye; however, the curve plotted is the best-fit *Planck* ΛCDM model.

29.6 Current Temperature Anisotropy Data

Steady improvement in CMB data quality has led to the present-day cosmological model. The most robust constraints currently available come from *Planck* satellite [47–49] data, although the latest results from ACT [50] and SPT [51] provide constraints

Int. J. Mod. Phys. A 2026.41. Downloaded from www.worldscientific.com
by UNIVERSITY OF CALIFORNIA @ BERKELEY on 09/16/26. Re-use and distribution is strictly not permitted, except for Open Access articles.

that are almost as strong (and the next set of ground-based experimental results should surpass *Planck*). Although there are some minor shifts in the best-fitting models of ACT and SPT, the main message is one of close agreement. We plot power spectrum estimates from these experiments in Fig. 29.2, along with *WMAP* data [5] for comparison (see previous versions of this review for data from earlier experiments). These independent observations show consistency, both in maps and in derived power spectra (up to systematic uncertainties in the overall calibration for some). This implies that systematic effects are largely under control.

The band-powers shown in Fig. 29.2 are in very good agreement with a 'ΛCDM' model. As described earlier, several (at least seven) of the peaks and troughs are quite apparent. The original papers present the details on how these estimates were made, on the band-power correlation strengths, and on the other information needed for their proper interpretation.

29.7 CMB Polarization

Thomson scattering of an anisotropic radiation field also generates linear polarization and the CMB is predicted to be polarized, at the level of roughly 5% of the temperature anisotropies [52]. Polarization is a spin-2 field on the sky, and the algebra of the modes in multipole space is strongly analogous to spin-orbit coupling in quantum mechanics [53]. The linear polarization pattern can be decomposed in a number of ways, with two quantities required for each pixel in a map, often given as the Q and U Stokes parameters. However, the most intuitive and physical decomposition is a geometrical one, splitting the polarization pattern into a part that comes from a divergence (often referred to as the 'E mode') and a part with a curl (called the 'B mode') [54]. More explicitly, the modes are defined in terms of second derivatives of the polarization amplitude, with the Hessian for the E modes having principal axes in the same sense as the polarization, while the B-mode pattern can be thought of as a 45° rotation of the E-mode pattern. Globally one sees that the E modes have $(-1)^\ell$ parity (like the spherical harmonics), while the B modes have $(-1)^{\ell+1}$ parity.

The existence of this linear polarization allows for six different cross-power spectra to be determined from data that measure the full temperature and polarization anisotropy information. Parity considerations make two of these zero, and we are left with four potential observables, C_ℓ^{TT}, C_ℓ^{TE}, C_ℓ^{EE}, and C_ℓ^{BB} (see Fig. 29.1). Because scalar perturbations have no handedness, the B-mode power spectrum can only be sourced by vectors or tensors. Moreover, inflationary scalar perturbations give only E modes, while tensors generate roughly equal amounts of E and B, and therefore the determination of a non-zero B-mode signal is a way to measure the gravitational-wave contribution (and thus potentially derive the energy scale of inflation). However, because the signal is expected to be rather weak, one must first eliminate the foreground contributions and other systematic effects down to very low levels. In addition, CMB lensing creates B modes from E modes, further complicating the extraction of a tensor signal.

As with temperature, the polarization C_ℓs exhibit a series of acoustic peaks generated by the oscillating photon-baryon fluid. The main 'EE' power spectrum has peaks that are out of phase with those in the 'TT' spectrum because the polarization anisotropies are sourced by the fluid velocity. The 'TE' part of the polarization and temperature patterns comes from correlations between density and velocity perturbations on the last-scattering surface, which can be both positive and negative, and is of larger amplitude than the EE signal. There is no polarization Sachs-Wolfe effect, and hence no large-angle (low-ℓ) plateau. However, scattering on electrons during a recent period of reionization can create a polarization 'bump' at large angular scales (see Fig. 29.1).

Because the polarization anisotropies have only a small fraction of the amplitude of the temperature anisotropies, they took longer to detect. The first measurement of a polarization signal came in 2002 from the DASI experiment [55], which provided a convincing detection, confirming the general paradigm, but of low enough significance that it lent no real constraint to models. Despite dramatic progress since then, it is still the case that polarization data mainly support the basic paradigm, while reducing error bars on parameters by only around 20%. However, there are exceptions

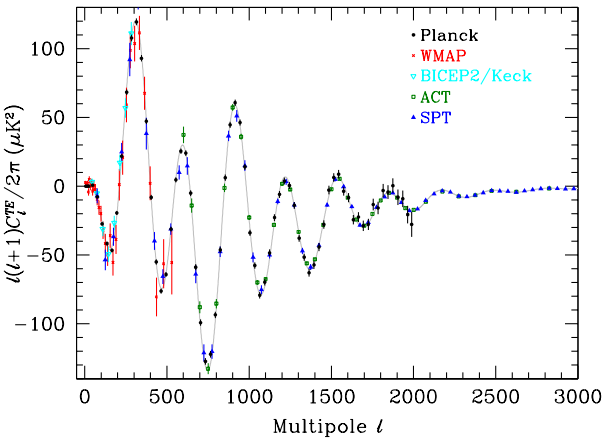

Figure 29.3: Cross-power spectrum band-powers of the temperature anisotropies and E-mode polarization signal from *Planck* (the low multipole data have been binned here), as well as *WMAP*, BICEP2/Keck, ACTPol, and SPTPol/SPT-3G. The curve is the best fit to the *Planck* temperature, polarization, and lensing band-powers. Note that each data point is an average over a band of multipoles, and hence to compare in detail with a model one has to integrate the theoretical curve through the band.

to this, specifically in the reionization optical depth, and the potential to constrain primordial gravitational waves. Moreover, the situation is expected to change dramatically as more of the available polarization modes are measured.

29.7.1 *T–E Power Spectrum*

Because the T and E skies are correlated, one has to measure the TE power spectrum, as well as TT and EE, in order to extract all the cosmological information [56]. This TE signal has been mapped out extremely accurately by *Planck* [48], with ACTPol [57] and SPTPol/-SPT-3G [51, 58] extending to smaller angular scales, and these band-powers are shown in Fig. 29.3, along with those from *WMAP* [59] and BICEP2/Keck [60], . The anti-correlation at $\ell \simeq 150$ and the peak at $\ell \simeq 300$ were the first features to become distinct, but now a whole series of oscillations is clearly seen in this power spectrum (including six or seven sets of peaks and troughs [10]). The measured shape of the cross-correlation power spectrum provides supporting evidence for the general cosmological picture, and also directly constrains the thickness of the last-scattering surface. Because the polarization anisotropies are generated in this scattering surface, the existence of correlations at angles above about a degree demonstrates that there were super-Hubble fluctuations at the recombination epoch. The sign of this correlation also confirms the adiabatic paradigm.

The overall picture of the source of CMB polarization and its oscillations has also been confirmed through tests that average the maps around both temperature hot spots and cold spots [61]. One sees precisely the expected patterns of radial and tangential polarization configurations, as well as the phase shift between polarization and temperature. This leaves no doubt that the oscillation picture is the correct one and that the polarization is coming from Thomson scattering at $z \simeq 1100$.

29.7.2 *E–E Power Spectrum*

Experimental band-powers for C_ℓ^{EE} from *Planck*, *WMAP*, BICEP2/Keck Array [60], ACTPol [50, 57], and SPTPol/SPT-3G [58, 62] are shown in Fig. 29.4. Without the benefit of correlating with the temperature anisotropies (*i.e.*, measuring C_ℓ^{TE}), the polarization anisotropies are very weak and challenging to measure. Nevertheless, the oscillatory pattern is now well established and the data closely match the TT-derived theoretical prediction. In Fig. 29.4 one can clearly see the 'shoulder' expected at $\ell \simeq 140$, the first main peak at $\ell \simeq 400$ (corresponding to the first trough in C_ℓ^{TT}), and the series of oscillations that is out of phase with those of the temperature anisotropy power spectrum (including

Int. J. Mod. Phys. A 2026.41. Downloaded from www.worldscientific.com by UNIVERSITY OF CALIFORNIA @ BERKELEY on 09/16/26. Re-
strictly not permitted, except for Open Access articles.

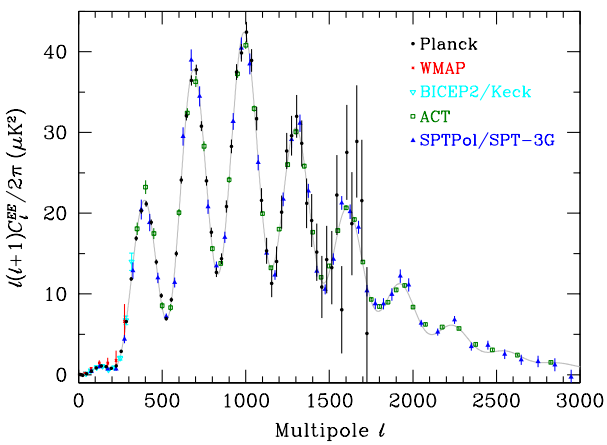

Figure 29.4: Power spectrum of E-mode polarization from *Planck*, together with *WMAP*, BICEP2/Keck, ACTPol, and SPTPol/SPT-3G. Note that some band-powers with larger uncertainties have been omitted and that the unbinned *Planck* low-ℓ data have been binned here. Also plotted is the best-fit theoretical model from *Planck* temperature + polarization + lensing data.

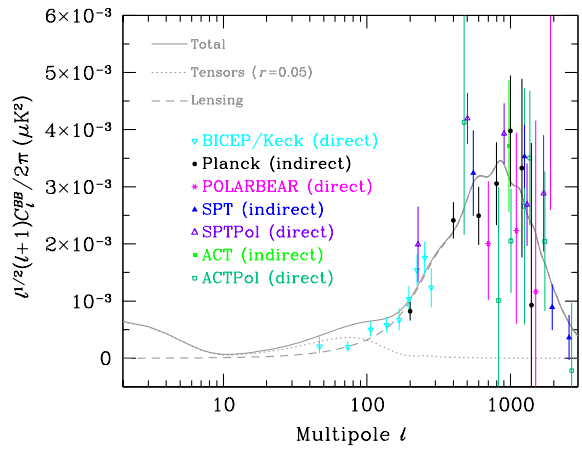

Figure 29.5: Power spectrum of B-mode polarization, including results from the BICEP2/BICEP3/Keck Array combined analysis, *Planck*, POLARBEAR, SPT, and ACT. Note that some of the measurements are direct estimates of B modes on the sky, while others are only sensitive to the lensing signal and come from combining E-mode and lensing potential measurements. Several earlier experiments reported upper limits, which are all off the top of this plot. A logarithmic horizontal axis is adopted here and the y-axis has been divided by a factor of $\sqrt{\ell}$ in order to show all three theoretically expected contributions: the low-ℓ reionization bump; the $\ell \simeq 100$ recombination peak; and the high-ℓ lensing signature. The dotted line is for a tensor (primordial gravitational wave) fraction $r = 0.05$, simply as an example, with all other cosmological parameters set at the best *Planck*-derived values, for which model the expected lensing B modes have also been shown with a dashed line.

six or seven sets of peaks and troughs [10]).

Perhaps the most unique result from the polarization measurements is at the largest angular scales ($\ell < 10$) in C_ℓ^{TE} and C_ℓ^{EE}, where there is evidence for an excess signal (not visible in Fig. 29.4) compared to that expected from the temperature power spectrum alone. This is precisely the signal anticipated from an early period of reionization, arising from Doppler shifts during the partial scattering at $z < z_{\rm i}$. The amplitude of the signal indicates that the first stars, presumably the source of the ionizing radiation, formed around $z \simeq 8$ (although the uncertainty is still quite large). This corresponds to a scattering optical depth $\tau \simeq 0.06$, so roughly 6% of CMB photons were re-scattered at the reionization epoch, with the other 94% last scattering at $z \simeq 1100$. Estimates of the amplitude of this reionization excess have come down since the first measurements by *WMAP* (indicating that this is an extremely difficult measurement to make) and the latest *Planck* results have reduced the value further [11,63].

29.7.3 *B–B Power Spectrum*

The expected amplitude of C_ℓ^{BB} is very small, so measurements of this polarization curl-mode are extremely challenging. The first indication of the existence of the BB signal came from the detection of the expected conversion of E modes to B modes by gravitational lensing, through a correlation technique using the lensing potential and polarization measurements from SPT [64]. However, the real promise of B modes lies in the detection of primordial gravitational waves at larger scales. This tensor signature could be seen either in the 'recombination bump' at around $\ell = 100$ (caused by an ISW effect as gravitational waves redshift away at the last-scattering epoch) or the 'reionization bump' at $\ell \lesssim 10$ (from additional scattering at low redshifts).

Results from the BICEP2 experiment [65] in 2014 suggested a detection of the primordial B-mode signature around the recombination peak. BICEP2 mapped a small part of the CMB sky with the best sensitivity level reached at that time (below 100 nK), but at a single frequency. Higher frequency data from *Planck* indicated that much of the BICEP2 signal was due to dust within our Galaxy, and a combined analysis by the BICEP2, Keck Array, and *Planck* teams [66] indicated that the data were consistent with no primordial B modes. The current constraint from *Planck* data alone is $r < 0.069$ (95% at $k = 0.05\,{\rm Mpc}^{-1}$ [11,63]) using all CMB power spectra, and this limit is reduced to $r < 0.044$ with the inclusion of BICEP2/Keck Array data [63,67]. The most constraining published limit is $r < 0.036$ from a combination of BICEP2, Keck Array, and BICEP3 data, using *WMAP* and *Planck* maps to help remove foregrounds [68].

Several experiments are continuing to push down the sensitivity of B-mode measurements, motivated by the enormous importance of a future detection of this telltale signature of inflation (or other physics at the highest energies). A compilation of experimental results for C_ℓ^{BB} is shown in Fig. 29.5, coming from a combination of direct estimates of the B modes (BICEP2/BICEP3/Keck Array [68], POLARBEAR [69], SPTPol/SPT-3G [70,71], and ACTPol [57]) and indirect determinations of the lensing B modes based on estimating the effect of measured lensing on measured E modes (*Planck* [72], SPT [64], and ACT [73]). Additional band-power estimates are expected from these and other experiments in the near future, with the Simons Observatory [74] and the *LiteBIRD* satellite [75] holding great promise for pushing down to a sensitivity level of $r \sim 0.001$.

29.8 CMB Lensing Power Spectrum

One further CMB observable is the gravitational lensing deflection, leading to the construction of a map of the lensing potential. The latest *Planck* results [76] give a map that is detected at the $> 40\sigma$ level using a minimum-variance procedure from the 4-point function of temperature and polarization data. From these maps, estimates can be constructed of $C_\ell^{\phi\phi}$, the lensing-potential power spectrum, which is found to be consistent with predictions from the best-fit temperature and polarization model. Recent results from both ACT [77] and SPT [78] give lensing power spectra that have similar overall signal-to-noise ratios. Figure 29.6 plots the *Planck*, ACT, and SPT estimates of $C_\ell^{\kappa\kappa}$, the lensing convergence power spectrum, which is proportional to $\ell^2(\ell+1)^2$ times the potential power spectrum $C_\ell^{\phi\phi}$.

We can think of each sky pixel as possessing three independent quantities that can be measured, namely T, E, and ϕ (and potentially B, if that becomes detectable). Determining the constraining power comes down to counting $Y_{\ell m}$ modes [56], as well as appreciating that some modes help to break particular parameter degeneracies. We have only scratched the surface of CMB lensing so far, and it is expected that future small-scale experiments will

Int. J. Mod. Phys. A 2026.41. Downloaded from www.worldscientific.com
by UNIVERSITY OF CALIFORNIA @ BERKELEY on 09/16/26. Re-use and distribution is strictly not permitted, except for Open Access articles.

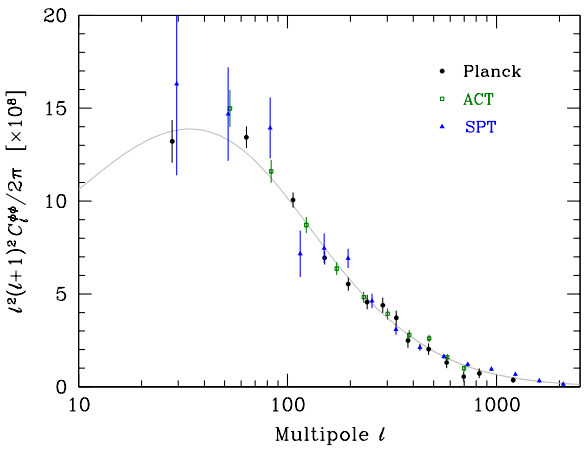

Figure 29.6: Power spectrum measurements for CMB lensing, including selected results from *Planck*, ACT, and SPT. The quantity plotted is the (dimensionless) potential power spectrum, scaled by $\ell^2(\ell+1)^2$ and multiplied by a factor of 10^8 to make the numbers more manageable. Some less reliable measurements have not been plotted. The best-fit *Planck* ΛCDM spectrum is plotted as a gray line.

be able to extract more of the cosmological information. Further constraints can also be derived on the lower-redshift Universe by cross-correlating CMB lensing with other cosmological tracers of large-scale structure. Additionally, small-scale lensing, combined with E-mode measurements, can be used to 'delens' CMB B-mode data, which will be important for pushing down into the $r \lesssim 0.01$ regime [79].

29.9 Complications

There are a number of issues that complicate the interpretation of CMB anisotropy data (and are considered to be *signal* by many astrophysicists), some of which we sketch out below.

29.9.1 *Foregrounds*

The microwave sky contains significant emission from our Galaxy and from extragalactic sources [80]. Fortunately, the frequency dependence of these various sources is in general substantially different from that of the CMB anisotropy signals. The combination of Galactic synchrotron, bremsstrahlung, and dust emission reaches a minimum at a frequency of roughly 100 GHz (or wavelength of about 3 mm). As one moves to greater angular resolution, the minimum moves to slightly higher frequencies, but becomes more sensitive to unresolved (point-like) sources.

At frequencies around 100 GHz, and for portions of the sky away from the Galactic plane, the foregrounds are typically 1 to 10% of the CMB anisotropies. By making observations at multiple frequencies, it is relatively straightforward to separate the various components and determine the CMB signal to the few per cent level. For greater sensitivity, it is necessary to use the spatial information and statistical properties of the foregrounds to separate them from the CMB. Furthermore, at higher ℓs it is essential to carefully model extragalactic foregrounds, particularly the clustering of infrared-emitting galaxies and scattering due to galaxy clusters, which dominate the measured power spectrum as we move into the damping tail.

The foregrounds for CMB polarization follow a similar pattern to those for temperature, but are intrinsically brighter relative to CMB anisotropies. *WMAP* showed that the polarized foregrounds dominate at large angular scales, and that they must be well characterized in order to be discriminated [81]. *Planck* has shown that it is possible to characterize the foreground polarization signals, with synchrotron dominating at low frequencies and dust at high frequencies [82]. On smaller scales there are no strongly-polarized foregrounds, and hence at high multipoles it is in principle easier to measure foreground-free modes in polarization than in temperature. Although foreground contamination will no doubt become more complicated as we push down in sensitivity, making analysis more difficult, for the time being, foreground contamination is not a fundamental limit for CMB experiments.

29.9.2 *Secondary Anisotropies*

With increasingly precise measurements of the primary anisotropies, there is growing theoretical and observational interest in 'secondary anisotropies,' pushing experiments to higher angular resolution and sensitivity. These secondary effects arise from the processing of the CMB due to ionization history and the evolution of structure, including gravitational lensing (which was already discussed) and patchy reionization effects [83]. Additional information can thus be extracted about the Universe at $z \ll 1000$ (the CMB 'mid-ground'). This tends to be most effectively done through correlating CMB maps with other cosmological probes of structure. Secondary signals are also typically non-Gaussian, unlike the primary CMB anisotropies.

A secondary signal of great current interest is the Sunyaev-Zeldovich (SZ) effect [84], which is Compton scattering ($\gamma e \to \gamma' e'$) of the CMB photons by hot electrons in intergalactic plasma. This creates spectral distortions by transferring energy from the hot electrons to the photons. For large clusters of galaxies, one observes a partially Comptonized spectrum, resulting in a decrement at radio wavelengths and an increment in the submillimeter.

The imprint on the CMB sky is of the form $\Delta T/T = y\, f(x)$, with the y parameter being the integral of Thomson optical depth times $kT_{\rm e}/m_{\rm e}c^2$ through the cluster, and $f(x)$ describing the frequency dependence. This is simply $x\coth(x/2) - 4$ for a non-relativistic gas (the electron temperature in a cluster is typically a few keV), where the dimensionless frequency $x \equiv h\nu/kT_\gamma$. As well as this 'thermal' SZ effect, there is also a smaller 'kinetic' effect due to the bulk motion of the cluster gas, giving $\Delta T/T \sim \tau(v/c)$, with either sign, but having the same spectrum as the primary CMB anisotropies.

A significant advantage in finding galaxy clusters via the SZ effect is that the signal is largely independent of redshift, so in principle clusters can be found to arbitrarily large distances. The SZ effect can be used to find and study individual clusters, and to obtain estimates of the Hubble constant. There is also the potential to constrain other cosmological parameters, such as the clustering amplitude σ_8 and the equation of state of the dark energy, through counts of detected clusters as a function of redshift. The promise of the method has been realized through detections of clusters purely through the SZ effect by SPT [85], ACT [86], and *Planck* [87]. Results from *Planck* clusters [88] suggest a somewhat lower value of σ_8 than inferred from CMB anisotropies, but there are still systematic uncertainties that might encompass the difference, and more recent analyses show better agreement [89]. Further analysis of scaling relations among cluster properties should enable more robust cosmological constraints to be placed in future, so that we can understand whether this 'tension' might be a sign of new physics.

29.9.3 *Higher-order Statistics*

Although most of the CMB anisotropy information is contained in the power spectra, there will also be weak signals present in higher-order statistics. These can measure any primordial non-Gaussianity in the perturbations, as well as non-linear growth of the fluctuations on small scales and other secondary effects (plus residual foreground contamination of course). There are an infinite variety of ways in which the CMB could be non-Gaussian [26]; however, there is a generic form to consider for the initial conditions, where a quadratic contribution to the curvature perturbations is parameterized through a dimensionless number $f_{\rm NL}$. This weakly non-linear component can be constrained in several ways, the most popular being through measurements of the bispectrum (or 3-point function).

The constraints depend on the shape of the triangles in harmonic space, and it has become common to distinguish the 'local' or 'squeezed' configuration (in which one side is much smaller than the other two) from the 'equilateral' configuration. Other configurations are also relevant for specific theories, such as 'orthogonal' non-Gaussianity, which has positive correlations for

Int. J. Mod. Phys. A 2026.41. Downloaded by UNIVERSITY OF CALIFORNIA @ BERKELEY on 09/16/26. Re-
orldscientific.com
strictly not permitted, except for Open Access articles.

$k_1 \simeq 2k_2 \simeq 2k_3$, and negative correlations for the equilateral configuration. The constraints from the *Planck* team [90] are $f_{\rm NL}^{\rm local} = 1 \pm 5$, $f_{\rm NL}^{\rm equil} = -26 \pm 47$, and $f_{\rm NL}^{\rm ortho} = -38 \pm 24$.

These results are consistent with zero, but are at a level that is now interesting for model predictions. The amplitude of $f_{\rm NL}$ expected is small, so that a detection of $f_{\rm NL} \gg 1$ would rule out all single-field, slow-roll inflationary models. It is still possible to improve upon these *Planck* results, and it certainly seems feasible that a measurement of primordial non-Gaussianity may yet be within reach. *Non*-primordial detections of non-Gaussianity from expected signatures have already been made. For example, the bispectrum and trispectrum contain evidence of gravitational lensing, the ISW effect, and Doppler boosting. For now the primordial signal is elusive, but should it be detected, then detailed measurements of non-Gaussianity will become a unique probe of inflationary-era physics. Because of that, much effort continues to be devoted to honing predictions and measurement techniques, with the expectation that we will need to go beyond the CMB (*e.g.*, 3D galaxy surveys) to dramatically improve the constraints.

29.9.4 *Anomalies*

Several features seen in the *Planck* data [29,61,91] confirm those found earlier with *WMAP* [28], showing mild deviations from a simple description of the sky; these are often referred to as 'anomalies.' One such feature is the lack of power in the multipole range $\ell \simeq 20$–30 [11, 48]. Other examples involve the apparent breaking of statistical anisotropy, caused by alignment of the lowest multipoles, as well as a somewhat excessive cold spot and a power asymmetry between hemispheres. No such feature is significant at more than the roughly 3σ level, and the importance of '*a posteriori*' statistics here has been emphasized by many authors. Since these effects are at large angular scales, where cosmic variance dominates, the results will not increase in significance with additional data, although there is the potential for more sensitive polarization measurements to provide independent tests.

29.10 Constraints on Cosmological Parameters

The most striking outcome of the last couple of decades of experimental results is that the standard cosmological paradigm continues to be in very good shape. A large amount of high-precision data on the CMB power spectra is adequately fit with fewer than 10 free parameters (and only six need non-trivial values). The framework is that of FRW models, which have nearly flat geometry, containing dark matter and dark energy, and with adiabatic perturbations having close to scale-invariant initial conditions.

Within this basic picture, the values of the cosmological parameters can be constrained. Of course, more stringent bounds can be placed on models that cover a restricted parameter space, *e.g.*, assuming that $\Omega_{\rm tot} = 1$ or $r = 0$. More generally, the constraints depend upon the adopted prior probability distributions, even if they are implicit, for example by restricting the parameter freedom or their ranges (particularly where likelihoods peak near the boundaries), or by using different choices of other data in combination with the CMB. As the data become even more precise, these considerations will be less important, but for now we caution that restrictions on model space and choice of non-CMB data sets and priors need to be kept in mind when adopting specific parameter values and uncertainties.

There are some combinations of parameters that fit the CMB anisotropies almost equivalently. For example, there is a nearly exact geometric degeneracy, where any combination of $\Omega_{\rm m}$ and Ω_Λ that provides the same angular-diameter distance to last scattering will give nearly identical C_ℓs. There are also other less exact degeneracies among the parameters. Such degeneracies can be broken when using the CMB results in combination with other cosmological data sets. Particularly useful are complementary constraints from baryon acoustic oscillations, galaxy clustering, the abundance of galaxy clusters, weak gravitational lensing measurements, and Type Ia supernova distances. For an overview of some of these other cosmological constraints, see The Cosmological Parameters—Sec. 25 of this *Review*.

Within the context of a 6-parameter family of models (which fixes $\Omega_{\rm tot} = 1$, $dn_{\rm s}/d\ln k = 0$, $r = 0$, and $w = -1$) the *Planck* results for TT, together with TE, EE, and CMB lensing, yield [11]: $\ln(10^{10}A_{\rm s}) = 3.044 \pm 0.014$; $n_{\rm s} = 0.965 \pm 0.004$; $\Omega_{\rm b}h^2 = 0.02237 \pm 0.00015$; $\Omega_{\rm c}h^2 = 0.1200 \pm 0.0012$; $100\theta_* = 1.04092 \pm 0.00031$; and $\tau = 0.054 \pm 0.007$. Other parameters can be derived from this basic set, including $h = 0.674 \pm 0.005$, $\Omega_\Lambda = 0.685 \pm 0.007$ $(= 1 - \Omega_{\rm m})$ and $\sigma_8 = 0.811 \pm 0.006$ (see also Astrophysical Constants and Parameters—Sec. 2). Somewhat different (although consistent) values are obtained using other data combinations, such as including BAO, supernova, H_0, or weak-lensing constraints (see Sec. 25 of this *Review*). However, the *Planck* results quoted above are currently the best available from CMB data alone. Results from other CMB experiments (*e.g.*, SPT-3G [62]) are consistent and becoming competitive.

The standard cosmological model still fits the data well, with the error bars on the parameters continuing to shrink. Improved measurement of higher acoustic peaks has dramatically reduced the uncertainty in the θ_* parameter, which is now detected at $> 3000\sigma$. The evidence for $n_{\rm s} < 1$ is now at the 8σ level from *Planck* data alone. The value of the reionization optical depth has decreased compared with earlier estimates; it is convincingly detected, but still not at very high significance.

The inferred value of H_0 is smaller than the most precise values derived from the cosmic distance ladder. This parameter tension is discussed more fully in other sections of this *Review*. The CMB anisotropies also provide the most precise estimate of the age of the Universe, with *Planck* giving the value $t_0 = 13.797 \pm 0.023\,{\rm Gyr}$.

Constraints can also be placed on parameters beyond the basic six, particularly when including other astrophysical data sets. Relaxing the flatness assumption, the constraint on $\Omega_{\rm tot}$ is 1.011 ± 0.006. Note that for h, the CMB data alone provide only a very weak constraint if spatial flatness is not assumed. However, with the addition of other data (particularly powerful in this context being a compilation of BAO measurements; see Sec. 25 of this *Review*), the constraints on the Hubble constant and curvature improve considerably, leading to $\Omega_{\rm tot} = 0.9993 \pm 0.0019$ [11].

For $\Omega_{\rm b}h^2$ the CMB-derived value is generally consistent with completely independent constraints from Big Bang nucleosynthesis (see Sec. 24 of this *Review*). Related are constraints on additional neutrino-like relativistic degrees of freedom, which lead to $N_{\rm eff} = 2.99 \pm 0.17$ (including BAO), *i.e.*, no evidence for extra neutrino species.

The current limit on the tensor-to-scalar ratio is $r \lesssim 0.04$ (measured at $k = 0.05\,{\rm Mpc}^{-1}$) from a combination of BICEP/Keck Array and *Planck* data [63, 68]. The detailed limit depends on how other parameters, especially $A_{\rm s}$, $n_{\rm t}$, and $dn_{\rm s}/d\ln k \neq 0$ are restricted. The joint constraints on $n_{\rm s}$ and r allow specific inflationary models to be tested [30, 92]. Looking at the $(n_{\rm s}, r)$ plane, this means that $m^2\phi^2$ (mass-term quadratic) inflation is disfavored by the data, as well as $\lambda\phi^4$ (self-coupled) inflation.

The addition of the dark-energy equation of state w adds the partial degeneracy of being able to fit a ridge in (w, h) space, extending to low values of both parameters. This degeneracy is broken when the CMB is used in combination with other data sets, *e.g.*, adding a compilation of BAO and supernova data gives $w = -1.028 \pm 0.031$ [11]. Constraints can also be placed on more general dark energy and modified-gravity models [93]. However, when extending the search space, one needs to be careful not to over-interpret some tensions between data sets as evidence for new physics.

For the reionization optical depth, a reanalysis of *Planck* data in 2016 resulted in a reduction in the value of τ, with the tightest result giving $\tau = 0.055 \pm 0.009$, and the newest analyses giving similar numbers. This corresponds to $z_{\rm i} = 7.8$–8.8 (depending on the functional form of the reionization history), with an uncertainty of ± 0.9 [94]. This redshift is only slightly higher that that suggested from studies of absorption lines in high-z quasar spectra [95] and Ly α-emitting galaxies [96], perhaps hinting that the process of reionization was not as complex as previously suspected. The important constraint provided by CMB polarization, in combination with astrophysical measurements, thus allows us to investigate how the first stars formed and brought about the end of the cosmic dark ages.

Int. J. Mod. Phys. A 2026.41. Downloaded from www.worldscientific.com
by UNIVERSITY OF CALIFORNIA @ BERKELEY on 09/16/26. Re-use and distribution is strictly not permitted, except for Open Access articles.

29.11 Particle Physics Constraints

CMB data place limits on parameters that are directly relevant for particle physics models. For example, there is a limit on the sum of the masses of the neutrinos, $\Sigma m_\nu < 0.12\,\mathrm{eV}$ (95%) [11] coming from *Planck* together with BAO measurements (although limits are weaker when considering both N_{eff} and Σm_ν as free parameters). This assumes the usual number density of fermions, which decoupled when they were relativistic. The limit is tantalizingly only a factor of a few higher than the minimum value coming from neutrino mixing experiments (see Neutrino Mixings—Secs. 14 and 26). As well as being an indirect probe of the neutrino background, *Planck* data also require that the neutrino fluid has perturbations, *i.e.*, that it possesses a sound speed $c_{\mathrm{s}}^2 \simeq 1/3$, as expected [9].

The current suite of data suggests that $n_{\mathrm{s}} < 1$, with a best-fitting value about 0.035 below unity. This is already quite constraining for inflationary models, particularly along with r limits. There is no current evidence for running of the spectral index, with $dn_{\mathrm{s}}/d\ln k = -0.004 \pm 0.007$ from *Planck* alone [11] (with a similar value when BAO data are included), although this is less of a constraint on models. Similarly, primordial non-Gaussianity is being probed to interesting levels, although tests of simple inflationary models will only come with significant reductions in uncertainty.

The large-angle anomalies, such as the hemispheric modulation of power and the dip in power at $\ell \simeq 20$–30, have the potential to be hints of new physics. Such effects might be expected in a Universe that has a large-scale power cut-off, or anisotropy in the initial power spectrum, or is topologically non-trivial. However, cosmic variance and *a posteriori* statistics limit the significance of these anomalies, absent the existence of a model that naturally yields some of these features (and ideally also predicting other phenomena that can be tested).

Constraints on 'cosmic birefringence' (*i.e.*, rotation of the plane of CMB polarization that generates non-zero TB and EB power) can be used to place limits on theories involving parity violation, Lorentz violation, or axion-photon mixing [97]. It is possible to place limits on additional areas of physics [98], for example annihilating dark matter [9], primordial magnetic fields [99], and time variation of the fine-structure constant [100], as well as the neutrino chemical potential, a contribution of warm dark matter, topological defects, or physics beyond general relativity. Further particle physics constraints will follow as the smaller-scale and polarization measurements continue to improve.

The CMB anisotropy measurements precisely pin down conditions at the time of last-scattering, and so any change of physics can be constrained if it affects the relevant energies or timescales. Future, higher sensitivity measurements of the CMB frequency spectrum will push the constraints back to cover energy injection at much earlier times ($\sim 1\,\mathrm{year}$). Comparison of CMB and BBN observables extend these constraints to timescales of order seconds, and energies in the MeV range. And to the extent that inflation provides an effective description of the generation of perturbations, the inflationary observables may constrain physics at GUT-type energy scales.

More generally, careful measurement of the CMB power spectra and non-Gaussianity can in principle put constraints on physics at the highest energies, including ideas of quantum gravity, string theory, extra dimensions, colliding branes, *etc.* At the moment any calculation of predictions appears to be far from definitive. However, there is a great deal of activity on implications of fundamental theories for the early Universe, and hence a chance that there might be observational implications for specific scenarios.

29.12 Fundamental Lessons

More important than the precise values of parameters is what we have learned about the general features that describe our observable Universe. Beyond the basic hot Big Bang picture, the CMB has taught us that:

- the (observable) Universe is very close to isotropic;
- the Universe recombined at $z \sim 1100$ and started to become ionized again at $z \sim 10$;
- the geometry of the Universe is close to flat;
- both dark matter and dark energy are required;
- gravitational instability is sufficient to grow all of the observed large structures in the Universe;
- topological defects were not important for structure formation;
- there were 'synchronized' super-Hubble modes generated in the early Universe;
- the initial perturbations were predominantly adiabatic in nature;
- the primordial perturbation spectrum has a slightly red tilt;
- the perturbations had close to Gaussian (*i.e.*, maximally random) initial conditions.

These features form the basis of the cosmological standard model, ΛCDM, for which it is tempting to make an analogy with the Standard Model of particle physics (see earlier Sections of this *Review*). In comparison, the cosmological model is much further from any underlying 'fundamental theory,' which might ultimately provide the values of the parameters from first principles. Nevertheless, any genuinely complete 'theory of everything' must include an explanation for the values of these cosmological parameters in addition to the parameters of the Standard Model of particle physics.

29.13 Future Directions

Given the significant progress in measuring the CMB sky, which has been instrumental in tying down the cosmological model, what can we anticipate for the future? There will be a steady improvement in the precision and confidence with which we can determine the appropriate cosmological parameters. Ground-based experiments operating at smaller angular scales will continue to place tighter constraints on the damping tail, lensing, and cross-correlations. New polarization experiments at small scales will probe further into the damping tail, without the limitation of extragalactic foregrounds. And polarization experiments at large angular scales will push down the limits on primordial B modes.

Planck, the third generation CMB satellite mission, was launched in 2009, and produced cosmological constraints based on Public Releases PR1 in 2013, PR2 in 2015, and PR3 in 2018. The 'legacy' products of 2018 give the results that we have used to define the current baseline cosmology. An enhanced set of products (PR4) have led to somewhat tighter constraints, while ACT and SPT data have extended the measurements to smaller angular scales. *Planck* data currently dominate constraints on models, but that situation will change soon.

A set of cosmological parameters is now known to percent-level accuracy, and that may seem sufficient for many people. However, we should certainly demand more of measurements that describe *the entire observable Universe!* Hence a lot of activity in the coming years will continue to focus on determining those parameters with increasing precision. This necessarily includes testing for consistency among different predictions of the cosmological Standard Model, and searching for signals that might require additional physics. On the horizon we have the Advanced Simons Observatory, as well as further developments of BICEP and the South Pole Telescope experiments, as well as the Taurus balloon experiment [101].

A second area of focus will be the smaller-scale anisotropies and 'secondary effects.' There is a great deal of information about structure formation at $z \ll 1000$ encoded in the CMB sky. This may involve higher-order statistics and cross-correlations with other large-scale structure tracers, as well as spectral signatures, with many experiments targeting the galaxy cluster SZ effect, for example. The current status of CMB lensing is similar (in terms of total signal-to-noise) to the quality of the first CMB anisotropy measurements by *COBE*, and thus we can expect that experimental probes of lensing will improve dramatically in the coming years. All of these investigations can provide constraints on the dark-energy equation of state, for example, which is a major area of focus for several cosmological surveys at optical wavelengths. CMB lensing also promises to yield a measurement of the sum of the neutrino masses.

A third direction is increasingly sensitive searches for specific

Int. J. Mod. Phys. A 2026.41. Downloaded from www.worldscientific.com by UNIVERSITY OF CALIFORNIA @ BERKELEY on 09/16/26. Re-[redacted]strictly not permitted, except for Open Access articles.

signatures of physics at the highest energies. The most promising of these may be the primordial gravitational wave signals in C_ℓ^{BB}, which could be a probe of the $\sim 10^{16}$ GeV energy range. There are several experiments underway or being developed that are designed to search for the polarization B modes, with the most ambitious being Simons Observatory and BICEP on the ground and *LiteBIRD* in space. Additionally, non-Gaussianity holds the promise of constraining models beyond single-field slow-roll inflation.

Anisotropies in the CMB have proven to be the premier probe of cosmology and the early Universe. Theoretically the CMB involves well-understood physics in the linear regime, and is under very good calculational control. A substantial and improving set of observational data now exists. Systematics appear to be under control and are not currently a limiting factor. And so for the next several years we can expect an increasing amount of cosmological information to be gleaned from CMB anisotropies, with the prospect also of some genuine surprises.

References

[1] A. A. Penzias and R. W. Wilson, Astrophys. J. **142**, 419 (1965); R. H. Dicke *et al.*, Astrophys. J. **142**, 414 (1965).

[2] M. White, D. Scott and J. Silk, Ann. Rev. Astron. Astrophys. **32**, 319 (1994); W. Hu and S. Dodelson, Ann. Rev. Astron. Astrophys. **40**, 171 (2002), [arXiv:astro-ph/0110414]; A. Challinor and H. Peiris, in M. Novello and S. Perez, editors, "American Institute of Physics Conference Series," volume 1132, 86–140 (2009), [arXiv:0903.5158].

[3] G. F. Smoot *et al.*, Astrophys. J. Lett. **396**, L1 (1992).

[4] C. L. Bennett *et al.*, Astrophys. J. Supp. **148**, 1 (2003), [arXiv:astro-ph/0302207].

[5] G. Hinshaw *et al.*, Astrophys. J. Supp. **208**, 19 (2013), [arXiv:1212.5226].

[6] Planck Collab. 2013 Results XVI, Astron. Astrophys. **571**, A16 (2014), [arXiv:1303.5076].

[7] J. A. Tauber *et al.*, Astron. Astrophys. **520**, A1 (2010); Planck Collab. 2013 Results I, Astron. Astrophys. **571**, A1 (2014), [arXiv:1303.5062].

[8] Planck Collab. 2015 Results I, Astron. Astrophys. **594**, A1 (2016), [arXiv:1502.01582].

[9] Planck Collab. 2015 Results XIII, Astron. Astrophys. **594**, A13 (2016), [arXiv:1502.01589].

[10] Planck Collab. 2018 Results I, Astron. Astrophys. **641**, A1 (2020), [arXiv:1807.06205].

[11] Planck Collab. 2018 Results VI, Astron. Astrophys. **641**, A6 (2020), [arXiv:1807.06209].

[12] D. S. Swetz *et al.*, Astrophys. J. Supp. **194**, 41 (2011), [arXiv:1007.0290].

[13] J. E. Carlstrom *et al.*, Proc. Astron. Soc. Pacific **123**, 568 (2011), [arXiv:0907.4445].

[14] V. V. Klimenko *et al.*, Astronomy Letters **46**, 11, 715 (2020), [arXiv:2106.00119]; D. A. Riechers *et al.*, Nature **602**, 7895, 58 (2022), [arXiv:2202.00693].

[15] D. J. Fixsen *et al.*, Astrophys. J. **734**, 5 (2011), [arXiv:0901.0555].

[16] J. Singal *et al.*, Proc. Astron. Soc. Pacific **130**, 985, 036001 (2018), [arXiv:1711.09979].

[17] A. Kogut *et al.*, J. Cosmology Astropart. Phys. **2011**, 7, 025 (2011), [arXiv:1105.2044]; P. André *et al.*, J. Cosmology Astropart. Phys. **2014**, 2, 006 (2014), [arXiv:1310.1554]; J. Delabrouille *et al.*, Experimental Astronomy **51**, 3, 1471 (2021), [arXiv:1909.01591].

[18] V. Desjacques *et al.*, Mon. Not. R. Astron. Soc. **451**, 4460 (2015), [arXiv:1503.05589].

[19] D. J. Fixsen, Astrophys. J. **707**, 916 (2009), [arXiv:0911.1955].

[20] J. C. Mather *et al.*, Astrophys. J. **512**, 511 (1999), [arXiv:astro-ph/9810373].

[21] Y. Hoffman, H. M. Courtois and R. B. Tully, Mon. Not. R. Astron. Soc. **449**, 4494 (2015), [arXiv:1503.05422].

[22] D. J. Fixsen *et al.*, Astrophys. J. **420**, 445 (1994).

[23] Planck Collab. 2013 Results XXVII, Astron. Astrophys. **571**, A27 (2014), [arXiv:1303.5087].

[24] S. Seager, D. D. Sasselov and D. Scott, Astrophys. J. Supp. **128**, 407 (2000), [arXiv:astro-ph/9912182].

[25] L. Knox, Phys. Rev. **D52**, 4307 (1995), [arXiv:astro-ph/9504054].

[26] N. Bartolo *et al.*, Phys. Rep. **402**, 103 (2004), [arXiv:astro-ph/0406398].

[27] Planck Collab. 2013 Results XXIV, Astron. Astrophys. **571**, A24 (2014), [arXiv:1303.5084].

[28] C. L. Bennett *et al.*, Astrophys. J. Supp. **192**, 17 (2011), [arXiv:1001.4758].

[29] Planck Collab. 2013 Results XXIII, Astron. Astrophys. **571**, A23 (2014), [arXiv:1303.5083].

[30] Planck Collab. 2018 Results X, Astron. Astrophys. **641**, A10 (2020), [arXiv:1807.06211].

[31] A. R. Liddle and D. H. Lyth, *Cosmological Inflation and Large-Scale Structure*, Cambridge University Press, Cambridge (2000).

[32] U. Seljak and M. Zaldarriaga, Astrophys. J. **469**, 437 (1996), [arXiv:astro-ph/9603033].

[33] A. Lewis, A. Challinor and A. Lasenby, Astrophys. J. **538**, 473 (2000), [arXiv:astro-ph/9911177].

[34] D. Blas, J. Lesgourgues and T. Tram, J. Cosmology Astropart. Phys. **7**, 034 (2011), [arXiv:1104.2933].

[35] U. Seljak *et al.*, Phys. Rev. **D68**, 083507 (2003), [arXiv:astro-ph/0306052].

[36] R. K. Sachs and A. M. Wolfe, Astrophys. J. **147**, 73 (1967).

[37] R. G. Crittenden and N. Turok, Phys. Rev. Lett. **76**, 575 (1996), [arXiv:astro-ph/9510072]; Planck Collab. 2015 Results XXI, Astron. Astrophys. **594**, A21 (2016), [arXiv:1502.01595].

[38] W. Hu *et al.*, Phys. Rev. **D59**, 2, 023512 (1998), [arXiv:astro-ph/9806362].

[39] W. Hu, N. Sugiyama and J. Silk, Nature **386**, 37 (1997), [arXiv:astro-ph/9604166].

[40] P. J. E. Peebles and J. T. Yu, Astrophys. J. **162**, 815 (1970); Sunyaev, R. A. and Zeldovich, Ya. B., Astron. Astrophys. Supp. **7**, 3 (1970).

[41] D. Scott, J. Silk and M. White, Science **268**, 829 (1995), [arXiv:astro-ph/9505015].

[42] D. J. Eisenstein, New Astron. Rev. **49**, 360 (2005).

[43] J. Silk, Astrophys. J. **151**, 459 (1968).

[44] M. Zaldarriaga and U. Seljak, Phys. Rev. **D58**, 023003 (1998), [arXiv:astro-ph/9803150].

[45] Planck Collab. 2013 Result XVII, Astron. Astrophys. **571**, A17 (2014), [arXiv:1303.5077].

[46] M. Kaplinghat, L. Knox and Y.-S. Song, Phys. Rev. Lett. **91**, 24, 241301 (2003), [arXiv:astro-ph/0303344].

[47] Planck Collab. 2013 Results XV, Astron. Astrophys. **571**, A15 (2014), [arXiv:1303.5075].

[48] Planck Collab. 2018 Results V, Astron. Astrophys. **641**, A5 (2020), [arXiv:1907.12875].

[49] E. Rosenberg, S. Gratton and G. Efstathiou, Mon. Not. R. Astron. Soc. **517**, 3, 4620 (2022), [arXiv:2205.10869]; M. Tristram *et al.*, Astron. Astrophys. **682**, A37 (2024), [arXiv:2309.10034].

[50] T. Louis *et al.*, J. Cosmology Astropart. Phys. **2025**, 11, 062 (2025), [arXiv:2503.14452].

[51] E. Camphuis *et al.*, arXiv e-prints arXiv:2506.20707 (2025), [arXiv:2506.20707].

Int. J. Mod. Phys. A 2026.41. Downloaded from www.worldscientific.com
by UNIVERSITY OF CALIFORNIA @ BERKELEY on 09/16/26. Re-use and distribution is strictly not permitted, except for Open Access articles.

[52] W. Hu and M. White, New Astron. **2**, 323 (1997), [arXiv:astro-ph/9706147].

[53] W. Hu and M. J. White, Phys. Rev. **D56**, 596 (1997), [arXiv:astro-ph/9702170].

[54] M. Zaldarriaga and U. Seljak, Phys. Rev. **D55**, 1830 (1997), [arXiv:astro-ph/9609170]; M. Kamionkowski, A. Kosowsky and A. Stebbins, Phys. Rev. **D55**, 7368 (1997), [arXiv:astro-ph/9611125].

[55] J. M. Kovac *et al.*, Nature **420**, 772 (2002), [arXiv:astro-ph/0209478].

[56] D. Scott *et al.*, J. Cosmology Astropart. Phys. **2016**, 6, 046 (2016), [arXiv:1603.03550].

[57] S. K. Choi *et al.*, J. Cosmology Astropart. Phys. **2020**, 12, 045 (2020), [arXiv:2007.07289].

[58] A. T. Crites *et al.*, Astrophys. J. **805**, 36 (2015), [arXiv:1411.1042].

[59] D. Larson *et al.*, Astrophys. J. Supp. **192**, 16 (2011), [arXiv:1001.4635].

[60] Keck Array and BICEP2 Collabs. V, Astrophys. J. **811**, 126 (2015), [arXiv:1502.00643].

[61] Planck Collab. 2018 Results VII, Astron. Astrophys. **641**, A7 (2020), [arXiv:1906.02552].

[62] L. Balkenhol *et al.*, Phys. Rev. **D108**, 2, 023510 (2023), [arXiv:2212.05642].

[63] M. Tristram *et al.*, Astron. Astrophys. **647**, A128 (2021), [arXiv:2010.01139].

[64] D. Hanson *et al.*, Phys. Rev. Lett. **111**, 14, 141301 (2013), [arXiv:1307.5830].

[65] BICEP2 Collab., Phys. Rev. Lett. **112**, 24, 241101 (2014), [arXiv:1403.3985].

[66] BICEP2/Keck and Planck Collabs., Phys. Rev. Lett. **114**, 10, 101301 (2015), [arXiv:1502.00612].

[67] BICEP2 and Keck Array Collab., Phys. Rev. Lett. **121**, 22, 221301 (2018), [arXiv:1810.05216].

[68] BICEP/Keck Collab., Phys. Rev. Lett. **127**, 151301 (2021), [arXiv:2110.00483].

[69] POLARBEAR Collab., Astrophys. J. **848**, 121 (2017), [arXiv:1705.02907].

[70] J. T. Sayre *et al.*, Phys. Rev. **D101**, 12, 122003 (2020), [arXiv:1910.05748].

[71] J. A. Zebrowski *et al.*, Phys. Rev. **D112**, 12, 123520 (2025), [arXiv:2505.02827].

[72] Planck Collab. 2015 Results XV, Astron. Astrophys. **594**, A15 (2016), [arXiv:1502.01591].

[73] A. van Engelen *et al.*, Astrophys. J. **808**, 7 (2015), [arXiv:1412.0626].

[74] P. Ade *et al.* (Simons Observatory Collab.), J. Cosmology Astropart. Phys. **2019**, 2, 056 (2019), [arXiv:1808.07445].

[75] LiteBIRD Collaboration, Prog. Theor. Exp. Phys. **2023**, 4, 042F01 (2023), [arXiv:2202.02773].

[76] Planck Collab. 2018 Results VIII, Astron. Astrophys. **641**, A8 (2020), [arXiv:1807.06210]; J. Carron, M. Mirmelstein and A. Lewis, J. Cosmology Astropart. Phys. **2022**, 9, 039 (2022), [arXiv:2206.07773].

[77] F. J. Qu *et al.*, Astrophys. J. **962**, 2, 112 (2024), [arXiv:2304.05202].

[78] F. Ge *et al.*, Phys. Rev. **D111**, 8, 083534 (2025), [arXiv:2411.06000].

[79] L. Knox and Y.-S. Song, Phys. Rev. Lett. **89**, 1, 011303 (2002), [arXiv:astro-ph/0202286]; M. Kesden, A. Cooray and M. Kamionkowski, Phys. Rev. Lett. **89**, 011304 (2002), [arXiv:astro-ph/0202434]; C. M. Hirata and U. Seljak, Phys. Rev. **D68**, 8, 083002 (2003), [arXiv:astro-ph/0306354].

[80] Planck Collab. 2013 Results XII, Astron. Astrophys. **571**, A12 (2014), [arXiv:1303.5072]; Planck Collab. 2015 Results X, Astron. Astrophys. **594**, A10 (2016), [arXiv:1502.01588]; Planck Collab. 2018 Results IV, Astron. Astrophys. **641**, A4 (2020), [arXiv:1807.06208].

[81] B. Gold *et al.*, Astrophys. J. Supp. **192**, 15 (2011), [arXiv:1001.4555].

[82] Planck Collab. Interm. Results XXX, Astron. Astrophys. **586**, A133 (2016), [arXiv:1409.5738].

[83] M. Millea *et al.*, Astrophys. J. **746**, 4 (2012), [arXiv:1102.5195].

[84] Sunyaev, R. A. and Zeldovich, Ya. B., Ann. Rev. Astron. Astrophys. **18**, 537 (1980).

[85] R. Williamson *et al.*, Astrophys. J. **738**, 139 (2011), [arXiv:1101.1290].

[86] M. Hilton *et al.*, Astrophys. J. Supp. **253**, 1, 3 (2021), [arXiv:2009.11043].

[87] Planck Collab. Early Results VIII, Astron. Astrophys. **536**, A8 (2011), [arXiv:1101.2024].

[88] Planck Collab. 2013 Results XX, Astron. Astrophys. **571**, A20 (2014), [arXiv:1303.5080].

[89] L. Salvati *et al.*, Astrophys. J. **934**, 2, 129 (2022), [arXiv:2112.03606]; E. Lee, R. Battye and B. Bolliet, Mon. Not. R. Astron. Soc. **538**, 4, 2768 (2025), [arXiv:2403.19542].

[90] Planck Collab. 2018 Results IX, Astron. Astrophys. **641**, A9 (2020), [arXiv:1905.05697].

[91] Planck Collab. 2015 Results XVI, Astron. Astrophys. **594**, A16 (2016), [arXiv:1506.07135].

[92] Planck Collab. 2013 Results XXII, Astron. Astrophys. **571**, A22 (2014), [arXiv:1303.5082]; Planck Collab. 2015 Results XX, Astron. Astrophys. **594**, A20 (2016), [arXiv:1502.02114].

[93] Planck Collab. 2015 Results XIV, Astron. Astrophys. **594**, A14 (2016), [arXiv:1502.01590].

[94] Planck Collab. Interm. Results XLVI, Astron. Astrophys. **596**, A107 (2016), [arXiv:1605.02985].

[95] X. Fan, C. L. Carilli and B. Keating, Ann. Rev. Astron. Astrophys. **44**, 415 (2006), [arXiv:astro-ph/0602375].

[96] M. Ouchi, Y. Ono and T. Shibuya, Ann. Rev. Astron. Astrophys. **58**, 617 (2020), [arXiv:2012.07960].

[97] Planck Collab. Interm. Results XLIX, Astron. Astrophys. **596**, A110 (2016), [arXiv:1605.08633]; E. Komatsu, Nature Reviews Physics **4**, 7, 452 (2022), [arXiv:2202.13919].

[98] M. Kamionkowski and A. Kosowsky, Ann. Rev. Nucl. Part. Sci. **49**, 77 (1999), [arXiv:astro-ph/9904108].

[99] Planck Collab. 2015 Results XIX, Astron. Astrophys. **594**, A19 (2016), [arXiv:1502.01594].

[100] Planck Collab. Interm. Results XXIV, Astron. Astrophys. **580**, A22 (2015), [arXiv:1406.7482].

[101] J. L. May *et al.*, in H. K. Marshall, J. Spyromilio and T. Usuda, editors, "Ground-based and Airborne Telescopes X," volume 13094 of *S.P.I.E. Conf. Ser.*, 1309432 (2024).

30. Cosmic Rays

Revised March 2026 by J. Alvarez-Muñiz (Santiago de Compostela U.), Z. Cao (IHEP Beijing), U.F. Katz (Erlangen U.), P. Mertsch (RWTH Aachen U.) and C. Spiering (DESY, Zeuthen).

30.1 Theory

Cosmic rays (CRs) are a non-thermal population of particles that pervade the Universe. Their salient characteristics can be inferred from their major observational properties: spectrum, composition, and arrival directions. For charged CRs, the energies extend from tens of MeV to close to 1 ZeV, the intensity is $\sim 10^4\,\mathrm{m}^{-2}\,\mathrm{s}^{-1}\,\mathrm{sr}^{-1}$ above 1 GeV, but the differential spectrum falls steeply with energy E, following a power-law dependence $E^{-\gamma}$. The most striking spectral features are the "knee" at a few PeV where the spectral index γ changes from ~ 2.7 to ~ 3, the "second knee" at ~ 100 PeV with a change to ~ 3.3 and the "ankle" at a few EeV where γ changes to ~ 2.5. The flux is largely suppressed above a few tens of EeV. (More detailed discussion of spectral features can be found below in Secs. 30.2.1 and 30.2.2.) Charged CRs are composed mostly of protons, helium, and other nuclei, as well as electrons, positrons and anti-protons. The arrival directions are mostly isotropic, but below and around the knee interesting $\mathcal{O}(10^{-4}\ldots10^{-3})$ anisotropies due to the distribution of sources and properties of the Galactic magnetic fields have been observed, reaching $\sim\mathcal{O}(10^{-1})$ at the highest energies. Gamma-rays can be resolved into those from astrophysical sources (~ 6660 [42] above 50 MeV, ~ 300 [43, 44] at TeV energies), plus diffuse fluxes of galactic and extra-galactic origin, predominantly showing power-law dependence on energy. The observation of high-energy neutrinos has opened a new window; while the distribution is largely isotropic, evidence for two extra-galactic sources as well as for a contribution from the galactic plane has been found. The energy spectra of charged CRs, diffuse gamma-rays and neutrinos are shown in Fig. 30.1. Combined observations of charged CRs, gamma-rays and neutrinos as well as gravitational waves (see Sec. 21.2.3) allow for valuable insights into the most extreme astrophysical environments and is referred to as multi-messenger astrophysics. Adding the contribution from all species results in the all-particle spectrum. While it was believed for a long-time that it was a featureless power law up to the knee at a few PeV, it has now been recognized that it has much more structure, mirroring the features in the individual species. These features carry important information on the acceleration and transport of CRs.

The energy variables used are kinetic energy E, kinetic energy per nucleon, $E_\mathrm{n} = E/A$ for a particle of mass number A, or rigidity $\mathcal{R} \equiv pc/(Ze)$ (given in units of volt) for a particle of charge number Z, p being the momentum of the particle; the term rigidity refers to the resistance against deflections in a magnetic field B: particles of low (high) rigidity have small (large) gyroradii $r_\mathrm{g} = 1\,\mathrm{kpc}\,(\mathcal{R}/\mathrm{EV})\,(B/\mu\mathrm{G})^{-1}$. Kinetic energy is closely related to the experimental signatures of a calorimetric instrument, while rigidity is the most natural one for a spectrometric one. Note also that relativistic nuclei suffer little energy losses and their transport is prescribed by magnetic fields, thus it can only depend on rigidity. The *intensity* J of CRs, also called the diffuse flux, is defined through the differential number $\mathrm{d}N$ of particles with energy in the interval $[E, E+\mathrm{d}E]$, crossing the area $\mathrm{d}A$ from a solid angle $\mathrm{d}\Omega$ in the time $\mathrm{d}t$: $\mathrm{d}N = J\,\mathrm{d}E\,\mathrm{d}A\,\mathrm{d}\Omega\,\mathrm{d}t$. Its isotropic part is related to the differential density $\psi = (4\pi/v)J$, v being the particle speed and to the phase-space density f as $J = p^2 f$. Note that the intensity can also be defined in reference to particle energy per nucleon or rigidity. To stress this, often the intensity is written as $\mathrm{d}J/\mathrm{d}E$, $\mathrm{d}J/\mathrm{d}E_\mathrm{n}$ or $\mathrm{d}J/\mathrm{d}\mathcal{R}$.

In the detection of CRs, two classes of techniques are distinguished [45]. *Direct observations*, see Sec. 30.2.1, make use of the interactions of CRs in particle physics detectors (e.g. trackers, spectrometers and calorimeters). Given the limited exposures of such instruments and the steeply falling spectra, this is currently only realistic below ~ 100 TeV. In *indirect observations*, see Sec. 30.2.2, showers of secondary particles initiated by charged CR interactions in natural materials (e.g. air, water or ice) are detected through fluorescence, air-Cherenkov, water-Cherenkov or scintillation effects. This allows for large instrumented surfaces or volumes. Historically, the two classes of techniques have been employed by two separate communities and we structure the review of charged CRs accordingly. For detection of gamma-rays, direct observations are relevant mostly below hundreds of GeV; for gamma-rays of higher energies and neutrinos of essentially all energies, indirect observations are required.

Charged CRs are deflected by magnetic fields and so generally speaking the observed events do not point back to sources. CRs can however reach the earth from galactic and even cosmological distances. Between hundreds of MeV and at least a few PeV, CRs are believed to be of galactic origin; above a few EeV, the sources are most likely extra-galactic. If CRs with energies in excess of ~ 1 EeV came from sources in the Galactic disk, the angular distribution at Earth would be very anisotropic, which is at variance with observations. And if CRs below ~ 1 PeV were dominantly of extra-galactic origin, this would result in a gamma-ray flux from objects like the Large Magellanic Cloud exceeding observations [46]. Direct and indirect observations therefore also largely refer to galactic/extra-galactic sources, respectively. CRs with energies in excess of 1 EeV are referred to as ultra-high energy cosmic rays (UHECRs).

Sources of non-thermal electromagnetic radiation are routinely observed, see Sec. 30.3, yet the dominant source of locally measured CRs have not been unambiguously identified. Source candidates are typically associated with endpoints of stellar evolution or supermassive black holes that release large amounts of gravitational or rotational energy [47]. In the Galaxy, the prime candidates are supernova remnants [48] where particles can be shock-accelerated by their blast waves [49]. Other candidates are star cluster winds [50,51], stellar wind binaries, micro quasars [52] (a source powered by accretion from a donor star onto a stellar mass black hole) or even the Galactic Center [53]. The candidate sources for extra-galactic CRs are Active Galactic Nuclei (AGN) [54], specifically blazars and radio galaxies, gamma-ray bursts [55], starburst galaxies [56, 57], pulsars [58] and magnetars [59]. These objects exhibit power-law spectra in electromagnetic radiation, albeit in limited wavelength ranges. The acceleration mechanisms considered in the literature are shock acceleration [49,60,61], stochastic acceleration [62], and reconnection [63]. A fundamental constraint on the maximum energy, the so-called Hillas criterion [64], follows from the requirement that the gyroradius must be smaller than the source size.

In the Milky Way, the dominant process in CR transport is diffusion as evidenced by the small anisotropies in CR arrival directions and by certain abundance ratios of nuclear species. This diffusive transport bears some resemblance with heat transport in that it smooths the spatial distribution of CRs. However, in contrast to heat transport, CR diffusion is not due to collisions, but interactions with turbulent magnetic fields. Generally, CRs interact "resonantly" with plasma waves, that is they get affected only by waves with a wavelength similar to the gyroradius of the CR particle. If this condition is satisfied, a CR particle will be deflected by the Lorentz force. Many random deflections lead to a random walk in space, that is diffusion [65]. Recently, scattering on non-wave-like perturbations has gained some attention [66].

There is a number of other processes contributing to the transport of charged CRs: momentum losses, i.e. radiative losses for electrons and positrons [68], ionization and Coulomb losses for nuclei, electrons and positrons [69]; spallation, that is production of (mostly) lighter nuclei by inelastic collisions of heavier ones; and other inelastic collisions, e.g. the production of light mesons. We note that progress in the study of CR transport is often limited by the nuclear interactions since many cross-sections are poorly known, if at all [70]. The various processes are encoded in the CR transport equation [71], also referred to as the Parker transport equation [72] in the space physics community. This partial differential equation is supplemented by the boundary condition of free escape on the surface of the (often cylindrical) confinement volume. Only in simplified cases can this equation be solved analytically. The most instructive case is the 1D approximation where only the direction perpendicular to the Galactic disk is retained. The solution differs for *primaries*, that is species present and accelerated in the CR sources, and *secondaries*, which are not present in CR sources, but pro-

Int. J. Mod. Phys. A 2026.41. Downloaded by UNIVERSITY OF CALIFORNIA @ BERKELEY on 09/16/26. Reproduction strictly not permitted, except for Open Access articles. worldscientific.com

Int. J. Mod. Phys. A 2026.41. Downloaded from www.worldscientific.com
by UNIVERSITY OF CALIFORNIA @ BERKELEY on 09/16/26. Re-use and distribution is strictly not permitted, except for Open Access articles.

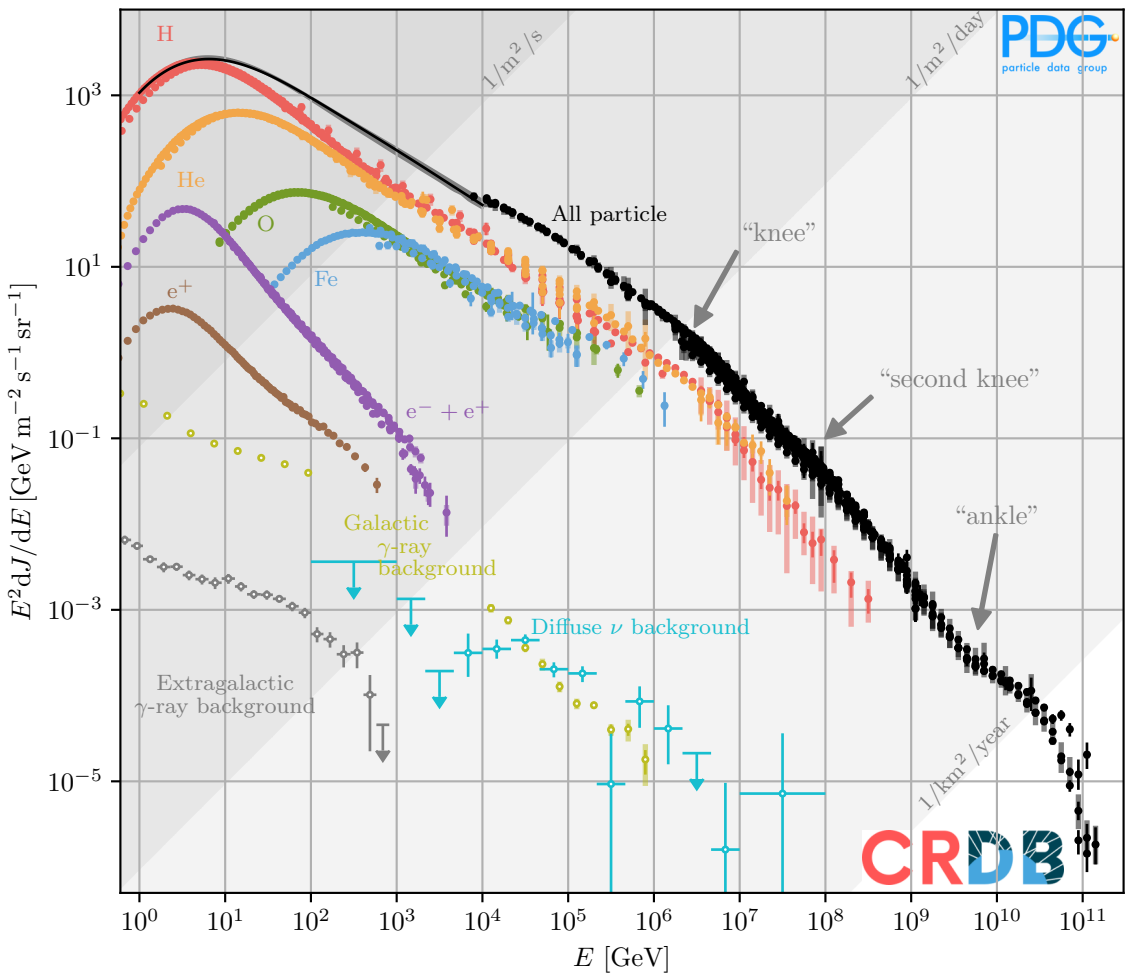

Figure 30.1: The spectrum of cosmic rays (CRs). Shown are measurements of the intensity of charged and neutral CRs, multiplied by kinetic energy squared. The data for the charged CRs [1–33] have been extracted from the Cosmic Ray Database (CRDB) [34] and we also include LHAASO data [35, 36]. Below 10^4 GeV, the all-particle spectrum is the sum of spline fits of the most important nuclear species. The diffuse γ-ray fluxes have been extracted from Refs. [37–40], measurements of the diffuse neutrino background from Ref. [41]. Energy-integrated intensities are indicated by the various diagonal lines.

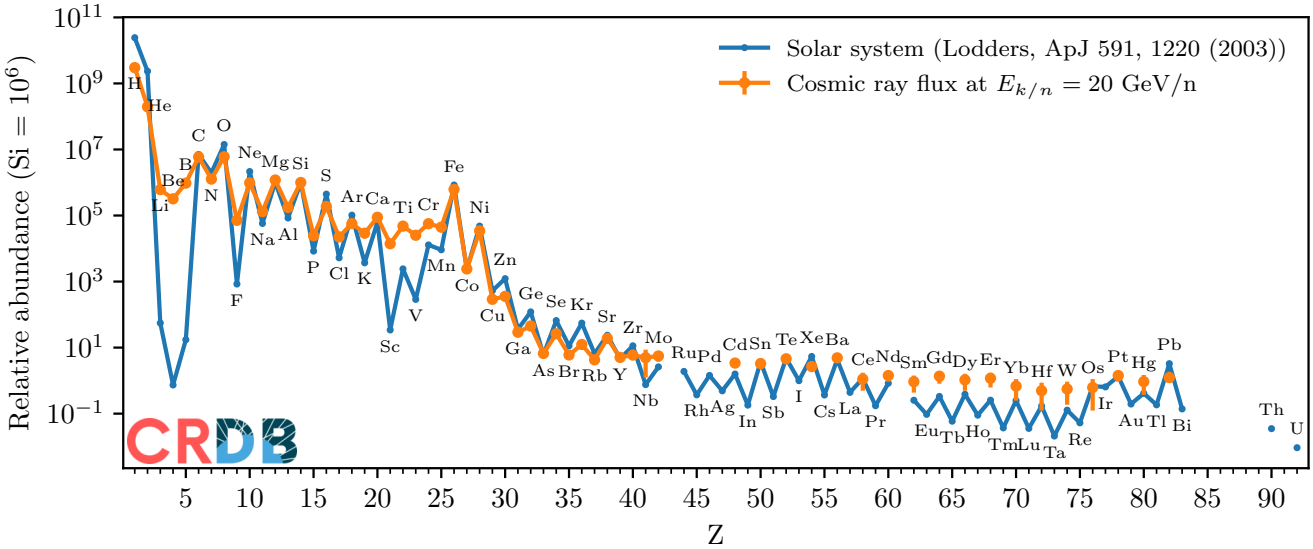

Figure 30.2: CR abundances compared with solar system ones [67]. Modified from [34].

Int. J. Mod. Phys. A 2026.41. Downloaded from www.worldscientific.com by UNIVERSITY OF CALIFORNIA @ BERKELEY on 09/16/26. Re- strictly not permitted, except for Open Access articles.

duced by inelastic collisions of primaries in the gaseous disk of the Galaxy. Diffusion in the Galaxy, characterized by a diffusion coefficient $\kappa(\mathcal{R})$, modifies the source spectrum $q(\mathcal{R})$, resulting in the steady-state spectrum $\psi(\mathcal{R}) \propto q(\mathcal{R})/\kappa(\mathcal{R})$. As the production spectrum of secondaries follows the steady-state spectrum of primaries, $q_2(\mathcal{R}) \propto \psi_1(\mathcal{R})$, the secondary steady-state spectrum is $\psi_2(\mathcal{R}) \propto q_2(\mathcal{R})/\kappa(\mathcal{R}) \propto \psi_1(\mathcal{R})/\kappa(\mathcal{R})$. As $\kappa(\mathcal{R})$ grows with $\mathcal{R}$, secondary spectra $\psi_2(\mathcal{R})$ fall more quickly with rigidity than primary spectra $\psi_1(\mathcal{R})$. Unstable secondaries provide additional constraints on the gas density and residence time of CRs. The solution of the transport equation in more realistic setups requires numerical codes [73–76].

Protons (iron nuclei) with energies in excess of $\sim 1\,\mathrm{EeV}$ ($\sim 26\,\mathrm{EeV}$) in a micro-Gauss magnetic field have gyroradii larger than the typical kiloparsec scales of the Galaxy, thus they cannot be confined. Their directions are however affected by so-called small-angle scattering, both in the Milky Way and possibly outside. As far as their spectrum and composition is concerned, protons and heavier nuclei suffer from inelastic collisions with the CMB and the extra-galactic background light at the highest energies. For protons above 10 EeV, photo-pion production limits the propagation distances to $\sim 100\,\mathrm{Mpc}$; for nuclei, heavier ones photo-disintegrate to lighter ones, also limiting their spatial reach. Both processes can lead to a suppression of the flux known as the GZK (Greisen, Zatsepin, Kuzmin) effect [77,78] and produce secondary gamma-rays and neutrinos. Other secondary particles include neutral and charged pions, which ultimately decay to photons, electrons, positrons and neutrinos, and electron-positron pairs which can also initiate a cascade of photons and lower energy electrons and positrons. The stable decay products, in particular gamma-rays and neutrinos can be used as an additional diagnostic tool for the study of the origin and transport of UHECRs.

In many astrophysical environments, the energy density of CRs constitutes a significant fraction of the total or is comparable to that of other ingredients. For instance, on galactic scales, the CR energy density is of the same order as that of magnetic fields, radiation fields or the turbulent gas. Due to their pressure, CRs can be dynamically important and shape their environments: Specifically, CRs contribute to the gravitational support of galaxies and can drive galaxy-scale outflows. They ionize neutral gas, thus determining coupling of gas and magnetic fields. CRs can generate turbulence by a variety of streaming instabilities [79, 80], which play a central role in shock acceleration and galactic transport [81]. Finally, CRs also produce diffuse emission through interactions with gas and radiation fields, an additional handle for CR studies.

CRs are also important probes of fundamental physics. If dark matter has interactions with the Standard Model, the products of self-annihilation or decay of DM particles can potentially be observed (DM, see Sec. 27.7). This is called DM indirect observation. Generically, one would expect similar rates of production of particles and antiparticles whereas astrophysical sources predominantly accelerate matter particles. It is therefore advisable to search for signals in CRs positrons, anti-protons and anti-nuclei [82, 83]. In fact, excesses have been reported of positrons and anti-protons, yet astrophysical pollutions and/or experimental systematic uncertainties cannot be excluded. There have also been searches in gamma-rays and neutrinos and a number of studies have indentified an excess of gamma-rays from the Galactic Center that is compatible with DM particles of weak-scale mass and weak annihilation cross-section [84]. Another target for exotic searches in CRs is anti-matter of primordial origin [85]. Most interestingly, the AMS-02 collaboration has claimed $\mathcal{O}(10)$ $\overline{\mathrm{He}}$ candidate events, but whether those are of primordial origin as opposed to instrumental effects is at this point not clear.

30.2 Charged cosmic rays

30.2.1 *Direct observations*

Direct observations [86] cover energies between a few MeV and a few tens of TeV, where CRs must be of Galactic origin. At energies lower than a few MeV, solar energetic particles [87] are dominating the flux; above a few tens of TeV, the fluxes are too low to be observed directly and instead indirect detection techniques [88] need to be used. Besides spectral information, direct observations enable identification of species on an event-by-event basis, certain experiments even provide isotopic discrimination. We present a compilation of direct observations of the most important primary and secondary nuclei in Fig. 30.3. These show broken power-law spectra in rigidity with $J \propto E^{-\gamma}$ in different rigidity ranges. The various changes in spectral slope contain valuable information on the rigidity-dependence of the diffusion coefficient κ and the primary source spectra q_1.

Protons are dominating the CR flux by number and by energy below $\sim 10\,\mathrm{TeV}$ and their spectrum has been measured with excellent precision. Measurements of the proton spectrum and other primaries are shown in the left panel of Fig. 30.3. Data from the AMS-02 experiment [8] show a $\mathcal{R}^{-2.8}$ spectrum above $\sim 10\,\mathrm{GeV}$ with a break to $\mathcal{R}^{-2.7}$ at $\sim 300\,\mathrm{GV}$. This feature had been observed by PAMELA earlier [2], and also with CREAM and ATIC for heavier nuclei [89, 90]. As a reminder, at energies above a few GeV, the measured spectrum can be interpreted as the ratio of the source spectrum $q(\mathcal{R}) \propto \mathcal{R}^{-\Gamma}$ divided by the diffusion coefficient $\kappa(\mathcal{R}) \propto \mathcal{R}^{\delta}$. Thus a spectral index of $\gamma = \Gamma + \delta \simeq 2.8$ can describe the data. On the basis of proton data alone, the degeneracy between the source spectral index Γ and the spectral index of the diffusion coefficient δ cannot be broken. Also, the break at $\sim 300\,\mathrm{GV}$ could be a break in the source spectrum or in the diffusion coefficient, but see below. At energies lower than $\sim 10\,\mathrm{GeV}$, the spectrum turns over because of energy losses and solar modulation. At energies beyond the reach of AMS-02, both DAMPE and CALET data show a softening at rigidity $\sim 10\,\mathrm{TV}$ [7, 10], confirming earlier indications [89, 90]. Indirect observations, see Sec. 30.2.2 are indicating another hardening at $\sim 200\,\mathrm{TeV}$ [32].

Most of the other primary species, that is helium, carbon, nitrogen, oxygen, neon, magnesium and silicon with the notable exception of iron, also show a spectral break at $\sim 300\,\mathrm{GV}$, but their spectra are generally harder than the proton one, e.g. $\gamma_{\mathrm{He}} < \gamma_{\mathrm{p}}$, both below and above the break. Suggested explanations for this difference in spectrum include gradients in the relative circumstellar abundances of protons and heavier nuclei or invoking different source populations for these two groups. At $\sim 10\,\mathrm{TV}$ a softening break mirrors the feature observed in protons [91]. Above an energy of $\sim 100\,\mathrm{TeV}$, elemental information is scarse, but a combined analysis of proton and helium by DAMPE extends to $\sim 300\,\mathrm{TeV}$ and indicates another spectral hardening [92]. (Note that this data are not included in Fig. 30.3 though.) Such a feature was to be expected to a certain degree in order to connect to the indirect measurements of proton and helium which start at $\sim 1\,\mathrm{PeV}$. Note that there exist some 20 % discrepancies between the oxygen and carbon data from AMS-02 [8], CALET [13] and PAMELA experiments [93] in normalization, possibly also in spectral shapes.

Iron constitutes an exception to the otherwise rather similar slopes of primary species heavier than proton. As is also the case for other nuclei, AMS-02 [15] and CALET [16] disagree on the normalization by $\sim 20\,\%$, but both measurements of the iron spectrum exhibit spectral shapes different from the oxygen ones. While the ratio of Fe/O could be accommodated if all nuclei traversed the same amount of matter (grammage) between source and observer (the so-called slab model), more realistic models cannot explain the observations [94]. Also, the AMS-02 data on Fe/O are in tension with earlier measurements [95, 96]. Most interestingly, if extrapolated to lower energies, the Fe/O could only be accommodated if solar modulation was negligible.

Measurements of *stable* secondary nuclei contribute two important pieces of information to the standard scenario of galactic CRs: First, their over-abundance in CRs (with respect to solar system values, see Fig. 30.2) indicates diffusion as the primary transport process; and second, their spectral shapes, or rather the difference in spectral shapes between secondaries and primaries allows inference of the diffusion coefficient. Specifically, at energies where energy losses can be ignored for nuclei, that is above a few GeV, the propagated spectra of primaries $\psi_1(\mathcal{R})$ are approximately $\propto \mathcal{R}^{-2.8\ldots-2.7}$, which is explained as a softening of the sources spectrum $q_1(\mathcal{R})$. Secondaries, however, are produced with a spectrum proportional to the propagated primary

Int. J. Mod. Phys. A 2026.41. Downloaded from www.worldscientific.com
by UNIVERSITY OF CALIFORNIA @ BERKELEY on 09/16/26. Re-use and distribution is strictly not permitted, except for Open Access articles.

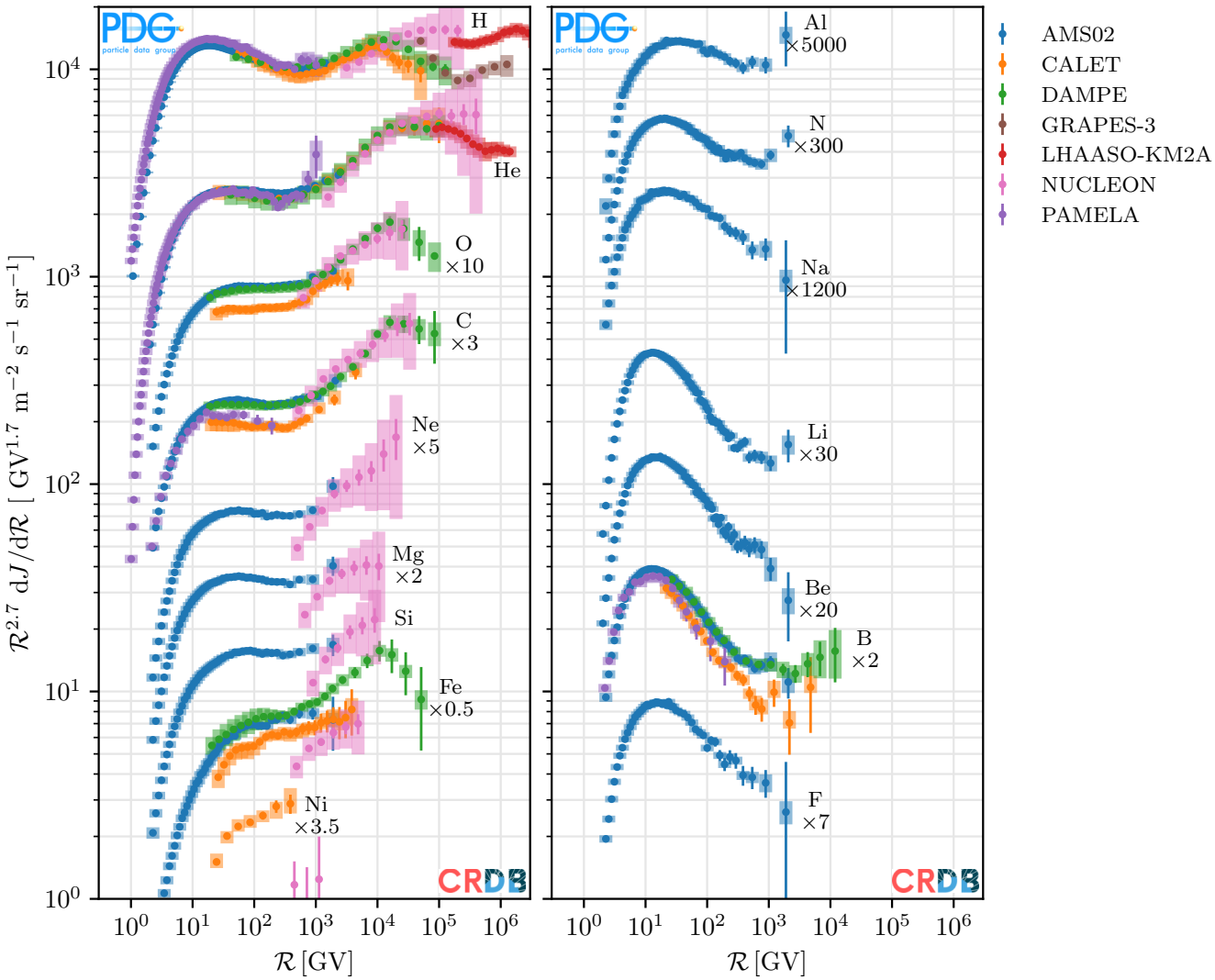

Figure 30.3: Rigidity spectra for a selection of CR nuclei. Primary species are shown in the left panel, (mostly) secondary species in the right panel. The error bars denote the statistical uncertainties, the shaded bars represent the systematic uncertainties. The spectra have been shifted and multiplied by $\mathcal{R}^{2.7}$ to better bring out spectral features. Here, we have constrained ourselves to data from space-borne experiments of the last ten years, that is AMS-02 [8,15,97–100], CALET [10,16,91,101,102], DAMPE [7,13,33,103], NUCLEON [5] and PAMELA [2,93], but also included the ground-based GRAPES-3 [32] experiment and LHAASO data [35,36]. Data have been extracted from [34].

spectrum, $q_2(\mathcal{R}) \propto \psi_1(\mathcal{R})$ which also gets further softened by the diffusion coefficient. The difference in spectral index can be clearly seen when comparing primary with secondary spectra. A compilation of such secondary spectra from AMS-02 [8, 98, 99], CALET [101], DAMPE [103] and PAMELA [93] is shown in the right panel of Fig. 30.3. Lithium, beryllium, boron and fluorine can be identified as almost pure secondaries by their soft spectra. Aluminium, sodium and neon, however, have harder spectra, somewhere intermediate between primaries and secondaries. This can be understood as being due to mixture of softer secondary contribution from spallation in the interstellar medium (ISM) and a harder primary source component. Secondaries also exhibit a hardening break at $\sim 300\,\mathrm{GV}$, but the change in spectral slope is about twice as big [104] when compared to that of the primaries. This fact serves as evidence for the break being due to a change in the rigidity-dependence of the diffusion coefficient, as opposed to a break in the source spectrum [105,106]. Recently, there have been some claims of excesses in low-energy intensities of Li, F, Al [107], however these claims are somewhat controversial. We note the importance of composition studies for shedding light on cosmic ray origin.

Unstable isotopes with a lifetime similar to the residence time of CRs can be used to study galactic propagation. Among these species, ^{10}Be, ^{26}Al and ^{60}Fe have been studied the most as their rest lifetime is close to the residence time of CRs at GV rigidities. Roughly speaking, the flux ratio of an unstable and a stable secondary that are both produced from similar primary species, reflects the ratio of production cross-section at high energies (where decay is suppressed by time-dilation). On the other hand, at low energies, this ratio is suppressed due to the decay of the unstable species. The transition takes place at energies where the decay time equals the residence time in the Galactic disk. At present, there is limited information on ratios at energies beyond 1 GeV/nucleon where the transition for the ratios of the above mentioned unstable nuclei is expected to take place.

CR electrons are also believed to be accelerated in the preferred candidate sources of nuclei, that is, SNRs. Other source candidates are pulsars and pulsar wind nebulae (PWNe); in the simplest models those also accelerate similar amounts of CR positrons. We show a compilation of the most recent and precise data from AMS-02 [8], CALET [108], DAMPE [17], *Fermi*-LAT [18], H.E.S.S. [109] and PAMELA [110] on CR electrons, positrons and the sum of electrons and positrons in Fig. 30.4. In addition to the processes at work in the propagation

Int. J. Mod. Phys. A 2026.41. Downloaded from www.worldscientific.com by UNIVERSITY OF CALIFORNIA @ BERKELEY on 09/16/26. Re-use strictly not permitted, except for Open Access articles.

of nuclei, electrons suffer significant radiative losses due to synchrotron emission and inverse Compton scattering. In fact, for the parameters determined in the standard scenario, the cooling time is shorter than the residence time above $\sim$ 10 GeV. For the same source spectral index, the spectra are predicted to be softer than those of primary nuclei. Indeed, the observed spectrum is roughly $\propto E^{-3.1}$ below ~ 1 TeV.

At energies above ~ 1 TeV, only calorimetric observations are currently available which cannot discriminate between electrons and positrons. Observations of the all-electron flux, that is the sum of electron and positron fluxes, find a break at $\sim$ 1 TeV, displayed in Fig. 30.4. This energy range is particularly interesting in the search for nearby source of (leptonic) CRs. Due to the increasingly important radiative losses, the distance to the sources which could significantly contribute to the total flux decreases with energy. Estimates at 1 TeV of this diffusion-loss length are only $\simeq 0.3$ kpc. The predicted spectrum therefore becomes rather sensitive to the exact distances and ages of young, nearby sources which manifest as individual bumps in the spectrum. Turning this around, observations can be used to search for young, nearby sources of CRs. The break by about one power in energy has been interpreted either as due to a break in the spectrum of a large number of sources, e.g. [111] or as a stochasticity effect from a small population of sources [112].

If positrons were only produced by spallation in the interstellar medium, the positron spectrum should be softer than the electron one. PAMELA [113] and more so AMS-02 have now measured the spectrum with great precision up to $\sim$ 1 TeV [8]. Between ~ 10 GeV and ~ 100 GeV its spectral index γ_{e^+} transitions from 3 to 2.7 before a spectral break or cut-off at a few hundred GeV as shown in Fig. 30.4. The origin of the harder positron spectrum remains unclear today, and most of the existing literature has entertained on of the follwoing three interpretations: The annihilation of weak-scale (WIMP) dark matter [114] can produce a hard spectrum of electrons and positrons that could *in principle* accommodate the observational data, if the annihilation cross-section was enhanced over the generic WIMP one by orders of magnitude. However, such interpretations are now severely constrained by observations of gamma-rays, anti-protons and the cosmic microwave background (CMB, see Chap. 29). Production of e^+ in pulsars or PWNe is an astrophysical explanation that had been hypothesized long before the PAMELA observations (e.g. [115]). Recently, there have been observations of extended emission of high-energy gamma-rays, so-called gamma-ray halos around PWNe [116], interpreted as evidence of the presence of high-energy electrons and positrons around these objects. Other astrophysical explanations include the production and subsequent acceleration of secondaries in old SNRs [117, 118].

In the standard scenario of galactic cosmic rays, anti-protons are also produced as secondary particles, but unlike secondary nuclei or electrons and positrons, their production is kinematically suppressed at lower energies. The spectrum of anti-protons observed by PAMELA (Fig. 3 in [119]) and AMS-02 (Fig. 62 in [8]) is close to $E^{-2.8}$, which is somewhat harder than predicted by earlier models. More recent models can accommodate the observations, in part due to a re-evaluation of the production cross-section. Note that there have been claims that the transport parameters obtained when fitting to proton and anti-proton data differ from those obtained by fitting to heavier nuclei [120]. An alternative explanation for the harder anti-proton spectrum is the acceleration of secondaries in old supernova remnants [118, 121]. At energies of a few GeV, there have been claims of an excess in the measured anti-proton spectrum. If interpreted as a sign of dark matter annihilation, such an excess could be explained by a weak-scale particle of mass of a few tens of GeV and annihilation cross-sections close to the thermal relic value. However, the significance of the signal is relatively low if correlations in the cross-section uncertainties and in the measurements are taken into account. Considering the spectra of anti-protons together with protons and positrons, it appears that all three have similar spectral indices between ~ 10 GV and ~ 300 GV. This is rather surprising, given that as secondaries positrons and anti-protons should have spectra softer than the primary protons, due to energy losses and diffusive losses, respectively. In the standard scenario this cannot be explained and thus must be considered a mere coincidence.

The only astrophysical mechanism for production of anti-nuclei like anti-deuterons ($\overline{\mathrm{D}}$) or anti-helium ($^3\overline{\mathrm{He}}$ or $^4\overline{\mathrm{He}}$) is coalescence of anti-nucleons produced in the spallation of primary nuclei in the interstellar medium. Due to kinematics, however, this is significantly suppressed at energies below a few GeV, thus rendering this an interesting channel for searches of dark matter, in particular for relatively light WIMPs with masses of a few GeV or less. The AMS-02 collaboration has reported some ten candidate events of anti-helium, yet the rate of $^3\overline{\mathrm{He}}$ or $^4\overline{\mathrm{He}}$ is incompatible with models of coalescence (e.g. [122]). Currently, the most constraining limits on $\overline{\mathrm{D}}$ are from the BESS balloon flights [123]. This should be improved on by the upcoming GAPS experiment, and also an upgrade of the AMS-02 experiment increasing the acceptance by a factor of three could help clarifying the situation.

Another important observable in the study of CRs are anisotropies, most commonly defined as the relative directional deviation of the CR intensity from the angular average. As the typical anisotropies are at the level of one part in 10^3 or 10^4, high statistics are required. At TeV and PeV energies, only ground-based experiments have enough statistics, yet they cannot constrain the component of the anisotropy that is aligned with the Earth's rotation axis. Traditionally, therefore, only the projection of the true 2D dipole into the equatorial plane has been reported in terms of an amplitude and phase. We show a compilation [34] in Fig. 30.5. The amplitude is at the level of $\simeq 10^{-4}$ at energies of hundreds of GeV and increases to $\simeq 10^{-3}$ at tens of TeV. At ~ 100 TeV there is a dip before the amplitude rises again. Beyond a few PeV upper limits exist at the level of 10^{-2}. The Compton-Getting effect [124, 125], that is a dipole anisotropy due to the relative motion of the solar system with respect to the Galactic rest frame has been experimentally confirmed [126]. The phase is relatively constant at a direction of 45° and switches to 250°, which is close to the Galactic Center direction, also around 100 TeV. For a description of anisotropies at the highest energies see Section 30.2.2. In addition, observations of anisotropies on scales smaller than the dipole have been reported (see Ref. [127]). These are not expected in standard diffusion theories that only predict a dipole. The leading explanation is the generation due to the specific realization of the turbulent magnetic field in our Galactic neighbourhood.

30.2.2 *Indirect observations*

In the energy range above $\simeq 1$ PeV the intensity of cosmic rays is so low that it prevents the collection of a statistically significant sample of these particles in a direct manner with detectors carried on balloons or satellites. Instead, cosmic rays are detected indirectly through the cascade of particles they produce in the atmosphere, the so-called extensive air showers (EAS). In this way, cosmic rays up to and even above 100 EeV have been observed [128–130], corresponding to about a hundred million times larger energy than that achieved by particles accelerated in human-made experiments.

Extensive Air Showers. Extensive air showers (EAS) are cascades of millions to billions of secondary particles initiated by a single primary particle (cosmic ray: proton, neutron, heavier nucleus, photon, or neutrino) of energy E in the atmosphere. Owing to the low air density $\rho \lesssim 10^{-3}\,\mathrm{g\,cm^{-3}}$, the shower develops throughout the atmosphere and, for a 10 EeV primary, extends laterally over $\sim 10\,\mathrm{km}^2$ at ground level, hence the name EAS.

When an energetic ($E \gtrsim 1$ PeV) cosmic proton or nucleus interacts with an air nucleus, it produces from a few to hundreds of secondaries depending on its energy. On average, $\sim 30\% - 40\%$ of the primary energy is carried by a leading baryon or nucleus, while the rest generates ultra-relativistic secondaries, mostly charged ($\pi^\pm$) and neutral (π^0) pions, with fewer hadrons and heavier mesons such as kaons and ρ-mesons. The primary energy quickly degrades into many secondaries that may interact or decay depending on their nature, energy, and the medium density, further feeding the shower development. If $\pi^\pm$ live long enough, they can interact with an air nucleus before decaying. At altitudes of a few

Int. J. Mod. Phys. A 2026.41. Downloaded from www.worldscientific.com
by UNIVERSITY OF CALIFORNIA @ BERKELEY on 09/16/26. Re-use and distribution is strictly not permitted, except for Open Access articles.

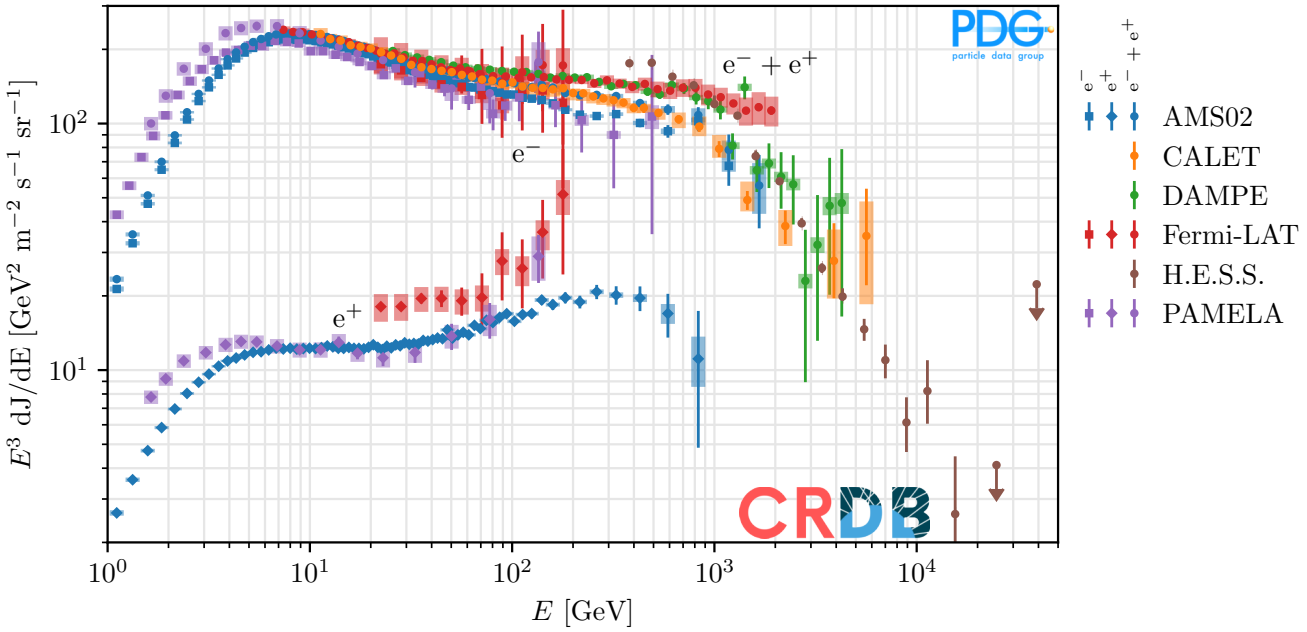

Figure 30.4: Intensities of cosmic ray electrons (squares), positrons (diamonds) and their sum (dots) as a function of kinetic energy E. We have included data from the most recent space experiments AMS-02 [8], CALET [108], DAMPE [17], *Fermi*-LAT [18] and PAMELA [110] as well as from the ground-based H.E.S.S. experiment [109]. The spectra have been multiplied by E^3 to enhance the visibility of the spectral features. Data have been extracted from [34].

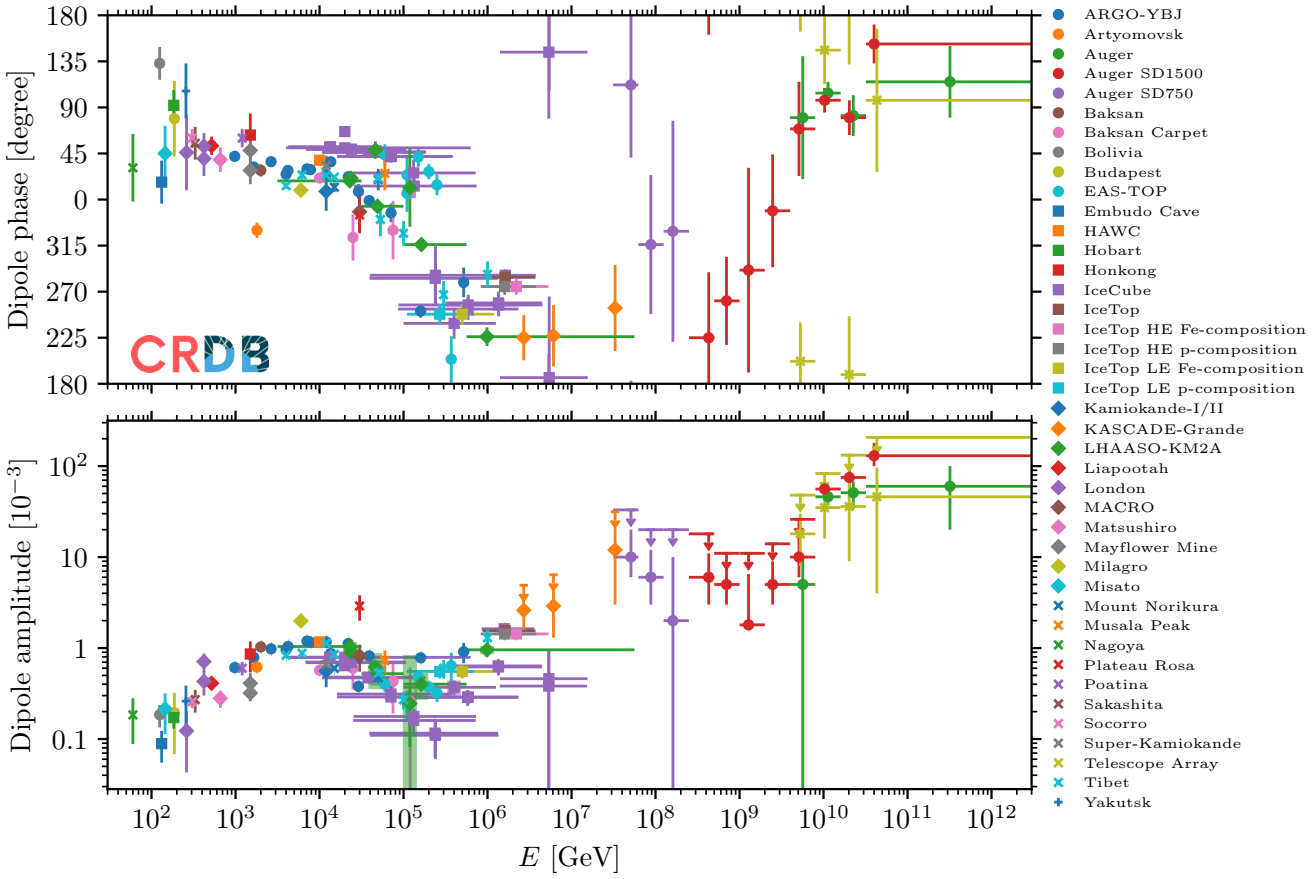

Figure 30.5: Phase and amplitude of the dipole anisotropy in CRs. Modified from Ref. [34].

Int. J. Mod. Phys. A 2026.41. Downloaded from www.worldscientific.com by UNIVERSITY OF CALIFORNIA @ BERKELEY on 09/16/26. Re-
strictly not permitted, except for Open Access articles.

km, where the air is less dense, most $\pi^{\pm}$ with $E_{\pi^{\pm}} \gtrsim 100\,\mathrm{GeV}$ interact, while lower-energy $\pi^{\pm}$ decay. Interacting $\pi^{\pm}$, together with the leading baryon and other hadrons, form a penetrating core of particles constituting the *hadronic component* (Fig. 30.6). Charged pions decaying into muons, $\pi^+ \to \mu^+ + \nu_\mu$ and $\pi^- \to \mu^- + \bar{\nu}_\mu$, provide the main contribution to the *muonic component* (Fig. 30.6) and generate most atmospheric neutrinos. Muons above a few GeV typically traverse the atmosphere without decaying, forming a penetrating component of the shower. Most π^0s, continuously produced in the hadronic core, decay almost immediately $\pi^0 \to \gamma\gamma$, as they seldom interact with air nuclei unless their energy exceeds $\sim 1\,\mathrm{EeV}$. They thus initiate electromagnetic subshowers. Neutral pions play a key role in generating the *electromagnetic component*, which dominates the shower (Fig. 30.6). It consists of e^- and e^+ with mean energy ~ 10 MeV mainly from photon pair production, and bremsstrahlung photons about an order of magnitude more numerous at 10 MeV [131]. Decaying muons also feed the electromagnetic component. The longitudinal development of the intertwined electromagnetic, muonic, and hadronic components is shown in Fig. 30.6. High-energy photons can occasionally photoproduce $\pi^{\pm}$, initiating hadronic subcascades and an additional muonic component.

As a cosmic-ray shower develops in the atmosphere, the number of particles increases along the shower axis. The traversed matter, X, is measured in $\mathrm{g\,cm^{-2}}$. The shower reaches the maximum of its electromagnetic component, $N_{\max}$, at a depth $X_{\max}$ (Fig. 30.6). After maximum, the number of electrons and positrons drops rapidly once their energy falls to the *critical energy* in air, $\sim 80\,\mathrm{MeV}$, where ionization losses dominate. Since neutrinos do not undergo electromagnetic interactions and high-energy muons reach the ground after losing only part of their energy, a fraction of the primary energy is not deposited in the atmosphere. This *invisible energy* accounts for $\approx 10\% - 20\%$ of the total shower energy above 0.1 EeV, decreasing with primary energy and increasing with its mass number [133]. Simultaneously, the shower expands laterally, as shown in Fig. 30.6, mainly due to the transverse momentum in hadronic interactions and the multiple Coulomb scattering of e^- and e^+.

Shower development is driven by the particles carrying most of the energy in the forward region of the kinematical phase space of the collisions with air nuclei. Particle production is dominated by non-perturbative QCD which is necessarily treated by using phenomenological approaches. Moreover, particle collisions occurring in the atmosphere at 0.1 EeV are equivalent to center-of-mass energies presently achieved at the LHC, and this energy scales up by a factor of approximately 30 at the highest cosmic ray energies observed. These two facts result in the need for extrapolations both in energy and phase space when modeling hadronic interactions [134]. The cosmic-ray community has developed sophisticated simulation packages such as AIRES [132] and CORSIKA [135, 136] to predict EAS observables as a function of primary energy and mass. These programs adopt models of hadronic interactions such as SIBYLL [137], QGSJET [138] and EPOS [139], tuned to a large data set including recent LHC data. Inferring fundamental properties of the primary particle initiating the shower, most notably its mass, requires the use of these air shower simulations. Large uncertainties remain, both due to theoretical limitations and the lack of data from existing collider experiments. A toy model to describe electromagnetic showers is due to Heitler [140], while for hadronic showers a model was developed by Matthews [141]. These oversimplified models shed light on the relation between the main shower observables and the nature of the primaries and predict that for the electromagnetic component, $N_{\max} \propto E$; $X_{\max} \propto \log E$ and $X_{\max} \propto \log A^{-1}$ with A the mass number of the primary nucleus; while for the muonic component, $N_\mu \propto A^{(1-\beta)} E^{\beta}$ with $\beta \simeq 0.85...0.95$. These important features of air showers constitute the basis for the identification of the primary particle with EAS (see next section). Similar features are also obtained in detailed Monte Carlo simulations of EAS development (Fig. 30.6), and have been observed experimentally.

Shower detection and cosmic-ray reconstruction. EAS have been detected with several techniques. Arrays of conventional particle detectors such as scintillators, water-Cherenkov stations or underground muon detectors, measure the lateral distribution of the shower front at ground, i.e., at a fixed depth. Due to the low cosmic-ray intensity especially at EeV energies (Figs. 30.1 and 30.7), the particle detectors are spread over large areas to compensate for the low flux, separated by distances that range from hundreds of meters to above 1 km. From the times at which the shower front hits several of these particle detectors, the arrival direction of the cosmic ray is measured with an accuracy typically better than $\sim 1°$. Shower arrays measure a shower size parameter, proportional to the number of secondary particles, that can be related to the energy E of the primary particle. With several types of detectors working together, it becomes possible to effectively separate the electromagnetic and muonic components of the shower, thereby providing an estimate of the mass of the primary. The main arrays of particle detectors for EAS observation above ~ 0.1 EeV currently in operation are the surface detector of water-Cherenkov stations and scintillators of the Pierre Auger Observatory in Argentina [142] spread over a total area of $\sim 3000\,\mathrm{km^2}$; the Telescope Array (TA) of scintillators in the USA ($\sim 700\,\mathrm{km^2}$) [143]; and the Yakutsk array of scintillators and underground muon detectors ($\sim 10\,\mathrm{km^2}$) in Russia [144]. Other arrays operating at energies $\gtrsim 1$ PeV include LHAASO in China [145] combining water-Cherenkov and scintillator detectors over $\sim 1\,\mathrm{km^2}$; IceTop at the South Pole [146] using ice-Cherenkov detectors ($\sim 1\,\mathrm{km^2}$) as the surface component of IceCube; and TAIGA in Siberia (Russia) [147] and GRAPES-3 [148] in India using scintillators. These arrays operate with nearly 100% duty cycle and have measured many properties of the cosmic-ray flux (see next section).

Other arrays can measure the radiation emitted when the shower develops in the atmosphere, namely, optical Cherenkov radiation, fluorescence light, or radio emission in the MHz to GHz frequency range. Cherenkov detectors measure the forward-beamed incoherent emission at optical wavelengths. This can be achieved with arrays of individual elements such as at the Yakutsk [149] and Tunka-133 [150] observatories. A fluorescence telescope can monitor a large volume of the atmosphere and detect the isotropic fluorescence radiation emitted by the nitrogen molecules of air excited by the passage of the charged particles of the shower. The fluorescence radiation is produced in proportion to the energy dissipation and the shower size $N(X)$, allowing a reconstruction of the longitudinal profile of the energy deposit dE/dX of the shower as a function of atmospheric depth X and, in particular, providing a measurement of $X_{\max}$. With the fluorescence detection technique, the atmosphere is used as a calorimeter, with the integral $E_{\mathrm{cal}} = \int (dE/dX) dX$ called the calorimetric energy of the shower. An estimation of the primary energy with the fluorescence detection technique is obtained by adding to E_{cal} a correction to account for the invisible energy introduced above. Fluorescence and optical Cherenkov detectors are limited by operation during clear and moonless nights which reduces their duty cycle to $\simeq 15\%$. The main fluorescence detectors at energies above ~ 0.1 EeV currently in operation are those of the Pierre Auger Observatory [142] and TA [143].

Arrays of detectors of radio emission employ cost-effective elements (antennas) to detect the radiation in the 10 MHz to GHz frequency range produced by the charged particles in the EAS. Radio emission is mainly due to two mechanisms: the transverse current induced by the magnetic field of the Earth that travels at the speed of light along shower axis, and the Askaryan effect i.e the radiation emitted by the excess of negative charge (e^-) that develops in the shower through Compton scattering of shower photons on e^- in the medium, as well as Möller and Bhabha scatterings. The measurement of the radiated energy in radio waves at ground also provides an estimate of the primary energy [151]. In a radio-quiet environment, these detectors can operate with a close to 100% duty cycle, only limited by thunderstorms and heavy rain. The principal arrays of radio antennas currently operating include the Auger Engineering Radio Array (AERA) [152] and the recently completed AugerPrime Radio Detector [153] which has begun collecting data, both at the site of the Pierre Auger Observatory in Argentina; the Tunka-Rex [154] and Yakutsk [155] radio

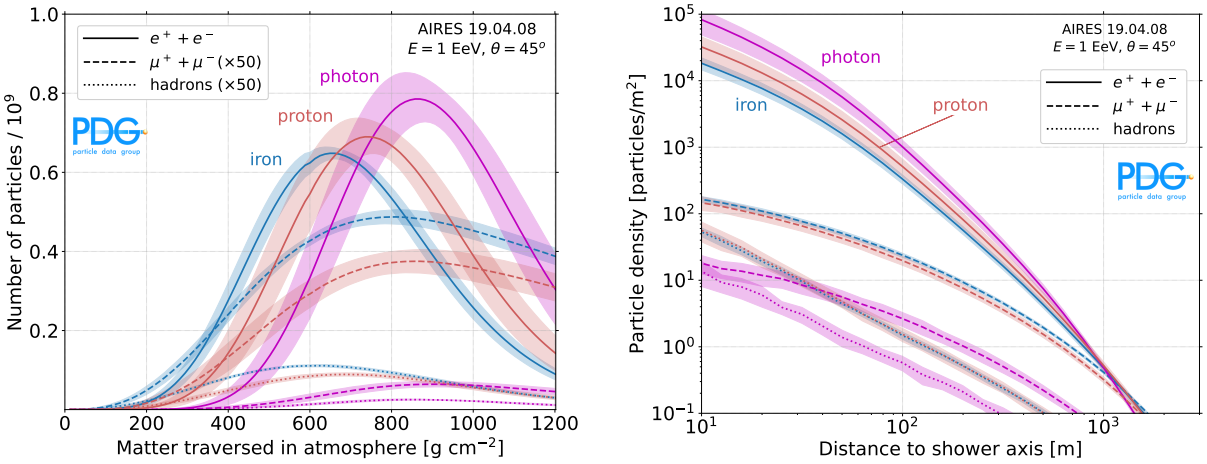

Figure 30.6: Left: Average number of $e^+ + e^-$, $\mu^+ + \mu^-$, and hadrons (lines), and their $\pm 1\,\sigma$ deviation (bands), as a function of matter (in g cm^{-2}) crossed in the atmosphere along the shower axis. The profiles are obtained with AIRES simulations [132] of proton, iron and photon-induced extensive air showers of energy $E = 1\,\text{EeV} = 10^{18}\,\text{eV}$ and zenith angle $\theta = 45°$ w.r.t. the vertical to ground (at depth 870 g cm^{-2}). Right: Lateral development (perpendicular to shower axis) at ground level of the same components as in the left panel as a function of distance to shower axis.

extensions in Russia; the LOw Frequency ARray (LOFAR) with its core detector in The Netherlands [156]; the Owens Valley Radio Observatory Long Wavelength Array (OVRO-LWA) [157] in the USA; and the Square Kilometer Array (SKA) in Australia [158].

Combining several types of detectors in the same array has proven very fruitful for increasing the accuracy in event reconstruction and energy calibration. Complementary measurements of the same event are expected to improve the determination of mass composition of the primary flux on an event-by-event basis. Projects under construction exploiting the simultaneous use of several detector kinds include, the nearly completed AugerPrime (water-Cherenkov stations, scintillators, underground muon detectors, fluorescence detectors and radio antennas) [159]; TAx4 (scintillators and fluorescence detectors) [160]; and the IceCube-Gen2 surface array (scintillators and radio antennas) [161]. Other arrays in the planning stages utilizing radio antennas, with some of them already reporting the detection of CR candidates, include: GRAND [162], BEACON [163], TAROGE [164]; HERON [165], and RNO-G [166].

Experimental results. Cosmic rays in the PeV to EeV energy range have been regularly detected for decades, with energies up to > 100 EeV. Despite the progress made in the field in the last 20 years, the nature and identity of their sources as well as the acceleration mechanisms that boost the particles to these extreme energies remain open questions. The understanding of CRs is mainly derived from analyzing their energy spectrum, several observables sensitive to their primary nature, and their arrival direction distribution. This is a challenging task mainly due to the small flux, with less than 1 particle per km^2 per year above 30 EeV (see Fig. 30.1), but also because the properties of CRs in this energy range can only be inferred indirectly from measurements of the EAS whose description relies on extrapolations of particle physics properties at energies several orders of magnitude above those achieved in terrestrial accelerators. Last but not least, since CRs are charged they are deflected by the galactic and intergalactic magnetic fields and their arrival directions at Earth point back only approximately to their actual sources.

Energy spectrum: The cosmic-ray spectrum observed at Earth (Fig. 30.1, with Fig. 30.7 highlighting the highest energies) can be characterized by a series of power-law functions proportional to $E^{-\gamma}$ with $\gamma \in (\simeq 2.5, \simeq 5.0)$ the spectral index that changes with energy. The production mechanism of CRs, mainly the unknown maximum CR energy achievable; the CR composition and spectral index at the sources; the source type and distribution in the Universe; and the propagation through the Galaxy and the intergalactic space, all leave distinct imprints on the spectrum giving rise to several observable features. The differential flux over 5 orders of magnitude in energy is shown in Fig. 30.7. The flux has been multiplied by E^3 to highlight the deviations from a pure power law with a single value of γ. Several features are apparent, namely: a steepening at $\simeq 5$ PeV known as the *knee* (Fig. 30.1); another steepening around 100 PeV dubbed the *second knee*; the *ankle*, a flattening of the spectrum at around 5 EeV; a feature recently identified with a significance exceeding 5σ [167] corresponding to a further flattening beginning at 10 EeV dubbed the *instep*; and the *suppression* of the spectrum starting around 50 EeV. These features are thought to be correlated with the observed changes on the average CR composition [168] (see *Primary composition* below).

Cosmic-ray experiments have systematic differences in their energy scales and this manifests itself in differences in the measured spectrum, not only on the energy axis but also on the normalization when the flux is scaled with a power of the energy. The diagonal uncertainty bars in Fig. 30.7 serve to visualize the impact of these systematic differences on the spectrum. In the energy range above ~ 100 PeV, the fluorescence technique is used to determine the primary cosmic-ray energy, with the atmosphere where the EAS develops functioning as a calorimeter. In the two state-of-the-art experiments for UHECRs, the Pierre Auger Observatory and the Telescope Array, a sub-sample of events is recorded simultaneously with the fluorescence (FD) and the surface detector (SD) arrays. With the SD, a shower size parameter is measured and corrected for atmospheric attenuation as the zenith angle varies. In Auger, this is fully data-driven with no assumptions on hadronic physics or primary mass, whereas in TA the ground signal is converted to shower energy using a Monte Carlo lookup table for a specific hadronic model assuming protons. In both cases, the signal in Auger and the estimated MC energy in TA are calibrated against the FD measurement, enabling a more direct determination of cosmic-ray energy without relying on simulations. Differences in the energy scale between Auger and TA remain, however, primarily due to the use of different measurements of the amount of fluorescence light emitted per unit of energy deposited, and to the different models for the invisible energy in EAS adopted. When these systematic uncertainties are accounted for, the spectra of the Pierre Auger Observatory and TA have been shown to agree within 4% below ~ 10 EeV, while in the energy region near the end of the instep

Int. J. Mod. Phys. A 2026.41. Downloaded from www.worldscientific.com by UNIVERSITY OF CALIFORNIA @ BERKELEY on 09/16/26. Re-use and distribution is strictly not permitted, except for Open Access articles.

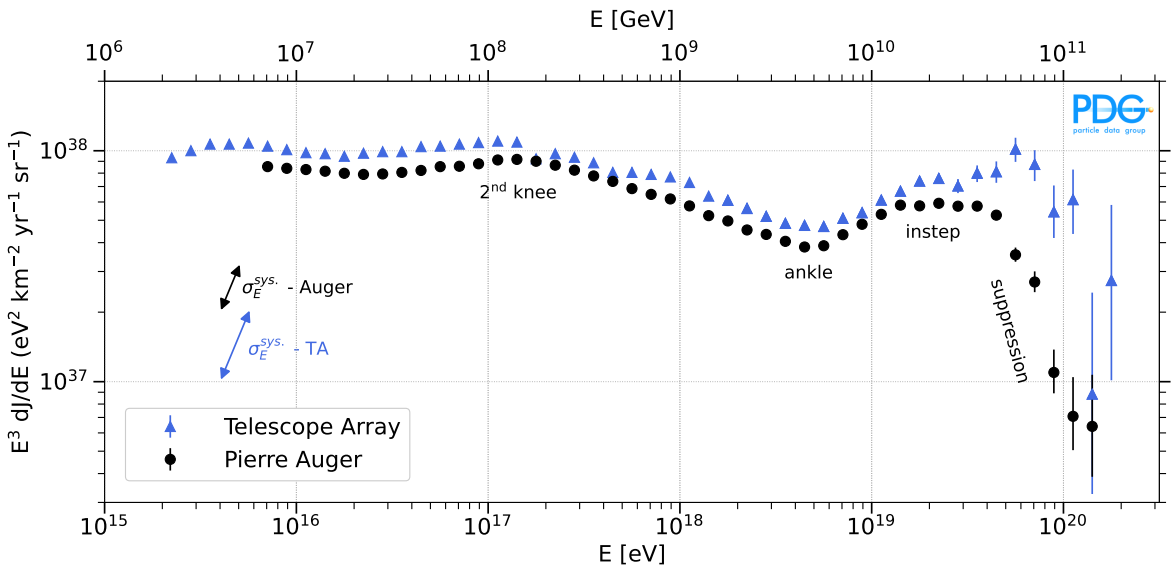

Figure 30.7: Measurements of the all-particle CR flux from Telescope Array (TA) [169] (blue triangles) and the Pierre Auger Observatory [29, 170] (black circles). The direction and magnitude of the systematic uncertainty on the flux due to the energy scale ($\sigma_E^{\rm sys}$) for TA and Auger is indicated by the corresponding arrows. For a comprehensive compilation of measurements see [171].

Int. J. Mod. Phys. A 2026.41. Downloaded from www.worldscientific.com by UNIVERSITY OF CALIFORNIA @ BERKELEY on 09/16/26. Re-[redacted] strictly not permitted, except for Open Access articles.

feature and at the suppression, a larger disagreement exists [178].

Primary composition: The main observable sensitive to CR composition is the depth in the atmosphere along shower axis ($X_{\rm max}$) at which the number of particles in the shower is maximum. Observatories capable of detecting Cherenkov and/or fluorescence light induced by the passage of the EAS through the atmosphere, can measure $X_{\rm max}$ on an event-by-event basis. With sufficient statistics, the distributions of $X_{\rm max}$ can be determined from which the average value $\langle X_{\rm max}\rangle$ and its fluctuations $\sigma(X_{\rm max})$ are obtained. A comparison with the $\langle X_{\rm max}\rangle$ and $\sigma(X_{\rm max})$ as predicted in simulations of EAS for different primaries and energies, as well as fits to the $X_{\rm max}$ distributions lead to the determination of the mean fractions of primary protons, helium, carbon-nitrogen-oxygen and iron in the cosmic-ray flux at Earth. However, the interpretation of any mass-sensitive observable relies on modeling hadronic interactions up to the highest energies where there are no data from terrestrial accelerators, and this introduces a considerable uncertainty in the determination of the mass. Also, due to intrinsic shower-to-shower fluctuations (see Fig. 30.6), an event-by-event determination of the mass of the primaries is not currently possible. Despite these limitations, the measurements presented in Fig. 30.8 alongside the predictions of EAS simulations for proton and iron primaries, reveal a broad trend toward a lighter composition at the knee, within the energy range of a few PeV. This is followed by a gradual rise in the average logarithm of the primary cosmic-ray mass, eventually leading to a heavier composition at around 100 PeV, although notable differences between experiments exist. As the energy increases from 100 PeV up to $\sim$ 2 EeV the measurements point consistently to a predominantly light composition with a large fraction of primary protons. Above that energy, the data from the largest statistical sample of events collected with the FD of the Pierre Auger Observatory indicate that the composition is mixed with the mean mass steadily growing. This observation is further supported by the shower-to-shower fluctuations of $X_{\rm max}$ also shown in Fig. 30.8. Though the data of the Telescope Array seem in apparent tension with this picture, they have been shown to be compatible with the results of the Pierre Auger and Yakutsk Observatories [179] within the current levels of statistics and understanding of systematic uncertainties. In particular, TA data are compatible with the mixed composition inferred by the Pierre Auger Collaboration up to 10 EeV [171].

The small duty cycle of the fluorescence technique combined with the steeply falling spectrum above $\simeq$ 50 EeV prevents a statistically significant determination of the composition in this energy range. Information on the distribution of nuclear masses can be obtained with the surface arrays alone that work with a high duty cycle. Exploiting the arrival times of particles in the SD stations, which are known to carry information on the shower penetration in the atmosphere, measurements of $X_{\rm max}$ with the Pierre Auger Observatory were extended up to 100 EeV, after calibrating the SD mass sensitivity with $X_{\rm max}$ measurements from the FD at lower energies [180]. In addition, deep-learning–based analyses applied to Auger SD data up to 100 EeV (Fig. 30.8) found evidence that the rate of change of $X_{\rm max}$ with the logarithm of energy exhibits three breaks, corresponding to the ankle, instep, and suppression features of the cosmic-ray flux [168]. The energy evolution of the mean and standard deviation of the measured $X_{\rm max}$ distributions indicates that the mass composition becomes progressively heavier and more pure. Additionally, the arrays of radio detectors are also sensitive to $X_{\rm max}$ through the measurement of the shape of the radio emission footprint on the ground induced mainly by the electromagnetic component of the EAS [177, 181]. The radio technique also exhibits significant potential at large zenith angles when combined with water-Cherenkov detectors to independently measure shower energy and muon number [182]. These demonstrated capabilities and scalability make the radio technique a cost-effective option for future UHECR observatories [183] such as the Global Cosmic-Ray Observatory (GCOS) initiative [184].

Arrival directions: Anisotropies in the arrival direction of CRs are a key to discovering their sources. This is in principle feasible if the charges of the CRs and the galactic and extragalactic magnetic fields are well-enough determined [185]. UHECRs are subject to the GZK effect, the energy loss of protons and heavier nuclei in interactions with the cosmic background. This imposes a horizon to possible sources of $\sim$ 250 Mpc for protons and Fe nuclei, but shorter for nuclei in between these two, for instance $\sim$ 5 Mpc for He and $\sim$ 100 Mpc for Si at energies above $\simeq$ 50 EeV [186]. Having only a limited range of source distances contributing to the signal makes it potentially feasible to identify sources or infer their properties statistically.

The Pierre Auger Collaboration has discovered a large-scale dipolar anisotropy at energies above 8 EeV with 6.8σ significance [187]. The amplitude of the dipolar anisotropy is $d = 0.074^{+0.010}_{-0.008}$ and the dipole points at a direction that is

Int. J. Mod. Phys. A 2026.41. Downloaded from www.worldscientific.com
by UNIVERSITY OF CALIFORNIA @ BERKELEY on 09/16/26. Re-use and distribution is strictly not permitted, except for Open Access articles.

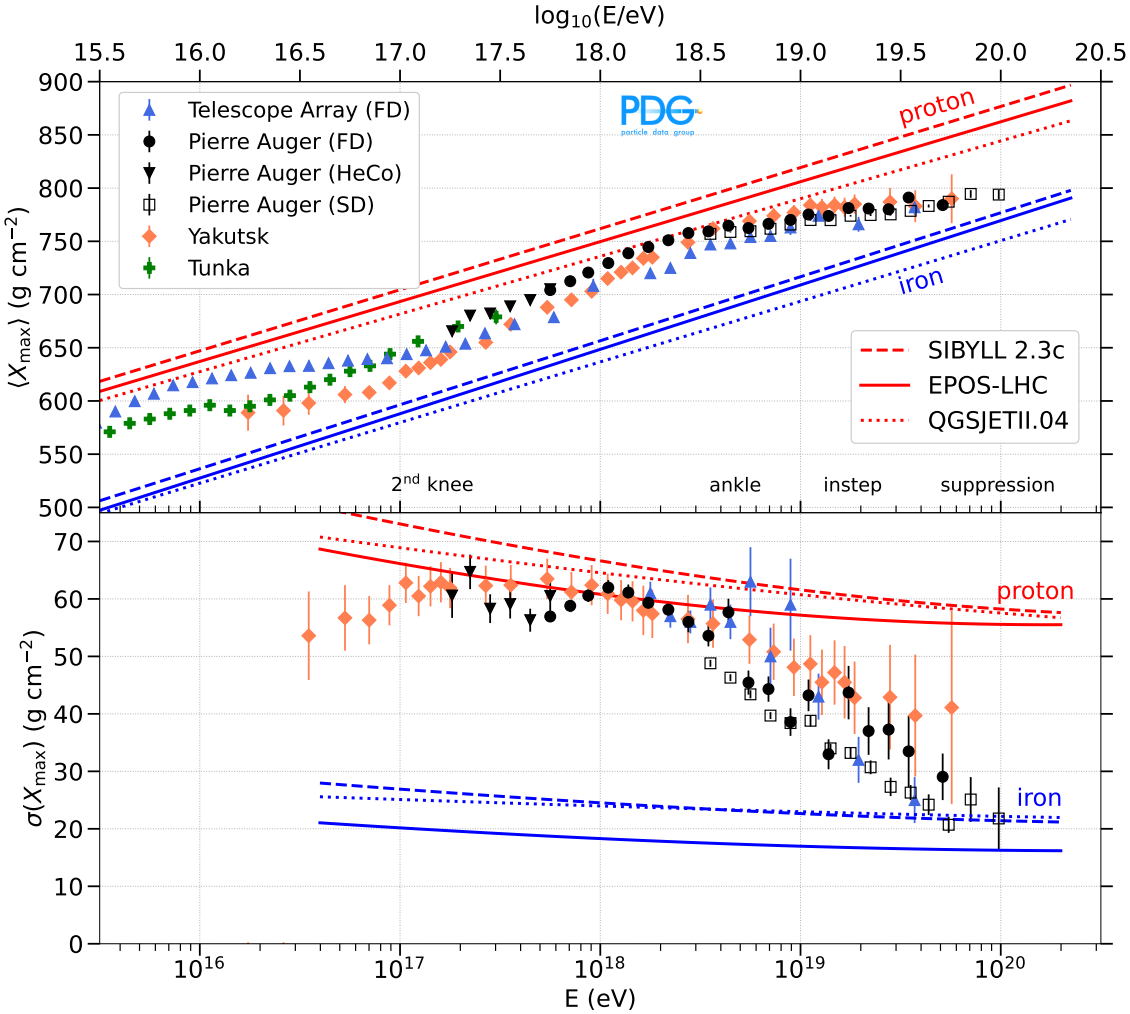

Figure 30.8: Measurements of the mean depth of shower maximum, $\langle X_{\max}\rangle$ (top), and its standard deviation, $\sigma(X_{\max})$ (bottom), obtained by the Telescope Array [172, 173]; Pierre Auger Observatory [168, 174, 175]; Yakutsk [149]; and Tunka [147] detectors. These measurements are compared to model predictions for proton and iron primaries using hadronic interaction models SIBYLL2.3c [176], EPOS-LHC [139], and QGSJET-II.04 [138]. The detection techniques include fluorescence (FD and HeCo), Cherenkov light detection (Yakutsk, Tunka, and Telescope Array below $\simeq 1$, EeV), and surface array measurements (Auger SD using deep-learning techniques). For a comprehensive compilation that includes experiments using radio detection techniques, see [171] and [177].

$\sim 113°$ away from the Galactic Center, evidencing the extragalactic origin of UHECRs above this energy threshold. The dipole direction is not aligned with any obvious individual source, or with the expected CMB dipole, and is instead consistent with the local distribution of stellar mass (2MASS Redshift Survey), after accounting for the deflections expected in the Galactic magnetic field. A compelling feature is the growth of the amplitude of the dipole with energy in agreement with the expectation that particles of higher rigidity are less deflected by magnetic fields. In the energy bin $8 - 16$ EeV the significance is at the level of 5.7σ. No time variation of the equatorial dipole modulation was found [187]. Combining the Pierre Auger Observatory data set in the southern hemisphere and the smaller statistical sample of events from Telescope Array in the north, a full-sky coverage is achieved. The combined results regarding the dipolar anisotropy are compatible with the Pierre Auger Observatory-only results with no evidence of the existence of a quadrupole component [188]. At energies between ~ 10 PeV and ~ 1 EeV the amplitude of the dipole is smaller (Fig. 30.5, bottom panel), but there is a trend for its direction to change from pointing close to the Galactic Center (GC) at low energy towards a direction away from the GC (Fig. 30.5, top panel) in the EeV energy range [187]. This suggests that there is a transition between the galactic and extragalactic origin of UHECRs around the ankle in the spectrum, at a few EeV.

Hints of correlation of arrival direction of UHECRs with potential sources have been confirmed in several analyses [171, 189, 190]. With data from the Pierre Auger Observatory, a 4σ excess of events above 38 EeV was found in a region of angular radius $\simeq 27°$ centered on the radio galaxy Centaurus A (CenA) [189], with the excess extending down to 20 EeV and no appreciable dependence of its position in the sky on the energy threshold chosen [191]. The Telescope Array Collaboration has also reported an excess of events with energies above 57 EeV (the so-called *hot spot*) in the northern sky in the direction of R.A. $= 144.0°$, Dec. $= 40.5°$, with a 2.9σ significance and in an angular window of $25°$ [192]. In contrast, the Pierre Auger Observatory data show no statistically significant excess in that region, despite having comparable integral exposure there [191]. Correlations with catalogs of potential UHECR sources have also been found. The sky viewed from the Pierre Auger Observatory is better modeled with a $\simeq 10\%$ flux excess in the directions of nearby starburst galaxies with a significance of 3.8σ and an energy threshold of 38 EeV with the correlation driven by the region of CenA where two prominent starburst galaxies are also located [189].

Despite the comprehensive observations made, it remains challenging to definitively ascertain the origin of UHECRs, primarily due to their deviation caused by the insufficiently constrained galactic and extragalactic magnetic fields. However, the constructed CR observatories designed to detect extensive air showers have the potential to also identify neutral particles of comparable

Int. J. Mod. Phys. A 2026.41. Downloaded from www.worldscientific.com
by UNIVERSITY OF CALIFORNIA @ BERKELEY on 09/16/26. Re- strictly not permitted, except for Open Access articles.

energies. These include neutrinos, neutrons, and photons. Such searches can be made provided that methods are devised to separate photon and neutrino-induced EAS from those produced by the more abundant charged CRs, or in the case of neutrons if excesses in the sky are found. No photon or neutrino candidates have been clearly identified in the energy range around and above 100 PeV and upper limits to their flux have been obtained (see Fig. 30.15). The neutrino limits are in tension with the observation of a candidate neutrino event in the KM3NeT detector with an estimated neutrino energy of 220^{+570}_{-110} PeV [193] (Fig. 30.15). UHECR observatories are thus also multi-messenger observatories of neutral particles [194]. These can be combined with gravitational wave detection and conventional radio, optical, X-ray and gamma-ray astronomy to greatly improve our knowledge about the most powerful objects in the Universe, as happened with the discovery of gravitational and electromagnetic radiation from the binary neutron star merger system in 2017 [195], with no neutrinos identified in temporal and spatial coincidence with it [196].

Astrophysical interpretation. A coherent picture of the nature and sources of CRs is emerging from the observations of the spectrum, composition and arrival directions, with many open questions. Cosmic rays below $\simeq 10$ PeV most likely have a galactic origin. The observed dipolar anisotropy in arrival directions imply that above 8 EeV they have their origin in extragalactic sources. One likely scenario is that the transition takes place at a few EeV, a hypothesis supported by the observed phase of the dipolar anisotropy changing around that energy from pointing to near the Galactic Center towards away from it (Fig. 30.5). Cosmic-ray rigidity $\mathcal{R} \equiv E/(Ze)$ determines the maximum energy at which different particle species can be accelerated in the sources $E_{\max}(Z) = Z \times E_{\max}(Z = 1)$. As a consequence, protons would cutoff first in the spectrum, followed by helium, carbon ... up to iron. The observed increase with energy of the mass below the *second knee* (Fig. 30.8) could be interpreted as the signature of the end of the Galactic contribution dominating up to that point [197]. As energy increases above a few times 100 PeV, the composition starts to become lighter. This could signify the emergence of an extragalactic component because no correlation with the densely populated Galactic plane is observed. A combined fit of the Pierre Auger Observatory measurements of the UHECR energy spectrum and composition [198] is compatible with the existence of this extragalactic component along with an additional component at higher energy responsible for the sharp decrease in spectral index at the *ankle* feature in the spectrum at $\simeq 5$ EeV (Fig. 30.7). Measurements of the energy spectrum and composition of UHECR, suggest that each accelerated nuclear species, from protons to iron, dominates in a narrow energy band, shaping the UHECR spectrum from the ankle up to the suppression. This is achieved through the contribution of distinct composition peaks: first protons; followed by lighter elements such as helium; then two groups of heavier elements, carbon-nitrogen-oxygen and magnesium to neon; ending with iron at the highest energies (see Fig. 5 in [198]). In particular, the *instep* reflects the interplay between the flux contributions of the helium and carbon-nitrogen-oxygen components, each injected at the source with distinct cutoff energies. This behavior is consistent with the observed *suppression* above $\simeq 50$ EeV, which can be attributed to the maximum energy ($E_{\max}$) achievable at cosmic accelerators, along with the GZK and photodisintegration effects during propagation. This comprehensive and unified understanding is continually evolving as additional data accumulates. Multi-messenger observations of the expected secondary neutrino and gamma-ray fluxes, or the lack thereof, will provide valuable constraints.

Hadronic interactions and Extensive Air Showers. EAS detectors probe energy and phase-space regions of hadronic interactions currently not accessible with terrestrial accelerators, although only in a very indirect manner. The tail of the distribution of $X_{\max}$ is sensitive to the attenuation length of primary p in the atmosphere, and the inelastic p-air cross-section can be inferred. In this manner, measurements of the p-air cross-section have been obtained at equivalent center-of-mass pp collision energy, $\sqrt{s_{pp}} > 40$ TeV, and are in agreement with model predictions within systematic uncertainties [171]. The muonic component in the air shower is generally used as a probe of the hadronic interactions during the shower development. Various measurements of muons with energies in the $\simeq 100$ MeV to $\simeq 10$ GeV range produced in EAS, have revealed that hadronic models of multiparticle production fall short in predicting the observed number of muons above cosmic-ray energies of $\simeq 100$ PeV [199]. On the other hand, the simulated shower-to-shower fluctuations in the muon number that are particularly sensitive to the first hadronic interactions in the shower, are in good agreement with the measurements [200]. This indicates that the shortage in the number of simulated muons builds-up in multiple soft-QCD processes throughout the EAS development rather than being driven by only the first few and highest-energy interactions of the EAS. This constrains possible explanations of the so-called *Muon Puzzle* based on new physics beyond the Standard Model. Recently, the Pierre Auger Observatory compared measured distributions of ground-particle signals and $X_{\max}$ with simulations based on different hadronic models, fitting primary mass fractions and allowing shifts in $X_{\max}$ and hadronic signal [201]. For $10^{18.5} - 10^{19.0}$ eV and $\theta < 60°$, the best fit requires $X_{\max}$ deeper by $20 - 50\,\mathrm{g/cm^2}$ and hadronic signals larger by $15-25\%$. These adjustments of the hadronic models would imply a heavier composition than currently inferred, helping to mitigate the muon deficit problem.

30.3 Gamma Rays

There is a well-studied flux of cosmic gamma rays (defined here as having energy greater than 1 MeV) present at the top of the atmosphere. Known as the diffuse gamma-ray flux, it has been measured with multiple space and ground-based instruments across a broad range of energy. On top of the diffuse one, many discrete sources have been found with either a steady gamma-ray flux or variability of many types.

30.3.1 *Observational Instruments: Space borne and Ground based*

Space borne γ-ray detectors, including AGILE [202], DAMPE [203], CALET [204], mainly Fermi-LAT [205], cover the energy range above 10 MeV up to 100 GeV. With the wide Field-of-View (FoV), they effectively survey the whole sky for steady γ-ray sources, and monitor all types of transient phenomena such as flares of Active Galactic Nuclei (AGN) and γ-ray bursts (GRBs). Above 100 GeV, ground-based Imaging Air Cherenkov telescope (IACT) experiments H.E.S.S [206], MAGIC [207], VERITAS [208] and CTA-LST [209] are very effective observational instruments. Using the stereo measurement technique, the IACT arrays achieve the angular resolution of the arrival direction of γ-rays at the level of 3 arc minute which is necessary for the high precision measurements of discrete sources. The small Field-of-View (FoV) of the telescopes and low-operation duty cycle make the all-sky surveys for new sources difficult. Only H.E.S.S scanned the region along the Galactic plane around the Galactic Center [210], as shown in Figure 30.9. Non-imaging Cherenkov light detection technique is also developed trying to cover wider FoV, e.g. in the TAIGA experiment [211]. The most suitable detectors for all-sky surveys are extensive air shower detector arrays at high altitudes, such as ARGO-YBJ [212], AS$_\gamma$ [213], HAWC [214] and LHAASO [215]. They are operated with very high duty cycle, typically $> 95\%$, have compatible sensitivity for discrete sources to IACT telescopes in much wider FoV in the same energy band, and higher sensitivity at higher energies above 10 TeV. In Table 30.1, the main features of the major facilities in γ-ray astronomy are listed.

30.3.2 *Diffuse Gamma Rays*

The majority of photons detected at high energies are characterized as diffuse emission that is not resolved as discrete sources. The observations of the diffuse emission are mainly carried out by wide FoV detectors, including space missions, OSO-3 [219], SAS-2 [220], COS-B [221], CGRO/EGRET [222], and Fermi-LAT [223] at energies below 1 TeV, and ground-based experiments Milagro [224], H.E.S.S [210], ARGO-YBJ [225], ASγ [226] and LHAASO [38] at energies up to 1 PeV. Evident in Figure 30.9, the

Int. J. Mod. Phys. A 2026.41. Downloaded from www.worldscientific.com
by UNIVERSITY OF CALIFORNIA @ BERKELEY on 09/16/26. Re-use and distribution is strictly not permitted, except for Open Access articles.

Instrument	**energy range**	**Effective area** (m^2)	**sensitivity** (milli-CU†)	**energy resolution** (%)	**PSF** (°)	**FoV** (sr)	**duty cycle** (%)
Fermi-LAT$^{a)}$	20 MeV - 300 GeV	~ 0.95	10 - 30	8 - 18	0.15 - 3.5	~ 2.4	~ 60
H.E.S.S.$^{b)}$	10 GeV - 50 TeV	$\sim 10^5$	~ 5	15	< 0.1	~ 0.03	$\sim$10
MAGIC$^{c)}$	$\geq$ 30 GeV	$\sim 10^5$	~ 7	16	≤ 0.07	0.02	$\sim$18
VERITAS$^{d)}$	50 GeV - 50 TeV	$\sim 10^5$	~ 5	10 - 15	0.08 - 0.13	0.02	10-14
CTA-LST1$^{e)}$	20 GeV - 300 GeV	$\sim 10^4$	~ 10	10 - 30	0.05 - 0.1	0.02	$\sim$10
AS$\gamma^{f)}$	10 TeV - 1 PeV	$\sim 7 \times 10^4$	~ 200	20 - 40	~ 0.8	~ 2.0	90
ARGO-YBJ$^{g)}$	50 GeV - 10 TeV	$\sim 0.8 \times 10^4$	~ 300	>13	~ 0.5	~ 2.0	86
HAWC$^{h)}$	100 GeV - 100 TeV	$\sim 3 \times 10^4$	~ 50	20 - 50	~ 0.69	> 1.5	95
LHAASO-WCDA$^{i)}$	100 GeV - 20 TeV	$\sim 0.8 \times 10^5$	~ 12	$\sim$33	0.2 - 0.84	~ 2.0	95
LHAASO-KM2A$^{i)}$	10 TeV - 4 PeV	$\sim 10^6$	~ 12	15 - 40	0.2 - 0.6	~ 2.0	95

Table 30.1: Facilities for γ-ray detection and their specifications in reference *a*) [205], *b*) [216], *c*) [217], *d*) [218], *e*) [209], *f*) [213], *g*) [212], *h*) [214], *i*) [215]. † milli-CU = 10^{-3} Crab Unit.

dominant component comes from the plane of the Galaxy (i.e., $|b| \lesssim 10°$, and is referred as the Galactic Diffuse Emission (GDE). Precise measurement of the GDE flux strongly depends on the subtraction of the contamination from discrete sources most of which are found spatially extended. With significantly improved sensitivity of source detection, Fermi-LAT and LHAASO largely reduce the contamination by removing the regions associated with known sources. In case of LHAASO, the flux in the Galactic plane with longitudes of $15° < l < 235°$ and latitudes of $|b| < 5°$ is well measured [38].

Three components are expected in GDE, namely γ-rays from the decay of neutral pions produced via inelastic collisions between energetic cosmic ray nuclei and the interstellar medium (ISM); bremsstrahlung radiation of electrons and positrons in ISM; and inverse Compton scattering of electrons and positrons off the interstellar radiation field. Possible annihilation or decay of dark matter (DM) particles might also give rise to diffuse γ-rays particularly in the densest region of the Galaxy. Therefore, GDE serves not only as a very important tool to probe the production, propagation, and interaction of cosmic rays, but also as a route to search for DM in any excess over the expectation, which is based on assumptions of the cosmic-ray spatial distribution, composition, energy spectrum and on the ISM column density along the line-of-sight. The search for DM also depends on the fraction of the contribution by the unresolved dim discrete sources in the GDE. Unfortunately, all of the assumptions have their own large uncertainties at present.

Evidence of an isotropic component of diffuse γ-ray emission, probably of extragalactic originated, was obtained with the measurement of its spectrum by CGRO/EGRET [227] and Fermi-LAT [228]. The Fermi-LAT spectrum covers the energy range from 0.1 GeV to 820 GeV and is well described by a power-law with an exponential cutoff. It is consistent with a scenario of a discrete source population, such as blazars with power-law spectral shape, dominating the emission and experiencing attenuation due to the extragalactic background light (EBL) [228]. Contributions from the cascade of very-high-energy gamma rays and UHECRs are not ruled out as a fraction of the extragalactic diffuse emission.

30.3.3 *Discrete Gamma Ray Sources*

As a neutral component of cosmic rays, γ-rays directly reach the earth from their sources, thus allowing us to identify the origin of the photons by association with known celestial objects or events. As shown in Figure 30.9, the source-associated contributions are revealed directly by the bright spots whose sizes are due to the point-spread-function (PSF) of the instruments and the intrinsic spatial extensions of the sources. It is also clearly shown that the sources are divided into two groups: *Galactic* and *extragalactic*.

Galactic Sources More than 6600 sources have been found emitting γ-rays in the Milky Way. Most of them have steady photon emissions over a wide energy range above 0.1 GeV up to 2 PeV. 43 of them have emission of γ-rays above 0.1 PeV referred as *PeVatrons* since the parent particles that emitted the photons must be accelerated above 1 PeV on average in the source regions. Variability of the photon fluxes has also been observed from known objects such as pulsars and binary systems or transient phenomena.

A. Sources with steady emissions are the majority of Galactic γ-ray emitters which are well documented in reviews [229–231] and in γ-ray source catalogs [232] (for < 100 MeV), 4FLCT (for 0.1-300 GeV) by Fermi-LAT [233], TeV-Catalog available on-line (http://tevcat.uchicago.edu) and the newly released 1LHAASO (for 1-2000 TeV) by LHAASO [44]. All associations with known celestial objects, such as SNRs, PWNe, young massive-star clusters (YMC) are discussed in the corresponding catalog papers (e.g. individual catalogs collected in http://tevcat.uchicago.edu). Most of the sources, particularly for their high-energy emission above tens of TeV, remain unidentified. Among the identified ones, the Crab [234] and RX J1713-3946 [235] are the most extensively studied objects and constitute paradigmatic examples of PWNe and SNRs.

The Crab has a compact PWN powered by the rotation energy of the pulsar in its heart. Electrons and positrons in the wind are accelerated at the termination shocks and emit γ-rays through synchrotron radiation at energies lower than 0.1 GeV. Simultaneously, accelerated electrons and positrons boost soft background photons, such as those in the cosmic microwave background, to energies well above 1 GeV via inverse Compton scattering. Figure 30.10 shows the spectral energy density (SED) of the Crab nebula with a fit using a simple one-zone leptonic model. It generally describes the radiation of the nebula over energies up to $E_\gamma \sim 1.1$ PeV, implying that electrons and positrons are confined in a small region of $\simeq 0.2$ pc by a magnetic field of intensity $B \simeq 110\,\mu$G and are accelerated to energies as high as $\simeq 2.3$ PeV. This requires a surprisingly high acceleration rate, $\eta = \bar{\epsilon}/B = 0.14(B/100\mu\text{G})(E_\gamma/1\text{ PeV})^{1.54}$ PeV, at the level of 15%, where $\bar{\epsilon}$ is projection of the electric field averaged over the particle trajectory. This rate is 3 orders of magnitude higher than that in the normal shock environment such as in SNRs, revealing the existence of a so-called 'extreme accelerator' in the middle of the nebula [234]. The flux of photons above 0.8 PeV indicates some deviation from the pure leptonic scenario implying that a hadronic component might be responsible. It could be a hint of the super PeVatron which may contribute to the Galactic cosmic rays above the knee [234] (see Fig. 30.1).

RX J1713.7-3946 is one of the brightest objects in the TeV sky, and is the first SNR shell to be confirmed as a TeV gamma-ray source [235]. The detailed TeV morphology reveals a shell structure similar to the X-ray observations, indicating that particles are accelerated to very high energy therein. The TeV gamma-ray spectrum extends to nearly 100 TeV. It is not determined yet whether the gamma-rays are produced via Inverse Compton scattering of relativistic electrons (leptonic process), or via neutral pion decay with the pions produced in the inelastic scattering of CR protons with ambient gas (hadronic process) [236]. Nevertheless, the spectral information demonstrates the efficient accel-

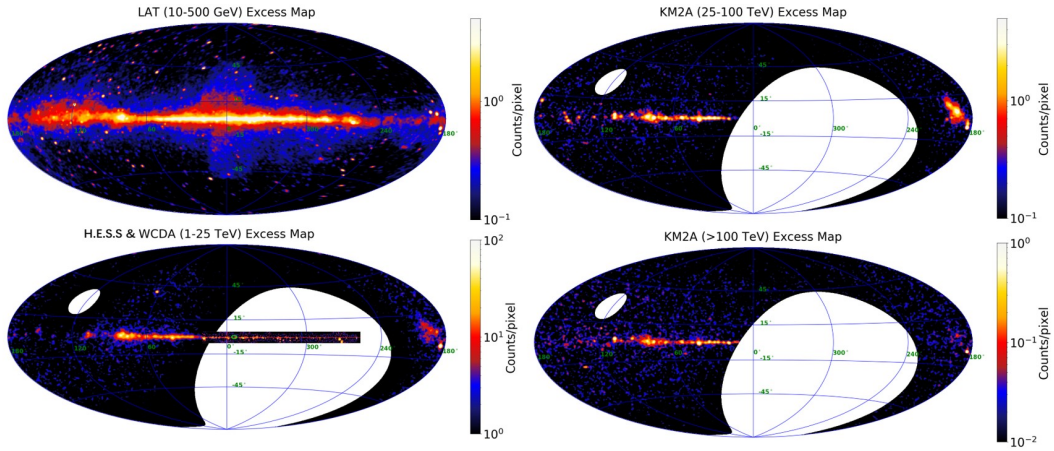

Figure 30.9: The GeV γ-ray sky maps surveyed by Fermi-LAT [223], LHAASO [44] and H.E.S.S [210] from 1 GeV to 100 TeV and above.

eration of charged particles to energies beyond 100 TeV in this object. The latest H.E.S.S observations also found that the TeV gamma-ray emission region extends significantly beyond the X-ray emitting shell [237], which may be due to either the escape of particles from the shell or to particle acceleration in the shock precursor region.

Another established population of gamma-ray sources is young massive clusters (YMCs). H.E.S.S collaboration have detected the extended gamma-ray emissions towards the YMC Westerlund 1 [238] and Westerlund 2 [239] in our Galaxy as well as 30C Doradus in the large Magellanic cloud (LMC) [240]. [241] also detected the GeV emissions from Cygnus-X region and attribute the gamma-ray emissions to the newly accelerated CRs in the star forming processes. Later on several YMCs are also found to be bright GeV gamma-ray emitters, such as W40 [242], W43 [243], Carina Nebular [244], G25 [245], NGC 3603 [246], NGC 6618 [247], and NGC 2244 [248]. The gamma-ray emissions in these regions reveal several universal spectral and spatial features. In GeV band these sources show similar power law spectra with the indices of $2.2 - 2.3$. Such a typical spectrum is similar to the widely predicted CR spectrum in acceleration sites and significantly harder than the Galactic diffuse gamma-ray emissions. Furthermore the gamma-ray emissions in YMCs are more extended than the physical size of these clusters themselves and can reach $\sim$ 100 pc in the most extreme case. Such a large extension allows the detailed morphological studies for those objects in gamma-ray band with moderate spatial resolution. Thus, combining the gas distributions derived from atomic/molecular spectral line emissions in radio band, the gamma-ray morphology can be used to derive the CR spatial distributions. In this regard, [249] have investigated the archival γ-ray data in Cygnus region, Westerlund 1 and central molecular zone (CMZ) as well as the gas information derived from CO/HI emissions. The derived CR radial distribution reveal a universal $1/r$ relation, in which r is the distance to the center of those YMCs. Such a profile indicates an continuous injection of CRs, which strongly favor a scenario in which CRs are accelerated by the stellar winds.

The H.E.S.S observations towards Westerlund 1 and CMZ, as well as the ARGO observations in Cygnus region, found no hint of spectral cutoff up to the energy of $\sim$ 20 TeV, which indicates that those objects would be plausible candidates of PeVatrons. A recent analysis using more than 3-years of LHAASO data revealed the UHE gamma-ray emissions in Cygnus region. An enormous γ-ray bubble extending more than 6° and hot spots associated with massive molecular clouds were detected, the γ-ray SEDs extend beyond 1 PeV. Figure 30.11 shows the contour map of γ-rays at energies from 2 to 20 TeV towards Cygnus X, and 66 dots mark the arrival directions of individual photon-like events of energies exceeding 400 TeV. The estimated cosmic ray background is about 9.5 among the 66 events. The contamination is smaller

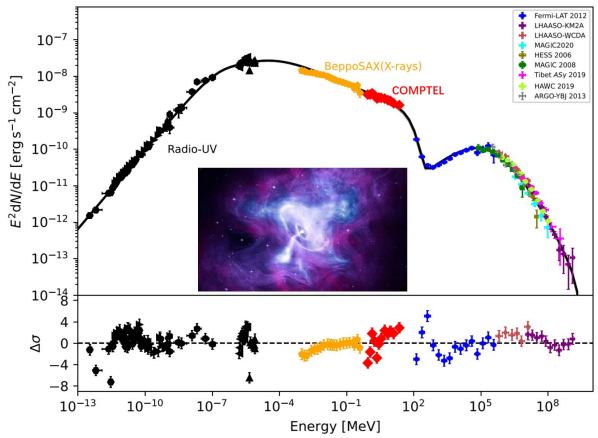

Figure 30.10: Spectral energy density (SED) of photons from the Crab from sub-μeV to 1.1 PeV. Above 1 TeV, data are collected from 7 experiments listed in legend in the upper panel. The lower panel shows the deviation between data and the model based on a widely accepted one-zone leptonic origin in the nebula. Only Fermi-LAT and LHAASO data are shown for simplicity. Inset is the X-ray image of the nebula by Chandra [250].

with the increase of energy benefitted from the improvement of rejection power, namely, 8 events are found above 1 PeV with only 0.75 background events in average. The surface density of these UHE photons is higher at a closer distance to the core. Especially within 0.5° radius around Cygnus OB2, 7 events above 400 TeV have been detected, including two photons of energies exceeding 1 PeV. This implies the operation of central CR accelerator(s) that injects relativistic protons and nuclei into the circumstellar medium. The γ-ray morphology and the SED of the bubble over six decades, from 1 GeV to 1 PeV, can be interpreted assuming the injection of relativistic protons and nuclei from PeVatron(s) located in the core . Gamma-rays are produced in interactions of these particles propagating diffusively through the circumstellar gas to at least 150 pc.

B. Variable sources Crab flares, binaries and pulsars are observed in the Galactic γ-ray sky. Their activity varies on timescales from a fraction of one second (pulsars), to days (Crab Nebula, Novae), weeks, months or even years (γ-ray binaries). Various analysis pipelines are developed mainly by the LAT collaboration to search for and monitor γ-ray transients.

The Crab Nebula shows flare activities on a timescale of days [251]. The instability is observed only in GeV band by AGILE and

Int. J. Mod. Phys. A 2026.41. Downloaded from www.worldscientific.com
by UNIVERSITY OF CALIFORNIA @ BERKELEY on 09/16/26. Re-
strictly not permitted, except for Open Access articles.

Int. J. Mod. Phys. A 2026.41. Downloaded from www.worldscientific.com
by UNIVERSITY OF CALIFORNIA @ BERKELEY on 09/16/26. Re-use and distribution is strictly not permitted, except for Open Access articles.

Fermi/LAT. The flaring mechanism is still unclear with a couple of models being under debate.

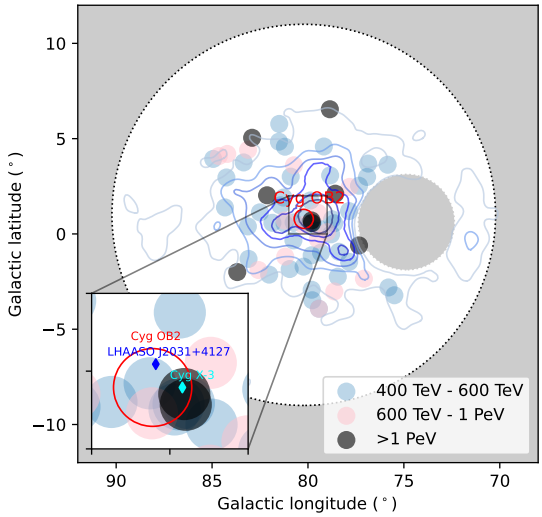

Figure 30.11: Photon distribution in the Cygnus-X region. The significance map of γ-rays from 2 to 20 TeV of the bubble is shown by gray contours starting from 3σ with a step of 3σ. The blue diamond marks LHAASO J2031 + 4127. There are 66 photon-like events within a radius of 6 degree with an estimated background of 9.5. Eight events with energy above 1 PeV are marked with black circles. Three interesting objects - Cygnus OB2 (red circle), Cyg X-3 (cyan diamond) and the powerful pulsar PSR J2031+4127 (blue diamond) are found in the central region. The larger circle in black dotted line represents the ROI used in this study, while the shaded circle within black dotted line marks the masked region near the bright source LHAASO J2018+3651.

Each γ-ray binary is composed of a compact object (pulsar or black hole) and a massive star. Their γ-ray emissions characterized by the orbital modulation, with time scales ranging from 3.9 days (LS 5039) to $\sim$ 47 years (PSR J2032+4127). Microquasars are also binary systems that launch powerful jets from the compact objects by accreting matter from their companions. Three microquasars have been detected namely, Cyg X-1, Cyg X-3, and SS 433. They have shown γ-ray activities correlated with orbital motion [252], jet precession [253], X-ray state changes [254], and flares [255]. Eta Carinae is the only colliding wind binary firmly detected, showing orbital modulation in the γ-ray emission in a period of 5.54 years [256].

Cygnus X-3 is a high-mass X-ray binary system consisting of a compact object, either a stellar-mass black hole or a neutron star, and a Wolf Rayet donor star [257]. It has a very short orbital period of 4.8 hours. The modulation of flux has been observed in infrared to GeV gamma-ray bands. The detection of relativistic jets during radio flares confirms its microquasar nature [258–262]. The source historically attracted significant interests in 1980s, when early ground based detector arrays reported periodic PeV γ-ray emission, though subsequent more sensitive experiments in TeV domain did not detect any signal from the binary [263]. During its flaring episode in the GeV domain, LHAASO has detected photons at energies above 60 TeV with a significance of 11.5σ from the point-like source at Cyg X-3, while no significant signal is found during its quiescent phases. The energy spectral distribution is a remarkably hard power law with the index of 2.18±0.17, up to 3.7 PeV, the hardest UHE spectrum among sources yet detected by LHAASO. Two events with energies of 3.73±0.41 PeV and 3.08±0.34 PeV represent the highest energy photons ever detected from an astrophysical source. The orbital modulation (4.8 hour period) is found with a statistical significance of 3.2σ. This indicates that the radiation zone is smaller than the scale of 10^{11} cm, where the magnetic field is so strong that PeV electrons would not survive from the severe synchrotron cooling. The extremely hard spectrum provides further evidence for the existence of a hadronic accelerator near the compact object. The intense ultraviolet radiation field of the companion star supplies sufficient targets for the proton-photon interactions, which naturally explain the sudden enhancement in the gamma ray spectrum above 1 PeV. This provides strong evidence for cosmic ray baryons being accelerated beyond tens of PeV inside the microquasar binary system during its flaring states [264].

Pulsars show steady pulsation on their spin periods ranging from several milliseconds to seconds in GeV band [265], thereby qualifying as γ-ray pulsars. Only the Crab and Vela pulsar are pulsating in TeV [266, 267]. PSR J2021+4026 is observed for the γ-ray flux variability on time scales of several years [268], making it the only variable γ-ray pulsar. Many millisecond pulsars themselves are γ-ray pulsars showing periodic variability in milliseconds [269]. γ-ray eclipses and orbital modulations have been detected in several binaries hosting millisecond pulsars, usually on the time scale of hours to days, arising from the intra binary shock between the pulsar wind and stellar wind [270, 271]. Millisecond pulsars could transit between spin-down-powered state and accretion-powered state. Variability in the γ-ray flux is observed accompanying these changes [272].

Novae outbursts have been detected in γ-rays, arising from the particle acceleration at shocks and last for months [273]. RS Ophiuchi is the first nova with its outburst detected in TeV up to 1 month [274].

Extragalactic Sources The majority of extragalactic γ-ray sources are active galactic nuclei (AGN). The fourth catalog of AGNs (4LAC) by LAT for 8 year observations contains 2863 objects located at high Galactic latitudes ($|b| > 10°$) while 344 others were found at lower latitudes [275]. 98% of them are blazars. The blazar population consists of Flat Spectrum Radio Quasars (FSRQs), BL Lac-type objects and unknown types [275]. The Data Release 3 adds 587 more blazars and 4 radio galaxies to the catalog [276]. More than 70 blazars and a few radio galaxies are detected in the very high-energy (VHE) band, namely photon energy greater than 0.1 TeV, by imaging atmospheric Cherenkov telescopes (IACT) (http://tevcat.uchicago.edu).

Blazars belong to a class of AGN where the jets are oriented at a relatively small angle with respect to the line of sight. This specific viewing angle allows us to observe the emission from those jets with significant Doppler boosting. The photon flux in the jets may enhance significantly with respect to that in quiet states, a phenomenon referred to as blazar flares. They are simultaneously observed over a wide energy band from radio to VHE γ-rays with timescales ranging from a few minutes to year [277, 278]. The broad-band SED of blazars typically shows two humps of non-thermal radiation. The one in the lower energy range from radio to X-rays is generally attributed to synchrotron emission from relativistic electrons and positrons in the jet, while the origin of the hump at higher energies is still under debate. Possible emission mechanisms are the IC scattering of accelerated leptons off low energy photons, which are inside jets or from outside regions [279], or decay of neutral pions produced in collisions of accelerated protons against ambient matter [280], or some combination of the two processes.

The ground-based EAS experiments are suitable γ-ray detectors for monitoring the flares of AGNs with the advantages of large FoV and full duty cycle of operation. The ARGO-YBJ collaboration reported a long-term continuous monitoring of Mrk 421 and Mrk 501 [281, 282, 287], the two brightest blazars in the TeV sky. The γ-ray flux shows a good long-term correlation with that in the X-ray band. HAWC detected the persistent emission from those two AGNs [288]. Recently, the LHAASO collaboration reported eight sources detected at Galactic latitude $|b| > 12°$, among which some are AGNs, including well-known emitters, such as the radio galaxy M87, VER J0521+211 and 1ES 1215+303 [44].

Using data for 4.5 years when ARGO-YBJ and Fermi-LAT si-

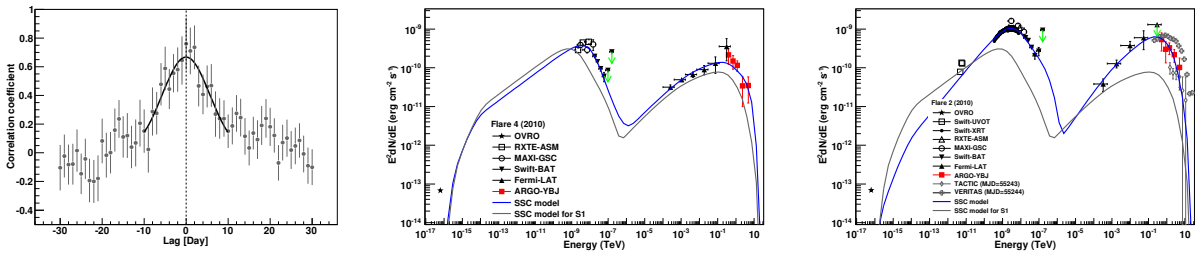

Figure 30.12: The multi wavelength analysis of Mrk 421 involving measurements over wide energy range from radio to TeV γ-ray during 4.5 years when ARGO-YBJ and LAT were operated [281]. The discrete correlation function between the light curves in X-ray band and TeV γ-ray band is calculated and clearly shows no time lag between emissions in the two bands [281] (left panel). The SED significantly changes from steady states (gray solid lines in middle and right panels) to flaring states depending on the strength of flares. Comparing a small flare in the middle panel and a larger one in right panel, the later has harder SED in VHE band [282].

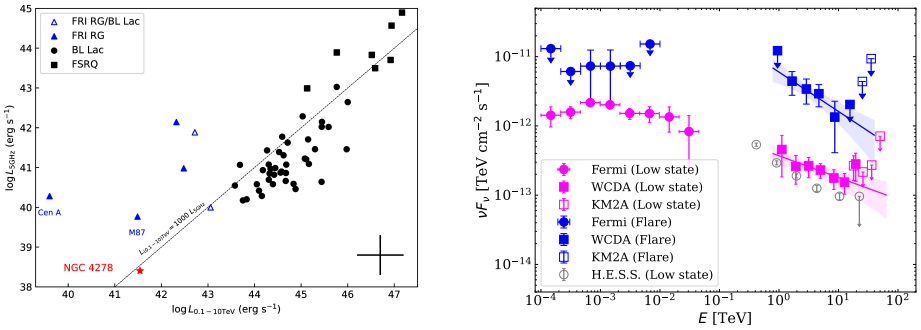

Figure 30.13: Upper panels: radio luminosity vs. TeV luminosity involving the detection of NGC 4278 (left), Gamma-ray SED of M87 for the low state and flare state (right)

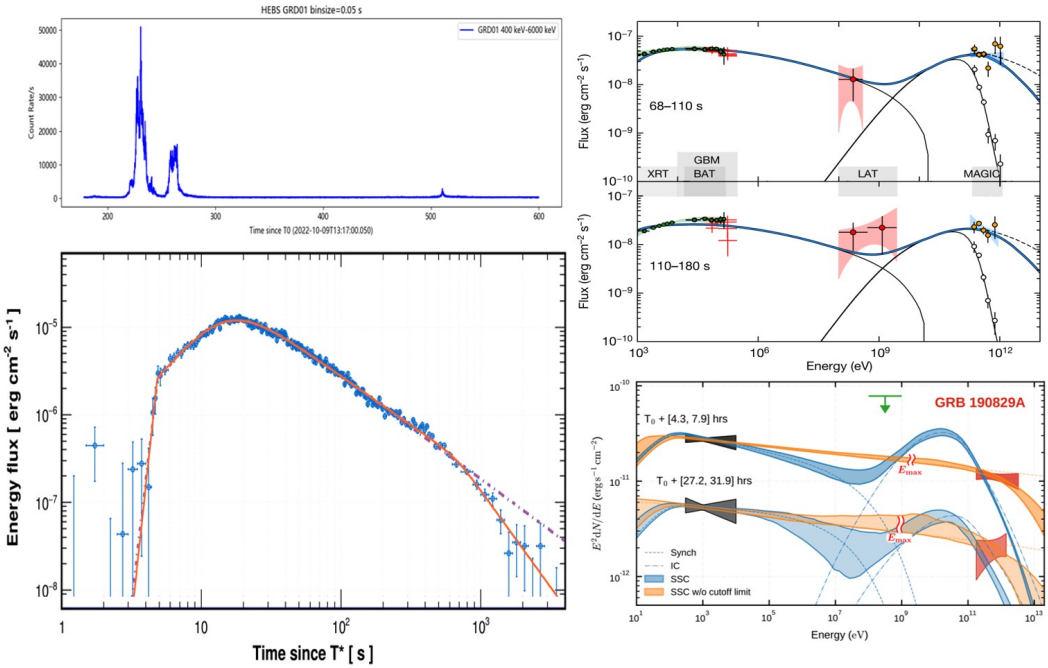

Figure 30.14: The typical multi-wavelength measurement of the light curves of the γ-ray burst GRB 221009A in the GeV band [283] (top left) and in the TeV band [284] (bottom left). The clear different structures of the brightness variation patterns indicate the different origins of the synchrotron radiation and inverse Compton scattering of leptons accelerated by the internal and external shock waves, respectively. The spectral energy distributions of the GRB 190114C and GRB 1908129A, respectively measured by MAGIC [285] (top right) and H.E.S.S [286] (bottom right). The Self-Synchrotron Compton scattering model of the afterglow is marginally supported in the observations covering a wide energy band from X-rays to TeV γ-rays.

Int. J. Mod. Phys. A 2026.41. Downloaded by UNIVERSITY OF CALIFORNIA @ BERKELEY on 09/16/26. Re-
worldscientific.com
strictly not permitted, except for Open Access articles.

Int. J. Mod. Phys. A 2026.41. Downloaded from www.worldscientific.com
by UNIVERSITY OF CALIFORNIA @ BERKELEY on 09/16/26. Re-use and distribution is strictly not permitted, except for Open Access articles.

multaneously operated from 2008 to 2013, the ARGO-YBJ collaboration realized the long-term multi wavelength observation of Mrk 421 in all bands of radio, optical, X-ray, GeV, and TeV gamma-rays [281]. The well-known correlation [289] between the photon fluxs in X-ray band and TeV γ-ray band is investigated in a quantitative way, namely the discrete correlation function between the light curves in two energy bands being calculated. No time lag in the scale of days is found(see Figure 30.12). This is regarded as evidence of favoring the one-zone Self-Synchrotron Compton scattering scenario [282].

Flares happened in that time window are systematically analyzed and clear correlation between the strength of flares and features of the SEDs are observed as an example shown in Figure 30.12. Detailed investigation of SEDs implies that various particle acceleration mechanisms, such as relativistic diffusive shock acceleration, might be responsible for different flares. A similar analysis is carried out with data during outbursts of Mrk 501. The SEDs in the VHE band are observed to be harder during flares than that in the quite period. The detection of energetic photons above 10 TeV and the hardness of the SED hint some exceeds over the expectation of one-zone SSC model [287].

The detection of TeV gamma-ray emissions from NGC 4278 [290] is remarkable since its luminosity is rather low, nearly 3 order of magnitudes lower than M87 (see the left panel in Fig. 30.13). The variability is found on a scale of few months in TeV band with the flux reaching as high as 50 milli-Crab Unit. The discovery of VHE emission from NGC 4278 indicates compact, weak radio jets being able to efficiently accelerate particles to multi-TeV level, thus reveals a new class of TeV γ-ray sources. The detection of TeV emission from nearby radio galaxy M87 [291] at very high energy of 20 TeV (see the right panel in Fig. 30.13) is long expected. The flux reaches 10^{-11}erg cm^{-2} s^{-1} during flares. A duty cycle of 1% for VHE flares is also found in the continuous monitoring of the source.

Gamma-Ray Bursts (GRBs) GRBs are violent explosions observed in distant galaxies, characterized by a rapid flash of γ-rays lasting from a fraction of a second up to several hundreds of seconds. The emission from GRBs occurs in two stages, namely the prompt emission phase and the afterglow phase, as can be seen in Figure 30.14.

In the second catalog of Fermi/LAT-detected GRBs, covering the first 10 yr of operations, 169 GRBs are detected above 100 MeV [292]. The high-energy emission generally lasts much longer than the prompt keV-MeV emission. The widely discussed scenario for the extended GeV emission is synchrotron radiation by relativistic electrons that are accelerated in shocks resulting from the interaction of the jet with the surrounding medium [293, 294].

VHE emission has been detected from just a few GRBs by IACTs during the afterglow decay phase. MAGIC slewed to the direction of GRB 190114C only $\simeq$ 60 seconds after the trigger and detected photons above 300 GeV from the burst for the first 20 minutes [295]. This VHE emission is explained by inverse Compton up-scattering of synchrotron photons by high energy electrons in the external shock [285], as shown in the right-upper panel of Figure 30.14. Two other events, GRB 180720B and GRB 190829A, were also detected during the afterglow decay phase by H.E.S.S [286,296], the unexpected SED is shown in the right-lower panel of Figure 30.14.

The brightest-of-all-time GRB 221009A serendipitously occurred within the FoV of LHAASO. More than 64,000 photons (above 0.2 TeV) were detected within the first 3000 seconds by LHAASO-WCDA [284]. The detection covers both the prompt emission phase and the early afterglow in the TeV band, revealing the onset of afterglow emission in the TeV band for the first time, as shown in the left panels of Figure 30.14. In addition, the unprecedented photon statistics of the TeV emission enabled identifying a jet break in the light curve, indicating an opening angle of GRB 221009A of $\sim$ 0.8°. This is consistent with the brightest core of a structured jet, explaining the unexpected high isotropic equivalent energy of this GRB. LHAASO-KM2A registered more than 140 photons with energies above 3 TeV from GRB 221009A [297]. The intrinsic energy spectrum of gamma-rays is well fitted by a power law after correcting for EBL absorption, with the highest energy photon above 13 TeV traveling over a distance with red shift $z \sim 0.152$ [297].

Tests on Lorentz Invariance Violation (LIV) Tests on LIV are feasible and thus, limits can be set using the highest energetic photons collected from remote sources. Any tiny violation of the invariance leads the fundamental dissipation relation to be rewritten [298] as $E^2 = m^2c^4 + p^2c^2(1 + A_1 pc/M_p c^2 + A_2(pc/M_p c^2)^2 + ...)$, where E, p are the energy and momentum of a particle with the mass m, the M_p is the Plank scale and A_1, A_2 are theoretic parameters of the violation at the first and second order levels. This must lead instability of photons that may decay on their way to the Earth [299]. The first order violation effect due to the decay channel $\gamma \to e^+ + e^-$ has not been found at energies $\sim$5 orders of magnitudes higher than the Planck scale, regarded as the null evidence of the quantum gravitational effect. However, the limit due to second-order effect caused by decay channel $\gamma \to 3\gamma$ is still found still $\sim$3 orders of magnitudes below the Planck scale, using the latest observations of photons up to 1.4 PeV from the Cygnus X direction [300].

30.4 Neutrinos

In contrast to charged particles, neutrinos are not deflected by electromagnetic fields and thus point back to their origin, making them appealing messengers for astronomical observations. In addition, neutrinos of cosmic origin, or produced in the atmosphere of the Earth, allow us to study particle physics in a kinematic regime not accessible to date to accelerator experiments. In the following, we will consider neutrinos with energies at the GeV energy scale and above.

30.4.1 *Production of high-energy neutrinos*

High-energy neutrinos can be produced in hadronic interactions in a variety of astrophysical objects (*astrophysical* or *cosmic* neutrinos), in scattering of extremely energetic protons (p) with the cosmic microwave background (*cosmogenic* neutrinos) and by cosmic-ray interactions in the Earth's atmosphere (*atmospheric* neutrinos). The main production chain is (A denoting atomic nuclei and X a hadronic system)

$$\begin{aligned} &p(A) + p(A,\gamma) \to \pi^{\pm} + X \\ &\quad \text{with subsequent decays} \quad \pi \to \mu\,\nu_\mu \text{ and } \mu \to e\,\nu_\mu\,\nu_e\ , \end{aligned} \tag{30.1}$$

resulting in a ratio $\nu_e : \nu_\mu : \nu_\tau = 1 : 2 : 0$ (not distinguishing here between ν and $\overline{\nu}$). If the source density is high, muons can lose most of their energy before decaying, yielding a ratio $0 : 1 : 0$ in the extreme case. If protons were kept in the source region by magnetic fields without interacting, and only neutrons could escape and then decay via $n \to p + e^- + \overline{\nu}_e$, the ratio would be $1 : 0 : 0$. Over cosmic distances, flavor mixing turns these ratios to 0.30:0.36:0.34 for the first source scenario (1:2:0), 0.17:0.45:0.37 for the second (0:1:0) and 0.55:0.17:0.28 for the third scenario (1:0:0) [301].

30.4.2 *Measurement methods*

Most experiments targeting high-energy cosmic neutrinos are based on the detection of Cherenkov light induced by charged secondary particles produced in neutrino interactions. This includes underground detectors like Super-Kamiokande with its fiducial volume of 22.5×10^3 m^3 (see Sect. 36.3.1) and underwater/ice detectors like ANTARES, KM3NeT (under construction) or IceCube, the latter with a volume of 10^9 m^3 (see Sect. 36.3.2). Neutrinos with energies exceeding some tens of PeV can be also detected via the coherent emission of Cherenkov radiation at radio wavelengths in ice or other radio-transparent media (e.g. ANITA or RNO-G, see Sect. 36.3.3). Neutrinos with EeV energies could be identified via extensive air showers starting too deep in the atmosphere to be due to particles with strong or electromagnetic interaction. Alternatively, they could be detected via slightly upward-directed air showers from the decay of tau leptons generated in interactions of Earth-skimming or mountain-traversing ν_τ [302]. These signatures could be observed by cosmic-ray experiments such as the Pierre Auger Observatory [303].

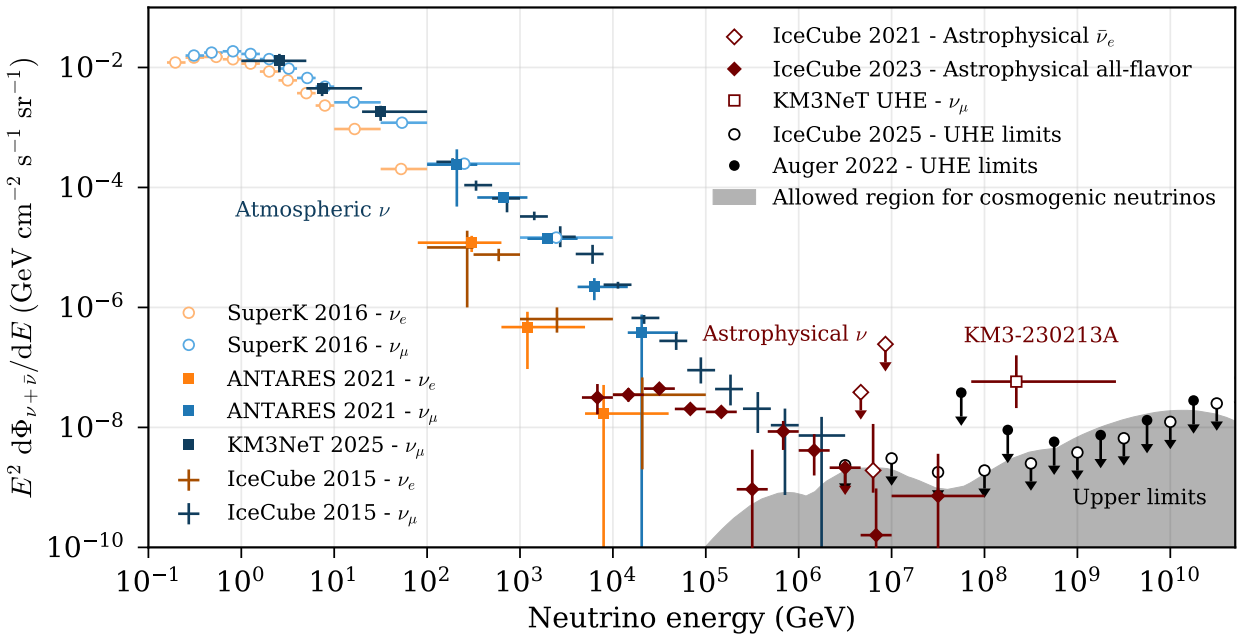

Figure 30.15: Measured energy spectra of atmospheric and cosmic diffuse neutrino fluxes. Experimental limits at highest energy are compared to model predictions for cosmogenic neutrinos [198]. All fluxes are normalized to one flavor ($\nu + \overline{\nu}$), assuming a ratio $\overline{\nu} : \nu = 1$ and, for cosmic neutrinos, a ratio $\nu_e : \nu_\mu : \nu_\tau = 1 : 1 : 1$ at Earth. Data sources: SuperK 2016 [304]; ANTARES 2021 [305]; KM3NeT 2025 ν_μ [306] IceCube 2015 ν_e [307]; IceCube 2015 ν_μ [308]; IceCube 2021 astrophysical $\bar{\nu}_e$ ($\nu + \overline{\nu}$ flux derived from a single candidate event for the Glashow resonance) [309]; IceCube 2023 astrophysical all flavor [41], KM3NeT-UHE ν_μ [193]. The limits at the highest energies are taken from [310] (IceCube) and [311] (Auger). They are shown in the energy bins used for the corresponding analyses and have been adjusted to bin widths of one decade. The region allowed for the expected cosmogenic neutrino fluxes is taken from [312] (see also Fig. 36.10).

30.4.3 *Diffuse fluxes*

Atmospheric neutrinos The flux of atmospheric neutrinos as measured by different experiments is shown in Fig. 30.15. The production chain for *conventional* atmospheric neutrinos follows eq. (30.1), with an observed ratio $\nu_e : \nu_\mu = 1 : 2$ at energies of a few GeV (where almost all muons decay in the atmosphere), and a ratio below 1 : 10 at TeV energies, where muons reach the ground before decaying. The flux of muon neutrinos with energies below 100 GeV from the lower hemisphere is modified due to neutrino oscillations, reducing the $\nu_e : \nu_\mu$ ratio at the lowest energies. The flux of ν_e is obtained by subtracting the number of neutral-current muon neutrino interactions (as deduced from the measured charged-current muon neutrino reactions) from the number of contained events without a muon track and converting the resulting E_{ν_e} distribution into the ν_e flux using the differential cross sections for CC and NC ν_e-nucleon scattering. The conventional atmospheric neutrino flux dominates in the GeV to TeV region, following an $E_\nu^{-3.7}$ power law.

Prompt atmospheric neutrinos are produced by the decay of hadrons containing a charm or bottom quark, the production of which is strongly suppressed. Since they are produced early in the air shower and decay before losing energy, however, the energy spectrum of prompt neutrinos is expected to be harder ($E_\nu^{-2.7}$) and to dominate the atmospheric neutrino flux at its highest energies. The corresponding theoretical prediction has large uncertainties related to the cosmic-ray spectrum and mass composition, the model for heavy-flavor production, and the parton distribution functions [313]. At present, experimental measurements only provide upper limits for the prompt flux (see e.g. Fig. 30.16 where the prompt component was fitted to zero).

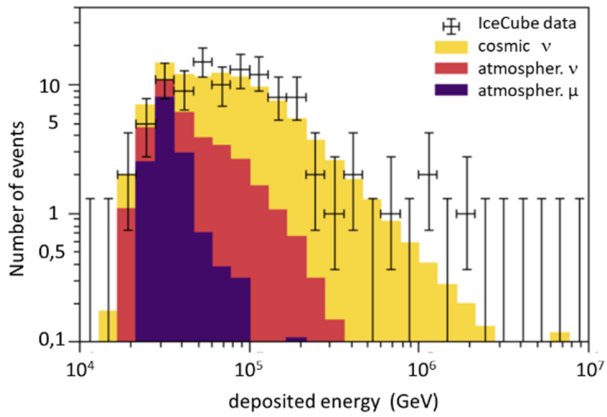

Figure 30.16: Measured (data points) and expected (histograms) distributions of the deposited energy measured in the IceCube detector for events passing the HESE selection, which strongly suppresses down-going atmospheric neutrinos by vetoing accompanying muons. The cosmic neutrino flux has been assumed to follow an unbroken power law in E_ν. Its normalization and spectral index, as well as the normalizations of the conventional and prompt atmospheric neutrino and the atmospheric muon contributions were fitted to the data, where only the region above 60 TeV was used to constrain the cosmic neutrino flux.

Diffuse extragalactic neutrino flux In 2013, a diffuse and isotropic flux of neutrinos of astrophysical origin was discovered with the IceCube Neutrino Observatory. The flux was identified with the so-called HESE (high-energy starting events) selection as an excess of neutrino events at high energies over atmospheric neutrinos and a background of misreconstructed atmospheric muons (see Fig. 30.16, for the 7.5-year HESE sample [316]). Similar high-energy excesses were also identified for tracks entering the detector from outside [317], and for fully contained cascade events. Evidence for this flux has meanwhile also been reported by ANTARES [318], albeit with much lower significance.

Int. J. Mod. Phys. A 2026.41. Downloaded by UNIVERSITY OF CALIFORNIA @ BERKELEY on 09/16/26. Re-[redacted]orldscientific.com strictly not permitted, except for Open Access articles.

Int. J. Mod. Phys. A 2026.41. Downloaded from www.worldscientific.com
by UNIVERSITY OF CALIFORNIA @ BERKELEY on 09/16/26. Re-use and distribution is strictly not permitted, except for Open Access articles.

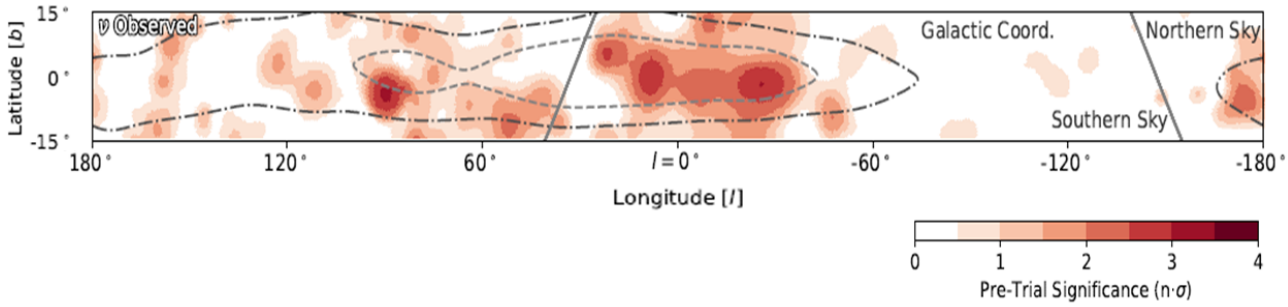

Figure 30.17: 829 The Milky Way plane in neutrinos (Galactic coordinates, with the origin being at the Galactic Center). Shown is the pre-trial significance of the IceCube observations using a cascade neutrino event sample, calculated from an all-sky scan for point-like sources [314]. Contours indicate the regions that contain 20% and 50% of the predicted diffuse neutrino emission according to an extrapolation of Fermi-LAT results. Gray lines indicate the Northern-Southern sky horizon line.

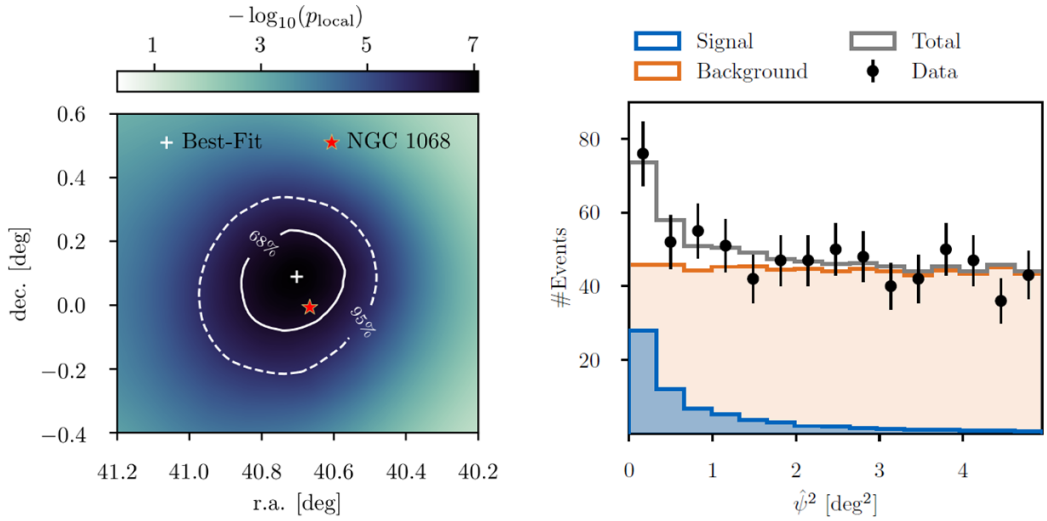

Figure 30.18: Left: The sky region around the most significant spot in the Northern Hemisphere and NGC 1068. Shown is a fine scan of the region around the hottest spot, marked by a white cross. The red circle shows the position of NGC 1068. The solid and dashed contours show the 68% and 95% confidence regions of the hot spot localization. Right: Distribution of the squared angular distance between NGC 1068 and the reconstructed event direction. Figures taken from [315].

Baikal-GVD observes an astrophysical diffuse flux of neutrinos at a significance of $5.1\,\sigma$, but with a substantially higher normalization than IceCube and ANTARES [319]. The measured fluxes are consistent with a parameterization as power-law functions proportional to $E_\nu^{-\gamma}$, with the normalization factor and the spectral index γ as parameters. The resulting γ values vary from 2.2 to 2.5 for different event classes covering different energy ranges. Recent IceCube studies [320,321] indicate that the energy spectrum is in fact well described by a broken power law, with spectral indices of $\gamma_1 = 1.7 \pm 0.3$ and $\gamma_2 = 2.8 \pm 0.1$ below and above the break at about 30 TeV, respectively.

Different production mechanisms result in different neutrino flavor compositions at sources and, after neutrino oscillations over astrophysical distances, at the Earth. An IceCube study of the event topologies [301] slightly favors $\nu_e : \nu_\mu : \nu_\tau = 1 : 2 : 0$ at the source (pion decay according to eq. (30.1) versus $0 : 1 : 0$ (damped muons) and disfavors a $1 : 0 : 0$ scenario (neutron decay).

A single event with energy 6.05 ± 0.72 PeV has been detected in IceCube [309]. It is compatible with having been generated by the resonant process $\bar{\nu}_e + e^- \to W^- \to$ hadrons at $E_\nu = 6.3$ PeV (Glashow resonance) [322]. A statistically significant observation of the Glashow resonance would reveal the presence of electron antineutrinos in the astrophysical flux and could provide information about their production process: the expected ratio $\bar{\nu}_e : \nu_e$ depends on the mass composition of cosmic rays and also on the photon density and the magnetic field strength of the source [323].

In February 2025, KM3NeT announced the observation of a neutrino event with an estimated neutrino energy of 220^{+570}_{-110} PeV in the ARCA detector, the highest-energy neutrino ever measured to date [193]. The diffuse neutrino flux corresponding to that event is indicated in Fig. 30.15. A possible astrophysical or cosmogenic origin of that neutrino, as well its potential association to blazars or a Galactic origin, are discussed in [324] and references therein.

Cosmogenic neutrinos Cosmogenic neutrinos stem from the decay of charged pions generated in interactions of ultra-high-energy cosmic rays with cosmic microwave (a) and infrared (b) background radiation ($p + \gamma \to n + \pi^+$) [325] and from the decays of neutrons produced in photodisintegration processes [326, 327] (c). The neutrino flux at EeV energies is expected to be dominated by (a) and (c).

Measurement methods and experimental data are described in Sect. 36.3.3. and Fig. 36.10. The expected flux can be estimated from the measured spectrum and composition of charged cosmic rays, using the CMB density and the well-measured properties of proton and nuclear interactions with photons at a center-of-mass energy in the GeV range. The current uncertainty of these predictions exceeds one order of magnitude. Figure 30.15 reproduces

Int. J. Mod. Phys. A 2026.41. Downloaded from www.worldscientific.com by UNIVERSITY OF CALIFORNIA @ BERKELEY on 09/16/26. Re- strictly not permitted, except for Open Access articles.

the presently tightest limits and compares them to the region for which cosmogenic neutrino fluxes would be consistent with those limits (as of 2019) and cosmic-ray analyses [312].

Neutrinos from the Galactic Plane The Milky Way is an emitter across the electromagnetic spectrum ranging from radio to gamma-rays. A large part of the observed gamma-ray flux is believed to consist of photons from the decays of π^0s produced by cosmic rays colliding with the interstellar medium. The TeV diffuse neutrino flux from the corresponding $\pi^\pm$ decays along the Galactic plane has been estimated with different models, ranging from a simple extrapolation of Fermi-LAT gamma-ray data to higher energies, to more sophisticated approaches (see e.g. [328]).

First hints for a TeV neutrino emission from the Galactic Ridge have been reported by the ANTARES collaboration [329]. IceCube has measured the flux of galactic neutrinos with a significance of 4.5σ against the only-background-hypothesis [314]. Baikal-GVD reports an excess of cascade events above 200 TeV from the Galactic plane [330]. Figure 30.17 shows a map of the Galactic plane with the point-by-point pre-trial significance of the IceCube neutrino observations. While the overall signal is consistent with the modeled diffuse emission from the Galactic plane, a significant part could also arise from a population of unresolved point sources. All individual "warm spots", however, are statistically consistent with background fluctuations.

30.4.4 *Neutrinos from astrophysical point sources*

Most point source candidates include Active Galactic Nuclei (AGN). In particular, blazars – AGN that have jets pointing towards the observer – are thought to be likely sources. In 2017, a spatial and temporal correlation was found between a flare of the electromagnetic emission from blazar TXS 0506+056 and the high-energy neutrino event IC170922A, detected by IceCube. An alert was sent to other observatories and a follow-up campaign in multiple wavelengths was started. At the moment of neutrino detection, the blazar was flaring in gamma rays, with an accidental coincidence excluded at the 3σ level [331]. Subsequent analyses of archival data revealed an excess in neutrino events with a significance of 3.5σ with respect to the expected atmospheric background, coincident with the position of TXS 0506+056, albeit not correlated with an electromagnetic flare [332].

In another analysis, the positions of 110 gamma-ray sources selected a priori were analyzed individually for a possible surplus of neutrinos over atmospheric and cosmic background expectations. An excess of 79^{+22}_{-20} neutrinos was found in the direction of the nearby AGN NGC 1068 (not a blazar, but a Seyfert-2 galaxy), at a significance of 4.2σ (see figure 30.18). The excess is spatially consistent with the direction of the strongest clustering of neutrinos in the Northern sky. The inferred flux exceeds the potential TeV gamma-ray flux by at least an order of magnitude [315], suggesting that the sight to the gamma-ray generation region is obscured, as expected for Seyfert-2 galaxies. A follow-up analysis by IceCube with more data confirms the excess, albeit at lower significance [333]. Several authors have argued that the neutrinos from NGC 1068 may originate from a region near its core, absorbing the gamma rays associated with the neutrinos, rather than from the blazar jet (see e.g. [334]). The general idea of such cocooned sources has first been discussed in [335].

Other potential sources include starburst galaxies, galaxy clusters, supernova remnants (steady emission) as well as Gamma Ray Bursts (GRBs) and Tidal Disruption Events, TDEs (transient emission). Indeed, using data from IceCube and the Zwicky Transient Facility ZTF, hints for a correlation of high-energy muon neutrinos with TDEs have been reported [336].

30.4.5 *Results on particle physics*

Investigating the attenuation of high-energy neutrinos as a function of energy and their path length through the Earth, the first measurement of the neutrino-nucleon cross section at energies between a few tens of TeV and ≈ 1 PeV (corresponding to center-of-mass energies between a few 100 GeV and about 1.4 TeV) has been achieved [337], giving access in deep-inelastic scattering in a kinematic region currently not accessible to accelerator-based experiments.

The study of atmospheric high-energy neutrinos allows for the investigation of oscillation physics (see Sect. 14) at higher energies and over longer baselines than Earth-bound experiments. Constraints ($\sin^2\theta_{23} = 0.51 \pm 0.050$ and $\Delta m^2_{32} = (2.41 \pm 0.07) \times 10^{-3}\,\mathrm{eV}^2$) have been obtained with IceCube and are compatible with corresponding results from accelerator experiments [338]. Both IceCube and KM3NeT/ORCA are sensitive to ν_τ appearance and have published results on the ν_τ normalization, *i.e.* the ratio between the number of observed and expected tau neutrino events that are consistent with the expectations [339, 340]. The KM3NeT/ORCA detector is furthermore expected to provide sensitivity to the neutrino mass hierarchy.

Also, Beyond-Standard-Model (BSM) physics is being tested. For instance, constraints by IceCube on 2/4 mixing (the fourth state being a sterile neutrino) are comparable to constraints from accelerator experiments [341]. Neutrinos may have BSM interactions, and if the coupling strengths are weak or if heavy mediators are involved, these interactions may only manifest themselves in the HE and UHE neutrino sector. Corresponding constraints from IceCube have been published in [342]. Additionally, possible oscillation-like effects induced by quantum gravity are investigated [343].

Acknowledgement Many thanks to team members, Prof. Q. Yuan, R.Z. Yang, J. Li, X.Y. Wang, S.Z. Chen and Dr. S.Q. Xu, L. Nie, R.F. Xu, who made substantial contributions to the γ-ray part of this section. We are grateful to C. Haack and L. Schumacher for their invaluable help in producing Fig. 30.15, and A. Coleman, E. Mayotte and A. Yushkov for help producing Figs. 30.7 and 30.8.

References

[1] Y. S. Yoon *et al.*, Astrophys. J. **728**, 122 (2011), [arXiv:1102.2575].

[2] O. Adriani *et al.* (PAMELA), Science **332**, 69 (2011), [arXiv:1103.4055].

[3] O. Adriani *et al.*, Adv. Space Res. **51**, 219 (2013).

[4] Y. S. Yoon *et al.*, Astrophys. J. **839**, 1, 5 (2017), [arXiv:1704.02512].

[5] N. Gorbunov *et al.*, Adv. Space Res. **64**, 12, 2546 (2019), [arXiv:1809.05333].

[6] M. G. Aartsen *et al.* (IceCube), Phys. Rev. D **100**, 8, 082002 (2019), [arXiv:1906.04317].

[7] Q. An *et al.* (DAMPE), Sci. Adv. **5**, 9, eaax3793 (2019), [arXiv:1909.12860].

[8] M. Aguilar *et al.* (AMS), Phys. Rept. **894**, 1 (2021).

[9] G. H. Choi *et al.*, Astrophys. J. **940**, 2, 107 (2022).

[10] O. Adriani *et al.* (CALET), Phys. Rev. Lett. **129**, 10, 101102 (2022), [arXiv:2209.01302].

[11] F. Alemanno *et al.*, Phys. Rev. Lett. **126**, 201102 (2021), [arXiv:2105.09073].

[12] H. S. Ahn *et al.*, Astrophys. J. **707**, 593 (2009), [arXiv:0911.1889].

[13] O. Adriani *et al.*, Phys. Rev. Lett. **125**, 251102 (2020), [arXiv:2012.10319].

[14] F. Aharonian *et al.* (H.E.S.S.), Phys. Rev. D **75**, 042004 (2007), [arXiv:astro-ph/0701766].

[15] M. Aguilar *et al.* (AMS), Phys. Rev. Lett. **126**, 4, 041104 (2021).

[16] O. Adriani *et al.* (CALET), Phys. Rev. Lett. **126**, 24, 241101 (2021), [arXiv:2106.08036].

[17] G. Ambrosi *et al.* (DAMPE), Nature **552**, 63 (2017), [arXiv:1711.10981].

[18] S. Abdollahi *et al.* (Fermi-LAT), Phys. Rev. D **95**, 8, 082007 (2017), [arXiv:1704.07195].

[19] O. Adriani *et al.*, Phys. Rev. Lett. **120**, 26, 261102 (2018), [arXiv:1806.09728].

Int. J. Mod. Phys. A 2026.41. Downloaded from www.worldscientific.com
by UNIVERSITY OF CALIFORNIA @ BERKELEY on 09/16/26. Re-use and distribution is strictly not permitted, except for Open Access articles.

[20] T. Antoni *et al.* (KASCADE), Astropart. Phys. **24**, 1 (2005), [arXiv:astro-ph/0505413].

[21] M. G. Aartsen *et al.* (IceCube), Phys. Rev. D **88**, 4, 042004 (2013), [arXiv:1307.3795].

[22] V. V. Prosin *et al.*, Nucl. Instrum. Meth. A **756**, 94 (2014).

[23] S. Schoo *et al.* (KASCADE-Grande), PoS **ICRC2015**, 263 (2016).

[24] K. Rawlins and T. Feusels (IceCube), PoS **ICRC2015**, 334 (2016).

[25] D. Ivanov, PoS **ICRC2015**, 349 (2016).

[26] A. Aab *et al.* (Pierre Auger), in "34th Int. Cosmic Ray Conf.", (2015), [arXiv:1509.03732].

[27] R. Alfaro *et al.* (HAWC), Phys. Rev. D **96**, 12, 122001 (2017), [arXiv:1710.00890].

[28] M. G. Aartsen *et al.* (IceCube), Phys. Rev. D **102**, 122001 (2020), [arXiv:2006.05215].

[29] P. Abreu *et al.* (Pierre Auger), Eur. Phys. J. C **81**, 11, 966 (2021), [arXiv:2109.13400].

[30] J. A. Morales-Soto *et al.* (HAWC), PoS **ICRC2021**, 330 (2021), [arXiv:2108.04748].

[31] Z. Cao *et al.* (LHAASO), Phys. Rev. Lett. **132**, 13, 131002 (2024), [arXiv:2403.10010].

[32] F. Varsi *et al.* (GRAPES-3), Phys. Rev. Lett. **132**, 5, 051002 (2024).

[33] F. Alemanno *et al.* (DAMPE) (2025), [arXiv:2511.05409].

[34] D. Maurin *et al.* (2023), [arXiv:2306.08901].

[35] Z. Cao *et al.* (LHAASO) (2025), [arXiv:2505.14447].

[36] Z. Cao *et al.* (LHAASO) (2025), [arXiv:2511.05013].

[37] M. Ackermann *et al.* (Fermi-LAT), Astrophys. J. **750**, 3 (2012), [arXiv:1202.4039].

[38] Z. Cao *et al.* (LHAASO), Physical Review Letters **131**, 15, 151001 (2023), [arXiv:2305.05372].

[39] M. Ackermann *et al.* (Fermi-LAT), Astrophys. J. **799**, 86 (2015), [arXiv:1410.3696].

[40] Z. Cao *et al.* (LHAASO), Physical Review Letters **134**, 8, 081002 (2025), [arXiv:2411.16021].

[41] R. Abbasi *et al.* (IceCube), PoS **ICRC2023**, 1064 (2023).

[42] S. Abdollahi *et al.* (Fermi-LAT), Astrophys. J. Supp. **260**, 2, 53 (2022), [arXiv:2201.11184].

[43] S. P. Wakely and D. Horan, in "30th Int. Cosmic Ray Conf.", volume 3, 1341–1344 (2007).

[44] Z. Cao *et al.* (LHAASO), Astrophys. J. Suppl. **271**, 1, 25 (2024), [arXiv:2305.17030].

[45] T. K. Gaisser, R. Engel and E. Resconi, *Cosmic Rays and Particle Physics: 2nd Edition*, Cambridge University Press (2016), ISBN 978-0-521-01646-9.

[46] P. Sreekumar *et al.*, Phys. Rev. Lett. **70**, 127 (1993).

[47] W. Baade and F. Zwicky, Proceedings of the National Academy of Science **20**, 259 (1934).

[48] D. Ter Haar, Reviews of Modern Physics **22**, 119 (1950).

[49] L. O. Drury, Rept. Prog. Phys. **46**, 973 (1983).

[50] C. J. Cesarsky and T. Montmerle, Space Sci. Rev. **36**, 2, 173 (1983).

[51] A. M. Bykov, Astron. Astrophys. Rev. **22**, 1, 77 (2014), [arXiv:1511.04608].

[52] V. Bosch-Ramon, F. A. Aharonian and J. M. Paredes, Astron. Astrophys. **432**, 609 (2005), [arXiv:astro-ph/0411508].

[53] V. S. Ptuskin and Y. M. Khazan, Soviet Astronomy **25**, 547 (1981).

[54] F. M. Rieger, Universe **8**, 11, 607 (2022), [arXiv:2211.12202].

[55] M. Milgrom and V. Usov, Astrophys. J. Lett. **449**, L37 (1995), [arXiv:astro-ph/9505009].

[56] L. A. Anchordoqui, G. E. Romero and J. A. Combi, Phys. Rev. D **60**, 103001 (1999), [arXiv:astro-ph/9903145].

[57] G. E. Romero, A. L. Müller and M. Roth, Astron. Astrophys. **616**, A57 (2018), [arXiv:1801.06483].

[58] P. Blasi, R. I. Epstein and A. V. Olinto, Astrophys. J. **533**, L123 (2000), [arXiv:astro-ph/9912240].

[59] J. Arons, Astrophys. J. **589**, 871 (2003), [arXiv:astro-ph/0208444].

[60] A. R. Bell, Mon. Not. Roy. Astron. Soc. **182**, 3, 443 (1978).

[61] D. Caprioli and A. Spitkovsky, Astrophys. J. **783**, 91 (2014), [arXiv:1310.2943].

[62] V. Petrosian, Space Sci. Rev. **173**, 535 (2012), [arXiv:1205.2136].

[63] E. G. Zweibel and M. Yamada, ARA&A **47**, 1, 291 (2009).

[64] A. M. Hillas, Ann. Rev. Astron. Astrophys. **22**, 425 (1984).

[65] J. R. Jokipii, Astrophys. J. **146**, 480 (1966).

[66] M. Lemoine, J. Plasma Phys. **89**, 5, 175890501 (2023), [arXiv:2304.03023].

[67] K. Lodders, Astrophys. J. **591**, 1220 (2003).

[68] G. B. Rybicki, *Radiative Processes in Astrophysics*, Wiley-VCH (2004), ISBN 978-0-471-82759-7, 978-3-527-61817-0.

[69] K. Mannheim and R. Schlickeiser, Astron. Astrophys. **286**, 983 (1994), [arXiv:astro-ph/9402042].

[70] Y. Genolini *et al.*, Phys. Rev. C **98**, 3, 034611 (2018), [arXiv:1803.04686].

[71] V. L. Ginzburg and S. I. Syrovatskii, *The Origin of Cosmic Rays*, Pergamon Press (1964).

[72] E. N. Parker, Planet. Space Sci. **13**, 1, 9 (1965).

[73] A. E. Vladimirov *et al.*, Comput. Phys. Commun. **182**, 1156 (2011), [arXiv:1008.3642].

[74] C. Evoli *et al.*, JCAP **10**, 018 (2008), [Erratum: JCAP 04, E01 (2016)], [arXiv:0807.4730].

[75] R. Kissmann, Astropart. Phys. **55**, 37 (2014), [arXiv:1401.4035].

[76] D. Maurin, Comput. Phys. Commun. **247**, 106942 (2020), [arXiv:1807.02968].

[77] K. Greisen, Phys. Rev. Lett. **16**, 748 (1966).

[78] G. T. Zatsepin and V. A. Kuzmin, JETP Lett. **4**, 78 (1966).

[79] R. Kulsrud and W. P. Pearce, Astrophys. J. **156**, 445 (1969).

[80] A. R. Bell and S. G. Lucek, Mon. Not. Roy. Astron. Soc. **321**, 3, 433 (2001).

[81] C. Evoli *et al.*, Phys. Rev. Lett. **121**, 2, 021102 (2018), [arXiv:1806.04153].

[82] J. Silk and M. Srednicki, Phys. Rev. Lett. **53**, 624 (1984).

[83] F. Donato, N. Fornengo and P. Salati, Phys. Rev. D **62**, 043003 (2000), [hep-ph/9904481].

[84] S. Murgia, Ann. Rev. Nucl. Part. Sci. **70**, 455 (2020).

[85] G. Steigman, Ann. Rev. Astron. Astrophys. **14**, 339 (1976).

[86] J. W. Mitchell and T. Hams, *Astrophysics and Space Instrumentation*, 559–592 (2012).

[87] D. V. Reames, Lect. Notes Phys. **978**, pp. (2021), [arXiv:2010.08517].

[88] R. Engel, *Indirect Detection of Cosmic Rays*, 593–632 (2012).

[89] A. D. Panov *et al.*, Bull. Russ. Acad. Sci. Phys. **71**, 494 (2007), [arXiv:astro-ph/0612377].

[90] H. S. Ahn *et al.*, Astrophys. J. Lett. **714**, L89 (2010), [arXiv:1004.1123].

[91] O. Adriani *et al.* (CALET), Phys. Rev. Lett. **130**, 17, 171002 (2023), [arXiv:2304.14699].

[92] F. Alemanno *et al.* (DAMPE) (2023), [arXiv:2304.00137].

[93] O. Adriani *et al.*, Astrophys. J. **791**, 2, 93 (2014), [arXiv:1407.1657].

Int. J. Mod. Phys. A 2026.41. Downloaded from www.worldscientific.com by UNIVERSITY OF CALIFORNIA @ BERKELEY on 09/16/26. Re-[redacted]strictly not permitted, except for Open Access articles.

[94] B. Schroer, C. Evoli and P. Blasi, Phys. Rev. D **103**, 123010 (2021), [arXiv:2102.12576].

[95] K. A. Lave *et al.*, Astrophys. J. **770**, 2, 117 (2013).

[96] J. J. Engelmann *et al.*, Astron. Astrophys. **233**, 96 (1990).

[97] M. Aguilar *et al.* (AMS), Phys. Rev. Lett. **124**, 21, 211102 (2020).

[98] M. Aguilar *et al.* (AMS), Phys. Rev. Lett. **126**, 8, 081102 (2021).

[99] M. Aguilar *et al.* (AMS), Phys. Rev. Lett. **127**, 2, 02101 (2021), [Erratum: Phys.Rev.Lett. 127, 159901 (2021)].

[100] M. Aguilar *et al.* (AMS), Phys. Rev. Lett. **130**, 21, 211002 (2023).

[101] O. Adriani *et al.* (CALET), Phys. Rev. Lett. **129**, 25, 251103 (2022), [arXiv:2212.07873].

[102] O. Adriani *et al.* (CALET), Phys. Rev. Lett. **128**, 13, 131103 (2022), [arXiv:2204.00845].

[103] F. Alemanno *et al.* (DAMPE), Phys. Rev. Lett. **134**, 19, 191001 (2025), [arXiv:2412.11460].

[104] M. Aguilar *et al.* (AMS), Phys. Rev. Lett. **120**, 2, 021101 (2018).

[105] A. E. Vladimirov *et al.*, Astrophys. J. **752**, 68 (2012), [arXiv:1108.1023].

[106] P. Blasi, E. Amato and P. D. Serpico, Phys. Rev. Lett. **109**, 061101 (2012), [arXiv:1207.3706].

[107] M. J. Boschini *et al.*, Astrophys. J. **889**, 167 (2020), [arXiv:1911.03108].

[108] O. Adriani *et al.* (CALET), Phys. Rev. Lett. **131**, 19, 191001 (2023), [arXiv:2311.05916].

[109] F. Aharonian *et al.* (H.E.S.S.), Phys. Rev. Lett. **133**, 22, 221001 (2024), [arXiv:2411.08189].

[110] O. Adriani *et al.* (PAMELA), Phys. Rev. Lett. **111**, 081102 (2013), [arXiv:1308.0133].

[111] C. Evoli *et al.*, Phys. Rev. D **103**, 8, 083010 (2021), [arXiv:2010.11955].

[112] P. Mertsch, JCAP **11**, 045 (2018), [arXiv:1809.05104].

[113] O. Adriani *et al.* (PAMELA), Nature **458**, 607 (2009), [arXiv:0810.4995].

[114] M. Klasen, M. Pohl and G. Sigl, Prog. Part. Nucl. Phys. **85**, 1 (2015), [arXiv:1507.03800].

[115] F. A. Aharonian, A. M. Atoyan and H. J. Volk, Astron. Astrophys. **294**, L41 (1995).

[116] A. U. Abeysekara *et al.* (HAWC), Science **358**, 6365, 911 (2017), [arXiv:1711.06223].

[117] P. Blasi, Phys. Rev. Lett. **103**, 051104 (2009), [arXiv:0903.2794].

[118] P. Mertsch, A. Vittino and S. Sarkar, Phys. Rev. D **104**, 103029 (2021), [arXiv:2012.12853].

[119] O. Adriani *et al.*, Pisma Zh. Eksp. Teor. Fiz. **96**, 693 (2012).

[120] G. Jóhannesson *et al.*, Astrophys. J. **824**, 1, 16 (2016), [arXiv:1602.02243].

[121] P. Blasi and P. D. Serpico, Phys. Rev. Lett. **103**, 081103 (2009), [arXiv:0904.0871].

[122] V. Poulin *et al.*, Phys. Rev. D **99**, 2, 023016 (2019), [arXiv:1808.08961].

[123] H. Fuke *et al.*, Phys. Rev. Lett. **95**, 081101 (2005), [arXiv:astro-ph/0504361].

[124] A. H. Compton and I. A. Getting, Phys. Rev. **47**, 11, 817 (1935).

[125] L. J. Gleeson and W. I. Axford, Astrophys. Sp. Sc. **2**, 4, 431 (1968).

[126] M. Aglietta *et al.* (EAS-TOP), Astrophys. J. **470**, 501 (1996).

[127] M. Ahlers and P. Mertsch, Prog. Part. Nucl. Phys. **94**, 184 (2017), [arXiv:1612.01873].

[128] A. Abdul Halim *et al.* (Pierre Auger), Astrophys. J. Suppl. **264**, 2, 50 (2023), [arXiv:2211.16020].

[129] R. U. Abbasi *et al.* (Telescope Array), Science **382**, 6673, abo5095 (2023), [arXiv:2311.14231].

[130] A. V. Glushkov *et al.*, Bull. Russ. Acad. Sci. Phys. **89**, 6, 894 (2025), [arXiv:2506.00517].

[131] E. W. Kellermann and L. Towers, J. Phys. A **3**, 284 (1970).

[132] S. Sciutto, AIRES User's Manual and Reference Guide; version 19.04.00 `http://aires.fisica.unlp.edu.ar/`.

[133] A. Aab *et al.* (Pierre Auger), Phys. Rev. D **100**, 8, 082003 (2019), [arXiv:1901.08040].

[134] J. Albrecht *et al.*, Nature Rev. Phys. **8**, 2, 98 (2026), [arXiv:2508.21796].

[135] D. Heck and T. Pierog, Extensive Air Shower Simulation with CORSIKA: A User's Guide (Version 7.7420) `https://www.iap.kit.edu/corsika/70.php`.

[136] J. M. Alameddine *et al.*, Astropart. Phys. **166**, 103072 (2025), [arXiv:2409.15999].

[137] F. Riehn *et al.*, Phys. Rev. D **102**, 6, 063002 (2020), [arXiv:1912.03300].

[138] S. Ostapchenko, EPJ Web Conf. **208**, 11001 (2019).

[139] T. Pierog *et al.*, Phys. Rev. C **92**, 3, 034906 (2015), [arXiv:1306.0121].

[140] W. Heitler, *The quantum theory of radiation*, volume 5 of *International Series of Monographs on Physics*, Oxford University Press, Oxford (1936).

[141] J. Matthews, Astropart. Phys. **22**, 387 (2005).

[142] A. Aab *et al.* (Pierre Auger), Nucl. Instrum. Meth. A **798**, 172 (2015), [arXiv:1502.01323].

[143] H. Kawai *et al.* (Telescope Array), Nucl. Phys. B Proc. Suppl. **175-176**, 221 (2008).

[144] S. P. Knurenko and A. V. Sabourov, Nucl. Phys. B Proc. Suppl. **151**, 92 (2006), yakutsk Array, Russia, 10^{15}–10^{19} eV range.

[145] Z. C. et al., Sci. China Phys. Mech. Astron. **64**, 1, 219501 (2021), lHAASO Collaboration, China, 10^{11}–10^{17} eV range.

[146] R. Abbasi *et al.* (IceCube), Nucl. Instrum. Meth. A **700**, 188 (2013), [arXiv:1207.6326].

[147] N. M. Budnev *et al.* (TAIGA), PoS **ICRC2021**, 731 (2021).

[148] S. K. Gupta *et al.* (GRAPES-3), Nucl. Instrum. Meth. A **540**, 311 (2005).

[149] S. Knurenko and I. Petrov, Adv. Space Res. **64**, 12, 2570 (2019), [arXiv:1908.01508].

[150] N. M. Budnev *et al.*, Astropart. Phys. **117**, 102406 (2020), [arXiv:2104.03599].

[151] A. Aab *et al.* (Pierre Auger), Phys. Rev. Lett. **116**, 24, 241101 (2016), [arXiv:1605.02564].

[152] A. Abdul Halim *et al.* (Pierre Auger), PoS **ICRC2025**, 275 (2025), [arXiv:2507.08510].

[153] J. Hörandel (Pierre Auger), PoS **ICRC2025**, 294 (2025).

[154] P. A. Bezyazeekov *et al.*, Phys. Rev. D **97**, 12, 122004 (2018), [arXiv:1803.06862].

[155] I. Petrov and S. Knurenko, PoS **ICRC2019**, 385 (2020).

[156] P. Schellart *et al.*, Astron. Astrophys. **560**, A98 (2013), [arXiv:1311.1399].

[157] R. Monroe *et al.*, Nucl. Instrum. Meth. A **953**, 163086 (2020), [arXiv:1907.10193].

[158] S. Buitink *et al.*, PoS **ICRC2023**, 503 (2023).

[159] A. Aab *et al.* (Pierre Auger) (2016), [arXiv:1604.03637].

[160] E. Kido (Telescope Array), EPJ Web Conf. **210**, 06001 (2019).

[161] M. G. Aartsen *et al.* (IceCube) (2014), [arXiv:1412.5106].

Int. J. Mod. Phys. A 2026.41. Downloaded from www.worldscientific.com
by UNIVERSITY OF CALIFORNIA @ BERKELEY on 09/16/26. Re-use and distribution is strictly not permitted, except for Open Access articles.

[162] J. Álvarez-Muñiz *et al.* (GRAND), Sci. China Phys. Mech. Astron. **63**, 1, 219501 (2020), [arXiv:1810.09994].

[163] D. Southall *et al.*, Nucl. Instrum. Meth. A **1048**, 167889 (2023), [arXiv:2206.09660].

[164] S.-H. Wang *et al.*, JCAP **11**, 022 (2022), [arXiv:2207.10616].

[165] K. Kotera *et al.*, PoS **ICRC2025**, 1078 (2025), [arXiv:2507.04382].

[166] S. Agarwal *et al.* (RNO-G), JINST **20**, 04, P04015 (2025), [arXiv:2411.12922].

[167] A. Abdul Halim *et al.* (Pierre Auger), Phys. Rev. Lett. **135**, 24, 241002 (2025), [arXiv:2506.11688].

[168] A. Abdul Halim *et al.* (Pierre Auger), Phys. Rev. Lett. **134**, 2, 021001 (2025), [arXiv:2406.06315].

[169] D. Ivanov (Telescope Array), PoS **ICRC2019**, 298 (2020).

[170] A. Aab *et al.* (Pierre Auger), Phys. Rev. D **102**, 6, 062005 (2020), [arXiv:2008.06486].

[171] A. Coleman *et al.*, Astropart. Phys. **149**, 102819 (2023), [arXiv:2205.05845].

[172] R. U. Abbasi *et al.* (Telescope Array), Astrophys. J. **858**, 2, 76 (2018), [arXiv:1801.09784].

[173] R. U. Abbasi *et al.* (Telescope Array), Astrophys. J. **909**, 2, 178 (2021), [arXiv:2012.10372].

[174] A. Abdul Halim *et al.* (Pierre Auger), PoS **ICRC2025**, 331 (2025), [arXiv:2507.10292].

[175] J. Bellido (Pierre Auger), PoS **ICRC2017**, 506 (2018).

[176] A. Fedynitch *et al.*, Phys. Rev. D **100**, 10, 103018 (2019), [arXiv:1806.04140].

[177] A. Abdul Halim *et al.* (Pierre Auger), Phys. Rev. Lett. **132**, 2, 021001 (2024), [arXiv:2310.19963].

[178] D. R. Bergman *et al.* (Pierre Auger, Telescope Array), PoS **ICRC2025**, 381 (2025), [arXiv:2509.05530].

[179] A. A. Watson, JHEAp **33**, 14 (2022), [arXiv:2112.06525].

[180] C. J. Todero Peixoto (Pierre Auger), PoS **ICRC2019**, 440 (2020).

[181] A. Corstanje *et al.*, Phys. Rev. D **103**, 10, 102006 (2021), [arXiv:2103.12549].

[182] A. Abdul Halim *et al.* (Pierre Auger), Phys. Rev. D **112**, 12, 123042 (2025), [arXiv:2507.02558].

[183] F. G. Schröder, Prog. Part. Nucl. Phys. **93**, 1 (2017), [arXiv:1607.08781].

[184] M. Ahlers *et al.* (2025), [arXiv:2502.05657].

[185] M. Unger and G. R. Farrar, Astrophys. J. **970**, 1, 95 (2024), [arXiv:2311.12120].

[186] D. Hooper, S. Sarkar and A. M. Taylor, Astropart. Phys. **27**, 199 (2007), [arXiv:astro-ph/0608085].

[187] A. A. Halim *et al.* (Pierre Auger), Astrophys. J. **976**, 1, 48 (2024), [arXiv:2408.05292].

[188] A. Abdul Halim *et al.* (Telescope Array, Pierre Auger), PoS **UHECR2024**, 009 (2025).

[189] G. Golup *et al.* (Pierre Auger), PoS **ICRC2023**, 252 (2023).

[190] J. Kim *et al.* (Telescope Array), PoS **ICRC2023**, 244 (2023).

[191] A. Abdul Halim *et al.* (Pierre Auger), Astrophys. J. **984**, 2, 123 (2025), [arXiv:2407.06874].

[192] J. Kim *et al.* (Telescope Array), PoS **ICRC2025**, 302 (2025), [arXiv:2510.02739].

[193] S. Aiello *et al.* (KM3NeT), Nature **638**, 8050, 376 (2025), [Erratum: Nature 640, E3 (2025)].

[194] A. Aab *et al.* (Pierre Auger), Front. Astron. Space Sci. **6**, 24 (2019), [arXiv:1904.11918].

[195] B. P. Abbott *et al.*, Astrophys. J. Lett. **848**, 2, L12 (2017), [arXiv:1710.05833].

[196] A. Albert *et al.*, Astrophys. J. Lett. **850**, 2, L35 (2017), [arXiv:1710.05839].

[197] S. Mollerach and E. Roulet, JCAP **03**, 017 (2019), [arXiv:1812.04026].

[198] A. A. Halim *et al.* (Pierre Auger), JCAP **05**, 024 (2023), [arXiv:2211.02857].

[199] J. C. Arteaga Velazquez, PoS **ICRC2023**, 466 (2023).

[200] A. Aab *et al.* (Pierre Auger), Phys. Rev. Lett. **126**, 15, 152002 (2021), [arXiv:2102.07797].

[201] A. Abdul Halim *et al.* (Pierre Auger), Phys. Rev. D **109**, 10, 102001 (2024), [arXiv:2401.10740].

[202] M. Tavani *et al.* (AGILE), Astron. Astrophys. **502**, 995 (2009), [arXiv:0807.4254].

[203] J. Chang *et al.* (DAMPE), Astroparticle Physics **95**, 6 (2017), [arXiv:1706.08453].

[204] S. Torii, C. Collaboration *et al.*, J. Jpn. Soc. Microgravity Appl. **24**, 1, 120 (2007).

[205] W. B. Atwood *et al.* (Fermi-LAT), Astrophys. J **697**, 2, 1071 (2009), [arXiv:0902.1089].

[206] F. Aharonian *et al.* (H.E.S.S.), Astron. Astrophys. **457**, 899 (2006), [arXiv:astro-ph/0607333].

[207] J. Sitarek *et al.* (MAGIC), in "International Cosmic Ray Conference," volume 33 of *International Cosmic Ray Conference*, 1116 (2013), [arXiv:1308.0141].

[208] D. B. Kieda (VERITAS), in "International Cosmic Ray Conference," volume 33 of *International Cosmic Ray Conference*, 1124 (2013), [arXiv:1308.4849].

[209] F. Di Pierro (CTA LST Project), Journal of Physics Conference Series **2429**, 012020 (2023).

[210] A. Abramowski *et al.* (H.E.S.S.), Physical Review D. **90**, 12, 122007 (2014), [arXiv:1411.7568].

[211] N. Budnev *et al.*, Nuclear Instruments and Methods in Physics Research A **958**, 162113 (2020).

[212] G. Aielli *et al.* (ARGO-YBJ), Nucl. Instrum. Meth. A **661**, S50 (2012).

[213] T. K. Sako *et al.*, volume 32, 177–184 (2009), [arXiv:0907.4589].

[214] B. M. Baughman, in "International Cosmic Ray Conference," volume 9 of *International Cosmic Ray Conference*, 123 (2011).

[215] Z. Cao, Nature Astron. **5**, 8, 849 (2021).

[216] J. A. Hinton (H.E.S.S.), New Astron. Rev. **48**, 331 (2004).

[217] C. Baixeras, Nuclear Physics B - Proceedings Supplements **114**, 247 (2003), ISSN 0920-5632.

[218] H. B. T.C Weekes *et al.*, Astroparticle Physics **17**, 2, 221 (2002), ISSN 0927-6505.

[219] G. W. Clark *et al.*, Astrophysical Journal, Letters **153**, L203 (1968).

[220] C. E. Fichtel *et al.*, Astrophysical Journal **198**, 163 (1975).

[221] H. A. Mayer-Hasselwander *et al.*, Astronomy and Astrophysics **105**, 1, 164 (1982).

[222] S. D. Hunter *et al.*, Astrophys. J. **481**, 205 (1997).

[223] M. Ackermann *et al.*, The Astrophysical Journal **750**, 1, 3 (2012), [arXiv:1202.4039].

[224] A. A. Abdo *et al.*, Astrophys. J. **688**, 1078 (2008), [arXiv:0805.0417].

[225] B. Bartoli *et al.* (ARGO-YBJ), Astrophys. J. **806**, 20 (2015), [arXiv:1507.06758].

[226] M. Amenomori *et al.* (Tibet ASgamma), Phys. Rev. Lett. **126**, 14, 141101 (2021), [arXiv:2104.05181].

[227] P. Sreekumar *et al.* (EGRET), Astrophys. J. **494**, 523 (1998), [arXiv:astro-ph/9709257].

[228] M. Ackermann *et al.* (Fermi-LAT), Astrophys. J. **799**, 86 (2015), [arXiv:1410.3696].

Int. J. Mod. Phys. A 2026.41. Downloaded from www.worldscientific.com by UNIVERSITY OF CALIFORNIA @ BERKELEY on 09/16/26. Re-[redacted]strictly not permitted, except for Open Access articles.

[229] Z. Cao *et al.*, Annual Review of Nuclear and Particle Science **73**, 341 (2023), [arXiv:2310.01744].

[230] S. Funk, Ann. Rev. Nucl. Part. Sci. **65**, 245 (2015).

[231] J. A. Hinton and W. Hofmann, Ann. Rev. Astron. Astrophys. **47**, 523 (2009), [arXiv:1006.5210].

[232] V. Schoenfelder (COMPTEL), Astron. Astrophys. Suppl. Ser. **143**, 145 (2000), [arXiv:astro-ph/0002366].

[233] S. Abdollahi *et al.* (Fermi-LAT), Astrophys. J. Suppl. **247**, 1, 33 (2020), [arXiv:1902.10045].

[234] Z. Cao *et al.* (LHAASO*†, LHAASO), Science **373**, 6553, 425 (2021).

[235] F. A. Aharonian *et al.* (H.E.S.S.), Nature **432**, 75 (2004), [arXiv:astro-ph/0411533].

[236] F. Aharonian (H.E.S.S.), Astron. Astrophys. **464**, 235 (2007).

[237] H. Abdalla *et al.* (H.E.S.S.), Astron. Astrophys. **612**, A6 (2018), [arXiv:1609.08671].

[238] A. Abramowski *et al.*, AAP **537**, A114 (2012), [arXiv:1111.2043].

[239] F. Aharonian *et al.*, AAP **467**, 3, 1075 (2007), [arXiv:astro-ph/0703427].

[240] F. Aharonian *et al.*, APJL **970**, 1, L21 (2024), [arXiv:2407.16219].

[241] X. Astiasarain *et al.*, Astron. Astrophys. **671**, A47 (2023), [arXiv:2301.04504].

[242] X.-N. Sun *et al.*, AAP **639**, A80 (2020), [arXiv:2006.00879].

[243] R.-Z. Yang and Y. Wang, AAP **640**, A60 (2020), [arXiv:2007.15295].

[244] T.-T. Ge *et al.*, Month. Not. Roy. Astr. Soc. **517**, 4, 5121 (2022), [arXiv:2210.01352].

[245] X.-N. Sun, R.-Z. Yang and X.-Y. Wang, MNRAS **494**, 3, 3405 (2020), [arXiv:2006.02052].

[246] R.-z. Yang and F. Aharonian, AAP **600**, A107 (2017), [arXiv:1612.02250].

[247] B. Liu, R.-z. Yang and Z. Chen, Monthly Notices of the Royal Astronomical Society **513**, 4, 4747 (2022), ISSN 0035-8711, URL `https://doi.org/10.1093/mnras/stac1252`.

[248] J.-h. Liu, B. Liu and R.-z. Yang, MNRAS **526**, 1, 175 (2023), [arXiv:2309.03577].

[249] F. Aharonian, R. Yang and E. de Oña Wilhelmi, Nature Astronomy **3**, 561 (2019), [arXiv:1804.02331].

[250] M. C. Weisskopf *et al.*, Astrophys. J. Lett. **536**, 2, L81 (2000), [arXiv:astro-ph/0003216].

[251] R. Bühler and R. Blandford, Rept. Prog. Phys. **77**, 066901 (2014), [arXiv:1309.7046].

[252] A. A. Abdo *et al.*, Science **326**, 5959, 1512 (2009).

[253] J. Li *et al.*, Nature Astron. **4**, 12, 1177 (2020), [arXiv:2008.10523].

[254] R. Zanin *et al.*, Astron. Astrophys. **596**, A55 (2016), [arXiv:1605.05914].

[255] J. Albert *et al.* (MAGIC), Astrophys. J. Lett. **665**, L51 (2007), [arXiv:0706.1505].

[256] G. Martí-Devesa and O. Reimer, Astron. Astrophys. **654**, A44 (2021), [arXiv:2109.05950].

[257] M. H. van Kerkwijk *et al.*, Natur **355**, 6362, 703 (1992).

[258] E. E. Becklin *et al.*, Natur **245**, 5424, 302 (1973).

[259] M. van der Klis and J. M. Bonnet-Bidaud, A&A **214**, 203 (1989).

[260] M. Tavani *et al.*, Natur **462**, 7273, 620 (2009), [arXiv:0910.5344].

[261] Fermi LAT Collaboration *et al.*, Sci **326**, 5959, 1512 (2009).

[262] A. A. Zdziarski *et al.*, MNRAS **479**, 4, 4399 (2018), [arXiv:1804.07460].

[263] J. M. Bonnet-Bidaud and G. Chardin, Phys. Rept. **170**, 6, 325 (1988).

[264] Z. Cao *et al.* (LHAASO) (2025), [arXiv:2512.16638].

[265] A. A. Abdo *et al.*, VizieR Online Data Catalog J/ApJS/208/17 (2013).

[266] S. Ansoldi *et al.* (MAGIC), Astron. Astrophys. **585**, A133 (2016), [arXiv:1510.07048].

[267] A. Djannati-Ataï, in "31st Texas Symposium on Relativistic Astrophysics," 33 (2022).

[268] A. Allafort *et al.* (Fermi-LAT), Astrophys. J. Lett. **777**, L2 (2013), [arXiv:1308.0358].

[269] A. A. Abdo *et al.* (Fermi-LAT), Astrophys. J. Suppl. **208**, 17 (2013), [arXiv:1305.4385].

[270] H. An, Astrophys. J. **924**, 2, 91 (2022), [arXiv:2111.02575].

[271] C. J. Clark *et al.*, Nature Astron. **7**, 4, 451 (2023), [arXiv:2301.10995].

[272] D. F. Torres *et al.*, Astrophys. J. **836**, 1, 68 (2017), [arXiv:1612.07083].

[273] A. Franckowiak *et al.*, Astron. Astrophys. **609**, A120 (2018), [arXiv:1710.04736].

[274] S. De Wolf *et al.* (H.E.S.S.), Science **376**, 6588, abn0567 (2022), [arXiv:2202.08201].

[275] M. Ajello *et al.* (Fermi-LAT), Astrophys. J. **892**, 105 (2020), [arXiv:1905.10771].

[276] M. Ajello *et al.* (Fermi-LAT), Astrophys. J. Suppl. **263**, 2, 24 (2022), [arXiv:2209.12070].

[277] M. Hayashida *et al.*, Astrophys. J. **807**, 1, 79 (2015), [arXiv:1502.04699].

[278] V. A. Acciari *et al.*, Astrophys. J. **738**, 25 (2011), [arXiv:1106.1210].

[279] M. Sikora, M. C. Begelman and M. J. Rees, Astrophys. J. **421**, 153 (1994).

[280] F. A. Aharonian, New Astron. **5**, 377 (2000), [arXiv:astro-ph/0003159].

[281] B. Bartoli *et al.* (ARGO-YBJ), Astrophys. J. Suppl. **222**, 1, 6 (2016), [arXiv:1511.06851].

[282] B. Bartoli *et al.* (ARGO-YBJ), Astrophys. J. **734**, 110 (2011), [arXiv:1106.0896].

[283] Z.-H. An *et al.* (Insight-HXMT, GECAM) (2023), [arXiv:2303.01203].

[284] Z. Cao *et al.* (LHAASO), Science **380**, 6652, 9328 (2023), [arXiv:2306.06372].

[285] V. A. Acciari *et al.* (MAGIC), Nature **575**, 7783, 459 (2019), [arXiv:2006.07251].

[286] H. Abdalla *et al.*, Nature **575**, 7783, 464 (2019), [arXiv:1911.08961].

[287] B. Bartoli, r. Xu *et al.* (ARGO-YBJ), Astrophys. J. **758**, 2 (2012), [arXiv:1209.0534].

[288] A. Albert *et al.* (HAWC), Astrophys. J. **929**, 2, 125 (2022), [arXiv:2106.03946].

[289] K. Katarzynski *et al.*, Astron. Astrophys. **433**, 479 (2005), [arXiv:astro-ph/0412405].

[290] Z. Cao, F. Aharonian and other sourcese (LHAASO), Astrophys. J. Lett. **971**, 2, L45 (2024), [arXiv:2405.07691].

[291] Z. Cao, F. Aharonian and other sourcese (LHAASO), Astrophys. J. Lett. **975**, 2, L44 (2024), [arXiv:2410.15353].

[292] M. Ajello *et al.*, Astrophys. J. **878**, 1, 52 (2019), [arXiv:1906.11403].

[293] P. Kumar and R. B. Duran, Mon. Not. Roy. Astron. Soc. **400**, 75 (2009), [arXiv:0905.2417].

[294] X.-Y. Wang *et al.*, Astrophys. J. **712**, 1232 (2010), [arXiv:0911.4189].

[295] V. A. Acciari *et al.* (MAGIC), Nature **575**, 7783, 455 (2019), [arXiv:2006.07249].

Int. J. Mod. Phys. A 2026.41. Downloaded from www.worldscientific.com
by UNIVERSITY OF CALIFORNIA @ BERKELEY on 09/16/26. Re-use and distribution is strictly not permitted, except for Open Access articles.

[296] H. Abdalla *et al.* (H.E.S.S.), Science **372**, 6546, 1081 (2021), [arXiv:2106.02510].

[297] Z. Cao *et al.* (LHAASA, LHAASO), Sci. Adv. **9**, 46, adj2778 (2023), [arXiv:2310.08845].

[298] S. R. Coleman and S. L. Glashow, Phys. Rev. D **59**, 116008 (1999), [hep-ph/9812418].

[299] F. W. Stecker and S. L. Glashow, Astropart. Phys. **16**, 97 (2001), [arXiv:astro-ph/0102226].

[300] Z. Cao *et al.* (LHAASO), Phys. Rev. Lett. **128**, 5, 051102 (2022), [arXiv:2106.12350].

[301] R. Abbasi *et al.* (IceCube), Eur. Phys. J. C **82**, 11, 1031 (2022), [arXiv:2011.03561].

[302] R. Mammen Abraham *et al.*, J. Phys. G **49**, 11, 110501 (2022), [arXiv:2203.05591].

[303] J. Abraham *et al.* (Pierre Auger), Phys. Rev. Lett. **100**, 211101 (2008), [arXiv:0712.1909].

[304] E. Richard *et al.* (Super-Kamiokande), Phys. Rev. D **94**, 052001 (2016), [arXiv:1510.08127].

[305] S. Adrian-Martinez *et al.* (ANTARES), Eur. Phys. J. C **73**, 2606 (2013), [arXiv:1308.1599].

[306] S. Aiello *et al.* (KM3NeT), Eur. Phys. J. C **85**, 8, 871 (2025), [arXiv:2504.09119].

[307] M. G. Aartsen *et al.* (IceCube), Phys. Rev. D **91**, 122004 (2015), [arXiv:1504.03753].

[308] M. Börner *et al.* (IceCube), PoS **ICRC2015**, 1098 (2016).

[309] M. Aartsen *et al.* (IceCube), Nature **591**, 220 (2021), [arXiv:2110.15051].

[310] R. Abbasi *et al.* ((IceCube Collaboration)§, IceCube), Phys. Rev. Lett. **135**, 3, 031001 (2025), [arXiv:2502.01963].

[311] M. Niechciol *et al.* (Pierre Auger), PoS **ICRC2023**, 1488 (2023).

[312] A. van Vliet, R. Alves Batista and J. R. Hörandel, Phys. Rev. D **100**, 2, 021302 (2019), [arXiv:1901.01899].

[313] S. Ostapchenko, M. V. Garzelli and G. Sigl, Phys. Rev. D **107**, 2, 023014 (2023), [arXiv:2208.12185].

[314] R. Abbasi *et al.* (IceCube), Science **380**, 6652 (2023), [arXiv:2307.04427].

[315] R. Abbasi *et al.* (IceCube), Science **378**, 538 (2022), [arXiv:2211.09972].

[316] R. Abbasi *et al.* (IceCube), Phys. Rev. D **104**, 02202 (2021), [arXiv:2011.03545].

[317] R. Abbasi *et al.* (IceCube), Astrophys. J. **928**, 50 (2022), [arXiv:2111.10299].

[318] L. A. Fusco and F. Versari (ANTARES), PoS **ICRC2019**, 891 (2020).

[319] V. A. Allakhverdyan *et al.* (GVD) (2025), [arXiv:2507.01893].

[320] R. Abbasi *et al.* (IceCube) (2025), [arXiv:2507.22233].

[321] A. Balagopal V. *et al.* (IceCube), PoS **ICRC2025**, 985 (2025), [arXiv:2507.06002].

[322] S. L. Glashow, Phys. Rev. **118**, 316 (1960).

[323] D. Biehl *et al.*, JCAP **01**, 033 (2017), [arXiv:1611.07983].

[324] R. Coniglione and M. Lamoureux, PoS **ICRC2025**, 1018 (2025).

[325] V. Berezinsky and G. Zatsepin, Phys. Lett. B **28**, 423 (1969).

[326] M. Ave *et al.*, Phys. Rev. Lett. **85**, 2244 (2000), [arXiv:astro-ph/0007386].

[327] D. Hooper, A. Taylor and S. Sarkar, Astropart. Phys. **23**, 11 (2005), [arXiv:astro-ph/0407618].

[328] D. Gaggero *et al.*, Phys. Rev. D **91**, 083012 (2014), [arXiv:1411.7623].

[329] A. Albert *et al.* (ANTARES), Phys. Lett. B **481**, 137951 (2023), [arXiv:2212.11876].

[330] V. A. Allakhverdyan *et al.* (Baikal-GVD), Astrophys. J. **982**, 2, 73 (2025), [arXiv:2411.05608].

[331] M. Aartsen *et al.* (IceCube, Fermi-LAT, MAGIC, AGILE, ASAS-SN, HAWC, H.E.S.S., INTEGRAL, Kanata, Kiso, Kapteyn, Liverpool Telescope, Subaru, Swift NuSTAR, VERITAS, VLA/17B-403), Science **361**, eaat1378 (2018), [arXiv:1807.08816].

[332] M. Aartsen *et al.* (IceCube), Science **361**, 147 (2018), [arXiv:1807.08794].

[333] R. Abbasi *et al.* (IceCube), Astrophys. J. **995**, 1, 11 (2025), [arXiv:2507.07275].

[334] P. Padovani *et al.*, Nature Astron. **8**, 9, 1077 (2024), [arXiv:2405.20146].

[335] V. S. Berezinsky and O. F. Prilutsky, in "International Neutrino Conference 1976," 650–653 (1976).

[336] R. Stein *et al.*, MNRAS **521,4**, 5046 (2023), [arXiv:2203.17135].

[337] M. G. Aartsen *et al.* (IceCube), Nature **551**, 596 (2017), [arXiv:1711.08119].

[338] R. Abbasi *et al.* (IceCube), Phys. Rev. D **108**, 1, 012014 (2023), [arXiv:2304.12236].

[339] M. G. Aartsen *et al.* (IceCube), Phys. Rev. D **99**, 3, 032007 (2019), [arXiv:1901.05366].

[340] S. Aiello *et al.* (KM3NeT), JHEP **07**, 213 (2025), [arXiv:2502.01443].

[341] M. G. Aartsen *et al.* (IceCube), Phys. Rev. Lett. **125**, 14, 141801 (2020), [arXiv:2005.12942].

[342] R. Abbasi *et al.* (IceCube), Phys. Rev. Lett. **129**, 1, 011804 (2022), [arXiv:2201.03566].

[343] A. Addazi *et al.*, Prog. Part. Nucl. Phys. **125**, 103948 (2022), [arXiv:2111.05659].

Int. J. Mod. Phys. A 2026.41. Downloaded from www.worldscientific.com
by UNIVERSITY OF CALIFORNIA @ BERKELEY on 09/16/26. Restrictions apply: Use is strictly not permitted, except for Open Access articles.

Experimental Methods and Colliders

31. Accelerator physics of colliders (rev.) 569
32. High-energy collider parameters (rev.) 580
33. Neutrino beam lines at high-energy proton synchrotrons (rev.) 585
34. Passage of particles through matter 586
35. Particle detectors at accelerators (rev.) 602
36. Particle detectors for non-accelerator phys. (rev.) 661
37. Radioactivity and radiation protection (rev.) 695
38. Commonly used radioactive sources 701

Int. J. Mod. Phys. A 2026.41. Downloaded from www.worldscientific.com
by UNIVERSITY OF CALIFORNIA @ BERKELEY on 09/16/26. Re-use and distribution is strictly not permitted, except for Open Access articles.

Int. J. Mod[redacted]wnloaded from www.worldscientific.com
by UNIVERSITY OF CALIFORNIA @ BERK[redacted]-use and distribution is strictly not permitted, except for Open Access articles.

31. Accelerator Physics of Colliders

Revised September 2025 by V. Shiltsev (NIU) and F. Zimmermann (CERN).

This article provides background for the High-Energy Collider Parameter Tables that follow and some additional information; see in-depth review and a comprehensive list of references in [1]; citations below are limited to widely used textbooks and open access seminal papers and reviews.

31.1 Energy and Luminosity

Collisions of two beams of particles accelerated to high energies $E_{1,2}$ provide access to center-of-mass energies (c.m.e.) of $E_{\rm cm} \approx 2\sqrt{E_1 E_2}$, assuming a typically small or zero crossing angle.

Among the 31 colliders that have ever reached the operational stage (seven remain in operation today), most used particles of equal mass and energy, yielding $E_{\rm cm} = 2E_{\rm b}$. Other machines collide beams of unequal energies—such as electron–proton, electron–ion or proton-ion colliders, or asymmetric B-factories, designed to produce short-lived particles whose decays are more easily detected and analyzed thanks to the resulting Lorentz boost.

In an accelerator, charged particles gain energy from an electric field, which typically oscillates at radio frequency (RF), ranging from hundreds of kHz to tens of GHz. With proper phasing relative to the RF field over a distance l, the energy gain of a particle with charge Ze is proportional to the average accelerating gradient G, i.e., $\Delta E_{\rm b} = ZeGl$. The highest beam accelerating gradients achieved to date in operational machines or dedicated test facilities ($G \approx 100$MV/m in 12GHz normal-conducting (NC) RF cavities and 31.5MV/m in 1.3GHz superconducting (SC) ones) make it possible, in principle, to reach very high energies over reasonably long linear accelerators (linacs), e.g. energies above 100 GeV with a length within 10s of kilometers. However, cost considerations often motivate minimization of RF acceleration via repeated use of the same RF system, which, in that case, would boost the energy in small portions $\Delta E_{\rm b} = ZeV_{\rm RF}$ per turn as the particles repeatedly traverse the total cavity voltage $V_{\rm RF}$. This concept underlies cyclotrons, synchrotrons and storage-ring circular colliders as well as more advanced schemes such as recirculating linear accelerators (RLAs), with or without energy recovery. Circular colliders are by far the most common; in such machines, the momentum and energy of ultra-relativistic particles are determined by the bending radius ρ of the particle trajectory inside the dipole magnets and by the average magnetic field B of these magnets:

$$p = ZeB\rho, \quad E \approx pc \quad \text{or} \quad E_{\rm b}\,[\text{GeV}] = 0.3Z(B\rho)\,[\text{Tm}]\,. \tag{31.1}$$

Such *synchrotron condition* assures approximately constant radius of the beam orbit during acceleration. Transverse focusing by quadrupole magnets is required to confine particles within the narrow aperture of the accelerator beam pipe that passes through the magnets. The maximum field of normal-conducting magnets is about 2 T, limited by the saturation of ferromagnetic materials. While this is sufficient for lower-energy colliders, such as most e^+e^- storage rings, it is inadequate for frontier-energy hadron (or muon) beams, since the implied accelerator tunnels would be excessively long and the total magnet power consumption prohibitively high.

The development of superconducting magnets, employing Nb-Ti wires carrying very high electric current and cooled by liquid helium below 5 K, opened the way to much higher magnetic fields and enabled record-energy hadron colliders [2]. For example, the 14 TeV c.m.e. LHC at CERN uses double-bore SC magnets with a maximum field of 8.3 T and a temperature of 1.9 K, installed in a tunnel of circumference $C \approx 26.7$ km (dipole-magnet bending radius $\rho \approx 2800$ m). The double-bore design permits acceleration of the same particle type in opposite directions, as well as operation with different particle species (e.g., protons and heavy ions) in the two apertures. In contrast, a single-bore design would generally imply counter-propagating beams of particles and antiparticles. Since antiparticle production is energy intensive and therefore limited, the double-aperture concept greatly expands the practical potential of high-performance hadron colliders.

The exploration of rare nuclear and high-energy particle physics phenomena requires not only sufficiently high collision energies but also a large number of detectable events. The expected number of events, $N_{\rm exp}$, is given by the product of the cross section for the reaction under study, $\sigma_{\rm exp}$, and the time integral of the instantaneous *luminosity*, $\mathcal{L}$:

$$N_{\rm exp} = \sigma_{\rm exp} \cdot \int \mathcal{L}(t)dt. \tag{31.2}$$

In the Tables, luminosity is stated in the units of cm^{-2}s^{-1}. The integral on the right is referred to as *integrated luminosity* $\mathcal{L}_{\rm int}$, and, reflecting the smallness of typical particle-interaction cross-sections is often reported in units of inverse femto- or attobarn, e.g., 1 ab^{-1}=10^{42} cm^{-2}. Colliders usually employ bunched beams of particles with approximately Gaussian distributions, and for two bunches containing N_1 and N_2 particles colliding head-on with frequency $f_{\rm coll}$, a basic expression for the luminosity is

$$\mathcal{L} = f_{\rm coll}\frac{N_1 N_2}{4\pi\sigma_x^*\sigma_y^*}\mathcal{F} \tag{31.3}$$

where σ_x^* and σ_y^* characterize the rms transverse beam sizes in the horizontal and vertical directions at the interaction point, and $\mathcal{F}$ is a factor of order 1, that accounts for inefficient geometric overlap of the beams due to a crossing angle, finite bunch length, and dynamic effects such as mutual focusing during the collision (see below). If each beam contains $n_{\rm b}$ bunches, the collision frequency increases to $f_{\rm coll} = n_{\rm b} f_0$, where f_0 is either the revolution frequency of a circular collider or the repetition rate of a linear collider. Achieving high luminosity therefore requires maximizing the bunch population and number of bunches, focusing them tightly, and colliding them at high frequencies at dedicated interaction points, where the products of the reactions can be registered by particle detectors.

Subsequent sections in this report briefly expand on the beam dynamics behind collider design, comment on the realization of collider performance in a selection of today's facilities, and end with some remarks on future possibilities.

31.2 Beam Dynamics

Given the enormous and highly concentrated power carried by modern high energy particle beams, the main concern of beam dynamics in colliders is stability of motion of i) individual particles in accelerators, ii) single high-intensity beams of many particles moving together, and iii) colliding beams [3–5].

31.2.1 *Single-Particle Dynamics*

While the reference particle at the nominal energy follows the design trajectory (the reference orbit) primarily determined by the transverse magnetic dipole fields, the other particles in the bunch are confined near it through the focusing action of quadrupole fields. We first focus on the transverse beam dynamics; the longitudinal dynamics—arising from the focusing effect of the RF system, which must remain powered even during steady-energy operation to maintain beam bunching—will be discussed next.

Assume that the reference particle carries a right-handed Cartesian coordinate system, with the co-moving z-coordinate pointed in the direction of motion along the reference trajectory, $z = s - vt$ (with v the reference particle velocity, and t time). The independent variable is the distance s of the reference particle along this trajectory, rather than time t, and for simplicity this reference path is taken to be planar. The transverse coordinates are x (horizontal) and y (vertical), where $\{x, z\}$ defines the plane of the reference trajectory.

Several time scales are involved, and this is reflected in the approximations used in formulating the equations of motion. All of today's high-energy colliders are alternating gradient synchrotrons or, respectively, storage rings and the shortest time scale is set by so-called *betatron oscillations*. The linearized equations of motion of a particle displaced from the reference trajectory are:

$$\begin{aligned} &x'' + K_x(s)x = 0\,, y'' + K_y(s)y = 0\,,\ z' = -x/\rho(s)\,, \\ &\text{with}\ \ K_x \equiv \frac{Ze}{p}\frac{\partial B_y}{\partial x} + \frac{1}{\rho^2}\ \text{and}\ K_y \equiv -\frac{Ze}{p}\frac{\partial B_y}{\partial x} \end{aligned} \tag{31.4}$$

Int. J. Mod. Phys. A 2026.41. Downloaded from www.worldscientific.com by UNIVERSITY OF CALIFORNIA @ BERKELEY on 09/16/26. Re-use and distribution is strictly not permitted, except for Open Access articles.

Int. J. Mod. Phys. A
by UNIVERSITY OF CALIFORNIA @ BERKE
nloaded from www.worldscientific.com
use and distribution is strictly not permitted, except for Open Access articles.

where $\rho = p/ZeB_y$ is the radius of curvature due to the field on the reference orbit. The prime denotes d/ds and the Maxwell equation in vacuum $\nabla \times \mathbf{B} = \mathbf{0}$ helps to eliminate $B_x(s)$ using the relation $\partial B_x/\partial y = \partial B_y/\partial x$. In this linear approximation, the vertical magnetic field $B_y(s)$ in the (x, z)-plane contains only dipole and quadrupole terms, which are treated as static in time, but s-dependent.

The solutions of the Hill's equations (31.4) for x and y with a restoring force periodic in s are those of quasi-harmonic oscillators:

$$x(s) = \sqrt{2J_x\beta_x}\ \cos\psi_x\ ,\ \ x'(s) = -\sqrt{\frac{2J_x}{\beta_x}}\,[\alpha_x\cos\psi_x + \sin\psi_x]\ , \tag{31.5}$$

where the *action* J_x is a constant of integration, $\alpha_x = \alpha_x(s) \equiv -(1/2)d\beta_x(s)/ds$, and the envelope of oscillations is modulated by the *beta-function* $\beta_x(s)$. A solution of the same form describes the motion in y. The betatron oscillation phase advances according to $d\psi_x/ds = 1/\beta_x$; that is, $2\pi\beta_x$ also plays the role of a local wavelength of oscillations along the orbit. An extremely important parameter for circular machines is the *tune*, Q_x, which is the number of such oscillations per turn about the closed path:

$$Q_x = \frac{1}{2\pi}\oint d\psi_x = \frac{1}{2\pi}\oint \frac{ds}{\beta_x(s)}. \tag{31.6}$$

While the integer part of the tune $[Q_{x,y}]$ generally characterizes the extent of the focusing lattice, it is the fractional part of the tune $\{Q_{x,y}\}$ that needs to be well defined and controlled by the machine operators in order to stay away from potentially detrimental resonances, which may occur under conditions of $kQ_x + lQ_y = m$, where k, l, and m are integers. For example, for the LHC a combination of horizontal and vertical tunes — also called the *working point* — equal to (Q_x, Q_y)=(64.31, 59.32) has been selected, such that resonances up to the order of $|k|+|l| = 10$ or 12 are avoided. These resonances are driven by high-order multipole components of the fields in the magnets, or by self-fields of the beam, or by the electromagnetic fields of the opposite bunch. Normally, the nonlinear components are very weak compared to linear ones, nevertheless, when the nonlinear resonance condition is encountered, the amplitudes of particle oscillations could grow over the beam lifetime, resulting in the escape of the particles to the machine aperture, in the increase of the average beam size, or in both; either of these is highly undesirable phenomena. Careful analysis of nonlinear beam dynamics is instrumental in determining and optimizing the *dynamic aperture*, which is defined as the maximum amplitude of a bounded particle motion.

Neglecting for now all nonlinear effects and usually small $x - y$ coupling, and considering only the linear dynamics, the beta-function is well defined and satisfies the following equation:

$$2\beta_x\beta_x'' - \beta_x'^2 + 4\beta_x^2 K_x = 4\,. \tag{31.7}$$

In a region free of magnetic fields, such as in the neighborhood of a collider interaction point (IP), usually occupied by particle detectors, a symmetric solution of Eq. (31.7) is a parabola:

$$\beta_x(s) = \beta_x^* + \frac{s^2}{\beta_x^*}\,, \tag{31.8}$$

where, in this case, s denotes the longitudinal distance from the IP. The location of the beam waist usually coincides with the IP and corresponds to the minimum value of the beta-function β_x^*; the asterisk is used to indicate IP parameters.

Note that individual quadrupole magnet focuses particles in one plane and defocuses in the orthogonal one, see Eq.(31.4), and a standard way to provide focusing in both planes is to employ an alternating gradient periodic focusing lattice, consisting of a sequence of equally-spaced quadrupoles with a magnetic field gradient equal in magnitude, but alternating in sign ("focusing quadrupole - drift space - defocusing quadrupole - drift space" – known as a *FODO cell*). Eq. (31.7) has stable periodic solutions $\beta_x(s), \beta_y(s)$ in both planes provided that the focal length of the quadrupoles is longer than half the focusing-lens spacing L, i.e., $f = p/(eB_2 l) > L/2$ (where l is the length of a quadrupole magnet, here assumed to be short $l \ll L$, and $B_2 \equiv |\partial B_y/\partial x|$ the quadrupoles' field gradient). In that case, the beta-functions have maxima at the focusing quadrupoles and minima at the defocusing ones, equal to, for example, $\beta_{\rm max,min} = (2 \pm \sqrt{2})L$ in the case of $f = L/\sqrt{2}$, which corresponds to a betatron phase advance $\Delta\psi_{x,y} = 90°$ per FODO cell.

Expressing the invariant J_x in terms of $x,\ x'$ yields

$$J_x = \frac{1}{2}\left(\gamma_x x^2 + 2\alpha_x x x' + \beta_x x'^2\right) = \frac{x^2 + (\alpha_x x + \beta_x x')^2}{2\beta_x} \tag{31.9}$$

with $\gamma_x = \gamma_x(s) \equiv (1 + \alpha_x^2(s))/\beta_x(s)$. In a periodic system, these *Courant-Snyder parameters* [6] (frequently referred to as *Twiss parameters*) $\alpha(s)$, $\beta(s)$, $\gamma(s)$ are usually defined by the focusing lattice; in a single pass system such as a linac, the parameters may be selected to match the x-x' distribution of the input beam. For a given position s in the ring, the transverse particle motion in $\{x, x' \equiv dx/ds\}$ phase space describes an ellipse, the area of which is $2\pi J_x$, where the horizontal action J_x is a constant of motion and independent of s. If the interior of that ellipse is populated by an ensemble of non-interacting and non-radiating particles, that area, given the name *emittance*, is constant over the trajectory as well and would only change with energy. In a typical case of the particle's energy change rate being much slower than betatron motion, and considering a Hamiltonian system (i.e., a hadron collider or a linear collider, either without significant synchrotron radiation), the adiabatic invariant $\int p_x dx$ is conserved, and given that for small angles $p_x = x' \cdot \beta\gamma mc^2$, it is common practice to consider an energy-independent *normalized beam emittance* that is equal to the product of the emittance and relativistic factor $\beta\gamma/\pi$ and denoted by $\varepsilon_{\rm n}$. For a beam with a Gaussian distribution in $\{x, x'\}$, average action value $\langle J_x\rangle$ and standard deviations σ_x, and $\sigma_{x'}$, the definition of the normalized rms beam emittance is

$$\varepsilon_{\rm nx} \equiv \beta\gamma\langle J_x\rangle = \beta\gamma\frac{\sigma_x^2(s)}{\beta_x(s)} = \beta\gamma\frac{\sigma_{x'}^2(s)}{\gamma_x(s)}\,, \tag{31.10}$$

with a corresponding expression for the other transverse direction, y. The angular brackets denote an average over the beam distribution. For 1D Gaussian beam, 95% of the particles are contained within $\{x, x'\}$ phase space area of $6\pi\varepsilon_{\rm n}/(\beta\gamma)$. Normalized beam emittances are conserved over the acceleration cycle in linear, static focusing lattices $K_{x,y}(s)$, and consequently, one would expect the same $\varepsilon_{\rm n}$ at the hadron (or linear) collider top energy as the one coming from the very initial low energy particle source. Unfortunately, that is rarely the case as many time-varying or nonlinear phenomena come into play. In an e^-/e^+ storage ring, the normalized emittance is not preserved during acceleration, but at each energy the beam's equilibrium emittance is determined by the effect of synchrotron radiation as a balance between radiation damping and quantum excitation [7]. In such a ring, for a given accelerator optics, the normalized equilibrium emittance increases with the third power of the beam energy [8].

As for the description of a particle's longitudinal motion, one takes the fractional momentum deviation $\Delta p/p$ from that of the reference particle as the variable conjugate to z. The factors $K_{x,y}$ and ρ in Hill's equations (31.4) are dependent on momentum p, leading to a number of effects: first, the trajectory of off-momentum particles deviates by $\Delta x(s) = D_x(s)(\Delta p/p)$, where the *dispersion function* $D_x(s)$ is determined by the magnetic lattice and is usually positive, periodic, and of the order of $\sim \rho/Q_x^2$. Second, the radius of curvature and orbit path-length C vary with the momentum and, to first order, are characterized by the momentum compaction factor $\alpha_{\rm c}$,

$$\alpha_{\rm c} \equiv \frac{\Delta C/C}{\Delta p/p} = \frac{1}{C}\oint \frac{D_x(s)}{\rho(s)}ds\,, \tag{31.11}$$

which typically is of order $1/Q_x^2$. Energy deviations also result in changes of machine focusing lattice properties and variations of the particle tunes, characterized by the *chromaticity* $Q'_{x,y} \equiv \Delta Q_{x,y}/(\Delta p/p)$. The natural chromaticity due to momentum dependence of the quadrupole focusing is negative and large

Int. J. Mod. Phys. A 2026.41. Downloaded from www.worldscientific.com
by UNIVERSITY OF CALIFORNIA @ BERKELEY on 09/16/26. Re-use and distribution is strictly not permitted, except for Open Access articles.

$\sim -Q_{x,y}$. Corresponding chromatic tune variations can, therefore, become unacceptably large even for relatively small energy deviations $(\Delta p/p) \sim (0.1-1)\cdot 10^{-3}$. To assure transverse particle stability, usually, the chromaticity is partially or fully compensated by additional sextupole magnets placed at locations of non-zero dispersion.

Radiofrequency electric fields in s direction provide a longitudinal focusing effect, allowing a stable increase of particle energy. The frequency f_s of such longitudinal *synchrotron oscillations* is (expressed in units of revolution frequency f_0, to become the synchrotron tune Q_s)

$$Q_s \equiv \frac{f_s}{f_0} = \sqrt{\frac{(\alpha_c - 1/\gamma^2)hZeV_{\rm RF}\sin\phi_s}{2\pi\beta cp}}\,, \tag{31.12}$$

where $h = f_{RF}/f_0$ denotes the harmonic number, $V_{\rm RF}$ the RF voltage, and $\phi_s = \cos^{-1}(\Delta E/ZeV_{\rm RF})$ the synchronous phase, with ΔE the average energy loss per turn (e.g. due to synchrotron radiation and impedance). The synchrotron tune Q_s determines the amplitude of longitudinal oscillations for a particle with an initial momentum offset, e.g., the rms bunch length σ_z relates to the rms momentum spread $\delta p/p$ as:

$$\sigma_z = \frac{c(\alpha_c - 1/\gamma^2)}{2\pi Q_s f_0}\left(\frac{\delta p}{p}\right). \tag{31.13}$$

Similarly to the case of transverse oscillations, the area of the longitudinal phase space $\{\Delta E, \Delta t\}$, or $\{\gamma\beta\delta p/p = (1/\beta)\Delta\gamma, z = \beta c\Delta t\}$, encircled by a moving particle is an adiabatic invariant, and the corresponding normalized *longitudinal emittance* $\varepsilon_{{\rm n},L} = \beta\gamma mc\sigma_z(\delta p/p)$ is a generally conserved quantity in hadron accelerators and also in linear accelerators. In the case of lepton storage rings, synchrotron radiation determines the equilibrium relative momentum spread, which grows linearly with beam energy [7, 8], and the corresponding bunch length follows from Eq. (31.13). In hadron synchrotrons, the longitudinal emittance sometimes is intentionally blown up during acceleration, so as to preserve longitudinal beam stability.

Longitudinal oscillations are the slowest of all the periodic processes which take place in the accelerators. For example, in the LHC, the frequency of synchrotron oscillations at the top energy of 7 TeV is about $f_s \approx 23$ Hz, the revolution frequency is $f_0 \approx 11.3$ kHz, the frequency of betatron oscillations is about $Q_{x,y}f_{\rm rev} \approx 700$ kHz and the RF frequency is $f_{\rm RF} = 400.8$ MHz ($h = 35640$). It should be noted that longitudinal motion is practically absent in linacs. In the absence of bending dipoles, dispersion $D_x(s)$ is zero and so are the momentum compaction factor α_c and the synchrotron tune Q_s. As a result, ultrarelativistic particles in a linac barely change their relative positions during acceleration despite significant energy spread.

Highest-energy circular colliders face a serious impediment in the form of synchrotron radiation (SR) that causes an energy loss per turn of

$$\Delta E_{\rm SR} = \frac{1}{3\varepsilon_0}\frac{Z^2e^2\beta^3\gamma^4}{\rho}\,, \tag{31.14}$$

here, ε_0 is the permittivity of vacuum. For electrons and positrons, the SR energy loss of the particles per turn can be expressed numerically as $\Delta E_{\rm SR} = 88.5$ [keV/turn] $E_{\rm b}^4$ [GeV]$/\rho$ [m]. Such losses must be fully compensated by a correspondingly high total RF voltage per turn. At beam energies above a few hundred GeV, the SR loss per turn of the particles becomes comparable to their energy ($\Delta E_{\rm SR} \sim E_{\rm b}$), which makes circular e^+e^- colliders impractical for center-of-mass energies above roughly 500 GeV.

Dynamics of the particle spin and sophisticated methods to maintain beam polarization along the acceleration chain, from the polarized sources to collisions, dedicated spin matching procedures to enable self polarization in e^+/e^- storage rings and the *resonant depolarization* method of ultra-precise c.m.e. calibration are described in [9].

31.2.2 *High Intensity Beams*

Ultimate collider luminosity calls for high beam currents $I_{\rm b} = Zef_0n_{\rm b}N$, where N is the intensity of a single bunch. Three related major difficulties include growing RF demands to compensate the synchrotron-radiation power loss $P = I_{\rm b}\Delta E_{\rm SR}$ in e^+/e^- beams, the advent of so-called *coherent (*or *collective) beam instabilities*, and growing demands for minimization of radiation due to inevitable particle losses. Many types of single- and multi-bunch instabilities are caused by beam interactions with electromagnetic fields induced by the beam itself due to the *impedance* of the vacuum chambers and RF cavities [4], or caused by unstable clouds of secondary particles, like electrons or ions, which are formed around the circulating beams [10]. These instabilities can develop as quickly as within tens to thousands of turns and need to be controlled. Mechanisms that are routinely employed to avoid coherent instabilities include the use of nonlinear magnets to generate sufficient spread of the tunes and therefore, provide *Landau damping*, fast beam-based transverse and longitudinal feedback systems, and electron/ion clearing (either by weak magnetic or electric fields or by modulation of the primary beam current profile rendering secondaries unstable, or by reducing the yield of secondary electrons via either a special coating or extensive *beam scrubbing* of the vacuum chamber walls). Careful control of the accelerator impedance during the design phase is another critical and routinely applied strategy for mitigating these instabilities.

High current beam operation is sensitive to even minuscule fractional intensity losses caused by particles' scattering at a large angle or with a large energy loss, sufficient for either the particle amplitudes $\sqrt{2J_{x,y}\beta_{x,y}(s)}$, or their dispersive position deviations $\Delta x = D_x(s)(\Delta p/p)$ to exceed the available transverse aperture, usually set by collimators (otherwise, by the vacuum chamber and magnet apertures). This can be due to residual vacuum molecules near the beam orbit or Compton scattering off thermal photons, due to Coulomb scattering off other particles within the same bunch (*Touschek effect*), or due to collisions with opposite beam particles and fields, such as inelastic interaction of protons, Bhabha scattering $e^+e^- \to e^+e^-$, or radiative Bhabha scattering $e^+e^- \to e^+e^-\gamma$ (see corresponding chapters in [11]).

Particles can also get lost on the aperture as a result of much slower mechanisms of diffusion caused either by the above processes with smaller scattering amplitudes, but stochastically repeated many times, such as intensity-dependent multiple Coulomb *intrabeam scattering* [12], by external noises such as ground motion or magnetic field fluctuations, or via chaotic mechanisms like *Arnold diffusion*, modulational diffusion, or resonance streaming in nonlinear fields, enhanced by minor tune modulations. Diffusion leads to a slow evolution of the beam distribution function and appearance of highly unwanted large-amplitude tails and beam emittance growth. The only way to counteract it is to arrange *beam cooling* (damping of particle oscillations). The cooling requires a reaction force opposite to particle momentum arranged such that, on average, the corresponding dissipative particle energy loss is compensated for by external power [13, 14].

In the case of electron or positron storage rings, such cooling occurs naturally due to synchrotron radiation and provides an automatic route to achieve small equilibrium emittances through a balance between radiation damping and excitation of oscillations by random radiation of individual photons. Fast radiation damping allows *top-up injection* of new particles without removing existing ones, a useful method to maximize the integrated luminosity of circular e^+e^- colliders. Synchrotron radiation damping will also be an important cooling mechanism for future energy-frontier hadron colliders, like the proposed FCC-hh and SPPC (see below). Four other methods of beam cooling have been developed and successfully employed to attain low emittances, namely *electron cooling* and *stochastic cooling* of heavy particles (ions and antiprotons), *laser cooling* of ion beams, and the *ionization cooling* of muons.

To prevent damage or excessive irradiation of accelerator components—ensuring they remain accessible for maintenance in the tunnel—sophisticated collimation systems are employed. These systems typically consist of a series of targets or primary collimators that scatter halo particles, followed by numerous absorbers (sometimes as many as a hundred) positioned at dedicated locations to intercept stray particles [15, Ch.9.7]. In the highest-energy modern and proposed future colliders, extreme to-

Int. J. Mod. Phys. A
by UNIVERSITY OF CALIFORNIA @ BERKE
Downloaded from www.worldscientific.com
use and distribution is strictly not permitted, except for Open Access articles.

tal beam energies, $n_\mathrm{b} N E_\mathrm{b}$, ranging from megajoules to gigajoules, and transverse energy densities reaching several GJ/mm^2 present one of the most significant challenges for achieving high-efficiency and robust particle collimation.

31.2.3 *High Luminosity Collisions*

Eq. (31.3) for luminosity can be recast in terms of normalized transverse emittances Eq. (31.10) and the beta-functions β^* at the IP as:

$$\mathcal{L} = f_0 \gamma n_\mathrm{b} \frac{N^2}{4\pi\sqrt{\varepsilon_{\mathrm{n}x}\beta_x^*\varepsilon_{\mathrm{n}y}\beta_y^*}}\mathcal{F}\,. \tag{31.15}$$

Here, equal bunch populations N are assumed in two Gaussian beams with identical emittances. To achieve high luminosity, one must maximize the total beam population $n_\mathrm{b}N$ while minimizing the emittances, and collide the beams at high frequency at locations where the focusing optics provides the lowest possible amplitude functions $\beta_{x,y}^*$. Achieving this requires sophisticated strong-focusing systems - the so-called *low-beta insertions* - sometimes occupying a significant fraction of the collider's total length. The minimum $\beta_{x,y}^*$ is limited by the maximum field gradients and apertures of the interaction region (IR) magnets, as well as by the effectiveness of chromatic and nonlinear aberration compensation.

The typical geometric reduction factor is $\mathcal{F} \approx 1$, it seldom drops below 0.5 for most colliders, except in cases dictated by specific physics processes under study. One source of reduction is the *hourglass effect*, arising from the growth of transverse beam sizes as the distance from the IP increases, where $\beta(s)$ expands parabolically as in Eq. (31.8). For long, round bunches, this effect can be approximated as $\mathcal{F} \approx \sqrt{\pi}A\exp(A^2)\mathrm{erfc}(A)$, with $A = \beta/\sigma_z$. Nonzero beam crossing angles, θ_c, for example in the horizontal plane, and long bunches with rms length σ_z, further reduce the luminosity by a factor $\mathcal{F} \approx 1/(1+\Phi^2)^{1/2}$, where $\Phi = \sigma_z \tan(\theta_\mathrm{c}/2)/\sigma_x^*$ is the so-called *Piwinski angle*.

One of the most common limits to producing high luminosity arises from electric and magnetic forces of the opposite bunch at the IPs, characterized by a dimensionless *beam-beam parameter* :

$$\xi_{x,y} = \frac{r_0 N \beta_{x,y}^*}{2\pi\gamma\sigma_{x,y}^*(\sigma_x^* + \sigma_y^*)}\,, \tag{31.16}$$

where $r_0 = Z^2e^2/(4\pi\varepsilon_0 mc^2)$ is the classical radius of the colliding particle (with charge Ze and mass m). From Eqs. (31.3) or (31.15) and (31.16), one can note that the path to higher luminosity via higher beam intensity and smaller beam sizes almost automatically calls for a higher beam-beam parameter as $\mathcal{L} \propto \xi$. Cited in the Tables, the beam-beam parameter is roughly equal to the betatron tune shift experienced by small-amplitude particles – positive in the case of opposite charge beams, like e^+e^-, and negative for same charge beams as in pp collisions. Beam-beam forces can lead to coherent effects, such as unstable beam oscillations or blow-up of one beam's size while the other beam remains small or even shrinks (*flip-flop effect*). The tune spread arising from ξ and the nonlinear nature of beam-beam interactions results in strong diffusion along high-order transverse resonances $kQ_x + lQ_y = m$ and, ultimately, in beam size growth and/or beam losses. Operational experience indicates that the aforementioned effects are tolerable below certain *beam-beam limit* of $\xi_{x,y} \approx 0.003 - 0.012$ in hadron colliders [16], and – due to strong synchrotron radiation damping – an order of magnitude higher one in e^+e^- colliders, with maximum $\xi_{x,y} \approx 0.03 - 0.12$ [17, 18]. The accessible beam-beam parameter range can also be restricted by coherent beam-beam instabilities. These various limits translate into a maximum allowed single bunch intensity N and call for an increase of the number of bunches n_b to achieve higher luminosities.

In linear colliders, where each bunch collides only once, with typically much smaller beam size and experiencing much stronger forces, the strength of the collision is measured by the ratio of the rms bunch length σ_z to the beam-beam focal length. This ratio, called *disruption parameter* D_y, is related to ξ_y via $D_y = 4\pi\sigma_z\xi_y/\beta_y^*$. Stronger beam-beam focusing and higher D_y lead to effectively smaller beam sizes and a resulting luminosity enhancement; but it also makes the collisions more sensitive to small offsets, resulting in a *kink instability*. Additional beam-beam effects arising in the collisions at linear colliders are the emission of *beamstrahlung* (synchrotron radiation in the field of the opposing beam), along with e^+e^- pair creation, and depolarization by various mechanisms.

Beamstrahlung is relevant for both linear colliders, where it may significantly degrade the luminosity spectrum, and for future highest-energy circular colliders, where it may limit the beam lifetime, and also increases the energy spread and bunch length of the stored beam. For both types of colliders, the beamstrahlung is mitigated by making the colliding beams as flat as possible at the interaction point ($\sigma_x^* \gg \sigma_y^*$) to lower the beams' EM fields. The photon energy spectrum of the beamstrahlung is characterized by the parameter $\Upsilon = (2/3)\hbar\omega_\mathrm{c}/E_\mathrm{b}$ [19], with $\hbar\omega_\mathrm{c}$ denoting the critical photon energy. The spectrum strongly deviates from the classical synchrotron radiation spectrum for Υ approaching or exceeding 1.

For hadron colliders, two fundamental luminosity limits are the beam lifetime, determined by burn-off in the collisions due to inelastic pp interaction $dN/dt = -\mathcal{L}\sigma_\mathrm{in}$, and the radiation from the collision debris, which may induce "quenches" (transitions to the normal-conducting state) of the superconducting final quadrupole magnets, and, in the long term, affect the equipment lifetime. Another limit on the achievable integrated luminosity in circular colliders is set by the minimum or average turnaround time (the time between the beam abort at the end of a physics fill and the start of the next physics collisions). Achieving practical filling times with many bunches in the collider requires either fast cycling injector machines and/or the top-up injection operation. The latter makes the average luminosity of circular electron-positron colliders approximately equal to the peak luminosity.

31.3 Recent High Energy Colliders

In this and the following section, elaboration is made on various issues associated with some of the recently operating colliders, particularly factors which impact integrated luminosity. Only general references are provided, where further information can be obtained. A more complete list of recent colliders and their parameters can be found in the High-Energy Collider Parameters tables.

31.3.1 *Tevatron*

The first superconducting synchrotron in history, the Tevatron [20], was converted into a proton-antiproton collider in 1985. Its 4.4 T dipole magnets employed Nb-Ti superconducting cable operating at 4.5 K, requiring what was then the world's largest cryogenic system. With $\sqrt{s}$ up to 1.96 TeV, it remained the highest-energy collider for 25 years and delivered more than 12 fb^{-1} of integrated luminosity to each $p\bar{p}$ detector experiment (CDF and D0) before being shut down in 2011. The route to high integrated luminosity in the Tevatron was governed by the antiproton production rate, the turnaround time to produce another store, and the resulting optimization of store duration [21]. The antiproton production complex consisted of three 8 GeV $\bar{p}$ accelerators (the Accumulator, Debuncher, and Recycler—the latter being the first high-energy accelerator built with permanent magnets) and employed 25 independent stochastic cooling systems along with a pioneering high-energy electron cooling setup, enabling accumulation of up to a record $25{\cdot}10^{10}$ $\bar{p}$ per hour. Despite severe parasitic long-range interactions between the two beams—each consisting of 36 bunches placed on helical orbits by two dozen ±150 kV high-voltage (HV) separators—a total beam-beam tune shift parameter of $n_\mathrm{IP}\xi \approx 0.025$–$0.03$ was achieved, a record for hadron beams, with $n_\mathrm{IP} = 2$ primary collision points. Other notable advances included sophisticated longitudinal beam manipulation techniques, such as *slip-stacking* and *momentum mining*, as well as the first operational use of *electron lenses* for beam collimation and for compensation of long-range beam-beam effects [22]. Ultimately, the Tevatron achieved luminosities a factor of 430 higher than its original design specification.

31.3.2 *HERA*

The first lepton–proton collider, the 6.4 km long Hadron–Elektron–Ring–Anlage (HERA) at DESY in Ger-

Int. J. Mod. Phys. A 2026.41. Downloaded from www.worldscientific.com by UNIVERSITY OF CALIFORNIA @ BERKELEY on 09/16/26. Re-use and distribution is strictly not permitted, except for Open Access articles.

many [23], operated between 1992 and 2007 and delivered nearly 1 fb^{-1} of integrated luminosity at $\sqrt{s} \approx 320$ GeV to the electron–proton collider experiments H1 and ZEUS [24, Ch.10.5]. HERA was the first facility to employ both major applications of superconductivity: 5 T magnets in the 920 GeV proton ring, and superconducting RF accelerating structures providing approximately 12 MW of power to compensate for synchrotron radiation losses of the 30 GeV lepton beams (electrons or positrons in a conventional-magnet ring). With precise orbit and optics control, the HERA lepton beam naturally became transversely polarized to about 60% within roughly 40 minutes via the *Sokolov–Ternov effect*. Special *spin rotator* magnets were installed on either side of the collider interaction points to provide 30–45% longitudinal polarization at the experiments

31.3.3 *LEP*

Installed in a 26.7 km circumference tunnel, LEP [25] was the largest circular e^+e^- collider constructed to date. It operated from 1989 to 2000 with beam energies ranging from 45.6 to 104.5 GeV. The synchrotron radiation loss per turn reached roughly 3% of the beam energy, making the total available RF voltage and power the limiting factors for LEP's maximum energy and luminosity of 10^{32} cm^{-2}s^{-1}. At a beam energy of 98 GeV, LEP ran with a beam-beam parameter $\xi \approx 0.083$, corresponding to a total beam-beam tune shift for four interaction points of $n_{\rm IP}\xi \approx 0.33$. In its final year of operation, 288 SRF cavities were powered by 36 klystrons, each delivering an average of 0.6 MW, providing a total $V_{\rm RF} = 3.63$ GV. For beam energies up to about 60 GeV, LEP employed the *resonant depolarization* technique to measure the beam energy with 0.001% accuracy.

31.3.4 *SLC*

Based on an existing 3-km long 2.85 GHz warm RF linac, the SLC [26] was the first and only linear collider. It was operated from 1987 to 1998 with a constant beam energy of 45.6 GeV, up to about 80% electron-beam polarization, quasi-flat beams, a final-focus optics with local chromatic correction based on four interleaved sextupoles and $\beta_y^* \approx 1$ mm. In its last year, SLC achieved a peak luminosity of about 3×10^{30} cm^{-2}s^{-1}, roughly half of the design value. The SLC had a high-efficiency positron source providing 5×10^{12} e^+ per s for 120 Hz injection into the linac. It also employed the *BNS damping* to suppress the single-bunch beam break up instability, and also demonstrated an about 2-fold increase of luminosity from *disruption enhancement* due to the mutual focusing of the colliding electron and positron bunches at the interaction point,

31.4 Presently Operating Colliders

31.4.1 *LHC*

With a beam energy of 6.8 TeV (to be raised to the design value of 7 TeV through consolidation and magnet training), the superconducting Large Hadron Collider [27] presently is the world's highest energy collider. In the latest runs, peak luminosities of up to 2.6×10^{34} cm^{-2}s^{-1} have been achieved at 13.6 TeV c.m.e. - more than twice the design value (the current status is best checked at the Web site [28]). To meet its luminosity goals, the LHC operates with a high beam current of approximately 0.5 A, leading to stored energies of about 330 MJ per beam. Controlled energy deposition and component protection are given a high priority and a sophisticated highly efficient system of more than 100 beam collimators is employed [29]. At the energy of about 7 TeV per particle, synchrotron radiation poses a challenge, as the cryogenic system must remove roughly 7 kW due to synchrotron radiation, intercepted with a specially designed *beamscreen* inside the vacuum chamber, at a temperature of about 5–20 K, to be compared with a temperature of 1.9 K for the magnet cold bore. The elevated temperature allows for a more energy-efficient removal of beam-induced heat. The beamscreen also provides an effective cryo-pump for the vacuum system. When synchrotron-radiation photons hit the beamscreen, they can generate photoelectrons. These photoelectrons, and also any other electrons generated in the vacuum system, e.g. by residual-gas ionization, are accelerated in the electric field of the beam and may multiply via secondary-electron emission, with consequent electron cloud development. To mitigate this issue, the beamscreen is regularly subjected to beam-induced surface conditioning (*scrubbing*), thereby lowering the secondary emission yield. The two proton beams of 2556 bunches spaced by 25 ns are contained in separate pipes throughout most of the circumference and are brought together into a single 130 m long beam pipe at the interaction points. To avoid approximately 30 head-on collisions a small crossing angle of about 0.3 mrad is employed, which reduces the luminosity by about 15%. Still, the bunches moving in one direction experience multiple long-range encounters with the counter-rotating bunches and the resulting perturbations of the particle motion substantially contribute to the beam lifetime reduction. The dominant source of approximately 8 hour characteristic luminosity decay time is proton burn-off due to inelastic *pp* interaction with $\sigma_{\rm in} \approx 81$ mb, corresponding to *pile-up* of up to 50 (number of events per individual bunch crossing). In special physics runs with a few bunches and large β^*, the LHC achieved a head-on beam-beam tune shift of $n_{\rm IP}|\xi| \approx 0.02$ with $n_{\rm IP} = 2$, about twice as high as in regular operation.

The Tables also show the LHC luminosity performance in Pb-Pb collisions, which for the ATLAS and CMS experiments well exceeded the design value, while for the ALICE experiment, the luminosity is *levelled* near the Pb-Pb design value of 10^{27} cm^{-2}s^{-1}. The LHC can also provide Pb-p collisions as it did in 2013 and 2016, and other ion-ion or ion-proton collisions, at different energies.

In the coming years, an ambitious luminosity upgrade program, HL-LHC [30], with the accompanying LHC Injectors Upgrade [31], has as its target an order-of-magnitude increase in integrated luminosity through doubling the proton beam current, the utilization of new larger aperture Nb_3Sn superconducting final quadrupoles to allow squeezing the β^* to as low as 15 cm, superconducting compact *crab cavities* and luminosity leveling also for ATLAS and CMS as its key ingredients.

31.4.2 *Electron-Positron Rings*

Asymmetric energies of the two colliding beams cause the fast-moving reaction products to travel measurable distances before decaying, enabling more precise studies in, for example, B-meson physics. High-luminosity colliders of this type (B-factories, such as the former PEP-II at SLAC and KEKB in Japan) require advanced interaction-region designs and face numerous additional challenges [32]. SuperKEKB operates with 7 GeV electron and 4 GeV positron beams since 2018 and is aiming for luminosities of $(6-8) \times 10^{35}$ cm^{-2}s^{-1} [33]. In 2024, a world record luminosity of 5.1×10^{34} cm^{-2}s^{-1} has been reached, still at rather low beam currents. Vertical beam-beam tune shifts of $\xi_y \approx 0.05$ for the 4 GeV positron beam, and $\xi_y \approx 0.03$ for the 7 GeV electron beam have been achieved. These values are still about a factor of two lower than at the previous KEKB. Since 2020 SuperKEKB operates with a virtual *crab-waist* collision scheme, first developed for the FCC-ee design [34]. The original crab-waist scheme, based on additional sextupole magnets, was earlier implemented at DAΦNE [35]. The general crab-waist concept combines a large Piwinski angle Φ, and an extremely low β_y^* ($\ll \sigma_z$) with the cancellation of the transverse betatron resonances which occur under conditions of $kQ_x + lQ_y = n$, where k, l, n are integers. The latter is achieved by means of existing or additional electromagnetic sextupoles with special betatron phase advances to the collision point [36]. The crab-waist collision scheme has become a design choice for all proposed future e^+e^- circular colliders.

Beside SuperKEKB and DAΦNE, three other e^+e^- ring colliders currently in operation are VEPP-2000 with $\sqrt{s}$ up to 2.0 GeV, BEPC-II with $\sqrt{s}$ up to 4.6 GeV and VEPP-4M with maximum c.m.e. of 12 GeV [1].

31.4.3 *RHIC*

The Relativistic Heavy Ion Collider [37] employs 3.45 T Nb-Ti superconducting magnets, and collides combinations of fully-stripped ions such as H-H ($p-p$), p-Al, p-Au, d-Au, h-Au, Cu-Cu, Cu-Au, Zr-Zr, Ru-Ru, Au-Au, and U-U over a wide energy range. The high charge per particle (+79 for gold, for instance) makes intra-beam scattering of particles within the bunch a special concern, even for seemingly moderate bunch intensities. In 2012,

Int. J. Mod. Phys. A 2020.
Downloaded from www.worldscientific.com
by UNIVERSITY OF CALIFORNIA @ BERKE
use and distribution is strictly not permitted, except for Open Access articles.

3-D stochastic cooling was successfully implemented in RHIC [38] and is now routinely used. With stochastic cooling, steady increases in the bunch intensity, and numerous other upgrades, RHIC now operates at 44 times the Au-Au design average luminosity. Unique among high energy colliders, RHIC heavy ions beams cross the *transition energy* $\gamma_{rmt} = 1/\sqrt{\alpha_c}$ during acceleration – see Eqs.(31.11, 31.12) – a point where the derivative with respect to momentum of the revolution period is zero. This period of time is kept as short as allowed by the magnet ramp rate and must be dealt with carefully.

RHIC is also unique in its ability to accelerate and collide polarized proton beams. As proton beam polarization must be maintained from its low-energy source, successful acceleration through the myriad of depolarizing resonance conditions in high energy circular accelerators has taken years to accomplish [39]. An energy of 255 GeV per proton with 60% final polarization per beam has been realized. As part of a scheme to compensate the head-on beam-beam effect, electron lenses operated routinely during the record high beam-beam parameter polarized proton operation at 100 GeV energy in 2015 [40].

31.5 Future High-Energy Colliders and Prospects

Modern nuclear physics and high energy particle physics face critical questions which require next-generation high-energy and high-intensity experiments using hadron-hadron, lepton-lepton, and lepton-proton colliding-beam facilities. Understanding the structure of the proton and neutron directly from the dynamics of their quarks and gluons governed by the quantum chromodynamics calls for new ion-ion and electron-ion colliders. Two types of colliders are generally aspired by the HEP community [41, 42]: i) Higgs factories with a c.m.e. of 240–250 GeV in e^+e^- collisions for precision studies of the Higgs boson ($m_H = 125$ GeV) and exploration of the Higgs sector in greater detail, including measurements of Higgs couplings to fermions and vector bosons, self-coupling, rare decays, mass and width, that can also deliver other electroweak precision physics, e.g., on the Z-pole (91 GeV c.m.e.), at the W-pair threshold (about 160 GeV), and when run as a top quark factory (365–380 GeV); and ii) colliders with c.m.e. levels significantly beyond those of the LHC to explore the energy frontier for potential discoveries through direct searches in pp, $\mu\mu$, and e^+e^- interactions. In addition, precision physics at future high-luminosity factories operating at the τ-charm energy also provides sensitivity to new physics at multi-TeV energies and beyond. A comprehensive review of the future colliders' projects, ideas, and R&D activities can be found in Ref. [1]; Ref. [43] presents comparative analysis of implementation challenges of numerous future HEP collider proposals. Below we only briefly summarize leading collider proposals for construction over the next several decades which rely mostly on currently available technologies, such as NC or SC RF and/or NC or SC magnets, some of them requiring reasonable scope and duration mission-oriented development programs, as well as advanced schemes based on plasma acceleration and other innovative ideas. Tentative parameters of some of the colliders discussed, or mentioned, in this section are summarized in Table 31.1 and Table 31.2.

31.5.1 *Ion-Ion and Electron-Ion Colliders*

NICA (Nuclotron-based Ion Collider fAcility) is a new accelerator complex under construction at the Joint Institute for Nuclear Research (JINR, Dubna, Russia) to study the properties of hot and dense baryonic matter, strong interactions among quarks and gluons, and spin physics [44]. NICA will provide a range of beam species, from protons and polarized deuterons to heavy bismuth ions. The 503 m circumference SC superferric-magnet collider is designed to deliver an average luminosity in heavy-ion interactions at $\sqrt{s_{NN}} = 4$–11 GeV/u of $1\times10^{27}\mathrm{cm}^{-2}\mathrm{s}^{-1}$ for a variety of nuclei up to $^{209}\mathrm{Bi}^{83+}$, and for polarized proton and deuteron collisions at $\sqrt{s} = 12$–27 GeV with $\mathcal{L} = (1$–$10) \times 10^{31}$ $\mathrm{cm}^{-2}\mathrm{s}^{-1}$. Major accelerator challenges at NICA include the suppression of strong intrabeam scattering and space-charge effects, which will be mitigated through extensive use of electron and stochastic cooling systems.

Also under construction is the Electron-Ion Collider (EIC) for nuclear physics research at Brookhaven National Laboratory in the US. It will collide a 41–275 GeV proton beam of the reconfigured RHIC with a 5–18 GeV electron beam circulating in a new storage ring [45]. The EIC physics requirements [46] call for electron and nucleon beams with high polarization, $P_{e,n} \sim 70\%$ (since the precision of measurements of interest scales as $\mathcal{L}P_e^2P_n^2$), a spectrum of ion beam species from deuterons to the heaviest nuclei (U or Pb), variable c.m.e. values from $\sqrt{s} = 20$ GeV to 140 GeV, high luminosities up to 10^{33-34} $\mathrm{cm}^{-2}\mathrm{s}^{-1}$, and the potential for multiple interaction regions. Major accelerator design challenges in achieving the required energy, luminosity, and polarization include the development of SRF crab cavities and advanced superconducting magnets for interaction region focusing, as well as high-intensity polarized particle sources complemented by specialized magnets and operational techniques—such as swap-out injection—to preserve polarization throughout acceleration and collision. Strong cooling of the EIC hadron beams is expected to be required if luminosity levels two orders of magnitude beyond those of the HERA *ep* collider are to be reached. To that end, ring-based or ERL-based electron and stochastic cooling systems are under consideration, including advanced concepts such as *coherent electron cooling*, and *optical stochastic cooling* (see review [47] and references therein).

31.5.2 *Higgs/Electroweak Factories*

Higgs factory proposals generally aim at improving the precision of coupling measurements of Higgs boson, top quark, W and Z by an order of magnitude or more compared with previous studies. Two proposals for ∼100 km circumference circular e^+e^- colliders have recently gained momentum: the Future Circular Collider (FCC-ee) at CERN [48] and the Circular Electron-Positron Collider (CEPC) in China [49]. Design philosophy of these machines assumes use of the maximum RF power available to compensate $O(100$ MW) synchrotron radiation losses $P_{\mathrm{SR}} = 2I \cdot \Delta E_{\mathrm{SR}}$ and operation at the beam-beam limit ξ_y that yields peak luminosity:

$$\mathcal{L} = \frac{3}{16\pi r_0^2(m_e c^2)} \frac{P_{\mathrm{SR}}\xi_y\rho}{\beta_y^*\gamma^3}\,, \tag{31.17}$$

that scales approximately as $1/E_{\mathrm{b}}^{3.5}$ for practical limits on P, ξ_y and β_y^*. At high target luminosities, the short beam lifetime caused by radiative Bhabha scattering necessitates the construction of a full-energy injector ring in the same tunnel, allowing continuous *top-up* injection of the electron and positron bunches in the collider rings operating at constant energy. Beamstrahlung imposes an additional limitation on beam lifetime, depending on momentum acceptance—making sufficient off-momentum dynamic aperture one of the design challenges—and also leads to some bunch lengthening.

These ambitious, large-scale projects based on well-established technologies are not extendable to TeV or multi-TeV energies, but they offer several important advantages that include the potential for much higher luminosities, and, thus, higher precision, the ability to operate multiple experiments simultaneously, and their ∼100 km circular tunnels that could later house $O(100$ TeV) hadron colliders. The high energy efficiency of circular e^+e^- colliders is further boosted by advances in RF power sources, by improved SC cavities, and by innovative low-power magnet systems including ones based on high-temperature superconductors (HTS) at moderate magnetic field.

These ambitious large-scale projects, though not extendable to TeV or multi-TeV energies, offer several important advantages: the potential for much higher luminosities—and thus higher precision—, the ability to operate multiple experiments simultaneously, and ∼100 km circular tunnels that could eventually host $O(100$ TeV) hadron colliders. The high energy efficiency of circular e^+e^- colliders will be further enhanced by advances in RF power sources, improved superconducting cavities, and innovative low-power magnet systems, including those based on high-temperature superconductors (HTS) operating at moderate magnetic fields.

For more than four decades, efforts have been devoted to developing high-gradient RF technology linear e^+e^- colliders in order to overcome the synchrotron radiation limitations of circular

Int. J. Mod. Phys. A 2026.41. Downloaded from www.worldscientific.com
by UNIVERSITY OF CALIFORNIA @ BERKELEY on 09/16/26. Re-use and distribution is strictly not permitted, except for Open Access articles.

Table 31.1: Tentative parameters of selected future e^+e^- high-energy colliders. Parameters associated with different beam energy scenarios are comma-separated; H and V indicate horizontal and vertical directions.

	FCC-ee	CEPC	ILC	CLIC
Species	e^+e^-	e^+e^-	e^+e^-	e^+e^-
Beam energy E_b (GeV)	46, 120, 183	45.5, 120, 180	125, 250	190, 1500
Circumference or length (km)	90.66	100	20.5, 31	11, 50
Interaction regions	4	2	1	2, 1
Est. integrated luminosity per experiment (ab^{-1}/year)	17, 0.9, 0.17	15, 0.65, 0.07	0.2, 0.3	0.27, 0.34
Peak lumi. $\mathcal{L}$/IP (10^{34}cm^{-2}s^{-1})	144, 7.5, 1.45	115, 5.0, 0.5	1.4, 1.8	2.25, 3.6
Rep.rate (Hz, f_rev for rings)	3307	3000	5	100, 50
Polarization (%)	$\geq$10, 0, 0	5–10, 0, 0	80/30 (e^-/e^+)	80/0 (e^-/e^+)
Time between collisions (μs)	0.025, 0.3, 2.5	0.025, 0.68, 2.6	0.55	0.0005
Energy spread (rms, 10^{-3})	1.15, 1.76, 1.86	1.3, 1.7, 2.0	e^-: 1.9, 1.2 e^+: 1.5, 0.7	3.5
Bunch length σ_z (rms, mm)	15.2, 5.6, 2.3	8.7, 4.1, 2.9	0.3	0.07, 0.044
IP beam size σ^* (rms, μm)	H: 9, 13, 37 V: 0.04, 0.03, 0.04	H: 6, 14, 39 V: 0.04, 0.04, 0.11	H: 0.52, 0.47 V: 0.008, 0.006	H: 0.15, 0.04 V: 0.003, 0.001
Emittance, ε_n (rms, μm)	H: 63, 155, 589 V: 0.19, 0.24, 0.47	H: 24, 150, 493 V: 0.12, 0.3, 1.7	H: 5, 10 V: 0.035, 0.035	H: 0.95, 0.66 V: 0.03, 0.02
β^* at interaction point (cm)	H: 11, 24, 90 V: 0.07, 0.1, 0.14	H: 13, 30, 104 V: 0.09, 0.1, 0.27	H: 1.3, 1.1 V: 0.041, 0.048	H: 0.8, 0.69 V: 0.01, 0.0068
Full crossing angle θ_c (mrad)	30	33	14	18/27, 21
Crossing scheme	crab waist	crab waist	crab crossing	crab crossing
Piwinski angle $\Phi = \sigma_z\theta_\mathrm{c}/(2\sigma_x^*)$	26, 6.6, 0.9	24, 4.9, 1.2	0	0
Beam-beam param. ξ_y (10^{-3})	98, 130, 144	127, 110, 100	n/a	n/a
Disruption parameter D_y	1.3, 0.9, 2.0	0.6, 1.3, 0.8	35, 25	13, 8
Average Upsilon Υ (10^{-2})	0.01, 0.04, 0.06	0.02, 0.04, 0.05	3, 6	17, 500
RF frequency f_RF (MHz)	400, 400, 800	650	1300	11994
Particles per bunch N (10^{10})	22, 17, 16	14, 13, 20	2	0.52, 0.37
Bunches per beam n_b	11200, 300, 60	11934, 268, 35	1312 (pulse)	352, 312 (trains at 50 Hz)
Average beam current I_b (mA)	1292, 27, 5.1	804, 16.7, 3.3	0.021	0.014, 0.009
Injection energy (GeV)	on E_b (top-up)	on E_b (top-up)	5.0 (linac)	9.0 (linac)
RF gradient G (MV/m)	10.6, 10.6, 20.2	17.4, 24.9, 27.6	31.5	72, 100
Total SR power loss (MW)	100	60	n/a	n/a
Total beam power (MW)	n/a	n/a	5.3, 10.5	5.6, 28
Key technology	—	—	high grad. SC RF	two-beam accel.

Table 31.2: Tentative parameters of selected future high-energy hadronic and muon colliders. Parameters associated with different particle species for NICA and EIC, and different beam-energy scenarios for a muon collider, are comma-separated. Quantities are, where appropriate, r.m.s.; unless noted otherwise, energies refer to beam energy; H and V indicate horizontal and vertical directions. Parameters of HL-LHC can be found in the High-Energy Collider Parameters review tables.

	NICA	EIC	FCC-hh	SPPC	$\mu\mu$ collider
Species	ion-ion, pp	ep, e-ion	pp	pp	$\mu^+\mu^-$
Beam energy E_b (TeV)	0.0045/u, 0.013	0.01(e), 0.275(p)	42.5	62.5	0.063, 5
Circumference C (km)	0.503	3.834	90.66	100	0.3, 10
Interaction regions	1+1	1(2)	4	2	1, 2
Est. integr. luminosity per exp. (ab^{-1}/year)	$10^{-8,-3}$ (ii, pp)	0.1	0.9	0.6	0.001, 2.0
Peak luminosity $\mathcal{L}$ (10^{34}cm^{-2}s^{-1})	$10^{-7,-2}$ (ii, pp)	1.05	30	4.3	0.008, 20
Rep. rate (Hz, f_rev for rings)	$5.9{\cdot}10^5$	$7.8{\cdot}10^4$	3307	3000	15, 5
Time between collisions (μs)	0.077	0.010	0.025	0.025	1, 33
Energy spread (rms, 10^{-3})	1.5	0.6(e), 1(p)	0.1	0.1	0.04, 1
Bunch length σ_z (rms, mm)	600	7(e), 70(p)	80	60	63, 1.5
IP beam size σ^* (H/V rms, μm)	660	95/8.5	3.8 (init.)	3.0 (init.)	75, 0.9
Emittance ε_n (H/V rms, mm mrad)	0.8(i), 4 (p)	20/1.3(e), 11.3/1(p)	2.2 (init.)	1.2 (init.)	200, 25
Beta function at IP β^* (H/V cm)	60	45/5.6(e), 80/7.2(p)	30	50	1.7, 0.15
Beam-beam param. ξ (10^{-3} H/V)	4(i), 15 (p)	72/100(e),12(p)	5–15	15	22, 78
RF frequency f_RF (MHz)	39	591	400	400/200	352/704/1300
Particles per bunch N (10^{10})	0.3(i), 50(p)	17.2(e), 6.9(p)	10	4	400, 180
Bunches per beam n_b	22	1160	9500	10082	1
Average beam current I_b (mA)	480(i), 1000(p)	2500(e),1000(p)	500	190	640, 9(peak)
Injection energy (GeV)	1-3.8(i), 2-10(p)	on E_b(e), 25(p)	$\geq$1300	3200	on E_b
Peak magnetic field B (T)	1.8	0.248(e), 3.80(p)	14	20	14
Polarization (%)	0(i), >50(p)	> 70(e), >70(p)	0	0	0
SR power loss/beam (MW)	10^{-6}	10(e), $< 10^{-6}$(p)	1.2	2.2	$< 10^{-5}$, 0.16
Key technology	electron and stoch. cooling	inj. cooling stoch. cooling	Nb_3Sn/HTS magnets	HTS magnets	μ prod./cool. HTS magnets

Int. J. Mod. Phys. A 2019.30:1930-1 Downloaded from www.worldscientific.com
by UNIVERSITY OF CALIFORNIA @ BERKE use and distribution is strictly not permitted, except for Open Access articles.

e^+e^- machines. The International Linear Collider (ILC), with a c.m.e. of 250 GeV in e^+e^- collisions, has been under consideration for more than two decades and could potentially be upgraded to $\sqrt{s}$=500 GeV and further to 1 TeV [50]. CERN's Compact Linear Collider (CLIC) design, developed since the mid-1980s, also includes possible upgrades, from an initial 380 GeV c.m.e. to ultimately 3 TeV, which would enable searches for new particles of significantly higher masses [51].

The primary challenge for a high-energy, high-luminosity single-pass collider design is the beam power requirement, so that measures must be taken to keep the power demand within bounds as illustrated in a transformed Eq.(31.15):

$$\mathcal{L} = \frac{1}{8\pi\alpha r_0}\,\frac{P_{\rm wall}}{\sqrt{s}}\,\frac{\eta}{\sigma_y^*}\,N_\gamma\,H_{\rm D}\,. \tag{31.18}$$

Here, $P_{\rm wall}$ is the total wall-plug power of the collider, to be converted into beam power $P_{\rm b} = 2f_0NE_{\rm b}$ with efficiency η, $N_\gamma \approx 2\alpha r_0 N/\sigma_x^*$ is the number of beamstrahlung photons emitted per $e^\pm$ ($\alpha \approx 1/137$ denotes the fine-structure constant), and the last factor $H_{\rm D}$, typically between 1 and 2, represents the enhancement of luminosity due to the *pinch effect*, the additional focusing occurring during the collision of oppositely charged bunches. The management of $P_{\rm wall}$ leads to an upward push on the bunch population N with an attendant rise in the energy radiated due to the electromagnetic field of one bunch acting on the particles of the other (beamstrahlung). Keeping a significant fraction of the luminosity close to the nominal energy represents a design goal, which is met if N_γ does not exceed a value of about 1. A consequence is the use of flat beams, where N_γ is managed by the beam width, and luminosity adjusted by the beam height, thus the explicit appearance of the vertical beam size σ_y^*.

The ILC [52] is based on 1.3 GHz standing-wave superconducting accelerating structures operating at 2 K with 31.5 MV/m average gradient, up to 8 nm vertical beam size at the IP, and luminosity comparable to the LHC. Progress toward higher field gradients and Q values continues to be made, with nitrogen-doping techniques being a recent example [53]. Taking advantage of such progress, a Linear Collider Facility (LCF) at CERN is proposed, which, in a first superconducting stage, could deliver two times the ILC luminosity to each of two experiments [54]. CLIC is based on a novel two-beam acceleration scheme [55]. Here, room-temperature NC copper high-gradient 12 GHz accelerating structures are powered by a high-current 1.9 GeV drive beam to efficiently enable accelerating gradients of up to 100 MV/m (though optimal G=70 MV/m for the first CLIC stage at $\sqrt{s}$=380 GeV, and for this stage an alternative RF power drive option with 12 GHz klystrons powering is also being considered).

To reach their design luminosities, linear colliders require unprecedented rates of positron production, about (20–100) times the world record set by the SLC positron source, mitigation of wakefield effects, advanced beam-based trajectory tuning, and very tight control of imperfections, misalignments, and jitter [56] (for example, for CLIC, this entails $O(10\ \mu\text{m})$ accuracy of pre-alignment of the main linac and beam delivery system components, and suppression of fast quadrupole vibrations from ground motion to the $O(1$ nm) level at frequencies above 1 Hz; the ILC tolerances are more relaxed, so that a linac pre-alignment of 200–300 μm suffices, and vibrations must be suppressed to the $O(1$ nm) level only above 1 MHz).

Recent developments in RF technologies offer the promise of more compact linear e^+e^- Higgs/Electroweak factories, based either on ∼70 MV/m traveling-wave 1.3 GHz SRF structures [57] or on 70–120 MV/m high-efficiency, distributed-RF-coupling, normal-conducting cold-copper 5.7 GHz accelerating cavities operated at liquid nitrogen temperature [58].

There are a number of alternative ideas proposed for studies of the Higgs/Electroweak physics, such as high-energy, high-luminosity e^+e^- collider in a 100 km tunnel using ERLs to accelerate particles to collision energy in 4 to 6 passes and return up to 81% of the energy back into the SRF cavities on deceleration turns, thus, lowering the required facility power several-fold; similar power recovery in one pass can greatly improve efficiency of linear colliders; an arrangement of $\gamma\gamma$ collision through near-IP conversion of high energy electron beams into intense photon beams by backward Compton scattering off a high-power laser or off an FEL photon pulse; $\mu\mu$ Higgs factory with unprecedented 0.004% energy resolution, and a high-energy lepton-hadron collider bringing into collision a 50- or 60-GeV electron beam from an ERL with the 7 TeV protons circulating in the LHC (LHeC) (see [1] and references therein). At lower energies, Super Tau-Charm Factory proposals aim at the production and precise study of charmonium states and of the tau lepton [59, 60].

31.5.3 *Energy Frontier Circular Colliders*

Several hadron and lepton colliders have been proposed to extend the energy reach beyond the LHC. As noted above, ambitious plans have been proposed to upgrade the FCC and CEPC to hadron colliders – FCC-hh at CERN and Super Proton Proton Collider (SPPC) in China, respectively – by means of next- or next-next generation SC magnets installed in the arc sections of the 100 km rings, so as to enable $\sqrt{s}$ of the order 100 TeV or above [48, 49, 61]. Comparable discovery reach is expected for a circular 10–14 TeV muon collider [62], significantly beyond that of practical e^+e^- linear colliders.

The maximum beam energy Eq.(31.1) is directly proportional to the magnetic field and to the ring circumference, hence, future hadron colliders like FCC-hh and SPPC rely on the development of the technology of 14–16 T Nb_3Sn dipole magnets [63] or dipole magnets based on high-temperature superconductors (HTS) with a field of up to 18-20 T, including iron-based HTS [64]. Though higher fields are possible with HTS, more cost-effective might be hybrid magnet designs incorporating Nb-Ti, Nb_3Sn, and an inner layer of HTS and providing fields of about 20 T. Another important technology is the cryogenic beam vacuum system, which has to cope with unusually high levels of synchrotron radiation (up to 15 MW in total, for FCC-hh) in a cold environment. The beam-screen intercepting the radiation inside the cold bore of the magnets should operate at or above 50 K — significantly higher temperature than in the LHC.

Design luminosities of these hadron colliders $O(10^{35}\ \text{cm}^{-2}\text{s}^{-1})$ will result in a pile-up of events per crossing $O(500)$ (from up to 60 in LHC) and fast intensity drop due to burn-off. Significant radiation damping of beam emittances will naturally level luminosity evolution, though the total beam-beam tune shift $n_{\rm IP}\xi \sim (0.01 - 0.03)$ might need a special control as it will increase during the store [65].

Future hadron colliders store enormous electromagnetic energy in their superconducting dipole magnets, posing a major challenge for quench protection. Moreover, the record-high stored beam energy — about ∼13 GJ in the FCC-hh — makes machine protection systems an equally critical concern. A very challenging multi-stage collimation system is needed to avoid local beam loss spikes near cold magnets, which would induce magnet quenches. The primary and secondary collimators of the LHC are based on carbon-carbon composite material. For the future hadron colliders, ever stronger materials are being developed and examined, which also feature higher conductivity and, hence, lower impedance. More advanced options include the use of short bent crystals as primary collimators [66] and the deployment of hollow electron-beam lenses as non-destructible collimators [67]. It is noteworthy that machines such as the FCC-hh or SPPC can also be employed for particle physics studies in ion-ion and ion-proton collisions as well as in lepton-hadron $(ep, \mu p)$ interactions with c.m.e. $O(3$–10 TeV), should the corresponding high-energy high-intensity electron or muon beam facilities (ring-based, ERL-based or linacs) be found feasible and practical.

The lifetime of the muon, $\gamma\tau_0$ (with $\tau_0 = 2.2\ \mu$s), is sufficient to allow rapid acceleration to high energies before the muons decay, and to permit storage in a ring for approximately $300 \times B$[T] turns, where B is the average dipole magnetic field in Tesla. The muon-to-electron mass ratio of 210 effectively eliminates the synchrotron radiation barrier, allowing a muon collider to be built at a scale compatible with existing accelerator laboratory sites. High-energy muon colliders, as presently conceived, are predicted to be more compact, more power-efficient and significantly less expensive than the equivalent energy-frontier hadron

Int. J. Mod. Phys. A 2026.41. Downloaded from www.worldscientific.com by UNIVERSITY OF CALIFORNIA @ BERKELEY on 09/16/26. Re-use and distribution is strictly not permitted, except for Open Access articles.

or e^+e^- machines [62], and a neutrino factory could potentially be realized in the course of their construction [68]. The Higgs production cross-section in the s-channel is enhanced by a factor of $(m_\mu/m_e)^2$ compared to that in e^+e^- collisions.

The average luminosity of a muon collider,

$$\langle\mathcal{L}\rangle = f_0\gamma^2\frac{c\tau_0}{2C}\frac{n_\mathrm{b}N^2}{4\pi\varepsilon_\mathrm{n}\beta^*}\mathcal{F} = BP_\mathrm{b}\frac{Nr_0}{4\pi\varepsilon_\mathrm{n}}\frac{\gamma}{\beta^*}\left(\frac{c\tau_0\mathcal{F}}{8\pi e}\right), \quad (31.19)$$

scales with B, the total beam power P_b, and the beam brightness – the third factor above is nothing but the muon beam-beam tune shift Eq. (31.16). There is an obvious incentive to have all the particles in just one bunch per beam. The beta-function at the two IPs $\beta^* \approx \sigma_z$ scales as $1/\gamma$ within certain range of energies, giving overall scaling $\langle\mathcal{L}\rangle \propto \gamma^2$ with other limiting parameters fixed. The main challenges to luminosity achievement with decaying particles are related to production and fast cooling and acceleration of $O(10^{12})$ muons per bunch without emittance degradation. A multi-TeV c.m.e. high luminosity $O(10^{34}\ \mathrm{cm}^{-2}\mathrm{s}^{-1})$ muon collider would consist of [69] : (i) a high power proton driver (e.g., 8 GeV 2-4 MW H^- SRF linac); (ii) pre-target accumulation and compressor rings, in which high intensity 1-3 ns long proton bunches are formed; (iii) a high-power target for converting the proton beam into a tertiary muon beam with energy of about 200 MeV; (iv) a multi-stage ionization cooling section that reduces transverse and longitudinal emittances by several orders of magnitude and creates a low emittance beam, similarly to that recently demonstrated [70]; (v) a multistage acceleration system, possibly employing either rapid cycling synchrotrons or RLAs to accelerate muons in a modest number of turns up to the final energy using superconducting RF technology; and, finally, (vi) a 3–14 km diameter collider ring, where counter-propagating muon beams are stored and collide over the roughly 3000 turns corresponding to the muon lifetime.

The intense neutrino flux originating from the multi-TeV muon beams decaying in the collider poses another challenge — the need to minimize the environmental impact. The collider complex is typically located underground, and when the produced neutrinos emerge at the surface, a small fraction interacts with the surrounding rock (and other materials), generating an ionizing radiation dose that scales approximately as γ^3 [71]. Proposed facility designs aim to fully mitigate the impact of this neutrino-induced radiation to remain within operationally permitted levels. This can be achieved through a combination of measures, such as continuously adjusting the beam orbits to spread the neutrino flux over a wider area, constructing deeper collider tunnels, or reducing the muon beam emittance so that the desired luminosity can be reached with a substantially smaller number of muons.

31.5.4 *Plasma Acceleration and Other Advanced Concepts*

Since about the mid-1950s, it has been understood that collective plasma-based accelerators promise extremely large accelerating gradients, approximately three orders of magnitude greater than ∼100 MV/m obtained in conventional breakdown-limited RF structures [72]. Ionized plasmas can sustain electron plasma density waves with electric fields in excess of $E_0 = cm_e\omega_\mathrm{p}/e$ or

$$E_0 \simeq 96\,[\mathrm{GV/m}]\sqrt{n_0[10^{18}\,\mathrm{cm}^{-3}]}, \quad (31.20)$$

where n_0 denotes the ambient electron number density and $\omega_p = \sqrt{e^2n_0/(m_e\varepsilon_0)}$ is the electron plasma frequency [73]. Such gradients can be effectively excited by either powerful external pulses of laser light or by electron bunches if they are shorter than the plasma wavelength $\lambda_p = c/\omega_p \simeq 33\ \mu\mathrm{m}\times\sqrt{10^{18}\,\mathrm{cm}^{-3}/n_0}$, or by longer beams of protons if their charge density is modulated with the period of λ_p.

In the past decade, impressive progress has been made in the plasma wakefield acceleration (PWA) of good-quality electron beams. Laser-driven electron energy gains of 10 GeV over 0.1-0.2 m of plasma with (1-6)$\times10^{17}\mathrm{cm}^{-3}$ density has been demonstrated by the UTA, UMD and CSU groups [74, 75], and at the BELLA facility at the Lawrence Berkeley National Laboratory (LBNL) [76]. Short electron bunches were used to boost the energy of externally injected electron bunches by 9 GeV over 1.3 m of $\sim10^{17}\mathrm{cm}^{-3}$ plasma at the FACET facility in SLAC [77]. The AWAKE experiment at CERN used long self-modulated 450 GeV proton bunches to accelerate electrons to 2 GeV over 10 m of $\sim10^{15}$ cm^{-3} plasma [78].

Despite recent advances, the applicability of plasma acceleration in a high-energy physics facility remains uncertain. The design of the most-sought multi-TeV PWA-based e^+e^- collider faces numerous challenges. The most fundamental issue is the acceleration of positively charged positrons, which, unlike electrons, are strongly defocused by the immobile ions in the electron-depleted plasma-wakefield channel. While several strategies to mitigate this defocusing are being explored, a few alternative plasma-based collider concepts have been proposed to circumvent the positron problem entirely, including asymmetric plasma–RF hybrid colliders, e^-e^- and $\gamma\gamma$ colliders (see [79] and references therein). Furthermore, the ultra-strong focusing gradients in the plasma—focusing for e^- and defocusing for e^+—make the transfer of highly divergent beams between PWA stages extremely challenging, requiring significant space for beam optics, and effectively reducing the net accelerating gradient [80]. The luminosity of PWA-based colliders, still described by Eq. (31.18), fundamentally hinges on high power efficiency η, and also requires excellent beam quality, tight control of coherent beam instabilities, and stringent alignment and vibration tolerances—yet by any metrics, it remains orders of magnitude below that projected for colliders based on conventional technology (e.g., CLIC) [79, 81].

In addition, many advanced approaches and innovative concepts have been proposed to extend the energy and physics reach of future particle colliders, reduce their cost, and enhance luminosity or energy efficiency. Among these are: i) *dielectric wakefield accelerators*, where resonant dielectric structures are powered by ultra-short RF wakefield pulses driven by collinear or preceding high-charge electron bunches, sustaining gradients up to ∼0.3 GV/m; ii) *dielectric laser accelerators*, micron-scale dielectric structures driven by laser pulses, supporting fields of order O(1 GV/m); iii) *linear muon crystal colliders*, exploiting O(10 TV/m) wakefield acceleration of muons channeling between crystal planes or inside carbon nanotubes with charge carrier densities $\sim10^{20-22}$ cm^{-3}, potentially enabling ultimate compact PeV-scale facilities; iv) the *Gamma Factory* concept, in which conventional laser pulses collide with partially stripped heavy-ion beams circulating in a hadron storage ring (e.g., the LHC or FCC-hh), producing intense bursts of double–Lorentz-boosted high-energy gamma rays that could enable the generation of positrons or muons at unprecedented rates. An overview of these and related concepts, along with extensive references, can be found, e.g., in Ch. V of [1].

The feasibility of applying PWA and other advanced technologies to future high-energy colliders is being explored through worldwide R&D programs.

References

[1] V. Shiltsev and F. Zimmermann, Reviews of Modern Physics **93**, 1, 015006 (2021).

[2] A. Tollestrup and E. Todesco, in "Reviews Of Accelerator Science And Technology: Volume 1," 185–210, World Scientific (2008).

[3] D. A. Edwards and M. J. Syphers, *An introduction to the physics of high energy accelerators*, John Wiley & Sons, New York, NY (2008).

[4] A. W. Chao, *Physics of collective beam instabilities in high energy accelerators*, Wiley, New York, NY (1993), URL `https://cds.cern.ch/record/246480`.

[5] S.-Y. Lee, *Accelerator physics*, World Scientific, Singapore (2018), URL `https://library.oapen.org/handle/20.500.12657/50490`.

[6] E. D. Courant and H. S. Snyder, Annals of Physics **3**, 1, 1 (1958).

[7] H. Wiedemann, *Particle accelerator physics*, Springer Nature (2015), URL `https://library.oapen.org/handle/20.500.12657/23641`.

[8] M. Sands, Conf. Proc. C **6906161**, 257 (1969).

Int. J. Mod. Phys. A Downloaded from www.worldscientific.com by UNIVERSITY OF CALIFORNIA @ BERKE use and distribution is strictly not permitted, except for Open Access articles.

[9] S.-Y. Lee, *Spin dynamics and snakes in synchrotrons*, World Scientific (1997).

[10] F. Zimmermann, Physical Review Special Topics-Accelerators and Beams **7**, 12, 124801 (2004).

[11] A. W. Chao *et al.*, editors, *Handbook of accelerator physics and engineering*, World Scientific (2023), URL `https://www.worldscientific.com/worldscibooks/10.1142/13229`.

[12] A. Piwinski, J. D. Bjorken and S. K. Mtingwa, Physical Review Accelerators and Beams **21**, 11, 114801 (2018).

[13] V. Parkhomchuk and A. Skrinsky, Reviews of Accelerator Science and Technology **1**, 01, 237 (2008).

[14] M. Minty and F. Zimmermann, *Measurement and control of charged particle beams*, Springer Nature (2003), URL `https://library.oapen.org/handle/20.500.12657/23642`.

[15] S. Myers, *Particle Physics Reference Library: Volume 3: Accelerators and Colliders*, volume 3, Springer Nature (2020), URL `https://library.oapen.org/handle/20.500.12657/39571`.

[16] V. Shiltsev *et al.*, Physical Review Special Topics-Accelerators and Beams **8**, 10, 101001 (2005).

[17] J. T. Seeman, in "Lecture Notes in Physics, vol.247," 121–153, Springer (1986).

[18] R. Assmann, M. Lamont and S. Myers, Nucl. Phys. B Proc. Suppl. **109**, 17 (2002).

[19] K. Yokoya and P. Chen, Lect. Notes Phys. **400**, 415 (1992).

[20] H. T. Edwards, Annual Review of Nuclear and Particle Science **35**, 1, 605 (1985).

[21] V. Lebedev and V. Shiltsev, *Accelerator physics at the Tevatron collider*, Springer (2014), URL `https://link.springer.com/book/10.1007/978-1-4939-0885-1`.

[22] S. D. Holmes and V. D. Shiltsev, Annual Review of Nuclear and Particle Science **63**, 435 (2013).

[23] G. Voss and B. Wiik, Annual Review of Nuclear and Particle Science **44**, 1, 413 (1994).

[24] S. Myers and H. Schopper, *Particle Physics Reference Library. Volume 3: Accelerators and Colliders*, Springer Nature (2020), URL `https://library.oapen.org/handle/20.500.12657/39571`.

[25] D. Brandt *et al.*, Reports on Progress in Physics **63**, 6, 939 (2000).

[26] N. Phinney, eConf **C00082**, MO102 (2000), [arXiv:physics/0010008].

[27] L. Evans, Annual Review of Nuclear and Particle Science **61**, 435 (2011).

[28] CERN, The Large Hadron Collider web site:URL `http://lhc.web.cern.ch/lhc/`.

[29] G. Valentino *et al.*, Physical Review Special Topics-Accelerators and Beams **15**, 5, 051002 (2012).

[30] G. Apollinari *et al.*, Technical Report CERN Yellow Report: 2017-007-M (2017).

[31] H. Damerau *et al.*, *LHC Injectors Upgrade, Technical Design Report* (2014), URL `https://cds.cern.ch/record/1976692`.

[32] J. T. Seeman, Annual Review of Nuclear and Particle Science **74**, 1, 613 (2024).

[33] Y. Ohnishi *et al.*, Progress of Theoretical and Experimental Physics **2013(3)**, 3 (2013).

[34] K. Oide *et al.*, Phys. Rev. Accel. Beams **19**, 111005 (2016).

[35] M. Zobov *et al.*, Physical Review Letters **104**, 17, 174801 (2010).

[36] P. Raimondi, D. N. Shatilov and M. Zobov (2007), [arXiv:physics/0702033].

[37] M. Harrison, S. Peggs and T. Roser, Annual Review of Nuclear and Particle Science **52**, 1, 425 (2002).

[38] M. Blaskiewicz, J. M. Brennan and K. Mernick, Phys. Rev. Lett. **105**, 094801 (2010).

[39] M. Bai *et al.*, Physical Review Letters **96**, 17, 174801 (2006).

[40] W. Fischer *et al.*, Phys. Rev. Lett. **115**, 26, 264801 (2015).

[41] 2020 Update of the European Strategy for Particle Physics, `https://home.cern/sites/home.web.cern.ch/files/2020-06/2020UpdateEuropeanStrategy.pdf` (2020).

[42] J. N. Butler *et al.*, Report of the 2021 US Community Study on the Future of Particle Physics (Snowmass 2021) (2023), [arXiv:2301.06581].

[43] T. Roser *et al.*, Journal of Instrumentation **18**, 05, P05018 (2023).

[44] V. Kekelidze *et al.*, The European Physical Journal A **52**, 8, 211 (2016).

[45] F. Willeke et al., Electron-Ion Collider Conceptual Design Report, BNL-221006-2021-FORE (2021), URL `https://www.osti.gov/biblio/1765663`.

[46] A. Accardi *et al.*, The European Physical Journal A **52**, 9, 268 (2016).

[47] V. Lebedev, Journal of Instrumentation **19**, 06, P06015 (2024).

[48] M. Benedikt *et al.*, FCC Feasibility Study Report. Vol. 2 (2025), [arXiv:2505.00274].

[49] CEPC Study Group, CEPC Technical Design Report. Vol.2. (2023), [arXiv:2312.14363].

[50] C. Adolphsen *et al.*, ILC Technical Design Report. Vol.3.II (2013), [arXiv:1306.6328].

[51] M. Aicheler *et al.*, CLIC Conceptual Design Report, CERN-2012-007 (2012), URL `https://cds.cern.ch/record/1500095`.

[52] L. Evans and S. Michizono, ILC Machine Staging Report (2017), [arXiv:1711.00568].

[53] A. Grassellino *et al.*, Supercond. Sci. Technol. **26**, 102001 (2013).

[54] H. Abramowicz *et al.*, The Linear Collider Facility (LCF) at CERN (2025), [arXiv:2503.24049], URL `https://arxiv.org/abs/2503.24049`.

[55] M. Aicheler *et al.*, CLIC Project Implementation Plan (2018), [arXiv:1903.08655].

[56] T. O. Raubenheimer, Physical Review Special Topics-Accelerators and Beams **3**, 12, 121002 (2000).

[57] S. Belomestnykh *et al.*, Journal of Instrumentation **18**, 09, P09039 (2023).

[58] C. Vernieri *et al.*, Journal of Instrumentation **18**, 07, P07053 (2023).

[59] P. Piminov, Physics of Particles and Nuclei Letters **15**, 7, 732 (2018).

[60] J. Bao *et al.*, Conceptual Design Report of Super Tau-Charm Facility: The Accelerator (2025), [arXiv:2509.11522], URL `https://arxiv.org/abs/2509.11522`.

[61] M. Benedikt *et al.*, The European Physical Journal Special Topics **228**, 4, 755 (2019).

[62] C. Accettura *et al.*, The European Physical Journal C **83**, 9, 864 (2023).

[63] D. Schoerling and A. V. Zlobin, *Nb_3Sn Accelerator Magnets*, Springer Nature (2019), URL `https://library.oapen.org/handle/20.500.12657/23335`.

[64] E. Kong *et al.*, International Journal of Modern Physics A **34**, 13n14, 1940003 (2019).

[65] M. Benedikt, D. Schulte and F. Zimmermann, Phys. Rev. ST Accel. Beams **18**, 101002 (2015).

[66] W. Scandale and A. Taratin, Physics Reports **815**, 1 (2019).

[67] V. Shiltsev, Journal of Instrumentation **16**, 03, P03039 (2021).

[68] S. Geer, Annual Review of Nuclear and Particle Science **59**, 347 (2009).

[69] C. Ankenbrandt *et al.*, Physical Review Special Topics-Accelerators and Beams **2**, 8, 081001 (1999).

[70] M. Bogomilov *et al.*, Nature **578**, 53 (2020).

[71] B. J. King, in "AIP Conference Proceedings," volume 530, 165–180, AIP (2000), URL `http://dx.doi.org/10.1063/1.1361675`.

[72] V. Veksler, The Soviet Journal of Atomic Energy **2**, 5, 525 (1957).

[73] T. Tajima and J. M. Dawson, Physical Review Letters **43**, 4, 267 (1979).

[74] C. Aniculaesei *et al.*, Matter and Radiation at Extremes **9**, 1 (2024).

[75] E. Rockafellow *et al.*, Nuclear Instruments and Methods A **1077**, 170586 (2025).

[76] A. Picksley *et al.*, Physical Review Letters **133**, 25, 255001 (2024).

[77] M. Litos *et al.*, Plasma Physics and Controlled Fusion **58**, 3, 034017 (2016).

[78] E. Adli *et al.*, Nature **561**, 7723, 363 (2018).

[79] G. J. Cao *et al.*, Physical Review Accelerators and Beams **27**, 3, 034801 (2024).

[80] C. A. Lindstrøm, Physical Review Accelerators and Beams **24**, 1, 014801 (2021).

[81] D. Schulte, Reviews of Accelerator Science and Technology **9**, 209 (2016).

Int. J. Mod. Phys. A 2026.41. Downloaded from www.worldscientific.com
by UNIVERSITY OF CALIFORNIA @ BERKELEY on 09/16/26. Re-use and distribution is strictly not permitted, except for Open Access articles.

32. High-Energy Collider Parameters

High-Energy Collider Parameters: e^+e^- Colliders (I)

Table 32.1: Updated in March 2026 with numbers received from representatives of the colliders (contact E. Pianori, LBNL). The table shows the parameter values achieved by December 2025. Quantities are, where appropriate, r.m.s.; unless noted otherwise, energies refer to beam energy; H and V indicate horizontal and vertical directions; s.c. stands for superconducting. Parameters for the defunct SPEAR, DORIS, PETRA, PEP, TRISTAN, and VEPP-2M colliders may be found in our 1996 edition (Phys. Rev. **D54**, 1 July 1996, Part I).

	VEPP-2000 (Novosibirsk)	VEPP-4M (Novosibirsk)	BEPC (China)	BEPC-II (China)	DAΦNE (Frascati)
Physics start date	2010	1994	1989	2008	1999
Physics end date	—	—	2005	—	—
Maximum beam energy (GeV)	1.0	6	2.5	1.89 (2.474 max)	0.510
Delivered integrated luminosity per exp. (fb^{-1})	1	0.05	0.11	53.5	$\approx$ 4.7 in 2001-2007 $\approx$ 2.7 w/crab-waist $\approx$ 6.8 2014-2018* $\approx$ 0.4 2021-2022† $\approx$ 1.1 2023-2024‡
Luminosity (10^{30} $\mathrm{cm}^{-2}\mathrm{s}^{-1}$)	90 at 890 MeV 42 at 550 MeV 4 at 300 MeV 0.4 at 200 MeV	20	12.6 at 1.843 GeV 5 at 1.55 GeV	1096	453
Time between collisions (μs)	0.04	0.6	0.8	0.006	0.0027
Full crossing angle (μ rad)	0	0	0	2.2×10^4	5×10^4
Energy spread (units 10^{-3})	0.71	1	0.58 at 2.2 GeV	0.52	0.40
Bunch length (cm)	4	5	$\approx$ 5	1.35	low current: 1 at 15mA: 2
Beam radius (10^{-6} m)	125 (round)	H:1000 V:30	H:890 V:37	H:347 V:4.5	H:260 V:4.8
Free space at interaction point (m)	$\pm$0.5	$\pm$2	$\pm$2.15	$\pm$0.63	$\pm$0.295
Luminosity lifetime (hr)	continuous	2	7–12	1.5	0.2
Turn-around time (min)	continuous	18	32	4 (topping up)	2 (topping up)
Injection energy (GeV)	on energy (0.16–1.0)	1.8	1.55	on energy	on energy
Transverse emittance (10^{-9} m)	H:150 V:150	H:200 V:20	H:660 V:28	H:121 V:1.56	H:260 V:2.6
β^*, amplitude function at interaction point (m)	H:0.04 - 0.11 V:0.04 - 0.11	H:0.75 V:0.05	H:1.2 V:0.05	H:1.0 V:0.0135	H:0.26 V:0.009
Beam-beam tune shift per crossing (units 10^{-4})	1100 at 890 MeV	500	350	383	440/894 (crab-waist run/test)
RF frequency (MHz)	172	180	199.53	499.8	368.667
Particles per bunch (units 10^{10})	12	15	20 at 2 GeV 11 at 1.55 GeV	3.8	e^-: 3.2 e^+: 2.1
Bunches per ring per species	1	2	1	119	100 to 110 (120 buckets)
Average beam current per species (mA)	240	80	40 at 2 GeV 22 at 1.55 GeV	910	e^-: 1250 e^+: 800
Circumference or length (km)	0.024	0.366	0.2404	0.23753	0.098
Interaction regions	2	1	2	1	1
Magnetic length of dipole (m)	1.1	2	1.6	outer ring: 1.6 inner ring: 1.41	outer ring: 1.2 inner ring: 1
Length of standard cell (m)	12	7.2	6.6	outer ring: 6.6 inner ring: 6.2	n/a
Phase advance per cell (deg)	H:745 V:385	65	$\approx$ 60	60–90 non-standard cells	—
Dipoles in ring	8	78	40 + 4 weak	84 + 8 weak	8
Quadrupoles in ring	24 + 4 s.c.	150	68	134+2 s.c.	48
Peak magnetic field (T)	2.4	0.6	0.903 at 2.8 GeV	outer ring: 0.677 inner ring: 0.766	1.2

*KLOE-2
†SIDDHARTINO
‡SIDDHARTA-2

Int. J. Mod. Phys. A
by UNIVERSITY OF CALIFORNIA @ BERKE
nloaded from www.worldscientific.com
use and distribution is strictly not permitted, except for Open Access articles.

Int. J. Mod. Phys. A 2026.41. Downloaded from www.worldscientific.com
by UNIVERSITY OF CALIFORNIA @ BERKELEY on 09/16/26. Re-use and distribution is strictly not permitted, except for Open Access articles.

High-Energy Collider Parameters: e^+e^- Colliders (II)

Table 32.2: Updated in March 2020 with numbers received from representatives of the colliders (contact E. Pianori, LBNL). The table shows the parameter values achieved. Quantities are, where appropriate, r.m.s.; unless noted otherwise, energies refer to beam energy; H and V indicate horizontal and vertical directions; s.c. stands for superconducting. ILC and CLIC parameters are documented in the Accelerator physics of colliders review.

	CESR (Cornell)	CESR-C (Cornell)	LEP (CERN)	SLC (SLAC)
Physics start date	1979	2002	1989	1989
Physics end date	2002	2008	2000	1998
Maximum beam energy (GeV)	6	6	100 - 104.6	50
Delivered integrated luminosity per experiment (fb^{-1})	41.5	2.0	0.221 at Z peak 0.501 at 65 − 100 GeV 0.275 at >100 GeV	0.022
Luminosity (10^{30} $\mathrm{cm}^{-2}\mathrm{s}^{-1}$)	1280 at 5.3 GeV	76 at 2.08 GeV	24 at Z peak 100 at > 90 GeV	2.5
Time between collisions (μs)	0.014 to 0.22	0.014 to 0.22	22	8300
Full crossing angle (μ rad)	±2000	±3300	0	0
Energy spread (units 10^{-3})	0.6 at 5.3 GeV	0.82 at 2.08 GeV	0.7→1.5	1.2
Bunch length (cm)	1.8	1.2	1.0	0.1
Beam radius (μm)	H:460 V:4	H:340 V:6.5	H:200→300 V:2.5→8	H:1.5 V:0.5
Free space at interaction point (m)	±2.2 (±0.6 to REC quads)	±2.2 (±0.3 to PM quads)	±3.5	±2.8
Luminosity lifetime (hr)	2–3	2–3	20 at Z peak 10 at > 90 GeV	—
Turn-around time (min)	5 (topping up)	1.5 (topping up)	50	120 Hz (pulsed)
Injection energy (GeV)	1.8–6	1.5–6	22	45.64
Transverse emittance (10^{-9} m)	210 1	120 3.5	H:20–45 V:0.25→1	H:0.5 V:0.05
β^*, amplitude function at interaction point (m)	1.0 0.018	0.94 0.012	1.5 0.05	0.0025 0.0015
Beam-beam tune shift per crossing (10^{-4}) or disruption	250 620	e^-: 420 (H), 280 (V) e^+: 410 (H), 270 (V)	830	0.75 (H) 2.0 (V)
RF frequency (MHz)	500	500	352.2	2856
Particles per bunch (units 10^{10})	1.15	4.7	45 in collision 60 in single beam	4.0
Bunches per ring per species	9 trains of 5 bunches	8 trains of 3 bunches	4 trains of 1 or 2	1
Average beam current per species (mA)	340	72	4 at Z peak 4→6 at > 90 GeV	0.0008
Beam polarization (%)	—	—	55 at 45 GeV 5 at 61 GeV	e^-: 80
Circumference or length (km)	0.768	0.768	26.66	1.45 +1.47
Interaction regions	1	1	4	1
Magnetic length of dipole (m)	1.6–6.6	1.6–6.6	11.66/pair	2.5
Length of standard cell (m)	16	16	79	5.2
Phase advance per cell (deg)	45–90 (no standard cell)	45–90 (no standard cell)	102/90	108
Dipoles in ring	86	84	3280 + 24 inj. + 64 weak	460+440
Quadrupoles in ring	101 + 4 s.c.	101 + 4 s.c.	520 + 288 + 8 s.c.	—
Peak magnetic field (T)	0.3 / 0.8 at 8 GeV	0.3 / 0.8 at 8 GeV, 2.1 wigglers at 1.9 GeV	0.135	0.597

High-Energy Collider Parameters: ep, e^+e^- Colliders (III)

Table 32.3: Updated in March 2026 with numbers received from representatives of the colliders (contact E. Pianori, LBNL). The table shows the parameter values achieved by December 2025. Design parameters for SuperKEKEB may be found in our 2018 edition (Phys. Rev. **D98**, 030001 (2018)) Quantities are, where appropriate, r.m.s.; unless noted otherwise, energies refer to beam energy; H and V indicate horizontal and vertical directions; s.c. stands for superconducting.

	HERA (DESY)	KEKB (KEK)	PEP-II (SLAC)	SuperKEKB (KEK)
Physics start date	1992	1999	1999	2018
Physics end date	2007	2010	2008	—
Particles collided	ep	e^+e^-	e^+e^-	e^+e^-
Maximum beam energy (TeV)	e: 0.030 p: 0.92	e^-: 8.33 (8.0 nominal) e^+: 3.64 (3.5 nominal)	e^-: 7–12 (9.0 nominal) e^+: 2.5–4 (3.1 nominal)	e^-: 7 e^+: 4
Delivered integrated luminosity per exp. (fb^{-1})	0.8	1040	557	712
Luminosity (10^{30} cm^{-2}s^{-1})	75	21083	12069 (design: 3000)	5.1×10^4
Time between collisions (ns)	96	5.9 or 7.86	4.2	4.2
Full crossing angle (μ rad)	0	$\pm$11000*	0	$\pm$41500
Energy spread (units 10^{-3})	e: 0.91 p: 0.2	e^-/e^+: 0.67/0.73	e^-/e^+: 0.61/0.77	e^-/e^+: 0.64/0.81
Bunch length (cm)	e: 0.83 p: 8.5	0.65	e^-/e^+: 1.1/1.0	e^-/e^+: 0.6/0.6
Beam radius (μm)	e: 110 (H), 30 (V) p: 111 (H), 30 (V)	H: 124 (e^-), 117 (e^+) V: 1.9	157 4.7	e^-: 16.6 (H), 0.27 (V) e^+: 15.5 (H), 0.27 (V)
Free space at interaction point (m)	$\pm$2	+0.75/−0.58 (+300/−500) mrad cone	$\pm$0.2, $\pm$300 mrad cone	e^- : +1.20/ − 1.28 e^+ : +0.78/ − 0.73 (+300/−500) mrad cone
Initial luminosity decay time, $-L/(dL/dt)$ (hr)	10	continuous	continuous	continuous
Turn-around time (min)	e: 75, p: 135	continuous	continuous	continuous
Injection energy (GeV)	e: 12 p: 40	e^-/e^+ : 8.0/3.5 (nominal)	e^-/e^+ : 9.0/3.1 (nominal)	e^-/e^+ : 7/4
Transverse emittance (10^{-9} m)	e: 20 (H), 3.5 (V) p: 5 (H), 5 (V)	e^-: 24 (57†) (H), 0.61 (V) e^+: 18 (55†) (H), 0.56 (V)	e^-: 48 (H), 1.8 (V) e^+: 24 (H), 1.8 (V)	e^-: 4.6 (H), 0.05 (V) e^+: 4.0 (H), 0.05 (V)
β^*, amplitude function at interaction point (m)	e: 0.6 (H), 0.26 (V) p: 2.45 (H), 0.18 (V)	e^-: 1.2 (0.27†) (H), 0.0059 (V) e^+: 1.2 (0.23†) (H), 0.0059 (V)	e^-: 0.50 (H), 0.012 (V) e^+: 0.50 (H), 0.012 (V)	e^-: 0.060 (H), 1×10^{-3} (V) e^+: 0.060 (H), 1×10^{-3} (V)
Beam-beam tune shift per crossing (units 10^{-4})	e:190 (H), 450 (V) p: 12 (H), 9 (V)	e^-: 1020 (H), 900 (V) e^+: 1270 (H), 1290 (V)	e^-: 703 (H), 498 (V) e^+: 510 (H), 727 (V)	e^-: 15 (H), 270 (V) e^+: 20 (H), 360 (V)
RF frequency (MHz)	e:499.7 p: 208.2/52.05	508.887	476	508.887
Particles per bunch (units 10^{10})	e:3 p:7	e^-/e^+: 4.7/6.4	e^-/e^+: 5.2/8.0	e^-/e^+: 3.37/4.37
Bunches per ring per species	e: 189 p: 180	1585	1732	2346
Average beam current per species (mA)	e:40 p:90	e^-/e^+: 1188/1637	e^-/e^+: 1960/3026	e^-/e^+: 1259/1632
Beam polarization (%)	—	—	—	—
Circumference or length (km)	6.336	3.016	2.2	3.016
Interaction regions	2 colliding beams 1 fixed target (e beam)	1	1	1
Magnetic length of dipole (m)	e:9.185; p: 8.82	e^-/e^+ : 5.86/0.915	e^-/e^+: 5.4/0.45	e^-/e^+ : 5.9/4.0
Length of standard cell (m)	e:23.5 p:47	e^-/e^+ : 75.7/76.1	15.2	e^-/e^+ : 75.7/76.1
Phase advance per cell (deg)	e:60 p:90	450	e^-/e^+: 60/90	450
Dipoles in ring	e: 396 p: 416	e^-/e^+ : 116/112	e^-/e^+: 192/192	e^-/e^+ : 116/112
Quadrupoles in ring	e:580 p:280	e^-/e^+ : 452/452	e^-/e^+: 290/326	e^-/e^+ : 466/460
Peak magnetic field (T)	e: 0.274; p: 5	e^-/e^+ : 0.25/0.72	e^-/e^+: 0.18/0.75	e^-/e^+ : 0.22/0.19

*KEKB was operated with crab crossing from 2007 to 2010.
†With dynamic beam-beam effect.

Int. J. Mod. Phys. A Downloaded from www.worldscientific.com
by UNIVERSITY OF CALIFORNIA @ BERKE use and distribution is strictly not permitted, except for Open Access articles.

Int. J. Mod. Phys. A 2026.41. Downloaded from www.worldscientific.com
by UNIVERSITY OF CALIFORNIA @ BERKELEY on 09/16/26. Re-use and distribution is strictly not permitted, except for Open Access articles.

High-Energy Collider Parameters: $\bar{p}p$, pp Colliders

Table 32.4: Updated in March 2026 with numbers received from representatives of the colliders (contact E. Pianori, LBNL). The table shows the parameter values achieved by December 2025. Parameters for the defunct S$p\bar{p}$S collider may be found in our 2002 edition (Phys. Rev. **D66**, 010001 (2002)). Quantities are, where appropriate, r.m.s.; unless noted otherwise, energies refer to beam energy; H and V indicate horizontal and vertical directions; s.c. stands for superconducting.

	TEVATRON* (Fermilab)	RHIC Brookhaven	LHC (CERN)			
Physics start date	1987	2001	2009 (Run 1)	2015 (Run 2)	2022 (Run 3)	2030 (HL-LHC)
Physics end date	2011	2026	—			
Particles collided	$p\bar{p}$	pp (polarized)	pp			
Maximum beam energy (TeV)	0.980	0.255 55% polarization	4.0	6.5	6.8	7.0
Max. delivered integrated luminosity per exp. (fb^{-1})	12	0.38 at 100 GeV 1.3 at 250/255 GeV	23.3 at 4.0 TeV 6.1 at 3.5 TeV	160	340	250/y
Luminosity (10^{30} $\text{cm}^{-2}\text{s}^{-1}$)	431	245 (pk) 160 (avg)	7.7×10^3	2.1×10^4	2.2×10^4 (leveled)	5.0×10^4 (leveled)
Time between collisions (ns)	396	107	49.90	24.95	24.95	24.95
Full crossing angle (μ rad)	0	0	290	$320 \to 260^\dagger$	$320 \to 240^\dagger$	500
Energy spread (units 10^{-3})	0.14	0.15	0.1445	0.11	0.11	0.11
Bunch length (cm)	p: 50 $\bar{p}$: 45	60	9.4	8	9.7	7.6
Beam radius (10^{-6} m)	p: 28 $\bar{p}$: 16	85	18.8	$8.5^\ddagger$	$5.7^\ddagger$	$7^\ddagger$
Free space at interaction point (m)	± 6.5	16	38	38	38	38
Initial luminosity decay time, $-L/(dL/dt)$ (hr)	6 (avg)	7.5	≈ 6	8.4	12 §	≈ 12 (leveled)
Turn-around time (min)	90	25	180	150	120¶	150
Injection energy (TeV)	0.15	0.023	0.450	0.450	0.450	0.450
Transverse emittance (10^{-9} m)	p: 3 $\bar{p}$: 1	11	0.59	0.29	0.22	0.33
β^*, ampl. function at interaction point (m)	0.28	0.65	0.6	$0.3 \to 0.25^\parallel$	$1.2/1.2 \to 0.5/0.15^{**}$	$1 \to 0.15^\parallel$
Beam-beam tune shift per crossing (units 10^{-4})	p: 120 $\bar{p}$: 120	73	72	45	$137^\S$	104
RF frequency (MHz)	53	accel: 9 store: 28	400.8	400.8	400.8	400.8
Particles per bunch (units 10^{10})	p:26 $\bar{p}$:9	18.5	16	11	18	22
Bunches per ring per species	36	111	1380	2556 2544 (i.r. $1/5^{\dagger\dagger}$)	2460 (total) 2464 (i.r. $1/5^{\dagger\dagger}$)	2760 2748 (i.r. $1/5^{\dagger\dagger}$)
Average beam current per species (mA)	p:70 $\bar{p}$:24	257	400	510	800	1094
Circumference (km)	6.28	3.834	26.659			
Interaction regions	2 high $\mathfrak{L}$	6 total, 2 high $\mathfrak{L}$	4 total, 2 high $\mathfrak{L}$			
Magnetic length of dipole (m)	6.12	9.45	14.3			
Length of standard cell (m)	59.5	29.7	106.90			
Phase advance per cell (deg)	67.8	84	90			
Dipoles in ring	774	192 per ring + 12 common	1232 main dipoles			
Quadrupoles in ring	216	246 per ring	482 2-in-1 24 1-in-1			
Magnet types	s.c., $\cos\theta$ warm iron	s.c., $\cos\theta$ cold iron	s.c., 2-in-1 cold iron			
Peak magnetic field (T)	4.4	3.5	$8.3^{\ddagger\ddagger}$			

*Other TEVATRON parameters: $\bar{p}$ source accum. rate: 25×10^{10} hr^{-1}; max. no. of $\bar{p}$ stored: 3.4×10^{12} (Accumulator), 6.1×10^{12} (Recycler).
†Variable crossing angle decreasing during the fill with the reduction in bunch population
‡Minimum beam radius during levelling
§Value at start of levelling
¶Most likely value as observed in 2025
‖ β^* levelling
**levelled, ×/|| values
††Number of bunches colliding at the interaction regions (i.r.) 1 (ATLAS) and 5 (CMS).
‡‡Value for design beam energy of 7 TeV.

High-Energy Collider Parameters: Heavy Ion Colliders

Table 32.5: Updated in March 2026 with numbers received from representatives of the collider (contact E. Pianori, LBNL) The table shows the parameter values achieved. For the LHC, only maximum values over all experiments per operational mode are provided. Quantities are, where appropriate, r.m.s.; unless noted otherwise, energies refer to beam energy; s.c. stands for superconducting. pk and avg denote peak and average values.

	RHIC (Brookhaven)		LHC (CERN)		
Physics start date	2000	2012 / 2018 / 2018 / 2012 / 2004 2021 / 2014 / 2002 / 2015 / 2015	2010	2012 / 2025	2017 / 2025
Physics end date	2026		—		
Particles collided	Au Au	U U / Zr Zr / Ru Ru / Cu Au / Cu Cu O O / h Au / d Au / p Au / p Al	Pb Pb	p-Pb / p-O	Xe-Xe / O-O / Ne-Ne
Max. beam energy (TeV/n)	0.1	0.1	2.68	p:6.5, Pb:2.56 p:6.8, O:3.4	2.72 / 2.68 / 2.68
$\sqrt{s_{NN}}$ (TeV)	0.2	0.2	5.36	8.16 / 9.62	5.44 / 5.36 / 5.36
Max. delivered int. nucleon-pair lumin. per exp. (pb^{-1})	2639 (at 100 GeV/n)	21 / 36 / 36.9 / 167 / 60 8.2 / 43 / 169 / 124 / 63 (all at 100 GeV/n)	125.5	40.4 / 0.77	0.05 / 2.4 / 0.4
Luminosity (10^{27} $\mathrm{cm}^{-2}\mathrm{s}^{-1}$)	pk: 15.5 avg: 8.7	pk: 0.4 / 4.8 / 3.8 / 12 / 21 450 / 170 / 850 / 880 / 7600 avg: 0.6 / 2.2 / 2.1 / 10 / 8 230 / 100 / 500 / 450 / 3800	6.4 (leveled)*	900 / 660	0.4 / 91 / 45
Time between collisions (ns)	107	107 / 107 / 107/ 107 / 321 107 / 107 / 107 / 107 / 107	49.9	99.8 / 149.7 / 998	5500 / 998 / 998
Full crossing angle (μ rad)	0	0	156	280 / 120	300 / 200 / 200
Energy spread (units 10^{-3})	0.75	0.75	0.13	0.11 / 0.16	0.11 / 0.16 / 0.16
Bunch length (cm)	30	30	9.6	p:9, Pb:11.5 p:9.9, O:9.9	11 / 9.9 / 9.9
Beam radius (10^{-6} m)	$114^{\dagger}$	$123^{\dagger}$ / $87^{\dagger}$ / $88^{\dagger}$ / $163^{\dagger}$ / $145^{\dagger}$ $100^{\dagger}$ / $136^{\dagger}$ / $124^{\dagger}$ / $147^{\dagger}$ / $128^{\dagger}$	20	p: 19, Pb:19 p:10, O:16	12 / 15 / 18
Free space at inter. point (m)	16	16	38	38	38
Initial luminosity decay time, $-L/(dL/dt)$ (hr)	1	$-0.35^{\ddagger}$ / $\infty^{\S}$ / $\infty^{\S}$ / $\infty^{\ddagger}$ / 1.8 ∞ / 0.6 / $\infty^{\ddagger}$ / 0.5 / 0.25	∞	$\approx$ 2 / 7	$\approx$ 6 / 17 / 25
Turn-around time (min)	30	$60^{\P}$ / $40^{\P}$ / $40^{\P}$ / $160^{\P}$ / $90^{\P}$ $45^{\P}$/ $45^{\P}$ / $90^{\P}$ / $60^{\P}$ / $50^{\P}$	134	150 / 335	180 / 107 / N/A
Injection energy (TeV/n)	0.011	0.011	0.177	p:0.45, Pb:0.177 p:0.45, O:0.225	0.188 / 0.225 / 0.225
Transverse emittance (10^{-9} m)	$19^{\dagger}$	$22^{\dagger}$ /$10.7^{\dagger}$ / $11.2^{\dagger}$ / $38^{\dagger}$ / $23^{\dagger}$ $12^{\dagger}$ / $19^{\dagger}$ / $22^{\dagger}$ / $26^{\dagger}$ / $21^{\dagger}$	0.80	p:0.29, Pb:0.29 p:0.18, O:0.51	0.3 / 0.46 / 0.62
β^*, ampl. function at interaction point (m)	0.7	0.7 / 0.7 /0.7 / 0.7 / 0.9 0.7 / 1.0 / 0.7 / 0.8 / 0.8	0.5	0.5 / 1.0	0.4 / 0.5 / 0.5
Beam-beam tune shift per crosssing (units 10^{-4})	$39^{\dagger}$	$6^{\dagger}$ / $18^{\dagger}$ /$21^{\dagger}$ / $14^{\dagger}$, $14^{\dagger}$ / $30^{\dagger}$ / $34^{\dagger}$ $42^{\dagger}$, $22^{\dagger}$ / $40^{\dagger}$, $27^{\dagger}$ / $53^{\dagger}$, $41^{\dagger}$ / $80^{\dagger}$, $59^{\dagger}$	4.26	15 / 20.6	$\approx$ 10 / 10.6 / 6.8
RF frequency (MHz)	accel: 28, store: 197		400.8	400.8 / 400.8	400.8 / 400.8 / 400.8
Particles per bunch (units 10^{10})	0.20	0.03 / 0.1 / 0.1 / 0.4, 0.13 / 0.45 / 0.85 4.5, 0.13 / 13, 0.20 / 22.5, 0.16 / 24, 1.1	0.0248 (r.m.s.)	p:2.6, Pb:0.022 p:3.0, O:0.39	0.027 / 0.29 / 0.20
Bunches per ring per species	111	111 / 111 / 111/ 111 / 37 106 / 111 /111 / 111 / 111	1240	p:540, Pb:684 p:52, O:52	16 / 62 / 62
Average beam current per species (mA)	224	38 / 56 / 61 / 160,138 / 60 / 95 125,143 / 181,213 / 313,176 / 334,199	45.4	p:16, Pb:15 p:2.21, O:2.83	0.54 / 2.56 / 2.20
Circumference (km)	3.834		26.659		
Interaction regions	6 total, 2 high $\mathfrak{L}$		4 total, 3 high $\mathfrak{L}$		
Magnetic length of dipole (m)	9.45		14.3		
Length of standard cell (m)	29.7		106.90		
Phase advance per cell (deg)	93	84 /84 / 84 / 84 / 84 / 84 93 / 84(d), 93 / 84(p), 93 / 84(p), 93	90		
Dipoles in ring	192 per ring, + 12 common		1232, main dipoles		
Quadrupoles in ring	246 per ring		482 2-in-1, 24 1-in-1		
Magnet Type	s.c. $\cos\theta$, cold iron		s.c., 2 in 1, cold iron		
Peak magnetic field (T)	3.5		8.3		

*Operational values in 2025 exceed HL-LHC projections from previous editions.
†Initial value, increases (descreases) without (with) cooling.
‡Negative or infinite decay time is effect of cooling.
§luminosity leveled to flat after set to target value, with cooling.
¶measured minimum, not theoretical.

Int. J. Mod. Phys. A
by UNIVERSITY OF CALIFORNIA @ BERKE
Downloaded from www.worldscientific.com
use and distribution is strictly not permitted, except for Open Access articles.

Int. J. Mod. Phys. A 2026.41. Downloaded from www.worldscientific.com
by UNIVERSITY OF CALIFORNIA @ BERKELEY on 09/16/26. Re-use and distribution is strictly not permitted, except for Open Access articles.

33. Neutrino Beam Lines at High-Energy Proton Synchrotrons

Revised August 2025 with numbers verified by representatives of the synchrotrons (contact C.-J. Lin, LBNL). For existing (future) neutrino beam lines the latest achieved (design) values are given.

The main source of neutrinos at proton synchrotrons is from the decay of pions and kaons produced by protons striking a nuclear target. There are different schemes to focus the secondary particles to enhance neutrino flux and/or tune the neutrino energy profile. In wide-band beams (WBB), the neutrino parent mesons are focused over a wide momentum range to obtain maximum neutrino intensity. In narrow-band beams (NBB), the secondary particles are first momentum-selected to produce a monochromatic parent beam. Another approach to generate a narrow-band neutrino spectrum is to select neutrinos that are emitted off-axis relative to the momentum of the parent mesons. For a comprehensive review of the topic, including other historical neutrino beam lines, see the article by S. E. Kopp, "Accelerator-based neutrino beams," Phys. Rept. **439**, 101 (2007).

	PS (CERN)				SPS (CERN)			PS (KEK)	Main Ring (JPARC)	
Date	1963	1969	1972	1983	1977	1995	2006	1999	2023	(2028)
Proton Kinetic Energy (GeV)	20.6	20.6	26	19	350	450	400	12	30	(30)
Protons per Cycle (10^{12})	0.7	0.6	5	5	10	36	48	6	153	(330)
Cycle Time (s)	3	2.3	-	-	-	14.4	6	2.2	1.36	(1.16)
Beam Power (kW)	0.8	0.9	-	-	-	180	510	5	540	(1300)
Target	-	-	-	-	-	Be	Graphite	Al	Graphite	(Graphite)
Target Length (cm)	-	-	-	-	-	290	130	66	91	(91)
Secondary Focussing	1-horn WBB	3-horn WBB	2-horn WBB	bare target	2-horn WBB	2-horn WBB	2-horn WBB	2-horn WBB	3-horn off-axis	(3-horn off-axis)
Decay Pipe Length (m)	-	-	-	-	-	110	1090	200	96	(96)
$\langle E_\nu \rangle$ (GeV)	1.5	1.5	1.5	1	20	24.3	17	1.3	0.6	(0.6)
Experiments	HLBC, Spark Ch.	HLBC, Spark Ch.	GGM, Aachen-Padova	CDHS, CHARM	GGM,CDHS, CHARM, BEBC	NOMAD, CHORUS	OPERA, ICARUS	K2K	T2K	Hyper-K

	Main Ring (Fermilab)					Booster (Fermilab)	Main Injector (Fermilab)			
Date	1974	1979	1976	1991	1998	2002, (2022)	2005	2017	2021	(2031)
Proton Kinetic Energy (GeV)	300	400	350	800	800	8	120	120	120	(60 – 120)
Protons per Cycle (10^{12})	10	10	13	10	12	4.5	37	54	55 (65)	(75)
Cycle Time (s)	-	-	-	60	60	0.2	2	1.333	1.2	(1.2)
Beam Power (kW)	-	-	-	20	25	29	350	720	840 (1000)	(1200)
Target	-	-	-	-	BeO	Be	Graphite	Graphite	Graphite	(Graphite)
Target Length (cm)	-	-	-	-	31	71	95	120	120	(150-180)
Secondary Focussing	dichromatic NBB	2-horn WBB	1-horn WBB	quad trip.	SSQT WBB	1-horn WBB	2-horn WBB	2-horn off-axis	2-horn off-axis	(3-horn WBB)
Decay Pipe Length (m)	400	400	400	400	400	50	675	675	675	(220)
$\langle E_\nu \rangle$ (GeV)	50,180†	25	100	90,260	70,180	1	3-20‡	2	2	(2.5)
Experiments	CITF, HPWF, 15' BC	15' BC	HPWF 15' BC	15' BC, CCFRR	NuTeV	MiniBooNE, SciBooNE, MicroBooNE, (SBND,ICARUS)	MINOS, MINERνA	NOνA, MINERνA, MINOS+	NOνA	DUNE

†Pion and kaon peaks in the momentum-selected channel.

‡Tunable WBB energy spectrum.

34. Passage of Particles Through Matter

Revised August 2023 by D.E. Groom (LBNL) and S.R. Klein (NSD LBNL; UC Berkeley).

34.1 Notation . . . 586
34.2 Electronic energy loss by heavy particles . . . 586
34.2.1 Moments and cross sections . . . 586
34.2.2 Maximum energy transfer to an electron in a single collision . . . 587
34.2.3 Stopping power at intermediate energies . . . 587
34.2.4 Mean excitation energy . . . 587
34.2.5 Density effect . . . 587
34.2.6 Energy loss at low energies . . . 588
34.2.7 Energetic knock-on electrons (δ rays) . . . 590
34.2.8 Restricted energy loss rates for relativistic ionizing particles . . . 590
34.2.9 Fluctuations in energy loss . . . 590
34.2.10 Energy loss in mixtures and compounds . . . 591
34.2.11 Ionization yields . . . 591
34.3 Multiple scattering through small angles . . . 591
34.4 Photon and electron interactions in matter . . . 592
34.4.1 Collision energy losses by $e^{\pm}$ . . . 592
34.4.2 Radiation length . . . 593
34.4.3 Bremsstrahlung energy loss by $e^{\pm}$ . . . 593
34.4.4 Critical energy . . . 594
34.4.5 Energy loss by photons . . . 594
34.4.6 Bremsstrahlung and pair production at very high energies . . . 595
34.4.7 Photonuclear and electronuclear interactions at still higher energies . . . 596
34.5 Electromagnetic cascades . . . 596
34.6 Muon energy loss at high energy . . . 597
34.7 Cherenkov and transition radiation . . . 598
34.7.1 Optical Cherenkov radiation . . . 598
34.7.2 Coherent radio Cherenkov radiation . . . 599
34.7.3 Transition radiation . . . 599

This review covers the interactions of photons and electrically charged particles in matter, concentrating on energies of interest for high-energy physics and astrophysics and processes of interest for particle detectors (ionization, Cherenkov radiation, transition radiation). Much of the focus is on particles heavier than electrons ($\pi^{\pm}$, p, etc.). Although the charge number z of the projectile is included in the equations, only $z = 1$ is discussed in detail. Muon radiative losses are discussed, as are photon/electron interactions at high to ultrahigh energies. Neutrons are not discussed.

34.1 Notation

The notation and important numerical values are shown in Table 34.1.

Table 34.1: Summary of variables used in this section. The kinematic variables β and γ have their usual relativistic meanings.

Symb.	Definition	Value or (usual) units
$m_e c^2$	electron mass $\times\, c^2$	0.510 998 950 00(15) MeV
r_e	classical electron radius $e^2/4\pi\epsilon_0 m_e c^2$	2.817 940 3227(19) fm
α	fine structure constant $e^2/4\pi\epsilon_0\hbar c$	1/137.035 999 139(31)
N_A	Avogadro's number	$6.022\,140\,76 \times 10^{23}$ mol^{-1}
ρ	density	g cm^{-3}
x	mass per unit area	g cm^{-2}
M	incident particle mass	MeV/c^2
E	incident part. energy γMc^2	MeV
T	kinetic energy, $(\gamma - 1)Mc^2$	MeV
W	energy transfer to an electron in a single collision	MeV
$W_{\max}$	Maximum possible energy transfer to an electron in a single collision	MeV
k	bremsstrahlung photon energy	MeV
z	charge number of incident particle	
Z	atomic number of absorber	
A	atomic mass of absorber	g mol^{-1}
K	$4\pi N_A r_e^2 m_e c^2$ (Coefficient for dE/dx)	0.307 075 MeV mol^{-1} cm^2
I	mean excitation energy	eV (*Nota bene!*)
$\delta(\beta\gamma)$	density effect correction to ionization energy loss	
$\hbar\omega_p$	plasma energy $\sqrt{4\pi N_e r_e^3}\; m_e c^2/\alpha$	$\sqrt{\rho\,\langle Z/A\rangle} \times 28.816$ eV, $\hookrightarrow \rho$ in g cm^{-3}
N_e	electron density	(units of r_e)$^{-3}$
w_j	weight fraction of the jth element in a compound or mixt.	
n_j	$\propto$ number of jth kind of atoms in a compound or mixture	
X_0	radiation length	g cm^{-2}
E_c	critical energy for electrons	MeV
$E_{\mu c}$	critical energy for muons	GeV
E_s	scale energy $\sqrt{4\pi/\alpha}\; m_e c^2$	21.2052 MeV
R_M	Molière radius	g cm^{-2}

34.2 Electronic energy loss by heavy particles

34.2.1 *Moments and cross sections*

The electronic interactions of fast charged particles with speed $v = \beta c$ occur in *single collisions with energy losses* W [1], leading to ionization, atomic, or collective excitation. Most frequently the energy losses are small (for 90% of all collisions the energy losses are less than 100 eV). In thin absorbers few collisions will take place and the total energy loss will show a large variance [1]; also see Sec. 34.2.9 below. For particles with charge ze more massive than electrons ("heavy" particles), scattering from free electrons is adequately described by the Rutherford differential cross section [2, 3].

$$\frac{d\sigma_R(W;\beta)}{dW} = \frac{2\pi r_e^2 m_e c^2 z^2}{\beta^2}\,\frac{(1-\beta^2 W/W_{\max})}{W^2}\ , \qquad (34.1)$$

where $W_{\max}$, the maximum energy transfer possible in a single collision, is discussed below. It differs from the classical cross section by the factor $(1 - \beta^2 W/W\max)$, which arises when the spin of the target electrons is taken into account.

Bethe's original theory applied only to energies above which atomic effects are not important. The free-electron cross section (Eq. (34.1)) was used to extend the cross section to $W_{\max}$. This free-electron approximation is not valid if W is not large compared to electron binding energies. For this energy regime Bethe [4, 5] used "Born Theorie" to obtain the differential cross section

$$\frac{d\sigma_B(W;\beta)}{dW} = \frac{d\sigma_R(W,\beta)}{dW} B(W)\ . \qquad (34.2)$$

Electronic binding is accounted for by the correction factor $B(W)$. Examples of $B(W)$ and $d\sigma_B/dW$ can be seen in Figs. 5 and 6 of Ref. [1]. For a given material, the correction results in introducing an *effective ionization energy* I "which is a geometric average of the excitation energies of the medium weighed by the corresponding oscillator strength." [6]. The nontrivial task of finding these values is discussed in Sec. 34.2.4.

At high energies the stopping power is further modified by polarization of the medium, and this "density effect," discussed in Sec. 34.2.5, must also be included.

The mean number of collisions with energy loss between W and $W + dW$ occurring in a distance δx is $N_e \delta x\,(d\sigma/dW)dW$, where $d\sigma(W;\beta)/dW$, where the cross section is the Rutherford formula if free electrons can be assumed and the Bethe form where binding energy is important. It is convenient to define the moments

$$M_j(\beta) = N_e\,\delta x \int W^j\,\frac{d\sigma(W;\beta)}{dW}dW\ , \qquad (34.3)$$

so that M_0 is the mean number of collisions in δx, M_1 is the

Int. J. Mod. Phys. A
Downloaded from www.worldscientific.com
by UNIVERSITY OF CALIFORNIA @ BERKE
use and distribution is strictly not permitted, except for Open Access articles.

Int. J. Mod. Phys. A 2026.41. Downloaded from www.worldscientific.com
by UNIVERSITY OF CALIFORNIA @ BERKELEY on 09/16/26. Re-use and distribution is strictly not permitted, except for Open Access articles.

mean energy loss in δx, $(M_2 - M_1)^2$ is the variance, *etc.* The number of collisions is Poisson-distributed with mean M_0. N_e is either measured in electrons/g ($N_e = N_A Z/A$) or electrons/cm^3 ($N_e = N_A\,\rho Z/A$). The former is used throughout this chapter, since quantities of interest (dE/dx, X_0, *etc.*) vary smoothly with composition when there is no density dependence.

34.2.2 *Maximum energy transfer to an electron in a single collision*

For a point-like particle with mass $M >> m_e$,

$$W_{\max} = \frac{2m_e c^2\,\beta^2\gamma^2}{1 + 2\gamma m_e/M + (m_e/M)^2}\ . \tag{34.4}$$

In older references [2, 9] the "low-energy" approximation $W_{\max} = 2m_e c^2\,\beta^2\gamma^2$, valid for $2\gamma m_e \ll M$, is often implicit. For a pion in copper, the error thus introduced into dE/dx is greater than 6% at 100 GeV. For $2\gamma m_e \gg M$, $W_{\max} = Mc^2\,\beta^2\gamma$.

At energies of order 100 GeV, the maximum 4-momentum transfer to the electron can exceed 1 GeV/c, where hadronic structure effects modify the cross sections. This problem has been investigated by J.D. Jackson [10], who concluded that for incident hadrons (but not for large nuclei) corrections to dE/dx are negligible below energies where radiative effects dominate. While the cross section for rare hard collisions is modified, the average stopping power, dominated by many softer collisions, is almost unchanged.

34.2.3 *Stopping power at intermediate energies*

The mean rate of energy loss by moderately relativistic charged heavy particles is well described by the "Bethe equation" [2,4,5,9],

$$\left\langle -\frac{dE}{dx} \right\rangle = Kz^2 \frac{Z}{A}\frac{1}{\beta^2}\left[\frac{1}{2}\ln\frac{2m_e c^2\beta^2\gamma^2 W_{\max}}{I^2} - \beta^2 - \frac{\delta(\beta\gamma)}{2}\right]. \tag{34.5}$$

Eq. (34.5) is valid in the region $0.1 \lesssim \beta\gamma \lesssim 1000$ with an accuracy of a few percent. At $\beta\gamma \sim 0.1$ the projectile speed is comparable to atomic electron "speed," and at $\beta\gamma \sim 1000$ radiative effects begin to be important (Sec. 34.6). Both limits are Z dependent. A minor dependence on M at high energies is introduced through $W_{\max}$, but for all practical purposes the stopping power in a given material is a function of β alone. Small corrections are discussed in Sec. 34.2.6.[1,2]

This is the *mass stopping power*; with the symbol definitions and values given in Table 34.1, the units are MeV g^{-1}cm^2. As can be seen from Fig. 34.2, dE/dx defined in this way is about the same for most materials, decreasing slowly with Z. The *linear stopping power*, in MeV/cm, is $\rho\,dE/dx$, where ρ is the density in g/cm^3.

The stopping power at first falls as $1/\beta^\alpha$ where $\alpha \approx 1.7$–1.5, decreasing with increasing Z, and reaches a broad minimum at $\beta\gamma = 3.8$–3.0 as Z rises from 6 to 82. It then inexorably rises as the argument of the logarithmic term increases. Two independent mechanisms contribute. Two thirds of the rise is produced by the explicit $\beta^2\gamma^2$ dependence through the relativistic flattening and extension of the particle's electric field. Rather than producing ionization at greater and greater distances, the field polarizes the medium, cancelling the increase in the logarithmic term at high energies. This is taken into account by the density-effect correction $\delta(\beta\gamma)$. The other third is introduced by the $\beta^2\gamma$ dependence of $W_{\max}$, the maximum possible energy transfer to a recoil electron. "Hard collision" events increasingly extend the tail of the energy loss distribution, increasing the mean but with little effect on the position of the maximum, the most probable energy loss.

Few concepts in high-energy physics are as misused as dE/dx, since the mean is weighted by rare events with large single-collision energy losses. Even with samples of hundreds of events in a typical detector, the mean energy loss cannot be obtained dependably. Far better and more easily measured is the most probable energy loss, discussed in Sec. 34.2.9. The most probable energy loss in a typical detector is considerably smaller than the mean given by the Bethe equation. It does not continue to rise with the mean stopping power, but approaches a "Fermi plateau."

In analysing TPC data (Sec. 35.6.4), the same end is often accomplished by using a restricted energy loss, the mean of 50%–70% of the samples with the smallest signals as the estimator.

Although it must be used with cautions and caveats, dE/dx as described in Eq. (34.5) still forms the basis of much of our understanding of energy loss by charged particles. Extensive tables are available [6, 7] and `pdg.lbl.gov/current/AtomicNuclearProperties/`.

For heavy projectiles, like ions, additional terms are required to account for higher-order photon coupling to the target, and to account for the finite target radius. These can change dE/dx by a factor of two or more for the heaviest nuclei in certain kinematic regimes [11].

The function as computed for muons on copper is shown as the "Bethe" region of Fig. 34.1. Mean energy loss behavior below this region is discussed in Sec. 34.2.6, and the radiative effects at high energy are discussed in Sec. 34.6. Only in the Bethe region is it a function of β alone; the mass dependence is more complicated elsewhere. The stopping power in several other materials is shown in Fig. 34.2. Except in hydrogen, particles with the same speed have similar rates of energy loss in different materials, although there is a slow decrease in the rate of energy loss with increasing Z. The qualitative behavior difference at high energies between a gas (He in the figure) and the other materials shown in the figure is due to the density-effect correction, $\delta(\beta\gamma)$, discussed in Sec. 34.2.5. The stopping power functions are characterized by broad minima whose position drops from $\beta\gamma = 3.5$ to 3.0 as Z goes from 7 to 100. The values of minimum ionization as a function of atomic number are shown in Fig. 34.3.

In practical cases, most relativistic particles (*e.g.*, cosmic-ray muons) have mean energy loss rates close to the minimum; they are "minimum-ionizing particles," or mip's.

Eq. (34.5) may be integrated to find the total (or partial) "continuous slowing-down approximation" (CSDA) range R for a particle which loses energy only through ionization and atomic excitation. Since dE/dx depends only on β, R/M is a function of E/M or pc/M. In practice, range is a useful concept only for low-energy hadrons ($R \lesssim \lambda_I$, where λ_I is the nuclear interaction length), and for muons below a few hundred GeV (above which radiative effects dominate). Fig. 34.4 shows R/M as a function of $\beta\gamma$ ($= p/Mc$) for a variety of materials.

The mass scaling of dE/dx and range is valid for the electronic losses described by the Bethe equation, but not for radiative losses.

34.2.4 *Mean excitation energy*

"The determination of the mean excitation energy is the principal non-trivial task in the evaluation of the Bethe stopping-power formula" [15]. Recommended values have varied substantially with time. Estimates based on experimental stopping-power measurements for protons, deuterons, and alpha particles and on oscillator-strength distributions and dielectric-response functions were given in ICRU 49 [6]. See also ICRU 37 [12]. These values, shown in Fig. 34.5, have since been widely used. Machine-readable versions can also be found [16].

34.2.5 *Density effect*

As the particle energy increases, its electric field flattens and extends, so that the distant-collision contribution to the logarithmic term in Eq. (34.5) increases as $\beta^2\gamma^2$. However, real media become polarized, limiting the field extension and effectively truncating this part of the logarithmic rise [2,3,6,17,18]. At very high energies,

$$\delta(\beta\gamma)/2 \to \ln(\hbar\omega_p/I) + \ln\beta\gamma - 1/2\ , \tag{34.6}$$

where $\delta(\beta\gamma)/2$ is the density effect correction introduced in Eq. (34.5) and $\hbar\omega_p$ is the plasma energy defined in Table 34.1. A comparison with Eq. (34.5) shows that dE/dx then grows as $\ln T_{\max}$ rather than $\ln\beta^2\gamma^2 T_{\max}$, and that the mean excitation

[1] For incident spin 1/2 particles, $(W_{\max}/E)^2/4$ is included in the square brackets. Although this correction is within the uncertainties in the total stopping power, its inclusion avoids a systematic bias.

[2] In this section, "dE/dx" will be understood to mean the mass stopping power "$\langle -dE/dx\rangle$."

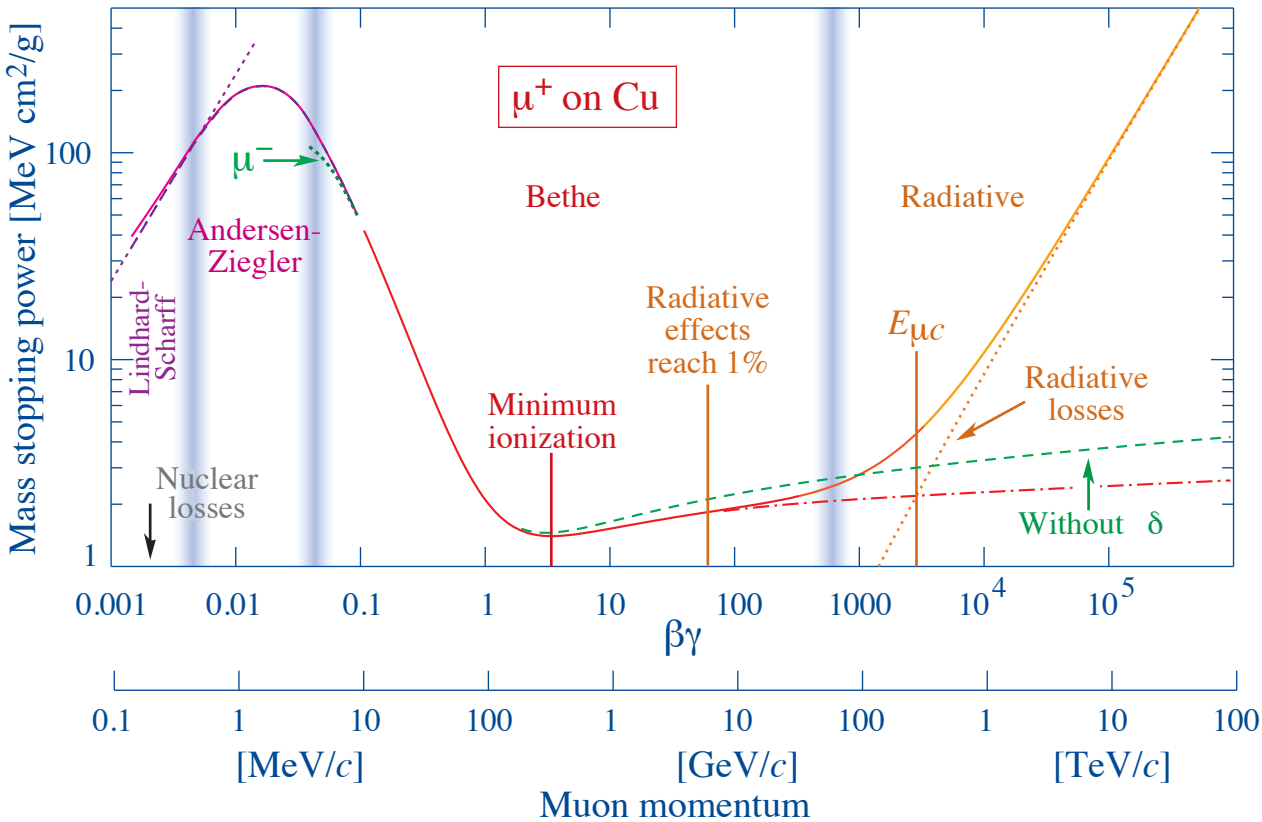

Figure 34.1: Mass stopping power (dE/dx) for positive muons in copper as a function of $\beta\gamma = p/Mc$ over nine orders of magnitude in momentum (12 orders of magnitude in kinetic energy). Solid curves indicate the total stopping power. Data below the break at $\beta\gamma \approx 0.1$ are taken from ICRU 49 [6] assuming only β dependence, and data at higher energies are from [7]. Vertical bands indicate boundaries between different approximations discussed in the text. The short dotted lines labeled "μ^-" illustrate the "Barkas effect," the dependence of stopping power on projectile charge at very low energies [8]. dE/dx in the radiative region is not simply a function of β.

energy I is replaced by the plasma energy $\hbar\omega_p$. An example of the ionization stopping power as calculated with and without the density effect correction is shown in Fig. 34.1. Since the plasma frequency scales as the square root of the electron density, the correction is much larger for a liquid or solid than for a gas, as is illustrated in Fig. 34.2.

The density effect correction is usually computed using Sternheimer's parameterization [17]:

$$\delta(\beta\gamma) = \begin{cases} 2(\ln 10)x - \overline{C} & \text{if } x \geq x_1; \\ 2(\ln 10)x - \overline{C} + a(x_1 - x)^k & \text{if } x_0 \leq x < x_1; \\ 0 & \text{if } x < x_0 \text{ (nonconductors)}; \\ \delta_0 10^{2(x-x_0)} & \text{if } x < x_0 \text{ (conductors)} \end{cases} \tag{34.7}$$

Here $x = \log_{10}\beta\gamma = \log_{10}(p/Mc)$. $\overline{C}$ (the negative of the C used in Ref. [17]) is obtained by equating the high-energy case of Eq. (34.7) with the limit given in Eq. (34.6). The other parameters are adjusted to give a best fit to the results of detailed calculations for momenta below $Mc\exp(x_1)$. For nonconductors the correction is 0 below $\beta\gamma = 10^{x_0}$, corresponding to 100–200 MeV for pions and 1–2 GeV for protons. For conductors it decreases rapidly below this point. Parameters for the elements and nearly 200 compounds and mixtures of interest are published in a variety of places, notably in Ref. [18]. A recipe for finding the coefficients for nontabulated materials is given by Sternheimer and Peierls [19] and is summarized in Ref. [7].

The remaining relativistic rise comes from the $\beta^2\gamma$ growth of $W_{\max}$, which in turn is due to (rare) large energy transfers to a few electrons. When these events are excluded, the energy deposit in an absorbing layer approaches a constant value, the Fermi plateau (see Sec. 34.2.8 below). At even higher energies (*e.g.*, > 332 GeV for muons in iron, and at a considerably higher energy for protons in iron), radiative effects are more important than ionization losses. These are especially relevant for high-energy muons, as discussed in Sec. 34.6.

34.2.6 *Energy loss at low energies*

The theory of energy loss by ionization and excitation as given by Bethe is based on a first-order Born approximation. It assumes free electrons, and should be valid when the projectile's speed is large compared to that of the atomic electrons. This presents a problem at low energies, where $W_{\max}$ is less than the K shell binding energy. However, Mott showed that the Born approximation can be applied at energies much smaller than atomic binding energies [20]; the incident particle can be treated by classical mechanics since its wavelength is shorter than atomic dimensions. The Born method is actually better justified when its speed is not large compared to the K electron speed [5].

Higher-order corrections must still be made to extend the Bethe equation (Eq. (34.5)) to low energies. An improved approximation for the terms in the square brackets of Eq. (34.5) at low energies is obtained with

$$L(\beta) = L_a(\beta) - \frac{C(\beta)}{Z} + zL_1(\beta) + z^2L_2(\beta)\ . \tag{34.8}$$

Here L_a is the square-bracketed terms of Eq. (34.5), C/Z is the sum of shell corrections and zL_1 and z^2L_2 are Barkas and Bloch correction terms [6, 21]. With these corrections, the Bethe treatment is accurate to about 1% down to $\beta \approx 0.05$, or about 1 MeV for protons (0.13 MeV for muons). Values of L_a, C/Z, L_1, and L_2 in the range $T = 0.3$–30 MeV for a proton traversing aluminum can be found in Table I of Ref. [21].

Shell correction $-C/Z$. As the speed of the projectile decreases, the contribution to the stopping power from K shell electrons decreases, and at even lower velocities contributions from L and

Downloaded from www.worldscientific.com
Int. J. Mod. use and distribution is strictly not permitted, except for Open Access articles.
by UNIVERSITY OF CALIFORNIA @ BERKE

Int. J. Mod. Phys. A 2026.41. Downloaded from www.worldscientific.com
by UNIVERSITY OF CALIFORNIA @ BERKELEY on 09/16/26. Re-use and distribution is strictly not permitted, except for Open Access articles.

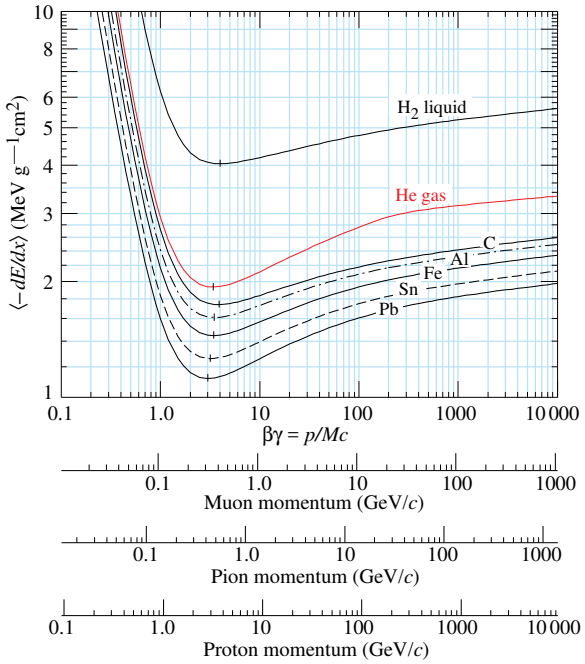

Figure 34.2: Mean energy loss rate in liquid (bubble chamber) hydrogen, gaseous helium, carbon, aluminum, iron, tin, and lead. Radiative effects, relevant for muons and pions, are not included. These become significant for muons in iron for $\beta\gamma \gtrsim 1000$, and at lower momenta for muons in higher-Z absorbers. See Fig. 34.23.

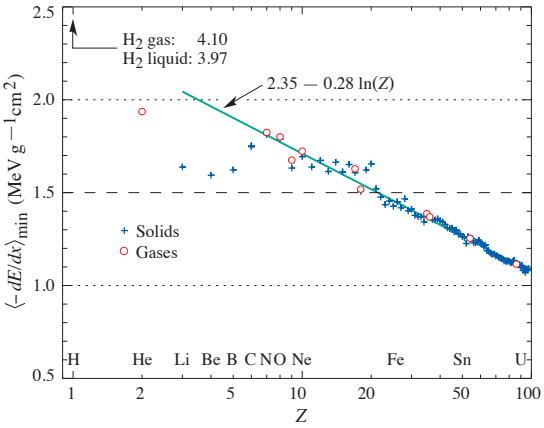

Figure 34.3: Mass stopping power at minimum ionization for the chemical elements. The straight line is fitted for $Z > 6$. A simple functional dependence on Z is not to be expected, since dE/dx also depends on other variables.

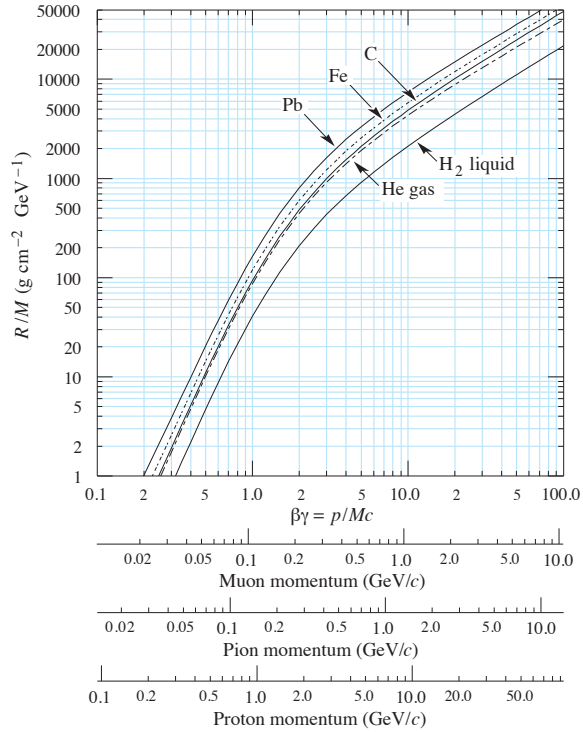

Figure 34.4: Range of heavy charged particles in liquid (bubble chamber) hydrogen, helium gas, carbon, iron, and lead. For example: For a K^+ whose momentum is 700 MeV/c, $\beta\gamma = 1.42$. For lead we read $R/M \approx 396$, and so the range is 195 g cm^{-2} (17 cm).

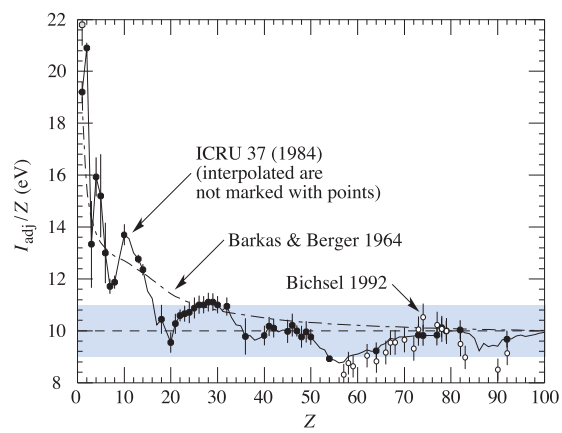

Figure 34.5: Mean excitation energies (divided by Z) as adopted by the ICRU [12]. Those based on experimental measurements are shown by symbols with error flags; the interpolated values are simply joined. The grey point is for liquid H_2; the black point at 19.2 eV is for H_2 gas. The open circles show more recent determinations by Bichsel [13]. The dash-dotted curve is from the approximate formula of Barkas [14] used in early editions of this *Review*.

higher shells further reduce it. The correction $(C_{\rm K} + C_{\rm L} + \ldots)/Z$ is should be included in the square brackets of Eq. (34.5). It is calculated and tabulated (for a few common materials) in a number of places; Refs. [6, 12, 21] are especially useful. As an example, the shell correction for a 30 MeV proton traversing aluminum is 0.6%, increasing to 9.9% as the proton's energy decreases to 0.3 MeV.

Barkas correction zL_1. Qualitatively, one might imagine an atom's electron cloud slightly recoiling at the approach of a negative projectile and being attracted toward an approaching positive projectile. Hence the stopping power for negative particles should be slightly smaller than the stopping power for positive particles. In a 1956 paper, Barkas *et al.* noted that negative pions possibly had a longer range than positive pions [8]. The effect has been measured for a number of negative/positive particle pairs, and more recently in detailed studies with antiprotons at the CERN LEAR facility [22]. Since no complete theory exists, an empirical approach is necessary. A 1972 harmonic-oscillator model by Ashley *et al.* [23] is often used; it has two parameters determined by experimental data. For protons in aluminum, L_1/L_a is less than 0.1% at 30 MeV, but increases to 17% as T decreases to 0.3 MeV. This correction is indicated in Fig. 34.1.

Bloch correction z^2L_2. Bloch's extension of Bethe's theory introduced a low-energy correction that takes account of perturbations of the atomic wave functions. The form obtained by Lindhard and Sørensen [11] is used *e.g.* in Refs. [6, 21]. For protons in aluminum, $-L_2/L_|$ is less than 0.3% at 3.0 MeV, but rises to 7% when the energy has fallen to 0.3 MeV.

Int. J. Mod. Phys. Lett. A 2014.78:1-10. Downloaded from www.worldscientific.com
by UNIVERSITY OF CALIFORNIA @ BERKE use and distribution is strictly not permitted, except for Open Access articles.

For the interval $0.01 < \beta < 0.05$ there is no satisfactory theory. For protons, one usually relies on the phenomenological fitting formulae developed by Andersen and Ziegler [6,24]. As tabulated in ICRU 49 [6], the nuclear plus electronic proton stopping power in copper is 113 MeV cm^2 g^{-1} at $T = 10$ keV ($\beta\gamma = 0.005$), rises to a maximum of 210 MeV cm^2 g^{-1} at $T \approx 120$ keV ($\beta\gamma = 0.016$), then falls to 118 MeV cm^2 g^{-1} at $T = 1$ MeV ($\beta\gamma = 0.046$). Above 0.5–1.0 MeV the corrected Bethe theory is adequate.

For particles moving more slowly than $\approx 0.01c$ (more or less the speed of the outer atomic electrons), Lindhard has been quite successful in describing electronic stopping power, which is proportional to β [25]. Finally, we note that at even lower energies, *e.g.*, for protons of less than several hundred eV, non-ionizing nuclear recoil energy loss dominates the total energy loss [6,25,26].

34.2.7 *Energetic knock-on electrons (δ rays)*

The distribution of secondary electrons with kinetic energies $T \gg I$ is [2]

$$\frac{d^2N}{dTdx} = \frac{1}{2}\,Kz^2\frac{Z}{A}\,\frac{1}{\beta^2}\,\frac{F(T)}{T^2} \tag{34.9}$$

for $I \ll T \le W_{\max}$, where $W_{\max}$ is given by Eq. (34.4). Here β is the speed of the primary particle. The factor F is spin-dependent, but is about unity for $T \ll W_{\max}$. For spin-0 particles $F(T) = (1-\beta^2 T/W_{\max})$; forms for spins 1/2 and 1 are also given by Rossi [2] (Sec. 2.3, Eqs. 7 and 8). Additional formulae are given in [27]. Equation Eq. (34.9) is inaccurate for T close to I [28].

δ rays of even modest energy are rare. For a $\beta \approx 1$ particle, for example, on average only one collision with $T_e > 10$ keV will occur along a path length of 90 cm of argon gas [1].

A δ ray with kinetic energy T_e and corresponding momentum p_e is produced at an angle θ given by

$$\cos\theta = (T_e/p_e)(p_{\max}/W_{\max})\ , \tag{34.10}$$

where $p_{\max}$ is the momentum of an electron with the maximum possible energy transfer $W_{\max}$.

34.2.8 *Restricted energy loss rates for relativistic ionizing particles*

Further insight can be obtained by examining the mean energy deposit by an ionizing particle when energy transfers are restricted to $T \le W_{\rm cut} \le W_{\max}$. The restricted energy loss rate is

$$-\frac{dE}{dx}\bigg|_{T<W_{\rm cut}} = Kz^2\frac{Z}{A}\frac{1}{\beta^2}\left[\frac{1}{2}\ln\frac{2m_ec^2\beta^2\gamma^2W_{\rm cut}}{I^2} - \frac{\beta^2}{2}\left(1+\frac{W_{\rm cut}}{W_{\max}}\right) - \frac{\delta}{2}\right]. \tag{34.11}$$

This form approaches the normal Bethe function (Eq. (34.5)) as $W_{\rm cut} \to W_{\max}$. It can be verified that the difference between Eq. (34.5) and Eq. (34.11) is equal to $\int_{W_{\rm cut}}^{W_{\max}} T(d^2N/dTdx)dT$, where $d^2N/dTdx$ is given by Eq. (34.9).

Since $W_{\rm cut}$ replaces $W_{\max}$ in the argument of the logarithmic term of Eq. (34.5), the $\beta\gamma$ term producing the relativistic rise in the close-collision part of dE/dx is replaced by a constant, and $|dE/dx|_{T<W_{\rm cut}}$ approaches the constant "Fermi plateau." (The density effect correction δ eliminates the explicit $\beta\gamma$ dependence produced by the distant-collision contribution.) This behavior is illustrated in Fig. 34.6, where restricted loss rates for two examples of $W_{\rm cut}$ are shown in comparison with the full Bethe dE/dx and the Landau-Vavilov most probable energy loss (to be discussed in Sec. 34.2.9 below).

"Restricted energy loss" is cut at the total mean energy, not the single-collision energy above $W_{\rm cut}$ It is of limited use. The most probable energy loss, discussed in the next Section, is far more useful in situations where single-particle energy loss is observed.

34.2.9 *Fluctuations in energy loss*

For detectors of moderate thickness x (*e.g.* scintillators or LAr cells),[3] the energy loss probability distribution $f(\Delta;\beta\gamma,x)$ is adequately described by the highly-skewed Landau (or Landau-Vavilov) distribution [29,30].

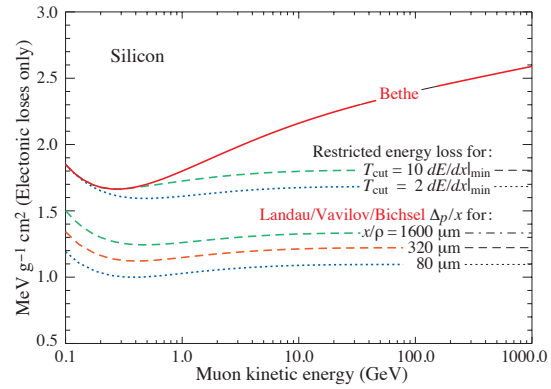

Figure 34.6: Bethe dE/dx, two examples of restricted energy loss, and the Landau most probable energy per unit thickness in silicon. The change of $\Delta_{\rm p}$/x with thickness x illustrates its $a\ln x + b$ dependence. Minimum ionization ($dE/dx|_{\rm min}$) is 1.664 MeV g^{-1} cm^2. Radiative losses are excluded. The incident particles are muons.

The most probable energy loss is [31][4]

$$\Delta_p = \xi\left[\ln\frac{2m_ec^2\beta^2\gamma^2}{I} + \ln\frac{\xi}{I} + j - \beta^2 - \delta(\beta\gamma)\right]\ , \tag{34.12}$$

where $\xi = (K/2)\,\langle Z/A\rangle\, z^2(x/\beta^2)$ MeV for a detector with a thickness x in g cm^{-2}, and $j = 0.200$ [31].[5] While dE/dx is independent of thickness, Δ_p/x scales as $a\ln x + b$. The density correction $\delta(\beta\gamma)$ was not included in Landau's or Vavilov's work, but it was later included by Bichsel [31]. The high-energy behavior of $\delta(\beta\gamma)$ (Eq. (34.6)) is such that

$$\Delta_p \underset{\beta\gamma\gtrsim 100}{\longrightarrow} \xi\left[\ln\frac{2m_ec^2\xi}{(\hbar\omega_p)^2} + j\right]\ . \tag{34.13}$$

Thus the Landau-Vavilov most probable energy loss, like the restricted energy loss, reaches a Fermi plateau. The Bethe dE/dx and Landau-Vavilov-Bichsel Δ_p/x in silicon are shown as a function of muon energy in Fig. 34.6. The energy deposit in the 1600 μm case is roughly the same as in a 3 mm thick plastic scintillator.

The distribution function for the energy deposit by a 10 GeV muon going through a detector of about this thickness is shown in Fig. 34.7. In this case the most probable energy loss is 62% of the mean ($M_1(\langle\Delta\rangle)/M_1(\infty)$). Folding in experimental resolution displaces the peak of the distribution, usually toward a higher value. 90% of the collisions ($M_1(\langle\Delta\rangle)/M_1(\infty)$) contribute to energy deposits below the mean. It is the very rare high-energy-transfer collisions, extending to $W_{\max}$ at several GeV, that drives the mean into the tail of the distribution. The large weight of these rare events makes the mean of an experimental distribution consisting of a few hundred events subject to large fluctuations and sensitive to cuts. *The mean of the energy loss given by the Bethe equation, Eq. (34.5), is thus ill-defined experimentally and is not useful for describing energy loss by single particles.*[6] It rises as $\ln\gamma$ because $W_{\max}$ increases as γ at high energies. *The most probable energy loss should be used.*

A practical example: For muons traversing 0.25 inches (0.64 cm) of PVT (polyvinyltolulene) based plastic scintillator,

[3] "Moderate thickness" means $G \lesssim 0.05$–0.1, where G is given by Rossi Ref. [2], Eq. 2.7(10). It is Vavilov's κ [29]. G is proportional to the absorber's thickness, and as such parameterizes the constants describing the Landau distribution. These are fairly insensitive to thickness for $G \lesssim 0.1$, the case for most detectors.

[4] Practical calculations can be expedited by using the tables of δ and β from the text versions of the muon energy loss tables to be found at `pdg.lbl.gov/curremt/AtomicNuclearProperties`.

[5] Rossi [2], Talman [32], and others give somewhat different values for j. The most probable loss is not sensitive to its value.

[6] It does find application in dosimetry, where only bulk deposit is relevant.

Int. J. Mod. Phys. A 2026.41. Downloaded from www.worldscientific.com
by UNIVERSITY OF CALIFORNIA @ BERKELEY on 09/16/26. Re-use and distribution is strictly not permitted, except for Open Access articles.

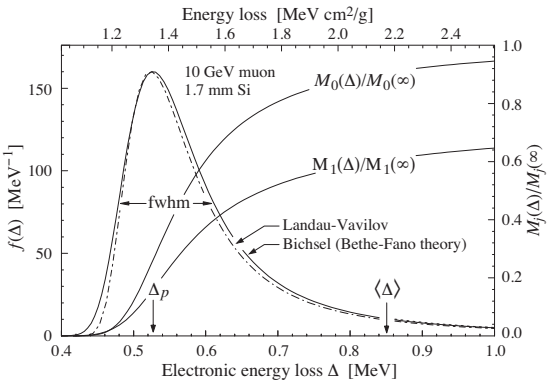

Figure 34.7: Electronic energy deposit distribution for a 10 GeV muon traversing 1.7 mm of silicon, the stopping power equivalent of about 0.3 cm of PVT-based scintillator [1, 13, 33]. The Landau-Vavilov function (dot-dashed) uses a Rutherford cross section without atomic binding corrections but with a kinetic energy transfer limit of $W_{\max}$. The solid curve was calculated using Bethe-Fano theory. $M_0(\Delta)$ and $M_1(\Delta)$ are the cumulative 0th moment (mean number of collisions) and 1st moment (mean energy loss) in crossing the silicon. (See Sec. 34.2.1). The fwhm of the Landau-Vavilov function is about 4ξ for detectors of moderate thickness. Δ_p is the most probable energy loss, and $\langle\Delta\rangle$ divided by the thickness is the Bethe dE/dx.

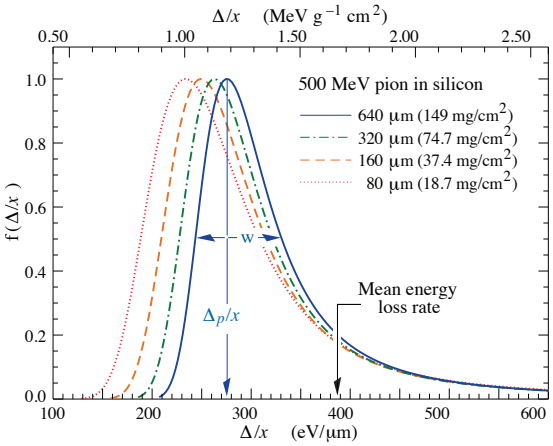

Figure 34.8: Straggling functions in silicon for 500 MeV pions, normalized to unity at the most probable value Δ_p/x. The width w is the full width at half maximum.

the ratio of the most probable E loss rate to the mean loss rate via the Bethe equation is $[0.69, 0.57, 0.49, 0.42, 0.38]$ for $T_\mu = [0.01, 0.1, 1, 10, 100]$ GeV. Radiative losses add less than 0.5% to the total mean energy deposit at 10 GeV, but add 7% at 100 GeV. The most probable E loss rate rises slightly beyond the minimum ionization energy, then is essentially constant.

The Landau distribution fails to describe energy loss in thin absorbers such as gas TPC cells [1] and Si detectors [31], as can be seen *e.g.* in Fig. 1 of Ref. [1] for an argon-filled TPC cell. Also see Talman [32]. While Δ_p/x may be calculated adequately with Eq. (34.12), the distributions are significantly wider than the Landau width $w = 4\xi$ Ref. [31], Fig. 15. Examples for 500 MeV pions incident on thin silicon detectors are shown in Fig. 34.8. For very thick absorbers the distribution is less skewed but never approaches a Gaussian.

The most probable energy loss, scaled to the mean loss at minimum ionization, is shown in Fig. 34.9 for several silicon detector thicknesses.

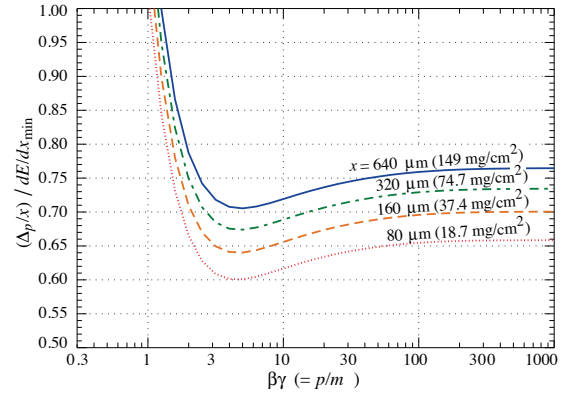

Figure 34.9: Most probable energy loss in silicon, scaled to the mean loss of a minimum ionizing particle, 388 eV/μm (1.66 MeV g^{-1}cm^2).

34.2.10 *Energy loss in mixtures and compounds*

A mixture or compound can be thought of as made up of thin layers of pure elements in the right proportion (Bragg additivity). In this case,

$$\left\langle \frac{dE}{dx} \right\rangle = \sum w_j \left\langle \frac{dE}{dx} \right\rangle_j , \tag{34.14}$$

where $dE/dx|_j$ is the mean rate of energy loss (in MeV g cm^{-1}) in the jth element. Eq. (34.5) can be inserted into Eq. (34.14) to find expressions for $\langle Z/A\rangle$, $\langle I\rangle$, and $\langle\delta\rangle$; for example, $\langle Z/A\rangle = \sum w_j Z_j/A_j = \sum n_j Z_j / \sum n_j A_j$. However, $\langle I\rangle$ as defined this way is an underestimate, because in a compound electrons are more tightly bound than in the free elements, and $\langle\delta\rangle$ as calculated this way has little relevance, because it is the electron density that matters. If possible, one uses the tables given in Refs. [18, 34], or the recipes given in [19] (repeated in Ref. [7]), that include effective excitation energies and interpolation coefficients for calculating the density effect correction for the chemical elements and nearly 200 mixtures and compounds. Otherwise, use the recipe for δ given in Refs. [7, 19], and calculate $\langle I\rangle$ following the discussion in Ref. [15]. (Note the "13%" rule!)

34.2.11 *Ionization yields*

The Bethe equation describes energy loss via excitation and ionization. Many gaseous detectors (proportional counters or TPCs) or liquid ionization detectors count the number of electrons or positive ions from ionization, rather than the ionization energy. As a further complication, the electron liberated in the initial ionization often has enough energy to ionize other atoms or molecules; this process can happen several times. The number of electron-ion pairs per unit length is typically three or more times the original number. Ion or electron counting is a proxy for a direct dE/dx measurement. Calibrations link the number of observed ions to the traversing particle's dE/dx.

The details depend on the gases (or liquids) and the particular detector involved. A useful discussion of the physics is provided in Sec.35.6 of this Review.

34.3 Multiple scattering through small angles

A charged particle traversing a medium is deflected by many small-angle scatters. Most of this deflection is due to Coulomb scattering from nuclei as described by the Rutherford cross section. (However, for hadronic projectiles, the strong interactions also contribute to multiple scattering.) For many small-angle scatters the net scattering and displacement distributions are Gaussian via the central limit theorem. Less frequent "hard" scatters produce non-Gaussian tails. These Coulomb scattering distributions are well-represented by the theory of Molière [35]. Accessible discussions are given by Rossi [2] and Jackson [3], and exhaustive reviews have been published by Scott [36] and Motz *et al.* [37]. Experimental measurements have been published by Bichsel [38] (low energy protons) and by Shen *et al.* [39] (relativistic pions,

Int. J. Mod. Phys. A 2011.Downloaded from www.worldscientific.com
by UNIVERSITY OF CALIFORNIA @ BERKE use and distribution is strictly not permitted, except for Open Access articles.

kaons, and protons).[7]

If we define

$$\theta_0 = \theta^{\,\mathrm{rms}}_{\,\mathrm{plane}} = \frac{1}{\sqrt{2}}\,\theta^{\mathrm{rms}}_{\mathrm{space}}\,, \tag{34.15}$$

then it is sufficient for many applications to use a Gaussian approximation for the central 98% of the projected angular distribution, with an rms width given by Lynch & Dahl [40]:

$$\begin{aligned}\theta_0 &= \frac{13.6\ \mathrm{MeV}}{\beta cp}\, z\sqrt{\frac{x}{X_0}}\left[1+0.088\log_{10}\!\left(\frac{x\,z^2}{X_0\beta^2}\right)\right]\\ &= \frac{13.6\ \mathrm{MeV}}{\beta cp}\, z\sqrt{\frac{x}{X_0}}\left[1+0.038\ln\!\left(\frac{x\,z^2}{X_0\beta^2}\right)\right]\end{aligned} \tag{34.16}$$

Here p, βc, and z are the momentum, speed, and charge number of the incident particle, and x/X_0 is the thickness of the scattering medium in radiation lengths (defined below). This takes into account the p and z dependence quite well at small Z, but for large Z and small x the β-dependence is not well represented. Further improvements are discussed in Ref. [40].

Eq. (34.16) describes scattering from a single material, while the usual problem involves the multiple scattering of a particle traversing many different layers and mixtures. Since it is from a fit to a Molière distribution, it is incorrect to add the individual θ_0 contributions in quadrature; the result is systematically too small. It is much more accurate to apply Eq. (34.16) once, after finding x and X_0 for the combined scatterer.

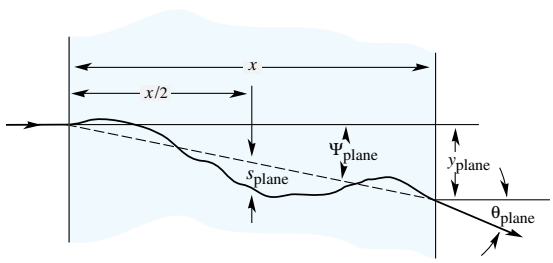

Figure 34.10: Quantities used to describe multiple Coulomb scattering. The particle is incident in the plane of the figure.

The nonprojected (space) and projected (plane) angular distributions are given approximately by [35]

$$\frac{1}{2\pi\,\theta_0^2}\,\exp\left(-\frac{\theta^2_{\mathrm{space}}}{2\theta_0^2}\right)\,d\Omega, \tag{34.17}$$

$$\frac{1}{\sqrt{2\pi}\,\theta_0}\,\exp\left(-\frac{\theta^2_{\mathrm{plane}}}{2\theta_0^2}\right)\,d\theta_{\mathrm{plane}}, \tag{34.18}$$

where θ is the deflection angle. In this approximation, $\theta^2_{\mathrm{space}} \approx (\theta^2_{\mathrm{plane},x} + \theta^2_{\mathrm{plane},y})$, where the x and y axes are orthogonal to the direction of motion, and $d\Omega \approx d\theta_{\mathrm{plane},x}\,d\theta_{\mathrm{plane},y}$. Deflections into $\theta_{\mathrm{plane},x}$ and $\theta_{\mathrm{plane},y}$ are independent and identically distributed. Fig. 34.10 shows these and other quantities sometimes used to describe multiple Coulomb scattering. They are

$$\psi^{\,\mathrm{rms}}_{\,\mathrm{plane}} = \frac{1}{\sqrt{3}}\,\theta^{\,\mathrm{rms}}_{\,\mathrm{plane}} = \frac{1}{\sqrt{3}}\,\theta_0, \tag{34.19}$$

$$y^{\,\mathrm{rms}}_{\,\mathrm{plane}} = \frac{1}{\sqrt{3}}\,x\,\theta^{\,\mathrm{rms}}_{\,\mathrm{plane}} = \frac{1}{\sqrt{3}}\,x\,\theta_0, \tag{34.20}$$

$$s^{\,\mathrm{rms}}_{\,\mathrm{plane}} = \frac{1}{4\sqrt{3}}\,x\,\theta^{\,\mathrm{rms}}_{\,\mathrm{plane}} = \frac{1}{4\sqrt{3}}\,x\,\theta_0. \tag{34.21}$$

All the quantitative estimates in this section apply only in the limit of small $\theta^{\,\mathrm{rms}}_{\,\mathrm{plane}}$ and in the absence of large-angle scatters. The random variables s, ψ, y, and θ in a given plane are correlated. Obviously, $y \approx x\psi$. In addition, y and θ have the correlation coefficient $\rho_{y\theta} = \sqrt{3}/2 \approx 0.87$. For Monte Carlo generation of a joint $(y_{\,\mathrm{plane}}, \theta_{\mathrm{plane}})$ distribution, or for other calculations, it may be most convenient to work with independent Gaussian random variables (z_1, z_2) with mean zero and variance one, and then set

$$y_{\mathrm{plane}} = z_1\,x\,\theta_0(1-\rho^2_{y\theta})^{1/2}/\sqrt{3} + z_2\,\rho_{y\theta}x\,\theta_0/\sqrt{3} \tag{34.22a}$$

$$= z_1\,x\,\theta_0/\sqrt{12} + z_2\,x\,\theta_0/2; \tag{34.22b}$$

$$\theta_{\mathrm{plane}} = z_2\,\theta_0. \tag{34.22c}$$

Note that the second term for $y_{\,\mathrm{plane}}$ equals $x\,\theta_{\mathrm{plane}}/2$ and represents the displacement that would have occurred had the deflection θ_{plane} all occurred at the single point $x/2$.

For heavy ions the multiple Coulomb scattering has been measured and compared with various theoretical distributions [41].

34.4 Photon and electron interactions in matter

At low energies electrons and positrons primarily lose energy by ionization, although other processes (Møller scattering, Bhabha scattering, e^+ annihilation) contribute, as shown in Fig. 34.11. While ionization loss rates rise logarithmically with energy, bremsstrahlung losses rise nearly linearly (fractional loss is nearly independent of energy), and dominates above the critical energy (Sec. 34.4.4 below), a few tens of MeV in most materials.

34.4.1 *Collision energy losses by* $e^{\pm}$

Stopping power differs somewhat for electrons and positrons, and both differ from stopping power for heavy particles because of the kinematics, spin, charge, and the identity of the incident electron with the electrons that it ionizes. Complete discussions and tables can be found in Refs. [12, 15, 34].

For electrons, large energy transfers to atomic electrons (taken as free) are described by the Møller cross section. From Eq. (34.4), the maximum energy transfer in a single collision should be the entire kinetic energy, $W_{\max} = m_e c^2(\gamma-1)$, but because the particles are identical, the maximum is half this, $W_{\max}/2$. (The results are the same if the transferred energy is ϵ or if the transferred energy is $W_{\max}-\epsilon$. The stopping power is by convention calculated for the faster of the two emerging electrons.) The first moment of the Møller cross section [27] (divided by dx) is the stopping power:

$$\begin{aligned}\left\langle -\frac{dE}{dx}\right\rangle = \frac{1}{2}K\frac{Z}{A}\frac{1}{\beta^2}\Bigg[&\ln\frac{m_e c^2\beta^2\gamma^2\{m_e c^2(\gamma-1)/2\}}{I^2} + (1-\beta^2)\\ &-\frac{2\gamma-1}{\gamma^2}\ln 2 + \frac{1}{8}\left(\frac{\gamma-1}{\gamma}\right)^2 - \delta\Bigg]\end{aligned} \tag{34.23}$$

The logarithmic term can be compared with the logarithmic term in the Bethe equation (Eq. (34.2)) by substituting $W_{\max} = m_e c^2(\gamma-1)/2$. Electron-positron scattering is described by the fairly complicated Bhabha cross section [27]. There is no identical particle problem, so $W_{\max} = m_e c^2(\gamma-1)$. The first moment of the Bhabha equation yields

$$\begin{aligned}\left\langle -\frac{dE}{dx}\right\rangle = \frac{1}{2}K\frac{Z}{A}\frac{1}{\beta^2}\Bigg[&\ln\frac{m_e c^2\beta^2\gamma^2\{m_e c^2(\gamma-1)\}}{2I^2} + 2\ln 2\\ &-\frac{\beta^2}{12}\left(23+\frac{14}{\gamma+1}+\frac{10}{(\gamma+1)^2}+\frac{4}{(\gamma+1)^3}\right) - \delta\Bigg]\,.\end{aligned} \tag{34.24}$$

Following ICRU 37 [12], the density effect correction δ has been added to Uehling's equations [27] in both cases.

For heavy particles, shell corrections were developed assuming that the projectile is equivalent to a perturbing potential whose center moves with constant speed. This assumption has no sound theoretical basis for electrons. The authors of ICRU 37 [12] estimated the possible error in omitting it by assuming the correction was twice as great as for a proton of the same speed. At $T = 10$ keV, the error was estimated to be ≈2% for water, ≈9% for Cu, and ≈21% for Au.

[7] Shen *et al.*'s measurements show that Bethe's simpler methods of including atomic electron effects agrees better with experiment than does Scott's treatment.

Int. J. Mod. Phys. A 2026.41. Downloaded from www.worldscientific.com
by UNIVERSITY OF CALIFORNIA @ BERKELEY on 09/16/26. Re-use and distribution is strictly not permitted, except for Open Access articles.

As shown in Fig. 34.11, stopping powers for e^-, e^+, and heavy particles are not dramatically different. In silicon, the minimum value for electrons is 1.50 MeV cm^2/g (at $\gamma = 3.3$); for positrons, 1.46 MeV cm^2/g (at $\gamma = 3.7$), and for muons, 1.66 MeV cm^2/g (at $\gamma = 3.58$).

34.4.2 *Radiation length*

High-energy electrons predominantly lose energy in matter by bremsstrahlung, and high-energy photons by e^+e^- pair production. The characteristic amount of matter traversed for these related interactions is called the radiation length X_0, usually measured in g cm^{-2}. It is the mean distance over which a high-energy electron loses all but $1/e$ of its energy by bremsstrahlung. It is also the appropriate scale length for describing high-energy electromagnetic cascades. X_0 has been calculated and tabulated by Y.S. Tsai [42]:

$$\frac{1}{X_0} = 4\alpha r_e^2 \frac{N_A}{A}\left\{Z^2\left[L_{\rm rad} - f(Z)\right] + Z\,L'_{\rm rad}\right\} . \tag{34.25}$$

For $A = 1$ g mol^{-1}, $4\alpha r_e^2 N_A/A = (716.408 \text{ g cm}^{-2})^{-1}$. $L_{\rm rad}$ and $L'_{\rm rad}$ are given in Table 34.2. The function $f(Z)$ is an infinite sum, but for elements up to uranium can be represented to 4-place accuracy by

$$f(Z) = a^2\Big[(1+a^2)^{-1} + 0.20206 - 0.0369\,a^2 + 0.0083\,a^4 - 0.002\,a^6\Big], \tag{34.26}$$

where $a = \alpha Z$ [43].

Table 34.2: Tsai's $L_{\rm rad}$ and $L'_{\rm rad}$, for use in calculating the radiation length in an element using Eq. (34.25).

Element	Z	$L_{\rm rad}$	$L'_{\rm rad}$
H	1	5.31	6.144
He	2	4.79	5.621
Li	3	4.74	5.805
Be	4	4.71	5.924
Others	> 4	$\ln(184.15\,Z^{-1/3})$	$\ln(1194\,Z^{-2/3})$

The radiation length in a mixture or compound may be approximated by

$$1/X_0 = \sum w_j/X_j, \tag{34.27}$$

where w_j and X_j are the fraction by weight and the radiation length for the jth element.

34.4.3 *Bremsstrahlung energy loss by* $e^\pm$

At very high energies and except at the high-energy tip of the bremsstrahlung spectrum, the cross section can be approximated in the "complete screening case" as [42]

$$d\sigma/dk = (1/k)4\alpha r_e^2\Big\{(\tfrac{4}{3} - \tfrac{4}{3}y + y^2)[Z^2(L_{\rm rad} - f(Z)) + Z\,L'_{\rm rad}] + \tfrac{1}{9}(1-y)(Z^2+Z)\Big\} , \tag{34.28}$$

where $y = k/E$ is the fraction of the electron's energy transferred to the radiated photon. At small y (the "infrared limit") the term on the second line ranges from 1.7% (low Z) to 2.5% (high Z) of the total. If it is ignored and the first line simplified with the definition of X_0 given in Eq. (34.25), we have

$$\frac{d\sigma}{dk} = \frac{A}{X_0 N_A k}\left(\tfrac{4}{3} - \tfrac{4}{3}y + y^2\right) . \tag{34.29}$$

This cross section (times k) is shown by the top curve in Fig. 34.12.

This formula is accurate except near $y = 1$, where screening may become incomplete, and near $y = 0$, where the infrared divergence is removed by the interference of bremsstrahlung amplitudes from nearby scattering centers (the LPM effect) [44, 45] and dielectric suppression [46, 47]. These and other suppression effects in bulk media are discussed in Sec. 34.4.6.

With decreasing energy ($E \lesssim 10$ GeV) the high-y cross section drops and the curves become rounded as $y \to 1$. Curves of this familar shape can be seen in Rossi [2] (Figs. 2.11.2,3); see also the review by Koch & Motz [48].

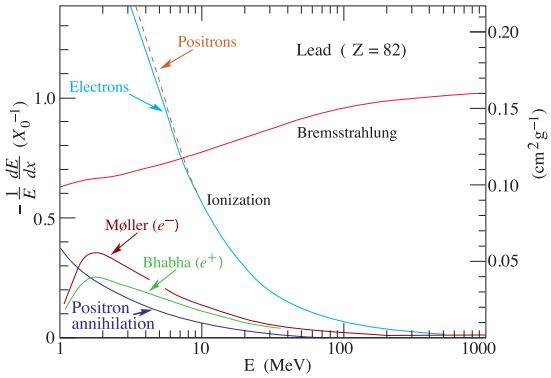

Figure 34.11: Fractional energy loss per radiation length in lead as a function of electron or positron energy. Electron (positron) scattering is considered as ionization when the energy loss per collision is below 0.255 MeV, and as Møller (Bhabha) scattering when it is above. Adapted from Fig. 3.2 from Messel and Crawford, *Electron-Photon Shower Distribution Function Tables for Lead, Copper, and Air Absorbers*, Pergamon Press, 1970. Messel and Crawford use X_0(Pb) = 5.82 g/cm^2, but we have modified the figures to reflect the value given in the Table of Atomic and Nuclear Properties of Materials (X_0(Pb) = 6.37 g/cm^2).

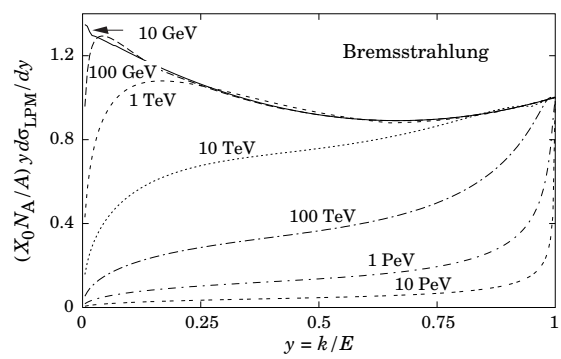

Figure 34.12: The normalized bremsstrahlung cross section $k\,d\sigma_{LPM}/dk$ in lead versus the fractional photon energy $y = k/E$. The vertical axis has units of photons per radiation length.

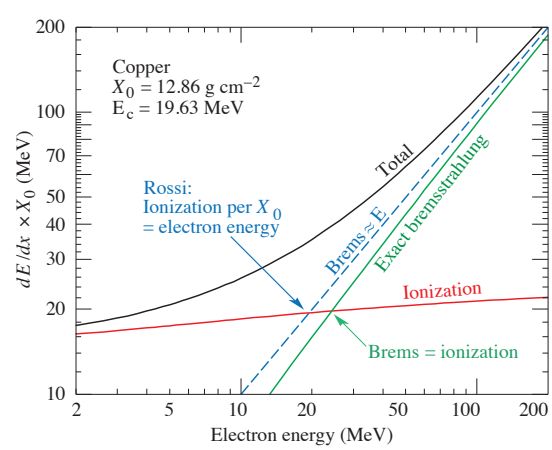

Figure 34.13: Two definitions of the critical energy E_c.

Int. J. Mod. Phys. A. Downloaded from www.worldscientific.com
by UNIVERSITY OF CALIFORNIA @ BERKE use and distribution is strictly not permitted, except for Open Access articles.

Except at these extremes, and still in the complete-screening approximation, the number of photons with energies between $k_{\min}$ and $k_{\max}$ emitted by an electron travelling a distance $d \ll X_0$ is

$$N_\gamma = \frac{d}{X_0}\left[\frac{4}{3}\ln\left(\frac{k_{\max}}{k_{\min}}\right) - \frac{4(k_{\max}-k_{\min})}{3E} + \frac{k_{\max}^2 - k_{\min}^2}{2E^2}\right]. \tag{34.30}$$

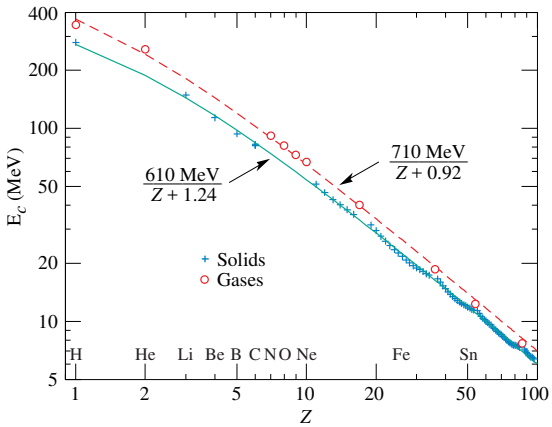

Figure 34.14: Electron critical energy for the chemical elements, using Rossi's definition [2]. The fits shown are for solids and liquids (solid line) and gases (dashed line). The rms deviation is 2.2% for the solids and 4.0% for the gases.

34.4.4 *Critical energy*

An electron loses energy by bremsstrahlung at a rate nearly proportional to its energy, while the ionization loss rate varies only logarithmically with the electron energy. The *critical energy* E_c is sometimes defined as the energy at which the two loss rates are equal [49]. Among alternate definitions is that of Rossi [2], who defines the critical energy as the energy at which the ionization loss per radiation length is equal to the electron energy. Equivalently, it is the same as the first definition with the approximation $|dE/dx|_{\text{brems}} \approx E/X_0$. This form has been found to describe transverse electromagnetic shower development more accurately (see below). These definitions are illustrated in the case of copper in Fig. 34.13.

The accuracy of approximate forms for E_c has been limited by the failure to distinguish between gases and solid or liquids, where there is a substantial difference in ionization at the relevant energy because of the density effect. We distinguish these two cases in Fig. 34.14. Fits were also made with functions of the form $a/(Z+b)^\alpha$, but α was found to be essentially unity. Since E_c also depends on A, I, and other factors, such forms are at best approximate.

Values of E_c for both electrons and positrons in more than 300 materials at
`pdg.lbl.gov/current/AtomicNuclearProperties.`

34.4.5 *Energy loss by photons*

Contributions to the photon cross section in a light element (carbon) and a heavy element (lead) are shown in Fig. 34.15. At low energies it is seen that the photoelectric effect dominates, although Compton scattering, Rayleigh scattering, and photonuclear absorption also contribute. The photoelectric cross section is characterized by discontinuities (absorption edges) as thresholds for photoionization of various atomic levels are reached. Photon attenuation lengths for a variety of elements are shown in Fig. 34.16, and data for 30 eV$< k <$100 GeV for all elements are available from the web pages given in the caption. Here k is the photon energy.

The increasing domination of pair production as the energy increases is shown in Fig. 34.17. Using approximations similar to those used to obtain Eq. (34.29), Tsai's formula for the differential

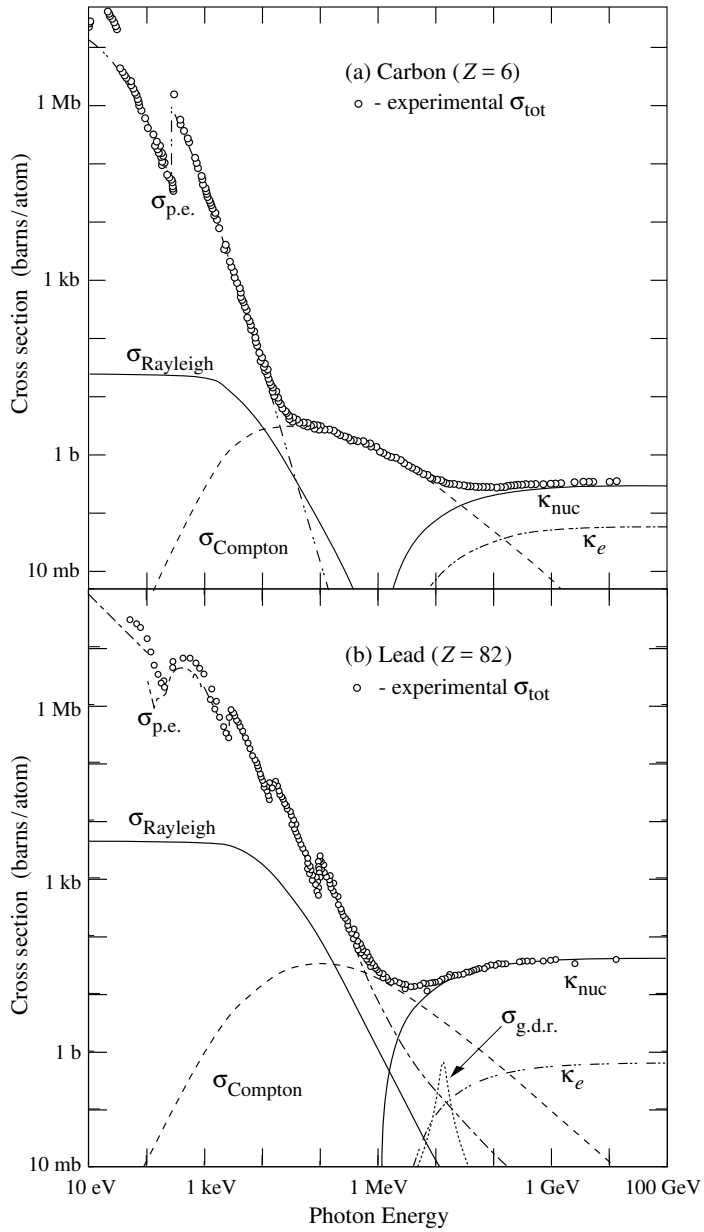

Figure 34.15: Photon total cross sections as a function of energy in carbon and lead, showing the contributions of different processes [50]:

$\sigma_{\text{p.e.}}$ = Atomic photoelectric effect (electron ejection, photon absorption)
σ_{Rayleigh} = Rayleigh (coherent) scattering–atom neither ionized nor excited
σ_{Compton} = Incoherent scattering (Compton scattering off an electron)
κ_{nuc} = Pair production, nuclear field
κ_e = Pair production, electron field
$\sigma_{\text{g.d.r.}}$ = Photonuclear interactions, most notably the Giant Dipole Resonance [51]. In these interactions, the target nucleus is usually broken up.

Original figures through the courtesy of John H. Hubbell (NIST).

cross section [42] reduces to

$$\frac{d\sigma}{dx} = \frac{A}{X_0 N_A}\left[1 - \tfrac{4}{3}x(1-x)\right] \tag{34.31}$$

in the complete-screening limit valid at high energies. Here $x = E/k$ is the fractional energy transfer to the pair-produced electron (or positron), and k is the incident photon energy. The cross

Int. J. Mod. Phys. A 2026.41. Downloaded from www.worldscientific.com
by UNIVERSITY OF CALIFORNIA @ BERKELEY on 09/16/26. Re-use and distribution is strictly not permitted, except for Open Access articles.

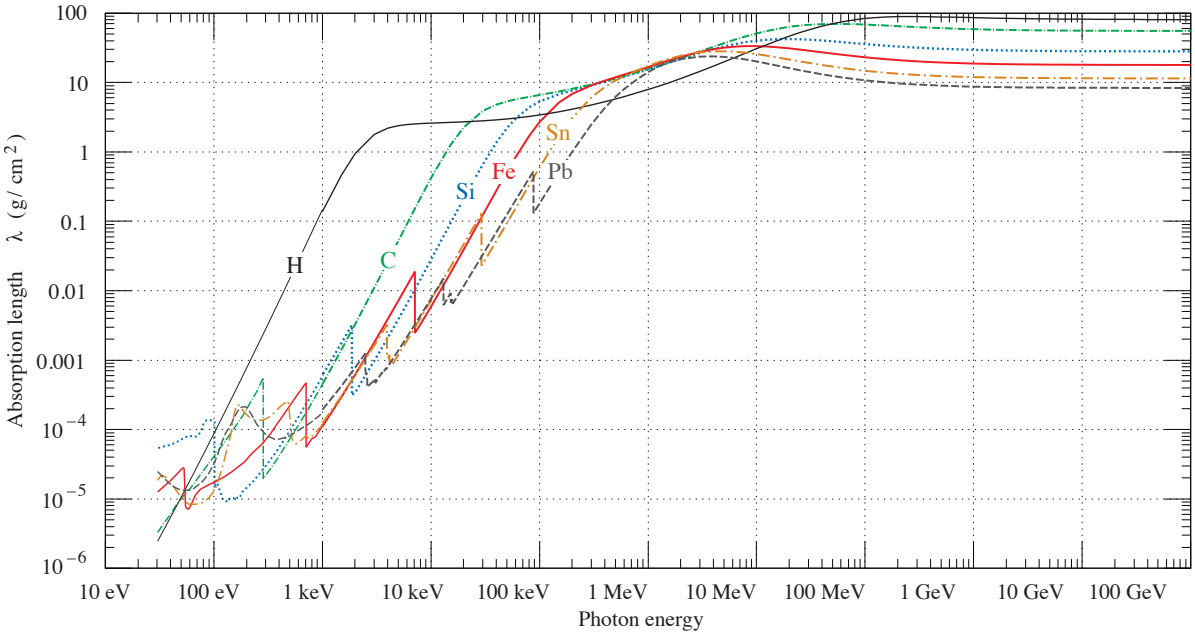

Figure 34.16: The photon mass attenuation length (or mean free path) $\lambda = 1/(\mu/\rho)$ for various elemental absorbers as a function of photon energy. The mass attenuation coefficient is μ/ρ, where ρ is the density. The intensity I remaining after traversal of thickness t (in mass/unit area) is given by $I = I_0 \exp(-t/\lambda)$. The accuracy is a few percent. For a chemical compound or mixture, $1/\lambda_{\rm eff} \approx \sum_{\rm elements} w_Z/\lambda_Z$, where w_Z is the proportion by weight of the element with atomic number Z. The processes responsible for attenuation are given in Fig. 34.11. Since coherent processes are included, not all these processes result in energy deposition. The data for 30 eV $< E <$ 1 keV are from Ref. [52], those for 1 keV $< E <$ 100 GeV from Ref. [53].

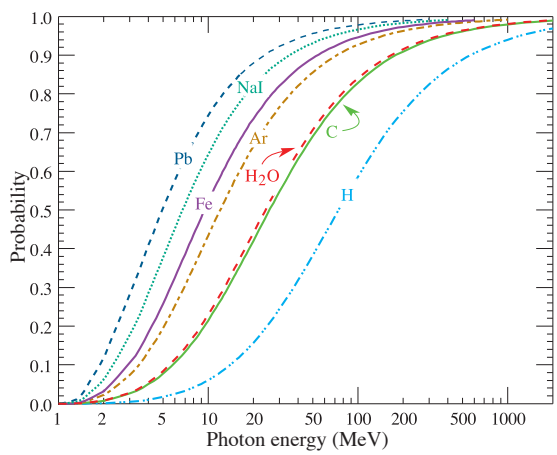

Figure 34.17: Probability P that a photon interaction will result in conversion to an e^+e^- pair. Except for a few-percent contribution from photonuclear absorption around 10 or 20 MeV, essentially all other interactions in this energy range result in Compton scattering off an atomic electron. For a photon attenuation length λ (Fig. 34.16), the probability that a given photon will produce an electron pair (without first Compton scattering) in thickness t of absorber is $P[1 - \exp(-t/\lambda)]$.

section is very closely related to that for bremsstrahlung, since the Feynman diagrams are variants of one another. The cross section is of necessity symmetric between x and $1 - x$, as can be seen by the solid curve in Fig. 34.18. See the review by Motz, Olsen, & Koch for a more detailed treatment [54]. Eq. (34.31) may be integrated to find the high-energy limit for the total e^+e^- pair-production cross section:

$$\sigma = \tfrac{7}{9}(A/X_0 N_A). \tag{34.32}$$

Equation Eq. (34.32) is accurate to within a few percent down to energies as low as 1 GeV, particularly for high-Z materials.

34.4.6 *Bremsstrahlung and pair production at very high energies*

At ultrahigh energies, Eqns. 34.28–34.32 will fail because of quantum mechanical interference between amplitudes from different scattering centers. Since the longitudinal momentum transfer to a given center is small ($\propto k/E(E-k)$, in the case of bremsstrahlung), the interaction is spread over a comparatively long distance called the formation length ($\propto E(E-k)/k$) via the uncertainty principle. In alternate language, the formation length is the distance over which the highly relativistic electron and the photon "split apart." The interference is usually destructive. Calculations of the "Landau-Pomeranchuk-Migdal" (LPM) effect may be made semi-classically based on the average multiple scattering, or more rigorously using a quantum transport approach [44, 45].

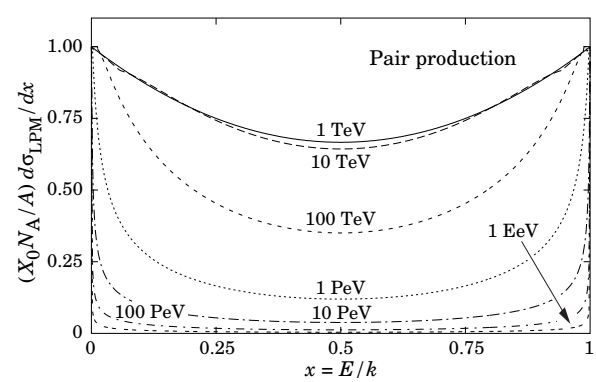

Figure 34.18: The normalized pair production cross section $d\sigma_{LPM}/dx$, versus fractional electron energy $x = E/k$.

In amorphous media, bremsstrahlung is suppressed if the pho-

Int. J. Mod. Phys. A. Downloaded from www.worldscientific.com
by UNIVERSITY OF CALIFORNIA @ BERKE use and distribution is strictly not permitted, except for Open Access articles.

ton energy k is less than $E^2/(E + E_{LPM})$ [45], where[8]

$$E_{LPM} = (m_e c^2)^2 \alpha \frac{X_0}{4\pi\hbar c\rho} = (7.7 \text{ TeV/cm}) \times \frac{X_0}{\rho} \ . \qquad (34.33)$$

Since physical distances are involved, X_0/ρ, in cm, appears. The energy-weighted bremsstrahlung spectrum for lead, $k\, d\sigma_{LPM}/dk$, is shown in Fig. 34.12. With appropriate scaling by X_0/ρ, other materials behave similarly.

For photons, pair production is reduced for $E(k - E) > k\, E_{LPM}$. The pair-production cross sections for different photon energies are shown in Fig. 34.18.

If $k \ll E$, several additional mechanisms can also produce suppression. When the formation length is long, even weak factors can perturb the interaction. For example, the emitted photon can coherently forward scatter off of the electrons in the media. Because of this, for $k < \omega_p E/m_e \sim 10^{-4}$, bremsstrahlung is suppressed by a factor $(km_e/\omega_p E)^2$ [47]. Magnetic fields can also suppress bremsstrahlung.

In crystalline media, the situation is more complicated, with coherent enhancement or suppression possible. The cross section depends on the electron and photon energies and the angles between the particle direction and the crystalline axes [56].

34.4.7 *Photonuclear and electronuclear interactions at still higher energies*

At still higher photon and electron energies, where the bremsstrahlung and pair production cross-sections are heavily suppressed by the LPM effect, photonuclear and electronuclear interactions predominate over electromagnetic interactions.

At photon energies above about 10^{20} eV, for example, photons usually interact hadronically. The exact cross-over energy depends on the model used for the photonuclear interactions. These processes are illustrated in Fig. 34.19. At still higher energies ($\gtrsim 10^{23}$ eV), photonuclear interactions can become coherent, with the photon interaction spread over multiple nuclei. Essentially, the photon coherently converts to a ρ^0, in a process that is somewhat similar to kaon regeneration [57].

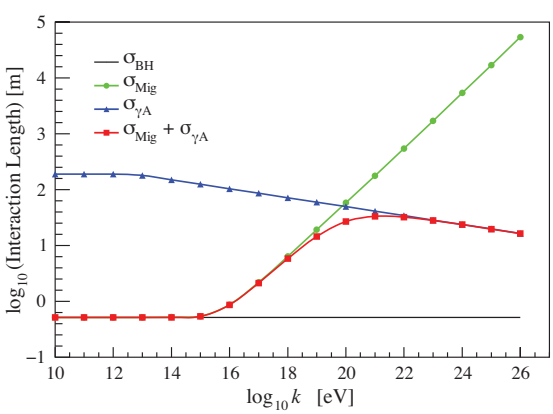

Figure 34.19: Interaction length for a photon in ice as a function of photon energy for the Bethe-Heitler (BH), LPM (Mig) and photonuclear (γA) cross sections [57]. The Bethe-Heitler interaction length is $9X_0/7$, and X_0 is 0.393 m in ice.

Similar processes occur for electrons. As electron energies increase and the LPM effect suppresses bremsstrahlung, electronuclear interactions become more important. At energies above 10^{21}eV, these electronuclear interactions dominate electron energy loss [57].

34.5 Electromagnetic cascades

When a high-energy electron or photon is incident on a thick absorber, it initiates an electromagnetic cascade as pair production and bremsstrahlung generate more electrons and photons with lower energy. The longitudinal development is governed by the high-energy part of the cascade, and therefore scales as the radiation length in the material. Electron energies eventually fall below the critical energy, and then dissipate their energy by ionization and excitation rather than by the generation of more shower particles. In describing shower behavior, it is therefore convenient to introduce the scale variables

$$t = x/X_0, \qquad y = E/E_c, \qquad (34.34)$$

so that distance is measured in units of radiation length and energy in units of critical energy.

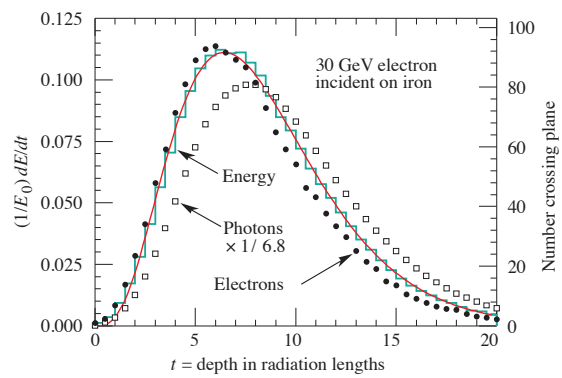

Figure 34.20: An EGS4 simulation of a 30 GeV electron-induced cascade in iron. The histogram shows fractional energy deposition per radiation length, and the curve is a gamma-function fit to the distribution. Circles indicate the number of electrons with total energy greater than 1.5 MeV crossing planes at $X_0/2$ intervals (scale on right) and the squares the number of photons with $E \geq$ 1.5 MeV crossing the planes (scaled down to have same area as the electron distribution).

Longitudinal profiles from an EGS4 [58] simulation of a 30 GeV electron-induced cascade in iron are shown in Fig. 34.20. The number of particles crossing a plane (very close to Rossi's Π function [2]) is sensitive to the cutoff energy, here chosen as a total energy of 1.5 MeV for both electrons and photons. The electron number falls off more quickly than energy deposition. This is because, with increasing depth, a larger fraction of the cascade energy is carried by photons. Exactly what a calorimeter measures depends on the device, but it is not likely to be exactly any of the profiles shown. In gas counters it may be very close to the electron number, but in glass Cherenkov detectors and other devices with "thick" sensitive regions it is closer to the energy deposition (total track length). In such detectors the signal is proportional to the "detectable" track length T_d, which is in general less than the total track length T. Practical devices are sensitive to electrons with energy above some detection threshold E_d, and $T_d = T\, F(E_d/E_c)$. An analytic form for $F(E_d/E_c)$ obtained by Rossi [2] is given by Fabjan in Ref. [59]; see also Amaldi [60].

The mean longitudinal profile of the energy deposition in an electromagnetic cascade is reasonably well described by a gamma distribution [61]:

$$\frac{dE}{dt} = E_0\, b\, \frac{(bt)^{a-1} e^{-bt}}{\Gamma(a)} \qquad (34.35)$$

The maximum $t_{\max}$ occurs at $(a-1)/b$. We have made fits to shower profiles in elements ranging from carbon to uranium, at energies from 1 GeV to 100 GeV. The energy deposition profiles are well described by Eq. (34.35) with

$$t_{\max} = (a-1)/b = 1.0 \times (\ln y + C_j), \qquad j = e, \gamma, \qquad (34.36)$$

where $C_e = -0.5$ for electron-induced cascades and $C_\gamma = +0.5$ for photon-induced cascades. To use Eq. (34.35), one finds $(a-1)/b$ from Eq. (34.36) and Eq. (34.34), then finds a either by assuming $b \approx 0.5$ or by finding a more accurate value from Fig. 34.21. The results are very similar for the electron number profiles, but there

[8] This definition differs from that of Ref. [55] by a factor of two. E_{LPM} scales as the 4th power of the mass of the incident particle, so that $E_{LPM} = (1.4 \times 10^{10}$ TeV/cm$) \times X_0/\rho$ for a muon.

Int. J. Mod. Phys. A 2026.41. Downloaded from www.worldscientific.com
by UNIVERSITY OF CALIFORNIA @ BERKELEY on 09/16/26. Re-use and distribution is strictly not permitted, except for Open Access articles.

is some dependence on the atomic number of the medium. A similar form for the electron number maximum was obtained by Rossi in the context of his "Approximation B," [2] (see Fabjan's review in Ref. [59]), but with $C_e = -1.0$ and $C_\gamma = -0.5$; we regard this as superseded by the EGS4 result.

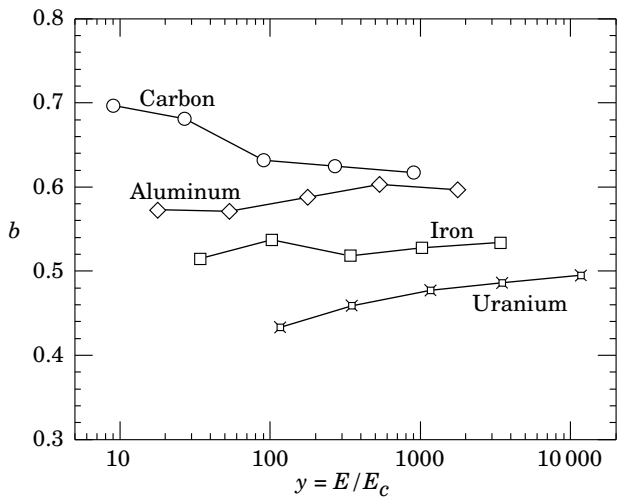

Figure 34.21: Fitted values of the scale factor b for energy deposition profiles obtained with EGS4 for a variety of elements for incident electrons with $1 \leq E_0 \leq 100$ GeV. Values obtained for incident photons are essentially the same.

The "shower length" $X_s = X_0/b$ is less conveniently parameterized, since b depends upon both Z and incident energy, as shown in Fig. 34.21. As a corollary of this Z dependence, the number of electrons crossing a plane near shower maximum is underestimated using Rossi's approximation for carbon and seriously overestimated for uranium. Essentially the same b values are obtained for incident electrons and photons. For many purposes it is sufficient to take $b \approx 0.5$.

The length of showers initiated by ultra-high energy photons and electrons is somewhat greater than at lower energies since the first or first few interaction lengths are increased via the mechanisms discussed above.

The gamma function distribution is very flat near the origin, while the EGS4 cascade (or a real cascade) increases more rapidly. As a result Eq. (34.35) fails badly for about the first two radiation lengths; it was necessary to exclude this region in making fits.

Because fluctuations are important, Eq. (34.35) should be used only in applications where average behavior is adequate. Grindhammer *et al.* have developed fast simulation algorithms in which the variance and correlation of a and b are obtained by fitting Eq. (34.35) to individually simulated cascades, then generating profiles for cascades using a and b chosen from the correlated distributions [62].

The transverse development of electromagnetic showers in different materials scales fairly accurately with the *Molière radius* R_M, given by [63, 64]

$$R_M = X_0\, E_s/E_c, \tag{34.37}$$

where $E_s \approx 21$ MeV (Table 34.1), and the Rossi definition of E_c is used.

In a material containing a weight fraction w_j of the element with critical energy E_{cj} and radiation length X_j, the Molière radius is given by

$$\frac{1}{R_M} = \frac{1}{E_s} \sum \frac{w_j\, E_{cj}}{X_j}\ . \tag{34.38}$$

Measurements of the lateral distribution in electromagnetic cascades are shown in Refs. [63, 64]. On the average, only 10% of the energy lies outside the cylinder with radius R_M. About 99% is contained inside of $3.5R_M$, but at this radius and beyond composition effects become important and the scaling with R_M fails. The distributions are characterized by a narrow core, and broaden as the shower develops. They are often represented as the sum of two Gaussians.

At high enough energies, the LPM effect (Sec. 34.4.6) reduces the cross sections for bremsstrahlung and pair production, and hence can cause significant elongation of electromagnetic cascades [45].

34.6 Muon energy loss at high energy

At sufficiently high energies, radiative processes become more important than ionization for all charged particles. For muons and pions in materials such as iron, this "critical energy" occurs at several hundred GeV. (There is no simple scaling with particle mass, but for protons the "critical energy" is much, much higher.) Radiative effects dominate the energy loss of energetic muons found in cosmic rays or produced at the newest accelerators. These processes are characterized by small cross sections, hard spectra, large energy fluctuations, and the associated generation of electromagnetic and (in the case of photonuclear interactions) hadronic showers [65–73] As a consequence, at these energies the treatment of energy loss as a uniform and continuous process is for many purposes inadequate.

It is convenient to write the average rate of muon energy loss as [74]

$$\langle -dE/dx \rangle = a(E) + b(E)\, E. \tag{34.39}$$

Here $a(E)$ is the ionization energy loss given by Eq. (34.5), and $b(E)$ is the sum of e^+e^- pair production, bremsstrahlung, and photonuclear contributions. To the approximation that these slowly-varying functions are constant, the mean range x_0 of a muon with initial energy E_0 is given by

$$x_0 \approx (1/b) \ln(1 + E_0/E_{\mu c}), \tag{34.40}$$

where $E_{\mu c} = a/b$.

Fig. 34.22 shows contributions to $b(E)$ for iron. Since $a(E) \approx 0.002$ GeV g^{-1} cm^2, $b(E)E$ dominates the energy loss above several hundred GeV, where $b(E)$ is nearly constant. The rates of energy loss for muons in hydrogen, uranium, and iron are shown in Fig. 34.23 [7].

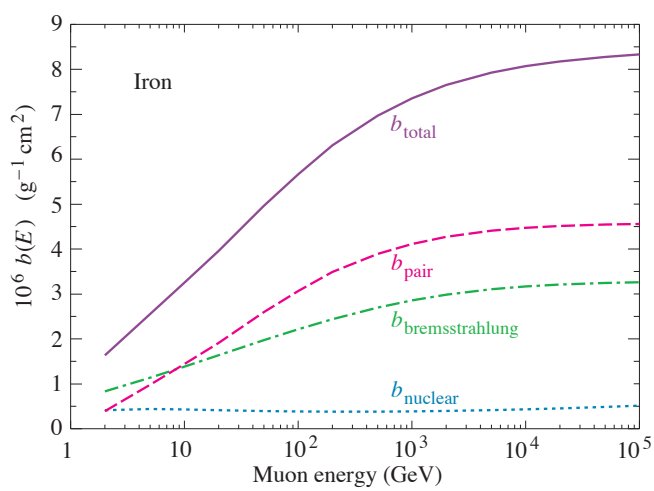

Figure 34.22: Contributions to the fractional energy loss by muons in iron due to e^+e^- pair production, bremsstrahlung, and photonuclear interactions, as obtained from Groom *et al.* [7] except for post-Born corrections to the cross section for direct pair production from atomic electrons.

The "muon critical energy" $E_{\mu c}$ can be defined more exactly as the energy at which radiative and ionization losses are equal, and can be found by solving $E_{\mu c} = a(E_{\mu c})/b(E_{\mu c})$. This definition corresponds to the solid-line intersection in Fig. 34.13, and is different from the Rossi definition we used for electrons. It serves the same function: below $E_{\mu c}$ ionization losses dominate, and above $E_{\mu c}$ radiative effects dominate. The dependence of $E_{\mu c}$ on atomic number Z is shown in Fig. 34.24.

Int. J. Mod. Phys. A 2012.27:1230024-1-1230024-20
by UNIVERSITY OF CALIFORNIA @ BERKE
nloaded from www.worldscientific.com
use and distribution is strictly not permitted, except for Open Access articles.

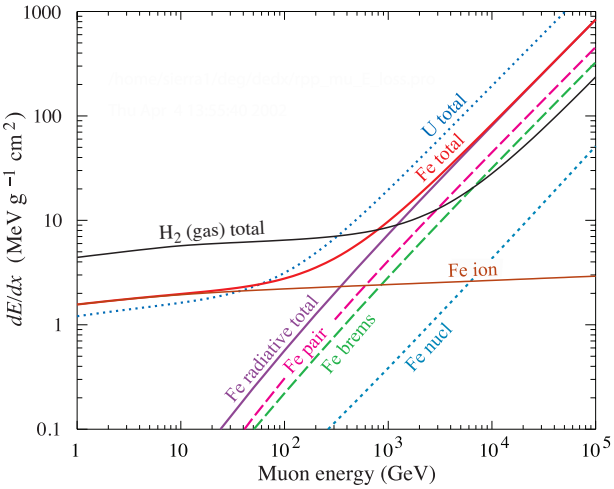

Figure 34.23: The average energy loss of a muon in hydrogen, iron, and uranium as a function of muon energy. Contributions to dE/dx in iron from ionization and pair production, bremsstrahlung and photonuclear interactions are also shown.

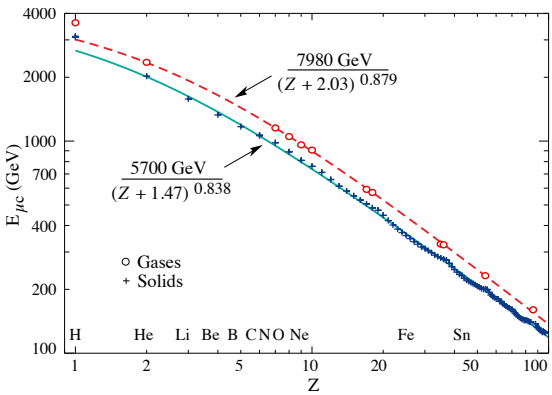

Figure 34.24: Muon critical energy for the chemical elements, defined as the energy at which radiative and ionization energy loss rates are equal [7]. The equality comes at a higher energy for gases than for solids or liquids with the same atomic number because of a smaller density effect reduction of the ionization losses. The fits shown in the figure exclude hydrogen. Alkali metals fall 3–4% above the fitted function, while most other solids are within 2% of the function. Among the gases the worst fit is for radon (2.7% high).

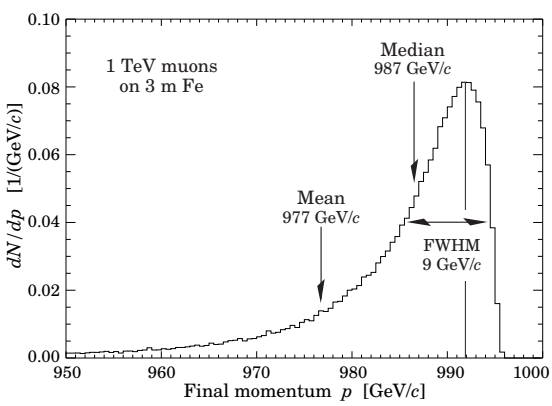

Figure 34.25: The momentum distribution of 1 TeV/c muons after traversing 3 m of iron as calculated by S.I. Striganov [7].

The radiative cross sections are expressed as functions of the fractional energy loss ν. The bremsstrahlung cross section goes roughly as $1/\nu$ over most of the range, while for the pair production case the distribution goes as ν^{-3} to ν^{-2} [75]. "Hard" losses are therefore more probable in bremsstrahlung, and in fact energy losses due to pair production may very nearly be treated as continuous. The simulated momentum distribution of an incident 1 TeV/c muon beam after it crosses 3 m of iron is shown in Fig. 34.25 [7]. The most probable loss is 8 GeV, or 3.4 MeV g^{-1}cm^2. The full width at half maximum is 9 GeV/c, or 0.9%. The radiative tail is almost entirely due to bremsstrahlung, although most of the events in which more than 10% of the incident energy lost experienced relatively hard photonuclear interactions. The latter can exceed detector resolution [76], necessitating the reconstruction of lost energy. Tables in Ref. [7] list the stopping power as 9.82 MeV g^{-1}cm^2 for a 1 TeV muon, so that the mean loss should be 23 GeV ($\approx$ 23 GeV/c), for a final momentum of 977 GeV/c, far below the peak. This agrees with the indicated mean calculated from the simulation. Electromagnetic and hadronic cascades in detector materials can obscure muon tracks in detector planes and reduce tracking efficiency [77].

34.7 Cherenkov and transition radiation [3, 78, 79]

A charged particle radiates if its speed is greater than the local phase speed of light (Cherenkov radiation) or if it crosses suddenly from one medium to another with different optical properties (transition radiation). Neither process is important for energy loss, but both are used in high-energy and cosmic-ray physics detectors.

34.7.1 *Optical Cherenkov radiation*

The angle θ_c of Cherenkov radiation, relative to the particle's direction, for a particle with speed βc in a medium with index of refraction n is

$$\begin{aligned} & \cos\theta_c = (1/n\beta) \\ \text{or} \quad & \tan\theta_c = \sqrt{\beta^2 n^2 - 1} \\ & \approx \sqrt{2(1 - 1/n\beta)} \quad \text{for small } \theta_c, \textit{e.g.} \text{ in gases.} \end{aligned} \tag{34.41}$$

The threshold speed β_t is $1/n$, and $\gamma_t = 1/(1-\beta_t^2)^{1/2}$. Therefore, $\beta_t\gamma_t = 1/(2\delta + \delta^2)^{1/2}$, where $\delta = n - 1$. Values of δ for various commonly used gases are given as a function of pressure and wavelength in Ref. [80]. See its Table 6.1 for values at atmospheric pressure. Data for other commonly used materials are given in Ref. [81].

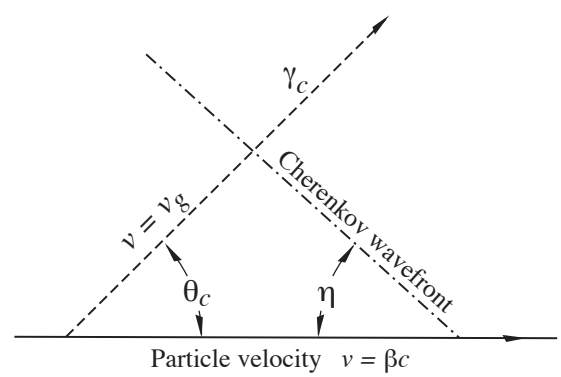

Figure 34.26: Cherenkov light emission and wavefront angles. In a dispersive medium, $\theta_c + \eta \neq 90^0$.

Practical Cherenkov radiator materials are dispersive. Let ω be the photon's frequency, and let $k = 2\pi/\lambda$ be its wavenumber. The photons propage at the group speed $v_g = d\omega/dk = c/[n(\omega) + \omega(dn/d\omega)]$. In a non-dispersive medium, this simplies to $v_g = c/n$.

In his classical paper, Tamm [82] showed that for dispersive media the radiation is concentrated in a thin conical shell whose

Int. J. Mod. Phys. A 2026.41. Downloaded from www.worldscientific.com
by UNIVERSITY OF CALIFORNIA @ BERKELEY on 09/16/26. Re-use and distribution is strictly not permitted, except for Open Access articles.

vertex is at the moving charge, and whose opening half-angle η is

$$\cot\eta = \left[\frac{d}{d\omega}(\omega\tan\theta_c)\right]_{\omega_0} = \left[\tan\theta_c + \beta^2\omega\, n(\omega)\,\frac{dn}{d\omega}\cot\theta_c\right]_{\omega_0}, \qquad (34.42)$$

where ω_0 is the central value of the small frequency range under consideration. (See Fig. 34.26.) This cone has a opening half-angle η, and, unless the medium is non-dispersive ($dn/d\omega = 0$), $\theta_c + \eta \neq 90^0$. The Cherenkov wavefront 'sideslips' along with the particle [83]. This effect has timing implications for ring imaging Cherenkov counters [84], but it is probably unimportant for most applications.

The number of photons produced per unit path length of a particle with charge ze and per unit energy interval of the photons is

$$\frac{d^2N}{dEdx} = \frac{\alpha z^2}{\hbar c}\sin^2\theta_c = \frac{\alpha^2 z^2}{r_e\, m_e c^2}\left(1 - \frac{1}{\beta^2 n^2(E)}\right) \approx 370\,\sin^2\theta_c(E)\ \mathrm{eV}^{-1}\mathrm{cm}^{-1} \qquad (z=1)\,, \qquad (34.43)$$

or, equivalently,

$$\frac{d^2N}{dxd\lambda} = \frac{2\pi\alpha z^2}{\lambda^2}\left(1 - \frac{1}{\beta^2 n^2(\lambda)}\right). \qquad (34.44)$$

The index of refraction n is a function of photon energy $E = \hbar\omega$, as is the sensitivity of the transducer used to detect the light. For practical use, Eq. (34.43) must be multiplied by the the transducer response function and integrated over the region for which $\beta\, n(\omega) > 1$. Further details are given in the discussion of Cherenkov detectors in the Particle Detectors section (Sec. 35.5 of this *Review*).

When two particles are close together (lateral separation $\lesssim 1$ wavelength), the electromagnetic fields from the particles may add coherently, affecting the Cherenkov radiation. Because of their opposite charges, the radiation from an e^+e^- pair at close separation is suppressed compared to two independent leptons [85].

34.7.2 *Coherent radio Cherenkov radiation*

Coherent Cherenkov radiation is produced by many charged particles with a non-zero net charge moving through matter on an approximately common "wavefront"—for example, the electrons and positrons in a high-energy electromagnetic cascade. The signals can be visible for energies above 10^{16} eV; see Sec. 36.3.3 for more details. The phenomenon is called the Askaryan effect [86]. Near the end of a shower, when typical particle energies are below E_c (but still relativistic), a charge imbalance develops. Photons can Compton-scatter atomic electrons, and positrons can annihilate with atomic electrons to contribute even more photons which can in turn Compton scatter. These processes result in a roughly 20% excess of electrons over positrons in a shower. The net negative charge leads to coherent radio Cherenkov emission. The radiation includes a component from the decelerating charges (as in bremsstrahlung). Because the emission is coherent, the electric field strength is proportional to the shower energy, and the signal power increases as its square. The electric field strength also increases linearly with frequency, up to a maximum frequency determined by the lateral spread of the shower. This cutoff occurs at about 1 GHz in ice, and scales inversely with the Moliere radius. At low frequencies, the radiation is roughly isotropic, but, as the frequency rises toward the cutoff frequency, the radiation becomes increasingly peaked around the Cherenkov angle. The radiation is linearly polarized in the plane containing the shower axis and the photon direction. A measurement of the signal polarization can be used to help determine the shower direction. The characteristics of this radiation have been nicely demonstrated in a series of experiments at SLAC [87]. A detailed discussion of the radiation can be found in Ref. [88].

34.7.3 *Transition radiation*

The energy radiated when a particle with charge ze crosses the boundary between vacuum and a medium with plasma frequency ω_p is

$$I = \alpha z^2\gamma\hbar\omega_p/3, \qquad (34.45)$$

where

$$\hbar\omega_p = \sqrt{4\pi N_e r_e^3}\; m_e c^2/\alpha = \sqrt{\rho\ (\text{in g/cm}^3)\ \langle Z/A\rangle} \times 28.81\ \text{eV}. \qquad (34.46)$$

For styrene and similar materials, $\hbar\omega_p \approx 20$ eV; for air it is 0.7 eV.

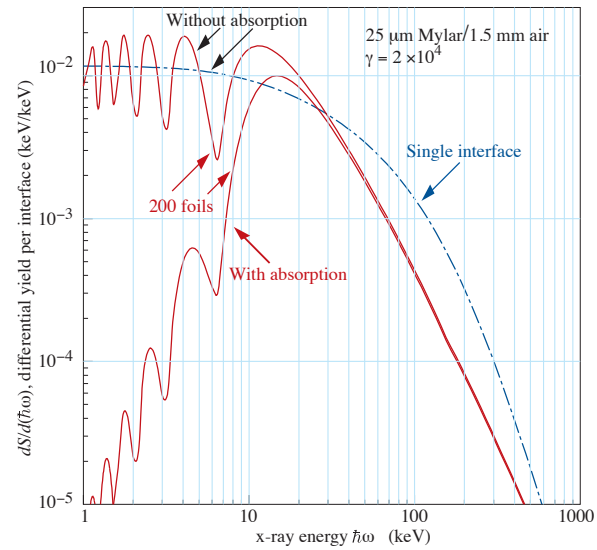

Figure 34.27: X-ray photon energy spectra for a radiator consisting of 200 25 μm thick foils of Mylar with 1.5 mm spacing in air (solid lines) and for a single surface (dashed line). Curves are shown with and without absorption. Adapted from Ref. [89].

The number spectrum $dN_\gamma/d(\hbar\omega$ diverges logarithmically at low energies and decreases rapidly for $\hbar\omega/\gamma\hbar\omega_p > 1$. About half the energy is emitted in the range $0.1 \le \hbar\omega/\gamma\hbar\omega_p \le 1$. Inevitable absorption in a practical detector removes the divergence. For a particle with $\gamma = 10^3$, the radiated photons are in the soft x-ray range 2 to 40 keV. The γ dependence of the emitted energy thus comes from the hardening of the spectrum rather than from an increased quantum yield.

The number of photons with energy $\hbar\omega > \hbar\omega_0$ is given by the answer to problem 13.15 in Ref. [3],

$$N_\gamma(\hbar\omega > \hbar\omega_0) = \frac{\alpha z^2}{\pi}\left[\left(\ln\frac{\gamma\hbar\omega_p}{\hbar\omega_0} - 1\right)^2 + \frac{\pi^2}{12}\right], \qquad (34.47)$$

within corrections of order $(\hbar\omega_0/\gamma\hbar\omega_p)^2$. The number of photons above a fixed energy $\hbar\omega_0 \ll \gamma\hbar\omega_p$ thus grows as $(\ln\gamma)^2$, but the number above a fixed fraction of $\gamma\hbar\omega_p$ (as in the example above) is constant. For example, for $\hbar\omega > \gamma\hbar\omega_p/10$, $N_\gamma = 2.519\,\alpha z^2/\pi = 0.59\% \times z^2$.

The particle stays "in phase" with the x ray over a distance called the formation length, $d(\omega) = (2c/\omega)(1/\gamma^2 + \theta^2 + \omega_p^2/\omega^2)^{-1}$. Most of the radiation is produced in this distance. Here θ is the x-ray emission angle, characteristically $1/\gamma$. For $\theta = 1/\gamma$ the formation length has a maximum at $d(\gamma\omega_p/\sqrt{2}) = \gamma c/\sqrt{2}\,\omega_p$. In practical situations it is tens of μm.

Since the useful x-ray yield from a single interface is low, in practical detectors it is enhanced by using a stack of N foil radiators—foils L thick, where L is typically several formation lengths—separated by gas-filled gaps. The amplitudes at successive interfaces interfere to cause oscillations about the single-interface spectrum. At increasing frequencies above the position of the last interference maximum ($L/d(w) = \pi/2$), the formation zones, which have opposite phase, overlap more and more and the

spectrum saturates, $dI/d\omega$ approaching zero as $L/d(\omega) \to 0$. This is illustrated in Fig. 34.27 for a realistic detector configuration.

For regular spacing of the layers fairly complicated analytic solutions for the intensity have been obtained [89, 90]. Although one might expect the intensity of coherent radiation from the stack of foils to be proportional to N^2, the angular dependence of the formation length conspires to make the intensity $\propto N$.

References

[1] H. Bichsel, Nucl. Instrum. Meth. **A562**, 154 (2006).

[2] B. Rossi, *High Energy Particles*, Prentice-Hall, Inc., Englewood Cliffs, NJ, 1952.

[3] J.D. Jackson, *Classical Electrodynamics*, 3rd edition, (John Wiley and Sons, New York, 1998).

[4] H.A. Bethe, *Zur Theorie des Durchgangs schneller Korpuskularstrahlen durch Materie,* H. Bethe, Ann. Phys. **5**, 325 (1930).

[5] M. S. Livingston and H. A. Bethe, Rev. Mod. Phys. **9**, 245 (1937).

[6] "Stopping Powers and Ranges for Protons and Alpha Particles," ICRU Report No. 49 (1993); Tables and graphs are available at `physics.nist.gov/PhysRefData/Star/Text/PSTAR.html` and `physics.nist.gov/PhysRefData/Star/Text/ASTAR.html`.

[7] D.E. Groom, N.V. Mokhov, and S.I. Striganov, "Muon stopping-power and range tables: 10 MeV–100 TeV," Atomic Data and Nuclear Data Tables **78**, 183–356 (2001). Since submission of this paper it has become likely that post-Born corrections to the direct pair production cross section should be made. Code used to make Figs. 34.22–34.24 included these corrections [D.Yu. Ivanov *et al.*, Phys. Lett. **B442**, 453 (1998)]. The effect is negligible except at high Z. (It is less than 1% for iron.); The introductory text of the paper can be found at `pdg.lbl.gov/current/AtomicNuclearProperties/adndt.pdf`

Extensive printable and machine-readable tables for muons are given at `pdg.lbl.gov/current/AtomicNuclearProperties/`.

[8] W. H. Barkas, W. Birnbaum and F. M. Smith, Phys. Rev. **101**, 778 (1956).

[9] U. Fano, Ann. Rev. Nucl. Part. Sci. **13**, 1 (1963).

[10] J. D. Jackson, Phys. Rev. **D59**, 017301 (1999).

[11] J. Lindhard and A. H. Sørensen, Phys. Rev. **A53**, 2443 (1996).

[12] "Stopping Powers for Electrons and Positrons," ICRU Report No. 37 (1984); Tables and graphs are available at `physics.nist.gov/PhysRefData/Star/Text/ESTAR.html` .

[13] H. Bichsel, Phys. Rev. **A46**, 5761 (1992).

[14] W.H. Barkas and M.J. Berger, *Tables of Energy Losses and Ranges of Heavy Charged Particles*, NASA-SP-3013 (1964).

[15] S.M. Seltzer and M.J. Berger, Int. J. of Applied Rad. **33**, 1189 (1982).

[16] `physics.nist.gov/PhysRefData/XrayMassCoef/tab1.html`.

[17] R. M. Sternheimer, Phys. Rev. **88**, 851 (1952).

[18] R. M. Sternheimer, M. J. Berger and S. M. Seltzer, Atom. Data Nucl. Data Tabl. **30**, 261 (1984); Minor errors are corrected in Ref. 5. Chemical composition for the tabulated materials is given in Ref. 10.

[19] R. M. Sternheimer and R. F. Peierls, Phys. Rev. **B3**, 3681 (1971).

[20] N. F. Mott, Proceedings of the Cambridge Philosophical Society **27**, 553 (1931).

[21] H. Bichsel, Phys. Rev. **A65**, 5, 052709 (2002).

[22] S. P. Møller *et al.*, Phys. Rev. **A56**, 4, 2930 (1997).

[23] J. C. Ashley, R. H. Ritchie and W. Brandt, Phys. Rev. B **5**, 2393 (1972).

[24] H.H. Andersen and J.F. Ziegler, *Hydrogen: Stopping Powers and Ranges in All Elements.* Vol. 3 of *The Stopping and Ranges of Ions in Matter* (Pergamon Press 1977).

[25] J. Lindhard, Kgl. Danske Videnskab. Selskab, Mat.-Fys. Medd. **28**, No. 8 (1954); J. Lindhard, M. Scharff, and H.E. Schiøtt, Kgl. Danske Videnskab. Selskab, Mat.-Fys. Medd. **33**, No. 14 (1963).

[26] J.F. Ziegler, J.F. Biersac, and U. Littmark, *The Stopping and Range of Ions in Solids*, Pergamon Press 1985.

[27] E.A. Uehling, Ann. Rev. Nucl. Sci. **4**, 315 (1954) (For heavy particles with unit charge, but $e^{\pm}$ cross sections and stopping powers are also given).

[28] N.F. Mott and H.S.W. Massey, *The Theory of Atomic Collisions*, Oxford Press, London, 1965.

[29] P. V. Vavilov, Sov. Phys. JETP **5**, 749 (1957), [Zh. Eksp. Teor. Fiz.32,920(1957)].

[30] L.D. Landau, J. Exp. Phys. (USSR) **8**, 201 (1944).

[31] H. Bichsel, Rev. Mod. Phys. **60**, 663 (1988).

[32] R. Talman, Nucl. Instrum. Meth. **159**, 189 (1979).

[33] H. Bichsel, Ch. 87 in the Atomic, Molecular and Optical Physics Handbook, G.W.F. Drake, editor (Am. Inst. Phys. Press, Woodbury NY, 1996).

[34] S.M. Seltzer and M.J. Berger, Int. J. of Applied Rad. **35**, 665 (1984). This paper corrects and extends the results of Ref. [15].

[35] H. A. Bethe, Phys. Rev. **89**, 1256 (1953).

[36] W. T. Scott, Rev. Mod. Phys. **35**, 231 (1963).

[37] J. W. Motz, H. Olsen and H. W. Koch, Rev. Mod. Phys. **36**, 881 (1964).

[38] H. Bichsel, Phys. Rev. **112**, 182 (1958).

[39] G. Shen *et al.*, Phys. Rev. **D20**, 1584 (1979).

[40] G. R. Lynch and O. I. Dahl, Nucl. Instrum. Meth. **B58**, 6 (1991).

[41] M. Wong *et al.*, Med. Phys. **17**, 163 (1990).

[42] Y.-S. Tsai, Rev. Mod. Phys. **46**, 815 (1974), [Erratum: Rev. Mod. Phys.49,521(1977)].

[43] H. Davies, H. A. Bethe and L. C. Maximon, Phys. Rev. **93**, 788 (1954).

[44] L. D. Landau and I. Pomeranchuk, Dokl. Akad. Nauk Ser. Fiz. **92**, 535 (1953); **92**, 735 (1953). These papers are available in English in L. Landau, *The Collected Papers of L.D. Landau*, Pergamon Press, 1965; A. B. Migdal, Phys. Rev. **103**, 1811 (1956).

[45] S. Klein, Rev. Mod. Phys. **71**, 1501 (1999).

[46] M.L. Ter-Mikaelian, SSSR **94**, 1033 (1954); M.L. Ter-Mikaelian, *High Energy Electromagnetic Processes in Condensed Media* (John Wiley and Sons, New York, 1972).

[47] P. L. Anthony *et al.*, Phys. Rev. Lett. **76**, 3550 (1996).

[48] H. W. Koch and J. W. Motz, Rev. Mod. Phys. **31**, 920 (1959).

[49] M.J. Berger and S.M. Seltzer, "Tables of Energy Losses and Ranges of Electrons and Positrons," National Aeronautics and Space Administration Report NASA-SP-3012 (Washington DC 1964).

[50] Curves for these and other elements, compounds, and mixtures may be obtained from `nist.gov/pml/xcom-photon-cross-sections-database`. The photon total cross section is approximately flat for at least two decades beyond the energy range shown.

[51] B. L. Berman and S. C. Fultz, Rev. Mod. Phys. **47**, 713 (1975).

[52] `www.cxro.lbl.gov/optical_constants/pert_form.html`.

[53] `physics.nist.gov/PhysRefData/XrayMassCoef/tab3.html`.

[54] J. W. Motz, H. A. Olsen and H. W. Koch, Rev. Mod. Phys. **41**, 581 (1969).

Int. J. Mod. Phys. E
by UNIVERSITY OF CALIFORNIA @ BERKE
nloaded from www.worldscientific.com
use and distribution is strictly not permitted, except for Open Access articles.

Int. J. Mod. Phys. A 2026.41. Downloaded from www.worldscientific.com
by UNIVERSITY OF CALIFORNIA @ BERKELEY on 09/16/26. Re-use and distribution is strictly not permitted, except for Open Access articles.

[55] P. L. Anthony *et al.*, Phys. Rev. Lett. **75**, 1949 (1995).

[56] U. I. Uggerhøj, Rev. Mod. Phys. **77**, 1131 (2005).

[57] L. Gerhardt and S. R. Klein, Phys. Rev. **D82**, 074017 (2010).

[58] W.R. Nelson, H. Hirayama, and D.W.O. Rogers, "The EGS4 Code System," SLAC-265, Stanford Linear Accelerator Center (Dec. 1985).

[59] *Experimental Techniques in High Energy Physics*, ed. T. Ferbel (Addison-Wesley, Menlo Park CA 1987).

[60] U. Amaldi, Phys. Scripta **23**, 409 (1981).

[61] E. Longo and I. Sestili, Nucl. Instrum. Meth. **128**, 283 (1975), [Erratum: Nucl. Instrum. Meth.135,587(1976)].

[62] G. Grindhammer *et al.*, in *Proceedings of the 1988 Summer Study on High Energy Physics in the 1990's*, Snowmass, CO, June 27 – July 15, 1990, edited by F.J. Gilman and S. Jensen, (World Scientific, Teaneck, NJ, 1989) p. 151.

[63] W. R. Nelson *et al.*, Phys. Rev. **149**, 201 (1966).

[64] G. Bathow *et al.*, Nucl. Phys. **B20**, 592 (1970).

[65] H. Bethe and W. Heitler, Proc. Roy. Soc. Lond. **A146**, 83 (1934); H.A. Bethe, *Proc. Cambridge Phil. Soc.* **30**, 542 (1934).

[66] A.A. Petrukhin and V.V. Shestakov, Can. J. Phys. **46**, S377 (1968).

[67] V.M. Galitskii and S.R. Kel'ner, Sov. Phys. JETP **25**, 948 (1967).

[68] S.R. Kel'ner and Yu.D. Kotov, Sov. J. Nucl. Phys. **7**, 237 (1968).

[69] R.P. Kokoulin and A.A. Petrukhin, in *Proceedings of the International Conference on Cosmic Rays*, Hobart, Australia, August 16–25, 1971, Vol. **4**, p. 2436 .

[70] A. I. Nikishov, Sov. J. Nucl. Phys. **27**, 677 (1978), [Yad. Fiz.27,1281(1978)].

[71] Yu. M. Andreev, L. B. Bezrukov and E. V. Bugaev, Phys. Atom. Nucl. **57**, 2066 (1994), [Yad. Fiz.57,2146(1994)].

[72] L. B. Bezrukov and E. V. Bugaev, Yad. Fiz. **33**, 1195 (1981), [Sov. J. Nucl. Phys.33,635(1981)].

[73] N.V. Mokhov and C.C. James, The MARS Code System User's Guide, Fermilab-FN-1058-APC (2018), `mars.fnal.gov/`; N. Mokhov *et al.*, Prog. Nucl. Sci. Tech. **4**, 496 (2014).

[74] P. H. Barrett *et al.*, Rev. Mod. Phys. **24**, 3, 133 (1952).

[75] A. Van Ginneken, Nucl. Instrum. Meth. **A251**, 21 (1986).

[76] U. Becker *et al.*, Nucl. Instrum. Meth. **A253**, 15 (1986).

[77] J.J. Eastman and S.C. Loken, in *Proceedings of the Workshop on Experiments, Detectors, and Experimental Areas for the Supercollider*, Berkeley, CA, July 7–17, 1987, edited by R. Donaldson and M.G.D. Gilchriese (World Scientific, Singapore, 1988), p. 542.

[78] *Methods of Experimental Physics*, L.C.L. Yuan and C.-S. Wu, editors, Academic Press, 1961, Vol. 5A, p. 163.

[79] W.W.M. Allison and P.R.S. Wright, "The Physics of Charged Particle Identification: dE/dx, Cherenkov Radiation, and Transition Radiation," p. 371 in *Experimental Techniques in High Energy Physics*, T. Ferbel, editor, (Addison-Wesley 1987).

[80] E.R. Hayes, R.A. Schluter, and A. Tamosaitis, "Index and Dispersion of Some Cherenkov Counter Gases," ANL-6916 (1964).

[81] T. Ypsilantis, in "Proceedings of the Symposium on Particle Identification at High Luminosity Hadron Colliders, Apr 5-7, 1989 Batavia, Ill.", 0661–676 (1989).

[82] I. Tamm, J. Phys. U.S.S.R., **1**, 439 (1939).

[83] H. Motz and L.I. Schiff, Am. J. Phys. **21**, 258 (1953).

[84] B. N. Ratcliff, Nucl. Instrum. Meth. **A502**, 211 (2003).

[85] S. K. Mandal, S. R. Klein and J. D. Jackson, Phys. Rev. **D72**, 093003 (2005).

[86] G. A. Askar'yan, Sov. Phys. JETP **14**, 2, 441 (1962), [Zh. Eksp. Teor. Fiz.41,616(1961)].

[87] P. W. Gorham *et al.*, Phys. Rev. **D72**, 023002 (2005).

[88] E. Zas, F. Halzen and T. Stanev, Phys. Rev. **D45**, 362 (1992).

[89] M. L. Cherry *et al.*, Phys. Rev. **D10**, 3594 (1974); M. L. Cherry, Phys. Rev. **D17**, 2245 (1978).

[90] B. Dolgoshein, Nucl. Instrum. Meth. **A326**, 434 (1993).

35. Particle Detectors at Accelerators

Revised March 2026. See the various sections for authors.

35.1 Introduction . . . 602
35.2 Photon detectors . . . 602
35.2.1 Vacuum photodetectors . . . 603
35.2.2 Gaseous photon detectors . . . 604
35.2.3 Solid-state photon detectors . . . 604
35.2.4 Superconducting photon detectors . . . 605
35.3 Organic scintillators . . . 605
35.3.1 Scintillation mechanism . . . 605
35.3.2 Plastic scintillator practicalities . . . 606
35.3.3 Organic glass scintillators . . . 607
35.3.4 Liquid scintillator practicalities . . . 607
35.3.5 Summary . . . 607
35.4 Inorganic scintillators . . . 607
35.5 Cherenkov detectors . . . 610
35.6 Gaseous detectors . . . 612
35.6.1 Energy loss and charge transport in gases . 612
35.6.2 Multi-Wire Proportional and Drift Chambers 615
35.6.3 Micro-Pattern Gas Detectors . . . 616
35.6.4 Time-projection chambers . . . 619
35.6.5 Transition radiation detectors (TRD's) . . . 621
35.6.6 Resistive-plate chambers . . . 623
35.7 LAr Time Projection Chamber . . . 625
35.7.1 Introduction . . . 625
35.7.2 Ultra-pure Liquid Argon . . . 626
35.7.3 Charge and Light Signals . . . 626
35.7.4 LAr TPC topologies . . . 627
35.7.5 Data Acquisition . . . 628
35.7.6 Event reconstruction . . . 628
35.7.7 Developments . . . 628
35.8 Semiconductor detectors . . . 629
35.8.1 Signal generation in semiconductors . . . 630
35.8.2 Junction detectors . . . 631
35.8.3 Detectors with structured electrodes . . . 632
35.8.4 Precise timing with silicon detectors . . . 634
35.8.5 Radiation damage in silicon detectors . . . 635
35.9 Low-noise detector readout . . . 637
35.9.1 Principal noise origins . . . 638
35.9.2 Noise in MOS devices . . . 638
35.9.3 Equivalent noise analysis . . . 639
35.9.4 Timing measurements . . . 641
35.9.5 Digital signal processing . . . 641
35.9.6 What to use when? . . . 642
35.10 Calorimeters . . . 642
35.10.1 Introduction . . . 642
35.10.2 Electromagnetic calorimeters . . . 644
35.10.3 Hadronic calorimeters . . . 646
35.10.4 Free electron drift velocities in liquid ionization chambers . . . 649
35.11 Superconducting magnets for collider detectors . 650
35.11.1 Solenoid Magnets . . . 650
35.11.2 Properties of collider detector magnets . . 651
35.11.3 Toroidal magnets . . . 652
35.12 Measurement of particle momenta in a uniform magnetic field . . . 652

35.1 Introduction

This review summarizes the detector technologies employed at accelerator particle physics experiments. Several of these detectors are also used in a non-accelerator context and examples of such applications will be provided. The detector techniques which are specific to non-accelerator particle physics experiments are the subject of Chap. 36. More detailed discussions of detectors and their underlying physics can be found in books by Kolanoski & Wermes [1], Ferbel [2], Kleinknecht [3], Knoll [4], Green [5], Leroy & Rancoita [6], and Grupen [7].

In Table 35.1 are given typical resolutions and deadtimes of common charged particle detectors. The quoted numbers are usually based on typical devices, and should be regarded only as rough approximations for new designs. The spatial resolution refers to the intrinsic detector resolution, i.e. without multiple scattering. We note that analog detector readout can provide better spatial resolution than digital readout by measuring and averaging the deposited charge in neighboring channels. Quoted ranges attempt to be representative of both possibilities. The time resolution is defined by how accurately the time at which a particle crossed the detector can be determined. The deadtime is the minimum separation in time between two resolved hits on the same channel. Typical performance of calorimetry and particle identification are provided in the relevant sections below.

Table 35.1: Typical resolutions and deadtimes of common charged particle detectors in tracking applications. See respective sections for details on R&D efforts and their achieved performances. Revised September 2025.

Detector Type	Intrinsinc Spatial Resolution (rms)	Time Resolution	Dead Time
Resistive plate chamber	50 μm	50–1000 ps*	10 ns†
Liquid argon TPC	0.5–1 mm‡	0.01-1 μs§	—¶
Scintillation tracker	$\sim$100 μm	100 ps/n‖	10 ns
Bubble chamber	10–150 μm	1 ms	50 ms**
Wire chambers (proportional and drift chambers)	50–100 μm	5–10 ns††	20–200 ns‡‡
Micro-pattern gas detector	30–40 μm	5–10 ns††	20–200 ns‡‡
Silicon strips/pixels	$\lesssim$ 10 μm§§	few ns¶¶ ‡‡	$\lesssim$ 50 ns‡‡

*LHC: $\sim$2 mm gap, $\sim$1 ns. HL-LHC: $\sim$1 mm gap, $\sim$350 ps. Timing RPC: $\sim$50 ps
†Limited by amplifier and discriminator bandwidth, usually around 100 MHz
‡Detector geometry dependent
§Using the scintillation signal
¶No deadtime for medium
‖n = index of refraction.
**Multiple pulsing time.
††For MIPs
‡‡Depending/limited by the analog and digital front-end electronics (see [8] and 35.9)
§§Depending on electrode pitch, best values around a few μm have been achieved
¶¶Resolutions < 30 ps are reached in dedicated developments

35.2 Photon detectors

Revised August 2023 by P. Križan (Ljubljana U; Jozef Stefan Inst.).

Most detectors in high-energy, nuclear, and astrophysics rely on the detection of photons in or near the visible range, 100 nm $\lesssim \lambda \lesssim$ 1000 nm, or 1 eV $\lesssim E \lesssim$ 10 eV. This range covers scintillation and Cherenkov radiation as well as the light detected in many astronomical observations.

Generally, photodetection involves generating a detectable electrical signal proportional to the (usually very small) number of incident photons. The process involves three distinct steps:

1. generation of a primary photoelectron or electron-hole (e-h) pair by an incident photon by the photoelectric or photoconductive effect,
2. multiplication of the photoelectron or electron-hole pair signal to detectable levels, usually by one or more multiplicative bombardment steps and/or an avalanche process, and,
3. detection of charges induced by secondary electrons.

The important characteristics of a photodetector include the following:

1. quantum efficiency (QE or ϵ_Q): the average number of primary photoelectrons generated per incident photon ($0 \leq \epsilon_Q \leq 1$; in silicon more than one e-h pair per incident photon can be generated for $\lambda \lesssim 165$ nm),
2. collection efficiency (CE or ϵ_C): the overall acceptance factor other than the generation of photoelectrons ($0 \leq \epsilon_C \leq 1$),
3. gain (G): the number of electrons collected for each photoelectron generated,
4. dark current or dark noise: the electrical signal when there is no incident photon,
5. precision of measuring the intensity I of the incoming light: electronic noise (ENC or N_e) and statistical fluctuations in the amplification process compound the Poisson distribution

Int. J. Mod. Phys. A Downloaded from www.worldscientific.com by UNIVERSITY OF CALIFORNIA @ BERKE use and distribution is strictly not permitted, except for Open Access articles.

Int. J. Mod. Phys. A 2026.41. Downloaded from www.worldscientific.com by UNIVERSITY OF CALIFORNIA @ BERKELEY on 09/16/26. Re-use and distribution is strictly not permitted, except for Open Access articles.

of n_γ photons from a given source:

$$\frac{\sigma(I)}{\langle I\rangle} = \sqrt{\frac{f_N}{n_\gamma \epsilon_Q \epsilon_C} + \left(\frac{N_e}{G n_\gamma \epsilon_Q \epsilon_C}\right)^2}, \qquad (35.1)$$

where f_N, or the excess noise factor (ENF), is the contribution to the intensity distribution variance due to multiplication statistics [9],

6. dynamic range, linearity and saturation: relation between the number of incident photons and the sensor output in the pulsed mode,
7. time dependence of the response: this includes the transit time, which is the time between the arrival of the photon and the electrical pulse, and the transit time spread, and
8. rate capability: maximal rate of light pulses at which detection is still possible.

The QE is a strong function of the photon wavelength (λ), and is usually quoted at maximum, together with a range of λ where the QE is comparable to its maximum. Spatial uniformity and linearity with respect to the number of photons are highly desirable in a photodetector response.

Optimization of these factors involves many trade-offs and varies widely between applications. For example, while a large gain is desirable, attempts to increase the gain for a given device also increases the ENF and after-pulsing ("echos" of the main pulse). In solid-state devices, a higher QE often requires a compromise in the timing properties. In other types, coverage of large areas by focusing photoelectrons increases the transit time spread.

Other important considerations also are highly application-specific. These include the photon flux and wavelength range, the total area to be covered, and the efficiency required, the volume available to accommodate the detectors, characteristics of the environment such as chemical composition, temperature, magnetic field, ambient background, as well as ambient radiation of different types, mode of operation (continuous or triggered), bias (high-voltage) requirements, power consumption, calibration needs, aging, cost, and so on. Several technologies employing different phenomena for the three steps described above, and many variants within each, offer a wide range of solutions to choose from. The salient features of the main technologies and the common variants are described below. Some key characteristics are summarized in Table 35.2.

35.2.1 *Vacuum photodetectors*

Vacuum photodetectors can be broadly subdivided into three types: photomultiplier tubes, microchannel plate photomultiplier tubes, and hybrid photodetectors.

35.2.1.1 *Photomultiplier tubes*

A versatile class of photon detectors, vacuum photomultiplier tube (PMT) has been employed by a vast majority of all particle physics experiments to date [9]. Both "transmission-" and "reflection-type" PMTs are widely used. In the former, the photocathode material is deposited on the inside of a transparent window through which the photons enter, while in the latter, the photocathode material rests on a separate surface that the incident photons strike. The cathode material has a low work function, chosen for the wavelength band of interest. When a photon hits the cathode and liberates an electron (the photoelectric effect), the latter is accelerated and guided by electric fields to impinge on a secondary-emission electrode, or dynode, which then emits several($\sim$ 5) secondary electrons. The multiplication process is repeated typically about 10 times in series to generate a sufficient number of electrons, which are collected at the anode for delivery to the external circuit. The total gain of a PMT depends on the applied high voltage V as $G = AV^{kn}$, where $k \approx 0.7$–0.8 (depending on the dynode material), n is the number of dynodes in the chain, and A a constant (which also depends on n). Typically, G is in the range of 10^5–10^7; time resolution is $O(1ns)$ but can be as good as $\approx$ 100 ps for certain PMT types.

A large variety of PMTs covers a wide span of wavelength ranges from infrared (IR) to extreme ultraviolet (XUV) [10]. They are categorized by the window materials, photocathode materials, dynode structures, and anode configurations. Common window materials are borosilicate glass for IR to near-UV, fused quartz and sapphire (Al_2O_3) for UV, and MgF_2 or LiF for XUV. The choice of photocathode materials include a variety of mostly Cs- and/or Sb-based compounds such as CsI, CsTe, bi-alkali (SbRbCs, SbKCs), multi-alkali (SbNaKCs), GaAs(Cs), GaAsP(Cs), *etc.* Sensitive wavelengths and peak quantum efficiencies for these materials are summarized in Table-35.3. Typical dynode structures used in PMTs are circular cage, line focusing, box-and-grid, venetian blind, and fine mesh.

Multianode PMTs (MaPMTs) of up to 5×5 cm^2 in size are based on the parallel (side-by-side) arrangement of several dynode channels and anodes in the same tube, requiring advanced micro-machining and processing techniques. Fast PMTs with very large windows—measuring up to 508 mm across—have been developed for detection of Cherenkov radiation in neutrino experiments such as Super-Kamiokande and KamLAND among many others. Specially prepared low-radioactivity glass is used to make these PMTs, and they are also able to withstand the high pressure of the surrounding liquid.

PMTs are vulnerable to magnetic fields—sometimes even the geomagnetic field causes large orientation-dependent gain changes. A high-permeability metal shield is often necessary. However, proximity-focused PMTs, *e.g.* the fine-mesh types, can be used even in a high magnetic field ($\geq$ 1 T) if the direction of electric field of the tube is close to the direction of the external magnetic field. CMS uses custom-made vacuum phototriodes (VPT) mounted on the back face of projective lead tungstate crystals to detect scintillation light in the endcap sections of its electromagnetic calorimeters, which are inside a 3.8 T superconducting solenoid. A VPT employs a single dynode (thus, $G \approx 10$) placed close to the photocathode, and a mesh anode plane between the two, to help it cope with the strong magnetic field, which is not too unfavorably oriented with respect to the photodetector axis in the endcaps (within 25°), but where the radiation level is too high for Avalanche Photodiodes (APDs) like those used in the barrel section.

35.2.1.2 *Microchannel plate photomultiplier tubes*

A typical microchannel plate photomultiplier tube (MCP-PMT) consists of two or more $\sim$1 mm thick glass plates with densely packed $O(10\ \mu\text{m})$-diameter cylindrical holes, or "microchannels", sitting between the transmission-type photocathode and anode planes, separated by $O(1$ mm) gaps. Instead of discrete dynodes, the inner surface of each cylindrical hole with a length-to-diameter ratio of 40-100 serves as a continuous dynode for the entire cascade of multiplicative bombardments initiated by a photoelectron. Gain fluctuations are reduced by operating each of the MCPs in the saturation mode. MCPs are stacked in a "chevron" configuration that alternates their bias angle; this reduces ion and photon feed-back effects and optimizes the overall amplification gain.

MCP-PMTs are thin, offer good spatial resolution, have excellent time resolution ($\sim$20 ps), and can tolerate magnetic fields up to 0.1 T and axial fields up to $1-2$ T. The technology has significantly evolved over the past 10 years [11]. A main breakthrough was the introduction of the atomic layer deposition (ALD) coatings on the MCP surfaces to increase the lifetime (>20 C/cm^2 of charge accumulated on the anode) and gain. The Large Area Picosecond Photo-Detector (LAPPD) project [12] is an important attempt to produce at a reasonable cost large (20 by 20 cm^2) sensors with a transit time spread of 50-70 ps.

35.2.1.3 *Hybrid photon detectors*

Hybrid photon detectors (HPD) combine the sensitivity of a vacuum PMT with the excellent spatial and energy resolutions of a silicon sensor [13]. A single photoelectron ejected from the photocathode is accelerated through a large potential difference of $\sim$20 kV before it impinges on the silicon sensor/anode. The gain nearly equals the maximum number of e-h pairs that could be created from the entire kinetic energy of the accelerated electron: $G \approx$ eV$/w$, where e is the electronic charge, V is the applied potential difference, and $w \approx 3.7$ eV is the mean energy required

Table 35.2: Representative characteristics of some photodetectors commonly used in particle physics.

Type	λ (nm)	$\epsilon_Q\,\epsilon_C$	Gain	Risetime (ns)	Single photon time resol. (ps)	Area (mm^2)	1-p.e noise * (Hz/mm^2)	HV (V)
PMT †	115–1700	0.15–0.25	10^5–10^7	0.7–10	∼200	10–10^5	10^{-2}–10^2	500–3000
MCP-PMT†	115–650	0.01–0.10	10^3–10^7	0.15–0.3	∼20	1–10^4	1–10	500–3500
HPD†	115–850	0.1–0.3	10^3–10^4	$O(1)$	∼1000	10–10^5	10–100	$\sim 2\times 10^4$
HAPD†	115–850	0.1–0.3	10^4–10^5	$O(1)$	∼30	10–10^5	∼1	$\sim 1\times 10^4$
GPD†	115–500	0.15–0.3	10^3–10^6	$O(0.1)$	∼100	$O(10)$	∼1	300–2000
APD	300–1700	∼0.7	10–10^8	$O(1)$	- ‡	1–10^3	$O(10^7)$ §	400–1400
SiPM	125–1000	0.15–0.4	10^5–10^6	∼ 1	∼50	1–36	10^4–10^5	30–60

*Normalized to photocathode/sensor area; room temperature operation assumed.
†These devices often come in multi-anode configurations. In such cases, the area is to be considered on a "per readout-channel" basis.
‡No single photon detection possible.
§Since in an APD no single photon detection is possible, dark current is usually quoted instead of the dark count rate; here we assumed a gain of 50 to convert from the dark current to the dark count rate.

to create an *e*-*h* pair in Si at room temperature. Since the gain is achieved in a single step, one can expect to have the excellent resolution of a simple Poisson statistic with large mean, but in fact it is even better, thanks to the Fano effect discussed in Sec. 35.8.

Low-noise electronics must be used to read out HPDs if one intends to take advantage of the low fluctuations in gain, *e.g.* when counting small numbers of photons. HPDs can have the same $\epsilon_Q\,\epsilon_C$ and window geometries as PMTs and can be segmented down to ∼50 μm. However, they require rather high biases and will not function in a magnetic field. The exception is proximity-focused devices (⇒ no (de)magnification) in an axial field. With time resolutions of ∼10 ps and superior rate capability, proximity-focused HPDs can be an alternative to MCP-PMTs. Applications of HPDs include the CMS hadronic calorimeter and the RICH detector in LHCb. Large-size HPDs with sophisticated focusing may be suitable for future water Cherenkov experiments.

Hybrid APDs (HAPDs) add an avalanche multiplication step following the electron bombardment to boost the gain by a factor of ∼50. This affords a higher gain and/or a lower bias voltage, but also increases the detector capacitance and fluctuations in multiplication. The forward RICH detector of Belle II uses a 144-channel device of this type [14].

Table 35.3: Properties of photocathode and window materials commonly used in vacuum photodetectors. [10]

Photocathode material	λ (nm)	Window material	Peak ϵ_Q (λ/nm)
CsI	115–200	MgF_2	0.13 (130)
CsTe	115–320	MgF_2	0.17 (200)
Bi-alkali	300–650	Borosilicate	0.27 (390)
	160-650	Synthetic Silica	0.27 (390)
"Ultra Bi-alkali"	300–650	Borosilicate	0.43 (350)
	160-650	Synthetic Silica	0.43 (350)
Multi-alkali	300–850	Borosilicate	0.20 (375)
	160-850	Synthetic Silica	0.25 (380)
GaAsP(Cs)	280-720	Borosilicate	0.40 (480-530)

35.2.2 *Gaseous photon detectors*

In a gaseous photon detector (GPD) a photoelectron in a suitable gas mixture initiates an avalanche in a high-field region, producing a large number of secondary impact-ionization electrons. In principle the charge multiplication and collection processes are identical to those employed in gaseous tracking detectors such as multiwire proportional chambers (MWPC), micromesh gaseous detectors (Micromegas), or gas electron multipliers (GEM). These are discussed in Sec. 35.6.3.

The devices can be divided into two types depending on the photosensitive material. One type uses solid photocathode materials much in the same way as PMTs. Since it is resistant to gas mixtures typically used in tracking chambers, CsI is a common choice. In the other type, photoionization occurs on suitable molecules vaporized and mixed in the drift volume. Most gases have photoionization work functions in excess of 10 eV, which would limit their sensitivity to wavelengths far too short. However, vapors of tetrakis dimethyl-amine ethylene (TMAE) or triethyl-amine (TEA), which have smaller work functions (5.3 eV for TMAE and 7.5 eV for TEA), are suited for XUV photon detection [15]. Since devices like GEMs offer sub-mm spatial resolution, GPDs are often used as position-sensitive photon detectors. They can be made into flat panels to cover large areas ($O(1\ m^2)$), can operate in high magnetic fields, and are relatively inexpensive. Many of the ring imaging Cherenkov (RICH) detectors have used GPDs for the detection of Cherenkov light [16–19]. Special care must be taken to suppress the ion-feedback and photon-feedback processes in GPDs. It is also important to maintain high purity of the gas as minute traces of O_2 or H_2O can significantly degrade the detection efficiency.

35.2.3 *Solid-state photon detectors*

In a phase of rapid development, solid-state photodetectors are competing with vacuum- or gas-based devices for many existing applications and making way for a multitude of new ones. Compared to traditional vacuum- and gaseous photodetectors, solid-state devices are more compact, lightweight, rugged, tolerant to magnetic fields, and often cheaper. They also allow fine pixelization, are easy to integrate into large systems, and can operate at low electric potentials, while matching or exceeding most performance criteria.

Silicon photodiodes (PD) are widely used in high-energy physics as particle detectors and in a large number of applications as photon detectors. The structure is discussed in some detail in Sec. 35.8. In its simplest form, the PD is a reverse-biased *p*-*n* junction. Photons with energies above the indirect bandgap energy (wavelengths shorter than about 1050 nm, depending on the temperature) can create *e*-*h* pairs (the photoconductive effect), which are collected on the *p* and *n* sides, respectively. Often, as in the PDs used for crystal scintillator readout in CLEO, L3, Belle, BaBar, and GLAST, intrinsic silicon is doped to create a *p*-*i*-*n* structure. The reverse bias increases the thickness of the depleted region; in the case of these particular detectors, to full depletion at a depth of about 100 μm. Increasing the depletion depth decreases the capacitance (and hence electronic noise) and extends the red response. Quantum efficiency can exceed 90%, but falls toward the red because of the decrease of the light absorption probability in silicon; the absorption length reaches 100 μm at 985 nm. However, since $G = 1$, electronic signal amplification is necessary. Optimal low-noise amplifiers are slow, but, even so, noise limits the minimum detectable signal in room-temperature devices to several hundred photons.

In APDs, an exponential cascade of impact ionizations initiated by the original photogenerated *e*-*h* pair under a large reverse-bias voltage leads to an avalanche multiplication [20–23], and even-

Int. J. Mod. Phys. A
Downloaded from www.worldscientific.com
by UNIVERSITY OF CALIFORNIA @ BERKE
use and distribution is strictly not permitted, except for Open Access articles.

Int. J. Mod. Phys. A 2026.41. Downloaded from www.worldscientific.com by UNIVERSITY OF CALIFORNIA @ BERKELEY on 09/16/26. Re-use and distribution is strictly not permitted, except for Open Access articles.

tually to breakdown in Geiger-mode APDs. As a result, detectable electrical response can be obtained from low-intensity optical signals down to single photons. Excellent junction uniformity is critical, and a guard ring is generally used as a protection against edge breakdown. Well-designed APDs, such as those used in CMS crystal-based electromagnetic calorimeter, have achieved $\epsilon_Q\,\epsilon_C \approx 0.7$ with sub-ns response time. The sensitive wavelength window and gain depend on the semiconductor used. The gain is typically 10–200 in linear and up to 10^8 in Geiger mode of operation. Stability and close monitoring of the operating temperature are important for linear-mode operation, and substantial cooling is often necessary.

One of the most promising recent developments in the field is SiPMs ("Silicon Photomultiplier"), a device consisting of large arrays ($O(10^3)$) of tiny APDs packed over a small area ($O(1\ \mathrm{mm}^2)$) and operated in a limited Geiger mode [24–26]. Although each cell only offers a binary output, linearity with respect to the number of photons is achieved by summing the cell outputs. The sum of all cells is proportional to the number of photons received so long as the probability of an individual cell receiving multiple photons during a single time gate is negligible. SiPMs are being adopted as the preferred solution for various purposes including medical imaging, *e.g.* positron emission tomography (PET). These compact, rugged, and economical devices allow auto-calibration through decent separation of photoelectron peaks and offer gains of $O(10^6)$ at a moderate bias voltage (∼30 V). However, the single-photoelectron noise of a SiPM, being the logical "or" of $O(10^3)$ Geiger APDs, is rather large: O(10-100 kHz/mm^2) at room temperature. Intensive R&D in recent years [27] led to a substantial reduction in dark count rates and in correlated noise levels, resulting in coverage of larger areas and in a wider range of applications. One way to further improve the signal-to-noise ratio in SiPMs is by using dedicated light collectors, either as quartz Winston cone like arrays [28] or suitably designed meta-materials [29]. In this way, photons propagate from a larger entry window to a considerably smaller semiconductor sensor, resulting in an improved signal photon to dark-count ratio. Intense R&D is expected to improve radiation hardness of these sensors. The fabrication of the sensors and the front-end electronics combined in the same process with the goal of making SiPMs extremely easy to use has already been successful (digital SiPMs) [30], and remains a topic of intense R&D.

More solid-state light sensors have either been developed or are potentially interesting for use in HEP experiments. The Run 2 DØ detector used 86000 Visible-light photon counters (VLPC) to read the optical signal from its scintillating-fiber tracker and scintillator-strip preshower detectors. These light sensors utilize the formation of an impurity band only 50 meV below the conduction band in As-doped Si to generate strong ($G \approx 5 \times 10^4$) yet sharp response to single photons with $\epsilon_Q \approx 0.9$ [31–33]. Only a very small bias (∼7 V) is needed, but high sensitivity to infrared photons requires cooling below 10 K. Another interesting light sensor that has not yet found its use in HEP instrumentation are quantum dots, realized by nanometer-sized semiconductor 'particles' embedded in a semiconductor bulk.

35.2.4 *Superconducting photon detectors*

In this rapidly developing technology field, three most established technologies are the superconducting nano-wire single photon detector (SNSPD), the transition edge sensor (TES), and the microwave kinetic inductance detector (MKID). An SNSPD consists of a thin (4 nm) and narrow (100-250 nm) superconducting nanostrip that is current-biased just below its critical current. Absorption of a photon generates a resistive domain in the superconducting nanostrip, which leads to a transient voltage signal that can be detected. SNSPDs offer a unique combination of speed, both in terms of count rate (∼GHz) and low timing jitter ($<$ 3 ps [34]), large range of wavelength sensitivity from VUV (120 nm) to mid-IR (10 μm), high detection efficiencies (approaching 100% for UV to near-IR), and low dark count rates (∼5-10 Hz), making them appealing for a wide variety of demanding applications.

Examples of present use in particle physics are small nanowire detectors for dark matter and dark photons. Work is in progress that could make these sensors relevant to HEP applications by increasing the area (using 300 mm wafers and larger) and pixel size, coupling via windows to cryogenic stages, and readout of arrays (superconducting electronics for data processing). While the performance of these sensors is impressive, an application in large accelerator-based detectors would require an extensive R&D program because of the severe cryogenic requirements.

35.3 Organic scintillators

Revised August 2025 by S.C. Eno (U. Maryland) and M. Hamel (Paris-Saclay U. CEA, LIST).

Organic scintillators produce light when transversed by a charged particle. They can be broadly categorized into four types: single crystal, liquid, plastic, and a recently emerged organic glass [35]. The most useful scintillators produce photons with wavelengths between 370-750 nm (ultraviolet to red), typically peaking at 425 nm [36] via a series of processes that are initialized when charged particles interact with the material via both excitation and ionization/recombination (see Sec. 34.2 of this *Review*). Typical light yields are about 1 photon per 100 eV of energy deposit [37], although the collected and transduced signal can be much lower. Methods to guide the light towards the photon-electron converter, such as diffusive paint, reflectors, photonic crystals, or light guides, may be required to optimize light yield.

Organic scintillators have found use in a wide variety of detectors [38]. Plastics are mostly used in collider detectors, and liquids in neutrino experiments. Ease of fabrication into desired shapes and low cost has made plastic scintillator ideal for large detectors. In the form of scintillating fiber, it has found widespread use in tracking and calorimetry. Demand for large volume detectors (e.g. neutrino detectors: MiniBooNE, NOvA) has led to increased use of liquid scintillator, which can be very low cost.

35.3.1 *Scintillation mechanism*

Plastic and liquid scintillators are based on an aromatic "matrix" such as benzene. The p electrons form both "pi" and "sigma" bonds between the atoms; the pi bonds are responsible for scintillation. Scintillation is produced via standard photophysical interactions, shown schematically in Fig. 35.1. Via radiation-matter interactions, the matrix is excited to various singlet states. By internal conversion (which is non radiative), the system relaxes to the S_1 state. Vibrational relaxation can also lead to non-radiative decays from excited singlet states. Intersystem crossing occurs primarily for particles with large energy deposition per unit path length dE/dx, and can be be used for their identification. While there have been claims of delayed light production on long time scales (labeled "phosphorescence" in the figure), this is still a subject of active debate in the community. As aromatic molecules scintillate in the ultraviolet (UV), useful scintillators have one or several fluorophores dissolved into the matrix as dopants. Common fluorophores include 2,5-diphenyloxazole, *p*-terphenyl, 9,10-diphenylanthracene (9,10-DPA), 1,4-bis(2-methylstyryl)benzene (bis-MSB) and 1,4-bis(5-phenyl-2-oxazolyl)benzene (POPOP). The key aspects of their molecular structure include pi-conjugated systems and steric effects; in particular functional groups located on the aromatic rings strongly influence their scintillation performance. Each molecule has its own role: the matrix (whether liquid or plastic) is where most of the radiation/matter interaction occurs. Numerous publications have demonstrated the strong dependence of the scintillator's response to the fluorophores concentration. At high concentrations, the probability of quenching increases, and the light output generally plateaus. After radiation interaction, ions may recombine giving birth to excited molecules (excitons). Excitons in the matrix are transferred to a "primary fluorophore", whose concentration is typically 1-3 weight % in commercial plastic and liquid scintillators. This concentration is large enough to ensure exciton transfer – primarily via the Förster mechanism, a resonant dipole-dipole interaction which decreases at sixth the power of the distance between molecules. The concentration, however, can be up to the solubility limit. Transfer via the Förster mechanism increases both speed and light output of the organic scintillator. To

Int. J. Mod. Phys. A 2020.
Downloaded from www.worldscientific.com
by UNIVERSITY OF CALIFORNIA @ BERKE
use and distribution is strictly not permitted, except for Open Access articles.

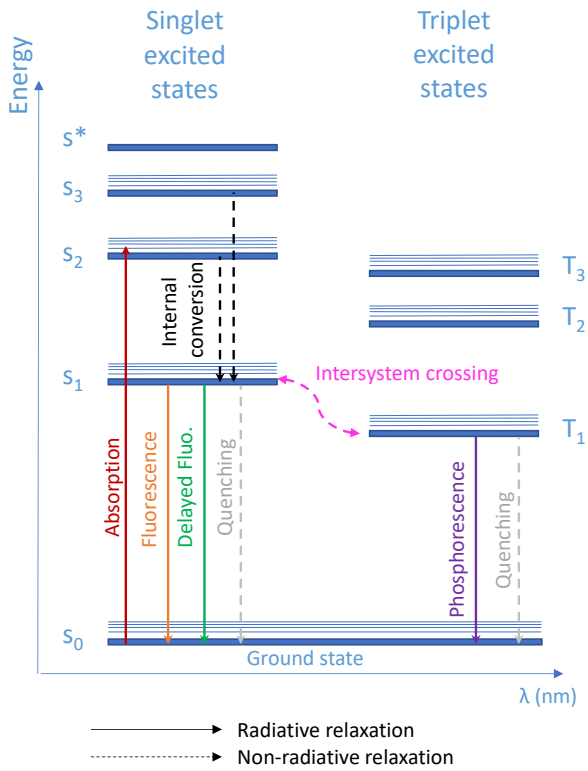

Figure 35.1: Schematic of scintillation mechanism. Schematic of typical excitation and de-excitation of matrix modules.

reduce reabsorption of the emitted light by the matrix or the primary fluorophore, and the resulting shortened attenuation length, a "secondary fluorophore" is also used to shift the light to longer wavelengths. Transfer from the primary to the secondary is generally radiative. Typical secondary concentrations in plastic and liquids are 0.01-0.2 weight %. The chain of emission and absorption from the matrix to the subsequent fluorophores is shown in Fig. 35.2.

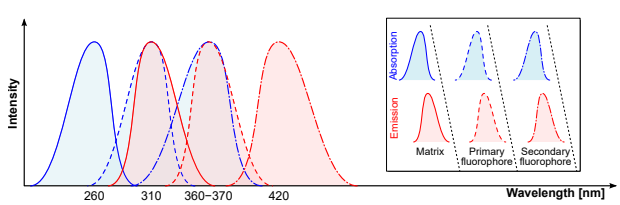

Figure 35.2: Schematic of scintillation mechanism. Typical emission and absorption spectra for the matrix, the primary, and the secondary fluorophore.

Scintillators with two fluorophores typically have absorption lengths of several meters. The longest attenuation lengths require a third fluorophore: when the matrix is transparent up to 1 cm, adding a primary fluorophore increases the light transmission up to ≈ 10 cm, whereas the ternary cocktail is transparent up to 2 m and longer [39].

For most scintillators, decay times are in the ns range; rise times are much faster. Sub-ns timing resolutions have been achieved [40].

Organic scintillators do not respond linearly to the ionization density. Very dense ionization tracks, with large dE/dx, emit less light than expected compared to minimum-ionizing particles. A widely used semi-empirical model by Birks posits that recombination and quenching effects between the excited molecules reduce the light yield [41]. These effects are more pronounced when the density of excited molecules is larger. Birks' formula is

$$\frac{d\mathcal{L}}{dx} = \mathcal{L}_0 \frac{dE/dx}{1 + kB\, dE/dx}, \tag{35.2}$$

where $\mathcal{L}$ is the luminescence, $\mathcal{L}_0$ is the luminescence at low specific ionization density, and the product kB is known as Birks' constant, which must be determined for each scintillator by measurement. The value of kB for polystyrene is 0.126 mm/MeV, which is large enough to play an important role in compensation in scintillator-based calorimetry. The high hydrogen content of plastic, which enhances the neutron interaction cross section, as well as its large mass stopping power, also contributes to calorimetry compensation. In the case of large or small [42] dE/dx values (e.g. with alpha particles or tritium, respectively), ion recombination may lead to the creation of triplet excited states instead of singlet excited states. If two triplet states are close enough (typically in the order of 10Å), then triplet-triplet annihilation may occur following the Dexter process [43], leading to delayed fluorescence. This phenomenon is useful for α/β or neutron/γ discrimination and is more efficient in liquid scintillators than in plastics due to the molecular motion.

Extensive research for new efficient molecules that can act as matrix, primary, or secondary fluorophores, is ongoing [44]. Other chemical modifications can affect the scintillator emission wavelength and decay time, or be used *e.g.* as stabilizers or to enhance thermal neutron sensitivity. Other parameters that can be modified are the density and the effective atomic number. Recently a new chemical formulation was developed for the search for double beta plus decays at the NuDoubt^{++} experiment. The new scintillator is a combination of hybrid ("slow" plastic scintillator for Cherenkov rejection) and opaque scintillator (to confine scintillation light through Mie scattering of optical photons) [45]. Also of note is a development related to the Mobile Antineutrino Demonstrator Project: embedding ^{6}Li-doped pulse shape discriminating plastic scintillators into 1 m long segments at 6 cm $\times$6,cm cross section assembled as a 2D array [46].

A major issue is efficiently choosing the most promising molecules, and so usually new organic scintillators are found via a lengthy trial-and-error procedure. A neural architecture built for organic molecule selection for sub-GeV dark matter detection [47] obtained promising results, notably by confirming the backbone of well-known fluorophores.

35.3.2 *Plastic scintillator practicalities*

Plastic scintillators are cheap, can be prepared at large volumes and purity, are reliable, robust, and convenient. Their high chemical versatility allows innovations in material science to open new research fields in high-energy physics. Most commercial plastic scintillators use either polystyrene (PS) or poly(vinyltoluene) (PVT) as matrix. A variety of manufacturing techniques [44] are used in the production of plastic scintillator. Cast plastic has the highest light yield, while extruded scintillator is less expensive and allows creation of the scintillator and coating with a diffusive reflector in a single process. 3D printing of plastic scintillator has also emerged as a reliable production method. The technique has been applied to plastics for pulse-shape discrimination [48] and 3D tracking [49]. However, large-scale production (10+ liters) has not yet been achieved. Plastic scintillator is also used to produce scintillating, wavelength-shifting, and clear fibers. These fibers can be useful to guide light to photodetectors, and as the active element in the type of calorimeter pioneered by the RD52/DREAM collaboration [50]. They have even been used in the construction of trackers [51,52]. A 3D-segmented detector for particle tracking and calorimetry has been achieved. SuperCube is a $5 \times 5 \times 5$ configuration of 1 cm^3 PS-based plastic scintillators prepared by additive manufacturing (fused deposition modeling) with embedded Kuraray Y11 wavelength-shifting fibers connected to Multi-Pixel Photon Counters [53].

Plastic scintillators are reliable, robust, and convenient. However, exposure to solvent vapors, high temperatures, mechanical flexing, irradiation, or rough handling will cause degradation. The surface is a particularly fragile region and can "craze" – develop microcracks which degrade transmission of light by total internal

Int. J. Mod. Phys. A 2026.41. Downloaded from www.worldscientific.com
by UNIVERSITY OF CALIFORNIA @ BERKELEY on 09/16/26. Re-use and distribution is strictly not permitted, except for Open Access articles.

Table 35.4: Typical properties of plastic, liquid, and organic glass scintillators.

Property	Plastic	Liquid	Organic glass
Light output (ph/MeV)	up to 10,000	up to 12,000	17,000 - 20,000
Stability	Generally stable; partial fogging with moisture	Stable if properly encapsulate; otherwize oxygen sensitive	Improved when blended with polymers
Density	1.04-1.56	$\approx$ 1.0 - $\approx$ 1.3	not available
Emission wavelength	Highly tunable	Highly tunable	Usually around 430 nm; should be tunable
Decay Time	0.3-280 ns, low after glow	fast, down to sub-ns	1.3-1.6 ns prompt
Loading with elements	Easy	Easy	B or Sn loading performed so far
Radiopurity	Highly pure	Highly pure	Highly pure
Achievable volumes	Bulk up to ca. 100 L	Virtually no limit	Ca. 0.3 L for pure OGS, larger volumes for OGS blended with polymers
Fast neutron/gamma discrimination	Moderate to good	Good to excellent	Excellent

reflection. Crazing is particularly likely where oils, solvents, or fingerprints have contacted the surface or when mechanical stresses are present. The light yield is influenced by several environmental factors: it decreases with the partial pressure of oxygen [54] and increases with increasing magnetic field [55]. In particular, the combination of elevated temperature with relative humidity accelerates aging. This apparent fogging is typically observed in radiation portal monitors, which are exposed to harsh environmental conditions. The aging can become irreversible after multiple cycles. Recently the T2K collaboration reported a 10-year light-yield measurement showing damage due to aging [56].

Plastics are susceptible to radiation damage [57, 58]. At high enough dose, the visible color of the plastic can change to yellow or even brown. The amount of damage for a fixed dose is higher at lower dose rates [59–61]. During irradiation, the transparency of the plastic decreases. When the irradiation ends, this can reverse and the transparency can increase ("anneal"). This process is faster in the presence of oxygen, which can diffuse into the plastic. Oxygen can also suppress temporary damage during irradiation, although this mechanism can be strongly suppressed at low enough temperatures [62]. The ratio of the light output to the unirradiated light output can roughly be parameterized as an exponential. For dose rates typical of current collider detectors at the Large Hadron Collider (from a few 10^{-3} to 10 Gy/hr), an exponential dose constant of tens of kGy is observed.

35.3.3 *Organic glass scintillators*

Starting in 2016, extensive research by Sandia National Laboratories lead to a new organic scintillator family: organic glasses (OGSs) [63]. Whereas polymers are long-chain molecules built from a standard unit called a monomer, OGSs consist of small organic molecules. In addition, polymers such as PS or PVT require dopants, when OGSs are intrinsically good scintillators. This new material has the useful properties present in inorganic single crystals (light yield, pulse-shape discrimination properties, along with fast-timing properties), without the poor mechanical characteristics seen in single crystals. The maintenance of the amorphous state of these bulk optical materials was achieved mainly either by using molecules with high configurational disorder or by introducing compositional disorder. OGSs can be prepared in medium to large scales when they are blended with polymers, or pixelated for neutron detection systems, and they can eventually be loaded with heavy elements. In 2021 Blueshift Optics secured a license from Sandia National Laboratories for the industrial production of OGSs.

35.3.4 *Liquid scintillator practicalities*

Liquid scintillators have been used in large scale neutrino experiments 36.3.1.1 due to their low cost. They can hermetically fill any vessel shape. Liquid scintillators are also, due to the mobility of the molecules, much less susceptible to radiation damage.

Care must be taken to avoid dissolved water, solvents such as isopropyl alcohol, and oxygen, which reduce light yield. As they can dissolve many materials (e.g. plastics, adhesives, paints..) care must be taken in their handling. Flammability concerns limit their use in practical experiments in intense radiation fields.

35.3.5 *Summary*

Table 35.4 summarizes some of the characteristics of and differences between plastic, liquid and organic glass scintillators.

35.4 Inorganic scintillators

Revised August 2025 by C.L. Woody (BNL) and R.-Y. Zhu (HEP California Inst. of Technology).

Inorganic crystals form a class of scintillating materials with much higher densities than organic plastic scintillators (typically $\sim$ 4–8 g/cm^3) with a variety of different properties for use as scintillation detectors. Due to their high density and high effective atomic number, they can be used in applications where high stopping power or a high conversion efficiency for electrons or photons is required. These include total absorption electromagnetic calorimeters (see Sec. 35.10.2), which consist of a totally active absorber (as opposed to a sampling calorimeter), and time of flight detectors as well as serving as gamma-ray detectors over a wide range of energies. Many of these crystals also have very high light output, and can therefore provide excellent energy resolution down to very low energies ($\sim$ few hundred keV).

Some crystals are intrinsic scintillators in which the luminescence is produced by a part of the crystal lattice itself. However, other crystals require the addition of a dopant, typically fluorescent ions such as thallium (Tl) or cerium (Ce), which is responsible for producing the scintillation light. However, in both cases, the scintillation mechanism is the same. For charged particles, energy is deposited in the crystal by ionization. For photons, energy is deposited by Compton electrons, photoelectrons, and electron-positron pairs, and the corresponding cross sections depend on the photon energy and the scintillator material. This energy is transferred to the luminescent centers which then radiate scintillation photons. The light yield LY in terms of the number of scintillation photons produced per MeV of energy deposited in the crystal can be expressed as [64]

$$LY = 10^6 \; S \cdot Q/(\beta \cdot E_g), \tag{35.3}$$

where $\beta \cdot E_g$ is the energy required to create an e-h pair expressed as a multiple of the band gap energy Eg (eV), S is the efficiency of energy transfer to the luminescent center and Q is the quantum efficiency of the luminescent center. The values of β, S and Q are crystal dependent and are the main factors in determining the intrinsic light yield of the scintillator. The decay time of the scintillator is mainly dominated by the decay time of the luminescent center.

Table-35.5 lists the basic properties of inorganic crystals commonly used in high energy or nuclear physics experiments. A

Table 35.5: Properties of several inorganic crystals used in high-energy or nuclear physics experiments. Most of the notation is defined in Sec. 6 of this *Review*.

Parameter:	ρ	MP	X_0*	R_M*	dE/dx*	λ_I*	$\tau_{\rm decay}$	$\lambda_{\rm max}$	$n^\dagger$	Relative light yield	Hygro-scopic?	$d(\mathrm{LY})/dT$
Units:	g/cm^3	°C	cm	cm	MeV/cm	cm	ns	nm		%‡		%/°C§
NaI(Tl)	3.67	651	2.59	4.13	4.8	42.9	245	410	1.85	100	yes	−0.2
BGO	7.13	1050	1.12	2.23	9.0	22.8	300	480	2.15	21	no	−0.9
BaF_2	4.89	1280	2.03	3.10	6.5	30.7	650^s	300^s	1.50	36^s	no	-1.9^s
							$<0.6^f$	220^f		4.1^f		0.1^f
CsI(Tl)	4.51	621	1.86	3.57	5.6	39.3	1220	550	1.79	165	slight	0.4
CsI(Na)	4.51	621	1.86	3.57	5.6	39.3	690	420	1.84	88	yes	0.4
CsI(pure)	4.51	621	1.86	3.57	5.6	39.3	30^s	310	1.95	3.6^s	slight	−1.4
							6^f			1.1^f		
$PbWO_4$	8.30	1123	0.89	2.00	10.1	20.7	30^s	425^s	2.20	0.3^s	no	−2.5
							10^f	420^f		0.077^f		
LSO(Ce)	7.40	2050	1.14	2.07	9.6	20.9	40	402	1.82	85	no	−0.2
PbF_2	7.77	824	0.93	2.21	9.4	21.0	-	-	-	Cherenkov	no	-
CeF_3	6.16	1460	1.70	2.41	8.42	23.2	30	340	1.62	7.3	no	0
$LaBr_3$(Ce)	5.29	783	1.88	2.85	6.90	30.4	20	356	1.9	180	yes	0.2
$CeBr_3$	5.23	722	1.96	2.97	6.65	31.5	17	371	1.9	165	yes	−0.1

*Numerical values calculated using formulae in this review.

†Refractive index at the wavelength of the emission maximum.

‡Relative light yield measured for samples of 1.5 X_0 cube with a Tyvek paper wrapping and a full end face coupled to a photodetector. The quantum efficiencies of the photodetector are taken out.

§Variation of light yield with temperature evaluated at room temperature.

f = fast component, s = slow component

more extensive list of organic and inorganic scintillators and their properties can be found in [65], which describes the open access library https://scintillator.lbl.gov/.

NaI(Tl) is one of the most common and widely used scintillators, with an emission that is well matched to a bialkali photomultiplier tube, but it is highly hygroscopic and difficult to work with, and has a rather low density. CsI(Tl) and CsI(Na) have high light yield, low cost, and are mechanically robust (high plasticity and resistance to cracking). However, they need careful surface treatment and are slightly and highly hygroscopic respectively. Pure CsI has identical mechanical properties as CsI(Tl), but has a faster emission at shorter wavelength and a much lower light yield.

Undoped BaF_2 has a fast component with a less than 0.6 ns decay time, and is the fastest known scintillator. However, it also has a slow component with a much longer decay time ($\sim$ 630 ns). Bismuth gemanate ($Bi_4Ge_3O_{12}$ or BGO) has a high density, and consequently a short radiation length X_0 and Molière radius R_M. Similar to CsI(Tl), BGO's emission is well-matched to the spectral sensitivity of silicon photodiodes, and it is easy to handle and not hygroscopic. Lead tungstate ($PbWO_4$ or PWO) has a very high density, with a very short X_0 and R_M, but its intrinsic light yield is rather low.

Cerium doped lutetium oxyorthosilicate (Lu_2SiO_5:Ce, or LSO:Ce) [66] and cerium doped lutetium-yttrium oxyorthosilicate ($Lu_{2(1-x)}Y_{2x}SiO_5$, LYSO:Ce) [67] are dense crystal scintillators which have a high light yield and a fast decay time. Only the properties of LSO:Ce are listed in Table-35.5 since the properties of LYSO:Ce are similar to that of LSO:Ce except a slightly lower density than LSO:Ce depending on the yttrium fraction (typically 5 to 10%) in LYSO:Ce. This material also exhibits excellent radiation hardness [68, 69], and can be used where extraordinary radiation hardness is required, such as the HL-LHC and FCC-hh.

Also listed in Table-35.5 are other fluoride crystals such as PbF_2 , which is a Cherenkov material, and CeF_3, which has been shown to provide excellent energy resolution in calorimeter applications [70, 71]. Table-35.5 also includes lanthanum tri-halides, such as $LaBr_3$(Ce) [72] and $CeBr_3$ [73], which are brighter and faster than LSO:Ce, but are highly hygroscopic and have a lower density. The FWHM energy resolution measured for these materials coupled to a PMT with bi-alkali photocathode for 0.662 MeV γ-rays from a ^{137}Cs source is about 3%, and has been improved to 2% by co-doping with calcium and strontium [74], which is the best among all inorganic crystal scintillators. For this reason, $LaBr_3$(Ce) and $CeBr_3$ are used in applications where good energy resolution for low energy photons are required, such as homeland security.

Beside the crystals listed in Table-35.5, a number of newer crystals are being investigated that may have potential applications in high energy or nuclear physics. Of particular interest is the family of yttrium and lutetium perovskites and garnets, which include YAP ($YAlO_3$:Ce), LuAP ($LuAlO_3$:Ce), YAG ($Y_3Al_5O_{12}$:Ce), LuAG ($Lu_3Al_5O_{12}$:Ce), GAGG ($Gd_3Al_2Ga_3O_{12}$:Ce) and their mixed compositions. These have been shown to be linear over a large energy range [75], and have the potential for providing good intrinsic energy resolution. Cerium doped garnets (YAG, LuAG and GAGG) are also radiation hard [76–80], and have been proposed for future applications in a severe radiation environment.

Aiming at the best jet-mass resolution, inorganic scintillators are being investigated for HEP calorimeters with dual readout for both Cherenkov and scintillation light to be used at future lepton colliders. These materials may be used for an electromagnetic calorimeter [81] or a homogeneous hadronic calorimetry (HHCAL) detector concept, including both electromagnetic and hadronic parts [82, 83]. Because of the unprecedented volume (70 to 100 m^3) foreseen for the HHCAL detector concept, the materials must be dense to minimize the leakage and also cost-effective. It should also be UV transparent (for effective collection of the Cherenkov light) and allow for a clear discrimination between the Cherenkov and scintillation light. The preferred scintillation light is thus at a longer wavelength, and not necessarily bright or fast.

Scintillating glasses [84] offer a very attractive option where large volumes of scintillating material are required, such as for the HHCAL detector concept, and are currently under development for future collider applications. Recent investigations of cerium doped ABS (Aluminoborosilicate) [85,86] and DSB (BaO • 2SiO2) [87, 88] show high density (6 and 4.3 g/cc respectively) for large samples heavily loaded with Gd. Their main limitation is a poorer optical quality, with light attenuation lengths at a level $\sim$ ten cm, as compared to longer than a meter for scintillating crystals used in total absorption calorimeters.

Fast scintillation light also provides timing information about electromagnetic interactions and showers, which may be used to mitigate pile-up effects and/or for particle identification, since the time development of electromagnetic and hadronic showers, as well as minimum ionizing particles, are different. The timing information is primarily determined by the scintillator rise time and decay time, and the number of photons produced. For fast timing, it is important to have a large number of photons emitted in the initial part of the scintillation pulse, e.g. in the first ns, since one is often measuring the arrival time of the particle

Int. J. Mod. Phys. A Downloaded from www.worldscientific.com
by UNIVERSITY OF CALIFORNIA @ BERKE use and distribution is strictly not permitted, except for Open Access articles.

Int. J. Mod. Phys. A 2026.41. Downloaded from www.worldscientific.com
by UNIVERSITY OF CALIFORNIA @ BERKELEY on 09/16/26. Re-use and distribution is strictly not permitted, except for Open Access articles.

in the crystal using the leading edge of the light pulse. A good example of this is BaF_2, which has $\sim 10\%$ of its light in its fast component with a decay time of less than 0.6 ns. Investigations also show that doping BaF_2 with yttrium reduces its slow component significantly, while keeping its ultrafast scintillation component unchanged [89, 90]. Ultrafast crystals of this type provide the best timing resolution [91, 92]. However, light propagation can spread out the arrival time of the scintillation photons at the photodetector due to time dispersion [93]. The time response of the photodetector also plays a major role in achieving good time resolution with fast scintillating crystals.

In summary, the timing precision of a scintillation detector generally depends on five parameters: the rise and decay times of the scintillator, the time dispersion of optical photons in the scintillator, the time response and jitter of the photodetector signal for single photons, and the number of photons that produce the photodetector signal. The numerical formulas that estimate the timing precision as a function of these parameters can be found in [64].

Table-35.5 gives the light yield of other crystals relative to NaI(Tl) and their dependence to temperature variations. The light output was measured for 1.5 X_0 cube crystal samples with a Tyvek paper wrapping and a full end face coupled to a photodetector [94]. The quantum efficiency of the photodetector is taken out to facilitate a direct comparison of crystal's light yield. However, the measured light output produced by a scintillator is usually quoted in terms of the number of photoelectrons per MeV produced by a given photodetector. The relationship between the light yield (LY) in number of photons/MeV produced (N_{photons}/MeV) and the light output (LO) in number of photoelectrons/MeV detected involves the factors for the light collection efficiency (LCE) and the quantum efficiency (QE) of the photodetector:

$$LO = LY \cdot LCE \cdot QE. \tag{35.4}$$

LCE depends on the size and shape of the crystal sample, and includes effects such as the transmission of scintillation light within the crystal (i.e., the bulk attenuation length of the material), scattering from within the crystal, reflections and scattering from the crystal surfaces, and reflections back into the crystal by wrapping materials. These factors can vary considerably depending on the sample, but can be in the range of $\sim$10–60%. The internal light transmission depends on the intrinsic properties of the material, e.g. the density and type of scattering centers and defects that can produce internal absorption within the crystal, and can be highly affected by factors such as radiation damage, as discussed below.

The quantum efficiency depends on the type of photodetector used to detect the scintillation light, which is typically $\sim$15–30% for photomultiplier tubes and higher for silicon photodetectors for visible wavelengths. The response of the detector is usually highly wavelength dependent and should be matched to the particular crystal of interest to give the highest quantum yield at the wavelength corresponding to the peak of the scintillation emission. Fig. 35.3 shows the quantum efficiency for a Hamamatsu R2059 PMT with bi-alkali cathode and quartz window, and the photon detection efficiency (PDE) for a Hamamatsu S14160-3015ps multi-pixel photon counter (MPPC), which is also called a silicon photomultiplier (SiPM), as a function of wavelength. Also shown in the figure are emission spectra of three crystal scintillators, BGO, LSO:Ce/LYSO:Ce and CsI(Tl), and the numerical values of the emission weighted quantum efficiency. The area under each emission spectrum is proportional to crystal's light yield, as shown in Table-35.5, where the quantum efficiencies of the photodetector has been taken out. Results with different photodetectors can be significantly different. For example, the response of CsI(Tl) relative to NaI(Tl) with a standard photomultiplier tube with a bi-alkali photo-cathode (e.g. Hamamatsu R2059) would be 45% rather than 165% because of the photomultiplier's low quantum efficiency at longer wavelengths. For scintillators which emit in the UV, a detector with a quartz window should be used.

For very low energy applications (typically below 1 MeV), the non-proportionality of the scintillation light yield may be important. It has been known for a long time that the number of photons produced is not proportional to the absorbed energy. It is also known that the energy resolution measured by all crystal scintillators for low energy γ-rays is significantly worse than the contribution from photo-electron statistics alone, indicating an intrinsic contribution from the scintillator itself. Precision measurements using a low energy electron beam show that this non-proportionality is crystal dependent [95, 96]. Followup investigations have greatly improved our understanding on this issue [97–102].

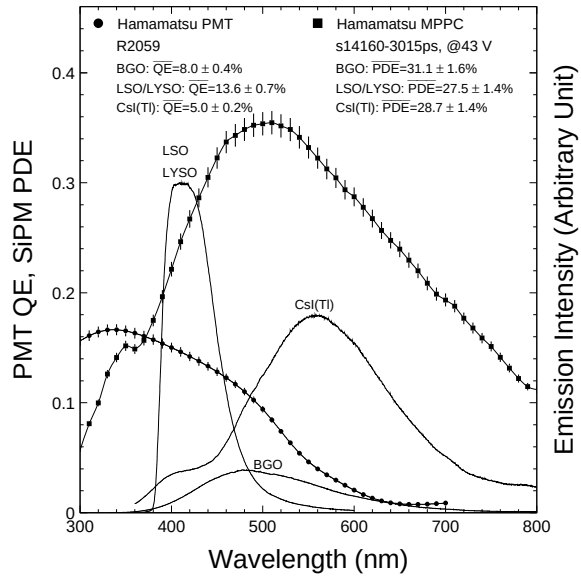

Figure 35.3: The quantum efficiency for a Hamamatsu R2059 PMT with bi-alkali cathode and quartz window and the particle detection efficiency (PDE) for a Hamamatsu S14160-3015ps multi-pixel photon counter (MPPC), which is also called a silicon photomultiplier (SiPM), are shown as a function of wavelength. Also shown in the figure are emission spectra of three crystal scintillators, BGO, LSO and CsI(Tl), and the numerical values of the emission weighted quantum efficiencies. The area under each emission spectrum is proportional to crystal's light yield.

One important issue related to the application of a crystal scintillator is its radiation hardness. Stability of its light output, or the ability to track and monitor the variation of its light output in a radiation environment, is required for high resolution and precision calibration [103]. All known crystal scintillators suffer from ionization dose induced radiation damage [104], where a common damage phenomenon is the appearance of radiation induced absorption caused by the formation of color centers originating from the impurities or point defects in the crystal. This radiation induced absorption reduces the light attenuation length in the crystal, and hence its light output. For crystals with high defect density, a severe reduction of light attenuation length may cause a distortion of the light response uniformity, leading to a degradation of the energy resolution. Additional radiation damage effects may include a reduced intrinsic scintillation light yield (damage to the luminescent centers) and an increased phosphorescence (afterglow). For crystals to be used in a high precision calorimeter in a radiation environment, its scintillation mechanism must not be damaged and its light attenuation length in the expected radiation environment must be long enough so that its light response uniformity, and thus its energy resolution, does not change.

While radiation damage induced by ionization dose is well understood [105], further investigations have been carried out to understand radiation damage caused by hadrons, including both charged hadrons [106] and neutrons [107]. Hadrons may cause damage by two additional fundamental processes: displacement damage and nuclear breakup. Charged hadrons can produce all three types of damage (and it's often difficult to separate them), but neutrons can only produce damage from the last two, and

Int. J. Mod. Phys. A
Downloaded from www.worldscientific.com
by UNIVERSITY OF CALIFORNIA @ BERKE
use and distribution is strictly not permitted, except for Open Access articles.

electrons and photons only produce ionization damage. Studies on hadron induced radiation damage in lead tungstate [108] show a proton-specific damage component caused by fragments from fission induced in lead and tungsten by particles in the hadronic shower. The fragments cause severe, local damage to the crystalline lattice due to their extremely high energy loss over a short distance [108]. An investigation also shows evidence of neutron-specfic damage in various crystals [107]. A more extensive list of investigations on this topic can be found in https://www.its.caltech.edu/~rzhu/.

Most of the crystals listed in Table-35.5 have been used in high energy or nuclear physics experiments when the ultimate energy resolution for electrons and photons is desired, as discussed in Sec. 35.10.2. Examples are the Crystal Ball NaI(Tl) calorimeter at SPEAR, the L3 BGO calorimeter at LEP, the CLEO CsI(Tl) calorimeter at CESR, the KTeV CsI calorimeter at the Tevatron, and the BaBar, BELLE and BES III CsI(Tl) calorimeters at PEP-II, KEK and BEPC II, respectively. Because of their high density and relatively low cost, PWO calorimeters have been used by CMS and ALICE at LHC, by CLAS and PrimEx at CEBAF, and by PANDA at GSI, and is planned to be used for the Backward Endcap Calorimeter for the ePIC experiment at the EIC. Similarly, PbF_2 calorimeters are used by the A4 experiment at MAINZ and by the g-2 experiment at Fermilab. CsI calorimeters are used by KTeV at Fermilab and by the Mu2e experiment at Fermilab. LYSO:Ce crystals are used by the COMET experiment at J-PARC, and by the CMS experiment to build a precision timing layer for the HL-LHC. GAGG:Ce crystals are considered as a candidate scintillator for the LHCb ECAL upgrade for the HL-LHC. Heavy scintillating glass, BaF_2:Y crystal and LuAG:Ce ceramics are considered for CEPC/FCC-ee, Mu2e-II and FCC-hh, respectively.

35.5 Cherenkov detectors

Revised March 2026 by J. Schwiening (GSI Darmstadt).

Although devices using Cherenkov radiation are often thought of as only particle identification (PID) detectors, in practice they are used over a much broader range of applications including; (1) fast particle counters; (2) hadronic PID; (3) electromagnetic calorimeters (EMC); and (4) tracking detectors performing complete event reconstruction. Examples of applications from each category include; (1) the BaBar luminosity detector [109] and the Quartic fast timing counter for the ATLAS Forward Proton Detector, designed to measure small angle scatters at the LHC [110]; (2) the hadronic PID detectors at the B factory detectors—DIRC in BaBar [111], and the modern Imaging Aerogel and TOP counters at Belle II [112]; (3) the CMS Hadron Forward calorimeter based on Cherenkov light emitted in quartz fibers embedded in a steel absorber [113]; and (4) large water Cherenkov counters such as Super-Kamiokande [114].

Cherenkov counters contain two main elements; (1) a radiator through which the charged particle passes, and (2) a photodetector. As Cherenkov radiation is a weak source of photons, light collection and detection must be as efficient as possible. The refractive index n and the particle's path length through the radiator L appear in the Cherenkov relations allowing the tuning of these quantities for particular applications. One or more of the properties of Cherenkov radiation discussed in the Passages of Particles through Matter section (Sec. 34 of this *Review*) are utilized in Cherenkov detectors: the prompt emission of a light pulse; the existence of a velocity threshold for radiation; and the dependence of the Cherenkov cone half-angle θ_c and the number of emitted photons on the velocity of the particle v_p and the refractive index n of the medium. The Cherenkov angle can be calculated as

$$\cos\theta_c = \frac{1}{n(E)\beta}, \tag{35.5}$$

where $\beta = v_p/c$ with c being the speed of light, and E the photon energy. The number of photoelectrons ($N_{\text{p.e.}}$) detected in a given device with radiator of length L is

$$N_{\text{p.e.}} = L\frac{\alpha^2 z^2}{r_e\, m_e c^2}\int \epsilon(E)\,\sin^2\theta_c(E)dE, \tag{35.6}$$

where $\epsilon(E)$ is the efficiency for collecting the Cherenkov light and transducing it into photoelectrons, and $\alpha^2/(r_e\, m_e c^2) = 370\ \text{cm}^{-1}\text{eV}^{-1}$. The quantities ϵ and θ_c are functions of the photon energy. As the typical energy dependent variation of the index of refraction is modest, a quantity called the *Cherenkov detector quality factor* N_0 can be defined as

$$N_0 = \frac{\alpha^2 z^2}{r_e\, m_e c^2}\int \epsilon\, dE, \tag{35.7}$$

so that, taking the charge number $z = 1$ (the usual case in high-energy physics),

$$N_{\text{p.e.}} \approx L N_0 \langle\sin^2\theta_c\rangle. \tag{35.8}$$

This definition of the quality factor N_0 is not universal, nor, indeed, very useful for those common situations where ϵ factorizes as $\epsilon = \epsilon_{\text{coll}}\epsilon_{\text{det}}$ with the geometrical photon collection efficiency (ϵ_{coll}) varying substantially for different tracks while the photon detector efficiency (ϵ_{det}) remains nearly track independent. In this case, it can be useful to explicitly remove (ϵ_{coll}) from the definition of N_0. A typical value of N_0 for a photomultiplier (PMT) detection system working in the visible and near UV, and collecting most of the Cherenkov light, is about 100 cm^{-1}. Practical counters, utilizing a variety of different photodetectors, have values ranging between about 30 and 180 cm^{-1}. Radiators can be chosen from a variety of transparent materials (Sec. 34 of this *Review* and Table 6). In addition to refractive index, the choice requires consideration of factors such as material density, radiation length and radiation hardness, transmission bandwidth, absorption length, chromatic dispersion, optical workability (for solids), availability, environmental impact, and cost. When the momenta of particles to be identified is high, the refractive index must be set close to one, so that the photon yield per unit length is low and a long particle path in the radiator is required. In recent years, the gap in refractive index that has traditionally existed between gases and liquid or solid materials has been partially closed with transparent *silica aerogels* with indices that range between about 1.003 and 1.26. Due to the potential ability to tune the refractive index to the exact requirements of an experiment, metamaterials, including photonic crystals, are being investigated as radiators for future Cherenkov counters [115–117].

Cherenkov counters may be classified as either *imaging* or *threshold* types, depending on whether they do or do not make use of Cherenkov angle (θ_c) information. Imaging counters may be used to track particles as well as identify them. The recent development of very fast photodetectors such as micro-channel plate PMTs (MCP-PMT) (see 35.2 of this *Review*) also potentially allows very fast Cherenkov based time of flight (TOF) detectors of either class [115–117]. The track timing resolution of imaging detectors can be extremely good as it scales approximately as $\frac{1}{\sqrt{N_{\text{p.e.}}}}$.

Threshold Cherenkov detectors [118], in their simplest form, make a yes/no decision based on whether the particle is above or below the Cherenkov threshold velocity $\beta_t = 1/n$. A straightforward enhancement of such detectors uses the number of observed photoelectrons (or a calibrated pulse height) to discriminate between species or to set probabilities for each particle species [119]. This strategy can increase the momentum range of particle separation by a modest amount (to a momentum some 20% above the threshold momentum of the heavier particle in a typical case).

Careful designs give $\langle\epsilon_{\text{coll}}\rangle \gtrsim 90\%$. For a photomultiplier with a typical bialkali cathode, $\int \epsilon_{\text{det}} dE \approx 0.27$ eV, so that

$$N_{\text{p.e.}}/L \approx 90\ \text{cm}^{-1}\,\langle\sin^2\theta_c\rangle \qquad (\textit{i.e.},\ N_0 = 90\ \text{cm}^{-1}). \tag{35.9}$$

Suppose, for example, that n is chosen so that the threshold for species a is p_t; that is, at this momentum species a has velocity

Int. J. Mod. Phys. A 2026.41. Downloaded from www.worldscientific.com
by UNIVERSITY OF CALIFORNIA @ BERKELEY on 09/16/26. Re-use and distribution is strictly not permitted, except for Open Access articles.

$\beta_a = 1/n$. A second, lighter, species b with the same momentum has velocity β_b, so $\cos\theta_c = \beta_a/\beta_b$, and

$$N_{\rm p.e.}/L \approx 90\ {\rm cm}^{-1}\ \frac{m_a^2 - m_b^2}{p_t^2 + m_a^2}. \tag{35.10}$$

For K/π separation at $p = p_t = 1(5)$ GeV/c, $N_{\rm p.e.}/L \approx 16(0.8)$ cm^{-1} for π's and (by design) 0 for K's.

For limited path lengths $N_{\rm p.e.}$ will usually be small. The overall efficiency of the device is controlled by Poisson fluctuations, which can be especially critical for separation of species where one particle type is dominant. Moreover, the effective number of photoelectrons is often less than the average number calculated above due to additional equivalent noise from the photodetector (see the discussion of the excess noise factor in 35.2 of this *Review*). It is common to design for at least 10 photoelectrons for the high velocity particle in order to obtain a robust counter. As rejection of the particle that is below threshold depends on *not* seeing a signal, electronic and other background noise, especially overlapping tracks, can be important. Physics sources of light production for the below threshold particle, such as decay to an above threshold particle, scintillation light, or the production of delta rays in the radiator, often limit the separation attainable, and need to be carefully considered. Well designed, modern multi-channel counters, such as the ACC at Belle [120], can attain adequate particle separation performance over a substantial momentum range.

Imaging counters make the most powerful use of the information available by measuring the ring-correlated angles of emission of the individual Cherenkov photons. They typically provide positive ID information both for the "wanted" and the "unwanted" particles, thus reducing mis-identification substantially. Since low-energy photon detectors can measure only the position (and, perhaps, a precise detection time) of the individual Cherenkov photons (not the angles directly), the photons must be "imaged" onto a detector so that their angles can be derived [121]. Typically the optics map the Cherenkov cone onto (a portion of) a distorted "circle" at the photodetector. Though the imaging process is directly analogous to familiar imaging techniques used in telescopes and other optical instruments, there is a somewhat bewildering variety of methods used in a wide variety of counter types with different names. Some of the imaging methods used include (1) focusing by a lens or mirror; (2) proximity focusing (i.e., focusing by limiting the emission region of the radiation); and (3) focusing through an aperture (a pinhole). In addition, the prompt Cherenkov emission coupled with the speed of some modern photon detectors allows the use of (4) time imaging, a method which is little used in conventional imaging technology, and may allow some separation with particle TOF. Finally, (5) correlated tracking (and event reconstruction) can be performed in large water counters by combining the individual space position and time of each photon together with the constraint that Cherenkov photons are emitted from each track at the same polar angle (Sec. 36.3.1of this *Review*).

In a simple model of an imaging PID counter, the fractional error on the particle velocity (δ_β) is given by

$$\delta_\beta = \frac{\sigma_\beta}{\beta} = \tan\theta_c \sigma(\theta_c)\ , \tag{35.11}$$

where

$$\sigma(\theta_c) = \frac{\langle\sigma(\theta_i)\rangle}{\sqrt{N_{\rm p.e.}}} \oplus C, \tag{35.12}$$

and $\langle\sigma(\theta_i)\rangle$ is the average single photoelectron resolution, as defined by the optics, detector resolution and the intrinsic chromaticity spread of the radiator index of refraction averaged over the photon detection bandwidth. C combines a number of other contributions to resolution including, (1) correlated terms such as tracking, alignment, and multiple scattering, (2) hit ambiguities, (3) background hits from random sources, and (4) hits coming from other tracks. The actual separation performance is also limited by physics effects such as decays in flight and particle interactions in the material of the detector. In many practical cases, the performance is limited by these effects.

For a $\beta \approx 1$ particle of momentum (p) well above threshold entering a radiator with index of refraction (n), the number of σ separation (N_σ) between particles of mass m_1 and m_2 is approximately

$$N_\sigma \approx \frac{|m_1^2 - m_2^2|}{2p^2\sigma(\theta_c)\sqrt{n^2-1}}. \tag{35.13}$$

In practical counters, the angular resolution term $\sigma(\theta_c)$ varies between about 0.1 and 5 mrad depending on the size, radiator, and photodetector type of the particular counter. The range of momenta over which a particular counter can separate particle species extends from the point at which the number of photons emitted becomes sufficient for the counter to operate efficiently as a threshold device ($\sim$20% above the threshold for the lighter species) to the value in the imaging region given by the equation above. For example, for $\sigma(\theta_c)$ =2 mrad, a fused silica radiator ($n = 1.474$), or a fluorocarbon gas radiator (C_5F_{12}, $n = 1.0017$), would separate π/K's from the threshold region starting around 0.15(3) GeV/c through the imaging region up to about 4.2(18) GeV/c at better than 3σ.

Many different imaging counters have been built during the last several decades [115–117]. Among the earliest examples of this class of counters are the very limited acceptance *Differential Cherenkov detectors*, designed for particle selection in high momentum beam lines. These devices use optical focusing and/or geometrical masking to select particles having velocities in a specified region. With careful design, a velocity resolution of $\sigma_\beta/\beta \approx 10^{-4}$–$10^{-5}$ can be obtained [118].

Practical multi-track *Ring-Imaging Cherenkov detectors* (generically called RICH counters) are a more recent development. RICH counters are sometimes further classified by 'generations' that differ based on historical timing, performance, design, and photodetection techniques. Prototypical examples of first generation RICH counters are those used in the DELPHI and SLD detectors at the LEP and SLC Z factory e^+e^- colliders [115–117]. They have both liquid (C_6F_{14}, $n = 1.276$) and gas (C_5F_{12}, $n = 1.0017$) radiators, the former being proximity imaged with the latter using mirrors. The phototransducers are a TPC/wire-chamber combination. They are made sensitive to photons by doping the TPC gas (usually, ethane/methane) with $\sim$ 0.05% TMAE (tetrakis(dimethylamino)ethylene). Great attention to detail is required, (1) to avoid absorbing the UV photons to which TMAE is sensitive, (2) to avoid absorbing the single photoelectrons as they drift in the long TPC, and (3) to keep the chemically active TMAE vapor from interacting with materials in the system. In spite of their unforgiving operational characteristics, these counters attained good $e/\pi/K/p$ separation over wide momentum ranges (from about 0.25 to 20 GeV/c) during several years of operation at LEP and SLC. Related but smaller acceptance devices include the OMEGA RICH at the CERN SPS, and the RICH in the balloon-borne CAPRICE detector [115–117]. Despite their excellent match to the radiator requirement for gaseous RICHes, saturated fluorocarbons may soon need to be replaced due to their high global warming impact. Possible alternatives for a similar refractive index include hydrofluoroolefins or Argon, pressurized at a few bar [115–117].

Later generation counters [115–117] generally operate at much higher rates, with more detection channels, than the first generation detectors just described. They also utilize faster, more forgiving photon detectors, covering different photon detection bandwidths. Radiator choices have broadened to include materials such as lithium fluoride, fused silica, and aerogel.

Vacuum-based photodetection systems (*e.g.*, single or multi anode PMTs, MCP-PMTs, or hybrid photodiodes (HPD)) have become increasingly common (see 35.2 of this *Review*). They handle high rates, and can be used with a wide choice of radiators. Examples include (1) the SELEX RICH at Fermilab, which mirror focuses the Cherenkov photons from a neon radiator onto a camera array made of $\sim$ 2000 PMTs to separate hadrons over a wide momentum range (to well above 200 GeV/c for heavy hadrons);(2) the NA62 RICH at CERN, which uses a 17 m long tank filled with neon gas as radiator and spherical mirrors to focus the photons on two arrays of 2 000 PMTs to separate pions from muons for momenta between 15 and 35 GeV/c; (3) the CBM RICH under

Int. J. Mod. Phys. A
Downloaded from www.worldscientific.com
by UNIVERSITY OF CALIFORNIA @ BERKE
use and distribution is strictly not permitted, except for Open Access articles.

construction at FAIR where the Cherenkov photons, produced in about 30 m^3 of CO_2 radiator gas, are mirror-focused on arrays of multi-anode PMTs (MaPMTs) with a total of about 55,000 pixels, to identify electrons with momenta up to 8 GeV/c; and (4) the LHCb detector now running at the LHC. It uses two separate counters. One volume contains C_4F_{10} (originally in combination with aerogel, which was removed in 2015) while the second volume contains CF_4. Photons are mirror-focused onto arrays of photon detectors to cover a π/K separation momentum range between 1 and 150 GeV/c. Additional upgrades, including the replacement of the HPDs by MaPMTs and improved readout electronics, were performed to deal with increases in luminosity.

Other fast detection systems that use solid cesium iodide (CsI) photocathodes or triethylamine (TEA) doping in proportional chambers are useful with certain radiator types and geometries. Examples include (1) the CLEO-III RICH at CESR that uses a LiF radiator with TEA doped proportional chambers; (2) the ALICE detector at the LHC that uses proximity focused liquid (C_6F_{14} radiators and solid CsI photocathodes (similar photodectors have been used for several years by the HADES and COMPASS detectors), and the hadron blind detector (HBD) in the PHENIX detector at RHIC that couples a low index CF_4 radiator to a photodetector based on electron multiplier (GEM) chambers with reflective CsI photocathodes [115–117].

Recent technological advances in the production of aerogel with improved transparency in the UV range and finely tuned refractive indices enable several new RICH designs. The innovative hybrid geometry of the CLAS12 RICH, with complex photon paths that feature multiple passes through the aerogel tiles, is only possible due to the improved scattering length of the aerogel. It minimizes the material inside of the detector acceptance as well as the size and cost of the photon sensor array. Beam tests have demonstrated that the counter will be able to provide clean π/K separation up to 8 GeV/c. The forward endcap Aerogel RICH (ARICH) for the Belle II upgrade at KEKB, designed to provide clean π/K separation for momenta up to 3.5 GeV/c, is an example of the so-called focusing aerogel approach [122]. The radiator is a dual-layer aerogel, with a thickness of 20 mm for each layer and increasing refractive indices of $n = 1.045$ and $n = 1.055$ along the particle path. The Cherenkov ring images from the two layers overlap on the array of Hybrid Avalanche Photo Detectors (HAPDs), which provide efficient single photon detection in the 1.5 T magnetic field.

A DIRC (Detection [of] Internally Reflected Cherenkov [light]) is a distinctive, compact RICH subtype first used in the BaBar detector [111]. A DIRC "inverts" the usual RICH principle for use of light from the radiator by collecting and imaging the total internally reflected light rather than the transmitted light. It utilizes the optical material of the radiator in two ways, simultaneously: as a Cherenkov radiator and as a light pipe. The magnitudes of the photon angles are preserved during transport by the flat, rectangular cross section radiators, allowing the photons to be efficiently transported to a detector outside the path of the particle where they may be imaged in up to three independent dimensions (the usual two in space and, due to the long photon paths lengths, one in time). Because the index of refraction in the radiator is large ($n \sim 1.47$ for fused silica), the momentum range with good π/K separation goes up to 4–5 GeV/c. It is plausible, but difficult, to extend it up to about 10 GeV/c with an improved design.

The BaBar experiment at the asymmetric PEP-II e^+e^- collider studied CP violation in $\Upsilon(4S)$ decays. Excellent pion/kaon separation for particle momenta up to 4 GeV/c was required. The BaBar DIRC used 4.9 m long, rectangular bars made from synthetic fused silica as radiator and light guide. The photons were imaged via a "pin-hole" through an expansion region filled with 6 000 liters of purified water onto an array of 10 752 densely packed photomultiplier tubes placed at a distance of about 1.2 m from the bar end. During more than 8 years of operation, the BaBar DIRC achieved π/K separation of 2.5 standard deviations or more up to 4 GeV/c momentum. For a pion identification rate around 85% the DIRC provided a kaon misidentification rate well below 1% up to 3 GeV/c.

The next generation of DIRC detectors [123] takes advantage of the new, very fast, pixelated photodetectors becoming available, such as MaPMTs and MCP-PMTs. They typically utilize either time imaging or lens/mirror-focused optics, or both, leading not only to a precision measurement of the Cherenkov angle, but in some cases, to a precise measurement of the particle time of flight, and/or to correction of the chromatic dispersion in the radiator. Examples [115–117] include (1) the Belle II Time of Propagation (TOP) counter that emphasizes precision timing for both Cherenkov imaging and TOF to perform π/K separation of at least 3 standard deviations up to 4 GeV/c; (2) the DIRC upgrade of the GlueX experiment at Jefferson Lab that places four decommissioned BaBar DIRC modules, coupled to upgraded optics and readout, perpendicular to the beamline, the first application of a DIRC in a detector endcap; (3) the high-performance DIRC for the ePIC detector at the EIC, to be installed in 2032, that will combine lens focusing with fast photon time imaging and is expected to provide more than 3 standard deviations π/K separation up to 6 GeV/c; and (4) the TORCH counter being developed for an LHCb upgrade in 2034 which uses DIRC imaging for individual photons with fast photon detectors to provide π/K separation up to 10 GeV/c via particle TOF with a precision of 10-15 ps per particle over a flight path length of 9.5 m.

35.6 Gaseous detectors

35.6.1 *Energy loss and charge transport in gases*

Revised August 2025 by P. Gasik (GSI Darmstadt; FAIR Darmstadt; Technische U., Darmstadt).

Gas-filled detectors rely on localized ionization produced by ionizing particles—charged particles or photons (via photoelectrons)—typically followed by charge multiplication. The statistics of ionization processes, which exhibit asymmetries in the ionization trails, impact the coordinate determination derived from measurements of drift time or the center of gravity of the collected charge. For thin gas layers, the width of the energy loss distribution can be larger than its average, requiring multi-sampling devices or truncated mean analysis for reliable particle identification. In the truncated mean method for calculating $\langle dE/dx \rangle$, the ionization measurements along the particle track are divided into many samples, and a fixed fraction of high-side (and sometimes low-side) values are discarded [124].

Table 35.6: Properties of noble and molecular gases at normal temperature and pressure (NTP: 20° C, 1 atm). E_X, E_I: first excitation, ionization energy; W_I: average energy for creation of electron-ion pair; $dE/dx|_{min}$, N_P, N_T: differential energy loss, primary and total number of electron-ion pairs per cm, for unit-charge minimum ionizing particles. Values often vary, depending on the source, and those in the table should be considered approximate.

Gas	Density, mg cm^{-3}	E_X eV	E_I eV	W_I eV	$dE/dx\|_{min}$ keV cm^{-1}	N_P cm^{-1}	N_T cm^{-1}
H_2	0.084	10.8	15.4	37	0.34	5.2	9.2
He	0.179	19.8	24.6	41.3	0.32	3.5	8
Ne	0.839	16.7	21.6	37	1.45	13	40
Ar	1.66	11.6	15.7	26	2.53	25	97
Xe	5.495	8.4	12.1	22	6.87	41	312
CH_4	0.667	8.8	12.6	30	1.61	28	54
C_2H_6	1.26	8.2	11.5	26	2.91	48	112
iC_4H_{10}	2.49	6.5	10.6	26	5.67	90	220
CO_2	1.84	7.0	13.8	34	3.35	35	100
CF_4	3.78	10.0	16.0	35-52	6.38	52-63	120

The energy loss of charged particles and photons in matter is discussed in Sec. 34. Every ionization process is a quantum mechanical transition initiated by the Coulomb field of the particle and the field created by neighbouring polarizable atoms. The average energy losses are described by the Bethe-Bloch formula with Sternheimer's density effect corrections. The fluctuations caused by Rutherford scattering on quasi-free electrons follow a Landau distribution and the influence of atomic shells is described by the

Int. J. Mod. Phys. A 2026.41. Downloaded from www.worldscientific.com
by UNIVERSITY OF CALIFORNIA @ BERKELEY on 09/16/26. Re-use and distribution is strictly not permitted, except for Open Access articles.

photoabsorption ionization (PAI) model, which allows simulation of each energy transfer [125], with relaxation cascades and simulation of delta-electrons [126]. Table 35.6 provides values of relevant parameters in some commonly used gases at NTP for unit-charge minimum ionizing particles (MIPs) [127] [128]. When an ionizing particle passes through a gas, it produces electron-ion pairs. In many cases, the ejected (primary) electrons possess enough energy to further ionize the medium, giving rise to secondary ionizations. These secondary electrons are generated in the immediate vicinity of the primary ionization site, and together with the primary electrons, they form clusters consisting of one, several, or sometimes many electron-ion pairs. The probability distribution describing the number of electron-ion pairs – both primary and secondary – produced in a single ionization encounter is referred to as the cluster-size distribution. As shown in Table 35.6, the total number of pairs ($N_{\rm T}$) is a few times larger than the number of primaries ($N_{\rm P}$). For different conditions and for mixtures, and neglecting energy transfer processes (*e.g.* Penning effect), one can scale the density, $N_{\rm P}$, and $N_{\rm T}$ with temperature and pressure assuming a perfect gas law.

The probability for a released electron to have an energy E or larger follows an approximate $1/E^2$ dependence (Rutherford law), shown in Fig. 35.4 for Ar at NTP (dotted line, left scale). More detailed estimates taking into account the electronic structure of the medium are shown in the figure, for three values of the particle velocity factor $\beta\gamma$ [129]. The dot-dashed line provides, on the right scale, the practical range of electrons (including scattering) of energy E. As an example, about 0.6% of released electrons have 1 keV or more energy, substantially increasing the total ionization loss. The practical range of 1 keV electrons in argon is approximately 70 μm, which can contribute to the uncertainty in the coordinate determination.

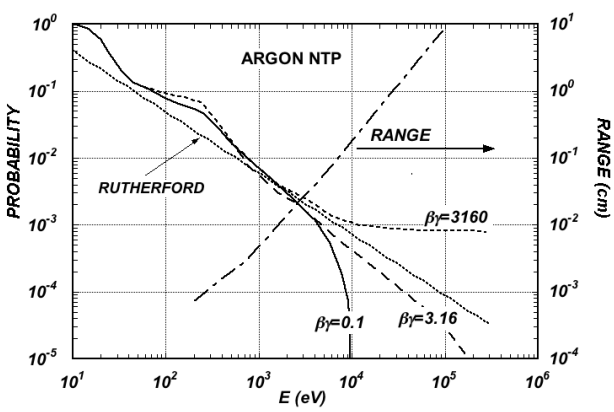

Figure 35.4: Probability of single collisions in which released electrons have an energy E or larger (left scale) and practical range of electrons in Ar at NTP (dot-dashed curve, right scale) [129].

Garfield^{++} [130], together with HEED [126], Degrad [131], Magboltz [132,133], SRIM, ANSYS, COMSOL, and neBEM [134] software packages represent the core simulation tools for microscopic modeling of gaseous detector response. The number of electron-ion pairs per primary ionization, or cluster size, depends little on the medium; it can be computed with the programs mentioned above or experimentally measured. For example, there is about 3% probability for primary clusters to contain ten or more electron-ion pairs in argon [135].

Once released into the gas, electrons and ions drift in opposite directions under the influence of an applied electric field, while simultaneously undergoing diffusion. The electron-molecule collision cross sections are determined by the details of atomic and molecular structure and depend strongly on the electron energy and therefore on the electric field $\boldsymbol{E}$ for most gases. High values of the total electron scattering cross section reduce the electron diffusion and increase the drift velocity; a large inelasticity implies that high fields are required to raise the electron energy. For noble gases, the inelastic cross section is zero until the electrons reach the first excitation and ionization energies, which are on the order of 10 eV; on the contrary, for molecular gases, like CH_4, inelastic channels, involving rotational and vibrational levels, open up at energies above ~0.1 eV. Large drift velocities are achieved by adding polyatomic gases (usually hydrocarbons $C_x H_y$, CO_2, CF_4) which have significant inelastic scattering components at moderate electron energies of a few electronvolts; this results in the electron "cooling" into the energy range of the Ramsauer-Townsend minimum (~0.3 eV in argon) of the elastic ("momentum-transfer") cross-section [128]. Similar to argon, krypton, and xenon also show the Ramsauer-Townsend minimum, while helium and neon do not. Under these circumstances, it is clear that the addition of very small quantities of one gas to another can dramatically modify the average electron energy and alter the dependence of the drift velocity ($v_{\rm d}$) on $\boldsymbol{E}/p$, where p is the gas pressure, and temperature T; this has a particularly strong effect for noble gases, as illustrated in Fig. 35.5 for argon. Carbon tetrafluoride (CF_4) has the largest drift velocity and the lowest electron diffusion among known gases due to the sizeable Ramsauer-Townsend dip in the elastic cross-section, which coincides with very large vibrational modes. Another principal role of the polyatomic gas is to absorb the ultraviolet photons emitted by the excited noble gas atoms. Addition of molecular gases (hydrocarbons or CO_2 is widely used in the proportional counters as a quencher) to noble gas allows to dissipate a good fraction of energy through rotational and vibrational radiationless transitions without the creation of photons or ions. On the contrary, CF_4 has a small quenching cross-section of excited Ar states and light emission in CF_4 (from the far UV to the visible light) is a complex process, involving the creation of CF_3^+ excited states [136].

Extensive collections of experimental data [137] and theoretical calculations based on transport theory permit evaluation of drift and diffusion properties in pure gases and their mixtures. Modern compilations of the electron-molecule cross sections are available at the open-access website LXCAT [138]. Fig. 35.5 and Fig. 35.6 show the drift velocity as well as transverse and longitudinal diffusion for some commonly used gases at NTP, computed with the Magboltz program [132, 133]. For different conditions, the horizontal axis must be scaled inversely with the gas density. The standard deviations for longitudinal ($\sigma_{\rm L}$) and transverse diffusion ($\sigma_{\rm T}$) are specified per centimeter of drift and scale with the square root of the drift distance.

In a simple approximation, gas kinetic theory provides the drift velocity $v_{\rm d}$ as a function of the mean collision time τ and the electric field E: $v_{\rm d} = eE\tau/m_e$ (Townsend's expression). In the presence of an external magnetic field, the Lorentz force acting on electrons between collisions deflects the drifting electrons and modifies the drift properties. The electron trajectories, velocities and diffusion parameters can be computed with Magboltz. The friction force model provides an approximate expression for the vector drift velocity $\boldsymbol{v_{\rm d}}$ as a function of electric and magnetic field vectors $\boldsymbol{E}$ and $\boldsymbol{B}$, of the Larmor frequency $\omega = eB/m_e$, and of the mean collision time τ (a more precise calculation is available in Magboltz, which computes the drift velocity by tracing electrons at the microscopic level through numerous collisions with gas molecules):

$$\boldsymbol{v_{\rm d}} = \frac{e}{m_e}\,\frac{\tau}{1+\omega^2\tau^2}\left(\boldsymbol{E} + \frac{\omega\tau}{B}(\boldsymbol{E}\times\boldsymbol{B}) + \frac{\omega^2\tau^2}{B^2}(\boldsymbol{E}\cdot\boldsymbol{B})\boldsymbol{B}\right) \quad (35.14)$$

To a good approximation, and for moderate fields, one can assume that the energy of the electrons is not affected by the magnetic field, and use for τ the values deduced from the drift velocity at $B = 0$ (Townsend's expression). For $\boldsymbol{E}$ perpendicular to $\boldsymbol{B}$, the drift angle relative to the electric field vector is $\tan\theta_{\rm B} = \omega\tau$ and $v_{\rm d} = (E/B)(\omega\tau/\sqrt{1+\omega^2\tau^2})$. For parallel electric and magnetic fields, the drift velocity and longitudinal diffusion are not affected, whereas the transverse diffusion can be strongly reduced: $\sigma_{\rm T}(B) = \sigma_{\rm T}(B=0)/\sqrt{1+\omega^2\tau^2}$. As an example, the dotted line in Fig. 35.6 represents $\sigma_{\rm T}$ for the classic Ar-CH_4 (90-10) mixture at 4 T. Large values of $\omega\tau \approx 20$ at 5 T are consistent with the measurement of the diffusion coefficient in Ar-CF_4-iC_4H_{10} (95-3-2). This reduction is exploited to substantially improve spatial resolution in the Drift (Sec. 35.6.2) and Time Projection Chambers (Sec. 35.6.4).

Int. J. Mod. Phys. A. Downloaded from www.worldscientific.com
by UNIVERSITY OF CALIFORNIA @ BERKE use and distribution is strictly not permitted, except for Open Access articles.

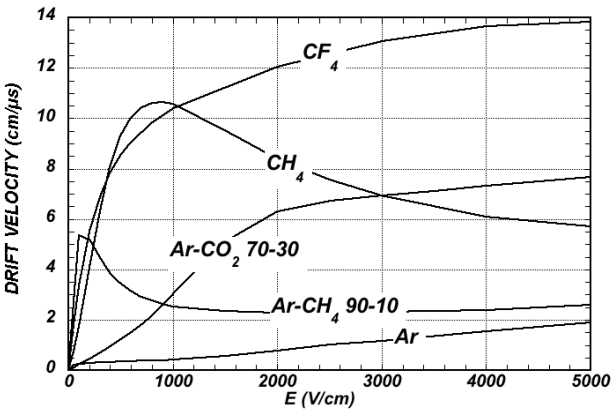

Figure 35.5: Computed electron drift velocity as a function of electric field in several gases at NTP and $B = 0$ [132, 133].

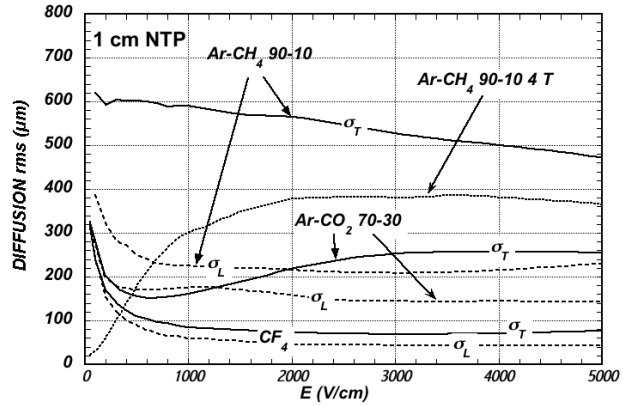

Figure 35.6: Electron longitudinal diffusion ($\sigma_{\rm L}$) (dashed lines) and transverse diffusion ($\sigma_{\rm T}$) (full lines) for 1 cm of drift at NTP and $B = 0$. The dotted line shows $\sigma_{\rm T}$ for the P10 mixture at 4 T [132, 133].

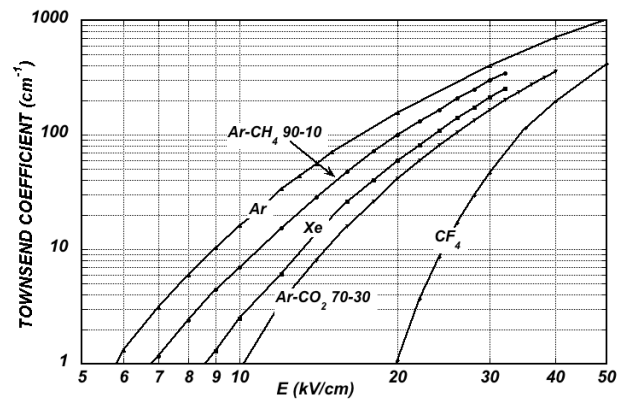

Figure 35.7: Computed first Townsend coefficient α as a function of the electric field in several gases at NTP [132, 133].

In some mixtures containing molecules with electronic affinity, electrons can be captured to form negative ions. Capture cross sections vary considerably with energy and, hence, the electric field. As a consequence, the three-body electron attachment coefficients may differ significantly for the same additive in different mixtures. As an example, at moderate fields (up to 1 kV/cm), the addition of 0.1% of oxygen to an Ar-CO_2 mixture results in an electron capture probability about twenty times larger than in Ar-CH_4. Among common molecules, the largest electron affinities are found for the halogenides, O_2 and H_2O. The attachment probability in O_2 or H_2O is large at low fields and electron energies close to thermal, but decreases at increasing fields. On the contrary, CF_4 is not electronegative at low and moderate fields, but has a large electron capture cross section at fields above ~8 kV/cm, before reaching the avalanche field strengths. Depending on the exact mixture and detector geometry, some signal reduction and energy resolution loss is expected in this gas.

If the electric field is increased sufficiently, electrons gain enough energy between collisions to excite and ionize molecules. Above a gas-dependent threshold, the mean free path for ionization, λ_i, decreases exponentially with the field; its inverse, $\alpha = 1/\lambda_i$, is named the first Townsend coefficient. Free charges originally deposited in the chamber volume are multiplied in the electron avalanche process. Gains of the order of 10^5–10^6 can be achieved, and the detected charge is proportional, via the multiplication factor, to the primary charge liberated by the incoming particle. The detector is operated in the proportional counter mode. In uniform fields, N_0 initial electrons multiply over a length x forming an electron avalanche of size $N = N_0\, e^{\alpha x}$; N/N_0 is the gain of the detector. Fig. 35.7 shows examples of Townsend coefficients for several gas mixtures, computed with Magboltz [132, 133].

Additional ionizing energy transfer mechanisms due to the excited noble gas atoms, called collisional Penning energy transfers, occur when the excitation energy of a noble gas is higher than the ionization potential of an admixture gas. The energy transfer rate, the probability that an excited atom ionizes a quenching agent, is a priori not known for a mixture, but can be extracted from the fits of the experimental gas gain data [139] using the Magboltz simulations [132, 133]. In the gain calculations, the Penning adjusted Townsend coefficient is defined in terms of the total production frequencies of the noble gas excitations and direct ionizations of the mixture. Systematic gas gain measurements for varying mixing ratios and pressures are critical for determining the efficiency of the different mechanisms involved in the transfers. Collisional energy transfer mostly scales linearly with the gas pressure and the fraction of quenching gas in the mixture, while ionization by photons emitted from excitations is independent of the medium [140]. In addition, collisional Penning transfers of some higher excited states can occur before they decay at atmospheric pressure and are not restricted to metastable states of the excited noble gas. For example, the impact of the Penning effect on gas gain is roughly a factor of 10 in Ar-CO_2 mixtures and exceeding a factor of 100 in Ar-C_2H_2 mixtures [140].

The proportionality of the amplification process is gradually lost at continuously increasing voltages, due to the electric field distortions (screening) resulting from the large charge densities around the wire. At the end of the region of limited proportionality, the gain is saturated and does not depend on the initial value of the deposited charge anymore. This is a region of the Geiger-Müller counter where the photon-mediated avalanche over the full length of the anode wire takes place. Finally, after reaching the so-called breakdown voltage $V_{\rm b}$, a discharge region is reached, corresponding to the self-sustaining discharges in which a steady discharge current flows between the electrodes. The voltage beyond $V_{\rm b}$ is so high that, once ionization takes place in the gas, a continuous discharge develops, and the detector can not be used for radiation detection anymore.

Positive ions originating from primary ionization or generated in avalanches undergo drift and diffusion under the influence of the electric field. Negatively charged ions may also be produced by electron attachment to gas molecules. The drift velocity of ions in the fields encountered in gaseous detectors (up to a few kV/cm) is typically about three orders of magnitude smaller than for electrons. The ion mobility μ, the ratio of drift velocity to electric field, is constant for a given ion type up to very high fields. Values of ion mobility at NTP are given in Table 35.7 [141]. For different temperatures and pressures, the mobility can be scaled inversely with the density, assuming an ideal gas law. Both the longitudinal and transverse diffusion of ions are proportional to the square root of the drift time, with a coefficient that depends on temperature but not on the ion mass. Historically, it was assumed that, due to efficient charge-transfer processes, only the ions with the lowest ionization potential would survive after a short drift

Int. J. Mod. Phys. A 2026.41. Downloaded from www.worldscientific.com
by UNIVERSITY OF CALIFORNIA @ BERKELEY on 09/16/26. Re-use and distribution is strictly not permitted, except for Open Access articles.

path in a gas mixture. Recent experimental data, however, indicate that in CO_2-quenched Ar or Ne mixtures the actual signal carriers are $CO_2^+!\cdot(CO_2)_n$ cluster ions rather than bare CO_2^+ or noble-gas ions [142]. Since such cluster ions drift more slowly than the primary ions, the time structure of the induced signals is correspondingly modified. The effect can be present in constant-field detectors and TPCs (see Sec. 35.6.4), and might affect devices such as Micromegas (see Sec. 35.6.3) and drift tubes.

Negative ions, formed through the capture of primary ionization electrons by highly electronegative gas components (e.g., CS_2), can be utilized in negative-ion time projection chambers (TPCs). In such detectors, the negative ions drift toward the anode under the influence of an electric field, with their diffusion reduced to the thermal limit. This technique enables high spatial resolution and can extend the sensitivity of directional dark matter searches [143].

Table 35.7: Mobility of ions in gases and mixtures at NTP [141].

Gas	Mobility μ ($cm^2\ V^{-1}\ s^{-1}$)
He	10.4
Ne	4.7
Ar	1.54
Ar-CH_4	1.87
Ar-CO_2	1.72
CH_4	2.26
CO_2	1.09

35.6.2 *Multi-Wire Proportional and Drift Chambers*

Revised August 2025 by P. Gasik (GSI Darmstadt; FAIR Darmstadt; Technische U., Darmstadt).

Single-wire counters that detect the ionization produced in a gas by a charged particle, followed by charge multiplication and collection around a thin (typically 20 – 50 µm diameter) wire, have been used for decades. Good energy resolution is obtained in the proportional amplification mode, while very large saturated pulses can be detected in the streamer and Geiger modes [144].

35.6.2.1 *Multi-wire proportional chamber, MWPC*

Modern fully electronic devices, multiwire proportional chambers (MWPCs) [145, 146] introduced in the late 1960s, detect, localize, and measure energy deposit by charged particles over large areas. A plane of parallel anode wires at a suitable potential, inserted between two cathodes, can be regarded as a set of independent proportional counters (see Fig. 35.8a). Electrons released in the gas volume drift towards the anodes and produce avalanches in the increasing field. Analytic expressions for the electric field can be found in many textbooks. The fields close to the wires $E(r)$, in the drift region E_D, and the capacitance C per unit length of anode wire is approximately given by

$$E(r) = \frac{CV_0}{2\pi\epsilon_0}\frac{1}{r} \qquad E_D = \frac{CV_0}{2\epsilon_0 s} \qquad C = \frac{2\pi\epsilon_0}{\pi(\ell/s) - \ln(2\pi a/s)}\ , \tag{35.15}$$

where r is the distance from the center of the anode, s is the wire spacing, ℓ and V_0 are the distance and potential difference between anode and cathode, and a is the anode wire radius.

In wire chambers, most of the increase of avalanche particle density occurs very close to the anode wires, and a simple electrostatic consideration shows that the largest fraction of the detected signal is due to the motion of positive ions receding from the wires. The electron component, although very fast, contributes very little to the signal. This determines the characteristic shape of the detected signals in the proportional mode: an extremely sharp onset followed by a long "ion tail". The latter limits the time resolution of the detector, and is usually removed by differentiation of the signal.

Because of electrostatic forces, anode wires are in equilibrium only for a perfect geometry. Small deviations result in forces displacing the wires alternatively below and above the symmetry plane, sometimes with catastrophic results [147]. These displacement forces are countered by the mechanical tension of the wire, up to a maximum unsupported stable length, L_M [148], above which the wire displaces:

$$L_M = \frac{s}{CV_0}\sqrt{4\pi\epsilon_0 T_M} \tag{35.16}$$

The maximum tension T_M depends on the wire diameter and modulus of elasticity. Internal supports and spacers can be used in the construction of longer detectors to overcome limits on the wire length imposed by Eq. (35.16).

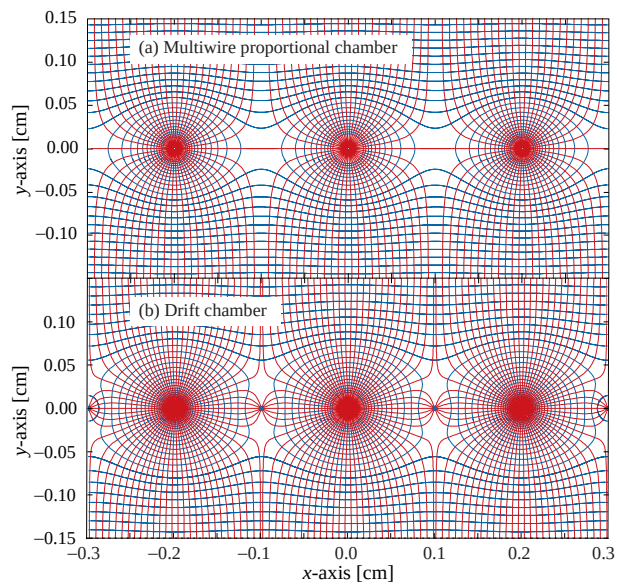

Figure 35.8: Electric field lines and equipotentials in (a) a multiwire proportional chamber and (b) a drift chamber.

Detection of charge on the wires over a predefined threshold provides the transverse coordinate to the wire with an accuracy comparable to that of the wire spacing. The coordinate along each wire can be obtained by measuring the ratio of the collected charge at the two ends of the resistive wires. The cathode planes can be fabricated in the form of a group of wires or isolated strips, which are often patterned in orthogonal directions. By exploiting the charge profile induced by avalanches on segmented cathodes, the so-called electronic center-of-gravity (COG) method enables track localization with sub-millimeter accuracy. Due to the statistics of energy loss and asymmetric ionization clusters, the position accuracy is ∼50 µm rms for fast particles perpendicular to the wire plane, but degrades to ∼250 µm at 30° to the normal [149].

35.6.2.2 *Drift chambers*

Drift chambers, developed in the early '70s, can be used to estimate the space coordinate perpendicular to the wires by exploiting the arrival time of electrons at the anodes if the time of interaction is known [150]. The distance between anode wires is typically several centimeters, enabling the coverage of large areas at reduced cost. In the original design, a thicker wire (the field wire, often from Cu-Be or Al) at the proper voltage, placed between the anode wires (e.g., gold-plated tungsten), removes the low-field region at the mid-point between anodes and improves charge collection (Fig. 35.8b). In some drift chamber designs, and with the help of suitable voltages applied to field-shaping electrodes, the electric field structure is adjusted to improve the linearity of the space-to-drift-time relation, resulting in better spatial resolution [151].

Drift chambers can achieve a longitudinal spatial resolution from timing measurements on the order of 100 µm (rms) or better for minimum ionizing particles, depending on the geometry and operating conditions. However, a degradation of resolution is observed due to primary ionization statistics for tracks close to the anode wires, caused by the spread in arrival time of the nearest

Int. J. Mod. Phys. A. Downloaded from www.worldscientific.com
by UNIVERSITY OF CALIFORNIA @ BERKE use and distribution is strictly not permitted, except for Open Access articles.

ionization clusters [152]. The effect can be reduced by operating the detector at higher pressures. Sampling the drift time on rows of anodes led to the concept of multiple arrays, such as the multi-drift module [153] and the JET chamber [154]. A measurement of drift time, together with the recording of charge sharing from the two ends of the anode wires, provides the coordinates of segments of tracks. An ultimate drift chamber design is the Time Projection Chamber (TPC) concept [155], which provides 3D precision tracking with low material budget and enables particle identification through differential energy loss $\mathrm{d}E/\mathrm{d}x$ measurement or cluster counting $\mathrm{d}N_{\mathrm{cl}}/\mathrm{d}x$ techniques (see Sec. 35.6.4). In all cases, a good knowledge of electron drift velocity and diffusion properties is required. This has to be combined with the knowledge of the electric fields in the structures [133]. For an overview of detectors exploiting the drift time for coordinate measurement, see Refs. [148, 156].

Multiwire and drift chambers have been operated with a variety of gas fillings and operating modes, depending on experimental requirements. For example, a mixture of argon, isobutane and freon in the volume proportions 70-29.6-0.4 [146], permits very high and saturated gains ($\sim 10^6$), i.e., a pulse-height distribution independent of the number of primary ionization charges. While this mixture was successfully used in early wire chambers, it was later found to suffer from severe aging effects. Similarly, light mixtures based on helium and hydrocarbons, although commonly employed, do not provide the reliability needed for long-term, high-rate operation [157]. To meet the demands of future colliders, dedicated R&D is required to identify suitable hydrocarbon-free gas mixtures that can ensure both stable operation and the desired detector performance.

The next generation of ultralight central trackers for future colliders aims at minimizing material budget, where the dominant contribution to the radiation length originates from tungsten wires. Significant progress has been achieved through the development of alternative wire materials (e.g., carbon monofilaments) and novel wiring and assembly procedures, building on experience from detectors such as the DAFNE KLOE Drift Chamber and its recent evolution for the MEG2 experiment [158].

35.6.2.3 *Straw and drift tubes*

Although very powerful in terms of performance, multi-wire structures can have reliability issues, as a single broken wire can disable a larger part or even the entire detector. Introduced in the 1980s, straw and drift tube systems make use of large arrays of proportional counters where each wire is encased and protected in a tube and acts as an independent wire counter [159]. Techniques for low-cost mass production of these detectors have been developed for large experiments, such as the Transition Radiation Tracker and the Drift Tubes arrays for CERN's LHC experiments [160]. The state-of-the-art straw trackers utilize new construction techniques of ultrasonic welding of the straw film tube, keeping it straight and withstanding the surrounding vacuum pressure without breaking (see [161], for example). Future efforts for straw detectors, e.g., COMET Phase-II at JPARC, Mu2e-II at Fermilab, or SHiP at CERN, will focus on ultra-thin wall developments, smaller tube diameters, long and thin wire handling, precise mechanics, and innovative designs.

35.6.2.4 *High-rate effects*

The production of positive ions in the avalanches and their slow drift before neutralization result in a rate-dependent accumulation of positive charge in the detector. This may result in significant field distortion, gain reduction, and degradation of spatial resolution. As shown in Fig. 35.9 [162], the proportional gain drops above a charge production rate around 10^9 electrons per second per millimeter of wire, independently of the avalanche size. For a proportional gain of 10^4 and 100 electrons per track, this corresponds to a particle flux of $10^3\,\mathrm{s}^{-1}\mathrm{mm}^{-1}$ (1 kHz/mm^2 for 1 mm wire spacing). Improvement of rate capability can be achieved by reducing the anode-to-cathode distance.

During the operation of gaseous detectors in particle accelerator experiments, performance degradation due to the formation of polymer deposits (so-called ageing) on electrode surfaces is often observed. Ageing phenomena can lead to operational instabilities and even total malfunctioning of the detectors operated under increasing charge density doses [163]. This process has been extensively investigated both in operating experiments and in dedicated laboratory studies. In general, gas polymerisation originates from the use of hydrocarbons as quenchers as well as from the outgassing of organic pollutants from certain insulators, glues, and silicon oils. Since the deposited layers are usually insulating, the addition of water vapour can sometimes mitigate performance degradation, although it does not necessarily stop the polymerisation process. Modern detectors, therefore, rely on a strict selection of construction materials and carefully controlled gas mixtures and purities, allowing the collection of several C/cm^2 on the relevant electrodes without observable ageing effects.

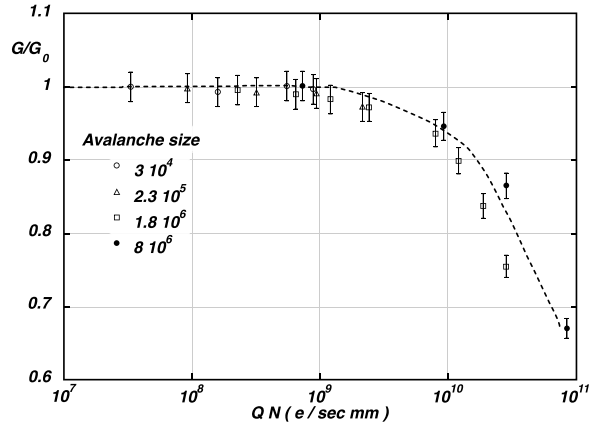

Figure 35.9: Charge rate dependence of normalized gas gain G/G_0 (relative to zero counting rate) in proportional thin-wire detectors [162]. Q is the total charge in a single avalanche; N is the particle rate per wire length.

35.6.3 *Micro-Pattern Gas Detectors*

Revised August 2025 by P. Gasik (GSI Darmstadt; FAIR Darmstadt; Technische U., Darmstadt).

Despite continuous improvements, position-sensitive detectors based on wire structures remain fundamentally limited by diffusion processes and space-charge effects, which restrict localization accuracies to about 50–100 µm [164]. Advances in microelectronics and photolithographic technology on flexible and standard PCB substrates enabled, toward the end of the 20th century, the development of novel Micro-Pattern Gaseous Detectors (MPGD) [165–167]. From the outset, the objective was to design devices combining high-rate capability (up to 10^6 Hz/mm^2), excellent spatial resolution (down to 30 µm), single-photoelectron timing in the nanosecond range, large sensitive area and dynamic range, superior radiation hardness, and cost-effectiveness for large-area coverage. Today, a broad family of MPGD technologies is being developed and optimized for a wide spectrum of applications, including [168, 169]: the Micro-Strip Gas Chamber (MSGC), Gas Electron Multiplier (GEM), Micro-Mesh Gaseous Structure (Micromegas), THick GEMs (THGEM, also referred to as Large Electron Multipliers, LEM), Resistive Plate WELL (RPWELL), GEM-derived architectures such as the µ-RWELL, the Micro-Pixel Gas Chamber (µ-PIC), and integrated gaseous detector readout concepts (GridPix, InGrid) that couple amplification stages with solid-state pixel detector ASICs (e.g., Medipix or Timepix).

The **MSGC** concept, invented in 1988, was the first of the micro-structure gas chambers [165]. It consists of a set of tiny parallel metal strips laid on a thin resistive support, alternatively connected as anodes and cathodes, and resembles a multi-anode proportional counter. Through an accurate and simple photolithography process, the anode strips can be made very narrow ($\sim$10 µm) with a typical pitch (distance between strips) of $\sim$100 µm. When appropriate potentials are applied to the electrodes, electrons released in the drift volume move toward the strips and multiply in the high-field region. Owing to the small

Int. J. Mod. Phys. A 2026.41. Downloaded from www.worldscientific.com
by UNIVERSITY OF CALIFORNIA @ BERKELEY on 09/16/26. Re-use and distribution is strictly not permitted, except for Open Access articles.

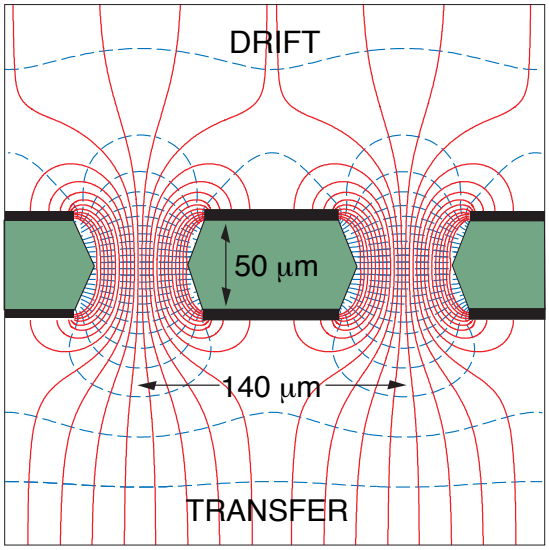

Figure 35.10: Schematic view and typical dimensions of the hole structure in the GEM amplification cell. Electric field lines (solid) and equipotentials (dashed) are shown. Electron trajectories do not strictly follow the electric field lines, since drifting electrons undergo isotropic scattering with gas molecules and, consequently, diffuse transversely.

anode-to-cathode distance, the fast removal of positive ions by nearby cathode strips reduces space charge build-up and significantly improves the rate capability, compared to the wire counter. Despite their promising performance, experience with MSGCs has raised serious concerns about their long-term behavior. There are several major processes, particularly at high rates, leading to the MSGC operational instabilities: substrate charging-up and time-dependent distortions of the electric field, surface deposition of polymers ("ageing") during sustained irradiation, and destructive discharges under exposure to heavily ionizing particles [170]. The physical parameters used to manufacture and operate these detectors (substrate material, metal of strips, type and purity of the gas mixture) appeared to play dominant roles in determining the medium- and long-term stability. The problems encountered inspired the development of novel structures, using modern photolithographic processes: GEM, Micromegas, and others, having increased reliability and radiation hardness.

A **GEM** detector consists of a thin-foil copper-insulator-copper sandwich chemically perforated to obtain a high density of holes in which avalanches occur [166, 171]. The hole diameter is typically of $\mathcal{O}(50\ \mu\text{m})$, with a hole pitch of 140 µm, which can be further optimized depending on the application. The central insulator is usually (in the original design) a polyimid foil, with a thickness of 50 µm. Application of a potential difference between the two metal sides of the GEM generates the electric fields indicated in Fig. 35.10. Each hole acts as an independent proportional counter. Electrons created by primary ionization in the drift gap above the GEM foil drift into its holes, where they undergo avalanche multiplication in the strong electric field (50–70 kV/cm). A significant fraction of the avalanche electrons exits the multiplication region and is extracted into the transfer gap below the foil, from where it can either be collected by an electrode or injected into a subsequent amplification stage. Systematic measurements with cascaded multi-GEM structures confirm that the gains and charge transfer processes are predictable from electrostatic considerations and avalanche development models; an overall gas gain well above 10^4 can be reached in the presence of highly ionizing particles, while strongly reducing the risk of discharges [172]. Other important parameters, such as attachment or diffusion, depend on the gas mixture composition and the reduced electric field E/p, where E is the electric field and p is the gas pressure. The majority of charges created in the avalanche process follow the electric field lines and are collected by the metallic electrodes. Owing to diffusion, however, a fraction may instead deposit on dielectric surfaces, thereby modifying the field configuration and affecting both the gain and the transparency of the structures [173]. This phenomenon is known as the "charging-up" effect; its time constant and amplitude depend strongly on the hole geometry.

The negative signal on the readout anode (below the last GEM in a multi-GEM structure) is primarily induced by the motion of electrons, with only a minor contribution from the ions produced in the amplification process. As a result, the signal is very fast, with a width determined by the drift of the high-mobility electrons over a distance of a few millimetres. Depending on the gas mixture, this enables time resolutions better than 10 ns. The achievable energy resolution is comparable to that of conventional proportional counters, around 17% FWHM for 5.9 keV X-rays [169].

For position measurements, the readout anode can be segmented into strips or pads. Because of the diffusion of the electron cloud in the transfer gaps between GEM foils and in the induction gap above the anode, the charge is shared among several neighbouring readout elements. A centre-of-gravity reconstruction of this charge distribution yields a spatial resolution that surpasses the segmentation pitch. In practice, resolutions well below 100 µm can be obtained, reaching 30 µm with finely segmented electrodes.

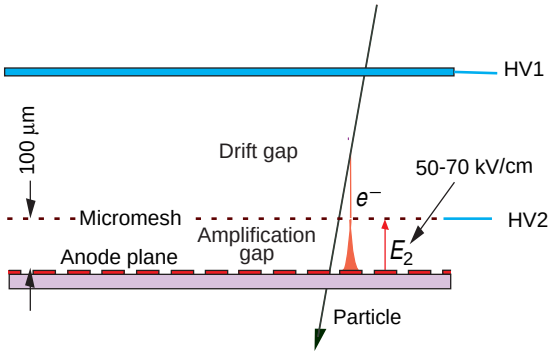

Figure 35.11: Schematic drawing of the Micromegas detector.

A **Micromegas** is a thin parallel-plate avalanche counter, as illustrated in Fig. 35.11 [167]. It employs a stretched metallic mesh, suspended on insulating pillars at a distance of $\mathcal{O}(100\ \mu\text{m})$ above a readout electrode, consisting of strips or pads of conductor printed on an insulating board. The pillars are attached to the mesh and patterned regularly using photolithography techniques. Electrons from the primary ionization drift through the mesh into the narrow multiplication gap, where they are amplified. The electric field is largely homogeneous in both the drift region (∼1 kV/cm) and the amplification region (50–70 kV/cm), but assumes a funnel-like shape near the micromesh openings: the field lines are compressed into a diameter of only a few micrometers, depending on the field ratio between the two gaps. The electron transparency, i.e. the fraction of ionization electrons transmitted into the amplification gap, is determined by the mesh geometry and the ratio of drift to amplification fields. High collection efficiency is obtained when the drift field exceeds the amplification field by a factor of 30–40 [169]. In the narrow multiplication region, small variations of the amplification gap are approximately compensated by the inverse dependence of the Townsend coefficient on the electric field, resulting in a more uniform gain. The transverse size of the electron avalanche due to diffusion is on the order of 10–15 µm, depending on the gas mixture, the electric field, and the gap width. This results in excellent spatial resolution, reaching about 12 µm for MIPs [174]. Most positive ions created in the avalanche process are quickly removed by the micromesh. This prevents space-charge accumulation and leads to very fast signals (∼100 ns), dominated by the electrons, with a small tail contribution from the ions.

Employment of photolithography and etching techniques allows for an improved spatial resolution and improved rate capabilities

Int. J. Mod. Phys. A
by UNIVERSITY OF CALIFORNIA @ BERKE
nloaded from www.worldscientific.com
use and distribution is strictly not permitted, except for Open Access articles.

(up to a few MHz/cm^2). For the same reason, the $E \times B$ effects can be neglected. The absence of space-charge effects in GEMs at the highest rates reached so far, thanks to its fine-pitch structure of a few hundred microns, improves the maximum rate capability by more than two orders of magnitude compared to MWPC (see Fig.35.12) [175] [176]. Even larger rate capability has been reported for Micromegas [177]. In addition, the peculiar shape of the electric field lines obtained in MPGD structures provides intrinsic ion feedback reduction capabilities (see also Sec. 35.6.4).

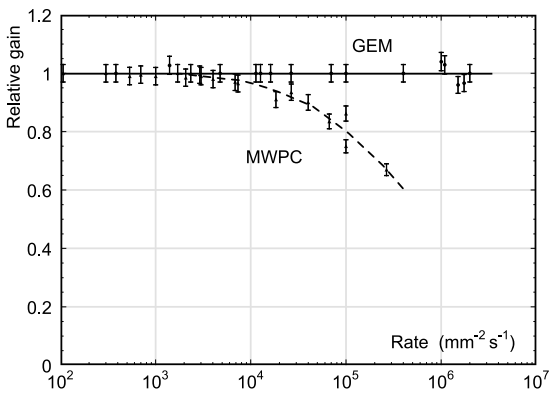

Figure 35.12: Normalized gas gain as a function of particle rate for MWPC [175] and GEM [176].

The fine granularity and high-rate capability of GEM and Micromegas can be fully exploited by using high-density pixel readout with a size corresponding to the intrinsic width of the detected avalanche charge. An elegant solution is the use of a CMOS pixel ASIC, assembled directly below the GEM or Micromegas amplification structure. Modern wafer post-processing technology allows an integration of a small-scale micromesh grid directly on top of a Timepix chip, thus forming an integrated MPGD readout, called GridPix concept (see Fig.35.13) [178]. With this arrangement, avalanche electrons are collected on the metalized input pads, exposed to the gas, and signals are induced at the input gate of a charge-sensitive preamplifier. Every pixel is then directly connected to the amplification and digitization circuits, integrated in the underlying CMOS layers. A thin insulating layer, e.g., a few µm of silicon nitride, is usually deposited on top of CMOS ASIC to protect against destructive discharges across the $\mathcal{O}(50$ µm) amplification gap. The GridPix concept provides the high granularity needed to resolve individual electron clusters (separated by an average distance of a few hundred µm) and to determine energy loss by the cluster counting technique ($\mathrm{d}N/\mathrm{d}x$), rather than by the charge measurement, with a precision better than 3 %. New structures, where a GEM foil is facing the Medipix chip, forming the GEMpix detector, are in use for medical applications [179] as well as for monitoring the radioactive waste [180].

Gaseous detectors represent the most cost-effective solution to cover very large areas with photosensitive elements. MPGD-based gaseous photomultipliers, conceived to overcome the limitations of MWPCs, with semi-transparent or reflective photocathodes (PC), allow for minimizing PC aging due to the ion and photon feedback and to avoid secondary effects causing electrical instability. For RICH applications requiring large-area coverage and moderate spatial resolution, coarser macro-patterned structures such as THGEM offer an interesting, cheaper solution [181].

Following the same principles, a **THGEM** shares a structural similarity with a GEM foil but features dimensions larger by roughly an order of magnitude in all directions. Instead of a thin polyimide sheet, it employs a thick PCB substrate as the dielectric, with holes produced through mechanical drilling and subsequent chemical rim etching of the metal cladding. While the spatial resolution of a THGEM is reduced compared to that of GEMs, it offers a robust alternative for large-area cryogenic detectors or photodetectors. Notably, MPGDs are already applied in single-photon detection—for instance, in the COMPASS RICH detector, which uses a hybrid architecture composed of two THGEM layers (one coated with a CsI photocathode) followed by a Micromegas as the final amplification stage.

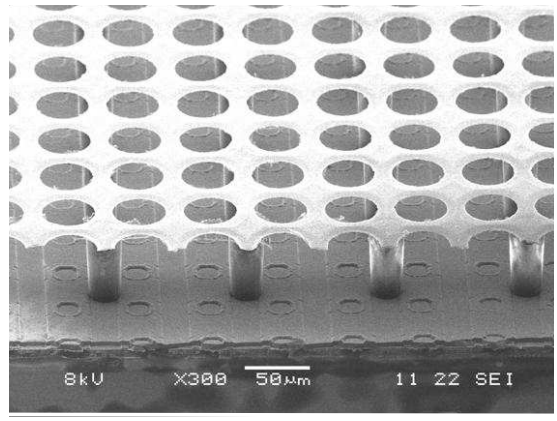

Figure 35.13: Photo of the Micromegas ('GridPix") detector. The grid holes can be accurately aligned with the readout pixels of the Timepix CMOS chip. The insulating pillars are centered between the grid holes, thus avoiding dead regions.

Resistive electrodes are increasingly employed in MPGD-based detectors to enhance spatial resolution and reduce the number of readout channels via charge sharing. Moreover, they provide effective spark protection for front-end electronics and reduce the discharge probability. When used as a high-voltage electrode or as a resistive layer capacitively coupled to the readout elements (e.g., strips or pads), they introduce a self-quenching mechanism that suppresses discharge development.

As an example, closed-geometry THGEM-based structures, known as **RPWELL** [182], have been developed, incorporating resistive anodes and combining features of THGEMs with those of Resistive Plate Chambers (RPCs, see Sec. 35.6.6). The concept consists of a single-faced THGEM, copper-clad only on its top side, placed directly on a resistive film deposited on a thin insulating sheet. Compared to a standard THGEM with an induction gap, the RPWELL configuration allows higher gains to be reached at lower applied voltages across the THGEM electrode, owing to the stronger electric field inside the closed holes.

With the gas discharge quenching capabilities, on the other hand, gain reduction comes into play at higher rates. In one of the pioneering studies with resistive Micromegas it was shown that the signal amplitude slowly decreases with increasing rate, reaching a drop of ∼20% at the rate of 10 kHz/cm^2 [183, 184].

Further improvements in resistive-electrode technology continue. A diamond-like carbon (DLC), a class of meta-stable amorphous carbon material that contains both diamond-structure and graphite-structure, has recently attracted much attention in the MPGD community and is exploited to make resistive electrodes to suppress discharges occurring in MPGDs [185, 186]). The DLC coating can also reduce gain variations over time and minimize charging-up effects.

One such implementation is the **µ-PIC** structure, an industrially manufactured PCB featuring anode strips on one side and orthogonal cathode strips on the opposite side. Along the cathode strips, a regular pattern of uncoated regions is formed; at the center of each, a conductive "dot" connected via a buried electrode in the thin substrate transmits the anode potential. Electron avalanches develop in the high-electric-field region surrounding these point-like anodes. Compared to MSGCs, the electric field near the cathode edges is significantly reduced, leading to a lower discharge probability. Furthermore, a DLC coating on the cathode strips ensures tolerance to occasional discharges [187].

A very promising GEM-derived architecture is the **µ-RWELL** [188], featuring a pitch approximately seven times smaller than that of the RPWELL. Various configurations of the

Int. J. Mod. Phys. A 2026.41. Downloaded from www.worldscientific.com
by UNIVERSITY OF CALIFORNIA @ BERKELEY on 09/16/26. Re-use and distribution is strictly not permitted, except for Open Access articles.

resistive stage (DLC) have been explored during the detector's development, culminating in a high-rate-optimized design that incorporates 3D charge evacuation through conductive vias [189]. This layout enables the detector to achieve gains up to 10^4 in a single amplification stage, and a rate capability exceeding $10\,\mathrm{MHz/cm^2}$.

A major step toward large-scale applications has been achieved through both conceptual consolidation and the development of industrial, cost-effective MPGD manufacturing techniques, such as resistive Micromegas [183] and single-mask or self-stretching GEM methods [190]. The successful scaling of MPGDs to very large single-unit detectors of $\mathcal{O}(\mathrm{m}^2)$ has enabled their deployment in the High-Luminosity LHC upgrades: Micromegas now cover an area of about $1000\,\mathrm{m}^2$ in the New Small Wheel of the ATLAS muon endcaps, GEMs are employed in the CMS muon system and the ALICE TPC readout, and a GEM+µRWELL hybrid is foreseen for the upgrade of the innermost regions of the LHCb muon system.

Exploiting the Micromegas, GEM, and µ-RWELL ability to measure both position and arrival time of the charge released in the drift gap, a novel µ-TPC concept has been developed. It permits achieving nearly constant spatial resolution over a wide range of particle incident angles and allows 3D track reconstruction with a single MPGD layer [191]

The consolidation of well-established technologies has been accompanied by the emergence of novel ones, often tailored to specific applications. Building on the Micromegas and GEM concepts, modern developments increasingly adopt hybrid approaches that integrate different elements within a single device – for instance, combining gaseous with non-gaseous detectors, as in optically read out detectors. Hybrid structures, combining various MPGD technologies, aimed at enhancing detector performance, remains a valuable strategy to address future experimental challenges such as high granularity and picosecond-level timing (e.g., the PICOSEC-Micromegas concept [192]). Moreover, GEMs, Micromegas, and µ-RWELLs can be bent to form cylindrically curved, ultra-light inner tracking systems that operate without support or cooling structures [193].

A clear direction for future MPGD developments is the use of resistive materials and related detector architectures. Their introduction enhances detector stability and allows higher gain to be reached within a single multiplication stage. Beyond resistive electrodes, further progress requires novel materials and advanced fabrication techniques. Contributions to detector concepts are needed in several areas, including resistive layers, solid-state photon and neutron converters, and innovative nanotechnology components. Material studies are particularly relevant for meeting stringent requirements such as low outgassing, radiation hardness, radio-purity, converter robustness, and compatibility with eco-friendly gases. The next generation of MPGDs can also profit from emerging technologies, such as Micro-Electro-Mechanical Systems (MEMS), advanced sputtering methods, novel photoconverters, and 3D-printed amplification structures or cooling circuits. These developments are being actively pursued in the framework of the world-wide CERN-DRD1 collaboration and its broad program of R&D on gaseous detector technologies [194].

35.6.4 *Time-projection chambers*

Revised August 2023 by C. Lippmann (GSI Darmstadt).

The Time Projection Chamber (TPC) concept was invented by David Nygren in the 1970's [195]. It consists of a cylindrical or square field cage that is filled with a gaseous (or liquid) detection medium. Charged particles produce tracks of ionization electrons that drift in a uniform electric field towards a position-sensitive amplification stage which provides a 2D projection of the particle trajectories. The third coordinate can be calculated from the arrival times of the drifted electrons. The start for this drift time measurement is usually derived from an external detector, e.g. a fast interaction trigger detector.

This section focuses on the gas-filled TPCs that are often used in particle or nuclear physics experiments at accelerators on account of their low material budget. For neutrino physics (Sec. 36) or for detecting rare events (Sec. 36.4), on the contrary, usually high density and large active mass are required, and a liquid detection medium is favored.

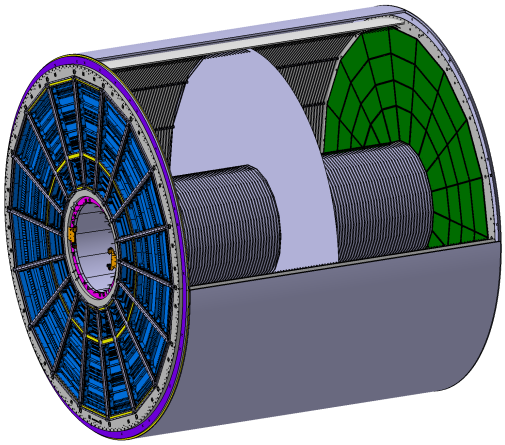

Figure 35.14: Schematic view of the ALICE TPC [196, 197]. The drift volume with 5 m diameter is divided into two halves, each providing 2.5 m drift length. The amplification stage has recently been upgraded from wire planes to GEMs.

The TPC enables full 3D measurements of charged particle tracks, which gives it a distinct advantage over other tracking detector designs which record information only in two-dimensional detector planes and have less overall segmentation. The track points recorded in a TPC are basically adjacent, which facilitates the track finding enormously. This advantage is often exploited for pattern recognition in events with large numbers of particles, e.g. heavy-ion collisions. Two examples of modern large-volume gaseous TPCs are shown in (Figure 35.14) and (Figure 35.15).

Identification of the charged particles crossing the TPC is possible by simultaneously measuring their momentum and specific energy deposit through ionisation ($\mathrm{d}E/\mathrm{d}x$). The momentum, as well as the charge sign, are calculated from a helix fit to the particle trajectory in the presence of a magnetic field (typically parallel to the drift field). For this application, precise spatial measurements in the plane transverse to the magnetic field are most important. The specific energy deposit is estimated from many charge measurements along the particle trajectory (e.g. one measurement per anode wire or per row of readout pads). As the charge collected per readout segment depends on the track angle and on the ambient conditions, the measured values are corrected for the effective length of the track segments and for variations of the gas temperature and pressure. The most probable value of the corrected signal amplitudes for a given track provides the best estimator for the specific energy deposit (see Sec. 34.2.3); it is usually approximated by the truncated mean, i.e. the average of the 50%–70% smallest values. The resulting particle identification performance is illustrated in (Figure 35.16), for the ALICE TPC.

The dependence of the achievable energy resolution on the number of measurements N, on the thickness of the sampling layers t, and on the gas pressure P can be estimated using an empirical formula [199]:

$$\sigma_{dE/dx} = 0.41\ N^{-0.43}(t\,P)^{-0.32}. \tag{35.17}$$

Typical values at nominal pressure are $\sigma_{dE/dx} = 4.5$ to 7.5%, with $t = 0.4$ to 1.5 cm and $N = 40$ up to more than 300. The record, with an unprecedented energy resolution of 3%, is held by the PEP-4/9 TPC [200], due to the high gas pressure of 8.5 bar.

The greatest challenges for a large TPC are due to the length of the drift of up to a few meters. In particular, it can make the device sensitive to small distortions in the electric field. Such distortions can arise from a number of sources, e.g. imperfections in the field cage construction or the presence of ions in the drift volume. The electron drift in a TPC in the presence of a magnetic

Int. J. Mod. Phys. A
by UNIVERSITY OF CALIFORNIA @ BERKE
nloaded from www.worldscientific.com
use and distribution is strictly not permitted, except for Open Access articles.

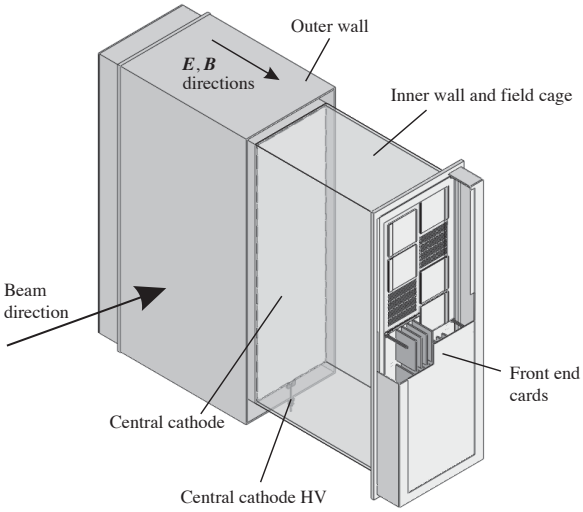

Figure 35.15: One of the 3 TPC modules for the near detector of the T2K experiment [198]. The size is $2 \times 2 \times 0.8\,\mathrm{m}^3$. Micromegas devices are used for gas amplification and readout.

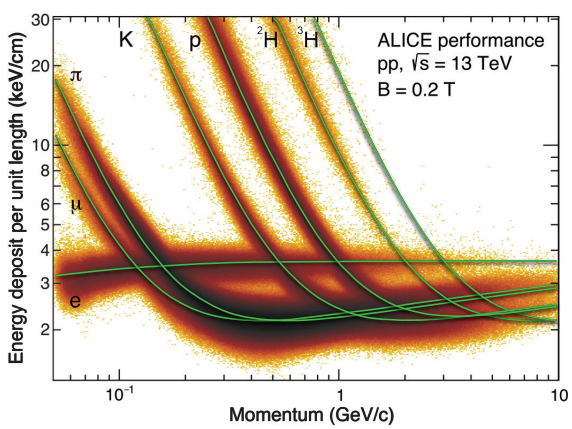

Figure 35.16: Energy deposit versus momentum measured in the ALICE TPC.

field is defined by Eq. (35.14). The $E \times B$ term of Eq. (35.14) vanishes for perfectly aligned electric and magnetic fields, which can however be difficult to achieve in practice. Furthermore, the electron drift depends on the $\omega\tau$ factor, which is defined by the gas mixture and the magnetic field strength. The electrons will tend to follow the magnetic field lines for $\omega\tau > 1$, or the electric field lines for $\omega\tau < 1$. The former mode of operation makes the TPC less sensitive to non-uniformities of the electric field, which is usually desirable.

The drift of the ionization electrons is superposed with a random diffusion motion which degrades their position information. The ultimate resolution of a single position measurement is limited to around

$$\sigma_x = \frac{\sigma_D \sqrt{L}}{\sqrt{n}}\,, \tag{35.18}$$

where σ_D is the transverse diffusion coefficient for 1 cm drift, L is the drift length in cm and n is the effective number of electrons collected. Without a magnetic field, $\sigma_{D,B=0}\sqrt{L}$ is typically a few mm after a drift of $L = 100\,\mathrm{cm}$. However, in a strong magnetic field parallel to the drift field, a large value of $\omega\tau$ can significantly reduce diffusion:

$$\frac{\sigma_{D,B>0}}{\sigma_{D,B=0}} = \frac{1}{\sqrt{1+\omega^2\tau^2}}\,. \tag{35.19}$$

This factor can reach values of up to 10. In practice, the final resolution limit due to diffusion typically lies around $\sigma_x = 100\,\mu\mathrm{m}$.

The drift and diffusion of electrons depend strongly on the gas mixture. The optimal gas mixture varies according to the environment in which the TPC operates. In all cases, the oxygen concentration must be kept very low (few ten parts per million in a large TPC) in order to avoid electron loss through attachment.

Ideally, the drift velocity should depend only weakly on the electric field at the nominal operating condition. The classic Ar/CH_4 (90:10) mixture, known as P10, has a drift velocity maximum of $5\,\mathrm{cm}/\mu\mathrm{s}$ at an electric field of only $125\,\mathrm{V/cm}$ (Figure 35.5). In this regime, the electron arrival time is not affected by small variations in the ambient conditions. Moreover, low electric fields simplify the design and operation of the field cage. The mixture has a large transverse diffusion at $B = 0$, but this can be reduced significantly in a strong magnetic field due to the relatively large value of $\omega\tau$.

For some applications organic gases like CH_4 are not desirable since they may cause aging. An alternative is to replace CH_4 with CO_2. An Ar/CO_2 (90:10) mixture has a low transverse diffusion at all magnetic field strengths, but does not provide a saturated drift velocity for the typical electric fields used in TPCs (up to a few $100\,\mathrm{V/cm}$). As a consequence, it is quite sensitive to the ambient conditions. Freon admixtures like CF_4 can be an attractive option for a TPC as well, since the resulting gas mixtures provide high drift velocities at low electric fields. However, the use of CF_4 always needs to be thoroughly validated for compatibility with all materials of the detector and the gas system.

Historically, the amplification stages used in gaseous TPCs have been planes of anode wires operated in proportional mode. The performance is limited by effects related to the feature size (wire spacing) of a few mm. Since near the wires the electric and magnetic fields are not parallel, the incoming ionisation electrons are displaced in the direction of the wires ("wire $E \times B$ effect"), which degrades the resolution. The smaller feature sizes of Micro-Pattern Gas Detectors (MPGDs) like GEMs and Micromegas lead to many advantages as compared to wire planes (see Sec. 35.6.3). In particular, $E \times B$ effects in the amplification stage are much smaller. Moreover, the signal induction process in MPGDs leads to a very narrow pad response, allowing for a much finer segmentation, which improves the separation for two very close tracks. Combinations of MPGDs with silicon sensors have resulted in the highest granularity readout systems so far (see Sec. 35.6.3). These devices make it possible to count the number of ionization clusters along the length of a track, which can, in principle, improve the particle identification capability. However, the big challenge for such a system is the huge number of readout channels for a TPC of a typical size.

The accumulation of the positive ions created by the ionization from the particle tracks can lead to time-dependent distortions of the drift field. Due to their low drift velocity, ions from many events may coexist in the drift volume. To reduce the effect of such a build-up of space charge, Argon can be replaced by Neon as the main component of the gas mixture. Neon features a lower number of ionisation electrons per unit of track length (see 35.6) and a higher ion mobility (see 35.7).

Of greater concern are the ions produced in the gas amplification stage. In order to prevent them from entering the drift volume, large TPCs built until now have a gating grid. The gating grid can be switched to transparent mode (usually in the presence of an interaction trigger) to allow the ionization electrons to pass into the amplification region. After all electrons have reached the amplification region, it is usually closed such that it is rendered opaque to electrons and ions. For triggered operation, a combination of a MPGD and a gating structure may be an attractive solution. However, a gating grid implies a principal rate limitation to a few kHz.

A next generation of TPCs (e.g. ALICE [197], sPHENIX [201]) has been developed for applications where a triggered operation would lead to inacceptable data loss. The employed readout

Int. J. Mod. Phys. A 2026.41. Downloaded from www.worldscientific.com
by UNIVERSITY OF CALIFORNIA @ BERKELEY on 09/16/26. Re-use and distribution is strictly not permitted, except for Open Access articles.

schemes are based on MPGDs, as these can be optimised in order to drastically reduce the ion back-flow. Extensive work has been carried out during the 2010's to design such readout structures. In ALICE and sPHENIX ion back-flow values below 1 % are achieved with a thorough adjustment of the various fields in a quadruple GEM system. Similar levels of ion back-flow can be reached with Micromegas detectors [202].

35.6.5 *Transition radiation detectors (TRD's)*

Revised August 2025 by P. Nevski (BNL) and A. Romaniouk (Innsbruck U.; Istinye U.).

Transition radiation (TR) x-rays are produced when a highly relativistic particle with Lorentz factor $\gamma \gtrsim 10^3$ crosses a refractive index interface, as discussed in Sec. 34.7. Since the TR yield is about a few % per boundary crossing, radiation from multiple surface crossings (e.g., a stack of foils) is used in practical detectors. The x-rays, ranging from a few keV to a few dozen keV or more, are emitted in a forward direction at small angles (within few mrad) to the particle trajectory. The TR intensity for a single boundary crossing always increases with γ, but, for multiple boundary crossings, interference leads to saturation above $\gamma_{\rm sat} = 0.6\ \omega_1\sqrt{\ell_1\ell_2}/c$ [203], where ω_1 is the radiator material plasma frequency, ℓ_1 is its thickness, and ℓ_2 the spacing between material elements. The probability density function of TR is a fairly complex function of γ, radiator parameters, photon energy (ω) and its emission angle (θ). For well defined radiator parameters a measured two-dimensional distribution of photon energy vs its reconstructed emission angle is in very good agreement with the theory predictions [204].

Integration over the angle yields the TR spectrum, which typically features many maxima (see Sec. 34.7). Most of the TR energy is emitted near the last maximum of the spectra determined by radiator material parameters at $\omega_{max} = \ell_1\omega_1^2/2\pi c$. The effective TR photon emission starts at about $\gamma_{thr} = \ell_1\omega_1/c$. By varying radiator parameters one may optimize the particle separation for a given range of the γ-factor. The angular distribution of TR photons has a few maxima and extends up to $\theta_{max} = (1/\gamma^2 + \omega_1^2/\omega^2)^{1/2}$ [205]. For a single foil the largest part of the TR energy is emitted around the most probable angle $\theta = (1/\gamma^2 + \omega_2^2/\omega^2)^{1/2}$, where ω_2 is the plasma frequency of the gas surrounding the radiator material elements. However, in case of multiple interfaces, interference effects may significantly change this angle and more realistic expression for the angle which corresponds to the last interference maximum of the energy spectra is $\theta \approx \sqrt{1.4\pi^2/\gamma_{\rm sat}^2 - 1/\gamma^2}$ [204]. The higher is the gamma-factor, the larger is the angle of the first interference maximum. It reaches almost its asymptotic limit at $\gamma = \gamma_{sat}$. This effect is illustrated in Fig. 35.17 [204] which shows two-dimensional distribution of the TR photon energy versus the reconstructed production angle obtained in 20 GeV electron beam with the radiator containing a stack of foils of 15.5 μm thickness spaced by 210 μm (the left plot) using a Si-pixel detector. TR produced by 20 GeV electrons is emitted mostly around $\theta \sim 0.9$ mrad. All features of this distribution are well reproduced with MC simulations (the right plot).

The simplified numerical expressions can be used for practical estimation of the main TR production parameters [204]: $\theta \sim 1.2/\omega_1\sqrt{l_1 l_2}$, $\gamma_{thr} \sim 3\times10^3\ \omega_1\ell_1$, $\gamma_{\rm sat} \sim 3\times10^3\ \omega_1\sqrt{\ell_1\ell_2}$ and $\omega_{max} = 0.65\ \ell_1\omega_1^2$, where θ in mrad, ω_1 in eV, ω_{max} in keV and l_1 and l_2 in mm.

In the simplest concept, a detector module might consist of a low-Z TR radiator followed by a high-Z active layer made of proportional counters filled with a Xe-rich gas mixture. The atomic number considerations follow from the dominant photoelectric absorption cross section per atom going roughly as Z^n/ω^3, where n varies between 4 and 5 over the region of interest.[1] To minimize self-absorption, materials such as polypropylene, Mylar, carbon, and (rarely) lithium in the form of foils, fibers or foams are used as radiators. The TR signal in the active regions is in most cases superimposed upon the particle ionization losses, which are proportional to Z. In most of the detectors used in particle physics the radiator parameters are chosen to provide $\gamma_{\rm sat} \approx 3000$. Those detectors normally work as threshold devices, ensuring the best electron/pion separation in the momentum range 1 GeV/$c \lesssim p \lesssim$ 150 GeV/c.

One can distinguish two design concepts—"thick" and "thin" detectors. In "thick" detectors the radiator, optimized for a fixed total radiation length at maximum TR yield and maximum TR absorption in the detector, consists of few hundred foils (for instance 300 20 μm thick polypropylene foils). Most of the TR photons are absorbed in the radiator itself. To maximise the number of TR photons reaching the detector, part of the radiator far from the active layers is often made of thicker foils, which shifts the x-ray spectrum to higher energies. The detector thickness, about 2-4 cm for Xe-filled gas chambers, is optimized to absorb most of the incoming x-ray spectrum. A classical detector is composed of several similar modules which respond nearly independently. Such detectors were used in the UA2, NA34 and other experiments [206], are being used in the ALICE experiment [207, 208] and are built for the CBM experiment [209]. In another TRD concept a fine granular radiator/detector structure exploits the soft part of the TR spectrum more efficiently. This can be achieved, for instance, by distributing small-diameter straw-tube detectors uniformly or in thin layers throughout the radiator material. This approach allows to realise a TRD as an integral part of a tracking detector providing many points of measurements on the particle track. Even with a relatively thin radiator stack, radiation below 4 keV is mostly lost in the radiators themselves. However, for photon energies above this value, the absorption is reduced and the radiation can be registered by several consecutive detector layers, thus creating a strong TR build-up effect. Descriptions of detectors using this approach in both accelerator and space experiments can be found in [207, 210–213]. For example, in the ATLAS TR tracker (TRT), charged particles on average cross about 35 straw tube layers embedded in the radiator material [210]. The effective thickness of the Xe gas per straw is about 2.5 mm and the average number of foils per straw is about 40 with an effective foil thickness of about 18 μm. In this approach straw walls also act as radiator and make some contribution to the TR spectrum.

Although the radiator parameters mentioned above are typical, they can vary significantly depending on the specific requirements of the detector. Careful simulations are usually needed to build a detector optimized for a particular application. For TRD simulations the codes are based on well understood TR emission formulas (see for instance [205] for regular radiators and [214] for irregular radiators). They are realised as the stand-alone simulation programs [204, 215, 216] or GEANT4 based ones [217] and give both a good agreement of the TR energy spectra and of the angular distributions with data [204, 218, 219].

Discrimination between electrons and pions can be based on the total energy deposition measured in each detection module, the number of clusters – defined as energy depositions exceeding an optimal threshold (typically 5—7 keV) – or on more sophisticated methods, such as pulse-shape analysis as a function of time. The total energy measurement technique is more suitable for thick gas volumes, which absorb most of the TR radiation and where the ionization loss fluctuations are relatively small. The cluster-counting method works better for detectors with thin gas layers, where the fluctuations of the ionization losses are bigger. Cluster-counting replaces the Landau-Vavilov distribution of background ionization energy losses with the Poisson statistics of δ-electrons, responsible for the distribution tails. The latter distribution is narrower than the Landau-Vavilov distribution. In practice, most of the experiments use a likelihood method, which exploits detailed knowledge of the detector response for different particles and gives the best separation. The neural network method is the most powerful tool. When used by the ALICE TRD (ALICE point in Fig. 35.18), it led to an increase in rejection power by a factor of 2–3 compared to the likelihood method [207]. However, the more parameters are included in the likelihood method, the better the achievable separation power, approaching the performance level of the neural network method [208].

Once the detector structure is optimized, the particle separa-

[1] Photon absorption coefficients for the elements (via a NIST link), and $dE/dx|_{\rm min}$ and plasma energies for many materials are given in https://pdg.lbl.gov/current/AtomicNuclearProperties.

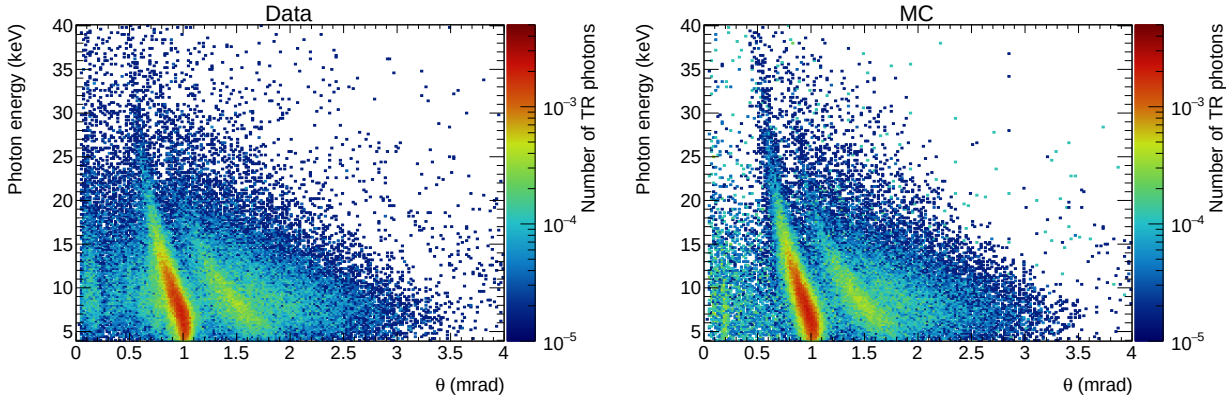

Figure 35.17: Two dimensional distributions of photon energy versus reconstructed production angle obtained with the polypropylene radiator with 20 GeV/c electron beam. Data - the left plot, MC - the right plot. Z-axis is a number of photons per particle [204]

tion power critically depends on the overall detector length. This is illustrated in Fig. 35.18, which shows, for a variety of detectors, the pion efficiency at a fixed electron efficiency of 90% as a function of the overall detector length. As TRD performance depends on particle energy, the experimental data in this figure covering a range of particle energies from 1 GeV to 40 GeV, are rescaled to an energy of 10 GeV when possible. Phenomenologically, the rejection power against pions increases as $5 \cdot 10^{L/38}$, where the range of validity is $L \approx$ 20–100 cm. Apart from the beam energy variations, the observed scattering of the points in the plot reflects how effectively the detector space is used and how well the exact response to different particles is taken into account in the analysis. For instance, the ATLAS TRT was built as a compromise between TR and tracking requirements; that is why the test-beam prototype result (lower point) is better than the real End-Cap TRT performance at the LHC shown in Fig. 35.18 for different regions in the detector (in agreement with MC).

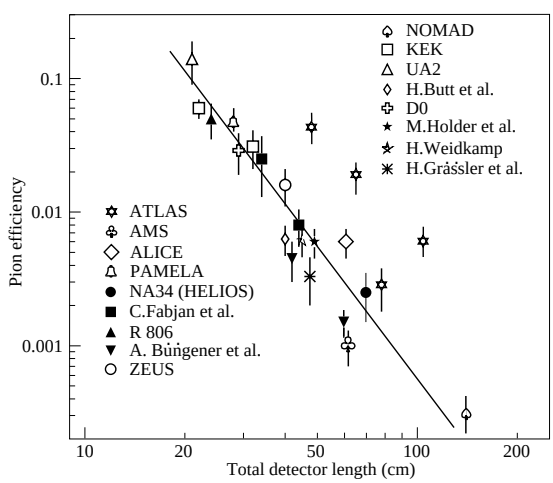

Figure 35.18: Pion efficiency measured (or predicted) for different TRDs as a function of the detector length for a fixed electron efficiency of 90%. The plot is based on the table given in [206]. Results from more recent detectors are added from [207, 211–213, 220].

In most cases, recent TRDs combine particle identification with charged-track measurement in the same detector [207, 209, 212]. This is particularly important for collider experiments, where the available space for the inner detector is very limited and the primary function of all detectors is particle tracking. For a modest increase of the radiation length due to the radiator (∼4% X0), a significant enhancement of the electron identification was obtained in the case of the ATLAS TRT. Here, the combination of the two detector functions provides a powerful tool for electron identification even at very high particle densities.

In addition to the enhancement of the electron identification during offline data analysis, TRD signatures are often used in the trigger algorithms at collider experiments. The ALICE experiment [208] is a good example for the use of the TRD in a First Level Trigger. In the ATLAS experiment, the TRT information is used in the High Level Trigger (HLT) algorithms. At increasing luminosities, the electron trigger output rate becomes so high that special measures must be taken to keep it at an acceptable level. Even a very soft TR cut at the HLT level, which preserves high electron efficiency (98%), allows to suppress a significant part of fake triggers and enhance the purity for physics events with electrons in a final state. The TRT also plays a crucial role in the studies where an electron suppression is required (e.g. hadronic mode of τ–decays). TR information is a completely independent tool for electron identification and allows to study systematic uncertainties of other electron reconstruction methods.

Electron identification is not the only application of TRDs. They are also sometimes used for hadron separation, which is a more challenging task, as the mass ratio of the particles involved is smaller. In the past, the TRD technique was successfully used to separate pions from protons and kaons at momenta up to 200 GeV/c (see, for example, [221]). In the TeV energy range, TRD remains the only viable technique for hadron separation [222]. For particle astrophysics some TRDs are designed to directly measure the Lorentz factor of high-energy nuclei by using the quadratic dependence of the TR yield on nuclear charge; see, for instance, in [223]. The radiator configuration (ℓ_1, ℓ_2) is tuned to extend the TR yield rise up to $\gamma \approx 10^5$ using the more energetic part of the TR spectrum (up to 100 keV). High density radiator materials (such as Al) are the best for this purpose. Direct absorption of the TR-photons of these energies with thin detectors becomes problematic and TR detection methods based on Compton scattering have been proposed, see in [224].

New detector techniques for TRDs are also under consideration. GasPixel detectors allow to reconstruct a track segment with a space point accuracy of $< 30\ \mu m$ and exploit all details of the particle tracks to highlight individual TR clusters in the gas, see in [225]. However, their ability to separate TR clusters from the energy losses of particles in space is limited by electron cloud diffusion in the gas. Semiconductor pixel or microstrip detectors with high granularity are promising candidates for the spatial separation of TR photons and dE/dx signals at relatively short distances between the radiator and the detector. This capability allows for the reconstruction of the TR production angle, which – together with the TR energy measurements – can help improve the particle identification (PID) performance of the TRD. Such detectors may be the basis for novel devices which combine precise tracking and PID properties [204, 216, 226]. The presence of a magnetic field could enhance the separation between TR photons and dE/dx losses [227]. Thin films of heavy scintillators might be a very attractive option for non-gas based TRD [228].

Int. J. Mod. Phys. A
by UNIVERSITY OF CALIFORNIA @ BERKE
nloaded from www.worldscientific.com
use and distribution is strictly not permitted, except for Open Access articles.

Int. J. Mod. Phys. A 2026.41. Downloaded from www.worldscientific.com
by UNIVERSITY OF CALIFORNIA @ BERKELEY on 09/16/26. Re-use and distribution is strictly not permitted, except for Open Access articles.

35.6.6 *Resistive-plate chambers*

Revised August 2025 by G. Aielli (Rome U. Tor Vergata).

The resistive-plate chamber (RPC) is a gaseous detector working at atmospheric pressure developed by R. Santonico and R. Cardarelli in the early 1980's [229]. A precursor of the RPC was the Pestov spark chamber [230] [231], which had a metallic plate cathode and a thick glass plate anode, designed to work at 12 bar to obtain an outstanding 0.1 ns time resolution. Although the original purpose of RPCs was to provide a competitive alternative to large scintillator counters, the RPC's potential for timing tracker systems was quickly recognized given its high detection efficiency (>95%), excellent temporal and spatial resolutions and ease of constructing large-format single frame detectors. The RPC, as sketched in Fig. 35.19, is a large planar capacitor with two parallel high bulk resistivity electrode plates (10^9–10^{13} Ω·cm) separated by a set of insulating spacers. The spacers define a gap in the range from a few millimeters down to 0.1 mm with a precision of a few μm. The gap is filled with a suitable atmospheric-pressure gas mixture which serves as a target for ionizing radiation. A thinner gas gap corresponds practically to an higher time resolution, on the other hand, the minimum gaseous target for reaching full detection efficiency at atmospheric pressure is typically 1 mm (also influenced by the gas molecular weight). Since the primary ionization released in sub-millimeter gas gaps is limited, multiple gaps can be combined to effectively obtain a high detection efficiency [232]. The electrodes are most commonly made of high pressure phenolic-melaminic laminate (HPL), commonly referred to as "bakelite", or glass. In the last case, typically soda-lime or alumino-silicate glass types are used, having a lower resistivity than borosilicate glass. An uniform electric field of several kV/mm is established on the gas gap, sufficient to promptly start an avalanche multiplication of the primary electrons. The electric field is typically applied through a moderately conductive ($\sim 10^5 to 10^8$ $\Omega/\square$) graphite varnish, forming an ohmic contact with the external faces of the electrodes. Its conductivity is sufficiently low to be transparent to the fast avalanche signal transients, and high enough to suppress surface voltage gradients arising from the working current flowing in it. Due to the high electrode resistivity in RPCs, the time constant of the equivalent RC circuit ($\tau = \rho\epsilon_r$ being ρ the electrode resistivity and ϵ_r its dielectric constant) is much longer than the discharge processes duration. Therefore only the locally-stored electrostatic energy contributes to the discharge, preventing the formation of sparks and leaving the rest of the detector field unaffected. The gas-facing surface of HPL electrodes are commonly coated with $\sim$ μm-thick layer of polymerized linseed oil [233] with the function of smoothing the electrode surface, improving the electric field uniformity. It also has the function of protecting the electrode from the being eventually etched by free radicals generated in the discharge e.g. in presence of fluorocarbons. Glass-based RPCs don't require such treatment. In RPCs the gaseous target and the multiplication region coincide. In the early stage of the avalanche multiplication the uniform electric field exponentially amplifies each primary ionization cluster, as the avalanche progresses away from the location of the primary ionization. Since the ionization clusters generated by the incident MIP are randomly distributed along the ionizing particle track, for low gains the observed RPC charge spectrum is broad and approximately exponentially distributed[2] with the mode close to zero. Because of this, it is difficult to separate noise from signals using a discrimination threshold. This is not the case in gaseous detectors where ionization and amplification occur in separate regions.

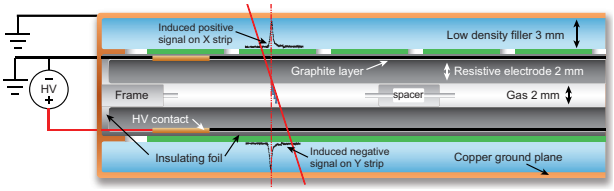

Figure 35.19: Schematic cross section of a generic single gap RPC. The thickness values shown are given just as an example.

For increasingly larger avalanches, the space-charge progressively saturates the avalanche growth from exponential to almost linear, producing a peaked charge spectrum, essential to efficiently separate the signal from the noise [235]. For large gains[3] the avalanche, with increasing probability, onsets a transition to "streamer" [236], a plasma filament connecting the electrodes, depleting all the locally-available energy [237], and generating an almost fixed amplitude signal. This prevents any further evolution of the discharge. This streamer mode was the first ever used by RPCs, until the introduction of very electronegative gases and more sensitive front end electronics made it possible to detect the precursor avalanche independently on the streamer [238, 239] Any of this operating regimes can be used in RPC detectors, depending on the application.

As with other gaseous detectors, the gas mixture is optimized for each specific application. In general it needs to contain a UV photons quencher suppressing the photon-mediated feedback that can lead to self generated after-pulse discharges, and one or more electronegative components, to extend the avalanche growth limit before increasing significantly the probability of generating a streamer. Even though there is not yet an accepted and robust avalanche-to-streamer-transition model, this effect is commonly explained as a delay in the growth of the electron density of the avalanche front, which perturbates the electric field driving the transition to streamer. The addition of small fractions of electronegative molecules with a very high capture cross section for slow electrons, such as SF_6, was proven [240] to inhibit the transition to streamer over a wide electric field range above the working point. Having such a wide interval is crucial in real applications, to cope with all the unavoidable gas gaps size fluctuations and surface quality, stabilizing and making uniform the detector response. In the last decades ATLAS and CMS adopted as a standard the mixture $C_2H_2F_4$/i-C_4H_10/SF_6=94.5%/5%/0.3% for stable avalanche operation (ATLAS changed it since 2023 as explained in Section 35.6.6.4).

The avalanche induces a fast electron signal on a set of metallic readout electrodes (e.g. pads or strips) commonly placed externally and electrically insulated from the resistive electrodes. The induced charge is isotropically distributed on the electrode plans with equal but opposite amplitude on both sides of the RPC. This symmetry makes both sides of the RPC functionally equivalent for the signal readout. The induced charge density distribution can be calculated for a simplified RPC model [241] [242] as: $\sigma(x) = A/\cosh[(r)/\delta]$ where A is a normalization constant, r is the distance from the center of the avalanche axis and $\delta = (g + 2d)/\pi$ depends on the gap and electrode width (g and d, respectively). Depending on the specific RPC layout and geometry, the interplay between conductive coating and pick-up electrodes typically broadens, by means of a diffusion-like process (see [242] [243]). This effect mostly preserves the information on the avalanche position, which can be obtained using the charge centroid method, with the drawback of increasing the signal space occupancy. A fast detector response, requires to preserve sensitivity to the high-end of electron avalanche signal frequency spectrum, and guaranteeing this across large RPC areas, requires a correspondingly adequate Faraday cage and readout design. At the same time, to preserve the excellent timing features of the RPC signal, the front end electronics should have a short rise time (ideally $\ll$ than the signal rise time) and low noise, although these are competing requirements [244].

35.6.6.1 *RPC types and applications*

RPCs are generally classified in two categories depending on the gas gap structure: single gap RPCs (described above) and multiple gap RPCs [232] (typically referred as MRPCs). While they are

[2] An analytic treatment of the low gain avalanche process shows that the charge distribution is well described by the Γ function [234]

[3] A multiplicity of the order of 10^8 electrons is classically referred as Raether/Meek limit for on-setting a streamer

Int. J. Mod. Phys. A
by UNIVERSITY OF CALIFORNIA @ BERKE
nloaded from www.worldscientific.com
use and distribution is strictly not permitted, except for Open Access articles.

both based on the same principle they have different construction techniques, performance and limitations, making them suitable for different applications. Due to its simplicity and robustness, the single gap RPC is ideal for covering very large surfaces. Typical detector systems can have sensitive surface areas up to $\sim 10^4$ m^2, with single module areas of a few m^2, a space resolution up to 100 μm [245] and a time resolution up to $\sim$0.4 ns [246]. Representative examples are the muon systems of ATLAS [247] and CMS [248] or ground and underground based cosmic rays [249] and neutrino arrays [250]. It is interesting to note that CMS implemented a bi-gap structure, i.e. the pickup signal is sandwiched by 2 single gas gaps, both contributing to the signal induction, improving efficiency and time resolution with respect to the single gas gap. Relevant new trends for single gap RPC applications are represented by new Dark Matter search experiments such as CODEX-B [251] and ANUBIS [252], in both cases exploiting RPCs to enclose and instrument large detection volumes with a good space-time tracker. Single gap RPCs have also recently demonstrated good candidates for application in tracking calorimetry [253].

The MRPC [254], as sketched in Fig. 35.20, segments the gaseous target by means of a stack of floating glass electrodes separated by a monofilament (i.e. fishing line) sandwiched between two external electrodes providing the high-voltage bias. Since the current flowing in between the gas gaps must be in average equal, the difference of potential between each couple of adjacent floating electrodes will tend to be the same. An extensive description can be found in [255]. It has been observed that higher time resolution is inversely correlated to the gas gap size, so this configuration allows for smaller gas thicknesses while maintaining a sufficient total gas thickness. This tends to separate primary clusters avalanches in different gas gaps, treating them independently, and determines a shorter avalanche growth time, increasing time resolution by one order of magnitude with respect to the classic RPCs [256]. The mechanical fragility of sub-mm-gap structures makes this technique less suitable for very large detector areas. Moreover the only material nowadays practically suitable for building such structures is glass with resistivity above 10^{12} Ω·cm, limiting the rate capability to about 500 Hz/cm^2 [257].

MRPCs have been largely used in Time of Flight systems such as ALICE [258], HADES [259], FOPI [260] and BESSIII [261], and in applications such as timing PET [262]. In perspective MRPC will be used for upgraded and new nuclear physics experiments such as CBM@FAIR [263] and SoLID [264].

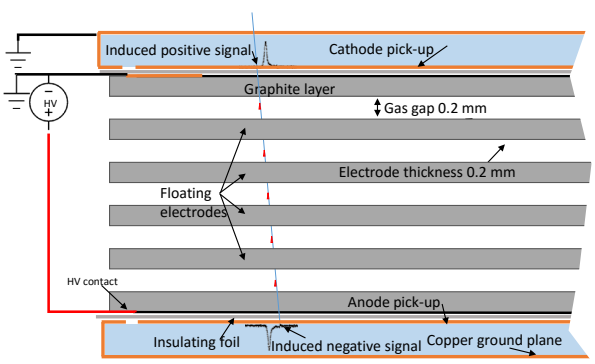

Figure 35.20: Schematic cross section of a generic multi gap RPC.

35.6.6.2 *Time and space resolution*

Space-time uncertainties in RPCs are intrinsically determined by the statistical fluctuations of the primary and secondary ionization, the avalanche multiplication rate and drift velocity, which are both a function of the electric field and gas composition. The Signal/Noise ratio of the front end electronics is crucial to preserve this information. The intrinsic signal latency (time lapsed between the ionizing event and the growth of the signal above detection threshold) is commonly in a few ns range, making the RPC suitable for applications where a low latency is essential.

The gas gap size is a crucial feature for the RPC timing performance: producing the same total charge (for a detectable signal) in a smaller gas gap implies the necessity of increasing the first Townsend coefficient by increasing the electric field, reducing at the same time the total signal duration and the related time fluctuations. Moreover, a thinner gas gap reduces the number on effective clusters participating to the signal formation, for an unknown amount of time, corresponding to their distance from the anode, thus decreasing the charge collection fluctuations [265]. Another important factor is the gas mixture, affecting both the drift velocity and multiplication rate. Depending on the gas mixture and on applied voltage, typical intrinsic resolution, ranges between $\sim$ 1 ns and $\sim$1.5 ns, for a 2 mm gas, and between $\sim$0.3 ns and $\sim$0.4 ns for a 1 mm gas gap [266].

The intrinsic position sensitivity of an RPC is in the range of tens of μm depending on the lateral spread of the avalanche induced charge distribution, influenced also by the gap size. In typical RPC applications the pick up electrodes pitch L ($\sim$1 cm) is much broader than the intrinsic resolution, and being readout via a discriminator, the spatial resolution is geometrically limited in the range of $L/\sqrt{12}$. A much better result is obtained by using a finer electrodes granularity and measuring the charge in each strip collecting the avalanche charge, so to reconstruct the charge centroid. It has been demonstrated, through charge centroid techniques, that the RPC avalanche space-time localization can be as good as $\sim$50 ps $\times$ 40 μm [267] [268]. Nevertheless, the high space resolution for large size RPCs, as well for any other planar detector structure, is often practically limited by the extensive mechanical precision of the readout electrode (which bulk is typically made of plastic), challenging to be kept negligible with respect to the intrinsic local resolution of the detector.

35.6.6.3 *Rate capability and ageing*

RPC rate capability is limited by the voltage drop on resistive electrodes, $\Delta V = V_{\rm a} - V_{\rm gas} = I \cdot R$ [269]. Here $V_{\rm a}$ is the applied voltage, $V_{\rm gas}$ is the effective voltage on the gas, $R = \rho \cdot d/S$ is the total electrode resistance, ρ being the resistivity and d,S the sample thickness and surface respectively, and I is the working current. Assuming uniform irradiation we can express $I = \phi \cdot S \cdot \langle Q \rangle$ where ϕ is the particle fluence and $\langle Q \rangle$ is average charge per avalanche. So we obtain a state equation for the RPC rate capability:

$$\Delta V/\phi = \rho \cdot d \cdot \langle Q \rangle$$

A large I not only limits the rate capability but also affects the long term performance of the detector, for three leading effects. Firstly, the working current, depletes the ionic electrode's carriers [270]. Secondly, the current builds up an electric field RI/d in the electrode bulk, accelerating the drif of internal ionic components to opposite surfaces. Thirdly, in presence of fluorocarbons and water, discharges generate hydrofluoric acid (HF) and other fluorinated compounds, which may damage internal detector surfaces. In case of electrodes made of glass, known to be not resistant to HF [271], it is necessary to suppress HF formation preventing water vapor contamination. Conversely, HPL electrodes, coated with linseed oil, notwithstanding the necessary presence of water which drives the conduction mechanism, demonstrated to be tolerant to HF in moderate concentrations, obtained by removing it with a forced flow of clean gas through the gas gap. Several ageing test have been carried out [272–275], confirming that measurable ageing effects were limited to a controlled increase of the ohmic current, of the electrode resistance and of the spontaneous counts. However, in extreme conditions, etching and surface damage have also been observed.

Operating in streamer regime places low requirements on the front end electronics sensitivity, but generally limits the counting rate capability to $\sim$100 Hz/cm^2. Higher-rate operation can be achieved by reducing gas gain in favor of electronic amplification, operating the detector in avalanche mode. Increasing concentrations of electronegative gases, such as $C_2H_2F_4$ and SF_6 [240], extends the avalanche signal distribution, requiring the front-end electronics a high sensitivity to the low end signal distribution and stability in presence of large signals. By further lowering the avalanche mode gas gain, efficient and stable performance at high

Int. J. Mod. Phys. A 2026.41. Downloaded from www.worldscientific.com
by UNIVERSITY OF CALIFORNIA @ BERKELEY on 09/16/26. Re-use and distribution is strictly not permitted, except for Open Access articles.

rates (e.g. 10 kHz/cm^2) has been achieved for large area single gap RPCs [244].

Further increasing the rate capability, can be achieved with complementary strategies: increasing the front end sensitivity to smaller signals and operating with a smaller amplification, relying on redundancy and higher signal yield of multiple micro gap structures [276] or lowering the electrodes resistivity [277]. The last strategy is increasingly difficult to be pursued, in presence of high electric field, since high resistivity limits the appearance of larger discharge events and increase of spurious counts, induced by the effect of local electrode defects on the field gradient. It seems in this case, that lowering the electrodes resistivity would require at the same time to reduce the operating electric field, achieving at the same time a lower average charge per count.

35.6.6.4 *Alternative gas mixtures*

The standard gas mixture mentioned above is based on Hydrofluorocarbon (HFC), specifically the R134a, and SF6, both extensively used in the industry. R134a features matches very well the RPCs performance requirements: high primary ionization yield; electronegative, limiting secondary discharge phenomena; not flammable; the absence of saturated bonds makes it robust to UV degradation, which is responsible for the production of fluoride radicals. SF6, as mentioned above is crucial to extend the streamer-free avalanche regime. The drawback is the high Global Warming Potential (GWP) of these gases (1430 and 24300 respectively), for which reason, their industrial application will be progressively limited in future according to the European Regulation [278]. In the last years the search for a possible replacement of R134a, relied on the Hydro-Fluoro-Olefins [279, 280], a category of gases recently proposed for industrial applications. However, HFOs exhibit important limitations with respect to HFCs, if used as main component of the mixture: for its electronegativity (higher than for R134a [281]) increasing the HV working point, and the charge per count, due to a large fraction of negative ions produced by electron capture [282, 283]. Moreover it is expected to produce a larger amount of fluoride radicals by UV decomposition of the gas, increasing the operative current and worsening the detector longevity [284, 285]. To contrast the ageing acceleration, driven by the effects stated above, the proposed strategy was to largely dilute HFO with a neutral gas, such as CO_2, compatibly with keeping an enough dense gaseous target, and, for future systems, operate at a lower gain by using very performing front end electronics. It has to be said that increasing of CO_2 finds its limits in the correspondingly increasing probability of inducing streamers [282, 283], which is further worsened by operating the RPC with an high discrimination threshold. A representative example of the several variants tested [286] is $CO_2/C_3H_2F_4$/i-C_4H_{10}/SF_6=59%/35%/5%/1%. This mixture with a large fraction of CO_2 is suitable for thicker (2mm) gas gap. The presence of CO_2 in 1 mm gas gaps reduces the amount of primary electrons, practically limiting its fraction to no more than 30% to keep the efficiency above 95%. Thus for a safe operation a reduction of the charge per count by an order of magnitude is necessary to compensate the expected stronger ageing phenomena. Detector performance and physics summaries can be found in [287, 288], not yet conclusive results about the detector longevity [284] confirm that the HFO based mixtures are more impacting than the standard one. On the base of the known results, LHC experiments conservatively opted either to hold on the standard gas mixture (CMS) or replace part of the R134a with an equivalent amount of CO2 (ATLAS). Several variants of this type of mixture have been tested, observing an improved longevity, with respect to the standard gas mixture, for lower fractions both of R134a and SF_6 [289, 290]. After this test,ATLAS decided to modify the standard gas mixture in two steps: first using $CO_2/C_2H_2F_4$/i-C_4H_{10}/SF_6=30%/64%/5%/1% in 2024 run. Then experimental confirmation of the expectations about ageing, lead to halve in 2025 run the fraction of SF_6, observing a further improvement (ATLAS internal). This allowed to safely lower the ATLAS CO_2 equivalent emissions by 25%. Given the very high GWP of SF_6 a dedicated investigation pointed out various alternatives [287, 291], in particular $C_3H_2ClF_3$ has been tested both for performance and longevity with very encouraging preliminary results [291].

35.6.6.5 *A new detector: the **R**esistive **C**ylindrical **C**ounter*

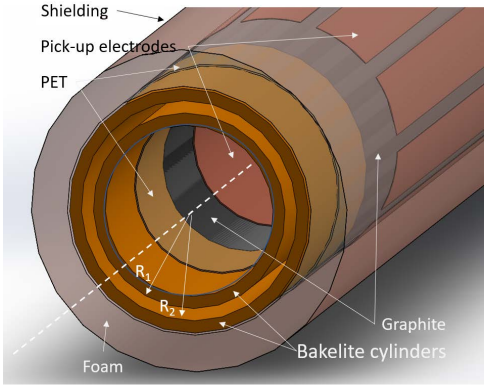

Figure 35.21: Schematic drawing of an RCC.

The RCC, illustrated in fig. 35.20, has been recently proposed as an evolution of the RPC [292] and is essentially an RPC warped to a cylindrical shape. The idea is to combine the advantages of parallel plate geometry and high pressure drift tubes in a single detector. The electric field $E(r)$, which is uniform in RPCs, here depends instead on the distance from the axis r, according to $E(r) = -\frac{V}{r\ln(R_1/R_2)}$. By choosing appropriate values for R_1, R_2, V and its polarization (the innermost cylinder is the cathode), it is possible to virtually segment the cylindrical gap in a innermost sensitive layer, where the field is sufficiently high to start the avalanche multiplication, and an outermost layer where the drift happens, increasing the induced signal with lower or no multiplication at all. This effect is called geometrical quenching and limits the avalanche growth without the necessity of electronegative gases. Moreover a geometrically quenched avalanche would have a much better prompt to total charge ratio, lowering the total operative current, hence increasing the rate capability. The cylindrical structure has a further major advantage with respect to the planar one, it can be easily pressurized overcoming the RPC limitation of working at atmospheric pressure only. Pressurization on one side increases the gaseous target density, thus increasing the efficiency of narrow gaps, on the other, it could largely improve RPC time resolution since the Townsend coefficient $\alpha = A\,p{\cdot}\exp(-Bp/E)$ (where p is the pressure, E the electric field and A,B are constants), as we learn from the RPC precursor, the Pestov spark chamber [231]. The preliminary performance of the first RCC prototypes in terms of efficiency, time resolution and counting rates are reported in [293] using the standard gas mixture. Further test will be needed to show the full potential of this device, such as its ability to work without fluorinated gases, and at high internal and external pressure, potentially extending its applicability range to space and under water applications.

35.7 LAr Time Projection Chamber

Written in October 2021 by F. Pietropaolo (CERN; INFN, Padova) and S. Pordes (FNAL). Revised in August 2025 by A. Fava (FNAL) and F. Pietropaolo (CERN; INFN, Padova).

35.7.1 *Introduction*

Liquid argon (LAr) is an attractive medium for particle detection. The most relevant physical properties of LAr are listed in Table 35.8; additional details can be found in [294]. In LAr, the energy deposited by charged particles is converted into ionization electrons and scintillation light; several tens of thousands scintillation photons and a similar number of ionization electrons are generated per MeV of deposited energy.

The LAr's high density (relative density ∼1.4), the electron drift over long distances with minimal diffusion, and the commercial availability as a by-product of air distillation make LAr especially suitable for large time projection chambers (TPCs) aimed at rare event detection, as first proposed in [296, 297]. Since then, LAr TPC technology has matured into a high-resolution (∼mm^3), fully

Int. J. Mod. by UNIVERSITY OF CALIFORNIA @ BERKE nloaded from www.worldscientific.com use and distribution is strictly not permitted, except for Open Access articles.

Table 35.8: Some physical properties of liquid argon from [295].

Property	Unit	Value
Boiling Point *(BP)* at 1013 hPa	K	87.3
Density (ρ) at 1013 hPa	kg m^{-3}	1395
d*(BP)*/dP	K hPa^{-1}	9×10^{-3}
dρ/dT	kg m^{-3} K^{-1}	-6.2
Latent Heat of Evaporation	kJ kg^{-1}	161
Freezing Point (1013 hPa)	K	83.8

active detector offering excellent particle identification, calorimetric capabilities, and nearly 100% live-time. Operating a liquid argon TPC requires the following core components:

1. A cryostat and cryogenics system to maintain ultra-pure liquid argon,
2. An electric field to drift ionization electrons toward the readout,
3. Charge readout sensors and electronics to amplify and digitize the signals,
4. Photodetectors and associated electronics to capture scintillation light,
5. A data acquisition (DAQ) system for readout and storage,
6. Reconstruction and analysis software.

This article discusses the challenges and practical solutions related to items 1–4. Topics 5 and 6 —DAQ and data processing— are also briefly introduced due to their critical role in realizing the full potential of LAr TPCs [298–300]. A number of auxiliary systems have been developed to enhance LAr TPC performance, including: in-argon cameras [301], purity monitors for fast assessment of argon quality [302, 303], and UV lasers for mapping drift field distortions due to space charge or electric field irregularities [304].

Detectors of up to 800 tons of LAr have been constructed and operated, and designs for tens-of-kiloton-scale detectors are underway. Extensive reviews of existing and planned LAr TPC detectors can be found in [305,306], as well as in detailed experiment reports [301, 307–316]. A summary of current and proposed LAr TPC experiments and their respective detector masses is provided in Table 35.9.

35.7.2 *Ultra-pure Liquid Argon*

A core requirement of the LAr TPC is the ability to maintain a large volume of ultra-pure liquid argon at stable temperature and pressure. This is achieved through a combination of cryostat design and cryogenic purification systems. For detectors with masses on the order of 100 tons, double-walled, vacuum-insulated, evacuable cryostats are practical. However, for larger detectors, this approach becomes impractical. The development of techniques to achieve ultra-high purity without prior evacuation [303] has enabled the use of non-evacuable, foam-insulated cryostats—adapted from liquefied natural gas (LNG) transport technology [301]. These cryostats are modular and designed for underground assembly. Furthermore, their passive insulation offers improved safety over vacuum insulation, as the insulation performance cannot abruptly change, as it would happen in case of vacuum loss.

Maintaining an extremely low level of electronegative impurities —primarily oxygen and water— is critical to preserving ionization electrons as they drift to the charge sensors. These contaminants capture free electrons, forming negative ions that drift too slowly to be detected. The argon purity is quantified by the electron lifetime τ, which describes the average time an electron can drift before being captured. For example, at an oxygen concentration of 0.1 ppb (by volume), the electron lifetime is approximately 3 ms [317, 318]. Since electron drift times in large detectors are often in the millisecond range, achieving oxygen concentrations well below 0.1 ppb is essential.

To reach these purity levels, the cryostat is first purged with argon gas to displace air, typically reducing oxygen and nitrogen concentrations to ppm levels [319]. During filling, commercial liquid argon —often containing oxygen and water at ppm levels— is passed through purification filters. Molecular sieves and activated copper on alumina [320] are widely used to remove water and oxygen, respectively. The realization that these purification materials remain effective at cryogenic temperatures [321] allowed for high-throughput liquid-phase purification, a major advancement over earlier gas-phase methods. Once the detector is operational, continuous recirculation of both liquid and boil-off gas through the purification system ensures the removal of contaminants introduced through outgassing or micro-leaks. Cryogenic system schematics are available in [301, 309, 311]. While the ultimate measure of argon purity comes from track reconstruction, dedicated "purity monitors" —double-gridded ionization chambers— are commonly employed for rapid, real-time feedback [301].

Nitrogen is another possible contaminant. While it does not significantly impact electron lifetime at concentrations up to several ppm, it degrades scintillation light yield and transmission with the few ppm N2 concentration [322, 323]. Oxygen at ppm concentrations also affects scintillation light [324], but in TPCs, this effect is typically negligible due to the stricter requirements imposed by charge readout.

35.7.3 *Charge and Light Signals*

Charged particles traversing liquid argon (LAr) deposit energy, producing both ionization electrons and scintillation light. Figure 35.22 (left) illustrates how these yields vary with applied electric field for a minimum ionizing particle (m.i.p.). The number of free electrons produced per unit energy is determined by the average energy required to form an electron-ion pair, $W_{el} = 23.6$ eV [325], the particle's energy loss rate (dE/dx), and the recombination factor R, which quantifies the fraction of electrons that escape recombination. Although several models have been proposed to describe recombination dynamics [326,327], the "box model" [328], which assumes mobile electrons and stationary ions, is widely used for its realistic assumptions [329], and has very recently been further improved to include an angular dependent effect [330]. Measurements of electron yield across various fields and ionization densities show good agreement [330–335]. One commonly used parameterization, based on ICARUS data [334], is $R = \frac{0.8}{(1+0.049(dE/dx)/\mathcal{E})}$ with dE/dx in MeV/cm and $\mathcal{E}$ in kV/cm. At a field of 500 V/cm, this yields $R \approx 0.70$ for m.i.p.s. corresponding to about 30,000 electrons/MeV escaping recombination. A detailed review of charge yield and recombination models is given in [336]. Under a uniform electric field, free electrons drift toward the charge readout system. This process is characterized by:

1. **Drift velocity**, which depends on electric field and slightly on temperature (see Table 35.10). A widely used parametrization [337,338] gives a drift velocity of 1.55 mm/μs at 500 V/cm and 89 K, shown in Figure 35.22 (right).
2. **Charge attenuation**, caused by capture on residual impurities. The surviving fraction after a drift time t is $\exp(-t/\tau)$, where τ is the electron lifetime. Lifetimes exceeding tens of milliseconds have been demonstrated [339–341].
3. **Diffusion**, which broadens the charge cloud. The spatial spread after time t is $\sigma_D^2 = 2Dt$, where D is the diffusion coefficient. Longitudinal diffusion measurements typically yield $D_L \approx 0.4$ mm^2/ms [333, 342–344], corresponding to a spread of ~1.5 mm over a 3 ms drift.

Scintillation light in LAr arises from the decay of excited argon dimers (excimers), Ar_2^*, produced via both direct excitation and electron-ion recombination [356]. The recombination contribution decreases with increasing electric field, as shown in Figure 35.22 (left). At a field of 500 V/cm, about 30,000 photons/MeV are emitted after recombination.

Excimers form in either singlet or triplet states, with lifetimes of approximately 6 ns and 1.5 μs, respectively. These nearly degenerate states decay radiatively, emitting vacuum ultraviolet (VUV) photons centered at 128 nm with a ~16 nm FWHM [349]. The singlet-to-triplet ratio depends on ionization density: 1:3 for m.i.p.s and up to 3:1 for highly ionizing tracks [353]. The long-lived triplet component is particularly sensitive to quenching by

Int. J. Mod. Phys. A 2026.41. Downloaded from www.worldscientific.com
by UNIVERSITY OF CALIFORNIA @ BERKELEY on 09/16/26. Re-use and distribution is strictly not permitted, except for Open Access articles.

Table 35.9: Summary of current and proposed accelerator-based LAr TPC experiments. For experiments on neutrino beams, the average energy is indicated.

Name	Total (fiducial) mass [t]	Beam type	$\langle E_\nu \rangle$ [GeV]	Location	Dates
ArCS	0.98(0.24)	p, μ, e, p, k	-	FNAL	2026
Argoneut	0.025	ν	3	FNAL	2009-10
DUNE 2x2	8.4(2.2)	ν	6	FNAL	2024-
DUNE ND-LAr	147(67)	ν	3	FNAL	2030-
DUNE FD	70k(40k)	ν	3	SURF	2027-
ICARUS	760(476)	ν	17	LNGS	2006-12
ICARUS	760(476)	ν	0.8	FNAL	2020-
LArIAT	0.76(0.24)	p, μ, e, p, k	-	FNAL	2015-17
MicroBooNE	170(85)	ν	0.8	FNAL	2014-21
ProtoDUNE	770(417)	p, μ, e, p, k	-	CERN	2018-
SBND	220(112)	ν	0.8	FNAL	2024-

Table 35.10: Some Detector Relevant Properties of liquid argon.

Property	Unit	Value
Stopping Power (m.i.p.)	MeV g^{-1} cm^2	1.51
Radiation Length	g cm^{-2}	19.6
Nuclear Interaction / Collision Length	g cm^{-2}	120 / 76
W_{el}, Energy to form one electron-ion pair	eV	23.6 ($\pm$0.3) [325, 345]
Ion mobility	cm^2 V^{-1} s^{-1}	1.6 $\times 10^{-3}$ [346]
Temperature dependence of drift velocity	% K^{-1}	-1.7 [338]
Longitudinal diffusion coefficient, D_L	mm^2 ms^{-1}	0.4 (see text)
W_{ph}, Energy to produce one scint. photon	eV	25 [347, 348]
Scintillation photon wavelength (vacuum)	nm	128 $\pm$8 (FWHM) [349]
Scintillation light inverse velocity	ns m^{-1}	7.46 ($\pm$0.08) [350]
Rayleigh scattering length (predicted)	m	0.9 ($\pm$0.2) [350–352]
Scintillation Decay times fast/slow	ns	6 ($\pm$1)/1500 ($\pm$100) [322, 353, 354]
Dielectric strength	kV cm^{-1}	>40 [314, 355]

impurities such as nitrogen and oxygen, which can non-radiatively absorb the excimer energy [322, 324].

Scintillation light propagation is influenced by **absorption** and **Rayleigh scattering**. Pure LAr is transparent to its own light due to a large Stokes shift [357], but trace levels of methane (ppb) [358] and nitrogen (ppm) [323] can significantly attenuate light. Rayleigh scattering, with a short mean free path in LAr, increases the photon path length and degrades spatial resolution in large detectors. To mitigate these effects, **wavelength-shifting dopants** have been proposed and tested. Xenon is a leading candidate: at tens of ppm concentrations, it efficiently absorbs excitation energy from argon dimers and re-emits photons at longer wavelengths, improving transparency and reducing scattering losses [359, 360].

35.7.4 *LAr TPC topologies*

Single-phase detectors, ranging from small-scale prototypes to large multi-kiloton systems, share a common layout: a cathode and surrounding field cage establish a uniform electric field across the active volume, directing electrons toward anode planes at ground potential. To maximize mass for a given readout complexity, long drift distances are favored. As a result, TPCs are often built with single drift regions, dual-drift volumes sharing a central cathode, or multiple drift modules. A notable exception is the DUNE Near Detector, where high event rates necessitate segmentation into many small TPCs [313].

The electric field is typically established by a planar cathode held at high negative voltage (up to -300 kV), a field cage that linearly degrades the potential, and sense planes at a voltage around 0 V. Uniformity of the field is essential, though it can be distorted in surface detectors by the accumulation of slow-moving positive ions produced by cosmic ray interactions [336, 341, 361–363]. Key challenges in high-voltage delivery include designing robust feedthroughs that transport the HV into the cryostat without breakdown [309, 364], preventing damage from possible discharges [301], and ensuring the integrity of the field cage resistor chains [365]. Maintaining HV stability in a medium designed for long-distance electron transport is one of the most demanding aspects of TPC design.

Figure 35.23 illustrates the typical single-phase geometry using wire planes with a horizontal drift field. Charge readout is performed by wire planes arranged perpendicularly to the drift direction, typically with two or three planes at different wire angles to enable 3D reconstruction. Although only two planes are strictly necessary to reconstruct the three-dimensional event topology, a third plane improves pattern recognition and mitigates inefficiencies due to noisy or dead channels. Wire pitch and inter-plane spacing are typically a few millimeters. The biasing scheme ensures that the drifting electrons pass through the intermediate planes and are collected on the final (collection) plane. Bipolar signals are induced on the induction planes, and a unipolar signal is recorded on the collection plane [366]. The condition for transparency is discussed in [367].

Signals are digitized at 2–2.5 MHz sampling rates over the full drift window. The 3D position of the charge deposit is reconstructed from the wire intersections and the drift time, converted to spatial coordinate via the known drift velocity.

Large-scale TPCs face intrinsic electrical design constraints: long cables between the sensing elements and amplifiers introduce capacitance and thus noise, while attempts to shorten cables can restrict sensor layout [366]. This challenge has been addressed by the development of cryogenic CMOS-based ASIC amplifiers that can operate directly in liquid argon [368, 369]. These cold electronics minimize noise and enable close proximity to the sensing elements, whether wires, strips, or pixels. The issue of routing hundreds of thousands of signals through the cryostat is further mitigated by implementing digitization and multiplexing within the cryostat itself [370], reducing the number and complexity of feedthroughs.

These developments have enabled equivalent noise levels of a few hundred electrons [341, 371], compared to expected charge yields of ~30,000 electrons/MeV, or 60,000 electrons/cm for min-

Int. J. Mod. Phys. A
Downloaded from www.worldscientific.com
by UNIVERSITY OF CALIFORNIA @ BERKE
use and distribution is strictly not permitted, except for Open Access articles.

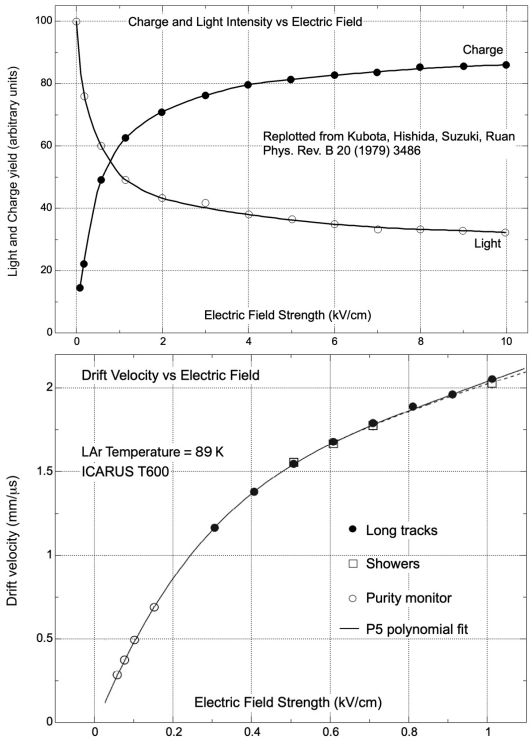

Figure 35.22: (*top*) the form of the light yield and the charge yield vs electric field redrawn from [356]; (*bottom*) electron drift velocity vs electric field redrawn from [337].

imum ionizing particles. This signal-to-noise ratio allows reliable detection of sub-MeV depositions and enables sub-centimeter spatial resolution with wire or pixel pitches below 5 mm.

Most large LAr TPCs also incorporate systems to detect primary scintillation light, which provides crucial timing information for 3D reconstruction [372], triggers [373, 374], complementary calorimetric information [341], and additional localization capability [298]. Given the VUV nature of LAr scintillation (128 nm), wavelength shifters are commonly employed to convert light into the visible range [375]. Photomultiplier tubes capable of cryogenic operation were originally developed for ICARUS [376], and recent systems increasingly use silicon photomultipliers (SiPMs). This allows for decoupling of the light collection and light detection components, and various strategies are being explored for each [301, 377, 378].

35.7.5 *Data Acquisition*

Operating large-mass LAr TPCs requires managing and processing immense volumes of data from digitized charge waveforms and scintillation light channels. For example, in the DUNE experiment, the data throughput is expected to reach up to 1.7 TB/s per detector module (with a 10 kt fiducial mass). To cope with this, several data reduction strategies are typically employed [379,380]:

1. **Zero suppression**: Applied channel-by-channel to digitized waveforms to discard time samples below a given threshold (generally related to the electronic noise level).
2. **Triggered readout**: Fast signals from photon detectors or external sources (e.g., a neutrino beam) trigger the readout of the TPC over a predefined time window. The trigger rate is tuned to match the DAQ throughput capabilities.

Historically, DAQ systems could not afford to buffer or process the full complement of TPC data. However, recent advances in computing and high-speed networking have reshaped this paradigm. It is now possible to read out and buffer the complete digitized TPC data in commercial off-the-shelf (COTS) computers, enabling online processing [381,382] to identify regions with significant charge or light activity. These "trigger primitives" can be used by higher-level software triggers to selectively store data from all or parts of the TPC, similarly to how external triggers are used. Additionally, trigger primitives can be saved as a separate, low-volume data stream, enabling continuous activity monitoring with minimal bias.

This approach permits significant data reduction—up to a factor of 300 for DUNE's four 10 kt modules—while maintaining sensitivity to low-energy signals. It also allows for complementary integration of charge and photon detector information in real-time. This combined readout enhances detection capabilities, particularly for low-energy depositions at the MeV scale, such as supernova neutrino bursts or rare decay signatures.

35.7.6 *Event reconstruction*

The goal of LAr TPC event reconstruction is to extract the physics content of interactions: event topology, particle identification, and energy measurement. Reconstruction generally proceeds in the following stages:

1. **Signal Processing**: Raw waveforms, which reflect the charge collected over time on each readout channel, are processed to correct for pedestal shifts, suppress noise, and deconvolve the detector and electronics response. The result is a set of "hit" objects representing localized energy depositions in space and time [383–385].
2. **Pattern Recognition (PR)**: In wire-readout TPCs, the signal from each wire plane forms a 2D image (drift time vs. position). Typically, three planes at different orientations allow stereo reconstruction of 3D structures. PR can be performed either by matching objects across 2D planes (as in Pandora [386]) or directly in 3D using tomographic reconstruction (as in WireCell [387]). The goal is to identify tracks, showers, common vertices, and the global event topology.
3. **Calorimetry and Particle Identification (PID)**: Reconstructed tracks and showers are calibrated and used to compute energy deposition per unit length (dQ/dx), which is further converted into dE/dx. This enables estimation of total energy and particle type [388].

Recent developments have made **machine learning (ML)** integral to LArTPC reconstruction. Early ML efforts included simple multivariate classifiers and boosted decision trees. More advanced techniques now dominate many tasks, particularly **convolutional neural networks (CNNs)**, which are applied for signal processing assistance [389,390], semantic segmentation [391–393], and vertex reconstruction [394]. CNNs are also used for high-level reconstruction tasks such as PID [300, 395] and energy estimation [396].

Beyond CNNs, newer architectures include **Recurrent Neural Networks (RNNs)** for time-series energy reconstruction [397], **Graph Neural Networks (GNNs)** for hit clustering and labeling [398], and hybrid CNN-GNN models for full event reconstruction pipelines [399]. These developments are accelerated by the availability of public datasets [400] and integration of ML tools within GPU-accelerated software frameworks [299, 401].

35.7.7 *Developments*

The successful operation of the ICARUS T600 detector [402] provided a milestone in demonstrating the feasibility of large-scale liquid argon TPCs. Since then, the technology has rapidly evolved, with the community expanding significantly. Notable advancements include:

- **Cold electronics**: CMOS-based amplifiers now operate reliably within liquid argon.
- **Modern photon detectors**: Silicon Photomultipliers (SiPMs) and novel light collection designs and readout are increasingly replacing traditional photomultiplier tubes.
- **Improved light performance**: Dopants (e.g., xenon, TMG) and advanced wavelength shifters improve light yield and timing.
- **Scalable cryostat technology**: Membrane cryostats, as adopted in DUNE, enable safe and cost-effective scaling to tens of kilotons.

Int. J. Mod. Phys. A 2026.41. Downloaded from www.worldscientific.com
by UNIVERSITY OF CALIFORNIA @ BERKELEY on 09/16/26. Re-use and distribution is strictly not permitted, except for Open Access articles.

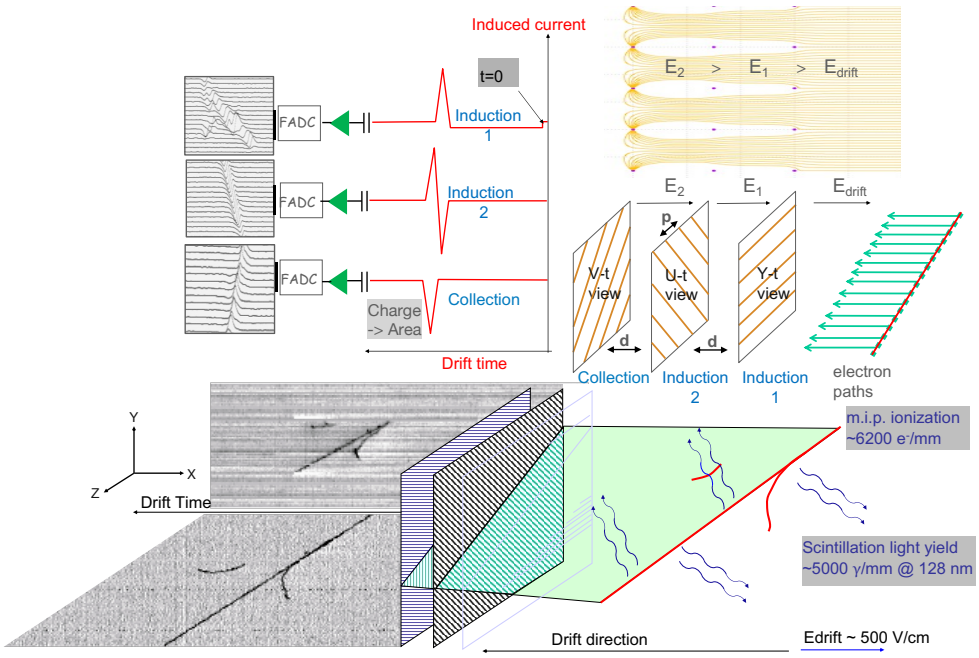

Figure 35.23: Schematic of an event in the ICARUS 3 t LAr TPC; *Top (from right to left)*: field lines from drift region to collection wires, electron flow & arrangement of wire-planes, signal shapes on the wires, and wave-forms from the continuous readout and digitization; *Bottom*: the passage of a muon. The gray scale on the track indicates the ionization density.

- **Pixelated readout**: Replaces traditional wire planes in high-rate or high-occupancy environments, allowing unambiguous 3D charge localization [403].
- **LAr Purification**: novel techniques to capture not only electronegative impurities but also Nitrogen dissolved in LAr through specific molecular sieves [404].

Several new directions are under exploration. These include the **vertical drift** single-phase TPC, proposed for the second DUNE far detector module, which uses perforated PCB strips for charge readout [405]; **optical-only dual-phase readout**, where the electroluminescence light is imaged by fast cameras [406]; and **photon sensors powered and readout by optical systems** (Power over Fiber, Signal over Fiber) [407] which enable light detection at arbitrary electric potentials and positions. In parallel, efforts are underway to **build high voltages in-situ** using Greinacher-style multipliers, eliminating the need for ultra-high-voltage feedthroughs [408]. Operation of a small **LAr-TPC in a magnetic field** of up to 0.7T is also being pursued [307] to investigate benefits of distinguishing particle's charge sign (enabling electron/positron discrimination and increasing electron/photon separation) and measuring momentum of particles via curvature (especially important for muons and pions exiting the detector).

Simultaneously, extensive datasets from current experiments are enabling deeper insights into the argon medium [336, 409] and revealing novel phenomena. These range from the detailed understanding of light propagation, scattering, and absorption, to the behavior of impurities and their impact on charge and light transport. Emerging topics—including the measurement of Rayleigh scattering, precise determination of water capture time, and the role of dopants—highlight the continuing richness of this research area.

The field is active, rapidly advancing, and full of opportunity.

35.8 Semiconductor detectors

Revised November 2025 by G. Kramberger (Jozef Stefan Inst.) and N. Wermes (Bonn U.).

Semiconductor detectors offer outstanding detection opportunities in terms of position, energy and also time resolution, often in combination. In accelerator experiments, they are most widely used as position-sensing devices, *e.g.* in tracking detectors, or as photodetectors (Sec. 35.2), for example in calorimeters (Sec. 35.10) or in imaging Cherenkov detectors (Sec. 35.5). In recent years, also precise time measurement ($\mathcal{O}$(10–30 ps)) with silicon detectors has come into the focus of developments. When comparing semiconductor detectors, particularly with gaseous detectors, the main features are high density and low ionisation threshold, providing in depleted substrates comparatively large signals even without intrinsic amplification. Silicon detectors with active layers only 50–300 µm thick provide adequately large and fast signals on a typical time scale[4] of 10–50 ns. Challenges are the purity of the semiconductor material, characterised by its mobility-lifetime ($\mu\tau$) product, and its radiation resistance. The development of modern semiconductor detectors is closely tied to integrated circuit (IC) technology. Micro-processing and microelectronics technologies enable fabrication of high-density micron-scale electrodes on large wafers (6–8 in $\approx$15–20 cm diameter of sensor wafers) and allow for high-density amplification and readout circuits connected to them (chip-wafer sizes are up to 12 in $\approx$ 30 cm with typical reticles of 26×33 mm^2). For larger than reticle-size area stitching over the reticle boundary is mandatory. In recent years stitching has been demonstrated even for wafer-scale area-sizes.

Some important material properties of common semiconductors used as detectors are summarised in Tab. 35.11. While for particle tracking the excellent position resolution is the main (but not the only) interest, high stopping power and high energy resolution are key parameters in X-ray, γ-ray, and β spectroscopy, for example, in neutrino-less double-beta decay searches. Due to its small bandgap, germanium excels in energy resolution but needs to be operated at very low temperatures (liq. N_2) to reduce thermally generated reverse bias current. Besides Ge, also GaAs, CdTe and CdZnTe (CZT) feature high atomic numbers and hence much higher stopping power and shorter absorption length than Si, which is important, especially for X-ray detection. Diamond, fabricated by chemical vapour deposition (CVD) and strictly speaking classified as an insulator with a large bandgap (Tab. 35.11), features low Z and large radiation length X_0. Thanks to its radiation hardness (Sec. 35.8.5), it is used for particle detection in

[4] Characterised here by the peaking time of the signal pulse.

Int. J. Mod. Phys. A
by UNIVERSITY OF CALIFORNIA @ BERKE
nloaded from www.worldscientific.com
use and distribution is strictly not permitted, except for Open Access articles.

dedicated applications, especially in zones with high particle flux (see *e.g.* [410] and references therein).

Materials R&D for radiation sensors extends to other bulk semiconductors as well, for example, ZnS, SiC, GaN or InP. SiC, in particular, shares most of the beneficial properties of diamond for particle detection and is available in high-quality, large-diameter wafers (see Tab. 35.11). Also, new material structures and metamaterials have come into focus. Examples are semiconductor Quantum Dots, realised by nanometer-sized semiconductor "particles" embedded in a semiconductor bulk, or graphene, which—as a zero-bandgap 2D material—features extraordinarily high conductivity (electrical and thermal) and outstanding photonic properties. A bandgap can be introduced by employing doped bi- or multi-layer graphene structures, thus rendering transistor and sensor realisations possible. The interested reader is referred to references [411] or [412], for example.

Operating usually without intrinsic amplification, semiconductor detectors crucially depend on low-noise electronics (see Sec. 35.9), so the detection sensitivity is determined largely by signal charge and input capacitance. Reviews of semiconductor detectors and electronics can be found, for example, in refs. [1, 8, 413–415].

35.8.1 *Signal generation in semiconductors*

35.8.1.1 *Creation of charges*

Semiconductor detectors are solid-state ionisation chambers. Absorbed energy forms electron-hole (*e*-*h*) pairs, *i.e.* negative and positive charge carriers which—when moving e.g. in an applied electric field—generate a signal current on the electrodes by electrostatic induction (see Sec. 35.8.1.2). For the signal charge carriers to (freely) drift in the electric field and become detectable, a semiconductor must feature a small intrinsic charge-carrier density (as exists, for example, in diamond and SiC, and to some extent also in GaAs and CZT) or they must be depleted by reverse-bias junction configurations (as for Si, Ge or CdTe). In addition, they should feature a low intrinsic density of defects which can act as trapping or generation/recombination centers (see Sec. 35.8.5).

The minimum energy required to form an *e*-*h* pair is the bandgap energy (1.12 eV in Si, 0.66 eV in Ge, 5.5 eV in diamond). However, impinging radiation or particles also release energy to lattice vibrations (phonons) such that the average energy for *e*-*h* pair creation is higher. In an "indirect" semiconductor like Si, the valence-band maximum is not at the same position in k-space (crystal-momentum space) as the conduction-band minimum and additional momentum transfer is required for a band transition to occur. Since the "direct" bandgap energy without k-transfer in Si is 3.4 eV, photons with energies less than 3.4 eV must receive momentum from lattice phonons. Because phonons are Bose-Einstein distributed, the needed momentum kick causes a steep rise in photon absorption probability between 1.12 eV and about 3.4 eV (see e.g. [1]). For larger energy deposits, the average energy $w_{\rm i}$ needed to produce an *e*-*h* pair assumes a constant value of 3.65 eV at room temperature. For other semiconductors consult Tab. 35.11.

For minimum-ionising particles, the most probable charge deposition in a 300 µm thick silicon detector is about 3.7 fC (∼23 000 electrons). In tracking detectors, a particle's energy loss and scattering in the detector material should be minimal (large X_0), whereas, for energy spectroscopy, *e.g.* of X-ray photons, the stopping power should be maximised by choosing high-Z semiconductors[5]. A smaller bandgap (in fact a smaller w_i) leads to a larger signal per deposited energy and improves the energy resolution, but also (exponentially) increases thermally excited carrier generation. To cope with excessive leakage currents at room temperature, Ge diodes are typically operated at liquid nitrogen temperature (77 K). In pure Si at 300 K, the intrinsic carrier concentration is $n_i \simeq 10^{10}\,\mathrm{cm}^{-3}$ (Tab. 35.11), corresponding to a resistivity in the order of $\rho \simeq (e\mu n)^{-1} \approx 400\,\mathrm{k\Omega\,cm}$. In reality, crystal imperfections and minute impurity concentrations limit Si carrier concentrations to about $10^{11}\,\mathrm{cm}^{-3}$ at 300 K ($\rho \approx 40\,\mathrm{k\Omega\,cm}$). In practice, wafer resistivities up to 20 kΩ cm are available, with mass production ranging from 1 to 10 kΩ cm.

[5]The cross section for photo effect scales as Z^5 (see Sec. 34)

The energy released in a semiconductor is absorbed by electronic excitations (e/h) and lattice excitations (phonons) in an anti-correlated way. Therefore, for a fixed released energy E (for example, of an X-ray photon), the variance in the number of charge carriers $N = E/w_i$ follows binomial statistics. Due to the energy constraint, this variance is reduced by the Fano factor F relative to Poisson statistics (F ≈ 0.1 in Si and Ge). Thus, $\sigma_N = \sqrt{FN}$ and the energy resolution is $\sigma_E/E = \sqrt{Fw_i/E}$. However, for semiconductors, the measured fluctuations of a detected energy signal are usually dominated by electronic noise rather than by signal fluctuations. The electronic noise contribution depends much on the detector leakage current and the electrode capacitance as well as on pulse shaping (*i.e.* the shaping time) in the signal processing electronics (see Sec. 35.9).

For X-ray detection, a major effort is made to find high-Z materials with a bandgap that is sufficiently large to allow for room-temperature operation while still providing good energy resolution. Compound semiconductors, *e.g.* CZT, can allow this, but typically suffer from charge collection problems, which are characterised by the product $\mu\tau$ of mobility and carrier lifetime; this is the depth per field strength that generated carriers can drift before being trapped.

In Si and Ge, $\mu\tau$ is orders of magnitude larger than in compound semiconductors for both electrons and holes (see Tab. 35.11). Since for holes $\mu\tau$ is typically much smaller than for electrons, detector configurations where the electron contribution to the charge signal near the readout electrode dominates (as *e.g.* in strip or pixel structures with electron collection) usually provide better performance (see also next section).

35.8.1.2 *Signal formation*

The signal and its pulse shape depend on the instantaneous carrier velocity $\vec{v}(\vec{x}) = \mu\vec{E}(\vec{x})$, μ = mobility, and on the electrode configuration and its geometry, which determine the form of the induced current according to the Shockley-Ramo theorem

$$i_S(t) = N_{e/h}\, e\, \vec{E}_w(\vec{x})\, \vec{v}(\vec{x}(t))\,, \qquad (35.20)$$

where $N_{e/h}\, e$ represents a drifting charge cloud of $N_{e/h}$ elementary charges, $\vec{E}_w(\vec{x})$ is the "weighting field", which accounts for the coupling of the charge to a specific electrode and depends on the electrode configuration, and $\vec{v}$ is the drift velocity. Note the difference between the electric field $\vec{E}$ and the weighting field $\vec{E}_w$ and take account of the fact that the mobility is, in general, field-dependent, $\mu = \mu(E)$, with $v \approx const$ at high fields (velocity saturation, for electrons in Si approaching 10^7 cm/s at $E > 10^4$ V/cm). Both electron and hole movements contribute to an electrode's signal. Hence, if the carrier mobility is very different for electrons and holes, like *e.g.* in CdTe where $\mu_h \ll \mu_e$ (Tab. 35.11), a photon signal, for example, can become absorption-point dependent.

Integration of the induced current signal on an electrode yields the "collected charge". The average time to collect the created charge decreases with increasing bias voltage (*i.e.* field strength) until velocity saturation occurs.

For a simple parallel-plate geometry with two electrodes, the weighting field is constant, whereas for structured electrode geometries, like for example strips or pixels, $\vec{E}_w$ is position dependent, which for small electrodes (compared to the sensor thickness) strongly enhances the contribution of the movement close to the electrode ("small-pixel effect"). More details and practical accounts of the Shockley-Ramo theorem and its usage can be found in [1, 8] and references therein.

Position resolution is ultimately limited by transverse diffusion of the moving charge cloud (typically 3–5 µm for 200–300 µm thickness) and by the emission of δ electrons. The performance then depends on optimal usage of charge sharing between neighbouring electrodes and on the noise. In magnetic fields, Lorentz drift deflects the electron and hole trajectories by an angle $\tan\alpha_L = \mu\, r_H B$, thus increasing the spatial spreading. The factor r_H accounts for the mobility difference with and without a magnetic field. For silicon at room temperature and small B-fields, $r_H \approx 1.15$ for electrons and $r_H \approx 0.8$ for holes; for large magnetic fields $r_H \approx 1$. The total spreading and hence charge sharing between electrodes can be tuned (increased or decreased) by tilting

Int. J. Mod. Phys. A 2026.41. Downloaded from www.worldscientific.com
by UNIVERSITY OF CALIFORNIA @ BERKELEY on 09/16/26. Re-use and distribution is strictly not permitted, except for Open Access articles.

Table 35.11: Properties of some detector-relevant semiconductors; temperature-dependent quantities given at 300 K (from [1, 416] and references therein).

Property	Si	Ge	GaAs	CdTe (CZT*)	Diamond	4H-SiC†
atomic number (Z)	14	32	31/33	48/(30)/52	6	14/6
density ρ (g/cm^3)	2.328	5.327	5.32	5.85	3.51	3.21
dielectric constant ϵ	11.9	16.0	13.1	10.2	5.7	9.72
semiconductor type	indirect	indirect	direct	direct	indirect	indirect
bandgap E_G (eV)	1.12	0.66	1.424	1.44(1.44–2.2)	5.5	3.26
intr. carrier density (cm^{-3})	1.09×10^{10}	2.4×10^{13}	2.1×10^{6}	10^7	≈ 0	≈ 0
radiation length X_0 (cm)	9.36	2.30	2.29	1.52	12.15	10.58
average energy w_i for (e/h) creation (eV)	3.65	2.96	4.35	4.43	13.1	7.8
mobility (cm^2/Vs)						
electrons μ_n	1450	3900	8500	1050	$\approx$1800‡	950
holes μ_h	500	1800	400	90	$\approx$2300‡	125
lifetime						
electrons τ_e	>100 µs	∼ms	1–10 ns	0.1–2 µs	$\approx$100 ns	0.1–2 µs
holes τ_h	>100 µs	∼ms	20 ns	0.1–1 µs	$\approx$ 50 ns	0.7 µs

*CZT = CdZnTe with the bandgap depending on the Cd to Zn ratio.
†4H-SiC = hexagonal silicon carbide with a 4-layer repeat structure.
‡Approximate averages. Mobility values for diamond quoted in the literature vary strongly.

the detector relative to the incoming (average) particle direction. Overall spatial resolutions of 2–4 µm (rms) have been obtained.

35.8.2 *Junction detectors*

Si and Ge detector substrates must be—others like CdTe, GaAs should be, and CZT can be—depleted of free charge carriers by operating them as reverse-bias junctions (p-n or Schottky) to be sensitive to the charge created by impinging particles. SiC, although intrinsically almost free of charge carriers, usually comes as wafers with doped epitaxial layers of thickness $\lesssim 100$ µm and SiC detectors are hence built as junction detectors.

A typical cross-section of a junction detector is shown in Fig. 35.24, here with structured electrodes at the top. A p-n junction—even without external voltage—forms a sensitive space-charge region across itself, depleted of mobile charges, hence also called "depletion region". The space charge establishes an electric field corresponding to a "built-in" voltage V_{bi}. An additional reverse-bias voltage V, applied externally, increases the space-charge region, allowing radiation-generated charge to be swept to the electrodes by the existing field. Detectors typically use an asymmetric structure, for example, a thin and highly doped p^+ electrode[6] region and a lightly doped n^- substrate region – or vice versa, so that the depletion region extends predominantly into the more lightly doped bulk volume.

In such planar Si (or Ge) devices, the thickness of the depleted region is

$$d = \sqrt{2\epsilon\,(V+V_{bi})/Ne} = \sqrt{2\rho\mu\epsilon\,(V+V_{bi})} \tag{35.21}$$

$$\approx \frac{0.5}{\mu\text{m}} \times \sqrt{\frac{\rho\,V}{\Omega\,\text{cm}\cdot\text{V}}} \qquad \text{for } n\text{-type Si bulk}$$

$$\approx \frac{0.3}{\mu\text{m}} \times \sqrt{\frac{\rho\,V}{\Omega\,\text{cm}\cdot\text{V}}} \qquad \text{for } p\text{-type Si bulk}$$

with (values for Si)

V = external bias voltage
V_{bi} = "built-in" voltage (≈ 0.5 V for typ. used resistivities)
N = doping concentration
e = elementary charge
ϵ = dielectric constant = $11.9\,\epsilon_0 \approx 1$ pF/cm
ρ = resistivity (typically 1–10 kΩ cm)
μ = charge carrier mobility ($\sim$ 1450 cm^2/Vs (electrons), $\sim$ 500 cm^2/Vs (holes) [417])

The conductive p and n regions together with the depleted volume form a capacitor with capacitance per unit area

$$C' = \frac{\epsilon}{d} \approx \frac{1\,\text{pF/cm}}{d} \qquad \text{in Si.} \tag{35.22}$$

The depletion depth d becomes as large as the sensor's thickness at the "full depletion voltage" $V = V_{fd}$ for which the sensor capacitance reaches a minimum (about 35 pF/cm^2 for $d = 300$ µm). In strip and pixel detectors (see next section), the capacitance is dominated by the fringing capacitance to neighbouring electrodes as the electrode pitch is typically much smaller than the sensor thickness. For example, the strip-to-strip Si fringing capacitance is about 1–1.5 pF per cm of strip length at a strip pitch of 25–50 µm, depending also on the electrode width.

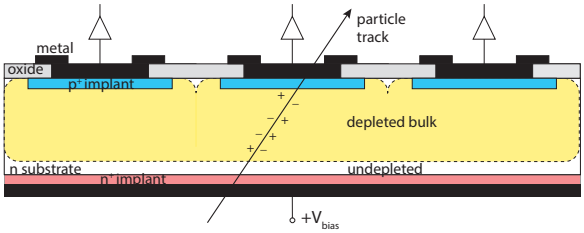

Figure 35.24: Reverse-bias junction detector with planar readout electrodes at the top in a standard sensor configuration (p^+-in-n): lightly doped n-type substrate with p^+ implants forming the diode junction at the top side. Electrons move to the bottom electrode and holes to the top. Both movements contribute to the (induced) signal at the top electrodes with amounts as specified by the weighting field (see Sec. 35.8.1.2). The n^+ implant at the bottom side forms an ohmic contact between bulk and metal.

The electric field strength and shape inside the semiconductor bulk are important for efficient signal-charge collection. Governed not only by the applied external voltage, but also by the space charge inside the semiconductor bulk, the field strength decreases linearly (for constant space charge) from its maximum at the junction's boundary into the depleted semiconductor bulk. Apart from

[6] $n^{+/++}$, $p^{+/++}$ as well as n^-, p^- qualitatively denote relative doping-concentration levels.

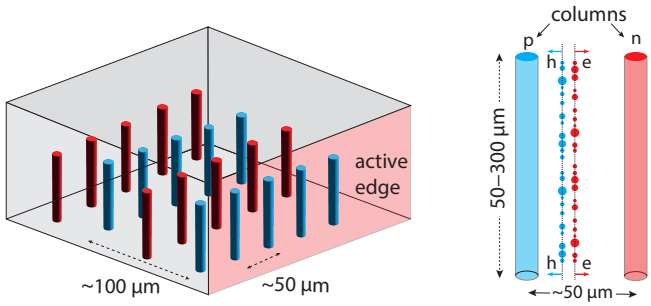

Figure 35.25: Junction detector with vertical electrodes, n (red) and p (blue), and "active" edges called 3D-Si. Dimensions given are typical. This electrode configuration provides short drift paths for moving charges while keeping a large sensing thickness. An active edge minimises dead areas at the sensor boundaries. This geometry has also been employed in CVD diamond substrates.

the doping atoms, space charge can also occur from ionised lattice defects which either naturally exist for example in GaAs or can be created by irradiation in any semiconductor material (see Sec. 35.8.5). This can lead to low-field regions as well as to changes in the field's shape (deviating from linear), both of which usually deteriorate the charge collection properties of a detector.

In partial depletion (*i.e.* $V < V_{fd}$), the field decreases to zero at the end of the depletion zone. Overbias ($V > V_{fd}$) adds a constant electric field component, which avoids a vanishing field region and also provides faster charge collection as long as the carrier drift velocity has not yet saturated. At an average field of $E = 10^4$ V/cm, the onset of velocity saturation, where $\mu_e \approx 7{\times}10^2\,\mathrm{cm}^2/\mathrm{Vs}$, $\mu_h \approx 3.5{\times}10^2\,\mathrm{cm}^2/\mathrm{Vs}$, the collection times for Si are about 15 ps/µm for electrons and 30 ps/µm for holes. In typical fully-depleted detectors, 100–300 µm thick, electrons are collected within less than about 5 ns, and holes within less than about 10 ns.

Large volume ($\sim 10^2 - 10^3\,\mathrm{cm}^3$) germanium detectors, especially for gamma-ray detection, are commonly configured in cylindrical or hexagonal rod shapes, for example, a 10 cm long cylindrical n-type crystal with 5–10 cm diameter with an inner 5–10 mm diameter n^+ electrode and an outer p^+ layer forming the diode junction. Germanium can be grown with fairly low impurity levels, 10^9–$10^{10}\,\mathrm{cm}^{-3}$ (HPGe, high-purity germanium), so these large volumes can be depleted with several kilovolts.

Diamond, featuring free charge carrier densities close to zero, needs no further depletion and is operated as a parallel plate capacitor with an insulator dielectric inside. Still, a substantial bias voltage is required to overcome charge trapping.

35.8.3 *Detectors with structured electrodes*

35.8.3.1 *Microstrip-, Si-drift- and hybrid-pixel detectors*

In HEP experiments semiconductor detectors usually aim at good position resolution achieved with electrodes patterned in "strips" or "pixels" with typical dimension scales (electrode pitch) of 50–100 µm, or in "pads" (mm^2–cm^2) if coarser granularity is affordable for the benefit of fewer channels.

Electrodes are usually placed "planar", *i.e.* at the surface of the sensing Si bulk (Fig. 35.24). In an alternative, but more elaborate way, electrodes can be shaped as columns or trenches running orthogonally to the surface and hence parallel to the average direction of impinging particles (Fig. 35.25) [418]. This geometry which is termed "3D-Si", but is also exercised with diamond, enhances the radiation tolerance due to shorter drift distances of charges at the same thickness, hence decreasing the probability for carrier trapping (see also Sec. 35.8.5).

The 3D technology offers a large variety of cell geometries usually optimized for a given task, realized with column electrodes, trench electrodes (plane parallel-trench cells) or a combination of both. In recent years, manufacturing the vertical electrodes has advanced to simpler single-sided processing, reaching aspect ratios (diameter to depth) of up to 70, thus enabling smaller cells and thicker detectors. The processing techniques employed for 3D devices also enable the creation of continuous trenches with conductive sensor side-walls ("active edge" in Fig. 35.25), which are useful for laterally extending the depleted volume up to the physical edges.

In strip detectors, the strip ends are connected to dedicated readout ICs where the signals are amplified and processed. Two-dimensional readout is realised either by angled double-layers of strip detectors or by "double-sided" strip sensors, structured by readout strips on either side (see *e.g.* [1, 414] and references therein). For the latter, one electrode surface features n^+n or p^+p strip junctions (rather than pn), respectively, which require dedicated measures, *e.g.* intermediate strips or special doping profiles to break the electron accumulation layer that occurs at an n^+n interface. For p^+p, intermediate n strips or similar are not necessary, owing to positive oxide charges residing at the Si/SiO$_2$ interface, thus preventing the formation of a hole accumulation layer.

Following the concept of gaseous drift chambers, silicon drift chambers provide the position of a hit orthogonal to a strip's coordinate from a measurement of the charge cloud's drift time, drifting over centimeter-long paths inside the silicon bulk (Fig. 35.26a). For this to work, the bulk is "sidewards depleted" by using junction strip-implants of the same polarity on both sides of the sensor (p in n or n in p, respectively), *i.e.* different to standard double-sided strip detectors (see *e.g.* [1]). This way, a quadratic potential minimum for electrons is created, confining them amidst the sensor bulk; holes, instead, drift to the sides. A constant potential (linear field) is superimposed in drift direction (Fig. 35.26c); near the anodes, electrons are pushed towards n-strip collection electrodes by appropriate biasing (Fig. 35.26d). Unlike strip detectors, far fewer electrodes are necessary for the same active area coverage. A drawback is the low rate capability of Si-drift detectors caused by the long drift path of the created charges. Arranged with only one small electrode with low capacitance in the center of a cylindrical disk, so-called silicon drift-diodes (SDD, Fig. 35.26b) are low-noise single-channel devices with large area coverage (typically cm^2), used for example in X-ray fluorescence analysis, electron microscopy and space applications.

Very small pixel structures for particle detection were first realised with CCDs (Charge Coupled Device) [419]. Most current applications, particularly those for high-rate applications such as at the LHC, employ the "hybrid-pixel" concept in which both the sensing diode structure as well as the readout IC have equal electrode structures and patterns (pixels). The connection is made by two-dimensional arrays of solder or indium bumps that mate the two parts by employing the flip-chip technology (Fig. 35.27, usually chip-to-(sensor)chip or several-chips-to-sensor; more details in [414,420,421]). Further advancements in bonding-technique development especially address chip-to-wafer or even wafer-to-wafer placements [420]. Attractive in this context of particle detectors are Cu–Cu, Cu–Sn, or oxide–oxide (SiO$_2$) diffusion bonding without solder. Also, SLID (Solid Liquid Interface Diffusion), which employs a very thin liquid metal layer (Sn) in between metals with higher melting points (*e.g.* Cu) is an option.

The hybrid approach excels in optimally utilising chip and sensor materials and technologies for radiation hardness and rate capability (see *e.g.* [420]). It is, therefore, the technology of choice for pixel trackers in high-rate, high-radiation environments optimised for that purpose by employing very thin modules ($\mathcal{O}(300\,\mu\mathrm{m})$ total). A disadvantage is the complex and cost-intensive module assembly.

35.8.3.2 *Monolithic pixels*

Partially or fully monolithic pixel detectors directly connect the generated signal charge with an embedded active electronics device (*i.e.* one or several transistors). An example of a partially monolithic device is the DEPFET (depleted p-channel FET) pixel sensor (see *e.g.* [422]), employed in the Belle-II pixel-vertex detector and—with circular cells—also developed for satellite experiments as shown in Fig. 35.28a. A single transistor (pMOSFET) is implemented in every pixel. The sensor substrate is "sidewards depleted"—as done similarly in Si driftchambers (Sec. 35.8.3.1)—employing the backside p-contact and several p regions near the transistor. Depletion is provided by the n^+ *clear* contact (see

Int. J. Mod. Phys. A
by UNIVERSITY OF CALIFORNIA @ BERKE
nloaded from www.worldscientific.com
use and distribution is strictly not permitted, except for Open Access articles.

Int. J. Mod. Phys. A 2026.41. Downloaded from www.worldscientific.com
by UNIVERSITY OF CALIFORNIA @ BERKELEY on 09/16/26. Re-use and distribution is strictly not permitted, except for Open Access articles.

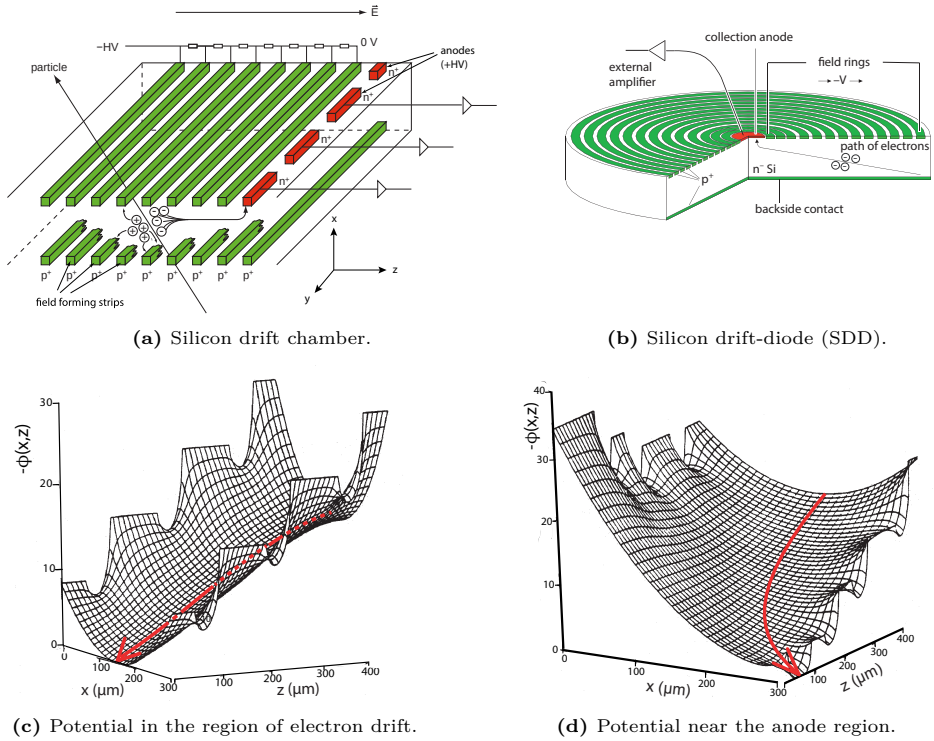

(a) Silicon drift chamber. **(b)** Silicon drift-diode (SDD).

(c) Potential in the region of electron drift. **(d)** Potential near the anode region.

Figure 35.26: Silicon drift detector: (a) Principle layout of an n-bulk Si drift chamber featuring field-forming p-strips on both sides and charge-collecting n-strip anodes. A linear field gradient, applied by a resistor chain, provides drift of electrons towards the anodes. (c) Shape of the electric potential in the drift region of the detector shown in (a). (d) Electric potential near the anode region. (b) Si drift diode featuring circular field rings and only one small collection anode in the center of the diode, constituting very low capacitance for the readout electronics.

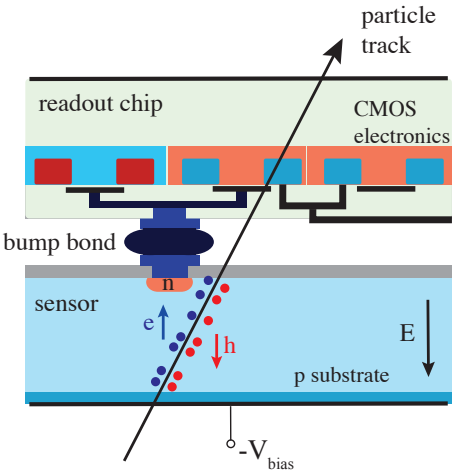

Figure 35.27: Cross-sectional view of a hybrid-pixel detector cell (one pixel) consisting of sensor (bottom) and readout chip (top) with CMOS circuitry illustrated by three transistors (red and blue implant areas plus metal lines). The sensor is a depleted diode structure (here p substrate with n electrode). Both parts are mated by a microbond (bump bond), typically solder or indium.

below) plus a bulk n-implant outside the matrix. In addition, the structure features a deep n-implant located a few micrometers underneath the transistor channel on floating potential. This implant becomes the most positive point of the structure, hence being an electron accumulation point which acts as an "internal gate" of the transistor. The gate voltage changes by an amount $\alpha q_S/C$, with signal charge q_S, gate-oxide capacitance $C = C_{ox}\,WL$ where $W\times L$ = gate area, and with $\alpha \lesssim 1$ accounting for stray capacitance. The gate voltage changes due to an accumulated signal charge q_S in the internal gate, leading to a detectable change in drain current (in saturation):

$$I_D = \frac{W}{2L}\,\mu C_{ox}\left(V_G + \frac{\alpha\, q_S}{C} - V_{th}\right)^2 . \qquad (35.23)$$

Other elements in Fig. 35.28a like the external FET gate and the *clear* implant provide control and reset of the structure. The device gain $g_q = dI_D/dq_S \approx \alpha g_m/C$, with transconductance $g_m = \mu C_{ox}\frac{W}{L}(V_G - V_{th})$, is of order 500 pA/e$^-$. The small capacitance of the internal gate (few fF) enables very low-noise operation ($\lesssim 2\mathrm{e}^-$) when operating with long shaping times (cf. Sec. 35.9).

Fully monolithic pixels combine the sensing task and the complete readout circuitry, *i.e.* the two separated parts of hybrid pixels, in one chip. Both functions must be properly shielded from each other, which is achieved by exploiting multi-well IC technology. Realised as MAPS (monolithic active pixel sensors, see Fig. 35.28b), standard CMOS wafers can be used for pixel detector fabrication. CMOS wafers often feature a Si epitaxial layer where the transistors are implanted. It is possible to use this epi-layer as a sensitive detection volume for particle detection. However, in such detectors, usually only the immediate regions near the collection nodes are depleted. Outside these confined regions, there is no or little electric field and charge collection is dominantly governed by slow and non-directional charge diffusion, a problem for high-rate applications. Depleted MAPS (DMAPS) exploit non-standard high resistivity wafers or high-ohmic epi-layers, typically with resistivities >1 kΩ cm, as well as high bias voltage (up to $\gtrsim$ 300 V), resulting in charge collection by directed drift motion. Charge collecting electrodes are deep wells (n-wells in Fig. 35.28b), either formed as large (typ. 50×100 μm^2) structures to fully contain the CMOS circuitry (Fig. 35.28b, top) or as small nodes, set aside the electronics (Fig. 35.28b, bottom), with obvious pros and cons resulting from shorter average drift distance (large electrode) versus much smaller capacitance (small

Int. J. Mod. by UNIVERSITY OF CALIFORNIA @ BERKE nloaded from www.worldscientific.com use and distribution is strictly not permitted, except for Open Access articles.

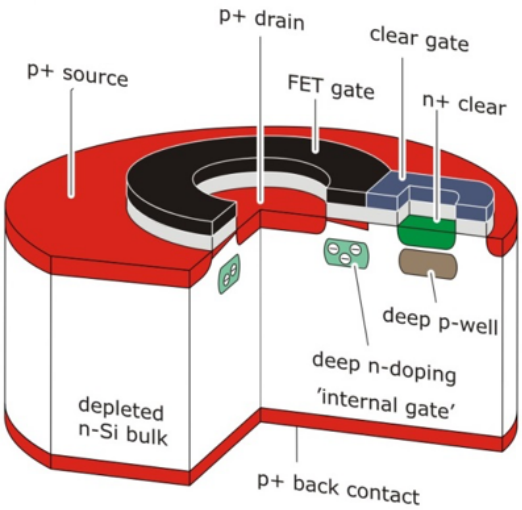

(a) DEPFET pixel structure.

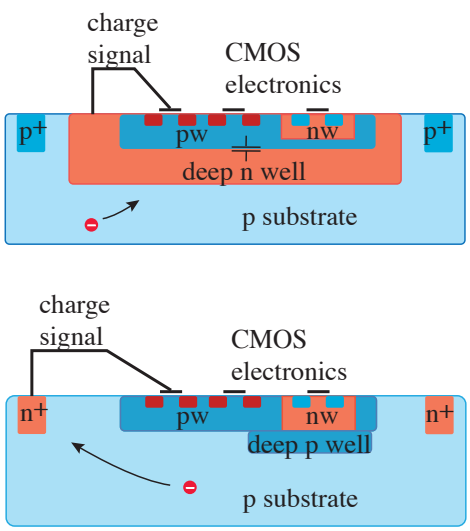

(b) DMAPS pixel structures.

Figure 35.28: Partially (a) and fully (b) monolithic pixels: (a) DEPFET pixel structure with an embedded pMOSFET transistor; source and drain are p implants (red), gate metal (black), oxide (grey), deep-n internal gate (light green), other metal (blue), clear contact (green), and deep p-well (brown). (b) Depleted MAPS (DMAPS) with joint sensing and electronics volumes: (top) charge collection by a *large-electrode* housing the electronics in a deep-n well; (bottom) charge collection by a *small electrode* set aside from the electronics area.

electrode). The former features a more uniform shape of the electric and the weighting field as well as short drift paths, benefiting radiation tolerance and timing performance in charge collection, whereas the latter allows for smaller pixels and benefits in noise and rise time from the small sensor capacitance. Yet, in both approaches radiation tolerance levels of $\gtrsim 10^{15}\,\mathrm{n_{eq}/cm^2}$ (fluence) and 1 MGy (ion. dose) have been demonstrated.

A variant of the monolithic approach are SOI (silicon-on-insulator) pixel devices, providing high spatial resolution, but less radiation tolerance: A high-resistivity supporting wafer, employed for particle sensing, connects through an embedded insulator (a buried oxide layer, BOX) to the CMOS readout circuitry. The BOX separates the sensing volume from the electronics layer and provides shielding. Because the area between the BOX and the transistor layer acts as a "back-gate", transistor operation can be affected, requiring careful considerations of radiation tolerance (see *e.g.* [423]).

35.8.4 *Precise timing with silicon detectors*

Typical time scales for silicon detector output signals are several tens of nanoseconds (*e.g.* rise times, shaping times, etc.) accompanied by a typical time mark precision in the order of nanoseconds. Essential for achieving precision time resolution ($\sigma_t < 100\,\mathrm{ps}$) are a large and steep signal as well as low noise, because time jitter (σ_{jitter}) relates to signal-amplitude fluctuations as:

$$\sigma_{\mathrm{jitter}} = \frac{\sigma_n}{(dS/dt)_{\mathrm{trig}}} \approx \frac{t_r}{SNR}, \tag{35.24}$$

where σ_n is the rms noise, t_r the rise time, SNR the signal-to-noise ratio, and dS/dt the "slew rate" evaluated at trigger threshold (see also Sec. 35.9), in which S is the "signal", *e.g.* an induced current or a voltage. This, in turn, requires fast charge collection, *e.g.* in thin planar or 3D-Si detectors with high E-fields, as well as fast and high amplification, both together yielding large slew rates. Important parameters that influence timing precision are the detector capacitance (including stray contributions), leakage current and—if present—the size of the amplification gain.

Among the detectors that have achieved precise time measurement are so-called LGADs (low gain avalanche detectors, Fig. 35.29). Their planar electrode geometry includes an implanted low-gain ($g = 10$–50) amplification structure on either the top or bottom electrode side to maximise the slew rate. Electrons created from impinging ionising particles drift towards a very high field created by an amplification layer near the (here) top electrode, where impact ionisation creates a multitude of e-h pairs. They induce a fast and large signal rise, mainly governed by the holes' movement away from the amplification layer. Sufficiently low amplification gain minimises excess noise contributions and avoids the creation of hole-induced avalanches moving in the opposite direction to electron avalanches.

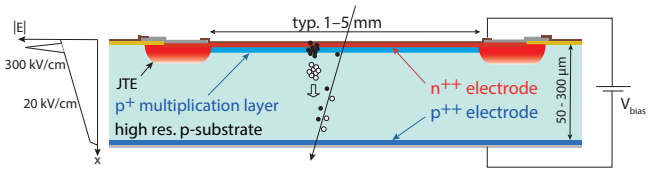

Figure 35.29: LGAD amplification structure for precision timing. Amplification (typ. $\times$ 10–50) occurs at the structure boundary in a highly doped p-n junction near the (here: top) surface (JTE = Junction Termination Extension, deep n-well).

The achievable time resolution has several contributions:

$$\sigma_t^2 \approx \left(\frac{\sigma_S^{thr}}{dS/dt}\right)^2 + \left(\frac{\sigma_n}{dS/dt}\right)^2 + \sigma^2_{\mathrm{arrival}}(V_{thr}) + \sigma^2_{\mathrm{dist}} + \sigma^2_{\mathrm{TDC}}\,. \tag{35.25}$$

The first term represents "time walk" coming from Landau fluctuations, defined as originating from number and energy-transfer fluctuations in the energy-loss process with σ_S^{thr} being the signal-height variations at discriminator threshold (V_{thr}). This term can be kept minimal, *e.g.* by employing constant-fraction discrimination or by applying corrections using amplitude information. The second term is the contribution of noise to the time jitter. Both first terms are kept small by large signal slew rates. An irreducible contribution comes from fluctuations in non-uniform depositions of charge along the particle path (including fluctuations in the amplification process), which causes an intrinsic jitter in the arrival time (third term)[7]. The smaller the threshold and the thinner

[7] In LGAD literature, these fluctuations are sometimes also referred to as "Landau fluctuations".

Int. J. Mod. Phys. A 2026.41. Downloaded from www.worldscientific.com
by UNIVERSITY OF CALIFORNIA @ BERKELEY on 09/16/26. Re-use and distribution is strictly not permitted, except for Open Access articles.

the detector, the less disturbing the effect is. If the amplification gain is mandatory for crossing V_{thr}, this term can become dominant as it explicitly depends on the gain. The fourth contribution is signal distortion due to non-uniform weighting-field regions and variations in (non-saturated) drift velocities. "Junction Termination Extensions" (JTE, see Fig. 35.29) serve to lower this term; it is usually marginal for LGADs with pitch/thickness $\gg 1$. The final term denotes time fluctuations due to uncertainties in digitisation, which can, however, be made negligible with GHz digital time conversion. Timing precision down to 15-20 ps for minimum-ionising particles has been reached for thin LGADs with relatively high gain (>40). Improving the time resolution for tracks beyond this value is possible by employing LGADs in multiple-layer structures.

Structural and operational variants to improve charge collection (uniform and efficient over the entire surface), position and also time resolution, are "resistive AC-coupled LGADs" (capacitively coupled electrodes on top of the gain layer), "inverse LGADs" (backside is segmented), "trench-isolated LGADs" (an oxide trench separates the electrodes) and other less mature ones like "deep junction LGADs". The LGAD technology is not limited to silicon detectors, but is also applicable, for example, in SiC: due to the doping profiles used in SiC, which are swapped compared to those in Fig. 35.29, dominantly holes are multiplied instead of electrons, albeit at higher electric fields. More details on LGADs can be found in [424] and [425].

Columnar electrode geometries such as shown in Fig. 35.25 with small diameter and small pitch are by design a very suitable choice for precision timing due to short collection paths and strong fields. Employing a trench-like shape of the columns, field- and weighting-field distortions are minimised and time resolutions in the order of 10 ps have been measured in prototypes [426].

High precision timing can also be approached by exploiting the benefits of SiGe BiCMOS technology: The strain mismatch of Si-Ge alloy layers results in a smaller bandgap as well as higher mobility, and hence larger transconductance. This benefits the speed in hetero-junction bipolar transistors (HBTs), which also feature less 1/f noise than MOS transistors. Resolutions of order 20 ps have been reached in a monolithic pixel matrix using this technology [427]. More elaborate discussions on timing with silicon detectors can be found *e.g.* in [428].

35.8.5 *Radiation damage in silicon detectors*

High channel density and response times in the nanosecond range render micro-patterned semiconductor detectors particularly suited for high particle rates. This is usually accompanied by high radiation, which causes damage to sensors and front-end electronics. We restrict ourselves here to the description of damage mechanisms typical in Si detectors and their electronics. Radiation damage occurs in semiconductor detectors through two basic mechanisms:

1. *Bulk damage* due to the displacement of atoms from their lattice sites, resulting in defect energy levels inside the bandgap. This leads to increased leakage current, carrier trapping, and build-up of space charge that changes the required operating voltage. Displacement damage results from non-ionising energy loss (NIEL). The energy imparted to the recoil atoms can initiate a chain of subsequent displacements, including "damage clusters". For NIEL scaling (see below), it is critical to consider both particle type and energy: conventionally, for silicon, the received NIEL is normalised to the damage level caused by 1 MeV neutrons and specified in units of neutron-equivalent fluence Φ_{eq} with units n_{eq}/cm^2.
2. *Surface damage* due to charge build-up in surface layers and formation of interface traps at *e.g.* Si–SiO_2 boundaries. These influence transistor currents and thresholds or cause thin charge carrier layers at a silicon surface. This leads to increased surface leakage currents in sensors as well as circuits, affects the insulation of electrode implants and changes the characteristics of transistors. The effects of charge build-up are strongly dependent on the device structure and on fabrication details. The damage is mainly due to the ionising energy loss (IEL) and is hence proportional to the absorbed total ionisation dose (TID) measured in Gy (or rad), independent of the irradiating particle type.

We note that the increase in reverse bias generation current (leakage current) due to bulk damage is $\Delta I_L = \alpha_I \Phi_{eq} V$, where V is the depleted volume under an electrode and $\alpha_I \simeq 4 \times 10^{-17}$ A/cm, a universal constant when normalised to temperature (conventionally 20°C), and measured after annealing for 80 min at 60 °C. Note that for devices with intrinsic amplification, the generation current is amplified accordingly. Reverse bias leakage current depends strongly on temperature

$$I_L(T) \propto T^2 \exp\left(-\frac{E_a}{2kT}\right) , \tag{35.26}$$

where $E_a \approx 1.2$ eV (activation energy), so rather modest cooling can reduce the current substantially (∼7-fold reduction in cooling from room temperature to 0 °C).

For bulk damage in silicon, the *NIEL hypothesis* is a good first-order description of the observed damage (especially regarding I_L). It states that all lattice radiation damage in silicon linearly scales with NIEL and can be traced back to the abundance of primary defects (point defects and clusters), irrespective of their initial distribution over energy and space, that is, regardless of the damage's topology and origin. Under the NIEL hypothesis, the observed differences in damage caused by neutrons, protons, pions and electrons are therefore usually scaled to each other. For other damage manifestations besides I_L, the NIEL hypothesis is moderately violated.

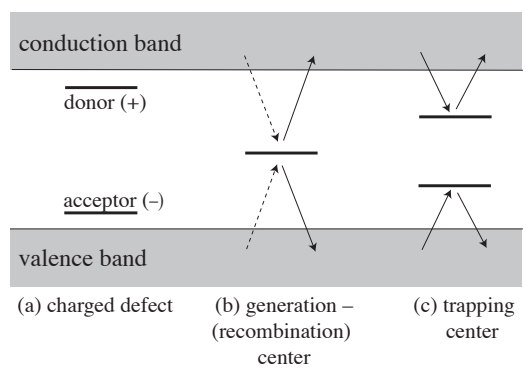

Figure 35.30: Characteristic locations of energy levels caused by bulk radiation damage and their main action effects.

Three main bulk displacement damage effects are sketched in Fig. 35.30: (a) defects acting as charged donors/acceptors, (b) deep defects (near the middle of the bandgap) causing increased leakage current, and (c) carrier trapping centers. Another consequence of deep defects is that any non-depleted bulk becomes more resistive, hence impacting the electric and the weighting field distributions. At very high fluences ($\Phi_{\mathrm{eq}} > 10^{16}$ cm^{-2}) also carrier mobilities decrease, leading to resistivities even lower than intrinsic.

Damage effects are not constant with time; for example, in n-type bulk, radiation-induced negative space charge anneals at first reaching a stable space charge minimum (beneficial annealing), but later electrically active defects (negative space charge from acceptor-type damage) build up over the time scale of months (reverse annealing) at room temperature and much longer at lower temperatures.

Acceptor- (usually dominant) or donor-like (deep) defects, when ionised, build up space charge (dominantly negative), which in turn normally requires an increase in the applied voltage to deplete the active volume of the detector and sweep the signal charge through the detector thickness. For n-type bulk starting material, however, shallow donor (*e.g.* phosphorus) removal is initiated by incipient radiation (production of lattice vacancies V) through formation of electrically inactive vacancy-phosphorus (V-P) complexes. This leads to a faster decrease in depletion voltage (faster

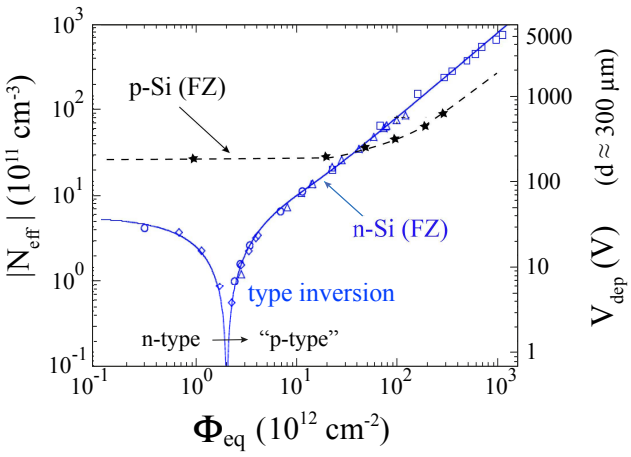

Figure 35.31: Effective space charge concentration $N_{\rm eff}$ (left axis) and required voltage for full depletion $V_{\rm dep}$ (right axis) of approximately 300 µm thick Si sensors as a function of neutron-equivalent radiation fluence for typical n-type (blue) and p-type (black) silicon float zone (FZ) material before annealing. While initial n-type Si inverts to effectively p-type Si, this is not observed for initial p-type silicon. Bias voltage supply for large systems is usually limited to less than 600–1000 V. Figure adapted using [429, 430] and [431].

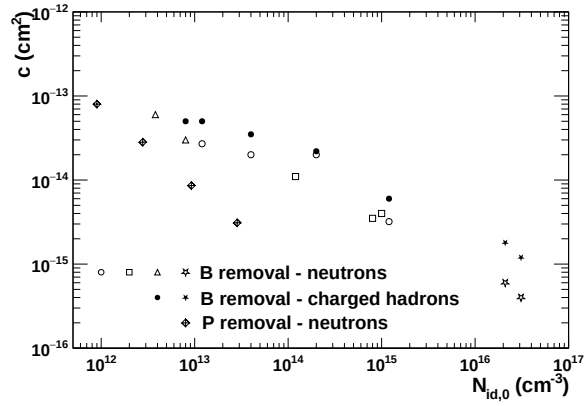

Figure 35.32: Initial dopant-removal (B boron, P phosphorous) constant c (immediately after irradiation) measured at different initial concentrations $N_{\rm id,0}$ for silicon irradiated with charged hadrons and with neutrons. Different markers indicate different types of devices. Data from CERN RD48/RD50 studies.

than only by the compensation of donors through generated deep acceptors) until positive and negative space charges effectively balance; only small bias voltage is then required for efficient operation (point of effective space charge inversion, also called "type inversion" (Fig. 35.31)). At larger fluences, the negative space charge dominates, and the required operating voltage increases proportionally to the increasing effective space charge density $N_{\rm eff}$, also called effective doping concentration.

The drift of thermally generated electrons and holes (generation current) in opposite directions and their (partial) trapping leads to a surplus of these carriers at the electrodes on either side. This affects the charge state of the deep energy levels (more carriers are trapped) and hence the space charge distribution, which can no longer be regarded as constant and homogeneous over the detector volume. Hence, the linear slope of the electric field from the junction to the backside, as was introduced in Sec. 35.8.2, is distorted; instead "double-junction"-like field distributions typically occur. The magnitude of the effect depends on the material and the type of radiation.

Today, p-type bulk silicon with n^+ electrode-implants is the preferred choice for sensors operating in high-radiation environments for reasons of cost-effectiveness in production as well as high radiation hardness due to fast (high mobility) electron collection in high electric- and high weighting-field regions at small segmented n^+ electrodes. Space charge inversion is usually not observed since the initial space charge is negative already (Fig. 35.31).

Removal of initial shallow dopants (donor or acceptor) through irradiation plays a major role in the property changes of various detector technologies. The decrease of initial doping concentration ($N_{id,0}$) is exponential $N_{id} = N_{id,0}\,\exp(-c\,\Phi_{\rm eq})$, with the removal constant c depending on $N_{id,0}$, particle type and on impurities in the semiconductor (see Fig. 35.32). Removal of acceptors (*i.e.* substitution of electrically active boron at its lattice site) in p material is found to be dominantly caused by interstitial silicon replacing boron on its lattice position. The highly active interstitial boron then can cause the formation of other defects such as interstitial oxygen-boron complexes (B_iO_i, subscript i for "interstitial") which absorb boron atoms into electrically active defects, dominantly as donors, that means that space charge can be changed twice.

Different techniques have been explored to neutralise radiation damage effects by defect engineering. For n-type material, oxygen enrichment, introduced during the Si growth, to a larger abundance than phosphorus, successfully reduces the formation of multi-vacancy, acceptor-like complexes, which are dominantly produced by charged-hadron irradiation. Instead, the oxygen enhances the formation of electrically neutral V-O complexes. For p-type Si, carbon enrichment reduces acceptor-dopant removal by building stable C_i-S_i complexes, thus trapping the Si interstitials, which could otherwise remove boron as described above.

Dopant removal plays a particularly important role in more complex sensor structures, such as DMAPS or LGADs. In particular, the high p-doping concentration in the LGAD's gain layer is vulnerable to acceptor removal, causing a drastic gain decrease with increasing fluence.

Deep level defects (Fig. 35.30b) typically are the origin of leakage current increase, whereas trapping centers (Fig. 35.30c) affect carrier trapping times and cause signal loss. The cumulative effect of different trapping centers can be expressed by effective trapping times of electrons and holes $\tau_{{\rm eff},e/h}$. The induced current equation Eq. (35.20) is multiplied by $\exp(-\frac{t}{\tau_{{\rm eff},e/h}})$, describing the reduction of the number of charge carriers $N_{e/h}$ due to trapping. The effective trapping probability of electrons and holes in silicon, proportional to $1/\tau_{{\rm eff},e/h}$, increases linearly with fluence up to around 10^{15} n$_{\rm eq}$/cm^2, where $\tau_{{\rm eff},e/h}$ is of order 1 ns, and then exhibits saturation [432]. Performance implications of trapping mainly reduce the charge collection efficiency and affect charge sharing among electrodes. Due to their larger drift velocity and smaller trapping probability, electron collection is favoured in irradiated silicon devices.

The safe limit on the operating voltage ultimately limits the detector lifetime. Strip and pixel detectors, specifically designed for high voltages, have been extensively operated at bias voltages of 500–600 V. The limit of operation voltage in highly energetic particle environment is set by single event effects (SEE), which occur when highly ionising nuclear fragments originating from the impinging particle cause permanent detector breakdown, happening at average electric fields approaching ∼12 V/µm. Sensors with columnar electrodes normal to the surface (3D-Si, Fig. 35.25) need significantly lower voltages for full depletion and are prime contenders for radiation-hard sensors.

Synthetic CVD diamond has proven strong against radiation damage due to its large bandgap (see Tab. 35.11) and strong lattice binding with a roughly twice higher threshold (∼40 eV) for the displacement of lattice atoms than silicon (see *e.g.* [410]). Even for polycrystalline material, charge collection distances (sum of the mean free paths $\mu\tau E$ of e and h over which charges reach the electrodes) of 300–400 µm have been achieved. The cost of diamond wafers, however, is very high in comparison. Smaller-scale diamond trackers acting *e.g.* as beam monitors have been built.

GaAs has received interest as a potentially radiation-hard material in the 1990s. For particle detection, it must still be depleted

Int. J. Mod. Phys. A 2020.
Downloaded from www.worldscientific.com
by UNIVERSITY OF CALIFORNIA @ BERKE
use and distribution is strictly not permitted, except for Open Access articles.

Int. J. Mod. Phys. A 2026.41. Downloaded from www.worldscientific.com by UNIVERSITY OF CALIFORNIA @ BERKELEY on 09/16/26. Re-use and distribution is strictly not permitted, except for Open Access articles.

from charge carriers despite comparatively small intrinsic carrier densities (see Tab. 35.11). It suffers from a strong loss in charge collection efficiency when irradiated, dominantly because of electron trapping. Other semiconductor materials such as SiC or GaN feature wider bandgaps (3.26 eV and 3.39 eV, respectively) than Si (but smaller than diamond) and possess other suitable properties relevant to high-fluence operation, such as density, *e-h* ionisation energy, and displacement energies. They have regained attention after the material quality has improved much due to an industrial push coming from power devices and LEDs. So far, charge collection degrades faster with radiation fluence than for Si and diamond, however.

Strip and pixel detectors have remained functional in large detectors even at particle fluences well beyond $10^{15}\,\mathrm{n_{eq}/cm^2}$ where charge loss due to recombination and trapping becomes significant. Thin planar ($\sim$100 µm) and 3D silicon detectors have been successfully operated at fluences of 2 and $3 \times 10^{16}\,\mathrm{n_{eq}/cm^2}$, respectively, and measurements indicate that operation above $10^{17}\,\mathrm{n_{eq}/cm^2}$ does not seem impossible. The large SNR obtainable with low capacitance pixel structures extends the detector lifetime. The higher mobility of electrons makes them less sensitive to carrier lifetime than holes, so detector configurations that emphasize the electron contribution to the charge signal are advantageous, *i.e.* n^+ strips or pixels on *p*- or *n*-substrates. The occupancy of the defect charge states is strongly temperature dependent; competing processes can increase or decrease space charge and the required operating voltage. It is critical to choose the operating temperature judiciously (−30 °C to 0 °C in typical collider detectors) and to limit warm-up periods during maintenance. Detailed discussions of radiation damage and its effects on semiconductor detectors can be found *e.g.* in [430, 433]; an introduction to the subject is given in [1].

Tolerance against surface damage, especially in SiO_2 layers as in gates and in oxide trenches of CMOS transistor structures, largely depends on the feature size of a technology and on appropriately designed circuitry. Deep submicron technology nodes of 130 nm and 65 nm sustain total ionisation doses of up to 5 MGy (500 Mrad), corresponding to fluences of up to $5 \times 10^{15}\,\mathrm{cm^{-2}}$ of minimum ionising pions or protons.

35.9 Low-noise detector readout

Revised November 2025 by J. Kaplon (CERN), revised November 2021 by N. Wermes (Bonn U.)

Many detectors rely critically on low-noise readout electronics for the best energy resolution or to allow low thresholds. A typical detector front-end is shown in Fig. 35.33.

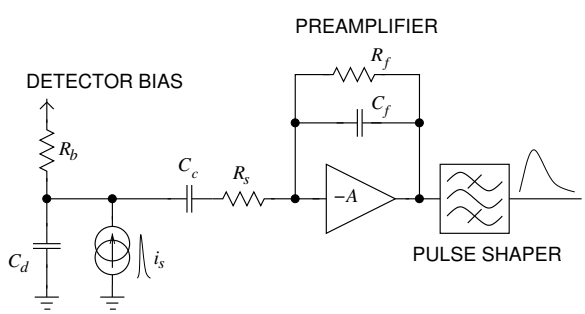

Figure 35.33: A typical front-end amplifier for a detector, with the shaper represented as an idealized band-pass filter. The operation of a charge-sensitive amplifier (CSA) relies on the feedback capacitor C_f, which determines the gain of the preamplifier.

In a model relevant to most readout applications, the detector, represented by a capacitance C_d, delivers a delta-function-shaped current signal, represented by a current source in parallel. Bias voltage is applied through resistor R_b, and the signal is (often) coupled to the amplifier through a blocking capacitor C_c. The series resistance R_s represents the sum of all resistances present in the input signal path, *e.g.* the electrode resistance, connection lines, any input protection network, and parasitic series resistances in the input transistor.

The amplification stage contains the preamplifier providing gain and a pulse shaper, which tailors the overall frequency response to optimise the signal-to-noise ratio (SNR), while limiting the duration of the signal pulse to accommodate the signal-pulse rate.

Detectors are often segmented with a granularity that matches the spatial resolution requirements of the experiment. In this case, the input stage must ensure efficient readout of the charge despite the presence of parasitic capacitances between adjacent detector electrodes. In order to minimise the cross-talk to adjacent channels, a low input impedance of the preamplifier is required. The basic solution for the input stage, which effectively addresses cross-talk and ensures efficient signal collection, is the charge-sensitive amplifier (CSA). This amplifier features high open-loop gain and employs shunt-shunt feedback through an integrating capacitor C_f, along with either an active or a passive discharging circuitry (for example, resistor R_f in Fig. 35.33) to prevent saturation of this stage within the signal processing chain. The CSA gain is primarily determined by the value of the feedback capacitor and does not depend on the detector capacitance.

In addition to the widely used charge-sensitive amplifiers in traditional tracking detectors, other low-noise architectures are employed for different applications. Transimpedance amplifiers (TIA) and wide-band voltage amplifiers are used when very high timing precision is required and the power budget is less constrained. Low-power voltage amplifiers are also employed in circuits with extremely low input capacitance—in the femtofarad range—where they can achieve adequate gain, avoiding significant power consumption. A typical example is monolithic active pixel sensors with small charge collection nodes. Although the following analysis focuses on the noise performance of CSA amplifiers, the applied methodology as well as conclusions *i.e.*, formulas for the equivalent input noise, are equally applicable to TIA and voltage preamplifiers working with capacitive sensors.

The classical theory of noise filtering, outlined in [434, 435] for nuclear spectroscopy systems, aims to maximise the signal-to-noise ratio, introducing the concept of the optimal noise filter. In modern high-energy physics experiments, front-end electronics must provide both amplitude measurement and precise timing requirements. Additionally, for multi-channel systems, minimizing power consumption and maintaining design simplicity are critical goals, which translates to enhanced robustness, particularly given the radiation-prone environments in which these chips typically operate. To balance performance with power consumption and design complexity, conventional band-pass filters, such as CR-$(\mathrm{RC})^m$, are often preferred for multi-channel front-end chips. These filters consist of a differentiating stage to filter low-frequency noise, followed by m integrator stages that attenuate high-frequency components.

In high data-rate applications, avoiding CSA saturation requires a low feedback impedance, typically achieved by employing a low-value feedback resistor. In these configurations, the feedback resistor R_f and capacitor C_f usually constitute the first CR (differentiation) stage of the pulse shaper, placing the charge-sensitive amplifier in what is referred to as transimpedance mode. This mode is commonly employed in the front-end input stages of modern detector readout electronics, as it accommodates high signal rates and reduces input impedance, thereby minimising cross-talk and offering advantages over a basic CSA configuration. It is essential to note that placing the high-pass CR filter—either in the preamplifier feedback loop or within the shaper stage—has no impact on the input noise analysis and is equivalent in terms of signal processing.

Assuming an ideal amplifier with infinite open-loop gain A and unlimited bandwidth to facilitate analysis, the Laplace-domain transfer function $H(s)$ of a charge-sensitive amplifier followed by an m-order CR-RC filter with equal differentiation and integration time constants τ is given by

$$H(s) = \frac{1}{s\,C_f}\,\frac{s\,\tau}{(1+s\,\tau)^{m+1}}\,, \qquad (35.27)$$

Int. J. Mod. Phys. A 2010.
Downloaded from www.worldscientific.com
by UNIVERSITY OF CALIFORNIA @ BERKE
use and distribution is strictly not permitted, except for Open Access articles.

where s denotes the complex frequency variable in the Laplace domain, and τ represents the time constant of the filter. The response in the time domain to the Dirac delta function of the preamplifier connected to a CR-(RC)$^{\rm m}$ filter is given by the formula

$$V_{out}(t) = \mathcal{L}^{-1}\Big\{H(s)\Big\} = \frac{\left(\frac{t}{\tau}\right)^m \; e^{-\frac{t}{\tau}}}{C_f \; \Gamma(1+m)} \,, \tag{35.28}$$

where $\mathcal{L}^{-1}$ is the inverse Laplace transform and Γ is the Euler Gamma-function. The signal reaches its peak at the time $t_p = m\,\tau$, commonly referred to as the shaping time. The response amplitude, G_{FE}, representing the overall gain of the processing chain, is given by

$$G_{FE} = \frac{m^m \; e^{-m}}{C_f \; \Gamma(1+m)} \tag{35.29}$$

35.9.1 *Principal noise origins*

It is useful to distinguish between noise inherent to a detector's signal amplification and processing circuitry (per channel) on the one hand, and — on the other hand — external noise sources propagated as a radiated or conducted electromagnetic interference (EMI) introduced *e.g.* by systems external to a specific readout circuit often resulting in "common-mode" noise, *i.e.* common to all channels. External noise can be introduced by power supplies, digital signal switching, RF pick-up, or effects due to "common grounding" allowing noise to couple to the current loop connecting the detector to the preamplifier. These noise sources differ from setup to setup and must be addressed individually, ideally to be eliminated. In the following, therefore, only the noise inherent to typical detector signal processing is discussed.

As principal noise origins in circuit elements, we distinguish *thermal noise*, *shot noise*, and *low-frequency* $1/f$ *noise*. Generally, noise is a fluctuation of current or voltage around a base level. Since the average value of noise is zero, noise is quantified by the variance of this fluctuation, $\langle v^2\rangle$ or $\langle i^2\rangle$. Noise sources are characterised by their power spectral densities, *i.e.*, $d\langle v^2\rangle/df$ and $d\langle i^2\rangle/df$, where f is the frequency.

Thermal noise results from the thermal random motion of charge carriers in a conductor (Brownian motion). In any conductor or resistor at a temperature $T > 0$, the random motion of electrons leads to current fluctuations giving rise to a voltage appearing across its terminals. For a resistor R, the (power) spectral density is proportional to the Boltzmann constant k and the temperature T. In electronic circuits, it can be represented either by a current or a voltage source with spectral densities given as:

$$d\langle i^2\rangle = 4\,k\,T\,\frac{1}{R}\;df \qquad\qquad d\langle v^2\rangle = 4\,k\,T\,R\;df \tag{35.30}$$

The spectral density distribution of thermal noise is $'$white$'$, *i.e.*, all frequencies contribute equally to the total noise intensity.

Shot noise arises from the discrete nature of charge carriers, creating discrete current fluctuations when crossing a potential barrier in electronic devices. Examples include fluctuations in the current flowing through a semiconductor junction or a metal-semiconductor junction. In contrast, a simple conductor or resistor lacks such a barrier and therefore does not exhibit shot noise.

The current spectral density is described as

$$d\langle i^2\rangle = 2\,q\,I\;df \;, \tag{35.31}$$

where q is the elementary charge and I is the DC current. Shot noise also exhibits a $'$white$'$ frequency spectrum.

Low frequency $1/f$ *noise*, also known as flicker noise, or pink noise, is a widespread phenomenon that appears not only in electronic devices but also in a variety of natural systems other than electronics. Common to all is a similar spectral density behaviour which is proportional to $1/f^{\alpha_f}$ with α_f between 0.5 and 2. In metal-oxide-semiconductor (MOS) devices, $1/f$ noise primarily arises from two mechanisms. The first involves the surface properties of the material, specifically, charge trapping and detrapping at the interface between the transistor channel and the gate insulating layer. The second mechanism, which becomes more significant in deep-submicron technologies, is due to mobility fluctuations caused by the scattering of charge carriers within the MOS channel. Enhanced surface treatment during manufacturing and the overall size of the transistor gate are key factors influencing the level of flicker noise.

35.9.2 *Noise in MOS devices*

In the following, we focus on the noise sources in MOSFETs, as the majority of front-end circuits used in today's HEP experiments are based on MOS transistor technology.

The primary noise source observed in MOSFETs is *thermal noise* in the transistor channel, which acts as a conductor. To calculate its spectral density, we employ the model proposed by Van der Ziel [436], adapted for devices implemented in integrated circuits that share a common substrate—thereby accounting for the noise contribution from the bulk transconductance g_{mb}—and operating in any inversion [8] region [437]. The current noise generator i_{nd} is placed between the drain and source of the input transistor, with its noise spectral density given by[9]

$$d\langle i_{nd}^2\rangle = 4\,k\,T\;n\;\gamma\;g_m\;df\;. \tag{35.32}$$

The noise contribution from the bulk transconductance, g_{mb}, is represented by a technology-dependent parameter n, known as the slope factor, which typically ranges from 1.25 to 1.45. It is defined as the ratio $n = (g_m + g_{mb})/g_m$, where g_m is the gate transconductance, hereafter referred to simply as transconductance.

The bias-dependent parameter γ ranges from 1/2 in weak inversion to 2/3 in strong inversion for an ideal long-channel transistor. While this assumption holds well for long-channel devices, it does not account for short-channel effects, which introduce excess noise. A practical approach to this issue is to use an excess noise factor α_w, which is usually characterised for a given technology and transistor length. In submicron technologies used today for HEP applications, transistors with channel lengths approximately twice the minimum feature size—thus avoiding short-channel effects—typically exhibit an excess noise factor α_w below 1.1 when operating in the weak to moderate inversion region.

The next source of noise taken into account in this analysis is *1/f noise*. In the commonly used model of 1/f noise, the current noise generator is placed between the drain and source of the MOS transistor. The power spectral density is given by:

$$d\langle i_{nf}^2\rangle = \frac{K_f}{f}\;\frac{g_m^2}{C_{ox}}\;df\;. \tag{35.33}$$

The technology-dependent parameter K_f is highly sensitive to the fabrication process, typically ranging from 1×10^{-24} to 1×10^{-25} Joule. Its value also depends on the device type and is typically lower for PMOS transistors. The values of K_f are also affected by transistor bias conditions and short-channel effects. C_{ox} represents the so-called gate-oxide capacitance of the transistor, defined as

$$C_{ox} = W\,L\,\frac{\varepsilon_{ox}}{t_{ox}}\;, \tag{35.34}$$

where W and L denote the gate's width and length; ε_{ox} is the permittivity of the silicon oxide, and t_{ox} represents the gate oxide

[8] Inversion in a MOS device occurs when the gate voltage attracts minority carriers to the semiconductor surface, forming a conductive channel under the gate that enables current flow between the source and drain—a fundamental principle of MOSFET operation. In strong inversion, where the gate voltage exceeds the threshold and a well-defined channel is formed, conduction is drift-dominated, and transconductance is given by $g_m = \sqrt{2\,K_p\,I_d\,W/(n\,L)}$, where K_p is the technology-dependent transconductance parameter, n is the slope factor, I_d is the drain current, and W and L are the transistor's width and length respectively. Here, g_m scales with the square root of current and depends on device dimensions. In weak inversion (sub-threshold operation), the device conducts a small diffusion-driven current even below the threshold voltage. The transconductance is given as $g_m = I_d/(n\,V_T)$, where V_T is the thermal voltage ($\sim$26 mV at room temperature), so it scales linearly with current and is independent of transistor geometry. In the moderate inversion region (between weak and strong inversion), transconductance is typically modeled using semi-empirical interpolation functions, such as those found in the EKV model.

[9] Here and in the following, the subscript part n always denotes *noise*, whereas further subscript letters denote specifics of this noise density.

Int. J. Mod. Phys. A 2026.41. Downloaded from www.worldscientific.com
by UNIVERSITY OF CALIFORNIA @ BERKELEY on 09/16/26. Re-use and distribution is strictly not permitted, except for Open Access articles.

thickness. Thus, the 1/f noise is inversely proportional to the transistor gate area.

Further noise nomenclature, such as *RTS (random telegraph signal) noise*, also known as burst noise or popcorn noise, is also related to its origin to trapping/detrapping processes in small MOS devices, where a single trap can cause a considerable variation in the channel current. For larger devices with many trapping centers, the popping-up nature of individual RTS bursts eventually leads to the $1/f$ noise spectral density when the noise from multiple traps with a wide range of trapping time constants is superimposed. Noise optimisation in front-end circuits typically involves using relatively large-area MOS transistors, where RTS noise is usually not observed. Consequently, the RTS noise is omitted in the following for simplicity reasons.

Another noise phenomenon observed in MOS devices at higher frequencies is known as *gate-induced current noise (GIC)*. Thermal fluctuations of current within the device channel couple to the transistor gate via the gate-oxide capacitance, resulting in an induced frequency-dependent current that acts as an additional noise source correlated with the channel thermal noise. Noise expressions for GIC have been derived in [436] for an ideal MOS transistor operating in strong inversion. Adapted to apply across all inversion regions and including also the noise contribution from the bulk transconductance, the GIC power spectral density is expressed as:

$$d\langle i_{ng}^2\rangle = 8\,\gamma\,k\,T\,g_g\,df \qquad \text{with} \qquad g_g = \frac{4}{45}\,\frac{\omega^2\,C_{ox}^2}{n\,g_m}\ , \tag{35.35}$$

where γ and n parametrise transistor operation modes and technology features, respectively and $\omega = 2\pi f$. The correlation between channel thermal noise and gate-induced noise is given by:

$$d\langle i_{ng}\ i_{nd}^*\rangle = \frac{\gamma}{6}\ j\ \omega\ C_{ox}\ 4\,k\,T\ df\ , \tag{35.36}$$

where j denotes the imaginary unit and i_{nd}^* is the complex conjugate of i_{nd}.

35.9.3 *Equivalent noise analysis*

The equivalent circuit used for noise analysis (Fig. 35.34) illustrates the contributions of all previously discussed noise sources at various points in the circuit.

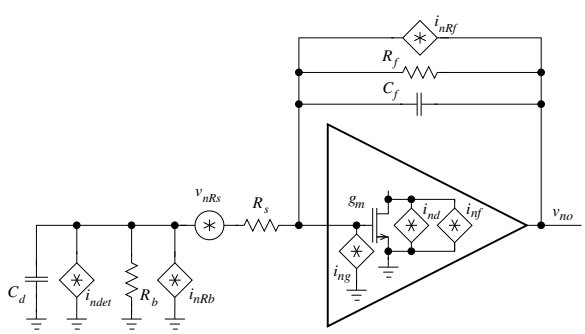

Figure 35.34: Equivalent front-end circuit diagram of the CSA showing the basic noise sources.

Shot noise, arising from fluctuations in detector leakage current, is modelled as a current noise source placed at the amplifier input in parallel with the detector. Its spectral density depends entirely on the magnitude of the leakage current I_{det} and can be expressed as

$$d\langle i_{ndet}^2\rangle = 2\ q\ I_{det}\ df\ . \tag{35.37}$$

Although any voltage source in series with a resistor can be transformed into an equivalent current source in parallel with a resistor (according to Norton's theorem), it is a common practice to represent (parallel) input-shunting resistors as noise current sources and series resistors at the amplifier input as noise voltage sources. These are typically referred to as equivalent input *parallel* and *series* noise sources, respectively. The noise spectral densities for the detector bias resistor R_b (parallel noise) and the series resistor R_s (series noise) are respectively given by:

$$d\langle i_{nRb}^2\rangle = \frac{4\,k\,T}{R_b}\,df \qquad \text{and} \qquad d\langle v_{nRs}^2\rangle = 4\,k\,T R_s\,df\ . \tag{35.38}$$

The value of the detector bias resistor is typically chosen such that its noise contribution to the overall noise can be neglected. The feedback resistor R_f also acts as a parallel noise source. It is particularly relevant for preamplifiers operating in transimpedance mode, contributing with a noise spectral density as in Eq. (35.38) (left) with R_b being replaced by R_f.

An important noise source is the preamplifier input stage, specifically the active devices operating within the circuit. In a well-designed input stage—characterised by high gain and degenerated active loads—the dominant noise source is the input transistor. Both flicker and channel thermal current noise generators are internal to the preamplifier structure (see Fig. 35.34). To evaluate their contribution to the output noise—without requiring knowledge of the amplifier's internal details—they are represented as equivalent noise sources at the preamplifier input, exploiting the definition of the input transistor's transconductance, $g_m = \partial I_d\ /\partial V_{gs}$, where I_d and V_{gs} are drain current and gate-to-source voltage, respectively. This leads to:

$$\begin{aligned} d\langle v_{nd}^2\rangle &= d\langle i_{nd}^2\rangle\frac{1}{g_m^2} = \frac{4\,k\,T\ n\ \gamma}{g_m}\,df \qquad \text{and} \\ d\langle v_{nf}^2\rangle &= d\langle i_{nf}^2\rangle\frac{1}{g_m^2} = \frac{K_f}{f\,C_{ox}}\,df\ . \end{aligned} \tag{35.39}$$

Noise spectrum calculation is simplified by assuming that filtering takes place in the shaper stage treating the feedback resistor solely as a noise source. The CSA output noise spectral density is obtained by accounting for all parallel and series noise sources. Series noise at the input is first converted to equivalent parallel noise via the input conductance $s\,C_{in}$, then all contributions are transferred to the output through the feedback impedance $1/s\,C_f$, yielding:

$$\frac{d\langle v_{no}^2\rangle}{df} = \frac{d\langle v_{ns}^2\rangle}{df}\,\frac{C_{in}^2}{C_f^2} + \frac{d\langle i_{np}^2\rangle}{df}\,\frac{1}{\omega^2\,C_f^2}\ , \tag{35.40}$$

where C_{in} represents the total input capacitance (including detector capacitance C_d, input transistor gate capacitance C_g, and any additional parasitic capacitance at the preamplifier input), the term $d\langle v_{ns}^2\rangle/df$ represents the noise spectral density of any series-noise source as shown in Eq. (35.39) and Eq. (35.38) (right equation), whereas $d\langle i_{np}^2\rangle/df$ is the noise spectral density of any parallel-noise source as in Eq. (35.35), Eq. (35.37) and Eq. (35.38) (left equation). The transfer function of the CR-(RC)^{m} filter in the Laplace domain is given by Eq. (35.41).

$$T(s) = \frac{s\,\tau}{(1+s\,\tau)^{m+1}}\ . \tag{35.41}$$

Consequently, the RMS value of noise at the shaper output can be obtained by integrating the preamplifier output noise spectra density, coming from all partial contributions, over the entire frequency range, taking into account the frequency characteristic of the applied filter:

$$\sigma_n^2 = \int_0^\infty \frac{d\langle v_{no}^2\rangle}{df}\,\frac{\omega^2\,\tau^2}{(1+\omega^2\,\tau^2)^{m+1}}\,df\ . \tag{35.42}$$

Dividing the result by the signal gain given by Eq. (35.29) we obtain the equivalent input noise charge:

$$ENC = \frac{\sigma_n}{G_{FE}} = \sigma_n\,\frac{C_f\ \Gamma(1+m)}{m^m\ e^{-m}}\ . \tag{35.43}$$

It is convenient to perform the above integral and ENC calculation for the individual noise sources separately. Table 35.12 summarises the individual contributions to the total ENC, where the

Int. J. Mod. Phys. A. Downloaded from www.worldscientific.com
by UNIVERSITY OF CALIFORNIA @ BERKE use and distribution is strictly not permitted, except for Open Access articles.

coefficients F_V, F_I, F_F, F_G, and F_C depend on the filter characteristic. The table also includes the GIC–thermal noise correlation term; however, its calculation is omitted here for brevity. In particle physics, ENC is often quoted in units of electrons (e^-) by dividing (35.43) by the elementary charge q.

Table 35.12: Partial contributions to the total ENC.

k		ENC_k
1	channel thermal	$F_V \frac{C_{in}}{\sqrt{t_p}} \sqrt{\frac{4\,k\,T\,\gamma\,n}{g_m}}$
2	series resistor	$F_V \frac{C_{in}}{\sqrt{t_p}} \sqrt{4\,k\,T\,R_s}$
3	flicker	$F_F\,C_{in} \sqrt{\frac{K_f}{C_{ox}}}$
4	feedback resistor	$F_I \sqrt{t_p} \sqrt{\frac{4\,k\,T}{R_f}}$
5	detector leakage	$F_I \sqrt{t_p} \sqrt{2\,q\,I_{det}}$
6	GIC	$F_G \frac{C_{ox}}{\sqrt{t_p}} \sqrt{\frac{4\,k\,T\,\gamma}{n\,g_m}}$
7	GIC-thermal corr.	$F_C \frac{\sqrt{C_{ox}\,C_{in}}}{\sqrt{t_p}} \sqrt{\frac{4\,k\,T\,\gamma}{g_m}}$

For the example of a first-order CR-RC filter, the filter coefficients F_V, F_I, F_F, F_G, and F_C are evaluated to be 0.96, 0.96, 1.92, 0.41, and 0.56, respectively. Finally, the total ENC squared is obtained by the quadrature sum of the individual contributions:

$$ENC^2 = \sum_{k=1}^{7} ENC_k^2 \,. \tag{35.44}$$

The formulas in Table 35.12 show that the first three contributions from series noise sources are directly proportional to the input capacitance and, except for 1/f noise, inversely proportional to the square root of the signal shaping time. Often, the dominant contribution comes from channel thermal noise (first entry in Table 35.12). Large thermal noise contribution must be compensated by a large transconductance g_m, or longer shaping time. Since g_m is determined by both the bias current and the transistor's dimensions, the first step in optimisation of the preamplifier involves sizing the input transistor appropriately to the detector capacitance and the target bias current. Furthermore, flicker noise as well as GIC and the GIC-thermal correlation term are also affected by the transistor's dimensions through its gate capacitance. A compact model like EKV [437] is essential, providing accurate, temperature-aware expressions for transconductance and gate capacitances across all inversion regions. Finally, noise optimisation can be achieved by selecting a shaping time that balances series and parallel noise contributions (series noise decreases with longer shaping time, while parallel noise increases; see Table 35.12). This optimisation is limited by the time resolution requirements of the front-end electronics, which impose an upper bound on the shaping time. In systems with high parallel noise and low series noise, the theoretically optimal very short shaping time may be unattainable due to technological constraints, such as the transistor transit frequency that limits the maximum operational speed of the electronics. If balancing parallel and series noise sources fails to meet noise specifications, the front-end design requirements may need to be revised. Increasing the bias current of the input transistor can improve transconductance and help suppress thermal noise. If excessive parallel noise is caused by radiation-induced leakage current, it may be necessary to adjust the detector segmentation—which will also impact the contribution from series noise—or improve cooling efficiency to operate at lower temperatures.

Figure 35.35 shows an example of the noise analysis for a preamplifier designed in 130 nm CMOS technology and developed for the ATLAS ITK strip tracker (ABCStar chip). The design is intended for short silicon strips with lengths ranging from 1.8 cm to 5.5 cm, corresponding to input capacitances between 2 pF and 7 pF. The ENC is shown as a function of shaping time, with individual contributions explicitly illustrated for two detector capacitance values representing different strip lengths. The optimal shaping time

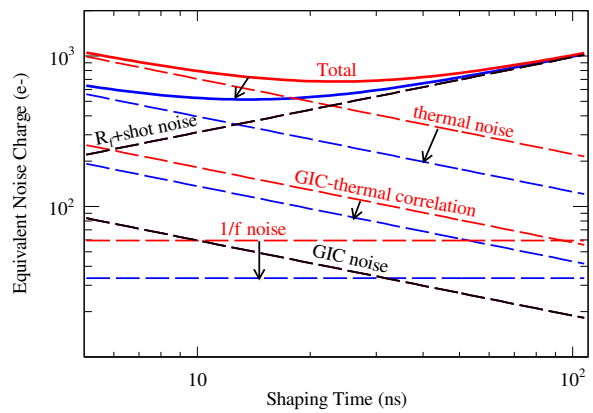

Figure 35.35: Equivalent noise charge as a function of the shaping time for the ABCstar front-end. Individual contributions include series channel thermal and 1/f noise, parallel shot and thermal R_f noise, as well as GIC noise and the GIC-thermal correlation. The contributions are shown for two detector capacitance values: 6 pF (RED traces), for which the input transistor was optimized, and 3 pF (BLUE traces), corresponding to the 2.4 cm strips. Noise contributions independent of the input capacitance, namely from the feedback resistor (105 kΩ), shot noise from detector leakage current (1 μA), and GIC noise, are shown in BLACK.

depends strongly on the detector capacitance. In particular, the contributions from series noise, flicker noise, and the GIC–thermal noise correlation term scale with input capacitance, whereas parallel noise and GIC contributions are independent of it. In the presented example, a shaping time of 22 ns is chosen, as it meets timing requirements, optimizes noise for the longer strips, and satisfies the stricter ENC limits for shorter strips, imposed by higher expected radiation damage. Analysing the individual contributions to the ENC from various noise sources reveals that, in the example under consideration—front-end designed for high signal rates and operation in radiation environments with significant sensor leakage—the dominant noise contributors are the input transistor channel thermal noise and the parallel noise resulting from the shot noise of the sensor leakage current and the preamplifier feedback resistor. However, in low-rate, low-radiation applications where the contribution from the feedback resistor can be minimised and sensor leakage current is negligible, longer shaping times can be employed. Then, flicker noise becomes the primary factor limiting the minimum achievable noise level.

The impact of GIC noise on the front-end amplifier's overall noise performance can be assessed by analysing the expressions for GIC noise and the correlation term, each normalized to the originating thermal noise. These normalised contributions are roughly $\approx 0.42\,C_{ox}/(n\,C_{in})$ and $\approx 0.58\,\sqrt{C_{ox}/(n\,C_{in})}$, respectively. It can be observed that when the front-end is connected to the sensor and $C_{in} \gg C_{ox}$, both contributions become negligible, since they combine with the thermal noise and finally with the total ENC in quadrature. In contrast, these contributions may become visible when evaluating the amplifier without a connected sensor, particularly in scenarios where the parallel noise from the feedback circuit is negligible.

Int. J. Mod. Phys. A 2026.41. Downloaded from www.worldscientific.com
by UNIVERSITY OF CALIFORNIA @ BERKELEY on 09/16/26. Re-use and distribution is strictly not permitted, except for Open Access articles.

35.9.4 *Timing measurements*

In timing measurements, the slope-to-noise ratio must be optimized, rather than the signal-to-noise ratio alone, so the rise time t_r of the pulse is important. The "jitter" σ_t of the timing distribution is

$$\sigma_t = \frac{\sigma_n}{(dS/dt)_{\text{trig}}} \approx \frac{t_r}{SNR}, \tag{35.45}$$

where σ_n is the rms noise, SNR the signal-to-noise ratio—defined for a CSA as the ratio of a MIP signal to the ENC—, and the slope dS/dt, *i.e.* the derivative of the signal, is evaluated at the discrimination level. The rise time of an amplifier, t_r, in the absence of a shaper, is limited by internal parasitic capacitances, which reduce its bandwidth and effectively act as a low-pass filter. Approximating the amplifier's behaviour with a CR-RC response, we find that linearly decreasing t_p leads to an ENC increase proportional to $\sqrt{t_p}$ from series noise sources, while the ENC contributions from parallel noise sources decrease (see Table 35.12). Therefore, from a jitter perspective, enhancing the amplifier's response time—even if it results in a noise increase—can be beneficial. However, preserving an adequate signal-to-noise ratio, which is critical for maintaining acceptable noise occupancy, imposes a fundamental constraint. Another undesired effect of increasing the front-end speed and input stage bandwidth will be higher susceptibility to the EMI interferences. From an EMI sensitivity standpoint, systems and detectors that employ higher-granularity sensors characterized by low parasitic capacitance offer an advantage.

For timing measurements with standard or 3D sensors, the preferred preamplifier is typically a CSA based on a buffered cascode [10] featuring high open-loop gain, operating in transimpedance mode. The rise time of the preamplifier response—more precisely, the integration time constant—is given by:

$$\tau_i = \frac{C_0}{g_m}\,\frac{C_{in}}{C_f}\,, \tag{35.46}$$

where the C_0 is the parasitic capacitance at the cascode output defining its bandwidth, g_m is the transconductance of the input transistor, C_{in} is the total capacitance at the preamplifier input and C_f is the feedback capacitance. As Eq. (35.46) shows, good timing performance can be achieved by minimizing the total input capacitance, which aligns well with the characteristics of pixel sensors. While increasing C_f can enhance timing performance, it is constrained by the requirement to maximise the stage gain, which is inversely proportional to C_f. Increasing g_m by raising the bias current improves the timing response. However, to maintain all transistors within their proper operating region, it eventually becomes necessary to increase the transistor dimensions, which in turn raises the parasitic capacitance C_0. The optimal g_m/C_0 ratio defines the maximum achievable Gain-Bandwidth-Product (GBP) of the cascode. For a given architecture, the GBP reaches a limit that can only be improved through technology scaling. The discharge time constant (τ_d), in turn, is defined by the product $R_f\,C_f$. The advantage of the CSA is that GBP optimisation can be achieved without necessarily increasing power consumption; the transistor dimensions and bias current can be scaled down according to the power budget and noise performance requirements.

For timing measurements with low-gain sensors of a few picofarad capacitance (LGAD, [424]), a common approach is a transimpedance amplifier based on a non-buffered cascode, featuring a resistive or active load (R_l) and resistive feedback through R_f. The input impedance R_{in} is determined by the g_m of the input transistor and the resistances R_f and R_l, and is approximately given by $R_f/[g_m\,(R_l \parallel R_f)]$. In contrast to the CSA, the rise time of the TIA amplifier is independent of the input capacitance, which is a significant advantage for timing detectors using sensors with higher capacitance. The integration time constant expressed by:

$$\tau_i = C_0\,(R_l \parallel R_f)\,, \tag{35.47}$$

is instead determined by the parasitic capacitance at the cascode output C_0 and the resistance formed by the parallel combination of the feedback and load resistances. The discharge time constant is set by the input capacitance C_{in} and input impedance R_{in}. The response amplitude scales inversely with C_{in} and is amplified by the cascode gain $g_m\,(R_l \parallel R_f)$. Although the front-end amplifier is a typical TIA in topology, it behaves more like a voltage amplifier sensing current integrated on the input capacitance. This results from the resistive feedback defining a constant input impedance, while the sensor's capacitance dominates at high frequencies, presenting a lower impedance path for fast and prompt signals.

Optimal noise filtering is achieved when the integration (τ_i) and discharge (τ_d) time constants are matched, yielding a CR-RC-like shaping response. In this case, the timing jitter can be estimated by applying the ENC formulas from Table 35.12 in conjunction with Eq. (35.45). It is important to note that, to optimise the signal-to-noise ratio, the intrinsic response time of the amplifier should not be significantly faster than the rise time of the signal from the sensor. This consideration is particularly important for the TIA architecture presented here, which is capable of providing a very fast intrinsic rise time. To align the amplifier's response with the sensor signal, the practical implementations usually incorporate a switchable capacitive matrix at the cascode output, slowing down the integration time constants.

The time resolution of binary electronics with a leading-edge discriminator is limited by signal jitter and time walk, *i.e.*, timing variations due to amplitude-dependent threshold crossing. These amplitude fluctuations arise from the Landau signal distribution and charge sharing in segmented sensors. Time walk can be corrected using the time-over-threshold (ToT) value, which is correlated with pulse height. In systems with a high signal-to-noise ratio, constant-fraction discriminators can be used to provide timing information independent of signal amplitude.

35.9.5 *Digital signal processing*

The filtering principles apply to both analog and digital signal processing. In digital signal processing, the pulse shaper shown in Fig. 35.33 is replaced by an analog to digital converter (ADC) followed by a digital processor that determines the pulse shape. Digital signal processing allows great flexibility in implementing filtering functions. The software can be changed readily to adapt to a wide variety of operating conditions and it is possible to implement filters that are impractical or even impossible using analog circuitry. However, this comes at the expense of increased circuit complexity and increased demands on the ADC compared to analog shaping.

If the sampling rate of the ADC is too low, high-frequency components will be transferred to lower frequencies ("aliasing"). The sampling rate of the ADC must be high enough to capture the maximum frequency component of the input signal. Apart from missing information on the fast components of the pulse, undersampling introduces spurious artefacts. If the frequency range of the input signal is much larger than the sampling rate, the noise at the higher frequencies will be transferred to lower frequencies and will increase the noise level in the frequency range of pulses formed in the subsequent digital shaper. The Nyquist criterion states that the sampling frequency must be at least twice the maximum relevant input frequency. This requires that the bandwidth of the circuitry preceding the ADC must be limited. The most reliable technique is to insert a low-pass filter.

The digitisation process also introduces inherent noise, since the voltage range ΔV corresponding to a minimum bit step introduces quasi-random fluctuations relative to the exact amplitude

$$\sigma_n = \frac{\Delta V}{\sqrt{12}}\,. \tag{35.48}$$

When the Nyquist condition is fulfilled, the noise bandwidth Δf_n is spread nearly uniformly and extends to 1/2 the sampling fre-

[10] The cascode amplifier is a two-stage topology—comprising a common-source stage followed by a common-gate stage—widely used in analog design for its high gain-bandwidth product. Behaving like a single-stage amplifier, it exhibits one dominant pole, which simplifies frequency compensation in feedback systems such as charge-sensitive amplifiers. In CSA applications, the cascode topology enables the use of large input transistors—optimized for low noise—while preserving high-speed performance by suppression of the Miller effect thanks to a low input impedance of the common-gate stage.

Int. J. Mod. Phys. A 2025.40:1-2. Downloaded from www.worldscientific.com
by UNIVERSITY OF CALIFORNIA @ BERKE use and distribution is strictly not permitted, except for Open Access articles.

quency f_S, so the spectral noise density is

$$\frac{\sigma_n}{\sqrt{\Delta f_n}} = \frac{\Delta V}{\sqrt{12}} \cdot \frac{1}{\sqrt{f_S/2}} = \frac{\Delta V}{\sqrt{6 f_S}} \,. \tag{35.49}$$

Sampling at a higher frequency spreads the total noise over a larger frequency range, so oversampling can be used to increase the effective resolution. In practice, this quantisation noise is increased by the ADC's differential non-linearity (DNL). Furthermore, the equivalent input noise of ADCs is often rather high, so the overall gain of the stages preceding the ADC must be sufficiently large for the preamplifier to override the ADC input noise.

35.9.6 *What to use when?*

When implemented properly, digital signal processing provides significant advantages in systems where the shape of detector signal pulses changes greatly, for example, in large semiconductor detectors for gamma rays or in gaseous detectors (*e.g.* TPCs) where the duration of the current pulse varies with drift time, which can range over orders of magnitude. Analog signal processing is best or most efficient in systems that require a fast time response, but the high power requirements of high-speed ADCs are prohibitive. Systems that are not sensitive to pulse shape can use fixed shaping time constants and rather simple filters (like CR–RC), which can be either continuous or sampled. In high-density systems that require small circuit area and low power (*e.g.*, in strip and pixel detectors), analog filtering often yields the required response and tends to be most efficient.

As stressed already in the introduction, it is important to consider that additional noise is often introduced externally. Recognising additional noise sources and minimising cross-coupling to the detector current loop is often essential to obtain the best overall noise performance. Understanding basic physics and its practical effects is important in forming a broad view of the detector system and recognising potential problems (*e.g.* modified data), rather than merely following standard recipes. More comprehensive treatments of low-noise detector readout and signal processing can be found, for example, in [1, 8, 421, 438–440].

35.10 Calorimeters

35.10.1 *Introduction*

Revised August 2023 by F. Sefkow (DESY, Hamburg) and F. Simon (KIT).

A calorimeter measures the energy and direction of particles by absorption in the detector material and registration of the energy deposited in an (ideally) contained electromagnetic (EM) or hadronic shower. Calorimeters are central components of modern high energy physics experiments, due to their ability to measure not only the energy of charged particles (with the exception of muons), but also of photons and neutral hadrons, thus enabling the reconstruction of π^0 and η decays and of exclusive final states involving long-lived neutral kaons, or neutrons. They are indispensable for the measurement of particle jets and for the reconstruction of total event properties, which, via the measurement of missing energy (or missing transverse energy in hadron colliders). enable the detection of the presence of "invisible" particles such as neutrinos and hypothetical particles such as dark-matter candidates. Calorimeters are also important for the identification of particle species, using information on the longitudinal and transverse shape of the energy deposition to separate electrons, photons, hadrons and muons. While the performance of calorimeters is typically assessed by the quality of their energy measurements, position resolution, both for EM and hadronic showers, is also highly relevant, for example for the reconstruction of effective jet masses. The capability to measure high-level observables that serve to classify events, such as particle and jet energies, missing energy and isolated leptons, makes calorimeters central components of the trigger systems in high-energy physics experiments.

In collider experiments, the importance of calorimeters tends to increase with increasing collision energies since the relative energy resolution improves with increasing particle energy while the depth required for full containment of the showers shows only logarithmic growth with energy. This is in contrast to the precision of track-based measurements, which is decreasing with increasing momentum. With recent advances in timing capabilities calorimeters are also contributing to the rejection of pile-up from multiple interactions within the same bunch crossings at colliders.

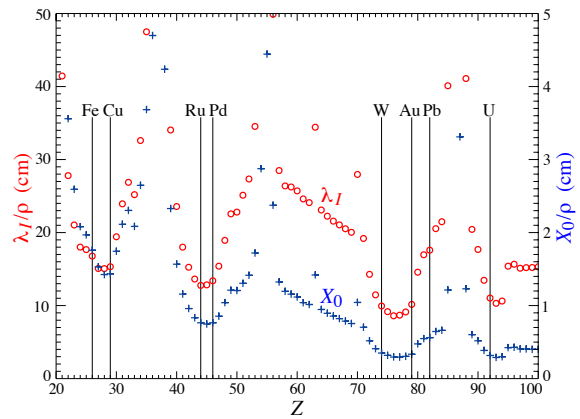

Figure 35.36: Nuclear interaction length λ_I/ρ (circles) and radiation length X_0/ρ (+'s) in cm for the chemical elements with $Z > 20$ and $\lambda_I < 50$ cm.

The characteristic length scale for EM showers is the radiation length X_0, which ranges from 1.8 cm (13.8 g cm^{-2}) in iron to 3.2 mm (6.0 g cm^{-2}) in uranium for materials used to generate showers in calorimeters.[11] Similarly, the characteristic nuclear interaction length λ_I varies from 16.8 cm (132.1 g cm^{-2}) (Fe) to 11.0 cm (209 g cm^{-2}) (U).[12] There is a premium on small λ_I/ρ and X_0/ρ (both with units of length). These quantities are shown for elements with $Z > 20$ in Fig. 35.36. The minima for both X_0 and λ_I correspond to elements between W and Au. Some of these elements are very difficult to work with (e.g. W) or expensive (e.g. Au), so, depending on the application (size of the required calorimeter) other materials, such as Fe, Cu, Pb, and different alloys like brass and CuW are often chosen. For EM calorimeters high Z is preferred; here Pb is a popular choice, while W provides even higher density and is generally affordable due to the limited volume of EM systems.

Most existing calorimeters are subdivided into a front EM section (ECAL) and a hadronic part (HCAL) behind; electrons and photons are measured in the ECAL, while hadrons and jets are measured in the combined ECAL and HCAL system. The detailed design depends on energy range and performance requirements as well as on size and cost constraints for the entire system. EM calorimeters tend to be 15–30 X_0 deep, while hadronic calorimeters are usually optimised for cost and performance at 5–8 λ_I. The depth of the ECAL typically corresponds to approximately 1 λ_I, with the exact value depending on the material. This means that approximately 70% of all hadronic showers will already begin in the electromagnetic calorimeter, making its response to a hadronic cascade highly relevant for the overall performance of the system. The choice of the calorimeter technology for the ECAL is thus a result of simultaneous optimisation for EM and hadronic performance of the overall system.

Sampling calorimeters consist of a high-density, normally metallic absorber sandwiched (or threaded) with an active material which generates a signal in response to shower particles. The active medium may be a scintillator, a noble liquid, a gas, silicon, or a Cherenkov radiator. These active media all have a relatively low Z, a significantly lower density, and larger X_0 and λ_I values than typical absorber materials. The average radiation and interaction lengths in the full detector are thus larger than those of the absorber alone.

There are also *homogeneous calorimeters*, in which the entire volume contributes to the signal. Homogeneous calorime-

[11] $X_0 = 120\ \mathrm{g\,cm^{-2}}\ Z^{-2/3}$ to better than 5% for $Z > 23$.
[12] $\lambda_I = 37.8\ \mathrm{g\,cm^{-2}}\ A^{0.312}$ to within 0.8% for $Z > 15$.
See https://pdg.lbl.gov/current/AtomicNuclearProperties for actual values.

Int. J. Mod. Phys. A 2026.41. Downloaded from www.worldscientific.com
by UNIVERSITY OF CALIFORNIA @ BERKELEY on 09/16/26. Re-use and distribution is strictly not permitted, except for Open Access articles.

ters may be built with inorganic heavy scintillating crystals or non-scintillating Cherenkov radiators such as lead glass and lead fluoride. Nuclear interaction lengths in inorganic crystals range from 17.8 cm ($LuAlO_3$) to 42.2 cm (NaI). Materials with low X_0 used in large systems are for example BGO with $\lambda_I = 22.3\,\text{cm}$ and $X_0 = 1.12\,\text{cm}$, and $PbWO_4$ (20.3 cm and 0.89 cm). Properties of these and other commonly used inorganic crystal scintillators can be found in Table 35.5. Cryogenic noble liquids, where scintillation light and/or inonization can be detected, are also suitable materials for homogeneous detectors.

Homogeneous calorimeters at colliders are usually only used for the EM section. For the use of homogeneous calorimeters for hadron energy measurement, the large differences in the response to EM and hadronic parts of the shower are a significant challenge, as is the three-dimensional segmentation. This is still requiring substantial R&D, including the search for affordable materials. In non-accelerator physics experiments or at neutrino beams, homogeneous calorimeters, where the sensitive medium can be water or ice, scintillator, a noble liquid or the atmosphere itself, are used to detect both EM and hadronic showers.

Comprehensive tables of particle-physics calorimeters are given as Appendix C in Ref. [441].

35.10.1.1 *Energy Resolution and System Performance*

The energy resolution of calorimeters is a complex observable, due to the variety of contributing processes with different energy dependencies, and response functions often not perfectly Gaussian. Nevertheless, a simplified picture is useful in practice, and in particular for EM calorimeters also numerically accurate. For hadronic calorimeters additional complications must be taken into account. In such a simplified picture, due to the stochastic nature of shower evolution, the intrinsic calorimeter energy resolution, σ, is proportional to $\sqrt{E}$, as the number of charged particles, or the total ionising track length in a shower are on average proportional to the incident particle energy E. The relative resolution σ/E therefore improves with $A/\sqrt{E}$, where A denotes the so-called *stochastic term*. The readout system of the active medium will contribute noise to the resolution, $\sigma_N = B$, which in general is not energy-dependent. Effects that are proportional to the total deposited energy result in a *constant term*, $\sigma_C = C \cdot E$. Different sources contribute to this term, depending on the type of calorimeter. For both EM and hadronic calorimeters, imperfections of the detector, inhomogeneities such as density variations or those introduced by the detector mechanics, instabilities in time, imperfections of the readout or incorrect calibration of channels contribute. Shower leakage, which depends on particle energy, also contributes to the resolution with approximately linear dependence on energy. In non-compensating hadronic calorimeters, fluctuations of the EM fraction f_{em} from shower to shower, together with the energy dependence of the average f_{em} value, can lead to a significant constant term that often dominates over the instrumental effects. Adding up all contributions in quadrature yields the standard parameterisation of the relative energy resolution of a calorimeter:

$$\frac{\sigma}{E} = \frac{A}{\sqrt{E}} \oplus \frac{B}{E} \oplus C\,. \tag{35.50}$$

In particular the effects specific to hadronic showers give rise to non-Gaussian distributions of the energy response. Therefore care must be used in performance comparisons, as different parameterisations of the line shape and different definitions of the resolution are in use. In some cases, a linear rather than a quadratic addition of the stochastic and constant term may provide a better description of the energy resolution as a function of energy. It should be noted that the individual terms then lose the simplified interpretation discussed above, and care has to be taken when comparing performance based on fits to the energy dependence of the resolution.

Typically, primarily the stochastic term — which is determined by the calorimeter design in terms of material and geometry — is considered in order to describe the overall properties of a calorimeter. For the calorimeters of the multi-purpose experiments at the LHC, the stochastic terms are $3 - 10\%$ for electromagnetic and $50 - 80\%$ for hadronic calorimeters. In practice, the energy resolution of a calorimeter at high energies is limited by the constant term C, which in the EM case mainly reflects the precision and stability of the mechanical construction, electronic readout system and calibration. Typical constant terms are a few per-mil for EM and a few percent for hadronic calorimeters. For concrete examples and references see Tables 35.13 and 35.15.

For sampling calorimeters, the stochastic term depends on the *sampling fraction* f_{samp}, i.e. the ratio of energies deposited in the active and passive material. Also the *sampling frequency* enters, which is determined by the number N of different sampling elements present in the region in which the shower develops. The stochastic term A scales approximately with $1/\sqrt{f_{\text{samp}}}$, and for given f_{samp} and total depth, with $1/\sqrt{N}$.

While the energy resolution for single hadrons (most commonly pions) is often used as the key performance criterion for a hadronic calorimeter, it has to be noted that this value is only of limited relevance in high-energy physics experiments. In most experiments, the calorimetric measurement of hadrons is based on the combined system consisting of ECAL and HCAL. Moreover, for the physics capabilities of a detector at a high-energy particle collider, also the combined calorimetric resolution for single hadrons is not a sufficient criterion to fully characterise hadronic performance, but rather the jet energy resolution, the resolution for missing (transverse) energy, and the capability to cope with high background and pile-up levels. These quantities cannot be measured directly with prototypes in beam tests, and strongly depend on overall system aspects and reconstruction tools. However, the performance in these observables can be reliably inferred from system simulations once the simulated response to single particles and the simulated topology of showers has been validated in detail by beam tests.

Besides energy resolution, response linearity is an important factor in the design of calorimeters. While a non-linear response for single particles can be corrected for if appropriate calibration measurements exist, such corrections deteriorate the energy resolution, in particular in the case of superposition of several showers, as it often occurs in jets. Sources for non-linearities can be intrinsic to the design, for example due to saturation effects in the active medium with increasing energy density, due to leakage, or connected to shower physics as discussed in section 35.10.3.

The energy resolution for hadrons is intrinsically limited by large event-to-event fluctuations of the shower evolution and of "invisible" components not contributing to the detector signal. It remains the limiting factor for single particles and for the high-level performance for jets and total event properties. This has motivated intense research in the past decades. One direction aims at improving the hadronic resolution by extracting additional signals to disentangle the shower composition, e.g.with so-called dual read-out methods, and is explained in the hadron calorimeter section 35.10.3. Another, so-called "particle flow" approach described below optimises the combination of measurements of individual particles in different detector components. Ideally, both methods can be combined.

35.10.1.2 *Role of Simulations*

Simulations have become indispensable for the design of detectors and the development of reconstruction algorithms. Since event-to-event fluctuations drive calorimeter performance, Monte Carlo techniques that accurately model the evolution of particle cascades in material are required. By far the most common computer code in use today is the *GEANT4* toolkit [442, 443], which provides a step-based simulation of the passage of particles through matter. Thanks to the relative simplicity of EM cascades, simulations of EM showers are typically highly accurate. The modelling of hadronic showers is more complex, and suffers from larger uncertainties. Significant improvement has been achieved in this area, moving from simpler parameterised models to physics-driven interaction models. From early on, detailed codes and data describing nuclear break-up and neutron transport like *CALOR* [444] or *FLUKA* [445, 446] contributed crucially to the understanding of hadron calorimetry. The simulations reproduce the general features of the substructure of hadronic showers,

Int. J. Mod. [redacted] by UNIVERSITY OF CALIFORNIA @ BERKE[redacted]nloaded from www.worldscientific.com use and distribution is strictly not permitted, except for Open Access articles.

characterised by dense shower activity and sparser ionising track segments, and their accuracy is adequate for most purposes of quantitative design optimisations. Details of the implementation of physics models in *GEANT4* are discussed in [447].

35.10.1.3 *Particle flow approach*

In a typical collider experiment, the EM and hadronic calorimeter system surrounds a charged-particle tracking volume devised for momentum measurement in a magnetic field. Matching tracks to calorimetric energy deposits provides corrections for the magnetic deflection of the charged particles, necessary for the reconstruction of invariant masses in multi-jet final states, or of the total momentum imbalance. Furthermore, for charged particles the track-based measurements are far more precise for particles in jets with energies of up to several hundred GeV, so using these instead of calorimeter energies may optimise the jet energy resolution. This so-called "particle flow" approach aims at reconstructing each particle individually, using a combination of the best measurements from the detector.

About 60% of the energy in a typical jet is carried by charged particles, predominantly hadrons, 30% by photons and only 10% by long-lived neutral hadrons (K_L^0 and n), for which hadronic calorimetry is unavoidable. Assuming, as motivated by detector designs proposed for a future Higgs factory, $15\%/\sqrt{E(\mathrm{GeV})}$ for photons and $55\%/\sqrt{E(\mathrm{GeV})}$ for hadrons, then, in the ideal case, where each particle is resolved, a jet energy resolution of $19\%/\sqrt{E(\mathrm{GeV})}$ could be obtained. Here the dominant part $(18\%/\sqrt{E(\mathrm{GeV})})$ is still due to the calorimeter resolution for neutral hadrons.

The particle flow method places high demands on the imaging capabilities of the calorimeters, and on the pattern recognition performance of the reconstruction algorithms. Only energy deposits not associated with charged particles and not identified as photons, will be interpreted as neutral hadrons. In practice, this cannot always be done unambiguously, and mis-assignments give rise to an additional measurement uncertainty, which is called *confusion*. For simulated detectors at proposed future Higgs factories jet energy resolutions of 3-4% have been demonstrated, significantly larger than in the ideal case, but sufficient for the required efficient separation of W and Z hadronic final states.

Particle flow-like techniques were first applied in the ALEPH detector [448], which achieved a jet energy resolution of $60\%/\sqrt{E}$, or 6.2 GeV for hadronic Z decays. More recently, particle flow techniques are successfully used in the CMS experiment [449], for example improving the missing energy resolution by one third over a wide range.

The Pandora particle flow algorithm (PFA) [450] is the most developed and best performing today in the context of future lepton colliders. The algorithms make use of topological information, including the sub-structure of showers, as well as the compatibility of calorimetric and track-based measurements. In this way the purely calorimetric performance for the jet is either retained or improved. In the framework of studies for CLIC [451], it was shown that the required jet energy resolution of 3.5% can be achieved with the PF technique for jet energies up to 1500 GeV.

For the use of energy-momentum matching in the assignment of energy depositions, and for energy flow treatment of dense jets, particle flow calorimeters with their emphasis on imaging must still feature a good energy resolution. Furthermore, the neutral hadron energy uncertainty is the dominant contribution to the jet resolution for low energy jets, where particles are well separated, while at higher energies the confusion effects take over.

High granularity in all three space dimensions comparable to or smaller than the length scales of particle showers given by X_0 and ρ_M for both ECAL and HCAL brings additional advantages; for example it offers ideal conditions for the application of software compensation methods, which improves the intrinsic resolution and also reduces "confusion" [452]. A particular strength is the possibility to use topological information such as the reconstructed starting point of the shower for the estimation of leakage. Moreover, the combination of fine-grained topological reconstruction and cuts on cluster-wise timing with a precision of few tens of pico-seconds allows for powerful pile-up rejection. This extends the application range of particle flow methods towards collider environments with less benign background conditions, like multi-TeV e^+e^- collisions, and it is an asset on its own for high-intensity hadron colliders, even if particle flow methods are difficult to apply.

The performance of highly granular calorimeters depends, among others, on the particle separation and pattern recognition capabilities and on the single particle energy and timing resolution. They are thus not only optimised for energy measurement, but also for multi-dimensional shower reconstruction and particle separation in space and time. The potential of such calorimeters can be further enhanced by combining a fine spatial segmentation with maximised information on energy, time, and possibly the nature of the energy deposition, for example by using dual-readout methods. This may be achieved, for example, by combining multiple optical materials sensitive to different components in the shower in finely segmented sandwich calorimeters, or by using timing information to extract the position of the energy deposition along a fibre. For future collider experiments, different approaches based on silicon, scintillator, noble liquid, fibre and crystal readout are being pursued [453]. They all foresee, with different level of emphasis, high granularity to enable the application of particle flow methods, and in some cases to further enhance their performance by additional information not exploited in current algorithms. One such example is the proposal [454] to benefit from the superior electromagnetic energy performance of crystals to pair photons from π^0 decays and thereby resolve jet finding ambiguities to improve the jet energy resolution.

35.10.2 *Electromagnetic calorimeters*

Revised August 2025 by C.L. Woody (BNL) and R.-Y. Zhu (HEP California Inst. of Technology).

The development of electromagnetic showers is discussed in the section on "Passage of Particles Through Matter" (Sec. 34 of this *Review*). Formulae are given which approximately describe average showers, but since the physics of electromagnetic showers is well understood, a detailed and reliable Monte Carlo simulation is possible. EGS4 [455] and GEANT [442] have emerged as the standards.

Electromagnetic calorimeters are devices that are designed to measure the total energy of electrons and photons by total absorption. They come in two general categories: homogeneous and sampling. In a homogeneous calorimeter, all of the particle's energy is deposited in the active detector volume and is used to produce a measurable signal (either scintillation light, Cherenkov light or charge). Homogeneous electromagnetic calorimeters are typically constructed using high density, high Z inorganic scintillating crystals such as BaF_2, BGO, CsI, CsI(Tl), LYSO, NaI(Tl) and PWO, non-scintillating Cherenkov radiators such as lead glass and lead fluoride (PbF_2), or ionizing noble liquids such as liquid argon, liquid krypton or liquid xenon. The properties of some commonly used inorganic crystal scintillators can be found in Table 35.5. Total absorption homogeneous calorimeters, such as those built with heavy crystal scintillators, provide the best energy resolution for measuring electromagnetic showers and are generally used when the best possible performance is required, particularly at lower energies. Attention, however, needs to be paid to radiation damage in inorganic scintillators when exposed to the typical environment of high luminosity proton colliders, as discussed below and in Section 35.4. In addition, it is often challenging to achieve high segmentation with homogeneous radiator materials, both longitudinal and transverse, which is necessary for techniques such as particle flow analysis.

A sampling calorimeter consists of an active medium which generates a signal and a passive medium which functions as an absorber. In this case, most of the particle's energy is deposited in the absorber and only a fraction of the energy is detected in the active medium. The ratio of energy in the sampling medium to the total enegy in calorimeter is called the sampling fraction. The active medium may be a scintillator, an ionizing noble liquid, a semiconductor, or a gas ionization detector. The absorber is typically a heavy metal with a high Z such as lead, tungsten, iron,

Int. J. Mod. Phys. A 2026.41. Downloaded from www.worldscientific.com
by UNIVERSITY OF CALIFORNIA @ BERKELEY on 09/16/26. Re-use and distribution is strictly not permitted, except for Open Access articles.

Table 35.13: Resolution of typical electromagnetic calorimeters. E is in GeV.

Technology (Experiment)	Depth	Energy resolution	Date
NaI(Tl) (Crystal Ball)	$20X_0$	$2.7\%/\mathrm{E}^{1/4}$	1983
$Bi_4Ge_3O_{12}$ (BGO) (L3)	$22X_0$	$2\%/\sqrt{E} \oplus 0.7\%$	1993
CsI (KTeV)	$27X_0$	$2\%/\sqrt{E} \oplus 0.45\%$	1996
CsI(Tl) (BaBar)	16–$18X_0$	$2.3\%/E^{1/4} \oplus 1.4\%$	1999
CsI(Tl) (BELLE)	$16X_0$	1.7% for $E_\gamma > 3.5$ GeV	1998
CsI(Tl) (BES III)	$15X_0$	2.5% for $E_\gamma = 1$ GeV	2010
$PbWO_4$ (PWO) (CMS)	$25X_0$	$3\%/\sqrt{E} \oplus 0.5\% \oplus 0.2/E$	1997
$PbWO_4$ (PWO) (ALICE)	$19X_0$	$3.6\%/\sqrt{E} \oplus 1.2\%$	2008
Lead glass (OPAL)	$20.5X_0$	$5\%/\sqrt{E}$	1990
PbF_2 (g-2)	$15X_0$	$3.6\%/\sqrt{E} \oplus 1.9\%$	2019
Liquid Kr (NA48)	$27X_0$	$3.2\%/\sqrt{E} \oplus 0.42\% \oplus 0.09/E$	1998
Scintillator/depleted U (ZEUS)	20–$30X_0$	$18\%/\sqrt{E}$	1988
Scintillator/Pb (CDF)	$18X_0$	$13.5\%/\sqrt{E}$	1988
SciFi/Pb spaghetti (KLOE)	$15X_0$	$5.7\%/\sqrt{E} \oplus 0.6\%$	1995
SciFi/W (sPHENIX)	$20X_0$	$13\%/\sqrt{E}$	2022
Liquid Ar/Pb (NA31)	$27X_0$	$7.5\%/\sqrt{E} \oplus 0.5\% \oplus 0.1/E$	1988
Liquid Ar/Pb (SLD)	$21X_0$	$8\%/\sqrt{E}$	1993
Liquid Ar/Pb (H1)	20–$30X_0$	$12\%/\sqrt{E} \oplus 1\%$	1998
Liquid Ar/depl. U (DØ)	$20.5X_0$	$16\%/\sqrt{E} \oplus 0.3\% \oplus 0.3/E$	1993
Liquid Ar/Pb accordion (ATLAS)	$25X_0$	$10\%/\sqrt{E} \oplus 0.4\% \oplus 0.3/E$	1996

copper, or depleted uranium. The active material is interspersed with the passive absorber in a variety of ways, e.g. by using alternating plates of active material and absorber, or embedding the active material, such as scintillating fibers, into the absorber.

The main difficulty in this approach is extracting the signal from the active material. One possibility is a simple stack of alternating absorber and active material. However, this usually leads to gaps for the readout and services and hence non-uniformities. This can be improved by using a so-called "spaghetti" design, where scintillating fibers are brought to the front or back of the detector and read out. This can also be done with either wavelength shifting plates or fibers, such as in a so-called "shashlik" design where wavelength shifting fibers run through the stack of alternating scintillator and absorber plates and are read out at one or both ends, or embedding wavelength shifting fibers in the scintillating plates which are then brought out to the edges or back of the detector and read out. Another similar design is the Tungsten SciFi (W/SciFi) configuration, which consists of a matrix of tungsten powder and epoxy with embedded scintillating fibers that are brought out to the back and form a bundle that is read out with silicon photomultipliers (SiPMs). This design was utilized for the sPHENIX EMCAL at RHIC and will be used for the Forward EMCAL for the ePIC Experiment at the EIC.

For sampling calorimeters that use ionizing liquids as the sampling medium, there is also an "accordion" design which avoids all gaps for services, where the absorber plates are folded into an accordion shape along with interspersed electrodes to collect the ionization charge [456]. While these readout schemes are generally more complicated than those for homogeneous calorimeters, the sampling calorimeter design allows more flexibility in terms of segmentation and the construction of very large calorimeters at much lower cost than homogeneous calorimeters.

The energy resolution σ_E/E of a calorimeter can be parameterized as $a/\sqrt{E} \oplus b \oplus c/E$, where $\oplus$ represents the square root of the sum in quadrature of the three terms, and E and σ_E are in GeV. The stochastic term a represents statistics-related fluctuations such as intrinsic shower fluctuations, photoelectron statistics, dead material at the front of the calorimeter, and sampling fluctuations for minimum ionizing particles. For a fixed number of radiation lengths, the stochastic term a for a sampling calorimeter is expected to be proportional to $\sqrt{t/f}$, where t is plate thickness and f is sampling fraction [457–459]. The stochastic term a is typically of the order of a few percent for a homogeneous calorimeter, and is generally in the range of 8 to 20% for sampling calorimeters, depending on the sampling fraction.

The main contributions to the systematic, or constant, term b are detector non-uniformity and calibration uncertainties. In the case of hadronic cascades discussed below, non-compensation also contributes deviations from $\sqrt{E}$ scaling. Another important contribution to the energy resolution of calorimeters that are used in high radiation environments such as high lumnosity colliders is radiation damage of the active medium. Radiation damage can induce optical absorption in scintillating materials which reduces the measured light output and produces non-uniformities in light collection. This can be mitigated by developing radiation-hard active media [460], by reducing the signal path length [461] and by frequent *in situ* calibration and monitoring [103,459]. With effort, the constant term b can be reduced to below one percent. The term c is due mainly to electronic noise summed over the readout channels required to measure the shower energy (typically a few Molière radii).

The position resolution depends on the effective Molière radius and the transverse granularity of the calorimeter. Like the energy resolution, it can be factored as $a/\sqrt{E} \oplus b$, where a is the stochastic term, typically of the order of a few mm to 20 mm, and b can be as small as a fraction of mm for a dense calorimeter with fine granularity. Fine granularity also helps particle flow analysis discussed in the hadron calorimeters section below.

Electromagnetic calorimeters may also provide angular and pointing measurements for electrons and photons. This is particularly important for photon-related physics to identify the correct primary vertex, since photons are not detected by the tracking system of the overall experiment. The typical photon angular resolution is about 45 mrad/$\sqrt{E}$, which can be achieved by implementing longitudinal segmentation [456] for a sampling calorimeter or by adding a preshower detector [462] for a homogeneous calorimeter without longitudinal segmentation.

There have been many electromagnetic calorimeters built and used in particle physics experiments for a variety of applications. Table 35.13 provides a short list of the major ones used in some of the larger experiments. Also listed are calorimeter depths in radiation lengths (X_0) and the achieved energy resolution. Whenever possible, the performance of the calorimeters *in situ* is quoted, which is usually in good agreement with prototype test beam results as well as EGS or GEANT simulations, provided that all systematic effects are properly included. Details about detector design and performance can be found in Appendix C of refer-

Int. J. Mod. Phys. A 2026.
Downloaded from www.worldscientific.com
by UNIVERSITY OF CALIFORNIA @ BERKE
use and distribution is strictly not permitted, except for Open Access articles.

ence [459] and Proceedings of the International Conference series on Calorimetry in High Energy Physics.

35.10.3 *Hadronic calorimeters*

Revised August 2025 by F. Sefkow (DESY, Hamburg) and F. Simon (KIT).

Hadronic calorimetry [441, 463, 464] is considerably more complex than electromagnetic (EM) calorimetry due to the wider range and different nature of physical processes contributing to shower development and energy deposition, which in turn are characterised by different length and time scales. Hadronic showers are initiated by inelastic strong interactions of highly-energetic charged and neutral hadrons with atomic nuclei. These interactions result in the production of secondary particles, which drive the development of the shower. Among these are energetic hadrons, as well as lower-energy nucleons, photons and nuclear fragments. Energy transferred to nuclear break-up, excitation or recoil does not, in general, produce a signal, but remains *invisible*, and event-to-event fluctuations of this invisible energy deposit ultimately limit the resolution of hadronic calorimeters (HCALs).

The length scale of the interaction of relativistic hadrons is given by the nuclear interaction length λ_I. As discussed in Section 35.10.1, λ_I is a factor 10 to 30 larger than X_0 for common materials used in the construction of calorimeters. HCALs thus require a significantly larger geometrical depth for full containment than electromagnetic calorimeters (ECALs), albeit not by the factor suggested by the ratio of λ_I/X_0 due to the different nature of the showers. A key role is played by the production of π^0s and their subsequent decay into two photons. These result in the formation of electromagnetic sub-showers which evolve on the scale given by the radiation length X_0, and thus require sufficiently fine sampling of the shower activity to capture also this electromagnetic component. The two different length scales occurring in hadronic showers, and the large fluctuations of hadronic, electromagnetic and invisible activity, result in significant event-to-event variations of the energy response and of the shower topology. This topology is characterized by a lumpy structure, with compact regions of high local energy density originating from electromagnetic sub-showers, and sparser hadronic activity with minimum-ionizing hadrons.

Figure 35.37 (top) shows the distribution of the longitudinal position of the first inelastic interaction measured for pion-induced hadronic showers with the highly-granular scintillator-steel HCAL of the CALICE collaboration [465]. The figure illustrates the exponential distribution, with a slope consistent with the pion interaction length expected from the geometry and material composition of the calorimeter. This distribution is well reproduced by simulations using GEANT4 [442, 447]. Figure 35.37 (bottom) shows the mean longitudinal shower profile, given by the mean energy deposition in each calorimeter layer, both relative to the front face of the calorimeter (dots, without corrections for dead cells) and relative to the measured shower starting point given by the first inelastic interaction (filled histogram). The latter is much more compact than the former, which is a convolution of the latter with the distribution of shower starting point shown in the left panel of the figure. This shows that the detector depth required for adequate shower containment is significantly influenced by the fluctuations of the position of the first hadronic interaction. Detection of this position allows for an estimate of leakage from a finite calorimeter volume, and it enables stringent tests of shower evolution models. In the past years, motivated by precision needs at the next generation of e^+e^- colliders, the CALICE collaboration has constructed a number of prototypes with high 3-dimensional spatial granularity and recorded large sets of data at test beams, allowing for studies of shower evolution processes in unprecedented detail. The refined simulations support the trend to proceed from research focused on understanding the global intrinsic properties of showers, e.g. for the purpose of compensation, towards the study of detailed information, in space, time, and energy deposition type, through many and multiple readout channels.

In an inelastic hadronic collision a significant fraction f_{em} of the energy is removed from further hadronic interaction by the production of secondary π^0/η's, whose decay photons generate high-energy electromagnetic showers. Charged secondaries ($\pi^\pm$, p, ...) deposit energy via ionization and excitation, but also interact with nuclei, producing evaporation neutrons, spallation protons and neutrons, and heavier spallation fragments. The charged collision products produce detectable ionization, as do the showering γ-rays from the prompt de-excitation of highly excited nuclei. The recoiling nuclei generate little or no detectable signal, as mentioned previously. The neutrons lose kinetic energy in elastic collisions which generate ionization signals via recoiling protons, thermalize on a time scale of several μs, and are finally captured, with the production of more γ-rays—usually outside the acceptance gate of the electronics. Between endothermic spallation losses, nuclear recoils, and late neutron capture, a significant fraction of the hadronic energy (20%–40%, depending on the absorber

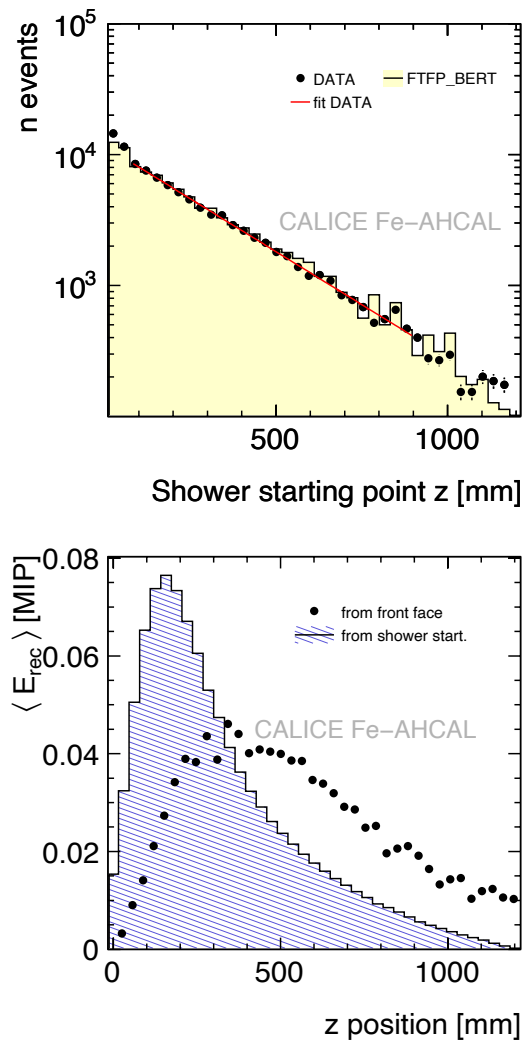

Figure 35.37: Longitudinal profile of hadronic showers induced by 45 GeV negative pions measured in he CALICE highly-granular steel-scintillator sampling calorimeter [465]. Top: Reconstructed position of the first inelastic interaction, compared to simulations (GEANT4 9.4p03, FTFP_BERT), and an exponential fit yielding a slope consistent with the expected pion interaction length. Bottom: Longitudinal shower profile measured from the front face of the calorimeter (dots, without corrections for dead cells) and relative to the position of the shower start given by the first inelastic interaction (filled histogram). The visible energy is given in units of the most probable energy loss of a minimum-ionizing particle (MIP). The integrals of the distributions are normalized to unity.

Int. J. Mod. Phys. A 2026.41. Downloaded from www.worldscientific.com
by UNIVERSITY OF CALIFORNIA @ BERKELEY on 09/16/26. Re-use and distribution is strictly not permitted, except for Open Access articles.

and energy of the incident particle) is used to overcome nuclear binding energies and is therefore lost or "invisible."

In a hadron-nucleus collision a large fraction of the incident energy is carried by a "leading particle" with the same quark content as the incident hadron. If the projectile is a charged pion, the leading particle is usually a pion, which can be neutral and hence contributes to the EM sector. This is not true for incident protons. The result is an increased mean hadronic fraction for incident protons.

The complexity of hadronic showers also has a significant impact on the energy measurement. In contrast to EM showers, hadronic cascade processes are characterised by the production of relatively few high-energy particles. The number multiplicity of these particles produced in hadronic interactions increases only logarithmically with energy. The lost energy and f_{em} are highly variable from event to event, and on average increase with increasing energy [466]. Electromagnetic sub-showers typically result in a higher response than the hadronic parts of the cascade, where undetectable energy loss due to nuclear dissociation, the long time scales and the material dependence of neutron signals, as well as other effects reduce the measured signal. This difference in response is often expressed by the $\langle h/e \rangle$ ratio, a calorimeter-dependent quantity which is smaller than unity for many, but not all, HCALs. The increase of the electromagnetic fraction with energy thus introduces a non-linear contribution to the response. Combined with the significant event-by-event fluctuations between electromagnetic and hadronic fractions of the showers and between different hadronic processes the non-equality of h and e deteriorates the energy resolution of HCALs. Different strategies to address this exist, as discussed further below.

Most large HCALs are parts of complex 4π detectors at colliding beam facilities. To date, all these HCALs are sampling calorimeters. This choice is imposed by the physics of hadronic showers, both by the required depth for containment which favours high-density materials with short λ_I, and by the differences in response to electromagnetic and hadronic parts of the cascade, which are particularly severe for homogeneous calorimeters. Common absorber materials are Fe, Cu, Pb, and U, with W also used occasionally. A large variety of different active materials are used, depending on application and optimisation, from plastic scintillators (plates, tiles, bars, fibers), crystals and Cherenkov media, silicon, liquid argon (LAr), to gaseous detectors. The energy loss of particles in the active medium is either detected directly by collecting charge, or via scintillation or Cherenkov light observed with conventional photomultipliers (PMTs), photodiodes or silicon photomultipliers (SiPMs). The choice of both active and passive materials is driven by different, sometimes conflicting, constraints, including performance requirements, space and other mechanical boundary conditions, radiation tolerance, and cost considerations.

A wide range of different geometries of absorbers and sensors is used, with design choices depending on the chosen priorities of addressing these constraints, also considering the need to bring the signals to the outside of the detector while achieving a hermetic coverage and other constraints. In this context it is important to note that a classic sandwich structure with absorber plates and active elements approximately perpendicular to the particle incidence is not required, and arbitrary orientations are viable for good calorimetric measurements, as long as channelling, meaning the extended passage of primary particles through low-density active regions, is excluded. Figure 35.38 shows two examples of plastic scintillator-based calorimeters to illustrate differences in design between coarsely-segmented and highly-granular calorimeters. The ATLAS tile calorimeter [467] uses scintillator tiles coupled to wavelength-shifting fibers which collect the light from the tiles and guide them to PMTs outside of the active region of the calorimeter. The calorimeter is segmented in ϕ (azimuthal angle) and η (pseudorapidity, defined as $\eta = -\ln\tan(\theta/2)$, where θ is the angle relative to the beam axis), with coarse longitudinal segmentation. The technological prototype of the CALICE analog HCAL, a highly granular SiPM-on-tile calorimeter is based on scintillator tiles directly coupled to SiPMs, which, together with the front-end electronics, are embedded inside of the the active

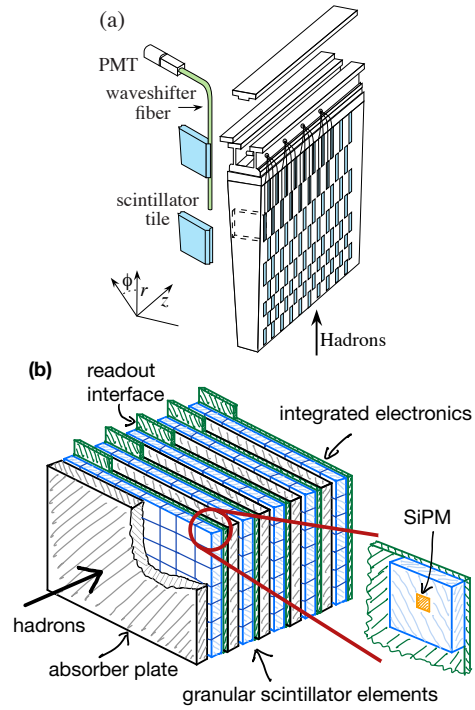

Figure 35.38: Two examples of geometrical structures of scintillator-based HCALs. (a) A wedge of the ATLAS central tile calorimeter consisting of scintillator tiles in iron, read out via wavelength-shifting fibers and PMTs [467]. The coordinate system is that of the ATLAS calorimeter within the experiment, with the z axis along the beam direction, r pointing radially outward, and ϕ being the azimuthal angle. (b) An illustration of the "SiPM-on-tile" structure used in the CALICE analogue HCAL prototype, and in the CMS High-Granularity Calorimeter (HGCAL), highly granular calorimeters with steel absorbers and small scintillator tiles directly read out via SiPMs with embedded electronics [464, 468–470].

volume of the calorimeter. The CMS HGCAL [470] uses the same concept in part of the detector, and in addition embeds elements for digital data concentration and power distribution in the active volume. Other detector solutions include scintillating fibres threading an absorber [471], liquid-argon-filled tubes [472] and the "accordion" LAr detector [473]. The latter has zig-zag absorber plates to minimize channeling effects; the calorimeter is hermetic (no cracks), and plates are oriented so that cascades cross the same plate repeatedly.

In particular, but not exclusively, the combination of heavy absorber materials (Pb, U) with plastic scintillators allows the construction of HCALs that have a near-equal response to electromagnetic and hadronic parts of the cascade, so-called compensating calorimeters [474]. In this first study, it was recognized that nuclear fission can amplify the hadronic signal when using uranium absorbers. However, the key drivers of compensation are the reduction of the electromagnetic response with high-Z absorbers and an increased sensitivity to neutrons, which are strongly correlated to otherwise invisible energy loss due to nuclear dissociation, with a hydrogeneous active medium [475–479]. Since the electromagnetic cross section increases, and the critical energy decreases with Z, and since most of the energy of an electromagnetic shower is deposited by low-energy, short-range electrons, a disproportionate fraction of the total electromagnetic energy is deposited in the absorber in the high-Z case. Hydrogenous active media, such as organic scintillators, have a high sensitivity to spallation neutrons via elastic $n-p$ scattering. The number of produced neutrons is highly correlated with the invisible energy of the hadronic cascade. Increasing the sensitivity to these particles can thus boost the visible hadronic signal. Achieving compensation requires carefully-chosen sampling fractions and frequencies, with the response to

Int. J. Mod. Phys. A
by UNIVERSITY OF CALIFORNIA @ BERKE
nloaded from www.worldscientific.com
use and distribution is strictly not permitted, except for Open Access articles.

the hadronic parts of the shower also sensitive to the integration time of the electronics due to the time structure of the neutron component of the signal.

Since Cherenkov light, for example in quartz plates or fibers, or in crystals, is produced only by relativistic particles in the cascade and thus predominantly by the electromagnetic component of the shower, such media are less common in hadronic than in ECALs. Notable exceptions are applications that require high radiation tolerance, and dual-readout calorimeters which specifically exploit this feature, as discussed below.

Silicon offers high compactness, high granularity, high radiation tolerance, long-term stability and fast charge collection, and is thus an interesting active material for sampling calorimeters. A thorough overview of the development and of the features of this technology can be found in a recent review paper [480]. The first silicon-based calorimeter in a collider experiment was a HCAL, the H1 PLUG calorimeter [481] covering the very forward region of the H1 experiment at HERA. The SICAPO collaboration has demonstrated the conceptual possibility of constructing compensating HCALs using silicon sensors [482]. Silicon is currently the technology of choice for several ECALs for future Higgs factories [483–485]. It is also being used extensively in the CMS HGCAL [470] in both electromagnetic and hadronic sections, complemented by scintillator tiles with on-tile SiPM readout where the radiation levels allow.

More generally, high-granularity calorimeters play an increasingly important role, in particular motivated by the use of particle-flow algorithms for global event reconstruction (see Section 35.10.1). The associated technologies for both electromagnetic and HCALs have been pioneered by the CALICE collaboration, which has built and tested an increasingly sophisticated series of "imaging" calorimeters with a highly granular readout [486]. In the area of HCALs, this includes the scintillator-based analog HCAL [487] with the latest SiPM-on-tile technological prototype with fully-integrated electronics having approximately 22,000 channels [468, 469], as well as digital [488] and semidigital [489] calorimeters using gas detectors, such as RPCs (Sec. 35.6.6) and micropattern gas detectors (Sec. 35.6.3), with channel counts of up to 500,000. The large numbers of channels of high-granularity calorimeters presents a significant integration challenge for full detector systems, and requires the full integration of the front-end electronics inside of the active volume of the detector, as well as very compact data concentration and interface units. The first such detector in construction for a collider experiment is the CMS HGCAL [470]. Beam tests with a combined prototype using both silicon and scintillator-SiPM instrumented active layers have confirmed simulation-based expectations [490]. The timing resolution is found to be 60ps for single-channel measurements and better than 20ps for full showers at the highest energies [491], setting excellent perspectives for the HGCAL calorimeter performance at the HL-LHC. The total silicon area of the full HGCAL amounts to about 600 m^2, and about 240,000 SiPMs are foreseen. The calibration of such calorimeters requires the monitoring of a large number of cells, which is achieved in-situ using reconstructed track segments within hadronic showers [470,492] or externally identified muons. For this method, the capability to detect the most probable energy loss of a minimum-ionizing particle in a single cell is essential. This is required over the full lifetime of the detector, also after the active elements have received significant radiation damage, resulting in increased noise and reduced charge or signal collection efficiency. Due to the large number of cells contributing to the measurement of one shower, the requirements on the precision of the calibration of individual cells is relaxed relative to the global energy calibration of the calorimeter.

The energy resolution of HCALs is severely affected by fluctuations between different components of the cascade, exacerbated by differences in response to purely hadronic and to electromagnetic sub-showers. In many detectors, fluctuations in the electromagnetic energy fraction, $f_{\rm em}$, and the related, consequential variations in nuclear energy dissociation losses, represent the biggest single contribution to the hadron energy resolution. One strategy to address this problem is the construction of intrinsically-compensating calorimeters, which imposes stringent constraints on materials and geometries as discussed above. Compensating calorimeters are not used in current large collider experiments, and are at the moment not considered for future collider detectors. Two different strategies are presently followed to improve the energy resolution in non-compensating calorimeters: Offline weighting or software compensation in longitudinally-segmented or in highly-granular calorimeters; and dual-readout calorimetry.

Software compensation and *Machine Learning* techniques exploit the fact that electromagnetic sub-showers typically have a higher spatial density than the purely hadronic parts of the cascade. Amplitude (or energy-density) dependent weights are applied in the reconstruction to reduce the effects of shower-to-shower fluctuations. These techniques were pioneered by the CDHS collaboration for a longitudinally segmented steel-plastic scintillator calorimeter [493], where an improvement of the energy resolution of 10% (at 10 GeV) to 30% (at 140 GeV) for charged pion showers was achieved. Similar techniques were successfully applied in the H1 [494] liquid argon calorimeter system resulting in a stochastic term of $51\%/\sqrt{E}$, and in the ATLAS [495] endcap calorimeters, also based on liquid argon, with an energy resolution of $84\%/\sqrt{E}$. Inspired by these approaches, a software compensation technique using the detailed spatial information provided by highly-granular calorimeters of the CALICE collaboration has been developed, achieving up to 25% improvement of the energy resolution compared to the resolution without software compensation, resulting in a stochastic term of $45\%/\sqrt{E}$ [496] in a scintillator tile calorimeter with steel absorbers. This technique has also been successfully transferred to particle-flow reconstruction [497], resulting in an improvement of the jet-energy resolution in simulated events by 8% - 15%, depending on jet energy. Highly-granular calorimeters with software compensation and particle-flow reconstruction are currently studied as the baseline configuration for several Higgs-factory detectors.

The wealth of detailed information provided by highly granular calorimeters with timing capabilities suggests the application of machine learning (ML) methods to optimise their performance. Using test beam data collected with CALICE and CMS HGCAL prototypes, significant improvements have been demonstrated for the hadron shower energy resolution [498, 499] as well as for the separation of showers [500] in multi-particle events for particle flow reconstruction.

The *dual-readout method*, originally proposed by Mockett in 1983 [501], measures $f_{\rm em}$ event by event in parallel to the total deposited energy. It uses the fact that most of the relativistic particles in the shower originate from the electromagnetic part, and that only those produce Cherenkov light, while the signal of the hadronic part is mostly due to non-relativistic protons. In practice either two different active media, e.g. scintillator and quartz, are used to register scintillation and Cherenkov light, respectively, or the optical signals from the two processes occurring in heavy crystals are disentangled, using their different spectral, directional or timing properties.

The Cherenkov and scintillation signals, normalised to the response for electrons, are given by

$$C = [f_{\rm em} + (h/e)_C(1 - f_{\rm em})]E\,, \tag{35.51}$$

$$S = [f_{\rm em} + (h/e)_S(1 - f_{\rm em})]E\,, \tag{35.52}$$

respectively, which can be solved for the fraction $f_{\rm em}$ and the energy

$$E = (\xi S - C)/(\xi - 1)\,, \tag{35.53}$$

where $\xi = [1 - (h/e)_C]/[1 - (h/e)_S]$ and $(h/e)_{C,S}$ denote the average ratios of hadronic to electromagnetic response in the Cherenkov and scintillator parts, respectively. This is illustrated in Figure 35.39, which shows their correlation for a set of simulated negative pion events [502] using FLUKA [446].

It was noted that the method demands a steep slope ξ, which implies that the scintillator read-out should be as compensating as possible, which however reduces the room for improvement by adding Cherenkov information.

The method was tested by the DREAM/RD52 collaboration [503,504], using a 1 ton copper matrix with embedded quartz and

Int. J. Mod. Phys. A 2026.41. Downloaded from www.worldscientific.com
by UNIVERSITY OF CALIFORNIA @ BERKELEY on 09/16/26. Re-use and distribution is strictly not permitted, except for Open Access articles.

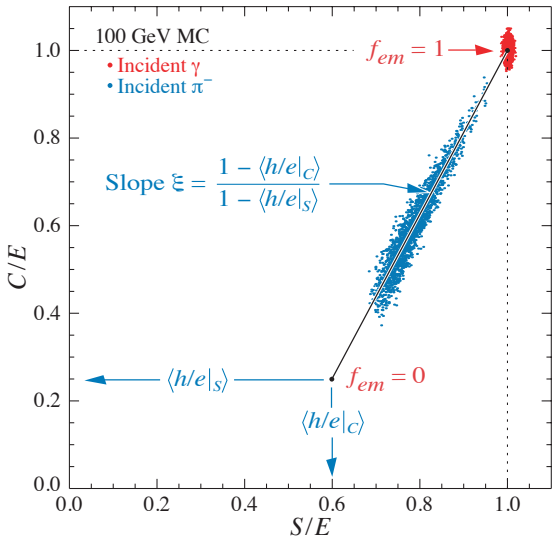

Figure 35.39: Scatter plot of Monte Carlo C/E (Cherenkov) vs S/E (scintillator) signals for individual events in a dual-readout calorimeter for 100 GeV negative pions and photons. Hadronic events are shown in blue, and scatter about the indicated event locus. Electromagnetic events cluster about $(C/E, S/E) = (1,1)$. In this case worse resolution (fewer p.e.'s) was assumed for the Cherenkov events, leading to the "elliptical" distribution.

scintillating fibers. The value of ξ was about 3 in this detector. With this detector, a resolution of $70\%/\sqrt{E(\mathrm{GeV})}$ was obtained for single hadrons [505]. Due to the small size of the module, this includes contributions from transverse leakage which prevent the full exploitation of key features of dual readout, and thus underestimates the potential of the method.

The separate Cherenkov read-out evidently provides excellent pion-electron separation for particle identification. In another RD52 prototype, each fiber is read out individually by SiPMs, giving also a superior transverse granularity. A fiber-based calorimeter with full solid-angle coverage requires a pointing geometry due to the limited or missing longitudinal segmentation. The resulting challenges for a mechanical design are studied in the framework of the IDEA detector concept [506].

Table 35.14 shows selected examples of the energy resolution of HCALs for single charged pions achieved in beam tests. The examples are selected to illustrate the performance achieved with different designs ranging from intrinsic compensation to software compensation and dual readout, with a focus on results by R&D projects. It should be noted that the exact values of the different resolution terms depend on the functional form used in the fit, here the addition in quadrature is used for the cases where more than just the stochastic term is quoted. The results shown in the table illustrate that (close to) compensating calorimeters with optimized sampling fraction and frequency, such as HELIOS (U-plastic scintillator) and SPACAL (Pb-plastic scintillator), achieve a very good energy resolution. The comparison with Bernardi *et al.*, which has the same Pb/scintillator ratio by volume as SPACAL, but coarser sampling in a sandwich structure, illustrates the importance of the geometrical details. Beyond the examples shown in the table, liquid argon has also been explored as an active medium, for example in the context of the SLD detector with different absorber options [511]. Due to the reduced sensitivity to neutrons in the shower, not the same resolution as for plastic-scintillator-based systems is achieved. This technology has also been used in the D0 experiment, as discussed below. The dual-readout method has the potential to reach or surpass this performance, but would require a prototype sufficiently large for full longitudinal and transverse shower containment for an experimental demonstration. The two CALICE calorimeters shown, which use the same active elements (5 mm thick scintillator tiles) but different absorbers (21.4 mm Fe vs 10 mm W + 4 mm Fe) per layer, illustrate the impact of the absorber choice on energy resolution and reconstruction possibilities. While the tungsten-based W-AHCAL setup is very close to compensating, the steel-based AHCAL achieves a better energy resolution when software compensation is applied, profiting from the finer sampling of the electromagnetic parts of the cascade and the correction for shower-to-shower fluctuations of the electromagnetic fraction in the reconstruction. In the case of tungsten, software compensation does not significantly improve the energy resolution, as expected. The comparison of the CALICE AHCAL performance with the one of CDHS illustrates the benefits of higher granularity for software compensation techniques, but it should be noted that the absorber thickness of the latter is 25 mm, with the same scintillator thickness as in the case of CALICE.

As explained in the introduction, in most high-energy physics experiments, the HCAL follows after an ECAL, making the response of the latter to hadronic cascades highly relevant for the overall performance of the combined ECAL HCAL system. For scenarios where the electromagnetic and the HCAL have very different $\langle h/e \rangle$, as is typically the case for crystal-based ECALs, the fluctuations of the fraction of the hadronic shower contained within the ECAL result in a significant deterioration of the energy resolution for hadrons. A deterioration of the hadronic performance also results from larger amounts of not-instrumented material, e.g. supports and services, between electromagnetic and hadronic sections. In particle-flow calorimeters, a large value of the λ_I/X_0 ratio of the absorber material, like in tungsten, maximises the longitudinal separation of electromagnetic and hadronic showers. This is reflected in the design of particle-flow-based detector concepts for future Higgs Factories.

Table 35.15 summarizes the single hadron energy resolution obtained from test beams of the combined ECAL and HCAL systems of the large multi-purpose experiments at HERA, the Tevatron and at the LHC. These systems are examples of different optimization strategies. D0 and ZEUS are near-compensating systems with the same technology in ECAL and HCAL emphasizing hadronic performance. ATLAS and H1 use sampling ECALs with good electromagnetic resolution and weighting techniques exploiting longitudinal and transverse shower information for hadronic energy reconstruction. CMS, with a crystal ECAL and a scintillator-brass HCAL, prioritizes electromagnetic performance, with very different $\langle h/e \rangle$ in the electromagnetic and hadronic system. Of the detectors shown in the table, CMS has the best electromagnetic resolution by a comfortable margin, but consequently the weakest hadronic resolution. The best hadronic performance is achieved with the compensating calorimeter of ZEUS, which however has a weaker electromagnetic performance than the other calorimeter systems shown here. It should be noted that an excellent single-hadron resolution in general does not fully propagate into the jet-energy performance. Inactive material in front of the calorimeter can significantly worsen the energy resolution for jets, with an impact in particular on lower-energy particles. For example, the core of the invariant mass distribution of hadronically-decaying Z^0 bosons measured in ZEUS, which had a superconducting coil in front of the calorimeter, is well described by a Gaussian with a σ of 6 GeV [518], approximately 40% wider than would be expected for a jet-energy resolution that is identical to the single-hadron performance.

35.10.4 *Free electron drift velocities in liquid ionization chambers*

Revised August 2009 by W. Walkowiak (Siegen U.).

Drift velocities of free electrons in LAr [338] are given as a function of electric field strength for different temperatures of the medium in Fig. 35.40. The drift velocites in LAr have been measured using a double-gridded drift chamber with electrons produced by a laser pulse on a gold-plated cathode. The average temperature gradient of the drift velocity of the free electrons in LAr is described [338] by

$$\frac{\Delta v_d}{\Delta T\, v_d} = (-1.72 \pm 0.08)\ \%/\mathrm{K}. \tag{35.54}$$

Previous measurements [519, 520, 522, 523] range from 13%

Int. J. Mod. Phys. A
Downloaded from www.worldscientific.com
by UNIVERSITY OF CALIFORNIA @ BERKE
use and distribution is strictly not permitted, except for Open Access articles.

Table 35.14: Energy resolution of selected hadron calorimeters for single charged hadrons obtained in beam tests.

Calorimeter	Passive	Active	Resolution	Ref.
Bernardi *et al.*	Pb	Scintillator layers	$44.2\%/\sqrt{E}$ §	[507]
CALICE AHCAL	Fe	Scintillator tiles	$44.3\%/\sqrt{E} \oplus 1.8\%$ †	[496]
CALICE W-AHCAL	W	Scintillator tiles	$57.9\%/\sqrt{E} \oplus 4.6\% \oplus 0.065/E$ §	[508]
CDHS	Fe	Scintillator layers	$58\%/\sqrt{E}$ ♯	[493]
DREAM/RD52	Pb	Scint.+ Quartz fibers	$70\%/\sqrt{E}$ *	[505]
HELIOS	U	Scintillator layers	$34\%/\sqrt{E}$ §	[509]
SPACAL	Pb	Scintillating fibers	$33.3\%/\sqrt{E} \oplus 2.2\%$ §	[510]

§ Bernardi *et al.*, CALICE W-AHCAL, HELIOS, SPACAL: (near-)compensating calorimeters.
† CALICE AHCAL: Local software compensation exploiting the high granularity of the calorimeter.
♯ CDHS: Offline weighting using longitudinal information.
* DREAM/RD52: Due to the relatively small transverse size of the detector lateral leakage was significant, deteriorating the energy resolution with respect to the full potential of the dual readout method.

Table 35.15: Energy resolution of selected combined electromagnetic and hadronic calorimeter systems in past and present high-energy collider experiments for single hadrons. The results are taken from beam tests of prototypes with the electromagnetic calorimeter upstream of the hadronic calorimeter.

Experiment	technology (ECAL, HCAL)	Combined hadronic resolution	Reference
H1	Pb/LAr, Steel / LAr	$46\%/\sqrt{E} \oplus 2.6\% \oplus 0.73/E$	[512]
ZEUS	depleted U / plastic scintillator	$35\%/\sqrt{E}$	[513]
CDF	Pb/plastic scint., Steel/plastic scint.	$68\%/\sqrt{E} \oplus 4.1\%$	[514]
D0	depleted U / LAr	$44.6\%/\sqrt{E} \oplus 3.9\%$	[515]
ATLAS	Pb/LAr, Steel/plastic scintillator	$52\%/\sqrt{E} \oplus 3.0\% \oplus 1.6/E$	[516]
CMS	$PbWO_4$, brass/plastic scintillator	$84.7\%/\sqrt{E} \oplus 7.4\%$	[517]

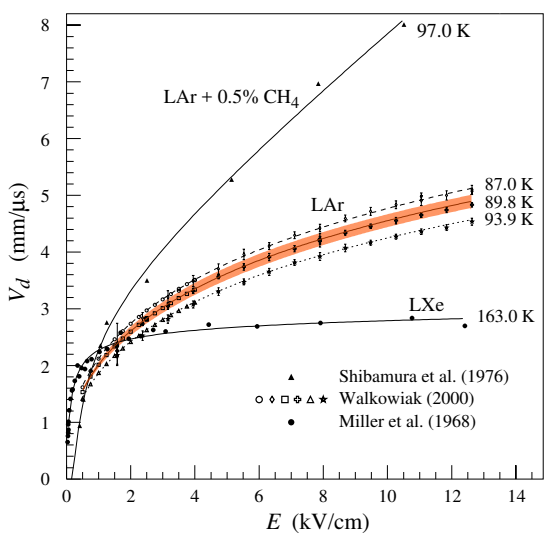

Figure 35.40: Drift velocity of free electrons as a function of electric field strength for LAr [338], LAr + 0.5% CH_4 [519] and LXe [520]. The average temperatures of the liquids are indicated. Results of a fit to an empirical function [521] are superimposed. In case of LAr at 91 K the error band for the global fit [338] including statistical and systematic errors as well as correlations of the data points is given. Only statistical errors are shown for the individual LAr data points.

higher [520] to 18% lower [522] than these measurements. They used different techniques and show drift velocities for free electrons which cannot be explained by the temperature dependence mentioned above.

Drift velocities of free electrons in LXe [519] as a function of electric field strength are also displayed in Fig. 35.40. The drift velocity saturates for $|E| > 3$ kV/cm, and decreases with increasing temperature for LXe as well as measured e.g. by [524].

The addition of small concentrations of other molecules like N_2, H_2 and CH_4 in solution to the liquid typically increases the drift velocities of free electrons above the saturation value [519, 522], see example for CH_4 admixture to LAr in Fig. 35.40. Therefore, actual drift velocities are critically dependent on even small additions or contaminations.

35.11 Superconducting magnets for collider detectors

Revised August 2025 by Y. Makida (KEK).

35.11.1 *Solenoid Magnets*

In all cases SI unit are assumed, so that the magnetic field, B, is in Tesla, the stored energy, E, is in joules, the dimensions are in meters, and vacuum permeability of $\mu_0 = 4\pi \times 10^{-7}$.

The magnetic field (B) in an simple solenoid with a flux return iron yoke, in which the magnetic field is lower than magnetic saturation of < 2 T, is given by

$$B = \frac{\mu_0\, n\, I}{L} \tag{35.55}$$

where n is the number of turns, I is the current and L is the coil length.

In an air-core solenoid case, the central field is given by

$$B(0,0) = \mu_0\, n\, I \frac{1}{\sqrt{L^2 + 4R^2}}\ , \tag{35.56}$$

where R is the coil radius.

In most cases, momentum analysis is made by measuring the circular trajectory of the passing particles according to $p = mv = qrB$, where p is the momentum, m the mass, q the charge, r the bending radius. By using the sagitta, s, of the trajectory, p is given by

$$s = q\, B\, \ell^2/8p\ , \tag{35.57}$$

where ℓ is the path length in the magnetic field as shown in Fig. 35.41 .

Int. J. Mod. Phys. A 2026.41. Downloaded from www.worldscientific.com
by UNIVERSITY OF CALIFORNIA @ BERKELEY on 09/16/26. Re-use and distribution is strictly not permitted, except for Open Access articles.

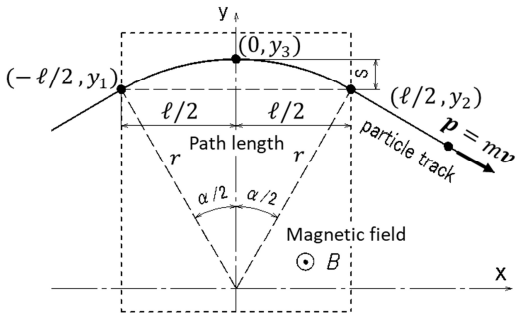

Figure 35.41: Geometric relation of sagitta between path length.

In a practical momentum measurement in colliding beam detectors, it is more effective to increase the magnetic volume than the field strength, since

$$dp/p \propto p/B\,\ell^2 \ , \tag{35.58}$$

where ℓ corresponds to the solenoid coil radius R. The energy stored in the magnetic field of any magnet is calculated by integrating B^2 over all space:

$$E = \frac{1}{2\mu_0}\int B^2 dV \tag{35.59}$$

If the coil thin and inside an iron return yoke , (which is the case if it is to superconducting coil), then

$$E \approx (B^2/2\mu_0)\pi R^2 L \ . \tag{35.60}$$

For a detector in which the calorimetry is outside the aperture of the solenoid, the coil must be transparent in terms of radiation and absorption lengths. This usually means that the superconducting solenoid and its cryostat is of minimum real thickness and is made of a material with long radiation length. There are two major contributors to the thickness of a thin solenoid:

1. The conductor consisting of the current-carrying superconducting material (usually Nb-Ti/Cu) and the quench protecting stabilizer (usually aluminum) are wound on the inside of a structural support cylinder (usually aluminum alloy). The coil thickness scales as B^2R, so the thickness in radiation lengths (X_0) is

$$t_{\rm coil}/X_0 = (R/\sigma_h X_0)(B^2/2\mu_0) \ , \tag{35.61}$$

   where $t_{\rm coil}$ is the physical thickness of the coil, X_0 the average radiation length of the coil/stabilizer material, and σ_h is the hoop stress in the coil [525]. $B^2/2\mu_0$ is the magnetic pressure. In large detector solenoids, the aluminum stabilizer and support cylinders dominate the thickness; the superconductor (Nb-TI/Cu) contributes a smaller fraction. The main coil and support cylinder components typically contribute about 2/3 of the total thickness in radiation lengths.
2. Another contribution to the material comes from the outer cylindrical shell of the vacuum vessel. Since this shell is susceptible to buckling collapse, its thickness is determined by the diameter, length and the modulus of the material of which it is fabricated. The outer vacuum shell represents about 1/3 of the total thickness in radiation length.

35.11.2 *Properties of collider detector magnets*

The physical dimensions, central field stored energy and thickness in radiation lengths normal to the beam line of the superconducting solenoids associated with the major collider are given in Table 35.16 [526]. Fig. 35.42 shows thickness in radiation lengths as a function of B^2R in various collider detector solenoids.

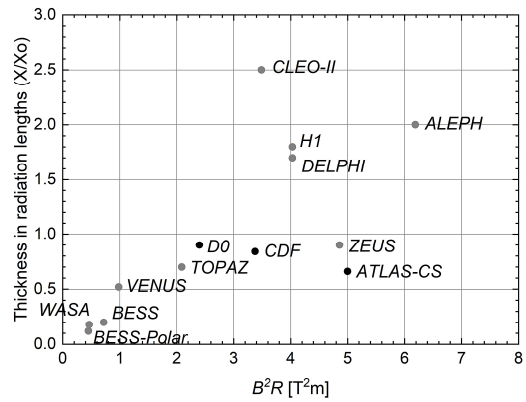

Figure 35.42: Magnet wall thickness in radiation length as a function of B^2R for various detector solenoids. Gray entries are for magnets no longer in use.

The ratio of stored energy to cold mass (E/M) is a useful performance measure. It can also be expressed as the ratio of the stress, σ_h, to twice the equivalent density, ρ, in the coil [525]:

$$\frac{E}{M} = \frac{(B^2/2\mu_0)\pi R^2 L}{\rho\, 2\pi t_{\rm coil} RL} \approx \frac{\sigma_h}{2\rho} \tag{35.62}$$

The E/M ratio in the coil is approximately equivalent to H,[†††] the enthalpy of the coil, and it determines the average coil temperature rise after energy absorption in a quench:

$$E/M = H(T_2) - H(T_1) \approx H(T_2) \tag{35.63}$$

where T_2 is the average coil temperature after the full energy absorption in a quench, and T_1 is the initial temperature. E/M ratios of 5, 10, and 20 kJ/kg correspond to ∼65, ∼80, and ∼100 K, respectively. The E/M ratios of various detector magnets are shown in Fig. 35.43 as a function of total stored energy. One would like the cold mass to be as small as possible to minimize the thickness, but temperature rise during a quench must also be minimized. An E/M ratio as large as 12 kJ/kg is designed into the CMS solenoid, with the possibility that about half of the stored energy can go to an external dump resistor. Thus the coil temperature can be kept below 80 K if the energy extraction system works well. The limit is set by the maximum temperature that the coil design can tolerate during a quench. This maximum local temperature should be <130 K (50 K + 80 K), so that thermal expansion effects, which are remarkable beyond 80 K, in the coil are manageable less than 50 K.

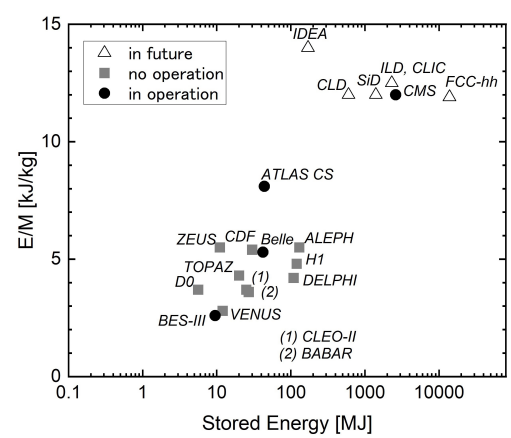

Figure 35.43: Ratio of stored energy to cold mass for major detector solenoids. Gray indicates magnets no longer in operation.

[†††]The enthalpy, or heat content, is called H in the thermodynamics literature. It is not to be confused with the magnetic field intensity B/μ.

Int. J. Mod. Phys. A 2017.01.0030 Downloaded from www.worldscientific.com
by UNIVERSITY OF CALIFORNIA @ BERKE use and distribution is strictly not permitted, except for Open Access articles.

Table 35.16: Progress of superconducting magnets for particle physics detectors.

Experiment	Laboratory	B [T]	Radius [m]	Length [m]	Energy [MJ]	X/X_0	E/M [kJ/kg]
TOPAZ*	KEK	1.2	1.45	5.4	20	0.70	4.3
CDF*	Tsukuba/Fermi	1.5	1.5	5.07	30	0.84	5.4
VENUS*	KEK	0.75	1.75	5.64	12	0.52	2.8
AMY*	KEK	3	1.29	3	40	†	
CLEO-II*	Cornell	1.5	1.55	3.8	25	2.5	3.7
ALEPH*	Saclay/CERN	1.5	2.75	7.0	130	2.0	5.5
DELPHI*	RAL/CERN	1.2	2.8	7.4	109	1.7	4.2
ZEUS*	INFN/DESY	1.8	1.5	2.85	11	0.9	5.5
H1*	RAL/DESY	1.2	2.8	5.75	120	1.8	4.8
BaBar*	INFN/SLAC	1.5	1.5	3.46	27	†	3.6
D0*	Fermi	2.0	0.6	2.73	5.6	0.9	3.7
BELLE*	KEK	1.5	1.8	4	42	†	5.3
BES-III	IHEP	1.0	1.475	3.5	9.5	†	2.6
ATLAS-CS	ATLAS/CERN	2.0	1.25	5.3	38	0.66	7.0
ATLAS-BT	ATLAS/CERN	1	4.7–9.75	26	1080	(Toroid)†	
ATLAS-ET	ATLAS/CERN	1	0.825–5.35	5	2×250	(Toroid)†	
CMS	CMS/CERN	4	6	12.5	2600	†	12
SiD**	ILC	5	2.9	5.6	1560	†	12
ILD**	ILC	4	3.8	7.5	2300	†	13
SiD**	CLIC	5	2.8	6.2	2300	†	14
ILD**	CLIC	4	3.8	7.9	2300	†	13
FCC**		6	6	23	54000	†	12

* No longer in service
** Conceptual design in future
† EM calorimeter is inside solenoid, so small X/X_0 is not a goal

35.11.3 *Toroidal magnets*

Toroidal coils uniquely provide a closed magnetic field without the necessity of an iron flux-return yoke. Because no field exists at the collision point and along the beam line, there is, in principle, no effect on the beam. On the other hand, the field profile generally has $1/R$ dependence. R is the distance from the center of the toroid. The particle momentum may be determined by measurements of the deflection angle combined with the sagitta. The deflection (bending) power BL is

$$BL \approx \int_{R_i}^{R_0} \frac{B_i R_i \, dR}{R \sin\theta} = \frac{B_i \, R_i}{\sin\theta} \ln(R_0/R_i) \ , \tag{35.64}$$

where R_i is the inner coil radius, R_0 is the outer coil radius, and θ is the angle between the particle trajectory and the beam line axis . The momentum resolution given by the deflection may be expressed as

$$\frac{\Delta p}{p} \propto \frac{p}{BL} \approx \frac{p \sin\theta}{B_i R_i \ \ln(R_0/R_i)} \ . \tag{35.65}$$

The momentum resolution is better in the forward/backward (smaller θ) direction. The geometry has been found to be optimal when $R_0/R_i \approx 3$–4. In practical designs, the coil is divided into 6–12 lumped coils in order to have reasonable acceptance and accessibility. This causes the coil design to be much more complex. The mechanical structure needs to sustain the decentering force between adjacent coils, and the peak field in the coil is 3–5 times higher than the useful magnetic field for the momentum analysis [527].

35.12 Measurement of particle momenta in a uniform magnetic field

The trajectory of a particle with momentum p (in GeV/c) and charge ze in a constant magnetic field $\vec{B}$ is a helix, with radius of curvature R and pitch angle λ. The radius of curvature and momentum component perpendicular to $\vec{B}$ are related by

$$p \cos\lambda = 0.3 \, z \, B \, R \ , \tag{35.66}$$

where B is in tesla and R is in meters.

The distribution of measurements of the curvature $k \equiv 1/R$ is approximately Gaussian. The curvature error for a large number of uniformly spaced measurements on the trajectory of a charged particle in a uniform magnetic field can be approximated by

$$(\delta k)^2 = (\delta k_{\rm res})^2 + (\delta k_{\rm ms})^2, \tag{35.67}$$

where δk = curvature error
$\delta k_{\rm res}$ = curvature error due to finite measurement resolution
$\delta k_{\rm ms}$ = curvature error due to multiple scattering.

If many (≥ 10) uniformly spaced position measurements are made along a trajectory in a uniform medium,

$$\delta k_{\rm res} = \frac{\epsilon}{L'^2} \sqrt{\frac{720}{N+4}}, \tag{35.68}$$

where N = number of points measured along track
L' = the projected length of the track onto the bending plane
ϵ = measurement error for each point, perpendicular to the trajectory.

If a vertex constraint is applied at the origin of the track, the coefficient under the radical becomes 320.

For arbitrary spacing of coordinates s_i measured along the projected trajectory and with variable measurement errors ϵ_i the curvature error $\delta k_{\rm res}$ is calculated from:

$$(\delta k_{\rm res})^2 = \frac{4}{w} \ \frac{V_{ss}}{V_{ss} V_{s^2 s^2} - (V_{ss^2})^2}, \tag{35.69}$$

where V are covariances defined as $V_{s^m s^n} = \langle s^m s^n - \rangle s^m \langle s^n$ with $\rangle s^m = w^{-1} \sum (s_i{}^m/\epsilon_i{}^2)$ and $w = \sum \epsilon_i{}^{-2}$.

The contribution due to multiple Coulomb scattering is approximately

$$\delta k_{\rm ms} \approx \frac{(0.016)({\rm GeV}/c) z}{L p \beta \cos^2\lambda} \sqrt{\frac{L}{X_0}}, \tag{35.70}$$

where p = momentum (GeV/c)
z = charge of incident particle in units of e
L = the total track length
X_0 = radiation length of the scattering medium (in units of length; the X_0 defined elsewhere must be multiplied by density)
β = the kinematic variable v/c.

More accurate approximations for multiple scattering may be found in the section on Passage of Particles Through Matter

Int. J. Mod. Phys. A 2026.41. Downloaded from www.worldscientific.com
by UNIVERSITY OF CALIFORNIA @ BERKELEY on 09/16/26. Re-use and distribution is strictly not permitted, except for Open Access articles.

(Sec. 34 of this *Review*). The contribution to the curvature error is given approximately by $\delta k_{\rm ms} \approx 8 s^{\rm rms}_{\rm plane}/L^2$, where $s^{\rm rms}_{\rm plane}$ is defined there.

References

[1] H. Kolanoski and N. Wermes, *Particle Detectors - Fundamentals and Applications*, Oxford University Press (2020), ISBN 978-0-19-885836-2.

[2] T. Ferbel, *Experimental techniques in high energy physics; 1st ed.*, Frontiers in physics, Addison-Wesley, Menlo Park, CA (1987), URL https://cds.cern.ch/record/110951.

[3] K. Kleinknecht, *Detectors for particle radiation* (1998), ISBN 978-0-521-64854-7.

[4] G. Knoll, *Radiation Detection and Measurement (4th ed.)*, John Wiley, Hoboken, NJ (2010), ISBN 978-0-470-13148-0.

[5] D. Green, *The physics of particle detectors*, Cambridge University Press, Cambridge, UK (2000), ISBN 9780521675680.

[6] C. Leroy and P.-G. Rancoita, *Principles of radiation interaction in matter and detection*, World Scientific, Singapore (2011), ISBN 978-981-238-909-1.

[7] C. Grupen and B. Schwartz, *Particle detectors*, Cambridge University Press, Cambridge, UK (2008), ISBN 9780521187954.

[8] H. Spieler, *Semiconductor Detector Systems*, Oxford University Press, Oxford (2005), ISBN 978-0-19-852784-8.

[9] K. Arisaka, Nucl. Instrum. Meth. **A442**, 80 (2000).

[10] N. Matsunaga (ed.), *Photomultiplier Tubes: Basics and Applications*, 4th edition, Hamamatsu Photonics K.K., Hamamatsu (2017), https://www.hamamatsu.com/resources/pdf/etd/PMT_handbook_v4E.pdf.

[11] M. Böhm *et al.*, JINST **15**, 11, C11015 (2020).

[12] M. J. Minot *et al.*, Nuovo Cim. C **43**, 1, 11 (2020).

[13] A. Braem *et al.*, Nucl. Instrum. Meth. **A518**, 574 (2004).

[14] S. Korpar *et al.*, Nucl. Instrum. Meth. A **766**, 145 (2014).

[15] R. Arnold *et al.*, Nucl. Instrum. Meth. **A314**, 465 (1992).

[16] P. Mangeot *et al.*, Nucl. Instrum. Methods **A216**, 79 (1983).

[17] R. Apsimon *et al.*, IEEE Trans. **NS33**, 112 (1986).

[18] R. Arnold *et al.*, Nucl. Instrum. Meth. **A270**, 255 (1988).

[19] D. Aston *et al.*, Nucl. Instrum. Meth. **A283**, 582 (1989).

[20] R. Haitz *et al.*, J. Appl. Phys. **36**, 3123 (1965).

[21] R. McIntyre, IEEE Trans. Electron Devices **13**, 164 (1966).

[22] H. Dautet *et al.*, Applied Optics, **32**, 3894 (1993).

[23] Perkin-Elmer Optoelectronics, *Avalanche Photodiodes: A User's Guide*, (2003).

[24] P. Buzhan *et al.*, Nucl. Instrum. Meth. **A504**, 48 (2003).

[25] Z. Sadygov *et al.*, Nucl. Instrum. Methods **A504**, 301 (2003).

[26] V. Golovin and V. Savelev, Nucl. Instrum. Meth. **A518**, 560 (2004).

[27] F. Simon, Nuclear Instruments and Methods in Physics Research Section A: Accelerators, Spectrometers, Detectors and Associated Equipment **926**, 85–100 (2019), ISSN 0168-9002, URL http://dx.doi.org/10.1016/j.nima.2018.11.042.

[28] S. Korpar *et al.*, Nucl. Instrum. Meth. **A766**, 107 (2014).

[29] R. H. Pots *et al.*, Nucl. Instrum. Meth. **A940**, 254 (2019).

[30] D. R. Schaart *et al.*, Nuclear Instruments and Methods in Physics Research Section A: Accelerators, Spectrometers, Detectors and Associated Equipment **809**, 31 (2016).

[31] M. Petrov, M. Stapelbroek, and W. Kleinhans, Appl. Phys. Lett. **51**, 406 (1987).

[32] M. Atac and M. Petrov, IEEE Trans. **NS36**, 163 (1989).

[33] M. Atac *et al.*, Nucl. Instrum. Meth. **A314**, 56 (1992).

[34] B. Korzh *et al.*, Nature Photonics **14**, 250 (2020).

[35] J. S. Carlson *et al.*, J. Am. Chem. Soc. **139**, 28, 9621 (2017).

[36] J.B. Birks, *The Theory and Practice of Scintillation Counting*, Pergamon, London (1964).

[37] D. Clark, Nucl. Instrum. Meth. **117**, 1, 295 (1974).

[38] Y. Kharzheev, J. Laser Opt. Photonics **4**, 1 (2017).

[39] S. Moser *et al.*, Rad. Phys. and Chem. **41**, 1, 31 (1993).

[40] M. Moszyński and B. Bengtson, Nucl. Instrum. Methods **158**, 1 (1979).

[41] J. B. Birks, Proc. Phys. Soc. **A64**, 874 (1951).

[42] T. Gangwer and J. K. Thomas, Radiation Research **54**, 192 (1973).

[43] D. Dexter, J. Chem. Phys. **21**, 836 (1953).

[44] C. Dujardin and M. Hamel, *Introduction—Overview on Plastic and Inorganic Scintillators*, 3–33, Springer International Publishing, Cham (2021), URL 10.1007/978-3-030-73488-6_1.

[45] M. Böhles *et al.* (NuDoubt++), Eur. Phys. J. C **85**, 2, 121 (2025), [arXiv:2407.05999].

[46] O. B. Rodrigues *et al.*, A prototype reactor-antineutrino detector based on ^{6}Li-doped pulse-shaping-discriminating plastic scintillator (2025), [arXiv:2505.05696], URL https://arxiv.org/abs/2505.05696.

[47] C. Cook, C. Blanco and J. Smirnov, Phys. Rev. D **112**, 083005 (2025).

[48] C. Chandler *et al.*, Addit. Manuf. **73**, 103688 (2023).

[49] B. Li *et al.*, J. Instrum. **20**, 04, P04008 (2025).

[50] S. Lee, M. Livan and R. Wigmans, Rev. Mod. Phys. **90**, 025002 (2018).

[51] R. C. Ruchti, Ann. Rev. Nucl. Part. **46**, 281 (1996).

[52] C. Joram, G. Haefeli and B. Leverington, JINST **10**, 08, C08005 (2015).

[53] T. Weber *et al.*, Commun. Eng. **4**, 41 (2025).

[54] D. Horstmann and U. Holm, Radiat. Phys. Chem. **41**, 1, 395 (1993).

[55] J. Cumalat *et al.*, Nucl. Instrum. Meth. **A293**, 3, 606 (1990).

[56] K. Abe *et al.* (T2K), JINST **17**, P10028 (2022).

[57] Y. Kharzheev, Phys. Part. Nucl. **50**, 1, 42 (2019).

[58] C. Zorn, in F. Sauli, editor, "Instrumentation in high-energy physics, Advanced Series on Directions in High Energy Physics," volume 9, 218, World Scientific (1992), URL 10.1142/9789814360333_0004.

[59] CMS Collaboration, J. Instrum. **15**, 06, P06009 (2020).

[60] K. Gillen and R. Clough, Polymer **33**, 4358 (1992).

[61] T. Seguchi *et al.*, Radiat. Phys. Chem. **17**, 195 (1981).

[62] B. Kronheim *et al.*, NIM **A1059**, 168922 (2024).

[63] P. Feng and et al., *Organic glass scintillators*, 243–283, Springer International Publishing, Cham (2021), URL 10.1007/978-3-030-73488-6_1.

[64] S.E. Derenzo, W.-S. Choong and W.W. Moses, Phys. Med. Biol. **59**, 3261 (2014).

[65] L. Shook, T.A. Laplace, M.S. Boswell, E.D. Bourret, S.E. Derenzo and B.L. Goldblum, Nucl. Instrum. Methods **A1075**, 170389S (2025) database of inorganic and organic scintillator properties",.

[66] C. Melcher and J. Schweitzer, Nucl. Instrum. Methods **A314**, 212 (1992).

[67] D.W. Cooke *et al.*, J. Appl. Phys. **88**, 7360 (2000).

[68] J.M. Chen *et al.*, IEEE Trans. **NS54**, 718 (2007).

[69] J.M. Chen *et al.*, IEEE Trans. **NS54**, 1319 (2007).

[70] M. Nicl and C. Pedrini, Sol.St.Comm. 90, 155 (1994) (2015).

[71] E. Auffray *et al.*, Nucl. Instrum. Methods **A380**, 524 (1996).

Int. J. Mod. [redacted] nloaded from www.worldscientific.com
by UNIVERSITY OF CALIFORNIA @ BERKE use and distribution is strictly not permitted, except for Open Access articles.

[72] E.V.D. van Loef *et al.*, Nucl. Instrum. Methods **A486**, 254 (2002).

[73] W. Drozdowski *et al.*, IEEE Trans. **NS55**, 1391 (2008).

[74] M.S. Alekhin *et al.*, Appl. Phys. Lett. **102**, 161915 (2013).

[75] C. Kuntner *et al.* (Crystal Clear), Nucl. Instrum. Meth. **A493**, 131 (2002).

[76] M. Nicl *et al.*, Adv. Optical Mater. 3 463 (2015).

[77] M.T. Lucchini *et al.*, Nucl. Instrum. Methods **A816**, 176 (2016).

[78] E. Auffray *et al.*, Rad. Phys. Chem. 164, 108365 (2019).

[79] C. Hu *et al.*, Nucl. Instrum. Methods **A954**, 161723 (2020).

[80] C. Hu *et al.*, IEEE Trans. **NS69**, 181 (2022).

[81] N. Akchurin *et al.*, Nucl. Instrum. Meth. **A595**, 359 (2008).

[82] H. Wenzel, Journal of Physics: Conference Series **404**, 012049 (2012).

[83] A. Benaglia *et al.*, IEEE Transactions on Nuclear Science **63**, 2, 574 (2016).

[84] R.H. Mao, L.Y. Zhang and R.-Y. Zhu, IEEE Trans. **NS59**, 2229 (2012).

[85] G. Tang *et al.*, Optical Materials 130 112585 (2022).

[86] L. Zhang and R.-Y. Zhu, EPJ Web of Conferences 320, 00062 (2025).

[87] E. Auffray *et al.*, J. Phys.:Conf.Ser.587. 012062 (2015).

[88] V. Dormenev *et al.*, IEEE Trans. **NS72**, 2007 (2025).

[89] R.-Y. Zhu, TIPP 2017, SPPHY 213, 70 (2018).

[90] C. Hu *et al.*, IEEE Transactions on Nuclear Science **66**, 7, 1854 (2019).

[91] S Gundacker *et al.*, Phys. Med. Biol. 66, 114002 (2021).

[92] R. Cala' *et al.* JINST 20 P04004 (2025).

[93] W.W. Moses, W.-S. Choong and S.E. Derenzo, Acta Physica Polonica **B7**, 725 (2014).

[94] R.H. Mao, L.Y. Zhang and R.-Y. Zhu, IEEE Trans. **NS55**, 2425 (2008).

[95] P. Dorenbos, J. T. M. de Haas, and C. W. E. van Eijk, IEEE Trans. **NS42**, 2190 (1995).

[96] B.D. Rooney and J.D. Valentine, IEEE Trans. **NS44**, 509 (1997).

[97] W.W. Moses *et al.*, IEEE Trans. **NS55**, 1049 (2008).

[98] A.N. Vasilev *et al.*, IEEE Trans. **NS55**, 1054 (2008).

[99] R.T. Williams *et al.* Phys. Status Solidi B, vol. 248, 426 (2011).

[100] Q. Li *et al.* J. Appl. Phys., vol. 109, 123716 (2011).

[101] S.A. Payne *et al.*, IEEE Trans. **NS58**, 3392 (2011).

[102] I. V. Khodyuk and P. Dorenbos, IEEE Trans. **NS42**, 3320 (2012).

[103] G. Gratta, H. Newman and R.-Y. Zhu, Ann. Rev. Nucl. Part. Sci. **44**, 453 (1994).

[104] R.-Y. Zhu, in "Handbook of Particle Detection and Imaging," 1–25, Springer International Publishing (2020).

[105] F. Yang *et al.*, IEEE Trans. **NS63**, 612 (2016).

[106] F. Yang *et al.*, IEEE Trans. **NS64**, 665 (2017).

[107] C. Hu *et al.*, IEEE Transactions on Nuclear Science **67**, 6, 1086 (2020).

[108] G. Dissertori *et al.*, Nucl. Instrum. Methods **745**, 1 (2014), and references therein.

[109] S. Ecklund, C. Field and G. Mazaheri, Nucl. Instr. and Meth. Res. Sect. **A463**, 68 (2001).

[110] M. G. Albrow *et al.*, JINST **7**, P10027 (2012), [arXiv:1207.7248].

[111] B. Aubert *et al.* (BaBar), Nucl. Instr. and Meth. Res. Sect. **A479**, 1 (2002), [hep-ex/0105044].

[112] E. Torassa (Belle-II PID Group), Nucl. Instr. and Meth. Res. Sect. **A824**, 152 (2016).

[113] G. Bayatian *et al.* (CMS), Eur. Phys. J. **C53**, 139 (2008).

[114] Y. Fukuda *et al.* (Super-Kamiokande), Nucl. Instr. and Meth. Res. Sect. **A501**, 418 (2003).

[115] Proceedings of the International Workshops on Ring Imaging Cherenkov Detectors, Nucl. Instr. and Meth. Res. Sect. **A343**, 1 (1993); Nucl. Instr. and Meth. Res. Sect. **A371**, 1 (1996); Nucl. Instr. and Meth. Res. Sect. **A433**, 1 (1999); Nucl. Instr. and Meth. Res. Sect. **A502**, 1 (2003); Nucl. Instr. and Meth. Res. Sect. **A553**, 1 (2005); Nucl. Instr. and Meth. Res. Sect. **A595**, 1 (2008); Nucl. Instr. and Meth. Res. Sect. **A639**, 1 (2011); Nucl. Instr. and Meth. Res. Sect. **A766**, 1 (2014); Nucl. Instr. and Meth. Res. Sect. **A876**, 1 (2017); Nucl. Instr. and Meth. Res. Sect. **A 952**, 1 (2019).

[116] https://www.sciencedirect.com/special-issue/10TGK7NM7NB.

[117] https://www.sciencedirect.com/special-issue/10S11JC46SX.

[118] J. Litt and R. Meunier, Ann. Rev. Nucl. Part. Sci. **23**, 1 (1973).

[119] D. Bartlett *et al.*, Nucl. Instr. and Meth. Res. Sect. **A260**, 55 (1987).

[120] A. Abashian *et al.*, Nucl. Instr. and Meth. Res. Sect. **A479**, 117 (2002).

[121] B. N. Ratcliff, Nucl. Instr. and Meth. Res. Sect. **A502**, 211 (2003).

[122] T. Iijima *et al.*, Nucl. Instr. and Meth. Res. Sect. **A548**, 383 (2005), [arXiv:physics/0504220].

[123] B. Ratcliff and J. Va'vra, Nucl. Instrum. Meth. **A**, 163442 (2020).

[124] W. Blum, W. Riegler, and L. Rolandi, *Particle Detection with Drift Chambers*, Springer-Verlag, Berlin (2008).

[125] R. M. Sternheimer and R. F. Peierls, Phys. Rev. B **3**, 3681 (1971); L. Landau, J. Phys. (USSR) **8**, 201 (1944); W. W. M. Allison and J. H. Cobb, Ann. Rev. Nucl. Part. Sci. **30**, 253 (1980).

[126] I. Smirnov, Nucl. Instrum. Meth. **A554**, 474 (2005); I. Smirnov, HEED - High Energy Electro Dynamics, http://ismirnov.web.cern.ch/ismirnov/heed.

[127] L.G. Christophorou, *Atomic and Molecular Radiation Physics*, John Wiley & Sons, Hoboken (1971); J. Berkowitz, *Atomic and Molecular Photoabsorption*, Academic Press, Cambridge (2015).

[128] F. Sauli, *Gaseous Radiation Detectors: Fundamentals and Applications*, Cambridge University Press (2014).

[129] H. Bichsel, Nucl. Instrum. Meth. **A562**, 154 (2006).

[130] R. Veenhof, Garfield - Simulation of Gaseous Detectors, http://garfield.web.cern.ch/garfield/.

[131] Degrad - cluster size distribution and primary cluster distribution in gas mixtures for minimum ionising particles and X-rays, http://magboltz.web.cern.ch/magboltz/.

[132] S. F. Biagi, Nucl. Instrum. Meth. **A421**, 1-2, 234 (1999).

[133] S. Biagi, R. Veenhof, Magboltz - Boltzmann transport equations for electrons in gas mixtures under the influence of electric and magnetic fields, http://magboltz.web.cern.ch/magboltz/.

[134] S. Mukhopadhyay and N. Majumdar, in "17th DAE-BRNS High Energy Physics Symposium," (2007), [arXiv:physics/0703009].

[135] H. Fischle, J. Heintze and B. Schmidt, Nucl. Instrum. Meth. **A301**, 202 (1991).

[136] M. M. F. R. Fraga *et al.*, Nucl. Instrum. Meth. A **504**, 88 (2003).

Int. J. Mod. Phys. A 2026.41. Downloaded from www.worldscientific.com
by UNIVERSITY OF CALIFORNIA @ BERKELEY on 09/16/26. Re-use and distribution is strictly not permitted, except for Open Access articles.

[137] A. Peisert and F. Sauli, Drift and Diffusion of Electrons in Gases: A Compilation (With an Introduction to the Use of Computing Program)CERN-84-08, CERN-YELLOW-84-08 (1984).

[138] https://us.lxcat.net/.

[139] O. Şahin, T. Z. Kowalski and R. Veenhof, Nucl. Instrum. Meth. A **768**, 104 (2014).

[140] O. Şahin *et al.*, JINST **5**, 05, P05002 (2010); O. Şahin, JINST **16**, 03, P03026 (2021).

[141] E. McDaniel and E. Mason, *The Mobility and Diffusion of Ions in Gases*, John Wiley & Sons, Hoboken (1973); G. Schultz, G. Charpak and F. Sauli, Rev. Phys. Appl. **12**, 1, 67 (1977).

[142] Y. Kalkan *et al.*, JINST **10**, 07, P07004 (2015).

[143] T. Ikeda *et al.*, JINST **15**, 07, P07015 (2020), [arXiv:2004.09706].

[144] G.F. Knoll, *Radiation Detection and Measurement*, 3nd edition, John Wiley & Sons, New York (1999).

[145] G. Charpak *et al.*, Nucl. Instrum. Methods **A62**, 262 (1968).

[146] G. Charpak and F. Sauli, Ann. Rev. Nucl. Sci. **34**, 285 (1984).

[147] G. Charpak *et al.*, Nucl. Instrum. Methods **A97**, 377 (1971).

[148] W. Blum, W. Riegler, and L. Rolandi, *Particle Detection with Drift Chambers*, Springer-Verlag, Berlin (2008).

[149] G. Charpak *et al.*, Nucl. Instrum. Methods **A167**, 455 (1979).

[150] A.H. Walenta *et al.*, Nucl. Instrum. Methods **A92**, 373 (1971).

[151] A. Breskin *et al.*, Nucl. Instrum. Methods **A124**, 189 (1975).

[152] A. Breskin *et al.*, Nucl. Instrum. Methods **A156**, 147 (1978).

[153] R. Bouclier *et al.*, Nucl. Instrum. Meth. **A265**, 78 (1988), [,556(1987)].

[154] H. Drumm *et al.*, Nucl. Instrum. Methods **A176**, 333 (1980).

[155] D.R. Nygren and J.N. Marx, Phys. Today **31N10**, 46 (1978).

[156] C. Grupen, *Particle Detectors*, Cambridge Monographs on Particle Physics, Nuclear Physics and Cosmology, Cambridge University Press (2008).

[157] M. P. Titov, ICFA Instrum. Bull. **26**, 002 (2004), [,199(2004)], [arXiv:physics/0403055]; M. P. Titov *et al.*, ICFA Instrum. Bull. **24**, 22 (2002), [hep-ex/0204005].

[158] G. F. Tassielli *et al.*, JINST **15**, 09, C09051 (2020), [arXiv:2006.02378].

[159] P. S. Baringer *et al.*, Nucl. Instrum. Meth. **A254**, 542 (1987).

[160] J. Virdee, Phys. Reports **403**, 401 (2004).

[161] A. Sergi, Phys. Procedia **37**, 530 (2012).

[162] A. H. Walenta, Phys. Scripta **23**, 354 (1981).

[163] J. A. Kadyk, Nucl. Instrum. Meth. A **300**, 436 (1991); J. Va'vra, ICFA Instrum. Bull. **24**, 1 (2002).

[164] M. Aleksa *et al.*, Nucl. Instrum. Meth. **A446**, 435 (2000).

[165] A. Oed, Nucl. Instrum. Meth. **A263**, 351 (1988).

[166] F. Sauli, Nucl. Instrum. Meth. **A386**, 531 (1997).

[167] Y. Giomataris *et al.*, Nucl. Instrum. Meth. **A376**, 29 (1996).

[168] Input to the European Particle Physics Strategy no. 87 (2019), S. Dalla Torre, E. Oliveri, L. Ropelewski, M. Titov, Development of the Micro-Pattern Gaseous Detector Technologies: an overview of the CERN-RD51 Collaboration, https://indico.cern.ch/event/765096/contributions/3295721.

[169] F. Sauli, *Micro-pattern gaseous detectors principles of operation and applications*, World Scientific, Singapore (2020).

[170] R. Bouclier *et al.*, Nucl. Instrum. Meth. A **381**, 289 (1996); Y. Bagaturia *et al.*, Nucl. Instrum. Meth. A **490**, 223 (2002).

[171] A. Bressan *et al.*, Nucl. Instrum. Meth. **A425**, 262 (1999).

[172] S. Bachmann *et al.*, Nucl. Instrum. Meth. **A479**, 294 (2002); A. Bressan *et al.*, Nucl. Instrum. Meth. **A424**, 321 (1999).

[173] M. Alfonsi *et al.*, Nucl. Instrum. Meth. A **671**, 6 (2012).

[174] J. Derre *et al.*, Nucl. Instrum. Meth. A **459**, 523 (2001).

[175] A. Breskin *et al.*, Nucl. Instrum. Meth. **124**, 189 (1975).

[176] J. Benlloch *et al.*, IEEE Trans. Nucl. Sci. **45**, 234 (1998).

[177] Y. Giomataris, Nucl. Instrum. Meth. **A419**, 239 (1998).

[178] M. Chefdeville *et al.*, Nucl. Instrum. Meth. A **556**, 490 (2006).

[179] J. Leidner, F. Murtas and M. Silari, Applied Sciences **11**, 1 (2021).

[180] A. Curioni *et al.*, Nucl. Instrum. Meth. A **849**, 60 (2017).

[181] R. Chechik *et al.*, Nucl. Instrum. Meth. A **535**, 303 (2004); M. Alexeev *et al.*, JINST **8**, C12005 (2013).

[182] L. Moleri *et al.*, JINST **12**, 10, P10017 (2017), [arXiv:1707.00125].

[183] T. Alexopoulos *et al.*, Nucl. Instrum. Meth. A **640**, 110 (2011).

[184] Y. Bilevych *et al.*, Nucl. Instr. and Meth. A **629**, 66 (2011), ISSN 0168-9002, URL https://www.sciencedirect.com/science/article/pii/S016890021002663X.

[185] A. Ochi, PoS **TIPP2014**, 351 (2015).

[186] Y. Lv *et al.*, Nucl. Instr. and Meth. A **958**, 162759 (2020), ISSN 0168-9002, URL https://www.sciencedirect.com/science/article/pii/S0168900219312148.

[187] F. Yamane *et al.*, Nucl. Instrum. Meth. A **951**, 162938 (2020), [arXiv:1901.03836].

[188] G. Bencivenni *et al.*, JINST **10**, 02, P02008 (2015), [arXiv:1411.2466].

[189] G. Bencivenni *et al.*, Nuclear Instruments and Methods in Physics Research Section A: Accelerators, Spectrometers, Detectors and Associated Equipment **1069**, 169725 (2024), ISSN 0168-9002, URL https://www.sciencedirect.com/science/article/pii/S016890022400651X.

[190] D. Abbaneo *et al.*, Nucl. Instrum. Meth. A **718**, 383 (2013).

[191] T. Alexopoulos *et al.*, Nucl. Instrum. Meth. A **617**, 161 (2010); L. Lavezzi *et al.*, in "2017 IEEE Nuclear Science Symposium and Medical Imaging Conference," (2017), [arXiv:1803.07266].

[192] J. Bortfeldt *et al.*, Nucl. Instrum. Meth. A **903**, 317 (2018), [arXiv:1712.05256].

[193] A. Balla *et al.*, Nucl. Instrum. Meth. A **732**, 221 (2013).

[194] DRD1 Collaboration: https://drd1.web.cern.ch ; A. Colaleo, L. Ropelewski *et al.* (2024), URL https://cds.cern.ch/record/2885937.

[195] D.R. Nygren and J.N. Marx, Phys. Today **31N10**, 46 (1978).

[196] J. Alme *et al.*, Nucl. Instrum. Meth. **A622**, 316 (2010), [arXiv:1001.1950].

[197] J. Adolfsson *et al.*, Journal of Instrumentation **16**, 03, P03022 (2021), URL https://doi.org/10.1088/1748-0221/16/03/p03022.

[198] N. Abgrall *et al.* (T2K ND280 TPC), Nucl. Instrum. Meth. A **637**, 25 (2011), [arXiv:1012.0865].

[199] A. H. Walenta *et al.*, Nucl. Instrum. Meth. **161**, 45 (1979).

[200] H. Aihara *et al.*, IEEE Trans. **NS30**, 63 (1983).

[201] K. Dehmelt (sPHENIX), PoS **MPGD2017**, 044 (2019).

[202] P. Colas, I. Giomataris and V. Lepeltier, Nucl. Instrum. Meth. **A535**, 226 (2004).

Int. J. Mod. Phys. A
by UNIVERSITY OF CALIFORNIA @ BERKE
nloaded from www.worldscientific.com
use and distribution is strictly not permitted, except for Open Access articles.

[203] X. Artru, G. B. Yodh and G. Mennessier, Phys. Rev. **D12**, 1289 (1975).

[204] J. Alozy *et al.*, Nucl. Instrum. Meth. **A961**, 163681 (2020).

[205] M. L. Cherry *et al.*, Phys. Rev. **D10**, 3594 (1974).

[206] B. Dolgoshein, Nucl. Instrum. Meth. **A326**, 434 (1993).

[207] A. Andronic and J. P. Wessels, Nucl. Instrum. Meth. **A666**, 130 (2012).

[208] S. Acharya *et al.* (ALICE), Nucl. Instrum. Meth. **A881**, 88 (2018), [arXiv:1709.02743].

[209] M. Petris *et al.*, Nucl. Instrum. Meth. **A714**, 17 (2013).

[210] T. Akesson *et al.* (ATLAS TRT), Nucl. Instrum. Meth. **A522**, 131 (2004).

[211] M. Ambriola *et al.*, Nucl. Instrum. Meth. **A522**, 77 (2004).

[212] J. Adelman (ATLAS), Nucl. Instrum. Meth. **A706**, 33 (2013).

[213] T. Kirn (AMS 02 TRD), Nucl. Instrum. Meth. **A706**, 43 (2013).

[214] G. M. Garibian, L. A. Gevorgian and C. Yang, Nucl. Instrum. Meth. **125**, 133 (1975).

[215] P. Nevski, Nucl. Instrum. Meth. **A522**, 116 (2004).

[216] J. Alozy *et al.*, Nucl. Instrum. Meth. **A927**, 1 (2019), [arXiv:1901.11265].

[217] V. M. Grishin and S. S. Sadilov, Nucl. Instrum. Meth. **A522**, 122 (2004).

[218] B. Beischer *et al.*, Nucl. Instrum. Meth. **A583**, 485 (2007).

[219] A. A. Savchenko *et al.*, JINST **15**, 06, C06024 (2020).

[220] T. Akesson *et al.* (ATLAS TRT), Nucl. Instrum. Meth. **A412**, 200 (1998).

[221] D. Errede *et al.*, Nucl. Instrum. Meth. A **309**, 386 (1991).

[222] M. Albrow *et al.*, Nucl. Instrum. Meth. A **1055**, 168535 (2023).

[223] M. Ave *et al.*, Nucl. Instrum. Meth. **A654**, 140 (2011).

[224] M. L. Cherry, Nucl. Instrum. Meth. **A706**, 39 (2013).

[225] F. Hartjes *et al.*, Nucl. Instrum. Meth. **A706**, 59 (2013).

[226] J. Alozy *et al.*, J. Phys. Conf. Ser. **1690**, 1, 012041 (2020).

[227] M. Brigida *et al.*, Nucl. Instrum. Meth. **A706**, 69 (2013).

[228] V. V. Berdnikov *et al.*, Nucl. Instrum. Meth. **A706**, 65 (2013).

[229] R. Santonico and R. Cardarelli, Nucl. Instrum. Meth. **187**, 377 (1981).

[230] V. Parkhomchuck, Y. Pestov and N. Petrovykh, Nucl. Instrum. Meth. **93**, 2, 269 (1971).

[231] G. V. Fedotovich, Y. N. Pestov and K. N. Putilin, in "International Conference on Instrumentation for Colliding Beam Physics," 127–131 (1982).

[232] E. Cerron Zeballos *et al.*, Nucl. Instrum. Meth. **A374**, 132 (1996).

[233] J. Juita *et al.*, Fire Science Reviews **1** (2012).

[234] P. Fonte, JINST **8**, 04, P04017 (2013).

[235] G. Aielli *et al.*, Nucl. Instrum. Meth. **A508**, 6 (2003).

[236] J. M. Meek, Phys. Rev. **57**, 722 (1940).

[237] R. Cardarelli, R. Santonico and V. Makeev, Nucl. Instrum. Meth. **A382**, 470 (1996).

[238] R. Cardarelli, A. Di Ciaccio and R. Santonico, Nucl. Instrum. Meth. **A333**, 399 (1993).

[239] R. Cardarelli, Sci Acta **8**, 159 (1993).

[240] P. Camarri *et al.*, Nucl. Instrum. Meth. **A414**, 317 (1998).

[241] L. Pontecorvo, ATLAS Muon Internal note **20** (1993).

[242] W. Riegler, JINST **11**, 11, P11002 (2016).

[243] R. Santonico, Nucl. Instrum. Meth. **A456**, 1 (2000).

[244] R. Cardarelli *et al.*, JINST **8**, P01003 (2013).

[245] G. Aielli *et al.*, JINST **9**, 09, C09030 (2014).

[246] S. Simsek (ATLAS Muon), Nucl. Instrum. Meth. A **1063**, 169298 (2024).

[247] G. Aad *et al.* (ATLAS), JINST **3**, S08003 (2008).

[248] S. Chatrchyan *et al.* (CMS), JINST **3**, S08004 (2008).

[249] G. Aielli *et al.*, Nucl. Instrum. Meth. A **562**, 92 (2006).

[250] A. Bertolin *et al.*, Nucl. Instrum. Meth. A **602**, 631 (2009).

[251] Aielli, Giulio *et al.*, Eur. Phys. J. C **80**, 12, 1177 (2020).

[252] M. Bauer *et al.*, ANUBIS: Proposal to search for long-lived neutral particles in CERN service shafts (2019), [arXiv:1909.13022].

[253] M. Bedjidian *et al.*, JINST **6**, P02001 (2011), [arXiv:1011.5969].

[254] P. Fonte, A. Smirnitsky and M. C. S. Williams (ALICE), Nucl. Instrum. Meth. **A443**, 201 (2000).

[255] M. Abbrescia, V. Peskov and P. Fonte, *Resistive Gaseous Detectors: Designs, Performance, and Perspectives*, Wiley (2018), ISBN 9783527340767.

[256] W. Riegler and C. Lippmann, Nucl. Instrum. Meth **A508**, 14 (2003).

[257] P. Fonte (2018), URL https://cds.cern.ch/record/2319919.

[258] A. Akindinov *et al.*, Eur. Phys. J. Plus **128**, 44 (2013).

[259] D. Belver *et al.*, Nucl. Instrum. Meth. A **602**, 687 (2009).

[260] A. Schuttauf (FOPI), Nucl. Instrum. Meth. A **533**, 65 (2004).

[261] M. Ablikim *et al.*, Nucl. Instrum. Meth. A **614**, 3, 345 (2010).

[262] e. a. P. Fonte, Nucl.Instrum.Meth.A **1051** (2023).

[263] I. Deppner and N. Herrmann, JINST **15**, 10, C10030 (2020).

[264] J. P. Chen *et al.*, A White Paper on SoLID (Solenoidal Large Intensity Device) (2014), [arXiv:1409.7741].

[265] M. Benoit *et al.*, JINST **11** (2015).

[266] G. Proto, Nucl. Instrum. Meth. **1070**, 170014 (2025).

[267] A. Blanco *et al.*, JINST **7**, P11012 (2012).

[268] C. Iacobaeus *et al.*, Nucl. Instrum. Meth. **A513**, 244 (2003), [arXiv:physics/0210006].

[269] G. Aielli *et al.*, Nucl. Instrum. Meth. **A456**, 82 (2000).

[270] G. Aielli *et al.*, Nucl. Instrum. Meth. **533**, 1, 86 (2004).

[271] H. Sakai *et al.*, Nucl. Instrum. Meth. **A484**, 153 (2002).

[272] G. A. et al., Nucl. Instrum. Meth. **515**, 1, 335 (2003), ISSN 0168-9002, proceedings of the International Workshop on Aging Phenomena in Gaseous Detectors.

[273] G. A. et al., Nuclear Science, IEEE Transactions on **53**, 567 (2006).

[274] M. A. et al., Nucl. Instrum. Meth. **533**, 1, 102 (2004), ISSN 0168-9002.

[275] M. C. et al., Nucl. Instrum. Meth. **661**, S214 (2012), ISSN 0168-9002, x. Workshop on Resistive Plate Chambers and Related Detectors (RPC 2010).

[276] R. Santonico, JINST **8**, P04023 (2013).

[277] L. Lopes *et al.*, Nucl. Instrum. Meth. **A533**, 69 (2004).

[278] European Commission website (2024), URL https://eur-lex.europa.eu/legal-content/EN/TXT/PDF/?uri=OJ:L_202400573.

[279] B. Liberti *et al.*, JINST **11**, 09, C09012 (2016).

[280] S. Pisano *et al.* (EEE), JINST **14**, 08, C08008 (2019), [arXiv:1806.03918].

[281] X. Fan *et al.*, Nucl. Instrum. Meth. **1024**, 166124 (2022), ISSN 0168-9002.

[282] L. Q. et al., Nucl. Instrum. Meth. **1080**, 170770 (2025).

[283] G. Proto, Il Nuovo Cimento C **2-3** (2021).

Int. J. Mod. Phys. A 2026.41. Downloaded from www.worldscientific.com
by UNIVERSITY OF CALIFORNIA @ BERKELEY on 09/16/26. Re-use and distribution is strictly not permitted, except for Open Access articles.

[284] L. Quaglia and e. a. Ramos, D, The European Physical Journal Plus **140** (2025).

[285] R. G. et al., Nucl. Instrum. Meth. **1054**, 168393 (2023), ISSN 0168-9002.

[286] G. Rigoletti, B. Mandelli and R. Guida, JINST **15**, 11, C11003 (2020).

[287] R. Guida, B. Mandelli and G. Rigoletti, Nucl. Instrum. Meth. **1039**, 167045 (2022).

[288] G. Proto *et al.*, JINST **17**, 05, P05005 (2022).

[289] S. Simsek, Nucl. Instrum. Meth. **1079**, 170618 (2025).

[290] G. Rigoletti *et al.*, Nucl. Instrum. Meth. **1075**, 170331 (2025).

[291] G. Proto, O. Kortner and H. Kroha, JINST **20**, 06, P06031 (2025).

[292] R. Cardarelli, JINST **16**, 05, C05004 (2021).

[293] R. Cardarelli *et al.*, Nucl. Instrum. Meth. **1058**, 168822 (2024).

[294] Summary of Liquid Argon PropertiesAccessed August 2021, URL https://lar.bnl.gov/properties/.

[295] E. W. Lemmon *et al.*, NIST Standard Reference Database 23: Reference Fluid Thermodynamic and Transport Properties-REFPROP, Version 10.0, National Institute of Standards and Technology (2018), URL https://www.nist.gov/srd/refprop.

[296] C. Rubbia, "The liquid-argon time projection chamber: a new concept for neutrino detectors: CERN-EP-INT-77-8," (1977), URL https://cds.cern.ch/record/117852.

[297] H. H. Chen and J. F. Lathrop, Nucl. Instrum. Meth. **150**, 585 (1978).

[298] P. Abratenko *et al.* (MicroBooNE), JINST **16**, 06, P06043 (2021), [arXiv:2011.01375].

[299] M. Wang *et al.*, Front. Big Data **3**, 604083 (2021), [arXiv:2009.04509].

[300] B. Abi *et al.* (DUNE), Phys. Rev. D **102**, 9, 092003 (2020), [arXiv:2006.15052].

[301] A. A. Abud *et al.* (DUNE (protoDUNE-SP)) (2021), [arXiv:2108.01902].

[302] G. Carugno *et al.* (ICARUS), Nucl. Instrum. Meth. A **292**, 580 (1990).

[303] M. Adamowski *et al.*, JINST **9**, P07005 (2014), [arXiv:1403.7236].

[304] C. Adams *et al.* (MicroBooNE), JINST **15**, 07, P07010 (2020), [arXiv:1910.01430].

[305] A. Marchionni, Ann. Rev. Nucl. Part. Sci. **63**, 269 (2013), [arXiv:1307.6918].

[306] K. Majumdar and K. Mavrokoridis, Appl. Sciences **11**, 6, 2455 (2021), [arXiv:2103.06395].

[307] M. Del Tutto, ArCS: A Magnetized Liquid Argon Time Projection Chamber for Neutrino Physics and Beyond (2025), URL https://indico.cern.ch/event/1488822/contributions/6480006/.

[308] F. Arneodo *et al.* (The ICARUS-Milano Collaboration), Phys. Rev. D **74**, 112001 (2006).

[309] S. Amerio *et al.* (ICARUS), Nucl. Instrum. Meth. A **527**, 329 (2004).

[310] C. Anderson *et al.* (ArgoNeuT), JINST **7**, P10019 (2012), [arXiv:1205.6747].

[311] R. Acciarri *et al.* (MicroBooNE), JINST **12**, 02, P02017 (2017), [arXiv:1612.05824].

[312] R. Acciarri *et al.* (LArIAT), JINST **15**, 04, P04026 (2020), [arXiv:1911.10379].

[313] A. Abed Abud *et al.* (DUNE) (2021), [arXiv:2103.13910].

[314] B. Abi *et al.* (DUNE), JINST **15**, 08, T08010 (2020), [arXiv:2002.03010].

[315] B. Russell (DUNE), PoS **TAUP2023**, 221 (2024).

[316] S. Collaboration *et al.*, The Short-Baseline Near Detector at Fermilab (2025), [arXiv:2504.00245], URL https://arxiv.org/abs/2504.00245.

[317] G. Bakale, U. Sowada and W. F. Schmidt, The Journal of Physical Chemistry **80**, 23, 2556 (1976).

[318] A. Bettini *et al.* (ICARUS), Nucl. Instrum. Meth. A **305**, 177 (1991).

[319] W. Jaskierny *et al.* (Fermilab-TM-2384-E), Technical report (2006), URL https://lss.fnal.gov/archive/test-tm/2000/fermilab-tm-2384-e.pdf.

[320] Sigma-Aldrich 4A, BASF Copper Getter CU-0226S.

[321] P. Cennini *et al.*, Nucl. Instrum. Meth. A **333**, 567 (1993).

[322] R. Acciarri *et al.* (WArP), JINST **5**, P06003 (2010), [arXiv:0804.1217].

[323] B. J. P. Jones *et al.*, JINST **8**, P07011 (2013), [Erratum: JINST 8, E09001 (2013)], [arXiv:1306.4605].

[324] R. Acciarri *et al.* (WArP), JINST **5**, P05003 (2010), [arXiv:0804.1222].

[325] M. Miyajima *et al.*, Phys. Rev. A **9**, 1438 (1974).

[326] G. Jaffe, Annalen der Physik **42**, 12, 303 (1913).

[327] L. Onsager, Phys. Rev. **54**, 554 (1938).

[328] J. Thomas and D. A. Imel, Phys. Rev. A **36**, 614 (1987).

[329] C. Adams *et al.* (MicroBooNE), JINST **15**, 03, P03022 (2020), [arXiv:1907.11736].

[330] P. Abratenko *et al.*, Journal of Instrumentation **20**, 01, P01033 (2025), URL https://dx.doi.org/10.1088/1748-0221/20/01/P01033.

[331] R. T. Scalettar *et al.*, Phys. Rev. A **25**, 2419 (1982).

[332] E. Aprile *et al.*, Nucl. Instrum. Meth. A **261**, 519 (1987).

[333] P. Cennini *et al.* (ICARUS), Nucl. Instrum. Meth. A **345**, 230 (1994).

[334] S. Amoruso *et al.* (ICARUS), Nucl. Instrum. Meth. A **523**, 275 (2004).

[335] R. Acciarri *et al.* (ArgoNeuT), JINST **8**, P08005 (2013), [arXiv:1306.1712].

[336] T. Yang, Instruments **5**, 1, 2 (2020), [arXiv:2012.01319].

[337] S. Amoruso *et al.* (ICARUS), Nucl. Instrum. Meth. A **516**, 68 (2004).

[338] W. Walkowiak, Nucl. Instrum. Meth. A **449**, 288 (2000).

[339] M. Antonello *et al.* (ICARUS), JINST **9**, 12, P12006 (2014), [arXiv:1409.5592].

[340] V. Meddage (MicroBooNE), in "Meeting of the APS Division of Particles and Fields," (2017), [arXiv:1710.00396].

[341] B. Abi *et al.* (DUNE), JINST **15**, 12, P12004 (2020), [arXiv:2007.06722].

[342] Y. Li *et al.*, Nucl. Instrum. Meth. A **816**, 160 (2016), [arXiv:1508.07059].

[343] P. Agnes *et al.* (DarkSide), Nucl. Instrum. Meth. A **904**, 23 (2018), [arXiv:1802.01427].

[344] P. Abratenko *et al.* (MicroBooNE), JINST **16**, 09, P09025 (2021), [arXiv:2104.06551].

[345] M. Miyajima *et al.*, Phys. Rev. A **10**, 1452 (1974).

[346] N. Gee *et al.*, Journal of Applied Physics **57**, 4, 1097 (1985).

[347] T. Doke *et al.*, Nucl. Instrum. Meth. A **269**, 291 (1988).

[348] T. Doke, K. Masuda and E. Shibamura, Nucl. Instrum. Meth. A **291**, 617 (1990).

[349] T. Heindl *et al.*, EPL **91**, 6, 62002 (2010), [arXiv:1511.07718].

[350] M. Babicz *et al.*, JINST **15**, 09, P09009 (2020), [arXiv:2002.09346].

[351] G. M. Seidel, R. E. Lanou and W. Yao, Nucl. Instrum. Meth. A **489**, 189 (2002), [hep-ex/0111054].

Int. J. Mod. [redacted] nloaded from www.worldscientific.com
by UNIVERSITY OF CALIFORNIA @ BERKE use and distribution is strictly not permitted, except for Open Access articles.

[352] E. Grace and J. A. Nikkel, Nucl. Instrum. Meth. A **867**, 204 (2017), [arXiv:1502.04213].

[353] A. Hitachi *et al.*, Phys. Rev. B **27**, 5279 (1983).

[354] P. Adhikari *et al.* (DEAP), Eur. Phys. J. C **80**, 4, 303 (2020), [arXiv:2001.09855].

[355] M. Auger *et al.*, JINST **11**, 03, P03017 (2016), [arXiv:1512.05968].

[356] S. Kubota *et al.*, Phys. Rev. B **20**, 8, 3486 (1979).

[357] F. Spiegelmann and J.-P. Malrieu, Chemical Physics Letters **57**, 2, 214 (1978), ISSN 0009-2614.

[358] B. Jones *et al.*, JINST **8**, P12015 (2013), [arXiv:1308.3658].

[359] A. Buzulutskov, EPL **117**, 3, 39002 (2017), [arXiv:1702.03612].

[360] J. Soto-Oton (DUNE), in "International Conference on Technology and Instrumentation in Particle Physics," (2021), [arXiv:2109.05858].

[361] P. Abratenko *et al.* (MicroBooNE), JINST **15**, 12, P12037 (2020), [arXiv:2008.09765].

[362] M. Antonello *et al.* (ICARUS), JINST **15**, 07, P07001 (2020), [arXiv:2001.08934].

[363] S. Palestini, Instruments **5**, 1, 9 (2021), [arXiv:2102.06082].

[364] C. Cantini *et al.*, JINST **12**, 03, P03021 (2017), [arXiv:1611.02085].

[365] J. Asaadi *et al.*, JINST **9**, P09002 (2014), [arXiv:1406.5216].

[366] V. Radeka *et al.*, J. Phys. Conf. Ser. **308**, 012021 (2011).

[367] O. Bunemann, T. E. Cranshaw and J. A. Harvey, Canadian Journal of Research **27a**, 5, 191 (1949).

[368] H. Chen *et al.*, Phys. Procedia **37**, 1287 (2012).

[369] S. Li *et al.*, IEEE Transactions on Nuclear Science **60**, 6, 4737 (2013).

[370] H. Chen *et al.*, Nucl. Instrum. Meth. A **936**, 271 (2019).

[371] R. Acciarri *et al.* (MicroBooNE), JINST **12**, 08, P08003 (2017), [arXiv:1705.07341].

[372] P. Cennini *et al.* (ICARUS), Nucl. Instrum. Meth. A **432**, 240 (1999).

[373] D. Caratelli (MicroBooNE), JINST **15**, 03, C03023 (2020).

[374] B. Ali-Mohammadzadeh *et al.* (ICARUS), JINST **15**, 10, T10007 (2020), [arXiv:2006.05261].

[375] M. Kuźniak and A. M. Szelc, Instruments **5**, 1, 4 (2020), [arXiv:2012.15626].

[376] A. Ankowski *et al.* (ICARUS), Nucl. Instrum. Meth. A **556**, 146 (2006).

[377] N. Anfimov *et al.*, JINST **15**, 07, C07022 (2020).

[378] E. Segreto *et al.*, JINST **15**, 05, C05045 (2020).

[379] M. Antonello *et al.*, JINST **9** (2014), URL https://iopscience.iop.org/article/10.1088/1748-0221/9/08/P08003/pdf.

[380] H. Chen *et al.*, 16th IEEE-NPSS Real Time Conference 159–162 (2009), URL https://ieeexplore.ieee.org/document/5322032.

[381] B. Abi *et al.* (DUNE) (2018), [arXiv:1807.10327].

[382] B. Abi *et al.* (DUNE) (2018), [arXiv:1807.10340].

[383] R. Acciarri *et al.*, JINST **12**, 08, P08003 (2017), [arXiv:1705.07341].

[384] C. Adams *et al.*, JINST **13**, 07, P07006 (2018), [arXiv:1802.08709].

[385] B. Abi *et al.*, JINST **15**, 12, P12004 (2020), [arXiv:2007.06722].

[386] R. Acciarri *et al.* (MicroBooNE), Eur. Phys. J. C **78**, 1, 82 (2018), [arXiv:1708.03135].

[387] X. Qian *et al.*, JINST **13**, 05, P05032 (2018), [arXiv:1803.04850].

[388] P. Abratenko *et al.* (MicroBooNE), JHEP **2021**, 153 (2021), [arXiv:2109.02460].

[389] L. Uboldi *et al.*, Nucl. Instrum. Meth. A **1028**, 166371 (2022), [arXiv:2106.09911].

[390] R. Acciarri *et al.* (ArgoNeuT), JINST **17**, 01, P01018 (2022), [arXiv:2103.06391].

[391] A. Abed Abud *et al.* (DUNE), Eur. Phys. J. C **82**, 10, 903 (2022), [arXiv:2203.17053].

[392] C. Adams *et al.* (MicroBooNE), Phys. Rev. D **99**, 9, 092001 (2019), [arXiv:1808.07269].

[393] P. Abratenko *et al.* (MicroBooNE), Phys. Rev. D **103**, 5, 052012 (2021), [arXiv:2012.08513].

[394] A. A. Abud *et al.* (DUNE), Eur. Phys. J. C **85**, 697, 697 (2025), [arXiv:2502.06637].

[395] P. Abratenko *et al.* (MicroBooNE), Phys. Rev. D **103**, 9, 092003 (2021), [arXiv:2010.08653].

[396] J. Liu *et al.* (DUNE) (2020), [arXiv:2012.06181].

[397] P. Abratenko *et al.* (MicroBooNE), Phys. Rev. D **110**, 9, 092010 (2024), [arXiv:2406.10123].

[398] A. Aurisano *et al.*, Phys. Rev. D **110**, 3, 032008 (2024), [arXiv:2403.11872].

[399] F. Drielsma *et al.*, in "34th Conference on Neural Information Processing Systems," (2021), [arXiv:2102.01033].

[400] G. Cerati (MicroBooNE), EPJ Web Conf. **295**, 08012 (2024), [arXiv:2309.15362].

[401] T. Cai *et al.*, Comput. Softw. Big Sci. **7**, 1, 11 (2023), [arXiv:2301.04633].

[402] C. Rubbia *et al.* (ICARUS), JINST **6**, P07011 (2011), [arXiv:1106.0975].

[403] D. A. Dwyer *et al.*, JINST **13**, 10, P10007 (2018), [arXiv:1808.02969].

[404] D. Cardoso *et al.*, JINST **19**, 08, C08001 (2024).

[405] B. Baibussinov *et al.* (ICARUS), JINST **13**, 03, T03001 (2018), [arXiv:1711.06781].

[406] A. Lowe *et al.*, Instruments **4**, 4, 35 (2020), [arXiv:2011.02292].

[407] M. Arroyave *et al.*, JINST **19**, 10, P10019 (2024), [arXiv:2405.16816].

[408] A. Ereditato *et al.*, JINST **8**, 07, P07002 (2013), [arXiv:1304.6961].

[409] E. Segreto, Phys. Rev. D **103**, 4, 043001 (2021), [arXiv:2012.06527].

[410] L. Bäni *et al.* (RD42), J. Phys. Conf. Ser. **2374**, 1, 012172 (2022).

[411] A. Rogalski, Adv. Opt. Photon. **11**, 2, 314 (2019).

[412] V. Saraswat, R. Jacobberger and M. Arnold, ACS Nano 15:3, 3674–3708 (2021).

[413] G. Lutz, *Semiconductor Radiation Detectors*, Springer (1999), ISBN 978-3-540-64859-8.

[414] F. Hartmann, *Evolution of Silicon Sensor Technology in Particle Physics: Basics and Applications*, volume 293, Springer (2024), ISBN 978-3-031-59719-0, 978-3-031-59720-6.

[415] G. Lutz and R. Klanner, *Particle Physics Reference Library (Vol. 2, Ch. 5., Solid State Detectors), Eds. Fabjan, C. W. and Schopper, H.*, Springer Nature (2020), ISBN 978-3-030-35317-9, 978-3-030-35318-6.

[416] T. Kimoto and J. A. Cooper, *Fundamentals of Silicon Carbide Technology: Growth, Characterization, Devices, and Applications*, John Wiley & Sons (2014), ISBN 9781118313527.

[417] Landolt-Börnstein, Springer (Berlin), 2002, https://doi.org/10.1007/10832182_456 and https://doi.org/10.1007/10832182_458.

Int. J. Mod. Phys. A 2026.41. Downloaded from www.worldscientific.com
by UNIVERSITY OF CALIFORNIA @ BERKELEY on 09/16/26. Re-use and distribution is strictly not permitted, except for Open Access articles.

[418] C. Da Via *et al.*, Nucl. Instrum. Meth. **587**, 243 (2008).

[419] C. Damerell, Nucl. Instrum. Meth. A **342**, 78 (1994).

[420] M. Garcia-Sciveres and N. Wermes, Rept. Prog. Phys. **81**, 6, 066101 (2018).

[421] L. Rossi *et al.*, *Pixel Detectors – From Fundamentals to Applications*, Springer, Berlin (2006), ISBN 978-3-540-28332-4, 978-3-540-28333-1, URL https://doi.org/10.1007/3-540-28333-1.

[422] H.-G. Moser *et al.*, PoS **VERTEX2007**, 022 (2007).

[423] Y. Arai *et al.*, Nucl. Instrum. Meth. A **623**, 186 (2010).

[424] H. Sadrozinski, A. Seiden and N. Cartiglia, Rept. Prog. Phys. **81**, 2, 026101 (2018).

[425] M. Ferrero *et al.*, *Ultra-Fast Silicon Detectors*, CRC Press, Open Access, Creative Commons (2021), ISBN 978-1-003-13194-6.

[426] A. Lampis *et al.*, JINST **18**, 01, C01051 (2023).

[427] S. Zambito *et al.*, JINST **18**, 03, P03047 (2023).

[428] W. Riegler and G. Aglieri Rinella, JINST **12**, 11, P11017 (2017).

[429] R. Wunstorf, *Systematische Untersuchungen zur Strahlenresistenz von Silizium-Detektoren für die Verwendung in Hohenergiephysikexperimenten*, Ph.D. thesis, Universität Hamburg (1992), URL https://www-library.desy.de/preparch/desy/int_rep/fh1k-92-01.pdf.

[430] M. Moll, IEEE Trans. Nucl. Sci. **65**, 8, 1561 (2018).

[431] G. Kramberger, Initial acceptor removal in p-type silicon-Talk at 26th CERN-RD50 Workshop, Santander (2015), https://indico.cern.ch/event/381195/contributions/905665/.

[432] W. Adam *et al.*, JINST **11**, P04023 (2016).

[433] G. Kramberger, *Particle Physics Reference Library (Vol. 2, Ch. 21., Solid State Detectors for High Radiation Environments), Eds. Fabjan, C. W. and Schopper, H.*, Springer Nature (2020), ISBN 978-3-030-35317-9, 978-3-030-35318-6.

[434] V. Radeka and N. Karlovac, Nuclear Instruments and Methods **52**, 1, 86 (1967), ISSN 0029-554X, URL https://www.sciencedirect.com/science/article/pii/0029554X67905617.

[435] V. Radeka, IEEE Transactions on Nuclear Science **15**, 3, 455 (1968), URL https://doi.org/10.1109/TNS.1968.4324970.

[436] A. van der Ziel, *Noise in Solid State Devices and Circuits*, John Wiley & Sons, Inc. (1986), ISBN 978-0471832348.

[437] C. C. Enz, F. Krummenacher and E. A. Vittoz, Analog Integr Circ Sig Process **8**, 83 (1995), URL https://doi.org/10.1007/BF01239381.

[438] W. Blum, L. Rolandi and W. Riegler, *Particle detection with drift chambers*, Particle Acceleration and Detection, Springer (2008), ISBN 978-3-540-76683-4, 978-3-540-76684-1, URL https://doi.org/10.1007/978-3-540-76684-1.

[439] V. Radeka, Ann. Rev. Nucl. Part. Sci. **38**, 217 (1988), URL https://doi.org/10.1146/annurev.ns.38.120188.001245.

[440] A. Rivetti, *CMOS: Front-End Electronics for Radiation Sensors*, CRC Press (2015), URL https://doi.org/10.1201/b18599.

[441] R. Wigmans, *Calorimetry*, International Series of Monographs on Physics, Oxford University Press (2017).

[442] S. Agostinelli *et al.* (GEANT4), Nucl. Instrum. Meth. A **506**, 250 (2003).

[443] J. Allison *et al.*, IEEE Trans. Nucl. Sci. **53**, 270 (2006).

[444] T. Gabriel and L. Charlton (1997).

[445] T. T. Böhlen *et al.*, Nucl. Data Sheets **120**, 211 (2014).

[446] A. Ferrari *et al.* (2005).

[447] J. Allison *et al.*, Nucl. Instrum. Meth. A **835**, 186 (2016).

[448] D. Buskulic *et al.* (ALEPH), Nucl. Instrum. Meth. A **360**, 481 (1995).

[449] A. M. Sirunyan *et al.* (CMS), JINST **12**, 10, P10003 (2017), [arXiv:1706.04965].

[450] M. A. Thomson, Nucl. Instrum. Meth. A **611**, 25 (2009), [arXiv:0907.3577].

[451] L. Linssen *et al.* (2012), [arXiv:1202.5940].

[452] H. L. Tran *et al.*, Eur. Phys. J. C **77**, 10, 698 (2017), [arXiv:1705.10363].

[453] M. Aleksa *et al.*, Eur. Phys. J. Plus **136**, 10, 1066 (2021), [arXiv:2109.00391].

[454] M. T. Lucchini *et al.*, JINST **15**, 11, P11005 (2020), [arXiv:2008.00338].

[455] W.R. Nelson, H. Hirayama, and D.W.O. Rogers, SLAC-265 (1985) .

[456] ATLAS Collab., CERN/LHCC 96-41 (1996).

[457] D. Hitlin *et al.*, Nucl. Instrum. Meth. **137**, 225 (1976).

[458] W. J. Willis and V. Radeka, Nucl. Instrum. Meth. **120**, 221 (1974).

[459] R. Wigmans, *Calorimetry: Energy Measurement in Particle Physics*, Inter. Series of Monographs on Phys. **107**, Second Edition, Oxford Schlarship Online (2017).

[460] R.-Y. Zhu, Nucl. Instrum. Meth. **A413**, 297 (1998).

[461] R.-Y. Zhu, Journal of Physics: Conference Series **587**, 012055 (2015).

[462] CMS Collab., CERN/LHCC 97-33 (1997).

[463] C. Leroy and P. Rancoita, Rept. Prog. Phys. **63**, 505 (2000).

[464] F. Sefkow and F. Simon, *Calorimeters*, in Fleck I., Titov M., Grupen C., Buvat I. (eds) Handbook of Particle Detection and Imaging, Springer (2021), ISBN 978-3-319-47999-6.

[465] C. Adloff *et al.* (CALICE), JINST **8**, 07005 (2013).

[466] T. A. Gabriel *et al.*, Nucl. Instrum. Meth. **A338**, 336 (1994).

[467] F. Ariztizabal *et al.* (RD-34), Nucl. Instrum. Meth. **A349**, 384 (1994).

[468] F. Sefkow and F. Simon (CALICE), J. Phys. Conf. Ser. **1162**, 1, 012012 (2019), [arXiv:1808.09281].

[469] A. White *et al.* (CALICE), JINST **18**, 11, P11018 (2023), [arXiv:2209.15327].

[470] CMS, CERN-LHCC-2017-023, CMS-TDR-019 (2017).

[471] N. Akchurin *et al.*, Nucl. Instrum. Meth. **A399**, 202 (1997).

[472] A. Artamonov *et al.*, JINST **3**, P02010 (2008).

[473] B. Aubert *et al.*, Nucl. Instrum. Meth. **A321**, 467 (1992).

[474] C. W. Fabjan *et al.*, Nucl. Instrum. Meth. **141**, 61 (1977).

[475] J. Brau *et al.*, Nucl. Instrum. Meth. **A238**, 489 (1985).

[476] H. Brückmann and H. Kowalski, ZEUS Int. Note 86/026 DESY, Hamburg (1986).

[477] R. Wigmans, Nucl. Instrum. Meth. **A259**, 389 (1987).

[478] R. Wigmans, Nucl. Instrum. Meth. **A265**, 273 (1988).

[479] J. E. Brau and T. A. Gabriel, Nucl. Instrum. Meth. A **275**, 190 (1989).

[480] J. C. Brient, R. Rusack and F. Sefkow, Ann. Rev. Nucl. Part. Sci. **68**, 271 (2018).

[481] E. Fretwurst *et al.* (1989), URL http://cds.cern.ch/record/368113.

[482] E. Borchi *et al.* (SICAPO), Nucl. Instrum. Meth. **A279**, 57 (1989).

[483] H. Abramowicz *et al.* (2013), [arXiv:1306.6329].

[484] N. Alipour Tehrani *et al.* (CLICdp) (2017), CLICdp-Note-2017-001.

[485] N. Bacchetta *et al.* (2019), [arXiv:1911.12230].

[486] https://twiki.cern.ch/twiki/bin/view/CALICE/CaliceDetectors.

[487] C. Adloff *et al.* (CALICE), JINST **5**, P05004 (2010), [arXiv:1003.2662].

[488] M. Chefdeville *et al.* (CALICE), Nucl. Instrum. Meth. A **939**, 89 (2019), [arXiv:1901.08818].

[489] G. Baulieu *et al.*, JINST **10**, 10, P10039 (2015), [arXiv:1506.05316].

[490] B. Acar *et al.* (CMS, CALICE), JINST **18**, 08, P08014 (2023), [arXiv:2211.04740].

[491] B. Acar *et al.* (CMS HGCAL), JINST **19**, 04, P04015 (2024), [arXiv:2312.14622].

[492] C. Adloff *et al.* (CALICE), JINST **8**, P09001 (2013), [arXiv:1305.7027].

[493] H. Abramowicz *et al.*, Nucl. Instrum. Meth. **180**, 429 (1981).

[494] B. Andrieu *et al.* (H1 Calorimeter Group), Nucl. Instrum. Meth. A **336**, 499 (1993).

[495] C. Cojocaru *et al.* (ATLAS Liquid Argon EMEC/HEC), Nucl. Instrum. Meth. A **531**, 481 (2004), [arXiv:physics/0407009].

[496] C. Adloff *et al.* (CALICE), J. Instr. **7**, 09, P09017 (2012).

[497] H. L. Tran *et al.*, The European Physical Journal C **77**, 10, 698 (2017).

[498] S. Lai *et al.* (CALICE), JINST **19**, P04037 (2024), [arXiv:2403.04632].

[499] M. Aamir *et al.* (CMS HGCAL, CALICE AHCAL), JINST **19**, 11, P11025 (2024), [arXiv:2406.11937].

[500] S. Lai *et al.* (CALICE), JINST **19**, 10, P10027 (2024), [arXiv:2407.00178].

[501] P. Mockett, SLAC-267, 335 (1983).

[502] D. E. Groom, Nucl. Instrum. Meth. **A572**, 633 (2007), erratum: Nucl. Instrum. Meth. **A593**, 628 (2008).

[503] R. Wigmans, *Proc. 7th Inter. Conf. on Calorimetry in High Energy Physics*, 182 World Scientific, River Edge, NJ, (1998);.

[504] S. Lee, M. Livan and R. Wigmans, Rev. Mod. Phys. **90**, 2, 025002 (2018).

[505] S. Lee *et al.*, Nucl. Instrum. Meth. A **866**, 76 (2017), [arXiv:1703.09120].

[506] M. Antonello *et al.*, JINST **15**, 06, C06015 (2020).

[507] E. Bernardi *et al.*, Nucl. Instrum. Meth. **A262**, 229 (1987).

[508] M. Chefdeville *et al.* (CALICE), JINST **10**, 12, P12006 (2015), [arXiv:1509.00617].

[509] T. Akesson *et al.*, Nucl. Instrum. Meth. **A262**, 243 (1987).

[510] D. Acosta *et al.*, Nucl. Instrum. Meth. **A308**, 481 (1991).

[511] R. Dubois *et al.*, IEEE Trans. Nucl. Sci. **33**, 194 (1986).

[512] B. Andrieu *et al.* (H1 Calorimeter Group), Nucl. Instrum. Meth. A **336**, 460 (1993).

[513] A. Bernstein *et al.* (ZEUS Barrel Calorimeter Group), Nucl. Instrum. Meth. A **336**, 23 (1993).

[514] J.-b. Liu (CDF), in "7th International Conference on Calorimetry in High-Energy Physics (ICCHEP 97)," 237–240 (1997).

[515] S. Abachi *et al.* (D0), Nucl. Instrum. Meth. A **324**, 53 (1993).

[516] G. Aad *et al.* (ATLAS), JINST **3**, S08003 (2008).

[517] S. Abdullin *et al.* (USCMS, ECAL/HCAL), Eur. Phys. J. C **60**, 359 (2009), [Erratum: Eur.Phys.J.C 61, 353–356 (2009)].

[518] H. Abramowicz *et al.* (ZEUS), Phys. Lett. B **718**, 915 (2013), [arXiv:1210.5511].

[519] E. Shibamura *et al.*, Nucl. Instrum. Methods **A316**, 184 (1975).

[520] L. S. Miller, S. Howe and W. E. Spear, Phys. Rev. **166**, 871 (1968).

[521] A.M. Kalinin *et al.*, ATLAS-LARG-NO-058 (1996).

[522] K. Yoshino, U. Sowada and W. F. Schmidt, Phys. Rev. **A14**, 438 (1976).

[523] A.O. Allen *et al.*, NSRDS-NBS-58 (1976).

[524] P. Benetti *et al.*, Nucl. Instrum. Methods **A32**, 361 (1993).

[525] A. Yamamoto, Nucl. Instrum. Meth. **A453**, 445 (2000).

[526] A. Yamamoto and Y. Makida, Nucl. Instrum. Meth. **A494**, 255 (2002).

[527] T. M. Taylor, Phys. Scripta **23**, 459 (1981).

[528] R. L. Gluckstern, Nucl. Instrum. Meth. **24**, 381 (1963).

[529] V. Karimaki, Nucl. Instrum. Meth. **A410**, 284 (1998).

Int. J. Mod. Phys. A Downloaded from www.worldscientific.com
by UNIVERSITY OF CALIFORNIA @ BERKE use and distribution is strictly not permitted, except for Open Access articles.

36. Particle Detectors for Non-Accelerator Physics

Revised March 2026. See the various sections for authors.

36.1 Introduction . . . 661
36.2 High-energy cosmic-ray hadron and gamma-ray detectors . . . 661
36.2.1 Atmospheric fluorescence detectors . . . 661
36.2.2 Atmospheric Cherenkov telescopes for high-energy gamma ray astronomy . . . 663
36.3 Large neutrino detectors . . . 665
36.3.1 Deep liquid detectors for rare processes . . . 665
36.3.2 Neutrino telescopes . . . 668
36.3.3 Radio emission from (ultra-)high energy particle showers . . . 670
36.4 Large time-projection chambers for rare event detection . . . 675
36.4.1 Dark matter and other low energy signals . . . 677
36.4.2 $0\nu\beta\beta$ Decay . . . 678
36.5 Sub-kelvin detectors . . . 679
36.5.1 Motivation for Sub-kelvin Detectors . . . 679
36.5.2 Detector Types . . . 680
36.5.3 Experimental Applications . . . 682
36.6 Low-radioactivity background techniques . . . 684
36.6.1 Introduction . . . 684
36.6.2 Radio-purity assay . . . 685
36.6.3 Radon and its progeny . . . 685
36.6.4 Surface backgrounds . . . 685
36.6.5 Mitigation of backgrounds and active background discrimination . . . 686

36.1 Introduction

Non-accelerator experiments have become increasingly important in particle physics and astrophysics. From them comes the evidence of physics beyond the SM, with the discovery of neutrino oscillations and adiabatic flavor conversion. Explored energies range from the meV scale to above the EeV, some 24 orders of magnitude. The physics and the design of the detectors vary as a consequence. Some experiments look at astrophysical high-energy phenomena using the atmosphere as a detector in the fluorescence and Cherenkov observatories or the polar ice and the ocean water in neutrino telescopes. Experiments on extremely rare events, such as neutrino-less double beta decay, solar neutrinos and dark matter induced scattering, need dedicated fully equipped deep underground laboratories, existing in different countries. Critical is the research to push back the ultra-low radioactive background frontier, with dedicated facilities in these laboratories. Detectors range from hyper-pure liquid scintillators, both organic and not, to thermalized and ballistic phonon detectors at the sub-Kelvin temperature, to dual phase noble fluid TPCs, etc. Space-based detectors also use some unique instrumentation, but these are beyond the present scope of this review. Gravitational wave detectors are not included as well.

36.2 High-energy cosmic-ray hadron and gamma-ray detectors

36.2.1 *Atmospheric fluorescence detectors*

Revised October 2025 by F. Salamida (L'Aquila U.; INFN, LNGS).

Cosmic-ray fluorescence detectors (FDs) use the atmosphere as a giant calorimeter to measure isotropic scintillation light that traces the development profiles of extensive air showers. An extensive air shower (EAS) is produced by the interactions of ultra high-energy ($E > 10^{17}$ eV) subatomic particles in the stratosphere and upper troposphere. The amount of scintillation light generated by an EAS is proportional to the energy deposited in the atmosphere and nearly independent of the primary species. With energies extending beyond 10^{20} eV, ultra high energy cosmic rays (UHECRs) are the highest energy subatomic particles known to exist. In addition to particle arrival directions, energy spectra and primary composition, the astroparticle science investigated with FDs also includes multi-messenger studies, searches for high energy photons, neutrinos, monopoles and deeply penetrating forms of dark matter. The Pierre Auger Observatory FD also measures UV scintillation that traces the development of ring-shaped atmospheric transient luminous events, called Elves, in the ionosphere that are initiated by strong lightning [1]. Similar phenomena have also been observed from space by Mini-EUSO [2].

Previous experiments with FDs included the pioneering Fly's Eye [3, 4], and the High Resolution Fly's Eye (HiRes and HiRes prototype) [5]. The use of atmospheric nitrogen fluorescence to detect extensive air showers was proposed in the 1950's by Greisen and Chudakov, and further developed in the 1960's through the systematic studies of Bunner [6, 7]. The current generation of experiments include the Telescope Array (TA) [8] in the northern hemisphere, and the larger Pierre Auger Observatory (Auger) [9] in the southern hemisphere. (Discussion, with extensive references, of current and possible future UHECR experiments can be found[in [10].) Auger and TA are hybrid observatories. Their FD telescopes overlook sparse arrays of particle detectors on the ground. Select parameters are listed in Table 36.1. TA and Auger have each one FD site populated with additional telescopes that view up to 60° in elevation to measure lower EASs using a combination of scintillation and direct Cherenkov light. As part of a fourfold coverage upgrade of TA (TAx4), 12 HiRes refurbished telescopes have been installed at the north and south-east sites of TA. A set of prototype fluorescence telescopes, known as FAST [11], has been developed as a cost-effective design for next-generation ultra-high energy cosmic ray observatories. These small-aperture telescopes, equipped with a single wide field-of-view photomultiplier and simple optics, have been successfully deployed and operated at both the Telescope Array site and the Pierre Auger Observatory, where they have detected air showers and validated the concept. A similar approach is being pursued by the CRAFFT [12] project in Japan, which uses Fresnel lenses and single-PMT readout to achieve comparable goals of simplicity and scalability.

The fluorescence light is emitted primarily between 290 and 430 nm (Figure 36.1) with major lines at 337, 357, and 391 nm, when relativistic charged particles, primarily electrons and positrons, excite nitrogen molecules in air, resulting in transitions of the 1P and 2P systems. Reviews and references for the pioneering and recent laboratory measurements of fluorescence yield, $Y(\lambda, P, T, u)$, including dependence on wavelength (λ), temperature (T), pressure (p), and humidity (u) may be found in Refs. [13–15]. The results of various laboratory experiments have been combined (Figure 36.2) to obtain an absolute average and uncertainty for Y(337 nm, 800 hPa, 293 K, dry air) of 7.04 ± 0.24 ph/ MeV after corrections for different electron beam energies and other factors. The units of ph/ MeV correspond to the number of fluorescence photons produced per MeV of energy deposited in the atmosphere by the electromagnetic component of an EAS.

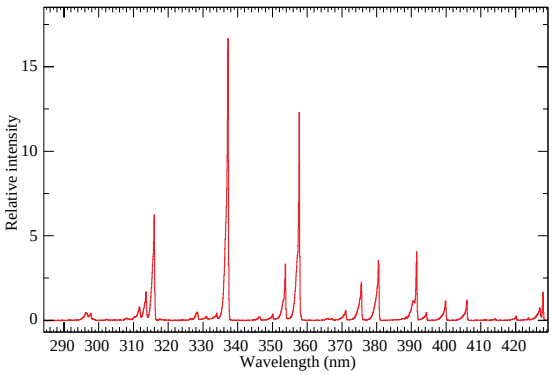

Figure 36.1: Measured fluorescence spectrum excited by 3 MeV electrons in dry air at 800 hPa and 293 K. Airfly experiment. Figure from Ref [16].

Int. J. Mod. Phys. A 2026.41. Downloaded from www.worldscientific.com by UNIVERSITY OF CALIFORNIA @ BERKELEY on 09/16/26. Re-use and distribution is strictly not permitted, except for Open Access articles.

Int. J. Mod. Phys. A. Downloaded from www.worldscientific.com
by UNIVERSITY OF CALIFORNIA @ BERKE... use and distribution is strictly not permitted, except for Open Access articles.

Table 36.1: Parameters of major fluorescence detectors. Note 1: Year when all FD sites were operational. Note 2: At TA 1 of the 3 FD sites features 24 telescopes from the HiRes experiment. Note 3: A-C for one telescope where A is the full area and C the area obscured by the camera and support structures. Thus A-C is the effective light collecting area. For the modified Schmidt design at Auger, the area of the entrance pupil, A, is listed because the pupil is smaller than the mirror and thus defines the entrance aperture. For the other experiments, the area of the mirror, A, is listed

Observatory	Fly's Eye	HiRes	Telescope Array	Pierre Auger
Location	Dugway UT US	Dugway UT US	Delta UT US	Malargüe AR
Start-End	1981-1992	1996-2006	2008-present	2005-present
Sites (note 1)	2 (1986)	2 (1999)	3 (2008)	4 (2008)
Separation	3.3 km	12.6 km	31-40 km	39-62 km
Telescopes/site	67,18	21,42	12+8,12,14+10+4	6, 6, 6, 6+3
Pixel FOV	5.5°	1°	1°	1.5°
Telescope FOV Azi×Elv	≈18°×≈18°	16°×13.5°	18°×15° (note 2)	30°×28.1°
Light collection area (note 3)	1.95 m^2 - 0.25 m^2	3.72 m^2 - 0.5 m^2	6.8 m^2 - 0.85 m^2 (for 2 sites)	3.80 m^2 - 0.80 m^2 (modified schmidt)
Energy Scale Uncertainty	≤40%	≈20%	≈20%	14%

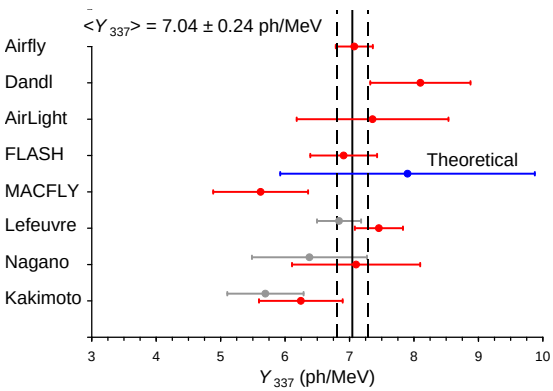

Figure 36.2: Fluorescence yield values and associated uncertainties at 337 nm (Y_{337}) in dry air at 800 hPa and 293 K The methodology and corrections that were applied to obtain the average and the uncertainty are discussed extensively in this reference. The vertical axis denotes different laboratory experiments that measured FY. The gray bars show three of the original measurements to illustrate the scale of the corrections applied. Figure from Ref [17].

An FD element (telescope) consists of a non-tracking spherical mirror of less than astronomical quality, a"camera" of photomultiplier tubes (PMTs) near the focal plane, and a flash ADC readout system with a pulse and track-finding trigger scheme [9, 18]. The major experiments listed in Table 36.1 all use conventional PMTs (for example, Hamamatsu R9508 or Photonis XP3062) with grounded cathodes and AC coupled readout. Segmented mirrors have been fabricated from slumped or slumped/polished glass with an anodized aluminum coating or fabricated using shaped aluminum that was then chemically anodized with $AlMgSiO_5$. A broadband UV filter (custom fabricated, BG-3, or Schott MUG-6) reduces background light such as starlight, airglow, man-made light pollution, and airplane strobe-lights.

At 10^{20} eV, where the flux drops below 1 EAS/km^2 century, the aperture for an eye of adjacent FD telescopes that span the horizon can reach 10^4 km^2 sr. FD operation requires (nearly) moonless nights and clear atmospheric conditions, which typically imposes a duty cycle of about 10%. Arrangements of LEDs, calibrated diffuse sources [19], pulsed UV lasers [20], LIDARs [1] and IR detectors that are sensitive to clouds are used for photometric calibration, atmospheric calibration [21], and determination of exposure [22]. For purposes of optical transmission, the atmosphere is treated as having a dominant molecular component and a secondary aerosol component. The latter is well described [23] by molecular scattering theory and models derived from radiosonde measurements. The aerosol component can include dust, haze and pollution and the aerosol optical depth profile must be measured on site in the UV during FD data taking.

The EAS generates a track consistent with a light source moving at $v = c$ across the FOV. The number of photons (N_γ) as a function of atmospheric depth (X) can be expressed as [14]

$$\frac{\mathrm{d}N_\gamma}{\mathrm{d}X} = \frac{dE^{\mathrm{tot}}_{\mathrm{dep}}}{dX} \int Y(\lambda, P, T, u) \cdot \tau_{\mathrm{atm}}(\lambda, X) \cdot \varepsilon_{\mathrm{FD}}(\lambda)\mathrm{d}\lambda, \quad (36.1)$$

where $\tau_{atm}(\lambda, X)$ is the atmospheric transmission, including wavelength (λ) dependence, and $\varepsilon_{\mathrm{FD}}(\lambda)$ is the FD efficiency. $\varepsilon_{\mathrm{FD}}(\lambda)$ includes geometric factors and collection efficiency of the optics, quantum efficiency of the PMTs, and other throughput factors. The typical systematic uncertainties, τ_{atm} (10%) and $\varepsilon_{\mathrm{FD}}$ (photometric calibration 10%), currently dominate the systematic uncertainty the absolute EAS energy scale. FD energy resolution, defined as event-to-event statistical uncertainty, is typically less than 10% for final data samples used for science analysis.

Analysis methods to reconstruct the EAS profile and deconvolve the contributions of re-scattered scintillation light, and direct and scattered Cherenkov light are described in [3] and more recently in [25]. The EAS energy is typically obtained by integrating over the Gaisser-Hillas function [26]

$$E_{\mathrm{cal}} = \int_0^\infty [w_{\max} \left(\frac{X - X_0}{X_{\max} - X_0}\right)^{(X_{\max}-X_0)/\lambda} e^{(X_{\max}-X)/\lambda}]\mathrm{d}X, \quad (36.2)$$

where E_{cal} is the energy of electromagnetic energy component of the EAS and $X_{\max}$ is the atmospheric slant depth at which the shower reaches its maximum energy deposit rate. This maximum dE/dX is denoted as $w_{\max}$. X_0 and λ are two shape parameters. Recent analyses adopt a modified Gaisser–Hillas parameterization that decouples the width L and asymmetry R, improving the robustness of the fit [27].

The energy of the primary cosmic ray is obtained by correcting E_{cal} upward by about 10% to account for the invisible energy carried by particles that do not interact in the atmosphere. Auger reported a data-driven method to estimate the invisible energy from the muon number at ground level and Xmax to reduce systematic uncertainties [28]. Energy resolution, $\Delta E/E$, of 15-20% is achievable, provided the geometric fit of the EAS axis is constrained, typically by multi-eye stereo projection or hybrid observations, and the profile fit of EAS development along the track is constrained by the observed rise and fall about $X_{\max}$. An example of a recorded EAS light profile and its corresponding dE/dX development profile are shown in Fig. 36.3. In 2023, the Pierre Auger Collaboration released a public dataset [29] of the

[1] LIDAR stands for "Light Detection and Ranging" and refers here to systems that measure atmospheric properties from the light scattered backwards from laser pulses directed into the sky.

Int. J. Mod. Phys. A 2026.41. Downloaded from www.worldscientific.com
by UNIVERSITY OF CALIFORNIA @ BERKELEY on 09/16/26. Re-use and distribution is strictly not permitted, except for Open Access articles.

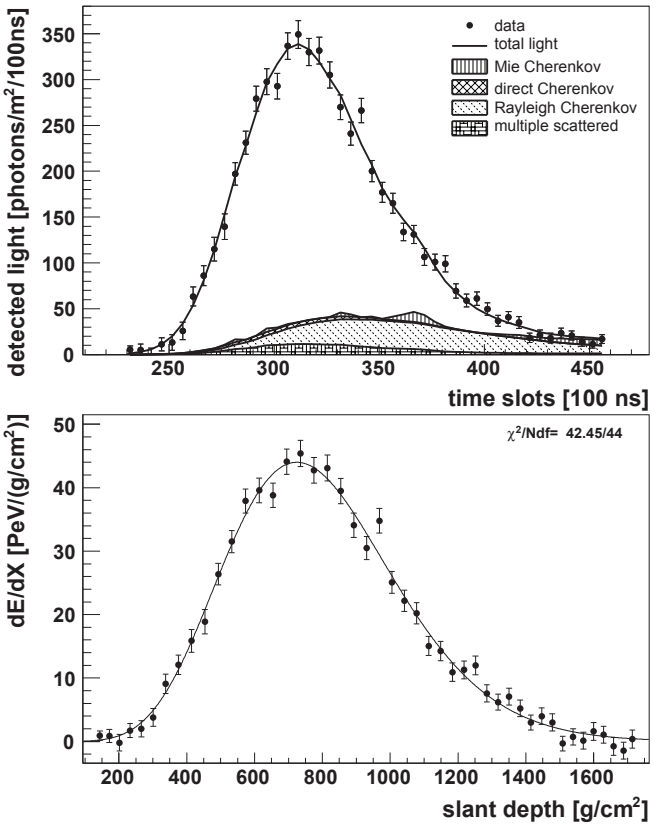

Figure 36.3: Example light profile (left) of one EAS recorded by the Pierre Auger FD and the corresponding profile (right) of energy deposited in the atmosphere vs atmospheric slant depth. The light profiles include the estimated components of Cherenkov light that have been scattered out of the forward beam by the molecular and aerosol (Mie) components of the atmosphere. The reconstructed energy of this EAS was $3.0 \pm 0.2 \times 10^{19}$ eV. Figure from Ref [24].

100 highest energy cosmic ray events collected over a 17-year span through 2020 with an additional 9 energetic hybrid events used in the calibration procedure. In 2024 the Pierre Auger Collaboration published the first systematic comparison of $X_{\max}$ measured with radio and fluorescence techniques for the same set of 53 air showers, finding no significant bias (-3.9 ± 11.2 g/cm^2) and a resolution better than 15 g/cm^2 [30]. These results also benefit from the ongoing *AugerPrime* upgrade [31]. Besides enhancing the surface-detector array with the installation of Surface Scintillator Detectors (SSD) and dedicated radio antennas, AugerPrime also deploys new front-end electronics that provide higher sampling speed and dynamic range, thereby enabling a more accurate time synchronisation of FD–SD coincident events. Recent results also show excellent agreement between the radio and FD-based energy scales, providing a strong and independent validation of the energy scale determined by the FD [32].

An FD that would look down on the Earth's atmosphere from orbit, and thus monitor a far larger area than any ground-based instrument, is an active area of R&D. Prototypes already flown include the pioneering TUS instrument [33,34] (2016–2018 on the Lomonosov satellite). The JEM-EUSO collaboration has tested balloon pathfinders in 2014 (EUSO-Balloon) [35], 2017 (EUSO-SPB1) [36], and 2023 (EUSO-SPB2) [37]. During its 2023 flight the EUSO-SPB2 mission recorded UV signals compatible with extensive air showers using both a fluorescence and a Cherenkov telescope, providing a critical validation of the optical and trigger systems planned for future orbital detectors [37, 38]. The Mini-EUSO [39] FD continues recording terrestrial UV emission by looking down through a 25 cm diameter UV-transmitting window inside the International Space Station since 2019.

Looking ahead, the Probe of Extreme Multi-Messenger Astrophysics (POEMMA) is in the NASA Probe-class pre-proposal phase. Its baseline design foresees two wide-field Schmidt satellites flying in formation to observe UHECRs and cosmogenic tau neutrinos from space [40, 41].As a precursor to the satellite mission, the POEMMA collaboration is developing a super-pressure balloon pathfinder (PBR), combining fluorescence, Cherenkov, and radio detectors, with a launch planned in 2027 [42].

36.2.2 *Atmospheric Cherenkov telescopes for high-energy gamma ray astronomy*

Revised October 2025 by W. Hofmann (MPIK).

A wide variety of astrophysical objects produce high-energy γ-ray photons. Leptonic or hadronic particles, accelerated to relativistic energies, produce γ-rays typically through inverse Compton boosting of ambient photons or through the decay of neutral pions produced in hadronic interactions. Below some 10s of GeV, γ-ray emission can be efficiently detected using satellite or balloon-borne instrumentation, with an effective area approximately equal to the size of the detector (typically $< 1\,\mathrm{m}^2$). At higher energies, a technique with much larger effective collection area is required to measure astrophysical γ-ray fluxes, which decrease rapidly with increasing energy. Atmospheric Cherenkov detectors achieve effective collection areas of $> 10^5\,\mathrm{m}^2$ by using the Earth's atmosphere as an intrinsic part of the detection technique. A hadronic cosmic ray or high energy γ-ray incident on the Earth's atmosphere induces a particle cascade, or air shower. Relativistic charged particles in the air shower generate Cherenkov radiation, which is emitted along the shower direction. For vertically incident γ-rays in the TeV range, the maximum emission occurs at an altitude of $\sim$10 km [43]. Following absorption and scattering in the atmosphere [43], the Cherenkov light at ground level peaks at a wavelength $\lambda \approx$ 300–350 nm. At typical observatory altitudes of 1-2 km a.s.l., Cherenkov light illuminates a light pool with a radius of $\sim$120-130 m, with roughly uniform light intensity across the light pool [43, 44]. Beyond the light pool radius, the intensity of Cherenkov light decreases rapidly. More deeply penetrating higher-energy γ-ray showers generate a peaked intensity distribution, distant showers at large zenith angles a larger light pool [43, 44]. The intensity is approximately proportional to the energy of the primary γ-ray, and is typically $\sim$100 photons/m^2 for a vertical 1 TeV primary, arriving in a brief flash of a few nanoseconds. The light yield varies with the seasonal atmospheric density profile, by 10% or more [43]. The Cherenkov pulse can be detected by using large reflecting surfaces to focus the Cherenkov light onto fast photo sensors. See [45, 46] for accounts of the historical development of the technique, [47] for a recent overview, and [48] for an exhaustive compilation of materials.

Imaging atmospheric Cherenkov telescopes (IACTs), such as H.E.S.S., MAGIC and VERITAS, use large ($> 100\,\mathrm{m}^2$) segmented mirrors on steerable mounts to focus the Cherenkov light onto arrays of photosensors (referred to as the "cameras") that record a Cherenkov image of each air shower. The intensity, shape and orientation of the Cherenkov images are used to reconstruct the γ-ray energy and arrival direction, and to discriminate γ-ray primaries from cosmic rays that provide a uniform background. Images resulting from purely electromagnetic γ-ray induced cascades appear as narrow, elongated ellipses in the camera. The long axis of the ellipse corresponds to the vertical extension of the air shower, and points back towards the source position in the field-of-view. If multiple telescopes are used to view the same shower ("stereoscopy"), the source position is simply the intersection point of the various image axes. Cosmic-ray primaries produce secondaries with large transverse momenta, which initiate sub-showers. Their images are consequently wider and less regular than those with γ-ray primaries. Reflecting the distance to the air shower maximum ($\sim$10 km for vertical incidence) and the scale of transverse structures in γ-ray showers (some 10 meters), IACT cameras mostly use relatively coarse pixel sizes in the range of $0.08^\circ - 0.19^\circ$ (Table 36.2). The image of a $\sim$10 km long air shower viewed at $\sim$100 m impact distance extends over roughly one degree, hence cameras need to provide fields of view of few degrees. Most modern instruments have larger fields of view, up to 10°, to cover extended γ-ray

Int. J. Mod. Phys. A
Downloaded from www.worldscientific.com
by UNIVERSITY OF CALIFORNIA @ BERKE
use and distribution is strictly not permitted, except for Open Access articles.

sources and enable sky surveys. Table 36.2 lists major IACT systems operating or under construction; all are stereoscopic systems, that provide improved resolution of the γ-ray direction and higher background rejection compared to single telescopes. Whereas in the operating few-telescope stereoscopic systems the telescopes are distributed over an area of the scale of the light pool radius – to ensure that multiple telescopes are illuminated by a given shower – the systems under construction use larger numbers of IACTs, covering areas larger than the light pool, and providing effective detection areas on the scale of 10^6 m^2.

IACTs are deployed at sites with dark skies and a large number of clear nights. Most IACT sites are well above sea level, at 1-2 km elevation (VERITAS, H.E.S.S., MAGIC, CTAO). Altitudes in the 4-5 km range provide lower energy thresholds [58]; for example, the MACE telescope [59] is located at 4.3 km a.s.l. IACTs benefit from sites with low geomagnetic field; large transverse fields spread the shower and reduce performance by $\sim 1\%$ per μG field [44]. At typical sites, IACTs log about 1000 - 1500 h per year, also depending on the level of moon light up to which telescopes are operated.

Traditionally, IACTs use single-mirror optics for imaging; for cost reasons, segmented mirrors are used. Mirror facet size ranges from $\sim 0.3\,\mathrm{m}^2$ to ~ 2 m^2, increasingly moving from aluminized ground-glass mirrors to lightweight composite sandwich structures. For mirror diameters d up to 10 - 15 m (VERITAS, H.E.S.S. CT1-4, CTAO MST), mostly Davies-Cotton optics is used, with facets of focal length f arranged on a shell of radius f, whereas larger mirrors use a parabolic shape (MAGIC, H.E.S.S. CT5, CTAO LST). Davies-Cotton optics provides better imaging over an extended field of view, but is not isochronous; for large telescopes the time dispersion is significant compared to the (ns) Cherenkov signal time scales. The off-axis point spread function (PSF) of single-mirror telescopes deteriorates rapidly with decreasing f/d [60, 61]; large f on the other hand results in large cameras and heavy support structures. As a compromise, $f/d \approx 1.0 - 1.3$ is typically chosen. Dual-mirror Schwarzschild-Coulder optics was proposed [62] to provide a near-uniform PSF across fields of view up to 10°, and a small plate scale suitable for silicon photo multipliers (SiPM). The first IACTs to implement Schwarzschild-Couder optics are the pSCT prototype telescope [63], and the ASTRI and CTAO SST telescopes. IACTs are usually focused on the height of shower maximum (about 10 km for vertical TeV γ-rays). For very large telescopes (d beyond 25 - 30 m), the finite depth of field limits telescope performance; Plenoscope optics [64] has been proposed as a way out. Alt-az mounts are generally employed to point IACTs, either using a central positioner (e.g. VERITAS, CTAO MSTs) or – in particular for larger telescopes - a cradle on a circular rail (e.g. H.E.S.S., MAGIC). Positioning speeds range from 20 s (CTAO LST) to 1-2 minutes. Cameras use mostly photomultipliers (PMTs), with a peak quantum efficiency (QE) approaching 40%, but silicon sensors (SiPM) as pioneered in the FACT telescope [65] are increasingly used (pSCT, ASTRI, CTAO SST, LACT) since they can operate under high illumination (moonlight) and provide higher QE, but not necessarily a better performance (signal to noise) for detecting the Cherenkov photons; see [66] for a comparison. A disadvantage of SiPMs is their red-sensitivity resulting in high night-sky background (NSB) rates unless filtered. Even with the blue-sensitive PMT response, night-sky background rates are in the range of few 100 MHz per pixel, for large mirrors. To avoid pile-up of NSB, exposure time for Cherenkov images should not exceed a few ns. For signal recording, either fast Flash-ADC systems used, or 1-2 GHz analog capacitor pipelines that store signals until a trigger decision is obtained. In most modern cameras, the full readout electronics is housed in the camera body. Triggering is usually multi-level, with a first-level decision based on the camera image using a coincidence or signal sum of neighboring pixels, followed by a second-level decision requesting a coincidence of multiple telescopes and initiating data transfer to storage. Camera-level triggers typically require about 50-100 detected photons in an air shower image; readout rates are in the kHz range.

For an overview of data analysis techniques, see e.g. [67]. The simplest form of image reconstruction parametrizes images by an ellipse (Hillas parameters) and reconstructs the shower direction from the intersection of image ellipses [68]. A wide range of improved reconstruction algorithms is used, in particular fits of the image distribution using semi-analytical [69] or MC-generated [70] image templates. Cosmic-ray rejection in its simplest form uses the size of the minor axis of the image ellipse to remove cosmic-ray showers; advanced techniques use the quality-of-fit of gamma-ray image templates, and/or machine learning using a wide range of image parameters. For optimizing the analysis, and determining effective detection areas, extensive Monte Carlo simulations are used, frequently based on the CORSIKA [71] air shower simulator. Lacking a "test beam" and relying on the atmosphere as detection medium, the absolute calibration of IACTs is challenging. Intensity of muon rings is one means for calibrating the telescope response [72], and atmospheric monitoring by independent devices (e.g. LIDARs [73]) or via the telescope trigger rates serves to monitor atmospheric transmission. Low-level image and air shower reconstruction is usually performed using custom software, but high-level analysis is increasingly relying on open-source packages such as Gammapy [74]. While cosmic rays are effectively rejected, still background remains that must be subtracted in the study of γ-ray sources. Techniques for background determination [75] include pointing the telescope offset from the source, and using off-regions distributed symmetrically to the telescope axis; using event rates in a ring around the source; globally fitting a background level from the full field of view; or using dedicated off-runs pointing towards an empty region of sky.

At low energies, where the light intensity in the Cherenkov light pool is below the trigger threshold of a telescope, IACTs only trigger because of fluctuations in shower development or light yield, and the trigger probability and hence the effective detection areas increase steeply with energy. Once the intensity in the light pool matches the trigger threshold, the effective area starts to saturate at $\sim 10^5$ m^2 (for vertical incidence on a single telescope or telescope array with size not larger than the light pool). Typical angular resolutions of telescope systems are $\sim$5 arc-min, but arc-min scale resolution can be achieved for well-reconstructed high-energy events. Typical γ-ray energy resolution is $\sim$10%. In the image analysis, 99% or more of the cosmic rays can be rejected based on image shapes; an additional factor of $\gg 100$ suppression can be gained from an angular cut around the (point) source position. Sensitivity is usually quoted as the minimally detectable point-source γ-ray energy flux $E^2 F_{min}(E)$ in a 0.2 decade energy band. Fig. 36.4 illustrates the flux sensitivity of IACT systems. At low energy, sensitivity is governed by the strong energy dependence of the effective area, but often starts to be limited by background systematics. At mid-energy, with roughly constant effective area, background statistics limits the sensitivity, resulting in a roughly constant $E^2 F_{min}(E)$. At high energy, telescopes are γ-ray rate limited, with $E^2 F_{min}(E) \sim E$. Currently operating systems reach peak sensitivities around 10^{-12} erg cm^{-2}s^{-1} for 50 h of observations, the larger next-generation systems approach 10^{-13} erg cm^{-2}s^{-1}. A special mode are observations at large zenith angles, of 60° and beyond. At these angles, the distance to the shower maximum is increased by factors of a few, and the size of the light pool is increased correspondingly. Effective detection areas can be increased by up to an order of magnitude compared to observations near zenith, at the expense of an increase in energy threshold (e.g. [76, 77]) and potentially increased systematic errors.

The first astrophysical source to be convincingly detected using the imaging atmospheric Cherenkov technique was the Crab Nebula, in 1989 [80]. Modern imaging atmospheric Cherenkov telescopes have sensitivity sufficient to detect sources at 1% of the Crab Nebula flux in about 10 hours, can measure the spectrum of the Crab pulsar and the nebula from $\sim$20 GeV to $\sim$100 TeV [76, 81], and can resolve the $\sim$1 arc-min size of the Crab Nebula [82]. Well over 200 TeV γ-ray sources – both galactic and extragalactic – were discovered using IACTs [83]. A significant fraction of the galactic sources were detected by scanning the Galactic plane from the southern hemisphere with the H.E.S.S. telescope array [84]. The CTAO IACT arrays – the first IACT system to be operated as an open observatory – are expected to

Int. J. Mod. Phys. A 2026.41. Downloaded from www.worldscientific.com
by UNIVERSITY OF CALIFORNIA @ BERKELEY on 09/16/26. Re-use and distribution is strictly not permitted, except for Open Access articles.

Table 36.2: Parameters of major IACT systems, operating or under construction. In the optics line, DC stands for Davies-Cotton, DC' for modified DC, P for parabolic, SC' for modified Schwarzschild-Couder. "Max. tel. dist." is the maximum distance between pairs of telescopes, as a measure for the extent of the array. The CTAO telescope numbers refer to the "alpha" configuration.

	H.E.S.S.		MAGIC	VERITAS	ASTRI	CTAO			LACT
Site	Namibia		La Palma	Arizona, US	Tenerife	La Palma and Chile			Sichuan, China
Altitude [m]	1800		2200	1300	2400	2200 / 2100			4400
Max. tel. dist. [m]	170		85	170	500	600 / 1800			1200
Status (2025)	Operational		Operational	Operational	Construction	Construction			Construction
Reference	[49]		[50, 51]	[52, 53]	[54]	[55]			[56, 57]
Telescopes	CT1-4	CT5				SST	MST	LST	
Number	4	1	2	4	9	0 / 37	9 / 14	4 / 0	32
Mirror dia. [m]	12	28	17	12	4.3	4.3	11.5	23	6
Focal len. [m]	15	36	18	12	2.2	2.2	16	28	8
Optics	DC	P	P	DC	SC'	SC'	DC'	P	DC
FoV [deg.]	5.0	3.4	3.5	3.5	10.5	8.8	7.7 / 7.5	4.3	8
Pixel size [deg.]	0.16	0.08	0.1	0.15	0.19	0.16	0.17	0.1	0.19
Pixel number	960	1758	1039	499	2368	2048	1855/1764	1855	1616
Photodet.	PMT	PMT	PMT	PMT	SiPM	SiPM	PMT	PMT	SiPM

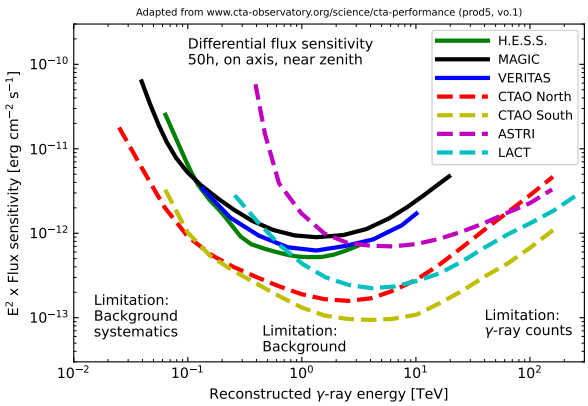

Figure 36.4: Differential flux sensitivity for IACT systems, in operation (solid lines) or under construction (dashed). Adapted from CTAO; sensitivity curves from [78](H.E.S.S.), [51](MAGIC), [79](VERITAS), [54](ASTRI), [57](LACT). Differences at the level of 20-30% may arise from slight differences in definition of sensitivity.

boost the number of detected sources to 500 or more; see [85] for a discussion of science with CTAO. The first 23 m diameter CTAO-LST is already operational on La Palma (e.g. [86]); the "alpha" configuration of CTAO (Table 36.2) should become operational around 2030. On the same time scale, the LACT telescopes at the LHAASO site will provide a significant step in sensitivity.

A recent development is the use of IACT arrays for intensity interferometry, using either dedicated photon detectors or special pixels in the camera. The multiple baselines provided by IACT arrays allow imaging of stars on milli-arc-sec scales, and first results are highly promising (e.g. [87–89]).

36.3 Large neutrino detectors

36.3.1 *Deep liquid detectors for rare processes*

Revised October 2025 by J. Cao (IHEP Beijing).

Deep, large detectors for rare processes tend to be multi-purpose with physics reach that includes not only solar, reactor, supernova and atmospheric neutrinos, but also searches for baryon number violation and lepton number violation, searches for exotic particles and beyond-the-standard-model physics, and neutrino and cosmic-ray astrophysics in different energy regimes. The detectors may also serve as targets for long-baseline neutrino beams for neutrino oscillation studies. In general, detector design considerations can be divided into high- and low-energy regimes, for which background and event reconstruction issues differ. The high-energy regime, from about 100 MeV to a few hundred GeV, is relevant for proton decay searches, atmospheric neutrinos and high-energy astrophysical neutrinos. The low-energy regime (a few tens of MeV or less) is relevant for supernova, solar, reactor and geological neutrinos.

Large water Cherenkov and scintillator detectors (see Table 36.3) usually consist of a volume of transparent liquid viewed by photosensors (see Section 35.2); the liquid serves as active target. While some early detectors are segmented into subvolumes individually viewed by photosensors, monolithic detectors usually have better performance and are cost-effective for large volume. A typical detector configuration is shown in Figure 36.5.

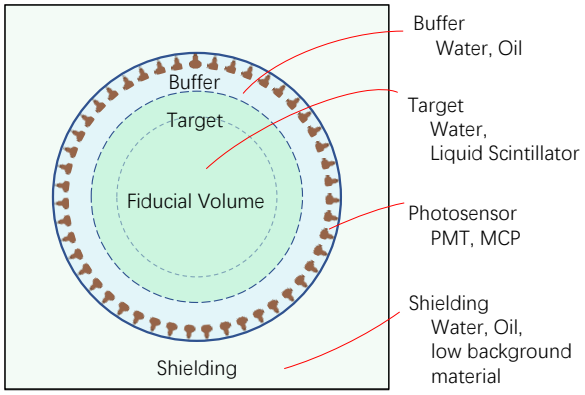

Figure 36.5: Schematic illustration of a typical water Cherenkov or liquid scintillator detector. An array of photosensors view the active target volume to detect the Cherenkov and/or scintillation light. For a liquid scintillator detector, usually there is a non-scintillating buffer between the target and the photosensors. The whole detector is usually surrounded by shielding materials and equipped with muon veto detectors.

A "fiducial volume" is usually defined within the target volume, some distance away from the photosensors, to have relatively uniform detector response and to suppress ambient backgrounds. A nonscintillating buffer is necessary only for liquid scintillator (LS) detectors to shield the active target from natural radioactivities from the photosensors and detector structures. The liquid volume usually requires purification and there may be continuous recirculation of liquid.

Photomultiplier tubes (PMTs) commonly used as photosensors for such large detectors have typical sizes ranging from 20 cm to 51 cm in diameter, quantum efficiencies in the 20–31% range, and time responses at nano-second level. PMTs are usually potted to be water-proof or oil-proof to protect the bases containing high voltage dividers. Protection covers may be needed to avoid chain reaction of implosion. Earth magnetic field can be shielded either for individual PMTs by wrapping high magnetic permeabil-

Int. J. Mod. Phys. A
by UNIVERSITY OF CALIFORNIA @ BERKE
Downloaded from www.worldscientific.com
use and distribution is strictly not permitted, except for Open Access articles.

Table 36.3: Properties of large detectors for rare processes. If total target mass is divided into modules, the number of modules is indicated in parentheses. Projects with first data expected in 2025 or later are indicated in italics.

Detector	Mass, kton (modules)	PMTs (diameter, cm)	Photocathode Coverage	p.e./MeV	Dates
BUST	0.33, scint (3150)	1/module (15)	segmented	40	1980–
MACRO	0.56, scint (476)	2-4/module (20)	segmented	18	1989–2000
LVD	1, scint (840)	3/module (15)	segmented	15	1992–2023
KamLAND	0.41*, scint	1325 (43) + 554 (51)†	34%	460	2002–
Borexino	0.1*, scint	2212 (20)	30%	500	2007–2021
CHOOZ	0.005, scint (Gd)	192 (20)	15%	130	1997–1998
Double Chooz	0.017, scint (Gd)(2)	390/detector (25)	13%	200	2011–2017
Daya Bay	0.160, scint (Gd)(8)	192/detector (20)	5.6%‡	163	2011–2020
RENO	0.032, scint (Gd)(2)	354/detector (25)	14%	230	2011–2023
SNO+	0.78, scint§	9362 (20)	31%¶	400–600	2021–
JUNO	18.3*, scint	17596 (51) + 25587 (8)	77.9%	1780	2025–
IMB-1	3.3*, H_2O	2048 (12.5)	1%	0.25	1982–1985
IMB-2	3.3*, H_2O	2048 (20)	4.5%	1.1	1987–1990
Kam I	0.88/0.78*, H_2O	1000/948 (51)	20%	3.4	1983–1985
Kam II	1.04*, H_2O	948 (51)	20%	3.4	1986–1990
Kam III	1.04*, H_2O	948 (51)	20%‖	4.3	1990–1995
SK I	22.5*, H_2O	11146 (51)	40%	6	1996–2001
SK II	22.5*, H_2O	5182 (51)	19%	3	2002–2005
SK III-V	22.5*, H_2O	11129 (51)	40%	6	2006–2020
SK-Gd	22.5*, H_2O (Gd)	11129 (51)	40%	6	2020–
Hyper-K	188*, H_2O	20000 (51) + 800 (mPMT)	20%	6	2028 (exp.)
SNO	1, D_2O	9438 (20)	31%¶	9	1999–2006
DUNE	40*, Ar (4)	TBD**	TBD**	TBD**	2028 (exp.)††

*Indicates typical fiducial mass used for data analysis; this may vary by physics topic.
†Measurements made before 2003 only considered data from the 43-cm PMTs.
‡The effective Daya Bay coverage is 12% with top and bottom reflectors.
§SNO+ ran with water fill from May 2017 to July 2019.
¶The effective SNO and SNO+ coverage is 54% with light collectors.
‖The effective Kamiokande III coverage was 25% with light collectors.
**Photodetector technology and coverage varies according to TPC type and is not yet fully determined.
††Modules will be constructed in a phased approach.

ity material or for the whole detector with compensating coils, to diminish the impact to the PMT collection efficiency. Devices to increase light collection, *e.g.*, reflectors or waveshifter plates, may be employed. Silicon Photomultipliers (SiPMs) and Microchannel Plates (MCPs) are new optional photosensors. Comparing with PMTs, SiPMs have higher quantum efficiency but much higher dark noise, and MCPs have faster time response.

Charges and times, sometimes the full waveforms, of photosensors are recorded and digitized. Triggering is usually based on coincidence of hits within a time window comparable to the detector's light-crossing time. For large homogeneous detectors, the event interaction vertex and energy deposition are determined using relative timing and/or charge distribution of photosensors in the detector. Usually, arbitrary light reflection is minimized to understand the light propagation and improve vertex and energy reconstruction. This can be achieved by placing black sheets between photosensors or blackening the inner surface of the detector. Meanwhile, light reflection is usually maximized to increase muon detection efficiency for outer veto detectors.

Because in most cases one is searching for rare events, large detectors are usually sited underground to reduce cosmic-ray-related background (see Chapter 30). The minimum depth required varies according to the physics goals [90]. To shield the cosmogenic backgrounds (for both water and LS detectors) and ambient natural radioactivities (for LS detectors), detectors are usually surrounded by water, oil, or other shielding material and equipped with muon veto detectors.

36.3.1.1 *Liquid scintillator detectors*

Past and current large underground detectors based on hydrocarbon scintillator include BUST, MACRO, LVD, KamLAND, Borexino, SNO+ and JUNO. Experiments at nuclear reactors include CHOOZ, Double CHOOZ, Daya Bay, and RENO. As shown in Figure 36.5, a nonscintillating buffer hosting the photosensors is necessary. A large LS detector usually consists of two or even three concentric liquid layers, separating by concentric thin acrylic vessels or balloons made of nylon transparent to scintillation light.

Organic liquid scintillators (see Section 35.3) for large detectors are chosen for high light yield and attenuation length, good stability, compatibility with other detector materials, high flash point, low toxicity, and low cost. They are made by dissolving a few gram per litre fluor into solvent. The most popular solvents are 1,2,4-trimethylbenzene (pseudocumene) and linear alkylbenzene (LAB). LAB is an ideal choice especially with very good transparency for a gigantic detector. Pseudocumene has a low flash point and is relatively aggressive to detector materials; thus is often diluted with alkane. Xylene is more volatile but has very good pulse shape discrimination power. The most popular fluor is 2,5-diphenyloxazole (PPO). Besides the primary fluor, a secondary fluor, aka waveshifter, is usually added to shift the scintillation light to longer wavelength where the LS is more transparent; thus the light yield increases. The most popular waveshifters include p-bis-(o-methylstyryl)-benzene (bis-MSB) and 1,4-bis(5-phenyl-2-oxazolyl)benzene (POPOP). Antioxidant may be added into LS for long-term stability.

Liquid scintillators have a typical light yield of $\sim 10^4$ photons/MeV. The attenuation length ranges from 5 to 20 meters when measured at $\sim$ 430 nm wavelength. Some solvents such as LAB have strong Rayleigh scattering, which contributes significantly to the attenuation length. The absorption length of LS can be as long as 70 meters. With current highest photocathode coverage 78% and 30% PMT photon detection efficiency (PDE, defined as the peak quantum efficiency times collection efficiency), about 1,780 pe/MeV of energy deposition can be obtained. The energy resolution reaches 3% at 1 MeV [91] and is still dominated by photon statistics. With a typical 20–40% coverage and $\sim$ 20% PDE, the energy resolution is about $5 - 7\%/\sqrt{E(\mathrm{MeV})}$. The energy response of LS is not linear and depends on particle types due to ionization quenching. Careful calibration with multiple sources at

Int. J. Mod. Phys. A 2026.41. Downloaded from www.worldscientific.com
by UNIVERSITY OF CALIFORNIA @ BERKELEY on 09/16/26. Re-use and distribution is strictly not permitted, except for Open Access articles.

multiples energy points is needed. Other quenching effects, such as oxygen and temperature, may reduce the light yield at 10% level. Light is emitted with a time response consisting of several exponential components, depending on the solvents and fluors. Usually most light is emitted in tens of nanoseconds. Typical resolution of position reconstruction, using charges and times of PMT hits, is a few tens of cm at ~ 1 MeV.

Radioactive backgrounds from photosensors, detector materials, LS itself, and immediate environment are serious issues for LS detectors. Dedicated detector design, careful selection of materials, purification of the scintillator, and well controlled assembly environment and procedure are essential (see Section 36.6). Radon and Krypton in air as well as Radon decay daughters may impose serious challenges to the experiment. The lower detection threshold of a LS detector is often determined by the ^{14}C content in LS with the 156 keV β-decay endpoint energy. Fiducialization helps to reduce the backgrounds originating from the outer part of the detector. The intrinsic backgrounds from the LS itself have been purified to $< 9.4 \times 10^{-20}$ g/g for ^{238}U and $< 5.7 \times 10^{-19}$ g/g for ^{232}Th [92].

For $\bar{\nu}_e$ detection via inverse beta decay on free protons, $\bar{\nu}_e + p \to n + e^+$, the time coincidence of the prompt positron signal and the delayed neutron capture signal suppresses significantly the radioactive backgrounds. Doping a small fraction of Gadolinium (or other elements with high neutron capture cross section, such as Cadmium and Lithium) in the LS, *e.g.* $\sim 0.1\%$ by mass, the neutron capture time could be reduced from ~ 200 μs to ~ 30 μs. Futhermore, the total gamma energy released from the neutron capture increases from 2.2 MeV to 8 MeV, well above the radioactive background energy thus providing a clean tag for antineutrino. Doping inorganic Gadolinium (as well as other elements) into organic scintillator requires specialized formulation to ensure adequate transparency and stability.

One can also dissolve neutrinoless double beta decay ($0\nu\beta\beta$) isotopes in scintillator. This has been realized by KamLAND-Zen, which deployed a 1.9 m-radius balloon containing enriched Xe dissolved in scintillator inside KamLAND, and ^{130}Te is planned for SNO+.

Liquid scintillator is especially suitable for detection of low-energy events. However, scintillation light emission is nearly isotropic, and therefore directional capabilities are relatively weak. Developing technology such as water-based liquid scintillator with reduced scintillation light yield [93] or liquid scintillator with slow fluors [94] provides the directional capability by separating the Cherenkov light from the scintillation.

36.3.1.2 *Water Cherenkov detectors*

Very large imaging water detectors reconstruct ten-meter-scale Cherenkov rings produced by charged particles (see Section 35.5). The first such large detectors were IMB and Kamiokande. Currently, the only operational detector of this kind is Super-Kamiokande (Super-K, SK), which has a fiducial mass of 22.5 kton and a total mass of 50 kton. Hyper-Kamiokande (Hyper-K) is under construction and will have a fiducial mass of 188 kton and a total mass of 258 kton.

Super-K is instrumented with 11,129 20-inch PMTs of a peak quantum efficiency $\sim 20\%$, corresponding to a photocathode coverage of $\sim 40\%$. Hyper-K will be equipped with at least 20,000 20-inch PMTs and 800 mPMTs, a module about 20-inch in size and assembled with multiple 3-inch PMTs, corresponding to $\sim 20\%$ photocathode coverage. Hyper-K PMTs have a quantum efficiency $\sim 31\%$ and a higher collection efficiency than Super-K, resulting in similar pe yields for the two detectors.

For volumes of this scale, absorption and scattering of Cherenkov light are non-negligible. Attenuation length of the high purity water have been achieved at the order of 100 meters with continuous recirculation and purification. Radon need be carefully stripped from water to reduce the detector noise during both the water production and recirculation. Maintaining a temperature gradient in the detector to avoid water convection helps to further reduce such noise. Given the giant detector size, PMT readout electronics works usually underwater to avoid signal attenuation; thus requires high reliability. Degassing may be a serious issue that causes high voltage breakdown when air in the underwater electronics boxes or cracks in connectors is gradually removed by the degassed pure water. A solution is to regas the pure water with nitrogen [95].

Cherenkov detectors are excellent electromagnetic calorimeters. The number of Cherenkov photons produced by an e/γ is nearly proportional to its kinetic energy, ~ 6 pe/MeV for Super-K. For massive particles, the number of photons produced is also related to the energy, but not linearly. The directionality of Cherenkov light allows individual particle tracks to be reconstructed. Vertex and direction fits are performed using PMT hit charges and times, requiring that the hit pattern be consistent with a Cherenkov ring.

High-energy ($\sim$100 MeV or more) neutrinos from the atmosphere or beams interact with nucleons; for the nucleons bound inside the ^{16}O nucleus, nuclear effects must be considered. Various event topologies, with final-state particles contained, exiting, or entering the detector, can be distinguished by their timing and fit patterns, and by presence or absence of light in a veto. At high energies, the energy resolution is approximately $3\%/\sqrt{E_{\rm vis}({\rm GeV})}$ for Super-K. The absolute energy scale in this regime can be known to $\sim$ 2–3% using cosmic-ray muon energy deposition, Michel electrons and π^0 from atmospheric neutrino interactions. Typical vertex resolutions for GeV energies are a few tens of cm. Angular resolution for determination of the direction of a charged particle track is a few degrees. For a neutrino interaction, because some final-state particles are usually below Cherenkov threshold, knowledge of direction of the incoming neutrino direction itself is generally worse, depending on neutrino energy.

Multiple particles in an interaction (so long as they are above Cherenkov threshold) may be reconstructed, allowing for the exclusive reconstruction of final states. In searches for proton decay, multiple particles can be kinematically reconstructed to form a decaying nucleon. Particle identification can be done with high reliability with pattern recognition: γ rays and electrons shower, and electrons scatter, which results in fuzzy rings, whereas muons, pions and protons make sharp rings.

In spite of the fairly low light yield, large water Cherenkov detectors may be employed for reconstructing low-energy events, down to *e.g.* $\sim$ 4-5 MeV for Super-K. Using an electron LINAC and/or nuclear sources, approximately 0.5% determination of the absolute energy scale has been achieved at solar neutrino energies. Angular resolution is limited by multiple scattering in this energy regime (25–30°). At these energies, radioactive backgrounds become a dominant issue. In the few to few tens of MeV range, radioactive products of cosmic-ray-muon-induced spallation are troublesome, and are removed by proximity in time and space to preceding muons. Gadolinium doping using $Gd_2(SO_4)_3$ has now been initiated for Super-K to improve selection of low-energy $\bar{\nu}_e$ and other events with accompanying neutrons.

The Sudbury Neutrino Observatory (SNO) detector was the only instance of a large heavy water detector. In addition to an outer 1.7 kton of light water, SNO contained 1 kton of D_2O, giving it unique sensitivity to neutrino neutral current ($\nu_x + d \to \nu_x + p + n$), and charged current ($\nu_e + d \to p + p + e^-$) deuteron breakup reactions. The neutrons were detected in three ways: via capture on deuterons, via capture on dissolved ^{35}Cl, and via specialized ^{3}He counters.

36.3.1.3 *Noble liquid detectors*

Noble liquids scintillate and can be used as the active medium for particle detection. Detectors employing argon and xenon are also used as time-projection chambers (TPCs), either as dual-phase low-energy recoil detectors, or as track-imaging detectors. Noble-liquid detectors with low energy (few to few tens of keV) capability for detecting electronic and nuclear recoils are employed for dark matter and other rare event searches and are described in Sec. 36.4. These detectors can also be employed for some of the same physics (solar neutrino, baryon number violation, astrophysical neutrino transient searches, etc.) as for the other large detectors described here, especially as they approach tens of ton scale and higher (e.g., XLZD, DarkSide-20k, ARGO). Track-imaging time-projection chambers, which are described in detail Section 36.4, have a dynamic range reaching down to the few to

Int. J. Mod. Phys. A. Downloaded from www.worldscientific.com
by UNIVERSITY OF CALIFORNIA @ BERKE use and distribution is strictly not permitted, except for Open Access articles.

few tens of MeV scale, enabling sensitivity to e.g., solar and supernova burst neutrinos. Surface LArTPCs have significant cosmic backgrounds, but may still have sensitivity to astrophysical transients such as supernova burst neutrinos. DUNE will be sufficiently deep to have sensitivity to steady-state low-energy neutrino sources such as solar neutrinos.

36.3.2 *Neutrino telescopes*

Revised March 2026 by U.F. Katz (Erlangen U.) and C. Spiering (DESY, Zeuthen).

The primary goal of neutrino telescopes (NTs) is the detection of astrophysical neutrinos, in particular those which are expected to accompany the production of high-energy cosmic rays in astrophysical accelerators. NTs in addition address a variety of other fundamental physics issues like the indirect search for dark matter, studies of neutrino oscillations, searches for exotic particles like magnetic monopoles or study of cosmic rays and their interactions [96–98]. Electromagnetic radio frequency detectors for high energy neutrinos are discussed in "Radio emission from (ultra-) high energy particle showers" section 36.3.3.

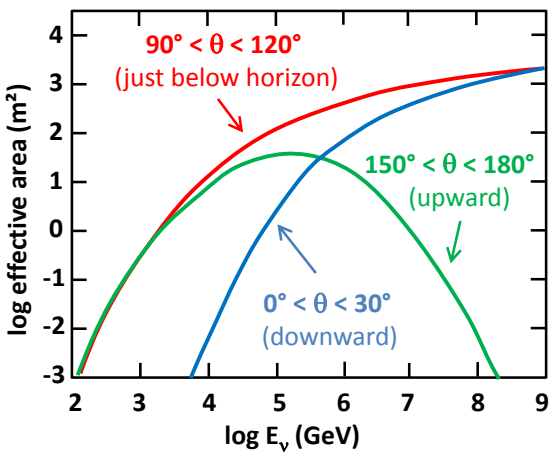

Figure 36.6: Average over the effective ν_μ and $\overline{\nu}_\mu$ areas for IceCube as an example of a cubic-kilometre NT, as a function of neutrino energy for three intervals of the zenith angle θ. The values shown here correspond to a specific event selection for point source searches.

NTs are large-volume arrays of "optical modules" (OMs) installed in open transparent media like water or ice, at depths that completely block the daylight. The OMs are sensitive to individual photons of the Cherenkov light induced by charged secondary particles produced in reactions of high-energy neutrinos in or around the instrumented volume. The time of photon-induced signals ("hits") is registered with a precision of a few nanoseconds. The neutrino energy, E_ν, and direction can be reconstructed from the hit pattern recorded. NTs typically target an energy range $E_\nu \gtrsim 100\,\mathrm{GeV}$; sensitivity to lower energies is achieved in dedicated setups with denser instrumentation.

In detecting cosmic neutrinos, three sources of backgrounds have to be considered: (i) *atmospheric neutrinos* from cosmic-ray interactions in the atmosphere, which can be separated from cosmic neutrinos on a statistical basis, or, for down-going neutrinos, by vetoing accompanying muons; (ii) down-going punch-through *atmospheric muons* from cosmic-ray interactions, which are suppressed by several orders of magnitude with respect to the ground level due to the large detector depths and can be further reduced by selecting upward-going or high-energy neutrinos or by self-veto methods; (iii) random backgrounds due to photomultiplier (PMT) dark counts, ^{40}K decays (mainly in sea water) or bioluminescence (only water). Atmospheric neutrinos and muons allow for investigating neutrino oscillations and cosmic ray anisotropies, respectively. Since 2012, it has become obvious that a precise measurement of the energy-zenith-distribution of atmospheric neutrinos in the energy range from a few to about 100 GeV may allow for determining the neutrino mass hierarchy by exploiting matter-induced oscillation effects in the Earth [99, 100].

Neutrinos can interact with target nucleons N through charged current ($\overset{(-)}{\nu}_\ell N \to \ell^\mp X$, CC) or neutral current ($\overset{(-)}{\nu}_\ell N \to \overset{(-)}{\nu}_\ell X$, NC) processes. A CC reaction of a $\overset{(-)}{\nu}_\mu$ produces a muon track and a hadronic particle cascade, whereas all NC reactions and CC reactions of $\overset{(-)}{\nu}_e$ produce particle cascades only. CC interactions of $\overset{(-)}{\nu}_\tau$ can have either signature, depending on the τ decay mode. Of particular interest is the so-called double-bang signature, where the τ decays sufficiently far away from the primary interaction to create a second, distinguishable cascade (typically at PeV energies and above). In most astrophysical models, neutrinos are expected to be produced through the $\pi/K \to \mu \to e$ decay chain, *i.e.*, with a flavour ratio $\nu_e : \nu_\mu : \nu_\tau \approx 1 : 2 : 0$. For sources outside the solar system, neutrino oscillations turn this ratio to $\nu_e : \nu_\mu : \nu_\tau \approx 1 : 1 : 1$ upon arrival on Earth.

The total neutrino-nucleon cross section is about $10^{-34}\,\mathrm{cm}^2$ at $E_\nu = 20\,\mathrm{TeV}$ and rises roughly linearly with E_ν below this energy and as $E_\nu^{0.3-0.5}$ above, flattening out towards high energies. The CC:NC cross-section ratio is about 2:1. At energies above several TeV, neutrino absorption in the Earth becomes noticeable; for vertically upward-moving neutrinos (zenith angle $\theta = 180°$), the survival probability is $74\,(27, < 2)\%$ for $10\,(100, 1000)$ TeV. The energy transferred to the final-state lepton varies between 0 and 100% of E_ν, with a mean of 50% (65%) for neutrinos (antineutrinos) at 100 GeV and 75% for both neutrinos and antineutrinos at 10 PeV.

The final-state lepton follows the initial (anti)neutrino direction with an average mismatch angle of about $\langle\phi_{\nu\ell}\rangle \approx 1°/(E_\nu/\mathrm{TeV})^{0.55}$, with a steeper decrease beyond 10 TeV, reaching 0.005° at 1 PeV [101]. These values indicate the intrinsic kinematic limit to the angular resolution of NTs. For CC $\overset{(-)}{\nu}_\mu$ reactions at energies above about 10 TeV, the angular resolution is dominated by the muon reconstruction accuracy of a few times 0.1° at most. For muon energies $E_\mu \gtrsim 1\,\mathrm{TeV}$, the increasing light emission due to radiative processes allows for reconstructing E_μ from the measured Cherenkov light intensity with an accuracy of $\sigma(\log E_\mu) \approx 0.3$; at lower energies, E_μ can be estimated from the length of the muon track if it is contained in the detector. These properties make CC $\overset{(-)}{\nu}_\mu$ reactions the prime channel for the identification of individual astrophysical neutrino sources.

Hadronic and electromagnetic particle cascades at the relevant energies are 5–20 m long, *i.e.*, short compared to typical OM spacings. The total amount of Cherenkov light provides a direct measurement of the cascade energy with an accuracy of about 20% at energies above 10 TeV and 10% beyond 100 TeV for events contained in the instrumented volume. Except for double-bang events, the neutrino flavour and reaction mechanism can, however, be determined on a statistical basis at best, and neutrinos from NC reactions or τ decays may carry away significant "invisible" energy. Above 100 TeV, the average directional reconstruction accuracy of cascades is better than 10 (2) degrees in polar ice (sea water), the difference being due to the inhomogeneity of the ice and stronger light scattering in ice. These features, together with the small background of atmospheric $\overset{(-)}{\nu}_e$ and $\overset{(-)}{\nu}_\tau$ events, makes the cascade channel particularly interesting for searches for a diffuse, high-energy excess of extraterrestrial over atmospheric neutrinos. Cascade events can also be used to complement the muon channel in searches for point sources or transient signals, albeit with inferior angular accuracy compared to muon tracks.

The detection efficiency of a NT is quantified by its effective area, *e.g.*, the fictitious area for which the full incoming neutrino flux would be recorded (see Figure 36.6). The increase with E_ν is due to the rise of neutrino cross section and muon range, while neutrino absorption in the Earth causes the decrease at large θ for large E_ν. Identification of downward-going neutrinos requires stringent event selection to suppress atmospheric muons, hence the cut-off towards low E_ν at low θ. Due to the small cross section, the effective area is many orders of magnitude smaller than the geometrical dimension of the detector; a $\overset{(-)}{\nu}_\mu$ with 1 TeV can, *e.g.*, be detected with a probability of the order 10^{-6} if the NT is on its path.

Due to the long muon range, CC interactions of up-going $\overset{(-)}{\nu}_\mu$ can be detected from far outside the instrumented volume. This

Int. J. Mod. Phys. A 2026.41. Downloaded from www.worldscientific.com
by UNIVERSITY OF CALIFORNIA @ BERKELEY on 09/16/26. Re-use and distribution is strictly not permitted, except for Open Access articles.

method also works for horizontal neutrinos up to about 10° above the horizon (depth dependent), where the background from atmospheric muons become prohibitive. Alternatively, one can select events that start inside the instrumented volume and thus remove incoming muons that generate early hits in the outer layers of the detector. Such a veto-based event selection is sensitive to neutrinos of all flavours from all directions, albeit with a reduced efficiency since a part of the instrumented volume is sacrificed for the veto. Such a muon veto, or vetoing events with a coincident signal in the surface array, also rejects down-going atmospheric neutrinos that are accompanied by muons from the same air shower and thus reduces the atmospheric-neutrino background. Actually, the breakthrough in detecting high-energy cosmic neutrinos was first achieved with this technique.

Note that the fields of view of NTs at the South Pole and in the Northern hemisphere are complementary for each reaction channel and neutrino energy.

36.3.2.1 *The Projects*

Table 36.4 lists past, present and future neutrino telescope projects and their main parameters.

Table 36.4: Past, present and future NT projects and their main parameters. The milestone years give the times of project start, of first data taking with partial configurations, of detector completion, and of project termination. Projects with first data expected past 2026 are indicated in italics. The size refers to the largest instrumented volume reached during the project development. The status of projects under construction is reported at the time of writing. See [98] for references to the different projects where unspecified.

Experiment	Milestones	Location	Size (km^3)	Remarks
DUMAND	1978/–/–/1995	Pacific Ocean		Terminated due to technical/funding problems
NT-200	1980/1993/1998/2015	Lake Baikal	10^{-4}	First proof of principle
GVD [102]	2012/2015/–/–	Lake Baikal	ca. 1	High-energy ν astronomy data taking with 14 clusters
AMANDA	1990/1996/2000/2009	South Pole	0.015	First deep-ice NT
IceCube [103]	2001/2005/2010/–	South Pole	1.0	First km^3-sized detector 6 additional strings installed 2025/26 (IceCube Upgrade)
IceCube-Gen2 [104]	2014/–/–/–	South Pole	5–10	Planned future extension of IceCube covering low and high energies, a surface array and radio detection
NESTOR	1991/–/–/2012	Med. Sea		2004 data taking with prototype
NEMO	1998/–/–/–	Med. Sea		R&D project, prototype tests
ANTARES	1997/2006/2008/2022	Med. Sea	0.010	First deep-sea NT
KM3NeT/ARCA [100]	2013/2021/–/–	Med. Sea	ca. 1	High-energy configuration for neutrino astronomy. Under construction, data taking with 45 strings
KM3NeT/ORCA [100]	2014/2020/–/–	Med. Sea	0.007	Low-energy configuration for neutrino mass hierarchy. Under construction, data taking with 33 strings
KM3NeT Phase 3	2013/–/–/–	Med. Sea	ca. 3	Possible future extension, 6 ARCA blocks + ORCA
P-ONE [105]	2018/–/–/–	Pacific Ocean	$\mathcal{O}(1)$	Planned future NT, R&D phase
TRIDENT [106]	2021/–/–/–	South China Sea	$\mathcal{O}(10)$	Planned future NT, R&D phase
HUNT [107]	2022/–/–/–	South China Sea or Lake Baikal	$\mathcal{O}(30)$	Planned future NT, R&D phase Prototype tests in Lake Baikal
NEON [108]	2023/–/–/–	South China Sea	$\mathcal{O}(10)$	Planned future NT, R&D phase

36.3.2.2 *Properties of media*

The efficiency and quality of event reconstruction depend strongly on the optical properties (absorption and scattering length, intrinsic optical activity) of the medium in the spectral range of bialkali photocathodes (300–550 nm). Large absorption lengths result in a better light collection, large scattering lengths in superior angular resolution. Deep-sea sites typically have effective scattering lengths of > 100 m and, at their peak transparency around 450 nm, absorption lengths of 50–65 m. The absorption length for Lake Baikal is 22–24 m. The properties of South Polar ice vary strongly with depth; at the peak transparency wave length (400 nm), the scattering length is between 5 and 75 m and the absorption length between 15 and 250 m, with the best values in the depth region 2200–2450 m and the worst ones in the layer 1950–2100 m.

Noise rates measured by PMTs with a diameter of 25 cm in deep polar ice are about 0.5 kHz per PMT and almost entirely due to radioactivity in the OM components. The corresponding rates in sea water are typically 60 kHz, mostly due to ^{40}K decays. Bioluminescence activity can locally cause rates on the MHz scale for seconds; the frequency and intensity of such "bursts" depends strongly on the sea current, the season, the geographic location, and the geometry of the detector elements. Experience from ANTARES shows that these backgrounds are manageable without a major loss of efficiency or experimental resolution.

36.3.2.3 *Technical realisation*

Optical modules (OMs) and PMTs: An OM is a pressure-tight glass sphere housing one or several PMTs with a time resolution in the nanosecond range, and in most cases also electronics for control, high-voltage generation, operation of calibration LEDs, time synchronisation and signal digitisation.

Hybrid PMTs with 37 cm diameter have been used for NT-200, conventional hemispheric PMTs with 20 cm diameter for AMANDA and with 25 cm diameter for ANTARES, IceCube and Baikal-GVD. A novel concept has been chosen for KM3NeT. Each OM (43 cm) is equipped with 31 PMTs (7.5 cm), plus control, calibration and digitisation electronics. Advantages are that (i) the overall photocathode area exceeds that of a 25 cm PMT by more

Int. J. Mod. Downloaded from www.worldscientific.com
by UNIVERSITY OF CALIFORNIA @ BERKE use and distribution is strictly not permitted, except for Open Access articles.

than a factor of 3; (ii) the individual readout of the PMTs results in a very good separation between one- and two-photoelectron signals which is essential for online data filtering and random background suppression; (iii) the hit pattern on an OM provides directional information; (iv) no mu-metal shielding against the Earth magnetic field is required. A multi-PMT optical module is also one of the two selected options for the IceCube Upgrade (see below). It contains 24 3-inch PMTs in a smaller-diameter glass vessel matching the maximal size of the ice holes. The second OM type for the Upgrade features two 8-inch PMTs (one upward- and one downward-pointing). See [104] for details. Figure 36.7 shows the OM designs currently used in IceCube and KM3NeT.

Readout and data filtering: In current NTs the PMT data are digitised in situ: for ANTARES and Baikal-GVD in special electronics containers close to the OMs, for IceCube and KM3NeT inside the OMs. For IceCube, data are transmitted via electrical cables of up to 3.3 km length, depending on the location of the strings and the depth of the OMs; for ANTARES, KM3NeT and Baikal-GVD optical fibre connections have been chosen (several 10 km for the first two and 4 km for GVD).

The full digitised waveforms of the IceCube OMs are transmitted to the surface for pulses appearing in local coincidences on a string; for other pulses, only time and charge information is provided. For ANTARES (time and charge) and KM3NeT (time and time over threshold), all PMT signals above an adjustable threshold are sent to shore.

The data are subsequently processed on online computer farms, where multiplicity- and topology-driven filter algorithms are applied to select event candidates. The filter output data rate is about 10 GByte/day for ANTARES and of the order 1 TByte/day for IceCube (100 GByte/day transferred via satellite) and KM3NeT.

Calibration: For efficient event recognition and reconstruction, the OM timing must be synchronised at the few-nanosecond level and the OM positions and orientations must be known to a few 10 cm and a few degrees, respectively. Time calibration is achieved by sending synchronisation signals to the OM electronics and also by light calibration signals emitted in situ at known times by LED or laser flashers (ANTARES, KM3NeT). Precise position calibration is achieved by measuring the travel time of light calibration signals sent from OM to OM (IceCube) or acoustic signals sent from transducers at the sea floor to receivers on the detector strings (ANTARES, KM3NeT, Baikal-GVD). Absolute pointing and angular resolution can be determined by measuring the "shadow of the moon" (*i.e.*, the directional depletion of muons generated in cosmic-ray interactions). IceCube and ANTARES have both shown that they have angular resolution below 1°, confirming MC calculations which indicate a precision of $\approx 0.5°$ for energies above 10 TeV. For KM3NeT, simulations indicate that sub-degree precision in the absolute pointing can be reached; for ORCA, 0.5° accuracy has been demonstrated..

Detector configurations: IceCube [103] (see Figure 36.8) consists of 5160 Digital OMs (DOMs) installed on 86 strings at depths of 1450 to 2450 m in the Antarctic ice; except for the DeepCore region, string distances are 125 m and vertical distances between OMs 17 m. 324 further DOMs are installed in IceTop, an array of detector stations on the ice surface above the strings. DeepCore is a high-density sub-array at large depths (*i.e.*, in the best ice layer) at the centre of IceCube.

The NT200 detector in Lake Baikal at a depth of 1100 m consisted of 8 strings attached to an umbrella-like frame, with 12 pairs of OMs per string. The diameter of the instrumented volume was 42 m, its height 70 m. Meanwhile, at the time of writing, the Baikal collaboration has installed and is operating the first 14 clusters of a future cubic-kilometre array, GVD [102]. It will consist of 20 clusters, each with 288 OMs at 8 strings, plus several single strings between the clusters; its completion is scheduled for 2028.

The operation of ANTARES (see [98, 109] and references therein) was terminated in 2022. It comprised 12 strings with lateral distances of 60–70 m, each carrying 25 triplets of OMs at vertical distances of 14.5 m, located at depths of 2.1–2.4 km, starting 100 m above the sea floor. An additional string held devices for calibration and environmental monitoring. A system to investigate the feasibility of acoustic neutrino detection was also implemented.

KM3NeT will consist of building blocks of 115 strings each, with 18 OMs per string. Operation of the first strings deployed has successfully verified the KM3NeT technology and sensitivity. In the upcoming phase of its staged implementation, KM3NeT aims at two building blocks for neutrino astronomy, with vertical distances between OMs of 36 m and a lateral distance between adjacent strings of 90 m (ARCA, for *Astroparticle Research with Cosmics in the Abyss*) and at one block for the measurement of the neutrino mass hierarchy, with vertical distances between OMs of 9 m and a lateral distance between adjacent strings of about 20 m (ORCA, for *Oscillation Research with Cosmics in the Abyss*) [100]. The installation of ARCA near Capo Passero, East of Sicily (depth 3440 m) and of ORCA near Toulon (depth 2450 m) is ongoing and as of now (March 2026) 45/33 strings have been deployed for ARCA/ORCA and are continuously taking data. Completion of the full ARCA and ORCA arrays is planned for 2030.

P-ONE (*Pacific Ocean Neutrino Experiment*) [105] is a new initiative in its R&D phase, envisaging a large NT in the Pacific Ocean off the Canadian coast. It is intended to use an existing deep-sea cable infrastructure and to optimise the sensitivity for horizontal neutrinos with energies beyond about 100 TeV.

Three Chinese collaborations are currently working towards projects on the 10 km^3 scale. TRIDENT (*Tropical Deep-Sea Neutrino Telescop*) is a proposed neutrino telescope in the South China Sea with an instrumented volume of 7.5 km^3. R&D and site exploration efforts are ongoing and a pathfinder (TRIDENT Phase-1) is planned to be commissioned around 2026 [110]. HUNT (*High-energy Underwater Neutrino Telescope*) aims at an instrumented volume of 30 km^3, either in the South China Sea or in Lake Baikal [107]. NEON (*NEutrino Observatory in the Nahnhai*) envisages another detector of 10 km^3 in the South China Sea [108]. Whether there will be a process convergence among these three projects appears open at present.

36.3.2.4 *Results*

See Sect. 30.4 for a summary of the results from neutrino telescopes.

36.3.2.5 *Plans beyond 2025*

The IceCube Upgrade project serves to create a very densely instrumented region by deploying additional strings in the DeepCore volume. Main objectives are to inclease the low-energy sensitivity, to improve the calibration of ice properties and thus also the archival data, and to test new technologies. In the Antarctic summer season 2025/26, six strings for the Upgrade have been deployed and are currently in their commissioning phase.

Within the future IceCube-Gen2 project, it is planned to extend the sensitivity of IceCube towards higher energies by installing a large-volume extension, combined with a radio array for highest-energy neutrinos and a surface array providing also a powerful veto against atmospheric events [104].

More information on the future extensions of GVD and KM3NeT and on P-ONE and the Chinese projects TRIDENT, HUNT and NEON are given above and in Table 36.4.

36.3.3 *Radio emission from (ultra-)high energy particle showers*

Revised March 2026 by S.R. Klein (NSD LBNL; UC Berkeley) and A. Nelles (DESY, Zeuthen; Erlangen U.).

Coherent radio-frequency (RF) electromagnetic radiation is an attractive signature to search for particle cascades produced by interactions of high-energy particles. RF signatures have been used to study both cosmic-ray air showers and to search for neutrino-induced showers. This article will discuss the radio signal generation in neutrino-induced showers. Radio signals from cosmic rays are discussed elsewhere [111,112]. The density of the medium (i.e. ice, air, lunar regolith, salt) determines how rapidly a shower develops. This, in turn, affects the radio emission mechanisms. In dense media, radio Cherenkov radiation dominates, while in air, geomagnetic radiation is dominant.

Int. J. Mod. Phys. A 2026.41. Downloaded from www.worldscientific.com
by UNIVERSITY OF CALIFORNIA @ BERKELEY on 09/16/26. Re-use and distribution is strictly not permitted, except for Open Access articles.

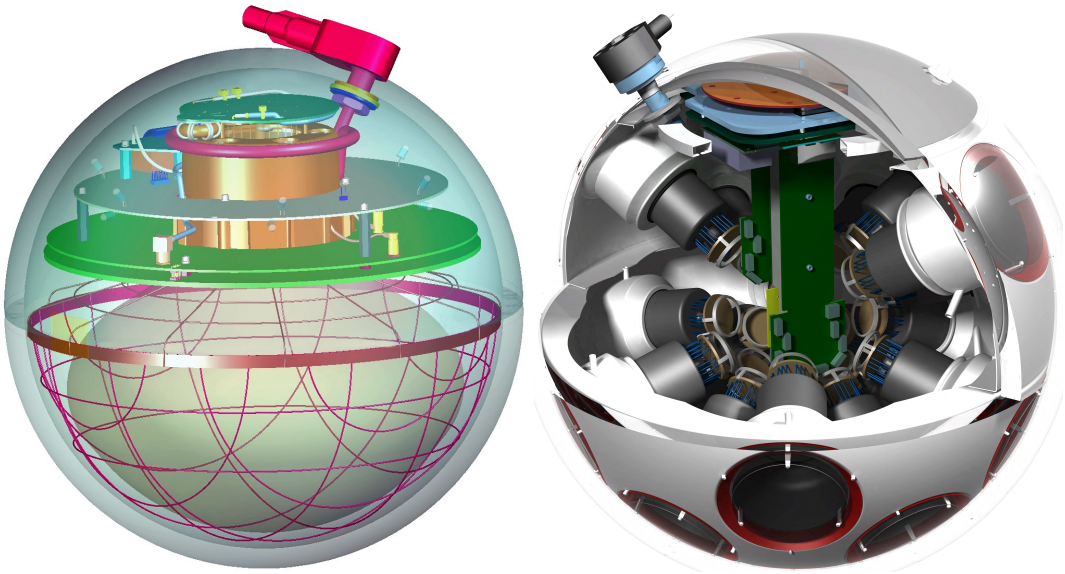

Figure 36.7: Schematic views of the digital OMs of IceCube (left) and KM3NeT (right).

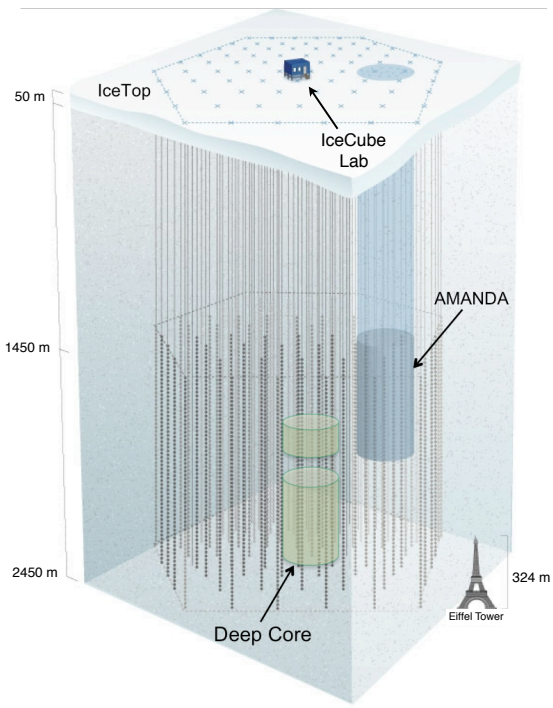

Figure 36.8: Schematic view of the IceCube neutrino observatory comprising the deep-ice detector including its nested dense part DeepCore, and the surface air shower array IceTop. Six strings of the IceCube Upgrade are installed in the DeepCore volume. The IceCube Lab houses data acquisition electronics and the computer farm for online processing. Operation of AMANDA was terminated in 2009.

At lower energies, incoherent optical Cherenkov radiation is frequently used, as discussed in "Neutrino telescopes" section 36.3.2. This article uses the general definitions and properties of neutrino telescopes as described in 36.3.2.

36.3.3.1 *Signal generation and its characteristics*

As discussed in the "Passage of Particles Through Matter" review Sec. 34 the electromagnetic component of a high energy shower gives rise to radio emission. The signal generation depends on the particle energy and the medium; the type of primary particle is unimportant. The medium must be non-conducting and transparent at RF frequencies. The shower develops over a length scale given by the radiation length X_0, which is much larger for air than for solids.

Coherent radio Cherenkov-like emission occurs because the shower contains more electrons than positrons. The coherent radio Cherenov emission, also known as Askaryan effect comes from the net current due to this excess [113–115].

In air, during propagation through the geomagnetic field, the relative motion of electrons and positrons is affected, which leads to a varying transverse current, usually referred to as the geomagnetic effect [111]. All effects may be described more generally as being due to radiation from a time-varying net charge [116]. Their relative importance is governed by the density of the medium, as the electric field of the Askaryan component scales as the net charge excess, and a lower density allows the geomagnetic effect to gain importance. Thus, in solid materials the emission from the Askaryan effect dominates, but it is a $< 20\%$ correction in air showers.

The net charge excess comes at the tail end of the shower, when the particles are mostly low-energy (< 100 MeV). There, positrons in the bean can annihilate on atomic electrons and inverse Compton scattering can accelerate atomic electrons into the shower. Even initially hadronic showers will have a low-energy tail that largely consists of $e^{\pm}$ and photons.

Coherent radiation is possible at wavelengths longer than the instantaneous thickness of the shower along an observer's line of sight. Since air showers have a larger extent than showers in solid media, their coherent radiation appears at lower frequencies [117]. If the density get too low, e.g. in very horizontal air showers, coherence is lost [118].

High-frequency radiation is concentrated around the Cherenkov angle θ_C. Viewed directly on the Cherenkov cone, the electric field strength, $\epsilon_{\rm Ch}$ at a frequency f from an electromagnetic shower from a ν_e with energy E_ν in ice may be roughly parameterized as [119, 120]

$$\epsilon_{\rm Ch}(V/{\rm mMHz}) = 2.53 \times 10^{-7} \frac{E_\nu}{1{\rm TeV}} \frac{f}{f_c} \left[\frac{1}{1 + (f/f_c)^{1.44}} \right] . \quad (36.3)$$

The electric field strength increases linearly with frequency, up to a cut-off frequency f_c, which is set by the transverse size of the shower [121, 122]. The maximum wavelength c/f_c is roughly the Molière radius divided by $\cos(\theta_C)$ where θ_C is the Cherenkov angle. The cutoff frequencies depend on the density (which affects the Molière radius). They are about 1 GHz in ice, about 3 GHz in the lunar regolith, and below 100 MHz in air, except exactly

Int. J. Mod. Downloaded from www.worldscientific.com
by UNIVERSITY OF CALIFORNIA @ BERKE use and distribution is strictly not permitted, except for Open Access articles.

on the Cherenkov angle, where all frequencies are coherent by definition.

Near f_c, radiation is narrowly concentrated around θ_C [121, 122]. At lower frequencies, the limited length of the emitting region leads to a broadening in emission angle around the Cherenkov cone. Away from θ_C, the electric field from Eq. (36.3) is reduced by [119],

$$\frac{\epsilon}{\epsilon_{\rm Ch}} = \exp\left(-\frac{1}{2}\frac{(\theta-\theta_C)^2}{(2.2^\circ \times [1{\rm GHz}/f])^2}\right). \qquad (36.4)$$

The angular distribution of the signal around θ_C can be parameterized by a Gaussian peak modulated by a $\sin\theta$. In both ice and the lunar regolith, θ_C is about 56°, in air only 1°. Close to θ_C, the 1 GHz maximum frequency in ice/regolith leads to a generated pulse width of ≈ 1 ns.

These equations are appropriate for ice. More general parameterizations can be found in [120, 123].

More accurate calculations of the predicted radio signal, in particular air showers are not easily parameterized, but require detailed Monte Carlo simulations. For air showers, these are built on microscopic air shower simulations, calculate the emission from all individual particles in the shower development and add them for different observer positions [111]. For neutrinos, most approaches calculate (directly or from a parameterization) the Askaryan signal from a shower profile. The signal is then propagated through the medium and into an antenna model [120].

At energies above 10^{16} eV in ice, the Landau-Pomeranchuk-Migdal effect lengthens electromagnetic showers, by reducing the cross-sections for bremsstrahlung and pair production [124]. The lengthening of the shower leads to a narrowing of the radio emission around the Cherenkov cone, and a reduction in high-frequency emission away from the cone [120]. At higher energies, this leads to two separate components of the Askaryan radiation from a neutrino interaction: an un-altered component from the hadronic portion of the shower and an angularly narrowed component from the LPM-lengthened electromagnetic shower. The width of the narrowed component scales as $E_\nu^{1/3}$. If these two components can be observed separately, they could, in principle, be combined to determine the inelasticity of the neutrino interaction [125], allowing for improved measurements of low$-x$ parton distributions and searches for beyond-standard-model interactions.

Similarly, energetic outgoing $\mu^\pm$ and $\tau^\pm$ from neutrino interactions dominantly lose energy via stochastic pair production and photonuclear interactions. These secondary particles will produce electromagnetic showers that can be detected by radio detectors, if they are above threshold energy. This will enable multiple detections of the same particle track and thus present interesting reconstruction opportunities and flavor sensitivity [126].

At still higher energies, above 10^{20} eV, the LPM effect strengthens, and the electromagnetic shower splits into multiple subshowers with significant separation. When these separations become large enough, the subshowers will effectively become independent radiators, with the total emission showing substantial event-by-event variation, depending on the division into subshowers [124]. Because of this, many experiments that study higher energy (well above 10^{20} eV) neutrinos focus on the hadronic shower from the struck nucleus. This contains an average of only about 20% of the energy, but with fewer large fluctuations [127].

36.3.3.2 *Energy regime of radio detectors*

In the coherent regime, the electric field amplitude is linearly proportional to the shower energy. Since the signal is a radio wave, the field amplitude decreases as $1/R$, plus potential absorption in the intervening medium, while the energy fluence decreases as $1/R^2$, again, plus potential absorption. The detection threshold depends on the distance to the antenna and the bandwidth and noise characteristics of the antenna and detector. For an antenna located in the detection medium, at a distance of 1 km the typical threshold is around 10^{17} eV. For stand-off (remote sensing) detectors, the threshold rises roughly linearly with the distance. These thresholds can be reduced by using directional antennas and/or combining the signals from multiple antennas using beam-forming techniques.

RF detectors are used to search for energetic neutrinos from three types of sources: astrophysical objects (*i.e.* extending measurements of the neutrino energy spectrum observed at TeV to PeV energies upward in energy), cosmogenic neutrinos associated with cosmic-ray-cosmic microwave background radiation (CMBR) interactions, and neutrinos from beyond-standard-model physics. These three types are very roughly associated with energies below 10^{18} eV, the energy range 10^{18} to 10^{20} eV, and above 10^{20} eV, albeit with considerable overlap.

Cosmogenic neutrinos are produced when ultra-high energy (UHE) protons with energy $E \gtrsim 5\times10^{19}$ eV interact with photons from the CMBR, infrared light from old stars, and other extragalactic background light. These protons are excited to a Δ^+ resonance which may decay via $\Delta^+ \to n\pi^+$, leading to neutrinos with energies above 10^{18} eV [128, 129]. The cosmogenic neutrino signal depends heavily on the fraction of UHE cosmic-rays that are protons. For a 100% proton composition (strongly disfavored by most data [130]), observing a cosmogenic neutrino signal of at least a few events per year requires a solid or liquid detector with an active volume of about 100 km^3 [131].

To reach the effective volumes necessary to observe the expected low fluxes of UHE neutrinos, common, naturally occurring, non-conducting solid (or potentially liquid) media, with a long absorption length for radio waves are needed. Optical Cherenkov detectors are limited by short (< 100 m) attenuation lengths [132] so would require a prohibitively expensive number of sensors. The radio detection technique has been used to detect air showers, targeting neutrinos as well as cosmic rays, and to search for neutrino showers in ice, salt domes and the lunar regolith.

36.3.3.3 *Reconstruction of particle energy and direction and background suppression*

Since radio detectors view the interaction from afar, the reconstruction techniques differ from optical neutrino telescopes.

Radio detection is a calorimetric measurement, thus provides good energy estimates of the shower energy. The energy fluence (time-integrated pulse power) of the signal scales quadratically with shower energy. It also depends on the distance to the shower, through potential attenuation losses and the usual $1/R$ loss in electric field amplitude. The arrival times in antennas and a spherical wave approximation can be used to determine the interaction vertex, although some uncertainty due to the viewing angle with respect to the Cherenkov angle may remain, if not corrected for by using the frequency information. If the radio signal travels through media where the index of refraction varies (like the firn of glacial ice), then ray-tracing techniques may be required to follow the signal back to the interaction point. For buried antennas, the bending of the signal trajectories due to the depth-dependent index of refraction creates an opportunity. For some geometries, there are two paths to the detector: a 'direct' path, with minor bending, and a second where the signal is bent beyond horizontal, bouncing off the surface before reaching the antenna. By measuring the time difference between the two paths, the distance to the interaction vertex may be determined; this greatly simplifies the energy determination [133, 134]. For most neutrino interactions (except for ν_e charged-current interactions), the shower energy is less than the neutrino energy. The uncertainty on the interaction inelasticity is a major contributor to the uncertainty in the neutrino energy, along with uncertainties on the distance between the antenna(s) and the interaction vertex [135].

Reconstruction of the neutrino arrival direction depends on several aspects of the signal and on a good understanding of the properties of the medium. First, the direction from the antenna to the interaction site must be determined. This can be done by using the relative timing from separated antennas, or using beam-forming techniques with multi-element arrays. For air showers, the signal arrival direction is (almost) equal to the particle arrival direction, with corrections being obtainable by fitting a hyperbolic wavefront [111, 112].

For showers in solid/liquid media, the arrival direction with respect to the interaction point - antenna vector is determined from two additional angles. The frequency spectrum can be used to de-

Int. J. Mod. Phys. A 2026.41. Downloaded from www.worldscientific.com
by UNIVERSITY OF CALIFORNIA @ BERKELEY on 09/16/26. Re-use and distribution is strictly not permitted, except for Open Access articles.

termine the angle between signal arrival direction and Cherenkov cone according to Eq. (36.4). The second angle can be determined from the polarization of the signal. The radio signal is produced with a linear polarization in the plane containing both the particle direction and the radio wave direction. These two angles can be combined to determine the direction, subject to a (usually) four-fold ambiguity, due to uncertainty as to whether the antenna is inside or outside the Cherenkov cone, and because the particle direction can be flipped 180° without affecting the observed signal [136]. Often, some of these solutions can be rejected because they correspond to long path lengths through the Moon or the Earth, where the neutrino would be absorbed. Spectral information is crucial for the reconstruction and background rejection. However, large bandwidth antennas typically disperse (i.e. broaden) the pulses. As long as the dispersion can be compensated for in the trigger and backgrounds controlled, a large bandwidth detector is the most sensitive.

All radio experiments must contend with background. Common sources are anthropogenic noise, antenna/preamp noise, charge generated by blowing snow, lightning, and, at low frequencies, radiation from the Milky Way. While narrowband noise impacts triggering and contaminates signal quality, impulsive backgrounds could mimic a signal. One of the major issues for radio-detection experiments is anthropogenic noise. Most anthropogenic noise has distinctive characteristics (such as being narrow-band, and coming from near the horizon) which makes it possible to reject during data analysis, via narrow-band filters and other techniques. However, these factors pose a challenge for triggering on the radio signal and reduce data purity. This is even an issue in Antarctica, where communication radios and passing satellites can mimic showers, at least at the trigger level. The need to limit anthropogenic noise has led most experimental groups to select remote locations for their detectors. Still, experiments need to reduce trigger-level noise, and/or to reject background at the analysis level. At this point, no robust and generally applicable strategy has been reported. For example, for multi-element arrays, the threshold drops as the square root of number of antennas, since the signal adds in-phase while the backgrounds add with random phases [137]. It seems, however, that e.g. triboelectric signals recorded in periods with winds exceeding 10 m/s are a problematic trigger-level background, for experiments in polar regions [138] and will require removal during analysis.

Most dedicated air shower experiments have used radio antennas in combination with at least one other detector technology, such as scintillation counters, if the site suffers from significant RF backgrounds and/or computing power on autonomous stations is limited. Exceptions are neutrino experiments with sensitivity to air showers, which are located in uninhabited polar regions, enabling them to relatively efficiently self-trigger on air showers [139, 140].

Lunar experiments (discussed below) use different techniques to reduce the anthropogenic background. Some experiments use multiple antennas, separated by at least hundreds of meters; by requiring a coincidence within a small time window, anthropogenic noise can be rejected. With good enough timing, beam-forming techniques can be used to further reduce the background. An alternative approach is to use beam forming with multiple feed antennas viewing a single reflector, to ensure that the signal points back to the moon.

Due to the similarity in the radio emission of air showers and neutrino showers, the more abundant cosmic rays can act as background to neutrino searches. In-ice detectors need to suppress in-air emission that is refracted into the ice, emission that is created from developing air showers continuing in the ice, as well as from stochastic energy-losses of atmospheric muons. Lunar experiments may faces challenges in separating neutrino interactions from cosmic ray interactions.

36.3.3.4 *Recent experiments*

Figure 36.9 shows some current limits from neutrino searches, including those from prototype arrays. Except for LOFAR, which is fully operational, projected limits from future experiments are not shown in the figure. Notably, the KM3NeT collaboration has observed an event with an energy above 100 PeV (with a central energy of 220 PeV) [141]. This observation is in tension (2.9σ) with the IceCube flux limit [142]. Various origin scenarios are being discussed.

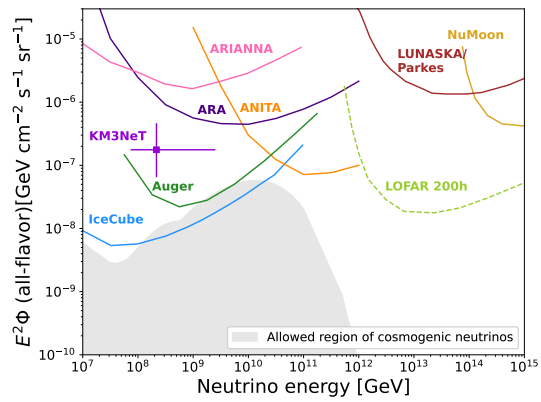

Figure 36.9: Representative 3-flavor (summed, assuming equal fluxes of each flavor) differential (over one decade in energy) limits from different experiments and prototype experiments. Shown are limits from the IceCube ultra-high energy ν search [142], the Auger search for earth-skimming ν_τ [143], the LUNASKA/-Parkes [144] and NuMoon lunar searches [145], the ANITA balloon experiment [146], ARA [147] and ARIANNA prototypes [148], along with projections for the LOFAR array [149]. Also shown is the flux implied by the event seen by KM3NeT [141]. The ARA and ARIANNA limits are from prototype arrays, and indicate the energy range that might be covered, with far higher sensitivity by larger arrays (see 36.3.3.5). The shaded area is the allowed region for cosmogenic neutrinos from a recent global analysis as published in [104] following the methods from [150].

i. *Ice*

The most common dense medium transparent to radio waves is ice. Natural ice is an attractive medium for neutrino detection with radio attenuation lengths from over 300 m to 1 km [151]. The attenuation length varies with frequency and ice temperature, with higher attenuation in warmer ice. Although glacial ice is mostly uniform, the top $\approx$ 100 m of ice, the 'firn,' exhibits a gradual transition from packed snow at the surface (typically $\rho = 0.35$ g/cm^3) to solid ice ($\rho = 0.92$ g/cm^3) below [152]. The thickness of the firn varies with location; it is thicker in central Antarctica than in the coastal ice sheets or in Greenland. The density variation has several implications.

The index of refraction depends linearly on the density, so radio waves curve downward in the firn. This bending reduces the effective volume of shallow or aerial antennas. A shallow antenna cannot see near-surface interactions at large horizontal distances. There are also indications that the increase in firn density is slightly non-monotonic [153, 154]. This leads to non-monotonic changes in index of refraction which may create waveguides that trap a small fraction of the radio energy and propagate it horizontally.

In one type of experiment, antennas mounted on high-altitude balloons observe the ice from above. Radio signals from in-ice neutrino interactions propagate to the surface, traverse the ice-air interface, and then travel to the balloon. The surface roughness of the ice can affect signals as they transition from the ice to the atmosphere. The best known example, ANITA, has made four flights around Antarctica, floating at an altitude around 35 km [155]. Its 32/40/48 (depending on the flight) dual-polarization horn antennas scanned the surrounding ice, out to the horizon (650 km away). Because of the small angle of incidence, ANITA could use polarization information to separate signals from background; ν signals should be vertically polarized, while most background from cosmic-ray air showers should be horizontally polarized.

Int. J. Mod. [redacted] nloaded from www.worldscientific.com
by UNIVERSITY OF CALIFORNIA @ BERKE use and distribution is strictly not permitted, except for Open Access articles.

As with all radio-detection experiments, ANITA had to contend with anthropogenic backgrounds. The ANITA collaboration uses their multiple antennas as a phased array to achieve good pointing accuracy, with a resolution of 0.2-0.4° in elevation, and 0.5-1.1° in azimuth. They rejected all events that pointed toward known or suspected areas of human activity. ANITA has set the most stringent flux limits yet on neutrinos with energies above 10^{20} eV [146]. The ANITA experiment has also reported several anomalous events, matching cosmic ray signals, but with unexpected polarization signature, which the collaboration has indicated might be from Earth-skimming ν_τ [156, 157]. However, this interpretation is controversial and firmly excluded by both Auger [158] and IceCube [142].

Because of the significant source-detector separation, ANITA is most sensitive at energies above 10^{19} eV. A lower energy threshold requires a smaller antenna-target separation.

Other ice based experiments use antennas located within the active volume, allowing them to reach thresholds around 10^{17} eV, or lower with phased array antennas. This approach was pioneered by the RICE experiment [159] which buried 18 half-wave dipole antennas in holes drilled for AMANDA at the South Pole, at depths from 100 to 300 m. The hardware was sensitive from 200 MHz to 1 GHz. Each antenna fed an in-situ preamplifier which transmitted the signals to surface digitizing electronics.

Following RICE, two groups have deployed prototype arrays which have explored different detector concepts. The Askaryan Radio Array (ARA) deployed surface and buried antennas at the South Pole [160], while the Antarctic Ross Iceshelf Antenna Neutrino Array (ARIANNA) installed shallow antennas on the Ross Ice Shelf [148], about 110 km north of McMurdo station. ARIANNA offered the possibility of detecting downward-going ν, from the radio waves reflected off the ice-sea water interface on the bottom of the Ross Ice Shelf, while ARA took advantage of the colder, deeper ice at the South Pole, with its longer radio attenuation length. ARA buried antennas up to 200 m deep to be able to observe a larger portion of ice, due to the refraction of the signal in the firn. In contrast, ARIANNA deployed antennas just below the surface, allowing them to use high-gain, but large log periodic dipole antennas. At ARA, phased-array trigger techniques have been demonstrated that can reduce the energy threshold by a factor of several [137, 161].

Both experiments use stations which operate independently, spaced far enough to maximize sensitivity, but where only a small fraction of neutrino events will be visible in multiple stations. Each station includes multiple antennas, which will be sensitive to both horizontal and vertical polarization. The expected angular resolution is a few degrees [136].

The Radio Neutrino Observatory Greenland (RNO-G) is under construction at Summit Station, Greenland, where the ice is about 3,000 m thick. RNO-G is planned to consist of 35 stations, which employ ARIANNA-style shallow antennas, an ARA-style phased array and deep antennas, and draws on ANITA's electronics heritage [162]. Installation speed is limited by the drill speed. In July, 2025, 8 stations were operational with holes for 4 additional stations prepared for installation.

ii. *The Moon*

Because of its large size and non-conducting regolith, and the availability of large radio-telescopes, the Moon is an attractive target [163]. Conventional radio-telescopes are quite well suited to lunar neutrino searches, with natural beam widths not too dissimilar from the size of the Moon. Still, there are experimental challenges. The attenuation length is typically estimated to be 9 m/f(GHz) [164], so only near-surface interactions can be studied. The composition of the lunar regolith is not well known, and there are significant uncertainties due to this uncertainty. One big limitation of lunar experiments is that the 385,000 km target-antenna separation leads to energy thresholds above 10^{20} eV.

The effective volume probed by experiments depends on the geometry, which itself depends on the frequency range used. At high frequencies f, the electric field strength is high, leading to a lower energy threshold, but the sensitive volume is limited because the Cherenkov cone only points toward the Earth for a narrow range of geometries. Lower frequency radiation is more isotropic, so the effective volume is larger, but, because the electric field is weaker, the energy threshold is higher. The $1/f$ dependence of the attenuation length in the lunar regolith further increases the effective volume at low frequencies. The frequency range affects the energy dependence of the sensitivity. As can be seen in Fig. 36.9, a low-frequency experiment like NuMoon (which covered 115-180 MHz) has good sensitivity, but only above about 10^{14} GeV, while Lunaska/Parkes, which observed in the range 1200-1500 MHz, has a higher flux limit, but is sensitive above about $10^{12.5}$ GeV.

Current limits and projected sensitivities are sensitive to many details. A recent review [165] compared different radio-detection experiments using a common framework, and found some significant shifts in sensitivities due to, e.g. different assumptions about lunar composition and inelasticities.

With modern technology, it is increasingly viable to search over very broad frequency ranges [166]. One technical challenge is due to dispersion (frequency dependent time delays) in the ionosphere. Dispersion can be largely removed with a de-dispersion filter, using either analog circuitry or post-collection digital processing.

iii. *Air*

Radio detection in air is sensitive to all particles inducing air showers. Radio-detection can be used to determine the energy of cosmic rays, as done by e.g. the Auger and Tunka-Rex experiments [167, 168]. Radio signals can also be used to infer the atmospheric depth for shower-maximum, where the shower contains the most particles, as done by e.g. the LOFAR and Tunka-Rex collaborations [168, 169]. This depth is sensitive to the cosmic-ray composition. Reconstructing the particle arrival direction is much easier in air since the Cherenkov angle, and thus the radio wavefront, aligns with the axis to 1°. Radio-detection is also useful for energy cross-calibrations between different experiments. The Pierre Auger collaboration has recently shown that radio can provide an independent energy scale calibration, in good agreement with the other detectors of the observatory [170].

One variation on the radio-detection approach is to look for radio emission from Earth-skimming ν_τ [171, 172]. Although ν_τ are much less commonly produced than ν_μ and ν_e, over astrophysical distances, oscillations lead to a $\nu_e : \nu_\mu : \nu_\tau$ ratio near $1 : 1 : 1$, for almost all non-exotic acceleration and propagation mechanisms.

If the ν_τ traverse the Earth and interact while traveling upward, the resulting $\tau^\pm$ may exit the Earth before decaying. 83% of the time, the decay produces a hadronic or electromagnetic shower in the atmosphere [173]. Experiments have searched for these upgoing showers, and for the resulting optical Cherenkov and coherent RF radiation. The threshold energy dependence for these searches depends on several factors, notably including the average $\tau^\pm$ decay length, which increases linearly with energy. For somewhat lower energy ν_τ, with shorter decay lengths, a mountain may serve as a target, with $\tau^\pm$ expected to emerge from the other side. The Pierre Auger observatory sets stringent limits on this neutrino flux at energies above 10^{17} eV [143]. The Pierre Auger Collaboration has recently upgraded their surface array to include radio antennas at all water Cherenkov detectors. This array will improve the sensitivity of the instrument to horizontal showers, both for composition sensitivity for cosmic rays and for the detection of Earth skimming neutrinos [174].

36.3.3.5 *Future experiments*

Looking ahead, RNO-G [162] will continue deployment in the next years and has reached the largest yearly sensitivity of any radio array thus far. Further out, the proposed IceCube-Gen2 expansion includes a substantial radio array component [104], which will be sensitive to both neutrinos from the ice and air showers from cosmic rays. PUEO, a successor of ANITA, with significantly improved sensitivity, completed its first flight early 2026 [175].

For lunar neutrino detection, several large radio detector arrays should reach significantly lower energies in the near future. The LOFAR array is taking data with 36 detector clusters spread over Northern Europe [149]. Also, the Square Kilometer Array (SKA) with its roughly 60,000 antennas will push thresholds down to near 10^{20} eV [166]. The SKA will also study air showers [176].

Int. J. Mod. Phys. A 2026.41. Downloaded from www.worldscientific.com
by UNIVERSITY OF CALIFORNIA @ BERKELEY on 09/16/26. Re-use and distribution is strictly not permitted, except for Open Access articles.

A number of dedicated prototype ν_τ radio-detection experiments exist. The GRAND Collaboration, e.g., is proposing to deploy a large array of simple autonomous radio stations optimized for near-horizontal signals [177]. As of 2025 a first proto-array is operational.

36.4 Large time-projection chambers for rare event detection

Written October 2025 by L. Baudis (Zurich U.).

Initially developed for particle physics experiments at accelerators (see *Section 35.6.5*), the concept of a Time Projection Chamber (TPC) [178] evolved and is now tailored to a large range of applications, most notably to experiments in astroparticle physics searching for rare interactions deep underground. Present and proposed experiments designed to observe interactions of dark matter and other exotic particles, second order weak nuclear decays, as well as neutrinos from a variety of sources are based on TPCs operated with pure noble elements, either in gaseous or liquid form. The detectors aim for large target masses, low energy thresholds (keV-scale) and ultra-low levels of backgrounds from radioactivity and cosmic rays. Historical introductions, reviews of the operation principles, instrumentation and technological aspects, as well as applications, are found in Refs. [179–184].

The two most common noble fluids employed as detector media in present TPCs for rare event searches are argon and xenon, either as a high-pressure gas, or in liquid phase, or in liquid and gas phase (dual-phase). An interaction within the active volume of a TPC will create ionisation electrons and scintillation photons. The prompt scintillation signal is detected with one or two arrays of photosensors, while the ionisation electrons, which drift in the pure medium under the influence of an external, uniform electric field, are observed either directly with charge sensors, or via proportional scintillation, or electroluminescence. Since transverse electron diffusion is small, albeit non-negligible, the ionisation signal provides the $x-y$ information of the interaction site, with the $z-$information coming from the drift time measurement. The TPC thus yields a three-dimensional event localisation, enabling fiducial volume selections and differentiation between single- and multiple-scatters in the active volume. These features are crucial for filtering out rare events from the much higher backgrounds due to residual radioactivity of detector components. The specific energy loss (dE/dx) depends on the primary interacting particle, and leads to a distinct ratio of scintillation to ionisation for gammas/electrons, alphas and fast neutrons, allowing for further background discrimination. Two examples for the operation principle of TPCs for rare event detection are shown in Fig. 36.10.

The properties of liquid argon as detection medium in a TPC are reviewed in *Section 35.7*. Here some properties for xenon are given in Tab. 36.5. In the liquid phase, the high xenon density allows for compact, large and homogeneous detector geometries with efficient self-shielding against external radiation, given that the cross sections for the photoelectric effect, Compton scattering and pair production scale as $Z^5/E_\gamma^{7/2}$, Z/E_γ and $Z^2 \ln(2E_\gamma)$, respectively, for incoming X-rays and gammas with energy E_γ. The radioactive isotopes ^{124}Xe, ^{126}Xe, ^{134}Xe and ^{136}Xe have very long half-lives, and their second-order weak decay modes are subject to investigation (see *Section 36.4.2*).

In an argon or xenon detector, the energy loss of an incident particle is shared between ionisation, excitation and sub-excitation electrons liberated in the ionisation process. The average energy loss in ionisation is slightly larger than the ionisation potential, as it includes multiple ionisation processes. In their condensed phases, argon and xenon exhibit a band structure of electronic states, with the band gap energy being around 14.3 eV and 9.3 eV for liquid argon and xenon, respectively. In gaseous xenon, the ionisation potential is about 12.1 eV. Scintillation arises from excited atoms (excitons) and from ions, via recombination, with the emitted vacuum-ultraviolet (VUV) photons in single bands centred at $\lambda = 128$ nm for argon and $\lambda = 175$ nm for xenon. The excited dimers (or excimers), at their lowest excited level, de-excite to the dissociative ground state by the emission of a single VUV photon. This comes from the large energy gap between the lowest excitation and the ground levels, forbidding other decay channels such as non-radiative transitions. The scintillation light has two decay components due to de-excitation of spin singlet and spin triplet states of the excited dimers to the ground state. The singlet and triplet states refer to the total spin quantum number (s=0 or s=1) of the excited Rydberg electron and the angular momentum due to the molecular orbit, with the shorter and longer decay shapes being produced by the de-excitation of s=0 states (spin-allowed) and s=1 states (spin-forbidden), respectively. The different pulse decay time for different type of particle interactions, and thus ionisation densities, is employed to discriminate electronic from nuclear recoils. While this is very effective in liquid argon, due to the large time separation of (6 ± 1) ns versus (1500 ± 100) ns, it is more difficult to put in practice for xenon [185], considering the much smaller separation, (2.2 ± 0.3) ns versus (27 ± 1) ns, of the two components.

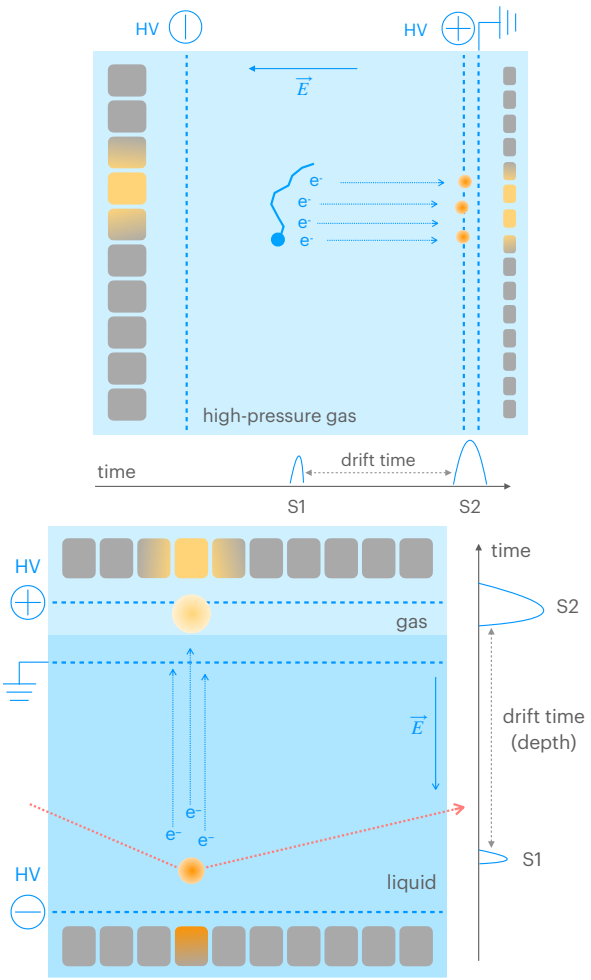

Figure 36.10: Operation principle of TPCs for rare event detection: a high-pressure gas (top) and a dual (liquid/gas) phase (bottom) TPC. A particle interaction yields a prompt scintillation signal (S1) and a delayed, amplified proportional scintillation signal (S2). The latter is caused by ionisation electrons drifted in a homogeneous electric field (and, for dual phase TPCs, extracted into the gas phase above the liquid). In these examples, both S1 and S2 signals are observed with photosensor arrays placed behind the anode and cathode (left), or at the top and bottom (bottom) of the TPC. The position information along the drift field is inferred from the time difference between the two light signals, while the position in the transverse plane to the field is derived from the S2 light pattern in the photosensor plane close to the electroluminiscent light production site.

The recombination-independent, mean energy required to produce a single detectable quantum (photon or electrons), called

Int. J. Mod. [redacted] by UNIVERSITY OF CALIFORNIA @ BERKE[redacted]nloaded from www.worldscientific.com use and distribution is strictly not permitted, except for Open Access articles.

Table 36.5: Physical properties, volume fraction in the atmosphere, radioactive isotopes of the noble element xenon.

Property [unit]	Xe
Atomic number, mean atomic mass [g/mol]	54, 131.29
Boiling T_b and melting T_m point at 1 atm [K]	165.0, 161.4
Gas density at 1 atm and 298 K (T_b) [g/l]	5.40 (9.99)
Liquid density at T_b [g/cm^3]	2.94
Volume ratio ($\rho_{\rm liduid}/\rho_{\rm gas}$)	526
Dielectric constant of liquid	1.95
Scintillation light yield (in liquid, at 122 keV) [186]	63 photons/keV
Wavelength (peak centred at)	175 nm
Decay time constants (s=0, s=1)	2.2 ns, 27 ns
Refractive index	1.69
Electron mobility* [188]	0.29 mm^2/(μs V) ($\lesssim$100 V/cm)
	0.01 mm^2/(μs V) ($\gtrsim$100 V/cm)
Volume fraction in Earth's atmosphere [ppb]	87
Isotopes with spin, abundance [%]	^{129}Xe, 26.44; ^{131}Xe, 21.18
Radioactive isotopes,	^{136}Xe, 8.87; 2.2×10^{21} [189, 190]
abundance [%] and $T_{1/2}$ [y]	^{124}Xe, 0.095; 1.1×10^{22} [191–193]
	^{134}Xe, 10.4; $>8.7\times10^{20}$ (90% C.L.) [194]
	^{126}Xe, 0.089; $>1.9\times10^{22}$ (90% C.L.) [195]

*Measured values in two benchmark regimes, so-called "cold" and "hot" electrons [187]. In the first case, the electron energies are due to thermal bath of the xenon fluid and they rapidly gain energy with increasing field; in the second case, the electrons have gained most of their energy through acceleration in the field and experience increased energy loss on their path due to collisions with Xe atoms.

the W-value, assumes that each recombining electron-ion pair produces an exciton, which leads to a photon. In liquid argon, the W-value is (19.5 ± 1.0) eV [196]. In liquid xenon, the widely-adopted W-value is (13.7 ± 0.2) eV, measured with 122 keV γ-rays from an external ^{57}Co source [197]. Recently, a lower value of $11.5^{+0.2}_{-0.3}$ (syst.) eV was obtained in a small TPC with internal sources at energies between 2.8 keV and 42 keV [198], consistent with the value measured at the MeV-scale, 11.5 ± 0.5(syst.) $\pm$ 0.1(stat.) eV with the EXO-200 detector [199]. The ionisation and scintillation W-values in gaseous xenon are 24.8 eV and (76 ± 6) eV, respectively [200].

The partition between excitation and ionisation depends on the density of the electron-ion pairs produced along the track of a particle, and the recombination fraction depends on the applied electric field, as well as on the ionisation density in the track. While several phenomenological models exist to describe electron-ion recombination as a function of stopping power and electric drift field (see [179] and discussions therein), a solid theory of energy loss of low-energy ions in noble fluids is still missing. For nuclear recoils as generated by interactions of neutrons, neutrinos or hypothetical WIMPs, an energy-dependent quenching is introduced via the Lindhard factor $\mathcal{L}$ [201], with $\mathcal{L}$ being around $0.2 - 0.25$ and $0.15 - 0.2$ in liquid argon [202] and xenon [203], respectively, at nuclear recoil energies in the range 3-100 keV. A comprehensive framework to simulate scintillation and ionisation yields in argon and xenon as a function of interaction type, energy and electric field in a TPC is the Noble Element Simulation Technique (NEST) [204].

To calibrate the energy scale and determine the energy resolution of low-background TPCs, mono-energetic lines from external (e.g., ^{57}Co, ^{60}Co, ^{137}Cs, ^{228}Th, etc) and internal (^{83m}Kr, ^{37}Ar) calibration sources, as well as from neutron activation lines (e.g., ^{129m}Xe, ^{131m}Xe in xenon) are used. Relative energy resolutions (σ/μ) at the level of 4-6% at energies of a few tens of keV and 2-3% at energies of a few 100 keV were reached in argon and xenon TPCs, respectively. At higher energies, relevant for the neutrinoless double beta decay of ^{136}Xe, relative resolutions of 0.67%, 0.8% and 1.2% around 2.5 MeV were obtained by LZ [205], XENON1T [206] and EXO-200 [207], respectively. Superior energy resolutions are attained in high-pressure gas TPCs with electroluminiscent amplification [208], with a relative resolution of 0.4% obtained in the NEXT-White detector [209]. This is due to the fact that the Fano factor in pure gaseous xenon, $F_{\rm GXe}$ = 0.15$\pm$0.02, is about two orders of magnitude smaller than in the liquid phase.

To achieve a high collection efficiency for both ionisation and scintillation signals, the concentration of impurities is reduced and maintained at a level below one part per 10^9 (ppb) oxygen equivalent. While the light can be strongly reduced by the presence of water vapour, the ionisation signal also requires high purity in terms of molecules with high electronegative affinity. The purity is commonly expressed via the electron drift lifetime, τ_e, which is the time over which the number of drifting electrons, n_e, is reduced by a factor e: $n_e(t) = n_e(t_0)\exp(-t/\tau_e)$. Ideally, τ_e should be a few times larger than the total drift time in a TPC, to prevent charge losses. Lifetimes > 10 ms were achieved both in argon and xenon (corresponding to impurity concentrations $\ll$1 ppb O_2 equivalent) via continuous recirculation and purification in the liquid or gas phase.

The drift velocity of electrons, which depends on the drift field E_d and the electron mobility μ as $v_d = \mu \cdot E_d$, has been measured for drift fields between $\sim (10 - 10^4)$ V/cm. It also depends on the temperature in the medium and the impurity concentration, often making the comparison between different measurements difficult. In general, the drift velocity raises from about 0.25 mm/μs at low fields to 2 mm/μs at high fields in both argon and xenon. As electrons drift in the electric field, the initial electron cloud spreads both in longitudinal and transversal direction to the field, expressed in terms of longitudinal D_L and transversal D_T diffusion coefficients, with $D_L < D_T$ and $D_L/D_T \approx 1$ for fields approaching zero. In argon, D_L was measured as $\sim$4.2 cm^2/s at 200 V/cm [210], $\sim$3.7 cm^2/s at 274 V/cm [211], $\sim$7.2 cm^2/s at 500 V/cm and D_T as $\sim$12 cm^2/s [212]. In xenon, D_L is around 100 cm^2/s at low fields, reaching $\sim$25 cm^2/s at higher drift fields [188], while D_T has been measured to be $\sim$55 cm^2/s at fields between (20-600) V/cm [213]. As an example, the spatial distribution of an initially point-like electron cloud, after a drift time t, is $\sigma_D = \sqrt{2Dt}$, resulting in a value of $\sim$20 mm for 1 ms drift and a 25 cm^2/s diffusion coefficient.

The scintillation light can be attenuated by absorption on impurities or due to Rayleigh scattering, the latter depending strongly on the wavelengths of the photons and the optical properties of the materials. Since only the combined effect is observed, it is non-trivial to disentangle the two contributions. A combination of measurements and theoretical calculations yield total attenuation and Rayleigh scattering lengths between 55-110 cm and 60-99 cm for argon and 30-50 cm and 30-50 cm for xenon detectors, with refractive indexes between 1.34 and 1.57-1.72, respectively, and absorption lengths $>$100 cm [179, 214].

Background sources for rare-event searches, their mitigation

Int. J. Mod. Phys. A 2026.41. Downloaded from www.worldscientific.com
by UNIVERSITY OF CALIFORNIA @ BERKELEY on 09/16/26. Re-use and distribution is strictly not permitted, except for Open Access articles.

techniques and radio-purity assays are discussed in *Section 36.6* of this *Review*. The main backgrounds in large TPCs are due to decays of other noble isotopes mixed with the argon and xenon (^{39}Ar, ^{85}Kr, ^{222}Rn), from natural, anthropogenic or cosmogenic radioactivity of detector materials in close proximity to the target (^{238}U, ^{232}Th, ^{40}K, ^{60}Co), and from muons and their secondary particles, including *in situ* production of isotopes which are sufficiently long-lived to render their vetoing difficult (e.g., ^{137}Xe in xenon TPCs). Astrophysical neutrinos cause largely irreducible backgrounds in dark matter detectors, but deliver exciting physics signatures in their own right. To mitigate the ^{39}Ar background, argon is extracted from underground sources (CO_2 wells), ^{85}Kr and ^{222}Rn are reduced by cryogenic distillation, exploiting the different vapour pressures of the different noble gases, or with gas chromatography using synthetic charcoal. In xenon detectors, ^{nat}Kr concentrations of < 50 ppq [215] and ^{222}Rn concentrations of $0.8\,\mu$Bq/kg were achieved by cryogenic distillation In argon TPCs, ^{39}Ar concentrations of (0.73 ± 0.11) mBq/kg were demonstrated [216].

An overview of large TPCs for rare event searches is given in Table 36.6.

36.4.1 *Dark matter and other low energy signals*

TPCs built to search for particle dark matter are based on the two-phase principle. Starting with total masses of a few kilogram the detectors evolved and reached active target masses at the tonne- and more recently multi-tonne scale. Concomitantly, the background levels in the most inner regions constantly decreased, with current electronic recoil rates of 15 events/(t y keV) in the energy region below 100 keV for xenon detectors [217]. Typically, the TPCs contain two arrays of photosensors, one immersed in the liquid, and one in the gas phase above the liquid at similar low temperature. The xenon scintillation light can be observed directly by PMTs with synthetic silica (quartz) windows or with VUV-sensitive SiPMs, while for argon detectors, tetraphenyl butadiene (TPB) is used to shift the 128 nm light to 420 nm, given that it is absorbed by quartz windows.

The DarkSide-50 experiment [216] operated a 50 kg TPC with liquid argon depleted in ^{39}Ar until 2019. DarkSide-20k [218], to operate 51.1 t of underground LAr in an octogonal TPC, the walls made of gadolinium-loaded acrylic panels, with two arrays of SiPMs, is under construction in Hall C of the Laboratori Nazionali del Gran Sasso (LNGS) in Italy. The first filling with liquid argon is planned for the end of 2026, with data taking starting in 2027. A larger, 400 t LAr detector, Argo, has been proposed for SNOLAB in Canada. After the successful operation of TPCs for LUX, PandaX-II and XENON1T, the current generation of xenon detectors, LUX-ZEPLIN (LZ) [219] at the Sanford Underground Facility (SURF) in USA, PandaX-4T [220] at the China Jinping Laboratory (CJPL) and XENONnT [221] at LNGS, employ several tons of LXe as active target mass. Their overall TPC design is rather similar, with cylindrical, polytetrafluoroethylene (PTFE) enclosed target regions viewed by two arrays of low-radioactivity, 3-inch diameter Hamamatsu R11410 PMTs. The PTFE has a high reflectivity for the Xe scintillation light [222]. Next-generation detectors, at the 50 t LXe scale or beyond, have been proposed with XLZD [223] and PandaX-xT [224], while DARWIN [225,226] continues the R&D towards XLZD. Recent constraints on various dark matter candidates are presented in *Section 27.6*. The search for WIMP dark matter is ongoing, with the sensitivity goal of current experiments to the spin-independent WIMP-nucleon cross section around $1.5\times10^{-48}\,\mathrm{cm}^2$ at 40-50 GeV/c^2 mass [219,221].

Owing to low electronic recoil backgrounds and low energy thresholds in noble liquid TPCs, high-sensitivity searches for dark matter electron scattering with particle candidates from a hidden sector, for keV-scale axion-like-particles (ALPs) and dark photons via absorption in LXe, as well as searches for solar axions, became feasible (see *Section 27.6*). Looking at ionisation-only signals allows for a further reduction of the energy threshold, given the much higher efficiency to detect an ionisation electron compared to a primary scintillation photon (typically 90% versus 10%). While this gain comes at the expense of higher backgrounds, it allows nonetheless to set stringent limits on light dark matter electron interactions at masses from a few tens of MeV to a few GeV, as shown by DarkSide-50 [227], PandaX-4T [228], XENONnT [229] and LZ [230]. Further, current-generation dual-phase TPCs have reached target masses which will allow for the first time the detection of solar *pp* neutrinos via elastic neutrino-electron scattering at energies down to 1 keV. Recently, the first detection of ^{8}B neutrinos via coherent elastic neutrino-nucleus scattering (CEνNS) was reported by PandaX-4T [231] and XENONnT [232].

Dual-phase TPCs were successful in gradually scaling up their target mass and in reducing the background levels for each iteration, while maintaining a low-energy threshold of $\sim$1 keV for electronic recoils. Notwithstanding, the construction of next-generation detectors at the multi-ten-tons scale poses multiple technological challenges. The background goals are such that electronic and nuclear recoils rates are below the ones from irreducible astrophysical neutrino interactions. This requirement sets the goals for the intrinsic ^{222}Rn and ^{85}Kr concentrations: the background from the decay of these isotopes should be significantly lower than the solar pp-neutrino elastic scattering rate. This translates into 0.1μBq/kg for ^{222}Rn[2] and 0.1 ppt (parts per billion, or 10^{-9}) for ^{nat}Kr, assuming a ^{85}Kr/^{nat}Kr ratio of 2×10^{-11}mol/mol. While ^{nat}Kr concentrations of < 50 ppq (parts per quadrillion, or 10^{-15}) were already achieved, for ^{222}Rn a factor of about 10 reduction compared to the current values [233] is needed. This calls for a high liquid throughput (close to 1 t/hour) with efficient cooling power based on cryogenic heat pumps and radon-free heat exchangers. Cryogenic distillation or charcoal chromatography must go hand in hand with selection of low radon emanation materials and new coating techniques to prevent radon emanation from surfaces.

Other challenges related to the liquid target are the continuous purification for electronegative impurities and water, to maintain high charge and light yields, while not introducing radon into the TPCs, as well as new solutions for reliable storage and recuperation at large scales. A dedicated single-closed-loop cryogenic system capable of handling 100 t of underground argon was designed and constructed for DarkSide-20k [234]. Liquid phase purification powered by a liquid xenon pump, as demonstrated in [235], was employed to achieve an electron drift lifetime above 15 ms in about 8.6 t of xenon in XENONnT. A system capable of handling 30 t of xenon in liquid phase, including long-term storage and and transfer of the cryogenic liquid between storage module and detectors was constructed for PandaX-xT [224, 236].

Regarding the detector design, electrodes with large (>2.5 m) diameters, with high transparency, minimal sagging and low spurious electron emission, as well as high-voltage feed-throughs that can safely deliver 50 kV or more to the cathode must be employed. DarkSide-20k will use for the first time anode and cathode plates made out of acrylic coated with a commercial conductive polymer and with TPB. LZ successfully built custom-woven wire-mesh grids with 1.5 m diameter, produced with an in-house built loom to weave the wire meshes [237]. Finally the cryostat design must ensure stability, while reducing as much as possible the amount of material, and thus gamma and neutron emitters in proximity to the TPCs.

Besides Ar and Xe TPCs, detectors using superfluid ^{4}He, targeted at low-mass dark matter, are under development within the HeRALD [238] and DELight [239] programs, based on the basic principles demonstrated by the HERON solar neutrino project [240]. The detectors will be instrumented with transition edge sensors or magnetic micro-calorimeters to observe both atomic signals, such as scintillation light, and quasiparticle (phonon and roton) excitations. As in other noble elements, the He_2^* dimers appear in a short-lived (<10 ns) singlet and long-lived (13 s) triplet state. The former decay promptly, emitting photons with energies peaked around 16 eV, while the triplet states can propagate through the fluid and de-excite at surfaces. Liquid helium is transparent to its VUV photons, since the first excited state of atomic helium is at 20 eV. Quasiparticles will propagate

[2] A ^{222}Rn concentration of 0.1μBq/kg corresponds to less than one radon atom per 100 mol of xenon. The main background is due to ^{214}Bi β-decays which are not accompanied by an α-decay and thus cannot be tagged in the TPC.

Int. J. Mod. Phys. A
by UNIVERSITY OF CALIFORNIA @ BERKE
nloaded from www.worldscientific.com
use and distribution is strictly not permitted, except for Open Access articles.

Table 36.6: Experiments using large TPCs for rare event searches. Shown are current, soon-to-be-operating and proposed experiments. UAr stands for underground argon; HP-GXe stands for high-pressure gaseous xenon. For some of the proposed experiments, the location or the readout scheme is not yet decided (marked as "TBD").

Experiment	Location	TPC type	Total (active) mass	Readout
Dark matter				
DarkSide-20k	LNGS	Dual-phase, UAr	50 t (50 t)	SiPMs, TPB
Argo	SNOLAB	Dual-phase*, UAr	∼400 t (∼400 t)	SiPMs, TPB
LUX-ZEPLIN	SURF	Dual-phase, Xe	10 t (7 t)	3″ PMTs
PandaX-4T	CJPL	Dual-phase, Xe	5.6 t (3.7 t)	3″ PMTs
PandaX-xT	CJPL	Dual-phase, Xe	47 t (43 t)	2″ PMTs
XENONnT	LNGS	Dual-phase, Xe	8.6 (5.9 t)	3″ PMTs
XLZD	TBD	Dual-phase, Xe	50-100 t (40-80 t)	3″ PMTs
$0\nu\beta\beta$ decay				
nEXO	SNOLAB	LXe, ^{136}Xe 90%	4.8 t (3.65 t)	SiPMs, charge pads
NEXT-100	LSC	HP-GXe, ^{136}Xe 90%	100 kg (80 kg)	3″ PMTs, SiPMs, TPB
NEXT-HD	TBD	HP-GXe, ^{136}Xe 90%	1.2 t (1 t)	Fibres + SiPMs, TPB
PandaX-III†	CJPL	HP-GXe, ^{136}Xe 90%	140 kg (100 kg)	Micromegas

*The option to build Argo as a single-phase detector is also under consideration.
†This is an R&D program for a future larger, enriched PandaX-xT detector.

ballistically through the liquid without decaying, and can also be detected via the evaporation of ^{4}He atoms from the surface of the liquid, with the helium binding energy being ∼0.7 meV.

Large volume, low-background TPCs are also developed for directional dark matter searches. An example is CYGNO [241] which aims to built a TPC with 50 cm drift, filled with a He:CF_4 gas mixture at room temperature and atmospheric pressure at LNGS. The liberated charge in a particle interaction is drifted towards an amplification stage consisting of a triple GEM structure, where the charge is multiplied and also light is produced. The readout will consist of light detectors, PMTs and scientific CMOS cameras, yielding the energy and z-position of events and the 2D track projections, respectively. The combined information thus allows for a 3D track reconstruction, with the goal being to achieve energy thresholds for electronic recoils around 1 keV.

36.4.2 $0\nu\beta\beta$ *Decay*

Experiments built to search for the $0\nu\beta\beta$-decay of ^{136}Xe, at a Q-values of 2457.8 keV, are based on single-phase TPCs, filled either with liquid or gas xenon at high pressure. The drift region is horizontal (EXO-200, NEXT-100) or vertical (nEXO, NEXT-HD, PandaX-xT-enriched).The TPCs are enclosed by radio-pure, thin-walled Cu vessels in a cryofluid, hydro-fluoro ether, or in a cold liquid scintillator, acting as a thermal bath, radiation shield and active veto in the latter case. In EXO-200, which took data at the Waste Isolation Pilot Plant (WIPP) until 2018, the charge drifted to crossed-wire planes at each anode, while the light was collected by arrays of large area avalanche photodiodes placed behind the wire planes at both ends. In nEXO, the TPC vessel is planned as a vertical Cu cylinder with 130 cm height and diameter (for 118.3 cm drift), with the charge collected at the anode by 0.6 cm pitch and 9.6 m long electrode strips, and the scintillation light observed by SiPMs arranged in a barrel configuration. Unlike for dark matter TPCs, there are no reflector panels and the field rings and cathode are coated with reflective aluminium deposition. The design drift field is 400 V/cm and the goal for the relative energy resolution is 0.8%. EXO-200 set a lower limit on the half-life of $0\nu\beta\beta$-decay of 3.5×10^{25} y with a total exposure of 231.4 kg y [242]. The proposed nEXO aims for a sensitivity of 1.35×10^{28} y with 5 t of enriched xenon and ten years of data taking [243].

TPCs using high-pressure xenon gas aim to reconstruct the tracks from the two electrons emitted in double beta decays, and the decay vertex, thus providing also a topological signature. In the NEXT project at the Laboratorio Subterráneo de Canfranc (LSC), the horizontal TPC, to be operated at 10-15 bar, features a single drift region. The primary (S1) and secondary (S2) scintillation light, the latter due to electroluminescence when the ionisation electrons cross a high-field region close to the anode, are collected by arrays of PMTs and SiPMs placed behind the cathode and anode, respectively, for energy measurements and tracking. The surfaces facing the active volume are coated with TPB to shift the VUV light to the visible spectrum. An inner Cu shield absorbs radiation from the high-pressure vessel of the cryostat.

The NEXT-White experiment, a prototype for NEXT-100 and for the proposed tonne-scale NEXT-HD, has operated a TPC with 20.8 cm radius and 53 cm drift, with 4.3 kg of xenon at 10 bar until 2023. It demonstrated excellent energy resolution (< 1% FWHM [209]) and background rejection using the capability to reconstruct the trajectories of ionising charges in the gas, thus separating the two-electron signature of $\beta\beta$-decay from single electrons due to background sources [244, 245]. Using data collected with xenon enriched and depleted in ^{136}Xe, it measured the half-life of the $2\nu\beta\beta$-decay and demonstrated clear Bragg peaks for the two electrons emitted in the decay [246]. NEXT-100 is currently acquiring data at LSC 5 bar [247], and will operate with >10 bar in 2026-2027. NEXT-HD will operate a vertical-drift TPC, 2.6 m in diameter and height, to accommodate ∼1.1 t of enriched xenon at 15 bar [248]. An intense R&D programe for the *in situ* identification of the barium ions ($^{136}Ba^{2+}$, $^{136}Ba^{+}$) produced in the $0\nu\beta\beta$-decay (called Ba-tagging) is ongoing [249–251]. PandaX-III, an R&D program for a future, enriched PandaX-xT detector, operates a high-pressure Xe gas TPC, where the xenon is mixed with 1% trimethylamine (TMA) to ensure stable operation of the Micromegas employed in the readout planes, and to minimise electron diffusion [252, 253]. Experimental searches for $0\nu\beta\beta$-decay are discussed in more detail in *Section 14.9*.

Apart from enriched xenon detectors, large TPCs using xenon in its natural isotopic abundance are also sensitive to second-order weak decays, such as the double beta decay of ^{134}Xe and ^{136}Xe, and the double electron capture process in ^{124}Xe and ^{126}Xe. In its electronic recoil channel, XENON1T observed for the first time the 2νECEC process in ^{124}Xe by detecting the simultaneously emitted K-shell X-rays/Auger electrons of the daughter atom ^{124}Te with a combined energy of 64.33 keV, which is twice the K-shell binding energy [191, 254]. The decay has also been observed by LZ [192] and PandaX-4T [193]. With a half-life around 1×10^{22} y, this is the slowest process ever measured directly. The double electron capture in ^{124}Xe can also be studied with high-pressure xenon gas TPCs, as demonstrated by NEXT [255]. LZ, PandaX-4T and XENONnT will improve upon existing results and will also search for the $2\nu\beta^+$EC decay. This channel has a distinct signature due to the two 511 keV gammas emitted after the positron annihilates with an electron in the medium. With a predicted half-life around 1.6×10^{23} y [256] its first observa-

Int. J. Mod. Phys. A 2026.41. Downloaded from www.worldscientific.com by UNIVERSITY OF CALIFORNIA @ BERKELEY on 09/16/26. Re-use and distribution is strictly not permitted, except for Open Access articles.

tion is within reach of these running experiments, which will also measure the half-life and in particular also the shape of the $2\nu\beta\beta$-decay of ^{136}Xe with high statistics and at low energies not previously accessed. The current generation of dark matter detectors can also set constraints on the $0\nu\beta\beta$-decays of ^{136}Xe and ^{134}Xe, as predicted or shown in [191, 257–261], delivering proof-of-principle methods towards higher sensitivity searches in XLZD and PandaX-xT. As an example, with 80 t of natural xenon in a TPC, a ^{136}Xe half-life exclusion sensitivity of 1.3×10^{28} y (90% C.L.) can be reached after ten years of operation [262, 263], fully probing the inverted neutrino mass ordering scenario.

36.5 Sub-kelvin detectors

Revised October 2025 by O. Cremonesi (INFN, Milano-Bicocca), L. Hsu (FNAL) and G. Signorelli (Pisa U.; INFN, Pisa).

36.5.1 *Motivation for Sub-kelvin Detectors*

Detectors operating below 1 K are referred to as low-temperature detectors (LTDs). The advantage of using LTDs over conventional detectors resides in their better energy resolutions, lower noise, and improved energy thresholds, which can all be achieved with a versatile choice in materials. In certain applications, these advantages outweigh the potential drawbacks of cooling and reading out a detector payload at sub-kelvin temperatures, and thus enable exploration of new frontiers in fundamental physics, astrophysics and cosmology. Among the endeavors enabled by LTDs are direct searches for dark matter over a wide mass range, precision experiments to measure the electron neutrino mass, searches for neutrinoless double-beta decay, and X-ray observation of the Universe. Large arrays of LTDs are also employed to measure the properties of the cosmic microwave background (CMB) spectrum whose parameters are determined by fundamental physics. These include dark matter and dark energy densities, the sum of neutrino masses and the number of light relativistic species, as well as probing the physics of inflation at energy scales of $\sim 10^{16}$ GeV. This article presents a brief overview of LTDs, their features, and several applications. More detailed treatment of this subject is available in the literature [264–267].

The advantages of LTDs are enabled by the detection of very low energy excitations (e.g. phonons and quasiparticles). In a typical interaction, energy from an incident particle is dissipated through excitation of secondary particles such as electrons, ions, holes, photons, phonons etc. These particles will in turn produce their own secondaries. Thus there is a cascade down in energy until the original energy deposit is converted entirely into heat and the detector reaches thermal equilibrium. Prior to the equilibrium phase, the energy at any given moment is partitioned among multiple excitation modes. Conventional particle detectors work by sensing the higher energy excitation modes, such as ionization and scintillation, which require an average minimum energy of few eV to 10's of eV to produce. For such detectors, a large fraction of the deposited energy remains undetected in the form of heat. Furthermore, the measurements are subject to the fluctuations inherent in the partition of energy across different excitation modes. Secondaries that don't eventually escape the detector, will de-excite or recombine to dissipate their energy in the form of phonons and quasiparticles, which are characterized by energies in the range of meV down to μeV. These can be detected by LTDs at various stages of their final degradation towards thermal equilibrium. Thus LTDs allow for energy resolutions and operational thresholds much lower than detectors that only sense scintillation and ionization. Furthermore, LTDs provide a precise energy measurement owing to the relatively large number of excitation quanta that can be detected. In fact, LTDs designed to measure thermal phonons achieve the highest possible energy resolutions with optimal noise performance.

At thermal equilibrium, energy E deposited in an LTD causes a temperature rise $\Delta T = E/C$ where C is the heat capacity. Thermal equilibrium is characterized by the condition where the average heat flowing to an LTD equals the average heat flowing from the LTD (into a proper heat sink or bath). In this state, the ideal intrinsic energy resolution is determined by the statistical fluctuations in the phonon system. Fluctuations in the total number of phonons in the LTD absorber have variance C/k_B, which yields a minimum resolution of $\Delta E^2 = k_B T^2 C$ to the device energy resolution, where k_B is Boltzmann's constant. Thus, the smaller the heat capacity, the more sensitive the response of the calorimeter and the better the energy resolution. The most relevant feature of this result is that the latter is independent of the energy deposition. The heat capacity itself is the product of the detector volume (V) and the specific heat (c_p). Optimization of LTD response can be achieved by using small detector volumes and materials with low specific heat. Noise contributions from additional sources will increase the variance and are generally parameterized as a multiplicative factor ($\xi \gtrsim 1$) to the variance expression above.

Similarly, the power P from incident particles or radiation can be measured through a temperature rise given by $\Delta T = P/G$, where G is the thermal conductance to a weakly linked bath held at constant temperature. Power fluctuations are limited by G and have a spectral density of $S_P = NEP^2 = 4k_{\rm B}T^2G$, where NEP is the noise equivalent power, defined as the power in a 1 Hz bandwidth that gives a response signal with an amplitude equal to the noise. Hence lower conductance yields better sensitivities. To minimize thermal conductance in precise power measurements, weak thermal links can be realized by using thin membranes or by decoupling the electron and phonon systems. However, a compromise must be made. While lower G yields better noise metrics, conversely, larger G is needed to dissipate all incident power (which can be large in the case of CMB detectors) or to have a faster detector response (the characteristic response time being $\tau = C/G$).

LTDs that measure power are sometimes referred to as *bolometers* in literature, as opposed to *calorimeters* that measure energy, generating some confusion. In principle, there is no clear distinction between a calorimeter and a bolometer. The operation mode is generally determined by the ratio of the characteristic time constant and the average time between the arrival of incident particles or quanta [268].Yet another convention is to refer to *non-equilibrium* LTDs as those detectors that measure incident energy or power by counting excitations that have energy $\gg k_B T$. In such detectors, energy resolution is determined by the statistical fluctuations of the energy partition, similar to conventional ionization detectors but with a much lower average excitation energy and hence a larger number of excitation quanta.

Table 36.7: Low temperature dependence on temperature (T) for specific heat, based on different material classes. In the table below Θ_D is the Debye temperature and T_C is the transition temperature of the superconductor.

Heat Capacity	Material
$\propto \left(\frac{T}{\Theta_D}\right)^3$	Dielectric and diamagnetic
$\propto T$	Conductor
$\propto \exp\left(-\frac{2T_C}{T}\right)$	Superconductor
$\propto \left(\frac{\mu_B B}{k_B T}\right)^2 \operatorname{sech}^2\left(\frac{\mu_B B}{k_B T}\right)$	Paramagnet (in magnetic field **B**)

A variety of possible detector materials and sensor technologies makes LTDs very versatile and highly customizable. Dielectric, superconducting and paramagnetic materials are often used owing to the fact that at very low temperatures, the specific heat decreases strongly as a function of T (see table 36.7). Superconductors offer additional advantages: the abrupt change in resistance when a material transitions from its normal to superconducting state enables highly sensitive measures of temperature changes. Additionally, the existence of a small (less than a meV) but distinct energy gap that is required to break a Cooper pair, provides a means to measure energy deposits by counting the resulting quasiparticles (QP). QP relaxation processes are typically faster than thermal processes making these detectors suitable for high-rate photo-counting. In summary, both the sensitivity and

Int. J. Mod. Phys. A 2026.40:1-2. Downloaded from www.worldscientific.com
by UNIVERSITY OF CALIFORNIA @ BERKE use and distribution is strictly not permitted, except for Open Access articles.

energy resolution of an LTD benefit greatly from low temperature operation.

36.5.2 *Detector Types*

A generalized LTD calorimeter consists of an absorber in thermal contact with a phonon or quasiparticle sensor, and a thermal link to a heat bath at a constant temperature (see figure 36.11). The absorber provides the mass necessary for the interaction of the particle and a fast and complete thermalization of the deposited energy. The sensor accomplishes the task of translating the particle interaction into measurable parameters. It is generally sensitive to equilibrium phonons (e.g. thermistors and MMCs) and thus provides a precise measurement of the temperature. However, non-equilibrium (e.g. STJ's or KIDs) and mixed (e.g. TES) phonon sensors have been devised and implemented in many applications as well. The goal of the thermal link is to cool the absorber down to its equilibrium temperature after the absorption of a particle. In monolithic detectors the thermometer and absorber are identical, while in composite detectors the thermometer is attached to a separate absorber. This basic design applies to single-event particle detection as well as for continuous radiation measurement devices. In the case of the latter, a suitable absorber whose mass is irrelevant, *e.g.* an antenna at the end of a waveguide, collects the incident power and dissipates it onto a resistive (*e.g.* Au) film, which is put in contact with a sensor capable of detecting tiny temperature changes (e.g. semiconductor thermistors, transition-edge sensors, and kinetic inductance detectors, to name a few).

Superconducting Tunnel Junctions (STJs) and Kinetic Inductance Detectors (KIDs) are examples of non-equilibrium detectors. STJs exploit tunnelling of particles and QPs between two superconductors. The superconductors act as radiation absorbers, and are separated by a thin insulating layer. When such a junction is DC biased at a voltage just below the gap voltage, the excess quasiparticles generated by the incoming radiation are detected as a tunneling-current proportional to the incoming energy. Statistical fluctuations in the tunnelling process limit the energy resolution which is given by:

$$\sigma_E = \sqrt{\varepsilon(F+G)E_0}, \tag{36.5}$$

where $\varepsilon \sim \Delta$, the band-gap, while $F \sim 0.2$ and $G > 1$ are the Fano factor and tunnelling fluctuation respectively. STJs have been proven to be excellent single photon and UV-VIS spectroscopic detectors with near theoretical energy resolutions, high detection efficiencies and excellent time resolution. In astrophysics they are used as mixers to detect radiation in the 100 GHz to 1 THz range by exploiting the non-linear behaviour of their current versus voltage characteristic curve. Despite their extremely good energy resolutions, STJs cannot be scaled-up to produce sensors with large observing volumes due to readout complexity and the difficulty in uniformly suppressing the superconducting Josephson current, which is superimposed on the QP current.

Qubits share similar design elements as STJs. Using a Josephson Junction (JJ, a thin normal layer separating two superconductors) as a non-linear inductor in a superconducting LC circuit, it is possible to realize a two-level system whose status can be read out by a suitable superconducting circuit [269]. When qubits are coupled to a resonant cavity, they can be used as ultra-sensitive detectors of electromagnetic radiation, especially in the microwave regime. Incident radiation can interact with the cavity field, inducing a measurable shift in the qubit's energy levels through dispersive coupling. This interaction alters the qubit's transition frequency or induces excitation, depending on the setup, which can be read out via high-fidelity quantum measurement techniques. Similarly, qubits can be patterned onto large absorbers such as silicon or sapphire in order to detect energy depositions of less than an eV, which may arise from scatters of dark matter or neutrinos [270–272]. A particle interaction in the absorber will downconvert to sub-ballistic phonons. Those that diffuse into the JJ may tunnel across it, thus altering the qubit's state. Such qubit systems are particularly useful for detecting weak signals, such as single microwave photons or very low energy particle interactions, making them powerful tools in quantum sensing for astrophysical or dark matter detection experiments [273].

KIDs exploit the variation of the kinetic energy T stored in a superconductor by Cooper pairs whose inertia acts as an effective inductance, given by:

$$T = \frac{1}{2}nm^*v^2 = \frac{1}{2}LI^2 \tag{36.6}$$

where n is the number density of Cooper pairs, $m^* = 2m_e$ is the Cooper pair mass and $I = 2nev$ is the Cooper pair current. $L = m_e/2ne$ is defined as Kinetic Inductance and is inversely proportional to the number of Cooper pairs [274]. When a KID is placed in series with a superconducting capacitor, the resonance frequency of the circuit will be temporarily shifted by incident radiation, which converts Cooper pairs to QPs, thus changing the effective inductance. The presence and amount of radiation is observed as a change in amplitude or phase of a tuned sinusoidal signal that is sent through the circuit. In practice the change in L is small, and very high Q microwave resonance circuits are needed to sense this variation (hence the name MKIDs, for Microwave-KIDs). Furthermore, only areas of the film where large currents are flowing will be sensitive to pair breaking, thus making the response of a distributed KID position dependent. To overcome this issue, QP trapping (by coupling two superconductors with different band-gaps) is used for absorbing optical photons and X-rays. To detect lower frequencies (*e.g.* in the 100-1000 GHz range for CMB) a lumped element resonator (LEKID), with little current variation across the device, is used. The device itself, based on a series LC circuit inductively coupled to a microstrip feed line, can act as the absorber as well as the sensing element in a detector system. Macroscopic devices (few mm^2) can be fabricated by shaping the inductor in the form of a meander coupled to an inter-digitated capacitor [275]. The theoretical noise limit of these devices is governed by generation-recombination noise and takes the form:

$$NEP_{QP} = 2\Delta\sqrt{\frac{n_{QP}}{\tau_{QP}}}, \tag{36.7}$$

where n_{QP} and τ_{QP} are the QP number and lifetime respectively. KIDs are easy to fabricate, very sensitive, broad band and easily multiplexable: they can be coupled with a single microstrip that simultaneously reads 1000s of detectors resonating at different frequencies. They provide therefore a promising solution for deploying large arrays of detectors with applications to high-energy physics, astronomy or CMB measurements, although there are still some challenges, especially at frequencies below 100 GHz, related to their worse noise performance when compared to other LTDs, and to the choice of materials with a sufficiently small energy-gap.

Semiconductor thermistors are resistive elements characterised by a strong dependence of the resistance on the temperature. Usually, they consist of small crystals of germanium or silicon with a dopant concentration slightly below the metal-to-insulator transition. However, they can also be realized in the form of amorphous films such as NbSi. At low temperatures, their resistivity (ρ) is governed by variable range hopping (VRH) conduction and is described by the expression $\rho(T) = \rho_0\ \exp\left((T_0/T)^\gamma\right)$, where T_0 and ρ_0 are parameters controlled by the doping level, while γ depends on the compensation level K (ratio of acceptor to donor concentrations). For low values of K, γ is well approximated by 1/4 while it converges to 1/2 as K increases.

Semiconductor thermistors are high impedance devices (1–100 MΩ) whose performance is usually parameterized in terms of the logarithmic sensitivity $\alpha = \mathrm{d}\log R/\mathrm{d}\log T$, typically in the range of 1–10. Silicon thermistors are fabricated using a multiple ion implantation process in high purity silicon wafers to produce a thin and uniformly doped box-like volume. The best germanium thermistors are fabricated starting from bulk, high-purity germanium crystals doped by means of neutron irradiation in the core of a nuclear reactor, referred to as nuclear transmutation doping (NTD). Individual sensors are then produced by dicing the irradiated samples and finishing them by hand. The great advantage of NTDs is the highly uniform doping level over large volumes which results in a better signal to noise ratio with respect to other doping

Int. J. Mod. Phys. A 2026.41. Downloaded from www.worldscientific.com
by UNIVERSITY OF CALIFORNIA @ BERKELEY on 09/16/26. Re-use and distribution is strictly not permitted, except for Open Access articles.

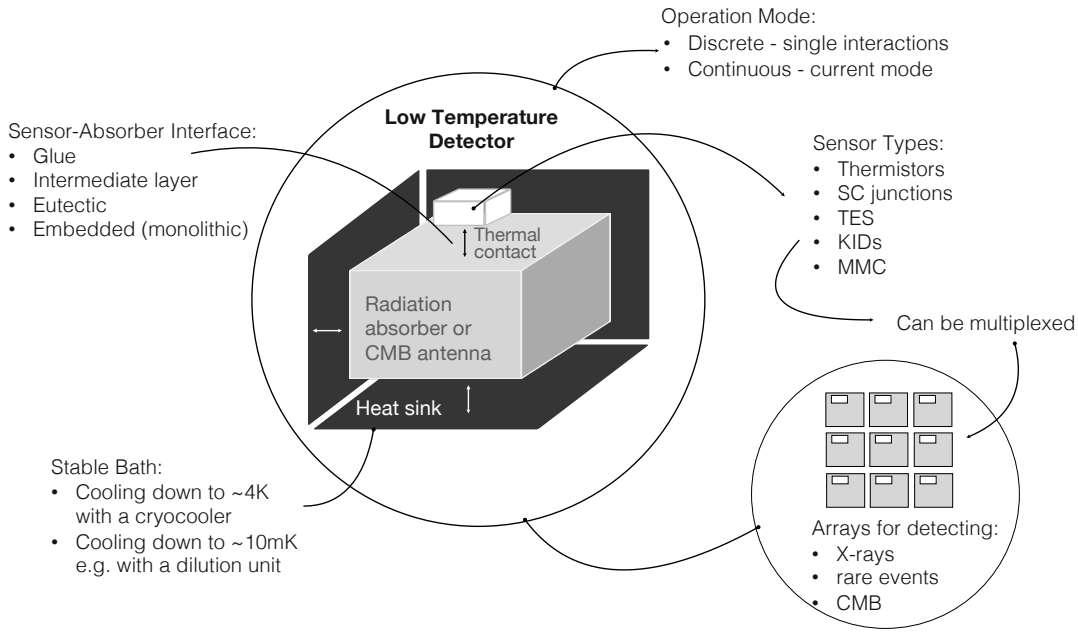

Figure 36.11: A generalized LTD consists of an absorber, a sensor and a thermal link to a stable-temperature bath. Biasing schemes and readout is described in detail in the text for individual sensor types.

techniques. The doping level depends on the isotopic composition of the starting material and the irradiation time.

The weak coupling to the heat sink can be provided by the electrical leads used for the read-out. However, nowadays microelectronic planar technologies and silicon micromachining are more commonly preferred, and sensors are suspended on thin silicon nitride membranes or thin silicon beams. Thermistors are read-out in an approximately constant current biasing configuration obtained by inserting large load resistors in the bias circuit, which allows for direct conversion of the thermal signal (ΔT) into a voltage signal (ΔV).

Semiconductor thermistors are very practical to use with some drawbacks. One of these is related to their high impedance which requires a JFET front-end placed as close as possible to the device in order to minimize the signal integration on parasitic electrical capacitances. This can represent a technical challenge, because JFETs must be maintained at significantly higher temperatures ($\gtrapprox$100 K). Furthermore, deviations from the exponential behaviour of the conductivity have been observed at low temperatures. They are usually described in terms of a finite thermal coupling between electrons and phonons which results in an intrinsic limit to the signal rise times, which is of the order of hundreds of milliseconds at temperatures below 100 mK. Nevertheless, semiconductor thermistors are an established and robust technology, and arrays of detectors based on these devices have been widely used for neutrinoless double beta decay searches, neutrino mass measurements and X-ray spectroscopy. Energy resolutions lower than 5 eV have been achieved with Sn or HgTe absorbers.

Superconducting Transition Edge Sensors (TESs) exploit the sharp transition between superconducting and normal conducting phases, yielding a high sensitivity to temperature variations. Temperature perturbations, and hence resistance changes, are sensed as modulations in the current through the TES. TESs are operated in a constant voltage biasing configuration where Joule heating, arising from the current flowing in the TES, decreases with a rise in resistance, which then brings the TES back to its nominal operating temperature. This electrothermal feedback (ETF) is achieved by providing a TES with a voltage bias whose power, $P_J = V_{\rm bias}^2/R(T)$, heats the TES to its nominal operation point, the superconducting transition temperature. Operation in ETF mode improves linearity, speeds up response (to faster than $\tau = C/G$), and in some cases it provides tolerance for $T_{\rm C}$ (critical temperature) variation between multiple TESs in a large array. The low impedance in this configuration makes them well-suited for readout by SQUID (Superconducting QUantum Interference Device) based amplifiers. Logarithmic sensitivities $\alpha = {\rm d}\log R/{\rm d}\log T$ of the order of several hundreds can be achieved. By using different superconductors, or superconductor-metal pairs patterned in suitable shapes, a wide range of resistances, transition temperatures and time constants are obtainable to meet the requirements of the desired application [276].

Nano-TESs are fabricated by lithographic techniques in the form of long (few μm) and narrow (nm) wires that exhibit extremely small NEPs due to their reduced C and G, enabling single-photon sensing. Superconducting Nanowire Single-Photon Detectors (SNSPDs) are similarly patterned superconductors or superconducting bilayers maintained at a temperature well below their $T_{\rm C}$. When a DC current just below the critical current is driven through the nanowire, the absorption of a single photon causes the formation of a hot spot that drives the superconductor to a normal conducting state, resulting in a very fast (tens of picoseconds) current pulse through a shunt resistor. For this reason, nano-TESs and SNSPDs are used as single photon detectors for light dark matter and axion searches in applications where large detecting mass is not critical [277].

Magnetic Metallic Calorimeters (MMC) exploit paramagnetic sensors exposed to a weak magnetic field with a weak thermal link to a heat bath. A temperature rise causes a change in the sensor magnetization, which is sensed by a SQUID magnetometer. A common material is an Au:Er mixture, with the addition of a few hundred ppm of enriched ^{166}Er, which is needed to reduce the unwanted contribution of nuclear magnetic moments of other Er isotopes. The read-out is non-dissipative and avoids the noise sources common to the dissipative devices. The use of a metallic host ensures relatively fast time response, since the typical spin-electron relaxation times are of the order of 0.1 microseconds at ~50 mK [278]. For an optimized MMC, the energy resolution is given by $\Delta_E = \sqrt{2k_B T^2 C}\,(\tau_0/\tau_1)^{1/4}$, where τ_0 (order of micro second) and τ_1 (order of milli second) denote the signal rising and decay times respectively [264]. In order to obtain a fast and efficient energy thermalization, MMC are typically fabricated from gold. The intrinsically large heat capacity of the paramagnet does

Int. J. Mod. Phys. A
by UNIVERSITY OF CALIFORNIA @ BERKE
nloaded from www.worldscientific.com
use and distribution is strictly not permitted, except for Open Access articles.

not spoil the temperature sensitivity and allows the use of relatively large gold absorbers without degrading the device performance. Furthermore, thermal isolation from the heat sink is not generally an issue. Owing to the simple concept of these devices, MMC can be precisely customized and fabricated by employing standard microtechnology. Planar MMC arrays characterized by an excellent energy resolution, large dynamic range and good linearity have been successfully used for the detection of soft X-rays.

Performance and technological constraints limit the maximum size of LTDs. To improve overall experimental sensitivities, a large number of sensors must be deployed, typically at temperatures of a few tens of mK, where cooling power is limited to a few μW. To reduce the readout complexity and the heat load at the colder stages, multiplexing (MUX) techniques are often employed. Multiplexing consists of reading multiple detectors out through a limited number of lines that traverse room temperature to cryogenic temperatures [279]. In frequency-domain multiplexing (FDM), a tuned superconducting LC circuit is placed in series with each sensor, and a frequency comb of AC biases (usually in the MHz range) is sent to a group of sensors in parallel. A synchronous demodulation of the amplified current signal allows the recovery of the resistance variation of each detector. Microwave-multiplexing (μMUX) represents a variation of this concept, based on the usage of rf-SQUIDs, where the frequency comb is in the GHz range. Alternatively, the signal from a single detector can be recovered by readout of one detector at a time (time-domain multiplexing, TDM). KIDs have been gaining popularity owing to the fact that they naturally form resonant circuits, hence multiplexing in the frequency domain is readily achieved by adjusting their capacitance.

36.5.3 *Experimental Applications*

LTDs are sensitive over a wide range of energy, from centimetre wavelength ($\sim$ meV) through the visible spectrum ($\sim$ eV) up to the X-ray domain ($\sim$ keV) and beyond. Several broad categories of LTD applications towards measurements of fundamental physics are described in more detail in the text below and summarized in tables 36.8 and 36.9.

Bolometric detectors are favored as microwave detectors owing to their nearly constant response over frequency, playing an important role in far-infrared astronomy and in the survey of the cosmic background radiation. The high-frequency instrument of the Planck satellite (HFI) used spiderweb bolometers read by NTD-Ge thermistors, but current experiments use mainly TESs or, more recently, KIDs. Depending on the objective of the experiment, antenna coupling or absorber coupling is used. In the former case, the bolometer detects one polarization and one (or a few) modes of the radiation, while absorber-coupled bolometers do not distinguish between polarizations. In order to avoid the absorption or emission from Earth's atmosphere, many (CMB) instruments are operated by observatories located at high altitude, dry places (such as the Atacama desert or Antarctica), balloon-borne platforms, or from space. In Table 36.8, we list a subset of the ongoing or planned CMB experiments (see Section 29 of this Review for the details on present challenges).

In the Atacama Desert, CLASS continues to collect data and has recently reported large scale E-mode polarization measurements and constraints on reionization [280], while Advanced ACT-Pol observations (2017–2022) continue to yield new maps and cosmology results [281]. POLARBEAR-2 (PB2-A), part of the Simons Array [282]. The Simons Observatory has achieved first light and is operating [283]. At the South Pole, SPT-3G, BICEP3, and the BICEP Array remain active with new results and ongoing receiver deployments. The CMB-S4 project, initially envisioned as the next-generation ground-based CMB survey with unprecedented sensitivity and scale, has been cancelled, and the project is proceeding with an orderly shutdown. In the Canary Islands, QUIJOTE and GroundBIRD are operating, while LSPE-STRIP is nearing construction [284, 285]. In Argentina, QUBIC resumed operations in 2025 and began sky calibration [286]. In Tibet, AliCPT-1 completed its first phase and captured initial 150 GHz images of the Moon and Jupiter. Among stratospheric balloon experiments, SPIDER has flown twice (2015 and 2022/23), EBEX flew in 2012–13, and LSPE/SWIPE remains in advanced development. Finally, in space, LiteBIRD remains in development with a launch targeted for the 2030s [287], and PICO (Probe of Inflation and Cosmic Origins) has been proposed as a NASA flagship mission concept to provide complementary full-sky, high-sensitivity CMB polarization measurements.

The incoming radiation couples directly to the antenna probes (as in BICEP/Keck) or through micro-machined horn waveguides (AdvancedACT-Pol, CLASS) or lenslets (Simons Array, SPT-3G), depending on the frequency range. All of these experiments have focal planes with hundreds to hundreds of thousands of sensors. To optimize focal plane occupancy, multi-mode or multi-chroic, dual polarization sensitive detectors are used. In the former case, the sensitivity is enhanced by collecting power from a larger number of modes at the expense of angular resolution. In the latter, one single mode of the radiation is focused on a broad band antenna, and on-chip polarization separation and band-pass filters split the signal in different frequency bands directing the power to different absorbers and sensors.

Experimental design is driven by a trade-off between the sensitivity and the complexity of the production processes and readout. On the one front, single-sensor NEP at the level of 10^{-21} W/$\sqrt{\text{Hz}}$ has been achieved in laboratories and research centers. Meanwhile, efforts are in place for the industrialization of the fabrication processes, which is essential for scaling up production for the large number of detectors needed for future experiments.

Massive cryogenic calorimeters have been proposed since the 1980's as particle detectors for the search of rare processes (e.g. dark matter, neutrinoless double beta decay) [288]. Almost simultaneously, the use of arrays of small mass calorimeters was suggested for X-ray astrophysics [289] and precision measurements of the neutrino mass [290, 291]. Although essential to understanding the nature of neutrinos, neutrinoless double beta decay (NDBD) has eluded discovery (or definitive exclusion) for over 50 years. Calorimeteric techniques provide the best sensitivities to NDBD. However, before the advent of low temperature calorimeters (LTC), only a few isotopes (^{48}Ca, ^{136}Xe and ^{76}Ge) could be utilized for NDBD studies with the calorimetric approach. This limitation was removed by the advancement of LTC's, and in particular by CUORE, which takes advantage of the naturally high abundance of ^{130}Te in TeO_2 crystals. Additionally, the operation of CUORE at LNGS [292] has demonstrated that the technical challenges of operating ton-sized LTD detectors in a deep, underground location are surmountable. Currently, the most promising future approach is based on the hybrid approach of scintillating LTCs, which unfortunately cannot be used for ^{130}Te. Now, new projects are being proposed based on different scintillating compounds. In particular ^{100}Mo is the choice of CUPID [293, 294] (NTD thermistors glued to $Li_2{}^{100}MoO_4$ crystals), which will use the same infrastracture of CUORE and follows from the successful operation of several demonstrators (CUPID-0 [295] and CUPID-Mo [296]), and AMORE (MMC sensors on $Ca^{100}MoO_4$ or $Li_2{}^{100}MoO_4$ crystals) [297]. With an energy resolution comparable to germanium diodes and a mass of the order of a ton, these experiments aim to probe the inverted hierarchy of neutrino masses. Extremely pure materials, careful assembly procedures, and deep underground laboratories are therefore necessary. These detectors are characterised by relatively slow responses, which still represent a major limitation for some of the proposed applications.

In the 1980's, the calorimetric technique was recognized as a feasible approach to make a direct measurement of the neutrino mass from the end-point of a beta spectrum. Thus, LTCs were proposed as a possible alternative to the standard spectrometric measurements [298]. Calorimetric measurements offer a number of advantages [299]: i) a weak dependence on the final excited states, ii) no source effects (e.g. self-absorption), and iii) lack of back-scattering from the detector. Therefore LTCs provide a faithful reconstruction of the beta spectral shape over a broad energy range below the end-point. However, the difficulty in resolving a small fraction of the spectrum near the end-point is a serious limitation that strongly constrains the source strength and the statistics that need to be accumulated. Such an inconvenience can be mitigated by selecting beta emitters with a small Q value, owing to the fact that the fraction of counts in an interval,

Int. J. Mod. Phys. A 2026.41. Downloaded from www.worldscientific.com
by UNIVERSITY OF CALIFORNIA @ BERKELEY on 09/16/26. Re-use and distribution is strictly not permitted, except for Open Access articles.

Table 36.8: Some selected experiments using LTDs to measure the CMB. These experiments constrain the physics of inflation and the absolute mass, hierarchy, and number of neutrino species. The experiment location determines the part of the sky that is observed. The size of the aperture determines the angular resolution. The table also indicates the type of sensor used, the number of sensors, the frequency range, and the number of frequency bands. Data for planned upgrades or future experiments are provided in parentheses.

Sub-K CMB Experiment	Location	Aperture	Sensor type	# Sensors (planned)	Frequency (planned)	Bands (planned)
Ground-based						
Atacama Cosmology Telescope (2007–)	Chile	6 m	TES	5,614	30–230 GHz	5
BICEP/Keck (2006–)	South Pole	26/68 cm	TES	2,500	95–270 GHz	6
CLASS (2015–)	Chile	60 cm	TES	3,488	40–220 GHz	4
GroundBIRD (2021-)	Canary Island	30 cm	MKID	322	145–220 GHz	2
POLARBEAR / Simons Array (2012–)	Chile	3.5 m	TES	1,274 (22,764)	150 GHz (90–280 GHz)	1 (4)
South Pole Telescope (2007–)	South Pole	10 m	TES	16,260	90–220 GHz	3
Simons Observatory (2022–)	Chile	6 m/0.5 m	TES	(60,000)	(27–280 GHz)	(6)
CMB-S4 (cancelled)	Chile + South Pole	21 telescopes	TES	(500,000)	(20–280 GHz)	(11)
Balloon						
EBEX (2013–)	McMurdo	1.5 m	TES	∼1,000	150–410 GHz	3
PIPER (2016–)	New Mexico	2 m	TES	5,120	200–600 GHz	4
SPIDER (2014–)	McMurdo	30 cm	TES	1,959	90–280 GHz	3
LSPE (2026–)	Longyearbyen	60 cm	TES	(326)	(140–270 GHz)	(3)
Satellite						
Planck HFI (2003-2013)	L2	1.5 m	NTD	52	100-857 GHz	9
LiteBIRD (2030s)	L2	80 cm	TES	(4,508)	(34–448 GHz)	(15)
PICO (2040s)	L2	1.4 m	TES	(12,996)	(21–799 GHz)	(21)

δ close to Q, scales as $(\delta/\mathrm{Q})^3$. However, this is generally at the cost of choosing decays with more complex nuclear transitions. In addition, LTCs may be affected by specific systematics (e.g. solid state effects). Ultimately it is recognized that spectrometers and calorimeters have complicated but different systematic effects. It is therefore critical to develop complementary experiments exploiting both techniques.

LTCs were initially proposed as perfect calorimeters to measure the energy spectrum of a low Q beta emitter embedded in an absorber. However, the requirements of excellent energy resolution and a low rate (to avoid pileup) requires a very large number, $\mathrm{O}(10^4 - 10^6)$, of small mass devices (micro-calorimeters). Early experiments used ^{187}Re, which is a long-lived beta emitter that is naturally abundant in rhenium samples and is characterised by a very low Q value (2.4709 keV [300]). A large number of ^{187}Re based experiments have been developed over the years (MANU [301], MIBETA [302], MARE [303]). Nowadays a different approach is preferred and is based on the measurement of the atomic radiation following electron capture, typically in ^{163}Ho which is also characterized by a very low Q (2.837 keV [304]). Different experiments have been proposed to face the challenge: ECHo in Germany [305] (using MMC sensors), HOLMES in Italy [306] and NUMECS [307] in the US (using TESs). LTCs are also included in PTOLEMY's proposal, whose main purpose is to detect relic neutrinos, but which also includes an initial stage dedicated to measuring the mass of neutrinos [308]. The very large number of microcalorimeters needed to obtain sensitivities comparable to spectrometric measurements is a serious challenge, both for the readout and the thermal heat load. An alternative readout based on the use of KIDs, for their multiplexing capability, has been proposed and is presently under development.

Traditional searches for WIMP-like dark matter aim to measure the scatter of a massive (>10 GeV/c^2) dark matter particle off of a target nucleus. Similar to detectors employed for neutrinoless double beta decay, these searches benefit from large-mass absorbers for the target because the dark matter interaction rate scales directly with the number of nuclei in the target and hence its mass. Among the most successful experiments to date, are those that combine the detection of phonons with another channel such as ionization energy (EDELWEISS [309] and SuperCDMS [310]) or scintilation light (CRESST [311]). This simultaneous, dual measurement takes advantage of the fact that the energy deposited in the absorber is partitioned into these channels differently depending on whether the initial particle interaction produces electron or nuclear recoils (or both). This particle identification allows for the rejection of background from natural sources of radiation, which most commonly manifest themselves as electron recoils in the detector.

In recent years, multi-ton liquid noble detectors have outclassed LTD-based technologies in searches for heavy dark matter owing to their ability to more easily and cheaply scale to large target masses. However, the lower thresholds achieved by LTDs continue to make them the technology of choice for low-mass dark matter searches. New advances have enabled these detectors to reach much lower energy thresholds than previously obtained, albeit sometimes at the cost of being able to detect energy in more than one channel as described above. For example, the use of an electric field to generate Neganov-Trofimov-Luke [317, 318] phonons in proportion to the applied voltage, has enabled the detection of single electron hole pairs in detectors with thresholds as low as a few eV (SuperCDMS HVeV [319], EDELWEISS_SubGeV [320]) and is proposed for the CUPID light detectors [321]. These advances have enabled sensitive searches for dark photons and dark matter that scatters off electrons. Next generation experiments such as TESSERACT aim to further optimize the intrinsic energy resolution of TES detectors, coupled with a strategic choice of target materials (He, GaAs) to enable sensitivites to dark matter with masses below an MeV/c^2 [322]. KIDs can be also applied to readout silicon dice to be sensitive to GeV DM, as in the BULLKID [323] proposal. Current state-of-the-art axion searches use SQUID based quantum amplifiers such as Josephson Parametric Amplifiers along with resonant cavities operating below 100 mK to look for a signal above fluctuations in the thermal noise [324, 325]. Future axion experiments are also working to close the sensitivity gap between particle and wave-like dark matter with the help of LTDs. Broad-band axion searches in the THz range are being

Table 36.9: Selected experiments using low temperature calorimeters. The table shows currently or soon-to-be operating experiments that will search for dark matter or neutrino properties. The dates refer to the start of the program.

Sub-K Experiment	Location	Detection mode	Absorber (Total mass)	Sensor type	# Sensor # Crystal
WIMPs					
CRESST [312] (upgrade 2026)	LNGS Italy	Athermal phonon and scint.	$CaWO_4$, Al_2O_3, Si, $LiAlO_2$	TES	variable
SuperCDMS (2025)	SNOLAB Canada	Athermal phonon and ion.	Ge/Si	TES	24
TESSERACT† (2029)	LSM Modane France	Athermal phonon quantum evaporation	GaAs, He, Si, Ge	TES	-
Neutrino mass					
ECHo [305] (2012)	Heidelberg Germany	Thermal phonon	Au:^{163}Ho (0.2μg)	MMC	16
HOLMES [306] (2015)	Milan Italy	Thermal phonon	implanted ^{163}Ho (18 μg)	TES	1000
NUMECS† [307] (2015)	LANL USA	Thermal phonon	implanted ^{163}Ho	TES	4096
$0\nu\beta\beta$ decay					
CUORE [313, 314] (2015)	LNGS Italy	Thermal phonon	$^{nat}TeO_2$ (741 kg)	NTD Ge	988
CUPID [294] (2015)	LNGS Italy	Phonon and scint.	$Li_2^{100}MoO_4$ (450 kg)	NTD Ge	1596
AMoRe-I [315] (2022)	Y2L South Korea	Phonon and scint.	$Ca^{100}MoO_4/Li_2{}^{100}MoO_4$ (6.2 kg)	MMC	18
AMoRe-II [316] (2026)	Yemilab South Korea	Phonon and scint.	$Li_2{}^{100}MoO_4$ (157 kg)	MMC	360

†No payload size quoted for experiments that are primarily in R&D or design phase.

proposed, which will make use of TES, SNSPDs or KIDs for single photon detection [326]. Finally, LTD-based dark matter detectors are also actively employed to study coherent neutrino scattering, owing to the fact that the hypothesized signal from dark matter-nucleus scattering is nearly identical to that from neutrino-nucleus scattering, with both inducing nuclear recoils in a similar energy range [327–330].

36.6 Low-radioactivity background techniques

Revised October 2025 by Al. Ianni (INFN, LNGS) and S. Schönert (TU Munich).

36.6.1 *Introduction*

The study of rare phenomena in fundamental physics, such as proton decay, neutrinoless double beta decay, dark matter, and MeV-scale neutrino interactions, requires extremely low levels of background radiation. Experiments searching for these rare events record electron recoils or nuclear recoils in the energy scale from a few eV to several MeV. The detector technologies used are multiple from organic and cryogenic liquid scintillators, to bolometers, solide state calorimeters, gaseous detectors, and crystal scintillators. As far as the background contamination is concerned at some extent the application defines the requirements, although the common denominator is that an extreme reduction of all background sources is essential. Leading experiments in rare events search have obtained in the region-of-interest (ROI) a background as low as $\sim 10^{-4}$ cts/kg/y/keV. As a first and crucial step, a dedicated radio-purity assay of the detector set-up components has to be carried out. Over the last fifty years, special screening and cleaning techniques have been developed to measure and mitigate ultra-low levels of background. In order to characterize the background sources we refer to Heusser [331] and identify the following five main categories:

- environmental radioactivity in the location where the detector is installed;
- radioimpurities in the detector and shielding;
- radon and its progenies;
- cosmic rays and induced radioactivity;
- neutrons from natural fission, (α,n) reactions, and from cosmic-ray muons interactions.

The energy range affected by these background sources is mainly <10 MeV. All materials contain traces of long-lived primordial radioimpurities, such as ^{238}U, ^{232}Th, ^{235}U (^{238}U/^{235}U ~ 138), and ^{40}K (^{40}K/K$^{nat} \sim 1.17 \times 10^{-4}$). We recall that 1 *ppt* of ^{238}U and ^{232}Th corresponds to 12.36 and 4.06 μBq/kg, respectively; 1 *ppb* of K^{nat} corresponds to 30.25 μBq/kg. In the Earth's crust the abundance of uranium and thorium is of the order of $1-10$ ppm which corresponds to about $10-100$ Bq/kg. Taking into account these contamination levels and the low background requirements, a fundamental background reduction and mitigation is essential to carry out rare phenomena research.

Besides primordial radionuclides other radioactive elements are produced through interactions with matter of secondary cosmic ray particles. Among these so-called cosmogenic radionuclides we recall, in particular, ^{3}H, ^{14}C, ^{7}Be, ^{39}Ar, ^{42}Ar , and, in copper, steel and iron often used as shielding materials, ^{57,60}Co.

A third category of background source in our environment consists of anthropogenic radionuclides. These are artificially produced mainly through nuclear reactions in nuclear power plants, nuclear fuel reprocessing plants, and nuclear weapons testing. Anthropogenic background elements of concern for rare phenomena are ^{85}Kr, ^{137}Cs, ^{241}Am, ^{60}Co, and ^{90}Sr. The concentration of ^{85}Kr ($T_{1/2}$=10.76 y, Q_β=687 keV) in air has been slowly increasing since World War Two with a present activity of order 1 Bq/m^3. As a consequence ^{85}Kr is a crucial background in experiments making use of nitrogen, xenon, and argon from air.

Once detector components radioactive backgrounds have been assayed and reduced by a careful selection campaign, which can last several years, a further step to push the background level beyond the screening possibilities is needed to reach the required sensitivity. For this purpose special active vetos, purification methods, and offline analyses have been developed. A meticulous background understanding and mitigation is crucial to explain any possible signal excess which may be detected. Background mitigation techniques are based on:

- use of radio-pure materials that absorb ionizing radiation;
- identify radio-pure material for detector construction;
- perform advanced surface and sub-surface cleaning treatment;
- reduce muon flux with underground detector deployment and

Int. J. Mod. Phys. A Downloaded from www.worldscientific.com by UNIVERSITY OF CALIFORNIA @ BERKE... use and distribution is strictly not permitted, except for Open Access articles.

Int. J. Mod. Phys. A 2026.41. Downloaded from www.worldscientific.com by UNIVERSITY OF CALIFORNIA @ BERKELEY on 09/16/26. Re-use and distribution is strictly not permitted, except for Open Access articles.

using active vetos;

- exploit advanced detection and tagging techniques to discriminate signal from background.

In the following we describe radio-assay and background mitigation techniques developed and exploited in the framework of rare phenomena searches in deep underground laboratories.

36.6.2 *Radio-purity assay*

The radio-purity assay of detector components is a basic prerequisite to be carried out in low counting experiments. Several techniques are exploited for radio-purity assay. They are complementary to characterise the radio-purity of materials for shielding or core detector components. Next generation experiments radioassay campaign requires a considerable effort and organization for several years [332–335].

Gamma spectroscopy (GS) via high purity germanium (HPGe) detectors is a powerful and crucial technique [331]. It is nondestructive and thanks to the energy resolution allows to distinguish various radionuclides elements. Radiation from ^{238}U and ^{232}Th comes with all decay products in the radioactive chains. However, if secular equilibrium is broken, this crucial information can be addressed by separating different gamma-ray lines characterizing elements in the decay chains. In the ^{238}U chain one can have three sub-chains out of equilibrium. The first sub-chain can be assessed through ^{234}Th direct progeny of ^{238}U. The second sub-chain, which originates from ^{226}Ra, can be probed by ^{214}Pb and ^{214}Bi. A third sub-chain, which starts from ^{210}Pb, cannot be efficiently probed by GS, yet is of crucial importance and alternative methods must be used. In the ^{232}Th chain again one can probe two sub-chains which can be out of secular equilibrium: the first one through ^{228}Ac from ^{228}Ra; the second from ^{228}Th can be measured through ^{212}Pb, ^{212}Bi and ^{208}Tl. The technology for HPGe operated in deep underground counting facilities [336, 337] or in shallow laboratories with an efficient active veto shielding [338] has been boosted to sensitivities of the order of 10-100 μBq/kg by carefully selecting detector components, electronics and sample handling systems. The HPGe screening method requires order of $\sim$ 0.1-a few kg of material, and weeks of acquisition to produce a reliable measurement.

A second crucial technique is based on inductively coupled plasma mass spectrometry (ICP-MS) [339]. This technique can probe primordial parent activities at the level of 1 μBq/kg. It is a destructive method and often needs special sample preparation on a small quantity of material. The ICP-MS does not measure the radioactive decay of isotopes but determines their concentration. At present, it is the most sensitive and rapid screening technique which allows to select materials at sub-ppt level of impurities. The drawback is that ICP-MS cannot assess whether the uranium and thorium chains are out of equilibrium and to reach ultra-high sensitivities one needs to carefully prepare and handle the samples in a cleanroom environment. ICP-MS screening must be coupled with other methods to properly assess the radio-purity of materials in the context of rare events searches. The Glow Discharge Mass Spectroscopy (GDMS) is a trace element analysis technique somehow alternative to ICP-MS. An advantage of GDMS is the possibility to determine the bulk composition of the sample, assuming homogeneity. Sensitivities of the order of 10 ppt can be achieved.

A third screening technique is based on neutron activation analysis (NAA) [340]. A sample exposed to a neutrons flux can be activated to form radioactive isotopes which can be detected using HPGe detectors or ICP-MS. Considering the difficulties to irradiate samples, this method is less often used. NAA can probe sensitivities at the level of 0.01 μBq/kg.

In case out of secular equilibrium conditions are measured for uranium and thorium from GS screening, a rigorous assessment cannot avoid radon emanation measurements. This matter is discussed in Section 36.6.3.

Complementarity between radio-purity assay techniques is a crucial parameter to design detectors for rare phenomena searches. As it has been pointed out above, requirements can be more stringent than the best sensitivity which can be obtained with the current radioassay techniques. In these cases, a number of prototype detectors have been built and operated to prove the feasibility to reach ultra-low backgrounds.

36.6.3 *Radon and its progeny*

Radon is considered to be rare in nature because most of its isotopes are short-lived. However, ^{222}Rn ($T_{1/2}$=3.82 d) is of particular concern in our context. ^{222}Rn is produced by ^{226}Ra and is a radioactive noble gas which can move within active detector components. ^{222}Rn daughters are heavy metals which can deposit on surfaces. Diffusive ^{222}Rn, supported by ^{226}Ra, can deposit on surfaces the long-lived ^{210}Pb, which is a major concern for low counting experiments. In addition, due to $\sim$100 keV nuclear recoil energies from alpha decays in the ^{226}Ra sub-chain, eventually ^{210}Pb can be implanted into a sub-surface layer of a material exposed to radon. This sub-surface contamination can remain even after surface cleaning. Surface contamination of ^{210}Pb is a serious background for direct dark matter experiments through alpha decay of ^{210}Po, which can generate neutrons by (α,n) reactions. Low energy beta/gamma emissions from ^{210}Pb are also a concern. Therefore, radon-free cleanrooms are essential for the assembly of the detector components. Effective radon abatement systems are available for this purpose. Air at the level of 1 mBq/m^3 of ^{222}Rn can be produced with such systems.

In assembling and commissioning rare events experiments, special care must be dedicated to the estimate of radon emanation of the materials and continuous radon monitoring. For this purpose different methods for radon assay have been developed and exploited since the beginning of solar neutrino observations. ^{222}Rn atoms are collected inside an exhalation chamber for several half-lives before adsorption and counting. Detection limits of the order of 100 μBq (about 50 ^{222}Rn atoms) can be obtained with $\sim$50 l stainless steel electro-polished chambers [341]. This limit can be pushed down to 30 μBq for 1-liter scale chamber. Emanation of large vessels (cryostats, storage tanks, purification columns) can be determined by collecting exhaled radon into transportable charcoal traps [342]. The same method can be used for liquid samples. In this case instead of evacuating the exhalation chamber into a charcoal trap, He is flushed through a sparger tube for about 10 times the volume of the liquid used. Sensitivities of the order of 10 μBq/kg have been reached. A novel technique of Rn emanation measurement developed in the framework of nEXO allows continuous gas transport and detection in a recirculation gas loop with an electrostatic chamber [343]. Another innovative method has been developed by using cryogenic physisorption traps [344]. Surface treatments can be exploited to enhance significantly the emanation measurement sensitivity and surface treatment with epoxy coating or covering it with alluminized Mylar is also shown to reduce emanation [345].

Nitrogen or synthetic air is often used in rare events experiments for purging, stripping, and assembling the experimental apparatus. These gases might contain radon. In gases ^{222}Rn can also be detected using electrostatic collection of ^{218}Po and ^{214}Po [346, 347]. Sensitivities of the order of mBq/m^3 can be obtained. In Borexino three grades of nitrogen purity were used: regular purity, high purity, and low argon and krypton purity. The regular purity is obtained from boil-off gas and has radon, measured with the method reported above, at the level of $< 100\mu$Bq/m^3. For nitrogen stripping the purified liquid scintillator a higher purity is needed. To remove radon from regular purity nitrogen a dedicated absorber plant has been built. This system can reduce radon by a factor of 100. Finally, we mention that not only radon is found in nitrogen. For specific applications the long-lived ^{39}Ar and ^{85}Kr in nitrogen are an important source of background.

36.6.4 *Surface backgrounds*

Surface contamination of long-lived ^{222}Rn daughters can be challenging in low-counting experiments. Considering required sensitivities of the next generation experiments, this source of background has to be properly quantified and mitigated. Therefore, exposure to ^{222}Rn should be monitored and limited to reduce build-up of ^{210}Pb on surfaces. In addition, ^{222}Rn exposure could also produce sub-surface contamination as discussed in Section 36.6.3. For one cannot avoid radon contamination in many circumstances during production of detectors components, it is

Int. J. Mod. [redacted] by UNIVERSITY OF CALIFORNIA @ BERKE
nloaded from www.worldscientific.com
use and distribution is strictly not permitted, except for Open Access articles.

crucial to quantify the effectiveness of cleaning aiming at removing surface contamination of ^{210}Pb, ^{210}Bi, and ^{210}Po. Depending on material, progeny are deposited deeper into the subsurface. A simple cleaning procedure, which implies degreasing, wiping, and rinsing the material surfaces is not effective in removing these surface contaminants. Studies of cleaning procedures have been carried out exposing stainless steel, copper and other materials (PTFE a common used material) to a strong radon source. Etching, leaching, and electropolishing with subsequential passivation and rinsing have been investigated in great details. Several recipes have been proposed [348,349]. Electropolishing has been shown to be very effective in reducing ^{210}Pb, ^{210}Bi, and ^{210}Po from both copper and stainless steel by a factor greater than 100. Etching, which is easier to perform than electropolishing, followed by passivation and rinsing with deionized water is effective in reducing ^{210}Pb and ^{210}Bi by a factor between 50 and 100. However, it is less effective for ^{210}Po, which in copper is very poorly reduced. Removing ^{210}Po from surfaces is crucial, therefore, naturally ^{210}Po contaminated copper and stainless steel surfaces have been deeply investigated with a high sensitivity ($1\,\mathrm{mBq/m^2}$) alpha spectrometer [350]. After multi-etching steps (≥ 3), followed by a passivation, a reduction of order 100 has been obtained. On the contrary, static etching (single step) is poorly effective. Electropolishing, or multi-etching are recommended in case copper is in direct contact with the active core of the detector and ultra-high radio-purity is essential or when copper electroforming cannot be used. Electroplating of a thin layer of high radio-pure copper onto the surface of less radio-pure copper has also been investigate to mitigate surface background [350]. This technique is shown to be efficient in reducing surface activity of ^{210}Po when electroformed copper is used [350].

Besides copper and steel other materials often used, such as polyethylene and teflon, have been investigated to understand how to reduce radon plate-out contaminations [351].

As far as surface contamination is concerned particulate fallout in cleanroom environments could be of concern. In general, chemical composition of dust reflects local composition of soil and dust. This is not necessarily true in cleanroom spaces, where the composition of dust depends on ongoing activities and handled materials [352]. The rate of fallout is an important information in the framework of rare events experiments, where assembling is performed in cleanrooms. The ^{210}Pb contamination, inferred from stable lead measured by ICP-MS, due to dust fallout has been investigated [352]. This contamination has a different origin with respect to ^{210}Pb from radon progeny implantation. Ultimately, one can conclude that radon exposure is more crucial than dust fallout. Therefore, the best practice for rare events experiments to face surface background contamination is to perform cleaning and assembling in a radon-free cleanroom environment.

36.6.5 *Mitigation of backgrounds and active background discrimination*

In this Section we discuss a selection of different background mitigation techniques used in experiments to search for rare events in deep underground laboratories. This includes both the avoidance or reduction of specific radioactive contamination, as well as active background suppression techniques based on specific event features and topologies.

- *Mitigation of ^{222}Rn daughters deposition.* In dark matter direct search radiogenic (α,n) reactions due to radioactive decays are of great concern. The emitted neutron can mimic a nuclear recoil induced by a dark matter particle interaction. In the DarkSide-50 and LUX-ZEPLIN (LZ) experiments to mitigate this background, cleaning of parts and assembling of the dual-phase Time Projection Chamber have been carried out in a radon-free cleanroom with ^{222}Rn activity of the order of $\lesssim 50\,\mathrm{mBq/m^3}$.
- *Underground argon.* Liquid argon is an excellent scintillator to search for dark matter interactions due to the high electron-recoils rejection power through pulse shape discrimination. Events from $\beta-\gamma$ background can be rejected at the level of 10^7 or better with respect to nuclear-recoils. Liquid argon is very effective as active shield and has been used in experiments for neutrinoless double beta decay. However, a major drawback for dark matter search using argon as a target is due to the fact that atmospheric argon contains about 1 Bq/kg of cosmogenic ^{39}Ar ($T_{1/2}$=269 y, Q_β=565 keV) [353]. For neutrinoless double beta decay search using argon as an active veto, ^{42}Ar ($T_{1/2}$=32.9 y, Q_β=599 keV) with its short lived progeny ^{42}K ($T_{1/2}$=12 h, Q_β=3525 keV) is a major source of background. ^{39}Ar limits significantly the dark matter and ^{42}Ar the neutrinoless double beta decay sensitivity search. Therefore, a source of argon with reduced ^{39}Ar and ^{42}Ar is crucial. Centrifugation or differential thermal diffusion are established methods to separate $^{39/42}$Ar and ^{40}Ar. However, this is an expensive method for a large fiducial mass. Argon from underground natural gas reservoirs is shown to contain low ^{39}Ar [354], and it is expected that ^{42}Ar is similar or even strongly reduced. Therefore, the use of underground argon mitigates the $^{39/42}$Ar backgrounds. DarkSide-50, with a mass of 150 kg of underground argon, has shown that this source of argon contains ^{39}Ar at a level reduced by a factor of $(1.4 \pm 0.3) \times 10^3$ with respect to atmospheric argon [355]. DarkSide-20k and LEGEND-1000 are planning to exploit underground argon from the Urania facility with a production capacity of order 300 kg/day [356]. The former to reduce ^{39}Ar and the latter ^{42}Ar.
- *Electro-formed copper.* High radio-purity copper is often used as shielding and as core detectors components. The radioimpurities in the copper can be a dominant source of external background. Copper electro-forming is a technique used to reduce this background component in rare events experiments. Copper electro-forming is a well known process to obtain ultra-high radio-purity copper. This technique has been used in the framework of the Majorana and LEGEND-200 experiments to search for neutrinoless double beta decay and in ANAIS to search for dark matter annual modulation. Sub-ppt levels in uranium and thorium have been achieved with electro-formed copper [334, 357].
- *Background suppression using topological event information.* In addition to rigorous selection of high-purity target and shielding materials from external radiation, additional active suppression techniques must usually be employed in low background experiments to achieve the appropriate experimental sensitivities. While signal and background events may be indistinguishable if only their energy deposition is measured, their event features may differ significantly in time and space. Liquid scintillators use the characteristic photon emission time distributions to distinguish between electron- and alpha-like signals [358] and nuclear recoils [359], respectively. High-purity germanium detectors use the time evolution of the induced charges to separate point-like signal candidates for neutrinoless double-beta decay events from background signals induced, for example, by gamma interactions with multiple interactions within a crystal, or from β or α events on the n+ or p+ electrodes [360]. The operation of bare high-purity germanium detectors in an instrumented liquid argon shield enabled the GERDA and LEGEND experiments to identify backgrounds with signal-like event topology within the HPGe detectors, but with characteristic energy deposition in the surrounding liquid argon. These synergistic background suppression techniques enabled for a first time ever a quasi background-free search for neutrinoless double beta decays with GERDA [361] and LEGEND-200 [362].

  EXO-200 [242] exploited topological event information distinghuishing single-site against multi-site events with a liquid xenon TPC for neutrinoless double beta decay in ^{136}Xe to reject background and threby enhancing signal discovery sensitivity. With a gas xenon TPC the NEXT experiment will fully exploit the differences in the spatial ionization patterns of double beta decay and single electron events [363]. The former is characterized by two Bragg peaks at opposite ends of the tracks, the latter on the contrary displays only one peak. The combination of topology information and good

Int. J. Mod. Phys. A 2026.41. Downloaded from www.worldscientific.com
by UNIVERSITY OF CALIFORNIA @ BERKELEY on 09/16/26. Re-use and distribution is strictly not permitted, except for Open Access articles.

energy resolution offer a powerful tool for background rejection. In general, the 3D reconstruction of detected events in a multivariate fit, which accounts for spacial surface and bulk distributions of signal and background together with other properties, such as pulse shape and topological features, is a powerful tool for background mitigation [364].

- *Signal selection in direct Dark Matter experiments.* In direct dark matter experiments electron recoil events have to be mitigated with respect to nuclear recoil events. In semiconductor bolometers, operating at a few tens of mK under a bias electric field and used as calorimeters, drifting charges produce a large phonon signal proportional to the ionization, which allows to discriminate electron recoils by the combination of charge and phonon signals [365]. In scintillating bolometers the phonon and light signals are used for the same purpose [366]. Cryogenic scintillators, such as xenon and argon, in time projection chambers offer a strong electron recoils background mitigation through the detection of a primary scintillation signal in liquid and a secondary signal in gas from the drift and extraction of ionization electrons. This background mitigation technique is also being used for neutrinoless double beta decay with ^{136}Xe. The accurate fiducialization and good rejection of multiple-scattering events allow dark matter optimized experiments to attempt a search for this very rare phenomenon.
- *Neutron tagging.* Present and next generation experiments need large neutron tagging detectors. In DarkSide-50 a dedicated active veto has been developed to both suppress and measure *in situ* the rate of neutron-induced background events [367]. The detector consisted of a boron-loaded liquid scintillator, which served both as shielding against γ-rays and as a tag for neutrons. Neutrons are thermalised and captured on ^{10}B. Experimental data has shown a neutron rejection power greater than 99.1% with 5% concentration of TMB in 30 tonnes pseudocumene-based liquid scintillator. The LZ direct dark matter detector with a central TPC of 7 tonnes of liquid xenon makes use of an outer Gd-loaded liquid scintillator neutron tagging veto, which works similarly to the DarkSide-50 veto, replacing boron with gadolinium. The 22 tonnes liquid scintillator is based on linear alkyl benzene (LAB) as solvent. This detector has been designed to operate with a neutron tagging efficiency greater than 95%. The nuclear-recoil background is reduced by a factor of 10. The XENONnT detector is making use of a cylindrical stainless steel tank filled with Gd-loaded water, which surrounds the cryostat with a TPC of 5.9 tonnes of active liquid xenon. The Gd concentration in water is 0.2% in mass. Neutrons leaving the TPC volume will be moderated and captured by the Gd with a probability of 91%. The gamma-rays emitted after the capture are detected from Cherenkov photons, providing a neutron tagging [368]. When operated with only demineralized water the efficiency for detecting neutrons is (82±1)% [369].

  Neutron tagging techniques are also crucial for coherent neutrino-nucleus elastic scattering detection from pion-decay-at-rest neutrino source at spallation sources [370, 371]. Neutrons can be produced in the Pb shielding from CC and NC interactions and propagate into the nuclear recoil sensitive volume, generating a beam-related background. Careful shielding design and implementation of neutron tagging is crucial.
- *Mitigation of cosmogenic background.* In recent years the required sensitivity to search for dark matter and neutrinoless double beta decay asks for a strong reduction of cosmogenic background. Muons can produce neutrons that can enter the active volume of the detector from the surrounding rock or from external detector components. The yield of these so-called *cosmogenic neutrons* depend on the muon energies and the material properties of the medium the muon passes through. In addition, muons can produce by spallation radioisotopes inside the detector active volume. Cosmogenic backgrounds are a function of depth and experimental design, and can limit the sensitivity to search for rare events. Most of these radioisotopes are short-lived and their effect can be easily removed by an active veto based on the time correlation with a crossing muon. However, a number of cosmogenic radioisotopes are long-lived and they require an important consideration. Mitigation of these cosmogenic backgrounds produced in-situ deep underground are a major challenge for upcoming and future experiments. Optimizing the detector design and analysis strategies at a given depth equals an effective muon flux reduction. In particular, we mention two discrimination techniques for muon-induced isotopes: 1) ^{11}C tagging by a three-fold coincidence between the crossing muon, the capture of the ejected neutron from ^{12}C, and the ^{11}C decay [372]; 2) similar delayed coincidence tagging can be exploited to mitigate the background due to ^{77}Ge and its metastable state ^{77m}Ge, which have been identified as dominant cosmogenic background in the search for neutrinoless double beta decay of ^{76}Ge [373].
- *Purification.* A number of high efficiency specific purification methods have been developed for different detectors in order to remove long-lived radio-isotopes, ^{39}K, ^{85}Kr, and ^{210}Pb progeny. For organic liquid scintillators, distillation and water extraction have been shown to be very effective to reach radiopurity levels of the order of $10^{-5}\mu$Bq/kg or better in uranium and thorium, and $10^{-3}\mu$Bq/kg in ^{210}Pb [374]. Distillation has been used to reduce ^{85}Kr in xenon by a factor of 10^3 [375]. Cryogenic distillation can be used to reduce the isotopic abundance of ^{39}Ar in argon extracted from underground with a 350 m column in the ARIA project [376]. Cryogenic distillation has been used in XENONnT to reduce online radon reaching a level of order 1 μBq/kg in the inner 5.9 tonne of liquid xenon [233]. For semiconductors [377] and scintillating crystals [378] zone-refining followed by single-crystal growth has been exploited to remove impurities at the cost of a small fraction of material kept after the purification.
- *Direct isotope tagging.* In neutrinoless double beta decay in order to explore half-lives greater than 10^{28} y one needs an almost background-free detector. The most robust signature is the identification of the daughter atom in the decay: for example, for ^{136}Xe, the $^{136}Ba^{2+}$. Important step forwards to establish a valid and promising method for this tagging have been recently made [379, 380].

References

[1] A. Aab *et al.* (the Pierre Auger Collaboration), Earth and Space Science **7**, 4, e2019EA000582 (2020), URL `https://agupubs.onlinelibrary.wiley.com/doi/abs/10.1029/2019EA000582`.

[2] S. Bacholle and the EUSO Collaboration, The Astrophysical Journal Supplement Series **253**, 2, 36 (2021), URL `https://doi.org/10.3847/1538-4365/abd93d`.

[3] R. M. Baltrusaitis *et al.*, Nucl. Instrum. Meth. **A240**, 410 (1985).

[4] D. J. Bird *et al.* (the HiRes Collaboration), Astrophys. J. **424**, 491 (1994).

[5] T. Abu-Zayyad *et al.* (the HiRes Collaboration), Nucl. Instrum. Meth. **A450**, 253 (2000).

[6] A. Watson, European Phys. J. Web of Confs. **210**, 00001 (2019), [arXiv:1901.06676].

[7] P. Sokolsky, European Phys. J. Web of Confs. **283**, 01003 (2023).

[8] H. Tokuno *et al.*, Nucl. Instrum. Meth. **A676**, 54 (2012), [arXiv:1201.0002].

[9] J. Abraham *et al.* (the Pierre Auger Collaboration), Nucl. Instrum. Meth. **A620**, 227 (2010), [arXiv:0907.4282].

[10] A. Coleman *et al.*, Astroparticle Physics **149**, 102819 (2023), ISSN 0927-6505, URL `https://www.sciencedirect.com/science/article/pii/S0927650523000051`.

Int. J. Mod. Phys. A Downloaded from www.worldscientific.com by UNIVERSITY OF CALIFORNIA @ BERKE use and distribution is strictly not permitted, except for Open Access articles.

[11] M. Malacari *et al.* (the FAST Collaboration), Astroparticle Physics **119**, 102430 (2020), ISSN 0927-6505, URL `https://www.sciencedirect.com/science/article/pii/S0927650520300037`.

[12] Y. Tameda *et al.* (the CRAFFT Collaboration), in "Proc. 38th Int. Cosmic Ray Conf. (ICRC 2023)," 329 (2023), [arXiv:2309.03325].

[13] F. Arqueros, J. R. Hoerandel and B. Keilhauer, Nucl. Instrum. Meth. **A597**, 23 (2008), [arXiv:0807.3844].

[14] F. Arqueros, J. R. Hoerandel and B. Keilhauer, Nucl. Instrum. Meth. **A597**, 1 (2008), [arXiv:0807.3760].

[15] J. Rosado, F. Blanco and F. Arqueros, Astropart. Phys. **34**, 164 (2010), [arXiv:1004.3971].

[16] M. Ave *et al.* (the AIRFLY Collaboration), Astropart. Phys. **28**, 41 (2007), [arXiv:astro-ph/0703132].

[17] J. Rosado, F. Blanco and F. Arqueros, Astropart. Phys. **55**, 51 (2014), [arXiv:1401.4310].

[18] J. H. Boyer *et al.*, Nucl. Instrum. Meth. **A482**, 457 (2002).

[19] J. T. Brack *et al.*, Astropart. Phys. **20**, 653 (2004).

[20] B. Fick *et al.*, JINST **1**, 11, P11003 (2006).

[21] J. Abraham *et al.* (the Pierre Auger Collaboration), Astropart. Phys. **33**, 108 (2010), [arXiv:1002.0366].

[22] P. Abreu *et al.* (the Pierre Auger Collaboration), Astropart. Phys. **34**, 368 (2011), [arXiv:1010.6162].

[23] R. Thalman *et al.* Journal of Quantitative Spectroscopy and Radiative Transfer , **147**, 171 (2014), Erratum-ibid. **189**, 281 (2017).

[24] Abraham, J. *et al.* (the Pierre Auger Collaboration), Nucl. Instrum. Methods **A789**, 172 (2015).

[25] M. Unger *et al.*, Nucl. Instrum. Meth. **A588**, 433 (2008), [arXiv:0801.4309].

[26] Gaisser, T. K. and Hillas, A. M. *Proc. 15th Int. Cosmic Ray Conf.* Bulgarska Akademiia na Naukite, Conf. Papers **8**, 353 (1978), (archived at http://adsabs.harvard.edu/abs/1977ICRC....8..353G).

[27] A. Aab *et al.* (the Pierre Auger Collaboration), Journal of Cosmology and Astroparticle Physics **2019**, 03, 018 (2019), [arXiv:1806.07422], URL `https://dx.doi.org/10.1088/1475-7516/2019/03/018`.

[28] A. Aab *et al.* (the Pierre Auger Collaboration), Phys. Rev. D **100**, 082003 (2019), URL `https://link.aps.org/doi/10.1103/PhysRevD.100.082003`.

[29] A. Abdul Halim *et al.* (the Pierre Auger Collaboration), "Astrophys. J. Suppl." **264**, 2, 50 (2023).

[30] A. Abdul Halim *et al.* (the Pierre Auger Collaboration), Phys. Rev. Lett. **132**, 021001 (2024), URL `https://link.aps.org/doi/10.1103/PhysRevLett.132.021001`.

[31] A. Abdul Halim *et al.* (the Pierre Auger Collaboration), The Pierre Auger Observatory Upgrade – Preliminary Design Report (2016), [arXiv:1604.03637].

[32] T. Huege *et al.* (the Pierre Auger Collaboration), in "Proc. 39th Int. Cosmic Ray Conf. (ICRC 2025)," (2025), [arXiv:2507.08500], URL `https://arxiv.org/abs/2507.08500`.

[33] P. A. Klimov *et al.*, Space Sci. Rev. **212**, 3-4, 1687 (2017), [arXiv:1706.04976].

[34] B. A. Khrenov *et al.*, Cosmic Research **58**, 5, 317 (2020).

[35] G. Abdellaoui *et al.* (the JEM-EUSO Collaboration), Journal of Instrumentation **13**, 5 (2018), ISSN 17480221.

[36] G. Abdellaoui *et al.* (the JEM-EUSO Collaboration), Astroparticle Physics **154**, 102891 (2024).

[37] J. Eser *et al.* (the JEM-EUSO Collaboration), Proceedings of Science **444**, 397 (2023).

[38] G. Filippatos *et al.*, arXiv preprint (2024), [arXiv:2406.13673], URL `https://arxiv.org/abs/2406.13673`.

[39] F. Capel *et al.*, Advances in Space Research **62**, 2954 (2018).

[40] A. V. Olinto (the POEMMA Collaboration), Journal of Cosmology and Astroparticle Physics **2021**, 06, 007 (2021), URL `https://dx.doi.org/10.1088/1475-7516/2021/06/007`.

[41] J. F. Krizmanic *et al.* (the POEMMA Collaboration), POEMMA (Probe of Extreme Multi-Messenger Astrophysics) Roadmap Update (2023), [arXiv:2309.14561].

[42] M. Battisti *et al.*, Nuclear Instruments and Methods in Physics Research Section A: Accelerators, Spectrometers, Detectors and Associated Equipment **1069**, 169819 (2024), ISSN 0168-9002, URL `http://dx.doi.org/10.1016/j.nima.2024.169819`.

[43] K. Bernlohr, Astropart. Phys. **12**, 255 (2000), [arXiv:astro-ph/9908093].

[44] T. Hassan *et al.*, Astropart. Phys. **93**, 76 (2017), [arXiv:1705.01790].

[45] T. C. Weekes, in "International WE - Heraeus Summer School: Physics with Cosmic Accelerators," (2005), [arXiv:astro-ph/0508253].

[46] R. Mirzoyan, in "Handbook of X-ray and Gamma-ray Astrophysics," (2024), [arXiv:2406.15037].

[47] J. Cortina and C. Delgado, in C. Bambi and A. Santangelo, editors, "Handbook of X-ray and Gamma-ray Astrophysics," Springer (2024), ISBN 978-981-16-4544-0, [arXiv:2306.06415].

[48] C. Bambi and A. Santangelo, editors, *Handbook of X-ray and Gamma-ray Astrophysics*, Springer (2024), ISBN 978-981-16-4544-0.

[49] G. Pühlhofer, F. Leuschner and H. Salzmann, in C. Bambi and A. Santangelo, editors, "Handbook of X-ray and Gamma-ray Astrophysics," Springer (2024), ISBN 978-981-16-4544-0, [arXiv:2405.11104].

[50] J. Albert *et al.* (MAGIC), Astrophys. J. **674**, 1037 (2008), [arXiv:0705.3244].

[51] O. Blanch and J. Sitarek, in C. Bambi and A. Santangelo, editors, "Handbook of X-ray and Gamma-ray Astrophysics," Springer (2024), ISBN 978-981-16-4544-0, [arXiv:2507.22585].

[52] J. Holder *et al.*, AIP Conf. Proc. **1085**, 657 (2009), [arXiv:0810.0474].

[53] D. Hanna and R. Mukherjee, in C. Bambi and A. Santangelo, editors, "Handbook of X-ray and Gamma-ray Astrophysics," Springer (2024), ISBN 978-981-16-4544-0, [arXiv:2507.09813].

[54] G. Pareschi (ASTRI), EPJ Web Conf. **319**, 01003 (2025).

[55] W. Hofmann and R. Zanin, in C. Bambi and A. Santangelo, editors, "Handbook of X-ray and Gamma-ray Astrophysics," Springer (2024), ISBN 978-981-16-4544-0, [arXiv:2305.12888].

[56] S. Zhang, PoS **ICRC2023**, 808 (2023).

[57] Z. Zhang, R. Yang and S. Zhang, arXiv e-prints arXiv:2509.20694 (2025), [arXiv:2509.20694].

[58] F. A. Aharonian *et al.*, Astropart. Phys. **15**, 335 (2001), [arXiv:astro-ph/0006163].

[59] C. Borwankar *et al.*, Astropart. Phys. **159**, 102960 (2024), [arXiv:2404.01649].

[60] A. Schliesser and R. Mirzoyan, Astropart. Phys. **24**, 382 (2005), [arXiv:astro-ph/0507617].

[61] S. Fegan, Astropart. Phys. **158**, 102948 (2024), [arXiv:2411.16434].

[62] V. Vassiliev, P. F. Brousseau and S. J. Fegan, Astropart. Phys. **28**, 10 (2007), [arXiv:astro-ph/0612718].

[63] L. Di Venere (CTA-SCT project), Nucl. Instrum. Meth. A **1056**, 168432 (2023).

Int. J. Mod. Phys. A 2026.41. Downloaded from www.worldscientific.com
by UNIVERSITY OF CALIFORNIA @ BERKELEY on 09/16/26. Re-use and distribution is strictly not permitted, except for Open Access articles.

[64] S. A. Mueller *et al.*, Astropart. Phys. **158**, 102933 (2024), [arXiv:2401.16148].

[65] D. Neise *et al.*, Nucl. Instrum. Meth. A **876**, 17 (2017).

[66] A. Hahn *et al.*, Nucl. Instrum. Meth. A **1064**, 169350 (2024), [arXiv:2404.14346].

[67] D. Malyshev and L. Mohrmann, in C. Bambi and A. Santangelo, editors, "Handbook of X-ray and Gamma-ray Astrophysics," Springer (2024), ISBN 978-981-16-4544-0, [arXiv:2309.02966].

[68] W. Hofmann *et al.*, Astropart. Phys. **122**, 135 (1999), [arXiv:astro-ph/9904234].

[69] M. de Naurois and L. Rolland, Astropart. Phys. **32**, 231 (2009), [arXiv:0907.2610].

[70] R. D. Parsons and J. A. Hinton, Astropart. Phys. **56**, 26 (2014), [arXiv:1403.2993].

[71] D. Heck *et al.*, FZKA-6019 (1998).

[72] M. Gaug *et al.*, Astrophys. J. Suppl. **243**, 1, 11 (2019), [arXiv:1907.04375].

[73] F. Schmuckermaier *et al.*, Astron. Astrophys. **673**, A2 (2023), [arXiv:2302.12072].

[74] A. Donath *et al.* (Gammapy), Astron. Astrophys. **678**, A157 (2023), [arXiv:2308.13584].

[75] D. Berge, S. Funk and J. Hinton, Astron. Astrophys. **466**, 1219 (2007), [arXiv:astro-ph/0610959].

[76] V. A. Acciari *et al.* (MAGIC), Astron. Astrophys. **635**, A158 (2020), [arXiv:2001.09566].

[77] Z. Zhang *et al.*, Chin. Phys. C **49**, 3, 035001 (2025), [arXiv:2409.14382].

[78] M. Holler *et al.* (H.E.S.S.), PoS **ICRC2015**, 847 (2016), [arXiv:1509.02902].

[79] N. Park (VERITAS), PoS **ICRC2015**, 771 (2016), [arXiv:1508.07070].

[80] T. C. Weekes *et al.*, Astrophys. J. **342**, 379 (1989).

[81] E. Aliu *et al.* (MAGIC), Science **322**, 1221 (2008), [arXiv:0809.2998].

[82] F. Aharonian *et al.* (H.E.S.S.), Astron. Astrophys. **686**, A308 (2024), [arXiv:2403.12608].

[83] `http://tevcat.org/`.

[84] F. Aharonian *et al.* (H.E.S.S.), Astrophys. J. **636**, 777 (2006), [arXiv:astro-ph/0510397].

[85] B. S. Acharya *et al.* (CTA Consortium), *Science with the Cherenkov Telescope Array*, WSP (2018), ISBN 978-981-327-008-4, [arXiv:1709.07997].

[86] K. Abe *et al.* (CTA-LST Project), Astron. Astrophys. **690**, A167 (2024), [arXiv:2407.02343].

[87] S. Abe *et al.* (MAGIC), Mon. Not. Roy. Astron. Soc. **529**, 4, 4387 (2024), [arXiv:2402.04755].

[88] A. Acharyya *et al.* (VERITAS), Astrophys. J. **966**, 1, 28 (2024), [arXiv:2401.01853].

[89] N. Vogel *et al.*, Mon. Not. Roy. Astron. Soc. **537**, 3, 2334 (2025), [arXiv:2411.16471].

[90] A. Bernstein *et al.*, *Report on the Depth Requirements for a Massive Detector at Homestake* (2009), [arXiv:0907.4183].

[91] A. Abusleme *et al.* (JUNO), Chin. Phys. C **49**, 1, 013003 (2025), [arXiv:2405.17860].

[92] G. Bellini *et al.* (BOREXINO), Nature **512**, 7515, 383 (2014).

[93] M. Yeh *et al.*, Nucl. Instrum. Meth. A **660**, 51 (2011).

[94] S. D. Biller, E. J. Leming and J. L. Paton, Nucl. Instrum. Meth. A **972**, 164106 (2020), [arXiv:2001.10825].

[95] J. Boger *et al.* (SNO), Nucl. Instrum. Meth. A **449**, 172 (2000), [arXiv:nucl-ex/9910016].

[96] T. K. Gaisser, F. Halzen and T. Stanev, Phys. Rept. **258**, 173 (1995), [Erratum: Phys. Rept. 271, 355 (1996)], [hep-ph/9410384].

[97] J. G. Learned and K. Mannheim, Ann. Rev. Nucl. Part. Sci. **50**, 679 (2000).

[98] U. F. Katz and C. Spiering, Prog. Part. Nucl. Phys. **67**, 651 (2012), [arXiv:1111.0507].

[99] M. G. Aartsen *et al.* (IceCube), J. Phys. **G44**, 5, 054006 (2017), [arXiv:1607.02671].

[100] S. Adrián-Martínez *et al.* (KM3NeT), J. Phys. **G43**, 8, 084001 (2016), [arXiv:1601.07459].

[101] A. Gazizov and M. P. Kowalski, Comput. Phys. Commun. **172**, 203 (2005), [arXiv:astro-ph/0406439].

[102] A. D. Avrorin *et al.*, Phys. Part. Nucl. **46**, 2, 211 (2015).

[103] M. G. Aartsen *et al.* (IceCube), JINST **12**, 03, P03012 (2017), [arXiv:1612.05093].

[104] M. G. Aartsen *et al.* (IceCube-Gen2), J. Phys. G **48**, 6, 060501 (2021), [arXiv:2008.04323].

[105] M. Agostini *et al.* (P-ONE), Nature Astron. **4**, 10, 913 (2020), [arXiv:2005.09493].

[106] Z. P. Ye *et al.* (TRIDENT), Nature Astron. **7**, 12, 1497 (2023), [arXiv:2207.04519].

[107] T.-Q. Huang *et al.*, PoS **ICRC2023**, 1080 (2023).

[108] H. Zhang *et al.*, Astropart. Phys. **171**, 103123 (2025), [arXiv:2408.05122].

[109] A. Albert *et al.* (ANTARES), Phys. Rept. **1121-1124**, 1 (2025), [arXiv:2504.09473].

[110] F. Hu, PoS **ICRC2023**, 1203 (2023).

[111] T. Huege, Phys. Rept. **620**, 1 (2016), [arXiv:1601.07426].

[112] F. G. Schroder, Prog. Part. Nucl. Phys. **93**, 1 (2017), [arXiv:1607.08781].

[113] G. A. Askar'yan, Sov. Phys. JETP **14**, 2, 441 (1962), [Zh. Eksp. Teor. Fiz.41,616(1961)].

[114] G.A. Askaryan, Sov. Phys. JETP **21**, 658 (1965).

[115] E. Zas, F. Halzen and T. Stanev, Phys. Rev. D **45**, 362 (1992).

[116] C. W. James *et al.*, Phys. Rev. **E84**, 056602 (2011), [arXiv:1007.4146].

[117] C. W. James, Phys. Rev. D **105**, 2, 023014 (2022), [arXiv:2201.01298].

[118] S. Chiche *et al.*, Phys. Rev. Lett. **132**, 23, 231001 (2024), [arXiv:2404.14541].

[119] J. Alvarez-Muniz, R. A. Vazquez and E. Zas, Phys. Rev. **D62**, 063001 (2000), [arXiv:astro-ph/0003315].

[120] C. Glaser *et al.*, Eur. Phys. J. C **80**, 77 (2020), [arXiv:1906.01670].

[121] D. Saltzberg *et al.*, Phys. Rev. Lett. **86**, 2802 (2001), [hep-ex/0011001].

[122] O. Scholten *et al.*, J. Phys. Conf. Ser. **81**, 012004 (2007).

[123] J. Alvarez-Muñiz *et al.*, Phys. Rev. D **74**, 023007 (2006), URL `https://link.aps.org/doi/10.1103/PhysRevD.74.023007`.

[124] L. Gerhardt and S. R. Klein, Phys. Rev. **D82**, 074017 (2010), [arXiv:1007.0039].

[125] J. Alvarez-Muniz, R. A. Vazquez and E. Zas, Phys. Rev. **D61**, 023001 (2000), [arXiv:astro-ph/9901278].

[126] D. García-Fernández, A. Nelles and C. Glaser, Phys. Rev. D **102**, 8, 083011 (2020), [arXiv:2003.13442].

[127] S. R. Klein, *Probing high-energy interactions of atmospheric and astrophysical neutrinos* (2020), [arXiv:1906.02221].

[128] K. Greisen, Phys. Rev. Lett. **16**, 748 (1966).

[129] G. T. Zatsepin and V. A. Kuzmin, JETP Lett. **4**, 78 (1966), [Pisma Zh. Eksp. Teor. Fiz.4,114(1966)].

Int. J. Mod. [redacted] by UNIVERSITY OF CALIFORNIA @ BERKE
nloaded from www.worldscientific.com
use and distribution is strictly not permitted, except for Open Access articles.

[130] A. A. Halim *et al.* (Pierre Auger), JCAP **05**, 024 (2023), [arXiv:2211.02857].

[131] A. Connolly and A. G. Vieregg, *Radio Detection of High Energy Neutrinos*, chapter 15, 217–240, World Scientific (2017), URL `https://www.worldscientific.com/doi/abs/10.1142/9789814759410_0015`.

[132] R. Abbasi *et al.* (IceCube), Astropart. Phys. **34**, 382 (2011), [arXiv:1004.1694].

[133] P. Allison *et al.* (ARA), Astropart. Phys. **108**, 63 (2019), [arXiv:1712.03301].

[134] A. Anker *et al.* (ARIANNA), JCAP **1911**, 030 (2019), [arXiv:1909.02677].

[135] J. A. Aguilar *et al.* (RNO-G), Eur. Phys. J. C **82**, 2, 147 (2022), [arXiv:2107.02604].

[136] I. Plaisier, S. Bouma and A. Nelles, Eur. Phys. J. C **83**, 5, 443 (2023), [arXiv:2302.00054].

[137] A. G. Vieregg, K. Bechtol and A. Romero-Wolf, JCAP **1602**, 02, 005 (2016), [arXiv:1504.08006].

[138] J. A. Aguilar *et al.*, Astropart. Phys. **145**, 102790 (2023), [arXiv:2103.06079].

[139] S. W. Barwick *et al.* (ARIANNA), Astropart. Phys. **90**, 50 (2017), [arXiv:1612.04473].

[140] S.-H. Wang *et al.* (TAROGE, Arianna), JCAP **11**, 022 (2022), [arXiv:2207.10616].

[141] S. Aiello *et al.* (KM3NeT), Nature **638**, 8050, 376 (2025), [Erratum: Nature 640, E3 (2025)].

[142] R. Abbasi *et al.* ((IceCube Collaboration)§, IceCube), Phys. Rev. Lett. **135**, 3, 031001 (2025), [arXiv:2502.01963].

[143] A. Aab *et al.* (Pierre Auger), JCAP **1910**, 10, 022 (2019), [arXiv:1906.07422].

[144] J. D. Bray *et al.*, Phys. Rev. **D91**, 6, 063002 (2015), [arXiv:1502.03313].

[145] O. Scholten *et al.*, Phys. Rev. Lett. **103**, 191301 (2009), [arXiv:0910.4745].

[146] P. W. Gorham *et al.* (ANITA), Phys. Rev. **D99**, 12, 122001 (2019), [arXiv:1902.04005].

[147] P. Allison *et al.* (ARA), Phys. Rev. D **102**, 4, 043021 (2020), [arXiv:1912.00987].

[148] A. Anker *et al.* (ARIANNA), JCAP **03**, 053 (2020), [arXiv:1909.00840].

[149] T. Winchen *et al.*, J. Phys. Conf. Ser. **1181**, 1, 012077 (2019), [arXiv:1903.08472].

[150] A. van Vliet, R. Alves Batista and J. R. Hörandel, Phys. Rev. D **100**, 2, 021302 (2019), [arXiv:1901.01899].

[151] S. Barwick *et al.*, Journal of Glaciology **51**, 173, 231–238 (2005).

[152] J.A. Dowdeswell and S. Evans, Rept. on Prog. in Phys. **67**, 1821 (2004).

[153] S. W. Barwick *et al.*, JCAP **1807**, 07, 055 (2018), [arXiv:1804.10430].

[154] C. Deaconu *et al.*, Phys. Rev. **D98**, 4, 043010 (2018), [arXiv:1805.12576].

[155] P. W. Gorham *et al.* (ANITA), Phys. Rev. Lett. **103**, 051103 (2009), [arXiv:0812.2715].

[156] P. W. Gorham *et al.* (ANITA), Phys. Rev. Lett. **121**, 16, 161102 (2018), [arXiv:1803.05088].

[157] P. W. Gorham *et al.* (ANITA), Phys. Rev. Lett. **126**, 7, 071103 (2021), [arXiv:2008.05690].

[158] A. Abdul Halim *et al.* (Pierre Auger), Phys. Rev. Lett. **134**, 12, 121003 (2025), [arXiv:2502.04513].

[159] I. Kravchenko *et al.* (RICE), Phys. Rev. **D73**, 082002 (2006), [arXiv:astro-ph/0601148].

[160] P. Allison *et al.* (ARA), Phys. Rev. **D93**, 8, 082003 (2016), [arXiv:1507.08991].

[161] J. Avva *et al.*, Nucl. Instrum. Meth. **A869**, 46 (2017), [arXiv:1605.03525].

[162] J. A. Aguilar *et al.* (RNO-G), JINST **16**, 03, P03025 (2021), [arXiv:2010.12279].

[163] R.D. Dagkesamanskii and I.M. Zheleznykh, Sov. Phys. JETP Lett. **50**, 233 (1989).

[164] G. R. Olhoeft and D. W. Strangway, Earth and Planetary Science Letters **24**, 3, 394 (1975).

[165] J. D. Bray, Astropart. Phys. **77**, 1 (2016), [arXiv:1601.02980].

[166] C. W. James *et al.*, EPJ Web Conf. **135**, 04001 (2017), [arXiv:1704.05336].

[167] A. Aab *et al.* (Pierre Auger), Phys. Rev. Lett. **116**, 24, 241101 (2016), [arXiv:1605.02564].

[168] P. A. Bezyazeekov *et al.* (Tunka-Rex), Phys. Rev. **D97**, 12, 122004 (2018), [arXiv:1803.06862].

[169] S. Buitink *et al.* (LOFAR), Phys. Rev. **D90**, 8, 082003 (2014), [arXiv:1408.7001].

[170] A. Abdul Halim *et al.* (Pierre Auger), Phys. Rev. Lett. **132**, 2, 021001 (2024), [arXiv:2310.19963].

[171] D. Fargion, Astrophys. J. **570**, 909 (2002), [arXiv:astro-ph/0002453].

[172] X. Bertou *et al.*, Astropart. Phys. **17**, 183 (2002), [arXiv:astro-ph/0104452].

[173] J. L. Feng *et al.*, Phys. Rev. Lett. **88**, 161102 (2002), [hep-ph/0105067].

[174] P. Abreu *et al.* (Pierre Auger), PoS **ICRC2021**, 262 (2021).

[175] Q. Abarr *et al.* (PUEO), JINST **16**, 08, P08035 (2021), [arXiv:2010.02892].

[176] A. Corstanje *et al.*, Phys. Rev. D **112**, 2, 023017 (2025), [arXiv:2504.16873].

[177] J. Álvarez Muñiz *et al.* (GRAND), Sci. China Phys. Mech. Astron. **63**, 1, 219501 (2020), [arXiv:1810.09994].

[178] D. Nygren, eConf **C740805**, 58 (1974).

[179] V. Chepel and H. Araujo, JINST **8**, R04001 (2013), [arXiv:1207.2292].

[180] E. Aprile and T. Doke, Rev. Mod. Phys. **82**, 2053 (2010), [arXiv:0910.4956].

[181] D. Gonzalez-Diaz, F. Monrabal and S. Murphy, Nucl. Instrum. Meth. A **878**, 200 (2018), [arXiv:1710.01018].

[182] E. Aprile *et al.*, *Noble Gas Detectors*, Wiley (2008), ISBN 978-3-527-40597-8, 978-3-527-61002-0.

[183] A. I. Bolozdynya, *Emission detectors*, World Scientific (2010).

[184] L. Baudis, Phil. Trans. Roy. Soc. Lond. A **382**, 2266, 20230083 (2023), [arXiv:2311.05320].

[185] D. S. Akerib *et al.* (LUX), Phys. Rev. D **97**, 11, 112002 (2018), [arXiv:1802.06162].

[186] B. Lenardo *et al.*, IEEE Trans. Nucl. Sci. **62**, 6, 3387 (2015), [arXiv:1412.4417].

[187] W. F. Schmidt, IEEE Trans. Electric. Insul. **19**, 389 (1984).

[188] L. Baudis *et al.*, Eur. Phys. J. C **83**, 8, 717 (2023), [arXiv:2303.13963].

[189] J. Albert *et al.* (EXO-200), Phys. Rev. C **89**, 1, 015502 (2014), [arXiv:1306.6106].

[190] A. Gando *et al.* (KamLAND-Zen), Phys. Rev. Lett. **122**, 19, 192501 (2019), [arXiv:1901.03871].

[191] E. Aprile *et al.* (XENON), Phys. Rev. C **106**, 2, 024328 (2022), [arXiv:2205.04158].

[192] J. Aalbers *et al.* (LZ), J. Phys. G **52**, 1, 015103 (2025), [arXiv:2408.17391].

[193] Z. Bo *et al.* (PandaX-4T, PandaX), JHEP **05**, 119 (2025), [arXiv:2411.14355].

Int. J. Mod. Phys. A 2026.41. Downloaded from www.worldscientific.com
by UNIVERSITY OF CALIFORNIA @ BERKELEY on 09/16/26. Re-use and distribution is strictly not permitted, except for Open Access articles.

[194] J. B. Albert *et al.* (EXO-200), Phys. Rev. D **96**, 9, 092001 (2017), [arXiv:1704.05042].

[195] K. Abe *et al.* (XMASS), PTEP **2018**, 5, 053D03 (2018), [arXiv:1801.03251].

[196] T. Doke *et al.*, Jap. J. Appl. Phys. **41**, 1538 (2002).

[197] C. E. Dahl, *The Physics of Background Discrimination in Liquid Xenon, and First Results from XENON10 in the Hunt for WIMP Dark Matter*, Ph.D. thesis, Princeton University (2009).

[198] L. Baudis, P. Sanchez-Lucas and K. Thieme, Eur. Phys. J. C **81**, 12, 1060 (2021), [arXiv:2109.07151].

[199] G. Anton *et al.* (EXO-200), Phys. Rev. C **101**, 6, 065501 (2020), [arXiv:1908.04128].

[200] J. J. Gomez-Cadenas, F. Monrabal Capilla and P. Ferrario, Front. in Phys. **7**, 51 (2019), [arXiv:1903.02435].

[201] M. S. J. Lindhard, V. Nielsen and P. Thomsen, Kgl. Danske Videnskab., Selskab. Mat. Fys. Medd **33**, 1 (1963).

[202] A. Hitachi and A. Mozumder (2019), [arXiv:1903.05815].

[203] P. Sorensen and C. E. Dahl, Phys. Rev. D **83**, 063501 (2011), [arXiv:1101.6080].

[204] M. Szydagis *et al.*, JINST **6**, P10002 (2011), [arXiv:1106.1613].

[205] G. Pereira, C. Silva and V. N. Solovov (LZ), JINST **18**, 04, C04007 (2023).

[206] E. Aprile *et al.* (XENON), Eur. Phys. J. C **80**, 8, 785 (2020), [arXiv:2003.03825].

[207] G. Anton *et al.* (EXO-200), Phys. Rev. Lett. **123**, 16, 161802 (2019), [arXiv:1906.02723].

[208] D. Nygren, Nucl. Instrum. Meth. A **603**, 337 (2009).

[209] J. Renner *et al.* (NEXT), JHEP **10**, 230 (2019), [arXiv:1905.13110].

[210] P. Agnes *et al.* (DarkSide), Nucl. Instrum. Meth. A **904**, 23 (2018), [arXiv:1802.01427].

[211] P. Abratenko *et al.* (MicroBooNE), JINST **16**, 09, P09025 (2021), [arXiv:2104.06551].

[212] Y. Li *et al.*, Nucl. Instrum. Meth. A **816**, 160 (2016), [arXiv:1508.07059].

[213] J. B. Albert *et al.* (EXO-200), Phys. Rev. C **95**, 2, 025502 (2017), [arXiv:1609.04467].

[214] M. Babicz *et al.*, JINST **15**, 09, P09009 (2020), [arXiv:2002.09346].

[215] E. Aprile *et al.* (XENON), PTEP **2022**, 5, 053H01 (2022), [arXiv:2112.12231].

[216] P. Agnes *et al.* (DarkSide), Phys. Rev. D **98**, 10, 102006 (2018), [arXiv:1802.07198].

[217] E. Aprile *et al.* (XENON), Phys. Rev. Lett. **129**, 16, 161805 (2022), [arXiv:2207.11330].

[218] P. Agnes (DarkSide), EPJ Web Conf. **280**, 06003 (2023).

[219] D. S. Akerib *et al.* (LZ), Nucl. Instrum. Meth. A **953**, 163047 (2020), [arXiv:1910.09124].

[220] Y. Meng *et al.* (PandaX-4T), Phys. Rev. Lett. **127**, 26, 261802 (2021), [arXiv:2107.13438].

[221] E. Aprile *et al.* (XENON), JCAP **11**, 031 (2020), [arXiv:2007.08796].

[222] S. Kravitz *et al.*, Eur. Phys. J. C **80**, 3, 262 (2020), [arXiv:1909.08730].

[223] J. Aalbers *et al.* (XLZD), Eur. Phys. J. C (2024), [arXiv:2410.17137].

[224] X. Wang *et al.*, JINST **18**, 05, P05028 (2023), [arXiv:2301.06044].

[225] J. Aalbers *et al.* (DARWIN), JCAP **1611**, 11, 017 (2016), [arXiv:1606.07001].

[226] J. Aalbers *et al.*, J. Phys. G **50**, 1, 013001 (2023), [arXiv:2203.02309].

[227] P. Agnes *et al.* (DarkSide), Phys. Rev. Lett. **130**, 10, 101002 (2023), [arXiv:2207.11968].

[228] S. Li *et al.* (PandaX), Phys. Rev. Lett. **130**, 26, 261001 (2023), [arXiv:2212.10067].

[229] E. Aprile *et al.* (XENON), Phys. Rev. Lett. **129**, 16, 161805 (2022), [arXiv:2207.11330].

[230] J. Aalbers *et al.* (LZ), Phys. Rev. D **108**, 7, 072006 (2023), [arXiv:2307.15753].

[231] Z. Bo *et al.* (PandaX), Phys. Rev. Lett. **133**, 19, 191001 (2024), [arXiv:2407.10892].

[232] E. Aprile *et al.* (XENON), Phys. Rev. Lett. **133**, 19, 191002 (2024), [arXiv:2408.02877].

[233] E. Aprile *et al.* (XENON), Phys. Rev. X **15**, 3, 031079 (2025), [arXiv:2502.04209].

[234] T. N. Thorpe (DarkSide-20k), SciPost Phys. Proc. **12**, 069 (2023), [arXiv:2210.00322].

[235] G. Plante *et al.*, Eur. Phys. J. C **82**, 10, 860 (2022), [arXiv:2205.07336].

[236] A. Abdukerim *et al.* (PandaX), Sci. China Phys. Mech. Astron. **68**, 2, 221011 (2025), [arXiv:2402.03596].

[237] K. Stifter (LZ), J. Phys. Conf. Ser. **1468**, 1, 012016 (2020).

[238] R. Anthony-Petersen *et al.* (SPICE, HeRALD), Phys. Rev. D **110**, 7, 072006 (2024), [arXiv:2307.11877].

[239] B. von Krosigk *et al.*, SciPost Phys. Proc. **12**, 016 (2023), [arXiv:2209.10950].

[240] R. E. Lanou, H. J. Maris and G. M. Seidel, Phys. Rev. Lett. **58**, 2498 (1987).

[241] F. D. Amaro *et al.*, Phys. Lett. B **855**, 138759 (2024).

[242] G. Anton *et al.* (EXO-200), Phys. Rev. Lett. **123**, 16, 161802 (2019), [arXiv:1906.02723].

[243] G. Adhikari *et al.* (nEXO), J. Phys. G **49**, 1, 015104 (2022), [arXiv:2106.16243].

[244] A. Simón *et al.* (NEXT), JHEP **07**, 146 (2021), [arXiv:2102.11931].

[245] P. Ferrario *et al.* (NEXT), JHEP **10**, 052 (2019), [arXiv:1905.13141].

[246] P. Novella *et al.* (NEXT), Phys. Rev. C **105**, 5, 055501 (2022), [arXiv:2111.11091].

[247] C. Adams *et al.* (NEXT) (2025), [arXiv:2505.17848].

[248] C. Adams *et al.* (NEXT), JHEP **2021**, 08, 164 (2021), [arXiv:2005.06467].

[249] A. D. McDonald *et al.*, Phys. Rev. Lett. **120**, 13, 132504 (2018), [arXiv:1711.04782].

[250] P. Herrero-Gómez *et al.* (NEXT), Nature Commun. **13**, 1, 7741 (2022), [arXiv:2201.09099].

[251] H. Rasiwala *et al.* (nEXO Ba-tagging group), Nucl. Instrum. Meth. B **541**, 298 (2023), [arXiv:2303.04698].

[252] W. Zhang *et al.* (PandaX-III), JINST **18**, 12, C12001 (2023), [arXiv:2311.13396].

[253] S. Wen *et al.*, Nucl. Instrum. Meth. A **1062**, 169206 (2024).

[254] E. Aprile *et al.* (XENON), Nature **568**, 7753, 532 (2019), [arXiv:1904.11002].

[255] G. Martínez-Lema *et al.* (NEXT), JHEP **21**, 203 (2020), [arXiv:2006.07320].

[256] C. Wittweg *et al.*, Eur. Phys. J. C **80**, 12, 1161 (2020), [arXiv:2002.04239].

[257] S. Zhang *et al.* (PandaX), Sci. Bull. **70**, 1779 (2025), [arXiv:2412.13979].

[258] L. Luo *et al.* (PANDA-X), JHEP **05**, 089 (2025), [arXiv:2502.03017].

[259] X. Yan *et al.* (PandaX), Phys. Rev. Lett. **132**, 15, 152502 (2024), [arXiv:2312.15632].

[260] D. S. Akerib *et al.* (LZ), Phys. Rev. C **102**, 1, 014602 (2020), [arXiv:1912.04248].

Int. J. Mod. [redacted] nloaded from www.worldscientific.com
by UNIVERSITY OF CALIFORNIA @ BERKE use and distribution is strictly not permitted, except for Open Access articles.

[261] D. S. Akerib *et al.* (LZ), Phys. Rev. C **104**, 6, 065501 (2021), [arXiv:2104.13374].

[262] F. Agostini *et al.* (DARWIN), Eur. Phys. J. C **80**, 9, 808 (2020), [arXiv:2003.13407].

[263] J. Aalbers *et al.* (XLZD), J. Phys. G **52**, 4, 045102 (2025), [arXiv:2410.19016].

[264] C. Enss, editor, *Cryogenic particle detection*, volume 99 of *Topics in applied physics*, Springer, Berlin, Germany (2005).

[265] K. Pretzl, *Cryogenic Detectors* (2020).

[266] *Proc. of the Low Temperature Detectors for Neutrinos and Dark Matter*, Low Temperature Detectors for Neutrinos and Dark Matter (start 1987).

[267] G. H. Rieke, *Detection of Light*, Cambridge University Press, 3rd edition (2021).

[268] H. Kraus, Superconductor Science and Technology **9**, 10, 827 (1996), URL `https://doi.org/10.1088/0953-2048/9/10/001`.

[269] M. H. Devoret, A. Wallraff and J. M. Martinis, Superconducting Qubits: A Short Review (2004), [arXiv:cond-mat/0411174], URL `https://arxiv.org/abs/cond-mat/0411174`.

[270] R. Linehan *et al.*, Phys. Rev. D **111**, 063047 (2025), URL `https://link.aps.org/doi/10.1103/PhysRevD.111.063047`.

[271] C. Fink *et al.*, Physical Review Applied **22**, 5 (2024), ISSN 2331-7019, URL `http://dx.doi.org/10.1103/PhysRevApplied.22.054009`.

[272] K. Ramanathan *et al.* (2024), [arXiv:2405.17192].

[273] A. V. Dixit *et al.*, Phys. Rev. Lett. **126**, 14, 141302 (2021), [arXiv:2008.12231].

[274] J. Zmuidzinas, Annual Review of Condensed Matter Physics **3**, 1, 169 (2012), URL `https://doi.org/10.1146/annurev-conmatphys-020911-125022`.

[275] S. Doyle *et al.*, Journal of Low Temperature Physics **151**, 1, 530 (2008), URL `https://doi.org/10.1007/s10909-007-9685-2`.

[276] K. Irwin and G. Hilton, *Transition-Edge Sensors*, 63–150, Springer Berlin Heidelberg, Berlin, Heidelberg (2005), ISBN 978-3-540-31478-3, URL `https://doi.org/10.1007/10933596_3`.

[277] F. Paolucci and F. Giazotto, Instruments **5**, 2 (2021), ISSN 2410-390X, URL `https://www.mdpi.com/2410-390X/5/2/14`.

[278] S. B. Bandler *et al.*, J. Low Temp. Phys. **93**, 709 (1993).

[279] D. Prele, Journal of Instrumentation **10**, 08, C08015 (2015), URL `https://doi.org/10.1088/1748-0221/10/08/c08015`.

[280] Y. Li *et al.* (CLASS), Astrophys. J. **986**, 2, 111 (2025), [arXiv:2501.11904].

[281] S. e. a. A. C. Naess, arXiv e-prints (2025), aCT data from 2017–2022; Accessed 2025-08-13, URL `https://arxiv.org/abs/2503.14451`.

[282] B. Westbrook and the POLARBEAR/Simons Array Collaboration, Journal of Low Temperature Physics **193**, 5?6, 758?770 (2018), ISSN 1573-7357, URL `http://dx.doi.org/10.1007/s10909-018-2059-0`.

[283] N. Galitzki *et al.* (SO), Astrophys. J. Suppl. **274**, 2, 33 (2024), [arXiv:2405.05550].

[284] S. e. a. Thoen, arXiv e-prints (2024), accessed 2025-08-13, URL `https://arxiv.org/abs/2407.17019`.

[285] F. e. a. Paonessa, arXiv e-prints (2025), URL `https://arxiv.org/abs/2506.22617`.

[286] A. Mennella *et al.* (QUBIC), EPJ Web Conf. **293**, 00030 (2024), [arXiv:2311.02779].

[287] E. Allys *et al.* (LiteBIRD), PTEP **2023**, 4, 042F01 (2023), [arXiv:2202.02773].

[288] E. Fiorini and T. Niinikoski, Nucl. Instrum. Meth. A **224**, 83 (1984).

[289] S. H. Moseley, J. C. Mather and D. McCammon, Thermal detectors as x-ray spectrometers (1984).

[290] V. Barger and D. Cline (1985), telemark, 1984.

[291] A. Blasi *et al.* (1985), `I.N.F.N./BE-85/2`, internal report.

[292] D. Q. Adams *et al.* (CUORE), Science **0**, 0, eadp6474, URL `https://www.science.org/doi/abs/10.1126/science.adp6474`.

[293] W. R. Armstrong *et al.* (CUPID) (2019), [arXiv:1907.09376].

[294] K. Alfonso *et al.* (CUPID) (2025), [arXiv:2504.14369].

[295] O. Azzolini *et al.* (CUPID), Phys. Rev. Lett. **129**, 11, 111801 (2022), [arXiv:2206.05130].

[296] C. Augier *et al.*, Eur. Phys. J. C **82**, 11, 1033 (2022), [arXiv:2202.08716].

[297] A. Agrawal *et al.* (AMoRE), Eur. Phys. J. C **85**, 2, 172 (2025), [Erratum: Eur.Phys.J.C 85, 256 (2025)], [arXiv:2407.12227].

[298] D. Mccammon *et al.* (1984).

[299] G. Drexlin *et al.*, Adv. High Energy Phys. **2013**, 293986 (2013), [arXiv:1307.0101].

[300] P. Filianin *et al.*, Phys. Rev. Lett. **127**, 7, 072502 (2021), [arXiv:2108.07039].

[301] D. Pergolesi *et al.*, Nucl. Instrum. Meth. A **559**, 349 (2006).

[302] M. Sisti *et al.*, Nuclear Instruments and Methods in Physics Research Section A: Accelerators, Spectrometers, Detectors and Associated Equipment **520**, 1, 125 (2004), ISSN 0168-9002, proceedings of the 10th International Workshop on Low Temperature Detectors, URL `https://www.sciencedirect.com/science/article/pii/S0168900203031814`.

[303] E. Ferri *et al.*, Phys. Procedia **61**, 227 (2015).

[304] C. Velte, *Measurement of a high energy resolution and high-statistics 163Ho electron capture spectrum for the ECHo experiment.*, Ph.D. thesis, U. Heidelberg (main) (2020).

[305] F. Mantegazzini *et al.*, Nucl. Instrum. Meth. A **1055**, 168564 (2023), [arXiv:2301.06455].

[306] B. K. Alpert *et al.* (2025), [arXiv:2503.19920].

[307] M. P. Croce *et al.*, J. Low Temp. Phys. **184**, 3-4, 958 (2016), [arXiv:1510.03874].

[308] M. Farino *et al.* (PTOLEMY) (2025), [arXiv:2503.10025].

[309] E. Armengaud *et al.* (EDELWEISS), Phys. Rev. D **86**, 051701 (2012), [arXiv:1207.1815].

[310] R. Agnese *et al.* (SuperCDMS), Phys. Rev. D **95**, 8, 082002 (2017), [arXiv:1610.00006].

[311] G. Angloher *et al.* (CRESST), Phys. Rev. D **110**, 8, 083038 (2024), [arXiv:2405.06527].

[312] G. Angloher *et al.* (2025), [arXiv:2505.01183].

[313] R. Ardito *et al.* (2005), [hep-ex/0501010].

[314] D. Q. Adams *et al.* (CUORE) (2024), [arXiv:2404.04453v1].

[315] A. Agrawal *et al.* (AMoRE), Phys. Rev. Lett. **134**, 8, 082501 (2025), [arXiv:2407.05618].

[316] S. Kim (AMoRE), PoS **TIPP2023**, 014 (2025).

[317] P. Luke *et al.*, Nucl. Instrum. Meth. A **289**, 406 (1990).

[318] B. Neganov *et al.*, J Low Temp Phys **93**, 417–422 (1993), URL `https://doi.org/10.1007/BF00693454`.

[319] M. F. Albakry *et al.* (SuperCDMS), Phys. Rev. D **111**, 1, 012006 (2025), [arXiv:2407.08085].

[320] E. Armengaud *et al.* (EDELWEISS), Phys. Rev. D **106**, 6, 062004 (2022), [arXiv:2203.03993].

[321] A. Armatol *et al.* (2025), [arXiv:2507.15732].

Int. J. Mod. Phys. A 2026.41. Downloaded from www.worldscientific.com
by UNIVERSITY OF CALIFORNIA @ BERKELEY on 09/16/26. Re-use and distribution is strictly not permitted, except for Open Access articles.

[322] *Snowmass2021-Letter of Interest The TESSERACT Dark Matter Project* (2020).

[323] A. Cruciani *et al.*, Appl. Phys. Lett. **121**, 21, 213504 (2022), [arXiv:2209.14806].

[324] T. Braine *et al.* (ADMX), Phys. Rev. Lett. **124**, 10, 101303 (2020), [arXiv:1910.08638].

[325] S. Ahn *et al.* (CAPP), Phys. Rev. X **14**, 3, 031023 (2024), [arXiv:2402.12892].

[326] *Snowmass2021-Letter of Interest Opening the Terahertz Axion Window* (2020).

[327] C. Augier *et al.* (Ricochet), Eur. Phys. J. C **84**, 2, 186 (2024), [arXiv:2306.00166].

[328] C. Bellenghi *et al.*, Eur. Phys. J. C **79**, 9, 727 (2019), [arXiv:1905.10611].

[329] I. Colantoni *et al.*, J. Low Temp. Phys. **199**, 3-4, 593 (2020).

[330] L. Pattavina *et al.* (RES-NOVA), JCAP **10**, 064 (2021), [arXiv:2103.08672].

[331] G. Heusser, Ann. Rev. Nucl. Part. Sci. **45**, 543 (1995).

[332] D. S. Akerib *et al.*, The European Physical Journal C **80**, 11 (2020), URL `https://doi.org/10.1140%2Fepjc%2Fs10052-020-8420-x`.

[333] D. S. Leonard *et al.*, Nucl. Instrum. Meth. A **871**, 169 (2017), [arXiv:1703.10799].

[334] N. Abgrall *et al.*, Nucl. Instrum. Methods Phys. Res. A **828**, 22 (2016).

[335] E. Aprile *et al.* (XENON), Eur. Phys. J. C **82**, 7, 599 (2022), [arXiv:2112.05629].

[336] M. Laubenstein, International Journal of Modern Physics A **32**, 30, 1743002 (2017), URL `https://doi.org/10.1142/s0217751x17430023`.

[337] P. Scovell *et al.*, Astroparticle Physics **97**, 160 (2018), URL `https://doi.org/10.1016/j.astropartphys.2017.11.006`.

[338] G. Heusser *et al.*, The European Physical Journal C **75**, 11 (2015), URL `https://doi.org/10.1140%2Fepjc%2Fs10052-015-3704-2`.

[339] N. Jakubowski, Analytical and Bioanalytical Chemistry **392**, 5, 775 (2008), URL `https://doi.org/10.1007%2Fs00216-008-2374-4`.

[340] M. Clemenza, J. Radioanal. Nucl. Chem. **318**, 3, 1765 (2018).

[341] G. Heusser *et al.*, Applied Radiation and Isotopes **52**, 3, 691 (2000), URL `https://doi.org/10.1016%2Fs0969-8043%2899%2900231-6`.

[342] M. Wojcik, G. Zuzel and H. Simgen, International Journal of Modern Physics A **32**, 30, 1743004 (2017), URL `https://doi.org/10.1142%2Fs0217751x17430047`.

[343] A. Anker *et al.*, Nucl. Instrum. Methods Phys. Res. A **1081**, 170876, 170876 (2026).

[344] D. Wiebe, S. Lindemann and M. Schumann, Journal of Instrumentation **19**, 04, P04014 (2024), ISSN 1748-0221, URL `http://dx.doi.org/10.1088/1748-0221/19/04/P04014`.

[345] Y. Wu *et al.*, Nuclear Instruments and Methods in Physics Research Section A: Accelerators, Spectrometers, Detectors and Associated Equipment **1080**, 170771 (2025), ISSN 0168-9002, URL `http://dx.doi.org/10.1016/j.nima.2025.170771`.

[346] Y. Takeuchi *et al.*, Nuclear Instruments and Methods in Physics Research Section A: Accelerators, Spectrometers, Detectors and Associated Equipment **421**, 1-2, 334 (1999), URL `https://doi.org/10.1016%2Fs0168-9002%2898%2901204-2`.

[347] J. Kiko, Nuclear Instruments and Methods in Physics Research Section A: Accelerators, Spectrometers, Detectors and Associated Equipment **460**, 2-3, 272 (2001), URL `https://doi.org/10.1016%2Fs0168-9002%2800%2901082-2`.

[348] E. Hoppe *et al.*, Nuclear Instruments and Methods in Physics Research Section A: Accelerators, Spectrometers, Detectors and Associated Equipment **579**, 1, 486 (2007), URL `https://doi.org/10.1016%2Fj.nima.2007.04.101`.

[349] A. D. C.D. Christofferson, V.E. Giuseppe, in "Low Radiation Techniques, Jaca, Spain, 2019," (2019).

[350] R. Bunker *et al.*, Nuclear Instruments and Methods in Physics Research Section A: Accelerators, Spectrometers, Detectors and Associated Equipment **967**, 163870 (2020), URL `https://doi.org/10.1016/j.nima.2020.163870`.

[351] S. Bruenner *et al.*, The European Physical Journal C **81**, 4 (2021), URL `https://doi.org/10.1140/epjc/s10052-021-09047-2`.

[352] M. L. di Vacri *et al.*, Nucl. Instrum. Meth. A **994**, 165051 (2021), [arXiv:2006.12746].

[353] H. Loosli, Earth and Planetary Science Letters **63**, 1, 51 (1983), URL `https://doi.org/10.1016%2F0012-821x%2883%2990021-3`.

[354] D. Acosta-Kane *et al.*, Nuclear Instruments and Methods in Physics Research Section A: Accelerators, Spectrometers, Detectors and Associated Equipment **587**, 1, 46 (2008), URL `https://doi.org/10.1016%2Fj.nima.2007.12.032`.

[355] P. Agnes *et al.* (DarkSide), Phys. Rev. D **93**, 8, 081101 (2016), [Addendum: Phys.Rev.D 95, 069901 (2017)], [arXiv:1510.00702].

[356] H. O. Back *et al.*, in "Snowmass 2021," (2022), [arXiv:2203.09734].

[357] I. Bandac *et al.*, Appl. Radiat. Isot. **126**, 127 (2017).

[358] G. Ranucci, in "IEEE Symposium Conference Record Nuclear Science 2004.", volume 2, 804–809 Vol. 2 (2004).

[359] P. Adhikari *et al.*, The European Physical Journal C **80**, 4 (2020), URL `https://doi.org/10.1140%2Fepjc%2Fs10052-020-7789-x`.

[360] D. Budjáš *et al.*, Journal of Instrumentation **4**, 10, P10007 (2009), URL `https://doi.org/10.1088/1748-0221/4/10/p10007`.

[361] M. Agostini *et al.* (GERDA), Phys. Rev. Lett. **125**, 25, 252502 (2020), [arXiv:2009.06079].

[362] H. Acharya *et al.* (LEGEND) (2025), [arXiv:2505.10440].

[363] A. Simón *et al.* (NEXT), JHEP **21**, 146 (2020), [arXiv:2102.11931].

[364] G. Adhikari *et al.*, J. Phys. G Nucl. Part. Phys. **49**, 1, 015104 (2022).

[365] R. Agnese *et al.* (SuperCDMS Collaboration), Phys. Rev. Lett. **120**, 061802 (2018), URL `https://link.aps.org/doi/10.1103/PhysRevLett.120.061802`.

[366] W. Westphal *et al.*, Nucl. Instrum. Meth. A **559**, 372 (2006).

[367] S. Westerdale, E. Shields and F. Calaprice, Astroparticle Physics **79**, 10 (2016), URL `https://doi.org/10.1016%2Fj.astropartphys.2016.01.005`.

[368] Marco Selvi, The XENONnT Neutron Veto (2023), URL `https://indico.cern.ch/event/1188759/`.

[369] E. Aprile *et al.*, Eur. Phys. J. C Part. Fields **85**, 6 (2025).

[370] D. Akimov *et al.* (COHERENT), Science **357**, 6356, 1123 (2017), [arXiv:1708.01294].

[371] D. Akimov *et al.*, in "Snowmass 2021," (2022), [arXiv:2204.04575].

[372] H. Back *et al.* (Borexino Collaboration), Phys. Rev. C **74**, 045805 (2006), URL `https://link.aps.org/doi/10.1103/PhysRevC.74.045805`.

[373] C. Wiesinger, L. Pandola and S. Schönert, Eur. Phys. J. C **78**, 7, 597 (2018), [arXiv:1802.05040].

[374] J. Benziger *et al.*, Nuclear Instruments and Methods in Physics Research Section A: Accelerators, Spectrometers, Detectors and Associated Equipment **587**, 2-3, 277 (2008), URL `https://doi.org/10.1016/j.nima.2007.12.043`.

[375] K. Abe *et al.*, Nucl. Instrum. Meth. A **716**, 78 (2013), [arXiv:1301.2815].

[376] E. Aaron *et al.* (DarkSide-20k), Eur. Phys. J. C **83**, 5, 453 (2023), [arXiv:2301.09639].

[377] K.-P. Gradwohl *et al.*, Journal of Instrumentation **15**, 12, P12010 (2020), URL `https://doi.org/10.1088/1748-0221/15/12/p12010`.

[378] B. Suerfu, F. Calaprice and M. Souza, Physical Review Applied **16**, 1 (2021), URL `https://doi.org/10.1103/physrevapplied.16.014060`.

[379] I. Rivilla *et al.*, Nature **583**, 7814, 48 (2020), URL `https://doi.org/10.1038/s41586-020-2431-5`.

[380] A. McDonald *et al.*, Physical Review Letters **120**, 13 (2018), URL `https://doi.org/10.1103/physrevlett.120.132504`.

Int. J. Mod. Phys. A Downloaded from www.worldscientific.com
by UNIVERSITY OF CALIFORNIA @ BERKE use and distribution is strictly not permitted, except for Open Access articles.

Int. J. Mod. Phys. A 2026.41. Downloaded from www.worldscientific.com by UNIVERSITY OF CALIFORNIA @ BERKELEY on 09/16/26. Re-use and distribution is strictly not permitted, except for Open Access articles.

37. Radioactivity and Radiation Protection

Revised August 2025 by S. Roesler (CERN) and M. Silari (CERN).

37.1 Definitions [1–3]

It would be desirable if legal protection limits could be expressed in directly measurable *physical quantities*. However, this does not allow quantifying biological effects of the exposure of the human body and its detriment to ionizing radiation.

For this reason, dose limits are expressed in terms of so-called *protection quantities* which, although calculable, are not measurable. Protection quantities are used to quantify the extent of exposure of the human body to ionizing radiation from both whole and partial body external irradiation and from intakes of radionuclides.

In order to demonstrate compliance with dose limits, so-called *operational quantities* are typically used, which aim at providing conservative estimates of protection quantities. Often radiation protection detectors used for individual and area monitoring are calibrated in terms of operational quantities and, thus, these quantities become "measurable".

37.1.1 *Physical quantities*

• **Fluence,** Φ (unit: $1/\mathrm{m}^2$): The fluence is the quotient of the sum of the particle track lengths dl in the volume dV

$$\Phi = dl/dV \ .$$

It can also be expressed in terms of number of particles dN incident upon a small sphere of cross-sectional area da

$$\Phi = dN/da \ .$$

• **Absorbed dose,** D (unit: gray, 1 Gy=1 J/kg=100 rad): The absorbed dose is the energy imparted by ionizing radiation in a volume element of a specified material divided by the mass of this volume element.

• **Kerma,** K (unit: gray): Kerma is the sum of the initial kinetic energies of all charged particles set in motion by indirectly ionizing radiation in a volume element of the specified material divided by the mass of this volume element.

• **Linear energy transfer,** L **or** LET (unit: J/m, often given in keV/μm, 1 keV/μm $\approx 1.602 \times 10^{-10}$ J/m): The linear energy transfer is the mean energy, dE, lost by a charged particle owing to collisions with electrons in traversing a distance dl in matter. *Low-LET radiation:* X rays and gamma rays (accompanied by charged particles due to interactions with the surrounding medium) or light charged particles such as electrons that produce sparse ionizing events far apart at a molecular scale ($L < 10$ keV/μm). *High-LET radiation:* neutrons and heavy charged particles that produce ionizing events densely spaced at a molecular scale ($L > 10$ keV/μm). While the above LET definition refers to electronic stopping power only, at low energy nuclear stopping power could be a significant fraction of the total stopping power.

• **Activity,** A (unit: Becquerel, 1 Bq=1/s=27 pCi): Activity is the expectation value of the number of nuclear decays occurring in a given quantity of material per unit time.

37.1.2 *Protection quantities*

• **Organ absorbed dose,** D_T (unit: gray): The mean absorbed dose in an organ or tissue T of mass m_T is defined as

$$D_T = \frac{1}{m_T} \int_{m_T} D dm \ .$$

• **Equivalent dose,** H_T (unit: sievert, 1 Sv=1 J/kg=100 rem):

The equivalent dose H_T in an organ or tissue T is equal to the sum of the absorbed doses $D_{T,R}$ in the organ or tissue caused by different radiation types R weighted with so-called radiation weighting factors w_R:

$$H_T = \sum_R w_R \times D_{T,R} \ .$$

It expresses long-term risks (primarily cancer and leukemia) from low-level chronic exposure. The values for w_R recommended by ICRP [2] are given in Table 37.1.

Table 37.1: Radiation weighting factors, w_R.

Radiation type	w_R
Photons, electrons and muons	1
Neutrons, $E_n < 1$ MeV	$2.5 + 18.2 \times \exp[-(\ln E_n)^2/6]$
1 MeV $\leq E_n \leq$ 50 MeV	$5.0 + 17.0 \times \exp[-(\ln(2E_n))^2/6]$
$E_n > 50$ MeV	$2.5 + 3.25 \times \exp[-(\ln(0.04E_n))^2/6]$
Protons and charged pions	2
Alpha particles, fission fragments, heavy ions	20

• **Effective dose,** E (unit: sievert): The sum of the equivalent doses, weighted by the tissue weighting factors w_T ($\sum_T w_T = 1$) of several organs and tissues T of the body that are considered to be most sensitive [2], is called "effective dose":

$$E = \sum_T w_T \times H_T \ . \tag{37.1}$$

37.1.3 *Operational quantities*

• **Dose equivalent,** H (unit: sievert): The dose equivalent at a point in tissue is given by:

$$H = D \times Q \tag{37.2}$$

where D is the absorbed dose and Q is the quality factor at that point. The quality factor at a point in tissue, is given by:

$$Q = \frac{1}{D} \int_{L=0}^{\infty} Q(L) D_L dL$$

where D_L is the distribution of D in unrestricted linear energy transfer L at the point of interest, and $Q(L)$ is the quality factor as a function of L. The integration is to be performed over D_L, due to all charged particles, excluding their secondary electrons.

• **Ambient dose equivalent,** $H^*(10)$ (unit: sievert): The dose equivalent at a point in a radiation field that would be produced by the corresponding expanded and aligned field in a 30 cm diameter sphere of unit density tissue (so-called ICRU sphere/tissue with a mass composition of 76.2% oxygen, 11.1% carbon, 10.1% hydrogen and 2.6% nitrogen) at a depth of 10 mm on the radius vector opposing the direction of the aligned field. Ambient dose equivalent is the operational quantity for *area monitoring*.

• **Personal dose equivalent,** $H_p(d)$ (unit: sievert): The dose equivalent in ICRU tissue at an appropriate depth, d, below a specified point on the human body. The specified point is normally taken to be where the individual dosimeter is worn. For the assessment of effective dose, $H_p(10)$ with a depth $d = 10$ mm is chosen, and for the assessment of the dose to the skin and to the hands and feet the personal dose equivalent, $H_p(0.07)$, with a depth $d = 0.07$ mm, is used. Personal dose equivalent is the operational quantity for *individual monitoring*.

37.1.4 *Dose conversion coefficients*

Dose conversion coefficients allow direct calculation of protection or operational quantities from particle fluence and are functions of particle type, energy and irradiation configuration. The most common coefficients are those for effective dose and ambient dose equivalent. The former are based on simulations in which the dose to organs of anthropomorphic phantoms is calculated for approximate actual conditions of exposure, such as irradiation of the front of the body (antero-posterior irradiation) or isotropic irradiation.

Conversion coefficients from fluence to effective dose are given for anterior-posterior irradiation and various particle types in Fig. 37.1 [4]. For example, the effective dose from an anterior-posterior irradiation in a field of 1-MeV neutrons with a fluence of 1 neutron per cm^2 is about 290 pSv. In Monte Carlo simulations such coefficients allow multiplication with fluence at scoring

Int. J. Mod. Phys. A 2000.
Downloaded from www.worldscientific.com
by UNIVERSITY OF CALIFORNIA @ BERKE
use and distribution is strictly not permitted, except for Open Access articles.

time such that effective dose to a human body at the considered location is directly obtained.

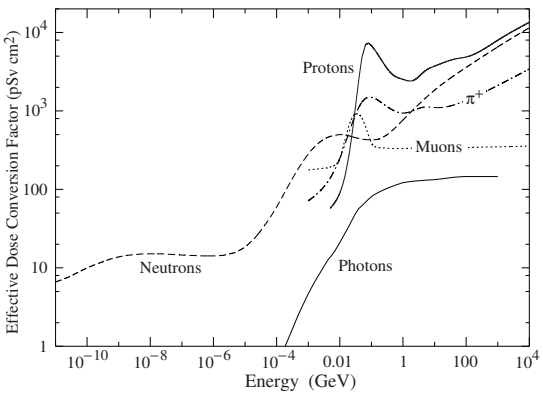

Figure 37.1: Fluence to effective dose conversion coefficients for anterior-posterior irradiation and various particle types [4].

37.2 Radiation levels [5]

• **Natural background radiation**:

On a worldwide average, the annual whole-body dose equivalent due to all sources of natural background radiation ranges from 1.0 to 13 mSv (0.1–1.3 rem) with an annual average of 2.4 mSv [6]. In certain areas values up to 50 mSv (5 rem) have been measured. A large fraction (typically more than 50%) originates from inhaled natural radioactivity, mostly radon and radon daughters [7]. The latter can vary by more than one order of magnitude: it is 0.1–0.2 mSv in open areas, 2 mSv on average in a house and more than 20 mSv in poorly ventilated mines.

• **Cosmic ray background radiation**: At sea level, the whole-body dose equivalent due to cosmic ray background radiation is dominated by muons; at higher altitudes also nucleons contribute. Dose equivalent rates range from less than 0.1 μSv/h at sea level to a few μSv/h at aircraft altitudes. Details on cosmic ray fluence levels are given in the Cosmic Rays section (Sec. 30 of this *Review*).

37.3 Health effects of ionizing radiation

Radiation can cause two types of health effects, deterministic and stochastic:

• **Deterministic effects** are tissue reactions which cause injury to a population of cells if a given threshold of absorbed dose is exceeded. The severity of the reaction increases with dose. The quantity in use for tissue reactions is the absorbed dose, D. When particles other than photons and electrons (low-LET radiation) are involved, a Relative Biological Effectiveness (RBE)-weighted dose may be used. The RBE of a given radiation is the reciprocal of the ratio of the absorbed dose of that radiation to the absorbed dose of a reference radiation (usually X rays) required to produce the same degree of biological effect. It is a complex quantity that depends on many factors such as cell type, dose rate, fractionation, etc.

• **Stochastic effects** are malignant diseases and heritable effects for which the probability of an effect occurring, but not its severity, is a function of dose without threshold.

• **Lethal dose**: The whole-body dose from penetrating ionizing radiation resulting in 50% mortality in 30 days (assuming no medical treatment) is 2.5–4.5 Gy (250–450 rad)[1], as measured internally on the body longitudinal center line. The surface dose varies due to variable body attenuation and may be a strong function of energy.

• **Cancer induction**:

The cancer induction probability is about 5% per Sv on average for the entire population [3].

• **Recommended effective dose limits**: The International Commission on Radiological Protection (ICRP) recommends a limit for radiation workers of 20 mSv effective dose per year averaged over 5 years, with the provision that the dose should not exceed 50 mSv in any single year [3]. The limit in the EU-countries and Switzerland is 20 mSv per year, in the U.S. it is 50 mSv per year (5 rem per year). Many physics laboratories in the U.S. and elsewhere set lower limits. The effective dose limit for the general public is typically 1 mSv per year.

[1] RBE-weighted when necessary

37.4 Prompt neutrons at accelerators

Neutrons dominate the radiation environment outside thick shielding (*e.g.*, > 1 m of concrete) for high energy (> a few hundred MeV) electron and hadron accelerators. In addition, for accelerators with energies above about 10 GeV, muons contribute significantly at small angles with regard to the beam, even behind several meters of shielding. Another special case are synchrotron light sources where particular care has to be taken to shield the very intense low-energy photons extracted from the electron synchrotron into the experimental areas. Due to its importance at high energy accelerators this section focuses on prompt neutrons.

37.4.1 *Electron accelerators*

At electron accelerators, neutrons are generated via photonuclear reactions from bremsstrahlung photons. Neutron production takes place above a threshold value which varies from 10 to 19 MeV for light nuclei (with important exceptions, such as 2.23 MeV for deuterium and 1.67 MeV for beryllium) and from 4 to 6 MeV for heavy nuclei. It is commonly described by different mechanisms depending on the photon energy: the giant dipole resonance interactions (from threshold up to about 30 MeV, often the dominant process), the quasi-deuteron effect (between 30 MeV and a few hundred MeV), the delta resonance mechanism (between 200 MeV and a few GeV) and the vector meson dominance model at higher energies.

The giant dipole resonance reaction consists in a collective excitation of the nucleus, in which neutrons and protons oscillate in the direction of the photon electric field. The oscillation is damped by friction in a few cycles, with the photon energy being transferred to the nucleus in a process similar to evaporation. Nucleons emitted in the dipolar interaction have an anisotropic angular distribution, with a maximum at 90°, while those leaving the nucleus as a result of evaporation are emitted isotropically with a Maxwellian energy distribution described as [8]:

$$\frac{dN}{dE_n} = \frac{E_n}{T^2} e^{-E_n/T} \ , \tag{37.3}$$

where T is a nuclear 'temperature' (in units of MeV) characteristic of the particular target nucleus and its excitation energy. For heavy nuclei the 'temperature' generally lies in the range of $T =$ 0.5–1.0 MeV. Neutron yields from semi-infinite targets per kW of electron beam power are plotted in Fig. 37.2 as a function of the electron beam energy [8].

While for thick targets neutron production is mainly due to photonuclear interactions, for thin targets (thickness of fractions of the radiation length) electronuclear interactions are the dominating process.

Typical neutron energy spectra outside of concrete (80 cm thick, 2.35 g/cm^3) and iron (40 cm thick) shields are shown in Fig. 37.3. In order to compare these spectra to those caused by proton beams (see below) the spectra are scaled by a factor of 100, which roughly corresponds to the difference in the high energy hadronic cross sections for photons and hadrons (*e.g.*, the fine structure constant). The shape of these spectra are generally characterized by a low-energy peak at around 1 MeV (evaporation neutrons) and a high-energy shoulder at around 70–80 MeV. In case of concrete shielding, the spectrum also shows a pronounced peak at thermal neutron energies.

37.4.2 *Proton accelerators*

At proton accelerators, neutron yields emitted per incident proton by different target materials are roughly independent of proton energy between 20 MeV and 1 GeV, and are given by the ratio C : Al : Cu-Fe : Sn : Ta-Pb = 0.3 : 0.6 : 1.0 : 1.5 : 1.7 [11]. Above about 1 GeV, the neutron yield is proportional to E^m, where $0.80 \leq m \leq 0.85$ [12].

Int. J. Mod. Phys. A 2026.41. Downloaded from www.worldscientific.com
by UNIVERSITY OF CALIFORNIA @ BERKELEY on 09/16/26. Re-use and distribution is strictly not permitted, except for Open Access articles.

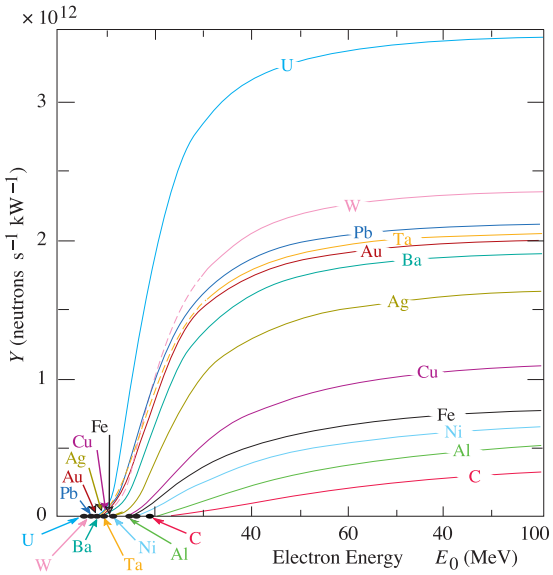

Figure 37.2: Neutron yields from semi-infinite targets per kW of electron beam power, as a function of the electron beam energy, disregarding target self-shielding [8].

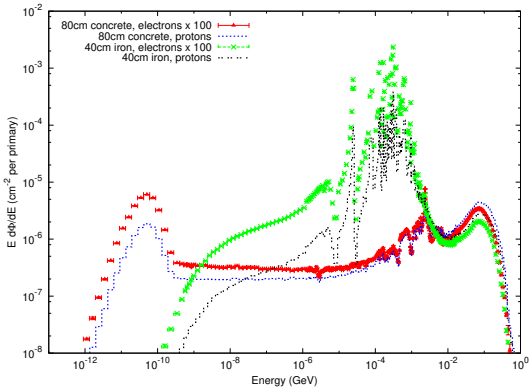

Figure 37.3: Neutron energy spectra calculated with the FLUKA code [9, 10] from 25 GeV proton and electron beams on a thick copper target. Spectra are evaluated at 90° to the beam direction behind 80 cm of concrete or 40 cm of iron. All spectra are normalized per beam particle. For better visualization, spectra for electron beam are multiplied by a factor of 100.

Typical neutron energy spectra outside of concrete and iron shielding are shown in Fig. 37.3. Here, the radiation fields are caused by a 25 GeV proton beam interacting with a thick copper target. The comparison of these spectra with those for an electron beam of the same energy reflects the difference in the hadronic cross sections between photons and hadrons above a few 100 MeV. Differences are increasing towards lower energies because of different interaction mechanisms. Furthermore, the slight shift in energy above about 100 MeV follows from the fact that the energies of the interacting photons are lower than 25 GeV. Apart from this the shapes of the two spectra are similar.

The neutron-attenuation length is shown in Fig. 37.4 for concrete and mono-energetic broad-beam conditions. It reaches an asymptotic value of about 117 g/cm^2 above 200 MeV. As the cascade through thick shielding is carried by particles with energies between about 100 MeV and 300 MeV (in this energy range non-elastic cross sections are at minimum and are dominated by quasi-elastic processes leading to low attenuation) this value is equal to the equilibrium attenuation length for particles emitted at 90° in concrete.

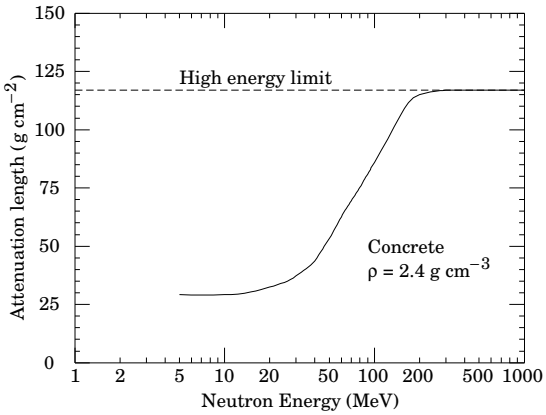

Figure 37.4: The variation of the attenuation length for mono-energetic neutrons in concrete as a function of neutron energy [11].

37.5 Photon sources

The dose equivalent rate in tissue (in mSv/h) from a gamma point source emitting one photon of energy E (in MeV) per second at a distance of 1 m is $4.6\times10^{-9}\ \mu_{en}/\rho\, E$, where μ_{en}/ρ is the mass energy absorption coefficient. The latter has a value of 0.029 ± 0.004 cm^2/g for photons in tissue over an energy range between 60 keV and 2 MeV (see Ref. [13] for tabulated values).

Similarly, the dose equivalent rate in tissue (in mSv/h) at the surface of a semi-infinite slab of uniformly activated material containing 1 Bq/g of a gamma emitter of energy E (in MeV) is $2.9 \times 10^{-4}\, R_\mu\, E$, where R_μ is the ratio of the mass energy absorption coefficients of the photons in tissue and in the material.

37.6 Accelerator-induced radioactivity

Typical medium- and long-lived activation products in metallic components of accelerators are ^{22}Na, ^{46}Sc, ^{48}V, ^{51}Cr, ^{54}Mn, ^{55}Fe, ^{59}Fe, ^{56}Co, ^{57}Co, ^{58}Co, ^{60}Co, ^{63}Ni and ^{65}Zn. Gamma-emitting nuclides dominate doses from external irradiation at longer decay times (more than one day) while at short decay times β^+ emitters are also important (through photons produced by β^+ annihilation). Due to their short range, β^- emitters are relevant, for example, only for dose to the skin and eyes or for doses due to inhalation or ingestion. Fig. 37.5 and Fig. 37.6 illustrate the contributions of gamma and β^+ emitters to the total dose rate at 12.4 cm distance to a copper sample [14]. The sample was activated by the stray radiation field created by a 120 GeV mixed hadron beam dumped in a copper target during about 8 hours at intensities between $10^7 - 10^8$ hadrons per second. Here, the contributions by individual nuclides were calculated analytically assuming exponential decay of the nuclide inventory present at 20 minute cooling time. The total dose rate, however, also includes decay chains and as such also contributions from daughter nuclides.

Typically, dose rates at a certain decay time are mainly determined by radionuclides having a half-life of the order of the decay time. Extended irradiation periods might be an exception to this general rule as in this case the activity of long-lived nuclides can build up sufficiently so that it dominates that one of short-lived even at short cooling times.

Activation in concrete is dominated by ^{24}Na (short decay time) and ^{22}Na (long decay time). Both nuclides can be produced either by low-energy neutron reactions on the sodium-component in the concrete or by spallation reactions on silicon, calcium and other constituents such as aluminum. At long decay times nuclides of radiological interest in activated concrete can also be ^{60}Co, ^{152}Eu, ^{154}Eu and ^{134}Cs, all of which produced by (n,γ)-reactions with traces of natural cobalt, europium and cesium, Thus, such trace elements might be important even if their content in concrete is only a few parts per million or less by weight.

The explicit simulation of radionuclide production with general-purpose Monte Carlo codes has become the most commonly applied method to calculate induced radioactivity and its radiologi-

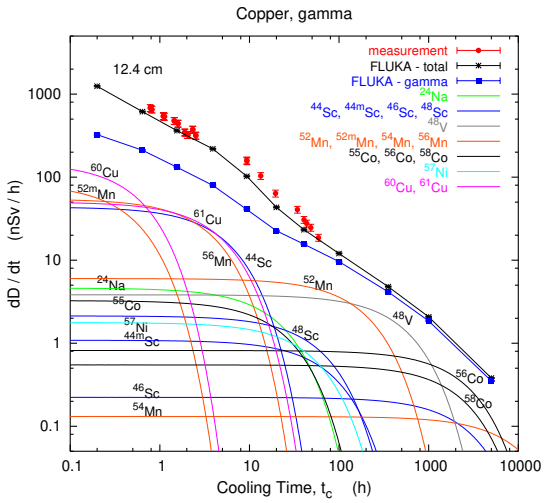

Figure 37.5: Contribution of individual gamma-emitting nuclides to the total dose rate at 12.4 cm distance to an activated copper sample [14].

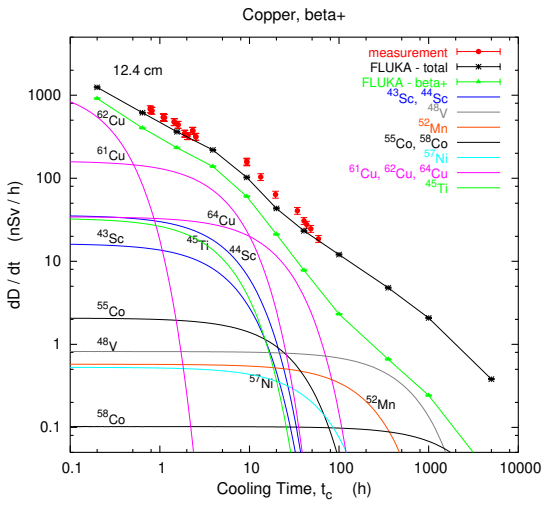

Figure 37.6: Contribution of individual positron-emitting nuclides to the total dose rate at 12.4 cm distance to an activated copper sample [14].

cal consequences [14] (see also Sec. 37.8). They are complemented by analytical codes based on folding particle fluence spectra with nuclide production cross sections. ActiWiz [15, 16] is an example of such a code targeting the domain of radiological characterization and material optimization. It allows for calculating nuclide inventories by convolution of fluence spectra with nuclide production data for 85 chemical elements and arbitrary compounds from threshold to an energy of 100 TeV.

37.7 Radiation protection instrumentation

The capacity to distinguish and measure the high-LET (mostly neutrons) and the low-LET components (photons, electrons, muons) of the radiation field at workplaces is of primary importance to evaluate the exposure of personnel. At proton accelerators the prompt dose equivalent outside a shield is mainly due to neutrons, with some contribution from photons and, to a minor extent, charged particles. At high-energy electron accelerators the dominant stray radiation during operation consists also of neutrons, because the shielding is normally thick enough to absorb most of the bremsstrahlung photons. Most of the personnel exposure at accelerator facilities is often received during maintenance interventions, and is due to gamma/beta radiation coming from residual radioactivity in accelerator components.

Radiation detectors used both for radiation surveys and area monitoring are normally calibrated in ambient dose equivalent $H^*(10)$.

37.7.1 *Neutron detectors*

• **Rem counters:** A rem counter [17] is a portable detector consisting of a thermal neutron counter embedded in a polyethylene moderator, with a response function that approximately follows the curve of the conversion coefficients from neutron fluence to $H^*(10)$ over a wide energy range. Conventional rem counters provide a response to neutrons up to approximately 10-15 MeV, extended-range units are heavier as they include a converter consisting of a material with high mass number to correctly measure $H^*(10)$ up to several hundred MeV [18].

• **Bonner Sphere Spectrometer (BSS):** A BSS [19] consists of a thermal neutron detector at the centre of moderating spheres of different diameters made of polyethylene (PE) or a combination of PE and a high-A material to enhance its response to high energy neutrons (similar to rem counters). Each sphere has a different response function versus neutron energy, and the neutron energy, at which the sensitivity peaks, increases with sphere diameter. The energy resolution of the system is rather low but satisfactory for radiation protection purposes. The neutron spectrum is obtained by unfolding the experimental counts of the BSS with its response matrix by a computer code that is often based on an iterative algorithm such as GRAVEL [20] and MAXED [21]. BSS exist in active (using ^{3}He or BF_3 proportional counters or ^{6}LiI scintillators) and passive versions (using CR-39 track detectors or LiF), for use *e.g.* in strongly pulsed fields. With ^{3}He counters the discrimination with respect to gamma rays and noise is excellent.

• **Bubble detectors:** A bubble detector [22] is a dosimeter based on a super-heated emulsion (super-heated droplets suspended in a gel) contained in a vial and acting as a continuously sensitive, miniature bubble chamber. The total number of bubbles evolved from the radiation-induced nucleation of drops gives an integrated measure of the total neutron exposure. Various techniques exist to record and count the bubbles, *e.g.*, visual inspection, automated reading with video cameras or acoustic counting. Bubble detectors are insensitive to low-LET radiation. Super-heated emulsions are used as personal, area and environmental dosimeters, as well as neutron spectrometers.

• **Track etched detectors:** Track etched detectors (TEDs) [23] are based on the preferential dissolution of suitable, mostly insulator, materials along the damage trails of charged particles of sufficiently high-energy deposition density. The detectors are effectively not sensitive to radiation which deposits the energy through the interactions of particles with low LET. These dosimeters are generally able to determine neutron ambient dose equivalent down to around 100 μSv. They are used both as personal dosimeters and for area monitoring, *e.g.*, in BSS.

37.7.2 *Photon detectors* [24]

• **Geiger Müller (GM) counters:** GM counters are low cost devices simple to operate. They work in pulse mode and since they only count radiation-induced events, any spectrometric information is lost. In general they are calibrated in terms of air kerma, for instance in a ^{60}Co field. The response of GM counters to photons is constant within 15% for energies up to 2 MeV and shows considerable energy dependence above.

• **Ionization chambers:** Ionization chambers are gas-filled detectors used both as hand-held instruments (*e.g.*, for radiation surveys) and environmental monitors. They are normally operated in current mode although pulse-mode operation is also possible. They possess a relatively flat response to a wide range of X- and gamma ray energies (typically from 10 keV to several MeV), can measure radiation over a wide intensity range and are capable of discriminating between the beta and gamma components of a radiation field (by use of, *e.g.*, a beta window). Pressurized ion chambers (filled, *e.g.*, with Ar or H gas to several tens of bars) are used for environmental and stray radiation monitoring applications. They have good sensitivity to neutrons and charged hadrons in addition to low LET radiation (gammas and muons),

Int. J. Mod. [redacted] by UNIVERSITY OF CALIFORNIA @ BERKE
nloaded from www.worldscientific.com
use and distribution is strictly not permitted, except for Open Access articles.

Int. J. Mod. Phys. A 2026.41. Downloaded from www.worldscientific.com by UNIVERSITY OF CALIFORNIA @ BERKELEY on 09/16/26. Re-use and distribution is strictly not permitted, except for Open Access articles.

with the response function to the former being strongly non-linear with energy.

• **Proportional counters:** Proportional counters are another type of gas-filled detector, operated in pulse mode. They are normally of cylindrical geometry, with a thin central wire (the anode) on the axis of a hollow tube (the cathode). The initial electron charge created by the interaction of the radiation with the gas is amplified by the multiplication process (Townsend avalanche) produced by the strong electric field in a narrow volume around the anode. The generated pulses are still proportional to the original number of ion pairs but are much larger than in an ionization chamber, yielding a much improved signal-to-noise ratio. Proportional counters are also used for neutron detection: the rem counter and BSS discussed in the previous sections typically employ ^{3}He or BF_3 filled tubes with a large sensitivity to thermal neutrons.

• **Scintillators:** Scintillation-based detectors are used in radiation protection as hand-held probes and in fixed installations, *e.g.*, portal monitors. A scintillation detector or counter is obtained coupling a scintillator to an electronic light sensor such as a photomultiplier tube (PMT), a photodiode or a silicon photomultiplier (SiPM). There is a wide range of scintillating materials, inorganic (such as CsI and BGO), organic or plastic; they find application in both photon dosimetry and spectrometry.

37.7.3 *Operation in pulsed radiation fields*

There are many practical situations with particle accelerators used for scientific, industrial and medical applications where the time structure of the stray radiation limits the use of active monitors or requires specifically designed electronics. Pulsed neutron and gamma fields may be present because of beam losses at, *e.g.*, targets, collimators and beam dumps. The time duration of a single burst can range from a few ns to about 1 ms with a typical repetition rate in the range 0.1–100 Hz. Conventional detectors generally suffer from dead time effects and have strong limitations in the measurements of pulsed fields. Severe under response has been observed, *e.g.*, in commercial rem counters, with tremendous underestimation of the ambient dose equivalent, $H^*(10)$, up to three orders of magnitude [25]. The common techniques used to correct the response of radiation detectors which include dead-time corrections operate properly in a steady-state radiation field, whereas it is much more difficult to cope with dead time losses in a pulsed radiation field of unknown time structure and burst dose. Generally speaking the monitoring instrumentation must be chosen on the basis of the knowledge of the radiation field. Detectors with specifically designed electronics must be employed in pulsed field conditions in place of conventional rem counters for neutrons, such as the LUPIN detector [26]. If real-time monitoring is not required, passive detectors or dosimeters such as TEDs mentioned in Sec. 37.7.1 or LiF mentioned in Sec. 37.7.5 can be employed, as they are insensitive to the time structure of the radiation.

37.7.4 *Operation in presence of magnetic fields*

There may be circumstances in which a radiation survey needs to be performed in the presence of a magnetic field. This may be the case for example for measurements on activated detector components in the underground experimental areas of CERN LHC experiments without switching off the intense magnetic field ofthe detectors; or measurements of the residual radioactivity of permanent magnets sometimes used in particle accelerators. In hospitals, one of most advanced diagnostic modalities is PET-MRI, in which PET imaging uses radioactive substances (radiopharmaceuticals) in proximity of the strong magnetic field of the MRI scanner. Another emerging technology is MR-Linac for image-guided adaptive radiation therapy. Most of the commercial survey meters do not operate correctly or do not function at all in the presence of even comparatively weak magnetic fields below 0.3 T, and often already at 0.1 T. This is either because of the presence of components in their electronics sensitive to magnetic field (e.g. inductive elements), ferromagnetic materials in general (such as shells, screws and frames), battery drain/heating or LCD screen failure. An instrument called B-RAD has recently been developed [27] that overcomes the above limitations and is now commercially available. It is a hand-held instrument for gamma dose rate and gamma spectrometry measurements, consisting of a central unit (housing a microcontroller, magnetic field insensitive electronic circuitry, the battery and two displays) and a probe connected through a cable, certified to operate up to 3 T fields. The probe uses a $LaBr_3$(Ce) crystal coupled to an array of silicon photomultipliers. The excellent scintillation properties and the high photon resolution of the scintillator (3.3% FWHM at 662 keV) make the device capable of operating in the energy range from 30 keV to 2 MeV photons with a very fast response.

37.7.5 *Personal dosimeters*

Personal dosimeters, calibrated in $H_p(10)$, are worn by persons exposed to ionizing radiation for professional reasons to record the dose received. They are typically passive detectors, either film, track etched detectors, ^{6}Li/^{7}Li-based dosimeters (*e.g.* LiF), optically stimulated luminescence (OSL) or radiophotoluminescence detectors (RPL) but semi-active dosimeters using miniaturized ion-chambers also exist, like the Direct Ion Storage (DIS) dosimeters in use at CERN.

Electronic personal dosimeters are small active units for on-line monitoring of individual exposure, designed to be worn on the body. They can give an alarm on both the integral dose received or dose rate once a pre-set threshold is exceeded.

37.8 Monte Carlo codes for radiation protection studies

The use of general-purpose particle interaction and transport Monte Carlo codes is often the most accurate and efficient choice for assessing radiation protection quantities at accelerators. Due to the vast spread of such codes to all areas of particle physics and the associated extensive benchmarking with experimental data, the modeling has reached an unprecedented accuracy. Furthermore, most codes allow the user to simulate all aspects of a high energy particle cascade in one and the same run: from the first interaction of a TeV nucleus over the transport and re-interactions (hadronic and electromagnetic) of the produced secondaries, to detailed nuclear fragmentation, the calculation of radioactive decays and even of the electromagnetic shower caused by the radiation from such decays. A brief account of the codes most widely used for radiation protection studies at high energy accelerators is given in the following.

• **FLUKA [9, 10, 28, 29]:** FLUKA is a general-purpose particle interaction and transport code. It comprises all features needed for radiation protection, such as detailed hadronic and nuclear interaction models up to 10 PeV, full coupling between hadronic and electromagnetic processes and numerous variance reduction options. The latter include weight windows, region importance biasing, and leading particle, interaction, and decay length biasing (among others). The capabilities of FLUKA are unique for studies of induced radioactivity, especially with regard to nuclide production, decay, and transport of residual radiation. In particular, particle cascades by prompt and residual radiation are simulated in parallel based on the microscopic models for nuclide production and a solution of the Bateman equations for activity build-up and decay.

• **GEANT4 [30–32]:** GEANT4 is an object-oriented toolkit consisting of a kernel that provides the framework for particle transport, including tracking, geometry description, material specifications, management of events and interfaces to external graphics systems. The kernel also provides interfaces to physics processes. It allows the user to freely select the physics models that best serve the particular application needs. Implementations of interaction models exist over an extended range of energies, from optical photons and thermal neutrons to high-energy interactions required for the simulation of accelerator and cosmic ray experiments. To facilitate the use of variance reduction techniques, general-purpose biasing methods such as importance biasing, weight windows, and a weight cut-off method have been introduced directly into the toolkit. Other variance reduction methods, such as leading particle biasing for hadronic processes, come with the respective physics packages.

• **MARS15 [33,34]:** The MARS15 code system is a set of Monte Carlo programs for the simulation of hadronic and electromagnetic cascades. It covers a wide energy range: 1 keV to 100 TeV for

Int. J. Mod. Phys. A
by UNIVERSITY OF CALIFORNIA @ BERKE
nloaded from www.worldscientific.com
use and distribution is strictly not permitted, except for Open Access articles.

muons, charged hadrons, heavy ions and electromagnetic showers; and 0.00215 eV to 100 TeV for neutrons. Hadron-nucleus interactions as well as practically all other strong, weak and electromagnetic interactions in the entire energy range can be simulated either inclusively or exclusively. MARS15 uses ENDFB-VII nuclear data to handle interactions of neutrons with energies below 14 MeV. Several variance reduction techniques, such as weight windows, particle splitting, and Russian roulette, are available. A tagging module allows tagging the origin of a given signal for source term or sensitivity analyses. The geometry module allows either a basic solid body representation option or a ROOT-based powerful engine. Further features of MARS15 include a MAD-MARS merge for a convenient creation of accelerator models and multi-turn tracking and cascade simulation in accelerator and beamline lattices.

• **MCNP6 [35, 36]:** MCNP6 is the latest version of the Monte Carlo N-Particle transport (MCNP) family of neutron interaction and transport codes and, therefore, features one of the most comprehensive and detailed descriptions of the related physical processes. It transports 37 different particle types, including ions and electromagnetic particles. The neutron interaction and transport modules use standard evaluated data libraries mixed with physics models where such libraries are not available. The transport is continuous in energy. MCNP6 contains one of the most powerful implementations of variance reduction techniques. Spherical mesh weight windows can be created by a generator in order to focus the simulation time on certain spatial regions of interest. In addition, a more generalized phase space biasing is also possible through energy- and time-dependent weight windows. Other biasing options include pulse-height tallies with variance reduction and criticality source convergence acceleration.

• **PHITS [37, 38]:** The Particle and Heavy-Ion Transport code System PHITS was among the first general-purpose codes to simulate the transport and interactions of heavy ions in a wide energy range, from 10 MeV/nucleon to 100 GeV/nucleon. It is based on the high-energy hadron transport code NMTC/JAM that was extended to heavy ions. The transport of low-energy neutrons employs cross sections from evaluated nuclear data libraries such as ENDF and JENDL below 20 MeV. Electromagnetic interactions are simulated based on the ITS code in the energy range between 1 keV and 100 MeV for electrons and positrons and between 1 keV and 100 GeV for photons. Several variance reduction techniques, including weight windows and region importance biasing, are available.

References

[1] International Commission on Radiation Units and Measurements, *Fundamental Quantities and Units for Ionizing Radiation*, ICRU Report 60 (1998).

[2] ICRP, 2010. *Conversion Coefficients for Radiological Protection Quantities for External Radiation Exposures*, ICRP Publication 116, Annals of the ICRP 40(2-5).

[3] ICRP Publication 103, *The 2007 Recommendations of the International Commission on Radiological Protection*, Annals of the ICRP, Elsevier (2007).

[4] M. Pelliccioni, Rad. Protection Dosimetry **88**, 279 (2000).

[5] E. Pochin, *Nuclear Radiation: Risks and Benefits*, Clarendon Press, Oxford, 1983.

[6] United Nations, *Report of the United Nations Scientific Committee on the Effect of Atomic Radiation*, General Assembly, Official Records A/63/46 (2008).

[7] G. Cinelli *et al.*, *European Atlas of Natural Radiation*, G. Cinelli, M. De Cort, and T. Tollefsen, editor(s), Publications Office of the European Union, Luxembourg, 2019, ISBN 978-92-76-08259-0, JRC116795.

[8] W. P. Swanson, *Radiological Safety Aspects of the Operation of Electron Linear Accelerators,* IAEA Technical Reports Series No. 188 (1979) (1979).

[9] A. Ferrari, *et al.*, FLUKA:, A Multi-particle Transport Code, CERN-2005-010 (2005), SLAC-R-773, INFN-TC-05-11, `http://www.fluka.org`.

[10] G. Battistoni *et al.*, Annals of Nuclear Energy **82**, 10 (2015).

[11] R.H. Thomas and G.R. Stevenson, *Radiological Safety Aspects of the Operation of Proton Accelerators,* SSC-N-354 (1986), IAEA Technical Report Series No. 283 (1988).

[12] T. Gabriel *et al.*, Nucl. Instrum. Meth. A **338**, 336 (1994).

[13] `http://physics.nist.gov/PhysRefData/XrayMassCoef/cover.html`.

[14] S. Roesler, *et al.*, "Simulation of Remanent Dose Rates and Benchmark Measurements at the CERN-EU High Energy Reference Field Facility," in *Proceedings of the Sixth International Meeting on Nuclear Applications of Accelerator Technology,* San Diego, CA, 1-5 June 2003, 655–662 (2003).

[15] C. Theis and H. Vincke, "The use of ActiWiz in operational radiation protection," in *Proceedings of the Twelfth Meeting of Task-Force on Shielding Aspects of Accelerators, Targets and Irradiation Facilities of Accelerator Technology, SATIF12* FNAL, 28-30 April 2014, Nuclear Science Report NEA/NSC/R 3, (2015).

[16] C. Theis and H. Vincke, "ActiWiz3 an overview of the concepts, architecture and new features," CERN Technical Note CERN-RP-2016-117-REPORTS-TN (2016), `http://actiwiz.web.cern.ch`.

[17] I.O. Andersson and J. Braun, "A neutron rem counter with uniform sensitivity from 0.025 eV to 10 MeV" in *Proceedings of the IAEA Symposium on Neutron dosimetry,* IAEA, Vienna, Vol. II, 87–95, (1963).

[18] C. Birattari, *et al.*, Radiation Protection Dosimetry **76**, 135 (1998).

[19] R.L. Bramblett, R.I. Ewing and T.W. Bonner, Nucl. Instrum. Methods **9**, 1 (1960).

[20] M. Matzke, PTB, Braunschweig PTBN-19, (1994).

[21] M. Reginatto and P. Goldhagen, Health Physics **77**, 579 (1999).

[22] F. d'Errico, Nucl. Instrum. Methods **B184**, 229 (2001).

[23] K. Becker, Dosimetric applications of track etching, in *Topics in Radiation Dosimetry* Ed. F.H. Attix, Academic Press, London, 79–143, (1972).

[24] G.F. Knoll, *Radiation detection and measurements,* Wiley (2010).

[25] M. Caresana *et al.*, Nucl. Instrum. Meth. A **737**, 203 (2014).

[26] M. Caresana, *et al.*, A new version of the LUPIN detector: Improvements and latest experimental verification, Review of Scientific Instruments **85**, 065102 (2014).

[27] F. Ferrulli and M. Silari, Nucl. Instrum. Meth. A **1042**, 167430 (2022).

[28] C. Ahdida, *et al.*, New Capabilities of the FLUKA Multi-Purpose Code, Frontiers in Physics **9**, 788253 (2022), `http://fluka.cern`.

[29] T. T. Böhlen *et al.*, Nucl. Data Sheets **120**, 211 (2014).

[30] S. Agostinelli *et al.* (GEANT4), Nucl. Instrum. Meth. A **506**, 250 (2003).

[31] J. Allison *et al.*, IEEE Trans. Nucl. Sci. **53**, 270 (2006).

[32] J. Allison *et al.*, Nucl. Instrum. Meth. A **835**, 186 (2016), `http://geant4.cern.ch`.

[33] N. Mokhov *et al.*, Prog. Nucl. Sci. Tech. **4**, 496 (2014), [arXiv:1409.0033].

[34] N. Mokhov *et al.*, in "15th Workshop on Shielding aspects of Accelerators, Targets, and Irradiation Facilities, SATIF-15," 3–14 (2022).

[35] J.T. Goorley, *et al.*, Nuclear Technology **180**, 298 (2012).

[36] J.A. Kulesza *et al.*, MCNP Code Version 6.3.0 Theory and User Manual, Los Alamos National Laboratory report, LA-UR-22-30006 (2022), `https://mcnp.lanl.gov`.

[37] T. Sato, *et al.*, Journal of Nuclear Science and Technology **55**, 684 (2018).

[38] T. Sato, *et al.*, PHITS Particle and Heavy Ion Transport code System, Version 3.31 (2023), `https://phits.jaea.go.jp`.

38. Commonly Used Radioactive Sources

Revised September 2023 by D.E. Groom (LBNL).

Table 38.1: Radioactive sources

Nuclide	Half-life	Type of Decay	Particle Energy (MeV)	Particle Emission prob.	Photon Energy (MeV)	Photon Emission prob.
$^{22}_{11}$Na	2.603 y	β^+,	0.546	90%	0.511	Annih.
		EC			1.275	100%
$^{51}_{24}$Cr	27.70 d	EC			0.320	10%
					V K x rays	100%
Neutrino calibration source						
$^{54}_{25}$Mn	0.855 y	EC			0.835	100%
					Cr K x rays	26%
$^{55}_{26}$Fe	2.747 y	EC			Mn K x rays:	
					0.00590	24.4%
					0.00649	2.86%
$^{57}_{27}$Co	271.8 d	EC			0.014	9%
					0.122	86%
					0.136	11%
					Fe K x rays	58%
$^{60}_{27}$Co	5.271 y	β^-	0.317	99.9%	1.173	99.9%
					1.333	99.9%
$^{68}_{32}$Ge	271.0 d	EC			Ga K x rays	42%
$\rightarrow {}^{68}_{31}$Ga						
	67.8 m	β^+,	1.899	90%	0.511	Annih.
		EC			1.077	3%
$^{90}_{38}$Sr	28.8 y	β^-	0.546	100%		
$\rightarrow {}^{90}_{39}$Y	2.67 d	β^-	2.279	100%		
$^{106}_{44}$Ru	371.5 d	β^-	0.039	100%		
$\rightarrow {}^{106}_{45}$Rh						
	30.1 s	β^-	3.546	79%	0.512	21%
					0.622	10%
$^{109}_{48}$Cd	1.265 y	EC	0.063 e^-	42%	0.088	3.7%
			0.084 e^-	44%	Ag K x rays	100%
$^{113}_{50}$Sn	115.1 d	EC	0.364 e^-	28%	0.392	65%
			0.388 e^-	6%	In K x rays	97
$^{137}_{55}$Cs	30.0 y	β^-	0.514	94%	0.662	85%
			1.176	6%		
$^{133}_{56}$Ba	10.55 y	EC	0.045 e^-	50%	0.081	33%
			0.075 e^-	6%	0.356	62%
					Cs K x rays	121%
$^{152}_{63}$Eu	13.537 y	EC		72.1%	Many γ's	
		β^-		27.9%	0.1218–1.408 MeV	
$^{207}_{83}$Bi	32.9 y	EC	0.481 e^-	2%	0.569	98%
			0.975 e^-	7%	1.063	75%
			1.047 e^-	2%	1.770	7%
					Pb K x rays	78%
$^{228}_{90}$Th	1.912 y	6α:	5.341 – 8.785		0.239	44%
		$3\beta^-$:	0.334 – 2.246		0.583	31%
					2.614	36%
($\rightarrow {}^{224}_{88}$Ra 361 d	$\rightarrow {}^{220}_{86}$Rn 55.8 s	$\rightarrow {}^{216}_{84}$Po 0.148 s	$\rightarrow {}^{212}_{82}$Pb 10.64 h	$\rightarrow {}^{212}_{83}$Bi 60.54 m	$\rightarrow {}^{212}_{84}$Po 300 ns)	
$^{241}_{95}$Am	432.6 y	α	5.433	13%	0.0595409	36%
			5.486	85%	Np L x rays	38%
$^{241}_{95}$Am/Be	432.6 y	neutrons ($\langle E \rangle = 4$ MeV) and γ's (4.43 MeV from ${}^{9}_{4}$Be(α, n))				
$^{244}_{96}$Cm	18.11 y	α	5.763	24%	Pu L x rays	$\sim 9\%$
			5.805	76%		
$^{252}_{98}$Cf	2.645 y	α	6.076	15%		
		(97%)	6.118	82%		
Fission (3.1%): Average 7.8 γ's/fission; $\langle E_\gamma \rangle = 0.88$ MeV ≈ 4 neutrons/fission; $\langle E_n \rangle = 2.14$ MeV						

"Emission probability" is the probability per decay of a given emission; because of cascades these may total more than 100%. Only principal emissions are listed. EC means electron capture, and e^- means monoenergetic internal conversion (Auger) electron. The intensity of 0.511 MeV e^+e^- annihilation photons depends upon the number of stopped positrons. Endpoint $\beta^\pm$ energies are listed. In some cases when energies are closely spaced, the γ-ray values are approximate weighted averages. Radiation from short-lived daughter isotopes is included where relevant.

Isotopic data may be found at `https://physics.nist.gov/cgi-bin/Compositions/stand_alone.pl`.

Neutron sources: See *e.g.* J. Liu *et al.*, "Neutron Calibration Sources in the Daya Bay Experiment" [1]. ${}^{51}_{24}$Cr calibration of neutrino detectors is discussed in *e.g.* J.N. Abdurashitov *et al.*, "Measurement of the response of a gallium metal solar neutrino experiment to neutrinos from a ^{51}Cr source" [2]. The use of ${}^{75}_{34}$Se and other isotopes has also been proposed.

References

[1] J. Liu *et al.*, Nucl. Instrum. Meth. A **797**, 260 (2015), [arXiv:1504.07911].

[2] J. N. Abdurashitov *et al.* (SAGE), Phys. Rev. C **59**, 2246 (1999), [hep-ph/9803418].

Int. J. Mod. Phys. A 2026.41. Downloaded from www.worldscientific.com by UNIVERSITY OF CALIFORNIA @ BERKELEY on 09/16/26. Re-use and distribution is strictly not permitted, except for Open Access articles.

Int. J. Mod.
nloaded from www.worldscientific.com
by UNIVERSITY OF CALIFORNIA @ BERKE
use and distribution is strictly not permitted, except for Open Access articles.

Mathematical Tools or Statistics, Monte Carlo, Group Theory

39. Probability (rev.) 705
40. Statistics (rev.) 710
41. Machine Learning (rev.) 727
42. Monte Carlo techniques (rev.) 768
43. Monte Carlo event generators (rev.) 772
44. Monte Carlo neutrino event generators (rev.) 784
45. Monte Carlo particle numbering scheme (rev.) 789
46. Clebsch-Gordan coefficients, spherical harmonics, and d functions 794
47. SU(3) isoscalar factors and representation matrices 795
48. SU(n) multiplets and Young diagrams 796

Int. J. Mod. Phys. A 2026.41. Downloaded from www.worldscientific.com
by UNIVERSITY OF CALIFORNIA @ BERKELEY on 09/16/26. Re-use and distribution is strictly not permitted, except for Open Access articles.

Phys. A 2026.41. Downloaded from www.worldscientific.com
by UNIVERSITY OF CA[redacted]ELEY on 09/16/26. Re-use and distribution is strictly not permitted, except for Open Access articles.

Int. J. Mod. Phys. A 2026.41. Downloaded from www.worldscientific.com
by UNIVERSITY OF CALIFORNIA @ BERKELEY on 09/16/26. Re-use and distribution is strictly not permitted, except for Open Access articles.

39. Probability

Revised August 2025 by G. Cowan (RHUL).

39.1 General

Further discussion of probability can be found, *e.g.*, in Refs. [1–8].

An abstract definition of probability can be given by considering a set S, called the sample space, and possible subsets $A, B, \ldots$, the interpretation of which is left open. The probability P is a real-valued function defined by the following axioms due to Kolmogorov [9]:

1. For every subset A in S, $P(A) \geq 0$;
2. For disjoint subsets (*i.e.*, $A \cap B = \emptyset$), $P(A \cup B) = P(A) + P(B)$;
3. $P(S) = 1$.

In addition, one defines the conditional probability $P(A|B)$ (read as P of A given B) as

$$P(A|B) = \frac{P(A \cap B)}{P(B)} \ . \tag{39.1}$$

From this definition and using the fact that $A \cap B$ and $B \cap A$ are the same, one obtains *Bayes' theorem*,

$$P(A|B) = \frac{P(B|A)P(A)}{P(B)} \ . \tag{39.2}$$

From the three axioms of probability and the definition of conditional probability, one obtains the *law of total probability*,

$$P(B) = \sum_i P(B|A_i)P(A_i) \ , \tag{39.3}$$

for any subset B and for disjoint A_i with $\cup_i A_i = S$. This can be combined with Bayes' theorem (Eq. (39.2)) to give

$$P(A|B) = \frac{P(B|A)P(A)}{\sum_i P(B|A_i)P(A_i)} \ , \tag{39.4}$$

where the subset A could, for example, be one of the A_i.

The most commonly used interpretation of the elements of the sample space are outcomes of a repeatable experiment. The probability $P(A)$ is assigned a value equal to the limiting frequency of occurrence of A. This interpretation forms the basis of *frequentist statistics*.

The elements of the sample space might also be interpreted as *hypotheses*, *i.e.*, statements that are either true or false, such as 'The mass of the W boson lies between 80.3 and 80.5 GeV.' Upon repetition of a measurement, however, such statements are either always true or always false, *i.e.*, the corresponding probabilities in the frequentist interpretation are either 0 or 1. Using *subjective probability*, however, $P(A)$ is interpreted as the degree of belief that the hypothesis A is true. Subjective probability is used in *Bayesian* (as opposed to frequentist) statistics. Bayes' theorem can be written

$$P(\text{theory}|\text{data}) \propto P(\text{data}|\text{theory})P(\text{theory}) \ , \tag{39.5}$$

where 'theory' represents some hypothesis and 'data' is the outcome of the experiment. Here $P(\text{theory})$ is the *prior* probability for the theory, which reflects the experimenter's degree of belief before carrying out the measurement, and $P(\text{data}|\text{theory})$ is the probability to have gotten the data actually obtained, given the theory, which is also called the *likelihood*.

Bayesian statistics provides no fundamental rule for obtaining the prior probability, which may depend on previous measurements, theoretical prejudices, *etc.* Once this has been specified, however, Eq. (39.5) tells how the probability for the theory must be modified in the light of the new data to give the *posterior* probability, $P(\text{theory}|\text{data})$. As Eq. (39.5) is stated as a proportionality, the probability must be normalized by summing (or integrating) over all possible hypotheses.

39.2 Random variables

A *random variable* is a numerical characteristic assigned to an element of the sample space. In the frequency interpretation of probability, it corresponds to an outcome of a repeatable experiment. Let x be a possible outcome of an observation. If x can take on any value from a continuous range, we write $f(x;\theta)dx$ as the probability that the measurement's outcome lies between x and $x + dx$. The function $f(x;\theta)$ is called the *probability density function* (p.d.f.), which may depend on one or more parameters θ. If x can take on only discrete values (*e.g.*, the non-negative integers), then we use $f(x;\theta)$ to denote the probability to find the value x. In the following the term p.d.f. is often taken to cover both the continuous and discrete cases, although technically the term density should only be used in the continuous case.

The p.d.f. is always normalized to unity. Both x and θ may have multiple components and are then often written as vectors. If θ is unknown, we may wish to estimate its value from a given set of measurements of x; this is a central topic of *statistics* (see Sec. 40).

The *cumulative distribution function* $F(a)$ is the probability that $x \leq a$:

$$F(a) = \int_{-\infty}^{a} f(x)\, dx \ . \tag{39.6}$$

Here and below, if x is discrete-valued, the integral is replaced by a sum. The endpoint a is expressly included in the integral or sum. Then $0 \leq F(x) \leq 1$, $F(x)$ is nondecreasing, and $P(a < x \leq b) = F(b) - F(a)$. If x is discrete, $F(x)$ is flat except at allowed values of x, where it has discontinuous jumps equal to $f(x)$.

Any function of random variables is itself a random variable, with (in general) a different p.d.f. The *expectation value* of any function $u(x)$ is

$$E[u(x)] = \int_{-\infty}^{\infty} u(x)\, f(x)\, dx \ , \tag{39.7}$$

assuming the integral is finite. The expectation value is linear, *i.e.*, for any two functions u and v of x and constants c_1 and c_2, $E[c_1 u + c_2 v] = c_1 E[u] + c_2 E[v]$.

The nth moment of a random variable x is

$$\alpha_n \equiv E[x^n] = \int_{-\infty}^{\infty} x^n f(x)\, dx \ , \tag{39.8a}$$

and the nth central moment of x (or moment about the mean, α_1) is

$$m_n \equiv E[(x - \alpha_1)^n] = \int_{-\infty}^{\infty} (x - \alpha_1)^n f(x)\, dx \ . \tag{39.8b}$$

The most commonly used moments are the mean μ and variance σ^2:

$$\mu \equiv \alpha_1 \ , \tag{39.9a}$$

$$\sigma^2 \equiv V[x] \equiv m_2 = \alpha_2 - \mu^2 \ . \tag{39.9b}$$

The mean is the location of the "center of mass" of the p.d.f., and the variance is a measure of the square of its width. Note that $V[cx + k] = c^2 V[x]$. It is often convenient to use the *standard deviation* of x, σ, defined as the square root of the variance.

Any odd moment about the mean is a measure of the skewness of the p.d.f. The simplest of these is the dimensionless coefficient of skewness $\gamma_1 = m_3/\sigma^3$.

The fourth central moment m_4 provides a convenient measure of the tails of a distribution. For the Gaussian distribution (see Sec. 39.4), one has $m_4 = 3\sigma^4$. The *kurtosis* is defined as $\gamma_2 = m_4/\sigma^4 - 3$, *i.e.*, it is zero for a Gaussian, positive for a *leptokurtic* distribution with longer tails, and negative for a *platykurtic* distribution with tails that die off more quickly than those of a Gaussian.

The *quantile* x_α is the value of the random variable x at which the cumulative distribution is equal to α. That is, the quantile

Phys. A 2026.41. Downloaded from www.worldscientific.com
by UNIVERSITY OF CA LEY on 09/16/26. Re-use and distribution is strictly not permitted, except for Open Access articles.

is the inverse of the cumulative distribution function, *i.e.*, $x_\alpha = F^{-1}(\alpha)$. An important special case is the *median*, $x_{\rm med}$, defined by $F(x_{\rm med}) = 1/2$, *i.e.*, half the probability lies above and half lies below $x_{\rm med}$. (More rigorously, $x_{\rm med}$ is a median if $P(x \geq x_{\rm med}) \geq 1/2$ and $P(x \leq x_{\rm med}) \geq 1/2$. If only one value exists, it is called '*the* median.')

Under a monotonic change of variable $x \to y(x)$, the quantiles of a distribution (and hence also the median) obey $y_\alpha = y(x_\alpha)$. In general the expectation value and *mode* (most probable value) of a distribution do not, however, transform in this way.

Let x and y be two random variables with a *joint* p.d.f. $f(x,y)$. The *marginal* p.d.f. of x (the distribution of x with y unobserved) is

$$f_1(x) = \int_{-\infty}^{\infty} f(x,y)\,dy\ , \tag{39.10}$$

and similarly for the marginal p.d.f. $f_2(y)$. The *conditional* p.d.f. of y given fixed x (with $f_1(x) \neq 0$) is defined by $f_3(y|x) = f(x,y)/f_1(x)$, and similarly $f_4(x|y) = f(x,y)/f_2(y)$. From these, we immediately obtain Bayes' theorem (see Eqs. (39.2) and (39.4)),

$$f_4(x|y) = \frac{f_3(y|x)f_1(x)}{f_2(y)} = \frac{f_3(y|x)f_1(x)}{\int f_3(y|x')f_1(x')\,dx'}\ . \tag{39.11}$$

The mean of x is

$$\mu_x = \int_{-\infty}^{\infty}\int_{-\infty}^{\infty} x\,f(x,y)\,dx\,dy = \int_{-\infty}^{\infty} x\,f_1(x)\,dx\ , \tag{39.12}$$

and similarly for y. The *covariance* of x and y is

$$\mathrm{cov}[x,y] = E[(x-\mu_x)(y-\mu_y)] = E[xy] - \mu_x\mu_y\ . \tag{39.13}$$

A dimensionless measure of the covariance of x and y is given by the *correlation coefficient*,

$$\rho_{xy} = \mathrm{cov}[x,y]/\sigma_x\sigma_y\ , \tag{39.14}$$

where σ_x and σ_y are the standard deviations of x and y. It can be shown that $-1 \leq \rho_{xy} \leq 1$.

Two random variables x and y are *independent* if and only if

$$f(x,y) = f_1(x)f_2(y)\ . \tag{39.15}$$

If x and y are independent, then $\rho_{xy} = 0$; the converse is not necessarily true. If x and y are independent, $E[u(x)v(y)] = E[u(x)]E[v(y)]$, and $V[x+y] = V[x]+V[y]$; otherwise, $V[x+y] = V[x]+V[y]+2\mathrm{cov}[x,y]$, and $E[uv]$ does not necessarily factorize.

Consider a set of n continuous random variables $\boldsymbol{x} = (x_1,\ldots,x_n)$ with joint p.d.f. $f(\boldsymbol{x})$, and a set of n new variables $\boldsymbol{y} = (y_1,\ldots,y_n)$, related to $\boldsymbol{x}$ by means of a function $\boldsymbol{y}(\boldsymbol{x})$ that is one-to-one, *i.e.*, the inverse $\boldsymbol{x}(\boldsymbol{y})$ exists. The joint p.d.f. for $\boldsymbol{y}$ is given by

$$g(\boldsymbol{y}) = f(\boldsymbol{x}(\boldsymbol{y}))|J|\ , \tag{39.16}$$

where $|J|$ is the absolute value of the determinant of the square matrix $J_{ij} = \partial x_i/\partial y_j$ (the Jacobian determinant). If the transformation from $\boldsymbol{x}$ to $\boldsymbol{y}$ is not one-to-one, the $\boldsymbol{x}$-space must be broken into regions where the function $\boldsymbol{y}(\boldsymbol{x})$ can be inverted, and the contributions to $g(\boldsymbol{y})$ from each region summed.

Given a set of functions $\boldsymbol{y} = (y_1,\ldots,y_m)$ with $m < n$, one can construct $n-m$ additional independent functions, apply the procedure above, then integrate the resulting $g(\boldsymbol{y})$ over the unwanted y_i to find the marginal distribution of those of interest.

Transformation of p.d.f.s of continuous random variables of any dimension can also be formulated using the Dirac delta function. Starting from an n-dimensional vector random variable $\boldsymbol{x} = (x_1,\ldots,x_n)$ that follows $f(\boldsymbol{x})$ and given m functions $\boldsymbol{a}(\boldsymbol{x}) = (a_1(\boldsymbol{x}),\ldots,a_m(\boldsymbol{x}))$, the p.d.f. of $\boldsymbol{y} \equiv \boldsymbol{a}(\boldsymbol{x})$ can be expressed as

$$g(\boldsymbol{y}) = \int d^n\boldsymbol{x}\,f(\boldsymbol{x})\,\delta^{(m)}(\boldsymbol{y}-\boldsymbol{a}(\boldsymbol{x}))\ , \tag{39.17}$$

where $\delta^{(m)}(\boldsymbol{y}-\boldsymbol{a}(\boldsymbol{x})) = \prod_{i=1}^m \delta(y_i - a_i(\boldsymbol{x}))$. A proof and examples can be found in Ref. [10].

For a one-to-one transformation of discrete random variables, the probability is obtained by simple substitution; no Jacobian is necessary because in this case f is a probability rather than a probability density. If the transformation is not one-to-one, then one must sum the probabilities for all values of the original variable that contribute to a given value of the transformed variable. If f depends on a set of parameters $\boldsymbol{\theta}$, a change to a different parameter set $\boldsymbol{\eta}(\boldsymbol{\theta})$ is made by simple substitution; no Jacobian is used.

39.2.1 *Propagation of errors*

Consider n random variables $\boldsymbol{x} = (x_1,\ldots,x_n)$ and m functions $\boldsymbol{y}(\boldsymbol{x}) = (y_1(\boldsymbol{x}),\ldots,y_m(\boldsymbol{x}))$. Suppose here that the mean values $\boldsymbol{\mu} = (\mu_1,\ldots,\mu_n) = E[\boldsymbol{x}]$ are known, although in practice they will only be estimated, and suppose we also know or have estimated the covariance matrix $V_{ij} = \mathrm{cov}[x_i,x_j]$. The goal of *error propagation* is to determine the covariance matrix for the functions, $U_{ij} = \mathrm{cov}[y_i,y_j]$. In particular, the diagonal elements $U_{ii} = V[y_i]$ give the variances. The new covariance matrix can be found by expanding the functions $\boldsymbol{y}(\boldsymbol{x})$ about the means $\boldsymbol{\mu}$ to first order in a Taylor series. Using this one finds

$$U_{ij} \approx \sum_{k,l} \frac{\partial y_i}{\partial x_k}\frac{\partial y_j}{\partial x_l}\bigg|_{\boldsymbol{\mu}} V_{kl}\ . \tag{39.18}$$

This can be written in matrix notation as $U \approx AVA^T$ where the matrix of derivatives A is

$$A_{ij} = \frac{\partial y_i}{\partial x_j}\bigg|_{\boldsymbol{\mu}}\ , \tag{39.19}$$

and A^T is its transpose. The approximation is exact if $\boldsymbol{y}(\boldsymbol{x})$ is linear. If this is not the case, the approximation can break down if, for example, $\boldsymbol{y}(\boldsymbol{x})$ is significantly nonlinear close to $\boldsymbol{\mu}$ in a region of a size comparable to the standard deviations of $\boldsymbol{x}$.

39.3 Characteristic functions

The characteristic function $\phi(u)$ associated with the p.d.f. $f(x)$ is essentially its Fourier transform, or the expectation value of e^{iux}:

$$\phi(u) = E\left[e^{iux}\right] = \int_{-\infty}^{\infty} e^{iux} f(x)\,dx\ . \tag{39.20}$$

Once $\phi(u)$ is specified, the p.d.f. $f(x)$ is uniquely determined and vice versa; knowing one is equivalent to the other. Characteristic functions are useful in deriving a number of important results about moments and sums of random variables.

It follows from Eqs. (39.8) and (39.20) that the nth moment of a random variable x that follows $f(x)$ is given by

$$i^{-n}\ \frac{d^n\phi}{du^n}\bigg|_{u=0} = \int_{-\infty}^{\infty} x^n f(x)\,dx = \alpha_n\ . \tag{39.21}$$

Thus it is often easy to calculate all the moments of a distribution defined by $\phi(u)$, even when $f(x)$ cannot be written down explicitly.

If the p.d.f.s $f_1(x)$ and $f_2(y)$ for independent random variables x and y have characteristic functions $\phi_1(u)$ and $\phi_2(u)$, then the characteristic function of the weighted sum $ax+by$ is $\phi_1(au)\phi_2(bu)$. The rules of addition for several important distributions (*e.g.*, that the sum of two Gaussian distributed variables also follows a Gaussian distribution) easily follow from this observation.

Let the (partial) characteristic function corresponding to the conditional p.d.f. $f_2(x|z)$ be $\phi_2(u|z)$, and the p.d.f. of z be $f_1(z)$. The characteristic function after integration over the conditional value is

$$\phi(u) = \int \phi_2(u|z)f_1(z)\,dz\ . \tag{39.22}$$

Suppose we can write ϕ_2 in the form

$$\phi_2(u|z) = A(u)e^{ig(u)z}\ . \tag{39.23}$$

Int. J. Mod. Phys. A 2026.41. Downloaded from www.worldscientific.com
by UNIVERSITY OF CALIFORNIA @ BERKELEY on 09/16/26. Re-use and distribution is strictly not permitted, except for Open Access articles.

Then

$$\phi(u) = A(u)\phi_1(g(u)) \ . \tag{39.24}$$

The cumulants (semi-invariants) κ_n of a distribution with characteristic function $\phi(u)$ are defined by the relation

$$\phi(u) = \exp\left[\sum_{n=1}^{\infty} \frac{\kappa_n}{n!}(iu)^n\right] = \exp\left(i\kappa_1 u - \frac{1}{2}\kappa_2 u^2 + \ldots\right) \ . \tag{39.25}$$

The values κ_n are related to the moments α_n and m_n. The first few relations are

$$\begin{aligned} \kappa_1 &= \alpha_1 \ (= \mu, \text{ the mean}) \\ \kappa_2 &= m_2 \ = \alpha_2 - \alpha_1^2 \ (= \sigma^2, \text{ the variance}) \\ \kappa_3 &= m_3 = \alpha_3 - 3\alpha_1\alpha_2 + 2\alpha_1^3. \end{aligned} \tag{39.26}$$

39.4 Commonly used probability distributions

Table 39.1 gives a number of common probability density functions and corresponding characteristic functions, means, and variances. Further information may be found in Refs. [1–8], [11] and [12], which has particularly detailed tables. Monte Carlo techniques for generating each of them may be found in our Sec. 42.4 and in Ref. [11]. We comment below on all except the trivial uniform distribution.

39.4.1 *Binomial and multinomial distributions*

A random process with exactly two possible outcomes which occur with fixed probabilities is called a *Bernoulli* process. If the probability of obtaining a certain outcome (a "success") in an individual trial is p, then the probability of obtaining exactly r successes ($r = 0, 1, 2, \ldots, N$) in N independent trials, without regard to the order of the successes and failures, is given by the binomial distribution $f(r; N, p)$ in Table 39.1. If r and s are binomially distributed with parameters (N_r, p) and (N_s, p), then $t = r + s$ follows a binomial distribution with parameters $(N_r + N_s, p)$. If there are are m possible outcomes for each trial having probabilities $p_1, p_2, \ldots, p_m$, then the joint probability to find $r_1, r_2, \ldots, r_m$ of each outcome after a total of N independent trials is given by the multinomial distribution as shown in Table 39.1. We can regard outcome i as "success" and all the rest as "failure", so individually, any of the r_i follow a binomial distribution for N trials and a success probability p_i.

39.4.2 *Poisson distribution*

The Poisson distribution $f(n; \nu)$ gives the probability of finding exactly n events in a given interval of x (*e.g.*, space or time) when the events occur independently of one another and of x at an average rate of ν per the given interval. The variance σ^2 equals ν. It is the limiting case $p \to 0$, $N \to \infty$, $Np = \nu$ of the binomial distribution. The Poisson distribution approaches the Gaussian distribution for large ν.

For example, a large number of radioactive nuclei of a given type will result in a certain number of decays in a fixed time interval. If this interval is small compared to the mean lifetime, then the probability for a given nucleus to decay is small, and thus the number of decays in the time interval is well modeled as a Poisson variable.

39.4.3 *Normal or Gaussian distribution*

The normal (or Gaussian) probability density function $f(x; \mu, \sigma^2)$ given in Table 39.1 has mean $E[x] = \mu$ and variance $V[x] = \sigma^2$. Comparison of the characteristic function $\phi(u)$ given in Table 39.1 with Eq. (39.25) shows that all cumulants κ_n beyond κ_2 vanish; this is a unique property of the Gaussian distribution. Some other properties are:

$$\begin{aligned} &P(x \text{ in range } \mu \pm \sigma) = 0.6827, \\ &P(x \text{ in range } \mu \pm 0.6745\sigma) = 0.5, \\ &E[|x - \mu|] = \sqrt{2/\pi}\,\sigma = 0.7979\sigma, \\ &\text{half-width at half maximum} = \sqrt{2\ln 2}\,\sigma = 1.177\sigma. \end{aligned}$$

For a Gaussian with $\mu = 0$ and $\sigma^2 = 1$ (the *standard normal*) the cumulative distribution, often written $\Phi(x)$, is related to the error function erf by

$$F(x; 0, 1) \equiv \Phi(x) = \frac{1}{2}\left[1 + \mathrm{erf}(x/\sqrt{2})\right] \ . \tag{39.27}$$

For a mean μ and variance σ^2, replace x by $(x - \mu)/\sigma$. The probability of x in a given range can be calculated with Eq. (40.78).

For x and y independent and normally distributed, $z = ax + by$ follows a normal p.d.f. $f(z; a\mu_x + b\mu_y, a^2\sigma_x^2 + b^2\sigma_y^2)$; that is, the weighted means and variances add.

The Gaussian derives its importance in large part from the *central limit theorem*:

If independent random variables $x_1, \ldots, x_n$ are distributed according to *any* p.d.f. with finite mean and variance, then the sum $y = \sum_{i=1}^{n} x_i$ will have a p.d.f. that approaches a Gaussian for large n. If the p.d.f.s of the x_i are not identical, the theorem still holds under somewhat more restrictive conditions. The mean and variance are given by the sums of corresponding terms from the individual x_i. Therefore, the sum of a large number of fluctuations x_i will be distributed as a Gaussian, even if the x_i themselves are not.

For a set of n Gaussian random variables $\boldsymbol{x}$ with means $\boldsymbol{\mu}$ and covariances $V_{ij} = \mathrm{cov}[x_i, x_j]$, the p.d.f. for the one-dimensional Gaussian is generalized to

$$f(\boldsymbol{x}; \boldsymbol{\mu}, V) = \frac{1}{(2\pi)^{n/2}\sqrt{|V|}} \exp\left[-\frac{1}{2}(\boldsymbol{x} - \boldsymbol{\mu})^T V^{-1}(\boldsymbol{x} - \boldsymbol{\mu})\right] \ , \tag{39.28}$$

where the determinant $|V|$ must be greater than 0. For diagonal V (independent variables), $f(\boldsymbol{x}; \boldsymbol{\mu}, V)$ is the product of the p.d.f.s of n Gaussian distributions.

For $n = 2$, $f(\boldsymbol{x}; \boldsymbol{\mu}, V)$ is

$$\begin{aligned} f(x_1, x_2;\ \mu_1, \mu_2, \sigma_1, \sigma_2, \rho) &= \frac{1}{2\pi\sigma_1\sigma_2\sqrt{1-\rho^2}} \\ \times\ \exp\Bigg\{ \frac{-1}{2(1-\rho^2)} \Bigg[\frac{(x_1-\mu_1)^2}{\sigma_1^2} &- \frac{2\rho(x_1-\mu_1)(x_2-\mu_2)}{\sigma_1\sigma_2} \\ &+ \frac{(x_2-\mu_2)^2}{\sigma_2^2} \Bigg] \Bigg\} . \end{aligned} \tag{39.29}$$

The characteristic function for the multivariate Gaussian is

$$\phi(\boldsymbol{u}; \boldsymbol{\mu}, V) = \exp\left[i\boldsymbol{\mu}\cdot\boldsymbol{u} - \frac{1}{2}\boldsymbol{u}^T V \boldsymbol{u}\right] \ . \tag{39.30}$$

If the components of $\boldsymbol{x}$ are independent, then Eq. (39.30) is the product of the characteristic functions of n Gaussians.

For an n-dimensional Gaussian distribution for $\boldsymbol{x}$ with mean $\boldsymbol{\mu}$ and covariance matrix V, the marginal distribution for any single x_i is is a one-dimensional Gaussian with mean μ_i and variance V_{ii}. The equation $(\boldsymbol{x} - \boldsymbol{a})^T V^{-1}(\boldsymbol{x} - \boldsymbol{a}) = C$, where C is any positive number, defines an n-dimensional ellipse centered about $\boldsymbol{a}$. If $\boldsymbol{a}$ is equal to the mean $\boldsymbol{\mu}$, then C is a random variable obeying the χ^2 distribution for n degrees of freedom, which is discussed in the following section. The probability that $\boldsymbol{x}$ lies outside the ellipsoid for a given value of C is given by $1 - F_{\chi^2}(C; n)$, where F_{χ^2} is the cumulative χ^2 distribution. This may be read from Fig. 40.2. For example, the "s-standard-deviation ellipsoid" occurs at $C = s^2$. For the two-variable case ($n = 2$), the point $\boldsymbol{x}$ lies outside the one-standard-deviation ellipsoid with 61% probability. The use of these ellipsoids as indicators of probable error is described in Sec. 40.4.2.3; the validity of those indicators assumes that $\boldsymbol{\mu}$ and V are correct.

39.4.4 *Log-normal distribution*

If a random variable y follows a Gaussian distribution with mean μ and variance σ^2, then $x = e^y$ follows a log-normal distribution, as given in Table 39.1. As a consequence of the central limit theorem described in Sec. 39.4.3, the distribution of the product of a large number of positive random variables approaches a log-normal. It is bounded below by zero and is thus well suited

by UNIVERSITY OF CA LEY on 09/16/26. Re-use and distribution is strictly not permitted, except for Open Access articles. Phys. A 2026.41. Downloaded from www.worldscientific.com

Table 39.1: Some common probability density functions, with corresponding characteristic functions and means and variances. In the Table, $\Gamma(k)$ is the gamma function, equal to $(k-1)!$ when k is an integer; ${}_1F_1$ is the confluent hypergeometric function of the 1st kind [12].

Distribution	Probability density function f (variable; parameters)	Characteristic function $\phi(u)$	Mean	Variance
Uniform	$f(x;a,b) = \begin{cases} 1/(b-a) & a \le x \le b \\ 0 & \text{otherwise} \end{cases}$	$\frac{e^{ibu}-e^{iau}}{(b-a)iu}$	$\frac{a+b}{2}$	$\frac{(b-a)^2}{12}$
Binomial	$f(r;N,p) = \frac{N!}{r!(N-r)!}\, p^r q^{N-r}$ $r = 0,1,2,\ldots,N;\quad 0 \le p \le 1;\quad q = 1-p$	$(q+pe^{iu})^N$	Np	Npq
Multinomial	$f(r_1,\ldots,r_m;N,p_1,\ldots,p_m) = \frac{N!}{r_1!\cdots r_m!} p_1^{r_1}\cdots p_m^{r_m}$	$\left(\sum_{k=1}^m p_k e^{iu_k}\right)^N$	$E[r_i] = Np_i$	$\mathrm{cov}[r_i,r_j] = Np_i(\delta_{ij}-p_j)$
Poisson	$f(n;\nu) = \frac{\nu^n e^{-\nu}}{n!};\ n = 0,1,2,\ldots;\ \nu > 0$	$\exp[\nu(e^{iu}-1)]$	ν	ν
Normal (Gaussian)	$f(x;\mu,\sigma^2) = \frac{1}{\sigma\sqrt{2\pi}}\ \exp(-(x-\mu)^2/2\sigma^2)$	$\exp(i\mu u - \frac{1}{2}\sigma^2u^2)$	μ	σ^2
Multivariate Gaussian	$f(\boldsymbol{x};\boldsymbol{\mu},\boldsymbol{V}) = \frac{1}{(2\pi)^{n/2}\sqrt{\lvert V\rvert}}$ $\times \exp\left[-\frac{1}{2}(\boldsymbol{x}-\boldsymbol{\mu})^T V^{-1}(\boldsymbol{x}-\boldsymbol{\mu})\right]$ $-\infty < x_j < \infty;\quad -\infty < \mu_j < \infty;\quad \lvert V\rvert > 0$	$\exp\left[i\boldsymbol{\mu}\cdot\boldsymbol{u} - \frac{1}{2}\boldsymbol{u}^T V\boldsymbol{u}\right]$	$\boldsymbol{u}$	V_{jk}
Log-normal	$f(x;\mu,\sigma^2) = \frac{1}{\sigma\sqrt{2\pi}}\frac{1}{x}\ \exp(-(\ln x-\mu)^2/2\sigma^2)$ $0 < x < \infty;\quad -\infty < \mu < \infty;\quad \sigma > 0$	—	$\exp(\mu+\sigma^2/2)$	$\exp(2\mu+\sigma^2)$ $\times[\exp(\sigma^2)-1]$
χ^2	$f(z;n) = \frac{z^{n/2-1}e^{-z/2}}{2^{n/2}\Gamma(n/2)};\quad z \ge 0$	$(1-2iu)^{-n/2}$	n	$2n$
Student's t	$f(t;n) = \frac{1}{\sqrt{n\pi}}\ \frac{\Gamma[(n+1)/2]}{\Gamma(n/2)}\left(1+\frac{t^2}{n}\right)^{-(n+1)/2}$ $-\infty < t < \infty;\quad$ n not required to be integer	—	0 for $n > 1$	$n/(n-2)$ for $n > 2$
Gamma	$f(x;\lambda,k) = \frac{x^{k-1}\lambda^k e^{-\lambda x}}{\Gamma(k)};\quad 0 \le x < \infty$; k not required to be integer	$(1-iu/\lambda)^{-k}$	k/λ	k/λ^2
Beta	$f(x;\alpha,\beta) = \frac{\Gamma(\alpha+\beta)}{\Gamma(\alpha)\Gamma(\beta)}x^{\alpha-1}(1-x)^{\beta-1}$ $0 \le x \le 1$	${}_1F_1(\alpha;\alpha+\beta;iu)$	$\frac{\alpha}{\alpha+\beta}$	$\frac{\alpha\beta}{(\alpha+\beta)^2(\alpha+\beta+1)}$

for modeling quantities that are intrinsically non-negative such as an efficiency. One can implement a log-normal model for a random variable x by defining $y = \ln x$ so that y follows a Gaussian distribution.

39.4.5 χ^2 *distribution*

If $x_1,\ldots,x_n$ are independent Gaussian random variables, the sum $z = \sum_{i=1}^n (x_i-\mu_i)^2/\sigma_i^2$ follows the χ^2 p.d.f. with n *degrees of freedom*, which we denote by $\chi^2(n)$. More generally, for n correlated Gaussian variables as components of a vector $\boldsymbol{X}$ with covariance matrix V, $z = \boldsymbol{X}^T V^{-1}\boldsymbol{X}$ follows $\chi^2(n)$ as in the previous section. For a set of z_i, each of which follows $\chi^2(n_i)$, $\sum z_i$ follows $\chi^2(\sum n_i)$. For large n, the χ^2 p.d.f. approaches a Gaussian with a mean and variance given by $\mu = n$ and $\sigma^2 = 2n$, respectively (here the formulae for μ and σ^2 are valid for all n).

The χ^2 p.d.f. is often used in evaluating the level of compatibility between observed data and a hypothesis for the p.d.f. that the data might follow. This is discussed further in Sec. 40.3.2 on significance tests.

39.4.6 *Student's t distribution*

Suppose that y and $x_1,\ldots,x_n$ are independent and Gaussian distributed with mean 0 and variance 1. We then define

$$z = \sum_{i=1}^n x_i^2 \quad \text{and} \quad t = \frac{y}{\sqrt{z/n}}\,. \tag{39.31}$$

The variable z thus follows a $\chi^2(n)$ distribution. Then t is distributed according to Student's t distribution with n degrees of freedom, $f(t;n)$, given in Table 39.1.

If defined through gamma functions as in Table 39.1, the parameter n is not required to be an integer. As $n \to \infty$, the distribution approaches a Gaussian, and for $n = 1$ it is a *Cauchy* or *Breit–Wigner* distribution.

As an example, consider the *sample mean* $\overline{x} = \sum x_i/n$ and the *sample variance* $s^2 = \sum(x_i-\overline{x})^2/(n-1)$ for normally distributed x_i with unknown mean μ and variance σ^2. The sample mean has a Gaussian distribution with a variance σ^2/n, so the variable $(\overline{x}-\mu)/\sqrt{\sigma^2/n}$ is normal with mean 0 and variance 1. The quantity $(n-1)s^2/\sigma^2$ is independent of this and follows $\chi^2(n-1)$. The ratio

$$t = \frac{(\overline{x}-\mu)/\sqrt{\sigma^2/n}}{\sqrt{(n-1)s^2/\sigma^2(n-1)}} = \frac{\overline{x}-\mu}{\sqrt{s^2/n}} \tag{39.32}$$

is distributed as $f(t;n-1)$. The unknown variance σ^2 cancels, and t can be used to test the hypothesis that the true mean is some particular value μ.

39.4.7 *Gamma distribution*

For a process that generates events as a function of x (*e.g.*, space or time) according to a Poisson distribution, the distance in x from an arbitrary starting point (which may be some particular event) to the kth event follows a *gamma* distribution, $f(x;\lambda,k)$. The Poisson parameter μ is λ per unit x. The special case $k = 1$ (*i.e.*, $f(x;\lambda,1) = \lambda e^{-\lambda x}$) is called the *exponential* distribution. A sum of k' exponential random variables x_i is distributed as $f(\sum x_i;\lambda,k')$.

The parameter k is not required to be an integer. For $\lambda = 1/2$ and $k = n/2$, the gamma distribution reduces to the $\chi^2(n)$ distribution.

39.4.8 *Beta distribution*

The beta distribution describes a continuous random variable x in the interval $[0,1]$. By scaling and translation one can easily generalize it to have arbitrary endpoints. In Bayesian inference about the parameter p of a binomial process, if the prior p.d.f. is a beta distribution $f(p;\alpha,\beta)$ then the observation of r successes out of N trials gives a posterior beta distribution $f(p;r+\alpha,N-r+\beta)$ (Bayesian methods are discussed further in Sec. 40). The uniform distribution is a beta distribution with $\alpha = \beta = 1$.

Int. J. Mod. Phys. A 2026.41. Downloaded from www.worldscientific.com
by UNIVERSITY OF CALIFORNIA @ BERKELEY on 09/16/26. Re-use and distribution is strictly not permitted, except for Open Access articles.

References

[1] H. Cramér, *Mathematical Methods of Statistics,* (Princeton Univ. Press, New Jersey, 1958).

[2] A. Stuart and J.K. Ord, *Kendall's Advanced Theory of Statistics*, Vol. 1 *Distribution Theory* 6th Ed., (Halsted Press, New York, 1994), and earlier editions by Kendall and Stuart.

[3] F.E. James, *Statistical Methods in Experimental Physics*, 2nd Ed., (World Scientific, Singapore, 2006).

[4] L. Lyons, *Statistics for Nuclear and Particle Physicists*, (Cambridge University Press, New York, 1986).

[5] B.R. Roe, *Probability and Statistics in Experimental Physics,* 2nd Ed., (Springer, New York, 2001).

[6] R.J. Barlow, *Statistics: A Guide to the Use of Statistical Methods in the Physical Sciences*, (John Wiley, New York, 1989).

[7] S. Brandt, *Data Analysis*, 3rd Ed., (Springer, New York, 1999).

[8] G. Cowan, *Statistical Data Analysis*, (Oxford University Press, Oxford, 1998).

[9] A.N. Kolmogorov, *Grundbegriffe der Wahrscheinlichkeitsrechnung*, (Springer, Berlin, 1933); *Foundations of the Theory of Probability*, 2nd Ed., (Chelsea, New York 1956).

[10] D. T. Gillespie, American Journal of Physics **51**, 6, 520 (1983).

[11] Ch. Walck, *Hand-book on Statistical Distributions for Experimentalists*, University of Stockholm Internal Report SUF-PFY/96-01, available from `staff.fysik.su.se/~walck/`.

[12] M. Abramowitz and I. Stegun, eds., *Handbook of Mathematical Functions*, (Dover, New York, 1972).

40. Statistics

Revised June 2025 by G. Cowan (RHUL) and L. Lista (UNINA; INFN, Napoli).

40.1 Fundamental concepts . . . 710
40.2 Parameter estimation . . . 710
40.2.1 Estimators for mean, variance, and median 711
40.2.2 The method of maximum likelihood . . . 711
40.2.2.1 Large-sample properties and variance of the MLE . . . 711
40.2.2.2 MLE with different likelihood functions: binned and unbinned data samples . . . 712
40.2.3 The method of least squares . . . 713
40.2.4 Parameter estimation with constraints . . . 713
40.2.5 The Bayesian approach . . . 714
40.2.5.1 Priors . . . 714
40.2.6 Nuisance parameters . . . 715
40.2.6.1 Frequentist treatment of nuisance parameters . . . 715
40.2.6.2 Bayesian treatment of nuisance parameters . . . 715
40.2.7 Unfolding . . . 715
40.3 Statistical tests . . . 716
40.3.1 Hypothesis tests . . . 716
40.3.2 Tests of significance, p-values . . . 717
40.3.2.1 Frequentist treatment of nuisance parameters and asymptotic methods for tests . . . 717
40.3.2.2 The look-elsewhere effect . . . 718
40.3.3 Goodness of fit . . . 718
40.3.3.1 Goodness-of-fit with chi-square or likelihood ratio . . . 719
40.3.3.2 Goodness-of-fit with the empirical distribution function . . . 720
40.3.4 Bayes factors . . . 720
40.4 Intervals and limits . . . 720
40.4.1 Bayesian credible intervals . . . 721
40.4.2 Frequentist confidence intervals . . . 721
40.4.2.1 The Neyman construction for confidence intervals . . . 721
40.4.2.2 Confidence interval from a hypothesis test . . . 722
40.4.2.3 Confidence regions from the likelihood function . . . 722
40.4.2.4 Limits for Poisson or binomial data 723
40.4.2.5 Parameter exclusion in cases of low sensitivity . . . 723
40.5 Experimental sensitivity . . . 724
References . . . 726

This chapter gives an overview of statistical methods used in high-energy physics. In statistics, we are interested in using a given sample of data to make inferences about a probabilistic model, *e.g.*, to assess the model's validity or to determine the values of its parameters. There are two main approaches to statistical inference, which we may call frequentist and Bayesian.

In frequentist statistics, probability is interpreted as the limiting frequency of the outcome of a repeatable experiment. The most important tools in this framework are parameter estimation, covered in Section 40.2, statistical tests, discussed in Section 40.3, and confidence intervals, which are constructed so as to cover the true value of a parameter with a specified probability, as described in Section 40.4.2. Note that in frequentist statistics one does not define a probability for a hypothesis or for the value of a parameter.

In Bayesian statistics, the subjective interpretation of probability is used to quantify one's *degree of belief* in a hypothesis. This allows one to define a probability density function (p.d.f.) for a parameter, which reflects one's knowledge about where its true value lies.

Bayesian methods provide a natural means to include additional information, which in general may be subjective; in fact they *require* prior probabilities for the hypotheses (or parameters) in question, *i.e.*, the degree of belief about the parameters' values, before carrying out the measurement. Using Bayes' theorem (Eq. (39.4)), the prior degree of belief is updated by the data from the experiment. Bayesian methods for interval estimation are discussed in Sections 40.4.1 and 40.4.2.5.

For many inference problems, the frequentist and Bayesian approaches give similar numerical values, even though they answer different questions and are based on fundamentally different interpretations of probability. In some important cases, however, the two approaches may yield very different results. For a discussion of Bayesian vs. non-Bayesian methods, see references written by a statistician [1], by a physicist [2], or the detailed comparison in Ref. [3].

40.1 Fundamental concepts

Consider an experiment whose outcome is characterized by one or more data values, which we can write as a vector $\boldsymbol{x}$. A *hypothesis* H is a statement about the probability for the data, often written $P(\boldsymbol{x}|H)$. (We will usually use a capital letter for a probability and lower case for a probability density. Often the term p.d.f. is used loosely to refer to either a probability or a probability density). This could, for example, define completely the p.d.f. for the data (a *simple* hypothesis), or it could specify only the functional form of the p.d.f., with the values of one or more parameters not determined (a *composite* hypothesis).

If the probability $P(\boldsymbol{x}|H)$ for data $\boldsymbol{x}$ is regarded as a function of the hypothesis H, then it is called the *likelihood* of H, usually written $L(H)$. Often the hypothesis is characterized by one or more parameters $\boldsymbol{\theta}$, in which case $L(\boldsymbol{\theta}) = P(\boldsymbol{x}|\boldsymbol{\theta})$ is called the likelihood function.

In some cases one can obtain at least approximate frequentist results using the likelihood evaluated only with the data obtained, for example, when determining confidence regions with Eq. (40.78). In general, however, the frequentist approach requires a full specification of the probability model $P(\boldsymbol{x}|H)$ both as a function of the data $\boldsymbol{x}$ and hypothesis H.

In the Bayesian approach, inference is based on the posterior probability for H given the data $\boldsymbol{x}$, which represents one's degree of belief that H is true given the data. This is obtained from Bayes' theorem (39.4), which can be written

$$P(H|\boldsymbol{x}) = \frac{P(\boldsymbol{x}|H)\pi(H)}{\int P(\boldsymbol{x}|H')\pi(H')\,dH'} \,. \tag{40.1}$$

Here $P(\boldsymbol{x}|H)$ is the likelihood for H, which depends only on the data actually obtained. The quantity $\pi(H)$ is the prior probability for H, which represents one's degree of belief for H before carrying out the measurement. The integral in the denominator (or sum, for discrete hypotheses) serves as a normalization factor. If H is characterized by a continuous parameter θ then the posterior probability is a p.d.f. $p(\theta|\boldsymbol{x})$. Note that the likelihood function itself is not a p.d.f. for θ.

40.2 Parameter estimation

Here we review *point estimation* of parameters, first with an overview of the frequentist approach and its two most important methods, maximum likelihood and least squares, treated in Sections 40.2.2 and 40.2.3. The Bayesian approach is outlined in Sec. 40.2.5. In both approaches it is useful to define the *Fisher Information* for a set of parameters $\boldsymbol{\theta} = (\theta_1, \ldots, \theta_M)$ as the matrix

$$I_{ij}(\boldsymbol{\theta}) = E\left[\left(\frac{\partial \ln L}{\partial \theta_i}\right)\left(\frac{\partial \ln L}{\partial \theta_j}\right)\right] = -E\left[\frac{\partial^2 \ln L}{\partial \theta_i \partial \theta_j}\right] \,, \tag{40.2}$$

where the operator $E[\,]$ is the expectation value with respect to the data. For the final equality to hold, the range of allowed data values must not depend on $\boldsymbol{\theta}$.

An *estimator* $\widehat{\theta}$ (written with a hat) is a function of the data used to estimate the value of the parameter θ. Sometimes the

Phys. A 2026.41. Downloaded from www.worldscientific.com
by UNIVERSITY OF CA LEY on 09/16/26. Re-use and distribution is strictly not permitted, except for Open Access articles.

Int. J. Mod. Phys. A 2026.41. Downloaded from www.worldscientific.com by UNIVERSITY OF CALIFORNIA @ BERKELEY on 09/16/26. Re-use and distribution is strictly not permitted, except for Open Access articles.

word "estimate" is used to denote the value of the estimator when evaluated with given data. There is no fundamental rule dictating how an estimator must be constructed. One tries, therefore, to choose that estimator which has the best properties. The most important of these are (a) *consistency*, (b) *bias*, (c) *efficiency*, and (d) *robustness*.

(a) An estimator is said to be *consistent* if the estimate $\widehat{\theta}$ converges in probability (see Ref. [3]) to the true value θ as the amount of data increases. This property is so important that it is possessed by all commonly used estimators.

(b) The *bias*, $b = E[\widehat{\theta}] - \theta$, is the difference between the expectation value of the estimator and the true value of the parameter. The expectation value is taken over a hypothetical set of similar experiments in which $\widehat{\theta}$ is constructed in the same way. When $b = 0$, the estimator is said to be unbiased. The bias depends on the chosen metric, *i.e.*, if $\widehat{\theta}$ is an unbiased estimator of θ, then $\widehat{\theta}^2$ is not in general an unbiased estimator for θ^2.

(c) *Efficiency* is the ratio of the minimum possible variance for any estimator of θ to the variance $V[\widehat{\theta}]$ of the estimator $\widehat{\theta}$. For the case of a single parameter, under rather general conditions, the variance of any estimator satisfies the *information* (or *Rao-Cramér-Fréchet*) *inequality*,

$$V[\hat{\theta}] \geq \left(1 + \frac{\partial b}{\partial \theta}\right)^2 / I(\theta) \ , \tag{40.3}$$

where $I(\theta) = I_{11}(\theta)$ is the only element of the Fisher information from Eq. (40.2).

The *mean-squared error*,

$$\mathrm{MSE} = E[\,(\widehat{\theta} - \theta)^2\,] = V[\widehat{\theta}] + b^2 \ , \tag{40.4}$$

is a measure of an estimator's quality which combines bias and variance.

(d) *Robustness* is the property of being insensitive to departures from assumptions about the p.d.f., *e.g.*, owing to uncertainties in the distribution's tails.

It is not in general possible to optimize simultaneously for all the measures of estimator quality described above. For some common estimators, the properties above are known exactly. More generally, it is possible to evaluate them by Monte Carlo simulation. Note that they will in general depend on the unknown θ.

40.2.1 *Estimators for mean, variance, and median*

Suppose we have a set of n independent measurements, $x_1, \ldots, x_n$, each assumed to follow a p.d.f. with unknown mean μ and unknown variance σ^2 (the measurements do not necessarily have to follow a Gaussian distribution). Then

$$\widehat{\mu} = \frac{1}{n} \sum_{i=1}^{n} x_i \tag{40.5}$$

$$\widehat{\sigma^2} = \frac{1}{n-1} \sum_{i=1}^{n} (x_i - \widehat{\mu})^2 \tag{40.6}$$

are unbiased estimators of μ and σ^2. The variance of $\widehat{\mu}$ is σ^2/n and the variance of $\widehat{\sigma^2}$ is

$$V\left[\widehat{\sigma^2}\right] = \frac{1}{n}\left(m_4 - \frac{n-3}{n-1}\sigma^4\right) \ , \tag{40.7}$$

where m_4 is the 4th central moment of x (see Eq. (39.8)). For Gaussian distributed x_i, this becomes $2\sigma^4/(n-1)$ for any $n \geq 2$, and for large n the standard deviation of $\widehat{\sigma}$ is $\sigma/\sqrt{2n}$. For any n and Gaussian x_i, $\widehat{\mu}$ is an efficient estimator for μ, and the estimators $\widehat{\mu}$ and $\widehat{\sigma^2}$ are uncorrelated. Otherwise the arithmetic mean (40.5) is not necessarily the most efficient estimator; this is discussed further in Sec. 8.7 of Ref. [4].

If σ^2 is known, it does not improve the estimate $\widehat{\mu}$, as can be seen from Eq. (40.5); however, if μ is known, one can substitute it for $\widehat{\mu}$ in Eq. (40.6) and replace $n-1$ by n to obtain an estimator of σ^2 still with zero bias but smaller variance. If the x_i have different, known variances σ_i^2, then the weighted average

$$\widehat{\mu} = \frac{1}{w} \sum_{i=1}^{n} w_i x_i \ , \tag{40.8}$$

where $w_i = 1/\sigma_i^2$ and $w = \sum_i w_i$, is an unbiased estimator for μ with a smaller variance than an unweighted average. The standard deviation of $\widehat{\mu}$ is $1/\sqrt{w}$.

As an estimator for the median x_{med}, one can use the sample median defined as the value $\widehat{x}_{\mathrm{med}}$ such that half of the x_i are below and half above, if n is odd, or the arithmetic mean of the two consecutive values such that half of the remaining half of the x_i are below and half above those two values.

If the p.d.f. of x has the form $f(x-\mu)$ and μ is both mean and median, then for large n the variance of the sample median approaches $1/[4nf^2(0)]$, provided $f(0) > 0$ [5]. Although estimating the median can often be more difficult computationally than the mean, the resulting estimator is generally more robust, as it is insensitive to the exact shape of the tails of a distribution.

40.2.2 *The method of maximum likelihood*

Suppose we have a set of measured quantities $\boldsymbol{x}$ and the likelihood $L(\boldsymbol{\theta}) = P(\boldsymbol{x}|\boldsymbol{\theta})$ for a set of parameters $\boldsymbol{\theta} = (\theta_1, \ldots, \theta_M)$. The *maximum likelihood estimators* (MLEs) for $\boldsymbol{\theta}$ are defined as the values that give the maximum of L. Because of the properties of the logarithm, it is usually easier to work with $\ln L$, and since both are maximized for the same parameter values $\boldsymbol{\theta}$, the MLEs can be found by solving the *likelihood equations*,

$$\frac{\partial \ln L}{\partial \theta_i} = 0 \ , \qquad i = 1, \ldots, M \ . \tag{40.9}$$

Often the solution must be found numerically.

In general the likelihood function is obtained from the probability of the data under assumption of the parameters $\boldsymbol{\theta}$. In evaluating the likelihood function, it is important that any normalization factors in the p.d.f. that involve $\boldsymbol{\theta}$ be included. However, we will only be interested in the maximum of L and in ratios of L at different values of the parameters; hence any multiplicative factors that do not involve the parameters that we want to estimate may be dropped, including factors that depend on the data but not on $\boldsymbol{\theta}$.

Under a one-to-one change of parameters from $\boldsymbol{\theta}$ to $\boldsymbol{\eta}$, the MLEs $\widehat{\boldsymbol{\theta}}$ transform to $\boldsymbol{\eta}(\widehat{\boldsymbol{\theta}})$. That is, the maximum-likelihood solution is invariant under change of parameter. However, other properties of MLEs, in particular the bias, are not invariant under change of parameter.

40.2.2.1 *Large-sample properties and variance of the MLE*

The method of maximum likelihood has particularly attractive properties when the size of the data sample (number of events) is very large. This situation is called the large-sample or asymptotic limit. The asymptotic properties emerge only if certain regularity conditions are satisfied. A complete statement of these conditions can be found, e.g., in [3]; they include the requirements that the range of possible data values not depend on the model parameters, and the true value of a parameter cannot lie on the boundary of its allowed values. For small samples the properties hold only in special cases, e.g., where the means of Gaussian distributed data are linear functions of the parameters.

Provided the regularity conditions are satisfied, in the large-sample limit the bias of the MLEs goes to zero and the information inequality becomes an equality. For a multi-parameter model, the inverse of the covariance matrix $V_{ij} = \mathrm{cov}[\widehat{\theta}_i, \widehat{\theta}_j\,]$ for a set of MLEs becomes approximately equal to the Fisher Information (40.2), i.e.,

$$V_{ij}^{-1} \approx I_{ij} = -E\left[\frac{\partial^2 \ln L}{\partial \theta_i \partial \theta_j}\right] \ . \tag{40.10}$$

To obtain a numerical estimate for V^{-1} one can use the matrix

by UNIVERSITY OF CA Phys. A 2026.41. Downloaded from www.worldscientific.com LEY on 09/16/26. Re-use and distribution is strictly not permitted, except for Open Access articles.

of second derivatives of $\ln L$ evaluated at its maximum:

$$(\widehat{V}^{-1})_{ij} = -\left.\frac{\partial^2 \ln L}{\partial\theta_i \partial\theta_j}\right|_{\widehat{\boldsymbol{\theta}}} . \tag{40.11}$$

In addition, in the large-sample limit the likelihood function itself takes on a Gaussian shape, so that the log-likelihood becomes a quadratic function of the form

$$\ln L(\boldsymbol{\theta}) = \ln L_{\max} - \frac{1}{2}(\boldsymbol{\theta} - \hat{\boldsymbol{\theta}})^T V^{-1}(\boldsymbol{\theta} - \hat{\boldsymbol{\theta}}) . \tag{40.12}$$

One therefore finds s times the standard deviations σ_i of the MLEs from their distances to the tangents of the hypersurface defined by

$$\ln L(\boldsymbol{\theta}) = \ln L_{\max} - \frac{s^2}{2} , \tag{40.13}$$

where $\ln L_{\max}$ is the value of $\ln L$ at the MLE. This formula relates the standard deviations to a log-likelihood contour and holds for any number of parameters. This is in contrast to a similar formula for a confidence region given in Eq. (40.78), which does depend on the number of parameters.

Equation (40.13) represents an ellipsoid in the M-dimensional parameter space. For $M = 2$ and $s = 1$, it gives the ellipse in the parameters space (θ_1, θ_2) centered about the estimated values $(\widehat{\theta}_1, \widehat{\theta}_2)$ shown in Fig. 40.1. The tangents to the ellipse give the standard deviations of the estimators, σ_1 and σ_2, and the angle of the major axis of the ellipse is given by

$$\tan 2\phi = \frac{2\rho_{12}\,\sigma_1\sigma_2}{\sigma_1^2 - \sigma_2^2} , \tag{40.14}$$

where $\rho_{12} = \mathrm{cov}[\,\widehat{\theta}_1, \widehat{\theta}_2\,]/\sigma_1\sigma_2$ is the correlation coefficient.

The correlation coefficient can be visualized as the fraction of the distance σ_2 from the ellipse's horizontal center-line at which the ellipse becomes tangent to vertical, *i.e.*, at the distance $\rho_{12}\sigma_2$ below the center-line as shown. As ρ_{12} goes to $+1$ or -1, the ellipse thins to a diagonal line.

If one considers one of the parameters, say θ_1, as known and its value is $\hat{\theta}_1$, then the quantity $\sigma_{\text{inner}} = \sqrt{1-\rho_{12}^2}\,\sigma_2$ represents the statistical error of the estimate $\hat{\theta}_2$. It corresponds to the intercept of the vertical center-line with the ellipse, as shown in the figure. This illustrates that constraining θ_1 decreases the statistical uncertainty of the estimate of θ_2, as long as $\hat{\theta}_1$ and $\hat{\theta}_2$ are correlated, i.e., the ellipse is tilted. The corresponding principle applies also to problems with more parameters.

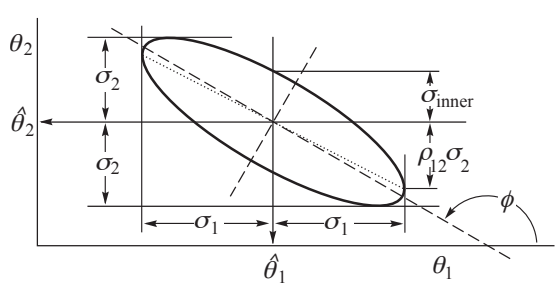

Figure 40.1: Standard error ellipse for the estimators $\widehat{\theta}_1$ and $\widehat{\theta}_2$. In the case shown the correlation is negative.

40.2.2.2 *MLE with different likelihood functions: binned and unbinned data samples*

An important special case is when the data consist of *i.i.d.* (independent and identically distributed) values. Here one has a set of n statistically independent quantities $\boldsymbol{x} = (x_1, \ldots, x_n)$, where each component follows the same p.d.f. $f(x;\boldsymbol{\theta})$. In this case the joint p.d.f. of the data sample factorizes and the likelihood function is

$$L(\boldsymbol{\theta}) = P(\boldsymbol{x}|\boldsymbol{\theta}) = \prod_{i=1}^{n} f(x_i;\boldsymbol{\theta}) . \tag{40.15}$$

Here the number n of observations is regarded as fixed.

If, however, the probability to observe n events itself depends on the parameters $\boldsymbol{\theta}$, then this dependence should be included in the likelihood. For example, if n follows a Poisson distribution with mean μ and the independent x values all follow $f(x;\boldsymbol{\theta})$, then the likelihood becomes

$$L(\boldsymbol{\theta}) = P(\boldsymbol{x}, n|\boldsymbol{\theta}) = P(n)P(\boldsymbol{x}|n) = \frac{\mu^n}{n!}e^{-\mu}\prod_{i=1}^{n} f(x_i;\boldsymbol{\theta}) . \tag{40.16}$$

Equation (40.16) is often called the *extended likelihood* (see, *e.g.*, Refs. [6, 7]).

If μ is given as a function of $\boldsymbol{\theta}$, then including the probability for n given $\boldsymbol{\theta}$ in the likelihood provides additional information about the parameters. This therefore leads to a reduction in their statistical uncertainties and in general changes their estimated values.

If the total number of data values is small, the unbinned maximum-likelihood method, *i.e.*, use of Equation (40.15) (or (40.16) for extended maximum likelihood), is preferred since binning can only result in a loss of information, and hence larger statistical errors for the parameter estimates. If the sample is large, it can be convenient to bin the values in a histogram with N bins, so that one obtains a vector of data $\boldsymbol{n} = (n_1, \ldots, n_N)$ with expectation values $\boldsymbol{\mu} = E[\,\boldsymbol{n}\,]$ and probabilities $f(\boldsymbol{n};\boldsymbol{\mu})$. Suppose the mean values $\boldsymbol{\mu}$ can be determined as a function of a set of parameters $\boldsymbol{\theta}$. Then one may maximize the likelihood function based on the contents of the bins.

As mentioned in Sec. 40.2.2, the total number of entries $n_{\text{tot}} = \sum_i n_i$ can be regarded either as fixed or as a random variable. If it is fixed, the histogram's values $\boldsymbol{n}$ follow a multinomial distribution,

$$f_{\text{M}}(\boldsymbol{n};\boldsymbol{\theta}) = \frac{n_{\text{tot}}!}{n_1!\cdots n_N!}\,p_1^{n_1}\cdots p_N^{n_N} , \tag{40.17}$$

where we assume the probabilities p_i are given functions of the parameters $\boldsymbol{\theta}$. The distribution can be written equivalently in terms of the expected number of entries in each bin, $\mu_i = n_{\text{tot}}p_i$. If the n_i are regarded as independent and Poisson distributed, then the data are instead described by a product of Poisson probabilities,

$$f_{\text{P}}(\boldsymbol{n};\boldsymbol{\theta}) = \prod_{i=1}^{N}\frac{\mu_i^{n_i}}{n_i!}e^{-\mu_i} , \tag{40.18}$$

where the mean values μ_i are given functions of $\boldsymbol{\theta}$. The total number of entries n_{tot} thus follows a Poisson distribution with mean $\mu_{\text{tot}} = \sum_i \mu_i$.

When using maximum likelihood with binned data, one can find the estimators and at the same time obtain a statistic usable for a test of goodness of fit (see Sec. 40.3.3.1). For independent Poisson distributed data, maximizing the likelihood $L(\boldsymbol{\theta}) = f_{\text{P}}(\boldsymbol{n};\boldsymbol{\theta})$ is equivalent to maximizing the likelihood ratio $\lambda(\boldsymbol{\theta}) = f_{\text{P}}(\boldsymbol{n};\boldsymbol{\theta})/f_{\text{sat}}(\boldsymbol{n};\hat{\boldsymbol{\mu}})$, where in the denominator $f_{\text{sat}}(\boldsymbol{n};\boldsymbol{\mu})$ is the corresponding model with an adjustable parameter for each bin, $\boldsymbol{\mu} = (\mu_1, \ldots, \mu_N)$, with estimators $\hat{\boldsymbol{\mu}} = (n_1, \ldots, n_N)$ (called the "saturated model"). Equivalently one often minimizes the quantity $-2\ln\lambda(\boldsymbol{\theta})$. For independent Poisson distributed n_i this is [8]

$$-2\ln\lambda(\boldsymbol{\theta}) = 2\sum_{i=1}^{N}\left[\mu_i(\boldsymbol{\theta}) - n_i + n_i \ln\frac{n_i}{\mu_i(\boldsymbol{\theta})}\right] , \tag{40.19}$$

where for bins with $n_i = 0$, the last term in (40.19) is zero. The expression (40.19) without the terms $\mu_i - n_i$ also gives $-2\ln\lambda(\boldsymbol{\theta})$ for multinomially distributed n_i, *i.e.*, when the total number of entries is regarded as fixed. In the limit of zero bin width, minimizing (40.19) is equivalent to maximizing the unbinned extended likelihood function (40.16); in the corresponding multinomial case without the $\mu_i - n_i$ terms one obtains Eq. (40.15).

A smaller value of $-2\ln\lambda(\widehat{\boldsymbol{\theta}})$ corresponds to better agreement between the data and the hypothesized form of $\boldsymbol{\mu}(\boldsymbol{\theta})$. The value of $-2\ln\lambda(\widehat{\boldsymbol{\theta}})$ can thus be translated into a p-value as a measure of

Int. J. Mod. Phys. A 2026.41. Downloaded from www.worldscientific.com
by UNIVERSITY OF CALIFORNIA @ BERKELEY on 09/16/26. Re-use and distribution is strictly not permitted, except for Open Access articles.

goodness-of-fit, as described in Sec. 40.3.3.1. Provided the model is correct and the same regularity conditions as needed for the asymptotic properties of the MLE are satisified (see Sec. 40.2.2.1), Wilks' theorem [9] states that the minimum of $-2\ln\lambda$, as defined by Eq. (40.19), follows a chi-square distribution (see, *e.g.*, Ref. [8]). If there are N bins and M fitted parameters, then the number of degrees of freedom for the chi-square distribution is $N-M$ if the data are treated as Poisson-distributed, and $N-M-1$ if the n_i are multinomially distributed.

Suppose the n_i are Poisson-distributed and the overall normalization $\mu_{\rm tot}=\sum_i \mu_i$ is taken as an adjustable parameter, so that $\mu_i=\mu_{\rm tot}\,p_i(\boldsymbol{\theta})$, where the probability to be in the ith bin, $p_i(\boldsymbol{\theta})$, does not depend on $\mu_{\rm tot}$. Then by minimizing Eq. (40.19), one obtains that the area under the fitted function is equal to the sum of the histogram contents, *i.e.*, $\sum_i \hat{\mu}_i=\sum_i n_i$. This is a property not possessed by the estimators from the method of least squares (see, *e.g.*, Sec. 40.2.3 and Ref. [10]).

40.2.3 *The method of least squares*

In the special case of a set of N independent measurements y_i at known points x_i where the measurements y_i are assumed to be Gaussian distributed with mean $\mu(x_i;\boldsymbol{\theta})$ and known variance σ_i^2, the method of maximum likelihood assumes a simplified form called *method of least squares* (LS). The log-likelihood function contains the sum of squares

$$\chi^2(\boldsymbol{\theta})=-2\ln L(\boldsymbol{\theta})+\text{ constant }=\sum_{i=1}^{N}\frac{(y_i-\mu(x_i;\boldsymbol{\theta}))^2}{\sigma_i^2}\ . \quad (40.20)$$

The parameter values that maximize L are the same as those which minimize χ^2. This method can also be used to build estimators of the unknown parameters $\boldsymbol{\theta}$ in the more general case where measurements are not necessarily Gaussian distributed.

The minimum of the chi-square function in Eq. (40.20) defines the least-squares estimators $\widehat{\boldsymbol{\theta}}$ for the more general case where the y_i are not Gaussian distributed as long as they are independent. If they are not independent but rather have a covariance matrix $V_{ij}=\text{cov}[\,y_i,y_j\,]$, then the LS estimators are determined by the minimum of

$$\chi^2(\boldsymbol{\theta})=(\boldsymbol{y}-\boldsymbol{\mu}(\boldsymbol{\theta}))^T V^{-1}(\boldsymbol{y}-\boldsymbol{\mu}(\boldsymbol{\theta}))\ , \quad (40.21)$$

where $\boldsymbol{y}=(y_1,\ldots,y_N)$ is the (column) vector of measurements, $\boldsymbol{\mu}(\boldsymbol{\theta})$ is the corresponding vector of predicted values, and the superscript T denotes the transpose. If the y_i are not Gaussian distributed, then the least-squares and maximum-likelihood estimators will not in general coincide.

Often one further restricts the problem to the case where $\mu(x_i;\boldsymbol{\theta})$ is a linear function of the parameters, *i.e.*,

$$\mu(x_i;\boldsymbol{\theta})=\sum_{j=1}^{M}\theta_j h_j(x_i)\ . \quad (40.22)$$

Here the $h_j(x)$ are M linearly independent functions, *e.g.*, $1,x,x^2,\ldots,x^{M-1}$ or Legendre polynomials. We require $M<N$ and at least m of the x_i must be distinct.

Minimizing χ^2 in this case with m parameters reduces to solving a system of M linear equations. Defining $H_{ij}=h_j(x_i)$ and minimizing χ^2 by setting its derivatives with respect to the θ_i equal to zero gives the LS estimators,

$$\widehat{\boldsymbol{\theta}}=(H^TV^{-1}H)^{-1}H^TV^{-1}\boldsymbol{y}\equiv D\boldsymbol{y}\ . \quad (40.23)$$

The covariance matrix for the estimators $U_{ij}=\text{cov}[\,\widehat{\theta}_i,\widehat{\theta}_j\,]$ is given by

$$U=DVD^T=(H^TV^{-1}H)^{-1}\ , \quad (40.24)$$

or equivalently, its inverse U^{-1} can be found from

$$(U^{-1})_{ij}=\frac{1}{2}\frac{\partial^2\chi^2}{\partial\theta_i\partial\theta_j}\bigg|_{\boldsymbol{\theta}=\widehat{\boldsymbol{\theta}}}=\sum_{k,\,l=1}^{N}h_i(x_k)(V^{-1})_{kl}\,h_j(x_l)\ . \quad (40.25)$$

The LS estimators can also be found from the expression

$$\widehat{\boldsymbol{\theta}}=U\boldsymbol{g}\ , \quad (40.26)$$

where the vector $\boldsymbol{g}$ is defined by

$$g_i=\sum_{j,\,k=1}^{N}y_j\,h_i(x_k)(V^{-1})_{jk}\ . \quad (40.27)$$

For the case of uncorrelated y_i, for example, one can use (40.26) with

$$(U^{-1})_{ij}=\sum_{k=1}^{N}\frac{h_i(x_k)h_j(x_k)}{\sigma_k^2}\ , \quad (40.28)$$

$$g_i=\sum_{k=1}^{N}\frac{y_k\,h_i(x_k)}{\sigma_k^2}\ . \quad (40.29)$$

Expanding $\chi^2(\boldsymbol{\theta})$ about $\widehat{\boldsymbol{\theta}}$, one finds that the contour in parameter space defined by

$$\chi^2(\boldsymbol{\theta})=\chi^2(\widehat{\boldsymbol{\theta}})+1=\chi^2_{\rm min}+1 \quad (40.30)$$

has tangent planes located at plus-or-minus-one standard deviation $\sigma_{\widehat{\theta}_i}$ from the LS estimates $\widehat{\theta}_i$ (the relation is approximate if the fit function $\mu(x;\boldsymbol{\theta})$ is nonlinear in the parameters).

In constructing the quantity $\chi^2(\boldsymbol{\theta})$ one requires the variances or, in the case of correlated measurements, the covariance matrix. Often these quantities are not known *a priori* and must be estimated from the data. In this case the least-squares and maximum-likelihood methods are no longer exactly equivalent even for Gaussian distributed measurements. An important example is where the measured value y_i represents the number of entries in a histogram bin. If, for example, y_i represents a Poisson variable, for which the variance is equal to the mean, then one can either estimate the variance from the predicted value, $\mu(x_i;\boldsymbol{\theta})$, or from the observed number itself, y_i. In the first option, the variances become functions of the parameters, and as a result the estimators may need to be found numerically. The second option can be undefined if y_i is zero, and for small y_i, the variance will be poorly estimated. In either case, one should constrain the normalization of the fitted curve to the correct value, *i.e.*, one should determine the area under the fitted curve directly from the number of entries in the histogram (see Ref. [10], Section 7.4). As noted in Sec. 40.2.2.2, this issue is avoided when using the method of extended maximum likelihood with binned data by minimizing Eq. (40.19). In that case if the expected number of entries $\mu_{\rm tot}$ does not depend on the other fitted parameters $\boldsymbol{\theta}$, then its extended MLE is equal to the observed total number of entries.

As the minimum value of the χ^2 represents the level of agreement between the measurements and the fitted function, it can be used for assessing the goodness-of-fit; this is discussed further in Section 40.3.3.1.

40.2.4 *Parameter estimation with constraints*

In some applications one is interested in using a set of measured quantities $\boldsymbol{y}=(y_1,\ldots,y_N)$ to estimate parameters $\boldsymbol{\theta}=(\theta_1,\ldots,\theta_M)$ subject to a number of constraints. For example, one may have measured coordinates from two tracks, and the goal is to estimate their momentum vectors subject to the constraint that the tracks have a common vertex. The parameters can also include momenta of undetected particles such as neutrinos, as long as the constraints from conservation of energy and momentum and from known masses of particles involved in the reaction chain provide enough information for these quantities to be inferred.

A set of K constraints can be given in the form of equations

$$c_k(\boldsymbol{\theta})=0\ ,\quad k=1,\ldots,K\ . \quad (40.31)$$

In some problems it may be possible to define a new set of parameters $\boldsymbol{\eta}=(\eta_1,\ldots,\eta_L)$ with $L=M-K$ such that every point

Phys. A 2026.41. Downloaded from www.worldscientific.com
by UNIVERSITY OF CA LEY on 09/16/26. Re-use and distribution is strictly not permitted, except for Open Access articles.

in $\boldsymbol{\eta}$-space automatically satisfies the constraints. If this is possible then the problem reduces to one of estimating $\boldsymbol{\eta}$ with, *e.g.*, maximum likelihood or least squares and then transforming the estimators back into $\boldsymbol{\theta}$-space.

In many cases it may be difficult or impossible to find an appropriate transformation $\boldsymbol{\eta}(\boldsymbol{\theta})$. Suppose that the parameters are determined by minimizing an objective function such as $\chi^2(\boldsymbol{\theta})$ in the method of least squares. Here one may enforce the constraints by finding the stationary points of the *Lagrange function*

$$\mathcal{L}(\boldsymbol{\theta}, \boldsymbol{\lambda}, \boldsymbol{y}) = \chi^2(\boldsymbol{\theta}, \boldsymbol{y}) + \sum_{k=1}^{K} \lambda_k c_k(\boldsymbol{\theta}) \tag{40.32}$$

with respect to both the parameters $\boldsymbol{\theta}$ and a set of *Lagrange multipliers* $\boldsymbol{\lambda} = (\lambda_1, \ldots, \lambda_K)$. Combining the parameters and Lagrange multipliers into an $(M+K)$-component vector $\boldsymbol{\gamma} = (\theta_1, \ldots, \theta_M, \lambda_1, \ldots, \lambda_K)$, the solutions for $\boldsymbol{\gamma}$, *i.e.*, the estimators $\hat{\boldsymbol{\gamma}}$, are found (*e.g.*, numerically) from the system of equations

$$F_i(\boldsymbol{\gamma}, \boldsymbol{y}) \equiv \frac{\partial \mathcal{L}}{\partial \gamma_i} = 0 \ , \quad i = 1, \ldots, M+K \ . \tag{40.33}$$

To obtain the covariance matrix of the estimated parameters one can find solutions $\tilde{\boldsymbol{\gamma}}$ corresponding to the expectation values of the data $\langle \boldsymbol{y} \rangle$ and expand $F_i(\hat{\boldsymbol{\gamma}}, \boldsymbol{y})$ to first order about these values. This gives (see, e.g., Sec. 11.6 of Ref. [10]) linearized approximations for the estimators, $\hat{\boldsymbol{\gamma}}(\boldsymbol{y}) \approx \tilde{\boldsymbol{\gamma}} + C(\boldsymbol{y} - \langle \boldsymbol{y} \rangle)$, where the matrix $C = -A^{-1}B$, and A and B are given by

$$A_{ij} = \left[\frac{\partial F_i}{\partial \gamma_j} \right]_{\tilde{\boldsymbol{\gamma}}, \langle \boldsymbol{y} \rangle} \quad \text{and} \quad B_{ij} = \left[\frac{\partial F_i}{\partial y_j} \right]_{\tilde{\boldsymbol{\gamma}}, \langle \boldsymbol{y} \rangle} \ . \tag{40.34}$$

In practice the values $\langle \boldsymbol{y} \rangle$ and corresponding solutions $\tilde{\boldsymbol{\gamma}}$ are estimated using the data from the actual measurement. Using this approximation for $\hat{\boldsymbol{\gamma}}(\boldsymbol{y})$, one can find the covariance matrix $U_{ij} = \mathrm{cov}[\,\hat{\gamma}_i, \hat{\gamma}_j\,]$ of the estimators for the γ_i in terms of that of the data $V_{ij} = \mathrm{cov}[\,y_i, y_j\,]$ using error propagation (cf. Eqs. (39.18) and (39.19)),

$$U = CVC^T \ . \tag{40.35}$$

The upper-left $M \times M$ block of the matrix U gives the covariance matrix for the estimated parameters $\mathrm{cov}[\,\hat{\theta}_i, \hat{\theta}_j\,]$. One can show for linear constraints that $\mathrm{cov}[\,\hat{\theta}_i, \hat{\theta}_j\,]$ is also given by the upper-left $M \times M$ block of $2A^{-1}$. If the parameters are estimated using the method of least squares, then the number of degrees of freedom for the distribution of the minimized χ^2 is increased by the number of constraints, *i.e.*, it becomes $N - M + K$. Further details can be found in, *e.g.*, Ch. 8 of Ref. [4] and Ch. 7 of Ref. [11].

40.2.5 *The Bayesian approach*

In the frequentist methods discussed above, probability is associated only with data, not with the value of a parameter. This is not the case in Bayesian statistics, however, which we introduce in this section. For general introductions to Bayesian statistics see, *e.g.*, Refs [12–15].

Suppose the outcome of an experiment is characterized by a vector of data $\boldsymbol{x}$, whose probability distribution depends on an unknown parameter (or parameters) $\boldsymbol{\theta}$ that we wish to determine. In Bayesian statistics, all knowledge about $\boldsymbol{\theta}$ is summarized by the posterior p.d.f. $p(\boldsymbol{\theta}|\boldsymbol{x})$, whose integral over any given region gives the degree of belief for $\boldsymbol{\theta}$ to take on values in that region, given the data $\boldsymbol{x}$. It is obtained by using Bayes' theorem,

$$p(\boldsymbol{\theta}|\boldsymbol{x}) = \frac{P(\boldsymbol{x}|\boldsymbol{\theta})\pi(\boldsymbol{\theta})}{\int P(\boldsymbol{x}|\boldsymbol{\theta}')\pi(\boldsymbol{\theta}')\, d\boldsymbol{\theta}'} \ , \tag{40.36}$$

where $P(\boldsymbol{x}|\boldsymbol{\theta})$ is the likelihood function, *i.e.*, the joint p.d.f. for the data viewed as a function of $\boldsymbol{\theta}$, evaluated with the data actually obtained in the experiment, and $\pi(\boldsymbol{\theta})$ is the prior p.d.f. for $\boldsymbol{\theta}$. Note that the denominator in Eq. (40.36) serves to normalize the posterior p.d.f. to unity.

As it can be difficult to report the full posterior p.d.f. $p(\boldsymbol{\theta}|\boldsymbol{x})$, one would usually summarize it with statistics such as the mean, mode or median value and covariance matrix. In addition one may construct intervals with a given probability content, as is discussed in Sec. 40.4.1 on Bayesian interval estimation.

40.2.5.1 *Priors*

Bayesian statistics supplies no unique rule for determining the prior $\pi(\boldsymbol{\theta})$; this reflects the analyst's subjective degree of belief (or state of knowledge) about $\boldsymbol{\theta}$ before the measurement was carried out. For the result to be of value to the broader community, whose members may not share these beliefs, it is important to carry out a *sensitivity analysis*, that is, to show how the result changes under a reasonable variation of the prior probabilities.

One might like to construct $\pi(\boldsymbol{\theta})$ to represent complete ignorance about the parameters by setting it equal to a constant. A problem here is that if the prior p.d.f. is flat in $\boldsymbol{\theta}$, then it is not flat for a nonlinear function of $\boldsymbol{\theta}$, and so a different parametrization of the problem would lead in general to a non-equivalent posterior p.d.f.

For the special case of a constant prior, one can see from Bayes' theorem (40.36) that the posterior is proportional to the likelihood, and therefore the mode (peak position) of the posterior is equal to the maximum-likelihood estimator. The posterior mode, however, will change in general upon a transformation of parameter. One may use as the Bayesian estimator a summary statistic other than the mode, such as the median, which is invariant under parameter transformation. But this will not in general coincide with the MLE.

The difficult and subjective nature of encoding personal knowledge into priors has led to what is called *objective Bayesian statistics*, where prior probabilities are based not on an actual degree of belief but rather derived from formal rules. These give, for example, priors which are invariant under a transformation of parameters, or ones which result in a maximum gain in information for a given set of measurements. For an extensive review see, *e.g.*, Ref. [16].

Objective priors do not in general reflect degree of belief, but they could in some cases be taken as possible subjective priors. The posterior probabilities as well therefore do not necessarily reflect a degree of belief. However one may regard investigating a variety of objective priors to be an important part of the sensitivity analysis. Furthermore, use of objective priors with Bayes' theorem can be viewed as a recipe for producing estimators or intervals which have desirable frequentist properties.

An important procedure for deriving objective priors is due to Jeffreys. According to *Jeffreys' rule* one takes the prior as

$$\pi(\boldsymbol{\theta}) \propto \sqrt{\det(I(\boldsymbol{\theta}))} \ , \tag{40.37}$$

where $I(\boldsymbol{\theta})$ is the Fisher information matrix from Eq. (40.2). One can show that the Jeffreys prior leads to inference that is invariant under a transformation of parameters. One should note that the Jeffreys prior does not in general correspond to one's degree of belief about the value of a parameter. As examples, the Jeffreys prior for the mean μ of a Gaussian distribution is a constant, and for the mean of a Poisson distribution one finds $\pi(\mu) \propto 1/\sqrt{\mu}$.

Neither the constant nor $1/\sqrt{\mu}$ priors can be normalized to unit area and are therefore said to be *improper*. This can be allowed because the prior always appears multiplied by the likelihood function, and if the likelihood falls to zero sufficiently quickly then one may have a normalizable posterior density.

An important type of objective prior is the reference prior due to Bernardo and Berger [17–19]. To find the reference prior for a given problem one considers the Kullback-Leibler divergence $D_n[\,\pi, p\,]$ of the posterior $p(\boldsymbol{\theta}|\boldsymbol{x})$ relative to a prior $\pi(\boldsymbol{\theta})$, obtained from a set of i.i.d. data $\boldsymbol{x} = (x_1, \ldots, x_n)$:

$$D_n[\,\pi, p\,] = \int p(\boldsymbol{\theta}|\boldsymbol{x}) \ln \frac{p(\boldsymbol{\theta}|\boldsymbol{x})}{\pi(\boldsymbol{\theta})}\, d\boldsymbol{\theta} \ . \tag{40.38}$$

This is effectively a measure of the gain in information provided by the data. The reference prior is chosen so that the expectation value of this information gain is maximized for the limiting case of $n \to \infty$, where the expectation is computed with respect to the marginal distribution of the data,

Int. J. Mod. Phys. A 2026.41. Downloaded from www.worldscientific.com
by UNIVERSITY OF CALIFORNIA @ BERKELEY on 09/16/26. Re-use and distribution is strictly not permitted, except for Open Access articles.

$$p(\boldsymbol{x}) = \int p(\boldsymbol{x}|\boldsymbol{\theta})\pi(\boldsymbol{\theta})\, d\boldsymbol{\theta} \; . \tag{40.39}$$

For a single, continuous parameter the reference prior is usually identical to the Jeffreys prior. In the multiparameter case an iterative algorithm exists, which requires sorting the parameters by order of inferential importance. Often the result does not depend on this order, but when it does, this can be part of a sensitivity analysis. Further discussion and applications to particle physics problems can be found in Ref. [20].

40.2.6 *Nuisance parameters*

Suppose we want to determine the values of parameters $\boldsymbol{\theta}$ using a set of measurements $\boldsymbol{x}$ described by a probability model $P(\boldsymbol{x}|\boldsymbol{\theta})$. In general the model is not perfect, which is to say it cannot provide an accurate description of the data even at the most optimal point of its parameter space. As a result, the estimated parameters can have a systematic bias.

One can improve the model by including in it additional parameters. That is, $P(\boldsymbol{x}|\boldsymbol{\theta})$ is replaced by a more general model $P(\boldsymbol{x}|\boldsymbol{\theta},\boldsymbol{\nu})$, which depends on parameters of interest $\boldsymbol{\theta}$ and *nuisance parameters* $\boldsymbol{\nu}$. The additional parameters are not of intrinsic interest but must be included for the model to be sufficiently accurate for some point in the enlarged parameter space.

40.2.6.1 *Frequentist treatment of nuisance parameters*

Although including additional parameters may eliminate or at least reduce the effect of systematic uncertainties, their presence will result in increased statistical uncertainties for the parameters of interest. This occurs because the estimators for the nuisance parameters and those of interest will in general be correlated, which results in an enlargement of the contour defined by Eq. (40.13).

To reduce the impact of the nuisance parameters one often tries to constrain their values by means of control or calibration measurements, say, having data $\boldsymbol{y}$. For example, some components of $\boldsymbol{y}$ could represent estimates of the nuisance parameters, often from separate experiments. Suppose the measurements $\boldsymbol{y}$ are statistically independent from $\boldsymbol{x}$ and are described by a model $P(\boldsymbol{y}|\boldsymbol{\nu})$. The joint model for both $\boldsymbol{x}$ and $\boldsymbol{y}$ is in this case therefore the product of the probabilities for $\boldsymbol{x}$ and $\boldsymbol{y}$, and thus the likelihood function for the full set of parameters is

$$L(\boldsymbol{\theta},\boldsymbol{\nu}) = P(\boldsymbol{x}|\boldsymbol{\theta},\boldsymbol{\nu})P(\boldsymbol{y}|\boldsymbol{\nu}) \; . \tag{40.40}$$

Note that in this case if one wants to simulate the experiment by means of Monte Carlo, both the primary and control measurements, $\boldsymbol{x}$ and $\boldsymbol{y}$, must be generated for each repetition under assumption of fixed values for the parameters $\boldsymbol{\theta}$ and $\boldsymbol{\nu}$.

Using all of the parameters $(\boldsymbol{\theta},\boldsymbol{\nu})$ in Eq. (40.13) to find the statistical errors in the parameters of interest $\boldsymbol{\theta}$ is equivalent to using the *profile likelihood*, which depends only on $\boldsymbol{\theta}$. It is defined as

$$L_{\rm p}(\boldsymbol{\theta}) = L(\boldsymbol{\theta},\widehat{\widehat{\boldsymbol{\nu}}}(\boldsymbol{\theta})), \tag{40.41}$$

where the double-hat notation indicates the profiled values of the parameters $\boldsymbol{\nu}$, defined as the values that maximize L for the specified $\boldsymbol{\theta}$. The profile likelihood is discussed further in Section 40.3.2.1 in connection with hypothesis tests.

40.2.6.2 *Bayesian treatment of nuisance parameters*

As discussed in Sec. 40.2.2, a model may depend on parameters of interest $\boldsymbol{\theta}$ as well as on nuisance parameters $\boldsymbol{\nu}$, which must be included for an accurate description of the data. Knowledge about the values of $\boldsymbol{\nu}$ may be supplied by control measurements, theoretical insights, physical constraints, etc. Suppose, for example, one has data $\boldsymbol{y}$ from a control measurement which is characterized by a probability $p(\boldsymbol{y}|\boldsymbol{\nu})$. Suppose further that before carrying out the control measurement one's state of knowledge about $\boldsymbol{\nu}$ is described by an initial prior $\pi_0(\boldsymbol{\nu})$, which in practice is often taken to be a constant or in any case very broad. By using Bayes' theorem (40.1) one obtains the updated prior $\pi(\boldsymbol{\nu})$ (*i.e.*, now $\pi(\boldsymbol{\nu}) = \pi(\boldsymbol{\nu}|\boldsymbol{y})$, the probability for $\boldsymbol{\nu}$ given $\boldsymbol{y}$),

$$\pi(\boldsymbol{\nu}|\boldsymbol{y}) \propto p(\boldsymbol{y}|\boldsymbol{\nu})\pi_0(\boldsymbol{\nu}) \; . \tag{40.42}$$

In the absence of a model for $P(\boldsymbol{y}|\boldsymbol{\nu})$ one may make some reasonable but *ad hoc* choices in order to approximate $\pi(\boldsymbol{\nu})$. For a single nuisance parameter ν, for example, one might characterize the uncertainty by a p.d.f. $\pi(\nu)$ centered about its nominal value with a certain standard deviation σ_ν. Often a Gaussian p.d.f. provides a reasonable model for one's degree of belief about a nuisance parameter; in other cases, more complicated shapes may be appropriate. If, for example, the parameter represents a non-negative quantity then a log-normal or gamma p.d.f. can be a more natural choice than a Gaussian truncated at zero. Note also that truncation of the prior of a nuisance parameter ν at zero will in general make $\pi(\nu)$ nonzero at $\nu = 0$, which can lead to an unnormalizable posterior for a parameter of interest that appears multiplied by ν.

The likelihood function, prior, and posterior p.d.f.s all depend on both $\boldsymbol{\theta}$ and $\boldsymbol{\nu}$, and are related by Bayes' theorem, as usual. Note that the likelihood here only refers to the primary measurement $\boldsymbol{x}$. Once any control measurements $\boldsymbol{y}$ are used to find the updated prior $\pi(\boldsymbol{\nu})$ for the nuisance parameters, this information is fully encapsulated in $\pi(\boldsymbol{\nu})$ and the control measurements do not appear further.

One can obtain the posterior p.d.f. for $\boldsymbol{\theta}$ alone by integrating over the nuisance parameters, *i.e.*,

$$p(\boldsymbol{\theta}|\boldsymbol{x}) = \int p(\boldsymbol{\theta},\boldsymbol{\nu}|\boldsymbol{x})\, d\boldsymbol{\nu} \; . \tag{40.43}$$

Such integrals can often not be carried out in closed form, and if the number of nuisance parameters is large, then they can be difficult to compute with standard Monte Carlo methods. *Markov Chain Monte Carlo* (MCMC) techniques are often used for computing integrals of this type (see Sec. 42.6).

40.2.7 *Unfolding*

An important class of parameter estimation problem involves measurement of the differential distribution of a kinematic variable in the form of a histogram with N bins. The data thus consist of the vector of measured data values $\boldsymbol{n} = (n_1, \ldots n_N)$, with expectation values $\nu_i = E[\, n_i \,]$. The n_i are usually independent and often modeled as Poisson distributed, from which it follows that the maximum-likelihood estimators are $\hat{\nu}_i = n_i$ for all i.

Because of the limited acceptance and resolution of the experiment, however, the measured values of the kinematic variable in question differ in general from their true values, and as a consequence the form of the data histogram is distorted relative to what would be obtained with perfect resolution. The desired parameters are not, therefore, the ν_i but rather one wants to estimate the expected number of entries in a given bin that would be found with a perfect detector. We call this the "true histogram" and denote it with $\boldsymbol{\mu} = (\mu_1, \ldots, \mu_M)$, where the number of bins M is not required to equal that of the observed histogram. The μ_i are related to the expected numbers of entries in the observed histogram by

$$\nu_i = \sum_{j=1}^{M} R_{ij}\mu_j + \beta_i \; , \tag{40.44}$$

where β_i here represents the expected number of entries in bin i due to background processes and the $N \times M$ *response matrix* R_{ij} gives the probability for an event to be observed in bin i of $\boldsymbol{\nu}$ given that the true value of the variable was in bin j of $\boldsymbol{\mu}$. For purposes of this discussion let us suppose that the response matrix and expected background values are known. There are two main approaches to this type of problem, which we can call *unfolding* and *folding*.

In unfolding, one treats the true histogram $\boldsymbol{\mu}$ as the parameters of interest. The result is thus given by estimators $\hat{\boldsymbol{\mu}}$ and the corresponding covariance matrix $U_{ij} = \mathrm{cov}[\, \hat{\mu}_i, \hat{\mu}_j \,]$. Provided the response matrix can be inverted, the maximum-likelihood solution is easily found as $\hat{\boldsymbol{\mu}} = R^{-1}(\boldsymbol{n} - \boldsymbol{\beta})$. If the response matrix allows for significant migration of entries between bins, then the variances of these estimators can be very large, sometimes to the point where the $\hat{\boldsymbol{\mu}}$ bear essentially no resemblance to the true

by UNIVERSITY OF CA Phys. A 2026.41. Downloaded from www.worldscientific.com LEY on 09/16/26. Re-use and distribution is strictly not permitted, except for Open Access articles.

$\boldsymbol{\mu}$. In such cases the estimators can be found by maximizing a linear combination of the log-likelihood and a regularization function that imposes some degree of smoothness on the unfolded distribution. In achieving a reduction in variance one inevitably introduces some bias into the estimators.

In the approach of folding, by contrast, to test a given model prediction for the true histogram $\boldsymbol{\mu}$ it is first "folded" with the response matrix and corrected for expected background to give the corresponding $\boldsymbol{\nu}$ according to Eq. (40.44), and these are compared to the corresponding $\boldsymbol{n}$ using, e.g., a likelihood ratio as shown in Sec. 40.2.2.2. In this way, one avoids any bias due to regularization.

To account for systematic uncertainties, the response matrix and background values may not be expressed as constants but rather as functions of nuisance parameters $\boldsymbol{\theta}$. These may be constrained by auxiliary measurements $\boldsymbol{u}$ with p.d.f. $p(\boldsymbol{u}|\boldsymbol{\theta})$ so that the full likelihood becomes (as in Eq. (40.40) but with different notation)

$$L(\boldsymbol{\mu}, \boldsymbol{\theta}) = P(\boldsymbol{n}|\boldsymbol{\nu}(\boldsymbol{\mu}, \boldsymbol{\theta}))\, p(\boldsymbol{u}|\boldsymbol{\theta}) \; . \tag{40.45}$$

Here the mean values $\boldsymbol{\nu} = R(\boldsymbol{\theta})\boldsymbol{\mu} + \boldsymbol{\beta}(\boldsymbol{\theta})$ now depend on both the true histogram parameters $\boldsymbol{\mu}$ as well as the nuisance parameters $\boldsymbol{\theta}$. Thus to record enough information for a future analysis using folding one must provide all of the ingredients used above: the primary data $\boldsymbol{n}$, the auxiliary measurements $\boldsymbol{u}$, and also the response matrix $R(\boldsymbol{\theta})$ and expected backgrounds $\boldsymbol{\beta}(\boldsymbol{\theta})$ as functions of the nuisance parameters. If unfolding is used, then future model tests or comparisons with other experiments can be carried out directly using the estimators $\hat{\boldsymbol{\mu}}$ and their covariance matrix.

If several distributions are unfolded, then to combine these in a test of a given model one should know how estimators for bins of different distributions are correlated, as can arise, e.g., through common systematic effects. If only the unfolded distributions and their separate covariance matrices are reported, however, then information on such correlations is not retained. In folding, one can include information on correlated systematic effects if the ingredients (R and $\boldsymbol{\beta}$) are known in terms of nuisance parameters that are common to different distributions.

In unfolding, the estimators for $\boldsymbol{\mu}$ can be constructed either by maximizing the log-likelihood using Eq. (40.45) or in the case where regularization is required one can maximize $\varphi(\boldsymbol{\mu}, \boldsymbol{\theta}) = \ln L(\boldsymbol{\mu}, \boldsymbol{\theta}) + \tau S(\boldsymbol{\mu})$, where the *regularization function* $S(\boldsymbol{\mu})$ reflects the smoothness of the true histogram and serves to reduce the variances of the estimators. Possible functions are based on the mean squared second derivative (a commonly used type of Tikhonov regularization) or the entropy of the true histogram. The parameter τ fixes the relative weighting of the log-likelihood and the regularization function and thus determines the balance between the bias and variance of the resulting estimators. Further discussion of the unfolding problem including methods for choosing the regularization function and parameter, as well as techniques that employ other types of regularization such as the iterative Bayes (Richardson-Lucy) method, can be found in Refs. [10, 11, 21, 22] and references therein.

40.3 Statistical tests

In addition to estimating parameters, one often wants to assess the validity of certain statements concerning the data's underlying distribution. Frequentist *hypothesis tests*, described in Sec. 40.3.1, provide a rule for accepting or rejecting hypotheses depending on the outcome of a measurement. In *significance tests*, covered in Sec. 40.3.2, one gives the probability to obtain a level of incompatibility with a certain hypothesis that is greater than or equal to the level observed with the actual data. Goodness-of-fit tests that quantify the general level of compatibility between data and a hypothesis are described in Sec. 40.3.3. In the Bayesian approach, the corresponding procedure is based fundamentally on the posterior probabilities of the competing hypotheses. In Sec. 40.3.4 we describe a related construct called the Bayes factor, which can be used to quantify the degree to which the data prefer one or another hypothesis.

40.3.1 *Hypothesis tests*

A frequentist *test* of a hypothesis (often called the null hypothesis, H_0) is a rule that states for which data values $\boldsymbol{x}$ the hypothesis is rejected. A region of $\boldsymbol{x}$-space called the critical region, w, is specified such that there is no more than a given probability under H_0, α, called the *size* or *significance level* of the test, to find $\boldsymbol{x} \in w$. If the data are discrete, it may not be possible to find a critical region with exact probability content α, and thus we require $P(\boldsymbol{x} \in w|H_0) \leq \alpha$. If the data are observed in the critical region, H_0 is rejected.

The data $\boldsymbol{x}$ used to construct a test could be, for example, a set of values that characterizes an individual event. In this case the test corresponds to classification as, *e.g.*, signal or background. Alternatively the data could represent a set of values from a collection of events. Often one is interested in knowing whether all of the events are of a certain type (background), or whether the sample contains at least some events of a new type (signal). Here the background-only hypothesis plays the role of H_0, and in the alternative H_1 both signal and background are present. Rejecting H_0 is, from the standpoint of frequentist statistics, the required step to establish discovery of the signal process.

The choice of the critical region is not unique. Its choice should take into account the probabilities for the data predicted by some alternative hypothesis (or set of alternatives) H_1. Rejecting H_0 if it is true is called a *type-I error*, and occurs by construction with probability no greater than α. Not rejecting H_0 if an alternative H_1 is true is called a *type-II error*, and for a given test this will have a certain probability $\beta = P(\boldsymbol{x} \notin w|H_1)$. The quantity $1 - \beta$ is called the *power* of the test of H_0 with respect to the alternative H_1. A strategy for defining the critical region can therefore be to maximize the power with respect to some alternative (or alternatives) given a fixed size α.

To maximize the power of a test of fixed size α of H_0 with respect to the alternative H_1, the *Neyman–Pearson lemma* states that the critical region w should be chosen such that for all data values $\boldsymbol{x}$ inside w, the likelihood ratio

$$\lambda(\boldsymbol{x}) = \frac{f(\boldsymbol{x}|H_1)}{f(\boldsymbol{x}|H_0)} \tag{40.46}$$

is greater than or equal to a given constant c_α, and everywhere outside the critical region one has $\lambda(\boldsymbol{x}) < c_\alpha$, where the value of c_α is determined by the size of the test α. The hypotheses H_0 and H_1 must be simple, *i.e.*, they should not contain undetermined parameters.

It is convenient to define the test using a scalar function of the data $\boldsymbol{x}$ called a *test statistic*, $t(\boldsymbol{x})$, such that the boundary of the critical region is given by a surface of constant $t(\boldsymbol{x})$. The Neyman–Pearson lemma is equivalent to the statement that the likelihood ratio (40.46) represents the optimal test statistic. It can be difficult in practice, however, to determine $\lambda(\boldsymbol{x})$, since this requires knowledge of the joint p.d.f.s $f(\boldsymbol{x}|H_0)$ and $f(\boldsymbol{x}|H_1)$. Often one does not have explicit formulae for these, but rather Monte Carlo models that allow one to generate instances of $\boldsymbol{x}$ that follow the p.d.f.s.

In the case where the likelihood ratio (40.46) cannot be used explicitly, there exist a variety of other multivariate methods for constructing a test statistic that may approach its performance. These are based on machine-learning algorithms that use samples of *training data* corresponding to the hypotheses in question, often generated from Monte Carlo models. Further information on Machine Learning can be found in Sec. 41 of this Review.

The multivariate algorithms designed to classify events into signal and background types also form the basis of tests of the hypothesis that a sample of events consists of background only. Such a test can be constructed using the distributions of the test statistic $t(\boldsymbol{x})$ for event classification obtained from a multivariate algorithm such as a Neural Network output. The distributions $p(t|s)$ and $p(t|b)$ for signal and background events, respectively, are used to construct the likelihood ratio of the signal-plus-background hypothesis relative to that of background only. To the extent that the test statistic $t(\boldsymbol{x})$ approximates the likelihood ratio (or a monotonic function thereof) for individual events given by (40.46), the resulting test of the background-only hypothesis for the event

Int. J. Mod. Phys. A 2026.41. Downloaded from www.worldscientific.com
by UNIVERSITY OF CALIFORNIA @ BERKELEY on 09/16/26. Re-use and distribution is strictly not permitted, except for Open Access articles.

sample will have maximum power with respect to the signal-plus-background alternative (see Ref. [23]).

40.3.2 *Tests of significance, p-values*

A frequentist *significance test* allows one to assign a numerical value, called the p-value, that reflects the level of agreement between a hypothesis H_0 and the observed data $\boldsymbol{x}$. To carry out a significance test one must specify a subset of the data space, whose boundary includes the observed data point $\boldsymbol{x}_{\rm obs}$, that is deemed to have equal or lesser compatibility with H_0 relative to $\boldsymbol{x}_{\rm obs}$. The p-value of H_0 is the probability, assuming data distributed according to H_0, to find $\boldsymbol{x}$ in the region of equal or lesser compatibility.

For continuous data, one can show that the p-value of H_0, here called p_0, follows a uniform distribution for data generated under H_0. Therefore, one has $P(p_0 \leq \alpha|H_0) = \alpha$ for any constant α in $[0,1]$. In this way the region of data space where $p_0 \leq \alpha$ gives a critical region w of a test of size α, as it satisfies $P(\boldsymbol{x} \in w|H_0) \leq \alpha$. Thus rejecting H_0 if $p_0 \leq \alpha$ is equivalent to the hypothesis test of Sec. 40.3.1 above. For the critical region w defined by $p_0 \leq \alpha$ one can find the power $P(\boldsymbol{x} \in w|H_1)$ with respect to an alternative hypothesis H_1, as defined in Sec. 40.3.1. In general the region of low compatibility with H_0 is defined so as to have a high probability for data generated under H_1, so that the distribution of p_0, assuming data $\boldsymbol{x}$ that follows H_1, will be concentrated at low values, and the critical region w derived from $p_0 \leq \alpha$ will have a high power with respect to H_1.

Similar to construction of a test's critical region in Sec. 40.3.1, finding the p-value is generally done by defining a statistic $t(\boldsymbol{x})$ whose value corresponds to better or worse levels of agreement with the hypothesis. The hypothesis being tested, H_0, will determine the p.d.f. $f(t|H_0)$ for the statistic. If, for example, t is defined such that large values correspond to poor agreement with the hypothesis, then the p-value is

$$p = \int_{t_{\rm obs}}^{\infty} f(t|H_0)\, dt \ , \tag{40.47}$$

where $t_{\rm obs} = t(\boldsymbol{x}_{\rm obs})$ is the value of the statistic obtained in the actual experiment.

Note that the p-value is not the probability of the hypothesis, which in frequentist statistics is not defined. The p-value should also not be confused with the size of a test, or the confidence level of a confidence interval (Section 40.4), both of which are pre-specified constants.

When searching for a new phenomenon, one tries to reject the hypothesis H_0 that the data are consistent with known (*e.g.*, Standard Model) processes. If the p-value of H_0 is sufficiently low, then one is willing to accept that some alternative hypothesis is true. Often one converts the p-value into an effective significance Z, defined as an equivalent number of standard deviations of a Gaussian distributed random variable. In a search for an intrinsically positive signal, *i.e.*, where only upward fluctuations of the estimated rate appear signal like, this is defined as

$$Z = \Phi^{-1}(1-p) \ . \tag{40.48}$$

Here Φ is the cumulative distribution of the standard Gaussian, and Φ^{-1} is its inverse (quantile) function. In this way, a p-value of $1/2$ gives $Z = 0$, *i.e.*, having an estimated signal rate of zero corresponds to zero significance. Under assumption of H_0, the p-value is uniformly distributed in $[0,1]$ and Z follows $\varphi(Z)$, the standard (zero mean and unit variance) Gaussian. If either positive or negative data fluctuations would indicate evidence of the signal, then one defines

$$Z = \Phi^{-1}(1-p/2) \ . \tag{40.49}$$

In this case an estimated signal rate of zero gives $p = 1$ and $Z = 0$. The p.d.f. of Z is $2\varphi(Z)$ for $Z \geq 0$.

Often in particle physics the level of significance where an effect is said to qualify as a discovery is $Z = 5$, *i.e.*, a 5σ effect, corresponding to a p-value of 2.87×10^{-7}. One's actual degree of belief that a new process is present, however, will depend in general on other factors as well, such as the plausibility of the new signal hypothesis and the degree to which it can describe the data, one's confidence in the model that led to the observed p-value, and possible corrections for multiple observations out of which one focuses on the smallest p-value obtained (the "look-elsewhere effect", discussed in Section 40.3.2.2).

40.3.2.1 *Frequentist treatment of nuisance parameters and asymptotic methods for tests*

Suppose one wants to test hypothetical values of parameters $\boldsymbol{\theta}$, but the model also contains nuisance parameters $\boldsymbol{\nu}$. To find a p-value for $\boldsymbol{\theta}$ we can construct a test statistic $q_{\boldsymbol{\theta}}$ such that larger values constitute increasing incompatibility between the data and the hypothesis. Then for an observed value of the statistic $q_{\boldsymbol{\theta},\rm obs}$, the p-value of $\boldsymbol{\theta}$ is

$$p_{\boldsymbol{\theta}}(\boldsymbol{\nu}) = \int_{q_{\boldsymbol{\theta},\rm obs}}^{\infty} f(q_{\boldsymbol{\theta}}|\boldsymbol{\theta},\boldsymbol{\nu})\, dq_{\boldsymbol{\theta}} \ , \tag{40.50}$$

which depends in general on the nuisance parameters $\boldsymbol{\nu}$. In the strict frequentist approach, $\boldsymbol{\theta}$ is rejected only if the p-value is less than α for all possible values of the nuisance parameters.

The test of $\boldsymbol{\theta}$ becomes easy to carry out if we can define the test statistic $q_{\boldsymbol{\theta}}$ such that its distribution $f(q_{\boldsymbol{\theta}}|\boldsymbol{\theta})$ is known and is independent of the nuisance parameters. Although exact independence is only found in special cases, it can be achieved approximately by using the *profile likelihood ratio*. This is given by the profile likelihood from Eq.(40.41) divided by the value of the likelihood at its maximum, *i.e.*, when evaluated with the maximum-likelihood estimators $\widehat{\boldsymbol{\theta}}$ and $\widehat{\boldsymbol{\nu}}$:

$$\lambda_p(\boldsymbol{\theta}) = \frac{L(\boldsymbol{\theta}, \widehat{\widehat{\boldsymbol{\nu}}}(\boldsymbol{\theta}))}{L(\widehat{\boldsymbol{\theta}}, \widehat{\boldsymbol{\nu}})} \ . \tag{40.51}$$

In the large-sample limit and assuming the same regularity conditions needed for the asymptotic properties of the MLE (cf. Sec. 40.2.2.1), Wilks' theorem [9] states that the distribution of $q_{\boldsymbol{\theta}} = -2\ln\lambda_{\rm p}(\boldsymbol{\theta})$, under assumption of $\boldsymbol{\theta}$, approaches a chi-square distribution where the number of degrees of freedom is equal to M, the number of components of $\boldsymbol{\theta}$. More details on use of the profile likelihood are given in Refs. [24–26] and in contributions to the PHYSTAT conferences [27]; explicit formulae for special cases can be found in Ref. [28, 29]. Further discussion on how to incorporate systematic uncertainties into p-values can be found in Ref. [30].

Even with use of the profile likelihood ratio, for a finite data sample, the p-value of hypothesized parameters $\boldsymbol{\theta}$ will retain in general some dependence on the nuisance parameters $\boldsymbol{\nu}$. Ideally one would find the the maximum of $p_\theta(\boldsymbol{\nu})$ from Eq. (40.50) explicitly, but that is often impractical. An approximate and computationally feasible technique is to use $p_\theta(\widehat{\widehat{\boldsymbol{\nu}}}(\theta))$, where $\widehat{\widehat{\boldsymbol{\nu}}}(\theta)$ are the profiled values of the nuisance parameters as defined in Section 40.2.6.1. The resulting p-value is correct if the true values of the nuisance parameters are equal to the profiled values used; otherwise it could be either too high or too low. This is discussed further in Section 40.4.2 on confidence intervals.

The methods above based on the profile likelihood ratio are useful in practice because, provided one has a sufficiently large data sample, the distributions of the test statistics are related through Wilks' theorem to the chi-square distribution. If the data sample is not large enough to justify use of the asymptotic formulae, then some adjustments can be made to the test statistics so that their distributions are better approximated by the asymptotic ones; these improvements go under the general name of "higher-order asymptotics", which are discussed briefly below. Using these methods one may obtain p-values using the asymptotic formulae even for smaller data samples, avoiding costly Monte Carlo simulation to find distributions of test statistics.

The chi-square distribution for the profile likelihood ratio relies on having a Gaussian distribution for estimators of the model's parameters. An important type of corrected statistic relies on an improved distribution for the maximum-likelihood estimator due to Barndorff–Nielsen [31] (the p^* approximation). Another class

Phys. A 2026.41. Downloaded from www.worldscientific.com by UNIVERSITY OF CALIFORNIA BERKELEY on 09/16/26. Re-use and distribution is strictly not permitted, except for Open Access articles.

of improved statistic due to Bartlett [32,33] starts with a statistic t which, asymptotically, should be chi-square distributed with $n_{\rm d}$ degrees of freedom. A new statistic is defined as $t' = t\, n_{\rm d}/E[\,t\,]$, which by construction has mean $E[\,t'\,] = n_{\rm d}$, as for the chi-square distribution. Further details and applications of these methods are described in Refs. [34, 35].

One may also treat model uncertainties in a Bayesian manner but then use the resulting model in a frequentist test. Suppose the uncertainty in a set of nuisance parameters $\boldsymbol{\nu}$ is characterized by a Bayesian prior p.d.f. $\pi(\boldsymbol{\nu})$. This can be used to construct the marginal (also called the prior predictive) model for the data $\boldsymbol{x}$ and parameters of interest $\boldsymbol{\theta}$,

$$P_{\rm m}(\boldsymbol{x}|\boldsymbol{\theta}) = \int P(\boldsymbol{x}|\boldsymbol{\theta},\boldsymbol{\nu})\pi(\boldsymbol{\nu})\, d\boldsymbol{\nu}\ . \tag{40.52}$$

The marginal model does not represent the probability of data that would be generated if one were really to repeat the experiment, as in that case one would assume that the nuisance parameters do not vary. Rather, the marginal model represents a situation in which every repetition of the experiment is carried out with new values of $\boldsymbol{\nu}$, randomly sampled from $\pi(\boldsymbol{\nu})$. It is in effect an average of models each with a given $\boldsymbol{\nu}$, where the average is carried out with respect to the prior p.d.f. $\pi(\boldsymbol{\nu})$.

The marginal model for the data $\boldsymbol{x}$ can be used to determine the distribution of a test statistic Q, which can be written

$$P_{\rm m}(Q|\boldsymbol{\theta}) = \int P(Q|\boldsymbol{\theta},\boldsymbol{\nu})\pi(\boldsymbol{\nu})\, d\boldsymbol{\nu}\ . \tag{40.53}$$

In a search for a new signal process, the test statistic can be based on the ratio of likelihoods corresponding to the experiments where signal and background events are both present, L_{s+b}, to that of background only, L_b. Often the likelihoods are evaluated with the profiled values of the nuisance parameters, which may give improved performance. It is important to note, however, that it is through use of the marginal model for the distribution of Q that the uncertainties related to the nuisance parameters are incorporated into the result of the test. Different choices for the test statistic itself only result in variations of the power of the test with respect to different alternatives. Studies of marginalization versus profiling of nuisance parameters and the effects on coverage for specific problems, e.g., related to a Poisson counting experiment, can be found in Refs. [36, 37].

40.3.2.2 *The look-elsewhere effect*

The "look-elsewhere effect" relates to multiple measurements used to test a single hypothesis. The classic example is when one searches in a distribution for a peak whose position is not predicted in advance. Here the no-peak hypothesis is tested using data in a given range of the distribution. In the frequentist approach the correct p-value of the no-peak hypothesis is the probability, assuming background only, to find a signal as significant as the one found or more so anywhere in the search region. This can be substantially higher than the probability to find a peak of equal or greater significance in the particular place where it appeared. There is in general some ambiguity as to what constitutes the relevant search region or even the broader set of relevant measurements. Although the desired p-value is well defined once the search region has been fixed, an exact treatment can require extensive computation.

The "brute-force" solution to this problem by Monte Carlo involves generating data under the background-only hypothesis and for each data set, fitting a peak of unknown position and recording a measure of its significance. To establish a discovery one often requires a p-value smaller than 2.87×10^{-7}, corresponding to a 5σ or larger effect. Determining this with Monte Carlo thus requires generating and fitting a very large number of experiments, perhaps several times 10^7. In contrast, if the position of the peak is fixed, then the fit to the distribution is much easier, and furthermore one can in many cases use formulae valid for sufficiently large samples that bypass completely the need for Monte Carlo (see, *e.g.*, Ref. [28, 29]). However, this fixed-position or "local" p-value would not be correct in general, as it assumes the position of the peak was known in advance.

A method that allows one to modify the local p-value computed under assumption of a fixed position to obtain an approximation to the correct "global" value using a relatively simple calculation is described in Ref. [38]. Suppose a model contains a nuisance parameter such as the peak position that is only defined under the signal model (there is no peak in the background-only model). Furthermore, suppose a test statistic q_0 is defined using the profile likelihood ratio, so that by Wilks' theorem it would be asymptotically chi-square distributed if the peak position were to be fixed. The asymptotic distribution no longer holds if the peak position is adjustable, however, as this violates the regularity conditions of Wilks' theorem. If the statistic has an observed value u, then an approximation for the global p-value is found to be

$$p_{\rm global} \approx p_{\rm local} + \langle N_u \rangle\ , \tag{40.54}$$

where $\langle N_u \rangle$, which is much smaller than one in cases of interest, is the mean number of "upcrossings" (as defined in Ref. [38]) of the statistic q_0 above the level u in the range of the nuisance parameter considered (*e.g.*, the mass range). The value of $\langle N_u \rangle$ can be estimated from the number of upcrossings $\langle N_{u_0} \rangle$ above some much lower value, u_0, by using a relation due to Davis [39],

$$\langle N_u \rangle \approx \langle N_{u_0} \rangle\, e^{-(u-u_0)/2}\ . \tag{40.55}$$

By choosing u_0 sufficiently low, the value of $\langle N_u \rangle$ can be estimated by simulating only a very small number of experiments, or even from the observed data, rather than of the order 10^7 needed if one is dealing with a 5σ effect.

In some cases, more than one parameter is determined from data. For instance, when both the mass and the width of a particle are fitted from a spectrum. In those cases, the number of upcrossing can be generalized by the Euler characteristic $\varphi(u)$, equal to the number of disconnected components minus the number of "holes" in the multidimensional set of the parameter space defined by $q_0(\boldsymbol{\theta}) > u$ [40], which reduces to N_u for one fitted parameter. For instance, when two parameters are determined from a one-dimensional spectrum, the scaling law in Eq. (40.55) can be extended as

$$\langle \varphi(u) \rangle = 1 - F_{\chi^2_1}(u) + (N_1 + N_2\sqrt{u}\,)e^{-u/2}\ , \tag{40.56}$$

where N_1 and N_2 can be evaluated using two convenient values for u. In the above equation, $F_{\chi^2_M}$ denotes the cumulative chi-square distribution for M degrees of freedom, M is equal to one in this case.

40.3.3 *Goodness of fit*

At times one wants to quantify the level of agreement between the data $\boldsymbol{x}$ and a hypothesis H_0 without explicit reference to alternative hypotheses. In the frequentist approach this is done using a *goodness-of-fit test*. The result is quantified with a p-value, in general obtained from a statistic $t(\boldsymbol{x})$ as done in Sec. 40.3.2 with a significance test. Here, however, the *goodness-of-fit statistic* is defined using general considerations of what constitutes greater or lesser compatibility between data and hypothesis and not with reference to alternative hypotheses or power. Nevertheless, for a given statistic $t(\boldsymbol{x})$, the power of the resulting test with respect to an alternative can be found, so that types of alternatives to which one is sensitive (*i.e.*, to which the test has high power) can be investigated.

The Neyman–Pearson lemma (see Sec. 40.3.1) states that a test of H_0 that has maximum power with respect to an alternative H_1 should be based on a statistic that is monotonic in the likelihood ratio $P(\boldsymbol{x}|H_1)/P(\boldsymbol{x}|H_0)$. Therefore, a goodness-of-fit statistic derived without reference to a specific H_1 will not in general attain this maximum power. And even if a given $t(\boldsymbol{x})$ happens to be optimal or nearly so for some alternative H_1, there may be other relevant alternatives for which its power is lower. In practice, goodness-of-fit statistics are defined so as to provide sensitivity to a broad class of alternatives, e.g., those that differ in the location of the bulk of the distribution's probability or the distribution's

Int. J. Mod. Phys. A 2026.41. Downloaded from www.worldscientific.com
by UNIVERSITY OF CALIFORNIA @ BERKELEY on 09/16/26. Re-use and distribution is strictly not permitted, except for Open Access articles.

width or the nature of the tails. It may therefore be useful to use several goodness-of-fit tests that are sensitive to different aspects of the data distribution in question.

The most important application of goodness-of-fit tests is no doubt in conjunction with the method of least squares, which we describe in Sec. 40.3.3.1 below. Other types of tests, particularly those based on the *empirical distribution function* are described in Sec. 40.3.3.2. Further discussion of goodness of fit can be found in Refs. [4, 41] and references therein.

40.3.3.1 *Goodness-of-fit with chi-square or likelihood ratio*

An important type of goodness-of-fit test arises when a set of measurements $\boldsymbol{y} = (y_1, \ldots, y_N)$ are used to test the hypothesis that the values are Gaussian distributed with given mean values $E[\,y_i\,] = \mu_i$ and variances $V[\,y_i\,] = \sigma_i^2$ (or covariance $V_{ij} = \mathrm{cov}[\,y_i, y_j\,]$ if the values are correlated). The general procedures also hold when the data are Poisson or multinomially distributed with sufficiently large mean values so that the Gaussian represents an adequate approximation. The Gaussian hypothesis may be simple (all parameters fully specified), or the mean values μ_i may be given as functions of some other parameters $\boldsymbol{\theta} = (\theta_1, \ldots, \theta_M)$, with $M < N$. The (co)variances are treated as fixed.

The test statistic derived from the likelihood ratio has already been introduced in Sec. 40.2.3 in connection with the method of least squares, and is given by the minimum of the function $\chi^2(\boldsymbol{\theta})$ with respect to $\boldsymbol{\theta}$, i.e., $t = \chi^2_{\min} = \chi^2(\hat{\boldsymbol{\theta}})$, *e.g.*, in the case of uncorrelated measurements

$$t = \sum_{i=1}^{N} \frac{(y_i - \mu_i(\hat{\boldsymbol{\theta}}))^2}{\sigma_i^2} \ . \tag{40.57}$$

For Gaussian distributed $\boldsymbol{y}$, the statistic t follows a chi-square distribution for $N - M$ degrees of freedom. From Eq. (40.57) one sees that greater t corresponds to increasing incompatibility between the measured y_i and predicted μ_i. The p-value of the Gaussian hypothesis is therefore taken to be

$$p = \int_{\chi^2_{\min}}^{\infty} f(t; n_\mathrm{d})\, dt \ , \tag{40.58}$$

where $f(t; n_\mathrm{d})$ is the chi-square distribution and $n_\mathrm{d} = N - M$ is the appropriate number of degrees of freedom. Values are shown in Fig. 40.2 or obtained from standard computer libraries. If the asymptotic conditions for using the chi-square distribution do not hold, the statistic can still be defined as before, but its p.d.f. must be determined by other means in order to obtain the p-value, *e.g.*, using a Monte Carlo calculation.

Often the data represent numbers of events in N bins of a histogram, *i.e.*, $\boldsymbol{n} = (n_1, \ldots, n_N)$. An important case is when $\boldsymbol{n}$ follows a multinomial distribution with $n_\mathrm{tot} = \sum_{i=1}^{N} n_i$ total entries and mean values μ_i, or equivalently bin probabilities $p_i = \mu_i / n_\mathrm{tot}$. Alternatively one may model the n_i as independent and Poisson distributed with means μ_i. If there are no adjustable parameters in the hypotheses, then the goodness-of-fit can be quantified with *Pearson's* χ^2 *statistic*, defined for multinomial data as

$$t_\mathrm{M} = \sum_{i=1}^{N} \frac{(n_i - n_\mathrm{tot} p_i)^2}{n_\mathrm{tot} p_i} \ , \tag{40.59}$$

or for the independent Poisson data as

$$t_\mathrm{P} = \sum_{i=1}^{N} \frac{(n_i - \mu_i)^2}{\mu_i} \ . \tag{40.60}$$

In the limit where the means μ_i are large, the statistics t_M and t_P are found to follow chi-square distributions for $N - 1$ and N degrees of freedom, respectively. Having one fewer degrees of freedom in the multinomial case is related to the fact that n_tot is fixed and thus the n_i are correlated.

Alternatively one can use the test statistic based on the likelihood ratio $t = -2 \ln \lambda(\hat{\boldsymbol{\theta}})$ given previously in Eq. (40.19). Here the likelihood ratio λ is chosen to correspond to the multinomial or Poisson model as appropriate, as described in Sec. 40.2.2.2. One finds that the distribution of the likelihood-ratio statistic approaches the asymptotic limit faster than does Pearson's χ^2 and thus when using the chi-square p.d.f. to compute a p-value one obtains in general a more accurate result from $-2 \ln \lambda$ (see [8]).

Since the mean of the chi-square distribution is equal to n_d, one expects in a "reasonable" experiment to obtain $\chi^2 \approx n_\mathrm{d}$ (here χ^2 refers to the minimized value). Hence the quantity χ^2/n_d is sometimes reported. Since the p.d.f. of χ^2/n_d depends on n_d, however, one must report n_d as well if one wishes to determine the p-value. The p-values obtained for different values of χ^2/n_d are shown in Fig. 40.3.

If the minimized χ^2 value indicates a low level of agreement between data and hypothesis, one may be tempted to expect a high degree of uncertainty for any fitted parameters. Poor goodness-of-fit, however, does not mean that one will have large statistical errors for parameter estimates. If, for example, the error bars (or covariance matrix) used in constructing the χ^2 are underestimated, then this will lead to underestimated statistical errors for the fitted parameters and an increased value of the minimized χ^2. The standard deviations of estimators that one finds from, say, Eq. (40.13) reflect how widely the estimates would be distributed if one were to repeat the measurement many times, assuming that the hypothesis and measurement errors used in the χ^2 are also correct. They do not include the systematic error which may result from an incorrect hypothesis or incorrectly estimated measurement errors in the χ^2.

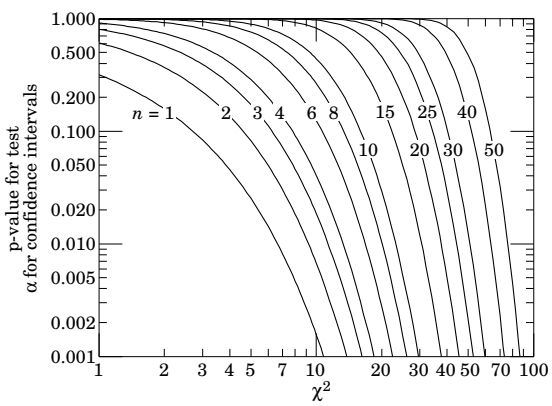

Figure 40.2: One minus the chi-square cumulative distribution, $1 - F_{\chi^2_n}(\chi^2)$, for n degrees of freedom, for n from one to fifty. This gives the p-value for the chi-square goodness-of-fit test as well as one minus the coverage probability for confidence regions (see Sec. 40.4.2.3).

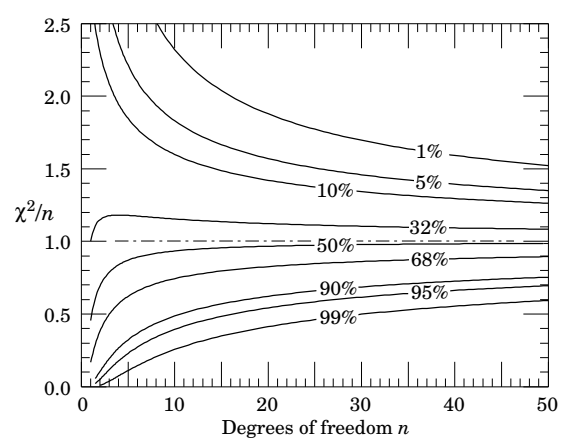

Figure 40.3: The "reduced" χ^2, equal to χ^2/n, for n degrees of freedom, corresponding to different values of the p-value.

by UNIVERSITY OF CA Phys. A 2026.41. Downloaded from www.worldscientific.com LEY on 09/16/26. Re-use and distribution is strictly not permitted, except for Open Access articles.

40.3.3.2 *Goodness-of-fit with the empirical distribution function*

Suppose a measurement yields a sample of independent and identically distributed (i.i.d.) values $\boldsymbol{x} = (x_1, \ldots, x_n)$. Often the values may be summarized by creating a histogram, but this inevitably results in a loss of information, since the position of the x values within each bin is not retained. Particularly with small numbers of observations n one therefore may prefer to keep the values of each of the x_i (*i.e.*, "unbinned"). The sample may be displayed graphically using the *empirical distribution function* (e.d.f.)

$$F_n(x) = \frac{\text{number of elements in sample with value } \leq x}{n} \; . \tag{40.61}$$

The e.d.f. $F_n(x)$ begins at zero for x less than the lowest observed value, increases by $1/n$ at each observed x_i, and saturates at unity for x equal to the highest value in the sample.

Given an i.i.d. data sample $\boldsymbol{x} = (x_1, \ldots, x_n)$, suppose one wants to test the hypothesis H_0 that x follows the p.d.f. $f(x)$ using a goodness-of-fit test, *i.e.*, without reference to a specific alternative. The hypothesis of the p.d.f. $f(x)$ is equivalent to saying the cumulative distribution function (c.d.f.) is $F(x) = \int_{-\infty}^{x} f(x')\, dx'$. As the e.d.f. $F_n(x)$ can be viewed as an estimator for the c.d.f. $F(x)$, we can derive a goodness-of-fit statistic by some appropriately defined measure of the "distance" between the two.

A widely used example is the Kolmogorov–Smirnov (K–S) test, based on

$$D_n = \sup_x |F_n(x) - F(x)| \; , \tag{40.62}$$

where sup denotes the supremum. That is, D_n is the greatest vertical distance between $F_n(x)$ and $F(x)$ for any x. In the limit of large sample size n, one can show that the distribution of D_n, assuming the data follows the c.d.f. $F(x)$, approaches the Kolmogorov distribution, which is independent of the specific form of $F(x)$ and is provided in many software packages. A larger value of D_n corresponds to greater incompatibility between data and hypothesis, so the p-value is the probability $P(D_n \geq D_{n,\mathrm{obs}}|H_0)$. The K–S test is sensitive in particular to differences in location (*i.e.*, in the mean of x), as this corresponds to a horizontal shift between $F_n(x)$ and $F(x)$, giving a large maximum vertical distance D_n.

The Cramér-von Mises family of tests is based on the squared difference between $F_n(x)$ and $F(x)$ through an integral of the form

$$W^2 = \int_{-\infty}^{\infty} (F(x) - F_n(x))^2 w(x) f(x)\, dx \; , \tag{40.63}$$

where $f(x) = dF/dx$ is the p.d.f. of x and $w(x)$ is a weight function that must be specified. Two important choices are the classic Cramér-von Mises test with $w(x) = 1$, and the Anderson-Darling test with $w(x) = [F(x)(1 - F(x))]^{-1}$, which gives increased sensitivity to departures in the tails of the distribution. For cases such as these, where the weight function depends on x only through the cumulative distribution $F(x)$, one can show (see, *e.g.*, Refs. [4,41]) that the distribution of W^2, assuming data that follows $F(x)$, is independent of the form of $F(x)$. The distributions of the Smirnov-Cramér-von Mises and Anderson-Darling statistics are available in standard computer libraries.

40.3.4 *Bayes factors*

In Bayesian statistics, all of one's knowledge about a model is contained in its posterior probability, which one obtains using Bayes' theorem (Eq. (40.36)). Thus one could reject a hypothesis H if its posterior probability $P(H|\boldsymbol{x})$ is sufficiently small. The difficulty here is that $P(H|\boldsymbol{x})$ is proportional to the prior probability $P(H)$, and there will not be a consensus about the prior probabilities for the existence of new phenomena. Nevertheless one can construct a quantity called the Bayes factor (described below), which can be used to quantify the degree to which the data prefer one hypothesis over another, and is independent of their prior probabilities.

Consider two models (hypotheses), H_i and H_j, described by vectors of parameters $\boldsymbol{\theta}_i$ and $\boldsymbol{\theta}_j$, respectively. Some of the components will be common to both models and others may be distinct. The full prior probability for each model can be written in the form

$$\pi(H_i, \boldsymbol{\theta}_i) = P(H_i)\pi(\boldsymbol{\theta}_i|H_i) \; . \tag{40.64}$$

Here $P(H_i)$ is the overall prior probability for H_i, and $\pi(\boldsymbol{\theta}_i|H_i)$ is the normalized p.d.f. of its parameters. For each model, the posterior probability is found using Bayes' theorem,

$$P(H_i|\boldsymbol{x}) = \frac{\int P(\boldsymbol{x}|\boldsymbol{\theta}_i, H_i) P(H_i) \pi(\boldsymbol{\theta}_i|H_i)\, d\boldsymbol{\theta}_i}{P(\boldsymbol{x})} \; , \tag{40.65}$$

where the integration is carried out over the internal parameters $\boldsymbol{\theta}_i$ of the model. The ratio of posterior probabilities for the models is therefore

$$\frac{P(H_i|\boldsymbol{x})}{P(H_j|\boldsymbol{x})} = \frac{\int P(\boldsymbol{x}|\boldsymbol{\theta}_i, H_i)\pi(\boldsymbol{\theta}_i|H_i)\, d\boldsymbol{\theta}_i}{\int P(\boldsymbol{x}|\boldsymbol{\theta}_j, H_j)\pi(\boldsymbol{\theta}_j|H_j)\, d\boldsymbol{\theta}_j} \frac{P(H_i)}{P(H_j)} \; . \tag{40.66}$$

The *Bayes factor* is defined as

$$B_{ij} = \frac{\int P(\boldsymbol{x}|\boldsymbol{\theta}_i, H_i)\pi(\boldsymbol{\theta}_i|H_i)\, d\boldsymbol{\theta}_i}{\int P(\boldsymbol{x}|\boldsymbol{\theta}_j, H_j)\pi(\boldsymbol{\theta}_j|H_j)\, d\boldsymbol{\theta}_j} \; . \tag{40.67}$$

This gives what the ratio of posterior probabilities for models i and j would be if the overall prior probabilities for the two models were equal. If the models have no nuisance parameters, *i.e.*, no internal parameters described by priors, then the Bayes factor is simply the likelihood ratio. The Bayes factor therefore shows by how much the probability ratio of model i to model j changes in the light of the data, and thus can be viewed as a numerical measure of evidence supplied by the data in favor of one hypothesis over the other.

Although the Bayes factor is by construction independent of the overall prior probabilities $P(H_i)$ and $P(H_j)$, it does require priors for all internal parameters of a model, *i.e.*, one needs the functions $\pi(\boldsymbol{\theta}_i|H_i)$ and $\pi(\boldsymbol{\theta}_j|H_j)$. In a Bayesian analysis where one is only interested in the posterior p.d.f. of a parameter, it may be acceptable to take an unnormalizable function for the prior (an improper prior) as long as the product of likelihood and prior can be normalized. Improper priors are, however, only defined up to an arbitrary multiplicative constant, and so the Bayes factor would depend on this constant. Furthermore, although the range of a constant normalized prior is unimportant for parameter determination (provided it is wider than the likelihood), this is not so for the Bayes factor when such a prior is used for only one of the hypotheses. So to compute a Bayes factor, all internal parameters must be described by normalized priors that represent meaningful probabilities over the entire range where they are defined.

Both integrals in Equation (40.67) are of the form

$$m = \int P(\boldsymbol{x}|\boldsymbol{\theta})\pi(\boldsymbol{\theta})\, d\boldsymbol{\theta} \; , \tag{40.68}$$

which is similar to the marginal likelihood seen previously in Eq. (40.52) (in some fields this quantity is called the *evidence*). Computing marginal likelihoods can be difficult; in many cases it can be done with the nested sampling algorithm [42]. A review of Bayes factors can be found in Ref. [43].

40.4 Intervals and limits

When the goal of an experiment is to determine a parameter θ, the result is usually expressed by quoting, in addition to the point estimate, some sort of interval which reflects the statistical precision of the measurement. In the simplest case, this can be given by the parameter's estimated value $\widehat{\theta}$ plus or minus an estimate of the standard deviation of $\widehat{\theta}$, $\widehat{\sigma}_{\widehat{\theta}}$. If, however, the p.d.f. of the estimator is not Gaussian or if there are physical boundaries on the possible values of the parameter, then one usually quotes instead an interval according to one of the procedures described below.

In reporting an interval or limit, the experimenter may wish to

Int. J. Mod. Phys. A 2026.41. Downloaded from www.worldscientific.com
by UNIVERSITY OF CALIFORNIA @ BERKELEY on 09/16/26. Re-use and distribution is strictly not permitted, except for Open Access articles.

- communicate as objectively as possible the result of the experiment;
- provide an interval that is constructed to cover on average the true value of the parameter with a specified probability;
- provide the information needed by the consumer of the result to draw conclusions about the parameter or to make a particular decision;
- draw conclusions about the parameter that incorporate stated prior beliefs.

With a sufficiently large data sample, the point estimate and standard deviation (or for the multiparameter case, the parameter estimates and covariance matrix) satisfy essentially all of these goals. For small data samples, no single method for quoting an interval will achieve all of them.

In addition to the goals listed above, the choice of method may be influenced by practical considerations such as ease of producing an interval from the results of several measurements. Of course the experimenter is not restricted to quoting a single interval or limit; one may choose, for example, first to communicate the result with a confidence interval having certain frequentist properties, and then in addition to draw conclusions about a parameter using a judiciously chosen subjective Bayesian prior. It is recommended, however, that there be a clear separation between these two aspects of reporting a result. In the remainder of this section, we assess the extent to which various types of intervals achieve the goals stated here.

40.4.1 *Bayesian credible intervals*

As described in Sec. 40.2.5, a Bayesian posterior probability may be used to determine regions that will have a given probability of containing the true value of a parameter. In the single parameter case, for example, an interval (called a Bayesian or credible interval) $[\theta_{\rm lo}, \theta_{\rm up}]$ can be determined which contains a given fraction $1-\alpha$ of the posterior probability, *i.e.*,

$$1-\alpha = \int_{\theta_{\rm lo}}^{\theta_{\rm up}} p(\theta|\boldsymbol{x})\, d\theta \; . \tag{40.69}$$

Sometimes an upper or lower limit is desired, *i.e.*, $\theta_{\rm lo}$ or $\theta_{\rm up}$ can be set to a physical boundary or to plus or minus infinity. In other cases, one might be interested in the set of θ values for which $p(\theta|\boldsymbol{x})$ is higher than for any θ not belonging to the set, which may constitute a single interval or a set of disjoint regions; these are called highest posterior density (HPD) intervals. Note that HPD intervals are not invariant under a nonlinear transformation of the parameter.

An important case is when we have a Poisson variable n which counts signal events with unknown mean s as well as background with mean b, assumed known. To obtain an upper limit on s, one may proceed as follows. The likelihood for s is given by the Poisson distribution for n with mean $s+b$,

$$P(n|s) = \frac{(s+b)^n}{n!} e^{-(s+b)} \; . \tag{40.70}$$

Assuming a uniform prior in the allowed range $s \geq 0$, Eq. (40.36) gives the posterior density for s. An upper limit $s_{\rm up}$ at confidence level (or here, rather, *credibility* level) $1-\alpha$ can be obtained by requiring

$$1-\alpha = \int_0^{s_{\rm up}} p(s|n) ds = \frac{\int_0^{s_{\rm up}} P(n|s)\, \pi(s)\, ds}{\int_0^{\infty} P(n|s)\, \pi(s)\, ds} \; . \tag{40.71}$$

By relating the integrals in Eq. (40.71) to incomplete gamma functions, the solution for the upper limit is found to be

$$s_{\rm up} = \frac{1}{2} F_{\chi^2}^{-1}(p; 2(n+1)) - b \; , \tag{40.72}$$

where F_{χ^2} is the cumulative chi-square distribution here for $2(n+1)$ degrees of freedom and $F_{\chi^2}^{-1}$ its inverse, i.e.: the quantile of the chi-square distribution. The p-value is

$$p = 1-\alpha \left(1 - F_{\chi^2}(2b; 2(n+1))\right) \; , \tag{40.73}$$

For the special case of $b=0$, the limit reduces to

$$s_{\rm up} = \frac{1}{2} F_{\chi^2}^{-1}(1-\alpha; 2(n+1)) \; . \tag{40.74}$$

It happens that for the case of $b=0$, the upper limit from Eq. (40.74) coincides numerically with the frequentist upper limit discussed in Section 40.4.2.4. Values of $\mu_{\rm up}$ for $1-\alpha = 0.9$ and 0.95 are given in Table 40.2. The frequentist properties of confidence intervals for the Poisson mean found in this way are discussed in Refs. [2] and [44].

As in any Bayesian analysis, it is important to show how the result changes under assumption of different prior probabilities. For example, one could consider the Jeffreys prior as described in Sec. 40.2.5. For this problem one finds the Jeffreys prior $\pi(s) \propto 1/\sqrt{s+b}$ with $s \geq 0$. As with the constant prior, one would not regard this as representing one's prior beliefs about s, both because it is improper and also as it depends on b. Rather it is used with Bayes' theorem to produce an interval whose frequentist properties can be studied.

If the model contains nuisance parameters then these are eliminated by marginalizing, as in Eq. (40.43), to obtain the p.d.f. for the parameters of interest. For example, if the parameter b in the Poisson counting problem above were to be characterized by a prior p.d.f. $\pi(b)$, then one would first use Bayes' theorem to find $p(s,b|n)$. This is then marginalized to find $p(s|n) = \int p(s,b|n)\pi(b)\, db$, from which one may determine an interval for s. One may not be certain whether to extend a model by including more nuisance parameters. In this case, a Bayes factor may be used to determine to what extent the data prefer a model with additional parameters, as described in Section 40.3.4.

40.4.2 *Frequentist confidence intervals*

The unqualified phrase "confidence intervals" refers to frequentist intervals obtained with a procedure due to Neyman [45], described below. The boundary of the interval (or in the multiparameter case, region) is given by a specific function of the data, which would fluctuate if one were to repeat the experiment many times. The *coverage probability* refers to the fraction of intervals in such an ensemble that contain the true parameter value. Confidence intervals are constructed so as to have a coverage probability greater than or equal to a given *confidence level*, regardless of the true parameter's value. It is important to note that in the frequentist approach, such a probability is not meaningful for a fixed interval. In this section we discuss several techniques for producing intervals that have, at least approximately, this property of coverage.

40.4.2.1 *The Neyman construction for confidence intervals*

Consider a p.d.f. $f(x;\theta)$ where x represents the outcome of the experiment and θ is the unknown parameter for which we want to construct a confidence interval. The variable x could (and often is) used to build an estimator for θ if it monothonically depends on θ. Using $f(x;\theta)$ we can find, using a pre-defined rule and probability $1-\alpha$ for every value of θ, a set of values $x_1(\theta,\alpha)$ and $x_2(\theta,\alpha)$ such that

$$P(x_1 < x < x_2; \theta) = \int_{x_1}^{x_2} f(x;\theta)\, dx \geq 1-\alpha \; . \tag{40.75}$$

If x is discrete, the integral is replaced by the corresponding sum where the extreme values x_1 and x_2 are excluded. In that case there may not exist a range of x values whose summed probability is exactly equal to a given value of $1-\alpha$, and one requires by convention $P(x_1 < x < x_2; \theta) \geq 1-\alpha$.

This is illustrated for continuous x in Fig. 40.4: a horizontal line segment $[x_1(\theta,\alpha), x_2(\theta,\alpha)]$ is drawn for representative values of θ. The union of such intervals for all values of θ, designated in the figure as $D(\alpha)$, is known as a *confidence belt*. Typically, the curves $x_1(\theta,\alpha)$ and $x_2(\theta,\alpha)$ are monotonic functions of θ, which we assume for this discussion.

Upon performing an experiment to measure x and obtaining a value x_0, one draws a vertical line through x_0. The confidence interval for θ is the set of all values of θ for which the corresponding line segment $[x_1(\theta,\alpha), x_2(\theta,\alpha)]$ is intercepted by this vertical line.

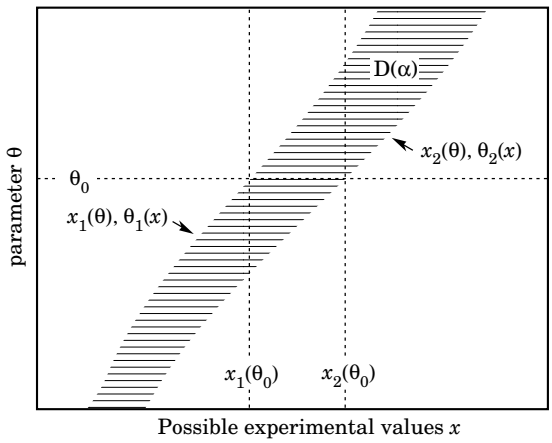

Figure 40.4: Construction of the confidence belt (see text).

Such confidence intervals are said to have a *confidence level* (CL) equal to $1-\alpha$.

Now suppose that the true value of θ is θ_0, indicated in the figure. We see from the figure that θ_0 lies between $\theta_1(x)$ and $\theta_2(x)$, where x is an outcome of our measurement, if and only if x lies between $x_1(\theta_0)$ and $x_2(\theta_0)$. The two events thus have the same probability, and since this is true for any value θ_0, we can drop the subscript 0 and obtain

$$1-\alpha = P(x_1(\theta) < x < x_2(\theta)) = P(\theta_2(x) < \theta < \theta_1(x)) \ . \quad (40.76)$$

In this probability statement, $\theta_1(x)$ and $\theta_2(x)$, *i.e.*, the endpoints of the interval, are the random variables and θ is an unknown constant. If the experiment were to be repeated a large number of times, the interval $[\theta_1, \theta_2]$ would vary, covering the fixed value θ in a fraction $1-\alpha$ of the experiments.

The condition of coverage in Eq. (40.75) does not determine x_1 and x_2 uniquely, and additional criteria are needed. One possibility is to choose *central intervals* such that the probabilities to find x below x_1 and above x_2 are each $\alpha/2$. In other cases, one may want to report only an upper or lower limit, in which case one of $P(x \le x_1)$ or $P(x \ge x_2)$ can be set to α and the other to zero. Another principle based on *likelihood ratio ordering* for determining which values of x should be included in the confidence belt is discussed below.

When the observed random variable x is continuous, the coverage probability obtained with the Neyman construction is $1-\alpha$, regardless of the true value of the parameter. Because of the requirement $P(x_1 < x < x_2) \ge 1-\alpha$ when x is discrete, one obtains in that case confidence intervals that include the true parameter with a probability greater than or equal to $1-\alpha$.

40.4.2.2 *Confidence interval from a hypothesis test*

An equivalent view of the Neyman construction from the previous section is to consider a test (see Sec. 40.3) of the hypothesis that the parameter's true value is θ (assume one constructs a test for all physical values of θ). One then excludes all values of θ where the hypothesis would be rejected in a test of size α or less. The remaining values constitute the confidence interval at confidence level $1-\alpha$. If the critical region of the test is characterized by having a p-value $p_\theta \le \alpha$, then the endpoints of the confidence interval are found in practice by solving $p_\theta = \alpha$ for θ. The confidence belt seen in Sec. 40.4.2.1 is a graphical representation of the complement of the critical region of the test of each θ.

In this view it is straightforward to generalize from scalar data x and single parameter θ to a vector of data values $\boldsymbol{x}$ that follow a probability $P(\boldsymbol{x}|\boldsymbol{\theta})$, which depends on a set of parameters $\boldsymbol{\theta} = (\theta_1, \ldots, \theta_M)$. We will refer to the result generically as a confidence interval or for multiple components a confidence *region*.

One is still free to choose the test to be used; this corresponds to the freedom in the Neyman construction as to which values of the data are included in the confidence belt. One possibility is to use a test statistic based on the *likelihood ratio*,

$$\lambda(\boldsymbol{\theta}) = \frac{P(\boldsymbol{x}|\boldsymbol{\theta})}{P(\boldsymbol{x}|\widehat{\boldsymbol{\theta}})} \ , \quad (40.77)$$

where $\widehat{\boldsymbol{\theta}}$ is the maximum-likelihood estimator. This results in the intervals described in Ref. [46] by Feldman and Cousins.

If the model contains nuisance parameters $\boldsymbol{\nu}$, then these can be incorporated into the test (or the p-values) used to determine the limit by profiling as discussed in Section 40.3.2.1. That is, the likelihood ratio (40.77) is replaced by the profile likelihood ratio of Eq. (40.51). As mentioned there, one excludes the parameter of interest $\boldsymbol{\theta}$ only if it is rejected for all possible values of $\boldsymbol{\nu}$. The resulting region for $\boldsymbol{\theta}$ will then cover the true value with a probability greater than or equal to the nominal confidence level for all points in $\boldsymbol{\nu}$-space.

If the p-value is based on the profiled values of the nuisance parameters, *i.e.*, with $\boldsymbol{\nu} = \widehat{\widehat{\boldsymbol{\nu}}}(\theta)$ used in Eq. (40.50), then the coverage probability of the resulting interval for the parameter of interest is approximate and may be too high or too low. This procedure has been called *profile construction* in particle physics [36] (see also Ref. [30]).

40.4.2.3 *Confidence regions from the likelihood function*

The procedure for determining confidence intervals or regions is greatly simplified in the large-sample limit with use of the profile likelihood ratio $\lambda_{\rm p}(\boldsymbol{\theta})$ from Eq. (40.51) to test each value of the parameters of interest $\boldsymbol{\theta}$, also in the case where the model contains nuisance parameters $\boldsymbol{\nu}$. In the large-sample limit and assuming the regularity conditions (see Sec. 40.2.2.1), the estimators for all of the parameters become Gaussian distributed. Wilks' theorem follows from this property and states that the asymptotic distribution of $-2\ln\lambda_{\rm p}(\boldsymbol{\theta})$ is chi-square for M degrees of freedom, where M is the number of parameters interest only. A test of $\boldsymbol{\theta}$ thus becomes independent of the nuisance parameters and the confidence region at confidence level $1-\alpha$ is therefore given by the set of $\boldsymbol{\theta}$ values satisfying

$$\ln L(\boldsymbol{\theta}) = \ln L(\hat{\boldsymbol{\theta}}) - \frac{1}{2} F^{-1}_{\chi^2_M}(1-\alpha) \ . \quad (40.78)$$

where F^{-1}_M is the quantile (inverse of the cumulative distribution) for a chi-square distribution with M degrees of freedom. This holds as long as the estimators for the parameters are Gaussian-distributed, which could hold even in a small-sample problem. One should be aware, however, of potential violations of the regularity conditions if, e.g., the true value of a parameter is at the boundary of the parameter space.

A common application of Eq. (40.78) is in the method of least squares, where the sum of squares to be minimized is related to the likelihood by $\chi^2(\boldsymbol{\theta}) = -2\ln L(\boldsymbol{\theta}) + C$, where the constant C does not depend on the parameters $\boldsymbol{\theta}$. In this case, Eq. (40.78) becomes

$$\chi^2(\boldsymbol{\theta}) = \chi^2(\hat{\boldsymbol{\theta}}) + F^{-1}_{\chi^2_M}(1-\alpha) \ . \quad (40.79)$$

The allowed departure of χ^2 or $\ln L$ from its optimized value is therefore found from $\Delta\chi^2 = 2\Delta\ln L = F^{-1}_{\chi^2_M}(1-\alpha)$. Values of $\Delta\chi^2$ or $2\Delta\ln L$ are given in Table 40.1 for several values of the coverage probability $1-\alpha$ and number of fitted parameters M.

For the special case of $M = 1$ and $1-\alpha = 0.683$ one has $F^{-1}_{\chi^2_1}(0.683) = 1$, so the formula for the 68.3% CL confidence interval coincides with Eq. (40.13) for the standard deviation of an estimator. The numerical factor $F^{-1}_{\chi^2_M}(1-\alpha)$ grows with M for fixed α, i.e., with more parameters, one needs a larger decrease in $\ln L$ from its maximum to obtain a region with a given confidence level. Comparison of Eqs. (40.13) and (40.78) gives the number of standard deviations from the MLE to the tangent of a $1-\alpha$ CL confidence region with N parameters as $s = [F^{-1}_{\chi^2_M}(1-\alpha)]^{1/2}$, e.g., for $M = 2$ and $1-\alpha = 0.95$, $s = 2.45$.

For small-sample problems, the likelihood ratio is no longer chi-square distributed and these are not exact confidence regions

Phys. A 2026.41. Downloaded from www.worldscientific.com
by UNIVERSITY OF CA LEY on 09/16/26. Re-use and distribution is strictly not permitted, except for Open Access articles.

Int. J. Mod. Phys. A 2026.41. Downloaded from www.worldscientific.com
by UNIVERSITY OF CALIFORNIA @ BERKELEY on 09/16/26. Re-use and distribution is strictly not permitted, except for Open Access articles.

Table 40.1: Values of $\Delta\chi^2$ or $2\Delta \ln L$ corresponding to a coverage probability $1-\alpha$ in the large data sample limit, for joint estimation of M parameters.

$(1-\alpha)$ (%)	$M=1$	$M=2$	$M=3$
68.27	1.00	2.30	3.53
90.	2.71	4.61	6.25
95.	3.84	5.99	7.82
95.45	4.00	6.18	8.03
99.	6.63	9.21	11.34
99.73	9.00	11.83	14.16

according to our previous definition, the coverage probability is no longer guaranteed to be equal to the nominal confidence level, and it will in general depend on $\boldsymbol{\theta}$. Nevertheless, they can still have a coverage probability only weakly dependent on the true parameter, and approximately as given in Table 40.1. In any case, the coverage probability of the intervals or regions obtained according to this procedure can in principle be determined as a function of the true parameter(s), for example, using a Monte Carlo calculation.

One of the practical advantages of intervals that can be constructed from the log-likelihood function or χ^2 is that it is relatively simple to produce the interval for the combination of several experiments. If N independent measurements result in log-likelihood functions $\ln L_i(\boldsymbol{\theta})$, then the combined log-likelihood function is simply the sum,

$$\ln L(\boldsymbol{\theta}) = \sum_{i=1}^{N} \ln L_i(\boldsymbol{\theta}) \; . \tag{40.80}$$

This can then be used to determine an approximate confidence interval or region with Eq. (40.78).

40.4.2.4 *Limits for Poisson or binomial data*

Another important class of measurements consists of counting a certain number of events, n. In this section, we will assume these are all events of the desired type, *i.e.*, there is no background. If n represents the number of events produced in a reaction with cross section σ and selection efficiency ε in a fixed integrated luminosity $\mathcal{L}$, then it follows a Poisson distribution with mean $\mu = \sigma\varepsilon\mathcal{L}$. If, on the other hand, one has selected a larger sample of N events and found n of them to have a particular property, then n follows a binomial distribution where the parameter p gives the probability for the event to possess the property in question. This is appropriate, *e.g.*, for estimates of branching ratios or selection efficiencies based on a given total number of events.

For the case of Poisson distributed n, limits on the mean value μ can be found from the Neyman procedure as discussed in Section 40.4.2.1 with n used directly as the statistic x . The upper and lower limits are found to be

$$\mu_{\rm lo} = \frac{1}{2} F^{-1}_{\chi^2}(\alpha_{\rm lo}; 2n) \; , \tag{40.81a}$$

$$\mu_{\rm up} = \frac{1}{2} F^{-1}_{\chi^2}(1-\alpha_{\rm up}; 2(n+1)) \; , \tag{40.81b}$$

where confidence levels of $1-\alpha_{\rm lo}$ and $1-\alpha_{\rm up}$ refer separately to the corresponding intervals $\mu \geq \mu_{\rm lo}$ and $\mu \leq \mu_{\rm up}$. For central confidence intervals at confidence level $1-\alpha$, set $\alpha_{\rm lo} = \alpha_{\rm up} = \alpha/2$.

It happens that the upper limit from Eq. (40.81b) coincides numerically with the Bayesian upper limit for a Poisson parameter, using a uniform prior p.d.f. for μ. Values for confidence levels of 90% and 95% are shown in Table 40.2.

For the case of binomially distributed n successes out of N trials with probability of success p, the upper and lower limits on p can be determined with a similar procedure due to Clopper and Pearson [47], which is available in computer libraries.

40.4.2.5 *Parameter exclusion in cases of low sensitivity*

An important example of a statistical test arises in the search for a new signal process. Suppose the parameter μ is defined such

Table 40.2: Lower and upper (one-sided) limits for the mean μ of a Poisson variable given n observed events in the absence of background, for confidence levels of 90% and 95%.

	$1-\alpha$ =90%		$1-\alpha$ =95%	
n	$\mu_{\rm lo}$	$\mu_{\rm up}$	$\mu_{\rm lo}$	$\mu_{\rm up}$
0	–	2.30	–	3.00
1	0.105	3.89	0.051	4.74
2	0.532	5.32	0.355	6.30
3	1.10	6.68	0.818	7.75
4	1.74	7.99	1.37	9.15
5	2.43	9.27	1.97	10.51
6	3.15	10.53	2.61	11.84
7	3.89	11.77	3.29	13.15
8	4.66	12.99	3.98	14.43
9	5.43	14.21	4.70	15.71
10	6.22	15.41	5.43	16.96

that it is proportional to the signal cross section. A statistical test may be carried out for hypothesized values of μ, which may be done by computing a p-value, p_μ, for all μ. Those values not rejected in a test of size α, *i.e.*, for which one does not find $p_\mu \leq \alpha$, constitute a confidence interval with confidence level $1-\alpha$.

In general one will find that for some regions in the parameter space of the signal model, the predictions for data are almost indistinguishable from those of the background-only model. This corresponds to the case where μ is very small, as would occur, *e.g.*, in a search for a new particle with a mass so high that its production rate in a given experiment is negligible. That is, one has essentially no experimental sensitivity to such a model.

One would prefer that if the sensitivity to a model (or a point in a model's parameter space) is very low, then it should not be excluded. Even if the outcomes predicted with or without signal are identical, however, the probability to reject the signal model will equal α, the type-I error rate. As one often takes α to be 5%, this would mean that in a large number of searches covering a broad range of a signal model's parameter space, there would inevitably be excluded regions in which the experimental sensitivity is very small, and thus one may question whether it is justified to regard such parameter values as disfavored.

Exclusion of models to which one has little or no sensitivity occurs, for example, if the data fluctuate very low relative to the expectation of the background-only hypothesis. In this case the resulting upper limit on μ may be anomalously low. As a means of controlling this effect one often determines the mean or median limit under assumption of the background-only hypothesis, as discussed in Sec. 40.5.

One way to mitigate the problem of excluding models to which one is not sensitive is the $\mathrm{CL_s}$ method, where the measure used to test a parameter is increased for decreasing sensitivity [48, 49].

The procedure is based on a statistic called $\mathrm{CL_s}$, which is defined as

$$\mathrm{CL_s} = \frac{p_\mu}{1-p_{\rm b}} \; , \tag{40.82}$$

where $p_{\rm b}$ is the p-value of the background-only hypothesis. In the usual formulation of the method, both p_μ and $p_{\rm b}$ are defined using a single test statistic, and the definition of $\mathrm{CL_s}$ above assumes this statistic is continuous; more details can be found in Refs. [48, 49].

A point in a model's parameter space is regarded as excluded if one finds $\mathrm{CL_s} \leq \alpha$. As the denominator in Eq. (40.82) is always less than or equal to unity, the exclusion criterion based on $\mathrm{CL_s}$ is more stringent than the usual requirement $p_\mu \leq \alpha$. In this sense the $\mathrm{CL_s}$ procedure is conservative, and the coverage probability of the corresponding intervals will exceed the nominal confidence level $1-\alpha$. If the experimental sensitivity to a given value of μ is very low, then one finds that as p_μ decreases, so does the denominator $1-p_{\rm b}$, and thus the condition $\mathrm{CL_s} \leq \alpha$ is effectively prevented from being satisfied. In this way the exclusion of parameters in the case of low sensitivity is suppressed.

The $\mathrm{CL_s}$ procedure has the attractive feature that the resulting intervals coincide with those obtained from the Bayesian method

by UNIVERSITY OF CA Phys. A 2026.41. Downloaded from www.worldscientific.com LEY on 09/16/26. Re-use and distribution is strictly not permitted, except for Open Access articles.

in two important cases: the mean value of a Poisson or Gaussian distributed measurement with a constant prior. The $\mathrm{CL_s}$ intervals overcover for all values of the parameter μ, however, by an amount that depends on μ.

The problem of excluding parameter values to which one has little sensitivity is particularly acute when one wants to set a one-sided limit, *e.g.*, an upper limit on a cross section. Here one tests a value of a rate parameter μ against the alternative of a lower rate, and therefore the critical region of the test is taken to correspond to data outcomes with a low event yield. If the number of events found in the search region fluctuates low enough, however, it can happen that all physically meaningful signal parameter values, including those to which one has very little sensitivity, are rejected by the test.

Another solution to this problem, therefore, is to replace the one-sided test by one based on the likelihood ratio, where the critical region is not restricted to low rates. This is the approach followed in the Feldman-Cousins procedure described in Section 40.4.2.1. The critical region for the test of a given value of μ contains data values characteristic of both higher and lower rates. As a result, for a given observed rate one can in general obtain a two-sided interval. If, however, the parameter estimate $\hat{\mu}$ is sufficiently close to the lower limit of zero, then only high values of μ are rejected, and the lower edge of the confidence interval is at zero. Note, however, that the coverage property of $1-\alpha$ pertains to the entire interval, not to the probability for the upper edge μ_{up} to be greater than the true value μ. For parameter estimates increasingly far away from the boundary, *i.e.*, for increasing signal significance, the point $\mu = 0$ is excluded and the interval has nonzero upper and lower edges.

An additional difficulty arises when a parameter estimate is not significantly far away from the boundary, in which case it is natural to report a one-sided confidence interval (often an upper limit). It is straightforward to force the Neyman prescription to produce only an upper limit by setting $x_2 = \infty$ in Eq. (40.75). Then x_1 is uniquely determined and the upper limit can be obtained. If, however, the data come out such that the parameter estimate is not so close to the boundary, one might wish to report a central confidence interval (*i.e.*, an interval based on a two-sided test with equal upper and lower tail areas). As pointed out by Feldman and Cousins [46], if the decision to report an upper limit or two-sided interval is made by looking at the data ("flip-flopping"), then in general there will be parameter values for which the resulting intervals have a coverage probability less than $1-\alpha$. With the confidence intervals suggested in Ref. [46], the prescription determines whether the interval is one- or two-sided in a way which preserves the coverage probability (and are thus said to be *unified*).

The intervals according to this method for the mean of Poisson variable in the absence of background are given in Table 40.3[1]. The values of $1-\alpha$ given here refer to the coverage of the true parameter by the whole interval $[\mu_1, \mu_2]$. In Table 40.2 for the one-sided upper limit, however, $1-\alpha$ refers to the probability to have $\mu_{\mathrm{up}} \geq \mu$ (or $\mu_{\mathrm{lo}} \leq \mu$ for lower limits).

A potential difficulty with unified intervals arises if, for example, one constructs such an interval for a Poisson parameter s of some yet to be discovered signal process with, say, $1-\alpha = 0.9$. If the true signal parameter is zero, or in any case much less than the expected background, one will usually obtain a one-sided upper limit on s. In a certain fraction of the experiments, however, a two-sided interval for s will result. Since, however, one typically chooses $1-\alpha$ to be only 0.9 or 0.95 when setting limits, the value $s = 0$ may be found below the lower edge of the interval before the existence of the effect is well established. It must then be communicated carefully that in excluding $s = 0$ at, say, 90% or 95% confidence level from the interval, one is not necessarily claiming to have discovered the effect, for which one would usually require a higher level of significance (*e.g.*, 5 σ).

Another possibility is to construct a Bayesian interval as described in Section 40.4.1. The presence of the boundary can be incorporated simply by setting the prior density to zero in the unphysical region. More specifically, the prior may be chosen using formal rules such as the reference prior or Jeffreys prior mentioned in Sec. 40.2.5.

[1] Note that α in Ref. [46] is defined following Neyman [45] as the coverage probability; this is opposite the modern convention used here in which the coverage probability is $1-\alpha$.

Table 40.3: Unified confidence intervals $[\mu_1, \mu_2]$ for a the mean of a Poisson variable given n observed events in the absence of background, for confidence levels of 90% and 95%.

	$1-\alpha$ =90%		$1-\alpha$ =95%	
n	μ_1	μ_2	μ_1	μ_2
0	0.00	2.44	0.00	3.09
1	0.11	4.36	0.05	5.14
2	0.53	5.91	0.36	6.72
3	1.10	7.42	0.82	8.25
4	1.47	8.60	1.37	9.76
5	1.84	9.99	1.84	11.26
6	2.21	11.47	2.21	12.75
7	3.56	12.53	2.58	13.81
8	3.96	13.99	2.94	15.29
9	4.36	15.30	4.36	16.77
10	5.50	16.50	4.75	17.82

In particle physics a widely used prior for the mean μ of a Poisson distributed measurement has been the uniform distribution for $\mu \geq 0$. This prior does not follow from any fundamental rule nor can it be regarded as reflecting a reasonable degree of belief, since the prior probability for μ to lie between any two finite values is zero. The procedure above can be more appropriately regarded as a way for obtaining intervals with frequentist properties that can be investigated. The resulting upper limits have a coverage probability that depends on the true value of the Poisson parameter, and is nowhere smaller than the stated probability content. Lower limits and two-sided intervals for the Poisson mean based on uniform priors undercover, however, for some values of the parameter, although to an extent that in practical cases may not be too severe [2, 44].

In any case, it is important to always report sufficient information so that the result can be combined with other measurements. Often this means giving an unbiased estimator and its standard deviation, even if the estimated value is in the unphysical region.

It can also be useful with a frequentist interval to calculate its subjective probability content using the posterior p.d.f. based on one or several reasonable guesses for the prior p.d.f. If it turns out to be significantly less than the stated confidence level, this warns that it would be particularly misleading to draw conclusions about the parameter's value from the interval alone.

40.5 Experimental sensitivity

In this section we describe methods for characterizing the sensitivity of a search for a new physics signal. As discussed in Sec. 40.3, an experimental analysis can often be formulated as a test of hypothetical model parameters. Therefore, we may quantify the sensitivity by giving the results that we expect from such a test under specific assumptions about the signal process.

Here to be concrete we will consider a parameter μ proportional to the rate of a signal process, although the concepts described in this section may be easily generalized to other parameters. One may wish to establish discovery of the signal process by testing and rejecting the hypothesis that $\mu = 0$, and in addition one often wants to test nonzero values of μ to construct a confidence interval (*e.g.*, limits) as described in Sec. 40.4. In the frequentist framework, the result of each tested value of μ is the p-value p_μ or equivalently the significance $Z_\mu = \Phi^{-1}(1-p_\mu)$, where as usual Φ is the standard Gaussian cumulative distribution and its inverse Φ^{-1} is the standard Gaussian quantile.

Prior to carrying out the experiment, one generally wants to quantify what significance Z_μ is expected under given assumptions for the presence or absence of the signal process. Specifically, for the significance of a test of $\mu = 0$ (the discovery significance) one usually quotes the Z_0 one would expect if the signal is present at a given nominal rate, which we can define in general to cor-

Int. J. Mod. Phys. A 2026.41. Downloaded from www.worldscientific.com by UNIVERSITY OF CALIFORNIA @ BERKELEY on 09/16/26. Re-use and distribution is strictly not permitted, except for Open Access articles.

respond to $\mu = 1$. For limits, one often gives the expected limit under assumption of the background-only ($\mu = 0$) model. These quantities are used to optimize the analysis and to quantify the experimental sensitivity, that is, to characterize how likely it is to make a discovery if the signal is present, and to say what values of μ one may be able to exclude if the signal is in fact absent.

First we clarify the notion of *expected significance*. Because the significance Z_μ is a function of the data, it is itself a random quantity characterized by a certain sampling distribution. This distribution depends on the assumed value of μ, which is not necessarily the same as the hypothesized value of μ being tested. We may therefore consider the distribution $f(Z_\mu|\mu')$, *i.e.*, the distribution of Z_μ that would be obtained by considering data samples generated under assumption of μ'. In a similar way one can talk about the sampling distribution of an upper limit for μ, $f(\mu_{\rm up}|\mu')$.

One can identify the expected significance or limit with either the mean or median of these distributions, but the median may be preferred since it is invariant under monotonic transformations. For example, the monotonic relation between p-value and significance, $p = 1-\Phi(Z)$, then gives $\mathrm{med}[\,p_\mu|\mu'\,] = 1-\Phi(\mathrm{med}[\,Z_\mu|\mu'\,])$, whereas the corresponding relation does not hold in general for the mean.

In some cases one may be able to write down approximate formulae for the distributions of Z_μ and for limits, but more generally they must be determined from Monte Carlo calculations. In many cases of interest, the significance Z_μ and the limits on μ will have approximate Gaussian distributions.

As an example, consider a Poisson counting experiment, where the result consists of an observed number n of events, modeled as a Poisson distributed variable with a mean of $\mu s+b$. Here s and b, the expected numbers of events from signal and background processes, are taken to be known. If we are interested in discovering the signal process we test and try to reject the hypothesis $\mu = 0$. To characterize the experimental sensitivity, we want to give the discovery significance expected under the assumption of $\mu = 1$.

In the limit where its mean value is large, the Poisson variable n can be approximated as an almost continuous Gaussian variable with mean $\mu s + b$ and standard deviation $\sigma = \sqrt{\mu s + b}$. In the usual case where a physical signal model corresponds to $\mu > 0$, the p-value of $\mu = 0$ is the probability to find n greater than or equal to the value observed,

$$p_0 = \Phi\left(\frac{n-b}{\sqrt{b}}\right) , \tag{40.83}$$

and the corresponding significance is $Z_0 = \Phi^{-1}(1-p_0) = (n-b)/\sqrt{b}$. The median (here equal to the mean) of n assuming $\mu = 1$ is $s + b$, and therefore the median discovery significance is

$$\mathrm{med}[\,Z_0|\mu = 1\,] = \frac{s}{\sqrt{b}} . \tag{40.84}$$

The figure of merit "$s/\sqrt{b}$" has been widely used in particle physics as a measure of expected discovery significance. A better approximation for the Poisson counting experiment, however, may be obtained by testing $\mu = 0$ using the likelihood ratio (40.51) $\lambda(0) = L(0)/L(\hat{\mu})$, where

$$L(\mu) = \frac{(\mu s + b)^n}{n!} e^{-(\mu s+b)} \tag{40.85}$$

is the likelihood function, and $\hat{\mu} = (n-b)/s$ is the estimator of μ. In this example there are no nuisance parameters, as s and b are taken to be known. For the case where the relevant signal models correspond to positive μ, one may test the $\mu = 0$ hypothesis with the statistic $q_0 = -2\ln\lambda(0)$ when $\hat{\mu} > 0$, *i.e.*, an excess is observed, and $q_0 = 0$ otherwise. One can show (see, *e.g.*, Ref. [28, 29]) that in the large-sample limit, the discovery significance is then $Z_0 = \sqrt{q_0}$, for which one finds

$$Z_0 = \sqrt{2\left(n\ln\frac{n}{b} + b - n\right)} \tag{40.86}$$

for $n > b$ and $Z_0 = 0$ otherwise. To approximate the expected discovery significance assuming $\mu = 1$, one may simply replace n with the expected value $E[\,n|\mu = 1\,] = s+b$, the so-called "Asimov data set" [28], giving

$$\mathrm{med}[Z_0|\mu = 1] = \sqrt{2\left((s+b)\ln\left(1+\frac{s}{b}\right) - s\right)} . \tag{40.87}$$

This has been shown in Ref. [28,29] to provide a good approximation to the median discovery significance for values of s of several and for b well below unity. The right-hand side of Eq. (40.87) reduces to $s/\sqrt{b}$ in the limit $s \ll b$.

Beyond the simple Poisson counting experiment, in general one may test values of a parameter μ with more complicated functions of the measured data to obtain a p-value p_μ, and from this one can quote the equivalent significance Z_μ or find, *e.g.*, an upper limit $\mu_{\rm up}$. In this case as well one may quantify the experimental sensitivity by giving the significance Z_μ expected if the data are generated with a different value of the parameter μ'. In some problems, finding the sampling distribution of the significance or limits may be possible using large-sample formulae as described, *e.g.*, in Ref. [28, 29]. In other cases a Monte Carlo study may be needed. Using whatever method of calculation is most appropriate, one usually quotes the expected (mean or, preferably, median) discovery significance or exclusion limit as the primary measure of experimental sensitivity.

Even if the true signal is present at its nominal rate, the actual discovery significance Z_0 obtained from the real data is subject to statistical fluctuations and will not in general be equal to its expected value. In an analogous way, the observed limit will differ from the expected limit even if the signal is absent. Upon observing such a difference one would like to know how large this is compared to expected statistical fluctuations. Therefore, in addition to the observed significance and limits it is useful to communicate not only their expected values but also a measure of the width of their distributions.

As the distributions of significance and limits are often well approximated by a Gaussian, one may indicate the intervals corresponding to plus-or-minus one and/or two standard deviations. If the distributions are significantly non-Gaussian, one may use instead the quantiles that give the same probability content, *i.e.*, $[0.159, 0.841]$ for $\pm 1\sigma$, $[0.0228, 0.9772]$ for $\pm 2\sigma$. An upper limit found significantly below the background-only expectation may indicate a strong downward fluctuation of the data, or perhaps as well an incorrect estimate of the background rate.

The procedures described above pertain to frequentist hypothesis tests and limits. Bayesian limits, just like those found from a frequentist procedure, are functions of the data and one may therefore find, usually with approximations or Monte Carlo studies, their sampling distribution and corresponding mean (or, preferably, median) and standard deviation.

When trying to establish discovery of a signal process, the Bayesian approach may employ a Bayes factor as described in Sec. 40.3.4. In the case of the Poisson counting experiment with the likelihood from Eq. (40.85), the log of the Bayes factor that compares $\mu = 1$ to $\mu = 0$ is $\ln B_{10} = \ln(L(1)/L(0)) = n\ln(1+s/b) - s$. That is, the expectation value, assuming $\mu = 1$, of $\ln B_{10}$ for this problem is

$$E[\,\ln B_{10}|\mu = 1\,] = (s+b)\ln\left(1+\frac{s}{b}\right) - s . \tag{40.88}$$

Comparing this to Eq. (40.87), one finds $\mathrm{med}[\,Z_0|1\,] = \sqrt{2E[\,\ln B_{10}|1\,]}$. Thus for this particular problem the frequentist median discovery significance can be related to the corresponding Bayes factor in a simple way.

In some analyses, the goal may not be to establish discovery of a signal process but rather to measure, as accurately as possible, the signal rate. If we consider again the Poisson counting experiment described by the likelihood function of Eq. (40.85), the maximum-likelihood estimator $\hat{\mu} = (n-b)/s$ has a variance, assuming $\mu = 1$, of

$$V[\,\hat{\mu}\,] = V\left[\frac{n-b}{s}\right] = \frac{1}{s^2}V[\,n\,] = \frac{s+b}{s^2} , \tag{40.89}$$

so that the standard deviation of $\hat{\mu}$ is $\sigma_{\hat{\mu}} = \sqrt{s+b}/s$. One may therefore use $s/\sqrt{s+b}$ as a figure of merit to be maximized in order to obtain the best measurement accuracy of a rate parameter. The quantity $s/\sqrt{s+b}$ is also the expected significance with which one rejects s assuming the signal is absent, and thus can be used to optimize the expected upper limit on s.

References

[1] B. Efron, Am. Stat. **40**, 1 (1986).

[2] R. D. Cousins, Am. J. Phys. **63**, 398 (1995).

[3] A. Stuart, J. K. Ord and S. Arnold, *Classical Inference and the Linear Model*, Kendall's Advanced Theory of Statistics, 6th ed. volume 2A, Arnold, London (1999), the likelihood-ratio ordering principle is described at the beginning of Ch. 23. Chapter 26 compares different schools of statistical inference.

[4] F. James, *Statistical methods in experimental physics*, World Scientific, Hackensack, USA (2006), ISBN 978-981-256-795-6, 978-981-270-527-3.

[5] P. R. Rider, Journal of the American Statistical Association **55**, 289, 148 (1960).

[6] L. Lyons, *Statistics for Nuclear and Particle Physicists*, Cambridge Univ. Pr., Cambridge, UK (1986), ISBN 978-0-521-37934-2.

[7] R. J. Barlow, Nucl. Instrum. Meth. A **297**, 496 (1990).

[8] S. Baker and R. D. Cousins, Nucl. Instrum. Meth. **221**, 437 (1984).

[9] S. S. Wilks, Annals Math. Statist. **9**, 1, 60 (1938).

[10] G. Cowan, *Statistical data analysis*, Clarendon press (1998), ISBN 978-0-19-850156-5.

[11] O. Behnke *et al.*, editors, *Data analysis in high energy physics: A practical guide to statistical methods*, Wiley-VCH, Weinheim, Germany (2013), ISBN 978-3-527-41058-3, 978-3-527-65344-7, 978-3-527-65343-0.

[12] A. O'Hagan and J. J. Forster, editors, *Bayesian Inference*, Kendall's Advanced Theory of Statistics, 2nd ed., volume 2B, Arnold, London (2004), ISBN 978-0-340-80752-1.

[13] D. Sivia and J. Skilling, editors, *Data Analysis: A Bayesian Tutorial*, Oxford University Press, Oxford (2006), ISBN 978-1-383-02981-9, 978-0-198-56831-5.

[14] P. C. Gregory, editor, *Bayesian Logical Data Analysis for the Physical Sciences*, Cambridge University Press, Cambridge (2005), ISBN 978-0-511-79127-7.

[15] J. M. Bernardo and A. F. M. Smith, editors, *Bayesian Theory*, Wiley, London (2000), ISBN 978-0-471-49464-5, 978-0-470-31687-0.

[16] R. E. Kass and L. Wasserman, J. Am. Stat. Assoc. **91**, 1343 (1996).

[17] J. M. Bernardo, J. R. Statist. Soc. B **41**, 113 (1979).

[18] J. M. Bernardo and J. O. Berger, J. Am. Stat. Assoc. **84**, 200 (1989).

[19] J. M. Bernardo, in D. Dey and C. Rao, editors, "Bayesian Thinking," volume 25 of *Handbook of Statistics*, 17–90, Elsevier (2005), URL `https://www.sciencedirect.com/science/article/pii/S0169716105250022`.

[20] L. Demortier, S. Jain and H. B. Prosper, Phys. Rev. **D82**, 034002 (2010), [arXiv:1002.1111].

[21] S. Schmitt, EPJ Web of Conferences **137**, 11008 (2017), ISSN 2100-014X.

[22] L. Brenner *et al.*, Int. J. Mod. Phys. A **35**, 24, 2050145 (2020), [arXiv:1910.14654].

[23] K. Cranmer, J. Pavez and G. Louppe, "Approximating Likelihood Ratios with Calibrated Discriminative Classifiers," (2015), unpublished, [arXiv:1506.02169].

[24] N. Reid, Proceedings of PHYSTAT: Statistical Problems in Particle Physics, Astrophysics, and Cosmology **C030908**, 265 (2003), URL `https://www.slac.stanford.edu/econf/C030908/papers/THAT001.pdf`.

[25] W. A. Rolke, A. M. Lopez and J. Conrad, Nucl. Instrum. Meth. **A551**, 493 (2005), [arXiv:physics/0403059].

[26] S. Algeri *et al.*, Nat. Rev. Phys. **2**, 245–252 (2020).

[27] Proceedings of the PHYSTAT Conference Series (Durham 2002, Stanford 2003, Oxford 2005, and Geneva 2007, 2011) can be found at `https://espace.cern.ch/phystat`.

[28] G. Cowan *et al.*, Eur. Phys. J. **C71**, 230 (2011), [arXiv:1007.1727].

[29] G. Cowan *et al.*, Eur. Phys. J. C **73**, 2501 (2013).

[30] L. Demortier, in "PHYSTAT-LHC Workshop on Statistical Issues for LHC Physics," 23–33 (2007), URL `https://cds.cern.ch/record/1099967/files/p23.pdf`.

[31] O. Barndorff-Nielsen, Biometrika **67**, 2, 293 (1980), ISSN 00063444, URL `http://www.jstor.org/stable/2335474`.

[32] M. S. Bartlett, Proceedings of the Royal Society of London. Series A - Mathematical and Physical Sciences **160**, 901, 268 (1937), URL `https://royalsocietypublishing.org/doi/abs/10.1098/rspa.1937.0109`.

[33] D. N. Lawley, Biometrika **43**, 3-4, 295 (1956), ISSN 0006-3444, URL `https://doi.org/10.1093/biomet/43.3-4.295`.

[34] A. R. Brazzale, A. C. Davison and N. Reid, *Applied Asymptotics: Case Studies in Small-Sample Statistics*, Cambridge University Press, Cambridge (2007), URL `http://infoscience.epfl.ch/record/104219`.

[35] G. Cordeiro and F. Cribari-Neto, *An Introduction to Bartlett Correction and Bias Reduction*, SpringerBriefs in Statistics, Springer Berlin Heidelberg (2014), ISBN 978-3-642-55255-7, URL `https://books.google.co.uk/books?id=MJyKAwAAQBAJ`.

[36] K. Cranmer, in "Statistical Problems in Particle Physics, Astrophysics and Cosmology (PHYSTAT 05): Proceedings, Oxford, UK, September 12-15, 2005," 112–123 (2005), [arXiv:physics/0511028].

[37] R. D. Cousins, J. T. Linnemann and J. Tucker, Nucl. Instrum. Meth. A **595**, 2, 480 (2008), URL `https://doi.org/10.1016%2Fj.nima.2008.07.086`.

[38] E. Gross and O. Vitells, Eur. Phys. J. **C70**, 525 (2010), [arXiv:1005.1891].

[39] R. B. Davies, Biometrika **74**, 33 (1987).

[40] O. Vitells and E. Gross, Astropart. Phys. **35**, 230– (2011), [arXiv:1105.4355].

[41] R. D. Cousins, Lectures on Statistics in Theory: Prelude to Statistics in Practice (2024), [arXiv:1807.05996].

[42] J. Skilling, AIP Conf. Proc. **735**, 395–405 (2004).

[43] R. E. Kass and A. E. Raftery, J. Am. Statist. Assoc. **90**, 430, 773 (1995).

[44] B. P. Roe and M. B. Woodroofe, Phys. Rev. **D63**, 013009 (2001), [hep-ex/0007048].

[45] J. Neyman, Phil. Trans. Roy. Soc. Lond. **A236**, 767, 333 (1937); Reprinted in *A Selection of Early Statistical Papers on J. Neyman*, (University of California Press, Berkeley, 1967).

[46] G. J. Feldman and R. D. Cousins, Phys. Rev. **D57**, 3873 (1998), [arXiv:physics/9711021].

[47] C. J. Clopper and E. S. Pearson, Biometrika **26**, 404–313 (1934).

[48] A. L. Read, in "Workshop on confidence limits, CERN, Geneva, Switzerland, 17-18 Jan 2000: Proceedings," 81–101 (2000), URL `http://weblib.cern.ch/record/451614`.

[49] T. Junk, Nucl. Instrum. Meth. **A434**, 435 (1999), [hep-ex/9902006].

Phys. A 2026.41. Downloaded from www.worldscientific.com by UNIVERSITY OF CA LEY on 09/16/26. Re-use and distribution is strictly not permitted, except for Open Access articles.

41. Machine Learning

Written August 2025 by J.M. Duarte (UC San Diego), U. Seljak (UC Berkeley; LBNL) and K. Terao (SLAC; Stanford U.).

41.1 Introduction . . . 727
41.1.1 A gentle introduction with a representative example . . . 727
41.2 Supervised learning . . . 728
41.2.1 Loss, risk, empirical risk . . . 728
41.2.2 Regression . . . 728
41.2.3 Classification . . . 729
41.2.4 Generalization and model complexity . . . 730
41.2.5 Regularization . . . 730
41.3 Unsupervised learning . . . 731
41.3.1 Representation learning, compression, and autoencoders . . . 731
41.3.2 Clustering . . . 732
41.3.3 Density estimation . . . 732
41.3.4 Generative models . . . 733
41.3.5 Anomaly detection and out-of-distribution detection . . . 736
41.4 Self-supervised learning . . . 737
41.5 Optimal control, reinforcement learning, and active learning . . . 738
41.5.1 Optimal control . . . 738
41.5.2 Reinforcement learning . . . 739
41.5.3 Multi-arm bandits . . . 739
41.5.4 Bayesian optimization . . . 739
41.5.5 Active learning . . . 739
41.6 Simulation-based inference . . . 739
41.6.1 Latent space reconstruction and unfolding . 740
41.7 Data representations, inductive bias, and example applications . . . 740
41.8 Flavors of ML models . . . 741
41.8.1 Support vector machines . . . 741
41.8.2 From Bayesian linear regression to kernel regression and Gaussian processes . . . 742
41.8.3 Decision trees . . . 743
41.8.4 Neural networks . . . 744
41.8.5 Model design with physics inductive bias . 751
41.9 Learning algorithms . . . 751
41.9.1 Gradient-based optimization . . . 751
41.9.2 Stochastic gradient descent . . . 751
41.9.3 Optimization algorithms . . . 751
41.9.4 Automatic differentiation and backpropagation . . . 752
41.9.5 The vanishing and exploding gradient problems . . . 752
41.9.6 Early stopping . . . 752
41.9.7 Initialization of model parameters . . . 753
41.9.8 Input normalization . . . 753
41.9.9 Batch normalization . . . 753
41.9.10 Transfer learning: pre-training and fine-tuning . . . 753
41.9.11 Foundation models . . . 753
41.10 Incorporating uncertainty . . . 754
41.10.1 Propagation of errors . . . 755
41.10.2 Domain adaptation . . . 755
41.10.3 Parameterized models . . . 756
41.10.4 Data augmentation . . . 756
41.10.5 Aleatoric and epistemic uncertainty . . . 756
41.10.6 Model averaging and Bayesian machine learning . . . 756
41.10.7 Connection to probabilistic machine learning 757
41.11 Model compression and deployment in experiments 758

41.1 Introduction

This chapter gives an overview of the core concepts of machine learning (ML)—the use of algorithms that learn from data, identify patterns, and make predictions or decisions without being explicitly programmed—that are relevant to particle physics with some examples of applications to the energy, intensity, cosmic, and accelerator frontiers. ML is an enormous field that has grown substantially in the last decade, largely driven by the emergence of so-called deep learning (DL) [1, 2]. ML has a long history in particle physics going back to the late 1980s and early 1990s; see Refs. [3–5] for recent reviews. ML is a subset of artificial intelligence (AI), which generally refers to computational systems that can perform tasks typically associated with human intelligence, such as learning, reasoning, problem-solving, perception, and decision-making.

Physicists are exploring and contributing to machine learning at an unprecedented rate, which poses a challenge for those who wish to have an up-to-date view of the field. This motivated an effort to create *A Living Review of Machine Learning for Particle and Nuclear Physics* [6], which can be accessed here: `https://iml-wg.github.io/HEPML-LivingReview/`. At the time of writing, the Living Review included more than 1,800 references organized hierarchically by topic. Although we make references to some of these papers, this chapter focuses on the methodology and does not attempt to give a comprehensive review of the applications.

Machine learning and artificial intelligence have a mathematical foundation that is closely tied to statistics (see Ch. 40), the calculus of variations, approximation theory, and optimal control theory. Nevertheless, there have been tremendous advances in recent years, driven by increased computational power, enormous datasets, and new insights, that are impacting physics and society.

The topic can be organized along a few axes, which we use to structure this section. First, there are different learning paradigms, for example, supervised learning, unsupervised learning, and reinforcement learning. Within these paradigms, there are various tasks; for example, classification and regression—which have been the primary use of ML in particle physics—are examples of supervised learning. In addition to the learning paradigm and tasks, there are various types of machine learning models that generically process some input and produce some output. The types of models vary based on what they are modeling (*e.g.*, so-called discriminative vs. generative models), as well as how they are implemented (*e.g.*, neural networks, decision trees, or kernel machines). Next, there are the issues around training or learning within the context of a given task and model class, which connects to optimization and regularization. We will briefly discuss the various considerations that emerge in the application of machine learning methods to physics, such as the treatment of systematic uncertainty, the interpretability of the models, and the incorporation of symmetry.

41.1.1 *A gentle introduction with a representative example*

We will use a specific, familiar example to introduce the various ingredients in context before factorizing and abstracting them. Consider the task of *classifying* energy deposits in a particle detector as coming from electrons or protons. For this example, let the detector data consist of energy deposits in d sensors so that the data can be represented as a *feature vector* $x \in \mathbb{R}^d$. Different components of x may correspond to physical quantities with different units (*e.g.*, units of energy, momentum, or position).

Due to the complex interactions of particles in the detector, we do not have an explicit probability model for the high-dimensional data for the electron and proton scenarios, but we do have a simulator that allows us to generate Monte Carlo samples for each. This allows us to assemble a *training dataset* $\{x_i, y_i\}_{i=1,\ldots,n}$, where y is a *label* that identifies how the example was generated (*e.g.*, $y = 0$ for electrons and $y = 1$ for protons). We would like to find a function that accurately *predicts* the label on new data. Because we have feature-label pairs, this is a *supervised learning* problem. We can use a *neural network* to provide a flexible family of functions $f_\phi : \mathbb{R}^d \to \mathbb{R}$, where ϕ denotes the internal parameters of the neural network (*i.e.*, the weights and biases that we will discuss in Sec. 41.8.4). The goal of *training* is to find

Int. J. Mod. Phys. A 2026.41. Downloaded from www.worldscientific.com by UNIVERSITY OF CALIFORNIA @ BERKELEY on 09/16/26. Re-use and distribution is strictly not permitted, except for Open Access articles.

Phys. A 2026.41. Downloaded from www.worldscientific.com
by UNIVERSITY OF CA LEY on 09/16/26. Re-use and distribution is strictly not permitted, except for Open Access articles.

the value of the parameters ϕ that provide the 'best' predictions. This is made concrete through a *loss function* $\mathcal{L}(y, f_\phi(x))$. Instead of the obvious zero-one loss, which is 0 if $f_\phi(x) = y$ and 1 if not, we use the squared-loss $\mathcal{L}_{\rm sq}(y, f_\phi(x)) = (y - f_\phi(x))^2$, which will be motivated in Sec. 41.2.3. We can evaluate the average of the loss on the training set of size n, known as the *empirical risk* or *training loss* $\mathcal{R}_{\rm emp}(f_\phi) = \sum_{i=1}^n \mathcal{L}(y_i, f_\phi(x_i))/n$. *Training* refers to numerically minimizing the empirical risk. We can numerically optimize the model through *gradient descent*, which iteratively adjusts the parameters of the network according to $\phi^{t+1} = \phi^t - \lambda \nabla_\phi \mathcal{R}_{\rm emp}(f_\phi)$, where λ is the *learning rate*.

Once the optimization is complete and we obtain the solution $\hat{\phi}$, it is natural to assess the quality of the trained model $f_{\hat{\phi}}$ on an independent *testing dataset*[1]. The empirical risk evaluated on the testing set is often larger than on the training set, and large differences indicate *overfitting*, meaning that the model does not generalize well to the unseen data. The ability to accurately predict on unseen data is referred to as *generalization* and the empirical risk on the test data provides a measure of the *generalization error*. In order to reduce the generalization error one might explore different model choices (*e.g.*, neural network architectures), additional regularization terms in the loss function, different learning rates, optimization algorithms, or early stopping criterion in the optimization.

In order to produce a binary electron vs. proton decision from the continuous output of the neural network, one typically chooses a threshold (*i.e.*, classify as proton if $f_{\hat{\phi}}(x) > c$). The choice of the threshold c is often referred to as a working point and it sets the tradeoff between electron and proton efficiencies, fake rates, and purities. A *receiver operating characteristic curve*, or ROC curve, is used to summarize the tradeoff between true positive rate (TPR) and false positive rate (FPR). Importantly, the characterization of the efficiency and rejection power (or equivalently the ROC curve) requires labeled data. In a particle physics context, it is recognized that the simulation is not perfect and the mismodeling is associated to the presence of systematic uncertainty. The discrepancy between the distribution of the training dataset and the distribution of the data where the model will be applied is referred to as *domain shift* or *distribution shift*. While mismodeling in the training dataset might lead to a suboptimal classifier, the real source of systematic uncertainty comes from the mismatch between the data used to characterize the performance of the classifier and the unlabeled data that the classifier is applied to. This motivates the use of data-driven methods to calibrate the resulting model.

This example provides a vertical slice through the various aspects of supervised machine learning in particle physics. Now we factorize and abstract the various ingredients in order to provide a more general treatment with a broader scope.

41.2 Supervised learning

Supervised learning generally refers to the class of problems where the training dataset are presented as input-output pairs $\{(x_i, y_i)\}_{i=1,\ldots,n}$, where $x_i \in \mathcal{X}$ are the input features and $y_i \in \mathcal{Y}$ are the corresponding target labels. Furthermore, it is typically the case that x_i and y_i are independent and identically distributed (i.i.d.) according to the data distribution $p(x, y)$, $(x_i, y_i) \overset{\text{i.i.d.}}{\sim} p(x, y)$, though $p(x, y)$ is usually not known explicitly.

The goal of supervised learning is find a function $f : \mathcal{X} \to Y$ that 'best' captures the relationship between the input features and the corresponding target labels, similar to parameter estimation described in Sec. 40.2 of the Statistics chapter. Section 41.2.1 discusses how we quantify which function is best.

41.2.1 *Loss, risk, empirical risk*

The term *learning* in machine learning generally refers to optimization of some objective, which can be thought of as minimizing *risk*. The risk brings together three main ingredients. The first is the *model family* $\mathcal{F}$ (where $f \in \mathcal{F}$ is the quantity that we vary during optimization), the second is the *loss function* $\mathcal{L}$, and the third is a data distribution $p(x, y)$. The *risk* for a model $f \in \mathcal{F}$ is defined as its expected loss

$$\mathcal{R}[f] \coloneqq \mathbb{E}_{p(x,y)}[\mathcal{L}(y, f(x))] \equiv \int \mathcal{L}(y, f(x))\, p(x, y)\, \mathrm{d}x\, \mathrm{d}y \ , \quad (41.1)$$

where $\mathbb{E}_p[\cdot]$ refers to the expectation with respect to the distribution p. Written this way, the risk is a functional, and the idealized goal for machine learning is to solve the optimization problem

$$f^* = \arg\min_{f \in \mathcal{F}} \mathcal{R}[f] \ , \quad (41.2)$$

where $\mathcal{F}$ would include all possible functions.

One of the defining characteristics of machine learning in practice is that one does not know the data distribution $p(x, y)$, but does have access to samples from that distribution, *i.e.* $\{x_i, y_i\}_{i=1,\ldots,n}$ with $(x_i, y_i) \overset{\text{i.i.d.}}{\sim} p(x, y)$. This leads to the corresponding *empirical risk*

$$\mathcal{R}_{\rm emp}[f] \coloneqq \mathbb{E}_{\hat{p}(x,y)}[\mathcal{L}(y, f(x))] \equiv \frac{1}{n} \sum_{i=1}^n \mathcal{L}(y_i, f(x_i)) \ , \quad (41.3)$$

where $\hat{p}(x, y) = \frac{1}{n} \sum_{i=1}^n \delta(x - x_i)\delta(y - y_i)$ is referred to as the empirical distribution of the dataset $\{(x_i, y_i)\}_{i=1,\ldots,n}$. The *empirical risk minimization* principle is a core idea in statistical learning theory [7], which approximates f^* with its empirical analogue

$$\hat{f} = \arg\min_{f \in \hat{\mathcal{F}}} \mathcal{R}_{\rm emp}[f] \ , \quad (41.4)$$

where $\hat{\mathcal{F}}$ is the set of all possible functions parametrized by the model parameters ϕ. In an idealized infinite parameter limit machine learning functions, such as neural networks, are often universal approximators, meaning they cover all functions and $\hat{\mathcal{F}} = \mathcal{F}$. For finite size models, this may not be a valid approximation. Expressivity of the network characterizes this universality property and is a function of the network architecture and its parameters such as width and depth of neural network layers. If the expressivity is too small it leads to underfitting. However, an equally important consideration is the risk of overfitting if we optimize Eq. 41.4 for too long or use an unrestricted model class (see Sec. 41.2.5).

While the loss function may quantify some well-motivated notion of risk, it is also common to design loss functions so that f^* has some desired property. In Secs. 41.2.2–41.2.5, we will consider several such loss functions where one can show that the corresponding f^* has the desired property even if the form of the loss is not obvious. Furthermore, there are often multiple loss functions that can lead to the same f^*. Thus, one can think of machine learning as solving Eq. 41.4 with a sufficiently flexible model, powerful optimization algorithms, and practical considerations to break the degeneracy between different loss functions that lead to the same f^*. As we shall see, commonly used loss functions can also be mathematically derived from a probabilistic approach.

41.2.2 *Regression*

The goal of regression is to predict a label $y \in \mathcal{Y}$ given an input feature vector $x \in \mathcal{X}$. Typically, the label is a real-valued scalar, but $\mathcal{X}$ can be $\mathbb{R}^d$ or some more structured target (*e.g.*, an image, sequence, graph, quantile, or distribution). When $\mathcal{Y}$ is discrete, the task is usually referred to as classification (see Sec. 41.2.3); however, the two are closely related and *logistic regression* is an example where the model predicts a continuous probability associated to the possible label values. In elementary statistical language, the target label y is often called a dependent variable, while the feature x is called the independent variable. In classical statistics, one often assumes a model for the data such as

$$y_i = f_\phi(x_i) + e_i \ , \quad (41.5)$$

where e_i is an additive error term that is often assumed to be independent of x and normally distributed. This leads to classic approaches like least-squares (see Sec. 40.2.3), and when the

[1] It is important to never use the testing dataset to make decisions about the model. For this purpose, another independent dataset, usually called the *validation dataset*, should be used (see Sec. 41.2.4).

Int. J. Mod. Phys. A 2026.41. Downloaded from www.worldscientific.com
by UNIVERSITY OF CALIFORNIA @ BERKELEY on 09/16/26. Re-use and distribution is strictly not permitted, except for Open Access articles.

model f_ϕ is linear in ϕ (not in x!) linear regression, which has a closed-form solution. However, we can relax these assumptions and consider the general case of an arbitrary joint distribution $p(x, y)$, which can be written as $p(y|x)p(x)$ without loss of generality (see Sec. 39.1). Consider the *squared error* as a loss function, which corresponds to the mean-squared error (MSE) empirical risk:

$$\mathcal{L}_{\text{MSE}}(y, f(x)) = (y - f(x))^2 \ . \tag{41.6}$$

One might expect that the squared error would only be appropriate in the case that the conditional distribution $p(y|x)$ is normally distributed, but one can use the calculus of variations to show that in general

$$f^*_{\text{MSE}}(x) = \mathbb{E}_{p(y|x)}[y] \ , \tag{41.7}$$

that is the optimal regressor for the MSE is the conditional expectation of y given x.

One issue with the squared-error as a loss function is that it is very sensitive to outliers. Alternatively, one can use the absolute error $|y - f(x)|$ as a loss function[2]. However, the discontinuous derivative of the absolute (L1) error leads to challenges in optimization. As a result there are various other loss functions, such as the Huber loss, that aim to be both robust and more amenable to optimization.

Note that this framing of regression yields a function $f(x)$ that only provides a point estimate for y. An alternative approach to regression is to model the full conditional distribution $p(y|x)$. One such example is Gaussian process regression, which is discussed in Sec. 41.8.2. In that probabilistic approach, one can still obtain a point estimator, such as the conditional expectation or the maximum a posteriori (MAP) estimator

$$f^*(x) = \arg\max_y p(y|x) \ , \tag{41.8}$$

and one can also derive uncertainty estimates on the predicted value y (see Sec. 41.10 for more details). In this setting, the prior distribution on the model family is closely related to the concept of regularization, which we touch on in Secs. 41.2.5 and 41.8.2.

When one directly models $p(y|x)$, or goes further to model the joint distribution $p(x, y) = p(y|x)p(x)$, then one can use maximum likelihood for the loss function. In that approach, the problem is really one of density estimation, which is a type of unsupervised learning that we discuss in Sec. 41.3.3. These two approaches are a classic examples of two different approaches to modeling. Regression with $f^*_{\text{MSE}}(x)$ is the prototypical example of *discriminative* modeling, while modeling the joint distribution is a prototypical example of *generative* modeling. Generally, discriminative approaches with supervised learning outperform generative approaches when there is sufficient data, but generative approaches can be beneficial in data-starved settings [8].

41.2.3 *Classification*

The goal of classification is to predict one of a finite number of class labels $y \in \mathcal{Y}$ given an input feature vector $x \in \mathbb{X}$. It is similar to regression in this way, but the focus is on discrete target space $\mathcal{Y}$. An important special case is when the label can only take on one of two values (*e.g.*, "signal" or "background"), which is referred to as binary classification and is equivalent to simple hypothesis testing in statistics. It is common for a classifier to be the composition of two functions: $f(g(x))$. The first function $g : \mathcal{X} \to \mathbb{R}^{|\mathcal{Y}|}$ predicts continuous probabilities for each class (*i.e.*, $g_c(x) \approx p(y = c|x)$). The second function $f : \mathbb{R}^{|\mathcal{Y}|} \to \mathcal{Y}$ then chooses the discrete label $y \in \mathcal{Y}$, such as $f(g(x)) = \arg\max_c g_c(x) \approx \arg\max_y p(y|x)$. This is the case for both classical methods like logistic regression and modern, deep learning approaches to classification; therefore, we will use the term probabilistic classifier for $g(x)$ or just classifier when it is clear in context.

An intuitive loss function for classification is the zero-one loss, which simply counts the number of mis-classifications:

$$\mathcal{L}_{0/1}(y, f(x)) = \begin{cases} 0, & \text{if } f(x) = y \\ 1, & \text{otherwise} \ . \end{cases} \tag{41.9}$$

[2]The absolute error and squared error are often denoted as L1 and L2 errors, respectively, in reference to the corresponding norms.

The zero-one loss can also be written as $\mathcal{L}_{0/1}(y, f(x)) = \mathbf{1}(y \neq f(x))$, where $\mathbf{1}(\cdot)$ is the indicator function. The zero-one loss is non-differentiable, so it does not pair well with gradient-based optimization.

For binary classification, one can use $y = \{0, 1\}$ as numerical values for the class labels and the *binary cross-entropy* loss function

$$\mathcal{L}_{\text{bxe}}(y, g(x)) = -\left[y \log(g(x)) + (1 - y) \log(1 - g(x))\right] \ . \tag{41.10}$$

The resulting model will approximate $f^*_{\text{bxe}}(x)$, which takes on the form

$$\begin{aligned} f^*_{\text{bxe}}(x) &= \mathbb{E}_{p(y|x)}[y] = p(y = 1|x) \\ &= \frac{p(x|y = 1)p(y = 1)}{p(x|y = 0)p(y = 0) + p(x|y = 1)p(y = 1)} \ . \end{aligned} \tag{41.11}$$

That is the binary cross-entropy loss for binary classification leads to the Bayesian posterior probability that the label $y = 1$ given the feature vector x (see Bayes theorem in Sec. 39.1).

Equation 41.11 highlights an important feature of supervised learning relevant for particle physics: the joint distribution $p(x, y)$ of the training dataset implies a prior distribution $p(y)$ on the labels or classes. This prior distribution reflects the frequency in the training dataset, not necessarily in the real data. When applying the resulting model to a different dataset with the same conditional distribution (data likelihood) $p(x|y)$ for the features and a different prior $p'(y)$ for the labels, the probabilistic interpretation of the result will not be properly calibrated, meaning $g(x) \not\approx p(y|x)$. A common choice for binary classification is to use a balanced training dataset with $p(y = 0) = p(y = 1) = \frac{1}{2}$, while in many cases the true $p'(y = 1)$ in the experimental data might be very small (*i.e.*, low signal-to-background), unknown, or zero (*i.e.*, a hypothetical particle that does not exist).

If $p'(y)$ and $p(y)$ are known then Bayes theorem can be used to re-calibrate the posterior $p(y|x)$ from one prior to another. One example of such re-calibration is the correspondence of binary classification to simple hypothesis tests in frequentist statistics discussed in Sec. 40.3.1 of the Statistics chapter. In that setting, the Neyman-Pearson lemma states that the optimal classifier is given by the likelihood ratio

$$f^*_{\text{NP}}(x) = \frac{p(x|y = 1)}{p(x|y = 0)} \ , \tag{41.12}$$

which does not depend on the prior probabilities $p'(y = 0)$ or $p'(y = 1)$ as in Eq. 41.11, or, equivalently, assumes equal priors $p'(y = 0) = p'(y = 1)$. Bayes theorem can be used to show that the two functions, $f^*_{\text{NP}}(x)$ and $f^*_{\text{bxe}}(x)$, are related by a one-to-one, monotonic transformation

$$f^*_{\text{NP}}(x) = \frac{p(y = 0)}{p(y = 1)} \frac{f^*_{\text{bxe}}(x)}{1 - f^*_{\text{bxe}}(x)} \ , \tag{41.13}$$

which is referred to as the *likelihood-ratio trick* and plays an important role in simulation-based inference (see Sec. 41.6).

A standard way to evaluate the performance of a classifier is to evaluate the true positive rate (TPR)—the proportion of $y = 1$ samples that are correctly identified based on a fixed threshold $g(x) > c$—as a function of the false positive rate (FPR)—the proportion of $y = 0$ samples that are misidentified based on the same fixed threshold. Plotting these values generates a graph known as the receiver operating characteristic (ROC) curve. Importantly, the monotonic transformation of Eq. 41.13 does not impact the tradeoff between FPR and TPR, therefore the ROC curves for $f^*_{\text{NP}}(x)$ and $f^*_{\text{bxe}}(x)$ are identical and do not depend on the prior probabilities $p(y)$. This property has been leveraged in *weakly supervised* approaches [9] to train a classifier in data without access to labels as long as one has two datasets with different $p(y = 1)/p(y = 0)$ ratios and the same conditional distribution $p(x|y)$ of the features given the labels.

A generalization of Eq. 41.10 that applies to multiple classes, is the *categorical cross-entropy* loss

$$\mathcal{L}_{\text{xe}}(y, f(x)) = -\sum_{c \in |\mathcal{Y}|} \mathbf{1}(y = c) \log(f_c(x)) \ , \tag{41.14}$$

by UNIVERSITY OF CA Phys. A 2026.41. Downloaded from www.worldscientific.com LEY on 09/16/26. Re-use and distribution is strictly not permitted, except for Open Access articles.

where $f : \mathcal{X} \to \mathbb{R}^{|\mathcal{Y}|}$ and the indicator function picks out the term in the sum for the corresponding class label y. This loss can be derived by maximizing the posterior of Eq. 41.25 using a discrete set of class labels y, which identifies $f_c(x) = \tilde{f}(y = c|x) = p(y = c|x)$ and thus assumes the constraint $\sum_c f_c(x) = 1$ and $f_c(x) \geq 0$ (see Sec. 41.8.4.2 for an activation function that enforces this). The function $\tilde{f}(y|x)$ can be interpreted as a conditional distribution, *i.e.*, an approximation to the true posterior $p(y|x)$. The risk associated to the cross entropy loss function is

$$\begin{aligned}\mathcal{R}_{\text{xe}}[f] &= \mathbb{E}_{p(x,y)}\left[-\sum_{c\in|\mathcal{Y}|}\mathbf{1}(y=c)\log f_c(x)\right] \\ &= -\sum_{c\in|\mathcal{Y}|} p(y=c)\mathbb{E}_{p(x|y)}[\log\tilde{f}(y=c|x)]\ .\end{aligned} \tag{41.15}$$

This is equivalent to $\mathcal{R}_{\text{xe}}[f] = \mathbb{E}_{p(x)}[H[p(y|x), \tilde{f}(y|x)]]$, where

$$H[p, f] \equiv \mathbb{E}_p[-\log f] = -\int p(x)\log(f(x))\,\mathrm{d}x \tag{41.16}$$

is the cross entropy between the two distributions. One can use a Lagrange multiplier to enforce the normalization constraint and the calculus of variations to show that

$$f^*_{\text{xe},c}(x) = p(y = c|x)\ , \tag{41.17}$$

which is equivalent to the solution in Eq. 41.11 in the binary case.

This approach is closely related to the loss functions that are used for density estimation, the forward Kullback-Leibler (KL) divergence, and the maximum likelihood estimation. Minimizing cross entropy $H[p, f_\phi]$ to ϕ is equivalent to minimizing the forward KL divergence

$$\text{KL}(p\|f_\phi) \coloneqq \mathbb{E}_p[\log p(x)) - \log f_\phi] = H[p, f_\phi] - H[p]\ , \tag{41.18}$$

where $H[p] \coloneqq \int p(x)\log p(x)dx$ is the entropy and independent of f_ϕ. The KL divergence $\text{KL}[p\|f] \geq 0$, and equal if and only if $p = f$.

Unlike in the binary classification case, the multi-class classifier is sensitive to the priors $p(y)$ used in training. This leads to complications as often the class proportions are unknown. For example, one might be interested in classifying a signal when multiple backgrounds are present and the relative proportion of those different background components is uncertain. Ideally one would like the class proportions for the background components used in training to match those in the data, which presents an additional training challenge if those proportions are heavily unbalanced.

41.2.4 *Generalization and model complexity*

With a sufficiently flexible model, it is possible to fit the training dataset very well, though the model might not *generalize* well to unseen data, a phenomenon known as *overfitting*. More concretely, for a nonnegative loss function one might have $\mathcal{R}_{\text{emp}}[\hat{f}] \to 0$, while the true risk $\mathcal{R}[\hat{f}]$ might be large. Conversely, *underfitting* occurs when a model is unable to capture the relationship between the inputs and labels accurately, resulting in large empirical and true risks. While it is generally not possible to evaluate $\mathcal{R}[\hat{f}]$ exactly because we do not know $p(u)$, we can use an independent dataset (also called validation dataset) to obtain an unbiased estimate of it. This *cross-validation* method motivates the test-train-validation split of the data.

Intuitively, a model with many parameters has more flexibility and is more prone to overfitting. However, some highly overparameterized models (that have large subspaces of their parameters where $\mathcal{R}_{\text{emp}}[\hat{f}_\phi] \to 0$) generalize well [10, 11]. Often this is achieved through *regularization*, both explicit and implicit (Sec. 41.2.5).

Two main sources of error prevent models from generalizing beyond their training dataset. One is *bias* arising from erroneous assumptions in the model and the other is *variance* arising from sensitivity to statistical fluctuations in the training dataset. The *bias-variance decomposition* is a way of analyzing a model's expected risk as a sum of bias and variance terms. Concretely, if $\mathcal{L}$ is the squared loss, one can decompose the expected risk $\mathbb{E}_{\mathcal{D}}[\mathcal{R}_{\text{emp}}[\hat{f}_\phi]]$ over all possible training datasets $\mathcal{D}$ into three terms [12, 13],

$$\begin{aligned}\mathbb{E}_{\mathcal{D}}\left[\mathcal{R}[\hat{f}^{\mathcal{D}}_\phi]\right] &= \mathbb{E}_{\mathcal{D}}\mathbb{E}_{p(x,y)}\left[(y - \hat{f}^{\mathcal{D}}_\phi(x))^2\right] \\ &= \mathbb{E}_{p(x)}\Bigg[\underbrace{\mathbb{E}_{p(y|x)}\left[(y-\bar{y})^2\right]}_{\text{noise}} + \underbrace{\mathbb{E}_{\mathcal{D}}\left[(\hat{f}_\phi(x) - \bar{f}(x))^2\right]}_{\text{variance}} \\ &\qquad + \underbrace{(\bar{y} - \bar{f}(x))^2}_{\text{bias}}\Bigg]\ ,\end{aligned} \tag{41.19}$$

where $\bar{f}(x) \equiv \mathbb{E}_{\mathcal{D}}\left[\hat{f}^{\mathcal{D}}_\phi(x)\right]$ is the "average" prediction of the model over different possible training datasets. In this expression, the first term is the inherent "noise" in the dataset, *i.e.*, the variance of y around its mean, which is zero if y is deterministically related to x. The second term is the variance of the model around its average when considering different training datasets, and the third term is the squared bias, *i.e.*, the difference between the average prediction and the true conditional mean.

Classically, there is a correspondence between overfitting and underfitting and the concepts of bias and variance discussed in Sec. 40.2 on parameter estimation. Overfitting implies high variance: the model class is too complex and retraining yields vastly different models. Variance tends to increase with model complexity and decrease with more training data. Underfitting implies high bias: the model class is too simple and has a large error rate. Thus, there exists a tradeoff between bias and variance, shown schematically in Fig. 41.1 (left).

However, in modern machine learning, very high-capacity models such as neural networks can be trained to exactly fit the data, and yet obtain high accuracy on test data [14], as shown in Fig. 41.1 (right). This phenomenon is known as "double descent." The apparent contradiction may be addressed by considering the regularizing (Sec. 41.2.5) effects of neural network training, specifically stochastic gradient descent (Sec. 41.9.2).

41.2.5 *Regularization*

The trained model $\hat{f}$, or equivalently, the parameters of the trained model $\hat{\phi}$ can be thought of as point estimates of f^*. The bias-variance tradeoff means that introducing a small bias can often lead to a significant reduction in variance. This motivates the explicit addition of a *regularization* term to the loss function, which will introduce some bias $f^*_{\text{reg}} \neq f^*$. A common form of regularization is to penalize by the L2 norm of the parameters (*i.e.* $\|\phi\|^2$), which is referred to as *L2 or Tikhonov regularization*. This appears in the form of penalized maximum likelihood, and it is also commonly used in unfolding [15]. Alternatively, one can penalize by the L1 norm $\|\phi\|$, which is known as *L1 regularization*. One can also interpret the regularization term as an explicit prior on the parameters, and the resulting model as the Bayesian maximum a posteriori (MAP) estimator. When L1 or L2 regularization is paired with linear regression, it is known as *LASSO regression* or *ridge regression*, respectively. In addition, L2 regularization paired with kernel machines gives rise to Gaussian process regression.

These two types of explicit regularization generally have solutions with different properties. For example, L1 regularization naturally induces sparsity, *i.e.*, a fraction of the parameters are nearly zero, whereas L2 regularization tends to keep all parameters nonzero but with lower magnitudes, as illustrated in Fig. 41.2. Because L1 regularization sets certain parameters to zero, it is often used as part of feature selection and model compression techniques, as discussed in Sec. 41.11.

Another form of regularization is to restrict the model class $\hat{\mathcal{F}}$. For example, a neural network and a sequence of narrow step functions (delta functions) can both be shown to be universal approximators in infinite parameter size limit, but on real world examples the former generalizes much better than the latter. Within the class of neural network models, convolutional neural networks are a subset of generic feedforward neural networks that approximately preserve translational symmetry (see Sec. 41.8.4.4 for more discussion). These types of choices are often encoded in

Int. J. Mod. Phys. A 2026.41. Downloaded from www.worldscientific.com
by UNIVERSITY OF CALIFORNIA @ BERKELEY on 09/16/26. Re-use and distribution is strictly not permitted, except for Open Access articles.

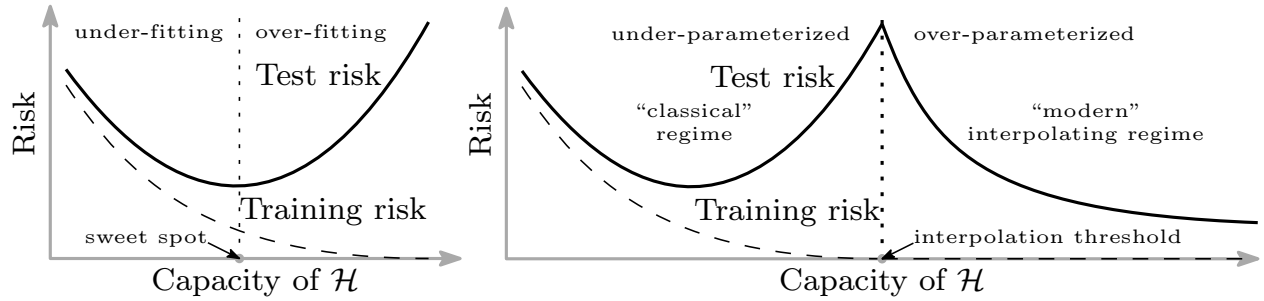

Figure 41.1: Curves for training risk (dashed line) and test risk (solid line) from Belkin et al. in Proceedings of the National Academy of Sciences, 2019. The classical U-shaped risk curve arising from the bias-variance trade-off (left) and the double descent risk curve (right), which incorporates the U-shaped risk curve (*i.e.*, the "classical" regime) together with the observed behavior from using high capacity function classes (*i.e.* the "modern" regime).

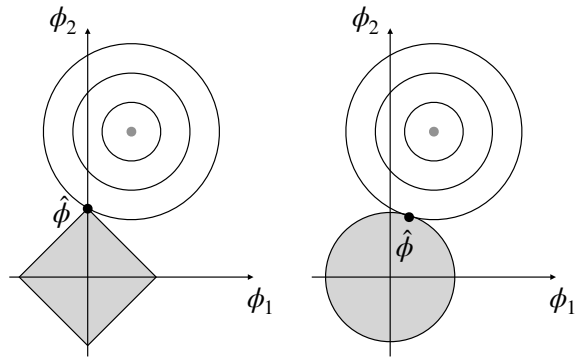

Figure 41.2: Depiction of L1 (left) and L2 (right) regularization constraint regions and the contours of an unregularized loss function. The intersection with the L1 constraint region gives an optimal value $\hat{\phi}$ that is sparse, *i.e.*, $\phi_1 = 0$, while the L2 contraint region yields an optimal value $\hat{\phi}$ where both ϕ_1 and ϕ_2 are small, but nonzero.

the architecture of a neural network and are broadly referred to as *inductive bias* in the model.

In addition to explicit regularization terms in the loss function or through restrictions to the model class, it is also possible to regularize implicitly. One implicit regularization is through early stopping [15,16], where we monitor the loss on the training dataset and the loss on held-out validation dataset. While the training loss continues to decrease with more gradient descent cycles, the validation loss may not, and early stopping stops the training when validation loss flattens out or begins to increase. Another powerful form of regularization used in deep learning models is known as *dropout* [17], which randomly removes some some parts of the model during training and can be thought of as implementing a type of model averaging [18].

The chosen numerical optimization procedure can also act as an implicit regularization. In the case of highly over-parameterized models where there is a large degenerate parameter space that achieves zero loss, $\Phi_0 = \{\phi | \mathcal{R}_{\text{emp}}[f_\phi]\} = 0$, the dynamics of the optimization algorithm will break the degeneracy and favor some particular $\hat{\phi} \in \Phi_0$ as if an additional regularization term was included. Despite zero loss and over-parametrization, the corresponding generalization error may be small, a phenomenon called *benign overfitting* [19]. Different optimization algorithms will have different implicit regularization effects, and thus favor different parameter points in Φ_0 that will have different generalization error [20]. Understanding this interaction is a topic of contemporary research in machine learning [21].

Some methods such as Gaussian process (GP) do not require optimization, and instead use linear algebra to obtain the solution. Benign overfitting is explicit for GP in that in the absence of noise the solution goes through all the training data, yet it generalizes well if the kernel is well chosen. Infinitely wide neural networks have an explicit correspondence to Gaussian process [22]. When applied to deep networks this leads to the concept of neural tangent kernel [23].

41.3 Unsupervised learning

Unsupervised learning generally refers to the class of problems that use unlabeled training dataset $\{x_i\}_{i=1,\ldots,n}$, where $x_i \in \mathcal{X}$ are the input features. Furthermore, it is typically assumed that $(x_i) \overset{\text{i.i.d.}}{\sim} p(x)$, though $p(x)$ is usually not known explicitly. Finally, the loss function in unsupervised learning takes on the special form $\mathcal{L}(x, f(x))$. This class of learning has many different applications, such as density estimation, anomaly detection, generative learning, representation learning and clustering, each with the corresponding set of methods. Some of these tasks can be achieved with the same methods, *e.g.* normalizing flows (see Sec. 41.3.4.3) can perform density estimation, generative sampling and anomaly detection.

41.3.1 *Representation learning, compression, and autoencoders*

A recurring topic in machine learning and statistics is how to represent the data. Much of classical statistics involves constructing a low-dimensional summary statistic that extracts the relevant information from the data for a particular task (a sufficient statistic in the language of classical statistics). There is a spectrum of representations with tradeoffs. At one end of this spectrum is lossless compression that allows one to encode the data into a smaller, intermediate representation that carries all the information since it can be decoded back into the original data. At the other end of the spectrum is something like the likelihood ratio, which is a single scalar that carries the relevant information needed for hypothesis testing for a single hypothesis, but it discards all the other information that might be needed for other tasks, such as testing other hypotheses. An intermediate point in this spectrum is the process of feature engineering, which refers to the creation of new features $\mathcal{X}'$ from the original features $\mathcal{X}$ in hopes that the downstream task will be easier with the new features. For example, instead of working directly with the energy and momentum of particles, one might compute invariant masses or angles between particles. This type of feature engineering generally improves performance for shallow neural networks and decision trees; however, with the rise of deep learning this is often no longer necessary and may limit performance compared to working with the original features [4]. One can think of the intermediate layers of a neural network between the input and the output a representation of the data that is good for the task at hand, and by training all the layers of the network simultaneously (or "end-to-end") one can see the intermediate layers as a learned representations. For a review, see Ref. [24].

An example of a linear dimensionality reduction representation and data compression is principal component analysis (PCA) of data $x \in \mathbb{R}^d$ at fixed latent space dimensionality k ($k < d$), which

Phys. A 2026.41. Downloaded from www.worldscientific.com
by UNIVERSITY OF CA LEY on 09/16/26. Re-use and distribution is strictly not permitted, except for Open Access articles.

finds the orthogonal linear transformation, O,

$$O : \mathbb{R}^k \to \mathbb{R}^d, z \mapsto Oz,\ OO^\intercal = I_d \tag{41.20}$$

that maximizes the data variance in the latent space. Maximizing the variance of the transformed data is equivalent to minimizing the average reconstruction error (the residual variance in data space),

$$\mathcal{L}_{\text{reco}}(x, f(x)) = \|x - f(x)\|^2 \ . \tag{41.21}$$

A PCA can thus be interpreted as a linear, orthogonal model that is trained to minimize the L_2-distance between the input data and the reconstructed data given the fixed dimensionality k. In practice, the PCA problem can be solved analytically without the use of optimization algorithms or the loss function: the principal components are given by the eigenvectors of the data covariance matrix.

A suitable latent space dimensionality, k, is chosen by ordering the eigenvalues, λ_i, of the data covariance in descending order, and keeping only the first few eigenvectors that correspond to the largest eigenvalues. The cut is often made at dimensionalities that capture around 90% of the data variance. For many data sets this results in $k \ll d$. The average reconstruction error that originates from the discarded eigenvalues is $\sigma^2_{\text{reco}} = \sum_{i=k+1}^{d} \lambda_i$.

Another common type of representation learning and nonlinear dimensionality reduction is based on the *autoencoder* $f = g \circ e : \mathcal{X} \to \mathcal{X}$, where $e : \mathcal{X} \to \mathcal{Z}$ is referred to as the *encoder* and $g : \mathcal{Z} \to \mathcal{X}$ is referred to as the *generator* or *decoder*. Typically the dimensionality of $\mathcal{Z}$ is much less than $\mathcal{X}$, and $z = e(x)$ can be thought of as a compressed representation of the input. The intermediate space $\mathcal{Z}$ is sometimes referred to as the bottleneck or the latent space of the autoencoder. If the bottleneck is sufficiently large and the encoder and decoder are sufficiently flexible, then the function f could just be the identity (*i.e.*, lossless compression). However, if the encoder and decoder are not sufficiently flexible or the dimensionality of the latent space is not large enough there will be some reconstruction error. Therefore, the reconstruction error of Eq. 41.21 serves as a natural loss function of an autoencoder.

Once trained, the encoder $e(x)$ can be used independently of the decoder to provide a generic low-dimensional representation of the data. The flexibility of this approach is attractive; however, there are no guarantees that this representation will be optimal for the other task. Indeed, the transition from pre-trained autoencoders to end-to-end learning is one of the important trends that characterized the onset of the deep learning era.

While achieving zero reconstruction error may seem good as it would imply lossless compression, it often performs poorly in practice. First, the encoder may be overfit to the training dataset and not generalize well to held out data. This can be addressed by adding a prior to the training, discussed in Sec. 41.3.4.1. Second, it may not be robust to domain shift (see Sec. 41.10.2).

41.3.2 *Clustering*

The goal of clustering is to group the data $\{x_i\}_{i=1,\ldots,n}$ into k groups, or *clusters*, usually with $k \ll n$. Intuitively, if two data points belong to the same cluster, then they should be similar in some sense. Conversely, if two data points are very different, then they should be assigned to different clusters. The notion of similarity usually is based on some heuristic, and there are a variety of algorithmic and probabilistic clustering algorithms. In some cases k is specified, while in others it is determined by the clustering algorithm. There is also a distinction between flat clustering that directly partitions the data into k clusters and hierarchical clustering where clusters are nested hierarchically as the name suggests. In many cases, clustering uses some notion of distance $d(x_i, x_j)$, which may be the L_p norm $\|x_i - x_j\|_p$.

One of the most common clustering algorithms is known as k-means, where k is specified by the user and results in sets $S = \{S_1, \ldots, S_k\}$ that minimize the variance of each cluster. Thus, the objective is

$$\begin{aligned} \arg\min_{\mathbf{S}} \sum_{i=1}^{k} \sum_{\mathbf{x} \in S_i} \|\mathbf{x} - \boldsymbol{\mu}_i\|^2 &= \arg\min_{\mathbf{S}} \sum_{i=1}^{k} |S_i| \operatorname{Var} S_i \\ &= \arg\min_{\mathbf{S}} \sum_{i=1}^{k} \frac{1}{2|S_i|} \sum_{\mathbf{x},\mathbf{y} \in S_i} \|\mathbf{x} - \mathbf{y}\|^2 \end{aligned} \tag{41.22}$$

where μ_i is the mean of points in S_i. k-means can be interpreted as a Gaussian mixture density estimation of $p(x)$, where all the Gaussians are isotropic. It can be generalized to a Gaussian mixture model, where both the means and the covariance matrix are estimated.

Among the other class of algorithms that determine k, density-based spatial clustering of applications with noise (DBSCAN) is one of the most frequently used. DBSCAN clusters points based on a distance metric (*e.g.*, Euclidean) defined for each application. Two hyperparameters are ϵ, the maximum distance threshold to determine whether a neighboring point belongs to the same cluster, and the minimum sample size for a group of close points to be identified as a valid cluster or noise. While DBSCAN is robust against irregularly shaped clusters with a simple distance-based metric, single threshold parameter ϵ shared to distinguish all clusters can be challenging. Hierarchical DBSCAN (HDBSCAN) generalizes to varying densities by building a hierarchy of density-based clusters across all ϵ via mutual-reachability distances, then extracts the most stable clusters from a condensed tree.

Finally, neural networks are often used for clustering in particle physics. One use case is to transform the data points into a latent space where clustering is performed using an unsupervised, traditional algorithm. For example, an input dataset may not follow an isotropic gaussian distribution which is assumed by k-means, but one can design a neural network to learn a transformation into the latent space where this assumption holds. Another use case is to use neural network directly for clustering operation. Examples include object detection [25] and segmentation [26, 27] in computer vision (see Sec. 41.8.4.4) as well as clustering of graph nodes via edge classification [28–32] (see Sec. 41.8.4.7).

41.3.3 *Density estimation*

The goal of density estimation is to estimate a distribution $p(x)$ based on samples $\{x_i\}_{i=1,\ldots,n}$ with $x_i \overset{\text{i.i.d.}}{\sim} p(x)$. Conceptually, this is the same goal as when fitting a parameterized distribution $f(x;\theta)$ to data using the method of maximum likelihood as described in Sec. 40.2.2 of the chapter on statistics. In practice, the difference in the machine learning context has to do with the flexibility of the model and the dimensionality of the data. A highly-flexible model, which can effectively approximate any distribution, is referred to as a non-parametric model (though, ironically, usually this means the model has many parameters). In contrast, typical maximum likelihood fits in particle physics are based on restricted families of distributions with relatively few parameters and the data is typically one- or two-dimensional, though occasionally five- or six-dimensional.

Maximizing the likelihood function in Eq. 40.10, $\mathcal{L}(\theta) = \prod_{i=1}^{n} f(x_i;\theta)$ is equivalent to minimizing the empirical risk:

$$\mathcal{R}_{\text{emp,xe}}[f_\phi] = -\frac{1}{n} \sum_{i=1}^{n} \log f_\phi(x) \ , \tag{41.23}$$

where we adopt the notation used in this chapter. The loss is simply $\mathcal{L}(x, f_\phi(x)) = -\log f_\phi(x)$, and the corresponding risk is

$$\mathcal{R}_{\text{xe}}[f_\phi] = \mathbb{E}_{p(x)}[-\log f_\phi(x)] \ , \tag{41.24}$$

which is the cross entropy $H[p, f_\phi]$. For density estimation, the model is usually constructed to enforce $\int f_\phi(x)dx = 1$ and $f_\phi(x) \geq 0$ so that it can be interpreted as a distribution. With this constraint, one can show that $f^*_{\text{xe}}(x) = p(x)$. This is not the only form of training: flow matching and diffusion methods train on a different objective, discussed further below.

Int. J. Mod. Phys. A 2026.41. Downloaded from www.worldscientific.com
by UNIVERSITY OF CALIFORNIA @ BERKELEY on 09/16/26. Re-use and distribution is strictly not permitted, except for Open Access articles.

The concepts of generalization and overfitting are particularly acute in *unsupervised* learning, where the likelihood maximization of equation 41.23, combined with universal approximator assumption, must converge onto $\hat{p}(x) = \frac{1}{n}\sum_{i=1}^{n}\delta(x - x_i)$, the empirical distribution of the dataset $\{x_i\}_{i=1,\ldots,n}$. This distribution has the highest likelihood on the training dataset and the lowest likelihood on the test data where it gives $\hat{p}(x) = 0$ as long as the test dataset are not identical to the training dataset. So the empirical distribution of the training dataset has the worst possible generalization property, yet it is the solution we converge to for sufficiently expressive architectures in the absence of any regularization. In contrast, in supervised learning we often observe the phenomenon of benign overfitting, where even zero loss can generalize well.

In addition to approaches to density estimation that involve learning in the sense of minimizing a loss or risk function, we note that there are also classical density estimation techniques such as histogramming and kernel density estimation [33–35]. These techniques often fail in very high dimensions.

41.3.4 *Generative models*

Deep generative models are powerful machine learning models that can learn complex, high-dimensional distributions and generate samples from them. Because of their inherently probabilistic formulation, generative models are rapidly becoming an indispensable tool for scientific data analysis in a range of domains. The goal of generative models is to draw samples from $p(x)$. For some formulations of learned $p(x)$, such as normalizing flows, the samples can be drawn directly. For other explicit formulations of $p(x)$, such as Boltzmann machines, one can use sampling techniques such as Monte Carlo Markov chain sampling. There are however many other approaches to drawing samples from $p(x)$ that do not rely on its explicit form.

Generative models can be contrasted against discriminative models that are primarily used for supervised learning tasks. Roughly, discriminative models are used for prediction and $f(x)$ provides a point estimate of the target y, and they are more closely connected to function approximation. In contrast, generative models describe the data distribution $p(x)$ (or the joint data distribution $p(x, y)$ in a supervised setting). An enlightening discussion of these two approaches can be found in Ref. [8].

There are a number of different types of deep generative models that have various pros and cons as they do not all have the same capabilities. We will focus on variational autoencoders (VAEs) [36, 37] , generative adversarial networks (GANs) [38, 39], normalizing flows (NFs) [40–44], and flow-matching and diffusion models [45–48], though other approaches have been explored in this quickly developing area of research. Consider these three distinct types of functionality:

- **generation:** ability to sample or "generate" a data point $x_i \sim p(x)$.
- **likelihood for generated data:** ability to evaluate the probability density (likelihood) $p(x_i)$ for a data point x_i sampled from the model $x_i \sim p(x)$.
- **likelihood for arbitrary data:** ability to evaluate the probability density $p(x_i)$ for an arbitrary data point $x_i \in \mathcal{X}$.

Each of the models above can be used for generation; however, only normalizing flows provide all three capabilities. For reasons that we will describe below, GANs and VAEs do not provide a tractable likelihood function, and they are sometimes referred to as *implicit models*. This establishes a connection to simulation-based inference where most scientific simulators are also implicit models with an intractable likelihood. Because normalizing flows have a tractable likelihood, they can be trained via maximum likelihood (Eq. 41.23) as described in Sec. 41.3.3. GANs and VAEs, on the other hand, need to employ some other loss function to be trained. In the case of VAEs, training is based on the ELBO used in variational inference (see Sec. 41.2.3 and the discussion around the reverse KL divergence below Eq. 41.18). While GANs are also implicit models they data they can generate is typically restricted to a lower-dimensional manifold $\mathcal{M} \subset \mathcal{X}$, meaning that almost all real training dataset doesn't "live on" the subspace of possibilities that the model can produce. In this case, the likelihood is for almost all data is zero, and so even ELBO-based training will not work. The breakthrough idea introduced in Ref. [38] was to use adversarial training where a classifier would be used to quantify how different the data generated from the model is from the data from the target distribution.

VAEs, GANs, and normalizing flows introduce a mapping $g(z, \theta)$ from a base random variable z to the space of the data $\mathcal{X}$. The map $g(z, \theta)$ is typically implemented with a neural network. The random variable z is sampled from some known base distribution $p(z)$ that is both easy to sample and has a density that is easy to evaluate. Typically, the base distribution is a multivariate normal.

In the literature on GANs and normalizing flows, this base random variable is often referred to as a latent variable and $p(z)$ is often referred to as a prior distribution. In the case of VAEs, one additionally adds some normally-distributed (Gaussian) random noise ϵ to the output so that $x = g(z, \theta) + \epsilon$. In this case, x and z are not deterministically related and z is a legitimate latent variable in the model and $p(z)$ can be interpreted as the prior on that latent variable. In this case, the model can populate the full space of the data. Unfortunately, the marginal likelihood $p(x) = \int p(x, z)dz$ involves an intractable integral, thus maximum likelihood training is infeasible. However, the likelihood term $p(x|z)$ is tractable (*i.e.* the Gaussian noise), so training with the ELBO is possible.

Note that the dimensionality of z need not be the same as that of x. If $z \in \mathbb{R}^q$ and $\mathcal{X} = \mathbb{R}^d$ with $q < d$, then all points $g(z, \theta)$ will lie on a d-dimensional surface in $\mathbb{R}^d$. In the case of a VAE, the Gaussian noise ϵ means that the generated data x will be distributed in a thin region around the surface defined by $g(z, \theta)$. The presence of a bottleneck (*i.e.* $q < d$) leads to advantages and disadvantages. The disadvantages for GANs is that the likelihood assigned to almost all real world data (*i.e.* data not generated by the model) will be zero, so training is more difficult and many tasks in probabilistic inference won't be applicable. However, often real world data is also effectively described by a low-dimensional subspace in the full space of the data – random images look like noise, while natural images are in some sense special. For this reason, images produced by GANs for instance often have better visual quality than those produced by other techniques. This points to the ambiguity encountered in quantifying how close two distributions are, and also motivates the use of distance measures such as the Earth movers distance or Wasserstein distance [49, 50]. Conversely, the lack of a bottleneck (*i.e.* $q = d$) leads to very large models and scalability issues when the data is high dimensional.

Recent work has also focused on combining ideas from VAEs, GANs, and normalizing flows so that the generative model does involve a bottleneck but can still provide tractable likelihoods for density estimation restricted to that manifold [40,51–54]. Some of these models can also be used in the context of anomaly detection and out of distribution detection by identifying data that is off the manifold.

The parametrization of the mapping (the architecture of the neural network) should match the structure of the data and be expressive enough. For problems with explicit symmetries it is beneficial to include them into the architecture of the network explicitly, which restricts the allowed space of the models and matches their inductive bias (implicit regularization inherently built into the choice of architecture of the network) to the data. Different architectures have been proposed [43, 55–57], and to achieve the best performance on a new dataset one needs extensive hyperparameter explorations [58].

41.3.4.1 *Variational autoencoders*

The autoencoder was described in Sec. 41.3.1 as model for compression and representation learning. The model is $f = g \circ e : \mathcal{X} \to \mathcal{X}$, where $e : \mathcal{X} \to \mathcal{Z}$ is referred to as the *encoder* and $g : \mathcal{Z} \to \mathcal{X}$ is referred to as the *generator* or *decoder*. The standard autoencoder is not a probabilistic model, but additional probabilitic structure can be added.

One approach is VAE mentioned above [36, 37]. By equipping the latent space with a prior distribution $p(z)$, the decoder of the autoencoder $g(z, \theta)$ implies a distribution on a manifold in the out-

by UNIVERSITY OF CA Phys. A 2026.41. Downloaded from www.worldscientific.com
LEY on 09/16/26. Re-use and distribution is strictly not permitted, except for Open Access articles.

put space $\mathcal{X}$. VAEs additionally add some normally-distributed (Gaussian) random noise ϵ to the output so that $x = g(z, \theta) + \epsilon$. This implies that $p_\theta(x|z)$ is a tractable quantity, and it is interpreted as the likelihood in this context.

In a VAE one also elevates the encoder to have a probabilistic form. Instead of encoding $z = e(x)$ in a deterministic way, one seeks a distribution over z given x. A natural target for the probabilistic encoder would be to probabilistically invert the decoder. This inverse problem is solved by the posterior distribution $p(z|x)$ via Bayes theorem

$$p(z|x) = \frac{p(x|z)p(z)}{p(x)} \ . \tag{41.25}$$

While the likelihood and the prior may both be tractable, the normalizing constant $p(x) = \int p(x, z)dz$ involves an intractable integral (the same intractable integral that makes maximum likelihood training of the VAE infeasible).

One approach to Bayesian inference in these settings is variational inference (VI). In VI one approximates the posterior with some parametric family $q_\phi(z|x)$ in a parametric form, and then optimizes the ELBO with respect to its parameters ϕ.

$$\begin{aligned} \text{ELBO} &= \mathbb{E}_{q(z)} \log p(x|z) - D_{\text{KL}}[q(z)||p(z)] \\ &\leq \log \mathbb{E}_{q(z)} \left[\frac{p(x, z)}{q(z)} \right] = \log p(x) \ , \end{aligned} \tag{41.26}$$

where we used Jensen's inequality for concave functions (log) and the reverse Kullback-Leibler (KL) divergence term is

$$D_{\text{KL}}[q(z)||p(z)] = \mathbb{E}_{q(z)}[\log q(z) - \log p(z)] \geq 0 \, . \tag{41.27}$$

In a VAE, the variational model for the posterior $q_\phi(z|x)$ is often assumed to be an uncorrelated Gaussian (this is often called mean field approximation) defined by the mean μ and variance Σ. Instead of optimizing the mean and variance independently for each x, VAEs use neural networks to predict the mean $\mu_\phi(x)$ and the variance $\Sigma_\phi(x)$. This is called *amortized inference*, since after an up-front training cost the approximate posterior $q_\phi(z|x)$ can be evaluated efficiently with a single forward pass of the neural network. Note the standard auto-encoder is recovered if one only used the mean $\mu_\phi(x)$ for the encoder and did not add noise ϵ to the decoder.

Both the probabilistic encoder $q_\phi(z|x)$ and the probabilistic decoder $p_\theta(x|z)$ are trained jointly by optimizing the ELBO. Unlike the standard autoencoder, which only minimizes the reconstruction error, ELBO optimization of Eq. 41.26 has a tradeoff between minimizing the reconstruction error in the first term (averaged over the approximate posterior $q(z)$), which encourages high quality reconstructions, and minimizing the KL divergence term, which forces the posterior $q(z)$ to be as close to the chosen prior $p(z)$, and thus controls the sample quality by matching the aggregate posterior with a chosen prior distribution [59]. This term regularizes the VAE latent space, such that every sample drawn from the prior $p(z)$ correspond to a valid sample. Successful VAE training requires to find a delicate balance between the two contributing terms to the ELBO. Whether the VAE training process succeeds in striking this balance depends on a number of factors, including the network architectures, the chosen prior and the class of allowed posterior distributions. Once trained, the VAE can be used as a generative model by sampling from the prior $z_i \sim p(z)$ and then decoding according to $p_\theta(x|z) = g(z, \theta) + \epsilon$.

VAEs allow for expressive architectures, enjoy the benefits of regularization through data compression and have a firm theoretical foundation. Compared to GANs [38] 41.3.4.2, VAEs are of particular interest to the scientific community as they provide a lower bound to the marginal likelihood (albeit potentially with a large gap) and a posterior distribution for the latent variables.

It is also interesting to consider a special case of the autoencoder and VAE where the encoder and decoder are restricted to be linear transformations, which is effectively PCA. In PCA the (linear) decoder can be written $g(z) = Oz$, where O is a matrix. As in the case of the autoencoder, PCA is not a probabilistic model, but probabilistic structure can be added. Probabilistic PCA [60] assumes that the latent variables follow a Gaussian distribution with mean zero and covariance Λ, where Λ is a diagonal matrix with the rank-ordered eigenvalues λ_i along its diagonal. The true distribution of the PCA components may be non-Gaussian, but a Gaussian is the maximum entropy approximation given their first two moments. Note that in probabilistic PCA these moments are measured on training dataset (when finding the principal components).

One can generalize probabilistic PCA to use nonlinear encoder and decoder as in an autoencoder. A Gaussian prior is a poor ansatz for the latent space distribution of data proceed by an autoencoder. Instead one can learn the density of the training samples in latent space using a normalizing flow. This model was introduced in $\mathcal{M}$-flows [53] and in probabilistic autoencoder (PAE) [54], which achieves similar performance to a VAE in terms of sample quality without explicit ELBO optimization. In all these cases the dimensionality of the latent space is a hyperparameter to be chosen or optimized by the user. Unlike a standard VAE, these models do not add noise to the decoded output, thus the data is strictly restricted to the manifold defined by the decoder $g(z, \theta)$. However, unlike a GAN there is a well defined way to take an arbitrary data point x, project it onto the manifold, and calculate the density of the data point projected onto the manifold. Thus these models can also be used in the context of anomaly detection and out of distribution detection by identifying data that is off the manifold.

41.3.4.2 *Generative adversarial networks*

GANs [38] also typically choose a low dimensional latent space z with a known prior distribution $p(z)$, typically a normal (Gaussian) distribution with zero mean and unit variance. GANs do not add noise to the output $g(z, \theta)$, so the likelihood $p(x|z)$ (and marginal likelihood $p(x)$) for almost all of the data space is 0, which precludes training by maximum likelihood and the ELBO. Instead of training on ELBO, GANs train on a dissimilarity measure defined implicitly by a discriminator $D(x)$ (also referred to as the critic). Calculating the dissimilarity often involves it's own learning problem (*i.e.*, adversarial training of the discriminator).

The training is usually framed as a mini-max game

$$\begin{aligned} &\min_g \max_D \mathcal{L}_{\text{GAN}} = \\ &\min_g \max_D \{\mathbb{E}_{x\sim p(x)} \log D(x) + \mathbb{E}_{z\sim p(z)} \log[1 - D(g(z))]\}. \end{aligned} \tag{41.28}$$

The goal of the discriminator is to distinguish between true and generated data, hence we want to maximize this loss with respect to D, assigning 1 to true data and 0 to generated data. The goal of generator is to fool the discriminator such that it cannot distinguish between true and generated data, hence we want to minimize this loss with respect to g at fixed D. This can be viewed as a game theoretical setup in a zero sum game between generator and discriminator.

Instead of this game theory interpretation we can view the internal objective $\max_D \mathcal{L}_{\text{GAN}}$ as an implicit loss function that measures the dissimilarity between the target and generated distributions. The loss of Eq. 41.28 corresponds to the Jensen-Shannon (JS) divergence, which is a symmetrized form of KL divergence. However, JS divergence is hard to directly work with, and the adversarial training could bring many problems such as vanishing gradient, mode collapse (tendency of generator to cluster the samples around the training samples, with holes between them) and non-convergence [49, 50]. One of the core issues is that the distribution generated by the GAN is not guaranteed to cover the entire space. To address these issues Wasserstein GANs train on

$$\min_g \max_D \mathcal{L}_{\text{WGAN}} = \min_g \max_D \{\mathbb{E}_{x\sim p(x)} D(x) - \mathbb{E}_{z\sim p(z)} D(g(z))\}. \tag{41.29}$$

Here again the goal of discriminator is to make the loss as large as possible between the true data and the generated data, while the goal of generator is to make it as small as possible, so that the discriminator cannot distinguish between the two. There is no requirement for $D(x)$ to be between 0 and 1, which helps with the above mentioned problems of JS divergence. Instead, this

Int. J. Mod. Phys. A 2026.41. Downloaded from www.worldscientific.com by UNIVERSITY OF CALIFORNIA @ BERKELEY on 09/16/26. Re-use and distribution is strictly not permitted, except for Open Access articles.

is replaced with a requirement that $D(x)$ is 1-Lipshitz, i.e. the absolute value of the norm of the gradient of the discriminator output with respect to the input has to be less or equal to 1.

Eq. 41.29 can be interpreted as the dual form of the 1-Wasserstein distance between the true and generated distribution [61]. Wasserstein distances are a measure of dissimilarity between two distributions used in the context of optimal transport, a mathematical theory of how to define a notion of distance between probability distributions. Since the transport distance increases with the separation between the two distributions when they are non-overlapping, there is no gradient collapse that plagues other measures. In its primal form p-Wasserstein distance, $p \in [1, \infty)$, between two probability distributions p_1 and p_2, is defined as $W_p(p_1, p_2) = \inf_{\gamma \in \Pi(p_1,p_2)} \left(\mathbb{E}_{(x,y)\sim\gamma}\left[|x-y|^p\right]\right)^{\frac{1}{p}}$, where $\Pi(p_1, p_2)$ is the set of all possible joint distributions $\gamma(x, y)$ with marginalized distributions p_1 and p_2. In 1D the Wasserstein distance has a closed form solution via cumulative distribution functions (CDFs), but this evaluation is intractable in high dimensions.

In the dual form of 1-Wasserstein distance, one instead maximizes Eq. 41.29 over all possible functions $D(x)$ that are 1-Lipschitz. One way to implement this is through weight clipping of the parameters of discriminator network, but a simpler solution is to add a gradient norm penalty term explicitly to the loss function [62].

Because of the discriminative nature of the dissimilarity measure defined in data space, GANs and Wasserstein GANs often generate more realistic samples than VAE or normalizing flows in high dimensions such as natural images (although flow matching and diffusion models can outperform GANs). However, GANs do not provide an encoder from data to latent space nor a tractable likelihood $p(x)$.

41.3.4.3 *Normalizing flows and autoregressive models*

Normalizing flows (NFs) provide a powerful framework for density estimation and sampling [40–44, 63]. These models map the data x to latent variables z through a sequence of invertible transformations $f = f_1 \circ f_2 \circ \cdots \circ f_n$, such that $z = f(x)$ or $x = g(z) = f^{-1}(x)$. As in the VAE and GAN, z is modeled as a random number with a simple base distribution $p_Z(z)$, which is typically chosen to be a standard normal (Gaussian) distribution. Since NFs are invertible the dimensionality of the latent space equals the dimensionality of the data space, in contrast to VAE and GANs where the latent space dimensionality is often lower. The probability density of the model be evaluated using the change of variables formula:

$$p_X(x) = p_Z(f(x)) \left|\det\left(\frac{\partial f(x)}{\partial x}\right)\right| = p_Z(f(x)) \prod_{l=1}^{n} \left|\det\left(\frac{\partial f_l(x)}{\partial x}\right)\right|, \tag{41.30}$$

where we have added subscripts to $p_X(x)$ and $p_Z(z)$ for clarity. The Jacobian determinant $\det(\frac{\partial f_l(x)}{\partial x})$ must be efficient to compute for density estimation to be practical, and the transformation f_l should be easy to invert for sampling. In contrast to VAE and GANs, standard normalizing flows preserve the dimensionality of the data space as they are invertible (though there are normalizing flows that are defined on lower dimensional manifolds embedded in the data space [40, 51–54]). As such, unlike GANs and VAEs, they can be trained via maximum likelihood (Eq. 41.23) as described in Sec. 41.3.3.

There are several popular architectures of NFs. A method used by NICE, RealNVP and Glow [41–43] is to split the space into two disjoint sets z_1 and z_2, and then use an identity forward map $z \to x$ for x_1, $x_1 = z_1$, and an affine transformation for x_2 of the form

$$x_2 = \exp(s(z_1)) \odot z_2 + m(z_1), \tag{41.31}$$

where $\odot$ is elementwise product and $m(z_1)$, $s(z_1)$ are neural networks. The Jacobian of this map is lower triangular, and its determinant is simply the product of elements along the diagonal, which is tractable, as is the inverse of the transformation. At the next layer one then performs a different split of dimensions into z_1 and z_2. The affine transformation can be further generalized to a nonlinear form using rational splines [64].

One can interpret the sequence of invertible transformations $f_1 \circ f_2 \circ \cdots \circ f_n$ as n discrete time steps in a continuous flow. In particular, one can think of a continuous-time flow described by an ordinary differential equation (ODE) and then interpret the discrete time steps as the result of a numerical integration of that ODE. This is the approach taken by the Ffjord algorithm [65] and other variants. A residual flow has an update $f_i(x) = x_i + \delta u_i(x)$, which for $\delta_i = n^{-1}$ and taking $n \to \infty$ limit gives rise to an ordinary differential equation (ODE)

$$dx_t = u_t(x_t)dt. \tag{41.32}$$

Here u_t is the velocity field that defines the flow and is a vector field. One can build the density estimator for all intermediate times t $p_t(x)$ using its divergence,

$$\ln p_t(x_t) = \ln p_0(x_0) - \int_0^t \nabla \cdot u_s(x_s)ds, \tag{41.33}$$

where p_0 at t_0 is the initial base distribution and p_1 at $t = 1$ is the target distribution. Continuous normalizing flows parametrize u_t as a neural network. They are very expressive, but expensive to train using maximum likelihood.

A different approach creating a deep generative model with a tractable likelihood is to model $p(x)$ autoregressively as

$$p(x) = \prod_{i=1}^{n} p(x_i|x_1, x_2, \ldots, x_{i-1}) \,. \tag{41.34}$$

This form describes each new dimension conditionally on all previous dimensions. It can model a general likelihood $p(x)$ as a sequence of conditional 1d distributions, whose conditional dependence on the parameters $x_1, x_2, \ldots, x_{i-1}$ can be modeled with neural networks. If x is a time series this form imposes a causal structure where x_i depends on all previous times x_j, $j < i$. WaveNet [66] and PixelCNN [67]) are two well known examples. Sampling from an autoregressive model is sequential, and can be slow in high dimensions. Inverse autoregressive flow reverses this process and makes sampling fast, but the likelihood evaluation is slow. Some normalizing flows have autoregressive coupling layers, such as masked autoregressive flow (MAF) [63].

All of the methods above use maximum likelihood training of likelihood $p(x)$ against network parameters, so the training is to minimize KL divergence between the data distribution and a Gaussian in latent space. This can be overly sensitive to small variance directions that dominate the likelihood, without being sensitive to the global structure of the data. An alternative is to use Optimal Transport Wasserstein distance between the density of the generated samples and the data, which can be evaluated either in data space or in latent space. As Wasserstein distance is difficult to evaluate in high dimensions, one can instead use slices, 1d projections of the data along different directions in high dimensional space, to build the flow [68]. Because this training is less sensitive to small variance directions than maximum likelihood training it achieves better results on anomaly detection tasks [68].

We end by noting that normalizing flows, autoregressive models, and other deep generative models that provide a tractable likelihood are powerful tools for simulation-based inference. They can provide surrogate models trained from large simulated datasets when the simulators have intractable likelihood functions, which is usually the case. As described in Sec. 41.6, one would like to work with models that can provide conditional density estimation in order to model either the likelihood $p(x|\theta)$ or the posterior $p(\theta|x)$ [69, 70]. These techniques are being actively explored and applied to a number of scientific problems.

41.3.4.4 *Flow-matching and diffusion models*

In flow-matching models, we start from a base distribution such as a Gaussian $p_0 = \mathcal{N}(0, I)$, and use ODEs to generate samples with a flow vector field $u_t^\theta(x)$ as in Eq. 41.32. As discussed above, continuous normalizing flows are expensive to train via maximum likelihood. Instead, one can learn directly the velocity

Phys. A 2026.41. Downloaded from www.worldscientific.com
by UNIVERSITY OF CA LEY on 09/16/26. Re-use and distribution is strictly not permitted, except for Open Access articles.

field parametrized as a neural network $u_t^\theta(x_t)$ with parameters θ via the flow-matching loss

$$\mathcal{L} = \mathbb{E}_{t\sim U(0,1),\ x\sim p_t}\left[u_t(x_t) - u_t^\theta(x_t)\right]^2, \tag{41.35}$$

where the expectation is uniform over time t and over all intermediate distributions p_t. This equation is however not practical since we do not know the target $u_t(x)$. Instead, one can take advantage of the target conditional velocity field $u_t(x_t|z)$, where $z \sim \hat{p}$ is a training data sample

$$\mathcal{L} = \mathbb{E}_{t\sim U(0,1),\ x\sim p_t,\ z\sim\hat{p}}\left[u_t(x|z) - u_t^\theta(x_t)\right]^2. \tag{41.36}$$

It has been shown that this conditional target velocity field training also leads to the correct distribution in the flow models [45,48]. Figure 41.3, taken from Ref. [71], illustrates the main idea, which is that training a conditional flow, and averaging over all the training data, is the same as training on unconditional flow.

The advantage of this formulation is that conditional velocity fields are a lot simpler to construct. A typical case is a flow from the initial Gaussian $p_0(x|z) = \mathcal{N}(0, I)$ to a delta function at z $p_1(x|z) = \delta_z(x)$. A very simple linear flow that achieves this is $p_t(x|z) = \mathcal{N}(tz, (1-t)^2 I)$. The flow itself moves from a random Gaussian variable $\epsilon \sim \mathcal{N}(0, I)$ to the data point z, so $x_t = \epsilon(1-t) + tz$. Finally, the conditional velocity field is given by $u(x_t|z) = z - \epsilon$, so the training loss is

$$\mathcal{L} = \mathbb{E}_{t\sim U(0,1),\ \epsilon\sim\mathcal{N}(0,I),\ z\sim\hat{p}}\left[z - \epsilon - u_t^\theta(\epsilon(1-t) + tz)\right]^2. \tag{41.37}$$

This leads to a simple training algorithm where one randomly chooses a minibatch of data z, random Gaussian variables ϵ, and a time t to update the parameters θ based on stochastic gradient descent using the loss of Eq. 41.37. The simplicity and efficiency of this training procedure has led flow matching to become one of the leading generative models for large image based data. Sampling from flow-matching models requires randomly choosing an initial condition $x_0 \sim N(0, I)$ and discretizing Eq. 41.32. Note that this is a deterministic ODE and all the randomness is in the initial conditions.

Diffusion models also start from a Gaussian base distribution, but also continuously add noise during the evolution in time, *i.e.*, they are based on a stochastic differential equation (SDE)

$$x_0 \sim p_0,\ \ dx_t = u_t^\theta(x_t)dt + \frac{\sigma_t^2}{2}s_t(x_t) + \sigma_t dW_t, \tag{41.38}$$

where we define score $s_t(x_t) = \nabla \ln p_t(x_t)$. Here, dW_t is the stochastic term, which adds Brownian motion (also called a Wiener process) in the form of uncorrelated Gaussian random noise. Note that with $\sigma_t = 0$, a diffusion model becomes a flow model. The noise variance σ_t is a free parameter that can be tuned for optimal performance. If our target is a static distribution so that $p_t = p$ then $u_t = 0$ and we obtain the Langevin equation.

In diffusion, we also need to learn the gradient field via the score function, and as before we can replace the marginal score with conditional score during the training to obtain score matching training procedure

$$\mathcal{L} = \mathbb{E}_{t\sim U(0,1),\ x\sim p_t,\ z\sim\hat{p}}\left[\nabla \ln p_t(x|z) - s_t^\theta(x_t)\right]^2. \tag{41.39}$$

In the simple Gaussian example with $p_t(x_t) = \mathcal{N}(\alpha_t z, \beta_t^2 I)$, where $\alpha_0 = \beta_1 = 0$ and $\alpha_1 = \beta_0 = 1$, we have a trajectory $x_t = \alpha_t z + \beta_t \epsilon$, and the score loss

$$\mathcal{L} = \mathbb{E}_{t\sim U(0,1),\ \epsilon\sim\mathcal{N}(0,I),\ z\sim\hat{p}}\left[\frac{\epsilon}{\beta_t} + s_t^\theta(\alpha_t z + \beta_t\epsilon)\right]^2. \tag{41.40}$$

It would appear that in diffusion, one must train both the flow and the score, but for simple linear models the two can be related to one another, and one can choose the flow-matching or score-matching training procedure. For the example in Eq. 41.38, the corresponding score-matching training is

$$x_0 \sim p_0,\ \ dx_t = \left[\left(\beta_t^2\frac{\dot{\alpha}}{\alpha} - \beta_t\dot{\beta}_t + \frac{\sigma_t^2}{2}\right)s_t(x_t) + \frac{\dot{\alpha}}{\alpha}x_t\right]dt + \sigma_t dW_t. \tag{41.41}$$

One of the advantages of score- and flow-based methods is that one can reduce the architectural restrictions imposed by normalizing flows or autoregressive models. Score- and flow-based training avoid the normalization requirement. Score-based models learn gradients of log probability density functions on a large number of noise-perturbed data distributions, and then generate samples by Langevin-type sampling.

The generative models described in this subsection are called flow-based models [45], score-based generative models [46], diffusion probabilistic models [47], or stochastic interpolants [48]. They have several advantages over other model families. They often outperform GAN-level sample quality without adversarial training, and enable exact log-likelihood computation through their connection to continuous-time flows, which can be represented as a probability flow ordinary differential equation [47]. The main advantage is that the distribution $p(x)$ can be specified solely by its score or flow. This in turn enables more flexible model architectures than what can be used in normalizing flows or autoregressive models.

41.3.5 *Anomaly detection and out-of-distribution detection*

Unsupervised anomaly detection techniques detect anomalies in an unlabeled test data set under the assumption that the majority of the in-distribution data are normal under some measure, while out-of-distribution (OOD) data are not. In the context of autoencoders a popular technique is to use the reconstruction error of Eq. 41.21 to identify an outlier as one with a large reconstruction error [72–74]. One issue with this method is that for higher dimensional latent space and flexible neural network architectures the encoder-decoder map become identity for any input data, $f(x) = x$, regardless of whether input x is from the in-distribution training dataset or from the out-of-distribution data. The choice of autoencoder latent space dimensionality is thus an important hyperparameter that must be tuned.

Another set of anomaly detection techniques construct a model representing normal behavior from a given in-distribution training dataset, and then evaluate the likelihood of a test instance to be generated by the utilized model. For instance, one can use density estimation methods such as normalizing flows (section 41.3.4.3) to learn the density (likelihood) of the in-distribution training dataset $p(x)$, and apply it to the test data. The expectation is that out-of-distribution data will have a lower density (likelihood) under the in-distribution density model. This expectation is however not always met in high dimensions and the method suffers because likelihood-based training is sensitive to the smallest variance directions [75]. Low-variance directions may contain little or no information on the global structure of the image, so there is a mismatch between the training objective and outlier detection objective. Lower dimensional autoencoders with NF in the latent space deal better with this issue [54].

A related issue is that of typicality: an in-distribution data sample likelihood will typically be lower than the maximum value, so an out-of-distribution data sample that is closer to the peak would have a higher likelihood. If this happens in low-variance directions that dominate the likelihood, normalizing flows can assign higher likelihoods to out-of-distribution data than to in-distribution training data [76]. A number of techniques have been proposed to circumvent these limitations, such as likelihood regret [77], likelihood-ratio [75], likelihood in autoencoder latent space [54], and Wasserstein distance training of the likelihood $p(x)$ [68,78]. These methods can achieve better anomaly detection performance than the autoencoder reconstruction error [53,54,78]. However, even perfect density estimation cannot guarantee good anomaly detection performance [79,80].

Supervised anomaly detection techniques require a data set that has been labeled as in-distribution and out-of-distribution and involves training a classifier (the key difference to many other statistical classification problems is the inherent unbalanced nature of outlier detection). These methods assume some form for what out-of-distribution data may look like, and their success relies on whether the assumed form is a realistic representation of actual out-of-distribution data. When this assumption is valid these methods can be more powerful than unsupervised methods, but the reverse is also true. A hybrid between the two approaches

Int. J. Mod. Phys. A 2026.41. Downloaded from www.worldscientific.com
by UNIVERSITY OF CALIFORNIA @ BERKELEY on 09/16/26. Re-use and distribution is strictly not permitted, except for Open Access articles.

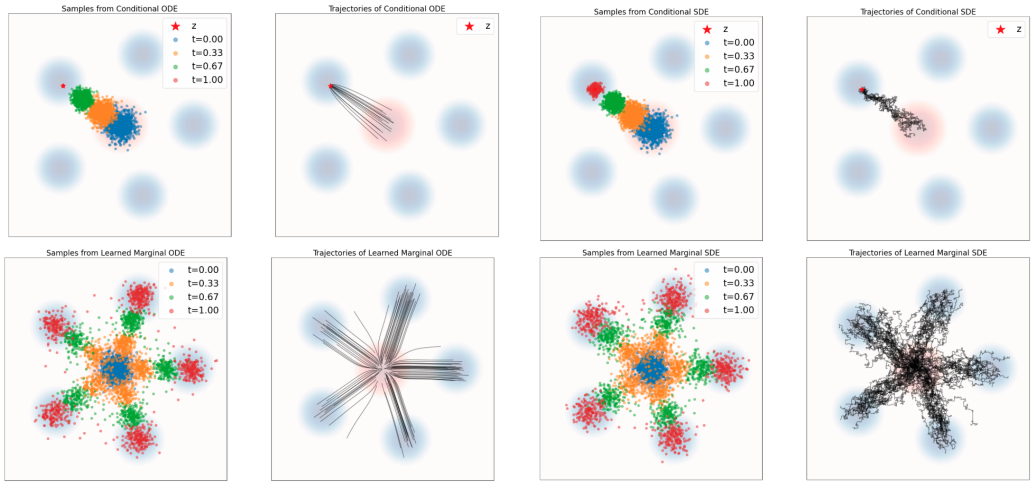

Figure 41.3: Illustration of the marginalization trick for flow-based models (left) and diffusion models (right), which simulate a probability path with ODEs or SDEs, respectively (Holderrieth and Erives, 2025). The data distribution $\hat{p}$ is the blue background, while the initial Gaussian distribution is the red background. The top graphs represent conditional probability paths, while the bottom graphs represent marginal probability paths. Both samples and trajectories are shown.

is to train a classifier without labels [81]. All these approaches are largely complementary to each other [82]. Examples of different anomaly detection methods applied to HEP are the LHC Olympics 2020 and Dark Machines challenges [83, 84].

41.4 Self-supervised learning

Self-supervised learning (SSL) also aims to distill useful features in the data without requiring supervision labels for every sample in the input data. Self-supervised methods make use of large unlabeled datasets to build meaningful representations. They can generally be categorized as *autoassociative*, where the model is trained to reproduce or reconstruct its own (masked) input or *contrastive*, where the model is trained to learn a mapping that is insensitive to different "views" of the data. These methods are often used to build "foundation models" (FMs) discussed in Sec. 41.9.11, which are pre-trained using self-supervised learning and fine-tuned using supervised learning for different downstream tasks. However, FMs are not the only possible use case.

A classic autoassociative task is masked language modeling popularized by the bidirectional encoder representations from transformers (BERT) model [85]. In this task, BERT ingests a sequence of words, a fraction of which are randomly masked, and tries to predict the original words that have been masked. For example, in the sentence "The Milky Way is a [MASK] galaxy," BERT would need to predict "spiral." This helps BERT learn bidirectional context. A variant of this approach is next token prediction, popularized by the generative pretrained transformer (GPT) [86]. A common theme in these methods is *tokenization*, in which elements of the input data are mapped to discrete vectors, known as tokens. These approaches have been applied in the context of particle jets [87–89], enabling the construction of backbone models that can be fine-tuned for different tasks and provide improvements for small training samples.

Sensory data (*e.g.*, 1D waveforms, 2D images, or 3D scenes) pose a significant challenge for autoassociative tasks compared to symbolic data such as language, math, and high-level physical concepts like jets and particles. For symbolic data, the masking unit is naturally defined (*e.g.*, a word for language) and associated with a strong semantic meaning, which yields a well-defined learning objective for mask-based self-supervision. On the contrary, sensory data captures raw information and a unit of data (*e.g.* a single pixel in an image) does not carry meaningful information alone. This challenge has resulted in in-depth R&D for self-supervision techniques in computer vision. The masked autoencoder (MAE) laid the initial ground work [90]: the authors discovered that a large fraction of masking (*i.e.*, 75%) is crucial for successful training using an asymmetric encoder-decoder architecture. Distillation with no labels (DINO) made another breakthrough by introducing a self-distillation technique where a student and teacher model pair—the teacher model typically being an exponential moving average of the student model—are forced to agree across different augmentations (*e.g.*, cropping, adding jitter, and rotating) of the same data instance [91, 92]. For effective representation learning of 3D geometrical shapes, multi-view projection matching techniques [93–95] are promising and a strong promise and relevant to time projection chamber (TPC) image data in high energy physics. Exploration of these specialized techniques in computer vision has impacted HEP applications [96, 97].

In contrastive learning, portions of the input data are paired together and the model is tasked to find matching pairs. Pairs can be constructed based on different data modalities, such as text and images, or based on data augmentations, that may be generic, such as adding noise, or domain-specific, like symmetry transformations. For example, the contrastive language-image pre-training (CLIP) [98] allows joint pretraining of a text encoder and an image encoder, such that a matching image-text pair have image encoding vector $\mathbf{z}_i$ and text encoding vector $\mathbf{z}_j$ that span a small angle, *i.e.*, have a large cosine similarity

$$c(\mathbf{z}_i, \mathbf{z}_j) = \frac{\mathbf{z}_i \cdot \mathbf{z}_j}{|\mathbf{z}_i||\mathbf{z}_j|} = \cos\theta_{ij} \ , \tag{41.42}$$

with θ_{ij} being the angle between the encoding vectors. This approach has been applied in astrophysics [99].

Positive pairs may also be constructed by applying data augmentations. For example, in the case of galaxy images, one may augment the data by performing image rotations, adding noise, size scaling, or adding point spread function smoothing, all of which are realistic transformations expected in a real galaxy image survey [100, 101]. For particle jets, tailored augmentations may include rotations about the jet axis, translations in the (η, ϕ) plane, smearing the positions of the soft jet constituents, and collinear splitting of the jet constituents [102–105]. Another augmentation strategy is based on re-simulating the stochastic shower and detector interactions, thus generating multiple physical realizations of a primary particle's evolution [106, 107].

A well-known approach for contrastive learning with augmentations is SimCLR [108]. In this approach, the contrastive loss for a positive pair of an input and its augmentation $(\mathbf{z}_i, \mathbf{z}'_i)$ is defined

Phys. A 2026.41. Downloaded from www.worldscientific.com
by UNIVERSITY OF CA LEY on 09/16/26. Re-use and distribution is strictly not permitted, except for Open Access articles.

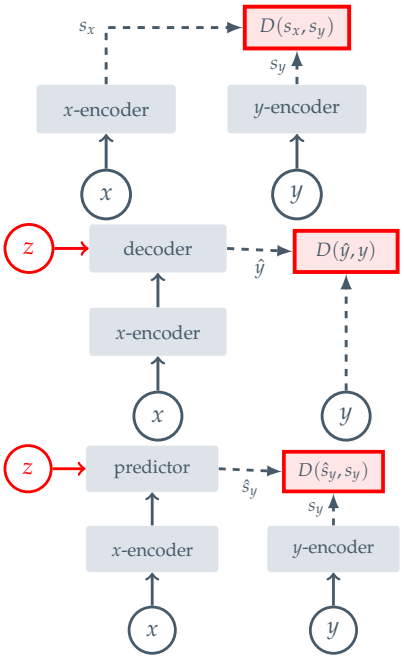

Figure 41.4: Common architectures for self-supervised learning, in which the system learns to assign a large scalar value to incompatible inputs, and a low scalar value to compatible inputs (M. Assran, et al. in ICCV, 2023). Joint-embedding architectures (left) learn to output similar embeddings for compatible inputs x, y and dissimilar embeddings for incompatible inputs. Generative architectures (center) learn to directly reconstruct a signal y from a compatible signal x, using a decoder network that is conditioned on additional (possibly latent) variables z to facilitate reconstruction. Joint-embedding predictive architectures (right) learn to predict the embeddings of a signal y from a compatible signal x, using a predictor network that is conditioned on additional (possibly latent) variables z to facilitate prediction.

in terms of the cosine similarity of Eq. 41.42 as

$$\mathcal{L}(\mathbf{z}, \mathbf{z}'_i) = -\ln \frac{\exp[c(\mathbf{z}_i, \mathbf{z}'_i)/\tau]}{\sum_{j \neq i \in \text{batch}} \left[\exp[c(\mathbf{z}_i, \mathbf{z}_j)/\tau] + \exp[c(\mathbf{z}_i, \mathbf{z}'_j)/\tau]\right]} , \tag{41.43}$$

and the total loss is given by the sum over all positive pairs in the batch, $\sum_{i \in \text{batch}} \mathcal{L}(\mathbf{z}_i, \mathbf{z}'_i)$. The loss decreases when the distance between positive pairs decreases or when the distance between negative pairs increases. The hyperparameter τ is known as temperature and controls the relative influence of positive and negative pairs. SimCLR has been applied in radio astronomy [109], neutrino physics [110], and collider physics [102]. Another application of contrastive regularization is self-distillation introduced in DINO discussed above. Self-distillation is a powerful technique that can be applied regardless of the target task, and improves the quality of self-supervision for many computer vision models for both image and point cloud data.

Finally, an alternative paradigm is the joint-embedding predictive architecture (JEPA) [111], which learns meaningful representations by modeling missing or unseen embeddings directly in the latent space without a decoder or full input reconstruction. The advantages of this approach are no data augmentations are required and unnecessary details of the input can be ignored. This approach has been applied to particle jets [112, 113] and Square Kilometer Array (SKA) light cones [114]. A comparison between the different self-supervised learning approaches can be found in Fig. 41.4, reproduced from Ref. [111].

41.5 Optimal control, reinforcement learning, and active learning

Many problems in science and engineering can be cast as a control problem, which comprises a cost functional that is a function of state and some control variables that specify some underlying dynamical system. This is relevant for the control of accelerators where the dynamical system is physical. This formalism can also be used to describe the design of experiments, planning of an observational survey, and other decision making processes relevant to the scientific method. It is closely connected to planning, dynamic programming, and reinforcement learning. Optimal control generalizes the framing of learning presented in Sec. 41.2.1.

41.5.1 *Optimal control*

Optimal control theory deals with finding a control for a dynamical system over a period of time such that the objective function is optimized. The underlying system can be discrete or continuous and may be deterministic or stochastic. The commonalities and differences between optimal control and reinforcement learning can be best understood through the formalism of a Markov decision process (MDP), which is a discrete-time stochastic control process.

A Markov decision process comprises four components often organized as a 4-tuple (S, A, P_a, R_a), where: S is a set of states called the state space, A is a set of actions called the action space, $P_a(s, s') = \Pr(s_{t+1} = s' \mid s_t = s, a_t = a)$ is the probability that action a in state s at time t will lead to state s' at time $t+1$, $R_a(s, s')$ is the immediate reward (or expected immediate reward) received after transitioning from state s to state s', due to action a.

The policy function π is a mapping from state space to action space that can be either deterministic or probabilistic. For examples, the policy that drives a computer chess playing system, decides which move to make given the current state of the board. Similarly, policies dictate which experiment should be built next, which field of the sky should be observed, or how to adjust the operational parameters of an accelerator. The dynamics of the resulting system are then fixed by combining the policy with the underlying MDP. The evolution of the resulting dynamical system behaves like a Markov chain since the action chosen in state s is completely determined by $\pi(s)$ and $\Pr(s_{t+1} = s' \mid s_t = s, a_t = a)$ implies the Markov transition matrix $\Pr(s_{t+1} = s' \mid s_t = s)$.

The objective optimal control is to choose a policy π that will maximize a cumulative function of the instantaneous rewards R_a. A common choice is the expected discounted sum:

$$\mathbb{E}\left[\sum_{t=0}^{\infty} \gamma^t R_{a_t}(s_t, s_{t+1})\right] , \tag{41.44}$$

where $a_t \sim \pi(s_t)$ are the actions given by the policy, the expectation computed with respect to the distribution $s_{t+1} \sim P_{a_t}(s_t, s_{t+1})$, and γ is the discount factor satisfying $0 \leq \gamma \leq 1$. The discount factor is usually close to 1 and sometimes reparameterized as $\gamma = 1/(1+r)$, where r is called the discount rate. A lower discount factor motivates the decision maker to favor taking actions early, rather than postpone them indefinitely.

A policy that maximizes the objective function is called an optimal policy and denoted π^*, though the optimal policy need not be unique. Importantly, the Markov property implies that the optimal policy is only a function of the current state. Dynamic programming can be used to find the optimal policy for MDPs with finite state and action spaces. For instance, in value iteration (a.k.a. backward induction) can be used to solve the "Bellman equation" [115]. For continuous-time systems, the optimal policy is defined by the Hamilton–Jacobi–Bellman equation [116].

In many settings, it is assumed that the state s is fully known when action is to be taken and there are no latent variables. When this assumption is not true, the problem is called a partially observable MDP. These problems are generally more difficult and the dynamic programming algorithms do not directly apply [117].

Int. J. Mod. Phys. A 2026.41. Downloaded from www.worldscientific.com by UNIVERSITY OF CALIFORNIA @ BERKELEY on 09/16/26. Re-use and distribution is strictly not permitted, except for Open Access articles.

41.5.2 *Reinforcement learning*

The main difference between the classical dynamic programming methods and reinforcement learning (RL) algorithms is that the latter do not assume knowledge of an exact mathematical model of the MDP and they target large MDPs where exact methods become infeasible. For example, RL was used in the context of jet physics to search for the most likely jet clustering when the number of constituents was too large for the exact dynamic programming algorithm to be used [118]. In addition, RL can be used when the probabilities or rewards are unknown. Instead, the transition probabilities are often accessed indirectly through interaction with a real or simulated environment.

Numerous variations to RL exist, which include so-called model-based and model-free approaches (referring to models of the instantaneous rewards and the state transitions) and on-policy and off-policy (which describes how the actions taken during learning are related to the current policy). See Ref. [119] for an introduction and Ref. [120] for a recent review. Some examples of RL use in particle physics are in Refs. [121–123].

41.5.3 *Multi-arm bandits*

Multi-arm bandit problems are a classic reinforcement learning problem where one tries to maximize the expected gain by allocating a limited set of resources to various alternatives. The name is a reference to a gambler with a fixed amount of money that must choose between multiple slot machines (or "one-armed" bandits) when the payoff for the individual machines is unknown. A hallmark of multi-arm bandit problems is that they involve a tradeoff between exploration (playing machines to estimate their payoff) and exploitation (playing machines with the highest estimated payoff). Multi-armed bandits are used to manage large projects, organizations, and scheduling problems. The theory has a long history going back to Robbins in 1952 that used it to study the sequential design of experiments [124] and Gittins who derived an optimal policy under some conditions [125].

41.5.4 *Bayesian optimization*

A closely related set of techniques involve optimizing some expensive black box function $f(x)$. For instance, the function may be computationally expensive to evaluate or low-latency, *e.g.* it may involve manually re-configuring a system. This is particularly relevant for analysis optimization in particle physics where evaluating $f(x)$ involves processing large numbers of simulated collisions. Another common use case involves optimizing the hyperparameters of a learning algorithm.

Without any assumptions about the function $f(x)$ this is hopeless; however, if one assumes something about the functions (*e.g.* some notion of smoothness) then one can leverage function evaluations evaluations $\{f(x_t)\}_{t=1,\ldots,T}$ to say something about what value the function might take on at other values of x. This is usually cast in Bayesian terms, and Gaussian processes (Section 41.8.2) are often used to model the distribution over $f(x)$. The optimization techniques that use this framing are generically referred to as Bayesian optimization [126].

Optimization in this context is usually characterized by an *exploration-exploitation* tradeoff, similar to what is found in multi-arm bandits. Here, exploration refers to function evaluations that characterize the function in regions that haven't been evaluated, while exploitation refers to evaluations near what is predicted to be its maximum. This setting is similar to reinforcement learning in that it involves sequential decisions (*i.e.*, where to evaluate the function next), but usually the target function $f(x)$ is assumed to be static. In that sense, the state referred to in the language of an MDP is the state of knowledge about the function after sequential evaluations $\{f(x_t)\}_{t=1,\ldots,T}$. The reward at time t is not the value of the function $f(x_t)$, but some quantity that characterizes what was learned about the function's maximum. In this literature, one often refers to the *acquisition function*, which plays a similar role as the expected value of the reward in RL. Common acquisition functions include the probability of improvement, the expected improvement, and an upper-confidence bound [127].

41.5.5 *Active learning*

Active learning is closely related to Bayesian optimization, described above. In Bayesian optimization one estimates the function $f(x)$ from some set of evaluations $\{y_t = f(x_t)\}_{t=1,\ldots,T}$; however, the goal is to find the maximum $x^* = \arg\max_x f(x)$. In active learning, the goal is not to find the maximum of $f(x)$, but to approximate the function as one does in supervised learning. The main difference compared to vanilla supervised learning is that the labeled training dataset isn't provided a priori in a passive way, but the learning algorithm actively decides where to generate $(x_t, y_t = f(x_t))$ pairs. The function $f(x)$ is sometimes referred to as an *oracle*. Active learning is particularly attractive when obtaining labeled data is a costly process.

More broadly, a challenge of many machine learning applications is obtaining labeled data, which can be a costly process. If a system could learn from small amounts of data, and choose by itself what data it would like the user to label via an external process called oracle, it would make machine learning more powerful. Such frameworks are also called experiment design or active learning. In active learning, a model is trained on a small amount of data (the initial training dataset), and an acquisition function (often based on the model's uncertainty) decides on which data points to ask for a label. The acquisition function selects one or more points from a pool of unlabeled data points, with the pool points lying outside of the training dataset. Once we label the selected data points, these are added to the training dataset, and a new model is trained on the updated training dataset. This process is then repeated, with the training dataset increasing in size over time. The advantage of such systems is that they often result in dramatic reductions in the amount of labeling required to train an ML system (and therefore cost and time).

41.6 Simulation-based inference

The goal of simulation-based inference (related to, but distinct from, likelihood-free inference) is to extend the statistical procedures described in the Chapter on Statistics (*e.g.* parameter estimation, hypothesis tests, confidence intervals, and Bayesian posterior distributions) to the situation where one does not know the explicit likelihood $p(x|\theta)$, the probability of the data given the parameters θ, but has access to a simulator that defines the likelihood $p(x|\theta)$ implicitly [128,129]. In a typical setup we would like to solve the so called inverse problem of getting the posterior of the parameters given the data, $p(\theta|x)$, but we cannot use Bayes theorem directly because we do not have explicit $p(x|\theta)$.

In particle physics and cosmology, the simulators usually use Monte Carlo event generators (see Sec. 43) to sample unobserved latent variables z, such as the z_p phase space of the hard scattering (see Sec. 49.4), z_s associated to showering and hadronization, z_d associated to the interaction of particles with the detector (see Sec. 34), or initial Gaussian modes of the universe realization. As such, the full simulation chain can be expressed approximately as

$$\begin{aligned} p(x|\theta) &= \int dz p(x,z|\theta) \\ &= \int \mathrm{d}z_d \int \mathrm{d}z_s \int \mathrm{d}z_p \, p(x|z_d)p(z_d|z_s)p(z_s|z_p)p(z_p|\theta) \,, \end{aligned} \tag{41.45}$$

where θ are the Lagrangian parameters that dictate the hard scattering. Evaluating the marginal likelihood $p(x|\theta)$ is intractable as it would require evaluating the integral above for each event.

While the marginal likelihood is intractable, simulators provide the ability to generate synthetic data $x_i \overset{\text{i.i.d.}}{\sim} p(x|\theta)$ for any value of the parameters θ. One can use a suitable proposal distribution $\tilde{p}(\theta)$, sample $\theta_i \overset{\text{i.i.d.}}{\sim} \tilde{p}(\theta)$, generate synthetic data $x_i \sim p(x|\theta_i)$, and then assemble a training dataset $\{x_i, \theta_i\}_{i=1,\ldots,n}$ that can be used to train various machine learning models.

There is thus a close analogy between simulation-based inference and data driven machine learning tasks discussed so far, replacing θ with y. One difference is that in simulation-based inference we can always generate new samples by running additional simulations, while we typically view training dataset in machine learning as fixed. This property of simulation-based inference enables active learning, where the additional simulations are chosen such as to minimize the error on the desired statistical inference

Phys. A 2026.41. Downloaded from www.worldscientific.com
by UNIVERSITY OF CA LEY on 09/16/26. Re-use and distribution is strictly not permitted, except for Open Access articles.

task. Another difference is that we often have access to the joint likelihood $p(x, z|\theta)$, where z are unobserved latent variables[3].

Typically in particle physics, one uses histograms or kernel density estimation to model the distribution of observables (low-dimensional summary statistics such as the invariant mass) of simulated data [130]. Alternatively, one can use an explicit parametric family (such as a falling exponential or a Gaussian distribution) to model $\hat{f}(x|\theta) \approx p(x|\theta)$. That model is then used as as a surrogate for the unknown density implicitly defined by the simulator. A related approach is known as approximate Bayesian computation (ABC), which approximates the likelihood through an acceptance probability that synthetic data is sufficiently close to the observed data [131, 132]. In practice, these techniques are limited to low-dimensional representations of the data. Thus the potential of recent machine learning approaches to simulation-based inference is to extend this approach to higher-dimensional data, while maintaining the already well-established statistical procedures.

For instance, one can use normalizing flows (see Sec. 41.3.4.3) and the loss functions for density estimation (see Sec. 41.3.3) to learn a surrogate model for the likelihood $\hat{f}(x|\theta) \approx p(x|\theta)$ [69]. Similarly, one can use conditional density estimation to learn a surrogate model for the posterior $\hat{f}(\theta|x) \approx p(\theta|x)$, which may involve including the prior-to-proposal ratio $\tilde{p}(\theta)/p(\theta)$ [70]. In addition to the unsupervised learning techniques, one can also use supervised learning to learn the likelihood-ratio $r(x|\theta_0, \theta_1) = p(x|\theta_0)/p(x|\theta_1)$ by leveraging the *likelihood-ratio trick* of Eq. 41.13 [133, 134].

In some cases one can also augment the training dataset to include the joint likelihood-ratio

$$r(x_i, z_i|\theta_0, \theta_1) \coloneqq p(x_i, z_i|\theta_0)/p(x_i, z_i|\theta_1) \ , \tag{41.46}$$

which can be used to reduce the variance for the squared-error or cross-entropy losses [134, 135]. While the marginal likelihood $p(x|\theta)$ is intractable due to the high-dimensional integral over the latent space, the joint likelihood is often tractable since no integration is necessary.

In some cases performing the marginal integral of Eq. 41.45 is tractable even for high dimensional latent space z. One of the approaches to make it feasible in high dimensional latent space is to make simulations differentiable with respect to all of its parameters, global variables θ and latent variables z. While differentiable simulations have not traditionally been developed for scientific applications, the success of machine learning based on backpropagation combined with gradient descent (see Sec. 41.9.1), has inspired a renewed interest. One example is FlowPM cosmological N-body simulation, which takes advantage of Mesh-Tensorflow to achieve a GPU-accelerated, distributed, and differentiable simulation [136]. Availability of simulation gradients in turn enables gradient based Monte Carlo Markov chain methods to perform high dimensional marginal integral over the latent space z and over parameter space θ [137].

Often SBI uses predetermined summary statistics, such as binned histograms in particle physics, or power spectrum in cosmology, to avoid the curse of dimensionality. It is however possible to train on uncompressed high dimensional data in cosmology by exploiting the symmetries [138]. Yet another alternative is to train the network to search for the best possible summary statistic. The summary statistic can then simply be $\hat{\theta}$, which is the estimate of the parameters θ that emerge from a supervised training on simulations. In SBI these can often be biased even after training, and one possible solution is to form a pseudo-likelihood to model the bias as a function of the true value of θ [139].

41.6.1 *Latent space reconstruction and unfolding*

While much of the work on simulation-based inference described above is aimed at inferring the parameters θ of the simulator, there is work that aims to infer the latent variables z. A common approach in particle physics is to think of the parameters θ as parameters of a theory, such as masses, coupling constants, or Lagrangian parameters, while z might describe the kinematics of a collision before the detector response. Inferring the distribution $p(z|\{x_1, \ldots, x_n\})$ from a dataset of multiple observations is commonly referred to as unfolding in particle physics, and deconvolution in other contexts. Unfolding is a classic inverse problem, and the collection of ideas being used for machine-learning based simulation-based inference are also being applied in this setting [140]. For example, the OmniFold method [141] iteratively reweights a dataset in an unbinned way using machine learning to produce a simultaneous measurement of many observables. In this method, samples $\vec{x}_r$ from detector-level MC simulation are first corrected by a learned weighting function $\omega(\vec{x}_r)$ to match data. Then, samples $\vec{x}_p$ from particle-level MC simulation are corrected by another learned weighting function $\nu(\vec{x}_p)$ to match the $\omega(\vec{x}_r)$-weighted MC simulation. The method is iterated multiple times, to achieve $\nu(\vec{x}_p)$-weighted MC events whose event yields and kinematics match those observed in data. The H1 [142] and ATLAS [143] Collaborations have used the OmniFold method in experimental measurements. It has also been applied to T2K [144] and CMS [145] open data.

In cosmology, a common task is to reconstruct initial density distribution of the dark matter, or its final distribution, from data such as galaxy positions. This can then be used for various downstream tasks such as cosmological parameter inference or making maps of dark matter in our universe. High dimensional SBI can be used for this task [146]. An alternative is Bayesian inverse problem inference using the forward model $g(z, \theta)$, which can be an N-body simulation with some simple galaxy formation model added to it [137, 147, 148]. Standard Bayesian methodology using for example MCMC can be used to solve this task and find the posterior $p(z, \theta|x)$, which specifies initial distribution of dark matter. To draw samples of final dark matter distribution, and of the reconstructed data, we can first draw samples from the posterior $p(z, \theta|x)$, and then evaluate forward model $g(z, \theta)$ for each sample.

41.7 Data representations, inductive bias, and example applications

In Sec. 41.2 we describe the input data as living in an abstract space $x_i \in \mathcal{X}$. In this section, we briefly discuss some of the common types of structured data that are encountered in physics and refer to the corresponding models classes that have been developed to work with them. We elaborate on the model classes in more detail in the following section.

The most basic and common type of data structure is when $\mathcal{X} = \mathbb{R}^d$. This is often referred to as *tabular data* since the entire data set $\{x_i\}_{i=1,\ldots,n}$ can be thought of as a table with n rows and d columns. It is common to think of an individual entry x_i as a vector in d-dimensional Euclidean space, where the coordinates correspond to the columns of this table. In some cases individual components of x_i might be integers or take on only discrete values, in which case describing the space of the data as real-valued is a slight abuse of notation and representation. For many years this was the dominant type of data in high energy physics as it is a natural input type for shallow neural networks, multilayer perceptrons, support vector machines, and tree-based methods found in popular tools such as `TMVA` [149].

For categorical data, one typically uses a numerical representation such as *integer encoding* where different categories are mapped to integers with a corresponding dictionary. Another common representation of categorical data is based on the so-called *one-hot encoding* (aka 'one-of-K' or 'dummy'), in which case the category is mapped to a k-dimensional binary vector where k is the number of categories and each component of this vector corresponds to a particular category. In the one-hot encoding, only one of the components is non-zero. Finally, there are approaches in one learns an *embedding* that maps discrete categories into $\mathbb{R}^d$; an example of this is `Word2Vec` [150]. Interestingly, such embeddings can preserve various types of semantics; for instance, the vector `walking - walk` is similar to the vector `swimming - swam` as are the vectors connecting countries and their capital cities. This allows for a loose sense of algebra on the word

[3]For this reason we prefer to use simulation-based inference instead of likelihood-free inference: joint likelihood $p(x, z|\theta)$ is often available, it is the marginal integral over latent space z that is assumed to be intractable.

Int. J. Mod. Phys. A 2026.41. Downloaded from www.worldscientific.com
by UNIVERSITY OF CALIFORNIA @ BERKELEY on 09/16/26. Re-use and distribution is strictly not permitted, except for Open Access articles.

embeddings such as `walking - swimming + swam = walk`. Similar types of embeddings have also been used in a number of scientific use-cases including biological sequences (*e.g.*, DNA, RNA, and proteins) for bioinformatics applications [151].

Particle physics data often is represented with an extension of the simple tabular data structure where the number of columns is not fixed. For instance, if the rows correspond to data for individual collisions, the number of electrons (and positrons) reconstructed in the event is variable. Thus the number of columns needed to represent the energy, momentum, and charge of these particles is also variable. A common solution to this problem is to fix a maximum number of particles and then *truncate* and *zero-pad* to fit the data into a fixed tabular representation, though this is not the natural representation of the data and it leads to a loss of information.

Sequential data is also commonly encountered in physics (*e.g.* in time series). Here an individual entry $x_i = (x_i^1, \ldots, x_i^t, \ldots x_i^{T_i})$ where t is index for the ordered sequence, T_i is the length of the sequence (which might be variable), and the data associated to each "time" $x_i^t \in \mathbb{R}^d$. This is similar to the previous example where the energy, momentum, and charge of the tth electron in the ith event would be x_i^t and the electrons might be sorted according to their energy or transverse momentum. Sequential data is also encountered in natural language processing, where x_i^t correspond to individual words in a sentence. Recurrent neural networks (see Sec. 41.8.4.5) are particularly well suited to sequential data. Examples applications from the Living Review include Refs. [152–157].

Image-like data is one of the most dominant forms of data in industrial applications of deep learning, is very relevant for astronomy and cosmology, and also appears in particle physics in various forms. Image-like data typically involves d-dimensional features associated to a regular grid or lattice that does not vary across the individual instances x_i. The canonical example is a standard image from a camera with $W \times H$ pixels where the pth pixel has data $x_i^p \in \mathbb{R}^3$ corresponding to the three *channels* in the RGB color model. It is important to recognize that the data corresponding to the 2-dimensional image is not 2-dimensional; instead, it is $(W \times H \times c)$-dimensional, where c is the number of channels. In astronomy, an image may be grey scale ($c = 1$) or there may be more *channels* ($c > 3$) corresponding to different color filters. In other applications, the grid or lattice might be 3- or 4-dimensional. For example, the data associated to a regularly segmented calorimeter can be thought of as a 3-dimensional image and the data associated to a lattice simulation of a classical or quantum system can be thought of as a 4-dimensional image. Convolutional neural networks, described in Sec. 41.8.4.4, are particularly well suited to image-like data. Example applications from the Living Review include Refs. [153, 158–180].

It is also possible that the data (or features) associated to one "pixel" or lattice site may itself be structured. For example, the single read-out plane of a liquid argon time projection chamber (LArTPC) may involve a 1-dimensional or 2-dimensional grid, but the data associated to each "pixel" is itself a sequence or waveform. Example applications in neutrino physics from the Living Review include Refs. [26, 27, 30, 181–208]. Similarly, in lattice quantum chromodynamics, the data associate to a particular site (or link) would be group valued (*e.g.* $x_i^p \in SU(3)$ as in Refs. [209, 210]).

Both sequential and image-like data have a notion of temporal or spatial structure. While it is possible to unroll an image into a $(W \times H \times c)$-dimensional vector, that would erase the spatial structure and obfuscate the fact that nearby pixels are highly correlated. Similarly, one could permute the time index for sequential data, but that would destroy the temporal structure of the data. The complementary point of view is that the model class should also be aware of the structure of the data. Recurrent and convolutional neural networks are good examples of *inductive bias* as the models incorporate the structure of the data. In some cases this can be formalized in terms of symmetry. For example, if we train model to classify images of cats and dogs, we would like it's prediction to be invariant to where in the image the cat is. This type of translational invariance can be enforced in the design of the model class.

While permuting the elements of a sequence destroys the temporal structure of a time series, attaching a temporal index t to a set of objects with features x_i^t can also be problematic. If the data corresponding to x_i are really a set $\{x_i^1, \ldots, x_i^{T_i}\}$ (*e.g.*, a point cloud), then we would like the output of the model to be *permutation invariant* or *permutation equivariant* depending on if the output is per-set or per-element, respectively. A standard sequential or convolutional model will not generally be permutation invariant, but models such as deep sets, various types of graph neural networks, and transformers can be made to enforce permutation symmetry. Example applications from the Living Review include Refs. [172, 211–222].

The temporal and spatial structure of sequences and image like data can also be generalized. For instance, a 1-dimensional sequence can be generalized to a tree structured data like one finds in the hierarchical clustering of jets or as in a directed-acyclic graph (DAG). Generalizations of recurrent neural networks have been constructed that can operate over these more complex data structures [223, 224]. More generally, one can considered graph-structured data composed of nodes and edges or multi-graphs that group together three nodes into faces or k nodes into k-edges. Graph neural networks are a class of models that work with this type of data. The emerging subfield of geometric deep learning aims to unify the notation, terminology, and theory that connect these considerations of the structure of the data and the corresponding model architecture. Example applications in the Living Review include Refs. [32, 190, 197, 200, 201, 203, 225–250].

If the data are expected to have a symmetry associated to them but one is working with a model class that does not enforce this symmetry, then *data augmentation* is a common procedure used to improve generalization performance. Here one starts with an initial dataset $\{x_i\}_{i=1,\ldots,n}$ and produces an augmented dataset $\{x_i'\}_{i'=1,\ldots,n'}$ through some data augmentation strategy. For example, one might apply a random rotation $R_{i'}$ to an image to produce $x_i' = R_{i'}(x_i)$ if one assumes rotational invariance in the underlying problem.

In some cases some of the individual features (components) of x are functions of other features. For instance, one may include components of a four-vector (E, p_x, p_y, p_z) as well as redundant information such as transverse momentum, azimuthal angles, rapidity, etc. In this case, the data is restricted to a lower-dimensional surface embedded in $\mathcal{X}$. Even if the features aren't redundant, statistically the data are often effectively restricted to a small subspace of statistically likely samples and those that are exceedingly unlikely. For instance, the space of natural images is a small and highly structured subspace of all possible images, which are dominated by what we would perceive visually as noise. The term *data manifold* is used to describe this restricted subspace where the data are to be found, even though it does not necessarily satisfy the formal requirements of a manifold in the mathematical sense.

These considerations on the structure of the data not only apply not to the input data $x_i \in \mathcal{X}$, but also to the output data $y_i \in \mathcal{Y}$. For instance, one might want a sequence-to-sequence model as in machine translation of written text [251] or to learn a function that takes sets as input and produces graphs as output as in the Set2Graph mode [252]. One might also want the input and output of the model to be different in representations of an underlying symmetry group and for the model to enforce group-equivariance [209, 210]. The development of the necessary modeling components to enable practitioners to compose and train these types of models is a significant development for the field of physics.

41.8 Flavors of ML models

41.8.1 *Support vector machines*

Support vector machines (SVMs) are a class of supervised learning models used for classification and regression. The learning algorithm involves a convex optimization problem that has a unique solution and can be solved with quadratic programming techniques. In this sense, they are robust and easier to characterize than neural networks that involve non-convex optimization.

by UNIVERSITY OF CA Phys. A 2026.41. Downloaded from www.worldscientific.com
LEY on 09/16/26. Re-use and distribution is strictly not permitted, except for Open Access articles.

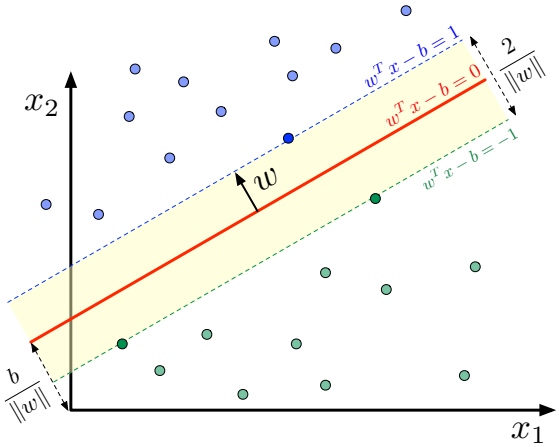

Figure 41.5: Illustration of a maximum margin classifier for a linear support vector machine in the separable case.

Linear support vector machines are used for binary classification, where $\mathcal{X} = \mathbb{R}^d$ and the target labels are conventionally defined as $\mathcal{Y} = \{-1, 1\}$. The classification is simply based on which side of a hyperplane the data lie. Any hyperplane can be written as the set of points x satisfying $w^T x - b = 0$, where $w, b \in \mathbb{R}^d$ are the parameters of the model. The vector w is normal to the hyperplane, but not necessarily normalized. The quantity $\frac{b}{\|w\|}$ quantifies the offset of the hyperplane from the origin along the normal vector w.

If the training dataset is linearly separable, then there is a region bounded by two parallel hyperplanes, called the *margin*, that separate the two classes of data. The maximum margin classifier is uniquely defined by making the distance between these two hyperplanes as large as possible. The boundaries of the margin can be defined by $w^T x_i - b = \pm 1$, and the width of the margin is given by $\frac{2}{\|w\|}$. Figure 41.5 illustrates this for $x \in \mathbb{R}^2$.

Since the width of the margin is maximized when $\|w\|$ is minimized, we can state the goal of the (hard) maximum-margin classifier in the linear separable case as the following constrained optimization problem: Minimize $\|w\|^2$ subject to the constraint $y_i(w^T x_i - b) \geq 1$ for $i = 1, \ldots, n$. The w and b that solve this problem uniquely determine the resulting classifier, $\hat{y}(x) = \mathrm{sgn}(w^T x - b)$. This geometric description makes it clear that the maximum-margin hyperplane is completely determined by those x_i that lie nearest to it: the eponymous *support vectors*.

41.8.2 *From Bayesian linear regression to kernel regression and Gaussian processes*

As discussed in Sec. 41.2.2, linear regression is a specific case of regression where the solution is parameterized as a linear combination of basis functions $\phi(x)$,

$$f_\phi(x) = \sum_k w_k \phi_k(x) = w^\intercal \phi, \tag{41.47}$$

using a short-hand vector notation. If we aggregate all the basis functions of the training data into $\Phi(x)$ and all x into X, and assuming a Gaussian noise model $\epsilon \sim \mathcal{N}(0, \sigma_n^2)$, we can write the noise probability distribution as

$$p(y|X, w) = \mathcal{N}(w^\intercal \Phi, \sigma_n^2 I). \tag{41.48}$$

In overparametrized models, this needs to be regularized, with explicit L2 norm of the weights, as discussed in Sec. 41.2.5. If we view the process in the Bayesian context, we add a weight prior $p(w) = \mathcal{N}(0, \Sigma_p)$ to the data likelihood. With this one can define the posterior of the weights as

$$p(w|X, y) \propto p(y|X, w)p(w) = \mathcal{N}(\sigma_n^{-2} A^{-1} \Phi y, A^{-1}), \tag{41.49}$$

where $A = \sigma_n^{-2} \Phi \Phi^\intercal + \Sigma_p^{-1}$.

Our main task is not to predict the weights themselves, but to predict f^* given some x^*. In the Bayesian view, one must model average over the weights,

$$\begin{aligned} p(f^*|x^*, X, y) &= \int \mathrm{d}w p(f^*|x^*, w) p(w|X, y) \\ &= \mathcal{N}(\sigma_n^{-2} \phi(x^*)^\intercal A^{-1} \Phi y, \phi(x^*)^T A^{-1} \phi(x^*)), \end{aligned} \tag{41.50}$$

where we used $p(f^*|x^*, w) = N(0, \sigma_n^2)$. This can be rewritten as

$$\begin{aligned} &p(f^*|x^*, X, y) \\ &= \mathcal{N}(\phi(x^*)^T \Sigma_p \Phi (K + \sigma_n^2 I)^{-1} y, \\ &\quad \phi(x^*)^\intercal \Sigma_p \phi(x^*)) - \phi(x^*) \Sigma_p \Phi (K + \sigma_n^2 I)^{-1} \Phi^T \Sigma_p \phi(x^*)), \end{aligned} \tag{41.51}$$

where $K = \Phi^T \Sigma_p \Phi$. In general we call $k(x, x') = \phi^T(x) \Sigma_p \phi(x')$ a kernel or covariance function between x and x'. The final expression for the regression mean and covariance has a form

$$f^* = K(x^*, X)[K(X, X) + \sigma_n I]^{-1} y, \tag{41.52}$$

with covariance

$$\mathrm{cov}(f^*) = K(x^*, x^*) - K(x^*, X)[K(X, X) + \sigma_n^2 I]^{-1} K(x^*, X). \tag{41.53}$$

One can see that the prediction takes the observed values y at the training data X, and predicts the value at x^* by incorporating the strength of their correlations via $K(x^*, X)$. In addition, the prediction also suppresses the training points with a small inverse covariance, a generalization of inverse noise weighting.

This expression simply rewrites the standard Bayesian regression, and the kernel is still defined as an inner product of the regression basis functions $\phi(x)$ with respect to Σ_p. However, the kernel can be replaced by any kernel form that describes the level of correlations between x and x', a process known as the *kernel trick*. A general condition for the kernel to be valid is that the covariance matrix is always invertible. In a Gaussian process the kernel is often stationary, defined as $k(x, x') = f(|x - x'|)$. This and many other kernels cannot be related to a finite set of basis functions $\phi(x)$, which is why it is often stated that Gaussian process corresponds to an infinite basis function expansion. Yet another form of the kernels are neural tangent kernels of neural networks in the infinitely wide network limit [23].

Another path to Gaussian processes is via kernel regression, where one makes kernel regression Bayesian [253]. Standard kernel regression, also called Nadaraya-Watson regression, is of the form $f^* = \sum_x k(x, x^*) y(x) / \sum_x k(x, x^*)$, which can be interpreted as a soft version of the k-nearest neighbors algorithm. Bayesian kernel regression in the form of a Gaussian process replaces kernel sums with matrix operations, and is closer to linear regression than to the nearest neighbor methods.

One advantage of Gaussian process is that one can work with a family of kernel functions parameterized by some hyperparameters η. One can then optimize the hyperparameters via gradient-ascent on the marginal likelihood function. In contrast, hyperparameter tuning in other models typically requires a grid search or some other black-box optimization procedure evaluated on held out data or some form of cross-validation.

While we only describe Gaussian process regression, there is a corresponding Gaussian process classification. Rasmussen and Williams provides an excellent review of Gaussian processes [254]. Numerically, Gaussian process libraries are confronted with computing the inverse of the covariance kernel, which scales like $\mathcal{O}(n^3)$ in computational complexity. Gaussian processes are often used as emulators or surrogate models, specially in the context of low dimensional input x and low number of training data n to avoid the steep $\mathcal{O}(n^3)$ scaling. They are used widely in cosmology, and there are a growing number of applications in (astro-)particle physics [255]. Recent works explore the design of physics-inspired kernels and use Gaussian processes to model the intensity for a Poisson point process like those found in experimental particle

Int. J. Mod. Phys. A 2026.41. Downloaded from www.worldscientific.com
by UNIVERSITY OF CALIFORNIA @ BERKELEY on 09/16/26. Re-use and distribution is strictly not permitted, except for Open Access articles.

physics and γ-ray and X-ray astronomy [256–258]. Gaussian processes are also extensively used in Bayesian optimization (Section 41.5), because the uncertainty quantification that is automatically provided by the Gaussian process enables exploration-exploitation strategies where to evaluate the function next.

41.8.3 *Decision trees*

Tree-based models Classification and regression trees (CART) typically partition the input space into J disjoint regions $\mathcal{X} = \mathcal{X}^1 \cup \cdots \cup \mathcal{X}^J$ through a sequence of $J-1$ binary splits based on an individual components of $x \in \mathcal{X}$ (*e.g.* $x_4 < 0.7$) [259]. The model is piecewise constant and assigns the value $b_j \in \mathcal{Y}$ to the jth terminal region $\mathcal{X}^j$. The model can be written

$$\hat{y}(x) = f_\phi(x) = \sum_j b_j \mathbf{1}(x \in \mathcal{X}^j) \ . \tag{41.54}$$

The parameters ϕ of the model comprise the components index and thresholds for the successive splittings and the coefficients b_j.

Tree learning refers to the algorithm used to choosing the tree structure and determining the predictions at leaf nodes. Optimization of the tree structure involves a difficult discrete optimization since the change in the loss with respect to the tree structure is non-differentiable and it is intractable to explore the combinatorially large space of possible trees with brute force. Therefore, the discrete optimization component of tree learning typically involves some approximate algorithm based on heuristics. In contrast, optimization of the b_j for a given tree structure can exploit gradient-based optimization algorithms.

Common approaches to building the decision tree start with a root node and grow with splits based on individual attributes (components of x). These are referred to as top-down induction strategies. There are various impurity heuristics used for choosing the best attribute to split on such as the Gini index, cross-entropy and mis-classification error. Generally they aim to find a split that will refine the the terminal nodes such that they have higher purity than the parent node.

Because most tree learning algorithms consider splits aligned with individual feature components, there are some failure modes for tree-based models. However, tree-based models work well with tabular data composed of a mix of continuous and discrete features. Tools such as `XGBoost` [260] and LightGBM [261] are competitive on tabular data benchmarks like TabArena [262] and are widely used in industry; the boosted decision trees (BDTs) implemented in
`StatPatternRecognition` [263] and `TMVA` [149] have been one of the most used techniques in particle physics [3].

Individual trees are often referred to as weak learners and they can be combined in various ways described below. Regularization is also an important consideration with tree-based models as one can always learn a tree that assigns exactly one training dataset point per terminal node and memorize the training dataset exactly. One approach to this is called *pre-pruning*, which simply terminates the growing of the trees if the number of training samples reaching the terminal node drops below some threshold, the purity of a terminal nodes is below some threshold, or if the improvement in purity due to a proposed split is not above a threshold. Another regularization approach is called *post-pruning*, which uses a validation data set that is disjoint from the training dataset to probe generalization performance. In this approach, after initially growing a tree with the training dataset, a sequence of pruned trees is considered where splits are removed based on some heuristic. The tree in this sequence of pruned trees that minimizes the generalization error on the validation set is chosen. Alternatively, in tools such as `XGBoost` there is an explicit regularization term included in the loss function (see Eq. 41.61).

Ensemble methods The idea of ensemble methods is to combine multiple models into a more performant one by exploiting the bias-variance tradeoff [264]. This is most commonly achieved through averaging (*e.g.* bagging and random forests), which primarily reduces variance, or boosting (*e.g.*, AdaBoost and gradient boosting), which primarily reduces bias. Here, bias refers to the difference between the Bayes optimal model and the average model produced by the learning procedure with different training sets and variance quantifies how much the learned model varies from one training set to another.

The motivation of boosting is to combine the outputs of many "weak" models to produce a more expressive model. Compared to averaging techniques like bagging and random forests, the model is built sequentially on modified versions of the data and the final predictions are combined through a weighted sum

$$\hat{y}(x) = \sum_{t=1}^{T} \beta_t \hat{y}_t(x) \ , \tag{41.55}$$

where β_t expand the parameters of the model ϕ.

Bagging The idea behind bagging (bootstrap aggregation) is to create T bootstrap training datasets $B_1, \ldots, B_T$ drawn from the training dataset $\{x_i, y_i\}_{i=1,\ldots,n}$, then learn a model $\hat{y}_t$ for each, and finally construct an average model $\hat{y}(x) = (1/T)\sum_t \hat{y}_t(x)$. If one had T independent training datasets each of size n, then the bias of the average model would be the same as the original model, but the variance would be reduced by a factor of T. By using bootstrap resampling, the bias may increase but the reduction in variance often dominates, which leads to improved performance.

Random forests Random forests refers to a type of "perturb and combine algorithm" that combines bagging and random attribute subset selection. Again one builds trees $\hat{y}_t(x)$ from bootstrap training datasets B_t, but instead of choosing the best split among all attributes, one select the best split among a random subset of k attributes. If k includes all attributes, then it is equivalent to bagging.

AdaBoost In AdaBoost (adaptive boost) the sequence of trees $\hat{y}_1, \ldots, \hat{y}_T$ are trained with reweighted versions of the original training dataset such that the weight of individual training sample is based on the prediction error in the previous iteration [265]. This requires working with a loss function that and learning procedure for the individual iterations that is amenable to weighted training dataset $\{x_i, y_i, w_i\}_{i=1,\ldots,n}$. Incorporating the weights w_i is straight forward when the risk is expressed as an expectation, since the emperical risk of Eq. 41.3 is just replaced with the weighted average. Similarly, the heuristic for many of the tree-based learning algorithms (*e.g.* the Gini index) also have natural generalizations with weighted events.

In the context of classification, the weighted error of the model $\hat{y}_t(x)$ is

$$\mathrm{err}_t = \frac{\sum_i w_i^{(t)} \mathbf{1}[y_i \neq \hat{y}_t(x_i)]}{\sum_i w_i^{(t)}} \ . \tag{41.56}$$

Based on this weighted error, the coefficient β_t of the component $\hat{y}_t(x)$ in Eq. 41.55 is given by

$$\beta_t = \log\left(\frac{1 - \mathrm{err}_t}{\mathrm{err}_t}\right) \ . \tag{41.57}$$

Then for the next iteration the weights of the misclassified events are updated as $w^{(t+1)} = w^{(t)} \exp(\beta_t)$ and then renormalized so that the sum of all weights is 1. This reweighted dataset is then used to train the next model $\hat{y}_{t+1}(x)$ and the entire procedure is initialized with uniform weights $w_i^{t=0} = 1/n$.

There is an analogous procedure for regression with the squared loss function based on the residuals $r_i = y_i - \hat{y}_t(x_i)$ (see for example Ref. [149] for details).

Gradient boosting One of the most powerful forms of tree based models, which is implemented in the tool `XGBoost` is referred to as *gradient boosting* [266]. In this setup, the model is purely additive as in the case of random forests, so the model is Eq. 41.55 with all $\beta_t = 1$. Note this is without loss of generality since the β_t can be absorbed into the b_j of Eq. 41.54. As with AdaBoost, the model is built sequentially through the sequence $\hat{y}_1, \ldots, \hat{y}_T$.

Phys. A 2026.41. Downloaded from www.worldscientific.com
by UNIVERSITY OF CA LEY on 09/16/26. Re-use and distribution is strictly not permitted, except for Open Access articles.

At each iteration, a new term f_t will be added to the sum in Eq. 41.55. For a given decision tree defined by splits on attributes, one can approximate the objective function (the loss function $\mathcal{L}$ plus a regularization term Ω) as a function of b_j in a second order Taylor series:

$$\text{obj}^{(t)} = \sum_{i=1}^{n} [\mathcal{L}(y_i, \hat{y}_i^{(t-1)}) + g_i f_t(x_i) + \frac{1}{2} h_i f_t^2(x_i)] + \Omega(f_t) + \text{constant} , \tag{41.58}$$

where

$$g_i = \partial_{\hat{y}_i^{(t-1)}} \mathcal{L}(y_i, \hat{y}_i^{(t-1)}) \tag{41.59}$$

and

$$h_i = \partial^2_{\hat{y}_i^{(t-1)}} \mathcal{L}(y_i, \hat{y}_i^{(t-1)}) \tag{41.60}$$

In `XGBoost`, the regularization term is taken to be

$$\Omega(f) = \gamma J + \frac{1}{2}\lambda \sum_{j=1}^{J} b_j^2 , \tag{41.61}$$

where J is the number of terminal nodes in the tree. With the second-order approximation of the objective, one can directly solve for the optimal b_j for the next tree and the corresponding value of the optimized objective function. The improvement in the objective function can then be used as a heuristic for choosing the best split. Specifically, define $G_j = \sum_{i \in I_j} g_i$ and $H_j = \sum_{i \in I_j} h_i$, where I_j is the set of indices of data points assigned to the jth leaf. The heuristic used in `XGBoost` for splitting a node is

$$\text{Gain} = \frac{1}{2}\left[\frac{G_L^2}{H_L + \lambda} + \frac{G_R^2}{H_R + \lambda} - \frac{(G_L + G_R)^2}{H_L + H_R + \lambda}\right] - \gamma . \tag{41.62}$$

This formula can be interpreted as the score on the new left leaf plus the score on the new right leaf minus the score on the original leaf minus a regularization penalty on the additional leaf. If the gain from splitting a leaf is smaller than γ, then the total Gain is negative and the split will not be added, which can be seen as implementing a form of pruning.

41.8.4 *Neural networks*

In this section we focus on the different types of components used in modern neural network architectures. Gradient-based optimization techniques are most commonly used for training neural networks, and they are described in Sec. 41.9.1. Similarly, other important aspects to effectively training neural network models such as parameter initialization and early stopping are discussed in Sec. 41.9.

The vanishing and exploding gradient problem is a common challenge for gradient-based optimization of neural networks and is described in Sec. 41.9.5. That problem is referred to repeatedly in this section because it has motivated the development of numerous architectural components described below.

41.8.4.1 *Feed-forward multilayer perceptron*

One of the core components in neural networks is the fully-connected, feedforward network or*multilayer perceptron* (MLP), which is composed of L *layers*: $f = f^{(L)} \circ \cdots \circ f^{(1)}$. The lth layer defines a function that maps a d_{l-1}-dimensional input vector, called *features*, to an d_l-dimensional output $f^{(l)} : \mathbb{R}^{d_{l-1}} \to \mathbb{R}^{d_l}$. A unit producing an individual component of the d_l-dimensional output is called a *neuron* or a *filter* interchangeably. For $l < L$, the functions f_l are called hidden layers, and the number of neurons (d_l) is referred to as the width of the hidden layers. The layers in an MLP take on the form:

$$f^{(l)}(u) = \sigma^{(l)}(W^{(l)} u + b^{(l)}) , \tag{41.63}$$

where $W^{(l)} \in \mathbb{R}^{d_l \times d_{l-1}}$ is called the *weight matrix*, the components of the vector $b^{(l)} \in \mathbb{R}^{d_l}$ are referred to as the *biases*, $u \in \mathbb{R}^{d_{l-1}}$ is the input from the previous layer, $W^{(l)}u$ denotes a matrix-vector product, and $\sigma^{(l)}$ is a non-linear *activation function* that is usually applied element-wise. The parameters of the network comprise the full collection of weights and biases, $\phi = (W^{(1)}, \ldots, W^{(L)}, b^{(1)}, \ldots, b^{(L)})$.

41.8.4.2 *Activation functions*

The activation functions σ in neural networks are nonlinear functions and key to the expressiveness of the resulting family of functions. Two traditionally used functions are the *logistic or sigmoid* function $\sigma(x) = 1/(1 + e^{-x})$ and *hyperbolic tangent* function $\tanh(x) = (e^x - e^{-x})/(e^x + e^{-x})$. These functions are bounded to be $(0, 1)$ and $(-1, 1)$ respectively, and are symmetric about the input value of zero. On the other hand, away from the zero input value, a gradient of both functions quickly vanishes and this poses a challenge in using gradient-based optimization method (see Sec. 41.9.1). This can be avoided, to some extent, by normalizing the input values and carefully initializing the values of $W^{(l)}$ and $b^{(l)}$. These are discussed in Sec. 41.9.7, 41.9.8 and 41.9.9. Yet, it becomes difficult to maintain a null input value for a *deep* neural network, a model with many layers. Instead, a popular choice for a deep neural network is the *rectified linear unit* (ReLU):

$$\text{ReLU}(x) = \begin{cases} x & \text{if } x > 0 \\ 0 & \text{otherwise} \end{cases} \tag{41.64}$$

whose computational cost is small and ensures that the gradient does not vanish for $x \in (0, +\infty)$ [267,268]. An alternative to preserve a non-zero gradient in negative input values are called *leaky ReLU* and modifies the output to $0.01x$ for $x \in (-\infty, 0)$ [269]. Another variant, called *parametric ReLU* (PReLU), turns the coefficient 0.01 into a variable that is optimized as a part of the model during optimization [270].

The choice of activation functions depends on the model architecture and applications. As described, while the use of ReLU types are a typical choice for a deep neural network, a logistic function is a popular choice at the final layer for classification tasks. In the area of neural scene representation, sinusoidal activation functions have been found to be surprisingly effective [271].

Recently, additional smooth loss functions have been found to work well with larger models, such as the Gaussian-error linear unit (GELU) [272],

$$\text{GELU}(x) = \frac{1}{2}\left(1 + \text{erf}\left(\frac{x}{\sqrt{2}}\right)\right) \tag{41.65}$$

and swish function [273]

$$\text{swish}_\beta(x) = \frac{x}{1 + e^{-\beta x}}, \tag{41.66}$$

which smoothly interpolates between a linear function ($\beta = 0$) and ReLU ($\beta = \infty$). In addition, the value of $\beta = 1$ corresponds to the sigmoid-weighted linear unit (SiLU) [274].

Softmax A softmax function is often used to normalize elements of a discrete vector u, or to interpret the output as a probability over a set of n discrete categories. Given a real-valued input vector $u \in \mathbb{R}^n$, the softmax function computes the output vector $v \in \mathbb{R}^n$ the ith component is given by:

$$v_i = \frac{\exp(u_i)}{\sum_{j=1}^{n} \exp(u_j)} . \tag{41.67}$$

The result has the property that $v_i \in (0, 1)$ and $\sum v_i = 1$. The components of the input vector u are often referred to as *logits* in reference to their connection to the logistic function used in logistic regression. The softmax function is commonly used as the last layer in multi-class classifier. The softmax is also used in the context of attention (see Sec. 41.8.4.6).

Int. J. Mod. Phys. A 2026.41. Downloaded from www.worldscientific.com
by UNIVERSITY OF CALIFORNIA @ BERKELEY on 09/16/26. Re-use and distribution is strictly not permitted, except for Open Access articles.

41.8.4.3 *Universal approximation and deep learning*

There are a number of universal approximation theorems in the theory of neural networks. One of the first was that even with one hidden layer ($L = 2$), an MLP can approximate any continuous function if the nonlinear activation function σ is not a polynomial and the width d_1 is large enough [275]. However, it is often more efficient (in terms of the number of parameters) to increase the *depth* of the network L [276].

Training a deep network (*i.e.* $L > 2$) that generalizes well can be difficult, requiring large training datasets, many gradient updates, and suitable regularization. The introduction of large labeled training sets, advances in computing (*e.g.* graphic processing units or GPUs which enabled orders of magnitude acceleration in parallel computation including matrix multiplies [277]), development of ReLU, research progress in initialization and optimization algorithms for model parameters, and regularization techniques like *dropout* [17] all played an important role in the rise of *deep learning* [2,278]. Though the name deep learning was originally a reference to the depth L of such networks, modern deep learning is characterized more by the composition of various types of modules that are trained through gradient-based optimization. Below we introduce some other common network architectures.

41.8.4.4 *Convolutional neural networks*

Convolutional neural networks (CNNs) are widely used for image-like data. They implement the convolution of the input image u and a *filter* W (also referred to as a kernel). The parameters of the filter are learnable and the convolution involves traversing over input and calculating the inner product of the filter W with the part of the input in the *receptive field*, which has the same spatial shape as the filter and is centered at the target pixel. At each location—indexed by i and j below—there is a pixel that may have a vector of features associated with it. In the context of CNNs, these components of these features—indexed by c and c' below—are often referred to as *channels* in reference to the red, green, and blue color channels in a traditional image. The convolution operation is often denoted with a $*$, and the result can be expressed as

$$v_c(j) = (W * u_c)(j) = \sum_{c'} \sum_{i} W_{c,c'}(i) u_{c'}(\text{“}j - i\text{”}) \,, \qquad (41.68)$$

where “$j - i$” is shorthand for the pixel index corresponding to the translation from pixel j to i. By repeating the operation over all pixels, the result of a kernel convolution is also an image as illustrated in Fig. 41.6. Note that the the number of channels in the output v does not need to be the same as in the input, and the collection of filters $W_{c,c'}$ is often referred to as a filter bank. The entire image for a fixed channel index is often referred to as a *feature map*.

A key feature of the CNN architecture is that it is *equivariant* to translations, meaning that if the input image is shifted (*e.g.*, $u(i) \to u'(i) = u(i-k)$), then the output is also shifted by the same amount (*e.g.*, $v(j) \to v'(j) = v(j-k)$). This equivariance property is a natural consequence of using convolutions. A fully connected MLP would not generally have this symmetry; however, it is enlightening to imagine transferring the computation performed by a CNN to the weights and biases of a fully connected MLP, which would result in duplicating the weights of the filters multiple times. In this view, the CNN can be interpreted as a fully connected MLP with *shared weights*, which would maintain the equivariance property. This view is helpful for gaining intuition about the inductive bias of models and makes clear that a CNN is a subset of the fully connected MLPs that satisfy the translation equivariance property.

One may wonder how CNNs identify features with a spatial size larger than a typical kernel size. One mechanism for this is by stacking multiple convolutional layers, *e.g.*, the composition of two 3×3 kernels will lead to an effective 5×5 kernel in terms of the receptive field. In addition, a typical CNN architecture uses pooling (described below), which effectively downsamples the image so that it can be processed at different resolutions. The effective receptive field in the input image may be much larger than the kernel size in this case. An alternative approach is to use an *inception module*, which is designed to extract features simultaneously using kernels of different size [279].

Pooling *Pooling* plays an important role in convolutional neural networks both practically and in terms of their mathematical properties. A pooling operation is a type of aggregation or downsampling that takes many pixels as input and produce one pixel for output. Typically, the pooling operation is applied independently for each channel or feature component. The most popular pooling operations are *max* and *average* pooling. Max pooling picks the highest activation pixel value within the specified receptive field, while the average pooling computes the average pixel value in the receptive field. The idea of pooling generalizes to other architectures, including graph neural networks where the receptive field includes the neighbors of a particular node in the graph (see Sec. 41.8.4.7). Pooling can make the model robust to small, local deformations in the input, a property called *geometric stability* [280–282]. This type of local deformation is important and distinct from the equivariance to rigid translations provided by the convolutional structure. Repeated pooling operations that eventually lead to a single feature vector with no spatial index is what gives rise to the invariance of common CNN architectures to translations (*i.e.*, an image with a dog will be labeled ‘dog’ regardless of where the dog is in the image).

CNN architectures for image analysis A typical CNN for extracting a 1-dimensional array of features is designed with repeating blocks of convolution layers and pooling operations [283]. Figure 41.7 shows an example evolution of a data tensor through the succession of convolution and pooling operations to extract a 1-dimensional array of features, which then can be fed into a block of MLP for an image classification (or a regression) task. This type of architecture is referred to as an *encoder* or *feature extractor*.

The reduction in the spatial size of an image is performed slowly, typically by a factor of 2, which is the minimum possible reduction factor. After the reduction of the spatial extent, the number of channels is typically increased (also by a factor of 2 in most cases), converging one set of feature maps into a larger number of downsampled feature maps. There may be more than one convolution layer within each spatial resolution (*i.e.*, between the grouping operations). Following these design principles, CNN encoders typically become *deep*, consisting of dozens or sometimes hundreds of convolution layers, and face challenges of vanishing gradient problem (see Sec. 41.9.5). A standard practice to mitigate this issue is to explicitly *normalize* the input tensor input in each convolution layer using algorithms such as *batch normalization*. This will be discussed in Sec. 41.9.9.

There are three main categories of computer vision tasks where CNNs are often used:

- *image classification or regression* requires a prediction of single value for the whole image (*i.e.*, a category or target value),
- *object detection* produces a list location information, typically as a rectangular shaped bounding box, for detecting arbitrary number of objects in the input image, and
- *semantic segmentation* brings a classification task down at the pixel-level (or regression although less common) to identify the class or a feature of every pixel in an image.

As discussed previously, a CNN feature extractor followed by MLP is often used for image classification and regression tasks in wide range of applications including particle physics. Many successful CNN architectures for object detection and semantic segmentation applications share key designs which we briefly discuss below.

Region convolutional neural network (R-CNN) is one of the most successful design for object detection [284]. R-CNN has been explored in HEP experiments where the number and location of signal (*e.g.*, neutrino interactions) are not known apriori in large image data such as neutrino detectors [3,25,187]. R-CNN consists of multiple CNNs. The first is a feature extractor which

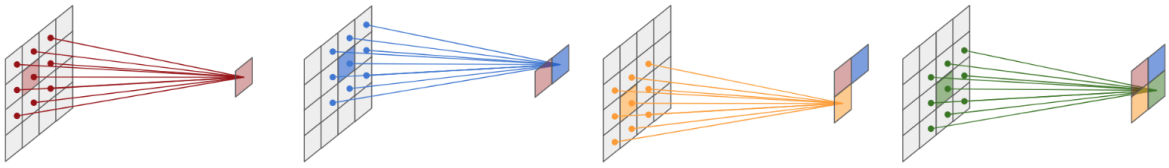

Figure 41.6: A pictorial description of a kernel convolution over four input pixels. It takes a product of the weight matrix (kernel) and the local input matrix centered at a target pixel. The operation is repeated over the input image using the same kernel. The size of the output image depends on the size of the kernel, stride, and padding. In this figure, the kernel size of 3, stride of 1, and padding of 0 is used.

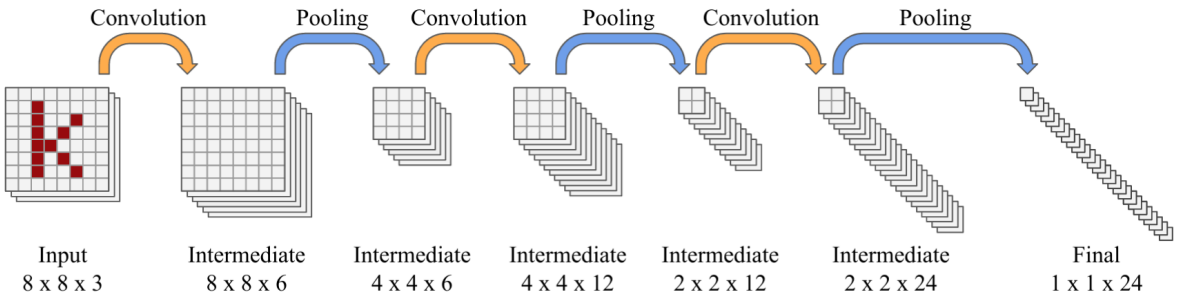

Figure 41.7: An example CNN architecture to extract a 1-dimensional array of features from an image via succession of convolution layers and pooling operations. The (square) kernel, stride, and padding size of a convolution operation are 3, 1, and 1 in respective order. The pooling operation uses a square kernel size of 2. The number of filters at the first convolution layer is 6, and is increased by a factor of 2 at subsequent convolution layers.

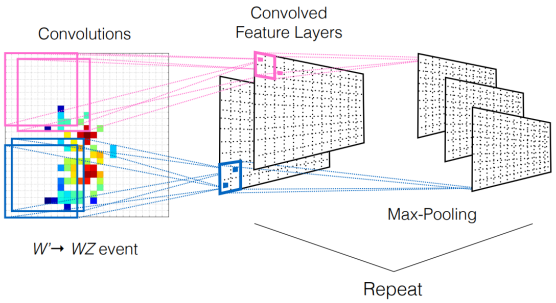

Figure 41.8: CNN classifier for identifying highly boosted W bosons at ATLAS.

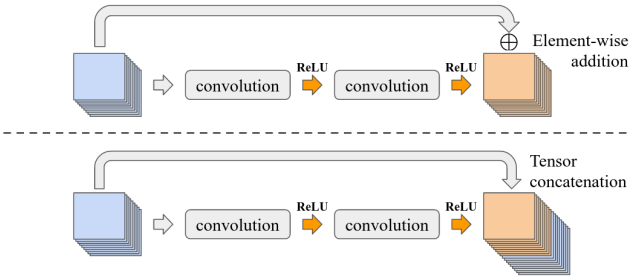

Figure 41.9: Two types of skip connections: the top is from ResNet where the input is element-wise added to the output tensor of a block of convolution layers while the bottom shows a concatenation of the input to the output tensor as employed in other models including U-Net and DenseNet.

produces a spatially compressed feature tensor. For every pixel in the compressed tensor, the second CNN applies 1×1 convolution to predict two information: an *object score* to inspect whether or not there is a target object in the (spatially compressed) pixel, and prediction of the location and size of a rectangular, axis-aligned bounding box that contains the object (if exists). This second CNN is called the *region proposal network* (RPN), and the bounding box is called the *region of interest* (ROI). For each ROI with an object score above threshold (hyperparameter), the third CNN operates in the corresponding sub-field of an already-compressed tensor (*i.e.* by the first CNN) to perform a classification for an object inside the ROI. This approach can produce multiple ROIs for the same object with a high overlap. Those predictions are reduced using non-maximum suppression (NMS) algorithm which computes the intersection-over-union (IoU) to combine overlapping ROIs that are likely detecting the same object.

Residual networks and skip connections

The expressivity of a neural network increases as more hidden layers are added, but gradient-based optimization of deep models can be notoriously difficult due to vanishing gradients (see Sec. 41.9.5). One powerful technique to address this challenge is a *residual network* (ResNet), which is a modular architecture design that can be applied to neural network models [285]. Suppose a $f(x)$ as the target transformation to be learned by a few stacked layers where x is the input to the first layer. The authors of ResNet hypothesized that it may be easier for a model to learn a residual transformation $\tilde{f}(x) \coloneqq f(x) - x$, thus the objective to learn is $\tilde{f}(x) + x$ where $\tilde{f}(x)$ denotes the output of stacked layers. This form assumes $\tilde{f}(x)$ and x share the same tensor dimension and size. If they differ in the feature dimension, equivalently the count of channels in an image tensor, one could use 1×1 convolutions to transform and match the dimension. Adding the input tensor x to the output of a convolution operation $\tilde{f}(x)$ in ResNet is a form of *skip connection*. For a residual block that outputs $y = \tilde{f}(x) + x$, the backpropagated gradient to the input x becomes

$$\frac{\partial \mathcal{L}}{\partial x} = \frac{\partial \mathcal{L}}{\partial y} \cdot \left(I + \frac{\partial \tilde{f}}{\partial x} \right), \tag{41.69}$$

Phys. A 2026.41. Downloaded from www.worldscientific.com
by UNIVERSITY OF CA LEY on 09/16/26. Re-use and distribution is strictly not permitted, except for Open Access articles.

Int. J. Mod. Phys. A 2026.41. Downloaded from www.worldscientific.com
by UNIVERSITY OF CALIFORNIA @ BERKELEY on 09/16/26. Re-use and distribution is strictly not permitted, except for Open Access articles.

meaning it sums an identity path with the gradient through the residual branch, helping prevent vanishing gradients. ResNet authors demonstrated performance improvement at depths exceeding 1000 layers where the non-residual counterpart could not improve beyond a few dozen layers. The ResNet design is widely used in many CNN architectures as it is modular, *i.e.*, a *residual block*, and can be applied per a stack of convolution layers (*e.g.*, U-ResNet introduced for LArTPC detectors uses ResNet modules within a U-Net architecture [26, 184]).

U-Net is one of the of most successful models used for semantic segmentation [286]. Since the output of U-Net is also an image, it is more interpretable compared to models for image-level classification or regression. The model is used widely in HEP experiments in both 2D and 3D image data [26, 27, 184, 194, 196]. The architecture of U-Net consists of a CNN encoder and *decoder*. A decoder consists of convolution and *transposed convolution* layers (also called deconvolution). The operation of a transposed convolution can be seen as the opposite of a convolution: for every input pixel, its value is multiplied by the kernel and copied to the output. In contrast to a regular convolution layer that reduces input pixels via the kernel, a transposed convolution layer broadcasts input pixels via the kernel, producing an output that is larger than the input. In the decoder of U-Net, transposed convolution layers are used to upsample spatially compressed feature tensors back to the original image resolution. Standard convolution layers are placed between upsampling operations. Features for every output pixel can be used for either a classification or a regression task. The idea behind encoder-decoder architecture is to extract features in the encoder, and the decoder interpolates those features back to the original spatial resolution. The downsampling operation (*e.g.*, max pooling) in the encoder is, however, a lossy process where spatial information is permanently lost. This is a major obstacle to achieve a high precision semantic segmentation task. The U-Net architecture overcomes this challenge by concatenating intermediate tensors in the encoder block with the tensors of the corresponding spatial size in the decoder block. This is a type of a *skip connection* discussed previously, which dramatically improves the performance of semantic segmentation.

41.8.4.5 *Recurrent neural networks*

Recurrent neural networks (RNNs) [287] are a family of neural networks designed for sequential data (*e.g.*, time series). Consider sequential data where x_t represents each step in a sequence with $t \in [1, n]$. A typical RNN takes the following form:

$$h_t = g_h(h_{t-1}, x_t, \theta) \tag{41.70}$$

where h_t and θ denote the *hidden state* of the system and parameters of g_h, the RNN model. The term *recurrent* refers the nature of the model operating on the previous state of the system (and hence the whole history). RNNs operate on three types of tasks:

- *One-to-many* takes a single input and generates a sequence (e.g. generates a sequence data, such as a sentence or waveform, given a category).
- *Many-to-one* takes a sequence and generates an output (e.g. sequence-labeling).
- *Many-to-many* takes a sequence and generates a sequence where the length of input and output sequence may be same (e.g. classification of individual element in a sequence) or different (e.g. sequence to sequence mapping).

Figure 41.10 shows an example for a many-to-many task, where $\{x_t\}_{t=1:n}$, $\{y_t\}_{t=1:n}$, and $\{h_t\}_{t=0:n}$ denote the inputs, outputs, and hidden states respectively. A set of operations at each time step is called a *cell*. A simple RNN cell may look like:

$$\begin{aligned} h_t &= g_h(Wx_t + Vh_{t-1} + b) \\ y_t &= g_o(Uh_t) \end{aligned} \tag{41.71}$$

where $W \in \mathbb{R}^{d_h \times d_i}$, $V \in \mathbb{R}^{d_h \times d_h}$, $U \in \mathbb{R}^{d_o \times d_h}$ are matrices g_h and g_o represent functions. d_i, d_h, and d_o are the dimension of input, hidden state, and output. $b \in \mathbb{R}^{d_h}$ is a bias term. An example application is sequence-labeling where the goal is for y_t to classify each input x_t in the sequence. In that case, one might use $g_h = \tanh$ and $g_o = \text{softmax}$ and use a loss function that averages classification accuracy over the sequence.

Variations in RNN architectures result from the design of cells (described below) and flow of information across the cells. For instance, a bidirectional RNN (Figure 41.11 left) employs two set of RNNs, one processing the sequence in the forward direction and the other in the backward direction, and the hidden states from both directions are then combined to capture the context from both parts of the sequence. An RNN encoder-decoder (Figure 41.11 right) use one RNN to generate a context vector that encodes the whole input sequence, and use a separate RNN to generate another sequence from the encoded context. This can be used for machine translation.

LSTM and GRU An RNN applies the same functions g_h and g_o in Eq. 41.71 repeatedly for each element of the sequence. This repeated component is similar to the shared weights for a convolutional filter in a CNN.

A hyperbolic tangent (tanh) is traditionally a popular choice for g_h as it regulates the magnitude of the hidden states and prevents it from diverging. Yet, this simple model is challenging to train for a long sequence of data [288, 289]. This is partially due to the fact that tanh contributes to the vanishing gradient problem and because repeated multiplication of the same weight matrices (i.e. V and W in Eq. 41.71) can lead to gradients that can either explode or vanish (see Sec. 41.9.5). Additionally, the way the signal accumulates means that changes early in the sequence have different impact from changes late in the sequence.

Long short-term memory (LSTM) [290] is a model designed to address the issue of vanishing gradient for RNNs. In this model, a *context* is introduced as a way to enable the model to hold long-term memory while the hidden states remain to hold short-term memory. The context c_t and hidden state h_t at step t are computed as follows:

$$\begin{aligned} c_t &= f_t \odot c_{t-1} + i_t \odot \tilde{c}_t \\ h_t &= o_t \odot c_t \\ &\text{where} \\ f_t &= \sigma\left(W^f x_t + V^f h_{t-1} + b^f\right) \\ i_t &= \sigma\left(W^i x_t + V^i h_{t-1} + b^i\right) \\ o_t &= \sigma\left(W^o x_t + V^o h_{t-1} + b^o\right) \\ \tilde{c}_t &= \tanh\left(W^c x_t + V^c h_{t-1} + b^c\right) \end{aligned} \tag{41.72}$$

where σ and $\odot$ denote logistic function and an element-wise (*i.e.*, Hadamard) product and f_t, i_t, and o_t are referred to as *gates*. Each gate outputs a value between 0 and 1, and is associated with unique weights, W and V, and a bias b. One can see c_t is a combination of the previous context vector c_{t-1} and a new context vector $\tilde{c}_t$. The *forget* gate f_t controls which and how much of the past context should be kept or forgotten. The *input* gate i_t controls how much of the present context $\tilde{c}_t$ should propagate to the current state c_t. The output gate o_t controls which and how much of the context vector should represent the present hidden state h_t. From Figure 41.12, one can see that the context vector c_t evolves with a gated addition operation. As such, it can be seen as an uninterrupted path for gradients to flow. This is similar to a residual connection (see ResNet in Sec. 41.8.4.4), which enabled training of CNNs with thousands of layers.

Another gated model to solve a vanishing gradient problem is the *gated recurrent unit* (GRU) [251]. The GRU is similar to the LSTM with a few simplifications: the GRU merges the context vector and the hidden states and combines three gates into two. As a result, it requires less computational resources while retaining a similar level of performance for long sequences. The GRU

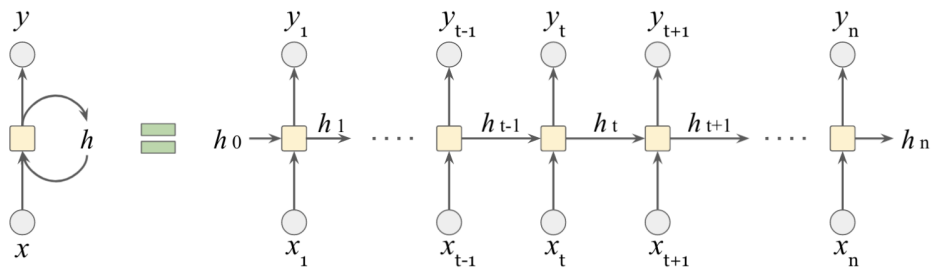

Figure 41.10: Pictorial description of a RNN (on the left) which takes an input and produces an output at every step with a hidden-to-hidden connection. The right diagram is unrolled over discrete steps. The yellow box represents a cell: a set of operations unique to each architecture.

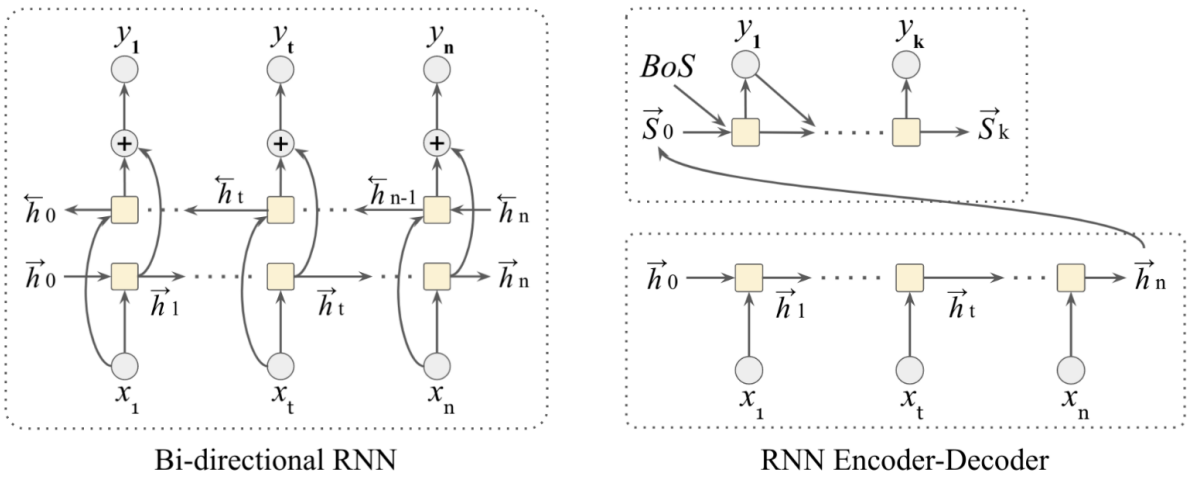

Figure 41.11: Bidirectional RNN (left) provides contexts in the preceding and subsequent parts of the input sequence. RNN encoder-decoder (right) can generate an output with a different sequence length from an input. Each cell in the decoder may take a previously generated element, starting from a special marker that signals the beginning of the sequence (BoS) and ending when the end of sequence is generated.

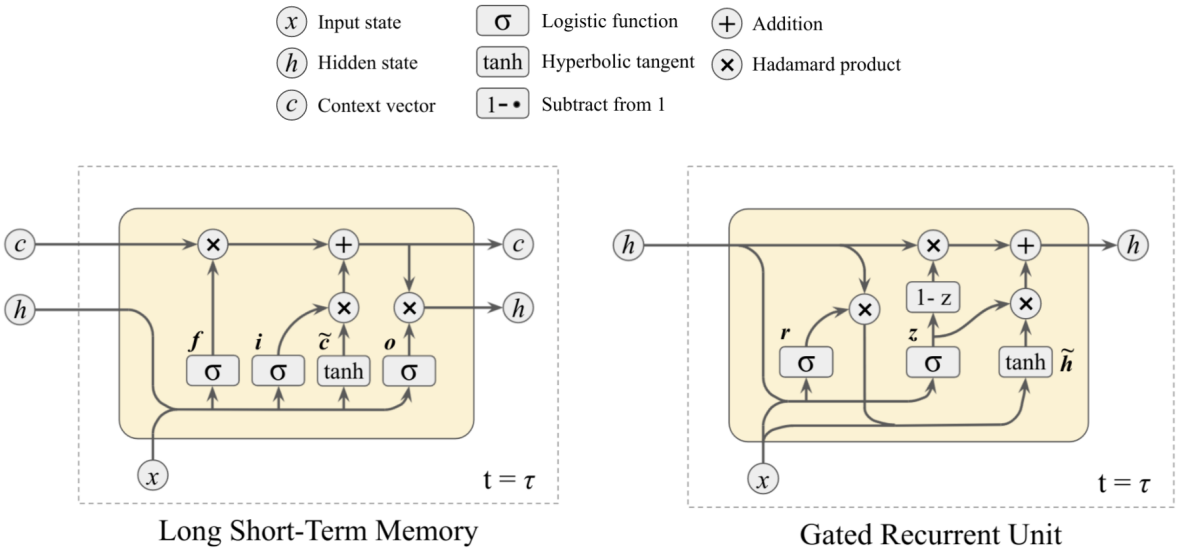

Figure 41.12: LSTM (left) and GRU (right) are both gated neural network designed to address a vanishing gradient problem for RNNs.

Phys. A 2026.41. Downloaded from www.worldscientific.com
by UNIVERSITY OF CA LEY on 09/16/26. Re-use and distribution is strictly not permitted, except for Open Access articles.

Int. J. Mod. Phys. A 2026.41. Downloaded from www.worldscientific.com
by UNIVERSITY OF CALIFORNIA @ BERKELEY on 09/16/26. Re-use and distribution is strictly not permitted, except for Open Access articles.

operations are defined as follows:

$$
\begin{aligned}
h_t &= z_t \bigodot h_{t-1} + (1 - z_t)\tilde{h}_t \\
&\quad \text{where} \\
r_t &= \sigma\left(W^r x_t + V^r h_{t-1} + b^r\right) \\
z_t &= \sigma\left(W^z x_t + V^z h_{t-1} + b^z\right) \\
\tilde{h}_t &= \tanh\left(W^h x_t + V^h \left(r_t \bigodot h_{t-1}\right) + b^h\right)
\end{aligned}
\tag{41.73}
$$

where r_t and z_t are referred to as *reset* and *update* gate. As one can see in Figure 41.10, the reset gate in GRU performs the same task as the forget gate in LSTM by removing or reducing the elements of its memory (*i.e.* the hidden state). The update gate z_t determines the relative proportion of the previous hidden state h_{t-1} and the new context $\tilde{h}_t$ to be mixed in producing the new hidden state.

In addition to sequential data, the LSTM and GRU units can be used for data that has a tree-like structure. In this setting, the networks are often referred to as recursive neural networks or TreeRNN and they have found applications in natural language processing and jet physics [223, 224, 291–293].

41.8.4.6 *Attention and transformers*

The idea behind *attention* is to form a representation for the input, but different parts of the input are weighted differently according to the task at hand. By making the weights learnable, the network can learn to attend to the relevant parts of the input. For the ith task, one can form a task-specific context c_i by computing the weighted average of the hidden state representations h_j for each component of the input. A softmax function is used to produce attention scores α_{ij} for the jth input and ith task because it assigns a positive value to each component of the input and sums to one, $\sum_j \alpha_{ij} = 1$. Putting these ingredients together, we have the *additive attention mechanism*

$$
c_i = \sum_{j=1}^{n} \alpha_{ij} h_j \qquad \text{where} \qquad \alpha_{ij} = \underset{j}{\text{softmax}}(\beta_{ij}) \ , \tag{41.74}
$$

where softmax_j indicates that normalizing sum runs over the index j and the logits β_{ij} can be computed from a neural network. In the case of a cell of an RNN encoder-decoder network (see Fig. 41.11) that is decoding element i with an incoming input state s_{i-1}, the logits for the attention mechanism can be computed as

$$
\beta_{ij} = U \tanh\left(W s_{i-1} + \widetilde{W} h_j + b_i\right) \ , \tag{41.75}
$$

where U, W, and $\widetilde{W}$ are the weights and b is the bias term of the model. Figure 41.13 from Ref. [294] illustrates the full attention mechanism. This idea was first implemented by a model called *RNNSearch* that made a breakthrough in machine translation by combining a bidirectional RNN with an additive attention mechanism [295].

The values α_{ij} can be used to visualize the influence of the jth input element on the ith output element, which improves interpretability of the model [294] as shown in Fig. 41.14.

In additive attention (Eq. 41.74), the hidden representations h_j, also called *values*, are combined through a weighted average based on the coefficients α_{ij}, resulting in a task-specific context vector c_i. These values are often arranged in a matrix labeled $V \in \mathbb{R}^{m \times d_v}$, where the m rows of the matrix correspond to individual hidden state vectors of length d_v. The α_{ij} can also be represented as a $n \times m$ matrix α resulting from applying the softmax function to the $n \times m$ matrix β, normalized independently for each row. With this notation, Eq. 41.74 could be rewritten as $c = \text{softmax}(\beta)V$, where the softmax is normalized per row.

One powerful and widely used variant of the attention mechanism is *scaled dot-product attention*. In scaled dot-product attention, instead of using an neural network to compute the logits β as in Eq. 41.75, the logits are computed by forming a dot product between an incoming *query* and *key*. The set of n query vectors can be arranged into the matrix $Q \in \mathbb{R}^{n \times d}$ and the set of d key

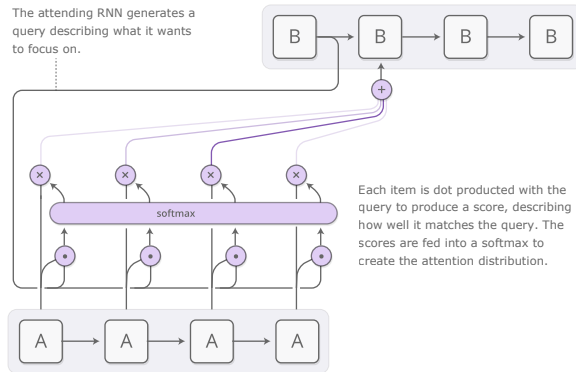

Figure 41.13: An illustration of the attention mechanism from Olah and Carter, "Attention and Augmented Recurrent Neural Networks." Lower boxes labeled `A` represent input elements in the sequence and upper boxes labeled `B` indicate output elements. The left-most line originating from the first `B` corresponds to the state s_{i-1} in the text.

vectors can be arranged into the matrix (transpose) $K^\intercal \in \mathbb{R}^{d \times m}$. One can interpret the keys as trying to detect certain types of queries and routing the attention to the relevant value. Typically, the dot-product is scaled by a factor of $1/\sqrt{d}$. The resulting task-dependent context is $c_i = \text{softmax}_j(q_i \cdot k_j/\sqrt{d})v_j$. A common, though confusing, notation is simply

$$
c = \text{Attention}\,(Q, K, V) = \text{softmax}\left(\frac{QK^\intercal}{\sqrt{d}}\right) V \ , \tag{41.76}
$$

where c is a $n \times d_v$ matrix organizing the n context vectors of length d_v that are tailored summaries of the input vector for each of the n tasks.

The *transformer* architecture is a powerful encoder-decoder model based on the scaled-dot product attention mechanism. It was originally designed for sequential data and subsequently used in other areas of research including computer vision. One advantage of scaled-dot product attention is that computing the attention weights does not involve any sequential processing. This allows the models to better leverage the parallelism of the hardware to train more expressive models faster than before. In place of the gated units of an RNN that are key to avoiding the vanishing gradient problem, the transformer architecture employs a residual connections at every attention module (*i.e.*, the input tensor is added to the output as in Fig. 41.9).

The second major ingredient in the transformer architecture is *multi-head attention*. A multi-head attention module executes multiple scaled dot-product attention modules in parallel. The query Q, key K, and value V matrices in each scaled dot-product attention module are obtained by applying linear transformations (with learnable weights) to the common Q, K, and V input matrices. Each of them can be considered a different (albeit related) *perspective* from which to derive attention.

For a sequence-to-sequence mapping task, the output of encoder is used to derive key K and value V matrices for the multi-head attention module in the decoder. The decoder is then responsible for mapping between the key-value features derived from the input (the encoder) and the queries from the decoder (which is still executed sequentially) in order to produce the final decoded output.

Finally, we note that the transformer architecture does not just employ an attention mechanism in the decoder. By employing attention in the encoder as well the model has more capacity to "interpret" the input—a concept referred to as *self-attention*. Transformer models have contributed to breakthroughs in many areas of scientific and industrial research [296]. While transformers are very powerful, they also require a larger number of training samples due to the weaker inductive bias than other models.

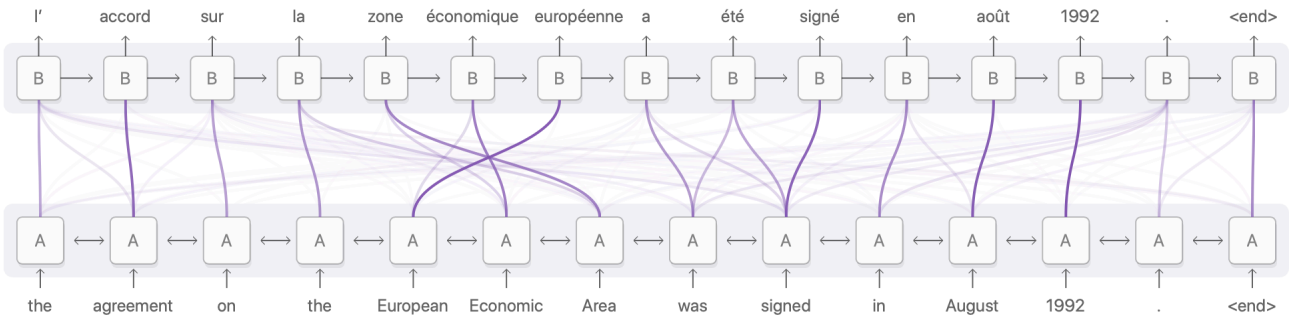

Figure 41.14: Visualization of the attention weights in a sequence-to-sequence problem from Olah and Carter, "Attention and Augmented Recurrent Neural Networks." The thickness of the lines is proportional to the attention weights α_{ij}.

41.8.4.7 *Graph networks and geometric deep learning*

Graphs are a powerful archetype for representing structure data. A graph consists of *nodes* as elements and *edges* between between them. Graphs are sufficiently flexible to describe many types of structured data including images and sequences. Graph-based neural networks can also be seen as a generalization of many common types of machine learning models such as recurrent and convolutional neural networks [282]. The term *geometric deep learning* refers to this recent formulation that focuses largely on the symmetries of the data.

An earlier attempt to organize the variations on different flavors of graph-based neural networks can be found in Ref. [297]. In their formalism, a graph network may be represented as $G(\mathbf{u}, V, E)$ where $\mathbf{u}$ represents an array of global features, $V = \{\mathbf{v}_i\}_{i=1:N^v}$ represents a set of N^v nodes with $\mathbf{v}_i$ as features for the ith node (e.g. such as RGB channels if a node represents a pixel in image data), and $E = \{(\mathbf{e}_k, r_k, s_k)\}_{k=1:N^e}$ represents a set of N^e edges with $\mathbf{e}_k$ as features for the kth edge. An edge may be (bi)directional where r_k and s_k denotes the destination and origin nodes respectively. The features of a graph may evolve with three *update* functions ϕ and three *aggregate* functions ρ:

$$
\begin{aligned}
&\mathbf{e}'_k = \phi^e(\mathbf{e}_k, \mathbf{v}_{r_k}, \mathbf{v}_{s_k}, \mathbf{u}) \quad \mathbf{e}'_i = \rho^{e\to v}(E'_i) \\
&\qquad \text{where} \quad E'_i = \{(\mathbf{e}'_k, r_k, s_k)\}_{r_k=i, k=1:N^e} \\
&\mathbf{v}'_i = \phi^v(\bar{\mathbf{e}}_i, \mathbf{v}_i, \mathbf{u}) \qquad \bar{\mathbf{e}}' = \rho^{e\to u}(E') \\
&\qquad \text{where} \quad E' = \cup_i E'_i = \{(\mathbf{e}'_k, r_k, s_k)\}_{k=1:N^e} \\
&\mathbf{u}' = \phi^u(\bar{\mathbf{e}}', \bar{\mathbf{v}}', \mathbf{u}) \qquad \bar{\mathbf{v}}' = \rho^{v\to u}(V') \\
&\qquad \text{where} \quad V' = \{\mathbf{v}'_i\}_{i=1:N^v}
\end{aligned}
\tag{41.77}
$$

where $\mathbf{e}'$, $\mathbf{v}'$, and $\mathbf{u}'$ denote the updated node, edge, and graph features. In Graph Networks, three types of information are updated in the following order. The first step is ϕ^e to update every edge. The second step updates every node: for ith node, compute $\rho^{e\to v}$ to aggregate updated attributes from the edges with $r_k = i$ then compute ϕ^v to update the node attributes. The third step updates the graph attributes through ϕ^u which takes the original state $\mathbf{u}$, aggregated node and edge attributes by $\rho^{v\to u}$ and $\rho^{e\to u}$ respectively.

Graph neural networks [298] (GNNs) are the class of neural networks that work on graph-structured data. A related data format in computer vision and physics is the *point cloud*, which is an unordered set of points (*i.e.*, a graph with no edges). Operations on point cloud need to be permutation invariant (*e.g.* min, max, $+$, $\cdot$), and analysis of 3-dimensional physical object represented by point cloud need to be rotation and translation invariant as in the case for an image. PointNet [299,300], a GNN that performs an object classification on point cloud of 3-dimensional positions, treats each point as a node, applies MLPs as ϕ^v to update node features, and global max-pooling operation as $\rho^{v\to u}$. There is no explicit edge definition in PointNet (though the model applies affine transformation to all points using spatial transformer network [301], which could be considered as a separate graph operation, to introduce rotation and translation invariance and to capture topological features). Deep sets [302] follow the same manner except ϕ^v takes the global entities $\mathbf{u}$. This is same for PointNet when performing point cloud segmentation: ϕ^v takes a step of simply concatenating $\mathbf{u}$ to node entities to combine a local and global features. Dynamic graph CNN [303] is a variant that (re)define edges dynamically using attention mechanism: $\rho^{e\to v}$ aggregates k neighbor nodes where the inter-node distance is defined as a Cartesian distance in the feature space. ϕ^v remains a MLP and, while edges are defined, there is no associated entity. A similar technique is used in nonlocal neural network [304] to efficiently propagate local feature information to points that may be far in the 3D cartesian coordinate. Message-passing neural network [305] (MPNN) explicitly defines a feature vector as edge entities. In MPNN, $\rho^{e\to v}$ performs element-wise sum of features and feed into ϕ^e, explicitly passing features across nodes as the name suggests. While these are representative models that are frequently used in particle physics applications [30,190,201,211,212,226,252,306–308,308], it is only a tiny fraction of GNN models developed over the past decade.

Graph-based models are particularly interesting for science applications because they offer a natural way to organize the entities in the data and encode how those components interact each other. This particular type of inductive bias is referred to as *relational inductive bias* in Ref. [298]. Graph edges may be intrinsically defined in the data (*e.g.*, when representing a social network) or not (*e.g.*, a point cloud). In the latter case, the graph structure must be chosen. A naive approach may be defining a fully-connected graph. However, for applications on hundreds of thousands of nodes (*e.g.*, high resolution 3D point cloud), this may require a prohibitive amount of memory and computation. On the other hand, if the graph is too sparse, it may negatively impact the performance. One may need to compare the model performance among differently constructed graphs and balance against computational burden. Ideally, the graph would be based on some knowledge of the interactions, but in the absence of such knowledge, popular graph construction methods include fully-connected, k-nearest neighbors, a Delaunay graph, minimum spanning tree, and locality-sensitive hashing [309].

Classification and regression tasks for graphs can be formulated such that the prediction is made for the entire graph or its individual nodes or edges. Graph-level prediction is like classifying an entire image, while node-level prediction is like semantic segmentation where individual pixels are classified. For clustering of points, GNNs can approximate a transformation function for nodes into the latent space where an optimal clustering of points can be performed. For instance, Ref. [310] proposes the *object condensation* approach to extract particle information from a graph of detector measurements as well as grouping of the measurements. The model predicts the properties of a smaller number of particles than there are measurements, in essence reducing the graph without explicit assumptions on the number of targeted particles. Certain nodes are chosen to be the "condensation" point of a particle, to which the target properties are attached. A special loss function mimics attractive and repulsive electromagnetic po-

Phys. A 2026.41. Downloaded from www.worldscientific.com
by UNIVERSITY OF CA LEY on 09/16/26. Re-use and distribution is strictly not permitted, except for Open Access articles.

Int. J. Mod. Phys. A 2026.41. Downloaded from www.worldscientific.com by UNIVERSITY OF CALIFORNIA @ BERKELEY on 09/16/26. Re-use and distribution is strictly not permitted, except for Open Access articles.

tentials to ensure nodes belonging to the same particle are close in the latent space. Alternatively, one can formulate clustering as an edge classification task [29–32]. See Ref. [311] for a comprehensive review on particle physics applications.

41.8.5 *Model design with physics inductive bias*

Designing neural networks that respect the structure of particle physics can materially improve sample efficiency, robustness to systematics, and physical interpretability. Rather than relying on generic inductive biases (*e.g.*, translation equivariance in image CNNs), particle-physics–informed models hard-wire symmetries, conservation laws, and kinematics into the architecture or loss. This reduces the hypothesis space to functions that are a priori plausible, which is particularly valuable when training data is scarce, for extrapolation outside the training distribution, and for tasks where trust and uncertainty quantification matter as much as raw accuracy.

Exploitation of symmetry groups and hence *equivariance* is arguably one of the most important forms of physics-informed approaches. At the constituent level, events and jets are sets of particles, so permutation symmetry is fundamental. Deep sets and graph neural networks implement this by aggregating over particles with symmetric operations [211]. Beyond permutation symmetry, Lorentz symmetry is the natural arena for high energy physics experiments. Networks can be built from Lorentz scalars and tensors or by representing features as four-vectors and ensuring intermediate outputs transform equivariantly under boosts and rotations [312–318]. Gauge symmetry offers another avenue where symmetry-aware design pays off. In lattice gauge theory, gauge-equivariant networks ensures locality and exact invariance under gauge transformations [209, 319–322].

While these models explicitly integrate laws of physics into mathematical operations and model architecture designs, it is also possible to implicitly enforce physics constraints through a loss definition and model optimization method. For instance, physics-informed neural networks (PINNs) introduce regularization terms that force predicted physics quantities to follow laws of physics in the form of partial differentiable equations (*e.g.*, acceleration as the time derivative of velocity) [323, 324]. Variants of PINNs incorporate differentiable physics models as a part of a model architectures [325]. Finally, it is also possible to introduce physics constraints in an optimization process. For example, for a machine learning model for data reconstruction, an output of the model may go through a forward physics simulator that infers the original input to the reconstruction model. By minimizing the difference between the original input and the inferred one, the reconstruction model is forced to learn a solution that is consistent with the forward physics model [326].

41.9 Learning algorithms

41.9.1 *Gradient-based optimization*

Given a parameterized model $f(x, \theta)$ and a loss function $\mathcal{L}(x, \theta)$, where x and θ denotes data and model parameters, one way to optimize θ is to first apply an appropriate initialization, $\theta_{t=0}$ (e.g. Sec. 41.9.7 for neural networks), and perform an iterative update:

$$\theta_t = \theta_{t-1} - \lambda \nabla_\theta \mathcal{L}(x, \theta), \tag{41.78}$$

where λ is a small, real valued hyperparameter called *learning rate*. To see how this works, define $\delta\theta \equiv \theta_t - \theta_{t-1}$ and consider $\delta(\nabla_\theta \mathcal{L}(x, \theta))$:

$$\delta\left(\nabla_\theta \mathcal{L}(x, \theta)\right) \approx \delta\theta \cdot \nabla_\theta \mathcal{L}(x, \theta) = -\lambda |\nabla_\theta \mathcal{L}(x, \theta)|^2 \tag{41.79}$$

which would monotonically decrease the loss function, and locally move the parameter values in the desired direction of loss function minimization. This algorithm is called *gradient descent* (GD). We note that λ needs to be sufficiently small for the approximation to hold. When λ is too large, this can be a cause of a gradient explosion discussed in Sec. 41.9.7.

41.9.2 *Stochastic gradient descent*

Stochastic gradient descent (SGD) follows GD but replaces the exact gradient term $\nabla_\theta \mathcal{L}(x, \theta)$ with a stochastic approximation, where we subsample the data in the loss function using N samples, where $N < n$,

$$\nabla_\theta \mathbb{E}_{\hat{p}(x)} \mathcal{L} \approx \frac{1}{N} \sum_i^N \nabla_\theta \mathcal{L}_i, \tag{41.80}$$

where $\mathcal{L}_i$ is the loss function for data sample i. It should be noted that N needs to be randomly and independently sampled for the approximation to hold. Implementation of SGD follows three steps: take new samples of size N, approximate the gradient, then update the parameters θ.

In the case of optimizing the loss using a static database (*i.e.* one cannot take new N samples for every update), *mini-batch learning* is often employed. This replaces the first step with a randomly sampled *batch* of data, which is a subset of all the samples in the database. In this case, however, since a batch of data used for each parameter update is not entirely independent, a model may overfit. In practice, a part of the whole dataset is reserved as a *validation* sample, and the model performance is carefully monitored during the optimization process to avoid overfitting via an early stopping criterion (see Sec. 41.9.6 and Fig. 41.15).

SGD with slowly decreasing learning rate can be shown to converge to a local minimum almost surely under mild conditions, and to a global minimum for unimodal loss functions. SGD may also prevent getting stuck in shallow local minima of the loss function, thereby reaching a better local minimum for multi-modal loss functions. The noise in SGD with a constant learning rate can be viewed as a form of Langevin dynamics, which under proper conditions on the learning rate and mini-batch size converges to the stationary posterior distribution of the weights [327]. Thus SGD at a constant learning rate can be viewed as a sampler bouncing around and exploring the posterior surface for better solutions, descending onto the best found solution as the learning rate is decreased, a process related to temperature annealing in global optimization.

Another advantage of SGD is simply the computational cost: rather than evaluating the loss over all the data samples at each update, we use a small subset of data instead at each update. Furthermore, mini-batching can take advantage of vectorization libraries and GPU architectures. Large batch training requires specialized methods of training, such as layer-wise adaptive rate scaling (LARS) [328].

41.9.3 *Optimization algorithms*

GD and SGD are the basic building blocks for more advanced optimization algorithms. One can improve the convergence rate of gradient based optimization by considering the learning rate λ to depend on individual θ_i. Second order algorithms such as Newton's method take into account second order derivatives (Hessian) to find the minimum, and give an exact solution in a single update when the loss is quadratic around the peak. However, this requires a matrix inversion of the Hessian, which is exceedingly expensive in ML applications, where the number of network parameters is very large. As a consequence, second order optimization is rarely used in ML.

There are several improvements to the basic SGD even in the absence of Hessian information. Momentum based optimization takes a physics perspective of a viscous fluid in an external potential, where one updates current velocity with the potential gradient (force), followed by an update in position based on velocity. This approach therefore uses previous gradients in addition to the current one to compute a running average of the gradient, with a forgetting factor that controls how far back the averaging goes. This helps move faster towards the minimum in ravines, where gradient descent is usually inefficient due to the high condition number of the Hessian.

Beyond SGD with momentum, modern optimizers adapt step sizes across parameters or layers using recent gradient statistics and decouple regularization from the update. RMSprop tracks a running RMS of gradients and scales steps inversely to damp oscillations. Adam adds momentum (first moment) and variance (second moment) estimates to provide per-parameter adaptive updates. AdamW [329] improves Adam [330] by decoupling weight decay from the adaptive step, applying true L2 regularization directly to weights, which typically yields better generalization and

Phys. A 2026.41. Downloaded from www.worldscientific.com
by UNIVERSITY OF CA LEY on 09/16/26. Re-use and distribution is strictly not permitted, except for Open Access articles.

has become a common default in vision and language models. For very large-batch regimes, layer-wise trust-ratio methods such as LARS (Layer-wise Adaptive Rate Scaling) [328] and LAMB (Layer-wise Adaptive Moments optimizer for Batch training) [331] scale each layer's effective learning rate by the ratio of parameter norm to gradient norm, enabling stable training with batch sizes of tens of thousands. More recently, Lion [332] uses the sign of the momentum update instead of a second-moment estimate, reducing memory and often improving speed and generalization; it can also be combined with decoupled weight decay. In practice, these optimizers are paired with warmup, cosine or exponential decay schedules, and sometimes gradient clipping; the best choice depends on model size, data regime, and whether you prioritize fast convergence, large-batch scalability, or final generalization.

41.9.4 *Automatic differentiation and backpropagation*

In practice, $f(x, \theta)$ might take a complex form and may include a large set of parameters. The term $\nabla_\theta \mathcal{L} = \nabla_\theta \mathcal{L}(f(x, \theta))$ requires computing partial derivatives with respect to individual parameter θ_i. If f is a composite model (i.e. $f = f_n(f_{n-1}(\cdots, \theta_{n-1}), \theta_n)$), and if all of $f_{i:1,n}$ are differentiable, a chain rule can be applied:

$$\nabla_{\theta_i} \mathcal{L} = \frac{\partial \mathcal{L}(f(x, \theta))}{\partial \theta_i} = \frac{\partial \mathcal{L}}{\partial x_n} \cdot \frac{\partial x_n}{\partial x_{n-1}} \cdots \frac{\partial x_i}{\partial \theta_i} \tag{41.81}$$

where x_n denotes the output of nth composite function f_n. In order to compute $\nabla_{\theta_i} \mathcal{L}$ for f_i, it needs computation of a gradient at all preceding (or subsequent if seen in the forward context) functions. As the gradients accumulate across differentiable functions in the reverse order of the model composition, this technique is called *backpropagation* [287]. An example of f that satisfies conditions to apply backpropagation is a neural network, which consists of repeating blocks of a (differentiable) activation function and an affine transformation.

When the model $f(x, \theta)$ is implemented as a computer program in practice, *automatic differentiation* (AD), also called *algorithmic differentiation*, is used to compute the derivatives. AD exploits the fact that any computer program consists of a sequence of elementary arithmetic operations (*i.e.*, addition, subtraction, multiplication, and division) and functions (*e.g.*, log, exp, sin, and cos) and apply chain rules to compute the target derivative. AD has advantages over traditional approaches including symbolic and numerical differentiation. The symbolic differentiation faces a serious difficulty of converting a program into a single expression, and the numerical differentiation suffers from round-off errors. Finally, both methods scale poorly in speed of computation for calculating partial derivatives with a large number of inputs. AD delivers much faster speed and does not suffer from increasing errors for calculating higher derivatives.

There are two modes of AD: the *forward* and *backward* mode. Consider a composite function $f(x, \theta) = f_n(f_{n-1}(\cdots f_1(x, \theta_1) \cdots), \theta_{n-1}), \theta_n)$. The forward mode applies the chain rule in the same order of the forward evaluation of f by computing $\partial f_1 / \partial x$ first, then $\partial f_2 / \partial f_1$, and continue to $\partial f_n / \partial f_{n-1}$. The backward mode traverses the reverse direction: starting from the last (outer-most) function $\partial f_n / \partial f_{n-1}$, next $\partial f_{n-1} / \partial f_{n-2}$, and continue to $\partial f_1 / \partial x$. Therefore, the backpropagation of gradients can be implemented using the backward AD, in which the target variable to be differentiated is fixed and the derivative is computed with respect to each sub-expression recursively as shown in Eq. 41.81. The forward mode is simpler to implement as the order of gradient calculation follows the order of composite functions to be executed. The reverse mode typically requires less amount of computation than the forward mode, but more memory is required to store intermediate function output values to calculate derivatives efficiently. Another consideration is the mapping of dimensionality $f : \mathbb{R}^k \to \mathbb{R}^\ell$ as it concerns the number of variables to sweep from each end. The forward mode is efficient when $k \ll \ell$ while the reverse mode takes an advantage if $\ell \ll k$. For instance, in the case of an image classification where $(k, \ell) = (\text{pixel count}, 1)$, the reverse AD is more efficient.

Development of a differentiable physics simulator is an active area of research and AD-enabled programming frameworks are at the core of those research work. AD-enabled simulator can be used to solve an inverse problem of inferring the physics model parameters (e.g. calibration) or the input (i.e. reconstruction) [333, 334]. A fully differentiable physics simulator often requires, however, a custom algorithm to approximate gradients to handle cases where gradient calculation is not straightforward (e.g. due to stochastic processes) [335]. Beyond AD, a specifically designed neural network that ensures accurate gradient calculation is also frequently used, sometimes in combination with AD-enabled framework [326, 336].

41.9.5 *The vanishing and exploding gradient problems*

Gradient based optimization crucially depends on the size of gradient with respect to each model parameter. If the magnitude of gradient is too large with respect to the distance to an optimal parameter value, it may repeatedly overshoot the target and cause an oscillation preventing convergence. If the gradient is too small, it may take an impractically long time to converge. As shown in Eq. 41.81, the gradient of ith function f_i is a product of gradients from the subsequent functions. If those gradients are too large or too small, the magnitude can can either increase or decrease exponentially in the number of layers. These are called *exploding* and *vanishing* gradient problem respectively.

Modern deep neural networks consist with many composite functions (*i.e.*, layers) and are particularly prone to this effect. Let us consider a simple RNN. From Eq. 41.71, we can write the backpropagating gradient:

$$\frac{\partial h_t}{\partial h_{t-1}} = \text{diagonal}\left(f'\left(Wx_t + Vh_{t-1} + b1\right)\right) W \tag{41.82}$$

where f' denotes the derivative of an activation function. The gradient of the contribution to the loss $\mathcal{L}_i$ from the ith element in the sequence with respect to the jth hidden state h_j is therefore:

$$\frac{\partial \mathcal{L}_i}{\partial h_j} = \frac{\partial \mathcal{L}_i}{\partial h_i} V^{i-j} \prod_{j<t\leq i} \text{diagonal}\left(f'\left(Wx_t + Vh_{t-1} + b1\right)\right) \tag{41.83}$$

where we can see that V contributes multiplicatively with $i - j$ powers when $i - j > 1$. This example is explored in depth for recurrent models [288, 289] but is common for all types of deep neural networks.

In practice, one may explicitly inspect the magnitude of gradients propagating across layers to ensure an effective optimization. One way to mitigate an exploding gradient is to set the maximum gradient value $\delta_{\max}$ as a model hyperparameter and *clip* any larger gradients δ where it appears in the backpropagation:

$$\delta = \frac{\delta_{\max}}{\|\delta\|} \delta \text{if} \|\delta\| > \delta_{\max}. \tag{41.84}$$

This is called *gradient clipping* [289].

Alternatively, there are many architecture designs that are motivated by the vanishing and exploding gradient problem or which aim to help propagate gradients across many layers. These considerations drove the design of gated models like the LSTM and GRU for sequential data and also motivated the ReLU non-linearity. Other example architectural designs or components motivated by these considerations include identity mapping and skip connections used in ResNet, U-Net, and DenseNet, which allow gradients to flow across many layers.

Other factors contributing to vanishing and exploding gradient include initialization of model parameters and normalization of input data. These factors contribute in keeping the magnitude of activation, which also concerns the magnitude of gradient, within a reasonable range. A recommended practice for a gradient-based optimization of a neural network is to maintain the input values centered around zero and a similar level of covariance across the inputs (and the outputs that are the inputs to the next layer) [337]. These factors are discussed in the following.

41.9.6 *Early stopping*

Early stopping is a form of regularization used to avoid overfitting when an iterative method, such as gradient descent, is used as a learning algorithm. Imagine a plot of the training loss and test

Int. J. Mod. Phys. A 2026.41. Downloaded from www.worldscientific.com
by UNIVERSITY OF CALIFORNIA @ BERKELEY on 09/16/26. Re-use and distribution is strictly not permitted, except for Open Access articles.

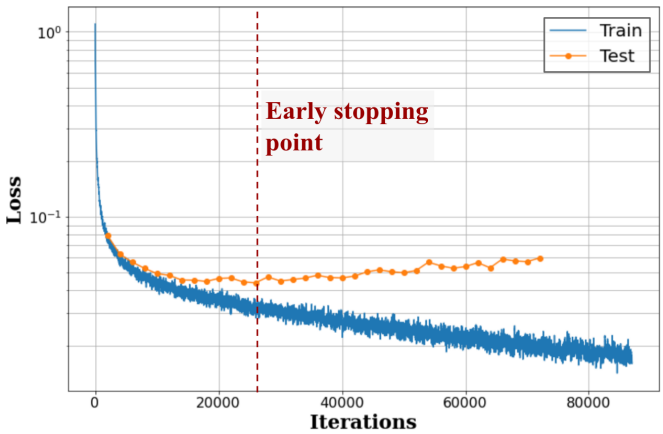

Figure 41.15: An example instance of overfitting. The training loss (vertical axis) shown in blue decreasing over iterations (horizontal axis) while the loss values evaluated on test samples shown in orange start to increase at around 26,000 iterations as indicated by the vertical line.

loss as a function of iterations (*i.e.* parameter updates). As learning proceeds, the training loss will generally decrease. However, the test loss will often decrease initially and then start to increase, which is the classic sign of overfitting as shown in Fig. 41.15. The basic idea of early stopping is simply to stop training before overfitting takes place. In some approaches to early stopping theoretical analysis of the learning problem provides a prescription for when to stop the training [338]; however, the most straight forward approaches use a held-out validation dataset to monitor the generalization performance [339].

41.9.7 *Initialization of model parameters*

An improper initialization can slow down the optimization process or even result in a loss of convergence. While $b^{(l)}$ is typically initialized to zero, $W^{(l)}$ values need to be stochastic to avoid identical updates during optimization. One way is to sample $W^{(l)}$ from a zero-centered Gaussian distribution with a small variance (e.g. 0.01) [340]. However, this method does not guarantee the same variance in the input to each layer, which depends on the size of the input layer, and makes it difficult to train a deep neural network [283]. The *Glorot* or *Xavier* initialization takes this into account and sets the variance of a Gaussian distribution to be $\sigma^2 = 1/d^{(l-1)}$ assuming a symmetric activation function around zero, such as a logistic function or hyperbolic tangent [341]. The *He* initialization uses the variance $\sigma^2 = 0.5/d^{(l-1)}$, and is a simple extension of Xavier initialization for leaky, parametric, and standard ReLU activation [270].

41.9.8 *Input normalization*

Input data to a neural network is often pre-processed for the same goals discussed previously: values are shifted to have the mean of zero and scaled to keep a similar covariance across features. Furthermore, a data may be transformed using techniques including PCA and whitening (sphering) to keep input features independent and uncorrelated from each other [337].

41.9.9 *Batch normalization*

Even with careful normalization of the input data and initialization of model parameters, the mean and covariance of the data representations in hidden layers will evolve during training and may pose challenges for learning for downstream layers. This is called an *internal covariate shift* [342] and may cause negative effects to an optimization process. Accordingly, techniques to explicitly normalize features in between hidden layers are often employed for a deep neural network. One of them is *batch normalization (BN)*, which shifts and scales the input to a hidden layer:

$$\tilde{u}^{(l)} = \gamma \frac{u^{(l)} - \mu_B}{\sqrt{\sigma_B^2 + \epsilon}} + \beta \tag{41.85}$$

where $u^{(l)}$ and $\tilde{u}^{(l)}$ refer to the raw and normalized input to the lth layer, μ_B and σ_B represent the mean and mean-squared-error of $u^{(l)}$ calculated using a *batch* of input data used to update the network parameters. γ and β are part of model parameters that are updated during the optimization. After optimization is complete, these parameters are fixed for model evaluation during production. ϵ is a small, fixed constant value to ensure numerical stability. While it is popular (especially in computer vision), a downside of BN is its dependency on the batch size. In situations where the batch size is limited to be a small number (*e.g.*, memory limitation for a large data or a model), the performance using BN could degrade since β and γ values may not be generalized for the dataset during training.

There are several variants to batch normalization with considerations on how to group a subset of values in u^l. For instance, an image naturally has three groupings: a set of pixels across spatial axis, features within one pixel (*i.e.*, image *channels*), alongside with a grouping across multiple images (*i.e.*, batch). Different groupings have been studied and found and some are found effective to particular type of applications: layer normalization groups values along the channel and spatial dimensions [343], instance normalization groups along the spatial dimension but not along the batch nor channel [344], and group normalization is similar to layer normalization but forms multiple sub-groups of channels [345]. These variants do not apply normalization across samples within a batch, and thus are agnostic to the batch size.

41.9.10 *Transfer learning: pre-training and fine-tuning*

Transfer learning is a technique to improve performance and accelerate optimization process by reusing a pre-trained machine learning model for a new task. The two tasks and corresponding datasets may differ, but fundamental features, such as implicitly learned symmetries in the underlying data, may be reusable across tasks and datasets. Transfer learning typically takes two steps: the first is to alter the model or data if necessary, then continue updating some or all of the model parameters on the new data or task, *fine-tuning* the model. The first step is required, for example, when solving a different task that requires a different architecture (*e.g.*, regression vs. classification), or when input data format requires a change (*e.g.*, original model trained on three channel image, such as RGB images, while new data has a single channel). Transfer learning has been widely practiced in the field of computer vision where large, labeled data sets are available [346–349]: a CNN trained for classifying images of an animal can be largely reused for object detection, or even for analyzing image data in science (*e.g.*, particle trajectories recorded by an imaging detector). It is a critical aspect for the development of general AI as well as interdisciplinary sharing of models across research fields.

While transformers were initially introduced for machine translation, later models such as GPT [86, 350] and BERT [85] showed that these models can be generalized to multiple NLP tasks through transfer learning by *pre-training* for several seemingly different tasks, including sentence classification, semantic similarity, question answering, and commonsense reasoning [350]. These models are collectively referred to as large language models (LLMs) and some have been fine-tuned for physics domains [351, 352].

41.9.11 *Foundation models*

A key to successful transfer learning is an effective pre-training process through which general (and thus re-usable) representations are learned by a model. When a large, comprehensive dataset within a certain domain is combined with an effective representation learning method, typically using self-supervision or multi-task supervision, which forces a model to learn foundational concepts, the resulting model may potentially be generalized for any task defined in the data domain. Such AI models are referred to as *foundation models* (FMs), which are a central theme of general AI research today [353]. The LLMs such as GPTs are the first and the most successful FMs to date. The core of LLM pre-training is based on self-supervised learning (see Sec. 41.4), where, *e.g.*, a model is tasked to predict the next or missing word in a sentence. To solve this task, a model must learn not only gram-

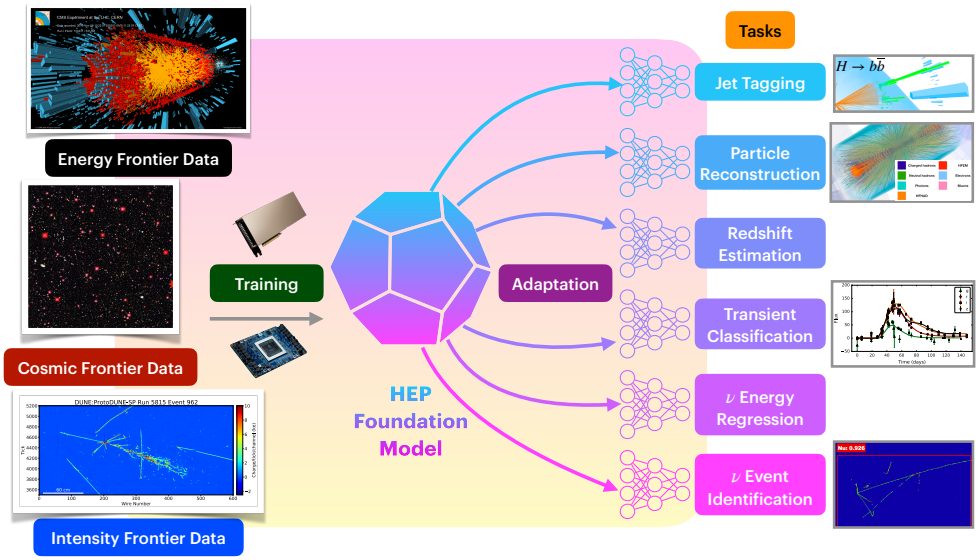

Figure 41.16: Schematic of a foundation model based on HEP data. Data is used to pre-train a large model, which can then be fine-tuned (or adapted) to various downstream tasks.

mar or parts of speech but also a concept of visual colors and the probability distribution over possible colors an apple can take. Using the vast online corpus as a training data, LLMs are trained to learn foundational representations of the world interpreted and generated by humans in the form of texts.

The critical properties of FMs include the *emergence*, *homogenization*, and *scalability* [353]. Emergence means the system behavior is implicitly induced rather than explicitly constructed (*e.g.*, a model's capability to generalize through self-supervised pre-training). Homogenization implies a single model or a system that can perform multiple tasks. Scalability is improvement in model performance when increasing the computing resources, number of model parameters, and size of training dataset. These properties are also used to evaluate the quality of FMs. Following the initial success of LLMs, R&D of FMs has expanded to computer vision and audio data domains.

Many modern FMs combine multiple data modalities (*e.g.*, image generation from text input, audio generation from text and image input) [98, 354, 355]. Multi-modal FMs are trained to correlate features from different data modalities either during a pre-training or fine-tuning stage. For example, the CLIP model achieves this by minimizing the distance between extracted features from an image and its corresponding caption (text) data [98]. It should be noted, however, pre-training FMs on sensory data (*e.g.*, 1D waveforms, 2D images, or 3D scenes) is more difficult compared to symbolic data (*e.g.*, language, math, or high-level physics data) as discussed in Sec. 41.4.

HEP datasets present unique R&D opportunities to advance understanding of FMs. Particles in high energy collisions follow well-established physics models and can be learned by FMs similar to words in natural language [87, 88]. Large public datasets of galaxies recorded in multiple modalities (*e.g.*, images and spectroscopy data) enable a contrastive learning approach based on CLIP [99]. Similarly, a high-fidelity simulator in HEP can be used to formulate contrastive learning objectives across different scenarios in a stochastic process [106]. Finally, HEP detectors offer big, high-precision data sets with challenging tasks to extract complicated physics information [96]. A schematic of a foundation model based on HEP data is shown in Fig. 41.16.

41.10 Incorporating uncertainty

A fundamental aspect of data analysis is the quantification of uncertainty. This broad topic includes the traditional distinction between statistical and systematic uncertainty, procedures for propagation of errors, and the incorporation of uncertainty in to the statistical models (*e.g.* with nuisance parameters) that are used in Bayesian or frequentist statistical procedures (see Sec. 40). Accounting for systematic uncertainty can be seen as a requirement, but ideally systematic uncertainties are also taken into account in the design of the analysis so as to mitigate their effect. The introduction of machine learning into the analysis pipeline requires revisiting the techniques used for uncertainty quantification and exposes many fundamental issues that have nothing to do with the use of machine learning per se. See Ref. [356] for a recent review on this topic.

In machine learning research and industrial settings, the mismatch between the data distribution $p_{\text{train}}(x, y)$ used for training and the data distribution $p_{\text{prod}}(x, y)$ that the model will be applied to in production is referred to as *covariate shift* or *domain shift*. For example, one might train a classifier to identify cats and dogs with images from a well lit studio and then apply the classifier on images taken in doors with poor lighting conditions and a scratched lens. Not surprisingly, the mis-classification rate of the classifier will be different between the two settings.

Physicists are keenly aware that the simulations that we use to describe the data are not perfect, and this mismodeling corresponds to a large fraction of the of systematic uncertainties accounted for in published works. Since simulated data is often used to train machine learning models (*i.e.* $p_{\text{train}}(x, y)$), it is important to understand and account for how this mismodeling will influence results when applied to real data (*i.e.* $p_{\text{prod}}(x, y)$).

One of the primary approaches to incorporating this type of uncertainty is to introduce nuisance parameters ν corresponding to the uncertain inputs to the simulation. One then parametrizes various types of perturbations (*e.g.*, corrections to efficiencies or energy scales) in the hopes that the resulting family of distributions $p(x|y, \nu)$ is flexible enough to encompass the true data distribution for class y. In this approach one does not have just two "domains" for the data (*i.e.*, p_{train} and p_{prod}), but a continuous family of domains parameterized by the nuisance parameters ν.

With this framing in mind, there are several approaches to incorporating uncertainty into an analysis that includes ML-based components:

- **propagation of errors:** one works with a model $f(x)$ and simply characterizes how uncertainty in the data distribution propagate through the function to the down-stream task irrespective of how it was trained.
- **domain adaptation:** one incorporates knowledge of the distribution for domains (or the parameterized family of distributions $p(x|y, \nu)$) into the training procedure so that the

Phys. A 2026.41. Downloaded from www.worldscientific.com
by UNIVERSITY OF CA LEY on 09/16/26. Re-use and distribution is strictly not permitted, except for Open Access articles.

Int. J. Mod. Phys. A 2026.41. Downloaded from www.worldscientific.com
by UNIVERSITY OF CALIFORNIA @ BERKELEY on 09/16/26. Re-use and distribution is strictly not permitted, except for Open Access articles.

performance of $f(x)$ for the down-stream task is robust or insensitive to the uncertainty in ν.

- **parameterized models:** instead of learning a single function of the data $f(x)$, one learns a family of functions $f(x;\nu)$ that is explicitly parameterized in terms of nuisance parameters and then accounts for the dependence on the nuisance parameters in the down-stream task.
- **data augmentation:** one trains a model $f(x)$ in the usual way using training dataset from multiple domains by sampling from some distribution over ν.

In this setting it is best to consider the trained model $f(x)$ or $f(x;\nu)$ to be a fixed function and decouple the variability associated to training or the choice of architecture. The fact that one could have chosen a different architecture or learning algorithm should be treated in the same way as other choices that are made in the data analysis pipeline. While it is reasonable to want downstream inference and decisions to be robust to these choices, they are of a different nature than the uncertainty in the modeling of the data distribution. We return to this point in Sections 41.10.5 and 41.10.6.

41.10.1 *Propagation of errors*

In this Section, we consider the common scenario in which one has used some machine learning technique to train a model $f(x)$ for classification or regression and wants to assess the sensitivity of the output of $f(x)$ to uncertainty in the input x. We regard the function $f(x)$ as fixed and we are not concerned with how the model was trained.

Propagating uncertainty through a ML-based model $f(x)$ is not fundamentally different than for any other function, and one can use the standard propagation of errors formula of Sec. 39.2.1. As always, it is important to recognize the limitations of the propagation of errors formula, which is accurate when the uncertainty on x is Gaussian and the function $f(x)$ is approximately linear within the region set by the uncertainty on x.

Similarly, classifiers are often used for particle identification or event selection. In that case, one is primarily interested in the efficiency ϵ to satisfy a cut on the classifier output. The efficiency depends on the distribution $p(x|y)$ through the equation $\epsilon_y = P(f(x) > f_{\rm cut}|y) = \int H(f(x) - f_{\rm cut})p(x|y)dx$, where H is the Heaviside step function and y is an index or label for the category of data that is being considered (*e.g.*, signal vs. background or electron vs. jet). Thus, the question in this context is what is the uncertainty on the efficiency ϵ_y due to uncertainty in the distribution $p(x|y)$. In practice, the quantification of the uncertainty in the efficiency ϵ_y is usually based on either a calibration measurement on real data or estimated with simulated data. These procedures typically treat the classifier as a black-box, and thus nothing precludes using those procedures on a ML-based classifier. An early example of this approach for b-tagging can be found in Ref. [357].

In the case where simulation is used to estimate the efficiency ϵ_y and its uncertainty, one usually varies nuisance parameters ν associated to the simulation. One then uses simulated samples to approximate $\epsilon_y(\nu) = P(f(x) > f_{\rm cut}|y,\nu) = \int H(f(x) - f_{\rm cut})p(x|y,\nu)dx$. Again, the procedure for incorporating uncertainty isn't fundamentally different if the classifier $f(x)$ is based on machine learning or a hand-crafted observable.

41.10.2 *Domain adaptation*

While estimating the uncertainty for a ML-based model is not fundamentally different than any other hand-crafted observable used for regression or classification, the worry of many physicists is that by working with a high-dimensional set of features x that one is more susceptible to mismodeling of subtle correlations. This is a valid concern, and it should be appreciated that a great deal of prior knowledge and physical insight goes into the construction of hand-crafted observables so that they will be robust to the most uncertain aspects of data. However, much of this craft is based on heuristics that are difficult to systematize. Furthermore, one can only validate that such an observable is robust if one can explicitly evaluate the performance for a perturbed distribution. Thus in the settings where one can validate the robustness to a perturbed scenario ν_0, one must have access to $p(x|y,\nu_0)$.

One approach to formalize this type of robustness is to consider the dependence on the distribution of the output of the model $f(x)$ to the nuisance parameters. In statistics, if the distribution of f is independent of the nuisance parameters, then f is referred to as a *pivotal quantity*. This is a property that we can incorporate directly into the training procedure to target a particular notion of robustness. The authors of Ref. [358] introduced an adversarial approach (similar to what is used in the generative adversarial network of Sec. 41.3.4.2) to penalize a model during training if the distribution of the output varies with the nuisance parameters. To construct the training dataset $\{x_i, y_i, \nu_i\}_{i=1,\ldots,n}$, one must sample y and ν according to some proposal distribution (similar to a prior, but only used for the creation of training dataset, not necessarily for statistical inference), corresponding to a joint distribution $p(x,y,\nu)$. Instead of minimizing the target loss $\mathcal{L}_f$ (*e.g.* cross-entropy or squared-error) with respect to the parameters ϕ_f that parameterize the model f, one trains with a minimax strategy that also includes an adversary q with parameters ϕ_r. The trained model is characterized by the saddle point

$$\hat{\phi}_f, \hat{\phi}_r = \arg\min_{\phi_f} \arg\max_{\phi_r} E_\lambda(\phi_f, \phi_r) \ , \tag{41.86}$$

where the value function E_λ includes the target loss as well as a regularization term associated to the adversary

$$E_\lambda(\phi_f, \phi_r) = \mathcal{L}_f(\phi_f) - \lambda \mathcal{L}_r(\phi_f, \phi_r) \ . \tag{41.87}$$

The constant λ is a hyperparameter, since generally there is a tradeoff between the two terms and only in special cases can the model that minimizes $\mathcal{L}_f$ also be a pivotal quantity. The regularization term

$$\mathcal{L}_r(\phi_f, \phi_r) = \mathbb{E}_{p(x,y,\nu)}[-\log q_{\phi_r}(\nu|f_{\phi_f}(x))] \tag{41.88}$$

is an example of conditional density estimation (see Sec. 41.3.3), where the model $q_{\phi_r}(\nu|f)$ is trying to predict the distribution of the nuisance parameter ν given the output of the model $f(x)$. This term is maximized when f is independent of ν. Earlier work had also used an adversarial technique for domain adaptation, but was limited to just two domains [359–361], while here ν parametrizes a continuous family of distributions and can have multiple components corresponding to different sources of uncertainty. Furthermore, the previous work aimed to make the distribution for a high-dimensional, intermediate representation of the data be invariant to the domain shift as opposed to just the final output $f(x)$.

One way of interpreting Eq. 41.86 is that the goal is to minimize a regularized loss function $\tilde{\mathcal{L}}(\phi_f) = \arg\max_{\phi_r} E_\lambda(\phi_f, \phi_r)$, where the optimization with respect to ϕ_r is not exposed. This motivates another approach in which the regularization is not achieved through a learned adversary, but by a measure of discrepancy between distributions that can be computed directly from samples. In particular, the authors of Ref. [362] proposed the use of *distance correlation* to avoid what can be a challenging min-max optimization problem.

In either case, the optimization of the hyperparameter λ is based on the downstream task. For example, in Ref. [358] considered the case where f was a signal vs. background binary classifier where the nuisance parameter ν was associated to uncertainty in the background model. The hyperparameter λ was then optimized to maximize the approximate median significance (AMS). Similarly, the authors of Refs. [363] and [362] considered new physics searches in the context of boosted jet tagging, where the hyperparameter controls the sculpting of the side-bands used for background estimation.

While these strategies modify the training procedure so that the sensitivity to the nuisance parameters is reduced, it does not typically eliminate it. As a result, one still needs to propagate the uncertainty in the data distribution through the learned model as described in the preceding section. Furthermore, care must be taken in interpreting the loss of sensitivity to the nuisance parameter. For example, for theoretical uncertainties estimated as the difference between two different calculations (*i.e.*, two-point

by UNIVERSITY OF CA Phys. A 2026.41. Downloaded from www.worldscientific.com
LEY on 09/16/26. Re-use and distribution is strictly not permitted, except for Open Access articles.

uncertainties), decorrelation methods may reduce the apparent uncertainty while the true uncertainty remains much larger [364].

Note, this adversarial technique has also been employed in other settings where one would like to decorrelate the output of the classifier with an observed quantity so that it can be used for background estimation [363], although other techniques like moment decomposition [365] may suffice without full decorrelation. Widely used alternative approaches to decorrelation include uboost [366], DDT [367], and using dedicated training samples that vary the chosen quantity to be decorrelated [368]. Other examples of the domain adaptation and decorrelation use cases from the Living Review include Refs. [358, 362–367, 369–378].

41.10.3 *Parameterized models*

An alternative to learning a model $f(x)$ that is pivotal—*i.e.*, whose distribution is independent of the nuisance parameter ν—is to learn a family of models $f(x;\nu)$ that is parameterized in terms of the nuisance parameters. In general, there is a tradeoff between the two terms of Eq. 41.87 for a single model $f(x)$. In a parameterized model, $f(x;\nu)$ optimizes the performance of the model for every value of ν. Parameterized classifiers were first advocated in Ref. [133] in the context of simulation-based inference (see Sec. 41.10.7) and in Ref. [379] for new physics searches. It has also been applied to simulation-based inference for effective field theory parameters in Ref. [380] and Ref. [381] provides additional pedagogical examples.

The training of a parameterized model is similar to the standard procedure. For example, if one originally wanted to minimize the squared loss function $\mathcal{L}(y, f(x)) = (y - f(x))^2$ with training dataset $\{x_i, y_i\}_{i=1,\ldots,n}$, then the corresponding training procedure for the parameterized model would be as follows. One would need to construct a training set $\{x_i, y_i, \nu_i\}_{i=1,\ldots,n}$ as described in the preceding section, construct a parameterized model $f(x;\nu)$ that takes as input the original feature vector x as well as the nuisance parameters ν, and then train using the same loss $\mathcal{L}(y, f(x;\nu)) = (y - f(x;\nu))^2$.

One complication of the parameterized approach is that it is no longer possible to evaluate the model on a dataset $\{x_i\}$ and pass on only $\{f_i\}$ for downstream analysis tasks since $f(x_i;\nu)$ still depends on ν. Instead, one delay evaluating the model to some down-stream stage when the dependence on ν would accounted for. For example, in the context of a likelihood based analysis where one is testing a hypothesis where the nuisance parameters take on a particular value ν_{test}, then one will consider the data distribution $p(x|\nu_{\text{test}})$, and at that point one would evaluate the model at the corresponding nuisance parameter value, *i.e.* $f(x;\nu_{\text{test}})$. Explicit examples are given in Refs. [133,356,380,381]. While this may seem complicated, it actually corresponds to what is done in a typical likelihood-based fit when the statistical model has nuisance parameters; *i.e.* the likelihood-ratio corresponds to the model $f(x;\nu)$ as in Eq. 41.13.

41.10.4 *Data augmentation*

An intuitive approach to building in robustness to systematic effects that can lead to domain shift, is simply to augment the training dataset so that it includes examples corresponding to several values of the nuisance parameter or systematic variations. As before one can construct a dataset $\{x_i, y_i, \nu_i\}_{i=1,\ldots,n}$, but instead of leveraging the information about ν_i, one simply discards this information. This corresponds to sampling from the marginal distribution $x_i, y_i \sim p(x,y) = \int d\nu p(x,y|\nu)p(\nu)$, and is often referred to as *smearing*. One can then use this smeared dataset for supervised learning in the traditional way. While it is possible that this approach will lead to improved robustness to systematic variations (*i.e.* generalization for ν other than the nominal value) than if systematic uncertainty weren't considered at all), this intuitive approach has several shortcomings. The approach does not yield a pivotal quantity as in the adversarial approach, so propagation of uncertainty through the network is still required. Moreover, there is no direct way to control the tradeoff between independence from the nuisance parameter and the original target loss as in the adversarial approach. Finally, it can lead to significant performance loss compared to what is possible with the parameterized approach. These tradeoffs were studied in Refs. [379, 381] with both pedagogical and physically-motivated examples.

41.10.5 *Aleatoric and epistemic uncertainty*

In the machine learning and risk assessment literature, uncertainty is often characterized in terms of *aleatoric* and *epistemic* uncertainty [382–385]. Familiarity with these terms is useful, but the distinction between the two can be ambiguous, the terms are not always consistently used, and they do not clearly map onto the concepts used physics.

For example, Ref. [384], states that "roughly speaking, aleatoric (*a.k.a.*, statistical) uncertainty refers to the notion of randomness, that is, the variability in the outcome of an experiment which is due to inherently random effects", while "epistemic (*a.k.a.*, systematic) uncertainty refers to uncertainty caused by a lack of knowledge (about the best model)." This seems clear enough, but in that same reference (and in Ref. [386]) the aleatoric uncertainty is considered irreducible, while the epistemic uncertainty could be reduced with additional information. This may seem backwards for many physicists since often in particle physics, we think of how uncertainties scale as we collect more data but keep the experimental design fixed. In that case, the statistical uncertainty will be reduced with time while the systematic uncertainty will remain constant[4]. There is no paradox here, it is simply a different point of view. The emphasis of the risk assessment community is not on collecting more data with the same experimental design, but collecting different types of data that will inform the models themselves. Clearly even for physicists, data from new experiments or calibration measurements could also reduce our systematic uncertainties. While there are exceptions in the literature, the bulk of it associates aleatoric uncertainty with the randomness of classical probability (*i.e.*, the statistical uncertainty associated to repeating the same experiment many times) and epistemic uncertainty with our state of knowledge.

Perhaps a more important distinction between the perspective of physicists and machine learning researchers has to do with the use of the term "model" and what exactly is uncertain. In physics, the systematic and epistemic uncertainty is typically associated to our understanding of the underlying physics and "the model" usually refers to the physics model, detector model encapsulated in a simulation. In contrast, for machine learning research, "the model" usually refers to the trained model $\hat{f} \in \mathcal{F}$ used as described in Section 41.2.1 (or the class of functions $\mathcal{F}$ itself). This makes sense if we recall that in the bulk of machine learning research, one has little insight into the process that generated the data (*e.g.*, images of cats and dogs, or natural language). In that sense, the epistemic uncertainty in machine learning is usually associated to uncertainty in the model parameters ϕ after training, which would be reduced if one could collect more training dataset (see Ref. [385] for this point of view).

In the literature on uncertainty quantification (UQ), which is more closely connected to physics given the role of computer simulations, the terminology is more fine grained and less ambiguous. That community uses the terms parameter uncertainty (*i.e.* nuisance parameters), structural uncertainty (*i.e.*, mismodelling), algorithmic uncertainty (*i.e.* numerical uncertainty), experimental uncertainty (*i.e.*, uncertainty from experimental resolution and statistical fluctuations), and interpolation uncertainty (*i.e.*, uncertainty due to interpolating between different parameter values due to lack of computational resources).

41.10.6 *Model averaging and Bayesian machine learning*

The core of Bayesian machine learning is the model averaging view. Here one often takes a more ambitious view of learning than described in Sec. 41.2.1, which is framed mainly as function approximation. While in Sec. 41.2.1, the goal is to find a function that minimizes the risk, in Bayesian machine learning one explicitly builds a probability model $q_\phi(x,y)$ for the training dataset $\mathcal{D} = \{x_i, y_i\}_{i=1,\ldots,n}$. It is the same change in perspective that one has when one views the squared error loss function $\mathcal{L}_{\text{MSE}} = (y - f_\phi(x))^2$ as the log-likelihood for a probability model

[4] Further complicating the relationship between the terms is that many experimental uncertainties that are characterized as systematic are actually statistical in nature as auxiliary measurements and control regions are used to constrain the corresponding nuisance parameters.

Int. J. Mod. Phys. A 2026.41. Downloaded from www.worldscientific.com
by UNIVERSITY OF CALIFORNIA @ BERKELEY on 09/16/26. Re-use and distribution is strictly not permitted, except for Open Access articles.

$y \sim N(f(x), \sigma)$. In addition, one assumes some prior on the model parameters $p(\phi)$, which is often a Gaussian distribution, and is analogous to Tikhonov regularization (see Sec. 41.2.5). In this way, a single trained model $\hat{f} = f_{\hat{\phi}}$ is the MAP point estimate and the more complete Bayesian solution is the entire posterior distribution over the model parameters $p(\phi|\mathcal{D})$. With this view, it is clear how increasing the number of training examples n will lead to a reduction in uncertainty on ϕ. However, this notion of epistemic uncertainty has little to do with the notion of systematic uncertainty as the term is used by particle physicists.

Bayesian methods can be applied to non-probabilistic regression problems, in which case they can provide uncertainty quantification. Consider the case of regression in traditional (non-Bayesian) machine learning. The trained model $f_{\hat{\phi}}(x)$ is used to predict the target label y. For a fixed x, the model does not provide any notion of uncertainty on the prediction. One could propagate uncertainty on x through $f(x)$, but that is also not the desired quantity to characterize the intrinsic spread $p(y|x)$ in the data, which may exist even if x has negligible uncertainty. In contrast, Gaussian process regression (a Bayesian method) does provide a natural way to communicate the uncertainty on the prediction, which is possible because one first had to specify a prior on the mean and covariance of the Gaussian process.

In the context of Bayesian deep learning and Bayesian neural networks, one would place a prior on the weights and biases of the neural network $p(\phi)$ and then use one of the many emerging techniques to calculate the approximate posterior $p(\phi|\mathcal{D})$. However, we should recognize that we have little-to-no insight into the parameters of a deep neural network, so the prior on ϕ is hardly well-justified. Furthermore, just as in all Bayesian approaches, the prior is not invariant to reparametrizing the model: $\phi \to \eta(\phi)$. While it is difficult to justify the choice of the prior on the parameters (and, thus, the resulting posterior), the resulting model may perform well empirically. In such high-dimensional parameter spaces, the bias-variance tradeoff can be dramatic.

Bayesian model averaging (BMA) performs Bayesian average over the posterior $p(\phi|\mathcal{D})$. This can be applied to any quantity f_ϕ, such as a regression or classification prediction y. Suppose we can draw from the posterior $\phi \sim p(\phi|\mathcal{D})$. For each draw we can evaluate the predicted regression variable $y = f_\phi(x) + \epsilon$, where ϵ is some noise to account for uncertainty in the predictions. We can denote this process as a draw from $p(y|x, \phi)$, $y \sim p(y|x, \phi) = N(f_\phi(x), \sigma_\epsilon^2)$, where σ_ϵ^2 is the noise variance. The BMA then performs

$$p(y|x, \mathcal{D}) = \int d\phi p(\phi|\mathcal{D}) p(y|x, \phi). \tag{41.89}$$

In practice $p(y|x, \phi)$ is evaluated by drawing samples of y and ϕ, so the posterior is defined implicitly by the samples. For example, the mean prediction is obtained by averaging $f_\phi(x)$ over the samples of ϕ, and the covariance matrix is similarly evaluated by averaging the second moments over the samples of ϕ.

Ref. [387] provides a different perspective on BMA analyzed in what are referred to as the $\mathcal{M}$-open and $\mathcal{M}$-closed settings [387]. The $\mathcal{M}$-closed setting refers to the situation where the true data generating process is in the space of models, even if it is unknown to us. In contrast, the $\mathcal{M}$-open setting refers to when the true data generating process is not in model space (*i.e.* the model is mis-specified). Interestingly, in the $\mathcal{M}$-open case one can potentially do better than any one model in the model class by considering an average over the models, since averaging can create a new model that is not in the model class. BMA provides one such averaging, but other averages, which are not weighted by $p(\phi|\mathcal{D})$, can be a better choice. When the weights of each model are optimized against appropriate loss the resulting procedure is called stacking, which has been shown to be superior to BMA in the $\mathcal{M}$-open setting [387]. Ref. [388] performed experiments indicating that in some cases model averaging can also improve predictive uncertainty estimates under domain shifts.

Neural network model averaging beyond BMA comes in several different flavors. Two successful model averaging procedures are Monte Carlo dropout [389], which uses dropout ensembling, and deep ensembles [390], which use random initialization ensembling. These methods may not only be superior to BMA, they are also often significantly faster than BMA. Whether these model averages are an approximation to BMA, or an alternative to it, remains a debated topic, and both views have been advocated. BMA itself can be accelerated using approximate methods, such as stochastic Variational Inference with reparametrization trick [391].

Finally, in the context of Bayesian model uncertainty estimation, there are two practical ways to capture: repulsive ensembles and evidential regression. Repulsive ensembles are standard deep ensembles trained with an extra diversity penalty so the ensemble members make deliberately different but plausible predictions, improving coverage with fewer models. Evidential regression uses one network to predict the parameters of a simple probabilistic family plus an "evidence" term; when data are ambiguous it learns low evidence and returns wider intervals, and when data are plentiful it narrows them. The latter has been studied for uncertainty quantification for neutrino applications [392]. In practice, both approaches can yield similarly well-calibrated uncertainties. An open direction is to bring such calibrated epistemic uncertainty into the density estimators of generative models (*e.g.*, flows, VAEs, or diffusion), for example via ensemble/Bayesian variants with diversity or evidential parameterizations, so we can represent and propagate uncertainty over whole distributions, not just point predictions.

41.10.7 *Connection to probabilistic machine learning*

We end this Section by reinforcing the connection between uncertainty quantification in traditional machine learning and the more probabilistic approaches to machine learning exemplified by simulation-based inference (see Sec 41.6) and deep generative models (see Sec. 41.3.4). In the standard approach to supervised learning (*e.g.* classification and regression) the model $f(x)$ provides a point estimate for y. Estimating an uncertainty on y goes a step further, but the complete picture would be to model the posterior distribution $p(y|x)$. Gaussian processes (see Sec. 41.8.2) are an example, but the form of the models is limited to Gaussian posteriors. In Sec 41.6 we discussed approaches to model $p(y|x)$ using conditional density estimation [69,70,128]. If we extend this task to include a family of distributions parameterized by some nuisance parameters ν, then the task is to model $p(y|x, \nu)$, which is structurally similar.

In the context of classification, the output is already probabilistic, and the interpretation of the resulting classifier is $\hat{f}_{\text{MSE}}(x) \approx p(y = 1|x)$ (see Eq. 41.11). Incorporating the dependence on the nuisance parameter, then connects to the likelihood-ratio trick (see Eq. 41.13), approaches to simulation-based inference that involve learning the likelihood-ratio, and the parameterized approaches described in Sec. 41.10.3.

If one pairs the training procedure for classification, regression, or density estimation used in the approaches above with model averaging techniques such as BMA, then it would be possible to incorporate both uncertainty associated to finite training dataset and the uncertainty associated to systematic uncertainties. However, as described in Sec. 41.10.5 and Sec. 41.10.1, it is not clear that in physics applications it is desirable to account for the variability associated to training when the more common practice is to regard the trained model $\hat{f}(x)$ as fixed.

While these probabilistic approaches to machine learning are attractive conceptually, it is known in the machine learning community that classifiers often are poorly calibrated and often overly confident in their predictions. This is a problem even if one regards the trained model $\hat{f}(x)$ as fixed. Various approaches, including model averaging, are being pursued to improve the calibration of trained models, but the problem is unlikely to be eliminated entirely. Miscalibration can be verified by evaluating the true positive and false positive rates on held out data. This is common practice in experimental particle physics, where the output of a binary classifier is rarely taken at face value. Instead, the true and false positive rates are estimated with simulated data or control samples as described in Sec. 41.10.1. Furthermore, the true and false positives can be characterized as a function of the nuisance parameters. These procedures can be used to help calibrate parameterized models based on the likelihood-ratio trick (see Refs. [133, 381]). Unfortunately, calibration in the con-

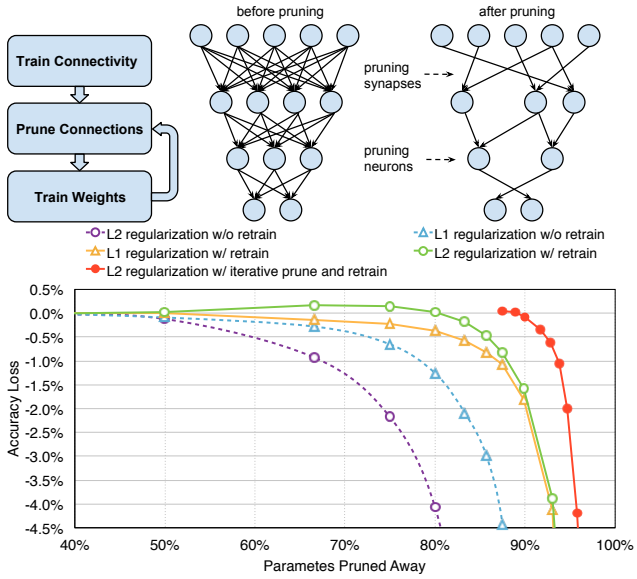

Figure 41.17: Illustration of the iterative magnitude-based parameter pruning and retraining with regularization procedure from Han et al. in NeurIPS, 2015. The top-5 accuracy loss is shown as a function of parameter reduction (sparsity) for VGG-16 on ImageNet following different pruning procedures. Without retraining, L1 regularization performs better than L2, but L2 performs better than L1 with retraining. Iterative pruning gives the best result.

text of density estimation is more challenging. This connects to topics and challenges in anomaly detection (see Sec. 41.3.5).

41.11 Model compression and deployment in experiments

The software and computing needs of training a machine learning model are different than those encountered when it is deployed for use. The two stages are referred to as *training* and *inference*, *i.e.* making a prediction $\hat{f}(x)$ given an input x and a trained model $\hat{f}$. Sometimes this transition also involves using different programming languages for implementing the trained model from the ones used for training them. Modern machine learning frameworks support various serialization formats to exchange trained models. For instance, `ONNX` [393] provides an open source format for many types of models, is widely supported, and can be found in many frameworks, tools, and hardware. This is important when integrating a trained model into the software frameworks used by the large experiments.

While hardware acceleration with GPUs is important for efficiently training modern machine learning techniques, there are also advantages of hardware acceleration at inference time. This may include GPUs or field programmable gate arrays (FPGAs), and the Living Review includes many example works focusing on efficient inference for a given hardware architecture [153, 180, 394–403]. Programming FPGAs requires the use of dedicated hardware description languages (HDLs) such as VHDL or Verilog as well as a design methodology that is aware of the limitations and nature of the relevant device. Recently, high-level synthesis (HLS) tools [404–406], which ingest algorithms written in C/C++ code, have lowered the barrier to entry for using FPGAs. Several tools, including hls4ml [407], FINN [408, 409], Conifer [410], and fwXmachina [411], have been developed to automatically create firmware from ML algorithms. These tools have been used for applications ranging from jet tagging [412–414] to muon transverse momentum regression [415], on-detector data compression [416], charged particle tracking [417, 418], calorimeter reconstruction [237], and anomaly detection [419–421].

For applications where latency is a key concern (*e.g.*, triggering at collider experiments), various accelerators have been investigated [237, 241, 407, 410, 411, 416, 419, 422–431]. To enable the use of an ML model in resource-constrained or latency-sensitive experimental settings, reducing the size and computational complexity of the model through *compression* is often essential. Compression techniques aim to improve the computational efficiency of models, while keeping the performance as close as possible to the original. The two most ubiquitous methods are *quantization* [432–448], which modifies the number of bits used to calculate and store results in the model, and *pruning* [433, 449–453], which removes model parameters. However, symbolic regression [454] and knowledge distillation [455] have also been explored to learn compact algorithms.

While it is common to use 32-bit floating-point precision, for many applications, this may not be required to ensure adequate performance. Reduced-precision formats, such as integer or fixed-point precision, may be used instead. We can distinguish *post-training quantization* (PTQ), in which model parameters are quantized after a traditional training is performed with 32-bit floating-point precision, and *quantization-aware training* (QAT), in which the training procedure is modified to emulate reduced precision formats. QAT results in better performance for a smaller bit width, but requires (re)training with a dedicated framework [447, 448, 456–458]. Serializing and exchanging quantized models is a challenge addressed by the `QONNX` format, which extends `ONNX` to represent arbitrary-precision quantized neural networks [459].

Pruning is the removal of unimportant weights, quantified in some way, from a neural network. The two main categories are *unstructured pruning*, where weights are removed without considering their location within a network, and *structured pruning*, where weights connected to a particular node, channel, or layer are removed. Pruning reduces the number of computations that must be performed to produce an inference result, thus reducing the hardware resources or algorithm latency. The development of pruning algorithms and understanding their behavior is an active area of research [453]. One relatively simple method is iterative, magnitude-based pruning [407, 460], as shown in Fig. 41.17. In this process, the model is trained with L1 or L2 regularization (discussed in Sec. 41.2.5), resulting in a set of optimal parameters, where some are close to zero. Those parameters with values below a certain threshold can be set to exactly zero (thereby removing them from the model), and training can be repeated. Successive iterations of this procedure can remove more parameters until the desired reduction in parameters, or *sparsity*, is achieved. This process usually results in models that have slightly reduced performance, although the performance loss is typically negligible for sparsities $\lesssim$90% [460]. Pruning and quantization can also be applied together [429].

Finally, some solutions for deployment of ML models involve using cloud resources [461, 462] or using hardware coprocessors, like GPUs and FPGAs, *as a service* [463–466]. In this approach, coprocessor resources are decoupled from CPUs, and CPU-based clients can send inference requests to coprocessor-based servers via network calls. The advantages of this approach are coprocessors can accept inference requests from local or remote CPUs, certain types of coprocessors can be allocated for specific tasks, the coprocessor-to-CPU ratio can be optimized, the separation of software support for coprocessor and CPU workflows reduces the maintenance burden, and developments from industry can be more easily leveraged [465].

References

[1] Y. Lecun, Y. Bengio and G. Hinton, Nature **521**, 7553, 436 (2015), ISSN 14764687.

[2] J. Schmidhuber, Neural Networks **61**, 85 (2015).

[3] A. Radovic *et al.*, Nature **560**, 7716, 41 (2018).

[4] D. Guest, K. Cranmer and D. Whiteson, Ann. Rev. Nucl. Part. Sci. **68**, 161 (2018), [arXiv:1806.11484].

[5] G. Carleo *et al.*, Rev. Mod. Phys. **91**, 4, 045002 (2019), [arXiv:1903.10563].

[6] M. Feickert and B. Nachman (2021), [arXiv:2102.02770].

Phys. A 2026.41. Downloaded from www.worldscientific.com
by UNIVERSITY OF CA LEY on 09/16/26. Re-use and distribution is strictly not permitted, except for Open Access articles.

Int. J. Mod. Phys. A 2026.41. Downloaded from www.worldscientific.com
by UNIVERSITY OF CALIFORNIA @ BERKELEY on 09/16/26. Re-use and distribution is strictly not permitted, except for Open Access articles.

[7] V. Vapnik, *The nature of statistical learning theory*, Springer science & business media (2013).

[8] A. Y. Ng and M. I. Jordan, in T. G. Dietterich, S. Becker and Z. Ghahramani, editors, "Advances in Neural Information Processing Systems 14 [Neural Information Processing Systems: Natural and Synthetic, NIPS 2001, December 3-8, 2001, Vancouver, British Columbia, Canada]," 841–848, MIT Press (2001), URL `https://proceedings.neurips.cc/paper/2001/hash/7b7a53e239400a13bd6be6c91c4f6c4e-Abstract.html`.

[9] E. M. Metodiev, B. Nachman and J. Thaler, JHEP **10**, 174 (2017), [arXiv:1708.02949].

[10] C. Zhang *et al.*, Communications of the ACM **64**, 3, 107 (2021).

[11] P. Nakkiran *et al.*, arXiv preprint arXiv:1912.02292 (2019).

[12] T. Hastie, R. Tibshirani and J. Friedman, *The Elements of Statistical Learning*, Springer, New York, NY, USA (2001).

[13] Y. S. Abu-Mostafa, M. Magdon-Ismail and H.-T. Lin, *Learning From Data*, AMLBook (2012).

[14] M. Belkin *et al.*, Proceedings of the National Academy of Sciences **116**, 32, 15849 (2019), [arXiv:1812.11118].

[15] M. Kuusela and V. M. Panaretos, Ann. Appl. Stat. **9**, 1671 (2015), [arXiv:1505.04768].

[16] L. Rosasco, A. Tacchetti and S. Villa, CoRR **abs/1405.0042** (2014), URL `http://arxiv.org/abs/1405.0042`.

[17] G. E. Hinton *et al.*, CoRR **abs/1207.0580** (2012), [arXiv:1207.0580], URL `http://arxiv.org/abs/1207.0580`.

[18] P. Baldi and P. J. Sadowski, Advances in neural information processing systems **26**, 2814 (2013).

[19] M. Belkin, S. Ma and S. Mandal, in J. G. Dy and A. Krause, editors, "Proceedings of the 35th International Conference on Machine Learning, ICML," volume 80, 540, PMLR (2018), URL `http://proceedings.mlr.press/v80/belkin18a.html`.

[20] S. Gunasekar *et al.*, in J. Dy and A. Krause, editors, "Proceedings of the 35th International Conference on Machine Learning," volume 80 of *Proceedings of Machine Learning Research*, 1832–1841, PMLR (2018), URL `http://proceedings.mlr.press/v80/gunasekar18a.html`.

[21] L. Zdeborová, Nature Physics **16**, 6, 602 (2020).

[22] R. M. Neal, University of Toronto (1994).

[23] A. Jacot, C. Hongler and F. Gabriel, in S. Bengio *et al.*, editors, "Advances in Neural Information Processing Systems 31: Annual Conference on Neural Information Processing Systems 2018, NeurIPS 2018, December 3-8, 2018, Montréal, Canada," 8580–8589 (2018), URL `https://proceedings.neurips.cc/paper/2018/hash/5a4be1fa34e62bb8a6ec6b91d2462f5a-Abstract.html`.

[24] Y. Bengio, A. Courville and P. Vincent, IEEE transactions on pattern analysis and machine intelligence **35**, 8, 1798 (2013).

[25] R. Acciarri *et al.* (MicroBooNE), JINST **12**, P03011 (2017), [arXiv:1611.05531].

[26] L. Dominé and K. Terao (DeepLearnPhysics), Phys. Rev. D **102**, 1, 012005 (2020), [arXiv:1903.05663].

[27] D. H. Koh *et al.* (DeepLearnPhysics) (2020), [arXiv:2007.03083].

[28] S. Farrell *et al.* (2017), URL `https://dl4physicalsciences.github.io/files/nips_dlps_2017_28.pdf`.

[29] S. Farrell *et al.*, in "4th International Workshop Connecting The Dots 2018 (CTD2018) Seattle, Washington, USA, March 20-22, 2018," (2018), [arXiv:1810.06111], URL `http://lss.fnal.gov/archive/2018/conf/fermilab-conf-18-598-cd.pdf`.

[30] F. Drielsma *et al.* (DeepLearnPhysics), Phys. Rev. D **104**, 7, 072004 (2021), [arXiv:2007.01335].

[31] X. Ju *et al.* (Exa.TrkX), Eur. Phys. J. C **81**, 10, 876 (2021), [arXiv:2103.06995].

[32] G. Dezoort *et al.* (2021), [arXiv:2103.16701].

[33] E. Parzen, The annals of mathematical statistics **33**, 3, 1065 (1962).

[34] R. A. Davis, K.-S. Lii and D. N. Politis, in "Selected Works of Murray Rosenblatt," 95–100, Springer (2011).

[35] K. S. Cranmer, Comput. Phys. Commun. **136**, 198 (2001), [hep-ex/0011057].

[36] D. P. Kingma and M. Welling, arXiv preprint arXiv:1312.6114 (2013).

[37] D. J. Rezende, S. Mohamed and D. Wierstra, in "Proceedings of the 31th International Conference on Machine Learning, ICML 2014, Beijing, China, 21-26 June 2014," volume 32 of *JMLR Workshop and Conference Proceedings*, 1278–1286, JMLR.org (2014), URL `http://proceedings.mlr.press/v32/rezende14.html`.

[38] I. J. Goodfellow *et al.*, in Z. Ghahramani *et al.*, editors, "Advances in Neural Information Processing Systems 27: Annual Conference on Neural Information Processing Systems 2014, December 8-13 2014, Montreal, Quebec, Canada," 2672–2680 (2014), URL `http://papers.nips.cc/paper/5423-generative-adversarial-nets`.

[39] A. Radford, L. Metz and S. Chintala, in Y. Bengio and Y. LeCun, editors, "4th International Conference on Learning Representations, ICLR 2016, San Juan, Puerto Rico, May 2-4, 2016, Conference Track Proceedings," (2016), URL `http://arxiv.org/abs/1511.06434`.

[40] D. Rezende and S. Mohamed, Proceedings of the 32nd International Conference on Machine Learning **37**, 1530 (2015), URL `http://proceedings.mlr.press/v37/rezende15.html`.

[41] L. Dinh, D. Krueger and Y. Bengio (2015), [arXiv:1410.8516].

[42] L. Dinh, J. Sohl-Dickstein and S. Bengio, in "5th International Conference on Learning Representations, ICLR 2017, Toulon, France, April 24-26, 2017, Conference Track Proceedings," OpenReview.net (2017), URL `https://openreview.net/forum?id=HkpbnH9lx`.

[43] D. P. Kingma and P. Dhariwal, in S. Bengio *et al.*, editors, "Advances in Neural Information Processing Systems 31: Annual Conference on Neural Information Processing Systems 2018, NeurIPS 2018, December 3-8, 2018, Montréal, Canada," 10236–10245 (2018).

[44] I. Kobyzev, S. Prince and M. Brubaker, IEEE Transactions on Pattern Analysis and Machine Intelligence (2020).

[45] Y. Lipman *et al.* (2023), [arXiv:2210.02747], URL `https://arxiv.org/abs/2210.02747`.

[46] Y. Song and S. Ermon, in H. Wallach *et al.*, editors, "Advances in Neural Information Processing Systems," volume 32, 11895, Curran Associates, Inc. (2019), URL `https://proceedings.neurips.cc/paper/2019/hash/3001ef257407d5a371a96dcd947c7d93-Abstract.html`.

[47] Y. Song *et al.*, CoRR **abs/2011.13456** (2020), [arXiv:2011.13456], URL `https://arxiv.org/abs/2011.13456`.

[48] M. S. Albergo and E. Vanden-Eijnden, in "The Eleventh International Conference on Learning Representations, ICLR 2023, Kigali, Rwanda, May 1-5, 2023," OpenReview.net (2023), URL `https://openreview.net/forum?id=li7qeBbCR1t`.

[49] M. Arjovsky and L. Bottou, in "5th International Conference on Learning Representations, ICLR 2017, Toulon, France, April 24-26, 2017, Conference Track Proceedings," OpenReview.net (2017), URL `https://openreview.net/forum?id=Hk4_qw5xe`.

Phys. A 2026.41. Downloaded from www.worldscientific.com
by UNIVERSITY OF CA LEY on 09/16/26. Re-use and distribution is strictly not permitted, except for Open Access articles.

[50] M. Wiatrak and S. V. Albrecht, arXiv preprint arXiv:1910.00927 (2019).

[51] D. J. Rezende *et al.*, in "International Conference on Machine Learning," 8083–8092, PMLR (2020).

[52] M. C. Gemici, D. Rezende and S. Mohamed, arXiv preprint arXiv:1611.02304 (2016).

[53] J. Brehmer and K. Cranmer (2020), [arXiv:2003.13913].

[54] V. Böhm and U. Seljak, arXiv preprint arXiv:2006.05479 (2020).

[55] A. van den Oord, O. Vinyals and K. Kavukcuoglu, in I. Guyon *et al.*, editors, "Advances in Neural Information Processing Systems 30: Annual Conference on Neural Information Processing Systems 2017, December 4-9, 2017, Long Beach, CA, USA," 6306–6315 (2017).

[56] T. Karras *et al.*, in "6th International Conference on Learning Representations, ICLR 2018, Vancouver, BC, Canada, April 30 - May 3, 2018, Conference Track Proceedings," OpenReview.net (2018), URL `https://openreview.net/forum?id=Hk99zCeAb`.

[57] T. Karras, S. Laine and T. Aila, in "IEEE Conference on Computer Vision and Pattern Recognition, CVPR 2019, Long Beach, CA, USA, June 16-20, 2019," 4401–4410, Computer Vision Foundation / IEEE (2019), URL `http://openaccess.thecvf.com/content_CVPR_2019/html/Karras_A_Style-Based_Generator_Architecture_for_Generative_Adversarial_Networks_CVPR_2019_paper.html`.

[58] M. Lucic *et al.*, in S. Bengio *et al.*, editors, "Advances in Neural Information Processing Systems 31: Annual Conference on Neural Information Processing Systems 2018, NeurIPS 2018, December 3-8, 2018, Montréal, Canada," 698–707 (2018).

[59] A. A. Alemi *et al.*, in J. G. Dy and A. Krause, editors, "Proceedings of the 35th International Conference on Machine Learning, ICML 2018, Stockholmsmässan, Stockholm, Sweden, July 10-15, 2018," volume 80 of *Proceedings of Machine Learning Research*, 159–168, PMLR (2018), URL `http://proceedings.mlr.press/v80/alemi18a.html`.

[60] M. E. Tipping and C. M. Bishop, Journal of the Royal Statistical Society: Series B (Statistical Methodology) **61**, 3, 611 (1999), URL `https://rss.onlinelibrary.wiley.com/doi/abs/10.1111/1467-9868.00196`.

[61] M. Arjovsky, S. Chintala and L. Bottou, arXiv preprint arXiv:1701.07875 (2017).

[62] L. Mescheder, S. Nowozin and A. Geiger, in I. Guyon *et al.*, editors, "Advances in Neural Information Processing Systems," volume 30, Curran Associates, Inc. (2017), URL `https://proceedings.neurips.cc/paper/2017/file/4588e674d3f0faf985047d4c3f13ed0d-Paper.pdf`.

[63] G. Papamakarios, I. Murray and T. Pavlakou, in "Advances in Neural Information Processing Systems," 2335–2344 (2017).

[64] C. Durkan *et al.*, in H. M. Wallach *et al.*, editors, "Advances in Neural Information Processing Systems," 7509 (2019).

[65] W. Grathwohl *et al.*, in "7th International Conference on Learning Representations, ICLR 2019, New Orleans, LA, USA, May 6-9, 2019," OpenReview.net (2019), URL `https://openreview.net/forum?id=rJxgknCcK7`.

[66] A. van den Oord *et al.*, arXiv:1609.03499 (2016), [arXiv:1609.03499], URL `http://arxiv.org/abs/1609.03499`.

[67] A. van den Oord *et al.*, in D. D. Lee *et al.*, editors, "Advances in Neural Information Processing Systems 29: Annual Conference on Neural Information Processing Systems 2016, December 5-10, 2016, Barcelona, Spain," 4790–4798 (2016), URL `https://proceedings.neurips.cc/paper/2016/hash/b1301141feffabac455e1f90a7de2054-Abstract.html`.

[68] B. Dai and U. Seljak, in M. Meila and T. Zhang, editors, "Proceedings of the 38th International Conference on Machine Learning, ICML 2021, 18-24 July 2021, Virtual Event," volume 139 of *Proceedings of Machine Learning Research*, 2352–2364, PMLR (2021), URL `http://proceedings.mlr.press/v139/dai21a.html`.

[69] K. Cranmer and G. Louppe, J. Brief Ideas (2016), 10.5281/zenodo.198541.

[70] G. Papamakarios and I. Murray, in "Advances in Neural Information Processing Systems," 1036–1044 (2016), ISSN 10495258, [arXiv:1605.06376].

[71] P. Holderrieth and E. Erives (2025), [arXiv:2506.02070].

[72] J. Hajer *et al.*, Phys. Rev. D **101**, 076015 (2020), URL `https://link.aps.org/doi/10.1103/PhysRevD.101.076015`.

[73] M. Farina, Y. Nakai and D. Shih, Phys. Rev. D **101** (2020), [arXiv:1808.08992].

[74] T. Heimel *et al.*, SciPost Phys. **6** (2019), [arXiv:1808.08979].

[75] J. Ren *et al.*, in H. M. Wallach *et al.*, editors, "Advances in Neural Information Processing Systems 32: Annual Conference on Neural Information Processing Systems 2019, NeurIPS 2019, December 8-14, 2019, Vancouver, BC, Canada," 14680–14691 (2019).

[76] E. T. Nalisnick *et al.*, in "7th International Conference on Learning Representations, ICLR 2019, New Orleans, LA, USA, May 6-9, 2019," OpenReview.net (2019), URL `https://openreview.net/forum?id=H1xwNhCcYm`.

[77] Z. Xiao, Q. Yan and Y. Amit, arXiv preprint arXiv:2003.02977 (2020).

[78] A. Hayrapetyan *et al.* (CMS) (2025), [arXiv:2510.02168].

[79] C. Le Lan and L. Dinh, Entropy **23**, 12, 1690 (2021), ISSN 1099-4300, URL `http://dx.doi.org/10.3390/e23121690`.

[80] G. Kasieczka *et al.*, Phys. Rev. D **107**, 1, 015009 (2023), [arXiv:2209.06225].

[81] J. H. Collins, K. Howe and B. Nachman, Phys. Rev. Lett. **121**, 24, 241803 (2018), [arXiv:1805.02664].

[82] J. H. Collins *et al.*, The European Physical Journal C **81**, 7 (2021), ISSN 1434-6052, URL `http://dx.doi.org/10.1140/epjc/s10052-021-09389-x`.

[83] G. Kasieczka *et al.* (2021), [arXiv:2101.08320].

[84] T. Aarrestad *et al.* (2021), [arXiv:2105.14027].

[85] J. Devlin *et al.*, in J. Burstein, C. Doran and T. Solorio, editors, "Proceedings of the 2019 Conference of the North American Chapter of the Association for Computational Linguistics: Human Language Technologies, Volume 1 (Long and Short Papers)," 4171, Association for Computational Linguistics, Minneapolis, Minnesota (2019), URL `https://aclanthology.org/N19-1423/`.

[86] T. Brown *et al.*, in H. Larochelle *et al.*, editors, "Advances in Neural Information Processing Systems," volume 33, 1877, Curran Associates, Inc. (2020), URL `https://proceedings.neurips.cc/paper/2020/file/1457c0d6bfcb4967418bfb8ac142f64a-Paper.pdf`.

[87] T. Golling *et al.*, Mach. Learn. Sci. Tech. **5**, 3, 035074 (2024), [arXiv:2401.13537].

[88] M. Leigh *et al.*, Mach. Learn. Sci. Tech. **6**, 2, 025075 (2025).

[89] J. Birk, A. Hallin and G. Kasieczka, Mach. Learn. Sci. Tech. **5**, 3, 035031 (2024), [arXiv:2403.05618].

[90] K. He *et al.*, in "CVPR," (2022), [arXiv:2111.06377].

[91] M. Caron *et al.*, in "Proceedings of the International Conference on Computer Vision (ICCV)," (2021), [arXiv:2104.14294].

[92] M. Oquab *et al.*, DINOv2: Learning Robust Visual Features without Supervision (2023).

[93] S. Wang *et al.*, in "CVPR," (2024).

Int. J. Mod. Phys. A 2026.41. Downloaded from www.worldscientific.com
by UNIVERSITY OF CALIFORNIA @ BERKELEY on 09/16/26. Re-use and distribution is strictly not permitted, except for Open Access articles.

[94] B. P. Duisterhof *et al.*, in "International Conference on 3D Vision 2025," (2025), URL `https://openreview.net/forum?id=5uw1GRBFoT`.

[95] J. Wang *et al.*, in "Proceedings of the IEEE/CVF Conference on Computer Vision and Pattern Recognition," (2025).

[96] S. Young, Y. jae Jwa and K. Terao, Particle Trajectory Representation Learning with Masked Point Modeling (2025), [arXiv:2502.02558], URL `https://arxiv.org/abs/2502.02558`.

[97] Z. Hao *et al.* (2025), [arXiv:2509.07486].

[98] A. Radford *et al.*, in M. Meila and T. Zhang, editors, "Proceedings of the 38th International Conference on Machine Learning," volume 139 of *Proceedings of Machine Learning Research*, 8748, PMLR (2021), [arXiv:2103.00020], URL `https://proceedings.mlr.press/v139/radford21a.html`.

[99] L. Parker *et al.*, Monthly Notices of the Royal Astronomical Society **531**, 4, 4990 (2024).

[100] M. A. Hayat *et al.*, ApJ Letters **911**, 2, L33 (2021).

[101] T. Chen *et al.*, in "Proceedings of the 37th International Conference on Machine Learning, ICML 2020, 13-18 July 2020, Virtual Event," volume 119 of *Proceedings of Machine Learning Research*, 1597–1607, PMLR (2020), URL `http://proceedings.mlr.press/v119/chen20j.html`.

[102] B. M. Dillon *et al.*, SciPost Phys. **12**, 188 (2022), [arXiv:2108.04253].

[103] B. M. Dillon, R. Mastandrea and B. Nachman, Phys. Rev. D **106**, 056005 (2022), URL `https://link.aps.org/doi/10.1103/PhysRevD.106.056005`.

[104] B. M. Dillon *et al.*, SciPost Phys. Core **7**, 056 (2024), URL `https://scipost.org/10.21468/SciPostPhysCore.7.3.056`.

[105] Z. Zhao *et al.*, in "22nd International Workshop on Advanced Computing and Analysis Techniques in Physics Research," (2024), [arXiv:2408.09343].

[106] P. Harris *et al.*, Phys. Rev. D **111**, 3, 032010 (2025), [arXiv:2403.07066].

[107] P. Rieck *et al.* (2025), [arXiv:2503.11632].

[108] T. Chen *et al.*, in H. D. III and A. Singh, editors, "Proceedings of the 37th International Conference on Machine Learning," volume 119, 1597 (2020), [arXiv:2002.05709], URL `https://proceedings.mlr.press/v119/chen20j.html`.

[109] N. Baron Perez *et al.*, Astron. Astrophys. **699**, A302 (2025), [arXiv:2503.19111].

[110] A. Wilkinson, R. Radev and S. Alonso-Monsalve, Phys. Rev. D **111**, 9, 092011 (2025), [arXiv:2502.07724].

[111] M. Assran *et al.*, in "2023 IEEE/CVF Conference on Computer Vision and Pattern Recognition (CVPR)," 15619 (2023), [arXiv:2301.08243].

[112] S. Katel *et al.*, in "7th Machine Learning and the Physical Sciences Workshop at the 38th Conference on Neural Information Processing Systems," (2024), [arXiv:2412.05333], URL `https://ml4physicalsciences.github.io/2024/files/NeurIPS_ML4PS_2024_222.pdf`.

[113] J. Bardhan *et al.* (2025), [arXiv:2502.03933].

[114] A. Ore, C. Heneka and T. Plehn, SciPost Phys. **18**, 5, 155 (2025), [arXiv:2410.18899].

[115] R. E. Bellman, *Dynamic Programming*, Princeton University Press, USA (1957), ISBN 069107951X.

[116] D. E. Kirk, *Optimal control theory: an introduction*, Courier Corporation (2004).

[117] K. J. Åström, Journal of Mathematical Analysis and Applications **10**, 174 (1965).

[118] J. Brehmer *et al.*, in "34th Conference on Neural Information Processing Systems," (2020), [arXiv:2011.08191].

[119] R. S. Sutton and A. G. Barto, Cambridge, MA **22447** (1998).

[120] K. Arulkumaran *et al.*, IEEE Signal Processing Magazine **34**, 6, 26 (2017).

[121] S. Carrazza and F. A. Dreyer, Phys. Rev. D **100**, 1, 014014 (2019), [arXiv:1903.09644].

[122] G. H. Mendizabal *et al.* (2025), [arXiv:2509.14894].

[123] G. N. Wojcik, S. T. Eu and L. L. Everett, Phys. Rev. D **111**, 3, 035007 (2025), [arXiv:2407.07203].

[124] H. Robbins, Bulletin of the American Mathematical Society **58**, 5, 527 (1952).

[125] J. C. Gittins, Journal of the Royal Statistical Society: Series B (Methodological) **41**, 2, 148 (1979).

[126] J. Mockus, *Bayesian approach to global optimization: theory and applications*, volume 37, Springer Science & Business Media (2012).

[127] E. Brochu, V. M. Cora and N. De Freitas (2010), [arXiv:1012.2599].

[128] K. Cranmer, J. Brehmer and G. Louppe, Proc. Nat. Acad. Sci. **117**, 48, 30055 (2020), [arXiv:1911.01429].

[129] J. Brehmer and K. Cranmer, *Artificial Intelligence for Particle Physics*, chapter Simulation-based inference methods for particle physics, World Scientific Publishing Co (2021).

[130] P. J. Diggle and R. J. Gratton, in "Journal of the Royal Statistical Society: Series B (Methodological)," volume 46, 193–212 (1984), ISSN 0035-9246.

[131] D. B. Rubin, The Annals of Statistics **12**, 4, 1151 (1984), ISSN 0090-5364, URL `https://doi.org/10.1214/aos/1176346785`.

[132] M. A. Beaumont, W. Zhang and D. J. Balding, Genetics **162**, 4, 2025 (2002), ISSN 00166731.

[133] K. Cranmer, J. Pavez and G. Louppe, arXiv:1506.02169 (2015), [arXiv:1506.02169], URL `http://arxiv.org/abs/1506.02169`.

[134] J. Brehmer *et al.*, Proc. Nat. Acad. Sci. 201915980 (2020), [arXiv:1805.12244].

[135] M. Stoye *et al.* (2018), [arXiv:1808.00973].

[136] C. Modi, F. Lanusse and U. Seljak, FlowPM: Distributed TensorFlow Implementation of the FastPM Cosmological N-body Solver (2020), [arXiv:2010.11847].

[137] J. Jasche and B. D. Wandelt, Mon. Not. Roy. Astron. Soc. **432**, 894 (2013), [arXiv:1203.3639].

[138] B. Dai and U. Seljak, Proceedings of the National Academy of Science **121**, 9, e2309624121 (2024).

[139] D. Ribli *et al.*, Monthly Notices of the Royal Astronomical Society **490**, 2, 1843 (2019).

[140] M. Arratia *et al.*, Journal of Instrumentation **17**, 1, P01024 (2022), [arXiv:2109.13243].

[141] A. Andreassen *et al.*, Phys. Rev. Lett. **124**, 18, 182001 (2020), [arXiv:1911.09107].

[142] V. Andreev *et al.* (H1) (2021), [arXiv:2108.12376].

[143] G. Aad *et al.* (ATLAS), Phys. Rev. Lett. **133**, 26, 261803 (2024), [arXiv:2405.20041].

[144] R. G. Huang *et al.*, Phys. Rev. D **112**, 1, 012008 (2025), [arXiv:2504.06857].

[145] P. T. Komiske, S. Kryhin and J. Thaler, Phys. Rev. D **106**, 9, 094021 (2022), [arXiv:2205.04459].

[146] L. Parker, A. E. Bayer and U. Seljak, Journal of Cosmology and Astroparticle Physics **2025**, 9, 039 (2025), [arXiv:2504.01092].

[147] H. Wang *et al.*, The Astrophysical Journal **794**, 1, 94 (2014), [arXiv:1407.3451].

[148] U. Seljak *et al.*, Journal of Cosmology and Astroparticle Physics **2017**, 12, 009 (2017), [arXiv:1706.06645].

[149] A. Hocker *et al.*, PoS **ACAT**, 040 (2007), [arXiv:physics/0703039].

by UNIVERSITY OF CA Phys. A 2026.41. Downloaded from www.worldscientific.com
LEY on 09/16/26. Re-use and distribution is strictly not permitted, except for Open Access articles.

[150] T. Mikolov *et al.*, arXiv preprint arXiv:1301.3781 (2013).

[151] E. Asgari and M. R. Mofrad, PloS one **10**, 11, e0141287 (2015).

[152] D. Guest *et al.*, Phys. Rev. **D94**, 11, 112002 (2016), [arXiv:1607.08633].

[153] T. Q. Nguyen *et al.*, Comput. Softw. Big Sci. **3**, 1, 12 (2019), [arXiv:1807.00083].

[154] E. Bols *et al.* (2020), [arXiv:2008.10519].

[155] K. Goto *et al.*, Development of a Vertex Finding Algorithm using Recurrent Neural Network (2021), [arXiv:2101.11906].

[156] R. T. de Lima (2021), [arXiv:2102.06128].

[157] Technical Report ATL-PHYS-PUB-2017-003, CERN, Geneva (2017), URL `http://cdsweb.cern.ch/record/2255226`.

[158] J. Pumplin, Phys. Rev. D **44**, 2025 (1991).

[159] J. Cogan *et al.*, JHEP **02**, 118 (2015), [arXiv:1407.5675].

[160] L. G. Almeida *et al.*, JHEP **07**, 086 (2015), [arXiv:1501.05968].

[161] L. de Oliveira *et al.*, JHEP **07**, 069 (2016), [arXiv:1511.05190].

[162] Technical Report ATL-PHYS-PUB-2017-017, CERN, Geneva (2017), URL `http://cds.cern.ch/record/2275641`.

[163] J. Lin *et al.*, JHEP **10**, 101 (2018), [arXiv:1807.10768].

[164] P. T. Komiske *et al.*, Phys. Rev. **D98**, 1, 011502 (2018), [arXiv:1801.10158].

[165] J. Barnard *et al.*, Phys. Rev. **D95**, 1, 014018 (2017), [arXiv:1609.00607].

[166] P. T. Komiske, E. M. Metodiev and M. D. Schwartz, JHEP **01**, 110 (2017), [arXiv:1612.01551].

[167] G. Kasieczka *et al.*, JHEP **05**, 006 (2017), [arXiv:1701.08784].

[168] S. Macaluso and D. Shih, JHEP **10**, 121 (2018), [arXiv:1803.00107].

[169] J. Li, T. Li and F.-Z. Xu (2020), [arXiv:2008.13529].

[170] J. Li and H. Sun (2020), [arXiv:2009.00170].

[171] J. S. H. Lee *et al.*, J. Korean Phys. Soc. **74**, 3, 219 (2019), [arXiv:2012.02531].

[172] J. Collado *et al.*, Learning to Isolate Muons (2021), [arXiv:2102.02278].

[173] Y.-L. Du, D. Pablos and K. Tywoniuk (2020), [arXiv:2012.07797].

[174] J. Filipek *et al.* (2021), [arXiv:2105.04582].

[175] Technical Report ATL-PHYS-PUB-2019-028, CERN, Geneva (2019), URL `http://cds.cern.ch/record/2684070`.

[176] M. Andrews *et al.* (2018), [arXiv:1807.11916].

[177] Y.-L. Chung, S.-C. Hsu and B. Nachman (2020), [arXiv:2009.05930].

[178] Y.-L. Du *et al.*, Eur. Phys. J. C **80**, 6, 516 (2020), [arXiv:1910.11530].

[179] M. Andrews *et al.* (2021), [arXiv:2104.14659].

[180] A. A. Pol *et al.* (2021), [arXiv:2105.05785].

[181] A. Aurisano *et al.*, JINST **11**, 09, P09001 (2016), [arXiv:1604.01444].

[182] R. Acciarri *et al.* (MicroBooNE), JINST **12**, 03, P03011 (2017), [arXiv:1611.05531].

[183] L. Hertel *et al.* (2017), URL `https://dl4physicalsciences.github.io/files/nips_dlps_2017_7.pdf`.

[184] C. Adams *et al.* (MicroBooNE), Phys. Rev. **D99**, 9, 092001 (2019), [arXiv:1808.07269].

[185] S. Aiello *et al.* (KM3NeT) (2020), [arXiv:2004.08254].

[186] C. Adams, K. Terao and T. Wongjirad (2020), [arXiv:2006.01993].

[187] L. Dominé *et al.* (DeepLearnPhysics), Phys. Rev. D **104**, 3, 032004 (2021), [arXiv:2006.14745].

[188] H. Yu *et al.*, JINST **16**, 01, P01036 (2021), [arXiv:2007.12743].

[189] F. Psihas *et al.* (2020), [arXiv:2008.01242].

[190] S. Alonso-Monsalve *et al.*, Phys. Rev. D **103**, 3, 032005 (2021), [arXiv:2009.00688].

[191] P. Abratenko *et al.* (MicroBooNE) (2020), [arXiv:2010.08653].

[192] B. Clerbaux *et al.* (2020), [arXiv:2011.08847].

[193] J. Liu *et al.* (2020), [arXiv:2012.06181].

[194] P. Abratenko *et al.* (MicroBooNE) (2020), [arXiv:2012.08513].

[195] S. Y.-C. Chen *et al.* (2020), [arXiv:2012.12177].

[196] R. Acciarri *et al.* (SBND) (2020), [arXiv:2012.01301].

[197] Z. Qian *et al.* (2021), [arXiv:2101.04839].

[198] R. Abbasi *et al.* (IceCube), A Convolutional Neural Network based Cascade Reconstruction for the IceCube Neutrino Observatory (2021), [arXiv:2101.11589].

[199] F. Drielsma *et al.*, in "34th Conference on Neural Information Processing Systems," (2021), [arXiv:2102.01033].

[200] M. Rossi and S. Vallecorsa, in "25th International Conference on Computing in High-Energy and Nuclear Physics," (2021), [arXiv:2103.01596].

[201] J. Hewes *et al.* (2021), [arXiv:2103.06233].

[202] R. Acciarri *et al.* (ArgoNeuT) (2021), [arXiv:2103.06391].

[203] V. Belavin, E. Trofimova and A. Ustyuzhanin (2021), [arXiv:2104.02040].

[204] D. Maksimović, M. Nieslony and M. Wurm (2021), [arXiv:2104.13426].

[205] A. Gavrikov and F. Ratnikov, in "25th International Conference on Computing in High-Energy and Nuclear Physics," (2021), [arXiv:2106.02907].

[206] J. García-Méndez *et al.* (ANTARES), JINST **16**, 09, C09018 (2021), [arXiv:2107.13654].

[207] K. Carloni *et al.* (2021), [arXiv:2110.10766].

[208] P. Abratenko *et al.* (MicroBooNE) (2021), [arXiv:2110.11874].

[209] D. Boyda *et al.*, Phys. Rev. D **103**, 7, 074504 (2021), [arXiv:2008.05456].

[210] G. Kanwar *et al.*, Phys. Rev. Lett. **125**, 12, 121601 (2020), [arXiv:2003.06413].

[211] P. T. Komiske, E. M. Metodiev and J. Thaler, JHEP **01**, 121 (2019), [arXiv:1810.05165].

[212] H. Qu and L. Gouskos, Phys. Rev. D **101**, 5, 056019 (2020), [arXiv:1902.08570].

[213] V. Mikuni and F. Canelli, Eur. Phys. J. Plus **135**, 6, 463 (2020), [arXiv:2001.05311].

[214] J. Shlomi *et al.*, Eur. Phys. J. C **81**, 6, 540 (2021), [arXiv:2008.02831].

[215] M. J. Dolan and A. Ore, Phys. Rev. D **103**, 7, 074022 (2021), [arXiv:2012.00964].

[216] M. J. Fenton *et al.*, Phys. Rev. D **105**, 11, 112008 (2022), [arXiv:2010.09206].

[217] J. S. H. Lee *et al.* (2020), [arXiv:2012.03542].

[218] V. Mikuni and F. Canelli, Mach. Learn. Sci. Tech. **2**, 035027 (2021), [arXiv:2102.05073].

[219] A. Shmakov *et al.*, SciPost Phys. **12**, 5, 178 (2022), [arXiv:2106.03898].

[220] C. Shimmin (2021), [arXiv:2107.02908].

[221] ATLAS Collaboration, ATLAS PUB Note ATL-PHYS-PUB-2020-014 (2020), URL `https://cds.cern.ch/record/2718948`.

Int. J. Mod. Phys. A 2026.41. Downloaded from www.worldscientific.com
by UNIVERSITY OF CALIFORNIA @ BERKELEY on 09/16/26. Re-use and distribution is strictly not permitted, except for Open Access articles.

[222] H. Qu, C. Li and S. Qian, in "Proceedings of the 39th International Conference on Machine Learning," 18281 (2022), [arXiv:2202.03772].

[223] G. Louppe *et al.*, JHEP **01**, 057 (2019), [arXiv:1702.00748].

[224] T. Cheng (2017), [arXiv:1711.02633].

[225] I. Henrion *et al.* (2017), URL `https://dl4physicalsciences.github.io/files/nips_dlps_2017_29.pdf`.

[226] X. Ju *et al.*, in "Machine Learning and the Physical Sciences at NeurIPS," (2020), [arXiv:2003.11603].

[227] M. Abdughani *et al.*, JHEP **08**, 055 (2019), [arXiv:1807.09088].

[228] J. Arjona Martínez *et al.*, Eur. Phys. J. Plus **134**, 7, 333 (2019), [arXiv:1810.07988].

[229] J. Ren, L. Wu and J. M. Yang, Phys. Lett. B **802**, 135198 (2020), [arXiv:1901.05627].

[230] E. A. Moreno *et al.*, Eur. Phys. J. C **80**, 1, 58 (2020), [arXiv:1908.05318].

[231] S. R. Qasim *et al.*, Eur. Phys. J. C **79**, 7, 608 (2019), [arXiv:1902.07987].

[232] A. Chakraborty, S. H. Lim and M. M. Nojiri, JHEP **19**, 135 (2020), [arXiv:1904.02092].

[233] A. Chakraborty *et al.* (2020), [arXiv:2003.11787].

[234] M. Abdughani *et al.* (2020), [arXiv:2005.11086].

[235] E. Bernreuther *et al.* (2020), [arXiv:2006.08639].

[236] J. Shlomi, P. Battaglia and J.-R. Vlimant, Machine Learning: Science and Technology **2**, 2, 021001 (2021), ISSN 2632-2153, URL `http://dx.doi.org/10.1088/2632-2153/abbf9a`.

[237] Y. Iiyama *et al.*, Front. Big Data **3**, 598927 (2020), [arXiv:2008.03601].

[238] X. Ju and B. Nachman, Phys. Rev. D **102**, 075014 (2020), [arXiv:2008.06064].

[239] N. Choma *et al.* (2020), [arXiv:2007.00149].

[240] Jun Guo and Jinmian Li and Tianjun Li (2020), [arXiv:2010.05464].

[241] A. Heintz *et al.*, 34th Conference on Neural Information Processing Systems (2020), [arXiv:2012.01563].

[242] Y. Verma and S. Jena (2020), [arXiv:2012.08515].

[243] F. A. Dreyer and H. Qu (2020), [arXiv:2012.08526].

[244] J. Pata *et al.* (2021), [arXiv:2101.08578].

[245] C. Biscarat *et al.*, in "25th International Conference on Computing in High-Energy and Nuclear Physics," (2021), [arXiv:2103.00916].

[246] S. Thais and G. DeZoort (2021), [arXiv:2103.06509].

[247] Y. Verma and S. Jena (2021), [arXiv:2103.14906].

[248] A. Hariri, D. Dyachkova and S. Gleyzer (2021), [arXiv:2104.01725].

[249] O. Atkinson *et al.* (2021), [arXiv:2105.07988].

[250] P. Konar, V. S. Ngairangbam and M. Spannowsky (2021), [arXiv:2109.14636].

[251] K. Cho *et al.*, in "Conference on Empirical Methods in Natural Language Processing (EMNLP 2014)," (2014).

[252] H. Serviansky *et al.*, in H. Larochelle *et al.*, editors, "Advances in Neural Information Processing Systems," volume 33, 22080–22091, Curran Associates, Inc. (2020), URL `https://proceedings.neurips.cc/paper/2020/file/fb4ab556bc42d6f0ee0f9e24ec4d1af0-Paper.pdf`.

[253] C. M. Bishop, *Pattern recognition and machine learning*, springer (2006).

[254] C. K. Williams and C. E. Rasmussen, *Gaussian processes for machine learning*, volume 2, MIT press Cambridge, MA (2006).

[255] A. Gandrakota *et al.*, JHEP **02**, 230 (2023), [arXiv:2202.05856].

[256] M. Frate *et al.* (2017), [arXiv:1709.05681].

[257] S. Mishra-Sharma and K. Cranmer, in "34th Conference on Neural Information Processing Systems," (2020), [arXiv:2010.10450].

[258] J. W. Foster *et al.*, Phys. Rev. Lett. **127**, 5, 051101 (2021), [arXiv:2102.02207].

[259] L. Breiman *et al.* (1984).

[260] XGBoost`https://xgboost.readthedocs.io/`.

[261] G. Ke *et al.*, in "Proceedings of the 31st International Conference on Neural Information Processing Systems," NIPS'17, 3149–3157, Curran Associates Inc., Red Hook, NY, USA (2017), ISBN 9781510860964.

[262] N. Erickson *et al.*, "Tabarena: A living benchmark for machine learning on tabular data," (2025), [arXiv:2506.16791].

[263] I. Narsky (2005), [arXiv:physics/0507143].

[264] G. Louppe, arXiv preprint arXiv:1407.7502 (2014).

[265] Y. Freund and R. E. Schapire, Journal of computer and system sciences **55**, 1, 119 (1997).

[266] J. H. Friedman, Annals of statistics 1189–1232 (2001).

[267] K. Fukushima, Biological Cybernetics **36**, 193 (1980).

[268] V. Nair and G. E. Hinton, in "ICML," (2010).

[269] A. L. Maas, A. Y. Hannun and A. Y. Ng, in "in ICML Workshop on Deep Learning for Audio, Speech and Language Processing," (2013).

[270] K. He *et al.*, IEEE International Conference on Computer Vision (ICCV 2015) **1502** (2015).

[271] V. Sitzmann *et al.*, in "Proc. NeurIPS," (2020).

[272] D. Hendrycks and K. Gimpel, Gaussian Error Linear Units (GELUs) (2023), [arXiv:1606.08415], URL `https://arxiv.org/abs/1606.08415`.

[273] P. Ramachandran, B. Zoph and Q. V. Le, Searching for Activation Functions (2017), [arXiv:1710.05941], URL `https://arxiv.org/abs/1710.05941`.

[274] S. Elfwing, E. Uchibe and K. Doya, Sigmoid-Weighted Linear Units for Neural Network Function Approximation in Reinforcement Learning (2017), [arXiv:1702.03118], URL `https://arxiv.org/abs/1702.03118`.

[275] G. Cybenko, Mathematics of control, signals and systems **2**, 4, 303 (1989).

[276] O. Delalleau and Y. Bengio, in J. Shawe-Taylor *et al.*, editors, "Advances in Neural Information Processing Systems," volume 24, Curran Associates, Inc. (2011), URL `https://proceedings.neurips.cc/paper/2011/file/8e6b42f1644ecb1327dc03ab345e618b-Paper.pdf`.

[277] R. Raina, A. Madhavan and A. Y. Ng, in "Proceedings of the 26th Annual International Conference on Machine Learning," ICML '09, 873–880, Association for Computing Machinery, New York, NY, USA (2009), ISBN 9781605585161, URL `https://doi.org/10.1145/1553374.1553486`.

[278] Y. LeCun, Deep Learning est mort. Vive Differentiable Programming!`https://www.facebook.com/yann.lecun/posts/10155003011462143` (2018), URL `https://www.facebook.com/yann.lecun/posts/10155003011462143`.

[279] C. Szegedy *et al.*, in "2015 IEEE Conference on Computer Vision and Pattern Recognition (CVPR)," 1–9 (2015).

[280] N. Cohen and A. Shashua, CoRR **abs/1605.06743** (2016), URL `http://arxiv.org/abs/1605.06743`.

[281] A. Bietti, L. Venturi and J. Bruna, arXiv preprint arXiv:2106.07148 (2021).

[282] M. M. Bronstein *et al.*, arXiv preprint arXiv:2104.13478 (2021).

[283] K. Simonyan and A. Zisserman, CoRR **abs/1409.1556** (2015).

Phys. A 2026.41. Downloaded from www.worldscientific.com
by UNIVERSITY OF CA LEY on 09/16/26. Re-use and distribution is strictly not permitted, except for Open Access articles.

[284] S. Ren *et al.*, in C. Cortes *et al.*, editors, "Advances in Neural Information Processing Systems," volume 28, Curran Associates, Inc. (2015), URL https://proceedings.neurips.cc/paper/2015/file/14bfa6bb14875e45bba028a21ed38046-Paper.pdf.

[285] K. He *et al.*, in "2016 IEEE Conference on Computer Vision and Pattern Recognition (CVPR)," 770–778 (2016).

[286] O. Ronneberger, P. Fischer and T. Brox, in N. Navab *et al.*, editors, "Medical Image Computing and Computer-Assisted Intervention – MICCAI 2015," 234–241, Springer International Publishing, Cham (2015), ISBN 978-3-319-24574-4.

[287] D. Rumelhart, G. Hinton and R. Williams .

[288] Y. Bengio, P. Simard and P. Frasconi, Neural Networks, IEEE Transactions on **5**, 2, 157 (1994).

[289] R. Pascanu, T. Mikolov and Y. Bengio, in S. Dasgupta and D. McAllester, editors, "Proceedings of the 30th International Conference on Machine Learning," volume 28 of *Proceedings of Machine Learning Research*, 1310–1318, PMLR, Atlanta, Georgia, USA (2013), URL https://proceedings.mlr.press/v28/pascanu13.html.

[290] S. Hochreiter and J. Schmidhuber, Neural Computation **9**, 8, 1735 (1997).

[291] R. Socher *et al.*, in "ICML," (2011).

[292] R. Socher *et al.*, in "Proceedings of the 2011 conference on empirical methods in natural language processing," 151–161 (2011).

[293] X. Chen *et al.*, in "Proceedings of the 2015 conference on empirical methods in natural language processing," 793–798 (2015).

[294] C. Olah and S. Carter, Distill (2016), URL http://distill.pub/2016/augmented-rnns.

[295] D. Bahdanau, K. Cho and Y. Bengio (2015), 3rd International Conference on Learning Representations, ICLR 2015 ; Conference date: 07-05-2015 Through 09-05-2015.

[296] R. Bommasani *et al.*, arXiv preprint arXiv:2108.07258 (2021).

[297] P. Battaglia *et al.*, arXiv (2018), URL https://arxiv.org/pdf/1806.01261.pdf.

[298] M. Gori, G. Monfardini and F. Scarselli, in "Proceedings. 2005 IEEE International Joint Conference on Neural Networks, 2005.", volume 2, 729–734 vol. 2 (2005).

[299] C. R. Qi *et al.*, in "Proceedings of the IEEE Conference on Computer Vision and Pattern Recognition (CVPR)," (2017).

[300] C. Qi *et al.*, in "NIPS," (2017).

[301] M. Jaderberg *et al.*, in C. Cortes *et al.*, editors, "Advances in Neural Information Processing Systems," volume 28, Curran Associates, Inc. (2015), URL https://proceedings.neurips.cc/paper/2015/file/33ceb07bf4eeb3da587e268d663aba1a-Paper.pdf.

[302] M. Zaheer *et al.*, in I. Guyon *et al.*, editors, "Advances in Neural Information Processing Systems," volume 30, Curran Associates, Inc. (2017), URL https://proceedings.neurips.cc/paper/2017/file/f22e4747da1aa27e363d86d40ff442fe-Paper.pdf.

[303] Y. Wang *et al.*, ACM Transactions on Graphics **38** (2018).

[304] X. Wang *et al.*, in "2018 IEEE/CVF Conference on Computer Vision and Pattern Recognition (CVPR)," 7794–7803, IEEE Computer Society, Los Alamitos, CA, USA (2018), URL https://doi.ieeecomputersociety.org/10.1109/CVPR.2018.00813.

[305] J. Gilmer *et al.*, in D. Precup and Y. W. Teh, editors, "Proceedings of the 34th International Conference on Machine Learning," volume 70 of *Proceedings of Machine Learning Research*, 1263–1272, PMLR (2017), URL https://proceedings.mlr.press/v70/gilmer17a.html.

[306] N. Choma *et al.* (IceCube) (2018), [arXiv:1809.06166].

[307] S. R. Qasim *et al.*, The European Physical Journal C **79**, 7 (2019), ISSN 1434-6052, URL http://dx.doi.org/10.1140/epjc/s10052-019-7113-9.

[308] E. A. Moreno *et al.*, Phys. Rev. D **102**, 1, 012010 (2020), [arXiv:1909.12285].

[309] J. Pata *et al.*, Commun. Phys. **7**, 1, 124 (2024), [arXiv:2309.06782].

[310] J. Kieseler, Eur. Phys. J. C **80**, 9, 886 (2020), [arXiv:2002.03605].

[311] J. Shlomi, P. Battaglia and J.-R. Vlimant, Machine Learning: Science and Technology **2**, 2, 021001 (2021), URL https://doi.org/10.1088/2632-2153/abbf9a.

[312] A. Bogatskiy *et al.*, in H. D. III and A. Singh, editors, "Proceedings of the 37th International Conference on Machine Learning," volume 119 of *Proceedings of Machine Learning Research*, 992–1002, PMLR (2020), URL https://proceedings.mlr.press/v119/bogatskiy20a.html.

[313] S. Gong *et al.*, JHEP **07**, 030 (2022), [arXiv:2201.08187].

[314] Z. Hao *et al.*, Eur. Phys. J. C **83**, 6, 485 (2023), [arXiv:2212.07347].

[315] A. Bogatskiy *et al.* (2022), [arXiv:2211.00454].

[316] A. Bogatskiy *et al.*, JHEP **03**, 113 (2024), [arXiv:2307.16506].

[317] J. Brehmer *et al.* (2024), [arXiv:2411.00446].

[318] J. Spinner *et al.* (2024), [arXiv:2405.14806].

[319] T. S. Cohen *et al.*, arXiv e-prints (2019), [arXiv:1902.04615].

[320] F. B. Fuchs *et al.*, in "Proceedings of the 34th International Conference on Neural Information Processing Systems," NIPS '20, Curran Associates Inc., Red Hook, NY, USA (2020), ISBN 9781713829546.

[321] D. Boyda *et al.*, Phys. Rev. D **103**, 074504 (2021), URL https://link.aps.org/doi/10.1103/PhysRevD.103.074504.

[322] S. Batzner *et al.*, Nature Communications **13**, 1 (2022), ISSN 2041-1723, URL http://dx.doi.org/10.1038/s41467-022-29939-5.

[323] M. Raissi, P. Perdikaris and G. Karniadakis, Journal of Computational Physics **378**, 686 (2019), ISSN 0021-9991, URL https://www.sciencedirect.com/science/article/pii/S0021999118307125.

[324] A. S. Krishnapriyan *et al.*, Advances in Neural Information Processing Systems **34** (2021).

[325] R. Newbury *et al.*, IEEE Access **12**, 97581 (2024), URL https://api.semanticscholar.org/CorpusID:271051266.

[326] S. Shirobokov *et al.*, in H. Larochelle *et al.*, editors, "Advances in Neural Information Processing Systems," volume 33, 14650–14662, Curran Associates, Inc. (2020), [arXiv:2002.04632], URL https://proceedings.neurips.cc/paper/2020/hash/a878dbebc902328b41dbf02aa87abb58-Abstract.html.

[327] S. Mandt, M. D. Hoffman and D. M. Blei, J. Mach. Learn. Res. **18**, 134:1 (2017), URL http://jmlr.org/papers/v18/17-214.html.

[328] Y. You, I. Gitman and B. Ginsburg (2017), [arXiv:1708.03888], URL https://arxiv.org/abs/1708.03888.

[329] I. Loshchilov and F. Hutter, Decoupled Weight Decay Regularization (2019), [arXiv:1711.05101], URL https://arxiv.org/abs/1711.05101.

[330] D. P. Kingma and J. Ba, Adam: A Method for Stochastic Optimization (2017), [arXiv:1412.6980], URL https://arxiv.org/abs/1412.6980.

[331] Y. You *et al.*, Large Batch Optimization for Deep Learning: Training BERT in 76 minutes (2020), [arXiv:1904.00962], URL https://arxiv.org/abs/1904.00962.

Int. J. Mod. Phys. A 2026.41. Downloaded from www.worldscientific.com
by UNIVERSITY OF CALIFORNIA @ BERKELEY on 09/16/26. Re-use and distribution is strictly not permitted, except for Open Access articles.

[332] X. Chen *et al.*, Symbolic Discovery of Optimization Algorithms (2023), [arXiv:2302.06675], URL `https://arxiv.org/abs/2302.06675`.

[333] S. Gasiorowski *et al.*, Machine Learning: Science and Technology **5**, 2, 025012 (2024), URL `https://doi.org/10.1088/2632-2153/ad2cf0`.

[334] L. Heinrich and M. Kagan, Journal of Physics: Conference Series **2438**, 1, 012137 (2023), ISSN 1742-6596, URL `http://dx.doi.org/10.1088/1742-6596/2438/1/012137`.

[335] M. Aehle *et al.*, Computer Physics Communications **309**, 109491 (2025), ISSN 0010-4655, URL `https://www.sciencedirect.com/science/article/pii/S0010465524004144`.

[336] M. Lei *et al.*, Implicit Neural Representation as a Differentiable Surrogate for Photon Propagation in a Monolithic Neutrino Detector (2022), [arXiv:2211.01505], URL `https://arxiv.org/abs/2211.01505`.

[337] Y. LeCun *et al.*, *Efficient backprop*, 9–48, Lecture Notes in Computer Science (including subseries Lecture Notes in Artificial Intelligence and Lecture Notes in Bioinformatics), Springer Verlag (2012), ISBN 9783642352881, copyright: Copyright 2021 Elsevier B.V., All rights reserved.

[338] Y. Yao, L. Rosasco and A. Caponnetto, Constructive Approximation **26**, 2, 289 (2007).

[339] L. Prechelt, in "Neural Networks: Tricks of the trade," 55–69, Springer (1998).

[340] A. Krizhevsky, I. Sutskever and G. Hinton, Neural Information Processing Systems **25** (2012).

[341] X. Glorot and Y. Bengio, in Y. W. Teh and M. Titterington, editors, "Proceedings of the Thirteenth International Conference on Artificial Intelligence and Statistics," volume 9 of *Proceedings of Machine Learning Research*, 249–256, PMLR, Chia Laguna Resort, Sardinia, Italy (2010), URL `http://proceedings.mlr.press/v9/glorot10a.html`.

[342] S. Ioffe and C. Szegedy, in F. Bach and D. Blei, editors, "Proceedings of the 32nd International Conference on Machine Learning," volume 37, 448, PMLR (2015), [arXiv:1502.03167], URL `https://proceedings.mlr.press/v37/ioffe15.html`.

[343] J. L. Ba, J. R. Kiros and G. E. Hinton, Layer Normalization (2016), [arXiv:1607.06450].

[344] D. Ulyanov, A. Vedaldi and V. Lempitsky, Instance Normalization: The Missing Ingredient for Fast Stylization (2017), [arXiv:1607.08022].

[345] Y. Wu and K. He, Group Normalization (2018), [arXiv:1803.08494].

[346] T.-Y. Lin *et al.*, in D. Fleet *et al.*, editors, "Computer Vision – ECCV 2014," 740–755, Springer International Publishing, Cham (2014), ISBN 978-3-319-10602-1.

[347] O. Russakovsky *et al.*, International Journal of Computer Vision (IJCV) **115**, 3, 211 (2015).

[348] M. Cordts *et al.*, in "Proc. of the IEEE Conference on Computer Vision and Pattern Recognition (CVPR)," (2016).

[349] L. Yi *et al.*, SIGGRAPH Asia (2016).

[350] A. Radford *et al.* (2018), URL `https://s3-us-west-2.amazonaws.com/openai-assets/research-covers/language-unsupervised/language_understanding_paper.pdf`.

[351] T. Hellert, J. Montenegro and A. Pollastro, APL Machine Learning **2**, 4, 046105 (2024), ISSN 2770-9019, URL `https://doi.org/10.1063/5.0238090`.

[352] T. Hellert *et al.*, Phys. Rev. Accel. Beams **28**, 044601 (2025), URL `https://link.aps.org/doi/10.1103/PhysRevAccelBeams.28.044601`.

[353] C. Tan *et al.* (2023), [arXiv:2312.17016].

[354] A. Ramesh *et al.*, in M. Meila and T. Zhang, editors, "Proceedings of the 38th International Conference on Machine Learning," volume 139, 8821 (2021), [arXiv:2102.12092], URL `https://proceedings.mlr.press/v139/ramesh21a.html`.

[355] A. Blattmann *et al.*, Retrieval-Augmented Diffusion Models (2022), URL `https://arxiv.org/abs/2204.11824`.

[356] T. Dorigo and P. De Castro Manzano (2020), [arXiv:2007.09121].

[357] R. Barate *et al.* (ALEPH), Phys. Lett. B **412**, 173 (1997).

[358] G. Louppe, M. Kagan and K. Cranmer, in I. Guyon *et al.*, editors, "Advances in Neural Information Processing Systems," volume 30, Curran Associates, Inc. (2017), [arXiv:1611.01046], URL `https://papers.nips.cc/paper/2017/hash/48ab2f9b45957ab574cf005eb8a76760-Abstract.html`.

[359] H. Edwards and A. Storkey, arXiv preprint arXiv:1511.05897 (2015).

[360] Y. Ganin and V. Lempitsky, in F. Bach and D. Blei, editors, "Proceedings of the 32nd International Conference on Machine Learning," volume 37 of *Proceedings of Machine Learning Research*, 1180, PMLR (2015), [arXiv:1409.7495], URL `https://proceedings.mlr.press/v37/ganin15.html`.

[361] Y. Ganin *et al.*, J. Mach. Learn. Res. **17**, 1 (2016), [arXiv:1412.4446], URL `http://jmlr.org/papers/v17/15-239.html`.

[362] G. Kasieczka and D. Shih, Phys. Rev. Lett. **125**, 12, 122001 (2020), [arXiv:2001.05310].

[363] C. Shimmin *et al.*, Phys. Rev. **D96**, 7, 074034 (2017), [arXiv:1703.03507].

[364] A. Ghosh and B. Nachman, Eur. Phys. J. C **82**, 46 (2022), [arXiv:2109.08159].

[365] O. Kitouni *et al.*, JHEP **21**, 070 (2020), [arXiv:2010.09745].

[366] J. Stevens and M. Williams, JINST **8**, P12013 (2013), [arXiv:1305.7248].

[367] J. Dolen *et al.*, JHEP **05**, 156 (2016), [arXiv:1603.00027].

[368] CMS Detector Performance Summary CMS-DP-2020-002 (2020), URL `https://cds.cern.ch/record/2707946`.

[369] I. Moult, B. Nachman and D. Neill, JHEP **05**, 002 (2018), [arXiv:1710.06859].

[370] L. Bradshaw *et al.* (2019), [arXiv:1908.08959].

[371] ATLAS Collaboration, ATLAS PUB Note ATL-PHYS-PUB-2018-014 (2018), URL `http://cds.cern.ch/record/2630973`.

[372] L.-G. Xia, Nucl. Instrum. Meth. A **930**, 15 (2019), [arXiv:1810.08387].

[373] C. Englert *et al.*, Eur. Phys. J. C **79**, 1, 4 (2019), [arXiv:1807.08763].

[374] S. Wunsch *et al.*, Comput. Softw. Big Sci. **4**, 5 (2020), [arXiv:1907.11674].

[375] A. Rogozhnikov *et al.*, JINST **10**, 03, T03002 (2015), [arXiv:1410.4140].

[376] A. M. Sirunyan *et al.* (CMS), Mach. Learn. Sci. Tech. **1**, 035012 (2020), [arXiv:1912.12238].

[377] J. M. Clavijo, P. Glaysher and J. M. Katzy (2020), [arXiv:2005.00568].

[378] G. Kasieczka *et al.* (2020), [arXiv:2007.14400].

[379] P. Baldi *et al.*, Eur. Phys. J. **C76**, 5, 235 (2016), [arXiv:1601.07913].

[380] J. Brehmer *et al.*, Phys. Rev. **D98**, 5, 052004 (2018), [arXiv:1805.00020].

[381] A. Ghosh, B. Nachman and D. Whiteson (2021), [arXiv:2105.08742].

Phys. A 2026.41. Downloaded from www.worldscientific.com
by UNIVERSITY OF CA LEY on 09/16/26. Re-use and distribution is strictly not permitted, except for Open Access articles.

[382] W. L. Oberkampf *et al.*, Reliability Engineering & System Safety **85**, 1, 11 (2004), ISSN 0951-8320, alternative Representations of Epistemic Uncertainty, URL https://www.sciencedirect.com/science/article/pii/S0951832004000493.

[383] A. O'Hagan and J. E. Oakley, Reliability Engineering & System Safety **85**, 1, 239 (2004), ISSN 0951-8320, alternative Representations of Epistemic Uncertainty, URL https://www.sciencedirect.com/science/article/pii/S0951832004000638.

[384] E. Hüllermeier and W. Waegeman, CoRR **abs/1910.09457** (2019), URL http://arxiv.org/abs/1910.09457.

[385] A. Kendall and Y. Gal, in I. Guyon *et al.*, editors, "Advances in Neural Information Processing Systems," volume 30, Curran Associates, Inc. (2017), URL https://proceedings.neurips.cc/paper/2017/file/2650d6089a6d640c5e85b2b88265dc2b-Paper.pdf.

[386] A. D. Kiureghian and O. Ditlevsen, Structural Safety **31**, 2, 105 (2009), ISSN 0167-4730, risk Acceptance and Risk Communication, URL https://www.sciencedirect.com/science/article/pii/S0167473008000556.

[387] Y. Yao *et al.*, Bayesian Analysis **13**, 3 (2018), ISSN 1936-0975, URL http://dx.doi.org/10.1214/17-BA1091.

[388] J. Snoek *et al.*, in "Advances in Neural Information Processing Systems," volume 32, 13969 (2019), URL https://proceedings.neurips.cc/paper/2019/hash/8558cb408c1d76621371888657d2eb1d-Abstract.html.

[389] Y. Gal and Z. Ghahramani, in M. Balcan and K. Q. Weinberger, editors, "Proceedings of the 33rd International Conference on Machine Learning," volume 48, 1050, JMLR.org (2016), URL http://proceedings.mlr.press/v48/gal16.html.

[390] B. Lakshminarayanan, A. Pritzel and C. Blundell, in I. Guyon *et al.*, editors, "Advances in Neural Information Processing Systems 30: Annual Conference on Neural Information Processing Systems 2017, December 4-9, 2017, Long Beach, CA, USA," 6402–6413 (2017), URL https://proceedings.neurips.cc/paper/2017/hash/9ef2ed4b7fd2c810847ffa5fa85bce38-Abstract.html.

[391] D. P. Kingma, T. Salimans and M. Welling, CoRR **abs/1506.02557** (2015), URL http://arxiv.org/abs/1506.02557.

[392] D. Koh, A. Mishra and K. Terao, Journal of Instrumentation **18**, 12, P12013 (2023), URL https://doi.org/10.1088/1748-0221/18/12/P12013.

[393] J. Bai *et al.*, Open Neural Network Exchangehttps://github.com/onnx/onnx (2017), URL https://github.com/onnx/onnx.

[394] G. C. Strong (2020), [arXiv:2002.01427].

[395] V. V. Gligorov and M. Williams, JINST **8**, P02013 (2013), [arXiv:1210.6861].

[396] D. W. III *et al.* (2017), URL https://dl4physicalsciences.github.io/files/nips_dlps_2017_3.pdf.

[397] D. Bourgeois, C. Fitzpatrick and S. Stahl (2018), [arXiv:1808.00711].

[398] J. Alimena, Y. Iiyama and J. Kieseler (2020), [arXiv:2004.10744].

[399] C. Balázs *et al.* (DarkMachines High Dimensional Sampling Group) (2021), [arXiv:2101.04525].

[400] F. Rehm *et al.* (2021), [arXiv:2103.10142].

[401] C. Mahesh *et al.*, in "34th Conference on Neural Information Processing Systems," (2021), [arXiv:2104.06622].

[402] S. Amrouche *et al.* (2021), [arXiv:2105.01160].

[403] P. Goncharov *et al.*, in "24th International Scientific Conference of Young Scientists and Specialists," (2021), [arXiv:2109.08982].

[404] Xilinx, Vitis Unified Software Platform Overview (2023), URL https://www.xilinx.com/products/design-tools/vitis/vitis-platform.html.

[405] Intel, Intel High Level Synthesis Compiler (2023), URL https://www.intel.com/content/www/us/en/software/programmable/quartus-prime/hls-compiler.html.

[406] Siemens, Catapult High-Level Synthesis and Verification (2023), URL https://eda.sw.siemens.com/en-US/ic/catapult-high-level-synthesis/.

[407] J. Duarte *et al.*, JINST **13**, 07, P07027 (2018), [arXiv:1804.06913].

[408] Y. Umuroglu *et al.*, in "Proceedings of the 2017 ACM/SIGDA International Symposium on Field-Programmable Gate Arrays," 65, ACM, New York, NY, USA (2017), ISBN 9781450343541, [arXiv:1612.07119].

[409] M. Blott *et al.*, ACM Trans. Reconfigurable Technol. Syst. **11**, 3 (2018), ISSN 1936-7406, [arXiv:1809.04570].

[410] S. Summers *et al.*, JINST **15**, 05, P05026 (2020), [arXiv:2002.02534].

[411] T. M. Hong *et al.*, JINST **16**, 08, P08016 (2021), [arXiv:2104.03408].

[412] E. E. Khoda *et al.*, Mach. Learn.: Sci. Technol. **4**, 2, 025004 (2023), [arXiv:2207.00559].

[413] P. Odagiu *et al.*, Mach. Learn.: Sci. Technol. **5**, 035017 (2024), [arXiv:2402.01876].

[414] CMS Collaboration, CMS Detector Performance Summary CMS-DP-2025-032 (2025), URL https://cds.cern.ch/record/2936315.

[415] CMS Collaboration, CMS Technical Design Report CERN-LHCC-2020-004. CMS-TDR-021 (2020), URL https://cds.cern.ch/record/2714892.

[416] G. Di Guglielmo *et al.* (2021), [arXiv:2105.01683].

[417] A. Elabd *et al.*, Front. Big Data **5** (2022), [arXiv:2112.02048].

[418] S.-Y. Huang *et al.*, in "33rd International Conference on Field-Programmable Logic and Applications," (2023), [arXiv:2306.11330].

[419] E. Govorkova *et al.*, Nature Mach. Intell. **4**, 154 (2022), [arXiv:2108.03986].

[420] CMS Collaboration, CMS Detector Performance Summary CMS-DP-2024-059 (2024), URL https://cds.cern.ch/record/2904695.

[421] CMS Collaboration, CMS Detector Performance Summary CMS-DP-2024-121 (2024), URL https://cds.cern.ch/record/2917884.

[422] J. Ngadiuba *et al.*, Mach. Learn.: Sci. Tech. **2**, 1, 015001 (2020), [arXiv:2003.06308].

[423] J. Krupa *et al.* (2020), [arXiv:2007.10359].

[424] L. R. M. Mohan *et al.* (2020), [arXiv:2008.09210].

[425] S. Carrazza, J. M. Cruz-Martinez and M. Rossi (2020), [arXiv:2009.06635].

[426] D. S. Rankin *et al.*, 2020 IEEE/ACM International Workshop on Heterogeneous High-performance Reconfigurable Computing (H2RC) 38 (2020), [arXiv:2010.08556].

[427] M. Rossi, S. Carrazza and J. M. Cruz-Martinez (2020), [arXiv:2012.08221].

[428] T. Aarrestad *et al.* (2021), [arXiv:2101.05108].

[429] B. Hawks *et al.* (2021), [arXiv:2102.11289].

[430] T. Teixeira, L. Andrade and J. M. de Seixas (2021), [arXiv:2103.12467].

[431] M. Migliorini *et al.* (2021), [arXiv:2105.04428].

[432] M. Nagel *et al.*, in "2019 IEEE/CVF International Conference on Computer Vision, Seoul, South Korea, October 27, 2019," 1325 (2019), [arXiv:1906.04721].

Int. J. Mod. Phys. A 2026.41. Downloaded from www.worldscientific.com
by UNIVERSITY OF CALIFORNIA @ BERKELEY on 09/16/26. Re-use and distribution is strictly not permitted, except for Open Access articles.

[433] S. Han, H. Mao and W. J. Dally, in Y. Bengio and Y. LeCun, editors, "4th International Conference on Learning Representations, San Juan, Puerto Rico, May 2, 2016," (2016), [arXiv:1510.00149].

[434] E. Meller *et al.*, in K. Chaudhuri and R. Salakhutdinov, editors, "Proceedings of the 36th International Conference on Machine Learning," volume 97, 4486, PMLR (2019), [arXiv:1902.01917], URL `http://proceedings.mlr.press/v97/meller19a.html`.

[435] R. Zhao *et al.*, in K. Chaudhuri and R. Salakhutdinov, editors, "Proceedings of the 36th International Conference on Machine Learning," volume 97, 7543, PMLR (2019), [arXiv:1901.09504], URL `http://proceedings.mlr.press/v97/zhao19c.html`.

[436] R. Banner *et al.*, in H. Wallach *et al.*, editors, "Advances in Neural Information Processing Systems," volume 32, 7950, Curran Associates, Inc. (2019), [arXiv:1810.05723], URL `https://proceedings.neurips.cc/paper/2019/file/c0a62e133894cdce435bcb4a5df1db2d-Paper.pdf`.

[437] B. Moons *et al.*, in M. B. Matthews, editor, "2017 51st Asilomar Conference on Signals, Systems, and Computers, Pacific Grove, CA, USA, October 29, 2017," 1921 (2017), [arXiv:1711.00215].

[438] M. Courbariaux, Y. Bengio and J.-P. David, in C. Cortes *et al.*, editors, "Advances in Neural Information Processing Systems," volume 28, 3123, Curran Associates, Inc. (2015), URL `https://proceedings.neurips.cc/paper/2015/file/3e15cc11f979ed25912dff5b0669f2cd-Paper.pdf`.

[439] D. Zhang *et al.*, in V. Ferrari *et al.*, editors, "Proceedings of the European Conference on Computer Vision, Munich, Germany, September 8, 2018," 373 (2018), [arXiv:1807.10029].

[440] F. Li and B. Liu, "Ternary weight networks," (2016), [arXiv:1605.04711].

[441] S. Zhou *et al.*, "DoReFa-Net: Training low bitwidth convolutional neural networks with low bitwidth gradients," (2016).

[442] I. Hubara *et al.*, J. Mach. Learn. Res. **18**, 187, 1 (2018), URL `http://jmlr.org/papers/v18/16-456.html`.

[443] M. Rastegari *et al.*, in "14th European Conference on Computer Vision (ECCV)," 525, Springer International Publishing, Cham, Switzerland (2016), [arXiv:1603.05279].

[444] P. Micikevicius *et al.*, in "6th International Conference on Learning Representations, Vancouver, BC, Canada, April 30, 2018," (2018), https://openreview.net/forum?id=r1gs9JgRZ, URL `https://openreview.net/forum?id=r1gs9JgRZ`.

[445] B. Zhuang *et al.*, in "2018 IEEE/CVF Conference on Computer Vision and Pattern Recognition, Salt Lake City, UT, USA, June 18, 2018," 7920 (2018), [arXiv:1711.00205].

[446] N. Wang *et al.*, in S. Bengio *et al.*, editors, "Advances in Neural Information Processing Systems," volume 31, 7675, Curran Associates, Inc. (2018), [arXiv:1812.08011], URL `https://proceedings.neurips.cc/paper/2018/file/335d3d1cd7ef05ec77714a215134914c-Paper.pdf`.

[447] Z. Dong *et al.*, in "2019 IEEE/CVF International Conference on Computer Vision, Seoul, South Korea, October 27, 2019," 293 (2019).

[448] Z. Dong *et al.*, in H. Larochelle *et al.*, editors, "Advances in Neural Information Processing Systems," volume 33, 18518, Curran Associates, Inc. (2020), [arXiv:1911.03852], URL `https://proceedings.neurips.cc/paper/2020/file/d77c703536718b95308130ff2e5cf9ee-Paper.pdf`.

[449] Y. LeCun, J. S. Denker and S. A. Solla, in D. S. Touretzky, editor, "Advances in Neural Information Processing Systems," volume 2, 598, Morgan-Kaufmann (1990), URL `http://papers.nips.cc/paper/250-optimal-brain-damage`.

[450] J. Frankle and M. Carbin, in "7th International Conference on Learning Representations," (2019), [arXiv:1803.03635], URL `https://openreview.net/forum?id=rJl-b3RcF7`.

[451] A. Renda, J. Frankle and M. Carbin, in "8th International Conference on Learning Representations, Addis Ababa, Ethiopia, April 26, 2020," (2020), https://openreview.net/forum?id=S1gSj0NKvB, [arXiv:2003.02389], URL `https://openreview.net/forum?id=S1gSj0NKvB`.

[452] H. Zhou *et al.*, in H. Wallach *et al.*, editors, "Advances in Neural Information Processing Systems," volume 32, 3597, Curran Associates, Inc. (2019), [arXiv:1905.01067], URL `https://proceedings.neurips.cc/paper/2019/file/1113d7a76ffceca1bb350bfe145467c6-Paper`.

[453] D. Blalock *et al.*, in I. Dhillon, D. Papailiopoulos and V. Sze, editors, "Proceedings of Machine Learning and Systems," volume 2, 129 (2020), [arXiv:2003.03033], URL `https://proceedings.mlsys.org/paper/2020/file/d2ddea18f00665ce8623e36bd4e3c7c5-Paper.pdf`.

[454] H. F. Tsoi *et al.*, EPJ Web Conf. **295**, 09036 (2024), [arXiv:2305.04099].

[455] A. Bal *et al.*, Mach. Learn. Sci. Tech. **5**, 2, 025033 (2024), [arXiv:2311.12551].

[456] C. N. Coelho *et al.*, Nat. Mach. Intell. (2021), [arXiv:2006.10159].

[457] C. Sun *et al.* (2024), [arXiv:2405.00645].

[458] A. Pappalardo, Xilinx/brevitas (2021), URL `https://github.com/Xilinx/brevitas`.

[459] A. Pappalardo *et al.*, in "4th Workshop on Accelerated Machine Learning at the High-performance Embedded Architecture and Compilation 2022 Conference," (2022), [arXiv:2206.07527], URL `https://accml.dcs.gla.ac.uk/papers/2022/4thAccML_paper_1(12).pdf`.

[460] S. Han *et al.*, in C. Cortes *et al.*, editors, "Advances in Neural Information Processing Systems 28," volume 28, 1135, Curran Associates, Inc. (2015), [arXiv:1506.02626], URL `https://papers.nips.cc/paper/2015/hash/ae0eb3eed39d2bcef4622b2499a05fe6-Abstract.html`.

[461] V. Kuznetsov, L. Giommi and D. Bonacorsi (2020), [arXiv:2007.14781].

[462] O. Sunneborn Gudnadottir *et al.*, EPJ Web Conf. **251**, 02054 (2021), [arXiv:2109.00264].

[463] J. Duarte *et al.*, Comput. Softw. Big Sci. **3**, 13 (2019), [arXiv:1904.08986].

[464] M. Wang *et al.*, Front. Big Data **3**, 604083 (2021), [arXiv:2009.04509].

[465] A. Hayrapetyan *et al.* (CMS), Comput. Softw. Big Sci. **8**, 1, 17 (2024), [arXiv:2402.15366].

[466] H. Zhao *et al.*, JINST **20**, 06, P06002 (2025), [arXiv:2501.05520].

42. Monte Carlo Techniques

Revised September 2025 by G. Cowan (RHUL).

Monte Carlo techniques are often the only practical way to evaluate difficult integrals or to sample random variables governed by complicated probability density functions. Here we describe an assortment of methods for sampling some commonly occurring probability density functions.

42.1 Sampling the uniform distribution

Most Monte Carlo sampling or integration techniques assume a "random number generator," which generates uniform statistically independent values on the half open interval $[0, 1)$; for reviews see, *e.g.*, Refs. [1, 2].

Uniform random number generators are available in software libraries such as CLHEP [3], and ROOT [4], as well as from the standard C++ library [5]. The ROOT generators are available in Python using the PyROOT interface [6]. All of the algorithms produce a periodic sequence of numbers, and to obtain effectively random values, one must not use more than a small subset of a single period. The performance of the generators can be investigated with tests such as DIEHARD [7] or TestU01 [8]. Many commonly available congruential generators fail these tests and often have sequences (typically with periods less than 2^{32}), which can be easily exhausted on modern computers.

The generators in ROOT can be accessed through the interface class `TRandom`. These include the widely used `TRandom3` generator, which implements the Mersenne twister algorithm of Matsumoto and Nishimura [9]. This is very fast and has an extremely long period of $2^{19937} - 1$, although it fails some of the more stringent TestU01 tests. Two somewhat slower generators available in ROOT that do not fail any TestU01 tests are the `Ranlux++` generator [10] based on the method of Lüscher [11], and the `MIXMAX` generator of Savvidy [12]. A recent review of high-quality random number generators can be found in Ref. [13].

42.2 Inverse transform method

If the desired probability density function is $f(x)$ on the range $-\infty < x < \infty$, its cumulative distribution function (expressing the probability that $x \leq a$) is given by Eq. (39.6). If a is chosen with probability density $f(a)$, then the integrated probability up to point a, $F(a)$, is itself a random variable which will occur with uniform probability density on $[0, 1]$. Suppose u is generated according to a uniformly distributed in $(0, 1)$. If x can take on any value, and ignoring the endpoints, we can then find a unique x chosen from the p.d.f. $f(x)$ for a given u if we set

$$u = F(x) \ , \tag{42.1}$$

provided we can find an inverse of F, defined by

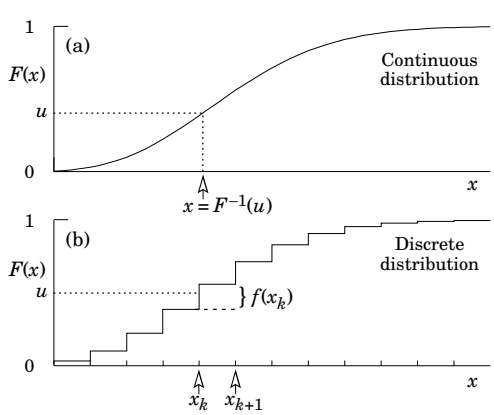

Figure 42.1: Use of a random number u chosen from a uniform distribution (0,1) to find a random number x from a distribution with cumulative distribution function $F(x)$.

$$x = F^{-1}(u) \ . \tag{42.2}$$

This method is shown in Fig. 42.1a. It is most convenient when one can calculate by hand the inverse function of the indefinite integral of f. This is the case for some common functions $f(x)$ such as $\exp(x)$, $(1 - x)^n$, and $1/(1 + x^2)$ (Cauchy or Breit-Wigner), although it does not necessarily produce the fastest generator. Standard libraries contain software to implement this method numerically, working from functions or histograms in one or more dimensions, *e.g.*, the UNU.RAN package [14], available in ROOT.

For a discrete distribution, $F(x)$ will have a discontinuous jump of size $f(x_k)$ at each allowed $x_k, k = 1, 2, \cdots$. Choose u from a uniform distribution on (0,1) as before. Find x_k such that

$$F(x_{k-1}) < u \leq F(x_k) \equiv \text{Prob}\ (x \leq x_k) = \sum_{i=1}^{k} f(x_i) \ ; \tag{42.3}$$

then x_k is the value we seek (note: $F(x_0) \equiv 0$). This algorithm is illustrated in Fig. 42.1b.

42.3 Acceptance-rejection method (Von Neumann)

Very commonly an analytic form for $F(x)$ is unknown or too complex to work with, so that obtaining an inverse as in Eq. (42.2) is impractical. We suppose that for any given value of x, the probability density function $f(x)$ can be computed, and further that enough is known about $f(x)$ that we can enclose it entirely inside a shape which is C times an easily generated distribution $h(x)$, as illustrated in Fig. 42.2. That is, $Ch(x) \geq f(x)$ must hold for all x.

Frequently $h(x)$ is uniform or is a normalized sum of uniform distributions. Note that both $f(x)$ and $h(x)$ must be normalized to unit area, and therefore, the proportionality constant $C > 1$. To generate $f(x)$, first generate a candidate x according to $h(x)$. Calculate $f(x)$ and the height of the envelope $C\,h(x)$; generate u and test if $uC\,h(x) \leq f(x)$. If so, accept x; if not reject x and try again. If we regard x and $uC\,h(x)$ as the abscissa and ordinate of a point in a two-dimensional plot, these points will populate the entire area $C\,h(x)$ in a smooth manner; then we accept those which fall under $f(x)$. The efficiency is the ratio of areas, which must equal $1/C$; therefore we must keep C as close as possible to 1.0. Therefore, we try to choose $C\,h(x)$ to be as close to $f(x)$ as convenience dictates, as in the lower part of Fig. 42.2.

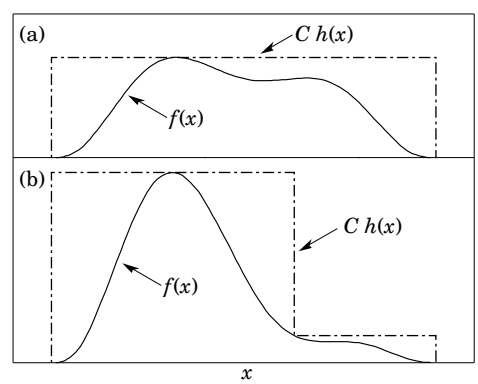

Figure 42.2: Illustration of the acceptance-rejection method. Random points are chosen inside the upper bounding figure, and rejected if the ordinate exceeds $f(x)$. The lower figure illustrates a method to increase the efficiency (see text).

42.4 Algorithms

Algorithms for generating random numbers belonging to many different distributions are given for example by Press [15], Ahrens and Dieter [16], Rubinstein [17], Devroye [18], Walck [19] and Gentle [20]. For many distributions, alternative algorithms exist, varying in complexity, speed, and accuracy. For time-critical applications, these algorithms may be coded in-line to remove the significant overhead often encountered in making function calls.

Phys. A 2026.41. Downloaded from www.worldscientific.com
by UNIVERSITY OF CA LEY on 09/16/26. Re-use and distribution is strictly not permitted, except for Open Access articles.

Int. J. Mod. Phys. A 2026.41. Downloaded from www.worldscientific.com
by UNIVERSITY OF CALIFORNIA @ BERKELEY on 09/16/26. Re-use and distribution is strictly not permitted, except for Open Access articles.

In the examples given below, we use the notation for the variables and parameters given in Table 39.1. Variables named "u" are assumed to be independent and uniform on [0,1). Denominators must be verified to be non-zero where relevant.

42.4.1 *Exponential decay*

This is a common application of the inverse transform method, and uses the fact that if u is uniformly distributed in $[0,1]$, then $(1-u)$ is as well. Consider an exponential p.d.f. $f(t) = (1/\tau)\exp(-t/\tau)$ that is truncated so as to lie between two values, a and b, and renormalized to unit area. To generate decay times t according to this p.d.f., first let $\alpha = \exp(-a/\tau)$ and $\beta = \exp(-b/\tau)$; then generate u and let

$$t = -\tau \ln(\beta + u(\alpha - \beta)). \tag{42.4}$$

For $(a,b) = (0,\infty)$, we have simply $t = -\tau \ln u$. (See also Sec. 42.4.6.)

42.4.2 *Isotropic direction in 3D*

Isotropy means the density is proportional to solid angle, the differential element of which is $d\Omega = d(\cos\theta)d\phi$. Hence $\cos\theta$ is uniform $(2u_1 - 1)$ and ϕ is uniform $(2\pi u_2)$. For alternative generation of $\sin\phi$ and $\cos\phi$, see the next subsection.

42.4.3 *Sine and cosine of random angle in 2D*

Generate u_1 and u_2. Then $v_1 = 2u_1 - 1$ is uniform on (−1,1), and $v_2 = u_2$ is uniform on (0,1). Calculate $r^2 = v_1^2 + v_2^2$. If $r^2 > 1$, start over. Otherwise, the sine (S) and cosine (C) of a random angle (*i.e.*, uniformly distributed between zero and 2π) are given by

$$S = 2v_1v_2/r^2 \quad \text{and} \quad C = (v_1^2 - v_2^2)/r^2 \ . \tag{42.5}$$

42.4.4 *Gaussian distribution*

If u_1 and u_2 are uniform on (0,1), then

$$z_1 = \sin(2\pi u_1)\sqrt{-2\ln u_2} \quad \text{and} \quad z_2 = \cos(2\pi u_1)\sqrt{-2\ln u_2} \tag{42.6}$$

are independent and Gaussian distributed with mean 0 and $\sigma = 1$.

There are many variants of this basic algorithm, which may be faster. For example, construct $v_1 = 2u_1 - 1$ and $v_2 = 2u_2 - 1$, which are uniform on (−1,1). Calculate $r^2 = v_1^2 + v_2^2$, and if $r^2 > 1$ start over. If $r^2 < 1$, it is uniform on (0,1). Then

$$z_1 = v_1\sqrt{\frac{-2\ln r^2}{r^2}} \quad \text{and} \quad z_2 = v_2\sqrt{\frac{-2\ln r^2}{r^2}} \tag{42.7}$$

are independent numbers chosen from a normal distribution with mean 0 and variance 1. $z_i' = \mu + \sigma z_i$ distributes with mean μ and variance σ^2.

For a multivariate Gaussian with an $n \times n$ covariance matrix V, one can start by generating n independent Gaussian variables, $\{\eta_j\}$, with mean 0 and variance 1 as above. Then the new set $\{x_i\}$ is obtained as $x_i = \mu_i + \sum_j L_{ij}\eta_j$, where μ_i is the mean of x_i, and L_{ij} are the components of L, the unique lower triangular matrix that fulfils $V = LL^T$. The matrix L can be easily computed by the following recursive relation (Cholesky's method):

$$L_{jj} = \left(V_{jj} - \sum_{k=1}^{j-1} L_{jk}^2\right)^{1/2} , \tag{42.8a}$$

$$L_{ij} = \frac{V_{ij} - \sum_{k=1}^{j-1} L_{ik}L_{jk}}{L_{jj}} \ , \ j = 1, ..., n \, ; \ i = j+1, ..., n, \tag{42.8b}$$

where $V_{ij} = \rho_{ij}\sigma_i\sigma_j$ are the components of V. For $n = 2$ one has

$$L = \begin{pmatrix} \sigma_1 & 0 \\ \rho\sigma_2 & \sqrt{1-\rho^2}\,\sigma_2 \end{pmatrix} , \tag{42.9}$$

and therefore the correlated Gaussian variables are generated as $x_1 = \mu_1 + \sigma_1\eta_1$, $x_2 = \mu_2 + \rho\sigma_2\eta_1 + \sqrt{1-\rho^2}\,\sigma_2\eta_2$.

42.4.5 $\chi^2(n)$ distribution

To generate a variable following the χ^2 distribution for n degrees of freedom, use the Gamma distribution with $k = n/2$ and $\lambda = 1/2$ using the method of Sec. 42.4.6.

42.4.6 *Gamma distribution*

All of the following algorithms are given for $\lambda = 1$. For $\lambda \neq 1$, divide the resulting random number x by λ.

- If $k = 1$ (the *exponential* distribution), accept $x = -\ln u$. (See also Sec. 42.4.1.)

- If $0 < k < 1$, initialize with $v_1 = (e+k)/e$ (with $e = 2.71828...$ being the natural log base). Generate u_1, u_2. Define $v_2 = v_1u_1$.

  Case 1: $v_2 \leq 1$. Define $x = v_2^{1/k}$. If $u_2 \leq e^{-x}$, accept x and stop, else restart by generating new u_1, u_2.

  Case 2: $v_2 > 1$. Define $x = -\ln([v_1 - v_2]/k)$. If $u_2 \leq x^{k-1}$, accept x and stop, else restart by generating new u_1, u_2. Note that, for $k < 1$, the probability density has a pole at $x = 0$, so that return values of zero due to underflow must be accepted or otherwise dealt with.

- Otherwise, if $k > 1$, initialize with $c = 3k - 0.75$. Generate u_1 and compute $v_1 = u_1(1-u_1)$ and $v_2 = (u_1 - 0.5)\sqrt{c/v_1}$. If $x = k + v_2 - 1 \leq 0$, go back and generate new u_1; otherwise generate u_2 and compute $v_3 = 64v_1^3u_2^2$. If $v_3 \leq 1 - 2v_2^2/x$ **or** if $\ln v_3 \leq 2\{[k-1]\ln[x/(k-1)] - v_2\}$, accept x and stop; otherwise go back and generate new u_1.

42.4.7 *Binomial distribution*

Begin with $k = 0$ and generate u uniform in $[0,1)$. Compute $P_k = (1-p)^n$ and store P_k into B. If $u \leq B$ accept $r_k = k$ and stop. Otherwise, increment k by one; compute the next P_k as $P_k \cdot (p/(1-p)) \cdot (n-k)/(k+1)$; add this to B. Again, if $u \leq B$, accept $r_k = k$ and stop, otherwise iterate until a value is accepted. If $p > 1/2$, it will be more efficient to generate r from $f(r; n, q)$, *i.e.*, with p and q interchanged, and then set $r_k = n - r$.

42.4.8 *Poisson distribution*

Iterate until a successful choice is made: Begin with $k = 1$ and set $A = 1$ to start. Generate u. Replace A with uA; if now $A < \exp(-\mu)$, where μ is the Poisson parameter, accept $n_k = k - 1$ and stop. Otherwise increment k by 1, generate a new u and repeat, always starting with the value of A left from the previous try.

Note that the Poisson generator used in ROOT's `TRandom` classes before version 5.12 (including the derived classes `TRandom1, TRandom2, TRandom3`) uses a Gaussian approximation when μ exceeds a given threshold. This may be satisfactory (and much faster) for some applications. To do this, generate z from a Gaussian with zero mean and unit standard deviation; then use $x = \max(0, [\mu + z\sqrt{\mu} + 0.5])$ where [ ] signifies the greatest integer $\leq$ the expression. The routines from Numerical Recipes [15] and CLHEP's routine `RandPoisson` do not make this approximation.

42.4.9 *Student's t distribution*

Generate u_1 and u_2 uniform in $(0,1)$; then $t = \sin(2\pi u_1)[n(u_2^{-2/n} - 1)]^{1/2}$ follows the Student's t distribution for $n > 0$ degrees of freedom (n not necessarily an integer).

Alternatively, generate x from a Gaussian with mean 0 and $\sigma^2 = 1$ according to the method of 42.4.4. Next generate y, an independent gamma random variate, according to 42.4.6 with $\lambda = 1/2$ and $k = n/2$. Then $z = x/\sqrt{y/n}$ is distributed as a t with n degrees of freedom.

For the special case $n = 1$, the Breit-Wigner distribution, generate u_1 and u_2; set $v_1 = 2u_1 - 1$ and $v_2 = 2u_2 - 1$. If $v_1^2 + v_2^2 \leq 1$ accept $z = v_1/v_2$ as a Breit-Wigner distribution with unit area, center at 0.0, and FWHM 2.0. Otherwise start over. For center M_0 and FWHM Γ, use $W = z\Gamma/2 + M_0$.

Phys. A 2026.41. Downloaded from www.worldscientific.com
by UNIVERSITY OF CA LEY on 09/16/26. Re-use and distribution is strictly not permitted, except for Open Access articles.

42.4.10 *Beta distribution*

The choice of an appropriate algorithm for generation of beta distributed random numbers depends on the values of the parameters α and β. For, *e.g.*, $\alpha = 1$, one can use the transformation method to find $x = 1 - u^{1/\beta}$, and similarly if $\beta = 1$ one has $x = u^{1/\alpha}$. For more general cases see, *e.g.*, Refs. [19, 20] and references therein.

42.5 Importance sampling and weighted Monte Carlo

Often the goal of a Monte Carlo calculation is to determine an expectation value of a function $h(x)$, where x is a (single or vector) random variable that follows a pdf $f(x)$,

$$E_f[h(x)] = \int h(x) f(x)\, dx \equiv \mu \; . \tag{42.10}$$

A Monte-Carlo estimator $\hat{\mu}_{\rm MC}$ for μ is the average of N values of $h(x)$ where x is sampled (generated) from $f(x)$, i.e., $\hat{\mu}_{\rm MC} = \frac{1}{N}\sum_{i=1}^{N} h(x_i)$. This has a variance

$$V[\hat{\mu}_{\rm MC}] = \frac{1}{N} V_f[h(x)] = \frac{1}{N}\left(E_f[h^2(x)] - \mu^2\right) \; . \tag{42.11}$$

By using the method of *importance sampling*, one can achieve a reduction in this variance and thus a more accurate determination of the expectation value for a given number of random values generated. The key idea is to rewrite the expectation value in Eq. (42.10) as

$$\mu = \int h(x) f(x)\, dx = \int \frac{h(x) f(x)}{g(x)}\, g(x)\, dx = E_g\left[\frac{h(x) f(x)}{g(x)}\right] \; , \tag{42.12}$$

where $g(x)$ is any other pdf of x with the same support as $f(x)$ (i.e., nonzero for the same region of x). Thus the desired quantity μ is the expectation value with respect to g of $h(x)f(x)/g(x)$. It can be estimated by generating N values of x sampled from g and computing

$$\hat{\mu}_{\rm IS} = \frac{1}{N}\sum_{i=1}^{N} \frac{h(x_i) f(x_i)}{g(x_i)} \; . \tag{42.13}$$

The variance of $\hat{\mu}_{\rm IS}$ is given by

$$V[\hat{\mu}_{\rm IS}] = \frac{1}{N} V_g\left[\frac{h(x) f(x)}{g(x)}\right] = \frac{1}{N}\left(E_g\left[\frac{h^2(x) f^2(x)}{g^2(x)}\right] - \mu^2\right) \; , \tag{42.14}$$

By choosing $g(x)$ such that $h(x)f(x)/g(x)$ is as constant as possible, the variance of $\hat{\mu}_{\rm IS}$ can be substantially reduced. One can show (see, e.g., Refs. [21,22]) that the variance is minimized when $g(x) \propto |h(x)| f(x)$.

An alternative importance sampling estimator can be constructed by replacing the number of generated values N in Eq. (42.13) by the sum $\sum_{i=1}^{N} f(x_i)/g(x_i)$. This can given an even smaller variance at the price of a small bias. It can be of further advantage in problems where the pdf $f(x)$ is known only up to a normalization constant, which then cancels (see Refs. [21, 22]).

A closely related application of importance sampling is the use of weighted Monte Carlo to compute the probability $P_f(x \in A)$ for x to be in a specified region A:

$$P_f(x \in A) = \int_A f(x)\, dx \; . \tag{42.15}$$

It may be, however, that one does not have an MC model capable of generating $x \sim f(x)$, but rather one can generate x according to a different density $g(x)$. The probability $P_f(x \in A)$ can be written

$$\begin{aligned} P_f(x \in A) &= \frac{\int_A \frac{f(x)}{g(x)}\, g(x)\, dx}{\int_A g(x)\, dx} \int_A g(x)\, dx \\ &= E_g[w(x) | x \in A]\, P_g(x \in A) \; , \end{aligned} \tag{42.16}$$

where $w(x) = f(x)/g(x)$ is the *weight function* and $P_g(x \in A) = \int_A g(x)\, dx$ is the probability to find $x \in A$ assuming $x \sim g(x)$. That is, $P_f(x \in A)$ is the conditional expectation value of $w(x)$ with respect to $g(x)$ given $x \in A$ multiplied by the probability to find $x \in A$ under assumption of $g(x)$.

Suppose N values of x are generated according to $g(x)$ and m of them are found in the region A. Then the probability to be in A for $x \sim g(x)$ can be estimated by m/N, and the expectation value above can be obtained from the average of the weights in A. Therefore the desired probability $P_f(x \in A)$ can be estimated using

$$\hat{P}_f(x \in A) = \frac{1}{m}\sum_{i=1}^{m} w_i \times \frac{m}{N} = \frac{1}{N}\sum_{i=1}^{m} w_i \; , \tag{42.17}$$

where $w_i = w(x_i)$ and the sum includes only the m values of x found in A. That is, when generating the x values according to $g(x)$ instead of $f(x)$, the number of events m found in A is replaced by the corresponding sum of weights. The variance of $\hat{P}_f(x \in A)$ can be found from

$$\widehat{V}[\hat{P}_f(x \in A)] = \frac{1}{N^2}\sum_{i=1}^{m} w_i^2 \; . \tag{42.18}$$

By choosing $g(x)$ so that a larger fraction of x values are sampled in the "important" region A, one can reduce the variance of the estimated probability for a given total number of generated values.

42.6 Markov Chain Monte Carlo

In applications involving generation of random numbers following a multivariate distribution with a high number of dimensions, the transformation method may not be possible and the acceptance-rejection technique may have too low of an efficiency to be practical. If it is not required to have independent random values, but only that they follow a certain distribution, then Markov Chain Monte Carlo (MCMC) methods can be used. In depth treatments of MCMC can be found, *e.g.*, in the texts by Robert and Casella [21], Liu [22], and the review by Neal [23]. HEP-oriented software for MCMC is available from the Bayesian Analysis Toolkit (BAT) [24, 25].

MCMC is particularly useful in connection with Bayesian statistics, where a p.d.f. $p(\boldsymbol{\theta})$ for an n-dimensional vector of parameters $\boldsymbol{\theta} = (\theta_1, \ldots, \theta_n)$ is obtained, and one needs the marginal distribution of a subset of the components. Here one samples $\boldsymbol{\theta}$ from $p(\boldsymbol{\theta})$ and simply records the marginal distribution for the components of interest.

A simple and broadly applicable MCMC method is the Metropolis-Hastings algorithm, which allows one to generate multidimensional points $\boldsymbol{\theta}$ distributed according to a target p.d.f. that is proportional to a given function $p(\boldsymbol{\theta})$. It is not necessary to have $p(\boldsymbol{\theta})$ normalized to unit area, which is useful in Bayesian statistics, as posterior probability densities are often determined only up to an unknown normalization constant.

To generate points that follow $p(\boldsymbol{\theta})$, one first needs a proposal p.d.f. $q(\boldsymbol{\theta}; \boldsymbol{\theta}_0)$, which can be (almost) any p.d.f. from which independent random values $\boldsymbol{\theta}$ can be generated, and which contains as a parameter another point in the same space $\boldsymbol{\theta}_0$. For example, a multivariate Gaussian centered about $\boldsymbol{\theta}_0$ can be used. Beginning at an arbitrary starting point $\boldsymbol{\theta}_0$, the Hastings algorithm iterates the following steps:

1. Generate a value $\boldsymbol{\theta}$ using the proposal density $q(\boldsymbol{\theta}; \boldsymbol{\theta}_0)$;

Int. J. Mod. Phys. A 2026.41. Downloaded from www.worldscientific.com
by UNIVERSITY OF CALIFORNIA @ BERKELEY on 09/16/26. Re-use and distribution is strictly not permitted, except for Open Access articles.

2. Form the Hastings test ratio, $\alpha = \min\left[1, \frac{p(\boldsymbol{\theta})q(\boldsymbol{\theta}_0;\boldsymbol{\theta})}{p(\boldsymbol{\theta}_0)q(\boldsymbol{\theta};\boldsymbol{\theta}_0)}\right]$;
3. Generate a value u uniformly distributed in $[0, 1]$;
4. If $u \leq \alpha$, take $\boldsymbol{\theta}_1 = \boldsymbol{\theta}$. Otherwise, repeat the old point, *i.e.*, $\boldsymbol{\theta}_1 = \boldsymbol{\theta}_0$.
5. Set $\boldsymbol{\theta}_0 = \boldsymbol{\theta}_1$ and return to step 1.

If one takes the proposal density to be symmetric in $\boldsymbol{\theta}$ and $\boldsymbol{\theta}_0$, then this is the *Metropolis*-Hastings algorithm, and the test ratio becomes $\alpha = \min[1, p(\boldsymbol{\theta})/p(\boldsymbol{\theta}_0)]$. That is, if the proposed $\boldsymbol{\theta}$ is at a value of probability higher than $\boldsymbol{\theta}_0$, the step is taken. If the proposed step is rejected, the old point is repeated.

Methods for assessing and optimizing the performance of the algorithm are discussed in, *e.g.*, Refs. [21–23]. One can, for example, examine the autocorrelation as a function of the lag k, *i.e.*, the correlation of a sampled point with that k steps removed. This should decrease as quickly as possible for increasing k.

Generally one chooses the proposal density so as to optimize some quality measure such as the autocorrelation. For certain problems it has been shown that one achieves optimal performance when the acceptance fraction, that is, the fraction of points with $u \leq \alpha$, is around 40%. This can be adjusted by varying the width of the proposal density. For example, one can use for the proposal p.d.f. a multivariate Gaussian with the same covariance matrix as that of the target p.d.f., but scaled by a constant.

References

[1] F. James and L. Moneta, Computing and Software for Big Science **4**, 1, 2 (2020).

[2] P. L'Ecuyer, *Proc. 1997 Winter Simulation Conference*, IEEE Press, Dec. 1997, 127–134.

[3] L. Lonnblad, Comput. Phys. Commun. **84**, 307 (1994).

[4] R. Brun and F. Rademakers, Nucl. Instrum. Meth. **A389**, 81 (1997); See also `root.cern.ch`.

[5] International Organization for Standardization/International Electrotechnical Commission, *Information technology – Programming languages – C++*, ISO/IEC 14882:2020, International Organization for Standardization, Geneva, Switzerland, sixth edition (2020).

[6] M. Galli, E. Tejedor and S. Wunsch, EPJ Web Conf. **245**, 06004 (2020).

[7] Much of DIEHARD is described in: G. Marsaglia, *A Current View of Random Number Generators*, keynote address, *Computer Science and Statistics: 16th Symposium on the Interface*, Elsevier (1985).

[8] P. L'Ecuyer and R. Simard, *ACM Transactions on Mathematical Software* 33, 4, Article 1, December 2007.

[9] M. Matsumoto and T. Nishimura, *ACM Transactions on Modeling and Computer Simulation*, Vol. 8, No. 1, January 1998, 3–30.

[10] Hahnfeld, Jonas and Moneta, Lorenzo, EPJ Web Conf. **251**, 03008 (2021).

[11] M. Luscher, Comput. Phys. Commun. **79**, 100 (1994), [hep-lat/9309020].

[12] K. G. Savvidy, Computer Physics Communications **196**, 161 (2015), ISSN 0010-4655.

[13] F. James and L. Moneta, Comput. Softw. Big Sci. **4**, 2. 12 p (2019), 4 figures, [arXiv:1903.01247], URL `http://cds.cern.ch/record/2678858`.

[14] UNU.RAN is described at `statmath.wu.ac.at/software/unuran`; See also W. Hörmann, J. Leydold, and G. Derflinger, *Automatic Nonuniform Random Variate Generation*, (Springer, New York, 2004).

[15] W.H. Press *et al.*, *Numerical Recipes*, 3rd edition, (Cambridge University Press, New York, 2007).

[16] J.H. Ahrens and U. Dieter, Computing **12**, 223 (1974).

[17] R.Y. Rubinstein, *Simulation and the Monte Carlo Method*, (John Wiley and Sons, Inc., New York, 1981).

[18] L. Devroye, *Non-Uniform Random Variate Generation*, (Springer-Verlag, New York, 1986); Available online at `luc.devroye.org/rnbookindex.html`.

[19] C. Walck, *Handbook on Statistical Distributions for Experimentalists*, University of Stockholm Report SUF-PFY/96-01, available from `www.fysik.su.se/~walck`.

[20] J.E. Gentle, *Random Number Generation and Monte Carlo Methods*, 2nd ed., (Springer, New York, 2003).

[21] C.P. Robert and G. Casella, *Monte Carlo Statistical Methods*, 2nd ed., (Springer, New York, 2004).

[22] J.S. Liu, *Monte Carlo Strategies in Scientific Computing*, (Springer, New York, 2001).

[23] R.M. Neal, *Probabilistic Inference Using Markov Chain Monte Carlo Methods*, Technical Report CRG-TR-93-1, Dept. of Computer Science, University of Toronto, available from `www.cs.toronto.edu/~radford/res-mcmc.html` .

[24] A. Caldwell, D. Kollar, K. Kroeninger, Comput. Phys. Commun. 180 (2009) pages 2197-2209.

[25] Schulz, O., Beaujean, F., Caldwell, A. et al., SN Computer Science 2, 210 (2021).

43. Monte Carlo Event Generators

Revised Oct 2025 by P. Nason (INFN, Milano-Bicocca; Milano-Bicocca U.) and P. Skands (Monash U.).

General-purpose Monte Carlo (GPMC) generators like HERWIG [1,2], PYTHIA [3,4], and SHERPA [5], provide detailed simulations of high-energy collisions. They play an essential role in QCD modeling (in particular for aspects beyond fixed-order perturbative QCD) and in data analysis and the planning of new experiments, where they are used together with detector simulation to estimate signals and backgrounds in high-energy processes. They are built from several components, that describe the physics starting from very short distance scales, up to the typical scale of hadron formation and decay. Since QCD is weakly interacting at short distances (below a femtometer), the components of the GPMC dealing with short-distance physics are based upon perturbation theory. At larger distances, all soft hadronic phenomena, like hadronization and the formation of the underlying event in hadron collisions, cannot be computed from first principles at present, and one must rely upon QCD-inspired models.

The purpose of this review is to illustrate the main components of these generators. It is divided into four sections. The first one deals with short-distance, perturbative phenomena. The basic concepts leading to the simulations of the dominant QCD processes are illustrated here. In the second section, the nonperturbative transition from partons to hadrons ("hadronization") is treated. The two most popular hadronization models, the string and cluster models, are illustrated. The basics of the implementation of decay chains of unstable "primary" hadrons into stable "secondaries" is also illustrated here. In the third section, models for soft hadron physics are discussed. These include models for the underlying event and for low-$p_\perp$ ("minimum-bias") interactions. Aspects of collective effects, such as Bose-Einstein and color-reconnection effects, are also discussed here. The fourth section briefly introduces the challenges of MC uncertainty estimates and tuning.

We use natural units throughout, such that $c = 1$ and $\hbar = 1$, with energies, momenta and masses measured in GeV, and times and distances measured in GeV^{-1}.

43.1 Short-distance physics in GPMC generators

The short-distance components of a GPMC generator deal with the computation of the primary process at hand, with decays of short-lived particles, and with the generation of QCD and QED radiation. QCD radiation is computable in perturbation theory as long as the time scales involved are well below $1/\Lambda$, where Λ is a typical hadronic scale of few hundred MeV. Because of the presence of logarithmic enhancements due to both collinear and soft emissions, this description involves an indefinite number of final-state particles that are emitted at time scales below $1/\Lambda$. In e^+e^- annihilation into hadrons, for example, the time scale of the primary process is of the order of the inverse of the annihilation energy Q. Collinear and soft emissions take place at all time scales between $1/Q$ and $1/\Lambda$, Technically, the computation of the dominant collinear and soft radiation is carried out by the so called shower algorithms. Historically, "Parton Shower" algorithms were first developed for resummation of collinear singularities. We will briefly describe this approach in this section. We stress, however, that many modern generators adopt approaches that focus initially upon soft singularities, leading to "Dipole Showers", discussed in Sec. 43.1.3.

Collinear singularities arise when the angle between two emitted light partons becomes small. For example, in a process in which a quark and a gluon are emitted, if the angle θ among them is very small (and is smaller than the angles among all other pairs of light partons in the process) the squared amplitude factorizes as follows

$$|M_{qg}|^2 \mathrm{d}\Phi_{qg} \approx |M_q|^2 \,\mathrm{d}\Phi_q \frac{\alpha_s}{2\pi} P_{q,qg}(z) \mathrm{d}z \frac{\mathrm{d}\phi}{2\pi} \frac{\mathrm{d}\theta^2}{\theta^2} \tag{43.1}$$

where M_{qg}, $\mathrm{d}\Phi_{qg}$ are the amplitude and phase space describing the emission of both the gluon and the quark; M_q, $\mathrm{d}\Phi_q$ are the amplitude and phase space when only the quark is emitted; $z = E_q/(E_q + E_g)$ is the fraction of energy carried by the quark; ϕ is the azimuth of the splitting plane, and $P_{q,qg}(z) = C_F(1+z^2)/(1-z)$ is the Altarelli-Parisi splitting kernel for gluon emission from a quark line, with color factor $C_F = 4/3$. The factorized form of Eq. (43.1) is due to the fact that for small angle the process is dominated by a single amplitude in which the splitting quark is almost on shell and hence propagates for long distances. We define the energy scale corresponding to the inverse of this distance as the *hardness* of the splitting process, so that larger hardness corresponds to shorter distance. We can define the hardness t as the product $E^2\theta^2$, or as the virtuality of the splitting parton p^2, or as a measure of the relative transverse momentum in the splitting such as the k_t of an emitted parton relative to its parent, defined by

$$\begin{aligned} p^2 &= 2E^2 z(1-z)(1-\cos\theta) \approx z(1-z)E^2\theta^2 \,, \\ k_t^2 &= z^2(1-z)^2 E^2\theta^2 \,. \end{aligned} \tag{43.2}$$

If the region of small values of z and $1-z$ was not important, these definitions would be equivalent. In QCD we also have soft divergences, arising when soft gluons are emitted. In Eq. (43.1) they appear as $z \to 1$, because of the $1/(1-z)$ singularity of $P_{q,qg}(z)$. Thus, we expect that the choice of the appropriate ordering variable will be relevant when dealing with soft divergences (see Sec. 43.3). The $\mathrm{d}\theta^2/\theta^2$ factor in Eq. (43.1) can be equivalently written in terms of the hardness $\mathrm{d}t/t$. After integration, it gives rise to a logarithmic factor $\log(Q^2/\Lambda^2)$. We can have many subsequent splittings, that we can describe by applying Eq. (43.1) recursively, as long as the splittings are strongly ordered in decreasing hardness. This means that, from a typical final-state configuration, by clustering together final-state parton pairs with the smallest hardness recursively, we can reconstruct a branching tree, that may be viewed as the splitting history of the event. We stress that all hardness values between the hardness of the primary process and the cutoff scale Λ are equally involved here. The collinear approximation is applied recursively to splitting processes that have much smaller hardness with respect to all previous ones.

By integrating over the phase space (and neglecting for the moment soft divergences), a process with n collinear splittings will be of order $(\alpha_S(Q^2)\log(Q^2/\Lambda^2))^n$ with respect to the primary process. Since $\alpha_S(Q^2) \propto 1/\log(Q^2/\Lambda^2)$ [6], these corrections are not small. The so-called KLN theorem [7,8] guarantees that large logarithmic enhancements arising from final-state collinear splitting cancel against the virtual corrections in inclusive cross sections, order by order in perturbation theory. Furthermore, the factorization theorem guarantees that initial-state collinear singularities can be factorized into the parton density functions (PDFs) [6]. Therefore, the cross section for the basic process remains accurate up to corrections of higher orders in $\alpha_\mathrm{S}(Q)$, provided it is interpreted as an inclusive cross section, rather than as a bare partonic cross section. For example, the leading order (LO) cross section for $e^+e^- \to q\bar{q}$ is a good estimate of the e^+e^- cross section for the production of a pair of quarks accompanied by an arbitrary number of collinear and soft gluons, but is not a good estimate of the cross section for the production of a $q\bar{q}$ pair with a veto on extra radiation. In summary, perturbation theory at fixed order can yield increasingly accurate predictions for inclusive observables, but cannot be used to describe the indefinite sequence of collinear and soft radiations that accompany the hard partons.

Parton-Shower algorithms are used to compute the cross section for generic hard processes including all dominant collinear radiation. These algorithms begin with the generation of the kinematics of the basic process, performed with a probability proportional to its LO partonic cross section. This is interpreted physically as the inclusive cross section for the basic process, followed by an arbitrary sequence of shower splittings. The algorithm then assigns a probability to each splitting sequence, so that the initial LO cross section is partitioned into the cross sections for a multitude of final states of arbitrary multiplicity, with their sum being equal to the cross section of the primary process. This property of the GPMCs reflects the KLN cancellation mentioned earlier, and it is often called "unitarity of the shower process", a name

Phys. A 2026.41. Downloaded from www.worldscientific.com by UNIVERSITY OF CALIFORNIA BERKELEY on 09/16/26. Re-use and distribution is strictly not permitted, except for Open Access articles.

Int. J. Mod. Phys. A 2026.41. Downloaded from www.worldscientific.com
by UNIVERSITY OF CALIFORNIA @ BERKELEY on 09/16/26. Re-use and distribution is strictly not permitted, except for Open Access articles.

that reminds us that the KLN cancellation itself is a consequence of unitarity. The fact that a quantum mechanical process can be described in terms of composition of probabilities, rather than amplitudes, follows from the collinear approximation. In fact, because of strong ordering, a radiated parton cannot be collinear to more than one parton in the amplitude, and this suppresses interference effects.

We now illustrate the basic parton-shower algorithm, as first introduced in Ref. [9]. (For more pedagogical introductions see Ref. [10] and references therein.) For simplicity, we consider the example of e^+e^- annihilation into $q\bar{q}$ pairs, where we only have to deal with final state radiation (FSR). We consider all final states that can be built by dressing the q and $\bar{q}$ partons with an indefinite number of splitting processes. By recursively clustering together final state parton pairs with the smallest relative hardness, from each final state configuration we can construct two trees rooted at the q and $\bar{q}$ partons. The momenta of all intermediate lines of the tree diagrams are then uniquely determined from the final-state momenta. Hardnesses in the trees are ordered. One assigns to each splitting vertex the hardness t, the energy fractions z and $1-z$ of the two generated partons, and the azimuth ϕ of the splitting process with respect to the momentum of the incoming parton. For definiteness, we assume that z and ϕ are defined in the center-of-mass (CM) frame of the e^+e^- collision. The differential cross section for a given final state is given by the product of the differential cross section for the initial $e^+e^- \to q\bar{q}$ process, multiplied by a factor

$$\Delta_i(t_m, t_n)\frac{\alpha_{\rm S}(t)}{2\pi}P_{i,jk}(z)\frac{dt_m}{t_m}dz\frac{d\phi}{2\pi} \tag{43.3}$$

for each intermediate line arising from the $n^{\rm th}$ and ending in the $m^{\rm th}$ splitting vertex. $\Delta(t_m, t_n)$ is the so-called Sudakov form factor

$$\Delta_i(t_m, t_n) = \exp\left[-\int_{t_m}^{t_n}\frac{dq^2}{q^2}\,\frac{\alpha_{\rm S}(q^2)}{2\pi}\int dz\frac{d\phi}{2\pi}\sum_{jk}P_{i,jk}(z)\right]. \tag{43.4}$$

The suffixes i and jk represent the parton species of the incoming and final partons, respectively, and $P_{i,jk}(z)$ are the Altarelli-Parisi [11] splitting kernels. Notice that the endpoints on the z integration depend upon the definition of hardness. For example, in case of virtuality or transverse momentum ordering, the z integration is automatically cut-off near the extremes, see eq. (1.2). When this is not the case (as, for example, for angular ordering) an explicit cut-off on z must be introduced, corresponding to the requirement that an emission must have some minimum energy to be distinguishable from no emission. For lines originating at the primary vertex, the scale t_n is replaced by the typical scale of the primary process and for lines ending without any further splitting the scale t_m is replaced by t_0, an infrared cutoff defined by the shower hadronization scale (at which the charges are screened by hadronization) or, for an unstable particle, its width (a source cannot emit radiation with a period exceeding its lifetime).

Eq. (43.3) can be obtained by iterating formula Eq. (43.1) recursively, with two important corrections: a) the strong coupling is evaluated at a scale corresponding to the hardness of the splitting process; b) the presence of the Sudakov form factor. Both these modifications arise from the inclusion of all collinear-dominant virtual corrections.

Notice that the Sudakov form factor for a small hardness interval $\Delta_i(t, t+\delta t)$ is equal to one minus the integrated emission probability of Eq. (43.3), i.e. it can be interpreted as the probability of no emission in the interval $t, t+\delta t$. From this, it immediately follows that $\Delta_i(t_m, t_n)$ can be interpreted as the no-emission probability in the full t_m, t_n interval. This interpretation allows one to formulate the shower process as a probabilistic algorithm. We first notice that $0 < \Delta_i(t_m, t_n) \leq 1$, where the upper extreme is reached for $t_m = t_n$, and the lower extreme is approached for $t_m = t_0$. Starting from each of the partons in the primary process (e.g., $e^+e^- \to q\bar{q}$), event generation then proceeds recursively as follows. Given a parton exiting a vertex with hardness t_n, (taken to be of order the annihilation scale Q^2 for the first branching) one seeks a solution of the equation $r = \Delta_i(t_m, t_n)$, with $r \in [0, 1]$ a uniform random number, and solves it for the hardness of the next branching t_m. If $t_m \leq t_0$, no splitting is generated and the line is interpreted as a final parton. If $t_m > t_0$, a branching is generated at the scale t_m. Its z value and the final parton species jk are generated with a probability proportional to $P_{i,jk}(z)$. If angular correlations are neglected (see Sec. 43.1.1) the azimuth can be generated uniformly. This procedure is started with each of the primary process partons, and is applied recursively to all generated partons. It may generate an arbitrary number of partons, and it stops when no final-state partons undergo further splitting.

The four-momenta of the final-state partons are reconstructed from the momenta of the initial ones, and from the whole sequence of splitting variables, subject to overall momentum conservation. Different algorithms employ different strategies to treat recoil effects due to momentum conservation, which may be applied either locally for each splitting, or globally for the entire set of partons (a procedure called *momentum reshuffling*).

We emphasize that the shower cross sections described above can be derived from perturbative QCD by keeping only the collinear-dominant real and virtual contributions to the cross section. As such it is unpredictive for large-angle radiation. It is thus unsafe to rely upon Parton Shower Monte Carlo alone to compute backgrounds to new physics signals that are characterized by several widely separated jets.

A Shower Monte Carlo builds its final state as if it developed from an iterative process, often with each intermediate stage made available to the user. It should be remarked that the meaning of these intermediate stages is only relevant within the approximation adopted by the generator, and could also differ in different implementations.

43.1.1 *Angular correlations*

In gluon-splitting processes ($g \to q\bar{q},\ g \to gg$) in the collinear approximation, the distribution of the split pair is not uniform in azimuth, and the Altarelli-Parisi splitting functions are recovered only after azimuthal averaging. This dependence is due to the interference of positive and negative helicity states for the gluon that undergoes splitting. Spin correlations propagate through the splitting process, and determine acausal correlations of the EPR kind [12]. A method to partially account for these effects was introduced in Ref. [13], in which the azimuthal correlation between two successive splittings is computed by averaging over polarizations. This can then be applied at each branching step. Acausal correlations are argued to be small, and are discarded with this method, that is still used in `PYTHIA` [3]. A method that fully includes spin correlation effects was later proposed [14], and has been implemented in `HERWIG` [2, 15]. For more recent developements, see Ref. [16] and references therein.

43.1.2 *Initial-state radiation*

Initial-state radiation (ISR) arises because incoming particles may undergo collinear radiation before entering the hard-scattering process. In doing so, they acquire a non-vanishing transverse momentum, and their virtuality becomes negative (spacelike). In order to efficiently sample the hard collision, it turns out to be convenient to develop the ISR shower starting with the highest hardness (i.e. with the hard process) and ending with the smallest (i.e. with the incoming parton in the hadron). Unlike the case of FSR, however, hardness ordering is opposite to time ordering in the ISR case. A corresponding backwards-evolution algorithm was formulated by Sjöstrand [17], and was basically adopted in all shower models. It can be illustrated by considering a primary interaction initiated by a quark where no collinear emissions of hardness $\geq t$ have taken place, and the same process where the quark also emits a collinear gluon of hardness t. The respective cross sections are proportional to

$$\begin{aligned} &|M_q(x)|^2 {\rm d}x f_q(x,t), \quad \text{and} \\ &|M_q(x)|^2\,{\rm d}x\frac{\alpha_s(t)}{2\pi}f_q(x/z,t)P_{q,qg}(z){\rm d}z\frac{{\rm d}\phi}{2\pi}\frac{{\rm d}t}{t}\,. \end{aligned} \tag{43.5}$$

Here f_q is the quark PDF in the incoming hadron, x is the fraction of momentum of the incoming quark that enters the basic

Phys. A 2026.41. Downloaded from www.worldscientific.com
by UNIVERSITY OF CA LEY on 09/16/26. Re-use and distribution is strictly not permitted, except for Open Access articles.

process, while x/z is the fraction of momentum of the incoming quark *before* it emits the collinear gluon. The elementary *emission probability* is the ratio of the second over the first expression in Eq. (43.5). In analogy with the final state radiation case, this ratio will appear in the exponent of the Sudakov form factor, that (after the inclusion of all splitting subprocesses) is given by

$$\Delta_i^{\mathrm{ISR}}(t,t') = \exp\left[-\int_{t'}^{t}\frac{dt''}{t''}\frac{\alpha_{\mathrm{S}}(t'')}{2\pi}\int_x^1\frac{dz}{z}\sum_{jk}P_{j,ik}(z)\frac{f_j(t'',x/z)}{f_i(t'',x)}\right]. \tag{43.6}$$

Notice that there are two uses of the PDFs: they are used to compute the cross section for the basic hard process, and they control ISR via backward evolution. Since the evolution is generated with leading-logarithmic accuracy, it is acceptable to use two different PDF sets for these two tasks, provided they agree at the LO level.

In the context of GPMC evolution, each ISR emission generates a finite amount of transverse momentum. Details on how the recoils generated by these transverse "kicks" are distributed among other partons in the event, in particular the ones involved in the hard process, constitute one of the main areas of difference between existing algorithms, see Ref. [10]. An additional $\mathcal{O}(1\,\mathrm{GeV})$ of "primordial k_T" is typically added, to represent the sum of unresolved and/or non-perturbative motion below the shower cutoff scale.

43.1.3 *Soft emissions and QCD coherence*

Soft singularities arise in QCD due to the real or virtual emission of soft gluons. For example, the cross section for the emission of a soft gluon in e^+e^- annihilation into hadrons is given by

$$\begin{aligned}\mathrm{d}\sigma_{q\bar{q}g} &\approx \mathrm{d}\sigma_{q\bar{q}}C_F(4\pi\alpha_s)\left[\frac{2\,p_q\cdot p_{\bar{q}}}{p_q\cdot l\;p_{\bar{q}}\cdot l}\right]\frac{\mathrm{d}^3 l}{2l^0(2\pi)^3}\\ &= \mathrm{d}\sigma_{q\bar{q}}\frac{\alpha_s}{2\pi}C_F\frac{\mathrm{d}l^0}{l^0}\frac{\mathrm{d}\phi}{2\pi}\frac{\mathrm{d}\cos\theta}{1-\cos^2\theta},\end{aligned} \tag{43.7}$$

where p_q, $p_{\bar{q}}$ and l are the quark, antiquark and gluon momentum, and θ and ϕ are the polar and azimuthal angle of the gluon momentum with respect to the quark direction. Since the gluon is soft, we may assume that p_q and $p_{\bar{q}}$ are unaffected by the gluon emission. The soft singularity is manifest in the $\mathrm{d}l^0/l^0$ factor. Notice that also collinear singularities are present at the same time when $\theta\to 0$ and $\theta\to\pi$, corresponding to the gluon becoming collinear to either the quark or the antiquark. It is easy to check that in the collinear limits Eq. (43.7) becomes equivalent to Eq. (43.1) with $P_{q,qg}(z) = C_F 2/(1-z)$, i.e. the limiting form of $P_{q,qg}(z)$ when z approaches 1. Thus, soft singularities coexist with collinear ones, so that two potentially large logarithms can arise simultaneously due to gluon emission.

Unlike the case of collinear emission, soft emission is not tied to a single emitting particle. The amplitude for the emission of a soft gluon from an external (incoming or outgoing) line with momentum p is proportional to $p\cdot\epsilon/p\cdot l$. When squaring the amplitude, products like the one appearing in the square bracket of Eq. (43.1) arise for all pairs of external particles, with the product of a single emission amplitude with itself appearing only if $p^2>0$, i.e. for massive colored particles. Thus, interference plays here a crucial role. This is unlike the case of collinear singularities, where because of strong ordering a radiated parton cannot be collinear to more than one other parton.

It was shown in a set of publications (see Ref. [18]) that, within the conventional parton-shower formalism based on collinear factorization, the region of collinear and soft emissions can be correctly described by using the angle of the emissions as the ordering variable, rather than the virtuality, and by setting the argument of α_{S} at the splitting vertex equal to the relative parton transverse momentum after the splitting. Physically, the ordering in angle approximates the coherent interference arising from large-angle soft emission from a bunch of collinear partons. Without this effect, the particle multiplicity would grow too rapidly with energy, in conflict with e^+e^- data. For this reason, angular ordering is used as the default evolution variable in all versions of `HERWIG` (see Ref. [19]). To partially account for soft interference effects, an angular veto is imposed on the virtuality-ordered evolution in `PYTHIA` 6 [20]. In modern designs this type of fix is avoided, the soft problem being addressed from the start.

A radical alternative formulation of QCD cascades first proposed in Ref. [21] focuses upon soft emission, rather than collinear emission, as the basic splitting mechanism. It then becomes natural to consider a branching process where it is a parton pair (i.e. a dipole) rather than a single parton, that emits a soft parton. Adding a suitable correction for non-soft, collinear partons, one can simultaneously achieve the correct logarithmic structure for both the collinear and soft emissions in the so called leading color approximation, i.e. when terms suppressed by a power of the number of colors are neglected. The `ARIADNE` [22] and `VINCIA` [23] programs are based on this approach. Dipole-type showers [24] are also used by default in `SHERPA` [25] and exist as an option in `HERWIG` [26]. The $p_\perp$-ordered showers in `PYTHIA` 6 and 8 represent a hybrid, combining collinear splitting kernels with dipole kinematics [27].

43.1.4 *Resummation*

Shower Monte Carlo generators perform resummation of all-order collinear- and/or soft-enhanced perturbative contributions, and it is thus natural to compare them to QCD resummation calculations [6]. The latter start from the definition of specific infrared-safe observables, that develop towers of large logarithms in certain regions of phase space, typically organized as

$$A(\alpha_{\mathrm{S}})\exp[Lg_0(\alpha_{\mathrm{S}}L)+g_1(\alpha_{\mathrm{S}}L)+\alpha_{\mathrm{S}}g_2(\alpha_{\mathrm{S}}L)+\ldots] \tag{43.8}$$

where L is the large logarithm, α_{S} is the strong coupling constant evaluated at some hard scale. The functions A has a power expansion in α_{S} starting with a constant, and the functions g_i have a power series expansion in their argument starting with the linear term. We talk about $\mathrm{N}^n\mathrm{LL}$ accuracy if all g_i functions for $i\le n$ are fully included in the resummation formula, and the A function is given up to the order $n-1$ in α_{S}. In particular we talk about LL accuracy if the function g_0 is included, NLL accuracy if also g_1 is included. In both cases only the constant term in A is needed, while for $\mathrm{N}^2\mathrm{LL}$ (or NNLL) g_0, g_1 and g_2 are included and A is given up to order α_{S}.

In general, a dedicated resummation calculation must be performed for each new observable. The predictions of shower MCs, on the other hand, are cast in terms of complete sets of final-state momenta, on which one can evaluate any observable; i.e., the shower algorithm itself is normally independent of the specific observable(s) under study. Because of this, it is not easy to qualifying the accuracy of a shower MC using the same criteria adopted in resummation calculation. In spite of this fact, shower MCs perform generally quite well in the description of observables that require resummation. This is related to their inclusion of several universal but formally subleading aspects. There is no guarantee, however, that the shower MC should perform to a certain level of accuracy for all distributions that require resummation. Thus, a more systematic treatment of subleading effects is quite desirable.

Several studies have appeared in the literature, aiming at either improving the current shower algorithms or formulate totally new ones, in such a way that the theoretical accuracy can be discussed in more precise terms [28–31]. Indeed, criteria for defining the accuracy of Shower Generators can be given on a quite general grounds. Two such criteria are [28]:

1. The approximations to multi-parton real matrix elements generated by the shower algorithm must be accurate in the region of phase space that are relevant for $\mathrm{N}^n\mathrm{LL}$ accuracy.
2. The implementation of the virtual corrections must be such that the shower MC agrees with resummed calculations at the $\mathrm{N}^n\mathrm{LL}$ level for a large class of shape variables.

The PanScales collaboration has constructed shower algorithms that are (with some restrictions) NLL accurate according to these criteria (see Ref. [32] and references therein). Other NLL accu-

Int. J. Mod. Phys. A 2026.41. Downloaded from www.worldscientific.com
by UNIVERSITY OF CALIFORNIA @ BERKELEY on 09/16/26. Re-use and distribution is strictly not permitted, except for Open Access articles.

rate (according to the same criteria) shower algorithms have been proposed in refs. [29] and [31].

43.1.5 *Massive quarks*

Quark masses act as a cut-off on collinear singularities. If the mass of a quark is below, or of the order of Λ, its effect in the shower is small. For larger quark masses, like in c, b, or t production, it is the mass, rather than the typical hadronic scale, that cuts off collinear radiation. For a quark with energy E and mass m_Q, the divergent behavior $d\theta/\theta$ of the collinear splitting process is regulated for $\theta \leq \theta_0 = m_Q/E$. We thus expect less collinear activity for heavy quarks than for light ones, which in turn is the reason why heavy quarks carry a larger fraction of the momentum acquired in the hard production process.

This feature can be implemented with different levels of sophistication. Using the fact that soft radiation is strongly suppressed at zero emission angle, older parton shower algorithms simply limited the shower emission to be not smaller than the angle θ_0. More modern approaches are used in both `PYTHIA`, where mass effects are included using a kind of matrix-element correction method [33], and in `HERWIG` and `SHERPA`, where a generalization of the Altarelli-Parisi splitting kernel is used for massive quarks [34]. For newer approaches for QCD evolution in processes with massive partons see ref. [35] and references therein.

43.1.6 *Color information*

In event generators, quarks and antiquarks are represented by color lines, with arrows indicating the direction of color flow. In the limit of infinitely many colors (called the leading color approximation), each such line can be associated with a unique label; the probability for two quarks (or antiquarks) to have the same color (anticolor) vanishes. Moreover, in the same limit gluons can be represented by a pair of color lines with opposite arrows, as can be realized e.g. from the SU(3) group relation $8 = 3 \otimes \bar{3} \ominus 1$. The rules for color propagation are:

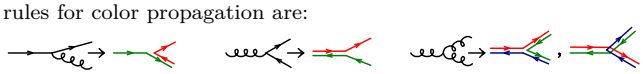

During the shower development, partons are connected by color lines. We can have a quark directly connected by a color line to an antiquark, or via an arbitrary number of intermediate gluons, as shown in Fig. 43.1. It is also possible for a set of gluons to be connected cyclically in color, as e.g. in the decay $\Upsilon \to ggg$. The color information is used in angular-ordered showers, where

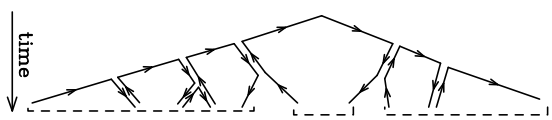

Figure 43.1: Color development of a shower in e^+e^- annihilation. Color-neutral clusters of partons are indicated by the dashed under-brackets.

the angle of color-connected partons (i.e. partons connected by the same color line) determines the initial angle for the shower development, and in dipole showers, where dipoles are formed by color-connected partons. It is also used in hadronization models, where the initial strings or clusters used for hadronization are formed by color-neutral clusters of partons.

43.1.7 *Electromagnetic (and weak) corrections*

The physics of photon emission from charged particles, and of photon splittings to pairs of charged fermions, can also be treated with a shower MC algorithm. High-energy electrons and quarks, for example, are accompanied by bremsstrahlung photons. Also here, similarly to the QCD case, electromagnetic corrections are of order $\alpha_{\rm em} \ln(Q/m)$, where m is the mass of the radiating particle, or even of order $\alpha_{\rm em} \ln(Q/m) \ln(E_\gamma/E)$ for soft γ emissions, so that, especially for the case of electrons, their inclusion in the simulation process is mandatory. This is done in most GPMCs (for a comparative study see [36]), which typically agree in collinear (DGLAP) limits but differ in whether and how soft (multipole) QED interference effects are handled. The specialized generator `PHOTOS` [37] is sometimes used as an afterburner for an improved treatment of QED radiation in non-hadronic resonance decays.

For photon emissions off leptons, the shower can be continued down to virtualities arbitrarily close to the lepton mass shell (unlike the case in QCD). In practice, an infrared cutoff is still required for the shower algorithm to terminate. Therefore, there is always an energy cut-off for emitted photons that depends upon the implementations [36]. In the case of electrons, this energy is typically of the order of its mass. Electromagnetic radiation below this scale is not enhanced by collinear singularities, and is thus bound to be soft, so that the electron momentum is not affected by it.

For photons emitted from quarks, there is instead the obvious limitation that the photon wavelength cannot exceed the typical hadronic size. Longer-wavelength photons are in fact emitted by hadrons, rather than quarks. This last effect is in practice never modeled by existing shower MC implementations. Thus, electromagnetic radiation from quarks is cut off at a typical hadronic scale. Finally, hadron (and τ) decays involving charged particles can produce additional soft bremsstrahlung. In `PYTHIA`, this is done via interfacing with `PHOTOS`, while `HERWIG` and `SHERPA` contain their own dedicated implementations [38,39] based upon the YFS formalism [40], which is also adopted in the KKMC-hh Monte Carlo [41].

At energies significantly above the electroweak (EW) scale, showers involving emissions (and splittings) of weak gauge and Higgs bosons can also be relevant, with recent implementations based on collinear limits ranging from weak-boson emissions from fermions in `PYTHIA` 8 [42], to triple-boson couplings in `HERWIG` 7 [43], to the full set of EW branching processes in `VINCIA` [44].

43.1.8 *Beyond-the-Standard-Model Physics*

The inclusion of processes for physics beyond the Standard Model (BSM) in event generators is to some extent only a matter of implementing the relevant hard processes and (chains of) decays, with the level of difficulty depending on the complexity of the model and the degree of automation [45,46]. Notable exceptions are long-lived colored particles [47], particles in exotic color representations, and particles showering under new gauge symmetries, with a growing set of implementations documented in the individual GPMC manuals. Further complications that may be relevant are finite-width effects (discussed in Sec. 43.1.9) and the assumed threshold behavior.

In addition to code-specific implementations [10], there are a few commonly adopted standards that are useful for transferring information and events between codes. Currently, the most important of these is the Les Houches Event File (LHEF) standard [48], normally used to transfer parton-level events from a hard-process generator to a shower generator. Another important standard is the Supersymmetry Les Houches Accord (SLHA) format [49], originally used to transfer information on supersymmetric particle spectra and couplings, but by now extended to apply also to more general BSM frameworks and incorporated within the LHEF standard [50]. Unfortunatly, at present no standard method for handling multiple shower starting scales has been define in the LHEF, so that further code, specific to the given GPMC, needs to be added to the interface in this case.

43.1.9 *Decay Chains and Particle Widths*

In most BSM processes and some SM ones, an important aspect of the event simulation is how decays of short-lived particles, such as top quarks, EW and Higgs bosons, and new BSM resonances, are handled. We here briefly summarize the spectrum of possibilities, but emphasize that there is no universal standard. Users are advised to check whether the treatment of a given code is adequate for the physics study at hand.

The appearance of an unstable resonance as a physical particle at an intermediate stage of the event generation implies that its production and decay processes are treated as being factorized. This is valid up to corrections of order Γ/m_0, with Γ the width and m_0 the pole mass. States whose widths are a substantial fraction of their mass should instead be treated as intrinsically off-shell internal propagator lines.

For states treated as physical particles, two aspects are relevant: the mass distribution of the decaying particle itself and the distributions of its decay products. For the former, matrix-

by UNIVERSITY OF CA LEY on 09/16/26. Re-use and distribution is strictly not permitted, except for Open Access articles. Phys. A 2026.41. Downloaded from www.worldscientific.com

element generators often use a simple δ function at m_0. The next level up, typically used in GPMCs, is to use a Breit-Wigner distribution, which formally resums higher-order virtual corrections to the mass distribution. Note, however, that this still only generates an improved picture for *moderate* fluctuations away from m_0. Similarly to above, particles that are significantly off-shell (in units of Γ) should not be treated as resonant, but rather as internal off-shell propagator lines. In most GPMCs, further refinements are included, for instance by letting Γ be a function of m ("running widths") and by limiting the magnitude of the allowed fluctuations away from m_0. We finally point out that NLO+PS generators have appeared that can deal with resonances including off-shell effects, non-resonance contributions and interference of radiation generated in resonance decay and production, see [51] and references therein. A new "interleaved" shower treatment also allows for interference between production and decay in the `VINCIA` model [44].

For the distributions of the decay products, the simplest treatment is again to assign them their respective m_0 values, with a uniform phase-space distribution. A more sophisticated treatment distributes the decay products according to the differential decay matrix elements, capturing at least the internal dynamics and helicity structure of the decay process, including EPR-like correlations. Further refinements include polarizations of the external states [52] and assigning the decay products their own Breit-Wigner distributions, the latter of which opens the possibility to include also intrinsically off-shell decay channels, like $H \to WW^*$.

GPMC manuals often give instructions on how to include new decay modes, at varying levels of sophistications ranging from simple uniform phase-space sampling (which the user can reweight a posteriori) and step-function thresholds, to fully matrix-element weighted decay implementations including potential off-shell / threshold effects.

During subsequent showering of the decay products, most parton-shower models will preserve the total invariant mass of the decayed resonance, so as not to skew the original resonance shape. In the context of passing externally generated LHEF files [48] to a GPMC for showering, note that this is only possible if the intermediate resonances are present (with status code 2) in the LHEF event record [53].

43.1.10 *Matching and Merging with Fixed-Order Matrix Elements*

Shower algorithms are based upon a combination of the collinear (small-angle) and soft (small-energy) approximations and are thus normally inaccurate for hard, wide-angle emissions (i.e., additional well-resolved jets). They also contain only the leading singular pieces of next-to-leading order (NLO) and higher corrections to the basic process.

Traditional GPMCs, like `HERWIG` and `PYTHIA`, have included for a long time the so called Matrix-Element Corrections (MEC), first formulated in Ref. [54] with later developments summarized in Ref. [10]. They are typically available for $2 \to 1$ or $1 \to 2$ processes, like DIS, vector boson and Higgs production and decays, and top decays. The MEC corrects the emission of the hardest jet at large angles, so that it becomes exact at LO. A generalization of the method to multiple emissions was formulated in Ref. [55].

Aside from MECs implemented directly in the GPMCs, the improvements on the parton-shower description of hard collisions have been made in two main directions: the so called Matrix Elements and Parton Shower matching (ME+PS from now on), and the matching of NLO calculations and Parton Showers (NLO+PS). We now discuss each of these, and then briefly summarize techniques becoming available for combining them.

The ME+PS method allows one to use tree-level matrix elements for hard, large-angle emissions. It was first formulated in the so-called CKKW paper [56], and several variants have appeared, including the CKKW-L, MLM, pseudoshower and MESS methods, see refs. [10, 57, 58] and references therein. So called "Truncated Showers" are required [59] to maintain color coherence when interfacing to angular-ordered parton showers, and care must be taken to use consistent α_S choices for the real (ME-driven) and virtual (PS-driven) corrections [60].

In the ME+PS method one typically starts by generating LO matrix elements for the production of the basic process plus a certain number $\leq n$ of other partons. A minimum separation is imposed on the produced partons, requiring, for example, that the relative transverse momentum in any pair of partons is above a given cut $Q_{\rm cut}$. One then reweights these amplitudes in such a way that, in the strongly ordered region, the virtual effects that are included in the shower algorithm (i.e. running couplings and Sudakov form factors) are also accounted for. At this stage, before parton showers are added, the generated configurations are tree-level accurate at large angle, and at small angle they match the results of the shower algorithm, except that there are no emissions below the scale $Q_{\rm cut}$, and no final states with more than n partons. These kinematic configurations are thus fed into a GPMC, that must generate all splittings with relative transverse momentum below the scale $Q_{\rm cut}$, for initial events with less than n partons, or below the scale of the smallest pair transverse momentum, for events with n partons. The matching parameter $Q_{\rm cut}$ must be chosen to be large enough for fixed-order perturbation theory to hold, but small enough so that the shower is accurate for emissions below it. Notice that the accuracy achieved with MEC is equivalent to that of ME+PS with $n = 1$, where MEC has the advantage of not having a matching parameter $Q_{\rm cut}$.

The popularity of the ME+PS method is due to the fact that processes with many jets often appear as backgrounds to new-physics searches. These jets are typically required to be well separated, and to have large transverse momenta. These kinematic configurations are exactly those for which pure shower algorithms are unreliable, hence it is mandatory to describe them using at least LO matrix elements.

Several ME+PS implementations use existing LO generators, like `ALPGEN` [61], `MADGRAPH` [62], and others summarized in Ref. [57], for the calculation of the matrix elements, and feed the partonic events to a GPMC like `PYTHIA` or `HERWIG` using the Les Houches Interface for User Processes (LHI/LHEF) [48, 53]. `SHERPA` and `HERWIG` also include their own matrix-element generators.

The NLO+PS methods promote the accuracy of the generation of the basic process from LO to NLO in QCD. They must thus include the radiation of one extra parton with tree-level accuracy, since this radiation constitutes a NLO correction to the basic process. They must also include NLO virtual corrections. They can be viewed as an extension of the MEC methods with the inclusion of NLO virtual corrections. They are however more general, since they are applicable to processes of arbitrary complexity. Two of these methods are now widely used: MC@NLO [63] and Powheg [59, 64], with several alternative methods now also being pursued [65]. For more recent proposals see refs. [66, 67] and references therein.

NLO+PS generators produce NLO accurate distributions for inclusive quantities, and generate the hardest jet with tree-level accuracy. Note also that the optimal tuning of an NLO+PS generator may well be different from that of the pure PS.

Several NLO+PS processes are implemented in the MC@NLO program [63], together with the `AMC@NLO` development [68], and in the Powheg-Box framework [64]. `HERWIG` supports its own variants of Powheg and MC@NLO for several processes. `SHERPA` instead implements a variant of the MC@NLO method.

For applications that require an accurate description of more than one hard, large-angle jet associated with the primary process, ME+PS schemes are still superior to NLO+PS ones. Ideally, one would like to improve NLO generators in such a way that also the production of associated jets achieves NLO accuracy. The FXFX [69], UNLOPS [70], MiNLO [71] and `MEPS@NLO` [72] methods address this problem. The solution of this problem is also a prerequisite for the construction of NNLO+PS generators, i.e. generators that, besides being NLO accurate for the production of an associated jet, are also NNLO accurate for fully inclusive observables. Three different approaches have appeared in the literature for dealing with this problem: the UN^{2}NLOPS, based upon UNLOPS method [73]; methods extending the MiNLO approach by reweigthting [74] and by the so called MiNNLO$_{\rm PS}$ technique [75]; and the GENEVA method [76]. Several processes have been implemented with the MiNLO related and GENEVA meth-

Int. J. Mod. Phys. A 2026.41. Downloaded from www.worldscientific.com
by UNIVERSITY OF CALIFORNIA @ BERKELEY on 09/16/26. Re-use and distribution is strictly not permitted, except for Open Access articles.

ods, mostly for the production of color singlet systems, with the exception of the recent $\mathrm{MiNNLO_{PS}}$ implementation of $t\bar{t}$ production (see refs. [65, 77, 78] for an extensive list of references).

43.2 Hadronization Models

In the context of GPMCs, *hadronization* denotes the process by which a set of colored partons (*after* showering) is transformed into a set of "primary hadrons", which may then subsequently decay further (to "secondary hadrons"). This non-perturbative transition takes place at the *hadronization scale* Q_{had}, which by construction is equal to the infrared cutoff of the parton shower. In the absence of a first-principles solution to the relevant dynamics, GPMCs use QCD-inspired phenomenological models to describe this transition.

An important result in "quenched" lattice QCD (see Chap. 17 of PDG book) is that the potential energy between two partons with opposite color charges grows linearly with their separation, at distances greater than about a femtometer. This is known as "linear confinement", and it forms the starting point for the *string model of hadronization*, discussed below in Sec. 43.2.1. Alternatively, a property of perturbative QCD called "preconfinement" is the basis of the *cluster model of hadronization*, discussed in Sec. 43.2.2.

A key difference between MC hadronization models and the fragmentation-function (FF) formalism used to describe inclusive hadron spectra in perturbative QCD (see Chap. 9 and Chap. 19 of PDG book) is that FFs can be defined at an arbitrary perturbative scale Q while MC hadronization models are intrinsically defined at the scale Q_{had}. Direct comparisons are therefore only meaningful if the perturbative evolution between Q and Q_{had} is taken into account. FFs are calculable in pQCD, given a non-perturbative initial condition obtained by fits to hadron spectra. In the MC context, one can prove that the correct QCD evolution of the FFs arises from the shower formalism, with the hadronization model providing an explicit parameterization of the non-perturbative component. However, the MC modeling of shower and hadronization includes much more information on the final state since it is fully exclusive (i.e., it addresses all particles in the final state explicitly), while FFs only describe inclusive spectra. This exclusivity also enables MC models to make use of the color-flow information coming from the perturbative shower evolution (see Sec. 43.1.6) to determine between which partons confining potentials should arise. E.g., in the string picture, the nonperturbative limit of a QCD dipole is a string piece [79].

Given an ideal, exact hadronization model, its dependence on the scale Q_{had} should in principle be compensated by the corresponding scale dependence of the shower algorithm, which stops generating branchings at the scale Q_{had}. However, due to their complicated and fully exclusive nature, it is generally not possible to enforce this compensation automatically in MC models. One must therefore be aware that the nonperturbative model parameters must be "retuned" by hand if the infrared cutoff is modified. Any other changes to the perturbative part of the calculation, such as matching to further (fixed-order or resummed) coefficients, may also necessitate a retuning. Tuning is discussed briefly in Sec. 43.4.

The impact of hadronization corrections in a GPMC can be estimated by switching off hadronization. It should be emphasized, however, that the so-called "parton level" obtained this way is not a fully universal concept. This is because Q_{had} is typically defined in a model-dependent way, via a cutoff in the respective shower model's evolution variable, sometimes with supplementary cutoffs, e.g., in invariant mass, p_{T}, or the like and different tunes possibly using different numerical values for the cutoff(s). Variations of the main shower cutoff scale (e.g., by a factor of 2) may give an indication of the level of model dependence, which may be mild for sufficiently inclusive observables. Nevertheless our recommendation is to avoid correcting experimental measurements to "parton level" as the intrinsic model dependence will always imply a loss of accuracy.

43.2.1 *The String Model*

Starting from early concepts [80], several hadronization models based on strings have been proposed [10]. Of these, the most widely used today is the so-called Lund model [81, 82], implemented in `PYTHIA` [3, 4]. We concentrate on that particular model here, though many of the overall concepts would be shared by any string-inspired method.

Consider a quark and an antiquark that have a large relative momentum and which are in an overall color-singlet state, such as the $\bar{q}q$ pair produced at the end of the shower in the center of Fig. 43.1. As the charges move apart, linear confinement implies that a potential $V(r) = \kappa\, r$ is reached for large distances r. (At short distances, there is a Coulomb term $\propto 1/r$ as well, but this is neglected in the Lund string.) This potential describes a string with tension $\kappa \sim 1\,\mathrm{GeV/fm} \sim 0.2\,\mathrm{GeV}^2$. The physical picture is that of a color flux tube being stretched between the q and the $\bar{q}$. As the string grows, the nonperturbative creation

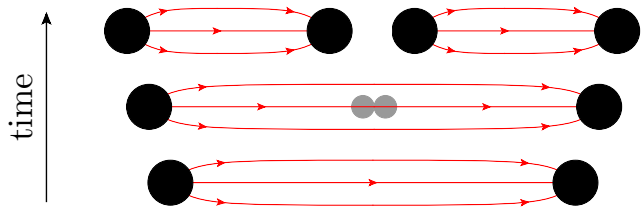

Figure 43.2: Illustration of string breaking by quark pair-creation in the string field.

of quark-antiquark pairs can break the string, via the process illustrated in Fig. 43.2. If either of the resulting string pieces after the break still has a large invariant mass, new breaks will then continue to occur until every piece has a mass of the order of that of a typical hadron. In nature, quantum mechanics ensures that these masses are (Breit-Wigner-distributed around) those of the physical hadron states in QCD, while in an algorithmic implementation, this is less trivial to impose. Within the Lund model, the constraint that each final string piece must have a mass consistent with that of physical hadron is addressed by first noting that each breakup vertex is spacelike separated from all others (the string cannot break again in the forward lightcone of a point where it has already broken); since the breakups are therefore causally disconnected, they do not have to be considered in any particular order. The Lund model exploits this to perform the fragmentation in an outwards-in manner [82], splitting off one physical hadron at a time from either the left or right endpoint (chosen randomly in each step).

The first hadron to be generated (starting either from the left or right) is thus the "outermost" one (sometimes called the "first-rank" hadron), formed by combining the original hadronizing endpoint quark (or antiquark) q_0 with an antiquark (or quark) $\bar{q}_1$ produced by the first breakup. The new leftover quark (or antiquark) q_1 becomes the string endpoint for the next iteration, in a Markov chain which continues, alternating randomly between the left and right ends of the string, until finally a small last bit of string is decayed directly to two hadrons, with no energy left over.

Not only does this allow for the hadron that is split off in each step to be assigned a physical mass, the fact that the fragmentation spectrum should be independent of whether one performs the fragmentation from left to right or vice versa places a strong constraint on the form of the nonperturbative *string fragmentation function*[1], $f(z)$, which governs the probability for the hadron produced in a given step to take a fraction $z \in [0, 1]$ of the remaining energy. Thus, in the Lund model, causality dictates that the fragmentation function should be of the form,

$$f(z) \propto \frac{1}{z}(1-z)^a \exp\left(-\frac{b\,(m_h^2 + p_{\mathrm{T},h}^2)}{z}\right) . \tag{43.9}$$

This is known as the Lund symmetric fragmentation function (normalized to unit integral). The dimensionless parameter a

[1] Note that the string fragmentation function differs from the parton-to-hadron fragmentation functions discussed earlier. In principle, the two kinds should be related (with the latter evolved to a low scale of the order of the hadronization scale), but the relationship is not trivial and goes beyond the scope of this review.

Phys. A 2026.41. Downloaded from www.worldscientific.com
by UNIVERSITY OF CALIFORNIA BERKELEY on 09/16/26. Re-use and distribution is strictly not permitted, except for Open Access articles.

dampens the hard tail of the fragmentation function, towards $z \to 1$, and may in principle be flavor-dependent, while b, with dimension GeV^{-2}, is a universal constant related to the string tension [82] which determines the behavior in the soft limit, $z \to 0$. Note that the dependence on the hadron mass, m_h, in $f(z)$ implies that heavier hadrons have higher $\langle z \rangle$. We return to the transverse momentum $p_{\mathrm{T},h}$ below.

The model is Lorentz invariant, so considerations involving boosted string systems are straightforward, involving the usual Lorentz effects.

As a by-product, the probability distribution in invariant time τ of $q'\bar{q}$ breakup vertices, or equivalently $\Gamma = (\kappa\tau)^2$, is also obtained, with $dP/d\Gamma \propto \Gamma^a \exp(-b\Gamma)$ implying an area law for the color flux, and the average breakup time lying along a hyperbola of constant invariant time $\tau_0 \sim 10^{-23}$s [82].

For massive endpoints (e.g. c and b quarks), which do not move along straight lightcone sections, the exponential suppression with string area leads to modifications of the form $f(z) \to f(z)/z^{b\,m_Q^2}$, with m_Q the mass of the heavy quark [83]. Although different forms, such as the Peterson formula [84], can also be used to describe inclusive heavy-meson spectra (see Sec 19.8 of PDG book), such choices are not strictly consistent with causality in the string framework. For a recent summary of heavy-quark hadronization, see Ref. [85].

43.2.1.1 *Strings with Gluons*

In the string model, energetic gluons lead to transverse "kinks" on strings, illustrated in Fig. 43.3. The order of these kinks follows from the color ordering produced by the parton shower, cf. the $\bar{q}gggq$ and $\bar{q}gq$ systems on the left and right part of Fig. 43.1. (Modifications to this order, by possible color reconnection/rearrangement effects, are discussed in Sec. 43.3.2.) Thus gluons

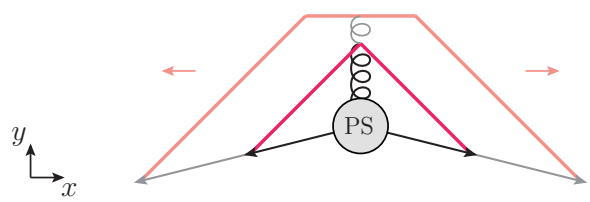

Figure 43.3: Schematic illustration of an $e^+e^- \to qg\bar{q}$ configuration emerging from the parton shower (PS). Snapshots of string positions are shown at two different times (full and shaded lines respectively). The gluon forms a transverse kink which grows in the y direction until all the gluon's kinetic energy has been used up.

effectively build up a transverse structure in the originally one-dimensional object, with infinitely soft ones smoothly absorbed into the string. Note: cyclic topologies made entirely of gluons (closed strings) are also possible, e.g. in decays such as $H \to gg$ or $\Upsilon \to ggg$. The space-time evolution is more involved when kinks are taken into account [82], but no additional free parameters need to be introduced. The main difference between quark and gluon hadronization stems from the fact that gluons are connected to two string pieces (one on either side), while quarks are only connected to a single string piece. Hence, the relative rate of energy loss per unit invariant time — and consequently also the rate of hadron production — is larger by a factor of 2 for gluons (analogously to the ratio of gluon to quark color charges $C_A/C_F = 2.25$).

43.2.1.2 *Transverse Momentum and Flavors*

For each breakup vertex, quantum mechanical tunneling is assumed to control the masses and p_T kicks (transverse to the string axis, in a frame in which the string itself has no transverse motion) that can be produced, leading to a Gaussian suppression

$$\mathrm{Prob}(m_q^2, p_{\mathrm{T},q}^2) \;\propto\; \exp\left(\frac{-\pi m_q^2}{\kappa}\right) \exp\left(\frac{-\pi p_{\mathrm{T},q}^2}{\kappa}\right) \;, \qquad (43.10)$$

where m_q is the mass of the produced quark flavor and p_T is the nonperturbative transverse momentum imparted to it by the breakup process, with a universal average value of $\left\langle p_{\mathrm{T},q}^2 \right\rangle = \kappa/\pi \sim (250\,\mathrm{MeV})^2$. The antiquark has the same mass and opposite p_T.

In an MC model with a fixed shower cutoff t_0, the effective amount of p_T in string breaks may be larger than the purely nonperturbative κ/π above, to account for effects of additional (unresolved) radiation below t_0.

From the mass term in Eq. (43.10), one concludes that charm and bottom quarks are too heavy to be produced in string breaks, while strange quarks will be suppressed relative to up and down ones. Lacking unambiguous and precise mass definitions for light quarks, however, the effective amount of strangeness suppression is normally extracted from experimental data, using observables such as K/π, K^*/ρ, and ϕ/K^* ratios.

Baryon production can also be incorporated, at various levels of sophistication. The simplest option is to allow string breaks to produce a diquark-antidiquark pair, where a diquark is a loosely bound states of two quarks in an overall $\bar{3}$ representation. Again, the relative rate of such pairs is extracted from data, e.g. using p/π or Λ/K ratios. Since the perturbative shower splittings do not produce diquarks, the optimal value for this parameter is mildly correlated with the amount of $g \to q\bar{q}$ splittings in the shower. More sophisticated options, including the so-called "popcorn" mechanism, are discussed in Ref. [82]. Finally, the `PYTHIA` framework also allows for baryon string junctions [86], in which three string pieces (which can be thought of as red, green, and blue, respectively) join together. These are used, e.g., to model the fragmentation of baryon beam remnants, and can also be created (in pairs of junctions and antijunctions) in some color-reconnection scenarios [87], making the effective baryon-to-meson ratios in such models dependent on the amount and type of color reconnections that occur in each event

The next step of the algorithm is the assignment of the produced quarks within hadron multiplets. Using a nonrelativistic classification of spin states, the hadronizing q may combine with the $\bar{q}'$ from a newly created breakup to produce a hadron of a given spin S and angular momentum L. The lowest-lying pseudoscalar and vector meson multiplets, and spin-1/2 and -3/2 baryons, are assumed to dominate in a string framework[2], but individual rates are not predicted by the model, and hence the ratios of spin-1 to spin-0 mesons and diquarks are free parameters (modulo a factor 3 from spin counting) which must be constrained by data.

43.2.2 *The Cluster Model*

The cluster hadronization model is based on *preconfinement*, i.e., on the observation [88, 89] that the color structure of a perturbative QCD shower evolution at any scale Q_0 is such that color-singlet subsystems of partons (labeled "clusters") occur with a universal invariant mass distribution which is power suppressed at large masses. For any starting scale $Q \gg Q_0 \gg \Lambda_\mathrm{QCD}$, only the number of such clusters depends on Q, while the shape of their mass distribution only depends on Q_0 and on Λ_QCD.

Following early models based on this universality [9, 90], the cluster model developed by Webber [91] has for many years been a hallmark of the `HERWIG` generators, with an alternative implementation [92] now available in the `SHERPA` generator. The key idea, in addition to preconfinement, is to force "by hand" all gluons to split into quark-antiquark pairs at the end of the parton shower. Compared with the string description, this effectively amounts to viewing gluons as "seeds" for string breaks, rather than as kinks in a continuous object. After the splittings, a new set of low-mass color-singlet clusters is obtained, formed only by quark-antiquark pairs. These can be decayed to on-shell hadrons in a simple manner, with the relative yields of different hadron species mainly governed by their masses and the size of the phase space.

The algorithm starts by generating the forced $g \to q\bar{q}$ breakups, and by assigning flavors and momenta to the produced quark

[2] In `PYTHIA`, the four $L = 1$ meson multiplets (scalar, tensor, and 2 pseudovectors) are also available but are disabled by default, since many states (and their decays) are poorly known.

Int. J. Mod. Phys. A 2026.41. Downloaded from www.worldscientific.com
by UNIVERSITY OF CALIFORNIA @ BERKELEY on 09/16/26. Re-use and distribution is strictly not permitted, except for Open Access articles.

pairs. For a typical shower cutoff corresponding to a gluon virtuality of $Q_{\rm had} \sim 1\,{\rm GeV}$, the $p_{\rm T}$ generated by the splittings can be neglected. The constituent light-quark masses, $m_{u,d} \sim 300\,{\rm MeV}$ and $m_s \sim 450\,{\rm MeV}$, imply a suppression (typically even an absence) of strangeness production. In principle, the model also allows for diquarks to be produced at this stage, but due to the larger constituent masses this would only become relevant for shower cutoffs larger than 1 GeV.

If a cluster formed in this way has an invariant mass above some cutoff value, typically 3–4 GeV, it is forced to undergo sequential $1 \to 2$ cluster breakups, along an axis defined by the constituent partons of the original cluster, until all sub-cluster masses fall below the cutoff value. Due to the preservation of the original axis in these breakups, this treatment has some resemblance to the string-like picture, though the nonperturbative $p_\perp$ kicks generated in this way are generally larger, up to half the allowed cluster mass.

Next, on the low-mass side of the spectrum, some clusters are allowed to decay directly to a single hadron, with nearby clusters absorbing any excess momentum. This improves the description of the high-z part of the spectrum — where the hadron carries almost all the momentum of its parent jet — at the cost of introducing one additional parameter, controlling the probability for single-hadron cluster decay.

Having obtained a final distribution of small-mass clusters, now with a strict cutoff at 3–4 GeV and with the component destined to decay to single hadrons already removed, the remaining clusters are interpreted as a smoothed-out spectrum of excited mesons, each of which decays isotropically to two hadrons, with relative probabilities proportional to the available phase space for each possible two-hadron combination that is consistent with the cluster's internal flavors, including spin degeneracy. It is important that all the light members (containing only uds) of each hadron multiplet be included, as the absence of members can lead to unphysical isospin or SU(3) flavor violation. Typically, the lightest pseudoscalar, vector, scalar, even and odd charge conjugation pseudovector, and tensor multiplets of light mesons are included. In addition, some excited vector multiplets of light mesons may be available. For baryons, usually only the lightest flavor-octet, -decuplet and -singlet baryons are present, although both the `HERWIG` and `SHERPA` implementations now include some heavier baryon multiplets as well.

Differently from the string model, the mechanism of phase-space suppression employed here leads to a natural enhancement of the lighter pseudoscalars, and no parameters beyond the spectrum of hadron masses need to be introduced at this point. The phase space also limits the transverse momenta of the produced hadrons relative to the jet axis.

Note that, since the masses and decays of excited heavy-flavor hadrons in particular are not well known, there is some freedom in the model to adjust these, which in turn will affect their relative phase-space populations.

43.2.3 *Hadron and τ Decays*

Of the so-called primary hadrons, originating directly from string breaks and/or cluster decays (see above), many are unstable and so decay further, until a set of particles is obtained that can be considered stable on time scales relevant to the given measurement. (A typical hadron-collider definition of a "stable particle" $c\tau \geq 10\,{\rm mm}$ includes weakly-decaying strange hadrons K, Λ, $\Sigma^\pm$, $\bar{\Sigma}^\pm$, Ξ, Ω.) The decay modeling can therefore have a significant impact on final particle yields and spectra, especially for the lowest-lying hadronic states, which receive the largest relative contributions from decays (feed-down). This interplay also implies that hadronization parameters may need to be retuned if significant changes to the decay treatment are made.

Particle summary tables, such as those given elsewhere in this *Review*, represent a condensed summary of the available experimental measurements and hence may be incomplete and/or exhibit inconsistencies within the experimental precision. In an MC decay package, on the other hand, all information must be quantified and consistent, with all branching ratios summing to unity. When adapting particle summary information for use in a decay package, a number of choices must therefore be made. The amount of ambiguity increases as more excited hadron multiplets are added to the simulation, about which less and less is known from experiment, with each GPMC making its own choices.

A related choice is how to distribute the decay products differentially in phase space, in particular which matrix elements to use. Historically, MC generators contained matrix elements only for selected (generator-specific) classes of hadron and τ decays, coupled with a Breit-Wigner smearing of the masses, truncated at the edges of the physical decay phase space (the treatment of decay thresholds can be important for certain modes [10]). A more sophisticated treatment can then be obtained by reweighting the generated events using the obtained particle four-momenta and/or by using specialized external packages such as `EVTGEN` [93] for hadron decays and `TAUOLA` [94] for τ decays.

More recently, `HERWIG` and `SHERPA` include helicity-dependence in τ decays [95, 96], with a more limited treatment available in `PYTHIA` 8 [4]. The `HERWIG` and `SHERPA` generators have also included significantly improved internal simulations of hadronic decays, which include spin correlations between those decays for which matrix elements are used. Photon-bremsstrahlung effects are discussed in Sec. 43.1.7.

`HERWIG` and `PYTHIA` include the probability for B mesons to oscillate into $\bar{B}$ ones before decay. `SHERPA` and `EVTGEN` also include CP-violating effects and, for common decay modes of the neutral meson and its antiparticle, the interference between the direct decay and oscillation followed by decay.

We end on a note of warning on double counting. This may occur if a particle can decay via an intermediate on-shell resonance. An example is $a_1 \to \pi\pi\pi$ which may proceed via $a_1 \to \rho\pi$, $\rho \to \pi\pi$. If these decay channels of the a_1 are both included, each with their full partial width, a double counting of the on-shell $a_1 \to \rho\pi$ contribution would result. Such cases are normally dealt with consistently in the default MC generator packages, so this warning is mostly for users that wish to edit decay tables on their own.

43.3 Models for Soft Hadron-Hadron Physics

43.3.1 *Underlying Event*

In the GPMC context, "underlying event" (UE) denotes any additional activity *beyond* the basic process and its associated ISR and FSR activity. The UE is thus only defined in the context of events selected with a "hard" (i.e., high-$p_\perp$) trigger which defines the basic process at hand. The dominant contribution to the UE is believed to come from additional color exchanges between the colliding hadronic states. These multiple exchanges can be modeled either as additional perturbative (mainly t-channel gluon) exchanges, called multiple parton-parton interactions (MPI), or nonperturbatively using so-called cut pomerons (roughly equivalent to exchange of gluons with $p_\perp \to 0$). The experimental observation that events with a hard trigger are accompanied by a higher-than-average level of associated activity is called the "jet pedestal" effect.

The most clearly identifiable consequence of MPI is arguably the possibility of observing several hard parton-parton interactions in one and the same hadron-hadron event. Typically, these are QCD $2 \to 2$ interactions, which produce additional back-to-back jet pairs, with each pair having a small value of sum($\vec{p}_\perp$). The fraction of MPI that give rise to additional reconstructible jets is, however, small. Soft interactions, that exchange color and a small amount of momentum without giving rise to observable jets, are much more plentiful, and can give significant corrections to the color flow and total scattered energy of the event. This affects the final-state activity in a more global way, increasing hadron-multiplicity and summed E_T distributions, and contributing to the break-up of the beam remnants in the forward direction.

The first detailed Monte Carlo model for perturbative MPI was proposed in Ref. [97], and with some variation this still forms the basis for most modern implementations. Some useful additional references can be found in Ref. [10]. The first crucial observation is that the t-channel propagators appearing in perturbative QCD $2 \to 2$ scattering almost go on shell at low $p_{\rm T}$, causing the

Phys. A 2026.41. Downloaded from www.worldscientific.com
by UNIVERSITY OF CA LEY on 09/16/26. Re-use and distribution is strictly not permitted, except for Open Access articles.

differential cross sections to behave roughly as

$$d\sigma_{2\to 2} \propto \frac{dt}{t^2} \sim \frac{dp_{\mathrm{T}}{}^2}{p_{\mathrm{T}}{}^4} \ . \tag{43.11}$$

This cross section represents the inclusive scattering of partons against partons in perturbative QCD, summed over all partons. Thus, if a single hadron-hadron scattering contains *two* parton-parton interactions, that event will contribute twice to the parton-parton cross section $\sigma_{2\to 2}$ but only once to the hadron-hadron one σ_{tot}, and so on. In the limit that all the parton-parton interactions are independent and equivalent, one has

$$\sigma_{2\to 2} = \langle n \rangle \ \sigma_{\mathrm{tot}} \ , \tag{43.12}$$

with $\langle n \rangle$ the average number of parton-parton interactions, typically defined with some minimal $p_{\mathrm{T}} > p_{\perp\mathrm{min}}$ to render the parton-parton cross section finite. The probability for n parton-parton scatterings then follows a Poisson distribution,

$$\mathcal{P}_n = \langle n \rangle^n \frac{\exp\left(-\langle n \rangle\right)}{n!} \ . \tag{43.13}$$

This simple argument expresses unitarity; instead of the total hadron-hadron interaction cross section diverging as the parton-parton $p_{\mathrm{T}} \to 0$ (which would violate unitarity), we have restated the problem so that it is now the *number of parton-parton interactions per hadron-hadron collision* that diverges, with the total hadron-hadron cross section remaining finite. At LHC energies, the parton-parton scattering cross sections computed using the LO QCD cross section folded with modern PDFs become larger than the total pp one for $p_{\perp\mathrm{min}}$ values of order 4–5 GeV (see e.g. [98, 99]). One therefore expects the average number of perturbative MPI to exceed unity at around that scale.

Two ingredients remain to fully regulate the remaining divergence. Firstly, the interactions cannot use up more momentum than is available in the parent hadron. This suppresses the large-n tail of the estimate above. In `PYTHIA`-based models, the MPI are ordered in p_{T}, and the parton densities for each successive interaction are explicitly constructed so that the sum of x fractions can never be greater than unity. In the `HERWIG` models, the Poisson estimate of $\langle n \rangle$ above is used as an initial guess, but the generation of actual MPI is stopped once the energy-momentum conservation limit is reached. Both of these approaches generate momentum (conservation) correlations among the MPI.

The second ingredient invoked to suppress the number of interactions, at low p_{T} and x, is color screening; if the wavelength $\sim 1/p_{\mathrm{T}}$ of an exchanged colored parton becomes larger than a typical color-anticolor separation distance, it will only see an *average* color charge that vanishes in the limit $p_{\mathrm{T}} \to 0$. This provides an infrared cutoff for MPI similar to that provided by the hadronization scale for parton showers. A first estimate of the color-screening cutoff would be the proton size, $p_{\perp\mathrm{min}} \approx \hbar/r_p \approx 0.3\,\mathrm{GeV} \approx \Lambda_{\mathrm{QCD}}$, but empirically this appears to be far too low. In current models, one replaces the proton radius r_p in the above formula by a "typical color screening distance," i.e., an average size of a region within which the net compensation of a given color charge occurs. This number is not known from first principles [100] and is perceived of simply as an effective cut-off parameter. The simplest choice is to introduce a step function $\Theta(p_{\mathrm{T}} - p_{\perp\mathrm{min}})$. Alternatively, one may note that the jet cross section is divergent like $\alpha_{\mathrm{S}}^2(p_{\mathrm{T}}{}^2)/p_{\mathrm{T}}{}^4$, cf. Eq. (43.11), and that therefore a factor

$$\frac{\alpha_{\mathrm{S}}^2(p_{\mathrm{T},0}^2 + p_{\mathrm{T}}{}^2)}{\alpha_{\mathrm{S}}^2(p_{\mathrm{T}}{}^2)} \frac{p_{\mathrm{T}}{}^4}{(p_{\mathrm{T},0}^2 + p_{\mathrm{T}}{}^2)^2} \tag{43.14}$$

would smoothly regulate the divergences, now with $p_{\mathrm{T},0}$ as the free parameter. Regardless of whether it is imposed as a smooth (`PYTHIA` and `SHERPA`) or step (`HERWIG`) function, this is effectively the main "tuning" parameter in such models.

Note that the numerical value obtained for the cross section depends upon the PDF set used, and therefore the optimal value to use for the cutoff will also depend on this choice. Note also that the cutoff does not have to be energy-independent. Higher energies imply that parton densities can be probed at smaller x values, where the number of partons rapidly increases. Partons then become closer packed and the color screening distance d decreases. The uncertainty on the energy and/or x scaling of the cutoff is a major concern when extrapolating between different collider energies [101].

We now turn to the origin of the observational fact that hard jets appear to sit on top of a higher "pedestal" of underlying activity than events with no hard jets. This is interpreted as a consequence of impact-parameter-dependence: in peripheral collisions, only a small fraction of events contain any high-p_{T} activity, whereas central collisions are more likely to contain at least one hard scattering; a high-p_{T} triggered sample will therefore be biased towards small impact parameters, b. The ability of a model to describe both the UE in events with a hard trigger as well as the activity in inclusive "minimum-bias" (MB) samples (see below) therefore depends upon its modeling of the b-dependence, and correspondingly the impact-parameter shape constitutes another main tuning parameter.

For each impact parameter b, the number of interactions $\tilde{n}(b)$ can still be assumed to be distributed according to Eq. (43.13), again modulo momentum conservation, but now with the mean value of the Poisson distribution depending on impact parameter, $\langle \tilde{n}(b) \rangle$. This causes the final n-distribution (integrated over b) to be wider than a Poissonian.

Finally, there are two perturbative modeling aspects which go beyond the introduction of MPI themselves: 1) parton showers off the MPI, and 2) perturbative parton-rescattering effects. Without showers, MPI models would generate very sharp peaks for back-to-back MPI jets, caused by unshowered partons passed directly to the hadronization model. However, with the exception of the oldest `PYTHIA6` model, all GPMC models do include such showers [10], and hence should exhibit more realistic (i.e., broader and more decorrelated) MPI jets. On the initial-state side, the main questions are whether and how correlated multi-parton densities are taken into account and, as discussed previously, how the showers are regulated at low p_{T} and/or low x. Although none of the general purpose MC models currently impose a rigorous correlated multi-parton evolution, all of them include some elementary aspects. The most significant for parton-level results is arguably momentum conservation, which is enforced explicitly in all the models. The so-called "interleaved" models [27] attempt to go a step further, generating an explicitly correlated multi-parton evolution in which flavor sum rules are imposed to conserve, e.g. the total numbers of valence and sea quarks [86]. Fully correlated double-parton evolution is so far only available in the more specialised code dShower [102]; see [103] for comparisons between this and Pythia's interleaved model.

Perturbative rescattering in the final state can occur if partons are allowed to undergo several distinct interactions, with showering activity possibly taking place in-between. This has so far not been studied extensively, but a first exploratory model is available [104]. In the initial state, parton rescattering/recombination effects have so far not been included in any of the GPMC models.

43.3.2 *Bose-Einstein and Color-Reconnection Effects*

In the context of e^+e^- collisions, Bose-Einstein (BE) correlations have mostly been discussed as a source of uncertainty on high-precision W mass determinations at LEP [105]. In hadron-hadron (and nucleus-nucleus) collisions, however, BE correlations are used extensively to study the space-time structure of hadronizing matter ("femtoscopy").

In MC models of hadronization, each string break or particle/-cluster decay is normally factorized from all other ones. This reduces the number of variables that must be considered in each step, but also makes it intrinsically difficult to introduce correlations among particles from different breaks/decays. In GPMCs, a few semi-classical models are available within the `PYTHIA` 6 and 8 generators [106], in which the BE effect is mimicked by an attractive interaction between pairs of identical particles in the final state, with no higher correlations included. Variants of this model differ mainly by the assumed shape of the correlation function and how overall momentum conservation is handled.

As discussed in Sec. 43.2, leading-color ("planar") color flows

Int. J. Mod. Phys. A 2026.41. Downloaded from www.worldscientific.com by UNIVERSITY OF CALIFORNIA @ BERKELEY on 09/16/26. Re-use and distribution is strictly not permitted, except for Open Access articles.

are used to set up the hadronizing systems (clusters or strings) at the hadronization stage. If the systems do not overlap significantly in space and time, subleading-color ambiguities and/or nonperturbative reconnections are expected to be small. However, if the density of displaced color charges is sufficiently high that several systems can overlap significantly, full-color and/or reconnection effects should become progressively larger.

In the specific context of MPI, a crucial question is how color is neutralized *between* different MPI systems, including the remnants. The large rapidity differences involved imply large invariant masses (though normally low p_{T}), and hence large amounts of (soft) particle production. Indeed, in the context of soft-inclusive physics, it is these "inter-system" strings/clusters that furnish the dominant particle-production mechanism, and hence their modeling is an essential part of the soft-physics description, affecting topics such as MB/UE multiplicity and p_{T} distributions, rapidity gaps, and precision mass measurements. Reviews of color-reconnection effects can be found in [10, 87].

43.3.3 *Minimum-Bias Events and Diffraction*

The term "minimum bias" (MB) originates from the experimental requirement of a minimal number of tracks (or hits) in a given instrumented region. In order to make MC predictions for such observables, all possible contributions to the relevant phase-space region must be accounted for. There are essentially four types of physics processes, which together make up the total hadron-hadron (hh) cross section: 1) elastic scattering[3]: $hh \to hh$, 2) single diffractive dissociation: $hh \to h + \mathrm{gap} + X$, with X denoting anything that is not the original beam particle, and "gap" denoting a rapidity region devoid of observed activity; 3) double diffractive dissociation: $hh \to X + \mathrm{gap} + X$, and 4) inelastic non-diffractive scattering: everything else. A fifth class may also be defined, called central diffraction ($hh \to h + \mathrm{gap} + X + \mathrm{gap} + h$). Note that different terminologies exist [107]: in experimental settings, diffraction is typically defined by an observable gap, of some minimal size in rapidity, while in the MC context, each diffractive physics process produces a whole spectrum of gaps, with small ones suppressed but not excluded.

The inelastic non-diffractive part of the cross section is typically modeled either by smoothly regulating and extending the perturbative QCD scattering cross sections all the way to zero $p_\perp$ [97] (`PYTHIA` and `SHERPA`), or by regulating the QCD cross sections with a sharp cutoff [108] and adding a separate class of nonperturbative scatterings below that scale [109] (`HERWIG`). See also Sec. 43.3.1. In all cases, the most important ingredients are: 1) the IR regularization of the perturbative scattering cross sections, including their PDF dependence, 2) the assumed matter distribution of the colliding hadrons, possibly including multi-parton correlations [86] and/or x dependence [110], and 3) additional soft-QCD effects such as color reconnections, discussed in Sec. 43.3.2.

Currently, there are essentially three methods for simulating diffraction in the main MC models: 1) in `PYTHIA` 6, one picks a diffractive mass according to parameterized cross sections $\propto \mathrm{d}M^2/M^2$ [111]. This mass is represented as a string, which is hadronized as described in Sec. 43.2.1, though differences in the effective scale of the hadronization may necessitate a (re)tuning of the hadronization parameters for diffraction; 2) in `PYTHIA` 8, the high-mass tail beyond $M \sim 10\,\mathrm{GeV}$ is augmented by a partonic description in terms of pomeron PDFs [112], allowing diffractive jet production including showers and underlying event [4]; 3) the `PHOJET` and `DPMJET` programs also include central diffraction and rely directly on a formulation in terms of pomerons (color-singlet multi-gluon states) [113–115]. Cut pomerons correspond to exchanges of soft gluons while uncut ones give elastic and diffractive topologies as well as virtual corrections that help preserve unitarity. So-called "hard pomerons" provide a transition to the perturbative regime. Hadronization is still handled using the Lund string model, so there is some overlap with the above models at the hadronization stage. In addition, a pomeron-based package exists for `HERWIG` [116], and an effort is underway to construct an MC implementation of the "KMR" model [100] within the `SHERPA` generator. Color reconnections (Sec. 43.3.2) may also play a role in creating rapidity gaps and the underlying event (Sec. 43.3.1) in filling them.

[3]The QED elastic cross section diverges and is normally a non-default option.

43.4 Uncertainties and Tuning

The accuracy that can be achieved by a GPMC model depends on the sophistication of the theory models it incorporates, on the available constraints on its free parameters, and on the nature of the observable(s) under study. Using existing data to constrain the model parameters is referred to as generator tuning. Although tuned models do tend to yield improved results also for observables that they have not been tuned to, the question of evaluating the remaining uncertainties reliably is still far from solved. It is worth noting, however, that all of the GPMCs now provide options for automatic evaluation of perturbative shower uncertainties (e.g., via renormalization-scale variations), in the form of vectors of alternative event weights [117–119]. One must be aware that these variations are not necessarily exhaustive and significant weight fluctuations can be a problem for processes with large shower phase spaces. Nonperturbative uncertainties are normally still evaluated by varying salient model parameters by hand, though this looks set to change with a new method based on reweighting [120]. A general method called eigentunes [121] is also available, based on global fits to data.

Typically, the overall event properties are determined by only a few, very important parameters, such as the effective value of α_{S}, for perturbative corrections, and the shape of the fragmentation functions, for nonperturbative ones. More parameters may then be introduced to describe successively more detailed aspects (e.g., the rates and decays of individual hadron species), but these should have progressively less impact on the overall modeling. One may therefore take a factorized approach, first constraining the perturbative parameters and thereafter the nonperturbative ones, in order of decreasing significance to the overall modeling. Furthermore, by identifying which measurements are most sensitive to each parameter, this ordering can be reflected in the way that data is selected and applied to constrain the models. Thus, measurements sensitive to global event properties would typically be applied first, to constrain the most inclusive parameters, and so on for progressively more exclusive aspects. For high-p_{T} processes, one should be aware that if the perturbative modelling is not adequate, there is a risk that one may end up effectively mistuning nonperturbative parameters to compensate for perturbative deficiencies. This is obviously wrong and care must be taken to avoid it. E.g., it would not make sense to tune to get the right total number of hadrons unless one also gets the right total number of jets. In this context, it may be more desirable to use ratios like the number of hadrons *per jet*.

Note also that the unitarity of shower and hadronization models implies that the Born-level cross-section normalization is not tunable, hence in tuning contexts one tends to focus on the shapes of distributions rather than their normalizations.

At LO×(N)LL, perturbation theory is doing well if it agrees with an IR safe shape measurement within $\sim 10\%$. It would therefore not make much sense to tune a GPMC to agree with individual data points beyond this level. To reflect this, and to protect against overfitting, a 5% sanity limit has sometimes been enforced in tuning studies [98, 122]. The advent of NLO Monte Carlos may reduce this number slightly, but only for quantities for which one expects NLO precision. For quantities governed by nonperturbative physics, uncertainties are larger. For some quantities, e.g. ones for which the underlying modeling is known to be poor, an order-of-magnitude agreement or worse may have to be accepted.

In the context of LO×LL GPMC tuning, subleading aspects of coupling-constant and PDF choices are relevant. In particular, one should be aware that the choice of QCD Λ parameter $\Lambda_{\mathrm{MC}} = 1.569\Lambda_{\overline{\mathrm{MS}}}$ (for 5 active flavors) improves the predictions of coherent shower algorithms at the NLL level for a class of relevant observables [123]. The question of LO vs. NLO PDFs is more involved [10], but it should be emphasized that the gluon PDF at (very) low x is important for determining the level of the underlying event in MPI models (Sec. 43.3.1), and hence the MB/UE tuning (and energy scaling [101]) is linked to the choice

Phys. A 2026.41. Downloaded from www.worldscientific.com
by UNIVERSITY OF CA LEY on 09/16/26. Re-use and distribution is strictly not permitted, except for Open Access articles.

of PDF in such models. Further issues and an example of a specific recipe that could be followed in a realistic set-up can be found in Ref. [98]. A useful online resource can be found at the mcplots.cern.ch website [124], based on the RIVET tool [125].

Recent years have seen the emergence of automated tools to reduce the amount of both computer and manpower required for tuning [121,126,127]. Automating the human expert input is more difficult. In the tools currently on the market, this is addressed by a combination of input solicited from the GPMC authors (e.g., which parameters and ranges to consider, which observables constitute a complete set, etc) and a set of weights determining the relative priority given to each bin in each distribution. The final result is therefore still subjective but at least reproducible. Backed by careful demonstrations of sensitivities, correlations, and uncertainties, competitive tunes can be produced. The field is still burgeoning, with future sophistications to be expected.

References

[1] G. Corcella *et al.*, JHEP **01**, 010 (2001), [hep-ph/0011363].

[2] G. Bewick *et al.*, Eur. Phys. J. C **84**, 10, 1053 (2024), [arXiv:2312.05175].

[3] T. Sjöstrand, S. Mrenna and P. Z. Skands, JHEP **05**, 026 (2006), [hep-ph/0603175].

[4] C. Bierlich *et al.*, SciPost Phys. Codebases **8** (2022), [arXiv:2203.11601].

[5] E. Bothmann *et al.* (Sherpa), JHEP **12**, 156 (2024), [arXiv:2410.22148].

[6] QCD summary, PDG.

[7] T. Kinoshita, J. Math. Phys. **3**, 650 (1962).

[8] T. Lee and M. Nauenberg, Phys. Rev. **133**, B1549 (1964).

[9] G. C. Fox and S. Wolfram, Nucl. Phys. B **168**, 285 (1980).

[10] A. Buckley *et al.*, Phys. Rept. **504**, 145 (2011), [arXiv:1101.2599].

[11] G. Altarelli and G. Parisi, Nucl. Phys. B **126**, 298 (1977).

[12] A. Einstein, B. Podolsky and N. Rosen, Phys. Rev. **47**, 777 (1935).

[13] B. Webber, Phys. Lett. B **193**, 91 (1987).

[14] J. C. Collins, Nucl. Phys. B **304**, 794 (1988).

[15] I. Knowles, Comput. Phys. Commun. **58**, 271 (1990).

[16] K. Hamilton *et al.*, JHEP **03**, 193 (2022), [arXiv:2111.01161].

[17] T. Sjöstrand, Phys. Lett. B **157**, 321 (1985).

[18] G. Marchesini and B. Webber, Nucl. Phys. B **310**, 461 (1988).

[19] S. Gieseke, P. Stephens and B. Webber, JHEP **12**, 045 (2003), [hep-ph/0310083].

[20] M. Bengtsson and T. Sjöstrand, Nucl. Phys. B **289**, 810 (1987).

[21] G. Gustafson and U. Pettersson, Nucl. Phys. B **306**, 746 (1988).

[22] L. Lönnblad, Comput. Phys. Commun. **71**, 15 (1992).

[23] H. Brooks, C. T. Preuss and P. Skands, JHEP **07**, 032 (2020), [arXiv:2003.00702].

[24] Z. Nagy and D. E. Soper, JHEP **10**, 024 (2005), [hep-ph/0503053].

[25] S. Schumann and F. Krauss, JHEP **03**, 038 (2008), [arXiv:0709.1027].

[26] S. Plätzer and S. Gieseke, Eur. Phys. J. C **72**, 2187 (2012), [arXiv:1109.6256].

[27] T. Sjöstrand and P. Z. Skands, Eur. Phys. J. C **39**, 129 (2005), [hep-ph/0408302].

[28] M. Dasgupta *et al.*, Phys. Rev. Lett. **125**, 5, 052002 (2020), [arXiv:2002.11114].

[29] J. R. Forshaw, J. Holguin and S. Plätzer, JHEP **09**, 014 (2020), [arXiv:2003.06400].

[30] Z. Nagy and D. E. Soper, Phys. Rev. D **99**, 5, 054009 (2019), [arXiv:1902.02105].

[31] F. Herren *et al.*, JHEP **10**, 091 (2023), [arXiv:2208.06057].

[32] G. Salam, PanScales web page, `https://gsalam.web.cern.ch/panscales/`.

[33] E. Norrbin and T. Sjöstrand, Nucl. Phys. B **603**, 297 (2001), [hep-ph/0010012].

[34] S. Catani *et al.*, Nucl. Phys. B **627**, 189 (2002), [hep-ph/0201036].

[35] B. Assi and S. Höche, Phys. Rev. D **109**, 11, 114008 (2024), [arXiv:2307.00728].

[36] J. Cembranos *et al.*, JHEP **09**, 077 (2013), [arXiv:1305.2124].

[37] N. Davidson, T. Przedzinski and Z. Was, Comput. Phys. Commun. **199**, 86 (2016), [arXiv:1011.0937].

[38] K. Hamilton and P. Richardson, JHEP **07**, 010 (2006), [hep-ph/0603034].

[39] M. Schonherr and F. Krauss, JHEP **12**, 018 (2008), [arXiv:0810.5071].

[40] D. R. Yennie, S. C. Frautschi and H. Suura, Annals Phys. **13**, 379 (1961).

[41] S. Jadach *et al.*, Phys. Rev. D **94**, 7, 074006 (2016), [arXiv:1608.01260].

[42] J. R. Christiansen and T. Sjöstrand, JHEP **04**, 115 (2014), [arXiv:1401.5238].

[43] M. R. Masouminia and P. Richardson, JHEP **04**, 112 (2022), [arXiv:2108.10817].

[44] H. Brooks, P. Skands and R. Verheyen, SciPost Phys. **12**, 3, 101 (2022), [arXiv:2108.10786].

[45] A. Semenov, Comput. Phys. Commun. **180**, 431 (2009), [arXiv:0805.0555].

[46] N. D. Christensen and C. Duhr, Comput. Phys. Commun. **180**, 1614 (2009), [arXiv:0806.4194].

[47] M. Fairbairn *et al.*, Phys. Rept. **438**, 1 (2007), [hep-ph/0611040].

[48] J. Alwall *et al.*, Comput. Phys. Commun. **176**, 300 (2007), [hep-ph/0609017].

[49] P. Z. Skands *et al.*, JHEP **07**, 036 (2004), [hep-ph/0311123].

[50] J. Alwall *et al.* (2007), [arXiv:0712.3311].

[51] T. Ježo *et al.*, Eur. Phys. J. C **76**, 12, 691 (2016), [arXiv:1607.04538].

[52] P. Richardson, JHEP **11**, 029 (2001), [hep-ph/0110108].

[53] E. Boos *et al.*, in "2nd Les Houches Workshop on Physics at TeV Colliders," (2001), [hep-ph/0109068].

[54] M. Bengtsson and T. Sjöstrand, Phys. Lett. B **185**, 435 (1987).

[55] W. Giele, D. Kosower and P. Skands, Phys. Rev. D **84**, 054003 (2011), [arXiv:1102.2126].

[56] S. Catani *et al.*, JHEP **11**, 063 (2001), [hep-ph/0109231].

[57] J. Alwall *et al.*, Eur. Phys. J. C **53**, 473 (2008), [arXiv:0706.2569].

[58] H. Brooks and C. T. Preuss, Comput. Phys. Commun. **264**, 107985 (2021), [arXiv:2008.09468].

[59] P. Nason, JHEP **11**, 040 (2004), [hep-ph/0409146].

[60] B. Cooper *et al.*, Eur. Phys. J. C **72**, 2078 (2012), [arXiv:1109.5295].

[61] M. L. Mangano *et al.*, JHEP **07**, 001 (2003), [hep-ph/0206293].

[62] J. Alwall *et al.*, JHEP **06**, 128 (2011), [arXiv:1106.0522].

[63] S. Frixione and B. R. Webber, JHEP **06**, 029 (2002), [hep-ph/0204244].

[64] S. Alioli *et al.*, JHEP **06**, 043 (2010), [arXiv:1002.2581].

Int. J. Mod. Phys. A 2026.41. Downloaded from www.worldscientific.com
by UNIVERSITY OF CALIFORNIA @ BERKELEY on 09/16/26. Re-use and distribution is strictly not permitted, except for Open Access articles.

[65] J. M. Campbell *et al.*, in "Snowmass 2021," (2022), [arXiv:2203.11110].

[66] M. van Beekveld *et al.* (2025), [arXiv:2504.05377].

[67] P. Sarmah, A. Siódmok and J. Whitehead, Acta Phys. Polon. Supp. **18**, 5, 5 (2025).

[68] J. Alwall *et al.*, JHEP **07**, 079 (2014), [arXiv:1405.0301].

[69] R. Frederix and S. Frixione, JHEP **12**, 061 (2012), [arXiv:1209.6215].

[70] L. Lönnblad and S. Prestel, JHEP **03**, 166 (2013), [arXiv:1211.7278].

[71] K. Hamilton, P. Nason and G. Zanderighi, JHEP **10**, 155 (2012), [arXiv:1206.3572].

[72] S. Hoeche *et al.*, JHEP **04**, 027 (2013), [arXiv:1207.5030].

[73] S. Höche, Y. Li and S. Prestel, Phys. Rev. D **91**, 7, 074015 (2015), [arXiv:1405.3607].

[74] K. Hamilton *et al.*, JHEP **05**, 082 (2013), [arXiv:1212.4504].

[75] P. F. Monni *et al.*, JHEP **05**, 143 (2020), [arXiv:1908.06987].

[76] S. Alioli *et al.*, JHEP **06**, 089 (2014), [arXiv:1311.0286].

[77] L. Buonocore *et al.* (2022), [arXiv:2203.07240].

[78] S. Alioli *et al.*, JHEP **05**, 128 (2023), [arXiv:2301.11875].

[79] G. Gustafson 193–198 (1986).

[80] X. Artru and G. Mennessier, Nucl. Phys. B **70**, 93 (1974).

[81] B. Andersson *et al.*, Phys. Rept. **97**, 31 (1983).

[82] B. Andersson, *The Lund model*, volume 7, Cambridge University Press (2005), ISBN 978-0-521-01734-3, 978-0-521-42094-5, 978-0-511-88149-7.

[83] M. Bowler, Z. Phys. C **11**, 169 (1981).

[84] C. Peterson *et al.*, Phys. Rev. D **27**, 105 (1983).

[85] J. Altmann *et al.*, Eur. Phys. J. C **85**, 1, 16 (2025), [arXiv:2405.19137].

[86] T. Sjöstrand and P. Z. Skands, JHEP **03**, 053 (2004), [hep-ph/0402078].

[87] J. R. Christiansen and P. Z. Skands, JHEP **08**, 003 (2015), [arXiv:1505.01681].

[88] D. Amati and G. Veneziano, Phys. Lett. B **83**, 87 (1979).

[89] A. Bassetto, M. Ciafaloni and G. Marchesini, Phys. Lett. B **83**, 207 (1979).

[90] R. D. Field and S. Wolfram, Nucl. Phys. B **213**, 65 (1983).

[91] B. Webber, Nucl. Phys. B **238**, 492 (1984).

[92] J.-C. Winter, F. Krauss and G. Soff, Eur. Phys. J. C **36**, 381 (2004), [hep-ph/0311085].

[93] D. Lange, Nucl. Instrum. Meth. A **462**, 152 (2001).

[94] S. Jadach *et al.*, Comput. Phys. Commun. **76**, 361 (1993).

[95] D. Grellscheid and P. Richardson (2007), [arXiv:0710.1951].

[96] T. Gleisberg *et al.*, JHEP **02**, 007 (2009), [arXiv:0811.4622].

[97] T. Sjöstrand and M. van Zijl, Phys. Rev. D **36**, 2019 (1987).

[98] P. Skands, S. Carrazza and J. Rojo, Eur. Phys. J. C **74**, 8, 3024 (2014), [arXiv:1404.5630].

[99] M. Bahr, J. M. Butterworth and M. H. Seymour, JHEP **01**, 065 (2009), [arXiv:0806.2949].

[100] M. Ryskin, A. Martin and V. Khoze, Eur. Phys. J. C **71**, 1617 (2011), [arXiv:1102.2844].

[101] H. Schulz and P. Skands, Eur. Phys. J. C **71**, 1644 (2011), [arXiv:1103.3649].

[102] B. Cabouat and J. R. Gaunt, JHEP **10**, 012 (2020), [arXiv:2008.01442].

[103] O. Fedkevych and J. R. Gaunt, JHEP **02**, 090 (2023), [arXiv:2208.08197].

[104] R. Casalbuoni *et al.*, JHEP **01**, 035 (2009), [arXiv:0812.1982].

[105] LEP Electroweak Working Group (2005), [hep-ex/0511027].

[106] L. Lönnblad and T. Sjöstrand, Eur. Phys. J. C **2**, 165 (1998), [hep-ph/9711460].

[107] V. Khoze *et al.*, Eur. Phys. J. C **69**, 85 (2010), [arXiv:1005.4839].

[108] J. Butterworth, J. R. Forshaw and M. Seymour, Z. Phys. C **72**, 637 (1996), [hep-ph/9601371].

[109] M. Bahr *et al.*, in "1st International Workshop on Multiple Partonic Interactions at the LHC," 239–248 (2009), [arXiv:0905.4671].

[110] R. Corke and T. Sjöstrand, JHEP **05**, 009 (2011), [arXiv:1101.5953].

[111] G. A. Schuler and T. Sjöstrand, Phys. Rev. D **49**, 2257 (1994).

[112] G. Ingelman and P. Schlein, Phys. Lett. B **152**, 256 (1985).

[113] P. Aurenche *et al.*, Comput. Phys. Commun. **83**, 107 (1994), [hep-ph/9402351].

[114] F. W. Bopp, R. Engel and J. Ranft, in "LAFEX International School on High-Energy Physics (LISHEP 98) Session A: Particle Physics for High School Teachers - Session B: Advanced School in HEP - Session C: Workshop on Diffractive Physics," 729–741 (1998), [hep-ph/9803437].

[115] S. Roesler, R. Engel and J. Ranft, in "International Conference on Advanced Monte Carlo for Radiation Physics, Particle Transport Simulation and Applications (MC 2000)," 1033–1038 (2000), [hep-ph/0012252].

[116] B. E. Cox and J. R. Forshaw, Comput. Phys. Commun. **144**, 104 (2002), [hep-ph/0010303].

[117] J. Bellm *et al.*, Phys. Rev. D **94**, 3, 034028 (2016), [arXiv:1605.08256].

[118] S. Mrenna and P. Skands, Phys. Rev. D **94**, 7, 074005 (2016), [arXiv:1605.08352].

[119] E. Bothmann, M. Schönherr and S. Schumann, Eur. Phys. J. C **76**, 11, 590 (2016), [arXiv:1606.08753].

[120] C. Bierlich *et al.*, SciPost Phys. **16**, 5, 134 (2024), [arXiv:2308.13459].

[121] A. Buckley *et al.*, Eur. Phys. J. C **65**, 331 (2010), [arXiv:0907.2973].

[122] A. Jueid *et al.*, JHEP **02**, 119 (2024), [arXiv:2303.11363].

[123] S. Catani, B. Webber and G. Marchesini, Nucl. Phys. B **349**, 635 (1991).

[124] N. Korneeva, A. Karneyeu and P. Skands, Eur. Phys. J. Plus **139**, 7, 653 (2024), [arXiv:2401.10621].

[125] C. Bierlich *et al.*, SciPost Phys. **8**, 026 (2020), [arXiv:1912.05451].

[126] J. Bellm and L. Gellersen, Eur. Phys. J. C **80**, 1, 54 (2020), [arXiv:1908.10811].

[127] M. Krishnamoorthy *et al.*, EPJ Web Conf. **251**, 03060 (2021), [arXiv:2103.05748].

44. Monte Carlo Neutrino Generators

Revised September 2025 by H. Gallagher (Tufts U.) and Y. Hayato (Kamioka Observatory, ICRR, UTokyo; Kavli IPMU (WPI), UTokyo).

Monte Carlo neutrino generators are programs or libraries which simulate neutrino interactions with electrons, nucleons and nuclei. In this capacity their usual task is to take an input neutrino and nucleus and produce a set of 4-vectors for particles emerging from the interaction, which are then input to full detector simulations. Since these generators have to simulate not only the initial interaction of neutrinos with target particles, but reinteractions of the generated particles in the nucleus, they contain a wide range of elementary particle and nuclear physics. Viewed more broadly, they are the access point for neutrino experimentalists to the theory inputs needed for analysis. Examples include cross section libraries for event rate calculations and parameter uncertainties and reweighting tools for systematic error evaluation.

Neutrino experiments typically operate in neutrino beams that are neither completely pure nor mono-energetic. Generators are a crucial component in the convolution of beam flux, neutrino interaction physics, and detector response that is necessary to make predictions about observable quantities. Generated events are used to define experimental analyses, like event selection criteria, for efficiency determination and background subtraction. Similarly they are used to relate reconstructed quantities back to true quantities. In these various capacities they are used from the detector design stage through the extraction of physics measurements from reconstructed observable. Monte Carlo neutrino generators play unique and important roles in the experimental study of neutrino interactions and oscillations.

There are several neutrino event generators available, such as ANIS [1], GENIE [2, 3], GiBUU [4, 5], MARLEY [6], NEGN [7], NEUT [8], NUANCE [9], the FLUKA routines NUNDIS/NUNRES [10, 11], NuWro [12], and ACHILLES [13] as well as tools to facilitate cross-generator comparisons, such as NUISANCE [14]. Historically, experiments would develop their own generators. This was often because they were focused on a particular measurement, energy range, or target, and wanted to ensure that the best physics was included for them. These 'homegrown' generators were often tuned primarily or exclusively to the neutrino data most similar to the data that the experiment would be collecting. A major advance in the field was the introduction of conference series devoted to the topic of neutrino interaction physics, NuINT (https://indico.cern.ch/event/703880/) and NuFACT (https://indico.cern.ch/event/855372/) in particular. Event generator comparisons have been a regular staple of the NuINT conference series from its inception, and a great deal of information on this topic can be found in the Proceedings of these meetings. These meetings have facilitated experiment-theory discussions leading to the first generator developed by a theory group (NuWro) [12], the extension of established nuclear interaction codes (FLUKA and GiBUU) to include neutrino-nuclear processes [4,5,10,11], and inclusion of theorists in existing generator development teams.

These activities have led to more careful scrutiny of the crucial hadron and nuclear theory inputs to these generators, which is evaluated in particular through comparisons to electron-scattering data. At this point in time all simulation codes face challenges in describing the full extent of the lepton scattering data, and the tension between incorporating the best available theory versus obtaining the best agreement with the data plays out in a variety of ways within the field. For the field to make progress, inclusion of state of the art theory needs to be coupled to global analyses that correctly incorporate correlations between measurements. Given the rapid pace of new data and the complexity of analyses, this is a significant challenge for the field in the coming years.

There are many neutrino experiments which use various sources of neutrinos, from reactors, accelerators33, the atmosphere, and astrophysical sources30,thereby covering a range of energies from MeV to TeV. Much of the emphasis has been on the few-GeV region in the generators, as this is the relevant energy range for short- and long-baseline neutrino oscillation experiments. Also, modern neutrino experiments utilize nuclei as interaction targets, such as scintillator (hydro-carbon), water, argon, and iron. Therefore, the generators must be capable of simulating neutrino interactions with various nuclear targets. Neutrino-nucleus interactions are separated in two stages: the initial neutrino interactions (ISI), and the final-state interactions (FSI) of the particles produced in the initial neutrino interaction. Traditionally, generators use the impulse approximation, which treats the nucleus as a collection of independent nucleons and the primary interaction, ISI, occurs between the probe and a single nucleon[1], for most of the initial interaction, and subsequently simulates the interactions of secondary particles in the nucleus (FSI) in semi-classical ways. However, the impulse approximation with simple nucleus modeling has limitations, and some interaction models in recent generators consider both the initial state and the final state of the nucleus when simulating ISI. Some of the generators go further and consider the correlation of ISI and FSI. Semi-classical hadron transport approaches are commonly used as they are able simulate a variety of nuclei in a single model, fully describe complex multi-particle final states, and for practical considerations as these approaches are fast. However, there are several challenges facing these simulations coming mainly from the complexity of the nuclear physics, and the need to avoid double counting in combining perturbative and non-perturbative models for the neutrino-nucleon scattering processes. One example of addressing this is in GiBUU, which treats the final state propagation using quantum-kinetic transport theory. The overall validity of impulse approximation-based scheme, and in particular the importance of scattering channels that involve more than one nucleon, is a crucial question that is the topic of much current work. While generators share many common ingredients, differences in implementation, parameter values, and approaches to avoid double counting can yield dramatically different predictions [15]. In the following sections, interaction models and their implementations, including final-state interactions of hadrons produced in the nuclei, are described.

In order to assure their validity, neutrino event generators are tuned and validated against a wide variety of data. This means that the quality of the outputs from generators is limited by the quality of experimental data. The existing neutrino-nucleon and neutrino-nucleus scattering data sets are not restrictive enough to eliminate many approaches. On the other hand, there are various precise data sets, which use photon, charged lepton, and hadron probes. These data sets are extensively used to validate the generators. The results from these external data tuning exercises are important for experiments as they quantify the uncertainty on model parameters, needed by experiments in the evaluation of generator-related systematic errors. Electron scattering data plays an important role in determining the vector contribution to the form-factors and structure functions, as well as in evaluating specific aspects of the nuclear model [16, 17]. Hadron scattering data is used in validating the nuclear model, in particular of interactions between hadrons produced in the primary interaction and the residual target nucleus (final state interactions). As mentioned, tuning of neutrino-nucleon scattering and hadronization models relies heavily on the previous generation of high energy neutrino scattering and hydrogen and deuterium bubble chamber experiments. More recent data from the K2K, MiniBooNE, NOMAD, SciBooNE, MINOS, T2K, ArgoNEUT, MINERvA, NOvA, MicroBooNE, ICARUS, SBND, Ninja and JSNS2 experiments has been, or will be, used for this purpose, although caution is advisable due to possible biases that mismodeled nuclear effects might introduce. In practice, there are often choices to be made about which models to include in an overall simulation, and which data sets to use for tuning. The process of developing a comprehensive tune in GENIE is discussed in Ref. [3].

However, all the recent experiments use nuclear targets and it is challenging to disentangle the neutrino-nucleon interaction from the effects of the nuclear environment. For example, it is diffi-

[1] Recently, importance of two nucleon processes are widely recognized and implemented in several generators. In such a case, two nucleons are involved in the ISI.

by UNIVERSITY OF CA Phys. A 2026.41. Downloaded from www.worldscientific.com LEY on 09/16/26. Re-use and distribution is strictly not permitted, except for Open Access articles.

Int. J. Mod. Phys. A 2026.41. Downloaded from www.worldscientific.com
by UNIVERSITY OF CALIFORNIA @ BERKELEY on 09/16/26. Re-use and distribution is strictly not permitted, except for Open Access articles.

cult to separate charged current quasi-elastic scattering from the multi-nucleon quasi-elastic like scattering or single pion production, in which a pion is absorbed in the nucleus. Sometimes, there are tensions between the data sets from different experiments. Data on multi-pion and meson production are limited, but are anticipated to be measured in the near future experiments. Next generation experiments are expected to provide better detection capabilities with higher statistics and these data will help in evaluating and validating the models implemented in the generators.

44.1 Neutrino-Nucleon Scattering

Event generators typically begin with free-nucleon cross sections which are then embedded into a nuclear physics model. The most important processes are quasi-elastic (elastic for neutral current (NC)) scattering, resonance production, and non-resonant inelastic scattering, which make comparable contributions for few-GeV interactions. The neutrino cross sections in this energy range can be seen in Figure 52.1 of this *Review*.

44.1.1 *Quasi-Elastic Scattering*

The cross section for the neutrino nucleon charged current quasi-elastic scattering is described in terms of the leptonic and hadronic weak currents, where dominant contributions to the hadronic current come from the vector (V) and axial-vector (A) form factors. Contributions from the pseudo-scalar form factor (P) are typically small for muon and electron neutrinos and are related to the axial form factor (A) assuming partially conserved axial currents (PCAC). Owing to isospin symmetry, the vector form factors are related to those measured by precise electron scattering experiments [18]. Therefore, most of the generators use parametrizations of these form factors taken directly from the data. For the axial form factor there is no such precise experiment, and most of the generators use a dipole form [19]. Generally, the value of axial form factor at $q^2 = 0$ (q is the four-momentum transfer) is extracted from the polarized nucleon beta decay experiment. The axial vector mass (M_A) has been determined to be ~ 1.0 GeV/c^2 by the results of bubble chamber neutrino scattering experiments and electro-pion production experiments. However, the selection of the axial vector mass parameter depends on the generator as the simulated results show significant differences from observations in several experiments. Nuclear modeling in the generators and missing interactions are thought to be the main causes. Recent LQCD axial form factor calculations indicate that the dipole axial-vector form factor with M_A =1.0 GeV/c^2 may not be appropriate [20]. The LQCD results provide better agreement with recent experiments. The MINERvA experiment measured the $\bar{\nu}_\mu$ differential cross-section on hydrogen, which also shows discrepancies in the large 4-momentum transfer region [21]. Recently, there are several attempts to use the new function forms of the axial form factors [20,22,23] and some generators have already implemented these form factors [8,24].

44.1.2 *Inelastic Production*

Most generators use the prescriptions of Rein-Sehgal [25], which is based on the relativistic harmonic oscillator model [26], to simulate neutrino-induced single pion production, or updated versions that incorporate lepton mass terms and pion pole contributions [27,28]. To obtain the cross section for a particular channel, they calculate the amplitude for the production of each resonance multiplied by the probability for the decay of that resonance into that particular channel. Implementation differences include the number of resonances included, whether the amplitudes are added coherently or incoherently, the invariant mass range over which the model is used, how non-resonant backgrounds are included, inclusion of lepton mass terms, and the model parameter values (in particular the axial mass). In this model it is also possible to calculate the cross-sections of single photon, and η production by changing the decay probability of the resonances, which are included in some of the programs. However, it is known that discrepancies exist between the recent pion electro/photo-production data and the results from the simulation data with the same framework, i.e. vector part of this model. There are several attempts to overcome this issue [29] and some of the generators started using more appropriate form factors. Recently, there are approaches that improve the theoretical description of non-resonant contributions in the resonance region, [30–32], and which account for interference between resonant and non-resonant amplitudes. GiBUU and NuWro generators do not use the Rein-Sehgal model, and instead rely directly on electro-production data for the vector contribution and fit bubble chamber data to determine the remaining parameters for the axial contribution [33–36]. These implementations do not include higher resonances explicitly. The dynamical coupled-channel model, which has been developed to simulate various electro- and photo-meson productions, was extended to simulate the neutrino single pion production [37]. In this approach pion-nucleon scattering is used to fix the form of the axial current at $q^2 = 0$. This model is also being implemented and is available in NEUT. Even with the new models, the axial-vector contributions must be determined experimentally; therefore, further experimental studies are essential to improve the prediction accuracy.

44.1.3 *Deep and Shallow Inelastic Scattering*

For this process the fundamental target shifts from the nucleon to its quark constituents. Therefore, the generators construct the nucleon structure functions F_2 and xF_3 from parton distributions for high Q^2 (the DIS regime: W$\gtrsim$ 2 GeV/c^2 and Q$^2 \gtrsim$ 1 GeV^2) to calculate the direction and momentum of the lepton. The first challenge is in extending this picture to the lower values of Q^2 and W that dominate the available phase space for few-GeV interactions (the so-called 'shallow inelastic scattering', or SIS regime). GRV98LO parton distribution functions [38] with the corrections proposed in [39,40] are widely used, while others [10] implement their own modifications to the parton distributions at low Q^2. Both DIS and SIS generate hadrons but their production depends on each generator's implementation of a hadronization model as described in the next section. There are various difficulties not only in the actual hadronization but the relation with the single meson production. It is necessary to avoid double counting between the resonance and SIS/DIS models, and all generators are different in this regard. The scheme chosen can have a significant impact on the results of simulations at a few-GeV neutrino energies. For simulating ultra-high energy interactions currently being studied with neutrino telescopes, fully partonic descriptions, which utilize beyond-leading-order pQCD calculations [41,42] are the norm [43].

44.2 Hadronization Models

For hadrons produced via baryonic resonances, the underlying model amplitudes and resonance branching fractions can be used to fully characterize the hadronic system. For shallow- and deep-inelastic scattering, a hadronization model is required. Most generators use PYTHIA [44] for this purpose, although some with modified parameters. In addition some implement their own models to handle invariant masses that are too low for PYTHIA, typically somewhere around 2.0 GeV/c^2. Such models rely heavily on measurements of neutrino hadro-production in high-resolution devices, such as bubble chambers and the CHORUS [45] and NOMAD experiments [46], to construct empirical parametrizations that reproduce the key features of the data [47,48]. The basic ingredients are the empirical observations that average charged particle multiplicities increase logarithmically with the invariant mass of the hadronic system, and that the distribution of charged particle multiplicities about this average are described by a single function (an observation known as KNO scaling [49]). The multiplicity of the neutral particles are usually obtained by scaling the charged particle multiplicity. Simple parametrizations to more accurately reproduce differences observed in the forward/backward hemispheres of hadronic systems are included in GENIE, NEUT, and NuWro.

44.3 Nuclear Physics

The nuclear physics relevant to neutrino-nucleus scattering at few-GeV energies is complicated, involving Fermi motion, nuclear binding, Pauli blocking, in-medium modifications of form factors and hadronization, intranuclear rescattering of hadrons, and many-body scattering mechanisms including long- and short-range nucleon-nucleon correlations.

by UNIVERSITY OF CA Phys. A 2026.41. Downloaded from www.worldscientific.com LEY on 09/16/26. Re-use and distribution is strictly not permitted, except for Open Access articles.

44.3.1 *Treatment of nuclear effects*

In order to obtain the cross-section off nucleons in the nucleus, it is necessary to take into account various in-medium effects. Most of the models used for neutrino-nuclear scattering kinematics were developed in the context of few-GeV inclusive electron scattering, by experiments going back nearly 50 years. The basic models employed in event generators rely on impulse approximation schemes, the most simple of which is the Relativistic Fermi Gas Model, such as the Smith-Moniz [50] and Bodek-Ritchie [51] models. However, the results from neutrino-nucleus scattering experiments in 2000 and afterwards, beginning with K2K, MiniBooNE have shown large discrepancies from the naive expectation from the models. Most striking differences are a suppression of forward going muons (low Q^2), a high Q^2 enhancement in the event rate, and an overall larger than expected number of observed events. In order to reproduce the data, the quasi-elastic axial mass was used as the effective parameter and increased by roughly 20% from the nominal values obtained by an earlier generation of bubble chamber experiments using hydrogen or deuterium [19]. Because the resolution and detection efficiencies of the detectors are limited, it is not possible to disentangle the contributions from the form factors of the neutrino (weak) interaction or nuclear in-medium effects. Recently, several LQCD groups have calculated the axial-vector nucleon form factor, and their results show different tendencies compared to the bubble-chamber data and are closer to the results of recent experiments. Therefore, the axial-vector form factor may be one reason for the discrepancies. However, it is known that the problem cannot be completely resolved by simply changing the axial-vector factor. Consequently, simple nuclear models are insufficient for recent and future neutrino experiments. Additionally, the discrepancies may indicate contributions from other interactions that are either not taken into account or are poorly modeled. Moreover, these simple Fermi-Gas models are not expected to describe the kinematical distributions of final state nucleons. Therefore, several generators have to implement better models, such as local Fermi-Gas model or more sophisticated models. Within the electron scattering community, the analogous calculations have for decades relied on spectral functions, which incorporate information about nucleon momenta and binding energies in the impulse approximation scheme [16]. Therefore, most of the generators have implemented the realistic spectral functions in their latest releases. Actually, the discrepancies in small q^2 could not be solved alone by just introducing the local Fermi-gas model nor spectral function models. This implies that appropriate medium correction effects are needed to be taken into account. One of the implemented solutions is the local Fermi-Gas model with medium correction calculated using the random phase approximation, which is known to give large suppression in small q^2 [52, 53]. Although, the fundamental parts of the models are same, actual implementations are quite different between the generators. Especially, the constructions of the final state hadron kinematics are quite different. Especially for the quasi-elastic scattering case, treatment of the nucleon masses in the nucleus, the binding and the separation energies are sometimes quite different [54]. Recently, Super-Scaling model with relativistic mean field theory effects (SuSAv2) [55, 56] is implemented in some of the generators. Different from the other generators, GiBUU treats various in-medium effects consistently, and ACHILLES is also designed to treat the nuclear modeling as consistent as possible.

Indications of the suppression in small q^2 in the single pion productions were also observed in K2K and MiniBooNE and it is clearly observed at the MINERνA and NOνA experiments. However, the models to explain the suppression have not been implemented, other than the phenomenological ones. Also, q^2 dependence of the cross-section is largely model and parameter dependent. Further studies of newly implemented single pion models and new data sets may give new insights. Also, there may be some interaction channels which are missing and not considered in the generators.

These led to a revisitation of the role played by excitation of multiple particle-hole states in the nucleus, and the experimental study of these scattering channels is an area of intense experimental interest [57]. The contribution of these scattering processes is an extremely active area of theoretical research as well, with significant implications for generators and analyses [58]. Several approaches, ranging from strictly phenomenological descriptions to full theoretical calculations, have recently been incorporated into generators [59–61]. One example of a phenomenological approach utilizes an Effective Spectral Function [62] and a Transverse Enhancement Model [63], which together encapsulate information derived from electron scattering experiments at relevant kinematics. The microscopic model of Nieves and collaborators is now available in GENIE and NEUT [64, 65]. SuSAv2 model [56] also has capability to simulate this multi-nucleon quasi-elastic like interaction and is also implemented in GENIE.

One of the challenges in incorporating full theoretical models of these processes is that they are typically slow, so generators have developed new approaches whereby much of the computation is done offline, and the generators simply read in the hadronic tensor components. This allows for a full prediction of the lepton kinematics, however the ability to simulate the hadronic component of these multinucleon states then relies on separate models. The other challenge is that the theoretical models are not designed to describe exclusive final states. These approaches, while making simulations computationally tractable, neglect correlations between the lepton and hadron kinematics. Also, there are limitations of the model itself to describe some of the kinematic regions. However, the generators need to simulate final all the state particles and thus, several assumptions are made by authors of the generators from time to time.

Also, it is known from photo and electro-nuclear scattering that the Delta width is affected by Pauli blocking and collisional broadening. These effects are included in some, but not all generators.

The remnant nucleus after the scattering is usually in an excited state. Therefore, the remnant may emit gamma-rays, additional nucleons or an alpha particle during the de-excitation process. This de-excitation gamma-ray is used in searching for proton decay in water Cherenkov detectors. Some generators have implemented this process. GENIE has deexcitation processes for various nuclei. Recently, a dedicated library, called NUCDEEX [66], which simulates de-excitation based on TALYS [67] was released. This library is designed to be used with any generators to simulate nuclear de-excitation processes. When scattering from a nucleus, coherent scattering of various kinds is possible. Most simulations incorporate, at least, coherent neutral and charged single pion production. While the interaction rate for these interactions is typically around a percent of the total yield, the unique kinematic features of these events can make them potential backgrounds for oscillation searches. Implemented in Monte Carlo are several PCAC-based methods [68, 69]. Microscopic models, valid at lower neutrino energies [70–73], have also been implemented in several generators. One commonly used model by Rein and Sehgal [68] predicts a cross section for charged-current coherent pion production that is much larger than what is observed by K2K, MINERvA and T2K. However, the cross-section is sensitive to the pion cross-section used in the model as parameters and improved models with lepton mass correction [69] give better agreement with the recent data. This improved model is implemented in most of the generators. In addition to coherent pion production, some generators can simulate coherent single photon production [74] and coherent elastic neutrino-nucleus scattering.

44.3.2 *Hadron Production in Nuclei*

Neutrino pion production is one of the dominant neutrino scattering mechanisms in the few-GeV region and the pions produced in the nucleus have quite large interaction cross sections. Therefore, pion intranuclear scattering can have sizable effects on the results of simulations at these energies. Also, recent neutrino oscillation experiments use the observed information of protons and pions more extensively, in addition to the charged leptons. Therefore, most generators implement this physics through an intranuclear cascade simulation. In generators which utilize cascade models, a hadron, which has been formed in the nucleus, is moved step by step until it interacts with a nucleon or escapes from the nucleus. The probabilities of each interaction in nucleus are usually given as the mean free paths and used to determine whether

Int. J. Mod. Phys. A 2026.41. Downloaded from www.worldscientific.com
by UNIVERSITY OF CALIFORNIA @ BERKELEY on 09/16/26. Re-use and distribution is strictly not permitted, except for Open Access articles.

the hadron has interacted or not. If the hadron is found to have interacted, appropriate final states are selected. Usually, absorption, elastic, charge exchange, and inelastic scatterings including particle productions are simulated as intranuclear interactions. The determination method of the kinematics for the final state particles heavily depends on the generators but most of them use experimentally validated models to simulate hadron interactions in nucleus. No two intranuclear cascade simulations implemented in neutrino event generators are the same [75]. In all cases hadrons propagate from an interaction vertex chosen based on the density distribution of the target nucleus. In determining the generated position of the hadrons in nucleus, the concept of the formation length is sometimes employed. Based on this idea, the hadronization process is not instantaneous and it takes some time before generating the hadrons [12]. The basis for formation times are measurements at relatively high energy and Q^2, and most generators that employ the concept do not apply them to resonance interactions.

GiBUU does not employ an intranuclear cascade simulation, instead, it utilizes a semi-classical transport model in coupled channels that describes the space-time evolution of a many body system in the presence of potentials and a collision term [4]. This approach assures consistency between nuclear effects in the initial state, such as Fermi motion, Pauli blocking, hadron self-energies [76], and modified cross sections, and the final state, such as particle re-interactions, since the two are derived from the same model. This model has been previously used to describe a wide variety of nuclear interaction data. Similarly, the hadronic simulation of the NUNDIS/NUNRES programs are handled by the well-established FLUKA hadronic simulation package [10]. Recently, GENIE included the interface to the external hadronic simulation package INCL++ [77].

References

[1] A. Gazizov and M. P. Kowalski, Comput. Phys. Commun. **172**, 203 (2005), [arXiv:astro-ph/0406439].

[2] C. Andreopoulos *et al.*, Nucl. Instrum. Meth. **A614**, 87 (2010), [arXiv:0905.2517].

[3] J. Tena-Vidal *et al.* (GENIE) (2021), [arXiv:2104.09179].

[4] O. Buss *et al.*, Phys. Rept. **512**, 1 (2012), [arXiv:1106.1344].

[5] K. Gallmeister, U. Mosel and J. Weil, Phys. Rev. **C94**, 3, 035502 (2016), [arXiv:1605.09391].

[6] S. Gardiner, C. Grant, E. Panic, and R. Svoboda, `http://www.marleygen.org`.

[7] D. Autiero, Nucl. Phys. Proc. Suppl. **139**, 253 (2005).

[8] Y. Hayato and L. Pickering, Eur. Phys. J. Spec. Top. (2021), [arXiv:2106.15809].

[9] D. Casper, Nucl. Phys. Proc. Suppl. **112**, 161 (2002), [hep-ph/0208030].

[10] G. Battistoni *et al.*, Acta Phys. Polon. **B40**, 2491 (2009).

[11] T. T. Böhlen *et al.*, Nucl. Data Sheets **120**, 211 (2014).

[12] T. Golan, C. Juszczak and J. T. Sobczyk, Phys. Rev. **C86**, 015505 (2012), [arXiv:1202.4197].

[13] J. Isaacson *et al.*, Phys. Rev. D **107**, 3, 033007 (2023), [arXiv:2205.06378].

[14] P. Stowell *et al.*, JINST **12**, 01, P01016 (2017), [arXiv:1612.07393].

[15] M. Betancourt *et al.*, Phys. Rept. **773-774**, 1 (2018), [arXiv:1805.07378].

[16] O. Benhar, D. day and I. Sick, Rev. Mod. Phys. **80**, 189 (2008), [arXiv:nucl-ex/0603029].

[17] B. Schmookler *et al.* (CLAS), Nature **566**, 7744, 354 (2019), [arXiv:2004.12065].

[18] A. Bodek *et al.*, Eur. Phys. J. **C53**, 349 (2008), [arXiv:0708.1946].

[19] H. Gallagher, G. Garvey and G. P. Zeller, Ann. Rev. Nucl. Part. Sci. **61**, 355 (2011).

[20] Y.-C. Jang *et al.* (Precision Neutron Decay Matrix Elements (PNDME)), Phys. Rev. D **109**, 1, 014503 (2024), [arXiv:2305.11330].

[21] T. Cai *et al.* (MINERvA), Nature **614**, 7946, 48 (2023).

[22] E. Tomasi-Gustafsson, G. I. Gakh and C. Adamuscin, Phys. Rev. **C73**, 045204 (2006), [arXiv:nucl-th/0512039].

[23] B. Bhattacharya, R. J. Hill and G. Paz, Phys. Rev. **D84**, 073006 (2011), [arXiv:1108.0423].

[24] A. S. Meyer *et al.*, Phys. Rev. **D93**, 11, 113015 (2016), [arXiv:1603.03048].

[25] D. Rein and L. M. Sehgal, Annals Phys. **133**, 79 (1981).

[26] R. P. Feynman, M. Kislinger and F. Ravndal, Phys. Rev. D **3**, 2706 (1971).

[27] K. S. Kuzmin, V. V. Lyubushkin and V. A. Naumov, Mod. Phys. Lett. A **19**, 2815 (2004), [hep-ph/0312107].

[28] C. Berger and L. M. Sehgal, Phys. Rev. D **76**, 113004 (2007), [arXiv:0709.4378].

[29] K. M. Graczyk and J. T. Sobczyk, Phys. Rev. **D77**, 053001 (2008), [Erratum: Phys. Rev.D79,079903(2009)], [arXiv:0707.3561].

[30] M. Kabirnezhad, Phys. Rev. **D97**, 1, 013002 (2018), [arXiv:1711.02403].

[31] M. Kabirnezhad, Phys. Rev. D **102**, 5, 053009 (2020), [arXiv:2006.13765].

[32] E. Hernandez, J. Nieves and M. Valverde, Phys. Rev. D **76**, 033005 (2007), [hep-ph/0701149].

[33] O. Lalakulich and E. A. Paschos, Phys. Rev. **D71**, 074003 (2005), [hep-ph/0501109].

[34] J. A. Nowak, Phys. Scripta **T127**, 70 (2006), [hep-ph/0607081].

[35] T. Leitner *et al.*, Phys. Rev. C **79**, 034601 (2009), [arXiv:0812.0587].

[36] L. Alvarez-Ruso, S. K. Singh and M. J. Vicente Vacas, Phys. Rev. **C57**, 2693 (1998), [arXiv:nucl-th/9712058].

[37] S. X. Nakamura, H. Kamano and T. Sato, Phys. Rev. **D92**, 7, 074024 (2015), [arXiv:1506.03403].

[38] M. Glück, E. Reya and A. Vogt, Eur. Phys. J. **C5**, 461 (1998), [hep-ph/9806404].

[39] A. Bodek and U. K. Yang, J. Phys. **G29**, 1899 (2003), [hep-ex/0210024].

[40] A. Bodek, U. K. Yang and Y. Xu (2021), [arXiv:2108.09240].

[41] A. Cooper-Sarkar, P. Mertsch and S. Sarkar, JHEP **08**, 042 (2011), [arXiv:1106.3723].

[42] V. Bertone, R. Gauld and J. Rojo, JHEP **01**, 217 (2019), [arXiv:1808.02034].

[43] A. Garcia and A. Heijboer (KM3NeT), PoS **ICRC2019**, 895 (2020), [arXiv:1908.10077].

[44] T. Sjostrand, S. Mrenna and P. Z. Skands, JHEP **05**, 026 (2006), [hep-ph/0603175].

[45] A. Kayis-Topaksu *et al.* (CHORUS), Eur. Phys. J. **C51**, 775 (2007), [arXiv:0707.1586].

[46] J. Altegoer *et al.* (NOMAD), Phys. Lett. **B445**, 439 (1999).

[47] T. Yang *et al.*, Eur. Phys. J. **C63**, 1 (2009), [arXiv:0904.4043].

[48] J. A. Nowak and J. T. Sobczyk, Acta Phys. Polon. **B37**, 2371 (2006), [hep-ph/0608108].

[49] Z. Koba, H. B. Nielsen and P. Olesen, Nucl. Phys. **B40**, 317 (1972).

[50] R. A. Smith and E. J. Moniz, Nucl. Phys. **B43**, 605 (1972), [Erratum: Nucl. Phys.B101,547(1975)].

[51] A. Bodek and J. L. Ritchie, Phys. Rev. **D24**, 1400 (1981).

[52] M. C. Martinez *et al.*, Phys. Rev. C **73**, 024607 (2006), [arXiv:nucl-th/0505008].

[53] J. Nieves, J. E. Amaro and M. Valverde, Phys. Rev. C **70**, 055503 (2004), [Erratum: Phys.Rev.C 72, 019902 (2005)], [arXiv:nucl-th/0408005].

[54] A. Bodek and T. Cai, Eur. Phys. J. C **79**, 4, 293 (2019), [arXiv:1801.07975].

[55] J. A. Caballero *et al.*, Phys. Lett. **B653**, 366 (2007), [arXiv:0705.1429].

[56] R. Gonzaléz-Jiménez *et al.*, Phys. Rev. C **90**, 3, 035501 (2014), [arXiv:1407.8346].

[57] X. G. Lu *et al.* (MINERvA) (2021), [arXiv:2107.02064].

[58] L. Alvarez-Ruso *et al.*, Prog. Part. Nucl. Phys. **100**, 1 (2018), [arXiv:1706.03621].

[59] T. Katori, AIP Conf. Proc. **1663**, 1, 030001 (2015), [arXiv:1304.6014].

[60] M. Alam *et al.* (2015), [arXiv:1512.06882].

[61] C. Wilkinson *et al.*, Phys. Rev. **D93**, 7, 072010 (2016), [arXiv:1601.05592].

[62] A. Bodek, M. E. Christy and B. Coopersmith, Eur. Phys. J. **C74**, 10, 3091 (2014), [arXiv:1405.0583].

[63] A. Bodek, H. S. Budd and M. E. Christy, Eur. Phys. J. **C71**, 1726 (2011), [arXiv:1106.0340].

[64] J. Nieves, I. Ruiz Simo and M. J. Vicente Vacas, Phys. Rev. **C83**, 045501 (2011), [arXiv:1102.2777].

[65] R. Gran *et al.*, Phys. Rev. **D88**, 11, 113007 (2013), [arXiv:1307.8105].

[66] S. Abe, Phys. Rev. D **109**, 3, 036009 (2024), [arXiv:2310.10394].

[67] A. Koning, S. Hilaire and S. Goriely, Eur. Phys. J. A **59**, 6, 131 (2023), [Erratum: Eur.Phys.J.A 59, 146 (2023)].

[68] D. Rein and L. M. Sehgal, Nucl. Phys. **B223**, 29 (1983).

[69] C. Berger and L. M. Sehgal, Phys. Rev. **D79**, 053003 (2009), [arXiv:0812.2653].

[70] L. Alvarez-Ruso *et al.*, Phys. Rev. **C75**, 055501 (2007), [Erratum: Phys. Rev.C80,019906(2009)], [arXiv:nucl-th/0701098].

[71] L. Alvarez-Ruso, L. S. Geng and M. J. Vicente Vacas, Phys. Rev. **C76**, 068501 (2007), [Erratum: Phys. Rev.C80,029904(2009)], [arXiv:0707.2172].

[72] J. E. Amaro *et al.*, Phys. Rev. D **79**, 013002 (2009), [arXiv:0811.1421].

[73] S. X. Nakamura *et al.*, Phys. Rev. C **81**, 035502 (2010), [arXiv:0910.1057].

[74] E. Wang, L. Alvarez-Ruso and J. Nieves, Phys. Rev. C **89**, 1, 015503 (2014), [arXiv:1311.2151].

[75] S. Dytman *et al.*, Phys. Rev. D **104**, 5, 053006 (2021), [arXiv:2103.07535].

[76] S. K. Singh, M. J. Vicente-Vacas and E. Oset, Phys. Lett. B **416**, 23 (1998), [Erratum: Phys.Lett.B 423, 428 (1998)].

[77] A. Boudard *et al.*, Phys. Rev. C **87**, 014606 (2013), URL `https://link.aps.org/doi/10.1103/PhysRevC.87.014606`.

by UNIVERSITY OF CA Phys. A 2026.41. Downloaded from www.worldscientific.com
LEY on 09/16/26. Re-use and distribution is strictly not permitted, except for Open Access articles.

Int. J. Mod. Phys. A 2026.41. Downloaded from www.worldscientific.com
by UNIVERSITY OF CALIFORNIA @ BERKELEY on 09/16/26. Re-use and distribution is strictly not permitted, except for Open Access articles.

45. Monte Carlo Particle Numbering Scheme

Revised August 2025 by A. Buckley (Glasgow U.), F. Krauss (Durham U.), S. Navas (Granada U.) and P. Richardson (Durham U.).

The Monte Carlo particle numbering scheme presented here is intended to facilitate interfacing between matrix-element generators, event generators, detector simulators, and analysis packages used in particle physics, and is widely accepted as the "industry standard".

The numbering scheme was introduced in 1988 [1], and has since been revised and expanded in the light of new information on hadronic resonances, and to encompass as yet undiscovered and hypothetical particles. The scheme was substantially updated and extended in 2012. Encodings have since been added for generic dark matter and for tetra- and penta-quark states; the 2026 update further refines the tetra/penta-quark schemes, and reserves ranges for user-specified states and PDG-node indexing. Further revisions and/or extensions of the numbering scheme are anticipated.

The general form for most particles is a 7-digit number:

$$\pm n\ n_r\ n_L\ n_{q1}\ n_{q2}\ n_{q3}\ n_J\ .$$

This encodes information about the particle's spin, flavor content, and internal quantum numbers. A 9–digit extension is used specifically for tetra- and penta-quark states, and a distinct 10-digit scheme is used for encoding (hyper)nuclear states. The details are as follows:

1. Particles are given positive numbers, antiparticles negative numbers. The PDG convention for mesons is used, so that K^+ and B^+ are particles.
2. Quarks and leptons are numbered consecutively starting from 1 and 11 respectively; to do this they are first ordered by family and within families by weak isospin.
3. In composite quark systems (diquarks, mesons, and baryons) $n_{q_{1-3}}$ are quark numbers used to specify the quark content, while the rightmost digit $n_J = 2J+1$ gives the system's spin (except for the K^0_S and K^0_L). The scheme does not cover particles of spin $J > 4$.
4. Diquarks have 4-digit numbers with $n_{q1} \geq n_{q2}$ and $n_{q3} = 0$.
5. The numbering of mesons is guided by the non-relativistic (L–S decoupled) quark model, as listed in Tables 15.2, 15.3, and 15.4.
   (a) The numbers specifying the meson's quark content conform to the convention $n_{q1} = 0$ and $n_{q2} \geq n_{q3}$. The special case K^0_L is the sole exception to this rule.
   (b) The quark numbers of flavorless, light (u, d, s) mesons are: 11 for the member of the isotriplet $(\pi^0, \rho^0, \ldots)$, 22 for the lighter isosinglet $(\eta, \omega, \ldots)$, and 33 for the heavier isosinglet $(\eta', \phi, \ldots)$. Since isosinglet mesons are often large mixtures of $u\bar{u} + d\bar{d}$ and $s\bar{s}$ states, 22 and 33 are assigned by mass and do not necessarily specify the dominant quark composition.
   (c) The special numbers 310 and 130 are given to the K^0_S and K^0_L respectively.
   (d) The fifth digit n_L is reserved to distinguish mesons of the same total (J) but different spin (S) and orbital (L) angular momentum quantum numbers. For $J > 0$ the numbers are: $(L, S) = (J-1, 1)$ $n_L = 0$, $(J, 0)$ $n_L = 1$, $(J, 1)$ $n_L = 2$ and $(J+1, 1)$ $n_L = 3$. For the exceptional case $J = 0$ the numbers are $(0, 0)$ $n_L = 0$ and $(1, 1)$ $n_L = 1$ (*i.e.* $n_L = L$). See Table 45.1.
   (e) If a set of physical mesons correspond to a (non-negligible) mixture of basis states, differing in their internal quantum numbers, then the lightest physical state gets the smallest basis state number. For example the $K_1(1270)$ is numbered 10313 (1^1P_1 K_{1B}) and the $K_1(1400)$ is numbered 20313 (1^3P_1 K_{1A}), using $n^{(2s+1)}L_J$ spectroscopic notation.
   (f) The sixth digit n_r is used to label mesons radially excited above the ground state.

Table 45.1: Meson numbering logic. Here qq stands for $n_{q2}\, n_{q3}$.

	$L=J-1, S=1$			$L=J, S=0$			$L=J, S=1$			$L=J+1, S=1$		
J	code	J^{PC}	L	code	J^{PC}	L	code	J^{PC}	L	code	J^{PC}	L
0	—	—	—	00qq1	0^{-+}	0	—	—	—	10qq1	0^{++}	1
1	00qq3	1^{--}	0	10qq3	1^{+-}	1	20qq3	1^{++}	1	30qq3	1^{--}	2
2	00qq5	2^{++}	1	10qq5	2^{-+}	2	20qq5	2^{--}	2	30qq5	2^{++}	3
3	00qq7	3^{--}	2	10qq7	3^{+-}	3	20qq7	3^{++}	3	30qq7	3^{--}	4
4	00qq9	4^{++}	3	10qq9	4^{-+}	4	20qq9	4^{--}	4	30qq9	4^{++}	5

   (g) Numbers have been assigned for complete $n_r = 0$ S- and P-wave multiplets, even where states remain to be identified.
   (h) In some instances assignments within the $q\bar{q}$ meson model are only tentative; here best guess assignments are made.
   (i) Many states appearing in the Meson Listings are not yet assigned within the $q\bar{q}$ model. Here $n_{q_{2-3}}$ and n_J are assigned according to the state's likely flavors and spin; all such unassigned light isoscalar states are given the flavor code 22. Within these groups $n_L = 0, 1, 2, \ldots$ is used to distinguish states of increasing mass. These states are flagged using $n = 9$. It is to be expected that these numbers will evolve as the nature of the states are elucidated. Codes are assigned to most mesons that are listed in the one-page table at the end of the Meson Summary Table as long as they have a preferred or established spin. Additional heavy meson states expected from heavy quark spectroscopy are also assigned codes.
6. The numbering of baryons is again guided by the non-relativistic quark model, see Table 15.6. This numbering scheme is illustrated through a few examples in Table 45.2.
   (a) The numbers specifying a baryon's quark content are generally ordered $n_{q1} \geq n_{q2} \geq n_{q3}$.
   (b) Two states exist for $J = 1/2$ baryons containing 3 distinct quark flavours. In the lighter state the light quarks are in an antisymmetric ($J = 0$) configuration, while for the heavier state they are in a symmetric ($J = 1$) configuration. In this situation n_{q2} and n_{q3} are reversed for the lighter state, so that the smaller number corresponds to the lighter baryon. For example, $uds \to \{\Lambda = 3122, \Sigma^0 = 3212\}$, the $udc = \{\Xi_c^+, \Xi_c^{'+}\}$ and $scb = \{\Omega^0_{bc}, \Omega^{'0}_{bc}\}$ baryon pairs, and equivalents in those families.
   (c) For excited baryons a scheme is adopted, where the n_r label is used to denote the excitation bands in the harmonic oscillator model, see Sec. 15.5. Using the notation employed there, n_r is given by the N-index of the D_N band identifier.
   (d) Further degeneracies of excited hadron multiplets with the same excitation number n_r and spin J are lifted by labelling such multiplets with the n_L index according to their mass, as given by its N or Δ-equivalent.
   (e) In such excited multiplets extra singlets may occur, the $\Lambda(1520)$ being a prominent example. In such cases the ordering is reversed such that the heaviest quark label is pushed to the last position: $n_{q3} > n_{q1} > n_{q2}$.
7. The gluon, when considered as a gauge boson, has code number 21. In codes for glueballs, however, 9 is used to allow a notation in close analogy with that of hadrons.
8. The pomeron and odderon trajectories and a generic reggeon trajectory of states in QCD are assigned codes 990, 9990, and 110 respectively, where the final 0 indicates the indeterminate nature of the spin, and the other digits reflect the expected "valence" flavor content. We do not attempt a complete classification of all reggeon trajectories, since there is currently no

Table 45.2: Some examples of octet (top) and decuplet (bottom) members for the numbering scheme for excited baryons. Here qqq stands for $n_{q_1}n_{q_2}n_{q_3}$. See the text for the definition of the notation. The numbers in parenthesis correspond to the mass of the baryons. The states marked as (?) are not experimentally confirmed.

J^P	(D, L_N^P)	$n_r n_L n_{q_1} n_{q_2} n_{q_3} n_J$	N	Λ_8	Σ	Ξ	Λ_1
Octet			211,221	312	311,321,322	331,332	213
$1/2^+$	$(\mathbf{56}, \mathbf{0_0^+})$	$00qqq2$	(939)	(1116)	(1193)	(1318)	—
$1/2^+$	$(\mathbf{56}, \mathbf{0_2^+})$	$20qqq2$	(1440)	(1600)	(1660)	(1690)	—
$1/2^+$	$(\mathbf{70}, \mathbf{0_2^+})$	$21qqq2$	(1710)	(1810)	(1880)	(?)	(?)
$1/2^-$	$(\mathbf{70}, \mathbf{1_1^-})$	$10qqq2$	(1535)	(1670)	(1620)	(1750)	(1405)
J^P	(D, L_N^P)	$n_r n_L n_{q_1} n_{q_2} n_{q_3} n_J$	Δ		Σ	Ξ	Ω
Decuplet			111,211,221,222		311,321,322	331,332	333
$3/2^+$	$(\mathbf{56}, \mathbf{0_0^+})$	$00qqq4$	(1232)		(1385)	(1530)	(1672)
$3/2^+$	$(\mathbf{56}, \mathbf{0_2^+})$	$20qqq4$	(1600)		(1690)	(?)	(?)
$1/2^-$	$(\mathbf{70}, \mathbf{1_1^-})$	$11qqq2$	(1620)		(1750)	(?)	(?)
$3/2^-$	$(\mathbf{70}, \mathbf{1_1^-})$	$12qqq4$	(1700)		(?)	(?)	(?)

need to distinguish a specific such trajectory from its lowest-lying member.

9. Two-digit numbers in the range 21–30 are provided for the Standard Model gauge and Higgs bosons.
10. Codes 81–100 are reserved for generator-specific pseudoparticles and concepts not corresponding to physical states. Codes 901–930, 1901–1930, 2901–2930, and 3901–3930 are for additional components of Standard Model parton distribution functions: the latter three ranges are intended to distinguish left/right/longitudinal components. Codes 998 and 999 are reserved for GEANT tracking purposes.
11. The search for physics beyond the Standard Model is an active area, so these codes are also standardized as far as possible.

    (a) A standard fourth generation of fermions is included by analogy with the first three.

    (b) The graviton and the boson content of a two-Higgs-doublet scenario and of additional SU(2)×U(1) groups are found in the range 31–40.

    (c) "One-of-a-kind" exotic particles are assigned numbers in the range 41–80. The subrange 61-80 is reserved for new heavier fermions in generic models, where partners to the SM fermions would have codes offset by 60. If required, however, other assignments could be made.

    (d) Fundamental supersymmetric particles are identified by adding a non-zero n to the particle number. The superpartner of a boson or a left-handed fermion has $n = 1$ while the superpartner of a right-handed fermion has $n = 2$. When mixing occurs, such as between the winos and charged Higgsinos to give charginos, or between left and right sfermions, the lighter physical state is given the smaller basis-state number.

    (e) Technicolor states have $n = 3$, with technifermions treated like ordinary fermions. States which are ordinary color singlets have $n_r = 0$. Color octets have $n_r = 1$. If a state has non-trivial quantum numbers under the top-color groups numbers are specified by tech,ij, where i and j are 1 or 2. n_L is then $2i + j$. The coloron, V_8, is a heavy gluon color octet and thus is 3100021.

    (f) Excited (composite) quarks and leptons are identified by setting $n = 4$ and $n_r = 0$.

    (g) Within several scenarios of new physics, it is possible to have colored particles sufficiently long-lived for color-singlet hadronic states to form around them. In the context of supersymmetric scenarios, these states are called R-hadrons, since they carry odd R-parity. R-hadron codes, defined here, should be viewed as templates for corresponding codes also in other scenarios, for any long-lived particle that is either an unflavored color octet or a flavored color triplet. The R-hadron code is obtained by combining the SUSY particle code with a code for the light degrees of freedom, with as many intermediate zeros removed from the former as required to make place for the latter at the end. (To exemplify, a sparticle $n00000n_{\tilde{q}}$ combined with quarks q_1 and q_2 obtains code $n00n_{\tilde{q}}n_{q_1}n_{q_2}n_J$.) Specifically, the new-particle spin decouples in the limit of large masses, so that the final n_J digit is defined by the spin state of the light-quark system alone. An appropriate number of n_q digits is used to define the ordinary-quark content. As usual, 9 rather than 21 is used to denote a gluon/gluino in composite states. The sign of the hadron agrees with that of the constituent new particle (a color triplet) where there is a distinct new antiparticle, and else is defined as for normal hadrons. Particle names are R with the flavor content as lower index.

    (h) A black hole in models with extra dimensions has code 5000040. Kaluza-Klein excitations in models with extra dimensions have $n = 5$ or $n = 6$, to distinquish excitations of left- or right-handed fermions or, in case of mixing, the lighter or heavier state (cf. 11d). The nonzero n_r digit gives the radial excitation number, in scenarios where the level spacings allow these to be distinguished. Should the model also contain supersymmetry, excited SUSY states would be denoted by an $n_r > 0$, with $n = 1$ or 2 as usual. Should some colored states be long-lived enough that hadrons would form around them, the coding strategy of Ref. 11g applies, with the initial two nn_r digits preserved in the combined code.

    (i) Magnetic monopoles and dyons are assumed to have one unit of Dirac monopole charge and a variable integer number $n_{q1}n_{q2}n_{q3}$ units of electric charge. Codes $411n_{q1}n_{q2}n_{q3}0$ are then used when the magnetic and electrical charge sign agree and $412n_{q1}n_{q2}n_{q3}0$ when they disagree, with the overall sign of the particle set by the magnetic charge. For now no spin information is provided.

    (j) The nature of dark matter (DM) is not known, and therefore a definitive classification would be premature. Candidates from specific BSM scenarios are classified within those ranges, such as 1000022 for the lightest neutralino. Generic fundamental states can be given temporary codes in the range 51–60, with 51, 52 and 53 reserved for spin 0, 1/2 and 1 DM states (this could also include axions). Generic mediators of s-channel DM pair creation of annihilation can be given codes 54 and 55 for spin-0 or 1 respectively. Separate antiparticles, with negative codes, may or may not exist. More elaborate new scenarios should be constructed with $n = 5$ and $n_r = 9$.

    (k) Hidden Valley particles have $n = 4$ and $n_r = 9$, and

Phys. A 2026.41. Downloaded from www.worldscientific.com
by UNIVERSITY OF CA LEY on 09/16/26. Re-use and distribution is strictly not permitted, except for Open Access articles.

Int. J. Mod. Phys. A 2026.41. Downloaded from www.worldscientific.com
by UNIVERSITY OF CALIFORNIA @ BERKELEY on 09/16/26. Re-use and distribution is strictly not permitted, except for Open Access articles.

trailing numbers in agreement with their nearest-analog standard particles, as far as possible. Thus 4900021 is the gauge boson g_v of a confining gauge field, $490000n_{q_v}$ and $490001n_{\ell_v}$ are fundamental constituents charged or not under this, 4900022 is the γ_v of a non-confining field, and $4900n_{q_{v1}}n_{q_{v2}}n_J$ a Hidden-Valley meson.

12. Occasionally users and program authors add their own states. These should be flagged by setting $nn_r = 99$, and $n_L = 0$ or 9 for user and program customisations respectively.

    In addition, the $nn_r = 99$ range may be used to provide an alternative classification of states by their PDG "node" identifier[1]. This non-decodeable approach is specifically intended for states with sufficiently tentative quantum numbers that they cannot yet be given unambiguous MC ID codes; where states are listed in the MC ID table at the end of this review, those explicit codes should be strongly preferred. For tentative states, the mapping of PDG nodes to MC custom IDs is as follows:

    991xxxx: S-nodes encoding, includes SM leptons, bosons, some hadrons, and BSM groups

    992xxxx: Q-node encoding, for quarks

    993xxxx: G-node encoding, currently only the gluon

    994xxxx: M-node encoding, for mesons and tetraquarks

    995xxxx: B-node encoding, for baryons and pentaquarks.

    where the xxxx placeholders are zero-padded, i.e. node Q005 maps to ID number 9920005. $n_L = 6$–8 codes are reserved for future expansion of the custom-state scheme.

13. Concerning the non-99 numbers, it may be noted that only quarks, excited quarks, squarks, and diquarks have $n_{q_3} = 0$; only diquarks, baryons, and the odderon have $n_{q_1} \neq 0$; and only mesons, the reggeon, and the pomeron have $n_{q_1} = 0$ and $n_{q_2} \neq 0$. Concerning mesons (not antimesons), if n_{q_1} is odd then it labels a quark and an antiquark if even.

14. Tetra-quark states are specified with 9-digit codes $\pm 1n_r n_L n_{q_1} n_{q_2} 0 n_{q_3} n_{q_4} n_J$. For the particle $q_1 q_2$ is a diquark and $\bar{q}_3\bar{q}_4$ an antidiquark, sorted such that $n_{q_1} \geq n_{q_2}$, $n_{q_3} \geq n_{q_4}$, $n_{q_1} \geq n_{q_3}$, and $n_{q_2} \geq n_{q_4}$ if $n_{q_1} = n_{q_3}$. For the antiparticle, given with a negative sign, $\bar{q}_1\bar{q}_2$ is an antidiquark and $q_3 q_4$ a diquark, with the same sorting except that either $n_{q_1} > n_{q_3}$ or $n_{q_2} > n_{q_4}$ (so that flavour-diagonal states are particles). The n_J number has the same meaning as for ordinary hadrons. The n_r and n_L numbers do not have physical meaning as the non-relativistic quark model and masses (as for baryon disambiguation) are less clear with these novel states; instead, they are to be used as a two-digit indexing, from 00 to 99 and incrementing with new additions to the tables at the end of this section.

15. Penta-quark states are specified with 9-digit codes $\pm 1n_r n_L n_{q_1} n_{q_2} n_{q_3} n_{q_4} n_{q_5} n_J$, sorted such that $n_{q_1} \geq n_{q_2} \geq n_{q_3} \geq n_{q_4}$. In the particle the first four are quarks and the fifth an antiquark while the opposite holds in the antiparticle, which is given with a negative sign. The n_J number has the same meaning as for ordinary hadrons. The n_r and n_L numbers do not have physical meaning as the non-relativistic quark model and masses (as for baryon disambiguation) are less clear with these novel states; instead, they are to be used as a two-digit indexing, from 00 to 99 and incrementing with new additions to the tables at the end of this section.

16. Nuclear codes are given as 10-digit numbers $\pm 10LZZZAAAI$. For a (hyper)nucleus consisting of n_p protons, n_n neutrons and n_Λ Λ's, $A = n_p + n_n + n_\Lambda$ gives the total baryon number, $Z = n_p$ the total charge and $L = n_\Lambda$ the total number of strange quarks. I gives the isomer level, with $I = 0$ corresponding to the ground state and $I > 0$ to excitations, see [2], where states denoted m, n, p, q translate to $I = 1$–4. As examples, the deuteron is 1000010020 and ^{235}U is 1000922350. To avoid ambiguities,

    nuclear codes should not be applied to a single hadron, like p, n or Λ^0, where quark-contents-based codes already exist.

The following tables give explicit codings for established states listed in the Summary Tables and unestablished states required for MC modelling, following the preceding rules. This list is not exhaustive, and further codes may be used following the rules.

QUARKS	
d	1
u	2
s	3
c	4
b	5
t	6
b'	7
t'	8

LEPTONS	
e^-	11
ν_e	12
μ^-	13
ν_μ	14
τ^-	15
ν_τ	16
τ'^-	17
$\nu_{\tau'}$	18

GAUGE AND HIGGS BOSONS	
g	(9) 21
γ	22
Z^0	23
W^+	24
h^0/H_1^0	25
Z'/Z_2^0	32
Z''/Z_3^0	33
W'/W_2^+	34
H^0/H_2^0	35
A^0/H_3^0	36
H^+	37
H^{++}	38
a^0/H_4^0	40

SPECIAL PARTICLES	
G (graviton)	39
R^0	41
LQ^c	42
DM ($S=0$)	51
DM ($S=\frac{1}{2}$)	52
DM ($S=1$)	53
reggeon	110
pomeron	990
odderon	9990

for MC internal, use 81–100, 901–930, 998-999, 1901–1930, 2901–2930, and 3901–3930;

for custom user-specified physical states, use 9900000–9909999;

for custom program-specified physical states use 9990000–9999999;

for reference to PDG database nodes, for tentative and untabulated states, use 99{1,2,3,4,5}xxxx.

DIQUARKS	
$(dd)_1$	1103
$(ud)_0$	2101
$(ud)_1$	2103
$(uu)_1$	2203
$(sd)_0$	3101
$(sd)_1$	3103
$(su)_0$	3201
$(su)_1$	3203
$(ss)_1$	3303
$(cd)_0$	4101
$(cd)_1$	4103
$(cu)_0$	4201
$(cu)_1$	4203
$(cs)_0$	4301
$(cs)_1$	4303
$(cc)_1$	4403
$(bd)_0$	5101
$(bd)_1$	5103
$(bu)_0$	5201
$(bu)_1$	5203
$(bs)_0$	5301
$(bs)_1$	5303
$(bc)_0$	5401
$(bc)_1$	5403
$(bb)_1$	5503

SUSY PARTICLES	
$\tilde{d}_L$	1000001
$\tilde{u}_L$	1000002
$\tilde{s}_L$	1000003
$\tilde{c}_L$	1000004
$\tilde{b}_1$	1000005[a]
$\tilde{t}_1$	1000006[a]
$\tilde{e}_L^-$	1000011
$\tilde{\nu}_{eL}$	1000012
$\tilde{\mu}_L^-$	1000013
$\tilde{\nu}_{\mu L}$	1000014
$\tilde{\tau}_1^-$	1000015[a]
$\tilde{\nu}_{\tau L}$	1000016
$\tilde{d}_R$	2000001
$\tilde{u}_R$	2000002
$\tilde{s}_R$	2000003
$\tilde{c}_R$	2000004
$\tilde{b}_2$	2000005[a]
$\tilde{t}_2$	2000006[a]
$\tilde{e}_R^-$	2000011
$\tilde{\mu}_R^-$	2000013
$\tilde{\tau}_2^-$	2000015[a]
$\tilde{g}$	1000021
$\tilde{\chi}_1^0$	1000022[b]
$\tilde{\chi}_2^0$	1000023[b]
$\tilde{\chi}_1^+$	1000024[b]
$\tilde{\chi}_3^0$	1000025[b]
$\tilde{\chi}_4^0$	1000035[b]
$\tilde{\chi}_2^+$	1000037[b]
$\tilde{G}$	1000039

LIGHT $I = 1$ MESONS	
π^0	111
π^+	211
$a_0(980)^0$	9000111
$a_0(980)^+$	9000211
$\pi(1300)^0$	100111
$\pi(1300)^+$	100211
$a_0(1450)^0$	10111
$a_0(1450)^+$	10211
$\pi(1800)^0$	9010111
$\pi(1800)^+$	9010211
$\rho(770)^0$	113
$\rho(770)^+$	213
$b_1(1235)^0$	10113
$b_1(1235)^+$	10213
$a_1(1260)^0$	20113
$a_1(1260)^+$	20213
$\pi_1(1400)^0$	9000113
$\pi_1(1400)^+$	9000213
$\rho(1450)^0$	100113
$\rho(1450)^+$	100213
$\pi_1(1600)^0$	9010113
$\pi_1(1600)^+$	9010213

Phys. A 2026.41. Downloaded from www.worldscientific.com
by UNIVERSITY OF CA LEY on 09/16/26. Re-use and distribution is strictly not permitted, except for Open Access articles.

$a_1(1640)^0$	9020113
$a_1(1640)^+$	9020213
$\rho(1700)^0$	30113
$\rho(1700)^+$	30213
$\rho(1900)^0$	9030113
$\rho(1900)^+$	9030213
$\rho(2150)^0$	9040113
$\rho(2150)^+$	9040213
$a_2(1320)^0$	115
$a_2(1320)^+$	215
$\pi_2(1670)^0$	10115
$\pi_2(1670)^+$	10215
$\boldsymbol{\pi_2(1880)^0}$	**110115**
$\boldsymbol{\pi_2(1880)^+}$	**110215**
$a_2(1700)^0$	9000115
$a_2(1700)^+$	9000215
$\pi_2(2100)^0$	9010115
$\pi_2(2100)^+$	9010215
$\rho_3(1690)^0$	117
$\rho_3(1690)^+$	217
$\rho_3(1990)^0$	9000117
$\rho_3(1990)^+$	9000217
$\rho_3(2250)^0$	9010117
$\rho_3(2250)^+$	9010217
$\boldsymbol{a_4(1970)^0}$	119
$\boldsymbol{a_4(1970)^+}$	219

LIGHT $I = 0$ MESONS
($u\bar{u}$, $d\bar{d}$, $s\bar{s}$ admixtures)

η	221
$\eta'(958)$	331
$f_0(500)$	9000221
$f_0(980)$	9010221
$\eta(1295)$	100221
$f_0(1370)$	10221
$\eta(1405)$	9020221
$\eta(1475)$	100331
$f_0(1500)$	9030221
$f_0(1710)$	10331
$\eta(1760)$	9040221
$f_0(2020)$	9050221
$f_0(2100)$	9060221
$f_0(2200)$	9070221
$\eta(2225)$	9080221
$\omega(782)$	223
$\phi(1020)$	333
$h_1(1170)$	10223
$f_1(1285)$	20223
$\boldsymbol{h_1(1415)}$	10333
$f_1(1420)$	20333
$\omega(1420)$	100223
$f_1(1510)$	9000223
$h_1(1595)$	9010223
$\omega(1650)$	30223
$\phi(1680)$	100333
$\boldsymbol{\phi(2170)}$	**230333**
$f_2(1270)$	225
$f_2(1430)$	9000225
$f_2'(1525)$	335
$f_2(1565)$	9010225
$f_2(1640)$	9020225
$\eta_2(1645)$	10225
$f_2(1810)$	9030225
$\eta_2(1870)$	10335
$f_2(1910)$	9040225
$f_2(1950)$	9050225
$f_2(2010)$	9060225
$f_2(2150)$	9070225
$f_2(2300)$	9080225
$f_2(2340)$	9090225
$\omega_3(1670)$	227
$\phi_3(1850)$	337
$f_4(2050)$	229
$f_J(2220)$	9000229
$f_4(2300)$	9010229

STRANGE MESONS

K_L^0	130
K_S^0	310
K^0	311
K^+	321
$K_0^*(700)^0$	9000311
$K_0^*(700)^+$	9000321
$K_0^*(1430)^0$	10311
$K_0^*(1430)^+$	10321
$K(1460)^0$	100311
$K(1460)^+$	100321
$K(1830)^0$	9010311
$K(1830)^+$	9010321
$K_0^*(1950)^0$	9020311
$K_0^*(1950)^+$	9020321
$K^*(892)^0$	313
$K^*(892)^+$	323
$K_1(1270)^0$	10313
$K_1(1270)^+$	10323
$K_1(1400)^0$	20313
$K_1(1400)^+$	20323
$K^*(1410)^0$	100313
$K^*(1410)^+$	100323
$K_1(1650)^0$	9000313
$K_1(1650)^+$	9000323
$K^*(1680)^0$	30313
$K^*(1680)^+$	30323
$K_2^*(1430)^0$	315
$K_2^*(1430)^+$	325
$K_2(1580)^0$	9000315
$K_2(1580)^+$	9000325
$K_2(1770)^0$	10315
$K_2(1770)^+$	10325
$K_2(1820)^0$	20315
$K_2(1820)^+$	20325
$K_2^*(1980)^0$	9010315
$K_2^*(1980)^+$	9010325
$K_2(2250)^0$	9020315
$K_2(2250)^+$	9020325
$K_3^*(1780)^0$	317
$K_3^*(1780)^+$	327
$K_3(2320)^0$	9010317
$K_3(2320)^+$	9010327
$K_4^*(2045)^0$	319
$K_4^*(2045)^+$	329
$K_4(2500)^0$	9000319
$K_4(2500)^+$	9000329

CHARMED MESONS

D^+	411
D^0	421
$\boldsymbol{D_0^*(2300)^+}$	10411
$\boldsymbol{D_0^*(2300)^0}$	10421
$D^*(2010)^+$	413
$D^*(2007)^0$	423
$D_1(2420)^+$	10413
$D_1(2420)^0$	10423
$(D_1(H)^+$	20413)
$D_1(2430)^0$	20423
$D_2^*(2460)^+$	415
$D_2^*(2460)^0$	425
D_s^+	431
$D_{s0}^*(2317)^+$	10431
D_s^{*+}	433
$D_{s1}(2536)^+$	10433
$D_{s1}(2460)^+$	20433
$\boldsymbol{D_{s1}^*(2700)^+}$	**100433**
$D_{s2}^*(2573)^+$	435
$\boldsymbol{D_3^*(2750)^+}$	**417**
$\boldsymbol{D_3^*(2750)^0}$	**427**
$\boldsymbol{D_{s3}^*(2860)^+}$	**437**

$c\bar{c}$ MESONS

$\eta_c(1S)$	441
$\chi_{c0}(1P)$	10441
$\boldsymbol{\chi_{c0}(3915)}$	**110441**
$\eta_c(2S)$	100441
$J/\psi(1S)$	443
$h_c(1P)$	10443
$\chi_{c1}(1P)$	20443
$\boldsymbol{\chi_{c1}(3872)}$	**120443**
$\boldsymbol{\chi_{c1}(4140)}$	**220443**
$\boldsymbol{\chi_{c1}(4274)}$	**320443**
$\psi(2S)$	100443
$\psi(4040)$	**200443**
$\boldsymbol{\psi(4230)}$	**300443**
$\boldsymbol{\psi(4360)}$	**400443**
$\psi(4415)$	**500443**
$\boldsymbol{\psi(4660)}$	**600443**
$\psi(3770)$	30443
$\psi(4160)$	**130443**
$\chi_{c2}(1P)$	445
$\chi_{c2}(3930)$	100445
$\boldsymbol{\psi_2(3823)}$	**20445**
$\boldsymbol{\psi_3(3842)}$	**447**

BOTTOM MESONS

B^0	511
B^+	521
$(B_0^{*0}$	10511)
$(B_0^{*+}$	10521)
B^{*0}	513
B^{*+}	523
$\boldsymbol{B_1(5721)^0}$	10513
$\boldsymbol{B_1(5721)^+}$	10523
$(B_1(H)^0$	20513)
$(B_1(H)^+$	20523)
$\boldsymbol{B_2^*(5747)^0}$	515
$\boldsymbol{B_2^*(5747)^+}$	525
B_s^0	531
$(B_{s0}^{*0}$	10531)
B_s^{*0}	533
$\boldsymbol{B_{s1}(5830)^0}$	10533
$(B_{s1}(H)^0$	20533)
$\boldsymbol{B_{s2}^*(5840)^0}$	535
B_c^+	541
$(B_{c0}^{*+}$	10541)
$\boldsymbol{B_c(2S)^+}$	**100541**
$[B_c^{*+}$	543]
$(B_{c1}(L)^+$	10543)
$(B_{c1}(H)^+$	20543)
$[B_{c2}^{*+}$	545]

$b\bar{b}$ MESONS

$\eta_b(1S)$	551
$\chi_{b0}(1P)$	10551
$\eta_b(2S)$	100551
$\chi_{b0}(2P)$	110551
$\eta_b(3S)$	200551
$\chi_{b0}(3P)$	210551
$\Upsilon(1S)$	553
$h_b(1P)$	10553
$\chi_{b1}(1P)$	20553
$\Upsilon_1(1D)$	30553
$\Upsilon(2S)$	100553
$h_b(2P)$	110553
$\chi_{b1}(2P)$	120553
$\Upsilon_1(2D)$	130553
$\Upsilon(3S)$	200553
$h_b(3P)$	210553
$\chi_{b1}(3P)$	220553
$\Upsilon(4S)$	300553
$\Upsilon(10860)$	9000553
$\Upsilon(11020)$	9010553
$\chi_{b2}(1P)$	555
$\eta_{b2}(1D)$	10555
$\Upsilon_2(1D)$	20555
$\chi_{b2}(2P)$	100555
$\eta_{b2}(2D)$	110555
$\Upsilon_2(2D)$	120555
$\chi_{b2}(3P)$	200555
$\Upsilon_3(1D)$	557
$\Upsilon_3(2D)$	100557

LIGHT BARYONS

p	2212
n	2112
Δ^{++}	2224
Δ^+	2214
Δ^0	2114
Δ^-	1114

STRANGE BARYONS

Λ	3122
Σ^+	3222
Σ^0	3212
Σ^-	3112
Σ^{*+}	3224^c
Σ^{*0}	3214^c
Σ^{*-}	3114^c
Ξ^0	3322
Ξ^-	3312
Ξ^{*0}	3324^c
Ξ^{*-}	3314^c
Ω^-	3334

CHARMED BARYONS

Λ_c^+	4122
Σ_c^{++}	4222
Σ_c^+	4212
Σ_c^0	4112
Σ_c^{*++}	4224
Σ_c^{*+}	4214
Σ_c^{*0}	4114
Ξ_c^+	4232
Ξ_c^0	4132
$\Xi_c'^+$	4322
$\Xi_c'^0$	4312
Ξ_c^{*+}	4324
Ξ_c^{*0}	4314
Ω_c^0	4332
Ω_c^{*0}	4334
Ξ_{cc}^+	4412
Ξ_{cc}^{++}	4422
Ξ_{cc}^{*+}	4414
Ξ_{cc}^{*++}	4424
Ω_{cc}^+	4432
Ω_{cc}^{*+}	4434
Ω_{ccc}^{++}	4444

BOTTOM BARYONS

Λ_b^0	5122
Σ_b^-	5112
Σ_b^0	5212
Σ_b^+	5222
Σ_b^{*-}	5114
Σ_b^{*0}	5214
Σ_b^{*+}	5224
Ξ_b^-	5132
Ξ_b^0	5232
$\Xi_b'^-$	5312
$\Xi_b'^0$	5322
Ξ_b^{*-}	5314
Ξ_b^{*0}	5324
Ω_b^-	5332
Ω_b^{*-}	5334
Ξ_{bc}^0	5142
Ξ_{bc}^+	5242
$\Xi_{bc}'^0$	5412
$\Xi_{bc}'^+$	5422
Ξ_{bc}^{*0}	5414
Ξ_{bc}^{*+}	5424
Ω_{bc}^0	5342
$\Omega_{bc}'^0$	5432
Ω_{bc}^{*0}	5434
Ω_{bcc}^+	5442
Ω_{bcc}^{*+}	5444
Ξ_{bb}^-	5512
Ξ_{bb}^0	5522
Ξ_{bb}^{*-}	5514
Ξ_{bb}^{*0}	5524
Ω_{bb}^-	5532
Ω_{bb}^{*-}	5534
Ω_{bbc}^0	5542
Ω_{bbc}^{*0}	5544
Ω_{bbb}^-	5554

TETRAQUARKS

$T_{c\bar{c}1}(3900)^+$	100420413
$T_{c\bar{c}1}(3900)^0$	100410413
$T_{c\bar{c}1}(4430)^+$	101420413
$T_{c\bar{c}1}(4430)^0$	101410413
$T_{b\bar{b}1}(10610)^+$	100520513
$T_{b\bar{b}1}(10610)^0$	100510513
$T_{b\bar{b}1}(10650)^+$	101520513
$T_{b\bar{b}1}(10650)^0$	101510513

Int. J. Mod. Phys. A 2026.41. Downloaded from www.worldscientific.com
by UNIVERSITY OF CALIFORNIA @ BERKELEY on 09/16/26. Re-use and distribution is strictly not permitted, except for Open Access articles.

Notes to the tables:

1) Numbers or names in **bold face** are new or have changed since the 2024 *Review*. Entries in square brackets are necessary multiplet states for consistent MC hadronisation models, which do not currently have experimentally evidenced entries in the RPP listings. Entries in parentheses do not currently have experimentally evidenced entries in the RPP listings.
2) All previously listed pentaquark states have been removed from the MC ID tables in the 2026 update due to not being considered experimentally established in the Summary Tables (Θ^+ [100221132] and Φ^{--} [100331122]).

a) Particularly in the third generation, the left and right sfermion states may mix, as shown. The lighter mixed state is given the smaller number.

b) The physical $\widetilde{\chi}$ states are admixtures of the pure $\widetilde{\gamma}$, $\widetilde{Z}^0$, $\widetilde{W}^+$, $\widetilde{H}_1^0$, $\widetilde{H}_2^0$, and $\widetilde{H}^+$ states.

c) Σ^* and Ξ^* are alternate names for $\Sigma(1385)$ and $\Xi(1530)$.

References

[1] G. P. Yost *et al.* (Particle Data Group), Phys. Lett. **B204**, 1 (1988).

[2] G. Audi *et al.*, Nucl. Phys. **A729**, 3 (2003).

46. Clebsch-Gordan Coefficients, Spherical Harmonics, and *d* Functions

Note: A square-root sign is to be understood over *every* coefficient, *e.g.*, for $-8/15$ read $-\sqrt{8/15}$.

Notation:

	J	J	…
M	M	…	
m_1 m_2	Coefficients		
m_1 m_2			
. .			
. .			
. .			

$$Y_1^0 = \sqrt{\frac{3}{4\pi}}\cos\theta$$

$$Y_1^1 = -\sqrt{\frac{3}{8\pi}}\sin\theta\, e^{i\phi}$$

$$Y_2^0 = \sqrt{\frac{5}{4\pi}}\Big(\frac{3}{2}\cos^2\theta - \frac{1}{2}\Big)$$

$$Y_2^1 = -\sqrt{\frac{15}{8\pi}}\sin\theta\cos\theta\, e^{i\phi}$$

$$Y_2^2 = \frac{1}{4}\sqrt{\frac{15}{2\pi}}\sin^2\theta\, e^{2i\phi}$$

$1/2\times1/2$

m_1	m_2	$J=1$	$J=0$
+1/2	+1/2	1	
+1/2	−1/2	1/2	1/2
−1/2	+1/2	1/2	−1/2
−1/2	−1/2	1	

$1\times1/2$

m_1	m_2	$J=3/2$	$J=1/2$
+1	+1/2	1	
+1	−1/2	1/3	2/3
0	+1/2	2/3	−1/3
0	−1/2	2/3	1/3
−1	+1/2	1/3	−2/3
−1	−1/2	1	

$2\times1/2$

m_1	m_2	$J=5/2$	$J=3/2$
+2	+1/2	1	
+2	−1/2	1/5	4/5
+1	+1/2	4/5	−1/5
+1	−1/2	2/5	3/5
0	+1/2	3/5	−2/5
0	−1/2	3/5	2/5
−1	+1/2	2/5	−3/5
−1	−1/2	4/5	1/5
−2	+1/2	1/5	−4/5
−2	−1/2	1	

2×1

m_1	m_2	$J=3$	$J=2$	$J=1$
+2	+1	1		
+2	0	1/3	2/3	
+1	+1	2/3	−1/3	
+2	−1	1/15	1/3	3/5
+1	0	8/15	1/6	−3/10
0	+1	2/5	−1/2	1/10
+1	−1	1/5	1/2	3/10
0	0	3/5	0	−2/5
−1	+1	1/5	−1/2	3/10
0	−1	2/5	1/2	1/10
−1	0	8/15	−1/6	−3/10
−2	+1	1/15	−1/3	3/5
−1	−1	2/3	1/3	
−2	0	1/3	−2/3	
−2	−1	1		

$3/2\times1/2$

m_1	m_2	$J=2$	$J=1$
+3/2	+1/2	1	
+3/2	−1/2	1/4	3/4
+1/2	+1/2	3/4	−1/4
+1/2	−1/2	1/2	1/2
−1/2	+1/2	1/2	−1/2
−3/2	+1/2	3/4	1/4
−3/2	−1/2	1/4	−3/4
−3/2	−1/2	1	

$3/2\times1$

m_1	m_2	$J=5/2$	$J=3/2$	$J=1/2$
+3/2	+1	1		
+3/2	0	2/5	3/5	
+1/2	+1	3/5	−2/5	
+3/2	−1	1/10	2/5	1/2
+1/2	0	3/5	1/15	−1/3
−1/2	+1	3/10	−8/15	1/6
+1/2	−1	3/10	8/15	1/6
−1/2	0	3/5	−1/15	−1/3
−3/2	+1	1/10	−2/5	1/2
−1/2	−1	3/5	2/5	
−3/2	0	2/5	−3/5	
−3/2	−1	1		

1×1

m_1	m_2	$J=2$	$J=1$	$J=0$
+1	+1	1		
+1	0	1/2	1/2	
0	+1	1/2	−1/2	
+1	−1	1/6	1/2	1/3
0	0	2/3	0	−1/3
−1	+1	1/6	−1/2	1/3
0	−1	1/2	1/2	
−1	0	1/2	−1/2	
−1	−1	1		

$$Y_\ell^{-m} = (-1)^m Y_\ell^{m*}$$

$$d^\ell_{m,0} = \sqrt{\frac{4\pi}{2\ell+1}}\, Y_\ell^m\, e^{-im\phi}$$

$$\langle j_1 j_2 m_1 m_2 | j_1 j_2 J M\rangle = (-1)^{J-j_1-j_2}\langle j_2 j_1 m_2 m_1 | j_2 j_1 J M\rangle$$

$$d^j_{m',m} = (-1)^{m-m'} d^j_{m,m'} = d^j_{-m,-m'}$$

$$d^1_{0,0} = \cos\theta \qquad d^{1/2}_{1/2,1/2} = \cos\frac{\theta}{2} \qquad d^1_{1,1} = \frac{1+\cos\theta}{2}$$

$$d^{1/2}_{1/2,-1/2} = -\sin\frac{\theta}{2} \qquad d^1_{1,0} = -\frac{\sin\theta}{\sqrt{2}}$$

$$d^1_{1,-1} = \frac{1-\cos\theta}{2}$$

$2\times3/2$

m_1	m_2	$J=7/2$	$J=5/2$	$J=3/2$	$J=1/2$
+2	+3/2	1			
+2	+1/2	3/7	4/7		
+1	+3/2	4/7	−3/7		
+2	−1/2	1/7	16/35	2/5	
+1	+1/2	4/7	1/35	−2/5	
0	+3/2	2/7	−18/35	1/5	
+2	−3/2	1/35	6/35	2/5	2/5
+1	−1/2	12/35	5/14	0	−3/10
0	+1/2	18/35	−3/35	−1/5	1/5
−1	+3/2	4/35	−27/70	2/5	−1/10
+1	−3/2	4/35	27/70	2/5	1/10
0	−1/2	18/35	3/35	−1/5	−1/5
−1	+1/2	12/35	−5/14	0	3/10
−2	+3/2	1/35	−6/35	2/5	−2/5
0	−3/2	2/7	18/35	1/5	
−1	−1/2	4/7	−1/35	−2/5	
−2	+1/2	1/7	−16/35	2/5	
−1	−3/2	4/7	3/7		
−2	−1/2	3/7	−4/7		
−2	−3/2	1			

$3/2\times3/2$

m_1	m_2	$J=3$	$J=2$	$J=1$	$J=0$
+3/2	+3/2	1			
+3/2	+1/2	1/2	1/2		
+1/2	+3/2	1/2	−1/2		
+3/2	−1/2	1/5	1/2	3/10	
+1/2	+1/2	3/5	0	−2/5	
−1/2	+3/2	1/5	−1/2	3/10	
+3/2	−3/2	1/20	1/4	9/20	1/4
+1/2	−1/2	9/20	1/4	−1/20	−1/4
−1/2	+1/2	9/20	−1/4	−1/20	1/4
−3/2	+3/2	1/20	−1/4	9/20	−1/4
+1/2	−3/2	1/5	1/2	3/10	
−1/2	−1/2	3/5	0	−2/5	
−3/2	+1/2	1/5	−1/2	3/10	
−1/2	−3/2	1/2	1/2		
−3/2	−1/2	1/2	−1/2		
−3/2	−3/2	1			

2×2

m_1	m_2	$J=4$	$J=3$	$J=2$	$J=1$	$J=0$
+2	+2	1				
+2	+1	1/2	1/2			
+1	+2	1/2	−1/2			
+2	0	3/14	1/2	2/7		
+1	+1	4/7	0	−3/7		
0	+2	3/14	−1/2	2/7		
+2	−1	1/14	3/10	3/7	1/5	
+1	0	3/7	1/5	−1/14	−3/10	
0	+1	3/7	−1/5	−1/14	3/10	
−1	+2	1/14	−3/10	3/7	−1/5	
+2	−2	1/70	1/10	2/7	2/5	1/5
+1	−1	8/35	2/5	1/14	−1/10	−1/5
0	0	18/35	0	−2/7	0	1/5
−1	+1	8/35	−2/5	1/14	1/10	−1/5
−2	+2	1/70	−1/10	2/7	−2/5	1/5
+1	−2	1/14	3/10	3/7	1/5	
0	−1	3/7	1/5	−1/14	−3/10	
−1	0	3/7	−1/5	−1/14	3/10	
−2	+1	1/14	−3/10	3/7	−1/5	
0	−2	3/14	1/2	2/7		
−1	−1	4/7	0	−3/7		
−2	0	3/14	−1/2	2/7		
−1	−2	1/2	1/2			
−2	−1	1/2	−1/2			
−2	−2	1				

$$d^{3/2}_{3/2,3/2} = \frac{1+\cos\theta}{2}\cos\frac{\theta}{2}$$

$$d^{3/2}_{3/2,1/2} = -\sqrt{3}\frac{1+\cos\theta}{2}\sin\frac{\theta}{2} \qquad d^2_{2,2} = \Big(\frac{1+\cos\theta}{2}\Big)^2$$

$$d^{3/2}_{3/2,-1/2} = \sqrt{3}\frac{1-\cos\theta}{2}\cos\frac{\theta}{2} \qquad d^2_{2,1} = -\frac{1+\cos\theta}{2}\sin\theta$$

$$d^{3/2}_{3/2,-3/2} = -\frac{1-\cos\theta}{2}\sin\frac{\theta}{2} \qquad d^2_{2,0} = \frac{\sqrt{6}}{4}\sin^2\theta \qquad d^2_{1,1} = \frac{1+\cos\theta}{2}(2\cos\theta-1)$$

$$d^{3/2}_{1/2,1/2} = \frac{3\cos\theta-1}{2}\cos\frac{\theta}{2} \qquad d^2_{2,-1} = -\frac{1-\cos\theta}{2}\sin\theta \qquad d^2_{1,0} = -\sqrt{\frac{3}{2}}\sin\theta\cos\theta$$

$$d^{3/2}_{1/2,-1/2} = -\frac{3\cos\theta+1}{2}\sin\frac{\theta}{2} \qquad d^2_{2,-2} = \Big(\frac{1-\cos\theta}{2}\Big)^2 \qquad d^2_{1,-1} = \frac{1-\cos\theta}{2}(2\cos\theta+1) \qquad d^2_{0,0} = \Big(\frac{3}{2}\cos^2\theta - \frac{1}{2}\Big)$$

Figure 46.1: The sign convention is that of Wigner (*Group Theory*, Academic Press, New York, 1959), also used by Condon and Shortley (*The Theory of Atomic Spectra*, Cambridge Univ. Press, New York, 1953), Rose (*Elementary Theory of Angular Momentum*, Wiley, New York, 1957), and Cohen (*Tables of the Clebsch-Gordan Coefficients*, North American Rockwell Science Center, Thousand Oaks, Calif., 1974).

Phys. A 2026.41. Downloaded from www.worldscientific.com
LEY on 09/16/26. Re-use and distribution is strictly not permitted, except for Open Access articles.
by UNIVERSITY OF CA

47. SU(3) Isoscalar Factors and Representation Matrices

Revised August 2019 by R. Kelly (LBNL).

The most commonly used SU(3) isoscalar factors, corresponding to the singlet, octet, and decuplet content of $8 \otimes 8$ and $10 \otimes 8$, are shown at the right. The notation uses particle names to identify the coefficients, so that the pattern of relative couplings may be seen at a glance. We illustrate the use of the coefficients below. See J.J de Swart, Rev. Mod. Phys. **35**, 916 (1963) for detailed explanations and phase conventions.

A $\sqrt{\ }$ is to be understood over every integer in the matrices; the exponent 1/2 on each matrix is a reminder of this. For example, the $\Xi \to \Omega K$ element of the $10 \to 10 \otimes 8$ matrix is $-\sqrt{6}/\sqrt{24} = -1/2$.

Intramultiplet relative decay strengths may be read directly from the matrices. For example, in decuplet $\to$ octet + octet decays, the ratio of $\Omega^* \to \Xi\overline{K}$ and $\Delta \to N\pi$ partial widths is, from the $10 \to 8 \times 8$ matrix,

$$\frac{\Gamma\,(\Omega^* \to \Xi\overline{K})}{\Gamma\,(\Delta \to N\pi)} = \frac{12}{6} \times \text{ (phase space factors) .} \tag{47.1}$$

Including isospin Clebsch-Gordan coefficients, we obtain, *e.g.*,

$$\frac{\Gamma(\Omega^{*-} \to \Xi^0 K^-)}{\Gamma(\Delta^+ \to p\,\pi^0)} = \frac{1/2}{2/3} \times \frac{12}{6} \times p.s.f. = \frac{3}{2} \times p.s.f. \tag{47.2}$$

Partial widths for $8 \to 8 \otimes 8$ involve a linear superposition of 8_1 (symmetric) and 8_2 (antisymmetric) couplings. For example,

$$\Gamma(\Xi^* \to \Xi\pi) \sim \left(-\sqrt{\frac{9}{20}}\, g_1 + \sqrt{\frac{3}{12}}\, g_2\right)^2 . \tag{47.3}$$

The relations between g_1 and g_2 (with de Swart's normalization) and the standard D and F couplings that appear in the interaction Lagrangian,

$$\mathscr{L} = -\sqrt{2}\; D\; Tr\,(\{\overline{B}, B\}M) + \sqrt{2}\; F\; Tr\,([\overline{B}, B]\,M) \;, \tag{47.4}$$

where $[\overline{B}, B] \equiv \overline{B}B - B\overline{B}$ and $\{\overline{B}, B\} \equiv \overline{B}B + B\overline{B}$, are

$$D = \frac{\sqrt{30}}{40}\, g_1 \;, \qquad F = \frac{\sqrt{6}}{24}\, g_2 \;. \tag{47.5}$$

Thus, for example,

$$\Gamma(\Xi^* \to \Xi\pi) \sim (F - D)^2 \sim (1 - 2\alpha)^2 \;, \tag{47.6}$$

where $\alpha \equiv F/(D + F)$. (This definition of α is de Swart's. The alternative $D/(D + F)$, due to Gell-Mann, is also used.)

The generators of SU(3) transformations, λ_a $(a = 1, 8)$, are 3×3 matrices that obey the following commutation and anticommutation relationships:

$$[\lambda_a,\ \lambda_b] \equiv \lambda_a\lambda_b - \lambda_b\lambda_a = 2if_{abc}\lambda_c \tag{47.7}$$

$$\{\lambda_a,\ \lambda_b\} \equiv \lambda_a\lambda_b + \lambda_b\lambda_a = \frac{4}{3}\delta_{ab}I + 2d_{abc}\lambda_c \;, \tag{47.8}$$

where I is the 3×3 identity matrix, and δ_{ab} is the Kronecker delta symbol. The f_{abc} are odd under the permutation of any pair of indices, while the d_{abc} are even. The nonzero values are:

$1 \to 8 \otimes 8$

$$\begin{pmatrix}\Lambda\end{pmatrix} \to \begin{pmatrix} N\overline{K} & \Sigma\pi & \Lambda\eta & \Xi K \end{pmatrix} = \frac{1}{\sqrt{8}}\begin{pmatrix}2 & 3 & -1 & -2\end{pmatrix}^{1/2}$$

$8_1 \to 8 \otimes 8$

$$\begin{pmatrix} N \\ \Sigma \\ \Lambda \\ \Xi \end{pmatrix} \to \begin{pmatrix} N\pi & N\eta & \Sigma K & \Lambda K \\ N\overline{K} & \Sigma\pi & \Lambda\pi & \Sigma\eta & \Xi K \\ N\overline{K} & \Sigma\pi & \Lambda\eta & \Xi K \\ \Sigma\overline{K} & \Lambda\overline{K} & \Xi\pi & \Xi\eta \end{pmatrix} = \frac{1}{\sqrt{20}}\begin{pmatrix} 9 & -1 & -9 & -1 \\ -6 & 0 & 4 & 4 & -6 \\ 2 & -12 & -4 & -2 \\ 9 & -1 & -9 & -1 \end{pmatrix}^{1/2}$$

$8_2 \to 8 \otimes 8$

$$\begin{pmatrix} N \\ \Sigma \\ \Lambda \\ \Xi \end{pmatrix} \to \begin{pmatrix} N\pi & N\eta & \Sigma K & \Lambda K \\ N\overline{K} & \Sigma\pi & \Lambda\pi & \Sigma\eta & \Xi K \\ N\overline{K} & \Sigma\pi & \Lambda\eta & \Xi K \\ \Sigma\overline{K} & \Lambda\overline{K} & \Xi\pi & \Xi\eta \end{pmatrix} = \frac{1}{\sqrt{12}}\begin{pmatrix} 3 & 3 & 3 & -3 \\ 2 & 8 & 0 & 0 & -2 \\ 6 & 0 & 0 & 6 \\ 3 & 3 & 3 & -3 \end{pmatrix}^{1/2}$$

$10 \to 8 \otimes 8$

$$\begin{pmatrix} \Delta \\ \Sigma \\ \Xi \\ \Omega \end{pmatrix} \to \begin{pmatrix} N\pi & \Sigma K \\ N\overline{K} & \Sigma\pi & \Lambda\pi & \Sigma\eta & \Xi K \\ \Sigma\overline{K} & \Lambda\overline{K} & \Xi\pi & \Xi\eta \\ \Xi\overline{K} \end{pmatrix} = \frac{1}{\sqrt{12}}\begin{pmatrix} -6 & 6 \\ -2 & 2 & -3 & 3 & 2 \\ 3 & -3 & 3 & 3 \\ 12 \end{pmatrix}^{1/2}$$

$8 \to 10 \otimes 8$

$$\begin{pmatrix} N \\ \Sigma \\ \Lambda \\ \Xi \end{pmatrix} \to \begin{pmatrix} \Delta\pi & \Sigma K \\ \Delta\overline{K} & \Sigma\pi & \Sigma\eta & \Xi K \\ \Sigma\pi & \Xi K \\ \Sigma\overline{K} & \Xi\pi & \Xi\eta & \Omega K \end{pmatrix} = \frac{1}{\sqrt{15}}\begin{pmatrix} -12 & 3 \\ 8 & -2 & -3 & 2 \\ -9 & 6 \\ 3 & -3 & -3 & 6 \end{pmatrix}^{1/2}$$

$10 \to 10 \otimes 8$

$$\begin{pmatrix} \Delta \\ \Sigma \\ \Xi \\ \Omega \end{pmatrix} \to \begin{pmatrix} \Delta\pi & \Delta\eta & \Sigma K \\ \Delta\overline{K} & \Sigma\pi & \Sigma\eta & \Xi K \\ \Sigma\overline{K} & \Xi\pi & \Xi\eta & \Omega K \\ \Xi\overline{K} & \Omega\eta \end{pmatrix} = \frac{1}{\sqrt{24}}\begin{pmatrix} 15 & 3 & -6 \\ 8 & 8 & 0 & -8 \\ 12 & 3 & -3 & -6 \\ 12 & -12 \end{pmatrix}^{1/2}$$

abc	f_{abc}	abc	d_{abc}	abc	d_{abc}
123	1	118	$1/\sqrt{3}$	355	1/2
147	1/2	146	1/2	366	−1/2
156	−1/2	157	1/2	377	−1/2
246	1/2	228	$1/\sqrt{3}$	448	$-1/(2\sqrt{3})$
257	1/2	247	−1/2	558	$-1/(2\sqrt{3})$
345	1/2	256	1/2	668	$-1/(2\sqrt{3})$
367	−1/2	338	$1/\sqrt{3}$	778	$-1/(2\sqrt{3})$
458	$\sqrt{3}/2$	344	1/2	888	$-1/\sqrt{3}$
678	$\sqrt{3}/2$				

The λ_a's are

$$\lambda_1 = \begin{pmatrix} 0 & 1 & 0 \\ 1 & 0 & 0 \\ 0 & 0 & 0 \end{pmatrix} \quad \lambda_2 = \begin{pmatrix} 0 & -i & 0 \\ i & 0 & 0 \\ 0 & 0 & 0 \end{pmatrix} \quad \lambda_3 = \begin{pmatrix} 1 & 0 & 0 \\ 0 & -1 & 0 \\ 0 & 0 & 0 \end{pmatrix}$$

$$\lambda_4 = \begin{pmatrix} 0 & 0 & 1 \\ 0 & 0 & 0 \\ 1 & 0 & 0 \end{pmatrix} \quad \lambda_5 = \begin{pmatrix} 0 & 0 & -i \\ 0 & 0 & 0 \\ i & 0 & 0 \end{pmatrix} \quad \lambda_6 = \begin{pmatrix} 0 & 0 & 0 \\ 0 & 0 & 1 \\ 0 & 1 & 0 \end{pmatrix}$$

$$\lambda_7 = \begin{pmatrix} 0 & 0 & 0 \\ 0 & 0 & -i \\ 0 & i & 0 \end{pmatrix} \quad \lambda_8 = \frac{1}{\sqrt{3}}\begin{pmatrix} 1 & 0 & 0 \\ 0 & 1 & 0 \\ 0 & 0 & -2 \end{pmatrix}$$

Equation (47.7) defines the Lie algebra of SU(3). A general d-dimensional representation is given by a set of $d \times d$ matrices satisfying Eq. (47.7) with the f_{abc} given above. Equation (47.8) is specific to the defining 3-dimensional representation.

Int. J. Mod. Phys. A 2026.41. Downloaded from www.worldscientific.com
by UNIVERSITY OF CALIFORNIA @ BERKELEY on 09/16/26. Re-use and distribution is strictly not permitted, except for Open Access articles.

48. SU(n) Multiplets and Young Diagrams

Revised August 2019 by C.G. Wohl (LBNL).

This note tells (1) how SU(n) particle multiplets are identified or labeled, (2) how to find the number of particles in a multiplet from its label, (3) how to draw the Young diagram for a multiplet, and (4) how to use Young diagrams to determine the overall multiplet structure of a composite system, such as a 3-quark or a meson-baryon system.

In much of the literature, the word "representation" is used where we use "multiplet," and "tableau" is used where we use "diagram."

48.1 Multiplet labels

An SU(n) multiplet is uniquely identified by a string of (n−1) nonnegative integers: $(\alpha, \beta, \gamma, \ldots)$. Any such set of integers specifies a multiplet. For an SU(2) multiplet such as an isospin multiplet, the single integer α is the number of *steps* from one end of the multiplet to the other (*i.e.*, it is one fewer than the number of particles in the multiplet). In SU(3), the two integers α and β are the numbers of steps across the top and bottom levels of the multiplet diagram. Thus the labels for the SU(3) octet and decuplet

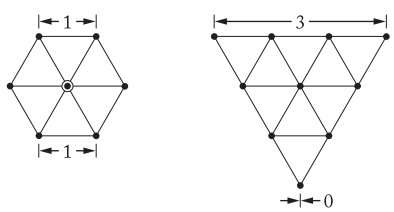

are (1,1) and (3,0). For larger n, the interpretation of the integers in terms of the geometry of the multiplets, which exist in an (n−1)-dimensional space, is not so readily apparent.

The label for the SU(n) singlet is $(0, 0, \ldots, 0)$. In a flavor SU(n), the n quarks together form a $(1, 0, \ldots, 0)$ multiplet, and the n antiquarks belong to a $(0, \ldots, 0, 1)$ multiplet. These two multiplets are *conjugate* to one another, which means their labels are related by $(\alpha, \beta, \ldots) \leftrightarrow (\ldots, \beta, \alpha)$.

48.2 Number of particles

The number of particles in a multiplet, $N = N(\alpha, \beta, \ldots)$, is given as follows (note the pattern of the equations). In SU(2), $N = N(\alpha)$ is

$$N = \frac{(\alpha+1)}{1} \ . \tag{48.1}$$

In SU(3), $N = N(\alpha, \beta)$ is

$$N = \frac{(\alpha+1)}{1} \cdot \frac{(\beta+1)}{1} \cdot \frac{(\alpha+\beta+2)}{2} \ . \tag{48.2}$$

In SU(4), $N = N(\alpha, \beta, \gamma)$ is

$$N = \frac{(\alpha+1)}{1} \cdot \frac{(\beta+1)}{1} \cdot \frac{(\gamma+1)}{1} \cdot \frac{(\alpha+\beta+2)}{2} \cdot \frac{(\beta+\gamma+2)}{2} \cdot \frac{(\alpha+\beta+\gamma+3)}{3} \ . \tag{48.3}$$

Note that in Eq. (48.3) there is no factor with $(\alpha+\gamma+2)$: only a *consecutive* sequence of the label integers appears in any factor. One more example should make the pattern clear for any SU(n). In SU(5), $N = N(\alpha, \beta, \gamma, \delta)$ is

$$N = \frac{(\alpha+1)}{1} \cdot \frac{(\beta+1)}{1} \cdot \frac{(\gamma+1)}{1} \cdot \frac{(\delta+1)}{1} \cdot \frac{(\alpha+\beta+2)}{2} \cdot \frac{(\beta+\gamma+2)}{2} \times \frac{(\gamma+\delta+2)}{2} \cdot \frac{(\alpha+\beta+\gamma+3)}{3} \cdot \frac{(\beta+\gamma+\delta+3)}{3} \cdot \frac{(\alpha+\beta+\gamma+\delta+4)}{4} \ . \tag{48.4}$$

From the symmetry of these equations, it is clear that multiplets that are conjugate to one another have the same number of particles, but so can other multiplets. For example, the SU(4) multiplets (3,0,0) and (1,1,0) each have 20 particles. Try the equations and see.

48.3 Young diagrams

A Young diagram consists of an array of boxes (or some other symbol) arranged in one or more *left-justified* rows, with each row being *at least as long* as the row beneath. The correspondence between a diagram and a multiplet label is: The top row juts out α boxes to the right past the end of the second row, the second row juts out β boxes to the right past the end of the third row, *etc.* A diagram in SU(n) has at most n rows. There can be any number of "completed" columns of n boxes buttressing the left of a diagram; these don't affect the label. Thus in SU(3) the diagrams

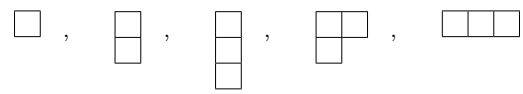

represent the multiplets (1,0), (0,1), (0,0), (1,1), and (3,0). In any SU(n), the quark multiplet is represented by a single box, the antiquark multiplet by a column of (n−1) boxes, and a singlet by a completed column of n boxes.

48.4 Coupling multiplets together

The following recipe tells how to find the multiplets that occur in coupling two multiplets together. To couple together more than two multiplets, first couple two, then couple a third with each of the multiplets obtained from the first two, *etc.*

First a definition: A sequence of the letters $a, b, c, \ldots$ is *admissible* if at any point in the sequence at least as many a's have occurred as b's, at least as many b's have occurred as c's, *etc.* Thus *abcd* and *aabcb* are admissible sequences and *abb* and *acb* are not. Now the recipe:

(a) Draw the Young diagrams for the two multiplets, but in one of the diagrams replace the boxes in the first row with a's, the boxes in the second row with b's, *etc.* Thus, to couple two SU(3) octets (such as the π-meson octet and the baryon octet), we start with and . The *unlettered* diagram forms the *upper left-hand corner* of all the enlarged diagrams constructed below.

(b) Add the a's from the lettered diagram to the right-hand ends of the rows of the unlettered diagram to form all possible legitimate Young diagrams that have no more than one a per column. In general, there will be several distinct diagrams, and all the a's appear in each diagram. At this stage, for the coupling of the two SU(3) octets, we have:

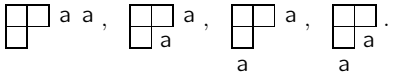

(c) Use the b's to further enlarge the diagrams already obtained, subject to the same rules. Then throw away any diagram in which the full sequence of letters formed by reading *right to left* in the first row, then the second row, *etc.*, is not admissible.

(d) Proceed as in (c) with the c's (if any), *etc.*

The final result of the coupling of the two SU(3) octets is:

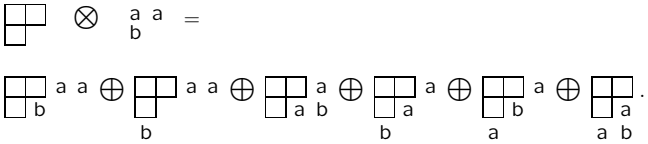

Here only the diagrams with admissible sequences of a's and b's and with fewer than four rows (since $n = 3$) have been kept. In terms of multiplet labels, the above may be written

$$(1,1) \otimes (1,1) = (2,2) \oplus (3,0) \oplus (0,3) \oplus (1,1) \oplus (1,1) \oplus (0,0) \ .$$

In terms of numbers of particles, it may be written

$$\mathbf{8} \otimes \mathbf{8} = \mathbf{27} \oplus \mathbf{10} \oplus \overline{\mathbf{10}} \oplus \mathbf{8} \oplus \mathbf{8} \oplus \mathbf{1} \ .$$

The product of the numbers on the left here is equal to the sum on the right, a useful check. (See also Sec. 15 on the Quark Model.)

Phys. A 2026.41. Downloaded from www.worldscientific.com
by UNIVERSITY OF CALIFORNIA, BERKELEY on 09/16/26. Re-use and distribution is strictly not permitted, except for Open Access articles.

Kinematics, Cross-Section Formulae, and Plots

49. Kinematics 799
50. Resonances (rev.) 803
51. Cross-section formulae for specific processes 815
52. Neutrino cross section measurements (rev.) 824
53. Plots of cross sections and related quantities 831

Int. J. Mod. Phys. A 2026.41. Downloaded from www.worldscientific.com
by UNIVERSITY OF CALIFORNIA @ BERKELEY on 09/16/26. Re-use and distribution is strictly not permitted, except for Open Access articles.

Int. J. Mod. Phys. A 2026.41. Downloaded from www.worldscientific.com
by [redacted]LIFORNIA @ BERKELEY on 09/16/26. Re-use and distribution is strictly not permitted, except for Open Access articles.

Int. J. Mod. Phys. A 2026.41. Downloaded from www.worldscientific.com
by UNIVERSITY OF CALIFORNIA @ BERKELEY on 09/16/26. Re-use and distribution is strictly not permitted, except for Open Access articles.

49. Kinematics

Reviewed August 2021 by D. Miller (Glasgow), D.R. Tovey (Sheffield), written January 2000 by J.D. Jackson (LBNL).

Throughout this section units are used in which $\hbar = c = 1$. The following conversions are useful: $\hbar c = 197.3$ MeV fm, $(\hbar c)^2 = 0.3894$ (GeV)^2 mb.

49.1 Lorentz transformations

The energy E and 3-momentum $\boldsymbol{p}$ of a particle of mass m form a 4-vector $p = (E, \boldsymbol{p})$ whose square $p^2 \equiv E^2 - |\boldsymbol{p}|^2 = m^2$. The velocity of the particle is $\boldsymbol{\beta} = \boldsymbol{p}/E$. The energy and momentum $(E^*, \boldsymbol{p}^*)$ viewed from a frame moving with velocity $\boldsymbol{\beta}_f$ are given by

$$\begin{pmatrix} E^* \\ p^*_\parallel \end{pmatrix} = \begin{pmatrix} \gamma_f & -\gamma_f\beta_f \\ -\gamma_f\beta_f & \gamma_f \end{pmatrix} \begin{pmatrix} E \\ p_\parallel \end{pmatrix} , \quad p^*_T = p_T , \tag{49.1}$$

where $\gamma_f = (1-\beta_f^2)^{-1/2}$ and p_T ($p_\parallel$) are the components of $\boldsymbol{p}$ perpendicular (parallel) to $\boldsymbol{\beta}_f$. Other 4-vectors, such as the space-time coordinates of events, of course transform in the same way. The scalar product of two 4-momenta $p_1 \cdot p_2 = E_1E_2 - \boldsymbol{p}_1 \cdot \boldsymbol{p}_2$ is invariant (frame independent).

49.2 Center-of-mass energy and momentum

In the collision of two particles of masses m_1 and m_2 the total center-of-mass energy can be expressed in the Lorentz-invariant form

$$\begin{aligned} E_{\rm cm} &= \left[(E_1+E_2)^2 - (\boldsymbol{p}_1+\boldsymbol{p}_2)^2\right]^{1/2} , \\ &= \left[m_1^2 + m_2^2 + 2E_1E_2(1-\beta_1\beta_2\cos\theta)\right]^{1/2} , \end{aligned} \tag{49.2}$$

where θ is the angle between the particles. In the frame where one particle (of mass m_2) is at rest (lab frame),

$$E_{\rm cm} = (m_1^2 + m_2^2 + 2E_{1\,\rm lab}\, m_2)^{1/2} . \tag{49.3}$$

The velocity of the center-of-mass in the lab frame is

$$\boldsymbol{\beta}_{\rm cm} = \boldsymbol{p}_{\rm lab}/(E_{1\,\rm lab} + m_2) , \tag{49.4}$$

where $\boldsymbol{p}_{\rm lab} \equiv \boldsymbol{p}_{1\,\rm lab}$ and

$$\gamma_{\rm cm} = (E_{1\,\rm lab} + m_2)/E_{\rm cm} . \tag{49.5}$$

The c.m. momenta of particles 1 and 2 are of magnitude

$$p_{\rm cm} = p_{\rm lab}\frac{m_2}{E_{\rm cm}} . \tag{49.6}$$

For example, if a 0.80 GeV/c kaon beam is incident on a proton target, the center of mass energy is 1.699 GeV and the center of mass momentum of either particle is 0.442 GeV/c. It is also useful to note that

$$E_{\rm cm}\, dE_{\rm cm} = m_2\, dE_{1\,\rm lab} = m_2\, \beta_{1\,\rm lab}\, dp_{\rm lab} . \tag{49.7}$$

49.3 Lorentz-invariant amplitudes

The matrix elements for a scattering or decay process are written in terms of an invariant amplitude $-i\mathscr{M}$. As an example, the S-matrix for $2 \to 2$ scattering is related to $\mathscr{M}$ by

$$\langle p_1' p_2' \,|S-1|\, p_1 p_2\rangle = i(2\pi)^4\, \delta^4(p_1+p_2-p_1'-p_2')\mathscr{M}(p_1,\, p_2;\, p_1',\, p_2') . \tag{49.8}$$

The state normalization is such that

$$\langle p'|p\rangle = (2\pi)^3\, 2E_p\, \delta^3(\boldsymbol{p}' - \boldsymbol{p}) , \tag{49.9}$$

with $E_p = \sqrt{\boldsymbol{p}^2 + m^2}$.

For a $2 \to 2$ scattering process producing unstable particles $1'$ and $2'$ decaying via $1' \to 3'4'$ and $2' \to 5'6'$ the matrix element for the complete process can be written in the narrow width approximation as:

$$\begin{aligned} &\mathscr{M}(12 \to 3'4'5'6') = \\ &\sum_{h_{1'},h_{2'}} \frac{\mathscr{M}(12 \to 1'2')\mathscr{M}(1' \to 3'4')\mathscr{M}(2' \to 5'6')}{(m^2_{3'4'} - m^2_{1'} + im_{1'}\Gamma_{1'})(m^2_{5'6'} - m^2_{2'} + im_{2'}\Gamma_{2'})} . \end{aligned} \tag{49.10}$$

Here, m_{ij} is the invariant mass of particles i and j, m_k and Γ_k are the mass and total width of particle k, and the sum runs over the helicities of the intermediate particles. This enables the cross section for such a process to be written as the product of the cross section for the initial $2 \to 2$ scattering process with the branching ratios (relative partial decay rates) of the subsequent decays. A more sophisticated treatment, beyond the narrow width approximation, can be found in the review on "Resonances".

49.4 Particle decays

The partial decay rate of a particle of mass M into n bodies in its rest frame is given in terms of the Lorentz-invariant matrix element $\mathscr{M}$ by

$$d\Gamma = \frac{(2\pi)^4}{2M}\, |\mathscr{M}|^2\, d\Phi_n\, (P;\, p_1,\, \ldots,\, p_n), \tag{49.11}$$

where $d\Phi_n$ is an element of n-body phase space given by

$$d\Phi_n(P;\, p_1,\, \ldots,\, p_n) = \delta^4\, (P - \sum_{i=1}^n p_i)\, \prod_{i=1}^n \frac{d^3p_i}{(2\pi)^3 2E_i} . \tag{49.12}$$

This phase space is reduced by combinatoric factors whenever there are identical particles in the final state. The phase space can be generated recursively, viz.

$$\begin{aligned} d\Phi_n(P;\, p_1,\, \ldots,\, p_n) &= d\Phi_j(q;\, p_1,\, \ldots,\, p_j) \\ &\times\ d\Phi_{n-j+1}\, (P;\, q,\, p_{j+1},\, \ldots,\, p_n)(2\pi)^3 dq^2 , \end{aligned} \tag{49.13}$$

where $q^2 = (\sum_{i=1}^j E_i)^2 - \left|\sum_{i=1}^j \boldsymbol{p}_i\right|^2$. This form is particularly useful in the case where a particle decays into another particle that subsequently decays.

49.4.1 *Survival probability*

If a particle of mass M has mean proper lifetime τ $(= 1/\Gamma)$ and has momentum $(E, \boldsymbol{p})$, then the probability that it lives for a time t_0 or greater before decaying is given by

$$P(t_0) = e^{-t_0\, \Gamma/\gamma} = e^{-Mt_0\, \Gamma/E} , \tag{49.14}$$

and the probability that it travels a distance x_0 or greater is

$$P(x_0) = e^{-Mx_0\, \Gamma/|\boldsymbol{p}|} . \tag{49.15}$$

49.4.2 *Two-body decays*

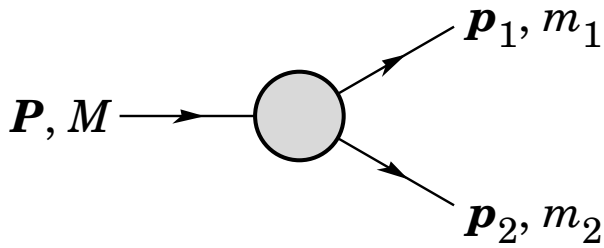

Figure 49.1: Definitions of variables for two-body decays.

In the rest frame of a particle of mass M, decaying into 2 particles labeled 1 and 2,

$$E_1 = \frac{M^2 - m_2^2 + m_1^2}{2M} , \tag{49.16}$$

$$|\boldsymbol{p}_1| = |\boldsymbol{p}_2| = \frac{1}{2M}\sqrt{\lambda(M^2, m_1^2, m_2^2)} , \tag{49.17}$$

Int. J. Mod. Phys. A 2026.41. Downloaded from www.worldscientific.com
by UNIVERSITY OF CALIFORNIA @ BERKELEY on 09/16/26. Re-use and distribution is strictly not permitted, except for Open Access articles.

and

$$d\Gamma = \frac{1}{32\pi^2}\,|\mathscr{M}|^2\,\frac{|\boldsymbol{p}_1|}{M^2}\,d\Omega\ , \tag{49.18}$$

where $\lambda(\alpha,\beta,\gamma) = \alpha^2+\beta^2+\gamma^2-2\alpha\beta-2\alpha\gamma-2\beta\gamma$ is the Källén function and $d\Omega = d\phi_1 d(\cos\theta_1)$ is the solid angle of particle 1. The invariant mass M can be determined from the energies and momenta using Eq. (49.2) with $M = E_{\rm cm}$.

49.4.3 *Three-body decays*

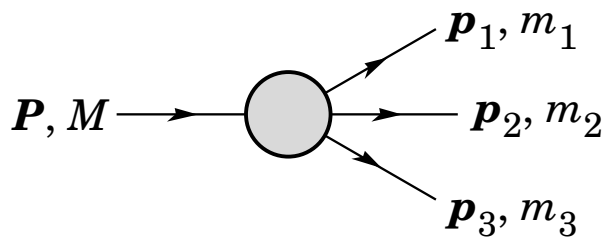

Figure 49.2: Definitions of variables for three-body decays.

Defining $p_{ij} = p_i + p_j$ and $m_{ij}^2 = p_{ij}^2$, then $m_{12}^2+m_{23}^2+m_{13}^2 = M^2+m_1^2+m_2^2+m_3^2$ and $m_{12}^2 = (P-p_3)^2 = M^2+m_3^2-2ME_3$, where E_3 is the energy of particle 3 in the rest frame of M. In that frame, the momenta of the three decay particles lie in a plane. The relative orientation of these three momenta is fixed if their energies are known. The momenta can therefore be specified in space by giving three Euler angles (α,β,γ) that specify the orientation of the final system relative to the initial particle. The direction of any one of the particles relative to the frame in which the initial particle is described can be specified in space by two angles (α,β) while a third angle, γ, can be set as the azimuthal angle of a second particle around the first [1]. Then

$$d\Gamma = \frac{1}{(2\pi)^5}\frac{1}{16M}\,|\mathscr{M}|^2\,dE_1\,dE_3\,d\alpha\,d(\cos\beta)\,d\gamma\ . \tag{49.19}$$

Alternatively

$$d\Gamma = \frac{1}{(2\pi)^5}\frac{1}{16M^2}\,|\mathscr{M}|^2\,|\boldsymbol{p}_1^*|\,|\boldsymbol{p}_3|\,dm_{12}\,d\Omega_1^*\,d\Omega_3\ , \tag{49.20}$$

where $(|\boldsymbol{p}_1^*|,\ \Omega_1^*)$ is the momentum of particle 1 in the rest frame of 1 and 2, and Ω_3 is the angle of particle 3 in the rest frame of the decaying particle. $|\boldsymbol{p}_1^*|$ and $|\boldsymbol{p}_3|$ are given by

$$|\boldsymbol{p}_1^*| = \frac{1}{2m_{12}}\sqrt{\lambda(m_{12}^2,m_1^2,m_2^2)}\ , \tag{49.21a}$$

and

$$|\boldsymbol{p}_3| = \frac{1}{2M}\sqrt{\lambda(M^2,m_{12}^2,m_3^2)}\ . \tag{49.21b}$$

[Compare with Eq. (49.17).]

If the decaying particle is a scalar, or we average over its spin states, then integration over the angles in Eq. (49.19) gives

$$\begin{aligned} d\Gamma &= \frac{1}{(2\pi)^3}\frac{1}{8M}\,\overline{|\mathscr{M}|^2}\,dE_1\,dE_3 \\ &= \frac{1}{(2\pi)^3}\frac{1}{32M^3}\,\overline{|\mathscr{M}|^2}\,dm_{12}^2\,dm_{23}^2\ . \end{aligned} \tag{49.22}$$

This is the standard form for the Dalitz plot.

49.4.3.1 *Dalitz plot*

For a given value of m_{12}^2, the range of m_{23}^2 is determined by its values when $\boldsymbol{p}_2$ is parallel or antiparallel to $\boldsymbol{p}_3$:

$$(m_{23}^2)_{\rm max} = (E_2^*+E_3^*)^2 - \left(\sqrt{E_2^{*2}-m_2^2}-\sqrt{E_3^{*2}-m_3^2}\right)^2\ , \tag{49.23a}$$

$$(m_{23}^2)_{\rm min} = (E_2^*+E_3^*)^2 - \left(\sqrt{E_2^{*2}-m_2^2}+\sqrt{E_3^{*2}-m_3^2}\right)^2\ . \tag{49.23b}$$

Here $E_2^* = (m_{12}^2-m_1^2+m_2^2)/2m_{12}$ and $E_3^* = (M^2-m_{12}^2-m_3^2)/2m_{12}$ are the energies of particles 2 and 3 in the m_{12} rest frame. The scatter plot in m_{12}^2 and m_{23}^2 is called a Dalitz plot. If $\overline{|\mathscr{M}|^2}$ is constant, the allowed region of the plot will be uniformly populated with events [see Eq. (49.22)]. A nonuniformity in the plot gives immediate information on $|\mathscr{M}|^2$. For example, in the case of $D\to K\pi\pi$, bands appear when $m_{(K\pi)} = m_{K^*(892)}$, reflecting the appearance of the decay chain $D\to K^*(892)\pi\to K\pi\pi$.

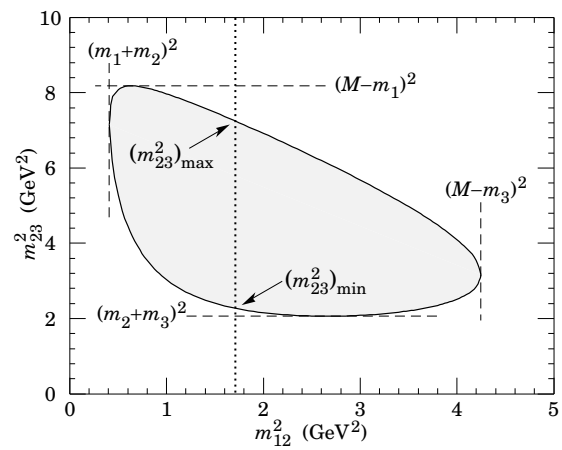

Figure 49.3: Dalitz plot for a three-body final state. In this example, the state is $\pi^+\overline{K}^0p$ at 3 GeV. Four-momentum conservation restricts events to the shaded region.

49.4.4 *Kinematic limits*

49.4.4.1 *Three-body decays*

In a three-body decay (Fig. 49.2) the maximum of $|\boldsymbol{p}_3|$, [given by Eq. (49.21)], is achieved when $m_{12} = m_1+m_2$, *i.e.*, particles 1 and 2 have the same vector velocity in the rest frame of the decaying particle. If, in addition, $m_3 > m_1, m_2$, then $|\boldsymbol{p}_3|_{\rm max} > |\boldsymbol{p}_1|_{\rm max}$, $|\boldsymbol{p}_2|_{\rm max}$. The distribution of m_{12} values possesses an end-point or maximum value at $m_{12} = M-m_3$. This can be used to constrain the mass difference of a parent particle and one invisible decay product.

49.4.4.2 *Sequential two-body decays*

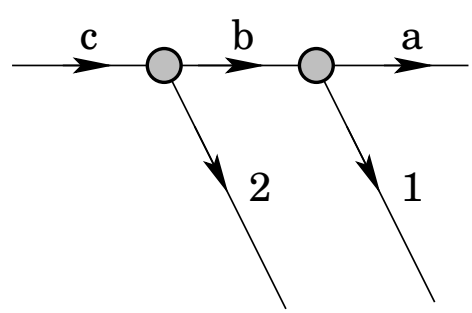

Figure 49.4: Particles participating in sequential two-body decay chain. Particles labeled 1 and 2 are visible while the particle terminating the chain (a) is invisible.

When a heavy particle initiates a sequential chain of two-body decays terminating in an invisible particle, constraints on the masses of the states participating in the chain can be obtained from end-points and thresholds in invariant mass distributions of the aggregated decay products. For the two-step decay chain depicted in Fig. 49.4 the invariant mass distribution of the two visible particles possesses an end-point given by:

$$(m_{12}^{\rm max})^2 = \frac{(m_{\rm c}^2-m_{\rm b}^2)(m_{\rm b}^2-m_{\rm a}^2)}{m_{\rm b}^2}\ , \tag{49.24}$$

Int. J. Mod. Phys. A 2026.41. Downloaded from www.worldscientific.com
by UNIVERSITY OF CALIFORNIA @ BERKELEY on 09/16/26. Re-use and distribution is strictly not permitted, except for Open Access articles.

provided particles 1 and 2 are massless. If visible particle 1 has non-zero mass m_1 then Eq. (49.24) is replaced by

$$(m_{12}^{\max})^2 = m_1^2 + \frac{(m_{\rm c}^2 - m_{\rm b}^2)}{2m_{\rm b}^2} \times \left(m_1^2 + m_{\rm b}^2 - m_{\rm a}^2 + \sqrt{(-m_1^2 + m_{\rm b}^2 - m_{\rm a}^2)^2 - 4m_1^2 m_{\rm a}^2}\right) \tag{49.25}$$

See Refs. [2] and [3] for other cases.

49.4.5 *Multibody decays*

The above results may be generalized to final states containing any number of particles by combining some of the particles into "effective particles" and treating the final states as 2 or 3 "effective particle" states. Thus, if $p_{ijk\ldots} = p_i + p_j + p_k + \ldots$, then

$$m_{ijk\ldots} = \sqrt{p^2{}_{ijk\ldots}} \ , \tag{49.26}$$

and $m_{ijk\ldots}$ may be used in place of *e.g.*, m_{12} in the relations in Sec. 49.4.3 or Sec. 49.4.4 above.

49.5 Cross sections

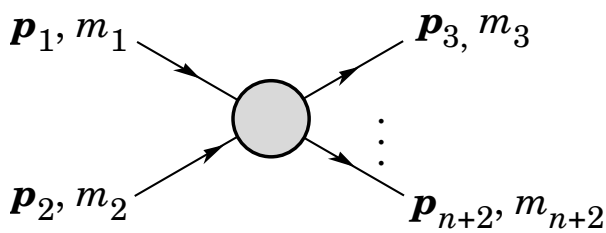

Figure 49.5: Definitions of variables for production of an n-body final state.

The differential cross section is given by

$$d\sigma = \frac{(2\pi)^4 |\mathscr{M}|^2}{4\sqrt{(p_1 \cdot p_2)^2 - m_1^2 m_2^2}} \times \ d\Phi_n(p_1 + p_2;\ p_3, \ldots, p_{n+2}) \ . \tag{49.27}$$

[See Eq. (49.12).] In the rest frame of m_2(lab),

$$\sqrt{(p_1 \cdot p_2)^2 - m_1^2 m_2^2} = m_2 p_{1\,\rm lab}; \tag{49.28a}$$

while in the center-of-mass frame

$$\sqrt{(p_1 \cdot p_2)^2 - m_1^2 m_2^2} = p_{1\rm cm}\sqrt{s} \ . \tag{49.28b}$$

49.5.1 *Two-body reactions*

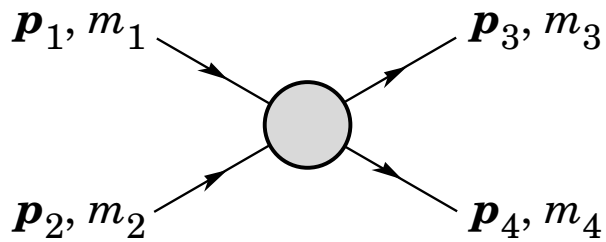

Figure 49.6: Definitions of variables for a two-body final state.

Two particles of momenta p_1 and p_2 and masses m_1 and m_2 scatter to particles of momenta p_3 and p_4 and masses m_3 and m_4; the Lorentz-invariant Mandelstam variables are defined by

$$\begin{aligned} s &= (p_1 + p_2)^2 = (p_3 + p_4)^2 \\ &= m_1^2 + 2E_1E_2 - 2\boldsymbol{p}_1 \cdot \boldsymbol{p}_2 + m_2^2 \ , \end{aligned} \tag{49.29}$$

$$\begin{aligned} t &= (p_1 - p_3)^2 = (p_2 - p_4)^2 \\ &= m_1^2 - 2E_1E_3 + 2\boldsymbol{p}_1 \cdot \boldsymbol{p}_3 + m_3^2 \ , \end{aligned} \tag{49.30}$$

$$\begin{aligned} u &= (p_1 - p_4)^2 = (p_2 - p_3)^2 \\ &= m_1^2 - 2E_1E_4 + 2\boldsymbol{p}_1 \cdot \boldsymbol{p}_4 + m_4^2 \ , \end{aligned} \tag{49.31}$$

and they satisfy

$$s + t + u = m_1^2 + m_2^2 + m_3^2 + m_4^2 \ . \tag{49.32}$$

The two-body cross section may be written as

$$\frac{d\sigma}{dt} = \frac{1}{64\pi s} \ \frac{1}{|\boldsymbol{p}_{1\rm cm}|^2} \ |\mathscr{M}|^2 \ . \tag{49.33}$$

In the center-of-mass frame

$$\begin{aligned} t &= (E_{1\rm cm} - E_{3\rm cm})^2 - (p_{1\rm cm} - p_{3\rm cm})^2 - 4p_{1\rm cm}\, p_{3\rm cm}\ \sin^2(\theta_{\rm cm}/2) \\ &= t_0 - 4p_{1\rm cm}\, p_{3\rm cm}\ \sin^2(\theta_{\rm cm}/2) \ , \end{aligned} \tag{49.34}$$

where $\theta_{\rm cm}$ is the angle between particle 1 and 3. The limiting values t_0 ($\theta_{\rm cm} = 0$) and t_1 ($\theta_{\rm cm} = \pi$) for $2 \to 2$ scattering are

$$t_0(t_1) = \left[\frac{m_1^2 - m_3^2 - m_2^2 + m_4^2}{2\sqrt{s}}\right]^2 - (p_{1\,\rm cm} \mp p_{3\,\rm cm})^2 \ . \tag{49.35}$$

In the literature the notation $t_{\min}$ ($t_{\max}$) for t_0 (t_1) is sometimes used, which should be discouraged since $t_0 > t_1$. The center-of-mass energies and momenta of the incoming particles are

$$E_{1\rm cm} = \frac{s + m_1^2 - m_2^2}{2\sqrt{s}} \ , \qquad E_{2\rm cm} = \frac{s + m_2^2 - m_1^2}{2\sqrt{s}} \ , \tag{49.36}$$

For $E_{3\rm cm}$ and $E_{4\rm cm}$, change m_1 to m_3 and m_2 to m_4. Then

$$p_{i\,\rm cm} = \sqrt{E_{i\,\rm cm}^2 - m_i^2} \text{ and } p_{1\rm cm} = \frac{p_{1\,\rm lab}\, m_2}{\sqrt{s}} \ . \tag{49.37}$$

Here the subscript lab refers to the frame where particle 2 is at rest. [For other relations see Eqs. (49.2)–(49.4).]

49.5.2 *Inclusive reactions*

Choose some direction (usually the beam direction) for the z-axis; then the energy and momentum of a particle can be written as

$$E = m_T \cosh y \ , \ p_x \ , \ p_y \ , \ p_z = m_T \sinh y \ , \tag{49.38}$$

where m_T, conventionally called the 'transverse mass', is given by

$$m_T^2 = m^2 + p_x^2 + p_y^2 \ . \tag{49.39}$$

and the rapidity y is defined by

$$\begin{aligned} y &= \frac{1}{2} \ln\left(\frac{E + p_z}{E - p_z}\right) \\ &= \ln\left(\frac{E + p_z}{m_T}\right) = \tanh^{-1}\left(\frac{p_z}{E}\right) \ . \end{aligned} \tag{49.40}$$

Note that the definition of the transverse mass in Eq. (49.39) differs from that used by experimentalists at hadron colliders (see Sec. 49.6.1 below). Under a boost in the z-direction to a frame with velocity β, $y \to y - \tanh^{-1}\beta$. Hence, the shape of the rapidity distribution dN/dy is invariant, as are differences in rapidity. The invariant cross section may also be rewritten

$$E\frac{d^3\sigma}{d^3p} = \frac{d^3\sigma}{d\phi\, dy\, p_T\, dp_T} \Longrightarrow \frac{d^2\sigma}{\pi\, dy\, d(p_T^2)} \ . \tag{49.41}$$

The second form is obtained using the identity $dy/dp_z = 1/E$, and the third form represents the average over ϕ.

Int. J. Mod. Phys. A 2026.41. Downloaded from www.worldscientific.com
by [redacted]LIFORNIA @ BERKELEY on 09/16/26. Re-use and distribution is strictly not permitted, except for Open Access articles.

Feynman's x variable is given by

$$x = \frac{p_z}{p_{z\,\max}} \approx \frac{E + p_z}{(E + p_z)_{\max}} \quad (p_T \ll |p_z|) \ . \tag{49.42}$$

In the c.m. frame,

$$x \approx \frac{2p_{z\,\mathrm{cm}}}{\sqrt{s}} = \frac{2m_T \sinh y_{\mathrm{cm}}}{\sqrt{s}} \tag{49.43}$$

and

$$= (y_{\mathrm{cm}})_{\max} = \ln(\sqrt{s}/m) \ . \tag{49.44}$$

The invariant mass M of the two-particle system described in Sec. 49.4.2 can be written in terms of these variables as

$$M^2 = m_1^2 + m_2^2 + 2[E_T(1)E_T(2)\cosh \Delta y - \boldsymbol{p}_T(1)\cdot\boldsymbol{p}_T(2)] \ , \tag{49.45}$$

where

$$E_T(i) = \sqrt{|\boldsymbol{p}_T(i)|^2 + m_i^2} \ , \tag{49.46}$$

and $\boldsymbol{p}_T(i)$ denotes the transverse momentum vector of particle i.

For $p \gg m$, the rapidity [Eq. (49.40)] may be expanded to obtain

$$y = \frac{1}{2}\ln\frac{\cos^2(\theta/2) + m^2/4p^2 + \ldots}{\sin^2(\theta/2) + m^2/4p^2 + \ldots} \approx -\ln\tan(\theta/2) \equiv \eta \tag{49.47}$$

where $\cos\theta = p_z/p$. The pseudorapidity η defined by the second line is approximately equal to the rapidity y for $p \gg m$ and $\theta \gg 1/\gamma$, and in any case can be measured when the mass and momentum of the particle are unknown. From the definition one can obtain the identities

$$\sinh\eta = \cot\theta \ , \ \ \cosh\eta = 1/\sin\theta \ , \ \ \tanh\eta = \cos\theta \ . \tag{49.48}$$

49.6 Transverse variables

At hadron colliders, a significant and unknown proportion of the energy of the incoming hadrons in each event escapes down the beam-pipe. Consequently, if invisible particles are created in the final state, their net momentum can only be constrained in the plane transverse to the beam direction. Defining the z-axis as the beam direction, this net momentum is equal to the missing transverse energy vector

$$\boldsymbol{E}_T^{\mathrm{miss}} = -\sum_i \boldsymbol{p}_T(i) \ , \tag{49.49}$$

where the sum runs over the transverse momenta of all visible final state particles.

49.6.1 *Single production with semi-invisible final state*

Consider a single heavy particle of mass M produced in association with visible particles which decays as in Fig. 49.1 to two particles, of which one (labeled particle 1) is invisible. The mass of the parent particle can be constrained with the quantity M_T defined by

$$\begin{aligned} M_T^2 &\equiv [E_T(1) + E_T(2)]^2 - [\boldsymbol{p}_T(1) + \boldsymbol{p}_T(2)]^2 \\ &= m_1^2 + m_2^2 + 2[E_T(1)E_T(2) - \boldsymbol{p}_T(1)\cdot\boldsymbol{p}_T(2)] \ , \end{aligned} \tag{49.50}$$

where

$$\boldsymbol{p}_T(1) = \boldsymbol{E}_T^{\mathrm{miss}} \ . \tag{49.51}$$

This quantity is called the 'transverse mass' by hadron collider experimentalists but it should be noted that it is quite different from that used in the description of inclusive reactions [Eq. (49.39)]. The distribution of event M_T values possesses an end-point at $M_T^{\max} = M$. If $m_1 = m_2 = 0$ then

$$M_T^2 = 2|\boldsymbol{p}_T(1)||\boldsymbol{p}_T(2)|(1 - \cos\phi_{12}) \ , \tag{49.52}$$

where ϕ_{ij} is defined as the angle between particles i and j in the transverse plane.

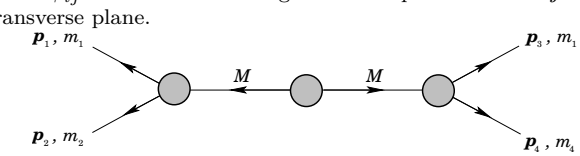

Figure 49.7: Definitions of variables for pair production of semi-invisible final states. Particles 1 and 3 are invisible while particles 2 and 4 are visible.

49.6.2 *Pair production with semi-invisible final states*

Consider two identical heavy particles of mass M produced such that their combined center-of-mass is at rest in the transverse plane (Fig. 49.7). Each particle decays to a final state consisting of an invisible particle of fixed mass m_1 together with an additional visible particle. M and m_1 can be constrained with the variables M_{T2} and M_{CT} which are defined in Refs. [4] and [5].

References

[1] J.D. Jackson in *High Energy Physics, Les Houches 1965 Summer School*, GORDON AND BREACH Science Publishers (1965), p. 348.

[2] I. Hinchliffe *et al.*, Phys. Rev. **D55**, 5520 (1997), [hep-ph/9610544].

[3] B. C. Allanach *et al.*, JHEP **09**, 004 (2000), [hep-ph/0007009].

[4] C. G. Lester and D. J. Summers, Phys. Lett. **B463**, 99 (1999), [hep-ph/9906349].

[5] D. R. Tovey, JHEP **04**, 034 (2008), [arXiv:0802.2879].

Int. J. Mod. Phys. A 2026.41. Downloaded from www.worldscientific.com
by UNIVERSITY OF CALIFORNIA @ BERKELEY on 09/16/26. Re-use and distribution is strictly not permitted, except for Open Access articles.

50. Resonances

Revised August 2025 by D.M. Asner (SNOLAB, Lively), C. Hanhart (FZ Jülich) and M. Mikhasenko (Ruhr U. Bochum).

50.1 General Considerations

Perturbative methods can be applied to systems of quarks and gluons only for large momentum transfers (see review on 'Quantum Chromodynamics') and, under certain conditions, to some properties of systems that contain heavy quarks or very large momentum scales (see review on "Heavy-quark and soft-collinear effective theory"). Dealing with Quantum Chromodynamics (QCD) in the low momentum transfer region is a very complicated, non-perturbative problem. Most hadrons are resonances, which means that they appear as poles of the $\mathcal{S}$-matrix in the complex energy plane, a notion further detailed in Sec. 50.2. These resonances can show up either in so-called formation experiments,

$$A + B \to \mathbf{R} \to C_1 + ... + C_n \ ,$$

where they become visible in an energy scan (for example, the R-function measured in e^+e^- annihilation, *cf.* the corresponding plots in the review on "Plots of Cross Sections and Related Quantities"), or together with a spectator particle S in production experiments of the kind

$$\begin{aligned} A + B \to \mathbf{R} + S \to [C_1 + ... + C_n] + S \ , \\ Z \to \mathbf{R} + S \to [C_1 + ... + C_n] + S \ , \end{aligned}$$

where the first reaction corresponds to an associated production, the second is a decay (see "Review of Multibody Charm Analyses"). In the latter case, the resonance properties are commonly extracted from a Dalitz-plot analysis (see review on "Kinematics") or projections thereof.

Resonance phenomena are very rich: while typical hadronic widths are of the order of 100 MeV (*e.g.*, for the meson resonances $\rho(770)$ or $\psi(4040)$ or the baryon resonance $\Delta(1232)$) corresponding to a lifetime of 10^{-23} s, the widths can also be as small as a few MeV (*e.g.* of $\phi(1020)$) or even a lot smaller (*e.g.* of J/ψ) or as large as several hundred MeV (*e.g.* of the meson resonances $f_0(500)$ or $D_1(2430)$ or the baryon resonance $N(2190)$).

Typically, a resonance appears as a peak in the total cross section, however, under certain conditions they can induce dips or become visible only after a partial wave decomposition. If the structure is narrow and if there are no relevant thresholds or other resonances nearby, the resonance properties may be extracted employing a Breit–Wigner parameterization, if necessary improved by using an energy-dependent width (*cf.* Sec. 50.3.1 of this review). However, in general, unitarity and analyticity call for the use of more refined tools as described in this manuscript, as well as in recent review articles [1,2]. When there are overlapping resonances with the same quantum numbers, the resonance terms should not simply be added but combined in a non-trivial way either in a $\mathcal{K}$-matrix approach (*cf.* Sec. 50.3.2 of this review) or using other advanced methods (*cf.* Sec. 50.3.5 of this review). Additional constraints from the $\mathcal{S}$-matrix allow one to build more reliable amplitudes and, in turn, to reduce the systematic uncertainties of the resonance parameters: pole locations and residues. In addition, for broad resonances there is no direct relation between pole location and the total width/lifetime — then, the pole residues need to be used in order to quantify the decay properties.

For simplicity, throughout this review we will primarily focus on the two-body kinematics. The formulas are given for resonances in a system of distinguishable, scalar particles. The additional complications that appear in the presence of spins can be controlled in the helicity framework developed by Jacob and Wick [3], or in a non-covariant [4] or covariant [5] tensor-operator formalisms. Within these approaches, sequential (cascade) decays are commonly treated as a coherent sum of two-body interactions.

50.1.1 *Properties of the $\mathcal{S}$-matrix*

The unitary operator that connects asymptotic *in* and *out* states is called the $\mathcal{S}$-matrix. The scattering amplitude is defined as the interacting part of the $\mathcal{S}$-matrix. For a two-particle scattering process, it is commonly defined via:

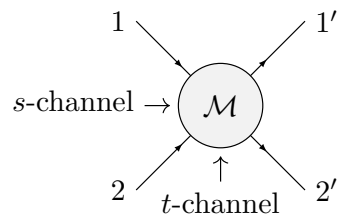

Figure 50.1: Illustration of the relation between s- and t-channel.

$$\begin{aligned} i(2\pi)^4\delta^4(p_1 + p_2 - p_{1'} - p_{2'})\,\mathcal{M}(p_1, p_2; p_{1'}, p_{2'})_{ba} \\ == {}_{\text{out}}\langle p_{1'}p_{2'}, b|\,\mathcal{S} - 1\,|p_1 p_2, a\rangle_{\text{in}} \end{aligned} \tag{50.1}$$

where $|p_1 p_2, a\rangle$ and $|p_{1'}p_{2'}, b\rangle$ are asymptotic states with on-shell four-momenta p_1, p_2 and $p_{1'}$, $p_{2'}$, respectively, that can be treated as non-interacting particles in the spirit of the Lehmann-Symanzik-Zimmermann (LSZ) reduction (for details see [6]).

The labels a and b are used to specify the *reaction channels*. In general terms, a reaction channel describes the possible outcome of a scattering event, characterized by the quantum numbers of the particles involved. Note that in general $\mathcal{M}_{ab}$ operates as a matrix in channel space and encodes both elastic transitions ($a = b$) and inelastic ones ($a \neq b$).

In many situations, however, the initial state is not itself part of the strongly interacting channel space. Typical examples are an electromagnetic current, e.g. e^+e^-, a weak decay, or a hadronic configuration with only a very small coupling to the system. Formally, such a source defines an additional row and column of the full scattering matrix, but its feedback on the hadronic submatrix is negligible. It is therefore advantageous to restrict attention to the strongly coupled channels, while collecting the source transitions into a *production amplitude* vector $\mathcal{A}_a$, with one component per hadronic channel. In Section 50.1.2, we make a great use of this distinction. The strong dynamics and rescattering are governed entirely by the coupled-channel matrix $\mathcal{M}_{ab}$, but the external source enters only as a driving term feeding into the hadronic system.

For a single-particle state, we employ the relativistic normalization,

$$\left\langle p' | p \right\rangle = (2\pi)^3 2E_p\,\delta^3(\vec{p}\,' - \vec{p}), \tag{50.2}$$

with $E_p = \sqrt{\vec{p}\,^2 + m^2}$.

Mandelstam variables are defined as $s = (p_1 + p_2)^2$, $t = (p_1 - p_{1'})^2$, and $u = (p_1 - p_{2'})^2$. They are not independent, since

$$s + t + u = m_1^2 + m_2^2 + m_{1'}^2 + m_{2'}^2$$

holds, where the m_i with $i \in \{1, 1', 2, 2'\}$ represent the masses of the particles involved. As a result, the reaction amplitude can be expressed as a function of two variables, $\mathcal{M}(s, t)$.

The Mandelstam variables represent a common choice of variables for characterizing particle scattering. Specifically, the process described in Eq. (50.1) is known as *s-channel*, referring to a reaction, $1, 2 \to 1', 2'$. Here, $\sqrt{s}$ represents the total energy of the interacting system in the center-of-momentum frame. The variable t corresponds to the *momentum transfer squared*, which is related to the scattering angle, the angle between the momenta of particles 1 and $1'$ in the center-of-momentum frame (see also the review on "Kinematics" in this Review of Particle Physics). The scattering process with particles 1 and the antiparticle of $1'$, denoted by $\overline{1'}$, incoming and the antiparticle of 2, denoted by $\overline{2}$, and $2'$ outgoing represents a different reaction, it is referred to as the *t-channel* reaction. The scattering amplitudes of s- and t-channel are related via the so-called *crossing symmetry*. The *u-channel* is introduced analogously as a reaction with the initial state of particles 1 and $\overline{2'}$ and the final state of particles $1'$ and $\overline{2}$. The t-channel and the u-channel are referred to as the *crossed*

Int. J. Mod. Phys. A 2026.41. Downloaded from www.worldscientific.com
by [redacted] LIFORNIA @ BERKELEY on 09/16/26. Re-use and distribution is strictly not permitted, except for Open Access articles.

channels relative to the reaction in Eq. (50.1). This relationship is illustrated in Fig. 50.1.

The analysis of resonance phenomena requires going deeper into the complex analysis of the amplitude: $\mathcal{M}(s,t)$ is a multivalued function due to the complex *branch points* associated with the Mandelstam variables. These branch points emerge whenever a new channel becomes accessible, that is, whenever s exceeds $s_{\mathrm{thr},a} = (m_{1,a}+m_{2,a})^2$, where $m_{i,a}$ denotes the masses of the two particles in channel a. Every two-particle threshold introduces a square-root singularity. The square-root function is inherently double-valued; for instance, the equation $x = y^2$ has two solutions: $\sqrt{x}$ and $-\sqrt{x}$. In the complex plane, these two solutions are represented as separate layers or surfaces, known as *Riemann sheets* or Riemann surfaces. Consequently, each square-root singularity causes the number of Riemann sheets of the scattering amplitude to double. If a channel opens that has an odd number of particles, the branch point at the threshold exhibits a logarithmic singularity [7]. Such a branch point gives rise to an infinite number of sheets. The branch points come with their associated branch cuts — by convention these are taken from the threshold to infinity along the real axis and accordingly called *right-hand cuts*. To explore a reaction amplitude in the complex energy plane, one can introduce a complex component to the Mandelstam variable s. The section of the complex plane that corresponds to a positive imaginary component of the relative momentum can be directly accessed from the physical region and is called the first Riemann sheet or the *physical sheet*. The other sheets are called *unphysical sheets*. The *physical axis* of an s-channel scattering amplitude represents a line for real values of the variable s larger than the lowest threshold to be evaluated on the physical sheet.

While the physical Riemann sheet is free of singularities off the real axis (which hosts the mentioned branch points and, in some cases, poles below the lowest threshold), the unphysical sheets may contain resonance poles and branch points. Branch points within the complex plane of an unphysical sheet appear, *e.g.*, when there is a resonance in a subsystem of involved particles [7,8] (for some in-depth discussion of the discontinuities, see Ref. [9]). The branch points related to thresholds in the crossed channels are located on the real axis to the left of the physical region, and, therefore, are referred to as the *left-hand cuts*. An illustrative example for a left-hand cut is the one-pion exchange in nucleon-nucleon scattering that is located in the unphysical domain at $s = 4m_N^2 - m_\pi^2$. Triangle topologies, which are Feynman diagrams characterized by a triangular loop of three propagators, can lead to logarithmic singularities in the scattering amplitude. These singularities, appearing on the unphysical sheets, are often termed *triangle singularities* (TS) [7,10,11].

The reaction amplitude has poles that can be categorized as bound states, virtual states, or resonances. Poles corresponding to bound and virtual states manifest at real values of s. Specifically, *bound state* poles are found on the physical sheet below the lowest threshold, while *virtual state* poles are situated on an unphysical sheet, below the threshold. *Resonance poles*, on the other hand, are located inside the complex plane of the unphysical sheets. Notably, those resonance poles that are on the unphysical sheet nearest to the physical region exert the most significant influence on experimental observables. Analyticity dictates that for every pole at a specific complex value of s_{p}, there must be a corresponding pole at its complex conjugate value s_{p}^*. This relationship is a direct consequence of the *Schwarz reflection principle*, a mathematical technique utilized for analytic continuation within scattering theory. For a single-channel case, the complex structure of an amplitude with a single resonance is illustrated in Fig. 50.2(a)-(c). Among the two poles, symmetrically positioned relative to the real axis on the second sheet, the one exhibiting a negative imaginary part seamlessly connects to the physical axis, which becomes especially clear in panel (c) of the figure where the physical axis is shown as the blue line. It therefore has a more pronounced effect on observables in the vicinity of the resonance region compared to its conjugate counterpart. The shortest continuous path from the physical region to the second sheet pole with the positive imaginary part is via a line that goes around the threshold. However, the effective distance to both poles becomes comparable for near threshold kinematics, thereby rendering the influence of both poles on observables similarly significant—in fact it is the interplay of the various resonance poles that renders scattering amplitudes real below the lowest threshold.

An alternative way to depict the complex sheet structure is through the momentum or k-plane, where k denotes the relative momentum of the two scattering particles in their center-of-momentum frame. For particles of equal mass, denoted as m (expression for unequal masses is given in Eq. (50.7)), one finds

$$k = \frac{1}{2}\sqrt{s - s_{\mathrm{thr}}}\,, \tag{50.3}$$

where $s_{\mathrm{thr}} = 4m^2$ is the threshold for two particles of mass m. Unlike the complex s-plane, in the single channel case the k-plane does not have a two-body threshold cut. Consequently, both the physical and unphysical Riemann sheets, which are linked along the branch cut in s, are mapped onto the upper and lower half of the complex k-plane, respectively. The k-plane is sketched in Fig. 50.2(d), including possible locations of resonance poles. In this representation it becomes especially clear that only one resonance pole drives the dynamics on the physical axis in the resonance region, while at the threshold, where $k = 0$, both poles are of equal significance.

In situations involving two relevant channels, we encounter four Riemann sheets. These are illustrated in the left panel of Fig. 50.3. For a system with two channels, the four-sheeted Riemann surface can also be transformed into a single plane free of cuts. For non-relativistic kinematics, it is represented by the new variable, ω, which is defined in relation to the channel-momenta, as detailed in references [12,13] (for a recent application, see Ref. [14]).

$$k_a = \sqrt{\frac{\mu_a \Delta}{2}}\left(\omega + \frac{1}{\omega}\right)\,, \quad k_b = \sqrt{\frac{\mu_b \Delta}{2}}\left(\omega - \frac{1}{\omega}\right)\,, \tag{50.4}$$

where Δ denotes the energy difference between the two thresholds and μ_a is the reduced mass of the particles in channel a, $\mu_a = m_{1,a}m_{2,a}/(m_{1,a}+m_{2,a})$. The lower threshold is located at $\omega = 0+i$, the higher at $\omega = 1+0i$. The mapping of the Riemann sheets and the different areas in the ω-plane is shown in the right panel of Fig. 50.3. The ω-plane nicely shows how the different sheets connect to each other.[1] The solid green line shows the physical axis in the physical regime. The thick black line shows its analytic continuation below the lowest threshold. The pronounced kinks in this line for the ω plane show the thresholds. Please observe that for $\omega \approx 0 + i$ the sheet structure agrees with panel (d) of Fig. 50.2, since in this kinematic regime the second channel does not matter.

In the context of a two-channel scenario, the proximity of a sheet to the physical axis varies with increasing energy. Specifically, for energies that exceed the first threshold, but remain below the second, sheet (21) is the one that smoothly connects to the upper half-plane of the physical sheet (11). Once the energy surpasses the second threshold, sheet (22) assumes this role. As a result, any pole on sheet (21) that lies above the second threshold will manifest in the data solely as a cusp right at the second threshold. Sheet (12), on the other hand, is remote for all energies, except those very close to the second threshold (for illustration see Ref. [15]).

Singularities, poles and branch points induce visible structures in observables. However, it is crucial to note that not every observable bump is indicative of a resonance as discussed in [16]. Under certain kinematic conditions, Triangle Singularities, in particular, can either mimic resonance signals, as suggested in Refs. [17–22], or significantly alter resonance signals [23] (see Ref. [24] for a review). Conversely, not all resonances produce a noticeable bump across all observables. For example, in the baryon sector, there is no clear trace of the $N(1440)1/2^+$, the so-called Roper resonance, in the πN observables or phase shifts, although careful analyses reveal a pole [25]. In the meson sector, the $f_0(500)$, also known as σ meson, was firmly established

[1] An alternative illustration for this two-channel case as well as an extension to three channels can be found in Ref. [2].

Int. J. Mod. Phys. A 2026.41. Downloaded from www.worldscientific.com
by UNIVERSITY OF CALIFORNIA @ BERKELEY on 09/16/26. Re-use and distribution is strictly not permitted, except for Open Access articles.

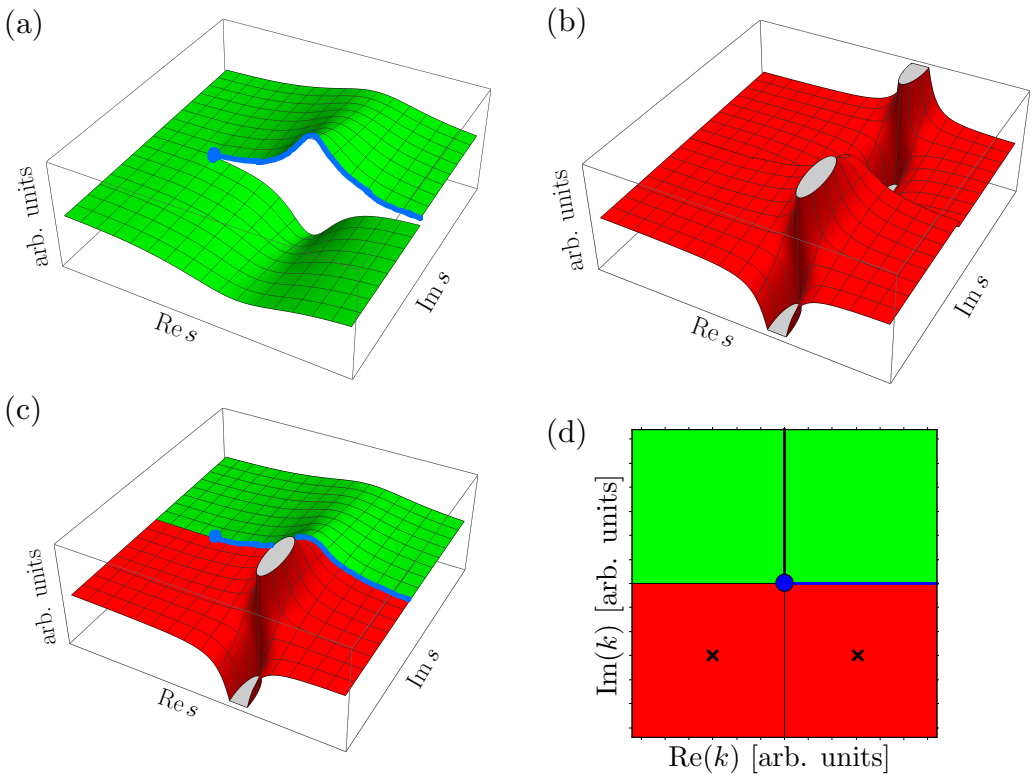

Figure 50.2: (a)-(c): Imaginary part of a typical scattering amplitude with an isolated resonance. The blue line shows the physical range of the Mandelstam variable s: it is real and starts from the threshold shown by the blue dot. Plot (a) shows the imaginary part of the amplitude in the complex s-plane that corresponds to the first or physical sheet (green surface), plot (b) shows the related unphysical or the second sheet (red surface) which contains the resonance poles, and plot (c) shows the analytic continuation of the same amplitude from the upper half plane of the physical sheet to the lower half plane of the unphysical sheet. The two sheets are connected smoothly along the real axis above the threshold. Panel (d) shows the k-plane, which is free of cuts. The upper (lower) half plane maps onto the physical (unphysical) sheet. Also here the blue line corresponds to the physically accessible values of the momentum k, which starts at threshold, where $k = 0$. The thick black line shows the analytic continuation of the on-shell momentum in the below threshold regime. The locations of the resonance poles are indicated by the black crosses.

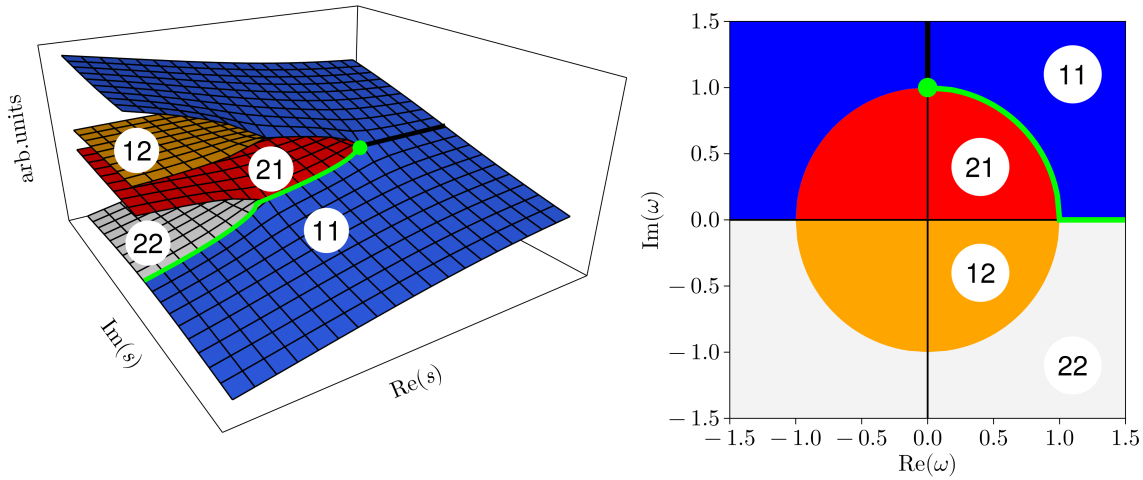

Figure 50.3: Cut structure of the $\mathcal{S}$-matrix with two channels present. The diagrams feature four sheets, labeled (ij), where both i and j can be 1 or 2. These labels indicate the doubling of the sheets at the first and second thresholds. The left panel displays the complex s plane, while the right panel represents the ω plane. The physical axis, along with its analytic continuation below the threshold, is highlighted with a thick solid line, green in the physical regime, black for the analytic continuation below the lowest threshold.

Int. J. Mod. Phys. A 2026.41. Downloaded from www.worldscientific.com
by [redacted]LIFORNIA @ BERKELEY on 09/16/26. Re-use and distribution is strictly not permitted, except for Open Access articles.

only after the application of very sophisticated theoretical analysis tools (see, *e.g.*, Ref. [26] for a review). This complexity arises since the approximate chiral symmetry of QCD calls for a zero in the scalar-isoscalar scattering amplitude right below threshold. Because of this, the scalar-isoscalar $\pi\pi$ phase shifts reach 90 degrees only near 800 MeV, which is approximately 400 MeV above the resonance mass. At this energy, the onset of the next resonance, the $f_0(980)$, is already visible.

The analyticity principle of the $\mathcal{S}$-matrix, germane to quantum scattering theories, dictates that only poles and branch points can exist on the real axis of the first Riemann sheet, excluding any singularities in the complex plane. This principle is closely linked to causality, ensuring that effects follow their causes in a chronological order. In non-relativistic scattering, the analyticity finds a solid mathematical base [27]. Similarly, perturbative relativistic theory maintains this analyticity through a series expansion of the $\mathcal{S}$-matrix, each term depicted by a Feynman diagram, representing processes with distinct analytical expressions. A deeper level of analyticity is proposed by the Mandelstam hypothesis, suggesting not only the analytic properties of the scattering amplitude within the complex plane of the first Riemann sheet but also a nuanced interconnection between crossed scattering processes through analytic continuation [28].

Unitarity further constrains the imaginary part of the amplitude on this real axis, a topic we will explore in the subsequent section. Additional constraints are introduced by principles such as crossing symmetry, duality [29] and positivity [30]. Approaches based on analyticity and crossing symmetry have been implemented through *dispersion theory*. Among the most notable are the Roy equations and their variants [31]. These have been applied to a range of processes, including $\pi\pi \to \pi\pi$ [32–34], πK scattering [35], $\gamma\gamma \to \pi\pi$ interactions [36], and pion-nucleon scattering [37–39].

50.1.2 *Consequences from unitarity*

Scattering amplitudes, denoted as $\mathcal{M}$, and production amplitudes, represented by $\mathcal{A}$, have distinct characteristics due to the different constraints imposed by unitarity. When considering the scattering amplitude, all coupled channels are treated equally within the formalism. In contrast, for production amplitudes, it is assumed that for the dynamics of the particles in the final state, the channel of the initial state does not play a role. Accordingly, the interactions in the final state among the produced particles are described by relevant scattering amplitudes of those particles only. Scattering processes are, for example, $\pi^+\pi^- \to K\bar{K}$ and $D^0\bar{D}^0 \to D^0\bar{D}^0$. Examples of production processes are $e^+e^- \to \gamma^* \to \pi^+\pi^-$, which provides access to the pion vector form factor, $\tau^- \to K^-\pi^0\nu_\tau$, and $B^0 \to J/\psi\pi^+\pi^-$.

The unitarity of the $\mathcal{S}$-matrix, represented by the equation $S^\dagger S = \mathbb{I}$, ensures the conservation of probability. This principle imposes a specific constraint on the imaginary part of the reaction amplitude. Below the lowest threshold (and above the first left-hand cut), the amplitude remains real. However, once the energy is higher than this threshold, there is a discontinuity associated with the threshold branch point. The $\mathcal{S}$-matrix unitarity relates the value of the discontinuity to the amplitude itself [6]:

$$\begin{aligned}\mathrm{Disc}\,\mathcal{M}_{ba} &= \mathcal{M}_{ba} - \mathcal{M}^*_{ab}\,,\\ &= i\,(2\pi)^4 \sum_c \int \mathrm{d}\Phi_c \mathcal{M}^*_{cb}\,\mathcal{M}_{ca}\,,\end{aligned} \tag{50.5}$$

where $\mathrm{d}\Phi_c$ denotes the Lorentz invariant phase space for a given channel, labeled as c. The factor $(2\pi)^4$ aligns with the convention for the phase space expression provided in the review on "Kinematics". It is essential to note that the summation only considers open channels, meaning those with a production threshold below the scattered system's energy. In the evaluation of an actual Feynman diagram, the discontinuity can be extracted by employing the Cutkosky rule, which comprises replacing the propagators in the pertinent intermediate state by delta-distributions. Eq. (50.5) is illustrated graphically in Fig. 50.4. The left part of the expression yields $2i\,\mathrm{Im}\,\mathcal{M}_{ba}$ in accordance to analytic properties of reaction amplitude [40]. For forward scattering, $t = 0$, the right part of Eq. (50.5) resembles the total cross section up to a kinematic factor, a relationship known as the optical theorem:

$$\mathrm{Im}\,\mathcal{M}_{aa}(s,0) = 2q_a\sqrt{s}\,\sigma_{\mathrm{tot}}(a \to \text{anything})\,. \tag{50.6}$$

In this equation, q_a represents the break-up momentum of the particles in the center-of-momentum frame,

$$q_a = \frac{\lambda^{1/2}(s, m^2_{1,a}, m^2_{2,a})}{2\sqrt{s}}\,, \tag{50.7}$$

where $\lambda(x,y,z) = x^2 + y^2 + z^2 - 2xy - 2yz - 2xz$ is the Källén function, and the masses of the two particles in the channel a, $m_{1,a}$ and $m_{2,a}$, *cf.* Eq. (17) of the review on "Kinematics".

The unitarity relation for a production amplitude in channel a is represented by:

$$\begin{aligned}\mathrm{Disc}\,\mathcal{A}_a &= \mathcal{A}_a - \mathcal{A}^*_a\,,\\ &= i\,(2\pi)^4 \sum_c \int \mathrm{d}\Phi_c \mathcal{M}^*_{ca}\mathcal{A}_c\,.\end{aligned} \tag{50.8}$$

Equation (50.8) is illustrated graphically in Fig. 50.4. A direct consequence of this equation is that the production amplitude shares its poles with the scattering amplitude. The relation between the production and scattering amplitudes is primarily explored for partial-wave amplitudes introduced in the next section. A common method to model the production amplitude that adheres to this unitary relation is to express it as a linear combination of scattering amplitudes. This approach, known as the $\mathcal{Q}$-vector method (see Sec 50.3.4), has its limitations. Specifically, in this way the production amplitude inherits the left-hand singularities of the scattering amplitude, while, in general, it has a different cut structure. To address this drawback, a more sophisticated method, known as *unitarization* is employed. This method, rooted in dispersion theory, offers a more refined approach to the problem and is detailed in [41]. A notable application of this method is the Khuri-Treiman framework [42, 43], which is frequently used to study three-body decays. This framework has been successfully applied to a range of decays, from light mesons [44–56] to heavy-flavour decays [57–61].

50.1.3 *Partial-wave decomposition*

It is often convenient to expand an amplitude in partial waves in using particle subsystems. Since resonances have a well-defined spin, they appear only in a specific partial wave of the reaction amplitude. For scalar particles, the expansion reads:

$$\mathcal{M}_{ba}(s,t) = \sum_{j=0}^{\infty}(2j+1)\mathcal{M}^j_{ba}(s)P_j(\cos(\theta))\,, \tag{50.9}$$

where j denotes the total angular momentum and the $P_j(\cos(\theta))$ denotes the Legendre polynomials. In the presence of spins an expansion more complicated than Eq. (50.9) is necessary — for a general discussion on how to handle spins see *e.g.* Ref. [62]. In the absence of spins, the parameter j coincides with the orbital angular momentum of the particle pairs in the initial and the final state. To simplify notation and since all amplitudes from here on are understood to be partial wave projected, we drop the label j for the single-argument function $\mathcal{M}_{ba}(s)$. Plugging Eq. (50.9) into Eq. (50.5), one finds the unitarity relation for the partial-wave amplitude $\mathcal{M}_{ba}(s)$, namely

$$\mathrm{Im}\,\mathcal{M}_{ba}(s) = \sum_c \mathcal{M}_{cb}(s)^*\,\rho_c(s)\,\mathcal{M}_{ca}(s)\,, \tag{50.10}$$

with $\rho_c(s)$ being a factor that is related to the two-body phase space in Eq. (12) of the review on "Kinematics",

$$\rho_c(s) = \frac{(2\pi)^4}{2}\int \mathrm{d}\Phi_2 = \frac{1}{16\pi}\frac{2|\vec{q}_c|}{\sqrt{s}}\,, \tag{50.11}$$

with the momentum q_c being defined in Eq. (50.7). Note that in the case of the two particles being identical, the inclusion of

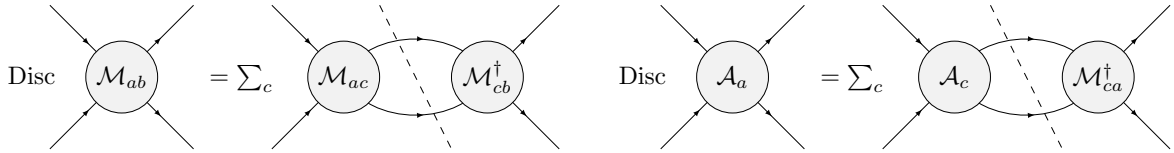

Figure 50.4: Graphical illustration of the discontinuity equations for the scattering and the production amplitude, respectively. The dashed line indicates that the intermediate state is to be put on-shell to find the discontinuity.

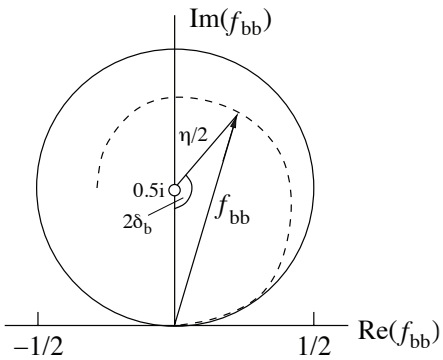

Figure 50.5: Argand plot showing a trajectory of the diagonal element of a partial-wave amplitude, f_{bb}, as a function of energy in the complex plane. As the energy increases the amplitude follows the line counter clockwise. The amplitude leaves the unitary circle (solid line) as soon as inelasticity sets in, $\eta < 1$ (dashed line).

symmetry factors becomes necessary. The partial-wave amplitude $f_{ba}(s)$ is introduced by normalizing the scattering amplitude with the phase space factors,

$$f_{ba}(s) = \sqrt{\rho_b}\,\mathcal{M}_{ba}(s)\,\sqrt{\rho_a}\,. \tag{50.12}$$

The unitarity condition for f_{ba} follows from Eq. (50.10):

$$\mathrm{Im}\, f_{ba}(s) = \sum_c f^*_{cb}(s) f_{ca}(s)\,. \tag{50.13}$$

It leads us to deduce that the imaginary part of $1/f_{ba}$ is equal to $-\delta_{ba}$. Moreover, $\mathcal{S} = \mathbb{I} + 2if$ is a unitary matrix. Hence, the diagonal elements of f can be parameterized as

$$f_{bb} = \frac{\eta_b \exp(2i\delta_b) - 1}{2i}\ , \tag{50.14}$$

where δ_b denotes the phase shift for the scattering from channel b to channel b and η_b is the elasticity parameter, also known as inelasticity. Building upon Eq. (50.13), we can further deduce that

$$\mathrm{Im}\, f_{bb}(s) = \frac{1 - \eta_b \cos(2\delta_b)}{2} = \sum_c |f_{cb}(s)|^2\ . \tag{50.15}$$

Using Eq. (50.14) for the last term in the sum, we obtain a relation highlighting the meaning of the inelasticity,

$$\frac{1}{4}(1 - \eta_b^2) = \sum_{c \neq b} |f_{cb}(s)|^2\ . \tag{50.16}$$

We note that the parameter η_b is confined within the range $[0, 1]$, where the case $\eta_b = 1$ is referred to as a purely elastic scattering. Thus, the function $\eta_b(s)$ is a direct measure of the contribution of the inelastic channels on the scattering amplitude in a given channel.

The evolution of the partial-wave amplitude f_{bb} with energy can be displayed as a trajectory in the Argand plot, as shown in Fig. 50.5. In the case of a two-channel problem, distinct channels a and b, $\eta_a = \eta_b = \eta$, and the off-diagonal element is $f_{ab} = \sqrt{1-\eta^2}/2\,\exp(i(\delta_1 + \delta_2))$. The unitarity condition Eq. (50.14) sets the limit to the squared amplitude f_{bb}:

$$|f_{bb}|^2 = \frac{1}{4}(\eta_b^2 - 2\eta_b \cos(2\delta_b) + 1) \leq \frac{1}{4}(\eta_b + 1)^2\ , \tag{50.17}$$

where the maximum value is reached for $\delta_b = \pi/2$. For the absolute square of the partial-wave-projected scattering amplitude the *unitarity bound* thus reads:

$$|\mathcal{M}_{bb}| \ \leq\ \frac{1}{2\rho_b}(\eta_b + 1)\ \leq\ \frac{8\pi}{q_b}\sqrt{s}\,, \tag{50.18}$$

where the second inequality comes from $\eta_b \leq 1$. For energies much larger than the masses of the scattering particles the upper bound for $|\mathcal{M}_{bb}|$ tends to 16π for large s.

The partial-wave projected production amplitude $\mathcal{A}(s)$ (note that the label j has been omitted for consistency) is also constrained by unitarity. As derived from Eq. (50.8):

$$\mathrm{Im}\,\mathcal{A}_a = \sum_b \mathcal{M}^*_{ba}\,\rho_b\,\mathcal{A}_b\ , \tag{50.19}$$

where the summation encompasses all open channels. For elastic scattering, only one channel, denoted by a, contributes to the sum. Consequently, the phase of $\mathcal{A}_a$ must align with the phase of $\mathcal{M}_{aa}$, given that the left-hand side of Eq. (50.19) represents a real value. This principle is recognized as the *Watson theorem* [63]. Accordingly, the phase of the pion vector form factor agrees with that of $\pi\pi$ scattering in the vector isovector channel (aside from effects of the isospin-violating $\rho - \omega$ mixing) up to about 1 GeV, where inelastic contributions start gaining significance.

50.2 Properties of resonances

A resonance is defined by its *pole position* in the complex s-plane, denoted as $s_{\rm R}$, and by the strength parameters of its couplings to various decay channels evaluated at this pole, known as the *pole residues*. The pole mass $M_{\rm R}$ and pole width $\Gamma_{\rm R}$ are defined via the pole parameters

$$\sqrt{s_{\rm R}} = M_{\rm R} - i\Gamma_{\rm R}/2\ . \tag{50.20}$$

For states where the relevant thresholds are situated significantly below the resonance location, the lifetime $\tau_{\rm R}$ of the resonance is given by $\tau_{\rm R} = 1/\Gamma_{\rm R}$ (refer to the review on "Kinematics" and for a recent discussion, see Ref. [64]). It is important to note that the conventional Breit–Wigner parameters $m_{\rm BW}$ and $\Gamma_{\rm BW}$, to be introduced in Eq. (50.31), differ from the pole parameters due to finite width effects and the influence of thresholds and background terms. It should be stressed that pole location $s_{\rm R}$ and pole residues are the only resonance properties that are model and parameterization independent.

When a resonance interacts with multiple channels, each channel contributes to the imaginary part of the pole position. However, these individual contributions do not simply sum up, calling for a careful definition of partial widths. This behavior is discussed using the example of the $f_0(980)$ in Refs. [65–68].

The pole residues are defined via

$$\mathcal{R}_{ba} = -\lim_{s \to s_{\rm R}} (s - s_{\rm R})\mathcal{M}_{ba}\ . \tag{50.21}$$

Int. J. Mod. Phys. A 2026.41. Downloaded from www.worldscientific.com
by UNIVERSITY OF CALIFORNIA @ BERKELEY on 09/16/26. Re-use and distribution is strictly not permitted, except for Open Access articles.

Int. J. Mod. Phys. A 2026.41. Downloaded from www.worldscientific.com
by [redacted]LIFORNIA @ BERKELEY on 09/16/26. Re-use and distribution is strictly not permitted, except for Open Access articles.

These can be conveniently calculated via an integration along a closed contour around the pole using

$$\mathcal{R}_{ba} = -\frac{1}{2\pi i}\oint \mathrm{d}s\mathcal{M}_{ba} \ . \tag{50.22}$$

Equivalently, the residue can also be computed using a derivative of inverted matrix element as (note element inversion, not the matrix inversion)

$$\mathcal{R}_{ba} = -\left(\frac{\mathrm{d}\mathcal{M}^{-1}_{ba}}{\mathrm{d}s}\bigg|_{s=s_\mathrm{R}}\right)^{-1} . \tag{50.23}$$

The residue adheres to the factorization relation, $(\mathcal{R}_{ba})^2 = \mathcal{R}_{aa} \times \mathcal{R}_{bb}$. This factorization emerges as a universal property stemming from the unitarity of scattering processes [7]. Building on this relation, one can define *pole couplings* as follows:

$$\tilde{g}_a^2 = \mathcal{R}_{aa} = \mathcal{R}_{ba}^2/\mathcal{R}_{bb} \, . \tag{50.24}$$

The pole couplings characterize the transition strength of a given resonance to some channel a independently of how the particular resonance was produced. They are in general complex valued.

In the baryon sector, it is customary to define the residue of the pole for the f_{ba} amplitude (as described in Eq. (50.13)) in terms of the variable $\sqrt{s}$ rather than s. This residue can be related to the residues mentioned earlier by:

$$r_{ba} = \frac{1}{2}\sqrt{\frac{\rho_a(s_\mathrm{R})\rho_b(s_\mathrm{R})}{s_\mathrm{R}}}\,\mathcal{R}_{ba} \ , \tag{50.25}$$

where the phase-space factors are to be continued analytically to the pole location. The residues quoted in the baryon listings are those for πN scattering (both a and b are πN channel).

Note that in general each resonance has various poles on different Riemann sheets with their own residues. For example, in a single channel reaction the Schwarz reflection principle calls for a pole at s_R to be accompanied by a pole at s_R^*. In this most simple case the residue of the one pole is the complex conjugate of that of the other. In multi-channel settings no simple relation can be given anymore. Thus, the equations discussed above are to be understood to refer to the physically most relevant pole—to ease notation we did not put a label specifying this.

The branching ratio of a resonance decay to a specific channel represents the fraction of the decay probability directed to that channel.

$$\mathrm{Br}_a = N_a/N_\mathrm{tot} \ . \tag{50.26}$$

Here, N_a is the experimental count of events for the decay channel $R \to a$, while N_tot represents the total number of events produced in the decay of the resonance. Since the amplitudes of decays to different final states add incoherently, we have $N_\mathrm{tot} = \sum_b N_b$. We note, however, that both N_a and N_tot may exhibit a dependence on the reaction through which the resonance is produced, due to the resonance's finite width. For a narrow resonance, the experimental count is determined by integrating the squared production amplitude over the decay channel's phase space:

$$N_a = N_0 \int |\mathcal{A}_a|^2 \, \mathrm{d}\Phi_a \ , \tag{50.27}$$

where N_0 is a normalization constant associated with the integrated luminosity, and $\mathcal{A}_a$ represents the amplitude of the resonance decay to channel a. When the decay rate's variation across the resonance width becomes significant, the resonance's lineshape must be considered:

$$N_a = N_0 \int_{s_{\mathrm{thr},a}}^{\infty} \mathrm{d}s\, \sigma_\mathrm{R}(s) \int |\mathcal{A}_a(s)|^2 \, \mathrm{d}\Phi_a(s) \ . \tag{50.28}$$

Here, $\sigma_\mathrm{R}(s)$ denotes a proper weight function of the resonance and $s_{\mathrm{thr},a}$ is the threshold value for the channel a. Additionally, the phase-space integral, $\mathrm{d}\Phi_a(s)$, puts the integrand to zero below the energy threshold of the decay channel a. This aspect is particularly crucial for the decays of broad resonances into channels with energy thresholds exceeding the resonance's nominal mass. This methodology is frequently employed in light-meson studies, as demonstrated in Ref. [69], and is also prevalent in light baryon research, as referenced in Ref. [67].

In the case of the decay of a state into multi-body final states, the transition amplitude can include resonances within subsystems of particles. When the total amplitude is decomposed as $\mathcal{A}_a = \sum_\mathrm{R} \mathcal{A}_{a(\mathrm{R})}$, the relative branching fraction for the decay of the given heavy state into final state a via resonance R in some subsystem, denoted as $\mathrm{Br}_{a(\mathrm{R})} \,/\, \mathrm{Br}_a$, is given by:

$$\mathrm{Br}_{a(\mathrm{R})} \,/\, \mathrm{Br}_a = \int \left|\mathcal{A}_{a(\mathrm{R})}\right|^2 \mathrm{d}\Phi_a \Big/ \int |\mathcal{A}_a|^2 \, \mathrm{d}\Phi_a \, . \tag{50.29}$$

The decomposition of the total amplitude, $\mathcal{A}_a$, into resonance amplitudes, $\mathcal{A}_{a(\mathrm{R})}$, is not a straightforward process. Beyond the differentiation of components based on distinct quantum numbers, this separation is inherently model-dependent. Furthermore, it is essential to be aware that the amplitudes $\mathcal{A}_{a(\mathrm{R})}$ can interfere with one another. As a result, their individual probabilities might not sum up to the total branching fraction of channel a. Nonetheless, in many scenarios, the interference contributions are small, making the fractions $\mathrm{Br}_{a(\mathrm{R})} \,/\, \mathrm{Br}_a$ indicative. For recent applications of these formulas in the context of B-decays see Refs. [70–73].

Lastly, an expression analogous to the branching fraction can be formulated using the pole parameters. For two-particle decays in the S-wave, one writes:

$$\mathrm{Br}_a = \frac{|\tilde{g}_a|^2}{M_\mathrm{R}\Gamma_\mathrm{R}}\rho_a(M_\mathrm{R}^2) \ , \tag{50.30}$$

where M_R and Γ_R are defined in Eq. (50.20) and the pole coupling $\tilde{g}_a$ in Eq. (50.24). This approach was utilized to define a two-photon width for the broad $f_0(500)$ resonance [74, 75]. Similarly, one should use residues to quantify the coupling of resonances to certain production channels [76]. For an application of this approach to the coupling of the $K_0^*(1430)$ resonance to a leptonic current, see Ref. [77]. Equation (50.30) provides a definition of branching fraction that remains independent of the reaction used to derive the quantity. For narrow resonances, this definition aligns well with Eq. (50.26) and Eq. (50.27). However, for broad, overlapping resonances, Eq. (50.30) is primarily used to convert residues into metrics that facilitate a more straightforward comparison of resonance transitions across different channels. For resonances with a coupling to a channel that remains closed at the resonance mass, Eq. (50.30) is not applicable due to the phase-space factor. In such scenarios, modification of the expression is required as elaborated upon in Refs. [67, 68], and in Sec. 50.3.5.

50.3 Common parameterizations

In general, there is no universal, model-independent recipe to build scattering amplitudes. However, a few approaches presented in this section are practical for extracting resonance properties in experimental analyses. The systematic theory uncertainties need to be assessed from a range of model variations that provide a sufficient quality of description of the available data and are permitted by general $\mathcal{S}$-matrix principles and the symmetries controlling the system at hand.

50.3.1 *The Breit–Wigner parameterization*

The relativistic Breit–Wigner parameterization represents a dressed propagator for an isolated resonance. An amplitude for a resonance observed in a channel a is given by

$$\mathrm{BW}(s) = \frac{1}{m_\mathrm{BW}^2 - s - i m_\mathrm{BW}\Gamma(s)} \tag{50.31}$$

where m_BW represents the Breit–Wigner mass, and $\Gamma_\mathrm{BW} = \Gamma(m_\mathrm{BW}^2)$ denotes the Breit–Wigner width. The function $\Gamma(s)$ is defined by the channels to which the resonance can decay. When

Int. J. Mod. Phys. A 2026.41. Downloaded from www.worldscientific.com
by UNIVERSITY OF CALIFORNIA @ BERKELEY on 09/16/26. Re-use and distribution is strictly not permitted, except for Open Access articles.

considering only two-body channels, it is given by

$$\Gamma(s) = \sum_b \Gamma_b(s) \text{ with } \Gamma_b(s) = \frac{1}{m_{\rm BW}} g_b^2 \rho_b(s) n_b^2(s)\,. \qquad (50.32)$$

Here the index b runs over all channels coupled to the resonance. The bare coupling constants are represented by g_b, and ρ_b is the phase-space factor as defined in Eq. (50.11). The expression for $n_a(s)$ is:

$$n_a = (q_a/q_0)^{l_a} F_{l_a}(q_a/q_0)\,, \qquad (50.33)$$

where l_a indicates the orbital angular momentum in channel a, $q_a(s)$ is the break-up momentum as defined in Eq. (50.7), and q_0 is a suitably selected momentum scale. The term $(q_a)^{l_a}$ ensures the amplitude's appropriate threshold behavior. The rapid growth of this factor for angular momenta $l_a > 0$ is offset at specific s values by a phenomenological form factor, represented here by $F_{l_a}(q_a/q_0)$. We note that the presence of these suppression factors is also a requirement from positivity which demands that the dressed propagator, the denominator of Eq. (50.31) and similar equations below, is not allowed to drop faster than $1/s$ [30]. The Blatt-Weisskopf form factors are frequently employed in the literature [78–80] to model F_j:

$$\begin{aligned} F_0^2(z) &= 1\,, \\ F_1^2(z) &= 1/(1+z^2)\,, \\ F_2^2(z) &= 1/(9+3z^2+z^4)\,, \end{aligned} \qquad (50.34)$$

where $z = q/q_0$, the scale parameter $1/q_0$ typically falls within the range of $1\,\text{GeV}^{-1}$ to $5\,\text{GeV}^{-1}$.

Bare coupling constants g_b do not have strict physical meaning, but rather serve as parameters reflecting the importance of a particular channel to the resonance lifetime. For narrow resonances with all coupled channel thresholds below the nominal mass, the coupling constant can be traded for the partial width $\Gamma_{{\rm BW},b}$.

$$g_b = \sqrt{\frac{m_{\rm BW}\,\Gamma_{{\rm BW},b}}{\rho_b(m_{\rm BW}^2) F_{l_b}^2(q_{b\,\rm r}/q_0)}} \left(\frac{q_0}{q_{b\,\rm r}}\right)^{l_b}\,. \qquad (50.35)$$

Here the $q_{b\,\rm r}$ are the values of the break-up momenta evaluated at $s = m_{\rm BW}^2$. It is essential to note that this substitution is valid only for channels where the decay channel's threshold is positioned below the nominal resonance mass. In other scenarios, Eq. (50.32) should be applied.

Equation (50.32) incorporates thresholds for each of the coupled channels. As an analytic function, it must remain valid in regions below any of these thresholds. Its evaluation in such regions, however, requires careful analytic continuation of the break-up momentum q_a that has a square root ambiguity. As outlined in Refs. [81, 82], it's done as

$$q_a = i\sqrt{-q_a^2} \quad \text{for} \quad q_a^2 < 0\,. \qquad (50.36)$$

The *Flatté parameterization* [81] describes the amplitude for two S-wave channels near the threshold of a heavier channel, evaluated in the physical region of the lighter channel using Eq. (50.36). When a resonance's coupling to the channel with a higher threshold is notably strong, the parameterization exhibits scaling invariance. This implies that individual partial decay widths cannot be extracted; only their ratios can be determined [83].

Commonly, one uses the Breit–Wigner amplitude to describe the production amplitude, then,

$$\mathcal{A}_a(s) = \mathcal{N}_a(s)\text{BW}(s)\,. \qquad (50.37)$$

The *numerator function* $\mathcal{N}_a(s) = \alpha\, g_a\, n_a(s)$ is tailored to the production process, encompassing kinematic factors and couplings pertinent to both the production and decay processes. The Breit–Wigner amplitude is an example of a unitary parameterization; it satisfies Eq. (50.10) with the scattering amplitude $\mathcal{M}_{ab}(s)$ given by

$$\mathcal{M}_{ab}(s) = g_a\, n_a(s)\,\text{BW}(s)\, g_b\, n_b(s)\,. \qquad (50.38)$$

The Breit–Wigner parameterization is an accurate representation of resonance phenomena strictly in the $\Gamma/\Delta \to 0$ limit, where Γ is the resonance width and Δ is the distance to the closest unaccounted singularity, be it a pole of a higher resonance or a kinematic threshold related to a channel that couples to the resonance. However, the situation is often more complex due to multiple singularities in the complex plane around the resonance with different importance. For instance, in P-wave $\pi\pi$ scattering, the Breit–Wigner parameterization aptly describes the ρ-meson resonance relatively well over an extensive range. Although the closest singularity to the ρ-meson pole is the ω-pole ($\Gamma_\rho/\Delta_\omega \gg 1$), this isospin breaking effect is insignificant for $\pi\pi$ scattering. However, in production reactions it can show a sizable effect—examples are $\chi_{c1}(3872) \to J/\psi\pi\pi$ [84], $e^+e^- \to \pi\pi$ [85], $B \to J/\psi\pi\pi$ [86] and $\eta' \to \pi\pi\gamma$ [87]. Subsequent singularities, namely the 3π, 4π, and 6π thresholds, can also be disregarded in the pertinent mass range. The two-pion threshold is incorporated in the Breit–Wigner parameterization through an energy-dependent width and can be improved further by using the Gounaris-Sakurai parameterization [88], which also includes dispersive corrections that will be discussed below in some detail. Finally, the parameterization's efficacy diminishes around 1.2 GeV due to the ρ' resonance, situated approximately at 1.4 GeV.

The extraction of the pole position from the Breit–Wigner amplitude is a straightforward technical task, achieved through analytic continuation. However, even if the applicability of the Breit–Wigner parameterization is established for a given resonance, it is crucial to recognize that its parameters will only align with the pole parameters if the width is small. Moreover, there can be sizable effects from non-resonant contributions, inducing some reaction dependence. Thus, neither the Breit–Wigner parameters nor the pole parameters deduced from those should be deemed reliable in general. If there is more than one resonance in one partial wave that significantly couples to the same channel, it is generally inappropriate to employ a sum of Breit–Wigner functions. Such an approach often results in a breach of unitarity constraints, potentially introducing an indeterminate bias to the inferred resonance properties from the reaction amplitude. For overlapping resonances in the same partial wave, more sophisticated methods, such as the $\mathcal{K}$-matrix approach detailed in the subsequent section, are recommended.

50.3.2 *$\mathcal{K}$-matrix approach*

The *$\mathcal{K}$-matrix* method offers a comprehensive framework for modeling coupled-channel amplitudes [89]. This method ensures two-particle unitarity. However, it traditionally omits the physical left-hand cuts, and introduces spurious branch points when using the phase space factor for particle loops (see *cf.* Sect. 50.3.3). The scattering amplitude $\mathcal{M}_{ba}(s)$ can be derived from the equation:

$$n_b\, \mathcal{M}_{ba}^{-1}\, n_a = \mathcal{K}_{ba}^{-1} - i\delta_{ba}\rho_a n_a^2\,. \qquad (50.39)$$

Here, $\mathcal{K}_{ba}$ represents a real function and is subject to modeling. The factor n_a is elaborated upon in Eq. (50.33). Since there is no unique recipe to build $\mathcal{K}$, it is essential to explore various parameterizations to gauge the theoretical systematic uncertainty—this idea is often used for the extraction of resonance poles of lattice studies; see e.g. Ref. [90]. A commonly adopted choice for the $\mathcal{K}$-matrix is given by:

$$\mathcal{K}_{ba}(s) = \sum_{\rm r} \frac{g_b^{\rm r} g_a^{\rm r}}{m_{\rm r}^2 - s} + \sum_n b_{ba}^{(n)} s^n\,, \qquad (50.40)$$

where $m_{\rm r}$ is referred to as the bare mass of the bare K-matrix pole r (not to be confused with the physical mass), and the $g_a^{\rm r}$ represents the bare couplings of the bare pole r to the channel a (not to be confused with the residues). The $b_{ba}^{(n)}$ are matrices that parameterize the non-pole components of the $\mathcal{K}$-matrix. Provided all parameters in Eq. (50.40) are real, the amplitude $\mathcal{M}_{ba}(s)$ remains unitary. We note that $\mathcal{K}$-matrix poles labeled by r produce the physical resonance poles labeled by R in the scattering amplitude, $\mathcal{M}$, but the converse is not true. Non-pole components of the $\mathcal{K}$-matrix can also produce poles in $\mathcal{M}$. From Eq. (50.39), the scattering amplitude $\mathcal{M}$ can be directly computed using its

Int. J. Mod. Phys. A 2026.41. Downloaded from www.worldscientific.com
by UNIVERSITY OF CALIFORNIA @ BERKELEY on 09/16/26. Re-use and distribution is strictly not permitted, except for Open Access articles.

matrix form:

$$\mathcal{M} = n[1 - \mathcal{K}\, i\rho\, n^2]^{-1}\mathcal{K}\, n\ , \tag{50.41}$$

where n and ρ are diagonal matrices, $n = \mathrm{diag}(n_a, n_b, \dots)$, and $\rho = \mathrm{diag}(\rho_a, \rho_b, \dots)$. As an alternative to Eq. (50.40), the same functional structure on the right side of Eq. (50.40) can be employed to parameterize the inverse $\mathcal{K}$-matrix, termed the M-matrix, by the authors of Ref. [91]. Numerous alternative formulations within the $\mathcal{K}$-matrix framework are utilized for amplitude studies related to lattice QCD calculations [90, 92–94].

A prevalent method to construct the production amplitude within the $\mathcal{K}$-matrix framework is the *$\mathcal{P}$-vector* parameterization [80, 89, 95]. The method utilizes the $\mathcal{K}$-matrix poles and bare couplings from Eq. (50.40):

$$\mathcal{A}_a(s) = n_a \sum_c \left[1 - \mathcal{K}\, i\rho n^2\right]^{-1}_{ac} \mathcal{P}_c\,, \tag{50.42}$$

$$\mathcal{P}_c = \sum_{\mathrm{r}} \frac{\alpha^{\mathrm{r}} g^{\mathrm{r}}_c}{m^2_{\mathrm{r}} - s} + \mathcal{B}_c. \tag{50.43}$$

The production vector, denoted as $\mathcal{P}_c$, comprises two main components. The first component represents a transition driven by the coupling of the bare resonance, r, to the channel c as well as the source. The coupling of the latter is characterized by a strength parameter, α^{r}. The second component, $\mathcal{B}_c$, signifies the direct transition from the source to the channel c. The formalism ensures that the complete production vector gets dressed via the final state interaction.

The *$\mathcal{Q}$-vector*, as discussed in Ref. [80, 91, 96], offers an alternative methodology for constructing a production amplitude:

$$\mathcal{A}_a(s) = \sum_c \mathcal{M}_{ac}(s)\mathcal{Q}_c(s)/n_c\ . \tag{50.44}$$

Here, $\mathcal{Q}_c(s)$ represents a smooth function of s and can be parameterized using a polynomial series. The unitarity condition of Eq. (50.19) is satisfied when $\mathcal{Q}_c(s)$ is a real function and in particular does not have singularities above the lowest threshold for all channels c. Besides these conditions, $\mathcal{Q}_c(s)$ is arbitrary. In a study of $\gamma\gamma \to \pi\pi$, *cf.* Ref. [74, 75] a low-order polynomial is claimed to be sufficient to parameterize the energy dependence of the function $\mathcal{Q}_c(s)$. The $\mathcal{Q}$-vector method is convenient if the full matrix $\mathcal{M}$ is known, *cf.* Ref. [91]. An important distinction between the $\mathcal{P}$-vector and the $\mathcal{Q}$-vector methods is highlighted in [95]. When the two-particle scattering amplitude approaches zero, the production amplitude in the $\mathcal{Q}$-vector construction unavoidably vanishes for finite values of $\mathcal{Q}_c$, whereas it can remain non-zero in the $\mathcal{P}$-vector approach.

Traditionally, amplitudes constructed using the $\mathcal{K}$-matrix technique exclude the left-hand cuts. Nevertheless, these can be customarily incorporated into the non-pole part of Eq. (50.40) for the scattering amplitude [97, 98], or via properly chosen background amplitudes [68]. Similarly, for the production amplitude, the functions $\mathcal{B}_c$ and $\mathcal{Q}_c$ from Eq. (50.43) and Eq. (50.44), respectively, might also encompass the left-hand cuts. These can often be parameterized by low order polynomials [74, 75, 99].

The position of the resonance poles can be determined by examining the zeros of the analytic function $\det[1 - \mathcal{K}\, i\rho\, n^2]$. Owing to the ρ factor, this determinant exhibits a complex multisheet structure. Nonetheless, the nearest unphysical sheet usually has the highest influence on the physical region. It is always the one which is determined by the heaviest threshold below the studied point in s (*cf.* Fig. 50.3). If for a given resonance the pole closest to the physical region is not located on a sheet that connects directly to the physical region, it is possible that $\mathcal{K}$-matrix fits do not allow one to fix the pole parameters, since a larger distance of the pole to the physical region can be balanced by increased residues—for a detailed discussion and a recent application see Ref. [83] and [100], respectively.

50.3.3 *Further improvements: Chew-Mandelstam function*

The $\mathcal{K}$-matrix framework often enables an accurate fit of physical amplitudes and is straightforward to handle. However, it does present a significant drawback: it breaches constraints imposed by analyticity. For instance, ρ_a, as defined in Eq. (50.11), is not well-defined at $s = 0$. Moreover, in cases of unequal masses, it manifests an unphysical cut, as depicted in the left panel of Fig. 50.6.

A method to improve the analytic properties has been suggested in Refs. [88, 101–104]. This approach replaces the term $i\rho_a(s)n_a^2$ from Eq. (50.39) with the analytic function $\Sigma_a(s)$, known as the Chew-Mandelstam function. This function produces the imaginary part $i\rho_a(s)n_a^2$ on the right-hand cut, while maintaining analyticity on the left-hand side, as represented by the once subtracted dispersion integral:

$$\Sigma_a(s + i0) = \frac{s - s_{\mathrm{thr},a}}{\pi} \int_{s_{\mathrm{thr},a}}^{\infty} \frac{\rho_a(s')n_a^2(s')}{(s' - s_{\mathrm{thr},a})(s' - s - i0)}\, \mathrm{d}s'. \tag{50.45}$$

Here, we chose the channel threshold, $s_{\mathrm{thr},a}$, as the subtraction point, and assumed that the subtraction constant is absorbed into the other parameters used for the amplitude. For an S-wave where $n_a = 1$, the integral has a closed form [41, 102]:

$$\Sigma_a(s) = \frac{1}{16\pi^2}\left[\frac{2q_a}{\sqrt{s}} \log \frac{m^2_{1,a} + m^2_{2,a} - s + 2\sqrt{s}q_a}{2m_{1,a}m_{1,a}}\,, \right.$$
$$\left. - (m^2_{1,a} - m^2_{2,a})\left(\frac{1}{s} - \frac{1}{s^2_{\mathrm{thr},a}}\right)\log\frac{m_{1,a}}{m_{2,a}}\right], \tag{50.46}$$

where $m_{1,a}$ and $m_{2,a}$ are masses of the final-state particles in channel a, with $s_{\mathrm{thr},a} = (m_{1,a} + m_{2,a})^2$. A closed form expression for the P-wave is provided in Ref. [105]. The behavior of $\Sigma_a(s)$ as given in Eq. (50.46) along the real axis is illustrated in the right panel of Fig. 50.6. A further discussion of the calculation of the Chew-Mandelstam function can be found in Refs. [106, 107].

If there is only a single resonance in a given channel, it is possible to feed the imaginary part of the Breit–Wigner function, Eq. (50.31) with an energy-dependent width, directly into a dispersion integral to get a resonance propagator with the correct analytic structure [108, 109].

50.3.4 *Effective-range expansion and scattering-length approximation*

For elastic scattering, $\eta_b = 1$, Eq. (50.14) simplifies to

$$f_{bb} = e^{i\delta}\sin(\delta) = \frac{q}{q\cot(\delta) - iq}\ , \tag{50.47}$$

where q is the relative momentum of the scattering particles. For S-waves one may then employ the *effective-range expansion* [110, 111] (ERE)

$$q\cot\delta = \frac{1}{a} + \frac{1}{2}rq^2 + O\left(R_f^3 q^4\right)\ , \tag{50.48}$$

whose radius of convergence is set by the closest non-analyticity, which may be the next threshold, a left-hand cut or a zero in the amplitude, which is equivalent to a pole in $q\cot\delta$. The ERE is understood to be an expansion in $R_f q$, where R_f denotes the range of forces provided by the inverse of the mass of the lightest exchange particle allowed. The *scattering length*, a, provides the strength of the scattering amplitude at threshold and is thus defined as the first term in an expansion of the real part of the inverse scattering amplitude. The sign convention used in Eq. (50.48) is the one commonly employed in particle physics. In this convention a positive scattering length indicates attraction; if, however, the attraction is strong enough to generate a bound state, the scattering length changes sign and turns negative. A negative scattering length also occurs for repulsive interactions. Note that in nuclear physics the leading term in the expansion of Eq. (50.48) is usually defined as $-1/a$ such that *e.g.* a bound state would be related to a positive scattering length. The parameter r is called the *effective range*. Especially, in cases where the scattering length is large, the ERE not only describes the low-energy scattering well, but also allows for an analytic continuation to find bound states below threshold by proper analytic continuation. This method was, *e.g.*, employed recently to analyze near threshold scattering

Int. J. Mod. Phys. A 2026.41. Downloaded from www.worldscientific.com
by UNIVERSITY OF CALIFORNIA @ BERKELEY on 09/16/26. Re-use and distribution is strictly not permitted, except for Open Access articles.

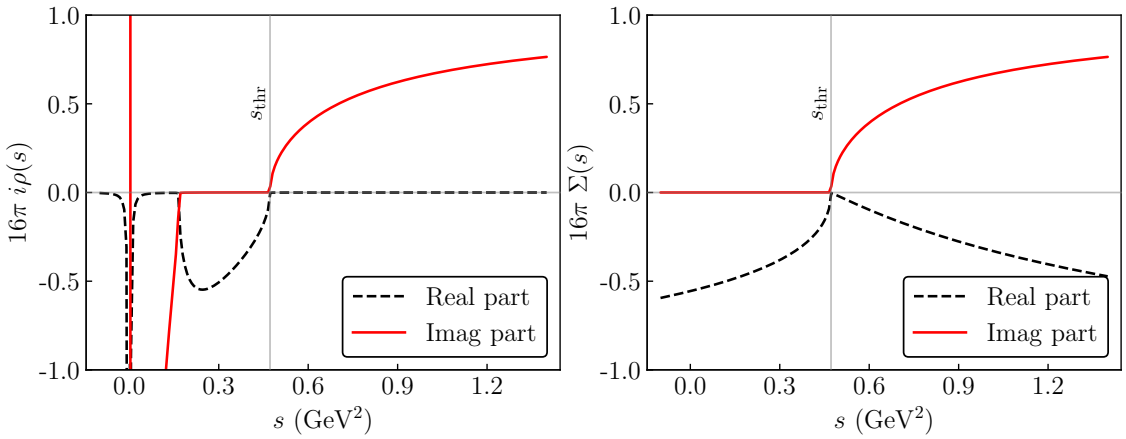

Figure 50.6: Comparison of the $i\rho$ function (left plot) to the *Chew-Mandelstam function* from Eq. (50.46) (right plot), evaluated for the case of S-wave $\eta\pi$ scattering. The values of s are taken slightly above the real axis, $s + i0$. The solid red line shows the imaginary part that is the same for both functions above threshold, $s_{\rm thr} = (m_\eta + m_\pi)^2$. The dashed black line presents the real part. One finds indications of the unphysical singularities, a branch point at the pseudothreshold $s_{\rm pth} = (m_\eta - m_\pi)^2$ and a pole at $s = 0$, of the function $i\rho$ on the left plot, while the Chew-Mandelstam function is analytic below the two-particle threshold.

phase shifts for $D^{*+}D^0$ scattering found in lattice analyses to extract properties of the $T_{cc}(3875)^+$ [112–114] at unphysical pion masses. It should be stressed that the analyses of the lattice data might call for a modification to account for the nearby left-hand cut which sets the radius of convergence of the ERE [115, 116].

When considering only the scattering length within the ERE, the scattering amplitude is represented as:

$$\mathcal{M}(s) = \frac{8\pi\sqrt{s}}{1/a - iq(s)}\,. \tag{50.49}$$

It is worth noting that the scattering length approximation is applicable only in a very limited energy range, however, it might well be appropriate to analyze the recently discovered narrow very near-threshold states [117, 118]. Examples of such analyses can be found in Refs. [119–121]. Moreover, it is possible to introduce the effect of a weakly coupled lower channel [122, 123]. Such coupling results in a positive imaginary part of the scattering length. It is also crucial to highlight that for large values of a, the amplitude of Eq. (50.49) develops a near-threshold pole located on the physical or unphysical sheet for negative or positive values of a, respectively. For readers interested in an exploration of how close-to-threshold poles interact with remote thresholds, we refer to Ref. [124].

While easy to use, it is important to stress, however, that the approximation in Eq. (50.49) is a specific choice of the dynamic function. This choice results in a single pole close to the physical region, suggesting that the state under study has the characteristics of a hadronic molecule, as discussed in references such as [121, 125–127]. Virtual states are discussed in this context in Ref. [128].

50.3.5 *Two-potential decomposition*

Another advanced technique to construct the scattering amplitude, which is widely used in the literature [61, 77, 129–133], is based on the two-potential formalism [134, 135]. While it is possible to formulate this method for the full unprojected amplitude $\mathcal{M}_{ba}(s,t)$, for clarity, we focus on presenting the equations in their partial-wave-projected form.

The scattering amplitude, $\mathcal{M}(s)$, can be broken down into two components: a background part and a pole part. This can be represented as:

$$\mathcal{M}(s) = \mathcal{M}^{\rm b.g.}(s) + \mathcal{M}^{\rm pole}(s)\,. \tag{50.50}$$

It is important to note that the division presented in Eq. (50.50) is not unique and model-dependent. This is further discussed in references such as [136, 137]. The background scattering matrix is assumed to satisfy the unitarity relations by itself. One approach to parameterize it, especially at lower energies, is by using phase shifts and inelasticities, as seen in [61, 77, 133]. Alternatively, it can be computed based on some potential, $V^{\rm b.g.}$, fed into a proper scattering equation [131, 132] or parameterized [68].

The complete amplitude, $\mathcal{M}$, from Eq. (50.50) satisfies the unitarity relations, if the pole part follows a specific construction. Namely,

$$\mathcal{M}^{\rm pole}_{ab}(s) = \sum_{c,d,e} n_a(s)\Omega_{ac}(s)\ [1 - V^{\rm pole}\Sigma^u(s)]^{-1}_{cd} V^{\rm pole}_{de}\ \Omega^T_{eb}(s) n_b(s)\,, \tag{50.51}$$

with the tamed centrifugal barrier factors introduced in Eq. (50.33). In this context, we introduce the vertex functions, denoted as $\Omega_{ab}(s)$, and the resonance potential, represented as $V^{\rm pole}(s)$. This potential operates as a matrix in the channel space and can be expressed as:

$$V^{\rm pole}_{ab}(s) = \sum_{\rm r} \frac{g^{\rm r}_a\ g^{\rm r}_b}{m^2_{\rm r} - s}\,. \tag{50.52}$$

The term Σ^u_{ab} represents the self-energy matrix. Additionally, $g^{\rm r}_a$ denotes the bare coupling of the resonance, labeled as r, to the channel a, and $m_{\rm r}$ is its bare mass. The vertex functions obey a unitarity relation similar to the production amplitude in Eq. (50.8). However, in this case, the final state interaction is determined by $\mathcal{M}^{\rm b.g.}$. This can be represented as:

$$\text{Disc}\,\Omega_{ab}(s) = 2i \sum_c \mathcal{M}^{\rm b.g.\,*}_{ca}(n_c(s)/n_a(s))\,\rho_c(s)\,\Omega_{cb}(s)\,. \tag{50.53}$$

When using low-energy phase shifts for the background term, it is practical to express the vertex functions in terms of an Omnès matrix, as discussed in [61]. The matrix reduces to the well-known Omnès function

$$\Omega(s) = \exp\left(\frac{s}{\pi}\int_{s_{\rm thr}}^{\infty} {\rm d}s' \frac{\delta^{\rm b.g.}(s')}{s'(s'-s-i\epsilon)}\right), \tag{50.54}$$

in the single-channel case [138], where $\delta^{\rm b.g.}(s)$ denotes the phase of the background scattering matrix $\mathcal{M}^{\rm b.g.}(s)$. The discontinuity associated with the self-energy matrix, $\Sigma^u(s)$, is given by:

$$\text{Disc}\,\Sigma^u_{ab}(s) = 2i \sum_c \Omega^*_{ca}(s)\,\rho_c(s) n_c(s)^2\,\Omega_{cb}(s)\,. \tag{50.55}$$

To determine the real part of Σ^u, one can use Eq. (50.55) with a properly subtracted dispersion integral — *cf.* Eq. (50.45).

Int. J. Mod. Phys. A 2026.41. Downloaded from www.worldscientific.com
by UNIVERSITY OF CALIFORNIA @ BERKELEY on 09/16/26. Re-use and distribution is strictly not permitted, except for Open Access articles.

When $\mathcal{M}^{\text{b.g.}}$ satisfies the unitarity relations, the full amplitude also does given Eq. (50.51). However, it is essential to note that the pole term alone does not satisfy the unitarity relation unless the background amplitude vanishes. Under such conditions, the described amplitude simplifies to the $\mathcal{K}$-matrix construction with improved analytic behavior as detailed in Sec. 50.3.3. Neglecting non-pole terms is not a good approximation for certain interactions, such as the scalar-isoscalar $\pi\pi$ at low energies, as discussed in Refs. [68, 139]. However, for higher partial waves, this approximation is generally effective.

A production amplitude consistent with Eq. (50.51) reads [61, 133]:

$$\mathcal{A}_a^{\text{pole}}(s) = n_a(s) \sum_{c,d} \Omega_{ac}(s)\, [1 - V^{(\text{r})}(s)\Sigma^u(s)]^{-1}_{cd} \mathcal{P}_d \ , \quad (50.56)$$

with function $\mathcal{P}_d$ given in Eq. (50.43). This form was employed in Refs. [61, 133] to treat the pion vector and scalar form factor, respectively, and in Ref. [77] for the scalar πK form factor.

The ideas presented above can be used to define branching fractions for broad resonances with minimal bias [68]. The starting point is the dressed resonance propagator for a single resonance that may be read off Eq. (50.56):

$$G_{\text{R}}(s) = \frac{1}{s - m_{\text{r}}^2 + \sum_a g_a^{\text{r}\,2} \Sigma_{aa}^u(s)} \ , \quad (50.57)$$

where the parameters m_{r}, g_a^{r} as well as those of the background interactions are to be adjusted such that pole locations and residues get reproduced. For this construction the background interactions contained in $\Sigma_{aa}^u(s)$ are taken diagonal, which implies diagonal vertex functions and therefore diagonal self energies, i.e. $\Sigma_{ab}^u(s)=\delta_{ab}\Sigma_{aa}^u(s)$. With this one can define branching ratios in line with Eq. (50.26) via

$$\text{Br}_a = \frac{g_a^{\text{r}\,2}}{2\pi i} \int_{s_{\text{thr},a}}^{\infty} \text{d}s\, |G_{\text{R}}(s)|^2\, \text{Disc}\, \Sigma_{aa}^u(s) = \frac{g_a^{\text{r}\,2}}{\pi} \int_{s_{\text{thr},a}}^{\infty} \text{d}s\, |G_{\text{R}}(s) \Omega_{aa}(s) n_a(s)|^2\, \rho_c(s) \ . \quad (50.58)$$

Thus, in this approach the weight function of Eq. (50.28) can be identified with

$$\sigma_{\text{R}}(s) = \frac{M_{\text{R}} \Gamma_{\text{R}}}{\pi} |G_{\text{R}}(s)|^2 \ . \quad (50.59)$$

The individual branching ratios automatically sum to one, since by construction

$$\sum_a \frac{g_a^{\text{r}\,2}}{2\pi i} \int_{s_{\text{thr},a}}^{\infty} \text{d}s\, |G_{\text{R}}(s)|^2\, \text{Disc}\Sigma_{aa}^u(s) = -\frac{1}{2\pi i} \int_{s_{\text{thr}}}^{\infty} \text{d}s\, \text{Disc}\, G_{\text{R}}(s) = 1 \ , \quad (50.60)$$

where s_{thr} denotes the lowest of the different thresholds. To see the last identity we follow Ref. [140] and use Cauchy's theorem as well as the fact that the resonance propagator has no non-analyticities on the physical sheet besides the threshold branch points, with the branch cuts extending to infinity along the positive real axis, to find

$$0 = \oint \text{d}s\, G_{\text{R}}(s) = \lim_{s_{\max}\to\infty} \left[\int_{s_{\text{thr}}}^{s_{\max}} \text{d}s\, \text{Disc}\, G_{\text{R}}(s) + i \int_0^{2\pi} \text{d}\phi\, s_{\max} e^{i\phi} G_{\text{R}}(s_{\max} e^{i\phi}) \right] \quad (50.61)$$

where the integration contour is chosen such that it encloses the branch cut from the lowest threshold and is closed by an arc of radius $s_{\max}$. Using that $\lim_{s\to\infty} \Sigma_{aa}(s)/s = 0$ such that $\lim_{s\to\infty} G_{\text{R}}(s) = 1/s$ the second integral above evaluates to $2\pi i$ which proves the identity from above. An alternative formal proof of Eq. (50.60) is provided in Ref. [30].

There has been considerable interest in the $3 \to 3$ scattering recently, particularly in light of new data on three-hadron interactions [141] and advancements in lattice calculations [142]. One finds that the methodologies devised for accounting for one-pion exchange bear a resemblance to the two-potential decomposition. For details see Ref. [143], also Eq. (93) in Ref. [144].

Acknowledgements

We thank Feng-Kun Guo for carefully reading the manuscript and for detailed and constructive suggestions.

References

[1] M. Albaladejo *et al.* (JPAC), Prog. Part. Nucl. Phys. **127**, 103981 (2022), [arXiv:2112.13436].

[2] M. Mai, U.-G. Meißner and C. Urbach, Phys. Rept. **1001**, 1 (2023), [arXiv:2206.01477].

[3] M. Jacob and G. C. Wick, Annals Phys. **7**, 404 (1959), [Annals Phys.281,774(2000)].

[4] C. Zemach, Phys. Rev. **140B**, 97, 109 (1965).

[5] A. V. Anisovich *et al.*, J. Phys. **G28**, 15 (2002), [hep-ph/0105330].

[6] M. E. Peskin and D. V. Schroeder, *An Introduction to quantum field theory*, Addison-Wesley, Reading, USA (1995), ISBN 978-0-201-50397-5.

[7] V. N. Gribov, Y. L. Dokshitzer and J. Nyiri, *Strong Interactions of Hadrons at High Energies – Gribov Lectures on Theoretical Physics*, Cambridge University Press, Cambridge (2009).

[8] M. Doring *et al.*, Nucl. Phys. A **829**, 170 (2009), [arXiv:0903.4337].

[9] H.-J. Jing, X.-H. Cao and F.-K. Guo (2025), [arXiv:2507.06175].

[10] L. Landau, Nucl. Phys. **13**, 181 (1959).

[11] R. Cutkosky, J. Math. Phys. **1**, 429 (1960).

[12] M. Kato, Annals Phys. **31**, 1, 130 (1965).

[13] A. M. Badalian *et al.*, Phys. Rept. **82**, 31 (1982).

[14] V. Baru *et al.*, Phys. Rev. D **99**, 9, 094013 (2019), [arXiv:1901.10319].

[15] Z.-H. Zhang and F.-K. Guo, Phys. Lett. B **863**, 139387 (2025), [arXiv:2407.10620].

[16] G. Calucci, L. Fonda and G. C. Ghirardi, Phys. Rev. **166**, 1719 (1968).

[17] S. Coleman and R. E. Norton, Nuovo Cim. **38**, 438 (1965).

[18] C. Schmid, Phys. Rev. **154**, 5, 1363 (1967).

[19] I. J. R. Aitchison and C. Kacser, Nuovo Cim. A **40**, 2, 576 (1965).

[20] M. Mikhasenko, B. Ketzer and A. Sarantsev, Phys. Rev. D **91**, 9, 094015 (2015), [arXiv:1501.07023].

[21] M. Bayar *et al.*, Phys. Rev. **D94**, 7, 074039 (2016), [arXiv:1609.04133].

[22] F. Aceti, L. R. Dai and E. Oset, Phys. Rev. **D94**, 9, 096015 (2016), [arXiv:1606.06893].

[23] J.-J. Wu *et al.*, Phys. Rev. Lett. **108**, 081803 (2012), [arXiv:1108.3772].

[24] F.-K. Guo, X.-H. Liu and S. Sakai, Prog. Part. Nucl. Phys. **112**, 103757 (2020), [arXiv:1912.07030].

[25] L. D. Roper, Phys. Rev. Lett. **12**, 340 (1964).

[26] J. R. Pelaez, Phys. Rept. **658**, 1 (2016), [arXiv:1510.00653].

[27] R. Omnès, *Introduction to Particle Physics*, Frontiers in physics, Wiley-Interscience (1971), ISBN 9780471653721.

[28] R. Omnès and M. Froissart, *Mandelstam Theory and Regge Poles: An Introduction for Experimentalists*, Frontiers in physics, W.A. Benjamin (1963), URL `https://books.google.fr/books?id=O8pEAAAAIAAJ`.

[29] M. Fukugita and K. Igi, Phys. Rept. **31**, 237 (1977).

[30] S. Weinberg, *The Quantum theory of fields. Vol. 1: Foundations*, Cambridge University Press (2005), ISBN 978-0-521-67053-1, 978-0-511-25204-4.

[31] S. M. Roy, Phys. Lett. **36B**, 353 (1971).

[32] B. Ananthanarayan *et al.*, Phys. Rept. **353**, 207 (2001), [hep-ph/0005297].

Int. J. Mod. Phys. A 2026.41. Downloaded from www.worldscientific.com
by UNIVERSITY OF CALIFORNIA @ BERKELEY on 09/16/26. Re-use and distribution is strictly not permitted, except for Open Access articles.

[33] G. Colangelo, J. Gasser and H. Leutwyler, Nucl. Phys. **B603**, 125 (2001), [hep-ph/0103088].

[34] R. Garcia-Martin *et al.*, Phys. Rev. D **83**, 074004 (2011), [arXiv:1102.2183].

[35] P. Buettiker, S. Descotes-Genon and B. Moussallam, Eur. Phys. J. **C33**, 409 (2004), [hep-ph/0310283].

[36] M. Hoferichter, D. R. Phillips and C. Schat, Eur. Phys. J. **C71**, 1743 (2011), [arXiv:1106.4147].

[37] G. E. Hite and F. Steiner, Nuovo Cim. A **18**, 237 (1973).

[38] M. Hoferichter *et al.*, Phys. Rept. **625**, 1 (2016), [arXiv:1510.06039].

[39] M. Hoferichter *et al.*, Phys. Lett. B **853**, 138698 (2024), [arXiv:2312.15015].

[40] D. I. Olive, Il Nuovo Cimento (1955-1965) **73**, 1, 73 (1962), ISSN 1827-6121, URL `https://doi.org/10.1007/BF02754344`.

[41] J. L. Basdevant and E. L. Berger, Phys. Rev. **D16**, 657 (1977).

[42] N. N. Khuri and S. B. Treiman, Phys. Rev. **119**, 1115 (1960).

[43] I. J. R. Aitchison and R. Pasquier, Phys. Rev. **152**, 4, 1274 (1966).

[44] J. Kambor, C. Wiesendanger and D. Wyler, Nucl. Phys. B **465**, 215 (1996), [hep-ph/9509374].

[45] A. V. Anisovich and H. Leutwyler, Phys. Lett. B **375**, 335 (1996), [hep-ph/9601237].

[46] P. Guo *et al.*, Phys. Lett. **B771**, 497 (2017), [arXiv:1608.01447].

[47] M. Albaladejo and B. Moussallam, Eur. Phys. J. **C77**, 8, 508 (2017), [arXiv:1702.04931].

[48] G. Colangelo *et al.*, Eur. Phys. J. **C78**, 11, 947 (2018), [arXiv:1807.11937].

[49] K. Kampf *et al.*, Phys. Rev. D **101**, 7, 074043 (2020), [arXiv:1911.11762].

[50] T. Isken *et al.*, Eur. Phys. J. **C77**, 7, 489 (2017), [arXiv:1705.04339].

[51] F. Niecknig, B. Kubis and S. P. Schneider, Eur. Phys. J. **C72**, 2014 (2012), [arXiv:1203.2501].

[52] I. V. Danilkin *et al.*, Phys. Rev. **D91**, 9, 094029 (2015), [arXiv:1409.7708].

[53] M. Dax, T. Isken and B. Kubis, Eur. Phys. J. C **78**, 10, 859 (2018), [arXiv:1808.08957].

[54] M. Albaladejo *et al.* (JPAC), Eur. Phys. J. C **80**, 12, 1107 (2020), [arXiv:2006.01058].

[55] M. Albaladejo *et al.* (JPAC), Phys. Rev. D **101**, 5, 054018 (2020), [arXiv:1910.03107].

[56] D. Stamen *et al.*, Eur. Phys. J. C **83**, 6, 510 (2023), [Erratum: Eur.Phys.J.C 83, 586 (2023)], [arXiv:2212.11767].

[57] F. Niecknig and B. Kubis, JHEP **10**, 142 (2015), [arXiv:1509.03188].

[58] F. Niecknig and B. Kubis, Phys. Lett. **B780**, 471 (2018), [arXiv:1708.00446].

[59] M. Albaladejo *et al.* (JPAC), Phys. Rev. D **108**, 1, 014035 (2023), [arXiv:2304.09736].

[60] Y.-H. Chen *et al.*, Phys. Rev. D **93**, 3, 034030 (2016), [arXiv:1512.03583].

[61] S. Ropertz, C. Hanhart and B. Kubis, Eur. Phys. J. **C78**, 12, 1000 (2018), [arXiv:1809.06867].

[62] M. Mikhasenko *et al.* (JPAC), Phys. Rev. D **101**, 3, 034033 (2020), [arXiv:1910.04566].

[63] K. M. Watson, Phys. Rev. **95**, 228 (1954).

[64] S. Willenbrock, Eur. Phys. J. Plus **139**, 6, 523 (2024), [arXiv:2203.11056].

[65] B. S. Zou and D. V. Bugg, Phys. Rev. D **48**, R3948 (1993).

[66] Z.-Q. Wang *et al.*, Phys. Rev. D **105**, 7, 074016 (2022), [arXiv:2201.00492].

[67] V. Burkert *et al.*, Phys. Lett. B **844**, 138070 (2023), [arXiv:2207.08472].

[68] L. A. Heuser *et al.*, Eur. Phys. J. C **84**, 6, 599 (2024), [arXiv:2403.15539].

[69] M. Aghasyan *et al.* (COMPASS), Phys. Rev. D **98**, 9, 092003 (2018), [arXiv:1802.05913].

[70] R. Aaij *et al.* (LHCb), Phys. Rev. D **94**, 7, 072001 (2016), [arXiv:1608.01289].

[71] R. Aaij *et al.* (LHCb), Phys. Rev. D **92**, 1, 012012 (2015), [arXiv:1505.01505].

[72] R. Aaij *et al.* (LHCb), Phys. Rev. D **91**, 9, 092002 (2015), [Erratum: Phys.Rev.D 93, 119901 (2016)], [arXiv:1503.02995].

[73] R. Aaij *et al.* (LHCb), Phys. Rev. D **102**, 112003 (2020), [arXiv:2009.00026].

[74] D. Morgan and M. R. Pennington, Z. Phys. **C37**, 431 (1988), [Erratum: Z. Phys.C39,590(1988)].

[75] D. Morgan and M. R. Pennington, Z. Phys. **C48**, 623 (1990).

[76] B. Moussallam, Eur. Phys. J. C **71**, 1814 (2011), [arXiv:1110.6074].

[77] L. Von Detten *et al.*, Eur. Phys. J. C **81**, 5, 420 (2021), [arXiv:2103.01966].

[78] J. M. Blatt and V. F. Weisskopf, *Theoretical nuclear physics*, Springer, New York (1952), ISBN 9780471080190.

[79] F. Von Hippel and C. Quigg, Phys. Rev. **D5**, 624 (1972).

[80] S. U. Chung *et al.*, Annalen Phys. **4**, 404 (1995).

[81] S. M. Flatte, Phys. Lett. **63B**, 224 (1976).

[82] V. V. Anisovich and A. V. Sarantsev, Eur. Phys. J. **A16**, 229 (2003), [hep-ph/0204328].

[83] V. Baru *et al.*, Eur. Phys. J. **A23**, 523 (2005), [arXiv:nucl-th/0410099].

[84] R. Aaij *et al.* (LHCb), Phys. Rev. D **108**, 1, L011103 (2023), [arXiv:2204.12597].

[85] J. P. Lees *et al.* (BaBar), Phys. Rev. D **86**, 032013 (2012), [arXiv:1205.2228].

[86] J. T. Daub, C. Hanhart and B. Kubis, JHEP **02**, 009 (2016), [arXiv:1508.06841].

[87] S. Holz *et al.*, Eur. Phys. J. C **82**, 5, 434 (2022), [Addendum: Eur.Phys.J.C 82, 1159 (2022)], [arXiv:2202.05846].

[88] G. J. Gounaris and J. J. Sakurai, Phys. Rev. Lett. **21**, 244 (1968).

[89] I. J. R. Aitchison, Nucl. Phys. **A189**, 417 (1972).

[90] G. Moir *et al.*, JHEP **10**, 011 (2016), [arXiv:1607.07093].

[91] K. L. Au, D. Morgan and M. R. Pennington, Phys. Rev. D **35**, 1633 (1987).

[92] J. J. Dudek, R. G. Edwards and D. J. Wilson (Hadron Spectrum), Phys. Rev. **D93**, 9, 094506 (2016), [arXiv:1602.05122].

[93] R. A. Briceno *et al.*, Phys. Rev. **D97**, 5, 054513 (2018), [arXiv:1708.06667].

[94] A. J. Woss *et al.*, Phys. Rev. D **100**, 5, 054506 (2019), [arXiv:1904.04136].

[95] I. J. R. Aitchison (2015), [arXiv:1507.02697].

[96] R. N. Cahn and P. V. Landshoff, Nucl. Phys. **B266**, 451 (1986).

[97] J. R. Pelaez, A. Rodas and J. Ruiz De Elvira, Eur. Phys. J. C **79**, 12, 1008 (2019), [arXiv:1907.13162].

[98] I. Danilkin *et al.*, Phys. Rev. D **107**, 7, 074021 (2023), [arXiv:2206.15223].

[99] B. Kubis and J. Plenter, Eur. Phys. J. C **75**, 6, 283 (2015), [arXiv:1504.02588].

[100] A. Asokan *et al.*, Eur. Phys. J. C **83**, 9, 850 (2023), [arXiv:2212.07856].

[101] M. R. Pennington *et al.*, Eur. Phys. J. **C56**, 1 (2008), [arXiv:0803.3389].

[102] J. A. Oller and E. Oset, Phys. Rev. **D60**, 074023 (1999), [hep-ph/9809337].

[103] N. N. Achasov and A. V. Kiselev, Phys. Rev. **D83**, 054008 (2011), [arXiv:1011.4446].

[104] A. V. Anisovich *et al.*, Phys. Rev. **D84**, 076001 (2011).

[105] C. Hanhart *et al.*, Eur. Phys. J. C **84**, 5, 483 (2024), [arXiv:2312.00619].

[106] J. H. Reid and N. N. Trofimenkoff, J. Math. Phys. **25**, 3540 (1984).

[107] J. A. Oller and U. G. Meissner, Phys. Lett. B **500**, 263 (2001), [hep-ph/0011146].

[108] E. L. Lomon and S. Pacetti, Phys. Rev. **D85**, 113004 (2012), [Erratum: Phys. Rev.D86,039901(2012)], [arXiv:1201.6126].

[109] B. Moussallam, Eur. Phys. J. **C73**, 2539 (2013), [arXiv:1305.3143].

[110] J. M. Blatt and J. D. Jackson, Phys. Rev. **76**, 18 (1949).

[111] H. A. Bethe, Phys. Rev. **76**, 38 (1949).

[112] M. Padmanath and S. Prelovsek, Phys. Rev. Lett. **129**, 3, 032002 (2022), [arXiv:2202.10110].

[113] S. Chen *et al.*, Phys. Lett. B **833**, 137391 (2022), [arXiv:2206.06185].

[114] Y. Lyu *et al.* (2023), [arXiv:2302.04505].

[115] M.-L. Du *et al.*, Phys. Rev. Lett. **131**, 13, 131903 (2023), [arXiv:2303.09441].

[116] M.-L. Du, F.-K. Guo and B. Wu, Phys. Rev. Lett. **135**, 1, 011903 (2025), [arXiv:2408.09375].

[117] S. K. Choi *et al.* (Belle), Phys. Rev. Lett. **91**, 262001 (2003), [hep-ex/0309032].

[118] R. Aaij *et al.* (LHCb), Phys. Rev. Lett. **122**, 22, 222001 (2019), [arXiv:1904.03947].

[119] E. Braaten and J. Stapleton, Phys. Rev. D **81**, 014019 (2010), [arXiv:0907.3167].

[120] V. Baru *et al.*, Eur. Phys. J. **A44**, 93 (2010), [arXiv:1001.0369].

[121] C. Fernández-Ramírez *et al.* (JPAC), Phys. Rev. Lett. **123**, 9, 092001 (2019), [arXiv:1904.10021].

[122] C. Hanhart *et al.*, Phys. Rev. Lett. **115**, 20, 202001 (2015), [arXiv:1507.00382].

[123] F. K. Guo *et al.*, Phys. Rev. D **93**, 7, 074031 (2016), [arXiv:1602.00940].

[124] X.-K. Dong, F.-K. Guo and B.-S. Zou, Phys. Rev. Lett. **126**, 15, 152001 (2021), [arXiv:2011.14517].

[125] D. Morgan, Nucl. Phys. **A543**, 632 (1992).

[126] V. Baru *et al.*, Phys. Lett. **B586**, 53 (2004), [hep-ph/0308129].

[127] F.-K. Guo *et al.*, Rev. Mod. Phys. **90**, 1, 015004 (2018), [arXiv:1705.00141].

[128] I. Matuschek *et al.*, Eur. Phys. J. A **57**, 3, 101 (2021), [arXiv:2007.05329].

[129] I. R. Afnan and B. Blankleider, Phys. Rev. **C22**, 1638 (1980).

[130] A. D. Lahiff and I. R. Afnan, Phys. Rev. **C60**, 024608 (1999), [arXiv:nucl-th/9903058].

[131] A. Matsuyama, T. Sato and T. S. H. Lee, Phys. Rept. **439**, 193 (2007), [arXiv:nucl-th/0608051].

[132] D. Ronchen *et al.*, Eur. Phys. J. **A49**, 44 (2013), [arXiv:1211.6998].

[133] C. Hanhart, Phys. Lett. **B715**, 170 (2012), [arXiv:1203.6839].

[134] M. Gell-Mann and M. L. Goldberger, Phys. Rev. **91**, 398 (1953).

[135] K. Nakano, Phys. Rev. **C26**, 1123 (1982).

[136] D. Djukanovic, J. Gegelia and S. Scherer, Phys. Rev. **D76**, 037501 (2007), [arXiv:0707.2030].

[137] M. Doring *et al.*, Phys. Lett. **B681**, 26 (2009), [arXiv:0903.1781].

[138] R. Omnes, Nuovo Cim. **8**, 316 (1958).

[139] J. Gasser and U. G. Meissner, Nucl. Phys. **B357**, 90 (1991).

[140] J. A. Oller (2025), [arXiv:2501.10000].

[141] B. Ketzer, B. Grube and D. Ryabchikov, Prog. Part. Nucl. Phys. **113**, 103755 (2020), [arXiv:1909.06366].

[142] B. Hörz and A. Hanlon, Phys. Rev. Lett. **123**, 14, 142002 (2019), [arXiv:1905.04277].

[143] M. Mikhasenko *et al.*, JHEP **08**, 080 (2019), [arXiv:1904.11894].

[144] M. T. Hansen and S. R. Sharpe, Phys. Rev. D **92**, 11, 114509 (2015), [arXiv:1504.04248].

Int. J. Mod. Phys. A 2026.41. Downloaded from www.worldscientific.com
by UNIVERSITY OF CALIFORNIA @ BERKELEY on 09/16/26. Re-use and distribution is strictly not permitted, except for Open Access articles.

Int. J. Mod. Phys. A 2026.41. Downloaded from www.worldscientific.com
by UNIVERSITY OF CALIFORNIA @ BERKELEY on 09/16/26. Re-use and distribution is strictly not permitted, except for Open Access articles.

51. Cross-Section Formulae for Specific Processes

Revised August 2019 by H. Baer (Oklahoma U.) and R.N. Cahn (LBNL).

PART I: STANDARD MODEL PROCESSES

Setting aside leptoproduction (for which, see Sec. 16 of this *Review*), the cross sections of primary interest are those with light incident particles, e^+e^-, $\gamma\gamma$, $q\overline{q}$, gq , gg, *etc.*, where g and q represent gluons and light quarks. The produced particles include both light particles and heavy ones - t, W, Z, and the Higgs boson H. We provide the production cross sections calculated within the Standard Model for several such processes.

51.1 Resonance Formation

Resonant cross sections are generally described by the Breit-Wigner formula (Sec. 50.3 of this *Review*).

$$\sigma(E) = \frac{2J+1}{(2S_1+1)(2S_2+1)}\frac{4\pi}{k^2}\left[\frac{\Gamma^2/4}{(E-E_0)^2+\Gamma^2/4}\right]B_{in}B_{out}, \tag{51.1}$$

where E is the c.m. energy, J is the spin of the resonance, and the number of polarization states of the two incident particles are $2S_1+1$ and $2S_2+1$. The c.m. momentum in the initial state is k, E_0 is the c.m. energy at the resonance, and Γ is the full width at half maximum height of the resonance. The branching fraction for the resonance into the initial-state channel is B_{in} and into the final-state channel is B_{out}. For a narrow resonance, the factor in square brackets may be replaced by $\pi\Gamma\delta(E-E_0)/2$.

51.2 Production of light particles

The production of point-like, spin-1/2 fermions in e^+e^- annihilation through a virtual photon, $e^+e^- \to \gamma^* \to f\overline{f}$, at c.m. energy squared s is given by

$$\frac{d\sigma}{d\Omega} = N_c\frac{\alpha^2}{4s}\beta\left[1+\cos^2\theta+(1-\beta^2)\sin^2\theta\right]Q_f^2 \ , \tag{51.2}$$

where β is v/c for the produced fermions in the c.m., θ is the c.m. scattering angle, and Q_f is the charge of the fermion. The factor N_c is 1 for charged leptons and 3 for quarks. In the ultrarelativistic limit, $\beta \to 1$,

$$\sigma = N_cQ_f^2\frac{4\pi\alpha^2}{3s} = N_cQ_f^2\frac{86.8\ \text{nb}}{s\,(\text{GeV}^2)} \ . \tag{51.3}$$

The cross section for the annihilation of a $q\overline{q}$ pair into a distinct pair $q'\overline{q}'$ through a gluon is completely analogous up to color factors, with the replacement $\alpha \to \alpha_s$. Treating all quarks as massless, averaging over the colors of the initial quarks and defining $t = -s\sin^2(\theta/2)$, $u = -s\cos^2(\theta/2)$, one finds [1]

$$\frac{d\sigma}{d\Omega}(q\overline{q} \to q'\overline{q}') = \frac{\alpha_s^2}{9s}\frac{t^2+u^2}{s^2} \ . \tag{51.4}$$

Crossing symmetry gives

$$\frac{d\sigma}{d\Omega}(qq' \to qq') = \frac{\alpha_s^2}{9s}\frac{s^2+u^2}{t^2} \ . \tag{51.5}$$

If the quarks q and q' are identical, we have

$$\frac{d\sigma}{d\Omega}(q\overline{q} \to q\overline{q}) = \frac{\alpha_s^2}{9s}\left[\frac{t^2+u^2}{s^2}+\frac{s^2+u^2}{t^2}-\frac{2u^2}{3st}\right] \ , \tag{51.6}$$

and by crossing

$$\frac{d\sigma}{d\Omega}(qq \to qq) = \frac{\alpha_s^2}{9s}\left[\frac{t^2+s^2}{u^2}+\frac{s^2+u^2}{t^2}-\frac{2s^2}{3ut}\right]. \tag{51.7}$$

Annihilation of e^+e^- into $\gamma\gamma$ has the cross section

$$\frac{d\sigma}{d\Omega}(e^+e^- \to \gamma\gamma) = \frac{\alpha^2}{2s}\frac{u^2+t^2}{tu} \ . \tag{51.8}$$

The related QCD process also has a triple-gluon coupling. The cross section is

$$\frac{d\sigma}{d\Omega}(q\overline{q} \to gg) = \frac{8\alpha_s^2}{27s}(t^2+u^2)\left(\frac{1}{tu}-\frac{9}{4s^2}\right) \ . \tag{51.9}$$

The crossed reactions are

$$\frac{d\sigma}{d\Omega}(qg \to qg) = \frac{\alpha_s^2}{9s}(s^2+u^2)(-\frac{1}{su}+\frac{9}{4t^2}) \tag{51.10}$$

and

$$\frac{d\sigma}{d\Omega}(gg \to q\overline{q}) = \frac{\alpha_s^2}{24s}(t^2+u^2)(\frac{1}{tu}-\frac{9}{4s^2}) \ . \tag{51.11}$$

Finally,

$$\frac{d\sigma}{d\Omega}(gg \to gg) = \frac{9\alpha_s^2}{8s}(3-\frac{ut}{s^2}-\frac{su}{t^2}-\frac{st}{u^2}) \ . \tag{51.12}$$

Lepton-quark scattering is analogous (neglecting Z exchange)

$$\frac{d\sigma}{d\Omega}(eq \to eq) = \frac{\alpha^2}{2s}e_q^2\frac{s^2+u^2}{t^2} \ . \tag{51.13}$$

where e_q is the charge of the quark. For neutrino scattering with the four-Fermi interaction

$$\frac{d\sigma}{d\Omega}(\nu d \to \ell^- u) = \frac{G_F^2 s}{4\pi^2} \ , \tag{51.14}$$

where the Cabibbo angle suppression is ignored. Similarly

$$\frac{d\sigma}{d\Omega}(\nu\overline{u} \to \ell^-\overline{d}) = \frac{G_F^2 s}{4\pi^2}\frac{(1+\cos\theta)^2}{4} \ . \tag{51.15}$$

To obtain the formulae for deep inelastic scattering (presented in more detail in Section 18) we consider quarks of type i carrying a fraction $x = Q^2/(2M\nu)$ of the nucleon's energy, where $\nu = E - E'$ is the energy lost by the lepton in the nucleon rest frame. With $y = \nu/E$ we have the correspondences

$$1+\cos\theta \to 2(1-y) \ ,$$

$$d\Omega_{cm} \to 4\pi f_i(x)dx\,dy \ , \tag{51.16}$$

where the latter incorporates the quark distribution, $f_i(x)$. In this way we find

$$\frac{d\sigma}{dx\,dy}(eN \to eX) = \frac{4\pi\alpha^2 xs}{Q^4}\frac{1}{2}\left[1+(1-y)^2\right] \times \left[\frac{4}{9}(u(x)+\overline{u}(x)+\ldots)+\frac{1}{9}(d(x)+\overline{d}(x)+\ldots)\right] \tag{51.17}$$

where now $s = 2ME$ is the cm energy squared for the electron-nucleon collision, and we have suppressed contributions from higher mass quarks.

Similarly,

$$\frac{d\sigma}{dx\,dy}(\nu N \to \ell^- X) = \frac{G_F^2 xs}{\pi}[(d(x)+\ldots)+(1-y)^2(\overline{u}(x)+\ldots)] \tag{51.18}$$

and

$$\frac{d\sigma}{dx\,dy}(\overline{\nu}N \to \ell^+ X) = \frac{G_F^2 xs}{\pi}[(\overline{d}(x)+\ldots)+(1-y)^2(u(x)+\ldots)] \ . \tag{51.19}$$

Quasi-elastic neutrino scattering ($\nu_\mu n \to \mu^- p$, $\overline{\nu}_\mu p \to \mu^+ n$) is directly related to the crossed reaction, neutron decay. The formula for the differential cross section is presented, for example, in N.J. Baker *et al.*, Phys. Rev. **D23**, 2499 (1981).

Int. J. Mod. Phys. A 2026.41. Downloaded from www.worldscientific.com
by [redacted] LIFORNIA @ BERKELEY on 09/16/26. Re-use and distribution is strictly not permitted, except for Open Access articles.

51.3 Hadroproduction of heavy quarks

For hadroproduction of heavy quarks $Q = c,\ b,\ t$, it is important to include mass effects in the formulae. For $q\bar{q} \to Q\bar{Q}$, one has

$$\frac{d\sigma}{d\Omega}(q\bar{q} \to Q\bar{Q}) = \frac{\alpha_s^2}{9s^3}\sqrt{1-\frac{4m_Q^2}{s}} \left[(m_Q^2-t)^2+(m_Q^2-u)^2+2m_Q^2 s\right], \quad (51.20)$$

while for $gg \to Q\bar{Q}$ one has

$$\begin{aligned}\frac{d\sigma}{d\Omega}(gg \to Q\bar{Q}) = \frac{\alpha_s^2}{32s}\sqrt{1-\frac{4m_Q^2}{s}}\Bigg[&\frac{6}{s^2}(m_Q^2-t)(m_Q^2-u)- \\ &-\frac{m_Q^2(s-4m_Q^2)}{3(m_Q^2-t)(m_Q^2-u)}+ \\ &\frac{4}{3}\frac{(m_Q^2-t)(m_Q^2-u)-2m_Q^2(m_Q^2+t)}{(m_Q^2-t)^2} \\ &+\frac{4}{3}\frac{(m_Q^2-t)(m_Q^2-u)-2m_Q^2(m_Q^2+u)}{(m_Q^2-u)^2} \\ &-3\frac{(m_Q^2-t)(m_Q^2-u)+m_Q^2(u-t)}{s(m_Q^2-t)} \\ &-3\frac{(m_Q^2-t)(m_Q^2-u)+m_Q^2(t-u)}{s(m_Q^2-u)}\Bigg]. \end{aligned} \quad (51.21)$$

51.4 Production of Weak Gauge Bosons

51.4.1 *W and Z resonant production*

Resonant production of a single W or Z is governed by the partial widths

$$\Gamma(W \to \ell_i \overline{\nu}_i) = \frac{\sqrt{2}G_F m_W^3}{12\pi} \quad (51.22)$$

$$\Gamma(W \to q_i \bar{q}_j) = 3\frac{\sqrt{2}G_F |V_{ij}|^2 m_W^3}{12\pi} \quad (51.23)$$

$$\Gamma(Z \to f\overline{f}) = N_c \frac{\sqrt{2}G_F m_Z^3}{6\pi} \times \left[(T_3 - Q_f \sin^2\theta_W)^2 + (Q_f \sin^2\theta_W)^2\right] \quad (51.24)$$

The weak mixing angle is θ_W. The CKM matrix elements are indicated by V_{ij} and N_c is 3 for $q\bar{q}$ final states and 1 for leptonic final states.

The full differential cross section for $f_i\bar{f}_j \to (W,Z) \to f_{i'}\bar{f}_{j'}$ is given by

$$\begin{aligned}\frac{d\sigma}{d\Omega} = &\frac{N_c^f}{N_c^i}\cdot\frac{1}{256\pi^2 s}\cdot\frac{s^2}{(s-M^2)^2+s\Gamma^2} \\ &\times\Big[(L^2+R^2)(L'^2+R'^2)(1+\cos^2\theta) \\ &+(L^2-R^2)(L'^2-R'^2)2\,cos\theta\Big] \end{aligned} \quad (51.25)$$

where M is the mass of the W or Z. The couplings for the W are $L = (8G_F m_W^2/\sqrt{2})^{1/2}V_{ij}/\sqrt{2}; R = 0$ where V_{ij} is the corresponding CKM matrix element, with an analogous expression for L' and R'. For Z, the couplings are $L = (8G_F m_Z^2/\sqrt{2})^{1/2}(T_3 - \sin^2\theta_W Q); R = -(8G_F m_Z^2/\sqrt{2})^{1/2}\sin^2\theta_W Q$, where T_3 is the weak isospin of the initial left-handed fermion and Q is the initial fermion's electric charge. The expressions for L' and R' are analogous. The color factors $N_c^{i,f}$ are 3 for initial or final quarks and 1 for initial or final leptons.

51.4.2 *Production of pairs of weak gauge bosons*

The cross section for $f\bar{f} \to W^+W^-$ is given in term of the couplings of the left-handed and right-handed fermion f, $\ell = 2(T_3 - Qx_W)$, $r = -2Qx_W$, where T_3 is the third component of weak isospin for the left-handed f, Q is its electric charge (in units of the proton charge), and $x_W = \sin^2\theta_W$:

$$\begin{aligned}\frac{d\sigma}{dt} = &\frac{2\pi\alpha^2}{N_c s^2}\Bigg\{\Bigg[\left(Q+\frac{\ell+r}{4x_W}\frac{s}{s-m_Z^2}\right)^2 \\ &+\left(\frac{\ell-r}{4x_W}\frac{s}{s-m_Z^2}\right)^2\Bigg]A(s,t,u) \\ &+\frac{1}{2x_W}\left(Q+\frac{\ell}{2x_W}\frac{s}{s-m_Z^2}\right) \\ &\qquad(\Theta(-Q)I(s,t,u)-\Theta(Q)I(s,u,t)) \\ &+\frac{1}{8x_W^2}\left(\Theta(-Q)E(s,t,u)+\Theta(Q)E(s,u,t)\right)\Bigg\}, \end{aligned} \quad (51.26)$$

where $\Theta(x)$ is 1 for $x > 0$ and 0 for $x < 0$, and where

$$\begin{aligned} A(s,t,u) &= \left(\frac{tu}{m_W^4}-1\right)\left(\frac{1}{4}-\frac{m_W^2}{s}+3\frac{m_W^4}{s^2}\right)+\frac{s}{m_W^2}-4, \\ I(s,t,u) &= \left(\frac{tu}{m_W^4}-1\right)\left(\frac{1}{4}-\frac{m_W^2}{2s}-\frac{m_W^4}{st}\right)+\frac{s}{m_W^2}-2+2\frac{m_W^2}{t}, \\ E(s,t,u) &= \left(\frac{tu}{m_W^4}-1\right)\left(\frac{1}{4}+\frac{m_W^4}{t^2}\right)+\frac{s}{m_W^2}, \end{aligned} \quad (51.27)$$

and s,t,u are the usual Mandelstam variables with $s = (p_f + p_{\bar{f}})^2, t = (p_f - p_{W^-})^2, u = (p_f - p_{W^+})^2$. The factor N_c is 3 for quarks and 1 for leptons.

The analogous cross-section for $q_i\bar{q}_j \to W^\pm Z^0$ is

$$\begin{aligned}\frac{d\sigma}{dt} = &\frac{\pi\alpha^2|V_{ij}|^2}{6s^2x_W^2}\Bigg\{\left(\frac{1}{s-m_W^2}\right)^2\Bigg[\left(\frac{9-8x_W}{4}\right)\left(ut-m_W^2m_Z^2\right) \\ &+(8x_W-6)\,s\left(m_W^2+m_Z^2\right)\Bigg] \\ &+\left[\frac{ut-m_W^2m_Z^2-s(m_W^2+m_Z^2)}{s-m_W^2}\right]\left[\frac{\ell_j}{t}-\frac{\ell_i}{u}\right] \\ &+\frac{ut-m_W^2m_Z^2}{4(1-x_W)}\left[\frac{\ell_j^2}{t^2}+\frac{\ell_i^2}{u^2}\right]+\frac{s(m_W^2+m_Z^2)}{2(1-x_W)}\frac{\ell_i\ell_j}{tu}\Bigg\}, \end{aligned} \quad (51.28)$$

where ℓ_i and ℓ_j are the couplings of the left-handed q_i and q_j as defined above. The CKM matrix element between q_i and q_j is V_{ij}.

The cross section for $q_i\bar{q}_i \to Z^0Z^0$ is

$$\frac{d\sigma}{dt} = \frac{\pi\alpha^2}{96}\frac{\ell_i^4+r_i^4}{x_W^2(1-x_W^2)^2s^2}\left[\frac{t}{u}+\frac{u}{t}+\frac{4m_Z^2s}{tu}-m_Z^4\left(\frac{1}{t^2}+\frac{1}{u^2}\right)\right]. \quad (51.29)$$

51.5 Production of Higgs Bosons

51.5.1 *Resonant Production*

The Higgs boson of the Standard Model can be produced resonantly in the collisions of quarks, leptons, W or Z bosons, gluons, or photons. The production cross section is thus controlled by the partial width of the Higgs boson into the entrance channel and its total width. The branching fractions for the Standard Model Higgs boson are shown in Fig. 1 of the "Searches for Higgs bosons"

Int. J. Mod. Phys. A 2026.41. Downloaded from www.worldscientific.com by UNIVERSITY OF CALIFORNIA @ BERKELEY on 09/16/26. Re-use and distribution is strictly not permitted, except for Open Access articles.

review in the Particle Listings section, as a function of the Higgs boson mass. The partial widths are given by the relations

$$\Gamma(H \to f\overline{f}) = \frac{G_F m_f^2 m_H N_c}{4\pi\sqrt{2}} \left(1 - 4m_f^2/m_H^2\right)^{3/2}, \qquad (51.30)$$

$$\Gamma(H \to W^+W^-) = \frac{G_F m_H^3 \beta_W}{32\pi\sqrt{2}} \left(4 - 4a_W + 3a_W^2\right), \qquad (51.31)$$

$$\Gamma(H \to ZZ) = \frac{G_F m_H^3 \beta_Z}{64\pi\sqrt{2}} \left(4 - 4a_Z + 3a_Z^2\right), \qquad (51.32)$$

where N_c is 3 for quarks and 1 for leptons and where $a_W = 1 - \beta_W^2 = 4m_W^2/m_H^2$ and $a_Z = 1 - \beta_Z^2 = 4m_Z^2/m_H^2$. The decay to two gluons proceeds through quark loops, with the t quark dominating [2]. Explicitly,

$$\Gamma(H \to gg) = \frac{\alpha_s^2 G_F m_H^3}{36\pi^3\sqrt{2}} \left| \sum_q I(m_q^2/m_H^2) \right|^2, \qquad (51.33)$$

where $I(z)$ is complex for $z < 1/4$. For $z < 2 \times 10^{-3}$, $|I(z)|$ is small so the light quarks contribute negligibly. For $m_H < 2m_t$, $z > 1/4$ and

$$I(z) = 3\left[2z + 2z(1-4z)\left(\sin^{-1}\frac{1}{2\sqrt{z}}\right)^2\right], \qquad (51.34)$$

which has the limit $I(z) \to 1$ as $z \to \infty$.

51.5.2 *Higgs Boson Production in W^* and Z^* decay*

The Standard Model Higgs boson can be produced in the decay of a virtual W or Z ("Higgstrahlung") [3,4]: In particular, if k is the c.m. momentum of the Higgs boson,

$$\sigma(q_i\overline{q}_j \to WH) = \frac{\pi\alpha^2|V_{ij}|^2}{36\sin^4\theta_W}\,\frac{2k}{\sqrt{s}}\,\frac{k^2+3m_W^2}{(s-m_W^2)^2} \qquad (51.35)$$

$$\sigma(f\bar{f} \to ZH) = \frac{2\pi\alpha^2(\ell_f^2 + r_f^2)}{48N_c\sin^4\theta_W\cos^4\theta_W}\,\frac{2k}{\sqrt{s}}\,\frac{k^2+3m_Z^2}{(s-m_Z^2)^2}, \qquad (51.36)$$

where ℓ and r are defined as above.

51.5.3 *W and Z Fusion*

Just as high-energy electrons can be regarded as sources of virtual photon beams, at very high energies they are sources of virtual W and Z beams. For Higgs boson production, it is the longitudinal components of the Ws and Zs that are important [5]. The distribution of longitudinal Ws carrying a fraction y of the electron's energy is [6]

$$f(y) = \frac{g^2}{16\pi^2}\,\frac{1-y}{y}, \qquad (51.37)$$

where $g = e/\sin\theta_W$. In the limit $s \gg m_H \gg m_W$, the partial decay rate is $\Gamma(H \to W_L W_L) = (g^2/64\pi)(m_H^3/m_W^2)$ and in the equivalent W approximation [7]

$$\sigma(e^+e^- \to \overline{\nu}_e\nu_e H) = \frac{1}{16m_W^2}\left(\frac{\alpha}{\sin^2\theta_W}\right)^3 \times \left[\left(1 + \frac{m_H^2}{s}\right)\log\frac{s}{m_H^2} - 2 + 2\frac{m_H^2}{s}\right]. \qquad (51.38)$$

There are significant corrections to this relation when m_H is not large compared to m_W [8]. For $m_H = 150$ GeV, the estimate is too high by 51% for $\sqrt{s} = 1000$ GeV, 32% too high at $\sqrt{s} = 2000$ GeV, and 22% too high at $\sqrt{s} = 4000$ GeV. Fusion of ZZ to make a Higgs boson can be treated similarly. Identical formulae apply for Higgs production in the collisions of quarks whose charges permit the emission of a W^+ and a W^-, except that QCD corrections and CKM matrix elements are required. Even in the absence of QCD corrections, the fine-structure constant ought to be evaluated at the scale of the collision, say m_W. All quarks contribute to the ZZ fusion process.

51.6 Inclusive hadronic reactions

One-particle inclusive cross sections $Ed^3\sigma/d^3p$ for the production of a particle of momentum p are conveniently expressed in terms of rapidity y (see above) and the momentum p_T transverse to the beam direction (in the c.m.):

$$E\frac{d^3\sigma}{d^3p} = \frac{d^3\sigma}{d\phi\,dy\,p_T\,dp_T}. \qquad (51.39)$$

In appropriate circumstances, the cross section may be decomposed as a partonic cross section multiplied by the probabilities of finding partons of the prescribed momenta:

$$\sigma_{\text{hadronic}} = \sum_{ij}\int dx_1\,dx_2\,f_i(x_1)\,f_j(x_2)\,d\widehat{\sigma}_{\text{partonic}}, \qquad (51.40)$$

The probability that a parton of type i carries a fraction of the incident particle's that lies between x_1 and $x_1 + dx_1$ is $f_i(x_1)dx_1$ and similarly for partons in the other incident particle. The partonic collision is specified by its c.m. energy squared $\hat{s} = x_1x_2s$ and the momentum transfer squared $\hat{t}$. The final hadronic state is more conveniently specified by the rapidities y_1, y_2 of the two jets resulting from the collision and the transverse momentum p_T. The connection between the differentials is

$$dx_1dx_2d\hat{t} = dy_1dy_2\frac{\hat{s}}{s}dp_T^2, \qquad (51.41)$$

so that

$$\frac{d^3\sigma}{dy_1dy_2dp_T^2} = \frac{\hat{s}}{s}\left[f_i(x_1)f_j(x_2)\frac{d\hat{\sigma}}{d\hat{t}}(\hat{s},\hat{t},\hat{u}) + f_i(x_2)f_j(x_1)\frac{d\hat{\sigma}}{d\hat{t}}(\hat{s},\hat{u},\hat{t})\right], \qquad (51.42)$$

where we have taken into account the possibility that the incident parton types might arise from either incident particle. The second term should be dropped if the types are identical: $i = j$.

51.7 Two-photon processes

In the Weizsäcker-Williams picture, a high-energy electron beam is accompanied by a spectrum of virtual photons of energies ω and invariant-mass squared $q^2 = -Q^2$, for which the photon number density is

$$dn = \frac{\alpha}{\pi}\left[1 - \frac{\omega}{E} + \frac{\omega^2}{E^2} - \frac{m_e^2\,\omega^2}{Q^2E^2}\right]\frac{d\omega}{\omega}\frac{dQ^2}{Q^2}, \qquad (51.43)$$

where E is the energy of the electron beam. The cross section for $e^+e^- \to e^+e^-X$ is then [9]

$$d\sigma_{e^+e^-\to e^+e^-X}(s) = dn_1dn_2d\sigma_{\gamma\gamma\to X}(W^2), \qquad (51.44)$$

where $W^2 = m_X^2$. Integrating from the lower limit $Q^2 = m_e^2\frac{\omega_i^2}{E_i(E_i-\omega_i)}$ to a maximum Q^2 gives

$$\sigma_{e^+e^-\to e^+e^-X}(s) = \frac{\alpha^2}{\pi^2}\int_{z_{th}}^1\frac{dz}{z} \times \left[\left(\ln\frac{Q^2_{max}}{zm_e^2} - 1\right)^2 f(z) + \frac{1}{3}(\ln z)^3\right]\sigma_{\gamma\gamma\to X}(zs), \qquad (51.45)$$

where

$$f(z) = \left(1 + \tfrac{1}{2}z\right)^2\ln(1/z) - \tfrac{1}{2}(1-z)(3+z). \qquad (51.46)$$

Int. J. Mod. Phys. A 2026.41. Downloaded from www.worldscientific.com
by [redacted]LIFORNIA @ BERKELEY on 09/16/26. Re-use and distribution is strictly not permitted, except for Open Access articles.

The appropriate value of Q^2_{max} depends on the properties of the produced system X. For production of hadronic systems, $Q^2_{max} \approx m^2_\rho$, while for lepton-pair production, $Q^2 \approx W^2$. For production of a resonance with spin $J \neq 1$, we have

$$\sigma_{e^+e^-\to e^+e^-R}(s) = (2J+1)\frac{8\alpha^2\Gamma_{R\to\gamma\gamma}}{m^3_R} \times \left[f(m^2_R/s)\left(\ln\frac{m^2_V s}{m^2_e m^2_R} - 1\right)^2 - \frac{1}{3}\left(\ln\frac{s}{M^2_R}\right)^3\right], \quad (51.47)$$

where m_V is the mass that enters into the form factor for the $\gamma\gamma \to R$ transition, typically m_ρ.

PART II: PROCESSES BEYOND THE STANDARD MODEL

51.8 Production of supersymmetric particles

In supersymmetric (SUSY) theories (see Supersymmetric Particle Searches in this *Review*), every boson has a fermionic superpartner, and every fermion has a bosonic superpartner. The minimal supersymmetric Standard Model (MSSM) is a direct supersymmetrization of the Standard Model (SM), although a second Higgs doublet is needed to avoid triangle anomalies [10]. Under *soft* SUSY breaking, superpartner masses are lifted above the SM particle masses. In weak scale SUSY, the superpartners are invoked to stabilize the weak scale under radiative corrections, so the superpartners are expected to have masses of order the TeV scale.

51.8.1 *Gluino and squark production*

The superpartners of gluons are the color octet, spin$-\frac{1}{2}$ gluinos ($\tilde{g}$), while each helicity component of quark flavor has a spin-0 *squark* partner, *e.g.* $\tilde{q}_L$ and $\tilde{q}_R$. Third generation left- and right- squarks are expected to have large mixing, resulting in mass eigenstates $\tilde{q}_1$ and $\tilde{q}_2$, with $m_{\tilde{q}_1} < m_{\tilde{q}_2}$ (here, q denotes any of the SM flavors of quarks and $\tilde{q}_i$ the corresponding flavor and type ($i = L, R$ or $1, 2$) of squark). Gluino pair production ($\tilde{g}\tilde{g}$) takes place via either glue-glue or quark-antiquark annihilation [11].

The subprocess cross sections are usually presented as differential distributions in the Mandelstam variables s, t and u. Note that for a $2 \to 2$ scattering subprocess $ab \to cd$, the Mandelstam variable $s = (p_a + p_b)^2 = (p_c + p_d)^2$, where p_a is the 4-momentum of particle a, and so forth. The variable $t = (p_c - p_a)^2$, where c and a are taken conventionally to be the most similar particles in the subprocess. The variable u would then be equal to $(p_d - p_a)^2$. Note that since s, t and u are squares of 4-vectors, they are invariants in any inertial reference frame.

Gluino pair production at hadron colliders is described by:

$$\frac{d\sigma}{dt}(gg \to \tilde{g}\tilde{g}) = \frac{9\pi\alpha^2_s}{4s^2}\left\{\frac{2(m^2_{\tilde{g}} - t)(m^2_{\tilde{g}} - u)}{s^2} + \frac{(m^2_{\tilde{g}} - t)(m^2_{\tilde{g}} - u) - 2m^2_{\tilde{g}}(m^2_{\tilde{g}} + t)}{(m^2_{\tilde{g}} - t)^2} + \frac{(m^2_{\tilde{g}} - t)(m^2_{\tilde{g}} - u) - 2m^2_{\tilde{g}}(m^2_{\tilde{g}} + u)}{(m^2_{\tilde{g}} - u)^2} + \frac{m^2_{\tilde{g}}(s - 4m^2_{\tilde{g}})}{(m^2_{\tilde{g}} - t)(m^2_{\tilde{g}} - u)} - \frac{(m^2_{\tilde{g}} - t)(m^2_{\tilde{g}} - u) + m^2_{\tilde{g}}(u - t)}{s(m^2_{\tilde{g}} - t)} - \frac{(m^2_{\tilde{g}} - t)(m^2_{\tilde{g}} - u) + m^2_{\tilde{g}}(t - u)}{s(m^2_{\tilde{g}} - u)}\right\}, \quad (51.48)$$

where α_s is the strong fine structure constant. Also,

$$\frac{d\sigma}{dt}(q\bar{q} \to \tilde{g}\tilde{g}) = \frac{8\pi\alpha^2_s}{9s^2}\left\{\frac{4}{3}\left(\frac{m^2_{\tilde{g}} - t}{m^2_{\tilde{q}} - t}\right)^2 + \frac{4}{3}\left(\frac{m^2_{\tilde{g}} - u}{m^2_{\tilde{q}} - u}\right)^2 + \frac{3}{s^2}\left[(m^2_{\tilde{g}} - t)^2 + (m^2_{\tilde{g}} - u)^2 + 2m^2_{\tilde{g}}s\right] - 3\frac{\left[(m^2_{\tilde{g}} - t)^2 + m^2_{\tilde{g}}s\right]}{s(m^2_{\tilde{q}} - t)} - 3\frac{\left[(m^2_{\tilde{g}} - u)^2 + m^2_{\tilde{g}}s\right]}{s(m^2_{\tilde{q}} - u)} + \frac{1}{3}\frac{m^2_{\tilde{g}}s}{(m^2_{\tilde{q}} - t)(m^2_{\tilde{q}} - u)}\right\}. \quad (51.49)$$

Gluinos can also be produced in association with squarks: $\tilde{g}\tilde{q}_i$ production, where $\tilde{q}_i$ represents any of the various types (left, right- or mixed) and flavors of squarks. The subprocess cross section is independent of whether the squark is the right-, left- or mixed type:

$$\frac{d\sigma}{dt}(gq \to \tilde{g}\tilde{q}_i) = \frac{\pi\alpha^2_s}{24s^2}\frac{\left[\frac{16}{3}(s^2 + (m^2_{\tilde{q}_i} - u)^2) + \frac{4}{3}s(m^2_{\tilde{q}_i} - u)\right]}{s(m^2_{\tilde{g}} - t)(m^2_{\tilde{q}_i} - u)^2} \times \left((m^2_{\tilde{g}} - u)^2 + (m^2_{\tilde{q}_i} - m^2_{\tilde{g}})^2 + \frac{2sm^2_{\tilde{g}}(m^2_{\tilde{q}_i} - m^2_{\tilde{g}})}{(m^2_{\tilde{g}} - t)}\right). \quad (51.50)$$

There are many different subprocesses for production of squark pairs. Since left- and right- squarks generally have different masses and different decay patterns, we present the differential cross section for each subprocess of $\tilde{q}_i$ ($i = L,\ R$ or $1,\ 2$) separately. (In early literature, the following formulae were often combined into a single equation which didn't differentiate the various squark types.) The result for $gg \to \tilde{q}_i\bar{\tilde{q}}_i$ is:

$$\frac{d\sigma}{dt}(gg \to \tilde{q}_i\bar{\tilde{q}}_i) = \frac{\pi\alpha^2_s}{4s^2}\left\{\frac{1}{3}\left(\frac{m^2_{\tilde{q}} + t}{m^2_{\tilde{q}} - t}\right)^2 + \frac{1}{3}\left(\frac{m^2_{\tilde{q}} + u}{m^2_{\tilde{q}} - u}\right)^2 + \frac{3}{32s^2}\left(8s(4m^2_{\tilde{q}} - s) + 4(u - t)^2\right) + \frac{7}{12} - \frac{1}{48}\frac{(4m^2_{\tilde{q}} - s)^2}{(m^2_{\tilde{q}} - t)(m^2_{\tilde{q}} - u)} + \frac{3}{32}\frac{\left[(t - u)(4m^2_{\tilde{q}} + 4t - s) - 2(m^2_{\tilde{q}} - u)(6m^2_{\tilde{q}} + 2t - s)\right]}{s(m^2_{\tilde{q}} - t)} + \frac{3}{32}\frac{\left[(u - t)(4m^2_{\tilde{q}} + 4u - s) - 2(m^2_{\tilde{q}} - t)(6m^2_{\tilde{q}} + 2u - s)\right]}{s(m^2_{\tilde{q}} - u)} + \frac{7}{96}\frac{\left[4m^2_{\tilde{q}} + 4t - s\right]}{m^2_{\tilde{q}} - t} + \frac{7}{96}\frac{\left[4m^2_{\tilde{q}} + 4u - s\right]}{m^2_{\tilde{q}} - u}\right\}, \quad (51.51)$$

which has an obvious $u \leftrightarrow t$ symmetry.

For $q\bar{q} \to \tilde{q}_i\bar{\tilde{q}}_i$ with the same initial and final state flavors, we have

$$\frac{d\sigma}{dt}(q\bar{q} \to \tilde{q}_i\bar{\tilde{q}}_i) = \frac{2\pi\alpha^2_s}{9s^2}\left\{\frac{1}{(t - m^2_{\tilde{g}})^2} + \frac{2}{s^2} - \frac{2/3}{s(t - m^2_{\tilde{g}})}\right\} \times \left[-st - (t - m^2_{\tilde{q}_i})^2\right], \quad (51.52)$$

while if initial and final state flavors are different ($q\bar{q} \to \tilde{q}'_i\bar{\tilde{q}}'_i$) we instead have

$$\frac{d\sigma}{dt}(q\bar{q} \to \tilde{q}'_i\bar{\tilde{q}}'_i) = \frac{4\pi\alpha^2_s}{9s^4}\left[-st - (t - m^2_{\tilde{q}'_i})^2\right]. \quad (51.53)$$

If the two initial state quarks are of different flavors, then we have

Int. J. Mod. Phys. A 2026.41. Downloaded from www.worldscientific.com
by UNIVERSITY OF CALIFORNIA @ BERKELEY on 09/16/26. Re-use and distribution is strictly not permitted, except for Open Access articles.

$$\frac{d\sigma}{dt}(q\bar{q}' \to \tilde{q}_i\bar{\tilde{q}}_i') = \frac{2\pi\alpha_s^2}{9s^2}\frac{-st-(t-m_{\tilde{q}_i}^2)^2}{(t-m_{\tilde{g}}^2)^2}. \tag{51.54}$$

If the initial quarks are of different flavor and final state squarks are of different type ($i \neq j$) then

$$\frac{d\sigma}{dt}(q\bar{q}' \to \tilde{q}_i\bar{\tilde{q}}_j') = \frac{2\pi\alpha_s^2}{9s^2}\frac{m_{\tilde{g}}^2 s}{(t-m_{\tilde{g}}^2)^2}. \tag{51.55}$$

For same-flavor initial state quarks, but final state unlike-type squarks, we also have

$$\frac{d\sigma}{dt}(q\bar{q} \to \tilde{q}_i\bar{\tilde{q}}_j) = \frac{2\pi\alpha_s^2}{9s^2}\frac{m_{\tilde{g}}^2 s}{(t-m_{\tilde{g}}^2)^2}. \tag{51.56}$$

There also exist cross sections for quark-quark annihilation to squark pairs. For same flavor quark-quark annihilation to same flavor/same type final state squarks,

$$\frac{d\sigma}{dt}(qq \to \tilde{q}_i\tilde{q}_i) = \\ = \frac{\pi\alpha_s^2}{9s^2}m_{\tilde{g}}^2 s\left\{\frac{1}{(t-m_{\tilde{g}}^2)^2}+\frac{1}{(u-m_{\tilde{g}}^2)^2}-\frac{2/3}{(t-m_{\tilde{g}}^2)(u-m_{\tilde{g}}^2)}\right\}, \tag{51.57}$$

while if the final type squarks are different ($i \neq j$), we have

$$\frac{d\sigma}{dt}(qq \to \tilde{q}_i\tilde{q}_j) = \\ \frac{2\pi\alpha_s^2}{9s^2}\times \\ \left\{\frac{[-st-(t-m_{\tilde{q}_i}^2)(t-m_{\tilde{q}_j}^2)]}{(t-m_{\tilde{g}}^2)}+\frac{[-su-(u-m_{\tilde{q}_i}^2)(u-m_{\tilde{q}_j}^2)]}{(u-m_{\tilde{g}}^2)}\right\}. \tag{51.58}$$

If initial/final state flavors are different, but final state squark types are the same, then

$$\frac{d\sigma}{dt}(qq' \to \tilde{q}_i\tilde{q}_i') = \frac{2\pi\alpha_s^2}{9s^2}\frac{m_{\tilde{g}}^2 s}{(t-m_{\tilde{g}}^2)^2}. \tag{51.59}$$

If initial quark flavors are different and final squark types are different, then

$$\frac{d\sigma}{dt}(qq' \to \tilde{q}_i\tilde{q}_j') = \frac{2\pi\alpha_s^2}{9s^2}\frac{-st-(t-m_{\tilde{q}_i}^2)(t-m_{\tilde{q}_j}^2)}{(t-m_{\tilde{g}}^2)^2}. \tag{51.60}$$

51.8.2 *Gluino and squark associated production*

In the MSSM, the charged spin-$\frac{1}{2}$ winos and higgsinos mix to make chargino states $\chi_1^\pm$ and $\chi_2^\pm$, with $m_{\chi_1^\pm} < m_{\chi_2^\pm}$. The spin$-\frac{1}{2}$ neutral bino, wino and higgsino fields mix to give four neutralino mass eigenstates $\chi_{1,2,3,4}^0$ ordered according to mass. We sometimes denote the charginos and neutralinos collectively as -inos for notational simplicity

For gluino and squark production in association with charginos and neutralinos [12], the quark-squark-neutralino couplings[1] are defined by the interaction Lagrangian terms

$$\mathcal{L}_{\tilde{f}f\tilde{\chi}_i^0} = \left[iA_{\tilde{\chi}_i^0}^f \tilde{f}_L^\dagger \bar{\tilde{\chi}}_i^0 P_L f + iB_{\tilde{\chi}_i^0}^f \tilde{f}_R^\dagger \bar{\tilde{\chi}}_i^0 P_R f + \text{h.c.}\right],$$

,where $A_{\tilde{\chi}_i^0}^f$ and $B_{\tilde{\chi}_i^0}^f$ are coupling constants involving gauge couplings, neutralino mixing elements and in the case of third generation fermions, Yukawa couplings. Their form depends on the conventions used for setting up the MSSM Lagrangian, and can be found in various reviews [14] and textbooks [13, 15]. P_L and P_R are the usual left- and right- spinor projection operators and f denotes any of the SM fermions u, d, e, $\nu_e, \cdots$. The fermion-sfermion- chargino couplings have the form $\mathcal{L} = \left[iA_{\tilde{\chi}_i^-}^d \tilde{u}_L^\dagger \overline{\tilde{\chi}_i^-} P_L d + iA_{\tilde{\chi}_i^-}^u \tilde{d}_L^\dagger \overline{\tilde{\chi}_i^{c-}} P_L u + \text{h.c.}\right]$ for u and d quarks, where the $A_{\tilde{\chi}_i^-}^d$ and $A_{\tilde{\chi}_i^-}^u$ couplings are again convention-dependent, and can be found in textbooks. The superscript c denotes "charge conjugate spinor", defined by $\psi^c \equiv C\bar{\psi}^T$.

The subprocess cross sections for chargino-squark associated production occur via squark exchange and are given by

$$\frac{d\sigma}{dt}(\bar{u}g \to \tilde{\chi}_i^-\bar{\tilde{d}}_L) = \frac{\alpha_s}{24s^2}|A_{\tilde{\chi}_i^-}^u|^2\psi(m_{\tilde{d}_L}, m_{\tilde{\chi}_i^-}, t), \tag{51.61}$$

$$\frac{d\sigma}{dt}(dg \to \tilde{\chi}_i^-\tilde{u}_L) = \frac{\alpha_s}{24s^2}|A_{\tilde{\chi}_i^-}^d|^2\psi(m_{\tilde{u}_L}, m_{\tilde{\chi}_i^-}, t), \tag{51.62}$$

while neutralino-squark production is given by

$$\frac{d\sigma}{dt}(qg \to \tilde{\chi}_i^0\tilde{q}) = \frac{\alpha_s}{24s^2}\left(|A_{\tilde{\chi}_i^0}^q|^2 + |B_{\tilde{\chi}_i^0}^q|^2\right)\psi(m_{\tilde{q}}, m_{\tilde{\chi}_i^0}, t), \tag{51.63}$$

where

$$\psi(m_1, m_2, t) = \frac{s+t-m_1^2}{2s} - \frac{m_1^2(m_2^2-t)}{(m_1^2-t)^2} \\ + \frac{t(m_2^2-m_1^2)+m_2^2(s-m_2^2+m_1^2)}{s(m_1^2-t)}. \tag{51.64}$$

Here, the variable t is given by the square of "squark-minus-quark" four-momentum. The neutralino-gluino associated production cross section also occurs via squark exchange and is given by

$$\frac{d\sigma}{dt}(q\bar{q} \to \tilde{\chi}_i^0\tilde{g}) = \frac{\alpha_s}{18s^2}\left(|A_{\tilde{\chi}_i^0}^q|^2 + |B_{\tilde{\chi}_i^0}^q|^2\right)\left[\frac{(m_{\tilde{\chi}_i^0}^2-t)(m_{\tilde{g}}^2-t)}{(m_{\tilde{q}}^2-t)^2} \right. \\ \left. + \frac{(m_{\tilde{\chi}_i^0}^2-u)(m_{\tilde{g}}^2-u)}{(m_{\tilde{q}}^2-u)^2} - \frac{2\eta_i\eta_{\tilde{g}}m_{\tilde{g}}m_{\tilde{\chi}_i^0}s}{(m_{\tilde{q}}^2-t)(m_{\tilde{q}}^2-u)}\right], \tag{51.65}$$

where η_i is the sign of the neutralino mass eigenvalue and $\eta_{\tilde{g}}$ is the sign of the gluino mass eigenvalue. We also have chargino-gluino associated production:

$$\frac{d\sigma}{dt}(\bar{u}d \to \tilde{\chi}_i^-\tilde{g}) = \frac{\alpha_s}{18s^2}\left[|A_{\tilde{\chi}_i^-}^u|^2\frac{(m_{\tilde{\chi}_i^-}^2-t)(m_{\tilde{g}}^2-t)}{(m_{d_L}^2-t)^2} \right. \\ \left. + |A_{\tilde{\chi}_i^-}^d|^2\frac{(m_{\tilde{\chi}_i^-}^2-u)(m_{\tilde{g}}^2-u)}{(m_{\tilde{u}_L}^2-u)^2} + \frac{2\eta_{\tilde{g}}Re(A_{\tilde{\chi}_i^-}^u A_{\tilde{\chi}_i^-}^d)m_{\tilde{g}}m_{\tilde{\chi}_i}s}{(m_{d_L}^2-t)(m_{\tilde{u}_L}^2-u)}\right], \tag{51.66}$$

where $\hat{t} = (\tilde{g}-d)^2$ and in the third term one must take the real part of the in general complex coupling constant product.

51.8.3 *Slepton and sneutrino production*

The subprocess cross section for $\tilde{\ell}_L\bar{\tilde{\nu}}_{\ell_L}$ production ($\ell = e$ or μ) occurs via s-channel W exchange and is given by

$$\frac{d\sigma}{dt}(d\bar{u} \to \tilde{\ell}_L\bar{\tilde{\nu}}_{\ell_L}) = \frac{g^4|D_W(s)|^2}{192\pi s^2}\left(tu - m_{\tilde{\ell}_L}^2 m_{\tilde{\nu}_{\ell_L}}^2\right), \tag{51.67}$$

where $D_W(s) = 1/(s-M_W^2+iM_W\Gamma_W)$ is the W-boson propagator denominator. The production of $\tilde{\tau}_1\bar{\tilde{\nu}}_\tau$ is given as above, but replacing $m_{\tilde{\ell}_L} \to m_{\tilde{\tau}_1}$, $m_{\tilde{\nu}_{\ell_L}} \to m_{\tilde{\nu}_\tau}$ and multiplying by an overall factor of $\cos^2\theta_\tau$ (where θ_τ is the tau-slepton mixing angle). Similar substitutions hold for $\tilde{\tau}_2\bar{\tilde{\nu}}_\tau$ production, except the overall factor is $\sin^2\theta_\tau$.

[1] The couplings $A_{\tilde{\chi}_i^0}^f$ and $B_{\tilde{\chi}_i^0}^f$ are given explicitly in Ref. [13] in Eq. (8.87). Also, the couplings $A_{\tilde{\chi}_i^-}^d$ and $A_{\tilde{\chi}_i^-}^u$ are given in Eq. (8.93). The couplings X_i^j and Y_i^j are given by Eq. (8.103), while the x_i and y_i couplings are given in Eq. (8.100). Finally, the couplings W_{ij} are given in Eq. (8.101).

Int. J. Mod. Phys. A 2026.41. Downloaded from www.worldscientific.com
by UNIVERSITY OF CALIFORNIA @ BERKELEY on 09/16/26. Re-use and distribution is strictly not permitted, except for Open Access articles.

Table 51.1: The constants α_f and β_f that appear in in the SM neutral current Lagrangian. Here $t \equiv \tan\theta_W$ and $c \equiv \cot\theta_W$.

f	q_f	α_f	β_f
ℓ	-1	$\frac{1}{4}(3t-c)$	$\frac{1}{4}(t+c)$
ν_ℓ	0	$\frac{1}{4}$(t+c)	$-\frac{1}{4}(t+c)$
u	$\frac{2}{3}$	$-\frac{5}{12}t+\frac{1}{4}c$	$-\frac{1}{4}(t+c)$
d	$-\frac{1}{3}$	$\frac{1}{12}t-\frac{1}{4}c$	$\frac{1}{4}(t+c)$

The subprocess cross section for $\tilde{\ell}_L\bar{\tilde{\ell}}_L$ production occurs via s-channel γ and Z exchange, and depends on the neutral current interaction, with fermion couplings to γ and Z^0 given by $\mathcal{L}_{\rm neutral} = -eq_f\bar{f}\gamma^\mu f A_\mu + e\bar{f}\gamma^\mu(\alpha_f+\beta_f\gamma_5)fZ_\mu$ (with values of q_f, α_f, and β_f given in Table-51.1.

The subprocess cross section is given by

$$\frac{d\sigma}{dt}(q\bar{q}\to\tilde{\ell}_L\bar{\tilde{\ell}}_L) = \frac{e^4}{24\pi s^2}\left(tu - m^4_{\tilde{\ell}_L}\right)\times$$
$$\left\{\frac{q_\ell^2 q_q^2}{s^2} + (\alpha_\ell-\beta_\ell)^2(\alpha_q^2+\beta_q^2)|D_Z(s)|^2\right.$$
$$\left. + \frac{2q_\ell q_q\alpha_q(\alpha_\ell-\beta_\ell)(s-M_Z^2)}{s}|D_Z(s)|^2\right\}, \qquad (51.68)$$

where $D_Z(s) = 1/(s-M_Z^2+iM_Z\Gamma_Z)$. The cross section for sneutrino production is given by the same formula, but with α_ℓ, β_ℓ, q_ℓ and $m_{\tilde{\ell}_L}$ replaced by α_ν, β_ν, 0 and $m_{\tilde{\nu}_L}$, respectively. The cross section for $\tilde{\tau}_1\bar{\tilde{\tau}}_1$ production is obtained by replacing $m_{\tilde{\ell}_L}\to m_{\tilde{\tau}_1}$ and $\beta_\ell\to\beta_\ell\cos 2\theta_\tau$. The cross section for $\tilde{\ell}_R\bar{\tilde{\ell}}_R$ production is given by substituting $\alpha_\ell-\beta_\ell\to\alpha_\ell+\beta_\ell$ and $m_{\tilde{\ell}_L}\to m_{\tilde{\ell}_R}$ in the equation above. The cross section for $\tilde{\tau}_2\bar{\tilde{\tau}}_2$ production is obtained from the formula for $\tilde{\ell}_R\bar{\tilde{\ell}}_R$ production by replacing $m_{\tilde{\ell}_R}\to m_{\tilde{\tau}_2}$ and $\beta_\ell\to\beta_\ell\cos 2\theta_\tau$.

Finally, the cross section for $\tilde{\tau}_1\bar{\tilde{\tau}}_2$ production occurs only via Z exchange, and is given by

$$\frac{d\sigma}{dt}(q\bar{q}\to\tilde{\tau}_1\bar{\tilde{\tau}}_2) = \frac{d\sigma}{dt}(q\bar{q}\to\bar{\tilde{\tau}}_1\tilde{\tau}_2) =$$
$$\frac{e^4}{24\pi s^2}(\alpha_q^2+\beta_q^2)\beta_\ell^2\sin^2 2\theta_\tau|D_Z(s)|^2(ut - m^2_{\tilde{\tau}_1}m^2_{\tilde{\tau}_2}). \qquad (51.69)$$

51.8.4 *Chargino and neutralino pair production*

51.8.4.1 $\tilde{\chi}_i^-\tilde{\chi}_j^0$ *production*

The subprocess cross section for $d\bar{u}\to\tilde{\chi}_i^-\tilde{\chi}_j^0$ depends on Lagrangian couplings

$$\mathcal{L}_{W\bar{u}d} = -\frac{g}{\sqrt{2}}\bar{u}\gamma_\mu P_L d W^{+\mu} \ + \text{h.c.},$$

$$\mathcal{L}_{W\tilde{\chi}_i^-\tilde{\chi}_j^0} = -g(-i)^{\theta_j}\overline{\tilde{\chi}^-}_i[X_i^j + Y_i^j\gamma_5]\gamma_\mu\tilde{\chi}_j^0 W^{-\mu} \ + \text{h.c.},$$

$$\mathcal{L}_{q\bar{q}\tilde{\chi}_i^-} = iA^d_{\tilde{\chi}_i^-}\tilde{u}_L^\dagger\overline{\tilde{\chi}_i^-}P_L d + iA^u_{\tilde{\chi}_i^-}\tilde{d}_L^\dagger\overline{\tilde{\chi}_i^c}P_L u \ + \text{h.c.}$$

and

$$\mathcal{L}_{q\bar{q}\tilde{\chi}_j^0} = iA^q_{\tilde{\chi}_j^0}\tilde{q}_L^\dagger\overline{\tilde{\chi}^0}_j P_L q \ + \text{h.c.}.$$

Contributing diagrams include W exchange and also $\tilde{d}_L$ and $\tilde{u}_L$ squark exchange. The X_i^j and Y_i^j couplings are new, and again convention-dependent: the cross section formulae works if the interaction Lagrangian is written in the above form, so that the couplings can be suitably extracted. The term $\theta_j = 0$ (1) if $m_{\tilde{\chi}_j^0} > 0$ (< 0); it comes about because the neutralino field must be re-defined by a $-i\gamma_5$ transformation if its mass eigenvalue is negative [13]. The subprocess cross section is given in terms of dot products of four momenta, where particle labels are used to denote their four-momenta; note that all mass terms in the cross section formulae are positive definite, so that the signs of mass eigenstates have been absorbed into the Lagrangian couplings, as for instance in Ref. [13]. We then have

$$\frac{d\sigma}{dt}(d\bar{u}\to\tilde{\chi}_i^-\tilde{\chi}_j^0) = \frac{1}{192\pi s^2}$$
$$\left[T_W + T_{\tilde{d}_L} + T_{\tilde{u}_L} + T_{W\tilde{d}_L} + T_{W\tilde{u}_L} + T_{\tilde{d}_L\tilde{u}_L}\right] \qquad (51.70)$$

where

$$T_W = 8g^4|D_W(s)|^2\left\{[X_i^{j2}+Y_i^{j2}](\tilde{\chi}_j^0\cdot d\tilde{\chi}_i^-\cdot\bar{u} + \tilde{\chi}_j^0\cdot\bar{u}\tilde{\chi}_i^-\cdot d)\right.$$
$$+ 2(X_i^jY_i^j)(\tilde{\chi}_j^0\cdot d\tilde{\chi}_i^-\cdot\bar{u} - \tilde{\chi}_j^0\cdot\bar{u}\tilde{\chi}_i^-\cdot d)$$
$$\left. + [X_i^{j2}-Y_i^{j2}]m_{\tilde{\chi}_i^-}m_{\tilde{\chi}_j^0}d\cdot\bar{u}\right\}, \qquad (51.71)$$

$$T_{\tilde{d}_L} = \frac{4|A^u_{\tilde{\chi}_i^-}|^2|A^d_{\tilde{\chi}_j^0}|^2}{[(\tilde{\chi}_i^- - \bar{u})^2 - m^2_{\tilde{d}_L}]^2}\ d\cdot\tilde{\chi}_j^0\tilde{\chi}_i^-\cdot\bar{u}, \qquad (51.72)$$

$$T_{\tilde{u}_L} = \frac{4|A^d_{\tilde{\chi}_i^-}|^2|A^u_{\tilde{\chi}_j^0}|^2}{[(\tilde{\chi}_j^0 - \bar{u})^2 - m^2_{\tilde{u}_L}]^2}\ \bar{u}\cdot\tilde{\chi}_j^0\tilde{\chi}_i^-\cdot d \qquad (51.73)$$

$$T_{W\tilde{d}_L} = \frac{-\sqrt{2}g^2 Re[A^{d*}_{\tilde{\chi}_j^0}A^u_{\tilde{\chi}_i^-}(-i)^{\theta_j}](s-M_W^2)|D_W(s)|^2}{(\tilde{\chi}_i^- - \bar{u})^2 - m^2_{\tilde{d}_L}}$$
$$\times\left\{8(X_i^j+Y_i^j)\tilde{\chi}_j^0\cdot d\bar{u}\cdot\tilde{\chi}_i^- + 4(X_i^j-Y_i^j)m_{\tilde{\chi}_i^-}m_{\tilde{\chi}_j^0}d\cdot\bar{u}\right\} \qquad (51.74)$$

$$T_{W\tilde{u}_L} = \frac{\sqrt{2}g^2 Re[A^{d*}_{\tilde{\chi}_i^-}A^u_{\tilde{\chi}_j^0}(-i)^{\theta_j}](s-M_W^2)|D_W(s)|^2}{(\tilde{\chi}_j^0 - \bar{u})^2 - m^2_{\tilde{u}_L}}$$
$$\times\left\{8(X_i^j-Y_i^j)\tilde{\chi}_j^0\cdot\bar{u}d\cdot\tilde{\chi}_i^- + 4(X_i^j+Y_i^j)m_{\tilde{\chi}_i^-}m_{\tilde{\chi}_j^0}d\cdot\bar{u}\right\} \qquad (51.75)$$

and

$$T_{\tilde{d}_L\tilde{u}_L} = -\frac{4Re[A^d_{\tilde{\chi}_j^0}A^{u*}_{\tilde{\chi}_i^-}A^{d*}_{\tilde{\chi}_i^-}A^u_{\tilde{\chi}_j^0}]m_{\tilde{\chi}_i^-}m_{\tilde{\chi}_j^0}d\cdot\bar{u}}{[(\tilde{\chi}_i^- - \bar{u})^2 - m^2_{\tilde{d}_L}][(\tilde{\chi}_j^0 - \bar{u})^2 - m^2_{\tilde{u}_L}]}. \qquad (51.76)$$

51.8.4.2 *Chargino pair production*

The subprocess cross section for $d\bar{d}\to\tilde{\chi}_i^-\tilde{\chi}_i^+$ $(i=1,2)$ depends on Lagrangian couplings $\mathcal{L} = e\overline{\tilde{\chi}_i^-}\gamma_\mu\tilde{\chi}_i^- A^\mu - e\cot\theta_W\overline{\tilde{\chi}_i^-}\gamma_\mu(x_i - y_i\gamma_5)\tilde{\chi}_i^- Z^\mu$ and also $\mathcal{L}\ni iA^d_{\tilde{\chi}_i^-}\tilde{u}_L^\dagger\overline{\tilde{\chi}_i^-}P_L d + iA^u_{\tilde{\chi}_i^-}\tilde{d}_L^\dagger\overline{\tilde{\chi}_i^{-c}}P_L u + \text{h.c.}$. Contributing diagrams include s-channel γ, Z^0 exchange and t-channel $\tilde{u}_L$ exchange [16, 17]. The couplings x_i and y_i are again new and as usual convention-dependent.

The subprocess cross section is given by

$$\frac{d\sigma}{dt}(d\bar{d}\to\tilde{\chi}_i^-\tilde{\chi}_i^+) =$$
$$\frac{1}{192\pi s^2}\left[T_\gamma + T_Z + T_{\tilde{u}_L} + T_{\gamma Z} + T_{\gamma\tilde{u}_L} + T_{Z\tilde{u}_L}\right] \qquad (51.77)$$

where

$$T_\gamma = \frac{32e^4q_d^2}{s^2}\left[d\cdot\tilde{\chi}_i^+\bar{d}\cdot\tilde{\chi}_i^- + d\cdot\tilde{\chi}_i^-\bar{d}\cdot\tilde{\chi}_i^+ + m^2_{\tilde{\chi}_i^-}d\cdot\bar{d}\right] \qquad (51.78)$$

$$T_Z = 32e^4\cot^2\theta_W|D_Z(s)|^2$$
$$\left\{(\alpha_d^2+\beta_d^2)(x_i^2+y_i^2)\left[d\cdot\tilde{\chi}_i^+\bar{d}\cdot\tilde{\chi}_i^- + d\cdot\tilde{\chi}_i^-\bar{d}\cdot\tilde{\chi}_i^+ + m^2_{\tilde{\chi}_i^-}d\cdot\bar{d}\right]\right.$$

Int. J. Mod. Phys. A 2026.41. Downloaded from www.worldscientific.com
by UNIVERSITY OF CALIFORNIA @ BERKELEY on 09/16/26. Re-use and distribution is strictly not permitted, except for Open Access articles.

$$\mp 4\alpha_d\beta_d x_i y_i \left[d\cdot\tilde{\chi}_i^+\bar{d}\cdot\tilde{\chi}_i^- - d\cdot\tilde{\chi}_i^-\bar{d}\cdot\tilde{\chi}_i^+\right] - 2y_i^2(\alpha_d^2+\beta_d^2)m^2_{\tilde{\chi}_i^-}\, d\cdot\bar{d}\Bigg\}, \tag{51.79}$$

$$T_{\tilde{u}_L} = \frac{4|A^d_{\tilde{\chi}_i^-}|^4}{[(d-\tilde{\chi}_i^-)^2 - m^2_{\tilde{u}_L}]^2}\; d\cdot\tilde{\chi}_i^-\bar{d}\cdot\tilde{\chi}_i^+ \tag{51.80}$$

$$T_{\gamma Z} = \frac{64e^4\cot\theta_W q_d(s-M_Z^2)|D_Z(s)|^2}{s}\times$$
$$\Bigg\{\alpha_d x_i\left(d\cdot\tilde{\chi}_i^+\bar{d}\cdot\tilde{\chi}_i^- + d\cdot\tilde{\chi}_i^-\bar{d}\cdot\tilde{\chi}_i^+ + m^2_{\tilde{\chi}_i^-}\, d\cdot\bar{d}\right)$$
$$\pm\beta_d y_i\left(d\cdot\tilde{\chi}_i^-\bar{d}\cdot\tilde{\chi}_i^+ - d\cdot\tilde{\chi}_i^+\bar{d}\cdot\tilde{\chi}_i^-\right)\Bigg\} \tag{51.81}$$

$$T_{\gamma\tilde{u}_L} = \mp\frac{8e^2 q_d}{s}\frac{|A^d_{\tilde{\chi}_i^-}|^2}{[(d-\tilde{\chi}_i^-)^2 - m^2_{\tilde{u}_L}]}\left\{2\bar{d}\cdot\tilde{\chi}_i^+ d\cdot\tilde{\chi}_i^- + m^2_{\tilde{\chi}_i^-}\, d\cdot\bar{d}\right\} \tag{51.82}$$

and

$$T_{Z\tilde{u}_L} = \mp 8e^2\cot\theta_W|D_Z(s)|^2\frac{|A^d_{\tilde{\chi}_i^-}|^2(s-M_Z^2)}{[(d-\tilde{\chi}_i^-)^2 - m^2_{\tilde{u}_L}]}(\alpha_d-\beta_d)$$
$$\times\left\{2(x_i\mp y_i)d\cdot\tilde{\chi}_i^-\bar{d}\cdot\tilde{\chi}_i^+ + m^2_{\tilde{\chi}_i^-}(x_i\pm y_i)d\cdot\bar{d}\right\} \tag{51.83}$$

using the upper of the sign choices.

The cross section for $u\bar{u}\to\tilde{\chi}_i^+\tilde{\chi}_i^-$ can be obtained from the above by replacing $\alpha_d\to\alpha_u$, $\beta_d\to\beta_u$, $q_d\to q_u$, $\tilde{u}_L\to\tilde{d}_L$, $A^d_{\tilde{\chi}_i^-}\to A^u_{\tilde{\chi}_i^-}$, $d\to\bar{u}$, $\bar{d}\to u$ and adopting the lower of the sign choices everywhere.

The cross section for $q\bar{q}\to\tilde{\chi}_1^-\tilde{\chi}_2^+$, $\tilde{\chi}_1^+\tilde{\chi}_2^-$ can occur via Z and $\tilde{q}_L$ exchange. It is usually much smaller than $\tilde{\chi}^-_{1,2}\tilde{\chi}^+_{1,2}$ production, so the cross section will not be presented here. It can be found in Appendix A of Ref. [13].

51.8.4.3 *Neutralino pair production*

Neutralino pair production via $q\bar{q}$ fusion takes place via s-channel Z exchange plus t- and u-channel left- and right- squark exchange (5 diagrams) [17, 18]. The Lagrangian couplings (see previous footnote*) needed include terms given above plus terms of the form $\mathcal{L} = W_{ij}\overline{\tilde{\chi}^0}_i\gamma_\mu(\gamma_5)^{\theta_i+\theta_j+1}\tilde{\chi}^0_j Z^\mu$. The couplings W_{ij} depend only on the *higgsino* components of the neutralinos i and j. The subprocess cross section is given by:

$$\frac{d\sigma}{dt}(q\bar{q}\to\tilde{\chi}_i^0\tilde{\chi}_j^0) = \frac{1}{192\pi s^2}\left[T_Z + T_{\tilde{q}_L} + T_{\tilde{q}_R} + T_{Z\tilde{q}_L} + T_{Z\tilde{q}_R}\right] \tag{51.84}$$

where

$$T_Z = 128e^2|W_{ij}|^2(\alpha_q^2+\beta_q^2)|D_Z(s)|^2$$
$$\left[q\cdot\tilde{\chi}_i^0\bar{q}\cdot\tilde{\chi}_j^0 + q\cdot\tilde{\chi}_j^0\bar{q}\cdot\tilde{\chi}_i^0 - \eta_i\eta_j m_{\tilde{\chi}_i^0}m_{\tilde{\chi}_j^0}q\cdot\bar{q}\right], \tag{51.85}$$

$$T_{\tilde{q}_L} = 4|A^q_{\tilde{\chi}_i^0}|^2|A^q_{\tilde{\chi}_j^0}|^2\Bigg\{\frac{q\cdot\tilde{\chi}_i^0\bar{q}\cdot\tilde{\chi}_j^0}{[(\tilde{\chi}_i^0-q)^2-m^2_{\tilde{q}_L}]^2} + \frac{q\cdot\tilde{\chi}_j^0\bar{q}\cdot\tilde{\chi}_i^0}{[(\tilde{\chi}_j^0-q)^2-m^2_{\tilde{q}_L}]^2}$$
$$-\ \eta_i\eta_j\frac{m_{\tilde{\chi}_i^0}m_{\tilde{\chi}_j^0}q\cdot\bar{q}}{[(\tilde{\chi}_i^0-q)^2-m^2_{\tilde{q}_L}][(\tilde{\chi}_j^0-q)^2-m^2_{\tilde{q}_L}]}\Bigg\} \tag{51.86}$$

$$T_{\tilde{q}_R} = 4|B^q_{\tilde{\chi}_i^0}|^2|B^q_{\tilde{\chi}_j^0}|^2\Bigg\{\frac{q\cdot\tilde{\chi}_i^0\bar{q}\cdot\tilde{\chi}_j^0}{[(\tilde{\chi}_i^0-q)^2-m^2_{\tilde{q}_R}]^2} + \frac{q\cdot\tilde{\chi}_j^0\bar{q}\cdot\tilde{\chi}_i^0}{[(\tilde{\chi}_j^0-q)^2-m^2_{\tilde{q}_R}]^2}$$
$$-\ \eta_i\eta_j\frac{m_{\tilde{\chi}_i^0}m_{\tilde{\chi}_j^0}q\cdot\bar{q}}{[(\tilde{\chi}_i^0-q)^2-m^2_{\tilde{q}_R}][(\tilde{\chi}_j^0-q)^2-m^2_{\tilde{q}_R}]}\Bigg\} \tag{51.87}$$

$$T_{Z\tilde{q}_L} = 16e(\alpha_q-\beta_q)(s-M_Z^2)|D_Z(s)|^2$$
$$\Bigg\{\frac{Re(W_{ij}A^{q*}_{\tilde{\chi}_i^0}A^q_{\tilde{\chi}_j^0})}{[(\tilde{\chi}_i^0-q)^2-m^2_{\tilde{q}_L}]}\left[2q\cdot\tilde{\chi}_i^0\bar{q}\cdot\tilde{\chi}_j^0 - \eta_i\eta_j m_{\tilde{\chi}_i^0}m_{\tilde{\chi}_j^0}q\cdot\bar{q}\right]$$
$$+\ \eta_i\eta_j\frac{Re(W_{ij}A^q_{\tilde{\chi}_i^0}A^{q*}_{\tilde{\chi}_j^0})}{[(\tilde{\chi}_j^0-q)^2-m^2_{\tilde{q}_L}]}\left[2q\cdot\tilde{\chi}_j^0\bar{q}\cdot\tilde{\chi}_i^0 - \eta_i\eta_j m_{\tilde{\chi}_i^0}m_{\tilde{\chi}_j^0}q\cdot\bar{q}\right]\Bigg\} \tag{51.88}$$

$$T_{Z\tilde{q}_R} = 16e(\alpha_q+\beta_q)(s-M_Z^2)|D_Z(s)|^2$$
$$\Bigg\{\frac{Re(W_{ij}B^{q*}_{\tilde{\chi}_i^0}B^q_{\tilde{\chi}_j^0})}{[(\tilde{\chi}_i^0-q)^2-m^2_{\tilde{q}_R}]}\left[2q\cdot\tilde{\chi}_i^0\bar{q}\cdot\tilde{\chi}_j^0 - \eta_i\eta_j m_{\tilde{\chi}_i^0}m_{\tilde{\chi}_j^0}q\cdot\bar{q}\right]$$
$$-\frac{Re(W_{ij}B^q_{\tilde{\chi}_i^0}B^{q*}_{\tilde{\chi}_j^0})}{[(\tilde{\chi}_j^0-q)^2-m^2_{\tilde{q}_R}]}\left[2q\cdot\tilde{\chi}_j^0\bar{q}\cdot\tilde{\chi}_i^0 - \eta_i\eta_j m_{\tilde{\chi}_i^0}m_{\tilde{\chi}_j^0}q\cdot\bar{q}\right]\Bigg\}. \tag{51.89}$$

As before, $\eta_i = \pm 1$ corresponding to whether the neutralino mass eigenvalue is positive or negative. When $i = j$ in the above formula, one must remember to integrate over just 2π steradians of solid angle to avoid double counting in the total cross section.

51.9 Universal extra dimensions

In the Universal Extra Dimension (UED) model of Ref. [19] (see Ref. [20] for a review of models with extra spacetime dimensions), the Standard Model is embedded in a five dimensional theory, where the fifth dimension is compactified on an S_1/Z_2 orbifold. Each SM chirality state is then the zero mode of an infinite tower of Kaluza-Klein excitations labeled by $n = 0-\infty$. A KK parity is usually assumed to hold, where each state is assigned KK-parity $P = (-1)^n$. If the compactification scale is around a TeV, then the $n = 1$ (or even higher) KK modes may be accessible to collider searches.

Of interest for hadron colliders are the production of massive $n \geq 1$ quark or gluon pairs. These production cross sections have been calculated in Ref. [21, 22]. We list here results for the $n = 1$ case only with $M_1 = 1/R$ (R is the compactification radius) and s, t and u are the usual Mandelstam variables; more general formulae can be found in Ref. [22]. The superscript $*$ stands for any KK excited state, while $\bullet$ stands for left chirality states and $\circ$ stands for right chirality states.

$$\frac{d\sigma}{dt} = \frac{1}{16\pi s^2}T \tag{51.90}$$

where

$$T(q\bar{q}\to g^*g^*) = \frac{2g_s^4}{27}\Bigg[M_1^2\left(-\frac{4s^3}{t'^2u'^2} + \frac{57s}{t'u'} - \frac{108}{s}\right)$$
$$+\frac{20s^2}{t'u'} - 93 + \frac{108t'u'}{s^2}\Bigg] \tag{51.91}$$

and

$$T(gg\to g^*g^*) =$$
$$\frac{9g_s^4}{27}\Bigg[3M_1^4\frac{s^2+t'^2+u'^2}{t'^2u'^2} - 3M_1^2\frac{s^2+t'^2+u'^2}{st'u'} + 1$$
$$+\frac{(s^2+t'^2+u'^2)^3}{4s^2t'^2u'^2} - \frac{t'u'}{s^2}\Bigg] \tag{51.92}$$

where $t' = t - M_1^2$ and $u' = u - M_1^2$.

Also,

$$T(q\bar{q}\to q_1^{*\prime}\bar{q}_1^{*\prime}) = \frac{4g_s^4}{9}\left[\frac{2M_1^2}{s} + \frac{t'^2+u'^2}{s^2}\right],$$

$$T(q\bar{q}\to q_1^*\bar{q}_1^*) = \frac{g_2^4}{9}\Bigg[2M_1^2\left(\frac{4}{s} + \frac{s}{t'^2} - \frac{1}{t'}\right)$$
$$+\frac{23}{6} + \frac{2s^2}{t'^2} + \frac{8s}{3t'} + \frac{6t'}{s} + \frac{8t'^2}{s^2}\Bigg],$$

Int. J. Mod. Phys. A 2026.41. Downloaded from www.worldscientific.com
by [redacted] LIFORNIA @ BERKELEY on 09/16/26. Re-use and distribution is strictly not permitted, except for Open Access articles.

$$T(qq \to q_1^* q_1^*) = \frac{g_s^4}{27}\left[M_1^2\left(6\frac{t'}{u'^2} + 6\frac{u'}{t'^2} - \frac{s}{t'u'}\right)\right.$$
$$\left. +2\left(3\frac{t'^2}{u'^2} + 3\frac{u'^2}{t'^2} + 4\frac{s^2}{t'u'} - 5\right)\right],$$

$$T(gg \to q_1^* \bar{q}_1^*) = g_s^4\left[M_1^4\frac{-4}{t'u'}\left(\frac{s^2}{6t'u'} - \frac{3}{8}\right)\right.$$
$$\left. +M_1^2\frac{4}{s}\left(\frac{s^2}{6t'u'} - \frac{3}{8}\right) + \frac{s^2}{6t'u'} - \frac{17}{24} + \frac{3t'u'}{4s^2}\right],$$

$$T(gq \to g^* q_1^*) = \frac{-g_s^4}{3}\left[\frac{5s^2}{12t'^2} + \frac{s^3}{t'^2u'} + \frac{11su'}{6t'^2} + \frac{5u'^2}{12t'^2} + \frac{u'^3}{st'^2}\right],$$

$$T(q\bar{q}' \to q_1^* \bar{q}_1^{*\prime}) = \frac{g_s^4}{18}\left[4M_1^4\frac{s}{t'^2} + 5 + 4\frac{s^2}{t'^2} + 8\frac{s}{t'}\right],$$

$$T(qq' \to q_1^* q_1^{*\prime}) = \frac{2g_s^4}{9}\left[-M_1^2\frac{s}{t'^2} + \frac{1}{4} + \frac{s^2}{t'^2}\right],$$

$$T(qq \to q_1^\bullet q_1^\circ) =$$
$$\frac{g_s^4}{9}\left[M_1^2\left(\frac{2s^3}{t'^2u'^2} - \frac{4s}{t'u'}\right) + 2\frac{s^4}{t'^2u'^2} - 8\frac{s^2}{t'u'} + 5\right],$$

$$T(q\bar{q}' \to q_1^\bullet \bar{q}_1^{\prime\circ}) = \frac{g_s^4}{9}\left[2M_1^2\left(\frac{1}{t'} + \frac{u'}{t'^2}\right) + \frac{5}{2} + \frac{4u'}{t'} + \frac{2u'^2}{t'^2}\right],$$

and

$$T(qq' \to q_1^\bullet q_1^{\prime\circ}) = \frac{g_s^4}{9}\left[-2M_1^2\left(\frac{1}{t'} + \frac{u'}{t'^2}\right) + \frac{1}{2} + \frac{2u'^2}{t'^2}\right].$$

51.10 Large extra dimensions

In the ADD theory [23] with large extra dimensions (LED), the SM particles are confined to a 3-brane, while gravity propagates in the bulk. It is assumed that the n extra dimensions are compactified on an n-dimensional torus of volume $(2\pi r)^n$, so that the fundamental $4+n$ dimensional Planck scale M_* is related to the usual 4-dimensional Planck scale M_{Pl} by $M_{Pl}^2 = M_*^{n+2}(2\pi r)^n$. If $M_* \sim 1$ TeV, then the $M_W - M_{Pl}$ hierarchy problem is just due to gravity propagating in the large extra dimensions.

In these theories, the KK-excited graviton states $G_{\mu\nu}^n$ for $n = 1-\infty$ can be produced at collider experiments. The graviton couplings to matter are suppressed by $1/M_{Pl}$, so that graviton emission cross sections $d\sigma/dt \sim 1/M_{Pl}^2$. However, the mass splittings between the excited graviton states can be tiny, so the graviton eigenstates are usually approximated by a continuum distribution. A summation (integration) over all allowed graviton emissions ends up cancelling the $1/M_{Pl}^2$ factor, so that observable cross section rates can be attained. Some fundamental production formulae for a KK graviton (denoted G) of mass m at hadron colliders include the subprocesses

$$\frac{d\sigma_m}{dt}(f\bar{f} \to \gamma G) = \frac{\alpha Q_f^2}{16N_f}\frac{1}{sM_{Pl}^2}F_1(\frac{t}{s}, \frac{m^2}{s}), \tag{51.93}$$

where Q_f is the charge of fermion f and N_f is the number of QCD colors of f. Also,

$$\frac{d\sigma_m}{dt}(q\bar{q} \to gG) = \frac{\alpha_s}{36}\frac{1}{sM_{Pl}^2}F_1(\frac{t}{s}, \frac{m^2}{s}), \tag{51.94}$$

$$\frac{d\sigma_m}{dt}(qg \to qG) = \frac{\alpha_s}{96}\frac{1}{sM_{Pl}^2}F_2(\frac{t}{s}, \frac{m^2}{s}), \tag{51.95}$$

$$\frac{d\sigma_m}{dt}(gg \to gG) = \frac{3\alpha_s}{16}\frac{1}{sM_{Pl}^2}F_3(\frac{t}{s}, \frac{m^2}{s}), \tag{51.96}$$

where

$$F_1(x,y) = \frac{1}{x(y-1-x)}\left[-4x(1+x)(1+2x+2x^2) + \right.$$
$$\left. y(1+6x+18x^2+16x^3) - 6y^2x(1+2x) + y^3(1+4x)\right] \tag{51.97}$$

$$F_2(x,y) = -(y-1-x)F_1\left(\frac{x}{y-1-x}, \frac{y}{y-1-x}\right) \tag{51.98}$$

and

$$F_3(x,y) = \frac{1}{x(y-1-x)}\left[1+2x+3x^2+2x^3+x^4\right.$$
$$\left. -2y(1+x^3) + 3y^2(1+x^2) - 2y^3(1+x) + y^4\right] \tag{51.99}$$

These formulae must then be multiplied by the graviton density of states formula $dN = S_{n-1}\frac{M_{Pl}^2}{M_*^{n+2}}m^{n-1}dm$ to gain the cross section

$$\frac{d^2\sigma}{dtdm} = S_{n-1}\frac{M_{Pl}^2}{M_*^{n+2}}m^{n-1}\frac{d\sigma_m}{dt} \tag{51.100}$$

where $S_n = \frac{(2\pi)^{n/2}}{\Gamma(n/2)}$ is the surface area of an n-dimensional sphere of unit radius.

Virtual graviton processes can also be searched for at colliders. For instance, in Ref. [24] the cross section for Drell-Yan production of lepton pairs via gluon fusion was calculated, where it is found that, in the center-of-mass system

$$\frac{d\sigma}{dz}(gg \to \ell^+\ell^-) = \frac{\lambda^2 s^3}{64\pi M_*^8}(1-z^2)(1+z^2) \tag{51.101}$$

where $z = \cos\theta$ and λ is a model-dependent coupling constant ~ 1. Formulae for Drell-Yan production via $q\bar{q}$ fusion can also be found in Refs. [24, 25].

51.11 Warped extra dimensions

In the Randall-Sundrum model [26] of warped extra dimensions, the arena for physics is a 5-d anti-deSitter (AdS_5) spacetime, for which a non-factorizable metric exists with a metric warp factor $e^{-2\sigma(\phi)}$. It is assumed that two opposite tension 3-branes exist within AdS_5 at the two ends of an S_1/Z_2 orbifold parameterized by co-ordinate ϕ which runs from $0-\pi$. The 4-D solution of the Einstein equations yields $\sigma(\phi) = kr_c|\phi|$, where r_c is the compactification radius of the extra dimension and $k \sim M_{Pl}$. The 4-D effective action allows one to identify $\overline{M}_{Pl}^2 = \frac{M^3}{k}(1-e^{-2kr_c\pi})$, where M is the 5-D Planck scale. Physical particles on the TeV scale (SM) brane have mass $m = e^{-kr_c\pi}m_0$, where m_0 is a fundamental mass of order the Planck scale. Thus, the weak scale-Planck scale hierarchy occurs due to the existence of the exponential warp factor if $kr_c \sim 12$.

In the simplest versions of the RS model, the TeV-scale brane contains only SM particles plus a tower of KK gravitons. The RS gravitons have mass $m_n = kx_ne^{-kr_c\pi}$, where the x_i are roots of Bessel functions $J_1(x_n) = 0$, with $x_1 \simeq 3.83$, $x_2 \simeq 7.02$ etc. While the RS zero-mode graviton couplings suppressed by $1/\overline{M}_{Pl}$ and are thus inconsequential for collider searches, the $n=1$ and higher modes have couplings suppressed instead by $\Lambda_\pi = e^{-kr_c\pi}\overline{M}_{Pl} \sim TeV$. The $n=1$ RS graviton should have width $\Gamma_1 = \rho m_1 x_1^2(k/\overline{M}_{Pl})^2$, where ρ is a constant depending on how many decay modes are open. The formulae for dilepton production via virtual RS graviton exchange can be gained from the above formulae for the ADD scenario via the replacement [27]

$$\frac{\lambda}{M_*^4} \to \frac{i^2}{8\Lambda_\pi^2}\sum_{n=1}^{\infty}\frac{1}{s - m_n^2 + im_n\Gamma_n}. \tag{51.102}$$

References

[1] J. F. Owens, E. Reya and M. Gluck, Phys. Rev. **D18**, 1501 (1978).

[2] F. Wilczek, Phys. Rev. Lett. **39**, 1304 (1977).

[3] B. L. Ioffe and V. A. Khoze, Sov. J. Part. Nucl. **9**, 50 (1978), [Fiz. Elem. Chast. Atom. Yadra9,118(1978)].

[4] J. R. Ellis, M. K. Gaillard and D. V. Nanopoulos, Nucl. Phys. **B106**, 292 (1976).

[5] R. N. Cahn and S. Dawson, Phys. Lett. **136B**, 196 (1984), [Erratum: Phys. Lett.138B,464(1984)].

[6] S. Dawson, Nucl. Phys. **B249**, 42 (1985).

[7] M. S. Chanowitz and M. K. Gaillard, Phys. Lett. **142B**, 85 (1984).

[8] R. N. Cahn, Nucl. Phys. **B255**, 341 (1985), [Erratum: Nucl. Phys.B262,744(1985)].

[9] V. M. Budnev *et al.*, Phys. Rept. **15**, 181 (1975), see for an exhaustive treatment.

[10] See *e.g.* H.Haber, *Supersymmetry, Part I (Theory), this Review.*

[11] P. R. Harrison and C. H. Llewellyn Smith, Nucl. Phys. **B213**, 223 (1983), [Erratum: Nucl. Phys.B223,542(1983)]; S. Dawson, E. Eichten and C. Quigg, Phys. Rev. **D31**, 1581 (1985); V. D. Barger *et al.*, Phys. Rev. **D31**, 528 (1985); H. Baer and X. Tata, Phys. Lett. **160B**, 159 (1985).

[12] H. Baer, D. D. Karatas and X. Tata, Phys. Rev. **D42**, 2259 (1990).

[13] Weak Scale Supersymmetry: From Superfields to Scattering Events, H. Baer and X. Tata (Cambridge University Press) 2006.

[14] H. E. Haber and G. L. Kane, Phys. Rept. **117**, 75 (1985).

[15] Theory and Phenomenology of Sparticles, M. Drees, R. Godbole, and P. Roy (World Scientific) 2005.

[16] A. Bartl, H. Fraas and W. Majerotto, Z. Phys. **C30**, 441 (1986).

[17] H. Baer *et al.*, Int. J. Mod. Phys. **A4**, 4111 (1989).

[18] A. Bartl, H. Fraas and W. Majerotto, Nucl. Phys. **B278**, 1 (1986).

[19] T. Appelquist, H.-C. Cheng and B. A. Dobrescu, Phys. Rev. **D64**, 035002 (2001), [hep-ph/0012100].

[20] For a review of models with extra spacetime dimensions, see G. Guidice and J. Wells, *Extra Dimensions, this Review.*

[21] J. M. Smillie and B. R. Webber, JHEP **10**, 069 (2005), [hep-ph/0507170].

[22] C. Macesanu, C. D. McMullen and S. Nandi, Phys. Rev. **D66**, 015009 (2002), [hep-ph/0201300].

[23] N. Arkani-Hamed, S. Dimopoulos and G. R. Dvali, Phys. Lett. **B429**, 263 (1998), [hep-ph/9803315]; N. Arkani-Hamed, S. Dimopoulos and G. R. Dvali, Phys. Rev. **D59**, 086004 (1999), [hep-ph/9807344].

[24] J. L. Hewett, Phys. Rev. Lett. **82**, 4765 (1999), [hep-ph/9811356].

[25] G. F. Giudice, R. Rattazzi and J. D. Wells, Nucl. Phys. **B544**, 3 (1999), [hep-ph/9811291]; E. A. Mirabelli, M. Perelstein and M. E. Peskin, Phys. Rev. Lett. **82**, 2236 (1999), [hep-ph/9811337]; T. Han, J. D. Lykken and R.-J. Zhang, Phys. Rev. **D59**, 105006 (1999), [hep-ph/9811350].

[26] L. Randall and R. Sundrum, Phys. Rev. Lett. **83**, 3370 (1999), [hep-ph/9905221].

[27] H. Davoudiasl, J. L. Hewett and T. G. Rizzo, Phys. Rev. Lett. **84**, 2080 (2000), [hep-ph/9909255].

Int. J. Mod. Phys. A 2026.41. Downloaded from www.worldscientific.com
by UNIVERSITY OF CALIFORNIA @ BERKELEY on 09/16/26. Re-use and distribution is strictly not permitted, except for Open Access articles.

52. Neutrino Cross Section Measurements

Revised August 2025 by G.P. Zeller (FNAL).

Neutrino cross sections are an essential ingredient in all neutrino experiments. Interest in neutrino scattering has increased due to the need for such information in the interpretation of neutrino data and given that uncertainties in neutrino-nucleus scattering remain a dominate source of systematic uncertainty in neutrino oscillation measurements. Historically, neutrino scattering results on both charged current (CC) and neutral current (NC) channels have been collected over many decades using a variety of targets, analysis techniques, and detector technologies. With the advent of intense neutrino sources constructed for neutrino oscillation investigations, experiments are now remeasuring such interaction cross sections with a renewed appreciation for nuclear effects[1] and the need for more precise neutrino flux estimations [1, 2]. This work summarizes neutrino cross section measurements performed in the $\sim 0.1-1000$ GeV range with an emphasis on inclusive, deep inelastic, quasi-elastic, and resonance production processes, areas where we have the most experimental input at present (Table 52.1). For a more comprehensive discussion of neutrino cross sections, including neutrino-electron scattering and lower energy measurements, the reader is directed to a review of this subject [3]. Here, we survey existing experimental data on neutrino interactions and do not attempt to provide a census of the associated theoretical calculations [4], which are both critical and plentiful. Companion electron-nucleus scattering data [5] are additionally playing an increased role in neutrino interaction predictions through such efforts as the e4ν Collaboration [6].

Table 52.1: List of properties of modern experiments measuring neutrino cross sections in the $\sim 0.1 - 1000$ GeV energy range.

Experiment	beam	$\langle E_\nu \rangle$, $\langle E_{\overline{\nu}} \rangle$ (GeV)	neutrino target(s)	run period
ArgoNeuT	$\nu, \overline{\nu}$	4.3, 3.6	Ar	2009 – 2010
FASERν	$\nu, \overline{\nu}$	1,000	W, emulsion	2021 –
ICARUS (at CNGS)	ν	20	Ar	2010 – 2012
ICARUS (at FNAL)	ν	0.8	Ar	2021 –
IceCube	$\nu, \overline{\nu}$	10^5	H_2O	2011 –
K2K	ν	1.3	CH, H_2O	2003 – 2004
MicroBooNE	ν	0.8	Ar	2015 – 2020
MINERvA	$\nu, \overline{\nu}$	3.5 (LE), 5.5 (ME)	He, C, CH, H_2O, Fe, Pb	2009 – 2019
MiniBooNE	$\nu, \overline{\nu}$	0.8, 0.7	CH_2	2002 – 2019
MINOS	$\nu, \overline{\nu}$	3.5, 6.1	Fe	2004 – 2016
NINJA	ν, $\overline{\nu}$	0.6, 0.6	Fe, emulsion	2015 –
NOMAD	$\nu, \overline{\nu}$	23.4, 19.7	C	1995 – 1998
NOvA	$\nu, \overline{\nu}$	2.0, 2.0	CH_2	2010 –
SBND	ν	0.8	Ar	2024 –
SciBooNE	$\nu, \overline{\nu}$	0.8, 0.7	CH	2007 – 2008
SND@LHC	$\nu, \overline{\nu}$	110	W, emulsion	2022 –
T2K	ν, $\overline{\nu}$	0.6, 0.6	CH, H_2O, Fe	2010 –

52.1 Inclusive Scattering

Over the years, many experiments have measured the total inclusive charged current cross section for neutrino ($\nu_\mu\, N \to \mu^-\, X$) and antineutrino ($\overline{\nu}_\mu\, N \to \mu^+\, X$) scattering covering a very broad range of energies. As can be seen in Fig. 52.1, which shows this data over decades of time and energy, the inclusive cross section approaches a linear dependence on neutrino energy. This behavior is expected for point-like scattering of neutrinos from quarks, an assumption which breaks down at lower energies.

To provide a more complete picture, differential cross sections for such inclusive scattering processes have also been reported. These include historical measurements on iron from NuTeV [7] and modern measurements on a variety of nuclear targets (Table 52.2). More recently, MINERvA has provided measurements in terms of longitudinal and transverse muon momenta [8, 9], MicroBooNE has measured the first triple differential cross sections in argon [10], and T2K has provided the first measurement of the antineutrino inclusive cross section at low energy [11] (Fig. 52.1).

At high energy, the inclusive cross section is dominated by deep inelastic scattering (DIS). Several neutrino experiments have measured DIS cross sections for specific targets and final states, for example, MINERvA has measured ratios of neutrino DIS cross sections on a variety of nuclear targets including lead, iron, and carbon [12, 13]. Other experiments have measured opposite-sign dimuon production, the most recent being from CHORUS [14], NOMAD [15], and NuTeV [16]. Multiple efforts are also now underway to measure inclusive neutrino scattering cross sections at significantly higher neutrino energies (in the TeV-PeV range), including at the LHC in FASERν [17] and SND@LHC [18], as well as using atmospheric neutrinos in IceCube [19–21].

Table 52.2: Published measurements of muon neutrino and antineutrino CC inclusive cross sections from modern neutrino experiments.

experiment	measurement	target
ArgoNeuT	ν_μ [22, 23], $\overline{\nu}_\mu$ [23]	Ar
FASERν	ν_μ [17], $\overline{\nu}_\mu$ [17]	W, emulsion
IceCube	$\nu + \overline{\nu}$ [20]	H_2O
MicroBooNE	ν_μ [10, 24–27]	Ar
MINERνA	ν_μ [8, 9, 12, 13, 28–31], $\overline{\nu}_\mu$ [28, 31], $\overline{\nu}_\mu/\nu_\mu$ [32]	C, CH, Fe, Pb
MINOS	ν_μ [33], $\overline{\nu}_\mu$ [33]	Fe
NINJA	ν_μ [34, 35], $\overline{\nu}_\mu$ [34]	H_2O, Fe
NOMAD	ν_μ [36]	C
NOvA	ν_μ [37–39]	CH_2
SciBooNE	ν_μ [40]	CH
T2K	ν_μ [41–45], $\overline{\nu}_\mu/\nu_\mu$ [11]	CH, H_2O, Fe

The reader is also referred to a recent review of the status of measurements and calculations in the shallow and deep inelastic scattering regions [46]. MINERvA has recently reported new measurements in the transition region between resonance production and DIS [31]. At lower neutrino energies, the inclusive cross section is an additionally complex combination of quasi-elastic scattering and resonance production processes, two areas we discuss next.

52.2 Quasi-elastic scattering

Quasi-elastic (QE) scattering is the dominant neutrino interaction for neutrino energies less than ~ 1 GeV and represents a large fraction of the signal samples in many neutrino oscillation experiments, which is why this process has received considerable attention in recent years. Historically, neutrino (antineutrino) quasi-elastic scattering refers to the process, $\nu_\mu\, n \to \mu^-\, p$ ($\overline{\nu}_\mu\, p \to \mu^+\, n$), where a charged lepton and single nucleon are ejected in the elastic interaction of a neutrino (or antineutrino) with a nucleon in the target material. This is the final state one would strictly observe, for example, in scattering off of a *free* nucleon target. There were many early measurements of neutrino QE scattering that span back to the 1970's [3]. In many of these initial measurements, bubble chamber experiments employed light targets (hydrogen or deuterium) and required both the detection of the final state muon and single nucleon[2]; thus the final state was clear and elastic kinematic conditions could be verified. The situation is more complicated, of course, for heavier nuclear targets used in modern neutrino experiments. In this case, nuclear effects can impact the size and shape of the cross section as well as the final state composition, kinematics, and topology. Due to intranuclear hadron rescattering and the effects of correlations between target nucleons, additional particles may be ejected in the final state; hence, a QE interaction on a nuclear target does not necessarily imply the ejection of a lepton and a *single* nucleon. One therefore needs to take care in

[1] Nuclear effects refer to kinematic, final state, and rate effects which impact neutrino scattering off nuclei. Such effects can be significant and are particularly relevant given that modern neutrino experiments use of nuclear targets to increase their event yields.

[2] In the case of deuterium, many experiments additionally observed the spectator proton.

Int. J. Mod. Phys. A 2026.41. Downloaded from www.worldscientific.com
by LIFORNIA @ BERKELEY on 09/16/26. Re-use and distribution is strictly not permitted, except for Open Access articles.

Int. J. Mod. Phys. A 2026.41. Downloaded from www.worldscientific.com
by UNIVERSITY OF CALIFORNIA @ BERKELEY on 09/16/26. Re-use and distribution is strictly not permitted, except for Open Access articles.

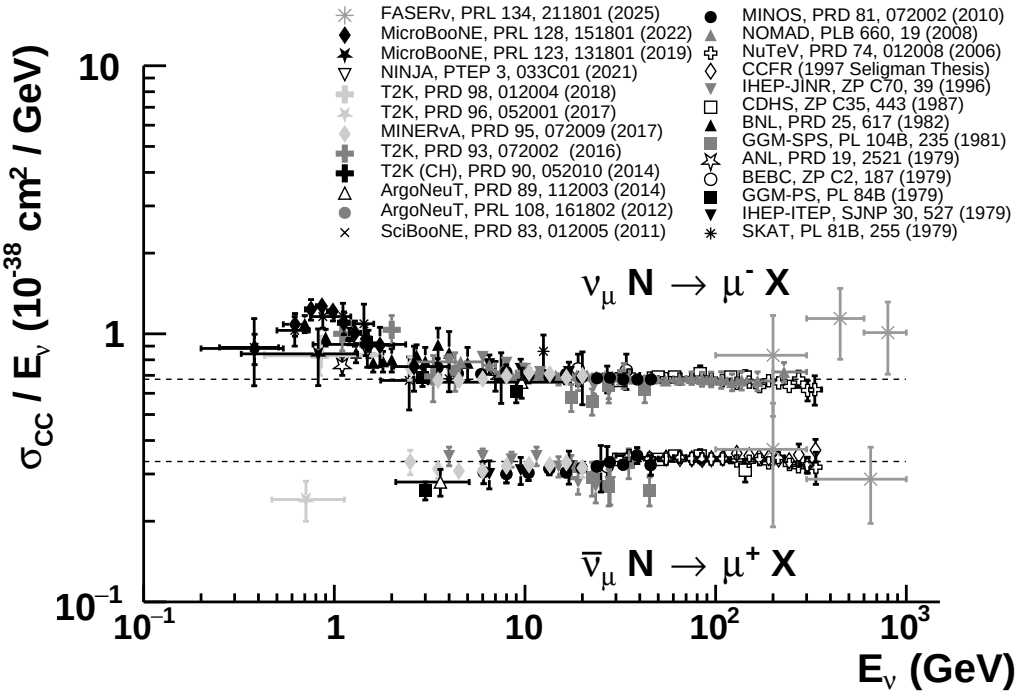

Figure 52.1: Measurements of per nucleon ν_μ and $\overline{\nu}_\mu$ CC inclusive scattering cross sections divided by neutrino energy as a function of neutrino energy. The data are on a variety of nuclear targets. The world-average values of $\sigma_{CC}/E_\nu = 0.677$ (neutrino) and 0.334 (antineutrino) $\times 10^{-38}$ cm^2/GeV are plotted as dashed lines. Neutrino cross sections are typically twice as large as their corresponding antineutrino counterparts, although this difference can be larger at lower energies. NC cross sections (not shown) are generally smaller compared to their CC counterparts.

defining what one means by neutrino QE scattering when scattering off targets heavier than hydrogen or deuterium. Because of this, modern experiments tend to instead report cross sections for processes involving pionless (e.g., nucleon-only) final states, often referred to as CC 0π or QE-like reactions in recent literature. Such measurements are summarized in Table 52.3. Many modern experiments have also recently opted to report QE-like cross sections as a function of observed final state particle (lepton, nucleon) kinematics. Such measurements can be more difficult to directly compare between experiments but have the advantage of being much less model-dependent and provide more stringent tests of the theory than historical cross sections as a function of derived quantities such as neutrino energy (E_ν) or 4-momentum transfer (Q^2). More recently, new thought has been given to the means for directly comparing experimental measurements produced in these less model-dependent forms [47].

The topic of neutrino QE scattering began drawing considerable attention following the first high statistics measurements of this process that revealed a significantly larger cross section than originally anticipated, predominantly in the backwards muon scattering region [75, 76]. Such an enhancement was observed many years prior in transverse electron-nucleus scattering [94] and was attributed to the presence of correlations between nucleons in the target nucleus. As a result, the impact of such nuclear effects on neutrino QE scattering has recently become the subject of intense experimental and theoretical scrutiny with implications on event rates, nucleon emission, neutrino energy reconstruction, and neutrino versus antineutrino cross sections. The reader is referred to reviews of the situation in [4, 95, 96]. To help drive further progress in understanding the underlying nuclear contributions, pionless (e.g., nucleon-only) cross sections have been reported for the first time in the form of double-differential distributions by MicroBooNE [56–58], MiniBooNE [75, 76], MINERvA [60–64, 70], and T2K [84–89]. Such double-differential cross sections in terms of final state particle kinematics reduce the model-dependence of the reported data, provide the most robust measurements available, and allow a more rigorous two-dimensional test of the underlying nuclear theory. MicroBooNE, MINERvA, and T2K have been especially prolific in recent years in probing this interaction process (Table 52.3). Neutrino experiments have also launched dedicated studies of the hadronic side of these interactions, including ArgoNeuT [48, 97], MicroBooNE [50, 51, 57], MINERvA [69, 98], and T2K [93]. MINERvA has been the first modern experiment to measure neutron emission in antineutrino interactions [99] and has simultaneously measured the A-dependence of neutrino QE cross sections on a variety of nuclear targets ranging from carbon to lead [64, 73]. ArgoNeuT [48], MicroBooNE [54], and NINJA [81] have explored two-proton final states. T2K has probed ratios of oxygen to carbon [87, 100], asymmetries between neutrino and antineutrino scattering [88], and simultaneous measurements both on and off axis to the neutrino beam [89]. In addition, the exploration of transverse kinematic variables and momentum imbalances in pionless neutrino scattering is allowing better constraints on the various nuclear contributions to the cross section. Such scrutiny includes important evaluations from MicroBooNE [52, 53, 59], MINERvA [60, 61, 65, 66] and T2K [93]. With the MiniBooNE results having first revealed these additional complexities in neutrino-nucleus QE scattering, measurements from multiple neutrino experiments, on multiple targets, and using a variety of kinematic information have been crucial in gaining a better handle on the underlying nuclear physics (2p2h, MEC, FSI) impacting neutrino-nucleus interactions. What we once thought was "simple" QE scattering is in fact not so simple.

Equally important, neutrino experiments such as MINERvA have revisited the extraction of the axial form factor from light target data using modern higher statistics data sets [72]. In addition to such charged current investigations, measurements of the neutral current counterpart of this channel have also been performed. The most recent NC elastic scattering cross section measurements include those from BNL E734 [101], MiniBooNE [78, 79], Super-K [83], and T2K [92]. A number of measurements of the Cabibbo-suppressed antineutrino QE hyperon (Λ) production cross section have additionally been reported [102,103], most recently by MicroBooNE [55]. As an exciting new addition, there have also been the

Int. J. Mod. Phys. A 2026.41. Downloaded from www.worldscientific.com
by [redacted] LIFORNIA @ BERKELEY on 09/16/26. Re-use and distribution is strictly not permitted, except for Open Access articles.

Table 52.3: Comprehensive summary of published modern measurements of muon neutrino QE-like cross sections with pionless final states.

experiment	measurement	target
ArgoNeuT	2p [48]	Ar
K2K	M_A [49]	H_2O
MicroBooNE	$\frac{d\sigma}{dp_\mu}$ $\frac{d\sigma}{dp_p}$ $\frac{d\sigma}{d\cos\theta_\mu}$ $\frac{d\sigma}{d\cos\theta_p}$ [50, 51], $\frac{d^2\sigma}{d\delta\alpha_T d\delta p_T}$ [52, 53], $\frac{d^2\sigma}{d\delta p_{Tx} d\delta p_{Ty}}$ [52], 2p [54], Λ [55], $\frac{d^2\sigma}{dp_\mu dcos\theta_\mu}$ [56], $\frac{d^2\sigma}{dp_p dcos\theta_p}$ [57], $\frac{d^2\sigma}{d\theta_{vis} dp_{miss}}$ [58], $\frac{d^2\sigma}{d\alpha_{3D} dp_n}$ [59]	Ar
MINERνA	$\frac{d^2\sigma}{dp_T dp_{\|\|}}$ [60–64], $\frac{d\sigma}{d\delta p_{Tx}}$ $\frac{d\sigma}{d\delta p_{Ty}}$ [65], $\frac{d\sigma}{dp_n}$ $\frac{d\sigma}{d\delta\alpha_T}$ [66], $\frac{d\sigma}{dQ^2}$ [67, 68], 1p [69], $\frac{d^2\sigma}{dE_{avail} dq_3}$ [70], $\frac{d\sigma}{dQ^2}$ [71], $F_A(Q^2)$ [72], A-dep [73], $\frac{d\sigma}{dp_T}(\overline{\nu})$ [74]	CH,Fe,Pb
MiniBooNE	$\frac{d^2\sigma}{dT_\mu d\theta_\mu}$ [75, 76], M_A [77], NC [78, 79]	CH_2
MINOS	M_A [80]	Fe
NINJA	2p [81]	Fe
NOMAD	M_A, $\sigma(E_\nu)$ [82]	C
Super-K	NC [83]	H_2O
T2K	$\frac{d^2\sigma}{dT_\mu d\theta_\mu}$ [84–89], $\sigma(E_\nu)$ [90], M_A [91], NC [92], $\frac{d\sigma}{d\delta p_T}$ $\frac{d\sigma}{d\delta\alpha_T}$ [93], O/C [87]	CH,H_2O

first observations of the very challenging-to-detect coherent elastic neutrino-nucleus scattering (CEνNS) process now in multiple nuclei by COHERENT [104].

52.3 Pion Production

In addition to such elastic scattering processes, neutrinos can also inelastically scatter producing a nucleon excited state (Δ, N^*). Such baryonic resonances quickly decay, most often to a nucleon and single-pion final state. Historically, experiments have measured various exclusive final states associated with these reactions, the majority of which have been on hydrogen and deuterium targets [3]. There have been several recent re-analyses of this data to better understand the consistency between data sets [105], nucleon form factors [106], and non-resonant contributions [107]. Also, modern measurements of neutrino-induced pion production have since been performed on a variety of nuclear targets (Table 52.4).

Table 52.4: Summary of modern measurements of NC and CC scattering cross sections involving a single pion or multiple pions in the final state.

experiment	$\pi^\pm$	π^0	target
ArgoNeuT	CC [108, 109]	NC [110]	Ar
K2K	CC[111, 112]	CC [113], NC [114]	CH, H_2O
MicroBooNE	–	CC [115, 116], NC [117, 118]	Ar
MINERνA	CC [119–126]	CC [120, 127–129], NC [130]	C, CH, Fe H_2O, Pb
MiniBooNE	CC [131, 132]	CC [133], NC [134, 135]	CH_2
MINOS	–	NC [136]	Fe
NOMAD	–	NC [137]	C
NOvA	–	NC [138, 139]	C
SciBooNE	CC [140]	NC [141, 142]	CH
T2K	CC [143–146], NC [147]	–	CH, H_2O

In addition to resonance production processes, neutrinos can also coherently scatter off of the entire nucleus and produce a distinctly forward-scattered single pion final state. Both CC ($\nu_\mu\, A \to \mu^-\, A\, \pi^+$, $\overline{\nu}_\mu\, A \to \mu^+\, A\, \pi^-$) and NC ($\nu_\mu\, A \to \nu_\mu\, A\pi^0, \overline{\nu}_\mu\, A \to \overline{\nu}_\mu\, A\pi^0$) processes are possible in this case. Even though the level of coherent pion production is small compared to their resonant counterpart, observations exist across a broad energy range and on multiple nuclear targets [148]. More recently, several modern neutrino experiments have either measured or set limits on coherent pion production cross sections including ArgoNeuT [108], K2K [112], MINERvA [121, 123, 125], MiniBooNE [135], MINOS [136], NOMAD [137], NOvA [138], SciBooNE [140,142], and T2K [112, 149].

As with inclusive and quasi-elastic scattering, a new appreciation for the significance of nuclear effects has also surfaced in pion production physics, again due to the use of heavy nuclear targets in modern neutrino experiments. Many experiments have been careful to report cross sections for various detected final states, thereby not correcting for large and uncertain nuclear effects (e.g., pion rescattering, charge exchange, and absorption) which can introduce significant sources of uncertainty and model dependence. Providing the most comprehensive survey of neutrino single-pion production to date, MiniBooNE has published a total of 16 single- and double-differential cross sections for both the final state muon (in the case of CC scattering) and pions in these interactions; thus, providing the first measurements of such final state kinematic distributions [131–134]. At similar neutrino energies, T2K has provided new data including the first measurement of the Adler angles in neutrino-nucleus scattering [145], the first exploration of transverse kinematic imbalances in pion production processes [146], and the first modern measurements of NC π^+ production [147]. MINERvA has produced a similar accompaniment of measurements at higher neutrino energies and uniquely on multiple nuclear targets [126]. Importantly, MINERvA has been working towards an improved nuclear model [129] that can potentially describe all of the pion reaction channels simultaneously, an issue that many experiments have struggled with up until now [120]. ArgoNeuT and MicroBooNE have since been adding new information on single pion production in argon. Regardless of the interaction channel or

Int. J. Mod. Phys. A 2026.41. Downloaded from www.worldscientific.com by UNIVERSITY OF CALIFORNIA @ BERKELEY on 09/16/26. Re-use and distribution is strictly not permitted, except for Open Access articles.

target material, differential cross section measurements in terms of observed final state particle (lepton, pion, nucleon) kinematics are preferred for their reduced model dependence and for the additional kinematic information they provide. Such a new direction has been the focus of modern measurements as opposed to the reporting of more model-dependent, historical cross sections as a function of E_ν or Q^2. Together with similar results for other interaction channels, a better understanding and modeling of nuclear effects will be possible moving forward. MINERvA [150] has already taken a large step in this direction by explicitly tuning the physics in existing neutrino event generators to best fit the experimental data on pion production.

It should be noted that baryonic resonances can also decay to multi-pion, other mesonic (K, η, ρ, etc.), and even photon final states. Experimental results for these channels are typically sparse or non-existent. More recently, MicroBooNE has produced the first measurement of neutrino-induced η [151] production on argon. Photon production processes can comprise an important background for $\nu_\mu \to \nu_e$ appearance searches in some detectors and thus have become the focus of recent experimental investigations, most notably in NOMAD [152] and T2K [153, 154]. There have also been several recent measurements of kaon final states by MicroBooNE [155] and MINERvA [156–158] that are providing needed background constraints for nucleon decay searches ($p \to K^+\overline{\nu}$).

52.4 Electron Neutrino Scattering

The aforementioned cross section measurements are all for either muon neutrino or muon antineutrino scattering. With the production of predominantly muon neutrino beams for neutrino oscillation studies, the availability of electron neutrino scattering data is by construction limited. However, for the first time, measurements of electron neutrino scattering cross sections are being produced by a variety of modern neutrino experiments (Table 52.5). Such measurements are important as they verify our assumptions about lepton universality and validate the use of muon neutrino data to constrain electron neutrino interaction predictions. For lower energy and historical electron neutrino cross section measurements, the reader is directed to reference [3].

Table 52.5: Published measurements of electron neutrino and antineutrino cross sections from modern neutrino experiments.

experiment	CC inclusive	QE-like	π production	target
ArgoNeuT	[159]	-	-	Ar
COHERENT	[160]	-	-	I
FASERν	[161]	-	-	W, emulsion
MicroBooNE	[162, 163]	[164]	[165]	Ar
MINERνA	[166]	[166, 167]	-	CH
NOvA	[168]	-	-	CH_2
T2K	[169–171]	-	[172]	CH, H_2O

52.5 Outlook

Neutrino experiments continue to produce critical neutrino scattering measurements on nuclei as they accumulate increased statistics and pursue new ways of reporting their measurements to reduce model dependencies. Analysis of a broad energy range of data from MINERvA is providing some of the most detailed analysis of nuclear effects in neutrino interactions by examining multiple nuclei in a single experiment. Data from ArgoNeuT, MicroBooNE, ICARUS and soon also SBND are probing deeper into complex neutrino final states using the superior capabilities of liquid argon time projection chambers, while the T2K and NOvA near detectors continue to collect high statistics samples in intense neutrino beams. Excitingly, new results from IceCube, FASERν, and SND@LHC are starting to probe up into the TeV region. Together with dedicated discussions between experiments on how best to report neutrino cross section measurements [173] and with accompanying work being advanced by theorists to further increase the sophistication of nuclear model calculations [4], we continue to advance our understanding of neutrino-nucleus scattering [174].

52.6 Acknowledgments

The author thanks Anne Schukraft (Fermilab) for help in preparing the plots and content of this review.

References

[1] L. Zazueta *et al.* (MINERvA), Phys. Rev. D **107**, 1, 012001 (2023), [arXiv:2209.05540].

[2] D. Ruterbories *et al.* (MINERvA), Phys. Rev. D **104**, 9, 092010 (2021), [arXiv:2107.01059].

[3] J. A. Formaggio and G. P. Zeller, Rev. Mod. Phys. **84**, 1307 (2012), [arXiv:1305.7513].

[4] L. Alvarez-Ruso *et al.*, Prog. Part. Nucl. Phys. **100**, 1 (2018), [arXiv:1706.03621].

[5] D. Drechsel and M. M. Giannini, Rept. Prog. Phys. **52**, 1083 (1989).

[6] M. Khachatryan *et al.* (CLAS, e4v), Nature **599**, 7886, 565 (2021).

[7] M. Tzanov *et al.* (NuTeV), Phys. Rev. **D74**, 012008 (2006), [hep-ex/0509010].

[8] A. Filkins *et al.* (MINERvA), Phys. Rev. D **101**, 11, 112007 (2020), [arXiv:2002.12496].

[9] D. Ruterbories *et al.* (MINERvA), Phys. Rev. D **104**, 9, 092007 (2021), [arXiv:2106.16210].

[10] P. Abratenko *et al.* (MicroBooNE) (2023), [arXiv:2307.06413].

[11] K. Abe *et al.* (T2K), Phys. Rev. **D96**, 5, 052001 (2017), [arXiv:1706.04257].

[12] B. G. Tice *et al.* (MINERvA), Phys. Rev. Lett. **112**, 23, 231801 (2014), [arXiv:1403.2103].

[13] J. Mousseau *et al.* (MINERvA), Phys. Rev. **D93**, 7, 071101 (2016), [arXiv:1601.06313].

[14] A. Kayis-Topaksu *et al.* (CHORUS), Nucl. Phys. **B798**, 1 (2008), [arXiv:0804.1869].

[15] O. Samoylov *et al.* (NOMAD), Nucl. Phys. **B876**, 339 (2013), [arXiv:1308.4750].

[16] D. Mason *et al.* (NuTeV), Phys. Rev. Lett. **99**, 192001 (2007).

[17] R. Mammen Abraham *et al.* (FASER), Phys. Rev. Lett. **134**, 21, 211801 (2025), [arXiv:2412.03186].

[18] R. Albanese *et al.* (SND@LHC), Phys. Rev. Lett. **131**, 3, 031802 (2023), [arXiv:2305.09383].

[19] M. G. Aartsen *et al.* (IceCube), Nature **551**, 596 (2017), [arXiv:1711.08119].

[20] R. Abbasi *et al.* (IceCube), Phys. Rev. D. **104**, 022001 (2021), [arXiv:2011.03560].

[21] M. Bustamante and A. Connolly, Phys. Rev. Lett. **122**, 4, 041101 (2019), [arXiv:1711.11043].

[22] C. Anderson *et al.* (ArgoNeuT), Phys. Rev. Lett. **108**, 161802 (2012), [arXiv:1111.0103].

[23] R. Acciarri *et al.* (ArgoNeuT), Phys. Rev. **D89**, 11, 112003 (2014), [arXiv:1404.4809].

[24] C. Adams *et al.* (MicroBooNE), Eur. Phys. J. **C79**, 3, 248 (2019), [arXiv:1805.06887].

[25] P. Abratenko *et al.* (MicroBooNE), Phys. Rev. Lett. **123**, 13, 131801 (2019), [arXiv:1905.09694].

[26] P. Abratenko *et al.* (MicroBooNE), Phys. Rev. Lett. **133**, 4, 041801 (2024), [arXiv:2402.19281].

[27] P. Abratenko *et al.* (MicroBooNE), Phys. Rev. D **110**, 1, 013006 (2024), [arXiv:2402.19216].

[28] J. Devan *et al.* (MINERvA), Phys. Rev. **D94**, 11, 112007 (2016), [arXiv:1610.04746].

[29] P. A. Rodrigues *et al.* (MINERvA), Phys. Rev. Lett. **116**, 071802 (2016), [Addendum: Phys. Rev. Lett.121,no.20,209902(2018)], [arXiv:1511.05944].

Int. J. Mod. Phys. A 2026.41. Downloaded from www.worldscientific.com
by [redacted]LIFORNIA @ BERKELEY on 09/16/26. Re-use and distribution is strictly not permitted, except for Open Access articles.

[30] M. V. Ascencio *et al.* (MINERvA), Phys. Rev. D **106**, 3, 032001 (2022), [arXiv:2110.13372].

[31] A. Lozano *et al.* (MINERvA) (2025), [arXiv:2503.20043].

[32] L. Ren *et al.* (MINERvA), Phys. Rev. **D95**, 7, 072009 (2017), [Addendum: Phys. Rev.D97,no.1,019902(2018)], [arXiv:1701.04857].

[33] P. Adamson *et al.* (MINOS), Phys. Rev. **D81**, 072002 (2010), [arXiv:0910.2201].

[34] A. Hiramoto *et al.* (NINJA), Phys. Rev. D **102**, 7, 072006 (2020), [arXiv:2008.03895].

[35] H. Oshima *et al.* (NINJA), PTEP **2021**, 3, 033C01 (2021), [arXiv:2012.05221].

[36] Q. Wu *et al.* (NOMAD), Phys. Lett. **B660**, 19 (2008), [arXiv:0711.1183].

[37] M. A. Acero *et al.* (NOvA), Phys. Rev. D **107**, 5, 052011 (2023), [arXiv:2109.12220].

[38] M. A. Acero *et al.* (NOvA) (2024), [arXiv:2410.10222].

[39] M. A. Acero *et al.* (NOvA), Phys. Rev. D **111**, 5, 052009 (2025), [arXiv:2410.05526].

[40] Y. Nakajima *et al.* (SciBooNE), Phys. Rev. **D83**, 012005 (2011), [arXiv:1011.2131].

[41] K. Abe *et al.* (T2K), Phys. Rev. **D87**, 9, 092003 (2013), [arXiv:1302.4908].

[42] K. Abe *et al.* (T2K), Phys. Rev. **D90**, 5, 052010 (2014), [arXiv:1407.4256].

[43] K. Abe *et al.* (T2K), Phys. Rev. **D93**, 7, 072002 (2016), [arXiv:1509.06940].

[44] K. Abe *et al.* (T2K), Phys. Rev. **D98**, 012004 (2018), [arXiv:1801.05148].

[45] K. Abe *et al.* (T2K), PTEP **2019**, 9, 093C02 (2019), [arXiv:1904.09611].

[46] M. Sajjad Athar and J. G. Morfín, J. Phys. G **48**, 3, 034001 (2021), [arXiv:2006.08603].

[47] K. Mahn, C. Marshall and C. Wilkinson, Ann. Rev. Nucl. Part. Sci. **68**, 105 (2018), [arXiv:1803.08848].

[48] R. Acciarri *et al.* (ArgoNeuT), Phys. Rev. **D90**, 1, 012008 (2014), [arXiv:1405.4261].

[49] R. Gran *et al.* (K2K), Phys. Rev. **D74**, 052002 (2006), [hep-ex/0603034].

[50] P. Abratenko *et al.* (MicroBooNE), Phys. Rev. D **102**, 11, 112013 (2020), [arXiv:2010.02390].

[51] P. Abratenko *et al.* (MicroBooNE), Phys. Rev. Lett. **125**, 20, 201803 (2020), [arXiv:2006.00108].

[52] P. Abratenko *et al.* (MicroBooNE), Phys. Rev. Lett. **131**, 10, 101802 (2023), [arXiv:2301.03706].

[53] P. Abratenko *et al.* (MicroBooNE), Phys. Rev. D **108**, 5, 053002 (2023), [arXiv:2301.03700].

[54] P. Abratenko *et al.* (MicroBooNE) (2022), [arXiv:2211.03734].

[55] P. Abratenko *et al.* (MicroBooNE), Phys. Rev. Lett. **130**, 23, 231802 (2023), [arXiv:2212.07888].

[56] P. Abratenko *et al.* (MicroBooNE) (2025), [arXiv:2507.00921].

[57] P. Abratenko *et al.* (MicroBooNE) (2024), [arXiv:2403.19574].

[58] P. Abratenko *et al.* (MicroBooNE), Phys. Rev. D **111**, 11, 113007 (2025), [arXiv:2504.17758].

[59] P. Abratenko *et al.* (MicroBooNE), Phys. Rev. D **109**, 9, 092007 (2024), [arXiv:2310.06082].

[60] D. Ruterbories *et al.* (MINERvA), Phys. Rev. **D99**, 1, 012004 (2019), [arXiv:1811.02774].

[61] C. E. Patrick *et al.* (MINERvA), Phys. Rev. **D97**, 5, 052002 (2018), [arXiv:1801.01197].

[62] M. F. Carneiro *et al.* (MINERvA), Phys. Rev. Lett. **124**, 12, 121801 (2020), [arXiv:1912.09890].

[63] A. Bashyal *et al.* (MINERvA), Phys. Rev. D **108**, 3, 032018 (2023).

[64] J. Kleykamp *et al.* (MINERvA), Phys. Rev. Lett. **130**, 16, 161801 (2023), [arXiv:2301.02272].

[65] T. Cai *et al.* (MINERvA), Phys. Rev. D **101**, 9, 092001 (2020), [arXiv:1910.08658].

[66] X. G. Lu *et al.* (MINERvA), Phys. Rev. Lett. **121**, 2, 022504 (2018), [arXiv:1805.05486].

[67] G. A. Fiorentini *et al.* (MINERvA), Phys. Rev. Lett. **111**, 022502 (2013), [arXiv:1305.2243].

[68] L. Fields *et al.* (MINERvA), Phys. Rev. Lett. **111**, 2, 022501 (2013), [arXiv:1305.2234].

[69] T. Walton *et al.* (MINERvA), Phys. Rev. **D91**, 7, 071301 (2015), [arXiv:1409.4497].

[70] R. Gran *et al.* (MINERvA), Phys. Rev. Lett. **120**, 22, 221805 (2018), [arXiv:1803.09377].

[71] M. Betancourt *et al.* (MINERvA), Phys. Rev. Lett. **119**, 8, 082001 (2017), [arXiv:1705.03791].

[72] T. Cai *et al.* (MINERvA), Nature **614**, 7946, 48 (2023).

[73] J. Kleykamp *et al.* (MINERvA) (2025), [arXiv:2503.15047].

[74] A. Olivier *et al.* (MINERvA), Phys. Rev. D **108**, 11, 112010 (2023), [arXiv:2310.17014].

[75] A. A. Aguilar-Arevalo *et al.* (MiniBooNE), Phys. Rev. **D81**, 092005 (2010), [arXiv:1002.2680].

[76] A. A. Aguilar-Arevalo *et al.* (MiniBooNE), Phys. Rev. **D88**, 3, 032001 (2013), [arXiv:1301.7067].

[77] A. A. Aguilar-Arevalo *et al.* (MiniBooNE), Phys. Rev. Lett. **100**, 032301 (2008), [arXiv:0706.0926].

[78] A. A. Aguilar-Arevalo *et al.* (MiniBooNE), Phys. Rev. **D82**, 092005 (2010), [arXiv:1007.4730].

[79] A. A. Aguilar-Arevalo *et al.* (MiniBooNE), Phys. Rev. **D91**, 1, 012004 (2015), [arXiv:1309.7257].

[80] P. Adamson *et al.* (MINOS), Phys. Rev. **D91**, 1, 012005 (2015), [arXiv:1410.8613].

[81] H. Oshima *et al.* (NINJA), Phys. Rev. D **106**, 3, 032016 (2022), [arXiv:2203.08367].

[82] V. Lyubushkin *et al.* (NOMAD), Eur. Phys. J. **C63**, 355 (2009), [arXiv:0812.4543].

[83] L. Wan *et al.* (Super-Kamiokande), Phys. Rev. **D99**, 3, 032005 (2019), [arXiv:1901.05281].

[84] K. Abe *et al.* (T2K), Phys. Rev. **D93**, 11, 112012 (2016), [arXiv:1602.03652].

[85] K. Abe *et al.* (T2K), Phys. Rev. **D97**, 1, 012001 (2018), [arXiv:1708.06771].

[86] K. Abe *et al.* (T2K), Phys. Rev. D **102**, 1, 012007 (2020), [arXiv:1908.10249].

[87] K. Abe *et al.* (T2K), Phys. Rev. D **101**, 11, 112004 (2020), [arXiv:2004.05434].

[88] K. Abe *et al.* (T2K), Phys. Rev. D **101**, 11, 112001 (2020), [arXiv:2002.09323].

[89] K. Abe *et al.* (T2K), Phys. Rev. D **108**, 11, 112009 (2023), [arXiv:2303.14228].

[90] K. Abe *et al.* (T2K), Phys. Rev. **D91**, 11, 112002 (2015), [arXiv:1503.07452].

[91] K. Abe *et al.* (T2K), Phys. Rev. **D92**, 11, 112003 (2015), [arXiv:1411.6264].

[92] K. Abe *et al.* (T2K), Phys. Rev. **D90**, 7, 072012 (2014), [arXiv:1403.3140].

[93] K. Abe *et al.* (T2K), Phys. Rev. **D98**, 3, 032003 (2018), [arXiv:1802.05078].

[94] J. Carlson *et al.*, Phys. Rev. **C65**, 024002 (2002), [arXiv:nucl-th/0106047].

Int. J. Mod. Phys. A 2026.41. Downloaded from www.worldscientific.com
by UNIVERSITY OF CALIFORNIA @ BERKELEY on 09/16/26. Re-use and distribution is strictly not permitted, except for Open Access articles.

[95] H. Gallagher, G. Garvey and G. P. Zeller, Ann. Rev. Nucl. Part. Sci. **61**, 355 (2011).

[96] G. T. Garvey *et al.*, Phys. Rept. **580**, 1 (2015), [arXiv:1412.4294].

[97] O. Palamara (ArgoNeuT), JPS Conf. Proc. **12**, 010017 (2016).

[98] D. Ruterbories *et al.* (MINERvA), Phys. Rev. Lett. **129**, 2, 021803 (2022), [arXiv:2203.08022].

[99] M. Elkins *et al.* (MINERvA), Phys. Rev. **D100**, 5, 052002 (2019), [arXiv:1901.04892].

[100] K. Abe *et al.* (T2K), PTEP **2021**, 4, 043C01 (2021), [arXiv:2004.13989].

[101] L. A. Ahrens *et al.*, Phys. Rev. **D35**, 785 (1987).

[102] J. Brunner *et al.* (SKAT), Z. Phys. **C45**, 551 (1990).

[103] V. V. Ammosov *et al.*, Z. Phys. **C36**, 377 (1987); O. Erriquez *et al.*, Phys. Lett. **70B**, 383 (1977); T. Eichten *et al.*, Phys. Lett. **40B**, 593 (1972).

[104] D. Akimov *et al.* (COHERENT), Phys. Rev. Lett. **126**, 1, 012002 (2021), [arXiv:2003.10630].

[105] C. Wilkinson *et al.*, Phys. Rev. **D90**, 11, 112017 (2014), [arXiv:1411.4482].

[106] A. S. Meyer *et al.*, Phys. Rev. **D93**, 11, 113015 (2016), [arXiv:1603.03048].

[107] P. Rodrigues, C. Wilkinson and K. McFarland, Eur. Phys. J. **C76**, 8, 474 (2016), [arXiv:1601.01888].

[108] R. Acciarri *et al.* (ArgoNeuT), Phys. Rev. Lett. **113**, 26, 261801 (2014), [erratum: Phys. Rev. Lett.114,no.3,039901(2015)], [arXiv:1408.0598].

[109] R. Acciarri *et al.* (ArgoNeuT), Phys. Rev. D **98**, 5, 052002 (2018), [arXiv:1804.10294].

[110] R. Acciarri *et al.* (ArgoNeuT), Phys. Rev. **D96**, 1, 012006 (2017), [arXiv:1511.00941].

[111] A. Rodriguez *et al.* (K2K), Phys. Rev. **D78**, 032003 (2008), [arXiv:0805.0186].

[112] M. Hasegawa *et al.* (K2K), Phys. Rev. Lett. **95**, 252301 (2005), [hep-ex/0506008].

[113] C. Mariani *et al.* (K2K), Phys. Rev. **D83**, 054023 (2011), [arXiv:1012.1794].

[114] S. Nakayama *et al.* (K2K), Phys. Lett. **B619**, 255 (2005), [hep-ex/0408134].

[115] C. Adams *et al.* (MicroBooNE), Phys. Rev. **D99**, 9, 091102 (2019), [arXiv:1811.02700].

[116] P. Abratenko *et al.* (MicroBooNE), Phys. Rev. D **110**, 9, 092014 (2024), [arXiv:2404.09949].

[117] P. Abratenko *et al.* (MicroBooNE), Phys. Rev. D **107**, 1, 012004 (2023), [arXiv:2205.07943].

[118] P. Abratenko *et al.* (MicroBooNE), Phys. Rev. Lett. **134**, 16, 161802 (2025), [arXiv:2404.10948].

[119] B. Eberly *et al.* (MINERvA), Phys. Rev. **D92**, 9, 092008 (2015), [arXiv:1406.6415].

[120] C. L. McGivern *et al.* (MINERvA), Phys. Rev. **D94**, 5, 052005 (2016), [arXiv:1606.07127].

[121] A. Higuera *et al.* (MINERvA), Phys. Rev. Lett. **113**, 26, 261802 (2014), [arXiv:1409.3835].

[122] T. Le *et al.* (MINERvA), Phys. Rev. **D100**, 5, 052008 (2019), [arXiv:1906.08300].

[123] A. Mislivec *et al.* (MINERvA), Phys. Rev. **D97**, 3, 032014 (2018), [arXiv:1711.01178].

[124] T. Le *et al.* (MINERvA), Phys. Rev. D **100**, 5, 052008 (2019), [arXiv:1906.08300].

[125] M. A. Ramírez *et al.* (MINERvA), Phys. Rev. Lett. **131**, 5, 051801 (2023), [arXiv:2210.01285].

[126] A. Bercellie *et al.* (MINERvA), Phys. Rev. Lett. **131**, 1, 011801 (2023), [arXiv:2209.07852].

[127] T. Le *et al.* (MINERvA), Phys. Lett. **B749**, 130 (2015), [arXiv:1503.02107].

[128] O. Altinok *et al.* (MINERvA), Phys. Rev. **D96**, 7, 072003 (2017), [arXiv:1708.03723].

[129] D. Coplowe *et al.* (MINERvA), Phys. Rev. D **102**, 7, 072007 (2020), [arXiv:2002.05812].

[130] J. Wolcott *et al.* (MINERvA), Phys. Rev. Lett. **117**, 11, 111801 (2016), [arXiv:1604.01728].

[131] A. A. Aguilar-Arevalo *et al.* (MiniBooNE), Phys. Rev. **D83**, 052007 (2011), [arXiv:1011.3572].

[132] A. A. Aguilar-Arevalo *et al.* (MiniBooNE), Phys. Rev. Lett. **103**, 081801 (2009), [arXiv:0904.3159].

[133] A. A. Aguilar-Arevalo *et al.* (MiniBooNE), Phys. Rev. **D83**, 052009 (2011), [arXiv:1010.3264].

[134] A. A. Aguilar-Arevalo *et al.* (MiniBooNE), Phys. Rev. **D81**, 013005 (2010), [arXiv:0911.2063].

[135] A. A. Aguilar-Arevalo *et al.* (MiniBooNE), Phys. Lett. **B664**, 41 (2008), [arXiv:0803.3423].

[136] P. Adamson *et al.* (MINOS), Phys. Rev. **D94**, 7, 072006 (2016), [arXiv:1608.05702].

[137] C. T. Kullenberg *et al.* (NOMAD), Phys. Lett. **B682**, 177 (2009), [arXiv:0910.0062].

[138] M. A. Acero *et al.* (NOvA), Phys. Rev. D **102**, 1, 012004 (2020), [arXiv:1902.00558].

[139] M. A. Acero *et al.* (NOvA), Phys. Rev. D **107**, 11, 112008 (2023), [arXiv:2306.04028].

[140] K. Hiraide *et al.* (SciBooNE), Phys. Rev. **D78**, 112004 (2008), [arXiv:0811.0369].

[141] Y. Kurimoto *et al.* (SciBooNE), Phys. Rev. **D81**, 033004 (2010), [arXiv:0910.5768].

[142] Y. Kurimoto *et al.* (SciBooNE), Phys. Rev. **D81**, 111102 (2010), [arXiv:1005.0059].

[143] K. Abe *et al.* (T2K), Phys. Rev. **D95**, 1, 012010 (2017), [arXiv:1605.07964].

[144] K. Abe *et al.* (T2K), Phys. Rev. Lett. **117**, 19, 192501 (2016), [arXiv:1604.04406].

[145] K. Abe *et al.* (T2K), Phys. Rev. D **101**, 1, 012007 (2020), [arXiv:1909.03936].

[146] K. Abe *et al.* (T2K), Phys. Rev. D **103**, 11, 112009 (2021), [arXiv:2102.03346].

[147] K. Abe *et al.* (T2K) (2025), [arXiv:2503.06849].

[148] P. Vilain *et al.* (CHARM-II), Phys. Lett. **B313**, 267 (1993); A compilation of historical coherent pion production data.

[149] K. Abe *et al.* (T2K), Phys. Rev. D **108**, 9, 092009 (2023), [arXiv:2308.16606].

[150] P. Stowell *et al.* (MINERvA), Phys. Rev. **D100**, 7, 072005 (2019), [arXiv:1903.01558].

[151] P. Abratenko *et al.* (MicroBooNE), Phys. Rev. D **108**, 5, 052010 (2023), [arXiv:2304.02076].

[152] C. T. Kullenberg *et al.* (NOMAD), Phys. Lett. **B706**, 268 (2012), [arXiv:1111.3713].

[153] K. Abe *et al.* (T2K), J. Phys. **G46**, 8, 08LT01 (2019), [arXiv:1902.03848].

[154] K. Abe *et al.* (T2K), Phys. Rev. D **100**, 11, 112009 (2019), [arXiv:1910.09439].

[155] P. Abratenko *et al.* (MicroBooNE) (2025), [arXiv:2503.00291].

[156] C. M. Marshall *et al.* (MINERvA), Phys. Rev. **D94**, 1, 012002 (2016), [arXiv:1604.03920].

[157] C. M. Marshall *et al.* (MINERvA), Phys. Rev. Lett. **119**, 1, 011802 (2017), [arXiv:1611.02224].

[158] Z. Wang *et al.* (MINERvA), Phys. Rev. Lett. **117**, 6, 061802 (2016), [arXiv:1606.08890].

[159] R. Acciarri *et al.* (ArgoNeuT), Phys. Rev. D **102**, 1, 011101 (2020), [arXiv:2004.01956].

[160] P. An *et al.* (COHERENT), Phys. Rev. Lett. **131**, 22, 221801 (2023), [arXiv:2305.19594].

[161] R. Mammen Abraham *et al.* (FASER), Phys. Rev. Lett. **133**, 2, 021802 (2024), [arXiv:2403.12520].

[162] P. Abratenko *et al.* (MicroBooNE), Phys. Rev. D **104**, 5, 052002 (2021), [arXiv:2101.04228].

[163] P. Abratenko *et al.* (MicroBooNE), Phys. Rev. D **105**, 5, L051102 (2022), [arXiv:2109.06832].

[164] P. Abratenko *et al.* (MicroBooNE), Phys. Rev. D **106**, 5, L051102 (2022), [arXiv:2208.02348].

[165] P. Abratenko *et al.* (MicroBooNE) (2025), [arXiv:2503.23384].

[166] S. Henry *et al.* (MINERvA), Phys. Rev. D **109**, 9, 092008 (2024), [arXiv:2312.16631].

[167] J. Wolcott *et al.* (MINERvA), Phys. Rev. Lett. **116**, 8, 081802 (2016), [arXiv:1509.05729].

[168] M. A. Acero *et al.* (NOvA), Phys. Rev. Lett. **130**, 5, 051802 (2023), [arXiv:2206.10585].

[169] K. Abe *et al.* (T2K), Phys. Rev. Lett. **113**, 24, 241803 (2014), [arXiv:1407.7389].

[170] K. Abe *et al.* (T2K), Phys. Rev. **D91**, 112010 (2015), [arXiv:1503.08815].

[171] K. Abe *et al.* (T2K), JHEP **10**, 114 (2020), [arXiv:2002.11986].

[172] K. Abe *et al.* (T2K) (2025), [arXiv:2505.00516].

[173] M. Betancourt *et al.*, Phys. Rept. **773-774**, 1 (2018), [arXiv:1805.07378].

[174] L. Alvarez-Ruso *et al.* (2025), [arXiv:2503.23556].

Int. J. Mod. Phys. A 2026.41. Downloaded from www.worldscientific.com
by UNIVERSITY OF CALIFORNIA @ BERKELEY on 09/16/26. Re-use and distribution is strictly not permitted, except for Open Access articles.

53. Plots of Cross Sections and Related Quantities

Updated in 2023. See various sections for details. For additional cross section results, please see earlier editions of the *Review of Particle Physics (https://pdg.lbl.gov/rpp-archive/)*.

53.1 Pseudorapidity Distributions in pp and $\overline{p}p$ Interactions . . . 831
53.2 Average Hadron Multiplicities in Hadronic e^+e^- Annihilation Events . . . 832
53.3 Annihilation Cross Section Near M_Z . . . 834

53.1 Pseudorapidity Distributions in pp and $\overline{p}p$ Interactions

Revised August 2013 by D.R. Ward (Cavendish Lab.).

Pseudorapidity Distributions in pp and $\overline{p}p$ Interactions

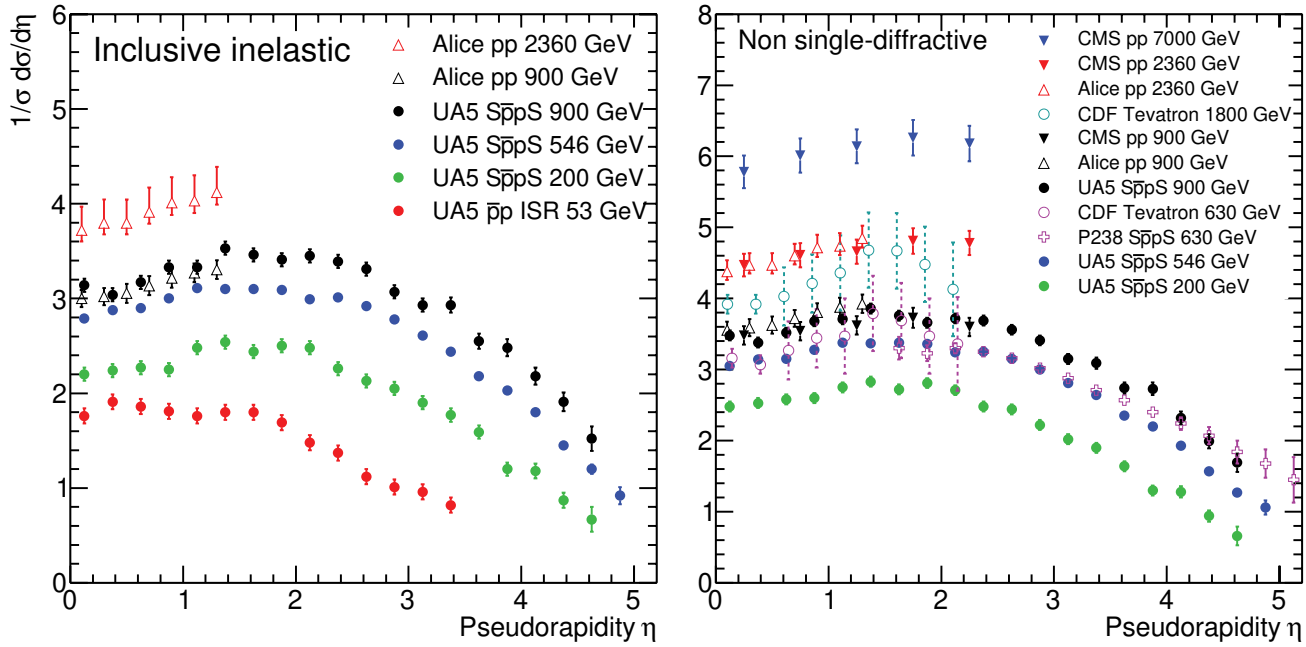

Figure 53.1: Charged particle pseudorapidity distributions in $p\overline{p}$ collisions for 53 GeV $\leq \sqrt{s} \leq$ 1800 GeV. UA5 data from the S$p\overline{p}$S are taken from [1], and from the ISR from [2]. The UA5 data are shown for both the full inelastic cross-section and with singly diffractive events excluded. Additional non single-diffractive measurements are available from CDF at the Tevatron [3] and from P238 at the S$p\overline{p}$S [4]. These may be compared with both inclusive and non single-diffractive measurements in pp collisions at the LHC from ALICE [5] and for non single-diffractive interactions from CMS [6, 7]. (Courtesy of D.R. Ward, Cambridge Univ., 2013)

Int. J. Mod. Phys. A 2026.41. Downloaded from www.worldscientific.com by UNIVERSITY OF CALIFORNIA @ BERKELEY on 09/16/26. Re-use and distribution is strictly not permitted, except for Open Access articles.

Int. J. Mod. Phys. A 2026.41. Downloaded from www.worldscientific.com
by [redacted]LIFORNIA @ BERKELEY on 09/16/26. Re-use and distribution is strictly not permitted, except for Open Access articles.

53.2 Average Hadron Multiplicities in Hadronic e^+e^- Annihilation Events

Revised August 2023 by O. Biebel (Ludwig-Maximilians U.).

Table 53.1: Average hadron multiplicities per hadronic e^+e^- annihilation event at $\sqrt{s} \approx 10$, 29–35, 91, and 130–200 GeV. The rates given include decay products from resonances with $c\tau < 10$ cm, and include the corresponding anti-particle state. Correlations of the systematic uncertainties were considered for the calculation of the averages. Quoted errors are not increased by scale factor S.

Particle	$\sqrt{s} \approx 10$ GeV	$\sqrt{s} = 29$–35 GeV	$\sqrt{s} = 91$ GeV	$\sqrt{s} = 130$–200 GeV	References
Pseudoscalar mesons:					
π^+	6.52 ± 0.11	0.3 ± 0.4	17.02 ± 0.19	21.24 ± 0.39	[8–17]
π^0	3.2 ± 0.3	5.83 ± 0.28	9.42 ± 0.32		[12, 18–23]
K^+	0.953 ± 0.018	1.48 ± 0.09	2.228 ± 0.059	2.82 ± 0.19	[9–17, 24, 25]
K^0	0.91 ± 0.05	1.48 ± 0.07	2.049 ± 0.026	2.10 ± 0.12	[12, 17, 20, 26–36]
η	0.20 ± 0.04	0.61 ± 0.07	1.049 ± 0.080		[12, 18, 19, 22, 23, 37–40]
$\eta'(958)$	0.03 ± 0.01	0.26 ± 0.10	0.152 ± 0.020		[20, 39, 41–43]
D^+	$0.194 \pm 0.019^{(a)}$	0.17 ± 0.03	0.175 ± 0.016		[12, 44–47]
D^0	$0.446 \pm 0.032^{(a)}$	0.45 ± 0.07	0.454 ± 0.030		[12, 44–47]
D_s^+	$0.063 \pm 0.014^{(a)}$	$0.45 \pm 0.20^{(b)}$	0.131 ± 0.021		[8, 39, 44, 47–49]
$B^{(c)}$	—	—	$0.134 \pm 0.016^{(d)}$		[46, 50]
B^+	—	—	$0.141 \pm 0.004^{(d)}$		[51]
B_s^0	—	—	$0.054 \pm 0.011^{(d)}$		[52, 53]
Scalar mesons:					
$f_0(980)$	0.024 ± 0.006	$0.05 \pm 0.02^{(e)}$	0.146 ± 0.012		[41, 54–56]
$a_0(980)^\pm$	—	—	$0.27 \pm 0.11^{(f)}$		[43]
Vector mesons:					
$\rho(770)^0$	0.35 ± 0.04	0.81 ± 0.08	1.231 ± 0.098		[9, 12, 55, 57, 58]
$\rho(770)^\pm$	—	—	$2.40 \pm 0.43^{(f)}$		[43]
$\omega(782)$	0.30 ± 0.08	—	1.016 ± 0.065		[40, 42, 43, 57]
$K^*(892)^+$	0.27 ± 0.03	0.64 ± 0.05	0.714 ± 0.055		[9, 12, 33, 57, 59, 60]
$K^*(892)^0$	0.29 ± 0.03	0.56 ± 0.06	0.738 ± 0.024		[9, 12, 36, 57, 58, 61, 62]
$\phi(1020)$	0.044 ± 0.003	0.085 ± 0.011	0.0963 ± 0.0032		[12, 36, 56–58, 61]
$D^*(2010)^+$	$0.177 \pm 0.022^{(a)}$	0.43 ± 0.07	$0.1937 \pm 0.0057^{(g)}$		[12, 44–46, 63, 64]
$D^*(2007)^0$	$0.168 \pm 0.019^{(a)}$	0.27 ± 0.11	—		[12, 44, 45]
$D_s^*(2112)^+$	$0.048 \pm 0.014^{(a)}$	—	$0.101 \pm 0.048^{(h)}$		[48, 65]
$B^{*\ (i)}$	—	—	0.288 ± 0.026		[66, 67]
$J/\psi(1S)$	$0.00050 \pm 0.00005^{(a)}$	—	$0.0052 \pm 0.0004^{(j)}$		[68–73]
$\psi(2S)$	—	—	$0.0023 \pm 0.0004^{(j)}$		[71, 73, 74]
$\Upsilon(1S)$	—	—	$0.00014 \pm 0.00007^{(j)}$		[75]
Pseudovector mesons:					
$f_1(1285)$	—	—	0.165 ± 0.051		[76]
$f_1(1420)$	—	—	0.056 ± 0.012		[76]
$\chi_{c1}(3510)$	—	—	$0.0041 \pm 0.0011^{(j)}$		[71, 74]
Tensor mesons:					
$f_2(1270)$	0.09 ± 0.02	0.14 ± 0.04	0.166 ± 0.020		[54–56, 77]
$f_2'(1525)$	—	—	0.012 ± 0.006		[55]
$K_2^*(1430)^+$	—	0.09 ± 0.03	—		[55, 78]
$K_2^*(1430)^0$	—	0.12 ± 0.06	0.084 ± 0.022		[54, 55, 79]
$B^{**\ (k)}$	—	—	0.118 ± 0.024		[80]
$D_{s1}^\pm$	—	—	$0.0052 \pm 0.0011^{(\ell)}$		[81]
$D_{s2}^{*\pm}$	—	—	$0.0083 \pm 0.0031^{(\ell)}$		[81]
Baryons:					
p	0.266 ± 0.008	0.640 ± 0.050	1.050 ± 0.032	1.41 ± 0.18	[10, 13–17, 24, 25, 77]
Λ	$0.093 \pm 0.006^{(a)}$	0.205 ± 0.010	0.3915 ± 0.0065	0.39 ± 0.03	[17, 20, 34, 36, 77, 82–85]
Σ^0	$0.0221 \pm 0.0018^{(a)}$	—	0.078 ± 0.010		[10, 59, 82, 86–88]
Σ^-	—	—	0.081 ± 0.010		[88, 89]
Σ^+	—	—	0.107 ± 0.011		[87, 88]
$\Sigma^\pm$	—	—	0.174 ± 0.009		[84, 88]
Ξ^-	$0.0055 \pm 0.0004^{(a)}$	0.0176 ± 0.0027	0.0262 ± 0.0009		[9, 59, 77, 82–85]
$\Delta(1232)^{++}$	0.040 ± 0.010	—	0.085 ± 0.014		[90–92]
$\Sigma(1385)^-$	0.006 ± 0.002	0.017 ± 0.004	0.0240 ± 0.0017		[59, 82, 84, 85, 93]
$\Sigma(1385)^+$	$0.0062 \pm 0.0011^{(a)}$	0.017 ± 0.004	0.0239 ± 0.0015		[59, 82–85, 93]
$\Sigma(1385)^\pm$	0.0106 ± 0.0020	0.033 ± 0.008	0.0472 ± 0.0027		[59, 82, 84, 85, 93]
$\Xi(1530)^0$	$0.00130 \pm 0.00010^{(a)}$	—	0.00694 ± 0.00049		[59, 82, 83, 85, 94]
Ω^-	$0.00060 \pm 0.00033^{(a)}$	0.014 ± 0.007	0.00124 ± 0.00018		[59, 77, 82, 83, 85, 86]
Λ_c^+	$0.0480 \pm 0.0036^{(a,m)}$	0.110 ± 0.050	$0.0591 \pm 0.0047^{(n)}$		[47, 49, 77, 83, 95, 96]
Λ_b^0	—	—	0.031 ± 0.016		[97]
Σ_c^0	$0.0025 \pm 0.0004^{(a)}$	—	—		[83]
$\Lambda(1520)$	$0.0046 \pm 0.0004^{(a)}$	—	0.0222 ± 0.0027		[83, 85, 89, 98]

(*a*) $\sigma_{\rm had} = 3.33 \pm 0.05 \pm 0.21$ nb (**CLEO**: [99]) has been used in converting the measured cross sections to average hadron multiplicities.
(*b*) $\mathrm{B}(D_s \to \eta\pi,\ \eta'\pi)$ was used (RPP 1994).

Int. J. Mod. Phys. A 2026.41. Downloaded from www.worldscientific.com
by UNIVERSITY OF CALIFORNIA @ BERKELEY on 09/16/26. Re-use and distribution is strictly not permitted, except for Open Access articles.

(c) Comprises both charged and neutral B meson states.
(d) The Standard Model $\mathrm{B}(Z \to b\bar{b}) = 0.217$ was used.
(e) $x_p = p/p_{\mathrm{beam}} > 0.1$ only.
(f) Both charge states.
(g) $\mathrm{B}(D^*(2010)^+ \to D^0\pi^+) \times \mathrm{B}(D^0 \to K^-\pi^+)$ has been used (RPP 2000).
(h) $\mathrm{B}(D_s^* \to D_S^+\gamma)$, $\mathrm{B}(D_s^+ \to \phi\pi^+)$, $\mathrm{B}(\phi \to K^+K^-)$ have been used (RPP 1998).
(i) Any charge state (*i.e.*, B_d^*, B_u^*, or B_s^*).
(j) $\mathrm{B}(Z \to \mathrm{hadrons}) = 0.699$ was used (RPP 1994).
(k) Any charge state (*i.e.*, B_d^{**}, B_u^{**}, or B_s^{**}).
(ℓ) Assumes $\mathrm{B}(D_{s1}^+ \to D^{*+}K^0 + D^{*0}K^+) = 100\%$ and $\mathrm{B}(D_{s2}^+ \to D^0K^+) = 45\%$.
(m) Derived from the production cross section of $\Lambda_c^+ \to p\pi K$ using (a) and using $\mathrm{B}(\Lambda_c^+ \to p\pi K) = (6.26 \pm 0.29)\%$ (RPP 2022).
(n) Derived from [96], updated with $\mathrm{B}(\Lambda_c^+ \to p\pi K) = (6.26 \pm 0.29)\%$ (RPP 2022), and complemented by the Λ_c^+ contribution from $g \to c\bar{c}$ of [47].

References grouped by collaboration for Table-53.1:

- **RPP**: [12]
- **ALEPH**: [13, 20, 40, 58, 59, 63, 70, 81],
- **ARGUS**: [8, 24, 37, 41, 57, 82, 90, 98],
- **BaBar**: [10, 48, 68, 95],
- **Belle**: [44, 69, 83],
- **CELLO**: [19, 26],
- **CLEO**: [9, 45, 49, 99],
- **Crystal Ball**: [38],
- **DELPHI**: [14, 17, 21, 25, 33, 46, 50–52, 55, 61, 66, 71, 76, 80, 84, 86, 89, 91, 94],
- **HRS**: [27, 54, 78, 93],
- **L3**: [22, 34, 42, 67, 72, 74, 87]
- **MARK II**: [29, 39],
- **JADE**: [18, 28],
- **OPAL**: [15, 23, 35, 43, 47, 53, 56, 60, 62, 64, 65, 73, 75, 79, 85, 88, 92, 97],
- **PLUTO**: [30]
- **SLD**: [16, 36],
- **TASSO**: [31]
- **TPC**: [32].

53.3 Annihilation Cross Section Near M_Z

Courtesy of M. Grünewald and the LEP Electroweak Working Group, 2007.

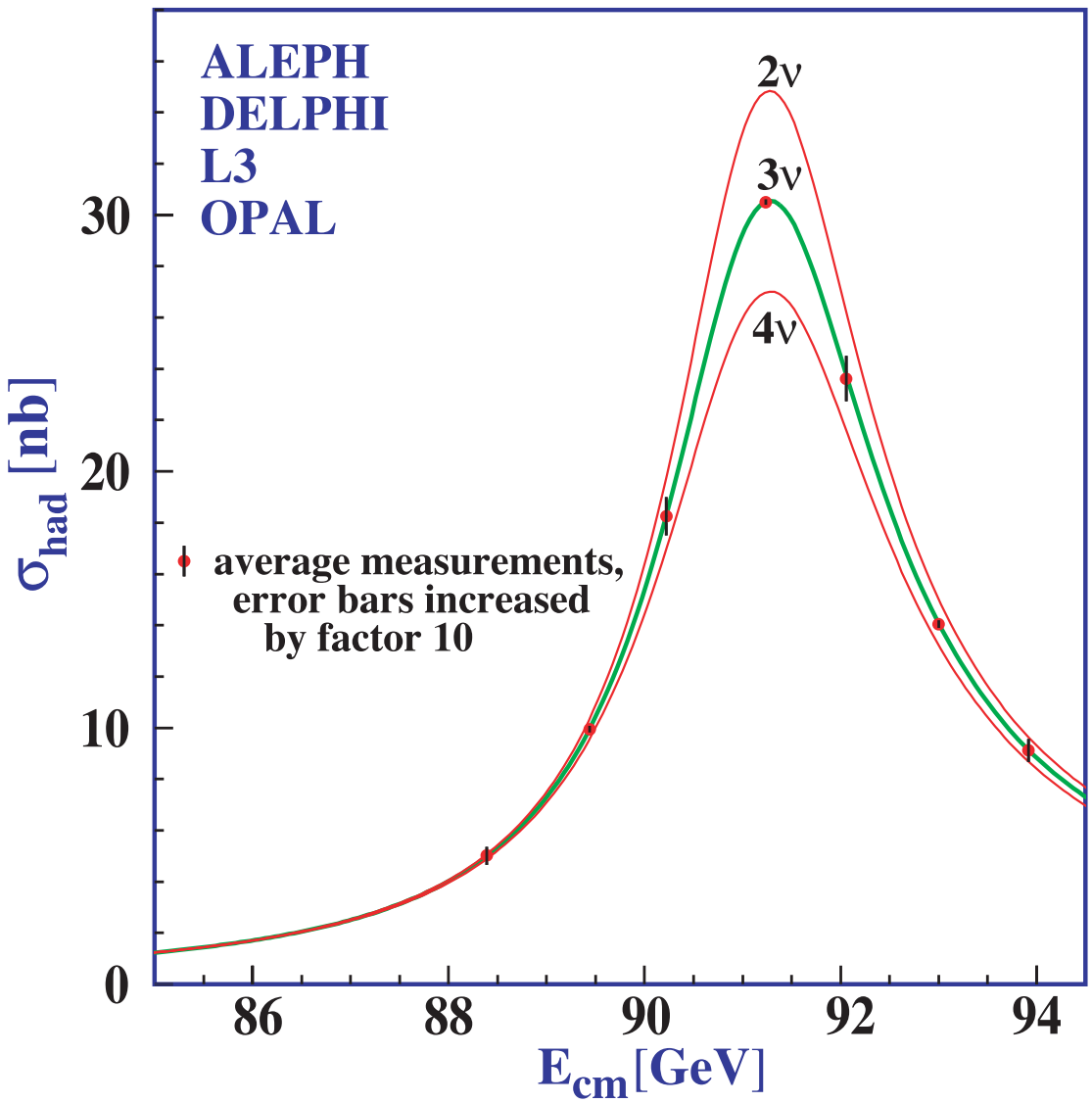

Figure 53.2: Combined data from the ALEPH, DELPHI, L3, and OPAL Collaborations for the cross section in e^+e^- annihilation into hadronic final states as a function of the center-of-mass energy near the Z pole. The curves show the predictions of the Standard Model with two, three, and four species of light neutrinos. The asymmetry of the curve is produced by initial-state radiation. Note that the error bars have been increased by a factor ten for display purposes. References: ALEPH [100], DELPHI [101], L3 [102], OPAL [103], Combination [104],

Int. J. Mod. Phys. A 2026.41. Downloaded from www.worldscientific.com
LIFORNIA @ BERKELEY on 09/16/26. Re-use and distribution is strictly not permitted, except for Open Access articles.
by

Int. J. Mod. Phys. A 2026.41. Downloaded from www.worldscientific.com
by UNIVERSITY OF CALIFORNIA @ BERKELEY on 09/16/26. Re-use and distribution is strictly not permitted, except for Open Access articles.

References

[1] G. J. Alner *et al.* (UA5), Z. Phys. **C33**, 1 (1986).

[2] K. Alpgard *et al.* (UA5), Phys. Lett. **112B**, 183 (1982).

[3] F. Abe *et al.* (CDF), Phys. Rev. **D41**, 2330 (1990), [,119(1989)].

[4] R. Harr *et al.*, Phys. Lett. **B401**, 176 (1997), [hep-ex/9703002].

[5] K. Aamodt *et al.* (ALICE), Eur. Phys. J. **C68**, 89 (2010), [arXiv:1004.3034].

[6] V. Khachatryan *et al.* (CMS), JHEP **02**, 041 (2010), [arXiv:1002.0621].

[7] V. Khachatryan *et al.* (CMS), Phys. Rev. Lett. **105**, 022002 (2010), [arXiv:1005.3299].

[8] H. Albrecht *et al.* (ARGUS), Z. Phys. **C54**, 1 (1992).

[9] S. Behrends *et al.* (CLEO), Phys. Rev. **D31**, 2161 (1985).

[10] J. P. Lees *et al.* (BaBar), Phys. Rev. **D88**, 032011 (2013), [arXiv:1306.2895].

[11] H. Albrecht *et al.*, Phys. Lett. **102B**, 291 (1981).

[12] K. Hikasa *et al.* (Particle Data Group), Phys. Rev. **D45**, S1 (1992), [Erratum: Phys. Rev.D46,5210(1992)].

[13] R. Barate *et al.* (ALEPH), Eur. Phys. J. **C5**, 205 (1998).

[14] P. Abreu *et al.* (DELPHI), Eur. Phys. J. **C5**, 585 (1998).

[15] R. Akers *et al.* (OPAL), Z. Phys. **C63**, 181 (1994).

[16] K. Abe *et al.* (SLD), Phys. Rev. **D69**, 072003 (2004), [hep-ex/0310017].

[17] P. Abreu *et al.* (DELPHI), Eur. Phys. J. **C18**, 203 (2000), [Erratum: Eur. Phys. J.C25,493(2002)], [hep-ex/0103031].

[18] D. D. Pitzl *et al.* (JADE), Z. Phys. **C46**, 1 (1990), [Erratum: Z. Phys.C47,676(1990)].

[19] H. J. Behrend *et al.* (CELLO), Z. Phys. **C47**, 1 (1990).

[20] R. Barate *et al.* (ALEPH), Eur. Phys. J. **C16**, 613 (2000).

[21] W. Adam *et al.* (DELPHI), Z. Phys. **C69**, 561 (1996).

[22] M. Acciarri *et al.* (L3), Phys. Lett. **B371**, 126 (1996).

[23] G. Abbiendi *et al.* (OPAL), Eur. Phys. J. **C17**, 373 (2000), [hep-ex/0007017].

[24] H. Albrecht *et al.* (ARGUS), Z. Phys. **C44**, 547 (1989).

[25] P. Abreu *et al.* (DELPHI), Nucl. Phys. **B444**, 3 (1995).

[26] H. J. Behrend *et al.* (CELLO), Z. Phys. **C46**, 397 (1990).

[27] M. Derrick *et al.*, Phys. Rev. **D35**, 2639 (1987).

[28] W. Bartel *et al.* (JADE), Z. Phys. **C20**, 187 (1983).

[29] H. Schellman *et al.*, Phys. Rev. **D31**, 3013 (1985).

[30] C. Berger *et al.* (PLUTO), Phys. Lett. **104B**, 79 (1981).

[31] M. Althoff *et al.* (TASSO), Z. Phys. **C27**, 27 (1985).

[32] H. Aihara *et al.* (TPC/Two Gamma), Phys. Rev. Lett. **53**, 2378 (1984).

[33] P. Abreu *et al.* (DELPHI), Z. Phys. **C65**, 587 (1995).

[34] M. Acciarri *et al.* (L3), Phys. Lett. **B407**, 389 (1997), [Erratum: Phys. Lett.B427,409(1998)].

[35] R. Akers *et al.* (OPAL), Z. Phys. **C67**, 389 (1995).

[36] K. Abe *et al.* (SLD), Phys. Rev. **D59**, 052001 (1999), [hep-ex/9805029].

[37] H. Albrecht *et al.* (ARGUS), Z. Phys. **C46**, 15 (1990).

[38] C. Bieler *et al.* (Crystal Ball), Z. Phys. **C49**, 225 (1991).

[39] G. Wormser *et al.*, Phys. Rev. Lett. **61**, 1057 (1988).

[40] A. Heister *et al.* (ALEPH), Phys. Lett. **B528**, 19 (2002), [hep-ex/0201012].

[41] H. Albrecht *et al.* (ARGUS), Z. Phys. **C58**, 199 (1993).

[42] M. Acciarri *et al.* (L3), Phys. Lett. **B393**, 465 (1997).

[43] K. Ackerstaff *et al.* (OPAL), Eur. Phys. J. **C5**, 411 (1998), [hep-ex/9805011].

[44] R. Seuster *et al.* (Belle), Phys. Rev. **D73**, 032002 (2006), [hep-ex/0506068].

[45] M. Artuso *et al.* (CLEO), Phys. Rev. **D70**, 112001 (2004), [hep-ex/0402040].

[46] P. Abreu *et al.* (DELPHI), Z. Phys. **C59**, 533 (1993), [Erratum: Z. Phys.C65,709(1995)].

[47] G. Alexander *et al.* (OPAL), Z. Phys. **C72**, 1 (1996).

[48] B. Aubert *et al.* (BaBar), Phys. Rev. **D65**, 091104 (2002), [hep-ex/0201041].

[49] D. Bortoletto *et al.* (CLEO), Phys. Rev. **D37**, 1719 (1988), [Erratum: Phys. Rev.D39,1471(1989)].

[50] P. Abreu *et al.* (DELPHI), Z. Phys. **C57**, 181 (1993).

[51] J. Abdallah *et al.* (DELPHI), Phys. Lett. **B576**, 29 (2003), [hep-ex/0311005].

[52] P. Abreu *et al.* (DELPHI), Z. Phys. **C61**, 407 (1994).

[53] R. Akers *et al.* (OPAL), Z. Phys. **C66**, 555 (1995).

[54] S. Abachi *et al.*, Phys. Rev. Lett. **57**, 1990 (1986).

[55] P. Abreu *et al.* (DELPHI), Phys. Lett. **B449**, 364 (1999).

[56] K. Ackerstaff *et al.* (OPAL), Eur. Phys. J. **C4**, 19 (1998), [hep-ex/9802013].

[57] H. Albrecht *et al.* (ARGUS), Z. Phys. **C61**, 1 (1994).

[58] D. Buskulic *et al.* (ALEPH), Z. Phys. **C69**, 379 (1996).

[59] R. Barate *et al.* (ALEPH), Phys. Rept. **294**, 1 (1998).

[60] P. D. Acton *et al.* (OPAL), Phys. Lett. **B305**, 407 (1993).

[61] P. Abreu *et al.* (DELPHI), Z. Phys. **C73**, 61 (1996).

[62] K. Ackerstaff *et al.* (OPAL), Phys. Lett. **B412**, 210 (1997), [hep-ex/9708022].

[63] R. Barate *et al.* (ALEPH), Eur. Phys. J. **C16**, 597 (2000), [hep-ex/9909032].

[64] K. Ackerstaff *et al.* (OPAL), Eur. Phys. J. **C1**, 439 (1998), [hep-ex/9708021].

[65] K. Ackerstaff *et al.* (OPAL), Eur. Phys. J. **C5**, 1 (1998), [hep-ex/9802008].

[66] P. Abreu *et al.* (DELPHI), Z. Phys. **C68**, 353 (1995).

[67] M. Acciarri *et al.* (L3), Phys. Lett. **B345**, 589 (1995).

[68] B. Aubert *et al.* (BaBar), Phys. Rev. Lett. **87**, 162002 (2001), [hep-ex/0106044].

[69] K. Abe *et al.* (Belle), Phys. Rev. Lett. **88**, 052001 (2002), [hep-ex/0110012].

[70] D. Buskulic *et al.* (ALEPH), Phys. Lett. **B295**, 396 (1992).

[71] P. Abreu *et al.* (DELPHI), Phys. Lett. **B341**, 109 (1994).

[72] M. Acciarri *et al.* (L3), Phys. Lett. **B453**, 94 (1999).

[73] G. Alexander *et al.* (OPAL), Z. Phys. **C70**, 197 (1996).

[74] M. Acciarri *et al.* (L3), Phys. Lett. **B407**, 351 (1997).

[75] G. Alexander *et al.* (OPAL), Phys. Lett. **B370**, 185 (1996).

[76] J. Abdallah *et al.* (DELPHI), Phys. Lett. **B569**, 129 (2003), [hep-ex/0309057].

[77] A. De Angelis, J. Phys. **G19**, 1233 (1993).

[78] S. Abachi *et al.*, Phys. Lett. **B199**, 151 (1987).

[79] R. Akers *et al.* (OPAL), Z. Phys. **C68**, 1 (1995).

[80] P. Abreu *et al.* (DELPHI), Phys. Lett. **B345**, 598 (1995).

[81] A. Heister *et al.* (ALEPH), Phys. Lett. **B526**, 34 (2002), [hep-ex/0112010].

[82] H. Albrecht *et al.* (ARGUS), Z. Phys. **C39**, 177 (1988).

[83] M. Niiyama *et al.* (Belle), Phys. Rev. **D97**, 7, 072005 (2018), [arXiv:1706.06791].

[84] P. Abreu *et al.* (DELPHI), Z. Phys. **C67**, 543 (1995).

[85] G. Alexander *et al.* (OPAL), Z. Phys. **C73**, 569 (1997).

[86] W. Adam *et al.* (DELPHI), Z. Phys. **C70**, 371 (1996).

[87] M. Acciarri *et al.* (L3), Phys. Lett. **B479**, 79 (2000), [hep-ex/0002066].

[88] G. Alexander *et al.* (OPAL), Z. Phys. **C73**, 587 (1997).

[89] P. Abreu *et al.* (DELPHI), Phys. Lett. **B475**, 429 (2000), [hep-ex/0103020].

[90] H. Albrecht *et al.* (ARGUS), Phys. Lett. **B230**, 169 (1989).

[91] P. Abreu *et al.* (DELPHI), Phys. Lett. **B361**, 207 (1995).

[92] G. Alexander *et al.* (OPAL), Phys. Lett. **B358**, 162 (1995).

[93] S. Abachi *et al.*, Phys. Rev. Lett. **58**, 2627 (1987), [Erratum: Phys. Rev. Lett.59,2388(1987)].

[94] J. Abdallah *et al.* (DELPHI), Eur. Phys. J. **C44**, 299 (2005), [hep-ex/0510023].

[95] B. Aubert *et al.* (BaBar), Phys. Rev. **D75**, 012003 (2007), [hep-ex/0609004].

[96] L. Gladilin, Eur. Phys. J. C **75**, 1, 19 (2015), [arXiv:1404.3888].

[97] P. D. Acton *et al.* (OPAL), Phys. Lett. **B281**, 394 (1992).

[98] H. Albrecht *et al.* (ARGUS), Phys. Rept. **276**, 223 (1996).

[99] R. Giles *et al.* (CLEO), Phys. Rev. **D29**, 1285 (1984).

[100] R. Barate *et al.* (ALEPH), Eur. Phys. J. **C14**, 1 (2000).

[101] P. Abreu *et al.* (DELPHI), Eur. Phys. J. **C16**, 371 (2000).

[102] M. Acciarri *et al.* (L3), Eur. Phys. J. **C16**, 1 (2000), [hep-ex/0002046].

[103] G. Abbiendi *et al.* (OPAL), Eur. Phys. J. **C19**, 587 (2001), [hep-ex/0012018].

[104] S. Schael *et al.* (ALEPH, DELPHI, L3, OPAL, SLD, LEP Electroweak Working Group, SLD Electroweak Group, SLD Heavy Flavour Group), Phys. Rept. **427**, 257 (2006), [hep-ex/0509008].

Int. J. Mod. Phys. A 2026.41. Downloaded from www.worldscientific.com
by [redacted]LIFORNIA @ BERKELEY on 09/16/26. Re-use and distribution is strictly not permitted, except for Open Access articles.

Int. J. Mod. Phys. A 2026.41. Downloaded from www.worldscientific.com
by UNIVERSITY OF CALIFORNIA @ BERKELEY on 09/16/26. Re-use and distribution is strictly not permitted, except for Open Access articles.

Particle Properties

Gauge Bosons
54. Mass and width of the W boson (rev.) 839
55. Z boson (rev.) 841

Charged Leptons
56. Muon anomalous magnetic moment (rev.) 846
57. Muon decay parameters 853
58. τ branching fractions (rev.) 856
59. τ-lepton decay parameters 859

Quarks
60. Quark masses 861
61. Top quark (rev.) 871

Mesons
62. Form factors for semileptonic kaon ($K_{\ell 3}$), radiative pion ($\pi_{\ell 2\gamma}$) & kaon ($K_{\ell 2\gamma}$) decays (rev.) 911
63. Spectroscopy of light meson resonances (rev.) 914
64. Scalar mesons below 1 GeV (rev.) 928
65. Rare kaon decays (rev.) 937
66. CPT invariance tests in neutral kaon decay 943
67. V_{ud}, V_{us}, Cabibbo angle, and CKM unitarity (rev.) 945
68. CP-violation in K_L decays 949
69. Review of multibody charm analyses (rev.) 952
70. D^0–$\overline{D}^0$ mixing (rev.) 958
71. Leptonic decays of charged pseudoscalar mesons (rev.) 969
72. Production and decay of b-flavored hadrons (rev.) 980
73. Polarization in B decays (rev.) 992
74. B^0–$\overline{B}^0$ mixing (rev.) 996
75. Semileptonic B decays, V_{cb} and V_{ub} (rev.) 1003
76. CKM angles from B hadrons, determination of (rev.) 1021
77. Spectroscopy of mesons containing two heavy quarks (rev.) 1026
78. Heavy non-$q\overline{q}$ mesons (rev.) 1035

Baryons
79. Baryon decay parameters 1046
80. N and Δ resonances 1047
81. Λ and Σ resonances 1052
82. Pole structure of the $\Lambda(1405)$ region (rev.) 1055
83. Pentaquarks (rev.) 1057

Notes in Volume 2

Triple gauge couplings (TGC's) 1247
Anomalous $ZZ\gamma$, $Z\gamma\gamma$, and ZZV couplings 1274
Anomalous W/Z quartic couplings 1276
Neutrino properties 1404
Sum of neutrino masses (rev.) 1407
Number of light neutrino types from collider experiments 1414
Charged kaon mass 1623
Dalitz plot parameters for $K \to 3\pi$ decays 1632
CP-violation in $K_S \to 3\pi$ 1642
Heavy Flavor Averaging Group (rev.) 1775
Charmonium system 2002
Branching ratios of $\psi(2S)$ and $\chi_{c0,1,2}$ (rev.) 2041
Bottomonium system 2142
Width determination of the Υ states 2142
Radiative hyperon decays 2348
Ξ and Ω resonances (rev.) 2352

Int. J. Mod. Phys. A 2026.41. Downloaded from www.worldscientific.com
UNIVERSITY OF CALIFORNIA @ BERKELEY on 09/16/26. Re-use and distribution is strictly not permitted, except for Open Access articles.

54. Mass and Width of the W Boson

Revised May 2026 by M. Grünewald (University Coll. Dublin), A. Gurtu (CERN; TIFR Mumbai) and J. Kretzschmar (Liverpool U.).

Precision determination of the W mass is of great importance in testing the internal consistency of the Standard Model. From the time of its discovery in 1983, the W boson has been studied and its mass determined in $p\bar{p}$, e^+e^- and pp interactions. The mass m_W and width Γ_W definition used in measurements corresponds to a Breit-Wigner with mass-dependent width with a propagator $\propto 1/(s - m_W^2 + is\Gamma_W/m_W)$.

At the e^+e^- collider LEP, the dependence of the W-pair production cross section on m_W is large close to the production threshold ($\sqrt{s} \approx 2m_W \approx 161$ GeV). Hence this was used for the mass measurement, together with the precise knowledge of the beam energy. At higher center-of-mass energies ($\sqrt{s} = 172$ to 209 GeV) this dependence is much weaker, thus W bosons were directly reconstructed and the mass determined as the invariant mass of the decay products, improving the resolution with a kinematic fit. The LEP average W mass was then determined in a combination of the measurements from each experiment for all channels ($q\bar{q}q\bar{q}$ and $q\bar{q}\ell\nu$, $\ell = e, \mu, \tau$) and centre-of-mass energies along with a detailed decomposition of uncertainty contributions [1]. This yielded a combined LEP average W mass of $m_W = 80.376 \pm 0.033$ GeV. Errors on m_W due to uncertainties in the LEP beam energy (9 MeV), and possible effect of color reconnection (CR) and Bose-Einstein correlations (BEC) between quarks from different W bosons (8 MeV) are included.

Currently the most precise measurements of the W mass are performed in hadron collisions at the Tevatron ($p\bar{p}$) and the LHC (pp). These analyses use the electron or muon decay modes of the W boson ($\ell\nu$, $\ell = e, \mu$) and tag the production of W bosons with the high p_T charged lepton and missing energy transverse to the beam direction arising from the neutrino. Owing to the unknown parton-parton effective energy and the unmeasured missing energy in the longitudinal direction, the hadron collider experiments reconstruct the transverse mass of the W boson, and derive the W mass from comparing the distribution with Monte Carlo predictions obtained for different values of m_W. The transverse momentum of the charged lepton itself and the transverse missing energy are also sensitive to the W mass and used in its determination. Specifically, measurements by the LHC experiments so far rely primarily on the charged lepton p_T distribution.

In the past, the two Tevatron experiments CDF [2] and D0 [3] provided a combined value for the W mass by identifying common systematic uncertainties due to the parton distribution functions (PDF), radiative corrections, and choice of the width [4]. With the first mass results from the two LHC experiments, ATLAS [5] and LHCb [6], a simplified W-mass average for the LHC was obtained, assuming a correlated uncertainty of 9 MeV (PDF) [7]. Similarly, assuming a correlated uncertainty of 7 MeV, a hadron collider average of the Tevatron and LHC measurements was obtained [7].

All measurements were in good agreement with each other, until the CDF collaboration published a result $m_W = 80.4335 \pm 0.0094$ GeV [8] in April 2022, based upon their full Run-II dataset of 8.8 fb^{-1}. This result is of higher precision than the 2022 world average, but the two values disagree significantly.[1] The LHC-TeV W-mass Working Group with W-mass experts from all hadron collider experiments, CDF, D0, ATLAS, CMS, LHCb, has been working to understand better the nature of this disagreement and suggest a new world average value of the W mass. Theoretical corrections, uncertainties and their correlations between different hadron collider experiments have been evaluated in detail and used in the combination: the central values are corrected to a common theory description and PDF set, and the uncertainties and correlations due to PDFs have been re-evaluated. The group reported in 2023 [9] that a combination of all W-mass measurements has a probability of compatibility of only 0.5%. A 91% probability of compatibility is obtained when the CDF Run-II measurement is removed.

Two new results have appeared since this combination. The ATLAS Collaboration published a refined analysis of their data used in [5] and obtained a more precise mass value of 80.3665 ± 0.0159 GeV [10]. The CMS Collaboration published their first measurement of $m_W = 80.3602 \pm 0.0099$ GeV [11], reaching a precision close to the CDF Run-II result.

In May 2026, LHC-TeV W-mass Working Group updated their combination with these new results [12], using the same combination strategy as previously in [9]. The ATLAS and CMS measurement uncertainties, resulting from profile-likelihood ratio fits, are decomposed using the prescription detailed in [13]. A combination of all W-mass measurements has a probability of compatibility of only 0.06%, and is therefore disfavoured. A 96.9% probability of compatibility is obtained when the CDF Run-II measurement is removed. The corresponding value of the W boson mass is $m_W = 80362.5 \pm 7.7$ MeV [12] which we quote as the World Average. More details can be found in [9, 12, 13].

The results on the W mass published by the experiments are shown in Figure 54.1.

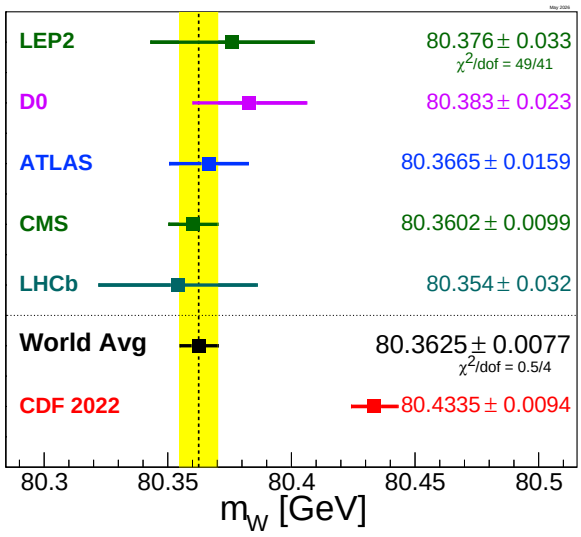

Figure 54.1: Measurements of the W-boson mass by the LEP, Tevatron and LHC experiments as well as their combination. Below the combination, the CDF 2022 result is shown which is currently not used in the world average.

Similarly, the W boson total width has been measured in e^+e^-, $p\bar{p}$ and pp collision data. The combined LEP average of the W boson total width was determined to be $\Gamma_W = 2.195 \pm 0.083$ GeV [1], with a good internal consistency of 27% χ^2 probability. The most recent width measurements from the Tevatron experiments CDF and D0 were combined to $\Gamma_W = 2.046 \pm 0.049$ GeV [14], also with very good internal compatibility of 84%. The latest and most precise measurement to date was performed by ATLAS yielding $\Gamma_W = 2.202 \pm 0.047$ GeV [10]. All results are shown in Figure 54.2 together with our weighted average of the three results of $\Gamma_W = 2.14 \pm 0.05$ GeV, where the error is scaled by a factor of 1.7 to account for a tension between the three width results (5.3% χ^2 probability) as shown in Figure 54.2.

The Standard Model prediction from an electroweak fit, including Z-pole data and the measured masses of the top quark and of the Higgs boson but excluding results on m_W and Γ_W, implies a W-boson mass of $m_W = 80.357 \pm 0.006$ GeV and a W-boson width of $\Gamma_W = 2.090 \pm 0.001$ GeV; see Section 10, Electroweak Model and Constraints on New Physics, J. de Blas, S. Dittmaier and R. Kogler, 2026, this review.

[1] The 2022 CDF result includes the 2.2 fb^{-1} of data used for the previous CDF Run-II result of 80.387 ± 0.019 GeV [2]. Incorporating the improved understanding of PDFs and track reconstruction , the central value of the 2.2 fb^{-1} result is increased by 0.0135 GeV to 80.4005 GeV [8].

Int. J. Mod. Phys. A 2026.41. Downloaded from www.worldscientific.com by UNIVERSITY OF CALIFORNIA @ BERKELEY on 09/16/26. Re-use and distribution is strictly not permitted, except for Open Access articles.

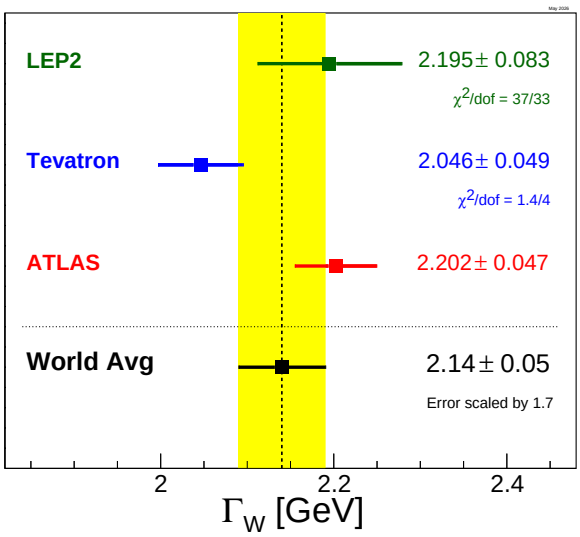

Figure 54.2: Measurements of the W-boson width by the LEP, Tevatron and LHC experiments.

References

[1] S. Schael *et al.* (ALEPH, DELPHI, L3, OPAL, LEP Electroweak Working Group), Phys. Rept. **532**, 119 (2013), [arXiv:1302.3415].

[2] T. Aaltonen *et al.* (CDF), Phys. Rev. Lett. **108**, 151803 (2012), [arXiv:1203.0275].

[3] V. M. Abazov *et al.* (D0), Phys. Rev. Lett. **108**, 151804 (2012), [arXiv:1203.0293].

[4] T. A. Aaltonen *et al.* (CDF, D0), Phys. Rev. D **88**, 5, 052018 (2013), [arXiv:1307.7627].

[5] M. Aaboud *et al.* (ATLAS), Eur. Phys. J. C **78**, 2, 110 (2018), [Erratum: Eur.Phys.J.C 78, 898 (2018)], [arXiv:1701.07240].

[6] R. Aaij *et al.* (LHCb), JHEP **01**, 166 (2022), [arXiv:2107.10090].

[7] R. L. Workman *et al.* (Particle Data Group), PTEP **2022**, 083C01 (2022).

[8] T. Aaltonen *et al.* (CDF), Science **376**, 6589, 170 (2022).

[9] S. Amoroso *et al.* (LHC-TeV MW Working Group), Eur. Phys. J. C **84**, 5, 451 (2024), [arXiv:2308.09417].

[10] G. Aad *et al.* (ATLAS), Eur. Phys. J. C **84**, 12, 1309 (2024), [arXiv:2403.15085].

[11] V. Chekhovsky *et al.* (CMS) (2024), [arXiv:2412.13872].

[12] LHC-TeVatron M_W Working Group, Compatibility and combination of world W-boson mass measurements (7 May 2026), URL `https://twiki.cern.ch/twiki/pub/LHCPhysics/LHC-TEV-MWWG/update_May2026.pdf`.

[13] A. Pinto *et al.*, Uncertainty components in profile likelihood fits (2024), [arXiv:2307.04007], URL `https://arxiv.org/abs/2307.04007`.

[14] The Tevatron Electroweak Working Group, for the CDF and D0 Collaborations, March 2010, [arXiv:1003.2826].

Int. J. Mod. Phys. A 2026.41. Downloaded from www.worldscientific.com
UNIVERSITY OF CALIFORNIA @ BERKELEY on 09/16/26. Re-use and distribution is strictly not permitted, except for Open Access articles.

Int. J. Mod. Phys. A 2026.41. Downloaded from www.worldscientific.com
by UNIVERSITY OF CALIFORNIA @ BERKELEY on 09/16/26. Re-use and distribution is strictly not permitted, except for Open Access articles.

55. Z Boson

Revised August 2025 by M. Grünewald (University Coll. Dublin), A. Gurtu (CERN; TIFR Mumbai) and J. Kretzschmar (Liverpool U.).

Precision measurements at the Z-boson resonance using electron–positron colliding beams began in 1989 at the SLC and at LEP. During 1989–95, the four LEP experiments (ALEPH, DELPHI, L3, OPAL) made high-statistics studies of the production and decay properties of the Z. Although the SLD experiment at the SLC collected much lower statistics, it was able to match the precision of LEP experiments in determining the effective electroweak mixing angle $\sin^2\overline{\theta}_W$ and the rates of Z decay to b- and c-quarks, owing to availability of polarized electron beams, small beam size, and stable beam spot. Measurements in $p\bar{p}$ and pp collisions at the Tevatron and the LHC have reached a precision competitive with the e^+e^- colliders in a limited set of observables.

The Z-boson properties reported in this section may broadly be categorized as:

- The standard 'lineshape' parameters of the Z consisting of its mass, M_Z, its total width, Γ_Z, and its partial decay widths, Γ(hadrons), and $\Gamma(\ell\bar{\ell})$ where $\ell = e, \mu, \tau, \nu$;
- Z asymmetries in leptonic decays and extraction of Z couplings to charged and neutral leptons;
- The b- and c-quark-related partial widths and charge asymmetries which require special techniques.

The effective vector and axial-vector coupling constants describing the Z-to-fermion coupling are also measured in $p\bar{p}$ and ep collisions at the Tevatron and at HERA. The corresponding cross-section formulae are given in Section 39 (Cross-section formulae for specific processes) and Section 16 (Structure Functions) in this *Review*. In this review, we concentrate on the measurements in e^+e^- collisions at LEP and SLC, mentioning hadron-collider measurements where relevant.

The standard 'lineshape' parameters of the Z are primarily determined from an analysis of the production cross sections of these final states in e^+e^- collisions. The $Z \to \nu\overline{\nu}$ state is identified directly by detecting single photon production (e^+e^-) or single jet production (pp) or indirectly by subtracting the visible partial widths from the total width. Inclusion of the forward-backward asymmetry of charged leptons, $A_{FB}^{(0,\ell)}$, of the τ polarization, $P(\tau)$, and its forward-backward asymmetry, $P(\tau)^{FB}$, enables the separate determination of the effective vector ($\overline{g}_V$) and axial vector ($\overline{g}_A$) couplings of the Z to these leptons and the ratio ($\overline{g}_V/\overline{g}_A$), which is related to the effective electroweak mixing angle $\sin^2\theta_{\rm eff}^{\rm lept}$ (see the "Electroweak Model and Constraints on New Physics" review).

Determination of the b- and c-quark-related partial widths and charge asymmetries involves tagging the b and c quarks for which various methods are employed: requiring the presence of a high momentum prompt lepton in the event with high transverse momentum with respect to the accompanying jet; impact parameter and lifetime tagging using precision vertex measurement with high-resolution detectors; application of neural-network techniques to classify events as b or non-b on a statistical basis using event–shape variables; and using the presence of a charmed meson (D/D^*) or a kaon as a tag.

55.1 Z-parameter determination

LEP was run at energy points on and around the Z mass (88–94 GeV) constituting an energy 'scan'. The shape of the cross-section variation around the Z peak can be described by a Breit-Wigner *ansatz* with an energy-dependent total width [1–3]. The **three** main properties of this distribution, viz., the **position** of the peak, the **width** of the distribution, and the **height** of the peak, determine respectively the values of M_Z, Γ_Z, and $\Gamma(e^+e^-) \times \Gamma(f\bar{f})$, where $\Gamma(e^+e^-)$ and $\Gamma(f\bar{f})$ are the electron and fermion partial widths of the Z. The quantitative determination of these parameters is done by writing analytic expressions for these cross sections in terms of the parameters, and fitting the calculated cross sections to the measured ones by varying these parameters, taking properly into account all the errors. Single-photon exchange (σ_γ^0) and γ-Z interference ($\sigma_{\gamma Z}^0$) are included, and the large ($\sim$25 %) initial-state radiation (ISR) effects are taken into account by convoluting the analytic expressions over a 'Radiator Function' [1–5] $H(s,s')$. Thus for the process $e^+e^- \to f\bar{f}$:

$$\sigma_f(s) = \int H(s,s')\ \sigma_f^0(s')\ ds' \tag{55.1}$$

$$\sigma_f^0(s) = \sigma_Z^0 + \sigma_\gamma^0 + \sigma_{\gamma Z}^0 \tag{55.2}$$

$$\sigma_Z^0 = \frac{12\pi}{M_Z^2}\ \frac{\Gamma(e^+e^-)\Gamma(f\bar{f})}{\Gamma_Z^2}\ \frac{s\ \Gamma_Z^2}{(s-M_Z^2)^2\ +\ s^2\Gamma_Z^2/M_Z^2} \tag{55.3}$$

$$\sigma_\gamma^0 = \frac{4\pi\alpha^2(s)}{3s}\ Q_f^2 N_c^f \tag{55.4}$$

$$\sigma_{\gamma Z}^0 = -\frac{2\sqrt{2}\alpha(s)}{3}\ (Q_f G_F N_c^f \mathcal{G}_V^e \mathcal{G}_V^f) \times \frac{(s-M_Z^2)M_Z^2}{(s-M_Z^2)^2 + s^2\Gamma_Z^2/M_Z^2} \tag{55.5}$$

where Q_f is the charge of the fermion, $N_c^f = 3$ for quarks and 1 for leptons, and $\mathcal{G}_V^f$ is the vector coupling of the Z to the fermion-antifermion pair $f\bar{f}$.

Since $\sigma_{\gamma Z}^0$ is expected to be much less than σ_Z^0, the LEP Collaborations have generally calculated the interference term in the framework of the Standard Model. This fixing of $\sigma_{\gamma Z}^0$ leads to a tighter constraint on M_Z, and consequently a smaller error on its fitted value. It is possible to relax this constraint and carry out the fit within the S-matrix framework, which is briefly described in the next section.

Hadron-collider experiments have shown the ability to measure M_Z by analysing the line shape of $pp/p\bar{p} \to Z/\gamma^* \to \mu^+\mu^-$ and comparing to simulation with an equivalent Breit-Wigner ansatz [6, 7]. While the LEP measurement depends most critically on the beam energy measurement (see Sec. 55.4 and 55.7), the hadron collider results rely on a precise calibration of the final-state muons using the masses of J/ψ and Υ resonances that are known to a precision significantly better than the current overall analysis uncertainties.

In the above framework, the QED radiative corrections have been explicitly taken into account by convoluting over the ISR and allowing the electromagnetic coupling constant to run [8]: $\alpha(s) = \alpha/(1-\Delta\alpha)$. On the other hand, weak radiative corrections that depend upon the assumptions of the electroweak theory and on the values of $M_{\rm top}$ and $M_{\rm Higgs}$ are accounted for by **absorbing them into the couplings**, which are then called the *effective* couplings $\mathcal{G}_V$ and $\mathcal{G}_A$ (or alternatively the effective parameters of the $\star$ scheme of Kennedy and Lynn [9].)

$\mathcal{G}_V^f$ and $\mathcal{G}_A^f$ are complex numbers with small imaginary parts. As experimental data does not allow simultaneous extraction of both real and imaginary parts of the effective couplings, the convention $g_A^f = {\rm Re}(\mathcal{G}_A^f)$ and $g_V^f = {\rm Re}(\mathcal{G}_V^f)$ is used and the imaginary parts are added in the fitting code [4].

Defining

$$A_f = 2\frac{g_V^f \cdot g_A^f}{(g_V^f)^2 + (g_A^f)^2} \tag{55.6}$$

the lowest-order expressions for the various lepton-related asymmetries on the Z pole are [10–12] $A_{FB}^{(0,\ell)} = (3/4)A_e A_f$, $P(\tau) = -A_\tau$, $P(\tau)^{fb} = -(3/4)A_e$, $A_{LR} = A_e$. The full analysis takes into account the energy-dependence of the asymmetries. Experimentally A_{LR} is defined as $(\sigma_L - \sigma_R)/(\sigma_L + \sigma_R)$, where $\sigma_{L(R)}$ are the $e^+e^- \to Z$ production cross sections with left- (right)-handed electrons.

The measurement of the effective leptonic electroweak mixing angle, $\sin^2\theta_{\rm eff}^{\rm lept}$, can be extracted from asymmetries measured in e^+e^- collisions, but also the from the forward-backward asymmetry in the $q\bar{q} \to Z/\gamma^* \to e^+e^-/\mu^+\mu^-$ process in hadronic collisions. It is related to the ratio of leptonic vector and axial-vector coupling constants, $\sin^2\theta_{\rm eff}^{\rm lept} = (1 - g_V^\ell/g_A^\ell)/4$. The ambi-

Int. J. Mod. Phys. A 2026.41. Downloaded from www.worldscientific.com
UNIVERSITY OF CALIFORNIA @ BERKELEY on 09/16/26. Re-use and distribution is strictly not permitted, except for Open Access articles.

guity regarding the direction of the initial quark and anti-quark can only be resolved on a statistical basis using the parton distribution functions. It results in significant uncertainties that are typically constrained using large event samples and ancillary measurements. The most recent measurements [13–17] approach a precision similar to the most sensitive e^+e^- collider results.

The definition of the partial decay width of the Z to $f\overline{f}$ includes the effects of QED and QCD final-state corrections, as well as the contribution due to the imaginary parts of the couplings:

$$\Gamma(f\overline{f}) = \frac{G_F M_Z^3}{6\sqrt{2}\pi}\, N_c^f \left(\left|\mathcal{G}_A^f\right|^2 R_A^f + \left|\mathcal{G}_V^f\right|^2 R_V^f\right) + \Delta_{ew/\mathrm{QCD}} \quad (55.7)$$

where R_V^f and R_A^f are radiator factors to account for final state QED and QCD corrections, as well as effects due to nonzero fermion masses, and $\Delta_{ew/\mathrm{QCD}}$ represents the non-factorizable electroweak/QCD corrections.

55.2 S-matrix approach to the Z

While most experimental analyses of LEP/SLC data have followed the 'Breit-Wigner' approach, an alternative S-matrix-based analysis is also possible. The Z, like all unstable particles, is associated with a complex pole in the S matrix. The pole position is process-independent and gauge-invariant. The mass, $\overline{M}_Z$, and width, $\overline{\Gamma}_Z$, can be defined in terms of the pole in the energy plane via [18–21]

$$\overline{s} = \overline{M}_Z^2 - i\overline{M}_Z\overline{\Gamma}_Z \quad (55.8)$$

leading to the relations

$$\begin{aligned}\overline{M}_Z &= M_Z/\sqrt{1+\Gamma_Z^2/M_Z^2} \\ &\approx M_Z \ - 34.1 \text{ MeV} \quad (55.9)\\ \overline{\Gamma}_Z &= \Gamma_Z/\sqrt{1+\Gamma_Z^2/M_Z^2} \\ &\approx \Gamma_Z \ - 0.9 \text{ MeV}\ . \quad (55.10)\end{aligned}$$

The LEP collaborations [22] have analyzed their data using the S–matrix approach as defined in Eq. (55.8), in addition to the conventional one. They observe a downward shift in the Z mass as expected.

55.3 Handling the large-angle e^+e^- final state

Unlike other $f\overline{f}$ decay final states of the Z, the e^+e^- final state has a contribution not only from the s-channel but also from the t-channel and s-t interference. The full amplitude is not amenable to fast calculation, which is essential if one has to carry out minimization fits within reasonable computer time. The usual procedure is to calculate the non-s channel part of the cross section separately using the Standard Model programs ALIBABA [23] or TOPAZ0 [24], with the measured value of M_{top}, and $M_{\mathrm{Higgs}} = 150$ GeV, and add it to the s-channel cross section calculated as for other channels. This leads to two additional sources of error in the analysis: firstly, the theoretical calculation in ALIBABA itself is known to be accurate to $\sim 0.5\%$, and secondly, there is uncertainty due to the error on M_{top} and the unknown value of M_{Higgs} (100–1000 GeV). These errors are propagated into the analysis by including them in the systematic error on the e^+e^- final state. As these errors are common to the four LEP experiments, this is taken into account when performing the LEP average.

55.4 Errors due to uncertainty in LEP energy determination

The systematic errors related to the LEP energy measurement, see [25–30], can be classified as:

- The absolute energy scale error;
- Energy-point-to-energy-point errors due to the nonlinear response of the magnets to the exciting currents;
- Energy-point-to-energy-point errors due to possible higher-order effects in the relationship between the dipole field and beam energy;
- Energy reproducibility errors due to various unknown uncertainties in temperatures, tidal effects, corrector settings, RF status, *etc.*

Precise energy calibration was done outside normal data-taking using the resonant depolarization technique. Run-time energies were determined every 10 minutes by measuring the relevant machine parameters and using a model which takes into account all the known effects, including leakage currents produced by trains in the Geneva area and the tidal effects due to gravitational forces of the Sun and the Moon. The LEP Energy Working Group has provided a covariance matrix from the determination of LEP energies for the different running periods during 1993–1995 [25].

55.5 Choice of fit parameters

The LEP Collaborations have chosen the following primary set of parameters for fitting:

$$M_Z, \Gamma_Z, \sigma^0_{\mathrm{hadron}}, R(\mathrm{lepton}), A_{FB}^{(0,\ell)},$$

where

$$\begin{aligned}R(\mathrm{lepton}) &= \Gamma(\mathrm{hadrons})/\Gamma(\mathrm{lepton}), \sigma^0_{\mathrm{hadron}} \\ &= 12\pi\Gamma(e^+e^-)\Gamma(\mathrm{hadrons})/M_Z^2\Gamma_Z^2.\end{aligned}$$

With a knowledge of these fitted parameters and their covariance matrix, any other parameter can be derived. The main advantage of these parameters is that they form a physics motivated set of parameters with much reduced correlations.

Thus, the most general fit carried out to cross section and asymmetry data determines the **nine parameters**: M_Z, Γ_Z, $\sigma^0_{\mathrm{hadron}}$, $R(e)$, $R(\mu)$, $R(\tau)$, $A_{FB}^{(0,e)}$, $A_{FB}^{(0,\mu)}$, $A_{FB}^{(0,\tau)}$. Assumption of lepton universality leads to a **five-parameter fit** determining M_Z, Γ_Z, $\sigma^0_{\mathrm{hadron}}$, $R(\mathrm{lepton})$, $A_{FB}^{(0,\ell)}$.

55.6 Combining results from LEP and SLC experiments

With a steady increase in statistics over the years and improved understanding of the common systematic errors between LEP experiments, the procedures for combining results have evolved continuously [31]. The Line Shape Sub-group of the LEP Electroweak Working Group investigated the effects of these common errors, and devised a combination procedure for the precise determination of the Z parameters from LEP experiments. Using these procedures, this note also gives the results after combining the final parameter sets from the four experiments, and these are the results quoted as the fit results in the Z listings below. Transformation of variables leads to values of derived parameters like partial decay widths and branching ratios to hadrons and leptons. Finally, transforming the LEP combined nine parameter set to (M_Z, Γ_Z, $\sigma^0_{\mathrm{hadron}}$, g_A^f, g_V^f, $f = e, \mu, \tau$) using the average values of lepton asymmetry parameters (A_e, A_μ, A_τ) as constraints, leads to the best fitted values of the vector and axial-vector couplings (g_V, g_A) of the charged leptons to the Z.

Brief remarks on the handling of common errors and their magnitudes are given below. The identified common errors are those coming from

(a) LEP energy-calibration uncertainties, and

(b) the theoretical uncertainties in (i) the luminosity determination using small angle Bhabha scattering, (ii) estimating the non-s channel contribution to large angle Bhabha scattering, (iii) the calculation of QED radiative effects, and (iv) the parametrization of the cross section in terms of the parameter set used.

55.7 Common LEP energy errors

All the collaborations incorporate in their fit the full LEP energy error matrix as provided by the LEP energy group for their intersection region [25]. The effect of these errors is separated out from that of other errors by carrying out fits with energy errors scaled up and down by $\sim 10\%$ and redoing the fits. From the observed changes in the overall error matrix, the covariance matrix of the common energy errors is determined. Common LEP energy errors lead to uncertainties on M_Z, Γ_Z, and $\sigma^0_{\mathrm{hadron}}$ of 1.7, 1.2 MeV, and 0.011 nb, respectively.

Int. J. Mod. Phys. A 2026.41. Downloaded from www.worldscientific.com
by UNIVERSITY OF CALIFORNIA @ BERKELEY on 09/16/26. Re-use and distribution is strictly not permitted, except for Open Access articles.

55.8 Common luminosity errors

BHLUMI 4.04 [32] is used by all LEP collaborations for small-angle Bhabha scattering leading to a common uncertainty in their measured cross sections of 0.061% [33]. BHLUMI does not include a correction for production of light fermion pairs. OPAL explicitly corrects for this effect and reduces their luminosity uncertainty to 0.054%, which is taken fully correlated with the other experiments. The other three experiments among themselves have a common uncertainty of 0.061%.

55.9 Common non-s channel uncertainties

The same standard model programs ALIBABA [23] and TOPAZ0 [24] are used to calculate the non-s channel contribution to the large angle Bhabha scattering [34]. As this contribution is a function of the Z mass, which itself is a variable in the fit, it is parameterized as a function of M_Z by each collaboration to properly track this contribution as M_Z varies in the fit. The common errors on R_e and $A_{FB}^{(0,e)}$ are 0.024 and 0.0014 respectively, and are correlated between them.

55.10 Common theoretical uncertainties: QED

There are large initial-state photon and fermion pair radiation effects near the Z resonance, for which the best currently available evaluations include contributions up to $\mathcal{O}(\alpha^3)$. To estimate the remaining uncertainties, different schemes are incorporated in the standard model programs ZFITTER [5], TOPAZ0 [24], and MIZA [35]. Comparing the different options leads to error estimates of 0.3 and 0.2 MeV on M_Z and Γ_Z respectively, and of 0.02% on $\sigma^0_{\rm hadron}$.

55.11 Common theoretical uncertainties: parametrization of lineshape and asymmetries

To estimate uncertainties arising from ambiguities in the model-independent parametrization of the differential cross-section near the Z resonance, results from TOPAZ0 and ZFITTER were compared by using ZFITTER to fit the cross sections and asymmetries calculated using TOPAZ0. The resulting uncertainties on M_Z, Γ_Z, $\sigma^0_{\rm hadron}$, R(lepton), and $A_{FB}^{(0,\ell)}$ are 0.1 MeV, 0.1 MeV, 0.001 nb, 0.004, and 0.0001 respectively.

Thus, the overall theoretical errors on M_Z, Γ_Z, $\sigma^0_{\rm hadron}$ are 0.3 MeV, 0.2 MeV, and 0.008 nb respectively; on each R(lepton) is 0.004 and on each $A_{FB}^{(0,\ell)}$ is 0.0001. Within the set of three R(lepton)'s and the set of three $A_{FB}^{(0,\ell)}$'s, the respective errors are fully correlated.

All the theory-related errors mentioned above utilize Standard Model programs which need the Higgs mass and running electromagnetic coupling constant as inputs; uncertainties on these inputs will also lead to common errors. All LEP collaborations used the same set of inputs for Standard Model calculations: $M_Z = 91.187$ GeV, the Fermi constant $G_F = (1.16637 \pm 0.00001) \times 10^{-5}$ GeV^{-2} [36], $\alpha^{(5)}(M_Z) = 1/128.877 \pm 0.090$ [37], $\alpha_s(M_Z) = 0.119$ [38], $M_{\rm top} = 174.3 \pm 5.1$ GeV [38] and $M_{\rm Higgs} = 150$ GeV. The only observable effect, on M_Z, is due to the variation of $M_{\rm Higgs}$ between 100–1000 GeV (due to the variation of the γ/Z interference term which is taken from the Standard Model): M_Z changes by +0.23 MeV per unit change in $\log_{10} M_{\rm Higgs}/{\rm GeV}$, which is not an error but a correction to be applied once $M_{\rm Higgs}$ is determined. The effect is much smaller than the error on M_Z ($\pm$2.1 MeV).

55.12 Methodology of combining the LEP experimental results

The LEP experimental results actually used for combination are slightly modified from those published by the experiments (which are given in the Listings below). This has been done in order to facilitate the procedure by making the inputs more consistent. These modified results are given explicitly in [31]. The main differences compared to the published results are (a) consistent use of ZFITTER 6.23 and TOPAZ0 (the published ALEPH results used ZFITTER 6.10); (b) use of the combined energy-error matrix, which makes a difference of 0.1 MeV on the M_Z and Γ_Z for L3 only as at that intersection the RF modeling uncertainties are the largest.

Thus, nine-parameter sets from all four experiments with their covariance matrices are used together with all the common errors correlations. A grand covariance matrix, V, is constructed and a combined nine-parameter set is obtained by minimizing $\chi^2 = \Delta^T V^{-1} \Delta$, where Δ is the vector of residuals of the combined parameter set to the results of individual experiments. Imposing lepton universality in the combination results in the combined five-parameter set.

55.13 Study of $Z \to b\bar{b}$ and $Z \to c\bar{c}$

In the sector of c- and b-physics, the LEP experiments have measured the ratios of partial widths $R_b = \Gamma(Z \to b\bar{b})/\Gamma(Z \to$ hadrons), and $R_c = \Gamma(Z \to c\bar{c})/\Gamma(Z \to$ hadrons), and the forward-backward (charge) asymmetries $A_{FB}^{b\bar{b}}$ and $A_{FB}^{c\bar{c}}$. The SLD experiment at SLC has measured the ratios R_c and R_b and, utilizing the polarization of the electron beam, was able to obtain the final state coupling parameters A_b and A_c from a measurement of the left-right forward-backward asymmetry of $b-$ and $c-$quarks. The high precision measurement of R_c at SLD was made possible owing to the small beam size and very stable beam spot at SLC, coupled with a highly precise CCD pixel detector. Several of the analyses have also determined other quantities, in particular the semileptonic branching ratios, B($b \to \ell^-$), B($b \to c \to \ell^+$), and B($c \to \ell^+$), the average time-integrated $B^0\overline{B}^0$ mixing parameter $\overline{\chi}$ and the probabilities for a c–quark to fragment into a D^+, a D_s, a D^{*+} , or a charmed baryon. These quantities are correlated with the electroweak parameters, and since the mixture of b hadrons is different from the one at the $\Upsilon(4S)$, their values might differ from those measured at the $\Upsilon(4S)$. As these measurements do not concern properties of the Z boson, they do not appear in the listing. Numerical values may be found in Ref. [31] and earlier versions of this review.

All the above quantities are correlated to each other since:

- Several analyses (for example the lepton fits) determine more than one parameter simultaneously;
- Some of the electroweak parameters depend explicitly on the values of other parameters (for example R_b depends on R_c);
- Common tagging and analysis techniques produce common systematic uncertainties.

The LEP Electroweak Heavy Flavour Working Group has developed [39] a procedure for combining the measurements taking into account known sources of correlation. The combining procedure determines fourteen parameters: the six parameters of interest in the electroweak sector, R_b, R_c, $A_{FB}^{b\bar{b}}$, $A_{FB}^{c\bar{c}}$, A_b and A_c and, in addition, B($b \to \ell^-$), B($b \to c \to \ell^+$), B($c \to \ell^+$), $\overline{\chi}$, $f(D^+)$, $f(D_s)$, $f(c_{\rm baryon})$ and $P(c \to D^{*+}) \times$ B($D^{*+} \to \pi^+ D^0$) Before the fit both the peak and off-peak asymmetries are translated to the common energy $\sqrt{s} = 91.26$ GeV using the predicted energy-dependence from ZFITTER [5].

55.13.1 *Summary of the measurements and of the various kinds of analysis*

The measurements of R_b and R_c fall into two classes. In the first, named single-tag measurement, a method for selecting b and c events is applied and the number of tagged events is counted. A second technique, named double-tag measurement, has the advantage that the tagging efficiency is directly derived from the data thereby reducing the systematic error on the measurement.

The measurements in the b- and c-sector can be essentially grouped in the following categories:

- Lifetime (and lepton) double-tagging measurements of R_b. These are the most precise measurements of R_b and obviously dominate the combined result. The main sources of systematics come from the charm contamination and from estimating the hemisphere b-tagging efficiency correlation;
- Analyses with $D/D^{*\pm}$ to measure R_c. These measurements make use of several different tagging techniques (inclusive/exclusive double tag, exclusive double tag, reconstruction of all weakly decaying charmed states) and no assumptions are made on the energy-dependence of charm fragmentation;

Int. J. Mod. Phys. A 2026.41. Downloaded from www.worldscientific.com
UNIVERSITY OF CALIFORNIA @ BERKELEY on 09/16/26. Re-use and distribution is strictly not permitted, except for Open Access articles.

- A measurement of R_c using single leptons and assuming $\mathrm{B}(b \to c \to \ell^+)$;
- Lepton fits which use hadronic events with one or more leptons in the final state to measure the asymmetries $A_{FB}^{b\bar{b}}$ and $A_{FB}^{c\bar{c}}$. Each analysis usually gives several other electroweak parameters. The dominant sources of systematics are due to lepton identification, to other semileptonic branching ratios and to the modeling of the semileptonic decay;
- Measurements of $A_{FB}^{b\bar{b}}$ using lifetime tagged events with a hemisphere charge measurement. These measurements dominate the combined result;
- Analyses with $D/D^{*\pm}$ to measure $A_{FB}^{c\bar{c}}$ or simultaneously $A_{FB}^{b\bar{b}}$ and $A_{FB}^{c\bar{c}}$;
- Measurements of A_b and A_c from SLD, using several tagging methods (lepton, kaon, D/D^*, and vertex mass). These quantities are directly extracted from a measurement of the left–right forward–backward asymmetry in $c\bar{c}$ and $b\bar{b}$ production using a polarized electron beam.

55.13.2 *Averaging procedure*

All the measurements are provided by the LEP and SLD Collaborations in the form of tables with a detailed breakdown of the systematic errors of each measurement and its dependence on other electroweak parameters.

The averaging proceeds via the following steps:

- Define and propagate a consistent set of external inputs such as branching ratios, hadron lifetimes, fragmentation models *etc.* All the measurements are checked to ensure that all use a common set of assumptions (for instance, since the QCD corrections for the forward–backward asymmetries are strongly dependent on the experimental conditions, the data are corrected before combining);
- Form the full (statistical and systematic) covariance matrix of the measurements. The systematic correlations between different analyses are calculated from the detailed error breakdown in the measurement tables. The correlations relating several measurements made by the same analysis are also used;
- Take into account any explicit dependence of a measurement on the other electroweak parameters. As an example of this dependence, we illustrate the case of the double-tag measurement of R_b, where c-quarks constitute the main background. The normalization of the charm contribution is not usually fixed by the data and the measurement of R_b depends on the assumed value of R_c, which can be written as:

$$R_b = R_b^{\mathrm{meas}} + a(R_c)\frac{(R_c - R_c^{\mathrm{used}})}{R_c} \ , \qquad (55.11)$$

  where R_b^{meas} is the result of the analysis which assumed a value of $R_c = R_c^{\mathrm{used}}$ and $a(R_c)$ is the constant which gives the dependence on R_c;
- Perform a χ^2 minimization with respect to the combined electroweak parameters.

After the fit the average peak asymmetries $A_{FB}^{c\bar{c}}$ and $A_{FB}^{b\bar{b}}$ are corrected for the energy shift from 91.26 GeV to M_Z and for QED (initial state radiation), γ exchange, and γZ interference effects, to obtain the corresponding pole asymmetries $A_{FB}^{0,c}$ and $A_{FB}^{0,b}$. The results of the averaging procedure are presented in the Z particle listing. Further information can be found in Ref. [31].

References

[1] R. N. Cahn, Phys. Rev. D **36**, 2666 (1987), [Erratum: Phys.Rev.D 40, 922 (1989)].

[2] D. Y. Bardin *et al.*, in "LEP Physics Workshop," 89–127 (1989).

[3] A. Borrelli *et al.*, Nucl. Phys. B **333**, 357 (1990).

[4] D. Y. Bardin and G. Passarino (1998), [hep-ph/9803425]; D. Y. Bardin, M. Grunewald and G. Passarino (1999), [hep-ph/9902452].

[5] D. Bardin *et al.*, Z. Phys. C **44**, 493 (1989); D. Bardin *et al.*, Comput. Phys. Commun. **59**, 303 (1990); D. Y. Bardin *et al.*, Nucl. Phys. B **351**, 1 (1991), [hep-ph/9801208]; D. Y. Bardin *et al.*, Phys. Lett. B **255**, 290 (1991), [hep-ph/9801209]; D. Y. Bardin *et al.* (1992), [hep-ph/9412201]; D. Y. Bardin *et al.*, Comput. Phys. Commun. **133**, 229 (2001), [hep-ph/9908433].

[6] T. Aaltonen *et al.* (CDF), Science **376**, 6589, 170 (2022).

[7] R. Aaij *et al.* (LHCb), Phys. Rev. Lett. **135**, 16, 161802 (2025), [arXiv:2505.15582].

[8] G. Burgers and F. Jegerlehner, Conf. Proc. C **8902201**, 55 (1989).

[9] D. Kennedy and B. Lynn, Nucl. Phys. B **322**, 1 (1989).

[10] M. Consoli, W. Hollik and F. Jegerlehner, in "LEP Physics Workshop," 7–54 (1989).

[11] M. Bohm *et al.*, in "LEP Physics Workshop," 203–234 (1989).

[12] P. Eberhard *et al.*, in "LEP Physics Workshop," 235–266 (1989).

[13] T. A. Aaltonen *et al.* (CDF, D0), Phys. Rev. D **97**, 11, 112007 (2018), [arXiv:1801.06283].

[14] (2018).

[15] A. M. Sirunyan *et al.* (CMS), Eur. Phys. J. C **78**, 9, 701 (2018), [arXiv:1806.00863].

[16] R. Aaij *et al.* (LHCb), JHEP **12**, 026 (2024), [arXiv:2410.02502].

[17] A. Hayrapetyan *et al.* (CMS), Phys. Lett. B **866**, 139526 (2025), [arXiv:2408.07622].

[18] R. G. Stuart, Phys. Lett. B **262**, 113 (1991).

[19] A. Sirlin, Phys. Rev. Lett. **67**, 2127 (1991).

[20] A. Leike, T. Riemann and J. Rose, Phys. Lett. B **273**, 513 (1991), [hep-ph/9508390].

[21] D. Bardin *et al.*, Phys. Lett. B **206**, 539 (1988).

[22] S. Schael *et al.* (ALEPH, DELPHI, L3, OPAL, LEP Electroweak), Phys. Rept. **532**, 119 (2013), [arXiv:1302.3415].

[23] W. Beenakker, F. A. Berends and S. van der Marck, Nucl. Phys. B **349**, 323 (1991).

[24] G. Montagna *et al.*, Nucl. Phys. B **401**, 3 (1993); G. Montagna *et al.*, Comput. Phys. Commun. **76**, 328 (1993); G. Montagna *et al.*, Comput. Phys. Commun. **93**, 120 (1996), [hep-ph/9506329]; G. Montagna *et al.*, Comput. Phys. Commun. **117**, 278 (1999), [hep-ph/9804211].

[25] R. Assmann *et al.*, Eur. Phys. J. C **6**, 187 (1999).

[26] R. Assmann *et al.* (Working Group on LEP Energy), Z. Phys. C **66**, 567 (1995).

[27] L. Arnaudon *et al.* (Working Group on LEP Energy, ALEPH, DELPHI, L3, OPAL), Phys. Lett. B **307**, 187 (1993).

[28] L. Arnaudon *et al.* (Working Group on LEP energy), in "26th International Conference on High-energy Physics," (1992).

[29] L. Arnaudon *et al.* (LEP Polarization), Phys. Lett. B **284**, 431 (1992).

[30] R. Bailey *et al.*, Conf. Proc. C **900612**, 1765 (1990).

[31] S. Schael *et al.* (ALEPH, DELPHI, L3, OPAL, SLD, LEP Electroweak Working Group, SLD Electroweak Group, SLD Heavy Flavour Group), Phys. Rept. **427**, 257 (2006), [hep-ex/0509008].

[32] S. Jadach *et al.*, Comput. Phys. Commun. **102**, 229 (1997); S. Jadach and O. Nicrosini, Event generators for Bhabha scattering, in Physics at LEP2, CERN-96-01 Vol. 2, February 1996.

[33] B. Ward *et al.*, Phys. Lett. B **450**, 262 (1999), [hep-ph/9811245].

[34] W. Beenakker and G. Passarino, Phys. Lett. B **425**, 199 (1998), [hep-ph/9710376].

[35] M. Martinez *et al.*, Z. Phys. C **49**, 645 (1991); M. Martinez and F. Teubert, Z. Phys. **C65**, 267 (1995), updated with results summarized in S. Jadach, B. Pietrzyk, and M. Skrzypek, Phys. Lett. **B456**, 77 (1999) and Reports of the working group on precision calculations for the Z resonance, CERN 95-03, ed. D. Bardin, W. Hollik, and G. Passarino, and references therein.

[36] T. van Ritbergen and R. G. Stuart, Phys. Lett. B **437**, 201 (1998), [hep-ph/9802341]; T. van Ritbergen and R. G. Stuart, Phys. Rev. Lett. **82**, 488 (1999), [hep-ph/9808283].

[37] S. Eidelman and F. Jegerlehner, Z. Phys. C **67**, 585 (1995), [hep-ph/9502298]; M. Steinhauser, Phys. Lett. B **429**, 158 (1998), [hep-ph/9803313].

[38] D. E. Groom *et al.* (Particle Data Group), Eur. Phys. J. C **15**, 1 (2000).

[39] Nucl. Instrum. Meth. A **378**, 101 (1996).

Int. J. Mod. Phys. A 2026.41. Downloaded from www.worldscientific.com
by UNIVERSITY OF CALIFORNIA @ BERKELEY on 09/16/26. Re-use and distribution is strictly not permitted, except for Open Access articles.

56. Muon Anomalous Magnetic Moment

Revised August 2025 by D.W. Hertzog (U. Washington) and M. Hoferichter (U. Bern).

56.1 Introduction and summary

The Dirac equation predicts a muon magnetic moment, $\boldsymbol{\mu} = g_\mu \frac{q}{2m_\mu}\mathbf{S}$, with gyromagnetic ratio $g_\mu = 2$, charge q, and mass m_μ. Quantum loop effects lead to a small calculable deviation from $g_\mu = 2$, parameterized by the anomalous magnetic moment of the muon $a_\mu \equiv (g_\mu - 2)/2$. This observable can be measured in storage-ring experiments and predicted within the Standard Model (SM) to high precision, testing the SM at its quantum loop level. In short, the current world average of the experimental determination after the final results of the FNAL E989 experiment reads [1–8]

$$a_\mu^{\rm exp} = 116\,592\,071.5(14.5) \times 10^{-11}\,, \tag{56.1}$$

to be compared with the SM prediction as compiled by the Muon $g-2$ Theory Initiative [9–69]

$$a_\mu^{\rm SM} = 116\,592\,033(62) \times 10^{-11}\,. \tag{56.2}$$

Accordingly, the difference

$$\Delta a_\mu \equiv a_\mu^{\rm exp} - a_\mu^{\rm SM} = 38(63) \times 10^{-11} \tag{56.3}$$

is compatible with zero, but the uncertainty is completely dominated by the SM prediction, allowing for a SM test at threefold improved precision once the experimental uncertainty can be matched. In Sec. 56.2 we briefly review the status of experiment, Eq. (56.1), in Sec. 56.3 the status of the SM prediction, Eq. (56.2), and conclude with some remarks on future improvements in Sec. 56.4.

56.2 Precision measurement of a_μ

The two most precise muon $g-2$ experiments—BNL E821 and FNAL E989—were developed based on the experiences of earlier storage ring experiments at CERN [70, 71]. The most significant improvements are related to the intensity and purity of muon delivery to the ring, which has led to the world average precision of 124 ppb in the determination of a_μ. Figure 56.1 displays the consistency of the individual BNL and FNAL run-period publications,[1] the final precision achieved, and the average. With the exception of BNL-01, all measurements used positive muons. Details of the combination procedure, including updated corrections since the original publication, can be found in Ref. [1].

Figure 56.1: Experimental values of a_μ from BNL E821 (blue triangles) [72–74],[1] FNAL E989 (red squares) [1, 2, 4], and the world average (black diamond). The uncertainties combine statistics and systematics. BNL values are rounded to the nearest 10 ppb. All measurements employed positive muons except BNL-01, which ran with negative muons (inverted triangle).

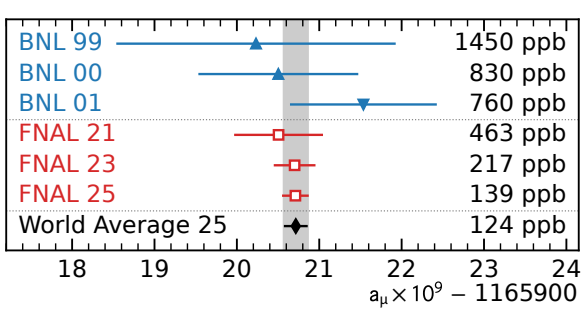

[1] The quoted BNL $\mathcal{R}'_\mu$ and a_μ values were computed by the FNAL Muon $g-2$ collaboration [1], converting the reported values for free protons in vacuum in the BNL references and using the converted $\mathcal{R}'_\mu$ values to recompute the a_μ values relying on CODATA 2022 [75] for the external inputs.

Table 56.1: $\mathcal{R}'_\mu$ values and uncertainties from BNL E821,[1] with uncertainties rounded to the nearest 10 ppb, and those from FNAL E989.

	$\mathcal{R}'_\mu$	Total (ppb)	Statistical (ppb)	Systematics (ppb)
BNL E821	0.00370730154	540	460	280
FNAL E989	0.00370730088	125	98	78
Combined	0.00370730091	122	96	75

In this compact description, we emphasize aspects of the common storage ring technique to determine a_μ to high precision, while also pointing out the relatively balanced final systematics table from FNAL that would have to be overcome for further improvements.

Polarized muon bunches are injected into a 7.1 m radius superconducting storage ring (SR) [76] having a highly uniform vertical magnetic field, $|\mathbf{B}| \approx 1.45$ T. A fast kicker magnet [77] deflects the muons during the first turn into a fiducial toroidal volume that is concentric with the SR center. Four regions containing electrostatic quadrupole (ESQ) plates provide weak vertical focusing. Approximately 5000 muons are stored in each "fill" of the ring.

The muons circulate in the ring at the cyclotron angular frequency $\boldsymbol{\omega}_c = -\frac{q}{m_\mu \gamma}\mathbf{B}$, $\gamma = 1/\sqrt{1-\beta^2}$ being the Lorentz factor, and their spins rotate at $\boldsymbol{\omega}_s = -g_\mu \frac{q}{2m_\mu}\mathbf{B} - (1-\gamma)\frac{q}{m_\mu\gamma}\mathbf{B}$. If g_μ were exactly equal to 2, the cyclotron and spin frequencies would be the same. For $g_\mu \neq 2$, and for the ideal case that $\boldsymbol{\beta}\cdot\mathbf{B} = 0$, the anomalous precession frequency $\boldsymbol{\omega}_a$ is simply given by

$$\boldsymbol{\omega}_a = \boldsymbol{\omega}_s - \boldsymbol{\omega}_c = -\frac{q}{m_\mu} a_\mu \mathbf{B}. \tag{56.4}$$

In practice, the betatron oscillations of the muon beam and the presence of the quadrupole electric field lead to a more complete expression [78]

$$\boldsymbol{\omega}_a = -\frac{q}{m_\mu}\left[a_\mu \mathbf{B} - a_\mu\left(\frac{\gamma}{\gamma+1}\right)(\boldsymbol{\beta}\cdot\mathbf{B})\boldsymbol{\beta} - \left(a_\mu - \frac{1}{\gamma^2-1}\right)\boldsymbol{\beta}\times\mathbf{E}\right]. \tag{56.5}$$

The second term accounts for the vertical betatron oscillations owing to the average value of $(\boldsymbol{\beta}\cdot\mathbf{B})^2$. A measurement of the vertical amplitude distribution leads to a "pitch" correction. The third term accounts for the motional magnetic field felt by the relativistic muons in the presence of the ESQ electric field $\mathbf{E}$. The CERN-III experiment [71] recognized that this term vanishes for $\gamma = \sqrt{1+1/a_\mu} \approx 29.3$, corresponding to a muon "magic momentum" of $P_0 \approx 3.094$ GeV.[2] The CERN-III, BNL, and FNAL experiments each operated at this momentum. The momentum spread with respect to P_0 ($\sim \Delta P/P_0 < 0.2\%$) requires an electric-field correction of order several hundred ppb, by far the largest correction in the experiment.

The magnetic field $\mathbf{B}$ in Eq. (56.5) is measured using pulsed proton NMR techniques and is expressed as $\tilde{\omega}'_p(T_r)$, which is the proton spin precession frequency inside a room-temperature spherical water sample and averaged over the stored muon distribution. Equation (56.5) demonstrates that $a_\mu \propto \omega_a/\tilde{\omega}'_p(T_r) \equiv \mathcal{R}'_\mu$, which is the quantity reported by all $g-2$ experiments. The muon anomaly is then determined from

$$a_\mu = \mathcal{R}'_\mu \frac{\mu'_p(T_r)}{\mu_B}\frac{m_\mu}{m_e}, \tag{56.6}$$

where $\mu'_p(T_r)/\mu_B$ is the ratio of the shielded proton magnetic moment to the Bohr magneton and m_μ/m_e is the muon-to-electron mass ratio [75]. Reporting this ratio allows a_μ to be recalculated if the fundamental constants are updated; see Table 56.1.

[2] The E34 experiment at J-PARC [79] plans to inject lower momentum muons with negligible transverse momentum components into a ring that does not include an electric quadrupole field. This will greatly reduce any needed electric field or pitch correction.

Int. J. Mod. Phys. A 2026.41. Downloaded from www.worldscientific.com
UNIVERSITY OF CALIFORNIA @ BERKELEY on 09/16/26. Re-use and distribution is strictly not permitted, except for Open Access articles.

Int. J. Mod. Phys. A 2026.41. Downloaded from www.worldscientific.com
by UNIVERSITY OF CALIFORNIA @ BERKELEY on 09/16/26. Re-use and distribution is strictly not permitted, except for Open Access articles.

Table 56.2: Corrections and uncertainties from combined FNAL running periods, and current uncertainties due to the external parameters. Here ω_a^m is the fit precession frequency. Corrections to ω_a^m yield ω_a, needed in the numerator of $\mathcal{R}_\mu^{'}$. Numerical summary courtesy of Alberto Lusiani, on behalf of the FNAL Muon $g-2$ Collaboration.

Quantity	Correction (ppb)	Uncertainty (ppb)
ω_a^m (statistical)	–	98
Beam dynamic (BD) corrections to ω_a^m to yield ω_a	+538	43
Net ω_a (statistical + BD + fitting uncertainties)	–	111
ω_p' (all systematics)	–	48
Magnetic field transient corrections to ω_p'	−58	31
Net ω_p' uncertainty	–	57
Total uncertainties for $\mathcal{R}_\mu'$	–	125
μ_p'/μ_B and m_μ/m_e external parameters	–	23
Total for a_μ		127

The absolute magnetic field [6] is established using custom high-purity water [80] and He-3 [81] probes measured in a special-purpose highly uniform MRI magnet. These probes cross-calibrate an in-ring movable "plunging" probe system, which in turn cross-calibrates one-by-one the 17 probes in an NMR trolley [82]. This device periodically maps the entire storage ring field *in situ*. The temporal variation of the field is continuously monitored using an additional set of 378 probes [83] placed above and below the fiducial volume.

Two arrays of in-vacuum straw Tracker detectors [84] located at two azimuthal positions in the SR record the inward bending trajectories of e^+ from muon decay. The fit tracks are then traced back to the approximate upstream decay location within the storage ring vs. time-in-fill. The measured stored muon distribution is folded with the azimuthally averaged field maps to give the muon-weighted field. Details are found in Refs. [3, 6].

Parity violation in weak $\mu^+ \to e^+\nu_e\bar{\nu}_\mu$ decay provides the polarimetry needed to deduce the average muon spin direction vs. time-in-fill. The decay positron energy in the boosted laboratory frame is related to the energy and angular distribution in the center-of-mass (CM) as in $E_{e,\mathrm{lab}} \approx \gamma E_{e,\mathrm{CM}}(1+\cos\theta_{\mathrm{CM}})$, and thus the highest-energy positrons are preferentially emitted in the direction of the muon spin. All decay positrons curl to the inside of the SR, where their time-of-arrival and energy are measured in calorimeters [85], forming a measured spectrum $N(t, E_e)$. In first order, this spectrum can be described by $N(t) = N_0 e^{-t/(\gamma\tau_\mu)}[1 + A\cos(\omega_a t - \phi)]$, where the asymmetry A depends on the energy threshold and the average polarization of the muons. The statistical precision of the experiment is optimized by fitting a histogram whose entries are weighted by the energy-dependent asymmetry $A(E)$; that is,

$$\frac{\delta\omega_a}{\omega_a} = \frac{1}{\omega_a\gamma\tau_\mu}\sqrt{\frac{2}{N\langle A(E)^2\rangle}}\,, \tag{56.7}$$

which emphasizes the importance of the higher-energy positrons.

The fit of $N(t, E_e)$ results in the measured precession frequency ω_a^m. To achieve a good χ^2, additional terms that account for the rate variations from the coupling of calorimeter acceptance to beam motions are required. The largest of these are associated with coherent betatron oscillations (CBO), which, if ignored, would pull ω_a^m from the true precession frequency ω_a by several hundred ppb. An RF modulation system [86], tuned to the CBO frequency and applied to the ESQ plates, creates a dipole field that significantly damps the intrinsic CBO effect. Details on the extraction of ω_a^m and the many independent checks and methods used can be found in Refs. [3, 5].

Table 56.2 lists the corrections and uncertainties reported for the entire FNAL E989 measurement [1, 2, 4]. For simplicity, this table combines the individual effects that impact ω_a^m or ω_p'. Corrections to the measured precession frequency, ω_a^m, are dominated by the effect of the electric field and pitch as expressed in Eq. (56.5). Several additional and much smaller corrections are needed because the stored muon phase space slightly evolves during the fill. Transient-magnetic-field corrections to ω_p' correspond to a residual eddy current from the fast kicker and a vibration-induced field perturbation from the charging of the ESQ plates. The systematic uncertainties are relatively balanced. The final precision on $\mathcal{R}_\mu^{'}$, and thus also on a_μ, is dominated by the statistical uncertainty.

Figure 56.2: Sample diagrams for a_μ in the SM: solid lines refer to the muon, wiggly lines to photons, and the red blobs to hadronic matrix elements. The first diagram gives the leading QED contribution by Schwinger, the second one represents a one-loop EW diagram with Z exchange, and the last two diagrams correspond to HVP and HLbL topologies, respectively.

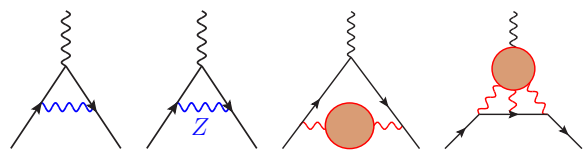

56.3 Standard Model prediction of a_μ

The SM prediction of a_μ decomposes into pure QED contributions, electroweak (EW) effects, and hadronic corrections

$$a_\mu^{\mathrm{SM}} = a_\mu^{\mathrm{QED}} + a_\mu^{\mathrm{EW}} + a_\mu^{\mathrm{had}}\,, \qquad a_\mu^{\mathrm{had}} = a_\mu^{\mathrm{HVP}} + a_\mu^{\mathrm{HLbL}}\,, \tag{56.8}$$

where the latter are further separated into topologies featuring hadronic vacuum polarization (HVP) and hadronic light-by-light scattering (HLbL), see Fig. 56.2 for representative diagrams in each category. In the subsequent sections we briefly discuss the status for each class of corrections, referring to Refs. [9, 87] for a thorough review, labeled as WP20 [87] and WP25 [9] below.[3] The resulting bottom line is summarized in Table 56.3.

56.3.1 *QED and electroweak contributions*

By far the dominant contribution to a_μ^{SM} arises from QED, including all diagrams with purely photonic and leptonic ($\ell = e, \mu, \tau$) loops. Starting from Schwinger's seminal result [89], the expansion can be expressed as

$$\begin{aligned} a_\mu^{\mathrm{QED}} &= \frac{\alpha}{2\pi} + 0.765\,857\,420(8)_e(11)_\tau[13]\left(\frac{\alpha}{\pi}\right)^2 \\ &\quad + 24.050\,509\,77(17)_e(16)_\tau[23]\left(\frac{\alpha}{\pi}\right)^3 \\ &\quad + 130.8782(60)_{\mathrm{MC}}\left(\frac{\alpha}{\pi}\right)^4 + 750.2(9)_{\mathrm{MC}}\left(\frac{\alpha}{\pi}\right)^5 + \mathcal{O}\left(\alpha^6\right), \end{aligned} \tag{56.9}$$

where the uncertainties derive from $m_\mu/m_e = 206.7682827(46)$, $m_\tau/m_\mu = 16.8170(11)$ [75], and Monte-Carlo (MC) integration,

[3] These white papers (WP) were compiled by the Muon $g-2$ Theory Initiative [88], reflecting a community consensus of the status of the SM prediction in 2020 and 2025, respectively.

Int. J. Mod. Phys. A 2026.41. Downloaded from www.worldscientific.com
UNIVERSITY OF CALIFORNIA @ BERKELEY on 09/16/26. Re-use and distribution is strictly not permitted, except for Open Access articles.

Table 56.3: Summary of all contributions to the SM prediction and comparison to experiment, adapted from Ref. [9].

Contribution	Value $\times 10^{11}$	References
Experiment (E989, E821)	116 592 071.5(14.5)	Refs. [1–8]
HVP LO (lattice)	7132(61)	Refs. [21–37]
HVP LO (e^+e^-, τ)	Estimates not provided at this point	
HVP NLO (e^+e^-)	−99.6(1.3)	Refs. [38, 39]
HVP NNLO (e^+e^-)	12.4(1)	Ref. [40]
HLbL (phenomenology)	103.3(8.8)	Refs. [19, 41–63]
HLbL NLO (phenomenology)	2.6(6)	Ref. [64]
HLbL (lattice)	122.5(9.0)	Refs. [65–69]
HLbL (phenomenology + lattice)	112.6(9.6)	Refs. [19, 41–63, 65–69]
QED	116 584 718.8(2)	Refs. [10–16]
EW	154.4(4)	Refs. [17–20]
HVP LO (lattice) + HVP N(N)LO (e^+e^-)	7045(61)	Refs. [21–40]
HLbL (phenomenology + lattice + NLO)	115.5(9.9)	Refs. [19, 41–69]
Total SM Value	116 592 033(62)	Refs. [10–69]
Difference: $\Delta a_\mu \equiv a_\mu^{\rm exp} - a_\mu^{\rm SM}$	38(63)	

respectively. Up to $\mathcal{O}(\alpha^3)$, analytical results are available, both for the mass-independent terms [90–92] and mass-dependent corrections [93–95], so that the uncertainties in the coefficients in Eq. (56.9) only depend on the input for the lepton mass ratios. At $\mathcal{O}(\alpha^4)$, the mass-independent term is known essentially analytically [96], and the uncertainty in the mass-dependent corrections is dominated by MC errors [10, 97]. Finally, at $\mathcal{O}(\alpha^5)$ both mass-independent and mass-dependent contributions are evaluated numerically, and the size of the mass-independent term recently decreased by $\simeq 0.8$ upon improved MC sampling [10–13], about the same size as the MC uncertainty in the mass-dependent correction. Numerically, the largest contributions to the coefficients arise from terms enhanced by powers of $\log \frac{m_\mu}{m_e}$ (and factors of π^2), explaining their rapid increase. For the evaluation of $a_\mu^{\rm QED}$, input for the fine-structure constant α is required, the current most precise determinations being [9]

$$\alpha^{-1}[\mathrm{Cs}] = 137.035\,999\,045(27)\,, \tag{56.10}$$

$$\alpha^{-1}[\mathrm{Rb}] = 137.035\,999\,2052(97)\,, \tag{56.11}$$

$$\alpha^{-1}[a_e] = 137.035\,999\,163(15)\,, \tag{56.12}$$

derived from atom-interferometry measurements in Cs [14], Rb [15], and the anomalous magnetic moment of the electron a_e [16], respectively. $\alpha^{-1}[\mathrm{Cs}]$ and $\alpha^{-1}[\mathrm{Rb}]$ disagree by 5.5σ, which translates to an uncertainty of about 0.14×10^{-11} in $a_\mu^{\rm QED}$. This is the same level at which $\mathcal{O}(\alpha^6)$ contributions are expected to enter, estimated based on the maximally possible enhancement with $\log \frac{m_\mu}{m_e}$ at six-loop order [10]. The combination of these two effects leads to the final uncertainty quoted for $a_\mu^{\rm QED}$ in Table 56.3.

Loop contributions that involve W, Z, or Higgs bosons are summarized in the EW contribution $a_\mu^{\rm EW}$. At one-loop order, the result can be expressed as [98–102]

$$\begin{aligned} a_\mu^{\rm EW}[\text{1-loop}] =& \frac{G_F}{\sqrt{2}}\frac{m_\mu^2}{8\pi^2}\left[\frac{5}{3} + \frac{1}{3}(1-4s_{\rm W}^2)^2 + \mathcal{O}\left(\frac{m_\mu^2}{M_W^2}, \frac{m_\mu^2}{M_H^2}\right)\right] \\ =& 194.79(1) \times 10^{-11}\,, \end{aligned} \tag{56.13}$$

with on-shell weak mixing angle $s_W^2 = \sin^2\theta_W = 1 - M_W^2/M_Z^2$ and the SM prediction expressed in terms of the Fermi constant G_F as measured in muon decay [103], M_Z, and α, while M_W is a derived quantity [18]. Two-loop contributions are sizable, $a_\mu^{\rm EW}[\text{2-loop}] = -40.4(4) \times 10^{-11}$, and are typically further separated into bosonic [104–106], Higgs-dependent [18, 107], and other fermionic contributions [17, 108, 109]. In particular, the latter include quark triangle loops, for which non-perturbative effects become important. Improvements in their evaluation [19, 20] together with the consideration of α_s corrections for the heavy quarks [110] and lattice-QCD input for γ–Z mixing [111] lead to the updated result [20]

$$a_\mu^{\rm EW} = 154.4(4) \times 10^{-11}\,, \tag{56.14}$$

where three-loop effects are estimated to be $\lesssim 0.2 \times 10^{-11}$ [17,112].

Figure 56.3: Summary of HLbL evaluations, from data-driven methods (green), lattice QCD (blue), and combinations (black). The averages are from WP20 and WP25, respectively, the other points refer to HSZ-24 [61, 113], RBC/UKQCD-19 [65], Mainz/CLS-21+22 [66, 67], RBC/UKQCD-23 [68], and BMW-24 [69]. Adapted from Ref. [9].

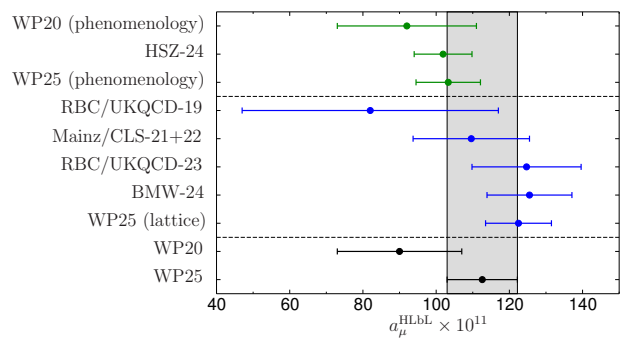

56.3.2 *Hadronic light-by-light scattering*

HLbL contributions enter at $\mathcal{O}(\alpha^3)$, involving the hadronic four-point function as indicated in Fig. 56.2, which can be determined with data-driven techniques or using lattice QCD. For a detailed review we refer to Ref. [9], while a summary of the present situation is shown in Fig. 56.3. Phenomenological [19, 41–63] and lattice-QCD [65–69] evaluations agree at a level of 1.5σ, leading to the overall average

$$a_\mu^{\rm HLbL}[\text{phenomenology + lattice}] = 112.6(9.6) \times 10^{-11}\,, \tag{56.15}$$

whose error includes a scale factor $S = 1.5$. Including an estimate for NLO HLbL topologies [64] then produces the final HLbL number quoted in Table 56.3.

56.3.3 *Hadronic vacuum polarization*

The leading, and most critical, hadronic effect already arises at $\mathcal{O}(\alpha^2)$ in the form of the HVP diagram shown in Fig. 56.2. Traditionally, this contribution has been evaluated using the master formula [114, 115]

$$a_\mu^{\rm HVP,\,LO} = \left(\frac{\alpha m_\mu}{3\pi}\right)^2 \int_{s_{\rm thr}}^{\infty} ds \frac{\hat{K}(s)}{s^2} R_{\rm had}(s)\,, \tag{56.16}$$

Int. J. Mod. Phys. A 2026.41. Downloaded from www.worldscientific.com
by UNIVERSITY OF CALIFORNIA @ BERKELEY on 09/16/26. Re-use and distribution is strictly not permitted, except for Open Access articles.

Figure 56.4: Summary of various determinations of $a_\mu^{\mathrm{HVP,\,LO}}$, propagated to a_μ^{SM}. The first two panels refer to data-driven determinations, where the three points for each e^+e^- experiment reflect the CHKLS [123,126–128] (triangle), DHMZ [121,125,129] (diamond), and KNTW [38,122,130] (square) methods, see WP25 for details. The gray band indicates the WP20 result, based on the e^+e^- experiments above the first dashed line. The second panel represents e^+e^- experiments that became available afterwards as well as the τ-based estimate from WP25. The last panel summarizes lattice-QCD determinations, including the hybrid evaluation by BMW/DMZ-24 [31], three individual lattice-QCD calculations by RBC/UKQCD-24+18 [33], Mainz/CLS-24 [34], BMW-20 [23], and five lattice HVP averages from WP25. The blue band refers to the final WP25 result, which coincides with "Avg. 1." In all cases, except for the gray WP20 band, the remaining contributions to a_μ^{SM} beyond $a_\mu^{\mathrm{HVP,\,LO}}$ are taken from WP25. The red band denotes the experimental world average. Adapted from Ref. [9].

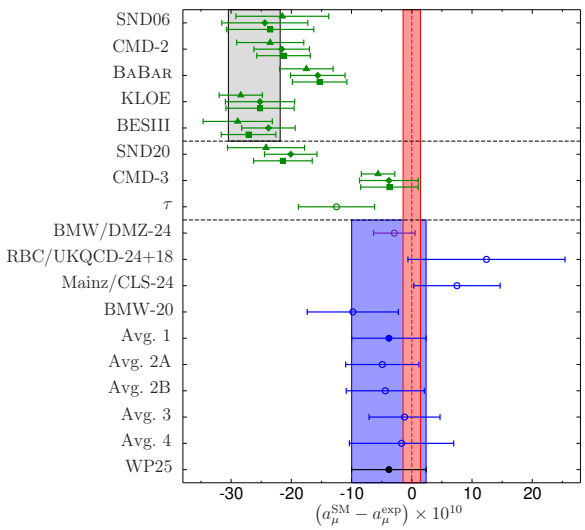

which allows one to express its effect via a dispersion integral in terms of the hadronic R-ratio,

$$R_{\mathrm{had}}(s) = \frac{3s}{4\pi\alpha^2}\sigma\left[e^+e^- \to \mathrm{hadrons}(+\gamma)\right], \tag{56.17}$$

and a kernel function $\hat{K}(s)$. In particular, the LO contribution is defined photon-inclusively, but removing vacuum-polarization effects in the photon propagator. Accordingly, the integration starts at the threshold of the $e^+e^- \to \pi^0\gamma$ channel, $s_{\mathrm{thr}} = M_{\pi^0}^2$. In WP20, the final result for the HVP contribution was based on e^+e^- data, including data for the by far numerically dominant $e^+e^- \to \pi^+\pi^-$ channel from the SND06 [116], CMD-2 [117], BaBar [118], KLOE [119], and BESIII [120] experiments. Moreover, different methodologies for the compilation of e^+e^- data were taken into account [38, 121–125], and an additional uncertainty beyond a simple scale factor was introduced to account for the tension between the BaBar and KLOE measurements, leading to the gray band in Fig. 56.4.

Subsequently, new $\pi^+\pi^-$ measurements from SND20 [131] and CMD-3 [132, 133] have become available, and while the former falls within the previous range, the latter increases tensions to a level that cannot be taken into account anymore by a meaningful inflation of uncertainties. For that reason, e^+e^- data are not used in WP25 for the LO HVP evaluation at this point, until the origin of the discrepancies among data sets is understood.[4]

An alternative data-driven evaluation relies on $\tau \to \nu_\tau +$ hadrons decays [136], in which case isospin symmetry provides access to the isovector part of the hadronic cross section as long as isospin-breaking corrections [137–142] can be controlled. A critical review of these corrections is provided in WP25, identifying several effects that currently preclude the use of τ data for the HVP evaluation due to a remaining model dependence that is difficult to quantify in a reliable manner. However, the current best estimate from WP25 (based on Refs. [126,129,140,142,143]) is included in the second panel of Fig. 56.4.

While the HVP evaluation from data-driven methods is thus inconclusive at this point, material progress has been achieved since WP20 in lattice QCD, based on the time-momentum representation of the hadronic two-point function [144]. In particular, detailed cross checks have been performed using windows in Euclidean time [21] as a tool to scrutinize the different systematic errors of the calculation. In total, the final average quoted in WP25,

$$a_\mu^{\mathrm{HVP,\,LO}}[\mathrm{lattice}] = 7132(61) \times 10^{-11}\,, \tag{56.18}$$

is based on 17 different papers from 8 independent lattice-QCD collaborations [21–37], from which three almost complete lattice calculations of the entire LO HVP contribution are derived [23, 33, 34], see Fig. 56.4. Moreover, different strategies to combine the individual results (corresponding to the five averages shown in Fig. 56.4) prove very stable, and additional systematic errors have been assigned to cover the most challenging aspects of the calculation related to the evaluation of isospin-breaking effects and the noisy contributions at long distances. Given this consolidation of lattice-QCD results, the final SM prediction in WP25, as reproduced in Table 56.3, is based on Eq. (56.18),[5] until the tensions among the data-driven evaluations are resolved.

56.4 Outlook

In the current situation, it is obvious that the SM prediction (56.2) needs to be improved by a factor of four to fully leverage the precision achieved in experiment (56.1), which would result in a three-fold improved precision of the SM test (56.3). Ongoing efforts include [145]:

- Data-driven and lattice-QCD evaluations of the HLbL contribution will be further scrutinized to better understand their slight tension and hopefully further improve the precision.
- Lattice-QCD calculations will be performed at increased precision, with focus on more precise evaluations of isospin-breaking effects and the noisy contributions at long distances.
- New e^+e^- results are expected from BaBar, KLOE (existing data that were never analyzed before) and Belle II, BESIII, SND (new data). In addition, the role of radiative corrections and MC generators will be carefully scrutinized [146–152].
- New data for τ decays are expected from Belle II, and improved determinations of the required isospin-breaking corrections will be developed using lattice QCD, dispersion relations, and data-driven techniques.
- An independent direct measurement of a_μ is the goal of the E34 experiment at J-PARC [79].
- The MUonE experiment [153–155] aims at a measurement of the HVP contribution in a spacelike process, yielding another independent determination with completely different systematics.

References

[1] D. P. Aguillard *et al.* (Muon $g-2$), Phys. Rev. Lett. **135**, 10, 101802 (2025), [arXiv:2506.03069].

[2] D. P. Aguillard *et al.* (Muon $g-2$), Phys. Rev. Lett. **131**, 16, 161802 (2023), [arXiv:2308.06230].

[3] D. P. Aguillard *et al.* (Muon $g-2$), Phys. Rev. D **110**, 3, 032009 (2024), [arXiv:2402.15410].

[4] B. Abi *et al.* (Muon $g-2$), Phys. Rev. Lett. **126**, 14, 141801 (2021), [arXiv:2104.03281].

[5] T. Albahri *et al.* (Muon $g-2$), Phys. Rev. D **103**, 7, 072002 (2021), [arXiv:2104.03247].

[4] The exception concerns higher-order HVP iterations [40,134], for which the increased uncertainty can be tolerated [38, 39]. Mixed leptonic and hadronic corrections at $\mathcal{O}(\alpha^4)$ are $\lesssim 1 \times 10^{-11}$ [135].

[5] This result agrees with the hybrid evaluation by BMW/DMZ-24 [31], using data input for the long-distance tail.

Int. J. Mod. Phys. A 2026.41. Downloaded from www.worldscientific.com
UNIVERSITY OF CALIFORNIA @ BERKELEY on 09/16/26. Re-use and distribution is strictly not permitted, except for Open Access articles.

[6] T. Albahri *et al.* (Muon $g-2$), Phys. Rev. A **103**, 4, 042208 (2021), [arXiv:2104.03201].

[7] T. Albahri *et al.* (Muon $g-2$), Phys. Rev. Accel. Beams **24**, 4, 044002 (2021), [arXiv:2104.03240].

[8] G. W. Bennett *et al.* (Muon $g-2$), Phys. Rev. D **73**, 072003 (2006), [hep-ex/0602035].

[9] R. Aliberti *et al.*, Phys. Rept. **1143**, 1 (2025), [arXiv:2505.21476].

[10] T. Aoyama *et al.*, Phys. Rev. Lett. **109**, 111808 (2012), [arXiv:1205.5370].

[11] S. Volkov, Phys. Rev. D **100**, 9, 096004 (2019), [arXiv:1909.08015].

[12] S. Volkov, Phys. Rev. D **110**, 3, 036001 (2024), [arXiv:2404.00649].

[13] T. Aoyama *et al.*, Phys. Rev. D **111**, 3, L031902 (2025), [arXiv:2412.06473].

[14] R. H. Parker *et al.*, Science **360**, 191 (2018), [arXiv:1812.04130].

[15] L. Morel *et al.*, Nature **588**, 7836, 61 (2020).

[16] X. Fan *et al.*, Phys. Rev. Lett. **130**, 7, 071801 (2023), [arXiv:2209.13084].

[17] A. Czarnecki, W. J. Marciano and A. Vainshtein, Phys. Rev. D **67**, 073006 (2003), [Erratum: Phys. Rev. D **73**, 119901 (2006)], [hep-ph/0212229].

[18] C. Gnendiger, D. Stöckinger and H. Stöckinger-Kim, Phys. Rev. D **88**, 053005 (2013), [arXiv:1306.5546].

[19] J. Lüdtke, M. Procura and P. Stoffer, JHEP **04**, 130 (2025), [arXiv:2410.11946].

[20] M. Hoferichter *et al.*, Phys. Rev. Lett. **134**, 20, 201801 (2025), [arXiv:2503.04883].

[21] T. Blum *et al.* (RBC, UKQCD), Phys. Rev. Lett. **121**, 2, 022003 (2018), [arXiv:1801.07224].

[22] D. Giusti *et al.* (ETM), Phys. Rev. D **99**, 11, 114502 (2019), [arXiv:1901.10462].

[23] S. Borsányi *et al.*, Nature **593**, 7857, 51 (2021), [arXiv:2002.12347].

[24] C. Lehner and A. S. Meyer, Phys. Rev. D **101**, 074515 (2020), [arXiv:2003.04177].

[25] G. Wang *et al.* (χQCD), Phys. Rev. D **107**, 3, 034513 (2023), [arXiv:2204.01280].

[26] C. Aubin *et al.*, Phys. Rev. D **106**, 5, 054503 (2022), [arXiv:2204.12256].

[27] M. Cè *et al.*, Phys. Rev. D **106**, 11, 114502 (2022), [arXiv:2206.06582].

[28] C. Alexandrou *et al.* (ETM), Phys. Rev. D **107**, 7, 074506 (2023), [arXiv:2206.15084].

[29] T. Blum *et al.* (RBC, UKQCD), Phys. Rev. D **108**, 5, 054507 (2023), [arXiv:2301.08696].

[30] S. Kuberski *et al.*, JHEP **03**, 172 (2024), [arXiv:2401.11895].

[31] A. Boccaletti *et al.* (2024), [arXiv:2407.10913].

[32] S. Spiegel and C. Lehner, Phys. Rev. D **111**, 11, 114517 (2025), [arXiv:2410.17053].

[33] T. Blum *et al.* (RBC, UKQCD), Phys. Rev. Lett. **134**, 20, 201901 (2025), [arXiv:2410.20590].

[34] D. Djukanovic *et al.*, JHEP **04**, 098 (2025), [arXiv:2411.07969].

[35] C. Alexandrou *et al.* (ETM), Phys. Rev. D **111**, 5, 054502 (2025), [arXiv:2411.08852].

[36] A. Bazavov *et al.* (Fermilab Lattice, HPQCD, MILC), Phys. Rev. D **111**, 9, 094508 (2025), [arXiv:2411.09656].

[37] A. Bazavov *et al.* (Fermilab Lattice, HPQCD, MILC), Phys. Rev. Lett. **135**, 1, 011901 (2025), [arXiv:2412.18491].

[38] A. Keshavarzi, D. Nomura and T. Teubner, Phys. Rev. D **101**, 014029 (2020), [arXiv:1911.00367].

[39] L. Di Luzio *et al.*, Phys. Rev. Lett. **134**, 1, 011902 (2025), [arXiv:2408.01123].

[40] A. Kurz *et al.*, Phys. Lett. B **734**, 144 (2014), [arXiv:1403.6400].

[41] G. Colangelo *et al.*, JHEP **09**, 074 (2015), [arXiv:1506.01386].

[42] P. Masjuan and P. Sánchez-Puertas, Phys. Rev. D **95**, 5, 054026 (2017), [arXiv:1701.05829].

[43] G. Colangelo *et al.*, JHEP **04**, 161 (2017), [arXiv:1702.07347].

[44] M. Hoferichter *et al.*, JHEP **10**, 141 (2018), [arXiv:1808.04823].

[45] G. Eichmann *et al.*, Phys. Lett. B **797**, 134855 (2019), [Erratum: Phys. Lett. B **799**, 135029 (2019)], [arXiv:1903.10844].

[46] J. Bijnens, N. Hermansson-Truedsson and A. Rodríguez-Sánchez, Phys. Lett. B **798**, 134994 (2019), [arXiv:1908.03331].

[47] J. Leutgeb and A. Rebhan, Phys. Rev. D **101**, 11, 114015 (2020), [arXiv:1912.01596].

[48] L. Cappiello *et al.*, Phys. Rev. D **102**, 1, 016009 (2020), [arXiv:1912.02779].

[49] P. Masjuan, P. Roig and P. Sánchez-Puertas, J. Phys. G **49**, 1, 015002 (2022), [arXiv:2005.11761].

[50] J. Bijnens *et al.*, JHEP **10**, 203 (2020), [arXiv:2008.13487].

[51] J. Bijnens *et al.*, JHEP **04**, 240 (2021), [arXiv:2101.09169].

[52] I. Danilkin, M. Hoferichter and P. Stoffer, Phys. Lett. B **820**, 136502 (2021), [arXiv:2105.01666].

[53] D. Stamen *et al.*, Eur. Phys. J. C **82**, 5, 432 (2022), [arXiv:2202.11106].

[54] J. Leutgeb, J. Mager and A. Rebhan, Phys. Rev. D **107**, 5, 054021 (2023), [arXiv:2211.16562].

[55] M. Hoferichter, B. Kubis and M. Zanke, JHEP **08**, 209 (2023), [arXiv:2307.14413].

[56] M. Hoferichter, P. Stoffer and M. Zillinger, JHEP **04**, 092 (2024), [arXiv:2402.14060].

[57] E. J. Estrada *et al.*, JHEP **12**, 203 (2024), [arXiv:2409.10503].

[58] O. Deineka, I. Danilkin and M. Vanderhaeghen, Phys. Rev. D **111**, 3, 034009 (2025), [arXiv:2410.12894].

[59] G. Eichmann *et al.*, Eur. Phys. J. C **85**, 4, 445 (2025), [arXiv:2411.05652].

[60] J. Bijnens, N. Hermansson-Truedsson and A. Rodríguez-Sánchez, JHEP **03**, 094 (2025), [arXiv:2411.09578].

[61] M. Hoferichter, P. Stoffer and M. Zillinger, JHEP **02**, 121 (2025), [arXiv:2412.00178].

[62] S. Holz *et al.*, JHEP **04**, 147 (2025), [arXiv:2412.16281].

[63] L. Cappiello *et al.*, JHEP **07**, 033 (2025), [arXiv:2501.09699].

[64] G. Colangelo *et al.*, Phys. Lett. B **735**, 90 (2014), [arXiv:1403.7512].

[65] T. Blum *et al.*, Phys. Rev. Lett. **124**, 13, 132002 (2020), [arXiv:1911.08123].

[66] E.-H. Chao *et al.*, Eur. Phys. J. C **81**, 7, 651 (2021), [arXiv:2104.02632].

[67] E.-H. Chao *et al.*, Eur. Phys. J. C **82**, 8, 664 (2022), [arXiv:2204.08844].

[68] T. Blum *et al.* (RBC, UKQCD), Phys. Rev. D **111**, 1, 014501 (2025), [arXiv:2304.04423].

[69] Z. Fodor *et al.*, Phys. Rev. D **111**, 11, 114509 (2025), [arXiv:2411.11719].

[70] H. R. P. Ferguson and D. H. Bailey, Technical report, RNR-91-032 (1992), URL `https://www.davidhbailey.com/dhbpapers/pslq.pdf`.

Int. J. Mod. Phys. A 2026.41. Downloaded from www.worldscientific.com
by UNIVERSITY OF CALIFORNIA @ BERKELEY on 09/16/26. Re-use and distribution is strictly not permitted, except for Open Access articles.

[71] J. Bailey *et al.* (CERN-Mainz-Daresbury), Nucl. Phys. B **150**, 1 (1979).

[72] H. N. Brown *et al.* (Muon $g-2$), Phys. Rev. Lett. **86**, 2227 (2001), [hep-ex/0102017].

[73] G. W. Bennett *et al.* (Muon $g-2$), Phys. Rev. Lett. **89**, 101804 (2002), [Erratum: Phys. Rev. Lett. **89**, 129903 (2002)], [hep-ex/0208001].

[74] G. W. Bennett *et al.* (Muon $g-2$), Phys. Rev. Lett. **92**, 161802 (2004), [hep-ex/0401008].

[75] P. J. Mohr *et al.*, Rev. Mod. Phys. **97**, 2, 025002 (2025), [arXiv:2409.03787].

[76] G. T. Danby *et al.*, Nucl. Instrum. Meth. A **457**, 151 (2001).

[77] A. P. Schreckenberger *et al.*, Nucl. Instrum. Meth. A **1011**, 165597 (2021), [arXiv:2104.07805].

[78] V. Bargmann, L. Michel and V. L. Telegdi, Phys. Rev. Lett. **2**, 435 (1959).

[79] M. Abe *et al.*, PTEP **2019**, 5, 053C02 (2019), [arXiv:1901.03047].

[80] D. Flay *et al.*, JINST **16**, 12, P12041 (2021), [arXiv:2109.08992].

[81] M. Farooq *et al.*, Phys. Rev. Lett. **124**, 22, 223001 (2020).

[82] S. Corrodi *et al.* (Muon $g-2$), JINST **15**, 11, P11008 (2020), [arXiv:2003.06244].

[83] E. Swanson *et al.*, Nucl. Instrum. Meth. A **1075**, 170338 (2025), [arXiv:2410.08279].

[84] B. T. King *et al.*, JINST **17**, 02, P02035 (2022), [arXiv:2111.02076].

[85] K. S. Khaw *et al.* (Muon $g-2$), Nucl. Instrum. Meth. A **945**, 162558 (2019), [arXiv:1905.04407].

[86] O. Kim *et al.*, New J. Phys. **22**, 6, 063002 (2020), [arXiv:1902.02959].

[87] T. Aoyama *et al.*, Phys. Rept. **887**, 1 (2020), [arXiv:2006.04822].

[88] Muon $g-2$ Theory Initiative `https://muon-gm2-theory.illinois.edu/`.

[89] J. S. Schwinger, Phys. Rev. **73**, 416 (1948).

[90] A. Petermann, Helv. Phys. Acta **30**, 407 (1957).

[91] C. M. Sommerfield, Ann. Phys. (N.Y.) **5**, 26 (1958).

[92] S. Laporta and E. Remiddi, Phys. Lett. B **379**, 283 (1996), [hep-ph/9602417].

[93] H. H. Elend, Phys. Lett. **20**, 682 (1966), [Erratum: Phys. Lett. **21**, 720 (1966)].

[94] S. Laporta and E. Remiddi, Phys. Lett. B **301**, 440 (1993).

[95] S. Laporta, Nuovo Cim. A **106**, 675 (1993).

[96] S. Laporta, Phys. Lett. B **772**, 232 (2017), [arXiv:1704.06996].

[97] T. Kinoshita and M. Nio, Phys. Rev. D **73**, 013003 (2006), [hep-ph/0507249].

[98] R. Jackiw and S. Weinberg, Phys. Rev. D **5**, 2396 (1972).

[99] I. Bars and M. Yoshimura, Phys. Rev. D **6**, 374 (1972).

[100] G. Altarelli, N. Cabibbo and L. Maiani, Phys. Lett. B **40**, 415 (1972).

[101] W. A. Bardeen, R. Gastmans and B. E. Lautrup, Nucl. Phys. B **46**, 319 (1972).

[102] K. Fujikawa, B. Lee and A. Sanda, Phys. Rev. D **6**, 2923 (1972).

[103] V. Tishchenko *et al.* (MuLan), Phys. Rev. D **87**, 5, 052003 (2013), [arXiv:1211.0960].

[104] A. Czarnecki, B. Krause and W. J. Marciano, Phys. Rev. Lett. **76**, 3267 (1996), [hep-ph/9512369].

[105] S. Heinemeyer, D. Stöckinger and G. Weiglein, Nucl. Phys. B **699**, 103 (2004), [hep-ph/0405255].

[106] T. Gribouk and A. Czarnecki, Phys. Rev. D **72**, 053016 (2005), [hep-ph/0509205].

[107] A. Czarnecki, B. Krause and W. J. Marciano, Phys. Rev. D **52**, 2619 (1995), [hep-ph/9506256].

[108] S. Peris, M. Perrottet and E. de Rafael, Phys. Lett. B **355**, 523 (1995), [hep-ph/9505405].

[109] M. Knecht *et al.*, JHEP **11**, 003 (2002), [hep-ph/0205102].

[110] K. Melnikov, Phys. Lett. B **639**, 294 (2006), [hep-ph/0604205].

[111] M. Cè *et al.*, JHEP **08**, 220 (2022), [arXiv:2203.08676].

[112] G. Degrassi and G. Giudice, Phys. Rev. D **58**, 053007 (1998), [hep-ph/9803384].

[113] M. Hoferichter, P. Stoffer and M. Zillinger, Phys. Rev. Lett. **134**, 6, 061902 (2025), [arXiv:2412.00190].

[114] C. Bouchiat and L. Michel, J. Phys. Radium **22**, 2, 121 (1961).

[115] S. J. Brodsky and E. de Rafael, Phys. Rev. **168**, 1620 (1968).

[116] M. N. Achasov *et al.* (SND), J. Exp. Theor. Phys. **103**, 380 (2006), [Zh. Eksp. Teor. Fiz. **130**, 437 (2006)], [hep-ex/0605013].

[117] R. R. Akhmetshin *et al.* (CMD-2), Phys. Lett. B **648**, 28 (2007), [hep-ex/0610021].

[118] J. P. Lees *et al.* (BaBar), Phys. Rev. D **86**, 032013 (2012), [arXiv:1205.2228].

[119] A. Anastasi *et al.* (KLOE-2), JHEP **03**, 173 (2018), [arXiv:1711.03085].

[120] M. Ablikim *et al.* (BESIII), Phys. Lett. B **753**, 629 (2016), [Erratum: Phys. Lett. B **812**, 135982 (2021)], [arXiv:1507.08188].

[121] M. Davier *et al.*, Eur. Phys. J. C **77**, 12, 827 (2017), [arXiv:1706.09436].

[122] A. Keshavarzi, D. Nomura and T. Teubner, Phys. Rev. D **97**, 11, 114025 (2018), [arXiv:1802.02995].

[123] G. Colangelo, M. Hoferichter and P. Stoffer, JHEP **02**, 006 (2019), [arXiv:1810.00007].

[124] M. Hoferichter, B.-L. Hoid and B. Kubis, JHEP **08**, 137 (2019), [arXiv:1907.01556].

[125] M. Davier *et al.*, Eur. Phys. J. C **80**, 3, 241 (2020), [Erratum: Eur. Phys. J. C **80**, 410 (2020)], [arXiv:1908.00921].

[126] G. Colangelo *et al.*, JHEP **10**, 032 (2022), [arXiv:2208.08993].

[127] P. Stoffer, G. Colangelo and M. Hoferichter, JINST **18**, 10, C10021 (2023), [arXiv:2308.04217].

[128] T. P. Leplumey and P. Stoffer (2025), [arXiv:2501.09643v1].

[129] M. Davier *et al.*, Eur. Phys. J. C **84**, 7, 721 (2024), [arXiv:2312.02053].

[130] A. Keshavarzi *et al.*, Phys. Rev. D **111**, 1, L011901 (2025), [arXiv:2409.02827].

[131] M. N. Achasov *et al.* (SND), JHEP **01**, 113 (2021), [arXiv:2004.00263].

[132] F. V. Ignatov *et al.* (CMD-3), Phys. Rev. D **109**, 11, 112002 (2024), [arXiv:2302.08834].

[133] F. V. Ignatov *et al.* (CMD-3), Phys. Rev. Lett. **132**, 23, 231903 (2024), [arXiv:2309.12910].

[134] J. Calmet *et al.*, Phys. Lett. **61B**, 283 (1976).

[135] M. Hoferichter and T. Teubner, Phys. Rev. Lett. **128**, 11, 112002 (2022), [arXiv:2112.06929].

[136] R. Alemany, M. Davier and A. Hoecker, Eur. Phys. J. C **2**, 123 (1998), [hep-ph/9703220].

[137] V. Cirigliano, G. Ecker and H. Neufeld, Phys. Lett. B **513**, 361 (2001), [hep-ph/0104267].

[138] V. Cirigliano, G. Ecker and H. Neufeld, JHEP **08**, 002 (2002), [hep-ph/0207310].

[139] F. Flores-Báez *et al.*, Phys. Rev. D **74**, 071301 (2006), [hep-ph/0608084].

[140] M. Davier *et al.*, Eur. Phys. J. C **66**, 127 (2010), [arXiv:0906.5443].

[141] J. A. Miranda and P. Roig, Phys. Rev. D **102**, 114017 (2020), [arXiv:2007.11019].

[142] G. López Castro, A. Miranda and P. Roig, Phys. Rev. D **111**, 7, 073004 (2025), [arXiv:2411.07696].

[143] M. Hoferichter *et al.*, Phys. Rev. Lett. **131**, 16, 161905 (2023), [arXiv:2307.02532].

[144] D. Bernecker and H. B. Meyer, Eur. Phys. J. A **47**, 148 (2011), [arXiv:1107.4388].

[145] G. Colangelo *et al.* (2022), [arXiv:2203.15810].

[146] F. Campanario *et al.*, Phys. Rev. D **100**, 7, 076004 (2019), [arXiv:1903.10197].

[147] F. Ignatov and R. N. Lee, Phys. Lett. B **833**, 137283 (2022), [arXiv:2204.12235].

[148] G. Colangelo *et al.*, JHEP **08**, 295 (2022), [Erratum: JHEP **03**, 217 (2025)], [arXiv:2207.03495].

[149] G. Abbiendi *et al.* (2022), [arXiv:2201.12102].

[150] J. P. Lees *et al.* (BaBar), Phys. Rev. D **108**, 11, L111103 (2023), [arXiv:2308.05233].

[151] E. Budassi *et al.*, JHEP **05**, 196 (2025), [arXiv:2409.03469].

[152] R. Aliberti *et al.*, SciPost Phys. Comm. Rep. **9**, 1 (2025), [arXiv:2410.22882].

[153] C. M. Carloni Calame *et al.*, Phys. Lett. B **746**, 325 (2015), [arXiv:1504.02228].

[154] G. Abbiendi *et al.* (MUonE), Eur. Phys. J. C **77**, 3, 139 (2017), [arXiv:1609.08987].

[155] P. Banerjee *et al.*, Eur. Phys. J. C **80**, 6, 591 (2020), [arXiv:2004.13663].

Int. J. Mod. Phys. A 2026.41. Downloaded from www.worldscientific.com
UNIVERSITY OF CALIFORNIA @ BERKELEY on 09/16/26. Re-use and distribution is strictly not permitted, except for Open Access articles.

Int. J. Mod. Phys. A 2026.41. Downloaded from www.worldscientific.com
by UNIVERSITY OF CALIFORNIA @ BERKELEY on 09/16/26. Re-use and distribution is strictly not permitted, except for Open Access articles.

57. Muon Decay Parameters

Revised August 2023 by W. Fetscher (ETH Zurich) and H.-J. Gerber (ETH Zurich).

57.1 Introduction:

All measurements in direct muon decay, $\mu^- \to e^- + 2$ neutrals, and its inverse, $\nu_\mu + e^- \to \mu^-$ + neutral, are successfully described by the "V-A interaction," which is a particular case of a local, derivative-free, lepton-number-conserving, four-fermion interaction [1]. As shown below, within this framework, the Standard Model assumptions, such as the V-A form and the nature of the neutrals (ν_μ and $\bar{\nu}_e$), and hence the doublet assignments $(\nu_e\, e^-)_L$ and $(\nu_\mu\, \mu^-)_L$, have been determined from experiments [2,3]. All considerations on muon decay are valid for the leptonic tau decays $\tau^- \to \ell^- + \nu_\tau + \bar{\nu}_\ell$ with the replacements $m_\mu \to m_\tau$, $m_e \to m_{ell}$, $\ell^- = e^-, \mu^-$.

57.2 Parameters:

The differential decay probability to obtain an $e^\pm$ with (reduced) energy between x and $x + \mathrm{d}x$, emitted in the direction $\widehat{\boldsymbol{x}}_3$ at an angle between ϑ and $\vartheta + \mathrm{d}\vartheta$ with respect to the muon polarization vector $\boldsymbol{P}_\mu$, and with its spin parallel to the arbitrary direction $\widehat{\boldsymbol{\zeta}}$, neglecting radiative corrections, is given by

$$\begin{aligned}\frac{\mathrm{d}^2\Gamma}{\mathrm{d}x\,\mathrm{d}\cos\vartheta} &= \frac{m_\mu}{4\pi^3}\, W_{e\mu}^4\, G_\mathrm{F}^2\, \sqrt{x^2 - x^{2_0}} \\ &\quad \times (F_\mathrm{IS}(x) \pm P_\mu \cos\vartheta F_\mathrm{AS}(x)) \\ &\quad \times \left[1 + \widehat{\boldsymbol{\zeta}} \cdot \boldsymbol{P}_e(x,\vartheta)\right] \ . \end{aligned} \tag{57.1}$$

Here, $W_{e\mu} = \max(E_e) = (m_\mu^2 + m_e^2)/2m_\mu$ is the maximum $e^\pm$ energy, $x = E_e/W_{e\mu}$ is the reduced energy, $x_0 = m_e/W_{e\mu} = 9.67 \times 10^{-3}$, and $P_\mu = |\boldsymbol{P}_\mu|$ is the degree of muon polarization. $\widehat{\boldsymbol{\zeta}}$ is the direction in which a perfect polarization-sensitive electron detector is most sensitive. The isotropic part of the spectrum, $F_\mathrm{IS}(x)$, the anisotropic part $F_\mathrm{AS}(x)$, and the electron polarization, $\boldsymbol{P}_e(x,\vartheta)$, may be parametrized by the Michel parameter ρ [1], by η [4], by ξ and δ [5,6], *etc.* These are bilinear combinations of the coupling constants $g^\gamma_{\varepsilon\mu}$, which occur in the matrix element (given below).

If the masses of the neutrinos as well as x_0^2 are neglected, the energy and angular distribution of the electron in the rest frame of a muon ($\mu^\pm$) measured by a polarization insensitive detector, is given by

$$\begin{aligned}\frac{\mathrm{d}^2\Gamma}{\mathrm{d}x\,\mathrm{d}\cos\vartheta} \sim x^2 \cdot \Big\{ & 3(1-x) + \frac{2\rho}{3}(4x-3) + 3\eta\, x_0(1-x)/x \\ & \pm P_\mu \cdot \xi \cdot \cos\vartheta \left[1 - x + \frac{2\delta}{3}(4x-3)\right]\Big\} \ . \end{aligned} \tag{57.2}$$

Here, ϑ is the angle between the electron momentum and the muon spin, and $x \equiv 2E_e/m_\mu$. For the Standard Model coupling, we obtain $\rho = \xi\delta = 3/4$, $\xi = 1$, $\eta = 0$ and the differential decay rate is

$$\frac{\mathrm{d}^2\Gamma}{\mathrm{d}x\,\mathrm{d}\cos\vartheta} = \frac{G_\mathrm{F}^2 m_\mu^5}{192\pi^3}\, [3 - 2x \pm P_\mu \cos\vartheta(2x-1)] \cdot x^2 \,. \tag{57.3}$$

The coefficient in front of the square bracket is the total decay rate.

If only the neutrino masses are neglected, and if the $e^\pm$ polarization is detected, then the functions in Eq. (57.1) become

$$F_\mathrm{IS}(x) = x\,(1-x) + \tfrac{2}{9}\,\rho\,(4x^2 - 3x - x_0^2) + \eta \cdot x_0\,(1-x) \tag{57.4a}$$

$$\begin{aligned}F_\mathrm{AS}(x) = \tfrac{1}{3}\,\xi\,\sqrt{x^2 - x_0^2} & \\ \times \left[(1-x) + \tfrac{2}{3}\delta\left\{(4x-3) + \left(\sqrt{1-x_0^2} - 1\right)\right\}\right] & \end{aligned} \tag{57.4b}$$

$$\boldsymbol{P}_e(x,\vartheta) = P_{\mathrm{T}_1} \cdot \widehat{\boldsymbol{x}}_1 + P_{\mathrm{T}_2} \cdot \widehat{\boldsymbol{x}}_2 + P_\mathrm{L} \cdot \widehat{\boldsymbol{x}}_3 \tag{57.4c}$$

Here $\widehat{\boldsymbol{x}}_1$, $\widehat{\boldsymbol{x}}_2$, and $\widehat{\boldsymbol{x}}_3$ are orthogonal unit vectors defined as follows:

$\widehat{\boldsymbol{x}}_3$	is along the e momentum $\boldsymbol{p}_e$
$\dfrac{\widehat{\boldsymbol{x}}_3 \times \boldsymbol{P}_\mu}{\lvert\widehat{\boldsymbol{x}}_3 \times \boldsymbol{P}_\mu\rvert} = \widehat{\boldsymbol{x}}_2$	is transverse to $\boldsymbol{p}_e$ and perpendicular to "the decay plane"
$\widehat{\boldsymbol{x}}_2 \times \widehat{\boldsymbol{x}}_3 = \widehat{\boldsymbol{x}}_1$	is transverse to $\boldsymbol{p}_e$ and in the decay plane

The components of $\boldsymbol{P}_e$ then are given by

$$P_{\mathrm{T}_1}(x,\vartheta) = P_\mu \sin\vartheta \cdot F_{\mathrm{T}_1}(x)/\left\{F_\mathrm{IS}(x) \pm P_\mu \cos\vartheta \cdot F_\mathrm{AS}(x)\right\} \tag{57.5a}$$

$$P_{\mathrm{T}_2}(x,\vartheta) = P_\mu \sin\vartheta \cdot F_{\mathrm{T}_2}(x)/\left\{F_\mathrm{IS}(x) \pm P_\mu \cos\vartheta \cdot F_\mathrm{AS}(x)\right\} \tag{57.5b}$$

$$P_\mathrm{L}(x,\vartheta) = \frac{\pm F_\mathrm{IP}(x) + P_\mu \cos\vartheta \cdot F_\mathrm{AP}(x)}{F_\mathrm{IS}(x) \pm P_\mu \cos\vartheta \cdot F_\mathrm{AS}(x)} \quad , \tag{57.5c}$$

where

$$\begin{aligned}F_{\mathrm{T}_1}(x) = \tfrac{1}{12}\Big\{ & -2\left[\xi'' + 12\left(\rho - \tfrac{3}{4}\right)\right](1-x)x_0 \\ & -3\,\eta\left(x^2 - x_0^2\right) + \eta''\left(-3x^2 + 4x - x_0^2\right)\Big\} \end{aligned} \tag{57.6a}$$

$$F_{\mathrm{T}_2}(x) = \tfrac{1}{3}\,\sqrt{x^2 - x_0^2} \cdot \left\{3\,\frac{\alpha'}{A}(1-x) + 2\,\frac{\beta'}{A}\sqrt{1-x_0^2}\right\} \tag{57.6b}$$

$$\begin{aligned}F_\mathrm{IP}(x) = \tfrac{1}{54}\sqrt{x^2 - x_0^2} \cdot \Big\{ & 9\,\xi'\left(-2x + 2 + \sqrt{1-x_0^2}\right) \\ & +4\,\xi\left(\delta - \tfrac{3}{4}\right)\left(4x - 4 + \sqrt{1-x_0^2}\right)\Big\} \end{aligned} \tag{57.6c}$$

$$\begin{aligned}F_\mathrm{AP}(x) = \tfrac{1}{6}\Big\{ & \xi''\left(2x^2 - x - x_0^2\right) + 4\left(\rho - \tfrac{3}{4}\right)\left(4x^2 - 3x - x_0^2\right) \\ & + 2\,\eta''(1-x)\,x_0\Big\} \,. \end{aligned} \tag{57.6d}$$

For the experimental values of the parameters ρ, ξ, ξ', ξ'', δ, η, η'', α/A, β/A, α'/A, β'/A, which are not all independent, see the Data Listings below. Experiments in the past have also been analyzed using the parameters a, b, c, a', b', c', α/A, β/A, α'/A, β'/A (and $\eta = (\alpha - 2\beta)/2A$), as defined by Kinoshita and Sirlin [5,6]. They serve as a model-independent summary of all possible measurements on the decay electron (see Listings below). The relations between the two sets of parameters are

$$\rho - \tfrac{3}{4} = \tfrac{3}{4}\,(-a + 2\,c)/A \tag{57.7a}$$

$$\eta = (\alpha - 2\beta)/A \tag{57.7b}$$

$$\eta'' = (3\,\alpha + 2\,\beta)/A \tag{57.7c}$$

$$\delta - \tfrac{3}{4} = \tfrac{9}{4} \cdot \frac{(a' - 2\,c')\,/A}{1 - [a + 3\,a' + 4\,(b + b') + 6\,c - 14\,c']\,/A} \tag{57.7d}$$

$$1 - \xi\frac{\delta}{\rho} = 4\,\frac{[(b + b') + 2\,(c - c')]\,/A}{1 - (a - 2\,c)/A} \tag{57.7e}$$

$$1 - \xi = \left[\left(a + a'\right) + 4\left(b + b'\right) + 6\left(c + c'\right)\right]/A \tag{57.7f}$$

$$1 - \xi'' = (-2\,a + 20\,c)/A \tag{57.7g}$$

$$\text{with} \qquad A = a + 4\,b + 6\,c \tag{57.7h}$$

The differential decay probability to obtain a *left-handed* ν_e with (reduced) energy between y and $y + dy$, neglecting radiative corrections as well as the masses of the electron and of the neutrinos, is given by [7]

$$\frac{\mathrm{d}\Gamma}{\mathrm{d}y} = \frac{m_\mu^5 G_\mathrm{F}^2}{16\,\pi^3} \cdot Q_L^{\nu_e} \cdot y^2 \left\{(1-y) - \omega_L \cdot \left(y - \tfrac{3}{4}\right)\right\} \,. \tag{57.8}$$

Int. J. Mod. Phys. A 2026.41. Downloaded from www.worldscientific.com
UNIVERSITY OF CALIFORNIA @ BERKELEY on 09/16/26. Re-use and distribution is strictly not permitted, except for Open Access articles.

Here, $y = 2\ E_{\nu_e}/m_\mu$. $Q_L^{\nu_e}$ and ω_L are parameters. ω_L is the neutrino analog of the spectral shape parameter ρ of Michel. Since in the Standard Model, $Q_L^{\nu_e} = 1$, $\omega_L = 0$, the measurement of $\mathrm{d}\Gamma/\mathrm{d}y$ has allowed a null-test of the Standard Model (see Listings below).

Table 57.1: Coupling constants $g^\gamma_{\varepsilon\mu}$ and some combinations of them. Ninety-percent confidence level experimental limits. The limits on $|g^S_{LL}|$ and $|g^V_{LL}|$ are from [8–10], and the others from a general analysis of muon decay measurements. Top three rows: [11], fourth row: [12], next three rows: [13], last row: [14]. The experimental uncertainty on the muon polarization in pion decay is included. Note that, by definition, $|g^S_{\varepsilon\mu}| \le 2$, $|g^V_{\varepsilon\mu}| \le 1$ and $|g^T_{\varepsilon\mu}| \le 1/\sqrt{3}$.

$\lvert g^S_{RR}\rvert < 0.035$	$\lvert g^V_{RR}\rvert < 0.017$	$\lvert g^T_{RR}\rvert \equiv 0$
$\lvert g^S_{LR}\rvert < 0.050$	$\lvert g^V_{LR}\rvert < 0.023$	$\lvert g^T_{LR}\rvert < 0.015$
$\lvert g^S_{RL}\rvert < 0.420$	$\lvert g^V_{RL}\rvert < 0.105$	$\lvert g^T_{RL}\rvert < 0.105$
$\lvert g^S_{LL}\rvert < 0.550$	$\lvert g^V_{LL}\rvert > 0.960$	$\lvert g^T_{LL}\rvert \equiv 0$
$\lvert g^S_{LR} + 6\,g^T_{LR}\rvert < 0.143$	$\lvert g^S_{RL} + 6\,g^T_{RL}\rvert < 0.418$	
$\lvert g^S_{LR} + 2\,g^T_{LR}\rvert < 0.108$	$\lvert g^S_{RL} + 2\,g^T_{RL}\rvert < 0.417$	
$\lvert g^S_{LR} - 2\,g^T_{LR}\rvert < 0.070$	$\lvert g^S_{RL} - 2\,g^T_{RL}\rvert < 0.418$	
$Q_{RR} + Q_{LR} < 8.2\times10^{-4}$		

57.3 Matrix element:

All results in direct muon decay (energy spectra of the electron and of the neutrinos, polarizations, and angular distributions), and in inverse muon decay (the reaction cross section) at energies well below $m_W c^2$, may be parametrized in terms of amplitudes $g^\gamma_{\varepsilon\mu}$ and the Fermi coupling constant G_F, using the matrix element

$$\frac{4G_\mathrm{F}}{\sqrt{2}} \sum_{\substack{\gamma=S,V,T\\ \varepsilon,\mu=R,L}} g^\gamma_{\varepsilon\mu}\, \langle \bar{e}_\varepsilon|\Gamma^\gamma|(\nu_e)_n\rangle\, \langle\bar{\nu}_\mu)_m|\Gamma_\gamma|\mu_\mu\rangle \tag{57.9}$$

We use the notation of Fetscher *et al.* [2], who in turn use the sign conventions and definitions of Scheck [15]. Here, $\gamma = S, V, T$ indicates a scalar, vector, or tensor interaction; and $\varepsilon, \mu = R, L$ indicate a right- or left-handed chirality of the electron or muon. The chiralities n and m of the ν_e and $\bar{\nu}_\mu$ are then determined by the values of γ, ε, and μ. The particles are represented by fields of definite chirality [16].

As shown by Langacker and London [17], explicit lepton-number nonconservation still leads to a matrix element equivalent to Eq. (57.9). They conclude that it is not possible, even in principle, to test lepton-number conservation in (leptonic) muon decay if the final neutrinos are massless and are not observed.

The ten complex amplitudes $g^\gamma_{\varepsilon\mu}$ (g^T_{RR} and g^T_{LL} are identically zero) and G_F constitute 19 independent (real) parameters to be determined by experiment. The Standard Model interaction corresponds to one single amplitude g^V_{LL} being unity and all the others being zero.

The (direct) muon decay experiments are compatible with an arbitrary mix of the scalar and vector amplitudes g^S_{LL} and g^V_{LL} – in the extreme even with purely scalar $g^S_{LL} = 2$, $g^V_{LL} = 0$. The decision in favour of the Standard Model comes from the quantitative observation of inverse muon decay, which would be forbidden for pure g^S_{LL} [2].

57.4 Experimental determination of $V{-}A$:

In order to determine the amplitudes $g^\gamma_{\varepsilon\mu}$ uniquely from experiment, the following set of equations, where the left-hand sides represent experimental results, has to be solved.

$$a = 16\left(|g^V_{RL}|^2 + |g^V_{LR}|^2\right) + \left|g^S_{RL} + 6\,g^T_{RL}\right|^2 + \left|g^S_{LR} + 6\,g^T_{LR}\right|^2 \tag{57.10a}$$

$$a' = 16\left(|g^V_{RL}|^2 - |g^V_{LR}|^2\right) + \left|g^S_{RL} + 6\,g^T_{RL}\right|^2 - \left|g^S_{LR} + 6\,g^T_{LR}\right|^2 \tag{57.10b}$$

$$\alpha = 8\,\mathrm{Re}\left\{g^V_{RL}\left(g^{S*}_{LR} + 6\,g^{T*}_{LR}\right) + g^V_{LR}\left(g^{S*}_{RL} + 6\,g^{T*}_{RL}\right)\right\} \tag{57.10c}$$

$$\alpha' = 8\,\mathrm{Im}\left\{-g^V_{RL}\left(g^{S*}_{LR} + 6\,g^{T*}_{LR}\right) + g^V_{LR}\left(g^{S*}_{RL} + 6\,g^{T*}_{RL}\right)\right\} \tag{57.10d}$$

$$b = 4\left(|g^V_{RR}|^2 + |g^V_{LL}|^2\right) + |g^S_{RR}|^2 + |g^S_{LL}|^2 \tag{57.10e}$$

$$b' = 4\left(|g^V_{RR}|^2 - |g^V_{LL}|^2\right) + |g^S_{RR}|^2 - |g^S_{LL}|^2 \tag{57.10f}$$

$$c = \tfrac{1}{2}\left\{|g^S_{RL} - 2\,g^T_{RL}|^2 + |g^S_{LR} - 2\,g^T_{LR}|^2\right\} \tag{57.10g}$$

$$c' = \tfrac{1}{2}\left\{|g^S_{RL} - 2\,g^T_{RL}|^2 - |g^S_{LR} - 2\,g^T_{LR}|^2\right\} \tag{57.10h}$$

and

$$Q_L^{\nu_e} = 1 - \left\{\tfrac{1}{4}|g^S_{LR}|^2 + \tfrac{1}{4}|g^S_{LL}|^2 + |g^V_{RR}|^2 + |g^V_{RL}|^2 + 3\,|g^T_{LR}|^2\right\}$$

$$\omega_L = \tfrac{3}{4}\,\frac{|g^S_{RR}|^2 + 4\,|g^V_{LR}|^2 + |g^S_{RL} + 2\,g^T_{LR}|^2}{|g^S_{RL}|^2 + |g^S_{RR}|^2 + 4\,|g^V_{LL}|^2 + 4\,|g^V_{LR}|^2 + 12\,|g^T_{RL}|^2}\,. \tag{57.10i}$$

It has been noted earlier by C. Jarlskog [18], that certain experiments observing the decay electron are especially informative if they yield the V-A values. The complete solution is now found as follows. Fetscher *et al.* [2] introduced four probabilities $Q_{\varepsilon\mu}(\varepsilon, \mu = R, L)$ for the decay of a μ-handed muon into an ε-handed electron, and showed that there exist upper bounds on Q_{RR}, Q_{LR}, and Q_{RL}, and a lower bound on Q_{LL}. These probabilities are given in terms of the $g^\gamma_{\varepsilon\mu}$'s by

$$Q_{\varepsilon\mu} = \tfrac{1}{4}|g^S_{\varepsilon\mu}|^2 + |g^V_{\varepsilon\mu}|^2 + 3\,(1 - \delta_{\varepsilon\mu})|g^T_{\varepsilon\mu}|^2 \tag{57.11}$$

where $\delta_{\varepsilon\mu} = 1$ for $\varepsilon = \mu$, and $\delta_{\varepsilon\mu} = 0$ for $\varepsilon \ne \mu$. They are related to the parameters $a,\ b,\ c,\ a', b'$, and c' by

$$Q_{RR} = 2\,(b + b')/A \tag{57.12a}$$

$$Q_{LR} = \left[(a - a') + 6\,(c - c')\right]/2A \tag{57.12b}$$

$$Q_{RL} = \left[(a + a') + 6\,(c + c')\right]/2A \tag{57.12c}$$

$$Q_{LL} = 2\,(b - b')/A \tag{57.12d}$$

with $A = 16$. In the Standard Model, $Q_{LL} = 1$ and the others are zero.

Since the upper bounds on Q_{RR}, Q_{LR}, and Q_{RL} are found to be small, and since the helicity of the ν_μ in pion decay is known from experiment [19, 20] to very high precision to be -1 [21], the cross section S of *inverse* muon decay, normalized to the V-A value, yields [2]

$$|g^S_{LL}|^2 \le 4(1 - S) \tag{57.13a}$$

and

$$|g^V_{LL}|^2 = S\,. \tag{57.13b}$$

Thus the Standard Model assumption of a pure V-A leptonic charged weak interaction of e and μ is derived (within errors) from experiments at energies far below the mass of the $W^\pm$: Eq. (57.13 b) gives a lower limit for V-A, and Eqs. (57.12 a, b, c)

and (57.13 a) give upper limits for the other four-fermion interactions. The existence of such upper limits may also be seen from $Q_{RR} + Q_{RL} = (1 - \xi')/2$ (e^+ longitudinal polarization) and $Q_{RR} + Q_{LR} = \frac{1}{2}(1 + \xi/3 - 16\,\xi\delta/9)$ (decay asymmetry). Table 57.1 gives the current experimental limits on the magnitudes of the $g^{\gamma}_{\varepsilon\mu}$'s. More stringent limits on the six coupling constants g^S_{LR}, g^V_{LR}, g^T_{LR}, g^S_{RL}, g^V_{RL}, and g^T_{RL} have been derived from upper limits on the neutrino mass [22]. Limits on the "charge retention" coordinates, as used in the older literature (*e.g.*, Ref. [23]), are given by Burkard *et al.* [24].

References

[1] L. Michel, Proc. Phys. Soc. **A63**, 514 (1950).

[2] W. Fetscher, H. J. Gerber and K. F. Johnson, Phys. Lett. **B173**, 102 (1986).

[3] P. Langacker, Comments Nucl. Part. Phys. **19**, 1, 1 (1989).

[4] C. Bouchiat and L. Michel, Phys. Rev. **106**, 170 (1957).

[5] T. Kinoshita and A. Sirlin, Phys. Rev. **107**, 593 (1957).

[6] T. Kinoshita and A. Sirlin, Phys. Rev. **108**, 844 (1957).

[7] W. Fetscher, Phys. Rev. **D49**, 5945 (1994).

[8] S. R. Mishra *et al.*, Phys. Lett. **B252**, 170 (1990).

[9] S. R. Mishra, private communication.

[10] P. Vilain *et al.* (CHARM-II), Phys. Lett. **B364**, 121 (1995).

[11] A. Hillairet *et al.* (TWIST), Phys. Rev. **D85**, 092013 (2012), [arXiv:1112.3606].

[12] R. P. MacDonald *et al.* (TWIST), Phys. Rev. **D78**, 032010 (2008), [arXiv:0807.1125].

[13] C. A. Gagliardi, R. E. Tribble and N. J. Williams, Phys. Rev. **D72**, 073002 (2005), [hep-ph/0509069].

[14] R. Bayes *et al.* (TWIST), Phys. Rev. Lett. **106**, 041804 (2011).

[15] F. Scheck, in *Electroweak and Strong Interactions* (Springer Verlag, 1996).

[16] K. Mursula and F. Scheck, Nucl. Phys. **B253**, 189 (1985).

[17] P. Langacker and D. London, Phys. Rev. **D39**, 266 (1989).

[18] C. Jarlskog, Nucl. Phys. **75**, 659 (1966).

[19] A. Jodidio *et al.*, Phys. Rev. **D34**, 1967 (1986), [Erratum: Phys. Rev.D37,237(1988)].

[20] L. P. Roesch *et al.*, Helv. Phys. Acta **55**, 74 (1982).

[21] W. Fetscher, Phys. Lett. **140B**, 117 (1984).

[22] G. Prezeau and A. Kurylov, Phys. Rev. Lett. **95**, 101802 (2005), [hep-ph/0409193].

[23] S. E. Derenzo, Phys. Rev. **181**, 1854 (1969).

[24] H. Burkard *et al.*, Phys. Lett. **160B**, 343 (1985).

Int. J. Mod. Phys. A 2026.41. Downloaded from www.worldscientific.com
by UNIVERSITY OF CALIFORNIA @ BERKELEY on 09/16/26. Re-use and distribution is strictly not permitted, except for Open Access articles.

58. τ Branching Fractions

Revised August 2025 by Sw. Banerjee (Louisville U.) and A. Lusiani (INFN, Pisa; SNS, Pisa).

58.1 τ Branching Fractions

The τ Listings contains 252 entries that correspond to either a τ partial decay fraction into a specific decay mode (branching fraction) or a ratio of two τ partial decay fractions (branching ratio). Experimental measurements provide values for 148 of these quantities, upper limits for 67 branching fractions to Lepton Family number, Lepton number, or Baryon number violating modes, and 37 additional upper limits for other modes. A total of 129 τ branching fractions and branching ratios are determined with a fit of 171 measurements. 85 quantities have at least one measurement in the fit.

58.2 The constrained fit to τ branching fractions

The τ branching fractions fit uses the reported values, uncertanties and statistical correlations of the τ branching fractions and branching ratios measurements. Asymmetric uncertainties are symmetrized as $\sigma^2_{\rm symm} = (\sigma^2_+ + \sigma^2_-)/2$. If only a few measurements are correlated, the correlation coefficients are listed in the footnote for each measurement (see for example $\Gamma(\text{particle}^- \geq 0\,\text{neutrals} \geq 0\,K^0\nu_\tau$ ("1-prong"))$/\Gamma_{\rm total}$). If a large number of measurements are correlated, then the full correlation matrix is listed in the footnote to the measurement that first appears in the τ Listings. Footnotes to the other measurements refer to the first one. For example, the large correlation matrices for the branching fraction or ratio measurements contained in Refs. [1] [2] are listed in Footnotes to the $\Gamma(e^-\overline{\nu}_e\nu_\tau)/\Gamma_{\rm total}$ and $\Gamma(h^-\nu_\tau)/\Gamma_{\rm total}$ measurements respectively. Additionally, the most precise experimental inputs are treated according to how they depend on external parameters on the basis of their documentation [3]. The τ measurements may depend on parameters such as the τ pair production cross-section in e^+e^- annihilations at the $\Upsilon(4S)$ peak. In some cases, measurements reported in different papers by the same collaboration may depend on common parameters like the estimate of the integrated luminosity or of particle identification efficiencies. For all the significant detected dependencies, the τ measurements and their uncertainties are updated to account for the updated values of the external parameters. The dependencies on common systematic effects are also determined in size and sign, and all the common systematic dependencies of different measurements are used together with the published statistical and systematic uncertainties and correlations in order to compute an updated all-inclusive variance and covariance matrix of the experimental inputs of the fit.

The fit parameters correspond to all measured τ branching fractions and ratios, to some non-measured branching fractions and ratios like for instance $\mathcal{B}(\tau^- \to \pi^- K^0_L K^0_L \nu_\tau)$ and to one nuisance variable. When discussing the fit results in the following, the fit χ^2, the number of degrees of freedom, the residuals and pulls all refer to the subset of fit parameters that correspond to τ branching fractions and ratios, excluding nuisance variables. Due to the small number of nuisance fit parameters with respect to the tau decay fit parameters, we assume that the "restricted" fit χ^2, residuals and pulls approximately share the statistical properties expected for a minimum χ^2 fit. The fit parameters are optimized while respecting relations described by a series of constraint equations. All the experimental inputs and all the constraint equations are reported in the τ Listings section that follows this review. In some cases, constraints describe approximate relations that nevertheless hold within the present experimental precision. For instance, the constraint $\mathcal{B}(\tau^- \to K^-K^-K^+\nu_\tau) = \mathcal{B}(\tau^- \to K^-\phi\nu_\tau) \times \mathcal{B}(\phi \to K^+K^-)$ is only empirically justified within the current experimental evidence. The constraint equations between the τ branching fractions and ratios include quantities other than τ branching fractions and branching ratios, like for instance the branching fractions of the η and ω mesons. We neglect the uncertainties on these values for all quantities except $\mathcal{B}(a_1^- \to \pi^-\gamma)$, whose value and uncertainty were estimated by ALEPH [1] to be $(0.21 \pm 0.08)\cdot 10^{-2}$, relying on a measurement of $\Gamma(a_1^- \to \pi^-\gamma)$ [4]. This quantity is included in the fit parameters as nuisance variable, with a χ^2 term corresponding to its estimate,

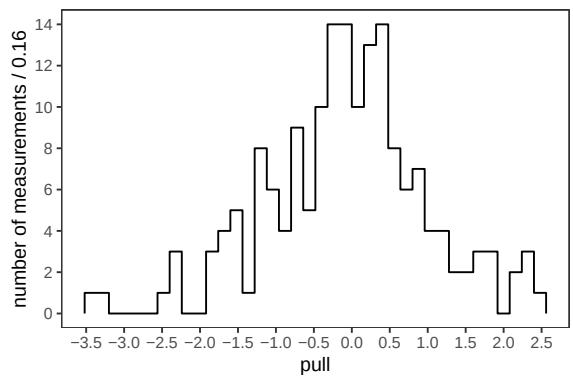

Figure 58.1: Pulls of individual measurements against the respective fitted quantity.

which is accomodated without a dedicated treatment in the general framework of the fit procedure described in Section 58.5. We assume that

$$\begin{aligned}\mathcal{B}(\tau^- \to a_1^-\nu_\tau) = {}& \mathcal{B}(\tau^- \to \pi^-\pi^+\pi^-\nu_\tau\ (\text{ex.}K^0,\omega))+ \\ & \mathcal{B}(\tau^- \to \pi^- 2\pi^0\nu_\tau\ (\text{ex.}K^0))+ \\ & \mathcal{B}(\tau^- \to a_1^-(\pi^-\gamma)\nu_\tau)\ ,\end{aligned} \tag{58.1}$$

neglecting the observed but negligible branching fractions to other modes, and that

$$\mathcal{B}(\tau^- \to a_1^-(\pi^-\gamma)\nu_\tau) = \mathcal{B}(\tau^- \to a_1^-\nu_\tau)\cdot\mathcal{B}(a_1^- \to \pi^-\gamma)\ . \tag{58.2}$$

The values of all other quantities in the constraint equations are taken from the 2024 edition of the Review of Particle Physics.

In the fit, uncertainty scale factors are applied to the published uncertainties of measurements only if significant inconsistency between different measurements remain after accounting for all relevant uncertainties and correlations. When performing the fit with no scale factors, the two measurements of $\mathcal{B}(\tau^- \to K^-K^-K^+\nu_\tau)$ have pulls exceeding $5\,\sigma$ from the fit values. There are 171 pulls, one per measurement. They are partially correlated, and the effective number of independent pulls is equal to the number of degrees of freedom of the fit, 126. The probability of getting pulls equal or larger than either one of the two very large pulls in a sample of 126 is smaller than the probability of a $3\,\sigma$ deviation for a Normal variable. Therefore, it has been decided to apply an uncertainty scale factor of 5.4 on all measurements of $\mathcal{B}(\tau^- \to K^-K^-K^+\nu_\tau)$ (one by BaBar and one by Belle). The scale factor has been computed according to the standard PDG procedure. After applying the scale factor, the pull distribution of the measurements in figure 58.1 is reasonably Normal and the pull probability distribution in figure 58.2 is reasonably flat.

Considering only the residuals with respect to τ branching fractions and ratios measurements, the constrained fit has a χ^2 of 138 for 126 degrees of freedom, corresponding to a χ^2 probability of 21.3%. We use 171 measurements and 84 constraints on the branching fractions and ratios to determine 129 quantities, consisting of 112 branching fractions and 17 branching ratios. The constraints include the unitarity constraint on the sum of all the exclusive τ decay modes, $\mathcal{B}_{\rm all} = 1$. If the unitarity constraint is released, the fit result for $\mathcal{B}_{\rm all}$ is consistent with unitarity with $1 - \mathcal{B}_{\rm all} = (0.07 \pm 0.11)\%$.

For the convenience of summarizing the fit results, we list in Table 58.1 the values and uncertainties for a set of 46 "basis" decay modes, from which all remaining branching fractions and ratios can be obtained using the constraints. The sum of all known τ branching fractions, which adds up to one according to the unitarity constraint, can be obtained by summing the fit values of all "basis" modes with a few adjustements:

- the modes $\mathcal{B}(\tau^- \to \pi^- K^0_S K^0_S \nu_\tau)$ and $\mathcal{B}(\tau^- \to \pi^- K^0_S K^0_S \pi^0 \nu_\tau)$ are both summed with a weight of 2, in or-

Int. J. Mod. Phys. A 2026.41. Downloaded from www.worldscientific.com
UNIVERSITY OF CALIFORNIA @ BERKELEY on 09/16/26. Re-use and distribution is strictly not permitted, except for Open Access articles.

Int. J. Mod. Phys. A 2026.41. Downloaded from www.worldscientific.com
by UNIVERSITY OF CALIFORNIA @ BERKELEY on 09/16/26. Re-use and distribution is strictly not permitted, except for Open Access articles.

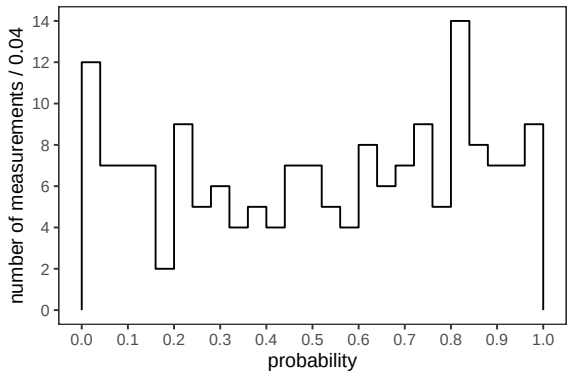

Figure 58.2: Probability of individual measurement pulls against the respective fitted quantity.

der to include the corresponding modes with K_L's, which are predicted to have the same respective branching fractions by the constraint equations;

- the mode $\mathcal{B}(\tau^- \to K^-\phi\nu_\tau)$ has a weight smaller than 1 because some of its final states are described by other "basis" modes;
- the modes $\mathcal{B}(\tau^- \to \pi^-2\pi^0\nu_\tau$ (ex.K^0)) and $\mathcal{B}(\tau^- \to \pi^-\pi^+\pi^-\nu_\tau$ (ex.K^0,ω)) have weights slighly larger than 1 to account for the $\mathcal{B}(\tau^- \to a_1^-(\pi^-\gamma)\nu_\tau)$ mode, which is predicted by them according to the constraint Eqs. 58.1 and 58.2.

Table 58.1 reports the weights with which the "basis" modes are summed to get the total τ branching fraction. The correlation matrix between the basis modes is reported in the τ Listings.

In defining the fit constraints and in selecting the modes that sum up to one we made some assumptions and choices. We assume that some channels, like $\tau^- \to \pi^-K^+\pi^- \geq 0\pi^0\nu_\tau$ and $\tau^- \to \pi^+K^-K^- \geq 0\pi^0\nu_\tau$, have negligible branching fractions as expected from the Standard Model, even if the experimental limits for these branching fractions are not very stringent. The 95% confidence level upper limits are $\mathcal{B}(\tau^- \to \pi^-K^+\pi^- \geq 0\pi^0\nu_\tau) < 0.25\%$ and $\mathcal{B}(\tau^- \to \pi^+K^-K^- \geq 0\pi^0\nu_\tau) < 0.09\%$, values not so different from measured branching fractions for allowed 3-prong modes containing charged kaons. For decays to final states containing one neutral kaon we assume that the branching fractions with the K^0_L are the same as the corresponding one with a K^0_S. On decays with two neutral kaons we assume that the branching fractions with $K^0_L K^0_L$ are the same as the ones with $K^0_S K^0_S$.

58.3 New measurements in this edition

With respect to the 2024 editions of the τ Listings and of this Review, a new precise measurement of the branching ratio $\mathcal{B}_\mu/\mathcal{B}_e = \mathcal{B}(\tau^- \to \mu^-\bar{\nu}_\mu\nu_\tau)/\mathcal{B}(\tau^- \to e^-\bar{\nu}_e\nu_\tau)$ by the Belle II collaboration [5] has been added. The updated fit has a slightly smaller value of $\mathcal{B}_\mu = \mathcal{B}(\tau^- \to \mu^-\bar{\nu}_\mu\nu_\tau)$ and a slightly larger value of $\mathcal{B}_e = \mathcal{B}(\tau^- \to e^-\bar{\nu}_e\nu_\tau)$, while $\mathcal{B}_\mu/\mathcal{B}_e$ has decreased and is closer to the Standard Model prediction. The other fit branching fractions and ratios have negligible changes.

58.4 Overconsistency of leptonic branching fraction and ratio measurements

As observed in the previous editions of this review, measurements of the leptonic branching fractions are more consistent with each other than expected from the quoted uncertainties on the individual measurements. When fitting all measurements of $\mathcal{B}_\mu$, $\mathcal{B}_e$ and $\mathcal{B}_\mu/\mathcal{B}_e$, the χ^2/n.d.o.f. is 2.6/11 and the probability of getting a smaller χ^2 is 0.53%.

58.5 Technical implementation of the fit

The fit computes a set of quantities denoted with q_i by minimizing a χ^2 while respecting a series of equality constraints on the q_i. The quantities q_i represent τ branching fractions and branching ratios, and nuisance variables. The fit minimization procedure is equivalent to choosing a set of basis fit variables, using functions of these basis variables to predict measurements, and determining these basis variables by minimizing the measurements' χ^2. The χ^2 is computed using the measurements m_i and their covariance matrix M_{ij} as $\chi^2 = (m_i - A_{ik}q_k)^t M^{-1}_{ij}(m_j - A_{jl}q_l)$, where the model matrix A_{ij} is used to get the vector of the predicted measurements m'_i from the vector of the fit parameters q_j as $m'_i = A_{ij}q_j$. There is one fit variable for each of the modes that have measurements, therefore $A_{ij} = 1$ when q_j corresponds to the τ branching fraction or branching ratio of the measurement m_i, and $A_{ij} = 0$ otherwise. The constraints are equations involving the fit parameters. The fit does not impose limitations on the functional form of the constraints. In summary, the fit requires:

$$\min\left[\chi^2(q_k)\right] = \min\left[(m_i - A_{ik}q_k)^t M^{-1}_{ij}(m_j - A_{jl}q_l)\right] \ , \quad (58.3)$$

$$\text{subjected to} \quad f_r(q_s) - c_r = 0 \ , \quad (58.4)$$

where the left term of Eq. 58.4 defines the constraint expressions. Using the method of Lagrange multipliers, a set of equations is obtained by taking the derivatives with respect to the fitted quantities q_k and the Lagrange multipliers λ_r of the sum of the χ^2 and the constraint expressions multiplied by the Lagrange multipliers

Table 58.1: Values, uncertainties and unitarity-constraint coefficients of the 46 "basis" modes of the τ branching fractions and ratios fit.

decay mode	fit result (%)	coefficient
$\mathcal{B}(\tau^- \to \mu^-\bar{\nu}_\mu\nu_\tau)$	0.1737 ± 0.0004	1.0000
$\mathcal{B}(\tau^- \to e^-\bar{\nu}_e\nu_\tau)$	0.1785 ± 0.0004	1.0000
$\mathcal{B}(\tau^- \to \pi^-\nu_\tau)$	0.1082 ± 0.0005	1.0000
$\mathcal{B}(\tau^- \to K^-\nu_\tau)$	0.00697 ± 0.00010	1.0000
$\mathcal{B}(\tau^- \to \pi^-\pi^0\nu_\tau)$	0.2549 ± 0.0009	1.0000
$\mathcal{B}(\tau^- \to K^-\pi^0\nu_\tau)$	0.00433 ± 0.00015	1.0000
$\mathcal{B}(\tau^- \to \pi^-2\pi^0\nu_\tau$ (ex.K^0))	0.0926 ± 0.0010	1.0022
$\mathcal{B}(\tau^- \to K^-2\pi^0\nu_\tau$ (ex.K^0))	$(0.65 \pm 0.22) \cdot 10^{-3}$	1.0000
$\mathcal{B}(\tau^- \to \pi^-3\pi^0\nu_\tau$ (ex.K^0))	0.0104 ± 0.0007	1.0000
$\mathcal{B}(\tau^- \to K^-3\pi^0\nu_\tau$ (ex.K^0,η))	$(0.48 \pm 0.21) \cdot 10^{-3}$	1.0000
$\mathcal{B}(\tau^- \to h^-4\pi^0\nu_\tau$ (ex.K^0,η))	0.0011 ± 0.0004	1.0000
$\mathcal{B}(\tau^- \to \pi^-\bar{K}^0\nu_\tau)$	0.00838 ± 0.00014	1.0000
$\mathcal{B}(\tau^- \to K^-K^0\nu_\tau)$	0.001486 ± 0.000034	1.0000
$\mathcal{B}(\tau^- \to \pi^-\bar{K}^0\pi^0\nu_\tau)$	0.00382 ± 0.00013	1.0000
$\mathcal{B}(\tau^- \to K^-K^0\pi^0\nu_\tau)$	0.00150 ± 0.00007	1.0000
$\mathcal{B}(\tau^- \to \pi^-\bar{K}^0 2\pi^0\nu_\tau$ (ex.K^0))	$(0.26 \pm 0.23) \cdot 10^{-3}$	1.0000
$\mathcal{B}(\tau^- \to \pi^-K^0_S K^0_S\nu_\tau)$	$(235 \pm 6) \cdot 10^{-6}$	2.0000
$\mathcal{B}(\tau^- \to \pi^-K^0_S K^0_L\nu_\tau)$	0.00108 ± 0.00024	1.0000
$\mathcal{B}(\tau^- \to \pi^-K^0_S K^0_S\pi^0\nu_\tau)$	$(18.2 \pm 2.1) \cdot 10^{-6}$	2.0000
$\mathcal{B}(\tau^- \to \pi^-K^0_S K^0_L\pi^0\nu_\tau)$	$(0.32 \pm 0.12) \cdot 10^{-3}$	1.0000
$\mathcal{B}(\tau^- \to \bar{K}^0h^-h^-h^+\nu_\tau)$	$(0.25 \pm 0.20) \cdot 10^{-3}$	1.0000
$\mathcal{B}(\tau^- \to \pi^-\pi^+\pi^-\nu_\tau$ (ex.K^0,ω))	0.0899 ± 0.0005	1.0022
$\mathcal{B}(\tau^- \to \pi^-\pi^+\pi^-\pi^0\nu_\tau$ (ex.K^0,ω))	0.0274 ± 0.0007	1.0000
$\mathcal{B}(\tau^- \to h^-h^-h^+2\pi^0\nu_\tau$ (ex.K^0,ω,η))	0.0010 ± 0.0004	1.0000
$\mathcal{B}(\tau^- \to \pi^-K^-K^+\nu_\tau)$	0.001435 ± 0.000027	1.0000
$\mathcal{B}(\tau^- \to \pi^-K^-K^+\pi^0\nu_\tau)$	$(61 \pm 18) \cdot 10^{-6}$	1.0000
$\mathcal{B}(\tau^- \to \pi^-\pi^0\eta\nu_\tau)$	0.00139 ± 0.00007	1.0000
$\mathcal{B}(\tau^- \to K^-\eta\nu_\tau)$	$(155 \pm 8) \cdot 10^{-6}$	1.0000
$\mathcal{B}(\tau^- \to K^-\pi^0\eta\nu_\tau)$	$(48 \pm 12) \cdot 10^{-6}$	1.0000
$\mathcal{B}(\tau^- \to \pi^-\bar{K}^0\eta\nu_\tau)$	$(94 \pm 15) \cdot 10^{-6}$	1.0000
$\mathcal{B}(\tau^- \to \pi^-\pi^+\pi^-\eta\nu_\tau$ (ex.K^0))	$(220 \pm 13) \cdot 10^{-6}$	1.0000
$\mathcal{B}(\tau^- \to K^-\omega\nu_\tau)$	$(0.41 \pm 0.09) \cdot 10^{-3}$	1.0000
$\mathcal{B}(\tau^- \to h^-\pi^0\omega\nu_\tau)$	0.0041 ± 0.0004	1.0000
$\mathcal{B}(\tau^- \to K^-\phi\nu_\tau)$	$(44 \pm 16) \cdot 10^{-6}$	0.8300
$\mathcal{B}(\tau^- \to \pi^-\omega\nu_\tau)$	0.0195 ± 0.0006	1.0000
$\mathcal{B}(\tau^- \to K^-\pi^-\pi^+\nu_\tau$ (ex.K^0,ω))	0.00293 ± 0.00007	1.0000
$\mathcal{B}(\tau^- \to K^-\pi^-\pi^+\pi^0\nu_\tau$ (ex.K^0,ω,η))	$(0.39 \pm 0.14) \cdot 10^{-3}$	1.0000
$\mathcal{B}(\tau^- \to \pi^-2\pi^0\omega\nu_\tau)$	$(72 \pm 16) \cdot 10^{-6}$	1.0000
$\mathcal{B}(\tau^- \to 2\pi^-\pi^+3\pi^0\nu_\tau$ (ex.K^0,η,ω,f_1))	$(14 \pm 27) \cdot 10^{-6}$	1.0000
$\mathcal{B}(\tau^- \to 3\pi^-2\pi^+\nu_\tau$ (ex.K^0,ω,f_1))	$(775 \pm 30) \cdot 10^{-6}$	1.0000
$\mathcal{B}(\tau^- \to K^-2\pi^-2\pi^+\nu_\tau$ (ex.K^0))	$(0.6 \pm 1.2) \cdot 10^{-6}$	1.0000
$\mathcal{B}(\tau^- \to 2\pi^-\pi^+\omega\nu_\tau$ (ex.K^0))	$(84 \pm 6) \cdot 10^{-6}$	1.0000
$\mathcal{B}(\tau^- \to 3\pi^-2\pi^+\pi^0\nu_\tau$ (ex.K^0,η,ω,f_1))	$(38 \pm 9) \cdot 10^{-6}$	1.0000
$\mathcal{B}(\tau^- \to K^-2\pi^-2\pi^+\pi^0\nu_\tau$ (ex.K^0))	$(1.1 \pm 0.6) \cdot 10^{-6}$	1.0000
$\mathcal{B}(\tau^- \to \pi^-f_1(2\pi^-2\pi^+)\nu_\tau)$	$(52 \pm 4) \cdot 10^{-6}$	1.0000
$\mathcal{B}(\tau^- \to \pi^-2\pi^0\eta\nu_\tau$ (ex.K^0))	$(0.19 \pm 0.04) \cdot 10^{-3}$	1.0000

λ_r, one for each constraint:

$$\min\left[(m_i - A_{ik}q_k)^t M_{ij}^{-1}(m_j - A_{jl}q_l) + 2\lambda_r(f_r(q_s) - c_r)\right] = \\ = \min\left[\tilde{\chi}^2(q_k, \lambda_r)\right] \ , \\ (\partial/\partial q_k, \partial/\partial\lambda_r)\left[\tilde{\chi}^2(q_k, \lambda_r)\right] = 0 \ . \qquad (58.5)$$

Eq. 58.5 defines a set of equations for the vector of the unknowns (q_k, λ_r), some of which may be non-linear, in case of non-linear constraints. An iterative minimization procedure approximates at each step the non-linear constraint expressions by their first order Taylor expansion around the current values of the fitted quantities, $\bar{q}_s$:

$$f_r(q_s) - c_r = f_r(\bar{q}_s) + \left.\frac{\partial f_r(q_s)}{\partial q_s}\right|_{\bar{q}_s}(q_s - \bar{q}_s) - c_r \ ,$$

which can be written as

$$B_{rs}q_s - c'_r \ ,$$

where c'_r are the resulting known terms, independent of q_s at first order. After the linearization of the constraint expressions in $\tilde{\chi}^2(q_k, \lambda_r)$, the differentiation by q_k and λ_r is trivial and leads to a set of linear equations

$$A^t_{ki}M^{-1}_{ij}A_{jl}q_l + B^t_{kr}\lambda_r = A^t_{ki}M^{-1}_{ij}m_j \ , \qquad (58.6)$$

$$B_{rs}q_s = c'_r \ , \qquad (58.7)$$

which can be expressed as

$$F_{ij}u_j = v_i \ , \qquad (58.8)$$

where $u_j = (q_k, \lambda_r)$ and v_i is the vector of the known constant terms running over the index k and then r in the right terms of Eq. 58.6 and Eq. 58.7, respectively. Solving the equation set in Eq. 58.8 by matrix inversion gives the the fitted quantities and their variance and covariance matrix, using the measurements and their variance and covariance matrix. The fit procedure starts by computing the linear approximation of the non-linear constraint expressions around the quantities seed values. With an iterative procedure, the unknowns are updated at each step by solving the equations and the equations are then linearized around the updated values, until the variation of the fitted unknowns is reduced below a numerically small threshold.

References

[1] S. Schael *et al.* (ALEPH), Phys. Rept. **421**, 191 (2005), [hep-ex/0506072].

[2] J. Abdallah *et al.* (DELPHI), Eur. Phys. J. **C46**, 1 (2006), [hep-ex/0603044].

[3] D. Asner *et al.* (Heavy Flavor Averaging Group) (2010), [arXiv:1010.1589].

[4] M. Zielinski *et al.*, Phys. Rev. Lett. **52**, 1195 (1984).

[5] I. Adachi *et al.* (Belle-II), JHEP **08**, 205 (2024), [arXiv:2405.14625].

Int. J. Mod. Phys. A 2026.41. Downloaded from www.worldscientific.com
UNIVERSITY OF CALIFORNIA @ BERKELEY on 09/16/26. Re-use and distribution is strictly not permitted, except for Open Access articles.

Int. J. Mod. Phys. A 2026.41. Downloaded from www.worldscientific.com by UNIVERSITY OF CALIFORNIA @ BERKELEY on 09/16/26. Re-use and distribution is strictly not permitted, except for Open Access articles.

59. τ-Lepton Decay Parameters

Revised February 2024 by A. Stahl (RWTH Aachen U.).

The purpose of the measurements of the decay parameters (also known as Michel parameters) of the τ is to determine the structure (spin and chirality) of the current mediating its decays.

59.1 Leptonic Decays:

The Michel parameters are extracted from the energy spectrum of the charged daughter lepton $\ell = e, \mu$ in the decays $\tau \to \ell\nu_\ell\nu_\tau$. Ignoring radiative corrections, neglecting terms of order $(m_\ell/m_\tau)^2$ and $\left(m_\tau/\sqrt{s}\right)^2$, and setting the neutrino masses to zero, the spectrum in the laboratory frame reads

$$\frac{d\Gamma}{dx} = \frac{G^2_{\tau\ell}\, m^5_\tau}{192\,\pi^3} \times \left\{ f_0\,(x) + \rho f_1\,(x) + \eta \frac{m_\ell}{m_\tau} f_2\,(x) - P_\tau\,[\xi g_1\,(x) + \xi\delta g_2\,(x)] \right\} \tag{59.1}$$

with

$$\begin{aligned} f_0(x) &= 2 - 6\,x^2 + 4\,x^3 \\ f_1(x) &= -\tfrac{4}{9} + 4x^2 - \tfrac{32}{9}x^3 \qquad g_1(x) = -\tfrac{2}{3} + 4x - 6x^2 + \tfrac{8}{3}x^3 \\ f_2(x) &= 12\,(1-x)^2 \qquad\qquad g_2(x) = \tfrac{4}{9} - \tfrac{16}{3}x + 12x^2 - \tfrac{64}{9}\,x^3\,. \end{aligned} \tag{59.2}$$

The quantity x is the fractional energy of the daughter lepton ℓ, *i.e.*, $x = E_\ell/E_{\ell,max} \approx E_\ell/(\sqrt{s}/2)$ and P_τ is the polarization of the tau leptons. The integrated decay width is given by

$$\Gamma = \frac{G^2_{\tau\ell}\, m^5_\tau}{192\,\pi^3}\left(1 + 4\,\eta\,\frac{m_\ell}{m_\tau}\right)\,. \tag{59.3}$$

The situation is similar to muon decays $\mu \to e\nu_e\nu_\mu$. The generalized matrix element with the couplings $g^\gamma_{\varepsilon\mu}$ and their relations to the Michel parameters ρ, η, ξ, and δ have been described in the "Note on Muon Decay Parameters". The Standard Model expectations are 3/4, 0, 1, and 3/4, respectively. For more details, see [1].

More information can be extracted from the decays, if the polarization of the daughter lepton is measured. Belle presented a first result (see [2]). A new parameter ξ' is introduced. Its relation to the couplings is given by (see [3]):

$$\xi' = 1 - 2\sum_{\omega=L,R}\left(\frac{1}{4}\left|g^S_{R\omega}\right|^2 + \left|g^V_{R\omega}\right|^2\right) + 3\left|g^T_{RL}\right|^2\,. \tag{59.4}$$

The new measurement improves the limit on g^T_{RL} by about a factor of two.

Additional Michel parameters can be defined in radiative decays $\tau \to \ell\nu_\ell\nu_\tau\gamma$, see [4]. A first measurement is presented in [5]. The experimental precision does not provide a significant impact on the knowledge about the couplings, yet.

59.2 Hadronic Decays:

In the case of hadronic decays $\tau \to h\nu_\tau$, with $h = \pi$, ρ, or a_1, the ansatz is restricted to purely vectorial currents. The matrix element is

$$\frac{G_{\tau h}}{\sqrt{2}}\sum_{\lambda=R,L} g_\lambda\,\langle\,\overline{\Psi}_\omega(\nu_\tau)\mid\gamma^\mu\mid\Psi_\lambda(\tau)\,\rangle\;\;J^h_\mu \tag{59.5}$$

with the hadronic current J^h_μ. The neutrino chirality ω is uniquely determined from λ. The spectrum depends only on a single parameter ξ_h

$$\frac{d^n\Gamma}{dx_1 dx_2\ldots dx_n} = f\,(\vec{x}) + \xi_h P_\tau\, g\,(\vec{x})\;\;, \tag{59.6}$$

with f and g being channel-dependent functions of the n observables $\vec{x} = (x_1, x_2, \ldots, x_n)$ (see [6]). The parameter ξ_h is related to the couplings through

$$\xi_h = |g_L|^2 - |g_R|^2\,. \tag{59.7}$$

ξ_h is the negative of the chirality of the τ neutrino in these decays. In the Standard Model, $\xi_h = 1$. Also included in the Data Listings for ξ_h are measurements of the neutrino helicity which coincide with ξ_h, if the neutrino is massless (ASNER 00 [7], ACKERSTAFF 97R [8], AKERS 95P [9], ALBRECHT 93C [10], and ALBRECHT 90I [11]).

59.3 Combination of Measurements:

The individual measurements are combined, taking into account the correlations between the parameters. In a first fit, universality between the two leptonic decays, and between all hadronic decays, is assumed. A second fit is made without these assumptions. The results of the two fits are provided as OUR FIT in the Data Listings below in the tables whose title includes "(e or mu)" or "(all hadronic modes)", and "(e)", "(mu)" *etc.*, respectively. The measurements show good agreement with the Standard Model. The χ^2 values with respect to the Standard model predictions are 24.1 for 41 degrees of freedom and 26.8 for 56 degrees of freedom, respectively. The correlations are reduced through this combination to less than 20%, with the exception of ρ and η which are correlated by +23%, for the fit with universality and by +70% for $\tau \to \mu\nu_\mu\nu_\tau$.

59.4 Model-independent Analysis:

From the Michel parameters, limits can be derived on the couplings $g^\kappa_{\varepsilon\lambda}$ without further model assumptions. In the Standard model $g^V_{LL} = 1$ (leptonic decays), and $g_L = 1$ (hadronic decays) and all other couplings vanish. First, the partial decay widths have to be compared to the Standard Model predictions to derive limits on the normalization of the couplings $A_x = G^2_{\tau x}/G^2_F$ with Fermi's constant G_F:

$$\begin{aligned} A_e &= 1.0022 \pm 0.0041\;, \\ A_\mu &= 0.983 \pm 0.017\;, \\ A_\pi &= 0.9957 \pm 0.0049\;. \end{aligned} \tag{59.8}$$

Then limits on the couplings (95% CL) can be extracted (see [12] and [13]). Without the assumption of universality, the limits given in Table 59.1 are derived.

Table 59.1: Coupling constants $g^\gamma_{\varepsilon\mu}$. 95% confidence level experimental limits. The limits include the quoted values of A_e, A_μ, and A_π and assume $A_\rho = A_{a_1} = 1$.

$\tau \to e\nu_e\nu_\tau$		
$\lvert g^S_{RR}\rvert < 0.70$	$\lvert g^V_{RR}\rvert < 0.17$	$\lvert g^T_{RR}\rvert \equiv 0$
$\lvert g^S_{LR}\rvert < 0.99$	$\lvert g^V_{LR}\rvert < 0.13$	$\lvert g^T_{LR}\rvert < 0.082$
$\lvert g^S_{RL}\rvert < 2.01$	$\lvert g^V_{RL}\rvert < 0.52$	$\lvert g^T_{RL}\rvert < 0.51$
$\lvert g^S_{LL}\rvert < 2.01$	$\lvert g^V_{LL}\rvert < 1.004$	$\lvert g^T_{LL}\rvert \equiv 0$
$\tau \to \mu\nu_\mu\nu_\tau$		
$\lvert g^S_{RR}\rvert < 0.72$	$\lvert g^V_{RR}\rvert < 0.18$	$\lvert g^T_{RR}\rvert \equiv 0$
$\lvert g^S_{LR}\rvert < 0.95$	$\lvert g^V_{LR}\rvert < 0.12$	$\lvert g^T_{LR}\rvert < 0.079$
$\lvert g^S_{RL}\rvert < 2.01$	$\lvert g^V_{RL}\rvert < 0.52$	$\lvert g^T_{RL}\rvert < 0.27$
$\lvert g^S_{LL}\rvert < 2.01$	$\lvert g^V_{LL}\rvert < 1.006$	$\lvert g^T_{LL}\rvert \equiv 0$
$\tau \to \pi\nu_\tau$		
$\lvert g^V_R\rvert < 0.15$	$\lvert g^V_L\rvert > 0.984$	
$\tau \to \rho\nu_\tau$		
$\lvert g^V_R\rvert < 0.10$	$\lvert g^V_L\rvert > 0.995$	
$\tau \to a_1\nu_\tau$		
$\lvert g^V_R\rvert < 0.16$	$\lvert g^V_L\rvert > 0.987$	

59.5 Model-dependent Interpretation:

More stringent limits can be derived assuming specific models. For example, in the framework of a two Higgs doublet model, the measurements correspond to a limit of $m_{H^\pm} > 2.0$ GeV $\times \tan\beta$ on the mass of the charged Higgs boson, or a limit of 500 GeV on the mass of the second W boson in left-right symmetric models for arbitrary mixing (both 95% CL). See [13] and [14].

References

[1] F. Scheck, Phys. Rept. **44**, 187 (1978); W. Fetscher and H.J. Gerber in *Precision Tests of the Standard Model*, edited by P. Langacker, World Scientific, 1993; A. Stahl, *Physics with τ Leptons*, Springer Tracts in Modern Physics, **160**, 1, (2000).

[2] D. Bodrov *et al.* (Belle), Phys. Rev. D **108**, 1, 012003 (2023), [arXiv:2303.10574].

[3] D. Bodrov and P. Pakhlov, JHEP **10**, 035 (2022), [arXiv:2203.12743].

[4] A. Arbuzov and T. Kopylova, JHEP 109 (2016).

[5] N. Shimizu *et al.* (Belle), Prog. Theo. Exp. Phys. **2**, 023C01 (2018).

[6] M. Davier *et al.*, Phys. Lett. B **306**, 411 (1993).

[7] D. Asner *et al.* (CLEO), Phys. Rev. D **61**, 012002 (2000), [hep-ex/9902022].

[8] K. Ackerstaff *et al.* (OPAL), Z. Phys. C **75**, 593 (1997).

[9] R. Akers *et al.* (OPAL), Z. Phys. C **67**, 45 (1995).

[10] H. Albrecht *et al.* (ARGUS), Z. Phys. C **58**, 61 (1993).

[11] H. Albrecht *et al.* (ARGUS), Phys. Lett. B **250**, 164 (1990).

[12] K. Ackerstaff *et al.* (OPAL), Eur. Phys. J. C **8**, 3 (1999), [hep-ex/9808016].

[13] A. Stahl, Nucl. Phys. B Proc. Suppl. **76**, 173 (1999).

[14] M.-T. Dova, J. Swain and L. Taylor, Phys. Rev. D **58**, 015005 (1998), [hep-ph/9712384]; T. Hebbeker and W. Lohmann, Z. Phys. C **74**, 399 (1997); A. Pich and J. P. Silva, Phys. Rev. D **52**, 4006 (1995), [hep-ph/9505327].

Int. J. Mod. Phys. A 2026.41. Downloaded from www.worldscientific.com
UNIVERSITY OF CALIFORNIA @ BERKELEY on 09/16/26. Re-use and distribution is strictly not permitted, except for Open Access articles.

Int. J. Mod. Phys. A 2026.41. Downloaded from www.worldscientific.com
by UNIVERSITY OF CALIFORNIA @ BERKELEY on 09/16/26. Re-use and distribution is strictly not permitted, except for Open Access articles.

60. Quark Masses

Revised August 2023 by R.M. Barnett (LBNL), L.P. Lellouch (CNRS & Aix-Marseille U.) and A.V. Manohar (UC San Diego).

60.1 Introduction

This note discusses some of the theoretical issues relevant for the determination of quark masses, which are fundamental parameters of the Standard Model of particle physics. Unlike the leptons, quarks are confined inside hadrons and are not observed as physical particles. Quark masses therefore cannot be measured directly, but must be determined indirectly through their influence on hadronic properties. Although one often speaks loosely of quark masses as one would of the mass of the electron or muon, any quantitative statement about the value of a quark mass must make careful reference to the particular theoretical framework that is used to define it. It is important to keep this *scheme dependence* in mind when using the quark mass values tabulated in the data listings.

Historically, the first determinations of quark masses were performed using quark models. These are usually called constituent quark masses and are of order 350 MeV for the u and d quarks. Constituent quark masses model the effects of dynamical chiral symmetry breaking discussed below, and are not directly related to the quark mass parameters m_q of the QCD Lagrangian of Eq. (60.1). The resulting masses only make sense in the limited context of a particular quark model, and cannot be related to the quark mass parameters, m_q, of the Standard Model. In order to discuss quark masses at a fundamental level, definitions based on quantum field theory must be used, and the purpose of this note is to discuss these definitions and the corresponding determinations of the values of the masses.

60.2 Mass parameters and the QCD Lagrangian

The QCD [1] Lagrangian is

$$\mathcal{L} = \sum_{q=u,d,s,\ldots,t} \overline{q}\,(i\not{D} - m_q)\,q - \tfrac{1}{2}\mathrm{tr}\,G_{\mu\nu}G^{\mu\nu}, \tag{60.1}$$

where the sum runs over the quark flavors u, d, s, c, b and t. $\not{D} = (\partial_\mu - igA_\mu)\,\gamma^\mu$ is the gauge covariant derivative, A_μ is the SU(3)-valued gluon field, $G_{\mu\nu} = \frac{i}{g}[D_\mu, D_\nu]$ is the gluon field strength, m_q is the mass parameter of quark flavor q, and q is the quark Dirac field. After renormalization, the QCD Lagrangian Eq. (60.1) gives finite values for physical quantities, such as scattering amplitudes. Renormalization is a procedure that invokes a subtraction scheme to render the amplitudes finite, and requires the introduction of a dimensionful scale parameter μ. The mass parameters in the QCD Lagrangian Eq. (60.1) depend on the renormalization scheme used to define the theory, and also on the scale parameter μ. The most commonly used renormalization scheme for QCD perturbation theory is the $\overline{\mathrm{MS}}$ scheme.

The QCD Lagrangian has a chiral symmetry in the limit that the quark masses vanish. This symmetry is spontaneously broken by dynamical chiral symmetry breaking, and explicitly broken by the quark masses. The nonperturbative scale of dynamical chiral symmetry breaking, Λ_χ, is around 1 GeV [2]. It is conventional to call quarks heavy if $m_q > \Lambda_\chi$, so that explicit chiral symmetry breaking dominates (c, b, and t quarks are heavy), and light if $m_q < \Lambda_\chi$, so that spontaneous chiral symmetry breaking dominates (the u and d are light and the s is considered to be light when using $\mathrm{SU}(3)_L \times \mathrm{SU}(3)_R$ chiral perturbation theory). The determination of light- and heavy-quark masses is considered separately in Sec. 60.5 and Sec. 60.6 below.

At high energies or short distances, nonperturbative effects, such as chiral symmetry breaking, become small and one can, in principle, determine quark masses by analyzing mass-dependent effects using QCD perturbation theory. Such computations are conventionally performed using the $\overline{\mathrm{MS}}$ scheme at a scale $\mu \gg \Lambda_\chi$, and give the $\overline{\mathrm{MS}}$ "running" mass $\overline{m}(\mu)$. We use the $\overline{\mathrm{MS}}$ scheme when reporting quark masses; one can readily convert these values into other schemes using perturbation theory.

The μ dependence of $\overline{m}(\mu)$ at short distances can be calculated using the renormalization group (RG) equation,

$$\mu^2 \frac{\mathrm{d}\overline{m}\,(\mu)}{\mathrm{d}\mu^2} = -\gamma(\overline{\alpha}_s\,(\mu))\;\overline{m}\,(\mu)\,, \tag{60.2}$$

where γ is the anomalous dimension which is now known to four-loop order in perturbation theory [3] [4]. $\overline{\alpha}_s$ is the coupling constant [1] in the $\overline{\mathrm{MS}}$ scheme. Defining the expansion coefficients γ_r by

$$\gamma\,(\overline{\alpha}_s) \equiv \sum_{r=1}^{\infty} \gamma_r \left(\frac{\overline{\alpha}_s}{4\pi}\right)^r, \tag{60.3}$$

the first four coefficients are given by

$$\begin{aligned}
\gamma_1 &= 4,\\
\gamma_2 &= \frac{202}{3} - \frac{20N_L}{9},\\
\gamma_3 &= 1249 + \left(-\frac{2216}{27} - \frac{160}{3}\zeta\,(3)\right) N_L - \frac{140}{81}N_L^2,\\
\gamma_4 &= \frac{4603055}{162} + \frac{135680}{27}\zeta\,(3) - 8800\zeta\,(5)\\
&\quad + \left(-\frac{91723}{27} - \frac{34192}{9}\zeta\,(3) + 880\zeta\,(4) + \frac{18400}{9}\zeta\,(5)\right) N_L\\
&\quad + \left(\frac{5242}{243} + \frac{800}{9}\zeta\,(3) - \frac{160}{3}\zeta\,(4)\right) N_L^2\\
&\quad + \left(-\frac{332}{243} + \frac{64}{27}\zeta\,(3)\right) N_L^3,
\end{aligned}$$

where N_L is the number of active light quark flavors at the scale μ, i.e. flavors with masses $\leq \mu$, and ζ is the Riemann zeta function ($\zeta(3) \simeq 1.2020569$, $\zeta(4) \simeq 1.0823232$, and $\zeta(5) \simeq 1.0369278$). Eq. (60.2) must be solved in conjunction with the RG equation for $\overline{\alpha}_s\,(\mu)$ given in [1]. In addition, as the renormalization scale crosses quark mass thresholds one needs to match the scale dependence of $\overline{m}$ below and above the threshold. There are finite threshold corrections; the necessary formulae can be found in Ref. [5].

60.3 Lattice QCD

Ab initio lattice QCD calculations of the fundamental parameters of QCD, i.e. the coupling constant and quark masses (except for the top-quark mass), has become a precision science (see also the sections on Lattice Quantum Chromodynamics and on Quantum Chromodynamics in this *Review*). Here we only briefly recall those features which are required for the determination of quark masses. For more details on lattice QCD, please see the section on Lattice Quantum Chromodynamics.

The inputs into lattice calculations are bare, dimensionless versions of the fundamental parameters of QCD: the bare strong coupling and the bare quark masses in lattice units, i.e. multiplied by the lattice spacing a, the distance between neighboring points of the lattice. The physical values of the quark masses are determined by computing as many physical quantities as there are parameters, including one for the gauge coupling. In practice, the computations are performed for multiple lattice spacings, determined by the bare coupling via dimensional transmutation, and a number of bare quark masses. After renormalizing these masses and converting them to physical units, the resulting renormalized masses are interpolated to their physical values. This is achieved by requiring that the computed physical quantities reproduce their measured values as the $a \to 0$ limit to our continuum world is taken. Such a tuning of fundamental parameters is required in any regularization of QCD: lattice QCD is simply a tool to perform QCD calculations in the low-energy, nonperturbative domain.

As discussed in the previous paragraph, one must renormalize the bare quark masses of lattice QCD simulations. The values of these bare masses refer to a particular discretization of QCD with the lattice spacing as the ultraviolet cut-off. In order for the resulting physical masses to be useful in phenomenological applications, it is necessary to give their values in some standard

Int. J. Mod. Phys. A 2026.41. Downloaded from www.worldscientific.com
UNIVERSITY OF CALIFORNIA @ BERKELEY on 09/16/26. Re-use and distribution is strictly not permitted, except for Open Access articles.

renormalization scheme such as $\overline{\text{MS}}$. Provided that both the ultraviolet cut-off a^{-1} and the renormalization scale μ are much greater than Λ_{QCD}, the bare masses can be renormalized in perturbation theory. However, in order to avoid uncertainties due to the unknown higher-order coefficients in lattice perturbation theory, most results obtained recently use *nonperturbative renormalization*. This procedure relates the bare masses to those defined in renormalization schemes which can be realized directly in lattice and continuum QCD, e.g. those obtained from quark and gluon Green functions at specified momenta in the Landau gauge [6] or those defined using finite-volume techniques and the Schrödinger functional [7], but not $\overline{\text{MS}}$ that is only defined for dimensional regularization. These methods require $\mu \gg \Lambda_{\text{QCD}}$ so that unwanted (nonperturbative) corrections proportional to inverse powers of μ, which appear in some approaches, remain small corrections that can be identified and removed. This condition is also necessary so that matching to other schemes can be performed reliably in perturbation theory. Moreover these methods require $a^{-1} \gg \mu$ so that cutoff effects are small enough to be extrapolated away when the continuum limit is taken. The conversion to the $\overline{\text{MS}}$ scheme is then performed using continuum perturbation theory, which is more readily obtained to higher orders and is usually better behaved than its lattice counterpart.

It is important to note that the final renormalized values for the quark masses must be the same in the continuum limit for any valid discretization of QCD and for any sensible choice of the physical quantities used for calibration, as long as the calculation is performed with a sufficient number of sea-quark flavors and with the relevant electromagnetic and strong-isospin breaking corrections for the claimed precision. It is also worth noting that issues surrounding the renormalization of quark masses disappear when considering pairwise ratios of these masses in QCD alone. Indeed, if the same renormalization scheme and scale are implemented, also for the definition of QCD in the absence or electromagnetism,[1] QCD renormalization factors are identical for all quark flavors, and these factors therefore cancel exactly in quark-mass ratio [2]. In particular, this means that these ratios are scheme and scale independent up to possible QED corrections. Moreover these ratios may suffer less from the uncertainties in the determination of the lattice scale, in particular in cases where the quantities used to fix the two quarks masses depend on these masses in a similar way, because these ratios are dimensionless. Thus, quark-mass ratios are often determined with significantly higher precision using lattice QCD than are the individual masses.

The determination of quark masses using lattice simulations is well established and the current emphasis is on the reduction and control of uncertainties. With better methods, improved algorithms and access to more powerful computing resources, the precision of the results has improved significantly in recent years. Vacuum polarization effects are included with $N_f = 2,\ 2+1$ or $N_f = 2+1+1$ flavors of sea quarks. The number 2 here indicates that the up and down quarks are degenerate. The first $+1$ corresponds to the inclusion of strange sea-quark effects and the second $+1$ to those of the charm. Simulations with $2+1$ and $2+1+1$ flavors represent controlled approximations to physical QCD at the low energies considered for quark mass determinations, up to corrections of $O((\Lambda_{\text{QCD}}/m_c)^2/N_c)$ and $O((\Lambda_{\text{QCD}}/m_b)^2/N_c)$, respectively. This is not the case for simulations with $N_f = 2$ or in which vacuum polarization effects are treated as a mean field (this is the so-called *quenched* approximation) and results obtained in those frameworks will not enter the discussion here.

Particularly pleasing is the observation that different formulations of lattice QCD and different approaches, with different systematic uncertainties, yield results which are largely consistent with each other. This gives us broad confidence in the estimates of the systematic errors. As the precision of the results approaches (or even exceeds in some cases) 1%, isospin breaking effects, including electromagnetic corrections need to be considered and this is beginning to be done as will be discussed below. In particular, a reliable estimate of these effects is required for determining the individual u and d quark masses.

Members of the lattice QCD community have organized a Flavour Lattice Averaging Group (FLAG) which, against stated quality criteria, critically reviews quantities computed in lattice QCD that are relevant to flavor physics and presents its view of the current status of the results. This includes the determination of quark masses. The latest edition reviews lattice results that appeared in print before April 30th 2021 [8]. Since that deadline and the writing of the previous edition of the present review, the only new results on quark masses that have been published are those of Ref. [9].

60.4 Averaging procedure for lattice QCD results

In this review we present summary numbers for each quark mass which are solely based on averages of lattice results. Those summary numbers differ from those presented in the particle listings, for three reasons. The first is that they do not include non-lattice estimates of the quark masses. The second is that they may differ slightly in the lattice results retained, as made explicit here and in the listings. The third difference comes from the averaging procedures, which are described in the listings and below. In the listings, summary numbers are obtained from averages of the individual quark-mass estimates, weighted by their total errors. Moreover, the resulting one-standard-deviation errors are rescaled by the usual $\sqrt{\chi^2/\text{dof}}$ factor, which is further multiplied by 1.645 to obtain the uncertainty corresponding to a 90% confidence interval. Nevertheless, the averages presented here and in the listings are fully consistent, with comparable uncertainties, signalling the robustness of the two combination procedure.

The results on which the lattice summary numbers presented here are those used in the FLAG reviews, supplemented by any new calculations that satisfy their selection criteria. The methodology that we use is also close to that of FLAG, but here we make an attempt to separate uncertainties into their statistical and systematic components, to provide some idea of what the relative weight of each is for different quark masses. In some cases, also, slightly different choices are also made. Thus, agreement between the results obtained is a further sign of the robustness of the combination procedures used here, as well as in FLAG.

We now lay out our averaging procedure. For each of m_{ud}, m_s or m_s/m_{ud}, and for each of $N_f = 2+1$ or $N_f = 2+1+1$, we perform averages of the relevant, individual lattice results with weights that include the sum in quadrature of the statistical and systematic uncertainties. The weights also account for correlations by assuming that they are 100% on any uncertainty components that may be correlated. This procedure yields a central value and a total error for each of the quantities of interest. The total uncertainty is rescaled by the usual factor of $\sqrt{\chi^2/\text{dof}}$ if that factor is larger than 1, where χ^2 is the one corresponding to the weighted average procedure. To isolate the statistical component of the uncertainty on any given average, like for the total uncertainty we use the standard error formula for correlated data, this time only taking into account the statistical uncertainties on the different collaborations' results. If the total error has been rescaled, this statistical uncertainty is multiplied by the same factor. The candidate systematic error on an average is then obtained by subtracting in quadrature the statistical uncertainty from the total one. For each quantity, the final systematic error on the average is the largest of two uncertainties: the candidate systematic error and the minimum of the systematic uncertainties on the individual lattice determinations. This guarantees that the final systematic error is no smaller than the one of any given calculation. We then repeat this whole procedure to average the $N_f = 2+1$ and $N_f = 2+1+1$ averages, for reasons discussed below. In cases where the error separation is not explicit in a particular collaboration's result, we assume that the quoted error is statistical and take, as the minimum of systematic error, the smallest non-vanishing one among those of the other individual results. While this procedure may change the balance between statistical and systematic errors, it does change the average (which

[1] Since QCD without QED is not the real world, it makes a difference, for example, which hadron mass is used to tune a quark mass and the QED correction will differ for different choices.

[2] The same remains true in the presence of QED if the two quarks in the ratio have the same charge.

Int. J. Mod. Phys. A 2026.41. Downloaded from www.worldscientific.com by UNIVERSITY OF CALIFORNIA @ BERKELEY on 09/16/26. Re-use and distribution is strictly not permitted, except for Open Access articles.

is weighted by the total errors of the individual entries and the correlations between them) and does not decrease the total error. When quantities involving m_c or m_b are averaged, we consider only the averages of $N_f = 2+1+1$ calculations, for reasons also explained below.

The values of the individual results used in the averages obtained below can be found in the quark properties listings of this *Review*.

60.5 Light quarks

In this section we review the determination of the masses of the light quarks u, d and s from lattice simulations and then discuss the consequences of the approximate chiral symmetry.

60.5.1 *Lattice QCD results*

The most reliable determinations of the strange quark mass, m_s, and of the up and down quark masses, m_u and m_d, are obtained from lattice simulations. This is reflected in part by the uncertainties of individual determinations of these masses given in this *Review's* listings of quark properties: lattice results typically have smaller error bars than phenomenological extractions. As explained in the previous section, the simulations are generally performed in the isospin-symmetric limit of QCD, i.e. with degenerate up and down quarks ($m_u = m_d$) and the electromagnetic coupling α set to zero. Thus, it is initially $m_{ud} = (m_u + m_d)/2$ which is obtained from the computations. The numerical values of these masses depend on the choice of renormalization scale and scheme. [3]

Below we discuss the derivation of m_u and m_d separately, but we start by briefly presenting our estimates for m_{ud}, m_s and their ratio, using the latest lattice results. FLAG [8] bases its summary numbers on references that the authors consider to have the most reliable estimates of systematic uncertainties, i.e. [12–18] for $N_f = 2+1$ and [19–24] for $N_f = 2+1+1$ flavors of sea quarks. Note that the $N_f = 2+1+1$ results of Ref. [9] did not make the FLAG deadline. In the estimates given below, we use the fact that Ref. [9] supersedes Ref. [22].

Applying the averaging procedure described in the previous section and the results of Refs. [12–18], for $N_f = 2+1$ we obtain $\overline{m}_{ud} = (3.382 \pm 0.026 \pm 0.040[\pm 0.050])$ MeV, $\overline{m}_s = (92.24 \pm 0.24 \pm 1.00[\pm 1.03])$ MeV and $(\overline{m}_s/\overline{m}_{ud}) = 27.42 \pm 0.05 \pm 0.12[\pm 0.12]$. These numbers are $\overline{m}_{ud} = (3.421 \pm 0.035 \pm 0.049[\pm 0.060])$ MeV, $\overline{m}_s = (92.93 \pm 0.51 \pm 0.37[\pm 0.063])$ MeV and $(\overline{m}_s/\overline{m}_{ud}) = 27.25 \pm 0.03 \pm 0.07[\pm 0.08]$ using the latest $N_f = 2+1+1$ calculations [9, 19–21, 23, 24]. The masses are given in the $\overline{\text{MS}}$ scheme at a renormalization scale of 2 GeV. In these averages, the first error is statistical, the second systematic and the third one in brackets is the sum in quadrature of the first two. Also, QED corrections have been accounted for only to the extent that they have been removed from the hadron mass inputs phenomenologically.

A few comments are in order concerning the compatibility of the results which enter these averages. We begin with the case of $N_f = 2+1$. For m_{ud} the results show a good degree of compatibility with a $\chi^2/\text{dof} = 5.7/4$ and the final systematic uncertainty is given by the one of Ref. [17]. The level of compatibility is similar in the case of m_s and the final systematic uncertainty is also given by the one of Ref. [17]. For m_s/m_{ud} the results are even more compatible and here the final systematic error is derived from the averaging procedure. In the case of $N_f = 2+1+1$, there are only two results for m_{ud} [9, 20] and their level of compatibility is poor, with $\chi^2/\text{dof} = 6.4/1$. This is due to the value of Ref. [9], $m_{ud} = (3.636 \pm 0.066 \pm 0.059)$ MeV, which is significantly larger than all other determinations, including those obtained in $N_f = 2+1$ determinations. The scenario repeats for m_s, but is diluted by the fact that there are four results [9, 19–21] which enter the average. However, compatibility is recovered for m_s/m_{ud}, suggesting a problem in the determination of the renormalization constants or the lattice spacing in at least one of the calculations. Since the different collaborations use different formulations of lattice QCD, the (relatively) small variations of the results between the groups provides important information about the reliability of the estimates. Furthermore, the conservative nature of our method for estimating uncertainties is confirmed by the excellent agreement of the averages obtained for $N_f = 2+1$ and $N_f = 2+1+1$ calculations.

Despite being reported in the $\overline{\text{MS}}$ scheme at a renormalization scale of 2 GeV, the schemes in simulations with $2+1$ and $2+1+1$ sea-quark flavors actually differ. This is because the former are renormalized with $N_L = 3$ and the latter with $N_L = 4$. Thus for a comparison one should convert the results to the same scheme. That is not the case for (m_s/m_{ud}), where renormalization factors cancel in the absence of electromagnetic corrections. The conversion of the $N_f = 2+1$ results to the $N_L = 4$ scheme can be performed, for instance, by running them down to the charm threshold in the $N_L = 3$ theory, matching the results to the $N_L = 4$ theory at that scale, and running them back up to 2 GeV with four active flavors. Such a conversion leads to an upward shift in the values of the quark masses of only around 0.3%, well within the quoted uncertainties on the quark masses themselves. Quark-mass ratios are not concerned by this upward shift, because it is identical for the numerator and denominator. There are also nonperturbative contributions to this procedure, of $O((\Lambda_{\text{QCD}}/m_c)^2/N_c) \sim 2\%$. However lattice QCD studies of these effects have shown that they are typically an order of magnitude smaller on hadronic quantities or on Λ_{QCD} [25, 26]. Given that the total errors on the $N_f = 2+1$ results for $\overline{m}_{ud}$ and $\overline{m}_s$ are larger than 1%, we consider these matching effects negligible. In addition, for m_{ud} in particular there are six $N_f = 2+1$ calculations in which all sources of uncertainty have been accounted for, while there are only two for $N_f = 2+1+1$. Thus, we average the averages from the two frameworks in the same way as above (see Sec. 60.4), yielding as a final lattice QCD estimate in the $\overline{\text{MS}}$ scheme at $\mu = 2$ GeV in the $N_L = 4$ theory:

$$\overline{m}_{ud} = (3.397 \pm 0.021 \pm 0.040[\pm 0.045])\,\text{MeV}, \tag{60.4}$$

$$\overline{m}_s = (92.74 \pm 0.22 \pm 0.49[\pm 0.54])\,\text{MeV}, \tag{60.5}$$

and

$$r_s \equiv \frac{\overline{m}_s}{\overline{m}_{ud}} = 27.30 \pm 0.03 \pm 0.07[\pm 0.08]. \tag{60.6}$$

In these averages, the first error is statistical, the second systematic and the third one in brackets is the sum in quadrature of the first two. QED corrections have been accounted for only to the extent that they have been removed from the hadron mass inputs phenomenologically. It is worth noting that the result for r_s in Eq. (60.6) is identical to the ratio of m_s and m_{ud} from Eqs. (60.4) and (60.5), within the four digits for r_s given in Eq. (60.6), albeit with a significantly smaller total uncertainty.

To obtain the individual values of $\overline{m}_u$ and $\overline{m}_d$ requires the introduction of isospin breaking effects, including electromagnetism. This is now being done completely using lattice field theory, albeit neglecting electromagnetic effects in the sea in most cases (for an exception, see Ref. [27] which includes a calculation of the valence and sea QED contributions to $\Delta M_K^2 = M_{K^0}^2 - M_{K^+}^2$ that is critical for determining $\overline{m}_d - \overline{m}_u$). The effect of neglecting QED contributions from the sea on the u and d quark masses has been estimated in Ref. [28] to induce a contribution to the uncertainty that ranges from about 3% in $\overline{m}_u/\overline{m}_d$ to less than 1% in $\overline{m}_d$. FLAG has also reviewed results for these masses [8]. Again, they separate results obtained from $N_f = 2+1$ and $N_f = 2+1+1$ simulations. For the former, they use the results of Ref. [28] and for the latter, those of Refs. [20, 29, 30].

To obtain our estimates, we proceed as for the light quark masses above. For $N_f = 2+1$, our estimates are the results

[3] If QED is not included, then quark masses also depend on the conditions used to match isospin-symmetric QCD to the low energy effective theory of the Standard Model, which includes QCD and QED with $m_u \neq m_d$. Those matching conditions, which define a matching scheme, are quite similar in the calculations reported on below. Moreover, they have been designed to minimize the impact of isospin-breaking effects on isospin-symmetric combinations of quark masses, such m_{ud} and m_s here, and m_c and m_b below. Thus, as does FLAG [8], we generally assume that any remaining differences between schemes are within the quoted errors. Such an assumption is certainly true for $\overline{m}_c(\overline{m}_c)$ [10], where QED effects have been studied explicitly. On the other hand, in the case of m_b/m_c, where the effects of QED have also been studied explicitly [11] and where uncertainties are less than 0.3%, these effects are no longer negligible.

Int. J. Mod. Phys. A 2026.41. Downloaded from www.worldscientific.com
UNIVERSITY OF CALIFORNIA @ BERKELEY on 09/16/26. Re-use and distribution is strictly not permitted, except for Open Access articles.

of the only calculation in which all sources of uncertainty are accounted for [28]. These are $\overline{m}_u = (2.27 \pm 0.06 \pm 0.06[\pm 0.09])$ MeV, $\overline{m}_d = (4.67 \pm 0.06 \pm 0.06[\pm 0.09])$ MeV and $\overline{m}_u/\overline{m}_d = (0.485 \pm 0.011 \pm 0.016[\pm 0.020])$. For $N_f = 2+1+1$, they rely on Refs. [20, 29, 30]. Our estimates are $\overline{m}_u = (2.14 \pm 0.04 \pm 0.07[\pm 0.08])$ MeV, $\overline{m}_d = (4.70 \pm 0.03 \pm 0.04[\pm 0.05])$ MeV and $\overline{m}_u/\overline{m}d = (0.460 \pm 0.008 \pm 0.018[\pm 0.020])$. These masses are given the the $\overline{\text{MS}}$ scheme at 2 GeV in the $N_L = 3$ and 4 theories, respectively. Given the size of the uncertainties on these averages, tiny corrections due to QED effects in the renormalization constants have been neglected.

In obtaining the $N_f = 2+1+1$ averages, there is a significant $\chi^2/1 = 4.7$ tension between the two results for m_u [20, 29] and a $\chi^2/1 = 3.4$ one between those for m_u/m_d [29, 30]. These tensions are accounted for by the usual rescaling of uncertainties. However, agreement is found between the two results for m_d [20, 29]. Moreover, at the level of our conservative uncertainties, agreement is found with the $N_f = 2+1$ results.

Again, given the small number of results and the few percent uncertainties, we average the $N_f = 2+1$ and $N_f = 2+1+1$ results, as explained in Sec. 60.4, to obtain our final estimates:

$$\overline{m}_u = (2.20 \pm 0.04 \pm 0.06[\pm 0.07])\,\text{MeV}, \tag{60.7}$$

$$\overline{m}_d = (4.69 \pm 0.03 \pm 0.04[\pm 0.05])\,\text{MeV}, \tag{60.8}$$

$$r \equiv \frac{\overline{m}_u}{\overline{m}_d} = (0.473 \pm 0.007 \pm 0.016[\pm 0.017]), \tag{60.9}$$

where the three uncertainties have the same meaning as described after Eq. 60.6. r in Eq. (60.9) is the combination of direct lattice computations of that ratio in which some systematics cancel. The averages are given in the $\overline{\text{MS}}$ scheme at 2 GeV in the $N_L = 4$ theory and, as above, tiny corrections due to QED effects in the renormalization constants have been neglected. Within one standard deviation it agrees with the ratio of $\overline{m}_u$ over $\overline{m}_d$ from Eqs. (60.7) and (60.8).

It is also worth noting that m_u differs from zero by more than 30 times the quoted error, making a scenario in which $m_u = 0$ very unlikely. This is important because there would be no strong CP problem if m_u were to vanish.

60.5.2 *Chiral Perturbation Theory*

For light quarks, one can use the techniques of chiral perturbation theory [31–33] to extract quark mass ratios. The mass term for light quarks in the QCD Lagrangian is

$$\overline{\Psi} M \Psi = \overline{\Psi}_L M \Psi_R + \overline{\Psi}_R M^\dagger \Psi_L, \tag{60.10}$$

where M is the light quark mass matrix,

$$M = \begin{pmatrix} m_u & 0 & 0 \\ 0 & m_d & 0 \\ 0 & 0 & m_s \end{pmatrix}, \tag{60.11}$$

$\Psi = (u, d, s)$, and L and R are the left- and right-chiral components of Ψ given by $\Psi_{L,R} = P_{L,R}\Psi$, $P_L = (1-\gamma_5)/2$, $P_R = (1+\gamma_5)/2$. The mass term is the only term in the QCD Lagrangian that mixes left- and right-handed quarks. In the limit $M \to 0$, there is an independent SU(3)×U(1) flavor symmetry for the left- and right-handed quarks. The vector U(1) symmetry is baryon number; the axial U(1) symmetry of the classical theory is broken in the quantum theory due to the anomaly. The remaining $G_\chi = \text{SU}(3)_L \times \text{SU}(3)_R$ chiral symmetry of the QCD Lagrangian is spontaneously broken to $\text{SU}(3)_V$, which, in the limit $M \to 0$, leads to eight massless Goldstone bosons, the π's, K's, and η.

The symmetry G_χ is only an approximate symmetry, since it is explicitly broken by the quark mass matrix M. The Goldstone bosons acquire masses which can be computed in a systematic expansion in M, in terms of low-energy constants, which are unknown nonperturbative parameters of the effective theory, and are not fixed by the symmetries. One treats the quark mass matrix M as a uniform, external field that transforms under G_χ as $M \to LMR^\dagger$, where $\Psi_L \to L\Psi_L$ and $\Psi_R \to R\Psi_R$ are the $\text{SU}(3)_L$ and $\text{SU}(3)_R$ transformations, and writes down the most general Lagrangian invariant under G_χ. Then one sets M to its given constant value Eq. (60.11), which implements the symmetry breaking. To first order in M one finds that [34]

$$\begin{aligned} m^2_{\pi^0} &= B\,(m_u + m_d)\,, \\ m^2_{\pi^\pm} &= B\,(m_u + m_d) + \Delta_{\text{em}}, \\ m^2_{K^0} &= m^2_{\overline{K}^0} = B\,(m_d + m_s)\,, \\ m^2_{K^\pm} &= B\,(m_u + m_s) + \Delta_{\text{em}}, \\ m^2_\eta &= \frac{1}{3} B\,(m_u + m_d + 4m_s)\,, \end{aligned} \tag{60.12}$$

with two unknown constants B, related to the light quark condensate, and Δ_{em}, the electromagnetic mass difference. From Eq. (60.12), one can determine the quark mass ratios [34]

$$\begin{aligned} \frac{m_u}{m_d} &= \frac{2m^2_{\pi^0} - m^2_{\pi^+} + m^2_{K^+} - m^2_{K^0}}{m^2_{K^0} - m^2_{K^+} + m^2_{\pi^+}} = 0.56, \\ \frac{m_s}{m_d} &= \frac{m^2_{K^0} + m^2_{K^+} - m^2_{\pi^+}}{m^2_{K^0} + m^2_{\pi^+} - m^2_{K^+}} = 20.2, \end{aligned} \tag{60.13}$$

to lowest order in chiral perturbation theory, with an error which will be estimated below. Since the mass ratios extracted using chiral perturbation theory use the symmetry transformation property of M under the chiral symmetry G_χ, it is important to use a renormalization scheme for QCD that does not change this transformation law. Any mass-independent subtraction scheme such as $\overline{\text{MS}}$ is suitable. The ratios of quark masses are scale independent in such a scheme (up to electromagnetic corrections), and Eq. (60.13) can be taken to be the ratio of $\overline{\text{MS}}$ masses. Chiral perturbation theory cannot determine the overall scale of the quark masses, since it uses only the symmetry properties of M, and any multiple of M has the same G_χ transformation law as M.

Chiral perturbation theory is a systematic expansion in powers of the light quark masses. The typical expansion parameter is $m^2_K/\Lambda^2_\chi \sim 0.25$ if one uses SU(3) chiral symmetry, and $m^2_\pi/\Lambda^2_\chi \sim 0.02$ if instead one uses SU(2) chiral symmetry. Electromagnetic effects at the few percent level also break SU(2) and SU(3) symmetry. The mass formulæ Eq. (60.12) were derived using SU(3) chiral symmetry, and are expected to have approximately a 25% uncertainty due to second order corrections. This estimate of the uncertainty yields results consistent with the lattice results summarized in Eq. (60.5)–(60.6).

There is a subtlety which arises when one tries to determine quark mass ratios at second order in chiral perturbation theory. The second order quark mass term [35]

$$\left(M^\dagger\right)^{-1} \det M^\dagger \tag{60.14}$$

(which can be generated by instantons) transforms in the same way under G_χ as M. Chiral perturbation theory cannot distinguish between M and $(M^\dagger)^{-1} \det M^\dagger$; one can make the replacement $M \to M(\lambda) = M + \lambda M (M^\dagger M)^{-1} \det M^\dagger$ in the chiral Lagrangian,

$$\begin{aligned} M(\lambda) &= \text{diag}\,(m_u(\lambda),\ m_d(\lambda),\ m_s(\lambda)) \\ &= \text{diag}\,(m_u + \lambda m_d m_s,\ m_d + \lambda m_u m_s,\ m_s + \lambda m_u m_d)\,, \end{aligned} \tag{60.15}$$

and leave all observables unchanged.

The combination

$$\left(\frac{m_u}{m_d}\right)^2 + \frac{1}{Q^2}\left(\frac{m_s}{m_d}\right)^2 = 1 \tag{60.16}$$

where

$$Q^2 = \frac{m_s^2 - m_{ud}^2}{m_d^2 - m_u^2}, \qquad m_{ud} = \frac{1}{2}\,(m_u + m_d)\,,$$

is insensitive to the transformation in Eq. (60.15). Eq. (60.16) gives an ellipse in the m_u/m_d-m_s/m_d plane. The ellipse is well-determined by chiral perturbation theory, but the location on the

Int. J. Mod. Phys. A 2026.41. Downloaded from www.worldscientific.com
by UNIVERSITY OF CALIFORNIA @ BERKELEY on 09/16/26. Re-use and distribution is strictly not permitted, except for Open Access articles.

ellipse, and the absolute normalization of the quark masses, have larger uncertainties.

A leading-order result for Q in SU(3) chiral perturbation theory can be derived using Eq. (60.12) and the values for the relevant meson masses. This result actually holds to next-to-leading order, yielding $Q \overset{\text{NLO}}{=} 24.3$. Phenomenologically, the preferred way to determine Q is from $\eta \to 3\pi$ decay, giving the smaller value $Q = 22.1(7)$ [36]. Lattice QCD collaborations have also reported determinations of Q. Using $N_f = 2+1$ simulations, Ref. [28] obtains $Q = 23.4 \pm 0.6$ and Ref. [29] determines $Q = 23.8 \pm 1.1$ with $N_f = 2+1+1$ simulations, results which are fully compatible. These results are also compatible with $Q = 23.4 \pm 0.5$, obtained from $Q^2 = (r_s^2 - 1)(1+r)/[4(1-r)]$ and from our lattice averages for r_s and r from Eqs. (60.6) and (60.9), respectively. Given the size of the uncertainties on the lattice results for Q, it is safe to neglect effects due to the definition of isosymmetric QCD (see footnote 3). On the whole, the lattice results are larger than the one from phenomenology [36]. This difference could be due to surprisingly large corrections to the NLO substitution of meson masses by Q in the phenomenological determination, as suggested by the authors of [36].

The absolute normalization of the quark masses cannot be determined using chiral perturbation theory. Other methods, such as lattice simulations discussed above, or spectral function sum rules [37,38] for hadronic correlation functions reviewed next, are necessary.

60.5.3 *Sum rules*

Sum rule methods have been used extensively to determine quark masses and for illustration we briefly discuss here their application to hadronic τ decays [39]. Other applications involve very similar techniques.

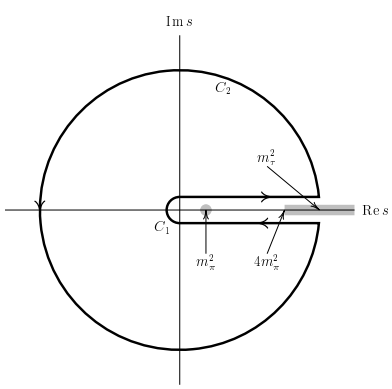

Figure 60.1: The analytic structure of $\Pi(s)$ in the complex s-plane. The contours C_1 and C_2 are the integration contours discussed in the text, and the integral over the closed contour C_1+C_2 vanishes. m_τ^2 has not been drawn to scale; $m_\tau^2 \sim 40(4m_\pi^2)$.

The experimentally measured quantity is R_τ,

$$\frac{\mathrm{d}R_\tau}{\mathrm{d}s} = \frac{\mathrm{d}\Gamma/\mathrm{d}s\left(\tau^- \to \text{hadrons} + \nu_\tau(\gamma)\right)}{\Gamma\left(\tau^- \to e^-\overline{\nu}_e\nu_\tau(\gamma)\right)} \tag{60.17}$$

the hadronic invariant mass spectrum in semihadronic τ decay, normalized to the leptonic τ decay rate. It is useful to define q as the total momentum of the hadronic final state, so $s = q^2$ is the hadronic invariant mass. The total hadronic τ decay rate R_τ is then given by integrating $\mathrm{d}R_\tau/\mathrm{d}s$ over the kinematically allowed range $0 \le s \le M_\tau^2$.

R_τ can be written as

$$R_\tau = 12\pi \int_0^{M_\tau^2} \frac{\mathrm{d}s}{M_\tau^2}\left(1 - \frac{s}{M_\tau^2}\right)^2 \times \left[\left(1 + 2\frac{s}{M_\tau^2}\right)\mathrm{Im}\,\Pi^T(s) + \mathrm{Im}\,\Pi^L(s)\right] \tag{60.18}$$

where the hadronic spectral functions $\Pi^{L,T}$ are defined from the time-ordered correlation function of two weak currents ($j^\mu(x)$ and $j^\nu(0)$) by

$$\Pi^{\mu\nu}(q) = i\int \mathrm{d}^4x\, e^{iq\cdot x}\,\langle 0|\,T\left(j^\mu(x)j^\nu(0)^\dagger\right)|0\rangle\,, \tag{60.19}$$

$$\Pi^{\mu\nu}(q) = \left(-g^{\mu\nu} + q^\mu q^\nu\right)\Pi^T(s) + q^\mu q^\nu \Pi^L(s), \tag{60.20}$$

and the decomposition Eq. (60.19) is the most general possible structure consistent with Lorentz invariance.

By the optical theorem, the imaginary part of $\Pi^{\mu\nu}$ is proportional to the total cross-section for the current to produce all possible states. A detailed analysis including the phase space factors leads to Eq. (60.18). The spectral functions $\Pi^{L,T}(s)$ are analytic in the complex s plane, with singularities along the real axis. There is an isolated pole at $s = m_\pi^2$, and single- and multi-particle singularities for $s \ge 4m_\pi^2$, the two-particle threshold. The discontinuity along the real axis is $\Pi^{L,T}(s+i0^+) - \Pi^{L,T}(s-i0^+) = 2i\mathrm{Im}\,\Pi^{L,T}(s)$. As a result, Eq. (60.18) can be rewritten with the replacement $\mathrm{Im}\,\Pi^{L,T}(s) \to -i\Pi^{L,T}(s)/2$, and the integration being over the contour C_1. Finally, the contour C_1 can be deformed to $-C_2$ without crossing any singularities, and so leaving the integral unchanged, i.e. the integral over the closed contour $C_1 + C_2$ vanishes. One can derive a series of sum rules analogous to Eq. (60.18) by weighting the differential τ hadronic decay rate by different powers of the hadronic invariant mass [40],

$$R_\tau^{kl} = \int_0^{M_\tau^2} \mathrm{d}s\,\left(1 - \frac{s}{M_\tau^2}\right)^k \left(\frac{s}{M_\tau^2}\right)^l \frac{\mathrm{d}R_\tau}{\mathrm{d}s}\,. \tag{60.21}$$

This leads to the final form of the sum rule(s),

$$R_\tau^{kl} = -6\pi i \int_{C_2} \frac{\mathrm{d}s}{M_\tau^2}\left(1 - \frac{s}{M_\tau^2}\right)^{2+k}\left(\frac{s}{M_\tau^2}\right)^l \times \left[\left(1 + 2\frac{s}{M_\tau^2}\right)\Pi^T(s) + \Pi^L(s)\right]. \tag{60.22}$$

The manipulations so far are completely rigorous and exact, relying only on the general analytic structure of quantum field theory. The left-hand side of the sum rule Eq. (60.22) is obtained from experiment. The right hand-side can be computed for s far away from any physical cuts using the operator product expansion (OPE) for the time-ordered product of currents in Eq. (60.18), and QCD perturbation theory. The OPE is an expansion in a series of local operators, and is an expansion about the $q \to \infty$ limit. It gives $\Pi^{L,T}(s)$ as an expansion in powers of $\alpha_s(s)$ and Λ_{QCD}^2/s, and is valid when s is far (in units of Λ_{QCD}^2) from any singularities in the complex s-plane.

The OPE gives $\Pi^{L,T}(s)$ as a series in α_s, quark masses, and various nonperturbative vacuum matrix elements. By computing $\Pi^{L,T}(s)$ theoretically, and comparing with the experimental values of R_τ^{kl}, one determines various parameters such as α_s and the quark masses. The theoretical uncertainties in using Eq. (60.22) arise from neglected higher order corrections (both perturbative and nonperturbative), and because the OPE is no longer valid near the real axis, where $\Pi^{L,T}$ have singularities. The contribution of neglected higher order corrections can be estimated as for any other perturbative computation. The error due to the failure of the OPE is more difficult to estimate. In Eq. (60.22), the OPE fails on the endpoints of C_2 that touch the real axis at $s = M_\tau^2$. The weight factor $(1 - s/M_\tau^2)$ in Eq. (60.22) vanishes at this point, so the importance of the endpoint can be reduced by choosing larger values of k.

Light quark masses are often determined using QCD sum rules [38], which are similar to the τ sum rules. One takes the correlator of two light-quark-bilinear operators (e.g. an axial vector current), as in Eq. (60.18), and computes their Laplace transforms or moments

$$\mathcal{L}_n(\tau) = \int_0^\infty \mathrm{d}s\, s^n\, e^{-\tau s}\,\mathrm{Im}\,\Pi(s),$$

$$\mathcal{M}_n(Q^2) = \int_0^\infty \frac{\mathrm{d}s}{(s+Q^2)^n}\,\mathrm{Im}\,\Pi(s)$$

Int. J. Mod. Phys. A 2026.41. Downloaded from www.worldscientific.com
UNIVERSITY OF CALIFORNIA @ BERKELEY on 09/16/26. Re-use and distribution is strictly not permitted, except for Open Access articles.

to get Laplace or moment sum rules, respectively. The quark masses are extracted by comparing the theoretical and experimental values of $\mathcal{L}_n(\tau)$ and $\mathcal{M}_n(Q^2)$. Considerable theoretical effort has gone into optimizing n and Q^2 to improve the precision of the resulting light quark masses.

60.6 Heavy quarks

60.6.1 *Continuum approaches and results*

For heavy quark physics one can exploit the fact that $m_Q \gg \Lambda_{\rm QCD}$ to construct effective theories (m_Q is the mass of the heavy quark Q). The masses and decay rates of hadrons containing a single heavy quark, such as the B and D mesons can be determined using the heavy quark effective theory (HQET) [41]. The theoretical calculations involve radiative corrections computed in perturbation theory with an expansion in $\alpha_s(m_Q)$ and nonperturbative corrections with an expansion in powers of $\Lambda_{\rm QCD}/m_Q$. Due to the asymptotic nature of the QCD perturbation series, the two kinds of corrections are intimately related; an example of this are renormalon effects in the perturbative expansion which are associated with nonperturbative corrections.

Systems containing two heavy quarks such as the Υ or J/Ψ are treated using non-relativistic QCD (NRQCD) [42]. The typical momentum and energy transfers in these systems are $\alpha_s m_Q$, and $\alpha_s^2 m_Q$, respectively, so these bound states are sensitive to scales much smaller than m_Q. However, smeared observables, such as the cross-section for $e^+e^- \to \bar{b}b$ averaged over some range of s that includes several bound state energy levels, are better behaved and only sensitive to scales near m_Q. For this reason, most determinations of the c, b quark masses using perturbative calculations compare smeared observables with experiment [43–45]. The method is similar to that outlined for τ decays. The current correlator in Eq. (60.18) is the electromagnetic current, and the experimental data is the value of $R(s)$ in the threshold region for $e^+e^- \to Q\overline{Q}$. The theoretical values for the moments are computed using renormalization group improved calculations in non-relativistic QCD.

There are many continuum extractions of the c and b quark masses, some with quoted errors of 10 MeV or smaller. There are systematic effects of comparable size, which are typically not included in these error estimates. Reference [46], for example, shows that even though the error estimate of m_c using the rapid convergence of the α_s perturbation series is only a few MeV, the central value of m_c can differ by a much larger amount depending on which algorithm (all of which are formally equally good) is used to determine m_c from the data. This leads to a systematic error from perturbation theory of around 20 MeV for the c quark and 25 MeV for the b quark. Electromagnetic effects, which also are important at this precision, are often not included. For this reason, we inflate the errors on the continuum extractions of m_c and m_b. The average values of m_c and m_b from continuum determinations are (see Sec. 60.7 for the 1S scheme)

$$\overline{m}_c(\overline{m}_c) = (1.280 \pm 0.025)\text{GeV},$$

$$\overline{m}_b(\overline{m}_b) = (4.18 \pm 0.03)\,\text{GeV}, \quad m_b^{1\text{S}} = (4.65 \pm 0.03)\,\text{GeV}.$$

60.6.2 *Lattice approaches and results*

Lattice QCD simulations of a heavy quark Q, described in a relativistic fermion formulation, lead to potentially large discretization errors which are powers of am_Q (modulated by logarithms); the leading power depends on the formulation of lattice QCD being used and in most cases is quadratic. Clearly those errors can be reduced by performing simulations at smaller lattice spacings a, but also by using *improved* discretizations of the theory, in which the leading discretization errors are systematically eliminated. Recently, with more powerful computing resources, better algorithms and improved discretizations of QCD, it has become possible to perform simulations with quarks more massive than the charm and even up to the b [11], decreasing or eliminating the extrapolation which has to be performed to reach the m_b. It is worth noting that computations using a relativistic fermion formulation for the valence charm with $N_f = 2+1$ sea-quark flavors, or with $N_f = 2+1+1$ flavors and a relativistic b, suffer from partial-quenching effects. This is because the heavy valence quarks are absent from the sea. While these effects are not expected to be large in $N_f = 2+1+1$ computations, they should be investigated when quoting results below the percent level in the case of $N_f = 2+1$ sea-quark flavors. For that reason we will omit heavy-quark results obtained with $N_f = 2+1$ sea-quark flavors from our averages and, more generally focus on $N_f = 2+1+1$ results. Note that these partial-quenching effects are accounted for systematically in lattice calculations in which the heavy valence quarks are described by HQET or NRQCD.

Traditionally the charm quark mass is obtained by tuning its bare, simulation input value to reproduce the physical mass of charmonium mesons or of the D, D_s mesons (requiring a more precise tuning of the light quark masses and the computation of larger QED effects in some cases). This mass can then be renormalized and matched to the $\overline{\rm MS}$ scheme using the methods discussed for the light quarks.

An alternative approach for obtaining the $\overline{\rm MS}$ mass was proposed in [47]. Euclidean-time moments of pseudoscalar, two-point functions of $c\bar{c}$ quark-bilinear operators can readily be computed on the lattice and extrapolated to the continuum limit where they can be compared to perturbative calculations of the same quantities at 4-loop order. In this way, both the strong coupling constant and the charm quark mass can be determined with remarkably small errors. As this approach uses the same perturbative expressions for two-point correlators as the continuum determinations discussed in Sec. 60.6.1, it suffers from similar perturbation-theory, systematic errors. FLAG [8] has reviewed lattice determinations of the charm-quark mass obtained using both approaches. For their $N_f = 2+1$ average they retain the results [13, 48–50], with [51] being published after their deadline. As stated above, we focus here on $N_f = 2+1+1$ results. For these, FLAG uses the results of Refs. [10, 19, 20, 22, 52].

Since the FLAG review, Refs. [22, 52] have been superseded by Ref. [9]. In that reference, only $\overline{m}_c(3\,\text{GeV})$ is given and we multiply it by the running factor 0.7739 ± 0.0060 from $\mu = 3\,\text{GeV}$ to $\overline{m}_c$ [8]. With this substitution and using the combination method described in Sec. 60.4, we obtain:

$$\overline{m}_c(\overline{m}_c) = (1.275 \pm 0.004 \pm 0.008[\pm 0.009])\,\text{GeV} \qquad (60.23)$$

where the three uncertainties have the same meaning as described after Eq. (60.6). This result is in good agreement with the continuum result given above, but with a smaller error.

It is worth noting that three [10, 19, 20] of the four results entering this average agree, while the other [9] is over 2 standard deviations larger than the average. This is taken into account by stretching errors in the usual way, but the total uncertainty on the lattice average of $\overline{m}_c$ will not significantly be reduced until this discrepancy is resolved. It should also be noted that [10] includes QED directly in the lattice calculation, albeit only for valence quarks, while some of the other computations account for these effects using phenomenology. For $\overline{m}_c(\overline{m}_c)$ considered above, these effects are below the permil [10] and are therefore neglected here.

Historically, the main approach to controlling the discretization errors in lattice studies of b-quark physics was to perform simulations of effective theories such as HQET and NRQCD. This remains an important technique, both in its own right and in providing additional information for extrapolations from lower masses to the bottom region. Using effective theories, m_b is obtained from what is essentially a computation of the difference of $M_{H_b} - m_b$, where M_{H_b} is the mass of a hadron H_b containing a b quark. The relative error on m_b is therefore much smaller than that for $M_{H_b} - m_b$. The principal systematic errors are the matching of the effective theories to QCD and the presence of power divergences in a^{-1} in the $1/m_b$ corrections which have to be subtracted numerically. A procedure for performing these subtractions fully nonperturbatively was proposed and implemented for the first time in [53].

The most recent $N_f = 2+1+1$ lattice QCD determinations of the b quark mass rely on a variety of approaches, including Euclidean-time moments of correlation functions with [54] or without NRQCD [19] and interpolations [55, 56] (using results from HQET simulations) or extrapolations [11, 20] from above the

Int. J. Mod. Phys. A 2026.41. Downloaded from www.worldscientific.com
by UNIVERSITY OF CALIFORNIA @ BERKELEY on 09/16/26. Re-use and distribution is strictly not permitted, except for Open Access articles.

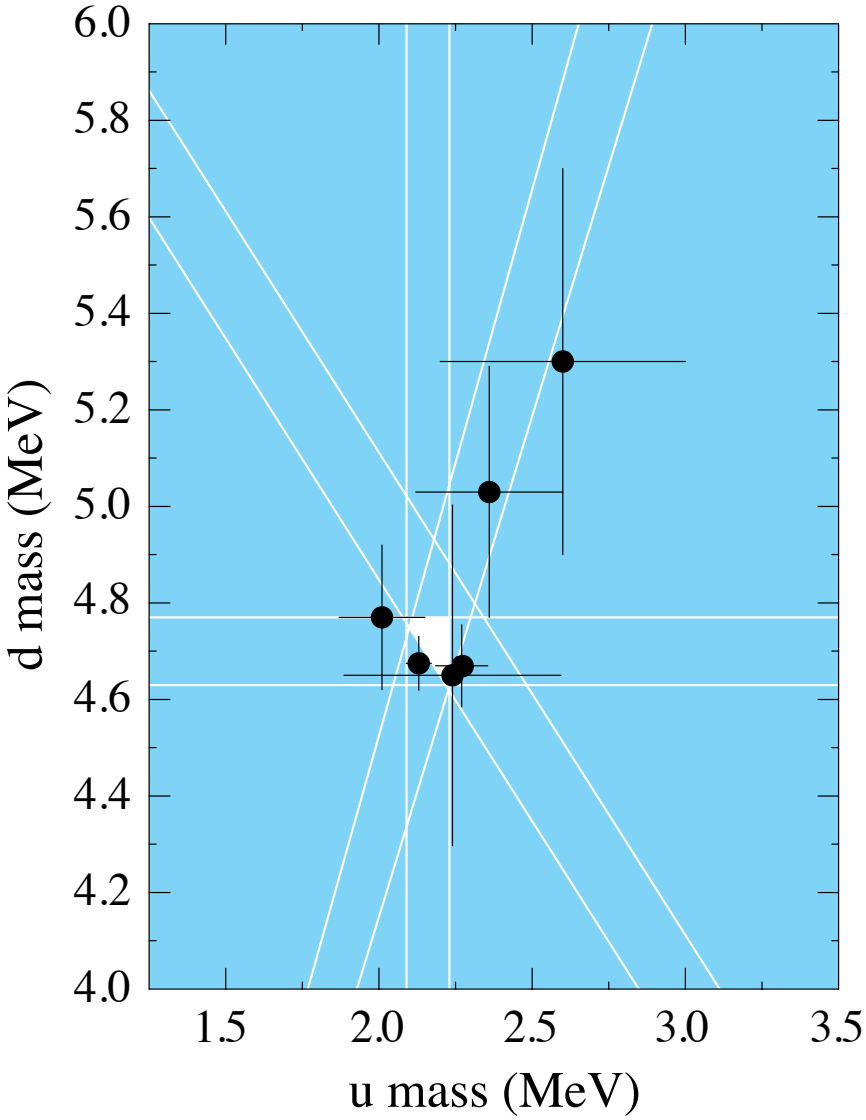

Figure 60.2: The allowed region (shown in white) for up quark and down quark masses renormalized in the $\overline{\text{MS}}$ scheme at 2 GeV, determined from the allowed ranges of mass parameters (see Fig. 60.3). The parameter $(m_u + m_d)/2$ yields the two downward-sloping white lines, while m_u/m_d yields the two rising white lines originating at $(0, 0)$. The white region is the remaining allowed parameter space after applying the limits on m_u, m_d, $(m_u + m_d)/2$ and m_u/m_d, where those limits are 90% confidence levels including the scale factors shown in the ideograms in the Data Listings.

charm mass to that of the b. One calculation [11] even includes simulations performed with a heavy quark whose mass is very near that of the b quark. The overall agreement of the results obtained using these very different approaches, which have different systematic errors, is a confirmation that the various groups control these uncertainties. As the range of heavy-quark masses which can be used in numerical simulations increases, the extrapolation or interpolation of results to the physical b mass, possibly including some obtained directly at that mass, are becoming ever more reliable (see e.g. Refs. [11, 20]).

Using the results from Refs. [11, 19, 20, 55, 56], converting those given in the $N_L = 4$ theory to the $N_L = 5$ one and applying the averaging method described in Sec. 60.4, we obtained the estimate:

$$\overline{m}_b(\overline{m}_b) = (4.196 \pm 0.009 \pm 0.009[\pm 0.012])\,\text{GeV}\ , \qquad (60.24)$$

where the three uncertainties have the same meaning as in the estimates given above for light-quark masses.

Among the results entering this average, only one [11] accounts for electromagnetic effects. Using Refs. [10, 11], it is straightforward to show that QED effects on the value of $\overline{m}_b$ at $\mu = 3\,\text{GeV}$, and thus at $\mu = \overline{m}_b$, are smaller than one permil in the separation scheme of those two references. Assuming that the same is true for the other results, we neglect these corrections here.

The lattice result of Eq. (60.24) is compatible with the average value of continuum results, but with a significantly smaller uncertainty. Note that FLAG [8] also provides an average of $N_f = 2+1$ results, taken from [13, 50]. It is about one combined, standard deviations lower that the result quoted above.

As explained in Sec. 60.3, ratios of quark masses can have significantly smaller errors than the individual masses if they are determined within the same lattice QCD framework. This led HPQCD to leverage their precise determination of m_c [47] to determine m_s and m_{ud} [57], through a precise computation of m_c/m_s [57] and of m_s/m_{ud} [58]. The $N_f = 2 + 1$ calculation [57] was updated using $N_f = 2 + 1 + 1$ simulations in [19]. The ratio m_c/m_s was also computed in Refs [48, 59] with $N_f = 2 + 1$ simulations and in Refs. [20, 22] with $N_f = 2 + 1 + 1$ ones. On the basis of those references, FLAG [8] gives average results from $N_f = 2 + 1$ and $N_f = 2+1+1$ simulations. Here we focus on $N_f = 2+1+1$ results and we replace the results of Ref. [22] by the collaboration's update [9]. Applying to the modern $N_f = 2+1+1$ computations of

Int. J. Mod. Phys. A 2026.41. Downloaded from www.worldscientific.com
UNIVERSITY OF CALIFORNIA @ BERKELEY on 09/16/26. Re-use and distribution is strictly not permitted, except for Open Access articles.

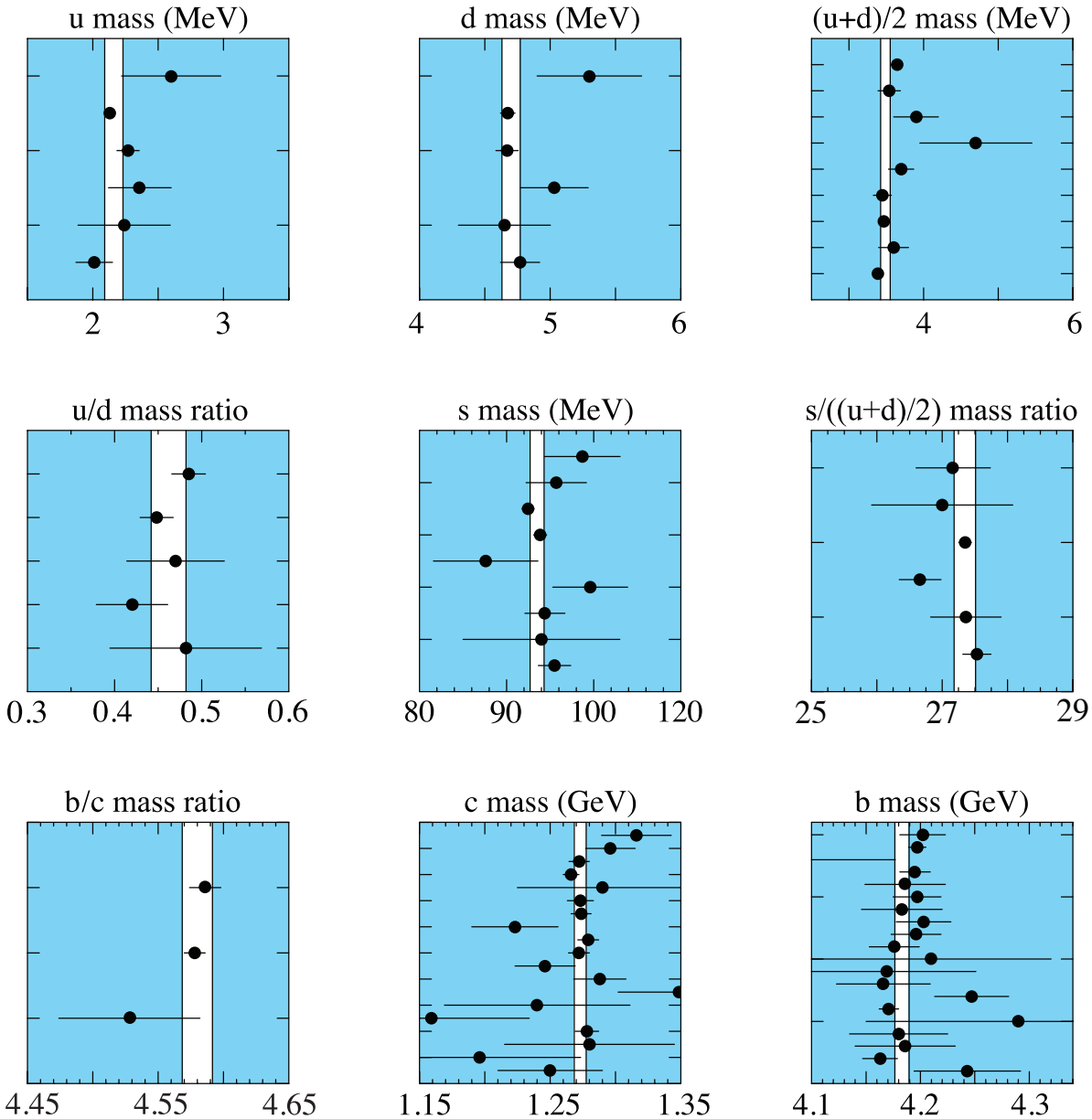

Figure 60.3: The allowed regions (shown in white) for quark masses renormalized in the $\overline{\text{MS}}$ scheme at 2 GeV. The points (taken from the Data Listings) are in chronological order with the more recent measurements shown at the top. The white regions indicate values allowed at the 90% confidence level including the scale factors shown in the ideograms in the Data Listings.

Refs. [9, 19, 20] the combination procedure described in Sec. 60.4, we obtain the following lattice average:

$$\overline{m}_c/\overline{m}_s = 11.769 \pm 0.021 \pm 0.028[\pm 0.035],$$

where the three uncertainties have the some meaning as described after Eq. 60.6. The average is dominated by Ref. [20] that has a substantially smaller error than the other results. The result of Ref. [9] is a little more that 1 standard deviation below that average and the one of Ref. [19] close to 2σ above, for a total $\chi^2/\text{dof} = 5.0/2$ and a rescaling factor of ~ 1.6 in the statistical and systematic errors.

The above ratio is renormalization scheme and scale independent, in the absence of electromagnetic corrections. None of the calculations above estimates the size of those corrections. Nevertheless, they are expected to still be smaller than the total uncertainty quoted above in a standard scheme for defining QCD in the isospin limit.

The ratio m_b/m_c has also been computed on the lattice. The two $N_f = 2+1$ results which satisfy FLAG's criteria are [13, 50]. As explained above, we focus on $N_f = 2+1+1$ calculations [11, 20, 55]. Ref. [11] is the only calculation which accounts for QED directly in the lattice simulations, albeit only for valence quarks, and thus must specify the renormalization scheme and scale of its result, which it chooses to be $\overline{\text{MS}}$ at 3 GeV. Here we correct the results of Refs. [20, 55] by the QED factor 1.0017 obtained in Ref. [11], and ascribe to it a 100% systematic uncertainty with 100% correlation. This means that we assume that the differences due to the separation schemes used in each calculation lies within that error. Averaging the resulting numbers, as prescribed in Sec. 60.4, yields

$$\overline{m}_b/\overline{m}_c = 4.584 \pm 0.006 \pm 0.010[\pm 0.012],$$

where exceptionally the bar indicates that the masses are renormalized in the $\overline{\text{MS}}$ at 3 GeV in the four-flavor theory. Here a scale factor of $\sqrt{\chi^2/\text{dof}} = 1.30$ has been applied to the error bar. Indeed, [55] contributes 3.3 to the total χ^2.

Int. J. Mod. Phys. A 2026.41. Downloaded from www.worldscientific.com
by UNIVERSITY OF CALIFORNIA @ BERKELEY on 09/16/26. Re-use and distribution is strictly not permitted, except for Open Access articles.

60.6.3 *Warnings concerning the use of the pole mass*

For an observable particle such as the electron, the position of the pole in the propagator is the definition of its mass. In QCD this definition of the quark mass is known as the pole mass. It is known that the on-shell quark propagator has no infrared divergences in perturbation theory [60,61], so this provides a perturbative definition of the quark mass. However, the pole mass cannot be used to arbitrarily high accuracy because of nonperturbative infrared effects in QCD. In fact the full quark propagator has no pole because the quarks are confined, so that the pole mass cannot be defined outside of perturbation theory. The relation between the pole mass m_Q and the $\overline{\rm MS}$ mass $\overline{m}_Q$, used throughout this review, is known to three loops [62–65]

$$m_Q = \overline{m}_Q(\overline{m}_Q)\Bigg\{1 + \frac{4\overline{\alpha}_s(\overline{m}_Q)}{3\pi} + \left[-1.0414\sum_q\left(1-\frac{4}{3}\frac{\overline{m}_q}{\overline{m}_Q}\right)+13.4434\right]\left[\frac{\overline{\alpha}_s(\overline{m}_Q)}{\pi}\right]^2 + \left[0.6527N_L^2 - 26.655N_L + 190.595\right]\left[\frac{\overline{\alpha}_s(\overline{m}_Q)}{\pi}\right]^3\Bigg\}, \tag{60.25}$$

where $\overline{\alpha}_s(\mu)$ is the strong interaction coupling constants in the $\overline{\rm MS}$ scheme, and the sum over q extends over the N_L flavors lighter than Q. The complete mass dependence of the α_s^2 term can be found in [62]; the mass dependence of the α_s^3 term is not known. For the b-quark, Eq. (60.25) reads

$$m_b = \overline{m}_b\,(\overline{m}_b)\,[1 + 0.10 + 0.05 + 0.03]\,, \tag{60.26}$$

where the contributions from the different orders in α_s are shown explicitly. The two and three loop corrections are comparable in size and have the same sign as the one loop term. This is a signal of the asymptotic nature of the perturbation series (there is a renormalon in the pole mass [66]). Such a badly behaved perturbation expansion can be avoided by directly extracting, from data, the mass defined in the $\overline{\rm MS}$ (used in this review) or other short-distance schemes (see below), without invoking the pole mass as an intermediate step.

60.7 Numerical values and caveats

The quark masses in the particle data listings have been obtained by using a wide variety of methods. Each method involves its own set of approximations and uncertainties. In most cases, the errors are an estimate of the size of neglected higher-order corrections or other uncertainties. The expansion parameters for some of the approximations are not very small (for example, they are $m_K^2/\Lambda_\chi^2 \sim 0.25$ for the SU(3) chiral expansion and $\Lambda_{\rm QCD}/m_b \sim 0.1$ for the heavy-quark expansion), so an unexpectedly large coefficient in a neglected higher-order term could significantly alter the results. Thus, before using a particular result, it is important to understand the possible limitations of the approach used to obtain it. It is also important to note that the quark mass values can be significantly different in the different schemes.

We have specified all masses in the $\overline{\rm MS}$ scheme. For light quarks, the renormalization scale has been chosen to be $\mu = 2$ GeV. Quoting these masses at smaller values of μ, where perturbative corrections become significantly larger, would introduce unnecessary uncertainties in the results. In fact, as lattice calculations, performed on finer and finer lattices, allow to determine quark masses, fully nonperturbatively, at larger and larger values of μ, it may become advantageous to quote quark mass results at renormalization scales above 2 GeV, where perturbative uncertainties are smaller.

The heavy quark masses obtained using HQET, QCD sum rules, or lattice gauge theory are consistent with each other if they are all converted into the same scheme and scale. For these quarks it is conventional to choose the renormalization scale equal to the quark mass, so we have quoted $\overline{m}_Q(\mu)$ at $\mu = \overline{m}_Q$ for the c and b quarks. Given the small size of the charm quark mass, in the future it may become advantageous to quote its value at larger values of μ so as not to introduce unnecessary perturbative uncertainties (see discussion above). Analyses of inclusive B meson decays have shown that other mass definitions lead to a better behaved perturbation series than for the $\overline{\rm MS}$ mass, and hence to more accurate mass values [67–70]. Thus, we have chosen to also give values for one of these, the b quark mass in the 1S scheme [67, 68]. Other schemes that have been proposed are the PS-scheme [69], the kinetic scheme [71] and, most recently, the minimal renormalon-subtracted mass (MRS) [70] used in the lattice calculation [20].

If necessary, we have converted values in the original papers to our chosen scheme using two-loop formulæ. It is important to realize that our conversions introduce significant additional errors. In converting to the $\overline{\rm MS}$ b-quark mass, for example, the three-loop conversions from the 1S and pole masses give values about 35 MeV and 135 MeV lower than the two-loop conversions. The uncertainty in $\alpha_s(M_Z) = 0.1179 \pm 0.0010$ [1] gives an uncertainty of ± 9 MeV and ± 21 MeV respectively in the same conversions. We have not added these additional errors when we do our conversions. The α_s value in the conversion is correlated with the α_s value used in determining the quark mass, so the conversion error is not a simple additional error on the quark mass.

References

[1] See the review of QCD in this volume.

[2] A. Manohar and H. Georgi, Nucl. Phys. B **234**, 189 (1984).

[3] K. Chetyrkin, Phys. Lett. B **404**, 161 (1997), [hep-ph/9703278].

[4] J. Vermaseren, S. Larin and T. van Ritbergen, Phys. Lett. B **405**, 327 (1997), [hep-ph/9703284].

[5] K. Chetyrkin, B. A. Kniehl and M. Steinhauser, Nucl. Phys. B **510**, 61 (1998), [hep-ph/9708255].

[6] G. Martinelli *et al.*, Nucl. Phys. B **445**, 81 (1995), [hep-lat/9411010].

[7] K. Jansen *et al.*, Phys. Lett. B **372**, 275 (1996), [hep-lat/9512009].

[8] Y. Aoki *et al.* (Flavour Lattice Averaging Group (FLAG)), Eur. Phys. J. C **82**, 10, 869 (2022), [arXiv:2111.09849].

[9] C. Alexandrou *et al.* (Extended Twisted Mass), Phys. Rev. D **104**, 7, 074515 (2021), [arXiv:2104.13408].

[10] D. Hatton *et al.* (HPQCD), Phys. Rev. D **102**, 5, 054511 (2020), [arXiv:2005.01845].

[11] D. Hatton *et al.*, Phys. Rev. D **103**, 11, 114508 (2021), [arXiv:2102.09609].

[12] A. Bazavov *et al.* (MILC), PoS **CD09**, 007 (2009), [arXiv:0910.2966].

[13] C. McNeile *et al.*, Phys. Rev. D **82**, 034512 (2010), [arXiv:1004.4285].

[14] A. Bazavov *et al.*, PoS **LATTICE2010**, 083 (2010), [arXiv:1011.1792].

[15] S. Durr *et al.*, Phys. Lett. B **701**, 265 (2011), [arXiv:1011.2403].

[16] S. Durr *et al.*, JHEP **08**, 148 (2011), [arXiv:1011.2711].

[17] T. Blum *et al.* (RBC, UKQCD), Phys. Rev. D **93**, 7, 074505 (2016), [arXiv:1411.7017].

[18] M. Bruno *et al.* (ALPHA), Eur. Phys. J. C **80**, 2, 169 (2020), [arXiv:1911.08025].

[19] B. Chakraborty *et al.*, Phys. Rev. D **91**, 5, 054508 (2015), [arXiv:1408.4169].

[20] A. Bazavov *et al.* (Fermilab Lattice, MILC, TUMQCD), Phys. Rev. D **98**, 5, 054517 (2018), [arXiv:1802.04248].

[21] A. Lytle *et al.* (HPQCD), Phys. Rev. D **98**, 1, 014513 (2018), [arXiv:1805.06225].

[22] N. Carrasco *et al.* (European Twisted Mass), Nucl. Phys. B **887**, 19 (2014), [arXiv:1403.4504].

[23] A. Bazavov *et al.* (Fermilab Lattice, MILC), Phys. Rev. D **90**, 7, 074509 (2014), [arXiv:1407.3772].

[24] A. Bazavov *et al.*, Phys. Rev. D **98**, 7, 074512 (2018), [arXiv:1712.09262].

[25] M. Bruno *et al.* (ALPHA), Phys. Rev. Lett. **114**, 10, 102001 (2015), [arXiv:1410.8374].

[26] A. Athenodorou *et al.* (ALPHA), Nucl. Phys. B **943**, 114612 (2019), [arXiv:1809.03383].

[27] S. Borsanyi *et al.*, Science **347**, 1452 (2015), [arXiv:1406.4088].

[28] Z. Fodor *et al.*, Phys. Rev. Lett. **117**, 8, 082001 (2016), [arXiv:1604.07112].

[29] D. Giusti *et al.*, Phys. Rev. D **95**, 11, 114504 (2017), [arXiv:1704.06561].

[30] S. Basak *et al.* (MILC), Phys. Rev. D **99**, 3, 034503 (2019), [arXiv:1807.05556].

[31] S. Weinberg, Physica A **96**, 1-2, 327 (1979).

[32] J. Gasser and H. Leutwyler, Annals Phys. **158**, 142 (1984).

[33] A. Pich, Rept. Prog. Phys. **58**, 563 (1995), [hep-ph/9502366].

[34] S. Weinberg, Trans. New York Acad. Sci. **38**, 185 (1977).

[35] D. B. Kaplan and A. V. Manohar, Phys. Rev. Lett. **56**, 2004 (1986).

[36] G. Colangelo *et al.*, Eur. Phys. J. C **78**, 11, 947 (2018), [arXiv:1807.11937].

[37] S. Weinberg, Phys. Rev. Lett. **18**, 507 (1967).

[38] M. A. Shifman, A. Vainshtein and V. I. Zakharov, Nucl. Phys. B **147**, 385 (1979).

[39] E. Braaten, S. Narison and A. Pich, Nucl. Phys. B **373**, 581 (1992).

[40] F. Le Diberder and A. Pich, Phys. Lett. B **286**, 147 (1992).

[41] N. Isgur and M. B. Wise, Phys. Lett. B **237**, 527 (1990).

[42] G. T. Bodwin, E. Braaten and G. Lepage, Phys. Rev. D **51**, 1125 (1995), [Erratum: Phys.Rev.D 55, 5853 (1997)], [hep-ph/9407339].

[43] A. Hoang, Phys. Rev. D **61**, 034005 (2000), [hep-ph/9905550].

[44] K. Melnikov and A. Yelkhovsky, Phys. Rev. D **59**, 114009 (1999), [hep-ph/9805270].

[45] M. Beneke and A. Signer, Phys. Lett. B **471**, 233 (1999), [hep-ph/9906475].

[46] B. Dehnadi *et al.*, JHEP **09**, 103 (2013), [arXiv:1102.2264].

[47] I. Allison *et al.* (HPQCD), Phys. Rev. D **78**, 054513 (2008), [arXiv:0805.2999].

[48] Y.-B. Yang *et al.*, Phys. Rev. D **92**, 3, 034517 (2015), [arXiv:1410.3343].

[49] K. Nakayama, B. Fahy and S. Hashimoto, Phys. Rev. D **94**, 5, 054507 (2016), [arXiv:1606.01002].

[50] P. Petreczky and J. Weber, Phys. Rev. D **100**, 3, 034519 (2019), [arXiv:1901.06424].

[51] J. Heitger, F. Joswig and S. Kuberski (ALPHA), JHEP **05**, 288 (2021), [arXiv:2101.02694].

[52] C. Alexandrou *et al.*, Phys. Rev. D **90**, 7, 074501 (2014), [arXiv:1406.4310].

[53] J. Heitger and R. Sommer (ALPHA), JHEP **02**, 022 (2004), [hep-lat/0310035].

[54] B. Colquhoun *et al.*, Phys. Rev. D **91**, 7, 074514 (2015), [arXiv:1408.5768].

[55] A. Bussone *et al.* (ETM), Phys. Rev. D **93**, 11, 114505 (2016), [arXiv:1603.04306].

[56] P. Gambino, A. Melis and S. Simula, Phys. Rev. D **96**, 1, 014511 (2017), [arXiv:1704.06105].

[57] C. Davies *et al.*, Phys. Rev. Lett. **104**, 132003 (2010), [arXiv:0910.3102].

[58] A. Bazavov *et al.* (MILC), Rev. Mod. Phys. **82**, 1349 (2010), [arXiv:0903.3598].

[59] Y. Maezawa and P. Petreczky, Phys. Rev. D **94**, 3, 034507 (2016), [arXiv:1606.08798].

[60] R. Tarrach, Nucl. Phys. B **183**, 384 (1981).

[61] A. S. Kronfeld, Phys. Rev. D **58**, 051501 (1998), [hep-ph/9805215].

[62] N. Gray *et al.*, Z. Phys. C **48**, 673 (1990).

[63] D. J. Broadhurst, N. Gray and K. Schilcher, Z. Phys. C **52**, 111 (1991).

[64] K. Chetyrkin and M. Steinhauser, Phys. Rev. Lett. **83**, 4001 (1999), [hep-ph/9907509].

[65] K. Melnikov and T. v. Ritbergen, Phys. Lett. B **482**, 99 (2000), [hep-ph/9912391].

[66] M. Beneke and V. M. Braun, Nucl. Phys. B **426**, 301 (1994), [hep-ph/9402364].

[67] A. H. Hoang, Z. Ligeti and A. V. Manohar, Phys. Rev. Lett. **82**, 277 (1999), [hep-ph/9809423].

[68] A. H. Hoang, Z. Ligeti and A. V. Manohar, Phys. Rev. D **59**, 074017 (1999), [hep-ph/9811239].

[69] M. Beneke, Phys. Lett. B **434**, 115 (1998), [hep-ph/9804241].

[70] N. Brambilla *et al.* (TUMQCD), Phys. Rev. D **97**, 3, 034503 (2018), [arXiv:1712.04983].

[71] P. Gambino and N. Uraltsev, Eur. Phys. J. C **34**, 181 (2004), [hep-ph/0401063].

Int. J. Mod. Phys. A 2026.41. Downloaded from www.worldscientific.com
UNIVERSITY OF CALIFORNIA @ BERKELEY on 09/16/26. Re-use and distribution is strictly not permitted, except for Open Access articles.

Int. J. Mod. Phys. A 2026.41. Downloaded from www.worldscientific.com
by UNIVERSITY OF CALIFORNIA @ BERKELEY on 09/16/26. Re-use and distribution is strictly not permitted, except for Open Access articles.

61. Top Quark

Revised September 2025 by F. Canelli (Zurich U.), A. Knue (TU Dortmund) and F. Maltoni (CP3 U. catholique de Louvain; Bologna U.).

61.1 Introduction and SM theory overview

In the Standard Model (SM), the left-handed top quark is the $Q = 2/3$, $T_3 = +1/2$ member of the weak-isospin doublet containing the bottom quark, while the right-handed top quark is an $SU(2)_L$ singlet. The phenomenology of the top quark is driven by its large mass, $m_t \simeq v/\sqrt{2}$, where $v = 246$ GeV is the Higgs vacuum expectation value, implying a Yukawa coupling of order unity. Being heavier than the W boson, it is the only quark that can decay weakly into a real W boson and a b quark. Its lifetime is shorter than the timescale of non-perturbative strong interactions, which prevents hadronization and preserves properties such as its spin, allowing the top to behave almost as a free quark. Through loop effects, it gives important contributions to SM precision observables, and its unique role makes it central to many extensions of the SM, often linked to new particles or interactions. These features strongly motivate increasingly precise studies of top-quark physics, providing a unique laboratory for testing the SM at the electroweak symmetry-breaking scale (EWSB) and beyond. At the same time, the abundant production of top quarks at the LHC enables precision measurements of their mass, couplings, production cross sections, and decay branching ratios. This review summarizes the experimental and theoretical issues in determining these properties and reports on recent progress.

61.1.1 *Mass*

The top-quark mass largely determines its unique phenomenology. In the SM, quark masses are derived parameters that are determined by the Yukawa coupling and the vacuum expectation value. At the loop level, with the Higgs boson discovery and better than per mil measurement of its mass, the values of the W-boson and top-quark mass are correlated, so that their precise determinations provide a strong test of the SM (see Section 10 "Electroweak Model and constraints on new physics" of this *Review*). At present, there is some tension at the $1.7\,\sigma$ level, between the indirect top-quark (pole) mass determination from electroweak (EW) precision data of 175.2 ± 1.8 GeV (see Section 10 in this *Review*) and the combination of direct measurements at the LHC that yields 172.52 ± 0.33 GeV [1].

The top-quark mass value is also crucial in the issue of vacuum stability in the SM [2–4]. At high scales, the Higgs quartic coupling λ evolves to increasingly small values as m_t grows. Above $m_t = 171$ GeV, i.e., very close to the most precise measurements, λ becomes negative at the Planck scale, leading to a meta-stable EW vacuum, while for slightly larger values, $m_t > 176$ GeV, the EW vacuum would become unstable. Current top-quark measurements therefore point to a Higgs quartic coupling that is nearly vanishing at the Planck scale. While being quite suggestive, in the absence of a clear UV picture, this argument allows only to conclude that comparison between our best SM predictions and the data does not imply new physics below the Planck scale (see Section 11.2.3 of "Status of Higgs Boson Physics" in this *Review*).

Due to its fundamental importance, precisely determining the top-quark mass has been a central objective of precision measurement programs carried out by the ATLAS and CMS collaborations at the LHC, and previously by the CDF and DØ collaborations at the Tevatron. The basic methodology rests on the idea of fitting m_t-dependent kinematic distributions to fully-exclusive (Monte Carlo) predictions, via the full or partial reconstruction of the system of the t and $\bar{t}$ decay products. These are called "direct measurements" and aim for a target accuracy in the per-mil range. With an absolute uncertainty of order or better than $\Lambda_{\rm QCD}$, however, a clear relation between the extracted mass and a well-defined quantum field theory parameter of the underlying theory has become necessary.

Several mass parameter definitions exist with a precise field-theoretical meaning, which can be organized into two broad classes: the long-distance ones, such as the "pole mass", and short-distance masses, such as the $\overline{\rm MS}$ mass. An additional mass definition [5] interpolates between the two.

Direct determinations rely on mass-sensitive observables constructed from the kinematics of the top-quark decay products. Monte Carlo generators enforce the invariant mass of this system to follow, as closely as possible, the virtuality of the top quark, which is modeled by a Breit–Wigner distribution centered on the Monte Carlo mass parameter. In this framework, the latter acts as an effective proxy for the pole mass. At e^+e^- colliders, one can define a short-distance mass, e.g., the "potential mass" that can be determined by measurements at the $t\bar{t}$ threshold, and it does not suffer from non-perturbative ambiguities. At hadron colliders, all observables that can be connected to the top-quark mass involve a top-quark reconstruction from the final state, and at the end are connected to the pole mass.

A top-quark mass measurement cannot be defined solely in terms of the mass of the system of its decay products: the top quark is a colored object; therefore, it cannot be an asymptotic state of the theory, and no final-state hadronic system can be unambiguously associated with it. On the other hand, final state observables, such as those arising from its decay, can be related to the top-quark mass through computations that have both perturbative and non-perturbative components, as seen in Monte Carlo generators.

From a purely theoretical (calculational) point of view, the top-quark mass parameter is defined within a given renormalization scheme, since divergent perturbative corrections arise order by order in perturbation theory and need to be subtracted. The pole mass scheme prescribes to subtract the divergent mass corrections so that the pole in the quark propagator remains fixed order by order in perturbation theory. The $\overline{\rm MS}$ scheme prescribes to employ dimensional regularization and subtract the pure $1/\epsilon$ pole in the divergent mass correction. In doing so, the corresponding mass becomes scale-dependent. In this scheme, the pole in the top quark propagator receives corrections at all orders in perturbation theory. This scheme has the advantage of making the relation between the mass and the Yukawa coupling straightforward in the SM and independent of non-perturbative corrections.

The relation between the top quark pole mass $m_t^{\rm pole}$ and $m_t^{\overline{\rm MS}}$ up to four loops reads [6]

$$m_t^{\rm pole} = m_t^{\overline{\rm MS}}(m_t)[1 + 0.4244\,\alpha_s + 0.8345\,\alpha_s^2 + 2.375\,\alpha_s^3 + (8.49 \pm 0.25)\,\alpha_s^4]\,, \tag{61.1}$$

which for strong coupling constant $\alpha_s = \alpha_s^{(6)}(m_t) = 0.1088$ and $m_t^{\rm pole} = 172.5$ GeV gives $m_t^{\overline{\rm MS}}(m_t) = 162.69 \pm 0.006$ GeV. The two definitions lead to perturbatively equivalent theories: the perturbative expression of the pole mass in terms of the $\overline{\rm MS}$ can be used to turn a result expressed in the pole mass scheme into the corresponding one in the $\overline{\rm MS}$ scheme. However, the relation above has only a perturbative meaning, as the two masses differ by non-perturbative, long-distance effects. The difference between the top-quark pole mass and the mass extracted in direct measurements arises due to non-perturbative effects, which are currently modeled by shower Monte Carlo programs. It is expected to be of order $Q_0 \cdot \alpha_s(Q_0)$ with $Q_0 \sim 1$ GeV, i.e., of order 0.5 GeV. Recent efforts to precisely define and estimate the uncertainties of the top-quark mass can be found in Refs. [7, 8].

61.1.2 *Width*

Like other unstable elementary particles in the SM, the top-quark lifetime, and thus its decay width, can be perturbatively calculated within the SM. With a mass exceeding the Wb production threshold and given that $|V_{tb}| \gg |V_{td}|, |V_{ts}|$, the top-quark decay width is dominated by the two-body decay channel $t \to Wb$. At next-to-leading order (NLO) prediction for the width within the SM is given by [9]:

$$\Gamma_t = \frac{G_F m_t^3}{8\pi\sqrt{2}} \left(1 - \frac{M_W^2}{m_t^2}\right)^2 \left(1 + 2\frac{M_W^2}{m_t^2}\right) \left[1 - \frac{2\alpha_s}{3\pi}\left(\frac{2\pi^2}{3} - \frac{5}{2}\right)\right], \tag{61.2}$$

where m_t refers to the top-quark pole mass (to keep the formula simple, known m_b^2/m_t^2, α_s^2, and $(\alpha_s/\pi)(M_W^2/m_t^2)$ are not

Int. J. Mod. Phys. A 2026.41. Downloaded from www.worldscientific.com
UNIVERSITY OF CALIFORNIA @ BERKELEY on 09/16/26. Re-use and distribution is strictly not permitted, except for Open Access articles.

included). The known quantum chromodynamics (QCD) corrections of order α_s^2 to Γ_t, and the EW NLO corrections [10, 11] improve the overall theoretical accuracy to better than 1%. As a result, between $m_t = 170$ GeV and 175 GeV, the width changes from 1.258 GeV to 1.394 GeV, with a linear dependence on m_t assuming $\alpha_s(M_Z) = 0.1179$ and $M_W = 80.377$ GeV. At the reference value of $m_t = 172.5$ GeV, one finds $\Gamma_t = 1.326$ GeV.

With its correspondingly short lifetime of about 0.5×10^{-24} s, the top quark is expected to decay before top-flavored hadrons or $t\bar{t}$ quarkonium-like bound states can form [12]. However, in the latter case, since the decay time is very close to the would-be-resonance binding time, a peak is predicted in e^+e^- scattering at the $t\bar{t}$ threshold [13] (whose position and width are linked to the "potential mass" of the top quark and its width, respectively), and it is also present in hadron collisions [14–16]. The short lifetime of the top quark also prevents strong interactions from efficiently scrambling its spin, as such processes would require a much longer timescale. Moreover, the purely left-handed structure of the weak interaction dictates that the top-quark decays predominantly via $t \to Wb$, followed by $W \to f\bar{f}'$, with the direction of the fermion f (the charged lepton or down-type quark component) being almost 100% correlated with the top-quark spin. Taken together, these features render the top quark unique among quarks, as they allow for direct experimental access to its spin properties through the angular distributions of its decay products.

Other decay modes of the top quark provide negligible contributions to the total width. For example, flavor-changing neutral current (FCNC) interactions, which are allowed starting at the one-loop level, give [17, 18]:

$$\begin{aligned}
&\mathrm{Br}^{\mathrm{SM}}(t \to gc) = 5 \cdot 10^{-12},\ \mathrm{Br}^{\mathrm{SM}}(t \to gu) = 4 \cdot 10^{-14},\\
&\mathrm{Br}^{\mathrm{SM}}(t \to \gamma c) = 5 \cdot 10^{-14},\ \mathrm{Br}^{\mathrm{SM}}(t \to \gamma u) = 4 \cdot 10^{-16},\\
&\mathrm{Br}^{\mathrm{SM}}(t \to Zc) = 1 \cdot 10^{-14},\ \mathrm{Br}^{\mathrm{SM}}(t \to Zu) = 7 \cdot 10^{-17},\\
&\mathrm{Br}^{\mathrm{SM}}(t \to Hc) = 3 \cdot 10^{-15},\ \mathrm{Br}^{\mathrm{SM}}(t \to Hu) = 2 \cdot 10^{-17}\,.
\end{aligned}$$

61.1.3 *Couplings*

The SM couplings involving top quarks are of two types: gauge couplings, which are universal, and Yukawa couplings, which instead depend on the generation. Following the notation of Sections 9 and 10 of this *Review*, after EWSB the top-quark interactions read

$$\begin{aligned}
\mathcal{L}_t^{\mathrm{SM}} = {}& \bar{\psi}_t \left[i\partial\!\!\!/ - m_t \right] \psi_t - g_s \bar{\psi}_t \gamma^\mu t^C \psi_t \mathcal{A}_\mu^C - e Q_t \bar{\psi}_t \gamma^\mu \psi_t A_\mu\\
&- \frac{g}{2\sqrt{2}} \bar{\Psi} \gamma^\mu (1-\gamma^5)(T^+ W_\mu^+ + T^- W_\mu^-) \Psi\\
&- \frac{g}{2\cos\theta_W} \bar{\psi}_t \gamma^\mu \left(g_V^t - g_A^t \gamma^5 \right) \psi_t Z_\mu\\
&- \frac{m_t}{v} H \bar{\psi}_t \psi_t\,,
\end{aligned} \tag{61.3}$$

where in the first line we include the kinetic term, the coupling to the $SU(3)$ field $\mathcal{A}_\mu^C$, to the EM field A_μ, to the weak bosons, $W_\mu^\pm, Z_\mu$ and to the Higgs boson ($\Psi = (t, b')$ with $b' = V_{tb}\, b + V_{ts}\, s + V_{td}\, d$). As mentioned above, there are no neutral flavor-changing interactions in the SM at tree level.

In the absence of evidence for physics beyond the SM at the weak scale or below, the SM Effective Field Theory (SMEFT) [19–21] provides a simple and consistent framework to systematically parameterize possible deviations from the SM predictions in the interactions among the known particles, using minimal theoretical assumptions. It amounts to extending the Lagrangian of the SM by all higher-dimensional operators that respect the gauge symmetry

$$\mathcal{L}^{\mathrm{SMEFT}} = \mathcal{L}^{\mathrm{SM}} + \sum_{D>4} \sum_i^{N_D} \frac{C_i^{(D)} O_i^{(D)}}{\Lambda^{D-4}}\,, \tag{61.4}$$

where D is the dimension of the operator $O_i^{(D)}$ and Λ provides an upper bound for the scale of new physics. An EFT model is generally characterized by power counting rules that identify a hierarchy among operators. In the case of the SMEFT, a minimal approach is considered, where the large-scale Λ provides a universal suppression factor for the higher-dimensional operators.

The currently adopted parametrization for SMEFT interpretations of top-quark measurements relies on the Warsaw basis of gauge-invariant dimension-six operators [21] and it is detailed in Ref. [22] (see [23, 24] for early discussions of top-quark related operators). For convenience, often specific degrees of freedom are identified from combinations of Warsaw-basis operator coefficients aligned with the directions of the EFT parameter space, which appear in given processes, in interferences with SM amplitudes, and top-quark interactions with some of the gauge boson mass eigenstates. Model implementations are available for tree-level and even one-loop Monte Carlo simulations [25, 26].

The definitions of the SMEFT operators can be organized in four categories: Four-quark, two-quark-two-bosons, two-quark-two-lepton, and baryon-lepton-number-violating operators. The overwhelming number of four-fermion operators is tamed by adopting simplifying assumptions about beyond-the-standard-model flavor structures. A baseline flavor scenario in the quark sector and motivated by the minimal flavor violation ansatz [27–29] corresponds to imposing a $U(2)_q \times U(2)_u \times U(2)_d$ symmetry among the first two generations (q refers to the SU(2) left-handed doublet, while u, d are right-handed singlets). In this case, the following numbers of degrees of freedom are produced for the operators of each category of field content:

four heavy quarks	$11 + 2$ CPV
two light and two heavy quarks	14
two heavy quarks and bosons	$9 + 6$ CPV
two heavy quarks and two leptons	$(8 + 3$ CPV$)\times$ 3 lepton flavors

where we counted separately CP-conserving and CP-violating (CPV) parameters. These operators are collected in Tab. 61.1. Other less restricted scenarios, such as that obtained by imposing $U(2)_{q+u+d}$ symmetry featuring additional $10 + 10$ CPV degrees of freedom, or more restricted ones, such as *top-philic* scenario where it is assumed that new physics couples dominantly to the left-handed doublet and right-handed up-type quark singlet of the third generation as well as to bosons, featuring only 19+6 (CPV) degrees of freedom, are often considered. It is also customary to analyze top-quark FCNCs separately, as at the tree level, they enter only quadratically.

61.1.4 *Production*

Top-quark production provides a powerful probe of QCD and the EW theory. Precise measurements of production rates and kinematic distributions constrain PDFs, α_s, and m_{t}. Since its discovery in 1995 at the Tevatron, direct measurements of top-quark production have been extensively performed. At the LHC, the broad range of center-of-mass energies, large production cross sections, and the ability to study forward production and heavy-ion collisions make top-quark measurements a uniquely sensitive tool for testing the SM and probing the partonic structure of matter.

Top-quark production processes are classified according to the underlying interaction mechanism. The primary categories include: *top-antitop quark pair production* through QCD interactions ($t\bar{t}$), *single top-quark production* via EW interactions (t or $\bar{t}$), and *associated production* involving the creation of a single top quark or a top-quark pair alongside gauge bosons or other particles via EW or QCD interactions ($t\bar{t} + X$, $t/\bar{t} + X$). Associated production also encompasses the rare scenarios where multiple top quarks are produced, specifically three-top ($tt\bar{t}/\bar{t}\bar{t}t$) and four-top ($t\bar{t}t\bar{t}$) production. Among these, pair production is the most abundant mode of top-quark production.

A key aspect of top-quark phenomenology is the study of its spin through the angular distributions of decay products, which directly reflect the production mechanism. In single-top-quark production via the weak interaction, the top quark is predicted to be fully polarized. In contrast, in $t\bar{t}$ production dominated by QCD interactions, individual top quarks are nearly unpolarized, but their spins exhibit nontrivial correlations. These spin effects are known up to NNLO in QCD and NLO in EW theory [30, 31]. In specific kinematic regimes, such as near threshold or at high transverse momentum (p_{T}), the correlations are strong enough that the $t\bar{t}$ spin system becomes entangled [32]. Recent

Int. J. Mod. Phys. A 2026.41. Downloaded from www.worldscientific.com
by UNIVERSITY OF CALIFORNIA @ BERKELEY on 09/16/26. Re-use and distribution is strictly not permitted, except for Open Access articles.

Table 61.1: List of SMEFT operators at dimension six, assuming $U(2)_q \times U(2)_u \times U(2)_d$ flavor symmetry. For more details on notation and conventions, see the reference in the text.

Operator	Field content	Operator	Field content
Four-quark		Two-quark-two-lepton	
$O_{qq}^{1(ijkl)}$	$(\bar{q}_i\gamma^\mu q_j)(\bar{q}_k\gamma_\mu q_l)$	$O_{lq}^{1(ijkl)}$	$(\bar{l}_i\gamma^\mu l_j)(\bar{q}_k\gamma^\mu q_l)$
$O_{qq}^{3(ijkl)}$	$(\bar{q}_i\gamma^\mu\tau^I q_j)(\bar{q}_k\gamma_\mu\tau^I q_l)$	$O_{lq}^{3(ijkl)}$	$(\bar{l}_i\gamma^\mu\tau^I l_j)(\bar{q}_k\gamma^\mu\tau^I q_l)$
$O_{qu}^{1(ijkl)}$	$(\bar{q}_i\gamma^\mu q_j)(\bar{u}_k\gamma_\mu u_l)$	$O_{lu}^{(ijkl)}$	$(\bar{l}_i\gamma^\mu l_j)(\bar{u}_k\gamma^\mu u_l)$
$O_{qu}^{8(ijkl)}$	$(\bar{q}_i\gamma^\mu T^A q_j)(\bar{u}_k\gamma_\mu T^A u_l)$	$O_{eq}^{(ijkl)}$	$(\bar{e}_i\gamma^\mu e_j)(\bar{q}_k\gamma^\mu q_l)$
$O_{qd}^{1(ijkl)}$	$(\bar{q}_i\gamma^\mu q_j)(\bar{d}_k\gamma_\mu d_l)$	$O_{eu}^{(ijkl)}$	$(\bar{e}_i\gamma^\mu e_j)(\bar{u}_k\gamma^\mu u_l)$
$O_{qd}^{8(ijkl)}$	$(\bar{q}_i\gamma^\mu T^A q_j)(\bar{d}_k\gamma_\mu T^A d_l)$	‡$O_{lequ}^{1(ijkl)}$	$(\bar{l}_i e_j)\ \varepsilon\ (\bar{q}_k u_l)$
$O_{uu}^{(ijkl)}$	$(\bar{u}_i\gamma^\mu u_j)(\bar{u}_k\gamma_\mu u_l)$	‡$O_{lequ}^{3(ijkl)}$	$(\bar{l}_i\sigma^{\mu\nu} e_j)\ \varepsilon\ (\bar{q}_k\sigma_{\mu\nu} u_l)$
$O_{ud}^{1(ijkl)}$	$(\bar{u}_i\gamma^\mu u_j)(\bar{d}_k\gamma_\mu d_l)$	‡$O_{ledq}^{(ijkl)}$	$(\bar{l}_i e_j)(\bar{d}_k q_l)$
$O_{ud}^{8(ijkl)}$	$(\bar{u}_i\gamma^\mu T^A u_j)(\bar{d}_k\gamma_\mu T^A d_l)$		
‡$O_{quqd}^{1(ijkl)}$	$(\bar{q}_i u_j)\ \varepsilon\ (\bar{q}_k d_l)$		
‡$O_{quqd}^{8(ijkl)}$	$(\bar{q}_i T^A u_j)\ \varepsilon\ (\bar{q}_k T^A d_l)$		
Two-quark operators		Baryon- and lepton-number-violating	
‡$O_{u\varphi}^{(ij)}$	$\bar{q}_i u_j \tilde{\varphi}\ (\varphi^\dagger\varphi)$	‡$O_{qqu}^{(ijkl)}$	$(\overline{q^c}_{i\alpha}\varepsilon q_{j\beta})(\overline{u^c}_{k\gamma} e_l)\ \epsilon^{\alpha\beta\gamma}$
$O_{\varphi q}^{1(ij)}$	$(\varphi^\dagger i\overleftrightarrow{D}_\mu\varphi)(\bar{q}_i\gamma^\mu q_j)$	‡$O_{qqq}^{1(ijkl)}$	$(\overline{q^c}_{i\alpha}\varepsilon q_{j\beta})(\overline{q^c}_{k\gamma}\varepsilon l_l)\ \epsilon^{\alpha\beta\gamma}$
$O_{\varphi q}^{3(ij)}$	$(\varphi^\dagger i\overleftrightarrow{D}^I_\mu\varphi)(\bar{q}_i\gamma^\mu\tau^I q_j)$	‡$O_{qqq}^{3(ijkl)}$	$(\overline{q^c}_{i\alpha}\tau^I\varepsilon q_{j\beta})(\overline{q^c}_{k\gamma}\tau^I\varepsilon l_l)\ \epsilon^{\alpha\beta\gamma}$
$O_{\varphi u}^{(ij)}$	$(\varphi^\dagger i\overleftrightarrow{D}_\mu\varphi)(\bar{u}_i\gamma^\mu u_j)$	‡$O_{duu}^{(ijkl)}$	$(\overline{d^c}_{i\alpha} u_{j\beta})(\overline{u^c}_{k\gamma} e_l)\ \epsilon^{\alpha\beta\gamma}$
‡$O_{\varphi ud}^{(ij)}$	$(\tilde{\varphi}^\dagger iD_\mu\varphi)(\bar{u}_i\gamma^\mu d_j)$		
‡$O_{uW}^{(ij)}$	$(\bar{q}_i\sigma^{\mu\nu}\tau^I u_j)\ \tilde{\varphi} W^I_{\mu\nu}$		
‡$O_{dW}^{(ij)}$	$(\bar{q}_i\sigma^{\mu\nu}\tau^I d_j)\ \varphi W^I_{\mu\nu}$		
‡$O_{uB}^{(ij)}$	$(\bar{q}_i\sigma^{\mu\nu} u_j)\quad \tilde{\varphi} B_{\mu\nu}$		
‡$O_{uG}^{(ij)}$	$(\bar{q}_i\sigma^{\mu\nu} T^A u_j)\ \tilde{\varphi} G^A_{\mu\nu}$		

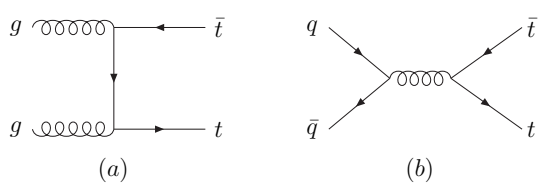

Figure 61.1: Representative Feynman diagrams for $t\bar{t}$ production (a) via gluon-gluon fusion and (b) via quark-antiquark annihilation.

LHC measurements at threshold by ATLAS and CMS have provided experimental confirmation of this phenomenon [33–35], see Sec. 61.2.5.3. Fully exclusive predictions via Monte Carlo generators for the $t\bar{t}$ and single top production processes at NLO accuracy in QCD are available, including top-quark decays and possibly off-shell effects [36–39] through the MC@NLO [40] and POWHEG [41] methods. The first Monte Carlo implementation of the NNLO QCD computation is also available [42, 43].

61.1.4.1 *Pair production*

The dominant production mode for top quarks in hadron collisions is top-antitop pair production via QCD interactions. Due to its significantly higher event rates compared to other production modes, this process is primarily used to extract top-quark properties. Additionally, it constitutes a significant background for many other collider physics measurements, making its thorough understanding and accurate modeling a key priority.

At leading order in QCD, the two principal partonic subprocesses that contribute to $t\bar{t}$ production are: gluon-gluon fusion ($gg \to t\bar{t}$) and quark-antiquark annihilation ($q\bar{q} \to t\bar{t}$), as shown in Fig. 61.1.

The relative contributions of these subprocesses depend on the collision energy and the PDFs of the incoming hadrons. At the Tevatron, where the initial state is proton-antiproton, and the energy is lower, the production of $t\bar{t}$ is dominated by quark-antiquark annihilation (approximately 85%), with gluon-gluon fusion contributing the remaining 15%. At the LHC, where protons collide at higher energies, the parton composition at low momentum fraction x is dominated by gluons, resulting in gluon-gluon fusion being the dominant production mechanism. At $\sqrt{s} = 13$ TeV, around 90% of $t\bar{t}$ pairs originate from gluon–gluon fusion, decreasing to approximately 80% at $\sqrt{s} = 7$ TeV.

Theoretical predictions for the inclusive $t\bar{t}$ production cross sections are available at NNLO in QCD, supplemented by next-to-next-to-leading logarithmic (NNLL) resummation of soft-gluon emissions [44, 45]. A combination of NNLO in QCD and NLO EW corrections is also available [46].

Assuming a top-quark mass of 173.3 GeV, the NNLO+NNLL prediction for the $t\bar{t}$ cross section at the Tevatron at $\sqrt{s} = 1.96$ TeV is:

$$\sigma_{t\bar{t}} = 7.16^{+0.11}_{-0.20}\,(\text{scale})^{+0.17}_{-0.12}\,(\text{PDF})\ \text{pb},$$

where the first uncertainty reflects variations in the renormalization and factorization scales, and the second arises from PDF uncertainties [44].

The $t\bar{t}$ cross sections for pp collisions at various center-of-mass energies for a top quark mass of 172.5 GeV and $\alpha_s = 0.118$ are presented in Tab. 61.2. They are calculated with the Top++2.0 program to NNLO in perturbative QCD (pQCD), including soft-gluon resummation to NNLL order (see [47] and references therein). The first uncertainty comes from the independent variation of the factorization and renormalization scales. In contrast, the second one is associated with variations in the PDF and α_s, following the PDF4LHC prescription with the MSTW2008 68% C.L. NNLO, CT10 NNLO and NNPDF2.3 5f FFN PDF sets (see [48] and references therein, and [49–51]).

The $t\bar{t}$ production is typically accompanied by additional QCD radiation, primarily driven by the initial states. Events with high jet multiplicities offer sensitivity to higher-order QCD radiation and to the accuracy of parton shower modeling. The exclusive $t\bar{t} + n-$jet cross sections are known at NLO in QCD. Inclusive samples matched with parton shower (PS) can be obtained by merging samples that are accurate at NLO in QCD at fixed jet multiplicities [52, 53].

Int. J. Mod. Phys. A 2026.41. Downloaded from www.worldscientific.com
UNIVERSITY OF CALIFORNIA @ BERKELEY on 09/16/26. Re-use and distribution is strictly not permitted, except for Open Access articles.

Table 61.2: Theoretical predictions for top quark pair production at LHC calculated at NNLO+NNLL in QCD. Results collected by the LHCTopWG, see `https://twiki.cern.ch/twiki/bin/view/LHCPhysics/TtbarNNLO`.

$\sqrt{s}$ (TeV)	$\sigma_{t\bar{t}}$ (pb)
5.02	$69.5^{+2.0}_{-2.3}$ (scale)$^{+2.9}_{-2.9}$(PDF)
7	$179.6^{+4.8}_{-6.2}$ (scale)$^{+6.1}_{-6.1}$(PDF)
8	$256.0^{+6.7}_{-8.9}$ (scale)$^{+8.0}_{-8.0}$(PDF)
13	$833.9^{+20.5}_{-30.0}$ (scale)$^{+21.0}_{-21.0}$(PDF)
13.6	$923.6^{+22.6}_{-33.4}$ (scale)$^{+22.8}_{-22.8}$(PDF)

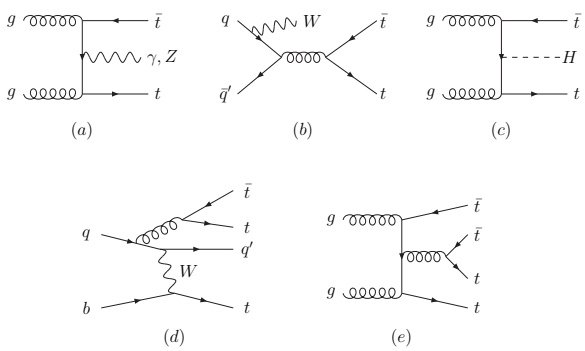

Figure 61.2: Representative Feynman diagrams for $t\bar{t}$ associated production with (a) γ, Z, (b) W, (c) Higgs, (d) a single-top, (e) an extra $t\bar{t}$ pair.

Additional jets may originate from heavy quarks, such as b and c quarks. Predictions for these processes can be obtained in different flavor schemes. For example, in the 4-flavor (3-flavor) scheme, b (c) quarks are treated as massive and not included as initial-state partons [54], while in the 5-flavor (4-flavor) scheme they are treated as massless and included on the same footing as the light quarks [55]. Matching or merging with parton showers can also be applied [39]. Despite these advances, theoretical predictions still carry sizable uncertainties. In particular, measurements of $t\bar{t}$+heavy-flavor production reveal moderate mismodeling, often requiring data-driven corrections in the background estimation for precise measurements.

61.1.4.2 *Pair production in heavy-ion collisions*

The top quark constitutes a novel and theoretically precise probe of the nuclear parton distribution functions (nuclear PDFs, or nPDFs), in the poorly explored region where partons have a significant fraction of the nucleon momentum, as well as of the properties of the produced quark-gluon plasma (QGP).

First, precise knowledge of nPDFs is a key prerequisite for extracting detailed information on QGP properties from experimental data. Second, on average, top quarks decay on a timescale similar to the formation of the QGP, offering a unique opportunity to study its time evolution [56].

For lead-lead ($PbPb$) collisions at center-of-mass energy of 5.02 TeV, the prediction for $t\bar{t}$ cross section is given by

$$\sigma^{t\bar{t}}_{\text{theory}} = \sigma^{\text{NNLO+NNLL}}_{\text{PbPb}\to t\bar{t}+X} = 3.22^{+0.38}_{-0.35}\,(\text{nPDF4 PDF})\,^{+0.09}_{-0.10}\,(\text{scale})\,\mu\text{b},$$

calculated with the Top++2.0 program at NNLO in QCD, including soft-gluon resummation at NNLL accuracy, with the nuclear EPPS16 and free-nucleon CT14 PDFs [47]. Results with a central value lower than about 7% are obtained from free-nucleon CT14 and NNPDF30 NNLO PDFs (scaled by the square of the number of nucleons in the Pb nucleus, $A^2 = 208^2$). A small difference between the cross sections obtained with nuclear and free-nucleon PDFs arises from the nPDF "antishadowing" effect, which is only mildly dependent on the center of mass energy.

61.1.4.3 *Associated pair production*

The $t\bar{t}$ production in association with other particles has substantially smaller cross sections compared to standard top-quark production modes. Nevertheless, these associated production processes offer valuable possibilities for precise tests of the SM, specifically enabling detailed studies of the top-quark couplings and EW interactions. Representative diagrams for each production channel are given in Fig. 61.2.

$t\bar{t}V$ ($V = W, Z, \gamma$): Associated $t\bar{t}$ production with vector bosons. Processes with γ and Z bosons in the final state test the neutral EW couplings of the top quark, see Fig. 61.2 (a). In $t\bar{t}W$, , on the other hand, the W-boson couples to the initial $q\bar{q}'$ state, see Fig. 61.2 (b). Predictions for $t\bar{t}W$ and $t\bar{t}Z$ are computed at complete NLO accuracy, including both QCD and EW effects, with resummation of soft emissions to NNLL accuracy in QCD [57]. Additionally, motivated by the large NLO QCD corrections, approximate NNLO QCD predictions have been obtained for $t\bar{t}W$ [58, 59]. Approximate NNLO and N^{3}LO predictions for $t\bar{t}Z$ production include, respectively, second- and third-order soft-gluon corrections added to the exact NLO QCD calculation, together with NLO EW contributions [60]. Predictions for $t\bar{t}\gamma$ are available at NLO in QCD [61].

$t\bar{t}H$: This process directly explores the top-quark Yukawa coupling. Predictions have been computed similarly to the $t\bar{t}W$ and $t\bar{t}Z$ processes, incorporating NLO corrections with soft-gluon emission resummation [57]. Recently, approximate NNLO QCD predictions have also been derived for $t\bar{t}H$ production [62].

$tt\bar{t}/\bar{t}\bar{t}t$: EW production of single t or $\bar{t}$ can be accompanied by the QCD emission of a $t\bar{t}$ pair. This leads to a final state with three top quarks. Depending on the EW single-top-quark production channel, predictions can be calculated either at LO (for tW) or at NLO (for $s-$ and t-channels) through automated codes. The LO expectation for the cross section at 14 TeV LHC is around 2 fb [63].

$t\bar{t}t\bar{t}$: The production of four top quarks at hadron colliders probes very high scales and is sensitive to higher-order EW and QCD effects [64]. Predictions have been computed to next-to-leading logarithmic (NLL') accuracy, matched to full NLO QCD and EW corrections. The NLL' corrections enhance the total production rate by approximately 26%, significantly reducing theoretical uncertainties from scale variations, which are now smaller than current experimental uncertainties [65].

Theoretical predictions for these processes are implemented in Monte Carlo event generators to at least NLO accuracy, and discussed in detail in the corresponding section in this *Review*. Many of these processes have already been observed at the LHC, and their computed cross sections are summarized in Tab. 61.3 at $\sqrt{s} = 13$ TeV.

Table 61.3: Predictions for inclusive cross sections at LHC at $\sqrt{s} = 13$ TeV for $t\bar{t}$ production in association with additional particles. The first uncertainty comes from scale variation, while the second (when present) comes from the PDF. The perturbative order refers to the highest order in QCD and EW available (aNNLO=approximated NNLO).

Process	Cross section [fb]	Perturbative order	Ref.
$t\bar{t}W$	745.3^{+37+14}_{-48-14}	aNNLO QCD +EW NLO	[59]
$t\bar{t}Z$	811^{+89+19}_{-78-19}	NLO+NNLL QCD	[57]
$t\bar{t}\gamma$	$1720^{+207+16}_{-208-16}$	NLO QCD + EW NLO	
(w/cuts)			[66]
$t\bar{t}H$	529^{+8}_{-12}	aNNLO+NNLL QCD +EW NLO	[67]
$t\bar{t}t\bar{t}$	$14.7^{+1.2}_{-2.5}$	NLO+NLL' QCD + EW NLO	[65]

61.1.4.4 *Single production*

There are three main mechanisms to produce top quarks singly in pp and $p\bar{p}$ collisions, see Fig. 61.3: t-channel ($qb \to q't$), mediated by a space-like (virtual) W boson [68], s-channel production

Int. J. Mod. Phys. A 2026.41. Downloaded from www.worldscientific.com
by UNIVERSITY OF CALIFORNIA @ BERKELEY on 09/16/26. Re-use and distribution is strictly not permitted, except for Open Access articles.

($q\bar{q}' \to t\bar{b}$) [69] mediated by a time-like W boson, and tW production ($bg \to tW^-$) [70], where the W boson is on-shell. These processes have smaller cross sections than QCD-driven $t\bar{t}$ production but offer unique sensitivity to the EW sector and top-quark couplings. Separate measurements of the s- and t-channel processes provide sensitivity to physics beyond the SM [71]. Additionally, the production of single top-quarks associated with a Z or Higgs boson is classified as *associated single top-quark production.*

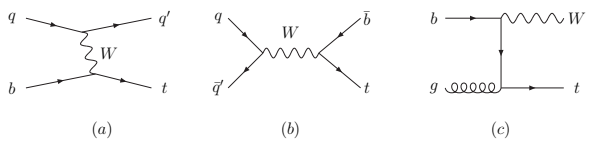

Figure 61.3: Representative Feynman diagrams for single top production (a) via t-channel, (b) via s-channel, and (c) via tW-channel.

Assuming $|V_{tb}| \gg |V_{td}|, |V_{ts}|$ (see the Section "The CKM Quark-Mixing Matrix" in this *Review*), the cross sections for single-top-quark production are proportional to $|V_{tb}|^2$. This brings the unique possibility that no additional assumptions about the number of quark families or CKM unitarity are required to extract $|V_{tb}|$.

While suppressed by the weak coupling relative to QCD $t\bar{t}$ production, t-channel single-top-quark production is kinematically enhanced, leading to sizeable cross sections at both Tevatron and LHC energies. At the Tevatron, the s-channel production is symmetric, while t-channel exhibits a forward–backward asymmetry; at the LHC, the symmetric pp initial state yields different top and antitop production rates in the t-channel.

For $m_t = 173.2$ GeV, the NNLO prediction for t-channel single top ($t + \bar{t}$) in $p\bar{p}$ collisions at $\sqrt{s} = 1.96$ TeV is [72]:

$$\sigma^{t+\bar{t}}_{t\text{-ch}} = 2.08^{+0.04}_{-0.03}\,(\text{scale})^{+0.08}_{-0.10}\,(\text{PDF})\,\text{pb}.$$

Updated NNLO predictions for $m_t = 172.5$ GeV at the LHC are given in Tab. 61.4, where the first uncertainty reflects scale variation and the second PDF and α_s uncertainties [72–74].

Finite-order expansions of resummed cross sections, including soft and collinear gluon corrections, have been computed through NNLO for single-top-quark production in the s-channel. At the Tevatron, the results for single top and antitop quarks are identical. For $\sqrt{s} = 1.96$ TeV and $m_t = 173$ GeV, the NNLO prediction is [75]:

$$\sigma^{t+\bar{t}}_{s\text{-ch}} = 1.05^{+0.001}_{-0.005}\,(\text{scale})^{+0.030}_{-0.028}\,(\text{PDF})\,\text{pb}.$$

At the LHC, the NNLO cross sections are summarized in Tab. 61.4, with uncertainties quoted from scale variation only.

Although negligible at Tevatron energies, tW production becomes sizeable at the LHC. Accurate predictions for this process are difficult to obtain as, starting at NLO in QCD, it interferes with $t\bar{t}$ production. Several schemes to proper account for this effect have been proposed [76] and implemented in MC generators [37, 77]. Approximate NNLO predictions, obtained from NNLL-resummed calculations, are available for the combined ($t + \bar{t}$) production rates, which are expected to be equal for top and antitop quarks. These predictions, summarized in Tab. 61.4, include uncertainties from scale variation and PDFs [70]. The approximate NNLO corrections enhance the cross section by about 8% relative to the NLO result.

61.1.4.5 *Associated single production*

These rare processes can probe the EW interactions of the top quark and are sensitive to potential contributions from new physics, such as anomalous couplings or effective operators. (Note that in this section, with t we mean both top and antitop quarks). Representative diagrams for each production channel are given in Fig. 61.4.

tZ: In this process, a Z boson is radiated from the top quark, the initial-state quark, or an internal W-boson line, and it can occur in all three single-top-quark production channels, with the t-channel contribution dominating. It provides direct sensitivity to anomalous tqZ and FCNC couplings [79]. At the LHC, the cross section for t-channel+Z production at $\sqrt{s} = 13$ TeV has been computed at NLO in QCD and EW [80] and is listed in Tab. 61.5.

Table 61.4: Predictions for inclusive cross sections of single top-quark production at the LHC. The first uncertainty corresponds to renormalization and factorization scale dependence, while the second is due to PDF+α_s variations.

$\sqrt{s}$ (TeV) *pp*	$\sigma^{t+\bar{t}}_{t-ch}$ (pb) (NNLO) [72–74]	$\sigma^{t+\bar{t}}_{s-ch}$ (pb) (NNLO) [78]	$\sigma^{t+\bar{t}}_{Wt-ch}$ (pb) (approx. NNLO) [70]
5.02	$30.3^{+0.4\,+0.6}_{-0.3\,-0.4}$	NA	$6.54^{+0.16\,+0.33}_{-0.14\,-0.33}$
7	$63.7^{+0.9\,+1.1}_{-0.5\,-0.7}$	$3.00^{+0.03}_{-0.03}$	$17.1^{+0.4\,+0.7}_{-0.3\,-0.7}$
8	$84.3^{+1.1\,+1.4}_{-0.7\,-0.9}$	$5.63^{+0.03}_{-0.03}$	$24.4^{+0.6\,+0.9}_{-0.5\,-0.9}$
13	$214.2^{+2.4\,+3.3}_{-1.7\,-2.0}$	$11.07^{+0.06}_{-0.03}$	$79.3^{+1.9\,+2.2}_{-1.8\,-2.2}$
13.6	$232.2^{+2.6\,+3.4}_{-1.7\,-2.2}$	$11.78^{+0.06}_{-0.04}$	$87.9^{+2.0\,+2.3}_{-1.9\,-2.4}$

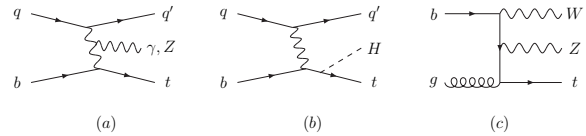

Figure 61.4: Representative Feynman diagrams for single top-quark associated production with (a) γ, Z (b) Higgs, and (c) WZ.

$t\gamma$: Photon emission in association with single-top-quark production or decay gives rise to this process, which probes the electromagnetic structure of the top-quark coupling. It is sensitive to anomalous $tq\gamma$ and dipole interactions. At the LHC, the cross section for t-channel+γ production at $\sqrt{s} = 13$ TeV has been calculated at NLO in QCD and EW [66] (see Tab. 61.5), with predictions depending on photon identification ($p_{\text{T}} > 25$ GeV, $|\eta| < 1.44$) and isolation requirements (see [66] for details).

tH: The associated production of a Higgs boson can occur through radiation from either the top quark or the intermediate W bosons. Non-trivial unitarity cancellations among diagrams make this final state highly sensitive to anomalous interactions [79], thereby playing a crucial role in global fits of top-quark EW couplings. At the LHC, the cross section for t-channel+H production at $\sqrt{s} = 13$ TeV has been calculated at NLO in QCD and EW [80] and is reported in Tab. 61.5.

tWZ: A rare mode, this process produces a single top quark together with a W and a Z boson, radiated from either initial-state quarks or intermediate propagators. The tWZ final state is sensitive to a broad range of anomalous interactions [81] and contributes to global analyses of top-quark EW couplings. At the LHC, the cross section for tWZ production at $\sqrt{s} = 13$ TeV has been computed at NLO in QCD [81] (see Tab. 61.5).

Table 61.5: Cross sections at $\sqrt{s} = 13$ TeV for $t(+\bar{t})$ in association with additional particles.

Process	Cross section [fb]	Perturbative order	Ref.
tZ (t-channel only)	805^{+45}_{-89} (scale) $^{+3}_{-3}$ (PDF)	NLO QCD+EW	[80]
$t\gamma$ (t-channel only	806^{+57}_{-66} (scale) $^{+4}_{-4}$ (PDF)	NLO QCD+EW	[66]
w/cuts)	806^{+57}_{-66} (scale) $^{+4}_{-4}$ (PDF)	NLO QCD+EW	[66]
tH (t-channel only)	$71.3^{+5.2}_{-7.7}$ (scale) $^{+0.3}_{-0.3}$ (PDF)	NLO QCD+EW	[80]
tWZ	$106.8^{+5.3}_{-6}$(scale)	NLO QCD	[81]

Int. J. Mod. Phys. A 2026.41. Downloaded from www.worldscientific.com
UNIVERSITY OF CALIFORNIA @ BERKELEY on 09/16/26. Re-use and distribution is strictly not permitted, except for Open Access articles.

61.2 Top-quark and precision SM tests

The first direct observation of the top quark was made in 1995 at the Tevatron in $p\bar{p}$ collisions at $\sqrt{s} = 1.8$ TeV by the CDF and DØ experiments [82, 83], followed by more precise measurements at $\sqrt{s} = 1.96$ TeV. Since 2010, the ATLAS and CMS experiments at the LHC have extended top-quark studies to higher energies, performing measurements in pp collisions at $\sqrt{s} = 5.02, 5.36, 7, 8, 13$, and 13.6 TeV. The LHCb experiment has further contributed by observing top-quark production in the forward region [84], a phase-space domain inaccessible to other detectors. Dedicated low-energy runs at $\sqrt{s} = 5.02$ TeV and $\sqrt{s} = 5.36$ TeV in $PbPb$ collisions [85–87] and at $\sqrt{s} = 8.16$ TeV in proton–lead (pPb) collisions [88, 89] have provided a novel and theoretically precise probe of nuclear parton distribution functions.

The experiments have collected approximately 10 fb^{-1} of data at the Tevatron and substantial datasets at the LHC: 255 pb^{-1} at 5 TeV, nearly 5 fb^{-1} at 7 TeV, 20 fb^{-1} at 8 TeV, 139 fb^{-1} at 13 TeV, and about 250 fb^{-1} at 13.6 TeV to date. These diverse datasets enable unprecedented precision in a wide range of top-quark measurements, including production mechanisms mediated by EW and QCD interactions, precise determinations of the top-quark mass, detailed studies of production dynamics such as $t\bar{t}$ spin correlations and charge asymmetries, extensive measurements of differential cross sections, investigations of the tWb vertex, and constraints on Wilson coefficients describing physics beyond the SM.

The top-quark mass has now been measured with a precision better than 0.2%, making it the most accurately determined quark mass to date [1]. Combined with precision measurements of the W-boson mass and Higgs-boson properties, these results provide stringent and comprehensive tests of the SM.

Significant progress has also been achieved in associated production processes involving the top quark, such as $t\bar{t}b\bar{b}$, $t\bar{t}t\bar{t}$, $t\bar{t}\gamma$, $t\bar{t}Z$, $t\bar{t}H$, tH, tZq, $t\gamma q$, and tWZ. Most of these processes have now been observed, including the recent observation of tWZ production, while tH associated production remains beyond current experimental reach. These channels probe novel aspects of top-quark physics, including its EW couplings to neutral gauge bosons and possible four-top production mediated by new contact interactions. The measurements of tH and $t\bar{t}H$ production are discussed in the *Review* "Status of Higgs Boson Physics" in Sec. 11.3.5.

Recent pioneering analyses have begun to explore quantum entanglement phenomena in top-quark pair production, and an excess has been reported compatible with a pseudoscalar quasi-bound state [90, 91], discussed further in chapters 61.2.5.3 and 61.2.5.5. In parallel, numerous searches for BSM physics exploit the top quark as a sensitive probe, either through its production dynamics or through decays involving hypothetical new particles.

The following sections review the current status of top-quark measurements and discuss their implications for our broader understanding of fundamental particle physics.

61.2.1 *Cross-section measurements of pair production*

Top quarks decay before they hadronize, and their presence is inferred from detecting their decay products. Each top quark decays almost exclusively to a W boson and a b quark. The $t\bar{t}$ final states are categorized based on the decays of the W bosons:

- **All-hadronic (AH) channel (45.7%):** $t\bar{t} \to W^+ b\, W^- \bar{b} \to q\bar{q}'\, b\, q''\bar{q}'''\bar{b}$
- **Lepton+jets (LJ) channel (43.8%):** $t\bar{t} \to W^+ b\, W^- \bar{b} \to q\bar{q}'\, b\, \ell^- \bar{\nu}_\ell\, \bar{b}$ or $\ell^+ \nu_\ell b\, q\bar{q}'\bar{b}$
- **Dilepton (DL) channel (10.5%):** $t\bar{t} \to W^+ b\, W^- \bar{b} \to \ell^+ \nu_\ell b\, \ell'^- \bar{\nu}_{\ell'}\, \bar{b}$

The branching fractions in parentheses are computed assuming lepton universality for the decay of the W-boson. The symbol ℓ refers to any charged lepton (e, μ, or τ). However, most analyses focus on electrons and muons due to the challenges associated with reconstructing τ leptons. The symbol q refers to any quark flavor other than a b quark. Final-state quarks hadronize into jets, whose reconstruction depends on the decay kinematics and the analysis algorithm. Neutrinos are not detected directly but are inferred as an imbalance in the event transverse momentum.

In general, the top-quark measurements extracted from $t\bar{t}$ are categorized depending on the number of leptons in the final state as dilepton (DL), lepton+jets (LJ), and all-hadronic (AH) decay channels. The DL channel offers the highest signal purity but is affected by larger statistical uncertainties due to its small branching ratio. The DL($e\mu$) channel specifically refers to events containing one electron and one muon in the final state. In contrast, the LJ channel benefits from a larger branching ratio and better statistical precision, although it is more susceptible to background contamination and larger systematic uncertainties. As data samples increased from the Tevatron to the LHC, the relative precision of these channels improved, with the DL channel often becoming the most precise. Measurements in the AH channel are less common due to the overwhelming QCD multijet background, which is challenging to model and suppress.

In some events, the top quarks are produced with high transverse momentum ($p_{\mathrm{T}} > 400$–500 GeV), resulting in a **boosted** topology where the decay products become collimated. In this case, traditional **resolved** analyses, which reconstruct separate jets, may not resolve individual decay products. Instead, jet substructure techniques are employed to identify large-radius jets consistent with hadronic top decays. Consequently, $t\bar{t}$ final states are further classified into *resolved* and *boosted* categories depending on the top-quark p_{T}.

Experimentally, the measurement of the $t\bar{t}$ production cross section begins with the selection of collision events consistent with the expected $t\bar{t}$ signatures described above. After event selection, background contributions from processes that mimic the signal, such as W/Z+jets, single-top production, QCD multijet and nonprompt-lepton events, and diboson production, are carefully estimated. These estimates are typically obtained using data-driven techniques or Monte Carlo simulations, which are validated against control regions in the data.

To distinguish genuine $t\bar{t}$ events from background processes, analyses employ a variety of discriminating methods, ranging from simple event-counting or kinematic selections to advanced multivariate classifiers such as boosted decision trees, neural networks, or matrix-element techniques. Once suitable discriminants are defined, the signal yield and corresponding cross section are extracted using statistical inference methods, including template fits, profile likelihood fits, or simultaneous maximum-likelihood fits across analysis categories. These inference techniques optimize the use of information in the data and improve the overall precision of the measurement.

Subsequently, detector effects such as trigger efficiency, acceptance, and event-selection efficiency must be corrected to obtain the true $t\bar{t}$ production rate. In simple event-counting analyses, these corrections are typically applied multiplicatively to the observed signal yield, using factors derived from detailed detector simulations calibrated with data. In more sophisticated analyses, such effects are incorporated directly into the signal modeling used for the statistical inference, through templates or parameterized response functions, which allows the fit to constrain the corresponding uncertainties from data and improves the overall measurement precision.

Cross-section measurements rely on a specific Monte Carlo model of $t\bar{t}$ production and decay, which defines the kinematic properties, acceptance, and efficiency of the signal. These simulations assume a value for the top-quark mass, typically 172.5GeV, and a particular modeling of QCD radiation, hadronization, and parton showering. The assumed mass and modeling both affect the acceptance corrections and, in some cases, the shapes of key kinematic and topological distributions used in the analysis. The precision of the measurements, therefore, benefits greatly from Monte Carlo generators that accurately reproduce the observables studied in data.

Comprehensive evaluations of systematic uncertainties, including detector performance and object reconstruction, background and signal modeling uncertainties, and luminosity measurement accuracy, are integral to ensuring the reliability and robustness of the measurement.

Systematic uncertainties related to object reconstruction include the jet energy scale (JES), b-tagging, and lepton identifi-

Int. J. Mod. Phys. A 2026.41. Downloaded from www.worldscientific.com
by UNIVERSITY OF CALIFORNIA @ BERKELEY on 09/16/26. Re-use and distribution is strictly not permitted, except for Open Access articles.

cation. The JES uncertainty accounts for possible mismatches between the true jet energy and its reconstructed value in the detector, affecting all measurements that rely on jet kinematics. The b-tagging systematic reflects differences between data and simulation in the efficiency of correctly identifying b-jets or misidentifying other jet flavors. Since nearly all top-quark measurements rely on b-tagging, this uncertainty appears prominently in most analyses. The lepton identification uncertainty accounts for potential discrepancies between data and simulation in the efficiency of reconstructing and identifying electrons or muons, and tends to dominate in analyses with multiple leptons.

A dominant source of systematic uncertainty in these measurements is the integrated luminosity, which is typically quoted separately from other systematic uncertainties. To mitigate this, some analyses have measured the $t\bar{t}$ production cross section relative to the Z boson production cross section, thus reducing the dependence on the absolute luminosity estimate. This is typically done in the early stages of data-taking, when the luminosity uncertainty is still large.

Finally, the measured $t\bar{t}$ cross section is interpreted by comparing it with theoretical predictions. Agreement or deviation from these predictions provides essential tests of the SM and opens opportunities to explore potential new physics phenomena.

Figure 61.5 summarizes the measured $t\bar{t}$ production cross sections from Tevatron and LHC collisions at various center-of-mass energies, compared to theoretical predictions at NNLO+NNLL accuracy.

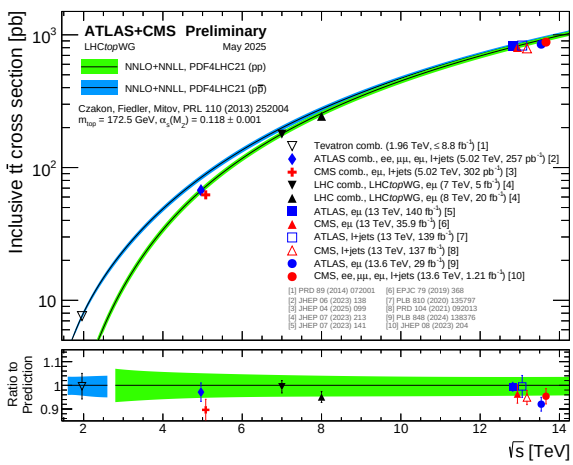

Figure 61.5: Measured and predicted $t\bar{t}$ production cross sections from Tevatron energies in $p\bar{p}$ collisions to LHC energies in pp collisions. The LHCtopWG working group kindly provides the plot, status as of May 2025, see `https://twiki.cern.ch/twiki/bin/view/LHCPhysics/LHCTopWGSummaryPlots`.

Studies of $t\bar{t}$ production in single-, double-, or, more recently, even triple-differential measurements are essential. Such measurements allow increasingly stringent tests of perturbative QCD as a description of the production mechanism and, in combination with other data, facilitate the extraction of PDFs. Measurements of the differential $t\bar{t}$ cross section also allow for the extraction of m_t, α_s, and the top Yukawa coupling to the Higgs boson. Moreover, such measurements enhance sensitivity to possible new physics contributions, particularly now that NNLO predictions for the main differential observables in $t\bar{t}$ production are available [92] and have been independently confirmed [45]. Finally, precise differential results also reduce uncertainties in modeling $t\bar{t}$ production as a background in other SM measurements and in searches for rare processes or physics beyond the SM.

Differential cross sections are typically determined by selecting candidate events, reconstructing their kinematics, and unfolding the measured event to the parton level, binned in kinematic variables to correct for detector resolution, acceptance, and migration effects. While bin-by-bin unfolding is used in some analyses, others apply more sophisticated approaches. The most commonly employed methods include iterative Bayesian unfolding (IBU) [93], often implemented through the `RooUnfold` package [94], and profile-likelihood unfolding [95,96]. Alternative techniques, such as singular value decomposition [97] and maximum likelihood fits [98], are also utilized. A general observation of $t\bar{t}$ differential measurements is that the measured top-quark p_{T} spectrum tends to be significantly softer than the corresponding NLO+PS theoretical predictions presented in the existing literature, while the agreement improves significantly when compared to NNLO+PS predictions [43].

At the Tevatron, both the CDF and DØ collaborations evolved from an initial search program aimed at discovering the top quark to performing precise measurements of the inclusive $t\bar{t}$ production cross section. Table 61.6 summarizes the earliest $t\bar{t}$ measurements, the most precise individual results, and the final combination.

The latest measurements of the $t\bar{t}$ production cross section from the DØ collaboration [101] and the CDF collaboration [102] assume a top-quark mass of 172.5 GeV, while earlier measurements assumed 175 GeV. Combining these measurements using the Best Linear Unbiased Estimator (BLUE) method, the Tevatron collaborations report a combined cross section: $\sigma_{t\bar{t}} = 7.60 \pm 0.20\,(\text{stat.}) \pm 0.29\,(\text{syst.}) \pm 0.21\,(\text{lumi.})$ pb, which is in agreement with the SM prediction calculated at the same top-quark mass [44]. The correlation coefficient between the measurements from the two experiments is determined to be 17%.

Additionally, CDF has measured the $t\bar{t}$ production cross section in the DL channel, including one hadronically decaying τ lepton, obtaining $\sigma_{t\bar{t}} = 8.1 \pm 2.1$ pb. By separately identifying the single-τ and di-τ leptons, CDF extracted the branching fraction of the top quark into a τ lepton, τ neutrino, and b-quark as $(9.6 \pm 2.8)\%$ [104]. CDF has also measured the $t\bar{t}$ production cross section normalized to the Z boson production cross section, thus reducing the impact of luminosity uncertainties [105].

The ATLAS and CMS experiments at the LHC employ similar techniques to measure the $t\bar{t}$ production cross section in pp collisions. The most precise determinations are typically obtained in the DL channel, particularly in the $e\mu$ final state, owing to the large statistical yield and high purity of this channel. Numerous measurements have been performed across a wide range of center-of-mass energies, including pPb and $PbPb$ collisions, in different channels, and using a variety of techniques. The uncertainties are divided into statistical, systematic, luminosity, and beam components. In CMS measurements, the uncertainty associated with the beam energy is typically included within the quoted systematic uncertainty. As the beam energy determination improved, this convention was also adopted in later ATLAS measurements. The systematic uncertainties strongly depend on the final state and include experimental contributions, related to the identification of objects and background estimates, as well as theoretical contributions that rely on the modeling assumptions used to extract the measurement.

Most results are summarized in Tab. 61.7 and found to be consistent with theoretical predictions. A description of the measurements at different collision energies follows.

61.2.1.1 *Measurements at* $\sqrt{s} = 5.02$ *TeV*

In a dedicated LHC run at this energy, both ATLAS and CMS measured the $t\bar{t}$ production cross section in the DL and LJ channels. Each experiment subsequently combined the results from its individual channels. The ATLAS combination yields $\sigma_{t\bar{t}} = 67.5 \pm 0.9\,(\text{stat.}) \pm 2.3\,(\text{syst.}) \pm 1.1\,(\text{lumi.}) \pm 0.2\,(\text{beam})$ pb, with the dominant uncertainty arising from background modeling [106]. The corresponding CMS combination gives $\sigma_{t\bar{t}} = 62.3 \pm 1.5\,(\text{stat.}) \pm 2.4\,(\text{syst.}) \pm 1.2\,(\text{lumi.})$ pb, where the main contributions to the uncertainty come from the integrated luminosity and from the b-tagging scale factors for b-jets [107]. The two measurements are consistent with each other and with the SM prediction within two standard deviations. These measurements provide important constraints on the proton PDFs at large Bjorken-x.

61.2.1.2 *Measurements at* $\sqrt{s} = 7$ *TeV*

At this energy, a wide variety of final states and methods were explored. The ATLAS measurement in the DL($e\mu$) chan-

Int. J. Mod. Phys. A 2026.41. Downloaded from www.worldscientific.com
UNIVERSITY OF CALIFORNIA @ BERKELEY on 09/16/26. Re-use and distribution is strictly not permitted, except for Open Access articles.

Table 61.6: Summary of $t\bar{t}$ cross-section measurements at the Tevatron.

Experiment [Ref.]	Lumi. (fb^{-1})	$\sqrt{s}$ (TeV)	Topology	Measurement (pb)
CDF (first observation) [82]	0.0067	1.8	LJ	$6.8^{+3.6}_{-2.4}$
DØ (first observation) [83]	0.0050	1.8	LJ	5.9 ± 1.7
CDF [99]	0.00109	1.8	DL+LJ	$6.5^{+1.7}_{-1.4}$
DØ [100]	0.00125	1.8	DL+LJ	5.9 ± 1.4
DØ [101]	9.7	1.96	DL+LJ	$7.26^{+0.58}_{-0.51}$
CDF [102]	8.8	1.96	DL	7.09 ± 0.84
CDF [103]	4.3–8.8	1.96	DL+LJ+AH	7.63 ± 0.50
DØ [103]	5.3–9.7	1.96	DL+LJ+AH	7.56 ± 0.59
Tevatron [103]	4.3–9.7	1.96	DL+LJ+AH	7.60 ± 0.41

nel yields $\sigma_{t\bar{t}} = 182.9 \pm 3.1(\text{stat.}) \pm 4.2(\text{syst.}) \pm 3.6(\text{lumi.}) \pm 3.3(\text{beam})$ pb [108], with the dominant uncertainty arising from the modeling of $t\bar{t}$ production, evaluated by comparing different Monte Carlo generators and hadronization models. CMS obtained its most precise measurement also in the DL($e\mu$) final state, using a binned likelihood fit to multi-dimensional distributions related to b-quark jets and other jets identified in the event. The measured cross-section is $\sigma_{t\bar{t}} = 173.6 \pm 2.1(\text{stat.})^{+4.5}_{-4.0}(\text{syst.}) \pm 3.8(\text{lumi.})$pb [109].

In the LJ channel, ATLAS utilized a three-class, multidimensional event classifier based on support vector machines to distinguish $t\bar{t}$ from $W/Z+b\bar{b}$ and other background processes, obtaining $\sigma_{t\bar{t}} = 168.5 \pm 0.7(\text{stat.})^{+6.2}_{-5.9}(\text{syst.})^{+3.4}_{-3.2}(\text{lumi.})$ pb [110].

Additional measurements using partial datasets by ATLAS and CMS played a crucial role in refining techniques and enhancing data understanding. These studies were carried out in several channels, including e/μ+jets [111], DL [112] [113], AH [114], lepton+τ [115], hadronic τ+lepton [116], and τ+jets [117] [118]. These results are consistent with theoretical predictions, although they are characterized by larger uncertainties due to limited data statistics and systematic effects.

Furthermore, both collaborations have jointly published a combined "legacy" cross-section measurement at $\sqrt{s} = 7$ TeV, which is also included in Tab. 61.7.

The first observation of $t\bar{t}$ production in the forward region of pp collisions was performed by LHCb using the e+jets and μ+jets channels. The inclusive $t\bar{t}$ production cross section measured in the fiducial region is $\sigma_{t\bar{t}} = 239 \pm 53(\text{stat.}) \pm 33(\text{syst.}) \pm 24(\text{theo.})$fb [84]. This result is in agreement with the SM predictions of 180^{+51}_{-41} fb at 7 TeV obtained at NLO using MCFM program [119].

ATLAS and CMS measured single-differential $t\bar{t}$ cross sections for the jet multiplicity, the top-quark p_{T}, and m_t, and the rapidity of the top quark as well as of the $t\bar{t}$ system or kinematic properties of the final-state charged leptons and jets associated with b-quarks. While CMS finds in general good agreement with the pQCD calculations [120–122], ATLAS finds the data to be softer, in particular in the $t\bar{t}$ mass and the top-quark p_{T} than the ALPGEN+HERWIG generator. Also, some disagreement in the rapidity spectrum is observed, indicating a preference for the HERAPDF1.5 PDF set over CT10 [123–125].

61.2.1.3 *Measurements at $\sqrt{s} = 8$ TeV*

The DIL($e\mu$) channel provided the most precise measurements of the $t\bar{t}$ production cross section at this energy, which is included in Tab. 61.7. ATLAS determined $\sigma_{t\bar{t}} = 242.9 \pm 1.7(\text{stat.}) \pm 5.5(\text{syst.}) \pm 5.1(\text{lumi.}) \pm 4.2(\text{beam})$ pb through a simultaneous extraction of the b-tagging efficiency [126]. CMS conducted a measurement by fitting multidimensional final-state distributions involving identified b-quark jets and other jets, obtaining $\sigma_{t\bar{t}} = 244.9 \pm 1.4(\text{stat.})^{+6.3}_{-5.5}(\text{syst.}) \pm 6.4(\text{lumi.})$ pb [109,127]. This measurement was also used to determine the m_t^{pole} and set constraints on potential new physics models.

In the LJ channel, ATLAS modeled the W+jets background using Z+jets data and employed neural networks to classify events across three regions defined by jet and b-jet multiplicities. This analysis resulted in $\sigma_{t\bar{t}} = 248.3 \pm 0.7(\text{stat.}) \pm 13.4(\text{syst.}) \pm 4.7(\text{lumi.})$ pb [128]. CMS performed a template fit to the invariant mass distribution M_{lb}, extracting from it $\sigma_{t\bar{t}} = 228.5 \pm 3.8(\text{stat.}) \pm 13.7(\text{syst.}) \pm 6.0(\text{lumi.})$ pb [129].

Additionally, both ATLAS and CMS measured the cross section in the hadronic τ+jets channel, producing consistent but less precise results [130, 131]. CMS also obtained a measurement in the AH final state [132].

ATLAS and CMS combined their DL($e\mu$) channel results [133], performing cross-section ratio studies to verify the internal consistency of the measurements and to reduce sensitivity to specific systematic uncertainties. Ratios of measurements taken at $\sqrt{s} = 7$ TeV and 8 TeV provided precise tests of perturbative QCD and constraints on PDFs. Additionally, ratios between $t\bar{t}$ and Z-boson production cross sections were analyzed to minimize luminosity uncertainties while maintaining sensitivity to the gluon-to-quark PDF ratio. These combined analyses also enabled the extraction of m_t^{pole} and the determination of α_s.

LHCb measured $t\bar{t}$ production in the forward region of pp collisions at 8 TeV in the e+jets and μ+jets channels. The measured cross section is $\sigma_{t\bar{t}} = 289 \pm 43(\text{stat.}) \pm 40(\text{syst.}) \pm 29(\text{theo.})$ fb [84], which agrees with the NLO SM prediction of 312^{+83}_{-68} fb calculated using MCFM. Additionally, the measured differential yield distributions and charge asymmetry are consistent with SM predictions.

ATLAS measured single-differential cross sections in the DL and LJ channels, analyzing observables such as m_t, top-quark p_{T}., rapidity of the $t\bar{t}$ system, and other event-level kinematic variables [134,135]. These measurements demonstrate good or fair agreement with theoretical predictions across a wide kinematic range, with predictions beyond NLO accuracy notably improving the consistency at high p_{T}.

CMS performed extensive measurements of normalized differential cross sections for $t\bar{t}$ production in the LJ channel, examining kinematic variables such as missing transverse energy, scalar sums of jet p_{T}, scalar sums of the p_{T} of all event objects, and the p_{T} of the leptonically decaying W bosons originating from top-quark decays [121]. Furthermore, CMS has measured differential cross sections in both the LJ and DL decay channels, focusing on kinematic properties of charged leptons, jets associated with b quarks, top quarks, and the entire $t\bar{t}$ system, comparing the results to predictions at approximate NNLO precision [136]. Notably, in the DL($e\mu$) channel, CMS's normalized double-differential cross-section measurements as a function of paired kinematic observables significantly impacted the determination of gluon distributions in PDF fits [137].

Additionally, ATLAS and CMS carried out targeted differential $t\bar{t}$ measurements in the boosted topology using the LJ channel. In these analyses, the hadronically decaying top quark was reconstructed as a single large-radius jet and identified as a top candidate through jet substructure techniques. ATLAS focused on events with hadronic top quarks of $p_{\mathrm{T}} > 300$ GeV [138], while CMS used a threshold of $p_{\mathrm{T}} > 400$ GeV [139]. Predictions from NLO and LO matrix-element calculations interfaced with parton-shower Monte Carlo generators generally overestimate the measured cross sections. This can be explained by the softer p_{T} spectra in the data compared to the simulation.

Int. J. Mod. Phys. A 2026.41. Downloaded from www.worldscientific.com by UNIVERSITY OF CALIFORNIA @ BERKELEY on 09/16/26. Re-use and distribution is strictly not permitted, except for Open Access articles.

61.2.1.4 *Measurements at* $\sqrt{s} = 13$ *TeV*

The most precise measurement of the $t\bar{t}$ cross section is obtained in the DL($e\mu$) final state with b-tagged jets by ATLAS, yielding $\sigma_{t\bar{t}} = 829 \pm 1(\text{stat.}) \pm 13(\text{syst.}) \pm 8(\text{lumi.}) \pm 2(\text{beam})$ pb [140]. This analysis includes differential and double-differential measurements of kinematic variables of leptons from top-quark decays, comparing results against predictions from several Monte Carlo generators. Although no single prediction matches all distributions, reweighting the simulated $t\bar{t}$ events to align with the top-quark p_{T} distribution calculated at NNLO significantly improves agreement, especially for lepton p_{T} distributions.

CMS measured the $t\bar{t}$ cross section in the DL channel using a likelihood fit, reporting $\sigma_{t\bar{t}} = 803 \pm 2(\text{stat.}) \pm 25(\text{syst.}) \pm 20(\text{lumi.})$ pb [141]. This result facilitated the extraction of the m_t^{pole} and $\overline{\text{MS}}$ schemes at NNLO and allowed the determination of α_s.

In the LJ channel, ATLAS measured the inclusive $t\bar{t}$ cross section using a profile-likelihood fit, obtaining $\sigma_{t\bar{t}} = 830 \pm 0.4(\text{stat.}) \pm 36(\text{syst.}) \pm 14(\text{lumi.})$ pb [142]. CMS measured this channel, dividing events into regions based on top-quark p_{T} and b-tag scores, and employed a combined χ^2 fit with migration matrices, measuring $\sigma_{t\bar{t}} = 791 \pm 1(\text{stat.}) \pm 21(\text{syst.}) \pm 14(\text{lumi.})$ pb, noting generally good agreement with SM predictions except for certain double-differential distributions [143].

ATLAS utilized partial datasets in the DL $e\mu$ channel with one or two b-tags to determine the m_t^{pole}, compute ratios and double ratios of $t\bar{t}$ to Z cross sections across different energies, and measure absolute and normalized differential cross sections as functions of LJ and DL kinematic variables [144]. A pioneering measurement of inclusive and normalized differential cross sections in the LJ channel was also conducted by CMS [145]. Other significant results using partial datasets include CMS measurements in the DL channel featuring a hadronically decaying τ [146].

CMS-TOTEM performed the first search for the central exclusive production of $t\bar{t}$ pairs using proton-tagged events with an integrated luminosity of 29.4 fb^{-1}. The top-quark pair decay products were reconstructed by the central CMS detector, while forward protons were measured using the TOTEM precision proton spectrometer. An observed (expected) upper limit on the production cross section of 0.59 (1.14) pb was established at a 95% C.L. for proton collisions with fractional momentum losses ranging from 2% to 20% [147].

LHCb measured the forward production of $t\bar{t}$ in the μeb final state, consisting of a muon, an electron, and a b-jet. The cross section is measured in a fiducial region defined by both leptons p_{T} and pseudorapidities as well as their angular separation, the b-jet p_{T} and its angular separation from the leptons, yielding $\sigma_{t\bar{t}} = 126 \pm 19(\text{stat.}) \pm 16(\text{syst.}) \pm 5(\text{lumi.})$fb [148].

Single- and double-differential cross-section measurements for $t\bar{t}$ production have been extensively performed in various channels. Both ATLAS and CMS have performed high-precision measurements of these cross sections in the DL and LJ channels, probing the kinematic properties of leptons, b-quark jets, top quarks, top-quark pairs, and jet multiplicities [149–153]. All results are compared with SM predictions from Monte Carlo simulations with NLO accuracy in QCD at matrix-element level interfaced to parton-shower simulations. While these measurements generally agree well with theoretical predictions, notable discrepancies have been observed in specific DL analyses. CMS has used these results to constrain the top-quark chromomagnetic dipole moment [154] within an EFT framework at NLO QCD, and to extract $t\bar{t}$ and leptonic charge asymmetries [155].

CMS performed the first triple-differential measurement of the $t\bar{t}$ production cross section in the dilepton (DL) channel, as a function of the invariant mass and rapidity of the $t\bar{t}$ system and the multiplicity of additional jets, using a partial Run 2 dataset. From this measurement, α_s, m_t^{pole}, and PDFs were extracted [156]. With the full Run 2 dataset, CMS measured differential $t\bar{t}$ and $t\bar{t}$+jets cross sections as functions of up to three kinematic variables, unfolded to both parton and particle levels. Comparisons with QCD predictions show that theoretical calculations do not consistently reproduce the data, with the most considerable deviations appearing in multi-differential observables. Predictions beyond NLO provide similar or improved agreement for top-quark and $t\bar{t}$ observables, while improvements for lepton and b-jet variables remain limited. The observed dependence on PDF choice indicates that these measurements can provide valuable input to future global PDF fits [157].

ATLAS measured absolute and normalized differential cross sections for the $t\bar{t}$ process in the $e\mu$ DL channel as functions of different observables. Also, it provided complementary measurements of $e\mu b\bar{b}$ production, treating both $t\bar{t}$ and Wt as signal. Comparisons with event generator predictions show that state-of-the-art generators such as Powheg MiNNLO or Powheg bb4l better model the lepton kinematics than the Powheg hvq process traditionally used for LHC physics analyses. These precise measurements provide input that can be used to further refine the modeling of the top quark production at hadron colliders [158].

ATLAS has performed measurements in the AH channel, examining the resolved regime with individually reconstructed jets [159], and measuring differential cross sections as a function of various kinematic properties of the top quarks and the overall $t\bar{t}$ system, both at the stable-particle level within a fiducial phase space and at the parton level in the full phase space.

In boosted topologies, CMS and ATLAS have performed dedicated analyses of $t\bar{t}$ cross sections as a function of top-quark and $t\bar{t}$ system kinematics. CMS measured these cross sections in the AH and LJ channels using large-radius jets with b-tags, finding absolute cross sections notably lower than theoretical predictions [160]. ATLAS carried out similar measurements in these channels, focusing on high-p_{T} hadronic decays, characterizing additional radiation, and setting limits on Wilson coefficients describing potential physics beyond the SM [161]. Mild discrepancies with the data were observed in the modeling of additional radiation. ATLAS has also measured differential $t\bar{t}$ cross sections in AH events in boosted topologies [162]. CMS has further performed single- and double-differential measurements in the LJ channel, categorized by top-quark p_{T}, boosted versus resolved topologies, and b-tagging scores, extending momentum measurements well into the TeV range [143].

Several differential $t\bar{t}$ cross-section measurements have been performed to aid in the tuning of Monte Carlo generators. ATLAS measured one- and two-dimensional differential cross sections for eight jet substructure variables, defined using charged jet components and corrected for detector effects [140, 163]. QCD predictions agree well with measured energy-flow variables, whereas discrepancies arise for variables sensitive to the three-body structure of top-quark jets. Additionally, observables sensitive to color reconnection effects in top-quark pair-production events, such as charged-particle multiplicity and scalar sums of charged-particle p_{T}, were measured and unfolded to the stable-particle level. These data disfavor certain color reconnection models, informing future Monte Carlo parameter optimizations [164].

Furthermore, ATLAS measured observables related to b-quark fragmentation into b-hadrons. Observables characterizing longitudinal and transverse momentum distributions of b-hadrons within jets were corrected for detector effects. The unfolded results were compared to various Monte Carlo generators, showing varying levels of agreement. These measurements complement similar results from e^+e^- collider experiments, where b-quarks originate from color-singlet Z/γ^* states [165].

61.2.1.5 *Measurements at* $\sqrt{s} = 13.6$ *TeV*

The LHC began colliding protons at $\sqrt{s} = 13.6$ TeV in 2022 and is expected to continue until mid-2026. ATLAS and CMS have already performed inclusive $t\bar{t}$ cross-section measurements using partial Run 3 datasets at this energy.

The first result was reported by the CMS collaboration using 1.21 fb^{-1} of data in events in the LJ channel [166]. Events were categorized according to lepton flavor and multiplicity, the number of jets, and the number of b-tagged jets, and the cross section was extracted from a profile-likelihood fit. CMS measured $\sigma_{t\bar{t}} = 881 \pm 23$ (stat+syst) ± 20 (lumi) pb.

ATLAS performed a complementary measurement in the DIL($e\mu$) final state with b-tagged jets using 29 fb^{-1} of data [167]. The result, $\sigma_{t\bar{t}} = 850 \pm 3$ (stat.) ± 18 (syst.) ± 20 (lumi.) pb, corresponds to a relative uncertainty of 3.2%, dominated by the

Int. J. Mod. Phys. A 2026.41. Downloaded from www.worldscientific.com
UNIVERSITY OF CALIFORNIA @ BERKELEY on 09/16/26. Re-use and distribution is strictly not permitted, except for Open Access articles.

luminosity calibration. To reduce its impact, ATLAS also extracted the ratio of $t\bar{t}$ to Z+jets production, obtaining $R_{t\bar{t}/Z} = 1.145 \pm 0.003$ (stat.) ± 0.021 (syst.) ± 0.002 (lumi.) with a relative uncertainty of 1.9%, benefitting from cancellations of common systematic effects.

Both ATLAS and CMS results are consistent with SM expectations and the NNLO+NNLL prediction, and already achieve percent-level precision despite being based on early Run 3 datasets.

61.2.2 *Cross-section measurements of associated pair production*

The associated production of a $t\bar{t}$ pair with an additional particle ($t\bar{t}X$, with $X = \gamma$, W, Z, H, top quarks or jets) provides direct probes of the top-quark couplings. The $t\bar{t}H$ process offers the most direct access to the top–Higgs Yukawa coupling, while $t\bar{t}Z$ and $t\bar{t}W$ test the EW couplings of the top quark and are sensitive to anomalous interactions in the EFT framework.

Measurements typically require the reconstruction of a $t\bar{t}$ final state in the DL or LJ channels, together with the specific signature of the associated particle (isolated photon, additional leptons, $b\bar{b}$ pair from $H \to b\bar{b}$, or extra jets), and employ multivariate techniques to separate signal from background. CDF reported the first measurement of the associated $t\bar{t}\gamma$ production, while studies of $t\bar{t}W$, $t\bar{t}Z$, $t\bar{t}H$, and $t\bar{t}t\bar{t}$ processes were initiated at the LHC. Evidence and subsequent observations of several of these processes began to emerge during Run 1.

This has become a very active area of research, with many new associated production processes observed in recent years. As larger datasets are collected, these measurements are becoming increasingly precise, and analyses are moving toward differential cross sections, which provide enhanced sensitivity to EFT coefficients.

The next section is organized by associated production processes, beginning with the most common production channel and progressing to increasingly rare ones.

61.2.2.1 *Associated pair production with jets*

The production of $t\bar{t}$ in association with jets, denoted as $t\bar{t}$+jets, where the additional jets originate from the fragmentation of quarks of any flavor or gluons, offers a valuable probe of QCD radiation in a multi-scale environment. Within this context, the subset of events involving additional b-quarks, $t\bar{t}+b$-jets, is of particular interest due to the added complexity introduced by heavy-flavor production. Although NLO QCD calculations are available for both $t\bar{t}$+jets and $t\bar{t} + b\bar{b}$ final states [170], these predictions are subject to sizable theoretical uncertainties. A major source of uncertainty lies in the choice of factorization and renormalization scales, which is complicated by the presence of at least two relevant physical scales: the m_t and the p_{T} of the additional jets. The measurements of $t\bar{t}$+jets offer useful constraints for tuning theoretical models of QCD radiation in $t\bar{t}$ events.

Measurements are usually performed in fiducial regions and unfolded to the particle level to enable direct comparisons with NLO calculations and Monte Carlo simulations.

At $\sqrt{s} = 7$ TeV, ATLAS performed a study of $t\bar{t}$ production with a veto on central jet activity, measuring the fraction of events that pass the jet veto as a function of the p_{T} threshold across multiple rapidity intervals [171]. Following, ATLAS measured the fiducial $t\bar{t}$ production cross section as a function of jet multiplicity, including up to eight jets, in both the LJ and DL decay channels [172]. The precision of these measurements ranged from approximately 10% to 30%, with the dominant uncertainties arising from background modeling at low jet multiplicities and uncertainties in the jet energy scale at higher multiplicities.

CMS conducted similar measurements of normalized differential $t\bar{t}$ cross sections as a function of jet multiplicity in the LJ and DL channels [122]. In the LJ channel, the cross section was studied as a function of the number of additional jets, while in the DL channel, the fraction of events with no additional jets above a specified threshold was measured. Comparisons with perturbative QCD predictions revealed no significant deviations.

At $\sqrt{s} = 8$ TeV, CMS extended these studies with measurements of absolute and normalized differential $t\bar{t}$+jets cross sections in the DL channel, exploring various jet p_{T} thresholds and the kinematics of the leading additional jets [173]. The fraction of events without additional jets was also determined as a function of the p_{T} of the leading additional jet and the scalar sum of the transverse momenta of all additional jets. These results were compared with predictions from a range of perturbative QCD event generators and NLO calculations, and were found to agree within uncertainties.

ATLAS performed studies in the DL($e\mu$) channel with two identified b-jets and measured the multiplicity and kinematic properties of additional jets for several p_{T} thresholds [174]. Normalized differential cross sections were reported for the five highest-p_{T} additional jets, as well as gap fraction observables, defined as the fraction of events lacking additional jets in a central rapidity region, as functions of jet p_{T} thresholds or the scalar p_{T} sum. These observables were also explored in different regions of the $e\mu b\bar{b}$ system invariant mass. After correcting for detector effects, the results were found to be largely consistent with LO and NLO event generator predictions, provided suitable parameter settings were used.

At $\sqrt{s} = 13$ TeV, both ATLAS and CMS significantly extended the study of $t\bar{t}$+jets, offering more precise tests of QCD radiation patterns and generator modeling. These analyses focused on inclusive and differential cross sections in both the LJ and DL decay channels, probing jet multiplicities and detailed jet kinematics.

ATLAS measured normalized differential $t\bar{t}$+jets cross sections in the LJ channel as functions of jet multiplicity and the properties of the leading additional jets [175]. These measurements, unfolded to particle level, were compared to predictions from several Monte Carlo event generators. While the Monte Carlo simulations described the general features of the data, notable discrepancies appeared in high jet multiplicity regions and in specific jet kinematic distributions.

In the DL channel, ATLAS performed a complementary study of $t\bar{t}$+jets production [176], which included differential measurements of jet multiplicities, transverse momenta, and gap fractions, defined as the fraction of events without additional jet activity above a given threshold. The results provided sensitivity to soft and collinear QCD radiation and were used to test both leading-order and NLO predictions matched to parton showers. Although broad agreement was observed, no single generator configuration consistently described all observables.

CMS measured differential and double-differential $t\bar{t}$+jets cross sections in the DL channel across a wide range of observables, including additional-jet momenta, angular separations, and global event variables [177]. This extended set of observables provides tighter constraints on parton-shower modeling and on the treatment of initial- and final-state radiation. Normalized $t\bar{t}$+jets cross sections were also measured as a function of jet multiplicity and the kinematics of additional jets in both the DL and LJ channels [178]. The measurements are performed in a fiducial phase space and extrapolated to the full phase space. The values of $\sigma_{t\bar{t}b\bar{b}}$ are extracted from the product of $\sigma_{t\bar{t}jj}$ and the measured cross-section ratio. Results unfolded to the particle level are broadly consistent with NLO+PS predictions, although some tension is observed in observables sensitive to hard radiation and color-reconnection effects.

Together, the ATLAS and CMS results at 13 TeV form a comprehensive dataset for validating QCD predictions in top-quark production with jets. They highlight the strengths and limitations of current theoretical tools and serve as benchmarks for improving Monte Carlo simulations used throughout top-quark physics and beyond.

61.2.2.2 *Associated pair production with b-jets*

The production of $t\bar{t}$ in association with additional b-jets arising from gluon radiation provides a stringent test of perturbative QCD. This process is particularly challenging to predict due to the interplay of multiple mass scales: the large mass of the top quark, the smaller but non-negligible b-quark mass, and the energy scale associated with gluon splitting into $b\bar{b}$ pairs. The hierarchy among these scales introduces significant theoretical uncertainties, especially in modeling the emission of heavy-flavor jets in the presence of top quarks.

Int. J. Mod. Phys. A 2026.41. Downloaded from www.worldscientific.com
by UNIVERSITY OF CALIFORNIA @ BERKELEY on 09/16/26. Re-use and distribution is strictly not permitted, except for Open Access articles.

Table 61.7: Summary of $t\bar{t}$ cross-section measurements at LHC.

Experiment [Ref.]	**Lumi.** (fb^{-1})	$\sqrt{s}$ **(TeV)**	**Topology**	**Measurement** (pb)
ATLAS [106]	0.257	5.02	DL+LJ	67.5 ± 2.7
CMS [168], [169]	0.302, 0.0274	5.02	DL($e\mu$)+LJ	63.0 ± 5.1
ATLAS [108]	4.6	7	DL($e\mu$)	182.9 ± 7.1
ATLAS [110]	4.6	7	LJ	$168.5^{+7.1}_{-6.7}$
CMS [109]	5	7	DL($e\mu$)	$173.6^{+6.3}_{-5.9}$
ATLAS+CMS [133]	5	7	DL,LJ	178.5 ± 4.7
LHCb [84]	1	7	LJ (fwd)	0.239 ± 0.067
ATLAS [126]	20.3	8	DL($e\mu$)	242.9 ± 8.8
ATLAS [128]	20.2	8	LJ	248.3 ± 14.2
CMS [109]	19.7	8	DL($e\mu$)	$244.9^{+9.1}_{-8.6}$
CMS [129]	19.6	8	LJ	228.5 ± 15.4
ATLAS+CMS [133]	20	8	DL	$243.3^{+6.0}_{-5.9}$
LHCb [84]	2	8	LJ (fwd)	0.289 ± 0.065
ATLAS [126]	140	13	DL($e\mu$)	829 ± 15.4
ATLAS [142]	139	13	LJ	830 ± 38.6
CMS [141]	35.9	13	DL	803 ± 32.1
CMS [143]	137	13	LJ	791 ± 25.3
LHCb [148]	1.93	13	DL($e\mu$) (fwd)	126 ± 25.3
ATLAS [167]	29	13.6	DL	850 ± 27
CMS [166]	1.21	13.6	DL+LJ	881 ± 30

Beyond its theoretical significance, $t\bar{t}$ production with additional b-jets is also an important background in several key analyses, such as those targeting $t\bar{t}H$ and $t\bar{t}t\bar{t}$ production, where its modeling uncertainty can significantly impact the overall sensitivity. The most precise theoretical predictions for these final states rely on fixed-order calculations at NLO accuracy in pQCD, typically matched to parton showers. These calculations are still limited by significant uncertainties from missing higher-order corrections, making direct experimental measurements of these processes especially valuable for improving the theoretical modeling.

To reduce the model dependence, experimental measurements are often performed in fiducial phase-space regions that are closely aligned with the detector acceptance. This strategy enables a more robust comparison with theoretical predictions, which are evaluated within the same fiducial region, thereby minimizing extrapolation uncertainties into unmeasured regions.

The first measurements of $t\bar{t}$ production with b-jets were performed by ATLAS at $\sqrt{s} = 7$ TeV [179]. Events with at least three b-tagged jets were selected, where two b-jets are attributed to top-quark decays and the third to additional heavy-flavor jets, defined to include both b- and c-jets. The result was expressed as the ratio of events with heavy-flavor jets to the total number of $t\bar{t}$ events with additional jets.

At $\sqrt{s} = 8$ TeV, CMS measured fiducial cross sections in the DL channel, requiring at least four jets, of which two were identified as b-jets [180]. ATLAS performed similar measurements in both the LJ and DL channels, targeting $t\bar{t}$ production in association with one or two additional b-jets [181].

CMS extended these studies with the first differential measurements of $t\bar{t}$ cross sections as functions of the jet multiplicity, exploring various jet transverse momentum thresholds and the kinematics of the leading additional jets. Furthermore, it provided differential cross-section measurements for $t\bar{t} + b$ and $t\bar{t} + b\bar{b}$ final states as a function of the kinematic properties of the leading additional b-jets [173].

At $\sqrt{s} = 13$ TeV, ATLAS measured inclusive and differential cross sections for $t\bar{t} + b\bar{b}$ production in both DL and LJ channels using a partial dataset [182]. The measured inclusive fiducial cross sections were generally found to exceed theoretical predictions from various NLO matrix element generators matched to parton showers.

CMS has performed complementary measurements of $t\bar{t} + b\bar{b}$ production across diverse event topologies: first in the DL channel [183], later in both the DL and LJ channels [184], and in the AH channel [185] using partial datasets. In the AH final state, events with at least eight jets, including at least two b-jets, were analyzed. A combination of multivariate techniques was used to suppress the substantial multijet background and to discriminate jets from top-quark decays from those originating from additional radiation. A two-dimensional likelihood fit yielded a $\sim 25\%$ precision on the $t\bar{t} + b\bar{b}$ cross section in this channel.

CMS reported comprehensive measurements of inclusive and normalized differential $t\bar{t} + b\bar{b}$ cross sections using the full dataset in the LJ channel [186], providing results in four distinct fiducial phase-space regions optimized to probe different aspects of the process. Distributions were unfolded to the particle level using maximum likelihood fits, enabling direct comparisons with theoretical predictions from a range of event generators. The measured inclusive cross sections tend to exceed the predictions obtained with the default settings of these generators. At the differential level, the data exhibit varying degrees of agreement, with discrepancies observed particularly in regions sensitive to additional b-jet radiation.

ATLAS performed differential measurements in the DL final state, analyzing events with exactly one electron and one muon and requiring at least three or four identified b-jets [187]. Results were unfolded to the particle level and reported for both inclusive and normalized differential cross sections. The differential measurements encompass global event properties, individual jet kinematics, and observables sensitive to correlations among b-jets, including those stemming from top-quark decays as well as those originating from additional heavy-flavor radiation. After correcting for detector effects, the measured integrated fiducial cross sections are generally consistent with predictions from various NLO matrix-element calculations matched to parton showers, within the quoted theoretical and experimental uncertainties.

In both ATLAS and CMS results, the unfolded differential measurements are compared with state-of-the-art theoretical predictions. While some event generators describe certain kinematic distributions well, none achieves a fully consistent agreement across all observables. The differences among the various theoretical predictions are generally smaller than the experimental uncertainties for most measured quantities, underscoring the need for further theoretical improvements and more precise data to better discriminate between modeling approaches.

61.2.2.3 *Associated pair production with c-jets*

Predicting and detecting production of $t\bar{t}$ in association with additional c-jets arising from gluon radiation is even more challenging than with additional b-jets. Both ATLAS and CMS have published such measurements using the 13 TeV dataset. The first measurement was performed by the CMS collaboration using a

Int. J. Mod. Phys. A 2026.41. Downloaded from www.worldscientific.com
UNIVERSITY OF CALIFORNIA @ BERKELEY on 09/16/26. Re-use and distribution is strictly not permitted, except for Open Access articles.

partial 13 TeV dataset [188]. The measurement is based on events with dileptonic $t\bar{t}$ final states and differentiates the three processes $t\bar{t}$+light, $t\bar{t}+b\bar{b}$ and $t\bar{t}+c\bar{c}$. The events are categorised using a neural-network approach that utilises charm-jet tagging information. The output probabilities of the different classes are then used to construct a two-dimensional discriminator that is used in a binned profile-likelihood fit to extract the cross-sections for the three processes. The measurement is performed in a fiducial and in the inclusive phase space. Also the ratios of cross-sections are extracted, which benefit from the cancellation of several uncertainties. The measured cross-sections agree with the MC generator predictions within the uncertainties. The cross-section of the $t\bar{t}+c\bar{c}$ process has an uncertainty of 18%, which is dominated by statistical uncertainties as well as uncertainties in the c-tagging calibration and the ME-PS matching uncertainties.

The ATLAS measurement based on the full 13 TeV datasets uses top-quark pairs with either one or two charged leptons in the final state [189]. The cross-sections are extracted for two $t\bar{t}$+charm categories, namely $t\bar{t}+\geq 2c$ and $t\bar{t}+1c$. A new flavour-tagging algorithm is employed that allows to tag b and c jets simultaneously. The discriminating variables in this approach are either the invariant masses of the two closest c-jets or b-jets, or the number of events in the specific region. Seven signal-enriched regions are included in the fit alongside 12 control regions. The cross-sections of the two signal processes as well as for the $t\bar{t}$ and $t\bar{t}+\bar{b}$ processes are extracted simultaneously, both for the fiducial and the inclusive cross-sections. Also ratios of cross-sections are measured. The signal cross-sections have uncertainties of 20% and 14% for $\sigma(t\bar{t}+\geq 2c)$ and $\sigma(t\bar{t}+1c)$, respectively. They are consistent with the predictions within the uncertainties, but are all slightly below the predictions. The precision is limited by data statistics as well as the tagger calibration and the modelling of the signal process.

61.2.2.4 *Associated pair production with massive vector bosons*

The associated production of $t\bar{t}$ with a vector boson V ($V = W, Z$) is a rare but powerful probe of the SM, accessible only at high energies and luminosities. These heavy final states allow precision studies of EW couplings in the top sector and offer unique sensitivity to new physics. In particular, $t\bar{t}W$ production features complex QCD and EW corrections, charge asymmetry from the initial state, and same-sign dilepton signatures, key ingredients in many beyond-the-SM searches. It also forms a major background in rare processes such as $t\bar{t}H$ and $t\bar{t}t\bar{t}$ production. Meanwhile, $t\bar{t}Z$ production provides the most direct probe of the t–Z coupling. In the SM, the W boson is expected to arise primarily from initial-state radiation. In contrast, the Z boson can also be emitted from a final-state top quark, offering direct sensitivity to the top-quark neutral-current interactions and, in particular, to the third component of its weak isospin, a property not yet directly measured. Together, $t\bar{t}V$ processes are central to both precision tests of the SM and the ongoing search for new phenomena at the LHC.

Experimental measurements of $t\bar{t}Z$ and $t\bar{t}W$ typically rely on leptonic decays of the Z and W bosons to suppress the large backgrounds from $t\bar{t}$+jets and $t\bar{t}$+b-jets. The most sensitive channels are final states with three or more charged leptons and events with two same-sign leptons (electrons or muons), which provide substantial background reduction. These analyses require lepton identification with high efficiency and purity to maximize the signal and minimize systematic uncertainties from misidentified leptons.

A summary of the LHC measurements of the inclusive $t\bar{t}V$ cross sections is given in Tab. 61.8.

The first measurement of $t\bar{t}V$ in pp collisions was performed by CMS at $\sqrt{s} = 7$ TeV using two independent analysis channels: a trilepton analysis targeting $t\bar{t}Z$ events and a same-sign dilepton analysis sensitive to $t\bar{t}V$ production. The trilepton channel enabled a direct measurement of the $t\bar{t}Z$ production rate, observed with a significance of 3.3 standard deviations above the background-only hypothesis. The same-sign dilepton analysis yielded evidence for $t\bar{t}V$ production with a significance of 3.0 standard deviations. In both cases, the measured rates were found to be consistent with NLO SM predictions within uncertainties [190].

At $\sqrt{s} = 8$ TeV, both ATLAS and CMS observed the production of $t\bar{t}$ with a W or Z boson. Both collaborations made simultaneous measurements of the $t\bar{t}W$ and $t\bar{t}Z$ cross sections using final states with two same-sign leptons, three leptons, and four leptons. ATLAS obtained significances of 5.0 and 4.2 standard deviations above the background-only hypothesis for $t\bar{t}W$ and $t\bar{t}Z$, respectively [191]. CMS also reported significances of 4.8 standard deviations for $t\bar{t}W$ and 6.4 for $t\bar{t}Z$ [192]. All results were found to be consistent with NLO SM predictions. In addition, the CMS analysis was used to set constraints on five dimension-six operators in the framework of EFT that could modify the $t\bar{t}W$ and $t\bar{t}Z$ production rates.

At $\sqrt{s} = 13$ TeV, the SM cross sections for $t\bar{t}Z$ and $t\bar{t}W$ production increase by factors of approximately 3.5 and 2.4, respectively, compared to 8 TeV. As Tab. 61.3 shows, these cross sections, calculated at different orders in EW and QCD, carry an uncertainty of about 10%, primarily from renormalization and factorization scale variations. At this center-of-mass energy, ATLAS and CMS performed various measurements in final states with two same-sign leptons or three and four leptons. Using partial datasets, ATLAS simultaneously measured the $t\bar{t}Z$ and $t\bar{t}W$ cross sections via a combined fit across multiple analysis regions [193]. The results are consistent with SM predictions and were used to set constraints on dimension-six SMEFT operators involving the top quark and the Z boson. CMS also reported measurements of the $t\bar{t}V$ cross section using similar final states. For $t\bar{t}W$ production in the same-sign dilepton channel, the observed (expected) significance reached 5.3 (4.5) standard deviations. In the three- and four-lepton channels targeting $t\bar{t}Z$, both observed and expected significances exceeded 5 standard deviations. These results agree with SM predictions and were further used to constrain Wilson coefficients of eight dimension-six EFT operators that would modify $t\bar{t}W$ and $t\bar{t}Z$ production [194].

The first differential $t\bar{t}Z$ measurement by CMS used events with three or four leptons, with the Z boson reconstructed from an oppositely charged lepton pair [195]. Results were presented as functions of the Z p_{T} and the angular distribution of the negatively charged decay lepton, providing a detailed characterization of the process and enabling stringent limits on anomalous tZ couplings.

ATLAS measured inclusive and differential $t\bar{t}Z$ cross sections [196] also using events with three or four isolated leptons. Differential results were unfolded at both the particle and parton levels in specific fiducial regions and are reported as absolute and normalized cross sections. A range of kinematic observables was studied to probe the dynamics of the $t\bar{t}Z$ system. The measurements were compared with predictions from several fixed-order calculations and Monte Carlo generators, showing good overall agreement.

An updated and extended $t\bar{t}Z$ measurement by ATLAS was later performed using the same dataset [197]. This analysis introduced an additional final state targeting the AH decay of the $t\bar{t}$, alongside the multilepton channels. The measurement benefits from improved calibrations, better background modeling, and reduced experimental and theoretical uncertainties. The inclusive and differential cross sections were extracted using a simultaneous profile-likelihood fit across all analysis regions. Unfolding was performed at both particle and parton levels using a consistent fiducial volume, yielding robust and precise results. These measurements were further interpreted in the EFT framework to constrain dimension-six operators relevant to the tZ interaction. Additionally, the spin density matrix coefficients of the $t\bar{t}Z$ system were extracted for the first time, offering a new perspective on the polarization structure of this process.

CMS measured inclusive and differential cross sections of $t\bar{t}Z$ simultaneously with tWZ and tZq in events with three or more leptons. A multiclass deep neural network was employed to separate $t\bar{t}Z$+tWZ, tZq, and background processes. The inclusive cross sections for $70 < m_{\ell\ell} < 110$ GeV are measured to be 1.14 ± 0.07 pb for $t\bar{t}Z$+tWZ and 0.81 ± 0.10 pb for tZq, both consistent with SM predictions [198].

A pioneering study of $t\bar{t}Z$ and $t\bar{t}H$ production in the LJ final state has been performed by CMS to probe potential effects of BSM in top-quark interactions with the Z and Higgs bosons [199]. The analysis selected events with a single charged lepton, multiple

Int. J. Mod. Phys. A 2026.41. Downloaded from www.worldscientific.com
by UNIVERSITY OF CALIFORNIA @ BERKELEY on 09/16/26. Re-use and distribution is strictly not permitted, except for Open Access articles.

jets, two of which are b-tagged, and an additional large-radius jet with high p_{T}, identified as a boosted Z or Higgs boson decaying into a $b\bar{b}$ pair. Signal strengths for boosted $t\bar{t}Z$ and $t\bar{t}H$ production were measured, and upper limits are set on their differential cross sections as functions of the boson p_{T}. These results are translated into constraints on eight dimension-six EFT operators. Limits are also placed on eight leading-order EFT parameters that significantly impact boosted $t\bar{t}Z$ and $t\bar{t}H$ production.

Using the full Run 2 datasets, both ATLAS and CMS have measured the $t\bar{t}W$ production cross section. CMS determined the inclusive cross section and the separate contributions from $t\bar{t}W^+$ and $t\bar{t}W^-$ production [200], obtaining values slightly higher than but consistent with SM predictions within two standard deviations. It also measured differential cross sections in final states with two same-sign or three leptons, using multivariate and selection-based methods. The normalized results agree with SM expectations, while the absolute cross sections are somewhat higher, in line with previous measurements [201].

ATLAS performed both inclusive and differential measurements of $t\bar{t}W$ production [202]. The inclusive result lies slightly above the NNLO QCD prediction. At the same time, the unfolded differential cross sections show good overall agreement with various theoretical models and provide detailed insight into the $t\bar{t}W$ process. In addition, ATLAS reported separate measurements of the $t\bar{t}W^+$ and $t\bar{t}W^-$ cross sections.

61.2.2.5 *Associated pair production with one or two photons*

The $t\bar{t}\gamma$ production provides a direct probe of the top-quark EM interactions. In particular, deviations in the p_T spectrum of the photon from the SM prediction could point to new physics through anomalous dipole moments of the top quark or the production of excited top quarks decaying radiatively via $t^* \to t\gamma$ [203–206].

The EM coupling of the top quark can be accessed experimentally by studying final states where a photon is radiated in $t\bar{t}$ events via measurements of the absolute cross sections, cross section ratios (e.g. $\sigma_{t\bar{t}\gamma}/\sigma_{t\bar{t}}$), or through fits within the framework of EFT using differential distributions.

In $t\bar{t}\gamma$ measurements, the cross section must be defined within a well-specified fiducial phase space because the photon can originate from different parts of the event, such as top-quark decay products or initial-state radiation. A clear fiducial selection area is required to unambiguously define which phase-space region and photon kinematics are included in the measurement.

A summary of the Tevatron and LHC measurements of the inclusive $t\bar{t}\gamma$ cross sections is given in Tab. 61.9.

The first evidence for $t\bar{t}\gamma$ production was reported by the CDF collaboration [207]. The analysis targeted events with a lepton, a photon, significant missing transverse momentum, at least one b-tagged jet, three or more additional jets, and large total transverse energy. The first observation of the $t\bar{t}\gamma$ process was reported by ATLAS in pp collisions at $\sqrt{s} = 7$ TeV, using events with an electron or muon and a high-p_{T} photon, with results consistent with LO theoretical predictions [208]. At $\sqrt{s} = 8$ TeV, ATLAS measured the $t\bar{t}\gamma$ cross section for photons with $p_{\mathrm{T}} > 15$ GeV and $|\eta| < 2.37$, selecting events with an isolated high-p_{T} lepton, large missing transverse momentum, and at least four jets, including at least one b-tagged jet [209]. The results are in good agreement with the NLO prediction [210]. CMS performed a similar measurement in the LJ channel, requiring photons with $p_{\mathrm{T}} > 25$ GeV and $|\eta| < 1.44$ [211]. When the measured cross-section is extrapolated to the cross-section times branching fraction by dividing by the kinematic acceptance, it is also consistent with theoretical predictions.

At $\sqrt{s} = 13$ TeV, ATLAS measured the fiducial and differential cross sections for $t\bar{t}\gamma$ production in LJ and DL final states containing exactly one isolated photon [212]. Differential cross sections were extracted as functions of the photon p_{T}, $|\eta|$, and the angular distance between the photon and the nearest lepton ($\Delta R(\gamma, \ell)$) in both channels. In the DL channel, additional observables include the azimuthal opening angle and the absolute pseudorapidity difference between the two leptons. All results are found to be consistent with theoretical predictions.

ATLAS measured the inclusive and differential cross-sections of combined $t\bar{t}\gamma$ and $tW\gamma$ in $e\mu + \gamma$ events with at least two jets, including at least one b-tagged jet [213]. Differential cross sections were measured as functions of the photon p_{T}, $|\eta|$, and angular correlations between the photon and leptons, as well as between the two leptons. The results are in good agreement with NLO predictions and state-of-the-art Monte Carlo simulations.

A subsequent ATLAS analysis measured inclusive and differential $t\bar{t}\gamma$ cross sections in both the LJ and DL channels [214], focusing on events where the photon was radiated in the production stage. The combined measurement achieves a relative uncertainty of 5.2%. Differential distributions were further used to set limits on EFT parameters related to the EW dipole moments of the top quark, with a significant improvement obtained when combining $t\bar{t}\gamma$ and $t\bar{t}Z$ differential measurements in a joint interpretation.

CMS measured $t\bar{t}\gamma$ production in the LJ channel in a fiducial phase space defined at particle level [215], requiring an isolated high-p_{T} lepton, at least three jets (including one or more b-tagged jets), and a single isolated photon. For photons with $p_{\mathrm{T}}^{\gamma} > 20$ GeV and $|\eta^{\gamma}| < 1.4442$, the inclusive fiducial cross section agrees with NLO QCD predictions. Differential cross sections were measured as functions of the photon p_{T} and η, and the angular separation between the photon and the lepton, and were interpreted in the EFT framework to constrain the Wilson coefficients c_{tZ} and c_{tZ}^{I}.

CMS also measured the inclusive $t\bar{t}\gamma$ cross section in the DL channel [216], selecting events with exactly one isolated photon with $p_{\mathrm{T}}^{\gamma} > 20$ GeV and at least one b-tagged jet. Differential cross sections were extracted as functions of observables related to the photon, leptons, and jets, and combined with the LJ results in a joint EFT interpretation, further improving the constraints on c_{tZ} and c_{tZ}^{I}. In addition, CMS measured in the DL channel the ratios of the inclusive and differential $t\bar{t}\gamma$ to $t\bar{t}$ cross sections, performed differential studies including the kinematics of the top quarks, and extracted the top-quark charge asymmetry, A_C, in $t\bar{t}\gamma$ events [217].

The production of a $t\bar{t}$ pair in association with two photons has been observed by ATLAS [218]. This process constitutes an important background to $t\bar{t}H(\gamma\gamma)$ and provides sensitivity to the top-quark chromomagnetic and electric dipole moments [154], the latter also probed through the ratio of $t\bar{t}$ events with one or two photons. The measurement includes both the fiducial cross-section and the cross-section ratio, extracted using a boosted decision tree as the final discriminant in a profile-likelihood fit. In the fiducial phase space at stable-particle level, events with at least one high-p_{T} electron or muon are selected, requiring two photons with $p_{\mathrm{T}}^{\gamma} > 20$ GeV. ATLAS measured a fiducial cross section of $\sigma_{t\bar{t}\gamma\gamma} = 2.42^{+0.46}_{-0.38}\,(\mathrm{stat})^{+0.35}_{-0.38}\,(\mathrm{syst})$ fb, with an observed significance of $5.2\,\sigma$.

61.2.2.6 *Four top quarks*

BSM effects that modify top-quark couplings are particularly relevant in rare processes with small SM cross sections, such as $t\bar{t}t\bar{t}$ production, where they can notably enhance the rate or distort kinematic distributions. Because of its tiny SM cross section, this process is highly sensitive to such effects and is widely used in EFT fits to constrain four-fermion operators, especially the four-top-quark operator. While $t\bar{t}t\bar{t}$ production offers the cleanest and most sensitive probe due to its low SM background, other processes—such as high-energy tails of $t\bar{t}$ production and other rare top-quark final states—also exhibit sensitivity to the same operators. Owing to this, the study of $t\bar{t}t\bar{t}$ production has attracted substantial theoretical and experimental interest in recent years.

Given its heavy final state and extremely low production rate, the first searches for $t\bar{t}t\bar{t}$ production were conducted at a center-of-mass energy of 13 TeV. Similar to $t\bar{t}V$ analyses, these studies target multilepton channels to improve signal purity and rely extensively on multivariate techniques to separate signal from background. The large number of b-jets in the final state makes efficient and well-calibrated b-tagging crucial, together with high reconstruction efficiency and small systematic uncertainties for all final-state objects.

Table 61.10 summarizes recent measurements. Throughout this review, quoted signal significances are taken directly from the corresponding publications; however, it should be noted that these are sometimes evaluated relative to different theoretical hypothe-

Int. J. Mod. Phys. A 2026.41. Downloaded from www.worldscientific.com
UNIVERSITY OF CALIFORNIA @ BERKELEY on 09/16/26. Re-use and distribution is strictly not permitted, except for Open Access articles.

Table 61.8: Summary of $t\bar{t}V$ cross-section measurements from LHC.

Experiment [Ref.]	$\sqrt{s}$ (TeV)	Measurement	Comment
CMS [190]	7	$\sigma_{t\bar{t}Z} = 280^{+152.3}_{-114.0}$ fb	3.3σ
CMS [190]	7	$\sigma_{t\bar{t}V} = 430^{+192.4}_{-165.5}$ fb	3.0σ
ATLAS [191]	8	$\sigma_{t\bar{t}W} = 369^{+100}_{-91}$ fb	5.0σ (3.2σ expected)
ATLAS [191]	8	$\sigma_{t\bar{t}Z} = 176^{+58}_{-52}$ fb	4.2σ (4.5σ expected)
CMS [192]	8	$\sigma_{t\bar{t}W} = 382^{+117}_{-102}$ fb	4.8σ (3.5σ expected)
CMS [192]	8	$\sigma_{t\bar{t}Z} = 242^{+65}_{-55}$ fb	6.4σ (5.7σ expected)
ATLAS [193]	13	$\sigma_{t\bar{t}W} = 870 \pm 191$ fb	4.3σ (3.4σ expected)
ATLAS [193]	13	$\sigma_{t\bar{t}Z} = 950 \pm 128$ fb	$>5\sigma$
CMS [195]	13	$\sigma_{t\bar{t}Z} = 950 \pm 78$ fb	first differential, EFT limits
ATLAS [196]	13	$\sigma_{t\bar{t}Z} = 990 \pm 94$ fb	
ATLAS [197]	13	$\sigma_{t\bar{t}Z} = 860 \pm 57$ fb	updated result, EFT limits
CMS [199]	13	$\mu(t\bar{t}Z) = 0.65^{+1.04}_{-0.98}$ $\mu(t\bar{t}H) = 0.27^{+0.86}_{-0.83}$	EFT limits
CMS [200]	13	$\sigma_{t\bar{t}W} = 868 \pm 65$; $R_{t\bar{t}W^+/t\bar{t}W^-} = 1.61^{+0.17}_{-0.16}$	
ATLAS [202]	13	$\sigma_{t\bar{t}W} = 880 \pm 80$ fb;$R_{t\bar{t}W^+/t\bar{t}W^-} = 1.96 \pm 0.22$	first differential

Table 61.9: Summary of $t\bar{t}\gamma$ cross-section measurements from Tevatron and LHC (see text for photon selection criteria).

Experiment [Ref.]	$\sqrt{s}$ (TeV)	Measurement
CDF [207]	1.96 ($p\bar{p}$)	Evidence for $t\bar{t}\gamma$ production $\sigma_{t\bar{t}\gamma} = 0.18 \pm 0.08$ pb $\sigma_{t\bar{t}\gamma}/\sigma_{t\bar{t}} = 0.024 \pm 0.009$
ATLAS [208]	7	Observation of $t\bar{t}\gamma$ production with 5.3σ significance $\sigma^{\text{fid.}}(t\bar{t}\gamma) \times BR = 63^{+19}_{-15}$ pb per lepton flavor
ATLAS [209]	8	Fiducial cross section: $\sigma_{t\bar{t}\gamma} = 139 \pm 18$ fb
CMS [211]	8	Normalized cross sections: $\mathcal{R}_{e+\text{jets}} = (5.7 \pm 1.8) \times 10^{-4}$ $\mathcal{R}_{\mu+\text{jets}} = (4.7 \pm 1.3) \times 10^{-4}$ Fiducial cross section: $\sigma_{t\bar{t}\gamma} = 244.9^{+9.1}_{-8.6}$ pb
ATLAS [212]	13	Fiducial cross section: $\sigma_{t\bar{t}\gamma} = 521 \pm 42$ fb LJ channel $\sigma_{t\bar{t}\gamma} = 69 \pm 5$ fb DL channel
ATLAS [213]	13	Fiducial cross section: $\sigma_{t\bar{t}\gamma} = 39.6^{+2.7}_{-2.3}$ fb DL $e\mu + \gamma$ channel
ATLAS [214]	13	Fiducial cross section (LJ+DL): $\sigma_{t\bar{t}\gamma} = 319^{+16}_{-15}$ fb – γ only radiated in production $\sigma_{t\bar{t}\gamma} = 788^{+38}_{-37}$ fb c_{tZ}, c_{tB} and $c_{t\gamma}$ limits
CMS [215]	13	Fiducial cross section: $\sigma_{t\bar{t}\gamma} = 798 \pm 49$ fb LJ channel c_{tZ} and c^I_{tZ} limits
CMS [216]	13	Fiducial cross section: $\sigma_{t\bar{t}\gamma} = 174.4 \pm 6.6$ fb DL channel c_{tZ} and c^I_{tZ} limits
CMS [217]	13	Fiducial cross section: $\sigma_{t\bar{t}\gamma} = 54 \pm 5$ fb DL channel $R(t\bar{t}\gamma/t\bar{t}) = 0.0125 \pm 0.0005$ $A_C = (-0.012 \pm 0.042)\%$

ses. While this caveat applies broadly, it is particularly relevant for $t\bar{t}t\bar{t}$ production, where variations in the assumed signal theoretical cross section can lead to notably different significance estimates.

CMS initiated the effort with a search in the one-lepton and two-lepton opposite-sign channels [219]. This was followed by the first measurement using events with two same-sign leptons or at least three leptons, which benefit from relatively low backgrounds but cover only a small fraction of the total branching ratio [220], achieving an observed (expected) significance of 2.6σ (2.7σ), approaching the threshold for evidence.

ATLAS measured $t\bar{t}t\bar{t}$ production in the same-sign dilepton and trilepton channels [221]. The analysis was extended to include the one-lepton and opposite-sign dilepton channels, which are dominated by $t\bar{t}+$heavy-flavor backgrounds [222]. The combination of these channels yielded an observed (expected) significance of 4.7σ (2.6σ), providing the first evidence for the $t\bar{t}t\bar{t}$ production.

CMS later reported evidence for $t\bar{t}t\bar{t}$ production using a complementary approach targeting the traditional $t\bar{t}$ channels: DL, LJ, and AH final states [223]. Combining this result with the previous multilepton measurements further increased the overall significance to 4.0σ (expected 3.2σ).

The first observations of $t\bar{t}t\bar{t}$ production were made following improvements in object reconstruction and analysis techniques. ATLAS reported the observation in events with two same-sign leptons or at least three leptons [224]. A graph neural network was employed to enhance signal-to-background discrimination, and dedicated control regions were used to constrain dominant backgrounds. The observed (expected) significance reached 6.1σ (4.3σ). In addition, the measurement was interpreted to constrain

Int. J. Mod. Phys. A 2026.41. Downloaded from www.worldscientific.com
by UNIVERSITY OF CALIFORNIA @ BERKELEY on 09/16/26. Re-use and distribution is strictly not permitted, except for Open Access articles.

the top-Higgs Yukawa coupling and EFT operator coefficients.

CMS reported the observation of the $t\bar{t}t\bar{t}$ production process using events with two same-sign, three, or four charged leptons and multiple jets [225]. The analysis featured improved lepton and b-jet identification, as well as a multivariate classification based on a multi-class boosted decision tree, and achieved an observed (expected) significance of 5.6σ (4.9σ).

The cross-sections measured by ATLAS and CMS are almost twice the SM prediction and compatible with it within 2 standard deviations.

61.2.3 *Cross-section measurements of single production*

The traditionally considered mechanisms for single-top-quark production are the t-channel exchange of a virtual W boson ($qb \to q't$) and the s-channel process ($q\bar{q}' \to t\bar{b}$). Additionally, the associated production with a W boson tW-channel ($b\bar{q} \to tW$) is also regarded as a main production mode. The primary motivation for precise measurements of single-top production is that they enable a direct determination of the CKM matrix element V_{tb}, without relying on assumptions about the number of quark generations or the unitarity of the CKM matrix.

At the Tevatron, the t-channel dominates, with a cross section approximately twice that of the s-channel. At the LHC, the t-channel is further enhanced by the large gluon and light-quark parton fluxes, while the s-channel rate is more than a factor of three smaller. Associated production of a single top quark with a vector boson (W, Z, γ) is negligible at the Tevatron but becomes non-negligible at the LHC.

In t-channel production, the final state contains a single top quark and a light spectator quark. A characteristic signature is a forward, high-$|\eta|$ spectator jet, typically well separated in rapidity from the b-jet originating from the top-quark decay. Events generally have little additional jet activity, and the absence of a second central b-jet provides further discrimination from $t\bar{t}$ production.

In s-channel production, the final state consists of a single top quark produced together with a second b-quark from the hard interaction. This process is of particular interest because deviations from the SM cross section could signal physics beyond the SM, as predicted in scenarios involving non-SM mediators such as a W' boson or a charged Higgs boson.

In tW channel, the signal is difficult to isolate because of its close resemblance to the $t\bar{t}$ signature. Its definition is also non-trivial, as at NLO a subset of diagrams leads to the same final state as $t\bar{t}$ production, resulting in interference between the two processes [77]. The tW channel is particularly interesting since it probes the Wtb vertex in a kinematic regime different from that of the s- and t-channels, and because of its similarity to the associated production of a charged Higgs boson with a top quark.

The top-quark decays almost exclusively via $t \to Wb$, producing a high-p_{T} central b-jet accompanied by an isolated lepton and missing transverse momentum in leptonic W decays, or by two additional jets in hadronic decays. Because the t-, s-, and tW-channel final states are relatively simple and contain only a few reconstructed objects, they are easily mimicked by background processes. Consequently, measurements of the t- and s-channels primarily use the single-lepton plus jets (LJ) final state, where the lepton is an electron or muon, which provides a favorable signal-to-background ratio. In contrast, the presence of two W bosons in the tW final state makes dileptonic topologies (DL), characterized by two leptons, missing transverse energy, and jets, the most sensitive channel for this mode.

61.2.3.1 *Measurements at the Tevatron*

The single-top production process was first observed in 2009 by the DØ collaboration [226–228] and by CDF [229–231] at the Tevatron. Although the single-top production cross section at the Tevatron is about half that of $t\bar{t}$ production, its final states are more difficult to isolate due to large backgrounds from W+jets and other processes. Comprehensive reviews of these early measurements and the analysis strategies employed to extract the signal from background-dominated datasets are provided in [232, 233].

At the Tevatron, searches targeted single-top production in both the t-channel and s-channel modes. These processes can in principle be separated kinematically, which is of particular interest since various new-physics scenarios—such as a fourth-generation quark, heavy W'/Z' bosons, flavor-changing neutral currents [71], or a charged Higgs boson—affect the two channels differently. In practice, however, this separation proved challenging, and the initial Tevatron results focused on the combined s and t contributions.

Due to the diverse backgrounds, the experiments developed multiple parallel analyses to optimize signal discrimination, employing advanced multivariate techniques, including likelihood fits, artificial neural networks, matrix-element methods, and BDTs. Each approach provided an independent cross-section measurement and statistical assessment of the excess over background expectations. To maximize sensitivity, the analyses were combined using a higher-level discriminant that took as input the outputs of the individual analysis discriminants for each event [231].

The CDF and DØ collaborations later combined their results, first for the $s+t$ channel using partial datasets [234], and subsequently with the full Run 2 dataset to measure the t-channel cross section [235]. In the latter publication, simultaneous extractions of the s-, t-, and combined $s+t$ cross sections were reported. The measurements were consistent with theoretical predictions at $\sqrt{s} = 1.96$ TeV and $m_t = 172.5$ GeV, yielding for both t and $\bar{t}$ production $\sigma_{s+t} = 2.08 \pm 0.13$ pb [75, 236].

These results were also used to extract the CKM matrix element $|V_{tb}|$, again in agreement with theoretical expectations. It is worth noting that theoretical cross sections are typically quoted separately for top and antitop quarks, whereas the Tevatron results refer to their sum. Since the two contributions are equal in $p\bar{p}$ collisions, the quoted theory predictions include a factor of two.

Finally, CDF and DØ combined their data to achieve the first observation of single-top production in the s-channel, with an observed significance of 6.3 standard deviations [237].

A summary of Tevatron single-top measurements is provided in Tab. 61.11.

61.2.3.2 *Measurements at the LHC*

At the LHC, single-top-quark production is enhanced by the higher energy and gluon-rich initial state with respect to the Tevatron. The t channel dominates, exceeding the combined rates of the s channel and tW production by a factor of more than three. While the t and tW channels have been observed, the s-channel process still has significance below 4σ.

Figure 61.6 summarizes the measured single-top-quark production cross sections in the t-channel, s-channel, and tW-channel from LHC collisions at various center-of-mass energies, compared to theoretical predictions at NNLO+NNLL accuracy. The following sections provide a detailed description of these measurements.

t-channel at the LHC

Studies of the t-channel process focus on precise measurements of the single top-quark (σ_t) and top-antiquark ($\sigma_{\bar{t}}$) production cross sections, which differ at the LHC, as well as their ratio (R_t) and the inclusive cross section ($\sigma_{t+\bar{t}}$). Comparing these measured cross sections with theoretical predictions allows the extraction of $|V_{tb}|^2$. The measurements are performed separately for each production mode and center-of-mass energy..

Measurements of t-channel single-top-quark production have been performed at several LHC energies and are summarized in Tab. 61.12. Figure 61.7 summarizes the ATLAS and CMS measurements of R_t compared to NLO QCD calculations using the PDF4LHC21 and CT18 PDF sets.

At $\sqrt{s} = 5.02$ TeV, ATLAS and CMS reported the observation of single-top production in the t-channel [238, 239]. Separate measurements of top and antitop quark production allowed the determination of their production ratio and an extraction of $|V_{tb}|$. This lower-energy result provides an independent test of the SM, with backgrounds and systematic uncertainties distinct from those at higher LHC energies.

At $\sqrt{s} = 7$ TeV, ATLAS measured the t-channel cross section in the LJ channel with one b-tagged jet, relying on a neural-network discriminant [240, 241]. Differential cross sections for top- and antitop-quark production were reported as functions of p_{T} and

Int. J. Mod. Phys. A 2026.41. Downloaded from www.worldscientific.com
UNIVERSITY OF CALIFORNIA @ BERKELEY on 09/16/26. Re-use and distribution is strictly not permitted, except for Open Access articles.

Table 61.10: Chronological summary of $t\bar{t}t\bar{t}$ production measurements at LHC at $\sqrt{s} = 13$ TeV.

Experiment [Ref.]	Lumi. (fb^{-1})	Topology	Measurement (fb)	Significance (obs/exp)
CMS [219]	35.8	LJ, DL	Search only	—
CMS [220]	137	Same-sign DL, ≥ 3 leptons	$\sigma = 12.6^{+5.8}_{-5.2}$	2.6σ / 2.7σ
ATLAS [221]	139	Same-sign DL, ≥ 3 leptons	$\sigma = 24^{+7}_{-6}$	4.3σ / 2.4σ
ATLAS [222]	139	LJ, DL	$\sigma = 26^{+17}_{-15}$	1.9σ / 1.0σ
ATLAS [222]	139	Combined channels	$\sigma = 24^{+7}_{-6}$	4.7σ / 2.6σ
CMS [223]	137	LJ, DL, AH	$\sigma = 36^{+12}_{-11}$	3.9σ / 1.5σ
CMS [223]	137	Combined channels	$\sigma = 17 \pm 5$	4.0σ / 3.2σ
ATLAS [224]	140	Same-sign DL, ≥ 3 leptons	$\sigma = 22.5^{+6.6}_{-5.5}$	6.1σ / 4.3σ
CMS [225]	137	Same-sign DL, 3 and 4 leptons	$\sigma = 17.7^{+4.4}_{-4.0}$	5.6σ / 4.9σ

Table 61.11: Single-top-quark production measurements from the Tevatron at $\sqrt{s} = 1.96$ TeV.

Experiment [Ref.]	Luminosity (fb^{-1})	Measurement	Note
DØ [226]	2.3	$\sigma_{s+t} = 3.94 \pm 0.88$ pb	Observation single top
CDF [229, 231]	up to 3.2	$\sigma_{s+t} = 2.3^{+0.6}_{-0.5}$ pb $\sigma_s = 1.8^{+0.7}_{-0.5}$ pb $\sigma_t = 0.8^{+0.4}_{-0.4}$ pb	Observation single top
Tevatron [235]	up to 9.7	$\sigma_t = 2.25^{+0.29}_{-0.31}$ pb $\sigma_{s+t} = 3.30^{+0.52}_{-0.40}$ pb $\lvert V_{tb}\rvert = 1.02^{+0.06}_{-0.05}$ $\lvert V_{tb}\rvert > 0.92$ at 95% C.L	t-channel only without assuming the SM ratio of σ_s/σ_t
Tevatron [237]	up to 9.7	$\sigma_s = 1.29^{+0.26}_{-0.24}$ pb	Observation s-channel

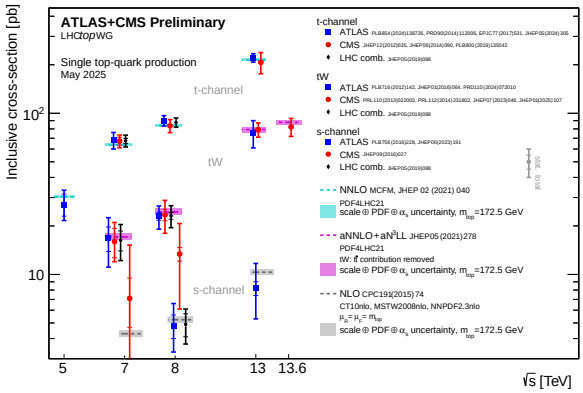

Figure 61.6: The LHC measured and predicted single-top-quark production cross sections as a function of the center-of-mass energy. The measurements are compared to theoretical calculations based on: NLO QCD, aNNLO QCD complemented with aN^{3}LL resummation and NNLO QCD. The LHCtopWG working group kindly provides the plot, status as of May 2025, see `https://twiki.cern.ch/twiki/bin/view/LHCPhysics/LHCTopWGSummaryPlots`.

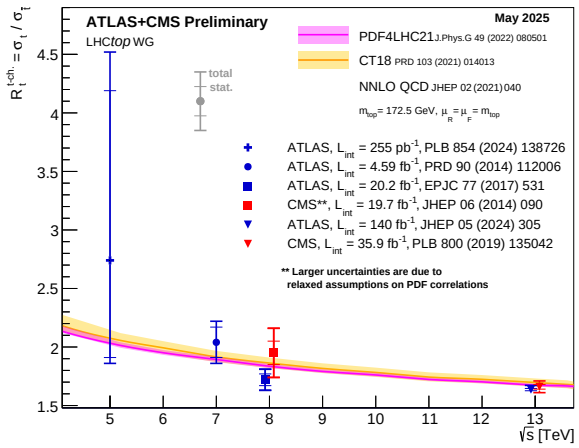

Figure 61.7: Summary of the ATLAS and CMS measurements of R_t, the ratio of the t-channel top-quark production cross section to the t-channel top-antiquark production cross section. The data measurements are compared to NLO QCD calculations using the PDF4LHC21 and CT18 PDF sets. The colored bands represent the uncertainties on the theoretical predictions (scale and PDF uncertainties). The plot is kindly provided by the LHCtopWG working group, status as of May 2025, see `https://twiki.cern.ch/twiki/bin/view/LHCPhysics/LHCTopWGSummaryPlots`

$|y|$. CMS carried out analogous measurements in the same channel [242]. One approach used the η distribution of the recoil jet and the reconstructed m_t with background estimates from data control samples, while another employed multivariate techniques. A combined ATLAS+CMS result at this energy shows good agreement with SM predictions [243].

At $\sqrt{s} = 8$ TeV, both experiments extended and refined their studies. ATLAS measured total, fiducial, and differential cross sections for top- and antitop-quark production evaluated at both the parton and particle levels, extracting $|V_{tb}|$ [244], and probed the structure of the Wtb vertex using polarization observables, with asymmetries in angular distributions consistent with the SM [245]. CMS performed measurements in the LJ channel, extracting the signal yield through maximum-likelihood fits to the $|\eta_j|$ distribution of the recoil jet [246], and reported separate fits for top and antitop quark cross sections. Combined ATLAS+CMS results again confirmed SM expectations [243]. CMS measured the top-quark spin asymmetry to be $A_\mu = 0.26 \pm 0.03$ (stat.) $\pm$ 0.10 (syst.), derived from the angular distribution of the charged lepton relative to the top-quark spin axis, defined by the spectator quark direction in t-channel production [247]. The measurement assumes the SM spin-analyzing power of 100% for the charged lepton and corresponds to a p-value of 4.6% (a 2.0σ deviation from the SM prediction, corresponding to $A_\mu^{\rm TH} = 0.44$ with very small uncertainty). The asymmetry probes the correlation between the lepton direction and the top-quark spin, providing sensitivity to

Int. J. Mod. Phys. A 2026.41. Downloaded from www.worldscientific.com by UNIVERSITY OF CALIFORNIA @ BERKELEY on 09/16/26. Re-use and distribution is strictly not permitted, except for Open Access articles.

the polarization and chiral structure of the top-quark interaction.

At $\sqrt{s} = 13$ TeV, the first analyses were performed with partial datasets. ATLAS extracted cross sections and their ratio using a binned maximum-likelihood fit to the output of a neural-network discriminant [248], while CMS employed simultaneous fits to the transverse W-mass and the output of a neural network to measure the cross section and determine $|V_{tb}|$ [249]. CMS later refined the measurement with a larger dataset, categorizing events by jet and b-jet multiplicity and applying multivariate discriminators [250]. From these data, cross sections and their ratio were measured, differential distributions obtained [251], and constraints placed on $|V_{tb}|$ and other CKM elements in a model-independent framework [252]. The spin asymmetry was measured as 0.440 ± 0.070, consistent with the SM but in tension with the 8 TeV result. Using the full dataset, ATLAS measured top and antitop quark cross sections with precisions of 6% and 8%, respectively [253], in agreement with NNLO QCD predictions. These results are also sensitive to PDFs, interpreted in terms of EFT operators, and used to measure $|V_{tb}|$ and set 95% C.L. limits on $|V_{td}|$ and $|V_{ts}|$. ATLAS further determined the three components of the polarization vectors for top and antitop quarks in t-channel events [254], reporting values consistent with SM expectations, and presented normalized differential cross sections as functions of charged-lepton angles, used to bound the complex Wilson coefficient of the dimension-six O_{tW} operator.

s-channel at the LHC

The growth of the s-channel cross section from $\sqrt{s} = 8$ to 13 TeV is slightly larger than that of W-boson production, the second most important background, but smaller than that of $t\bar{t}$ production, which remains dominant. Theory predicts that the ratio of the s-channel single-top cross section to the W-boson cross section is 1.4×10^{-4} (1.7×10^{-4}) at $\sqrt{s} = 8$ (13) TeV, and its ratio to the $t\bar{t}$ cross section is 2.1×10^{-2} (1.2×10^{-2}). Consequently, the analysis of this process becomes increasingly challenging as the center-of-mass energy rises.

A summary of results at different center-of-mass energies is given in Tab. 61.13.

At $\sqrt{s} = 7$ TeV, CMS analyzed events in the LJ channel using a maximum-likelihood fit to a BDT discriminant, presenting results that were later combined with those at 8 TeV [255].

At $\sqrt{s} = 8$ TeV, ATLAS reported the first evidence for s-channel single-top-quark production at the LHC [256], employing a discriminant based on the Matrix Element Method optimized against the dominant $t\bar{t}$ and W+jets backgrounds. CMS measured the s-channel cross section using a maximum-likelihood fit to a BDT discriminant [255] and combined the result with the 7 TeV measurement, obtaining a best-fit value of 2.0 ± 0.9 for the ratio of the measured to the expected cross section. A joint ATLAS+CMS combination confirmed consistency with the SM [243], but did not allow for observing the process.

At $\sqrt{s} = 13$ TeV, ATLAS studied the s-channel cross section using the full Run 2 dataset in events with an electron or muon, missing transverse momentum, and exactly two b-tagged jets. A discriminant based on Matrix-Element Method calculations was used to separate the s-channel signal from $t\bar{t}$ and W+jets backgrounds. The result was found to be consistent with the SM prediction [257], but the significance of the result is still below 4σ.

61.2.3.3 *tW-channel at LHC*

The tW signal is difficult to isolate because of its similarity to the $t\bar{t}$ final state. Its definition is further complicated at NLO, where part of the contributing diagrams lead to identical final states as $t\bar{t}$ production, giving rise to interference between the two processes [77]. The standard approach is to define the signal using the diagram-removal technique [76], in which the interfering diagrams are removed at the amplitude level. An alternative method, diagram subtraction, removes these contributions at the cross-section level, leading to similar results [76]. Both techniques are valid provided that the event selection cuts are chosen to keep interference effects small, which is typically the case.

Experimentally, the presence of two W bosons in the final state makes dileptonic topologies the most sensitive, requiring two leptons, missing transverse energy, and jets. A summary of results is given in Tab. 61.14.

At $\sqrt{s} = 7$ TeV, both ATLAS and CMS reported evidence for this process [259, 260]. ATLAS employed template fits to BDT classifiers, while CMS used a multivariate analysis. Both of them used events in the DL channel with exactly one b-tagged jet. The combination of ATLAS and CMS results is consistent with SM predictions [243].

At $\sqrt{s} = 8$ TeV, the two experiments strengthened their measurements. ATLAS observed tW production with a significance of 7.7σ using a BDT discriminant and extracted the cross section with a profile-likelihood fit; a fiducial cross section was also reported [261]. In a separate analysis, ATLAS studied the LJ channel with at least three jets, training a neural network to discriminate signal from $t\bar{t}$ and extracting the cross section with a two-dimensional fit involving the neural network output and the invariant mass of the hadronic W boson [262]. CMS analyzed the DL channel with a b-tagged jet, employing a multivariate discriminant to suppress the $t\bar{t}$ background and observing the signal with a significance of 6.1σ [263]. ATLAS and CMS combined their results to determine σ_{tW} and extract $|V_{tb}|f_{\rm LV}$, where $f_{\rm LV}$ is a real form factor parameterizing potential anomalous left-handed vector couplings. The extraction is based on the ratio of the measured to the predicted cross section, under the assumption that $|V_{td}|, |V_{ts}| \ll |V_{tb}|$. The combined result shows good agreement with the NLO+NNLL SM prediction [243].

At $\sqrt{s} = 13$ TeV, analyses progressed with increasingly larger datasets. ATLAS first studied the DL channel, defining signal and control regions by jet and b-tag multiplicities and employing BDTs to separate the tW signal from backgrounds, measuring a cross section consistent with the SM [264]. Differential cross sections were also obtained as functions of the b-jet energy, the energy of the $\ell\ell b$ system, and various invariant and transverse masses involving the leptons, b-jet, and neutrinos [265].

A subsequent ATLAS analysis using the full Run 2 dataset improved precision by employing a BDT discriminant in three jet and b-tag–defined signal regions, with the cross section extracted from a profile-likelihood fit [266]. The measurement is dominated by systematic uncertainties, and a value of V_{tb} was also extracted.

CMS performed measurements in the DL channel with a partial dataset, selecting events with one tight and one loose lepton and at least one b-tagged jet. A BDT was used to separate signal from background, and the cross section was extracted with a likelihood fit [267]. The same dataset enabled a preliminary differential measurement in a fiducial region requiring exactly one b-tagged jet [268]. CMS also analyzed the LJ channel, where a BDT was employed to discriminate tW from $t\bar{t}$, with other backgrounds constrained using data-driven methods. This led to the first observation of tW production in the LJ final state, with a significance exceeding 5σ [269].

Finally, using the full Run 2 dataset, CMS measured inclusive and normalized differential cross sections in $e\mu$ events [270]. A multivariate discriminant was used to isolate the signal for the inclusive measurement, yielding a cross section consistent with the SM. The differential distributions were unfolded to the particle level in a fiducial region requiring exactly one b jet and were found to agree with NLO QCD predictions.

At $\sqrt{s} = 13.6$ TeV, CMS measured tW production using a partial dataset of 34.7 fb^{-1} [271]. The analysis includes both inclusive and differential cross sections in the DL($e\mu$) channel. For the differential measurements at the stable-particle level in a fiducial phase space, good agreement was observed with the predictions. The inclusive cross section is consistent with the NNLO QCD prediction, with the overall precision limited by systematic uncertainties.

61.2.4 *Cross-section measurements of associated single production*

Beyond the primary single-top-quark production channels, rarer processes occur in association with EW bosons, such as tZ, $t\gamma$, tH, and tWZ. Although their cross sections are much smaller, these modes provide unique sensitivity to the couplings of the top quark to the Z boson, photon, and Higgs boson. They thus serve as precision tests of the SM and impose powerful constraints on

Int. J. Mod. Phys. A 2026.41. Downloaded from www.worldscientific.com
UNIVERSITY OF CALIFORNIA @ BERKELEY on 09/16/26. Re-use and distribution is strictly not permitted, except for Open Access articles.

Table 61.12: Single top-quark t-channel production measurements from the LHC.

Experiment [Ref.]	$\sqrt{s}$ (TeV)	Measurement
ATLAS [238]	5.02	$\sigma_{t+\bar{t}} = 27.1^{+6.2}_{-5.5}$pb $R_t = 2.73^{+1.75}_{-0.87}$ $f_{LV} \cdot \lvert V_{tb}\rvert = 0.94^{+0.11}_{-0.10}$
CMS [239]	5.02	$\sigma_{t+\bar{t}} = 30.2^{+5.8}_{-5.6}$pb $R_t = 2.6^{+1.3}_{-0.7}$
ATLAS [240]	7	$\sigma_t = 46 \pm 6$pb; $\sigma_{\bar{t}} = 23 \pm 4$pb $R_t = 2.04 \pm 0.18$ $\sigma_{t+\bar{t}} = 68 \pm 8$pb
CMS [242]	7	$\sigma_{t+\bar{t}} = 67.2 \pm 6.1$pb $\lvert V_{tb}\rvert = 1.020 \pm 0.049$
LHC [243]	7	$\sigma_{t+\bar{t}} = 67.5 \pm 5.7$pb
ATLAS [244]	8	$\sigma_t = 56.7^{+4.3}_{-3.8}$pb; $\sigma_{\bar{t}} = 32.9^{+3.0}_{-2.7}$pb $R_t = 1.72 \pm 0.09$ $f_{LV} \cdot \lvert V_{tb}\rvert = 1.029 \pm 0.048$ $\lvert V_{tb}\rvert > 0.92$ at 95% C.L.
CMS [246]	8	$\sigma_t = 53.8 \pm 4.6$pb; $\sigma_{\bar{t}} = 27.6 \pm 3.9$pb $R_t = 1.95 \pm 0.21$ $\sigma_{t+\bar{t}} = 83.6 \pm 7.7$pb $\lvert V_{tb}\rvert = 0.998 \pm 0.041$
LHC [243]	8	$\sigma_{t+\bar{t}} = 87.7 \pm 5.8$pb
CMS [250] [252]	13	$\sigma_t = 130 \pm 19$ pb; $\sigma_{\bar{t}} = 77 \pm 12$ pb $R_t = 1.68 \pm 0.054$ $\lvert V_{tb}\rvert > 0.970$ $\lvert V_{tb}\rvert = 0.988 \pm 0.024$ $\lvert V_{td}\rvert^2 + \lvert V_{ts}\rvert^2 = 0.06 \pm 0.06$
ATLAS [253]	13	$\sigma_t = 137^{+8}_{-8}$pb; $\sigma\bar{t} = 84^{+6}_{-5}$pb $R_t = 1.636^{+0.036}_{-0.034}$ $\sigma_{t+\bar{t}} = 221 \pm 13$pb $f_{LV} \cdot \lvert V_{tb}\rvert = 1.015 \pm 0.031$ $f_{LV} \cdot \lvert V_{td}\rvert < 0.13$ $f_{LV} \cdot \lvert V_{ts}\rvert < 0.31$ EFT coefficients constraints

Table 61.13: Single top-quark s-channel production measurements from the LHC.

Experiment [Ref.]	$\sqrt{s}$ (TeV)	Measurement
ATLAS [258]	7	$\sigma_s < 26.5$ (20.5) pb
CMS [255]	7	$\sigma_s = 7.1 \pm 8.1$ pb
ATLAS [256]	8	$\sigma_s = 4.8^{+1.8}_{-1.5}$ pb 3.2σ obs. (3.9σ exp.)
CMS [255]	8	$\sigma_s = 13.4 \pm 7.3$ pb $R_s = 2.0 \pm 0.9$ combining 7 and 8 TeV 2.5σ obs. (1.1σ exp.)
LHC [243]	8	$\sigma_s = 4.9 \pm 1.4$ pb
ATLAS [257]	13	$\sigma_s = 8.2^{+3.5}_{-2.9}$ pb 3.3σ obs. (3.9σ exp.)

anomalous couplings and possible effects of new physics [272,273]. The Tevatron lacked the sensitivity to observe these processes, and only with the increased energy and luminosity of the 13 TeV LHC dataset has evidence for them been obtained. The following sections summarize these measurements in order of decreasing production rate, and Fig. 61.8 presents an overview of the ATLAS and CMS results for associated single-top-quark production at 13 TeV.

61.2.4.1 *Associated single production with a photon*

As in the case of $t\bar{t} + \gamma$, the measurement of single-top+γ production requires a well-defined fiducial phase-space definition that specifies the photon kinematic and isolation criteria, as well as its separation from other objects, to ensure that the measured cross section corresponds to a clearly defined and reproducible region of phase space.

The first evidence for the associated production of a single top quark with a photon was reported by CMS at $\sqrt{s} = 13$ TeV using a partial dataset [274]. A multivariate discriminant was applied to events containing a muon, a photon, and jets. For isolated photons with $p_{\mathrm{T}} > 25$ GeV in the central detector region ($|\eta_\gamma| < 1.44$), the measured cross section times branching fraction was found to be consistent with the SM expectation. At the same center-of-mass energy, ATLAS achieved the first observation of this process [275], exploiting the presence of a forward jet and using neural networks for signal discrimination. Requiring a photon with $p_{\mathrm{T}} > 20$ GeV within the detector acceptance ($|\eta_\gamma| < 2.37$), ATLAS measured a fiducial cross section consistent with the NLO QCD prediction of 515^{+36}_{-42} fb, with $t\bar{t}\gamma$ modeling among the leading sources of uncertainty. The results are summarized in Table 61.15.

61.2.4.2 *Associated single production with a Z boson*

The tZq process probes both the WWZ coupling, when the Z boson is emitted from the t-channel W in single-top production, and the tZ coupling, when the Z is radiated from the top quark.

At $\sqrt{s} = 8$ TeV, CMS searched for tZq production in trilepton

Int. J. Mod. Phys. A 2026.41. Downloaded from www.worldscientific.com
by UNIVERSITY OF CALIFORNIA @ BERKELEY on 09/16/26. Re-use and distribution is strictly not permitted, except for Open Access articles.

Table 61.14: Single top-quark tW-channel measurements from the LHC. Unless indicated, measurements are extracted in the DL channel.

Experiment [Ref.]	$\sqrt{s}$ (TeV)	Measurement
ATLAS [259]	7	$\sigma_{tW} = 16.8 \pm 5.7$ pb $\lvert V_{tb}\rvert = 1.03^{+0.16}_{-0.19}$ 3.3σ obs. (3.4σ exp.)
CMS [260]	7	$\sigma_{tW} = 16^{+5}_{-4}$ pb 4.0σ obs. (3.6σ exp.)
LHC [243]	7	$\sigma_{tW} = 16.3 \pm 4.1$ pb
ATLAS [261]	8	$\sigma_{tW} = 23.0^{+3.6}_{-3.9}$ pb $\lvert V_{tb}\rvert = 1.01 \pm 0.10$ at 95% C.L.
ATLAS [262]	8	$\sigma_{tW} = 26 \pm 7$ pb (LJ channel)
CMS [263]	8	$\sigma_{tW} = 23.4 \pm 5.4$ pb $\lvert V_{tb}\rvert = 1.03 \pm 0.13$
LHC [243]	8	$\sigma_{tW} = 23.1 \pm 3.6$ pb $\lvert V_{tb}\rvert = 1.02 \pm 0.045 > 0.79$, with 7 and 8 TeV
ATLAS [264]	13	$\sigma_{tW} = 94^{+30}_{-24}$ pb
ATLAS [266]	13	$\sigma_{tW} = 75^{+15}_{-14}$ pb $\quad \lvert V_{tb}\rvert = 0.97 \pm 0.10$
CMS [267]	13	$\sigma_{tW} = 63.1 \pm 7.0$ pb
CMS [269]	13	$\sigma_{tW} = 89 \pm 13$ pb (LJ channel)
CMS [270]	13	$\sigma_{tW} = 79.2^{+7.8}_{-8.1}$ pb
CMS [271]	13.6	$\sigma_{tW} = 82.3^{+10.6}_{-10.5}$ pb

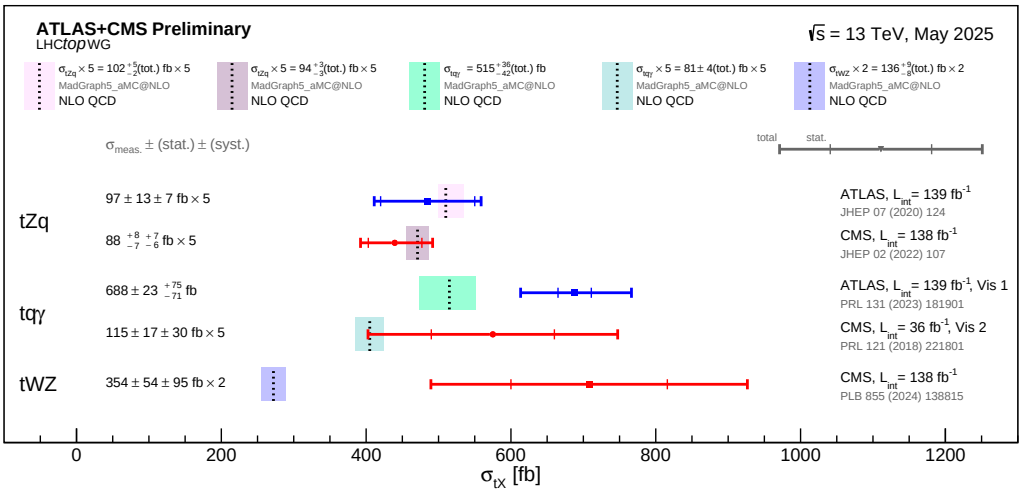

Figure 61.8: Summary of ATLAS and CMS measurements of $t + WZ$, $t + Z$ and $t + \gamma$ cross sections at 13 TeV. The cross-section measurements are compared to the NLO QCD theoretical calculation. "Vis 1" and "Vis 2" highlight that the relevant phase space used for the ATLAS and CMS $t\gamma$ measurements is different. The theory prediction and experimental results of tZ, and those of the CMS $t\gamma$ measurement, are multiplied by a factor of 5 to allow for easy visualization on the same scale; those of the CMS tWZ measurement are multiplied by a factor of 2. The theory bands represent uncertainties due to renormalization and factorization scales and parton density functions. The LHCtopWG working group kindly provides the plot, status as of May 2025, see `https://twiki.cern.ch/twiki/bin/view/LHCPhysics/LHCTopWGSummaryPlots`.

Table 61.15: Associated single top-quark production with a photon measurements from the LHC.

Experiment [Ref.]	$\sqrt{s}$ (TeV)	Measurement
CMS [274]	13	$\sigma_{t\gamma} = 115 \pm 34$fb ($p_T^\gamma > 25$ GeV; $\lvert\eta_\gamma\rvert < 1.44$) 4.4σ obs. (3.0σ exp.)
ATLAS [275]	13	$\sigma_{t\gamma} = 688^{+78}_{-75}$fb ($p_T^\gamma > 20$ GeV; $\lvert\eta_\gamma\rvert < 2.37$) 9.3σ obs. (6.8σ exp.)

events and reported a hint of signal with a significance of 2.4σ relative to the background-only hypothesis [276].

At $\sqrt{s} = 13$ TeV, both CMS and ATLAS measured tZq production in events with three leptons from $Z \to \ell^+\ell^-$ and top quark decay. CMS reported evidence using a partial dataset [274], followed by an observation with the full dataset [277], and later a comprehensive analysis of inclusive and differential cross sections [278]. The latter included the ratio of cross sections for top-and antitop-associated production, as well as the first differential measurements at both parton and particle levels. The spin asymmetry, sensitive to top-quark polarization, was also determined from the parton-level distribution of the polarization angle. All results were consistent with NLO SM predictions. ATLAS employed a simultaneous binned maximum-likelihood fit with neural-network discriminants to improve background rejection, extracting a signal also consistent with the SM expectation [279].

Int. J. Mod. Phys. A 2026.41. Downloaded from www.worldscientific.com
UNIVERSITY OF CALIFORNIA @ BERKELEY on 09/16/26. Re-use and distribution is strictly not permitted, except for Open Access articles.

These results are summarized in Tab. 61.16.

61.2.4.3 *Associated single production with a W and Z boson*

At $\sqrt{s} = 13$ TeV, CMS reported the first evidence for single-top-quark production in association with a W and a Z boson in multilepton final states [280], with the Z reconstructed from e^+e^- or $\mu^+\mu^-$ pairs. The analysis made extensive use of multivariate techniques applied across multiple regions and event categories to suppress backgrounds and extract the signal. A key challenge was separating the tWZ signal from the dominant $t\bar{t}Z$ background, which was addressed using improved tWZ modeling.

This result was recently updated using both 13 and 13.6 TeV datasets, corresponding to an integrated luminosity of about 200 fb^{-1} [281]. Events with three or four leptons were divided into distinct signal regions based on the output of a machine-learning classifier with multiple output nodes, and the distributions in these categories were used in a profile-likelihood fit. For the 13 TeV dataset alone, the expected significance increased from 1.4σ in the first analysis to approximately 3σ. Combining the 13 and 13.6 TeV results, summarized in Tab. 61.17, led to the first observation of the tWZ process.

61.2.5 *Properties*

The following sections provide an overview of experimental results on **top-quark properties**, that is, the intrinsic or fundamental characteristics of the particle itself, rather than how it is produced or which process it participates in. In this context, "top-quark properties" serves as an umbrella term for all observables that characterize the nature of the top quark itself, independent of the particular process used to measure them. Measurements of these properties provide stringent tests of the SM and sensitivity to new physics.

Intrinsic properties are quantities that define the top quark as a fundamental particle in the SM, including its mass (m_t), electric charge ($+2/3\,e$), spin (1/2), and lifetime or decay width (Γ_t). Interaction properties describe how the top quark couples to other SM particles, its couplings to the W, Z, and Higgs bosons, as well as to gluons and photons. These reflect the particle's gauge and Yukawa interactions, which are part of its defining characteristics within the SM. Derived properties, such as polarization, spin correlations, and charge asymmetries, characterize the behavior of the top quark in production and decay and reveal how its intrinsic features manifest dynamically.

This section begins with measurements of m_t and Γ_t, followed by studies of its decay and spin structure, including polarization, spin correlations in $t\bar{t}$ pairs, and the observation of quantum entanglement in $t\bar{t}$ events. In this context, results on the production of a pseudo-bound state at the $t\bar{t}$ threshold are also reviewed. The V–A structure of the Wtb vertex is examined through measurements in both single-top-quark and $t\bar{t}$ events. Finally, results on asymmetries in $t\bar{t}$ and $t\bar{t} + X$ production are summarized and compared with theoretical expectations.

Most results are obtained from $t\bar{t}$ events, with analyses categorized according to the final state: lepton+jets (LJ), dilepton (DL), and all-hadronic (AH), as described in Sect. 61.2.1.

61.2.5.1 *Mass*

In the early 1990s, indirect constraints from precision measurements at CERN's LEP collider suggested that m_t lay between about 150 and 200 GeV, based on radiative corrections to EW observables involving the Z boson. In 1995, the top quark was directly discovered by the CDF and D0 collaborations at the Tevatron $p\bar{p}$ collider at Fermilab, with an initial mass estimate in the range of 151–197 GeV. Subsequent measurements at the Tevatron rapidly improved the precision, establishing the top-quark mass near 175 GeV. With the start of the LHC program, measurements by ATLAS and CMS further reduced the uncertainty to below 1 GeV, making m_t one of the most precisely determined parameters of the SM.

Final state topologies The top-quark mass has been determined in both top-quark pair and single-top-quark production, exploiting a variety of decay channels, each with distinct sensitivities to systematic uncertainties. This diversity enables internal consistency checks and improved precision when results are combined. The "standard" analyses use inclusive $t\bar{t}$ final states, classified into the DL, LJ, and AH channels, and further distinguished as **resolved**, when all decay products can be individually reconstructed, or **boosted**, when the large p_{T} of the top quarks causes two or more decay products to merge into a single reconstructed object in the detector, as described in Sec. 61.2.1. Since final states with many jets lead to larger overall systematic uncertainties, alternative channels have also been explored for measuring the m_t. Examples include events in which the b hadron decays semileptonically and produces a low-p_{T} ("soft") lepton, which can be combined with other objects to form an observable sensitive to m_t, or decays containing a J/ψ meson. These approaches benefit from a reduced impact of jet-related uncertainties but suffer from the low branching ratios of the relevant b-hadron decays, resulting in larger statistical uncertainties.

Reconstruction of observables

The first step in a top-quark mass measurement is to identify an observable sensitive to m_t and reconstruct it from the event. The calculation of such observables requires assigning the parton-level objects to the reconstructed objects in the detector. An assignment is considered correct ("matched") if $\Delta R(\text{parton}, \text{detector object}) < 0.3$ or 0.4. Three categories are defined: correctly matched events, incorrectly matched events, and unmatched events, the latter occurring when at least one parton cannot be matched to a reconstructed object, for example, because it fails the selection criteria or lies outside the detector acceptance. While leptons are matched with very high efficiency, the matching efficiency for jets is significantly lower.

Several methods exist for jet–parton assignment. Kinematic fits are widely used, as they both improve the resolution of reconstructed observables and provide a goodness-of-fit estimator, which helps identify correctly matched events [282]. Matching can be further enhanced using machine-learning techniques, such as deep neural networks trained with correct assignments as signal and incorrect assignments as background. Since combinatorial mismatches worsen mass resolution and increase overall uncertainty, removing unmatched or incorrectly matched events is crucial. One common strategy is to reject events in the tails of reconstructed mass distributions, which are rarely populated by correctly matched events. The goodness-of-fit from kinematic fits also enables event selection with high probability of correct assignment [283–286]. In another approach, a BDT was trained to distinguish correctly from incorrectly or unmatched events, and events were selected by applying a cut on the classifier output [282].

In the LJ and AH final states, the invariant mass of the objects assigned to their parton-level particles, m_t^{reco}, is often used for the measurement. In the DL channel, a full reconstruction of the events is more challenging due to the presence of two neutrinos in the final state. To address this, several methods have been developed, such as full kinematic reconstruction [287,288]. At the Tevatron, the neutrino-weighting and matrix-element-weighting techniques were introduced [289–291].

In the neutrino-weighting method, for each assumed value of m_t, energy and momentum conservation is applied to the decay, yielding up to four possible solutions for the neutrino and antineutrino momenta. The missing transverse energy calculated from these solutions is then compared with the observed missing E_T to assign a weight. In the matrix-element weighting method, the neutrino momenta are likewise solved up to a fourfold ambiguity, but each solution is assigned a weight proportional to the likelihood of the kinematics arising from $t\bar{t}$ production and decay at that mass hypothesis. By scanning over m_t values (typically in the range 80–280 GeV), one obtains a weight distribution that reflects the production kinematics, decay distributions, and available phase space, which is then used to extract m_t.

Alternatively, without requiring full event reconstruction, several observables directly sensitive to the top-quark mass can be used, albeit with larger systematic uncertainties. One example is the invariant mass of the b-jet–lepton pair, $m_{\ell b}^{\mathrm{reco}}$ [292], or event variables such as the scalar sum of jet transverse energies and the missing transverse energy [293], both of which reduce the depen-

Int. J. Mod. Phys. A 2026.41. Downloaded from www.worldscientific.com
by UNIVERSITY OF CALIFORNIA @ BERKELEY on 09/16/26. Re-use and distribution is strictly not permitted, except for Open Access articles.

Table 61.16: Associated single top-quark production with a Z boson measurements from the LHC.

Experiment [Ref.]	$\sqrt{s}$ (TeV)	Measurement
CMS [278]	13	$\sigma_{tZq} = 87.9^{+10.5}_{-9.5}$ fb for $m(\ell\ell) > 30$ GeV $R_t = 2.37^{+0.62}_{-0.44}$ $A_l = 0.58^{+0.16}_{-0.17}$
ATLAS [279]	13	$\sigma_{tZq} = 97 \pm 15$ fb for $m(\ell\ell) > 30$ GeV

Table 61.17: Associated single top-quark production with a W and Z bosons measurements from the LHC.

Experiment [Ref.]	$\sqrt{s}$ (TeV)	Measurement
CMS [280]	13	$\sigma_{tWZ} = 354 \pm 109$ fb 3.5σ obs. (1.4σ exp.)
CMS [281]	13	$\sigma_{tWZ} = 248 \pm 52$ fb
	13.6	$\sigma_{tWZ} = 244 \pm 74$ fb 5.8σ obs. (3.5σ exp.) in combination

dence on jet-related uncertainties. In final states with additional leptons from b-hadron decays, the invariant mass of all leptons can be used [294–296]. Another approach exploits the invariant mass of a charged lepton from the W decay and the tracks forming a secondary vertex from the b hadron [297].

In addition to observables directly sensitive to the top-quark mass, auxiliary observables are often employed to reduce specific groups of uncertainties. The invariant mass of the hadronically decaying W boson, m_W^{reco}, is widely used to constrain the jet-energy scale (JES). This can be achieved either by extracting a dedicated jet-energy scale factor (JSF) simultaneously with m_t [298,299], or by using the ratio of the jet energies assigned to the top quark and to the W boson [300,301].

When the uncertainty in the b-JES is also relevant, an additional observable can be introduced to determine the b-to-light jet scale factor (bJSF) [282]. To ensure sensitivity primarily to the bJSF rather than the overall JSF, the ratio of jet momenta assigned to the W boson and to the b jets is used, denoted R_{bq}^{reco} in the following.

Measurement techniques

A wide range of techniques has been developed to extract m_t, many of which have subsequently found applications in other areas of particle physics. The most precise determinations proceed by reconstructing an observable in data and comparing it to the same observable obtained from Monte Carlo simulations generated with different input values of m_t. This so-called *template method* has been the most widely used approach, see for example Refs. [283, 284,302,303]. The template method has been used to extract m_t since the first direct measurement at the Tevatron. It remains in use today, now often fitting multiple observables simultaneously to constrain the main systematic uncertainties.

Owing to its good signal-to-background ratio and the ability to use the hadronic W decay to constrain the dominant JES uncertainty, the LJ channel is considered the golden channel for top-quark mass measurements.

At the Tevatron, considerable effort was devoted to improving the statistical precision of m_t measurements, leading to the development of new techniques. In the DL channel, methods were introduced that fit the dynamics of the decay products and evaluate per-event weights (matrix-element weighting) as mentioned above. In the LJ channel, the so-called *matrix-element method* was pioneered [304]. In this approach, a probability density is calculated for each event as a function of m_t, using a leading-order matrix element for $t\bar{t}$ production and decay. The probability densities are calculated using the four-momenta of the reconstructed objects, taking into account all possible jet–parton assignments. An *in situ* calibration of dijet pairs to the $W \to jj$ hypothesis is simultaneously performed to constrain the JES uncertainty [299]. The top-quark mass is then extracted from a likelihood fit to the ensemble of events, with each event contributing its own likelihood distribution, in contrast to the template method, where each event contributes a single number.

In the template method, templates are constructed from simulated samples generated with different input values of m_t for the observables used in the measurement. Typically, only one jet–parton permutation is considered per event. The top-quark mass is then extracted from a binned or unbinned maximum-likelihood fit. In the LJ channel, simultaneous fits of m_t together with the JSF and bJSF parameters have also been performed [282, 298].

The *ideogram* m_t method [305] is an unbinned likelihood fit that incorporates up to four jet–parton permutations, weighted to reduce the impact of incorrect assignments. The weights are derived from the goodness-of-fit probabilities obtained from the kinematic reconstruction. CMS employed this method to measure m_t simultaneously with an overall JSF, where the JSF was constrained by a Gaussian prior whose width was set to the total uncertainty of the JES corrections [306].

As the available statistics increased, methods aimed at reducing systematic uncertainties became more widely developed. In recent years, the use of *profile-likelihood fits* has grown. These are maximum-likelihood fits in which systematic uncertainties are incorporated as nuisance parameters. The nuisance parameters can be constrained in the fit, resulting in a reduction in overall uncertainty compared to traditional methods. However, greater care is required for uncertainties derived from comparisons of different Monte Carlo setups, which combine the effects of multiple variations. A notable example is the modeling uncertainty associated with hadronization, which is often evaluated by comparing simulations based on string and cluster models.

Results from the Tevatron

Both the DØ and CDF experiments performed numerous top-quark mass measurements, exploring various strategies to reduce the overall uncertainty in different final states. These included the use of matrix-element and template techniques, as well as alternative approaches such as exploiting soft-muon decays [294], the transverse momentum of the lepton [307], and global event variables like the scalar sum of jet transverse energies and the missing transverse energy [293].

The most precise results from both experiments are summarized in Tab. 61.18, which also shows their combination. This average incorporates published Run 1 (1992–1996) results together with the most precise published and preliminary Run 2 (2001–2011) measurements, based on up to 9.7 fb^{-1} of Tevatron data. Accounting for correlations among uncertainties, and combining statistical and systematic contributions in quadrature, the Tevatron average yields $m_t = 174.30 \pm 0.65$ GeV, corresponding to a relative precision of 0.37% [308].

Results from the LHC

In the following, the precision of top-quark mass measurements at the LHC is examined across different decay topologies and anal-

Int. J. Mod. Phys. A 2026.41. Downloaded from www.worldscientific.com
UNIVERSITY OF CALIFORNIA @ BERKELEY on 09/16/26. Re-use and distribution is strictly not permitted, except for Open Access articles.

Table 61.18: Summary of Tevatron top-quark mass measurements.

Experiment [Ref.]	**Lumi.** (fb^{-1})	**Topology**	m_t **(GeV)**
CDF (Run 1) [283]	0.1	LJ	176.1 ± 5.1 (stat) ± 5.3 (syst)
CDF (Run 1) [291]	0.1	DL	167.4 ± 10.3 (stat) ± 4.9 (syst)
CDF (Run 1) [309]	0.1	AH	186.0 ± 10.0 (stat) ± 5.7 (syst)
DØ(Run 1) [304]	0.1	LJ	180.1 ± 3.6 (stat) ± 3.9 (syst)
DØ(Run 1) [290]	0.1	DL	168.4 ± 12.3 (stat) ± 3.9 (syst)
CDF (Run 2) [310]	8.7	LJ	172.9 ± 0.5 (stat) ± 1.0 (syst)
CDF (Run 2) [311]	1.9	L_{XY}	166.9 ± 9.0 (stat) ± 2.8 (syst)
CDF (Run 2) [312]	8.7	E_T	173.9 ± 1.3 (stat) ± 1.4 (syst)
CDF (Run 2) [313]	9.1	DL	171.5 ± 1.3 (stat) ± 2.5 (syst)
CDF (Run 2) [314]	9.3	AH	175.1 ± 1.2 (stat) ± 1.6 (syst)
DØ(Run 2) [315]	9.7	LJ	175.0 ± 0.4 (stat) ± 0.6 (syst)
DØ(Run 2) [316]	9.7	DL	173.5 ± 1.3 (stat) ± 0.8 (syst)
CDF+DØ [308]	0.1-9.7	all	174.30 ± 0.35 (stat) ± 0.54 (syst)

ysis methods. Due to the large number of measurements that were carried out at the LHC, the focus will be on the most precise ones. Further measurements and more detailed discussions can be found in the reviews of the ATLAS and CMS experiments, published in Refs. [288, 317].

For the direct measurements, the most precise individual result is presented in Tab. 61.19 for each topology. Except for the measurement using J/ψ mesons in b-hadron decays, performed with the 8 TeV dataset, all results are based on 13 TeV data. Owing to the very large $t\bar{t}$ dataset available at the LHC (the 13 TeV sample alone contains more than 115 million events per experiment), statistical uncertainties are negligible for most analyses and become relevant only in rare topologies that exploit additional leptons from b-hadron decays.

The use of auxiliary observables in combination with profile-likelihood fits has substantially reduced the overall uncertainty in the LJ channel. In the resolved analysis [286], several auxiliary variables are included, such as m_W^{reco} and R_{bq}^{reco}. The former helps constrain uncertainties from JES corrections and final-state radiation (FSR). These sources, however, still dominate the overall uncertainty, with jet-flavor–dependent jet-energy corrections being the largest component.

In the boosted analysis [318], the observable sensitive to m_t is the average mass of the large-R jets, $\bar{m}_J$. As in the resolved analysis, m_W^{reco} is used to reduce sensitivity to jet-related uncertainties. A significant uncertainty in this channel arises from modeling the recoil scheme in Pythia for secondary and subsequent gluon emissions. This effect is mitigated by introducing a third observable, m_{tj}, defined as the invariant mass of the leptonically decaying top quark and the nearest additional jet. After these improvements, the dominant remaining uncertainties stem from the JES and $t\bar{t}$ modeling, particularly FSR and color-reconnection effects.

The systematic models used by ATLAS and CMS are not identical, leading to different dominant uncertainties in the measurements discussed here.

Each experiment has produced a combined measurement of the top-quark mass using its individual results. The CMS combination gives $m_t = 172.44 \pm 0.13$ (stat.) ± 0.47 (syst.) GeV [319], while the ATLAS combination yields $m_t = 172.69 \pm 0.25$ (stat.) $\pm$ 0.41 (syst.) GeV [282].

Global combinations from the Tevatron and the LHC account for correlations both within individual experiments and between different experiments. A Tevatron–LHC combination released in 2014 reported $m_t = 173.34 \pm 0.76$ GeV (0.44%) [320], but this result, based only on the 7 TeV LHC data, has since been superseded by the most recent LHC combination [1]. In this latest combination, ATLAS and CMS included fifteen individual measurements in leptonic and hadronic top-quark decays, as well as a measurement in events enriched with single-top production via the EW t-channel. The datasets correspond to the full 7 and 8 TeV samples. The combination was performed using the BLUE method [321], incorporating estimator correlations both within and across experiments. The impact of correlation choices on the final result was investigated and found to be small. The combined result is $m_t = 172.52 \pm 0.33$ GeV, corresponding to a relative precision of 0.2%, and is limited primarily by the b-jet energy scale (b-JES) uncertainty.

The direct measurements of the top-quark mass correspond to the parameter used in Monte Carlo generators, which is closely related to the pole mass [8]. The relation between the pole mass and short-distance mass definitions, such as $\overline{\mathrm{MS}}$, is affected by non-perturbative effects. Recent calculations estimate the renormalon ambiguity to be below 250 MeV, which remains smaller than the current measurement uncertainty [322, 323]. Other ambiguities, for example, the one related to the parton-shower cut-off value, can be of the order of 500 MeV [8, 324]. A calibration of the top-quark mass parameter in Powheg+Pythia 8 with respect to the MSR mass scheme [325] was performed by ATLAS. Using simulated $t\bar{t}$ events in the LJ channel and the mass distribution of large-radius jets containing the three quarks from the hadronic top decay, a difference between the Monte Carlo mass and the MSR mass of about 80 MeV was obtained, with large associated uncertainties [326].

As a result of renormalization at higher orders in perturbation theory, m_t depends on the scale at which it is defined. The first measurement of the running of the top-quark mass in the $\overline{\mathrm{MS}}$ scheme was reported by CMS [327]. The running mass was extracted from the differential cross section as a function of the $t\bar{t}$ invariant mass, unfolded to parton level in DL($e\mu$) final states. The result shows a variation of about 15% between $M_{t\bar{t}} = 400$ GeV and $M_{t\bar{t}} \approx 1$ TeV, in good agreement with the one-loop renormalization-group prediction. Relative to the hypothesis of no running, the significance of the observed effect is 2.6σ, although the interpretation is subject to large theoretical uncertainties [328].

Measurements of m_{t} based on inclusive and differential cross sections of $t\bar{t}$ and $t\bar{t}$+jet final states are summarized in Fig. 61.9. These have been performed at center-of-mass energies between 7 and 13 TeV using observables related to the production cross section. The most recent result, not yet included in this comparison, obtained by ATLAS at 13 TeV in the DL channel with $t\bar{t}$+jet final states, yields $m_{\mathrm{t}} = 170.9 \pm 1.5$ GeV [329].

Vacuum stability

With the discovery of a Higgs boson at the LHC with a mass of about 125 GeV [330, 331], the precise determination of the top-quark mass has taken a central role in assessing the stability of the EW vacuum. Radiative corrections from the top quark tend to drive the Higgs quartic coupling λ negative, potentially leading to vacuum instability. An NNLO calculation [2] indicates vacuum stability for a Higgs mass satisfying $M_H \geq 129.4 \pm 5.6$ GeV [332]. Within this uncertainty, a Higgs boson mass of 125 GeV is compatible with stability, although the central values of the Higgs boson and top-quark masses still allow for a metastable scenario.

In the context of the European Strategy for Particle Physics 2025 update, ATLAS and CMS prepared projections of future Higgs boson and m_t determinations [333], shown in Fig. 61.10. These projections are based on two m_t measurements at 8 and

Int. J. Mod. Phys. A 2026.41. Downloaded from www.worldscientific.com
by UNIVERSITY OF CALIFORNIA @ BERKELEY on 09/16/26. Re-use and distribution is strictly not permitted, except for Open Access articles.

Table 61.19: Comparison of the most precise individual measurements of m_t per decay topology. The uncertainties displayed are the statistical and systematic uncertainties. In the soft-muon-tag and the boosted topology, an additional uncertainty related to recoil effects in the simulation is also considered. The * indicates that the measurement was performed using 8 TeV data, while all others use 13 TeV datasets. The last row shows the LHC combination of 7 and 8 TeV results.

Exp. [Ref.]	m_t **(GeV)**	**Topology**	**Method**	**Dominant uncert.**
CMS [286]	$171.77 \pm 0.04 \pm 0.37$	Resolved (LJ)	profile LH (5D)	JES, FSR
CMS [141]	$172.33 \pm 0.14\ ^{+0.66}_{-0.72}$	Resolved (DL)	profile LH	JES, MC statistics
CMS [285]	$172.34 \pm 0.20 \pm 0.70$	Resolved (AH)	ideogram	JES, color reconnection
ATLAS [318]	$172.95 \pm 0.27 \pm 0.46$	Boosted (LJ)	profile LH (3D)	JES, $t\bar{t}$ modelling
CMS [296]	$173.5 \pm 3.0 \pm 0.9$	J/Ψ (LJ)*	template	data statistics
ATLAS [295]	$174.41 \pm 0.39 \pm 0.66 \pm 0.25$	Soft muon tag (LJ)	profile LH	b fragmentation/decay, data statistics
CMS [267]	$172.13 \pm 0.32\ ^{+0.69}_{-0.71}$	Single top	particle-level profiled	JES
LHC [1]	$172.52 \pm 0.14 \pm 0.30$	7 and 8 TeV results	BLUE	b-JES

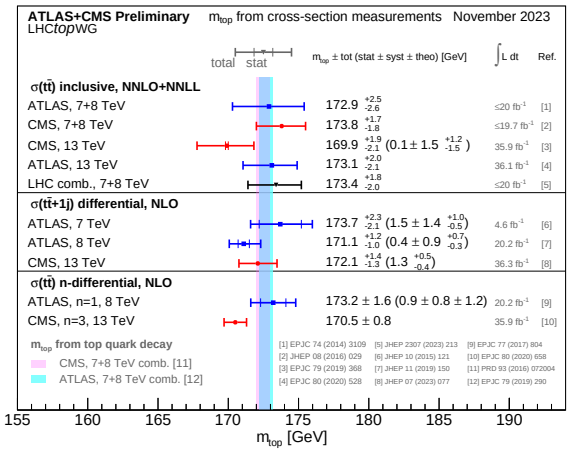

Figure 61.9: Comparison of ATLAS and CMS measurements of the top-quark mass using observables related to $t\bar{t}$ and $t\bar{t}$+jet production. The LHCtopWG working group kindly provides the plot, status as of November 2023, see `https://twiki.cern.ch/twiki/bin/view/LHCPhysics/LHCTopWGSummaryPlots`.

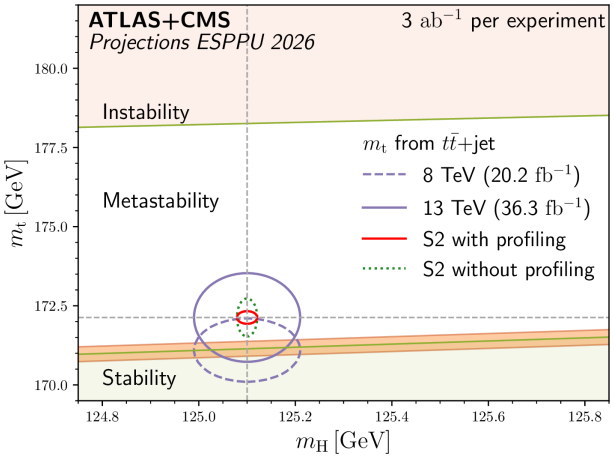

Figure 61.10: Regions of stability, metastability and instability of the SM potential as a function of the top-quark and the Higgs-boson masses [333]. The input measurements from ATLAS and CMS were used to extrapolate the size of the dataset to 3 ab^{-1}, using different assumptions on the systematic uncertainties and analysis methods.

13 TeV, obtained from differential cross-section measurements in $t\bar{t}$+jets final states. For the projections, different scenarios for reducing systematic uncertainties and employing alternative analysis methods are explored. Further projections can be found in the same document.

CPT test based on m_t measurements

The CPT theorem requires that particles and their antiparticles have identical masses, lifetimes, and absolute charges. A test of this symmetry has been performed by measuring the mass difference between the top and antitop quarks, $\Delta m_t = m_t - m_{\bar{t}}$, which is expected to vanish if CPT is conserved. The top and antitop quarks are distinguished through the charge of the decay lepton, and such measurements have been performed at both the Tevatron and the LHC. The results, summarized in Tab. 61.20, are consistent with the SM expectation of no mass difference, with a current sensitivity at the level of a few hundred MeV.

61.2.5.2 *Width*

The top-quark width, inversely proportional to its lifetime, is expected to be of order 1 GeV (Eq. 1). Early measurements made at CDF [340] and CMS [341] established confidence-level intervals for the width but lacked the sensitivity to make a direct measurement.

The total width of the top quark can be inferred from the partial decay width $\Gamma(t \to Wb)$ and the branching fraction $B(t \to Wb)$. DØ extracted $\Gamma(t \to Wb)$ from the measured t-channel single-top-quark production cross section, and $B(t \to Wb)$ from the ratio $R = B(t \to Wb)/B(t \to Wq)$ in $t\bar{t}$ events in the LJ channel with 0, 1, and 2 b-tags. Assuming $B(t \to Wq) = 1$ for any kinematically allowed quark q, the result was $\Gamma_t = 2.00^{+0.47}_{-0.43}$ GeV, corresponding to a top-quark lifetime of $\tau_t = (3.29^{+0.90}_{-0.63}) \times 10^{-25}$ s. Under the assumption of a heavy fourth-generation b' quark and unitarity of the four-generation mixing matrix, an upper limit of $|V_{tb'}| < 0.59$ at 95% C.L. was obtained [342].

The first direct measurement of the top-quark width was performed by ATLAS at $\sqrt{s} = 8$ TeV, fitting reconstructed LJ events, and yielded $\Gamma_t = 1.76 \pm 0.33$ (stat.)$^{+0.79}_{-0.68}$ (syst.) GeV [343]. A more recent ATLAS analysis at $\sqrt{s} = 13$ TeV, based on a template fit to the lepton–b-quark invariant mass in DL final states, obtained $\Gamma_t = (1.9 \pm 0.5)$ GeV [344].

A similar analysis performed by CMS at $\sqrt{s} = 8$ TeV provided a more precise determination of the width, yielding $\Gamma_t = 1.36 \pm 0.02$ (stat.) $^{+0.14}_{-0.11}$ (syst.) GeV [345].

61.2.5.3 *Top Quark Spin Correlations, Polarization, and Entanglement*

One of the unique features of the top quark is that it decays before QCD interactions can flip its spin. Thus, the top quark polarization is directly observable via the angular distribution of its decay products, and it is possible to define and measure observables sensitive to the top quark spin and its production mechanism. Although the top and antitop-quarks produced by QCD interactions in hadron collisions are essentially unpolarized, the spins of t and $\bar{t}$ are correlated. For QCD production at threshold, the $t\bar{t}$ system is produced in a $^3S_1$ state with parallel spins for $q\bar{q}$ annihilation or in a $^1S_0$ state with antiparallel spins for gluon-gluon fusion, as shown in Fig. 61.11.

The production mechanisms at the Tevatron, where $t\bar{t}$ pairs

Int. J. Mod. Phys. A 2026.41. Downloaded from www.worldscientific.com
UNIVERSITY OF CALIFORNIA @ BERKELEY on 09/16/26. Re-use and distribution is strictly not permitted, except for Open Access articles.

Table 61.20: Comparison of the measurements of $\Delta m_t = m_t - m_{\bar{t}}$ in $t\bar{t}$ and single-top events.

Exp. [Ref]	$\sqrt{s}$ (TeV)	Δm_t [GeV]	Topology
CDF [334]	1.96	$-1.95 \pm 1.11(stat.) \pm 0.59(syst.)$	$t\bar{t}$ LJ
DØ [335]	1.96	$0.84 \pm 1.81(stat.) \pm 0.48(syst.)$	$t\bar{t}$ LJ
ATLAS [336]	7	$0.67 \pm 0.61(stat.) \pm 0.41(syst.)$	$t\bar{t}$ LJ
CMS [337]	7	$-0.44 \pm 0.46(stat.) \pm 0.27(syst.)$	$t\bar{t}$ LJ
CMS [338]	8	$-0.15 \pm 0.19(stat.) \pm 0.09(syst.)$	$t\bar{t}$ LJ
CMS [339]	13	$0.83^{+1.79}_{-1.35}(stat. + syst.)$	single-top LJ

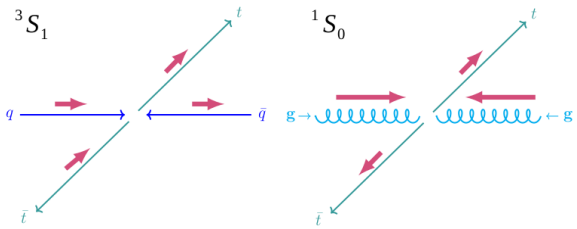

Figure 61.11: Spin state of the $t\bar{t}$ system at the production threshold for $q\bar{q}$ annihilation (left) and gluon-gluon fusion (right). The thin arrows describe the momentum direction of the particles, while the thicker arrows reflect the spin direction of the gluons (long arrows) and the quarks (short arrows).

are predominantly produced via $q\bar{q}$ annihilation, and at the LHC, where gluon–gluon fusion dominates, are therefore complementary. At the LHC, $t\bar{t}$ production at large invariant mass arises mainly from gluons with opposite helicities, resulting in $t\bar{t}$ pairs with parallel spins, similar to the configuration produced at the Tevatron through $q\bar{q}$ annihilation.

The top-quark spin is fully correlated with the angular distributions of the down-type fermion (charged lepton or d-type quark) in the decay. The corresponding joint angular distribution is given in Refs. [346–348]

$$\frac{1}{\sigma}\frac{d^2\sigma}{d(\cos\theta^i_+)d(\cos\theta^j_-)} = \frac{1}{4}(1 + B^i_+\cos\theta^i_+ + B^j_-\cos\theta^j_- + C_{ij}\cdot\cos\theta^i_+\cdot\cos\theta^j_-), \tag{61.5}$$

where θ^i_+ and θ^j_- are the angles of the daughters in the top-quark (antitop-quark) rest frame with respect to a particular spin quantization axis i (j). The maximum value for C, 0.782 at NLO at the Tevatron [349], is found in the off-diagonal basis [346], while at the LHC the value at NLO is 0.326 in the helicity basis [349]. The coefficients B_+ and B_- are near zero in the SM because the top quarks are unpolarized in $t\bar{t}$ production. In place of C, $A\alpha_+\alpha_-$ is often used, where α_i is the spin analyzing power, and A is the spin correlation coefficient, defined as

$$A = \frac{N(\uparrow\uparrow) + N(\downarrow\downarrow) - N(\uparrow\downarrow) - N(\downarrow\uparrow)}{N(\uparrow\uparrow) + N(\downarrow\downarrow) + N(\uparrow\downarrow) + N(\downarrow\uparrow)}, \tag{61.6}$$

where the first arrow represents the direction of the top quark spin along a chosen quantization axis, and the second arrow represents the same for the antitop-quark. The spin analyzing power α_i at parton level is +0.998 for positively charged leptons, -0.966 for down-type quarks from W decays, and -0.393 for bottom quarks [350]. The sign of α flips for the respective antiparticles. The spin correlation could be modified by a new $t\bar{t}$ production mechanism such as through a Z' boson, Kaluza-Klein gluons, a dark-matter mediator, or a Higgs boson.

Measurement of SM spin correlation fraction

The experiments typically use Monte Carlo simulation to provide templates for the measured distributions, or a matrix-element method, and fit a parameter $f_{\rm SM}$, representing the fraction of events with the expected SM correlation, with $(1 - f_{\rm SM})$ the fraction with no correlation. The correlation coefficient is extracted via $A_{\rm meas} = f \cdot A_{\rm SM}$. A 'fraction' $f_{\rm SM} > 1$ means that the measured correlation coefficient is larger than the SM expectation. DØ pioneered the study of spin correlations in $t\bar{t}$ production during Run 1 [351], setting the first limits of $\kappa > -0.25$ at the 68% confidence level using the DL channel. In Run 2, both CDF and DØ extended the studies to the DL and LJ channels. Although the sensitivity was limited, these analyses provided the first evidence for spin-correlation effects [352–355].

Spin correlations have been conclusively established at the LHC by both ATLAS and CMS. In the dominant gluon-gluon-fusion production mode for $t\bar{t}$ pairs, the angular separation between the two leptons in the DL channel is sensitive to the degree of spin correlation [356].

Measurements have been performed at $\sqrt{s} = 7$, 8, and 13 TeV, with the corresponding values of $f_{\rm SM}$ summarized in Tab. 61.21. While the $\sqrt{s}$ dependence of the correlations is of interest as a probe of the production mechanism ($q\bar{q}$ annihilation versus gluon-gluon fusion) and as a potential window to new physics, the 7 and 8 TeV results [357–363] were limited by relatively large uncertainties. These have since been superseded by the high-statistics measurements at 13 TeV, which are reviewed here in more detail.

At $\sqrt{s} = 13$ TeV, the most recent ATLAS measurement of $f_{\rm SM}$ is based on $\Delta\phi$, the azimuthal angle between the two charged leptons in $e\mu$ events, within an analysis that also measures the differential cross sections in $\Delta\phi$ and $\Delta\eta$ [364]. The comparison with NLO Monte Carlo generators yields $f = 1.249 \pm 0.024$ (stat.) $\pm$ 0.061 (syst.)$^{+0.067}_{-0.090}$ (theo.). While earlier measurements were statistically consistent with the SM expectation of $f = 1.0$, the current result lies above this value by about 2.2σ. The NLO predictions considered are based on QCD corrections only and correspond to the production level. When EW corrections are included, the SM prediction becomes compatible with the measurement within uncertainties, although it is affected by a relatively large uncertainty, $f = 1.03 \pm 0.13$.

The CMS measurement at $\sqrt{s} = 13$ TeV was obtained from DL events by measuring parton-level normalized differential cross sections, which are sensitive to each of the independent coefficients of the spin-dependent parts of the $t\bar{t}$ production density matrix. These measured distributions and extracted coefficients were compared with SM predictions from simulations at NLO accuracy in QCD, and from NLO QCD calculations including EW corrections. The comparison with the simulation yields $f = 0.98 \pm 0.03$ (stat.) $\pm$ 0.04 (syst.) $\pm$ 0.01 (theo.). The normalized differential cross sections are used in fits to constrain the anomalous chromomagnetic and chromoelectric dipole moments of the top quark [154]: $-0.24 < C_{tG}/\Lambda^2 < 0.07$ TeV^{-2} and $-0.33 < C^I_{tG}/\Lambda^2 < 0.20$ TeV^{-2}, respectively, at 95% C.L. [365].

These results are part of a comprehensive study of the top quark spin density matrix at $\sqrt{s} = 13$ TeV, as measured through the coefficients of Eq. 61.5, which will be discussed further below.

Measurement of the full spin density matrix

Instead of extracting a single overall correlation coefficient or the fraction of SM-like spin correlation, the full spin density matrix can be measured. This requires determining the top- and antitop-quark polarizations P in the three spatial directions and the nine components of the spin-correlation matrix C[1]. An introduction to the spin-density-matrix formalism is given in Ref. [30].

[1]Some publications denote the polarizations by P instead of B, and the correlations by C instead of A, as the notation has varied over time.

Int. J. Mod. Phys. A 2026.41. Downloaded from www.worldscientific.com
by UNIVERSITY OF CALIFORNIA @ BERKELEY on 09/16/26. Re-use and distribution is strictly not permitted, except for Open Access articles.

Table 61.21: Measurements of the SM spin correlation fraction $f_{\rm SM}$ in $t\bar{t}$ events at the LHC, performed at $\sqrt{s} = 7$, 8 TeV and 13 TeV. The results are shown together with their overall uncertainties. The precision is mainly limited by the systematic uncertainties. For the 13 TeV results, the precision is mainly limited by signal-modeling uncertainties. Only the most precise measurement per channel and publication is listed below. Further results are given in the individual publications.

Exp. [Ref.]	**Lumi.** [fb^{-1}]	**Measurement Value ± Unc.**	**Channel**	**Observable**
		7 TeV results		
ATLAS [357]	2.1	$f_{\rm SM} = 1.30 \pm^{+0.30}_{-0.26}$	DL	$\Delta\Phi(\ell^+, \ell^-)$
ATLAS [358]	4.6	$f_{\rm SM} = 1.19 \pm 0.20$	DL	$\Delta\Phi(\ell^+, \ell^-)$
ATLAS [358]	4.6	$f_{\rm SM} = 0.87 \pm 0.18$	DL	S-ratio of matrix-elements
ATLAS [358]	4.6	$f_{\rm SM} = 1.12 \pm 0.25$	SL	$\Delta\Phi(\ell, d) + \Delta\Phi(\ell, b)$
CMS [361]	5.0	$f_{\rm SM} = 0.98 \pm 0.15$	DL	From asymmetry $A_{\Delta\Phi}$ measurement
		8 TeV results		
ATLAS [359]	20.3	$f_{\rm SM} = 1.20 \pm 0.14$	DL	$\Delta\Phi(\ell^+, \ell^-)$
CMS [362]	19.7	$f_{\rm SM} = 0.72^{+0.17}_{-0.15}$	DL	matrix-element method
CMS [363]	19.5	$f_{\rm SM} = 1.12^{+0.12}_{-0.15}$	DL	$A_{\Delta\phi}$ measurement as function of $m_{t\bar{t}}$
		13 TeV results		
ATLAS [364]	36.1	$f_{\rm SM} = 1.249^{+0.094}_{-0.111}$	DL	$\Delta\Phi(\ell^+, \ell^-)$
ATLAS [197]	140	$f_{\rm SM} = 1.20 \pm 0.68$	$t\bar{t}Z$ ev.	combination of 9 observables
CMS [365]	35.9	$f_{\rm SM} = 0.98 \pm 0.05$	DL	From D measurement

To extract all coefficients, spin-quantization axes must first be defined. A full reconstruction of the $t\bar{t}$ final state is required. In the notation of the first ATLAS measurement [366], the helicity axis is denoted k, the transverse axis n, and the r axis orthogonal to both. Spin analyzers are boosted into the rest frames of the respective top or antitop quark, and the angular distribution $\cos\theta$ of their momenta relative to the chosen axis is reconstructed. The 15 parameters are then obtained from data using one observable per parameter, as listed in Fig. 61.12 from Ref. [366].

The most precise individual measurement of these 15 coefficients has recently been performed by CMS in LJ events at $\sqrt{s} = 13$ TeV [35], using the down-type quark and the charged lepton as spin analyzers. In this analysis, the coefficients are extracted from a combined fit to data. Events are categorized according to $m_{t\bar{t}}$, $p_{\rm T}^{\rm top}$, and the absolute value of the top-quark scattering angle $|\cos\theta|$. The templates are parametrized as functions of the angular distributions of the top- and antitop-quark decay products. The setup achieving the best precision is based on event categories in bins of $p_{\rm T}^{\rm top}$ and $|\cos\theta|$.

Expectation values	NLO predictions	Observables
B_+^k	0.0030 ± 0.0010	$\cos\theta_+^k$
B_-^k	0.0034 ± 0.0010	$\cos\theta_-^k$
B_+^n	0.0035 ± 0.0004	$\cos\theta_+^n$
B_-^n	0.0035 ± 0.0004	$\cos\theta_-^n$
B_+^r	0.0013 ± 0.0010	$\cos\theta_+^r$
B_-^r	0.0015 ± 0.0010	$\cos\theta_-^r$
$C(k,k)$	0.318 ± 0.003	$\cos\theta_+^k \cos\theta_-^k$
$C(n,n)$	0.332 ± 0.002	$\cos\theta_+^n \cos\theta_-^n$
$C(r,r)$	0.055 ± 0.009	$\cos\theta_+^r \cos\theta_-^r$
$C(n,k) + C(k,n)$	0.0023	$\cos\theta_+^n \cos\theta_-^k + \cos\theta_+^k \cos\theta_-^n$
$C(n,k) - C(k,n)$	0	$\cos\theta_+^n \cos\theta_-^k - \cos\theta_+^k \cos\theta_-^n$
$C(n,r) + C(r,n)$	0.0010	$\cos\theta_+^n \cos\theta_-^r + \cos\theta_+^r \cos\theta_-^n$
$C(n,r) - C(r,n)$	0	$\cos\theta_+^n \cos\theta_-^r - \cos\theta_+^r \cos\theta_-^n$
$C(r,k) + C(k,r)$	-0.226 ± 0.004	$\cos\theta_+^r \cos\theta_-^k + \cos\theta_+^k \cos\theta_-^r$
$C(r,k) - C(k,r)$	0	$\cos\theta_+^r \cos\theta_-^k - \cos\theta_+^k \cos\theta_-^r$

Figure 61.12: Expected values and corresponding observables for the measurement of spin correlations and polarizations of the top and antitop quarks [366].

61.2.5.4 *Measurement of spin entanglement in pair production*

Entanglement, such as between the spin states of two particles, is a fundamental property of quantum mechanics [367–369]. Two particles are entangled if the state of one cannot be described independently of the state of the other. While entanglement has been observed in many physical systems, its study at high-energy colliders has been limited until recently. Notable examples include flavor entanglement in $\Upsilon(4S) \to B_0\bar{B}_0$ decays [370] and tests of Bell non-locality in $B_0 \to J/\psi K^*(892)^0$ decays [371]. The idea of probing entanglement in top-quark pairs through their spin correlations was first proposed in 2020 [32, 372–378].

At the LHC, $t\bar{t}$ pairs are predominantly produced via gluon–gluon fusion. Near production threshold ($m_{t\bar{t}} \approx 2m_t \approx$ 350 GeV), they are expected to form dominantly a spin-singlet state ($^1S_0$), which is maximally entangled. The different spin states are illustrated in Fig. 61.11. Since the spin state of an individual top quark cannot be determined directly in a collision experiment, the presence of quantum entanglement must be inferred statistically from ensembles of $t\bar{t}$ events. The spin singlet is rotationally invariant, which motivates the use of the trace of the spin-correlation matrix C as an entanglement witness. A sufficient condition for entanglement is given by $\mathrm{tr}[C]+1 < 0$, measuring entanglement, a natural extension of spin-correlation studies. This can be rewritten as

$$D = tr[C]/3, \tag{61.7}$$

which can be experimentally measured as:

$$D = -3 \cdot \langle\cos\varphi\rangle. \tag{61.8}$$

Here $\langle\cos\varphi\rangle$ is the average of the opening angle between the two spin analyzers in their respective parent-top rest frames. If $D < -1/3$, the top quarks are entangled [32].

The first measurement of D at $\sqrt{s} = 13$ TeV was performed by CMS using a partial dataset [365]. In that analysis, the full $m_{t\bar{t}}$ spectrum was included, which reduced the sensitivity and prevented a significant deviation from zero.

The first observation of quantum entanglement in $t\bar{t}$ events was reported by ATLAS using the full Run 2 dataset at 13 TeV [33]. The analysis employed the mean value of the $\cos\phi$ distribution to construct a calibration curve relating detector-level to particle-level observables. This calibration was then applied to the detector-level measurement of D in data, and the resulting particle-level value was compared with theoretical predictions. Since entanglement effects are expected to be most pronounced near threshold, the analysis was restricted to events with

Int. J. Mod. Phys. A 2026.41. Downloaded from www.worldscientific.com
UNIVERSITY OF CALIFORNIA @ BERKELEY on 09/16/26. Re-use and distribution is strictly not permitted, except for Open Access articles.

$340 < m_{t\bar{t}} < 380$ GeV. The precision of the measurement is limited by signal-modeling uncertainties, particularly those arising from differences between parton-shower algorithms.

Subsequently, CMS observed entanglement in $t\bar{t}$ events in both the DL channel [34] and the LJ channel [35]. In the DL analysis, a template fit to the full $\cos\phi$ spectrum was performed using a partial Run 2 dataset, with phase-space selections listed in Tab. 61.22. Non-relativistic bound-state effects were included in the prediction, improving agreement with the data. The LJ result forms part of the measurement of the full spin density matrix discussed above. Although the sensitivity to entanglement near threshold in this channel is insufficient for an observation, it provides access to a second phase space where entanglement is present: events at high $m_{t\bar{t}}$, where the top quarks are produced more widely separated in a $^3S_1$ state. Since in this region C_{rr} and C_{kk} become negative, the entanglement witness $\tilde{D}$ is defined as

$$\tilde{D} = \frac{1}{3}(C_{nn} - C_{rr} - C_{kk}) \tag{61.9}$$

and has to fulfill the criterion: $3\tilde{D} > 1$ [375]. This was achieved for events with $m_{t\bar{t}} > 800$ GeV and $|\cos\theta| < 0.4$. The ATLAS and CMS experiments have observed entanglement at the highest energy to date, both for $t\bar{t}$ events almost at rest and for more space-like separated top quarks. The measured values are summarized in Tab. 61.22.

61.2.5.5 *Pseudo-bound $t\bar{t}$ states at the production threshold*

During the development of quantum entanglement measurements, it became clear that modeling of the $t\bar{t}$ threshold region required improvements. As shown in the CMS analyses [34, 35], the inclusion of threshold effects leads to better agreement between the data and the prediction. Because the top quark decays before forming hadrons, bound states cannot occur in the usual sense. However, a $t\bar{t}$ pair produced nearly at rest can exchange gluons before one quark decays weakly [16, 379].

Threshold effects from non-relativistic QCD (NRQCD) have two main contributions: the potential has an attractive component from $t\bar{t}$ pairs in a color-singlet configuration (produced in gg fusion), corresponding to the $^1S_0^{[1]}$ spin–angular-momentum–color state. The second component of the potential is repulsive and originates from $t\bar{t}$ pairs produced in a color-octet configuration. The latter component is small and not included in the measurements discussed here. The resummation of Coulomb gluon exchange enhances $t\bar{t}$ production just below threshold. For $m_t = 172.5$ GeV and a binding energy of about 2 GeV, the expected mass of this state is $\simeq 343$ GeV, with a width of $2\Gamma_t$.

Standard Monte Carlo $t\bar{t}$ samples do not include these pseudo-bound-state effects, or other QCD effects occurring at the production threshold and discussed in Ref. [380]. Although these contributions amount to less than 1% of the total cross section and have negligible impact on most top-quark measurements, they become important for precision studies close to threshold, such as entanglement or top-quark Yukawa coupling measurements using the $m_{t\bar{t}}$ spectrum, and for new-physics searches in the low-$m_{t\bar{t}}$ region. To address this, CMS developed a dedicated cross-section measurement of this contribution using the full Run 2 dataset [90]. The analysis, performed in the DL channel, fitted the full $m_{t\bar{t}}$ spectrum, which was divided into nine signal regions defined by angular variables. This strategy significantly improved sensitivity compared with a single inclusive distribution. The signal was simulated with MG5_AMC@NLO using a simplified resonance model ($\eta_{t\bar{t}}$) decaying into $t\bar{t}$. The predicted cross section is 6.43 pb, and the measurement, limited by systematic uncertainties, yielded $\sigma(\eta_{t\bar{t}}) = 8.8^{+1.2}_{-1.4}$ pb with a significance greater than 5σ.

ATLAS carried out a similar analysis [91], also extracting the cross section from the $m_{t\bar{t}}$ distribution split into angular regions. The fit range was restricted to 300–500 GeV to avoid potential mis-modeling at high invariant masses. A more complete pseudo-bound state model was employed, in which LO $t\bar{t}$ matrix elements were reweighted using the NRQCD-resummed Green's function [16, 379]. The ATLAS result, also limited by systematic uncertainties, is $\sigma(t\bar{t}_{\mathrm{NRQCD}}) = 9.0 \pm 1.3$ pb with an observed significance of 7.7σ.

Both measurements are consistent with the production of a pseudo-bound color-singlet state. However, with the current invariant-mass resolution, a clear observation of the peak structure predicted by NRQCD cannot yet be claimed, and the enhancement can also be described within more inclusive approaches [380]. Further theoretical and experimental studies will be needed to clarify the nature of this enhancement.

61.2.5.6 *W-boson helicity in top-quark decay*

In the SM, the top quark couples to the W boson through the vector-minus-axial-vector ($V-A$) charged-current interaction, $-i\frac{g}{\sqrt{2}}V_{tb}\gamma^\mu\frac{1}{2}(1-\gamma_5)$. Because the fraction of decays to longitudinally polarized W bosons is proportional to the top-quark Yukawa coupling, it is enhanced relative to the weak coupling. The expected fraction is [381] $\mathcal{F}_0^{\mathrm{SM}} \approx x/(1+x)$, with $x = m_t^2/(2M_W^2)$, giving $\mathcal{F}_0^{\mathrm{SM}} \simeq 70\%$ for $m_t = 173$ GeV. The fractions of left-handed, right-handed, and longitudinal W bosons are denoted $\mathcal{F}_-$, $\mathcal{F}_+$, and $\mathcal{F}_0$, with SM expectations $\mathcal{F}_- \simeq 30\%$ and $\mathcal{F}_+ \simeq 0\%$. Predictions at NNLO in QCD are available [382].

Measurements of the W helicity in top-quark decays have been performed by both Tevatron and LHC experiments, in $t\bar{t}$ events reconstructed in the LJ and DL channels. As for the extraction of the top-quark mass, the template technique is widely used, although the matrix-element method and its variants have also been employed to determine the helicity fractions $\mathcal{F}$.

In Run 1 at the Tevatron, the charged-lepton p_{T} spectrum [383] and the invariant mass $M^2_{\ell b}$ of the lepton–b-quark system [384] in top-quark decays were used as template observables. In Run 2, both of these observables [385] the helicity angle $\cos\theta^*$, defined as the angle between the lepton and the b quark in the W-boson rest frame, became the primary observable [386–388]. In the DL channel, reconstruction is further improved by applying the neutrino-weighting technique (see Sec. 61.2.5.1), or both. The matrix element method has also been developed for this measurement, in which a likelihood is constructed from event probabilities expressed as functions of the W-helicity fractions $\mathcal{F}$ [389]. CDF and DØ combined their Run 2 results, based on 2.7–5.4 fb^{-1} of data [390], assuming a top-quark mass of 172.5 GeV. From the combination of measurements that simultaneously determined the fractions of W bosons, the results are $\mathcal{F}_0 = 0.722 \pm 0.081$ [± 0.062 (stat.) $\pm$ 0.052 (syst.)] and $\mathcal{F}_+ = -0.033 \pm 0.046$ [± 0.034 (stat.) $\pm$ 0.031 (syst.)]. In an alternative combination, where one of the helicity fractions was fixed to the SM expectation, the results are $\mathcal{F}_0 = 0.682 \pm 0.057$ [± 0.035 (stat.) $\pm$ 0.046 (syst.)] and $\mathcal{F}_+ = -0.015 \pm 0.035$ [± 0.018 (stat.) $\pm$ 0.030 (syst.)]. Both sets of results are consistent with SM predictions.

The large LHC datasets make it possible to perform simultaneous fits of $\mathcal{F}0$, $\mathcal{F}-$, and $\mathcal{F}_+$; the corresponding ATLAS and CMS results are summarized in Fig. 61.13.

At $\sqrt{s} = 7$ TeV, ATLAS used a template method for the $\cos\theta^*$ distribution and extracted angular asymmetries from the unfolded $\cos\theta^*$ distribution in both the LJ and DL channels [391]. CMS performed a similar measurement in the LJ channel, also based on template fits to the $\cos\theta^*$ distribution [392].

Since the polarization of W bosons in top-quark decays is directly sensitive to the Lorentz structure of the Wtb vertex and to possible anomalous couplings, both collaborations derived limits on non-SM contributions to the Wtb interaction. ATLAS and CMS also combined their 7 TeV results, also assuming a top-quark mass of 172.5 GeV, to obtain joint values of the W-boson helicity fractions and corresponding limits on anomalous couplings [393].

At $\sqrt{s} = 8$ TeV, ATLAS measured the W-boson helicity fractions in LJ events with at least one b tag [394]. CMS carried out complementary measurements: in LJ events with two b-tags [395] Using the same dataset, CMS also presented the first measurement of W-boson helicity in EW single-top production [396], obtaining results of similar precision and in agreement with the SM. The 8 TeV results from ATLAS and CMS in both $t\bar{t}$ and single-top events were subsequently combined [397]. The combined analysis, consistent with the SM predictions at NNLO in QCD, improved the precision by 25% (29%) for F_0 (F_L) compared to the most precise individual measurement, and set limits on anoma-

Int. J. Mod. Phys. A 2026.41. Downloaded from www.worldscientific.com
by UNIVERSITY OF CALIFORNIA @ BERKELEY on 09/16/26. Re-use and distribution is strictly not permitted, except for Open Access articles.

Table 61.22: Measurements of different entanglement witnesses at $\sqrt{s} = 13$ TeV. The results are shown together with their overall uncertainties. The precision for the threshold measurements is mainly limited by signal-modeling uncertainties, while the measurement in the boosted phase-space is limited by statistical uncertainties. The CMS results include the modeling of threshold effects. Only the most precise measurement per channel and publication is listed below. Further results are given in the individual publications.

Exp. [Ref.]	Measurement	Significance Obs. (Exp.)	Topology	Method/Phase space
CMS [365]	$D = -0.237 \pm 0.011$		DL	Fit to $\cos\phi$ distribution inclusive in $m_{t\bar{t}}$
ATLAS [33]	$D = -0.547 \pm 0.021$	$> 5\sigma$ ($> 5\sigma$)	DL	Calibration curve $340 < m_{t\bar{t}} < 380$ GeV Particle level
CMS [34]	$D = -0.480^{+0.026}_{-0.029}$	5.1σ (4.7σ)	DL	Fit to $\cos\phi$ distribution $\beta_z^{t\bar{t}} < 0.9$, $m_{t\bar{t}} < 400$ GeV Parton level
CMS [35]	$\tilde{D} = 0.652 \pm 0.052$	6.7σ (5.6σ)	SL	Fit to multi-differential distr. $m_{t\bar{t}} > 800$ GeV, $\lvert\cos\theta\rvert < 0.4$

lous right-handed vector (V_R) and left- and right-handed tensor (g_L, g_R) tWb couplings, as well as on the corresponding Wilson coefficients.

At $\sqrt{s} = 8$ TeV, ATLAS analyzed DL events with at least two b tags, measuring the normalized differential $t\bar{t}$ cross section with respect to $\cos\theta^*$ at parton level and, from template fits, extracting the W-boson helicity fractions [398]. The results are complementary to earlier measurements and consistent with SM expectations, with the precision limited by systematic uncertainties.

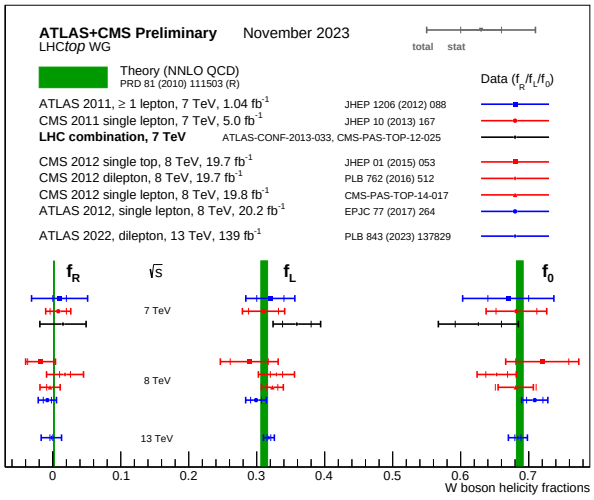

Figure 61.13: W-boson helicity fractions measured at the ATLAS and CMS experiments at different center-of-mass energies, compared to the theoretical NNLO predictions. The LHCtopWG working group kindly provides the plot, status as of November 2023, see `https://twiki.cern.ch/twiki/bin/view/LHCPhysics/LHCTopWGSummaryPlots`.

61.2.5.7 *Yukawa coupling*

The top-Higgs Yukawa coupling is expected to be the largest among all Yukawa couplings. It can be accessed directly by measurements of the $t\bar{t}$ cross section in association with a Higgs boson, $t\bar{t}H$, or indirectly via loop processes in $gg \to H$ production as well as $H \to \gamma\gamma$ or $H \to WW$ decays or in the rare process of $t\bar{t}t\bar{t}$ production. A discussion of the former can be found in Chapter 11 of this review. Searches for and recent observations of $t\bar{t}t\bar{t}$ production are discussed in Sec. 61.2.2. Measurements of y_t in kinematic distributions of $t\bar{t}$ production are providing additional information [399, 400].

61.2.5.8 *Top-quark asymmetries*

In $t\bar{t}$ production at hadron colliders, the SM predicts different predicts characteristic angular distributions that differ between the top and antitop quarks. Unlike most observables in the top-quark sector, measurements of asymmetries are still largely limited by statistical precision. This is particularly true for analyses probing the extreme regions of phase space, such as those targeting boosted top quarks, and for rare production modes like $t\bar{t}W$ and $t\bar{t}\gamma$. With the increasing luminosity delivered during Run 3 of the LHC and in future runs, significant improvements in these measurements are anticipated. Theoretical predictions for these asymmetries, however, have already reached a high level of precision.

Measurement of the forward-backward asymmetry A_{FB}

In $p\bar{p}$ collisions at the Tevatron collider, a forward-backward asymmetry arises in $t\bar{t}$ production starting at order α_S^3 in QCD. The asymmetry originates from the interference between the Born amplitude $q\bar{q} \to t\bar{t}$ with 1-loop box production diagrams and between diagrams with initial- and final-state gluon radiation. The asymmetry, A_{FB}, is defined by

$$A_{FB} = \frac{N(x > 0) - N(x < 0)}{N(x > 0) + N(x < 0)}. \tag{61.10}$$

Three types of asymmetries are discussed in the following:

- $A_{FB}^{t\bar{t}}$, where x is the rapidity difference between the top- and the antitop quark: $\Delta y = y_t - y_{\bar{t}}$. This asymmetry requires the full reconstruction of the $t\bar{t}$ final state.
- A_{FB}^{ℓ}, where x is the product of the charge and the rapidity of the lepton: $q_\ell \cdot \eta_\ell$.
  This asymmetry is only defined in the SL channel.
- $A_{FB}^{\ell\ell}$, where x is the rapidity difference between the two charged leptons: $\Delta\eta = \eta_{\ell^+} - \eta_{\ell^-}$. This asymmetry is only defined in the DL channel.

Calculations at α_S^3 predict a measurable A_{FB} at the Tevatron. Both CDF and DØ measured asymmetry values exceeding the SM prediction, which prompted considerable interest and speculation about possible contributions from new physics (see, for example, [401] and references therein). An overview of the early Tevatron measurements and the combined CDF and DØ results is given in Tab. 61.23. More recent calculations, extended to order α_S^4 and including EM and EW corrections, predict $A_{FB} \approx 0.095 \pm 0.007$ [402]. This value is about 10% larger than the previous NLO prediction [403, 404], leading to improved agreement with experimental results.

The first measured values at DØ and CDF were higher, though statistically consistent, with the SM expectation. With the addition of more data, the uncertainties were reduced, and the central values, if somewhat smaller, have remained consistent with the

Table 61.23: Forward-backward asymmetry measurements in $t\bar{t}$ events at the Tevatron, performed at $\sqrt{s} = 1.96$ TeV. If only one uncertainty is given, it reflects the total uncertainty on the measurement or prediction.

Experiment [Ref.]	**Luminosity (fb^{-1})**	**Measurement Value ± (stat.) ± (syst.)**	**Note**
DØ [405]	0.9	$A_{FB}^{t\bar{t}} = 0.12 \pm 0.08$	first DØ result
CDF [406]	1.9	$A_{FB}^{t\bar{t}} = 0.24 \pm 0.14$	first CDF result, parton level
Theory [402]		$A_{FB}^{t\bar{t}} = 0.095 \pm 0.007$	NNLO QCD + NLO EW
Comb. [407]	9-10	$A_{FB}^{t\bar{t}} = 0.128 \pm 0.021 \pm 0.014$	DØ+CDF combination
Theory [404]		$A_{FB}^{\ell} = 0.038 \pm 0.003$	NLO QCD + NLO EW
Comb. [407]	9-10	$A_{FB}^{\ell} = 0.073 \pm 0.016 \pm 0.012$	DØ+CDF combination
Theory [404]		$A_{FB}^{\ell\ell} = 0.048 \pm 0.004$	NLO QCD + NLO EW
Comb. [407]	9-10	$A_{FB}^{\ell\ell} = 0.108 \pm 0.043 \pm 0.016$	DØ+CDF combination

first measurements. At the same time, the improved calculations based on theory have increased the predicted asymmetry values, thereby improving the agreement between theory and experiment. Both experiments have also measured differential asymmetries, in bins of $m_{t\bar{t}}$, Δy, $q_\ell \cdot \eta_\ell$, and $\Delta\eta_{\ell\ell}$, with consistent results, though the growth of $A_{FB}^{t\bar{t}}$ with increasing $m_{t\bar{t}}$ and Δy appears somewhat more rapid than the SM prediction [407].

Charge asymmetry A_C

At the LHC, where $t\bar{t}$ production is dominated by charge-symmetric gluon–gluon fusion, the measurement is intrinsically different from that at the Tevatron. In the subdominant $q\bar{q}$ production mode, the symmetry of the pp initial state does not provide a natural definition of forward and backward directions. Instead, charge and energy asymmetries are defined based on Eq. 61.10 as follows:

- $A_C^{t\bar{t}}$, where x is the difference between the absolute rapidities of the top- and antitop quark: $\Delta|y| = |y_t| - |y_{\bar{t}}|$. The asymmetry requires the full $t\bar{t}$ event reconstruction.
- $A_C^{\ell\ell}$, where x is the difference between absolute pseudorapidities of the two charged leptons: $\Delta|\eta| = |\eta_{\ell^+}| - |\eta_{\ell^-}|$. This asymmetry is only defined in the DL channel and is referred to as "leptonic charge asymmetry."
- A_E, which is defined as the difference between the top- and antitop-quark energies, and can be measured as a function of the associated high-p_{T} jet angle, θ_j. The energies and jet angle are measured in the $t\bar{t}j$ rest frame. This asymmetry is referred to as "energy asymmetry" [408].

Both CMS and ATLAS have measured the charge asymmetry in different channels and at various center-of-mass energies. Results from the individual experiments at 7 and 8 TeV, as well as their combination, are summarized in Tab. 61.24. Statistical uncertainties primarily limit the precision; however, in some measurements, the statistical and systematic components are of comparable size. In addition to inclusive values, differential measurements as functions of $m_{t\bar{t}}$, and of the p_{T} and rapidity y of the $t\bar{t}$ system, have also been performed.

To reduce model dependence, CMS performed a measurement in a reduced fiducial phase space [409], obtaining $A_C = (-0.35 \pm 0.72\ (\mathrm{stat.}) \pm 0.31\ (\mathrm{syst.}))\%$, consistent with the SM prediction. To probe the $m_{t\bar{t}}$ dependence, ATLAS carried out a measurement in boosted $t\bar{t}$ events with $m_{t\bar{t}} > 0.75$ TeV, and also reported results in three bins of $m_{t\bar{t}}$ [410].

Overall, the measurements from both experiments are in agreement with SM expectations.

At 13 TeV, the measurements are more diverse, targeting not only $t\bar{t}$ events but also $t\bar{t}$+jet and $t\bar{t}$+boson final states [217, 411–413]. The size and sign of the asymmetries differ for the various final states. While the $t\bar{t}$ asymmetry is diluted in inclusive measurements at the LHC owing to the large fraction of gluon–gluon-initiated $t\bar{t}$ events which increases as a function of the center-of-mass energy, it is enhanced in other topologies such as $t\bar{t}\gamma$ due to an increased fraction of the quark initiated production mode. Another interesting quantity is the leptonic charge asymmetry in $t\bar{t}W$ events using final states with exactly three charged light leptons (electrons or muons). Here, the events are also enhanced in quark-initiated production processes. Additionally, the W boson in the initial state causes polarization of the $t\bar{t}$ pair, which further leads to a sizeable asymmetry. The results for the $t\bar{t}$+boson and $t\bar{t}$+jet final states are still strongly limited by statistical uncertainties and will benefit from the increased dataset at 13.6 TeV and beyond.

The most precise measurement to date was performed by ATLAS at $\sqrt{s} = 13$ TeV, combining LJ and DL channels with reconstruction techniques for both resolved and boosted topologies [424]. Differential results are reported as functions of the invariant mass, p_{T}, and longitudinal boost of the $t\bar{t}$ system. Both inclusive and differential measurements are compatible with SM predictions at NLO QCD with NLO EW corrections. The results are also interpreted in SMEFT, setting bounds on several Wilson coefficients.

CMS measured the charge asymmetry in $t\bar{t}$ events with highly Lorentz-boosted top quarks for $m_{t\bar{t}} > 0.75$ TeV, a phase space particularly relevant for BSM searches [425]. The measurement, corrected for detector and acceptance effects using a binned maximum-likelihood fit, was performed in three $m_{t\bar{t}}$ ranges. The results are in good agreement with the SM.

A model-independent comparison of the Tevatron and LHC results is made difficult by the differing $t\bar{t}$ production mechanisms at work at the two accelerators and by the symmetric nature of the pp collisions at the LHC. An early analysis from the CMS collaboration [427] using LJ events at $\sqrt{s} = 13$ TeV, uses a likelihood analysis to separate the $q\bar{q}$ process from production via gluon-gluon and gluon-quark interactions. The values found for the asymmetry parameters are $A_{FB} = 0.048^{+0.095}_{-0.087}\ (\mathrm{stat.})\ ^{+0.020}_{-0.029}\ (\mathrm{syst.})$, for the anomalous chromomagnetic dipole moment $\mu^t = -0.024^{+0.013}_{-0.009}\ (\mathrm{stat.})\ ^{+0.016}_{-0.011}\ (\mathrm{syst.})$, and a limit is placed on the magnitude of a possible anomalous chromoelectric dipole moment $|d^t| < 0.03$ at 95% C.L. [427].

61.2.5.9 *Electric charge*

The top quark is the only quark whose electric charge has not been measured through threshold production in e^+e^- collisions, and its electromagnetic coupling has only recently been studied in detail. Early CDF and DØ analyses of top-quark production did not uniquely associate the b, $\bar{b}$, and $W^\pm$ to the top or antitop quark, so that exotic decays such as $t \to W^+\bar{b}$ and $\bar{t} \to W^-b$ could not be excluded. A quark with charge 4/3 is, in fact, compatible with EW precision data. In particular, the $Z \to \ell^+\ell^-$ and $Z \to b\bar{b}$ measurements, including the discrepancy between A_{LR} at SLC and $A_{FB}^{0,b}$ and $A_{FB}^{0,\ell}$ at LEP, can be fitted with a 270 GeV quark of charge 4/3, provided the right-handed b mixes with the isospin $+1/2$ component of an exotic doublet $(Q_1, Q_4)_R$ with charges $-1/3$ and $-4/3$ [428, 429]. The third component of the top-quark weak isospin has likewise not been measured directly.

DØ studied the top-quark charge in double-tagged LJ events, while CDF analyzed single-tagged LJ and DL events. Assuming the top and antitop quarks carry equal and opposite charges, the b-quark charge was reconstructed using jet-charge discrimination to

Int. J. Mod. Phys. A 2026.41. Downloaded from www.worldscientific.com
UNIVERSITY OF CALIFORNIA @ BERKELEY on 09/16/26. Re-use and distribution is strictly not permitted, except for Open Access articles.

Int. J. Mod. Phys. A 2026.41. Downloaded from www.worldscientific.com
by UNIVERSITY OF CALIFORNIA @ BERKELEY on 09/16/26. Re-use and distribution is strictly not permitted, except for Open Access articles.

Table 61.24: Charge asymmetry measurements in $t\bar{t}$ events at the LHC, performed at $\sqrt{s} = 7$ and 8 TeV. The results are shown together with their overall uncertainties and are compared to the theoretical prediction. The precision is primarily limited by the dataset's size.

Exp./Pred. [Ref.]	**Lumi. [fb^{-1}]**	**Measurement**	**Note**
		7 TeV results	
Theory [404]		$A_C^{t\bar{t}} = (1.23 \pm 0.05)\%$	NLO QCD + NLO EW
ATLAS [414]	4.7	$A_C^{t\bar{t}} = (0.6 \pm 1.0)\%$	LJ
CMS [415]	5.0	$A_C^{t\bar{t}} = (0.4 \pm 1.5)\%$	LJ
ATLAS [416]	4.6	$A_C^{t\bar{t}} = (2.1 \pm 3.0)\%$.	DL, neutrino weighting
CMS [417]	5.0	$A_C^{t\bar{t}} = (1.0 \pm 1.6)\%$,	DL, matrix weighting technique
Combin. [418]		$A_C^{t\bar{t}} = (0.5 \pm 0.9)\%$	LJ, ATLAS+CMS combination
Theory [404]		$A_C^{\ell\ell} = (0.70 \pm 0.03)$ %	NLO QCD + NLO EW
ATLAS [416]	4.6	$A_C^{\ell\ell} = (2.4 \pm 1.8)\%$	DL
CMS [417]	5.0	$A_C^{\ell\ell} = (0.9 \pm 1.2)\%$	DL
		8 TeV results	
Theory [404]		$A_C^{t\bar{t}} = (1.11 \pm 0.04)\%$	NLO QCD + NLO EW
Theory [419]		$A_C^{t\bar{t}} = (0.95^{+0.05}_{-0.07})\%$	NNLO QCD + NLO EW
ATLAS [420]	20.3	$A_C^{t\bar{t}} = (0.9 \pm 0.5)$	LJ
CMS [421]	19.7	$A_C^{t\bar{t}} = (0.33 \pm 0.43)\%$	LJ (*) stat=syst
ATLAS [422]	20.3	$A_C^{t\bar{t}} = (2.1 \pm 1.6)\%$	DL
CMS [423]	19.5	$A_C^{t\bar{t}} = (1.1 \pm 1.3)\%$	DL
Combin. [418]		$A_C^{t\bar{t}} = (0.55 \pm 0.34)\%$	LJ, ATLAS+CMS combination (*)
Theory [404]		$A_C^{\ell\ell} = (0.64 \pm 0.03)\%$	NLO QCD + NLO EW
ATLAS [422]	20.3	$A_C^{\ell\ell} = (0.8 \pm 0.6)\%$	DL
CMS [423]	19.5	$A_C^{\ell\ell} = (0.3 \pm 0.7)\%$	DL

Table 61.25: Asymmetry measurements in $t\bar{t}$ and $t\bar{t} + X$ events at the LHC, performed at 13 TeV. The results are shown together with their overall uncertainties and are compared to the theoretical prediction. The dataset's size primarily limits the precision.

Exp./Pred. [Ref.]	**Lumi. [fb^{-1}]**	**Measurement**	**Note**
		$t\bar{t}$	
Theory [419]		$A_C^{t\bar{t}} = (0.64^{+0.05}_{-0.06})$ %	NNLO (QCD) + NLO (EW)
ATLAS [424]	139	$A_C^{t\bar{t}} = (0.68 \pm 0.15)$ %	DL+LJ, resolved+boosted Bayesian unfolding, 4.7σ
Theory [404]		$A_C^{\ell\ell} = (0.40^{+0.02}_{-0.01})$ %	NLO (QCD + EW)
ATLAS [424]	139	$A_C^{\ell\ell} = (0.54 \pm 0.26)$ %	
Theory [419]		$A_C^{t\bar{t}} = (0.94^{+0.05}_{-0.07})$ %	NNLO (QCD) + NLO (EW)
CMS [425]	138	$A_C^{t\bar{t}} = (0.42^{+0.64}_{-0.69})$ %	LJ, boosted topology, $m_{t\bar{t}} > 750$ GeV
		$t\bar{t}$+jet	
Theory		$A_E = (-3.7 \pm 0.3)$ %	MG5_aMC@NLO
ATLAS [426]	139	$A_E = (-4.3 \pm 2.0)$ %	Bayesian unfolding, EFT interpretation
		$t\bar{t}\gamma$	
Theory		$A_C^{t\bar{t}} = (-1.4 \pm 0.1)$ %	MG5_aMC@NLO
ATLAS [411]	139	$A_C^{t\bar{t}} = (-0.3 \pm 2.9)$ %	stat limited, PL unfolding
Theory		$A_C^{t\bar{t}} = (-0.5 \pm 0.2)$ %	MG5_aMC@NLO
CMS [217]	138	$A_C^{t\bar{t}} = (-1.2 \pm 4.2)$ %	
		$t\bar{t}W$	
Theory		$A_C^{\ell\ell} = (-8.4^{+0.8}_{-0.7})$ %	Sherpa 2.2.10 (NLO QCD +EW)
ATLAS [412]	139	$A_C^{\ell\ell} = (-12 \pm 15)$ %	PL fit, reco level, 3ℓ events
Theory		$A_C^{\ell\ell} = (-9^{+12}_{-14})$ %	NLO simulation
CMS [413]	138	$A_C^{\ell\ell} = (-19^{+16}_{-18})$ %	3ℓ events
Theory		$A_C^{\ell\ell} = (-6.3^{+0.8}_{-0.6})$ %,	Sherpa 2.2.10 (NLO QCD +EW)
ATLAS [412]	139	$A_C^{\ell\ell} = (-11 \pm 18)$ %	PL fit, particle level

test the $|Q_{top}| = 2/3$ SM scenario against the exotic $|Q_{top}| = 4/3$ hypothesis. Within the framework of the exotic model of Chang

Int. J. Mod. Phys. A 2026.41. Downloaded from www.worldscientific.com
UNIVERSITY OF CALIFORNIA @ BERKELEY on 09/16/26. Re-use and distribution is strictly not permitted, except for Open Access articles.

et al. [429], CDF excluded $Q_{top} = 4/3$ at 99% C.L. [430], while DØ excluded it at more than 5σ and limited the fraction of such quarks in the data to below 0.46 [431]. These results firmly established that the observed particle is consistent with the SM quark of charge $+2/3$. At the LHC, ATLAS performed a similar measurement at $\sqrt{s} = 7$ TeV using jet-charge techniques and soft-lepton tagging in b decays combined with a kinematic likelihood fit. The measured top-quark charge was 0.64 ± 0.02 (stat.) $\pm\, 0.08$ (syst.), excluding the exotic $Q = -4/3$ hypothesis at more than 8σ [432]. CMS also tested the exotic-charge scenario at $\sqrt{s} = 7$ TeV in the muon+jets channel, exploiting the correlation between high-p_{T} muons from W decays and soft muons from B-hadron decays inside b-jets. Using an asymmetry variable A, with $A = -1$ corresponding to $Q = -4/3$ and $A = +1$ to $Q = +2/3$, CMS preliminary measured $A = 0.97 \pm 0.12$ (stat.) $\pm\, 0.31$ (syst.), in agreement with the SM and excluding the exotic scenario at 99.9% C.L. [433].

61.2.6 *Physics beyond the SM*

The top quark plays a special role in the SM. Being the only quark with a coupling to the Higgs boson of order one, it provides the most important contributions to the quadratic radiative corrections to the Higgs mass exposing the issue of the naturalness of the SM. It is therefore very common for models where the naturalness problem is addressed to have new physics associated with the top quark. In SUSY, for instance, naturalness predicts the scalar top-quark partners to be the lightest among the squarks and to be accessible at the LHC energies (see the review "Supersymmetry: Theory"). In models where the Higgs is a pseudo-Goldstone boson, such as Little Higgs models, naturalness predicts the existence of partners of the top quarks with the same spin and color, but with different EW couplings, the so-called vectorial t'. Stops and t''s are expected to have sizeable branching ratios to top quarks. Another intriguing prediction of SUSY models with universal couplings at the unification scale is that for a top-quark mass close to the measured value, the running of the Yukawa coupling down to 1 TeV naturally leads to the radiative breaking of the EW symmetry [434]. In fact, the top quark plays a role in the dynamics of EW symmetry breaking in many models [435]. One example is topcolor [436], where a large top-quark mass can be generated through the formation of a dynamic $t\bar{t}$ condensate, X, which is formed by a new strong gauge force coupling preferentially to the third generation. Another example is topcolor-assisted technicolor [437], predicting the existence of a heavy Z' boson that couples preferentially to the third generation of quarks. If light enough, such a state might be directly accessible at the present hadron collider energies, or if too heavy, lead to four-top interactions possibly visible in the $t\bar{t}t\bar{t}$ final state.

61.2.6.1 *Direct searches for physics beyond the SM*

In this section, the most recent direct searches for effects beyond the SM in top-quark production and decay are reviewed. These searches can be broadly divided into two categories: (i) searches for $t\bar{t}$ resonances, and (ii) searches for rare non-SM interactions involving top quarks, including flavor-changing neutral currents (FCNC). Resonance searches in the top sector include (a) $t\bar{t}$ resonances, in which a hypothetical heavy particle X decays into a $t\bar{t}$ pair, and (b) searches where a non-SM decay product of the top quark is identified through its resonant signature. The most recent results belong to the latter class. For comprehensive discussions of $X \to t\bar{t}$ searches, see Refs. [438–440]. Searches for rare non-SM interactions and FCNC processes are interpreted within the EFT framework described in Section 61.1.3. Here we focus on the limits on branching ratios obtained from these searches, while the corresponding EFT interpretations are discussed in Section 61.2.6.2.

FCNC searches. The most recent FCNC searches target the decay $t \to qH$ in $t\bar{t}$ production, or an FCNC vertex in single-top-quark production associated with a Higgs boson.

ATLAS probes both processes using $H \to VV$ decays. Neural-network outputs are used to define four signal regions, two each for production and decay, further divided into categories with two same-sign leptons or three leptons [441]. Despite the small branching ratio, this channel provides the best sensitivity. The results are combined with complementary searches using Higgs-boson decays to $b\bar{b}$ [442], $\tau\tau$ [443], and $\gamma\gamma$ [444], accounting for correlations among parameters. The combined upper limits on the branching ratios are $\mathcal{B}(t \to Hu) < 2.6 \times 10^{-4}$ and $\mathcal{B}(t \to Hc) < 3.4 \times 10^{-4}$.

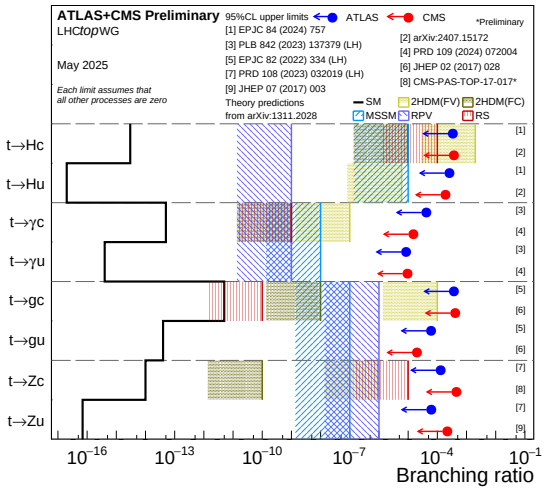

Figure 61.14: Overview of branching-ratio limits in searches for FCNCs in different production and decay channels, compared to different theory predictions. The LHCtopWG working group kindly provides the plot, status as of May 2025, see `https://twiki.cern.ch/twiki/bin/view/LHCPhysics/LHCTopWGSummaryPlots`.

CMS uses Higgs decays to vector bosons and $\tau\tau$ [445], and combines these results with analyses targeting $H \to b\bar{b}$ [446] and $H \to \gamma\gamma$ [447]. As in the ATLAS case, the $H \to VV$ decay mode yields the highest sensitivity. The combined limits are $\mathcal{B}(t \to Hu) < 1.9 \times 10^{-4}$ and $\mathcal{B}(t \to Hc) < 3.7 \times 10^{-4}$. A comparison of the ATLAS and CMS results with predictions from representative BSM models is shown in Fig. 61.14.

Searches targeting tZq couplings use leptonic decays of the Z-boson and a trilepton final state. In $t\bar{t}$ events, the signal occurs through the FCNC decay $t \to Zq$, in single-top quark the signal occurs through the associated production of a top quark and a Z-boson. The branching-ratio limits shown in Fig. 61.14 are for tZu and tZc left-handed couplings and assume, for tZu, that the tZc coupling is zero and vice versa. Reference [448] presents limits for right-handed couplings, which are close to the values quoted in Fig. 61.14 for left-handed couplings.

Searches targeting $t\gamma q$ couplings focus on a high-p_{T} photon in the final state. As with tZq couplings, signal events occur through top-quark decay in $t\bar{t}$ and through associated production of a top quark and a photon in single-top events. ATLAS has set limits on the corresponding EFT couplings, shown in Fig. 61.18 [449]. The limits are derived assuming left-handed couplings; those for right-handed couplings are also provided and are only slightly weaker.

FCNC couplings tgq between a top quark, a gluon, and an up or charm quark have been probed by ATLAS in single-top-quark production [450]. Such couplings enhance the single-top-quark production cross section and, in the case of the tgc interaction, modify the rapidity distribution of the top quark due to the different PDFs of valence and sea quarks.

Searches for charged-lepton flavor violation. CMS has searched for for charged-lepton-flavor-violating (CLFV) interactions in both production, $q \to e\mu t$, and decay, $t \to e\mu q$, with $q = u$ or c [451] in final states with two leptons. Additional searches have been performed in final states with three leptons [452] and, more recently, in single-lepton final states targeting $\mu\tau qt$ interactions [453]. Limits on scalar, vector, and tensor couplings are summarized in Tab. 61.26. These limits are also shown in Fig. 61.17 and compared with the corresponding ATLAS search for CLFV $\mu\tau qt$ interactions [454], which uses final states containing a same-sign dimuon pair.

Int. J. Mod. Phys. A 2026.41. Downloaded from www.worldscientific.com
by UNIVERSITY OF CALIFORNIA @ BERKELEY on 09/16/26. Re-use and distribution is strictly not permitted, except for Open Access articles.

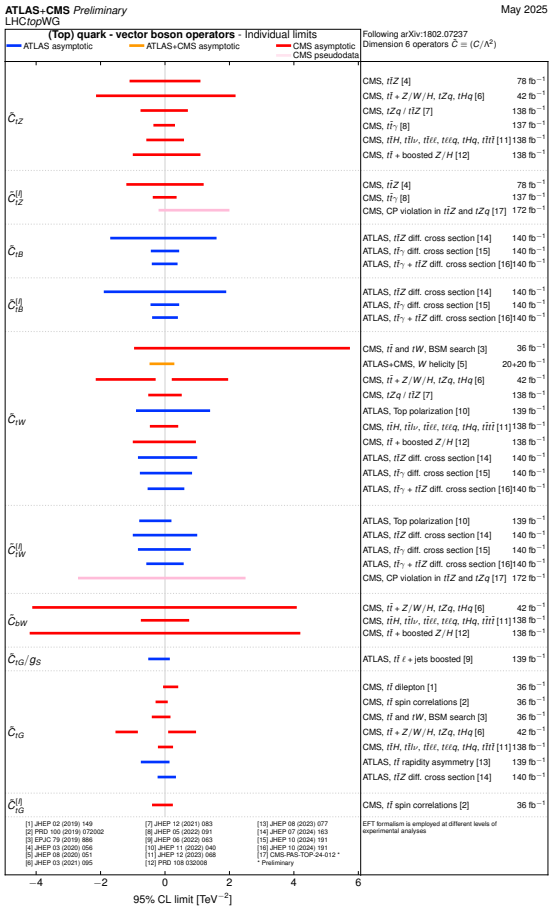

Figure 61.15: Wilson coefficients (WCs) corresponding to vector boson operators and related BSM search references. The LHCtopWG working group kindly provides the plot, status as of May 2025, see `https://twiki.cern.ch/twiki/bin/view/LHCPhysics/LHCTopWGSummaryPlots`.

Searches for baryon number violation. CMS recently reported a search for baryon-number violation (BNV) in top-quark production and decay [455], using events with two same-sign leptons and at least one b-tagged jet. Both single-top and top-quark-pair production modes are considered. Boosted decision trees are employed to discriminate signal from background processes. No significant excess is observed, and upper limits are set on the corresponding couplings. The obtained limits improve upon previous constraints by several orders of magnitude.

Resonance searches. While technically an FCNC search, a decay of the type $t \to qX$ where $q = u$ or c, could be missed when X is not the expected quark or boson. ATLAS has searched for $t \to qX$ where X is a light scalar with a mass below the top quark that decays to $b\bar{b}$ [442]. Such phenomena exist in composite Higgs models [456]. The ATLAS search used $t\bar{t}$ events and separated signal from background by categorizing events according to the number of jets and the number of jets tagged as originating from b-quarks. The observed limits correspond to the product of the BR $t \to qX$ and $X \to b\bar{b}$. The limit in the $t \to uX(t \to cX)$ channel is 0.019% (0.018%) for $M_X = 20$ GeV and 0.062% (0.078%) for $M_X = 160$ GeV.

There is a wide range of searches for new resonances decaying into $t\bar{t}$ events which are partially covered in the section "Hypothetical particles and concepts" of this review.

61.2.6.2 *Effective field theory*

As described in Sec. 61.1.3, EFTs have become an important tool to search for new physics processes. The EFT interpretations benefit from the increasing datasets, as this allows for very

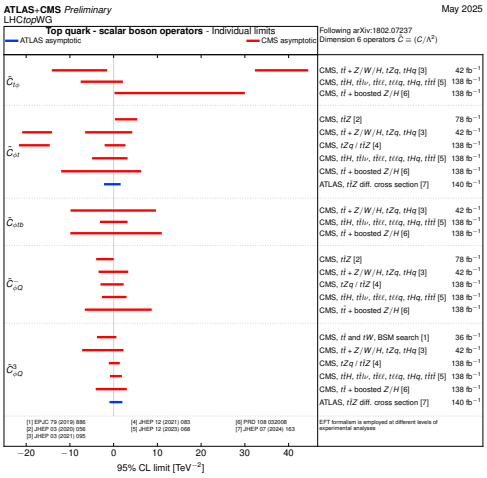

Figure 61.16: Wilson coefficients (WCs) corresponding to scalar boson operators and related BSM search references. The LHCtopWG working group kindly provides the plot, status as of May 2025, see `https://twiki.cern.ch/twiki/bin/view/LHCPhysics/LHCTopWGSummaryPlots`.

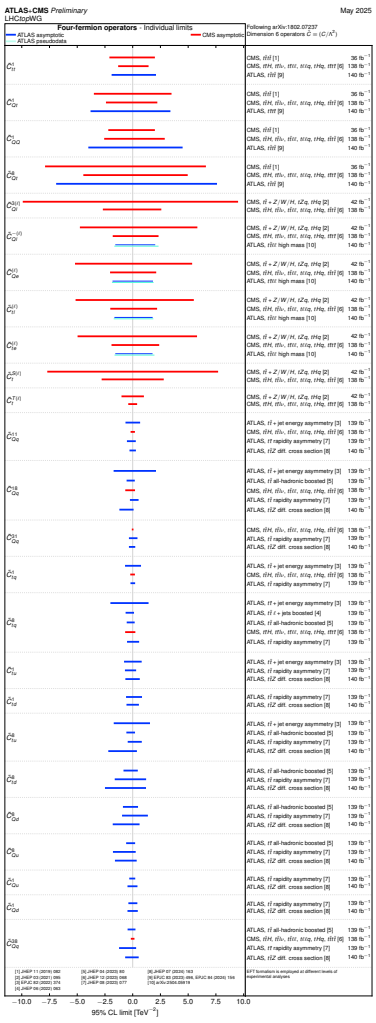

Figure 61.17: Wilson coefficients (WCs) corresponding to four-fermion operators and related BSM search references. The LHCtopWG working group kindly provides the plot, status as of May 2025, see `https://twiki.cern.ch/twiki/bin/view/LHCPhysics/LHCTopWGSummaryPlots`.

Int. J. Mod. Phys. A 2026.41. Downloaded from www.worldscientific.com
UNIVERSITY OF CALIFORNIA @ BERKELEY on 09/16/26. Re-use and distribution is strictly not permitted, except for Open Access articles.

Table 61.26: 95% C.L. limits on branching ratios (BR) of the top quark in searches for charged-lepton flavor violation. All searches were carried out at $\sqrt{s} = 13$ TeV.

Exp.	Process	N(ℓ)	BR limit	Reference
CMS	$t \to e\mu u$ (scalar)	2ℓ	0.07×10^{-6}	[451]
CMS	$t \to e\mu u$ (vector)	2ℓ	0.13×10^{-6}	[451]
CMS	$t \to e\mu u$ (tensor)	2ℓ	0.25×10^{-6}	[451]
CMS	$t \to e\mu c$ (scalar)	2ℓ	0.89×10^{-6}	[451]
CMS	$t \to e\mu c$ (vector)	2ℓ	1.31×10^{-6}	[451]
CMS	$t \to e\mu c$ (tensor)	2ℓ	2.59×10^{-6}	[451]
CMS	$t \to e\mu u$ (scalar)	3ℓ	0.012×10^{-6}	[452]
CMS	$t \to e\mu u$ (vector)	3ℓ	0.022×10^{-6}	[452]
CMS	$t \to e\mu u$ (tensor)	3ℓ	0.032×10^{-6}	[452]
CMS	$t \to e\mu c$ (scalar)	3ℓ	0.216×10^{-6}	[452]
CMS	$t \to e\mu c$ (vector)	3ℓ	0.369×10^{-6}	[452]
CMS	$t \to e\mu c$ (tensor)	3ℓ	0.498×10^{-6}	[452]
ATLAS	$t \to \mu\tau u$ (scalar)	2ℓSS	0.20×10^{-6}	[454]
CMS	$t \to \mu\tau u$ (scalar)	1ℓ	0.04×10^{-6}	[453]
ATLAS	$t \to \mu\tau u$ (vector)	2ℓSS	0.33×10^{-6}	[454]
CMS	$t \to \mu\tau u$ (vector)	1ℓ	0.08×10^{-6}	[453]
ATLAS	$t \to \mu\tau u$ (tensor)	2ℓSS	0.52×10^{-6}	[454]
CMS	$t \to \mu\tau u$ (tensor)	1ℓ	0.12×10^{-6}	[453]
ATLAS	$t \to \mu\tau c$ (scalar)	2ℓSS	3.40×10^{-6}	[454]
CMS	$t \to \mu\tau c$ (scalar)	1ℓ	0.81×10^{-6}	[453]
ATLAS	$t \to \mu\tau c$ (vector)	2ℓSS	5.30×10^{-6}	[454]
CMS	$t \to \mu\tau c$ (vector)	1ℓ	1.71×10^{-6}	[453]
ATLAS	$t \to \mu\tau c$ (tensor)	2ℓSS	6.70×10^{-6}	[454]
CMS	$t \to \mu\tau c$ (tensor)	1ℓ	2.05×10^{-6}	[453]

precise inclusive and differential measurements of top processes. These precision measurements of diverse sets of observables allows to improve the EFT interpretations by combining these measurements in a global analysis, as can be done using tools such as SMEFit [457]. In Ref. [458], Zhang and Willenbrock elucidate the advantages of the EFT approach compared to the vertex-function approach for searching for BSM effects in top-quark interactions, including the fact that the EFT approach incorporates the SM gauge symmetry and contact interactions that are neglected in the vertex-function approach. As a result of these advantages, EFTs have become the dominant technique for evaluating search limits, and the most recent results are reviewed in this section.

The top-EFT operators are categorized as follows: operators involving the contact-interaction of four fermions together (four-fermion operators), operators involving the interaction between top quarks and a vector boson (vector-boson operators) and between top quarks and scalar bosons (scalar-boson operators). Operators can change the overall rate of top-quark production, modify the kinematics of production and/or decay, or produce new interactions, such as FCNCs. To date, all results are consistent with the SM expectation of zero for each Wilson coefficient C. The bounds are set on C/Λ^2 and have a dimension of TeV$^{-}2$. Once the value for the unknown coupling strength C of the interaction is set, the size of the interval is inversely proportional to the square of the new physics scale.

The individual limits from the ATLAS and CMS results provided by the LHCtopWG can be found in Figs. 61.15–61.18. Marginalised limits and different representations can be found on the LHCtopWG page linked from the individual figure captions. Additional limits and references can be found in the listings and for example in the references [199, 216, 451, 459, 460, 460–468].

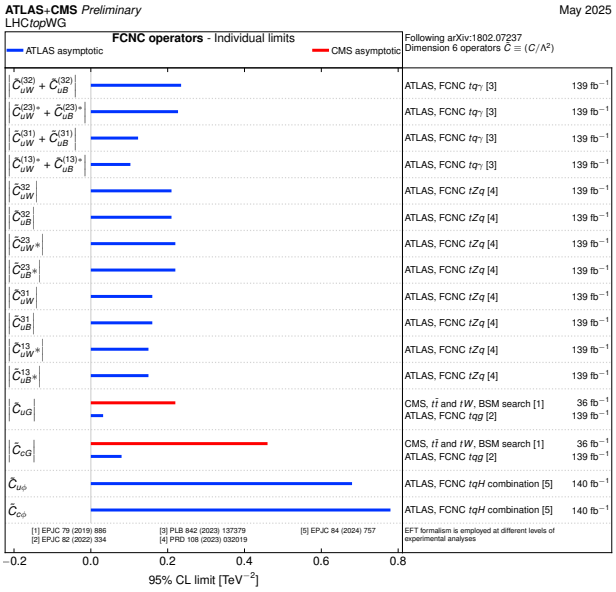

Figure 61.18: Wilson coefficients (WCs) corresponding to flavor-changing-neutral-current (FCNC) operators and related BSM search references. The LHCtopWG working group kindly provides the plot, status as of May 2025, see `https://twiki.cern.ch/twiki/bin/view/LHCPhysics/LHCTopWGSummaryPlots`.

61.3 Summary and outlook

In the three decades since its discovery, top-quark physics has evolved from the observation of a single particle into a precision field that probes the SM at the highest energy scales. With the large datasets collected at the LHC, a wide range of top-quark properties have been measured with unprecedented accuracy. Production cross sections and other $\sqrt{s}$-dependent quantities have been determined at multiple energies, enabling stringent tests of QCD and EW production mechanisms. All results to date are consistent with SM predictions, providing strong validation of the theory. The precision will continue to improve as larger datasets and refined theoretical and experimental techniques become available, enhancing sensitivity to potential deviations from the SM.

The large top-quark samples recorded in Run 2 have enabled detailed studies of both $t\bar{t}$ production and single-top processes, all now firmly established at the LHC. Many associated production modes have also become accessible: while Run 1 provided the first evidence and observations of processes such as $t\bar{t}\gamma$, $t\bar{t}Z$, $t\bar{t}W$, $t\bar{t}H$, and $t\bar{t}t\bar{t}$, Run 2 has opened the path to precision studies of these reactions. Rare single-top associated modes, including tZ, $t\gamma$, and tWZ, are now being measured as well, extending sensi-

Int. J. Mod. Phys. A 2026.41. Downloaded from www.worldscientific.com
by UNIVERSITY OF CALIFORNIA @ BERKELEY on 09/16/26. Re-use and distribution is strictly not permitted, except for Open Access articles.

tivity to the structure of top-quark couplings and to possible new physics. Many of these results are interpreted within the framework of EFT, providing global constraints on higher-dimensional operators that parameterize deviations from the SM.

The complexity of top-quark final states and the precision they demand have driven major advances in analysis techniques, notably multivariate methods and machine learning, which are now standard in collider physics. The large top-quark mass, its unique role in electroweak symmetry breaking, and its potential link to new dynamics continue to make it a central focus of particle physics.

For many measurements, uncertainties in event simulation remain the dominant limitation on precision. Differential measurements are essential to further reduce these uncertainties, particularly in complex final states such as $t\bar{t}$+heavy-flavor jets.

While most of the Run 2 dataset at $\sqrt{s} = 13$ TeV has been analyzed, Run 3 at $\sqrt{s} = 13.6$ TeV, with an expected integrated luminosity exceeding 300 fb^{-1}, will more than double the available statistics. The forthcoming High-Luminosity LHC (HL-LHC) phase, expected to deliver up to 3 ab^{-1} of data, will mark the next major step in this progression—from discovery to precision characterization. It will enable sub-percent precision in key measurements, stringent global EFT constraints, and unprecedented sensitivity to rare processes and possible new interactions. With many results already published and more to come, top-quark physics continues to provide one of the most powerful tools for testing the SM and exploring physics at the TeV scale.

CDF and DØ notes can be retrieved from
`https://inspirehep.net`
with the search command "find CDF-NOTE-XXXXX" or "find D0 Note XXXX",
and ATLAS note references from
`https://twiki.cern.ch/twiki/bin/view/AtlasPublic/TopPublicResults`,
and CMS note references from
`https://twiki.cern.ch/twiki/bin/view/CMSPublic/PhysicsResultsTOP`,
and plots provided by the LHC Top Working Group from
`https://twiki.cern.ch/twiki/bin/view/LHCPhysics/LHCTopWGSummaryPlots`.

References

[1] A. Hayrapetyan *et al.* (ATLAS, CMS), Phys. Rev. Lett. **132**, 26 (2024), [arXiv:2402.08713].

[2] G. Degrassi *et al.*, JHEP **08**, 098 (2012), [arXiv:1205.6497].

[3] D. Buttazzo *et al.*, JHEP **12**, 089 (2013), [arXiv:1307.3536].

[4] A. Andreassen, W. Frost and M. D. Schwartz, Phys. Rev. D **97**, 5, 056006 (2018), [arXiv:1707.08124].

[5] A. H. Hoang *et al.*, JHEP **04**, 003 (2018), [arXiv:1704.01580].

[6] P. Marquard *et al.*, Phys. Rev. Lett. **114**, 14, 142002 (2015), [arXiv:1502.01030].

[7] P. Nason, *The Top Mass in Hadronic Collisions*, 123–151 (2019), [arXiv:1712.02796].

[8] A. H. Hoang, Ann. Rev. Nucl. Part. Sci. **70**, 225 (2020), [arXiv:2004.12915].

[9] M. Jezabek and J. H. Kuhn, Nucl. Phys. **B314**, 1 (1989).

[10] A. Czarnecki and K. Melnikov, Nucl. Phys. **B544**, 520 (1999), [hep-ph/9806244]; K. G. Chetyrkin *et al.*, Phys. Rev. **D60**, 114015 (1999), [hep-ph/9906273].

[11] L.-B. Chen *et al.*, Phys. Rev. D **108**, 5, 054003 (2023), [arXiv:2212.06341].

[12] I. I. Y. Bigi *et al.*, Phys. Lett. **B181**, 157 (1986).

[13] A. H. Hoang *et al.*, Phys. Rev. **D65**, 014014 (2002), [hep-ph/0107144].

[14] K. Hagiwara, Y. Sumino and H. Yokoya, Phys. Lett. **B666**, 71 (2008), [arXiv:0804.1014].

[15] Y. Kiyo *et al.*, Eur. Phys. J. C **60**, 375 (2009), [arXiv:0812.0919].

[16] B. Fuks *et al.*, Phys. Rev. D **104**, 3, 034023 (2021), [arXiv:2102.11281].

[17] G. Eilam, J. L. Hewett and A. Soni, Phys. Rev. D **44**, 1473 (1991), [Erratum: Phys.Rev.D 59, 039901 (1999)].

[18] J. A. Aguilar-Saavedra, Acta Phys. Polon. B **35**, 2695 (2004), [hep-ph/0409342].

[19] S. Weinberg, Phys. Rev. Lett. **43**, 1566 (1979).

[20] W. Buchmuller and D. Wyler, Nucl. Phys. B **268**, 621 (1986).

[21] B. Grzadkowski *et al.*, JHEP **10**, 085 (2010), [arXiv:1008.4884].

[22] D. Barducci *et al.* (2018), [arXiv:1802.07237].

[23] J. A. Aguilar-Saavedra, Nucl. Phys. B **812**, 181 (2009), [arXiv:0811.3842].

[24] C. Zhang and S. Willenbrock, Phys. Rev. **D83**, 034006 (2011), [arXiv:1008.3869].

[25] I. Brivio, JHEP **04**, 073 (2021), [arXiv:2012.11343].

[26] C. Degrande *et al.*, Phys. Rev. D **103**, 9, 096024 (2021), [arXiv:2008.11743].

[27] R. S. Chivukula and H. Georgi, Phys. Lett. B **188**, 99 (1987).

[28] L. J. Hall and L. Randall, Phys. Rev. Lett. **65**, 2939 (1990).

[29] G. D'Ambrosio *et al.*, Nucl. Phys. B **645**, 155 (2002), [hep-ph/0207036].

[30] W. Bernreuther, D. Heisler and Z.-G. Si, JHEP **12**, 026 (2015), [arXiv:1508.05271].

[31] A. Behring *et al.*, Phys. Rev. Lett. **123**, 8, 082001 (2019), [arXiv:1901.05407].

[32] Y. Afik and J. R. M. de Nova, Eur. Phys. J. Plus **136**, 9, 907 (2021), [arXiv:2003.02280].

[33] G. Aad *et al.* (ATLAS), Nature **633**, 8030, 542 (2024), [arXiv:2311.07288].

[34] A. Hayrapetyan *et al.* (CMS), Rept. Prog. Phys. **87**, 11, 117801 (2024), [arXiv:2406.03976].

[35] A. Hayrapetyan *et al.* (CMS), Physical Review D **110**, 11 (2024), [arXiv:2409.11067].

[36] S. Frixione, P. Nason and B. R. Webber, JHEP **08**, 007 (2003), [hep-ph/0305252]; W. Kim and H. Shin, JHEP **07**, 070 (2007), [arXiv:0706.3563]; J. M. Campbell *et al.*, JHEP **04**, 114 (2015), [arXiv:1412.1828].

[37] T. Ježo *et al.*, Eur. Phys. J. **C76**, 12, 691 (2016), [arXiv:1607.04538].

[38] S. Frixione *et al.*, JHEP **03**, 092 (2006), [hep-ph/0512250]; V. Marotta and A. Naddeo, JHEP **08**, 029 (2008), [arXiv:0810.4759]; S. Alioli *et al.*, JHEP **09**, 111 (2009), [Erratum: JHEP02,011(2010)], [arXiv:0907.4076]; E. Re, Eur. Phys. J. **C71**, 1547 (2011), [arXiv:1009.2450]; R. Frederix, E. Re and P. Torrielli, JHEP **09**, 130 (2012), [arXiv:1207.5391]; R. Frederix *et al.*, JHEP **06**, 027 (2016), [arXiv:1603.01178].

[39] S. Frixione, P. Nason and G. Ridolfi, JHEP **09**, 126 (2007), [arXiv:0707.3088].

[40] S. Frixione and B. R. Webber, JHEP **06**, 029 (2002), [hep-ph/0204244].

[41] P. Nason, JHEP **11**, 040 (2004), [hep-ph/0409146].

[42] J. Mazzitelli *et al.*, Phys. Rev. Lett. **127**, 6, 062001 (2021), [arXiv:2012.14267].

[43] J. Mazzitelli *et al.*, JHEP **04**, 079 (2022), [arXiv:2112.12135], URL `https://doi.org/10.1007/JHEP04(2022)079`.

[44] M. Czakon, P. Fiedler and A. Mitov, Phys. Rev. Lett. **110**, 252004 (2013), [arXiv:1303.6254].

[45] S. Catani *et al.*, JHEP **07**, 100 (2019), [arXiv:1906.06535].

[46] M. Czakon *et al.*, JHEP **10**, 186 (2017), [arXiv:1705.04105].

Int. J. Mod. Phys. A 2026.41. Downloaded from www.worldscientific.com
UNIVERSITY OF CALIFORNIA @ BERKELEY on 09/16/26. Re-use and distribution is strictly not permitted, except for Open Access articles.

[47] M. Czakon and A. Mitov, Comput. Phys. Commun. **185**, 2930 (2014), [arXiv:1112.5675].

[48] M. Botje *et al.* (2011), [arXiv:1101.0538].

[49] A. D. Martin *et al.*, Eur. Phys. J. C **64**, 653 (2009), [arXiv:0905.3531].

[50] J. Gao *et al.*, Phys. Rev. D **89**, 3, 033009 (2014), [arXiv:1302.6246].

[51] R. D. Ball *et al.*, Nucl. Phys. B **867**, 244 (2013), [arXiv:1207.1303].

[52] L. Lönnblad and S. Prestel, JHEP **03**, 166 (2013), [arXiv:1211.7278].

[53] R. Frederix and S. Frixione, JHEP **12**, 061 (2012), [arXiv:1209.6215].

[54] A. Bredenstein *et al.*, JHEP **03**, 021 (2010), [arXiv:1001.4006].

[55] R. Frederix and T. Moskalets, Eur. Phys. J. C **84**, 7, 763 (2024), [arXiv:2403.14419].

[56] L. Apolinário *et al.*, Phys. Rev. Lett. **120**, 23, 232301 (2018), [arXiv:1711.03105].

[57] A. Broggio *et al.*, JHEP **08**, 039 (2019), [arXiv:1907.04343].

[58] S. Catani *et al.*, Phys. Rev. Lett. **130**, 11, 111902 (2023), [arXiv:2210.07846].

[59] L. Buonocore *et al.*, Phys. Rev. Lett. **131**, 23, 231901 (2023), [arXiv:2306.16311].

[60] N. Kidonakis and C. Foster, Physics Letters B **860**, 139146 (2025), revised to match the published version, [arXiv:2410.01214], URL `https://arxiv.org/abs/2410.01214`.

[61] D. Stremmer and M. Worek, JHEP **07**, 091 (2024), [arXiv:2403.03796].

[62] S. Devoto *et al.*, JHEP **03**, 189 (2025), [arXiv:2411.15340].

[63] E. Boos and L. Dudko, Int. J. Mod. Phys. A **37**, 05, 2250023 (2022), [arXiv:2107.07629].

[64] R. Frederix, D. Pagani and M. Zaro, JHEP **02**, 031 (2018), [arXiv:1711.02116].

[65] M. van Beekveld, A. Kulesza and L. M. Valero (2022), [arXiv:2212.03259].

[66] D. Pagani *et al.*, JHEP **09**, 155 (2021), [arXiv:2106.02059].

[67] R. Balsach *et al.* (2025), [arXiv:2503.15043].

[68] S. S. D. Willenbrock and D. A. Dicus, Phys. Rev. **D34**, 155 (1986).

[69] S. Cortese and R. Petronzio, Phys. Lett. **B253**, 494 (1991).

[70] N. Kidonakis, Phys. Rev. **D82**, 054018 (2010), [arXiv:1005.4451].

[71] T. M. P. Tait and C. P. Yuan, Phys. Rev. **D63**, 014018 (2000), [hep-ph/0007298].

[72] J. Campbell, T. Neumann and Z. Sullivan, JHEP **02**, 040 (2021), [arXiv:2012.01574].

[73] M. Brucherseifer, F. Caola and K. Melnikov, Phys. Lett. **B736**, 58 (2014), [arXiv:1404.7116].

[74] E. L. Berger, J. Gao and H. X. Zhu, JHEP **11**, 158 (2017), [arXiv:1708.09405].

[75] N. Kidonakis, Phys. Rev. **D81**, 054028 (2010), [arXiv:1001.5034].

[76] S. Frixione *et al.*, JHEP **07**, 029 (2008), [arXiv:0805.3067].

[77] C. D. White *et al.*, JHEP **11**, 074 (2009), [arXiv:0908.0631].

[78] Z. L. Liu and J. Gao, Phys. Rev. D **98**, 7, 071501 (2018), [arXiv:1807.03835].

[79] C. Degrande *et al.*, JHEP **10**, 005 (2018), [arXiv:1804.07773].

[80] D. Pagani, I. Tsinikos and E. Vryonidou, JHEP **08**, 082 (2020), [arXiv:2006.10086].

[81] H. E. Faham *et al.*, JHEP **01**, 100 (2022), [arXiv:2111.03080].

[82] F. Abe *et al.* (CDF), Phys. Rev. Lett. **74**, 2626 (1995).

[83] Abachi *et al.* (D0), Phys. Rev. Lett. **74**, 2632 (1995).

[84] R. Aaij *et al.* (LHCb), Phys. Rev. Lett. **115**, 11, 112001 (2015), [arXiv:1506.00903].

[85] A. M. Sirunyan *et al.* (CMS), Phys. Rev. Lett. **125**, 22, 222001 (2020), [arXiv:2006.11110].

[86] G. Aad *et al.* (ATLAS), Phys. Rev. Lett. **134**, 142301 (2025), [arXiv:2411.10186].

[87] (2025), cMS Collaboration, CMS-PAS-HIN-24-021, URL `https://inspirehep.net/literature/2970211`.

[88] A. M. Sirunyan *et al.* (CMS), Phys. Rev. Lett. **119**, 24, 242001 (2017), [arXiv:1709.07411].

[89] G. Aad *et al.* (ATLAS), JHEP **11**, 101 (2024), [arXiv:2405.05078].

[90] A. Hayrapetyan *et al.* (CMS), ROPP **88**, 8, 087801 (2025), [arXiv:2503.22382].

[91] ATLAS Collaboration, ATLAS-CONF-2025-008.

[92] M. Czakon, D. Heymes and A. Mitov, Phys. Rev. Lett. **116**, 8, 082003 (2016), [arXiv:1511.00549].

[93] G. D'Agostini, Nucl. Instrum. Meth. A **362**, 487 (1995).

[94] T. Adye, in "PHYSTAT 2011," 313–318, CERN, Geneva (2011), [arXiv:1105.1160].

[95] G. Aad *et al.* (ATLAS), Eur. Phys. J. C **80**, 10, 957 (2020), [Erratum: Eur.Phys.J.C 81, 29 (2021), Erratum: Eur.Phys.J.C 81, 398 (2021)], [arXiv:2004.03447].

[96] A. M. Sirunyan *et al.* (CMS), JHEP **01**, 183 (2019), [arXiv:1807.03825].

[97] A. Hocker and V. Kartvelishvili, Nucl. Instrum. Meth. A **372**, 469 (1996), [hep-ph/9509307].

[98] V. Blobel, in "Conference on Advanced Statistical Techniques in Particle Physics," 258–267 (2002), [hep-ex/0208022].

[99] T. Affolder *et al.* (CDF), Phys. Rev. D **64**, 032002 (2001), [hep-ex/0101036].

[100] V. M. Abazov *et al.* (D0), Phys. Rev. **D67**, 012004 (2003), [hep-ex/0205019].

[101] V. M. Abazov *et al.* (D0), Phys. Rev. **D94**, 092004 (2016), [arXiv:1605.06168].

[102] T. Aaltonen *et al.* (CDF), Phys. Rev. **D88**, 091103 (2013), [arXiv:1304.7961].

[103] T. A. Aaltonen *et al.* (CDF, D0), Phys. Rev. **D89**, 7, 072001 (2014), [arXiv:1309.7570].

[104] T. A. Aaltonen *et al.* (CDF), Phys. Rev. **D89**, 9, 091101 (2014), [arXiv:1402.6728].

[105] T. Aaltonen *et al.* (CDF), Phys. Rev. Lett. **105**, 012001 (2010), [arXiv:1004.3224].

[106] G. Aad *et al.* (ATLAS), JHEP **06**, 138 (2023), [arXiv:2207.01354].

[107] A. Hayrapetyan *et al.* (CMS), JHEP **04**, 099 (2025), [arXiv:2410.21631].

[108] G. Aad *et al.* (ATLAS), Eur. Phys. J. **C74**, 10, 3109 (2014), [Addendum: Eur. Phys. J.C76,no.11,642(2016)], [arXiv:1406.5375].

[109] V. Khachatryan *et al.* (CMS), JHEP **08**, 029 (2016), [arXiv:1603.02303].

[110] M. Aaboud *et al.* (ATLAS), Phys. Rev. D **108**, 3, 032014 (2023), [arXiv:2212.00571].

[111] S. Chatrchyan *et al.* (CMS), Phys. Lett. **B720**, 83 (2013), [arXiv:1212.6682].

[112] S. Chatrchyan *et al.* (CMS), JHEP **11**, 067 (2012), [arXiv:1208.2671].

Int. J. Mod. Phys. A 2026.41. Downloaded from www.worldscientific.com
by UNIVERSITY OF CALIFORNIA @ BERKELEY on 09/16/26. Re-use and distribution is strictly not permitted, except for Open Access articles.

[113] G. Aad *et al.* (ATLAS), JHEP **05**, 059 (2012), [arXiv:1202.4892].

[114] S. Chatrchyan *et al.* (CMS), JHEP **05**, 065 (2013), [arXiv:1302.0508].

[115] S. Chatrchyan *et al.* (CMS), Phys. Rev. **D85**, 112007 (2012), [arXiv:1203.6810].

[116] G. Aad *et al.* (ATLAS), Phys. Lett. **B717**, 89 (2012), [arXiv:1205.2067].

[117] S. Chatrchyan *et al.* (CMS), Eur. Phys. J. **C73**, 4, 2386 (2013), [arXiv:1301.5755].

[118] G. Aad *et al.* (ATLAS), Eur. Phys. J. **C73**, 3, 2328 (2013), [arXiv:1211.7205].

[119] J. Campbell *et al.*, MCFM: parton-level Monte Carlo program`https://mcfm.fnal.gov/`.

[120] S. Chatrchyan *et al.* (CMS), Eur. Phys. J. **C73**, 3, 2339 (2013), [arXiv:1211.2220].

[121] V. Khachatryan *et al.* (CMS), Phys. Rev. **D94**, 5, 052006 (2016), [arXiv:1607.00837].

[122] S. Chatrchyan *et al.* (CMS), Eur. Phys. J. **C74**, 3014 (2015), [Erratum: Eur. Phys. J.C75,no.5,216(2015)], [arXiv:1404.3171].

[123] G. Aad *et al.* (ATLAS), Eur. Phys. J. **C73**, 1, 2261 (2013), [arXiv:1207.5644].

[124] G. Aad *et al.* (ATLAS), Phys. Rev. **D90**, 7, 072004 (2014), [arXiv:1407.0371].

[125] G. Aad *et al.* (ATLAS), JHEP **06**, 100 (2015), [arXiv:1502.05923].

[126] G. Aad *et al.* (ATLAS), Eur. Phys. J. **C74**, 10, 3109 (2014), [Addendum: Eur. Phys. J.C76,no.11,642(2016)], [arXiv:1406.5375].

[127] S. Chatrchyan *et al.* (CMS), JHEP **02**, 024 (2014), [Erratum: JHEP02,102(2014)], [arXiv:1312.7582].

[128] M. Aaboud *et al.* (ATLAS), Eur. Phys. J. **C78**, 487 (2018), [arXiv:1712.06857].

[129] V. Khachatryan *et al.* (CMS), Eur. Phys. J. **C77**, 1, 15 (2017), [arXiv:1602.09024].

[130] M. Aaboud *et al.* (ATLAS), Phys. Rev. **D95**, 7, 072003 (2017), [arXiv:1702.08839].

[131] V. Khachatryan *et al.* (CMS), Phys. Lett. **B739**, 23 (2014), [arXiv:1407.6643].

[132] V. Khachatryan *et al.* (CMS), Eur. Phys. J. **C76**, 3, 128 (2016), [arXiv:1509.06076].

[133] G. Aad *et al.* (ATLAS, CMS), JHEP **07**, 213 (2023), [arXiv:2205.13830].

[134] M. Aaboud *et al.* (ATLAS), Phys. Rev. **D94**, 9, 092003 (2016), [arXiv:1607.07281].

[135] G. Aad *et al.* (ATLAS), Eur. Phys. J. **C76**, 10, 538 (2016), [arXiv:1511.04716].

[136] V. Khachatryan *et al.* (CMS), Eur. Phys. J. **C75**, 11, 542 (2015), [arXiv:1505.04480].

[137] A. M. Sirunyan *et al.* (CMS), Eur. Phys. J. **C77**, 7, 459 (2017), [arXiv:1703.01630].

[138] G. Aad *et al.* (ATLAS), Phys. Rev. **D93**, 3, 032009 (2016), [arXiv:1510.03818].

[139] V. Khachatryan *et al.* (CMS), Phys. Rev. **D94**, 7, 072002 (2016), [arXiv:1605.00116].

[140] G. Aad *et al.* (ATLAS), JHEP **07**, 141 (2023), [arXiv:2303.15340].

[141] A. M. Sirunyan *et al.* (CMS), Eur. Phys. J. **C79**, 5, 368 (2019), [arXiv:1812.10505].

[142] G. Aad *et al.* (ATLAS), Phys. Lett. B **810**, 135797 (2020), [arXiv:2006.13076].

[143] A. Tumasyan *et al.* (CMS) (2021), [arXiv:2108.02803].

[144] G. Aad *et al.* (ATLAS), Eur. Phys. J. C **80**, 6, 528 (2020), [arXiv:1910.08819].

[145] A. M. Sirunyan *et al.* (CMS), JHEP **09**, 051 (2017), [arXiv:1701.06228].

[146] A. M. Sirunyan *et al.* (CMS), JHEP **02**, 191 (2020), [arXiv:1911.13204].

[147] A. Tumasyan *et al.* (CMS, TOTEM) (2023), [arXiv:2310.11231].

[148] R. Aaij *et al.* (LHCb), JHEP **08**, 174 (2018), [arXiv:1803.05188].

[149] A. M. Sirunyan *et al.* (CMS), JHEP **04**, 060 (2018), [arXiv:1708.07638].

[150] V. Khachatryan *et al.* (CMS), Phys. Rev. **D95**, 9, 092001 (2017), [arXiv:1610.04191].

[151] A. M. Sirunyan *et al.* (CMS), JHEP **06**, 002 (2018), [arXiv:1803.03991].

[152] A. M. Sirunyan *et al.* (CMS), Phys. Rev. **D97**, 11, 112003 (2018), [arXiv:1803.08856].

[153] G. Aad *et al.* (ATLAS), Eur. Phys. J. C **79**, 12, 1028 (2019), [Erratum: Eur.Phys.J.C 80, 1092 (2020)], [arXiv:1908.07305].

[154] W. Bernreuther and Z.-G. Si, Physics Letters B **725**, 1–3, 115–122 (2013).

[155] A. M. Sirunyan *et al.* (CMS), JHEP **02**, 149 (2019), [arXiv:1811.06625].

[156] A. M. Sirunyan *et al.* (CMS), Eur. Phys. J. C **80**, 7, 658 (2020), [arXiv:1904.05237].

[157] A. Hayrapetyan *et al.* (CMS), JHEP **2025**, 2 (2025), [arXiv:2402.08486].

[158] G. Aad *et al.* (ATLAS) (2025), [arXiv:2509.15066].

[159] G. Aad *et al.* (ATLAS), JHEP **01**, 033 (2021), [arXiv:2006.09274].

[160] A. M. Sirunyan *et al.* (CMS), Phys. Rev. D **103**, 5, 052008 (2021), [arXiv:2008.07860].

[161] G. Aad *et al.* (ATLAS), JHEP **06**, 063 (2022), [arXiv:2202.12134].

[162] M. Aaboud *et al.* (ATLAS), Phys. Rev. **D98**, 1, 012003 (2018), [arXiv:1801.02052].

[163] G. Aad *et al.* (ATLAS), Phys. Rev. D **109**, 112016 (2024), [arXiv:312.03797].

[164] G. Aad *et al.* (ATLAS), Eur. Phys. J. C **83**, 6, 518 (2023), [arXiv:2209.07874].

[165] G. Aad *et al.* (ATLAS), Phys. Rev. D **106**, 3, 032008 (2022), [arXiv:2202.13901].

[166] A. Tumasyan *et al.* (CMS), JHEP **08**, 204 (2023), [arXiv:2303.10680].

[167] G. Aad *et al.* (ATLAS), Phys. Lett. B **848**, 138376 (2024), [arXiv:2308.09529].

[168] A. M. Sirunyan *et al.* (CMS), JHEP **03**, 115 (2018), [arXiv:1711.03143].

[169] A. Tumasyan *et al.* (CMS), JHEP **04**, 144 (2022), [arXiv:2112.09114].

[170] F. Buccioni *et al.*, JHEP **12**, 15 (2019), [arXiv:1907.13624].

[171] Aad, Georges and others, Eur. Phys. J. C **72**, 2043 (2012), [arXiv:1203.5015].

[172] G. Aad *et al.* (ATLAS), JHEP **01**, 020 (2015), [arXiv:1407.0891].

[173] V. Khachatryan *et al.* (CMS), Eur. Phys. J. C **76**, 7, 379 (2016), [arXiv:1510.03072].

[174] G. Aad *et al.* (ATLAS), Eur. Phys. J. C **76**, 642 (2016), [arXiv:1606.09490].

[175] G. Aad *et al.* (ATLAS), Eur. Phys. J. C **77**, 220 (2017), [arXiv:1610.09978].

Int. J. Mod. Phys. A 2026.41. Downloaded from www.worldscientific.com
UNIVERSITY OF CALIFORNIA @ BERKELEY on 09/16/26. Re-use and distribution is strictly not permitted, except for Open Access articles.

[176] G. Aad *et al.* (ATLAS), JHEP **10**, 159 (2018), [arXiv:1802.06572].

[177] A. M. Sirunyan *et al.* (CMS), Phys. Rev. D **97**, 112003 (2018), [arXiv:1803.08856].

[178] A. M. Sirunyan *et al.* (CMS), JHEP **07**, 125 (2020), [arXiv:2003.06467].

[179] G. Aad *et al.* (ATLAS), Phys. Rev. D **89**, 072012 (2014), [arXiv:1304.6386].

[180] V. Khachatryan *et al.* (CMS), Phys. Lett. **B746**, 132 (2015), [arXiv:1411.5621].

[181] G. Aad *et al.* (ATLAS), Eur. Phys. J. **C76**, 1, 11 (2016), [arXiv:1508.06868].

[182] M. Aaboud *et al.* (ATLAS), JHEP **04**, 046 (2019), [arXiv:1811.12113].

[183] A. M. Sirunyan *et al.* (CMS), Phys. Lett. **B776**, 355 (2018), [arXiv:1705.10141].

[184] A. M. Sirunyan *et al.* (CMS), JHEP **07**, 125 (2020), [arXiv:2003.06467].

[185] A. M. Sirunyan *et al.* (CMS), Phys. Lett. B **803**, 135285 (2020), [arXiv:1909.05306].

[186] A. Hayrapetyan *et al.* (CMS), JHEP **05**, 042 (2024), [arXiv:2309.14442].

[187] Aad, Georges and others (ATLAS), JHEP **01**, 068 (2025), [arXiv:2407.13473].

[188] A. M. Sirunyan *et al.* (CMS), Phys. Lett. B **820**, 136565 (2021), [arXiv:2012.09225].

[189] G. Aad *et al.* (ATLAS), Physics Letters B **860**, 139177 (2025), [arXiv:2409.11305].

[190] S. Chatrchyan *et al.* (CMS), Phys. Rev. Lett. **110**, 172002 (2013), [arXiv:1303.3239].

[191] G. Aad *et al.* (ATLAS), JHEP **11**, 172 (2015), [arXiv:1509.05276].

[192] V. Khachatryan *et al.* (CMS), JHEP **01**, 096 (2016), [arXiv:1510.01131].

[193] M. Aaboud *et al.* (ATLAS), Phys. Rev. **D99**, 7, 072009 (2019), [arXiv:1901.03584].

[194] A. M. Sirunyan *et al.* (CMS), JHEP **08**, 011 (2018), [arXiv:1711.02547].

[195] A. M. Sirunyan *et al.* (CMS), JHEP **03**, 056 (2020), [arXiv:1907.11270].

[196] G. Aad *et al.* (ATLAS), Eur. Phys. J. C **81**, 737 (2021), [arXiv:2103.12603].

[197] G. Aad *et al.* (ATLAS), JHEP **07**, 163 (2024), [arXiv:2312.04450].

[198] A. Hayrapetyan *et al.* (CMS), JHEP **02**, 177 (2025), [arXiv:2410.23475].

[199] A. Tumasyan *et al.* (CMS), Phys. Rev. D **108**, 032008 (2023), [arXiv:2208.12837].

[200] A. Tumasyan *et al.* (CMS), JHEP **07**, 219 (2023), [arXiv:2208.06485].

[201] A. Tumasyan *et al.*, JHEP **07**, 219 (2023), [arXiv:2208.06485].

[202] G. Aad *et al.* (ATLAS), JHEP **07**, 096 (2024), [arXiv:2401.05299].

[203] O. Bessidskaia Bylund *et al.*, JHEP **05**, 052 (2016), [arXiv:1601.08193].

[204] M. Schulze and Y. Soreq, Eur. Phys. J. C **76**, 466 (2016), [arXiv:1603.08911].

[205] A. O. Bouzas and F. Larios, Phys. Rev. D **87**, 074015 (2013), [arXiv:1212.6575].

[206] P.-F. Duan *et al.*, Phys. Lett. B **766**, 102 (2017), [arXiv:1612.00248].

[207] T. Aaltonen *et al.* (CDF), Phys. Rev. **D84**, 031104 (2011), [arXiv:1106.3970].

[208] G. Aad *et al.* (ATLAS), Phys. Rev. **D91**, 7, 072007 (2015), [arXiv:1502.00586].

[209] M. Aaboud *et al.* (ATLAS), JHEP **11**, 086 (2017), [arXiv:1706.03046].

[210] K. Melnikov, M. Schulze and A. Scharf, Phys. Rev. **D83**, 074013 (2011), [arXiv:1102.1967].

[211] A. M. Sirunyan *et al.* (CMS), JHEP **10**, 006 (2017), [arXiv:1706.08128].

[212] M. Aaboud *et al.* (ATLAS), Eur. Phys. J. **C79**, 5, 382 (2019), [arXiv:1812.01697].

[213] G. Aad *et al.* (ATLAS), JHEP **09**, 049 (2020), [arXiv:2007.06946].

[214] G. Aad *et al.* (ATLAS), JHEP **2024**, 10 (2024), [arXiv:2403.09452].

[215] A. Tumasyan *et al.* (CMS), JHEP **12**, 180 (2021), [arXiv:2107.01508].

[216] A. Tumasyan *et al.* (CMS), JHEP **05**, 091 (2022), [arXiv:2201.07301].

[217] CMS Collaboration, CMS-PAS-TOP-23-002.

[218] G. Aad *et al.* (ATLAS) (2025), [arXiv:2506.05018].

[219] A. M. Sirunyan *et al.* (CMS), JHEP **11**, 082 (2019), [arXiv:1906.02805].

[220] A. M. Sirunyan *et al.* (CMS), Eur. Phys. J. C **80**, 2, 75 (2020), [arXiv:1908.06463].

[221] G. Aad *et al.* (ATLAS), Eur. Phys. J. C **80**, 11, 1085 (2020), [arXiv:2007.14858].

[222] G. Aad *et al.* (ATLAS), JHEP **11**, 118 (2021), [arXiv:2106.11683].

[223] A. Tumasyan *et al.* (CMS), Phys. Lett. B **844**, 138076 (2023), [arXiv:2303.03864].

[224] G. Aad *et al.* (ATLAS), Eur. Phys. J. C **83**, 6, 496 (2023), [arXiv:2303.15061].

[225] A. Hayrapetyan *et al.* (CMS), Phys. Lett. B **847**, 138290 (2023), [arXiv:2305.13439].

[226] V. M. Abazov *et al.* (D0), Phys. Rev. Lett. **103**, 092001 (2009), [arXiv:0903.0850].

[227] V. M. Abazov *et al.* (D0), Phys. Rev. **D78**, 012005 (2008), [arXiv:0803.0739].

[228] V. M. Abazov *et al.* (D0), Phys. Rev. Lett. **98**, 181802 (2007), [hep-ex/0612052].

[229] T. Aaltonen *et al.* (CDF), Phys. Rev. Lett. **103**, 092002 (2009), [arXiv:0903.0885].

[230] T. Aaltonen *et al.* (CDF), Phys. Rev. **D81**, 072003 (2010), [arXiv:1001.4577].

[231] T. Aaltonen *et al.* (CDF), Phys. Rev. **D82**, 112005 (2010), [arXiv:1004.1181].

[232] A. Heinson and T. R. Junk, Ann. Rev. Nucl. Part. Sci. **61**, 171 (2011), [arXiv:1101.1275].

[233] A. Giammanco and R. Schwienhorst, Rev. Mod. Phys. **90**, 3, 035001 (2018), [arXiv:1710.10699].

[234] Tevatron Electroweak Working Group, (2009), [arXiv:0908.2171].

[235] T. A. Aaltonen *et al.* (CDF, D0), Phys. Rev. Lett. **115**, 15, 152003 (2015), [arXiv:1503.05027].

[236] N. Kidonakis, Phys. Rev. **D83**, 091503 (2011), [arXiv:1103.2792].

[237] T. A. Aaltonen *et al.* (CDF, D0), Phys. Rev. Lett. **112**, 231803 (2014), [arXiv:1402.5126].

[238] G. Aad *et al.* (ATLAS), Phys. Lett. B **854**, 138726 (2024), [arXiv:2310.01518].

[239] C. Collaboration (CMS), Technical Report CMS-PAS-TOP-24-011 (2024).

[240] G. Aad *et al.* (ATLAS), Phys. Rev. **D90**, 11, 112006 (2014), [arXiv:1406.7844].

Int. J. Mod. Phys. A 2026.41. Downloaded from www.worldscientific.com
by UNIVERSITY OF CALIFORNIA @ BERKELEY on 09/16/26. Re-use and distribution is strictly not permitted, except for Open Access articles.

[241] G. Aad *et al.* (ATLAS), Phys. Lett. **B717**, 330 (2012), [arXiv:1205.3130].

[242] S. Chatrchyan *et al.* (CMS), JHEP **12**, 035 (2012), [arXiv:1209.4533].

[243] M. Aaboud *et al.* (ATLAS, CMS), JHEP **05**, 088 (2019), [arXiv:1902.07158].

[244] M. Aaboud *et al.* (ATLAS), Eur. Phys. J. **C77**, 8, 531 (2017), [arXiv:1702.02859].

[245] M. Aaboud *et al.* (ATLAS), JHEP **04**, 124 (2017), [arXiv:1702.08309].

[246] V. Khachatryan *et al.* (CMS), JHEP **06**, 090 (2014), [arXiv:1403.7366].

[247] V. Khachatryan *et al.* (CMS), JHEP **04**, 073 (2016), [arXiv:1511.02138].

[248] M. Aaboud *et al.* (ATLAS), JHEP **04**, 086 (2017), [arXiv:1609.03920].

[249] A. M. Sirunyan *et al.* (CMS), Phys. Lett. **B772**, 752 (2017), [arXiv:1610.00678].

[250] A. M. Sirunyan *et al.* (CMS), Phys. Lett. B **800**, 135042 (2020), [arXiv:1812.10514].

[251] A. M. Sirunyan *et al.* (CMS), Eur. Phys. J. C **80**, 5, 370 (2020), [arXiv:1907.08330].

[252] A. M. Sirunyan *et al.* (CMS), Phys. Lett. B **808**, 135609 (2020), [arXiv:2004.12181].

[253] Aad, Georges and others, JHEP **05**, 305 (2024), [arXiv:2403.02126].

[254] G. Aad *et al.* (ATLAS), JHEP **11**, 040 (2022), [arXiv:2202.11382].

[255] V. Khachatryan *et al.* (CMS), JHEP **09**, 027 (2016), [arXiv:1603.02555].

[256] G. Aad *et al.* (ATLAS), Phys. Lett. **B756**, 228 (2016), [arXiv:1511.05980].

[257] G. Aad *et al.* (ATLAS), JHEP **06**, 191 (2023), [arXiv:2209.08990].

[258] ATLAS Collaboration, ATLAS-CONF-2011-118.

[259] G. Aad *et al.* (ATLAS), Phys. Lett. **B716**, 142 (2012), [arXiv:1205.5764].

[260] S. Chatrchyan *et al.* (CMS), Phys. Rev. Lett. **110**, 022003 (2013), [arXiv:1209.3489].

[261] G. Aad *et al.* (ATLAS), JHEP **01**, 064 (2016), [arXiv:1510.03752].

[262] G. Aad *et al.* (ATLAS), Eur. Phys. J. C **81**, 8, 720 (2021), [arXiv:2007.01554].

[263] S. Chatrchyan *et al.* (CMS), Phys. Rev. Lett. **112**, 23, 231802 (2014), [arXiv:1401.2942].

[264] M. Aaboud *et al.* (ATLAS), JHEP **01**, 063 (2018), [arXiv:1612.07231].

[265] M. Aaboud *et al.* (ATLAS), Eur. Phys. J. C **78**, 3, 186 (2018), [arXiv:1712.01602].

[266] G. Aad *et al.* (ATLAS), Physical Review D **110**, 7 (2024), [arXiv:2407.15594].

[267] A. M. Sirunyan *et al.* (CMS), JHEP **10**, 117 (2018), [arXiv:1805.07399].

[268] CMS Collaboration, CMS-PAS-TOP-19-003.

[269] CMS Collaboration, JHEP **11**, 111 (2021), [arXiv:2109.01706].

[270] A. Tumasyan *et al.* (CMS), JHEP **07**, 046 (2023), [arXiv:2208.00924].

[271] A. Hayrapetyan *et al.* (CMS), JHEP **2025**, 1 (2025), [arXiv:2409.06444].

[272] M. Fael and T. Gehrmann, Phys. Rev. D **88**, 033003 (2013), [arXiv:1307.1349].

[273] S. M. Etesami, S. Khatibi and M. Mohammadi Najafabadi, Eur. Phys. J. C **76**, 533 (2016), [arXiv:1606.02178].

[274] A. M. Sirunyan *et al.* (CMS), Phys. Rev. Lett. **121**, 22, 221802 (2018), [arXiv:1808.02913].

[275] G. Aad *et al.* (ATLAS), Phys. Rev. Lett. **131**, 161802 (2023), [arXiv:2302.01283].

[276] A. M. Sirunyan *et al.* (CMS), JHEP **07**, 003 (2017), [arXiv:1702.01404].

[277] A. M. Sirunyan *et al.* (CMS), Phys. Rev. Lett. **122**, 13, 132003 (2019), [arXiv:1812.05900].

[278] A. Tumasyan *et al.* (CMS), JHEP **02**, 107 (2022), [arXiv:2111.02860].

[279] G. Aad *et al.* (ATLAS), JHEP **07**, 124 (2020), [arXiv:2002.07546].

[280] CMS Collaboration, Phys. Lett. B **855**, 138815 (2024), [arXiv:2312.11668].

[281] CMS Collaboration, CMS-PAS-TOP-24-009.

[282] M. Aaboud *et al.* (ATLAS), Eur. Phys. J. **C79**, 4, 290 (2019), [arXiv:1810.01772].

[283] T. Affolder *et al.* (CDF), Phys. Rev. D **63**, 032003 (2001), [hep-ex/0006028].

[284] B. Abbott *et al.* (D0), Phys. Rev. D **58**, 052001 (1998), [hep-ex/9801025].

[285] A. M. Sirunyan *et al.* (CMS), Eur. Phys. J. **C79**, 4, 313 (2019), [arXiv:1812.10534].

[286] A. Tumasyan *et al.* (CMS), Eur. Phys. J. C **83**, 10 (2023), [arXiv:2302.01967].

[287] L. Sonnenschein, Phys. Rev. D **73**, 054015 (2006), [hep-ph/0603011].

[288] A. Hayrapetyan *et al.* (CMS), Physics Reports 116–218 (2025), [arXiv:2403.01313].

[289] B. Abbott *et al.* (D0), Phys. Rev. Lett. **80**, 2063 (1998), [hep-ex/9706014].

[290] B. Abbott *et al.* (D0), Phys. Rev. **D60**, 052001 (1999), [hep-ex/9808029].

[291] F. Abe *et al.* (CDF), Phys. Rev. Lett. **82**, 271 (1999), [Erratum: Phys. Rev. Lett.82,2808(1999)], [hep-ex/9810029].

[292] M. Aaboud *et al.* (ATLAS), Phys. Lett. **B761**, 350 (2016), [arXiv:1606.02179].

[293] A. Abulencia *et al.* (CDF), Phys. Rev. D **75**, 111103 (2007), [arXiv:0705.1594].

[294] T. Aaltonen *et al.* (CDF), Phys. Rev. **D80**, 051104 (2009), [arXiv:0906.5371].

[295] G. Aad *et al.* (ATLAS), JHEP **2023**, 6 (2023), [arXiv:2209.00583].

[296] V. Khachatryan *et al.* (CMS), JHEP **12**, 123 (2016), [arXiv:1608.03560].

[297] V. Khachatryan *et al.* (CMS), Phys. Rev. **D93**, 9, 092006 (2016), [arXiv:1603.06536].

[298] A. Abulencia *et al.* (CDF), Phys. Rev. Lett. **96**, 022004 (2006), [hep-ex/0512070].

[299] T. Aaltonen *et al.* (CDF), Phys. Rev. Lett. **99**, 182002 (2007), [arXiv:0707.3934].

[300] G. Aad *et al.* (ATLAS), Eur. Phys. J. C **75**, 4 (2015), [arXiv:1409.0832].

[301] G. Aad *et al.* (ATLAS), Eur. Phys. J. C **72**, 6 (2012), [arXiv:1203.5755].

[302] F. Abe *et al.* (CDF), Phys. Rev. Lett. **80**, 2767 (1998), [hep-ex/9801014].

[303] B. Abbott *et al.* (D0), Phys. Rev. Lett. **79**, 1197 (1997), [hep-ex/9703008].

[304] V. M. Abazov *et al.* (D0), Nature **429**, 638 (2004), [hep-ex/0406031].

[305] A. Abulencia *et al.* (CDF), Phys. Rev. D **73**, 092002 (2006), [hep-ex/0702018].

Int. J. Mod. Phys. A 2026.41. Downloaded from www.worldscientific.com
UNIVERSITY OF CALIFORNIA @ BERKELEY on 09/16/26. Re-use and distribution is strictly not permitted, except for Open Access articles.

[306] A. M. Sirunyan *et al.* (CMS), Eur. Phys. J. **C78**, 11, 891 (2018), [arXiv:1805.01428].

[307] T. Aaltonen *et al.* (CDF), Phys. Lett. **B698**, 371 (2011), [arXiv:1101.4926].

[308] The Tevatron Electroweak Working Group, arXiv:1608.01881, FERMILAB-CONF-16-298-E.

[309] F. Abe *et al.* (CDF), Phys. Rev. Lett. **79**, 1992 (1997).

[310] T. Aaltonen *et al.* (CDF), Phys. Rev. Lett. **105**, 252001 (2010), [arXiv:1010.4582].

[311] T. Aaltonen *et al.* (CDF), Phys. Rev. D **81**, 032002 (2010), [arXiv:0910.0969].

[312] T. Aaltonen *et al.* (CDF), Phys. Rev. D **88**, 011101 (2013), [arXiv:1305.3339].

[313] T. Aaltonen *et al.* (CDF), Phys. Rev. D **92**, 032003 (2015), [arXiv:1505.00500].

[314] T. Aaltonen *et al.* (CDF), Phys. Rev. D **88**, 091101 (2013), [arXiv:1309.7570].

[315] V. M. Abazov *et al.* (D0), Phys. Rev. Lett. **113**, 032002 (2014), [arXiv:1405.1756].

[316] V. M. Abazov *et al.* (D0), Phys. Rev. **D91**, 11, 112003 (2015), [arXiv:1501.07912].

[317] G. Aad *et al.* (ATLAS), Physics Reports 127–183 (2025), [arXiv:2404.10674].

[318] G. Aad *et al.* (ATLAS) (2025), [arXiv:2502.18216].

[319] V. Khachatryan *et al.* (CMS), Phys. Rev. **D93**, 7, 072004 (2016), [arXiv:1509.04044].

[320] [arXiv:1403.4427].

[321] R. Nisius, SoftwareX **11**, 100468 (2020).

[322] M. Beneke *et al.*, Phys. Lett. **B775**, 63 (2017), [arXiv:1605.03609].

[323] A. H. Hoang, C. Lepenik and M. Preisser, JHEP **09**, 099 (2017), [arXiv:1706.08526].

[324] A. H. Hoang, S. Plätzer and D. Samitz, JHEP **10**, 200 (2018), [arXiv:1807.06617].

[325] A. H. Hoang *et al.*, Phys. Rev. Lett. **101**, 151602 (2008), [arXiv:0803.4214].

[326] ATLAS Collaboration, ATL-PHYS-PUB-2021-034.

[327] A. M. Sirunyan *et al.*, Physics Letters B **803**, 135263 (2020), [arXiv:1909.09193].

[328] S. Catani *et al.*, JHEP **08**, 08, 027 (2020), [arXiv:2005.00557].

[329] G. Aad *et al.* (ATLAS) (2025), [arXiv:2507.02632].

[330] G. Aad *et al.* (ATLAS), Phys. Lett. **B716**, 1 (2012), [arXiv:1207.7214].

[331] S. Chatrchyan *et al.* (CMS), Phys. Lett. **B716**, 30 (2012), [arXiv:1207.7235].

[332] S. Alekhin, A. Djouadi and S. Moch, Phys. Lett. **B716**, 214 (2012), [arXiv:1207.0980].

[333] G. Aad *et al.* (ATLAS, CMS) (2025), [arXiv:2504.00672].

[334] T. Aaltonen *et al.* (CDF), Phys. Rev. **D87**, 5, 052013 (2013), [arXiv:1210.6131].

[335] V. M. Abazov *et al.* (D0), Phys. Rev. **D84**, 052005 (2011), [arXiv:1106.2063].

[336] G. Aad *et al.* (ATLAS), Phys. Lett. **B728**, 363 (2014), [arXiv:1310.6527].

[337] S. Chatrchyan *et al.* (CMS), JHEP **06**, 109 (2012), [arXiv:1204.2807].

[338] S. Chatrchyan *et al.* (CMS), Phys. Lett. **B770**, 50 (2017), [arXiv:1610.09551].

[339] A. Hayrapetyan *et al.* (CMS), JHEP **2021**, 12 (2021), [arXiv:2108.10407].

[340] T. A. Aaltonen *et al.* (CDF), Phys. Rev. Lett. **111**, 20, 202001 (2013), [arXiv:1308.4050].

[341] CMS Collaboration, CMS-PAS-TOP-16-019.

[342] V. M. Abazov *et al.* (D0), Phys. Rev. **D85**, 091104 (2012), [arXiv:1201.4156].

[343] M. Aaboud *et al.* (ATLAS), Eur. Phys. J. **C78**, 2, 129 (2018), [arXiv:1709.04207].

[344] ATLAS Collaboration, ATLAS-CONF-2019-038.

[345] V. Khachatryan *et al.* (CMS), Phys. Lett. **B736**, 33 (2014), [arXiv:1404.2292].

[346] G. Mahlon and S. J. Parke, Phys. Rev. **D53**, 4886 (1996), [hep-ph/9512264]; G. Mahlon and S. J. Parke, Phys. Lett. **B411**, 173 (1997), [hep-ph/9706304].

[347] G.R. Goldstein, in *Spin 96: Proceedings of the 12th International Symposium on High Energy Spin Physics,* ed. C.W. Jager (World Scientific, Singapore, 1997), p. 328.

[348] T. Stelzer and S. Willenbrock, Phys. Lett. **B374**, 169 (1996), [hep-ph/9512292].

[349] W. Bernreuther *et al.*, Nucl. Phys. **B690**, 81 (2004), [hep-ph/0403035].

[350] A. Brandenburg, Z. G. Si and P. Uwer, Phys. Lett. **B539**, 235 (2002), [hep-ph/0205023].

[351] B. Abbott *et al.* (D0), Phys. Rev. Lett. **85**, 256 (2000), [hep-ex/0002058].

[352] T. Aaltonen *et al.* (CDF), Phys. Rev. D **83**, 031104 (2011), [arXiv:1012.3093].

[353] V. M. Abazov *et al.* (D0), Phys. Lett. **B757**, 199 (2016), [arXiv:1512.08818].

[354] V. M. Abazov *et al.* (D0), Phys. Rev. **D95**, 1, 011101 (2017), [arXiv:1607.07627].

[355] V. M. Abazov *et al.* (D0), Phys. Rev. **D92**, 052007 (2015), [arXiv:1507.05666].

[356] G. Mahlon and S. J. Parke, Phys. Rev. **D81**, 074024 (2010), [arXiv:1001.3422].

[357] G. Aad *et al.* (ATLAS), Phys. Rev. Lett. **108**, 21 (2012), [arXiv:1203.4081].

[358] G. Aad *et al.* (ATLAS), Phys. Rev. **D90**, 11, 112016 (2014), [arXiv:1407.4314].

[359] G. Aad *et al.* (ATLAS), Phys. Rev. Lett. **114**, 14, 142001 (2015), [arXiv:1412.4742].

[360] G. Aad *et al.* (ATLAS), Phys. Rev. **D93**, 1, 012002 (2016), [arXiv:1510.07478].

[361] S. Chatrchyan *et al.* (CMS), Phys. Rev. Lett. **112**, 18, 182001 (2014), [arXiv:1311.3924].

[362] V. Khachatryan *et al.* (CMS), Phys. Lett. **B758**, 321 (2016), [arXiv:1511.06170].

[363] V. Khachatryan *et al.* (CMS), Phys. Rev. **D93**, 5, 052007 (2016), [arXiv:1601.01107].

[364] M. Aaboud *et al.* (ATLAS), Eur. Phys. J. C **80**, 8, 754 (2020), [arXiv:1903.07570].

[365] A. M. Sirunyan *et al.* (CMS), Phys. Rev. **D100**, 7, 072002 (2019), [arXiv:1907.03729].

[366] M. Aaboud *et al.* (ATLAS), JHEP **03**, 113 (2017), [arXiv:1612.07004].

[367] A. Einstein, B. Podolsky and N. Rosen, Phys. Rev. **47**, 777 (1935).

[368] E. Schrödinger, Mathematical Proceedings of the Cambridge Philosophical Society **31**, 4, 555–563 (1935).

[369] J. S. Bell, Physics Physique Fizika **1**, 195 (1964).

[370] A. Go *et al.* (Belle), Phys. Rev. Lett. **99**, 131802 (2007), [arXiv:quant-ph/0702267].

[371] M. Fabbrichesi *et al.* (2023), [arXiv:2305.04982].

[372] M. Fabbrichesi, R. Floreanini and G. Panizzo, Phys. Rev. Lett. **127**, 16, 161801 (2021), [arXiv:2102.11883].

[373] C. Severi *et al.*, Eur. Phys. J. C **82**, 4, 285 (2022), [arXiv:2110.10112].

Int. J. Mod. Phys. A 2026.41. Downloaded from www.worldscientific.com
by UNIVERSITY OF CALIFORNIA @ BERKELEY on 09/16/26. Re-use and distribution is strictly not permitted, except for Open Access articles.

[374] Y. Afik and J. R. M. n. de Nova, Quantum **6**, 820 (2022), [arXiv:2203.05582].

[375] J. A. Aguilar-Saavedra and J. A. Casas, Eur. Phys. J. C **82**, 8, 666 (2022), [arXiv:2205.00542].

[376] Y. Afik and J. R. M. n. de Nova, Phys. Rev. Lett. **130**, 22, 221801 (2023), [arXiv:2209.03969].

[377] R. Ashby-Pickering, A. J. Barr and A. Wierzchucka, JHEP **05**, 020 (2023), [arXiv:2209.13990].

[378] J. A. Aguilar-Saavedra (2023), [arXiv:2307.06991].

[379] B. Fuks *et al.*, The European Physical Journal C **85**, 2 (2025).

[380] P. Nason, E. Re and L. Rottoli (2025), [arXiv:2505.00096].

[381] G. L. Kane, G. A. Ladinsky and C. P. Yuan, Phys. Rev. **D45**, 124 (1992).

[382] A. Czarnecki, J. G. Korner and J. H. Piclum, Phys. Rev. **D81**, 111503 (2010), [arXiv:1005.2625].

[383] T. Affolder *et al.* (CDF), Phys. Rev. Lett. **84**, 216 (2000), [hep-ex/9909042].

[384] D. Acosta *et al.* (CDF), Phys. Rev. D **71**, 031101 (2005), [hep-ex/0411070].

[385] A. Abulencia *et al.* (CDF), Phys. Rev. D **73**, 111103 (2006), [hep-ex/0511023].

[386] V. M. Abazov *et al.* (D0), Phys. Rev. D **75**, 031102 (2007), [hep-ex/0609045].

[387] V. M. Abazov *et al.* (D0), Phys. Rev. Lett. **100**, 062004 (2008), [arXiv:0711.0032].

[388] T. Aaltonen *et al.* (CDF), Phys. Lett. B **674**, 160 (2009), [arXiv:0811.0344].

[389] V. M. Abazov *et al.* (D0), Phys. Rev. D **70**, 032004 (2004), [hep-ex/0404040].

[390] T. Aaltonen *et al.* (CDF, D0), Phys. Rev. **D85**, 071106 (2012), [arXiv:1202.5272].

[391] G. Aad *et al.* (ATLAS), JHEP **06**, 088 (2012), [arXiv:1205.2484].

[392] S. Chatrchyan *et al.* (CMS), JHEP **10**, 167 (2013), [arXiv:1308.3879].

[393] ATLAS and CMS Collaboration, ATLAS-CONF-2013-033, CMS-PAS-TOP-12-025.

[394] M. Aaboud *et al.* (ATLAS), Eur. Phys. J. **C77**, 4, 264 (2017), [Erratum: Eur. Phys. J.C79,no.1,19(2019)], [arXiv:1612.02577].

[395] V. Khachatryan *et al.* (CMS), Phys. Lett. **B762**, 512 (2016), [arXiv:1605.09047].

[396] V. Khachatryan *et al.* (CMS), JHEP **01**, 053 (2015), [arXiv:1410.1154].

[397] G. Aad *et al.* (CMS, ATLAS), JHEP **08**, 08, 051 (2020), [arXiv:2005.03799].

[398] G. Aad *et al.* (ATLAS), Phys. Lett. B **843**, 137829 (2023), [arXiv:2209.14903].

[399] G. Aad *et al.* (ATLAS) (2025), [arXiv:2509.16039], URL `https://arxiv.org/abs/2509.16039`.

[400] A. M. Sirunyan *et al.* (CMS), Physical Review D **102**, 9 (2020), [arXiv:2009.07123].

[401] S. Jung *et al.*, Phys. Rev. **D81**, 015004 (2010), [arXiv:0907.4112].

[402] M. Czakon, P. Fiedler and A. Mitov, Phys. Rev. Lett. **115**, 5, 052001 (2015), [arXiv:1411.3007].

[403] W. Hollik and D. Pagani, Phys. Rev. **D84**, 093003 (2011), [arXiv:1107.2606].

[404] W. Bernreuther and Z.-G. Si, Phys. Rev. **D86**, 034026 (2012), [arXiv:1205.6580].

[405] V. M. Abazov *et al.* (D0), Phys. Rev. Lett. **100**, 142002 (2008), [arXiv:0712.0851].

[406] T. Aaltonen *et al.* (CDF), Phys. Rev. Lett. **101**, 202001 (2008), [arXiv:0806.2472].

[407] T. A. Aaltonen *et al.* (CDF, D0), Phys. Rev. Lett. **120**, 4, 042001 (2018), [arXiv:1709.04894].

[408] S. Berge and S. Westhoff, JHEP **2013**, 7 (2013), ISSN 1029-8479, [arXiv:1305.3272].

[409] V. Khachatryan *et al.* (CMS), Phys. Lett. **B757**, 154 (2016), [arXiv:1507.03119].

[410] G. Aad *et al.* (ATLAS), Phys. Lett. **B756**, 52 (2016), [arXiv:1512.06092].

[411] G. Aad *et al.* (ATLAS), Phys. Lett. B **843**, 137848 (2023), [arXiv:2212.10552].

[412] G. Aad *et al.* (ATLAS), JHEP **07**, 033 (2023), [arXiv:2301.04245].

[413] A. Hayrapetyan *et al.* (CMS) (2025), [arXiv:2509.13512].

[414] G. Aad *et al.* (ATLAS), JHEP **02**, 107 (2014), [arXiv:1311.6724].

[415] S. Chatrchyan *et al.* (CMS), Phys. Lett. **B717**, 129 (2012), [arXiv:1207.0065].

[416] G. Aad *et al.* (ATLAS), JHEP **05**, 061 (2015), [arXiv:1501.07383].

[417] S. Chatrchyan *et al.* (CMS), JHEP **04**, 191 (2014), [arXiv:1402.3803].

[418] M. Aaboud *et al.* (ATLAS, CMS), JHEP **04**, 033 (2018), [arXiv:1709.05327].

[419] M. Czakon *et al.*, Phys. Rev. **D98**, 1, 014003 (2018), [arXiv:1711.03945].

[420] G. Aad *et al.* (ATLAS), Eur. Phys. J. **C76**, 2, 87 (2016), [Erratum: Eur. Phys. J.C77,564(2017)], [arXiv:1509.02358].

[421] V. Khachatryan *et al.* (CMS), Phys. Rev. **D93**, 3, 034014 (2016), [arXiv:1508.03862].

[422] G. Aad *et al.* (ATLAS), Phys. Rev. **D94**, 3, 032006 (2016), [arXiv:1604.05538].

[423] V. Khachatryan *et al.* (CMS), Phys. Lett. **B760**, 365 (2016), [arXiv:1603.06221].

[424] G. Aad *et al.* (ATLAS), JHEP **08**, 077 (2023), [arXiv:2208.12095].

[425] A. Tumasyan *et al.* (CMS), Phys. Lett. B **846**, 137703 (2023), [arXiv:2208.02751].

[426] G. Aad *et al.* (ATLAS), Eur. Phys. J. C **82**, 4, 374 (2022), [arXiv:2110.05453].

[427] A. M. Sirunyan *et al.* (CMS), JHEP **06**, 146 (2020), [arXiv:1912.09540].

[428] D. Choudhury, T. M. P. Tait and C. E. M. Wagner, Phys. Rev. **D65**, 053002 (2002), [hep-ph/0109097].

[429] D. Chang, W.-F. Chang and E. Ma, Phys. Rev. **D59**, 091503 (1999), [hep-ph/9810531]; D. Chang, W.-F. Chang and E. Ma, Phys. Rev. **D61**, 037301 (2000), [hep-ph/9909537].

[430] T. Aaltonen *et al.* (CDF), Phys. Rev. **D88**, 3, 032003 (2013), [arXiv:1304.4141].

[431] V. M. Abazov *et al.* (D0), Phys. Rev. **D90**, 5, 051101 (2014), [Erratum: Phys. Rev.D90,no.7,079904(2014)], [arXiv:1407.4837].

[432] G. Aad *et al.* (ATLAS), JHEP **11**, 031 (2013), [arXiv:1307.4568].

[433] CMS Collaboration, CMS-PAS-TOP-11-031.

[434] S. P. Martin 1–98 (1997), [Adv. Ser. Direct. High Energy Phys.18,1(1998)], [hep-ph/9709356].

[435] C. T. Hill and E. H. Simmons, Phys. Rept. **381**, 235 (2003), [Erratum: Phys. Rept.390,553(2004)], [hep-ph/0203079].

[436] C. T. Hill, Phys. Lett. **B266**, 419 (1991).

[437] C. T. Hill, Phys. Lett. **B345**, 483 (1995), [hep-ph/9411426].

[438] S. Chatrchyan *et al.* (CMS), Phys. Rev. D **87**, 072002 (2013), URL https://link.aps.org/doi/10.1103/PhysRevD.87.072002.

[439] S. Chatrchyan *et al.* (CMS), JHEP **12**, 015 (2012), [arXiv:1209.4397].

[440] G. Aad *et al.* (ATLAS), JHEP **10**, 061 (2020), [arXiv:2005.05138].

[441] G. Aad *et al.* (ATLAS), The European Physical Journal C **84**, 7 (2024).

[442] G. Aad *et al.* (ATLAS), JHEP **07**, 199 (2023), [arXiv:2301.03902].

[443] G. Aad *et al.* (ATLAS), JHEP **2306**, 155 (2023), [arXiv:2208.11415].

[444] G. Aad *et al.* (ATLAS), JHEP **2023**, 12 (2023), [arXiv:2309.12817].

[445] A. Hayrapetyan *et al.* (CMS), Physical Review D **112**, 3 (2025), [arXiv:2407.15172].

[446] A. Tumasyan *et al.* (CMS), JHEP **02**, 169 (2022), [arXiv:2112.09734].

[447] A. Tumasyan *et al.* (CMS), Phys. Rev. Lett. **129**, 032001 (2022), URL https://link.aps.org/doi/10.1103/PhysRevLett.129.032001.

[448] G. Aad *et al.* (ATLAS), Physical Review D **108**, 3 (2023), [arXiv:2301.11605].

[449] G. Aad *et al.* (ATLAS), Phys. Lett. B **842**, 137379 (2023), [arXiv:2205.02537].

[450] G. Aad *et al.* (ATLAS), Eur. Phys. J. C **82**, 4, 334 (2022), [arXiv:2112.01302].

[451] A. Tumasyan *et al.* (CMS), JHEP **06**, 082 (2022), [arXiv:2201.07859].

[452] A. Hayrapetyan (CMS), Physical Review D **111**, 1 (2025), [arXiv:2312.03199].

[453] A. Hayrapetyan *et al.* (CMS) (2025), [arXiv:2504.08532].

[454] G. Aad *et al.* (ATLAS), Physical Review D **110**, 1 (2024), [arXiv:2403.06742].

[455] A. Hayrapetyan *et al.* (CMS), Physical Review Letters **132**, 24 (2024), [arXiv:2402.18461].

[456] S. Banerjee, M. Chala and M. Spannowsky, Eur. Phys. J. C **78**, 8, 683 (2018), [arXiv:1806.02836].

[457] T. Giani, G. Magni and J. Rojo, EPJC **83**, 5 (2023).

[458] C. Zhang and S. Willenbrock, Nuovo Cim. C **033**, 4, 285 (2010), [arXiv:1008.3155].

[459] A. M. Sirunyan *et al.* (CMS), JHEP **03**, 095 (2021), [arXiv:2012.04120].

[460] A. Tumasyan *et al.* (CMS), JHEP **2021**, 12 (2021), [arXiv:2107.13896].

[461] A. Hayrapetyan *et al.* (CMS) (2025), [arXiv:2505.21206].

[462] A. Hayrapetyan *et al.* (CMS) (2025), [arXiv:2507.17498].

[463] A. Hayrapetyan, Physical Review D **109**, 7 (2024), [arXiv:2312.08229].

[464] A. a. Hayrapetyan, Physical Review D **111**, 1 (2025), [arXiv:2312.03199].

[465] A. Hayrapetyan, JHEP **2023**, 12 (2023), [arXiv:2307.15761].

[466] G. Aad *et al.* (ATLAS), JHEP **2025**, 2 (2025), [arXiv:2409.14982].

[467] G. Aad *et al.* (ATLAS) (2025), [arXiv:2504.05919].

[468] G. Aad *et al.* (ATLAS) (2025), [arXiv:2509.19038].

Int. J. Mod. Phys. A 2026.41. Downloaded from www.worldscientific.com
UNIVERSITY OF CALIFORNIA @ BERKELEY on 09/16/26. Re-use and distribution is strictly not permitted, except for Open Access articles.

Int. J. Mod. Phys. A 2026.41. Downloaded from www.worldscientific.com by UNIVERSITY OF CALIFORNIA @ BERKELEY on 09/16/26. Re-use and distribution is strictly not permitted, except for Open Access articles.

62. Form Factors for Semileptonic Kaon ($K_{\ell 3}$), Radiative Pion ($\pi_{\ell 2\gamma}$) and Kaon ($K_{\ell 2\gamma}$) Decays

Revised August 2025 by M.A. Bychkov (Virginia U.) and G. D'Ambrosio (INFN, Napoli).

62.1 $\pi^{\pm}_{\ell 2\gamma}$ and $K^{\pm}_{\ell 2\gamma}$ Form Factors

The radiative decays, $\pi^{\pm} \to l^{\pm}\nu\gamma$ and $K^{\pm} \to l^{\pm}\nu\gamma$, with l standing for an e or a μ, and γ for a real or virtual photon (e^+e^- pair), provide a powerful tool to investigate the hadronic structure of pions and kaons. The structure-dependent part SD_i of the amplitude describes the emission of photons from virtual hadronic states, and is parametrized in terms of form factors V, A, (vector, axial vector), in the standard description [1–4]. Note that in the Listings and some literature, equivalent nomenclature F_V and F_A for the vector and axial form factors is often used. Exotic, non-standard contributions like $i = T, S$ (tensor, scalar) have also been considered. Apart from the SD terms, there is also the Inner Bremsstrahlung amplitude, IB, corresponding to photon radiation from external charged particles and described by Low theorem in terms of the physical decay $\pi^{\pm}(K^{\pm}) \to l^{\pm}\nu$. Experiments try to optimize their kinematics so as to minimize the IB part of the amplitude.

The SD amplitude in its standard form is given as

$$M(\mathrm{SD}_V) = \frac{-eG_F U_{qq'}}{\sqrt{2}m_P}\epsilon^{\mu} l^{\nu} V^P \epsilon_{\mu\nu\sigma\tau} k^{\sigma} q^{\tau} \tag{62.1}$$

$$M(\mathrm{SD}_A) = \frac{-ieG_F U_{qq'}}{\sqrt{2}m_P}\epsilon^{\mu} l^{\nu}\{A^P[(qk-k^2)g_{\mu\nu} - q_{\mu}k_{\nu}] + R^P k^2 g_{\mu\nu}\}\ , \tag{62.2}$$

which contains an additional axial form factor R^P which only can be accessed if the photon remains virtual. $U_{qq'}$ is the Cabibbo-Kobayashi-Maskawa mixing-matrix element; ϵ^{μ} is the polarization vector of the photon (or the effective vertex, $\epsilon^{\mu} = (e/k^2)\overline{u}(p_-)\gamma^{\mu}v(p_+)$, of the e^+e^- pair); $\ell^{\nu} = \overline{u}(p_{\nu})\gamma^{\nu}(1-\gamma_5)v(p_{\ell})$ is the lepton-neutrino current; q and k are the meson and photon four-momenta ($k = p_+ + p_-$ for virtual photons); and P stands for π or K.

For decay processes where the photon is real, the partial decay width can be written in analytical form as a sum of IB, SD, and IB/SD interference terms INT [1, 4]:

$$\begin{aligned}\frac{d^2\Gamma_{P\to\ell\nu\gamma}}{dxdy} &= \frac{d^2\left(\Gamma_{\mathrm{IB}} + \Gamma_{\mathrm{SD}} + \Gamma_{\mathrm{INT}}\right)}{dxdy} \\ &= \frac{\alpha}{2\pi}\Gamma_{P\to\ell\nu}\frac{1}{(1-r)^2}\Bigg\{\mathrm{IB}(x,y) \\ &+ \frac{1}{r}\left(\frac{m_P}{2f_P}\right)^2\left[(V+A)^2\mathrm{SD}^+(x,y) + (V-A)^2\mathrm{SD}^-(x,y)\right] \\ &+ \epsilon_P\frac{m_P}{f_P}\left[(V+A)\mathrm{S}^+_{\mathrm{INT}}(x,y) + (V-A)\mathrm{S}^-_{\mathrm{INT}}(x,y)\right]\Bigg\}.\end{aligned} \tag{62.3}$$

Here

$$\begin{aligned}\mathrm{IB}(x,y) &= \left[\frac{1-y+r}{x^2(x+y-1-r)}\right] \\ &\quad \left[x^2 + 2(1-x)(1-r) - \frac{2xr(1-r)}{x+y-1-r}\right] \\ \mathrm{SD}^+(x,y) &= (x+y-1-r)\Big[(x+y-1)(1-x) - r\Big] \\ \mathrm{SD}^-(x,y) &= (1-y+r)\Big[(1-x)(1-y) + r\Big] \\ \mathrm{S}^+_{\mathrm{INT}}(x,y) &= \left[\frac{1-y+r}{x(x+y-1-r)}\right]\Big[(1-x)(1-x-y) + r\Big] \\ \mathrm{S}^-_{\mathrm{INT}}(x,y) &= \left[\frac{1-y+r}{x(x+y-1-r)}\right]\Big[x^2 - (1-x)(1-x-y) - r\Big]\end{aligned} \tag{62.4}$$

where $x = 2E_{\gamma}/m_P$, $y = 2E_{\ell}/m_P$, $r = (m_{\ell}/m_P)^2$, f_P is the meson decay constant, and ϵ_P is +1 for pions and -1 for kaons. The structure dependent terms SD^+ and SD^- are shown in Fig. 1. The SD^- term is maximized in the same kinematic region where overwhelming IB term dominates (along $x + y = 1$ diagonal). Thus experimental yields with less background are dominated by SD^+ contribution and proportional to $A^P + V^P$ making simultaneous precise determination of the form factors difficult.

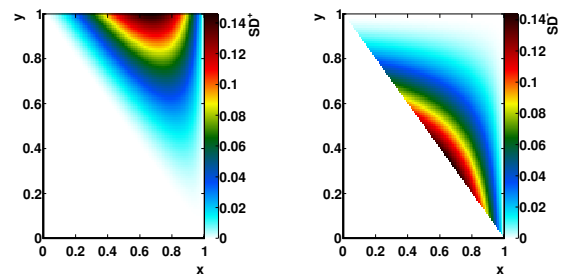

Figure 62.1: Components of the structure dependent terms of the decay width. Left: SD^+, right: SD^-

Recently, formulas 62.3 and 62.4 have been extended to describe polarized distributions in radiative meson and muon decays [5].

The "helicity" factor r is responsible for the enhancement of the SD over the IB amplitude in the decays $\pi^{\pm} \to e^{\pm}\nu\gamma$, while $\pi^{\pm} \to \mu^{\pm}\nu\gamma$ is dominated by IB. Interference terms are important for the decay $K^{\pm} \to \mu^{\pm}\nu\gamma$ [6], but contribute only a few percent correction to pion decays. However, they provide the basis for determining the signs of V and A. Radiative corrections to the decay $\pi^+ \to e^+\nu\gamma$ have to be taken into account in the analysis of the precision experiments. They make up to 4% corrections in the total decay rate [7]. In $\pi^{\pm} \to e^{\pm}\nu e^+e^-$ and $K^{\pm} \to \ell^{\pm}\nu e^+e^-$ decays, all three form factors, V^P, A^P, and R^P, can be determined [8, 9].

Theoretically, the first non-trivial χPT contributions to A^P and V^P appear at $\mathcal{O}(p^4)$ [4], respectively from Gasser-Leutwyler coefficients, L_i's, and the anomalous lagrangian:

$$A^P = \frac{4\sqrt{2}M_P}{F_{\pi}}(L^r_9 + L^r_{10}), \quad V^P = \frac{\sqrt{2}M_P}{8\pi^2 F_{\pi}}. \tag{62.5}$$

In case of the kaon $A^K = 0.042$ and $V^K = 0.096$. $\mathcal{O}(p^6)$ contributions to A^K can be predicted accurately: they are flat in the momentum dependence and shift the $\mathcal{O}(p^4)$ value to 0.034. $\mathcal{O}(p^6)$ contributions to V^K are model dependent and can be approximated by a form factor linearly dependent on momentum. For example, when looking at the spread of results obtained within two different models, the constant piece of this linear form factor is shifted to 0.078 ± 0.005 [1, 2, 4].

We give the experimental $\pi^{\pm}$ form factors V^{π}, A^{π}, and R^{π} in the Listings. In the $K^{\pm}$ Listings, we give the extracted sum $A^K + V^K$ and difference $A^K - V^K$, as well as V^K, A^K and R^K. In particular KLOE has measured for the constant piece of the form factor $A^K + V^K = 0.125 \pm 0.007 \pm 0.001$ [10] while ISTRA+, $V^K - A^K = 0.21 \pm 0.04 \pm 0.04$ [11].

The pion vector form factor, V^{π}, is related via CVC (Conserved Vector Current) to the $\pi^0 \to \gamma\gamma$ decay width. The constant term is given by $|V^{\pi}(0)| = (1/\alpha)\sqrt{2\Gamma_{\pi^0\to\gamma\gamma}/\pi m_{\pi^0}}$ [3]. The resulting value, $V^{\pi}(0) = 0.0259(9)$, has been confirmed by calculations based on chiral perturbation theory (χPT) [4], and by two experiments given in the Listings.

A recent experiment by the PIBETA collaboration [12] obtained a $V^{\pi}(0)$ that is in excellent agreement with the CVC hypothesis. It also measured the slope parameter a in $V^{\pi}(s) = V^{\pi}(0)(1 + a\cdot s)$, where $s = (1 - 2E_{\gamma}/m_{\pi})$, and E_{γ} is the gamma energy in the pion rest frame: $a = 0.095 \pm 0.058$. A functional dependence on s is expected for all form factors. It becomes non-negligible in the case of $V^{\pi}(s)$ when a wide range of photon momenta is recorded; proper treatment in the analysis of K decays is mandatory.

Int. J. Mod. Phys. A 2026.41. Downloaded from www.worldscientific.com
UNIVERSITY OF CALIFORNIA @ BERKELEY on 09/16/26. Re-use and distribution is strictly not permitted, except for Open Access articles.

The form factor, R^P, can be related to the electromagnetic radius, r_P, of the meson [2]: $R^P = \frac{1}{3} m_P f_P \langle r_P^2 \rangle$ using PCAC (Partial Conserved Axial vector Current).

In lowest order χPT, the ratio A^π/V^π is related to the pion electric polarizability $\alpha_E = [\alpha/(8\pi^2 m_\pi f_\pi^2)] \times A^\pi/V^\pi$ [13]. Direct experimental and theoretical status of pion polarizability studies currently is not settled. Most recent theoretical predictions from χPT at $\mathcal{O}(p^6)$ [14] and experimental results from COMPASS collaboration [15] favor a small value of pion polarizability $\alpha_\pi \sim (2 \div 3) \times 10^{-4}\,\mathrm{fm}^3$. Dispersive analysis of $\gamma\gamma \to \pi^+\pi^-$ crossection [16] and experimental results from MAMI collaboration [17] report a much larger value of $\alpha_\pi \sim 6 \times 10^{-4}\,\mathrm{fm}^3$. Precise measurement of the pion form factors by PIBETA collaboration favors smaller values of polarizability $\alpha_\pi = 2.7^{+0.6}_{-0.5} \times 10^{-4}\,\mathrm{fm}^3$.

Several searches for the exotic form factors F_T^π, F_T^K (tensor), and F_S^K (scalar) have been pursued in the past. In particular, F_T^π has been brought into focus by experimental as well as theoretical work [18]. New high-statistics data from the PIBETA collaboration have been re-analyzed together with an additional data set optimized for low backgrounds in the radiative pion decay. In particular, lower beam rates have been used in order to reduce the accidental background, thereby making the treatment of systematic uncertainties easier and more reliable. The PIBETA analysis now restricts F_T^π to the range $-5.2 \times 10^{-4} < F_T^\pi < 4.0 \times 10^{-4}$ at a 90% confidence limit [12]. This result is in excellent agreement with the most recent theoretical work [4].

Precision measurements of radiative pion and kaon decays are effective tools to study QCD in the non-perturbative region and are of interest beyond the scope of radiative decays. Meanwhile other processes such as $\pi^+ \to e^+\nu$ that seem to be better suited to search for new physics at the precision frontier are currently studied. The advantages of such process are the very accurate and reliable theoretical predictions and the more straightforward experimental analysis.

62.2 $K_{\ell 3}^\pm$ and $K_{\ell 3}^0$ Form Factors

Assuming that only the vector current contributes to $K \to \pi\ell\nu$ decays, we write the matrix element as

$$M \propto f_+(t)\left[(P_K + P_\pi)_\mu \bar{\ell}\gamma_\mu(1+\gamma_5)\nu\right] + f_-(t)\left[m_\ell \bar{\ell}(1+\gamma_5)\nu\right] , \tag{62.6}$$

where P_K and P_π are the four-momenta of the K and π mesons, m_ℓ is the lepton mass, and f_+ and f_- are dimensionless form factors which can depend only on $t = (P_K - P_\pi)^2$, the square of the four-momentum transfer to the leptons. If time-reversal invariance holds, f_+ and f_- are relatively real. $K_{\mu 3}$ experiments, discussed immediately below, measure f_+ and f_-, while K_{e3} experiments, discussed further below, are sensitive only to f_+ because the small electron mass makes the f_- term negligible.

62.2.1 $K_{\mu 3}$ *Decays*

Analyses of $K_{\mu 3}$ data frequently assume a linear dependence of f_+ and f_- on t, *i.e.*,

$$f_\pm(t) = f_\pm(0)\left[1 + \lambda_\pm (t/m_{\pi^+}^2)\right] . \tag{62.7}$$

Most $K_{\mu 3}$ data are adequately described by formula 62.7 for f_+ and a constant f_- (*i.e.*, $\lambda_- = 0$).

There are two equivalent parametrizations commonly used in these analyses: $\lambda_+, \xi(0)$ parametrization and λ_+, λ_0 parametrization.

Older analyses of $K_{\mu 3}$ data often introduce the ratio of the two form factors

$$\xi(t) = f_-(t)/f_+(t) . \tag{62.8}$$

The $K_{\mu 3}$ decay distribution is then described by the two parameters λ_+ and $\xi(0)$ (assuming time reversal invariance and $\lambda_- = 0$).

More recent $K_{\mu 3}$ analyses have parametrized in terms of the form factors f_+ and f_0, which are associated with vector and scalar exchange, respectively, to the lepton pair. f_0 is related to f_+ and f_- by

$$f_0(t) = f_+(t) + \left[t/(m_K^2 - m_\pi^2)\right] f_-(t) . \tag{62.9}$$

Here $f_0(0)$ must equal $f_+(0)$. The earlier assumption that f_+ is linear in t and f_- is constant leads to f_0 linear in t:

$$f_0(t) = f_0(0)\left[1 + \lambda_0 (t/m_{\pi^+}^2)\right] . \tag{62.10}$$

With the assumption that $f_0(0) = f_+(0)$, the two parametrizations, $(\lambda_+, \xi(0))$ and (λ_+, λ_0) are equivalent as long as correlation information is retained. (λ_+, λ_0) correlations tend to be less strong than $(\lambda_+, \xi(0))$ correlations.

Since the 2006 edition of the *Review* [19], we no longer quote results in the $(\lambda_+, \xi(0))$ parametrization. We have removed many older low statistics results from the Listings. See the 2004 version of this note [20] for these older results, and the 1982 version [21] for additional discussion of the $K_{\mu 3}^0$ parameters, correlations, and conversion between parametrizations.

More recent high-statistics experiments have included a quadratic term in the expansion of $f_+(t)$,

$$f_+(t) = f_+(0)\left[1 + \lambda_+^{'}(t/m_{\pi^+}^2) + \frac{\lambda_+^{''}}{2}(t/m_{\pi^+}^2)^2\right] . \tag{62.11}$$

If there is a non-vanishing quadratic term, then λ_+ of formula 62.7 represents the average slope, which is then different from $\lambda_+^{'}$. Our convention is to include the factor $\frac{1}{2}$ in the quadratic term, and to use m_{π^+} even for K_{e3}^+ and $K_{\mu 3}^+$ decays. We have converted other's parametrizations to match our conventions, as noted in the beginning of the "$K_{\ell 3}^\pm$ and $K_{\ell 3}^0$ Form Factors" sections of the Listings.

There are two alternatives to the Taylor parametrization: The Pole Parametrization and Dispersive Parametrization.

The pole model describes the t-dependence of $f_+(t)$ and $f_0(t)$ in terms of the exchange of the lightest vector and scalar K^* mesons with masses M_V and M_S, respectively:

$$f_+(t) = f_+(0)\left[\frac{M_V^2}{M_V^2 - t}\right] , \quad f_0(t) = f_0(0)\left[\frac{M_S^2}{M_S^2 - t}\right] . \tag{62.12}$$

The Dispersive Parametrization approach, valid in a much wider kinematic range and able to describe at the same time τ-decay data, [22] uses dispersive techniques and the known low-energy K-π phases to parametrize the vector and scalar form factors:

$$f_+(t) = f_+(0)\exp\left[\frac{t}{m_\pi^2}(\Lambda_+ + H(t))\right]; \tag{62.13}$$

$$f_0(t) = f_+(0)\exp\left[\frac{t}{(m_K^2 - m_\pi^2)}\,(ln[C] - G(t))\right], \tag{62.14}$$

where Λ_+ is the slope of the vector form factor, and $\ln C = \ln[f_0(m_K^2 - m_\pi^2)]$ is the logarithm of the scalar form factor at the Callan-Treiman point. The functions $H(t)$ and $G(t)$ are dispersive integrals.

62.2.2 K_{e3} *Decays*

Analysis of K_{e3} data is simpler than that of $K_{\mu 3}$ because the second term of the matrix element assuming a pure vector current [formula 62.6 above] can be neglected. Here f_+ can be assumed to be linear in t, in which case the linear coefficient λ_+ of formula 62.7 is determined, or quadratic, in which case the linear coefficient $\lambda_+^{'}$ and quadratic coefficient $\lambda_+^{''}$ of formula 62.11 are determined.

If we remove the assumption of a pure vector current, then the matrix element for the decay, in addition to the terms in formula 62.6, would contain

$$+2m_K\, f_S\, \bar{\ell}(1+\gamma_5)\nu + (2f_T/m_K)(P_K)_\lambda (P_\pi)_\mu\, \bar{\ell}\,\sigma_{\lambda\mu}(1+\gamma_5)\nu , \tag{62.15}$$

Int. J. Mod. Phys. A 2026.41. Downloaded from www.worldscientific.com
by UNIVERSITY OF CALIFORNIA @ BERKELEY on 09/16/26. Re-use and distribution is strictly not permitted, except for Open Access articles.

where f_S is the scalar form factor, and f_T is the tensor form factor. In the case of the K_{e3} decays where the f_- term can be neglected, experiments have yielded limits on $|f_S/f_+|$ and $|f_T/f_+|$.

For K_{e3} data, we determine best values for the three parametrizations: linear (λ_+), quadratic ($\lambda_+^{'}$, $\lambda_+^{''}$) and pole (M_V). For $K_{\mu 3}$ data, we determine best values for the three parametrizations: linear (λ_+, λ_0), quadratic ($\lambda_+^{'}, \lambda_+^{''}$, λ_0) and pole (M_V, M_S). We then assume $\mu - e$ universality so that we can combine K_{e3} and $K_{\mu 3}$ data, and again determine best values for the three parametrizations: linear (λ_+, λ_0), quadratic ($\lambda_+^{'}, \lambda_+^{''}$, λ_0), and pole (M_V, M_S). When there is more than one parameter, fits are done including input correlations. Simple averages suffice in the two K_{e3} cases where there is only one parameter: linear (λ_+) and pole (M_V).

A comprehensive global analysis of the semileptonic kaon decay data and its effect on the CKM unitarity debate can be found in [23, 24]. An update on experimental data including NA48/2 newest results can be found in [25].

Both KTeV and KLOE see an improvement in the quality of their fits relative to linear fits when a quadratic term is introduced, as well as when the pole parametrization is used. The quadratic parametrization has the disadvantage that the quadratic parameter $\lambda_+^{''}$ is highly correlated with the linear parameter $\lambda_+^{'}$, in the neighborhood of 95%, and that neither parameter is very well determined. The pole fit has the same number of parameters as the linear fit, but yields slightly better fit probabilities, so that it would be advisable for all experiments to include the pole parametrization as one of their choices.

The "Kaon Particle Listings" show the results with and without assuming μ-e universality. The "Meson Summary Tables" show all of the results assuming μ-e universality, but most results not assuming μ-e universality are given only in the Listings.

References

[1] D. A. Bryman, P. Depommier and C. Leroy, Phys. Rept. **88**, 151 (1982), see our note on "Decay Constants of Charged Pseudoscalar Mesons" elsewhere in this *Review*; S. G. Brown and S. A. Bludman, Phys. Rev. **136**, B1160 (1964); P. DeBaenst and J. Pestieau, Nuovo Cimento **A53**, 137 (1968).

[2] W. T. Chu, T. Ebata and D. M. Scott, Phys. Rev. **166**, 1577 (1968); D. Yu. Bardin and E. A. Ivanov, Sov. J. Part. Nucl. **7**, 286 (1976), [Fiz. Elem. Chast. Atom. Yadra7,726(1976)]; A. Kersch and F. Scheck, Nucl. Phys. **B263**, 475 (1986).

[3] V.G. Vaks and B.L. Ioffe, Nuovo Cimento **10**, 342 (1958); V.F. Muller, Z. Phys. **173**, 438 (1963).

[4] C. Q. Geng, I.-L. Ho and T. H. Wu, Nucl. Phys. **B684**, 281 (2004), [hep-ph/0306165]; J. Bijnens and P. Talavera, Nucl. Phys. **B489**, 387 (1997), [hep-ph/9610269]; V. Mateu and J. Portoles, Eur. Phys. J. **C52**, 325 (2007), [arXiv:0706.1039]; R. Unterdorfer and H. Pichl, Eur. Phys. J. **C55**, 273 (2008), [arXiv:0801.2482]; V. Cirigliano *et al.*, Rev. Mod. Phys. **84**, 399 (2012), [arXiv:1107.6001].

[5] E. Gabrielli and L. Trentadue, Nucl. Phys. **B792**, 48 (2008), [hep-ph/0507191].

[6] S. Adler *et al.* (E787), Phys. Rev. Lett. **85**, 2256 (2000), [hep-ex/0003019].

[7] E. A. Kuraev, Yu. M. Bystritsky and E. P. Velicheva, Phys. Rev. **D69**, 114004 (2004), [hep-ph/0310275]; R. Unterdorfer and H. Pichl have treated radiative corrections of the structure terms to lowest order within χPT for the first time. See the reference under [4].

[8] S. Egli *et al.* (SINDRUM), Phys. Lett. **B175**, 97 (1986).

[9] A. A. Poblaguev *et al.*, Phys. Rev. Lett. **89**, 061803 (2002), [hep-ex/0204006].

[10] F. Ambrosino *et al.* (KLOE), Eur. Phys. J. **C64**, 627 (2009), [Erratum: Eur. Phys. J.65,703(2010)], [arXiv:0907.3594].

[11] V. A. Duk *et al.* (ISTRA+), Phys. Lett. **B695**, 59 (2011), [arXiv:1005.3517].

[12] D. Pocanic *et al.*, Phys. Rev. Lett. **93**, 181803 (2004), [hep-ex/0312030]; E. Frlez *et al.*, Phys. Rev. Lett. **93**, 181804 (2004), [hep-ex/0312029]; M. Bychkov *et al.*, Phys. Rev. Lett. **103**, 051802 (2009), [arXiv:0804.1815].

[13] J. F. Donoghue and B. R. Holstein, Phys. Rev. **D40**, 2378 (1989).

[14] J. Gasser, M. A. Ivanov and M. E. Sainio, Nucl. Phys. **B745**, 84 (2006), [hep-ph/0602234].

[15] C. Adolph *et al.* (COMPASS), Phys. Rev. Lett. **114**, 062002 (2015), [arXiv:1405.6377].

[16] L. V. Fil'kov and V. L. Kashevarov, Phys. Rev. **C73**, 035210 (2006), [arXiv:nucl-th/0512047].

[17] J. Ahrens *et al.*, Eur. Phys. J. **A23**, 113 (2005), [arXiv:nucl-ex/0407011].

[18] A. A. Poblaguev, Phys. Lett. **B238**, 108 (1990); V. N. Bolotov *et al.*, Phys. Lett. **B243**, 308 (1990); V. M. Belyaev and I. I. Kogan, Phys. Lett. **B280**, 238 (1992); A. V. Chernyshev *et al.*, Mod. Phys. Lett. **A12**, 1669 (1997); A. A. Poblaguev, Phys. Rev. **D68**, 054020 (2003), [hep-ph/0307166]; M. V. Chizhov, Phys. Part. Nucl. Lett. **2**, 193 (2005), [Pisma Fiz. Elem. Chast. Atom. Yadra2005,no.4,7(2005)], [hep-ph/0402105].

[19] W. Yao *et al.*, Journal of Physics G: Nuclear and Particle Physics **33**, 1 (2006), ISSN 0954-3899.

[20] S. Eidelman *et al.*, Physics Letters B **592**, 1, 1 (2004), ISSN 0370-2693, review of Particle Physics, URL `https://www.sciencedirect.com/science/article/pii/S0370269304007579`.

[21] M. Roos *et al.*, Physics Letters B **111**, i (1982), ISSN 0370-2693, URL `https://www.sciencedirect.com/science/article/pii/0370269382912862`.

[22] V. Bernard *et al.*, Physics Letters B **638**, 5, 480 (2006), ISSN 0370-2693, URL `https://www.sciencedirect.com/science/article/pii/S0370269306006812`; A. Lai *et al.*, Physics Letters B **647**, 5, 341 (2007), ISSN 0370-2693, URL `https://www.sciencedirect.com/science/article/pii/S0370269307002432`.

[23] M. Antonelli *et al.* (FlaviaNet Working Group on Kaon Decays), Eur. Phys. J. C **69**, 399 (2010), [arXiv:1005.2323].

[24] C.-Y. Seng *et al.* (2021), [arXiv:2107.14708].

[25] J. R. Batley *et al.* (NA48/2), JHEP **10**, 150 (2018), [arXiv:1808.09041].

[26] L.-M. Chounet, J.-M. Gaillard and M. Gaillard, Physics Reports **4**, 5, 199 (1972), ISSN 0370-1573, URL `https://www.sciencedirect.com/science/article/pii/037015737290018X`.

[27] H. W. Fearing, E. Fischbach and J. Smith, Phys. Rev. D **2**, 542 (1970), URL `https://link.aps.org/doi/10.1103/PhysRevD.2.542`.

[28] N. Cabibbo and A. Maksymowicz, Phys. Lett. **9**, 352 (1964).

63. Spectroscopy of Light Meson Resonances

Revised September 2025 by C. Amsler (Marietta Blau Inst.), S. Giovannella (INFN, Frascati), A. Masoni (INFN, Cagliari) and G. Venanzoni (Liverpool U.; INFN, Pisa).

63.1 Introduction . . . 914
63.2 Scalar mesons . . . 915
63.3 Glueballs . . . 915
63.3.1 Scalar glueballs . . . 916
63.3.2 Tensor glueballs . . . 916
63.4 Pseudoscalar mesons . . . 917
63.4.1 Pseudoscalar glueballs . . . 918
63.5 Vector mesons . . . 918
63.5.1 $\rho(770)$ . . . 918
63.5.2 $\rho(770)$ excitations . . . 919
63.6 Axial-vector mesons . . . 919
63.7 Hybrid mesons . . . 920
63.8 Tetraquark states . . . 920
63.9 Baryonia . . . 921
63.10 Conclusions . . . 921

63.1 Introduction

According to the constituent quark model, a light meson consists of a color singlet quark-antiquark pair made of the u, d, or s quarks and the $\overline{u}$, $\overline{d}$, or $\overline{s}$ antiquarks, grouped into a flavor multiplet of SU(3). However, additional mesons made of bound gluons (glueballs) could exist in the same mass range, suggested by the self coupling of gluons in QCD. Multiquark structures are also possible, such as quark-antiquark pairs with an excited gluon (hybrid mesons). Tetraquarks are compact color singlets of diquark-antidiquark pairs ($qq\overline{q}\overline{q}$) or 'molecular' bound states of two mesons ($q\overline{q}q\overline{q}$). More complex systems such as $qqq\overline{q}\overline{q}\overline{q}$ (baryonia) are also predicted.

Fundamentals on the constituent quark model on light and heavy mesons and baryons (including hadrons with charm and bottom quarks), and on predictions from lattice gauge theories, are described in 'Quark Model' in this issue of the *Review of Particle Physics*, henceforth called the *Review*. In the present text we describe the experimental spectrum of light mesons and their classifications within the constituent quark model, with emphasis on states exhibiting properties incompatible with $q\overline{q}$ structures. The discussion is driven by the publications quoted in the *Listings* of the *Review*. The spectrum of kaon excitations is less well-defined and therefore deferred to a future edition, when further data might become available. More detailed discussions on exotic mesons – including those involving the c and b quarks – can be found in Refs. [1–8] and in 'Heavy Non-$q\overline{q}$ Mesons' of the *Review*. For more information on the meson (and baryon) spectrum of light (and heavy) quarks we refer to one of the textbooks [9].

Figure 63.1 shows the mass spectrum of $q\overline{q}$ mesons. The mass (vertical axis) increases with orbital excitation ℓ and radial excitation n. In the quark model one uses the notation nS, nP, nD... for the radial excitations ($n = 1$ for the ground states), in contrast to the usual $1s$, $2p$, $3d$... notation in atomic physics. Each box represents an SU(3) nonet containing multiplets of the isospin I, (*e.g.* for the pseudoscalar ground state nonet, one isotriplet (π^+, π^0, π^-), two strange isodoublets (K^-, $\overline{K}^0$ and K^0, K^+) and two isosinglets (η, η'). The spin, parity [$P = -(-1)^\ell$] and C-parity [$C = (-1)^{\ell+s}$] take the possible values $J^{PC} = 0^{++}$ (scalar), 0^{-+} (pseudoscalar), 1^{--} (vector), $1^{+\pm}$ (axial- or pseudovector), 2^{++} (tensor), etc. Therefore mesons with the *exotic* quantum numbers 0^{--}, 0^{+-}, 1^{-+}, 2^{+-}, 3^{-+}, etc. cannot be $q\overline{q}$ states. Note that the C-parity is defined only for the electrically neutral non-strange nonet members. The classification shown in fig. 63.1 is tentative for the radial excitations, in particular for those not fully established.

The two isosinglets in each nonet mix with an angle θ close to the *ideal* value of 35.3° for the 1^{--}, $1^{+\pm}$, 2^{++} and 3^{--} nonets, in which case the two isosinglets decouple to $u\overline{u} + d\overline{d}$ and $s\overline{s}$. The orbital excitations $\ell \geq 1$ consist of four nonets for each value of n, since $j = \ell$ for antiparallel quark spins and $j = \ell - 1, \ell$ or $\ell + 1$ for parallel spins. Since the C-parity is not defined for strange mesons, the K_{1A} and K_{1B} in the axial vector 1^{++} and 1^{+-} nonets of fig. 63.1 are mathematical constructs which mix to give the observed $K_1(1270)$ and $K_1(1400)$ mesons. A similar scenario occurs for the observed 2^{-+} $K_2(1770)$ and 2^{--} $K_2(1820)$ mesons, with a small mixing angle [10]. According to Ref. [11], the masses of radially excited mesons and baryons appear to grow logarithmically with quantum number n, a phenomenon that is not understood.

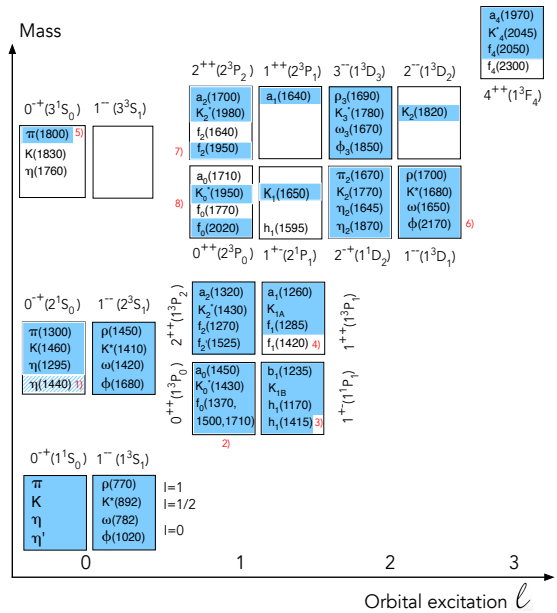

Figure 63.1: The mesons made of the u, d, and s light quarks are organised in $J^{PC}(n^{2s+1}\ell_j)$ nonets with isospin I. The established mesons (which appear in the *Summary Table* of the *Review*) are shown in the blue areas. The white areas contain those omitted in the *Summary Table* but reported in the *Listings*. States with the same J^{PC} mix, such as the 2^3S_1 and 1^3D_1 mesons. The states become broad and overlap with increasing masses, which complicates the determination of the masses, widths and spins. For a complete list of mesons see the *Listings*.

[1] The $\eta(1440)$ stands for the $\eta(1405)$ and the $\eta(1475)$ which may be manifestations of the same state, see section 63.4.
[2] The classification of the scalar nonet is controversial. In alternative schemes the 1^3P_0 nonet contains the light scalars below 1 GeV, section 63.2.
[3] Considered established, but more data would be desirable.
[4] An alternative to the $f_1(1420)$ is the $f_1(1510)$, section 63.6.
[5] The $\pi(1800)$ has also been proposed as a hybrid meson, section 63.7.
[6] The $\phi(2170)$ has also been proposed as a tetraquark state, section 63.8.
[7] The $f_2(1950)$ has also been proposed as a tensor glueball, section 63.3.2.
[8] Tentative assignment following Ref. [12].

As described in more detail below (section 63.2), it is hard to accommodate all the known scalar mesons in the lower $q\overline{q}$ nonets: The light scalar mesons $a_0(980)$, $K_0^*(700)$ (also known as κ), the $f_0(500)$ (also known as σ) and the $f_0(980)$, not shown in the figure, could build the lightest nonet, but could also be two-meson resonances or tetraquarks (section 63.8). Three isoscalars are known in the 1500 MeV region, the $f_0(1500)$ or $f_0(1710)$ being proposed as states with a large gluon content, mixing with the $f_0(1370)$ (section 63.3.1). The pseudoscalar labeled $\eta(1440)$ may consist of two states (section 63.4). The status of vector meson excitations is described in section 63.5. The axial-vector meson $f_1(1420)$ could be replaced in the 1^{++} nonet by the $f_1(1510)$ which, however, needs confirmation (see the *Listings* and section 63.6). Mesons with exotic quantum numbers are discussed in section 63.7.

Int. J. Mod. Phys. A 2026.41. Downloaded from www.worldscientific.com
UNIVERSITY OF CALIFORNIA @ BERKELEY on 09/16/26. Re-use and distribution is strictly not permitted, except for Open Access articles.

Int. J. Mod. Phys. A 2026.41. Downloaded from www.worldscientific.com
by UNIVERSITY OF CALIFORNIA @ BERKELEY on 09/16/26. Re-use and distribution is strictly not permitted, except for Open Access articles.

63.2 Scalar mesons

Scalar mesons decay dominantly into pairs of pseudoscalar mesons ($\pi\pi$, $K\overline{K}$, $\pi\eta$, $\eta\eta$ or $\eta\eta'$). The widths tend to be large for those decaying into $\pi\pi$, due to the absence of angular momentum barrier and the large available phase space. Broad overlapping states decaying into the same final state interfere, which complicates the determination of their masses and widths. Furthermore, the ground state glueball, a 0^{++} expected below 2 GeV, will mix with the isoscalar 0^{++} $q\bar{q}$ states. The onset of the $K\overline{K}$, $\eta\eta$ or $\eta\eta'$ thresholds also distorts the line shapes and produces cusps. This requires high statistics data from various production and decay channels, and the use of coupled channel analyses taking into account unitarity and analyticity (see 'Resonances' in the *Review*).

There is long-time evidence for the existence of two scalar nonets, one below 1 GeV, one around 1.4 GeV and one glueball below 1.7 GeV [13]. The lighter nonet consists of the $a_0(980)$, $f_0(980)$, $f_0(500)$ and $K_0^*(700)$, and the heavier one contains the mesons shown in Fig. 63.1. Two isovector scalars are established, the $a_0(980)$ and the $a_0(1450)$, together with five isoscalars: the very broad $f_0(500)$, the $f_0(980)$, the broad $f_0(1370)$, and the comparatively narrow $f_0(1500)$ and $f_0(1710)$. The strange partners are the $K_0^*(700)$ and the $K_0^*(1430)$. The $f_0(500)$ and $K_0^*(700)$ deserve a separate treatment and are discussed in 'Scalar Mesons below 1 GeV', which also contains more details on the $a_0(980)$ and $f_0(980)$ briefly reviewed in section 63.8, see also Ref. [1].

The $a_0(1450)$ was first reported by the Crystal Barrel experiment (see [14] for a review) in $\bar{p}p$ annihilation with stopped antiprotons [15, 16]. An isovector scalar, possibly the $a_0(1450)$ (albeit at a lower mass of 1317 MeV), is observed by Belle in $\gamma\gamma$ collisions leading to $\eta\pi^0$ [17]. A contribution from $a_0(1450) \to K\bar{K}$ is also found in the CLEO-c analysis of $D^\pm \to K^+K^-\pi^\pm$ [18] and $D^0 \to K_S^0 K^\pm\pi^\mp$ from LHCb [19]. The $a_0(1450)$ is reported at a lower mass in $\bar{p}p$ annihilation in flight, overlapping with the $a_2(1320)$ [20, 21].

The $f_0(1370)$ and $f_0(1500)$ were observed by Crystal Barrel [22–24] and by WA102 in central production with 450 GeV protons [25,26]. They decay mostly into 2π and 4π. The $f_0(1500)$ was also observed to decay into $\eta\eta$ [27–29] and $\eta\eta'$ [30]. All data agree that the 4π decay mode represents about half of the $f_0(1500)$ decay width, but is dominant for the $f_0(1370)$.

The determination of the $\pi\pi$ coupling of the very broad $f_0(1370)$ is complicated by its interference with the $f_0(500)$. The existence of the $f_0(1370)$ was questioned by COMPASS from $\pi^-p \to \pi^-\pi^-\pi^+p$ data [31] and by LHCb in $\overline{B}_s^0 \to J/\psi(1S)\pi^+\pi^-$ [32]. In $\overline{B}^0 \to J/\psi(1S)\pi^+\pi^-$ the $\pi\pi$ mass spectrum does not show any significant scalar component above $\sim$1.2 GeV [33] (an analysis that is challenged in [34]). The existence of the $f_0(1370)$ has also been disputed by a reassessment of various production modes [35] (with the $K_0^*(700)$ not needed in $K\pi$ scattering). This contrasts with its $\pi\pi$ decay analyzed in Ref. [36]. However, data from CLEO-c in $D^0 \to \pi^+\pi^-\pi^+\pi^-$ require a contribution from $f_0(500)f_0(1370) \to 4\pi$ [37]. A broad 2π signal is also observed by BaBar around 1400 MeV in the decay $B^\pm \to \pi^\pm\pi^\pm\pi^\mp$ [38] which is attributed to the $f_0(1370)$ (but could also be due to the $f_0(1500)$). The existence of the $f_0(1370)$ is confirmed by a recent dispersive analysis of $\pi\pi$ scattering data, which leads to a complex pole around 1245 MeV with a very large width of about 600 MeV [39].

While the $K\bar{K}$ decay branching ratio of the $f_0(1500)$ is small [25, 40], the $f_0(1710)$ decays dominantly into $K\overline{K}$. The $f_0(1710)$ is not observed in $p\bar{p}$ annihilation at rest [40] and only weakly produced in $p\bar{p}$ annihilation in flight [41], with a rate strongly suppressed compared to that of the $f_0(1500)$ ($\sim$7%). (For comparison, the rate for the $(s\bar{s})$ $f_2'(1525)$ production is about 9% that of the $(u\bar{u}+d\bar{d})$ $f_2(1270)$, as expected from the OZI rule [41].) On the other hand the $f_0(1370)$ does not couple strongly to $K\bar{K}$ [25]. This suggests an $n\bar{n}$ structure $(u\bar{u}+d\bar{d})$ for the $f_0(1370)$ and $s\bar{s}$ for the $f_0(1710)$. The $f_0(1500)$ would also qualify as an $n\bar{n}$ state, although it is very narrow compared to the other states. Occam's razor principle therefore suggests that the $f_0(1370)$, $a_0(1450)$, and the $f_0(1710)$ form the 1^3P_0 $q\bar{q}$ flavor nonet, the $f_0(1370)$ and $a_0(1450)$ being the two (mostly) $n\bar{n}$ states, and the $f_0(1710)$ the (dominantly) $s\bar{s}$ one. The nature of the $f_0(1500)$ is discussed along this scheme in section 63.3.1.

Other schemes have been proposed, for example a tetraquark for the $f_0(1500)$ [42] or flavor octets for the $f_0(1500)$ and $f_0(1710)$ [3]. In Refs. [43, 44] the $f_0(1370)$ and $f_0(1710)$ are interpreted as bound systems of two vector mesons, a view is challenged in Ref. [45]. In Ref. [46] the $a_0(1450)$, $f_0(1370)$, $f_0(1500)$ and $K_0^*(1430)$ are radial excitations of the scalar nonet below 1 GeV. In Ref. [47] the light tetraquark scalar nonet mixes with the $q\bar{q}$ 1^3P_0 nonet, while in Ref. [48] both nonets are made of mixing tetraquarks. In the unitarized quark model with coupled $q\bar{q}$ and meson-meson channels, the scalars below 1 GeV are manifestations of bare $q\bar{q}$ confinement states, mass shifted from the 1.4 GeV region and distorted by the strong $^3P_0$ coupling to S-wave two-meson decay channels [49, 50]. Thus, in these models the light scalar nonet comprising the light and 1^3P_0 scalar nonets are manifestations of the same bare input states (see also [51]). Surprisingly for a state decaying strongly into 2π and 4π, the $f_0(1370)$ is assumed to be an $s\bar{s}$ state in Ref. [52]. The $f_0(1500)$ is then a radial excitation.

There is evidence for two further 0^{++} mesons in the 1700 – 1800 MeV range, the isovector $a_0(1710)$ and the $f_0(1770)$, possibly the isoscalar partner of the $f_0(1710)$. The $f_0(1770)$, claimed by BESII/III [53–55], and also observed in $\pi^-p \to n\omega\phi$ by VES [56], could be a radial excitation [57]. Two isoscalars at 1700 and 1765 MeV are also reported by a re-analysis of BESIII radiative $J/\psi(1S)$ decay data [58, 59].

The evidence for the $a_0(1710)$ was inferred from the interference of the K^+K^- and $K_S^0K_S^0$ decays of the $f_0(1710)$ in $D_s^+ \to f_0(1710)\pi^+$, leading to a relative branching ratio an order of magnitude larger than expected from isospin symmetry [60,61]. The $a_0(1710)$ is now confirmed by LHCb in B^+ decays to $K_SK^+K^\pm\pi^\mp$ from an analysis of the $\eta(1S,2S) \to (K_SK^\pm\pi)^\mp$ Dalitz plots [62]. A signal for $a_0(1710)^\pm \to K_S^0K^\pm$ is also reported by BESIII [63], albeit at 1817 MeV, in contrast to the state observed by BaBar in $\eta\pi^\pm$ at 1704 MeV [64].

From a study of the vector-vector interaction the authors of Ref. [65], predict an isovector pole at 1780 MeV, while the $f_0(1710)$ is a $K^*\bar{K}^*$ molecule, a view also supported by Refs. [66–69]. Thus the $f_0(1710)$ and $a_0(1710)$ might be $K^*\bar{K}^*$ molecules, similar to the $f_0(980)$ and $a_0(980)$ which have been interpreted as $K\bar{K}$ molecules [70].

Scalar resonances near the D_0 mass such as the $f_0(1710)$ and the $f_0(1770)$ are also suggested to produce CP violation enhancements in the charm system [71].

63.3 Glueballs

Lattice calculations predict that the lightest glueball is a 0^{++} state with a mass in the 1600-1800 MeV range. The first and second excited states have 2^{++} and 0^{-+} with masses around 2300 and 2500 MeV, respectively, with large uncertainties. For more information and references on lattice calculations see 'Quark Model' in the *Review*, in particular fig. 15.3 for a mass spectrum. Predictions were made in the quenched approximation, neglecting $q\bar{q}$ loops. However quenched predictions and full QCD calculations lead to small mass shifts (see fig. 15.15 in the *Review*). The most recent prediction [72] quotes the more precise masses 1653 $\pm$ 26, 2376 $\pm$ 32 and 2561 $\pm$ 40 MeV for the 0^{++}, 2^{++} and 0^{-+} respectively. For an experimental review see Ref. [8].

The lightest glueballs lie in the same mass region as ordinary radial and orbital $q\bar{q}$ excitations, in the mass range of the 0^{++}, 2^{++} and 0^{-+} multiplets. Therefore, mixing of glueballs with nearby $q\bar{q}$ states of the same quantum numbers leads to supernumerary isoscalar state in the $q\bar{q}$ nonets.

Among the signatures naively expected for glueballs are (i) isoscalar states that do not fit in $q\bar{q}$ nonets, (ii) enhanced production in gluon-rich channels such as central production and radiative $J/\psi(1S)$ decay, (iii) decay branching fractions incompatible with SU(3) predictions for $q\bar{q}$ states, and (iv) small $\gamma\gamma$ couplings [73] (see however [74, 75]). Mixing effects with isoscalar $q\bar{q}$ mesons [35, 74, 76–83] and decay form factors [84] can obscure these simple signatures.

According to SU(3) the decay branching ratios for $q\bar{q}$ mesons and pure glueballs are different, and therefore useful to determine the internal structures of mesons. For pure glueballs with flavor

Int. J. Mod. Phys. A 2026.41. Downloaded from www.worldscientific.com
UNIVERSITY OF CALIFORNIA @ BERKELEY on 09/16/26. Re-use and distribution is strictly not permitted, except for Open Access articles.

symmetric couplings the decay ratios are $\pi\pi : K\bar{K} : \eta\eta : \eta\eta'$ = 3 : 4: 1 : 0, apart from phase space factors. The partial widths for the decay of a scalar (or a tensor) meson into a pair of pseudoscalar mesons are given in fig. 63.2 (for a derivation see e.g. [9]). The decay of a $q\bar{q}$ meson into a pair of mesons involves the creation of a $q\bar{q}$ pair, and SU(3) symmetry assumes that the matrix elements for the creation of $s\bar{s}$, $u\bar{u}$, and $d\bar{d}$ pairs are equal. (The generalization to unequal $s\bar{s}$, $u\bar{u}$, and $d\bar{d}$ couplings is given in Ref. [76].) An excellent fit to the tensor meson decay widths is obtained with $\beta \simeq 0.5$ GeV/c, $\theta_V \simeq 26\,^\circ$ and $\theta_P \simeq -17\,^\circ$ [76].

Note that the assumption of flavor symmetric couplings may not apply in models describing the scalar glueball by a dilaton field, which lead to mass dependent couplings [85, 86] (Ref. [87] predicts that a scalar glueball above 1 GeV would be unobservably wide).

Another way to determine the flavor contents of neutral mesons is the decay $B^0 \to J/\psi(1S)X$ which filters out the $d\bar{d}$ content of X, while $B^0_s \to J/\psi(1S)X$ selects its $s\bar{s}$ component [88]. More precise data on $B^0_{(s)} \to J/\psi(1S)[f_0(1370), f_0(1500), f_0(1710)]$ would help to pin down the nature of these scalar mesons [89].

63.3.1 *Scalar glueballs*

One of the three isoscalars, the $f_0(1370)$, $f_0(1500)$ or $f_0(1710)$, appears to be supernumerary. The branching ratios in fig. 63.2 can be used to deduce their structures, assuming that they are $q\bar{q}$. The comparison of decay branching ratios from Crystal Barrel annihilation and WA102 central collision data shows that the $f_0(1500)$ is compatible with an $n\bar{n}$ structure, while the $f_0(1710)$ is mostly $s\bar{s}$ [90]. However, the close vicinity of the very broad $n\bar{n}$ $f_0(1370)$, its narrow width and enhanced production at low transverse momentum transfer in central collisions [91–93] favor the $f_0(1500)$ to be the supernumerary non-$q\bar{q}$ state. According to [76, 82] the $f_0(1370)$ and $f_0(1710)$ would be dominantly $\bar{q}q$ states mixing with glue, while the $f_0(1500)$ would be dominantly a glueball mixing with $q\bar{q}$ states. Its suppressed $K\bar{K}$ decay would be due to interferences with the $f_0(1370)$ and $f_0(1710)$. In the analogous mixing scheme of Ref. [57], which uses central production data from WA102 and the hadronic $J/\psi(1S)$ decay data from BES [94, 95], glue is shared between the $f_0(1370)$ (mainly $n\bar{n}$), $f_0(1500)$(mainly glue) and $f_0(1710)$ (dominantly $s\bar{s}$). This agrees with the analyses [76, 82]. In the mixing scheme of Ref. [96] the QCD spectral sum rule also leads to a large gluonic component in the $f_0(1500)$ (satisfying the observed strong $\pi\pi$ and $f_0(500)f_0(500) \to 4\pi$ decays).

However, not everybody agrees that the strong $K\bar{K}$ signal is indicative of an $s\bar{s}$ structure for the $f_0(1710)$. The $f_0(1710)$ could still be the glueball, since the two-gluon coupling to $n\bar{n}$ appears to be suppressed by chiral symmetry [97], thus $K\bar{K}$ would be enhanced compared to $\pi\pi$. It was argued that chiral symmetry constraints in a multichannel analysis imply that the $f_0(1710)$ is an unmixed scalar glueball [98]. However, this view is challenged in [65].

The $K\bar{K}$ decay is also naturally enhanced in the extended linear sigma model with a dilaton as glueball [85] and in the holographic model of [86, 99] which both prefer the $f_0(1710)$ as the glueball. For a scalar glueball Ref. [86] finds a strong enhancement of the decays into $K\bar{K}$ and $\eta\eta$, in fairly close agreement with the measured branching ratios of the $f_0(1710)$, while Ref. [99] predicts the (so far not measured) rate into $\eta\eta'$ to be very small.

In $\gamma\gamma$ collisions leading to K_SK_S [100] and K^+K^- [101] a spin-0 signal is observed at the $f_0(1710)$ mass (together with a dominant spin-2 component), while the $f_0(1500)$ is not observed in $\gamma\gamma \to K\bar{K}$ nor $\pi^+\pi^-$ [102]. The $f_0(1500)$ is also not observed by Belle in $\gamma\gamma \to \pi^0\pi^0$, although a shoulder is seen which could also be due to the $f_0(1370)$ [103]. The absence of $f_0(1500)$ signal in the $\pi\pi$ channel in $\gamma\gamma$ collisions does not favor an $\overline{n}n$ interpretation for the $f_0(1500)$. The upper limit for $\Gamma_{2\gamma}$ (< 1.4 keV) in $\pi^+\pi^-$ [90]) excludes a large $n\overline{n}$ content, and hence points to a mainly $s\overline{s}$ content [90], which contradicts the small $K\overline{K}$ decay branching ratio of the $f_0(1500)$ [16, 25, 40]. Belle finds that in $\gamma\gamma \to K_SK_S$ collisions the 1500 MeV region is dominated by the $f_2'(1525)$. The $f_0(1710)$ is also observed with a production rate $\times$ branching ratio compatible with an $s\bar{s}$ state [104]. Ref. [74] predicts the glueball $\gamma\gamma$ partial width in the few keV range (comparable to that of $q\bar{q}$ mesons) due to couplings of vector mesons to γ via VDM, in agreement with holographic models [75], but this is disputed in Ref. [73] which predicts $\Gamma_{\gamma\gamma} \sim 1$ eV from lattice calculations of radiative glueball decay. Note, however, that the $\gamma\gamma$ couplings of glueballs are sensitive to glue mixing with $q\bar{q}$ [57].

Alternative assignments for the scalar glueball have been proposed:

- In Ref. [78] the gluonic signal is distributed over $f_0(1370)$, $f_0(1500)$ and another broad isoscalar around 1530 MeV, while the gluonic contribution to the $f_0(1710)$ is small.
- In Ref. [81, 85, 86] the $f_0(1710)$ is the glueball state, as in Ref. [83], where the $f_0(1500)$ is the $q\bar{q}$ octet state degenerate with the $a_0(1450)$.
- In the generalized linear sigma model [105] the $a_0(980)$ is dominantly a tetraquark and $a_0(1450)$ a $q\bar{q}$ state. The $f_0(980)$, $f_0(1370)$ and $f_0(1500)$ (or $f_0(1710)$) are dominantly tetraquark, $q\bar{q}$ and glue.
- In Ref. [80] the $f_0(500)$ and $f_0(1370)$ are signals from a single broad resonance proposed as the scalar glueball. The ground state scalar nonet then consists of the $f_0(980)$, $a_0(980)$, $K_0^*(1430)$ and $f_0(1500)$ [35]. The $f_0(980)$ and $f_0(1500)$ mix (similarly to the η and η' in the pseudoscalar nonet), while the $f_0(1500)$ mixes with a glueball in the 500 – 1000 MeV mass range, which is identified as the $f_0(500)$.
- In Ref. [106], a large K^+K^- scalar signal is reported by Belle in B decays into $KK\bar{K}$ [107], compatible with the $f_0(1500)$. It is due to constructive interference of a flavor octet with a broad glueball background. However, the Belle data are inconsistent with the BaBar measurements which show instead a broad scalar at this mass for B decays into both $K^\pm K^\pm K^\mp$ [108] and $K^+K^-\pi^0$ [109].

The $f_0(1500)$ is observed by BESII in $J/\psi(1S) \to \gamma\pi\pi$ [110] and by BESIII in $J/\psi(1S) \to \gamma\eta\eta$ [111] with a much smaller rate than for the $f_0(1710)$, which would speak against a glueball interpretation of the former, although the systematic uncertainties are large, and the $f_0(1500)$ appears at a lower mass and the $f_0(1710)$ at a higher mass than the accepted values.

The authors of Ref. [58] have analyzed the high statistics data from $J/\psi(1S)$ radiative decays into S-wave $\pi^0\pi^0$, $K^0_SK^0_S$, $\eta\eta$ and $\omega\phi$ from BESIII, including data on $\pi\pi$, $\eta\eta$ and $\eta\eta'$ from the CERN SPS, BNL data on $\pi\pi \to K^0_SK^0_S$ and $\bar{p}p$ annihilation data from LEAR into various final states. The coupled channel analysis requires ten scalar mesons, the established ones in the *Review* and the $f_0(2020)$, as well as the isoscalars $f_0(2100, 2200, 2330)$ so far omitted from the *Summary Table*. Comparable contributions from $f_0(1500)$ and $f_0(1710)$ are found, with a preference for $\pi\pi$ decay over $K\bar{K}$ for the former and $K\bar{K}$ over $\pi\pi$ for the latter. As a new feature, the $f_0(1710)$ splits into two states, one at about 1700 MeV, the former $f_0(1710)$, and the new $f_0(1770)$ discussed above, being mandatory to obtain a good fit. A broad ($\sim$370 MeV) enhancement is observed in $J/\psi(1S)$ radiative decays around 1865 MeV, attributed to the contribution of glue distributed among the scalar mesons, with a very strong contribution from the 1770 MeV state [59]. In this model there are no supplementary states as the glue 'fragments' between the various isoscalars.

Ref. [112] presents a re-analysis of the BESIII $J/\psi(1S)$ radiative decay data into S- and P-wave $\pi^0\pi^0$ and $K^0_SK^0_S$ between 1.0 and 2.5 GeV. A good fit is obtained with only two scalar resonances below 2 GeV, the $f_0(1500)$ and $f_0(1710)$. The latter is more strongly produced, which points to a sizeable glueball component.

63.3.2 *Tensor glueballs*

Above the well known $f_2(1270)$ and $f_2'(1525)$ $q\bar{q}$ mesons, the $f_2(1640)$ and $f_2(1950)$ are tentatively assigned to the 2^3P_2 nonet (fig. 63.1). The broad $f_2(1950)$ has been observed by several experiments, *e.g.* in central production [26] and in $\overline{p}p$ annihilation in flight [21] and is often identified as a glueball [113], the ground state of the pomeron [114, 115].

Four further isoscalar tensors, the $f_2(2010)$, $f_2(2150)$, $f_2(2300)$ and $f_2(2340)$, which are in the range of the 1^3F_2 and 3^3P_2

Int. J. Mod. Phys. A 2026.41. Downloaded from www.worldscientific.com
by UNIVERSITY OF CALIFORNIA @ BERKELEY on 09/16/26. Re-use and distribution is strictly not permitted, except for Open Access articles.

Isospin	Decay channel	γ^2
0	$\pi\pi$	$3\cos^2\alpha$
	$K\overline{K}$	$(\cos\alpha - \sqrt{2}\sin\alpha)^2$
	$\eta\eta$	$(\cos\alpha\cos^2\phi - \sqrt{2}\sin\alpha\sin^2\phi)^2$
	$\eta\eta'$	$\frac{1}{2}\sin^2 2\phi\ (\cos\alpha + \sqrt{2}\sin\alpha)^2$
1	$\eta\pi$	$2\ \cos^2\phi$
	$\eta'\pi$	$2\ \sin^2\phi$
	$K\overline{K}$	1
$\frac{1}{2}$	$K\pi$	$\frac{3}{2}$
	$K\eta$	$(\sin\phi - \frac{\cos\phi}{\sqrt{2}})^2$
	$K\eta'$	$(\cos\phi + \frac{\sin\phi}{\sqrt{2}})^2$

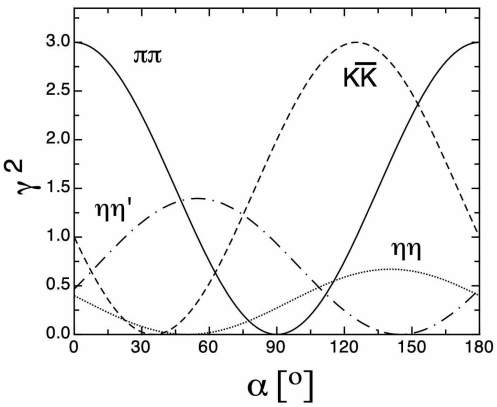

Figure 63.2: Left: SU(3) couplings γ^2 for scalar (or tensor) $q\bar{q}$ meson decays. The angles α and ϕ are defined as $\alpha = 54.7^\circ + \theta$ and $\phi = 54.7^\circ + \theta_P$, where θ is the mixing angle of the 0^{++} (2^{++}) isoscalars and θ_P the mixing angle in the 0^{-+} nonet. The partial decay width is given by $\Gamma = C \times \gamma^2 \times |F(q)|^2 \times q$, where C is a nonet constant, q the momentum of the decay products and $F(q)$ a form factor which may be taken as $|F(q)|^2 = q^{2\ell} \times \exp(-q^2/8\beta^2)$ with β= 0.5 GeV/c, and where ℓ is the relative angular momentum between the decay products ($\ell = 0$ for scalars and $\ell = 2$ for tensors). Right: SU(3) couplings γ^2 as a function of mixing angle α for isoscalar decays for $\theta_P = -17.3^\circ$ (from [76]).

nonets, exhibit a very large OZI breaking $\phi\phi$ production cross section in $\pi^- N \to \phi\phi n$ [116], in accord with earlier observations [117,118], which could be due to the production of the 2^{++} glueball. The enhanced $\phi\phi$ production is also observed in central collisions [119] and in $\overline{p}p \to \phi\phi$ just above threshold [120]. The $f_2(2010)$, $f_2(2300)$ and $f_2(2340)$ have been reported by BESIII in $J/\psi(1S) \to \gamma\phi\phi$ [121]. The production rate of a tensor glueball in $J/\psi(1S)$ radiative decay has been calculated in quenched lattice QCD to be large (around 1%) [122] and is claimed by BESIII to be compatible with their measured rates in $J/\psi(1S) \to \gamma f_2(2340)$, $f_2(2340) \to \eta\eta$ [111], and $f_2(2340) \to \phi\phi$ [121].

The authors of Ref. [123] have re-analyzed the $J/\psi(1S)$ radiative decay into $\pi^0\pi^0$ and $K_S K_S$ from BESIII and found as glueball candidate an enhancement described by a 360 MeV broad pole around 2210 MeV, possibly composed of the resonances observed earlier in $\phi\phi$. The relatively narrow $f_2(2300) \to \phi\phi$ (width of 150 MeV) is preferred by the holographic QCD model of Ref. [124]. However, the tensor glueball is predicted to be much broader (600-900 MeV) by the holographic model of Ref. [125].

There is no evidence for a narrow meson, $f_J(2220)$ (a tensor candidate) in $\overline{p}p$ annihilation (see the note under the $f_J(2220)$ in the 2004 issue of the *Review*). The measured partial width to $\overline{p}p$ in radiative $J/\psi(1S)$ decay [126] is too large and inconsistent with the upper limit from $\overline{p}p$ annihilation into $\pi\pi$ [127].

63.4 Pseudoscalar mesons

We now deal with the first radial excitations of the 0^{-+} nonet (fig. 63.1). The $\pi(1300)$ is a very broad resonance (200–600 MeV) decaying into 3π. The $K(1460)$ was confirmed with high statistics data from LHCb in $D^0 \to K3\pi$ decays [128] and has become an established kaon excitation.

The $\eta(1295)$ has been observed in various production mechanisms, in $\pi^- p$ experiments [129–132], and possibly in $\overline{p}p$ annihilation [133,134]. In $J/\psi(1S)$ radiative decay, a 0^{-+} signal is evident in the $\eta\pi\pi$ wave of the DM2 data, together with a 1^{++} of similar magnitude [135]. Also BaBar reports a signal around 1295 MeV in B decays into $\eta\pi\pi K$ [136]. The existence of the $\eta(1295)$ has been questioned [3, 137], being very close to the $f_1(1285)$. However, experimental evidences for a pseudoscalar in this mass region is reported by production mechanisms in which 1^{++} is suppressed, such as $\gamma\gamma$ production or $\overline{p}p$ annihilation at rest in liquid hydrogen. We therefore assume that the $\eta(1295)$ is one of the isoscalars in this nonet.

Two isoscalars were later observed in this mass region, the $\eta(1405)$ and $\eta(1475)$. The former decays mainly into $a_0(980)\pi$ (or direct $K\overline{K}\pi$) and the latter mainly into $K^*(892)\overline{K}$. The simultaneous observation of two pseudoscalars is reported in three production mechanisms: $\pi^- p$ [129, 138], radiative $J/\psi(1S)$ decay [135, 139], and $\overline{p}p$ annihilation at rest [140–143]. All of them give values for the masses, widths, and decay modes that are in reasonable agreement (except for Ref. [135] which favors a state decaying into $K^*(892)\overline{K}$ at a lower mass than the state decaying into $a_0(980)\pi$). In $J/\psi(1S)$ radiative decay, the $\eta(1405)$ decays into $K\overline{K}\pi$ through $a_0(980)\pi$, and hence a signal is also expected in the $\eta\pi\pi$ mass spectrum. This was indeed observed by MARK III in $\eta\pi^+\pi^-$ [144], which reported a mass of 1400 MeV, in line with the existence of the $\eta(1405)$ decaying into $a_0(980)\pi$. The $\eta(1405)$ decaying into $\eta\pi\pi$ was also observed by Crystal Barrel [134]. Two states were reported by BES: Around 1452 MeV BESII observed a $K\bar{K}\pi$ enhancement in $J/\psi(1S) \to \omega K\bar{K}\pi$ but not in $J/\psi(1S) \to \phi K\bar{K}\pi$ [145], while BESIII reported a 52 MeV broad state in $\psi(2S) \to \omega K^* K$ [146], both left without J^{PC} determination.

The $K\overline{K}\pi$ and $\eta\pi\pi$ channels were studied in $\gamma\gamma$ collisions by L3 [147]. (For the 2γ couplings of glueballs and $q\bar{q}$ mesons see [74, 75, 148, 149].) The analysis led to a clear $\eta(1475)$ signal in $K\overline{K}\pi$, decaying into $K^*\overline{K}$, well identified in the untagged data sample, where spin 1 resonances are not allowed. At the same time, L3 did not observe the $\eta(1405)$, neither in $K\overline{K}\pi$ nor in $\eta\pi\pi$ [147]. On the other hand, CLEO-II did not observe any pseudoscalar signal with tagged γ's in $\gamma\gamma \to \eta(1475) \to K^0_S K^\pm \pi^\mp$ [150], with an upper limit slightly smaller than the signal observed by L3. After the CLEO-II result, L3 performed a further analysis with full statistics [151], confirming their previous evidence for the $\eta(1475)$. The CLEO upper limit for $\Gamma_{\gamma\gamma}$ [150], and the L3 results [151], are consistent with the world average for the $\eta(1475)$ width. BaBar [136] also reported the $\eta(1475)$ in B decays into $K\bar{K}^*$ recoiling against a K, while upper limits only were given for the $\eta(1405)$.

Hence, in radiative $J/\psi(1S)$ decay, $\pi^- p$ and $\overline{p}p$ annihilation at rest two isoscalar signals are observed in the 1400 – 1500 MeV mass region, while the $\eta(1405)$ is not seen in $\gamma\gamma$ interactions nor in B decays. The $\eta(1475)$ could be the first radial excitation of the η', with the $\eta(1295)$ being the first radial excitation of the η. Ideal mixing, suggested by the $\eta(1295)$ and $\pi(1300)$ mass degeneracy, would then imply that the second isoscalar in the nonet is mainly $s\bar{s}$, and hence couples to $K^*\overline{K}$, in agreement with properties of the $\eta(1475)$. In addition, its width agrees with the expected one for the radially excited $s\bar{s}$ state [84, 91]. A study of radial excitations of pseudoscalar mesons [152] also favors the $s\bar{s}$ interpretation of the $\eta(1475)$. However, due to the strong kinematical suppression in $\eta(1405) \to K^*\overline{K}$ the data are not sufficient to exclude a sizeable $s\bar{s}$ admixture also in the $\eta(1405)$.

Here also, there are alternative explanations for the existence of two states:

Int. J. Mod. Phys. A 2026.41. Downloaded from www.worldscientific.com
UNIVERSITY OF CALIFORNIA @ BERKELEY on 09/16/26. Re-use and distribution is strictly not permitted, except for Open Access articles.

– The isoscalar $\eta(1405)$ would be a candidate for the 0^{-+} glueball (section 63.4.1).
– In Refs. [3,137], apart from questioning the mere existence of the $\eta(1295)$, the authors propose a single pseudoscalar meson at 1440 MeV, the first radial excitation of the η. According to Refs. [84,153] the splitting of the 1440 MeV state into $\eta(1405)$ and $\eta(1475)$ could be due to nodes in the decay amplitudes (which differ in $\eta\pi\pi$ and $K^*(892)\overline{K}$), nevertheless the following paper [154] underlines the relevance of $\gamma\gamma$ production and radiative decays to vector mesons to solve the $\eta(1440)$ riddle.
– The splitting could be due to a triangle singularity, hence the manifestation of one state only (fig. 63.3) [155–157]. The importance of the triangle singularity for the $\eta(1295)$ and $\eta(1405/1475)$ in the $\eta\pi\pi$ and $K\bar{K}\pi$ channels is stressed in Ref. [158]. In Ref. [159], using the triangle singularity approach of [155], the authors conclude that the BESIII results can be reproduced either with the $\eta(1405)$ or the $\eta(1475)$, or by a mixture of these two states.
– From a high statistics data sample in $J/\psi(1S) \to \gamma K_S K_S \pi^0$ BESIII reports the observation of both $\eta(1405)$ and $\eta(1475)$ using Breit-Wigner fits [160]. A one resonance parametrization is ruled out and triangle singularity models do not describe the data satisfactorily.
– The decay $J/\psi(1S) \to \gamma K_S K_S \pi^0$ has been studied in a three-body unitary coupled-channel analysis and compared to the BESIII data, including ratios of radiative branching ratios into $\eta\pi^+\pi^-$ and $K\bar{K}\pi$ through the $\eta(1405/1475)$ intermediate states [161]. Two poles emerge for $K^*\bar{K}$ in different Riemann sheets around 1400 MeV and only one pole around 1500 MeV.

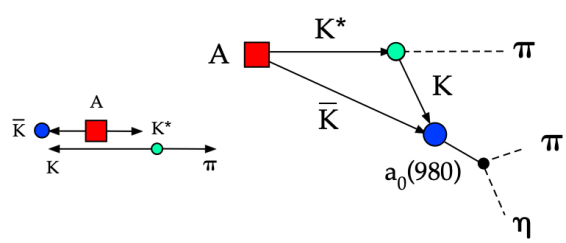

Figure 63.3: Triangle singularity: a state A decays into $K^*\overline{K}$. The K from K^* decay catches up with the $\overline{K}$ and excites the $a_0(980)$ resonance which in turn decays into $\eta\pi$. This mechanism can lead to two distinct peaks (depending on the width of A), one in $K^*\overline{K}$ and the other via rescattering in $\eta\pi\pi$. Similarly, the virtual $K^*\overline{K}$ loop can couple to $f_0(980)$ which, decaying into $\pi\pi$, leads to a peak in the 3π final state.

To summarise, the experimental data on the 1400 – 1500 MeV region span several decades, various production mechanisms and decay modes, with models for data analysis evolving with time. A coherent picture of all available data is therefore difficult. We believe that there is sufficient evidence to consider the 0^{-+} nonet with the $\eta(1440)$ in fig. 63.1 as established. Whether one or two different states – $\eta(1405)$ and $\eta(1475)$ – exist is an open question, in which case the $\eta(1405)$ would be supernumerary. The most recent high statistics data and their theoretical interpretation seem to favor the two-resonance scenario.

63.4.1 *Pseudoscalar glueballs*

The first observation of an isoscalar resonance around 1425 MeV – the E-meson – was made in $p\bar{p}$ annihilation at rest into $E\,\pi^+\pi^-$, $E \to K\overline{K}\pi$ [162]. This state was reported to decay into $a_0(980)\pi$ and $K^*(892)\overline{K}$ with roughly equal contributions. An isoscalar state, the ι meson, was observed in radiative $J/\psi(1S)$ decay into $K\overline{K}\pi$ [163–165] and $\gamma\rho$ [166], and was considered as a glueball candidate, owing to its strong signal in radiative $J/\psi(1S)$ decay. The E and ι were later assumed to be the same state, called $\eta(1440)$. For a historical survey see Ref. [167] and Ref. [168] for a review of the experimental status on the pseudoscalar glueball.

The $\eta(1405)$ would be a candidate for the 0^{-+} glueball in the fluxtube model [169], in which the 0^{++} glueball is also naturally related to a 0^{-+} glueball with mass degeneracy broken in QCD. The pseudoscalar glueball could lie at a lower mass than predicted from lattice calculation [170], see also Refs. [171–173]. The $\eta(1760)$, produced very strongly in radiative $J/\psi(1S)$ decay to $\omega\omega$ [174], has also been proposed for the 0^{-+} glueball mixed with the η and η' [175].

The holographic model of Ref. [75] predicts the pseudoscalar glueball below 2600 MeV, decaying dominantly into two vector mesons.

The $X(2370)$ has recently been studied by BESIII in radiative $J/\psi(1S)$ decay to $K_S K_S \eta'$ with $f_0(980) \to K_S K_S$ [176]. This channel is much less prone to γ background and more restrictive on the $X(2370)$ quantum numbers than $J/\psi(1S) \to \gamma K^+K^-\eta'$ and $\gamma\pi^+\pi^-\eta'$ reported earlier by BESIII. This state is determined to be 0^{-+} isoscalar (and therefore renamed $\eta(2370)$) with a (Breit-Wigner) mass of 2317±9 MeV and a width of 140^{+80}_{-28} MeV (averaged over all three decay channels). According to Ref. [177] the $\eta(2370)$ would be a candidate for the ground state pseudoscalar glueball, but in a region where many 0^{-+} $q\bar{q}$ broad and overlapping radial excitations are also expected. Progress above 2000 MeV requires larger data sets and coupled channel K-matrix analyses.

63.5 Vector mesons

In this section we restrict ourselves to the isovector spectrum which contains broad and overlapping states.

63.5.1 $\rho(770)$

The determination of the parameters of the $\rho(770)$ is beset with many difficulties because of its large width. Its line shape depends on the production process and is not described by a relativistic Breit-Wigner function with a P-wave width, but requires some additional shape parameters [178]. Bose-Einstein correlations are another source of shifts in the $\rho(770)$ line shape, particularly in multiparticle final-state systems [179].

The same model dependence afflicts any other source of resonance parameters, such as the energy dependence of the phase shift δ_1^1, or the pole position. It is, therefore, not surprising that a study of $\rho(770)$ dominance in the decays of the η and η' reveals the need for specific dynamical effects, in addition to the $\rho(770)$ pole [180,181].

The cleanest determination of the $\rho(770)$ mass and width comes from e^+e^- annihilation and τ-lepton decays. ALEPH data [182] showed that the charged $\rho(770)$ parameters measured from τ-lepton decays are consistent with those of the neutral one determined from e^+e^- data [183]. This conclusion is qualitatively supported by the later studies of CLEO [184] and Belle [185]. However, a comparison of the two-pion mass spectrum in τ decays from OPAL [186], CLEO [184], and ALEPH [187,188], and the $e^+e^- \to \pi^+\pi^-$ cross section from CMD-2 [189,190], showed significant discrepancies between the two shapes which can be as high as 10% above the ρ meson mass [191,192]. This discrepancy remains after measurements of the two-pion cross section in e^+e^- annihilation at KLOE [193–196], SND [197,198], BaBar [199] and BESIII [200]. The effect is not accounted for by isospin breaking [201–204], but the accuracy of its calculation may be overestimated [205,206].

Two recent measurements of the $e^+e^- \to \pi^+\pi^-$ cross section by SND [207] and CMD-3 [208,209] show discrepancies in the ρ region: while SND is consistent with previous e^+e^- experiments, CMD-3 finds differences as high as 5% around the ρ meson mass. In addition, in the fit of the $e^+e^- \to \pi^+\pi^-$ cross section CMD-3 reports values for the mass of the ω and the mass and width of the ϕ, which differ slightly from the PDG values, showing for the first time the effect of the $\phi \to \pi^+\pi^-$ interference.

The problem of the difference in the $\pi^+\pi^-$ shapes between e^+e^- and τ decays seems to be solved after the analysis of Ref. [210], which showed that, after correcting the τ data for the missing $\rho-\gamma$ mixing contribution, besides the other known isospin symmetry violating corrections, the $\pi\pi$ isospin 1 part of the hadronic vacuum polarization contribution to the muon $g-2$ is fully compatible between τ-based and e^+e^--based evaluations.

Int. J. Mod. Phys. A 2026.41. Downloaded from www.worldscientific.com
by UNIVERSITY OF CALIFORNIA @ BERKELEY on 09/16/26. Re-use and distribution is strictly not permitted, except for Open Access articles.

The global fit of the whole set of the ρ, ω, and ϕ decays, taking into account mixing effects in the hidden local symmetry model, also showed consistency of the two-pion data in τ decay and e^+e^- annihilation [211,212]. However, because of the progress in e^+e^- data, the τ input is now less precise and less reliable due to additional theoretical uncertainties [213] decreasing the importance of τ decay for the determination of the $\rho(770)$ parameters.

63.5.2 $\rho(770)$ *excitations*

In our 1988 edition, we replaced the $\rho(1600)$ entry with two new ones, the $\rho(1450)$ and the $\rho(1700)$, because there was emerging evidence that the 1600-MeV region actually contains two ρ-like resonances. This possibility was pointed out by a theoretical analysis [214] on the consistency of the 2π and 4π electromagnetic form factors and the $\pi\pi$ scattering length. A consistent picture of $e^+e^- \to 2\pi, 4\pi$ and diffractive photoproduction is obtained with two resonances [215]. The existence of the $\rho(1450)$ was supported by the analysis of $\eta\rho^0$ mass spectra obtained in photoproduction and e^+e^- annihilation [216], as well as that of $e^+e^- \to \omega\pi$ [217].

The analysis of [215] was further extended by [218, 219] to include new data on 4π-systems produced in e^+e^- annihilation, and in τ decays ($\tau \to 4\pi$ and $e^+e^- \to 4\pi$ are related by the Conserved Vector Current hypthesis). These systems were successfully analyzed using interfering contributions from two ρ-like states, and from the tail of the $\rho(770)$ two-body decay. While specific conclusions on $\rho(1450) \to 4\pi$ were obtained, little could be said about the $\rho(1700)$. Independent evidence for two 1^- states is provided by [220] in 4π electroproduction at $\langle Q^2\rangle = 1$ (GeV/c)^2, and by [221] in a high-statistics sample of the $\eta\pi\pi$ system in π^-p charge exchange.

This scenario with two overlapping resonances is supported by other data. DM2 [222] measured the pion form factor in the interval 1.35–2.4 GeV, and observed a deep minimum around 1.6 GeV. The best fit was obtained with the hypothesis of ρ-like resonances at 1420 and 1770 MeV, with widths of about 250 MeV. DM2 [223] found that the $e^+e^- \to \eta\pi^+\pi^-$ cross section is better fitted with two fully interfering Breit-Wigners, with parameters in fair agreement with those of [215] and [222]. Recent LHCb data in $D^+ \to \pi^+\pi^+\pi^-$ also require both interfering $\rho(1450)$ and $\rho(1700)$ [224].

Decisive evidence for the $\pi\pi$ decay mode of both $\rho(1450)$ and $\rho(1700)$ comes from $\overline{p}p$ annihilation at rest [225]. It has been shown that these resonances possess a $K\overline{K}$ decay mode [16, 226, 227]. This decay mode has also been studied in three-body hadronic B decays [228]. High-statistics studies of the decays $\tau \to \pi\pi\nu_\tau$ [182, 184], and $\tau \to 4\pi\nu_\tau$ [229] also require the $\rho(1450)$, but are not sensitive to the $\rho(1700)$, being too close to the τ mass. A high-statistics study of the $\tau \to \pi\pi\nu_\tau$ from Belle [185] reports the first observation of both $\rho(1450)$ and $\rho(1700)$ in τ decays. A clear picture of the two $\pi^+\pi^-$ resonances interfering with the $\rho(770)$ in e^+e^- annihilation was also reported by BaBar using the ISR (Initial State Radiation) method [230], and more recently by CMD-3 [208].

The structure of these ρ states is not yet completely clear. From $e^+e^- \to \omega\pi^0$ data and using the $^3P_0$ model the authors of Ref. [231] find that $\rho(1450)$ and $\rho(1700)$ mix, the former being mainly $2S$ and the latter mainly $3D$. The authors of Refs. [84,232] also claim that $\rho(1450)$ has a mass consistent with radial $2S$, but its decays show characteristics of hybrids, and suggest that this state may be a $2S$-hybrid mixture. Hybrid states could have a 4π decay mode dominated by the $a_1\pi$ [233]. Such behavior has been observed by [234] in $e^+e^- \to 4\pi$ in the energy range 1.05–1.38 GeV, and by [229] in $\tau \to 4\pi\nu_\tau$ decays. CLEO [235] and Belle [236] observe the $\rho(1450) \to \omega\pi$ decay mode in B-meson decays, however, do not find $\rho(1700) \to \omega\pi^0$. The $e^+e^- \to \omega\pi^0$ Born cross section between 1 and 2 GeV from SND (including data from BaBar and BESIII) is described by the $\rho(770)$, $\rho(1570)$, $\rho(1700)$ and $\rho(2150)$ in a vector dominance fit [237], while earlier data [238, 239] did not observe a statistically significant signal of the $\rho(1700)$.

Various decay modes of the $\rho(1450)$ and $\rho(1700)$ are observed in $\overline{p}n$ and $\overline{p}p$ annihilation [240, 241], but no definite conclusions can be drawn. More data should be collected to clarify the nature of the ρ states, particularly in the energy range above 1.6 GeV.

Under the $\rho(1570)$ we list the $\phi\pi$ state with $J^{PC} = 1^{--}$ earlier observed in [242] – referred to as $C(1480)$ – also reported in [243] and possibly seen in [244] which cannot exclude that the observation of the $\rho(1570)$ is due to an OZI-suppressed decay mode of the $\rho(1700)$. The $C(1480)$ has not been seen in $\overline{p}p$ [245] nor in other e^+e^- [246, 247] experiments, which cannot exclude that the observation of the $\rho(1570)$ is due to an OZI-suppressed decay mode of the $\rho(1700)$.

Several observations on the $\omega\pi$ system in the 1200 MeV region [248–254] may be interpreted in terms of either $J^P = 1^-$ $\rho(770) \to \omega\pi$ production [255], or $J^P = 1^+$ $b_1(1235)$ production [253, 254]. Evidence for a $\rho(1250)$ from a reanalysis of elastic scattering data is claimed in Ref. [256] and was reported earlier by LASS [257].

Ref. [258] finds a very broad 1^{--} resonance-like K^+K^- state in $J/\psi \to K^+K^-\pi^0$ decays with pole mass 1576 MeV and width 818 MeV, with possibly molecular or multiquark structure [259–261], or due to the $\rho(1450)$ and $\rho(1700)$ interference [262–265]. We quote this state as $X(1575)$ in the section 'Further States'. Another state observed in $J/\psi \to K^+K^-\pi^0$ is the $\phi(2170)$ [266] which has been interpreted as exotic, e.g. as tetraquark, see section 63.8.

Evidence for ρ-like mesons decaying into 6π was first noted in [267] in the analysis of $e^+e^- \to 6\pi$ [268, 269] and diffractive photoproduction [270]. The authors of Ref. [267] argued that two states at about 2.1 and 1.8 GeV exist: while the former is a candidate for the $\rho(2150)$, the latter could be a manifestation of the $\rho(1700)$ distorted by threshold effects. BaBar reported observations of the new decay modes of the $\rho(2150)$ in the channels $\eta'(958)\pi^+\pi^-$, $f_1(1285)\pi^+\pi^-$ [271] and $\pi^+\pi^-$ [272]. The decay of the $\rho(2150)$ into K^+K^- has been observed by BESIII [273] and confirmed by BaBar [274]. The relativistic quark model [12] predicts the 2^3D_1 state with $J^{PC} = 1^{--}$ at 2.15 GeV which can be identified with the $\rho(2150)$.

Under $\rho(1900)$ we list various observations of irregular behavior of the cross sections near the $N\bar{N}$ threshold. Dips of various widths around 1.9 GeV were reported by the E687 Collaboration (a narrow one in the $3\pi^+3\pi^-$ diffractive photoproduction [275, 276]), by the FENICE experiment reporting a narrow dip [277], by BaBar in ISR (a narrow structure in $e^+e^- \to \phi\pi$ final state [244], but much broader in $e^+e^- \to 3\pi^+3\pi^-$ and $e^+e^- \to 2(\pi^+\pi^-\pi^0)$ [278]), by CMD-3 (also a rather broad dip in $e^+e^- \to 3\pi^+3\pi^-$ [279]). A dedicated scan of the $N\bar{N}$-threshold region by CMD-3 confirms this effect in the $e^+e^- \to 3\pi^+3\pi^-$ and $e^+e^- \to K^+K^-\pi^+\pi^-$ final states, but does not see it in the cross section of $e^+e^- \to 2\pi^+2\pi^-$ [280]. Most probably, these structures emerge as a threshold effect due to the opening of the $N\bar{N}$ channel [281–283]. A similar enhancement is observed by BESIII in $e^+e^- \to \Lambda\bar{\Lambda}$ near the $\Lambda\bar{\Lambda}$ threshold [284, 285] which can be described as $\Lambda\bar{\Lambda}$ final state interaction [286].

63.6 Axial-vector mesons

The 1^{++} nonet consists of the isovector $a_1(1260)$, the isoscalars $f_1(1285)$ and $f_1(1420)$, and the K_{1A}, which is a superposition of the physical states $K_1(1270)$ and $K_1(1400)$ with a mixing angle θ_{K_1} of about 35°, according to the phenomenological analysis of Ref. [287]. The nonet mixing angle $\theta_{1^{++}}$ is around 23°. The orthogonal combination – the K_{1B} – belongs to the 1^{+-} nonet with a mixing angle $\theta_{1^{+-}}$ of about 28° [287]. However, a two-pole structure for the $K_1(1270)$ emerges when using the unitary extension of chiral perturbation theory [288].

The mass region above 1400 MeV is rather complex [289–291]. The $f_1(1420)$ was first reported in π^-p reactions at 4 GeV/c, decaying into $K^*\overline{K}$ [292]. The $K\overline{K}\pi$ decay was also observed in a reanalysis of the MARK III data [139], and a C=+1 state seen in tagged $\gamma\gamma$ collisions [293]. The $K^0_SK^0_S\pi^0$ decay mode of the $f_1(1420)$ establishes unambiguously C=+1. Axial-vector mesons are not observed in $\overline{p}p$ annihilation at rest in liquid hydrogen, which proceeds dominantly through S-wave annihilation. However, in gaseous hydrogen, P-wave annihilation is enhanced and the $f_1(1420)$ is observed, decaying into $K^*\overline{K}$ [141]. The $f_1(1420) \to K\overline{K}\pi$, is also seen in pp central production, together with the $f_1(1285)$. The latter decays via $a_0(980)\pi$, and the former only via $K^*\overline{K}$ which suggests an $s\bar{s}$ structure. Neither central

Int. J. Mod. Phys. A 2026.41. Downloaded from www.worldscientific.com
UNIVERSITY OF CALIFORNIA @ BERKELEY on 09/16/26. Re-use and distribution is strictly not permitted, except for Open Access articles.

production [294] nor $\pi^- p$ interactions at 100 GeV [131] find any evidence for a $\eta\pi\pi$ decay mode of the $f_1(1420)$. However, the $f_1(1420)$ is not seen in the $K^- p$ data [295], which would argue against this state being the $s\bar{s}$ member of the 1^{++} nonet.

The $f_1(1285)$ has been suggested to be a $K^*\overline{K}$ molecule [296]. However, LHCb has determined the 1^{++} nonet mixing angle to be consistent with a mostly $n\bar{n}$ structure for the $f_1(1285)$ from $\overline{B}^0/\overline{B}^0 \to J/\psi(1S)f_1(1285)$, independent of the identity of its isoscalar partner [297]. The mixing angle $\theta_{1^{++}} = 24°$ agrees with that of Ref. [287] quoted above. The $n\bar{n}$ structure is also suggested by ALICE [298] using a comparison of ϕ/π and $f_1(1285)/\pi$ yields in the canonical statistical hadronization model. The ratio of $\overline{B}^0/\overline{B}^0_s$ decay rates also excludes the tetraquark interpretation of the $f_1(1285)$ [297]. This is consistent with earlier determinations assuming that the $f_1(1420)$ is the other isoscalar in the nonet [299].

The $a_1(1420)$ decaying into 3π, reported earlier by COMPASS at 1420 MeV in $\pi^- p \to \pi^-\pi^-\pi^+ p$ [300,301], originates from a triangle singularity: the decay of the $a_1(1260)$ into $K^*(\to K\pi)\bar{K}$ is followed by rescattering into the $f_0(980)\pi$ channel, $f_0(980) \to \pi\pi$ [302] (see the caption of fig. 63.3). A similar triangle singularity is proposed for the $f_1(1420)$, resulting from the $K^*\overline{K}$ and $a_0(980)\pi$ decay modes of the $f_1(1285)$ [303,304].

The $f_1(1420)$ was also suggested to be a hybrid $q\bar{q}g$ meson [305] or a $K^*\overline{K}$ molecule, due to the proximity of the $K^*\overline{K}$ threshold [306]. Instead, the $s\bar{s}$ partner of the $f_1(1285)$ could be the $f_1(1510)$ [307] (omitted from the Summary Table). This state was seen to decay into $K\bar{K}\pi$ in $K^- p$ interactions at 4 and 11 GeV/c, recoiling against a Λ [295,308], which indeed points to an $s\bar{s}$ state. Evidence was reported in $\pi^- p$ interactions, based on the phase motion of the 1^{++} $K^*\overline{K}$ wave [291]. The $f_1(1510)$ is also needed by CMD-3 in $e^+e^- \to f_1(1285, 1420, 1510)\rho(770)$ to describe the shoulder in the $K_S K^\pm\pi^\mp$ mass around 1500 MeV [309]. A somewhat broader 1^{++} signal is observed in $J/\psi(1S) \to \gamma\eta\pi^+\pi^-$ [310] and a small signal in $J/\psi(1S) \to \gamma\eta'\pi^+\pi^-$ [311].

However, there is no evidence for the $f_1(1510)$ in other $K^- p$ experiments [312, 313]. The $f_1(1510)$ is not seen in central collisions [314], nor in $\gamma\gamma$ collisions [315], although surprisingly for an assumed $s\bar{s}$ meson, a signal is reported in 4π decays [316]. Data from LHCb in $B \to (K_S K\pi)K$ [317] require the $f_1(1420)$ and a much weaker $f_1(1510)$ signal. Given this confusing experimental situation, the isoscalar classification in the 1^{++} nonet is not yet settled.

63.7 Hybrid mesons

Hybrids may be viewed as $q\bar{q}$ mesons with a vibrating gluon flux tube. In contrast to glueballs, they have isospin 0 or 1 and can be electrically charged. The mass spectrum of hybrids with exotic (non-$q\bar{q}$) quantum numbers was predicted in Ref. [318], while Ref. [319] also deals with non-exotic quantum numbers. The ground-state hybrids with quantum numbers (0^{-+}, 1^{-+}, 1^{--}, and 2^{-+}) are expected around 1.7 to 1.9 GeV. Lattice calculations predict that the hybrid with exotic quantum numbers 1^{-+} lies at a mass of 1.9 ± 0.2 GeV [320,321]. Most hybrids are expected to be rather broad, but some can be as narrow as 100 MeV [322]. They prefer to decay into a pair of S- and P-wave mesons. The lattice study in [323, 324], based on full QCD with pion masses around 400 MeV, finds that several of the high-lying states observed in their spectrum show significant overlap with gluon rich source terms interpreted as hybrid states. A very broad 1^{-+} isovector structure is predicted by a recent lattice calculation [325]. The main decay mode is $b_1(1235)\pi$ (a pair of S- and P-wave mesons), while other modes, such as $\rho\pi$, $\eta\pi$ and $\eta'\pi$, are suppressed by at least an order of magnitude. For an experimental and theoretical review on hybrid mesons see Ref. [4, 326].

Two isovector 1^{-+} candidates have been reported, one around 1400 MeV (called earlier $\pi_1(1400)$) and the $\pi_1(1600)$. The ∼350–400 MeV broad $\pi_1(1400)$, was reported in $\pi^- p \to \eta\pi^- p$ [327,328] and in $\pi^- p \to \eta\pi^0 n$ [329]. It was observed as an interference between the angular momentum $L = 1$ and $L = 2$ $\eta\pi$ amplitudes, leading to a forward/backward asymmetry in the $\eta\pi$ angular distribution. This state had been reported earlier in $\pi^- p$ reactions [330], but ambiguous solutions in the partial wave analysis were pointed out [331,332]. A resonating 1^{-+} contribution to the $\eta\pi$ P-wave is also required in the Dalitz plot analysis of $\bar{p}n$ annihilation into $\pi^-\pi^0\eta$ [333], and in $\bar{p}p$ annihilation into $\pi^0\pi^0\eta$ [334]. Mass and width are consistent with the results of Ref. [327]. A coupled channel re-analysis of the $\pi^0\pi^0\eta$, $\pi^0\eta\eta$ and $K^+K^-\pi^0$ Crystal Barrel data at 900 MeV/c, supplemented with data from other collaboration in $\pi\pi \to \pi\pi, K\bar{K}, \eta\eta$ and $\eta\eta'$, leads to a single 1^{-+} ∼600 MeV broad state with a pole around 1400 MeV, decaying into $\eta\pi^0$ [20]. Ref. [335] suggested for the production in $\pi^- p$ that a Deck-generated $\eta\pi$ background from final state rescattering in $\pi_1(1600)$ decay could mimic $\pi_1(1400)$, a mechanism that is, however, absent in $\bar{p}p$ annihilation.

The $\pi_1(1600)$, decaying into $\rho\pi$, was reported by COMPASS with 190 GeV pions hitting a lead target [336,337]. It had already been observed in $\pi^- p$ interactions in the decay modes $\eta'\pi$ [338], $f_1(1285)\pi$ [339], and $\omega\pi\pi$ [340], $b_1(1235)\pi$, but not $\eta\pi$ [341]. A strong enhancement in the 1^{-+} $\eta'\pi$ wave, compared to $\eta\pi$, was reported at this mass in Ref. [342]. The enhancement is also observed by COMPASS in $\pi^- p \to \eta'\pi$ but in $\eta\pi$ a peak appears at 1400 MeV and in $\eta'\pi$ at 1600 MeV [343]. A coupled channel analysis of the $\eta\pi$ and $\eta'\pi$ COMPASS data leads to a single pole at 1564 ± 89 MeV, with a width of 492 ± 115 MeV [344]. The predicted width from the lattice calculation [325] is compatible with the COMPASS result. Furthermore, a combined analysis of the COMPASS and Crystal Barrel data at 900 MeV/c leads to similar results, a single pole around 1623 MeV, with a width of about 455 MeV, although a two-pole scenario cannot be completely excluded [345]. Accordingly, the $\pi_1(1400)$ data are listed in the $\pi_1(1600)$ section.

Very recently, BESIII reported a 188 MeV broad enhancement at 1855 MeV in $J/\psi(1S)$ radiative decay into the $\eta\eta'$ P-wave [346], hence with exotic quantum numbers 1^{-+}. This isoscalar resonance is needed with very high significance, albeit the contribution to $\gamma\eta\eta'$ is weak and several other isoscalars expected to contribute are absent [347]. Hence this state needs confirmation. We have listed claims for such a state decaying into $\eta\eta'$ in this mass range under the $f_2(1910)$ (see e.g. Ref. [30] from WA102 central production, suggesting 1^{-+} as an alternative to 2^{++}). If confirmed, the $\eta(1855)$ could be one of the isospin 0 partners of the $\pi_1(1600)$, a member of the 1^{-+} hybrid nonet [348–350] or a $K\bar{K}_1(1400)$ molecule [351]. In Ref. [348] this state is interpreted as the heavy isoscalar while its light partner is much narrower, with a mass of about 1660 MeV.

Hybrid candidates with the non-exotic quantum numbers 0^{-+}, 1^{--}, and 2^{-+} have also been reported: the $\pi(1800)$ is somewhat narrow if interpreted as the second radial excitation of the pion. It decays mostly into a pair of S- and P-wave mesons [352,353], in line with expectations for 0^{-+} hybrid mesons. The evidence for 1^{--} hybrids in e^+e^- annihilation and in τ decays has been discussed in [233]. The near degeneracy of the $\eta_2(1645)$ and $\pi_2(1670)$ suggests ideal mixing in the 2^{-+} $q\bar{q}$ nonet, and hence, the second isoscalar, presumably the $\eta_2(1870)$, should be mainly $s\bar{s}$ (fig. 63.1). However, the $\eta_2(1870)$ is also observed in $\bar{p}p$ annihilation and decays mainly into $a_2(1320)\pi$ and $f_2(1270)\pi$ [354], with a relative rate compatible with a hybrid state [319].

Evidence for another exotic $\pi_1(2015)$ has been claimed in $\pi^- p$ interactions [339, 340]. A flavor multiplet of vector hybrids between 2200 and 2300 MeV is predicted by the constituent gluon model [350]. Decays of light hybrids in the constituent model are discussed in Ref. [355].

Summarizing, there is evidence for a very broad 1^{-+} enhancement in the 1400–1600 MeV region, which consists of one (or possibly two) exotic states. As isovectors they cannot be glueballs. The coupling to $\eta\pi$ of the lighter one points to a four-quark state [356], while the $\eta'\pi$ coupling of the heavier one is favored for hybrid states [357, 358]. The mass of the latter, the $\pi_1(1600)$, is not far below the lattice and flux tube model predictions. The $\eta_1(1855)$ is an isoscalar candidate for the ground state 1^{-+} hybrid nonet.

63.8 Tetraquark states

The existence of multiquark states was suggested a long time ago, based on duality arguments [359, 360]. The most prominent light tetraquark candidates are the $a_0(980)$ and $f_0(980)$ [361–363].

Int. J. Mod. Phys. A 2026.41. Downloaded from www.worldscientific.com
by UNIVERSITY OF CALIFORNIA @ BERKELEY on 09/16/26. Re-use and distribution is strictly not permitted, except for Open Access articles.

A remarkable prediction for the existence of low-lying four quarks states is based on color hyperfine splitting. The lowest ground state ($L = 0$) tetraquark multiplet is predicted to be a scalar nonet. The scalar nonet lies just below 1 GeV when one assumes as mass scale the hyperfine color splitting between the ρ and the π (for a simple derivation see [9]). One then gets the nonet structure

$$\begin{aligned}
|a_0(980)\rangle &= |us\bar{d}\bar{s}\rangle, \frac{1}{\sqrt{2}}|(u\bar{u} - d\bar{d})s\bar{s}\rangle, |\bar{u}\bar{s}ds\rangle,\\
|f_0(980)\rangle &= \frac{1}{\sqrt{2}}|(u\bar{u} + d\bar{d})s\bar{s}\rangle,\\
|f_0(500)\rangle &= |\bar{u}\bar{d}ud\rangle,\\
|K_0^*(700)\rangle &= |\bar{s}\bar{d}ud\rangle, |\bar{s}\bar{u}ud\rangle \text{ and } |\bar{u}\bar{d}us\rangle, |\bar{u}\bar{d}ds\rangle. \qquad (63.1)
\end{aligned}$$

The two isoscalars are expected to mix with the angle φ:

$$\begin{aligned}
|f_0(980)\rangle &= \cos\varphi|s\bar{s}\rangle + \sin\varphi|n\bar{n}\rangle,\\
|f_0(500)\rangle &= -\sin\varphi|s\bar{s}\rangle + \cos\varphi|n\bar{n}\rangle. \qquad (63.2)
\end{aligned}$$

Table 63.1: Coupling amplitudes for $\bar{B}^0$ and $\bar{B}_s^0$ decays into $J/\psi(1S)f_0(500)/f_0(980)$, depending on the $q\bar{q}$ or tetraquark structures of the $f_0(500)$ and $f_0(980)$ (from [364] where illustrative decay diagrams can be found). The angle φ is defined in Eq. 63.2.

	$\bar{B}^0$		$\bar{B}_s^0$	
	$f_0(980)$	$f_0(500)$	$f_0(980)$	$f_0(500)$
$q\bar{q}$	$\sin\varphi/\sqrt{2}$	$\cos\varphi/\sqrt{2}$	$\cos\varphi$	$\sin\varphi$
$qq\bar{q}\bar{q}$	$1/\sqrt{2}$	1	$\sqrt{2}$	0

Whether these mesons are really tetraquark states or $q\bar{q}$ mesons, is still an open issue:

- The $f_0(980)$ is strongly produced in D_s^+ decay [365], which suggests a large $s\bar{s}$ component, due to the Cabibbo-favored $c \to s$ coupling. However, the mainly $n\bar{n}$ $f_0(1370)$ is also strongly produced in D_s^+ decay, hence additional graphs must contribute [366].
- The relative branching ratios for $\bar{B}^0$ and $\bar{B}_s^0 \to J/\psi(1S)f_0(500)$ and $J/\psi(1S)f_0(980)$ can be used to probe the $q\bar{q}$ or tetraquark natures of the $f_0(500)$ and $f_0(980)$ [364, 367]. LHCb observes the $f_0(980)$ in $\bar{B}_s^0$ decays, but not the $f_0(500)$ [32], as would be expected for tetraquarks (see Table 63.1). In contrast, LHCb also observes the $f_0(500)$ in $\bar{B}^0$ decays, but not the $f_0(980)$ with an upper limit eight standard deviations below the predicted value for a tetraquark state [33]. However, these contradicting findings have been challenged by a dispersive analysis [368], using a model independent inclusion of hadronic final state interactions, in which a substantial $f_0(980)$ contribution is nevertheless found in $\bar{B}^0$-decays, thus still leaving the tetraquark structure as an open possibility.
- The ALICE collaboration reports a much stronger K_SK_S femtoscopic correlation than for $K_SK^\pm$ in high energy pp collisions, indicative of the $a_0(980)$ being a tetraquark state [369].
- The $f_0(980)$ and $a_0(980)$ could also be $K\overline{K}$ molecular states [70, 370, 371], being close to the $K\overline{K}$ threshold and decaying strongly into $K\overline{K}$. For $q\bar{q}$ states, the expected $\gamma\gamma$ widths [372, 373] are not significantly larger than for molecular states [372, 374] and both predictions are consistent with data.
- Radiative decays of the $\phi(1020)$ into $a_0(980)$ and $f_0(980)$ were proposed to disentangle compact tetraquark structures from hadronic molecules. In Ref. [13] these states are made of four-quark cores and virtual $K\overline{K}$ clouds at the periphery, a view that is challenged in Ref. [375] showing that radiative ϕ decay data are consistent with molecular structures of light scalars. However, following Refs. [376, 377], the data from KLOE [378] and SND [379] in $\phi \to \gamma\eta\pi^0$, from KLOE [380] in $\phi \to \gamma\pi^0\pi^0$ and in $\phi \to \gamma\pi^+\pi^-$ from CMD-2 [381] favor these mesons to be tetraquark states. This is also supported by a BESIII analysis of $J/\psi(1S) \to \gamma\pi^0\pi^0$ [382] and by a measurement of $a_0(980) - f_0(980)$ mixing at BESIII [383].

More information on the $a_0(980)$, $f_0(980)$, $f_0(500)$ and $K_0^*(700)$ is provided by 'Scalar Mesons below 1 GeV' in the *Review*. For the $f_0(500)$ see also Ref. [384].

As mentioned already, the $f_0(1500)$ [42] and the $f_1(1285)$ [364] have been proposed as tetraquarks, the latter also as $K^*\overline{K}$ molecule [296], together with the $f_1(1420)$ [306]. Another potential candidate for a tetraquark is the $\phi(2170)$. As an excited $q\bar{q}$ state of the $\phi(1020)$, this meson should decay strongly into K^+K^- and $K_S^0K_L^0$, and also $K^*\bar{K}^*$. However, these decays are not observed. Hence, based on its observed decay into $f_0(980)\phi(1020)$ this meson could be an $ss\bar{s}\bar{s}$ tetraquark [385]. However, Refs. [386, 387] claim that the $\phi(2170)$ may not be a good candidate for the $ss\bar{s}\bar{s}$ state, predicted to lie higher in mass, but could qualify as an $su\bar{s}\bar{u}$ tetraquark.

63.9 Baryonia

Nucleon-antinucleon ($N\bar{N}$) bound states and resonances (baryonium) were predicted a long time ago [388, 389], based on the strongly attractive $N\bar{N}$ meson exchange potential, which is obtained from the NN one by multiplying with the G-parity of the exchanged meson. Several candidates had been reported in the seventies by experiments at CERN, BNL and KEK, some of them being indisputably statistically significant (for details on the model and on experiments, see [390, 391] and references therein). Most potential models predict a sequence of deeply bound isoscalar baryonia with quantum numbers $J^{PC} = 2^{++}$, 1^{--} and 0^{++}, the latter being the mostly bound [392, 393]. The $f_2(1565)$ which is observed in $\bar{p}p$ annihilation only [394, 395], is a good candidate for the 2^{++} $\bar{p}p$ bound state.

Enhancements close to the $\bar{p}p$ threshold have also been reported in B decays [396–398]. The strong signal near the $p\bar{p}$ threshold in $J/\psi(1S) \to \gamma\bar{p}p$ [399–401] could be due to a 0^{-+} baryonium [402], but could also be generated by the $N\bar{N}$ final state interaction [403–406]. The strong energy dependence of the cross section in $e^+e^- \to \bar{p}p$ [407, 408] and $\bar{p}p \to e^+e^-$ [409] is attributed to the $N\bar{N}$ final state interaction [410] (see also our comments on the $\rho(1900)$ at the end of section 63.5.2). Alternative explanations to baryonia have been proposed for the signals in $B \to \bar{p}pK$, such as the dynamics of the fragmentation mechanism [397].

63.10 Conclusions

The ground state nonets 1^1S_0, 1^3S_1, 1^1P_1, 1^3P_2, 1^1D_2 and 1^3D_3 (see fig. 63.1) are established (although more data are desirable for the $h_1(1415)$ in the 1^1P_1 nonet). There are uncertainties and ambiguities in all other nonets. In the pseudoscalar sector the $\eta(1440)$ may consist of two states, one at 1405 MeV, the other at 1475 MeV, which could also be the manifestation of a single resonance decaying into two different final states. In this case the 1475 one could be the radial excitation of the η' and the 1405 the pseudoscalar ground state glueball predicted a long time ago by the bag model, although the lattice puts it above 2 GeV. In the 1^{++} nonet two isoscalars – the $f_1(1420)$ and $f_1(1510)$ – compete for the $s\bar{s}$ slot. The first radial excitation 2^3S_1 is complete, but questions have been raised as to the nature of the $\rho(1450)$ and its relation to the $\rho(1700)$. The classification of scalar mesons is not settled, with the ones below 1 GeV being tetraquark states or building the ground state $q\bar{q}$ nonet. The nature of the scalars in the 1.5 – 1.8 GeV region is unclear, obscured by the interference with the ground state scalar glueball predicted in this mass region. For example, the $f_0(1500)$ and the $f_0(1710)$ could be $q\bar{q}$ states ($n\bar{n}$ and $s\bar{s}$, respectively) or made of gluons mixed with $q\bar{q}$. The $f_0(1500)$, or alternatively the $f_0(1710)$, have been proposed as mostly gluonic. Scalar mesons above the $f_0(1710)$ need experimental confirmation. Another pair of scalars, $a_0(1710)$ and $f_0(1770)$, has been reported. An isovector meson with exotic (1^{-+}) quantum numbers, $\pi_1(1600)$, is observed around 1.6 GeV with mass not far below theoretical predictions, although a further 1^{-+} state, decaying into $\eta\pi$, cannot be entirely excluded

around 1.4 GeV. An isoscalar partner, the $\eta_1(1855)$, has been reported, needing confirmation. Above 1.8 GeV mesons are broad and overlap, which complicates the data analyses. This makes the classification difficult, in particular the identification of the 2^{++} and 0^{-+} glueballs, expected above 2000 MeV.

Acknowledgements

We thank Paolo Gauzzi, Bertram Kopf and Curtis Meyer for carefully reading the manuscript and for detailed and constructive suggestions.

References

[1] C. Amsler and N. A. Tornqvist, Phys. Rept. **389**, 61 (2004).

[2] D. V. Bugg, Phys. Rept. **397**, 257 (2004), [hep-ex/0412045].

[3] E. Klempt and A. Zaitsev, Phys. Rept. **454**, 1 (2007), [arXiv:0708.4016].

[4] C. A. Meyer and E. S. Swanson, Prog. Part. Nucl. Phys. **82**, 21 (2015), [arXiv:1502.07276].

[5] R. De Vita, EPJ Web Conf. **66**, 01004 (2014).

[6] A. Esposito, A. Pilloni and A. D. Polosa, Phys. Rept. **668**, 1 (2017), [arXiv:1611.07920].

[7] F.-K. Guo *et al.*, Rev. Mod. Phys. **90**, 015004 (2018), [arXiv:1705.00141].

[8] V. Crede and C. A. Meyer, Prog. Part. Nucl. Phys. **63**, 74 (2009), [arXiv:0812.0600].

[9] C. Amsler, *The Quark Structure of Hadrons: An Introduction to the Phenomenology and Spectroscopy*, volume 949 of *Lecture Notes in Physics*, Springer (2018).

[10] L. Burakovsky and T. Goldman, Nuclear Physics A **625**, 1, 220 (1997).

[11] L. D. Roper and I. Strakovsky, The European Physical Journal A **61**, 5, 102 (2025), [arXiv:2410.11196].

[12] S. Godfrey and N. Isgur, Phys. Rev. **D32**, 189 (1985).

[13] F. E. Close and N. A. Tornqvist, J. Phys. **G28**, R249 (2002), [hep-ph/0204205].

[14] C. Amsler, Rev. Mod. Phys. **70**, 1293 (1998), [hep-ex/9708025].

[15] C. Amsler *et al.* (Crystal Barrel), Phys. Lett. **B333**, 277 (1994).

[16] A. Abele *et al.*, Phys. Rev. **D57**, 3860 (1998).

[17] S. Uehara *et al.* (Belle), Phys. Rev. **D80**, 032001 (2009), [arXiv:0906.1464].

[18] P. Rubin *et al.* (CLEO), Phys. Rev. **D78**, 072003 (2008), [arXiv:0807.4545].

[19] R. Aaij *et al.* (LHCb), Phys. Rev. **D93**, 052018 (2016), [arXiv:1509.06628].

[20] M. Albrecht *et al.* (Crystal Barrel), Eur. Phys. J. **C80**, 453 (2020), [arXiv:1909.07091].

[21] C. Amsler *et al.* (Crystal Barrel), Eur. Phys. J. **C23**, 29 (2002).

[22] C. Amsler *et al.* (Crystal Barrel), Phys. Lett. **B322**, 431 (1994).

[23] C. Amsler *et al.* (Crystal Barrel), Phys. Lett. **B342**, 433 (1995).

[24] A. Abele *et al.* (Crystal Barrel), Phys. Lett. **B380**, 453 (1996).

[25] D. Barberis *et al.* (WA102), Phys. Lett. **B462**, 462 (1999), [hep-ex/9907055].

[26] D. Barberis *et al.* (WA102), Phys. Lett. **B471**, 440 (2000), [hep-ex/9912005].

[27] C. Amsler *et al.* (Crystal Barrel), Phys. Lett. **B353**, 571 (1995).

[28] C. Amsler *et al.* (Crystal Barrel), Phys. Lett. **B355**, 425 (1995).

[29] D. Barberis *et al.* (WA102), Phys. Lett. **B479**, 59 (2000), [hep-ex/0003033].

[30] D. Barberis *et al.*, Physics Letters B **471**, 429 (2000), [hep-ex/9911041].

[31] C. Adolph *et al.* (COMPASS), Phys. Rev. **D95**, 032004 (2017), [arXiv:1509.00992].

[32] R. Aaij *et al.* (LHCb), Phys. Rev. **D89**, 092006 (2014), [arXiv:1402.6248].

[33] R. Aaij *et al.* (LHCb), Phys. Rev. **D90**, 012003 (2014), [arXiv:1404.5673].

[34] F. E. Close and A. Kirk, Phys. Rev. **D91**, 114015 (2015), [arXiv:1503.06942].

[35] W. Ochs, J. Phys. **G40**, 043001 (2013), [arXiv:1301.5183].

[36] D. V. Bugg, B. S. Zou and A. V. Sarantsev, Nucl. Phys. **B471**, 59 (1996).

[37] P. d'Argent *et al.*, JHEP **05**, 143 (2017), [arXiv:1703.08505].

[38] B. Aubert *et al.* (BaBar), Phys. Rev. **D79**, 072006 (2009), [arXiv:0902.2051].

[39] J. R. Pelaez, A. Rodas and J. R. de Elvira, Phys. Rev. Lett. **130**, 051902 (2023), [arXiv:2206.14822].

[40] A. Abele *et al.* (Crystal Barrel), Phys. Lett. **B385**, 425 (1996).

[41] C. Amsler *et al.* (Crystal Barrel), Phys. Lett. **B639**, 165 (2006).

[42] L. Zou *et al.*, Phys. Rev. D **99**, 114024 (2019), [arXiv:1901.11205].

[43] R. Molina, D. Nicmorus and E. Oset, Phys. Rev. **D78**, 114018 (2008), [arXiv:0809.2233].

[44] C. García-Recio *et al.*, Phys. Rev. **D87**, 096006 (2013), [arXiv:1304.1021].

[45] D. Gülmez, U. G. Meißner and J. A. Oller, Eur. Phys. J. **C77**, 460 (2017), [arXiv:1611.00168].

[46] E. Klempt, Physics Letters B **820**, 136512 (2021), [arXiv:2104.09922].

[47] D. Black, A. H. Fariborz and J. Schechter, Phys. Rev. **D61**, 074001 (2000), [hep-ph/9907516].

[48] H. Kim and K. S. Kim, The European Physical Journal C **82**, 1113 (2022), [arXiv:2209.02958].

[49] N. A. Tornqvist, Z. Phys. **C68**, 647 (1995), [hep-ph/9504372].

[50] E. van Beveren and G. Rupp, Eur. Phys. J. **C22**, 493 (2001), [hep-ex/0106077].

[51] M. Boglione and M. R. Pennington, Phys. Rev. **D65**, 114010 (2002), [hep-ph/0203149].

[52] L. S. Celenza *et al.*, Phys. Rev. C **61**, 035201 (2000).

[53] M. Ablikim *et al.* (BES), Phys. Lett. B **607**, 243 (2005), [hep-ex/0411001].

[54] M. Ablikim *et al.* (BES), Phys. Rev. D **72**, 092002 (2005), [hep-ex/0508050].

[55] M. Ablikim *et al.* (BESIII), Phys. Rev. D **87**, 032008 (2013), [arXiv:1211.5668].

[56] V. A. Dorofeev *et al.*, The European Physical Journal A **60**, 5, 105 (2024).

[57] F. E. Close and Q. Zhao, Phys. Rev. D **71**, 094022 (2005), [hep-ph/0504043].

[58] A. Sarantsev *et al.*, Physics Letters B **816**, 136227 (2021), [arXiv:2103.09680].

[59] E. Klempt and A. Sarantsev, Physics Letters B **826**, 136906 (2022), [arXiv:2112.04348].

[60] M. Ablikim *et al.* (BESIII), Phys. Rev. D **104**, 012016 (2021), [arXiv:2011.08041].

[61] M. Ablikim *et al.* (BESIII), Phys. Rev. D **105**, L051103 (2022), [arXiv:2110.07650].

[62] R. Aaij *et al.* (LHCb), Phys. Rev. D **108**, 3, 032010 (2023), [arXiv:2304.14891].

Int. J. Mod. Phys. A 2026.41. Downloaded from www.worldscientific.com
UNIVERSITY OF CALIFORNIA @ BERKELEY on 09/16/26. Re-use and distribution is strictly not permitted, except for Open Access articles.

Int. J. Mod. Phys. A 2026.41. Downloaded from www.worldscientific.com
by UNIVERSITY OF CALIFORNIA @ BERKELEY on 09/16/26. Re-use and distribution is strictly not permitted, except for Open Access articles.

[63] M. Ablikim *et al.* (BESIII), Phys. Rev. Lett. **129**, 182001 (2022), [arXiv:2204.09614].

[64] J. P. Lees *et al.* (BaBar), Phys. Rev. D **104**, 072002 (2021), [arXiv:2106.05157].

[65] L. S. Geng and E. Oset, Phys. Rev. D **79**, 074009 (2009), [arXiv:0812.1199].

[66] X. Zhu *et al.*, Phys. Rev. D **105**, 116010 (2022), [arXiv:2204.09384].

[67] X. Zhu *et al.*, Phys. Rev. D **107**, 034001 (2023), [arXiv:2210.12992].

[68] Z.-L. Wang and B.-S. Zou, Phys. Rev. D **104**, 114001 (2021), [arXiv:2107.14470].

[69] Z.-Y. Wang *et al.*, Phys. Rev. D **107**, 116018 (2023), [arXiv:2306.06395].

[70] J. D. Weinstein and N. Isgur, Phys. Rev. **D41**, 2236 (1990).

[71] S. Schacht and A. Soni, Physics Letters B **825**, 136855 (2022), [arXiv:arXiv:2110.07619].

[72] A. Athenodorou and M. Teper, Journal of High Energy Physics **2020**, 11, 172 (2020), [arXiv:2007.06422].

[73] J. Zou *et al.*, Science China Physics, Mechanics & Astronomy **67**, 11, 111012 (2024), [arXiv:2404.01564].

[74] S. R. Cotanch and R. A. Williams, Phys. Lett. B **621**, 269 (2005), [arXiv:nucl-th/0505074].

[75] F. Hechenberger, J. Leutgeb and A. Rebhan, Phys. Rev. D **107**, 114020 (2023), [arXiv:2302.13379].

[76] C. Amsler and F. E. Close, Phys. Rev. **D53**, 295 (1996), [hep-ph/9507326].

[77] N. A. Tornqvist and M. Roos, Phys. Rev. Lett. **76**, 1575 (1996), [hep-ph/9511210].

[78] A. V. Anisovich, V. V. Anisovich and A. V. Sarantsev, Phys. Lett. **B395**, 123 (1997), [hep-ph/9611333].

[79] M. Boglione and M. R. Pennington, Phys. Rev. Lett. **79**, 1998 (1997), [hep-ph/9703257].

[80] P. Minkowski and W. Ochs, Eur. Phys. J. **C9**, 283 (1999), [hep-ph/9811518].

[81] W.-J. Lee and D. Weingarten, Phys. Rev. **D61**, 014015 (2000), [hep-lat/9910008].

[82] F. E. Close and A. Kirk, Eur. Phys. J. **C21**, 531 (2001), [hep-ph/0103173].

[83] H.-Y. Cheng, C.-K. Chua and K.-F. Liu, Phys. Rev. **D74**, 094005 (2006), [hep-ph/0607206].

[84] T. Barnes *et al.*, Phys. Rev. **D55**, 4157 (1997), [hep-ph/9609339].

[85] S. Janowski, F. Giacosa and D. H. Rischke, Phys. Rev. **D90**, 114005 (2014), [arXiv:1408.4921].

[86] F. Brünner and A. Rebhan, Phys. Rev. Lett. **115**, 131601 (2015), [arXiv:1504.05815].

[87] J. Ellis and J. Lánik, Physics Letters B **150**, 289 (1985).

[88] C.-D. Lu *et al.*, Eur. Phys. J. **A49**, 58 (2013), [arXiv:1301.0225].

[89] J.-L. Ren *et al.*, The European Physical Journal C **84**, 4, 358 (2024), [arXiv:2311.16824].

[90] C. Amsler, Phys. Lett. **B541**, 22 (2002), [hep-ph/0206104].

[91] F. E. Close and A. Kirk, Phys. Lett. **B397**, 333 (1997), [hep-ph/9701222].

[92] F. E. Close, Phys. Lett. **B419**, 387 (1998), [hep-ph/9710450].

[93] A. Kirk, Phys. Lett. **B489**, 29 (2000), [hep-ph/0008053].

[94] M. Ablikim *et al.* (BES), Phys. Lett. **B603**, 138 (2004), [hep-ex/0409007].

[95] M. Ablikim *et al.* (BES), Phys. Lett. **B607**, 243 (2005), [hep-ex/0411001].

[96] S. Narison, Nuclear Physics B **509**, 312 (1998).

[97] M. Chanowitz, Phys. Rev. Lett. **95**, 172001 (2005), [hep-ph/0506125].

[98] M. Albaladejo and J. A. Oller, Phys. Rev. Lett. **101**, 252002 (2008), [arXiv:0801.4929].

[99] F. Brünner and A. Rebhan, Phys. Rev. D **92**, 121902 (2015), [arXiv:1510.07605].

[100] M. Acciarri *et al.* (L3), Phys. Lett. **B501**, 173 (2001), [hep-ex/0011037].

[101] K. Abe *et al.* (Belle), Eur. Phys. J. **C32**, 323 (2003), [hep-ex/0309077].

[102] R. Barate *et al.* (ALEPH), Phys. Lett. **B472**, 189 (2000), [hep-ex/9911022].

[103] S. Uehara *et al.* (Belle), Phys. Rev. **D78**, 052004 (2008), [arXiv:0805.3387].

[104] S. Uehara *et al.* (Belle), PTEP **2013**, 123C01 (2013), [arXiv:1307.7457].

[105] A. H. Fariborz *et al.*, Phys. Rev. **D90**, 033009 (2014), [arXiv:1407.3870].

[106] P. Minkowski and W. Ochs, Eur. Phys. J. **C39**, 71 (2005), [hep-ph/0404194].

[107] A. Garmash *et al.* (Belle), Phys. Rev. **D71**, 092003 (2005), [hep-ex/0412066].

[108] B. Aubert *et al.* (BaBar), Phys. Rev. **D74**, 032003 (2006), [hep-ex/0605003].

[109] B. Aubert *et al.* (BaBar), Phys. Rev. Lett. **99**, 161802 (2007), [arXiv:0706.3885].

[110] M. Ablikim *et al.*, Phys. Lett. **B642**, 441 (2006), [hep-ex/0603048].

[111] M. Ablikim *et al.* (BESIII), Phys. Rev. **D87**, 092009 (2013), [Erratum: Phys. Rev.D87, 119901(2013)], [arXiv:1301.0053].

[112] A. Rodas *et al.*, Eur. Phys. J. **C82**, 80 (2022), [arXiv:2110.00027].

[113] A. Vereijken *et al.*, Phys. Rev. D **108**, 014023 (2023), [arXiv:2304.05225].

[114] A. A. Godizov, Eur. Phys. J. C **76**, 361 (2016), [arXiv:1604.01689].

[115] S. Donnachie *et al.*, *Pomeron Physics and QCD*, Cambridge Monographs on Particle Physics, Nuclear Physics and Cosmology, Cambridge University Press, p. 85 (2002).

[116] R. S. Longacre and S. J. Lindenbaum, Phys. Rev. D **70**, 094041 (2004), [hep-ex/0407054].

[117] P. S. L. Booth *et al.*, Nucl. Phys. B **273**, 689 (1986).

[118] A. Etkin *et al.*, Phys. Lett. B **201**, 568 (1988).

[119] D. Barberis *et al.* (WA102), Phys. Lett. B **432**, 436 (1998), [hep-ex/9805018].

[120] C. Evangelista *et al.* (JETSET), Phys. Rev. D **57**, 5370 (1998), [hep-ex/9802016].

[121] M. Ablikim *et al.* (BESIII), Phys. Rev. D **93**, 112011 (2016), [arXiv:1602.01523].

[122] Y.-B. Yang *et al.* (CLQCD Collaboration), Phys. Rev. Lett. **111**, 091601 (2013), [arXiv:1304.3807].

[123] E. Klempt *et al.*, Phys. Lett. B **830**, 137171 (2022), [arXiv:2205.07239].

[124] I. Iatrakis, A. Ramamurti and E. Shuryak, Phys. Rev. D **94**, 045005 (2016), [arXiv:1602.05014].

[125] F. Brünner, D. Parganlija and A. Rebhan, Phys. Rev. D **91**, 106002 (2015), [Erratum: Phys.Rev. D93, 109903 (2016)], [arXiv:1501.07906].

[126] J. Z. Bai *et al.* (BES), Phys. Rev. Lett. **76**, 3502 (1996).

[127] C. Amsler *et al.* (Crystal Barrel), Phys. Lett. B **520**, 175 (2001).

[128] R. Aaij *et al.* (LHCb), Eur. Phys. J. C **78**, 443 (2018), [arXiv:1712.08609].

Int. J. Mod. Phys. A 2026.41. Downloaded from www.worldscientific.com
UNIVERSITY OF CALIFORNIA @ BERKELEY on 09/16/26. Re-use and distribution is strictly not permitted, except for Open Access articles.

[129] G. S. Adams *et al.* (E852), Phys. Lett. **B516**, 264 (2001), [hep-ex/0107042].

[130] S. Fukui *et al.*, Phys. Lett. **B267**, 293 (1991).

[131] D. Alde *et al.* (GAMS), Phys. Atom. Nucl. **60**, 386 (1997), [Yad. Fiz.60,458(1997)].

[132] J. J. Manak *et al.* (E852), Phys. Rev. **D62**, 012003 (2000), [hep-ex/0001051].

[133] A. V. Anisovich *et al.*, Nucl. Phys. **A690**, 567 (2001).

[134] C. Amsler *et al.*, Eur. Phys. J. **C33**, 23 (2004).

[135] J. E. Augustin *et al.* (DM2), Phys. Rev. **D46**, 1951 (1992).

[136] B. Aubert *et al.* (BaBar), Phys. Rev. Lett. **101**, 091801 (2008), [arXiv:0804.0411].

[137] E. Klempt, Int. J. Mod. Phys. **A21**, 739 (2006).

[138] M. G. Rath *et al.*, Phys. Rev. **D40**, 693 (1989).

[139] Z. Bai *et al.* (MARK-III), Phys. Rev. Lett. **65**, 2507 (1990).

[140] A. Bertin *et al.* (OBELIX), Phys. Lett. **B361**, 187 (1995).

[141] A. Bertin *et al.* (OBELIX), Phys. Lett. **B400**, 226 (1997).

[142] C. Cicalo *et al.* (OBELIX), Phys. Lett. **B462**, 453 (1999).

[143] F. Nichitiu *et al.* (OBELIX), Phys. Lett. **B545**, 261 (2002).

[144] T. Bolton *et al.*, Phys. Rev. Lett. **69**, 1328 (1992).

[145] M. Ablikim *et al.* (BES), Phys. Rev. **D77**, 032005 (2008), [arXiv:0712.1411].

[146] M. Ablikim *et al.* (BESIII), Phys. Rev. **D87**, 092006 (2013), [arXiv:1303.6360].

[147] M. Acciarri *et al.* (L3), Phys. Lett. **B501**, 1 (2001), [hep-ex/0011035].

[148] F. E. Close, G. R. Farrar and Z.-p. Li, Phys. Rev. **D55**, 5749 (1997), [hep-ph/9610280].

[149] D. M. Li, H. Yu and S. S. Fang, Eur. Phys. J. **C28**, 335 (2003).

[150] R. Ahohe *et al.* (CLEO), Phys. Rev. **D71**, 072001 (2005), [hep-ex/0501026].

[151] P. Achard *et al.* (L3), JHEP **03**, 018 (2007).

[152] T. Gutsche, V. E. Lyubovitskij and M. C. Tichy, Phys. Rev. **D79**, 014036 (2009), [arXiv:0811.0668].

[153] E. Klempt, in "32nd International Conference on High Energy Physics, Beijing," (2004), [hep-ph/0409148].

[154] T. Barnes, N. Black and P. R. Page, Phys. Rev. D **68**, 054014 (2003), [arXiv:nucl-th/0208072].

[155] J.-J. Wu *et al.*, Phys. Rev. Lett. **108**, 081803 (2012), [arXiv:1108.3772].

[156] X.-G. Wu *et al.*, Phys. Rev. **D87**, 014023 (2013), [arXiv:1211.2148].

[157] M.-C. Du and Q. Zhao, Phys. Rev. D **100**, 036005 (2019), [arXiv:1905.04207].

[158] Y. Cheng, L. Qiu and Q. Zhao [arXiv:2302.01210].

[159] F. Aceti *et al.*, Phys. Rev. **D86**, 114007 (2012), [arXiv:1209.6507].

[160] M. Ablikim *et al.* (BESIII), JHEP **03**, 121 (2023), [arXiv:2209.11175].

[161] S. X. Nakamura *et al.*, Phys. Rev. D **107**, L091505 (2023), [arXiv:2212.07904].

[162] P. H. Baillon *et al.*, Nuovo Cim. **A50**, 393 (1967).

[163] D. L. Scharre *et al.*, Phys. Lett. **97B**, 329 (1980).

[164] C. Edwards *et al.*, Phys. Rev. Lett. **49**, 259 (1982), [Erratum: Phys. Rev. Lett.50,219(1983)].

[165] J. E. Augustin *et al.* (DM2), Phys. Rev. **D42**, 10 (1990).

[166] J. Z. Bai *et al.* (BES), Phys. Lett. **B594**, 47 (2004), [hep-ex/0403008].

[167] C. Amsler [arXiv:2503.14689].

[168] A. Masoni, C. Cicalo and G. L. Usai, J. Phys. **G32**, R293 (2006).

[169] L. Faddeev, A. J. Niemi and U. Wiedner, Phys. Rev. **D70**, 114033 (2004), [hep-ph/0308240].

[170] H.-Y. Cheng, H.-n. Li and K.-F. Liu, Phys. Rev. **D79**, 014024 (2009), [arXiv:0811.2577].

[171] G. Li, Q. Zhao and C.-H. Chang, J. Phys. **G35**, 055002 (2008), [hep-ph/0701020].

[172] T. Gutsche, V. E. Lyubovitskij and M. C. Tichy, Phys. Rev. **D80**, 014014 (2009), [arXiv:0904.3414].

[173] B. A. Li, Phys. Rev. **D81**, 114002 (2010), [arXiv:0912.2323].

[174] M. Ablikim *et al.* (BES Collaboration), Phys. Rev. D **73**, 112007 (2006), [hep-ex/0604045].

[175] P. R. Page and X.-Q. Li, Eur. Phys. J. C **1**, 579 (1998), [hep-ph/9610250].

[176] M. Ablikim *et al.* (BESIII), Phys. Rev. Lett. **132**, 18, 181901 (2024), [arXiv:2312.05324].

[177] L.-C. Gui *et al.*, Phys. Rev. D **100**, 5, 054511 (2019), [arXiv:1906.03666].

[178] J. Pisut and M. Roos, Nucl. Phys. **B6**, 325 (1968).

[179] G. D. Lafferty, Z. Phys. **C60**, 659 (1993).

[180] A. Abele *et al.* (Crystal Barrel), Phys. Lett. **B402**, 195 (1997).

[181] M. Benayoun *et al.*, Eur. Phys. J. **C31**, 525 (2003), [arXiv:nucl-th/0306078].

[182] R. Barate *et al.* (ALEPH), Z. Phys. **C76**, 15 (1997).

[183] L. M. Barkov *et al.*, Nucl. Phys. **B256**, 365 (1985).

[184] S. Anderson *et al.* (CLEO), Phys. Rev. **D61**, 112002 (2000), [hep-ex/9910046].

[185] M. Fujikawa *et al.* (Belle), Phys. Rev. **D78**, 072006 (2008), [arXiv:0805.3773].

[186] K. Ackerstaff *et al.* (OPAL), Eur. Phys. J. **C7**, 571 (1999), [hep-ex/9808019].

[187] M. Davier and C.-Z. Yuan, Nucl. Phys. B - Proc. Suppl. **123**, 47 (2003), [hep-ex/0211057].

[188] S. Schael *et al.* (ALEPH), Phys. Rept. **421**, 191 (2005), [hep-ex/0506072].

[189] R. R. Akhmetshin *et al.* (CMD-2), Phys. Lett. **B527**, 161 (2002), [hep-ex/0112031].

[190] R. R. Akhmetshin *et al.* (CMD-2), Phys. Lett. **B578**, 285 (2004), [hep-ex/0308008].

[191] M. Davier *et al.*, Eur. Phys. J. **C27**, 497 (2003), [hep-ph/0208177].

[192] M. Davier *et al.*, Eur. Phys. J. **C31**, 503 (2003), [hep-ph/0308213].

[193] A. Aloisio *et al.* (KLOE), Phys. Lett. **B606**, 12 (2005), [hep-ex/0407048].

[194] F. Ambrosino *et al.* (KLOE), Phys. Lett. **B670**, 285 (2009), [arXiv:0809.3950].

[195] F. Ambrosino *et al.* (KLOE), Phys. Lett. **B700**, 102 (2011), [arXiv:1006.5313].

[196] D. Babusci *et al.* (KLOE), Phys. Lett. B **720**, 336 (2013), [arXiv:1212.4524].

[197] M. N. Achasov *et al.*, J. Exp. Theor. Phys. **101**, 1053 (2005), [hep-ex/0506076].

[198] M. N. Achasov *et al.*, J. Exp. Theor. Phys. **103**, 380 (2006), [hep-ex/0605013].

[199] B. Aubert *et al.* (BaBar), Phys. Rev. Lett. **103**, 231801 (2009), [arXiv:0908.3589].

[200] M. Ablikim *et al.* (BESIII), Phys. Lett. B **753**, 629 (2016), [Erratum: Phys.Lett.B 812, 135982 (2021)], [arXiv:1507.08188].

[201] R. Alemany, M. Davier and A. Hocker, Eur. Phys. J. **C2**, 123 (1998), [hep-ph/9703220].

[202] H. Czyz and J. H. Kuhn, Eur. Phys. J. **C18**, 497 (2001), [hep-ph/0008262].

Int. J. Mod. Phys. A 2026.41. Downloaded from www.worldscientific.com
by UNIVERSITY OF CALIFORNIA @ BERKELEY on 09/16/26. Re-use and distribution is strictly not permitted, except for Open Access articles.

[203] V. Cirigliano, G. Ecker and H. Neufeld, Phys. Lett. **B513**, 361 (2001), [hep-ph/0104267].

[204] V. Cirigliano *et al.*, Eur. Phys. J. **C23**, 121 (2002), [hep-ph/0110153].

[205] K. Maltman and C. E. Wolfe, Phys. Rev. **D73**, 013004 (2006), [hep-ph/0509224].

[206] C. E. Wolfe and K. Maltman, Phys. Rev. **D80**, 114024 (2009), [arXiv:0908.2391].

[207] M. N. Achasov *et al.*, Journal of High Energy Physics **2021**, 113 (2021), [arXiv:2004.00263].

[208] F. V. Ignatov *et al.* (CMD-3) (2023), [arXiv:2302.08834].

[209] F. V. Ignatov *et al.* (CMD-3) (2023), [arXiv:2309.12910].

[210] F. Jegerlehner and R. Szafron, Eur. Phys. J. **C71**, 1632 (2011), [arXiv:1101.2872].

[211] M. Benayoun *et al.*, Eur. Phys. J. **C72**, 1848 (2012), [arXiv:1106.1315].

[212] M. Benayoun *et al.*, Eur. Phys. J. C **73**, 2453 (2013), [arXiv:1210.7184].

[213] M. Davier *et al.*, Eur. Phys. J. C **77**, 827 (2017), [arXiv:1706.09436].

[214] C. Erkal and M. G. Olsson, Z. Phys. **C31**, 615 (1986).

[215] A. Donnachie and H. Mirzaie, Z. Phys. **C33**, 407 (1987).

[216] A. Donnachie and A. B. Clegg, Z. Phys. **C34**, 257 (1987).

[217] A. Donnachie and A. B. Clegg, Z. Phys. **C51**, 689 (1991).

[218] A. B. Clegg and A. Donnachie, Z. Phys. **C40**, 313 (1988).

[219] A. B. Clegg and A. Donnachie, Z. Phys. **C62**, 455 (1994).

[220] T. J. Killian *et al.*, Phys. Rev. **D21**, 3005 (1980).

[221] S. Fukui *et al.*, Phys. Lett. **B202**, 441 (1988).

[222] D. Bisello *et al.* (DM2), Phys. Lett. **B220**, 321 (1989).

[223] A. Antonelli *et al.* (DM2), Phys. Lett. **B212**, 133 (1988).

[224] R. Aaij *et al.*, Journal of High Energy Physics **2023**, 6, 44 (2023), [arXiv:2208.03300].

[225] A. Abele *et al.* (Crystal Barrel), Phys. Lett. **B391**, 191 (1997).

[226] A. Bertin *et al.* (OBELIX), Phys. Lett. **B434**, 180 (1998).

[227] A. Abele *et al.* (Crystal Barrel), Phys. Lett. **B468**, 178 (1999).

[228] W.-F. Wang, Phys. Rev. D **103**, 056021 (2021), [arXiv:2012.15039].

[229] K. W. Edwards *et al.* (CLEO), Phys. Rev. **D61**, 072003 (2000), [hep-ex/9908024].

[230] J. P. Lees *et al.* (BaBar), Phys. Rev. **D86**, 032013 (2012), [arXiv:1205.2228].

[231] K. Kittimanapun *et al.*, Phys. Rev. C **79**, 025201 (2009), [arXiv:0803.2028].

[232] F. E. Close and P. R. Page, Phys. Rev. **D56**, 1584 (1997), [hep-ph/9701425].

[233] A. Donnachie and Yu. S. Kalashnikova, Phys. Rev. **D60**, 114011 (1999), [hep-ph/9901334].

[234] R. R. Akhmetshin *et al.* (CMD-2), Phys. Lett. **B466**, 392 (1999), [hep-ex/9904024].

[235] J. P. Alexander *et al.* (CLEO), Phys. Rev. **D64**, 092001 (2001), [hep-ex/0103021].

[236] D. Matvienko *et al.* (Belle), Phys. Rev. **D92**, 012013 (2015), [arXiv:1505.03362].

[237] M. N. Achasov *et al.* (SND), Phys. Rev. D **108**, 9, 092012 (2023), [arXiv:2309.00280].

[238] R. R. Akhmetshin *et al.* (CMD-2), Phys. Lett. **B562**, 173 (2003), [hep-ex/0304009].

[239] M. N. Achasov *et al.*, Phys. Rev. D **94**, 112001 (2016), [arXiv:1610.00235].

[240] A. Abele *et al.* (CRYSTAL BARREL), Eur. Phys. J. **C21**, 261 (2001).

[241] M. Bargiotti *et al.* (Obelix), Phys. Lett. **B561**, 233 (2003).

[242] S. I. Bityukov *et al.*, Phys. Lett. **B188**, 383 (1987).

[243] M. N. Achasov *et al.*, Eur. Phys. J. C **80**, 1139 (2020), [arXiv:2007.04527].

[244] B. Aubert *et al.* (BaBar), Phys. Rev. **D77**, 092002 (2008), [arXiv:0710.4451].

[245] A. Abele *et al.* (Crystal Barrel), Phys. Lett. **B415**, 280 (1997).

[246] V. M. Aulchenko *et al.*, JETP Lett. **45**, 145 (1987), [Pisma Zh. Eksp. Teor. Fiz.45,118(1987)].

[247] D. Bisello *et al.*, Z. Phys. **C52**, 227 (1991).

[248] P. Frenkiel *et al.*, Nucl. Phys. **B47**, 61 (1972).

[249] G. Cosme *et al.*, Phys. Lett. **63B**, 352 (1976).

[250] D. P. Barber *et al.* (LAMP2 Group), Z. Phys. **C4**, 169 (1980).

[251] D. Aston *et al.*, Phys. Lett. **92B**, 211 (1980), [Erratum: Phys. Lett.95B,461(1980)].

[252] M. Atkinson *et al.* (Omega Photon), Nucl. Phys. **B243**, 1 (1984).

[253] J. E. Brau *et al.* (SLAC Hybrid Facility Photon), Phys. Rev. **D37**, 2379 (1988).

[254] C. Amsler *et al.* (Crystal Barrel), Phys. Lett. **B311**, 362 (1993).

[255] J. Layssac and F. M. Renard, Nuovo Cim. **A6**, 134 (1971).

[256] N. Hammoud *et al.*, Phys. Rev. D **102**, 054029 (2020), [arXiv:2009.06317].

[257] D. Aston *et al.*, Nucl. Phys. Proc. Suppl. **21**, 105 (1991).

[258] M. Ablikim *et al.* (BES), Phys. Rev. Lett. **97**, 142002 (2006), [hep-ex/0606047].

[259] G.-J. Ding and M.-L. Yan, Phys. Lett. **B643**, 33 (2006), [hep-ph/0607253].

[260] F.-K. Guo *et al.*, Nucl. Phys. **A773**, 78 (2006), [hep-ph/0509050].

[261] A. Zhang, T. Huang and T. G. Steele, Phys. Rev. **D76**, 036004 (2007), [hep-ph/0612146].

[262] B. A. Li, Phys. Rev. **D76**, 094016 (2007), [hep-ph/0701159].

[263] X. Liu *et al.*, Phys. Rev. **D75**, 074017 (2007), [hep-ph/0701022].

[264] J. P. Lees *et al.* (BaBar), Phys. Rev. D **88**, 032013 (2013), [arXiv:1306.3600].

[265] M. N. Achasov *et al.*, Phys. Rev. D **94**, 112006 (2016), [arXiv:1608.08757].

[266] M. Ablikim *et al.*, Journal of High Energy Physics **2022**, 45 (2022), and references therein, [arXiv:2202.06447].

[267] A. B. Clegg and A. Donnachie, Z. Phys. **C45**, 677 (1990).

[268] D. Bisello *et al.*, Phys. Lett. **107B**, 145 (1981).

[269] A. Castro *et al.*, LAL-88-58(1988), URL `https://doi.org/10.17182/hepdata.38181`.

[270] M. Atkinson *et al.* (Omega Photon), Z. Phys. **C29**, 333 (1985).

[271] B. Aubert *et al.* (BaBar), Phys. Rev. **D76**, 092005 (2007), [Erratum: Phys. Rev.D77,119902(2008)], [arXiv:0708.2461].

[272] J. P. Lees *et al.* (BABAR Collaboration), Phys. Rev. D **86**, 032013 (2012), [arXiv:1205.2228].

[273] M. Ablikim *et al.* (BESIII Collaboration), Phys. Rev. D **99**, 032001 (2019), [arXiv:1811.08742].

[274] J. P. Lees *et al.* (BaBar Collaboration), Phys. Rev. D **101**, 012011 (2020), [arXiv:1912.04512].

[275] P. L. Frabetti *et al.* (E687), Phys. Lett. **B514**, 240 (2001), [hep-ex/0106029].

[276] P. L. Frabetti *et al.*, Phys. Lett. **B578**, 290 (2004), [hep-ex/0310041].

[277] A. Antonelli *et al.* (FENICE), Phys. Lett. **B365**, 427 (1996).

Int. J. Mod. Phys. A 2026.41. Downloaded from www.worldscientific.com
UNIVERSITY OF CALIFORNIA @ BERKELEY on 09/16/26. Re-use and distribution is strictly not permitted, except for Open Access articles.

[278] B. Aubert *et al.* (BaBar), Phys. Rev. **D73**, 052003 (2006), [hep-ex/0602006].

[279] R. R. Akhmetshin *et al.* (CMD-3), Phys. Lett. **B723**, 82 (2013), [arXiv:1302.0053].

[280] R. R. Akhmetshin *et al.* (CMD-3), Phys. Lett. B **794**, 64 (2019), [arXiv:1808.00145].

[281] A. E. Obrazovsky and S. I. Serednyakov, JETP Lett. **99**, 315 (2014), [arXiv:1402.5225].

[282] J. Haidenbauer *et al.*, Phys. Rev. **D92**, 054032 (2015), [arXiv:1506.08120].

[283] A. I. Milstein and S. G. Salnikov, Nucl. Phys. A **977**, 60 (2018), [arXiv:1804.01283].

[284] M. Ablikim *et al.* (BESIII Collaboration), Phys. Rev. D **97**, 032013 (2018), [arXiv:1709.10236].

[285] M. Ablikim *et al.* (BESIII), Phys. Rev. D **107**, 072005 (2023), [arXiv:2303.07629].

[286] A. I. Milstein and S. G. Salnikov, JETP Lett. **117**, 905 (2023), [arXiv:2303.13551].

[287] H.-Y. Cheng, Phys. Lett. **B707**, 116 (2012), [arXiv:1110.2249].

[288] L. S. Geng *et al.*, Phys. Rev. D **75**, 014017 (2007), [hep-ph/0610217].

[289] S. U. Chung *et al.*, Phys. Rev. Lett. **55**, 779 (1985), [Erratum: Phys. Rev. Lett.55,2093(1985)].

[290] D. F. Reeves *et al.*, Phys. Rev. **D34**, 1960 (1986).

[291] A. Birman *et al.*, Phys. Rev. Lett. **61**, 1557 (1988), [Erratum: Phys. Rev. Lett.62,1577(1989)].

[292] C. Dionisi *et al.* (CERN-College de France-Madrid-Stockholm), Nucl. Phys. **B169**, 1 (1980).

[293] H. J. Behrend *et al.* (CELLO), Z. Phys. **C42**, 367 (1989).

[294] T. A. Armstrong *et al.* (WA76), Z. Phys. **C52**, 389 (1991).

[295] D. Aston *et al.*, Phys. Lett. **B201**, 573 (1988).

[296] F. Aceti, J.-J. Xie and E. Oset, Phys. Lett. **B750**, 609 (2015), [arXiv:1505.06134].

[297] R. Aaij *et al.* (LHCb), Phys. Rev. Lett. **112**, 091802 (2014), [arXiv:1310.2145].

[298] S. Acharya *et al.*, Physics Letters B **866**, 139562 (2025), [arXiv:2409.11936].

[299] G. Gidal *et al.*, Phys. Rev. Lett. **59**, 2012 (1987).

[300] C. Adolph *et al.* (COMPASS), Phys. Rev. Lett. **115**, 082001 (2015), [arXiv:1501.05732].

[301] M. Aghasyan *et al.* (COMPASS), Phys. Rev. **D98**, 092003 (2018), [arXiv:1802.05913].

[302] G. D. Alexeev *et al.*, Phys. Rev. Lett. **127**, 082501 (2021), [arXiv:2006.05342].

[303] V. R. Debastiani *et al.*, Phys. Rev. **D95**, 034015 (2017), [arXiv:1611.05383].

[304] J.-X. Lin *et al.*, The European Physical Journal C **84**, 1, 52 (2024), [arXiv:2310.19213].

[305] S. Ishida *et al.*, Prog. Theor. Phys. **82**, 119 (1989).

[306] R. S. Longacre, Phys. Rev. **D42**, 874 (1990).

[307] F. E. Close and A. Kirk, Z. Phys. **C76**, 469 (1997), [hep-ph/9706543].

[308] P. Gavillet *et al.*, Z. Phys. **C16**, 119 (1982).

[309] R. R. Akhmetshin *et al.*, Physics Letters B **836**, 137606 (2023), [arXiv:2207.04615].

[310] J. Z. Bai *et al.* (BES), Phys. Lett. **B446**, 356 (1999).

[311] M. Ablikim *et al.* (BESIII), Phys. Rev. Lett. **106**, 072002 (2011), [arXiv:1012.3510].

[312] P. F. Ermolov *et al.*, Sov. J. Nucl. Phys. **39**, 738 (1984), [Yad. Fiz.39,1170(1984)].

[313] E. King *et al.*, Nucl. Phys. Proc. Suppl. **21**, 11 (1991).

[314] D. Barberis *et al.* (WA102), Phys. Lett. **B413**, 225 (1997), [hep-ex/9707022].

[315] H. Aihara *et al.* (TPC/Two Gamma), Phys. Rev. **D38**, 1 (1988).

[316] D. A. Bauer *et al.* (TPC/Two Gamma), Phys. Rev. **D48**, 3976 (1993).

[317] R. Aaij *et al.* (LHCb Collaboration), Phys. Rev. D **111**, 092009 (2025), [arXiv:2501.06483].

[318] N. Isgur, R. Kokoski and J. Paton, Phys. Rev. Lett. **54**, 869 (1985).

[319] F. E. Close and P. R. Page, Nucl. Phys. **B443**, 233 (1995), [hep-ph/9411301].

[320] P. Lacock *et al.* (UKQCD), Phys. Lett. **B401**, 308 (1997), [hep-lat/9611011].

[321] C. W. Bernard *et al.* (MILC), Phys. Rev. **D56**, 7039 (1997), [hep-lat/9707008].

[322] P. R. Page, E. S. Swanson and A. P. Szczepaniak, Phys. Rev. **D59**, 034016 (1999), [hep-ph/9808346].

[323] J. J. Dudek *et al.*, Phys. Rev. **D83**, 111502 (2011), [arXiv:1102.4299].

[324] J. J. Dudek *et al.*, Phys. Rev. **D88**, 094505 (2013), [arXiv:1309.2608].

[325] A. J. Woss *et al.*, Phys. Rev. D **103**, 054502 (2021), [arXiv:2009.10034].

[326] C. A. Meyer and Y. Van Haarlem, Phys. Rev. C **82**, 025208 (2010), [arXiv:1004.5516].

[327] D. R. Thompson *et al.* (E852), Phys. Rev. Lett. **79**, 1630 (1997), [hep-ex/9705011].

[328] S. U. Chung *et al.* (E852), Phys. Rev. **D60**, 092001 (1999), [hep-ex/9902003].

[329] G. S. Adams *et al.* (E862), Phys. Lett. **B657**, 27 (2007), [hep-ex/0612062].

[330] D. Alde *et al.*, Phys. Lett. **B205**, 397 (1988).

[331] Yu. D. Prokoshkin and S. A. Sadovsky, Phys. Atom. Nucl. **58**, 606 (1995), [Yad. Fiz.58N4,662(1995)].

[332] Yu. D. Prokoshkin and S. A. Sadovsky, Phys. Atom. Nucl. **58**, 853 (1995), [Yad. Fiz.58,921(1995)].

[333] A. Abele *et al.* (Crystal Barrel), Phys. Lett. **B423**, 175 (1998).

[334] A. Abele *et al.* (Crystal Barrel), Phys. Lett. **B446**, 349 (1999).

[335] A. Donnachie and P. R. Page, Phys. Rev. **D58**, 114012 (1998), [hep-ph/9808225].

[336] M. Aghasyan *et al.* (COMPASS), Phys. Rev. D **98**, 092003 (2018), [arXiv:1802.05913].

[337] G. D. Alexeev *et al.*, Phys. Rev. D **105**, 012005 (2022), [arXiv:arXiv:2108.01744].

[338] E. I. Ivanov *et al.* (E852), Phys. Rev. Lett. **86**, 3977 (2001), [hep-ex/0101058].

[339] J. Kuhn *et al.* (E852), Phys. Lett. **B595**, 109 (2004), [hep-ex/0401004].

[340] M. Lu *et al.* (E852), Phys. Rev. Lett. **94**, 032002 (2005), [hep-ex/0405044].

[341] Yu.P. Gouz *et al.*, Proc. XXVI Int. Conf. on HEP, Dallas (1992).

[342] G. M. Beladidze *et al.* (VES), Phys. Lett. **B313**, 276 (1993).

[343] C. Adolph *et al.* (COMPASS), Phys. Lett. B **740**, 303 (2015), [Erratum: Phys.Lett.B 811, 135913 (2020)], [arXiv:1408.4286].

[344] A. Rodas *et al.* (JPAC), Phys. Rev. Lett. **122**, 042002 (2019), [arXiv:1810.04171].

[345] B. Kopf *et al.*, Eur. Phys. J. C **81**, 12, 1056 (2021), [arXiv:2008.11566].

Int. J. Mod. Phys. A 2026.41. Downloaded from www.worldscientific.com
by UNIVERSITY OF CALIFORNIA @ BERKELEY on 09/16/26. Re-use and distribution is strictly not permitted, except for Open Access articles.

[346] M. Ablikim *et al.* (BESIII), Phys. Rev. Lett. **129**, 192002 (2022), [Erratum: Phys.Rev.Lett. 130, 159901 (2023)], [arXiv:2202.00621].

[347] M. Ablikim *et al.* (BESIII), Phys. Rev. D **106**, 072012 (2022), [Erratum: Phys.Rev.D 107, 079901 (2023)], [arXiv:2202.00623].

[348] V. Shastry, C. S. Fischer and F. Giacosa, Phys. Lett. B **834**, 137478 (2022), [arXiv:2203.04327].

[349] L. Qiu and Q. Zhao, Chin. Phys. C **46**, 5, 051001 (2022), [arXiv:2202.00904].

[350] E. S. Swanson, Phys. Rev. D **107**, 074028 (2023), [arXiv:2302.01372].

[351] X.-K. Dong, Y.-H. Lin and B.-S. Zou, Sci. ChinaPhys. Mech. Astron. **65**, 261011 (2022), [arXiv:2202.00863].

[352] M. Alekseev *et al.* (COMPASS), Phys. Rev. Lett. **104**, 241803 (2010), [arXiv:0910.5842].

[353] D. V. Amelin *et al.* (VES), Phys. Lett. **B356**, 595 (1995).

[354] J. Adomeit *et al.* (Crystal Barrel), Z. Phys. **C71**, 227 (1996).

[355] C. Farina and E. S. Swanson, Phys. Rev. D **109**, 094015 (2024), [arXiv:2312.05370].

[356] S. U. Chung, E. Klempt and J. G. Korner, Eur. Phys. J. **A15**, 539 (2002), [hep-ph/0211100].

[357] F. E. Close and H. J. Lipkin, Phys. Lett. **B196**, 245 (1987).

[358] F. Iddir and A. S. Safir, Phys. Lett. **B507**, 183 (2001), [hep-ph/0010121].

[359] G. C. Rossi and G. Veneziano, Nucl. Phys. **B123**, 507 (1977).

[360] J. L. Rosner, Phys. Rev. Lett. **21**, 950 (1968).

[361] R. L. Jaffe, Phys. Rev. **D15**, 281 (1977).

[362] M. G. Alford and R. L. Jaffe, Nucl. Phys. **B578**, 367 (2000), [hep-lat/0001023].

[363] G. 't Hooft *et al.*, Phys. Lett. **B662**, 424 (2008), [arXiv:0801.2288].

[364] S. Stone and L. Zhang, Phys. Rev. Lett. **111**, 062001 (2013), [arXiv:1305.6554].

[365] E. M. Aitala *et al.* (E791), Phys. Rev. Lett. **86**, 765 (2001), [hep-ex/0007027].

[366] H.-Y. Cheng, Phys. Rev. **D67**, 054021 (2003), [hep-ph/0212361].

[367] R. Fleischer, R. Knegjens and G. Ricciardi, Eur. Phys. J. **C71**, 1832 (2011), [arXiv:1109.1112].

[368] J. T. Daub, C. Hanhart and B. Kubis, JHEP **02**, 009 (2016), [arXiv:1508.06841].

[369] S. Acharya *et al.* (ALICE), Physics Letters B **833**, 137335 (2022), [arXiv:2111.06611].

[370] G. Janssen *et al.*, Phys. Rev. **D52**, 2690 (1995), [arXiv:nucl-th/9411021].

[371] M. P. Locher, V. E. Markushin and H. Q. Zheng, Eur. Phys. J. **C4**, 317 (1998), [hep-ph/9705230].

[372] J. A. Oller and E. Oset, AIP Conf. Proc. **432**, 413 (1998), [hep-ph/9710557].

[373] R. Delbourgo, D.-s. Liu and M. D. Scadron, Phys. Lett. **B446**, 332 (1999), [hep-ph/9811474].

[374] C. Hanhart *et al.*, Phys. Rev. **D75**, 074015 (2007), [hep-ph/0701214].

[375] Yu. S. Kalashnikova *et al.*, Eur. Phys. J. **A24**, 437 (2005), [hep-ph/0412340].

[376] F. E. Close, N. Isgur and S. Kumano, Nucl. Phys. **B389**, 513 (1993), [hep-ph/9301253].

[377] N. N. Achasov, V. V. Gubin and V. I. Shevchenko, Phys. Rev. **D56**, 203 (1997), [hep-ph/9605245].

[378] F. Ambrosino *et al.*, Physics Letters B **681**, 5 (2009), [arXiv:0904.2539].

[379] M. N. Achasov *et al.*, Phys. Lett. **B479**, 53 (2000), [hep-ex/0003031].

[380] F. Ambrosino *et al.*, Eur. Phys. J. C **49**, 473 (2007), [hep-ex/0609009].

[381] R. R. Akhmetshin *et al.* (CMD-2), Phys. Lett. **B462**, 371 (1999), [hep-ex/9907005].

[382] N. N. Achasov *et al.*, Phys. Rev. D **103**, 014010 (2021), [arXiv:2009.04191].

[383] M. Ablikim *et al.* (BESIII Collaboration), Phys. Rev. Lett. **121**, 022001 (2018), [arXiv:1802.00583].

[384] J. R. Pelaez, Phys. Rept. **658**, 1 (2016), [arXiv:1510.00653].

[385] H.-W. Ke and X.-Q. Li, Phys. Rev. D **99**, 036014 (2019), [arXiv:1810.07912].

[386] F.-X. Liu *et al.*, Phys. Rev. D **103**, 016016 (2021), [arXiv:2008.01372].

[387] S. S. Agaev, K. Azizi and H. Sundu, Phys. Rev. D **101**, 074012 (2020).

[388] O. D. Dalkarov, V. B. Mandelzweig and I. S. Shapiro, Nucl. Phys. B **21**, 88 (1970).

[389] G. Rossi and G. Veneziano, Physics Reports **63**, 153 (1980).

[390] C. Amsler, Adv. Nucl. Phys. **18**, 183 (1987).

[391] L. Montanet, Phys. Rept. **63**, 201 (1980).

[392] C. B. Dover and J. M. Richard, Annals of Phys. **121**, 70 (1979).

[393] W. W. Buck, C. B. Dover and J. M. Richard, Annals of Phys. **121**, 47 (1979).

[394] B. May *et al.* (ASTERIX), Z. Phys. **C46**, 203 (1990).

[395] A. Bertin *et al.* (OBELIX), Phys. Rev. **D57**, 55 (1998).

[396] K. Abe *et al.* (Belle), Phys. Rev. Lett. **88**, 181803 (2002), [hep-ex/0202017].

[397] M. Z. Wang *et al.* (Belle), Phys. Lett. **B617**, 141 (2005), [hep-ex/0503047].

[398] K. Abe *et al.* (Belle), Phys. Rev. Lett. **89**, 151802 (2002), [hep-ex/0205083].

[399] J. Z. Bai *et al.* (BES), Phys. Rev. Lett. **91**, 022001 (2003), [hep-ex/0303006].

[400] J. P. Alexander *et al.* (CLEO), Phys. Rev. **D82**, 092002 (2010), [arXiv:1007.2886].

[401] M. Ablikim *et al.* (BESIII), Phys. Rev. Lett. **108**, 112003 (2012), [arXiv:1112.0942].

[402] G.-J. Ding and M.-L. Yan, Phys. Rev. **C72**, 015208 (2005), [hep-ph/0502127].

[403] B. Loiseau and S. Wycech, Phys. Rev. **C72**, 011001 (2005), [hep-ph/0501112].

[404] A. Sibirtsev *et al.*, Phys. Rev. **D71**, 054010 (2005), [hep-ph/0411386].

[405] X.-W. Kang, J. Haidenbauer and U.-G. Meissner, JHEP **02**, 113 (2014), [arXiv:1311.1658].

[406] X.-W. Kang, J. Haidenbauer and U.-G. Meissner, Phys. Rev. **D91**, 074003 (2015), [arXiv:1502.00880].

[407] J. P. Lees *et al.* (BaBar), Phys. Rev. **D87**, 092005 (2013), [arXiv:1302.0055].

[408] E. P. Solodov *et al.*, EPJ Web Conf. **212**, 07002 (2019).

[409] G. Bardin *et al.*, Nucl. Phys. **B411**, 3 (1994).

[410] J. Haidenbauer, X. W. Kang and U. G. Meissner, Nucl. Phys. **A929**, 102 (2014), [arXiv:1405.1628].

64. Scalar Mesons below 1 GeV

Revised October 2025 by T. Gutsche (Tübingen U.), C. Hanhart (FZ Jülich), R.E. Mitchell (Indiana U.) and S. Spanier (Tennessee U.).

64.1 Introduction

Scalar resonances are difficult to resolve experimentally, as they either have large decay widths, which cause a strong overlap between neighboring resonances, or several decay channels open up within a short mass range (*e.g.* at the $K\bar{K}$ and $\eta\eta$ thresholds), producing cusps in the line shapes of the nearby resonances. Furthermore, one expects non-$q\bar{q}$ scalar objects, such as hadronic molecules and multiquark states, in the mass range of interest (for reviews see, *e.g.*, Refs. [1–6]).

Light scalars are produced, for example, in πN scattering on polarized/unpolarized targets, $p\bar{p}$ annihilation, central hadronic production, $J/\psi(1S)$, ψ, B-, D- and K-meson decays, $\gamma\gamma$ formation, and ϕ radiative decays. Especially for the lightest scalar mesons, simple parameterizations like Breit-Wigner functions and variants thereof fail — this is demonstrated explicitly on the example of the $f_0(500)$ or σ, e.g., in Ref. [7]. Accordingly, more advanced theory tools are necessary to extract the resonance parameters from data.

The mass and width of a resonance are determined by the position of the corresponding pole of the process amplitude (S- or T-matrix) in the complex energy plane, specifically from the pole closest to the physical axis on an unphysical Riemann sheet. The pole's real part indicates the resonance mass M, and its imaginary part corresponds to half the width Γ:

$$\sqrt{s_{\rm Pole}} = M - i\,\Gamma/2\ . \tag{64.1}$$

It is important to note that, in general, the pole of a Breit-Wigner parameterization does not agree with the T-matrix pole. For a detailed discussion of this issue, we refer to the review on *Resonances* in this Review of Particle Physics (RPP).

In the analyses available in the literature, fundamental properties of the amplitudes, such as unitarity, analyticity, Lorentz invariance, and chiral and flavor symmetry are implemented at different levels of rigor. Especially, chiral symmetry implies the appearance of zeros, the so-called Adler zeros, close to the threshold in elastic S-wave scattering amplitudes involving Goldstone bosons [8, 9], which may be shifted or removed in associated production processes [10]. Moreover, especially for the lightest non-strange and strange scalar resonance, accurate extractions of pole parameters become complicated by the presence of both left-hand cuts as well as circular cuts (for a recent review on the subject see Ref. [5]). The methods employed are the K-matrix formalism, the N/D-method, the Dalitz-Tuan ansatz, the inverse amplitude method, unitarized quark models with coupled channels, effective chiral field theories, and the linear sigma model, *etc.* Dynamics near the lowest two-body thresholds in some analyses are described by crossed channel (t, u) meson exchange or with an effective range parameterization instead of, or in addition to, resonant features in the s-channel. Dispersion theory is applied to pin down the location of resonance poles for the low mass states [11–16] unambiguously — in particular, the existence of a nonet of light scalar mesons is not questioned anymore.

In parallel to the developments sketched above, lattice QCD also entered the field of precision spectroscopy, since it was acknowledged that a study of resonances calls for a proper treatment of the scattering process employing e.g. the Lüscher method [17], later extended to coupled channels in Refs. [18–23]. This allowed for determinations of the poles of the $I = 1/2$ [24], the $I = 1$ [25] as well as the $I = 0$ [26, 27] light scalar mesons—those findings were later confirmed and refined by sophisticated dispersive analyses of lattice data for the $I = 0$ and $I = 1/2$ sectors in Refs. [28, 29] and Refs. [30, 31], respectively. Besides an additional firm confirmation of the existence of a nonet of light scalar mesons, via the quark mass dependence of the pole locations, these studies allow for an alternative look on their nature [32–34].

In this review, we present proposed values for the mass parameters of the scalar resonances below 1 GeV. Note that those are labeled as 'our estimate' — it is not an average over the quoted analyses, but is chosen to include the bulk of the analyses. An averaging procedure is not justified, since the analyses use overlapping or sometimes even identical data sets so that they are not statistically independent.

In this note, we discuss the light scalars below 1 GeV organized in the *Listings* under the entries $K_0^*(700)$ (or κ) with isospin $I = 1/2$, $a_0(980)$ with $I = 1$, as well as $f_0(500)$ (or σ) and $f_0(980)$ both with $I = 0$. The $I = 2$ $\pi\pi$ and $I = 3/2$ $K\pi$ partial waves do not exhibit resonant behavior.

64.2 The $K_0^*(700)$, also known as κ ($I = 1/2$)

The $K_0^*(700)$ corresponds to a pole in the low-energy πK scattering. Its properties are challenging to establish, since it appears to have a large width ($\Gamma \approx 500$ MeV) and resides close to the $K\pi$ threshold. The widely used LASS parameterization [35] models the $K\pi$ S-wave amplitude with a Breit-Wigner function representing $K^\star(1430)$ together with an effective range non-resonant component. Hadronic D- and B-meson decays provide additional data points in the vicinity of the $K\pi$ threshold and are discussed in detail in the *Review on Multibody Charm Analyses* in this RPP. With a few exceptions discussed there, the multi-hadron final states are usually treated in the approximation of non-interacting two-body systems. Precise information from semileptonic D decays, where the strongly interacting two-particle final states could be treated without approximation, is not available. BES II [36] (re-analyzed in [37]) finds a $K_0^*(700)$-like structure in $J/\psi(1S)$ decays to $\bar{K}^{*0}(892)K^+\pi^-$ where $K_0^*(700)$ recoils against the $K^*(892)$. The decay $\tau^- \to K_S^0\pi^-\nu_\tau$ can be considered clean with respect to final-state interactions and is studied by Belle [38], with $K_0^*(700)$ parameters fixed to those of Ref. [36]. Some

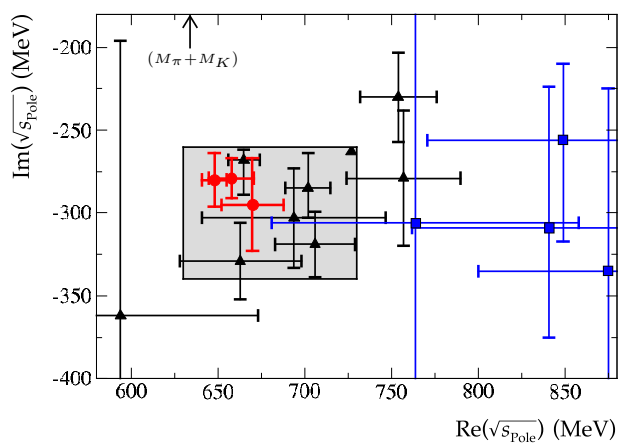

Figure 64.1: Location of the $K_0^*(700)$ (or κ) poles in the complex energy plane. Red circles denote the results of the analyses based on dispersion relations (see text for details), poles extracted from Breit-Wigner fits are shown as blue squares, while all other analyses quoted in the *Listings* are denoted by black triangles. The corresponding references are given in the listing. The arrow shows the location of the πK thresholds. The gray box indicates the range of pole locations classified as 'our estimate' .

authors find a $K_0^*(700)$ pole in their phenomenological analysis (see, *e.g.*, [39–48]), while others do not need to include it in their fits (see, *e.g.*, [49–52]; note that in Ref. [53] only a K_0^* meson above 825 MeV was discarded using scattering data fits and analyticity, which is not in conflict with the properties quoted below). All works including constraints from chiral symmetry at low energies naturally find a light $K_0^*(700)$ below 800 MeV, see, *e.g.*, [54–60]. The analyses of Ref. [15, 16] are based on the Roy-Steiner equations, which include analyticity and crossing symmetry constraints. Ref. [61] uses the Padé method to extract pole parameters after refitting scattering data constrained to satisfy forward dispersion relations. All three arrive at compatible pole positions for the $K_0^*(700)$ that are also consistent with the pole parameters deduced from other theoretical methods. Recently, the $K_0^*(700)$ was investigated using the femtoscopy technique at

Int. J. Mod. Phys. A 2026.41. Downloaded from www.worldscientific.com
UNIVERSITY OF CALIFORNIA @ BERKELEY on 09/16/26. Re-use and distribution is strictly not permitted, except for Open Access articles.

Int. J. Mod. Phys. A 2026.41. Downloaded from www.worldscientific.com
by UNIVERSITY OF CALIFORNIA @ BERKELEY on 09/16/26. Re-use and distribution is strictly not permitted, except for Open Access articles.

ALICE [62]. The data is shown to be consistent with the dispersive analyses quoted above and, in particular, with the established properties of the $K_0^*(700)$ in Ref. [63], albeit calling for unusual source parameters.

Due to their large uncertainties, the pole locations deduced from the Breit-Wigner fits agree with the other determinations' widths, but their masses are found to be systematically higher. Moreover, phase shifts extracted from the Breit-Wigner functions for the $K_0^*(700)$ are very different from the known scalar πK phase shifts. The various poles are shown in Fig. 64.1. The compilation in this figure motivates the pole parameters of the $K_0^*(700)$, which we quote as 'our estimate', namely,

$$\sqrt{s^{\kappa}_{\rm Pole}} = (630-730) - i(260-340)\ \text{MeV}\ . \qquad (64.2)$$

For an extensive discussion about the πK system in general and the κ meson in particular, see Ref. [64]. Applying the same strategy to only those pole locations determined with the sophisticated dispersive methods (solid red circles in the figure) the region narrows down to

$$\sqrt{s^{\kappa}_{\rm Pole}} = (640-680) - i(265-305)\ \text{MeV}\ . \qquad (64.3)$$

64.3 The $a_0(980)$ ($I=1$)

The $a_0(980)$ couples strongly to the channels $\pi\eta$ and $K\bar{K}$. The $K\bar{K}$ component must be large in the $a_0(980)$ wave function, since the mass of the $a_0(980)$ lies very close to the opening of the $K\bar{K}$ channel [65, 66]. This generates a pronounced cusp-like behavior in the resonant amplitude, and to reveal its properties, the presence of the $K\bar{K}$ channel cannot be ignored. All listed $a_0(980)$ measurements agree on a mass position value near 980 MeV, but the width deduced from the imaginary part of the pole location has values between 60 and 140 MeV. Note that the width of the $a_0(980)$ line shape is usually smaller than what is derived from the pole location because the aforementioned channel coupling heavily distorts the line shape. The relative coupling $K\bar{K}/\pi\eta$ is determined indirectly from $f_1(1285)$ [67–69] or $\eta(1410)$ decays [70–72], from the line shape observed in the $\pi\eta$ decay mode [73–76], or from the coupled-channel analysis of the $\pi\pi\eta$ and $K\bar{K}\pi$ final states of $p\bar{p}$ annihilation at rest [65]. The most recent data on the $a_0(980)$ come from measurements of different charge channels for $D \to a_0(980)\pi$ [77], from a measurement of $D^+ \to \pi^+\eta\eta$ [78], and from $\Lambda_c^+ \to \Lambda a_0^+(980)$ [79]. All three reactions are claimed to be driven by non-trivial production mechanisms [78, 80–82]. It remains to be checked if claims about the structure of the a_0 from, e.g., D-decay data [83] can be confirmed.

For the extraction of the $a_0(980)$ pole locations, Refs. [56, 57, 59, 84] use unitarized chiral perturbation theory. Ref. [85] uses a similar formalism, employing the amplitude fixed in Ref. [86]. A dispersion theoretical approach to the isovector scalar $\pi\eta - K\bar{K}$ system is presented in Ref. [87] that may be refined further from studies of heavy meson decays [88]. Those efforts lead to a rather precise determination of the $a_0(980)$ pole location [89]. A value consistent for the mass parameter, but with a larger width, is found in the analysis of $\bar{p}p$ annihilation in flight data employing a K-matrix [90]. The poles presented in Refs. [59, 65, 76, 89, 90] are shown in Fig. 64.2 together with the range of pole parameters estimated by us from this compilation, namely,

$$\sqrt{s^{a_0(980)}_{\rm Pole}} = (970-1020) - i(30-70)\ \text{MeV} \qquad (64.4)$$

indicated by the box. Two disclaimers are important here: First of all, both poles of $a_0(980)$ and of $f_0(980)$, to be discussed below, are located very close to the kaon thresholds, with the charged and neutral ones being only 8 MeV apart. To illustrate this point, the pertinent thresholds are shown explicitly in Figs. 64.2 and 64.4. Thus, pole extractions for the neutral $a_0(980)$ might be affected by the enhanced $a_0 - f_0$ mixing discussed in Refs. [91–94]. On the other hand, all analyses employed in the pole determinations quoted above are done assuming isospin symmetry. A second important remark is that the imaginary part of the pole location needs to be interpreted with care, in particular for those states that couple strongly to a near-by, yet closed threshold—for a detailed discussion see Refs. [95, 96] and the review "Resonances" in this *Review*.

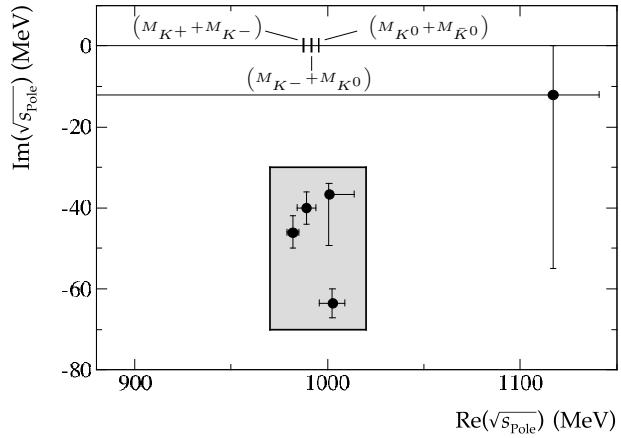

Figure 64.2: Location of the $a_0(980)$ poles from different extractions in the complex energy plane. The corresponding references are given in the *Listings*. Also shown are the thresholds for the K^+K^- and $K^0\bar{K}^0$ channels, relevant for $a_0(980)^0$, and for the K^-K^0 channel, relevant for the $a_0(980)^-$. The gray box indicates the range of pole locations classified as 'our estimate'. Note that by default, we take the pole located closest to the physical axis. Accordingly, not all poles shown are located on the same sheet. We refer to the original references for details.

64.4 The $f_0(500)$, also known as σ-meson ($I=0$)

For discussions of the $\pi\pi$ S-wave below the $K\bar{K}$ threshold and on the long history of the $f_0(500)$, which was suggested in studies of nuclear interactions almost 70 years ago, see the review [5]. Information on the $\pi\pi$ S-wave phase shift $\delta_J^I = \delta_0^0$ was already extracted many years ago from πN scattering [97–99], and near the $\pi\pi$ threshold from K_{e4} decays [100]. The kaon decays were later revisited, leading to consistent data with very much improved statistics [101, 102]. The reported $\pi\pi \to K\bar{K}$ cross sections [103–106] have large uncertainties. The πN datasets have been analyzed in combination with high-statistics data (see entries labeled as RVUE for re-analyses of the data). The $2\pi^0$ invariant mass spectra, extracted from $p\bar{p}$ annihilation at rest into $3\pi^0$ [107,108] and into $5\pi^0$ [109] and from central pp collision [109] do not show a distinct resonance structure below 900 MeV, but these data sets are consistently described with the standard solution for the $\pi\pi$ scalar isoscalar S-wave extracted from high energy $\pi N \to \pi\pi N$ data [98, 110], which allows for the broad $f_0(500)$, but also fits without it existing. An enhancement is observed in the $\pi^+\pi^-$ invariant mass near threshold in the decays $D^+ \to \pi^+\pi^-\pi^+$ [111–113] and $J/\psi(1S) \to \omega\pi^+\pi^-$ [114, 115], and in $\psi(2S) \to J/\psi(1S)\pi^+\pi^-$ with very limited phase space [116, 117].

To establish the pole location of the $f_0(500)$, sophisticated theoretical tools are necessary, mainly because of its large width. The $\pi\pi$ scattering amplitude shows an unusual energy dependence due to the presence of the Adler zero in the unphysical regime close to the threshold [8, 9], required by chiral symmetry. Most of the modern analyses listed under $f_0(500)$ agree on a pole position near $(500 - i\,250$ MeV). In particular, analyses of $\pi\pi$ data that include unitarity are consistent with the near threshold $\pi\pi$ data from K_{e4} decays, and the chiral symmetry constraints from Adler zeroes and/or scattering lengths find a light $f_0(500)$, see, *e.g.*, [118, 119]. Interestingly, the Roy-equation analysis of Ref. [28] also shows the reverse, namely all amplitudes that meet the acceptability criteria display an Adler zero below threshold. Analogously, an Adler zero appears automatically, when a parameterization of the spectral function for the $f_0(500)$ with proper pole location and residue is constructed [120].

Precise pole positions with an uncertainty of less than 20 MeV

Int. J. Mod. Phys. A 2026.41. Downloaded from www.worldscientific.com
UNIVERSITY OF CALIFORNIA @ BERKELEY on 09/16/26. Re-use and distribution is strictly not permitted, except for Open Access articles.

(see our table for the T-matrix pole in the *Listings*) are extracted using the Roy equations, which are twice-subtracted dispersion relations derived from crossing symmetry and analyticity. In Ref. [12], the subtraction constants are fixed to the S-wave scattering lengths a_0^0 and a_0^2 derived from matching the Roy equations and two-loop chiral perturbation theory [11]. The only additional relevant input to fix the $f_0(500)$ pole is the $\pi\pi$-wave phase shift at some higher energy point, chosen as 800 MeV. The analysis is improved further in Ref. [14]. Alternatively, in Ref. [13] Roy equations are used as constraints for a fit to data. In that reference, also once-subtracted Roy–like equations, called GKPY equations, are used, since the extrapolation into the complex plane based on the twice-subtracted equations leads to larger uncertainties, mainly due to the limited experimental information on the isospin-2 $\pi\pi$ scattering length. Ref. [121] uses Padé approximants for the analytic continuation. All these extractions find consistent results. Using only analyticity and unitarity to describe data from $K_{2\pi}$ and K_{e4} decays, Ref. [122] finds consistent values for the pole position and the scattering length a_0^0. The importance of the $\pi\pi$ scattering data for fixing the $f_0(500)$ pole is nicely illustrated by comparing analyses of $\bar{p}p \to 3\pi^0$ omitting [107, 123] or including [108, 124] information on $\pi\pi$ scattering: while the former analyses find an extremely broad structure above 1 GeV, the latter find $f_0(500)$ masses of the order of 400 MeV.

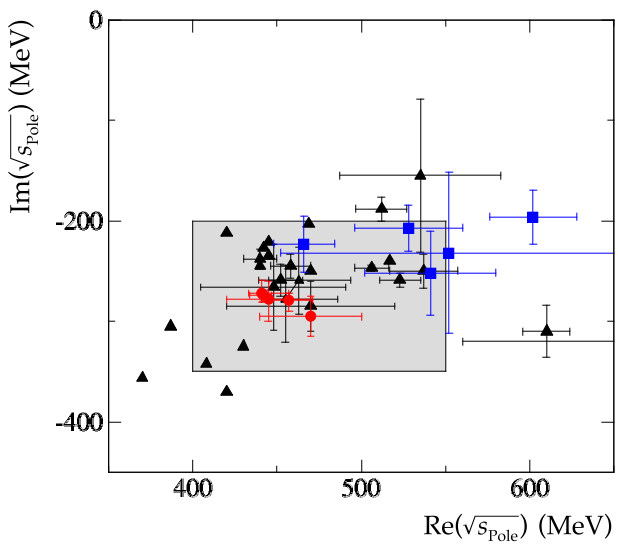

Figure 64.3: Location of the $f_0(500)$ (or σ) poles in the complex energy plane. Red circles denote the analyses based on Roy(-like) dispersion relations, poles extracted from Breit-Wigner fits are shown as blue squares, while all other analyses are denoted by triangles. The corresponding references are given in the *Listings*. The gray box indicates the range of pole locations classified as 'our estimate' .

From Fig. 64.3 we estimate the range of pole positions for the $f_0(500)$, namely,

$$\sqrt{s^{\sigma}_{\rm Pole}} = (400 - 550) - i(200 - 350)\ \text{MeV}\ . \qquad (64.5)$$

The plot contains the poles from Refs. [44, 55, 57, 59, 60, 75, 84, 97, 108, 113, 116–119, 122, 124–143] as well as the advanced dispersion analyses [11–14, 121]. The extracted $f_0(500)$ pole position is very sensitive to the high-accuracy low-energy $\pi\pi$ scattering data [101, 102]. In fact, all analyses consistent with this data find poles within the accepted range indicated in the figure. Similar to the case of the $K_0^*(700)$, we observe that poles identified through Breit-Wigner analyses usually appear at higher masses, although this effect is less noticeable here. One should not interpret this as justification for using Breit-Wigner functions in the case of the $f_0(500)$, since $\pi\pi$ phase shifts obtained from Breit-Wigners significantly differ from the measured scattering phase shifts.

If one uses just the most sophisticated dispersive analyses of Refs. [11–14], shown as red solid dots in Fig. 64.3 to determine the pole location of the $f_0(500)$, the range narrows down to

$$\sqrt{s^{\sigma}_{\rm Pole}} = (430 - 490) - i(260 - 310)\ \text{MeV}\ , \qquad (64.6)$$

which agrees in the central values to those provided in Ref. [5], however, with larger uncertainties.

Besides $\pi\pi$, the only other decay channel of the $f_0(500)$ is two photons. Due to the large width of $f_0(500)$ and the non-trivial phase motion connected to it, directly extracting its two-photon width from the data is not possible. Thus, the values for $\Gamma(\gamma\gamma)$ quoted in the literature as well as the in *Listings* are based on the expression in the narrow width approximation [144] $\Gamma(\gamma\gamma) \simeq \alpha^2|g_\gamma|^2/(4\mathrm{Re}(\sqrt{s^{\sigma}_{\rm Pole}}))$, where g_γ is derived from the residue at the $f_0(500)$ pole to two photons and α denotes the electromagnetic fine-structure constant (see also the review on *Resonances* in this issue of the RPP). The explicit form of the expression may vary between different authors due to different definitions of the coupling constant; however, the expression given for $\Gamma(\gamma\gamma)$ is free of ambiguities. This prescription leads to a two-photon branching ratio of 3×10^{-6}, which is about twice as large as the one derived from a formalism that accounts for the $f_0(500)$ line shape [120]. According to Refs. [145–148], $\pi\pi$ and $\gamma\gamma$ scattering data sets are consistently described including $f_0(500)$ via the two step process of $\gamma\gamma \to \pi^+\pi^-$ with pion exchange in the t- and u-channel, followed by a final-state interaction $\pi^+\pi^- \to \pi^0\pi^0$. The same conclusion is drawn in Ref. [149], where the $f_0(500) \to \gamma\gamma$ decay width is dominated by re-scattering. Therefore, it might be difficult to learn anything new about the nature of the $f_0(500)$ from its $\gamma\gamma$ coupling. For the recent work on $\gamma\gamma \to \pi\pi$, see Refs. [60, 84, 122–124, 131–144, 147–152]. There are strong indications (*e.g.*, [153–183]) that the $f_0(500)$ pole cannot be classified as a $q\bar{q}$ state.

64.5 The $f_0(980)$ $(I = 0)$

The $f_0(980)$ couples predominantly to the $\pi\pi$ and $K\bar{K}$ channels and its signal overlaps strongly with the background represented mainly by the $f_0(500)$ and the $f_0(1370)$. This can lead to a dip in the $\pi\pi$ spectrum at the $K\bar{K}$ threshold. It changes from a dip into a peak structure in the $\pi^0\pi^0$ invariant mass spectrum of the reaction $\pi^-p \to \pi^0\pi^0n$ [157], with increasing four momentum transfer to the $\pi^0\pi^0$ system, which means increasing the a_1 exchange contribution in the amplitude, while the π exchange decreases. Also, when a $(u\bar{u} + d\bar{d})$ source is switched to a $s\bar{s}$ source, as it appears when moving from $B_d \to J/\psi(1S)\pi\pi$ to $B_s \to J/\psi(1S)\pi\pi$, the f_0 signal switches from a dip to a peak [171] (similarly in D versus D_s meson decays; see, *e.g.,* Refs. [184, 185]). For a general discussion of the underlying mechanism of near-threshold dips vs. peaks, see Ref. [186]. The $f_0(500)$ and the $f_0(980)$ are also observed in the data for radiative ϕ decays ($\phi \to f_0\gamma$) from SND [158, 159], CMD2 [160], and KLOE [161, 162].

Unitarized chiral perturbation theory is employed to extract the pole of the $f_0(980)$ in Refs. [56, 57, 59, 84, 85]. Two different dispersive analyses are used in Ref. [13] to simultaneously pin down the pole parameters of both the $f_0(500)$ and the $f_0(980)$. The poles extracted in Refs. [13, 14, 59, 60, 90, 127, 187–189] are shown in Fig. 64.4, together with the range of pole parameters estimated by us from this compilation, namely,

$$\sqrt{s^{f_0(980)}_{\rm Pole}} = (980 - 1010) - i(20 - 35)\ \text{MeV} \qquad (64.7)$$

indicated by the box. A disclaimer is important here: Both the poles of $a_0(980)$ and of $f_0(980)$ are located very close to the kaon thresholds, with the charged and neutral thresholds being 8 MeV apart — to illustrate this point the pertinent thresholds are shown explicitly in Figs. 64.2 and 64.4. This observation leads to the prediction of an enhanced a_0–f_0 mixing [91–94]. On the other hand, all analyses employed in the pole determinations quoted above are done assuming isospin symmetry. Future studies need to show the impact of isospin violation on the extraction of the $a_0(980)/f_0(980)$ pole parameters.

It has also been recently shown [95, 96] that the proximity of the $f_0(980)$ pole to the $K\bar{K}$-threshold singularity does not always

Int. J. Mod. Phys. A 2026.41. Downloaded from www.worldscientific.com
by UNIVERSITY OF CALIFORNIA @ BERKELEY on 09/16/26. Re-use and distribution is strictly not permitted, except for Open Access articles.

allow for a direct identification of the total width with the imaginary part of the pole position as in Eq. (64.1). The correct relation is more subtle, when the pole lies in the unphysical sheet obtained from analytic continuation from below the $K\bar{K}$ threshold (second sheet) as it is the case of several poles in Fig. 64.4 [95]—see also the discussion in the section "Resonances" in this *Review*.

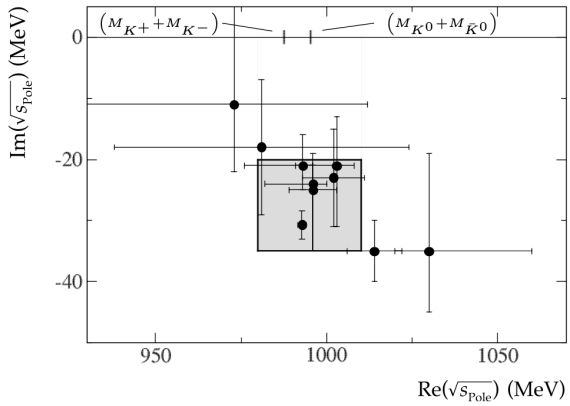

Figure 64.4: Location of the $f_0(980)$ poles from different extractions in the complex energy plane. The corresponding references are given in the *Listings*. Also shown are the thresholds for the K^+K^- and $K^0\bar{K}^0$ channels. The gray box indicates the range of pole locations classified as 'our estimate' .

Analyses of $\gamma\gamma \to \pi\pi$ data [163–165] underline the importance of the $K\bar{K}$ coupling of the $f_0(980)$, while the resulting two-photon width of the $f_0(980)$ cannot be determined precisely [166]. The prominent appearance of the $f_0(980)$ in the semileptonic D_s decays and decays of B and B_s mesons implies a dominant $(\bar{s}s)$ component: those decays occur via weak transitions that alternatively result in $\phi(1020)$ production. Ratios of decay rates of B and/or B_s mesons into $J/\psi(1S)$ plus $f_0(980)$ or $f_0(500)$ are proposed to extract the flavor mixing angle and to probe the tetraquark nature of those mesons within a certain model [167, 168]. The resulting phenomenological fits of the LHCb collaboration [169, 170] lead the authors to conclude that their data are incompatible with a model where $f_0(500)$ and $f_0(980)$ are formed from two quarks and two antiquarks (tetraquarks). However, a dispersive analysis of the same data that allows for a model-independent inclusion of the hadronic final-state interactions in Ref. [171] puts into question the conclusions of Ref. [169]. Moreover, the assumption underlying Ref. [169] that the production dynamics of $f_0(500)$ and $f_0(980)$ are equal such that they cancel in ratios appears not to be justified [5].

Ref. [190] investigates the p_T dependence of elliptic anisotropies for the production of $f_0(980)$ in proton-lead collisions. From the anticipated scaling of this observable with respect to the number of constitutents of the observed state, the authors conclude that the $f_0(980)$ is a $\bar{q}q$ state. However, this interpretation should also be re-examined critically, since the form factor $\langle\pi\pi|\bar{s}s|0\rangle$ probed here and discussed, e.g., in Ref. [171] is consistent also with other interpretations.

64.6 Interpretation of the scalars below 1 GeV

In the literature, various structures are discussed for light scalar mesons, such as conventional $q\bar{q}$ mesons, compact $(qq)(\bar{q}\bar{q})$ configurations (tetraquarks), or meson-meson bound states (hadronic molecules). In reality, these components can be superimposed, and identifying the dominant one is often model-dependent. Although progress has been made in recent years, this question remains unresolved. Here, we highlight some current conclusions.

The $f_0(980)$ and $a_0(980)$ are often interpreted as compact tetraquark states [180–183, 191] or $K\bar{K}$ bound states [192]. The insight into their internal structure using two-photon widths [159, 193–199] is not conclusive. The $f_0(980)$ appears as a peak structure in D_s decays without $f_0(500)$ background. Based on that observation, it is suggested that $f_0(980)$ has a large $s\bar{s}$ component, which according to Ref. [200] is surrounded by a virtual $K\bar{K}$ cloud (see also Ref. [201]). The relevance of a tetraquark flavor structure of the $a_0(980)$ in the decays $D \to a_0(980)P$ (P denotes a pseudoscalar meson) as opposed to a naive $q\bar{q}$ configuration is discussed in Ref. [83]. The inclusive production property of the $f_0(980)$ in Z^0 decays is consistent with mesons of other nonets [202]. However, as stated by the authors, the results should be taken as model-dependent measurements while presently no reliable predictions for production rates of non-$q\bar{q}$ states in Z^0 decay are available. Data sets on radiative decays ($\phi \to f_0\gamma$ and $\phi \to a_0\gamma$) from SND, CMD2, and KLOE (see above) are consistent with a prominent role of kaon loops. This observation is interpreted as evidence for a compact four-quark structure of the light scalars in Ref. [203], while it is claimed to point at a molecular nature in Ref. [204, 205]. Details of this controversy are given in the comments [206, 207]; see also Ref. [208]. There is now a rather broad consensus that the states $f_0(980)$ and $a_0(980)$, together with the $f_0(500)$ and the $K_0^*(700)$, form a nonet of predominantly four-quark states, where at larger distances the quarks recombine into a pair of pseudoscalar mesons creating a meson cloud (see, *e.g.,* Ref. [209]). Various QCD sum rule studies [210–215] do not agree on a tetraquark configuration for the same particle group.

Models that start directly from chiral Lagrangians, either in non-linear [56, 59, 118, 204] or in linear [216–222] realization, predict the existence of the $f_0(500)$ meson near 500 MeV. Here the $f_0(500)$, $a_0(980)$, $f_0(980)$, and $K_0^*(700)$ (in some models the $K_0^*(1430)$) would form a nonet (not necessarily $q\bar{q}$). In the linear sigma models, the lightest pseudoscalars appear as their chiral partners.

In the non-linear approaches of Refs. [56] and [118] the above resonances, together with the low mass vector states, are generated starting from chiral perturbation theory predictions near the first open channel, and then by shifting the states to the resonance locations, using unitarity and analyticity.

Ref. [216] uses a framework with explicit resonances that are unitarized and coupled to the light pseudoscalars in a chirally invariant way. Evidence for a dominant non-$\bar{q}q$ nature of the lightest scalar resonances is derived from their mixing scheme. In Ref. [217], the scheme is extended and applied to the decay $\eta' \to \eta\pi\pi$, which leads to the same conclusions. In Ref. [223], the large N_c behavior of the poles is studied to identify the nature of the resonances generated from scattering equations. This leads to the observation that, while the light vector states behave consistently with what is predicted for $\bar{q}q$ states, the light scalars behave very differently. This finding provides strong support for a dominant non-$\bar{q}q$ nature of the light scalar resonances. Note, the more refined study of Ref. [153] which finds, in the case of the $f_0(500)$, indications for a subdominant $\bar{q}q$ component located around 1 GeV in addition to a dominant non-$\bar{q}q$ nature. Additional support for the dominant non-$q\bar{q}$ nature of the $f_0(500)$ is given in Ref. [224], where the connection between the poles of resonances and their Regge trajectories is analyzed. All works including constraints from chiral symmetry at low energies naturally find a light $K_0^*(700)$ below 800 MeV and a $f_0(500)$ below 600 MeV, see, *e.g.*, [54–59]. In these works the $K_0^*(700)$, $f_0(500)$, $f_0(980)$, and $a_0(980)$ appear to form a nonet [55, 58]. Additional evidence for this assignment is presented in Ref. [14], where the couplings of the nine states to $\bar{q}q$ sources are compared. Similar conclusions are reached in Ref. [225] where in the analyzed data the $f_0(980)$ for example appears as a peak structure in $J/\psi(1S) \to \phi\pi^+\pi^-$ while in $J/\psi(1S) \to \omega\pi^+\pi^-$ the signal is suppressed. The same low mass scalar nonet is also found earlier in the unitarized quark model of Ref. [130]. A recent phenomenological study based on a $q\bar{q}$ flavor scheme for the light scalars concludes that their glueball content is ruled out because of low production rates in radiative $J/\psi(1S)$ decays [226]. This work was refined further in Ref. [188], where the $f_0(500)$ and the $f_0(980)$ are identified as mostly singlet and mostly octet, respectively.

There are, however, alternative interpretations of some of the light scalars. For example Ref. [227] (for a more recent, condensed discussion of the idea see Ref. [228]), also builds on chiral symmetry, but expands around an infrared fixed point such that the

Int. J. Mod. Phys. A 2026.41. Downloaded from www.worldscientific.com
UNIVERSITY OF CALIFORNIA @ BERKELEY on 09/16/26. Re-use and distribution is strictly not permitted, except for Open Access articles.

$f_0(500)$ appears as a QCD dilaton with a mass driven by the QCD scale anomaly. The phenomenology studied in that work appears consistent with this proposal. An updated discussion on the properties of the $f_0(500)$ as a QCD dilaton candidate and their relation to flavor singlet-octet mixing can be found in Ref. [229]. In Ref. [127, 149, 230, 231] data sets on $\pi\pi - \bar{K}K$ scattering, as well as $\gamma\gamma \to \pi\pi$, are analyzed and the authors conclude that especially the $f_0(500)$ should have a significant gluon content. An extensive analysis on mass, width, and decay couplings of the light scalars in a QCD spectral sum rule study [232] leads to ambiguous results for their internal structure. The $f_0(500)$ can equally well have tetraquark, molecular, or gluonic content, while the states $f_0(980)$ and $a_0(980)$ can be of molecular or tetraquark nature. A scenario where the $f_0(500)$ and $f_0(980)$ result from quarkonia-glueball mixing is also possible. Note, however, that the large similarities of the features of the κ and the σ meson put into question both a dilaton and a glueball contribution to the latter, since neither of them can be present in the former.

A model-independent method to identify hadronic molecules goes back to a proposal by Weinberg [233] (an extension of the formalism to virtual states is provided in Ref. [34]), which is shown to be equivalent to the pole counting arguments of [91–94, 234–239] in Ref. [237]. The formalism allows one to extract the amount of the molecular component in the wave function from the effective coupling constant of a physical state to a nearby continuum channel. It can be applied to near-threshold states only and provides strong evidence that the $f_0(980)$ is predominantly a $\bar{K}K$ molecule, while the situation turns out to be less clear for the $a_0(980)$ (see also Refs. [197,199]). This is in line with the findings of Ref. [85], which reports an important role of the $\pi\eta$ channel to the formation of the $a_0(980)$ in addition to the $\bar{K}K$ channel, while the $f_0(980)$ also in this work appears to be predominantly a $\bar{K}K$ molecule. The relevance of both the $\bar{K}K$ and the $\pi\eta$ channels in a dynamically generated $a_0(980)$ is also pointed out in the description of the $\chi_{c1} \to \eta\pi^+\pi^-$ and $D_s^+ \to \pi^+\pi^0\eta$ reactions [240, 241]. Dynamically generated $f_0(500)$, $f_0(980)$ and $K_0^*(700)$ resonances also give sizable contributions to the measured mass distributions in $D_s^+ \to K^+\pi^+\pi^-$ decay as pointed out in Ref. [242]. A recent analysis on the compositeness of the $\pi\pi - K\bar{K}$ and $\pi\eta - K\bar{K}$ channels for the $f_0(980)$ and $a_0(980)$ resonances based on pole values and decay branchings is performed in Ref. [95]. While the $K\bar{K}$ configuration dominates in the $f_0(980)$, the meson-meson components are subdominant in $a_0(980)$. Further insights into $a_0(980)$ and $f_0(980)$ are expected from their mixing [91–94]. A corresponding signal predicted in Refs. [92,93] is reported by BES III [243]. The importance of the molecular structure of $a_0(980)$, $f_0(980)$ and of their mixing in the reactions $\bar{B}_s^0 \to J/\psi(1S)\pi^+\pi^-$ and $\bar{B}_s^0 \to J/\psi(1S)\pi^0\eta$ is pointed out in Ref. [244].

In the unitarized quark model with coupled $q\bar{q}$ and meson-meson channels, the light scalars are interpreted as additional manifestations of bare $q\bar{q}$ confinement states, strongly mass shifted from the 1.3 - 1.5 GeV region and very distorted due to the strong $^3P_0$ coupling to S-wave two-meson decay channels [239, 245]. Thus, in these models, the light scalar nonet comprising the $f_0(500)$, $f_0(980)$, $K_0^*(700)$, and $a_0(980)$, as well as the nonet consisting of the $f_0(1370)$, $f_0(1500)$ (or $f_0(1710)$), $K_0^*(1430)$, and $a_0(1450)$, respectively, are seen as two manifestations of the same bare input states (see also Ref. [246]). It should not remain unmentioned, however, that the heavier nonet lies rather close to the input nonet, and that the light scalar one emerges only once the coupling to the two-meson channels is switched on, again highlighting that the meson-meson interaction is indispensable for the light scalars. A similar phenomenology emerges in a coupled two-quark four-quark treatment employing Dyson-Schwinger equations [247, 248]: Also here, the $f_0(500)$ is by far dominated by its two-pion component.

Acknowledgment

The authors would like to thank Eberhard Klempt, Mikhail Mikhasenko and José R. Peláez for helpful input and discussions in the preparation of the review.

References

[1] F. E. Close and N. A. Tornqvist, J. Phys. **G28**, R249 (2002), [hep-ph/0204205].

[2] C. Amsler and N. A. Tornqvist, Phys. Rept. **389**, 61 (2004).

[3] D. V. Bugg, Phys. Rept. **397**, 257 (2004), [hep-ex/0412045].

[4] E. Klempt and A. Zaitsev, Phys. Rept. **454**, 1 (2007), [arXiv:0708.4016].

[5] J. R. Pelaez, Phys. Rept. **658**, 1 (2016), [arXiv:1510.00653].

[6] J. R. Peláez, A. Rodas and J. R. de Elvira, Eur. Phys. J. ST **230**, 6, 1539 (2021), [arXiv:2101.06506].

[7] S. Gardner and U.-G. Meissner, Phys. Rev. D **65**, 094004 (2002), [hep-ph/0112281].

[8] S. L. Adler, Phys. Rev. **137**, B1022 (1965).

[9] S. L. Adler, Phys. Rev. **139**, B1638 (1965).

[10] J. A. Oller, Phys. Rev. **D71**, 054030 (2005), [hep-ph/0411105].

[11] G. Colangelo, J. Gasser and H. Leutwyler, Nucl. Phys. **B603**, 125 (2001), [hep-ph/0103088].

[12] I. Caprini, G. Colangelo and H. Leutwyler, Phys. Rev. Lett. **96**, 132001 (2006), [hep-ph/0512364].

[13] R. Garcia-Martin *et al.*, Phys. Rev. Lett. **107**, 072001 (2011), [arXiv:1107.1635].

[14] B. Moussallam, Eur. Phys. J. **C71**, 1814 (2011), [arXiv:1110.6074].

[15] S. Descotes-Genon and B. Moussallam, Eur. Phys. J. C **48**, 553 (2006), [hep-ph/0607133].

[16] J. R. Peláez and A. Rodas, Phys. Rev. Lett. **124**, 17, 172001 (2020), [arXiv:2001.08153].

[17] M. Luscher, Nucl. Phys. B **354**, 531 (1991).

[18] S. He, X. Feng and C. Liu, JHEP **07**, 011 (2005), [hep-lat/0504019].

[19] M. Doring *et al.*, Eur. Phys. J. A **47**, 139 (2011), [arXiv:1107.3988].

[20] M. Doring *et al.*, Eur. Phys. J. A **47**, 163 (2011), [arXiv:1108.0676].

[21] M. T. Hansen and S. R. Sharpe, Phys. Rev. D **86**, 016007 (2012), [arXiv:1204.0826].

[22] P. Guo *et al.*, Phys. Rev. D **88**, 1, 014501 (2013), [arXiv:1211.0929].

[23] R. A. Briceno and Z. Davoudi, Phys. Rev. D **88**, 9, 094507 (2013), [arXiv:1204.1110].

[24] J. J. Dudek *et al.* (Hadron Spectrum), Phys. Rev. Lett. **113**, 18, 182001 (2014), [arXiv:1406.4158].

[25] J. J. Dudek, R. G. Edwards and D. J. Wilson (Hadron Spectrum), Phys. Rev. D **93**, 9, 094506 (2016), [arXiv:1602.05122].

[26] R. A. Briceno *et al.*, Phys. Rev. Lett. **118**, 2, 022002 (2017), [arXiv:1607.05900].

[27] R. A. Briceno *et al.*, Phys. Rev. D **97**, 5, 054513 (2018), [arXiv:1708.06667].

[28] A. Rodas, J. J. Dudek and R. G. Edwards (Hadron Spectrum), Phys. Rev. D **109**, 3, 034513 (2024), [arXiv:2304.03762].

[29] X.-H. Cao *et al.*, Phys. Rev. D **108**, 3, 034009 (2023), [arXiv:2303.02596].

[30] X.-H. Cao *et al.*, Phys. Rev. D **112**, 3, L031503 (2025), [arXiv:2412.03374].

[31] X.-H. Cao *et al.*, Phys. Rev. D **112**, 3, 034042 (2025), [arXiv:2506.10619].

[32] C. Hanhart, J. R. Pelaez and G. Rios, Phys. Rev. Lett. **100**, 152001 (2008), [arXiv:0801.2871].

[33] C. Hanhart, J. R. Pelaez and G. Rios, Phys. Lett. B **739**, 375 (2014), [arXiv:1407.7452].

[34] I. Matuschek *et al.*, Eur. Phys. J. A **57**, 3, 101 (2021), [arXiv:2007.05329].

[35] D. Aston *et al.*, Nucl. Phys. **B296**, 493 (1988).

Int. J. Mod. Phys. A 2026.41. Downloaded from www.worldscientific.com
by UNIVERSITY OF CALIFORNIA @ BERKELEY on 09/16/26. Re-use and distribution is strictly not permitted, except for Open Access articles.

[36] M. Ablikim *et al.* (BES), Phys. Lett. **B633**, 681 (2006), [hep-ex/0506055].

[37] F.-K. Guo *et al.*, Nucl. Phys. **A773**, 78 (2006), [hep-ph/0509050].

[38] D. Epifanov *et al.* (Belle), Phys. Lett. **B654**, 65 (2007), [arXiv:0706.2231].

[39] C. Cawlfield *et al.* (CLEO), Phys. Rev. **D74**, 031108 (2006), [hep-ex/0606045].

[40] A. V. Anisovich and A. V. Sarantsev, Phys. Lett. **B413**, 137 (1997), [hep-ph/9705401].

[41] R. Delbourgo and M. D. Scadron, Int. J. Mod. Phys. **A13**, 657 (1998), [hep-ph/9807504].

[42] C. M. Shakin and H. Wang, Phys. Rev. **D63**, 014019 (2001).

[43] M. D. Scadron *et al.*, Nucl. Phys. **A724**, 391 (2003), [hep-ph/0211275].

[44] D. V. Bugg, Phys. Lett. **B572**, 1 (2003), [Erratum: Phys. Lett.B595,556(2004)].

[45] M. Ishida, Prog. Theor. Phys. Suppl. **149**, 190 (2003), [hep-ph/0212383].

[46] H. Q. Zheng *et al.*, Nucl. Phys. **A733**, 235 (2004), [hep-ph/0310293].

[47] Z. Y. Zhou and H. Q. Zheng, Nucl. Phys. **A775**, 212 (2006), [hep-ph/0603062].

[48] J. M. Link *et al.* (FOCUS), Phys. Lett. **B653**, 1 (2007), [arXiv:0705.2248].

[49] B. Aubert *et al.* (BaBar), Phys. Rev. **D76**, 011102 (2007), [arXiv:0704.3593].

[50] S. Kopp *et al.* (CLEO), Phys. Rev. **D63**, 092001 (2001), [hep-ex/0011065].

[51] J. M. Link *et al.* (FOCUS), Phys. Lett. **B535**, 43 (2002), [hep-ex/0203031].

[52] J. M. Link *et al.* (FOCUS), Phys. Lett. **B621**, 72 (2005), [hep-ex/0503043].

[53] S. N. Cherry and M. R. Pennington, Nucl. Phys. **A688**, 823 (2001), [hep-ph/0005208].

[54] M. Jamin, J. A. Oller and A. Pich, Nucl. Phys. **B587**, 331 (2000), [hep-ph/0006045].

[55] D. Black *et al.*, Phys. Rev. **D64**, 014031 (2001), [hep-ph/0012278].

[56] J. A. Oller, E. Oset and J. R. Pelaez, Phys. Rev. **D59**, 074001 (1999), [Erratum: Phys. Rev.D75,099903(2007)], [hep-ph/9804209].

[57] J. A. Oller and E. Oset, Phys. Rev. **D60**, 074023 (1999), [hep-ph/9809337].

[58] J. A. Oller, Nucl. Phys. **A727**, 353 (2003), [hep-ph/0306031].

[59] J. R. Pelaez, Mod. Phys. Lett. **A19**, 2879 (2004), [hep-ph/0411107].

[60] I. Danilkin, O. Deineka and M. Vanderhaeghen, Phys. Rev. D **103**, 11, 114023 (2021), [arXiv:2012.11636].

[61] J. R. Peláez, A. Rodas and J. Ruiz de Elvira, Eur. Phys. J. **C77**, 2, 91 (2017), [arXiv:1612.07966].

[62] S. Acharya *et al.* (ALICE), Phys. Lett. B **856**, 138915 (2024), [arXiv:2312.12830].

[63] M. Albaladejo *et al.*, Phys. Lett. B **866**, 139552 (2025), [arXiv:2503.19746].

[64] J. R. Peláez and A. Rodas, Phys. Rept. **969**, 1 (2022), [arXiv:2010.11222].

[65] A. Abele *et al.*, Phys. Rev. **D57**, 3860 (1998).

[66] M. Bargiotti *et al.* (OBELIX), Eur. Phys. J. **C26**, 371 (2003).

[67] D. Barberis *et al.* (WA102), Phys. Lett. **B440**, 225 (1998), [hep-ex/9810003].

[68] M. J. Corden *et al.*, Nucl. Phys. **B144**, 253 (1978).

[69] C. Defoix *et al.*, Nucl. Phys. **B44**, 125 (1972).

[70] Z. Bai *et al.* (MARK-III), Phys. Rev. Lett. **65**, 2507 (1990).

[71] T. Bolton *et al.*, Phys. Rev. Lett. **69**, 1328 (1992).

[72] C. Amsler *et al.* (Crystal Barrel), Phys. Lett. **B353**, 571 (1995).

[73] S. M. Flatte, Phys. Lett. **63B**, 224 (1976).

[74] C. Amsler *et al.* (Crystal Barrel), Phys. Lett. **B333**, 277 (1994).

[75] G. Janssen *et al.*, Phys. Rev. **D52**, 2690 (1995), [arXiv:nucl-th/9411021].

[76] D. V. Bugg, Phys. Rev. **D78**, 074023 (2008), [arXiv:0808.2706].

[77] M. Ablikim *et al.* (BESIII), Phys. Rev. D **110**, 11, L111102 (2024), [arXiv:2404.09219].

[78] J. Wu *et al.* (BESIII) (2025), [arXiv:2505.12086].

[79] M. Ablikim *et al.* (BESIII), Phys. Rev. Lett. **134**, 2, 021901 (2025), [arXiv:2407.12270].

[80] M. Bayar *et al.*, Phys. Rev. D **109**, 7, 076027 (2024), [arXiv:2312.12004].

[81] S. Rahmani *et al.*, Phys. Rev. D **112**, 3, 036001 (2025).

[82] M.-Y. Duan *et al.*, Phys. Rev. D **111**, 1, 016004 (2025), [arXiv:2410.16078].

[83] H.-Y. Cheng, C.-W. Chiang and F. Xu, Phys. Rev. D **110**, 9, 094052 (2024), [arXiv:2408.13942].

[84] J. A. Oller and E. Oset, Nucl. Phys. **A620**, 438 (1997), [Erratum: Nucl. Phys.A652,407(1999)], [hep-ph/9702314].

[85] H. A. Ahmed and C. W. Xiao, Phys. Rev. D **101**, 9, 094034 (2020), [arXiv:2001.08141].

[86] C. W. Xiao, U. G. Meißner and J. A. Oller, Eur. Phys. J. A **56**, 1, 23 (2020), [arXiv:1907.09072].

[87] M. Albaladejo and B. Moussallam, Eur. Phys. J. C **75**, 10, 488 (2015), [arXiv:1507.04526].

[88] M. Albaladejo *et al.*, JHEP **04**, 010 (2017), [arXiv:1611.03502].

[89] J. Lu and B. Moussallam, Eur. Phys. J. C **80**, 5, 436 (2020), [arXiv:2002.04441].

[90] M. Albrecht *et al.* (Crystal Barrel), Eur. Phys. J. C **80**, 5, 453 (2020), [arXiv:1909.07091].

[91] N. N. Achasov, S. A. Devyanin and G. N. Shestakov, Phys. Lett. **88B**, 367 (1979).

[92] J.-J. Wu, Q. Zhao and B. S. Zou, Phys. Rev. **D75**, 114012 (2007), [arXiv:0704.3652].

[93] C. Hanhart, B. Kubis and J. R. Pelaez, Phys. Rev. **D76**, 074028 (2007), [arXiv:0707.0262].

[94] L. Roca, Phys. Rev. **D88**, 014045 (2013), [arXiv:1210.4742].

[95] Z.-Q. Wang *et al.*, Phys. Rev. D **105**, 7, 074016 (2022), [arXiv:2201.00492].

[96] V. Burkert *et al.*, Phys. Lett. B **844**, 138070 (2023), [arXiv:2207.08472].

[97] S. D. Protopopescu *et al.*, Phys. Rev. **D7**, 1279 (1973).

[98] G. Grayer *et al.*, Nucl. Phys. **B75**, 189 (1974).

[99] H. Becker *et al.* (CERN-Cracow-Munich), Nucl. Phys. **B151**, 46 (1979).

[100] L. Rosselet *et al.*, Phys. Rev. **D15**, 574 (1977).

[101] S. Pislak *et al.* (BNL-E865), Phys. Rev. Lett. **87**, 221801 (2001), [Erratum: Phys. Rev. Lett.105,019901(2010)], [hep-ex/0106071].

[102] J. R. Batley *et al.* (NA48-2), Eur. Phys. J. **C70**, 635 (2010).

[103] W. Wetzel *et al.*, Nucl. Phys. **B115**, 208 (1976).

[104] V. A. Polychronakos *et al.*, Phys. Rev. **D19**, 1317 (1979).

[105] D. H. Cohen *et al.*, Phys. Rev. **D22**, 2595 (1980).

[106] A. Etkin *et al.*, Phys. Rev. **D25**, 1786 (1982).

Int. J. Mod. Phys. A 2026.41. Downloaded from www.worldscientific.com
UNIVERSITY OF CALIFORNIA @ BERKELEY on 09/16/26. Re-use and distribution is strictly not permitted, except for Open Access articles.

[107] C. Amsler *et al.*, Phys. Lett. **B342**, 433 (1995).

[108] C. Amsler *et al.* (Crystal Barrel), Phys. Lett. **B355**, 425 (1995).

[109] A. Abele *et al.* (Crystal Barrel), Phys. Lett. **B380**, 453 (1996).

[110] R. Kaminski, L. Lesniak and K. Rybicki, Z. Phys. **C74**, 79 (1997), [hep-ph/9606362].

[111] E. M. Aitala *et al.* (E791), Phys. Rev. Lett. **86**, 770 (2001), [hep-ex/0007028].

[112] J. M. Link *et al.* (FOCUS), Phys. Lett. **B585**, 200 (2004), [hep-ex/0312040].

[113] G. Bonvicini *et al.* (CLEO), Phys. Rev. **D76**, 012001 (2007), [arXiv:0704.3954].

[114] J. E. Augustin *et al.* (DM2), Nucl. Phys. **B320**, 1 (1989).

[115] M. Ablikim *et al.* (BES), Phys. Lett. **B598**, 149 (2004), [hep-ex/0406038].

[116] A. Gallegos, J. L. Lucio M. and J. Pestieau, Phys. Rev. **D69**, 074033 (2004), [hep-ph/0311133].

[117] M. Ablikim *et al.* (BES), Phys. Lett. **B645**, 19 (2007), [hep-ex/0610023].

[118] A. Dobado and J. R. Pelaez, Phys. Rev. **D56**, 3057 (1997), [hep-ph/9604416].

[119] I. Caprini, Phys. Rev. **D77**, 114019 (2008), [arXiv:0804.3504].

[120] L. A. Heuser *et al.*, Eur. Phys. J. C **84**, 6, 599 (2024), [arXiv:2403.15539].

[121] P. Masjuan, J. Ruiz de Elvira and J. J. Sanz-Cillero, Phys. Rev. D **90**, 9, 097901 (2014), [arXiv:1410.2397].

[122] R. Garcia-Martin, J. R. Pelaez and F. J. Yndurain, Phys. Rev. **D76**, 074034 (2007), [hep-ph/0701025].

[123] V. V. Anisovich, Phys. Usp. **41**, 419 (1998), [hep-ph/9712504].

[124] V. V. Anisovich, Int. J. Mod. Phys. **A21**, 3615 (2006), [hep-ph/0510409].

[125] M. Ablikim *et al.* (BESIII), Phys. Rev. Lett. **118**, 1, 012001 (2017), [arXiv:1606.03847].

[126] M. Albaladejo and J. A. Oller, Phys. Rev. D **86**, 034003 (2012), [arXiv:1205.6606].

[127] G. Mennessier, S. Narison and X. G. Wang, Phys. Lett. B **688**, 59 (2010), [arXiv:1002.1402].

[128] M. Ablikim *et al.* (BES), Phys. Lett. B **598**, 149 (2004), [hep-ex/0406038].

[129] P. Estabrooks, Phys. Rev. D **19**, 2678 (1979).

[130] E. van Beveren *et al.*, Z. Phys. **C30**, 615 (1986), [arXiv:0710.4067].

[131] B. S. Zou and D. V. Bugg, Phys. Rev. **D48**, R3948 (1993).

[132] N. A. Tornqvist and M. Roos, Phys. Rev. Lett. **76**, 1575 (1996), [hep-ph/9511210].

[133] R. Kaminski, L. Lesniak and J. P. Maillet, Phys. Rev. **D50**, 3145 (1994), [hep-ph/9403264].

[134] N. N. Achasov and G. N. Shestakov, Phys. Rev. **D49**, 5779 (1994).

[135] M. P. Locher, V. E. Markushin and H. Q. Zheng, Eur. Phys. J. **C4**, 317 (1998), [hep-ph/9705230].

[136] T. Hannah, Phys. Rev. **D60**, 017502 (1999), [hep-ph/9905236].

[137] R. Kaminski, L. Lesniak and B. Loiseau, Phys. Lett. **B413**, 130 (1997), [hep-ph/9707377].

[138] R. Kaminski, L. Lesniak and B. Loiseau, Eur. Phys. J. **C9**, 141 (1999), [hep-ph/9810386].

[139] M. Ishida *et al.*, Prog. Theor. Phys. **104**, 203 (2000), [hep-ph/0005251].

[140] Y. S. Surovtsev, D. Krupa and M. Nagy, Phys. Rev. D **63**, 054024 (2001), [hep-ph/0008317].

[141] M. Ishida *et al.*, Phys. Lett. **B518**, 47 (2001).

[142] Z. Y. Zhou *et al.*, JHEP **02**, 043 (2005), [hep-ph/0406271].

[143] D. V. Bugg, J. Phys. **G34**, 151 (2007), [hep-ph/0608081].

[144] D. Morgan and M. R. Pennington, Z. Phys. **C48**, 623 (1990).

[145] J. F. Donoghue, B. R. Holstein and Y. C. Lin, Phys. Rev. D **37**, 2423 (1988).

[146] A. Dobado and J. R. Pelaez, Z. Phys. C **57**, 501 (1993).

[147] M. R. Pennington, Phys. Rev. Lett. **97**, 011601 (2006).

[148] M. R. Pennington, Mod. Phys. Lett. **A22**, 1439 (2007), [arXiv:0705.3314].

[149] G. Mennessier, S. Narison and W. Ochs, Phys. Lett. **B665**, 205 (2008), [arXiv:0804.4452].

[150] R. Garcia-Martin and B. Moussallam, Eur. Phys. J. **C70**, 155 (2010), [arXiv:1006.5373].

[151] M. Hoferichter, D. R. Phillips and C. Schat, Eur. Phys. J. **C71**, 1743 (2011), [arXiv:1106.4147].

[152] L.-Y. Dai and M. R. Pennington, Phys. Rev. **D90**, 3, 036004 (2014), [arXiv:1404.7524].

[153] J. R. Pelaez and G. Rios, Phys. Rev. Lett. **97**, 242002 (2006), [hep-ph/0610397].

[154] H.-X. Chen, A. Hosaka and S.-L. Zhu, Phys. Lett. **B650**, 369 (2007), [hep-ph/0609163].

[155] F. Giacosa, Phys. Rev. **D75**, 054007 (2007), [hep-ph/0611388].

[156] L. Maiani *et al.*, Eur. Phys. J. **C50**, 609 (2007), [hep-ph/0604018].

[157] N. N. Achasov and G. N. Shestakov, Phys. Rev. **D58**, 054011 (1998), [hep-ph/9802286].

[158] M. N. Achasov *et al.*, Phys. Lett. **B479**, 53 (2000), [hep-ex/0003031].

[159] M. N. Achasov *et al.*, Phys. Lett. **B485**, 349 (2000), [hep-ex/0005017].

[160] R. R. Akhmetshin *et al.* (CMD-2), Phys. Lett. **B462**, 371 (1999), [hep-ex/9907005].

[161] A. Aloisio *et al.* (KLOE), Phys. Lett. **B536**, 209 (2002), [hep-ex/0204012].

[162] F. Ambrosino *et al.* (KLOE), Eur. Phys. J. **C49**, 473 (2007), [hep-ex/0609009].

[163] M. Boglione and M. R. Pennington, Eur. Phys. J. **C9**, 11 (1999), [hep-ph/9812258].

[164] T. Mori *et al.* (Belle), Phys. Rev. **D75**, 051101 (2007), [hep-ex/0610038].

[165] N. N. Achasov and G. N. Shestakov, Phys. Rev. **D77**, 074020 (2008), [arXiv:0712.0885].

[166] M. R. Pennington *et al.*, Eur. Phys. J. **C56**, 1 (2008), [arXiv:0803.3389].

[167] R. Fleischer, R. Knegjens and G. Ricciardi, Eur. Phys. J. **C71**, 1832 (2011), [arXiv:1109.1112].

[168] S. Stone and L. Zhang, Phys. Rev. Lett. **111**, 6, 062001 (2013), [arXiv:1305.6554].

[169] R. Aaij *et al.* (LHCb), Phys. Rev. **D90**, 1, 012003 (2014), [arXiv:1404.5673].

[170] R. Aaij *et al.* (LHCb), Phys. Rev. **D89**, 9, 092006 (2014), [arXiv:1402.6248].

[171] J. T. Daub, C. Hanhart and B. Kubis, JHEP **02**, 009 (2016), [arXiv:1508.06841].

[172] D. Barberis *et al.* (WA102), Phys. Lett. **B462**, 462 (1999), [hep-ex/9907055].

[173] D. Barberis *et al.* (WA102), Phys. Lett. **B479**, 59 (2000), [hep-ex/0003033].

[174] M. Gaspero, Nucl. Phys. **A562**, 407 (1993).

[175] A. Adamo *et al.*, Nucl. Phys. **A558**, 13C (1993).

Int. J. Mod. Phys. A 2026.41. Downloaded from www.worldscientific.com
by UNIVERSITY OF CALIFORNIA @ BERKELEY on 09/16/26. Re-use and distribution is strictly not permitted, except for Open Access articles.

[176] C. Amsler *et al.* (Crystal Barrel), Phys. Lett. **B322**, 431 (1994).

[177] A. Abele *et al.* (Crystal Barrel), Eur. Phys. J. **C19**, 667 (2001).

[178] A. Abele *et al.* (CRYSTAL BARREL), Eur. Phys. J. **C21**, 261 (2001).

[179] D. Barberis *et al.* (WA102), Phys. Lett. **B471**, 440 (2000), [hep-ex/9912005].

[180] R. L. Jaffe, Phys. Rev. **D15**, 267 (1977).

[181] M. G. Alford and R. L. Jaffe, Nucl. Phys. **B578**, 367 (2000), [hep-lat/0001023].

[182] L. Maiani *et al.*, Phys. Rev. Lett. **93**, 212002 (2004), [hep-ph/0407017].

[183] L. Maiani, A. D. Polosa and V. Riquer, Phys. Lett. **B651**, 129 (2007), [hep-ph/0703272].

[184] X.-H. Zhang *et al.*, Phys. Rev. D **110**, 114050 (2024).

[185] M. Ablikim *et al.* (BESIII), Phys. Rev. Lett. **132**, 14, 141901 (2024), [arXiv:2303.12927].

[186] X.-K. Dong, F.-K. Guo and B.-S. Zou, Phys. Rev. Lett. **126**, 15, 152001 (2021), [arXiv:2011.14517].

[187] V. V. Anisovich and A. V. Sarantsev, Int. J. Mod. Phys. A **24**, 2481 (2009).

[188] A. V. Sarantsev *et al.*, Phys. Lett. B **816**, 136227 (2021), [arXiv:2103.09680].

[189] M. Hoferichter *et al.*, Phys. Lett. B **853**, 138698 (2024), [arXiv:2312.15015].

[190] A. Hayrapetyan *et al.* (CMS), Nature Commun. **16**, 1, 7990 (2025), [arXiv:2312.17092].

[191] G. 't Hooft *et al.*, Phys. Lett. **B662**, 424 (2008), [arXiv:0801.2288].

[192] J. D. Weinstein and N. Isgur, Phys. Rev. **D41**, 2236 (1990).

[193] T. Barnes, Phys. Lett. **165B**, 434 (1985).

[194] Z. P. Li, F. E. Close and T. Barnes, Phys. Rev. **D43**, 2161 (1991).

[195] R. Delbourgo, D.-s. Liu and M. D. Scadron, Phys. Lett. **B446**, 332 (1999), [hep-ph/9811474].

[196] J. L. Lucio Martinez and M. Napsuciale, Phys. Lett. **B454**, 365 (1999), [hep-ph/9903234].

[197] C. Hanhart *et al.*, Phys. Rev. **D75**, 074015 (2007), [hep-ph/0701214].

[198] R. H. Lemmer, Phys. Lett. **B650**, 152 (2007), [hep-ph/0701027].

[199] T. Branz, T. Gutsche and V. E. Lyubovitskij, Eur. Phys. J. **A37**, 303 (2008), [arXiv:0712.0354].

[200] A. Deandrea *et al.*, Phys. Lett. **B502**, 79 (2001), [hep-ph/0012120].

[201] K. M. Ecklund *et al.* (CLEO), Phys. Rev. **D80**, 052009 (2009), [arXiv:0907.3201].

[202] K. Ackerstaff *et al.* (OPAL), Eur. Phys. J. C **4**, 19 (1998), [hep-ex/9802013].

[203] N. N. Achasov and V. N. Ivanchenko, Nucl. Phys. **B315**, 465 (1989).

[204] J. A. Oller, Nucl. Phys. **A714**, 161 (2003), [hep-ph/0205121].

[205] Yu. S. Kalashnikova *et al.*, Eur. Phys. J. **A24**, 437 (2005), [hep-ph/0412340].

[206] Yu. S. Kalashnikova *et al.*, Phys. Rev. **D78**, 058501 (2008), [arXiv:0711.2902].

[207] N. N. Achasov and A. V. Kiselev, Phys. Rev. **D78**, 058502 (2008), [arXiv:0806.2993].

[208] M. Boglione and M. R. Pennington, Eur. Phys. J. **C30**, 503 (2003), [hep-ph/0303200].

[209] F. Giacosa and G. Pagliara, Phys. Rev. **C76**, 065204 (2007), [arXiv:0707.3594].

[210] S. Narison, editor, *Quantum chromodynamics. Proceedings, 8th Conference, 5th Euroconference, QCD 2000, Montpellier, France, July 6-13, 2000* (2001).

[211] H.-J. Lee, Eur. Phys. J. **A30**, 423 (2006), [hep-ph/0512212].

[212] H.-X. Chen, A. Hosaka and S.-L. Zhu, Phys. Rev. **D76**, 094025 (2007), [arXiv:0707.4586].

[213] J. Sugiyama *et al.*, Phys. Rev. **D76**, 114010 (2007), [arXiv:0707.2533].

[214] T. Kojo and D. Jido, Phys. Rev. **D78**, 114005 (2008), [arXiv:0802.2372].

[215] H.-J. Lee, K. S. Kim and H. Kim, Phys. Rev. D **100**, 3, 034021 (2019), [arXiv:1904.12311].

[216] D. Black *et al.*, Phys. Rev. **D59**, 074026 (1999), [hep-ph/9808415].

[217] A. H. Fariborz *et al.*, Phys. Rev. **D90**, 3, 033009 (2014), [arXiv:1407.3870].

[218] M. D. Scadron, Eur. Phys. J. **C6**, 141 (1999), [hep-ph/9710317].

[219] M. Ishida, Prog. Theor. Phys. **101**, 661 (1999), [hep-ph/9902260].

[220] N. A. Tornqvist, Eur. Phys. J. **C11**, 359 (1999), [hep-ph/9905282].

[221] M. Napsuciale and S. Rodriguez, Phys. Lett. **B603**, 195 (2004), [hep-ph/0403072].

[222] M. Napsuciale and S. Rodriguez, Phys. Rev. **D70**, 094043 (2004), [hep-ph/0407037].

[223] J. R. Pelaez, Phys. Rev. Lett. **92**, 102001 (2004), [hep-ph/0309292].

[224] J. T. Londergan *et al.*, Phys. Lett. **B729**, 9 (2014), [arXiv:1311.7552].

[225] L. Roca *et al.*, Nucl. Phys. A **744**, 127 (2004), [hep-ph/0405228].

[226] E. Klempt, Phys. Lett. B **820**, 136512 (2021), [arXiv:2104.09922].

[227] R. J. Crewther and L. C. Tunstall, Phys. Rev. D **91**, 3, 034016 (2015), [arXiv:1312.3319].

[228] R. J. Crewther, Universe **6**, 7, 96 (2020), [arXiv:2003.11259].

[229] R. Zwicky, Phys. Rev. D **110**, 1, 014048 (2024), [arXiv:2312.13761].

[230] R. Kaminski, G. Mennessier and S. Narison, Phys. Lett. B **680**, 148 (2009), [arXiv:0904.2555].

[231] G. Mennessier, S. Narison and X. G. Wang, Phys. Lett. B **696**, 40 (2011), [arXiv:1009.2773].

[232] R. Albuquerque, S. Narison and D. Rabetiarivony, Nucl. Phys. A **1039**, 122743 (2023), [arXiv:2305.02421].

[233] S. Weinberg, Phys. Rev. **130**, 776 (1963).

[234] D. Morgan and M. R. Pennington, Phys. Lett. **B258**, 444 (1991), [Erratum: Phys. Lett.B269,477(1991)].

[235] D. Morgan, Nucl. Phys. **A543**, 632 (1992).

[236] N. A. Tornqvist, Phys. Rev. **D51**, 5312 (1995), [hep-ph/9403234].

[237] V. Baru *et al.*, Phys. Lett. **B586**, 53 (2004), [hep-ph/0308129].

[238] M. Ablikim *et al.* (BESIII), Phys. Rev. **D83**, 032003 (2011), [arXiv:1012.5131].

[239] N. A. Tornqvist, Z. Phys. **C68**, 647 (1995), [hep-ph/9504372].

[240] W.-H. Liang, J.-J. Xie and E. Oset, Eur. Phys. J. C **76**, 12, 700 (2016), [arXiv:1609.03864].

[241] R. Molina *et al.*, Phys. Lett. B **803**, 135279 (2020), [arXiv:1908.11557].

[242] L. R. Dai and E. Oset, Phys. Rev. D **109**, 5, 054008 (2024), [arXiv:2307.03014].

[243] M. Ablikim *et al.* (BESIII), Phys. Rev. Lett. **121**, 2, 022001 (2018), [arXiv:1802.00583].

[244] J.-T. Li *et al.*, Chin. Phys. C **46**, 8, 083108 (2022), [arXiv:2203.13786].

[245] E. van Beveren and G. Rupp, Eur. Phys. J. **C22**, 493 (2001), [hep-ex/0106077].

[246] M. Boglione and M. R. Pennington, Phys. Rev. **D65**, 114010 (2002), [hep-ph/0203149].

[247] G. Eichmann, C. S. Fischer and W. Heupel, Phys. Lett. B **753**, 282 (2016), [arXiv:1508.07178].

[248] N. Santowsky *et al.*, Phys. Rev. D **102**, 5, 056014 (2020), [arXiv:2007.06495].

Int. J. Mod. Phys. A 2026.41. Downloaded from www.worldscientific.com
UNIVERSITY OF CALIFORNIA @ BERKELEY on 09/16/26. Re-use and distribution is strictly not permitted, except for Open Access articles.

Int. J. Mod. Phys. A 2026.41. Downloaded from www.worldscientific.com
by UNIVERSITY OF CALIFORNIA @ BERKELEY on 09/16/26. Re-use and distribution is strictly not permitted, except for Open Access articles.

65. Rare Kaon Decays

Revised August 2025 by L. Littenberg (BNL) and G. Valencia (Monash U.).

65.1 Introduction

There are several useful reviews on rare kaon decays and related topics [1–13]. Activity in rare kaon decays can be divided roughly into four categories:

1. Searches for explicit violations of the Standard Model (SM)
2. The golden modes: $K \to \pi\nu\bar{\nu}$
3. Other constraints on SM parameters
4. Studies of strong interactions at low energy.

The paradigm of Category 1 is the lepton flavor violating decay $K_L \to \mu e$. Category 2 includes the two modes that can be calculated with negligible theoretical uncertainty, $K^+ \to \pi^+\nu\bar{\nu}$ and $K_L \to \pi^0\nu\bar{\nu}$. These modes can lead to precision determinations of CKM parameters or, in combination with other measurements of these parameters, they can constrain new interactions. They constitute the main focus of the current experimental kaon program. The search for new light particles through the reaction $K \to \pi X^0$ is a byproduct of these measurements. Category 3 is focused on decays with charged leptons, such as $K_L \to \pi^0\ell^+\ell^-$ or $K_L \to \ell^+\ell^-$ where $\ell \equiv e, \mu$. These modes are sensitive to CKM parameters, but they suffer from multiple hadronic uncertainties that can be addressed, at least in part, through a systematic study of the peripheral modes indicated in Fig. 65.1.

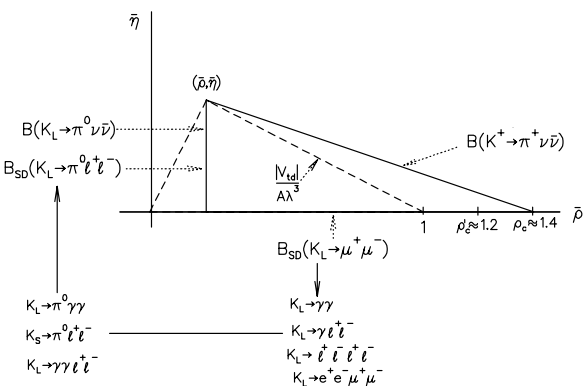

Figure 65.1: Role of rare kaon decays in determining the unitarity triangle. The solid arrows point to auxiliary modes needed to interpret the main results, or potential backgrounds to them.

The interplay between Categories 3-4 and their complementarity to Category 2 is illustrated in the figure. Category 4 includes reactions like $K^+ \to \pi^+\ell^+\ell^-$ those where long distance contributions are dominant and which constitute a testing ground for the ideas of chiral perturbation theory. Other decays in this category are $K_L \to \pi^0\gamma\gamma$ and $K_L \to \ell^+\ell^-\gamma$. The former is important in understanding a CP-conserving contribution to $K_L \to \pi^0\ell^+\ell^-$, whereas the latter could shed light on long distance contributions to $K_L \to \mu^+\mu^-$.

65.2 Explicit violations of the Standard Model

Much activity has focused on searches for lepton flavor violation (LFV). This is motivated by the fact that many extensions of the minimal Standard Model violate lepton flavor and by the potential to access very high energy scales. For example, the tree-level exchange of a LFV vector boson of mass M_X that couples to left-handed fermions with electroweak strength and without mixing angles yields $\mathrm{B}(K_L \to \mu e) = 4.7\times10^{-12}(148\ \mathrm{TeV}/M_X)^4$ [2]. This simple dimensional analysis may be used to read from Table 65.1 that the reaction $K_L \to \mu e$ is already probing scales of over 100 TeV. Table 65.1 summarizes the present experimental situation vis-à-vis LFV. The decays $K_L \to \mu^\pm e^\mp$ and $K^+ \to \pi^+ e^\mp \mu^\pm$ (or $K_L \to \pi^0 e^\mp \mu^\pm$) provide complementary information on potential family number violating interactions, since the former is sensitive to parity-odd couplings and the latter is sensitive to parity-even couplings.

Limits on certain lepton-number violating (LNV) kaon decays also have been obtained, with special interest arising from their role in constraining possible extensions of the neutrino sector [14, 15], and we list those in the table as well. Related searches in μ and τ processes are discussed in Section 5.

Table 65.1: Searches for lepton flavor and lepton number violation in K decay

LFV mode	90% CL upper limit	Experiment	Yr./Ref.	Type
$K^+ \to \pi^+ e^- \mu^+$	1.3×10^{-11}	BNL-865	2005/ [16]	LFV
$K^+ \to \pi^+ e^+ \mu^-$	6.6×10^{-11}	NA62	2021/ [17]	LFV
$K_L \to \mu e$	4.7×10^{-12}	BNL-871	1998/ [18]	LFV
$K_L \to \pi^0 e\mu$	7.6×10^{-11}	KTeV	2008/ [19]	LFV
$K_L \to \pi^0\pi^0 e\mu$	1.7×10^{-10}	KTeV	2008/ [19]	LFV
$K^+ \to \pi^- e^+ e^+$	5.3×10^{-11}	NA62	2022/ [20]	LNV
$K^+ \to \pi^-\pi^0 e^+ e^+$	8.5×10^{-10}	NA62	2022/ [20]	LNV
$K^+ \to \pi^- \mu^+ \mu^+$	4.2×10^{-11}	NA62	2019/ [21]	LNV
$K_L \to e^\pm e^\pm \mu^\mp \mu^\mp$	4.12×10^{-11}	KTeV	2003/ [22]	LNV
$K^+ \to \pi^- \mu^+ e^+$	4.2×10^{-11}	NA62	2021/ [17]	LNFV
$K^+ \to \mu^- \nu e^+ e^+$	8.1×10^{-11}	NA62	2023/ [23]	LNV/LFV
$K^+ \to \pi^0\pi^- \mu^+ e^+$	2.9×10^{-10}	NA62	2024/ [24]	LNV
$K^+ \to \pi^0\pi^+ \mu^- e^+$	3.1×10^{-10}	NA62	2024/ [24]	LFV
$K^+ \to \pi^0\pi^+ \mu^+ e^-$	5.0×10^{-10}	NA62	2024/ [24]	LFV

65.3 The golden modes: $K \to \pi\nu\bar{\nu}$

In the SM, the decay $K^+ \to \pi^+\nu\bar{\nu}$ is dominated by one-loop diagrams with top-quark intermediate states, while long-distance contributions are known to be quite small [25–27]. This permits a precise calculation of this rate in terms of SM parameters. Studies of this process are thus motivated by the possibility of detecting non-SM physics when comparing with the results of global fits [28, 29].

The branching ratio can be written in a compact form that exhibits the different ingredients that go into the calculation [30],

$$\mathrm{B}\left(K^+ \to \pi^+\nu\bar{\nu}(\gamma)\right) = \kappa_+(1+\Delta_{\mathrm{EM}})\left[\left(\frac{\mathrm{Im}(V_{ts}^\star V_{td})}{\lambda^5}X_t\right)^2 + \left(\frac{\mathrm{Re}(V_{cs}^\star V_{cd})}{\lambda}P_c + \frac{\mathrm{Re}(V_{ts}^\star V_{td})}{\lambda^5}X_t\right)^2\right]. \tag{65.1}$$

The parameters in Eq. 65.1 incorporate the *a priori* unknown hadronic matrix element in terms of the very well-measured K_{e3} rate [25] in κ_+; long distance QED corrections in Δ_{EM} [31]; the Inami-Lim function for the short distance top-quark contribution [32] , including NLO QCD corrections [33, 34] , and the two-loop electroweak correction [30], all in X_t; and the charm-quark contributions due to short distance effects, including NNLO QCD corrections [35, 36] and NLO electroweak corrections via P_c [37], which also includes certain long distance terms dubbed $\delta P_{c,u}$ [27, 38]. An interesting approximate way to cast this result in terms of the CKM parameters λ, V_{cb}, $\overline{\rho}$ and $\overline{\eta}$ (see Eq. 12.4) [9] is:

$$\mathrm{B}(K^+ \to \pi^+\nu\overline{\nu}) \approx 1.6\times10^{-5}|V_{cb}|^4[(\sigma\overline{\eta})^2 + (\rho_c - \overline{\rho})^2], \tag{65.2}$$

where $\rho_c \approx 1.45$ and $\sigma \equiv \frac{1}{(1-\frac{1}{2}\lambda^2)^2}$. Thus, $\mathrm{B}(K^+ \to \pi^+\nu\overline{\nu})$ determines an ellipse in the $\overline{\rho}$, $\overline{\eta}$ plane with center $(\rho_c, 0)$ and

Int. J. Mod. Phys. A 2026.41. Downloaded from www.worldscientific.com
UNIVERSITY OF CALIFORNIA @ BERKELEY on 09/16/26. Re-use and distribution is strictly not permitted, except for Open Access articles.

semiaxes $\approx \frac{1}{|V_{cb}|^2}\sqrt{\frac{\mathrm{B}(K^+\to\pi^+\nu\overline{\nu})}{1.6\times10^{-5}}}$ and $\frac{1}{\sigma|V_{cb}|^2}\sqrt{\frac{\mathrm{B}(K^+\to\pi^+\nu\overline{\nu})}{1.6\times10^{-5}}}$.

BNL-787 observed two candidate events [39,40] in the clean high π^+ momentum and one event [41] in the low-momentum region. The successor experiment BNL-949 observed one more in the high-momentum region [42] , and three more in the low-momentum region [43], yielding a branching ratio of $(1.73^{+1.15}_{-1.05})\times10^{-10}$ [44].

NA62 was commissioned in 2015 and took data in 2016, 2017, and 2018, and published results from those runs [45]. Data taking recommenced in 2021, and a result based on all data taken through 2022 was published in 2025 [46]. They resumed data taking in 2023 after some upgrades to the detector and in 2026 reported a result taking into account all data taken through 2024. They observed 84 events, including an estimated background of 30^{+4}_{-3} events, yielding $\mathrm{B}(K^+\to\pi^+\nu\overline{\nu}) = (9.6^{+1.9}_{-1.8})\times10^{-11}$ [47]. The experiment continues to run in 2025 and 2026.

Using values for the Wolfenstein parameters from Eq. 12.26, we estimate $\mathrm{B}(K^+\to\pi^+\nu\overline{\nu})_{SM} = (8.2\pm0.6)\times10^{-11}$, near the lower end of the measurements of BNL-787/949 and NA62. Current parametric uncertainty in the CKM angles can result in numbers with central values differing from this one by up to 10% [48].

The second golden mode is the neutral counterpart to our preceding discussion: $K_L\to\pi^0\nu\overline{\nu}$. It is dominantly CP-violating and free of hadronic uncertainties [25, 49, 50]. In the Standard Model, this mode is dominated by an intermediate top-quark state and does not suffer from the small uncertainty associated with the charm-quark intermediate state that affects $K^+\to\pi^+\nu\overline{\nu}$. The branching ratio is given by [9]:

$$\mathrm{B}(K_L\to\pi^0\nu\overline{\nu}) = \kappa_L\left(\frac{\mathrm{Im}(V_{ts}^\star V_{td})}{\lambda^5}X_t\right)^2 \approx 7.6\times10^{-5}|V_{cb}|^4\overline{\eta}^2\ . \tag{65.3}$$

As with the charged mode, the hadronic matrix element can be related to that measured in $K_{\ell3}$ decay and is incorporated into κ_L.

Our estimate for the branching ratio within the SM, again with parameters from Eq. 12.26, is $(2.9\pm0.3)\times10^{-11}$. Similarly to the charged kaon case, parametric uncertainty in the CKM angles can result in a central value that differs from this one by up to almost 20% [48].

Grossman and Nir (GN) [51] pointed out that, in a nearly model-independent manner, the two golden modes satisfy the relation $\mathrm{B}(K_L\to\pi^0\nu\overline{\nu})\lesssim 4.3\ \mathrm{B}(K^+\to\pi^+\nu\overline{\nu})$. Using the BNL 787/949 90% CL bound on $K^+\to\pi^+\nu\overline{\nu}$, GN then predict $B(K_L\to\pi^0\nu\overline{\nu})<1.46\times10^{-9}$. Using instead the latest NA62 result, the GN upper bound becomes $B(K_L\to\pi^0\nu\overline{\nu})<5.2\times10^{-10}$.

The KOTO experiment at J-PARC, whose goal is to make an initial observation of this decay, has been in operation since 2013. It has made a series of data collection runs and has reported on three data sets thus far. In 2018 it published a 90% CL upper limit of 3.0×10^{-9} [52], based on 2015 data. They have run almost every year since, making incremental improvements to the experimental configuration between runs. In 2021 they published a result on the data taken between 2016 and 2018 in which three events were observed in the signal region [53], whereas the expected background was 1.22 events, mainly from charged kaons produced by K_L interactions in the downstream collimator. Conservatively assuming the three events were due to background, they extracted a 90% CL upper limit of 4.9×10^{-9}. Subsequent hardware and analysis improvements reduced the expected background to 0.26 in a sample of similar sensitivity taken in 2021. No events were observed in the signal region, and a 90% CL upper limit of 2.2×10^{-9} was established [54]. An increase of 3-5 in sensitivity is anticipated from runs planned in the next three years.

The current theoretical and experimental situation for the golden modes is summarized in Fig. 65.2. The red area corresponds to the 1σ SM prediction we obtain with the CKM parameter values taken from Eq. 12.26. The yellow region shows the result established by the combined BNL-787 and BNL-949 results, whereas the green region marks the new NA62 result for $K^+\to\pi^+\nu\overline{\nu}$. The black shaded region marks the GN exclusion, which lies significantly above the SM expectation, leaving a large window for discovery of new physics contributions by experiments seeking to measure $\mathrm{B}(K_L\to\pi^0\nu\overline{\nu})$. The 90% CL upper bound on this mode from the KOTO result published in 2025 [54] is shown in orange, and is seen to still lie in the GN excluded zone.

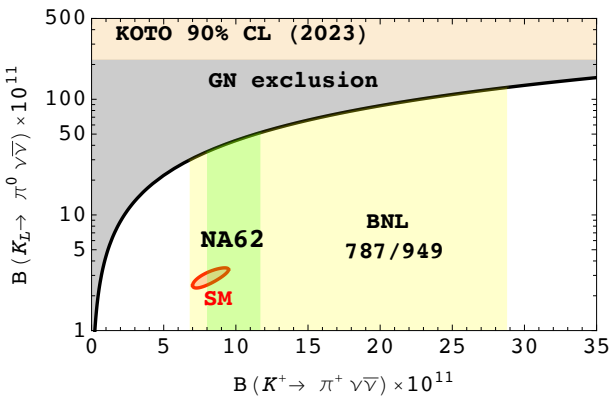

Figure 65.2: Summary of the current situation for the golden modes $K\to\pi\nu\overline{\nu}$. The red ellipse shows the 1σ SM prediction; the green (yellow) region corresponds to the NA62 (BNL787/949) 1σ measurement; and the orange region marks the 90% CL KOTO upper bound. The black shaded region shows the GN exclusion.

Much theoretical work has explored beyond the SM scenarios that can populate this window, as well as their correlations with other rare processes outside kaon physics. Although it would be relatively straightforward to establish the existence of new physics by observing deviations from their SM values in the $K\to\pi\nu\overline{\nu}$ rates, it would take much more extensive global fits to pinpoint the origin of any such deviation. Partial summaries with references focusing on quark flavor physics can be found in Refs. [9, 55–59]. Different possibilities emphasizing an interpretation of these modes as $K\to\pi+E_{\mathrm{miss}}$ can be found in Refs. [60–62].

There is a subtlety in converting the GN bound extracted from measurements of $K^+\to\pi^+\nu\overline{\nu}$ into an upper bound for $K_L\to\pi^0\nu\overline{\nu}$ as applied to KOTO [63]. This is due to a lack of sensitivity of the charged kaon experiments to a kinematic window near the pion mass. New physics appearing through a two body mode $K^+\to\pi^+X^0$, for an invisible X^0 particle with mass near the pion mass, has a much weaker constraint. The situation is illustrated in Fig. 65.3 which shows the BNL787/949 [44] (dashed black) and NA62 [64] (solid black) 90% c.l. limits on $K^+\to\pi^+X^0$ as a function of m_{X^0} assuming X^0 is stable. The implied GN bound for $K_L\to\pi^0X^0$, $B(K_L\to\pi^0X^0)\lesssim 4.3B(K^+\to\pi^+X^0)$ is shown as a blue line and can be compared with the actual KOTO [54] constraint on $K_L\to\pi^0X^0$ in red. Notice that the upper bound derived from NA62 is lower than that derived from BNL787/949 except for a small mass window. For $120\lesssim m_{X^0}\lesssim 150$ MeV, KOTO already has better sensitivity than that implied by the GN bound in this case. The possibility of new physics in this scenario has generated much theoretical speculation [65–75].

The search for a new light particle X^0 in $K^+\to\pi^+X^0$ has a long tradition covering both long-lived particles (*e.g.*, hyperphoton, axion, familon, *etc.*), and short-lived ones that decay to muon, electron, photon or neutrino pairs. The longstanding 90% CL upper limit on $K^+\to\pi^+X^0$ from BNL787/949 7.3×10^{-11} [42] for the case of massless X^0 has been slightly improved by NA62 to 5×10^{-11} as can be read from Fig. 65.3. These limits can also be reinterpreted in connection with a dark photon [76] or dark Z [77], and in this context, NA48/2 also constrained the mode $B(K^\pm\to\pi^\pm A'\to\pi^\pm e^+e^-)$ [78]. Complementary searches for new light particles in kaon experiments use modes with two pions and include the KTeV bound $B(K_L\to\pi^0\pi^0X^0\to\pi^0\pi^0\mu^+\mu^-)<1\times10^{-10}$ [79] and the E391a bound $B(K_L\to\pi^0\pi^0X^0\to\pi^0\pi^0\gamma\gamma)<2.4\times10^{-7}$ [80].

Neutrino pair modes with one extra pion, $K\to\pi\pi\nu\overline{\nu}$, are similarly dominated by short distance contributions in the SM [81–83]. Even though they are theoretically clean, they occur with very

Int. J. Mod. Phys. A 2026.41. Downloaded from www.worldscientific.com
by UNIVERSITY OF CALIFORNIA @ BERKELEY on 09/16/26. Re-use and distribution is strictly not permitted, except for Open Access articles.

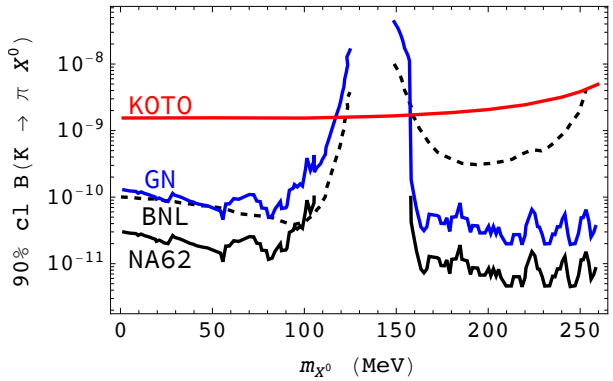

Figure 65.3: Summary of the current situation for $K \to \pi X^0$. The solid (dashed) black line shows the exclusion limit for $K^+ \to \pi^+ X^0$ from NA62 (BNL787/949) assuming X^0 is stable. The blue line marks the constraint implied for $K_L \to \pi^0 X^0$ by the Grossman-Nir relation and the red line marks the current KOTO limit on $K^+ \to \pi^+ X^0$.

low rates, with branching ratios of order 10^{-13}. The current best bound comes from KEK-391a, $B(K_L \to \pi^0\pi^0\nu\bar{\nu}) < 8.1 \times 10^{-7}$ at 90% CL [84]. There is also a bound for the charged kaon mode $B(K^+ \to \pi^+\pi^0\nu\bar{\nu}) < 4.3 \times 10^{-5}$ at 90% CL [85] from BNL-787. New physics contributions to these modes are discussed in [86].

65.4 Other constraints on Standard Model parameters

The decay $K_L \to \mu^+\mu^-$ has a short distance contribution sensitive to the CKM parameter $\bar{\rho}$, given by [5]:

$$\mathrm{B}_{\mathrm{SD}}(K_L \to \mu^+\mu^-) \approx 2.7 \times 10^{-4} |V_{cb}|^4 (1.2 - \bar{\rho})^2. \quad (65.4)$$

This decay, however, is dominated by a long-distance contribution from a two-photon intermediate state. The absorptive (imaginary) part of the long-distance component is determined by the measured rate for $K_L \to \gamma\gamma$ to be $\mathrm{B}_{\mathrm{abs}}(K_L \to \mu^+\mu^-) = (6.54 \pm 0.05) \times 10^{-9}$; and it almost completely saturates the observed rate $\mathrm{B}(K_L \to \mu^+\mu^-) = (6.84 \pm 0.11) \times 10^{-9}$ [87]. The difference between the observed rate and the absorptive component can be attributed to the (coherent) sum of the short-distance amplitude and the real part of the long-distance amplitude. A recent detailed evaluation that incorporates all known information from the ancillary modes in Fig. 65.1, finds $\mathrm{B}(K_L \to \mu^+\mu^-)_{SM} = (7.44^{+0.41}_{-0.34}) \times 10^{-9}$ [88].

By contrast, the decay $K_L \to e^+e^-$ is completely dominated by long distance physics and is easier to estimate. The result, $B(K_L \to e^+e^-) = (8.46 \pm 0.37) \times 10^{-12}$ [88], is in good agreement with the BNL-871 measurement, $(8.7^{+5.7}_{-4.1}) \times 10^{-12}$ [89].

The mode $K_S \to \mu^+\mu^-$ has a short distance contribution proportional to the square of the CKM parameter $\bar{\eta}$ entering at the 10^{-13} level [10]. It also has long distance contributions arising from the two photon intermediate state, which result in a rate $B(K_S \to \mu^+\mu^-)_{LD} = 5.1 \times 10^{-12}$ [10]. There is a 90% CL limit $B(K_S \to \mu^+\mu^-) < 2.1 \times 10^{-10}$ from LHCb [90, 91]. The interplay between $K_L \to \mu^+\mu^-$ and $K_S \to \mu^+\mu^-$ has been the subject of [92, 93], and it has been pointed out that a measurement of time-dependent interference effects could be used to extract information on CKM angles from $K \to \mu^+\mu^-$ measurements [94, 95].

The decay $K_L \to \pi^0 e^+e^-$ is sensitive to the CKM parameter η through its CP-violating component. There are both direct and indirect CP-violating amplitudes that can interfere. The direct CP-violating amplitude is short distance dominated and has been calculated in detail within the SM [5]. The indirect CP-violating amplitude can be inferred from a measurement of $K_S \to \pi^0 e^+e^-$. The complete CP-violating contribution to the rate can be written as [96–98]:

$$\mathrm{B}_{\mathrm{CPV}} \approx \left[15.7|a_S|^2 \pm 1.4 \left(\frac{|V_{cb}|^2\overline{\eta}}{10^{-4}} \right) |a_S| + 0.12 \left(\frac{|V_{cb}|^2\overline{\eta}}{10^{-4}} \right)^2 \right] \times 10^{-12} \quad (65.5)$$

where the three terms correspond to the indirect CP violation, the interference, and the direct CP violation, respectively. The parameter a_S has been extracted by NA48/1 from a measurement of $K_S \to \pi^0 e^+e^-$ with the result $|a_S| = 1.06^{+0.26}_{-0.21} \pm 0.07$ [99], as well as from a measurement of $K_S \to \pi^0\mu^+\mu^-$ with the result $|a_S| = 1.54^{+0.40}_{-0.32} \pm 0.06$ [100]. With current constraints on the CKM parameters, and assuming a positive sign for the interference term [98, 101], this implies that $\mathrm{B}_{\mathrm{CPV}}(K_L \to \pi^0 e^+e^-) \approx (3.1 \pm 0.9) \times 10^{-11}$, where the three contributions to the central value from indirect, interference and direct CP violation are $(1.76, 0.9, 0.45) \times 10^{-11}$ respectively. It should be noted that more recent studies suggest a much larger uncertainty in the value of a_S [102].

$K_L \to \pi^0 e^+e^-$ also has a CP-conserving component dominated by a two-photon intermediate state. This component can be decomposed into an absorptive and a dispersive part. The absorptive part can be extracted from the measurement of the low $m_{\gamma\gamma}$ region of the $K_L \to \pi^0\gamma\gamma$ spectrum. The rate and the shape of the distribution $d\Gamma/dm_{\gamma\gamma}$ in $K_L \to \pi^0\gamma\gamma$ are well described in chiral perturbation theory in terms of three (*a priori*) unknown parameters [103–106].

Both KTeV and NA48 have studied the mode $K_L \to \pi^0\gamma\gamma$, reporting similar results. KTeV finds $B(K_L \to \pi^0\gamma\gamma) = (1.29 \pm 0.03_{\mathrm{stat}} \pm 0.05_{\mathrm{sys}}) \times 10^{-6}$ [107], while NA48 finds $B(K_L \to \pi^0\gamma\gamma) = (1.36 \pm 0.03_{\mathrm{stat}} \pm 0.03_{\mathrm{sys}} \pm 0.03_{\mathrm{norm}}) \times 10^{-6}$ [108]. Both experiments are consistent with a negligible rate in the low $m_{\gamma\gamma}$ region, suggesting a very small CP-conserving component $B_{\mathrm{CP}}(K_L \to \pi^0 e^+e^-) \sim \mathcal{O}(10^{-13})$ [98, 106, 108]. There remains some model dependence in the estimate of the dispersive part of the CP-conserving $K_L \to \pi^0 e^+e^-$ [98].

The related process, $K_L \to \pi^0\gamma e^+e^-$, is potentially an additional background to $K_L \to \pi^0 e^+e^-$ in some region of phase space [109]. This process has been observed with a branching ratio of $(1.62 \pm 0.14_{\mathrm{stat}} \pm 0.09_{\mathrm{sys}}) \times 10^{-8}$ [110].

The decay $K_L \to \gamma\gamma e^+e^-$ constitutes the dominant background to $K_L \to \pi^0 e^+e^-$. It was first observed by BNL-845 [111], and subsequently confirmed with a much larger sample by KTeV [112]. It has been estimated that this background will enter at about the 10^{-10} level [113, 114], comparable to or larger than the signal level. Because of this, the observation of $K_L \to \pi^0 e^+e^-$ at the SM level will depend on background subtraction with good statistics. Possible alternative strategies are discussed in [98] and references cited therein.

The 90% CL upper bound for the process $K_L \to \pi^0 e^+e^-$ is 2.8×10^{-10} [114]. For the closely related muonic process, the published upper bound is $\mathrm{B}(K_L \to \pi^0\mu^+\mu^-) \leq 3.8 \times 10^{-10}$ [115], compared with the SM prediction of $(1.9 \pm 0.5) \times 10^{-11}$. The latter assumes positive interference between the direct- and indirect-CP violating components and includes a CP-conserving component which contributes about 30% of the total [10, 116].

A study of $K_L \to \pi^0\mu^+\mu^-$ has indicated that it might be possible to extract the direct CP-violating contribution by a joint study of the Dalitz plot variables and the components of the μ^+ polarization [117]. The latter tends to be quite substantial so that large statistics may not be necessary.

Combined information from $K_L \to \pi^0\ell^+\ell^-$ as well as $K_L \to \mu^+\mu^-$ complements the $K \to \pi\nu\bar{\nu}$ measurements in constraining physics beyond the SM [118].

65.5 Other long distance dominated modes

The rates and spectra for the decays $K^+ \to \pi^+\ell^+\ell^-$ ($\ell = e$ or μ) have been measured [119–124] and are successfully described with a parameterization inspired by chiral perturbation theory but with large corrections beyond leading order [96, 97] (see [102, 125] for a review). The most recent NA62 result shows

Int. J. Mod. Phys. A 2026.41. Downloaded from www.worldscientific.com
UNIVERSITY OF CALIFORNIA @ BERKELEY on 09/16/26. Re-use and distribution is strictly not permitted, except for Open Access articles.

good agreement between the electron and muon mode form factors [126]. NA62 has also obtained a first measurement of the forward-backward asymmetry in the muon mode [126].

The mode $K^+ \to \pi^+\pi^0 e^+ e^-$, analyzed by NA48/2 [127], is also dominated by long distance physics but it has been argued that measuring asymmetries can provide information on the short distance components [128]. The current status of these modes is discussed in [129]. Contributions to $K^+ \to \pi^+ e^+ e^- e^+ e^-$ beyond the double Dalitz decay in $K^+ \to \pi^+\pi^0$ are considered in [130], and have been measured by NA62 [131].

The decay $K^+ \to \pi^+\gamma\gamma$ can be predicted in terms of one unknown parameter to leading order in χPT, dubbed $\hat{c}$, resulting in a correlation between the rate and the diphoton mass spectrum [132]. Certain important corrections at the next order are also known [133]. The rate and spectrum were first measured by E787 [134], followed by NA48/2 [135] and NA62 [136]. The most recent measurement from NA62 [137], based on a sample of almost 4000 events, finds $B(K^+ \to \pi^+\gamma\gamma) = (9.61 \pm 0.17) \times 10^{-7}$ and a precise value for $\hat{c}$.

Much information was recorded by KTeV and NA48 on the rates and spectrum for the Dalitz pair conversion modes $K_L \to \ell^+\ell^-\gamma$ [138, 139], and $K_L \to \ell^+\ell^-\ell'^+\ell'^-$ for $\ell, \ell' = e$ or μ [22, 140], and LHCb has recently placed limits on $K_{L,S} \to \mu^+\mu^-\mu^+\mu^-$ [141]. All these results are used to test hadronic models and should eventually help unravel the underlying physics in $K_L \to \mu^+\mu^-$ [88, 92, 142, 143].

Despite the current theoretical uncertainties in $K^+ \to \pi^+\ell^+\ell^-$, $K_L \to \pi^0\ell^+\ell^-$ and $K_L \to \mu^+\mu^-$, these modes can serve to constrain new interactions, particularly when combined with $K \to \pi\nu\bar{\nu}$ and other observables. [86, 88, 93, 98, 118, 144–146].

References

[1] L. Littenberg and G. Valencia, Ann. Rev. Nucl. Part. Sci. **43**, 729 (1993), [hep-ph/9303225].

[2] J. L. Ritchie and S. G. Wojcicki, Rev. Mod. Phys. **65**, 1149 (1993).

[3] B. Winstein and L. Wolfenstein, Rev. Mod. Phys. **65**, 1113 (1993).

[4] A. Pich, Rept. Prog. Phys. **58**, 563 (1995), [hep-ph/9502366].

[5] G. Buchalla, A. J. Buras and M. E. Lautenbacher, Rev. Mod. Phys. **68**, 1125 (1996), [hep-ph/9512380].

[6] G. D'Ambrosio and G. Isidori, Int. J. Mod. Phys. **A13**, 1 (1998), [hep-ph/9611284].

[7] P. Buchholz and B. Renk, Prog. Part. Nucl. Phys. **39**, 253 (1997).

[8] A. R. Barker and S. H. Kettell, Ann. Rev. Nucl. Part. Sci. **50**, 249 (2000), [hep-ex/0009024].

[9] A. J. Buras, F. Schwab and S. Uhlig, Rev. Mod. Phys. **80**, 965 (2008), [hep-ph/0405132].

[10] V. Cirigliano *et al.*, Rev. Mod. Phys. **84**, 399 (2012), [arXiv:1107.6001].

[11] D. Bryman *et al.*, Ann. Rev. Nucl. Part. Sci. **61**, 331 (2011).

[12] T. K. Komatsubara, Prog. Part. Nucl. Phys. **67**, 995 (2012), [arXiv:1203.6437].

[13] A. Ceccucci, Annual Review of Nuclear and Particle Science **71**, 1 (2021), URL `https://doi.org/10.1146/annurev-nucl-102419-054905`.

[14] A. Atre *et al.*, JHEP **05**, 030 (2009), [arXiv:0901.3589].

[15] L. S. Littenberg and R. Shrock, Phys. Lett. **B491**, 285 (2000), [hep-ph/0005285].

[16] A. Sher *et al.*, Phys. Rev. **D72**, 012005 (2005), [hep-ex/0502020].

[17] E. Cortina Gil *et al.* (NA62), Phys. Rev. Lett. **127**, 13, 131802 (2021), [arXiv:2105.06759].

[18] D. Ambrose *et al.* (BNL), Phys. Rev. Lett. **81**, 5734 (1998), [hep-ex/9811038].

[19] E. Abouzaid *et al.* (KTeV), Phys. Rev. Lett. **100**, 131803 (2008), [arXiv:0711.3472].

[20] E. Cortina Gil *et al.* (NA62), Phys. Lett. B **830**, 137172 (2022), [arXiv:2202.00331].

[21] E. Cortina Gil *et al.* (NA62), Phys. Lett. **B797**, 134794 (2019), [arXiv:1905.07770].

[22] A. Alavi-Harati *et al.* (KTeV), Phys. Rev. Lett. **90**, 141801 (2003), [hep-ex/0212002].

[23] E. Cortina Gil *et al.* (NA62), Phys. Lett. B **838**, 137679 (2023), [arXiv:2211.04818].

[24] M. U. Ashraf *et al.* (NA62), Phys. Lett. B **859**, 139122 (2024), [arXiv:2409.12981].

[25] J. S. Hagelin and L. S. Littenberg, Prog. Part. Nucl. Phys. **23**, 1 (1989).

[26] M. Lu and M. B. Wise, Phys. Lett. **B324**, 461 (1994), [hep-ph/9401204].

[27] A. F. Falk, A. Lewandowski and A. A. Petrov, Phys. Lett. **B505**, 107 (2001), [hep-ph/0012099].

[28] J. Charles *et al.*, Phys. Rev. **D84**, 033005 (2011), [arXiv:1106.4041].

[29] M. Bona *et al.* (UTfit), JHEP **03**, 049 (2008), [arXiv:0707.0636].

[30] J. Brod, M. Gorbahn and E. Stamou, Phys. Rev. **D83**, 034030 (2011), [arXiv:1009.0947].

[31] F. Mescia and C. Smith, Phys. Rev. **D76**, 034017 (2007), [arXiv:0705.2025].

[32] T. Inami and C. S. Lim, Prog. Theor. Phys. **65**, 297 (1981), [Erratum: Prog. Theor. Phys. **65**, 1772 (1981)].

[33] G. Buchalla and A. J. Buras, Nucl. Phys. **B548**, 309 (1999), [hep-ph/9901288].

[34] M. Misiak and J. Urban, Phys. Lett. **B451**, 161 (1999), [hep-ph/9901278].

[35] A. J. Buras *et al.*, Phys. Rev. Lett. **95**, 261805 (2005), [hep-ph/0508165].

[36] A. J. Buras *et al.*, JHEP **11**, 002 (2006), [Erratum: JHEP **11**, 167 (2012)], [hep-ph/0603079].

[37] J. Brod and M. Gorbahn, Phys. Rev. **D78**, 034006 (2008), [arXiv:0805.4119].

[38] G. Isidori, F. Mescia and C. Smith, Nucl. Phys. **B718**, 319 (2005), [hep-ph/0503107].

[39] S. Adler *et al.* (E787), Phys. Rev. Lett. **88**, 041803 (2002), [hep-ex/0111091].

[40] S. Adler *et al.* (E787), Phys. Rev. Lett. **84**, 3768 (2000), [hep-ex/0002015].

[41] S. S. Adler *et al.* (E787), Phys. Lett. **B537**, 211 (2002), [hep-ex/0201037].

[42] V. V. Anisimovsky *et al.* (E949), Phys. Rev. Lett. **93**, 031801 (2004), [hep-ex/0403036].

[43] A. V. Artamonov *et al.* (E949), Phys. Rev. Lett. **101**, 191802 (2008), [arXiv:0808.2459].

[44] A. V. Artamonov *et al.* (BNL-E949), Phys. Rev. **D79**, 092004 (2009), [arXiv:0903.0030].

[45] E. Cortina Gil *et al.* (NA62), JHEP **06**, 093 (2021), [arXiv:2103.15389].

[46] E. Cortina Gil *et al.* (NA62), JHEP **02**, 191 (2025), [arXiv:2412.12015].

[47] R. Fiorenza (NA62), "New measurement of the $K^+ \to \pi^+\nu\bar{\nu}$ decay at NA62," (2026), Talk at Les Rencontres de Physique de la Vallée d'Aoste, URL `https://agenda.infn.it/event/48984/contributions/286360/attachments/146881/223788/Fiorenza_LaThuile2026.pdf`.

[48] A. J. Buras *et al.*, JHEP **11**, 033 (2015), [arXiv:1503.02693].

[49] L. S. Littenberg, Phys. Rev. **D39**, 3322 (1989).

[50] G. Buchalla and G. Isidori, Phys. Lett. **B440**, 170 (1998), [hep-ph/9806501].

Int. J. Mod. Phys. A 2026.41. Downloaded from www.worldscientific.com
by UNIVERSITY OF CALIFORNIA @ BERKELEY on 09/16/26. Re-use and distribution is strictly not permitted, except for Open Access articles.

[51] Y. Grossman and Y. Nir, Phys. Lett. **B398**, 163 (1997), [hep-ph/9701313].

[52] J. K. Ahn *et al.* (KOTO), Phys. Rev. Lett. **122**, 021802 (2019), [arXiv:1810.09655].

[53] J. K. Ahn *et al.* (KOTO), Phys. Rev. Lett. **126**, 121801 (2021), [arXiv:2012.07571].

[54] J. K. Ahn *et al.* (KOTO), Phys. Rev. Lett. **134**, 8, 081802 (2025), [arXiv:2411.11237].

[55] G. D'Ambrosio and G. Isidori, Phys. Lett. **B530**, 108 (2002), [hep-ph/0112135].

[56] D. Bryman *et al.*, Int. J. Mod. Phys. **A21**, 487 (2006), [hep-ph/0505171].

[57] A. J. Buras, D. Buttazzo and R. Knegjens, JHEP **11**, 166 (2015), [arXiv:1507.08672].

[58] X.-G. He, G. Valencia and K. Wong, Eur. Phys. J. **C78**, 472 (2018), [arXiv:1804.07449].

[59] J. Aebischer, A. J. Buras and J. Kumar, JHEP **12**, 097 (2020), [arXiv:2006.01138].

[60] M. Bordone *et al.*, Eur. Phys. J. **C77**, 618 (2017), [arXiv:1705.10729].

[61] F. F. Deppisch, K. Fridell and J. Harz, JHEP **12**, 186 (2020), [arXiv:2009.04494].

[62] X.-G. He, X.-D. Ma and G. Valencia, JHEP **03**, 037 (2023), [arXiv:2209.05223].

[63] K. Fuyuto, W.-S. Hou and M. Kohda, Phys. Rev. Lett. **114**, 171802 (2015), [arXiv:1412.4397].

[64] E. Cortina Gil *et al.* (NA62), JHEP **11**, 143 (2025), [arXiv:2507.17286].

[65] T. Kitahara *et al.*, Phys. Rev. Lett. **124**, 071801 (2020), [arXiv:1909.11111].

[66] D. Egana-Ugrinovic, S. Homiller and P. Meade, Phys. Rev. Lett. **124**, 191801 (2020), [arXiv:1911.10203].

[67] P. S. B. Dev, R. N. Mohapatra and Y. Zhang, Phys. Rev. D **101**, 075014 (2020), [arXiv:1911.12334].

[68] M. Fabbrichesi and E. Gabrielli, Eur. Phys. J. C **80**, 532 (2020), [arXiv:1911.03755].

[69] Y. Liao *et al.*, Phys. Rev. D **102**, 055005 (2020), [arXiv:2005.00753].

[70] R. Ziegler, J. Zupan and R. Zwicky, JHEP **07**, 229 (2020), [arXiv:2005.00451].

[71] T. Li, X.-D. Ma and M. A. Schmidt, Phys. Rev. D **101**, 055019 (2020), [arXiv:1912.10433].

[72] X.-G. He *et al.*, JHEP **08**, 034 (2020), [arXiv:2005.02942].

[73] M. Hostert, K. Kaneta and M. Pospelov, Phys. Rev. D **102**, 055016 (2020), [arXiv:2005.07102].

[74] S. Gori, G. Perez and K. Tobioka, JHEP **08**, 110 (2020), [arXiv:2005.05170].

[75] T. B. de Melo *et al.*, Phys. Rev. D **103**, 115001 (2021), [arXiv:2102.06262].

[76] M. Pospelov, Phys. Rev. **D80**, 095002 (2009), [arXiv:0811.1030].

[77] H. Davoudiasl, H.-S. Lee and W. J. Marciano, Phys. Rev. **D89**, 095006 (2014), [arXiv:1402.3620].

[78] J. R. Batley *et al.* (NA48/2), Phys. Lett. **B746**, 178 (2015), [arXiv:1504.00607].

[79] E. Abouzaid *et al.* (KTeV), Phys. Rev. Lett. **107**, 201803 (2011), [arXiv:1105.4800].

[80] Y. C. Tung *et al.* (E391a), Phys. Rev. Lett. **102**, 051802 (2009), [arXiv:0810.4222].

[81] L. S. Littenberg and G. Valencia, Phys. Lett. **B385**, 379 (1996), [hep-ph/9512413].

[82] C.-W. Chiang and F. J. Gilman, Phys. Rev. **D62**, 094026 (2000), [hep-ph/0007063].

[83] C. Q. Geng, I. J. Hsu and Y. C. Lin, Phys. Rev. **D50**, 5744 (1994), [hep-ph/9406313].

[84] R. Ogata *et al.* (E391a), Phys. Rev. **D84**, 052009 (2011), [arXiv:1106.3404].

[85] S. Adler *et al.* (E787), Phys. Rev. **D63**, 032004 (2001), [hep-ex/0009055].

[86] C.-Q. Geng and J. Tandean, Phys. Rev. D **102**, 115021 (2020), [arXiv:2009.00608].

[87] D. Ambrose *et al.* (E871), Phys. Rev. Lett. **84**, 1389 (2000).

[88] M. Hoferichter, B.-L. Hoid and J. R. de Elvira, JHEP **04**, 071 (2024), [arXiv:2310.17689].

[89] D. Ambrose *et al.* (BNL E871), Phys. Rev. Lett. **81**, 4309 (1998), [hep-ex/9810007].

[90] R. Aaij *et al.* (LHCb), Eur. Phys. J. **C77**, 678 (2017), [arXiv:1706.00758].

[91] R. Aaij *et al.* (LHCb), Phys. Rev. Lett. **125**, 231801 (2020), [arXiv:2001.10354].

[92] G. D'Ambrosio and T. Kitahara, Phys. Rev. Lett. **119**, 201802 (2017), [arXiv:1707.06999].

[93] V. Chobanova *et al.*, JHEP **05**, 024 (2018), [arXiv:1711.11030].

[94] A. Dery *et al.*, JHEP **07**, 103 (2021), [arXiv:2104.06427].

[95] A. Dery *et al.*, JHEP **03**, 014 (2023), [arXiv:2211.03804].

[96] G. D'Ambrosio *et al.*, JHEP **08**, 004 (1998), [hep-ph/9808289].

[97] C. Dib, I. Dunietz and F. J. Gilman, Phys. Rev. **D39**, 2639 (1989).

[98] G. Buchalla, G. D'Ambrosio and G. Isidori, Nucl. Phys. **B672**, 387 (2003), [hep-ph/0308008].

[99] J. R. Batley *et al.* (NA48/1), Phys. Lett. **B576**, 43 (2003), [hep-ex/0309075].

[100] J. R. Batley *et al.* (NA48/1), Phys. Lett. **B599**, 197 (2004), [hep-ex/0409011].

[101] S. Friot, D. Greynat and E. De Rafael, Phys. Lett. **B595**, 301 (2004), [hep-ph/0404136].

[102] G. D'Ambrosio, D. Greynat and M. Knecht, JHEP **02**, 049 (2019), [arXiv:1812.00735].

[103] G. Ecker, A. Pich and E. de Rafael, Phys. Lett. **B237**, 481 (1990).

[104] L. Cappiello, G. D'Ambrosio and M. Miragliuolo, Phys. Lett. **B298**, 423 (1993).

[105] A. G. Cohen, G. Ecker and A. Pich, Phys. Lett. **B304**, 347 (1993).

[106] F. Gabbiani and G. Valencia, Phys. Rev. **D66**, 074006 (2002), [hep-ph/0207189].

[107] E. Abouzaid *et al.* (KTeV), Phys. Rev. **D77**, 112004 (2008), [arXiv:0805.0031].

[108] A. Lai *et al.* (NA48), Phys. Lett. **B536**, 229 (2002), [hep-ex/0205010].

[109] J. F. Donoghue and F. Gabbiani, Phys. Rev. **D56**, 1605 (1997), [hep-ph/9702278].

[110] E. Abouzaid *et al.* (KTeV), Phys. Rev. **D76**, 052001 (2007), [arXiv:0706.4074].

[111] W. M. Morse *et al.*, Phys. Rev. **D45**, 36 (1992).

[112] A. Alavi-Harati *et al.* (KTeV), Phys. Rev. **D64**, 012003 (2001), [hep-ex/0010059].

[113] H. B. Greenlee, Phys. Rev. **D42**, 3724 (1990).

[114] A. Alavi-Harati *et al.* (KTeV), Phys. Rev. Lett. **93**, 021805 (2004), [hep-ex/0309072].

[115] A. Alavi-Harati *et al.* (KTEV), Phys. Rev. Lett. **84**, 5279 (2000), [hep-ex/0001006].

[116] G. Isidori, C. Smith and R. Unterdorfer, Eur. Phys. J. **C36**, 57 (2004), [hep-ph/0404127].

[117] M. V. Diwan, H. Ma and T. L. Trueman, Phys. Rev. **D65**, 054020 (2002), [hep-ph/0112350].

[118] F. Mescia, C. Smith and S. Trine, JHEP **08**, 088 (2006), [hep-ph/0606081].

[119] R. Appel *et al.* (E865), Phys. Rev. Lett. **83**, 4482 (1999), [hep-ex/9907045].

[120] J. R. Batley *et al.* (NA48/2), Phys. Lett. **B677**, 246 (2009), [arXiv:0903.3130].

[121] S. Adler *et al.* (E787), Phys. Rev. Lett. **79**, 4756 (1997), [hep-ex/9708012].

[122] H. Ma *et al.* (e865), Phys. Rev. Lett. **84**, 2580 (2000), [hep-ex/9910047].

[123] H. K. Park *et al.* (HyperCP), Phys. Rev. Lett. **88**, 111801 (2002), [hep-ex/0110033].

[124] J. R. Batley *et al.* (NA48/2), Phys. Lett. **B697**, 107 (2011), [arXiv:1011.4817].

[125] G. D'Ambrosio, D. Greynat and M. Knecht, Phys. Lett. B **797**, 134891 (2019), [arXiv:1906.03046].

[126] E. Cortina Gil *et al.* (NA62), JHEP **11**, 011 (2022), [Addendum: JHEP 06, 040 (2023)], [arXiv:2209.05076].

[127] J. R. Batley *et al.* (NA48/2), Phys. Lett. **B788**, 552 (2019), [arXiv:1809.02873].

[128] L. Cappiello *et al.*, Eur. Phys. J. **C72**, 1872 (2012), [Erratum: Eur. Phys. J. **C72**, 2208 (2012)], [arXiv:1112.5184].

[129] L. Cappiello, O. Catà and G. D'Ambrosio, Eur. Phys. J. **C78**, 265 (2018), [arXiv:1712.10270].

[130] T. Husek, Phys. Rev. D **106**, 7, L071301 (2022), [arXiv:2207.02234].

[131] E. Cortina Gil *et al.* (NA62), Phys. Lett. B **846**, 138193 (2023), [arXiv:2307.04579].

[132] G. Ecker, A. Pich and E. de Rafael, Nucl. Phys. **B303**, 665 (1988).

[133] G. D'Ambrosio and J. Portoles, Phys. Lett. **B386**, 403 (1996), [Erratum: Phys. Lett. **B395**, 389 (1997)], [hep-ph/9606213].

[134] P. Kitching *et al.* (E787), Phys. Rev. Lett. **79**, 4079 (1997), [hep-ex/9708011].

[135] J. R. Batley *et al.* (NA48/2), Phys. Lett. **B730**, 141 (2014), [arXiv:1310.5499].

[136] C. Lazzeroni *et al.* (NA62), Phys. Lett. **B732**, 65 (2014), [arXiv:1402.4334].

[137] E. Cortina Gil *et al.* (NA62), Phys. Lett. B **850**, 138513 (2024), [arXiv:2311.01837].

[138] A. Alavi-Harati *et al.* (KTeV), Phys. Rev. Lett. **87**, 071801 (2001).

[139] E. Abouzaid *et al.* (KTeV), Phys. Rev. Lett. **99**, 051804 (2007), [hep-ex/0702039].

[140] V. Fanti *et al.* (NA48), Phys. Lett. **B458**, 553 (1999).

[141] R. Aaij *et al.* (LHCb), Phys. Rev. D **108**, 3, L031102 (2023), [arXiv:2212.04977].

[142] G. Isidori and R. Unterdorfer, JHEP **01**, 009 (2004), [hep-ph/0311084].

[143] G. D'Ambrosio, D. Greynat and G. Vulvert, Eur. Phys. J. **C73**, 2678 (2013), [arXiv:1309.5736].

[144] A. Crivellin *et al.*, Phys. Rev. D **93**, 7, 074038 (2016), [arXiv:1601.00970].

[145] G. D'Ambrosio *et al.*, JHEP **09**, 148 (2022), [arXiv:2206.14748].

[146] A. Roy, J. Tandean and G. Valencia, Phys. Rev. D **111**, 1, 013003 (2025), [arXiv:2404.15268].

Int. J. Mod. Phys. A 2026.41. Downloaded from www.worldscientific.com
UNIVERSITY OF CALIFORNIA @ BERKELEY on 09/16/26. Re-use and distribution is strictly not permitted, except for Open Access articles.

Int. J. Mod. Phys. A 2026.41. Downloaded from www.worldscientific.com
by UNIVERSITY OF CALIFORNIA @ BERKELEY on 09/16/26. Re-use and distribution is strictly not permitted, except for Open Access articles.

66. *CPT* Invariance Tests in Neutral Kaon Decay

Revised August 2023 by M. Antonelli (INFN, Frascati), G. D'Ambrosio (INFN, Napoli) and M.S. Sozzi (Pisa U.; INFN, Pisa).

CPT theorem is based on three assumptions: quantum field theory, locality, and Lorentz invariance, and thus it is a fundamental probe of our basic understanding of particle physics. Strangeness oscillation in $K^0-\overline{K}^0$ system, described by the equation

$$i\frac{d}{dt}\begin{bmatrix}K^0\\ \overline{K}^0\end{bmatrix} = [M - i\Gamma/2]\begin{bmatrix}K^0\\ \overline{K}^0\end{bmatrix} ,$$

where M and Γ are hermitian matrices (see PDG review [1], references [2,3], and KLOE paper [4] for notations and previous literature), allows a very accurate test of CPT symmetry; indeed since CPT requires $M_{11} = M_{22}$ and $\Gamma_{11} = \Gamma_{22}$, the mass and width eigenstates, $K_{S,L}$, have a CPT-violating piece, δ, in addition to the usual CPT-conserving parameter ϵ:

$$K_{S,L} = \frac{1}{\sqrt{2\left(1+|\epsilon_{S,L}|^2\right)}}\left[\left(1+\epsilon_{S,L}\right)K^0 \pm \left(1-\epsilon_{S,L}\right)\overline{K}^0\right]$$

$$\epsilon_{S,L} = \frac{-i\Im\left(M_{12}\right) - \frac{1}{2}\Im\left(\Gamma_{12}\right) \mp \frac{1}{2}\left[M_{11} - M_{22} - \frac{i}{2}\left(\Gamma_{11}-\Gamma_{22}\right)\right]}{m_L - m_S + i(\Gamma_S - \Gamma_L)/2}$$

$$\equiv \epsilon \pm \delta. \tag{66.1}$$

Using the phase convention $\Im(\Gamma_{12}) = 0$, we determine the phase of ϵ to be $\varphi_{SW} \equiv \arctan\frac{2(m_L-m_S)}{\Gamma_S-\Gamma_L}$. Imposing unitarity to an arbitrary combination of K^0 and $\overline{K}^0$ wave functions, we obtain the Bell-Steinberger relation [5] connecting CP and CPT violation in the mass matrix to CP and CPT violation in the decay; in fact, neglecting $\mathcal{O}(\epsilon)$ corrections to the coefficient of the CPT-violating parameter, δ, we can write [4]

$$\left[\frac{\Gamma_S+\Gamma_L}{\Gamma_S-\Gamma_L} + i\tan\phi_{\rm SW}\right]\left[\frac{\Re(\epsilon)}{1+|\epsilon|^2} - i\Im(\delta)\right] = \frac{1}{\Gamma_S-\Gamma_L}\sum_f A_L(f)A_S^*(f), \tag{66.2}$$

where $A_{L,S}(f) \equiv A(K_{L,S} \to f)$. We stress that this relation is phase-convention-independent. The advantage of the neutral kaon system is that only a few decay modes give significant contributions to the r.h.s. in Eq. (66.2); in fact, defining for the hadronic modes

$$\alpha_i \equiv \frac{1}{\Gamma_S}\langle\mathcal{A}_L(i)\mathcal{A}_S^*(i)\rangle = \eta_i\ \mathcal{B}(K_S \to i),$$
$$i = \pi^0\pi^0, \pi^+\pi^-(\gamma), 3\pi^0, \pi^0\pi^+\pi^-(\gamma), \tag{66.3}$$

the recent data from CPLEAR, KLOE, KTeV, and NA48 have led to the following determinations (the analysis described in Ref. [4] has been updated by using the recent measurements of K_L branching ratios from KTeV [6, 7], NA48 [8, 9], the results described in the CP violation in K_L decays minireview, and the KLOE result [10])

$$\alpha_{\pi^+\pi^-} = ((1.121\pm0.010) + i(1.061\pm0.010))\times10^{-3} ,$$
$$\alpha_{\pi^0\pi^0} = ((0.493\pm0.005) + i(0.471\pm0.005))\times10^{-3} ,$$
$$\alpha_{\pi^+\pi^-\pi^0} = ((0\pm2) + i(0\pm2))\times10^{-6},$$
$$|\alpha_{\pi^0\pi^0\pi^0}| < 1.5\times10^{-6} \text{ at 95\% CL} . \tag{66.4}$$

The semileptonic contribution to the right-handed side of Eq. (66.2) requires the determination of several observables: we define [2, 3]

$$\mathcal{A}(K^0 \to \pi^- l^+\nu) = \mathcal{A}_0(1-y) ,$$
$$\mathcal{A}(K^0 \to \pi^+ l^-\nu) = \mathcal{A}_0^*(1+y^*)(x_+ - x_-)^* ,$$
$$\mathcal{A}(\overline{K}^0 \to \pi^+ l^-\nu) = \mathcal{A}_0^*(1+y^*) ,$$
$$\mathcal{A}(\overline{K}^0 \to \pi^- l^+\nu) = \mathcal{A}_0(1-y)(x_+ + x_-) , \tag{66.5}$$

where x_+ (x_-) describes the violation of the $\Delta S = \Delta Q$ rule in CPT-conserving (violating) decay amplitudes, and y parameterizes CPT violation for $\Delta S = \Delta Q$ transitions. Taking advantage of their tagged $K^0(\overline{K}^0)$ beams, CPLEAR has measured $\Im(x_+)$, $\Re(x_-)$, $\Im(\delta)$, and $\Re(\delta)$ [11]. These determinations have been improved in Ref. [4] by including the information $A_S - A_L = 4[\Re(\delta) + \Re(x_-)]$ (valid at first order in the small parameters), where $A_{L,S}$ are the K_L and K_S semileptonic charge asymmetries, respectively, from the PDG [12] and the new KLOE semileptonic measurement [13]. Here we are also including the T-violating asymmetry measurement from CPLEAR [14] with a finer binning than appearing in the published article.

Table 66.1: Values, errors, and correlation coefficients for $\Re(\delta)$, $\Im(\delta)$, $\Re(x_-)$, $\Im(x_+)$, and $A_S + A_L$ obtained from a combined fit, including KLOE [4, 13] and CPLEAR [14].

	value	Correlations coefficients				
$\Re(\delta)$	$(4.3\pm2.7)\ \times10^{-4}$	1				
$\Im(\delta)$	$(-0.9\pm0.6)\times10^{-2}$	−0.40	1			
$\Re(x_-)$	$(-0.22\pm0.10)\times10^{-2}$	−0.14	−0.30	1		
$\Im(x_+)$	$(0.06\pm0.19)\times10^{-2}$	−0.12	−0.02	0.34	1	
$A_S + A_L$	$(-0.23\pm0.38)\times10^{-2}$	−0.12	−0.29	0.94	0.18	1

The value $A_S + A_L$ in Table 66.1 can be directely included in the semileptonic contributions to the Bell Steinberger relations in Eq. (66.2)

$$\sum_{\pi\ell\nu}\langle\mathcal{A}_L(\pi\ell\nu)\mathcal{A}_S^*(\pi\ell\nu)\rangle$$
$$= 2\Gamma(K_L \to \pi\ell\nu)(\Re(\epsilon) - \Re(y) - i(\Im(x_+) + \Im(\delta)))$$
$$= 2\Gamma(K_L \to \pi\ell\nu)((A_S + A_L)/4 - i(\Im(x_+) + \Im(\delta))) . \tag{66.6}$$

Defining

$$\alpha_{\pi\ell\nu} \equiv \frac{1}{\Gamma_S}\sum_{\pi\ell\nu}\langle\mathcal{A}_L(\pi\ell\nu)\mathcal{A}_S^*(\pi\ell\nu)\rangle + 2i\frac{\tau_{K_S}}{\tau_{K_L}}\mathcal{B}(K_L \to \pi\ell\nu)\Im(\delta) , \tag{66.7}$$

we find:

$$\alpha_{\pi\ell\nu} = ((-0.1\pm0.2) + i(-0.1\pm0.5))\times10^{-5} . \tag{66.8}$$

Table 66.2: Summary of results: values, errors, and correlation coefficients for $\Re(\epsilon)$, $\Im(\delta)$, $\Re(\delta)$, and $\Re(x_-)$.

	value	Correlations coefficients			
$\Re(\epsilon)$	$(161.2\pm0.5)\times10^{-5}$	+1			
$\Im(\delta)$	$(-0.3\pm1.4)\times10^{-5}$	+0.08	1		
$\Re(\delta)$	$(2.6\pm2.5)\times10^{-4}$	+0.00	−0.05	1	
$\Re(x_-)$	$(-2.7\pm1.0)\times10^{-3}$	+0.05	0.13	−0.30	1

The analysis of semileptonic decay asymmetries implicitly assumes Lepton Flavour Universality (LFU) of any effect violating CPT or $\Delta S = \Delta Q$, through the use of a single set of x, y parameters, consistently with the availability of experimental information on A_S for the electron mode only. The explicit LFU assumption in the input BR measurements has been lifted exploiting the measurement of $BR(K_S \to \pi\mu\nu)$ Ref. [15], with no effect on the numerical results.

Int. J. Mod. Phys. A 2026.41. Downloaded from www.worldscientific.com
UNIVERSITY OF CALIFORNIA @ BERKELEY on 09/16/26. Re-use and distribution is strictly not permitted, except for Open Access articles.

Inserting the values of the α parameters into Eq. (66.2), we find

$$\Re(\epsilon) = (161.2 \pm 0.5) \times 10^{-5},$$
$$\Im(\delta) = (-0.3 \pm 1.4) \times 10^{-5}\,. \qquad (66.9)$$

The complete information on Eq. (66.9) is given in Table 66.2.

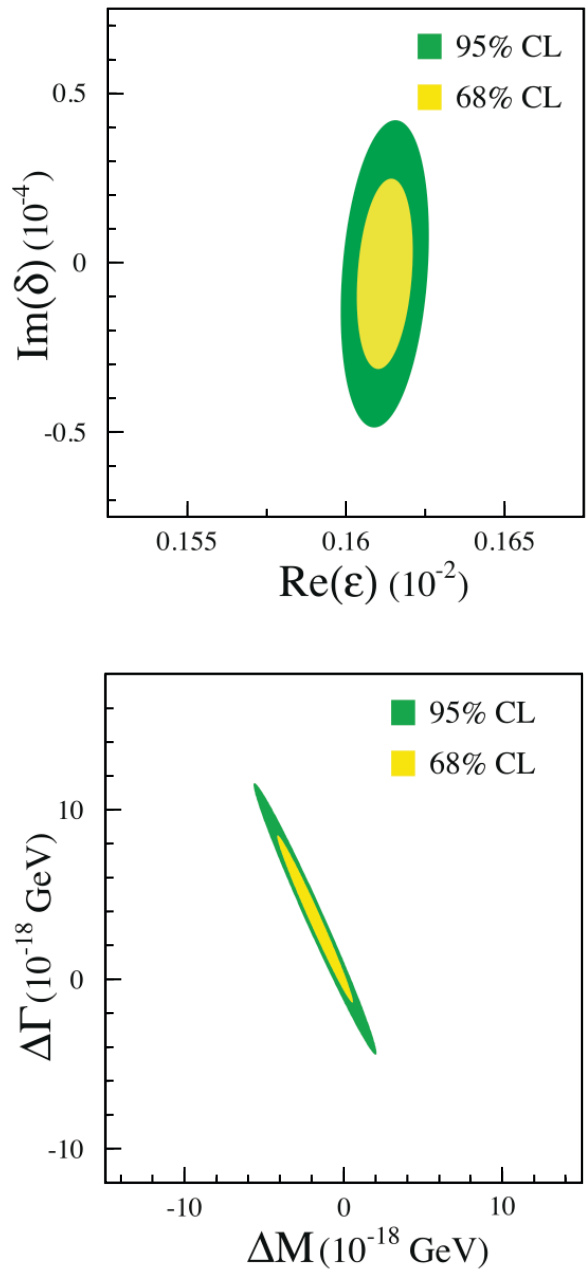

Figure 66.1: Top: allowed region at 68% and 95% C.L. in the $\Re(\epsilon)$, $\Im(\delta)$ plane. Bottom: allowed region at 68% and 95% C.L. in the $\Delta M, \Delta\Gamma$ plane.

Now the agreement with CPT conservation, $\Im(\delta) = \Re(\delta) = \Re(x_-) = 0$, is at 18% C.L.

The allowed region in the $\Re(\epsilon) - \Im(\delta)$ plane at 68% CL and 95% C.L. is shown in the top panel of Fig. 66.1.

The process giving the largest contribution to the size of the allowed region is $K_L \to \pi^+\pi^-$, through the uncertainty on ϕ_{+-}.

The limits on $\Im(\delta)$ and $\Re(\delta)$ can be used to constrain the $K^0 - \overline{K}^0$ mass and width difference

$$\delta = \frac{i(m_{K^0} - m_{\overline{K}^0}) + \frac{1}{2}(\Gamma_{K^0} - \Gamma_{\overline{K}^0})}{\Gamma_S - \Gamma_L} \cos\phi_{SW} e^{i\phi_{SW}} [1 + \mathcal{O}(\epsilon)]\,.$$

The allowed region in the $\Delta M = (m_{K^0} - m_{\overline{K}^0}), \Delta\Gamma = (\Gamma_{K^0} - \Gamma_{\overline{K}^0})$ plane is shown in the bottom panel of Fig. 66.1. As a result, we improve on the previous limits (see for instance, P. Bloch in Ref. [12]) and in the limit $\Gamma_{K^0} - \Gamma_{\overline{K}^0} = 0$ we obtain

$$-4.0\times10^{-19}\ \text{GeV} < m_{K^0} - m_{\overline{K}^0} < 4.0\times10^{-19}\ \text{GeV} \quad \text{at 95 \% C.L.}\,.$$

References

[1] See the "CP Violation in Meson Decays," in this *Review*.

[2] L. Maiani, "CP And CPT Violation in Neutral Kaon Decays," L. Maiani, G. Pancheri, and N. Paver, *The Second DAΦNE Physics Handbook,* Vol. 1,2.

[3] G. D'Ambrosio, G. Isidori and A. Pugliese, in "2nd DAΦNE Physics Handbook:63-96," 63–96 (1994), [hep-ph/9411389], URL `http://preprints.cern.ch/cgi-bin/setlink?base=preprint&categ=cern&id=th-7504-94`.

[4] G. D'Ambrosio and G. Isidori (KLOE), JHEP **12**, 011 (2006), [hep-ex/0610034].

[5] J. S. Bell and J. Steinberger, in "Wolfenstein, L. (eq.): CP violation, 42-57. (In Oxford International Symposium Conference on Elementary Particles) ," 195–208, 221–222 (1966), (See Book Index).

[6] T. Alexopoulos *et al.* (KTeV), Phys. Rev. **D70**, 092006 (2004), [hep-ex/0406002].

[7] E. Abouzaid *et al.* (KTeV), Phys. Rev. **D83**, 092001 (2011), [arXiv:1011.0127].

[8] A. Lai *et al.* (NA48), Phys. Lett. **B645**, 26 (2007), [hep-ex/0611052]; A. Lai *et al.* (NA48), Phys. Lett. **B602**, 41 (2004), [hep-ex/0410059].

[9] We thanks G. Isidori and M. Palutan for their contribution to the original analysis [4] performed with KLOE data.

[10] D. Babusci *et al.* (KLOE), Phys. Lett. **B723**, 54 (2013), [arXiv:1301.7623].

[11] A. Angelopoulos *et al.* (CPLEAR), Phys. Lett. **B444**, 52 (1998).

[12] W. M. Yao *et al.* (Particle Data Group), J. Phys. **G33**, 1 (2006).

[13] A. Anastasi *et al.* (KLOE-2), JHEP **09**, 021 (2018), [arXiv:1806.08654].

[14] P. Bloch, M. Fidecaro, private communication of the data in a finer binning format; A. Angelopoulos *et al.* (CPLEAR), Phys. Lett. **B444**, 43 (1998).

[15] D. Babusci *et al.* (KLOE-2), Phys. Lett. B **804**, 135378 (2020), [arXiv:1912.05990].

Int. J. Mod. Phys. A 2026.41. Downloaded from www.worldscientific.com
by UNIVERSITY OF CALIFORNIA @ BERKELEY on 09/16/26. Re-use and distribution is strictly not permitted, except for Open Access articles.

67. V_{ud}, V_{us} the Cabibbo Angle, and CKM Unitarity

Revised August 2025 by E. Blucher (Chicago U.), G. D'Ambrosio (INFN, Napoli) and W.J. Marciano (BNL).

The Cabibbo-Kobayashi-Maskawa (CKM) [1, 2] three-generation quark mixing matrix written in terms of the Wolfenstein parameters (λ, A, ρ, η) [3] nicely illustrates the orthonormality constraint of unitarity, as well as the central role played by λ.

$$V_{\rm CKM} = \begin{pmatrix} V_{ud} & V_{us} & V_{ub} \\ V_{cd} & V_{cs} & V_{cb} \\ V_{td} & V_{ts} & V_{tb} \end{pmatrix} = \begin{pmatrix} 1-\lambda^2/2 & \lambda & A\lambda^3(\rho - i\eta) \\ -\lambda & 1-\lambda^2/2 & A\lambda^2 \\ A\lambda^3(1-\rho-i\eta) & -A\lambda^2 & 1 \end{pmatrix} + \mathcal{O}(\lambda^4)\ . \tag{67.1}$$

That cornerstone parameter is a carryover from the two-generation Cabibbo angle, $\lambda = \sin(\theta_{\rm Cabibbo}) = V_{us}$. Its value is an important component in tests of CKM unitarity.

Up until 2003, the precise value of λ was controversial, with kaon decays (specifically $K \to \pi e \nu$) branching fractions suggesting [4] $\lambda \simeq 0.220$, while indirect determinations via V_{ud} obtained from nuclear β-decays combined with unitarity preferred a somewhat larger $\lambda \simeq 0.225 - 0.230$. This difference implied a 2 - 2.5 sigma deviation from the first row unitarity requirement

$$|V_{ud}|^2 + |V_{us}|^2 + |V_{ub}|^2 = 1, \tag{67.2}$$

a possible hint [5, 6] of new physics effects. Below, we describe the current status of V_{ud} and V_{us}, and their implication for the unitarity test in Eq. (67.2). (Since $|V_{ub}|^2 \simeq 1.7\times10^{-5}$ is negligibly small, it is ignored in this discussion.) Eq. (67.2) is currently the most stringent test of unitarity in the CKM matrix. As we shall see, it is again showing signs of a possible 2 to 3 sigma inconsistency.

67.1 V_{ud}

Precise values of V_{ud} have been obtained from superallowed nuclear, neutron, and pion beta decays. Currently, the best determination of V_{ud} comes from analysis of a set of 15 precisely measured superallowed nuclear beta-decays [5, 6] ($0^+ \to 0^+$ transitions). Measuring their half-lives, t, and Q values gives the decay rate factors, f, which lead to a precise determination of V_{ud} via [7–12]. Based on several decades of dedicated studies, Hardy and Towner recently updated the average of the half-life, $\overline{\mathcal{F}t}$, [6]

$$|V_{ud}|^2 = \frac{K}{2G_F^2(1+\Delta_{\rm R}^{\rm V})\overline{\mathcal{F}t}} = \frac{2912.95 \pm 0.54}{\overline{\mathcal{F}t}} = 0.94815 \pm 0.00060 \quad \text{for } \Delta_R^V = 2.454(19)\%, \tag{67.3}$$

where $K/(\hbar c)^6 = 2\pi^3\hbar \ln 2/(m_e c^2)^5 = 8120.27648(26) \times 10^{-10} GeV^{-4}s$, Δ_R^V denotes the so-called inner or universal electroweak radiative corrections (RC) to superallowed nuclear beta decays. A dispersion relation (DR) calculational approach [13] to quantum loop corrections, specifically the gamma-W box diagram, gives $\Delta_R^V = 0.02467(22)$. Actually the authors of Ref. [13–19] have combined the different theoretical calculations leading to $\Delta_R^V = 0.02467(27)$ and

$$V_{ud} = 0.97367(11)_{\rm exp}(13)_{\Delta_R^V}(27)_{\rm NS}\ (32)_{\rm total}\ \text{(superallowed)}\ . \tag{67.4}$$

As a result of its small uncertainty and more rigorous theoretical footing, we use this value below. A somewhat different approach [16] found $\Delta_R^V = 0.02426(32)$. These recent values are roughly consistent. Both are larger than the 2018 PDG value of 0.02361(38). Implications and possible nuclear physics modifications of those studies are still under scrutiny [20–24]. Note that an additional uncertainty $(54)_{\rm NS}$ from nuclear structure (NS) [21] has been recently included [6] in that master formula. This recent determination of V_{ud} has shifted significantly down compared to the 2018 PDG value of 0.97420(21). In addition, NS uncertainties are now the dominant contribution to the overall uncertainty. Taken at face value, along with current V_{us} determinations (see subsection 67.2), the reduced V_{ud} would seem to violate the first row unitarity requirement, and thus suggest the presence of deviations from unitarity or unaccounted uncertainties.

Measurements of the neutron lifetime, τ_n, and the ratio of axial-vector/vector couplings, $g_A \equiv G_A/G_V$, via neutron decay asymmetries combined with the inner radiative corrections can also be used to determine V_{ud} via the precise formula [14, 25]

$$|V_{ud}|^2 = \frac{5099.33\ \text{s}}{\tau_n(1+3{g_A}^2)(1+\Delta_R)}, \tag{67.5}$$

where $\Delta_R = 0.03983(27)$ represents radiative corrections [14]. We present the V_{ud} results using either the the current published world averages [26] or the best measured values for λ [27] and for τ_n [28]. The average leads to

$$\tau_n^{\rm ave} = 879.4(6)\ \text{s}\ \ (1.6\ \text{PDG scale factor})$$
$$g_A^{\rm ave} = 1.2756(13),\ \ (2.6\ \text{PDG scale factor}), \tag{67.6}$$

$$|V_{ud}^{n,PDG}| = 0.97441(28)_{\tau_n}(82)_\lambda(13)_{\Delta_R}(88)_{\rm TOT}, \tag{67.7}$$

while the best values lead to

$$|V_{ud}^{n,best}| = 0.97413(20)_{\tau_n}(35)_\lambda(13)_{\Delta_R}(42)_{\rm TOT}. \tag{67.8}$$

Both central values are similar to the superallowed nuclear beta decay result reported above. Reconciliation with CKM unitarity suggests a shorter neutron lifetime near 878.5 s or a smaller g_A. We note that the most precise recent neutron lifetime update reported [28], $\tau_n = 877.75(34)$ s, has an uncertainty about half as big as the average given in Eq. 67.6. It corresponds to $|V_{ud}| = 0.9746(8)$, a value more in keeping with unitarity expectations; but too large an uncertainty from g_A to be meaningful. Future neutron studies [29, 30] are expected to resolve any current inconsistencies and further reduce the uncertainties in g_A and τ_n making them a potentially better way to determine V_{ud} without the nuclear physics uncertainties.

The PIBETA experiment at PSI measured the very small ($\mathcal{O}(10^{-8})$) branching ratio for $\pi^+ \to \pi^o e^+ \nu_e$ with about $\pm 0.6\%$ precision. Its result gives [31]

$$|V_{ud}| = 0.9739(27)\left[\frac{BR(\pi^+ \to e^+\nu_e(\gamma))}{1.2325\times10^{-4}}\right]^{\frac{1}{2}}, \tag{67.9}$$

which is normalized using the very precisely measured $BR(\pi^+ \to e^+\nu_e(\gamma)) = 1.2325(23) \times 10^{-4}$ [7], rather than the theoretical branching ratio of $1.2350(2)\times10^{-4}$, which if used, would increase $|V_{ud}|$ to 0.9749(27). Theoretical uncertainties in pion beta decay are very small [32], leaving open more than an order of magnitude improvement of its experimental branching ratio before theory uncertainties become a problem. Although challenging, improved measurements of pion beta decay currently under discussion would allow this decay mode to compete with superallowed beta decays and future neutron decay efforts for the most precise direct $|V_{ud}|$ determination.

67.2 V_{us}

$|V_{us}|$ may be directly obtained from kaon decays, hyperon decays, and tau decays. Early determinations most often used $K\ell3$ decays:

$$\Gamma_{K\ell3} = \frac{G_F^2 M_K^5}{192\pi^3} S_{EW}(1+\delta_K^\ell+\delta_{SU2})C^2\,|V_{us}|^2\, f_+^2(0) I_K^\ell. \tag{67.10}$$

Here, ℓ refers to either e or μ, G_F is the Fermi constant, M_K is the kaon mass, S_{EW} is the short-distance radiative correction, δ_K^ℓ is the mode-dependent long-distance radiative correction, $f_+(0)$ is the calculated form factor at zero momentum transfer for the $\ell\nu$ system, and I_K^ℓ is the phase-space integral, which depends on measured semileptonic form factors. For charged kaon decays, δ_{SU2} is the deviation from one of the ratio of $f_+(0)$ for the charged to neutral kaon decay; it is zero for the neutral kaon. C^2 is 1 (1/2) for neutral (charged) kaon decays. Most early determinations of

Int. J. Mod. Phys. A 2026.41. Downloaded from www.worldscientific.com
UNIVERSITY OF CALIFORNIA @ BERKELEY on 09/16/26. Re-use and distribution is strictly not permitted, except for Open Access articles.

$|V_{us}|$ were based solely on $K \to \pi e \nu$ decays; $K \to \pi \mu \nu$ decays were not used because of large uncertainties in I_K^μ. The experimental measurements are the semileptonic decay widths (based on the semileptonic branching fractions and lifetime) and form factors (allowing calculation of the phase space integrals). Theory is needed for S_{EW}, δ_K^ℓ, δ_{SU2}, and $f_+(0)$.

Many measurements during the last 20 years have resulted in a shift in $|V_{us}|$. Most importantly, the $K \to \pi e \nu$ branching fractions are significantly different than much earlier PDG averages, probably as a result of inadequate treatment of radiation in older experiments. This effect was first observed by BNL E865 [33] in the charged kaon system and then by KTeV [34,35] in the neutral kaon system; subsequent measurements were made by KLOE [36–39], NA48 [40–42], and ISTRA+ [43]. Current averages (*e.g.*, by the PDG [44] or Flavianet [45]) of the semileptonic branching fractions are based only on recent, high-statistics experiments where the treatment of radiation is clear. In addition to measurements of branching fractions, new measurements of lifetimes [46] and form factors [47–51], have resulted in improved precision for all of the experimental inputs to $|V_{us}|$. Precise measurements of form factors for $K_{\mu 3}$ decay make it possible to use both semileptonic decay modes to extract V_{us}.

Following the analysis of Moulson [25, 52] and the Flavianet group [45, 53, 54], along with recent improvements in the QED radiative corrections [55], one finds [56], after including the isospin violating effect, δ_{SU2} , the values of $|V_{us}|f_+(0)$ in Table 67.1. The average of these measurements, including correlation effects [25, 56–58] gives [14]

$$f_+(0)|V_{us}| = 0.21656(35) \quad \text{FLAVIANET} \tag{67.11}$$

where the errors correspond to kaon experimental parameters and radiative corrections, respectively, leading, as we shall see, to $|V_{us}| = 0.22330(35)_{\rm exp}(39)_{\rm LAT}(8)_{\rm RC+IB}(53)_{TOT}$.

Lattice QCD calculations of $f_+(0)$ have been carried out for 2, 2+1, and 2+1+1 quark flavors and range from about 0.96 to 0.97. Here, we illustrate recent FLAG (2020) updated averages [59] for 2+1 and 2+1+1 flavors:

$$\begin{aligned} f_+(0) &= 0.9677(27) \quad N_f = 2+1 \\ f_+(0) &= 0.9698(17) \quad N_f = 2+1+1 \end{aligned} \tag{67.12}$$

Updating the result for $N_f = 2+1+1$ we obtain for V_{us} from Eq. (67.11) and Eq. (67.12),

$$\begin{aligned} |V_{us}| &= 0.2238(4)_{\rm exp+RC}(6)_{\rm lattice} \ (N_f = 2+1,\ K_{\ell 3} \text{ decays}) \\ &= 0.22330(4)_{\rm exp+RC}(4)_{\rm lattice} \ (N_f = 2+1+1,\ K_{\ell 3} \text{ decays}) \end{aligned} \tag{67.13}$$

based on ref. [25] and ref. [56]

Table 67.1: $|V_{us}|f_+(0)$ from $K\ell 3$, based on ref. [25, 56]

Decay Mode	$\lvert V_{us}\rvert f_+(0)$
$K^\pm e3$	0.2169(6)
$K^\pm \mu 3$	0.2168(10)
$K_L e3$	0.2162(5)
$K_L \mu 3$	0.2165(6)
$K_S e3$	0.2169(8)
$K_S \mu 3$	0.2125(47)
Average (including correlation effects [25, 56])	0.21656(35)

A value of V_{us} can also be obtained from a comparison of the radiative inclusive decay rates for $K \to \mu\nu(\gamma)$ and $\pi \to \mu\nu(\gamma)$ combined with a lattice gauge theory calculation of f_{K^+}/f_{π^+} via

$$\frac{|V_{us}|f_{K^+}}{|V_{ud}|f_{\pi^+}} = 0.23871(20) \left[\frac{\Gamma(K \to \mu\nu(\gamma))}{\Gamma(\pi \to \mu\nu(\gamma))}\right]^{\frac{1}{2}} \tag{67.14}$$

with the small error coming from electroweak radiative corrections [60–62]; these corrections were confirmed by direct lattice calculation of the kaon and pion leptonic decay rates [61, 62].

A recent fit [14, 25] gives

$$\frac{|V_{us}|f_{K^+}}{|V_{ud}|f_{\pi^+}} = 0.27679(28)_{\rm BR}(20)_{\rm corr}. \tag{67.15}$$

Employing the FLAG [59] lattice QCD averages for the isospin broken decay constants

$$\frac{f_{K^+}}{f_{\pi^+}} = 1.1978(22) \quad N_f = 2+1+1 \tag{67.16}$$

leading to

$$\frac{|V_{us}|}{|V_{ud}|} = 0.23108(51) \ (N_f = 2+1+1,\ K_{\mu 2} \text{ decays}). \tag{67.17}$$

Actually we can average the Cabibbo angle determinations from kaons: from $K_{\ell 3}$ decays in eqs. 67.11, 67.12 and from $K_{\mu 2}$ in eqs. 67.15, 67.16 with $N_f = 2+1+1$. Assuming 20% correlation between $(|V_{us}/V_{ud}|f_K/f_\pi)$ and (f_K/f_π) we obtain

$$V_{us} = 0.22431(85) \quad \text{S} = 2.5. \tag{67.18}$$

The result shown in Eq. 67.18 is what we use when we consider the first row test of CKM unitarity. The quoted uncertainty includes a scale factor of 2.5 to account for the discrepancies between the values of V_{us} obtained from $K\ell 3$ and $K\mu 2$ decays.

This is the current status of the Cabibbo Angle determination from the kaon sector, and theoretical and experimental progress is expected to clarify the situation soon.

It should be mentioned that hyperon decay fits suggest [63]

$$|V_{us}| = 0.2250(27) \ \text{(Hyperon Decays)} \tag{67.19}$$

modulo SU(3) breaking effects that could shift that value up or down. We note that a representative effort [64] that incorporates SU(3) breaking found $V_{us} = 0.226(5)$. Strangeness changing tau decays, averaging both inclusive and exclusive measurements, give [65, 66]

$$|V_{us}| = 0.2207(14) \ \text{(Tau Decays)} \ , \tag{67.20}$$

which differs by about 2 sigma from the kaon determination discussed above, and would, if combined with V_{ud} from super-allowed beta decays, lead to a 4 sigma deviation from unitarity. This discrepancy results mainly from the inclusive tau decay results that rely on Finite Energy Sum Rule techniques and assumptions, as well as experimental uncertainties. Recent investigation of that approach suggests a larger value for V_{us}, which is more in accord with other determinations [67].

Employing the values of V_{ud} and V_{us} with an error scale factor of 2 from Eq. (67.4) and the average obtained after rescaling the errors from mEq. 67.18 leads to the unitarity consistency check

$$|V_{ud}|^2 + |V_{us}|^2 + |V_{ub}|^2 = 0.9983(6)(4), \tag{67.21}$$

where the first error is the uncertainty from $|V_{ud}|^2$ and the second error is the uncertainty from the average $|V_{us}|^2$ in Eq. 67.18 . One finds about an overall 2 sigma deviation from unitarity. (The deviation increases to 3 sigma if nuclear structure uncertainties are ignored.) That deviation could be due a problem with $|V_{ud}|$ theory (RC or NS), the lattice determination of $f_+(0)$ or new physics.

67.3 CKM Unitarity Constraints

The current 2 sigma experimental disagreement with unitarity, $|V_{ud}|^2 + |V_{us}|^2 + |V_{ub}|^2 = 0.9983(7)$, still provides strong confirmation of Standard Model radiative corrections (which range between 3-4% depending on the nucleus used) at a high significance level [68]. In addition, it implies constraints on "New Physics" effects at both the tree and quantum loop levels. Those effects could be in the form of contributions to nuclear beta decays, K decays and/or muon decays, with the last of these providing normalization via the muon lifetime [69], which is used to obtain the Fermi constant, $G_\mu = 1.1663787(6) \times 10^{-5}\text{GeV}^{-2}$.

In the following examples, we illustrate the implications of CKM unitarity for (1) exotic muon decays [70] (beyond ordinary

Int. J. Mod. Phys. A 2026.41. Downloaded from www.worldscientific.com
by UNIVERSITY OF CALIFORNIA @ BERKELEY on 09/16/26. Re-use and distribution is strictly not permitted, except for Open Access articles.

muon decay $\mu^+ \to e^+\nu_e\bar{\nu}_\mu$) and (2) new heavy quark mixing V_{uD} [71]. Other examples in the literature [72, 73] include Z_χ boson quantum loop effects, supersymmetry, leptoquarks, compositeness etc.

References

[1] N. Cabibbo, Phys. Rev. Lett. **10**, 531 (1963).

[2] M. Kobayashi and T. Maskawa, Prog. Theor. Phys. **49**, 652 (1973).

[3] L. Wolfenstein, Phys. Rev. Lett. **51**, 1945 (1983).

[4] S. Eidelman *et al.* (Particle Data Group), Phys. Lett. B **592**, 1-4, 1 (2004).

[5] I. Towner and J. Hardy, Rept. Prog. Phys. **73**, 046301 (2010).

[6] J. C. Hardy and I. S. Towner, Phys. Rev. C **102**, 4, 045501 (2020).

[7] W. J. Marciano and A. Sirlin, Phys. Rev. Lett. **71**, 3629 (1993).

[8] A. Czarnecki, W. J. Marciano and A. Sirlin, Phys. Rev. D **70**, 093006 (2004), [hep-ph/0406324].

[9] W. J. Marciano and A. Sirlin, Phys. Rev. Lett. **96**, 032002 (2006), [hep-ph/0510099].

[10] I. Towner and J. Hardy, Phys. Rev. C **77**, 025501 (2008), [arXiv:0710.3181].

[11] J. Hardy and I. Towner, Phys. Rev. C **79**, 055502 (2009), [arXiv:0812.1202].

[12] J. Hardy and I. Towner, Phys. Rev. C **91**, 2, 025501 (2015), [arXiv:1411.5987].

[13] C.-Y. Seng *et al.*, Phys. Rev. Lett. **121**, 24, 241804 (2018), [arXiv:1807.10197].

[14] V. Cirigliano *et al.*, Phys. Lett. B **838**, 137748 (2023), [arXiv:2208.11707].

[15] C.-Y. Seng, M. Gorchtein and M. J. Ramsey-Musolf, Physical Review D **100**, 1 (2019), ISSN 2470-0029, URL `http://dx.doi.org/10.1103/PhysRevD.100.013001`.

[16] A. Czarnecki, W. J. Marciano and A. Sirlin, Phys. Rev. D **100**, 7, 073008 (2019), [arXiv:1907.06737].

[17] C.-Y. Seng *et al.*, Physical Review D **101**, 11 (2020), ISSN 2470-0029, URL `http://dx.doi.org/10.1103/PhysRevD.101.111301`.

[18] L. Hayen, Phys. Rev. D **103**, 113001 (2021), URL `https://link.aps.org/doi/10.1103/PhysRevD.103.113001`.

[19] K. Shiells, P. G. Blunden and W. Melnitchouk, Phys. Rev. D **104**, 033003 (2021), URL `https://link.aps.org/doi/10.1103/PhysRevD.104.033003`.

[20] C. Y. Seng, M. Gorchtein and M. J. Ramsey-Musolf, Phys. Rev. D **100**, 1, 013001 (2019), [arXiv:1812.03352].

[21] M. Gorchtein, Phys. Rev. Lett. **123**, 4, 042503 (2019), [arXiv:1812.04229].

[22] M. Gennari *et al.*, Phys. Rev. Lett. **134**, 1, 012501 (2025), [arXiv:2405.19281].

[23] V. Cirigliano *et al.*, Phys. Rev. Lett. **133**, 21, 211801 (2024), [arXiv:2405.18469].

[24] V. Cirigliano *et al.*, Phys. Rev. C **110**, 5, 055502 (2024), [arXiv:2405.18464].

[25] M. Moulson, talk at CKM2023, `https://indico.cern.ch/event/1184945/contributions/5540813/attachments/2717802/4721036/CKM202023.pdf`.

[26] R. L. Workman *et al.* (Particle Data Group), PTEP **2022**, 083C01 (2022).

[27] B. Märkisch *et al.*, Phys. Rev. Lett. **122**, 24, 242501 (2019), [arXiv:1812.04666].

[28] F. M. Gonzalez *et al.* (UCNτ) (2021), [arXiv:2106.10375].

[29] H. Abele, Prog. Part. Nucl. Phys. **60**, 1 (2008).

[30] D. Dubbers and B. Märkisch, Annual Review of Nuclear and Particle Science **71**, 1, 139–163 (2021), ISSN 1545-4134, URL `http://dx.doi.org/10.1146/annurev-nucl-102419-043156`.

[31] D. Pocanic *et al.*, Phys. Rev. Lett. **93**, 181803 (2004), [hep-ex/0312030]; A. Czarnecki, W. J. Marciano and A. Sirlin, Phys. Rev. D **101**, 9, 091301 (2020), [arXiv:1911.04685].

[32] X. Feng *et al.*, Phys. Rev. Lett. **124**, 19, 192002 (2020), [arXiv:2003.09798].

[33] A. Sher *et al.*, Phys. Rev. Lett. **91**, 261802 (2003), [hep-ex/0305042].

[34] T. Alexopoulos *et al.* (KTeV), Phys. Rev. Lett. **93**, 181802 (2004), [hep-ex/0406001].

[35] T. Alexopoulos *et al.* (KTeV), Phys. Rev. D **70**, 092006 (2004), [hep-ex/0406002].

[36] F. Ambrosino *et al.* (KLOE), Phys. Lett. B **632**, 43 (2006), [hep-ex/0508027].

[37] F. Ambrosino *et al.* (KLOE), Phys. Lett. B **638**, 140 (2006), [hep-ex/0603041].

[38] F. Ambrosino *et al.* (KLOE), Phys. Lett. B **636**, 173 (2006), [hep-ex/0601026].

[39] B. Sciascia (KLOE), PoS **HEP2005**, 287 (2006), [hep-ex/0510028].

[40] A. Lai *et al.* (NA48), Phys. Lett. B **602**, 41 (2004), [hep-ex/0410059].

[41] A. Lai *et al.* (NA48), Phys. Lett. B **645**, 26 (2007), [hep-ex/0611052].

[42] J. Batley *et al.* (NA48/2), Eur. Phys. J. C **50**, 329 (2007), [Erratum: Eur.Phys.J.C 52, 1021–1023 (2007)], [hep-ex/0702015].

[43] V. Romanovsky *et al.* (2007), [arXiv:0704.2052].

[44] K. Olive *et al.* (Particle Data Group), Chin. Phys. C **38**, 090001 (2014).

[45] M. Antonelli *et al.* (FlaviaNet Working Group on Kaon Decays), Eur. Phys. J. C **69**, 399 (2010), [arXiv:1005.2323]; For a detailed review, see; M. Antonelli *et al.*, Phys. Rept. **494**, 197 (2010), [arXiv:0907.5386].

[46] F. Ambrosino *et al.* (KLOE), Phys. Lett. B **626**, 15 (2005), [hep-ex/0507088].

[47] T. Alexopoulos *et al.* (KTeV), Phys. Rev. D **70**, 092007 (2004), [hep-ex/0406003].

[48] E. Abouzaid *et al.* (KTeV), Phys. Rev. D **74**, 097101 (2006), [hep-ex/0608058].

[49] F. Ambrosino *et al.* (KLOE), Phys. Lett. B **636**, 166 (2006), [hep-ex/0601038].

[50] A. Lai *et al.* (NA48), Phys. Lett. B **604**, 1 (2004), [hep-ex/0410065].

[51] O. Yushchenko *et al.*, Phys. Lett. B **589**, 111 (2004), [hep-ex/0404030].

[52] M. Moulson, PoS **CKM2016**, 033 (2017), [arXiv:1704.04104].

[53] E. Passemar, talk at CKM2018, `https://zenodo.org/record/2565480`.

[54] Y. Aoki *et al.* (Flavour Lattice Averaging Group (FLAG)), Eur. Phys. J. C **82**, 10, 869 (2022), [arXiv:2111.09849].

[55] C.-Y. Seng *et al.* (2021), [arXiv:2103.04843].

[56] C.-Y. Seng *et al.* (2021), [arXiv:2107.14708].

[57] C.-Y. Seng *et al.*, JHEP **07**, 071 (2022), [arXiv:2203.05217].

[58] V. Cirigliano, talk at Cabibbo 60 - Convegno, Accademia Nazionale dei Lincei , `https://www.lincei.it/it/manifestazioni/cabibbo-60-convegno`.

[59] S. Aoki *et al.* (Flavour Lattice Averaging Group), Eur. Phys. J. C **80**, 2, 113 (2020), [arXiv:1902.08191]; A. Bazavov *et al.*, Phys. Rev. Lett. **112**, 11, 112001 (2014), [arXiv:1312.1228]; N. Carrasco *et al.*, Phys. Rev. D **93**, 11, 114512 (2016), [arXiv:1602.04113]; A. Bazavov *et al.*, Phys. Rev. D **87**, 073012 (2013), [arXiv:1212.4993]; P. A. Boyle *et al.* (RBC/UKQCD), JHEP **06**, 164 (2015), [arXiv:1504.01692]; A. Bazavov *et al.*, Phys. Rev. D **98**, 7, 074512 (2018), [arXiv:1712.09262]; T. Blum *et al.* (RBC, UKQCD), Phys. Rev. D **93**, 7, 074505 (2016), [arXiv:1411.7017]; R. Dowdall *et al.*, Phys. Rev. D **88**, 074504 (2013), [arXiv:1303.1670]; N. Carrasco *et al.*, Phys. Rev. D **91**, 5, 054507 (2015), [arXiv:1411.7908]; E. Follana *et al.* (HPQCD, UKQCD), Phys. Rev. Lett. **100**, 062002 (2008), [arXiv:0706.1726]; A. Bazavov *et al.* (MILC), PoS **LATTICE2010**, 074 (2010), [arXiv:1012.0868]; S. Durr *et al.*, Phys. Rev. D **81**, 054507 (2010), [arXiv:1001.4692]; S. Dürr *et al.*, Phys. Rev. D **95**, 5, 054513 (2017), [arXiv:1601.05998]; V. Bornyakov *et al.* (QCDSF), Phys. Lett. B **767**, 366 (2017), [arXiv:1612.04798].

[60] V. Cirigliano and H. Neufeld, Phys. Lett. B **700**, 7 (2011), [arXiv:1102.0563]; W. J. Marciano, Phys. Rev. Lett. **93**, 231803 (2004), [hep-ph/0402299].

[61] D. Giusti *et al.*, Phys. Rev. Lett. **120**, 7, 072001 (2018), [arXiv:1711.06537].

[62] M. Di Carlo *et al.*, Phys. Rev. D **100**, 3, 034514 (2019), [arXiv:1904.08731].

[63] N. Cabibbo, E. C. Swallow and R. Winston, Phys. Rev. Lett. **92**, 251803 (2004), [hep-ph/0307214].

[64] V. Mateu and A. Pich, JHEP **10**, 041 (2005), [hep-ph/0509045].

[65] Y. S. Amhis *et al.* (HFLAV) (2019), [arXiv:1909.12524].

[66] Y. S. Amhis *et al.* (HFLAV), Phys. Rev. D **107**, 5, 052008 (2023), [arXiv:2206.07501].

[67] R. J. Hudspith *et al.*, Phys. Lett. B **781**, 206 (2018), [arXiv:1702.01767]; P. Boyle *et al.* (RBC, UKQCD), Phys. Rev. Lett. **121**, 20, 202003 (2018), [arXiv:1803.07228].

[68] A. Sirlin, Rev. Mod. Phys. **50**, 573 (1978), [Erratum: Rev.Mod.Phys. 50, 905 (1978)].

[69] D. Webber *et al.* (MuLan), Phys. Rev. Lett. **106**, 041803 (2011), [arXiv:1010.0991].

[70] K. Babu and S. Pakvasa (2002), [hep-ph/0204236].

[71] W. Marciano and A. Sirlin, Phys. Rev. Lett. **56**, 22 (1986); P. Langacker and D. London, Phys. Rev. D **38**, 886 (1988).

[72] W. Marciano and A. Sirlin, Phys. Rev. D **35**, 1672 (1987).

[73] R. Barbieri *et al.*, Phys. Lett. B **156**, 348 (1985); K. Hagiwara, S. Matsumoto and Y. Yamada, Phys. Rev. Lett. **75**, 3605 (1995), [hep-ph/9507419]; A. Kurylov and M. Ramsey-Musolf, Phys. Rev. Lett. **88**, 071804 (2002), [hep-ph/0109222]; S. Bauman, J. Erler and M. Ramsey-Musolf, Phys. Rev. D **87**, 3, 035012 (2013), [arXiv:1204.0035].

Int. J. Mod. Phys. A 2026.41. Downloaded from www.worldscientific.com
UNIVERSITY OF CALIFORNIA @ BERKELEY on 09/16/26. Re-use and distribution is strictly not permitted, except for Open Access articles.

Int. J. Mod. Phys. A 2026.41. Downloaded from www.worldscientific.com
by UNIVERSITY OF CALIFORNIA @ BERKELEY on 09/16/26. Re-use and distribution is strictly not permitted, except for Open Access articles.

68. CP Violation in K_L^0 Decays

Revised August 2023 by C.-J. Lin (LBNL).

The symmetries C (particle-antiparticle interchange) and P (space inversion) hold for strong and electromagnetic interactions. After the discovery of large C and P violation in the weak interactions, it appeared that the product CP was a good symmetry. In 1964 CP violation was observed in K^0 decays at a level given by the parameter $\epsilon \approx 2.3 \times 10^{-3}$.

A unified treatment of CP violation in K, D, B, and B_s mesons is given in "CP Violation in Meson Decays" by D. Kirkby and Y. Nir in this *Review*. A more detailed review including a thorough discussion of the experimental techniques used to determine CP violation parameters is given in a book by K. Kleinknecht [1]. Here we give a concise summary of the formalism needed to define the parameters of CP violation in K_L decays, and a description of our fits for the best values of these parameters.

68.1 Formalism for CP violation in Kaon decay

CP violation has been observed in the semi-leptonic decays $K_L^0 \to \pi^\mp \ell^\pm \nu$, and in the nonleptonic decay $K_L^0 \to 2\pi$. The experimental numbers that have been measured are

$$A_L = \frac{\Gamma(K_L^0 \to \pi^- \ell^+ \nu) - \Gamma(K_L^0 \to \pi^+ \ell^- \nu)}{\Gamma(K_L^0 \to \pi^- \ell^+ \nu) + \Gamma(K_L^0 \to \pi^+ \ell^- \nu)} \tag{68.1a}$$

$$\eta_{+-} = A(K_L^0 \to \pi^+\pi^-)/A(K_S^0 \to \pi^+\pi^-) = |\eta_{+-}|\, e^{i\phi_{+-}} \tag{68.1b}$$

$$\eta_{00} = A(K_L^0 \to \pi^0\pi^0)/A(K_S^0 \to \pi^0\pi^0) = |\eta_{00}|\, e^{i\phi_{00}} \ . \tag{68.1c}$$

CP violation can occur either in the K^0–$\overline{K}^0$ mixing or in the decay amplitudes. Assuming CPT invariance, the mass eigenstates of the K^0–$\overline{K}^0$ system can be written

$$|K_S\rangle = p|K^0\rangle + q|\overline{K}^0\rangle \ , \quad |K_L\rangle = p|K^0\rangle - q|\overline{K}^0\rangle \ . \tag{68.2}$$

If CP invariance held, we would have $q = p$ so that K_S would be CP-even and K_L CP-odd. (We define $|\overline{K}^0\rangle$ as $CP\ |K^0\rangle$). CP violation in K^0–$\overline{K}^0$ mixing is then given by the parameter $\widetilde{\epsilon}$ where

$$\frac{p}{q} = \frac{(1+\widetilde{\epsilon})}{(1-\widetilde{\epsilon})} \ . \tag{68.3}$$

CP violation can also occur in the decay amplitudes

$$A\Big(K^0 \to \pi\pi(I)\Big) = A_I e^{i\delta_I} \ , \quad A\Big(\overline{K}^0 \to \pi\pi(I)\Big) = A_I^* e^{i\delta_I} \ , \tag{68.4}$$

where I is the isospin of $\pi\pi$, δ_I is the final-state phase shift, and A_I would be real if CP invariance held. The CP-violating observables are usually expressed in terms of ϵ and ϵ' defined by

$$\eta_{+-} = \epsilon + \epsilon' \ , \quad \eta_{00} = \epsilon - 2\epsilon' \ . \tag{68.5a}$$

One can then show [2]

$$\epsilon = \widetilde{\epsilon} + i\ \Big(\mathrm{Im}\ A_0/\mathrm{Re}\ A_0\Big) \ , \tag{68.5b}$$

$$\sqrt{2}\epsilon' = ie^{i(\delta_2-\delta_0)}(\mathrm{Re}\,A_2/\mathrm{Re}\,A_0)\ \Big(\mathrm{Im}\,A_2/\mathrm{Re}\,A_2 - \mathrm{Im}\,A_0/\mathrm{Re}\,A_0\Big) \ , \tag{68.5c}$$

$$A_L = 2\mathrm{Re}\ \epsilon/(1+|\epsilon|^2) \approx 2\mathrm{Re}\ \epsilon \ . \tag{68.5d}$$

In Eq. (68.5a), small corrections [3] of order $\epsilon' \times \mathrm{Re}\ (A_2/A_0)$ are neglected, and Eq. (68.5d) assumes the $\Delta S = \Delta Q$ rule.

The quantities Im A_0, Im A_2, and Im $\widetilde{\epsilon}$ depend on the choice of phase convention, since one can change the phases of K^0 and $\overline{K}^0$ by a transformation of the strange quark state $|s\rangle \to |s\rangle\ e^{i\alpha}$; of course, observables are unchanged. It is possible by a choice of phase convention to set Im A_0 or Im A_2 or Im $\widetilde{\epsilon}$ to zero, but none of these is zero with the usual phase conventions in the Standard Model. The choice Im $A_0 = 0$ is called the Wu-Yang phase convention [4], in which case $\epsilon = \widetilde{\epsilon}$. The value of ϵ' is independent of phase convention, and a nonzero value demonstrates CP violation in the decay amplitudes, referred to as direct CP violation. The possibility that direct CP violation is essentially zero, and that CP violation occurs only in the mixing matrix, was referred to as the superweak theory [5].

By applying CPT invariance and unitarity the phase of ϵ is given approximately by

$$\phi_\epsilon \ \approx\ \tan^{-1}\frac{2(m_{K_L} - m_{K_S})}{\Gamma_{K_S} - \Gamma_{K_L}} \approx 43.52 \pm 0.05^\circ \ , \tag{68.6a}$$

while Eq. (68.5c) gives the phase of ϵ' to be

$$\phi_{\epsilon'} = \delta_2 - \delta_0 + \frac{\pi}{2} \approx 42.3 \pm 1.5^\circ \ , \tag{68.6b}$$

where the numerical value is based on an analysis of π–π scattering using chiral perturbation theory [6]. The approximation in Eq. (68.6a) depends on the assumption that direct CP violation is very small in all K^0 decays. This is expected to be good to a few tenths of a degree, as indicated by the small value of ϵ' and of η_{+-0} and η_{000}, the CP-violation parameters in the decays $K_S \to \pi^+\pi^-\pi^0$ [7], and $K_S \to \pi^0\pi^0\pi^0$ [8]. The relation in Eq. (68.6a) is exact in the superweak theory, so this is sometimes called the superweak-phase ϕ_{SW}. An important point for the analysis is that $\cos(\phi_{\epsilon'} - \phi_\epsilon) \simeq 1$. The consequence is that only two real quantities need be measured, the magnitude of ϵ and the value of (ϵ'/ϵ), including its sign. The measured quantity $|\eta_{00}/\eta_{+-}|^2$ is very close to unity so that we can write

$$|\eta_{00}/\eta_{+-}|^2 \approx 1 - 6\mathrm{Re}\ (\epsilon'/\epsilon) \approx 1 - 6\epsilon'/\epsilon \ , \tag{68.7a}$$

$$\mathrm{Re}(\epsilon'/\epsilon) \approx \frac{1}{3}(1 - |\eta_{00}/\eta_{+-}|) \ . \tag{68.7b}$$

From the experimental measurements in this edition of the *Review*, and the fits discussed in the next section, one finds

$$|\epsilon| = (2.228 \pm 0.011) \times 10^{-3}, \tag{68.8a}$$

$$\phi_\epsilon = (43.5 \pm 0.5)^\circ, \tag{68.8b}$$

$$\mathrm{Re}(\epsilon'/\epsilon) \approx \epsilon'/\epsilon = (1.66 \pm 0.23) \times 10^{-3}, \tag{68.8c}$$

$$\phi_{+-} = (43.4 \pm 0.5)^\circ, \tag{68.8d}$$

$$\phi_{00} - \phi_{+-} = (0.34 \pm 0.32)^\circ, \tag{68.8e}$$

$$A_L = (3.32 \pm 0.06) \times 10^{-3}. \tag{68.8f}$$

Direct CP violation, as indicated by ϵ'/ϵ, is expected in the Standard Model. However, the numerical value cannot be reliably predicted because of theoretical uncertainties [9]. The value of A_L agrees with Eq. (68.5d). The values of ϕ_{+-} and $\phi_{00} - \phi_{+-}$ are used to set limits on CPT violation [see "Tests of Conservation Laws"].

68.2 Fits for K_L^0 CP-violation parameters

In recent years, K_L^0 CP-violation experiments have improved our knowledge of CP-violation parameters,

and their consistency with the expectations of CPT invariance and unitarity. To determine the best values of the CP-violation parameters in $K_L^0 \to \pi^+\pi^-$ and $\pi^0\pi^0$ decay, we make two types of fits, one for the phases ϕ_{+-} and ϕ_{00} jointly with Δm and τ_S, and the other for the amplitudes $|\eta_{+-}|$ and $|\eta_{00}|$ jointly with the $K_L^0 \to \pi\pi$ branching fractions.

68.2.1 *Fits to ϕ_{+-}, ϕ_{00}, $\Delta\phi$, Δm, and τ_S data*

These are joint fits to the data on ϕ_{+-}, ϕ_{00}, the phase difference $\Delta\phi = \phi_{00} - \phi_{+-}$, the $K_L^0 - K_S^0$ mass difference Δm, and the K_S^0 mean life τ_S, including the effects of correlations.

Measurements of ϕ_{+-} and ϕ_{00} are highly correlated with Δm and τ_S. Some measurements of τ_S are correlated with Δm. The correlations are given in the footnotes of the ϕ_{+-} and ϕ_{00} sections of the K_L^0 Listings, and the τ_S section of the K_S^0 Listings.

In most cases, the correlations are quoted as 100%, with the value and error of ϕ_{+-} or ϕ_{00} given at a fixed value of Δm and τ_S, with additional terms specifying the dependence of the value on Δm and τ_S. These cases lead to diagonal bands in Figs. 68.1

Int. J. Mod. Phys. A 2026.41. Downloaded from www.worldscientific.com
UNIVERSITY OF CALIFORNIA @ BERKELEY on 09/16/26. Re-use and distribution is strictly not permitted, except for Open Access articles.

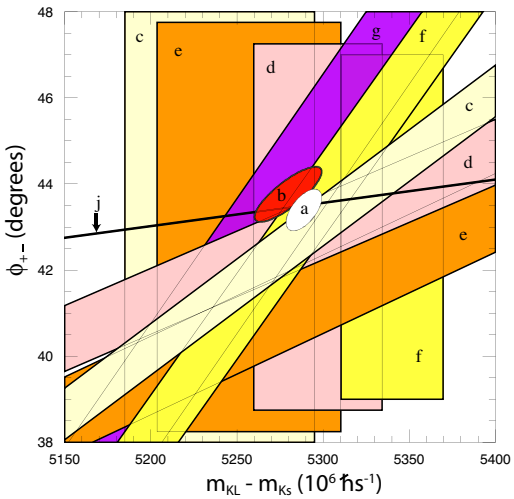

Figure 68.1: ϕ_{+-} vs Δm for experiments which do not assume CPT invariance. Δm measurements appear as vertical bands spanning $\Delta m \pm 1\sigma$, cut near the top and bottom to aid the eye. Most ϕ_{+-} measurements appear as diagonal bands spanning $\phi_{+-} \pm \sigma_\phi$. Data are labeled by letters: "b"–FNAL KTeV, "c"–CERN CPLEAR, "d"–FNAL E773, "e"–FNAL E731, "f"–CERN, "g"–CERN NA31, and are cited in Table 68.1. The narrow band "j" shows ϕ_{SW}. The ellipse "a" shows the $\chi^2 = 1$ contour of the fit result.

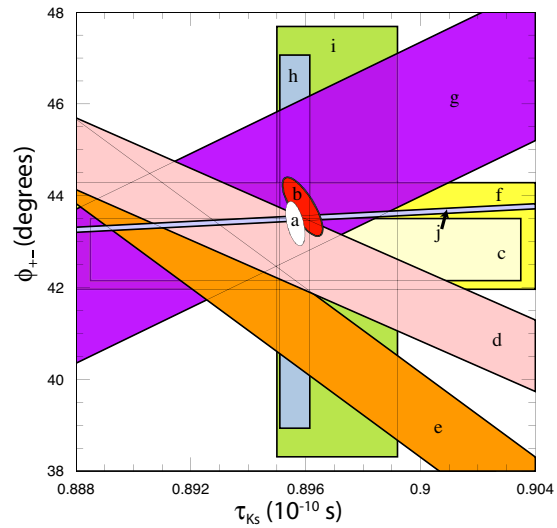

Figure 68.2: ϕ_{+-} vs τ_S. τ_S measurements appear as vertical bands spanning $\tau_S \pm 1\sigma$, some of which are cut near the top and bottom to aid the eye. Most ϕ_{+-} measurements appear as diagonal or horizontal bands spanning $\phi_{+-} \pm \sigma_\phi$. Data are labeled by letters: "b"–FNAL KTeV, "c"–CERN CPLEAR, "d"–FNAL E773, "e"–FNAL E731, "f"–CERN, "g"–CERN NA31, "h"–CERN NA48, "i"–CERN NA31, and are cited in Table 68.1. The narrow band "j" shows ϕ_{SW}. The ellipse "a" shows the fit result's $\chi^2 = 1$ contour.

and 68.2. The KTeV experiment [10] quotes its results as values of Δm, τ_S, ϕ_ϵ, Re(ϵ'/ϵ), and Im(ϵ'/ϵ) with correlations, leading to the ellipses labeled "b." The correlations for the KTeV measurements are given in the Im(ϵ'/ϵ) section of the K_L^0 Listings. For small $|\epsilon'/\epsilon|$, $\phi_{+-} \approx \phi_\epsilon + \mathrm{Im}(\epsilon'/\epsilon)$.

Table 68.1: References, Document ID's, and sources corresponding to the letter labels in the figures. The data are given in the ϕ_{+-} and Δm sections of the K_L Listings, and the τ_S section of the K_S Listings.

Label	Source	PDG Document ID	Ref.
a	This *Review*	OUR FIT	
b	FNAL KTeV	ABOUZAID 11	[10]
c	CERN CPLEAR	APOSTOLAKIS 99C	[11]
d	FNAL E773	SCHWINGENHEUER 95	[12]
e	FNAL E731	GIBBONS 93,93C	[13], [14]
f	CERN	GEWENIGER 74B,74C	[15], [16]
g	CERN NA31	CAROSI 90	[17]
h	CERN NA48	LAI 02C	[18]
i	CERN NA31	BERTANZA 97	[19]
j	This *Review*	SUPERWEAK 16	

The data on τ_S, Δm, and ϕ_{+-} shown in Figs. 68.1 and 68.2 are combined with data on ϕ_{00} and $\phi_{00} - \phi_{+-}$ in two fits, one without assuming CPT, and the other with this assumption. The results without assuming CPT are shown as ellipses labeled "a." These ellipses are seen to be in good agreement with the superweak phase

$$\phi_{SW} = \tan^{-1}\left(\frac{2\Delta m}{\Delta\Gamma}\right) = \tan^{-1}\left(\frac{2\Delta m \tau_S \tau_L}{\hbar(\tau_L - \tau_S)}\right) . \qquad (68.9)$$

In Figs. 68.1 and 68.2, ϕ_{SW} is shown as narrow bands labeled "j."

Table 68.2 column 2, "Fit w/o CPT," gives the resulting fitted parameters, while Table 68.3 gives the correlation matrix for this fit. The white ellipses labeled "a" in Figure 68.1 and 68.2 are the $\chi^2 = 1$ contours for this fit.

For experiments which have dependencies on unseen fit parameters, that is, parameters other than those shown on the x or y axis of the figure, their band positions are evaluated using the fit results and their band widths include the fitted uncertainty in the unseen parameters. This is also true for the ϕ_{SW} bands.

If CPT invariance and unitarity are assumed, then by Eq. (68.6a), the phase of ϵ is constrained to be approximately equal to

$$\phi_{SW} = (43.50258 \pm 0.00021)^\circ + 54.1(\Delta m - 0.5289)^\circ + 32.0(\tau_S - 0.89564) \qquad (68.10)$$

where we have linearized the Δm and τ_S dependence of Eq. (68.9). The error ± 0.00021 is due to the uncertainty in τ_L. Here Δm has units $10^{10}\,\hbar\,\mathrm{s}^{-1}$ and τ_S has units 10^{-10} s.

If in addition we use the observation that $Re(\epsilon'/\epsilon) \ll 1$ and $cos(\phi_{\epsilon'} - \phi_\epsilon) \simeq 1$, as well as the numerical value of $\phi_{\epsilon'}$ given in Eq. (68.6b), then Eqs. 68.5a, which are sketched in Fig 68.3, lead to the constraint

$$\begin{aligned} \phi_{00} - \phi_{+-} &\approx -3\ \mathrm{Im}\left(\frac{\epsilon'}{\epsilon}\right) \\ &\approx -3\ \mathrm{Re}\left(\frac{\epsilon'}{\epsilon}\right) \tan(\phi_{\epsilon'} - \phi_\epsilon) \\ &\approx 0.006^\circ \pm 0.008^\circ , \end{aligned} \qquad (68.11)$$

so that $\phi_{+-} \approx \phi_{00} \approx \phi_\epsilon \approx \phi_{SW}$.

Table 68.2: Fit results for ϕ_{+-}, Δm, τ_S, ϕ_{00}, $\Delta\phi = \phi_{00} - \phi_{+-}$, and ϕ_ϵ without and with the CPT assumption

Quantity(units)	Fit w/o CPT	Fit w/ CPT
$\phi_{+-}(^\circ)$	43.4 ± 0.5 (S=1.2)	43.51 ± 0.05 (S=1.2)
$\Delta m(10^{10}\hbar\,\mathrm{s}^{-1})$	0.5289 ± 0.0010	0.5293 ± 0.0009 (S=1.3)
$\tau_S(10^{-10}\mathrm{s})$	0.89564 ± 0.00033	0.8954 ± 0.0004 (S=1.1)
$\phi_{00}(^\circ)$	43.7 ± 0.6 (S=1.2)	43.52 ± 0.05 (S=1.3)
$\Delta\phi(^\circ)$	0.34 ± 0.32	0.006 ± 0.014 (S=1.7)
$\phi_\epsilon(^\circ)$	43.5 ± 0.5 (S=1.3)	43.52 ± 0.05 (S=1.2)
χ^2	16.4	20.0
# Deg. Free.	14	16

Int. J. Mod. Phys. A 2026.41. Downloaded from www.worldscientific.com
by UNIVERSITY OF CALIFORNIA @ BERKELEY on 09/16/26. Re-use and distribution is strictly not permitted, except for Open Access articles.

In the fit assuming CPT, we constrain $\phi_\epsilon = \phi_{SW}$ using the linear expression in Eq. (68.10), and constrain $\phi_{00} - \phi_{+-}$ using Eq. (68.11). These constraints are inserted into the Listings with the Document ID of SUPERWEAK 16. Some additional data for which the authors assumed CPT are added to this fit or substitute for other less precise data for which the authors did not make this assumption. See the Listings for details.

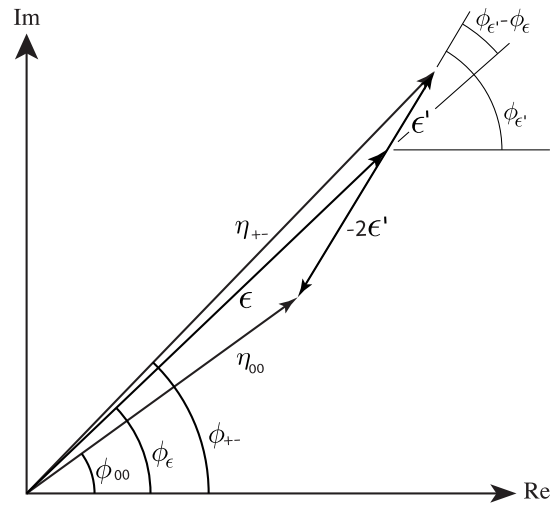

Figure 68.3: Sketch of Eqs. 68.5a. Not to scale

The results of this fit are shown in Table 68.2, column 3, "Fit w/CPT," and the correlation matrix is shown in Table 68.4. The Δm precision is improved by the CPT assumption.

Table 68.3: Correlation matrix for the results of the fit without the CPT assumption

	ϕ_{+-}	Δm	τ_S	ϕ_{00}	$\Delta\phi$	ϕ_ϵ
ϕ_{+-}	1.000	0.596	-0.488	0.827	-0.040	0.976
Δm	0.596	1.000	-0.572	0.487	-0.035	0.580
τ_S	-0.488	-0.572	1.000	-0.423	-0.014	-0.484
ϕ_{00}	0.827	0.487	-0.423	1.000	0.529	0.929
$\Delta\phi$	-0.040	-0.035	-0.014	0.529	1.000	0.178
ϕ_ϵ	0.976	0.580	-0.484	0.929	0.178	1.000

Table 68.4: Correlation matrix for the results of the fit with the CPT assumption

	ϕ_{+-}	Δm	τ_S	ϕ_{00}	$\Delta\phi$	ϕ_ϵ
ϕ_{+-}	1.000	0.972	-0.311	0.957	-0.105	0.995
Δm	0.972	1.000	-0.509	0.958	-0.007	0.977
τ_S	-0.311	-0.509	1.000	-0.306	0.004	-0.312
ϕ_{00}	0.957	0.958	-0.306	1.000	0.189	0.981
$\Delta\phi$	-0.105	-0.007	0.004	0.189	1.000	-0.006
ϕ_ϵ	0.995	0.977	-0.312	0.981	-0.006	1.000

68.2.2 *Fits for ϵ'/ϵ, $|\eta_{+-}|$, $|\eta_{00}|$, and $B(K_L \to \pi\pi)$*

We list measurements of $|\eta_{+-}|$, $|\eta_{00}|$, $|\eta_{00}/\eta_{+-}|$, and ϵ'/ϵ. Independent information on $|\eta_{+-}|$ and $|\eta_{00}|$ can be obtained from measurements of the K_L^0 and K_S^0 lifetimes (τ_L, τ_S), and branching ratios (B) to $\pi\pi$, using the relations

$$|\eta_{+-}| = \left[\frac{\mathrm{B}(K_L^0 \to \pi^+\pi^-)}{\tau_L}\ \frac{\tau_S}{\mathrm{B}(K_S^0 \to \pi^+\pi^-)}\right]^{1/2}, \quad (68.12a)$$

$$|\eta_{00}| = \left[\frac{\mathrm{B}(K_L^0 \to \pi^0\pi^0)}{\tau_L}\ \frac{\tau_S}{\mathrm{B}(K_S^0 \to \pi^0\pi^0)}\right]^{1/2}. \quad (68.12b)$$

For historical reasons, the branching ratio fits and the CP-violation fits are done separately, but we want to include the influence of $|\eta_{+-}|$, $|\eta_{00}|$, $|\eta_{00}/\eta_{+-}|$, and ϵ'/ϵ measurements on $\mathrm{B}(K_L^0 \to \pi^+\pi^-)$ and $\mathrm{B}(K_L^0 \to \pi^0\pi^0)$ and vice versa. We approximate a global fit to all of these measurements by first performing two independent fits: 1) BRFIT, a fit to the K_L^0 branching ratios, rates, and mean life, and 2) ETAFIT, a fit to the $|\eta_{+-}|$, $|\eta_{00}|$, $|\eta_{+-}/\eta_{00}|$, and ϵ'/ϵ measurements. The results from fit 1, along with the K_S^0 values from this edition, are used to compute values of $|\eta_{+-}|$ and $|\eta_{00}|$, which are included as measurements in the $|\eta_{00}|$ and $|\eta_{+-}|$ sections with a document ID of BRFIT 16. Thus, the fit values of $|\eta_{+-}|$ and $|\eta_{00}|$ given in this edition include both the direct measurements and the results from the branching ratio fit.

The process is reversed in order to include the direct $|\eta|$ measurements in the branching ratio fit. The results from fit 2 above (before including BRFIT 16 values) are used along with the K_L^0 and K_S^0 mean lives and the $K_S^0 \to \pi\pi$ branching fractions to compute the K_L^0 branching ratio $\Gamma(K_L^0 \to \pi^0\pi^0)/\Gamma(K_L^0 \to \pi^+\pi^-)$. This branching ratio value is included as a measurement in the branching ratio section with a document ID of ETAFIT 16. Thus, the K_L^0 branching ratio fit values in this edition include the results of the direct measurement of $|\eta_{00}/\eta_{+-}|$ and ϵ'/ϵ. Most individual measurements of $|\eta_{+-}|$ and $|\eta_{00}|$ enter our fits directly via the corresponding measurements of $\Gamma(K_L^0 \to \pi^+\pi^-)/\Gamma(\text{total})$ and $\Gamma(K_L^0 \to \pi^0\pi^0)/\Gamma(\text{total})$, and those that do not have too large errors to have any influence on the fitted values of these branching ratios. A more detailed discussion of these fits is given in the 1990 edition of this *Review* [20].

References

[1] K. Kleinknecht, *Uncovering CP violation: Experimental clarification in the neutral K meson and B meson*, volume 195, Spriger Verlag (2003).

[2] B. Winstein and L. Wolfenstein, Rev. Mod. Phys. **65**, 1113 (1993).

[3] M. S. Sozzi, Eur. Phys. J. **C36**, 37 (2004), [hep-ph/0401176].

[4] T. T. Wu and C.-N. Yang, Phys. Rev. Lett. **13**, 380 (1964).

[5] L. Wolfenstein, Phys. Rev. Lett. **13**, 562 (1964); L. Wolfenstein, Comments Nucl. Part. Phys. **21**, 5, 275 (1994).

[6] G. Colangelo, J. Gasser and H. Leutwyler, Nucl. Phys. **B603**, 125 (2001), [hep-ph/0103088].

[7] R. Adler *et al.* (CPLEAR), Phys. Lett. **B407**, 193 (1997); P. Bloch, *Proceedings of Workshop on K Physics* (Orsay 1996), ed. L. Iconomidou-Fayard, Edition Frontieres, Gif-sur-Yvette, France (1997) p. 307.

[8] A. Lai *et al.* (NA48), Phys. Lett. **B610**, 165 (2005), [hep-ex/0408053].

[9] G. Buchalla, A. J. Buras and M. E. Lautenbacher, Rev. Mod. Phys. **68**, 1125 (1996), [hep-ph/9512380]; S. Bosch *et al.*, Nucl. Phys. **B565**, 3 (2000), [hep-ph/9904408]; S. Bertolini, M. Fabbrichesi and J. O. Eeg, Rev. Mod. Phys. **72**, 65 (2000), [hep-ph/9802405].

[10] E. Abouzaid *et al.* (KTeV), Phys. Rev. **D83**, 092001 (2011), [arXiv:1011.0127].

[11] A. Apostolakis *et al.* (CPLEAR), Phys. Lett. **B458**, 545 (1999).

[12] B. Schwingenheuer *et al.*, Phys. Rev. Lett. **74**, 4376 (1995).

[13] L. K. Gibbons *et al.*, Phys. Rev. Lett. **70**, 1199 (1993).

[14] L.K. Gibbons, Thesis, RX-1487, Univ. of Chicago, 1993.

[15] C. Geweniger *et al.*, Phys. Lett. **48B**, 487 (1974).

[16] C. Geweniger *et al.*, Phys. Lett. **52B**, 108 (1974).

[17] R. Carosi *et al.* (NA31), Phys. Lett. **B237**, 303 (1990).

[18] A. Lai *et al.* (NA48), Phys. Lett. **B537**, 28 (2002), [hep-ex/0205008].

[19] L. Bertanza *et al.*, Z. Phys. **C73**, 629 (1997).

[20] J. J. Hernandez *et al.* (Particle Data Group), Phys. Lett. **B239**, 1 (1990), [Erratum: Phys. Lett.B253,524(1991)].

69. Multibody Charm Analyses

Revised August 2025 by J. Rademacker (Bristol U.); written with D.M. Asner (BNL)

69.1 Overview

The study of multibody charm decays is a vibrant field, with vast and fast-increasing datasets, new developments in theory and experimental technique, and implications reaching beyond charm. This review is structured as follows: Sec. 69.2 summarizes key aspects of amplitude models that describe multibody charm decays, their application to data, and theory progress; Sec. 69.3 reviews the special role of charm threshold data in model-independent approaches; and Sec. 69.4 describes applications of multi-body charm analyses, focusing on Charge-Parity (CP) violation, charm mixing and the role of threshold data in this context. In Sec. 69.5, we conclude.

69.2 Kinematics & Models

The differential decay rate to a point $\mathbf{s} = (s_1, \ldots, s_n)$ in n dimensional phase space can be expressed as

$$d\Gamma = |\mathcal{M}(\mathbf{s})|^2 \left| \frac{\partial^n \phi}{\partial(s_1 \ldots s_n)} \right| d^n s \,, \tag{69.1}$$

where $|\partial^n \phi/\partial(s_1 \ldots s_n)|$ represents the density of states at $\mathbf{s}$, and $\mathcal{M}$ the matrix element for the decay at that point in phase space, which is $2, 5, 8, \ldots$ dimensional for D decays to $3, 4, 5, \ldots$ spinless particles. Additional parameters are required to fully describe decays involving particles with non-zero spin in the initial or final state.

For the important case of D decays to three pseudoscalars, the decay kinematics can be represented in a two-dimensional Dalitz plot [1]. This is usually parameterized in terms of $s_{12} \equiv (p_1+p_2)^2$ and $s_{23} \equiv (p_2+p_3)^2$, where p_1, p_2, and p_3 are the four-momenta of the final-state particles. In terms of these variables, phase-space density is constant across the kinematically allowed region, so that any structure seen in the Dalitz plot is a direct consequence of the dynamics encoded in $|\mathcal{M}|^2$. Note that decays to four or more particles cannot be unambiguously described in terms of analogously-defined variables s_{ij} and s_{ijk}, as these cannot describe parity-odd kinematics; these are absent in the three-body case because the decay products are confined to a plane. See Sec. 69.4.4 for a discussion on the use of parity-odd variables in four-body decays.

In the widely-used isobar approach, the matrix element $\mathcal{M}$ is modeled as a sum of interfering decay amplitudes, each proceeding through resonant two-body decays [2–6]. See [2, 7, 8] for a review of resonance phenomenology. In most analyses, each resonance is described by a relativistic Breit–Wigner [9] or Flatté [10] lineshape, and the model includes a non-resonant term with a constant phase and magnitude. This approach has well-known theoretical limitations, such as the violation of unitarity and analyticity, which can break the relationship between magnitude and phase across phase space. This motivates the use of more sophisticated descriptions, especially for broad, overlapping resonances (frequently found in S-wave components) where these limitations are particularly problematic. In charm analyses, these approaches have included the K-matrix [11] which respects two-body unitarity; the use of LASS scattering data [12]; dispersive methods [13–16]; multi-meson models using chiral Lagrangians [17–20]; and methods based on chiral unitarity [21–24]; QCD factorization [25–28]; and quasi model-independent parametrizations that use generic lineshapes, with minimal theory input and many free parameters, for a subset of resonances [29–37].

An important example of a multibody charm decay is $D^0 \to K^0_S \pi^+ \pi^-$, which is a key channel in CP violation and charm-mixing analyses. A joint analysis by BaBar and Belle [38] describes a Dalitz plot with 1.1M $D^0 \to K^0_S \pi^+ \pi^-$ events (the largest sample analyzed in this way) with 18 resonant components, including four doubly Cabibbo suppressed ones. The model uses a K-matrix description for the $\pi\pi$ S-wave based on [39] and input from LASS scattering data [12,40] for the $K\pi$ S-wave, with no need to add a non-resonant component to describe the data. These data were reanalyzed by [25] in a QCD factorization framework, using line-shape parametrizations for the S [41, 42] and P wave [14] contributions that preserve two-body unitarity and analyticity. The analyses give compatible results for the components they share. Recently, BESIII studied both the $D^0 \to K^0_S \pi^+ \pi^-$ and the $D^0 \to K^0_L \pi^+ \pi^-$ Dalitz plot, providing insights into U-spin breaking effects [43].

The field of charm amplitude analyses remains very active. Publications since the last update of this review two years ago include Dalitz plot analyses of $D^+ \to \pi^+ \eta\eta$, $D_s^+ \to K^0_S K^0_L \pi^+$, $D^+ \to K^0_S K^0_S \pi^+$, $D^+ \to K^0_S \pi^+ \eta$, $D^0 \to \pi^+ \pi^- \eta$, $D^+ \to \pi^+ \pi^0 \eta$, by BESIII [44–48] and $D_s^+ \to \pi^- \pi^+ \pi^+$ by LHCb [36]. LHCb performed an amplitude analyses of the decay of an excited charm state, $D_{s1}(2460)^+ \to D_s^+ \pi^+ \pi^-$ [49]. The amplitude structure of charm baryon decays was studied by BESIII in $\Lambda_c \to \Lambda \pi^+ \eta$ and by LHCb in $\Lambda_c \to pK^- \pi^+$ [50, 51] and $\Xi_c^+ \to pK^- \pi^+$ [52]. BESIII continued its series of four-body amplitude analyses, investigating the hadronic decays $D^+ \to K^- \pi^+ \pi^+ \pi^0$, $D_s^+ \to \pi^+ \pi^+ \pi^- \pi^0$, $D^0 \to \pi^+ \pi^- \pi^+ \pi^-$, and $D^0 \to \pi^+ \pi^- \pi^0 \pi^0$ [53–55] as well as the semileptonic decays $D^+ \to K^0_S \pi^0 \mu^+ \nu_\mu$, $D^+ \to K^0_S \pi^0 e^+ \nu_e$, $D^0 \to \overline{K}^0 \pi^- \mu^+ \nu_\mu$, $D^0 \to \overline{K}^0 \pi^- e^+ \nu_e$, $D^+ \to \pi^+ \pi^- e^+ \nu_e$, and $D_s^+ \to K^+ K^- \mu^+ \nu_\mu$ [56–61]. BESIII published five-body amplitude analyses of the decays $D_s^+ \to \pi^+ \pi^+ \pi^- \pi^0 \pi^0$, $D^+ \to K^- \pi^+ \pi^0 e^+ \nu_e$, and $D^0 \to K^- \pi^+ \pi^- e^+ \nu_e$. [62, 63].

Noteworthy is the increasing sophistication of recent amplitude analyses, most of which go substantially beyond the isobar model with Breit–Wigner and Flatté lineshapes. However, with the notable exceptions of [15, 16, 23, 24, 64, 65], they remain within the isobar framework, which describes the decay as a series of two-body processes. This approach ignores long-range hadronic effects such as re-scattering, and does not respect three (or four)-body unitarity and analyticity. Recent quasi model-independent measurements of the $\pi^+ \pi^-$ lineshape emphasize the importance of such effects. Significant differences have been found between the $\pi^+ \pi^-$ S-wave components observed in $D_s^+ \to \pi^+ \pi^- \pi^+$ [31,35,36] and $D^+ \to \pi^+ \pi^- \pi^+$ [37], and between either of them and phase shifts observed in scattering data [66–68].

Several groups work on improved models and their application to data. Dispersive techniques, which respect three-body unitarity and analyticity, have been applied to regions of the $D^+ \to K^- \pi^+ \pi^+$ and $D^+ \to K^0_S \pi^0 \pi^+$ Dalitz plots below the $\eta' K$ threshold [15, 16], where they provide a good description of the data with fewer fit parameters than the isobar approach. Reference [64] uses a unitary coupled channel approach to describe $D^+ \to K^- \pi^+ \pi^+$, which has no restrictions on the kinematic range, but requires additional parameters to describe the Dalitz plot above the $\eta' K$ threshold. Using an effective chiral Lagrangian, the authors of reference [19] provide a description of the annihilation contribution to the decay amplitude which respects three-body unitarity. The approach provides a good description of LHCb's $D^+ \to K^+ K^- K^+$ data, with fewer parameters than an equivalent isobar model [65]. The same channel has more recently been re-analyzed by the authors of [23], who argue that the internal emission diagram should dominate and use a chiral unitarity-based approach to achieve a reasonable description of the data with two free parameters.

Limitations in the theoretical description of interfering resonances are the leading source of systematic uncertainty in many analyses. In some cases, the model uncertainty can be removed through model-independent methods, often relying on input from the charm threshold, as discussed in Sec. 69.3. The authors of [69] expand the scope and applicability of the quasi model-independent approach in amplitude fits. At the same time, increasingly sophisticated models are being developed, and applied to data. The authors of [20] and [70] provide valuable practical frameworks for sophisticated amplitude analyses.

69.3 Model Independent Methods and the Charm Threshold

Precision measurements of the CP-violation phase γ/ϕ_3 using $B^- \to DK^-$, $D \to K^0_S \pi^+ \pi^-$ and related decay modes, as well as precision measurements of charm-mixing parameters in decay modes such as $D^0 \to K^0_S \pi^+ \pi^-$, require input on the relative de-

Int. J. Mod. Phys. A 2026.41. Downloaded from www.worldscientific.com
UNIVERSITY OF CALIFORNIA @ BERKELEY on 09/16/26. Re-use and distribution is strictly not permitted, except for Open Access articles.

Int. J. Mod. Phys. A 2026.41. Downloaded from www.worldscientific.com by UNIVERSITY OF CALIFORNIA @ BERKELEY on 09/16/26. Re-use and distribution is strictly not permitted, except for Open Access articles.

cay amplitudes of D^0 and $\overline{D}^0$. In the above examples, $K^0_S\pi^+\pi^-$ can be replaced with other final states accessible to both D^0 and $\overline{D}^0$ [71–79]. While the magnitudes of the decay amplitudes can be measured precisely using the vast charm samples at the B factories and LHCb, obtaining the relative phases requires either amplitude models with reliable phase motion, or model-independent approaches. More details on the measurements of γ/ϕ_3 and charm mixing can be found in sections 69.4.1 and 69.4.2.

Model-independent measurements of relative phases between D^0 and $\overline{D}^0$ decay amplitudes rely on interference effects in the decays of well-defined coherent superpositions of D^0 and $\overline{D}^0$. These are accessible at the charm threshold [74, 77, 79–84], where CLEO–c and BESIII operate. There, quantum-correlated D-meson pairs are produced, which have opposite CP and flavor content. For example, if one (the tag) is identified as a CP eigenstate through its decay (e.g. to K^+K^- or $K_S\pi^0$), the other D meson is an eigenstate state with the opposite CP eigenvalue. (For a discussion of other potential sources of correlated charm with different characteristics, see [85].) The decay rate of a CP eigenstate $\frac{1}{\sqrt{2}}\left(D^0 \pm \overline{D}^0\right)$ is proportional to $|A_D|^2 + |\overline{A}_D|^2 \pm 2|A_D||\overline{A}_D|\cos(\delta_D)$, where A_D and $\overline{A}_D$ are the D^0 and $\overline{D}^0$ decay amplitudes, and δ_D is their sought-after phase difference. Other quantum correlations give access to $\sin(\delta_D)$. For multibody decays, A_D, $\overline{A}_D$ and δ_D vary across phase space. Model-independent phase information is measured either integrated over the entire phase space of the decay, or in subregions/bins. The results can be expressed in terms of one complex parameter $\mathcal{Z} = Re^{-i\delta_D} = c+is$ per pair of CP-conjugate bins; c and s are the average of $\cos(\delta_D)$ and $\sin(\delta_D)$ over that region of phase space. Amplitude models can be used to optimize the binning for sensitivity to γ/ϕ_3, without introducing a model-dependent bias in the result [86]; novel unbinned approaches have the potential to further increase the precision on γ/ϕ_3 in future analyses [87–89].

BESIII data have been analyzed to provide binned $\mathcal{Z}$ for $K_{S,L}\pi^+\pi^-$, $K_{S,L}K^+K^-$, $K^+\pi^-\pi^0$, $\pi^+\pi^-\pi^+\pi^-$, $K^+K^-\pi^+\pi^-$, and $K^+\pi^-\pi^+\pi^-$ final states [90–96]. Many of these analyses were first carried out with CLEO–c data [97–102].

For self-conjugate decays such as $D^0 \to \pi^+\pi^-\pi^0$, one can define the CP-even fraction F_+ which is +1 for a CP-even eigenstate and 0 for a CP-odd one [82]. F_+ is related to $Re(\mathcal{Z}) = c$, defined for a single CP-conjugate bin pair. For the purpose of γ/ϕ_3 measurements, this information allows the decay to be treated equivalently to a two-body decay, where γ/ϕ_3 is constrained from decay rates without the need to resolve the phase-space distribution. In the mathematical expressions for the decay rates, a factor $(2F_+ - 1)$ multiplies the γ/ϕ_3-sensitive term, leading to the best sensitivity for $F_+ = 1$ or $F_+ = 0$. The decay $D^0 \to \pi^+\pi^-\pi^0$ is found to be, with $F_+ = (94.2 \pm 0.7)\%$, very close to being completely CP-even [83, 103]. The decays $D^0 \to \pi^+\pi^-\pi^+\pi^-$ [83, 94, 99, 104] and $D^0 \to K^+K^-\pi^+\pi^-$ [95, 105] are predominantly CP even with F_+ of 75%, as is $D^0 \to K^+K^-\pi^0$ with 73% [82, 83]; on the other hand, $D^0 \to K^0_S\pi^+\pi^-\pi^0$ is predominantly CP odd with $F_+ = 23\%$ [100, 106]; these measurements have percent-level uncertainties. Additional measurements for decays to four, five, and six pions can be found in [107].

Comparing measured parameters like F_+ and $\mathcal{Z}$ with those predicted from amplitude models provides a test of the models' phase motion. The measured value for F_+ in $D^0 \to \pi^+\pi^-\pi^+\pi^-$ for example, $F_+ = (74.6 \pm 0.8)\%$ [99, 104], compares well with $(72.9 \pm 2.0)\%$ calculated from [32]. The coherence factor $|\mathcal{Z}^{3\pi}| = R^{K3\pi} = 0.430^{+0.043}_{-0.039}$ measured in $D^0 \to K^\pm\pi^\mp\pi^\pm\pi^\mp$ quantum correlated events at BESIII and CLEO–c [96, 102] and charm mixing at LHCb [108, 109], compares well with 0.459 ± 0.025 predicted by [33]. The bin-wise comparisons between model and data for $D^0 \to K^+K^-\pi^-\pi^+$, $\pi^+\pi^-\pi^+\pi^-$, $K_{L,S}\pi^+\pi^-$, $K^\pm\pi^\mp\pi^\pm\pi^\mp$, $K^\pm\pi^\mp\pi^0$, and $K^0_SK^+K^-$ can be found in [43, 91–96, 96, 99] and mostly show reasonable or good agreement. These results are a welcome surprise given the preceding discussion on the theoretical shortcomings of amplitude models.

69.4 Applications of multibody charm analyses for CP violation and mixing

Amplitude analyses provide sensitivity to both relative magnitudes and phases of the interfering decay amplitudes. It is especially the sensitivity to phases that makes amplitude analyses such a uniquely powerful tool for studying a wide range of phenomena. Here we concentrate on their critical role in CP violation and mixing measurements. Properties of light-meson resonances determined in D amplitude analyses are reported in the light-unflavored-meson section of this *Review*.

The closely related topics of multibody charm decays in measurements of CP violation in beauty decays to charm and charm mixing will be discussed in turn, followed by a review of searches for time-integrated CP violation in multibody charm decays.

69.4.1 *CP violation in decays of Beauty to Charm*

Neutral D mesons originating from $B^- \to DK^-$ (here denoted as D_{B^-}) are a superposition of D^0 and $\overline{D}^0$ with a relative phase that depends on the CKM unitarity triangle parameter γ/ϕ_3,

$$D_{B^-} \propto D^0 + r_B e^{i(\delta_B - \gamma)}\overline{D}^0,$$

where δ_B is a CP conserving strong phase, and $r_B \sim 0.1$ is the magnitude of the ratio of the $B^- \to \overline{D}^0K^-$ and $B^- \to D^0K^-$ decay amplitudes. In the corresponding CP-conjugate expression, γ/ϕ_3 changes sign. The amplitude analysis of the subsequent $D_{B^\pm}$ decay to a state accessible to both D^0 and $\overline{D}^0$ allows the measurement of γ/ϕ_3 [71–78]. The method generalizes to similar B hadron decays, such as $B^0 \to DK^{*0}$, and, albeit with reduced sensitivity, to decays where the kaon is replaced by a pion.

Measurements based on this technique have been reported by BaBar [110, 111], Belle [112–114], Belle II [115, 116], and LHCb [117–136]. Since it relies on $D^0 - \overline{D}^0$ interference, the phase differences between the relevant D^0 and $\overline{D}^0$ decay amplitudes are required in order to extract γ/ϕ_3. Because the theoretical shortcomings of amplitude models, discussed above, make their phases unreliable, most recent γ/ϕ_3 measurements use amplitude model-independent approaches to obtain this information [113, 114, 116–121, 123–129, 132, 135]. These depend critically on input from the charm threshold described in Sec. 69.3. Charm mixing also results in a (time-dependent) $D^0 - \overline{D}^0$ superposition, which can be used to measure the relevant phase information as input to γ/ϕ_3 measurements [137, 138]. This method is particularly powerful in doubly Cabibbo-suppressed decays such as $D^0 \to K^+\pi^-\pi^+\pi^-$, and when used in combination with threshold data.

Under some circumstances, with large data sets, the relevant strong phases and γ/ϕ_3 can be extracted without external input, for example in simultaneous analysis of the $B^0 \to DK^+\pi^-$ Dalitz plot and that of the subsequent $D \to K^0_S\pi^+\pi^-$ decay [139]. However, the global effort to measure γ/ϕ_3 to sub-degree precision will continue to rely critically on input from the charm threshold and the analysis of BESIII's full dataset [140].

The most precise individual γ/ϕ_3 measurement is $\gamma/\phi_3 = 68.5^{\circ}{}^{+5.2^\circ}_{-5.1^\circ}$ resulting from LHCb's amplitude model-independent study of $D_{B^-} \to K^0_S\pi^+\pi^-$ and $D_{B^-} \to K^0_SK^+K^-$ [141], using input from the charm threshold [90, 92, 97]. LHCb's analysis of $D_{B^-} \to K^+\pi^-\pi^+\pi^-$ decays leads to the second most precise individual γ/ϕ_3 measurement with $\gamma/\phi_3 = 54.8^{\circ}{}^{+6.0^\circ}_{-5.8^\circ} \pm 0.6^{\circ}{}^{+6.7^\circ}_{-4.3^\circ}$ [128]. This analysis benefits from an optimized model-informed partition of the five-dimensional $D^0 \to K^+\pi^-\pi^+\pi^-$ phase space [33, 102], and input from the charm threshold [96, 102]; the third uncertainty on γ/ϕ_3 in the result quoted above quantifies the impact of the uncertainty on the charm parameters measured at the threshold. These have recently been constrained further from charm mixing measurements [108, 109], leading to a significant improvement in the precision of γ/ϕ_3 [135].

The current world average on γ/ϕ_3 [142, 143] is dominated by LHCb who finds, combining its results with input from CLEO–c and BESIII in an amplitude-model-independent approach, $\gamma = 62.8^\circ \pm 2.6^\circ$ [135]. Belle II is also expected to reach excellent precision in γ/ϕ_3, benefiting from its strength in reconstructing decays with neutral particles in the final state. Combining Belle

Int. J. Mod. Phys. A 2026.41. Downloaded from www.worldscientific.com
UNIVERSITY OF CALIFORNIA @ BERKELEY on 09/16/26. Re-use and distribution is strictly not permitted, except for Open Access articles.

and Belle II data with charm threshold input, the collaborations find an average, dominated by model-independent results, of $\phi_3 = 75.2^\circ \pm 7.6^\circ$ [115].

The interference between mixing and decay in $B^0 \to D^0 h^0$ with $h^0 = \pi^0, \eta, \omega$ provides sensitivity to another CKM unitarity triangle parameter, β/ϕ_1, which can be extracted from the Dalitz plot of the subsequent $D^0 \to K^0_S \pi^+\pi^-$ decay [38, 144–147]. The combined BaBar/Belle analysis based on this technique resolved the ambiguity in β/ϕ_1 present in other measurements [38].

Further details on *CP* violation in beauty and charm can be found in [148, 149].

69.4.2 *Charm Mixing and CP violation*

Time-dependent amplitude analyses in decays to final states that are accessible to both D^0 and $\overline{D}^0$ have unique sensitivity to mixing parameters. A Dalitz plot analysis of a self-conjugate final state, such as $K^0_S\pi^+\pi^-$ and $K^0_S K^+K^-$, allows a direct measurement of x and y, the normalized mass and width difference of the $D^0 - \overline{D}^0$ system's mass eigenstates [150]. This is in contrast to decays like $D^0 \to K^+\pi^-$, which only provide access to decay-specific parameters x'^2, y'.

The phase differences between D^0 and $\overline{D}^0$ amplitudes across the Dalitz plot affect these measurements in the same way as those of γ/ϕ_3 in $B^+ \to DK^+$, and can be taken into account in an amplitude model-independent way using the same charm threshold results [74, 79–84, 148]. This approach resulted in the first observation of a non-zero mass difference between the neutral charm mass eigenstates by LHCb [151], using a model-independent analysis of $D^0 \to K^0_S\pi^+\pi^-$. Applying the same technique to their combined dataset, Belle and Belle II find consistent results, albeit with lower precision [152]. The "bin flip" technique applied in these measurements exploits that *CP*-conjugate regions of the $D^0 \to K^0_S\pi^+\pi^-$ Dalitz plot have near-identical experimental efficiencies [153]. This technique is also sensitive to *CP* violation in mixing and in the interference between mixing and decay, which is discussed further in [148, 149].

The simultaneous dependence on charm mixing parameters and the same relative phases that affect the measurement of γ/ϕ_3 can also be exploited to constrain those phases [137,138], using mixing parameters as external input. This led to an improvement in the measurement of the $D^0 \to K^+\pi^-\pi^+\pi^-$ coherence factor and relative strong phase from $R^{K3\pi} = 0.52^{+0.10}_{-0.09}$, $\delta^{K3\pi} = 167^{\circ\,+31^\circ}_{\;\;-19^\circ}$ measured at the charm threshold [96,102] to $R^{K3\pi} = 0.430^{+0.043}_{-0.039}$, $\delta^{K3\pi} = 163^{\circ\,+13.8^\circ}_{\;\;-14.8^\circ}$ when combined with LHCb charm mixing data [108, 109]. It is worth noting, though, that charm mixing alone is only sensitive to a linear combination of $R^{K3\pi}\cos(\delta^{K3\pi})$ and $R^{K3\pi}\sin(\delta^{K3\pi})$ - combining this with constraints from the threshold allows a measurement in terms of $R^{K3\pi}$ and $\delta^{K3\pi}$.

69.4.3 *Everything, Everywhere, All at Once*

The discussion above shows how closely related the measurements of γ/ϕ_3, charm mixing, and the analysis of charm threshold data are, due to the shared charm parameters. While above, the emphasis was on the importance of charm as input to γ/ϕ_3, and threshold data as input to charm mixing and γ/ϕ_3, these relationships are in fact omnidirectional. This is demonstrated by LHCb's combined analysis on beauty and charm data [135], as well as a global combination by UTfit members and collaborators [143]. Not only does charm input improve the precision on γ/ϕ_3, both analyses also show that input from beauty decays to charm (such as $B^- \to DK^-$) has a significant impact on charm parameters.

69.4.4 *Searches for time-integrated CPV in charm*

The recent observation of direct *CP* violation in LHCb's analysis of $D^0 \to \pi^+\pi^-$ and $D^0 \to K^+K^-$ decays [154,155], and the open question as to its Standard Model or beyond the Standard Model nature, add renewed interest in the search for *CP* violation in other decays.

Multibody decays, with their rich structure and varying strong phase across phase space, could potentially have particularly high sensitivity to *CP* violation. Comparing the results of amplitude fits for *CP*-conjugate decay modes provides a measure of *CP* violation, as for example done for $D^0 \to K^0_S K^\pm\pi^\mp$, $D^0 \to K^+K^-\pi^+\pi^-$, and $D^0 \to \pi^+\pi^-\pi^+\pi^-$ using LHCb and CLEO–c data [32, 156–158]. A widely-used amplitude model-independent technique to search for local *CP* violation in multibody phase space is based on performing a χ^2 comparison of *CP*-conjugate phase-space distributions. This method was pioneered by BaBar [159] and developed further in [160–162], with results reported by BaBar and LHCb in $D^\pm \to K^+K^-\pi^\pm$ [159, 163–166], CDF in $D^0 \to K^0_S\pi^+\pi^-$ [167], and LHCb in $D^0 \to K^0_S K^\pm\pi^\mp$, $D^+_{(s)} \to K^+K^-K^+$, $D^+ \to \pi^-\pi^+\pi^+$, $D^0 \to K^+K^-\pi^+\pi^-$, $D^0 \to \pi^+\pi^-\pi^+\pi^-$, and $\Xi^+_c \to pK^-\pi^+$ [162, 168–171]. Unbinned methods can increase sensitivity [172, 173] and have been applied by LHCb to $D^+ \to \pi^-\pi^+\pi^+$, $D^0 \to \pi^+\pi^-\pi^0$, $D^0 \to \pi^+\pi^-\pi^+\pi^-$, $D^0 \to K^0_S K^\pm\pi^\mp$, and $\Xi^+_c \to pK^-\pi^+$ [168, 170, 171, 174–176].

An alternative model-independent approach is based on observables in four body decays that are odd under motion reversal ("naïve T") [177–185], which is equivalent to P for scalar particles [185]. One such observable is $C_T = \vec{p}_2 \cdot (\vec{p}_3 \times \vec{p}_4)$, where $\vec{p}_i$ is the ith decay product's three momentum in the decay's center of mass frame. Comparing the P violating asymmetry $A_T \equiv \frac{\Gamma(C_T>0)-\Gamma(C_T<0)}{\Gamma(C_T>0)+\Gamma(C_T<0)}$ with its C-conjugate provides sensitivity to *CP* violation. Additional variables are proposed in [185], which also provides an excellent review of this topic. Searches for *CP* violation using P-odd variables have been carried out by BaBar, Belle, Belle II, FOCUS, and LHCb in $D^+ \to K^0_S K^-\pi^+\pi^+$,$D_s \to K^0_S K^-\pi^+\pi^+$ [186]; $D^0 \to K^+K^-\pi^+\pi^-$ [187–190]; $D^+ \to K^+K^0_S\pi^+\pi^-$, $D^+_s \to K^+K^0_S\pi^+\pi^-$ [191]; $D^0 \to K^0_S\pi^+\pi^-\pi^0$ [192]; and $D^0 \to \pi^+\pi^-\pi^+\pi^-$ [175].

LHCb's angular analysis of the rare decays $D^0 \to \pi^+\pi^-\mu^+\mu^-$, $D^0 \to K^+K^-\mu^+\mu^-$, and $\Lambda^+_c \to p\mu^+\mu^-$ yields several observables with sensitivity to physics beyond the Standard Model, including *CP*-violating ones. The results are in agreement with Standard-Model predictions [193–195].

All results of analyses mentioned in this section are compatible with *CP* conservation. The observation of *CP* violation in two body charm decays [154,155], and the vast data samples about to be collected, provide grounds for optimism that this may change in the foreseeable future.

69.5 Summary

Multibody charm decays offer a rich phenomenology, including unique sensitivity to *CP* violation and charm mixing. This is a highly dynamic field with many new results (some of which we presented here) and rapidly increasing, high quality datasets. These datasets constitute a huge opportunity, but also a challenge to improve the theoretical descriptions of soft hadronic effects in multibody decays. For some measurements, model-independent methods, many relying on input from the charm threshold, provide a way of removing model-induced uncertainties. At the same time, substantial progress in the theoretical description of multibody decays is being made.

References

[1] R. Dalitz, Phil. Mag. Ser. 7 **44**, 1068 (1953).

[2] M. Bauer, B. Stech and M. Wirbel, Z. Phys. C **34**, 103 (1987).

[3] L.-L. Chau and H.-Y. Cheng, Phys. Rev. D **36**, 137 (1987), [Addendum: Phys.Rev.D 39, 2788–2791 (1989)].

[4] P. F. Bedaque, A. K. Das and V. Mathur, Phys. Rev. D **49**, 269 (1994), [hep-ph/9307296].

[5] K. Terasaki, Int. J. Mod. Phys. A **10**, 3207 (1995).

[6] F. Buccella, M. Lusignoli and A. Pugliese, Phys. Lett. B **379**, 249 (1996), [hep-ph/9601343].

[7] J. D. Jackson, Nuovo Cim. **34**, 1644 (1964).

[8] See the note on Resonances in this *Review*.

[9] E. P. Wigner, Phys. Rev. **70**, 15 (1946).

[10] S. M. Flatte, Phys. Lett. B **63**, 224 (1976).

[11] I. Aitchison, Nucl. Phys. A **189**, 417 (1972).

Int. J. Mod. Phys. A 2026.41. Downloaded from www.worldscientific.com
by UNIVERSITY OF CALIFORNIA @ BERKELEY on 09/16/26. Re-use and distribution is strictly not permitted, except for Open Access articles.

[12] D. Aston *et al.*, Nucl. Phys. B **296**, 493 (1988).

[13] R. Omnes, Nuovo Cim. **8**, 316 (1958).

[14] C. Hanhart, Phys. Lett. B **715**, 170 (2012), [arXiv:1203.6839].

[15] F. Niecknig and B. Kubis, JHEP **10**, 142 (2015), [arXiv:1509.03188].

[16] F. Niecknig and B. Kubis, Phys. Lett. B **780**, 471 (2018), [arXiv:1708.00446].

[17] P. Magalhães and M. Robilotta, Phys. Rev. D **92**, 9, 094005 (2015), [arXiv:1504.06346].

[18] P. Magalhaes *et al.*, Phys. Rev. D **84**, 094001 (2011), [arXiv:1105.5120].

[19] R. Aoude *et al.*, Phys. Rev. D **98**, 5, 056021 (2018), [arXiv:1805.11764].

[20] P. C. Magalhães, A. C. dos Reis and M. R. Robilotta, Phys. Rev. D **102**, 7, 076012 (2020), [arXiv:2007.12304].

[21] J. A. Oller, Phys. Rev. D **71**, 054030 (2005), [hep-ph/0411105].

[22] G. Toledo, N. Ikeno and E. Oset, Eur. Phys. J. C **81**, 3, 268 (2021), [arXiv:2008.11312].

[23] L. Roca and E. Oset, Phys. Rev. D **103**, 3, 034020 (2021), [arXiv:2011.05185].

[24] J. Song, A. Feijoo and E. Oset, Phys. Rev. D **106**, 7, 074027 (2022), [arXiv:2205.04781].

[25] J.-P. Dedonder *et al.*, Phys. Rev. D **89**, 9, 094018 (2014), [arXiv:1403.2971].

[26] D. Boito *et al.*, Phys. Rev. D **96**, 11, 113003 (2017), [arXiv:1709.09739].

[27] R. Klein *et al.*, JHEP **10**, 117 (2017), [arXiv:1708.02047].

[28] J. P. Dedonder *et al.*, Phys. Rev. D **103**, 11, 114028 (2021), [arXiv:2105.03355].

[29] E. Aitala *et al.* (E791), Phys. Rev. D **73**, 032004 (2006), [Erratum: Phys. Rev.D 74, 059901 (2006)], [hep-ex/0507099].

[30] G. Bonvicini *et al.* (CLEO), Phys. Rev. D **78**, 052001 (2008), [arXiv:0802.4214].

[31] B. Aubert *et al.* (BaBar), Phys. Rev. D **79**, 032003 (2009), [arXiv:0808.0971].

[32] P. d'Argent *et al.*, JHEP **05**, 143 (2017), [arXiv:1703.08505].

[33] R. Aaij *et al.* (LHCb), Eur. Phys. J. C **78**, 6, 443 (2018), [arXiv:1712.08609].

[34] M. Ablikim *et al.* (BESIII), Phys. Rev. D **104**, 1, 012016 (2021), [arXiv:2011.08041].

[35] M. Ablikim *et al.* (BESIII), Phys. Rev. D **106**, 11, 112006 (2022), [arXiv:2108.10050].

[36] R. Aaij *et al.* (LHCb), JHEP **07**, 204 (2023), [arXiv:2209.09840].

[37] R. Aaij *et al.* (LHCb), JHEP **06**, 044 (2023), [arXiv:2208.03300].

[38] I. Adachi *et al.* (BaBar, Belle), Phys. Rev. Lett. **121**, 26, 261801 (2018), [arXiv:1804.06152]; I. Adachi *et al.* (BaBar, Belle), Phys. Rev. D **98**, 11, 112012 (2018), [arXiv:1804.06153].

[39] V. Anisovich and A. Sarantsev, Eur. Phys. J. A **16**, 229 (2003), [hep-ph/0204328].

[40] Z. Y. Zhou and H. Q. Zheng, Nucl. Phys. A **775**, 212 (2006), [hep-ph/0603062].

[41] B. El-Bennich *et al.*, Phys. Rev. D **79**, 094005 (2009), [Erratum: Phys. Rev. D 83, 039903 (2011)], [arXiv:0902.3645].

[42] J.-P. Dedonder *et al.*, Acta Phys. Polon. B **42**, 2013 (2011), [arXiv:1011.0960].

[43] M. Ablikim *et al.* (BESIII) (2022), [arXiv:2212.09048].

[44] M. Ablikim *et al.* (BESIII) (2025), [arXiv:2503.11383].

[45] J. Wu *et al.* (BESIII) (2025), [arXiv:2505.12086].

[46] M. Ablikim *et al.* (BESIII), Phys. Rev. D **110**, 9, 092006 (2024), [arXiv:2409.01419].

[47] M. Ablikim *et al.* (BESIII), Phys. Rev. Lett. **132**, 13, 131903 (2024), [arXiv:2309.05760].

[48] M. Ablikim *et al.* (BESIII), Phys. Rev. D **110**, 11, L111102 (2024), [arXiv:2404.09219].

[49] R. Aaij *et al.* (LHCb), Sci. Bull. **70**, 1432 (2025), [arXiv:2411.03399].

[50] R. Aaij *et al.* (LHCb), Phys. Rev. D **108**, 1, 012023 (2023), [arXiv:2208.03262].

[51] R. Aaij *et al.* (LHCb), JHEP **07**, 228 (2023), [arXiv:2301.07010].

[52] R. Aaij *et al.* (LHCb), Phys. Rev. D **112**, 9, 092003 (2025), [arXiv:2508.00492].

[53] M. Ablikim *et al.* (BESIII), JHEP **2025**, 195 (2025), [arXiv:2412.11040].

[54] M. Ablikim *et al.* (BESIII), Phys. Rev. Lett. **134**, 1, 011904 (2025), [arXiv:2406.17452].

[55] M. Ablikim *et al.* (BESIII), Chin. Phys. C **48**, 8, 083001 (2024), [arXiv:2312.02524].

[56] M. Ablikim *et al.* (BESIII), Phys. Rev. Lett. **135**, 171801 (2025), [arXiv:2506.05761].

[57] M. Ablikim *et al.* (BESIII), Phys. Rev. Lett. **135**, 111803 (2025), [arXiv:2504.10867].

[58] M. Ablikim *et al.* (BESIII), JHEP **03**, 197 (2025), [arXiv:2412.10803].

[59] M. Ablikim *et al.* (BESIII), Phys. Rev. D **110**, 9, 092008 (2024), [arXiv:2401.13225].

[60] M. Ablikim *et al.* (BESIII), JHEP **10**, 199 (2024), [arXiv:2408.04422].

[61] M. Ablikim *et al.* (BESIII), JHEP **12**, 072 (2023), [arXiv:2307.03024].

[62] M. Ablikim *et al.* (BESIII), Phys. Rev. Lett. **134**, 20, 201902 (2025).

[63] M. Ablikim *et al.* (BESIII) (2025), [arXiv:2503.02196].

[64] S. X. Nakamura, Phys. Rev. D **93**, 1, 014005 (2016), [arXiv:1504.02557].

[65] R. Aaij *et al.* (LHCb), JHEP **04**, 063 (2019), [arXiv:1902.05884].

[66] K. M. Watson, Phys. Rev. **88**, 1163 (1952).

[67] B. Hyams *et al.*, Nuclear Physics B **64**, 134 (1973), ISSN 0550-3213, URL `https://www.sciencedirect.com/science/article/pii/0550321373906184`.

[68] J. R. Batley *et al.* (NA48/2), Eur. Phys. J. C **70**, 635 (2010).

[69] F. Krinner *et al.*, Phys. Rev. D **97**, 11, 114008 (2018), [arXiv:1710.09849].

[70] M. Mikhasenko *et al.* (JPAC), Phys. Rev. D **101**, 3, 034033 (2020), [arXiv:1910.04566].

[71] M. Gronau and D. Wyler, Phys. Lett. B **265**, 172 (1991).

[72] M. Gronau and D. London, Phys. Lett. B **253**, 483 (1991).

[73] A. Bondar, Proceedings of BINP special analysis meeting on Dalitz analysis, 24–26 Sep. 2002, unpublished.

[74] A. Giri *et al.*, Phys. Rev. D **68**, 054018 (2003), [hep-ph/0303187].

[75] A. Poluektov *et al.* (Belle), Phys. Rev. D **70**, 072003 (2004), [hep-ex/0406067].

[76] D. Atwood, I. Dunietz and A. Soni, Phys. Rev. D **63**, 036005 (2001), [hep-ph/0008090].

[77] D. Atwood and A. Soni, Phys. Rev. D **68**, 033003 (2003), [hep-ph/0304085].

[78] J. Rademacker and G. Wilkinson, Phys. Lett. B **647**, 400 (2007), [hep-ph/0611272].

[79] A. Bondar, A. Poluektov and V. Vorobiev, Phys. Rev. D **82**, 034033 (2010), [arXiv:1004.2350].

Int. J. Mod. Phys. A 2026.41. Downloaded from www.worldscientific.com
UNIVERSITY OF CALIFORNIA @ BERKELEY on 09/16/26. Re-use and distribution is strictly not permitted, except for Open Access articles.

[80] S. Malde and G. Wilkinson, Phys. Lett. B **701**, 353 (2011), [arXiv:1104.2731].

[81] C. Thomas and G. Wilkinson, JHEP **10**, 185 (2012), [arXiv:1209.0172].

[82] M. Nayak *et al.*, Phys. Lett. B **740**, 1 (2015), [arXiv:1410.3964].

[83] S. Malde *et al.*, Phys. Lett. B **747**, 9 (2015), [arXiv:1504.05878].

[84] S. Malde, C. Thomas and G. Wilkinson, Phys. Rev. D **91**, 9, 094032 (2015), [arXiv:1502.04560].

[85] P. Naik, JHEP **03**, 038 (2023), [arXiv:2102.07729].

[86] A. Bondar and A. Poluektov, Eur. Phys. J. C **55**, 51 (2008), [arXiv:0801.0840].

[87] A. Poluektov, Eur. Phys. J. C **78**, 2, 121 (2018), [arXiv:1712.08326].

[88] J. V. Backus *et al.* (2022), [arXiv:2211.05133].

[89] J. Lane, E. Gersabeck and J. Rademacker, JHEP **09**, 007 (2023), [arXiv:2305.10787].

[90] M. Ablikim *et al.* (BESIII) (2025), [arXiv:2503.22126].

[91] M. Ablikim *et al.* (BESIII), Phys. Rev. Lett. **124**, 24, 241802 (2020), [arXiv:2002.12791].

[92] M. Ablikim *et al.* (BESIII), Phys. Rev. D **101**, 11, 112002 (2020), [arXiv:2003.00091].

[93] M. Ablikim *et al.* (BESIII), Phys. Rev. D **102**, 5, 052008 (2020), [arXiv:2007.07959].

[94] M. Ablikim *et al.* (BESIII), Phys. Rev. D **110**, 11, 112008 (2024), [arXiv:2408.16279].

[95] M. Ablikim *et al.* (BESIII), Phys. Rev. D **112**, 1, 012015 (2025).

[96] M. Ablikim *et al.* (BESIII), JHEP **05**, 164 (2021), [arXiv:2103.05988].

[97] J. Libby *et al.* (CLEO), Phys. Rev. D **82**, 112006 (2010), [arXiv:1010.2817].

[98] R. A. Briere *et al.* (CLEO), Phys. Rev. D **80**, 032002 (2009), [arXiv:0903.1681].

[99] S. Harnew *et al.*, JHEP **01**, 144 (2018), [arXiv:1709.03467].

[100] P. Resmi *et al.*, JHEP **01**, 082 (2018), [arXiv:1710.10086].

[101] J. Insler *et al.* (CLEO), Phys. Rev. D **85**, 092016 (2012), [Erratum: Phys. Rev. D 94, 099905 (2016)], [arXiv:1203.3804].

[102] T. Evans *et al.*, Phys. Lett. B **757**, 520 (2016), [Erratum: Phys. Lett. B 765, 402–403 (2017)], [arXiv:1602.07430].

[103] M. Ablikim *et al.* (BESIII), Phys. Rev. D **111**, 1, 012007 (2025), [arXiv:2409.07197].

[104] M. Ablikim *et al.* (BESIII), Phys. Rev. D **106**, 9, 092004 (2022), [arXiv:2208.10098].

[105] M. Ablikim *et al.* (BESIII), Phys. Rev. D **107**, 3, 032009 (2023), [arXiv:2212.06489].

[106] C. Rosner *et al.* (BESIII), Phys. Rev. D **108**, 3, 032003 (2023), [arXiv:2305.03975].

[107] M. Ablikim *et al.* (BESIII), Phys. Rev. D **106**, 9, 092005 (2022), [arXiv:2206.13864].

[108] R. Aaij *et al.* (LHCb) (2025), [arXiv:2510.04963].

[109] R. Aaij *et al.* (LHCb), Phys. Rev. Lett. **116**, 24, 241801 (2016), [arXiv:1602.07224].

[110] P. del Amo Sanchez *et al.* (BaBar), Phys. Rev. Lett. **105**, 121801 (2010), [arXiv:1005.1096].

[111] J. Lees *et al.* (BaBar), Phys. Rev. D **84**, 012002 (2011), [arXiv:1104.4472].

[112] A. Poluektov *et al.* (Belle), Phys. Rev. D **81**, 112002 (2010), [arXiv:1003.3360].

[113] H. Aihara *et al.* (Belle), Phys. Rev. D **85**, 112014 (2012), [arXiv:1204.6561].

[114] P. K. Resmi *et al.* (Belle), JHEP **10**, 178 (2019), [arXiv:1908.09499].

[115] I. Adachi *et al.* (Belle, Belle-II), JHEP **10**, 143 (2024), [arXiv:2404.12817].

[116] F. Abudinén *et al.* (Belle, Belle-II), JHEP **02**, 063 (2022), [Erratum: JHEP 12, 034 (2022)], [arXiv:2110.12125].

[117] R. Aaij *et al.* (LHCb), Phys. Lett. B **726**, 151 (2013), [arXiv:1305.2050].

[118] R. Aaij *et al.* (LHCb), Phys. Lett. B **723**, 44 (2013), [arXiv:1303.4646].

[119] R. Aaij *et al.* (LHCb), Phys. Lett. B **718**, 43 (2012), [arXiv:1209.5869].

[120] R. Aaij *et al.* (LHCb), JHEP **10**, 097 (2014), [arXiv:1408.2748].

[121] R. Aaij *et al.* (LHCb), Phys. Lett. B **733**, 36 (2014), [arXiv:1402.2982].

[122] R. Aaij *et al.* (LHCb), Nucl. Phys. B **888**, 169 (2014), [arXiv:1407.6211].

[123] R. Aaij *et al.* (LHCb), Phys. Rev. D **91**, 11, 112014 (2015), [arXiv:1504.05442].

[124] R. Aaij *et al.* (LHCb), JHEP **06**, 131 (2016), [arXiv:1604.01525].

[125] R. Aaij *et al.* (LHCb), JHEP **12**, 087 (2016), [arXiv:1611.03076].

[126] R. Aaij *et al.* (LHCb), JHEP **08**, 176 (2018), [Erratum: JHEP 10, 107 (2018)], [arXiv:1806.01202].

[127] R. Aaij *et al.* (LHCb), JHEP **07**, 099 (2022), [arXiv:2112.10617].

[128] R. Aaij *et al.* (LHCb), JHEP **07**, 138 (2023), [arXiv:2209.03692].

[129] R. Aaij *et al.* (LHCb), Eur. Phys. J. C **83**, 6, 547 (2023), [Erratum: Eur.Phys.J.C 83, 672 (2023)], [arXiv:2301.10328].

[130] R. Aaij *et al.* (LHCb), Eur. Phys. J. C **84**, 2, 206 (2024), [arXiv:2309.05514].

[131] R. Aaij *et al.* (LHCb), JHEP **02**, 118 (2024), [arXiv:2311.10434].

[132] R. Aaij *et al.* (LHCb), JHEP **12**, 013 (2023), [arXiv:2310.04277].

[133] R. Aaij *et al.* (LHCb), JHEP **02**, 113 (2025), [arXiv:2410.21115].

[134] R. Aaij *et al.* (LHCb), JHEP **05**, 025 (2024), [arXiv:2401.17934].

[135] R. Aaij *et al.* (LHCb), JHEP **12**, 141 (2021), [arXiv:2110.02350]; LHCb-CONF-2025-003 (2025), (update in LHCb-CONF-2025-003 (2025)), URL `https://cds.cern.ch/record/2946710`.

[136] R. Aaij *et al.* (LHCb) (2025), [arXiv:2509.15139].

[137] S. Harnew and J. Rademacker, Phys. Lett. B **728**, 296 (2014), [arXiv:1309.0134].

[138] S. Harnew and J. Rademacker, JHEP **03**, 169 (2015), [arXiv:1412.7254].

[139] D. Craik, T. Gershon and A. Poluektov, Phys. Rev. D **97**, 5, 056002 (2018), [arXiv:1712.07853].

[140] M. Ablikim *et al.* (BESIII), Chin. Phys. C **48**, 12, 123001 (2024), [arXiv:2406.05827].

[141] R. Aaij *et al.* (LHCb), JHEP **02**, 169 (2021), [arXiv:2010.08483].

[142] Y. S. Amhis *et al.* (HFLAV), Phys. Rev. D **107**, 5, 052008 (2023), updated results and plots available https://hflav-eos.web.cern.ch/hflav-eos/triangle/latest/., [arXiv:2206.07501].

[143] F. Betti *et al.*, Phys. Rev. D **112**, 1, 013004 (2025), [arXiv:2409.06449].

[144] A. Bondar, T. Gershon and P. Krokovny, Phys. Lett. B **624**, 1 (2005), [hep-ph/0503174].

Int. J. Mod. Phys. A 2026.41. Downloaded from www.worldscientific.com
by UNIVERSITY OF CALIFORNIA @ BERKELEY on 09/16/26. Re-use and distribution is strictly not permitted, except for Open Access articles.

[145] P. Krokovny *et al.* (Belle), Phys. Rev. Lett. **97**, 081801 (2006), [hep-ex/0605023].

[146] B. Aubert *et al.* (BaBar), Phys. Rev. Lett. **99**, 231802 (2007), [arXiv:0708.1544].

[147] V. Vorobyev *et al.* (Belle), Phys. Rev. D **94**, 5, 052004 (2016), [arXiv:1607.05813].

[148] See the note on D^0–$\overline{D}^0$ Mixing in this *Review*.

[149] See the note CP violation in the quark sector in this *Review*.

[150] D. Asner *et al.* (CLEO), Phys. Rev. D **72**, 012001 (2005), [hep-ex/0503045].

[151] R. Aaij *et al.* (LHCb), Phys. Rev. Lett. **127**, 11, 111801 (2021), [arXiv:2106.03744].

[152] I. Adachi *et al.* (Belle, Belle-II), Phys. Rev. D **111**, 11, 112011 (2025), [arXiv:2410.22961].

[153] A. Di Canto *et al.*, Phys. Rev. D **99**, 1, 012007 (2019), [arXiv:1811.01032].

[154] R. Aaij *et al.* (LHCb), Phys. Rev. Lett. **122**, 21, 211803 (2019), [arXiv:1903.08726].

[155] R. Aaij *et al.* (LHCb), Phys. Rev. Lett. **131**, 9, 091802 (2023), [arXiv:2209.03179].

[156] R. Aaij *et al.* (LHCb), Phys. Rev. D **93**, 5, 052018 (2016), [arXiv:1509.06628].

[157] R. Aaij *et al.* (LHCb), JHEP **02**, 126 (2019), [arXiv:1811.08304].

[158] M. Artuso *et al.* (CLEO), Phys. Rev. D **85**, 122002 (2012), [arXiv:1201.5716].

[159] B. Aubert *et al.* (BaBar), Phys. Rev. D **78**, 051102 (2008), [arXiv:0802.4035].

[160] I. Bediaga *et al.*, Phys. Rev. D **80**, 096006 (2009), [arXiv:0905.4233].

[161] I. Bediaga *et al.*, Phys. Rev. D **86**, 036005 (2012), [arXiv:1205.3036].

[162] R. Aaij *et al.* (LHCb), Phys. Lett. B **726**, 623 (2013), [arXiv:1308.3189].

[163] R. Aaij *et al.* (LHCb), Phys. Rev. Lett. **133**, 25, 251801 (2024), [arXiv:2409.01414].

[164] R. Aaij *et al.* (LHCb), JHEP **06**, 112 (2013), [arXiv:1303.4906].

[165] R. Aaij *et al.* (LHCb), Phys. Rev. D **84**, 112008 (2011), [arXiv:1110.3970].

[166] J. Lees *et al.* (BaBar), Phys. Rev. D **87**, 5, 052010 (2013), [arXiv:1212.1856].

[167] T. Aaltonen *et al.* (CDF), Phys. Rev. D **86**, 032007 (2012), [arXiv:1207.0825].

[168] R. Aaij *et al.* (LHCb), JHEP **03**, 107 (2024), [arXiv:2310.19397].

[169] R. Aaij *et al.* (LHCb), JHEP **07**, 067 (2023), [arXiv:2303.04062].

[170] R. Aaij *et al.* (LHCb), Phys. Lett. B **728**, 585 (2014), [arXiv:1310.7953].

[171] R. Aaij *et al.* (LHCb), Eur. Phys. J. C **80**, 10, 986 (2020), [arXiv:2006.03145].

[172] M. Williams, Phys. Rev. D **84**, 054015 (2011), [arXiv:1105.5338].

[173] A. Davis *et al.*, JHEP **06**, 098 (2023), [arXiv:2301.13211].

[174] R. Aaij *et al.* (LHCb), Phys. Lett. B **740**, 158 (2015), [arXiv:1410.4170].

[175] R. Aaij *et al.* (LHCb), Phys. Lett. B **769**, 345 (2017), [arXiv:1612.03207].

[176] R. Aaij *et al.* (LHCb), JHEP **09**, 129 (2023), [Erratum: JHEP 04, 040 (2024)], [arXiv:2306.12746].

[177] E. Golowich and G. Valencia, Phys. Rev. D **40**, 112 (1989).

[178] G. Valencia, Phys. Rev. D **39**, 3339 (1989).

[179] W. Bensalem and D. London, Phys. Rev. D **64**, 116003 (2001), [hep-ph/0005018].

[180] I. I. Bigi, in "KAON2001: International Conference on CP Violation," (2001), [hep-ph/0107102].

[181] W. Bensalem, A. Datta and D. London, Phys. Rev. D **66**, 094004 (2002), [hep-ph/0208054].

[182] W. Bensalem, A. Datta and D. London, Phys. Lett. B **538**, 309 (2002), [hep-ph/0205009].

[183] A. Datta and D. London, Int. J. Mod. Phys. A **19**, 2505 (2004), [hep-ph/0303159].

[184] M. Gronau and J. L. Rosner, Phys. Rev. D **84**, 096013 (2011), [arXiv:1107.1232].

[185] G. Durieux and Y. Grossman, Phys. Rev. D **92**, 7, 076013 (2015), [arXiv:1508.03054].

[186] L. Aggarwal *et al.* (Belle, Belle-II), JHEP **04**, 036 (2025), [arXiv:2409.15777].

[187] J. Link *et al.* (FOCUS), Phys. Lett. B **622**, 239 (2005), [hep-ex/0506012].

[188] P. del Amo Sanchez *et al.* (BaBar), Phys. Rev. D **81**, 111103 (2010), [arXiv:1003.3397].

[189] R. Aaij *et al.* (LHCb), JHEP **10**, 005 (2014), [arXiv:1408.1299].

[190] J. Kim *et al.* (Belle), Phys. Rev. D **99**, 1, 011104 (2019), [arXiv:1810.06457].

[191] J. Lees *et al.* (BaBar), Phys. Rev. D **84**, 031103 (2011), [arXiv:1105.4410].

[192] K. Prasanth *et al.* (Belle), Phys. Rev. D **95**, 9, 091101 (2017), [arXiv:1703.05721].

[193] R. Aaij *et al.* (LHCb), Phys. Rev. Lett. **128**, 22, 221801 (2022), [arXiv:2111.03327].

[194] R. Aaij *et al.* (LHCb), Phys. Rev. Lett. **121**, 9, 091801 (2018), [arXiv:1806.10793].

[195] R. Aaij *et al.* (LHCb), Phys. Rev. D **111**, 9, L091102 (2025), [arXiv:2502.04013].

Int. J. Mod. Phys. A 2026.41. Downloaded from www.worldscientific.com
UNIVERSITY OF CALIFORNIA @ BERKELEY on 09/16/26. Re-use and distribution is strictly not permitted, except for Open Access articles.

70. D^0-$\overline{D}^0$ Mixing

Revised September 2025 by A.J. Schwartz (U. of Cincinnati); written with D.M. Asner (SNOLAB, Lively).

The formalism for D^0-$\overline{D}^0$ mixing is closely related to that for CP violation; for further details on the latter, see the note "CP Violation in the Quark Sector" in this *Review*. The time evolution of the D^0–$\overline{D}^0$ system is described by the Schrödinger equation

$$i\frac{\partial}{\partial t}\begin{pmatrix}D^0(t)\\ \overline{D}^0(t)\end{pmatrix} = \left(\mathbf{M} - \frac{i}{2}\mathbf{\Gamma}\right)\begin{pmatrix}D^0(t)\\ \overline{D}^0(t)\end{pmatrix}, \tag{70.1}$$

where the $\mathbf{M}$ and $\mathbf{\Gamma}$ matrices are Hermitian, and CPT invariance requires that $M_{11} = M_{22} \equiv M$ and $\Gamma_{11} = \Gamma_{22} \equiv \Gamma$. The off-diagonal elements of $\mathbf{M}$ and $\mathbf{\Gamma}$ are referred to as the dispersive and absorptive parts, respectively, of the mixing. The mass eigenstates D_1 and D_2 of the Hamiltonian $\mathbf{M}$ - $i\mathbf{\Gamma}/2$ are defined as

$$|D_{1,2}\rangle \;\equiv\; p|D^0\rangle \pm q|\overline{D}^0\rangle\,, \tag{70.2}$$

where normalization imposes $|p|^2 + |q|^2 = 1$. Equation (70.1) implies that a charm meson created as a D^0 will time-evolve to a $\overline{D}^0$, and vice-versa. As shown in Eqs. (70.11) and (70.13) below, the probability for $D^0 \to \overline{D}^0 \propto |q/p|^2$, whereas the probability for $\overline{D}^0 \to D^0 \propto |p/q|^2$. Thus, if $|q/p| \neq 1$, CP is violated in mixing. If $\mathrm{Arg}(q/p) \neq 0$ or π, CP is violated in the interference between a mixed decay amplitude and a direct decay amplitude. These two types of CP violation are collectively referred to as *indirect* CP violation.

As the absolute phases of $|D^0\rangle$ and $|\overline{D}^0\rangle$ are arbitrary, the relative phase ξ between them is unphysical. This relative phase must appear in a CP transformation: $CP|D^0\rangle = e^{i\xi}|\overline{D}^0\rangle$ and $CP|\overline{D}^0\rangle = e^{-i\xi}|D^0\rangle$, resulting in $(CP)^2|D^0\rangle = |D^0\rangle$ and $(CP)^2|\overline{D}^0\rangle = |\overline{D}^0\rangle$. For definiteness we choose a phase convention $CP|D^0\rangle = -|\overline{D}^0\rangle$, which fixes $\xi = \pi$. In addition, for $\mathrm{Arg}(q/p)$ to have physical meaning it must be defined relative to a reference phase, i.e., only phase *differences* are physical. In Ref. [1], the reference phase is taken to be that of the $\Delta(U\text{-spin}) = 2$ component of $\langle\overline{D}^0|\Gamma|D^0\rangle$; this is equivalent to defining this component of Γ_{12} to be real and positive, and we retain this definition here. With these conventions, if $p = \pm q$ then D_1, D_2 are CP eigenstates, and there is no indirect CP violation ($|q/p| = 1$ and $\mathrm{Arg}(q/p) = 0$ or π).

The eigenvalues of the Hamiltonian $\mathbf{M}$ - $i\mathbf{\Gamma}/2$ are

$$\omega_{1,2} \;=\; \left(M - \frac{i}{2}\Gamma\right) \pm \frac{q}{p}\left(M_{12} - \frac{i}{2}\Gamma_{12}\right) \;\equiv\; m_{1,2} - \frac{i}{2}\Gamma_{1,2}\,, \tag{70.3}$$

where $m_{1,2}$ and $\Gamma_{1,2}$ are defined to be real and thus correspond to the masses and decay widths, respectively, of the eigenstates $D_{1,2}$. As the traces $M_{11} + M_{22} = 2M$ and $\Gamma_{11} + \Gamma_{22} = 2\Gamma$ are unchanged by diagonalizing $\mathbf{M}$ and $\mathbf{\Gamma}$, M must equal the mean value $(M_1 + M_2)/2$ and Γ must equal the mean value $(\Gamma_1 + \Gamma_2)/2$. Solving for the eigenstates of the Hamiltonian yields

$$\left(\frac{q}{p}\right)^2 = \frac{M_{12}^* - \frac{i}{2}\Gamma_{12}^*}{M_{12} - \frac{i}{2}\Gamma_{12}}\,. \tag{70.4}$$

If $\mathrm{Arg}(M_{12}) = \mathrm{Arg}(\Gamma_{12})$, then $|q/p| = 1$ and CP is conserved in mixing. In the more restrictive case that M_{12} and Γ_{12} are real, Eq. (70.4) implies that $\mathrm{Arg}(q/p) = 0$ or π and there is no indirect CP violation. In this case, Eq. (70.3) implies that the differences in eigenvalues $\Delta m \equiv m_2 - m_1 = 2M_{12}$ and $\Delta\Gamma \equiv \Gamma_2 - \Gamma_1 = \Gamma_{12}$. The magnitudes and signs of Δm and $\Delta\Gamma$ are difficult to predict from theory and must be determined experimentally.

It is advantageous to define dimensionless mixing parameters x and y as

$$x \;\equiv\; \frac{\Delta m}{\Gamma} \qquad y \;\equiv\; \frac{\Delta\Gamma}{2\Gamma}\,. \tag{70.5}$$

These parameters are measured in several ways; the most precise values are obtained by measuring the time dependence of D^0 decays. As an alternative to parameters x, y, one can define mixing parameters [2]

$$x_{12} \;\equiv\; \frac{2|M_{12}|}{\Gamma} \qquad y_{12} \;\equiv\; \frac{|\Gamma_{12}|}{\Gamma}\,. \tag{70.6}$$

As shown above, CP violation in mixing arises from $\mathrm{Arg}(M_{12}) \neq \mathrm{Arg}(\Gamma_{12})$, and CP violation due to interference arises from either $\mathrm{Arg}(M_{12}) \equiv \phi^M \neq 0, \pi$ or $\mathrm{Arg}(\Gamma_{12}) \equiv \phi^\Gamma \neq 0, \pi$. Defining $\phi \equiv \mathrm{Arg}(q/p) + n\pi$, the conversion between parameters $(x, y, |q/p|, \phi)$ and equivalent parameters $(x_{12}, y_{12}, \phi^M, \phi^\Gamma)$ is [1,3]

$$x^2 = \frac{x_{12}^2 - y_{12}^2 + \sqrt{(x_{12}^2 + y_{12}^2)^2 - 4x_{12}^2 y_{12}^2 \sin^2\phi_{12}}}{2} \tag{70.7}$$

$$y^2 = \frac{y_{12}^2 - x_{12}^2 + \sqrt{(x_{12}^2 + y_{12}^2)^2 - 4x_{12}^2 y_{12}^2 \sin^2\phi_{12}}}{2} \tag{70.8}$$

$$\left|\frac{q}{p}\right|^2 = \sqrt{\frac{x_{12}^2 + y_{12}^2 + 2x_{12}y_{12}\sin\phi_{12}}{x_{12}^2 + y_{12}^2 - 2x_{12}y_{12}\sin\phi_{12}}} \tag{70.9}$$

$$\tan(2\phi) = -\frac{x_{12}^2\sin(2\phi^M) + y_{12}^2\sin(2\phi^\Gamma)}{x_{12}^2\cos(2\phi^M) + y_{12}^2\cos(2\phi^\Gamma)}\,, \tag{70.10}$$

where $\phi_{12} \equiv \phi^M - \phi^\Gamma$. If CP is conserved in mixing ($|q/p| = 1$), then $\phi_{12} = 0, \pi$ and $|x| = x_{12}$, $|y| = y_{12}$. In this case, Eq. (70.10) implies $\phi = -\phi^{M,\Gamma}$ modulo π. It can be shown that the product $xy = x_{12}\,y_{12}\cos\phi_{12}$, and thus the fact that x and y are measured to be positive implies ϕ_{12} is close to zero rather than π. It can also be shown that the parameter $y_{CP}(K^+K^-, \pi^+\pi^-) \approx y_{12}\cos\phi^\Gamma$, and thus the fact that y_{CP} is measured to be positive implies ϕ^Γ (and hence ϕ^M) is close to zero rather then π.

To measure mixing, the initial flavor of the D^0 or $\overline{D}^0$ when produced must be determined. The most common method used to identify the initial flavor is to reconstruct $D^{*+} \to D^0\pi^+$ or $D^{*-} \to \overline{D}^0\pi^-$ decays; the charge of the accompanying pion (which has low momentum in the lab frame and is often referred to as the "soft" pion) determines the flavor of the neutral D. BABAR and LHCb have also identified the flavor of the neutral D by reconstructing the semileptonic decays $B^+ \to \overline{D}^0 X\ell^+\nu$, $B^0 \to D^{*-}X\ell^+\nu$, $B^- \to D^0X\ell^-\bar{\nu}$, and $\overline{B}^0 \to D^{*+}X\ell^-\bar{\nu}$;[1] in this case the charge of the accompanying lepton determines (or "tags") the D flavor. Both experiments have used these tags together to select "double-tagged" $B^0 \to D^{*-}X\ell^+\nu$, $D^{*-} \to \overline{D}^0\pi^-$ decays, which have especially high purity. At e^+e^- collider experiments such as Belle, Belle II, BABAR, and BESIII, the D flavor can also be determined by reconstructing a flavor-specific D decay on the "opposite side" of an event, i.e., recoiling against the signal-side D decay.

At BESIII, where $D\overline{D}$ pairs are produced near their threshold via $e^+e^- \to \psi(3770) \to D^0\overline{D}^0$, there is little background and the purity of opposite-side tagging is equivalent to that achieved using $D^{*\pm}$ decays. However, BESIII operates at a symmetric e^+e^- collider, and the $D\overline{D}$ pairs are produced almost at rest in the lab frame. As a consequence, the D's do not travel any appreciable distance before decaying, and time-dependent analyses are not possible. To overcome this, measurements of mixing at BESIII utilize the quantum coherence of the initial $\psi(3770) \to D^0\overline{D}^0$ state and time-integrated measurements [4–8].

70.1 Time-Dependent Analyses

Starting from a pure $|D^0\rangle$ state, after a time t there will exist a mixture of states:

$$|D^0(t)\rangle = g_+(t)|D^0\rangle + \left(\frac{q}{p}\right)g_-(t)|\overline{D}^0\rangle, \tag{70.11}$$

where

$$g_\pm(t) = \frac{1}{2}\left(e^{-i\omega_1 t} \pm e^{-i\omega_2 t}\right) \tag{70.12}$$

and $\omega_{1,2}$ are defined in Eq. (70.3). Similarly, a pure $|\overline{D}^0\rangle$ state will evolve to a mixture of states

$$|\overline{D}^0(t)\rangle = g_+(t)|\overline{D}^0\rangle + \left(\frac{p}{q}\right)g_-(t)|D^0\rangle. \tag{70.13}$$

[1] Charge-conjugate modes are implicitly included throughout this Review, unless noted otherwise.

Int. J. Mod. Phys. A 2026.41. Downloaded from www.worldscientific.com
by UNIVERSITY OF CALIFORNIA @ BERKELEY on 09/16/26. Re-use and distribution is strictly not permitted, except for Open Access articles.

The respective decay rates to a final state f are

$$r_f(t) \equiv \left|\langle f|H|D^0(t)\rangle\right|^2 = \left|g_+(t)\langle f|H|D^0\rangle + \frac{q}{p}\, g_-(t)\langle f|H|\overline{D}^0\rangle\right|^2 \tag{70.14}$$

$$\bar{r}_f(t) \equiv \left|\langle f|H|\overline{D}^0(t)\rangle\right|^2 = \left|g_+(t)\langle f|H|\overline{D}^0\rangle + \frac{p}{q}\, g_-(t)\langle f|H|D^0\rangle\right|^2. \tag{70.15}$$

In these expressions we have neglected phase-space factors, which divide out in ratios of D^0 and $\overline{D}^0$ decay rates to common final states. Denoting the decay amplitudes of pure D^0 and $\overline{D}^0$ states as $A_f \equiv \langle f|H|D^0\rangle$, $\overline{A}_f \equiv \langle f|H|\overline{D}^0\rangle$, $A_{\overline{f}} \equiv \langle \overline{f}|H|D^0\rangle$, and $\overline{A}_{\overline{f}} \equiv \langle \overline{f}|H|\overline{D}^0\rangle$, and defining the combinations of factors

$$\lambda_f \;\equiv\; \frac{q}{p}\frac{\overline{A}_f}{A_f} \qquad\qquad \lambda_{\overline{f}} \;\equiv\; \frac{q}{p}\frac{\overline{A}_{\overline{f}}}{A_{\overline{f}}}\,, \tag{70.16}$$

one obtains

$$r_f(t) = |A_f|^2\left[|g_+(t)|^2 + |\lambda_f|^2|g_-(t)|^2 + 2\mathrm{Re}\Big(\lambda_f\, g_+^*(t)\, g_-(t)\Big)\right] \tag{70.17}$$

$$= \frac{|A_f|^2}{2}\, e^{-\Gamma t}\Big[(1+|\lambda_f|^2)\cosh(y\Gamma t) + 2\mathrm{Re}(\lambda_f)\sinh(y\Gamma t) + (1-|\lambda_f|^2)\cos(x\Gamma t) - 2\mathrm{Im}(\lambda_f)\sin(x\Gamma t)\Big] \tag{70.18}$$

$$\bar{r}_f(t) = |\overline{A}_f|^2\left[|g_+(t)|^2 + |\lambda_f|^{-2}|g_-(t)|^2 + 2\mathrm{Re}\Big(\lambda_f^{-1}\, g_+^*(t)\, g_-(t)\Big)\right] \tag{70.19}$$

$$= \frac{|\overline{A}_f|^2}{2}\, e^{-\Gamma t}\Big[(1+|\lambda_f|^{-2})\cosh(y\Gamma t) + 2\mathrm{Re}(\lambda_f^{-1})\sinh(y\Gamma t) + (1-|\lambda_f|^{-2})\cos(x\Gamma t) - 2\mathrm{Im}(\lambda_f^{-1})\sin(x\Gamma t)\Big]\,. \tag{70.20}$$

The rates $r_{\overline{f}}$ and $\bar{r}_{\overline{f}}$ are identical to Eqs. (70.18) and (70.20), respectively, except that f is replaced by $\bar{f}$. We note that a change in convention for the relative phase between D^0 and $\overline{D}^0$ cancels between q/p and $\overline{A}_f/A_f$ or $\overline{A}_{\overline{f}}/A_{\overline{f}}$, leaving λ_f and $\lambda_{\overline{f}}$ unchanged.

As $x, y \ll 1$ and experiments typically measure t in the range $(1-8)/\Gamma$, the cosh, sinh, cosine, and sine functions can be expanded to second order in x and y. One obtains:

$$r_f(t) \approx |A_f|^2\, e^{-\Gamma t}\left\{1 + \Big[y\,\mathrm{Re}(\lambda_f) - x\,\mathrm{Im}(\lambda_f)\Big](\Gamma t) + |\lambda_f|^2\left(\frac{x^2+y^2}{4}\right)(\Gamma t)^2 + \left(\frac{y^2-x^2}{4}\right)(\Gamma t)^2\right\} \tag{70.21}$$

$$\bar{r}_f(t) \approx |\overline{A}_f|^2\, e^{-\Gamma t}\left\{1 + \Big[y\,\mathrm{Re}\Big(\frac{1}{\lambda_f}\Big) - x\,\mathrm{Im}\Big(\frac{1}{\lambda_f}\Big)\Big](\Gamma t) + \frac{1}{|\lambda_f|^2}\left(\frac{x^2+y^2}{4}\right)(\Gamma t)^2 + \left(\frac{y^2-x^2}{4}\right)(\Gamma t)^2\right\}. \tag{70.22}$$

For $r_{\overline{f}}$ and $\bar{r}_{\overline{f}}$, A_f, $\bar{A}_f$, and λ_f are replaced by $A_{\bar{f}}$, $\bar{A}_{\bar{f}}$, and $\lambda_{\overline{f}}$. In the sections below we discuss various final states f; our convention is that amplitudes A_f and $\overline{A}_{\overline{f}}$ are Cabibbo-favored (CF), whereas $\overline{A}_f$ and $A_{\overline{f}}$ are Cabibbo-suppressed. With this convention, $|\lambda_f| \ll 1$ and $|1/\lambda_{\overline{f}}| \ll 1$. For multibody final states, Eqs. (70.21) and (70.22) apply separately to each point in phase-space.

70.2 Semileptonic decays

Consider the semileptonic decay $D^0 \to K^-\ell^+\nu$. For this final state, $\overline{A}_f = A_{\overline{f}} = 0$ to excellent approximation.[2] Thus, the final state f is reached from a pure $\overline{D}^0$ state at $t = 0$ only via mixing. The parameters $\lambda_f = 1/\lambda_{\overline{f}} = 0$, and Eqs. (70.21) and (70.22) become

$$r_f(t) = \left|A_f\right|^2 e^{-\Gamma t}\,,$$
$$\bar{r}_f(t) = \left|A_f\right|^2 e^{-\Gamma t}\left|\frac{p}{q}\right|^2\left[\frac{x^2+y^2}{4}\right]\Gamma t)^2\,, \tag{70.23}$$

where the term proportional to $(y^2-x^2)(\Gamma t)^2$ in $r_f(t)$ is negligible and thus dropped. For $r_{\overline{f}}(t)$ and $\bar{r}_{\overline{f}}(t)$, the former equals the second expression in Eq. (70.23) with $|q/p|^2$ replacing $|p/q|^2$, and the latter equals the first expression. In the Standard Model, CP violation in charm mixing is tiny and $|q/p| \approx 1$. Assuming such CP violation is negligible, the time-integrated mixed decay rate relative to the time-integrated unmixed decay rate is

$$\frac{\displaystyle\int_0^\infty \bar{r}_f(t)\,dt}{\displaystyle\int_0^\infty r_f(t)\,dt} = \frac{\displaystyle\int_0^\infty r_{\overline{f}}(t)\,dt}{\displaystyle\int_0^\infty \bar{r}_{\overline{f}}(t)\,dt} = \frac{x^2+y^2}{2} \equiv R_M\,. \tag{70.24}$$

Measurements of R_M from semileptonic decays are listed in Table 70.1. The world average from the Heavy Flavor Averaging Group (HFLAV) [9] is $R_M = (1.30 \pm 2.69) \times 10^{-4}$.

70.3 Hadronic decays to non-CP eigenstates

Consider the hadronic decay $D^0 \to K^-\pi^+$, i.e., $\overline{A}_f$ and $A_{\overline{f}}$ are doubly Cabibbo-suppressed (DCS). Because these CF and DCS decays are dominated by tree-level amplitudes involving only the first two quark generations, direct CP violation is expected to be very small. The ratios of decay amplitudes can be written

$$\frac{\overline{A}_f}{A_f} = \sqrt{R_D^-}\, e^{-i\delta_f} \qquad\qquad \frac{A_{\overline{f}}}{\overline{A}_{\overline{f}}} = \sqrt{R_D^+}\, e^{-i\delta_f}\,, \tag{70.25}$$

where R_D^- and R_D^+ are the ratios of the DCS decay rate to the CF decay rate: $R_D^- \equiv |\overline{A}_f/A_f|^2$ and $R_D^+ \equiv |A_{\overline{f}}/\overline{A}_{\overline{f}}|^2$. A relative minus sign resulting from the weak phase difference between $V_{cd}^*V_{us}$ (for $\overline{A}_f$) and $V_{cs}^*V_{ud}$ (for A_f) is canceled by the phase difference π between D^0 and $\overline{D}^0$ resulting from our convention $CP|D^0\rangle = -|\overline{D}^0\rangle$. From the CKM matrix elements, one estimates R_D^-, $R_D^+ \approx \tan^4\theta_c$, where θ_c is the Cabibbo angle. The parameter δ_f is the strong phase difference between CF and DCS amplitudes: $\delta \equiv \mathrm{Arg}(A_f/\overline{A}_f) = \mathrm{Arg}(\overline{A}_{\overline{f}}/A_{\overline{f}})$. The amplitudes A_f and $\overline{A}_f$ can in principle involve higher-order (or sub-leading) diagrams with a different weak phase than the leading diagram. The phase differences φ_f would depend on the final state and contribute factors $e^{i\varphi_f}$ to Eq. (70.25). However, such amplitudes are highly suppressed and can be safely neglected here; this is referred to as "approximate universality." Eq. (70.25) implies

$$\lambda_f = \sqrt{R_D^-}\,\left|\frac{q}{p}\right|\, e^{-i(\delta_f-\phi)}\,, \quad \left(\lambda_{\overline{f}}\right)^{-1} = \sqrt{R_D^+}\,\left|\frac{p}{q}\right|\, e^{-i(\delta_f+\phi)}\,, \tag{70.26}$$

where $\phi = \mathrm{Arg}(q/p)$.

For convenience, we define the mean decay rate $R_D \equiv (R_D^+ + R_D^-)/2$ and the decay rate asymmetry $A_D \equiv (R_D^+ - R_D^-)/(R_D^+ + R_D^-)$. With these definitions, the rates for the mixed ("wrong-

[2] There exists a doubly Cabibbo-suppressed amplitude in which the c and $\bar{u}$ quarks exchange a W, and the resulting d quark from the c decays semileptonically. We neglect this higher-order process.

Int. J. Mod. Phys. A 2026.41. Downloaded from www.worldscientific.com
UNIVERSITY OF CALIFORNIA @ BERKELEY on 09/16/26. Re-use and distribution is strictly not permitted, except for Open Access articles.

Table 70.1: Results for $R_M = (x^2+y^2)/2$ in D^0 semileptonic decays. The HFLAV average assumes statistical and systematic uncertainties are uncorrelated. When a single uncertainty is listed, it corresponds to statistical and systematic uncertainties combined. The measurements with an asterisk (*) have been superseded and are not included in the HFLAV average.

Year	Experiment	Final state(s)	R_M ($\times 10^{-3}$)	90% C.L. ($\times 10^{-3}$)
2008	Belle (492 fb^{-1}) [10]	$K^{(*)+}e^-\overline{\nu}_e$	$0.13\pm0.22\pm0.20$	< 0.61
2007	BABAR (344 fb^{-1}) [11]	$K^{(*)+}e^-\overline{\nu}_e$	$0.04\,^{+0.70}_{-0.60}$	$(-1.3, 1.2)$
2005	CLEO (9.0 fb^{-1}) [12]	$K^{(*)+}e^-\overline{\nu}_e$	$1.6\pm2.9\pm2.9$	< 7.8
1996	E791 (2×10^{10} evts) [13]	$K^+\ell^-\overline{\nu}_\ell$	$1.1\,^{+3.0\,+0.0}_{-2.7\,-0.1}$	< 5.0
	HFLAV Average [14]		$\mathbf{0.130 \pm 0.269}$	
2005*	Belle (253 fb^{-1}) [15]	$K^{(*)+}e^-\overline{\nu}_e$	$0.02\pm0.47\pm0.14$	< 1.0
2004*	BABAR (87 fb^{-1}) [16]	$K^{(*)+}e^-\overline{\nu}_e$	$2.3\pm1.2\pm0.4$	< 4.2

sign") decays $D^0 \to K^+\pi^-$ and $\overline{D}^0 \to K^-\pi^+$ are [17, 18]:

$$r_{\overline{f}}(t) = \left|\overline{A}_{\overline{f}}\right|^2 e^{-\Gamma t}\Bigg[R_D(1+A_D) + \sqrt{R_D(1+A_D)}\left|\frac{q}{p}\right| y'_+(\Gamma t) + \left|\frac{q}{p}\right|^2 \frac{(x'^2_+ + y'^2_+)}{4}(\Gamma t)^2\Bigg] \tag{70.27}$$

$$\bar{r}_f(t) = \left|A_f\right|^2 e^{-\Gamma t}\Bigg[R_D(1-A_D) + \sqrt{R_D(1-A_D)}\left|\frac{p}{q}\right| y'_-(\Gamma t) + \left|\frac{p}{q}\right|^2 \frac{(x'^2_- + y'^2_-)}{4}(\Gamma t)^2\Bigg], \tag{70.28}$$

where

$$x'_\pm = x'\cos\phi \;\pm\; y'\sin\phi \tag{70.29}$$

$$y'_\pm = y'\cos\phi \;\mp\; x'\sin\phi\,, \tag{70.30}$$

and

$$x' \equiv x\cos\delta_f \;+\; y\sin\delta_f \tag{70.31}$$

$$y' \equiv y\cos\delta_f \;-\; x\sin\delta_f\,. \tag{70.32}$$

The parameters x', y' are obtained from x, y via a rotation by the strong phase δ; these are often referred to as "strong-phase-rotated" mixing parameters. The parameters $x'_\pm, y'_\pm$ are obtained from x', y' via a subsequent rotation by the weak phase $+\phi$ for D^0 decays and $-\phi$ for $\overline{D}^0$ decays. Note that $x'^2_+ + y'^2_+ = x'^2_- + y'^2_- = x'^2 + y'^2 = x^2 + y^2$. In Eqs. (70.27) and (70.28), a fourth term proportional to $R_D(1\pm A_D)(x^2_\pm - y^2_\pm)(\Gamma t)^2/4$ has been dropped, as it is negligible relative to the other terms for the range of decay times measured by experiments.

Comparing Eqs. (70.27) and (70.28), one sees that $r_{\overline{f}}(t) \neq \bar{r}_f(t)$ if either $A_D \neq 0$, $|q/p| \neq 1$, or $\phi \neq 0$. The first inequality corresponds to CP violation in the decay amplitudes ($R^+_D \neq R^-_D$), which is referred to as *direct* CP violation. The second inequality corresponds to CP violation in mixing, and the third inequality corresponds to CP violation due to interference between a mixed decay amplitude and an unmixed amplitude. Whereas CP violation in decay amplitudes is parameterized by A_D, CP violation in mixing is often parameterized by $A_M \equiv (|q/p| - |p/q|)/(|q/p| + |p/q|)$.

In the limit of CP conservation, $A_D = 0$, $|q/p| = 1$, and $\phi = 0$. In this case,

$$r_{\overline{f}}(t) = \bar{r}_f(t) = \left|A_f\right|^2 e^{-\Gamma t}\left[R_D + \sqrt{R_D}\,y'(\Gamma t) + \frac{x'^2 + y'^2}{4}(\Gamma t)^2\right]. \tag{70.33}$$

The time-integrated mixed decay rate relative to the time-integrated unmixed decay rate is

$$R = \frac{\displaystyle\int_0^\infty r_{\overline{f}}(t)\,dt}{\displaystyle\int_0^\infty \left|A_f\right|^2 e^{-\Gamma t}\,dt} = R_D + \sqrt{R_D}\,y' + \frac{x'^2 + y'^2}{2}\,. \tag{70.34}$$

The ratio R is straightforward to measure, as there is no decay-time dependence. Parameters R_D, x'^2, y' are measured by assuming CP conservation and fitting to the decay-time distribution of wrong-sign ($D^0 + \overline{D}^0$) decays. Experiments allow for CP violation and measure $x'^2, y', A_D, |q/p|, \phi$ by separately fitting the decay-time distributions of wrong-sign $D^0 \to K^+\pi^-$ and $\overline{D}^0 \to K^-\pi^+$ decays. Results for R, R_D, and A_D are listed in Table 70.2, and results for x'^2 and y' are listed in Table 70.3.

The LHCb experiment recently analyzed all Runs 1+2 data with a D^*-tag, fitting to the ratios $r_{\overline{f}}(t)/\bar{r}_{\overline{f}}(t) \equiv R^+_{K\pi}(t)$ and $\bar{r}_f(t)/r_f(t) \equiv R^-_{K\pi}(t)$ in bins of decay time [19]. The fitted functions are parameterized as

$$R^\pm_{K\pi}(t) = R_D(1\pm A_D) + \sqrt{R_D(1\pm A_D)}(c_{K\pi} \pm \Delta c_{K\pi})(\Gamma t) + (c'_{K\pi} \pm \Delta c'_{K\pi})(\Gamma t)^2\,. \tag{70.35}$$

Fit results for parameters $c_{K\pi}, \Delta c_{K\pi}, c'_{K\pi}$, and $\Delta c'_{K\pi}$ are listed also in Table 70.3.

Extraction of the mixing parameters x and y from measurements of x' and y' requires knowledge of the strong phase difference $\delta_{K\pi}$. This can be determined from the decay rates of $D_\pm \to K^+\pi^-$, where D_+ (D_-) denotes the CP-even (CP-odd) eigenstate. Since $|D_\pm\rangle = (|D^0\rangle \mp |\overline{D}^0\rangle)/\sqrt{2}$,

$$\sqrt{2}\,A(D_\pm \to K^+\pi^-) \;=\; A(D^0 \to K^+\pi^-) \mp A\big(\overline{D}^0 \to K^+\pi^-\big)\,. \tag{70.36}$$

Squaring this amplitude and using Eq. (70.25) yields the relation

$$\cos\delta_{K\pi} \;=\; \frac{|A(D_- \to K^+\pi^-)|^2 - |A(D_+ \to K^+\pi^-)|^2}{2\,|A(D^0 \to K^+\pi^-)|\,|A(\overline{D}^0 \to K^+\pi^-)|}\,. \tag{70.37}$$

Measuring the right-hand side is possible if one can identify pure D_+, D_-, D^0, and $\overline{D}^0$ initial states. This is accomplished at CLEOc and BESIII utilizing the processes $e^+e^- \to \psi(3770) \to \overline{D}^0 D^0 \to (f_{CP})(K^+\pi^-)$, or $\psi(3770) \to \overline{D}^0 D^0 \to (f_{\overline{D}^0})(K^+\pi^-)$, where f_{CP} denotes a CP-specific final state, and $f_{\overline{D}^0}$ denotes a $\overline{D}^0$-flavor-specific final state. In the first case, quantum coherence and CP symmetry ensures that the $K^+\pi^-$ state originates from a neutral D with CP opposite that of f_{CP}. In the second case, when the $\overline{D}^0$ decays, the opposite side must be D^0. However, it can potentially mix to $\overline{D}^0$ before decaying to $K^+\pi^-$, and this introduces some dependence on the mixing parameters x and y. This dependence is seen explicitly in the observable

$$A^{CP}_{K\pi} \;\equiv\; \frac{|A(D_- \to K^-\pi^+)|^2 - |A(D_+ \to K^-\pi^+)|^2}{|A(D_- \to K^-\pi^+)|^2 + |A(D_+ \to K^-\pi^+)|^2}\,. \tag{70.38}$$

To lowest order in the mixing parameters [34],

$$A^{CP}_{K\pi} \;=\; \frac{2\sqrt{R_D}\cos\delta_{K\pi} + y}{1+R}\,, \tag{70.39}$$

where R is defined in Eq. (70.34). Such measurements are discussed in Section 70.5.

Int. J. Mod. Phys. A 2026.41. Downloaded from www.worldscientific.com
by UNIVERSITY OF CALIFORNIA @ BERKELEY on 09/16/26. Re-use and distribution is strictly not permitted, except for Open Access articles.

Table 70.2: Results for R, R_D, and A_D measured using $D^0 \to K^\pm\pi^\mp$ decays. When a single uncertainty is listed, it corresponds to statistical and systematic uncertainties combined. The measurements with an asterisk (*) have been superseded and thus are not included in the HFLAV global fit (Section 70.7). The measurements with a dagger (†) are not included in the HFLAV global fit due to much poorer precision.

Year	Experiment	$R\,(\times10^{-3})$	$R_D\,(\times10^{-3})$	$A_D\,(\%)$
2025	LHCb (8.4 fb^{-1} D^* tag) [19]	—	3.427±0.019	−0.66±0.57
2025	LHCb (8.4 fb^{-1} $B{+}D^*$ double-tagged) [20]	—	3.470±0.051	0.9±1.5
2014	Belle (976 fb^{-1}) [21]	3.86±0.06	3.53±0.13	—
2013	CDF (9.6 fb^{-1}) [22]	4.30±0.05	3.51±0.35	—
2007	BABAR (384 fb^{-1}) [23]	3.53±0.08±0.04	3.03±0.16±0.10	−2.1±5.2±1.5
	HFLAV Fit Result [24]		**3.436 ± 0.012**	**−0.81 ± 0.88**
2018*	LHCb (5.0 fb^{-1} D^* tag) [25]	—	3.454±0.031	−0.01±0.91
2017*	LHCb (3.0 fb^{-1} $B{+}D^*$ double-tagged) [26]	—	3.48±0.10	−3.15±3.31
2013b*	LHCb (3.0 fb^{-1} D^* tag) [27]	—	3.568±0.066	−0.7±1.9
2013a*	LHCb (1.0 fb^{-1}) [28]	4.25±0.04	3.52±0.15	—
2008*	CDF (1.5 fb^{-1}) [29]	4.15±0.10	3.04±0.55	—
2006*	Belle (400 fb^{-1}) [30]	3.77±0.08±0.05	3.64±0.18	2.3±4.7
2005†	FOCUS (234 evts) [31]	$4.29\,^{+0.63}_{-0.61}\pm0.27$	$5.17\,^{+1.47}_{-1.58}\pm0.76$	$13\,^{+33}_{-25}\pm10$
2000†	CLEO (9.0 fb^{-1}) [32]	$3.32\,^{+0.63}_{-0.65}\pm0.40$	4.8±1.2±0.4	$-1\,^{+16}_{-17}\pm1$
1998†	E791 (5643 evts) [33]	$6.8\,^{+3.4}_{-3.3}\pm0.7$	—	—

Table 70.3: Results for mixing parameters measured using $D^0 \to K^\pm\pi^\mp$ decays. When a single uncertainty is listed, it corresponds to statistical and systematic uncertainties combined. The measurements with an asterisk (*) have been superseded and thus are not included in the HFLAV global fit. The measurements with a dagger (†) are not included in the HFLAV global fit due to much poorer precision.

Year	Experiment	No CP violation		Allowing for CP violation	
2025	LHCb (6, 8.4 fb^{-1} D^* tag) [19]	—	—	$c_{K\pi}$, $\Delta c_{K\pi}$ $(\times10^{-4})$: 52.8±3.3, 2.0±3.4	$c'_{K\pi}$, $\Delta c'_{K\pi}$ $(\times10^{-6})$: 12.0±3.5, −0.7±3.6
		$x'^2\,(\times10^{-3})$	$y'\,(\%)$	$x'^2\,(\times10^{-3})$	$y'\,(\%)$
2025	LHCb (5.4, 8.4 fb^{-1} $B{+}D^*$ double-tagged) [20]	0.00±0.12	0.58±0.16	D^0: 0.08±0.15 $\overline{D}^0$: −0.05±0.17	0.41±0.20 0.68±0.21
2014	Belle (976 fb^{-1}) [21]	0.09±0.22	0.46±0.34	—	—
2013	CDF (9.6 fb^{-1}) [22]	0.08±0.18	0.43±0.43	—	—
2007	BABAR (384 fb^{-1}) [23]	−0.22±0.37	0.97±0.54	D^0: −0.24±0.52 $\overline{D}^0$: −0.20±0.50	0.98±0.78 0.96±0.75
2006	Belle (400 fb^{-1}) [30]	$\left(0.18\,^{+0.21}_{-0.23}\right)^*$	$\left(0.06\,^{+0.40}_{-0.39}\right)^*$	< 0.72	$-2.8 < y' < 2.1$
2018*	LHCb $\begin{pmatrix}5.0\text{ fb}^{-1}\\ D^*\text{ tag}\end{pmatrix}$ [25]	0.039±0.027	0.528±0.052	D^0: 0.061±0.037 $\overline{D}^0$: 0.016±0.039	0.501±0.074 0.554±0.074
2017*	LHCb $\begin{pmatrix}3.0\text{ fb}^{-1}\\ B{+}D^*\\ \text{double tag}\end{pmatrix}$ [26]	0.028±0.310	0.46±0.37	D^0: −0.019±0.447 $\overline{D}^0$: 0.079±0.433	0.581±0.526 0.332±0.523
2013b*	LHCb $\begin{pmatrix}3.0\text{ fb}^{-1}\\ D^*\text{ tag}\end{pmatrix}$ [27]	0.055±0.049	0.48±0.10	D^0: 0.049±0.070 $\overline{D}^0$: 0.060±0.068	0.51±0.14 0.45±0.14
2013a*	LHCb (1.0 fb^{-1}) [28]	−0.09±0.13	0.72±0.24	—	—
2008*	CDF (1.5 fb^{-1}) [29]	−0.12±0.35	0.85±0.76	—	—
2005†	FOCUS (234 evts) [31]	< 8.3	$-7.2 < y' < 4.1$	< 8.0	$-11.2 < y' < 6.7$
2000†	CLEO (9.0 fb^{-1}) [32]	0.00±0.23	$-2.3\,^{+1.3}_{-1.4}$	0.00±0.23	$-2.5\,^{+1.4}_{-1.6}$
1998†	E791 (5643 evts) [33]	< 17	< 13	—	—

70.3.1 *Wrong-sign decays to multibody final states*

For multibody final states, Eqs. (70.25)-(70.34) apply to each point in phase-space. Although x and y do not vary across phase-space, knowledge of the resonant substructure is needed to determine the strong phase difference δ at each point in order to extract x and y. Alternatively, experimental knowledge of the strong phase difference between A_f and $\overline{A}_f$ or between $A_{\overline{f}}$ and $\overline{A}_{\overline{f}}$ in regions of phase space [35] allows one to determine x and y independent of the decay model of resonant substructure. This phase information can be measured in $e^+e^- \to \psi(3770) \to \overline{D}D$ reactions in a manner similar to that for measuring $\delta_{K\pi}$, i.e., applying Eq. (70.37) to regions of phase space.

A time-dependent analysis of DCS $D^0 \to K^+\pi^-\pi^0$ decays relative to CF $\overline{D}^0 \to K^+\pi^-\pi^0$ decays by BABAR [36, 37] fit for both mixing parameters and the strong phase variation across the Dalitz plot. They reported results $x'' = (2.61\,^{+0.57}_{-0.68} \pm 0.39)\%$ and $y'' = (-0.06\,^{+0.55}_{-0.64} \pm 0.34)\%$, where

$$x'' = x\cos\delta_{K\pi\pi^0} + y\sin\delta_{K\pi\pi^0} \tag{70.40}$$

$$y'' = y\cos\delta_{K\pi\pi^0} - x\sin\delta_{K\pi\pi^0}\,, \tag{70.41}$$

in analogy with x', y', and $\delta_{K\pi}$ for $D^0 \to K^+\pi^-$ decays. Here, $\delta_{K\pi\pi^0}$ is the "reference" strong phase difference between amplitudes $A(\overline{D}^0 \to K^+\rho^-)$ and $A(D^0 \to K^+\rho^-)$, which cannot be determined in this analysis. However, $\delta_{K\pi\pi^0}$ can be measured using Eq. (70.37) and quantum-correlated measurements in $e^+e^- \to \psi(3770) \to D\overline{D}$ events of the branching fractions

Int. J. Mod. Phys. A 2026.41. Downloaded from www.worldscientific.com
UNIVERSITY OF CALIFORNIA @ BERKELEY on 09/16/26. Re-use and distribution is strictly not permitted, except for Open Access articles.

$B(D_+ \to K^+\rho^-)$, $B(D_- \to K^+\rho^-)$, $B(D^0 \to K^+\rho^-)$, and $B(\overline{D}^0 \to K^+\rho^-)$.

For decays $(D^0, \overline{D}^0) \to K^+\pi^-\pi^+\pi^-$, Belle measured $R = (0.324 \pm 0.008 \pm 0.007)\%$ [38]. A phase-space-integrated analysis from LHCb [39] measured the product of a "coherence factor" $R_D^{K3\pi}$ and the mixing parameter $y''_{K3\pi}$ with high statistics. This resulted in an observation of charm mixing with a significance of 8.2σ.

Both the sign and magnitude of x and y without strong phases entering can be determined by measuring the time-dependence of resonance structure for multibody D^0 decays to self-conjugate final states [40, 41]. This method has been used extensively for $D^0 \to K_S^0\pi^+\pi^-$ decays, in which the DCS and CF amplitudes populate the same Dalitz plot. Assuming a decay model of intermediate resonances, this allows for fitting for strong phase differences and direct measurement of x and y. Alternatively, several LHCb $D^0 \to K_S^0\pi^+\pi^-$ analyses [42–45] use values of strong phase differences measured in bins of phase space by CLEO-c [46] and BESIII [47, 48]; these (x, y) measurements are independent of the decay model. The most recent LHCb analyses fit for CP-violating parameters Δx and Δy; the translation of these parameters to $|q/p|$ and ϕ is given in Ref. [49]. Belle II [50] also used values of strong phase differences measured by BESIII [47, 48] to determine decay-model-independent values of x and y. Table 70.4 summarizes results from time-dependent analyses of self-conjugate multibody final states. World average values for x and y are given later, when discussing results from the HFLAV global fit.

BESIII recently updated their measurements of strong-phase differences for $D^0 \to K_S^0\pi^+\pi^-$ decays using 7.9 fb^{-1} of data [51]; these are now the world's most precise values. BESIII has also measured strong-phase differences in bins of phase space for $(D^0, \overline{D}^0) \to K^+K^-\pi^+\pi^-$ decays [52] and $(D^0, \overline{D}^0) \to \pi^+\pi^-\pi^+\pi^-$ decays [53]. Strong phase differences for the latter mode have also been measured using a small sample (0.82 fb^{-1}) of CLEO-c data [54]. These multibody self-conjugate final states can all be used to determine x and y.

70.4 Hadronic decays to *CP* eigenstates

When the final state f is a CP eigenstate, there is no distinction between f and $\overline{f}$. Thus, $A_f = A_{\overline{f}}$, $\overline{A}_{\overline{f}} = \overline{A}_f$, and $\lambda_f = \lambda_{\overline{f}}$. We denote final states with CP eigenvalues ± 1 by $f_\pm$. Decays to CP eigenstates are singly Cabibbo-suppressed and can proceed via both a tree amplitude and an internal-loop amplitude. These two amplitudes have different weak phases, and thus their interference leads to direct CP violation. As loop amplitudes are suppressed, direct CP violation is expected to be very small, and the presence of a weak phase is often neglected. For a negligible weak phase in the decay amplitude, $\lambda_{f_\pm} = \mp|q/p|\, e^{i\phi}$, where the choice of signs corresponds to $\phi = 0$ (rather than π) if CP is conserved.

The mixing parameter y can be measured by comparing the rate for D^0 decays to CP eigenstates such as K^+K^- with the rate to flavor eigenstates such as $K^-\pi^+$ [18]. If decays to K^+K^- have a shorter effective lifetime than those to $K^-\pi^+$, then $\Gamma_+ > \Gamma_-$. Since CP violation is very small, $\Gamma_2 > \Gamma_1$ and y is positive. Since mixing is very small, i.e., $x, y \ll 1$, the $(\Gamma t)^2$ terms in Eqs. (70.27) and (70.28) are often neglected. In this case the decay rates for $D^0 \to f_\pm$ and $\overline{D}^0 \to f_\pm$ are approximately exponential:

$$r_\pm(t) \propto \exp(-\Gamma_\pm\, t) \tag{70.42}$$

$$\overline{r}_\pm(t) \propto \exp(-\overline{\Gamma}_\pm\, t)\,, \tag{70.43}$$

with effective decay widths

$$\Gamma_\pm = \Gamma\left(1 \pm \left|\frac{q}{p}\right| (y\cos\phi - x\sin\phi)\right) \tag{70.44}$$

$$\overline{\Gamma}_\pm = \Gamma\left(1 \pm \left|\frac{p}{q}\right| (y\cos\phi + x\sin\phi)\right). \tag{70.45}$$

The effective decay rate to a CP eigenstate for a data sample containing equal numbers of D^0 and $\overline{D}^0$ decays (e.g., an untagged sample with no production asymmetry) is

$$r_\pm(t) \;+\; \overline{r}_\pm(t) \;\propto\; e^{-(1\pm y_{CP})\Gamma t}\,, \tag{70.46}$$

where

$$y_{CP} = \frac{1}{2}\left(\left|\frac{q}{p}\right| + \left|\frac{p}{q}\right|\right) y\cos\phi - \frac{1}{2}\left(\left|\frac{q}{p}\right| - \left|\frac{p}{q}\right|\right) x\sin\phi \tag{70.47}$$

$$\approx y\cos\phi - A_M\, x\sin\phi\,. \tag{70.48}$$

If CP is conserved ($\phi = 0$), $y_{CP} = y$. Equation (70.46) implies that y_{CP} can be determined from the decay-time dependence of either CP-even or CP-odd decays:

$$y_{CP} \;=\; \frac{\Gamma_+}{\Gamma} - 1 \;=\; 1 - \frac{\Gamma_-}{\Gamma}\,. \tag{70.49}$$

Most y_{CP} measurements have used $D^0 \to K^+K^-$ and $D^0 \to \pi^+\pi^-$ decays, which are CP-even, measured relative to $D^0 \to K^-\pi^+$. Belle measured y_{CP} also using $D^0 \to K_S^0\,\omega$ decays [58], which are CP-odd, and $D^0 \to K_S^0\,K^+K^-$ decays [59], which are dominated by the CP-odd final state $K_S^0\,\phi$. Table 70.5 summarizes the status of measurements. The most recent y_{CP} measurement from LHCb has sufficient precision that the tiny effect of mixing upon $D^0(t) \to K^-\pi^+$ decays, which are used in the measurement to determine Γ, must be accounted for. The measurement directly yields

$$\frac{\Gamma_+}{\Gamma_{K^-\pi^+}} - 1 \;=\; \frac{1 + y_{CP}}{1 + y_{CP}^{K\pi}} - 1 \;\approx\; y_{CP} - y_{CP}^{K\pi}\,, \tag{70.50}$$

where the correction $y_{CP}^{K\pi}$ is $\sim 10^{-4}$. This correction was first pointed out in Ref. [60]; it is calculated in terms of parameters $(x, y, |q/p|, \phi)$ in Ref. [61].

In addition to y_{CP}, the asymmetry in decay rates to CP-even final states (A_Γ) has been measured [62–66]:

$$A_\Gamma \equiv \frac{\Gamma_+ - \overline{\Gamma}_+}{\Gamma_+ + \overline{\Gamma}_+} \;=\; \frac{(1/\tau_+) - (1/\overline{\tau}_+)}{(1/\tau_+) + (1/\overline{\tau}_+)} \;=\; \frac{\overline{\tau}_+ - \tau_+}{\overline{\tau}_+ + \tau_+} \tag{70.51}$$

$$\approx \frac{1}{2}\left(\left|\frac{q}{p}\right| - \left|\frac{p}{q}\right|\right) y\cos\phi - \frac{1}{2}\left(\left|\frac{q}{p}\right| + \left|\frac{p}{q}\right|\right) x\sin\phi \tag{70.52}$$

$$\approx A_M\, y\cos\phi - x\sin\phi\,. \tag{70.53}$$

If CP is conserved ($A_M = 0$, $\phi = 0$), then $A_\Gamma = 0$.

There is a contribution to Eq. (70.53) from direct CP violation, i.e., $|\overline{A}_f/A_f| \neq 1$ [1, 67]. For $f = K^+K^-$ and $\pi^+\pi^-$, this contribution can be estimated from measurements of $A_{CP}(K^+K^-)$ and $A_{CP}(\pi^+\pi^-)$ (see below) and is much smaller than the current uncertainty on A_M; thus we neglect it here. We note that, when averaging A_Γ measurements over K^+K^- and $\pi^+\pi^-$ final states, the contribution from direct CP violation nominally cancels, as it is expected to have the same magnitude for K^+K^- and $\pi^+\pi^-$ but opposite signs due to U-spin symmetry [1].

The observable A_Γ is an asymmetry in the full decay widths. An asymmetry in *partial* widths is referred to as A_{CP} and depends on the final state:

$$A_{CP} \;\equiv\; \frac{\Gamma(D^0 \to f) - \Gamma(\overline{D}^0 \to \overline{f})}{\Gamma(D^0 \to f) + \Gamma(\overline{D}^0 \to \overline{f})}\,. \tag{70.54}$$

Unlike A_Γ, which is measured by fitting decay-time distributions, A_{CP} is measured by fitting for signal yields and, aside from acceptance effects, does not require measuring decay times. For neutral D decays, A_{CP} receives contributions from both direct and indirect CP violation: $A_{CP}(D^0 \to f) = A_{CP}^f + A_{CP}^{\rm indirect}$. The indirect contribution depends on x and y:

$$A_{CP}^{\rm indirect} \;=\; \frac{1}{2}\left(\left|\frac{q}{p}\right| + \left|\frac{p}{q}\right|\right) x\sin\phi - \frac{1}{2}\left(\left|\frac{q}{p}\right| - \left|\frac{p}{q}\right|\right) y\cos\phi$$
$$=\; -A_\Gamma\,. \tag{70.55}$$

Numerous measurements of A_{CP} for decays to CP eigenstates are listed in this *Review* [68]. Table 70.6 summarizes the status of measurements of the *difference* in A_{CP} for $D^0 \to K^+K^-$ and $D^0 \to \pi^+\pi^-$ decays: $\Delta A_{CP} \equiv A_{CP}(K^+K^-) - A_{CP}(\pi^+\pi^-)$.

Int. J. Mod. Phys. A 2026.41. Downloaded from www.worldscientific.com
by UNIVERSITY OF CALIFORNIA @ BERKELEY on 09/16/26. Re-use and distribution is strictly not permitted, except for Open Access articles.

Table 70.4: Results from time-dependent multibody analyses. The errors are statistical, systematic, and, when a third error is listed, due to the decay-model, respectively. The measurement with an asterisk (*) has been superseded and thus is not included in the HFLAV global fit. The measurement with a dagger (†) is not included in the HFLAV global fit due to poorer precision. The 2019–2023 LHCb analyses fit for CP-violating parameters Δx and Δy; the translation of these parameters to $|q/p|$ and ϕ is given in Ref. [49].

No CP Violation				
Year	Experiment	Final state(s)	x ($\times 10^{-3}$)	y ($\times 10^{-3}$)
2025	Belle II (951+408 fb^{-1}) [50]	$K^0_S\,\pi^+\pi^-$	$4.0 \pm 1.7 \pm 0.4$	$2.9 \pm 1.4 \pm 0.3$
2023	LHCb (5.4 fb^{-1} B tag) [45]	$K^0_S\,\pi^+\pi^-$	$4.29 \pm 1.48 \pm 0.26$	$12.61 \pm 3.12 \pm 0.83$
2021	LHCb (5.4 fb^{-1} D^* tag) [44]	$K^0_S\,\pi^+\pi^-$	$3.97 \pm 0.46 \pm 0.29$	$4.59 \pm 1.20 \pm 0.85$
2019	LHCb (3.0 fb^{-1} B, D^* tags) [43]	$K^0_S\,\pi^+\pi^-$	$2.7 \pm 1.6 \pm 0.4$	$7.4 \pm 3.6 \pm 1.1$
2016	LHCb (1.0 fb^{-1} D^* tag) [42]	$K^0_S\,\pi^+\pi^-$	$-8.6 \pm 5.3 \pm 1.7$	$0.3 \pm 4.6 \pm 1.3$
2016	BABAR (468 fb^{-1}) [55]	$\pi^+\pi^-\pi^0$	$15 \pm 12 \pm 6$	$2 \pm 9 \pm 5$
2010	BABAR (469 fb^{-1}) [56]	$\begin{cases} K^0_S\,\pi^+\pi^- \\ K^0_S\,K^+K^- \end{cases}$	$1.6 \pm 2.3 \pm 1.2 \pm 0.8$	$5.7 \pm 2.0 \pm 1.3 \pm 0.7$
2014*	Belle (921 fb^{-1}) [57]	$K^0_S\,\pi^+\pi^-$	$5.6 \pm 1.9\,^{+0.3}_{-0.9}\,^{+0.6}_{-0.9}$	$3.0 \pm 1.5\,^{+0.4}_{-0.5}\,^{+0.3}_{-0.6}$
2007*	Belle (540 fb^{-1}) [41]	$K^0_S\,\pi^+\pi^-$	$8.0 \pm 2.9\,^{+0.9}_{-0.7}\,^{+1.0}_{-1.4}$	$3.3 \pm 2.4\,^{+0.8}_{-1.2}\,^{+0.6}_{-0.8}$
2005†	CLEO (9.0 fb^{-1}) [40]	$K^0_S\,\pi^+\pi^-$	$19\,^{+32}_{-33} \pm 4 \pm 4$	$-14 \pm 24 \pm 8 \pm 4$

With CP Violation				
Year	Experiment	Final state(s)	$\lvert q/p\rvert$	ϕ
2023	LHCb (5.4 fb^{-1} B tag) [45]	$K^0_S\,\pi^+\pi^-$	$\begin{cases} \Delta x \times 10^3 = \\ -0.77 \pm 0.93 \pm 0.28 \end{cases}$	$\begin{cases} \Delta y \times 10^3 = \\ 3.01 \pm 1.92 \pm 0.26 \end{cases}$
2021	LHCb (5.4 fb^{-1} D^* tag) [44]	$K^0_S\,\pi^+\pi^-$	$\begin{cases} 0.996 \pm 0.052 \\ \Delta x \times 10^3 = \\ -0.27 \pm 0.18 \pm 0.01 \end{cases}$	$\begin{cases} (3.2\,^{+2.7}_{-2.9})^\circ \\ \Delta y \times 10^3 = \\ 0.20 \pm 0.36 \pm 0.13 \end{cases}$
2019	LHCb (3.0 fb^{-1} B, D^* tags) [43]	$K^0_S\,\pi^+\pi^-$	$\begin{cases} 1.05\,^{+0.22}_{-0.17} \\ \Delta x \times 10^3 = \\ -0.53 \pm 0.70 \pm 0.22 \end{cases}$	$\begin{cases} (-5.2\,^{+6.3}_{-9.2})^\circ \\ \Delta y \times 10^3 = \\ 0.6 \pm 1.6 \pm 0.3 \end{cases}$
2014	Belle (921 fb^{-1}) [57]	$K^0_S\pi^+\pi^-$	$0.90\,^{+0.16}_{-0.15}\,^{+0.05}_{-0.04}\,^{+0.06}_{-0.05}$	$(-6 \pm 11 \pm 3\,^{+3}_{-4})^\circ$
2007*‡	Belle (540 fb^{-1}) [41]	$K^0_S\,\pi^+\pi^-$	$0.86\,^{+0.30}_{-0.29}\,^{+0.06}_{-0.03} \pm 0.08$	$(-14\,^{+16}_{-18}\,^{+5}_{-3}\,^{+2}_{-4})^\circ$

‡This result allows for all types of CP violation and is superseded by Ref. [57], which assumes no direct CP violation in CF or DCS decays.

U-spin symmetry predicts $A_{CP}(KK) = -A_{CP}(\pi\pi)$ [69]; consequently, even accounting for U-spin-breaking, ΔA_{CP} should increase any direct CP asymmetry present. The difference is also advantageous experimentally, as several systematic uncertainties cancel. As $A_{CP}^{\rm indirect}$ is independent of the final state, it subtracts out of ΔA_{CP}. However, at hadron experiments such as LHCb, there is a difference in efficiencies between K^+K^- and $\pi^+\pi^-$ such that $\langle t\rangle_{KK} \neq \langle t\rangle_{\pi\pi}$, i.e., the mean decay times differ slightly. This difference introduces a small contribution to ΔA_{CP} from $A_{CP}^{\rm indirect}$ [67]. A measurement of ΔA_{CP} from LHCb [70] based on 8.9 fb^{-1} of data differs from zero with a statistical significance of 5.3σ; this measurement constitutes the first (and only) observation of CP violation in charm decays. A subsequent measurement by LHCb of $A_{CP}(K^+K^-)$ [71] yielded $(0.068 \pm 0.056)\%$, which is consistent with zero. Taken together, these results suggest that the large value of ΔA_{CP} is due to $D^0 \to \pi^+\pi^-$ decays, and that the expectation $A_{CP}(KK) \approx -A_{CP}(\pi\pi)$ is violated. However, the uncertainty on $A_{CP}(K^+K^-)$ is sufficiently large that the central value can be explained as a statistical fluctuation at the level of $\sim 2.3\sigma$. These CP asymmetries are included in HFLAV's global fit for charm mixing parameters, as discussed below.

70.5 Quantum-correlated $D^0\overline{D}^0$ Analyses

Measurements of R_D, $\cos\delta_{K\pi}$, $\sin\delta_{K\pi}$, x, and y can be obtained from a combined fit to time-integrated yields of single-tagged (ST) and double-tagged (DT) $D^0\overline{D}^0$ events produced at the $\psi(3770)$ resonance. Single-tagged events are those in which either the D^0 or $\overline{D}^0$ decay is reconstructed (identified), and the other neutral D decays generically. Double-tagged events are those in which both the D^0 and $\overline{D}^0$ decays are identified. Due to quantum correlations, the decay of a D^0, $\overline{D}^0$, D_+, or D_- projects the other neutral D into a state $\overline{D}^0$, D^0, D_-, or D_+, respectively. Neglecting CP violation, states D_- and D_+ are 50% D^0 and 50% $\overline{D}^0$; thus the $D_\pm$ decay rates include an interference term proportional to $\sqrt{R_D}\cos\delta_{K\pi}$. The interference also includes contributions from D^0–$\overline{D}^0$ mixing and thus provides sensitivity to x and y. An example is the parameter $A_{K\pi}^{CP}$ in Eq. (70.39). For details of this method, see Refs. [4–8].

BESIII has reported results using 2.9 fb^{-1} of $e^+e^- \to \psi(3770)$ data, where the quantum-correlated $D^0\overline{D}^0$ pairs are produced in a $C=-1$ state. They measure $y_{CP} = (-2.0 \pm 1.3 \pm 0.7)\%$ [79] from DT yields using a CP-eigenstate tag for one D and a flavor-specific semileptonic tag for the other; and they measure $A_{K\pi}^{CP} = (13.2 \pm 1.1 \pm 0.7)\%$ [90] from DT yields using a CP tag for one D and a $K^\pm\pi^\mp$ tag for the other. For y_{CP}, the CP eigenstates used are K^-K^+ (f_+), $\pi^+\pi^-$ (f_+), $K^0_S\,\pi^0\pi^0$ (f_+), $K^0_S\,\pi^0$ (f_-), $K^0_S\,\eta$ (f_-), and $K^0_S\,\omega$ (f_-). For $A_{K\pi}^{CP}$, seven additional CP eigenstates are included: $\pi^0\pi^0$ (f_+), $K^0_S\,\eta'$ (f_-), $K^0_S\,\phi$ (f_-), $K^0_L\,\pi^0$ (f_+), $K^0_L\,\omega$ (f_+), $K^0_L\,\pi^0\pi^0$ (f_-), and $\pi^+\pi^-\pi^0$ (mixed CP). Using Eq. (70.39) and external inputs for the CP-even fraction of $D^0 \to \pi^+\pi^-\pi^0$ (from Ref. [72]) and values of R_D and y (from HFLAV [14]), BESIII obtains $\delta_{K\pi} = (7.6\,^{+10.4}_{-11.6})^\circ$ [90].

Recently, BESIII reported results (unpublished) using 7.13 fb^{-1} of data collected at center-of-mass energies in the range 4.13–4.12 GeV [91]. This range allows for the production of $D\overline{D}$, $D^*\overline{D}$, $\overline{D}^*D$, and $D^*\overline{D}^*$ pairs, and the resulting $D^0\overline{D}^0$ pair can be in either a CP-even or CP-odd state. The strong phase difference $\delta_{K\pi}$ is determined using $D^0\overline{D}^0$ pairs decaying to $K^-\pi^+$ versus K^+K^- (f_+), $\pi^+\pi^-$ (f_+), $K^0\pi^0$ (f_-), $\pi^+\pi^-\pi^0$ (nearly f_+), and $K^0_S\pi^+\pi^-$ (mixed CP) final states. Using external inputs for R_D and y, the analysis obtains similar precision for $\delta_{K\pi}$ as that of Ref. [90], with a higher central value of 12.8°.

CLEO-c has reported results using 0.82 fb^{-1} of $e^+e^- \to \psi(3770)$ data [92–94]. The values for y, R_M, $\cos\delta_{K\pi}$, and $\sin\delta_{K\pi}$ are obtained from a combined fit to the ST (hadronic only) and DT yields. The DT yields include events in which one D is reconstructed in a hadronic mode and the other D is partially reconstructed in flavor-specific $D \to K^\mp e^\pm\nu$ and $D \to K^\mp\mu^\pm\nu$ modes. The CLEO-c analysis obtains $\cos\delta_{K\pi} = 0.81\,^{+0.22}_{-0.18}\,^{+0.07}_{-0.05}$ and $\sin\delta_{K\pi} = -0.01 \pm 0.41 \pm 0.04$. These fits allow $\cos\delta_{K\pi}$ and

Int. J. Mod. Phys. A 2026.41. Downloaded from www.worldscientific.com
UNIVERSITY OF CALIFORNIA @ BERKELEY on 09/16/26. Re-use and distribution is strictly not permitted, except for Open Access articles.

Table 70.5: Results for y_{CP} and A_Γ from D^0 decays to CP eigenstates. When a single uncertainty is listed, it corresponds to statistical and systematic uncertainties combined. The measurements with an asterisk (*) have been superseded. The third row (8.4 fb^{-1} A_Γ) lists the LHCb combination of the LHCb measurements listed below it.

Year	Experiment	Final state(s)	y_{CP} (%)	A_Γ ($\times 10^{-3}$)
2024‡	LHCb (7.7 fb^{-1} D^* tag) [73]	$\pi^+\pi^-\pi^0$	—	$0.13\pm0.63\pm0.24$
2022§	LHCb (6 fb^{-1} D^* tag) [74]	$K^+K^-+\pi^+\pi^-$	$0.696\pm0.026\pm0.013$	—
2021	LHCb (8.4 fb^{-1} B, D^* tags) [66]	$K^+K^-+\pi^+\pi^-$	—	$0.10\pm0.11\pm0.03$
2021	LHCb (6 fb^{-1} D^* tag) [66]	$K^+K^-+\pi^+\pi^-$	—	$0.27\pm0.13\pm0.03$
2021	LHCb (6 fb^{-1} D^* tag) [66]	K^+K^-	—	$0.23\pm0.15\pm0.03$
2021	LHCb (6 fb^{-1} D^* tag) [66]	$\pi^+\pi^-$	—	$0.40\pm0.28\pm0.04$
2020	LHCb (5.4 fb^{-1} B tag) [75]	K^+K^-	—	$-0.43\pm0.36\pm0.05$
2020	LHCb (5.4 fb^{-1} B tag) [75]	$\pi^+\pi^-$	—	$0.22\pm0.70\pm0.08$
2020	Belle (976 fb^{-1}) [58]	$K^0_S\,\omega$	$0.96\pm0.91^{+0.64}_{-0.62}$	—
2019	LHCb (3 fb^{-1} B tag) [76]	$K^+K^-+\pi^+\pi^-$	$0.57\pm0.13\pm0.09$	—
2017	LHCb (3 fb^{-1} D^* tag) [77]	$K^+K^-+\pi^+\pi^-$	—	$-0.13\pm0.28\pm0.10$
2017	LHCb (3 fb^{-1} D^* tag) [77]	K^+K^-	—	$-0.30\pm0.32\pm0.10$
2017	LHCb (3 fb^{-1} D^* tag) [77]	$\pi^+\pi^-$	—	$0.46\pm0.58\pm0.12$
2016	Belle (976 fb^{-1}) [62]	$K^+K^-+\pi^+\pi^-$	$1.11\pm0.22\pm0.09$	$-0.3\pm2.0\pm0.7$
2015	LHCb (3 fb^{-1} B tag) [78]	$K^+K^-+\pi^+\pi^-$	—	-1.25 ± 0.73
2015	LHCb (3 fb^{-1} B tag) [78]	K^+K^-	—	$-1.34\pm0.77^{+0.26}_{-0.34}$
2015	LHCb (3 fb^{-1} B tag) [78]	$\pi^+\pi^-$	—	$-0.92\pm1.45^{+0.25}_{-0.33}$
2015	BES III (2.9 fb^{-1}) [79]	$\begin{cases} K^+K^-,\ \pi^+\pi^- \\ K^0_S\,\pi^0,\ K^0_S\,\pi^0\pi^0 \\ K^0_S\,\eta,\ K^0_S\,\omega \end{cases}$	$-2.0\pm1.3\pm0.7$	—
2014	CDF (9.7 fb^{-1}) [64]	$K^+K^-+\pi^+\pi^-$	—	-1.2 ± 1.2
2014	CDF (9.7 fb^{-1}) [64]	K^+K^-	—	$-1.9\pm1.5\pm0.4$
2014	CDF (9.7 fb^{-1}) [64]	$\pi^+\pi^-$	—	$-0.1\pm1.8\pm0.3$
2012	BABAR (468 fb^{-1}) [63]	$K^+K^-+\pi^+\pi^-$	$0.72\pm0.18\pm0.12$	$0.9\pm2.6\pm0.6$
2009	Belle (673 fb^{-1}) [59]	$K^0_S\,K^+K^-$	$0.11\pm0.61\pm0.52$	—
2002	CLEO (9.0 fb^{-1}) [80]	$K^+K^-+\pi^+\pi^-$	$-1.2\pm2.5\pm1.4$	—
2000	FOCUS (1×10^6 evts) [81]	K^+K^-	$3.42\pm1.39\pm0.74$	—
1999	E791 (2×10^{10} evts) [82]	K^+K^-	$0.73\pm2.89\pm1.03$	—
	HFLAV Average [83]		$\mathbf{0.697\pm0.028}$	$\mathbf{0.089\pm0.113}$
2013*	LHCb (1.0 fb^{-1} D^* tag) [84]	K^+K^-	—	$-0.35\pm0.62\pm0.12$
2013*	LHCb (1.0 fb^{-1} D^* tag) [84]	$\pi^+\pi^-$	—	$0.33\pm1.06\pm0.14$
2011*¶	LHCb (29 pb^{-1} D^* tag) [65]	K^+K^-	$0.55\pm0.63\pm0.41$	$-5.9\pm5.9\pm2.1$
2009*	BABAR (384 fb^{-1}) [85]	K^+K^-	$1.16\pm0.22\pm0.18$	—
2008*	BABAR (384 fb^{-1}) [86]	$K^+K^-+\pi^+\pi^-$	$1.03\pm0.33\pm0.19$	$2.6\pm3.6\pm0.8$
2007*	Belle (540 fb^{-1}) [87]	$K^+K^-+\pi^+\pi^-$	$1.31\pm0.32\pm0.25$	$0.1\pm3.0\pm1.5$
2003*	BABAR (91 fb^{-1}) [88]	$K^+K^-+\pi^+\pi^-$	$0.8\pm0.4^{+0.5}_{-0.4}$	—
2001*	Belle (23.4 fb^{-1}) [89]	K^+K^-	$-0.5\pm1.0^{+0.7}_{-0.8}$	—

‡This measurement uses the $D^0\to\pi^+\pi^-\pi^0$ CP-even fraction measured in Ref. [72].

§This measurement has sufficient precision that y_{CP} for the normalization channel $D^0\to K^-\pi^+$ must be accounted for. HFLAV accounts for this small correction in their global fit.

¶This result for y_{CP} is not superseded, but it is not included in the HFLAV average due to having some correlations with the result of Ref. [76] but much worse precision.

$\sin\delta_{K\pi}$ (and also x^2) to be unphysical. Constraining $\cos\delta_{K\pi}$ and $\sin\delta_{K\pi}$ to the physical range $[-1,+1]$ (i.e., interpreting $\delta_{K\pi}$ as an angle) and also using external inputs for x, y, and y_{CP} from HFLAV 2012 [95], CLEO-c obtains $\delta_{K\pi}=(18^{+11}_{-17})^\circ$ [94].

70.6 Summary of Experimental Results

The first evidence for D^0-$\overline{D}^0$ mixing was obtained in 2007 by Belle [87] and BABAR [23]. These results were confirmed by CDF [96] and, much later, by LHCb [28]. There are now numerous measurements of D^0-$\overline{D}^0$ mixing with various levels of precision. Using $D^0\to K^+\pi^-$ decays, CDF [22], LHCb [27,28], and Belle [21] each exclude the no-mixing hypothesis by more than five standard deviations. The most significant observation of mixing (8.2σ significance) was made by LHCb using $D^0\to K^+\pi^-\pi^+\pi^-$ decays [39]. However, strong phase differences for this multibody decay are not known, and thus x and y cannot be extracted. The most precise measurement of y is essentially LHCb's measurement of y_{CP} using $D^0\to(K^+K^-,\pi^+\pi^-)$ decays [74], and the most precise measurement of x is LHCb's measurement using $D^0\to K^0_S\,\pi^+\pi^-$ decays [44]. This measurement resulted in the first direct observation ($>5\sigma$ significance) of dispersive mixing ($x\neq0$).

These experimental measurements establish that D^0 and $\overline{D}^0$ mesons mix. In the Standard Model, this mixing is dominated by long-distance amplitudes, which are difficult to calculate. If one assumes the observed mixing is due to non-Standard Model processes, significant constraints on new physics models can be obtained [105]. A significant limitation to interpreting charm mixing in terms of new physics is the theoretical uncertainty on Standard Model predictions [106,107]. We note that the HFLAV global fit results for x and y (see below) indicate that charm mixing is at the upper end of the range of predictions. The current situation would benefit from knowledge of strong phase differences between $\overline{D}^0\to K^+\pi^-\pi^0$ and $D^0\to K^+\pi^-\pi^0$ decays, and between $\overline{D}^0\to K^+\pi^-\pi^+\pi^-$ and $D^0\to K^+\pi^-\pi^+\pi^-$ decays. Such knowledge would allow one to extract x and y from measurements of $(x''^2_{K2\pi}, y''_{K2\pi})$ and $(x''^2_{K3\pi}, y''_{K3\pi})$ performed for these modes.

With regard to CP violation, by combining separate measurements from two data sets totalling 8.9 fb^{-1} of data, LHCb observed CP violation in D decays for the first time [70]. The observable measured, $\Delta A_{CP}=A_{CP}(K^+K^-)-A_{CP}(\pi^+\pi^-)$, is dominated by direct CP violation; contributions from indirect CP violation mostly cancel. The amount of direct CP violation measured is small: $\Delta A_{CP}=(-0.154\pm0.029)\%$. Several theory

Int. J. Mod. Phys. A 2026.41. Downloaded from www.worldscientific.com
by UNIVERSITY OF CALIFORNIA @ BERKELEY on 09/16/26. Re-use and distribution is strictly not permitted, except for Open Access articles.

Table 70.6: Results for A_{CP} and the difference ΔA_{CP} between $D^0 \to K^+K^-$ and $D^0 \to \pi^+\pi^-$ decays. When a single uncertainty is listed, it corresponds to statistical and systematic uncertainties combined. The measurements with an asterisk (*) have been either superseded or combined with subsequent results and thus are not included in the HFLAV global fit.

Year	Experiment	A_{CP} ($\times 10^{-3}$)
2024	LHCb $D^0 \to K^+K^-$ (5.7 fb^{-1}) [71]	0.68 ± 0.56
		ΔA_{CP} ($\times 10^{-3}$)
2019	LHCb (8.9 fb^{-1} B, D^* tags) [70]	-1.54 ± 0.29
2013	CDF (9.7 fb^{-1} D^* tag) [97]	$-6.2 \pm 2.1 \pm 1.0$
2008	BABAR (386 fb^{-1}) [98]	$2.4 \pm 6.2 \pm 2.6$
2008	Belle (540 fb^{-1}) [99]	$-8.6 \pm 6.0 \pm 0.7$
2016*	LHCb (3.0 fb^{-1} D^* tag) [100]	$-1.0 \pm 0.8 \pm 0.3$
2014*	LHCb (3.0 fb^{-1} B tag) [101]	$1.4 \pm 1.6 \pm 0.8$
2013*	LHCb (1.0 fb^{-1} B tag) [102]	$4.9 \pm 3.0 \pm 1.4$
2012*	LHCb (0.62 fb^{-1} D^* tag) [103]	$-8.2 \pm 2.1 \pm 1.1$
2012‡	Belle (976 fb^{-1}) [104]	$-8.7 \pm 4.1 \pm 0.6$

‡This preliminary result was not published and thus is not included in the HFLAV global fit.

calculations [108–110] indicate that this value is consistent with the Standard Model, although new physics contributions cannot be excluded (see e.g., [111, 112]). A subsequent LHCb measurement of $A_{CP}(K^+K^-)$ differs from zero by only 1.2σ [71]; thus, the ΔA_{CP} value is interpreted as indicating direct CP violation in $D^0 \to \pi^+\pi^-$ decays. Among all measurements, there is no evidence so far of indirect CP violation in the D^0-$\overline{D}^0$ system.

70.7 HFLAV Global Fit for Charm Mixing Parameters

The Heavy Flavor Averaging Group (HFLAV) performs global fits to all relevant mixing measurements to obtain world average values for the following: mixing parameters x and y or alternatively x_{12} and y_{12}; strong phase differences $\delta_{K\pi}$ and $\delta_{K\pi\pi^0}$; the ratio R_D of $\Gamma(D^0 \to K^+\pi^-)$ and $\Gamma(\overline{D}^0 \to K^+\pi^-)$ partial widths; direct CP-violating parameters $A_D(K^+\pi^-)$, $A_{CP}(D^0 \to K^+K^-) \equiv A_K$, and $A_{CP}(D^0 \to \pi^+\pi^-) \equiv A_\pi$; and indirect CP-violating parameters $|q/p|$ and ϕ or alternatively ϕ^M, ϕ^Γ, and their difference $\phi_{12} \equiv \phi^M - \phi^\Gamma$. Three separate fits are performed: *(a)* assuming no indirect CP violation; *(b)* assuming no subleading amplitudes in indirect CP violation (the "superweak" model); *(c)* allowing for all CP violation. Details of these fits are given in Ref. [14]. For fit *(b)* in which there are no subleading amplitudes, one can derive the relation $\tan\phi = (x/y)\cdot(1-|q/p|^2)/(1+|q/p|^2)$ [2, 3, 113]; this reduces four fitted parameters to three. Alternatively, one can fit for the three parameters x_{12}, y_{12}, and ϕ_{12}. However, the direct CP violation observed in ΔA_{CP} implies that subleading amplitudes play a role in Γ_{12}, the off-diagonal element of the decay matrix.

The fits use Belle, BABAR, CDF, and LHCb measurements of $D^0 \to K^{(*)+}\ell^-\overline{\nu}$, K^+K^-, $\pi^+\pi^-$, $K^+\pi^-$, $K^+\pi^-\pi^0$, $K^+\pi^-\pi^+\pi^-$, $K^0_S\pi^+\pi^-$, $K^0_S K^+K^-$, and $\pi^+\pi^-\pi^0$ decays, as well as CLEO-c and BESIII measurements of $\cos\delta$, $\sin\delta$, and $A_{CP}(K^+\pi-)$ obtained from quantum-correlated measurements of branching fractions in $e^+e^- \to \psi(3770) \to D^0\overline{D}^0$ reactions. Correlations among observables are taken into account by using the error matrices provided by the experiments. Three observables input to the fit are themselves world average values calculated by HFLAV: $R_M = (x^2+y^2)/2$ from $D^0 \to K^{(*)+}\ell^-\overline{\nu}$ decays (Table 70.1), and y_{CP} and A_Γ from $D^0 \to f_{CP}$ decays (Table 70.5). A measurement of R_M by LHCb using $D^0 \to K^+\pi^-\pi^+\pi^-$ decays is input separately.

The results of the fit as of September, 2025 are listed in Table 70.7. Confidence contours in the two dimensions (x, y) and $(|q/p|, \phi)$ resulting from the fit are plotted in Fig. 70.1. These contours are obtained by allowing, for any point in the two-dimensional plane, all other floated parameters to take their preferred values. The 1σ–5σ boundaries drawn are the loci of points in which the χ^2 rises above the minimum by 2.30, 6.18, 11.83, 19.33, and 28.67 units. The fit excludes the no-mixing point $x = y = 0$ at more than 11.5σ. The fit is consistent with CP conservation ($|q/p| = 1$, $\phi = 0$) at the 2σ level. The χ^2 of the all-CP-violation-allowed fit is 70.7 for $59 - 10 = 49$ degrees of freedom, which is considered satisfactory. One-dimensional likelihood functions for parameters are obtained by allowing, for any value of the parameter, all other floated parameters to take their preferred values. The resulting likelihood functions give the 95% C.L. intervals listed in Table 70.7.

From the results of the HFLAV fit, one concludes the following: (1) since CP violation is small and y_{CP} is positive, the CP-even state is shorter-lived, as in the $K^0\overline{K}^0$ system; but since x is positive, the CP-even state is heavier, which is opposite to the $K^0\overline{K}^0$ system. (2) The strong phase difference $\delta_{K\pi}$ is nonzero: the 95% C.L. interval is $8.1^\circ < \delta_{K\pi} < 20.9^\circ$, with a preferred value of 14.8°. (3) While direct CP violation has been observed ($\Delta A_{CP} \neq 0$), there is still no evidence for indirect CP violation, i.e., $|q/p| \neq 1$ or $\phi \neq 0$ or $\phi^M \neq 0$ or $\phi^\Gamma \neq 0$. Observing such CP violation at the current level of experimental sensitivity would hint at new physics.

Finally, we note that the global fit to charm mixing measurements can be expanded to include $B \to (D^0, \overline{D}^0)K$ and $B \to (D^0, \overline{D}^0)\pi$ measurements; this larger fit is performed to determine the CKM angle ϕ_3 (or γ) [114,115]. When $D^0 \to K^\pm\pi^\mp$, the B decay data is sensitive to the strong phase $\delta_{K\pi}$, and the fit gives improved precision for $\delta_{K\pi}$ [115]. This improvement leads to a small improvement in the precision for y (from measurements of y' via $D^0 \to K^+\pi^-$ decays and Eq. (70.32)).

70.8 Future Data

Current mixing and CP violation results are based mainly upon the following:

- CLEO-c (0.82 fb^{-1}) and BESIII (2.9 fb^{-1}) data recorded in $e^+e^- \to \psi(3770)$ reactions;
- BABAR (384 fb^{-1}), Belle (976 fb^{-1}), and Belle II (408 fb^{-1}) data recorded in $e^+e^- \to \Upsilon(4S)$ reactions;
- CDF (9.6 fb^{-1}) data of $\bar{p}p$ collisions at $\sqrt{s} = 2$ TeV; and
- LHCb Run 1 (3.0 fb^{-1}, $\sqrt{s} = 7$, 8 TeV) and Run 2 (6 fb^{-1}, $\sqrt{s} = 13$ TeV) data of pp collisions.

BESIII has recently completed its goal of accumulating 20 fb^{-1} of $e^+e^- \to \psi(3770)$ data. These data should provide numerous strong phase measurements that would enable additional model-independent determinations of mixing parameters from Belle II and LHCb. In 2019 Belle II began a long-range program to accumulate 50 ab^{-1} of $e^+e^- \to \Upsilon(4S)$ data [116]. To date, the experiment has recorded about 0.6 ab^{-1} of data and is expected to record several ab^{-1} over the next few years. At LHCb, Run 2 was completed in 2018, Run 3 is now in progress, and Run 4 is planned for 2030-33 [117]. The goal for Runs $3+4$ is to accumulate an additional 50 fb^{-1} of pp data at $\sqrt{s} \approx 14$ TeV [118]. These data, along with the substantial e^+e^- dataset from Belle II, should provide more precise measurements of D^0-$\overline{D}^0$ mixing and direct

Table 70.7: HFLAV global fit results (see text and Ref. [24]). The upper two sections list mixing and indirect CP violation (CPV) parameters; the third section lists strong phases and the ratio of decay rates R_D; and the bottom section lists direct CP violation parameters.

Parameter	No indirect CPV Fit *(a)*	No subleading amplitudes in indirect CPV Fit *(b)*	All CPV allowed Fit *(c)*	95% C.L. Interval (all CPV)
x (%)	0.398 ± 0.044	0.405 ± 0.043	0.405 ± 0.043	[0.320, 0.489]
y (%)	0.636 ± 0.024	0.638 ± 0.023	0.636 ± 0.024	[0.590, 0.682]
$\|q/p\|$	1	1.002 ± 0.005	0.983 ± 0.015	[0.96, 1.01]
ϕ (°)	0	-0.08 ± 0.19	-1.51 ± 1.04	[−3.63, 0.51]
x_{12} (%)	0.398 ± 0.044	0.405 ± 0.043	0.406 ± 0.043	[0.321, 0.490]
y_{12} (%)	0.636 ± 0.024	0.638 ± 0.023	0.635 ± 0.024	[0.589, 0.682]
ϕ^M(°)	0	0.27 ± 0.66	-0.03 ± 0.70	[−1.48, 1.35]
ϕ^Γ(°)	0	0	2.03 ± 1.53	[−0.94, 5.08]
$\delta_{K\pi}$ (°)	14.9 ± 3.2	15.2 ± 3.2	14.8 ± 3.2	[8.1, 20.9]
$\delta_{K\pi\pi}$ (°)	24.7 ± 22.2	24.4 ± 22.0	24.2 ± 22.1	[−20.6, 65.5]
R_D (%)	0.344 ± 0.001	0.344 ± 0.001	0.344 ± 0.001	[0.341, 0.346]
A_D (%)	0	0	-0.81 ± 0.88	[−2.54, 0.92]
A_π(%)	0.212 ± 0.051	0.222 ± 0.057	0.225 ± 0.057	[0.11, 0.34]
A_K(%)	0.055 ± 0.043	0.065 ± 0.051	0.068 ± 0.051	[−0.03, 0.17]
χ^2/d.o.f.	$72.817/(59-7)$ $= 1.40$	$72.797/(59-8)$ $= 1.43$	$70.711/(59-10)$ $= 1.44$	

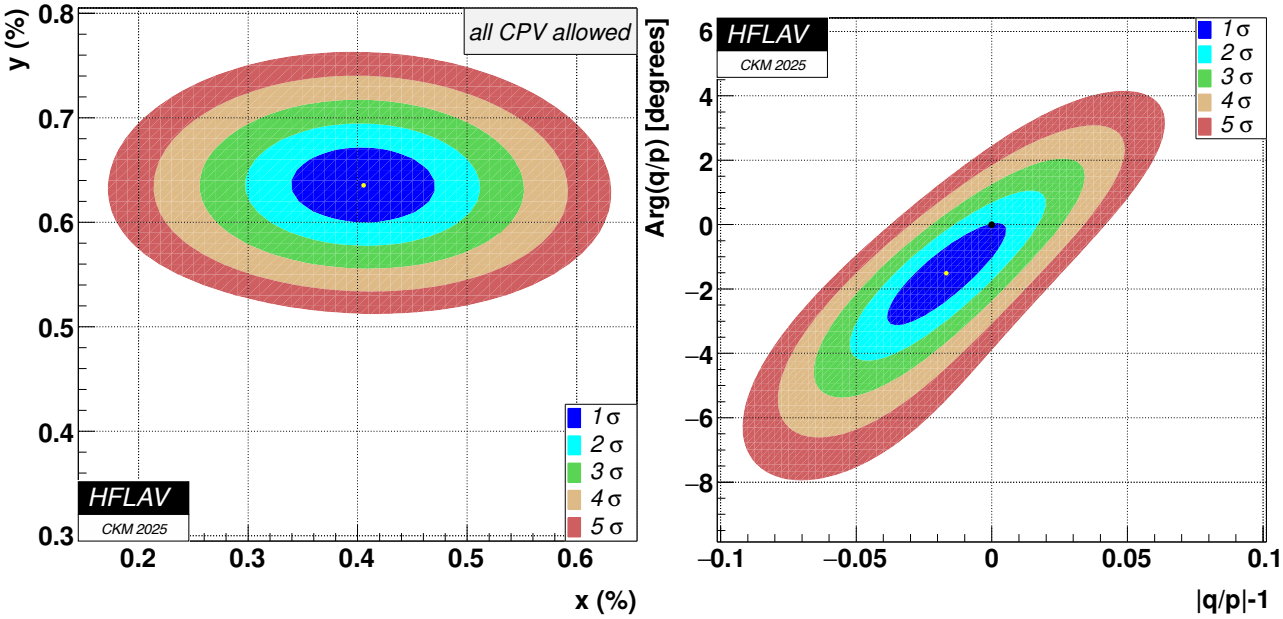

Figure 70.1: Two-dimensional 1σ-5σ contours for (x, y) (left) and for $(|q/p|, \phi)$ (right) from the HFLAV global fit [24]. The black dot in the right plot denotes the no-CP-violation point.

CP violation, and hopefully uncover indirect CP violation in the D^0-$\overline{D}^0$ system.

References

[1] A. L. Kagan and L. Silvestrini, Phys. Rev. D **103**, 5, 053008 (2021), [arXiv:2001.07207].

[2] Y. Grossman, Y. Nir and G. Perez, Phys. Rev. Lett. **103**, 071602 (2009), [arXiv:0904.0305].

[3] A. L. Kagan and M. D. Sokoloff, Phys. Rev. **D80**, 076008 (2009), [arXiv:0907.3917].

[4] D. M. Asner and W. M. Sun, Phys. Rev. **D73**, 034024 (2006), [Erratum: Phys. Rev. **D77**, 019901 (2008)], [hep-ph/0507238].

[5] D. Atwood and A. A. Petrov, Phys. Rev. **D71**, 054032 (2005), [hep-ph/0207165].

[6] M. Gronau, Y. Grossman and J. L. Rosner, Phys. Lett. **B508**, 37 (2001), [hep-ph/0103110].

[7] Z.-z. Xing, Phys. Rev. **D55**, 196 (1997), [hep-ph/9606422].

[8] M. Goldhaber and J. L. Rosner, Phys. Rev. **D15**, 1254 (1977).

[9] Y. S. Amhis *et al.* (HFLAV), Eur. Phys. J. C **81**, 3, 226 (2021), [arXiv:1909.12524].

[10] U. Bitenc *et al.* (Belle), Phys. Rev. **D77**, 112003 (2008), [arXiv:0802.2952].

[11] B. Aubert *et al.* (BaBar), Phys. Rev. **D76**, 014018 (2007), [arXiv:0705.0704].

[12] C. Cawlfield *et al.* (CLEO), Phys. Rev. **D71**, 077101 (2005), [hep-ex/0502012].

[13] E. M. Aitala *et al.* (E791), Phys. Rev. Lett. **77**, 2384 (1996), [hep-ex/9606016].

[14] S. Banerjee *et al.* (Heavy Flavor Averaging Group (HFLAV)) (2024), [arXiv:2411.18639].

[15] U. Bitenc *et al.* (Belle), Phys. Rev. **D72**, 071101 (2005), [hep-ex/0507020].

[16] B. Aubert *et al.* (BaBar), Phys. Rev. **D70**, 091102 (2004), [hep-ex/0408066].

Int. J. Mod. Phys. A 2026.41. Downloaded from www.worldscientific.com
UNIVERSITY OF CALIFORNIA @ BERKELEY on 09/16/26. Re-use and distribution is strictly not permitted, except for Open Access articles.

Int. J. Mod. Phys. A 2026.41. Downloaded from www.worldscientific.com
by UNIVERSITY OF CALIFORNIA @ BERKELEY on 09/16/26. Re-use and distribution is strictly not permitted, except for Open Access articles.

[17] Y. Nir, Lectures given at 27th SLAC Summer Institute on Particle Physics: "*CP* Violation in and Beyond the Standard Model (SSI 99)," Stanford, California, 7-16 July 1999. Published in Trieste 1999, *Particle Physics*, pp. 165-243.

[18] S. Bergmann *et al.*, Phys. Lett. **B486**, 418 (2000), [hep-ph/0005181].

[19] R. Aaij *et al.* (LHCb), Phys. Rev. D **111**, 1, 012001 (2025), [arXiv:2407.18001].

[20] R. Aaij *et al.* (LHCb), JHEP **03**, 149 (2025), [arXiv:2501.11635].

[21] B. R. Ko *et al.* (Belle), Phys. Rev. Lett. **112**, 11, 111801 (2014), [Addendum: Phys. Rev. Lett. **112**, 139903 (2014)], [arXiv:1401.3402].

[22] T. A. Aaltonen *et al.* (CDF), Phys. Rev. Lett. **111**, 23, 231802 (2013), [arXiv:1309.4078].

[23] B. Aubert *et al.* (BaBar), Phys. Rev. Lett. **98**, 211802 (2007), [hep-ex/0703020].

[24] Heavy Flavor Averaging Group, `https://hflav-eos.web.cern.ch/hflav-eos/charm/CKM25/results_mix_cpv.html`.

[25] R. Aaij *et al.* (LHCb), Phys. Rev. **D97**, 3, 031101 (2018), [arXiv:1712.03220].

[26] R. Aaij *et al.* (LHCb), Phys. Rev. **D95**, 5, 052004 (2017), [Erratum: Phys. Rev. **D96**, 099907 (2017)], [arXiv:1611.06143].

[27] R. Aaij *et al.* (LHCb), Phys. Rev. Lett. **111**, 25, 251801 (2013), [arXiv:1309.6534].

[28] R. Aaij *et al.* (LHCb), Phys. Rev. Lett. **110**, 10, 101802 (2013), [arXiv:1211.1230].

[29] T. Aaltonen *et al.* (CDF), Phys. Rev. Lett. **100**, 121802 (2008), [arXiv:0712.1567].

[30] L. M. Zhang *et al.* (Belle), Phys. Rev. Lett. **96**, 151801 (2006), [hep-ex/0601029].

[31] J. M. Link *et al.* (FOCUS), Phys. Lett. **B618**, 23 (2005), [hep-ex/0412034].

[32] R. Godang *et al.* (CLEO), Phys. Rev. Lett. **84**, 5038 (2000), [hep-ex/0001060].

[33] E. M. Aitala *et al.* (E791), Phys. Rev. **D57**, 13 (1998), [hep-ex/9608018].

[34] M. Ablikim *et al.* (BESIII), Phys. Lett. **B734**, 227 (2014), [arXiv:1404.4691].

[35] See "Review of Multibody Charm Analyses" in this *Review*.

[36] B. Aubert *et al.* (BaBar), Phys. Rev. Lett. **97**, 221803 (2006), [hep-ex/0608006].

[37] B. Aubert *et al.* (BaBar), Phys. Rev. Lett. **103**, 211801 (2009), [arXiv:0807.4544].

[38] E. White *et al.* (Belle), Phys. Rev. **D88**, 5, 051101 (2013), [arXiv:1307.5935].

[39] R. Aaij *et al.* (LHCb), Phys. Rev. Lett. **116**, 24, 241801 (2016), [arXiv:1602.07224].

[40] D. M. Asner *et al.* (CLEO), Phys. Rev. **D72**, 012001 (2005), [hep-ex/0503045].

[41] K. Abe *et al.* (Belle), Phys. Rev. Lett. **99**, 131803 (2007), [arXiv:0704.1000].

[42] R. Aaij *et al.* (LHCb), JHEP **04**, 033 (2016), [arXiv:1510.01664].

[43] R. Aaij *et al.* (LHCb), Phys. Rev. Lett. **122**, 23, 231802 (2019), [arXiv:1903.03074].

[44] R. Aaij *et al.* (LHCb), Phys. Rev. Lett. **127**, 11, 111801 (2021), [arXiv:2106.03744].

[45] R. Aaij *et al.* (LHCb), Phys. Rev. D **108**, 052005 (2023), [arXiv:2208.06512].

[46] J. Libby *et al.* (CLEO), Phys. Rev. **D82**, 112006 (2010), [arXiv:1010.2817].

[47] M. Ablikim *et al.* (BESIII), Phys. Rev. Lett. **124**, 24, 241802 (2020), [arXiv:2002.12791].

[48] M. Ablikim *et al.* (BESIII), Phys. Rev. D **101**, 11, 112002 (2020), [arXiv:2003.00091].

[49] A. Di Canto *et al.*, Phys. Rev. **D99**, 1, 012007 (2019), [arXiv:1811.01032].

[50] I. Adachi *et al.* (Belle, Belle-II), Phys. Rev. D **111**, 11, 112011 (2025), [arXiv:2410.22961].

[51] M. Ablikim *et al.* (BESIII) (2025), [arXiv:2503.22126].

[52] M. Ablikim *et al.* (BESIII) (2025), [arXiv:2502.12873].

[53] M. Ablikim *et al.* (BESIII), Phys. Rev. D **110**, 11, 112008 (2024), [arXiv:2408.16279].

[54] S. Harnew *et al.*, JHEP **01**, 144 (2018), [arXiv:1709.03467].

[55] J. P. Lees *et al.* (BaBar), Phys. Rev. **D93**, 11, 112014 (2016), [arXiv:1604.00857].

[56] P. del Amo Sanchez *et al.* (BaBar), Phys. Rev. Lett. **105**, 081803 (2010), [arXiv:1004.5053].

[57] T. Peng *et al.* (Belle), Phys. Rev. **D89**, 9, 091103 (2014), [arXiv:1404.2412].

[58] M. Nayak *et al.* (Belle), Phys. Rev. D **102**, 7, 071102 (2020), [arXiv:1912.10912].

[59] A. Zupanc *et al.* (Belle), Phys. Rev. **D80**, 052006 (2009), [arXiv:0905.4185].

[60] T. Pajero and M. J. Morello, JHEP **03**, 162 (2022), [arXiv:2106.02014].

[61] A. J. Schwartz (2022), [arXiv:2207.11867].

[62] M. Starič *et al.* (Belle), Phys. Lett. **B753**, 412 (2016), [arXiv:1509.08266].

[63] J. P. Lees *et al.* (BaBar), Phys. Rev. **D87**, 1, 012004 (2013), [arXiv:1209.3896].

[64] T. A. Aaltonen *et al.* (CDF), Phys. Rev. **D90**, 11, 111103 (2014), [arXiv:1410.5435].

[65] R. Aaij *et al.* (LHCb), JHEP **04**, 129 (2012), [arXiv:1112.4698].

[66] R. Aaij *et al.* (LHCb), Phys. Rev. D **104**, 7, 072010 (2021), [arXiv:2105.09889].

[67] M. Gersabeck *et al.*, J. Phys. G **39**, 045005 (2012), [arXiv:1111.6515].

[68] See the tabulation of A_{CP} results in the D^0 and D^+ Listings in this *Review*.

[69] Y. Grossman, A. L. Kagan and Y. Nir, Phys. Rev. D **75**, 036008 (2007), [hep-ph/0609178].

[70] R. Aaij *et al.* (LHCb), Phys. Rev. Lett. **122**, 21, 211803 (2019), [arXiv:1903.08726].

[71] R. Aaij *et al.* (LHCb), Phys. Rev. Lett. **131**, 9, 091802 (2023), [arXiv:2209.03179].

[72] S. Malde *et al.*, Phys. Lett. B **747**, 9 (2015), [arXiv:1504.05878].

[73] R. Aaij *et al.* (LHCb), Phys. Rev. Lett. **133**, 10, 101803 (2024), [arXiv:2405.06556].

[74] R. Aaij *et al.* (LHCb), Phys. Rev. D **105**, 9, 092013 (2022), [arXiv:2202.09106].

[75] R. Aaij *et al.* (LHCb), Phys. Rev. **D101**, 1, 012005 (2020), [arXiv:1911.01114].

[76] R. Aaij *et al.* (LHCb), Phys. Rev. Lett. **122**, 1, 011802 (2019), [arXiv:1810.06874].

[77] R. Aaij *et al.* (LHCb), Phys. Rev. Lett. **118**, 26, 261803 (2017), [arXiv:1702.06490].

[78] R. Aaij *et al.* (LHCb), JHEP **04**, 043 (2015), [arXiv:1501.06777].

[79] M. Ablikim *et al.* (BESIII), Phys. Lett. **B744**, 339 (2015), [arXiv:1501.01378].

[80] S. E. Csorna *et al.* (CLEO), Phys. Rev. **D65**, 092001 (2002), [hep-ex/0111024].

[81] J. M. Link *et al.* (FOCUS), Phys. Lett. **B485**, 62 (2000), [hep-ex/0004034].

[82] E. M. Aitala *et al.* (E791), Phys. Rev. Lett. **83**, 32 (1999), [hep-ex/9903012].

[83] Heavy Flavor Averaging Group, `https://hflav-eos.web.cern.ch/hflav-eos/charm/CKM25/results_mixing.html`.

[84] R. Aaij *et al.* (LHCb), Phys. Rev. Lett. **112**, 4, 041801 (2014), [arXiv:1310.7201].

[85] B. Aubert *et al.* (BaBar), Phys. Rev. **D80**, 071103 (2009), [arXiv:0908.0761].

[86] B. Aubert *et al.* (BaBar), Phys. Rev. **D78**, 011105 (2008), [arXiv:0712.2249].

[87] M. Staric *et al.* (BELLE), Phys. Rev. Lett. **98**, 211803 (2007), [,65(2007)], [hep-ex/0703036].

[88] B. Aubert *et al.* (BaBar), Phys. Rev. Lett. **91**, 121801 (2003), [hep-ex/0306003].

[89] K. Abe *et al.* (Belle), Phys. Rev. Lett. **88**, 162001 (2002), [hep-ex/0111026].

[90] M. Ablikim *et al.* (BESIII), Eur. Phys. J. C **82**, 11, 1009 (2022), [arXiv:2208.09402].

[91] M. Ablikim *et al.* (BESIII) (2025), [arXiv:2506.07907].

[92] J. L. Rosner *et al.* (CLEO), Phys. Rev. Lett. **100**, 221801 (2008), [arXiv:0802.2264].

[93] D. M. Asner *et al.* (CLEO), Phys. Rev. **D78**, 012001 (2008), [arXiv:0802.2268].

[94] D. M. Asner *et al.* (CLEO), Phys. Rev. **D86**, 112001 (2012), [arXiv:1210.0939].

[95] Heavy Flavor Averaging Group, `https://hflav-eos.web.cern.ch/hflav-eos/charm/March12/results_mix_cpv.html`.

[96] T. Aaltonen *et al.* (CDF), Phys. Rev. Lett. **100**, 121802 (2008), [arXiv:0712.1567].

[97] T. Aaltonen *et al.* (CDF), Phys. Rev. Lett. **109**, 111801 (2012), [arXiv:1207.2158].

[98] B. Aubert *et al.* (BaBar), Phys. Rev. Lett. **100**, 061803 (2008), [arXiv:0709.2715].

[99] M. Staric *et al.* (Belle), Phys. Lett. **B670**, 190 (2008), [arXiv:0807.0148].

[100] R. Aaij *et al.* (LHCb), Phys. Rev. Lett. **116**, 19, 191601 (2016), [arXiv:1602.03160].

[101] R. Aaij *et al.* (LHCb), JHEP **07**, 041 (2014), [arXiv:1405.2797].

[102] R. Aaij *et al.* (LHCb), Phys. Lett. **B723**, 33 (2013), [arXiv:1303.2614].

[103] R. Aaij *et al.* (LHCb), Phys. Rev. Lett. **108**, 111602 (2012), [arXiv:1112.0938].

[104] B. R. Ko (Belle), in "7th International Workshop on the CKM Unitarity Triangle (CKM 2012) Cincinnati, Ohio, USA, September 28-October 2, 2012," (2012), [arXiv:1212.5320].

[105] E. Golowich *et al.*, Phys. Rev. **D76**, 095009 (2007), [arXiv:0705.3650].

[106] G. Isidori *et al.*, Phys. Lett. **B711**, 46 (2012), [arXiv:1111.4987].

[107] E. Franco, S. Mishima and L. Silvestrini, JHEP **05**, 140 (2012), [arXiv:1203.3131].

[108] J. Brod, A. L. Kagan and J. Zupan, Phys. Rev. D **86**, 014023 (2012), [arXiv:1111.5000].

[109] Y. Grossman and S. Schacht, JHEP **07**, 020 (2019), [arXiv:1903.10952].

[110] M. Gavrilova, Y. Grossman and S. Schacht, Phys. Rev. D **109**, 3, 033011 (2024), [arXiv:2312.10140].

[111] M. Chala *et al.*, JHEP **07**, 161 (2019), [arXiv:1903.10490].

[112] A. Dery and Y. Nir, JHEP **12**, 104 (2019), [arXiv:1909.11242].

[113] M. Ciuchini *et al.*, Phys. Lett. **B655**, 162 (2007), [hep-ph/0703204].

[114] R. Aaij *et al.* (LHCb), JHEP **12**, 141 (2021), [arXiv:2110.02350].

[115] F. Betti *et al.*, Phys. Rev. D **112**, 1, 013004 (2025), [arXiv:2409.06449].

[116] W. Altmannshofer *et al.* (Belle-II), PTEP **2019**, 12, 123C01 (2019), [Erratum: PTEP 2020, 029201 (2020)], [arXiv:1808.10567].

[117] CERN LHC Schedule, `https://lhc-commissioning.web.cern.ch/schedule/LHC-long-term.htm`.

[118] R. Aaij *et al.* (LHCb) (2018), [arXiv:1808.08865].

Int. J. Mod. Phys. A 2026.41. Downloaded from www.worldscientific.com
UNIVERSITY OF CALIFORNIA @ BERKELEY on 09/16/26. Re-use and distribution is strictly not permitted, except for Open Access articles.

Int. J. Mod. Phys. A 2026.41. Downloaded from www.worldscientific.com
by UNIVERSITY OF CALIFORNIA @ BERKELEY on 09/16/26. Re-use and distribution is strictly not permitted, except for Open Access articles.

71. Leptonic Decays of Charged Pseudoscalar Mesons

Updated Aug. 2025 by R. A. Briere (Carnegie Mellon U.); written with J. L. Rosner (Chicago U.), S. L. Stone (Syracuse U.) and R. Van de Water (FNAL)

71.1 Introduction

This review updates one in Ref. [1]. Lattice QCD updates rely on the Flavor Lattice Averaging Group FLAG 24 update [2]; these updates were modest. The most significant updates involve D_s experimental results; some changes to the discussions of semileptonic decays in second-generation unitarity and inclusive-exclusive V_{ub} tension are also noted.

Charged mesons formed from a quark and antiquark can decay to a lepton-neutrino pair when these objects annihilate via a virtual W boson. Figure 71.1 illustrates this process for the purely leptonic decay of a D^+ meson.

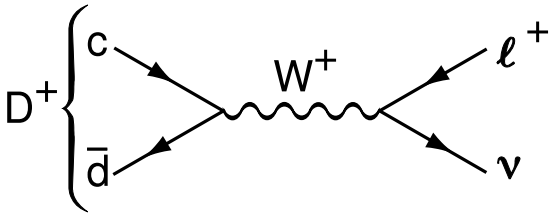

Figure 71.1: The annihilation process for pure D^+ leptonic decays in the standard model.

Similar quark-antiquark annihilations via a virtual W^+ to the $\ell^+\nu$ final states occur for the π^+, K^+, D_s^+, and B^+ mesons. (Whenever pseudoscalar-meson charges are specified in this article, use of the charge-conjugate particles and corresponding decays are also implied.) Let P be any of these pseudoscalar mesons. To lowest order, the decay width is

$$\Gamma^{(0)}(P \to \ell\nu) = \frac{G_F^2}{8\pi} f_P^2 \; m_\ell^2 M_P \left(1 - \frac{m_\ell^2}{M_P^2}\right)^2 |V_{q_1 q_2}|^2 \; . \quad (71.1)$$

Here M_P is the P mass, m_ℓ is the ℓ mass, $V_{q_1 q_2}$ is the Cabibbo-Kobayashi-Maskawa (CKM) matrix element between the quarks $q_1\bar{q}_2$ in P, and G_F is the Fermi coupling constant. The decay constant f_P is proportional to the matrix element of the axial current between the one-P-meson state and the vacuum:

$$\langle 0|\bar{q}_1\gamma_\mu\gamma_5 q_2|P(p)\rangle = ip_\mu f_P \; , \quad (71.2)$$

and can be thought of as proportional to the "wave function overlap" of the quark and antiquark. In this article, we use the convention in which $f_\pi \approx 130$ MeV. For brevity, we will often denote the purely leptonic decay width in Eq. (71.1) by $\Gamma^{(0)}$.

The decay of $P^\pm$ starts with a spin-0 meson, and ends up with a left-handed neutrino or right-handed antineutrino. By angular momentum conservation, the $\ell^\pm$ must then also be left-handed or right-handed, respectively. In the $m_\ell = 0$ limit, the decay is forbidden, and can only occur as a result of the finite ℓ mass. This helicity suppression is the origin of the m_ℓ^2 factor in the decay width.

Experimentally, it is difficult to isolate events in which there are *only* a lepton and neutrino in the final state from those with a lepton, neutrino, and soft photon. Thus, radiative contributions must be removed from the experimental measurements *a posteriori* to obtain $\Gamma^{(0)}$. The radiative contributions can be broken into three pieces: the short-distance contribution to leptonic and semileptonic decays mediated by a $W^\pm$ boson that accounts for electroweak corrections not included in the definition of G_F, the long-distance internal bremsstrahlung (IB) contribution, and the contribution from photon emission that depends upon the hadron's structure. The universal electroweak correction was calculated at $\mathcal{O}(\alpha)$ by Sirlin [3], and increases the purely leptonic decay rate by $\sim$ 1.8–2.2% depending on the decaying meson. The $\mathcal{O}(\alpha)$ IB contribution was calculated by Kinoshita [4], and again is universal for all leptonic decays at this order. Numerically, this universal long-distance contribution lowers the purely leptonic decay rate by $\sim$ 0.4–2.4%, where the correction is smallest for pions and largest for $D_{(s)}$ mesons. The structure-dependent contributions have been estimated within various effective theories and from lattice-QCD,QED calculations to increase the purely leptonic rate by one to a few percent [5–10].

In this review, we treat the radiative corrections differently for the light, charm, and bottom meson systems for several reasons. First, the experimental uncertainties on the decay widths vary substantially. Thus, while the inclusion of radiative corrections is essential for the pion, kaon, and $D_{(s)}$-meson decay widths, which have been measured to (sub)-percent precision, radiative corrections can be neglected (for now) for $B \to \tau\nu$ decay. Second, the photons are treated differently on the experimental side for the different decay processes. For pions and kaons, the experimental measurements of $\Gamma_{P\ell 2[\gamma]}$ are fully inclusive, while for $D_{(s)}$ mesons, the experiments impose cuts on the energy of any neutral cluster deposited in the calorimeter, which reduce the soft-photon background substantially. Some experiments also remove the QED bremsstrahlung in the leading-logarithmic approximation using the PHOTOS Monte-Carlo generator [11]. Third, the theoretical knowledge of the structure-dependent corrections varies for each meson system.

Once radiative corrections have been accounted for, measurements of purely leptonic decay branching fractions and lifetimes allow an experimental determination of the product $|V_{q_1 q_2}|\, f_P$. If the decay constant f_P is known to sufficient precision from theory, one can obtain the corresponding CKM element within the standard model. If, on the other hand, one takes the value of $|V_{q_1 q_2}|$ assuming CKM unitarity, one can infer an "experimental measurement" of the decay constant that can then be compared with theory.

The importance of measuring $\Gamma(P \to \ell\nu)$ depends on the particle being considered. Leptonic decays of charged pseudoscalar mesons occur at tree level within the standard model. Thus one does not expect large new-physics contributions to measurements of $\Gamma(P \to \ell\nu)$ for the lighter mesons $P = \pi^+, K^+$, and these processes, in principle, provide clean standard-model determinations of $|V_{ud}|$ and $|V_{us}|$. The situation is different for leptonic decays of charm and bottom mesons. The presence of new heavy particles such as charged Higgs bosons or leptoquarks could lead to observable effects in $\Gamma(P \to \ell\nu)$ for $P = D_{(s)}^+, B^+$ [12–16]. Thus, the determination of $|V_{ub}|$ from $B^+ \to \tau\nu$ decay, in particular, should be considered a probe of new physics. More generally, the ratio of leptonic decays to $\tau\nu$ over $\mu\nu$ final states probes lepton universality [12, 17].

The determinations of CKM elements from leptonic decays of charged pseudoscalar mesons provide complementary information to those from other decay processes. The decay $P \to \ell\nu$ proceeds in the standard model via the axial-vector current $\bar{q}_1\gamma_\mu\gamma_5 q_2$, whereas semileptonic pseudoscalar meson decays $P_1 \to P_2\ell\nu$ proceed via the vector current $\bar{q}_1\gamma_\mu q_2$. Thus the comparison of determinations of $|V_{q_1 q_2}|$ from leptonic and semileptonic decays tests the $V - A$ structure of the standard-model electroweak charged-current interaction. More generally, a small right-handed admixture to the standard-model weak current would lead to discrepancies between $|V_{q_1 q_2}|$ obtained from leptonic pseudoscalar-meson decays, exclusive semileptonic pseudoscalar-meson decays, exclusive semileptonic baryon decays, and inclusive semileptonic decays [18, 19].

Both measurements of the decay rates $\Gamma(P \to \ell\nu)$ and theoretical calculations of the decay constants f_P for $P = \pi^+, K^+, D_{(s)}^+$ from numerical lattice-QCD calculations are now quite precise. As a result, the elements of the first row of the CKM matrix $|V_{ud}|$ and $|V_{us}|$ can be obtained to sub-percent precision from $\pi^+ \to \ell\nu$ and $K^+ \to \ell\nu$, where the limiting error is from continuum theory radiative corrections. The elements of the second row of the CKM matrix $|V_{cd(s)}|$ can be obtained from leptonic decays of charmed pseudoscalar mesons to few-percent precision, where here the limiting error is from experiment. These enable stringent tests of the unitarity of the first and second rows of the CKM matrix.

Int. J. Mod. Phys. A 2026.41. Downloaded from www.worldscientific.com
UNIVERSITY OF CALIFORNIA @ BERKELEY on 09/16/26. Re-use and distribution is strictly not permitted, except for Open Access articles.

This review is organized as follows. Because the experimental and theoretical issues associated with measurements of pions and kaons, charmed mesons, and bottom mesons differ, we discuss each one separately. We begin with the pion and kaon system in Sec. 71.2. First, in Sec. 71.2.1, we review current measurements of the experimental decay rates. We provide tables of branching-ratio measurements and determinations of the product $|V_{ud(s)}|f_{\pi^+(K^+)}$, as well as average values for these quantities including correlations and other effects needed to combine results. Then, in Sec. 71.2.2, we summarize the status of theoretical calculations of the decay constants. We provide tables of recent lattice-QCD results for f_{π^+}, f_{K^+}, and their ratio from calculations including dynamical u, d, s, and (in some cases c) quarks, along with averages including correlations and strong SU(2)-isospin breaking corrections as needed. We next discuss the charmed meson system in Sec. 71.3, again reviewing current experimental rate measurements in Sec. 71.3.1 and theoretical decay-constant calculations in Sec. 71.3.2. Last, we discuss the bottom meson system in Sec. 71.4, following the same organization as the two previous sections. For almost all of the decay constants presented in Secs. 71.2.2, 71.3.2, and 71.4.2, we take as our preferred values the four-flavor averages from the FLAG 24 review [2], with isospin-breaking corrections as noted.

After having established the status of both experimental measurements and theoretical calculations of leptonic charged pseudoscalar-meson decays, we discuss some implications for phenomenology in Sec. 71.5. For each process discussed in Secs. 71.2–71.4, we combine the average $\mathcal{B}(P \to \ell\nu)$ with the decay constant f_P to infer the associated CKM matrix element. We then compare these results with determinations of the same CKM elements from other processes. We also use the CKM elements obtained from leptonic decays to test the unitarity of the first and second rows of the CKM matrix. Further, as in previous reviews, we combine the experimental $\mathcal{B}(P \to \ell\nu)$s with the associated CKM elements obtained from CKM unitarity to infer "experimental" values for the decay constants. The comparison of these values with theory provides a test of lattice and other QCD approaches, assuming that new-physics contributions to these processes are not significant.

71.2 Pions and kaons

71.2.1 *Experimental rate measurements*

Experimental rate measurements of pion and kaon leptonic decays are fully radiation inclusive. Following Refs. [20, 21], and references therein, we combine the $\mathcal{O}(\alpha)$ radiative corrections to the purely leptonic rate as follows:

$$\Gamma(P \to \ell\nu[\gamma]) = \Gamma^{(0)}(P \to \ell\nu)\left[1 + \frac{\alpha}{\pi}C_P\right], \tag{71.3}$$

where $P = \pi, K$. The full expressions for C_π and C_K are given in Eq. (114) of Ref. [7]. In addition to the universal short- [3] and long-distance [4] corrections, C_π and C_K include hadronic-structure dependent contributions [5] through $\mathcal{O}(\alpha p^4)$ in chiral perturbation theory (χPT), where p is the pion or kaon momentum. The inclusion of radiative corrections to the purely leptonic rates is numerically important given the level of precision achieved on the experimental measurements of the $\pi^\pm \to \mu^\pm\nu$ and $K^\pm \to \mu^\pm\nu$ decay widths.

We evaluate $\delta_P \equiv (\alpha/\pi)C_P$ using experimentally-measured meson and lepton masses and coupling constants from the Particle Data Group [22], and taking the low-energy constants (LECs) that parametrize the hadronic contributions from Refs. [7, 23, 24]. Because the finite non-logarithmic parts of the LECs were estimated within the large-N_C approximation assuming that contributions from the lowest-lying resonances dominate, we conservatively assign a 100% uncertainty to the LECs, which leads to a ± 0.9 error in $C_{\pi,K}$.[1] We obtain the following correction factors to the individual charged pion and kaon decay widths:

$$\delta_\pi = 0.0176(21) \quad \text{and} \quad \delta_K = 0.0107(21)\,. \tag{71.4}$$

The error on the ratio of kaon-to-pion leptonic decay widths is under better theoretical control because the hadronic contributions from low-energy constants estimated within the large-N_c framework cancel at lowest order in the chiral expansion. For the ratio, we use the correction factor

$$\delta_{K/\pi} = -0.0069(17)\,, \tag{71.5}$$

where we take the estimated error due to higher-order corrections in the chiral expansion from Ref. [26].

There have been no new measurements of the pion leptonic decay rate since the review of Ref. [27]. The sum of branching fractions for $\pi^- \to \mu^-\bar{\nu}$ and $\pi^- \to \mu^-\bar{\nu}\gamma$ is 99.98770(4)% [1]. Together with the lifetime 26.033(5) ns [1] this implies $\Gamma(\pi^- \to \mu^-\bar{\nu}[\gamma]) = 3.8408(7) \times 10^7\ \mathrm{s}^{-1}$. We then subtract the estimated radiative correction factor δ_π in Eq. (71.4) to obtain the purely leptonic rate $\Gamma^{(0)}(\pi^- \to \mu^-\bar{\nu})$. Using this rate and the PDG masses [1] in Eq. (71.1) gives

$$f_{\pi^+}|V_{ud}| = (127.13 \pm 0.01 \pm 0.13)\ \mathrm{MeV}\,, \tag{71.6}$$

where the errors are from the experimental rate measurement and the radiative correction factor, respectively.

The uncertainty on $f_{\pi^-}|V_{ud}|$ is dominated by that from theoretical estimate of the hadronic structure-dependent radiative corrections. The first direct lattice-QCD calculation of the radiative corrections to the pion and kaon leptonic decay rates was performed by the RM123-Soton Collaboration [10]. The results for both $\delta_\pi = 0.0153(19)$ and $\delta_K = 0.0088(9)$, which are given in the Gasser-Rusetsky-Scimemi scheme for separating strong and electromagnetic effects [28], are compatible with our chiral-perturbation-theory estimates above and have smaller quoted uncertainties, especially for δ_K. Less precise results have also been presented by RBC/UKQCD [29]. While further confirmation of these results is needed, they demonstrate a promising approach for reducing the theoretical uncertainties on the pion and kaon leptonic decay rates in the future.

The world average for the $K \to \mu\nu$ decay rate was previously obtained from a global fit of several kaon-decay branching ratios and lifetime measurements by the FlaviaNet Working Group on Kaon Decays in 2014 [42]; we have now updated to the PDG [1]. The radiation-inclusive branching ratio $\mathcal{B}(K^+ \to \mu^+\nu[\gamma]) = 63.56(11)\%$ and lifetime $\tau_{K^\pm} = 12.380(20)$ ns are now used; this is a very small change. These measurements imply $\Gamma(K^+ \to \mu^+\nu[\gamma]) = 5.134(12) \times 10^7\ \mathrm{s}^{-1}$. As before, we subtract δ_K in Eq. (71.4) from the radiation-inclusive decay width to obtain $\Gamma^{(0)}(K^+ \to \mu^+\nu)$. We then use Eq. (71.1) to obtain

$$f_{K^+}|V_{us}| = (35.083 \pm 0.042 \pm 0.037)\ \mathrm{MeV}\,, \tag{71.7}$$

where the errors are from the experimental rate measurement and the radiative correction factor, respectively.

Short-distance radiative corrections cancel in the ratio of pion-to-kaon decay rates [43]:

$$\frac{\Gamma_{K_{\ell 2[\gamma]}}}{\Gamma_{\pi_{\ell 2[\gamma]}}} = \frac{|V_{us}^2|f_{K^-}^2}{|V_{ud}|^2 f_{\pi^-}^2}\,\frac{m_K(1 - m_\ell^2/m_K^2)^2}{m_\pi(1 - m_\ell^2/m_\pi^2)^2}(1 + \delta_{K/\pi})\,, \tag{71.8}$$

where $\delta_{K/\pi}$ is given in Eq. (71.5). The left-hand side of Eq. (71.8) is 1.3367(32), which implies

$$\frac{|V_{us}|f_{K^+}}{|V_{ud}|f_{\pi^+}} = 0.27599 \pm 0.00033 \pm 0.00024\,, \tag{71.9}$$

where the first uncertainty is from the branching fractions and the second is from $\delta_{K/\pi}$. Here, the estimated error on the hadronic structure-dependent radiative corrections is commensurate with the experimental error.

[1] This uncertainty on $C_{\pi,K}$ is smaller than the error estimated by Marciano and Sirlin in Ref. [25], which predates the calculations of the hadronic-structure contributions in Refs. [5, 7, 23, 24]. The hadronic LECs incorporate the large short-distance electroweak logarithm discussed in Ref. [25], and their dependence on the chiral renormalization scale cancels the scale-dependence induced by chiral loops, thereby removing the dominant scale uncertainty of the Marciano–Sirlin analysis [25].

Int. J. Mod. Phys. A 2026.41. Downloaded from www.worldscientific.com
by UNIVERSITY OF CALIFORNIA @ BERKELEY on 09/16/26. Re-use and distribution is strictly not permitted, except for Open Access articles.

Table 71.1: Recent published lattice-QCD results for f_{π^+}, f_{K^+}, and their ratio. The upper and lower panels show $(2+1+1)$-flavor and $(2+1)$-flavor determinations, respectively. When two errors are shown, they are statistical and systematic, respectively. Results for f_π and f_K in the isospin symmetric limit $m_u = m_d$ are noted with a ‡; they are corrected for isospin breaking via Eq. (71.13) before computing the averages. The 2+1+1 FLAG 24 averages are dominated by the Fermilab/MILC values.

Reference	N_f	f_{π^+}(MeV)	f_{K^+}(MeV)	f_{K^+}/f_{π^+}
ETM 21 [30]	2+1+1	–	155.92(62)(9)	1.1957(44)(7)
CalLat 20 [31]	2+1+1	–	–	1.1942(32)(31)
Fermilab/MILC 17 [32] *	2+1+1	–	–	$1.1950(15)(^{+6}_{-18})$
ETM 14 [33] *	2+1+1	–	154.4(1.5)(1.3)	1.184(12)(11)
Fermilab/MILC 14 [9] * †	2+1+1	–	$155.92(13)(^{+42}_{-34})$	$1.1956(10)(^{+26}_{-18})$ † ‡
HPQCD 13 [34] *	2+1+1	–	155.37(20)(27)	1.1916(15)(16)
FLAG 24 average [2]	2+1+1	–	155.7(3)	1.1934(19)
CLQCD 23 [35]	2+1	130.7(0.9)(2.1)	155.6(0.8)(2.7)	11907(76)(17)
QCDSF/UKQCD 16 [36]	2+1	–	–	1.190(10)(13)
BMW 16 [37]	2+1	–	–	1.178(10)(26)
RBC/UKQCD 14 [38]‡	2+1	130.19(89)	155.51(83)	1.1945(45)
MILC 10 [39]	2+1	129.2(0.4)(1.4)	$156.1(4)(^{+6}_{-9})$	$1.197(2)(^{+3}_{-7})$
BMW 10 [40]‡	2+1	–	–	1.192(7)(6)
HPQCD/UKQCD 07 [41]‡	2+1	132(2)	157(2)	1.189(2)(7)
FLAG 24 average [2]	2+1	130.2(8)	155.7(7)	1.1916(34)

*PDG 2014 value of $f_{\pi^+} = 130.41(21)$ MeV used to set absolute lattice scale.
†Superseded by f_{K^+}/f_{π^+} from Fermilab/MILC 17.

In summary, the main experimental results pertaining to charged pion and kaon leptonic decays are

$$|V_{ud}|f_{\pi^+} = (127.13 \pm 0.01 \pm 0.13)\ \text{MeV}\,, \tag{71.10}$$

$$|V_{us}|f_{K^+} = (35.083 \pm 0.042 \pm 0.037)\ \text{MeV}\,, \tag{71.11}$$

$$\frac{|V_{us}|f_{K^+}}{|V_{ud}|f_{\pi^+}} = 0.27599 \pm 0.00033 \pm 0.00024\,, \tag{71.12}$$

where the errors are from the experimental uncertainties in the branching fractions and the theoretical uncertainties in the radiative correction factors δ_P, respectively. These values are unchanged since the last reviews [1].

71.2.2 *Theoretical decay-constant calculations*

Table 71.1 presents recent published results for the charged pion and kaon decay constants and their ratio from numerical lattice-QCD calculations with three ($N_f = 2+1$) or four flavors ($N_f = 2+1+1$) of dynamical quarks. The uncertainties on both the individual decay constants and their ratio are at the sub-percent level. The SU(3)-breaking ratio f_{K^+}/f_{π^+} can be obtained with especially small errors because statistical errors associated with the Monte Carlo calculations are correlated between the numerator and denominator, as are some systematics. The results in Table 71.1 were obtained using several independent sets of gauge-field configurations, and a variety of lattice fermion actions that are sensitive to different systematic uncertainties.[2][3] Thus, the good agreement between them indicates that the lattice-QCD uncertainties are controlled and the associated error estimates are reliable.[4]

Table 71.1 also shows the three- and four-flavor averages for the pion and kaon decay constants and their ratio from the FLAG 24 review [2] in the lines labeled "FLAG 24 average." There is no four-flavor average for the pion decay constant in Table 71.1 because all of the four-flavor calculations use the quantity $f_{\pi^+} =$ 130.41(20) MeV [22] as an input to fix the absolute lattice scale needed to convert from lattice-spacing units to GeV [9,33,34].

All of the results in Table 71.1 were obtained using isospin-symmetric gauge-field configurations, *i.e.*, the dynamical up and down quarks have the same mass. Fortunately, however, the leading effect of strong-isospin breaking is easily included in lattice-QCD calculations as follows. Because the up-down mass difference $\Delta m_{ud} \equiv (m_u - m_d) \sim -2.5$ MeV [49,51] is much less than typical hadronic scales, the strong-isospin breaking corrections to physical observables can be systematically expanded in the small parameter $\delta m_{ud} \equiv \Delta m_{ud}/\Lambda_{\rm QCD}$. The leading strong-isospin-breaking corrections to pseudoscalar-meson decay constants arise from the light *valence* quarks in the initial- and final-state hadrons. (See, *e.g.,* the discussion in Ref. [52], for a detailed discussion of isospin-breaking effects in pion and kaon observables.) Thus, to include the effect of non-degenerate up- and down-quark masses, most recent lattice-QCD calculations of f_{π^+} and f_{K^+} evaluate the masses of the valence quarks in the pion at the physical m_u and m_d, and the mass of the valence light quark in the kaon at the physical m_u. This procedure yields a correction to the kaon decay constant below 0.5%. Consequently, strong-isospin breaking corrections from the light sea-quark masses — which are suppressed by an additional power of δm_{ud} — can be neglected given present uncertainties.

Some earlier lattice-QCD calculations, however, only provide the decay constants and their ratio in the $SU(2)$ isospin-symmetric limit [38,40,41]. The Flavour Lattice Averaging Group corrects these results for strong-isospin breaking using chiral perturbation theory before including them in the averages. The leading strong-isospin-breaking corrections to the pion and kaon decay constants in χPT can be parametrized as [26,56]

$$f_{\pi^+} = f_\pi\,, \qquad f_{K^+} = f_K\sqrt{1+\delta_{\rm SU(2)}}\,, \tag{71.13}$$

where f_π and f_K denote the values of the decay constants in the isospin-symmetric limit. The pion decay constant does not receive corrections linear in $m_u - m_d$ because of the G-parity symmetry[5] of the pion triplet, so at first order the δm_{ud} expansion, strong-isospin breaking corrections are characterized by a single parameter, $\delta_{\rm SU(2)}$. Next-to-leading order χPT yields numerical

[2]See the PDG mini-review on "Lattice Quantum Chromodynamics" [44–46] for a general review of numerical lattice-QCD calculations. Details on the different methods used in modern lattice-QCD calculations are provided in Appendix A of the FLAG "Review[s] of lattice results concerning low energy particle physics" [47–49].

[3]Note that one must be careful concerning issues of scheme dependence, particularly in the ambiguous separation of QED and QCD effects; see, e.g., Sec. 3 of Ref. [2].

[4]See the review by Kronfeld [50] for a summary of the large body of evidence validating the methods employed in modern lattice-QCD calculations.

[5]This is a combination of charge conjugation, C, and an $e^{i\pi I_2}$ rotation in isospin space that maps the triplet onto itself.

Int. J. Mod. Phys. A 2026.41. Downloaded from www.worldscientific.com
UNIVERSITY OF CALIFORNIA @ BERKELEY on 09/16/26. Re-use and distribution is strictly not permitted, except for Open Access articles.

Table 71.2: Experimental results for $\mathcal{B}(D^+ \to \mu^+\nu[\gamma])$, $\mathcal{B}(D^+ \to \tau^+\nu[\gamma])$, and $|V_{cd}|f_{D^+}$. The first two uncertainties are experimental statistics and systematics, respectively. The third uncertainty on the extracted $|V_{cd}|f_{D^+}$ is from external inputs: masses, lifetimes, and radiative corrections. The uncertainty on the latter item dominates this third value. In the second CLEO line the τ^+ decays to $\mu^+\nu_\mu\bar{\nu}_\tau$.

Experiment	Mode	$\mathcal{B}$	$\lvert V_{cd}\rvert f_{D^+}$ (MeV)
CLEO-c [53]	$\mu^+\nu$	$(3.93 \pm 0.35 \pm 0.09) \times 10^{-4}$	$46.80 \pm 2.08 \pm 0.54 \pm 0.34$
CLEO-c [53]	$\mu^+\nu + \tau^+\nu$	$(3.82 \pm 0.32 \pm 0.09) \times 10^{-4}$	$46.14 \pm 1.93 \pm 0.54 \pm 0.34$
BESIII [54]	$\mu^+\nu$	$(4.034 \pm 0.080 \pm 0.040) \times 10^{-4}$	$47.42 \pm 0.47 \pm 0.24 \pm 0.35$
Our average	Lines 2+3	$(4.020 \pm 0.078 \pm 0.038) \times 10^{-4}$	$47.33 \pm 0.46 \pm 0.25 \pm 0.35$
CLEO-c [53]	$\tau^+\nu$ ($\pi^+\overline{\nu}$)	$< 1.2 \times 10^{-3}$	
BESIII [55]	$\tau^+\nu$ ($\pi^+\overline{\nu}$)	$(0.99 \pm 0.11 \pm 0.05) \times 10^{-3}$	$45.48 \pm 2.53 \pm 1.15 \pm 0.34$
Our average	$\mu^+\nu + \tau^+\nu$		$47.27 \pm 0.45 \pm 0.22 \pm 0.35$

values for $\delta_{\mathrm{SU}(2)}$ of approximately -0.004. Recent direct lattice-QCD calculations of $\delta_{\mathrm{SU}(2)}$ give larger values of around -0.005 to -0.008 [10, 32–34, 52, 57], but further studies are needed. Thus, to be conservative, FLAG includes an uncertainty of 100% on the χPT estimate for $\delta_{\mathrm{SU}(2)}$ when correcting those decay-constant values that are quoted in the isospin-symmetric limit.

The errors on the decay-constant results in Table 71.1 obtained from $(2+1)$-flavor lattice-QCD calculations do not include an estimate of the systematic uncertainty from the omission of charm sea quarks in the calculation. Consequently, when the uncertainty on the $(2+1+1)$-flavor FLAG average is comparable to or better than that on the $(2+1)$-flavor FLAG average, we simply use the four-flavor average as our preferred value. This is not possible, however, for the pion decay constant. To account for this, we first estimate the systematic uncertainty on pseudoscalar-meson decay constants associated with the omission of charm sea quarks. We then add this estimate in quadrature to the quoted error on the (2+1)-flavor FLAG average for f_{π^+} to obtain our preferred value.

The error introduced by omitting charm sea quarks can be roughly estimated by expanding the charm-quark determinant in powers of $1/m_c$ [58]; the resulting leading contribution is of order $\alpha_s \left(\Lambda_{\mathrm{QCD}}/2m_c\right)^2$ [59]. Taking the $\overline{\mathrm{MS}}$ values $\overline{m}_c(\overline{m}_c) = 1.275$ GeV, $\overline{\Lambda}_{\mathrm{QCD}} \sim 340$ MeV from FLAG [47], and $\overline{\alpha}_s(\overline{m}_c) \sim 0.4$, leads to an estimate of about 0.7% for the contribution to the decay constants from charm sea quarks. We can compare this power-counting estimate of charm sea-quark contributions with the observed differences between the (2+1)- and (2+1+1)-flavor lattice-QCD averages for kaon, $D_{(s)}$-meson, and $B_{(s)}$-decay constants in Tables 71.1, 71.4, and 71.6. Looking at Table 71.1, the three- and four-flavor averages for f_{K^+} agree to much better than our simple power-counting estimate. Inspection of Tables 71.4 and 71.6 shows, however, that charm sea-quark effects of this size are still allowed for both $D_{(s)}$-meson and $B_{(s)}$-meson decay constants.

Our final preferred theoretical values for the charged pion and kaon decay constants are

$$f_{\pi^+} = 130.2(1.2)\ \mathrm{MeV}\,, \quad f_{K^+} = 155.7(3)\ \mathrm{MeV}\,, \quad \frac{f_{K^+}}{f_{\pi^+}} = 1.193(2)\,, \tag{71.14}$$

where f_{K^+} and f_{K^+}/f_{π^+} are simply the four-flavor FLAG 2024 averages [2], and f_{π^+} is the three-flavor FLAG 2024 average with the error increased by the estimated 0.7% charm sea-quark contribution.

71.3 Charmed mesons

71.3.1 *Experimental rate measurements*

Measurements have been made of the branching fractions for D^+ and D_s^+ mesons decaying to both $\mu^+\nu$ and $\tau^+\nu$ final states. The CLEO-c and BESIII experiments have made measurements of D^+ decays using e^+e^- collisions at the $\psi(3770)$ resonant energy where D^-D^+ pairs are copiously produced. They fully reconstruct one of the D mesons; for concreteness, we will take this to be the D^-. Counting the number of these events provides the normalization for the branching fraction measurement. The experimental analyses then proceed by identifying a candidate μ^+ and forming the missing-mass squared, $MM^2 = (E_{\mathrm{cm}} - E_{D^-})^2 - \left(\vec{p}_{\mathrm{cm}} - \vec{p}_{D^-} - \vec{p}_{\mu^+}\right)^2$, where E_{cm} and p_{cm} are the center-of-mass energy (which is known) and momentum (which equals zero in e^+e^- collisions). A peak at zero MM^2 implies the existence of a missing neutrino, and hence the $\mu^+\nu$ decay of the D^+. CLEO-c does not explicitly identify the muon, so their data consists of a combination of $\mu^+\nu$ and $\tau^+\nu$, $\tau^+ \to \pi^+\nu$ events. This permits them to do two fits: in one they fit for the individual components, and in the other they fix the ratio of $\tau^+\nu/\mu^+\nu$ events to be that given by the standard-model expectation. Thus, the former measurement should be used for new-physics searches, and the latter for standard-model predictions. Our average uses the fixed-ratio value; this ratio is implied by Eq. 71.1 which is necessary to extract $|V_{cd}|f_{D^+}$.

Table 71.2 shows the available measurements of $D^+ \to \mu^+\nu$, an upper limit on $D^+ \to \tau^+\nu$ from CLEO-c, and the first measurement of this decay from BESIII. To extract the values of $|V_{cd}|f_{D^+}$ via Eq. (71.1), we use [1] the mass $m_{D^+} = 1.86966(5)$ GeV and the lifetime $\tau_{D^+} = 1.033(5)$ ps, and apply radiative corrections as described below. For calculating the average $\mu^+\nu$ number, we use the CLEO-c result from $\mu^+\nu + \tau^+\nu$.

To obtain the purely leptonic rates $\Gamma^{(0)}(D^+ \to \mu^+(\tau^+)\nu)$, we subtract the radiative contributions as in Sec. 71.2.1, but use numerical values for the corrections appropriate for D mesons. First, we reduce both the $\mu^+\nu$ and $\tau^+\nu$ branching fractions in Table 71.2 by 1.8%, which is the universal short-distance electroweak contribution of Sirlin [3] evaluated using the D-meson mass for the factorization scale. We do not adjust the experimental rates by the universal long-distance correction [4]. This is because QED bremsstrahlung contributions have already been subtracted at leading-log order from the measurements in Table 71.2 using Monte-Carlo estimates computed with PHOTOS [11]. The $\mu^+\nu$ rates should also be reduced by the 1% estimate of the structure-dependent contributions from Dobrescu and Kronfeld [16]. This correction accounts for tree-level radiative processes in which the D meson decays into a real photon and an off-shell vector meson, which subsequently decays weakly to a charged lepton and neutrino. It is estimated using Eq. (12) of Burdman *et al.* [6] with the CLEO-c cut on the photon energy from Ref. [72], which is typical of all the measurements. We do not need to apply the structure-dependent correction to the $\mu^+\nu$ branching fractions in Table 71.2, however, because the experiments have already included it in their quoted results. CLEO-c directly subtracts 1%, while BESIII simulates these structure- dependent radiative decays and adds a fit component describing them. Therefore, in summary, we reduce both the $D^+ \to \mu^+\nu$ and the $D^+ \to \tau^+\nu$ rates by 1.8% to account for radiative corrections. It is worth noting, however, that the universal long-distance electromagnetic contribution estimated for point-like charged mesons by Kinoshita [4], which we are not including because IB contributions are already subtracted from the measurements via PHOTOS, would *increase* both rates by about 2.5%.

We now discuss the D_s^+ decay process; there are significant updates since our previous review [1] due to new results from BESIII as well as our averaging strategy. Measurements of D_s^+

Int. J. Mod. Phys. A 2026.41. Downloaded from www.worldscientific.com
by UNIVERSITY OF CALIFORNIA @ BERKELEY on 09/16/26. Re-use and distribution is strictly not permitted, except for Open Access articles.

Table 71.3: Experimental results for $\mathcal{B}(D_s^+ \to \mu^+\nu[\gamma])$, $\mathcal{B}(D_s^+ \to \tau^+\nu[\gamma])$, and $|V_{cs}|f_{D_s^+}$. The uncertainties have the same meaning as in Table 71.2. The single-experiment average BFs are taken from the cited papers, for proper treatment of correlated systematic uncertainties.

Experiment	Mode	$\mathcal{B}(\%)$	$\lvert V_{cs}\rvert f_{D_s^+}$ (MeV)
CLEO-c [60]	$\mu^+\nu$	$0.565 \pm 0.045 \pm 0.017$	$248.2 \pm 9.9 \pm 3.7 \pm 1.8$
BaBar [61]	$\mu^+\nu$	$0.596 \pm 0.038 \pm 0.035$	$254.9 \pm 8.1 \pm 7.5 \pm 1.9$
Belle [62]	$\mu^+\nu$	$0.526 \pm 0.028 \pm 0.021$	$239.5 \pm 6.4 \pm 4.8 \pm 1.8$
BESIII [63]	$\mu^+\nu$	$0.517 \pm 0.075 \pm 0.021$	$237.4 \pm 17.2 \pm 4.9 \pm 1.7$
BESIII [64]	$\mu^+\nu$	$0.5294 \pm 0.0108 \pm 0.0085$	$240.3 \pm 2.5 \pm 1.9 \pm 1.8$
BESIII [65]	$\mu^+\nu$	$0.542 \pm 0.026 \pm 0.017$	$243.1 \pm 5.8 \pm 3.8 \pm 1.8$
BESIII [65]	average	$0.5304 \pm 0.0099 \pm 0.0090^*$	$240.5 \pm 2.2 \pm 2.0 \pm 1.8$
Our average	$\mu^+\nu$	$0.534 \pm 0.009 \pm 0.008$	$241.6 \pm 2.0 \pm 1.7 \pm 1.8$
CLEO-c [60]	$\tau^+\nu$ ($\pi^+\overline{\nu}$)	$6.42 \pm 0.81 \pm 0.18$	$268.0 \pm 16.9 \pm 3.8 \pm 2.0$
CLEO-c [66]	$\tau^+\nu$ ($e^+\nu\overline{\nu}$)	$5.30 \pm 0.47 \pm 0.22$	$243.5 \pm 10.8 \pm 5.1 \pm 1.8$
CLEO-c [67]	$\tau^+\nu$ ($\rho^+\overline{\nu}$)	$5.52 \pm 0.57 \pm 0.21$	$248.5 \pm 12.8 \pm 4.7 \pm 1.8$
CLEO-c [67]	average	$5.58 \pm 0.33 \pm 0.13$	$249.9 \pm 7.4 \pm 2.9 \pm 1.8$
BaBar [61]	$\tau^+\nu$ ($e^+(\mu^+)\nu\overline{\nu}$)	$4.96 \pm 0.37 \pm 0.57$	$235.6 \pm 8.8 \pm 13.5 \pm 1.7$
Belle [62]	$\tau^+\nu$ ($\pi^+\overline{\nu}$)	$6.04 \pm 0.43^{+0.46}_{-0.40}$	$260.0 \pm 9.3^{+9.9}_{-8.6} \pm 1.9$
Belle [62]	$\tau^+\nu$ ($e^+\nu\overline{\nu}$)	$5.37 \pm 0.33^{+0.35}_{-0.31}$	$245.1 \pm 7.5^{+8.0}_{-7.1} \pm 1.8$
Belle [62]	$\tau^+\nu$ ($\mu^+\nu\overline{\nu}$)	$5.86 \pm 0.37^{+0.34}_{-0.59}$	$256.1 \pm 8.1^{+7.4}_{-12.9} \pm 1.9$
Belle [62]	average	$5.70 \pm 0.21^{+0.31}_{-0.30}$	$252.5 \pm 4.7^{+6.9}_{-6.7} \pm 1.9$
BESIII [63]	$\tau^+\nu$ ($\pi^+\overline{\nu}$)	$3.28 \pm 1.83 \pm 0.37$	$192 \pm 53 \pm 11 \pm 1.4$
BESIII [68]	$\tau^+\nu$ ($\pi^+\pi^0\overline{\nu}$)	$5.29 \pm 0.25 \pm 0.20$	$243.3 \pm 5.8 \pm 4.6 \pm 1.8$
BESIII [69]	$\tau^+\nu$ ($e^+\nu\overline{\nu}$)	$5.27 \pm 0.10 \pm 0.12$	$242.8 \pm 2.3 \pm 3.0 \pm 1.8$
BESIII [70]	$\tau^+\nu$ ($\pi^+\overline{\nu}$)	$5.44 \pm 0.17 \pm 0.13$	$246.7 \pm 3.9 \pm 3.0 \pm 1.8$
BESIII [71]	$\tau^+\nu$ ($\mu^+\nu\overline{\nu}$)	$5.37 \pm 0.17 \pm 0.15$	$245.1 \pm 3.9 \pm 3.4 \pm 1.8$
BESIII [65]	$\tau^+\nu$ ($e, \mu, \pi, \pi\pi$)	$5.60 \pm 0.16 \pm 0.20$	$250.3 \pm 3.6 \pm 4.5 \pm 1.8$
BESIII [65]	average	$5.359 \pm 0.067 \pm 0.075$	$244.9 \pm 1.5 \pm 1.7 \pm 1.8$
Our average	$\tau^+\nu$	$5.388 \pm 0.063 \pm 0.068$	$245.5 \pm 1.4 \pm 1.6 \pm 1.8$
Our average	$\mu^+\nu + \tau^+\nu$		$244.0 \pm 1.2 \pm 1.2 \pm 1.8$

*An error in Ref. [65] has been corrected here; BESIII Collab., private communication.

leptonic decay branching fractions by several groups are listed in Table 71.3. We exclude older values obtained by normalizing to D_s^+ decay modes that are not well-defined. Many measurements, for example, used the $\phi\pi^+$ mode. This decay is a subset of the $D_s^+ \to K^+K^-\pi^+$ channel which has interferences from other modes populating the K^+K^- mass region near the ϕ, the most prominent of which is the $f_0(980)$. Thus, the extraction of the effective $\phi\pi^+$ rate is sensitive to the mass resolution of the experiment and the cuts used to define the ϕ mass region [73].[6]

To find D_s decays in the $\mu^+\nu$ signal channels, the experiments rely on fully reconstructing all of the final state particles except for the neutrino and use a missing-mass technique to infer the existence of the neutrino. CLEO and BESIII use $e^+e^- \to D_s D_s^*$ collisions at 4170 MeV, while BaBar and Belle use $e^+e^- \to DKn\pi D_s^*$ collisions at energies near the $\Upsilon(4S)$. CLEO and BESIII do a similar analysis as was done for the D^+ above. BaBar and Belle do a similar MM^2 calculation by using the reconstructed hadrons, the photon from the D_s^{*+} decay and a detected μ^+. To get the normalization they do a MM^2 fit without the μ^+ and use the signal at the D_s^+ mass squared to determine the total D_s^+ yield.

When selecting the $\tau^+ \to \pi^+\bar{\nu}$ and $\tau^+ \to \rho^+\bar{\nu}$ decay modes, CLEO uses both the calculation of the missing-mass and the fact that there should be no extra energy in the event beyond that deposited by the measured tagged D_s^- and the τ^+ decay products. The $\tau^+ \to e^+\nu\bar{\nu}$ mode, however, uses only extra energy. BaBar and Belle also use the extra energy to discriminate signal from background in their $\tau^+\nu$ measurements. BESIII uses $\tau^+ \to \pi^+\overline{\nu}$ decays, where they calculate the MM^2 and discriminate against μ^+ from $D_s^+ \to \mu^+\nu$ decays, and more recently $\tau^+ \to e^+\nu\overline{\nu}$ and $\tau^+ \to \pi^+\pi^0\overline{\nu}$ decays.

When extracting $|V_{cs}|f_{D_s^+}$ via Eq. (71.1), we first apply the -1.8% universal electroweak correction [3] to all of the $\mu^+\nu$ and $\tau^+\nu$ branching fractions in Table 71.3; this is the same as for D^+ mesons. We also decrease the BaBar, Belle, and third BESIII $\mu^+\nu$ branching fractions by the 1% structure-dependent correction [16]. This correction was already included in CLEO and other BESIII results for the $\mu^+\nu$ branching fractions in Table 71.3. We use the masses and lifetimes $m_{D_s^+} = 1.96835(7)$ GeV, $m_{\tau^+} = 1.77686(12)$ GeV, and $\tau_{D_s^+} = 0.5012(22)$ ps [1]. The inferred values for $f_{D_s^+}|V_{cs}|$ are in good agreement for the $\mu^+\nu$ and$\tau^+\nu$ decay modes.

It is clear from the discussion of radiative corrections in this section that they are less well understood theoretically for D^+ and D_s^+ meson decays than for pions and kaons. We therefore assign a 1.4% systematic uncertainty to the purely leptonic decay rates, which is half the size of the applied radiative corrections. This translates to a 0.7% error on the products of the decay constant times CKM matrix element. Putting everything together, the main experimental results pertaining to charmed meson leptonic decays are (see the bottom lines of Tables 71.2 and 71.3):

$$|V_{cd}|f_{D^+} = 47.27(45)(22)(35) = 47.27(0.61)\ \text{MeV}\,, \quad (71.15)$$

$$|V_{cs}|f_{D_s^+} = 244.0(1.2)(1.2)(1.8) = 244.0(2.4)\ \text{MeV}\,, \quad (71.16)$$

where the errors are the statistical and systematic uncertainties from the measured branching fractions, and the external inputs (including the applied radiative corrections), respectively.

71.3.2 *Theoretical decay-constant calculations*

Table 71.4 presents recent theoretical calculations of charmed heavy-light meson decay constants and their ratio in the isospin-symmetric limit $m_u = m_d$. (As in Sec. 71.2.2, we denote the physical D^+-meson decay constant by f_{D^+}, and use f_D for the isospin-symmetric value.) The upper two panels show results from lattice-QCD calculations with three ($N_f = 2+1$) or four flavors ($N_f = 2+1+1$) of dynamical quarks. Although there are fewer available results than for the pion and kaon sector, both f_D and f_{D_s} have been obtained using multiple sets of gauge-field configurations with different lattice fermion actions, providing independent confirmation. For comparison, the bottom panel of Table 71.4 shows QCD-model calculations of the D- and D_s-meson decay constants for which uncertainty estimates are provided. The lattice and non-lattice results agree, but numerical lattice-QCD calculations have now reached significantly greater precision than other approaches.

[6] We do not include two BaBar results [74, 75] for $\mathcal{B}(D_s^+ \to \mu^+\nu)$ and $\mathcal{B}(D_s^+ \to \tau^+\nu)$ that normalize to other D_S^+ decay modes.

Int. J. Mod. Phys. A 2026.41. Downloaded from www.worldscientific.com
UNIVERSITY OF CALIFORNIA @ BERKELEY on 09/16/26. Re-use and distribution is strictly not permitted, except for Open Access articles.

Table 71.4: Recent theoretical determinations of f_D, f_{D_s}, and their ratio in the isospin-symmetric limit. The upper panels show results from lattice-QCD calculations with $(2+1+1)$ and $(2+1)$ dynamical quark flavors, respectively. Statistical and systematic errors are quoted separately. The bottom panel shows estimates from QCD sum rules (QCD SR). These are not used to obtain our preferred decay-constant values. The 2+1+1 averages are dominated by the Fermilab/MILC values.

Reference	Method	N_f	f_D(MeV)	f_{D_s}(MeV)	f_{D_s}/f_D
Fermilab/MILC 17 [32]	LQCD	2+1+1	212.1(0.3)(0.5)	249.9(0.3)(0.3)	1.1782(06)(15)*
ETM 14 [33]	LQCD	2+1+1	207.4(3.7)(0.9)	247.2(3.9)(1.4)	1.192(19)(11)
FLAG 24 average [76]	LQCD	2+1+1	212.0(0.7)	249.9(0.5)	1.1783(16)
ALPHA 23 [77]	211.3(1.9)(0.6)	247.0(1.9)(0.7)	1.177(15)(5)		
χQCD 20A [78]	LQCD	2+1	213(5)	249(7)	1.16(3)
RBC/UKQCD 18A [79]†	LQCD	2+1	–	–	1.1740(51)(68)
RBC/UKQCD 17 [80]	LQCD	2+1	$208.7(2.8)(^{+2.1}_{-1.8})$	$246.4(1.3)(^{+1.3}_{-1.9})$	$1.1667(77)(^{+57}_{-43})$
χQCD 14 [81]	LQCD	2+1	–	254(2)(4)	–
HPQCD 12 [82]	LQCD	2+1	208.3(1.0)(3.3)	–	1.187(4)(12)
Fermilab/MILC 11 [83]	LQCD	2+1	218.9(9.2)(6.6)	260.1(8.9)(6.1)	1.188(14)(21)
HPQCD 10 [84]	LQCD	2+1	–	248.0(1.4)(2.1)	–
FLAG 24 average [76]	LQCD	2+1	210.4(1.5)	247.7(1.2)	1.174(7)
Pullin 21 [85]	QCD SR		190(15)	226(17)	1.19(7)
Wang 15 [86]‡	QCD SR		208(10)	240(10)	1.15(6)
Gelhausen 13 [87]	QCD SR		$201\left(^{+12}_{-13}\right)$	$238\left(^{+13}_{-23}\right)$	$1.15\left(^{+0.04}_{-0.05}\right)$
Narison 12 [88]	QCD SR		204(6)	246(6)	1.21(4)
Lucha 11 [89]	QCD SR		206.2(8.9)	245.3(16.3)	1.193(26)

*Ref. [32] provides values for f_D and f_{D_s} in the isopsin-symmetric limit, but not for their ratio. Here we infer the central value from those of the individual decay constants, and take the statistical and systematic errors to be the same as for the physical ratio f_{D_s}/f_{D^+}.

†Slight difference from preliminary value quoted in 2019 FLAG review.

‡Obtained using $m_c^{\overline{\rm MS}}$; results using $m_c^{\rm pole}$ are also given in the paper.

The lattice-QCD decay-constant results in Table 71.4 were all obtained using isospin-symmetric gauge-field configurations. As discussed in Sec. 71.2.2, however, the leading strong-isospin breaking corrections to heavy-light pseudoscalar-meson decay constants can be accounted for by using the physical down (or up) quark in the D (or B) meson. Strong-isospin breaking corrections to heavy-strange meson decay constants are roughly an order-of-magnitude smaller because there are no light valence quarks involved. Recently, the Fermilab Lattice and MILC Collaborations used this approach to calculate directly the leading strong-isospin breaking corrections to both f_D and f_B, finding [32]

$$\begin{aligned} f_{D^+} - f_D &= +0.58(1)(7)(1)\ \text{MeV}\,, \\ f_{B^+} - f_B &= -0.53(5)(7)(0)\ \text{MeV}\,, \end{aligned} \tag{71.17}$$

where the uncertainties are from statistics, systematics, and the EM scheme, respectively. These results agree with independent estimates of the strong-isospin-breaking corrections to heavy-light meson decay constants from QCD sum rules [90]. Combined with the determinations of f_D and f_B from the same work, Eq. (71.17) implies that the corrections to the SU(3)-flavor breaking ratios are

$$\frac{f_{D_s}}{f_{D^+}} = \frac{f_{D_s}}{f_D}\Big(1 - 0.0027(3)\Big)\,, \qquad \frac{f_{B_s}}{f_{B^+}} = \frac{f_{B_s}}{f_B}\Big(1 + 0.0028(5)\Big)\,. \tag{71.18}$$

These estimated strong-isospin-breaking corrections to f_D and f_{D_s}/f_D above are commensurate with the uncertainties on the (2+1+1)-flavor FLAG averages in Table 71.4. Consequently, it is important to account for isospin-breaking effects before combining the theoretical decay constants with the corresponding experimental decay rates.

To obtain the charged D^+-meson decay constant, we apply the correction in Eq. (71.17) to the (2+1+1)-flavor FLAG 2024 average for the D-meson decay constant in the isospin-symmetric limit. Similarly we use Eq. (71.18) to correct the (2+1+1)-flavor FLAG 2024 average for f_{D_s}/f_D. We take the four-flavor FLAG 2024 average for f_{D_s} directly. Our final preferred theoretical values for the charmed pseudoscalar-meson decay constants are

$$\begin{aligned} f_{D^+} &= 212.6(7)\ \text{MeV}\,, \\ f_{D_s} &= 249.9(5)\ \text{MeV}\,, \\ \frac{f_{D_s}}{f_{D^+}} &= 1.175(2)\,. \end{aligned} \tag{71.19}$$

71.4 Bottom mesons

71.4.1 *Experimental rate measurements*

The Belle and BaBar collaborations have found evidence for $B^- \to \tau^-\overline{\nu}$ decay in $e^+e^- \to B^-B^+$ collisions at the $\Upsilon(4S)$ energy. The analysis relies on reconstructing a hadronic or semileptonic B decay tag, finding a τ candidate in the remaining track and photon candidates, and examining the extra energy in the event which should be close to zero for a real τ^- decay to $e^-\nu\bar{\nu}$ or $\mu^-\nu\bar{\nu}$ opposite a B^+ tag. The results are listed in Table 71.5. These are unchanged since the previous review [1]. But we note a very recent result from Belle II using hadronic tagging [91] which gives $\mathcal{B}(B^+ \to \tau^+\nu_\tau) = (1.24 \pm 0.41 \pm 0.19) \times 10^{-4}$; this is not yet included in our averages pending an evaluation of correlated systematic uncertainties.

Table 71.5: Experimental results for $\mathcal{B}(B^- \to \tau^-\overline{\nu})$ and $|V_{ub}|f_{B^+}$. External systematic uncertainties from masses and lifetimes are negligible compared to current experimental uncertainties.

Experiment	Tag	$\mathcal{B}$ (units of 10^{-4})	$\lvert V_{ub}\rvert f_{B^+}$ (MeV)
Belle [92]	Hadronic	$0.72^{+0.27}_{-0.25} \pm 0.11$	
Belle [93]	Semileptonic	$1.25 \pm 0.28 \pm 0.27$	
Belle [93]	Average	0.91 ± 0.22	0.72 ± 0.09
BaBar [94]	Hadronic	$1.83\,^{+0.53}_{-0.49} \pm 0.24$	
BaBar [95]	Semileptonic	$1.7 \pm 0.8 \pm 0.2$	
BaBar [94]	Average	1.79 ± 0.48	1.01 ± 0.14
Our average		1.06 ± 0.20	0.77 ± 0.07

Because there are large backgrounds under the signals for these measurements, as well as substantial systematic errors, the significances of the individual results are still below the 5σ discovery threshold. Belle quotes 4.6σ for their combined hadronic and semileptonic tags, while BaBar quotes 3.3σ and 2.3σ, for hadronic and semileptonic tags. Greater precision is necessary to determine if any effects beyond the standard model are present.

We do not correct the measured branching ratios in Table 71.5 for radiative corrections because the experimental uncertainties are so large. The relative radiative corrections are expected to be larger, however, for $B \to \mu\nu$ leptonic decays because the corrections are no longer helicity suppressed [8], and may be a significant fraction of the purely leptonic rate. More theoretical work is

Int. J. Mod. Phys. A 2026.41. Downloaded from www.worldscientific.com
by UNIVERSITY OF CALIFORNIA @ BERKELEY on 09/16/26. Re-use and distribution is strictly not permitted, except for Open Access articles.

Table 71.6: Recent theoretical determinations of f_B, f_{B_s}, and their ratio in the isospin-symmetric limit. The upper panels show results from lattice-QCD calculations with $(2+1+1)$ and $(2+1)$ dynamical quark flavors, respectively. When available, statistical and systematic errors are quoted separately. The bottom panel shows estimates from the relativistic potential model (RPM) and QCD sum rules (QCD SR), which are not used to obtain our preferred decay-constant values. The 2+1+1 FLAG 24 averages are dominated by the Fermilab/MILC values.

Reference	Method	N_f	f_B(MeV)	f_{B_s}(MeV)	f_{B_s}/f_B
Frezzotti 24 [96]	LQCD	2+1+1	–	224.5(5.0)	–
Fermilab/MILC 17 [32]	LQCD	2+1+1	189.9(1.4)	230.7(1.2)	1.2146(49)
HPQCD 17 [97]*	LQCD	2+1+1	190(4)	229(5)	1.206(5)
ETM 16 [98]	LQCD	2+1+1	193(6)	229(5)	1.184(25)
HPQCD 13 [99]	LQCD	2+1+1	186(4)	224(5)	1.205(7)
FLAG 24 average [76]	LQCD	2+1+1	190.0(1.3)	230.3(1.3)	1.209(5)
Aoki 14 [100]†	LQCD	2+1	218.8(6.5)(30.8)	263.5(4.8)(36.7)	1.193(20)(44)
RBC/UKQCD 14 [101]‡	LQCD	2+1	195.6(6.4)(13.3)	235.4(5.2)(11.1)	1.223(14)(70)
HPQCD 12 [102]	LQCD	2+1	191(1)(8)	228(3)(10)	1.188(12)(13)
HPQCD 12 [102]	LQCD	2+1	189(3)(3)*	–	–
HPQCD 11 [103]	LQCD	2+1	–	225(3)(3)	–
Fermilab/MILC 11 [83]	LQCD	2+1	196.9(5.5)(7.0)	242.0(5.1)(8.0)	1.229(13)(23)
FLAG 24 average [76]	LQCD	2+1	192.0(4.3)	228.4(3.7)	1.201(16)
Pullin 21 [85]	QCD SR		192^{+20}_{-19}	225^{+21}_{-20}	1.17(7)
Sun 16 [104]§	RPM		219(15)	266(19)	1.21(9)
Wang 15 [86]§	QCD SR		194(15)	231(16)	1.19(10)
Baker 13 [105]	QCD SR		186(14)	222 (12)	1.19(4)
Lucha 13 [106]	QCD SR		192.0(14.6)	228.0(19.8)	1.184(24)
Gelhausen 13 [87]	QCD SR		$207\left(^{+17}_{-9}\right)$	$242\left(^{+17}_{-12}\right)$	$1.17\left(^{+3}_{-4}\right)$
Narison 12 [88]	QCD SR		206(7)	234(5)	1.14(3)

*Average of new HPQCD 17 and previous HPQCD 13 results allowing for correlations between the two sets of results.
†Obtained with static b quarks (*i.e.*, $m_b \to \infty$).
‡Ref. [101] does not provide results in the isospin-symmetric limit, so we show f_{B^+} and f_{B_s}/f_{B^+} for this work.
§Obtained using $m_b^{\overline{\rm MS}}$; results using $m_b^{\rm pole}$ are also given in the paper.

needed to understand radiative corrections to leptonic B decays in anticipation of future measurements with greater precision, and of new decay channels.

71.4.2 *Theoretical decay-constant calculations*

Table 71.6 presents recent theoretical calculations of bottom heavy-light meson decay constants and their ratio in the isospin-symmetric limit $m_u = m_d$. The upper two panels show results from lattice-QCD calculations with three ($N_f = 2+1$) or four flavors ($N_f = 2+1+1$) of dynamical quarks. For all decay constants, calculations using different gauge-field configurations, light-quark actions, and b-quark actions provide independent confirmation. For comparison, the bottom panel of Table 71.6 shows QCD-model calculations of the B- and B_s-meson decay constants for which uncertainty estimates are provided. These are consistent with the lattice values, but with much larger uncertainties.

The lattice-QCD decay-constant results in Table 71.6 were all obtained using isospin-symmetric gauge-field configurations. Some calculations, however, account for the leading effect of strong-isospin-breaking by using the correct value for the valence light-quark mass in the B meson (m_u for f_{B^+} and m_d for f_{B^0}). Early estimates of the strong-isospin-breaking correction obtained $f_{B^+} - f_B \sim -2$ MeV [99, 101], which would be significant given the present lattice-QCD uncertainties. It turns out, however, that these calculations inadvertently introduced a spurious sea-quark contribution, and therefore overestimated the size of the effect. A more recent calculation by the Fermilab/MILC Collaboration finds very little evidence for isospin violation ($f_{B^+} - f_B \sim -0.5$ MeV) [32], which is more than two times smaller than the total uncertainties on present lattice-QCD calculations. For this reason, we quote isospin averages in the current review. Our preferred theoretical values for the bottom pseudoscalar-meson decay constants are simply the $N_f = 2+1+1$ FLAG 2024 averages [2], after inclusion of the isospin-breaking corrections from Eq. (71.17) and Eq. (71.18):

$$\begin{aligned} f_{B^+} &= 189.5(1.3)\ \text{MeV}\,, \\ f_{B_s} &= 230.3(1.3)\ \text{MeV}\,, \\ \frac{f_{B_s}}{f_{B^+}} &= 1.212(5)\,. \end{aligned} \tag{71.20}$$

Because the uncertainties on the three-flavor results in Table 71.6 are substantially larger than those on the four-flavor results, including them in the average leaves the central values almost unchanged, and decreases the errors only slightly. Note that Ref. [96] is not included in the f_{B_s} average since it was published after the FLAG 24 deadline; including it would decrease f_{B_s} by about 0.3 MeV with little effect on the uncertainty.

71.5 Phenomenological implications

71.5.1 $|V_{ud}|$, $|V_{us}|$, *and status of first-row unitarity*

Using the average values for $f_{\pi^+}|V_{ud}|$, $f_{K^+}|V_{us}|$, and their ratio from Eqs. (71.10)–(71.12) and for f_{π^+}, f_{K^+}, and their ratio from Eq. (71.14), we obtain the following determinations of the CKM matrix elements $|V_{ud}|$, $|V_{us}|$, and their ratio from leptonic decays within the standard model:

$$\begin{aligned} &|V_{ud}| = 0.9763(1)(90)(10)\,, \quad |V_{us}| = 0.2253(3)(4)(2), \\ &\frac{|V_{us}|}{|V_{ud}|} = 0.2313(3)(4)(2)\,, \end{aligned} \tag{71.21}$$

where the errors are from the experimental branching fraction(s), the pseudoscalar decay constant(s), and radiative corrections, respectively. These results enable a test of the unitarity of the first row of the CKM matrix from leptonic decays alone (the contribution from $|V_{ub}|$ is negligible). Using the values of $|V_{ud}|$ and $|V_{us}|$ from Eq. (71.21), we find

$$|V_{ud}|^2 + |V_{us}|^2 + |V_{ub}|^2 - 1 = 0.004(18)\,, \tag{71.22}$$

which is consistent with three-generation unitarity at the few-percent level.

Int. J. Mod. Phys. A 2026.41. Downloaded from www.worldscientific.com
UNIVERSITY OF CALIFORNIA @ BERKELEY on 09/16/26. Re-use and distribution is strictly not permitted, except for Open Access articles.

The determinations of $|V_{ud}|$ and $|V_{us}|$ from leptonic decays in Eq. (71.21) can be compared to those obtained from other processes. The result above for $|V_{ud}|$ agrees with the determination from super-allowed β-decay (a previous value of $|V_{ud}| = 0.97420(21)$ [107] has been updated to $|V_{ud}| = 0.97373(31)$ [108]) but has a considerably larger error, primarily due to the uncertainty in the theoretical determination of f_{π^+}.

The CKM element $|V_{us}|$ can be determined from semileptonic $K^+ \to \pi^0\ell^+\nu$ decay. Here experimental measurements provide a value for the product $f_+^{K\pi}(0)|V_{us}|$, where $f_+^{K\pi}(0)$ is the form factor at zero four-momentum transfer between the initial state kaon and the final state pion. We quote a recent analysis by Seng *et al.* [109] which finds $|V_{us}|f_+^{K\pi}(0) = 0.21635(39)(3)$, with the first uncertainty from experiment and the second reflecting uncertainty in higher order corrections. This average involves detailed considerations of radiative corrections; these are taken from chiral perturbation theory with lattice-QCD inputs for some needed low-energy constants. Choosing the FLAG 2024 2+1+1-flavor average for $f_+(0)^{K\pi} = 0.9698(17)$ [2] based on the calculations of ETM [110] and Fermilab/MILC [111] gives $|V_{us}| = 0.22309(39)_{\rm exp}(39)_{\rm LQCD}(3)_{\rm HO}$ from semileptonic decay. The determinations of $|V_{us}|$ from leptonic and semileptonic kaon decays are both quite precise, with comparable errors, but the central values differ by 2.8σ.

Finally, the combination of the ratio $|V_{us}|/|V_{ud}|$ from leptonic decays [Eq. (71.21)] with $|V_{ud}|$ from β decay implies an alternative determination of $|V_{us}| = 0.2252(5)$ which agrees with the value from leptonic kaon decay, but again disagrees with the semileptonic-decay result at the 2.8σ level.

Given the roughly 3σ tension between $|V_{us}|$ from leptonic and semileptonic kaon decays, it is important to scrutinize the uncertainties on the theoretical and experimental inputs to $|V_{us}|$ and other elements of the first row of the CKM matrix. Seng *et al.* have introduced a new approach for calculating radiative corrections to neutron and nuclear beta decays using dispersion relations [112–115]. These calculations imply a value of $|V_{ud}| = 0.97395(23)$ [113], consistent with the updated analysis of Ref. [108]. An independent calculation of the radiative corrections by Czarnecki and Marciano using QCD sum rules yields similar results [116]. Using this value of $|V_{ud}|$ with the determination of $|V_{us}|$ from leptonic kaon decays in Eq. (71.21), we obtain $|V_{ud}|^2 + |V_{us}|^2 + |V_{ub}|^2 - 1 = -0.0007(5)$, again consistent with first-row unitarity.

Last, we combine the experimental measurement of $f_{\pi^+}|V_{ud}|$ in Eq. (71.10) with $|V_{ud}|$ from super-allowed β-decay [108] to infer an "experimental" value for the pion decay constant:

$$f_{\pi^-}^{\text{"exp"}} = 130.56(2)(4)(13)\ \text{MeV}\,, \tag{71.23}$$

where the uncertainties are from the errors on Γ, $|V_{ud}|$, and higher-order corrections, respectively. Many recent (2+1+1)-flavor lattice-QCD calculations use this quantity to set the overall physical scale in their simulations, *e.g.*, Refs. [9, 32–34]. Conversely, comparing $f_{\pi^-}^{\text{"exp"}}$ with the FLAG 2024 (2+1)-flavor average [2] $f_{\pi^+} = 130.2(8)$ MeV, which only includes lattice-QCD results that employ other observables to set the scale [36–41], provides a test of lattice-QCD methods. The values are in good agreement within present uncertainties. We do not quote an "experimental" value for the kaon decay constant because the value of $|V_{us}|$ is less clear given the approximately 3σ tension between the values of $|V_{us}|$ obtained from leptonic and semileptonic kaon decays.

71.5.2 $|V_{cd}|$, $|V_{cs}|$, *and status of second-row unitarity*

Using the average values for $|V_{cd}|f_{D^+}$ and $|V_{cs}|f_{D_s^+}$ from Eqs. (71.15) and (71.16), and for f_{D^+} and $f_{D_s^+}$ from Eq. (71.19), we obtain the following determinations of the CKM matrix elements $|V_{cd}|$ and $|V_{cs}|$ from leptonic decays within the standard model:

$$|V_{cd}| = 0.2223(24)(7)(17) \quad \text{and} \quad |V_{cs}| = 0.9764(66)(20)(72)\,, \tag{71.24}$$

where the errors are from the measured branching fractions, decay constants, and external inputs (radiative corrections and masses and lifetimes), respectively. These results enable a test of the unitarity of the second row of the CKM matrix. Taking $|V_{cb}| = 41.8(0.8)) \times 10^{-3}$ [1], we obtain

$$|V_{cd}|^2 + |V_{cs}|^2 + |V_{cb}|^2 - 1 = +0.005(20)\,, \tag{71.25}$$

in agreement with three-generation unitarity. Note that correlations among the external uncertainties in the $f|V|$ values have a negligible effect.

The uncertainty on $|V_{cd}|$ in Eq. (71.24) is limited by the measurement error on the $D^+ \to \mu^+\nu$ decay rate. For $|V_{cs}|$, however, the experimental and radiative-correction errors are commensurate. The value of $|V_{cs}|$ from leptonic D_s decays decreased substantially from the value of 1.007(17) in an earlier version of this review [27, 117], and is now below unity as expected in the three-generation CKM framework. This change is due to our more consistent treatment of the radiative corrections, which lower the purely leptonic decay rates for $D_s^+ \to \mu^+\nu$ and $D_s^+ \to \tau^+\nu$. We emphasize, however, that we have taken a generous uncertainty on these estimates, and that more theoretical work is needed to really pin down the sizes of the radiative corrections to $D_{(s)}$-meson leptonic decays.

The CKM matrix elements $|V_{cd}|$ and $|V_{cs}|$ can also be obtained from semileptonic $D^+ \to \pi^0\ell^+\nu$ and $D_s^+ \to K^0\ell^+\nu$ decays, respectively. Here experimental measurements determine the product of the form factor times the CKM element, and theory provides the value for the form factor at zero four-momentum transfer between the initial $D_{(s)}$ meson and the final pion or kaon.

The latest experimental averages (2023, with data as of 2021) from the Heavy Flavor Averaging Group (HFLAV) are $f_+^{D\pi}(0)|V_{cd}| = 0.1426(18)$ and $f_+^{DK}(0)|V_{cs}| = 0.7180(33)$ [118]. The FLAG 2024 $2+1+1$ lattice-QCD averages for the form-factors at $q^2 = 0$ are $f_+^{D\pi}(0) = 0.6295(50)$ and $f_+^{DK}(0) = 0.7430(27)$. The $D\pi$ number is an average of FNAL/MILC Collaborations [119] and ETM Collaboration [120] results, while the DK number includes these two plus the HPQCD Collaboration [121]. The older ETM results have lower precision than the others. Combining of the HFLAV $f(0)|V|$ products and the FLAG average for $f(0)$ gives results for $|V_{cd}|$ and $|V_{cs}|$ consistent with the leptonic decays in Eq. (71.24):

$$|V_{cd}| = 0.2265(29)(18) \quad \text{and} \quad |V_{cs}| = 0.9664(44)(35)\,, \tag{71.26}$$

However, as with the leptonic case, one must exercise some care with corrections; this is beyond the scope of the present review. We do note that Ref. [119] presents a detailed discussion of CKM element extractions using their lattice-QCD results, including consideration of QED, electroweak and isospin corrections; a comparison of leptonic and semileptonic results and unitarity tests is also included.

We can combine the experimental measurements of $f_{D^+}|V_{cd}|$ and $f_{D_s^+}|V_{cs}|$ from Tables 71.2 and 71.3 with $|V_{cd}| = 0.22487(68)$ and $|V_{cs}| = 0.97349(16)$ from the PDG 2024 global unitarity-triangle analysis [1] to infer "experimental" values for the decay constants within the standard model. We take the CKM elements from the global fit because they are based on many input quantities, thereby reducing the sensitivity to any one outlying measurement or calculation. We obtain for the decay constants

$$\begin{aligned} f_{D^+}^{\text{"exp"}} &= 210.2(2.2)(0.6)(1.6)\ \text{MeV}\,, \\ f_{D_s^+}^{\text{"exp"}} &= 250.6(1.7)(0.04)(1.8)\ \text{MeV}\,, \\ (f_{D_s^+}/f_{D^+})^{\text{"exp"}} &= 1.191(16)(4)(9)\,. \end{aligned} \tag{71.27}$$

where the uncertainties are from the errors on $f|V|$, CKM matrix elements, and external inputs (radiative corrections and masses and lifetimes), respectively. Here, the 0.7% radiative correction uncertainty is taken as the the same size on the ratio as on the first two results (as opposed to a quadrature sum), due to presumed partial cancellation. Recent improvements in experimental precision make an improved understanding of the degree of cancellation desirable. The "experimental" values f_{D^+} $(f_{D_s^+}/f_{D^+})$ are consistent within 1σ with the (2+1+1)-flavor lattice-QCD averages in Eq. (71.19). The CKM matrix element $|V_{cd}|$ is approximately

Int. J. Mod. Phys. A 2026.41. Downloaded from www.worldscientific.com
by UNIVERSITY OF CALIFORNIA @ BERKELEY on 09/16/26. Re-use and distribution is strictly not permitted, except for Open Access articles.

equal to $|V_{us}|$, as first shown by Wolfenstein [122,123]. Thus, resolving the inconsistencies between determinations of $|V_{us}|$ from leptonic and semileptonic decays discussed in Sec. 71.5.1 may benefit from the constraints observed here.

Last, we can test lepton-flavor universality in charm meson decays by checking the following relationship derived from Eq. (71.1):

$$\frac{\Gamma(D_s^+ \to \tau^+\nu)}{\Gamma(D_s^+ \to \mu^+\nu)} = \frac{m_\tau^2\left(1 - m_\tau^2/M_{D_s}^2\right)^2}{m_\mu^2\left(1 - m_\mu^2/M_{D_s}^2\right)^2} = 9.75\,, \qquad (71.28)$$

where the uncertainties from the masses are negligible to the number of digits quoted. The measured ratio of $\tau^+\nu$ to $\mu^+\nu$ rates is 10.06 ± 0.28 which, while 1.1σ high, is consistent with the standard-model expectation.

71.5.3 $|V_{ub}|$ *and other applications*

Using the average value for $|V_{ub}|f_{B^+}$ from Table 71.5, and for f_{B^+} from Eq. (71.20), we obtain the following determination of the CKM matrix element $|V_{ub}|$ from leptonic decays within the standard model:

$$|V_{ub}| = (4.06 \pm 0.37 \pm 0.003) \times 10^{-3}\,, \qquad (71.29)$$

where the errors are from experiment and theory, respectively. One should bear in mind when interpreting Eq. (71.29) that none of the experimental measurements of the branching fractions that enter the average for $|V_{ub}|f_{B^+}$ have individually reached the 5σ discovery level (see Sec. 71.4.1). Further, decays involving the third generation of quarks and leptons may be particularly sensitive to new physics associated with electroweak symmetry breaking due to their larger masses [12,14], so Eq. (71.29) is more likely to be influenced by new physics than the determinations of the elements of the first and second rows of the CKM matrix in the previous sections.

The CKM element $|V_{ub}|$ can also be obtained from semileptonic B-meson decays. A long-standing 2-3σ tension between the determinations of $|V_{ub}|$ from exclusive $B \to \pi\ell\nu$ decay and from inclusive $B \to X_u\ell\nu$ decay has diminished somewhat; here, X_u denotes all hadronic states populated by the $b \to u$ weak transition [22, 124–128]. The semileptonic review in the last PDG compilation [129] gives $|V_{ub}| = (3.70 \pm 0.10 \pm 0.12) \times 10^{-3}$ (exclusive) and $|V_{ub}| = (4.13 \pm 0.12\,^{+0.13}_{-0.14} \pm 0.18) \times 10^{-3}$ (inclusive). These agree now at the 1.4σ level; the difference is still only 1.8σ when dropping the third model uncertainty added to the inclusive value by the authors of Ref. [129]. The value of $|V_{ub}|$ from leptonic $B \to \tau\nu$ decay in Eq. (71.29) lies between these inclusive and exclusive determinations, and is compatible (within large uncertainties) with both.

Given the large uncertainties on the experimental measurements of $\mathcal{B}(B^- \to \tau^-\overline{\nu})$, and the evolving values of $|V_{ub}|$ obtained from inclusive and exclusive semileptonic B decays, we do not present an "experimental" value of the decay constant f_{B^+}.

71.6 Concluding remarks

The increasing precision of measurements of leptonic decays of charged pseudoscalar mesons has begun to require control over radiative corrections at a level superior to that presented here. Improvements will be called for both in theory and in experiment (for example, by BESIII and Belle II).

Unitarity of the CKM matrix is in reasonable shape. However, there is a lingering almost 3σ tension between the values of V_{us} determined by semileptonic and leptonic kaon decays. It will be interesting to follow experimental and theoretical developments on this quantity.

Acknowledgements

We thank V. Cirigliano, C. Davies, M. Di Carlo, S. Gottlieb, S. Hashimoto, A. Kronfeld, H.-L. Ma, W. Marciano, J. L. Rosner, and S. Stone for useful discussions on this and previous versions of the review.

References

[1] S. Navas *et al.* (Particle Data Group), Phys. Rev. D **110**, 3, 030001 (2024).

[2] Y. Aoki *et al.* (Flavour Lattice Averaging Group (FLAG)) (2024), [arXiv:2411.04268].

[3] A. Sirlin, Nucl. Phys. **B196**, 83 (1982).

[4] T. Kinoshita, Phys. Rev. Lett. **2**, 477 (1959).

[5] M. Knecht *et al.*, Eur. Phys. J. **C12**, 469 (2000), [hep-ph/9909284].

[6] G. Burdman, J. T. Goldman and D. Wyler, Phys. Rev. **D51**, 111 (1995), [hep-ph/9405425].

[7] V. Cirigliano and I. Rosell, JHEP **10**, 005 (2007), [arXiv:0707.4464].

[8] D. Becirevic, B. Haas and E. Kou, Phys. Lett. **B681**, 257 (2009), [arXiv:0907.1845].

[9] A. Bazavov *et al.* (Fermilab Lattice and MILC), Phys. Rev. **D90**, 074509 (2014), [arXiv:1407.3772].

[10] M. Di Carlo *et al.*, Phys. Rev. **D100**, 034514 (2019), [arXiv:1904.08731].

[11] E. Barberio and Z. Was, Comput. Phys. Commun. **79**, 291 (1994).

[12] W.-S. Hou, Phys. Rev. **D48**, 2342 (1993).

[13] A. G. Akeroyd and S. Recksiegel, Phys. Lett. **B554**, 38 (2003), [hep-ph/0210376].

[14] A. G. Akeroyd and S. Recksiegel, J. Phys. **G29**, 2311 (2003), [hep-ph/0306037].

[15] A. G. Akeroyd, Prog. Theor. Phys. **111**, 295 (2004), [hep-ph/0308260].

[16] B. A. Dobrescu and A. S. Kronfeld, Phys. Rev. Lett. **100**, 241802 (2008), [arXiv:0803.0512].

[17] J. L. Hewett, in "Heavy flavor physics. Proceedings, LISHEP 95, LAFEX International School on High-Energy Physics, session C, cbt Workshop, Rio de Janeiro, Brazil, February 21-23, 1995," 171–187 (1995), [hep-ph/9505246], URL `https://www.slac.stanford.edu/pubs/slacpubs/6750/slac-pub-6821.pdf`.

[18] A. Crivellin, Phys. Rev. **D81**, 031301 (2010), [arXiv:0907.2461].

[19] F. U. Bernlochner, Z. Ligeti and S. Turczyk, Phys. Rev. **D90**, 094003 (2014), [arXiv:1408.2516].

[20] W. J. Marciano, Phys. Rev. Lett. **93**, 231803 (2004), [hep-ph/0402299].

[21] V. Cirigliano *et al.*, Rev. Mod. Phys. **84**, 399 (2012), [arXiv:1107.6001].

[22] K. A. Olive *et al.* (Particle Data Group), Chin. Phys. **C38**, 090001 (2014).

[23] B. Ananthanarayan and B. Moussallam, JHEP **06**, 047 (2004), [hep-ph/0405206].

[24] S. Descotes-Genon and B. Moussallam, Eur. Phys. J. **C42**, 403 (2005), [hep-ph/0505077].

[25] W. J. Marciano and A. Sirlin, Phys. Rev. Lett. **71**, 3629 (1993).

[26] V. Cirigliano and H. Neufeld, Phys. Lett. **B700**, 7 (2011), [arXiv:1102.0563].

[27] J. L. Rosner, S. Stone and R. S. Van de Water (2015), review prepared for PDG 2015 edition, [arXiv:1509.02220].

[28] J. Gasser, A. Rusetsky and I. Scimemi, Eur. Phys. J. **C32**, 97 (2003), [hep-ph/0305260].

[29] P. Boyle *et al.*, JHEP **02**, 242 (2023), [arXiv:2211.12865].

[30] C. Alexandrou *et al.* (Extended Twisted Mass), Phys. Rev. D **104**, 7, 074520 (2021), [arXiv:2104.06747].

[31] N. Miller *et al.*, Phys. Rev. **D102**, 3, 034507 (2020), [arXiv:2005.04795].

[32] A. Bazavov *et al.*, Phys. Rev. **D98**, 7, 074512 (2018), [arXiv:1712.09262].

[33] N. Carrasco *et al.* (ETM), Phys. Rev. **D91**, 054507 (2015), [arXiv:1411.7908].

Int. J. Mod. Phys. A 2026.41. Downloaded from www.worldscientific.com
UNIVERSITY OF CALIFORNIA @ BERKELEY on 09/16/26. Re-use and distribution is strictly not permitted, except for Open Access articles.

[34] R. Dowdall *et al.* (HPQCD), Phys. Rev. **D88**, 074504 (2013), [arXiv:1303.1670].

[35] Z.-C. Hu *et al.* (CLQCD), Phys. Rev. D **109**, 5, 054507 (2024), [arXiv:2310.00814].

[36] V. G. Bornyakov *et al.* (QCDSF-UKQCD), Phys. Lett. **B767**, 366 (2017), [arXiv:1612.04798].

[37] S. Durr *et al.*, Phys. Rev. **D95**, 5, 054513 (2017), [arXiv:1601.05998].

[38] T. Blum *et al.* (RBC, UKQCD), Phys. Rev. **D93**, 074505 (2016), [arXiv:1411.7017].

[39] A. Bazavov *et al.* (MILC), PoS **LATTICE2010**, 074 (2010), [arXiv:1012.0868].

[40] S. Durr *et al.* (BMW), Phys. Rev. **D81**, 054507 (2010), [arXiv:1001.4692].

[41] E. Follana *et al.* (HPQCD, UKQCD), Phys. Rev. Lett. **100**, 062002 (2008), [arXiv:0706.1726].

[42] M. Moulson, in "8th International Workshop on the CKM Unitarity Triangle (CKM2014) Vienna, Austria, September 8-12, 2014," (2014), [arXiv:1411.5252].

[43] M. Antonelli *et al.* (FlaviaNet Working Group on Kaon Decays), Eur. Phys. J. **C69**, 399 (2010), [arXiv:1005.2323].

[44] S. Hashimoto, J. Laiho and S. R. Sharpe, Lattice Quantum Chromodynamics (2017), review prepared for PDG 2018 edition, URL `http://pdg.lbl.gov/2019/reviews/rpp2018-rev-lattice-qcd.pdf`.

[45] S. Hashimoto, J. Laiho and S. R. Sharpe, Lattice Quantum Chromodynamics (2020), review prepared for PDG 2020 edition, URL `http://pdg.lbl.gov/2020/reviews/rpp2020-rev-lattice-qcd.pdf`.

[46] S. Hashimoto, J. Laiho and S. R. Sharpe, Lattice Quantum Chromodynamics (2021), review prepared for PDG 2022 edition, URL `http://pdg.lbl.gov/2022/reviews/rpp2022-rev-lattice-qcd.pdf`.

[47] S. Aoki *et al.* (Flavour Lattice Averaging Group), Eur. Phys. J. **C74**, 2890 (2014), [arXiv:1310.8555].

[48] S. Aoki *et al.*, Eur. Phys. J. **C77**, 2, 112 (2017), [arXiv:1607.00299].

[49] S. Aoki *et al.* (Flavour Lattice Averaging Group), Eur. Phys. J. C **80**, 2, 113 (2020), [arXiv:1902.08191].

[50] A. S. Kronfeld, Ann. Rev. Nucl. Part. Sci. **62**, 265 (2012), [arXiv:1203.1204].

[51] A. V. Manohar, C. T. Sachrajda and R. M. Barnett, Quark Masses (2018), review prepared for PDG 2018 update, URL `http://pdg.lbl.gov/2019/reviews/rpp2018-rev-quark-masses.pdf`.

[52] G. M. de Divitiis *et al.*, JHEP **04**, 124 (2012), [arXiv:1110.6294].

[53] B. I. Eisenstein *et al.* (CLEO), Phys. Rev. **D78**, 052003 (2008), [arXiv:0806.2112].

[54] M. Ablikim *et al.* (BESIII), Phys. Rev. Lett. **135**, 061801 (2025), [arXiv:2410.07626].

[55] M. Ablikim *et al.* (BESIII), JHEP **01**, 089 (2025), [arXiv:2410.20063].

[56] J. Gasser and H. Leutwyler, Nucl. Phys. **B250**, 465 (1985).

[57] G. M. de Divitiis *et al.* (RM123), Phys. Rev. **D87**, 11, 114505 (2013), [arXiv:1303.4896].

[58] M. Nobes (2005), [hep-lat/0501009].

[59] A. Bazavov *et al.* (Fermilab Lattice, MILC), Phys. Rev. **D93**, 11, 113016 (2016), [arXiv:1602.03560].

[60] J. P. Alexander *et al.* (CLEO), Phys. Rev. **D79**, 052001 (2009), [arXiv:0901.1216].

[61] P. del Amo Sanchez *et al.* (BaBar), Phys. Rev. **D82**, 091103 (2010), [Erratum: Phys. Rev. **D91**, 019901 (2015)], [arXiv:1008.4080].

[62] A. Zupanc *et al.* (Belle), JHEP **1309**, 139 (2013), [arXiv:1307.6240].

[63] M. Ablikim *et al.* (BESIII), Phys. Rev. **D94**, 7, 072004 (2016), [arXiv:1608.06732].

[64] M. Ablikim *et al.* (BESIII), Phys. Rev. D **108**, 11, 112001 (2023), [arXiv:2307.14585].

[65] M. Ablikim *et al.* (BESIII), Phys. Rev. D **110**, 5, 052002 (2024), [arXiv:2407.11727].

[66] P. U. E. Onyisi *et al.* (CLEO), Phys. Rev. **D79**, 052002 (2009), [arXiv:0901.1147].

[67] P. Naik *et al.* (CLEO), Phys. Rev. **D80**, 112004 (2009), [arXiv:0910.3602].

[68] M. Ablikim *et al.* (BESIII), Phys. Rev. **D104**, 3, 032001 (2021), [arXiv:2105.07178].

[69] M. Ablikim *et al.* (BESIII), Phys. Rev. Lett. **127**, 17, 171801 (2021), [arXiv:2106.02218].

[70] M. Ablikim *et al.* (BESIII), Phys. Rev. D **108**, 9, 092014 (2023), [arXiv:2303.12600].

[71] M. Ablikim *et al.* (BESIII), JHEP **09**, 124 (2023), [arXiv:2303.12468].

[72] T. K. Pedlar *et al.* (CLEO), Phys. Rev. **D76**, 072002 (2007), [arXiv:0704.0437].

[73] J. P. Alexander *et al.* (CLEO), Phys. Rev. Lett. **100**, 161804 (2008), [arXiv:0801.0680].

[74] B. Aubert *et al.* (BaBar), Phys. Rev. Lett. **98**, 141801 (2007), [hep-ex/0607094].

[75] J. P. Lees *et al.* (BaBar) (2010), [arXiv:1003.3063].

[76] Y. Aoki *et al.* (Flavour Lattice Averaging Group (FLAG)) 2023 online web update.

[77] A. Bussone *et al.* (Alpha), Eur. Phys. J. C **84**, 5, 506 (2024), [arXiv:2309.14154].

[78] Y. Chen *et al.* (χQCD), Chin. Phys. C **45**, 2, 023109 (2021), [arXiv:2008.05208].

[79] P. A. Boyle *et al.* (RBC/UKQCD) (2018), [arXiv:1812.08791].

[80] P. A. Boyle *et al.*, JHEP **12**, 008 (2017), [arXiv:1701.02644].

[81] Y.-B. Yang *et al.* (χQCD), Phys. Rev. **D92**, 034517 (2015), [arXiv:1410.3343].

[82] H. Na *et al.* (HPQCD), Phys. Rev. **D86**, 054510 (2012), [arXiv:1206.4936].

[83] A. Bazavov *et al.* (Fermilab Lattice and MILC), Phys. Rev. **D85**, 114506 (2012), [arXiv:1112.3051].

[84] C. T. H. Davies *et al.* (HPQCD), Phys. Rev. **D82**, 114504 (2010), [arXiv:1008.4018].

[85] B. Pullin and R. Zwicky (2021), [arXiv:2106.13617].

[86] Z.-G. Wang, Eur. Phys. J. **C75**, 427 (2015), [arXiv:1506.01993].

[87] P. Gelhausen *et al.*, Phys. Rev. **D88**, 014015 (2013), [arXiv:1305.5432].

[88] S. Narison, Phys. Lett. **B718**, 1321 (2013), [arXiv:1209.2023].

[89] W. Lucha, D. Melikhov and S. Simula, Phys. Lett. **B701**, 82 (2011), [arXiv:1101.5986].

[90] W. Lucha, D. Melikhov and S. Simula, Eur. Phys. J. **C78**, 2, 168 (2018), [Erratum: Eur. Phys. J. **C78**, 936 (2018)], [arXiv:1702.07537].

[91] I. Adachi *et al.* (Belle-II), Phys. Rev. D **112**, 7, 072002 (2025), [arXiv:2502.04885].

[92] I. Adachi *et al.* (Belle), Phys. Rev. Lett. **110**, 131801 (2013), [arXiv:1208.4678].

[93] B. Kronenbitter *et al.* (Belle), Phys. Rev. **D92**, 051102 (2015), [arXiv:1503.05613].

[94] J. P. Lees *et al.* (BaBar), Phys. Rev. **D88**, 031102 (2013), [arXiv:1207.0698].

Int. J. Mod. Phys. A 2026.41. Downloaded from www.worldscientific.com
by UNIVERSITY OF CALIFORNIA @ BERKELEY on 09/16/26. Re-use and distribution is strictly not permitted, except for Open Access articles.

[95] B. Aubert *et al.* (BaBar), Phys. Rev. **D81**, 051101 (2010), [arXiv:0912.2453].

[96] R. Frezzotti *et al.*, Phys. Rev. D **109**, 11, 114506 (2024), [arXiv:2402.03262].

[97] C. Hughes, C. T. H. Davies and C. J. Monahan, Phys. Rev. **D97**, 5, 054509 (2018), [arXiv:1711.09981].

[98] A. Bussone *et al.* (ETM), Phys. Rev. **D93**, 11, 114505 (2016), [arXiv:1603.04306].

[99] R. Dowdall *et al.* (HPQCD), Phys. Rev. Lett. **110**, 222003 (2013), [arXiv:1302.2644].

[100] Y. Aoki *et al.*, Phys. Rev. **D91**, 114505 (2015), [arXiv:1406.6192].

[101] N. H. Christ *et al.* (RBC/UKQCD), Phys. Rev. **D91**, 054502 (2015), [arXiv:1404.4670].

[102] H. Na *et al.* (HPQCD), Phys. Rev. **D86**, 034506 (2012), [arXiv:1202.4914].

[103] C. McNeile *et al.* (HPQCD), Phys. Rev. **D85**, 031503 (2012), [arXiv:1110.4510].

[104] H.-K. Sun and M.-Z. Yang, Phys. Rev. **D95**, 11, 113001 (2017), [arXiv:1609.08958].

[105] M. J. Baker *et al.*, JHEP **07**, 032 (2014), [arXiv:1310.0941].

[106] W. Lucha, D. Melikhov and S. Simula, Phys. Rev. **D88**, 056011 (2013), [arXiv:1305.7099].

[107] J. Hardy and I. S. Towner, PoS **CKM2016**, 028 (2016).

[108] J. C. Hardy and I. S. Towner, Phys. Rev. **C102**, 4, 045501 (2020).

[109] C.-Y. Seng *et al.*, Phys. Rev. **D105**, 1, 013005 (2022), [arXiv:2107.14708].

[110] N. Carrasco *et al.*, Phys. Rev. **D93**, 11, 114512 (2016), [arXiv:1602.04113].

[111] A. Bazavov *et al.* (Fermilab Lattice and MILC), Phys. Rev. Lett. **112**, 112001 (2014), [arXiv:1312.1228].

[112] C.-Y. Seng *et al.*, Phys. Rev. Lett. **121**, 241804 (2018), [arXiv:1807.10197].

[113] C. Y. Seng, M. Gorchtein and M. J. Ramsey-Musolf, Phys. Rev. **D100**, 013001 (2019), [arXiv:1812.03352].

[114] M. Gorchtein, Phys. Rev. Lett. **123**, 042503 (2019), [arXiv:1812.04229].

[115] C.-Y. Seng and U.-G. Meissner, Phys. Rev. Lett. **122**, 211802 (2019), [arXiv:1903.07969].

[116] A. Czarnecki, W. J. Marciano and A. Sirlin, Phys. Rev. D **100**, 7, 073008 (2019), [arXiv:1907.06737].

[117] C. Patrignani *et al.* (Particle Data Group), Chin. Phys. **C40**, 10, 100001 (2016).

[118] Y. S. Amhis *et al.* (Heavy Flavor Averaging Group, HFLAV), Phys. Rev. D **107**, 5, 052008 (2023), [arXiv:2206.07501].

[119] A. Bazavov *et al.* (Fermilab Lattice, MILC), Phys. Rev. D **107**, 9, 094516 (2023), [arXiv:2212.12648].

[120] V. Lubicz *et al.* (ETM), Phys. Rev. **D96**, 5, 054514 (2017), [Errata: Phys. Rev. **D99**, 099902 (2019),Phys. Rev. **D100**, 079901 (2019)], [arXiv:1706.03017].

[121] B. Chakraborty *et al.* ((HPQCD Collaboration)), Phys. Rev. **D104**, 3, 034505 (2021), [arXiv:2104.09883].

[122] L. Wolfenstein, Phys. Rev. Lett. **51**, 1945 (1983).

[123] J. Charles *et al.* (CKMfitter Group), Eur. Phys. J. **C41**, 1 (2005), updated results and plots available at: `http://ckmfitter.in2p3.fr`, [hep-ph/0406184].

[124] M. Antonelli *et al.*, Phys. Rept. **494**, 197 (2010), [arXiv:0907.5386].

[125] J. N. Butler *et al.* (Quark Flavor Physics Working Group), in "Community Summer Study 2013: Snowmass on the Mississippi (CSS2013) Minneapolis, MN, USA, July 29-August 6, 2013," (2013), [arXiv:1311.1076], URL `http://www.slac.stanford.edu/econf/C1307292/docs/IntensityFrontier/QuarkFl-15.pdf`.

[126] Y. Amhis *et al.* (Heavy Flavor Averaging Group) (2014), [arXiv:1412.7515].

[127] A. J. Bevan *et al.* (Belle, BaBar), Eur. Phys. J. **C74**, 3026 (2014), [arXiv:1406.6311].

[128] Y. Amhis *et al.* (HFLAV), Eur. Phys. J. **C77**, 12, 895 (2017), [arXiv:1612.07233].

[129] A. X. El-Khadra and P. Urquiljo, Semileptonic b-Hadron Decays, Determination of V_{cb}, V_{ub} (2023), review prepared for PDG 2024 update, URL `http://pdg.lbl.gov/2024/reviews/rpp2024-rev-vcb-vub.pdf`.

Int. J. Mod. Phys. A 2026.41. Downloaded from www.worldscientific.com
UNIVERSITY OF CALIFORNIA @ BERKELEY on 09/16/26. Re-use and distribution is strictly not permitted, except for Open Access articles.

72. Production and Decay of b-flavored Hadrons

Revised March 2026 by P. Eerola (Research Council of Finland), M. Kreps (Warwick U.) and Y. Kwon (Yonsei U., Seoul).

The b quark belongs to the third generation of quarks and is the weak–doublet partner of the t quark. The existence of the third–generation quark doublet was proposed in 1973 by Kobayashi and Maskawa [1] in their model of the quark mixing matrix ("CKM" matrix), and confirmed four years later by the first observation of a $b\bar{b}$ meson [2]. In the KM model, CP violation is explained within the Standard Model (SM) by an irreducible phase of the 3×3 unitary matrix. The regular pattern of the three lepton and quark families is one of the most intriguing puzzles in particle physics. The existence of families gives rise to many of the free parameters in the SM, including the fermion masses, and the elements of the CKM matrix.

Since the b quark is the lighter element of the third–generation quark doublet, the decays of b-flavored hadrons occur via generation-changing processes through CKM matrix. Because of this, and the fact that the CKM matrix is close to a 3×3 unit matrix, many interesting features such as loop and box diagrams, flavor oscillations, as well as large CP asymmetries, can be observed in the weak decays of b-flavored hadrons.

The CKM matrix is parameterized by three real parameters and one complex phase. This complex phase is the source of CP violation in B meson decays in the Standard Model. A crucial milestone was the first observation of CP violation in the B meson system in 2001, by the BaBar [3] and Belle [4] collaborations. They measured a large value for the parameter $\sin 2\beta$ $(= \sin 2\phi_1)$ [5], almost four decades after the discovery of a small CP asymmetry in neutral kaons. A more detailed discussion of the CKM matrix and CP violation can be found elsewhere in this *Review* [6,7].

The structure of this mini-review is organized as follows. After a discussion of b-quark production and current results on spectroscopy, we discuss lifetimes of b-flavored hadrons. We then discuss some basic properties of B-meson decays, followed by summaries of dominant hadronic, rare hadronic, and electroweak penguin decays of B-mesons. There are separate mini-reviews for B^0–$\overline{B}^0$ mixing [8] and the extraction of the CKM matrix elements V_{cb} and V_{ub} from B-meson decays [9] in this *Review*.

72.1 Production and spectroscopy

The bound states of a $\bar{b}$ antiquark and a u, d, s, or c quark are referred to as the B_u (B^+), B_d (B^0), B_s (B_s^0), and B_c (B_c^+) mesons, respectively. The B_c^+ is the heaviest of the ground–state b-flavored mesons, and the most difficult to produce: it was observed for the first time in the semileptonic mode by CDF in 1998 [10], but its mass was accurately determined only in 2006, from the fully reconstructed mode $B_c^+ \to J/\psi\pi^+$ [11]. Many exclusive decay channels can now be used for the accurate mass measurements, given the large statistics available at the LHC. Currently the most precise measurement is made by LHCb and yields $m(B_c^+) = 6274.47 \pm 0.27 \pm 0.17$ MeV/c^2 [12], combining $B_c^+ \to J/\psi\pi^+$, $B_c^+ \to J/\psi\pi^+\pi^-\pi^+$, $B_c^+ \to J/\psi p\bar{p}\pi^+$, $B_c^+ \to J/\psi D_s^+$, $B_c^+ \to J/\psi D^0 K^+$ and $B_c^+ \to B_s^0\pi^+$ decay modes.

The first excited meson is called the B^* meson, while B^{**} is the generic name for the four orbitally excited $(L = 1)$ B-meson states that correspond to the P-wave mesons in the charm system, D^{**}. Excited states of the B_s^0 meson are similarly named B_s^* and B_s^{**}.

Of the possible bound $\bar{b}b$ states, the $\Upsilon(nS)$ and $\chi_{bJ}(nP)$ states are well studied. The pseudoscalar ground state η_b has been observed for the first time by BaBar [13] indirectly through the decay $\Upsilon(3S) \to \gamma\eta_b$, and then confirmed by Babar in $\Upsilon(2S)$ decays [14] and CLEO in $\Upsilon(3S)$ decays [15]. The most accurate mass and width measurements come now from Belle, using decays $\Upsilon(5S) \to h_b(1P)\pi^+\pi^-$, $h_b(1P) \to \gamma\eta_b(1S)$ [16], $\Upsilon(4S) \to \eta h_b(1P)$, $h_b(1P) \to \gamma\eta_b(1S)$ [17], and $\Upsilon(2S) \to \gamma\eta_b(1S)$ [18]. Belle has also reported first evidence for the $\eta_b(2S)$ in the $h_b(2P) \to \eta_b(2S)\gamma$ transition [16]. In addition, Belle has observed $T_{b\bar{b}1}(10610)$ (was $Z_b(10610)$) and $T_{b\bar{b}1}(10650)$ (was $Z_b(10650)$) states in the processes $\Upsilon(5S) \to \Upsilon(nS)\pi^+\pi^-$ $(n = 1, 2, 3)$ and $\Upsilon(5S) \to h_b(mP)\pi^+\pi^-$ $(m = 1, 2)$ [19]. These $T_{b\bar{b}1}$ states are observed to decay to $\Upsilon(nS)\pi^\pm$ and $h_b(mP)\pi^\pm$, hence electrically charged and do not belong to ordinary $q\bar{q}$ mesons. For classification and naming of these and other states, see Ref. [20].

Experimental studies of b decays have been performed in e^+e^- collisions at the $\Upsilon(4S)$ (ARGUS, CLEO, Belle, BaBar) and $\Upsilon(5S)$ (CLEO, Belle) resonances. The $e^+e^- \to b\bar{b}$ production cross-section at the $\Upsilon(4S)$ $(\Upsilon(5S))$ resonance is about 1.1 nb (0.3 nb). The full data samples of BaBar and Belle are 560 fb^{-1} and 1020 fb^{-1}, respectively, of which 433 fb^{-1} and 710 fb^{-1} are at the $\Upsilon(4S)$ resonance. Since the $\Upsilon(4S)$ decays dominantly to a pair of B mesons (either B^+B^- or $B^0\overline{B}^0$), a precise knowledge of the energy-momentum of one B meson (the 'tagging B') enables deducing the properties of the other B (the 'signal B'). This property has been exploited by both BaBar and Belle, in particular, to measure inclusive decay modes as well as final states with missing neutrinos. The Belle II experiment at SuperKEKB has started recording data in 2019, and the experiment has so far collected about 700 fb^{-1} of data by the March 2026. At the Z resonance (SLC, LEP) all species of b-flavored hadrons could be studied for the first time. The $e^+e^- \to b\bar{b}$ production cross-section at the Z resonance is about 6.6 nb.

High-energy $p\bar{p}$ (Tevatron) and pp collisions (LHC) produce b-flavored hadrons of all species with large cross-sections. At the Tevatron ($\sqrt{s} = 1.96$ TeV) the visible cross section $\sigma(p\bar{p} \to bX, |\eta| < 1)$ is about 30 μb. CDF and D0 experiments at the Tevatron have accumulated by the end of their running about 10 fb^{-1} each.

At the LHC pp collider at $\sqrt{s} = 7 - 13$ TeV, the visible b-hadron cross section at the LHCb experiment with pseudorapidity acceptance $2 < \eta < 5$ has been measured to be ~ 72 μb at 7 TeV and ~ 144 μb at 13 TeV [21] (cross section at 13 TeV corrected in Erratum). LHCb has collected about 1 fb^{-1} at 7 TeV, 2 fb^{-1} at 8 TeV, and close to 5.9 fb^{-1} at 13 TeV during LHC Runs 1 and 2. CMS and ATLAS have collected each about 5 fb^{-1} of data at $\sqrt{s} = 7$, 20 fb^{-1} at 8 TeV and about 150 fb^{-1} at 13 TeV during LHC Runs 1 and 2. The latest LHC Run 3 at 13.6 TeV started in summer 2022, with upgraded detectors. By the end of 2025, LHC has delivered about 330 fb^{-1} to ATLAS and CMS experiments, and about 24 fb^{-1} to the LHCb experiment.

In hadron collisions, production happens as $b\bar{b}$ pairs via leading order flavor creation or higher order processes such as gluon–splitting. Single b-quarks can be produced by flavor excitation. The total b-production cross section is an interesting test of our understanding of leading and higher order QCD processes. With a wealth of measurements at LHC and at Tevatron (see Ref. [21] and references therein), and improved calculations [22], there is a reasonable agreement between measurements and predictions.

Each quark of a $b\bar{b}$ pair produced in hadron collisions hadronizes separately and incoherently from the other, but it is still possible to obtain a statistical indication of the charge of a produced $b/\bar{b}$ quark ("flavor tag" or "charge tag") from the accompanying particles produced in the hadronization process, or from the decay products of the other quark. The momentum spectrum of produced b-quarks typically peaks near the b-quark mass, and extends to much higher momenta, dropping by about a decade for every ten GeV. Typical decay lengths are of the order of a centimeter at 13 TeV pp collisions; the resolution for the decay vertex must be more precise than this to resolve the fast oscillations of B_s^0 mesons.

In e^+e^- colliders, since the B mesons are very slow in the $\Upsilon(4S)$ rest frame, asymmetric beam energies are used to boost the decay products to allow time-dependent measurements that are crucial for the study of CP violation. At KEKB, the boost was $\beta\gamma = 0.43$, while PEP-II used a slightly larger boost, $\beta\gamma = 0.55$. The typical B-meson decay length is dilated from ≈ 20 μm to ≈ 200 μm. At SuperKEKB the boost is lower, $\beta\gamma = 0.28$, which puts more demanding requirements on the track reconstruction precision at Belle II to reach a resolution in decay time measurements similar to Belle. The two B mesons produced in $\Upsilon(4S)$ decay are in a coherent quantum state, which makes it easier than in hadron collisions to infer the charge state of one B meson from observation of the other; however, the coherence also requires determination

Int. J. Mod. Phys. A 2026.41. Downloaded from www.worldscientific.com by UNIVERSITY OF CALIFORNIA @ BERKELEY on 09/16/26. Re-use and distribution is strictly not permitted, except for Open Access articles.

of the decay time of both mesons, rather than just one, in order to perform time–dependent CP–violation measurements. For B_s^0, which can be produced at $\Upsilon(5S)$ the situation is less favourable, as boost is not high enough to provide sufficient time resolution to resolve the fast B_s^0 oscillations.

For the measurement of branching fractions, the initial composition of the data sample must be known. The $\Upsilon(4S)$ resonance decays predominantly to $B^0\overline{B}^0$ and B^+B^-; the current experimental upper limit for non-$B\overline{B}$ decays of the $\Upsilon(4S)$ is less than 4% at the 95% confidence level (CL) [23]. The observed hadronic modes of this category are decays to lower Υ states and a pion pair, η, or η', measured branching fractions being of order $10^{-4} - 10^{-5}$ [24], and decays to $h_b(1P)\eta$ with branching fraction of order 10^{-3} [17].

The ratio f_+/f_0 of the fractions of charged to neutral B productions from $\Upsilon(4S)$ decays has been measured by CLEO, BaBar, and Belle in various ways. They typically use pairs of isospin-related decays of B^+ and B^0, such that it can be assumed that $\Gamma(B^+ \to x^+) = \Gamma(B^0 \to x^0)$. In this way, the ratio of the number of events observed in these modes is proportional to $(f_+\tau_+)/(f_0\tau_0)$ [25]. BaBar has also performed an independent measurement of f_0 with a different method that does not require isospin symmetry or the value of the lifetime ratio, based on the number of events with one or two reconstructed $B^0 \to D^{*-}\ell^+\nu$ decays [26]. The combined result, from the current average of τ_+/τ_0, is $f_+/f_0 = 1.058 \pm 0.024$ [27]. The result is consistent within 2.4σ with equal production of B^+B^- and $B^0\overline{B}^0$ pairs, and we assume $f_+/f_0 = 1$ in this mini-review except where explicitly stated otherwise. This assumption is also supported by the near equality of the B^+ and B^0 masses: our fit yields $m(B^0) = 5279.72 \pm 0.08$ MeV/c^2, $m(B^+) = 5279.41 \pm 0.07$ MeV/c^2, and $m(B^0) - m(B^+) = 0.31 \pm 0.05$ MeV/c^2.

Data collected at the $\Upsilon(5S)$ resonance gave CLEO, Belle and BaBar access to B_s^0 decays. In $\Upsilon(5S)$ decays there are seven possible final states including a pair of non-strange B mesons and 0, 1 or 2 pions, and three final states with a pair of strange B mesons ($B_s^{*0}\overline{B}_s^{*0}$, $B_s^{*0}\overline{B}_s^0$, and $B_s^0\overline{B}_s^0$). The fraction of events with a pair of B_s^0 mesons over the total number of events with a pair of b-flavored hadrons has been measured to be $f_s[\Upsilon(5S)] = 0.199^{+0.030}_{-0.029}$ [28], of which 88% is $B_s^{*0}\bar{B}_s^{*0}$ events. However, the small boost of B_s^0 mesons produced in this way prevents resolution of their fast oscillations for time-dependent measurements; these are only accessible in hadron collisions (or at the Z peak).

In high-energy collisions, the produced b or $\bar{b}$ quarks can hadronize with different probabilities into the full spectrum of b-hadrons, either in their ground or excited states. The hadronization does not have to be identical in $p\overline{p}$ or pp collisions and in Z decay, because of the different momentum distributions of the b-quark in these processes; the sample used in the $p\overline{p}$ measurements has momenta close to the b mass, rather than $m_Z/2$ in Z decay. The available data from Tevatron and LHC show that the production fractions f_d, f_u, f_s, and f_{baryon} of B^0, B^+, B_s^0, and b baryons, respectively, of weakly decaying b hadrons depend on the kinematics of the produced b hadron. Recently LHCb experiment found evidence for dependence of b-quark hadronization on multiplicity in pp collisions [29]. The production fractions of b hadrons are discussed in more detail in the $B^0 - \overline{B}^0$ mixing section in this *Review* [8].

Excited B-meson states have been thoroughly studied by CLEO, LEP, CUSB, D0 and CDF (an admixture of B mesons) and LHCb (B^{*+}-meson). The current PDG fit of the B^*–B mass difference is 45.18 ± 0.20 MeV/c^2. Excited B_s^*-meson states have observed in $\Upsilon(5S)$ decays by CUSB, CLEO and Belle.

For orbitally excited $B_{(s)}$ meson states, with relative angular momentum L=1 of the two quarks, there exist four states $(J, j_q) = (0, 1/2), (1, 1/2), (1, 3/2), (2, 3/2)$, where j_q is the total angular momentum of the light u, d or s quark and J is the total angular momentum of the B meson. These states are collectively called as $B_{(s)}^{**}$ mesons. The $j_q = 1/2$ states are named $B_{(s)0}^*$ ($J = 0$) and $B_{(s)1}$ ($J = 1$) mesons, while the states with $j_q = 3/2$ are named $B_{(s)1}$ ($J = 1$) and $B_{(s)2}^*$ ($J = 2$) mesons. The states with $j_q = 1/2$ can decay through an S-wave transition and are expected to have a large width, but the $j_q = 3/2$ states are narrow D-wave decays. Evidence for B^{**} production has been initially obtained at LEP as a broad $B\pi$ resonance [30] or a B^+K^- enhancement [31]. Detailed results have been obtained for the narrow states $B_1(5721)^{0,+}$ and $B_2(5747)^{0,+}$ at the Tevatron and by LHCb, and clear enhancements compatible with the higher mass states $B_J(5840)^{0,+}$ and $B_J(5970)^{0,+}$ have been observed [32]. Also the narrow B_s^{**} states $B_{s1}(5830)^0$ and $B_{s2}(5840)^0$ have been measured at the CDF [32], LHCb [33], and CMS [34].

Excited states of B_c^+ mesons will provide important information about the strong potential. A $B_c^+\pi^+\pi^-$ resonance has been observed for the first time by ATLAS [35]. The mass of the resonance has been measured precisely by CMS and LHCb as 6871.2 ± 1.0 MeV/c^2 [36]. The resonance may be interpreted as the second S-wave state of the B_c^+ meson, $B_c^+(2S)$, but the quantum numbers are to be confirmed.

Baryon states containing a b quark are labeled according to the same scheme used for non-b baryons, with the addition of a b subscript [20]. The first observed b baryon was the Λ_b^0 (quark composition udb). Thanks to the large samples accumulated at the Tevatron and specially at the LHC many new b baryons have been found. The masses of all these new baryons have been measured to a precision of a few MeV/c^2, and found to be in agreement with predictions from Heavy Quark Effective Theory (HQET).

Clear signals of four strongly–decaying baryon states, Σ_b^+, Σ_b^{*+} (uub), Σ_b^-, Σ_b^{*-} (ddb) have been obtained by CDF [37] and LHCb [38]. LHCb has also observed two new mass peaks in the $\Lambda_b^0\pi^\pm$ systems, consistent with single resonances and named as $\Sigma_b^\pm(6097)$ [38]. The nature of these resonances is, however, not yet clear. The isodublet of strange b baryons Ξ_b^0 (usb) and $\Xi_b^\pm$ (dsb) has been observed by CDF and D0 [39]. Masses, lifetimes, and branching ratios have been accurately measured by LHCb [40–43], CDF [44], and CMS [45]. LHCb has also measured several parameters sensitive to P and CP violation [42,46]. Other observed Ξ_b baryons are spin-3/2 states $\Xi_b(5945)^0$ (Ξ_b^{*0}) [45, 47, 48], $\Xi_b^*(5955)^-$ [48, 49] and $\Xi_b(6100)^-$ [48, 50], a spin-1/2 state $\Xi_b'(5935)^-$ [48,49], and resonance states $\Xi_b^0(6087)$ [48], $\Xi_b^0(6095)$ [48], $\Xi_b^-(6227)$ [41, 51], $\Xi_b^0(6227)$ [41], $\Xi_b^0(6327)$ [52] and $\Xi_b^0(6333)$ [52]. The doubly–strange bottom baryon Ω_b^- has been observed first by D0 and CDF [53]. Mass and mean life have been measured precisely by LHCb [43, 54] and CDF [44]. LHCb has also observed four excited Ω_b^- states $\Omega_b^-(6316)$, $\Omega_b^-(6330)$, $\Omega_b^-(6340)$ and $\Omega_b^-(6350)$ [55].

The so-called exotic states have raised a lot of interest recently. While many exotic states were seen in the charm sector, in bottom sector there are fewer seen. The D0 Collaboration claimed a narrow state $X(5568)$ decaying into a $B_s^0\pi^\pm$ final state [56]. While this would be an interesting addition to the observed states as the first exotic state with constituent quarks with four different flavours (b, s, u, d), analyses by LHCb, CMS, CDF and ATLAS yield negative results [57–60].

72.2 Lifetimes

Precise lifetimes are key in extracting the weak parameters that are important for understanding the role of the CKM matrix in CP violation, such as the determination of V_{cb} and B_s^0–$\overline{B}_s^0$ mixing parameters. In the naive spectator model, the heavy-flavored hadrons can decay only via the external spectator mechanism, and thus, the lifetimes of all mesons and baryons containing b quarks would be equal. Non–spectator effects, such as the interference between contributing amplitudes, modify this simple picture and give rise to a lifetime hierarchy for b-flavored hadrons similar to the one in the charm sector. However, since the lifetime differences are expected to scale as $1/m_Q^2$, where m_Q is the mass of the heavy quark, the variations in the b system are expected to be only 10% or less [61, 62]. We expect:

$$\tau(B^+) \geq \tau(B^0) \approx \tau(B_s^0) > \tau(\Lambda_b^0) \gg \tau(B_c^+) \,. \qquad (72.1)$$

Int. J. Mod. Phys. A 2026.41. Downloaded from www.worldscientific.com
UNIVERSITY OF CALIFORNIA @ BERKELEY on 09/16/26. Re-use and distribution is strictly not permitted, except for Open Access articles.

For the B_c^+, both quarks decay weakly, so the lifetime is much shorter.

Measurements of the lifetimes of the different b-flavored hadrons thus provide a means to determine the importance of non-spectator mechanisms in the b sector. Availability of large samples of fully–reconstructed decays of different b-hadron species has resulted in precise measurements with small statistical and systematic uncertainties (∼1%). The world averages given in Table 72.1 have been determined by the Heavy Flavor Averaging Group (HFLAV) [63].

Table 72.1: Summary of the world-average b-hadron lifetime measurements. For the B_s^0 lifetimes, see text below.

Particle	Lifetime [ps]
B^+	1.637 ± 0.004
B^0	1.5113 ± 0.0027
B_s^0	1.515 ± 0.006
B_{sL}^0	1.430 ± 0.006
B_{sH}^0	1.611 ± 0.008
B_c^+	0.510 ± 0.009
Λ_b^0	1.465 ± 0.009
Ξ_b^-	1.575 ± 0.021
Ξ_b^0	1.472 ± 0.016
Ω_b^-	1.64 ± 0.16

The B_s^0 lifetime in Table 72.1 is defined as $1/\Gamma_s$, where Γ_s is the average width of the light (L) and heavy (H) mass eigenstates, $(\Gamma_L+\Gamma_H)/2$. In the absence of CP violation, the light (heavy) B_s^0 mass eigenstate is the CP-even (CP-odd) eigenstate. Thus, the lifetime of the light (heavy) mass eigenstate can be measured from CP-even (odd) final states. The lifetimes can also be obtained from time-dependent angular analysis of $B_s^0 \to J/\psi\phi$ decays.

The short B_c^+ lifetime is in good agreement with predictions [64]. With large samples of B_c^+ mesons at the LHC precision on the lifetimes can still improve. The measurement using semileptonic decays gives $\tau_{B_c^+} = 0.509 \pm 0.008 \pm 0.012$ ps [65] while using decays $B_c^+ \to J/\psi\pi^+$ yields $\tau_{B_c^+} = 0.5134 \pm 0.0110 \pm 0.0057$ ps [66]. Each of these is more precise than the combination of all previous experiments.

The recent Λ_b^0 lifetime measurements from LHC experiments and CDF are precise and favour lifetime close to the lifetime of B^0 meson, in agreement with theory.

For precision comparisons with theory, lifetime ratios are more sensitive. Experimentally it is found [67]:

$$\frac{\tau_{B^+}}{\tau_{B^0}} = 1.0832 \pm 0.0034\,, \quad \frac{\tau_{B_s^0}}{\tau_{B^0}} = 1.003 \pm 0.004\,, \quad \frac{\tau_{\Lambda_b^0}}{\tau_{B^0}} = 0.970 \pm 0.006\,,$$

$$\frac{\tau_{\Omega_b^-}}{\tau_{B^0}} = 1.09 \pm 0.11\,, \quad \frac{\tau_{\Xi_b^0}}{\tau_{\Xi_b^-}} = 0.934 \pm 0.014\,,$$

while recent Heavy Quark Expansion (HQE) predictions give [68–70]:

$$\frac{\tau_{B^+}}{\tau_{B^0}} = 1.086 \pm 0.022\,, \quad \frac{\tau_{B_s^0}}{\tau_{B^0}} = 1.003 \pm 0.006\,, \quad \frac{\tau_{\Lambda_b^0}}{\tau_{B^0}} = 0.955 \pm 0.014\,,$$

$$\frac{\tau_{\Omega_b^-}}{\tau_{B^0}} = 1.081 \pm 0.042\,, \quad \frac{\tau_{\Xi_b^0}}{\tau_{\Xi_b^-}} = 0.929 \pm 0.028.$$

The ratio of B^+ to B^0 lifetimes has a precision of better than 1%, and is significantly different from 1.0, in agreement with predictions [61, 68, 69]. The ratio of B_s^0 to B^0 lifetimes is predicted to be very close to 1.0 in scenario with small $SU(3)_F$ breaking from Ref. [71]. If on the other hand $SU(3)_F$ breaking is large as suggested by Ref. [72] the prediction is $\tau_{B_s^0}/\tau_{B^0} = 1.028 \pm 0.011$.

For a detailed discussion on neutral B^0 and B_s^0 oscillation and relevant CP violation measurements see Ref. [8].

72.3 Features of decays

The ground states of b-flavored hadrons decay via weak interactions. In most decays of the b-flavored hadrons, where the b-quark is accompanied by lighter partner quarks (d, u, s, or c), the decay modes are well described by the decay of the b quark (spectator model) [73]. The dominant decay mode of a b quark is $b \to cW^{*-}$ (referred to as a "tree" or "spectator" decay), where the virtual W materializes either into a pair of leptons $\ell\bar{\nu}$ ("semileptonic decay"), or into a pair of quarks which then hadronizes. The transition $b \to u$ is suppressed by $|V_{ub}/V_{cb}|^2 \sim (0.1)^2$ relative to $b \to c$ transitions. The decays in which the spectator quark combines with one of the quarks from W^* to form one of the final state hadrons are suppressed by a factor $\sim (1/3)^2$, because the colors of the two quarks from different sources must match ("color–suppression").

Semileptonic B decays $B \to X_c\ell\nu$ and $B \to X_u\ell\nu$ provide an excellent way to measure the magnitude of the CKM elements $|V_{cb}|$ and $|V_{ub}|$ respectively, because the strong interaction effects are much simplified due to the two leptons in the final state. Both exclusive and inclusive decays can be used with dominant uncertainties being complementary. For exclusive decay analysis, knowledge of the form factors for the exclusive hadronic system $X_{c(u)}$ is required. For inclusive analysis, it is usually necessary to restrict the available phase-space of the decay products to suppress backgrounds; subsequently uncertainties are introduced in the extrapolation to the full phase-space. Moreover, restriction to a small corner of the phase-space may result in breakdown of the operator-product expansion scheme, thus making theoretical calculations unreliable. A more detailed discussion of B semileptonic decays and the extraction of $|V_{cb}|$ and $|V_{ub}|$ is given elsewhere in this *Review* [9]. While traditionally B^0 and B^+ decays were used, over time also other B hadron studies became available. Most notably, determination of of $|V_{ub}|$ using $\Lambda_b^0 \to p\mu^-\bar{\nu}_\mu$ decays by LHCb [74] was more precise than expected. Besides, there have been measurements of inclusive semileptonic decay rates of B_s^0 [75] and B_c^+ [76] mesons. One of the latest additions in this area is the observation of the $B_s^0 \to K^-\mu^+\nu_\mu$ decays by LHCb using only a fraction of their available data [77].

On the other hand, hadronic B decays are complicated because of strong interaction effects caused by the surrounding cloud of light quarks and gluons. While this complicates the extraction of CKM matrix elements, it also provides a great opportunity to study perturbative and non-perturbative QCD, hadronization, and Final State Interaction (FSI) effects.

Many aspects of B decays can be understood through the Heavy Quark Effective Theory (HQET) [78]. This has been particularly successful for semileptonic decays. For further discussion of HQET, see for instance Ref. [79]. For hadronic decays, one typically uses effective Hamiltonian calculations that rely on a perturbative expansion with Wilson coefficients. In addition, some form of the factorization hypothesis is commonly used, where, in analogy with semileptonic decays, two-body hadronic decays of B mesons are expressed as the product of two independent hadronic currents, one describing the formation of a charm meson (in case of the dominant $b \to cW^{*-}$ decays), and the other describing the hadronization of the remaining $\bar{u}d$ (or $\bar{c}s$) system from the virtual W^-. Qualitatively, for B decays with a large energy release, e.g. $b \to uW^{*-}$ transitions, the $\bar{u}d$ pair (produced as a color singlet) travels fast enough to leave the interaction region without influencing the meson containing the spectator quark. This is known to work well for the dominant spectator decays [80]. There are several common implementations of these ideas for hadronic B decays, the most common of which are QCD factorization (QCDF) [81], perturbative QCD (pQCD) [82], and soft collinear effective theory (SCET) [83].

The transitions $b \to s$ and $b \to d$ are flavor-changing neutral-current (FCNC) processes. Although they are not allowed in the SM as a tree-process, they can occur via loop diagrams (denoted "penguin" decays). The rates for $b \to s$ penguin decays are comparable to the CKM-suppressed $b \to u$ tree processes. Pure-penguin decays were first established by the observation of $B \to K^*(892)\gamma$ [84]. Penguin processes involving $b \to d$ transitions are further suppressed by CKM, and have been observed for $B \to (\rho/\omega)\gamma$ decays [85, 86]. LHCb has observed a $b \to d$

Int. J. Mod. Phys. A 2026.41. Downloaded from www.worldscientific.com
by UNIVERSITY OF CALIFORNIA @ BERKELEY on 09/16/26. Re-use and distribution is strictly not permitted, except for Open Access articles.

penguin transition in the $B^+ \to \pi^+\mu^+\mu^-$ mode and measured its branching fraction to be $(1.83 \pm 0.24 \pm 0.05) \times 10^{-8}$ [87].

Other decay processes discussed in this *Review* include W–exchange (a W is exchanged between initial–state quarks), penguin annihilation (the gluon from a penguin loop attaches to the spectator quark, similar to an exchange diagram), and pure–annihilation (the initial quarks annihilate to a virtual W, which then decays). Some observed decay modes such as $B^0 \to D_s^- K^+$, may be interpreted as evidence of a W-exchange process [88]. The evidence for the purely leptonic decay $B^+ \to \tau^+\nu$ from Belle [89] and BaBar [90] is the first sign of a pure annihilation decay. The average branching fraction is $(1.09 \pm 0.24) \times 10^{-4}$, which is somewhat larger than, though consistent with, the value expected in the SM. A substantial region of parameter space of charged Higgs mass vs. $\tan\beta$ is excluded by the measurements of this mode. A dedicated discussion of purely leptonic decays of charged pseudoscalar mesons is given elsewhere in this *Review* [91].

72.4 Dominant hadronic decays

Most of the hadronic B decays involve $b \to c$ transition at the quark level, resulting in a charmed hadron or charmonium in the final state. Other types of hadronic decays are very rare and will be discussed separately in the next section. The experimental results on hadronic B decays have steadily improved over the years, and the measurements have reached sufficient precision to challenge our understanding of the dynamics of these decays. With good particle detection and hadron identification capabilities of B-factory detectors, a substantial fraction (roughly on the order of a few per mill) of hadronic B decay events can be fully reconstructed. In particular, good performances for detecting π^0 and other neutral particles helped Belle and BaBar to make comprehensive measurements of the decays $\overline{B}^0 \to D^{(*)0}h^0$ [92], where h^0 stands for light neutral mesons such as $\pi^0, \eta^{(\prime)}, \rho^0, \omega$. The measurements are being complemented by LHCb, in decays like $\overline{B^0} \to D^0\pi^+\pi^-$ [93], where no neutral particles reconstruction is needed. These decays proceed through color-suppressed diagrams, hence they provide useful tests on the factorization models.

Because of the kinematic constraint of $\Upsilon(4S) \to B\bar{B}$, the energy sum of the final-state particles of a B meson decay is always equal to one half of the total energy in the center of mass frame. As a result, the two variables, ΔE (energy difference) and M_B (B candidate mass with a beam-energy constraint) are very effective for reducing combinatorial background both from $\Upsilon(4S)$ and $e^+e^- \to q\bar{q}$ continuum events. In particular, the energy-constraint in M_B improves the signal resolution by almost an order of magnitude.

The kinematically clean environment of B meson decays provides an excellent opportunity to search for new states. For instance, quark-level $b \to c\bar{c}s$ decays have been used to search for new charmonium and charm-strange mesons and study their properties in detail. While narrow charm-strange states $D_{s0}^*(2317)$ [94] and $D_{s1}(2460)$ [95] were discovered by BaBar and CLEO, respectively, the properties of these new states were revealed by studying the B meson decays, $B \to DD_{s0}^*(2317)$ and $B \to DD_{s1}(2460)$ by Belle [96] and BaBar [97]. Another example is Dalitz plot analysis of decay $B_s^0 \to \bar{D}^0K^-\pi^+$ in which the decay to spin-3 resonance was observed for the first time [98]. One of the most significant improvements in the past decade is establishment of decays $B^+ \to D^0K^+$ and $B^+ \to D^0K^*(892)^+$ with D^0 decaying to final state common to D^0 and $\overline{D}^0$ [99]. This allows direct determination of CKM angle $\gamma(=\phi_3)$ to be $65.9^{+3.3}_{-3.5}$.

Information on B_s^0, B_c^+ and Λ_b^0 decays have been remarkably improved with recent studies of large samples from LHCb. Noticeable additions in B_s include decay modes to $D_s^{(*)+}D_s^{(*)-}$, $\bar{D}^0\bar{K}^0$, and $J/\psi\bar{K}^*(892)^0$. The $B_s^0 \to D_s^{(*)+}D_s^{(*)-}$ decays were first observed by CDF [100], followed by Belle [101]. LHCb has improved the precision with $\mathcal{B}(B_s^0 \to D_s^{(*)+}D_s^{(*)-}) = (3.07 \pm 0.22 \pm 0.33)\%$ [102], which suggests that $B_s^0 \to D_s^{(*)+}D_s^{(*)-}$ decays do not saturate the CP-even modes of the B_s decays. The $B_s^0 \to \bar{D}^0\bar{K}^0$ decay occurs mostly via a color-suppressed tree diagram, and has a small theoretical uncertainty in the SM, thus this mode can significantly improve the determination of the CP-violation angle ϕ_s. LHCb has observed this decay and the branching fraction is $(4.3 \pm 0.5 \pm 0.7) \times 10^{-4}$ [103]. The $B_s^0 \to J/\psi\bar{K}^*(892)^0$ decay can be used to constrain the penguin pollution in determining ϕ_s. LHCb has updated the branching fraction and measured the CP asymmetries of this decay, thereby constraining the penguin pollution in ϕ_s [104], although a much more stringent constraint on penguin pollution can come from $B^0 \to J/\psi\rho^0$ which has been observed by BaBar [105] and LHCb [106]. The $B_c^+ \to B_s^0\pi^+$ decay is unique as the only observed mode of b-flavored hadron decays where the partner quark decays (c in this case) while the b quark remains a spectator. LHCb has observed this mode [107] and measured $\mathcal{B}(B_c^+ \to B_s^0\pi^+)/\mathcal{B}(B_c^+ \to J/\psi\pi^+) = (91 \pm 10 \pm 8 \pm 3)$ [108]. In addition, LHCb [109] and ATLAS [110] have measured $B_c^+ \to J/\psi D_s^{(*)+}$, which, by comparing with $B_c^+ \to B_s^0\pi^+$, provides a ratio of exclusive $b \to c$ and $c \to s$ decays of B_c^+. For $\Lambda_b^0 \to \Lambda_c^+\pi^+\pi^-\pi^-$ [111], not only the total rate is measured, but also structure involving decays through excited Λ_c and Σ_c baryons.

In addition, a variety of exotic particles that do not fit the conventional meson spectroscopy have been discovered in B decays. Belle found the $X(3872)$ state by studying $B^+ \to J/\psi\pi^+\pi^-K^+$ [112], which was confirmed by CDF [113], D0 [114] and BaBar [115]. Production of $X(3872)$ has been studied by the LHC experiments, LHCb [116], CMS [117] and ATLAS [118].

A charged charmonium-like state $X(4430)^\pm$ that decays to $\psi(2S)\pi^\pm$ was observed by Belle in $B \to \psi(2S)K\pi^\pm$ [119]. Since it is charged, it could not be an ordinary charmonium state. A high-statistics study by LHCb confirmed the existence of the $X(4430)^\pm$ in decays $B \to \psi(2S)K\pi^\pm$ [120], demonstrated its resonance character by studying the phase motion, unambiguously determined its spin-parity, and saw evidence for another state. In a Dalitz plot analysis of $\bar{B}^0 \to J/\psi K^-\pi^+$ [121], Belle has found another state, labeled as $X(4200)^+$ in this *Review*, adding to the list of exotic charged charmonium-like states. In an amplitude analysis of the decay $\Lambda_b^0 \to J/\psi pK^-$, LHCb observed exotic structures, labeled as $P_c(4380)^+$ and $P_c(4450)^+$ in this *Review*, in the $J/\psi p$ channel [122]. The subsequent analysis with significantly increased statistics observed additional state and resolved the peak at 4450 MeV/c^2 as being due to the two states close in the mass [123]. The structure in the $J/\psi p$ channel was also seen in the $B_s^0 \to J/\psi p\bar{p}$ decays [124] and in the $J/\psi\Lambda$ channel in $B^+ \to J/\psi\Lambda p$ and $\Xi_b^- \to J/\psi\Lambda K^-$ decays [125]. They are referred to as charmonium-pentaquark states. More detailed discussions of exotic meson-like states and pentaquarks are given elsewhere in this *Review* [126].

72.5 Rare hadronic decays

All B-meson decays that do not occur through the $b \to c$ transition are usually called rare B decays. These include both semileptonic and hadronic $b \to u$ decays that are suppressed at leading order by the small CKM matrix element V_{ub}, as well as higher-order $b \to s(d)$ processes such as electroweak and gluonic penguin decays. In this section, we review hadronic rare B decays, while electroweak penguin decays and others are discussed in the next.

Charmless B meson decays into two-body hadronic final states such as $B \to \pi\pi$ and $K\pi$ are experimentally clean, and provide good opportunities to probe new physics and search for indirect and direct CP violations. Since the final state particles in these decays tend to have larger momenta than average B decay products, the event environment is cleaner than for $b \to c$ decays. Branching fractions are typically around 10^{-5}. Over the past decade, many such modes have been observed not only by e^+e^- collider experiments such as BaBar and Belle, but also by hadron collider experiments such as CDF ($p\bar{p}$) and LHCb (pp). In the latter cases, huge data samples of the modes with all charged final-state particles have been reconstructed by triggering on the impact parameter of the charged tracks. This has also allowed observation of charmless decays of the B_s, in final states such as $\phi\phi$ [127], K^+K^- [128, 129], and $K^-\pi^+$ [129, 130], and of charmless decays of the Λ_b^0 baryon [130]. The large samples available at LHCb experiment allow to perform also time-dependent CP violation measurements [131]. Charmless B_s modes are related to corresponding B^0 modes by U-spin symmetry, and are determined

Int. J. Mod. Phys. A 2026.41. Downloaded from www.worldscientific.com
UNIVERSITY OF CALIFORNIA @ BERKELEY on 09/16/26. Re-use and distribution is strictly not permitted, except for Open Access articles.

by similar amplitudes. Combining the observables from B_s^0 and B^0 modes is a further way of eliminating hadronic uncertainties and extracting relevant CKM information [132].

Because of relatively high-momenta for final state particles, the dominant source of background in e^+e^- collisions is $q\bar{q}$ continuum events; sophisticated background suppression techniques exploiting event shape variables are essential for these analyses. In hadron collisions, the dominant background comes from QCD or partially reconstructed heavy flavors, and is similarly suppressed by a combination of kinematic and isolation requirements. The results are in general consistent among the experiments.

Most rare decay modes including $B^0 \to K^+\pi^-$ have contributions from both $b \to u$ tree and $b \to sg$ penguin processes. If the size of the two contributions are comparable, the interference between them may result in direct CP violation, seen experimentally as a charge asymmetry in the decay rate measurement. BaBar [133], Belle [134], CDF [128], and LHCb [131, 135] have measured the direct CP violating asymmetry in $B^0 \to K^+\pi^-$ decays. Direct CP violation has been observed in this decay with a significance of more than 5σ. The world average value of the asymmetry is now rather precise, $A_{CP}(K^+\pi^-) = -0.0831 \pm 0.0031$. The CP asymmetry in $B^+ \to K^+\pi^0$ mode has been measured by BaBar [136], Belle [134], Belle II [137] and [138] with the average value $A_{CP}(K^+\pi^0) = 0.027 \pm 0.012$. These two asymmetries differ significantly, in contrast to a naive expectation based on simplified picture in the SM. For more detailed tests, there are sum rules [139] that relate the decay rates and decay-rate asymmetries between the four $K\pi$ charge states. A crucial ingredient of the sum rule test is $A_{CP}(K^0\pi^0)$. Currently, measured values are reported by both BaBar [140] and Belle [141]. Using the $A_{CP}(K^0\pi^0)$ value of Ref. [141], Belle reports the sum rule test result that is consistent with zero within 1.9σ [134]. With the future improvements via Belle II and upgraded LHCb, the measurements are expected to become precise enough to shape a definite conclusion. The CP asymmetry in the π^+K^- mode has also been measured in B_s^0 decays, by CDF [128] and LHCb [131, 135]. The combined value is $A_{CP}(B_s^0 \to \pi^+K^-) = 0.224 \pm 0.012$.

In addition to $B_{(s)} \to K\pi$ modes, significant ($> 3\sigma$) non-zero CP asymmetries have been measured in several other rare decay modes: $A_{CP}(B^+ \to \rho^0K^+) = 0.37 \pm 0.10$ [142], $A_{CP}(B^+ \to \eta K^+) = -0.37 \pm 0.08$ [143], $A_{CP}(B^0 \to \eta K^{*0}) = 0.19 \pm 0.05$ [144], and $A_{CP}(B^+ \to f_2(1270)K^+) = -0.68^{+0.19}_{-0.17}$ [142]. In at least the first two cases, a large direct CP violation might be expected since the penguin amplitude is suppressed so the tree and penguin amplitudes may have comparable magnitudes. There are also measurements by LHCb of CP asymmetries in several 3-body modes: $A_{CP}(B^+ \to \pi^+\pi^-\pi^+) = 0.057 \pm 0.013$, $A_{CP}(B^+ \to K^+\pi^-\pi^+) = 0.027 \pm 0.008$, $A_{CP}(B^+ \to K^+K^-\pi^+) = -0.122 \pm 0.0021$, and $A_{CP}(B^+ \to K^+K^-K^+) = -0.033 \pm 0.008$ [145]. Many of these analyses now include Dalitz plot treatments with many intermediate resonances.

BaBar [146] and Belle [134, 147] have observed the decays $B^+ \to \overline{K}^0K^+$ and $B^0 \to K^0\overline{K}^0$. The world-average branching fractions are $\mathcal{B}(B^0 \to K^0\overline{K}^0) = (1.21 \pm 0.16) \times 10^{-6}$ and $\mathcal{B}(B^+ \to \overline{K}^0K^+) = (1.31 \pm 0.17) \times 10^{-6}$. These are the first observations of hadronic $b \to d$ transitions, with significance bigger than 5σ for all four measurements. CP asymmetries have been measured for these modes, but with large errors. LHCb has observed $B^0 \to K^+K^-$ mode which occurs via a weak-annihilation process and is the rarest hadronic B-meson decay thus far observed, with $\mathcal{B}(B^0 \to K^+K^-) = (7.80 \pm 1.52) \times 10^{-8}$ [148]. $B_s^0 \to K^+K^-$ decay mode, which occurs mostly via $b \to s$ penguin process, has been observed by Belle [149], CDF [150] and LHCb [129]. The average branching fraction is $\mathcal{B}(B_s^0 \to K^+K^-) = (27.2 \pm 2.3) \times 10^{-6}$. Belle has also observed $B_s^0 \to K^0\overline{K}^0$ [151] which also occurs via $b \to s$ penguin transition in the SM. This was recently confirmed by LHCb [152]. The average branching fraction is $(1.76 \pm 0.31) \times 10^{-5}$.

The decay $B^0 \to \pi^+\pi^-$ can be used to extract the CKM angle α (for details see elsewhere in this *Review* [153]). This is complicated by the presence of significant contributions from penguin diagrams. An isospin analysis [154] can be used to untangle the penguin complications. The decay $B^0 \to \pi^0\pi^0$ is crucial in this analysis. Both BaBar and Belle have observed $B^0 \to \pi^0\pi^0$, with a mild tension in the measured branching fractions: $(1.83 \pm 0.25) \times 10^{-6}$ for BaBar [133] and $(1.31 \pm 0.26) \times 10^{-6}$ for Belle [155]. It turns out that the amount of penguin pollution in the $B \to \pi\pi$ system is rather large. In the past few years, measurements in the $B^0 \to \rho\rho$ system have produced more precise values of α, since penguin amplitudes are generally smaller for decays with vector mesons. An important ingredient in the analysis is the $B^0 \to \rho^0\rho^0$ branching fraction. The average of measurements from BaBar [156] and Belle [157] yields a branching fraction of $(0.96 \pm 0.15) \times 10^{-6}$. This is only 3% of the $\rho^+\rho^-$ branching fraction, much smaller than the corresponding ratio ($\gtrsim 20\%$) in the $\pi\pi$ system.

Since $B \to \rho\rho$ has two vector mesons in the final state, the CP eigenvalue of the final state depends on the longitudinal polarization fraction f_L for the decay. Therefore, a measurement of f_L is needed to extract the CKM angle α. Both BaBar and Belle have measured f_L for the decays $\rho^+\rho^-$ [158] and $\rho^+\rho^0$ [159] and in both cases the measurements show $f_L > 0.9$, making a complete angular analysis unnecessary. In $B^0 \to \rho^0\rho^0$, f_L is measured by BaBar [156], Belle [157] and LHCb [160], with the average value being $0.71^{+0.08}_{-0.09}$.

By analyzing the angular distributions of the B decays to two vector mesons, we can learn a lot about both weak- and strong-interaction dynamics in B decays. Decays that are penguin-dominated surprisingly have values of f_L near 0.5. The list of such decays has now grown to include $B \to \phi K^*(892)$, $B \to \rho K^*(892)$, and $B \to \omega K^*(892)$. The reasons for this "polarization puzzle" are not fully understood. A detailed description of the angular analysis of B decays to two vector mesons can be found in a separate mini-review [161] in this *Review* .

72.6 Electroweak penguin decays

Electroweak penguin decays are one-loop FCNC decays proceeding through penguin or box Feynman diagrams with final state including real photon or pair of leptons. Such decays were first observed by CLEO experiment when it observed decay $B \to K^*(892)\gamma$ [84]. Since then significant amount of experimental information was obtained. Branching fractions for these decays are 10^{-5} or less, which makes them excellent candidates for searches for new physics beyond SM. Often several observables are available, which allows for stringent tests of the SM.

Starting with radiative decays, experimentally easiest to study are exclusive decays with a fully reconstructed final state. The best studied decay in this class is $B \to K^*(892)\gamma$ seen by CLEO, Belle, BaBar experiments [162, 163] with world average branching fraction $\mathcal{B}(B^0 \to K^*(892)^0\gamma) = (41.8 \pm 2.5) \times 10^{-6}$. Decays through several other kaon resonances such as $B \to K_1(1270)\gamma$, $K_2^*(1430)\gamma$, *etc.* were studied at B-factories [164,165]. It is worth to mention decay $B^+ \to K^+\pi^+\pi^-\gamma$ for which besides measurements of the branching fraction [165, 166] one can also use the angular distribution to access photon polarization. Such a measurement was done by the LHCb experiment, which was able to clearly demonstrate that the photon in $B^+ \to K^+\pi^+\pi^-\gamma$ decay is polarized [167]. Unfortunately given non-trivial hadronic structure, more work is needed before turning this into test of the SM. The exclusive radiative decays $B_s^0 \to \phi\gamma$ was seen by the Belle and LHCb experiments [168] with an average branching fraction of $(3.4 \pm 0.4) \times 10^{-5}$ and more recently also decay $\Lambda_b \to \Lambda\gamma$ was observed by LHCb [169].

Compared to $b \to s\gamma$, the $b \to d\gamma$ transitions such as $B \to \rho\gamma$, are suppressed by the CKM elements ratio $|V_{td}/V_{ts}|^2$. Both Belle and BaBar have observed these decays [85,86]. The world average $\mathcal{B}(B \to (\rho,\omega)\gamma) = (1.30 \pm 0.23) \times 10^{-6}$. This can be used to calculate $|V_{td}/V_{ts}|$ [170]; the measured values are $0.195^{+0.025}_{-0.024}$ from Belle [85] and $0.233^{+0.033}_{-0.032}$ from BaBar [86].

The observed radiative penguin branching fractions can constrain a large class of SM extensions [171]. However, due to the uncertainties in the hadronization, only the inclusive $b \to s\gamma$ rate can be reliably compared with theoretical calculations. This rate can be measured from the endpoint of the inclusive photon spectrum in B decay. By combining the measurements of $B \to X_s\gamma$ from the CLEO, BaBar, and Belle experiments [172,173], HFLAV

Int. J. Mod. Phys. A 2026.41. Downloaded from www.worldscientific.com by UNIVERSITY OF CALIFORNIA @ BERKELEY on 09/16/26. Re-use and distribution is strictly not permitted, except for Open Access articles.

obtains the average: $\mathcal{B}(B \to X_s\gamma) = (3.49 \pm 0.19) \times 10^{-4}$ [67] for $E_\gamma \geq 1.6$ GeV, averaging over B^+ and B^0. Consistent but less precise results have been reported by ALEPH for inclusive b–hadrons produced at the Z, which includes also contribution from B_s^0 and Λ_b^0 hadrons. Using the sum of seven exclusive final states, the BaBar experiment measured the branching fraction of inclusive $b \to d\gamma$ decays to be $(9.2 \pm 2.0 \pm 2.3) \times 10^{-6}$ [174]. The measured branching fraction can be compared to theoretical calculations. Recent calculations of $\mathcal{B}(b \to s\gamma)$ at NNLO level predict for the $E_\gamma \geq 1.6$ GeV values of $(3.36 \pm 0.23) \times 10^{-4}$ for $b \to s\gamma$ and $(1.68 \pm 0.17) \times 10^{-5}$ for $b \to d\gamma$ decays [175].

The CP asymmetry in $b \to s\gamma$ is extensively studied theoretically both in the SM and beyond [176]. According to the SM, the CP asymmetry in $b \to s\gamma$ is smaller than 1%, but some non-SM models allow significantly larger CP asymmetry ($\sim 10\%$) without altering the branching fraction. The current world average is $A_{CP} = 0.015 \pm 0.011$, again dominated by BaBar and Belle [177, 178]. In addition to the CP asymmetry, BaBar and Belle also measured the isospin asymmetry $\Delta_{0-} = -0.005 \pm 0.020$ in $b \to s\gamma$ measured using sum of exclusive decays [177, 179]. An alternative measurement using full reconstruction of the companion B in the hadronic decay modes yields a consistent, but less precise result [180]. Both Belle and BaBar experiments measured the isospin asymmetry in exclusive $B \to K^*(892)\gamma$ decay with average of $6.3 \pm 1.7\%$ [163] and therefore providing evidence for the non-zero isospin asymmetry.

In addition, experiments have measured the inclusive photon energy spectrum for $b \to s\gamma$, and by analyzing the shape of the spectrum they obtain the first and second moments for photon energies. Belle has measured these moments covering the widest range in the photon energy ($1.7 < E_\gamma < 2.8$ GeV) [173]. The measurement by BaBar has slightly smaller range with lower limit at 1.8 GeV [181]. These results can be used to extract non-perturbative HQET parameters that are needed for precise determination of the CKM matrix element V_{ub} (see further discussion elsewhere in this *Review* [182]).

Additional information on FCNC processes can be obtained from $b \to s\ell^+\ell^-$ decays. These processes are studied as a function of dilepton invariant mass squared, q^2. Different q^2 regions are sensitive to different physics. Starting at the very low q^2 decays exhibit sensitivity to the same physics as the radiative decays. Then for the q^2 in region 1.1 to 6.0 GeV$^2/c^4$ the SM and new physics have best chance to compete. At the high q^2 above the $\psi(2S)$ mass, the interference of SM and new physics is to some extend complementary to that in lower q^2. Regions around J/ψ and $\psi(2S)$ is normally excluded from measurements as these are dominated by the $b \to c$ transitions to charmonia. For exclusive decays, theory predictions require calculations of hadronic form factors. With current theory predictions, the most useful are measurements within the q^2 regions 1.1 to 6.0 GeV$^2/c^4$ and from 16.0 GeV$^2/c^4$ up to the kinematic limit. From this reason in the listing we provide results mainly in those two regions.

Similar as for radiative decays, also for the $b \to s\ell^+\ell^-$ decays the inclusive measurements provide some benefits. Both Belle and BaBar performed such measurement without reconstructing hadronic part exclusively and measure a branching fraction of $(5.8 \pm 1.3) \times 10^{-6}$ [183]. Unfortunately this measurement is not trivially possible at hadron colliders and also does not easily allow the angular distributions of the decay products to be exploited. One alternative is to extract information on the inclusive decay as sum of exclusive decays. Such a measurement was performed by Belle [184], but in this case the difficulty lies in extrapolation for the missing hadronic states.

Turning to the exclusive decays, the initial measurements performed by B-factories typically averaged between charged and neutral B mesons as well as between e^+e^- and $\mu^+\mu^-$ finals states. The experiments CDF, LHCb, ATLAS and CMS are much better suited for the $\mu^+\mu^-$ finals states compared to the e^+e^- final states. As such most measurements at hadron colliders are done only with $\mu^+\mu^-$ pairs and by separating charged and neutral B mesons. Recently, however, with much increased statistics, LHCb measured several final states with e^+e^-, to make a series of tests of e/μ universality in $B \to K^{(*)}\ell^+\ell^-$ decays. At hadron colliders other b hadrons are produced and as such CDF and LHCb experiments did observe also $B_s^0 \to \phi\mu^+\mu^-$ [185, 186], $\Lambda_b^0 \to \Lambda\mu^+\mu^-$ [185, 187] and $\Lambda_b^0 \to pK^-\mu^+\mu^-$ decays [188]. The averages of the total branching fractions integrated over whole q^2 regions are $(5.6 \pm 0.6) \times 10^{-7}$ for $B^+ \to K^+e^+e^-$, $(4.53 \pm 0.35) \times 10^{-7}$ for $B^+ \to K^+\mu^+\mu^-$, $(1.03^{+0.19}_{-0.17}) \times 10^{-6}$ for $B^0 \to K^*(892)^0e^+e^-$ and $(0.94 \pm 0.05) \times 10^{-6}$ for $B^0 \to K^*(892)^0\mu^+\mu^-$ decays [189–193]. The total branching fractions for $B_s^0 \to \phi\mu^+\mu^-$ and $\Lambda_b^0 \to \Lambda\mu^+\mu^-$ decays are $(8.4 \pm 0.4) \times 10^{-7}$ [185, 186, 194] and $(1.08 \pm 0.28) \times 10^{-6}$ [185, 187] respectively. With increased precision of $B^0 \to K^*(892)^0\ell^+\ell^-$ decay, there is a question on what fraction of the seen branching fraction is due to the $K^*(892)^0$ resonance and what fraction is due to the $K\pi$ in s-wave. This has been studied by LHCb which found that the $K\pi$ in s-wave fraction varies between 1% and about 10% depending on the q^2 region [193]. It should be noted, that for all relevant B meson decays the branching fractions so far studied are consistently below the SM expectation.

In the $b \to s\ell^+\ell^-$ decays angular distributions offer rich source of information. The full angular analysis was performed for decays $B^+ \to K^+\ell^+\ell^-$, $B^0 \to K^0\ell^+\ell^-$, $B^+ \to K^*(892)^+\ell^+\ell^-$, $B^0 \to K^*(892)^0\ell^+\ell^-$, $B_s^0 \to \phi\mu^+\mu^-$ and $\Lambda_b^0 \to \Lambda\mu^+\mu^-$ decays [195–203]. An attempt to increase sensitivity to the NP was made by constructing observables, which have reduced theory uncertainties and measurements of these are done. Most notably the observable called P_5' [204] shows a discrepancy with the SM in the q^2 region which is highly sensitive to new physics [197–199]. Measurements of the CP asymmetries [188, 189, 192, 205, 206] and the isospin asymmetry [190–192, 205] were also performed. All these measurements are well consistent with the small A_{CP} and small isospin asymmetry expected in the SM [207]. With statistics available at the LHC, the measurement of phase difference between long- and short-distance contribution in $B^+ \to K^+\mu^+\mu^-$ decays became possible [208].

With the data samples available at LHC, the lepton universality in $b \to s\ell^+\ell^-$ can be tested. While in the SM decays to electron-positron and muon pairs are expected to be same up to small corrections due to the different masses of leptons, in extensions of the SM this does not have to hold. The angular analysis of $B^0 \to K^*(892)^0e^+e^-$ decays was performed by LHCb at low dilepton invariant masses [209] and Belle in several regions over whole q^2 range [199]. The LHCb measurement yields the most stringent constraint on the photon polarization. The result on lepton universality test which over past few years attracted most attention is the ratio of branching fractions between $B^+ \to K^+\mu^+\mu^-$ and $B^+ \to K^+e^+e^-$ and between $B^0 \to K^*(892)^0\mu^+\mu^-$ and $B^0 \to K^*(892)^0e^+e^-$ decays [190, 210]. The measurements by LHCb showed mild discrepancy from the SM, with significance of $3.1\,\sigma$ for $B^+ \to K^+\ell^+\ell^-$ and about $2.4\,\sigma$ for $B^0 \to K^*(892)^0\ell^+\ell^-$. The latest analysis in Ref. [211] identified previously missed hadronic misidentification background. With better handling of such background the results are now consistent with the SM. LHCb experiment performed similar test with $\Lambda_b^0 \to pK^-\ell^+\ell^-$ decays [212], $B^0 \to K_S^0\ell^+\ell^-$ and $B^+ \to K^*(892)^+\ell^+\ell^-$ [213].

While $b \to d\ell^+\ell^-$ decays are further suppressed, they recently became accessible. Signals were observed for $B^+ \to \pi^+\mu^+\mu^-$ [87], $B^0 \to \pi^+\pi^-\mu^+\mu^-$ [214] and $\Lambda_b^0 \to p\pi^-\mu^+\mu^-$ [215] decays. Search for the $B_s^0 \to \overline{K}^*(892)^0\mu^+\mu^-$ at LHCb is complicated by large background from $B^0 \to K^*(892)^0\mu^+\mu^-$ and current significance for the decay is 3.4σ [216]. The total branching fractions are only quantities measured and these are about 2×10^{-8} for the meson decays and about 7×10^{-8} for the Λ_b^0 decay.

A closely related process is $B \to X_s\nu\overline{\nu}$. Since the neutrinos are not detected, the final state is a strange hadron system X_s plus missing energy-momentum. Depending on X_s, the SM branching fraction is $\mathcal{O}(10^{-6})$. New physics effects beyond SM, e.g. those from dark sector models can greatly enhance the yield of X_s plus missing energy. BaBar [217], Belle [218], and Belle II [219] have searched for these decays and determined the upper limits in the range $\mathcal{O}(10^{-5})$.

Finally the decays $B_{(s)}^0 \to e^+e^-$ and $\mu^+\mu^-$ are interesting

Int. J. Mod. Phys. A 2026.41. Downloaded from www.worldscientific.com
UNIVERSITY OF CALIFORNIA @ BERKELEY on 09/16/26. Re-use and distribution is strictly not permitted, except for Open Access articles.

since they only proceed at second order in weak interactions in the SM, but may have large contributions from supersymmetric loops, proportional to $(\tan\beta)^6$. First limits were published more than 30 years ago and since then experiments at Tevatron, B-factories and LHC gradually improved those and effectively excluded whole models of new physics and significantly constrained allowed parameter space of others. For the decays to $\mu^+\mu^-$, Tevatron experiments pushed the limits down to roughly factor of 5-10 above the SM expectation [220]. The long journey in the search for these decays culminated in 2012, when first evidence for $B_s^0 \to \mu^+\mu^-$ decay was seen [221]. Subsequently, LHC experiments ATLAS [222], CMS [223] and LHCb [224] observed statistically significant signal for $B_s^0 \to \mu^+\mu^-$ decay. The current average branching fraction is $(3.34 \pm 0.27) \times 10^{-9}$. In experiments at hadron colliders searches for $B^0 \to \mu^+\mu^-$ decays are performed at the same time. The $B(B^0 \to \mu^+\mu^-)$ is extracted in simultaneously with $B(B_s^0 \to \mu^+\mu^-)$ and is found to be $(0.07^{+0.13}_{-0.11}) \times 10^{-9}$. The limits for the e^+e^- modes are: $< 9.4 \times 10^{-9}$ and $< 2.5 \times 10^{-9}$, respectively, for B_s^0 and B^0 [225]. The searches for decays to $\tau^+\tau^-$ are more challenging with current best limits of $B(B^0 \to \tau^+\tau^-) < 2.1 \times 10^{-3}$ and $B(B_s^0 \to \tau^+\tau^-) < 6.8 \times 10^{-3}$ at 95% C.L. [226]. All existing measurements of B^0 and B_s^0 decays to same flavour dilepton pair is consistent with SM expectation [227]. With $B_s^0 \to \mu^+\mu^-$ decay observed, it was suggested that the effective lifetime is useful further test of the decay [228]. Attempt was made by LHCb and CMS experiments, but its precision is not yet sufficient to provide test of the SM [223, 224]. It will take couple of years until interesting precision is reached. The searches were also performed for lepton flavour violating decays to two leptons with best limits in $e^\pm\mu^\mp$ channel, where limits are $< 1.3 \times 10^{-9}$ for B^0 and $< 6.3 \times 10^{-9}$ for B_s^0, at 95% confidence level [229].

Several theory groups performed global analysis of electroweak decays concluding that significant tension between data and SM is present [230]. The tension can be relieved by new physics beyond SM. For more detailed reviews see e.g. Ref. [231].

72.7 Summary and Outlook

The study of B mesons continues to be one of the most productive fields in particle physics. With the two asymmetric B-factory experiments Belle and BaBar, we now have a combined data sample of well over 1 ab^{-1}. CP violation has been firmly established in many decays of B mesons. Evidence for direct CP violation has been observed. Many rare decays resulting from hadronic $b \to u$ transitions and $b \to s(d)$ penguin decays have been observed, and the emerging pattern is still full of surprises. Despite the remarkable successes of the B-factory experiments, many fundamental questions in the flavor sector remain unanswered.

At Fermilab, CDF and D0 each has accumulated about 10 fb^{-1}, which is the equivalent of about 10^{12} b-hadrons produced. In spite of the low trigger efficiency of hadronic experiments, a selection of modes have been reconstructed in large quantities, giving a start to a program of studies on B_s and b-flavored baryons, in which a first major step has been the determination of the B_s oscillation frequency.

As Tevatron and B-factories finished their data taking few year ago, the experiments at the LHC have become very active. LHCb has collected about 1 fb^{-1} at 7 TeV, 2 fb^{-1} at 8 TeV, and close to 5.9 fb^{-1} at 13 TeV during LHC Runs 1 and 2. CMS and ATLAS have collected each about 5 fb^{-1} of data at $\sqrt{s} = 7$ TeV, 20 fb^{-1} at 8 TeV and about 150 fb^{-1} at 13 TeV during LHC Runs 1 and 2. The latest LHC Run 3 at 13.6 TeV started in summer 2022, with upgraded detectors. By the time of the writing (March 2026), LHC has delivered about 330 fb^{-1} to ATLAS and CMS experiments. LHCb, which is dedicated to the studies of b- and c-hadrons, has a data sample that is larger than the sum of all previous experiments. With it, we are entering to regime of precision physics even for many rare decays, which allows much more detailed measurements.

The Belle II experiment at the SuperKEKB has started recording data in 2019 and has by March 2026 collected about 700 fb^{-1} of data with successful restart of data taking after their long shutdown. The aim to increase sample to $\sim$ 50 ab^{-1} will make it possible to explore the indirect evidence of new physics beyond the SM in the heavy-flavor particles (b, c, and τ), in a way that is complementary to the LHC. The LHCb Collaboration successfuly commissioned upgrade of its detector and since 2024 is accummulating data as planned rate/ The aim of the upgrade was to increase flexibility of the trigger, which will allow about a factor of five increase in instantaneous luminosity and of about a factor of two in efficiencies on triggering on purely hadronic decays, which is being delivered. The plan is to integrate about 50 fb^{-1} of data during LHC runs 3 and 4.

These experiments promise a rich spectrum of rare and precise measurements that have the potential to fundamentally affecting our understanding of the SM and CP-violating phenomena.

References

[1] M. Kobayashi and T. Maskawa, Prog. Theor. Phys. **49**, 652 (1973).

[2] S. W. Herb *et al.*, Phys. Rev. Lett. **39**, 252 (1977).

[3] B. Aubert *et al.* (BaBar), Phys. Rev. Lett. **87**, 091801 (2001), [hep-ex/0107013].

[4] K. Abe *et al.* (Belle), Phys. Rev. Lett. **87**, 091802 (2001), [hep-ex/0107061].

[5] Currently two different notations (ϕ_1, ϕ_2, ϕ_3) and (α, β, γ) are used in the literature for CKM unitarity angles. In this mini-review, we use the latter notation following the other mini-reviews in this *Review*. The two notations are related by $\phi_1 = \beta$, $\phi_2 = \alpha$ and $\phi_3 = \gamma$.

[6] See the "CP Violation in Meson Decays" by D. Kirkby and Y. Nir in this *Review*.

[7] See the "CKM Quark Mixing Matrix," by A. Cecucci, Z. Ligeti, and Y. Sakai, in this *Review*.

[8] See the note on "$B^0 - \overline{B}^0$ mixing," by O. Schneider in this *Review*.

[9] See the "Determination of $|V_{cb}|$ and $|V_{ub}|$," by R. Kowalewski and T. Mannel in this *Review*.

[10] F. Abe *et al.* (CDF), Phys. Rev. Lett. **81**, 2432 (1998), [hep-ex/9805034]; F. Abe *et al.* (CDF), Phys. Rev. **D58**, 112004 (1998), [hep-ex/9804014].

[11] A. Abulencia *et al.* (CDF), Phys. Rev. Lett. **96**, 082002 (2006), [hep-ex/0505076].

[12] R. Aaij *et al.* (LHCb), JHEP **07**, 123 (2020), [arXiv:2004.08163].

[13] B. Aubert *et al.* (BaBar), Phys. Rev. Lett. **101**, 071801 (2008), [Erratum: Phys. Rev. Lett. 102, 029901 (2009)], [arXiv:0807.1086].

[14] B. Aubert *et al.* (BaBar), Phys. Rev. Lett. **103**, 161801 (2009), [arXiv:0903.1124].

[15] G. Bonvicini *et al.* (CLEO), Phys. Rev. **D81**, 031104 (2010), [arXiv:0909.5474].

[16] R. Mizuk *et al.* (Belle), Phys. Rev. Lett. **109**, 232002 (2012), [arXiv:1205.6351].

[17] U. Tamponi *et al.* (Belle), Phys. Rev. Lett. **115**, 14, 142001 (2015), [arXiv:1506.08914].

[18] B. Fulsom *et al.* (Belle), Phys. Rev. Lett. **121**, 232001 (2018), [arXiv:1807.01201].

[19] A. Bondar *et al.* (Belle), Phys. Rev. Lett. **108**, 122001 (2012), [arXiv:1110.2251].

[20] See the note on "Naming scheme for hadrons," by M. Roos and C.G. Wohl in this *Review*.

[21] R. Aaij *et al.* (LHCb), Phys. Rev. Lett. **118**, 5, 052002 (2017), [Erratum: Phys. Rev. Lett. 119, 169901 (2017)], [arXiv:1612.05140].

[22] M. Cacciari *et al.*, JHEP **10**, 137 (2012), [arXiv:1205.6344]; B. A. Kniehl *et al.*, Phys. Rev. **D84**, 094026 (2011), [arXiv:1109.2472]; M. Cacciari, M. L. Mangano and P. Nason, Eur. Phys. J. **C75**, 12, 610 (2015), [arXiv:1507.06197].

[23] B. Barish *et al.* (CLEO), Phys. Rev. Lett. **76**, 1570 (1996).

Int. J. Mod. Phys. A 2026.41. Downloaded from www.worldscientific.com
by UNIVERSITY OF CALIFORNIA @ BERKELEY on 09/16/26. Re-use and distribution is strictly not permitted, except for Open Access articles.

[24] E. Guido *et al.* (Belle), Phys. Rev. Lett. **121**, 062001 (2018), [arXiv:1803.10303]; E. Guido *et al.* (Belle), Phys. Rev. **D96**, 052005 (2017), [arXiv:1707.04973]; A. Sokolov *et al.* (Belle), Phys. Rev. **D79**, 051103 (2009), [arXiv:0901.1431]; B. Aubert *et al.* (BaBar), Phys. Rev. **D78**, 112002 (2008), [arXiv:0807.2014].

[25] J. P. Alexander *et al.* (CLEO), Phys. Rev. Lett. **86**, 2737 (2001), [hep-ex/0006002]; S. B. Athar *et al.* (CLEO), Phys. Rev. **D66**, 052003 (2002), [hep-ex/0202033]; N. C. Hastings *et al.* (Belle), Phys. Rev. **D67**, 052004 (2003), [hep-ex/0212033].

[26] B. Aubert *et al.* (BaBar), Phys. Rev. Lett. **95**, 042001 (2005), [hep-ex/0504001].

[27] Y. Amhis *et al.* (HFLAV), Eur. Phys. J. **C77**, 12, 895 (2017), [arXiv:1612.07233].

[28] Y. S. Amhis *et al.* (HFLAV), Eur. Phys. J. C **81**, 3, 226 (2021), [arXiv:1909.12524].

[29] R. Aaij *et al.* (LHCb), Phys. Rev. Lett. **131**, 061901 (2023), [arXiv:2204.13042], URL `https://link.aps.org/doi/10.1103/PhysRevLett.131.061901`.

[30] P. Abreu *et al.* (DELPHI), Phys. Lett. **B345**, 598 (1995).

[31] R. Akers *et al.* (OPAL), Z. Phys. **C66**, 19 (1995).

[32] T. A. Aaltonen *et al.* (CDF), Phys. Rev. **D90**, 1, 012013 (2014), [arXiv:1309.5961]; R. Aaij *et al.* (LHCb), JHEP **04**, 024 (2015), [arXiv:1502.02638].

[33] R. Aaij *et al.* (LHCb), Phys. Rev. Lett. **110**, 15, 151803 (2013), [arXiv:1211.5994].

[34] A. M. Sirunyan *et al.* (CMS), Eur. Phys. J. **C78**, 939 (2018), [arXiv:1809.03578].

[35] G. Aad *et al.* (ATLAS), Phys. Rev. Lett. **113**, 21, 212004 (2014), [arXiv:1407.1032].

[36] A. Sirunyan *et al.* (CMS), Phys. Rev. Lett. **122**, 132001 (2019), [arXiv:1902.00571]; R. Aaij *et al.* (LHCb), Phys. Rev. Lett. **122**, 232001 (2019), [arXiv:1904.00081].

[37] T. Aaltonen *et al.* (CDF), Phys. Rev. Lett. **99**, 202001 (2007), [arXiv:0706.3868]; T. Aaltonen *et al.* (CDF), Phys. Rev. **D85**, 092011 (2012), [arXiv:1112.2808].

[38] R. Aaij *et al.* (LHCb), Phys. Rev. Lett. **122**, 012001 (2019), [arXiv:1809.07752].

[39] V. M. Abazov *et al.* (D0), Phys. Rev. Lett. **99**, 052001 (2007), [arXiv:0706.1690]; T. Aaltonen *et al.* (CDF), Phys. Rev. Lett. **99**, 052002 (2007), [arXiv:0707.0589].

[40] R. Aaij *et al.* (LHCb), Phys. Rev. Lett. **113**, 032001 (2014), [arXiv:1405.7223]; R. Aaij *et al.* (LHCb), Phys. Lett. **B736**, 154 (2014), [arXiv:1405.1543]; R. Aaij *et al.* (LHCb), Phys. Rev. **D89**, 3, 032001 (2014), [arXiv:1311.4823]; R. Aaij *et al.* (LHCb), Phys. Rev. Lett. **113**, 24, 242002 (2014), [arXiv:1409.8568]; R. Aaij *et al.* (LHCb), Phys. Rev. Lett. **115**, 24, 241801 (2015), [arXiv:1510.03829]; R. Aaij *et al.* (LHCb), Phys. Rev. Lett. **118**, 7, 071801 (2017), [arXiv:1612.02244]; R. Aaij *et al.* (LHCb), Phys. Lett. **B722**, 265 (2017), [arXiv:1701.05274]; R. Aaij *et al.* (LHCb), JHEP **02**, 98 (2018), [arXiv:1711.05490]; R. Aaij *et al.* (LHCb), Phys. Rev. **D99**, 052006 (2019), [arXiv:1901.07075]; R. Aaij *et al.* (LHCb), Phys. Rev. Lett. **124**, 11, 111802 (2020), [arXiv:1912.02110]; R. Aaij *et al.* (LHCb Collaboration), Phys. Rev. D **108**, 072002 (2023), [arXiv:2307.09427], URL `https://link.aps.org/doi/10.1103/PhysRevD.108.072002`; R. Aaij *et al.* (LHCb), Eur. Phys. J. **C84**, 237 (2024), [arXiv:2310.13546], URL `https://arxiv.org/abs/2310.13546`; R. Aaij *et al.* (LHCb Collaboration), Phys. Rev. D **110**, 072002 (2024), [arXiv:2406.12111], URL `https://link.aps.org/doi/10.1103/PhysRevD.110.072002`.

[41] R. Aaij *et al.* (LHCb Collaboration), Phys. Rev. D **103**, 012004 (2021), [arXiv:2010.14485], URL `https://link.aps.org/doi/10.1103/PhysRevD.103.012004`.

[42] R. Aaij *et al.* (LHCb), Phys. Rev. **D104**, 052010 (2021), [arXiv:2104.15074].

[43] R. Aaij *et al.* (LHCb Collaboration), Journal of High Energy Physics **2024**, 8 (2024), ISSN 1029-8479, [arXiv:2405.12688], URL `http://dx.doi.org/10.1007/JHEP08(2024)132`.

[44] T. A. Aaltonen *et al.* (CDF), Phys. Rev. **D89**, 7, 072014 (2014), [arXiv:1403.8126].

[45] A. Hayrapetyan *et al.* (CMS Collaboration), Phys. Rev. D **110**, 012002 (2024), [arXiv:2402.17738], URL `https://link.aps.org/doi/10.1103/PhysRevD.110.012002`.

[46] R. Aaij *et al.* (LHCb), JHEP **08**, 039 (2018), [arXiv:1805.03941]; R. Aaij *et al.* (LHCb), Eur. Phys. J. C **79**, 9, 745 (2019), [arXiv:1903.06792]; R. Aaij *et al.* (LHCb), Eur. Phys. J. **C79**, 9, 745 (2019), [arXiv:1903.06792].

[47] S. Chatrchyan *et al.* (CMS), Phys. Rev. Lett. **108**, 252002 (2012), [arXiv:1204.5955]; R. Aaij *et al.* (LHCb), JHEP **1605**, 161 (2016), [arXiv:1604.03896].

[48] R. Aaij *et al.* (LHCb Collaboration), Phys. Rev. Lett. **131**, 171901 (2023), [arXiv:2307.13399], URL `https://link.aps.org/doi/10.1103/PhysRevLett.131.171901`.

[49] R. Aaij *et al.* (LHCb), Phys. Rev. Lett. **114**, 062004 (2015), [arXiv:1411.4849].

[50] A. M. Sirunyan *et al.* (CMS Collaboration), Phys. Rev. Lett. **126**, 252003 (2021), [arXiv:2102.04524], URL `https://link.aps.org/doi/10.1103/PhysRevLett.126.252003`.

[51] R. Aaij *et al.* (LHCb), Phys. Rev. Lett. **121**, 072002 (2018), [arXiv:1805.09418].

[52] R. Aaij *et al.* (LHCb Collaboration), Phys. Rev. Lett. **128**, 162001 (2022), [arXiv:2110.04497], URL `https://link.aps.org/doi/10.1103/PhysRevLett.128.162001`.

[53] V. M. Abazov *et al.* (D0), Phys. Rev. Lett. **101**, 232002 (2008), [arXiv:0808.4142]; T. Aaltonen *et al.* (CDF), Phys. Rev. **D80**, 072003 (2009), [arXiv:0905.3123].

[54] R. Aaij *et al.* (LHCb), Phys. Rev. Lett. **110**, 18, 182001 (2013), [arXiv:1302.1072]; R. Aaij *et al.* (LHCb), Phys. Lett. **B736**, 154 (2014), [arXiv:1405.1543]; R. Aaij *et al.* (LHCb), Phys. Rev. **D93**, 9, 092007 (2016), [arXiv:1604.01412]; R. Aaij *et al.* (LHCb), Phys. Rev. **D104**, L091102 (2021), [arXiv:2107.03419]; R. Aaij *et al.* (LHCb Collaboration), Phys. Rev. D **108**, 052008 (2023), [arXiv:2305.15329], URL `https://link.aps.org/doi/10.1103/PhysRevD.108.052008`.

[55] R. Aaij *et al.* (LHCb Collaboration), Phys. Rev. Lett. **124**, 082002 (2020), [arXiv:2001.00851], URL `https://link.aps.org/doi/10.1103/PhysRevLett.124.082002`.

[56] V. M. Abazov *et al.* (D0), Phys. Rev. Lett. **117**, 2, 022003 (2016), [arXiv:1602.07588]; V. M. Abazov *et al.* (D0), Phys. Rev. **D97**, 092004 (2018), [arXiv:1712.10176].

[57] R. Aaij *et al.* (LHCb), Phys. Rev. Lett. **117**, 15, 152003 (2016), [Addendum: Phys. Rev. Lett.118,no.10,109904(2017)], [arXiv:1608.00435].

[58] A. Sirunyan *et al.* (CMS), Phys. Rev. Lett. **120**, 202005 (2018), [arXiv:1712.06144].

[59] T. Aaltonen *et al.* (CDF Collaboration), Phys. Rev. Lett. **120**, 202006 (2018), [arXiv:1712.09620], URL `https://link.aps.org/doi/10.1103/PhysRevLett.120.202006`.

[60] M. Aaboud *et al.* (ATLAS Collaboration), Phys. Rev. Lett. **120**, 202007 (2018), [arXiv:1802.01840], URL `https://link.aps.org/doi/10.1103/PhysRevLett.120.202007`.

[61] C. Tarantino, Eur. Phys. J. **C33**, S895 (2004), [hep-ph/0310241]; F. Gabbiani, A. I. Onishchenko and A. A. Petrov, Phys. Rev. **D70**, 094031 (2004), [hep-ph/0407004]; F. Gabbiani, A. I. Onishchenko and A. A. Petrov, Phys. Rev. **D68**, 114006 (2003), [hep-ph/0303235].

[62] A. Lenz, Int. J. Mod. Phys. **A30**, 10, 1543005 (2015), [arXiv:1405.3601].

Int. J. Mod. Phys. A 2026.41. Downloaded from www.worldscientific.com
UNIVERSITY OF CALIFORNIA @ BERKELEY on 09/16/26. Re-use and distribution is strictly not permitted, except for Open Access articles.

[63] S. Banerjee *et al.* (Heavy Flavor Averaging Group (HFLAV)), Phys. Rev. D **113**, 1, 012008 (2026), [arXiv:2411.18639].

[64] C.-H. Chang *et al.*, Phys. Rev. **D64**, 014003 (2001), [hep-ph/0007162]; V. V. Kiselev, A. E. Kovalsky and A. K. Likhoded, Nucl. Phys. **B585**, 353 (2000), [hep-ph/0002127]; A. Yu. Anisimov *et al.*, Phys. Lett. **B452**, 129 (1999), [hep-ph/9812514]; M. Beneke and G. Buchalla, Phys. Rev. **D53**, 4991 (1996), [hep-ph/9601249].

[65] R. Aaij *et al.* (LHCb), Eur. Phys. J. **C74**, 5, 2839 (2014), [arXiv:1401.6932].

[66] R. Aaij *et al.* (LHCb), Phys. Lett. **B742**, 29 (2015), [arXiv:1411.6899].

[67] Y. S. Amhis *et al.* (Heavy Flavor Averaging Group, HFLAV), Phys. Rev. D **107**, 5, 052008 (2023), [arXiv:2206.07501].

[68] J. Albrecht *et al.*, Eur. Phys. J. ST **233**, 2, 359 (2024), [arXiv:2402.04224].

[69] A. Lenz, M. L. Piscopo and A. V. Rusov, JHEP **01**, 004 (2023), [arXiv:2208.02643].

[70] J. Gratrex *et al.*, JHEP **04**, 034 (2023), [arXiv:2301.07698].

[71] F. Bernlochner *et al.*, JHEP **10**, 068 (2022), [arXiv:2205.10274].

[72] M. Bordone, B. Capdevila and P. Gambino, Phys. Lett. B **822**, 136679 (2021), [arXiv:2107.00604].

[73] The B_c is a special case, where a weak decay of the c quark is also possible, but the spectator model still applies.

[74] R. Aaij *et al.* (LHCb), Nature Phys. **11**, 743 (2015), [arXiv:1504.01568].

[75] J. P. Lees *et al.* (BaBar), Phys. Rev. **D85**, 011101 (2012), [arXiv:1110.5600]; C. Oswald *et al.* (Belle), Phys. Rev. **D87**, 7, 072008 (2013), [Erratum: Phys. Rev. D90, 119901 (2014)], [arXiv:1212.6400]; C. Oswald *et al.* (Belle), Phys. Rev. **D92**, 7, 072013 (2015), [arXiv:1504.02004].

[76] T. A. Aaltonen *et al.* (CDF), Phys. Rev. **D93**, 5, 052001 (2016), [arXiv:1601.03819].

[77] R. Aaij *et al.* (LHCb), Phys. Rev. Lett. **126**, 8, 081804 (2021), [arXiv:2012.05143].

[78] B. Grinstein, Nucl. Phys. **B339**, 253 (1990); H. Georgi, Phys. Lett. **B240**, 447 (1990); A. F. Falk *et al.*, Nucl. Phys. **B343**, 1 (1990); E. Eichten and B. R. Hill, Phys. Lett. **B234**, 511 (1990).

[79] "Heavy-Quark and Soft-Collinear Effective Theory" by C.W. Bauer and M. Neubert in this *Review*.

[80] M. Neubert, "Aspects of QCD Factorization," `hep-ph/0110093`, *Proceedings of HF9*, Pasadena (2001) and references therein; Z. Ligeti, M. E. Luke and M. B. Wise, Phys. Lett. **B507**, 142 (2001), [hep-ph/0103020].

[81] M. Beneke *et al.*, Phys. Rev. Lett. **83**, 1914 (1999), [hep-ph/9905312]; M. Beneke *et al.*, Nucl. Phys. **B591**, 313 (2000), [hep-ph/0006124]; M. Beneke *et al.*, Nucl. Phys. **B606**, 245 (2001), [hep-ph/0104110]; M. Beneke and M. Neubert, Nucl. Phys. **B675**, 333 (2003), [hep-ph/0308039].

[82] Y.-Y. Keum, H.-n. Li and A. I. Sanda, Phys. Lett. **B504**, 6 (2001), [hep-ph/0004004]; Y. Y. Keum, H.-N. Li and A. I. Sanda, Phys. Rev. **D63**, 054008 (2001), [hep-ph/0004173]; Y.-Y. Keum and H.-n. Li, Phys. Rev. **D63**, 074006 (2001), [hep-ph/0006001]; C.-D. Lu, K. Ukai and M.-Z. Yang, Phys. Rev. **D63**, 074009 (2001), [hep-ph/0004213]; C.-D. Lu and M.-Z. Yang, Eur. Phys. J. **C23**, 275 (2002), [hep-ph/0011238].

[83] C. W. Bauer, S. Fleming and M. E. Luke, Phys. Rev. **D63**, 014006 (2000), [hep-ph/0005275]; C. W. Bauer *et al.*, Phys. Rev. **D63**, 114020 (2001), [hep-ph/0011336]; C. W. Bauer and I. W. Stewart, Phys. Lett. **B516**, 134 (2001), [hep-ph/0107001].

[84] R. Ammar *et al.* (CLEO), Phys. Rev. Lett. **71**, 674 (1993).

[85] N. Taniguchi *et al.* (Belle), Phys. Rev. Lett. **101**, 111801 (2008), [Erratum: Phys. Rev. Lett. 101, 129904 (2008)], [arXiv:0804.4770].

[86] B. Aubert *et al.* (BaBar), Phys. Rev. **D78**, 112001 (2008), [arXiv:0808.1379].

[87] R. Aaij *et al.* (LHCb), JHEP **10**, 034 (2015), [arXiv:1509.00414].

[88] P. Krokovny *et al.* (Belle), Phys. Rev. Lett. **89**, 231804 (2002), [hep-ex/0207077]; B. Aubert *et al.* (BaBar), Phys. Rev. Lett. **98**, 081801 (2007), [hep-ex/0604012].

[89] B. Kronenbitter *et al.* (Belle), Phys. Rev. **D92**, 5, 051102 (2015), [arXiv:1503.05613]; I. Adachi *et al.* (Belle), Phys. Rev. Lett. **110**, 13, 131801 (2013), [arXiv:1208.4678].

[90] J. P. Lees *et al.* (BaBar), Phys. Rev. **D88**, 3, 031102 (2013), [arXiv:1207.0698]; B. Aubert *et al.* (BaBar), Phys. Rev. **D81**, 051101 (2010), [arXiv:0912.2453].

[91] See the "Leptonic decays of charged pseudoscalar mesons," by R. Briere, J. Rosner, S. Stone, and R. Van de Water, in this *Review*.

[92] J. P. Lees *et al.* (BaBar), Phys. Rev. **D84**, 112007 (2011), [Erratum: Phys. Rev. D87, 039901 (2013)], [arXiv:1107.5751]; S. Blyth *et al.* (Belle), Phys. Rev. **D74**, 092002 (2006), [hep-ex/0607029].

[93] R. Aaij *et al.* (LHCb), Phys. Rev. D **92**, 3, 032002 (2015), [arXiv:1505.01710].

[94] B. Aubert *et al.* (BaBar), Phys. Rev. Lett. **90**, 242001 (2003), [hep-ex/0304021].

[95] D. Besson *et al.* (CLEO), Phys. Rev. **D68**, 032002 (2003), [Erratum: Phys. Rev.D75,119908(2007)], [hep-ex/0305100].

[96] P. Krokovny *et al.* (Belle), Phys. Rev. Lett. **91**, 262002 (2003), [hep-ex/0308019]; Y. Mikami *et al.* (Belle), Phys. Rev. Lett. **92**, 012002 (2004), [hep-ex/0307052].

[97] B. Aubert *et al.* (BaBar), Phys. Rev. Lett. **93**, 181801 (2004), [hep-ex/0408041].

[98] R. Aaij *et al.* (LHCb), Phys. Rev. Lett. **113**, 162001 (2014), [arXiv:1407.7574].

[99] R. Aaij *et al.* (LHCb), JHEP **12**, 141 (2021), [arXiv:2110.02350]; F. Abudinén *et al.* (Belle, Belle-II), JHEP **02**, 063 (2022), [Erratum: JHEP 12, 034 (2022)], [arXiv:2110.12125].

[100] T. Aaltonen *et al.* (CDF), Phys. Rev. Lett. **108**, 201801 (2012), [arXiv:1204.0536].

[101] S. Esen *et al.* (Belle), Phys. Rev. **D87**, 3, 031101 (2013), [arXiv:1208.0323].

[102] R. Aaij *et al.* (LHCb), Phys. Rev. **D93**, 9, 092008 (2016), [arXiv:1602.07543].

[103] R. Aaij *et al.* (LHCb), Phys. Rev. Lett. **116**, 16, 161802 (2016), [arXiv:1603.02408].

[104] R. Aaij *et al.* (LHCb), JHEP **11**, 082 (2015), [arXiv:1509.00400].

[105] B. Aubert *et al.* (BaBar), Phys. Rev. **D76**, 031101 (2007), [arXiv:0704.1266].

[106] R. Aaij *et al.* (LHCb), Phys. Rev. **D90**, 1, 012003 (2014), [arXiv:1404.5673].

[107] R. Aaij *et al.* (LHCb), Phys. Rev. Lett. **111**, 18, 181801 (2013), [arXiv:1308.4544].

[108] R. Aaij *et al.* (LHCb), JHEP **07**, 066 (2023), [arXiv:2210.12000].

[109] R. Aaij *et al.* (LHCb), Phys. Rev. **D87**, 11, 112012 (2013), [Addendum: Phys. Rev. D89, 019901 (2014)], [arXiv:1304.4530].

[110] G. Aad *et al.* (ATLAS), Eur. Phys. J. **C76**, 1, 4 (2016), [arXiv:1507.07099]; G. Aad *et al.* (ATLAS), JHEP **08**, 087 (2022), [arXiv:2203.01808].

Int. J. Mod. Phys. A 2026.41. Downloaded from www.worldscientific.com
by UNIVERSITY OF CALIFORNIA @ BERKELEY on 09/16/26. Re-use and distribution is strictly not permitted, except for Open Access articles.

[111] R. Aaij *et al.* (LHCb), Phys. Rev. **D84**, 092001 (2011), [Erratum: Phys. Rev.D85,039904(2012)], [arXiv:1109.6831]; T. Aaltonen *et al.* (CDF), Phys. Rev. **D85**, 032003 (2012), [arXiv:1112.3334].

[112] S. K. Choi *et al.* (Belle), Phys. Rev. Lett. **91**, 262001 (2003), [hep-ex/0309032].

[113] D. Acosta *et al.* (CDF), Phys. Rev. Lett. **93**, 072001 (2004), [hep-ex/0312021].

[114] V. M. Abazov *et al.* (D0), Phys. Rev. Lett. **93**, 162002 (2004), [hep-ex/0405004].

[115] B. Aubert *et al.* (BaBar), Phys. Rev. **D71**, 071103 (2005), [hep-ex/0406022].

[116] R. Aaij *et al.* (LHCb), Eur. Phys. J. **C72**, 1972 (2012), [arXiv:1112.5310].

[117] S. Chatrchyan *et al.* (CMS), JHEP **04**, 154 (2013), [arXiv:1302.3968].

[118] M. Aaboud *et al.* (ATLAS), JHEP **01**, 117 (2017), [arXiv:1610.09303].

[119] S. K. Choi *et al.* (Belle), Phys. Rev. Lett. **100**, 142001 (2008), [arXiv:0708.1790]; R. Mizuk *et al.* (Belle), Phys. Rev. **D80**, 031104 (2009), [arXiv:0905.2869].

[120] R. Aaij *et al.* (LHCb), Phys. Rev. Lett. **112**, 22, 222002 (2014), [arXiv:1404.1903]; R. Aaij *et al.* (LHCb), Phys. Rev. **D92**, 11, 112009 (2015), [arXiv:1510.01951].

[121] K. Chilikin *et al.* (Belle), Phys. Rev. **D90**, 11, 112009 (2014), [arXiv:1408.6457].

[122] R. Aaij *et al.* (LHCb), Phys. Rev. Lett. **115**, 072001 (2015), [arXiv:1507.03414].

[123] R. Aaij *et al.* (LHCb), Phys. Rev. Lett. **122**, 22, 222001 (2019), [arXiv:1904.03947].

[124] R. Aaij *et al.* (LHCb), Phys. Rev. Lett. **128**, 6, 062001 (2022), [arXiv:2108.04720].

[125] R. Aaij *et al.* (LHCb), Phys. Rev. Lett. **131**, 3, 031901 (2023), [arXiv:2210.10346]; R. Aaij *et al.* (LHCb), Sci. Bull. **66**, 1278 (2021), [arXiv:2012.10380].

[126] See the "Non-$q\bar{q}$ mesons," by C. Amsler and C. Hanhart, and "Pentaquarks," by M. Karliner and T. Skwarnicki, in this *Review*.

[127] T. Aaltonen *et al.* (CDF), Phys. Rev. Lett. **107**, 261802 (2011), [arXiv:1107.4999]; R. Aaij *et al.* (LHCb), JHEP **10**, 053 (2015), [arXiv:1508.00788].

[128] T. A. Aaltonen *et al.* (CDF), Phys. Rev. Lett. **113**, 24, 242001 (2014), [arXiv:1403.5586].

[129] R. Aaij *et al.* (LHCb), JHEP **10**, 037 (2012), [arXiv:1206.2794].

[130] T. Aaltonen *et al.* (CDF), Phys. Rev. Lett. **103**, 031801 (2009), [arXiv:0812.4271].

[131] R. Aaij *et al.* (LHCb), Phys. Rev. D **98**, 3, 032004 (2018), [arXiv:1805.06759]; R. Aaij *et al.* (LHCb), JHEP **12**, 155 (2019), [arXiv:1907.10003]; R. Aaij *et al.* (LHCb), Phys. Rev. Lett. **131**, 171802 (2023), [arXiv:2304.06198], URL `https://link.aps.org/doi/10.1103/PhysRevLett.131.171802`.

[132] R. Fleischer, Phys. Lett. **B459**, 306 (1999), [hep-ph/9903456]; D. London and J. Matias, Phys. Rev. **D70**, 031502 (2004), [hep-ph/0404009].

[133] J. P. Lees *et al.* (BaBar), Phys. Rev. **D87**, 5, 052009 (2013), [arXiv:1206.3525].

[134] Y. T. Duh *et al.* (Belle), Phys. Rev. **D87**, 3, 031103 (2013), [arXiv:1210.1348].

[135] R. Aaij *et al.* (LHCb), JHEP **03**, 075 (2021), [arXiv:2012.05319].

[136] B. Aubert *et al.* (BaBar), Phys. Rev. **D76**, 091102 (2007), [arXiv:0707.2798].

[137] I. Adachi *et al.* (Belle-II), Phys. Rev. D **109**, 1, 012001 (2024), [arXiv:2310.06381].

[138] R. Aaij *et al.* (LHCb), Phys. Lett. B **726**, 646 (2013), [arXiv:1308.1277]; R. Aaij *et al.* (LHCb), Phys. Rev. Lett. **126**, 9, 091802 (2021), [arXiv:2012.12789].

[139] M. Gronau and J. L. Rosner, Phys. Rev. **D71**, 074019 (2005), [hep-ph/0503131]; M. Gronau, Phys. Lett. **B627**, 82 (2005), [hep-ph/0508047].

[140] B. Aubert *et al.* (BaBar), Phys. Rev. D **79**, 052003 (2009), [arXiv:0809.1174].

[141] M. Fujikawa *et al.* (Belle), Phys. Rev. D **81**, 011101 (2010), [arXiv:0809.4366].

[142] B. Aubert *et al.* (BaBar), Phys. Rev. **D78**, 012004 (2008), [arXiv:0803.4451]; A. Garmash *et al.* (Belle), Phys. Rev. Lett. **96**, 251803 (2006), [hep-ex/0512066].

[143] C. T. Hoi *et al.* (Belle), Phys. Rev. Lett. **108**, 031801 (2012), [arXiv:1110.2000]; B. Aubert *et al.* (BaBar), Phys. Rev. **D80**, 112002 (2009), [arXiv:0907.1743].

[144] B. Aubert *et al.* (BaBar), Phys. Rev. Lett. **97**, 201802 (2006), [hep-ex/0608005]; C. H. Wang *et al.* (Belle), Phys. Rev. **D75**, 092005 (2007), [hep-ex/0701057].

[145] R. Aaij *et al.* (LHCb), Phys. Rev. **D90**, 11, 112004 (2014), [arXiv:1408.5373]; C.-L. Hsu *et al.* (Belle), Phys. Rev. D **96**, 3, 031101 (2017), [arXiv:1705.02640].

[146] B. Aubert *et al.* (BaBar), Phys. Rev. Lett. **97**, 171805 (2006), [hep-ex/0608036].

[147] K. Abe *et al.* (Belle), Phys. Rev. Lett. **98**, 181804 (2007), [hep-ex/0608049].

[148] R. Aaij *et al.* (LHCb), Phys. Rev. Lett. **118**, 8, 081801 (2017), [arXiv:1610.08288].

[149] C. C. Peng *et al.* (Belle), Phys. Rev. **D82**, 072007 (2010), [arXiv:1006.5115].

[150] T. Aaltonen *et al.* (CDF), Phys. Rev. Lett. **106**, 181802 (2011), [arXiv:1103.5762].

[151] B. Pal *et al.* (Belle), Phys. Rev. Lett. **116**, 16, 161801 (2016), [arXiv:1512.02145].

[152] R. Aaij *et al.* (LHCb), Phys. Rev. D **102**, 1, 012011 (2020), [arXiv:2002.08229].

[153] See the "Determination of CKM angles from B hadrons," by T. Gershon, M. Kenzie, and K. Trabelsi, in this *Review*.

[154] M. Gronau and D. London, Phys. Rev. Lett. **65**, 3381 (1990).

[155] T. Julius *et al.* (Belle), Phys. Rev. **D96**, 3, 032007 (2017), [arXiv:1705.02083].

[156] B. Aubert *et al.* (BaBar), Phys. Rev. **D78**, 071104 (2008), [arXiv:0807.4977].

[157] P. Vanhoefer *et al.* (Belle), Phys. Rev. **D89**, 072008 (2014), [Addendum: Phys. Rev. D89 119903 (2014)], [arXiv:1212.4015].

[158] B. Aubert *et al.* (BaBar), Phys. Rev. **D76**, 052007 (2007), [arXiv:0705.2157]; P. Vanhoefer *et al.* (Belle), Phys. Rev. D **93**, 3, 032010 (2016), [Addendum: Phys.Rev.D 94, 099903 (2016)], [arXiv:1510.01245].

[159] B. Aubert *et al.* (BaBar), Phys. Rev. Lett. **102**, 141802 (2009), [arXiv:0901.3522]; J. Zhang *et al.* (Belle), Phys. Rev. Lett. **91**, 221801 (2003), [hep-ex/0306007].

[160] R. Aaij *et al.* (LHCb), Phys. Lett. **B747**, 468 (2015), [arXiv:1503.07770].

[161] See the "Polarization in B Decays," by A. Gritsan in this *Review*.

[162] T. E. Coan *et al.* (CLEO), Phys. Rev. Lett. **84**, 5283 (2000), [hep-ex/9912057].

[163] B. Aubert *et al.* (BaBar), Phys. Rev. Lett. **103**, 211802 (2009), [arXiv:0906.2177]; T. Horiguchi *et al.* (Belle), Phys. Rev. Lett. **119**, 19, 191802 (2017), [arXiv:1707.00394].

[164] B. Aubert *et al.* (BaBar), Phys. Rev. **D70**, 091105 (2004), [hep-ex/0409035]; S. Nishida *et al.* (Belle), Phys. Lett. **B610**, 23 (2005), [hep-ex/0411065]; B. Aubert *et al.* (BaBar), Phys. Rev. **D74**, 031102 (2006), [hep-ex/0603054].

Int. J. Mod. Phys. A 2026.41. Downloaded from www.worldscientific.com
UNIVERSITY OF CALIFORNIA @ BERKELEY on 09/16/26. Re-use and distribution is strictly not permitted, except for Open Access articles.

[165] H. Yang *et al.* (Belle), Phys. Rev. Lett. **94**, 111802 (2005), [hep-ex/0412039].

[166] B. Aubert *et al.* (BaBar), Phys. Rev. Lett. **98**, 211804 (2007), [Erratum: Phys. Rev. Lett.100,199905(2008)], [hep-ex/0507031]; P. del Amo Sanchez *et al.* (BaBar), Phys. Rev. **D93**, 5, 052013 (2016), [arXiv:1512.03579].

[167] R. Aaij *et al.* (LHCb), Phys. Rev. Lett. **112**, 16, 161801 (2014), [arXiv:1402.6852].

[168] J. Wicht *et al.* (Belle), Phys. Rev. Lett. **100**, 121801 (2008), [arXiv:0712.2659]; D. Dutta *et al.* (Belle), Phys. Rev. **D91**, 1, 011101 (2015), [arXiv:1411.7771]; R. Aaij *et al.* (LHCb), Nucl. Phys. **B867**, 1 (2013), [arXiv:1209.0313].

[169] R. Aaij *et al.* (LHCb), Phys. Rev. Lett. **123**, 3, 031801 (2019), [arXiv:1904.06697].

[170] A. Ali, E. Lunghi and A. Ya. Parkhomenko, Phys. Lett. **B595**, 323 (2004), [hep-ph/0405075]; P. Ball, G. W. Jones and R. Zwicky, Phys. Rev. **D75**, 054004 (2007), [hep-ph/0612081].

[171] J. L. Hewett, Phys. Rev. Lett. **70**, 1045 (1993), [hep-ph/9211256].

[172] S. Chen *et al.* (CLEO), Phys. Rev. Lett. **87**, 251807 (2001), [hep-ex/0108032]; J. P. Lees *et al.* (BaBar), Phys. Rev. **D86**, 112008 (2012), [arXiv:1207.5772].

[173] A. Limosani *et al.* (Belle), Phys. Rev. Lett. **103**, 241801 (2009), [arXiv:0907.1384]; T. Saito *et al.* (Belle), Phys. Rev. **D91**, 5, 052004 (2015), [arXiv:1411.7198].

[174] P. del Amo Sanchez *et al.* (BaBar), Phys. Rev. **D82**, 051101 (2010), [arXiv:1005.4087].

[175] M. Misiak *et al.*, Phys. Rev. Lett. **114**, 22, 221801 (2015), [arXiv:1503.01789]; M. Czakon *et al.*, JHEP **04**, 168 (2015), [arXiv:1503.01791]; R. Bause *et al.*, Eur. Phys. J. C **83**, 5, 419 (2023), [arXiv:2209.04457].

[176] L. Wolfenstein and Y. L. Wu, Phys. Rev. Lett. **73**, 2809 (1994), [hep-ph/9410253]; G. M. Asatrian and A. Ioannisian, Phys. Rev. **D54**, 5642 (1996), [hep-ph/9603318]; M. Ciuchini, E. Gabrielli and G. F. Giudice, Phys. Lett. **B388**, 353 (1996), [Erratum: Phys. Lett.B393,489(1997)], [hep-ph/9604438]; S. Baek and P. Ko, Phys. Rev. Lett. **83**, 488 (1999), [hep-ph/9812229]; A. L. Kagan and M. Neubert, Phys. Rev. **D58**, 094012 (1998), [hep-ph/9803368]; K. Kiers, A. Soni and G.-H. Wu, Phys. Rev. **D62**, 116004 (2000), [hep-ph/0006280].

[177] S. Watanuki *et al.* (Belle), Phys. Rev. D **99**, 3, 032012 (2019), [arXiv:1807.04236].

[178] J. P. Lees *et al.* (BaBar), Phys. Rev. **D90**, 9, 092001 (2014), [arXiv:1406.0534].

[179] B. Aubert *et al.* (BaBar), Phys. Rev. **D72**, 052004 (2005), [hep-ex/0508004].

[180] B. Aubert *et al.* (BaBar), Phys. Rev. **D77**, 051103 (2008), [arXiv:0711.4889].

[181] J. P. Lees *et al.* (BaBar), Phys. Rev. Lett. **109**, 191801 (2012), [arXiv:1207.2690].

[182] See the "Semileptonic b-Hadron Decays, Determination of V_{cb}, V_{ub}," by T. Mannel and P. Urquijo in this *Review*.

[183] M. Iwasaki *et al.* (Belle), Phys. Rev. **D72**, 092005 (2005), [hep-ex/0503044]; J. P. Lees *et al.* (BaBar), Phys. Rev. Lett. **112**, 211802 (2014), [arXiv:1312.5364].

[184] Y. Sato *et al.* (Belle), Phys. Rev. **D93**, 3, 032008 (2016), [Addendum: Phys. Rev.D93,no.5,059901(2016)], [arXiv:1402.7134].

[185] T. Aaltonen *et al.* (CDF), Phys. Rev. Lett. **107**, 201802 (2011), [arXiv:1107.3753].

[186] R. Aaij *et al.* (LHCb), JHEP **07**, 084 (2013), [arXiv:1305.2168]; R. Aaij *et al.* (LHCb), JHEP **09**, 179 (2015), [arXiv:1506.08777].

[187] R. Aaij *et al.* (LHCb), Phys. Lett. **B725**, 25 (2013), [arXiv:1306.2577].

[188] R. Aaij *et al.* (LHCb), JHEP **06**, 108 (2017), [arXiv:1703.00256].

[189] B. Aubert *et al.* (BaBar), Phys. Rev. Lett. **102**, 091803 (2009), [arXiv:0807.4119].

[190] S. Choudhury *et al.* (BELLE), JHEP **03**, 105 (2021), [arXiv:1908.01848].

[191] R. Aaij *et al.* (LHCb), JHEP **06**, 133 (2014), [arXiv:1403.8044].

[192] J. T. Wei *et al.* (Belle), Phys. Rev. Lett. **103**, 171801 (2009), [arXiv:0904.0770].

[193] R. Aaij *et al.* (LHCb), JHEP **11**, 047 (2016), [Erratum: JHEP 04, 142 (2017)], [arXiv:1606.04731].

[194] R. Aaij *et al.* (LHCb), Phys. Rev. Lett. **127**, 15, 151801 (2021), [arXiv:2105.14007].

[195] T. Aaltonen *et al.* (CDF), Phys. Rev. Lett. **108**, 081807 (2012), [arXiv:1108.0695].

[196] R. Aaij *et al.* (LHCb), JHEP **05**, 082 (2014), [arXiv:1403.8045].

[197] A. M. Sirunyan *et al.* (CMS), Phys. Lett. B **781**, 517 (2018), [arXiv:1710.02846].

[198] R. Aaij *et al.* (LHCb), Phys. Rev. Lett. **125**, 1, 011802 (2020), [arXiv:2003.04831].

[199] S. Wehle *et al.* (Belle), Phys. Rev. Lett. **118**, 11, 111801 (2017), [arXiv:1612.05014].

[200] M. Aaboud *et al.* (ATLAS), JHEP **10**, 047 (2018), [arXiv:1805.04000].

[201] R. Aaij *et al.* (LHCb), Phys. Rev. Lett. **126**, 16, 161802 (2021), [arXiv:2012.13241].

[202] R. Aaij *et al.* (LHCb), JHEP **11**, 043 (2021), [arXiv:2107.13428].

[203] R. Aaij *et al.* (LHCb), JHEP **09**, 146 (2018), [arXiv:1808.00264].

[204] S. Descotes-Genon *et al.*, JHEP **01**, 048 (2013), [arXiv:1207.2753].

[205] J. P. Lees *et al.* (BaBar), Phys. Rev. **D86**, 032012 (2012), [arXiv:1204.3933].

[206] R. Aaij *et al.* (LHCb), JHEP **09**, 177 (2014), [arXiv:1408.0978].

[207] J. Lyon and R. Zwicky, Phys. Rev. **D88**, 9, 094004 (2013), [arXiv:1305.4797].

[208] R. Aaij *et al.* (LHCb), Eur. Phys. J. **C77**, 3, 161 (2017), [arXiv:1612.06764].

[209] R. Aaij *et al.* (LHCb), JHEP **12**, 081 (2020), [arXiv:2010.06011].

[210] R. Aaij *et al.* (LHCb), Phys. Rev. Lett. **122**, 19, 191801 (2019), [arXiv:1903.09252]; R. Aaij *et al.* (LHCb), JHEP **08**, 055 (2017), [arXiv:1705.05802]; R. Aaij *et al.* (LHCb), Nature Phys. **18**, 3, 277 (2022), [arXiv:2103.11769]; A. Abdesselam *et al.* (Belle), Phys. Rev. Lett. **126**, 16, 161801 (2021), [arXiv:1904.02440].

[211] R. Aaij *et al.* (LHCb), Phys. Rev. Lett. **131**, 5, 051803 (2023), [arXiv:2212.09152].

[212] R. Aaij *et al.* (LHCb), JHEP **05**, 040 (2020), [arXiv:1912.08139].

[213] R. Aaij *et al.* (LHCb), Phys. Rev. Lett. **128**, 19, 191802 (2022), [arXiv:2110.09501].

[214] R. Aaij *et al.* (LHCb), Phys. Lett. **B743**, 46 (2015), [arXiv:1412.6433].

[215] R. Aaij *et al.* (LHCb), JHEP **04**, 029 (2017), [arXiv:1701.08705].

[216] R. Aaij *et al.* (LHCb), JHEP **07**, 020 (2018), [arXiv:1804.07167].

[217] J. P. Lees *et al.* (BaBar), Phys. Rev. D **87**, 11, 112005 (2013), [arXiv:1303.7465].

Int. J. Mod. Phys. A 2026.41. Downloaded from www.worldscientific.com
by UNIVERSITY OF CALIFORNIA @ BERKELEY on 09/16/26. Re-use and distribution is strictly not permitted, except for Open Access articles.

[218] J. Grygier *et al.* (Belle), Phys. Rev. D **96**, 9, 091101 (2017), [Addendum: Phys. Rev. D97, 099902 (2018)], [arXiv:1702.03224].

[219] F. Abudinén *et al.* (Belle-II), Phys. Rev. Lett. **127**, 18, 181802 (2021), [arXiv:2104.12624].

[220] T. Aaltonen *et al.* (CDF), Phys. Rev. Lett. **107**, 191801 (2011), [Addendum: Phys. Rev. Lett. 107, 239903 (2011)], [arXiv:1107.2304]; V. M. Abazov *et al.* (D0), Phys. Rev. **D87**, 7, 072006 (2013), [arXiv:1301.4507].

[221] R. Aaij *et al.* (LHCb), Phys. Rev. Lett. **110**, 2, 021801 (2013), [arXiv:1211.2674].

[222] M. Aaboud *et al.* (ATLAS), JHEP **04**, 098 (2019), [arXiv:1812.03017].

[223] A. M. Sirunyan *et al.* (CMS), JHEP **04**, 188 (2020), [arXiv:1910.12127].

[224] R. Aaij *et al.* (LHCb), Phys. Rev. Lett. **118**, 19, 191801 (2017), [arXiv:1703.05747]; R. Aaij *et al.* (LHCb), Phys. Rev. Lett. **128**, 4, 041801 (2022), [arXiv:2108.09284].

[225] R. Aaij *et al.* (LHCb), Phys. Rev. Lett. **124**, 21, 211802 (2020), [arXiv:2003.03999].

[226] R. Aaij *et al.* (LHCb), Phys. Rev. Lett. **118**, 25, 251802 (2017), [arXiv:1703.02508].

[227] C. Bobeth *et al.*, Phys. Rev. Lett. **112**, 101801 (2014), [arXiv:1311.0903].

[228] K. De Bruyn *et al.*, Phys. Rev. Lett. **109**, 041801 (2012), [arXiv:1204.1737]; A. J. Buras *et al.*, JHEP **07**, 77 (2013), [arXiv:1303.3820].

[229] R. Aaij *et al.* (LHCb), JHEP **03**, 078 (2018), [arXiv:1710.04111].

[230] J. Aebischer *et al.*, Eur. Phys. J. C **80**, 3, 252 (2020), [arXiv:1903.10434]; F. Beaujean, C. Bobeth and D. van Dyk, Eur. Phys. J. **C74**, 2897 (2014), [Erratum: Eur. Phys. J. C74, 3179 (2014)], [arXiv:1310.2478]; M. Algueró *et al.*, JHEP **07**, 096 (2019), [arXiv:1902.04900]; M. Algueró *et al.*, Eur. Phys. J. C **79**, 8, 714 (2019), [Addendum: Eur.Phys.J.C 80, 511 (2020)], [arXiv:1903.09578]; M. Algueró *et al.*, Eur. Phys. J. C **82**, 4, 326 (2022), [arXiv:2104.08921]; A. Arbey *et al.*, Phys. Rev. D **100**, 1, 015045 (2019), [arXiv:1904.08399]; W. Altmannshofer and P. Stangl, Eur. Phys. J. C **81**, 10, 952 (2021), [arXiv:2103.13370]; T. Hurth *et al.*, Phys. Lett. B **824**, 136838 (2022), [arXiv:2104.10058].

[231] T. Blake, G. Lanfranchi and D. M. Straub, Prog. Part. Nucl. Phys. **92**, 50 (2017), [arXiv:1606.00916]; J. Albrecht, S. Reichert and D. van Dyk, Int. J. Mod. Phys. A **33**, 1830016 (2018), [arXiv:1806.05010]; J. Albrecht, D. van Dyk and C. Langenbruch, Prog. Part. Nucl. Phys. **120**, 103885 (2021), [arXiv:2107.04822].

Int. J. Mod. Phys. A 2026.41. Downloaded from www.worldscientific.com
UNIVERSITY OF CALIFORNIA @ BERKELEY on 09/16/26. Re-use and distribution is strictly not permitted, except for Open Access articles.

73. Polarization in B Decays

Revised August 2025 by A.V. Gritsan (Johns Hopkins U.).

We review the notation used in polarization measurements in particle production and decay, with a particular emphasis on the B decays and the CP-violating observables in polarization measurements. We look at several examples of vector-vector and vector-tensor B meson decays, while more details about the theory and experimental results in B decays can be found in a separate mini-review [1] in this *Review*.

Figure 73.1 illustrates angular observables in an example of the sequential process $ab \to X \to P_1 P_2 \to (p_{11}p_{12})(p_{21}p_{22})$ [2]. The angular distributions are of particular interest because they are sensitive to spin correlations and reveal properties of particles and their interactions, such as quantum numbers and couplings. In the case of a spin-zero particle X, such as B meson or a Higgs boson, there are no spin correlations in the production mechanism and the decay chain is to be analyzed. The angular distribution of decay products can be expressed as a function of three helicity angles which describe the alignment of the particles in the decay chain. The analyzer of the B-daughter polarization is normally chosen for two-body decays, as the direction of the daughters in the center-of-mass of the parent (*e.g.*, $\rho \to 2\pi$) [3], and for three-body decays as the normal to the decay plane (*e.g.*, $\omega \to 3\pi$) [4]. An equivalent set of transversity angles is sometimes used in polarization analyses [5]. The differential decay width depends on complex amplitudes $A_{\lambda_1\lambda_2}$, corresponding to the X-daughter helicity states λ_i.

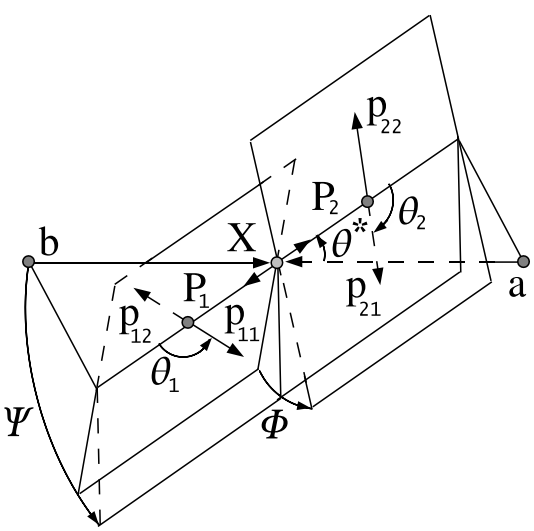

Figure 73.1: Definition of the production and helicity angles in the sequential process $ab \to X \to P_1 P_2 \to (p_{11}p_{12})(p_{21}p_{22})$. The three helicity angles include θ_1 and θ_2, defined in the rest frame of the two daughters P_1 and P_2, and Φ, defined in the X frame as the angle between the two decay planes. The two production angles θ^* and Ψ are defined in the X frame, where Ψ is the angle between the production plane and the average of the two decay planes.

In the case of a spin-zero B-meson decay, its daughter helicities are constrained to $\lambda_1 = \lambda_2 = \lambda$. Therefore we simplify amplitude notation as A_λ. Moreover, most B-decay polarization analyses are limited to the case when the spin of one of the B-meson daughters is 1. In that case, there are only three independent amplitudes corresponding to $\lambda = 0$ or ± 1 [6], where the last two can be expressed in terms of parity-even and parity-odd amplitudes $A_{\parallel,\perp} = (A_{+1} \pm A_{-1})/\sqrt{2}$. The overall decay amplitude involves three complex terms proportional to the above amplitudes and the Wigner d functions of helicity angles. The exact angular dependence would depend on the quantum numbers of the B-meson daughters and of their decay products, and can be found in the literature [6,7]. When both B-meson daughters are tensor mesons and the smaller of the two daughter spins is $J_1 > 1$, this formalism can be easily extended by introducing the parity-even and parity-odd amplitudes of higher order $A_{\parallel n,\perp n} = (A_{+n} \pm A_{-n})/\sqrt{2}$, with $1 < n \leq J_1$, while the general angular parameterization may be found in Ref. [7]. However, we limit the following discussion to $J_1 = 1$. The differential decay rate would involve six real quantities α_i, including interference terms,

$$\frac{d\Gamma}{\Gamma\, d\cos\theta_1\, d\cos\theta_2\, d\Phi} = \sum_i \alpha_i\ f_i\,(\cos\theta_1,\, \cos\theta_2,\, \Phi)\,, \qquad (73.1)$$

where each $f_i\,(\cos\theta_1,\, \cos\theta_2,\, \Phi)$ has unique angular dependence specific to particle quantum numbers, and the α_i parameters are defined as:

$$\alpha_1 = \frac{|A_0|^2}{\Sigma|A_\lambda|^2} = f_L\,, \qquad (73.2)$$

$$\alpha_2 = \frac{|A_\parallel|^2 + |A_\perp|^2}{\Sigma|A_\lambda|^2} = (1 - f_L)\,, \qquad (73.3)$$

$$\alpha_3 = \frac{|A_\parallel|^2 - |A_\perp|^2}{\Sigma|A_\lambda|^2} = (1 - f_L - 2\, f_\perp)\,, \qquad (73.4)$$

$$\alpha_4 = \frac{\Im m(A_\perp A_\parallel^*)}{\Sigma|A_\lambda|^2} = \sqrt{f_\perp(1 - f_L - f_\perp)}\ \sin(\phi_\perp - \phi_\parallel)\,, \qquad (73.5)$$

$$\alpha_5 = \frac{\Re e(A_\parallel A_0^*)}{\Sigma|A_\lambda|^2} = \sqrt{f_L\,(1 - f_L - f_\perp)}\ \cos(\phi_\parallel)\,, \qquad (73.6)$$

$$\alpha_6 = \frac{\Im m(A_\perp A_0^*)}{\Sigma|A_\lambda|^2} = \sqrt{f_\perp\, f_L}\ \sin(\phi_\perp)\,, \qquad (73.7)$$

where the amplitudes have been expressed with the help of polarization parameters f_L, $f_\perp$, $\phi_\parallel$, and $\phi_\perp$ defined in Table 73.1. Note that the terms proportional to $\Re e(A_\perp A_\parallel^*)$, $\Im m(A_\parallel A_0^*)$, and $\Re e(A_\perp A_0^*)$ are absent in Eqs. (2-7). However, these terms may appear for some three-body decays of a B-meson daughter, see Ref. [7].

Table 73.1: Rate, polarization, and CP-asymmetry parameters defined for the B-meson decays to mesons with non-zero spin. Numerical examples are shown for the average of the $B^0 \to \varphi K^*(892)^0$ decay measurements obtained from BABAR [8], Belle [9], and LHCb [10]. The first six parameters are defined under the assumption of no CP violation in decay, while they are averaged between the $\overline{B}$ and B parameters in general. The last six parameters involve differences between the $\overline{B}$ and B meson decay parameters. The phase convention δ_0 is chosen with respect to a single A_{00} amplitude from a reference B decay mode, which is $B^0 \to \varphi K_0^*(1430)^0$ for numerical results.

parameter	definition	average
$\mathcal{B}$	$\Gamma/\Gamma_{\rm total}$	$(10.1^{+0.6}_{-0.5}) \times 10^{-6}$
f_L	$\lvert A_0\rvert^2/\Sigma\lvert A_\lambda\rvert^2$	0.497 ± 0.017
$f_\perp$	$\lvert A_\perp\rvert^2/\Sigma\lvert A_\lambda\rvert^2$	0.225 ± 0.015
$\phi_\parallel - \pi$	$\arg(A_\parallel/A_0) - \pi$	-0.712 ± 0.058
$\phi_\perp - \pi$	$\arg(A_\perp/A_0) - \pi$	-0.615 ± 0.056
$\delta_0 - \pi$	$\arg(A_{00}/A_0) - \pi$	-0.26 ± 0.10
A_{CP}	$(\bar{\Gamma} - \Gamma)/(\bar{\Gamma} + \Gamma)$	-0.003 ± 0.038
A_{CP}^0	$(\bar{f_L} - f_L)/(\bar{f_L} + f_L)$	-0.007 ± 0.030
$A_{CP}^\perp$	$(\bar{f_\perp} - f_\perp)/(\bar{f_\perp} + f_\perp)$	-0.014 ± 0.057
$\Delta\phi_\parallel$	$(\bar{\phi_\parallel} - \phi_\parallel)/2$	$+0.051 \pm 0.053$
$\Delta\phi_\perp$	$(\bar{\phi_\perp} - \phi_\perp - \pi)/2$	$+0.075 \pm 0.050$
$\Delta\delta_0$	$(\bar{\delta_0} - \delta_0)/2$	$+0.13 \pm 0.08$

Overall, six real parameters describe three complex amplitudes A_0, $A_\parallel$, and $A_\perp$. These could be chosen to be the four polarization

Int. J. Mod. Phys. A 2026.41. Downloaded from www.worldscientific.com
by UNIVERSITY OF CALIFORNIA @ BERKELEY on 09/16/26. Re-use and distribution is strictly not permitted, except for Open Access articles.

parameters f_L, $f_\perp$, $\phi_\parallel$, and $\phi_\perp$, one overall size normalization, such as decay rate Γ, or branching fraction $\mathcal{B}$, and one overall phase δ_0. The phase convention is arbitrary for an isolated B decay mode. However, for several B decays, the relative phase could produce meaningful and observable effects through interference with other B decays with the same final states, such as for $B \to VK_J^*$ with $J = 0, 1, 2, 3, 4, ...$ The phase could be referenced to the single $B \to VK_0^*$ amplitude A_{00} in such a case, as shown in Table 73.1. Here V stands for any spin-one vector meson.

Moreover, *CP* violation can be tested in the angular distribution of the decay as the difference between the B and $\overline{B}$. Each of the six real parameters describing the three complex amplitudes would have a counterpart *CP*-asymmetry term, corresponding to three direct-*CP* asymmetries in three amplitudes, and three *CP*-violating phase differences, equivalent to the phase measurements from the mixing-induced *CP* asymmetries in the time evolution of B-decays [1]. In Table 73.1 and Ref. [11], these are chosen to be the direct-*CP* asymmetries in the overall decay rate $\mathcal{A}_{CP}$, in the f_L fraction $\mathcal{A}_{CP}^0$, and in the $f_\perp$ fraction $\mathcal{A}_{CP}^\perp$, and three weak phase differences:

$$\Delta\phi_\parallel = \frac{1}{2}\arg(\bar{A}_\parallel A_0/A_\parallel \bar{A}_0)\,, \tag{73.8}$$

$$\Delta\phi_\perp = \frac{1}{2}\arg(\bar{A}_\perp A_0/A_\perp \bar{A}_0) - \frac{\pi}{2}\,, \tag{73.9}$$

$$\Delta\delta_0 = \frac{1}{2}\arg(\bar{A}_{00} A_0/A_{00} \bar{A}_0)\,. \tag{73.10}$$

The $\frac{\pi}{2}$ term in Eq. (73.9) reflects the fact that $A_\perp$ and $\bar{A}_\perp$ differ in phase by π if *CP* is conserved. The two parameters $\Delta\phi_\parallel$ and $\Delta\phi_\perp$ are equivalent to triple-product asymmetries constructed from the vectors describing the decay angular distribution [12]. The *CP*-violating phase difference in the reference decay mode [11] is, in the Wolfenstein CKM quark-mixing phase convention,

$$\Delta\phi_{00} = \frac{1}{2}\arg(A_{00}/\bar{A}_{00})\,. \tag{73.11}$$

This can be measured only together with the mixing-induced phase difference for some of the neutral B-meson decays similar to other mixing-induced *CP* asymmetry measurements [1].

It may not always be possible to have a phase-reference decay mode which would define δ_0 and $\Delta\delta_0$ parameters. In that case, it may be possible to define the phase difference directly similarly to Eq. (73.11):

$$\Delta\phi_0 = \frac{1}{2}\arg(A_0/\bar{A}_0)\,. \tag{73.12}$$

One can measure the angles of the CKM unitarity triangle, assuming Standard Model contributions to the $\Delta\phi_0$ and B-mixing phases. Examples include measurements of $\beta = \phi_1$ with $B \to J/\psi K^*$ and $\alpha = \phi_2$ with $B \to \rho\rho$.

Most of the B decays that arise from tree-level $b \to c$ transitions have the amplitude hierarchy $|A_0| > |A_+| > |A_-|$ which is expected from analyses based on quark-helicity conservation [13]. The larger the mass of the vector-meson daughters, the weaker the inequality. The B meson decays to heavy vector particles with charm, such as $B \to J/\psi K^*$, $\psi(2S)K^*$, $\chi_{c1}K^*$, $D^*\rho$, D^*K^*, D^*D^*, and $D^*D_s^*$, show a substantial fraction of the amplitudes corresponding to transverse polarization of the vector mesons ($A_{\pm 1}$), in agreement with the factorization prediction. The detailed amplitude analysis of the $B \to J/\psi K^*$ decays has been performed by the BABAR [14], Belle [15], CDF [16], CLEO [17], D0 [18], and LHCb [19] collaborations. Most analyses are performed under the assumption of the absence of direct *CP* violation. The parameter values are given in the particle listing of this *Review*. The difference between the strong phases $\phi_\parallel$ and $\phi_\perp$ deviates significantly from zero. The measurements [14, 15] of *CP*-violating terms similar to those in $B \to \varphi K^*$ [8] shown in Table 73.1 are consistent with zero.

In addition, the mixing-induced *CP*-violating asymmetry is measured in the $B^0 \to J/\psi K^{*0}$ decay [1, 14, 15] where angular analysis allows one to separate *CP*-eigenstate amplitudes. This allows one to resolve the sign ambiguity of the $\cos 2\beta$ ($\cos 2\phi_1$) term that appears in the time-dependent angular distribution due to interference of parity-even and parity-odd terms. This analysis relies on the knowledge of discrete ambiguities in the strong phases $\phi_\parallel$ and $\phi_\perp$, as discussed below. The BABAR experiment used a method based on the dependence on the $K\pi$ invariant mass of the interference between the S- and P-waves to resolve the discrete ambiguity in the determination of the strong phases $(\phi_\parallel, \phi_\perp)$ in $B \to J/\psi K^*$ decays [14]. The result is in agreement with the amplitude hierarchy expectation [13]. The CDF [20], D0 [21], LHCb [22], ATLAS [23], and CMS [24] experiments have studied the $B_s^0 \to J/\psi(K^+K^-)$, $J/\psi(\pi^+\pi^-)$, $\psi(K^+\pi^-)$ decays and provided the lifetime, polarization, and phase measurements.

The amplitude hierarchy $|A_0| \gg |A_+| \gg |A_-|$ was expected in B decays to light vector particles in both penguin transitions [25, 26] and tree-level transitions [13]. There is confirmation by the BABAR and Belle experiments of predominantly longitudinal polarization in the tree-level $b \to u$ transition, such as $B^0 \to \rho^+\rho^-$ [27], $B^+ \to \rho^0\rho^+$ [28], and $B^+ \to \omega\rho^+$ [29]; this is consistent with the analysis of the quark helicity conservation [13]. Because the longitudinal amplitude dominates the decay, a detailed amplitude analysis is not possible with current B samples, and limits on the transverse amplitude fraction are obtained. The small branching fractions of $B^0 \to \rho^0\rho^0, \omega\rho^0, \omega\omega$ [29–32] indicate that $b \to d$ penguin pollution is small in the charmless, strangeless vector-vector B decays. There is a measurement of large longitudinal polarization in $B^0 \to \rho^0\rho^0$ [30–32] and $B^0 \to \omega\omega$ [33] decays. The fraction of transverse polarization is large in decays to heavier mesons such as $B^0 \to a_1(1260)^+ a_1(1260)^-$ [34].

The interest in the polarization and *CP*-asymmetry measurements in penguin transition, such as $b \to s$ decays $B \to \varphi K^*$, ρK^*, ωK^*, or $B_s^0 \to \varphi\varphi$, K^*K^*, and $b \to d$ decay $B \to K^*\bar{K}^*$, is motivated by their potential sensitivity to physics beyond the Standard Model. The decay amplitudes for $B \to \varphi K^*$ have been measured by the BABAR, Belle, and LHCb experiments [9–11, 35, 36]. The fractions of longitudinal polarization are $f_L = 0.50 \pm 0.05$ for the $B^+ \to \varphi K^{*+}$ decay and $f_L = 0.497 \pm 0.017$ for the $B^0 \to \varphi K^{*0}$ decay. These indicate significant departure from the naive expectation of predominant longitudinal polarization, suggesting other contributions to the decay amplitude, previously neglected, either within the Standard Model, such as penguin annihilation [37] or QCD rescattering [38], or from physics beyond the Standard Model [39]. The complete set of twelve amplitude parameters measured in the $B^0 \to \varphi K^{*0}$ decay is given in Table 73.1. Several other parameters could be constructed from the above twelve parameters, as suggested in Ref. [40].

The discrete ambiguity in the phase $(\phi_\parallel, \phi_\perp, \Delta\phi_\parallel, \Delta\phi_\perp)$ measurements has been resolved by BABAR in favor of $|A_+| \gg |A_-|$ through interference between the S- and P-waves of $K\pi$. The search for vector-tensor and vector-axialvector $B \to \varphi K_J^{(*)}$ decays with $J = 1, 2, 3, 4$ revealed a large fraction of longitudinal polarization in the decay $B \to \varphi K_2^*(1430)$ with $f_L = 0.90^{+0.06}_{-0.07}$ [11, 41], but large contribution of transverse amplitude in $B \to \varphi K_1(1270)$ with $f_L = 0.46^{+0.13}_{-0.15}$ [42].

Like $B \to \varphi K^*$, the decays $B \to \rho K^*$ and $B \to \omega K^*$ may be sensitive to New Physics. Measurements of the longitudinal polarization fraction in $B \to \rho K^*$ [43] and in both vector-vector and vector-tensor final states of $B \to \omega K_J^*$ [29] by BABAR and Belle reveal a large fraction of transverse polarization, indicating an anomaly similar to $B \to \varphi K^*$ except for a different pattern in vector-tensor final states. An angular analysis of the $B^0 \to \rho^0 K^{*0}$ decay mode by LHCb [44] provides much higher precision and indicates remarkably small longitudinal polarization fraction and a significant direct CP asymmetry observed in angular distributions of $B \to VV$ decays for the first time. A large transverse polarization is also observed in the $B_s^0 \to \varphi\varphi$ decay by CDF [45] and LHCb [46], $B_s^0 \to K^{*0}\bar{K}^{*0}$ decays by LHCb [47], and $B_s^0 \to \varphi K^{*0}$ decays by LHCb [48]. At the same time, measurement of the polarization in the $b \to d$ penguin decays $B \to K^*\bar{K}^*$ indicates a large fraction of longitudinal polarization [47, 49]. The LHCb experiment has also provided the very first polarization results on the tensor-tensor, as well as vector-tensor, decays of the B_s^0 meson in the $(K\pi)(K\pi)$ final state [47]. The polarization pattern in penguin-dominated B-meson decays is not fully understood [37–39].

Int. J. Mod. Phys. A 2026.41. Downloaded from www.worldscientific.com
UNIVERSITY OF CALIFORNIA @ BERKELEY on 09/16/26. Re-use and distribution is strictly not permitted, except for Open Access articles.

The three-body semileptonic B-meson decays, such as $B \to V\ell_1\ell_2$, share many features with the two-body $B \to VV$ decays. Their differential decay width can be parameterized with the two helicity angles defined in the V and $(\ell_1\ell_2)$ frames and with the azimuthal angle, as defined in Fig. 73.1. However, since the $(\ell_1\ell_2)$ pair does not come from an on-shell particle, the angular distribution is unique to each point in the dilepton mass $m_{\ell\ell}$ spectrum. The polarization measurements as a function of $m_{\ell\ell}$ provide complementary information on physics beyond the Standard Model, as discussed for $B \to K^*\ell^+\ell^-$ and $B_s \to \phi\ell^+\ell^-$ decays in Ref. [50]. The data in these modes have been analyzed by the BABAR, Belle, CDF, CMS, ATLAS, and LHCb experiments [51–56].

The examples of the angular distributions and observables in $B \to K^*\ell^+\ell^-$ are discussed in Ref. [50]. Two angular observables have been measured in this decay in certain ranges of the dilepton mass $m_{\ell\ell}$. One parameter is the fraction of longitudinal polarization F_L, which is determined by the K^* angular distribution and is similar to f_L defined for exclusive two-body decays. The other parameter is the forward-backward asymmetry of the lepton pair A_{FB}, which is the asymmetry of the decay rate with positive and negative values of $\cos\theta_1$. A complete set of observables and angular terms has been adopted by the LHCb collaboration [56] following Ref. [50] with the F_L, A_{FB}, and $S_3 - S_9$ coefficients in the angular distributions. Additional set of optimized observables $P_i^{(\prime)}$ is derived from those, for example $P_2 = 2A_{FB}/(3-3F_L)$ and $P_5' = S_5/\sqrt{F_L(1-F_L)}$. These observables have the advantage that the leading form-factor uncertainties cancel. There have been hints of deviations from SM in the measurement of P_5' and lepton flavor universality [51–56].

In summary, there has been considerable interest in the polarization measurements of B-meson decays because they reveal both weak- and strong-interaction dynamics [37–39, 57]. New measurements will further elucidate the pattern of spin alignment measurements in rare B decays, and further test the Standard Model and strong interaction dynamics, including the non-factorizable contributions to the B-decay amplitudes.

References

[1] P. Eerola, M. Kreps, and Y. Kwon, "Production and Decay of b-Flavored Hadrons," mini-review in this *Review*.

[2] Y. Gao *et al.*, Phys. Rev. D **81**, 075022 (2010), [arXiv:1001.3396].

[3] M. Jacob and G. Wick, Annals Phys. **7**, 404 (1959).

[4] S. Berman and M. Jacob, Phys. Rev. **139**, B1023 (1965).

[5] I. Dunietz *et al.*, Phys. Rev. D **43**, 2193 (1991).

[6] G. Kramer and W. Palmer, Phys. Rev. D **45**, 193 (1992).

[7] A. Datta *et al.*, Phys. Rev. D **77**, 114025 (2008), [arXiv:0711.2107].

[8] B. Aubert *et al.* (BaBar), Phys. Rev. D **78**, 092008 (2008), [arXiv:0808.3586].

[9] M. Prim *et al.* (Belle), Phys. Rev. D **88**, 7, 072004 (2013), [arXiv:1308.1830].

[10] R. Aaij *et al.* (LHCb), JHEP **05**, 069 (2014), [arXiv:1403.2888].

[11] B. Aubert *et al.* (BaBar), Phys. Rev. Lett. **93**, 231804 (2004), [hep-ex/0408017]; B. Aubert *et al.* (BaBar), Phys. Rev. Lett. **98**, 051801 (2007), [hep-ex/0610073]; B. Aubert *et al.* (BaBar), Phys. Rev. D **78**, 092008 (2008), [arXiv:0808.3586].

[12] G. Valencia, Phys. Rev. D **39**, 3339 (1989); A. Datta and D. London, Int. J. Mod. Phys. A **19**, 2505 (2004), [hep-ph/0303159].

[13] A. Ali *et al.*, Z. Phys. C **1**, 269 (1979); M. Suzuki, Phys. Rev. D **64**, 117503 (2001), [hep-ph/0106354].

[14] B. Aubert *et al.* (BaBar), Phys. Rev. D **71**, 032005 (2005), [hep-ex/0411016]; B. Aubert *et al.* (BaBar), Phys. Rev. D **76**, 031102 (2007), [arXiv:0704.0522].

[15] R. Itoh *et al.* (Belle), Phys. Rev. Lett. **95**, 091601 (2005), [hep-ex/0504030]; M. Prim *et al.* (Belle), Phys. Rev. D **88**, 7, 072004 (2013), [arXiv:1308.1830].

[16] T. Affolder *et al.* (CDF), Phys. Rev. Lett. **85**, 4668 (2000), [hep-ex/0007034]; D. Acosta *et al.* (CDF), Phys. Rev. Lett. **94**, 101803 (2005), [hep-ex/0412057].

[17] C. Jessop *et al.* (CLEO), Phys. Rev. Lett. **79**, 4533 (1997), [hep-ex/9702013].

[18] V. Abazov *et al.* (D0), Phys. Rev. Lett. **102**, 032001 (2009), [arXiv:0810.0037].

[19] R. Aaij *et al.* (LHCb), Phys. Rev. D **88**, 052002 (2013), [arXiv:1307.2782].

[20] T. Aaltonen *et al.* (CDF), Phys. Rev. Lett. **100**, 121803 (2008), [arXiv:0712.2348]; T. Aaltonen *et al.* (CDF), Phys. Rev. D **85**, 072002 (2012), [arXiv:1112.1726].

[21] V. Abazov *et al.* (D0), Phys. Rev. Lett. **98**, 121801 (2007), [hep-ex/0701012]; V. M. Abazov *et al.* (D0), Phys. Rev. D **85**, 032006 (2012), [arXiv:1109.3166].

[22] R. Aaij *et al.* (LHCb), Phys. Rev. Lett. **108**, 101803 (2012), [arXiv:1112.3183]; R. Aaij *et al.* (LHCb), Phys. Rev. Lett. **114**, 4, 041801 (2015), [arXiv:1411.3104]; R. Aaij *et al.* (LHCb), Phys. Lett. B **747**, 484 (2015), [arXiv:1503.07112]; R. Aaij *et al.* (LHCb), JHEP **11**, 082 (2015), [arXiv:1509.00400]; R. Aaij *et al.* (LHCb), JHEP **08**, 037 (2017), [arXiv:1704.08217]; R. Aaij *et al.* (LHCb) (2025), [arXiv:2506.22090].

[23] G. Aad *et al.* (ATLAS), Eur. Phys. J. C **81**, 4, 342 (2021), [arXiv:2001.07115].

[24] A. Hayrapetyan *et al.* (CMS) (2024), [arXiv:2412.19952].

[25] H.-Y. Cheng and K.-C. Yang, Phys. Lett. B **511**, 40 (2001), [hep-ph/0104090]; C.-H. Chen, Y.-Y. Keum and H.-n. Li, Phys. Rev. D **66**, 054013 (2002), [hep-ph/0204166].

[26] A. L. Kagan, Phys. Lett. B **601**, 151 (2004), [hep-ph/0405134]; Y. Grossman, Int. J. Mod. Phys. A **19**, 907 (2004), [hep-ph/0310229].

[27] B. Aubert *et al.* (BaBar), Phys. Rev. D **76**, 052007 (2007), [arXiv:0705.2157]; P. Vanhoefer *et al.* (Belle), Phys. Rev. D **93**, 3, 032010 (2016), [Erratum: Phys. Rev. D **94**, 099903 (2016)], [arXiv:1510.01245].

[28] J. Zhang *et al.* (Belle), Phys. Rev. Lett. **91**, 221801 (2003), [hep-ex/0306007]; B. Aubert *et al.* (BaBar), Phys. Rev. Lett. **102**, 141802 (2009), [arXiv:0901.3522].

[29] B. Aubert *et al.* (BaBar), Phys. Rev. D **74**, 051102 (2006), [hep-ex/0605017]; B. Aubert *et al.* (BaBar), Phys. Rev. D **79**, 052005 (2009), [arXiv:0901.3703].

[30] B. Aubert *et al.* (BaBar), Phys. Rev. D **78**, 071104 (2008), [arXiv:0807.4977].

[31] I. Adachi *et al.* (Belle), Phys. Rev. D **89**, 7, 072008 (2014), [Erratum: Phys. Rev. D **89**, 119903 (2014)], [arXiv:1212.4015].

[32] R. Aaij *et al.* (LHCb), Phys. Lett. B **747**, 468 (2015), [arXiv:1503.07770].

[33] Y. Guan *et al.* (Belle), Phys. Rev. Lett. **133**, 8, 081801 (2024), [arXiv:2401.04646].

[34] B. Aubert *et al.* (BaBar), Phys. Rev. D **80**, 092007 (2009), [arXiv:0907.1776].

[35] K.-F. Chen *et al.* (Belle), Phys. Rev. Lett. **94**, 221804 (2005), [hep-ex/0503013].

[36] B. Aubert *et al.* (BaBar), Phys. Rev. Lett. **99**, 201802 (2007), [arXiv:0705.1798].

[37] A. L. Kagan, Phys. Lett. B **601**, 151 (2004), [hep-ph/0405134]; H.-n. Li and S. Mishima, Phys. Rev. D **71**, 054025 (2005), [hep-ph/0411146]; C.-H. Chen *et al.*, Phys. Rev. D **72**, 054011 (2005), [hep-ph/0507012]; M. Beneke, J. Rohrer and D. Yang, Phys. Rev. Lett. **96**, 141801 (2006), [hep-ph/0512258]; C.-H. Chen and C.-Q. Geng, Phys. Rev. D **75**, 054010 (2007), [hep-ph/0701023]; A. Datta *et al.*, Phys. Rev. D **76**, 034015 (2007), [arXiv:0705.3915]; M. Beneke, J. Rohrer and D. Yang, Nucl. Phys. B **774**, 64 (2007), [hep-ph/0612290]; H.-Y. Cheng and K.-C. Yang, Phys. Rev. D **78**,

Int. J. Mod. Phys. A 2026.41. Downloaded from www.worldscientific.com
by UNIVERSITY OF CALIFORNIA @ BERKELEY on 09/16/26. Re-use and distribution is strictly not permitted, except for Open Access articles.

094001 (2008), [Erratum: Phys. Rev. D **79**, 039903 (2009)], [arXiv:0805.0329].

[38] C. W. Bauer *et al.*, Phys. Rev. D **70**, 054015 (2004), [hep-ph/0401188]; P. Colangelo, F. De Fazio and T. Pham, Phys. Lett. B **597**, 291 (2004), [hep-ph/0406162]; M. Ladisa *et al.*, Phys. Rev. D **70**, 114025 (2004), [hep-ph/0409286]; H.-Y. Cheng, C.-K. Chua and A. Soni, Phys. Rev. D **71**, 014030 (2005), [hep-ph/0409317]; H.-Y. Cheng and K.-C. Yang, Phys. Rev. D **83**, 034001 (2011), [arXiv:1010.3309].

[39] Y. Grossman, Int. J. Mod. Phys. A **19**, 907 (2004), [hep-ph/0310229]; E. Alvarez *et al.*, Phys. Rev. D **70**, 115014 (2004), [hep-ph/0410096]; P. K. Das and K.-C. Yang, Phys. Rev. D **71**, 094002 (2005), [hep-ph/0412313]; C.-H. Chen and C.-Q. Geng, Phys. Rev. D **71**, 115004 (2005), [hep-ph/0504145]; Y.-D. Yang, R.-M. Wang and G.-R. Lu, Phys. Rev. D **72**, 015009 (2005), [hep-ph/0411211]; K.-C. Yang, Phys. Rev. D **72**, 034009 (2005), [Erratum: Phys. Rev. D **72**, 059901 (2005)], [hep-ph/0506040]; S. Baek *et al.*, Phys. Rev. D **72**, 094008 (2005), [hep-ph/0508149]; C.-S. Huang *et al.*, Phys. Rev. D **73**, 034026 (2006), [hep-ph/0511129]; C.-H. Chen and H. Hatanaka, Phys. Rev. D **73**, 075003 (2006), [hep-ph/0602140]; A. Faessler *et al.*, Phys. Rev. D **75**, 074029 (2007), [hep-ph/0702020].

[40] D. London, N. Sinha and R. Sinha, Phys. Rev. D **69**, 114013 (2004), [hep-ph/0402214].

[41] B. Aubert *et al.* (BaBar), Phys. Rev. D **76**, 051103 (2007), [arXiv:0705.0398].

[42] B. Aubert *et al.* (BaBar), Phys. Rev. Lett. **101**, 161801 (2008), [arXiv:0806.4419].

[43] J. Zhang *et al.* (Belle), Phys. Rev. Lett. **95**, 141801 (2005), [hep-ex/0408102]; B. Aubert *et al.* (BaBar), Phys. Rev. Lett. **97**, 201801 (2006), [hep-ex/0607057]; P. del Amo Sanchez *et al.* (BaBar), Phys. Rev. D **83**, 051101 (2011), [arXiv:1012.4044]; J. Lees *et al.* (BaBar), Phys. Rev. D **85**, 072005 (2012), [arXiv:1112.3896].

[44] R. Aaij *et al.* (LHCb), JHEP **05**, 026 (2019), [arXiv:1812.07008].

[45] T. Aaltonen *et al.* (CDF), Phys. Rev. Lett. **107**, 261802 (2011), [arXiv:1107.4999].

[46] R. Aaij *et al.* (LHCb), Phys. Lett. B **713**, 369 (2012), [arXiv:1204.2813]; R. Aaij *et al.* (LHCb), Phys. Rev. D **90**, 5, 052011 (2014), [arXiv:1407.2222]; R. Aaij *et al.* (LHCb), JHEP **12**, 155 (2019), [arXiv:1907.10003]; R. Aaij *et al.* (LHCb), Phys. Rev. Lett. **131**, 17, 171802 (2023), [arXiv:2304.06198].

[47] R. Aaij *et al.* (LHCb), Phys. Lett. B **709**, 50 (2012), [arXiv:1111.4183]; R. Aaij *et al.* (LHCb), JHEP **07**, 166 (2015), [arXiv:1503.05362]; R. Aaij *et al.* (LHCb), JHEP **07**, 032 (2019), [arXiv:1905.06662].

[48] R. Aaij *et al.* (LHCb), JHEP **11**, 092 (2013), [arXiv:1306.2239].

[49] B. Aubert *et al.* (BaBar), Phys. Rev. Lett. **100**, 081801 (2008), [arXiv:0708.2248]; B. Aubert *et al.* (BaBar), Phys. Rev. D **79**, 051102 (2009), [arXiv:0901.1223].

[50] G. Burdman, Phys. Rev. D **52**, 6400 (1995), [hep-ph/9505352]; F. Kruger and J. Matias, Phys. Rev. D **71**, 094009 (2005), [hep-ph/0502060]; E. Lunghi and J. Matias, JHEP **04**, 058 (2007), [hep-ph/0612166]; W. Altmannshofer *et al.*, JHEP **01**, 019 (2009), [arXiv:0811.1214]; J. Matias *et al.*, JHEP **04**, 104 (2012), [arXiv:1202.4266]; S. Descotes-Genon *et al.*, JHEP **01**, 048 (2013), [arXiv:1207.2753].

[51] B. Aubert *et al.* (BaBar), Phys. Rev. D **79**, 031102 (2009), [arXiv:0804.4412]; J. Lees *et al.* (BaBar), Phys. Rev. D **93**, 5, 052015 (2016), [arXiv:1508.07960].

[52] J.-T. Wei *et al.* (Belle), Phys. Rev. Lett. **103**, 171801 (2009), [arXiv:0904.0770]; S. Wehle *et al.* (Belle), Phys. Rev. Lett. **118**, 11, 111801 (2017), [arXiv:1612.05014]; A. Abdesselam *et al.* (Belle), Phys. Rev. Lett. **126**, 16, 161801 (2021), [arXiv:1904.02440]; D. Ferlewicz *et al.* (Belle), Phys. Rev. D **110**, 7, 072005 (2024), [arXiv:2404.00201].

[53] T. Aaltonen *et al.* (CDF), Phys. Rev. Lett. **108**, 081807 (2012), [arXiv:1108.0695].

[54] S. Chatrchyan *et al.* (CMS), Phys. Lett. B **727**, 77 (2013), [arXiv:1308.3409]; V. Khachatryan *et al.* (CMS), Phys. Lett. B **753**, 424 (2016), [arXiv:1507.08126]; A. M. Sirunyan *et al.* (CMS), Phys. Lett. B **781**, 517 (2018), [arXiv:1710.02846]; A. M. Sirunyan *et al.* (CMS), JHEP **04**, 124 (2021), [arXiv:2010.13968]; A. Hayrapetyan *et al.* (CMS), Phys. Lett. B **864**, 139406 (2025), [arXiv:2411.11820].

[55] M. Aaboud *et al.* (ATLAS), JHEP **10**, 047 (2018), [arXiv:1805.04000].

[56] R. Aaij *et al.* (LHCb), JHEP **08**, 131 (2013), [arXiv:1304.6325]; R. Aaij *et al.* (LHCb), JHEP **04**, 064 (2015), [arXiv:1501.03038]; R. Aaij *et al.* (LHCb), JHEP **02**, 104 (2016), [arXiv:1512.04442]; R. Aaij *et al.* (LHCb), JHEP **11**, 047 (2016), [Erratum: JHEP **04**, 142 (2017)], [arXiv:1606.04731]; R. Aaij *et al.* (LHCb), JHEP **12**, 065 (2016), [arXiv:1609.04736]; R. Aaij *et al.* (LHCb), JHEP **08**, 055 (2017), [arXiv:1705.05802]; R. Aaij *et al.* (LHCb), Phys. Rev. Lett. **125**, 1, 011802 (2020), [arXiv:2003.04831]; R. Aaij *et al.* (LHCb), Phys. Rev. Lett. **126**, 16, 161802 (2021), [arXiv:2012.13241]; R. Aaij *et al.* (LHCb), JHEP **09**, 179 (2015), [arXiv:1506.08777]; R. Aaij *et al.* (LHCb), JHEP **11**, 043 (2021), [arXiv:2107.13428]; R. Aaij *et al.* (LHCb), Phys. Rev. Lett. **128**, 19, 191802 (2022), [arXiv:2110.09501]; R. Aaij *et al.* (LHCb), Phys. Rev. D **108**, 3, 032002 (2023), [arXiv:2212.09153]; R. Aaij *et al.* (LHCb), Phys. Rev. D **109**, 5, 052009 (2024), [arXiv:2312.09102]; R. Aaij *et al.* (LHCb), Phys. Rev. Lett. **132**, 13, 131801 (2024), [arXiv:2312.09115]; R. Aaij *et al.* (LHCb), JHEP **09**, 026 (2024), [arXiv:2405.17347]; R. Aaij *et al.* (LHCb), JHEP **06**, 140 (2025), [arXiv:2502.10291].

[57] C.-H. Chen and H.-N. Li, Phys. Rev. D **71**, 114008 (2005), [hep-ph/0504020].

Int. J. Mod. Phys. A 2026.41. Downloaded from www.worldscientific.com
UNIVERSITY OF CALIFORNIA @ BERKELEY on 09/16/26. Re-use and distribution is strictly not permitted, except for Open Access articles.

74. B^0–$\overline{B}^0$ Mixing

Revised March 2026 by O. Schneider (EPFL).

There are two neutral B^0–$\overline{B}^0$ meson systems, B_d^0–$\overline{B}_d^0$ and B_s^0–$\overline{B}_s^0$ (generically denoted B_q^0–$\overline{B}_q^0$, $q = s, d$), which exhibit particle-antiparticle mixing [1]. This mixing phenomenon is described in Ref. [2]. In the following, we adopt the notation introduced in Ref. [2], and assume CPT conservation throughout. In each system, the light (L) and heavy (H) mass eigenstates,

$$|B_{q\mathrm{L},q\mathrm{H}}\rangle = p|B_q^0\rangle \pm q|\overline{B}_q^0\rangle, \tag{74.1}$$

have a mass difference $\Delta m_q = m_{q\mathrm{H}} - m_{q\mathrm{L}} > 0$, a total decay-width difference $\Delta\Gamma_q = \Gamma_{q\mathrm{L}} - \Gamma_{q\mathrm{H}}$ and an average decay width $\Gamma_q = (\Gamma_{q\mathrm{L}}+\Gamma_{q\mathrm{H}})/2$. In the absence of CP violation in the mixing, $|q/p| = 1$, the differences are given by $\Delta m_q = 2|M_{12}|$ and $|\Delta\Gamma_q| = 2|\Gamma_{12}|$, where M_{12} and Γ_{12} are the off-diagonal elements of the mass and decay matrices [2]. The evolution of a pure $|B_q^0\rangle$ or $|\overline{B}_q^0\rangle$ state at $t = 0$ is given by

$$|B_q^0(t)\rangle = g_+(t)\,|B_q^0\rangle + \frac{q}{p}\,g_-(t)\,|\overline{B}_q^0\rangle, \tag{74.2}$$

$$|\overline{B}_q^0(t)\rangle = g_+(t)\,|\overline{B}_q^0\rangle + \frac{p}{q}\,g_-(t)\,|B_q^0\rangle, \tag{74.3}$$

which means that the flavor states remain unchanged (+) or oscillate into each other (−) with time-dependent probabilities proportional to

$$|g_\pm(t)|^2 = \frac{e^{-\Gamma_q t}}{2}\left[\cosh\left(\frac{\Delta\Gamma_q}{2}\,t\right) \pm \cos(\Delta m_q\,t)\right]. \tag{74.4}$$

In the absence of CP violation, the time-integrated mixing probability $\int |g_-(t)|^2\,dt/(\int |g_-(t)|^2\,dt + \int |g_+(t)|^2\,dt)$ is given by

$$\chi_q = \frac{x_q^2 + y_q^2}{2(x_q^2+1)}\,, \quad \text{where} \quad x_q = \frac{\Delta m_q}{\Gamma_q}\,, \quad y_q = \frac{\Delta\Gamma_q}{2\Gamma_q}\,. \tag{74.5}$$

74.1 Standard Model predictions and phenomenology

In the Standard Model, the transitions $B_q^0 \to \overline{B}_q^0$ and $\overline{B}_q^0 \to B_q^0$ are due to the weak interaction. They are described, at the lowest order, by box diagrams involving two W bosons and two up-type quarks (see Fig. 74.1), as is the case for $K^0 - \overline{K}^0$ mixing. However, the long range interactions arising from intermediate virtual states are negligible for the neutral B meson systems, because the large B mass is off the region of hadronic resonances. The calculation of the dispersive and absorptive parts of the box diagrams yields the following predictions for the off-diagonal element of the mass and decay matrices [3],

$$M_{12} = -\frac{G_F^2 m_W^2 \eta_B m_{B_q} B_{B_q} f_{B_q}^2}{12\pi^2}\, S_0(m_t^2/m_W^2)\,(V_{tq}^* V_{tb})^2\,, \tag{74.6}$$

$$\Gamma_{12} = \frac{G_F^2 m_b^2 \eta_B' m_{B_q} B_{B_q} f_{B_q}^2}{8\pi} \times \left[(V_{tq}^* V_{tb})^2 + V_{tq}^* V_{tb} V_{cq}^* V_{cb}\,\mathcal{O}\left(\frac{m_c^2}{m_b^2}\right) + (V_{cq}^* V_{cb})^2\,\mathcal{O}\left(\frac{m_c^4}{m_b^4}\right)\right], \tag{74.7}$$

where G_F is the Fermi constant, m_W the W boson mass, and m_i the mass of quark i; m_{B_q}, f_{B_q} and B_{B_q} are the B_q^0 mass, weak decay constant and bag parameter, respectively. The known function $S_0(x_t)$ can be approximated very well by $0.784\,x_t^{0.76}$ [4], and V_{ij} are the elements of the CKM matrix [5]. The QCD corrections η_B and η_B' are of order unity. The only non-negligible contributions to M_{12} are from box diagrams involving two top quarks. The phases of M_{12} and Γ_{12} satisfy

$$\phi_M - \phi_\Gamma = \pi + \mathcal{O}\left(\frac{m_c^2}{m_b^2}\right), \tag{74.8}$$

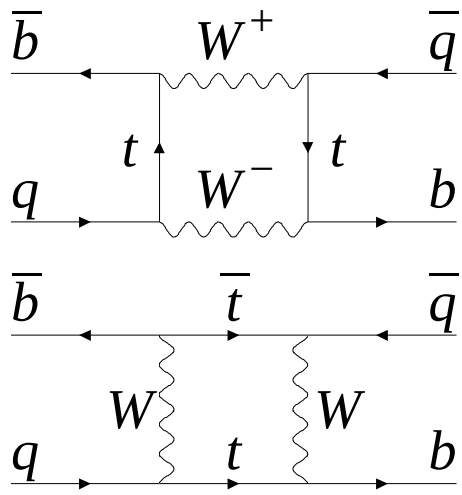

Figure 74.1: Dominant box diagrams for the $B_q^0 \to \overline{B_q}^0$ transitions ($q = d$ or s). Similar diagrams exist where one or both t quarks are replaced with c or u quarks.

implying that the mass eigenstates have mass and width differences of opposite signs. This means that, like in the K^0–$\overline{K}^0$ system, the heavy state is expected to have a smaller decay width than that of the light state: $\Gamma_\mathrm{H} < \Gamma_\mathrm{L}$. Hence, $\Delta\Gamma_q = \Gamma_\mathrm{L} - \Gamma_\mathrm{H}$ is expected to be positive in the Standard Model.

Furthermore, the quantity

$$\left|\frac{\Gamma_{12}}{M_{12}}\right| \simeq \frac{3\pi}{2}\,\frac{m_b^2}{m_W^2}\,\frac{1}{S_0(m_t^2/m_W^2)} \sim \mathcal{O}\left(\frac{m_b^2}{m_t^2}\right) \tag{74.9}$$

is small, and a power expansion of $|q/p|^2$ yields

$$\left|\frac{q}{p}\right|^2 = 1 + \left|\frac{\Gamma_{12}}{M_{12}}\right| \sin(\phi_M - \phi_\Gamma) + \mathcal{O}\left(\left|\frac{\Gamma_{12}}{M_{12}}\right|^2\right). \tag{74.10}$$

Therefore, considering both Eqs. (74.8) and (74.9), the CP-violating parameter

$$1 - \left|\frac{q}{p}\right|^2 \simeq \mathrm{Im}\left(\frac{\Gamma_{12}}{M_{12}}\right) \tag{74.11}$$

is expected to be very small: $\sim \mathcal{O}(10^{-3})$ for the B_d^0–$\overline{B}_d^0$ system and $\lesssim \mathcal{O}(10^{-4})$ for the B_s^0–$\overline{B}_s^0$ system [6].

In the approximation of negligible CP violation in mixing, the ratio $\Delta\Gamma_q/\Delta m_q$ is equal to the small quantity $|\Gamma_{12}/M_{12}|$ of Eq. (74.9); it is hence independent of CKM matrix elements, *i.e.*, the same for the B_d^0–$\overline{B}_d^0$ and B_s^0–$\overline{B}_s^0$ systems. Calculations [7] yield $\sim 5 \times 10^{-3}$ with a $\sim 15\%$ uncertainty. Given the published experimental knowledge [8] on the mixing parameter x_q

$$\begin{cases} x_d = 0.7659 \pm 0.0032 & (B_d^0\text{–}\overline{B}_d^0 \text{ system}) \\ x_s = 26.91 \pm 0.11 & (B_s^0\text{–}\overline{B}_s^0 \text{ system}) \end{cases}, \tag{74.12}$$

the Standard Model thus predicts that $\Delta\Gamma_d/\Gamma_d$ is very small (below 1%), but $\Delta\Gamma_s/\Gamma_s$ considerably larger ($\sim 10\%$). These width differences are caused by the existence of final states to which both the B_q^0 and $\overline{B}_q^0$ mesons can decay. Such decays involve $b \to c\bar{c}q$ quark-level transitions, which are Cabibbo-suppressed if $q = d$ and Cabibbo-allowed if $q = s$.

Complete sets of Standard Model predictions for all mixing parameters in both the B_d^0–$\overline{B}_d^0$ and B_s^0–$\overline{B}_s^0$ systems can be found in Refs. [7, 9].

Int. J. Mod. Phys. A 2026.41. Downloaded from www.worldscientific.com
by UNIVERSITY OF CALIFORNIA @ BERKELEY on 09/16/26. Re-use and distribution is strictly not permitted, except for Open Access articles.

74.2 Experimental issues and methods for oscillation analyses

Time-integrated measurements of B^0–$\overline{B}^0$ mixing were published for the first time in 1987 by UA1 [10] and ARGUS [11], and since then by other experiments. These measurements are typically based on counting same-sign and opposite-sign lepton pairs from the semileptonic decay of the produced $b\bar{b}$ pairs. Such analyses cannot easily separate the contributions from the different b-hadron species, therefore, the clean environment of $\Upsilon(4S)$ machines (where only B^0_d and charged B_u mesons are produced) is in principle best suited to measure χ_d.

However, better sensitivity is obtained from time-dependent analyses aiming at the direct measurement of the oscillation frequencies Δm_d and Δm_s, from the proper time distributions of B^0_d or B^0_s candidates identified through their decay in (mostly) flavor-specific modes, and suitably tagged as mixed or unmixed. This is particularly true for the B^0_s–$\overline{B}^0_s$ system, where the large value of x_s implies maximal mixing, *i.e.*, $\chi_s \simeq 1/2$. In such analyses, the B^0_d or B^0_s mesons are either fully reconstructed, partially reconstructed from a charm meson, selected from a lepton with the characteristics of a $b \to \ell^-$ decay, or selected from a reconstructed displaced vertex. At high-energy colliders (LEP, SLC, Tevatron, LHC), the proper time $t = \frac{m_B}{p} L$ is measured from the distance L between the production vertex and the B decay vertex, and from an estimate of the B momentum p. At asymmetric B factories (PEP-II, KEKB, SuperKEKB), producing $e^+e^- \to \Upsilon(4S) \to B^0_d\, \overline{B_d}^0$ events with a boost $\beta\gamma$ (= 0.55, 0.425, 0.28), the proper time difference between the two B candidates is estimated as $\Delta t \simeq \frac{\Delta z}{\beta\gamma c}$, where Δz is the spatial separation between the two B decay vertices along the boost direction. In all cases, the good resolution needed on the vertex positions is obtained with silicon detectors.

The average statistical significance $\mathcal{S}$ of a B^0_q oscillation signal can be approximated as [12]

$$\mathcal{S} \approx \sqrt{N/2}\, f_{\rm sig}\, (1-2\eta)\, e^{-(\Delta m_q\, \sigma_t)^2/2}\,, \qquad (74.13)$$

where N is the number of selected and tagged candidates, $f_{\rm sig}$ is the fraction of signal in that sample, η is the total mistag probability, and σ_t is the resolution on proper time (or proper time difference). The quantity $\mathcal{S}$ decreases very quickly as Δm_q increases; this dependence is controlled by σ_t, which is therefore a critical parameter for Δm_s analyses. At high-energy colliders, the proper time resolution $\sigma_t \sim \frac{m_B}{\langle p\rangle}\sigma_L \oplus t\frac{\sigma_p}{p}$ includes a constant contribution due to the decay length resolution σ_L (typically 0.04–0.3 ps), and a term due to the relative momentum resolution σ_p/p (typically 10–20% for partially reconstructed decays), which increases with proper time. At B factories, the boost of the B mesons is estimated from the known beam energies, and the term due to the spatial resolution dominates (typically 0.7–1.5 ps because of the much smaller B boost).

In order to tag a B^0_q candidate as mixed or unmixed, it is necessary to determine its flavor both in the initial state and in the final state. The initial and final state mistag probabilities, η_i and η_f, degrade $\mathcal{S}$ by a total factor $(1-2\eta) = (1-2\eta_i)(1-2\eta_f)$. In lepton-based analyses, the final state is tagged by the charge of the lepton from $b \to \ell^-$ decays; the largest contribution to η_f is then due to $\bar{b} \to \bar{c} \to \ell^-$ decays. Alternatively, the charge of a reconstructed charm meson (D^{*-} from B^0_d or D^-_s from B^0_s), or that of a kaon hypothesized to come from a $b \to c \to s$ decay [13], can be used. For fully-inclusive analyses based on topological vertexing, final-state tagging techniques include jet-charge [14] and charge-dipole [15, 16] methods. At high-energy colliders, the methods to tag the initial state (*i.e.*, the state at production), can be divided into two groups: the ones that tag the initial charge of the $\bar{b}$ quark contained in the B^0_q candidate itself (same-side tag), and the ones that tag the initial charge of the other b quark produced in the event (opposite-side tag). On the same side, the sign of a charged pion, kaon or proton from the primary vertex is correlated with the production state of the B^0_q meson if that particle is a decay product of a B^{**} state or the first in the fragmentation chain [17, 18]. Jet- and vertex-charge techniques work on both sides and on the opposite side, respectively. Finally, the charge of a lepton from $b \to \ell^-$, of a kaon from $b \to c \to s$ or of a charm hadron from $b \to c$ [19] can be used as an opposite-side tag, keeping in mind that its performance is degraded due to integrated mixing. At SLC, the beam polarization produced a sizeable forward-backward asymmetry in the $Z \to b\bar{b}$ decays, and provided another very interesting and effective initial state tag based on the polar angle of the B^0_q candidate [15]. Initial state tags have also been combined to reach $\eta_i \sim 26\%$ at LEP [18, 20] or 22% at SLD [15] with full efficiency. In the case $\eta_f = 0$, this corresponds to an effective tagging efficiency $Q = \epsilon D^2 = \epsilon(1-2\eta)^2$, where ϵ is the tagging efficiency, in the range $23-31\%$. The equivalent figure achieved by CDF during Tevatron Run I was $\sim 3.5\%$ (see tagging summary on page 160 of Ref. [21]), reflecting the fact that tagging is more difficult at hadron colliders. The CDF and DØ analyses of Tevatron Run II data reached $\epsilon D^2 = (1.8 \pm 0.1)\%$ [22] and $(2.5 \pm 0.2)\%$ [23] for opposite-side tagging, while same-side kaon tagging (for B^0_s analyses) contributed an additional $3.7-4.8\%$ at CDF [22], and pushed the combined performance to $(4.7 \pm 0.5)\%$ at DØ [24]. LHCb, operating in the forward region at the LHC where the environment is different in terms of track multiplicity and b-hadron production kinematics, has reported $\epsilon D^2 = (2.10 \pm 0.25)\%$ [25] for opposite-side tagging, $(1.80 \pm 0.26)\%$ [26] for same-side kaon tagging, and $(2.11 \pm 0.11)\%$ [27] for same-side pion and proton tagging: the combined figure ranges typically between $(3.73 \pm 0.15)\%$ [28] and $(6.3 \pm 0.5)\%$ [29] depending on the mode in which the tagged B^0_s meson is reconstructed, and reaches up to $(8.1 \pm 0.6)\%$ [30] for hadronic B^0_d modes. ATLAS [31] and CMS [32] have reported $\epsilon D^2 \sim 1.75\%$ and $\epsilon D^2 \sim 5.6\%$, respectively, using opposite-side tagging of $B^0_s \to J/\psi\phi$ decays.

At B factories, the flavor of a B^0_d meson at production cannot be determined, since the two neutral B mesons produced in a $\Upsilon(4S)$ decay evolve in a coherent P-wave state where they keep opposite flavors at any time. However, as soon as one of them decays, the other follows a time-evolution given by Eqs. (74.2) or (74.3), where t is replaced with Δt (which will take negative values half of the time). Hence, the "initial state" tag of a B can be taken as the final-state tag of the other B. Effective tagging efficiencies of 30% are achieved by BaBar and Belle [33], using different techniques including $b \to \ell^-$ and $b \to c \to s$ tags. It is worth noting that, in this case, mixing of the other B (*i.e.*, the coherent mixing occurring before the first B decay) does not contribute to the mistag probability.

Before the experimental observation of a decay-width difference, oscillation analyses typically neglected $\Delta\Gamma_q$ in Eq. (74.4), and described the time dependence with the functions $\Gamma_q e^{-\Gamma_q t}(1 \pm \cos(\Delta m_q t))/2$ (high-energy colliders) or $\Gamma_d e^{-\Gamma_d|\Delta t|}(1 \pm \cos(\Delta m_d \Delta t))/4$ (asymmetric $\Upsilon(4S)$ machines). As can be seen from Eq. (74.4), a non-zero value of $\Delta\Gamma_q$ would effectively reduce the oscillation amplitude with a small time-dependent factor that would be very difficult to distinguish from time resolution effects. Measurements of Δm_q are usually extracted from the data using a maximum likelihood fit.

74.3 Δm_d and $\Delta\Gamma_d$ measurements

Many B^0_d–$\overline{B}^0_d$ oscillation analyses have been published [34] by the ALEPH [35], DELPHI [16, 36], L3 [37], OPAL [38, 39], CDF [17], DØ [23], BaBar [40], Belle [41], Belle II [42], and LHCb [43–46] collaborations. Although a variety of different techniques have been used, the individual Δm_d results obtained at LEP and Tevatron have remarkably similar precision. Their average is compatible with the more precise measurements at the asymmetric B factories and the LHC. The systematic uncertainties are not negligible; they are often dominated by sample composition, mistag probability, or b-hadron lifetime contributions. Before being combined, the measurements are adjusted on the basis of a common set of input values, including the b-hadron lifetimes and fractions published in this *Review*. Some measurements are statistically correlated. Systematic correlations arise both from common physics sources (fragmentation fractions, lifetimes, branching ratios of b hadrons), and from purely experimental or algorithmic effects (efficiency, resolu-

Int. J. Mod. Phys. A 2026.41. Downloaded from www.worldscientific.com
UNIVERSITY OF CALIFORNIA @ BERKELEY on 09/16/26. Re-use and distribution is strictly not permitted, except for Open Access articles.

tion, tagging, background description). Combining all measurements [16, 17, 23, 35–46] and accounting for all identified correlations yields $\Delta m_d = 0.5068 \pm 0.0016(\text{stat}) \pm 0.0011(\text{syst})\ \text{ps}^{-1}$ [8], a result dominated by the latest LHCb measurement with $B^0 \to D^{(*)-}\mu^+\nu_\mu X$ decays [46].

The decay-width difference can be determined from the B^0 effective lifetimes [47, 48]

$$\tau_d^{\text{eff}} = \frac{1 + 2\mathcal{A}_{\Delta\Gamma}\, y_d + y_d^2}{\Gamma_d(1 - y_d^2)(1 + \mathcal{A}_{\Delta\Gamma}\, y_d)}\,, \tag{74.14}$$

where $\mathcal{A}_{\Delta\Gamma} = 0$ for a flavor-specific final state and $\mathcal{A}_{\Delta\Gamma} \simeq \eta_{CP}\cos(2\beta)$ for a CP eigenstate with eigenvalue η_{CP}. A fit to all available effective B^0 lifetime measurements using flavor-specific final states or the CP-odd $J/\psi K^0_{\text{S}}$ final state, as well as the dedicated measurements of $\Delta\Gamma_d/\Gamma_d$ by BaBar [49], Belle [50], LHCb [51], ATLAS [52] and CMS [53], using the external constraint $\beta \equiv \arg(-V_{cd}V_{cb}^*/(V_{td}V_{tb}^*)) = 22.63 \pm 0.45$ degrees [8], allows the simultaneous determination [8] of

$$\Delta\Gamma_d/\Gamma_d = +0.005 \pm 0.010 \quad \text{and} \quad 1/\Gamma_d = 1.5113 \pm 0.0027\ \text{ps}\,. \tag{74.15}$$

These results are compatible both with $\Delta\Gamma_d = 0$ and with the Standard Model prediction for $\Delta\Gamma_d$ of $0.00215 \pm 0.00013\ \text{ps}^{-1}$ [9].

The time-integrated mixing measurements published by ARGUS and CLEO [54–56] average to $\chi_d = 0.182 \pm 0.015$. Assuming no CP violation in mixing, the Δm_d, $1/\Gamma_d$, $\Delta\Gamma_d/\Gamma_d$ and χ_d results can be combined to yield the world average

$$\Delta m_d = 0.5068 \pm 0.0019\ \text{ps}^{-1} \tag{74.16}$$

or, equivalently,

$$\chi_d = 0.1849 \pm 0.0010\,. \tag{74.17}$$

This Δm_d value provides an estimate of $2|M_{12}|$, and can be used with Eq. (74.6) to extract $|V_{td}|$ within the Standard Model [57]. The main experimental uncertainties on the result come from m_t and Δm_d, but are still completely negligible with respect to the uncertainty due to the hadronic matrix element $f_{B_d}\sqrt{B_{B_d}} = 225 \pm 9$ MeV [58] obtained from three-flavor lattice QCD calculations.

74.4 Δm_s and $\Delta\Gamma_s$ measurements

After many years of intense search at LEP and SLC, B_s^0–$\overline{B}_s^0$ oscillations were first observed in 2006 by CDF using 1 fb^{-1} of Tevatron Run II data [22]. LHCb then observed B_s^0–$\overline{B}_s^0$ oscillations independently with $B_s^0 \to D_s^-\pi^+$ [43, 59], $B_s^0 \to D_s^-\mu^+\nu X$ [45] and $B_s^0 \to J/\psi K^+K^-$ [28] decays using up to 3 fb^{-1} of LHC Run 1 data. More recent measurements based on LHC Run 2 data have been published by CMS with $B_s^0 \to J/\psi\phi$ decays [32], and by LHCb with $B_s^0 \to D_s^-\pi^+\pi^-\pi^+$ [60], $B_s^0 \to D_s^-\pi^+$ [61] and $B_s^0 \to J/\psi K^+K^-$ [62] decays. Taking systematic correlations into account, the average [8] of all published measurements of Δm_s [22, 28, 32, 43, 45, 59–62] is

$$\Delta m_s = 17.766 \pm 0.004(\text{stat}) \pm 0.004(\text{syst})\ \text{ps}^{-1}\,, \tag{74.18}$$

with an impressive precision dominated by the recent $B_s^0 \to D_s^-\pi^+$ result [61] of Fig. 74.2.

The information on $|V_{ts}|$ obtained in the framework of the Standard Model is hampered by the hadronic uncertainty, as in the B_d^0 case. However, several uncertainties cancel in the frequency ratio

$$\frac{\Delta m_s}{\Delta m_d} = \frac{m_{B_s}}{m_{B_d}}\,\xi^2\left|\frac{V_{ts}}{V_{td}}\right|^2\,, \tag{74.19}$$

where the SU(3) flavor-symmetry breaking factor $\xi = (f_{B_s}\sqrt{B_{B_s}})/(f_{B_d}\sqrt{B_{B_d}})$ is obtained as 1.206 ± 0.017 from a combination of three-flavor lattice QCD calculations [58] dominated by the results of Ref. [63], or as $1.2014^{+0.0065}_{-0.0072}$ from QCD sum rules [64]. Using the measurements of Eqs. (74.16) and (74.18), one can extract

$$\left|\frac{V_{td}}{V_{ts}}\right| = \begin{cases} 0.2054 \pm 0.0004 \pm 0.0029\ (\text{lattice QCD}) \\ 0.2045 \pm 0.0004^{+0.0011}_{-0.0012}\ (\text{QCD sum rules}) \end{cases}\,, \tag{74.20}$$

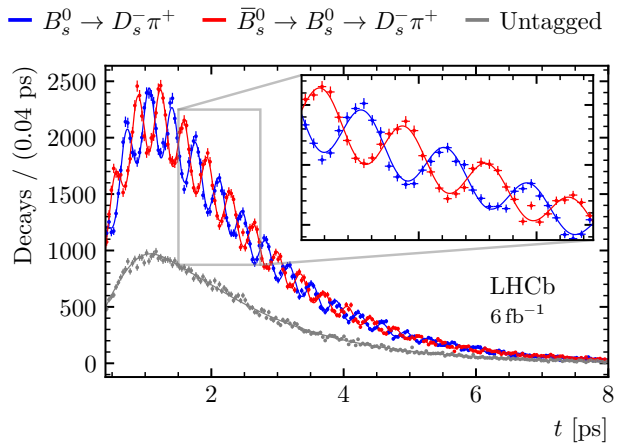

Figure 74.2: Proper decay-time distributions of background-subtracted $B_s^0 \to D_s^-\pi^+$ decays tagged as unmixed (blue), tagged as mixed (red) or untagged (grey) in the Run 2 data of the LHCb experiment, displaying B_s^0–$\overline{B}_s^0$ oscillations [61].

in good agreement with (but much more precise than) the value obtained from the ratio of the $b \to d\gamma$ and $b \to s\gamma$ transition rates observed at the B factories [57].

The CKM matrix can be constrained using experimental results on observables such as Δm_d, Δm_s, $|V_{ub}/V_{cb}|$, ϵ_K, and $\sin(2\beta)$ together with theoretical inputs and unitarity conditions [57, 65, 66]. The constraint from our knowledge on the ratio $\Delta m_s/\Delta m_d$ is more effective in limiting the position of the apex of the CKM unitarity triangle than the one obtained from the Δm_d measurements alone, due to the reduced hadronic uncertainty in Eq. (74.19). We also note that the experimental value of Δm_s from Eq. (74.18) is consistent with the Standard Model predictions obtained from CKM fits where no experimental information on Δm_s is used, *e.g.*, $17.26 \pm 0.58\ \text{ps}^{-1}$ [65] or $17.05^{+0.75}_{-0.44}\ \text{ps}^{-1}$ [66]. It is also consistent with the prediction $18.23 \pm 0.62\ \text{ps}^{-1}$ from Ref. [7].

Information on $\Delta\Gamma_s$ can be obtained from the study of the proper time distribution of untagged B_s^0 samples [47]. In the case of an inclusive B_s^0 selection [67], or a flavor-specific (semileptonic or hadronic) B_s^0 decay selection [20, 68–70], both the short- and long-lived components are present, and the proper decay-time distribution is a superposition of two exponentials with decay constants $\Gamma_{\text{L,H}} = \Gamma_s \pm \Delta\Gamma_s/2$. In principle, this provides sensitivity to both Γ_s and $(\Delta\Gamma_s/\Gamma_s)^2$. Ignoring $\Delta\Gamma_s$ and fitting for a single exponential leads to an estimate of $1/\Gamma_s$ (called effective lifetime) with a relative bias proportional to $(\Delta\Gamma_s/\Gamma_s)^2$. An alternative approach, sensitive to first order in $\Delta\Gamma_s/\Gamma_s$, is to determine the effective lifetime of untagged B_s^0 decays to pure CP eigenstates; measurements exist for $B_s^0 \to D_s^+D_s^-$ [69], $B_s^0 \to K^+K^-$ [70, 71], $B_s^0 \to J/\psi\eta$ [72, 73], $B_s^0 \to J/\psi f_0(980)$ [74], $B_s^0 \to J/\psi\pi^+\pi^-$ [53, 75, 76], $B_s^0 \to J/\psi K^0_{\text{S}}$ [77], and $B_s^0 \to \mu^+\mu^-$ [78]. The extraction of $1/\Gamma_s$ and $\Delta\Gamma_s$ from such measurements, discussed in detail in Ref. [48], requires additional information in the form of theoretical assumptions or external inputs on weak phases and hadronic parameters. In what follows, we only use the effective lifetimes of decays to CP-even ($D_s^+D_s^-$, $J/\psi\eta$) and CP-odd ($J/\psi f_0(980)$, $J/\psi\pi^+\pi^-$) final states where CP conservation can be assumed. In addition $\Delta\Gamma_s$ can be extracted from the decay-time distributions of B_s^0 decays to CP-even and CP-odd final states, as has been done by LHCb with $B_s^0 \to J/\psi\eta'$ and $B_s^0 \to J/\psi\pi^+\pi^-$, respectively [79].

The best sensitivity to $1/\Gamma_s$ and $\Delta\Gamma_s$ is achieved by the time-dependent measurements of the $B_s^0 \to J/\psi K^+K^-$ (including $B_s^0 \to J/\psi\phi$) and $B_s^0 \to \psi(2S)\phi$ decay rates performed at CDF [80], DØ [81], ATLAS [31, 82], CMS [32, 83] and LHCb [28, 62, 84–86], where the CP-even and CP-odd amplitudes are separated statistically through a full angular analysis (see Fig. 74.3). The LHCb collaboration analyzed the $B_s^0 \to J/\psi K^+K^-$ decay considering that the K^+K^- system can be in a P-wave or S-wave state, and measured the dependence of

Int. J. Mod. Phys. A 2026.41. Downloaded from www.worldscientific.com
by UNIVERSITY OF CALIFORNIA @ BERKELEY on 09/16/26. Re-use and distribution is strictly not permitted, except for Open Access articles.

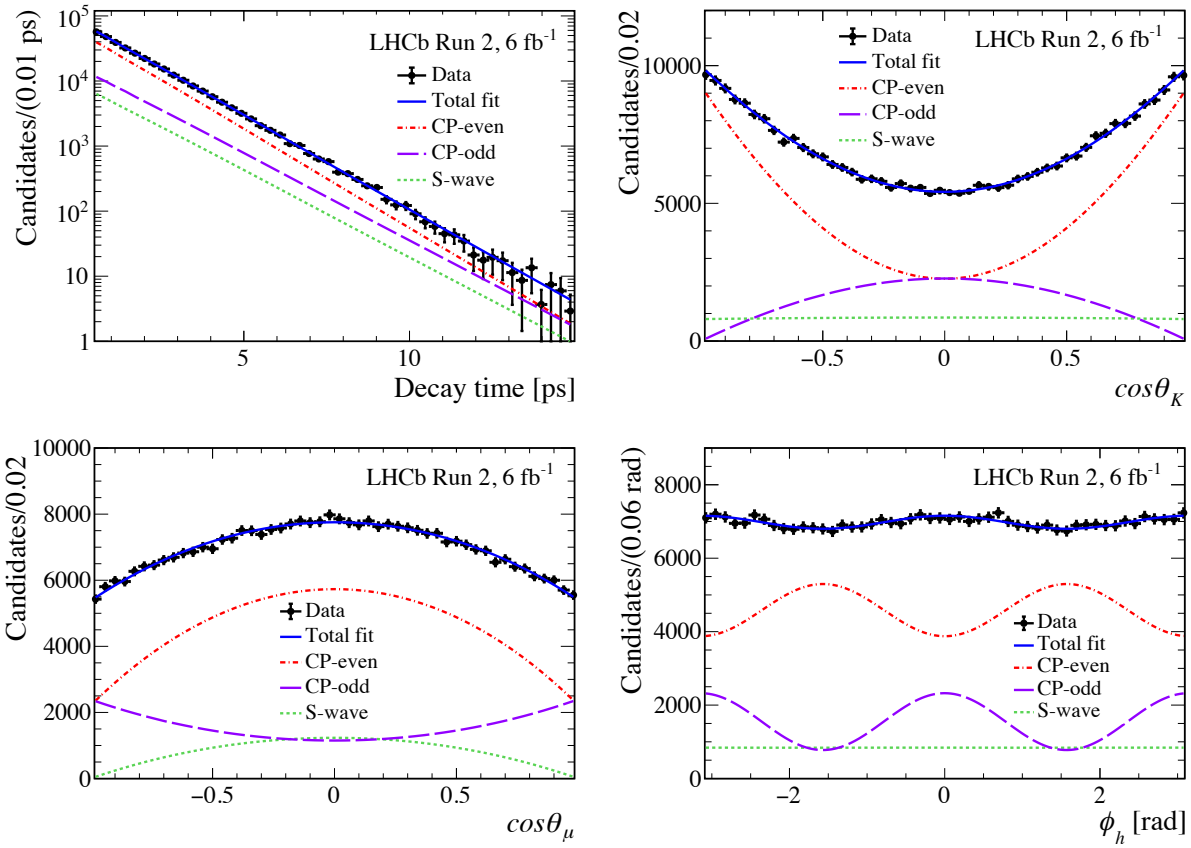

Figure 74.3: Distributions of the proper decay-time and of the three decay angles of background-subtracted $B_s^0 \to J/\psi K^+K^-$ decays reconstructed by LHCb in the vicinity of the ϕ resonance [62]. The kaon pair is predominantly in a P-wave state (from the ϕ decay) which can be CP-even or CP-odd, while a small S-wave state is CP-odd. The curves show the projections of a four-dimensional fit allowing the various components to be disentangled. The different lifetimes of the CP-even and CP-odd components are evident from the decay-time distribution.

the strong phase difference between the P-wave and S-wave amplitudes as a function of the K^+K^- invariant mass [28, 62, 87]; this allows the unambiguous determination of the sign of $\Delta\Gamma_s$, which is found to be positive. All these studies use both untagged and tagged B_s^0 candidates and are optimized for the measurement of the phase $\phi_s^{c\bar{c}s}$ that describes CP violation in the interference between B_s^0–$\overline{B}_s^0$ mixing and decay in $b \to c\bar{c}s$ transitions. The published $B_s^0 \to J/\psi K^+K^-$, $J/\psi\phi$ and $\psi(2S)\phi$ analyses [28, 31, 32, 62, 80–86] are combined in a multi-dimensional fit including all measured parameters and their correlations. To account for a tension in the time and angular parameters, scale factors are applied on the combined uncertainty of each parameter where a discrepancy arise. For example, the scale factors on the uncertainties of $\Delta\Gamma_s$, Γ_s and $\phi_s^{c\bar{c}s}$ are 1.65, 2.41 and 1.00, respectively. The averages are then further refined by applying constraints from the published lifetime measurements with flavor-specific [20, 68–70] and pure CP [53, 69, 72–76, 79] final states, to yield [8]

$$\Delta\Gamma_s = +0.0783 \pm 0.0035 \text{ ps}^{-1} \quad \text{and} \quad 1/\Gamma_s = 1.515 \pm 0.006 \text{ ps}\,, \tag{74.21}$$

or, equivalently,

$$1/\Gamma_{sL} = 1.430 \pm 0.006 \text{ ps} \quad \text{and} \quad 1/\Gamma_{sH} = 1.611 \pm 0.008 \text{ ps}\,, \tag{74.22}$$

in good agreement with the Standard Model predictions $\Delta\Gamma_s^{\rm SM} = +0.091 \pm 0.015$ ps^{-1} [7] and $\Delta\Gamma_s^{\rm SM} = +0.078 \pm 0.015$ ps^{-1} [9]. Estimates of $\Delta\Gamma_s/\Gamma_s$ obtained from measurements of the $B_s^0 \to D_s^{(*)+}D_s^{(*)-}$ branching fractions are not included in the average, since they are based on the questionable [88] assumption that these decays account for all CP-even final states.

From Eqs. (74.5), (74.18) and (74.21), one gets

$$\chi_s = 0.499313 \pm 0.000006\,. \tag{74.23}$$

74.5 CP-violation studies

Evidence for CP violation in B_q^0–$\overline{B}_q^0$ mixing has been searched for, both with flavor-specific and inclusive B_q^0 decays, in samples where the initial flavor state is tagged, usually with a lepton from the other b-hadron in the event. In the case of semileptonic (or other flavor-specific) decays, where the final-state tag is also available, the following asymmetry [2]

$$\mathcal{A}_{\rm SL}^q = \frac{N(\overline{B}_q^0(t) \to \ell^+\nu_\ell X) - N(B_q^0(t) \to \ell^-\overline{\nu}_\ell X)}{N(\overline{B}_q^0(t) \to \ell^+\nu_\ell X) + N(B_q^0(t) \to \ell^-\overline{\nu}_\ell X)} \simeq 1 - |q/p|_q^2 \tag{74.24}$$

has been measured either in time-integrated analyses at CLEO [56, 89], BaBar [90], CDF [91], DØ [92–94] and LHCb [95], or in time-dependent analyses at LEP [39, 96], BaBar [49, 97] and Belle [98]. In the inclusive case, also investigated at LEP [96, 99], no final-state tag is used, and the asymmetry [100]

$$\frac{N(\overline{B}_q^0(t) \to \text{all}) - N(B_q^0(t) \to \text{all})}{N(\overline{B}_q^0(t) \to \text{all}) + N(B_q^0(t) \to \text{all})} \simeq \mathcal{A}_{\rm SL}^q \left[\sin^2\left(\frac{\Delta m_q\, t}{2}\right) - \frac{x_q}{2}\sin(\Delta m_q\, t)\right] \tag{74.25}$$

must be measured as a function of the proper time to extract information on CP violation. In addition LHCb has studied the time dependence of the charge asymmetry of $B^0 \to D^{(*)-}\mu^+\nu_\mu X$ decays without tagging the initial state [101], which would be

Int. J. Mod. Phys. A 2026.41. Downloaded from www.worldscientific.com
UNIVERSITY OF CALIFORNIA @ BERKELEY on 09/16/26. Re-use and distribution is strictly not permitted, except for Open Access articles.

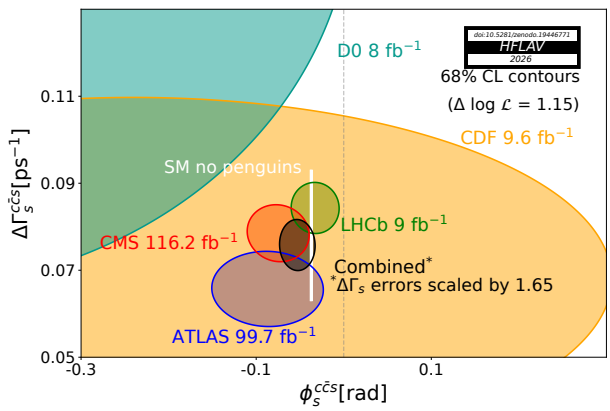

Figure 74.4: 68% CL contours in the $(\phi_s^{c\bar{c}s}, \Delta\Gamma_s)$ plane, showing all measurements from CDF [80], DØ [81], ATLAS [31, 82], CMS [32, 83] and LHCb [28, 62, 76, 84–86, 102–104] using B_s^0 decays governed by the $b \to c\bar{c}s$ transition. Their average [8] is represented as the black ellipse, where the combined uncertainty on $\Delta\Gamma_s$ has been multiplied by 1.65. The very thin white rectangle represents the Standard Model predictions of $-2\beta_s$ [65, 66] and $\Delta\Gamma_s$ [9].

equal to

$$\frac{N(D^{(*)-}\mu^+\nu_\mu X) - N(D^{(*)+}\mu^-\bar{\nu}_\mu X)}{N(D^{(*)-}\mu^+\nu_\mu X) + N(D^{(*)+}\mu^-\bar{\nu}_\mu X)} = \mathcal{A}_{\rm SL}^d \frac{1-\cos(\Delta m_d\, t)}{2} \tag{74.26}$$

in absence of detection and production asymmetries.

The DØ collaboration measured a like-sign dimuon charge asymmetry in semileptonic b decays that deviates by $2.8\,\sigma$ from the tiny Standard Model prediction and concluded, from a more refined analysis in bins of muon impact parameters, that the overall discrepancy is at the level of $3.6\,\sigma$ [92]. In all other cases, asymmetries compatible with zero have been found, with a precision limited by the available statistics. Several of the analyses at high energy don't disentangle the B_d^0 and B_s^0 contributions, and either quote a mean asymmetry or a measurement of $\mathcal{A}_{\rm SL}^d$ assuming $\mathcal{A}_{\rm SL}^s = 0$: we do not include these in the average. An exception is the dimuon DØ analysis [92], which separates the two contributions by exploiting their dependence on the muon impact parameter cut. The resulting measurements of $\mathcal{A}_{\rm SL}^d$ and $\mathcal{A}_{\rm SL}^s$ are then both compatible with the Standard Model. They are also correlated. We therefore perform a two-dimensional average of the measurements of Refs. [49, 56, 89, 90, 92–95, 97, 98, 101] and obtain [8]

$$\mathcal{A}_{\rm SL}^d = -0.0021 \pm 0.0017 \Leftrightarrow |q/p|_d = 1.0010 \pm 0.0008\,, \tag{74.27}$$
$$\mathcal{A}_{\rm SL}^s = -0.0006 \pm 0.0028 \Leftrightarrow |q/p|_s = 1.0003 \pm 0.0014\,, \tag{74.28}$$

with a correlation coefficient of -0.054 between $\mathcal{A}_{\rm SL}^d$ and $\mathcal{A}_{\rm SL}^s$. These results show no evidence of CP violation and are compatible with the very small Standard Model predictions, $\mathcal{A}_{\rm SL}^{d,\rm SM} = -(5.19 \pm 0.30) \times 10^{-4}$ and $\mathcal{A}_{\rm SL}^{s,\rm SM} = +(2.27 \pm 0.13) \times 10^{-5}$ [9], but have insufficient precision yet to constrain the Standard Model.

CP violation induced by B_s^0–$\overline{B}_s^0$ mixing in $b \to c\bar{c}s$ decays is controlled by the small weak phase $\phi_s^{c\bar{c}s}$. Measuring $\phi_s^{c\bar{c}s}$ requires tagging the initial flavor of the decaying B_s^0 meson. In addition to the previously mentioned $B_s^0 \to J/\psi K^+K^-$ (including $B_s^0 \to J/\psi\phi$) and $B_s^0 \to \psi(2S)\phi$ studies, the decay modes $B_s^0 \to J/\psi\pi^+\pi^-$ (including $B_s^0 \to J/\psi f_0(980)$) [76, 104] and $B_s^0 \to D_s^+D_s^-$ [102, 103] have also been analyzed by LHCb to measure $\phi_s^{c\bar{c}s}$, without the need for an angular analysis. The $J/\psi\pi^+\pi^-$ final state has been shown indeed to be (very close to) a pure CP-odd state [105]. In the $B_s^0 \to J/\psi\phi$ and $B_s^0 \to J/\psi K^+K^-$ analyses, $\phi_s^{c\bar{c}s}$ is obtained together with several other observables, including $\Delta\Gamma_s$, Γ_s, the longitudinal and perpendicular ϕ polarisation amplitudes, the S-wave amplitude, and strong phases. In order to account for all correlations, the full sets of measurements provided by the different analyses are combined in a multi-dimensional fit [8] of which $\phi_s^{c\bar{c}s}$ is just one of the free parameters. As already mentioned the $B_s^0 \to J/\psi\phi$ analyses of ATLAS, CMS and LHCb show a poor overall compatibility, mostly in the lifetime and angular parameters. Therefore, scale factors are applied on the combined uncertainty of each parameter where a discrepancy arises. For the parameters already in agreement, such as $\phi_s^{c\bar{c}s}$, no scale factor is applied. The combined result based on all published analyses [28, 31, 32, 62, 76, 80–86, 102–104] is

$$\phi_s^{c\bar{c}s} = -0.053 \pm 0.013\,. \tag{74.29}$$

A two-dimensional projection of the overall situation in the $(\phi_s^{c\bar{c}s}, \Delta\Gamma_s)$ plane is shown in Fig. 74.4. The experimental determination of $\phi_s^{c\bar{c}s}$ is still statistically limited. It is consistent with the Standard Model prediction, which is equal to $-2\beta_s = -2\arg(-(V_{ts}V_{tb}^*)/(V_{cs}V_{cb}^*)) = -0.0367 \pm 0.0010$ [65] or -0.0377 ± 0.0006 [66] assuming negligible Penguin pollution.

CP violation induced by B_s^0–$\overline{B}_s^0$ mixing in $b \to s\bar{s}s$ decays is controlled by the weak phase $\phi_s^{s\bar{s}s}$, which is an observable different from $\phi_s^{c\bar{c}s}$. In the Standard Model, such pure gluonic Penguin decays have an amplitude with a CKM phase that cancels that of the mixing amplitude, and hence $\phi_s^{s\bar{s}s}$ is expected to be essentially zero. LHCb has performed a flavor-tagged time-dependent angular analysis of $B_s^0 \to \phi\phi$ decays [29, 106], similar to that of $B_s^0 \to J/\psi\phi$ decays, and measured

$$\phi_s^{s\bar{s}s} = -0.074 \pm 0.069\,, \tag{74.30}$$

in agreement with the Standard Model prediction.

74.6 Summary

B^0–$\overline{B}^0$ mixing has been and still is a field of intense study. The mass differences in the B_d^0–$\overline{B}_d^0$ and B_s^0–$\overline{B}_s^0$ systems are known to relative precisions of 0.37% and 0.03%, respectively. The non-zero decay-width difference in the B_s^0–$\overline{B}_s^0$ system is well established, with a relative difference of $\Delta\Gamma_s/\Gamma_s = (11.8 \pm 0.6)\%$, meaning that the heavy state of the B_s^0–$\overline{B}_s^0$ system lives $\sim 13\%$ longer than the light state. In contrast, the relative decay-width difference in the B_d^0–$\overline{B}_d^0$ system, $\Delta\Gamma_d/\Gamma_d = (0.5 \pm 1.0)\%$, is still consistent with zero. CP violation in B_d^0–$\overline{B}_d^0$ or B_s^0–$\overline{B}_s^0$ mixing has not been observed yet, with precisions on the semileptonic asymmetries below 0.3%. CP violation induced by B_s^0–$\overline{B}_s^0$ mixing in B_s^0 decays has not yet been observed either, with uncertainties on the $\phi_s^{c\bar{c}s}$ and $\phi_s^{s\bar{s}s}$ phases of 13 mrad and 69 mrad, respectively. All observations so far remain consistent with the Standard Model expectations.

However, the measurements where New Physics might show up are still statistically limited. More results are awaited from the LHC experiments and Belle II, with promising prospects for the investigation of the CP-violating phase $\arg(-M_{12}/\Gamma_{12})$ and improved determination of the $\phi_s^{c\bar{c}s}$ and $\phi_s^{s\bar{s}s}$ phases.

Mixing studies have clearly reached the stage of precision measurements, where much effort is needed, both on the experimental and theoretical sides, in particular to further reduce the hadronic uncertainties of lattice QCD calculations. In the long term, a stringent check of the consistency of the B_d^0 and B_s^0 mixing amplitudes (magnitudes and phases) with all other measured flavor-physics observables will be possible within the Standard Model, leading to very tight limits on (or otherwise a long-awaited surprise about) New Physics.

References

[1] T. D. Lee and C. S. Wu, Ann. Rev. Nucl. Part. Sci. **16**, 511 (1966); I. I. Bigi and A. I. Sanda, Camb. Monogr. Part. Phys. Nucl. Phys. Cosmol. **9**, 1 (2009), second edition, first published in 2000; G. C. Branco, L. Lavoura and J. P. Silva, Int. Ser. Monogr. Phys. **103**, 1 (1999).

[2] See the review on CP violation in the quark sector by T. Gershon and Y. Nir in this publication.

[3] A. J. Buras, W. Slominski and H. Steger, Nucl. Phys. **B245**, 369 (1984).

Int. J. Mod. Phys. A 2026.41. Downloaded from www.worldscientific.com
by UNIVERSITY OF CALIFORNIA @ BERKELEY on 09/16/26. Re-use and distribution is strictly not permitted, except for Open Access articles.

[4] T. Inami and C. S. Lim, Prog. Theor. Phys. **65**, 297 (1981), erratum *ibid.* **65**, 1772 (1981); for the power-like approximation, see A. J. Buras and R. Fleischer, page 91 in "Heavy Flavours II," eds. A. J. Buras and M. Lindner, Singapore World Scientific (1998).

[5] M. Kobayashi and T. Maskawa, Prog. Theor. Phys. **49**, 652 (1973).

[6] I. I. Bigi *et al.*, in "*CP* violation," ed. C. Jarlskog, Singapore World Scientific (1989).

[7] J. Albrecht, F. Bernlochner, A. Lenz and A. Rusov (2024), [arXiv:2402.04224].

[8] Sw. Banerjee *et al.* (HFLAV), Phys. Rev. D **113**, 1, 012008 (2026), [arXiv:2411.18639]; the combined results on *b*-hadron lifetimes and mixing parameters published in this *Review* have been obtained by the corresponding sub-group of the Heavy Flavor Averaging (HFLAV) group in March 2026 as updates of the averages published in Chapter 5 of the above paper and submitted as a Zenodo record available at https://doi.org/10.5281/zenodo.19446771; for more information, see https://hflav.web.cern.ch/.

[9] U. Nierste, P. Reeck, V. Shtabovenko and M. Steinhauser, JHEP **03**, 094 (2026), [arXiv:2512.07949].

[10] C. Albajar *et al.* (UA1), Phys. Lett. **B186**, 247 (1987), erratum *ibid.* **B197**, 565 (1987).

[11] H. Albrecht *et al.* (ARGUS), Phys. Lett. **B192**, 245 (1987).

[12] H. G. Moser and A. Roussarie, Nucl. Instrum. Meth. **A384**, 491 (1997).

[13] SLD collab., SLAC-PUB-7228, SLAC-PUB-7229, and SLAC-PUB-7230, *28th Int. Conf. on High Energy Physics,* Warsaw (1996); J. L. Wittlin, *A measurement of the time dependence of B_d^0–$\overline{B}_d^0$ mixing with kaon tagging*, Ph.D. thesis, Massachusetts U., Amherst (2001).

[14] ALEPH collab., contrib. 596 to *Int. Europhysics Conf. on High Energy Physics,* Jerusalem (1997).

[15] K. Abe *et al.* (SLD), Phys. Rev. **D67**, 012006 (2003), [hep-ex/0209002].

[16] J. Abdallah *et al.* (DELPHI), Eur. Phys. J. **C28**, 155 (2003), [hep-ex/0303032].

[17] F. Abe *et al.* (CDF), Phys. Rev. Lett. **80**, 2057 (1998), [hep-ex/9712004]; F. Abe *et al.* (CDF), Phys. Rev. **D59**, 032001 (1998), [hep-ex/9806026]; F. Abe *et al.* (CDF), Phys. Rev. **D60**, 051101 (1999); F. Abe *et al.* (CDF), Phys. Rev. **D60**, 072003 (1999), [hep-ex/9903011]; T. Affolder *et al.* (CDF), Phys. Rev. **D60**, 112004 (1999), [hep-ex/9907053].

[18] R. Barate *et al.* (ALEPH), Eur. Phys. J. **C4**, 367 (1998); R. Barate *et al.* (ALEPH), Eur. Phys. J. **C7**, 553 (1999), [hep-ex/9811018].

[19] R. Aaij *et al.* (LHCb), JINST **10**, P10005 (2015), [arXiv:1507.07892].

[20] P. Abreu *et al.* (DELPHI), Eur. Phys. J. **C16**, 555 (2000), [hep-ex/0107077].

[21] K. Anikeev *et al.* (2002), [hep-ph/0201071].

[22] A. Abulencia *et al.* (CDF), Phys. Rev. Lett. **97**, 242003 (2006), [hep-ex/0609040].

[23] V. M. Abazov *et al.* (DØ), Phys. Rev. **D74**, 112002 (2006), [hep-ex/0609034].

[24] V. M. Abazov *et al.* (DØ), Phys. Rev. Lett. **101**, 241801 (2008), [arXiv:0802.2255].

[25] R. Aaij *et al.* (LHCb), Eur. Phys. J. **C72**, 2022 (2012), [arXiv:1202.4979].

[26] R. Aaij *et al.* (LHCb), JINST **11**, P05010 (2016), [arXiv:1602.07252].

[27] R. Aaij *et al.* (LHCb), Eur. Phys. J. **C77**, 238 (2017), [arXiv:1610.06019].

[28] R. Aaij *et al.* (LHCb), Phys. Rev. Lett. **114**, 041801 (2015), [arXiv:1411.3104].

[29] R. Aaij *et al.* (LHCb), Phys. Rev. Lett. **131**, 17, 171802 (2023), [arXiv:2304.06198].

[30] R. Aaij *et al.* (LHCb), Phys. Rev. Lett. **117**, 261801 (2016), [arXiv:1608.06620].

[31] G. Aad *et al.* (ATLAS), Eur. Phys. J. **C81**, 342 (2021), [arXiv:2001.07115].

[32] A. Hayrapetyan *et al.* (CMS), to appear in Phys. Rev. Lett. (2026), [arXiv:2412.19952].

[33] B. Aubert *et al.* (BaBar), Phys. Rev. Lett. **94**, 161803 (2005), [hep-ex/0408127]; K. F. Chen *et al.* (Belle), Phys. Rev. **D72**, 012004 (2005), [hep-ex/0504023].

[34] Throughout this document we omit references of results that have been replaced by new published measurements.

[35] D. Buskulic *et al.* (ALEPH), Z. Phys. **C75**, 397 (1997).

[36] P. Abreu *et al.* (DELPHI), Z. Phys. **C76**, 579 (1997).

[37] M. Acciarri *et al.* (L3), Eur. Phys. J. **C5**, 195 (1998).

[38] G. Alexander *et al.* (OPAL), Z. Phys. **C72**, 377 (1996); K. Ackerstaff *et al.* (OPAL), Z. Phys. **C76**, 417 (1997), [hep-ex/9707010]; G. Abbiendi *et al.* (OPAL), Phys. Lett. **B493**, 266 (2000), [hep-ex/0010013].

[39] K. Ackerstaff *et al.* (OPAL), Z. Phys. **C76**, 401 (1997), [hep-ex/9707009].

[40] B. Aubert *et al.* (BaBar), Phys. Rev. Lett. **88**, 221802 (2002), [hep-ex/0112044]; B. Aubert *et al.* (BaBar), Phys. Rev. **D66**, 032003 (2002), [hep-ex/0201020]; B. Aubert *et al.* (BaBar), Phys. Rev. Lett. **88**, 221803 (2002), [hep-ex/0112045]; B. Aubert *et al.* (BaBar), Phys. Rev. **D67**, 072002 (2003), [hep-ex/0212017]; B. Aubert *et al.* (BaBar), Phys. Rev. **D73**, 012004 (2006), [hep-ex/0507054].

[41] N. C. Hastings *et al.* (Belle), Phys. Rev. **D67**, 052004 (2003), [hep-ex/0212033]; Y. Zheng *et al.* (Belle), Phys. Rev. **D67**, 092004 (2003), [hep-ex/0211065]; K. Abe *et al.* (Belle), Phys. Rev. **D71**, 072003 (2005), erratum *ibid.* **D71**, 079903 (2005), [hep-ex/0408111].

[42] F. Abudinén *et al.* (Belle II), Phys. Rev. **D107**, L091102 (2023), [arXiv:2302.12791].

[43] R. Aaij *et al.* (LHCb), Phys. Lett. **B709**, 177 (2012), [arXiv:1112.4311].

[44] R. Aaij *et al.* (LHCb), Phys. Lett. **B719**, 318 (2013), [arXiv:1210.6750].

[45] R. Aaij *et al.* (LHCb), Eur. Phys. J. **C73**, 2655 (2013), [arXiv:1308.1302].

[46] R. Aaij *et al.* (LHCb), Eur. Phys. J. **C76**, 412 (2016), [arXiv:1604.03475].

[47] K. Hartkorn and H. G. Moser, Eur. Phys. J. **C8**, 381 (1999).

[48] R. Fleischer and R. Knegjens, Eur. Phys. J. **C71**, 1789 (2011), [arXiv:1109.5115].

[49] B. Aubert *et al.* (BaBar), Phys. Rev. Lett. **92**, 181801 (2004), [hep-ex/0311037]; B. Aubert *et al.* (BaBar), Phys. Rev. **D70**, 012007 (2004), [hep-ex/0403002].

[50] T. Higuchi *et al.*, Phys. Rev. **D85**, 071105 (2012), [arXiv:1203.0930].

[51] R. Aaij *et al.* (LHCb), JHEP **04**, 114 (2014), [arXiv:1402.2554].

[52] M. Aaboud *et al.* (ATLAS), JHEP **06**, 081 (2016), [arXiv:1605.07485].

[53] A. M. Sirunyan *et al.* (CMS), Eur. Phys. J. **C78**, 457 (2018), erratum *ibid.* **C78**, 561 (2018), [arXiv:1710.08949].

[54] H. Albrecht *et al.* (ARGUS), Z. Phys. **C55**, 357 (1992); H. Albrecht *et al.* (ARGUS), Phys. Lett. **B324**, 249 (1994).

[55] J. E. Bartelt *et al.* (CLEO), Phys. Rev. Lett. **71**, 1680 (1993).

[56] B. H. Behrens *et al.* (CLEO), Phys. Lett. **B490**, 36 (2000), [hep-ex/0005013].

Int. J. Mod. Phys. A 2026.41. Downloaded from www.worldscientific.com
UNIVERSITY OF CALIFORNIA @ BERKELEY on 09/16/26. Re-use and distribution is strictly not permitted, except for Open Access articles.

[57] See the review on the CKM quark-mixing matrix by A. Ceccucci, Z. Ligeti, and Y. Sakai in this publication.

[58] S. Aoki *et al.* (Flavour Lattice Averaging Group) (2019), [arXiv:1902.08191].

[59] R. Aaij *et al.* (LHCb), New J. Phys. **15**, 053021 (2013), [arXiv:1304.4741].

[60] R. Aaij *et al.* (LHCb), JHEP **03**, 137 (2021), [arXiv:2011.12041].

[61] R. Aaij *et al.* (LHCb), Nature Phys. **18**, 1 (2022), [arXiv:2104.04421].

[62] R. Aaij *et al.* (LHCb), Phys. Rev. Lett. **132**, 051802 (2024), [arXiv:2308.01468].

[63] A. Bazavov *et al.* (Fermilab Lattice and MILC), Phys. Rev. **D93**, 113016 (2016), [arXiv:1602.03560].

[64] D. King, A. Lenz and T. Rauh, JHEP **05**, 034 (2019), [arXiv:1904.00940].

[65] M. Bona *et al.* (UTfit), Rend. Lincei Sci. Fis. Nat. **34**, 37 (2023), [arXiv:2212.03894]; updated results at http://www.utfit.org/.

[66] J. Charles *et al.* (CKMfitter), Phys. Rev. **D91**, 073007 (2015), [arXiv:1501.05013]; updated results at http://ckmfitter.in2p3.fr/.

[67] M. Acciarri *et al.* (L3), Phys. Lett. **B438**, 417 (1998).

[68] D. Buskulic *et al.* (ALEPH), Phys. Lett. **B377**, 205 (1996); K. Ackerstaff *et al.* (OPAL), Phys. Lett. **B426**, 161 (1998), [hep-ex/9802002]; F. Abe *et al.* (CDF), Phys. Rev. **D59**, 032004 (1999), [hep-ex/9808003]; V. M. Abazov *et al.* (DØ), Phys. Rev. Lett. **114**, 062001 (2015), [arXiv:1410.1568]; T. Aaltonen *et al.* (CDF), Phys. Rev. Lett. **107**, 272001 (2011), [arXiv:1103.1864]; R. Aaij *et al.* (LHCb), Phys. Rev. Lett. **113**, 172001 (2014), [arXiv:1407.5873]; R. Aaij *et al.* (LHCb), Phys. Rev. Lett. **119**, 101801 (2017), [arXiv:1705.03475].

[69] R. Aaij *et al.* (LHCb), Phys. Rev. Lett. **112**, 111802 (2014), [arXiv:1312.1217].

[70] R. Aaij *et al.* (LHCb), Phys. Lett. **B736**, 446 (2014), [arXiv:1406.7204].

[71] R. Aaij *et al.* (LHCb), Phys. Lett. **B707**, 349 (2012), [arXiv:1111.0521].

[72] R. Aaij *et al.* (LHCb), Phys. Lett. **B762**, 484 (2016), [arXiv:1607.06314].

[73] R. Aaij *et al.* (LHCb), Eur. Phys. J. **C83**, 7, 629 (2023), [arXiv:2206.03088].

[74] T. Aaltonen *et al.* (CDF), Phys. Rev. **D84**, 052012 (2011), [arXiv:1106.3682]; V. M. Abazov *et al.* (DØ), Phys. Rev. **D94**, 012001 (2016), [arXiv:1603.01302].

[75] R. Aaij *et al.* (LHCb), Phys. Rev. **D87**, 112010 (2013), [arXiv:1304.2600].

[76] R. Aaij *et al.* (LHCb), Phys. Lett. **B797**, 134789 (2019), [arXiv:1903.05530].

[77] R. Aaij *et al.* (LHCb), Nucl. Phys. **B873**, 275 (2013), [arXiv:1304.4500].

[78] R. Aaij *et al.* (LHCb), Phys. Rev. Lett. **128**, 041801 (2022), [arXiv:2108.09284]; R. Aaij *et al.* (LHCb), Phys. Rev. **D105**, 012010 (2022), [arXiv:2108.09283]; A. Tumasyan *et al.* (CMS), Phys. Lett. **B842**, 137955 (2023), [arXiv:2212.10311]; G. Aad *et al.* (ATLAS), JHEP **09**, 199 (2023), [arXiv:2308.01171].

[79] R. Aaij *et al.* (LHCb), JHEP **05**, 253 (2024), [arXiv:2310.12649].

[80] T. Aaltonen *et al.* (CDF), Phys. Rev. Lett. **109**, 171802 (2012), [arXiv:1208.2967].

[81] V. M. Abazov *et al.* (DØ), Phys. Rev. **D85**, 032006 (2012), [arXiv:1109.3166].

[82] G. Aad *et al.* (ATLAS), Phys. Rev. **D90**, 052007 (2014), [arXiv:1407.1796]; G. Aad *et al.* (ATLAS), JHEP **08**, 147 (2016), [arXiv:1601.03297].

[83] V. Khachatryan *et al.* (CMS), Phys. Lett. **B757**, 97 (2016), [arXiv:1507.07527].

[84] R. Aaij *et al.* (LHCb), Eur. Phys. J. **C81**, 1026 (2021), [arXiv:2105.14738].

[85] R. Aaij *et al.* (LHCb), JHEP **08**, 037 (2017), [arXiv:1704.08217].

[86] R. Aaij *et al.* (LHCb), Phys. Lett. **B762**, 253 (2016), [arXiv:1608.04855].

[87] R. Aaij *et al.* (LHCb), Phys. Rev. Lett. **108**, 241801 (2012), [arXiv:1202.4717].

[88] A. Lenz and U. Nierste, JHEP **06**, 072 (2007), [hep-ph/0612167].

[89] D. E. Jaffe *et al.* (CLEO), Phys. Rev. Lett. **86**, 5000 (2001), [hep-ex/0101006].

[90] J. P. Lees *et al.* (BaBar), Phys. Rev. Lett. **114**, 081801 (2015), [arXiv:1411.1842].

[91] F. Abe *et al.* (CDF), Phys. Rev. **D55**, 2546 (1997).

[92] V. M. Abazov *et al.* (DØ), Phys. Rev. **D89**, 012002 (2014), [arXiv:1310.0447].

[93] V. M. Abazov *et al.* (DØ), Phys. Rev. **D86**, 072009 (2012), [arXiv:1208.5813].

[94] V. M. Abazov *et al.* (DØ), Phys. Rev. Lett. **110**, 011801 (2013), [arXiv:1207.1769].

[95] R. Aaij *et al.* (LHCb), Phys. Rev. Lett. **117**, 061803 (2016), erratum *ibid.* **118**, 129903 (2017), [arXiv:1605.09768].

[96] R. Barate *et al.* (ALEPH), Eur. Phys. J. **C20**, 431 (2001).

[97] J. P. Lees *et al.* (BaBar), Phys. Rev. Lett. **111**, 101802 (2013), erratum *ibid.* **111**, 159901 (2013), [arXiv:1305.1575].

[98] E. Nakano *et al.* (Belle), Phys. Rev. **D73**, 112002 (2006), [hep-ex/0505017].

[99] G. Abbiendi *et al.* (OPAL), Eur. Phys. J. **C12**, 609 (2000), [hep-ex/9901017].

[100] M. Beneke, G. Buchalla and I. Dunietz, Phys. Lett. **B393**, 132 (1997), [hep-ph/9609357]; I. Dunietz, Eur. Phys. J. **C7**, 197 (1999), [hep-ph/9806521].

[101] R. Aaij *et al.* (LHCb), Phys. Rev. Lett. **114**, 041601 (2015), [arXiv:1409.8586].

[102] R. Aaij *et al.* (LHCb), Phys. Rev. Lett. **113**, 211801 (2014), [arXiv:1409.4619].

[103] R. Aaij *et al.* (LHCb), JHEP **01**, 061 (2025), [arXiv:2409.03009].

[104] R. Aaij *et al.* (LHCb), Phys. Lett. **B736**, 186 (2014), [arXiv:1405.4140].

[105] R. Aaij *et al.* (LHCb), Phys. Rev. **D86**, 052006 (2012), [arXiv:1204.5643].

[106] R. Aaij *et al.* (LHCb), Phys. Rev. **D90**, 052011 (2014), [arXiv:1407.2222].

Int. J. Mod. Phys. A 2026.41. Downloaded from www.worldscientific.com
by UNIVERSITY OF CALIFORNIA @ BERKELEY on 09/16/26. Re-use and distribution is strictly not permitted, except for Open Access articles.

75. Semileptonic b-Hadron Decays, Determination of V_{cb}, V_{ub}

Revised March 2026 by A.X. El-Khadra (Physics, Illinois U.) and P. Urquijo (School of Phys. U. of Melbourne).

75.1 Introduction

Precision determinations of $|V_{ub}|$ and $|V_{cb}|$ are central to testing the CKM sector of the Standard Model, and complement the measurements of CP asymmetries in B decays. The length of the side of the unitarity triangle opposite the well-measured angle β is proportional to the ratio $|V_{ub}|/|V_{cb}|$; its precise determination is a high priority of the heavy-flavor physics program.

The transitions $b \to c\ell\bar{\nu}_\ell$ and $b \to u\ell\bar{\nu}_\ell$ ($\ell = e, \mu$) each provide two avenues for determining these CKM matrix elements, namely through measurements of inclusive decay rates, $\bar{B} \to X\ell\bar{\nu}_\ell$ with a sum over all possible hadronic states X or of exclusive rates, where the final state hadron is a specific meson ($X = D$, D^*, π, ρ etc.).

Purely leptonic decays, such as $B_c^- \to \tau\bar{\nu}$, $B^- \to \tau\bar{\nu}$, and $B^- \to \mu\bar{\nu}$, provide a third avenue that is theoretically very simple (see the RPP mini-review [1]). However, we do not use this information at present since none of the measurements have reached a competitive level of precision. Hence the results presented here are solely obtained from exclusive and inclusive semileptonic b-hadron decays. This article and the values quoted here update the previous review [2].

The theoretical methods underlying the different determinations of $|V_{qb}|$ are quite mature. The theoretical approach for inclusive determinations uses the fact that the mass m_b of the b quark is large compared to the scale $\Lambda_{\rm QCD}$ that determines low-energy hadronic physics. Thus the basis for precise calculations is a systematic expansion in powers of Λ/m_b, where $\Lambda \sim 500 - 700$ MeV is a hadronic scale of the order of $\Lambda_{\rm QCD}$. Such an expansion can be formulated in the framework of an effective field theory which is described in a separate RPP mini-review [3]. Exclusive determinations rely on non-perturbatively calculated form factors that encode the low-energy dynamics of the hadronic transition. Here, lattice QCD provides an, in principle, ab-initio method to calculate the non-perturbative QCD contributions to the exclusive decay amplitudes. Thanks to a combination of improved theoretical methods, better algorithms, and large increases in computational power, precise lattice QCD results are now available for the processes that are used in exclusive $|V_{ub}|$ and $|V_{cb}|$ determinations. State-of-the-art lattice QCD calculations are based on gauge-field ensembles that include realistic sea quark effects for degenerate up/down and strange quarks (aka $2+1$-flavor ensembles), and increasingly, also for charm (aka $2+1+1$-flavor ensembles). They employ ensembles generated at three (or more) lattice spacings, different spatial volumes, among other parameter variations to allow for quantification of the underlying systematic errors, and include detailed systematic error analyses. This is described in a separate RPP mini-review [4]. The lattice-QCD results discussed in this review are all state-of-the art with fully quantified uncertainties, and therefore play a central role in exclusive $|V_{qb}|$ determinations. In the case of exclusive $\bar{B} \to D^{(*)}\ell\bar{\nu}_\ell$ decays, heavy quark symmetry (HQS) and heavy quark effective theory (HQET) yield constraints on the form factors that can be used to test lattice results and refined constraints on the form factors. Light-cone sum rules (LCSR) provide another nonperturbative approach to compute form factors. However, while the lattice-QCD results employed in this review have well-quantified uncertainties, LCSR results suffer, in general, from hard-to-quantify systematic errors. The two methods typically provide results in opposite regions of phase space. Lattice-QCD calculations work best at low hadronic recoil or high momentum transfer (q^2) to the leptons, while LCSR calculations provide estimates at high recoil, near $q^2 = 0$. However, the kinematic range for which lattice-QCD calculations provide information is increasing and further enhanced with the aid of model-independent parameterizations and HQE constraints. In general, we do not use form factor inputs obtained from LCSR in this review.

The measurements discussed in this review are of branching fractions, ratios of branching fractions, and decay kinematic distributions. The determinations of $|V_{cb}|$ and $|V_{ub}|$ also require a measurement of the total decay widths of the corresponding b hadrons, determined from lifetimes, which is the subject of a separate RPP mini-review [5]. The measurements of inclusive semileptonic decays relevant to this review come primarily from e^+e^- B factories operating at the $\Upsilon(4S)$ resonance, while the measurements of exclusive semileptonic decays come from both the e^+e^- B factories and from the LHCb experiment at CERN.

Semileptonic B-meson decay amplitudes to electrons and muons are well measured and consistent with Standard Model W-boson exchange. As they are expected to be insensitive to the effects of non-Standard-Model physics, they are used to extract $|V_{qb}|$. However, semileptonic decays to tau-lepton final states, such as $\bar{B} \to D^{(*)}\tau\bar{\nu}_\tau$, may be sensitive to effects from beyond the Standard Model particles due to the large mass of the τ lepton. The currently observed tensions between Standard Model theory and experiment for these decays indicate that semitauonic decays must be studied further. For rare decays, tests of lepton-flavor universality violations (LFUV) in ratios involving μ/e final states provide CKM-free tests of the SM. These and other flavor dependent angular analyses are also included in this review.

Many of the numerical results quoted in this review have been provided by the Heavy Flavor Averaging Group (HFLAV) [6].

75.2 Determination of $|V_{cb}|$

Summary: The determination of $|V_{cb}|$ from inclusive decays has a relative uncertainty of about 1.2%; the limitations arise mainly from our ignorance of higher-order perturbative and non-perturbative corrections. Exclusive $\bar{B} \to D^*\ell\bar{\nu}_\ell$ decays provide a determination of $|V_{cb}|$ with a relative precision of about 1.6%, with comparable contributions from theory and experiment to the total uncertainty; the value determined from $\bar{B} \to D\ell\bar{\nu}_\ell$ decays is consistent and has an uncertainty of 1.8%. The values obtained from the inclusive and exclusive B decay determinations discussed below are:

$$|V_{cb}| = (42.0 \pm 0.5) \times 10^{-3} \quad \text{(inclusive)} \tag{75.1}$$

$$|V_{cb}| = (39.5 \pm 0.5) \times 10^{-3} \quad \text{(exclusive)}. \tag{75.2}$$

An average of these determinations has $p(\chi^2) < 1\%$, so we scale the error by $\sqrt{\chi^2/1} = 3.7$ to find

$$|V_{cb}| = (40.7 \pm 1.3) \times 10^{-3} \quad \text{(average)}. \tag{75.3}$$

Given the inconsistency this average should be treated with caution.

75.2.1 $|V_{cb}|$ *from exclusive decays*

Exclusive determinations of $|V_{cb}|$ make use of semileptonic B (or B_s) decays into the ground state charmed mesons D (D_s) and D^* (D_s^*). The corresponding hadronic matrix elements can be parameterized in terms of six independent form factors, which depend on the variable $w \equiv v \cdot v'$, where v and v' are the four velocities of the initial and final-state hadrons. In the rest frame of the decay this variable corresponds to the Lorentz factor of the final state $D^{(*)}$ meson. Determinations of $|V_{cb}|$ from experimental measurements of $\bar{B} \to D^{(*)}\ell\bar{\nu}_\ell$ decay rates require precise knowledge of these form factors. Fortunately, lattice QCD results for all relevant form factors, including their recoil dependence, are now available [7–13]. Additional, new lattice-QCD results are expected to become available in the coming years [14–17].

Heavy Quark Symmetry (HQS) [18, 19] predicts that in the infinite mass limit the six form factors collapse into a single one, which is normalized at the "zero recoil point" $w = 1$, the point of maximum momentum transfer to the leptons. Heavy Quark Effective Theory (HQET) provides a framework for obtaining the corrections to the HQS prediction in a systematic expansion in powers of $\Lambda_{\rm QCD}/m_c$ which is discussed in a separate RPP mini-review [3].

Int. J. Mod. Phys. A 2026.41. Downloaded from www.worldscientific.com
UNIVERSITY OF CALIFORNIA @ BERKELEY on 09/16/26. Re-use and distribution is strictly not permitted, except for Open Access articles.

75.2.2 $\bar{B} \to D^* \ell \bar{\nu}_\ell$

The decay rate for $\bar{B} \to D^* \ell \bar{\nu}_\ell$, assuming massless leptons, is given by

$$\frac{d\Gamma}{dw}(\bar{B} \to D^* \ell \bar{\nu}_\ell) = \frac{G_F^2 m_B^5}{48\pi^3} |V_{cb}|^2 |\eta_{\rm EW}|^2 (w^2-1)^{1/2} P(w) |\mathcal{F}(w)|^2, \tag{75.4}$$

where $P(w)$ is a phase space factor,

$$P(w) = r^3 (1-r)^2 (w+1)^2 \left(1 + \frac{4w}{w+1} \frac{1-2rw+r^2}{(1-r)^2}\right), \tag{75.5}$$

with $r = m_{D^*}/m_B$. The decay amplitude $\mathcal{F}(w)$ can be expressed in terms of the form factors which parametrize the vector and axial vector current matrix elements

$$\frac{\langle D^*(v',\epsilon)|\bar{c}\gamma^\mu b|B(v)\rangle}{\sqrt{m_B m_{D^*}}} = h_V(w)\, \varepsilon^{\mu\nu\rho\sigma} v_{B,\nu} v_{D^*,\rho} \epsilon^*_\sigma, \tag{75.6}$$

$$\frac{\langle D^*(v',\epsilon)|\bar{c}\gamma^\mu \gamma^5 b|B(v)\rangle}{\sqrt{m_B m_{D^*}}} = i h_{A_1}(w)\,(1+w)\epsilon^{*\mu} - i\left[h_{A_2}(w) v_B^\mu + h_{A_3}(w) v_{D^*}^\mu\right] \epsilon^* \cdot v_B, \tag{75.7}$$

and the ratios

$$R_1(w) = \frac{h_V(w)}{h_{A_1}(w)}, \quad R_2(w) = \frac{h_{A_3}(w) + r\, h_{A_2}(w)}{h_{A_1}(w)}, \tag{75.8}$$

as

$$P(w)|\mathcal{F}(w)|^2 = |h_{A_1}(w)|^2 \times \left\{ 2\frac{r^2-2rw+1}{(1-r)^2}\left[1 + \frac{w-1}{w+1} R_1^2(w)\right] + \left[1 + \frac{w-1}{1-r}(1-R_2(w))\right]^2 \right\}. \tag{75.9}$$

Note that $\mathcal{F}$ at $w = 1$ is unity by HQS in the infinite-mass limit [20–23]. The effect of assuming massless leptons is typically very small, but for the muon case can be non-negligible in fits to data at high hadronic recoil.

The factor $\eta_{\rm EW} = 1.0066 \pm 0.0050$ accounts for the leading electroweak corrections to the four-fermion operator mediating the semileptonic decay [24], and includes an estimated uncertainty for missing long-distance and structure-dependent QED corrections [25]. While some QED radiative corrections are included in the experimental analysis, the Coulomb correction, which arises when the final-state hadron is charged, is not taken into account.

The determination of $|V_{cb}|$ requires knowledge of the normalization, where one commonly uses a theoretical calculation of the zero recoil input, $\mathcal{F}(1)$. Theoretical knowledge of the shapes of the form factors provides crucial compatibility checks between theory and experiment, and improves the precision of the determinations.

Model-independent shape parametrizations of the form factors make use of analyticity and unitarity constraints and are expressed in terms of the variable

$$z = \frac{\sqrt{w+1} - \sqrt{2N}}{\sqrt{w+1} + \sqrt{2N}}, \tag{75.10}$$

originating from a conformal transformation, where $N = (t_+ - t_0)/(t_+ - t_-)$, $t_\pm = (m_B \pm m_{D^*})^2$, and the choice of t_0 determines the kinematic point at which $z = 0$. The form factors (generically denoted as F) may then be written as [26–30]

$$F(z) = \frac{1}{P_F(z)\phi_F(z)} \sum_{n=0}^{\infty} a_n z^n \tag{75.11}$$

where the sum is bounded, $\sum |a_n|^2 < 1$. Furthermore, the function $P_F(z)$ takes into account the resonances in the $(\bar{c}b)$ system below the $\bar{D}B$ threshold, and the weighting functions $\phi_F(z)$ are derived from the unitarity constraint on the corresponding form factor. With the conventional choice $N = 1$, $z = 0$ when $w = 1$ and kinematic range of the decay corresponds to $0 \le z \le 0.06$. As a result, only very few terms are needed in the series in z. We refer to Eq. (75.11) as the "BGL" expansion. The Caprini-Lellouch-Neubert (CLN) parametrization [31] yields a simple form with only two fit parameters (the slope ρ and normalization $h_{A_1}(1)$), albeit at the cost of introducing model dependence and neglecting higher-order corrections in the $1/m_{c/b}$ expansion, which are relevant at the current level of precision [30,32–38]. Thus, this report focuses on analyses that employ lattice form factors at non-zero recoil, the model-independent BGL expansion. and HQET expansions through $\mathcal{O}(\alpha_s/m_{b,c}, 1/m_{b,c}^2)$. Typical fits include up to three parameters a_n in Eq. (75.11) for the different form factors.

While lattice QCD results for the form factor at the zero-recoil point, $\mathcal{F}(1)$ have been available for over a decade [25, 39], there now exist three independent lattice QCD calculations by [10], [11], and [12] of the $\bar{B} \to D^* \ell \bar{\nu}_\ell$ form factors at non-zero recoil. The three groups each employ statistically independent gauge-field ensembles and use different lattice actions for the heavy and light quarks. To obtain results in the continuum and at the physical point, all three analyses first perform chiral-continuum fits and systematic error studies on the corresponding lattice form factor data. The resulting continuum form factors are smooth functions (bands) obtained over recoil ranges which depend on the respective simulation details. For the next step, the lattice-QCD form factors are presented as synthetic data points (including the statistical and systematic correlations), to be used as inputs in BGL-expansion fits to obtain the form factors over the entire recoil range. A comparison of the resulting $|\mathcal{F}(w)|^2$ amplitudes is shown in Fig. 75.1. While the lattice results are reasonably consistent in the low-recoil region, small variations in the slopes yield the observed spread between the bands at large recoil. Indeed, the

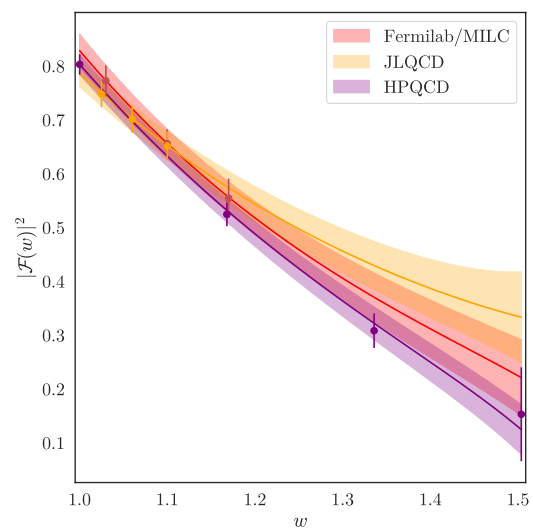

Figure 75.1: Comparison of lattice QCD results for $|\mathcal{F}(w)|^2$ obtained by the Fermilab Lattice and MILC collaborations (red), HPQCD (purple), and JLQCD (yellow). Plot courtesy of A. Vaquero.

FLAG collaboration [40] performs combined BGL fits using the form-factor results of Refs. [10,12], which both employ gauge field ensembles with three active flavors in the sea (representing light and strange quarks), with $\chi^2/\text{dof} < 1$. FLAG further finds that their BGL fits of the form factor results of Ref. [11], which employ gauge-field ensembles with four active flavors in the sea, are compatible with Refs. [10, 12].[1] Their BGL fits also yield results for the form factor at zero recoil, where they obtain $\mathcal{F}(1) = 0.894(10)$ for their three-flavor combination and $\mathcal{F}(1) = 0.899(14)$ for four-

[1] We note that as a matter of principle, the FLAG collaboration doesn't combine lattice-QCD results obtained from simulations with different numbers of sea-quark flavors.

Int. J. Mod. Phys. A 2026.41. Downloaded from www.worldscientific.com
by UNIVERSITY OF CALIFORNIA @ BERKELEY on 09/16/26. Re-use and distribution is strictly not permitted, except for Open Access articles.

flavors. A weighted average yields

$$\mathcal{F}(1) = 0.896 \pm 0.008\,. \tag{75.12}$$

Non-lattice estimates based on zero-recoil sum rules for the form factor tend to yield lower central values for $\mathcal{F}(1)$ [41–43]. The sum rules indicate that $\mathcal{F}(1) < 0.92$ [41, 42, 44, 45], while an explicit estimate that includes excited state contributions yields $\mathcal{F}(1) \approx 0.86$ [43, 46]. While Light Cone Sum Rules (LCSR) can provide constraints on the form factors near maximum recoil, the underlying systematic errors are not fully quantified. A modern LCSR calculation [47] quotes uncertainties in the $\lesssim 20\%$ range for the $\bar{B} \to D^{(*)}\ell\bar{\nu}_\ell$ form factors at $q^2 = 0$.

Dispersive methods [48] can also be used to provide additional constraints on form factors calculated in lattice QCD. Refs. [49,50] introduce the dispersive matrix method and a lattice-QCD calculation of the susceptibilities, which are required inputs to the dispersive matrix method and also needed in z-expansion fits. The susceptibilities of Ref. [50] differ from the perturbative-QCD results of Ref. [51], in some cases outside of the quoted error bars, with a significance of up to 2.5σ, while more recent results [52,53] are more compatible with pQCD. A test of the dispersive matrix approach for the $D \to K\ell\nu$ form factors, which can be computed in lattice-QCD over the entire kinematic range, is presented in Ref. [49]. The implementation of the dispersive matrix in Ref. [54] imposes unitarity constraints on the input data via a so-called unitarity filter. The filter has the effect of altering the shapes of the form factor bands while reducing the uncertainties from extrapolating the form factors over the entire kinematic range. Subsequently, the authors of Ref. [54] determine $|V_{cb}|$ from a bin-by-bin analysis of the experimental data, which avoids the common shape constraints in joint z-expansion fits. In follow-up work, this method has also been applied to other semileptonic decay channels [55–60]. Another approach [61] employs Bayesian inference to implement unitarity constraints, which allows for a straightforward combination of inputs from multiple lattice calculations while including experimental data in joint z-expansion fits. However, the correlations between lattice form factor results at different recoil momenta (or q^2 or z values) may not be preserved in these implementations of the dispersive constraints, for which further studies would be welcome.

Many experiments [62–75] have measured the differential decay rate as a function of w, employing a variety of methods: using either B^+ or B^0 decays, with or without B-tagging, and with or without explicit reconstruction of the transition pion from $D^* \to D$ decays. The leading experimental uncertainties are due to detection efficiencies and $D^{(*)}$ decay branching fractions.

The most commonly accepted approach for the determination of $|V_{cb}|$ is to fit the available data with the BGL form-factor parameterization [27–30, 34]. The BABAR and Belle experiments have published analyses with BGL based parametrizations at a given order in the expansion [71–74]. The main results from these measurements are summarised in Table 75.1 after multiplying through the value of $\mathcal{F}(1)$ quoted in the nominal result of each respective study. These results have not yet been combined by the Heavy Flavor Averaging Group.

The Belle analysis [71] and the Belle II analysis [74] are both based on untagged approaches in the mode $\bar{B}^0 \to D^{*+}\ell\bar{\nu}_\ell$ and measure 1-d projections in bins of the hadronic recoil w, and angular variables $\cos\theta_\ell$, $\cos\theta_V$, and χ. The BABAR analysis [72] and the recent Belle analyses [73,75] are based on hadronic tagged samples using both charged and neutral B decays. BABAR performs a full 4-d unbinned analysis of neutral and charged B decay modes, while Belle [73] uses unfolded 1-d projections of w, $\cos\theta_\ell$, $\cos\theta_V$, and χ, and Belle [75] fits to normalised angular coefficients as a function of w. The latter Belle measurements are performed on the same dataset. Only the BGL form factors are directly determined in these tagged analysis, not the normalization, which is taken from the world average $\bar{B} \to D^*\ell\bar{\nu}_\ell$ branching fractions.

The studies in Refs. [71,73–75] publish the fully-differential decay rate data and associated covariance matrices. Some studies report fit results at low order in the three BGL expansion terms when non-zero lattice data is not used as an additional constraint, ranging from zero-order to second-order. Studies of the impact of higher order expansions based on the Belle untagged published decay rate data have been reported in Refs. [35,36], as well as in the recent Belle and Belle II studies [73,74], where it is shown that the fit uncertainty on $|V_{cb}|$ increases substantially with respect to the results reported at lower order, while the parameter correlations approach 1. This is due to larger number of degrees of freedom allowed in the higher order expansions, which are not sufficiently constrained without lattice-QCD inputs at nonzero recoil.

In Ref. [10], BGL expansion fits to the FNAL/MILC lattice QCD form factors show that they are insensitive to truncation effects beyond quadratic order, and similar results were obtained in Refs. [11,12] as well as for the combined lattice-QCD form factor fits performed by the FLAG collaboration [40]. While each lattice group separately performs combined lattice+experiment BGL fits to extract $|V_{cb}|$, here we quote the results of Ref. [40], which uses the same experimental inputs as HFLAV [6]. In particular, Ref. [40] quotes values for $|V_{cb}|$ from $\bar{B} \to D^*\ell\bar{\nu}_\ell$ data of $|V_{cb}| = 39.23(65) \times 10^{-3}$ for their their three-flavor combination and $|V_{cb}| = 39.44(89) \times 10^{-3}$ for the four-flavor result.

There is some spread between predictions from the three lattice-QCD form factor sets for derived quantities, such as the $R_2(w)$ ratio [77]. Similarly, while the experimental results for $R_2(w)$ in Refs. [73,74] are in tension with Refs. [10,11], the recent measurement of angular coefficients in Ref. [75] yields results for $R_2(w)$ that are compatible with Refs. [10, 12] and in mild tension with Ref. [11]. Furthermore, an analysis of the lattice form factors within the framework of the HQE [78] finds them to be well compatible with it and with each other and (with some spread) with HQE expectations for $R_2(w)$.

For this review, we take results of a combination performed by HFLAV. Firstly, the average value of the $\overline{B}^0 \to D^{*+}\ell^-\bar{\nu}_\ell$ branching fraction is determined by assuming isospin symmetry from measurements of the decays $\overline{B}^0 \to D^{*+}\ell^-\bar{\nu}_\ell$ [62–66, 68, 71, 74, 79, 80] and $\overline{B}^- \to D^{*0}\ell^-\bar{\nu}_\ell$ [66, 68, 79]. A fit is then performed on an average of the normalised unfolded $\overline{B}^0 \to D^{*+}\ell^-\bar{\nu}_\ell$ differential measurements by the Belle [73] and Belle II [74] collaborations. The untagged Belle [71] measurement was not included as unfolded spectra were not provided. Using the BGL parametrization for the form factors, the branching fraction measurement is combined with normalised differential distributions in w, $\cos\theta_\ell$, $\cos\theta_V$ and χ as well as non-zero lattice QCD input from FNAL/MILC [10], HPQCD [11], JLQCD [12] a fit for $|V_{cb}|$. The nominal result for $|V_{cb}|$ is therefore

$$|V_{cb}| = (40.0 \pm 0.7) \times 10^{-3}\ (\bar{B} \to D^*\ell\bar{\nu}_\ell,\ \text{LQCD}, \text{BGL}), \tag{75.13}$$

where the uncertainty contains contributions from experimental, lattice QCD, and $\eta_{\rm EW}$ sources. We note that despite the improvements in the experimental data, theoretical inputs, and $|V_{cb}|$ extraction methods, this new exclusive determination of $|V_{cb}|$, while higher in central value compared to earlier ones, is still in tension with the inclusive determinations discussed in Section 75.2.5 and summarized in Eq. (75.27). However, we note that the new measurement of angular coefficients by the Belle collaboration [75], which is not yet included in the HFLAV average, yields a slightly higher value of $|V_{cb}| = (40.7 \pm 0.7) \times 10^{-3}$ when combined with the same lattice-QCD inputs.

75.2.3 $\bar{B} \to D\ell\bar{\nu}_\ell$

The differential rate for $\bar{B} \to D\ell\bar{\nu}_\ell$ is given by

$$\frac{d\Gamma}{dw}(\bar{B} \to D\ell\bar{\nu}_\ell) = \frac{G_F^2}{48\pi^3}|V_{cb}|^2(m_B + m_D)^2 m_D^3 (w^2-1)^{3/2}(\eta_{\rm EW}\mathcal{G}(w))^2. \tag{75.14}$$

The form factor is defined in terms of

$$\frac{\langle D(v')|\bar{c}\gamma^\mu b|B(v)\rangle}{\sqrt{m_B m_D}} = h_+(w)\,(v_B + v_D)^\mu + h_-(w)\,(v_B - v_D)^\mu \tag{75.15}$$

and reads

$$\mathcal{G}(w) = h_+(w) - \frac{m_B - m_D}{m_B + m_D} h_-(w), \tag{75.16}$$

Int. J. Mod. Phys. A 2026.41. Downloaded from www.worldscientific.com
UNIVERSITY OF CALIFORNIA @ BERKELEY on 09/16/26. Re-use and distribution is strictly not permitted, except for Open Access articles.

Table 75.1: $\mathcal{F}(1)\eta_{EW}|V_{cb}|$ results from $B \to D^*\ell\nu$ with BGL expansion fits. Note that the tagged analyses combine results from B^- and $\bar{B}^0$ decays, while the untagged analyses study only $\bar{B}^0$ decays. The final column listed the non-zero recoil lattice QCD data used in each result.

Measurement	Tag	$\mathcal{F}(1)\eta_{EW}\lvert V_{cb}\rvert \times 10^3$	Fit inputs
Belle [76]	Untagged	35.22 ± 0.95	FNAL/MILC [25]
Babar [72]	Tagged	34.98 ± 0.65	
Belle [73]	Tagged	37.12 ± 0.57	FNAL/MILC [10], HPQCD [11], JLQCD [12]
Belle [75]	Tagged	36.94 ± 0.56	FNAL/MILC [10], HPQCD [11], JLQCD [12]
Belle II [74]	Untagged	37.00 ± 0.91	FNAL/MILC [10]

where $h_+(1)$ is normalized to unity due to HQS and $h_-(1)$ vanishes in the infinite-mass limit. Thus

$$\mathcal{G}(1) = 1 + \mathcal{O}\left(\left(\frac{m_B - m_D}{m_B + m_D}\right)^2 \frac{\Lambda_{\rm QCD}}{m_c}\right) \tag{75.17}$$

and the corrections to the HQS prediction are of order $\Lambda_{\rm QCD}/m_c$ in contrast to the case of $\mathcal{F}(1)$. The lattice-QCD result for the normalization $\mathcal{G}(1)$, obtained in Ref. [7] is

$$\mathcal{G}(1) = 1.054 \pm 0.004 \pm 0.008\,. \tag{75.18}$$

For the $\bar{B} \to D\ell\bar{\nu}_\ell$ modes, theoretical input on the shape of the form factor, especially near $w \sim 1$, is especially beneficial to $|V_{cb}|$ determinations, since experimental measurements of the differential decays rate near zero recoil are affected by the more severe phase space suppression, compared to the D^* case. Hence the best $|V_{cb}|$ determinations from exclusive $\bar{B} \to D\ell\bar{\nu}_\ell$ decays employ lattice-QCD form factors obtained over a range of $w \geq 1$ [7, 8]. We take the result from Ref. [6] for $|V_{cb}|$. Firstly, the average value of the $\overline{B}^0 \to D^+\ell^-\bar{\nu}_\ell$ branching fraction is determined by assuming isospin asymmetry from measurements of the decays $\overline{B}^0 \to D^+\ell^-\bar{\nu}_\ell$ [62, 81–84] and $\overline{B}^- \to D^0\ell^-\bar{\nu}_\ell$ [81–84]. Using the BGL parametrization for the form factors, the branching fraction measurement is combined with normalised w spectrum from Belle [83] in a fit for $|V_{cb}|$. Only Ref. [83] published the full measurement covariance matrix, while Ref. [82] provides the statistical uncertainty covariance. Non-zero recoil lattice QCD inputs are included in the fit following the procedure outlined in Ref. [40] to give

$$|V_{cb}| = (38.9 \pm 0.7) \times 10^{-3} \quad (\bar{B} \to D\ell\bar{\nu}_\ell,\ \text{LQCD, BGL}). \tag{75.19}$$

We note that a similar analysis by FLAG [40], obtains $|V_{cb}| = 40.0(1.0) \times 10^{-3}$ using the same lattice and similar experimental inputs.

The $|V_{cb}|$ averages from $\bar{B} \to D^*\ell\bar{\nu}_\ell$ and $\bar{B} \to D\ell\bar{\nu}_\ell$ decays (Eq. (75.13)) and (Eq. (75.19)), respectively, are consistent. The correlations between the lattice uncertainties for $\bar{B} \to D^*\ell\bar{\nu}_\ell$ and $\bar{B} \to D\ell\bar{\nu}_\ell$ form factors are discussed in Ref. [40, 85]. The statistical uncertainties for the form factors obtained by Fermilab/MILC are conservatively taken to be 100% correlated. We assume an experimental uncertainty correlation of order 20% and combine the results of Eq. (75.13) and Eq. (75.19), giving

$$|V_{cb}| = (39.5 \pm 0.5) \times 10^{-3} \quad \text{(exclusive)}. \tag{75.20}$$

75.2.4 $B_s \to D_s^{(*)-}\mu^+\nu_\mu$

Semileptonic decays of B_s mesons are being studied extensively by the LHCb experiment. On the theory side, lattice QCD calculations of the corresponding form factors can proceed using the same methods and gauge-field ensembles as for B-meson decays. In fact, the presence of a strange spectator quark in the B_s-meson decay amplitudes tends to yield smaller statistical and systematic errors in the lattice computation. Nevertheless, to-date there are still fewer lattice-QCD results for B_s-meson form factors available than for the B-meson case, but this situation is expected to change [14, 16]. For the case of the $B_s \to D_s$ transition, two lattice QCD calculations of the form factors over a range of recoil momenta have been performed by the HPQCD collaboration, the first on $2+1$-flavor gauge field ensembles (generated by the MILC collaboration) using NRQCD b-quarks [86]. The second calculation uses the $2+1+1$-flavor gauge-field ensembles (also generated by MILC), employing the HISQ action for all valence quarks [9]. The all-HISQ approach avoids the need to compute renormalization factors separately, at the cost of requiring an extrapolation to the physical b-quark mass at the lattice spacings used in Ref. [9]. For the $B_s \to D_s^{*-}$ transition, Refs. [11, 13] provide lattice QCD results for the form factors at nonzero recoils, building on previous zero-recoil results [39, 87] and Ref. [40] quotes

$$\mathcal{F}^{B_s \to D_s^*}(1) = 0.8972(92)\,. \tag{75.21}$$

LHCb has extracted $|V_{cb}|$ from semileptonic B_s^0 decays [88]. The measurement uses both $B_s^0 \to D_s^-\mu^+\nu_\mu$ and $B_s^0 \to D_s^{*-}\mu^+\nu_\mu$ decays. The value of $|V_{cb}|$ is determined from the observed yields of B_s^0 decays normalized to those of B^0 decays after correcting for the relative reconstruction and selection efficiencies. The normalization channels are $B^0 \to D^-\mu^+\nu_\mu$ and $B^0 \to D^{*-}\mu^+\nu_\mu$ decays, where the D^- is reconstructed with the same decay mode of the D_s ($D_{(s)}^- \to [K^+K^-]_\phi\pi^-$). The shape of the form factors are extracted using $p_\perp(D_s)$, which is the component of the D_s^- momentum perpendicular to the B_s^0 flight direction. This variable is correlated with q^2 and the helicity angles in the $B_s^0 \to D_s^{*-}\mu^+\nu_\mu$ decay. For the $B_s \to D_s^-\mu^+\nu_\mu$ decay, for example, $|V_{cb}|$ is related to the measured ratio of signal yields, N_{sig}, and the normalization channel yields, N_{ref}, through the relation

$$\frac{N_{\rm sig}}{N_{\rm ref}} = \xi\, \frac{f_s}{f_d} \frac{\mathcal{B}(D_s^- \to K^+K^-\pi^-)}{\mathcal{B}(D^- \to K^+K^-\pi^-)} \frac{1}{\mathcal{B}(B^0 \to D^-\mu\nu_\mu)}\, \tau_s \times \int \frac{d\Gamma(B_s \to D_s\mu\nu_\mu)}{dw} dw\ ,$$

where τ_s is the B_s lifetime, and ξ is the efficiency ratio between the signal and the normalization. The analysis uses the lattice-QCD form factors obtained for $B_s \to D_s^-$ over the full kinematic range in Ref. [9] and the zero-recoil result for the $B_s \to D_s^{*-}$ form factor from Ref. [87]. Fits to both the CLN parameterization and a 5-parameter version of BGL were performed (although we will only quote the BGL results). The result for $|V_{cb}|$, updated with the most recent determination of f_s/f_d and $\mathcal{B}(D_s^- \to K^-K^+\pi^-)$ from Ref. [89], is $|V_{cb}|_{\rm BGL} = (41.7 \pm 0.8 \pm 0.9 \pm 1.1) \times 10^{-3}$, where the first uncertainty is statistical, the second systematic and the third due to the limited knowledge of the external inputs, in particular the constant $f_s/f_d \times \mathcal{B}(D_s^- \to K^+K^-\pi^-)$. The determination of $|V_{cb}|$ in Ref. [13], using the lattice form factors obtained therein combined with LHCb data yields a consistent result, $|V_{cb}| = 42.7(1.5)_{\rm latt}(1.7)_{\rm exp}(0.4)_{\rm EM} \times 10^{-3}$. The results obtained are consistent with the exclusive determinations of $|V_{cb}|$ using the B^0 and B^+ decays but are not used in the overall average in this review at this stage. These channels are important in the measurement of the ratio $|V_{ub}|/|V_{cb}|$, which cancels out the B_s normalisation uncertainties, discussed in Section 75.5. LHCb also perform measurements of the $B_s^0 \to D_s^{*-}\mu^+\nu_\mu$ differential decay rate [90]. Fits are performed to extract the form factors in CLN and BGL parametrizations.

75.2.5 $|V_{cb}|$ *from inclusive decays*

Measurements of the total semileptonic branching decay rate, along with moments of the lepton energy, lepton invariant mass squared, and hadronic invariant mass spectra in inclusive semileptonic $b \to c$ transitions, can be used for a precision determination

Int. J. Mod. Phys. A 2026.41. Downloaded from www.worldscientific.com
by UNIVERSITY OF CALIFORNIA @ BERKELEY on 09/16/26. Re-use and distribution is strictly not permitted, except for Open Access articles.

of $|V_{cb}|$. The total semileptonic decay rate can be calculated quite reliably in terms of non-perturbative parameters that can be extracted from the information contained in the moments.

75.2.6 *Inclusive semileptonic rate*

The theoretical foundation for the calculation of the total semileptonic rate is the Operator Product Expansion (OPE) which yields the Heavy Quark Expansion (HQE) [91, 92]. Details can be found in the RPP mini-review on Effective Theories [3].

The OPE result for the total rate can be written schematically (details can be found, *e.g.*, in Ref. [93]) as

$$\begin{aligned}\Gamma =&|V_{cb}|^2\frac{G_F^2 m_b^5(\mu)}{192\pi^3}|\eta_{\rm EW}|^2\times\\ &\Bigg[z_0^{(0)}(r)+\frac{\alpha_s(\mu)}{\pi}z_0^{(1)}(r)+\left(\frac{\alpha_s(\mu)}{\pi}\right)^2 z_0^{(2)}(r)+\cdots\\ &+\frac{\mu_\pi^2}{m_b^2}\left(z_2^{(0)}(r)+\frac{\alpha_s(\mu)}{\pi}z_2^{(1)}(r)+\cdots\right)\\ &+\frac{\mu_G^2}{m_b^2}\left(y_2^{(0)}(r)+\frac{\alpha_s(\mu)}{\pi}y_2^{(1)}(r)+\cdots\right)\\ &+\frac{\rho_{\rm D}^3}{m_b^3}\left(z_3^{(0)}(r)+\frac{\alpha_s(\mu)}{\pi}z_3^{(1)}(r)+\cdots\right)\\ &+\frac{\rho_{\rm LS}^3}{m_b^3}\left(y_3^{(0)}(r)+\frac{\alpha_s(\mu)}{\pi}y_3^{(1)}(r)+\cdots\right)+...\Bigg] \quad (75.22)\end{aligned}$$

where r is the ratio m_c/m_b and the y_i and z_i are perturbatively calculable Wilson coefficients functions that appear at different orders of the heavy mass expansion.

The parameters μ_π^2, μ_G^2, ρ_D^3 and ρ_{LS}^3 constitute the non-perturbative input into the heavy quark expansion; they correspond to certain matrix elements to be discussed below. In the same way the HQE can be set up for the moments of distributions of charged-lepton energy, hadronic invariant mass and hadronic energy, e.g.

$$\langle E_e^n\rangle_{E_e>E_{\rm cut}}=\int_{E_{\rm cut}}^{E_{\rm max}}\frac{d\Gamma}{dE_e}E_e^n dE_e\Bigg/\int_{E_{\rm cut}}^{E_{\rm max}}\frac{d\Gamma}{dE_e}dE_e\ . \quad (75.23)$$

The coefficients of the HQE are known up to order $1/m_b^5$ at tree level [94–97]. The leading term $z_0^{(i)}$ is the parton model, and is known completely through order α_s^2 [98–100] and now also at α_s^3 [101]. The terms of order $\alpha_s^{n+1}\beta_0^n$ (where β_0 is the first coefficient of the QCD β function, $\beta_0=(33-2n_f)/3$) have been included following the BLM procedure [93, 102–105]. Corrections of order $\alpha_s\mu_\pi^2/m_b^2$ have been computed in Ref. [106] and Ref. [107], while the $\alpha_s\mu_G^2/m_b^2$ terms have been calculated in Ref. [108] and Ref. [109], and the $\alpha_s\rho_D^3/m_b^3$ corrections in Refs. [110, 111].

Starting at order $1/m_b^3$ contributions with an infrared sensitivity to the charm mass, m_c, appear [94, 96, 112, 113]. At order $1/m_b^3$ this "intrinsic charm" contribution manifests as a $\log(m_c)$ in the coefficient of the Darwin term ρ_D^3. At higher orders, terms such as $1/m_b^3\times 1/m_c^2$ and $\alpha_s(m_c)1/m_b^3\times 1/m_c$ appear; numerically these terms may be comparable in size to the contributions of order $1/m_b^4$.

The HQE parameters are given in terms of forward matrix elements of local operators; the parameters entering the expansion for orders up to $1/m_b^3$ are ($D_\perp^\mu=(g_{\mu\nu}-v_\mu v_\nu)D^\nu$, where $v=p_B/M_B$ is the four-velocity of the B meson)

$$\begin{aligned}\overline{\Lambda}&=M_B-m_b\,,\\ \mu_\pi^2&=-\langle B|\bar b(iD_\perp)^2 b|B\rangle\,,\\ \mu_G^2&=\langle B|\bar b(iD_\perp^\mu)(iD_\perp^\nu)\sigma_{\mu\nu}b|B\rangle\,,\\ \rho_{\rm D}^3&=\langle B|\bar b(iD_{\perp\mu})(ivD)(iD_\perp^\mu)b|B\rangle\,,\\ \rho_{\rm LS}^3&=\langle B|\bar b(iD_\perp^\mu)(ivD)(iD_\perp^\nu)\sigma_{\mu\nu}b|B\rangle. \quad (75.24)\end{aligned}$$

These parameters still depend on the heavy quark mass. Sometimes the infinite mass limits of these parameters $\overline{\Lambda}\to\overline{\Lambda}_{\rm HQET}$, $\mu_\pi^2\to-\lambda_1$, $\mu_G^2\to 3\lambda_2$, $\rho_D^3\to\rho_1$ and $\rho_{LS}^3\to 3\rho_2$, are used instead. Beyond $1/m^3$ the number of independent HQE parameters starts to proliferate [97, 114]. In general, there are 13 parameters (at tree level) up to order $1/m^4$ and 31 (at tree level) up to order $1/m^5$, not including $\overline{\Lambda}$. A framework to compute observables at higher order in $1/m$ [97, 115] has been used to estimate the HQE parameters of the orders $1/m_b^4$ and $1/m_b^5$. Their their impact on the $|V_{cb}|$ determination has been studied in Ref. [116]. However, as pointed out in Ref. [117] one may reduce the number of independent parameters in the HQE by exploiting reparametrization invariance, which is a symmetry of the HQE stemming from Lorentz invariance of QCD. For a subset of observables this allows us to reduce the number of parameters to three up to order $1/m^3$ (ρ_{LS}^3 can be absorbed into μ_G^2 by a re-definition) and to 8 up to order $1/m^4$ [118].

The perturbative QCD expansion for the decay rate does not converge, in general. In addition, the expansion coefficients in the rates and spectra depend strongly on the scheme used for m_b (or equivalently on $\overline{\Lambda}$). It is well known (see eg. [119]) that using the pole mass definition for heavy quark masses leads to particularly badly behaved expansions. This motivates the use of "short-distance" mass definitions, such as the kinetic scheme [41] or the $1S$ scheme [120–122]. Both schemes are well suited for the HQE, since they allow the choice of the renormalization scale $\mu\le m_b$. Furthermore, in both schemes, the masses can be extracted from other observables with sufficient precision, enabling a precise determination of $|V_{cb}|$, despite of the strong quark-mass dependence of the total rate. Recent work has primarily been done in the kinetic scheme, so we will not discuss the 1S scheme results and further. In the kinetic scheme the "kinetic mass" $m_b^{\rm kin}(\mu)$ is introduced, which enters the non-relativistic expression for the kinetic energy of a heavy quark, and is defined using heavy-quark sum rules [41]. The relation between $m_b^{\rm kin}$ and $m_b^{\overline{MS}}$ is known through three-loop order [123]. .

Finally, we note that the theoretical description of inclusive decays employed here, is based on the assumption of quark-hadron duality. While there is no evidence of violations of quark-hadron duality, the theoretical uncertainties due to such violations are not well quantified [3]. Here, we note that a program to compute inclusive B-meson decay rates in lattice-QCD is being developed [124–126], and recent progress [127–131] shows promise for quantitative results with controlled systematic errors in the not-too-distant future.

75.2.7 *Determination of HQE Parameters and $|V_{cb}|$*

Several experiments have measured moments in $\bar B\to X_c\ell\bar\nu_\ell$ decays [132–140] as a function of the minimum lepton momentum. More recently, moments measurements have been performed as a function of lepton invariant mass squared, q^2 [141, 142]. The measurements of the moments of the electron energy spectrum ($0^{\rm th}$-$3^{\rm rd}$) and of the squared hadronic mass spectrum ($0^{\rm th}$-$2^{\rm nd}$) have statistical uncertainties that are roughly equal to their systematic uncertainties. The $3^{\rm rd}$ order hadronic mass spectrum moments have also been measured by some experiments, with relatively large statistical uncertainty. The sets of moments measured within each experiment have strong correlations; their use in a global fit requires fully specified statistical and systematic covariance matrices. Measurements of photon energy moments ($0^{\rm th}$-$2^{\rm nd}$) in $B\to X_s\gamma$ decays [143–147] as a function of the minimum accepted photon energy are also used in some fits; the dominant uncertainties on these measurements are statistical.

Global fits [140, 144, 148–155] to the moments of the electron energy spectrum and the squared hadronic mass spectrum have been performed in the $1S$ and kinetic schemes. The semileptonic moments alone determine a linear combination of m_b and m_c very accurately but leave the orthogonal combination poorly determined (See e.g. [156]); additional input is required to allow a precise determination of m_b. This additional information can come from the radiative $B\to X_s\gamma$ moments (with the caveat that the OPE for $b\to s\gamma$ breaks down beyond leading order in $\Lambda_{\rm QCD}/m_b$), which provide complementary information on m_b and μ_π^2, or from precise determinations of the charm and beauty quark masses [85, 157, 158]. The values obtained in the kinetic

Int. J. Mod. Phys. A 2026.41. Downloaded from www.worldscientific.com
UNIVERSITY OF CALIFORNIA @ BERKELEY on 09/16/26. Re-use and distribution is strictly not permitted, except for Open Access articles.

scheme fits [6, 152, 153] with these two constraints are consistent. Based on the charm and beauty quark mass constraints [85, 154] $\overline{m}_c(2\,\mathrm{GeV}) = 1.093 \pm 0.008\,\mathrm{GeV}$, and $m_{\mathrm{kin}}^{1\,\mathrm{GeV}} = 4.565 \pm 0.019)\mathrm{GeV}$ a fit in the kinetic scheme [154] obtains

$$|V_{cb}| = (42.16 \pm 0.51) \times 10^{-3} \tag{75.25}$$

where the error includes experimental and theoretical uncertainties. This analysis [154] includes calculations of the third-order corrections to the semi-leptonic $b \to c\ell\nu$ decay width [101] and mass relations [123, 159]. Theoretical uncertainties from higher orders in $1/m$ as well as in α_s are estimated and included in performing the fits. Similar values for the parameters are obtained with a variety of assumptions about the theoretical uncertainties and their correlations. The χ^2/dof is well below unity, which could suggest that the theoretical uncertainties may be overestimated. However, while one could obtain a satisfactory fit with smaller uncertainties, this would result in unrealistically small uncertainties on the extracted HQE parameters, which are used as input to other calculations (e.g. the determination of $|V_{ub}|$).

Measurements of higher order moments and moments of additional variables, such as q^2, can further improve the sensitivity of the fits to higher-order terms in the HQE [118]. The q^2 moments depend on a reduced set of operators, thereby possibly making it easier to extract higher-order terms from data. A fit to the q^2 moments measured by the Belle [141] and Belle II [142] experiments combined with the world average inclusive branching fractions, finds [160]:

$$|V_{cb}| = (41.69 \pm 0.63) \times 10^{-3}\ , \tag{75.26}$$

which is compatible with the fit to the other moments. Note there is a strong correlation with the other determinations due to the use of common inputs for the branching fractions.

Most recently, an updated calculation of the $\langle q^{2n} \rangle$ moments including $\mathcal{O}(\alpha_s^2\beta)$ corrections was published [155]. This work was used in a fit to the moments of the electron energy spectrum, the moments of the lepton invariant mass spectrum up to $\langle q^{2n} \rangle$, and the moments of the squared hadronic mass spectrum. These results are taken as the inclusive determination of $|V_{cb}|$

$$|V_{cb}| = (42.0 \pm 0.5) \times 10^{-3}\ \text{(inclusive)}. \tag{75.27}$$

75.3 Determination of $|V_{ub}|$

Summary: Currently the best determinations of $|V_{ub}|$ are from $\bar{B} \to \pi\ell\bar{\nu}_\ell$ decays, where combined fits to theory and experimental data as a function of q^2 provide a precision of about 4%; the uncertainties from experiment and theory are comparable in size. Determinations based on inclusive semileptonic B decays are based on different observables and use different strategies to suppress the $b \to c$ background. Most of the determinations are consistent and provide a precision of about 7%, with comparable contributions to the uncertainty from experiment and theory.

The values obtained from inclusive and exclusive B decay determinations are

$$|V_{ub}| = (4.06 \pm 0.11 \pm 0.13 \pm 0.18) \times 10^{-3} \quad \text{(inclusive)}, \tag{75.28}$$

$$|V_{ub}| = (3.75 \pm 0.06 \pm 0.19) \times 10^{-3} \quad \text{(exclusive)}, \tag{75.29}$$

where the last uncertainty on the inclusive result was added by the authors of this review and is discussed below. The exclusive and inclusive determinations are independent, and the dominant uncertainties are on multiplicative factors. The results from the two determinations are compatible to within one standard deviation.

This can be compared to the values derived from $|V_{ub}|/|V_{cb}|$ ratio measurements, described in the next section. Taking the value for this ratio from Eq. (75.49), and $|V_{cb}|$ from Eq. (75.3) we obtain.

$$|V_{ub}| = (3.43 \pm 0.32) \times 10^{-3} \qquad (\mathrm{B_s},\ \Lambda_\mathrm{b}), \tag{75.30}$$

We choose to combine only the direct determinations of $|V_{ub}|$, based on the inclusive and exclusive B measurements. In the combination they are weighted by their relative errors, where the uncertainties are treated as normally distributed. The resulting average has $p(\chi^2) = 29\%$, so we scale the error by $\sqrt{\chi^2/1} = 1.1$ to find

$$|V_{ub}| = (3.89 \pm 0.16) \times 10^{-3} \quad \text{(average)}. \tag{75.31}$$

In a future update we may consider the constraints in the $|V_{ub}|$-$|V_{cb}|$ plane from the direct determinations together with the LHCb $|V_{ub}/V_{cb}|$ results, although the agreement among all inputs is somewhat marginal.

75.3.1 $|V_{ub}|$ *from inclusive decays*

The theoretical description of inclusive $\bar{B} \to X_u\ell\bar{\nu}_\ell$ decays is based on the Heavy Quark Expansion and leads to a predicted total decay rate with uncertainties below 5% [121, 161]. However, the total decay rate is hard to measure due to the large background from CKM-favored $\bar{B} \to X_c\ell\bar{\nu}_\ell$ transitions, and hence the theoretical methods differ from the $\bar{B} \to X_c\ell\bar{\nu}_\ell$ case. For a calculation of the partial decay rate in regions of phase space where $\bar{B} \to X_c\ell\bar{\nu}_\ell$ decays are suppressed one cannot use the HQE as for $b \to c$, rather one needs to introduce non-perturbative distribution functions, the "shape functions" (SF) [162, 163]. Their exact form is not known, but its moments can be related to the HQE parameters known e.g from the $b \to c$ case.

The shape functions become important when the light-cone momentum component $P_+ \equiv E_X - |P_X|$ is not large compared to Λ_{QCD}, as is the case near the endpoint of the $\bar{B} \to X_u\ell\bar{\nu}_\ell$ lepton spectrum. Partial rates for $\bar{B} \to X_u\ell\bar{\nu}_\ell$ are predicted and measured in a variety of kinematic regions that differ in their sensitivity to shape-function effects.

At leading order in $1/m_b$ only a single shape function (SF) appears, which is universal for all heavy-to-light transitions [162, 163] and can be extracted in $\bar{B} \to X_s\gamma$ decays. At subleading order in $1/m_b$, several shape functions appear [164], along with small "resolved photon contributions" specific for $\bar{B} \to X_s\gamma$ [165–167], and thus the prescriptions that relate directly the partial rates for $\bar{B} \to X_s\gamma$ and $\bar{B} \to X_u\ell\bar{\nu}_\ell$ decays [168–176] are limited to leading order in $1/m_b$.

Existing approaches use parametrizations of the leading SF that respect constraints on the normalization and on the first and second moments, which are given in terms of the HQE parameters $\overline{\Lambda} = M_B - m_b$ and μ_π^2, respectively. The relations between SF moments and the HQE parameters are known to second order in α_s [177]; as a result, measurements of HQE parameters from global fits to $\bar{B} \to X_c\ell\bar{\nu}_\ell$ and $\bar{B} \to X_s\gamma$ moments can be used to constrain the SF moments, as well as to provide accurate values of m_b and other parameters for use in determining $|V_{ub}|$. Flexible parametrizations of the SF using orthogonal basis functions [178] or artificial neural networks [179] allow global fits to inclusive B meson decay data [167] that incorporate the known short-distance contributions and renormalization properties of the SF.

HFLAV performs fits on the basis of several approaches, with varying degrees of model dependence. We will consider here the approaches documented in Ref. [180] (BLNP), Ref. [181] (GGOU) and Ref. [182] (DGE).

The triple differential rate in the variables

$$P_\ell = M_B - 2E_\ell, \quad P_- = E_X + |\vec{P}_X|, \quad P_+ = E_X - |\vec{P}_X| \tag{75.32}$$

is

$$\frac{d^3\Gamma}{dP_+\,dP_-\,dP_\ell} = \frac{G_F^2|V_{ub}|^2}{16\pi^2}(M_B - P_+) \tag{75.33}$$
$$\Big\{(P_- - P_\ell)(M_B - P_- + P_\ell - P_+)\mathcal{F}_1 + (M_B - P_-)(P_- - P_+)\mathcal{F}_2 + (P_- - P_\ell)(P_\ell - P_+)\mathcal{F}_3\Big\}.$$

The "structure functions", $\mathcal{F}_i$, can be calculated using factorization theorems that have been proven to subleading order in the $1/m_b$ expansion [183].

The BLNP [180] calculation uses these factorization theorems to write the $\mathcal{F}_i$ terms as functions of perturbatively calculable hard coefficients and jet functions, which are convolved with the (soft) light-cone distribution functions. The calculation of $\mathcal{O}(\alpha_s^2)$

Int. J. Mod. Phys. A 2026.41. Downloaded from www.worldscientific.com
by UNIVERSITY OF CALIFORNIA @ BERKELEY on 09/16/26. Re-use and distribution is strictly not permitted, except for Open Access articles.

contributions [184,185] is not yet complete and is not included in the $|V_{ub}|$ determination given below.

The leading order term in the $1/m_b$ expansion of the $\mathcal{F}_i$ terms contains a single non-perturbative function and is calculated to subleading order in α_s, while at subleading order in the $1/m_b$ expansion there are several independent non-perturbative functions that have been calculated only at tree level in the α_s expansion.

A distinct approach (GGOU) [181] uses a hard, Wilsonian cutoff that matches the definition of the kinetic mass. The non-perturbative input is similar to what is used in BLNP, but the shape functions are defined differently. In particular, they are defined at finite m_b and depend on the light-cone component k_+ of the b quark momentum and on the momentum transfer q^2 to the leptons. These functions include subleading effects to all orders; as a result they are non-universal, with one shape function corresponding to each structure function in Eq. (75.33). Their k_+ moments can be computed in the OPE.

Going to subleading order in α_s requires the definition of a renormalization scheme for the HQE parameters and for the SF. The relation between the moments of the SF and the forward matrix elements of local operators appearing the HQE is plagued by ultraviolet problems and requires additional renormalization. A scheme for improving this behavior was suggested in Refs. [180,186], which introduce a definition of the quark mass (the so-called shape-function scheme) based on the first moment of the measured $\bar{B} \to X_s\gamma$ photon energy spectrum. Likewise, the HQE parameters can be defined from measured moments of spectra, corresponding to moments of the SF.

There are various ideas to model the SF, but this requires additional assumptions. One approach (DGE) is the so-called "dressed gluon exponentiation" [182], where the perturbative result is continued into the infrared regime using the renormalon structure obtained in the large β_0 limit, where β_0 has been defined following Eq. (75.22). Other approaches make even stronger assumptions, such as in Ref. [187], which assumes an analytic behavior for the strong coupling in the infrared to perform an extrapolation of perturbation theory.

In order to reduce sensitivity to SF uncertainties, measurements that use a combination of cuts on the leptonic momentum transfer q^2 and the hadronic invariant mass m_X, as suggested in Ref. [188, 189], have been made. In general, experimental measurements of $\bar{B} \to X_u\ell\bar{\nu}_\ell$ into charm-dominated regions (in order to reduce SF uncertainties) are sensitive to the modeling of $\bar{B} \to X_u\ell\bar{\nu}_\ell$ and $\bar{B} \to X_c\ell\bar{\nu}_\ell$ decays. The measurements quoted below have used a variety of functional forms to parametrize the leading SF; a specific error budget for one determination is quoted in the next section. In no case is the parametrization uncertainty estimated to be more than a 2% on $|V_{ub}|$.

Weak Annihilation [181, 190, 191] (WA) can in principle contribute significantly in the high-q^2 region of $\bar{B} \to X_u\ell\bar{\nu}_\ell$ decays. Estimates based on semileptonic D_s decays [113, 188, 189, 191] lead to a $\sim 2\%$ uncertainty on the total $\bar{B} \to X_u\ell\bar{\nu}_\ell$ rate from the $\Upsilon(4S)$. The q^2 spectrum of the WA contribution is not well known, but from the OPE it is expected to contribute predominantly at high q^2. Other theoretical investigations [113, 192, 193], a direct search [194], and $\mathcal{B}(B^0 \to X_u\ell\bar{\nu})/\mathcal{B}(B^+ \to X_u\ell\bar{\nu})$ ratio measurements [195–198] indicate that WA is a small effect, but may become a significant source of uncertainty for $|V_{ub}|$ measurements that accept only a small fraction of the full $\bar{B} \to X_u\ell\bar{\nu}_\ell$ phase space.

75.3.2 *Measurements*

We summarize the measurements used in the determination of $|V_{ub}|$ below. Given the improved precision and more rigorous theoretical interpretation of more recent measurements, determinations [199–202] done with LEP data are not considered in this review.

Inclusive electron momentum measurements [203, 204] reconstruct a single charged electron to determine a partial decay rate for $\bar{B} \to X_u\ell\bar{\nu}_\ell$ near the kinematic endpoint. This results in a selection efficiency of order 50% and only modest sensitivity to the modeling of detector response. The inclusive electron momentum spectrum from $B\bar{B}$ events, after subtraction of the $e^+e^- \to q\bar{q}$ continuum background, is fitted to a model $\bar{B} \to X_u\ell\bar{\nu}_\ell$ spectrum and several components ($D\ell\bar{\nu}_\ell$, $D^*\ell\bar{\nu}_\ell$, ...) of the $\bar{B} \to X_c\ell\bar{\nu}_\ell$ background; the dominant uncertainties are related to this subtraction and modeling. The decay rate can be cleanly extracted for $E_e > 2.3\,\text{GeV}$, but this is deep in the SF region, where theoretical uncertainties are large. More recent measurements have increased the accessed phase phase. The resulting $|V_{ub}|$ values for various E_e cuts are given in Table 75.2.

The final BABAR measurement [205] is based on the inclusive electron spectrum and determines the partial branching fraction and $|V_{ub}|$ for $E_e > 0.8\,\text{GeV}$. The analysis shows that the partial branching fraction measurements can have signal model dependence when the kinematic acceptance includes regions dominated by $\bar{B} \to X_c\ell\bar{\nu}_\ell$ background. The model dependence enters primarily through the partial branching fractions, and arises because the signal yield fit has sensitivity to $\bar{B} \to X_u\ell\bar{\nu}_\ell$ decays only in regions with good signal to noise.

An untagged "neutrino reconstruction" measurement [206] from BABAR uses a combination [207] of a high-energy electron with a measurement of the missing momentum vector. This allows S/B~ 0.7 for $E_e > 2.0\,\text{GeV}$ and a $\approx 5\%$ selection efficiency, but at the cost of a smaller accepted phase space for $\bar{B} \to X_u\ell\bar{\nu}_\ell$ decays and uncertainties associated with the determination of the missing momentum.

The large samples accumulated at the B factories allow studies in which one B meson is fully reconstructed and the recoiling B decays semileptonically [208–211]. The experiments can fully reconstruct a "tag" B candidate in about 0.5% (0.3%) of B^+B^- ($B^0\bar{B}^0$) events. An electron or muon with center-of-mass momentum above 1.0 GeV is required amongst the charged tracks not assigned to the tag B and the remaining particles are assigned to the X_u system. The full set of kinematic properties (E_ℓ, m_X, q^2, *etc.*) are available for studying the semileptonically decaying B, making possible selections that accept up to 90% of the full $\bar{B} \to X_u\ell\bar{\nu}_\ell$ rate; however, the sensitivity to $\bar{B} \to X_u\ell\bar{\nu}_\ell$ decays is still driven by the regions where $\bar{B} \to X_c\ell\bar{\nu}_\ell$ decays are suppressed. Despite requirements (e.g. on the square of the missing mass) aimed at rejecting events with additional missing particles, undetected or mis-measured particles from $\bar{B} \to X_c\ell\bar{\nu}_\ell$ decay (e.g., K_L^0 and additional neutrinos) remain an important source of uncertainty.

A recoil method measurement of partial branching fractions in three phase-space regions, covering about 31% to 86% of the accessible phase space, was performed by Belle [195], where machine learning techniques were used to reduce background levels. The measurement contains substantial decay model updates and supersedes previous measurements from Belle [209, 210]. The measurement of the partial branching fraction obtained in the $E_\ell^B > 1\text{GeV}$ region, the most precise one, is used to obtain $|V_{ub}|$ [195]. Belle also reports measurements of the background subtracted, and unfolded differential decay spectra in bins of m_X, m_X and q^2, P_+ and E_ℓ [212] for use in global fit analyses.

Earlier measurements by BABAR [208] were also performed with cuts on m_X, m_X and q^2, P_+ and E_ℓ using the recoil method. In each case the experimental systematic uncertainties have significant contributions from the modeling of $\bar{B} \to X_u\ell\bar{\nu}_\ell$ and $\bar{B} \to X_c\ell\bar{\nu}_\ell$ decays and from the detector response to charged particles, photons and neutral hadrons.

To reduce modeling uncertainties associated to $\bar{B} \to X_c\ell\bar{\nu}_\ell$ decays a recent Belle tagged measurement [198] uses a novel data driven approach to correct the kinematics and normalization of this background component, while using less restrictive event selection with higher efficiency than the other recent Belle result. In the analysis the ratio $|V_{ub}|/|V_{cb}|$ is directly extracted from inclusive decays for the first time. While a value for $|V_{ub}|$ is provided here, it is not yet included in the combination.

The corresponding $|V_{ub}|$ values are given in Table 75.2.

75.3.3 $|V_{ub}|$ *from inclusive partial rates*

The measured partial rates and theoretical calculations from BLNP, GGOU and DGE described previously are used to determine $|V_{ub}|$ from all measured partial $\bar{B} \to X_u\ell\bar{\nu}_\ell$ rates [213]; selected values are given in Table 75.2. The correlations amongst the multiple BABAR recoil-based measurements [208] are fully accounted for in the average. The statistical corre-

Int. J. Mod. Phys. A 2026.41. Downloaded from www.worldscientific.com
UNIVERSITY OF CALIFORNIA @ BERKELEY on 09/16/26. Re-use and distribution is strictly not permitted, except for Open Access articles.

lations amongst the other measurements used in the average are small (due to small overlaps among signal events and large differences in S/B ratios) and have been ignored. Correlated systematic and theoretical errors are taken into account, both within an experiment and between experiments. As an illustration of the relative sizes of the uncertainties entering $|V_{ub}|$ we give the error breakdown for the GGOU average: statistical—1.4%; experimental—1.6%; $\bar{B} \to X_c \ell \bar{\nu}_\ell$ modeling—0.9%; $\bar{B} \to X_u \ell \bar{\nu}_\ell$ modeling—1.7%; HQE parameters (m_b) —1.6%; higher-order corrections—1.5%; q^2 modeling—1.3%; Weak Annihilation—$^{+0.0}_{-1.0}$%; SF parametrization—0.2%.

The averages quoted here are based on the following m_b values: $m_b^{SF} = 4.600 \pm 0.022$ GeV for BLNP, $m_b^{\rm kin} = 4.573 \pm 0.012$ GeV for GGOU, and $m_b^{\overline{MS}} = 4.206 \pm 0.040$ GeV for DGE. The $m_b^{\rm kin}$ value is determined in a global fit to moments in the kinetic scheme [155]; this value is translated into m_b^{SF} and $m_b^{\overline{MS}}$ at fixed order in α_s.

Hadronization uncertainties also impact the $|V_{ub}|$ determination. The theoretical expressions are valid at the parton level and do not incorporate any resonant structure (*e.g.* $\bar{B} \to \pi \ell \bar{\nu}_\ell$); this must be added to the simulated $\bar{B} \to X_u \ell \bar{\nu}_\ell$ event samples, since the detailed final state multiplicity and structure impacts the estimates of experimental acceptance and efficiency. The experiments have adopted procedures to input resonant structure while preserving the appropriate behavior in the kinematic variables (q^2, E_ℓ, m_X) averaged over the sample, but these prescriptions are *ad hoc* and ultimately require *in situ* calibration. The resulting uncertainties have been estimated to be $\sim$ 1-2% on $|V_{ub}|$. A recent inclusive $|V_{ub}|$ Belle measurement is the first to perform a fit to final state pion multiplicity for *in situ* calibration of the hadronization models used. The measurement simultaneously extracts inclusive and exclusive $|V_{ub}|$, with compatible results [214].

All calculations yield compatible $|V_{ub}|$ values and similar error estimates. The arithmetic mean of the values and errors of the HFLAV combinations listed in Table 75.2 is $|V_{ub}| = (4.06 \pm 0.12_{\rm exp} \pm 0.13_{\rm theo}) \times 10^{-3}$, although there is a spread of approximately 10% in the evaluations with the three theoretical models. For reasons discussed below, we assign an additional uncertainty due to model dependence that is not reflected in the HFLAV averages. As highlighted in the BABAR analysis [195,205], model dependence entering measurement procedures can be sizeable, and is not consistently treated across analyses. Many of the analyses shown in Table 75.2 were based on partial branching fraction measurements determined in a single model (i.e. the one used by that analysis when simulating $\bar{B} \to X_u \ell \bar{\nu}_\ell$ decays), although in some cases simulated events were weighted to match the expected spectra in other models and the differences introduced as systematic uncertainties, e.g. Ref. [195]. The $|V_{ub}|$ value quoted by HFLAV for each model are, typically, derived from this unique partial branching fraction combined with another model-specific partial rate calculation. The model dependence in the partial branching fraction is sensitive to how the model predictions compare in the restricted region with good signal-to-noise, not by how they compare when integrated over the full kinematic range used in the fit. Ideally this effect needs to be accounted for by the experiments; the published information is insufficient to determine it. To account for the range in results using the different theoretical models, we take half of the spread of the averages as an additional systematic uncertainty, denoted Δmodel. With this addition, the inclusive $|V_{ub}|$ average is

$$|V_{ub}| = (4.06 \pm 0.12_{\rm exp} \pm 0.13_{\rm theo} \pm 0.19_{\Delta \rm model}) \times 10^{-3} \quad \text{(inclusive)}. \tag{75.34}$$

75.3.4 $|V_{ub}|$ *from exclusive decays*

Exclusive charmless semileptonic decays offer a complementary means of determining $|V_{ub}|$. For the experiments, the specification of the final state provides better background rejection, but the branching fraction to a specific final state is typically only a few percent of that for inclusive decays. For theory, the calculation of the form factors for decays of B-mesons into exclusive final states is challenging, but brings in a different set of uncertainties from those encountered in inclusive decays. In this review we focus on $\bar{B} \to \pi \ell \bar{\nu}_\ell$, as it is the most promising decay mode for both experiment and theory. However, we also discuss $\bar{B}_s \to K \ell \bar{\nu}_\ell$ decays, for which there are recent interesting results. Measurements of other exclusive $\bar{B} \to X_u \ell \bar{\nu}_\ell$ decays can be found in Refs. [215–228].

75.3.5 $\bar{B} \to \pi \ell \bar{\nu}_\ell$ *form factor calculations*

The relevant form factors for the decay $\bar{B} \to \pi \ell \bar{\nu}_\ell$ are usually defined as

$$\langle \pi(p_\pi) | V^\mu | B(p_B) \rangle = f_+(q^2) \left[p_B^\mu + p_\pi^\mu - \frac{m_B^2 - m_\pi^2}{q^2} q^\mu \right] + f_0(q^2) \frac{m_B^2 - m_\pi^2}{q^2} q^\mu \tag{75.35}$$

in terms of which the rate becomes (in the limit $m_\ell \to 0$)

$$\frac{d\Gamma}{dq^2} = \frac{G_F^2 |V_{ub}|^2}{24\pi^3} |p_\pi|^3 |f_+(q^2)|^2, \tag{75.36}$$

where p_π is the pion momentum in the B meson rest frame.

Lattice-QCD calculations of the form factors for the $B \to \pi \ell \bar{\nu}$ and $B_s \to K \ell \bar{\nu}$ transitions are available from the FNAL/MILC [229, 230], HPQCD [231], [232, 233], and JLQCD [234] collaborations. The lattice form factors are obtained in the large q^2 region, $q^2_{\rm max} > q^2 \gtrsim 15\,{\rm GeV}^2$ and the calculations differ in actions employed for the b quark. While HPQCD [231] is using lattice-nonrelativistic QCD, the results from FNAL/MILC [229, 230] and RBC/UKQCD [232] are obtained with relativistic b quark actions based on the Fermilab approach [235], albeit using independently generated gauge-field configurations. The JLQCD collaboration is using all-domain-wall-fermion set-up, The results agree within the quoted errors. For the $B \to \pi$ form factor $f_+(q^2 = 20\,{\rm GeV}^2)$, Ref. [229] quotes uncertainty of 3.4%, where the leading contribution is due to the chiral-continuum extrapolation fit, which includes statistical and heavy-quark discretization errors.

Similar to the case of $\bar{B} \to D^{(*)} \ell \bar{\nu}_\ell$ form factors, the extrapolation to small values of q^2 (large recoil) can be performed using guidance from analyticity and unitarity together with a conformal mapping of the kinematical variables onto the complex unit disc,

$$z = \frac{\sqrt{t_+ - q^2} - \sqrt{t_+ - t_0}}{\sqrt{t_+ - q^2} + \sqrt{t_+ - t_0}}\,, \tag{75.37}$$

where $t_\pm = (M_B \pm m_\pi)^2$ and the choice of t_0 determines the range of z that corresponds to the kinematic range of the decay. Setting $t_0 = t_-$ results in $z = 0$ when $q^2 = q^2_{\rm max}$. The choice $t_0 = (m_B + m_\pi)/(\sqrt{m_B} - \sqrt{m_\pi})^2$ centers the kinematic range around $z = 0$, so that $|z| < 0.3$.

We note that the $\bar{B}_s \to K \ell \bar{\nu}_\ell$ decay is an example were the implementation of unitarity bounds is complicated by the fact that the location of the cut in the q^2 plane is different from the $B_s K$ threshold, because the cut starts at $B\pi$ production threshold. Modifications of the unitarity constraints in this and similar examples are discussed in Refs. [233, 236–239].

The "BCL" parameterization of Ref. [240] is commonly used for these decays, as it is consistent with the asymptotic scaling ($q^2 \to \infty$) as well as near threshold, $q^2 = t_+$. As pointed out in Ref. [241] the unitarity sum of the z-expansion coefficients for f_+ is expected to be of order $(\Lambda/m)^3$, hence yielding a rapidly converging series. We note that relatively small differences in different lattice QCD form factor results can be amplified by a long extrapolation to the low-q^2 region. However, such extrapolations are not needed, when lattice form factors are combined with experimental measurements of the differential decay rate. The joint fits provide constraints on the shape of the form factor over the entire kinematic range, in addition to enabling precise determinations of $|V_{ub}|$ [242].

LCSR calculations provide estimates for the product $f_B f_+(q^2)$, valid in the region $0 < q^2 \lesssim 12$ GeV [47, 243–247] and unitarity constraints can be used to extrapolate the form factors away from the low-q^2 region [248, 249] where reasonable agreement with lattice QCD form factor predictions is found. However, in this review we do not pursue LCSR-based determinations of $|V_{ub}|$.

Int. J. Mod. Phys. A 2026.41. Downloaded from www.worldscientific.com
by UNIVERSITY OF CALIFORNIA @ BERKELEY on 09/16/26. Re-use and distribution is strictly not permitted, except for Open Access articles.

Table 75.2: $|V_{ub}|$ (in units of 10^{-5}) from inclusive $\bar{B} \to X_u \ell \bar{\nu}_\ell$ measurements. The first uncertainty on $|V_{ub}|$ is experimental, while the second includes both theoretical and HQE parameter uncertainties. The values are generally listed in order of increasing kinematic acceptance, f_u (0.19 to 0.90), except for the BABAR E_e >0.8 GeV measurement; those below the horizontal bar are based on recoil methods.

Ref.	cut (GeV)	BLNP	GGOU	DGE
CLEO [203]	$E_e > 2.1$	$410 \pm 48 \,^{+26}_{-30}$	$394 \pm 44 \,^{+17}_{-26}$	$377 \pm 46 \,^{+20}_{-24}$
BABAR [206]	$E_e - q^2$	$457 \pm 31 \,^{+29}_{-34}$	not available	$405 \pm 20 \,^{+22}_{-34}$
Belle [204]	$E_e > 1.9$	$483 \pm 45 \,^{+23}_{-25}$	$475 \pm 44 \,^{+14}_{-19}$	$473 \pm 44 \,^{+19}_{-20}$
BABAR [205]	$E_e > 0.8$	$438 \pm 12 \,^{+25}_{-26}$	$390 \pm 9 \,^{+18}_{-18}$	$379 \pm 10 \,^{+8}_{-9}$
BABAR [208]	$q^2 > 8$, $m_X < 1.7$	$400 \pm 23 \,^{+17}_{-19}$	$407 \pm 23 \,^{+7}_{-9}$	$412 \pm 22 \,^{+10}_{-11}$
BABAR [208]	$P_+ < 0.66$	$397 \pm 24 \,^{+21}_{-22}$	$398 \pm 24 \,^{+22}_{-22}$	$405 \pm 25 \,^{+25}_{-30}$
BABAR [208]	$m_X < 1.7$	$394 \pm 22 \,^{+19}_{-20}$	$393 \pm 22 \,^{+13}_{-13}$	$414 \pm 23 \,^{+20}_{-21}$
BABAR [208]	$E_\ell > 1.3$	$428 \pm 26 \,^{+18}_{-20}$	$435 \pm 24 \,^{+8}_{-9}$	$441 \pm 24 \,^{+11}_{-12}$
Belle [195]	$E_\ell > 1$	$400 \pm 23 \,^{+17}_{-19}$	$407 \pm 23 \,^{+7}_{-9}$	$412 \pm 23 \,^{+10}_{-11}$
HFLAV [6]	Combination	$425 \pm 13 \,^{+19}_{-19}$	$406 \pm 12 \,^{+11}_{-11}$	$387 \pm 10 \,^{+9}_{-10}$

75.3.6 $\bar{B} \to \pi \ell \bar{\nu}_\ell$ *measurements*

The $\bar{B} \to \pi \ell \bar{\nu}_\ell$ measurements fall into two broad classes: untagged, in which case the reconstruction of the missing momentum of the event serves as an estimator for the unseen neutrino, and tagged, in which the second B meson in the event is fully reconstructed in either a hadronic or semileptonic decay mode. The tagged measurements have better q^2 resolution, high and uniform acceptance, and S/B as high as 10, but lower statistical power. The untagged measurements have higher background (S/B < 1) and make slightly more restrictive kinematic cuts, but still provide statistical power precision on the q^2 dependence of the form factor.

CLEO has analyzed $\bar{B} \to \pi \ell \bar{\nu}_\ell$ and $\bar{B} \to \rho \ell \bar{\nu}_\ell$ using an untagged analysis [222–224]. Similar analyses have been done at BABAR [225–228] and Belle [250]. The leading systematic uncertainties in the untagged $\bar{B} \to \pi \ell \bar{\nu}_\ell$ analyses are associated with modeling the missing momentum reconstruction, with background from $\bar{B} \to X_u \ell \bar{\nu}_\ell$ decays and $e^+e^- \to q\bar{q}$ continuum events, and with varying the form factor used to model $\bar{B} \to \rho \ell \bar{\nu}_\ell$ decays.

Analyses [217,251] based on reconstructing a B in the $\bar{D}^{(*)} \ell^+ \nu_\ell$ decay mode and looking for a $\bar{B} \to \pi \ell \bar{\nu}_\ell$ or $\bar{B} \to \rho \ell \bar{\nu}_\ell$ decay amongst the remaining particles in the event make use of the fact that the B and $\bar{B}$ are back-to-back in the $\Upsilon(4S)$ frame to construct a discriminant variable that provides a signal-to-noise ratio above unity for all q^2 bins. A related technique was discussed in Ref. [252]. BABAR [251] and Belle [215] have used their samples of B mesons reconstructed in hadronic decay modes to measure exclusive charmless semileptonic decays, resulting in very clean but smaller samples. The dominant systematic uncertainties in the tagged analyses arise from tag calibration.

$|V_{ub}|$ can be obtained from the average $\bar{B} \to \pi \ell \bar{\nu}_\ell$ branching fraction and the measured q^2 spectrum. Fits to the q^2 spectrum using a theoretically motivated parametrization (e.g. "BCL" from Ref. [240]) remove most of the model dependence from theoretical uncertainties in the shape of the spectrum. The most sensitive method for determining $|V_{ub}|$ from $\bar{B} \to \pi \ell \bar{\nu}_\ell$ decays employs a simultaneous fit [6, 229, 232, 234, 241, 242, 253–255] to measured experimental partial rates and lattice points versus q^2 (or z) to determine $|V_{ub}|$ and the first few coefficients of the expansion of the form factor in z. We quote the result from Ref. [6], which uses as experimental input an average of the measurements in Refs. [215, 225, 228, 250] and an average [40] of the LQCD input from Refs. [229, 232, 234]. The p-value of the q^2 measurement average is 40%. The average for the total $B^0 \to \pi^- \ell^+ \nu_\ell$ branching fraction is obtained by summing up the partial branching fractions:

$$\mathcal{B}(B^0 \to \pi^- \ell^+ \nu_\ell) = (1.50 \pm 0.02_{\rm stat} \pm 0.05_{\rm syst}) \times 10^{-4} \quad (75.38)$$

The corresponding value of $|V_{ub}|$ with this approach is found to be

$$|V_{ub}| = (3.75 \pm 0.06 \pm 0.19\,) \times 10^{-3} \quad \text{(exclusive)}, \qquad (75.39)$$

where the first uncertainty is experimental and the second is from theory. The theory uncertainty is scaled in Ref. [40] to account for disagreements between inputs from Refs. [229, 232, 234]. We note that Ref. [40] obtains $|V_{ub}| = 3.61(16) \times 10^{-3}$ from the same lattice inputs and similar experimental inputs.

75.3.7 $\bar{B}_s \to K \ell \bar{\nu}_\ell$

The LHCb experiment have conducted the first observation of the decay $B_s^0 \to K^- \mu^+ \nu_\mu$ and the measurements of its branching fraction normalised to the $B_s^0 \to D_s^- \mu^+ \nu_\mu$ decays [256]. The measurement has been performed in two bins of q^2, derived using the B_s^0 flight direction and the known B_s^0 mass. The analysis uses a BDT classifier to suppress semileptonic b-hadron background. The results of the partial branching fractions have been translated into measurements of $|V_{ub}|/|V_{cb}|$ using form factor calculations from LCSR for $q^2 < 7$ GeV^2 [257], and a LQCD calculation for $q^2 > 7$ GeV^2 [230]. The results are

$$|V_{ub}|/|V_{cb}| = 0.0946 \pm 0.0041 \pm 0.0068, \; q^2 > 7 \text{ GeV}^2, \quad (75.40)$$

$$|V_{ub}|/|V_{cb}| = 0.0607 \pm 0.0021 \pm 0.0030, \; q^2 < 7 \text{ GeV}^2, \quad (75.41)$$

where the first uncertainties also include experimental and external input sources, and the latter are due to the form factor calculations. The discrepancy between the values of $|V_{ub}|/|V_{cb}|$ for the low and high q^2, requires further theoretical and experimental investigation. On the theory side, FLAG [40] perform a joint z-fit to the lattice QCD results in Refs. [230, 231, 233], with error inflation to account for the tensions between lattice results for f_0. They then combine the form factors for $\bar{B}_s \to K \ell \bar{\nu}_\ell$ with the $\bar{B}_s \to D_s^* \ell \bar{\nu}_\ell$ form factors from Ref. [9] to determine the ratio $|V_{ub}|/|V_{cb}|$ in combination with the LHCb measurements in the high- and low-q^2 regions, finding good agreement between the two:

$$|V_{ub}|/|V_{cb}| = \quad 0.0861 \pm 0.0038_{\rm exp} \pm 0.0057_{\rm lat}, \; q^2 > 7 \text{ GeV}^2 \quad (75.42)$$

$$|V_{ub}|/|V_{cb}| = \quad 0.0779 \pm 0.0028_{\rm exp} \pm 0.0098_{\rm lat}, \; q^2 < 7 \text{ GeV}^2. \quad (75.43)$$

While the experimental measurement has higher purity in the low q^2 region, the lattice QCD form factors are constrained more reliably in high-q^2 region. RBC/UKQCD presented in Ref. [233] a study the effect of different strategies for obtaining the form factors $f_{+,0}$ in the continuum limit, finding sizeable differences for f_0, but not f_+. This issue needs to be studied further. In particular, such differences were not seen in a similar study, albeit for D-meson decay form factors [258]. However, the resulting effect on $|V_{ub}|/|V_{cb}|$ is relatively small, as the f_0 form factor enters the determination only via the kinematic constraint at $q^2 = 0$.

Int. J. Mod. Phys. A 2026.41. Downloaded from www.worldscientific.com
UNIVERSITY OF CALIFORNIA @ BERKELEY on 09/16/26. Re-use and distribution is strictly not permitted, except for Open Access articles.

An analysis in Ref. [259] combines the lattice QCD form factors from Refs. [231,233] with the LHCb data in $|V_{ub}|/|V_{cb}|$ determinations that are compatible with Eq. (75.42). When they combine their updated LCSR results with the low-q^2 LHCb data, they find $|V_{ub}|/|V_{cb}| = 0.057 \pm 0.005$, compatible with Eq. (75.41), and hence also in tension with Eq. (75.42). Experimental measurements of the differential rates in smaller bins would provide valuable shape constraints and additional compatibility tests, improving the reliability of the $|V_{ub}|/|V_{cb}|$ determinations by reducing the need for extrapolations of form factors.

75.4 Semileptonic *b*-baryon decays

Summary: A significant sample of Λ_b^0 baryons is available at the LHCb experiment, and methods have been developed to study their semileptonic decays. Both $\Lambda_b^0 \to p\mu\bar{\nu}$ and $\Lambda_b^0 \to \Lambda_c^+\mu\bar{\nu}$ decays have been measured at LHCb, and the ratio of branching fractions to these two decay modes is used to determine the ratio $|V_{ub}/V_{cb}|$.

75.4.1 $\Lambda_b^0 \to \Lambda_c^+\mu\bar{\nu}$ and $\Lambda_b^0 \to p\mu\bar{\nu}$

The $\Lambda_b^0 \to \Lambda_c^+$ and $\Lambda_b^0 \to p$ semileptonic transitions are described in terms of six form factors each. The three form factors corresponding to the vector current can be defined as [260]

$$\begin{aligned}\langle F(p',s')|\bar{q}\,\gamma_\mu\, b|\Lambda_b^0(p,s)\rangle = \bar{u}_F(p',s')\Big\{ & f_0(q^2)\,(M_{\Lambda_b^0}-m_F)\,\frac{q_\mu}{q^2} \\ & +f_+(q^2)\,\frac{M_{\Lambda_b^0}+m_F}{s_+}\left(p_\mu+p'_\mu-\frac{q_\mu}{q^2}\,(M^2_{\Lambda_b^0}-m_F^2)\right) \\ & +f_\perp(q^2)\left(\gamma_\mu-\frac{2m_F}{s_+}\,p_\mu-\frac{2M_{\Lambda_b^0}}{s_+}\,p'_\mu\right)\Big\}\,u_{\Lambda_b^0}(p,s)\,,\end{aligned} \tag{75.44}$$

where $F = p$ or Λ_c^+ and where we define $s_\pm = (M_{\Lambda_b^0} \pm m_F)^2 - q^2$. At vanishing momentum transfer, $q^2 \to 0$, the kinematic constraint $f_0(0) = f_+(0)$ holds. The form factors are defined in such a way that they correspond to time-like (scalar), longitudinal and transverse polarization with respect to the momentum-transfer q^μ for f_0, f_+ and $f_\perp$, respectively. Likewise, the expression for the axial-vector current is

$$\begin{aligned}&\langle F(p',s')|\bar{q}\,\gamma_\mu\gamma_5\, b|\Lambda_b^0(p,s)\rangle = \\ &\quad -\bar{u}_F(p',s')\gamma_5\Big\{ g_0(q^2)\,(M_{\Lambda_b^0}+m_F)\,\frac{q_\mu}{q^2} \\ &\quad +g_+(q^2)\,\frac{M_{\Lambda_b^0}-m_F}{s_-}\left(p_\mu+p'_\mu-\frac{q_\mu}{q^2}\,(M^2_{\Lambda_b^0}-m_F^2)\right) \\ &\quad +g_\perp(q^2)\left(\gamma_\mu+\frac{2m_F}{s_-}\,p_\mu-\frac{2M_{\Lambda_b^0}}{s_-}\,p'_\mu\right)\Big\}\,u_{\Lambda_b^0}(p,s)\,,\end{aligned} \tag{75.45}$$

with the kinematic constraint $g_0(0) = g_+(0)$ at $q^2 \to 0$.

In the heavy-quark limit, where both the b and c quarks are treated as heavy, all the form factors reduce to the Isgur Wise function ξ_B for baryons [260]:

$$f_0 = f_+ = f_\perp = g_0 = g_+ = g_\perp = \xi_B \tag{75.46}$$

With a light baryon in the final state, the form factors are related through the heavy quark symmetries of the Λ_b^0, reducing the number of independent form factors to two. It should be noted that the differential $\Lambda_b^0 \to (p/\Lambda_c^+)\mu\bar{\nu}$ decay rates peak at high q^2, so that the kinematic regions where both lattice QCD calculations and experimental measurements are precise are well matched.

The form factors for Λ_b^0 decays have been studied with lattice QCD [261]. Based on these results the differential rates for both $\Lambda_b^0 \to \Lambda_c^+\mu\bar{\nu}$ as well as for $\Lambda_b^0 \to p\mu\bar{\nu}$ can be predicted in the full phase space. In particular, for the experimentally interesting region, they find the ratio of decay rates to be [261]

$$\frac{\mathcal{B}(\Lambda_b^0 \to p\mu\bar{\nu})_{q^2>15\,\mathrm{GeV}^2}}{\mathcal{B}(\Lambda_b^0 \to \Lambda_c^+\mu\bar{\nu})_{q^2>7\,\mathrm{GeV}^2}} = (1.471 \pm 0.095 \pm 0.109)\left|\frac{V_{ub}}{V_{cb}}\right|^2 \tag{75.47}$$

where the first uncertainty is statistical and the second systematic. We note that the FLAG review [40] of this calculation points out that the finite volume effects may not be under complete control due to the small valence-quark masses used in the calculation. Furthermore, the analysis of Ref. [261] is based on only three ensembles at two lattice spacing and with heavy sea-pion masses. An ongoing project [262] to calculate the Λ_b form factors includes a larger range of lattice spacings, volumes and ensembles with physical sea-pion masses.

75.4.2 *Measurements at LHCb*

The LHCb experiment has measured the branching fractions of the semileptonic decays $\Lambda_b^0 \to \Lambda_c^+\mu\bar{\nu}$ and $\Lambda_b^0 \to p\mu\bar{\nu}$, from which they determine $|V_{ub}|/|V_{cb}|$. This is the first such determination at a hadron collider, the first to use a b baryon decay, and the first observation of $\Lambda_b^0 \to p\mu\bar{\nu}$. Excellent vertex resolution allows the $p\mu$ and production vertices to be separated, which permits the calculation of the transverse momentum $p_\perp$ of the $p\mu$ pair relative to the Λ_b^0 flight direction. The corrected mass, $m_{\mathrm{corr}} = \sqrt{p_\perp^2 + m_{p\mu}^2} + p_\perp$, peaks at the Λ_b^0 mass for signal decays and provides good discrimination against background combinations. The topologically similar decay $\Lambda_b^0 \to \Lambda_c^+\mu\bar{\nu}$ is also measured, which eliminates the need to know the production cross-section or absolute efficiencies. Using vertex and Λ_b^0 mass constraints, q^2 can be determined up to a two-fold ambiguity. The LHCb analysis requires both solutions to be in the high q^2 region to minimise contamination from the low q^2 region. Their result [263], rescaled [6] to take into account the branching fraction measurement [264] $\mathcal{B}(\Lambda_c^+ \to pK^-\pi^+) = (6.28 \pm 0.32)\%$, is

$$\frac{\mathcal{B}(\Lambda_b^0 \to p\mu\bar{\nu})_{q^2>15\mathrm{GeV}^2}}{\mathcal{B}(\Lambda_b^0 \to \Lambda_c^+\mu\bar{\nu})_{q^2>7\mathrm{GeV}^2}} = (0.92 \pm 0.04 \pm 0.07) \times 10^{-2} \quad . \tag{75.48}$$

The largest systematic uncertainty is from the measured $\mathcal{B}(\Lambda_c^+ \to pK^-\pi^+)$; uncertainties due to trigger, tracking and the Λ_c^+ selection efficiency are each about 3%.

A LHCb analysis [265] measures the normalized q^2 spectrum and finds good agreement with the shape calculated with lattice QCD [261].

The decay rate for $\Lambda_b^0 \to p\mu\bar{\nu}$ peaks at high q^2 where the calculation of the associated form factors using lattice QCD is under good control. Using the measured ratio from Eq. (75.48) along with the calculated ratio from Ref. [261] (see Eq. (75.47)) results in [6]

$$|V_{ub}|/|V_{cb}| = 0.079 \pm 0.004 \pm 0.004(\Lambda_b). \tag{75.49}$$

where the first uncertainty is experimental and the second is from the LQCD calculation.

75.5 The ratio $|V_{ub}|/|V_{cb}|$

The ratio of matrix elements, $|V_{ub}|/|V_{cb}|$, is often required when testing the compatibility of a set of measurements with theoretical predictions. It can be determined from the ratio of branching fractions and has been directly measured by the LHCb (quoted in the previous sections) and Belle experiments. It can also be calculated based on the $|V_{ub}|$ and $|V_{cb}|$ values quoted earlier in this review.

The first direct extraction of this ratio from inclusive B decays was recently performed by Belle [198]. Belle measures the ratio of $\bar{B} \to X_u\ell\bar{\nu}_\ell$ and $\bar{B} \to X_c\ell\bar{\nu}_\ell$ branching fractions with a lepton energy threshold of 1.0 GeV. The partial decay widths, omitting the CKM factors, are taken from BLNP and GGOU for $|V_{ub}|$ and the kinetic scheme for $|V_{cb}|$ to extract the ratio of CKM factors. The results are found to be

$$|V_{ub}|/|V_{cb}| = 0.098 \pm 0.008 \quad \text{(BLNP)}, \tag{75.50}$$

$$|V_{ub}|/|V_{cb}| = 0.101 \pm 0.007 \quad \text{(GGOU)}. \tag{75.51}$$

Int. J. Mod. Phys. A 2026.41. Downloaded from www.worldscientific.com
by UNIVERSITY OF CALIFORNIA @ BERKELEY on 09/16/26. Re-use and distribution is strictly not permitted, except for Open Access articles.

These values are in excellent agreement with $|V_{ub}|/|V_{cb}|$ from independent inclusive determinations, given below, but involve nonzero correlations in both the theoretical and experimental uncertainties. We will therefore leave it out of the combination for this edition.

Given the similarities in the theoretical frameworks used for charmed and charmless decays, we choose to also quote separate ratios of $|V_{ub}|/|V_{cb}|$ for inclusive and exclusive B decays, as discussed earlier:

$$|V_{ub}|/|V_{cb}| = 0.097 \pm 0.005 \quad \text{(inclusive)}, \tag{75.52}$$
$$|V_{ub}|/|V_{cb}| = 0.095 \pm 0.005 \quad \text{(exclusive)}. \tag{75.53}$$

The respective determinations of $|V_{ub}|$ and $|V_{cb}|$ are taken to be uncorrelated in the ratio, although there could be some small cancellations of the uncertainties in both the experimental and the theoretical input. We average the B decay values, along with the B_s value weighting by relative errors to find

$$|V_{ub}|/|V_{cb}| = 0.093 \pm 0.003 \quad \text{(average)}, \tag{75.54}$$

where the uncertainty has been scaled by a factor $\sqrt{\chi^2/2} = 1.1$.

75.6 Lepton flavour universality violation

75.6.1 *Semitauonic decays*

Summary: Semileptonic decays to third-generation leptons provide sensitivity to non-Standard Model amplitudes, such as from a charged Higgs boson [266–269] and from leptoquarks [270–276]. The ratios of branching fractions of semileptonic decays involving tau leptons to those involving $\ell = e/\mu$, $R(D^{(*)}) \equiv \mathcal{B}(\bar{B} \to D^{(*)}\tau\bar{\nu}_\tau)/\mathcal{B}(\bar{B} \to D^{(*)}\ell\bar{\nu}_\ell)$, are predicted with good precision and consistency in the Standard Model [7,8,10–12,32,35,38,51,54,277], using a variety of different strategies. Because this ratio is independent of $|V_{cb}|$, it can, in principle, be computed entirely from within the Standard Model, without using experimental decay rate data. Indeed, the lattice-QCD form factor results of Refs. [7–11, 11–13] have been used for just that purpose. Ref. [40] obtains the three-flavor averages

$$R(D)^{\text{LQCD,FLAG2024}} = 0.2938 \pm 0.0054 \ ,$$
$$R(D^*)^{\text{LQCD,FLAG2024}} = 0.2582 \pm 0.0051 \ . \tag{75.55}$$

and the four-flavor average $R(D^*) = 0.275(15)$. Without constraints from experimental data at large recoil, such SM-theory only evaluations tend to be less precise than those obtained from joint fits that employ experimental data as well as Standard-Model theory inputs (lattice-QCD form factors, HQET constraints, etc.). Here we use the evaluations from Ref. [40], which are based on joint fits to (three-flavor) averages of lattice-QCD form factors and experimental data for $\bar{B} \to D^{(*)}\ell\bar{\nu}_\ell$ decays:

$$R(D)^{\text{LQCD+Exp}} = 0.2955 \pm 0.0032 \ ,$$
$$R(D^*)^{\text{LQCD+Exp}} = 0.2505 \pm 0.0011 \ . \tag{75.56}$$

Measurements [278–287], of these ratios yield higher values; averaging measurements of $R(D)$ and $R(D^*)$ at the $\Upsilon(4S)$ and at LHCb yields [288]

$$R(D)^{\text{meas}} = 0.347 \pm 0.025 \ ,$$
$$R(D^*)^{\text{meas}} = 0.288 \pm 0.012 \ , \tag{75.57}$$

with a linear correlation of -0.37. These values exceed the Standard Model predictions of Eq. (75.56) by 2.0σ and 2.2σ, respectively. A variety of new physics models have been proposed to explain this excess, see eg. Refs. [266–273] as well as reviews in Refs. [289–291].

75.6.2 *Sensitivity of $\bar{B} \to D^{(*)}\tau\bar{\nu}_\tau$ to additional amplitudes*

In addition to the helicity amplitudes present for decays to $e\bar{\nu}_e$ and $\mu\bar{\nu}_\mu$, decays proceeding through $\tau\bar{\nu}_\tau$ include a scalar amplitude H_s. The differential decay rate is given by [292]

$$\frac{d\Gamma}{dq^2} = \frac{G_F^2\,|V_{cb}|^2\,|\mathbf{p}^*_{D^{(*)}}|q^2}{96\pi^3 m_B^2}\left(1 - \frac{m_\tau^2}{q^2}\right)^2 \left[(|H_+|^2 + |H_-|^2 + |H_0|^2)\left(1 + \frac{m_\tau^2}{2q^2}\right) + \frac{3m_\tau^2}{2q^2}|H_s|^2\right], \tag{75.58}$$

where $|\mathbf{p}^*_{D^{(*)}}|$ is the 3-momentum of the $D^{(*)}$ in the $\bar{B}$ rest frame and the helicity amplitudes H depend on the four-momentum transfer q^2. All four helicity amplitudes contribute to $\bar{B} \to D^*\tau\bar{\nu}_\tau$, while only H_0 and H_s contribute to $\bar{B} \to D\tau\bar{\nu}_\tau$; as a result, new physics contributions can produce larger effects in the latter mode. Semi-leptonic B decays into a τ lepton provide a stringent test of the two-Higgs doublet model of type II (2HDMII), i.e. where the two Higgs doublets couple separately to up- and down-type quarks. The distinct feature of the 2HDMII is that the contributions of the charged scalars scale as $m_\tau^2/m_{H^+}^2$, since the couplings to the charged Higgs particles are proportional to the mass of the lepton. As a consequence, one may expect visible effects in decays into a τ, but only small effects for decays into e and μ. The present data disfavors the 2HDMII, see below.

75.6.3 *Measurement of $R(D^{(*)})$*

$\bar{B} \to D^{(*)}\tau\bar{\nu}_\tau$ decays have been studied at the $\Upsilon(4S)$ resonance and in pp collisions. At the $\Upsilon(4S)$, the majority of experimental measurements are based on signatures that consist of a D or D^* meson, an electron or muon (denoted here by ℓ) from the decay $\tau \to \ell\nu_\tau\bar{\nu}_\ell$, a fully-reconstructed decay of the second B meson in the event, and multiple missing neutrinos. One analysis reconstructs the τ in a hadronic mode. The analyses that use hadronic B tags separate signal decays from $\bar{B} \to D^{(*)}\ell\bar{\nu}_\ell$ decays using the lepton momentum and the measured missing mass squared; decays with only a single missing neutrino peak sharply at zero in this variable, while the signal is spread out to positive values. When a semileptonic B tag is used, the discrimination between signal and $\bar{B} \to D^{(*)}\ell\bar{\nu}_\ell$ decays comes from the calorimeter energy that is not associated with any particle used in the reconstruction of the B meson candidates, the measured missing mass squared and the cosine of the angle between the $D^*\ell$ system and its parent B meson, which is calculated under the assumption that only one particle (a neutrino) is missing. In both these approaches, background from $\bar{B} \to D^{**}\ell\bar{\nu}_\ell$ decays with one or more unreconstructed particles is challenging to separate from signal, as is background from $\bar{B} \to D^{(*)}H_{\bar{c}}X$ (where $H_{\bar{c}}$ is a hadron containing a $\bar{c}$ quark) decays. The leading sources of systematic uncertainty are due to the limited size of simulation samples used in constructing the PDFs, the composition of the D^{**} states, efficiency corrections, and cross-feed (swapping soft particles between the signal and tag B).

The most precise measurement from Belle [282] uses semileptonic B tags and leptonic τ decays to simultaneously measure $R(D^*)$ and $R(D)$. The measurement combines results from charged and neutral B decays for both $R(D^*)$ and $R(D)$, and is compatible with the Standard Model expectation to approximately 1σ. The first result from Belle II [283] uses a hadronic tag to measure $R(D^*)$ in $\bar{B} \to D^*\tau^-\bar{\nu}_\tau$ decays with a 189 fb^{-1} dataset. The statistical power of the Belle II dataset has been found to outperform that of Belle in this channel. A complementary measurement was recently published by Belle II, using semileptonic B^0 tags and leptonic τ decays [287] with a 365 fb^{-1} dataset. The neutral B tag was studied due to their lower combinatorial background than charged B tag events. A multiclass multivariate approach is used to isolate signal contributions.

In addition to the ratio measurements, the Belle experiment has performed polarization measurements of the τ [281] and D^* [293] respectively. The τ polarization measurement uses hadronic B tags and τ^- decays to $\pi^-\nu_\tau$ or $\rho^-\nu_\tau$. The main discriminant variables are the measured missing mass squared and the unassociated calorimeter energy. This measurement provides the first determination of the τ polarization in the $\bar{B} \to D^*\tau\bar{\nu}_\tau$ decay, $\mathcal{P}_\tau(D^*) = -0.38 \pm 0.51\,^{+0.21}_{-0.16}$, compatible with the Standard Model expectation [35], $\mathcal{P}_\tau(D^*) = -0.476^{+0.037}_{-0.034}$.

Int. J. Mod. Phys. A 2026.41. Downloaded from www.worldscientific.com
UNIVERSITY OF CALIFORNIA @ BERKELEY on 09/16/26. Re-use and distribution is strictly not permitted, except for Open Access articles.

Table 75.3: Measurements of $R(D)$ and $R(D^*)$, their correlations, ρ, and the combined averages [288].

		$R(D) \times 10^2$	$R(D^*) \times 10^2$	ρ
BABAR [278, 279]	B^0, B^+	$44.0 \pm 5.8 \pm 4.2$	$33.2 \pm 2.4 \pm 1.8$	-0.27
Belle^a [280]	B^0, B^+	$37.5 \pm 6.4 \pm 2.6$	$29.3 \pm 3.8 \pm 1.5$	-0.49
Belle^b [281, 294]	B^0, B^+		$27.0 \pm 3.5\ ^{+\ 2.8}_{-\ 2.5}$	
Belle^c [282]	B^0, B^+	$30.7 \pm 3.7 \pm 1.6$	$28.3 \pm 1.8 \pm 1.4$	-0.51
LHCb^a [285]	B^+ ($R(D)$), B^0	$44.1 \pm 6.0 \pm 6.6$	$28.1 \pm 1.8 \pm 2.4$	-0.43
LHCb^b [284]	B^0		$26.4 \pm 1.1 \pm 1.9$	
LHCb^c [286]	B^0	$24.9 \pm 4.3 \pm 4.7$	$40.2 \pm 8.1 \pm 8.5$	-0.39
Belle II^a [283]	B^0, B^+		$26.2^{+4.1+3.5}_{-3.9-3.2}$	
Belle II^b [287]	B^0	$41.8 \pm 7.4 \pm 5.1$	$30.6 \pm 3.4 \pm 1.8$	-0.22
Average	B^0, B^+	34.7 ± 2.5	28.8 ± 1.2	-0.39

The main uncertainties on the $R(D^*)$ measurement come from the composition of the hadronic B background and from modeling of semileptonic B decays and mis-reconstructed D^* mesons. The D^* polarization measurement uses an inclusive tag approach based on Refs. [295, 296], and reconstructs the τ decays in $\ell\nu_\tau\bar{\nu}_\ell$ and $\pi^+\bar{\nu}_\tau$ channels. The main discriminant variables are $X_{\rm miss}$, a quantity that approximates missing mass but does not depend on tag B reconstruction, the visible energy of the event, and the beam-energy constrained mass, $M_{\rm bc}$, of the inclusively reconstructed tag side B. This measurement provides the first determination of the D^* longitudinal polarization fraction in the $\bar{B} \to D^*\tau\bar{\nu}_\tau$ decay, $\mathcal{F}_L(D^*) = -0.38 \pm 0.60\ ^{+0.08}_{-0.04}$, compatible with the Standard Model expectation [297] within 1.7σ.

The LHCb experiment has performed a simultaneous analysis of $R(D^*)$ and $R(D)$ where $\tau \to \mu\nu_\tau\bar{\nu}_\mu$. The reconstructed decay modes are $\bar{B}^0 \to D^{*+}\tau^-\bar{\nu}_\tau$ with $D^{*+} \to D^0\pi^+$, $B^- \to D^{*0}\tau^-\bar{\nu}_\tau$ with $D^{*0} \to D^0\pi^0$ and $D^{*0} \to D^0\pi^0$, and $B^- \to D^0\tau^-\bar{\nu}_\tau$. Their analysis [285] takes advantage of the measurable flight lengths of b and c hadrons and τ leptons. A multivariate discriminant is used to select decays where no additional charged particles are consistent with coming from the signal decay vertices. The separation between the primary and B decay vertices is used to calculate the momentum of the B decay products transverse to the B flight direction. The longitudinal component of the B momentum can be estimated based on the visible decay products; this allows a determination of the B rest frame, with modest resolution, and enables the calculation of similar discrimination variables to those available at the e^+e^- B factories. The (rest frame) muon energy, missing mass-squared and q^2 are used in a 3-d fit.

A complementary LHCb result [284] on $R(D^*)$ uses three-prong τ decays that take advantage of their excellent vertex resolution to isolate the τ decay from hadronic background. A 3-d fit is performed to determine the signal yield, based on the τ-ν_τ pair q^2, the τ lifetime, as well as a boosted decision tree classifier based on isolation, invariant mass and flight distance information. The leading sources of systematic uncertainty are due to the size of the simulation sample used in constructing the fit templates, uncertainties in modelling the background from hadronic $\bar{B} \to D^{(*)}H_{\bar{c}}X$ decays, as well as reconstruction and trigger effects. The result is normalized to $B^0 \to D^{*-}\pi^+\pi^-\pi^+$ and found to be 1σ from the Standard Model expectation (using the expectation value quoted here). An analogous measurement of $B_c \to J/\psi\tau\bar{\nu}_\tau$ was performed by the LHCb measurement [298], in leptonic τ decays. The result, $R(J/\psi) = 0.71 \pm 0.17 \pm 0.18$, while relatively high is compatible to within 2σ of a recent Standard Model evaluation [299] based on a latttice-QCD calculation [300] of the form factors. Systematic uncertainties are dominated by form factors, as B_c decays are relatively unexplored.

Measurements from BABAR [278, 279], Belle [280–282], Belle II [283, 287] and LHCb [284–286] result in values for $R(D)$ and $R(D^*)$ that exceed Standard Model predictions. Table 75.3 lists these values and their average. Two early untagged Belle measurements [295, 296] are subject to larger systematic uncertainties, with a breakdown of the respective contributions that is inconsistent with the more recent determinations, hence they cannot be reliably combined in the average. All three experiments assume the Standard Model kinematic distributions for $\bar{B} \to D^{(*)}\tau\bar{\nu}_\tau$ in their determinations of the branching fraction ratios.

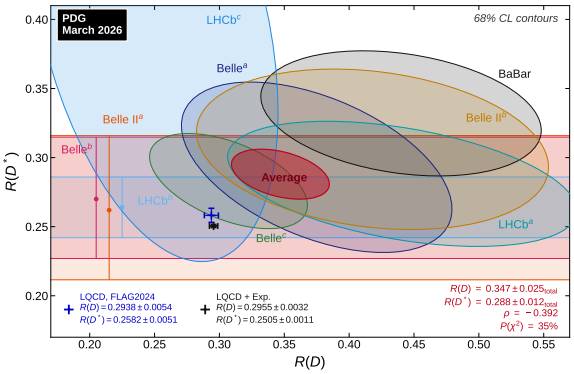

Figure 75.2: Measurements of $R(D)$ and $R(D^*)$ and their two-dimensional average compared with the average predictions for $R(D)$ and $R(D^*)$ given in Eq. 75.56. Contours correspond to 68% CL. The experiment-lattice QCD predictions and the experimental average deviate from each other by 4.4σ.

The measurement combination in the $R(D) - R(D^*)$ plane is shown in Fig. 75.2, compared with the predictions in Eq. (75.55) (LQCD) and Eq. (75.56) (Experiment+LQCD). The measurement combination is based on Ref. [6] with the inclusion of recent results from LHCb and Belle II. The tension between the Standard Model prediction in Eq. (75.56) and the measurements is at the level of 2.0σ ($R(D)$) and 3.1σ ($R(D^*)$); if one considers these deviations together the significance is 4.4σ. However, we note that the LQCD and LQCD+Exp. predictions don't include error estimates due to unknown QED effects, which are significant at this level of uncertainty and would reduce the significances reported above. Still, the observed tensions motivate speculation on possible new physics contributions. The measurements reported in Refs. [283, 284, 294] are all in reasonable agreement with the Standard-Model predictions. There is some tension in the combination coming from the BABAR [278, 279], Belle II [287] and LHCb [285] measurements. The BABAR measurement is the only one to claim a deviation from the Standard Model of more than 3σ, although the $p-$value of the full combination is an acceptable 35%.

The current discussion of $R(D)$ and $R(D^*)$ may be embedded in the theoretical analysis of the other anomalies that have been observed in semileptonic FCNC ($b \to s\ell\ell$) transitions. More sophisticated approaches fit the data to a general effective Hamiltonian. Matching this effective Hamiltonian to simplified models, the current situation of the anomalies seems to be compatible with scenarios with an additional Z' or a leptoquark scenario, see e.g. [270–276].

75.6.4 *Measurements of* $R(X)$

We note that in addition to exclusive modes, inclusive modes also offer an opportunity to test the presence of non-Standard Model contributions, although typically with lower precision. The first measurement of $R(X)$ from a B-factory was recently per-

Int. J. Mod. Phys. A 2026.41. Downloaded from www.worldscientific.com by UNIVERSITY OF CALIFORNIA @ BERKELEY on 09/16/26. Re-use and distribution is strictly not permitted, except for Open Access articles.

formed by Belle II [301], $R(X) = 0.228 \pm 0.039$, and found to be compatible with an average of Standard Model predictions $R(X) = 0.223 \pm 0.005$ [302–304]. Prior measurements of the branching fractions of $b \to X\tau\nu$ were performed by LEP experiments and also found to be compatible with Standard Model predictions.

75.6.5 *Ratios of semileptonic decay rates with e to μ final states*

Several tests of lepton flavor universality in semileptonic B decays have recently been undertaken at Belle and Belle II. This includes ratios of rates to electron and muon modes (i.e. $R(e/\mu)$) performed as part of CKM matrix element extraction analyses (Table 75.4), as well as dedicated flavour dependent angular analyses [305]. Refs. [71,73,74,287] provide measurements of LFUV in $\bar{B} \to D^{(*)}\ell\bar{\nu}$ decays at Belle (untagged, and hadron tagged) and Belle II (hadron and semileptonic tagged). The corresponding theoretical predictions are $\mathcal{B}(B \to De\nu)/\mathcal{B}(B \to D\mu\nu) = 1.0028 \pm 0.0001$ and $\mathcal{B}(B \to D^*e\nu)/\mathcal{B}(B \to D^*\mu\nu) = 1.0041 \pm 0.0001$ [38]. Refs. [198, 306] provide measurements of LFUV in $B \to X_c\ell\bar{\nu}$ in hadron tagged events at Belle and Belle II, where the theoretical expectation is $\mathcal{B}(B \to X_c e\nu)/\mathcal{B}(B \to X_c\mu\nu) = 1.006 \pm 0.001$ [303]. Finally, Ref. [195] provides a result for LFUV in $B \to X_u\ell\nu$ decays where the ratio is expected to be close to 1, as in the $B \to X_c\ell\nu$ case. With the exception of the charmless decay measurement, the experimental uncertainties are dominated by lepton identification uncertainties that do not cancel in the ratios. All results are found to be highly compatible with SM expectations.

Table 75.4: Selected measurements of $R(e/\mu) = \mathcal{B}(B \to Xe\nu)/\mathcal{B}(B \to X\mu\nu)$ where the specific decay process is listed.

Ref.	Decay	$R(e/\mu) \times 100$
Belle [73]	$\bar{B} \to D^*\ell\bar{\nu}$	$99.2 \pm 2.3 \pm 2.3$
Belle [71]	$B^0 \to D^{*+}\ell\nu$	$101 \pm 1 \pm 3$
Belle II [74]	$B^0 \to D^{*+}\ell\nu$	$99.8 \pm 0.9 \pm 2.0$
Belle II [287]	$B^0 \to D^+\ell\nu$	$106.8^{+5.0+2.4}_{-4.8-2.3}$
Belle II [306]	$B \to X_c\ell\nu$	$100.7 \pm 0.9 \pm 1.9$
Belle [198]	$B \to X_c\ell\nu$	$100.3 \pm 0.5 \pm 2.4$
Belle [195]	$B \to X_u\ell\nu$	$97 \pm 9 \pm 4$

75.7 Conclusion

The study of semileptonic B meson decays continues to be an active area for both theory and experiment. The application of HQE calculations to inclusive decays is well established, and fits to moments of $\bar{B} \to X_c\ell\bar{\nu}_\ell$ decays provide precise values for $|V_{cb}|$ and, in conjunction with input on m_c provide precise and consistent values for m_b. Recent developments will make use of more types of moments and better theoretical inputs to constrain higher order effects. Further into the future, new nonperturbative methods to compute inclusive decay rates, for example, in lattice QCD [124–126], may provide interesting new insights.

The determination of $|V_{ub}|$ from inclusive $\bar{B} \to X_u\ell\bar{\nu}_\ell$ decays is based on multiple calculational approaches and independent measurements over a variety of kinematic regions, all of which provide consistent results. Further progress in this area is possible, but will require better theoretical control over higher-order terms, improved experimental knowledge of the $\bar{B} \to X_c\ell\bar{\nu}_\ell$ background and improvements to the modeling of the $\bar{B} \to X_u\ell\bar{\nu}_\ell$ signal distributions.

In both $b \to u$ and $b \to c$ exclusive channels there has been significant recent progress in lattice-QCD calculations, resulting in improved precision on both $|V_{ub}|$ and $|V_{cb}|$, and further progress is expected. These calculations now provide information on the form factors well away from the high q^2 region, allowing better use of experimental data. For $|V_{cb}|$ recent measurements have provided binned data enabling model-independent fits.

While for $|V_{ub}|$ determinations from inclusive and exclusive processes are now compatible, for $|V_{cb}|$ they are only marginally consistent. This is a long-standing puzzle that the recent improvements have, unfortunately, not yet resolved.

Both $|V_{cb}|$ and $|V_{ub}|$ are indispensable inputs into unitarity triangle fits. In particular, knowing $|V_{ub}|$ with good precision allows a test of CKM unitarity in a most direct way, by comparing the length of the $|V_{ub}|$ side of the unitarity triangle with the measurement of $\sin(2\beta)$. This comparison of a "tree" process ($b \to u$) with a "loop-induced" process ($B^0 - \bar{B}^0$ mixing) provides sensitivity to possible contributions from new physics.

The observation of semileptonic decays into τ leptons has opened a new window to the physics of the third generation. The measurements indicate a tension between the data and Standard-Model predictions, which could be a hint for new physics, manifesting itself as a violation of lepton universality beyond the Standard-Model couplings to the Higgs. It should be noted that none of the most recent measurements alone claim discovery of a deviation from the Standard Model. Combining the data of the semitauonic decays with the anomalies observed in the FCNC $b \to s\ell\ell$ transitions allows an interpretation in terms of additional Z' or in terms of additional leptoquarks, but the current data does not allow us to draw a definite conclusion.

Acknowledgements

We thank L. Grillo, E. Lunghi, M. Rotondo, and A. Vaquero for assistance with figures and useful discussions and information. Previous assistance from D. Ferlewicz, J. Flynn, P. Gambino, S. Hashimoto, E. Kou, Z. Ligeti, and M. Rotondo, C. Schwanda, and K. Vos is also acknowledged.

References

[1] See"Leptonic Decays of Charged Pseudoscalar Mesons" by R.A. Briere Rosner, S.L. Stone, and R. Van de Water in this *Review*.

[2] S. Navas *et al.* (Particle Data Group), Phys. Rev. D **110**, 3, 030001 (2024).

[3] See"Heavy-Quark and Soft-Collinear Effective Theory" by C.W. Bauer and M. Neubert in this *Review*.

[4] See "Lattice Quantum Chromodynamics" by S. Hashimoto and S.R. Sharpe in this *Review*.

[5] See "Production and Decay of b-Flavored Hadrons" by P. Eerola, M. Kreps and Y. Kwon in this *Review*.

[6] S. Banerjee *et al.* (Heavy Flavor Averaging Group (HFLAV)), Phys. Rev. **D113**, 1, 012008 (2026), [arXiv:2411.18639].

[7] J. A. Bailey *et al.* (Fermilab Lattice and MILC), Phys. Rev. **D92**, 3, 034506 (2015), [arXiv:1503.07237].

[8] H. Na *et al.* (HPQCD), Phys. Rev. **D92**, 5, 054510 (2015), [Erratum: Phys. Rev.D93,no.11,119906(2016)], [arXiv:1505.03925].

[9] E. McLean *et al.*, Phys. Rev. D **101**, 7, 074513 (2020), [arXiv:1906.00701].

[10] A. Bazavov *et al.* (Fermilab Lattice, MILC), Eur. Phys. J. C **82**, 12, 1141 (2022), [Erratum: Eur.Phys.J.C 83, 21 (2023)], [arXiv:2105.14019].

[11] J. Harrison and C. T. H. Davies (HPQCD, (HPQCD Collaboration)‡), Phys. Rev. D **109**, 9, 094515 (2024), [arXiv:2304.03137].

[12] Y. Aoki *et al.* (JLQCD), Phys. Rev. D **109**, 7, 074503 (2024), [arXiv:2306.05657].

[13] J. Harrison and C. T. H. Davies (HPQCD), Phys. Rev. D **105**, 9, 094506 (2022), [arXiv:2105.11433].

[14] A. Lytle *et al.*, PoS **LATTICE2023**, 240 (2024), [arXiv:2403.03959].

[15] P. Mohanta, T. Kaneko and S. Hashimoto (JLQCD), PoS **LATTICE2023**, 267 (2024), [arXiv:2401.01570].

[16] A. Boushmelev, M. Black and O. Witzel (RBC, UKQCD), PoS **LATTICE2024**, 251 (2025), [arXiv:2412.17406].

[17] P. Butti *et al.*, PoS **LATTICE2024**, 255 (2025), [arXiv:2501.18969].

[18] N. Isgur and M. B. Wise, Phys. Lett. **B232**, 113 (1989); N. Isgur and M. B. Wise, Phys. Lett. **B237**, 527 (1990).

Int. J. Mod. Phys. A 2026.41. Downloaded from www.worldscientific.com
UNIVERSITY OF CALIFORNIA @ BERKELEY on 09/16/26. Re-use and distribution is strictly not permitted, except for Open Access articles.

[19] M. A. Shifman and M. B. Voloshin, Sov. J. Nucl. Phys. **47**, 511 (1988), [Yad. Fiz.47,801(1988)].

[20] A. V. Manohar and M. B. Wise, Camb. Monogr. Part. Phys. Nucl. Phys. Cosmol. **10**, 1 (2000).

[21] H. Georgi, Phys. Lett. **B240**, 447 (1990).

[22] A. F. Falk *et al.*, Nucl. Phys. **B343**, 1 (1990).

[23] E. Eichten and B. R. Hill, Phys. Lett. **B234**, 511 (1990).

[24] A. Sirlin, Nucl. Phys. **B196**, 83 (1982).

[25] J. A. Bailey *et al.* (Fermilab Lattice, MILC), Phys. Rev. D **89**, 11, 114504 (2014), [arXiv:1403.0635].

[26] C. G. Boyd, B. Grinstein and R. F. Lebed, Phys. Rev. Lett. **74**, 4603 (1995), [hep-ph/9412324].

[27] C. G. Boyd, B. Grinstein and R. F. Lebed, Phys. Lett. B **353**, 306 (1995), [hep-ph/9504235].

[28] C. G. Boyd, B. Grinstein and R. F. Lebed, Nucl. Phys. B **461**, 493 (1996), [hep-ph/9508211].

[29] C. G. Boyd, B. Grinstein and R. F. Lebed, Phys. Rev. D **56**, 6895 (1997), [hep-ph/9705252].

[30] B. Grinstein and A. Kobach, Phys. Lett. **B771**, 359 (2017), [arXiv:1703.08170].

[31] I. Caprini, L. Lellouch and M. Neubert, Nucl. Phys. **B530**, 153 (1998), [hep-ph/9712417].

[32] M. Bordone, M. Jung and D. van Dyk, Eur. Phys. J. C **80**, 2, 74 (2020), [arXiv:1908.09398].

[33] F. U. Bernlochner *et al.*, Phys. Rev. **D95**, 11, 115008 (2017), [erratum: Phys. Rev.D97,no.5,059902(2018)], [arXiv:1703.05330].

[34] D. Bigi, P. Gambino and S. Schacht, Phys. Lett. **B769**, 441 (2017), [arXiv:1703.06124].

[35] P. Gambino, M. Jung and S. Schacht, Phys. Lett. **B795**, 386 (2019), [arXiv:1905.08209].

[36] F. U. Bernlochner, Z. Ligeti and D. J. Robinson, Phys. Rev. **D100**, 1, 013005 (2019), [arXiv:1902.09553].

[37] F. U. Bernlochner *et al.*, Phys. Rev. **D96**, 9, 091503 (2017), [arXiv:1708.07134].

[38] F. U. Bernlochner *et al.*, Phys. Rev. D **106**, 9, 096015 (2022), [arXiv:2206.11281].

[39] J. Harrison, C. Davies and M. Wingate (HPQCD), Phys. Rev. **D97**, 5, 054502 (2018), [arXiv:1711.11013].

[40] Y. Aoki *et al.* (Flavour Lattice Averaging Group (FLAG)) (2024), [arXiv:2411.04268].

[41] I. I. Y. Bigi *et al.*, Phys. Rev. **D52**, 196 (1995), [hep-ph/9405410].

[42] A. Kapustin *et al.*, Phys. Lett. **B375**, 327 (1996), [hep-ph/9602262].

[43] P. Gambino, T. Mannel and N. Uraltsev, Phys. Rev. **D81**, 113002 (2010), [arXiv:1004.2859].

[44] M. A. Shifman, N. G. Uraltsev and A. I. Vainshtein, Phys. Rev. D **51**, 2217 (1995), [Erratum: Phys.Rev.D 52, 3149 (1995)], [hep-ph/9405207].

[45] A. Czarnecki, K. Melnikov and N. Uraltsev, Phys. Rev. D **57**, 1769 (1998), [hep-ph/9706311].

[46] P. Gambino, T. Mannel and N. Uraltsev, JHEP **10**, 169 (2012), [arXiv:1206.2296].

[47] N. Gubernari, A. Kokulu and D. van Dyk, JHEP **01**, 150 (2019), [arXiv:1811.00983].

[48] L. Lellouch, Nucl. Phys. B **479**, 353 (1996), [hep-ph/9509358].

[49] M. Di Carlo *et al.*, Phys. Rev. D **104**, 5, 054502 (2021), [arXiv:2105.02497].

[50] G. Martinelli, S. Simula and L. Vittorio (2021), [arXiv:2105.07851].

[51] D. Bigi and P. Gambino, Phys. Rev. **D94**, 9, 094008 (2016), [arXiv:1606.08030].

[52] J. Harrison, Phys. Rev. D **110**, 5, 054506 (2024), [arXiv:2405.01390].

[53] A. Melis, F. Sanfilippo and S. Simula, PoS **LATTICE2023**, 243 (2024), [arXiv:2401.03920].

[54] G. Martinelli, S. Simula and L. Vittorio, Phys. Rev. D **105**, 3, 034503 (2022), [arXiv:2105.08674].

[55] G. Martinelli, S. Simula and L. Vittorio, Eur. Phys. J. C **82**, 12, 1083 (2022), [arXiv:2109.15248].

[56] G. Martinelli, S. Simula and L. Vittorio, JHEP **08**, 022 (2022), [arXiv:2202.10285].

[57] G. Martinelli *et al.*, Phys. Rev. D **106**, 9, 093002 (2022), [arXiv:2204.05925].

[58] G. Martinelli, S. Simula and L. Vittorio, Eur. Phys. J. C **84**, 4, 400 (2024), [arXiv:2310.03680].

[59] G. Martinelli, S. Simula and L. Vittorio, Eur. Phys. J. C **85**, 3, 242 (2025), [arXiv:2410.17974].

[60] C. Radley-Scott, J. Flynn and N. Husung, PoS **LATTICE2024**, 253 (2025).

[61] J. M. Flynn, A. Jüttner and J. T. Tsang, JHEP **12**, 175 (2023), [arXiv:2303.11285].

[62] D. Buskulic *et al.* (ALEPH), Phys. Lett. **B395**, 373 (1997).

[63] G. Abbiendi *et al.* (OPAL), Phys. Lett. **B482**, 15 (2000), [hep-ex/0003013].

[64] P. Abreu *et al.* (DELPHI), Phys. Lett. **B510**, 55 (2001), [hep-ex/0104026].

[65] J. Abdallah *et al.* (DELPHI), Eur. Phys. J. **C33**, 213 (2004), [hep-ex/0401023].

[66] N. E. Adam *et al.* (CLEO), Phys. Rev. **D67**, 032001 (2003), [hep-ex/0210040].

[67] B. Aubert *et al.* (BaBar), Phys. Rev. **D77**, 032002 (2008), [arXiv:0705.4008].

[68] B. Aubert *et al.* (BaBar), Phys. Rev. Lett. **100**, 231803 (2008), [arXiv:0712.3493].

[69] B. Aubert *et al.* (BaBar), Phys. Rev. **D79**, 012002 (2009), [arXiv:0809.0828].

[70] W. Dungel *et al.* (Belle), Phys. Rev. **D82**, 112007 (2010), [arXiv:1010.5620].

[71] E. Waheed *et al.* (Belle), Phys. Rev. D **100**, 5, 052007 (2019), [Erratum: Phys.Rev.D 103, 079901 (2021)], [arXiv:1809.03290].

[72] J. P. Lees *et al.* (BaBar), Phys. Rev. Lett. **123**, 9, 091801 (2019), [arXiv:1903.10002].

[73] M. T. Prim *et al.* (Belle), Phys. Rev. D **108**, 1, 012002 (2023), [arXiv:2301.07529].

[74] I. Adachi *et al.* (Belle-II), Phys. Rev. D **108**, 9, 092013 (2023), [arXiv:2310.01170].

[75] M. T. Prim *et al.* (Belle), Phys. Rev. Lett. **133**, 13, 131801 (2024), [arXiv:2310.20286].

[76] D. Ferlewicz, P. Urquijo and E. Waheed, Phys. Rev. D **103**, 7, 073005 (2021), [arXiv:2008.09341].

[77] M. Bordone and A. Juttner, Eur. Phys. J. C **85**, 2, 129 (2025), [arXiv:2406.10074].

[78] M. Bordone *et al.*, JHEP **11**, 051 (2025), [arXiv:2507.03569].

[79] B. Aubert *et al.* (BaBar), Phys. Rev. Lett. **100**, 151802 (2008), [arXiv:0712.3503].

[80] F. Abudinén *et al.* (Belle-II) (2020), [arXiv:2008.10299].

[81] J. E. Bartelt *et al.* (CLEO), Phys. Rev. Lett. **82**, 3746 (1999), [hep-ex/9811042].

[82] B. Aubert *et al.* (BaBar), Phys. Rev. Lett. **104**, 011802 (2010), [arXiv:0904.4063].

[83] R. Glattauer *et al.* (Belle), Phys. Rev. **D93**, 3, 032006 (2016), [arXiv:1510.03657].

[84] F. Abudinén *et al.* (Belle-II) (2022), [arXiv:2210.13143].

Int. J. Mod. Phys. A 2026.41. Downloaded from www.worldscientific.com
by UNIVERSITY OF CALIFORNIA @ BERKELEY on 09/16/26. Re-use and distribution is strictly not permitted, except for Open Access articles.

[85] Y. Aoki *et al.* (Flavour Lattice Averaging Group (FLAG)), Eur. Phys. J. C **82**, 10, 869 (2022), [arXiv:2111.09849].

[86] C. J. Monahan *et al.*, Phys. Rev. D **95**, 11, 114506 (2017), [arXiv:1703.09728].

[87] E. McLean *et al.*, Phys. Rev. D **99**, 11, 114512 (2019), [arXiv:1904.02046].

[88] R. Aaij *et al.* (LHCb), Phys. Rev. D **101**, 7, 072004 (2020), [arXiv:2001.03225].

[89] R. Aaij *et al.* (LHCb), Phys. Rev. D **104**, 3, 032005 (2021), [arXiv:2103.06810].

[90] R. Aaij *et al.* (LHCb), JHEP **12**, 144 (2020), [arXiv:2003.08453].

[91] A. V. Manohar and M. B. Wise, Phys. Rev. **D49**, 1310 (1994), [hep-ph/9308246].

[92] I. I. Y. Bigi *et al.*, Phys. Rev. Lett. **71**, 496 (1993), [,201(1993)], [hep-ph/9304225]; I. I. Y. Bigi *et al.*, Phys. Lett. **B323**, 408 (1994), [hep-ph/9311339].

[93] D. Benson *et al.*, Nucl. Phys. **B665**, 367 (2003), [hep-ph/0302262].

[94] M. Gremm and A. Kapustin, Phys. Rev. **D55**, 6924 (1997), [hep-ph/9603448].

[95] B. M. Dassinger, T. Mannel and S. Turczyk, JHEP **03**, 087 (2007), [hep-ph/0611168].

[96] I. I. Bigi, N. Uraltsev and R. Zwicky, Eur. Phys. J. **C50**, 539 (2007), [hep-ph/0511158].

[97] T. Mannel, S. Turczyk and N. Uraltsev, JHEP **11**, 109 (2010), [arXiv:1009.4622].

[98] A. Pak and A. Czarnecki, Phys. Rev. **D78**, 114015 (2008), [arXiv:0808.3509].

[99] S. Biswas and K. Melnikov, JHEP **02**, 089 (2010), [arXiv:0911.4142].

[100] P. Gambino, JHEP **09**, 055 (2011), [arXiv:1107.3100].

[101] M. Fael, K. Schönwald and M. Steinhauser, Phys. Rev. D **104**, 1, 016003 (2021), [arXiv:2011.13654].

[102] P. Gambino and N. Uraltsev, Eur. Phys. J. **C34**, 181 (2004), [hep-ph/0401063].

[103] V. Aquila *et al.*, Nucl. Phys. **B719**, 77 (2005), [hep-ph/0503083].

[104] M. E. Luke, M. J. Savage and M. B. Wise, Phys. Lett. B **343**, 329 (1995), [hep-ph/9409287].

[105] M. E. Luke, M. J. Savage and M. B. Wise, Phys. Lett. B **345**, 301 (1995), [hep-ph/9410387].

[106] T. Becher, H. Boos and E. Lunghi, JHEP **12**, 062 (2007), [arXiv:0708.0855].

[107] A. Alberti *et al.*, Nucl. Phys. **B870**, 16 (2013), [arXiv:1212.5082].

[108] A. Alberti, P. Gambino and S. Nandi, JHEP **01**, 147 (2014), [arXiv:1311.7381].

[109] T. Mannel, A. A. Pivovarov and D. Rosenthal, Phys. Rev. **D92**, 5, 054025 (2015), [arXiv:1506.08167].

[110] T. Mannel and A. A. Pivovarov, Phys. Rev. D **100**, 9, 093001 (2019), [arXiv:1907.09187].

[111] T. Mannel, D. Moreno and A. A. Pivovarov, Phys. Rev. D **105**, 5, 054033 (2022), [arXiv:2112.03875].

[112] C. Breidenbach *et al.*, Phys. Rev. **D78**, 014022 (2008), [arXiv:0805.0971].

[113] I. Bigi *et al.*, JHEP **04**, 073 (2010), [arXiv:0911.3322].

[114] A. Kobach and S. Pal, Phys. Lett. **B772**, 225 (2017), [arXiv:1704.00008].

[115] J. Heinonen and T. Mannel, Nucl. Phys. **B889**, 46 (2014), [arXiv:1407.4384].

[116] P. Gambino, K. J. Healey and S. Turczyk, Phys. Lett. **B763**, 60 (2016), [arXiv:1606.06174].

[117] T. Mannel and K. K. Vos, JHEP **06**, 115 (2018), [arXiv:1802.09409].

[118] M. Fael, T. Mannel and K. Keri Vos, JHEP **02**, 177 (2019), [arXiv:1812.07472].

[119] I. I. Y. Bigi *et al.*, Phys. Rev. **D50**, 2234 (1994), [hep-ph/9402360].

[120] A. H. Hoang, Z. Ligeti and A. V. Manohar, Phys. Rev. Lett. **82**, 277 (1999), [hep-ph/9809423].

[121] A. H. Hoang, Z. Ligeti and A. V. Manohar, Phys. Rev. **D59**, 074017 (1999), [hep-ph/9811239].

[122] A. H. Hoang and T. Teubner, Phys. Rev. **D60**, 114027 (1999), [hep-ph/9904468].

[123] M. Fael, K. Schönwald and M. Steinhauser, Phys. Rev. Lett. **125**, 5, 052003 (2020), [arXiv:2005.06487].

[124] P. Gambino and S. Hashimoto, Phys. Rev. Lett. **125**, 3, 032001 (2020), [arXiv:2005.13730].

[125] P. Gambino *et al.*, JHEP **07**, 083 (2022), [arXiv:2203.11762].

[126] A. Barone *et al.*, JHEP **07**, 145 (2023), [arXiv:2305.14092].

[127] R. Kellermann *et al.*, PoS **LATTICE2024**, 245 (2025), [arXiv:2411.18058].

[128] Z. Hu *et al.*, PoS **LATTICE2024**, 241 (2025), [arXiv:2501.19284].

[129] R. Kellermann *et al.*, Phys. Rev. D **112**, 1, 014501 (2025), [arXiv:2504.03358].

[130] A. De Santis *et al.*, Phys. Rev. D **112**, 5, 054503 (2025), [arXiv:2504.06063].

[131] A. De Santis *et al.*, Phys. Rev. Lett. **135**, 12, 121901 (2025), [arXiv:2504.06064].

[132] S. E. Csorna *et al.* (CLEO), Phys. Rev. **D70**, 032002 (2004), [hep-ex/0403052].

[133] A. H. Mahmood *et al.* (CLEO), Phys. Rev. **D70**, 032003 (2004), [hep-ex/0403053].

[134] B. Aubert *et al.* (BaBar), Phys. Rev. **D69**, 111103 (2004), [hep-ex/0403031].

[135] B. Aubert *et al.* (BaBar), Phys. Rev. **D69**, 111104 (2004), [hep-ex/0403030].

[136] C. Schwanda *et al.* (Belle), Phys. Rev. **D75**, 032005 (2007), [hep-ex/0611044].

[137] P. Urquijo *et al.* (Belle), Phys. Rev. **D75**, 032001 (2007), [hep-ex/0610012].

[138] J. Abdallah *et al.* (DELPHI), Eur. Phys. J. **C45**, 35 (2006), [hep-ex/0510024].

[139] D. Acosta *et al.* (CDF), Phys. Rev. **D71**, 051103 (2005), [hep-ex/0502003].

[140] B. Aubert *et al.* (BaBar), Phys. Rev. **D81**, 032003 (2010), [arXiv:0908.0415].

[141] R. van Tonder *et al.* (Belle), Phys. Rev. D **104**, 11, 112011 (2021), [arXiv:2109.01685].

[142] F. Abudinén *et al.* (Belle-II), Phys. Rev. D **107**, 7, 072002 (2023), [arXiv:2205.06372].

[143] A. Limosani *et al.* (Belle), Phys. Rev. Lett. **103**, 241801 (2009), [arXiv:0907.1384].

[144] C. Schwanda *et al.* (Belle), Phys. Rev. **D78**, 032016 (2008), [arXiv:0803.2158].

[145] B. Aubert *et al.* (BaBar), Phys. Rev. **D72**, 052004 (2005), [hep-ex/0508004].

[146] B. Aubert *et al.* (BaBar), Phys. Rev. Lett. **97**, 171803 (2006), [hep-ex/0607071].

[147] S. Chen *et al.* (CLEO), Phys. Rev. Lett. **87**, 251807 (2001), [hep-ex/0108032].

[148] M. Battaglia *et al.*, eConf **C0304052**, WG102 (2003), [Phys. Lett.B556,41(2003)], [hep-ph/0210319].

Int. J. Mod. Phys. A 2026.41. Downloaded from www.worldscientific.com
UNIVERSITY OF CALIFORNIA @ BERKELEY on 09/16/26. Re-use and distribution is strictly not permitted, except for Open Access articles.

[149] B. Aubert *et al.* (BaBar), Phys. Rev. Lett. **93**, 011803 (2004), [hep-ex/0404017].

[150] O. Buchmüller and H. Flächer, `hep-ph/0507253` updated in Ref. [307].

[151] C. W. Bauer *et al.*, Phys. Rev. **D70**, 094017 (2004), updated in Ref. [307], [hep-ph/0408002].

[152] P. Gambino and C. Schwanda, Phys. Rev. **D89**, 1, 014022 (2014), [arXiv:1307.4551].

[153] A. Alberti *et al.*, Phys. Rev. Lett. **114**, 6, 061802 (2015), [arXiv:1411.6560].

[154] M. Bordone, B. Capdevila and P. Gambino, Phys. Lett. B **822**, 136679 (2021), [arXiv:2107.00604].

[155] G. Finauri and P. Gambino, JHEP **02**, 206 (2024), [arXiv:2310.20324].

[156] M. Antonelli *et al.*, Phys. Rept. **494**, 197 (2010), see section 5.4.2, [arXiv:0907.5386].

[157] S. Aoki *et al.* (Flavour Lattice Averaging Group) (2019), [arXiv:1902.08191].

[158] See"Quark Masses" by A.V. Manohar, L.P. Lellouch , and R.M. Barnett in this *Review*.

[159] M. Fael, K. Schönwald and M. Steinhauser, Phys. Rev. D **103**, 1, 014005 (2021), [arXiv:2011.11655].

[160] F. Bernlochner *et al.*, JHEP **10**, 068 (2022), [arXiv:2205.10274].

[161] N. Uraltsev, Int. J. Mod. Phys. **A14**, 4641 (1999), [hep-ph/9905520].

[162] M. Neubert, Phys. Rev. **D49**, 4623 (1994), [hep-ph/9312311]; M. Neubert, Phys. Rev. **D49**, 3392 (1994), [hep-ph/9311325].

[163] I. I. Y. Bigi *et al.*, Int. J. Mod. Phys. **A9**, 2467 (1994), [hep-ph/9312359].

[164] C. W. Bauer, M. E. Luke and T. Mannel, Phys. Rev. **D68**, 094001 (2003), [hep-ph/0102089].

[165] M. Benzke *et al.*, Phys. Rev. Lett. **106**, 141801 (2011), [arXiv:1012.3167].

[166] A. Gunawardana and G. Paz, JHEP **11**, 141 (2019), [arXiv:1908.02812].

[167] F. U. Bernlochner *et al.* (SIMBA), Phys. Rev. Lett. **127**, 10, 102001 (2021), [arXiv:2007.04320].

[168] M. Neubert, Phys. Lett. **B513**, 88 (2001), [hep-ph/0104280].

[169] M. Neubert, Phys. Lett. **B543**, 269 (2002), [hep-ph/0207002].

[170] A. K. Leibovich, I. Low and I. Z. Rothstein, Phys. Rev. **D61**, 053006 (2000), [hep-ph/9909404].

[171] A. K. Leibovich, I. Low and I. Z. Rothstein, Phys. Rev. **D62**, 014010 (2000), [hep-ph/0001028].

[172] A. K. Leibovich, I. Low and I. Z. Rothstein, Phys. Lett. **B486**, 86 (2000), [hep-ph/0005124].

[173] A. K. Leibovich, I. Low and I. Z. Rothstein, Phys. Lett. **B513**, 83 (2001), [hep-ph/0105066].

[174] A. H. Hoang, Z. Ligeti and M. Luke, Phys. Rev. **D71**, 093007 (2005), [hep-ph/0502134].

[175] B. O. Lange, M. Neubert and G. Paz, JHEP **10**, 084 (2005), [hep-ph/0508178].

[176] B. O. Lange, JHEP **01**, 104 (2006), [hep-ph/0511098].

[177] M. Neubert, Phys. Lett. **B612**, 13 (2005), [hep-ph/0412241].

[178] Z. Ligeti, I. W. Stewart and F. J. Tackmann, Phys. Rev. **D78**, 114014 (2008), [arXiv:0807.1926].

[179] P. Gambino, K. J. Healey and C. Mondino, Phys. Rev. **D94**, 1, 014031 (2016), [arXiv:1604.07598].

[180] B. O. Lange, M. Neubert and G. Paz, Phys. Rev. **D72**, 073006 (2005), [hep-ph/0504071].

[181] P. Gambino *et al.*, JHEP **10**, 058 (2007), [arXiv:0707.2493].

[182] J. R. Andersen and E. Gardi, JHEP **01**, 097 (2006), [hep-ph/0509360].

[183] M. Beneke *et al.*, JHEP **06**, 071 (2005), [hep-ph/0411395].

[184] C. Greub, M. Neubert and B. D. Pecjak, Eur. Phys. J. **C65**, 501 (2010), [arXiv:0909.1609].

[185] M. Brucherseifer, F. Caola and K. Melnikov, Phys. Lett. **B721**, 107 (2013), [arXiv:1302.0444].

[186] T. Mannel and S. Recksiegel, Phys. Rev. **D60**, 114040 (1999), [hep-ph/9904475].

[187] U. Aglietti *et al.*, Eur. Phys. J. **C59**, 831 (2009), [arXiv:0711.0860].

[188] C. W. Bauer, Z. Ligeti and M. E. Luke, Phys. Rev. **D64**, 113004 (2001), [hep-ph/0107074].

[189] C. W. Bauer, Z. Ligeti and M. E. Luke, Phys. Lett. **B479**, 395 (2000), [hep-ph/0002161].

[190] I. I. Y. Bigi and N. G. Uraltsev, Nucl. Phys. **B423**, 33 (1994), [hep-ph/9310285].

[191] M. B. Voloshin, Phys. Lett. **B515**, 74 (2001), [hep-ph/0106040].

[192] Z. Ligeti, M. Luke and A. V. Manohar, Phys. Rev. **D82**, 033003 (2010), [arXiv:1003.1351].

[193] P. Gambino and J. F. Kamenik, Nucl. Phys. **B840**, 424 (2010), [arXiv:1004.0114].

[194] J. L. Rosner *et al.* (CLEO), Phys. Rev. Lett. **96**, 121801 (2006), [hep-ex/0601027].

[195] L. Cao *et al.* (Belle), Phys. Rev. D **104**, 1, 012008 (2021), [arXiv:2102.00020].

[196] B. Aubert *et al.* (BaBar), in "23rd International Symposium on Lepton-Photon Interactions at High Energy (LP07)," (2007), [arXiv:0708.1753].

[197] J. P. Lees *et al.* (BaBar), Phys. Rev. D **86**, 032004 (2012), [arXiv:1112.0702].

[198] M. Hohmann *et al.* (Belle), Phys. Rev. D **111**, 9, 092016 (2025), [arXiv:2311.00458].

[199] R. Barate *et al.* (ALEPH), Eur. Phys. J. **C6**, 555 (1999).

[200] M. Acciarri *et al.* (L3), Phys. Lett. **B436**, 174 (1998).

[201] G. Abbiendi *et al.* (OPAL), Eur. Phys. J. **C21**, 399 (2001), [hep-ex/0107016].

[202] P. Abreu *et al.* (DELPHI), Phys. Lett. **B478**, 14 (2000), [hep-ex/0105054].

[203] A. Bornheim *et al.* (CLEO), Phys. Rev. Lett. **88**, 231803 (2002), [hep-ex/0202019].

[204] A. Limosani *et al.* (Belle), Phys. Lett. **B621**, 28 (2005), [hep-ex/0504046].

[205] J. P. Lees *et al.* (BaBar), Phys. Rev. **D95**, 7, 072001 (2017), [arXiv:1611.05624].

[206] B. Aubert *et al.* (BaBar), Phys. Rev. Lett. **95**, 111801 (2005), [Erratum: Phys. Rev. Lett.97,019903(2006)], [hep-ex/0506036].

[207] R. V. Kowalewski and S. Menke, Phys. Lett. **B541**, 29 (2002), [hep-ex/0205038].

[208] J. P. Lees *et al.* (BaBar), Phys. Rev. **D86**, 032004 (2012), [arXiv:1112.0702].

[209] I. Bizjak *et al.* (Belle), Phys. Rev. Lett. **95**, 241801 (2005), [hep-ex/0505088].

[210] P. Urquijo *et al.* (Belle), Phys. Rev. Lett. **104**, 021801 (2010), [arXiv:0907.0379].

[211] B. Aubert *et al.* (BaBar), Phys. Rev. Lett. **96**, 221801 (2006), [hep-ex/0601046].

[212] L. Cao *et al.* (Belle), Phys. Rev. Lett. **127**, 26, 261801 (2021), [arXiv:2107.13855].

Int. J. Mod. Phys. A 2026.41. Downloaded from www.worldscientific.com
by UNIVERSITY OF CALIFORNIA @ BERKELEY on 09/16/26. Re-use and distribution is strictly not permitted, except for Open Access articles.

[213] S. Banerjee *et al.* (Heavy Flavor Averaging Group (HFLAV)), Phys. Rev. **D113**, 1, 012008 (2026), with specific result from doi:10.5281/zenodo.19102822, [arXiv:2411.18639].

[214] L. Cao *et al.* (Belle), Phys. Rev. Lett. **131**, 21, 211801 (2023), [arXiv:2303.17309].

[215] A. Sibidanov *et al.* (Belle), Phys. Rev. **D88**, 3, 032005 (2013), [arXiv:1306.2781].

[216] B. Aubert *et al.* (BaBar), Phys. Rev. Lett. **90**, 181801 (2003), [eConfC0304052,WG117(2003)], [hep-ex/0301001].

[217] T. Hokuue *et al.* (Belle), Phys. Lett. **B648**, 139 (2007), [hep-ex/0604024].

[218] B. Aubert *et al.* (BaBar), Phys. Rev. **D79**, 052011 (2009), [arXiv:0808.3524].

[219] J. P. Lees *et al.* (BaBar), Phys. Rev. **D88**, 7, 072006 (2013), [arXiv:1308.2589].

[220] J. P. Lees *et al.* (BaBar), Phys. Rev. **D87**, 3, 032004 (2013), [Erratum: Phys. Rev.D87,no.9,099904(2013)], [arXiv:1205.6245].

[221] C. Schwanda *et al.* (Belle), Phys. Rev. Lett. **93**, 131803 (2004), [hep-ex/0402023].

[222] N. E. Adam *et al.* (CLEO), Phys. Rev. Lett. **99**, 041802 (2007), [hep-ex/0703041].

[223] S. B. Athar *et al.* (CLEO), Phys. Rev. **D68**, 072003 (2003), superceded by Ref. [224], [hep-ex/0304019].

[224] R. Gray *et al.* (CLEO), Phys. Rev. **D76**, 012007 (2007), [Addendum: Phys. Rev.D76,no.3,039901(2007)], [hep-ex/0703042].

[225] P. del Amo Sanchez *et al.* (BaBar), Phys. Rev. **D83**, 032007 (2011), supercedes Ref. [226], [arXiv:1005.3288].

[226] B. Aubert *et al.* (BaBar), Phys. Rev. **D72**, 051102 (2005), [hep-ex/0507003].

[227] P. del Amo Sanchez *et al.* (BaBar), Phys. Rev. **D83**, 052011 (2011), updated in Ref. [228], [arXiv:1010.0987].

[228] J. P. Lees *et al.* (BaBar), Phys. Rev. **D86**, 092004 (2012), [arXiv:1208.1253].

[229] J. A. Bailey *et al.* (Fermilab Lattice, MILC), Phys. Rev. **D92**, 1, 014024 (2015), [arXiv:1503.07839].

[230] A. Bazavov *et al.* (Fermilab Lattice, MILC), Phys. Rev. **D100**, 3, 034501 (2019), [arXiv:1901.02561].

[231] C. M. Bouchard *et al.*, Phys. Rev. **D90**, 054506 (2014), [arXiv:1406.2279].

[232] J. M. Flynn *et al.*, Phys. Rev. **D91**, 7, 074510 (2015), [arXiv:1501.05373].

[233] J. M. Flynn *et al.* (RBC/UKQCD), Phys. Rev. D **107**, 11, 114512 (2023), [arXiv:2303.11280].

[234] B. Colquhoun *et al.* (JLQCD), Phys. Rev. D **106**, 5, 054502 (2022), [arXiv:2203.04938].

[235] A. X. El-Khadra, A. S. Kronfeld and P. B. Mackenzie, Phys. Rev. D **55**, 3933 (1997), [hep-lat/9604004].

[236] A. Berns and H. Lamm, JHEP **12**, 114 (2018), [arXiv:1808.07360].

[237] N. Gubernari, D. van Dyk and J. Virto, JHEP **02**, 088 (2021), [arXiv:2011.09813].

[238] T. Blake *et al.*, Phys. Rev. D **108**, 9, 094509 (2023), [arXiv:2205.06041].

[239] N. Gubernari *et al.*, JHEP **09**, 133 (2022), [arXiv:2206.03797].

[240] C. Bourrely, I. Caprini and L. Lellouch, Phys. Rev. **D79**, 013008 (2009), [Erratum: Phys. Rev.D82,099902(2010)], [arXiv:0807.2722].

[241] T. Becher and R. J. Hill, Phys. Lett. **B633**, 61 (2006), [hep-ph/0509090].

[242] M. C. Arnesen *et al.*, Phys. Rev. Lett. **95**, 071802 (2005), [hep-ph/0504209].

[243] M. A. Shifman, A. I. Vainshtein and V. I. Zakharov, Nucl. Phys. **B147**, 385 (1979); M. A. Shifman, A. I. Vainshtein and V. I. Zakharov, Nucl. Phys. **B147**, 448 (1979).

[244] P. Ball and R. Zwicky, Phys. Rev. **D71**, 014015 (2005), [hep-ph/0406232].

[245] G. Duplancic *et al.*, JHEP **04**, 014 (2008), [arXiv:0801.1796].

[246] A. Bharucha, JHEP **05**, 092 (2012), [arXiv:1203.1359].

[247] A. V. Rusov, Eur. Phys. J. **C77**, 7, 442 (2017), [arXiv:1705.01929].

[248] I. Sentitemsu Imsong *et al.*, JHEP **02**, 126 (2015), [arXiv:1409.7816].

[249] D. Leljak, B. Melić and D. van Dyk, JHEP **07**, 036 (2021), [arXiv:2102.07233].

[250] H. Ha *et al.* (Belle), Phys. Rev. **D83**, 071101 (2011), [arXiv:1012.0090].

[251] B. Aubert *et al.* (BaBar), Phys. Rev. Lett. **101**, 081801 (2008), [arXiv:0805.2408].

[252] W. S. Brower and H. P. Paar, Nucl. Instrum. Meth. **A421**, 411 (1999), [hep-ex/9710029].

[253] P. Ball, eConf **C070512**, 016 (2007), [arXiv:0705.2290].

[254] J. M. Flynn and J. Nieves, Phys. Lett. **B649**, 269 (2007), [hep-ph/0703284].

[255] E. Dalgic *et al.*, Phys. Rev. **D73**, 074502 (2006), [Erratum: Phys. Rev.D75,119906(2007)], [hep-lat/0601021].

[256] R. Aaij *et al.* (LHCb), Phys. Rev. Lett. **126**, 8, 081804 (2021), [arXiv:2012.05143].

[257] A. Khodjamirian and A. V. Rusov, JHEP **08**, 112 (2017), [arXiv:1703.04765].

[258] A. Bazavov *et al.* (Fermilab Lattice, MILC), Phys. Rev. D **107**, 9, 094516 (2023), [arXiv:2212.12648].

[259] C. Bolognani, D. van Dyk and K. K. Vos, JHEP **11**, 082 (2023), [arXiv:2308.04347].

[260] T. Feldmann and M. W. Y. Yip, Phys. Rev. **D85**, 014035 (2012), [Erratum: Phys. Rev.D86,079901(2012)], [arXiv:1111.1844].

[261] W. Detmold, C. Lehner and S. Meinel, Phys. Rev. **D92**, 3, 034503 (2015), [arXiv:1503.01421].

[262] S. Meinel, PoS **LATTICE2023**, 275 (2024), [arXiv:2309.01821].

[263] R. Aaij *et al.* (LHCb), Nature Phys. **11**, 743 (2015), [arXiv:1504.01568].

[264] M. Ablikim *et al.* (BESIII), Phys. Rev. Lett. **116**, 5, 052001 (2016), [arXiv:1511.08380].

[265] R. Aaij *et al.* (LHCb), Phys. Rev. **D96**, 11, 112005 (2017), [arXiv:1709.01920].

[266] M. Tanaka, Z. Phys. **C67**, 321 (1995), [hep-ph/9411405].

[267] H. Itoh, S. Komine and Y. Okada, Prog. Theor. Phys. **114**, 179 (2005), [hep-ph/0409228].

[268] U. Nierste, S. Trine and S. Westhoff, Phys. Rev. **D78**, 015006 (2008), [arXiv:0801.4938].

[269] M. Tanaka and R. Watanabe, Phys. Rev. **D82**, 034027 (2010), [arXiv:1005.4306].

[270] A. Datta, M. Duraisamy and D. Ghosh, Phys. Rev. **D86**, 034027 (2012), [arXiv:1206.3760].

[271] D. Becirevic, N. Kosnik and A. Tayduganov, Phys. Lett. **B716**, 208 (2012), [arXiv:1206.4977].

[272] S. Fajfer *et al.*, Phys. Rev. Lett. **109**, 161801 (2012), [arXiv:1206.1872].

[273] A. Crivellin, C. Greub and A. Kokulu, Phys. Rev. **D86**, 054014 (2012), [arXiv:1206.2634].

[274] M. Bauer and M. Neubert, Phys. Rev. Lett. **116**, 14, 141802 (2016), [arXiv:1511.01900].

[275] I. Doršner *et al.*, Phys. Rept. **641**, 1 (2016), [arXiv:1603.04993].

[276] A. Celis *et al.*, Phys. Lett. **B771**, 168 (2017), [arXiv:1612.07757].

[277] I. Ray and S. Nandi, JHEP **01**, 022 (2024), [arXiv:2305.11855].

[278] J. P. Lees *et al.* (BaBar), Phys. Rev. Lett. **109**, 101802 (2012), [arXiv:1205.5442].

[279] J. P. Lees *et al.* (BaBar), Phys. Rev. **D88**, 7, 072012 (2013), [arXiv:1303.0571].

[280] M. Huschle *et al.* (Belle), Phys. Rev. **D92**, 7, 072014 (2015), [arXiv:1507.03233].

[281] S. Hirose *et al.* (Belle), Phys. Rev. Lett. **118**, 21, 211801 (2017), [arXiv:1612.00529].

[282] G. Caria *et al.* (Belle), Phys. Rev. Lett. **124**, 16, 161803 (2020), [arXiv:1910.05864].

[283] I. Adachi *et al.* (Belle-II), Phys. Rev. D **110**, 7, 072020 (2024), [arXiv:2401.02840].

[284] R. Aaij *et al.* (LHCb), Phys. Rev. D **108**, 1, 012018 (2023), [Erratum: Phys.Rev.D 109, 119902 (2024)], [arXiv:2305.01463].

[285] R. Aaij *et al.* (LHCb), Phys. Rev. Lett. **131**, 111802 (2023), [arXiv:2302.02886].

[286] R. Aaij *et al.* (LHCb), Phys. Rev. Lett. **134**, 6, 061801 (2025), [arXiv:2406.03387].

[287] I. Adachi *et al.* (Belle-II), Phys. Rev. D **112**, 3, 032010 (2025), [arXiv:2504.11220].

[288] S. Banerjee *et al.* (Heavy Flavor Averaging Group (HFLAV)), Phys. Rev. **D113**, 1, 012008 (2026), with specific result from `doi:10.5281/zenodo.19174281`, [arXiv:2411.18639].

[289] M. Blanke, PoS **LeptonPhoton2019**, 015 (2019), [arXiv:1908.09713].

[290] S. Descotes-Genon, PoS **ALPS2019**, 016 (2020).

[291] D. London and J. Matias, Ann. Rev. Nucl. Part. Sci. **72**, 37 (2022), [arXiv:2110.13270].

[292] J. G. Korner and G. A. Schuler, Z. Phys. **C46**, 93 (1990).

[293] A. Abdesselam *et al.* (Belle), in "10th International Workshop on the CKM Unitarity Triangle (CKM 2018) Heidelberg, Germany, September 17-21, 2018," (2019), [arXiv:1903.03102].

[294] S. Hirose *et al.* (Belle), Phys. Rev. **D97**, 1, 012004 (2018), [arXiv:1709.00129].

[295] A. Matyja *et al.* (Belle), Phys. Rev. Lett. **99**, 191807 (2007), [arXiv:0706.4429].

[296] A. Bozek *et al.* (Belle), Phys. Rev. **D82**, 072005 (2010), [arXiv:1005.2302].

[297] M. Tanaka and R. Watanabe, Phys. Rev. **D87**, 3, 034028 (2013), [arXiv:1212.1878].

[298] R. Aaij *et al.* (LHCb), Phys. Rev. Lett. **120**, 12, 121801 (2018), [arXiv:1711.05623].

[299] J. Harrison, C. T. H. Davies and A. Lytle (LATTICE-HPQCD), Phys. Rev. Lett. **125**, 22, 222003 (2020), [arXiv:2007.06956].

[300] J. Harrison, C. T. H. Davies and A. Lytle (HPQCD), Phys. Rev. D **102**, 9, 094518 (2020), [arXiv:2007.06957].

[301] I. Adachi *et al.* (Belle-II), Phys. Rev. Lett. **132**, 21, 211804 (2024), [arXiv:2311.07248].

[302] M. Freytsis, Z. Ligeti and J. T. Ruderman, Phys. Rev. D **92**, 5, 054018 (2015), [arXiv:1506.08896].

[303] M. Rahimi and K. K. Vos, JHEP **11**, 007 (2022), [arXiv:2207.03432].

[304] Z. Ligeti, M. Luke and F. J. Tackmann, Phys. Rev. D **105**, 7, 073009 (2022), [arXiv:2112.07685].

[305] I. Adachi *et al.* (Belle-II), Phys. Rev. Lett. **131**, 18, 181801 (2023), [arXiv:2308.02023].

[306] L. Aggarwal *et al.* (Belle-II), Phys. Rev. Lett. **131**, 5, 051804 (2023), [arXiv:2301.08266].

[307] Y. Amhis *et al.* (HFLAV), Eur. Phys. J. **C77**, 12, 895 (2017), [arXiv:1612.07233].

Int. J. Mod. Phys. A 2026.41. Downloaded from www.worldscientific.com
UNIVERSITY OF CALIFORNIA @ BERKELEY on 09/16/26. Re-use and distribution is strictly not permitted, except for Open Access articles.

Int. J. Mod. Phys. A 2026.41. Downloaded from www.worldscientific.com
by UNIVERSITY OF CALIFORNIA @ BERKELEY on 09/16/26. Re-use and distribution is strictly not permitted, except for Open Access articles.

76. Determination of CKM angles from B hadrons

Revised July 2025 by T. Gershon (Warwick U.), M. Kenzie (Cambridge U.) and K. Trabelsi (CPPM Marseille).

76.1 Introduction

The Cabibbo–Kobayashi–Maskawa (CKM) description of quark mixing [1, 2] leads to a number of triangle relations between pairs of CKM matrix elements. One of these,

$$V_{ud}V_{ub}^* + V_{cd}V_{cb}^* + V_{td}V_{tb}^* = 0 \,, \tag{76.1}$$

is of particular interest since (i) all its terms are of comparable magnitude, and (ii) its properties can be measured through studies of oscillations and decays of B mesons. As the area of this unitary triangle is a measure of the amount of CP violation in the Standard Model [3], it is of particular interest to determine the values of its angles and to test the consistency of the CKM paradigm with the experimental measurements. The angles are defined as

$$\begin{aligned} \alpha &= \arg\left[-\frac{V_{td}V_{tb}^*}{V_{ud}V_{ub}^*}\right] \,, \qquad \beta = \arg\left[-\frac{V_{cd}V_{cb}^*}{V_{td}V_{tb}^*}\right] \,, \\ \gamma &= \arg\left[-\frac{V_{ud}V_{ub}^*}{V_{cd}V_{cb}^*}\right] \,, \end{aligned} \tag{76.2}$$

with an alternative notation $(\phi_2, \phi_1, \phi_3) \equiv (\alpha, \beta, \gamma)$ also widely used in the literature.

In this mini-review, the most precise methods to determine the CKM angles are described, with a particular focus on nontrivial aspects of the combination of results. More detailed discussions of these points can be found in Ref. [4]. A similar mini-review on the side of the unitarity triangle adjacent to the angle γ can be found in Ref. [5]. A detailed overview of the CKM quark-mixing matrix is given in Ref. [6] while CP violation in the quark sector is discussed in Ref. [7].

76.2 β

The relative weak (*i.e.* CP-violating) phase between the amplitude for any CKM-favoured B^0 meson decay to a CP eigenstate and that for the decay following B^0–$\overline{B}^0$ oscillation is twice the angle β. The decay-time-dependent CP asymmetry can be expressed as

$$\mathcal{A}_{f_{CP}}(t) \equiv \frac{d\Gamma/dt\left[\overline{B}^0_{\rm phys}(t) \to f_{CP}\right] - d\Gamma/dt\left[B^0_{\rm phys}(t) \to f_{CP}\right]}{d\Gamma/dt\left[\overline{B}^0_{\rm phys}(t) \to f_{CP}\right] + d\Gamma/dt\left[B^0_{\rm phys}(t) \to f_{CP}\right]} \,, \tag{76.3a}$$

$$= S_f \sin(\Delta m t) - C_f \cos(\Delta m t) \,, \tag{76.3b}$$

where the notation $B^0_{\rm phys}(t)$ ($\overline{B}^0_{\rm phys}(t)$) denotes a neutral B meson that decays at time t into the final state f_{CP}, and is known ("tagged") at time $t = 0$ to have flavour content corresponding to B^0 ($\overline{B}^0$). In Eq. (76.3b), Δm denotes the mass difference between the two physical eigenstates of the B^0–$\overline{B}^0$ system, while the corresponding decay-width difference is assumed to be negligible [8]; moreover CPT symmetry and the absence of CP violation in B^0–$\overline{B}^0$ mixing is assumed throughout this mini-review.

In the general case, one can write

$$S_f \equiv \frac{2\,\mathcal{I}m(\lambda_f)}{1 + \left|\lambda_f\right|^2} \qquad \text{and} \qquad C_f \equiv \frac{1 - \left|\lambda_f\right|^2}{1 + \left|\lambda_f\right|^2} \,, \tag{76.4}$$

where the parameter $\lambda_f = \frac{q}{p}\frac{\overline{A}_f}{A_f}$ is defined in terms of p and q, which define the flavour content of the mass eigenstates of the B^0–$\overline{B}^0$ system [8], and the amplitudes $\overline{A}_f$ (A_f) for a $\overline{B}^0$ (B^0) decay to the final state f_{CP}. In the limit that the decay amplitude is dominated by a CKM-favoured transition, as is the case for $B^0 \to J/\psi K^0_{\rm S}$ decays, one obtains simple relations: $S_f = -\eta_{CP}\sin(2\beta)$ and $C_f = 0$, where η_{CP} is the CP eigenvalue of the final state [9,10]. This method has been pursued intensively by experiments. The current world averages, combining results for several charmonium-kaon final states but dominated by results on $B^0 \to J/\psi K^0_{\rm S}$ (CP odd) and $B^0 \to J/\psi K^0_{\rm L}$ (CP even), are [4]

$$-\eta_{CP}S_f = 0.710 \pm 0.011 \,, \qquad C_f = +0.004 \pm 0.010 \,. \tag{76.5}$$

Despite the large number of signal events in the data, the dominant uncertainties are still statistical. One important source of potential systematic correlation between results from different experiments is that due to "tag-side interference" [11], which is common to measurements exploiting production through the $e^+e^- \to \Upsilon(4S) \to B^0\overline{B}^0$ process, including the latest results from BaBar [12], Belle [13] and Belle II [14]. It does not, however, affect the results from LHCb [15] that now have better statistical sensitivity. Another common source of systematic uncertainty is due to knowledge of the value of Δm, but since this quantity has been measured precisely [8] the effect remains small.

The interpretation of the value of $-\eta_{CP}S_f$ from Eq. (76.5) as $\sin(2\beta)$ assumes negligible contributions from subleading amplitudes with a different weak phase to that of the tree diagram (*i.e.* to that of the CKM matrix elements $V_{cb}V_{cs}^*$). This potential additional contribution is often referred to as "penguin pollution". All existing data, including the value of C_f in Eq. (76.5), as well as several explicit calculations [16–19], are consistent with penguin pollution in B^0 meson decays to charmonium-kaon decays being negligible at the current level of precision. Therefore, the value of $-\eta_{CP}S_f$ is generally converted to $\sin(2\beta)$ without any correction or additional uncertainty being assigned due to this assumption. This gives [4]

$$\beta = \left(22.6\,^{+0.5}_{-0.4}\right)^\circ \,, \tag{76.6}$$

where only the solution consistent with the Standard Model is reported (methods to resolve the trigonometric ambiguity in the result are discussed below). It is also possible to use data-driven methods, typically based on flavour symmetries plus some additional assumptions, to constrain the effects of penguin pollution [20–22]. In this case it is necessary to consider each charmonium-kaon final state separately, since the penguin pollution to each may differ. The most common approach [20], which relies on experimental information on $B^0 \to J/\psi\pi^0$ decays, currently gives an additional uncertainty on $\sin(2\beta)$ from $B^0 \to J/\psi K^0_{\rm S}$ of around 0.01.

It is possible to avoid the issue of penguin pollution in the measurement of β by using B^0 meson decays to a charm- and light-meson final state, such as $D_{CP}\pi^0$ (where D_{CP} represents a D^0 meson decaying into a CP eigenstate), instead of the charmonium-kaon final states. These decays do have a CKM-suppressed contribution ($V_{ub}V_{cd}^*$ instead of $V_{cb}V_{ud}^*$), which can in principle bias the determination of $\sin(2\beta)$ from S_f, but this can be calculated and is known to be negligible at current precision. The requirement that the neutral D meson decays to a final state that is common to both D^0 and $\overline{D}^0$, such as the CP-even eigenstate K^+K^-, reduces the sample size that is available for analysis. Consequently, the world average [4], $\sin(2\beta) = 0.71 \pm 0.09$, with these channels is not as precise as that from the charmonium-kaon states.

Converting experimental results on $\sin(2\beta)$ into constraints on β leads to a trigonometric ambiguity in the range $[0^\circ, 180^\circ]$. This can be resolved with experimental measurements of $\cos(2\beta)$, which can be obtained from decay-time-dependent analyses of B^0 meson decays to multibody (non-CP-eigenstate) final states. Among the charmonium-kaon decays, study of $B^0 \to J/\psi K^*(892)^0$ with $K^*(892)^0 \to K^0_{\rm S}\pi^0$ is the most promising approach, but due to the limited sample size that has been analysed to date the precision is not sufficient to resolve the ambiguity conclusively. The charm- and light-meson channels such as $B^0 \to D\pi^0$ with $D \to K^0_{\rm S}\pi^+\pi^-$ have been shown to provide good statistical power for this purpose, with a joint analysis of BaBar and Belle data giving $\cos(2\beta) = 0.91 \pm 0.25$ [23, 24], sufficient to rule out the alternative solution for β.

76.3 α

In the limit that only tree amplitudes contribute to B^0 meson decays to light mesons, such as $B^0 \to \pi^+\pi^-$, then the observables of the decay-time-dependent CP asymmetry of Eq. (76.3) would allow a straight-forward determination of 2α: $S_f = +\eta_{CP}\sin(2\alpha)$

Int. J. Mod. Phys. A 2026.41. Downloaded from www.worldscientific.com
UNIVERSITY OF CALIFORNIA @ BERKELEY on 09/16/26. Re-use and distribution is strictly not permitted, except for Open Access articles.

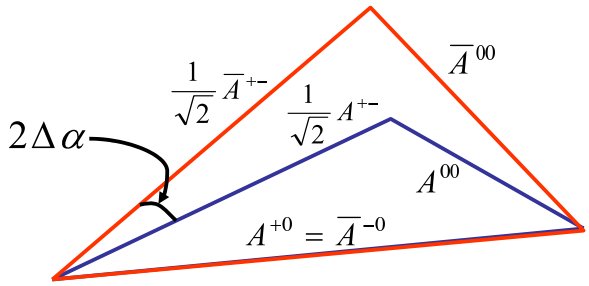

Figure 76.1: Isospin triangles for $B \to \pi\pi$ decays, reproduced from Ref. [25]. Here, the relative phase between A^{+0} and $\overline{A}^{-0}$ has been rotated away to simplify the picture. The total relative phase probed by $S_{\pi^+\pi^-}$ is $\arg\left(\frac{q}{p}\frac{\overline{A}^{+-}}{A^{+-}}\right) = 2\alpha - 2\Delta\alpha$, including contributions from B^0–$\overline{B}^0$ mixing, the tree-level amplitudes and the correction $\Delta\alpha$, and exploiting the unitarity requirement $\alpha + \beta + \gamma = 180°$.

and $C_f = 0$. In general, however, the determination of α is complicated by the presence of contributions from $b \to d(u\bar{u})$ neutral-current penguin transitions, which have a similar level of CKM-suppression as the $b \to u(\bar{u}d)$ charged-current tree amplitudes but have a different weak phase. Consequently, one obtains instead for $B^0 \to \pi^+\pi^-$

$$S_{\pi^+\pi^-} = \sqrt{1 - C^2_{\pi^+\pi^-}}\,\sin(2\alpha - 2\Delta\alpha), \qquad (76.7)$$

where $\Delta\alpha$ is the *a priori* unknown penguin contribution.

This contribution from the penguin amplitude can be accounted for in an analysis relating the amplitudes for isospin partner decays, *e.g.* A^{+-} for $B^0 \to \pi^+\pi^-$, A^{+0} for $B^+ \to \pi^+\pi^0$, A^{00} for $B^0 \to \pi^0\pi^0$ decays and $\left(\overline{A}^{+-}, \overline{A}^{-0}, \overline{A}^{00}\right)$ for their charge conjugates. The isospin analysis relies on the fact that there is no penguin contribution to A^{+0} and $\overline{A}^{-0}$, because $\pi^\pm\pi^0$ is a pure isospin-2 state, and the ($\Delta I = \frac{1}{2}$) QCD-penguin amplitudes only contribute to the isospin-0 final state. One therefore obtains the following isospin triangle relations [26]

$$A^{+0} = \frac{1}{\sqrt{2}}A^{+-} + A^{00} \quad \text{and} \quad \overline{A}^{-0} = \frac{1}{\sqrt{2}}\overline{A}^{+-} + \overline{A}^{00}\,, \qquad (76.8)$$

from which it is possible to determine $\Delta\alpha$, as shown in Fig. 76.1.

Since the determination of $\Delta\alpha$ and thus also α requires construction of amplitude-level relations, it is not appropriate to simply average results of α from different experiments. Instead, measurements of each of the observable quantities needed to determine α are input into a combination. For the $B \to \pi\pi$ system, the inputs are the branching fractions of $B^0 \to \pi^+\pi^-$, $B^+ \to \pi^+\pi^0$ and $B^0 \to \pi^0\pi^0$ decays, the lifetimes of the B^+ and B^0 mesons (which are needed to relate the branching fractions to amplitude-level quantities), and the $S_{\pi^+\pi^-}$, $C_{\pi^+\pi^-}$ and $C_{\pi^0\pi^0}$ observables. Potential sources of correlation must be taken into account, but these are predominantly systematic in origin and thus have a small effect on the combination, since the measurements are statistically limited. An exception is that the LHCb measurements of $(S_{\pi^+\pi^-}, C_{\pi^+\pi^-})$ [27, 28] have a significant statistical correlation due to the fact that the time variable of Eq. (76.3) is the difference between production and decay, and hence is in the range $[0, \infty]$. This correlation is largely absent for measurements from BaBar [29] and Belle [30], where the difference between the signal and tagging B meson decay times is measured, and hence $t \in [-\infty, \infty]$. The combination itself can be performed with different statistical approaches; the procedure described in detail in Ref. [31], based on a frequentist treatment, is used here. The knowledge of $C_{\pi^0\pi^0}$ [29, 32] is currently the limiting factor in the precision on α from the $B \to \pi\pi$ system, and is likely to remain so for some time due to the difficulty to reconstruct this final state.

In general, the isospin triangle construction gives a four-fold ambiguity on $2\Delta\alpha$ (each triangle can face either up or down), leading to an eight-fold ambiguity on α in the range $[0°, 180°]$. This is reduced if either or both of the triangles are flat, or if the two triangles have sides of identical length. The ambiguities can also be reduced if measurement of the $S_{\pi^0\pi^0}$ (or equivalent) observable is available, since this can be combined with the corresponding $\Delta\alpha$ parameter from the right-hand corner of the triangle in Fig. 76.1 to provide an additional constraint. None of these possibilities are realised in the $B \to \pi\pi$ system; in particular a decay-time-dependent analysis of $B^0 \to \pi^0\pi^0$ is extremely challenging experimentally due to the absence of any charged particle originating from the B decay position. Nonetheless, solutions consistent with $\alpha = 0$ can be rejected on physical grounds [25].

The isospin analysis can also be performed with the $B \to \rho\rho$ system, which contains two vector particles in the final state and so does not have a fixed *CP* eigenvalue. In principle the analysis can be performed separately for each $\rho\rho$ polarization state, but in practise it is found that the longitudinal polarization fraction, f_L, is close to unity, and hence the final state is approximately *CP*-even. Compared to $B^0 \to \pi\pi$, the $\rho\rho$ modes benefit experimentally from a higher branching fraction and smaller penguin contributions, so that the isospin triangles are flatter, reducing the ambiguities. (The value of $\Delta\alpha$ in the $B \to \rho\rho$ system, obtained from the isospin analysis, has a single solution in $[0, \pi]$ at $(3 \pm 5)°$, while for $B \to \pi\pi$ there are two solutions at 13° and 27° with $\Delta\alpha \in [7, 33]°$ at 68.3% confidence level (CL). The isospin analysis with either final state has an ambiguity under $\Delta\alpha \Leftrightarrow -\Delta\alpha$.) For the BaBar [33], Belle [34] and Belle II [35] experiments, the high branching fraction and smaller penguin contribution compensate for the increased difficulty to reconstruct the $\rho\rho$ final state relative to $\pi\pi$. Moreover, in contrast to $S_{\pi^0\pi^0}$, measurement of $S_{\rho^0\rho^0}$ is possible due to the four charged pion final state, following $\rho^0 \to \pi^+\pi^-$ decay, as has been demonstrated by BaBar [36].

In the $B \to \rho\pi$ system there are more amplitudes to consider, so that the isospin relation corresponds to a pentagon rather than a triangle and Eq. (76.8) is modified to become

$$\begin{aligned} \sqrt{2}(A^{+0} + A^{0+}) &= A^{+-} + A^{-+} + 2A^{00} \quad \text{and} \\ \sqrt{2}(\overline{A}^{-0} + \overline{A}^{0-}) &= \overline{A}^{+-} + \overline{A}^{-+} + 2\overline{A}^{00}\,. \end{aligned} \qquad (76.9)$$

As in Eq. (76.8), the left-hand sides of these expressions correspond to a pure isospin-2 final state, and therefore the ratio of the right-hand sides gives a pure phase term that, accounting for the B^0–$\overline{B}^0$ mixing phase that also contributes to the measured quantities, is 2α. The relative amplitudes for B^0 and $\overline{B}^0$ decays to $\rho^+\pi^-$, $\rho^-\pi^+$ and $\rho^0\pi^0$ can all be determined from a decay-time-dependent analysis of the $\pi^+\pi^-\pi^0$ Dalitz plot, so that study of this channel alone allows determination of α [37]. This analysis in principle leads to a single solution for α in $[0°, 180°]$, but the precision of current measurements [38–40] is limited.

The isospin analysis used to determine α is believed to be valid to high precision, and theoretical uncertainties in the procedure are usually neglected. Nonetheless, it should be noted that the analysis assumes the absence of electroweak penguin amplitudes, which can contribute to $\Delta I = \frac{3}{2}$ transitions with a different weak phase to that of the tree amplitudes [41, 42]. Moreover, isospin-breaking effects such as $\left(\pi^0, \eta, \eta'\right)$ mixing would impact on the relations of Eq. (76.8). A further complication in the $B \to \rho\rho$ system is the effect of the non-zero ρ meson width [43]. Estimates of the size of these effects on the determined value of α are typically at the 1° level or less [31]. By contrast, methods to determine α using SU(3) or other flavour symmetries are generally considered to have larger theoretical uncertainties and are not included here.

The world average obtained for the angle α from isospin analysis of $B \to \pi\pi$, $\rho\pi$ and $\rho\rho$ decays is [4]

$$\alpha = (84.1\,^{+3.7}_{-3.0})°\,, \qquad (76.10)$$

where the quoted uncertainty is at the 68.3% CL and does not include effects due to isospin-breaking. This world average, together with results split by decay mode, is shown in Fig. 76.2. The combination has a total of 61 experimental inputs from which 24 parameters are determined, and an overall χ^2 of 28.63, which corresponds to a p-value of 84%. Thus, there is excellent overall consistency between the inputs, despite the tension apparent in

Int. J. Mod. Phys. A 2026.41. Downloaded from www.worldscientific.com
by UNIVERSITY OF CALIFORNIA @ BERKELEY on 09/16/26. Re-use and distribution is strictly not permitted, except for Open Access articles.

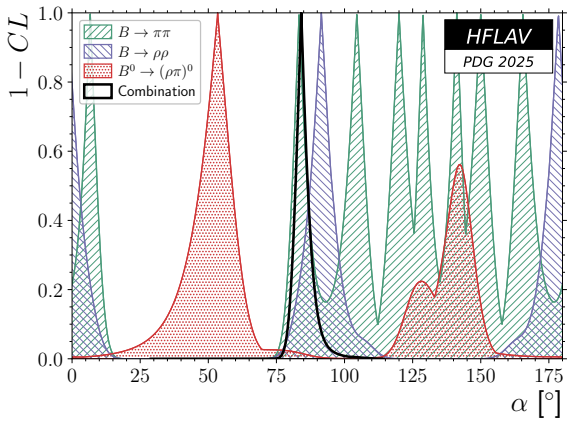

Figure 76.2: World average of α, as well as contributions from individual modes, in terms of 1−CL.

Fig. 76.2 between the results from $B^0 \to (\rho\pi)^0$ and the others. The combination gives a single best-fit for α in $[0°, 180°]$, but an ambiguous solution exists at $\alpha \Leftrightarrow \alpha{+}180°$. A secondary minimum close to zero is disfavoured [31].

76.4 γ

The angle γ is the weak phase between Cabibbo-favoured $b \to c$ and suppressed $b \to u$ quark transitions and can be determined by exploiting interference between them. Explicitly, the ratio of suppressed to favoured amplitudes is parameterized by

$$r_B e^{i(\delta_B \pm \gamma)} = \frac{A_{\rm sup}}{A_{\rm fav}} \ , \tag{76.11}$$

where r_B is the ratio of amplitude magnitudes, δ_B the strong phase difference and the + or − sign depends on whether the transition involves a $\bar{b}$ or b quark, respectively. Measurement of γ in this way has negligible theoretical uncertainty in the Standard Model [44], and therefore this approach provides a benchmark against which determinations from other methods, typically involving loop diagrams, can be compared.

Interference between these amplitudes is realised in $B^+ \to DK^+$ decays, where D represents an admixture of D^0 and $\overline{D}^0$ mesons. The simplest case is that of D decays to *CP*-eigenstates (GLW method [45, 46]), either *CP*-even such as K^+K^- (*CP*+) or *CP*-odd such as $K^0_{\rm S}\pi^0$ (*CP*−). The normalized decay rate and *CP* asymmetry are given by

$$\begin{aligned} R_{CP\pm} &= \frac{\Gamma(B^- \to D_{CP\pm}K^-) + \Gamma(B^+ \to D_{CP\pm}K^+)}{\Gamma(B^- \to D^0K^-) + \Gamma(B^+ \to \overline{D}^0K^+)} \\ &= 1 + r_B^2 \pm 2r_B\cos(\delta_B)\cos(\gamma) \ , \end{aligned} \tag{76.12a}$$

$$\begin{aligned} A_{CP\pm} &= \frac{\Gamma(B^- \to D_{CP\pm}K^-) - \Gamma(B^+ \to D_{CP\pm}K^+)}{\Gamma(B^- \to D_{CP\pm}K^-) + \Gamma(B^+ \to D_{CP\pm}K^+)} \\ &= \frac{\pm 2r_B\sin(\delta_B)\sin(\gamma)}{1 + r_B^2 \pm 2r_B\cos(\delta_B)\cos(\gamma)} \ . \end{aligned} \tag{76.12b}$$

These relations assume the absence of direct *CP* violation in the charm system; experimentally allowed deviations from this assumption are too small to cause a significant bias on γ [7, 47]. It is convenient to determine the $R_{CP\pm}$ quantities through a double ratio, normalizing to $B^+ \to D\pi^+$ decays involving the same final states, since this cancels potential sources of systematic uncertainty due to the branching fractions of the D decays that are used; small possible effects of *CP* violation in $B^+ \to D\pi^+$ decays are a source of systematic uncertainty in this procedure. The GLW method can be extended to include final states that are almost *CP*-eigenstates [48], as is the case in $D \to \pi^+\pi^-\pi^0$ and $D \to K^+K^-\pi^0$ decays, via inclusion of a factor encoding the fraction of *CP*-even (or *CP*-odd) content, $F_\pm$, which dilutes the sensitivity to γ by reducing the size of the interference terms (the terms linear with r_B) in Eq. (76.12).

For other D decays, the ratio of amplitudes for the D^0 and $\overline{D}^0$ decays to the final state of interest has to be accounted for in the formalism. The ADS method [49, 50] uses D decays to final states such as $K^\mp\pi^\pm$, which involve interference between Cabibbo-favoured (CF) and doubly-Cabibbo-suppressed (DCS) transitions. The observables in this case are

$$\begin{aligned} A_{\rm ADS} &= \frac{\Gamma(B^- \to [K^+\pi^-]_D K^-) - \Gamma(B^+ \to [K^-\pi^+]_D K^+)}{\Gamma(B^- \to [K^+\pi^-]_D K^-) + \Gamma(B^+ \to [K^-\pi^+]_D K^+)} \\ &= \frac{2r_B r_D \sin(\delta_B + \delta_D)\sin(\gamma)}{r_B^2 + r_D^2 + 2r_B r_D\cos(\delta_B + \delta_D)\cos(\gamma)} \ , \end{aligned} \tag{76.13a}$$

$$\begin{aligned} R_{\rm ADS} &= \frac{\Gamma(B^- \to [K^+\pi^-]_D K^-) + \Gamma(B^+ \to [K^-\pi^+]_D K^+)}{\Gamma(B^- \to [K^-\pi^+]_D K^-) + \Gamma(B^+ \to [K^+\pi^-]_D K^+)} \\ &= r_B^2 + r_D^2 + 2r_B r_D\cos(\delta_B + \delta_D)\cos(\gamma) \ , \end{aligned} \tag{76.13b}$$

where r_D and δ_D are the amplitude magnitude ratio and strong phase difference between the CF and DCS D decay. An alternative pair of observables, (R_-, R_+), is also sometimes used, where R_- (R_+) is the ratio of decay rates between the suppressed and favoured transitions for B^- (B^+) decays. The R_- and R_+ observables are statistically independent, while $A_{\rm ADS}$ and $R_{\rm ADS}$ are not (in particular, the uncertainty on $A_{\rm ADS}$ depends on the central value of $R_{\rm ADS}$). However, the pair (R_-, R_+) has more correlated sources of systematic uncertainty compared to $(A_{\rm ADS}, R_{\rm ADS})$. The observables of Eq. (76.13) are therefore usually preferred once a significant signal is established. The ADS method can also be extended to include decays to multibody final states, such as $D \to K^\pm\pi^\mp\pi^0$ and $D \to K^\pm\pi^\mp\pi^+\pi^-$, by addition of a coherence factor [51] which appears in the interference terms of Eq. (76.13) and accounts for dilution of the sensitivity due to variation of the decay amplitude across the phase space of the final state. A similar method can be used for singly Cabibbo-suppressed D decays to non-*CP* eigenstates such as K^*K [52].

For D decays to multibody self-conjugate final states (BPGGSZ method [53,54]), such as $D \to K^0_{\rm S}\pi^+\pi^-$, one can write the partial decay rate as a function of the position in the phase space in terms of the "Cartesian parameters" $x_\pm + iy_\pm = r_B e^{i(\delta_B \pm \gamma)}$:

$$\begin{aligned} d\Gamma(B^\pm \to [K^0_{\rm S}\pi^+\pi^-]_D K^\pm) &= A^2_{(\mp,\pm)} + r_B^2 A^2_{(\pm,\mp)} \\ &+ 2A_{(\pm,\mp)}A_{(\mp,\pm)}[x_\pm c_{D(\pm,\mp)} + y_\pm s_{D(\pm,\mp)}], \end{aligned} \tag{76.14}$$

where the notation $(+,-)$ is shorthand for the dependence on the Dalitz-plot position — the squared invariant masses of $K^0_{\rm S}\pi^+$ and $K^0_{\rm S}\pi^-$ combinations, respectively. The quantities $A_{(+,-)}$ and $A_{(-,+)}$ represent the magnitudes of the D^0 and $\overline{D}^0$ decay amplitudes at the position $(+,-)$ and are interchangable with their *CP* conjugate amplitudes because *CP* conservation is assumed in the D decay (*i.e.* $A_{(-,+)} = \overline{A}_{(+,-)}$). The quantities $c_{D(\pm,\mp)}$ and $s_{D(\pm,\mp)}$ are the cosine and sine of the strong phase difference, $\delta_{D(+,-)} = \arg(\overline{A}_{(+,-)}) - \arg(A_{(+,-)})$, between the $\overline{D}^0$ and D^0 amplitudes. These quantities can be determined from an amplitude model, although this leads to a hard-to-quantify systematic uncertainty associated to the composition of the model. An alternative, "model-independent", approach involves dividing the phase space into appropriate bins. In this case, the analysis benefits from external input on the values of c_D and s_D integrated over each bin. Measurements of these external parameters have been performed for the $D \to K^0_{\rm S}\pi^+\pi^-$ decay by the CLEO-c and BESIII collaborations [55–58]. The use of common input values for these parameters in model-independent determinations of γ with the BPGGSZ method by different experiments is a source of correlation between experiments that is currently negligible but will become more significant as the available B meson data samples increase in size.

The discussion above refers to $B^+ \to DK^+$ decays, but analogous measurements can be made also for additional channels such as $B^+ \to D^*K^+$ (with $D^* \to D\pi^0$, $D\gamma$) and $B^+ \to DK^{*+}$ (with $K^{*+} \to K^0_{\rm S}\pi^+$, $K^+\pi^0$). In the limit that these can be treated purely as two-body decays, the expressions for $B^+ \to DK^+$ are modified only by ensuring the r_B and δ_B parameters are specific to each B decay. Moreover, for $B^+ \to D^*K^+$ decays an effective

Int. J. Mod. Phys. A 2026.41. Downloaded from www.worldscientific.com
UNIVERSITY OF CALIFORNIA @ BERKELEY on 09/16/26. Re-use and distribution is strictly not permitted, except for Open Access articles.

shift of the strong phase by π between $D^* \to D\pi^0$ and $D\gamma$ decays [59] has to be taken into account. In case the finite width of the decaying resonance is non-negligible, as is the case for the $K^*(892)$ state, additional amplitudes can contribute leading to a dilution of the sensitivity, which can be accounted for in the formalism through the introduction of a relevant coherence factor. For the $B^0 \to DK^{*0}$ decay, full amplitude analysis of the $B^0 \to DK^+\pi^-$ Dalitz plot provides additional sensitivity compared to the quasi-two-body approach [60, 61].

It is also possible to measure γ using decay-time-dependent analysis of the B_s^0 meson [62]. The weak phase arising in the interference between direct decay of $B_s^0 \to D_s^\mp K^\pm$ and decay via mixing is $(\gamma - 2\beta_s)$, where β_s is the angle associated with $B_s^0 \to J/\psi\phi$ decays in a similar way to the relation between β and $B^0 \to J/\psi K_S^0$ decays described in Sec. 76.2. Sufficient information can be obtained from the tagged, decay-time-dependent rates of $B_s^0 \to D_s^\mp K^\pm$ decays that this weak phase can be determined, up to an ambiguity, together with the strong phase difference between, and the ratio of the magnitudes of, the suppressed and favoured amplitudes. Since β_s is known to good precision [8], measurements of the decay-time-dependent *CP*-asymmetry observables in $B_s^0 \to D_s^\mp K^\pm$ decays can be used to infer constraints on γ. Alternatively, if effects of penguin pollution in $B_s^0 \to J/\psi\phi$ decays [18, 19] are a concern, as they will become in the future, results from the $B_s^0 \to D_s^\mp K^\pm$ mode can be combined with an independent precise measurement of γ to provide a penguin-free determination of β_s.

The average for γ requires a non-trivial combination due the complicated relations between the observables and the physics parameters of interest, such as in Eqs. (76.12), (76.13) and (76.14). Moreover, hadronic parameters such as r_B and δ_B defined in Eq. (76.11) are common to all different D decay modes (but differ for each B decay mode). Thus, it is not correct to simply average results for γ obtained by different experiments or in different channels. Instead, measurements of rate asymmetries, rate ratios and the Cartesian parameters are taken as inputs to the combination, from which results are obtained not only for γ but also for the hadronic parameters. Independent measurements of auxiliary parameters such as r_D and δ_D are also treated as inputs to the combination. In some cases the B decay data can help to reduce uncertainties on these auxiliary parameters and therefore a simultaneous fit of charm and beauty data can provide stronger constraints [63]; this approach however is not currently used for the world average.

The precision to which γ can be measured with a particular B decay is approximately inversely proportional to the value of r_B. Thus, results from channels with smaller yields but larger values of r_B, such as $B^0 \to DK^{*0}$ and $B_s^0 \to D_s^\mp K^\pm$ ($r_B \approx 0.3$–0.4), can have a significant impact on the world average and are included in the combination. By contrast the $B^+ \to D\pi^+$ mode, for which large samples are available but $r_B \approx 0.005$, has little impact and is also more sensitive to potential systematic biases; hence it is not included. The sensitivity of the world average at present is dominated by results from $B^+ \to DK^+$, where $r_B \approx 0.1$, in particular results with the GLW [64], ADS [64] and BPGGSZ [65] methods.

The world average obtained for the angle γ, obtained by combining results from $B^+ \to DK^+$, D^*K^+, DK^{*+}, $DK^+\pi^+\pi^-$, $B^0 \to DK^+\pi^-$, $B_s^0 \to D_s^\mp K^\pm$ and $B_s^0 \to D_s^\mp K^\pm\pi^+\pi^-$ decays, is

$$\gamma = \left(66.4^{+2.7}_{-2.8}\right)^\circ \ , \tag{76.15}$$

where the quoted uncertainty is at the 68.3% CL.

Effects related to charm and kaon mixing and *CP* violation are generally negligible at the current level of precision, in particular for modes with $r_B \gtrsim 0.1$. An exception is that a dependence of the selection efficiency on the charm decay time can induce a dependence of the observables on charm mixing parameters [66]. Such effects can be important at hadron collider experiments such as LHCb, but can be and are corrected for. Interactions of neutral kaons with detector material can also cause a bias in determination of γ from modes with low values of r_B [67], such as the BPGGSZ method applied to $B^+ \to D\pi^+$, but are negligible in modes with larger r_B values. A further subtlety is that the identification of the weak phase between suppressed and favoured amplitudes in $B \to DK$ decays with γ, as defined in Eq. (76.2), assumes that the 2×2 submatrix of the CKM matrix is real, *i.e.* that $\arg\left[V_{ud}V_{us}^*/\left(V_{cd}V_{cs}^*\right)\right] = 0$. This is true to an excellent approximation in the Standard Model, and is known experimentally from independent studies of the charm system [47] to contribute negligible bias to current measurements. Nonetheless, in future it will be possible to test directly this assumption by comparing the value of γ obtained from the $B \to DK$ and $B \to D\pi$ systems.

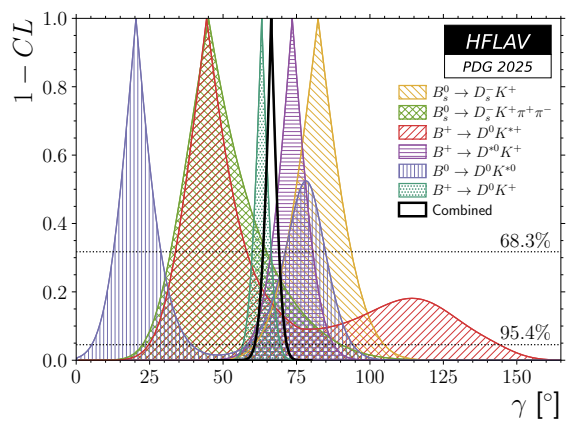

Figure 76.3: World average of $\gamma \equiv \phi_3$, as well as contributions from individual modes, in terms of 1−CL.

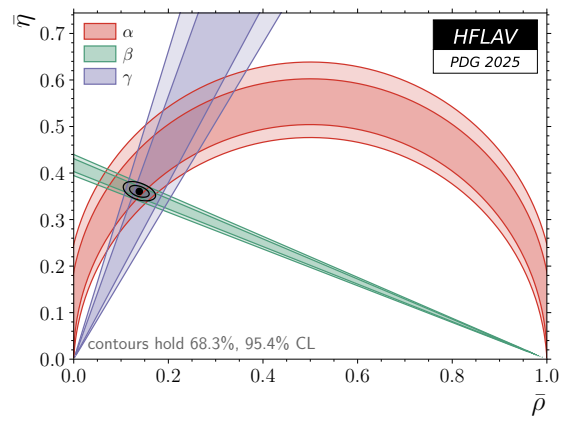

Figure 76.4: Constraints from the measurements of the angles of the CKM unitarity triangle in the $(\overline{\rho}, \overline{\eta})$ plane.

Effects from correlated uncertainties between amplitude models and strong phase differences in charm decays are negligible and are not explicitly accounted for in the combination, nor are effects related to charm and kaon mixing and *CP* violation. This world average, together with results split by decay mode, is shown in Fig. 76.3. The combination has a total of 178 experimental inputs from which 36 parameters are determined, and an overall χ^2 of 159.89, which corresponds to a p-value of 15% indicating reasonable agreement between the inputs. The combination gives a single solution for γ in $[0°, 180°]$, but an ambiguous solution exists at $\gamma \Leftrightarrow \gamma + 180°$.

76.5 Summary

Experimental progress has resulted in all three angles of the CKM unitarity triangle being measured with good accuracy, with β known to subdegree precision and both α and γ known to better than 5°. The constraints from these three measurements in the $(\overline{\rho}, \overline{\eta})$ plane are shown in Fig. 76.4; further discussion and comparison with constraints from independent measurements can be found in Ref. [6]. The determinations of all three angles remain statistically limited, but it will be a challenge for experiments to

Int. J. Mod. Phys. A 2026.41. Downloaded from www.worldscientific.com
by UNIVERSITY OF CALIFORNIA @ BERKELEY on 09/16/26. Re-use and distribution is strictly not permitted, except for Open Access articles.

ensure that this remains the case as the precision improves. Consequently, the correct treatment of sources of correlation between the measurements that go into the world average combinations is becoming increasingly important.

References

[1] N. Cabibbo, Phys. Rev. Lett. **10**, 531 (1963).

[2] M. Kobayashi and T. Maskawa, Prog. Theor. Phys. **49**, 652 (1973).

[3] C. Jarlskog, Phys. Rev. Lett. **55**, 1039 (1985).

[4] Y. S. Amhis *et al.* (HFLAV), Phys. Rev. **D107**, 5, 052008 (2023), updated averages are available online at hflav.web.cern.ch, [arXiv:2206.07501].

[5] See the review on "Semileptonic *b*-Hadron Decays, Determination of V_{cb}, V_{ub}" in this *Review*.

[6] See the review on "Cabibbo-Kobayashi-Maskawa Mixing Matrix," in this *Review*.

[7] See the review on "*CP* Violation in the Quark Sector," in this *Review*.

[8] See the review on "B^0–$\overline{B}^0$ Mixing" in this *Review*.

[9] A. Carter and A. Sanda, Phys. Rev. **D23**, 1567 (1981).

[10] I. Bigi and A. Sanda, Nucl. Phys. **B193**, 85 (1981).

[11] O. Long *et al.*, Phys. Rev. **D68**, 034010 (2003), [hep-ex/0303030].

[12] B. Aubert *et al.* (BaBar), Phys. Rev. **D79**, 072009 (2009), [arXiv:0902.1708].

[13] I. Adachi *et al.* (Belle), Phys. Rev. Lett. **108**, 171802 (2012), [arXiv:1201.4643].

[14] I. Adachi *et al.* (Belle-II), Phys. Rev. **D110**, 1, 012001 (2024), [arXiv:2402.17260].

[15] R. Aaij *et al.* (LHCb), Phys. Rev. Lett. **132**, 021801 (2024), [arXiv:2309.09728].

[16] H.-n. Li and S. Mishima, JHEP **03**, 009 (2007), [hep-ph/0610120].

[17] M. Jung, Phys. Rev. **D86**, 053008 (2012), [arXiv:1206.2050].

[18] K. De Bruyn and R. Fleischer, JHEP **1503**, 145 (2015), [arXiv:1412.6834].

[19] P. Frings, U. Nierste and M. Wiebusch, Phys. Rev. Lett. **115**, 061802 (2015), [arXiv:1503.00859].

[20] M. Ciuchini, M. Pierini and L. Silvestrini, Phys. Rev. Lett. **95**, 221804 (2005), [hep-ph/0507290].

[21] S. Faller *et al.*, Phys. Rev. **D79**, 014030 (2009), [arXiv:0809.0842].

[22] Z. Ligeti and D. Robinson, Phys. Rev. Lett. **115**, 251801 (2015), [arXiv:1507.06671].

[23] I. Adachi *et al.* (BaBar, Belle), Phys. Rev. Lett. **121**, 261801 (2018), [arXiv:1804.06152].

[24] I. Adachi *et al.* (BaBar, Belle), Phys. Rev. **D98**, 112012 (2018), [arXiv:1804.06153].

[25] M. Antonelli *et al.*, Phys. Rept. **494**, 197 (2010), [arXiv:0907.5386].

[26] M. Gronau and D. London, Phys. Rev. Lett. **65**, 3381 (1990).

[27] R. Aaij *et al.* (LHCb), Phys. Rev. **D98**, 032004 (2018), [arXiv:1805.06759].

[28] R. Aaij *et al.* (LHCb), JHEP **03**, 075 (2021), [arXiv:2012.05319].

[29] J. P. Lees *et al.* (BaBar), Phys. Rev. **D87**, 052009 (2013), [arXiv:1206.3525].

[30] I. Adachi *et al.* (Belle), Phys. Rev. **D88**, 092003 (2013), [arXiv:1302.0551].

[31] J. Charles *et al.*, Eur. Phys. J. **C77**, 574 (2017), [arXiv:1705.02981].

[32] T. Julius *et al.* (Belle), Phys. Rev. **D96**, 032007 (2017), [arXiv:1705.02083].

[33] B. Aubert *et al.* (BaBar), Phys. Rev. **D76**, 052007 (2007), [arXiv:0705.2157].

[34] P. Vanhoefer *et al.* (Belle), Phys. Rev. **D93**, 032010 (2016), [Addendum *ibid*: **D94** 099903 (2016)], [arXiv:1510.01245].

[35] I. Adachi *et al.* (Belle-II), Phys. Rev. D **111**, 9, 092001 (2025), [arXiv:2412.19624].

[36] B. Aubert *et al.* (BaBar), Phys. Rev. **D78**, 071104 (2008), [arXiv:0807.4977].

[37] A. E. Snyder and H. R. Quinn, Phys. Rev. **D48**, 2139 (1993).

[38] J. P. Lees *et al.* (BaBar), Phys. Rev. **D88**, 012003 (2013), [arXiv:1304.3503].

[39] A. Kusaka *et al.* (Belle), Phys. Rev. Lett. **98**, 221602 (2007), [hep-ex/0701015].

[40] A. Kusaka *et al.* (Belle), Phys. Rev. **D77**, 072001 (2008), [arXiv:0710.4974].

[41] M. Gronau and J. Zupan, Phys. Rev. **D71**, 074017 (2005), [hep-ph/0502139].

[42] S. Gardner, Phys. Rev. **D72**, 034015 (2005), [hep-ph/0505071].

[43] A. Falk *et al.*, Phys. Rev. **D69**, 011502 (2004), [hep-ph/0310242].

[44] J. Brod and J. Zupan, JHEP **01**, 051 (2014), [arXiv:1308.5663].

[45] M. Gronau and D. London, Phys. Lett. **B253**, 483 (1991).

[46] M. Gronau and D. Wyler, Phys. Lett. **B265**, 172 (1991).

[47] See the review on "D^0–$\overline{D}^0$ Mixing" in this *Review*.

[48] M. Nayak *et al.*, Phys. Lett. **B740**, 1 (2015), [arXiv:1410.3964].

[49] D. Atwood, I. Dunietz and A. Soni, Phys. Rev. Lett. **78**, 3257 (1997), [hep-ph/9612433].

[50] D. Atwood, I. Dunietz and A. Soni, Phys. Rev. **D63**, 036005 (2001), [hep-ph/0008090].

[51] D. Atwood and A. Soni, Phys. Rev. **D68**, 033003 (2003), [hep-ph/0304085].

[52] Y. Grossman, Z. Ligeti and A. Soffer, Phys. Rev. **D67**, 071301 (2003), [hep-ph/0210433].

[53] A. Giri *et al.*, Phys. Rev. **D68**, 054018 (2003), [hep-ph/0303187].

[54] A. Bondar, *Proceedings of BINP special analysis meeting on Dalitz analysis*, 24-26 Sep. 2002, unpublished.

[55] R. Briere *et al.* (CLEO), Phys. Rev. **D80**, 032002 (2009), [arXiv:0903.1681].

[56] J. Libby *et al.* (CLEO), Phys. Rev. **D82**, 112006 (2010), [arXiv:1010.2817].

[57] M. Ablikim *et al.* (BESIII), Phys. Rev. Lett. **124**, 241802 (2020), [arXiv:2002.12791].

[58] M. Ablikim *et al.* (BESIII), Phys. Rev. **D101**, 112002 (2020), [arXiv:2003.00091].

[59] A. Bondar and T. Gershon, Phys. Rev. **D70**, 091503 (2004), [hep-ph/0409281].

[60] T. Gershon, Phys. Rev. **D79**, 051301 (2009), [arXiv:0810.2706].

[61] T. Gershon and M. Williams, Phys. Rev. **D80**, 092002 (2009), [arXiv:0909.1495].

[62] R. Aleksan, I. Dunietz and B. Kayser, Z. Phys. **C54**, 653 (1992).

[63] R. Aaij *et al.* (LHCb), JHEP **12**, 141 (2021), [arXiv:2110.02350].

[64] R. Aaij *et al.* (LHCb), JHEP **04**, 081 (2021), [arXiv:2012.09903].

[65] R. Aaij *et al.* (LHCb), JHEP **02**, 169 (2021), [arXiv:2010.08483].

[66] M. Rama, Phys. Rev. **D89**, 014021 (2014), [arXiv:1307.4384].

[67] M. Bjørn and S. Malde, JHEP **07**, 106 (2019), [arXiv:1904.01129].

77. Spectroscopy of Mesons Containing Two Heavy Quarks

Revised October 2025 by J.J. Hernández-Rey (IFIC, Valencia), C. Lourenço (CERN), R.E. Mitchell (Indiana U.), S. Navas (Granada U.) and C. Patrignani (Bologna U.).

A golden age for heavy quarkonium physics dawned at the turn of this century, triggered by the confluence of new approaches to non-perturbative quantum chromodynamics (QCD) and a series of experimental results. The subsequent broad spectrum of breakthroughs, surprises, and continuing puzzles had not been anticipated. Indeed, CLEO-c, BESIII, and the B-factories, later joined by ATLAS, CMS and LHCb, have made a series of groundbreaking observations. For an extensive presentation of the status of heavy quarkonium physics, the reader is referred to several reviews [1–10]. This note focuses on experimental developments in heavy quarkonium spectroscopy with very few theoretical comments. Possible theoretical interpretations of the states with properties incompatible with the quark model are presented in the review "Heavy non-$q\bar{q}$ mesons". Note that in this review we follow the new naming scheme for hadrons (see the review "Naming scheme for hadrons" in the current edition of the RPP).

This review covers states discovered since 2003, the year that marked the unexpected discovery of the $X(3872)$ [11]. The $X(3872)$, now called $\chi_{c1}(3872)$, was the first of the mesons containing two heavy quarks that could not be easily accommodated by the $q\bar{q}$ quark model. Its discovery was a watershed event in meson spectroscopy. In earlier versions of this write-up the particles were sorted according to an assumed *conventional* or *unconventional* nature with respect to the quark model. However, since this classification is not always unambiguous, we here follow Ref. [12] and sort the states into three groups, namely states below (*cf.* Table 77.1), above (*cf.* Table 77.2), and near (*cf.* Table 77.3) the lowest open-flavor thresholds. Due to the presence of many open-flavor thresholds, we note that the division of states between "above" and "near" open-flavor thresholds is not absolute.

77.1 States Below Open-Flavor Threshold

Table 77.1 lists properties of recently observed heavy quarkonium states located below the lowest open-flavor thresholds. Those are expected to be (at least prominently) conventional quarkonia. The majority of charmonium ($c\bar{c}$) and bottomonium ($b\bar{b}$) states were established prior to 2003.

77.1.1 *Charmonium*

The $h_c(1P)$ is the 1^1P_1 charmonium state, the singlet partner of the long-known χ_{cJ} triplet 1^3P_J. After being firmly established in 2005 through the process $\psi(2S) \to \pi^0 h_c(1P)$ [13], it has since been studied extensively by BESIII using large samples of $\psi(2S)$ decays. Exclusive hadronic decays of the $h_c(1P)$, strongly suppressed relative to the dominant radiative transition $h_c(1P) \to \gamma\eta_c(1S)$, were first observed in 2019 [14] and additional decays were found in 2020 [15] and 2022 [16].

Belle reported an observation of the $\psi_2(1D)$ decaying to $\gamma\chi_{c1}(1P)$ with J^{PC} presumed to be 2^{--} [17]. This state is listed in Table 77.1 as $\psi_2(3823)$. Its existence was confirmed with high significance by BESIII [18, 19]. While the negative C-parity is indeed established by its observed decay channel, the assignment of $J = 2$ was made by matching to the closest quark model state (1^3D_2) and requires experimental confirmation.

The 1^1D_2 state, or the $\eta_{c2}(1D)$, with a mass expected near 3820 MeV, has not yet been observed. Recently Belle performed a search in $B \to \eta_{c2}(1D)K(\pi)$ decays in the mass range 3795–3845 MeV and found no signal [20]. Thus, the $\eta_{c2}(1D)$ remains the only unobserved conventional charmonium state that does not have open-charm decays.

77.1.2 *Bottomonium*

The ground state of bottomonium, $\eta_b(1S)$, is well established. After the initial reports from BaBar in radiative decays of the $\Upsilon(3S)$ (observation) [21] and $\Upsilon(2S)$ (evidence) [22], Belle confirmed the existence of the $\eta_b(1S)$ with more than 5σ significance in radiative decays of the newly discovered $h_b(1P)$ [23, 24] and $h_b(2P)$ [23] (see next paragraph), as well as in $\Upsilon(2S)$ radiative decays [25]. Belle has also reported strong evidence for the $\eta_b(2S)$ [23], but it still needs confirmation at the 5σ level. Note that there are hints of tension in the $\eta_b(1S)$ mass as measured in radiative M1 and E1 transitions. In the M1 transition $\Upsilon(2S) \to \gamma\eta_b(1S)$ Belle measures a mass of $9394.8^{+2.7+4.5}_{-3.1-2.7}$ MeV [25], while in the E1 transitions $h_b(1P, 2P) \to \gamma\eta_b(1S)$ Belle measures $9402.4 \pm 1.5 \pm 1.8$ MeV [23]. This tension may point to an incomplete understanding of the $\eta_b(1S)$ lineshape in different production mechanisms.

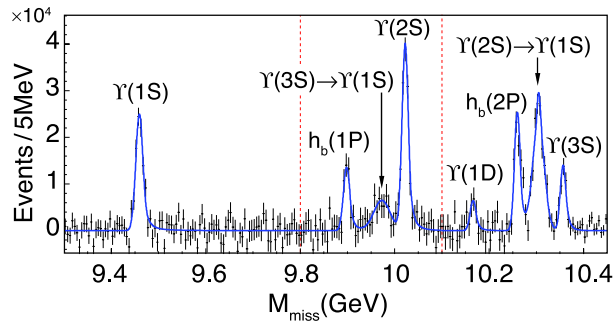

Figure 77.1: From Belle [26], the mass recoiling against $\pi^+\pi^-$ pairs, $M_{\rm miss}$, in e^+e^- collision data taken near the peak of the $\Upsilon(10860)$. The smooth combinatorial and $K^0_S \to \pi^+\pi^-$ background contributions have been subtracted. The fit to the various labeled signal contributions is overlaid (*curve*). The fit is performed separately in three regions with boundaries indicated by the vertical dashed lines.

The $h_b(1P)$, the bottomonium counterpart of the $h_c(1P)$, and the next excited state, the $h_b(2P)$, were simultaneously discovered by Belle using dipion transitions from the $\Upsilon(10860)$ [26] (Fig. 77.1). The same analysis also showed the $\Upsilon_J(1D)$, the lowest-lying D-wave triplet of the $b\bar{b}$ system, but did not resolve the $J = 1, 2, 3$ components. The search for the $h_b(1P)$ was directly inspired by a CLEO result [27], which found a surprisingly copious production of $e^+e^- \to \pi^+\pi^- h_c(1P)$ as well as an indication that $\psi(4230) \to \pi^+\pi^- h_c(1P)$ occurs at a comparable rate with the signature mode $\psi(4230) \to \pi^+\pi^- J/\psi(1S)$. The presence of $\Upsilon(nS)$ peaks in Fig. 77.1 at rates two orders of magnitude larger than expected, along with separate studies with exclusive decays $\Upsilon(nS) \to \mu^+\mu^-$, allow precise calibration of the $\pi^+\pi^-$ recoil mass spectrum and very accurate measurements of the $h_b(1P)$ and $h_b(2P)$ masses. Both corresponding hyperfine splittings are consistent with zero within an uncertainty of about 1.5 MeV (lowered to 1.1 MeV for the $h_b(1P)$ in Ref. [28]). Belle later observed the transition $\Upsilon(4S) \to h_b(1P)\eta$ [24] and the corresponding 1P hyperfine splitting was also found to be compatible with zero at a similar precision level.

Just before Christmas 2011, ATLAS offered the world a beautiful gift, in the form of the discovery of the $\chi_b(3P)$ quarkonium state [29], observed by combining dimuons from $\Upsilon(1S)$ or $\Upsilon(2S)$ decays with photons emitted in the radiative $\chi_b(3P)$ decays (Fig. 77.2, bottom left panel). The new resonance, with a mass of $10\,530 \pm 5(\text{stat}) \pm 9(\text{syst})$ MeV, was soon confirmed by D0 [30]. Also LHCb observed the $\chi_b(3P)$ peak, using the full Run 1 event sample, corresponding to an integrated luminosity of 3 fb^{-1} [31] (Fig. 77.2, middle left panel). Finally, CMS used 80 fb^{-1} of 13 TeV pp collisions, collected in 2016 and 2017, to show two well-resolved $\chi_{b1}(3P)$ and $\chi_{b2}(3P)$ peaks [32], separated by a mass difference of $10.60 \pm 0.64(\text{stat}) \pm 0.17(\text{syst})$ MeV (Fig. 77.2, top left panel). The remarkable precision of the individual mass measurements, with relative uncertainties as small as 50 ppm, shows that the LHC experiments can provide important results in the field of hadron spectroscopy, especially in the case of heavy particles, which require very high collision energies and large event samples.

77.1.3 B_c *System*

The $B_c^\pm$ family is quite special because these (charged) quarkonium states consist of two heavy quarks of different flavor. Among

Int. J. Mod. Phys. A 2026.41. Downloaded from www.worldscientific.com
UNIVERSITY OF CALIFORNIA @ BERKELEY on 09/16/26. Re-use and distribution is strictly not permitted, except for Open Access articles.

Int. J. Mod. Phys. A 2026.41. Downloaded from www.worldscientific.com
by UNIVERSITY OF CALIFORNIA @ BERKELEY on 09/16/26. Re-use and distribution is strictly not permitted, except for Open Access articles.

Table 77.1: New states below the open-flavor thresholds in the $c\bar{c}$, $b\bar{c}$, and $b\bar{b}$ regions, ordered by mass. Masses m and widths Γ represent the PDG25 weighted averages with statistical and systematic uncertainties added in quadrature. In the Production column, the state is always denoted by X. Ellipses (...) indicate inclusively selected event topologies, *i.e.*, additional particles not directly detected by experiment. A question mark (?) indicates an unmeasured value. The Discovery Year column gives the date of the first measurement cited. The Summary Table column indicates whether or not the state appears in the summary tables, usually requiring at least two independent experiments with significance of $>5\sigma$. Refer to the particle listings for references and further information.

PDG Name	Former Name	m (MeV)	Γ (MeV)	$I^G(J^{PC})$	Production	Decay	Discovery Year	Summary Table
$h_c(1P)$		3525.37 ± 0.14	$0.78^{+0.30}_{-0.27}$	$0^-(1^{+-})$	$\psi(2S) \to \pi^0 X$ $p\bar{p} \to X$ $e^+e^- \to \pi\pi X$	$\gamma\eta_c(1S)$ hadrons (see listings)	2004	YES
$\psi_2(3823)$	$X(3823)$	3823.51 ± 0.34	< 2.9	$0^-(2^{--})$	$B \to KX$ $e^+e^- \to \pi^+\pi^- X$	$\gamma\,\chi_{c1}(1P)$ $\pi^+\pi^- J/\psi(1S)$	2013	YES
B_c^+		6274.47 ± 0.32	stable*	$0(0^-)$	$\bar{p}p \to X...$ $pp \to X...$	$\pi^+ J/\psi(1S)$ (see listings)	2007	YES
$B_c^+(1P)^\dagger$		6704.8 ± 6.2 6752.4 ± 10.0	?	$0(?^?)$	$pp \to X...$	γB_c^+	2025	NO
$B_c^+(2S)$		6871.2 ± 1.0	?	$0(0^-)$	$pp \to X...$	$B_c^+\pi^+\pi^-$	2014	YES
$\eta_b(1S)$		9398.7 ± 2.0	10^{+5}_{-4}	$0^+(0^{-+})$	$\Upsilon(2S,3S) \to \gamma X$ $h_b(1P,2P) \to \gamma X$	hadrons (see listings)	2008	YES
$h_b(1P)$		9899.3 ± 0.8	?	$0^-(1^{+-})$	$\Upsilon(10860) \to \pi^+\pi^- X$ $\Upsilon(3S) \to \pi^0 X$ $\Upsilon(4S) \to \eta X$ $T_{b\bar{b}}(10610)^+ \to \pi^+ X$ $T_{b\bar{b}}(10650)^+ \to \pi^+ X$	$\gamma\eta_b(1S)$	2011	YES
$\eta_b(2S)$		$9999.0^{+4.5}_{-4.0}$	< 24	$0^+(0^{-+})$	$h_b(2P) \to \gamma X$	hadrons	2012	NO
$\Upsilon_2(1D)$		10163.7 ± 1.4	?	$0^-(2^{--})$	$\Upsilon(3S) \to \gamma\gamma X$ $\Upsilon(10860) \to \pi^+\pi^- X$	$\gamma\gamma\Upsilon(1S)$ $\pi^+\pi^-\Upsilon(1S)$	2004	YES
$h_b(2P)$		10259.8 ± 1.2	?	$0^-(1^{+-})$	$\Upsilon(10860) \to \pi^+\pi^- X$ $T_{b\bar{b}}(10610)^+ \to \pi^+ X$ $T_{b\bar{b}}(10650)^+ \to \pi^+ X$	$\gamma\eta_b(1S,2S)$	2011	YES
$\chi_{b1}(3P)$		10513.42 ± 0.67	?	$0^+(1^{++})$	$pp \to X...$	$\gamma\Upsilon(1S,2S,3S)$	2011	YES
$\chi_{b2}(3P)$		10524.02 ± 0.78	?	$0^+(2^{++})$	$pp \to X...$	$\gamma\Upsilon(3S)$	2011	YES

*The B_c^+ decays only weakly and has a lifetime of 0.510 ± 0.009 ps ($\Gamma \approx 1.3 \times 10^{-9}$ MeV).

†The observed structure in γB_c^+ is described by two Gaussian functions and is consistent with contributions from $^3P_0$, $^3P_2$, and mixed $^3P_1$ and $^1P_1$ states decaying to both γB_c^+ and γB_c^{*+}.

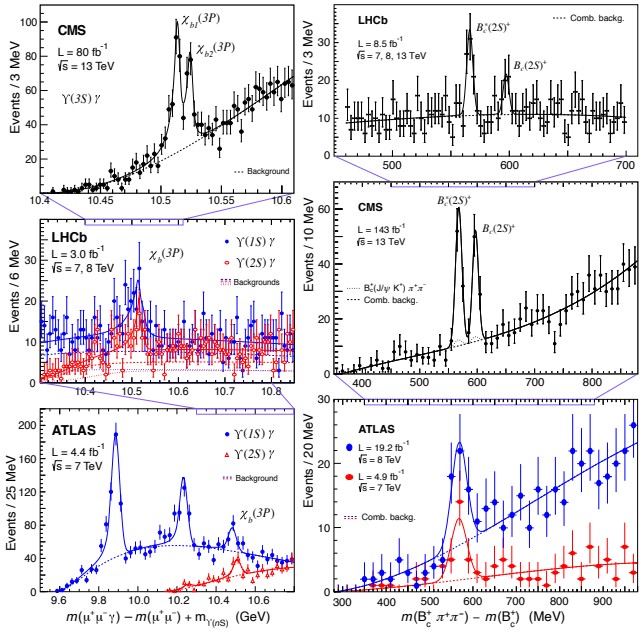

Figure 77.2: (Left Column) Invariant mass distributions measured by the ATLAS [29] (bottom), LHCb [31] (middle) and CMS [32] (top) experiments in their searches for the $\chi_b(3P)$ states through their radiative decays to one of the S-wave bottomonia. (Right Column) Invariant mass distributions measured by the ATLAS [33] (bottom), CMS [34] (middle) and LHCb [35] (top) experiments in their searches for $B_c^\pm$ excited states decaying to the $B_c^\pm$ ground state with the emission of two charged pions.

other interesting properties, this means that they cannot annihilate into gluons, the excited states only decaying to the pseudoscalar ground state, $B_c^\pm$, via electromagnetic and pionic transitions.

On the basis of an event sample collected in the Run 1 of the LHC, corresponding to an integrated luminosity of 24 fb^{-1}, adding the 7 and 8 TeV data, the ATLAS Collaboration observed a resonance in the $B_c^+\pi^+\pi^-$ invariant mass spectrum [33] (Fig. 77.2, bottom right panel). This peak, observed with a significance of 5.2 standard deviations and a mass of $6842 \pm 4(\text{stat}) \pm 5(\text{syst})$ MeV, was immediately recognized as the $B_c(2S)^\pm$ state, the first radial excitation in the $B_c^\pm$ family. Profiting from the much larger Run 2 event sample, corresponding to 143 fb^{-1} of 13 TeV pp collisions, as well as from a measurement resolution of around 6 MeV, the CMS Collaboration could observe *two* well-resolved peaks, separated by $29.1 \pm 1.5(\text{stat}) \pm 0.7(\text{syst})$ MeV [34] (Fig. 77.2, middle right panel). The existence of two peaks, rather than a single one, is established with a significance of 6.5 standard deviations. The "right peak" has a mass of $6871.0 \pm 1.2(\text{stat}) \pm 0.8(\text{syst}) \pm 0.8(B_c^+)$ MeV, where the last term is the uncertainty in the B_c^+ mass, and is identified as the $B_c(2S)^\pm$ state, which decays directly to the $B_c^\pm$, emitting two (easy to detect) pions. The CMS observation, reported a couple of months after the end of the LHC Run 2, was soon followed by the corresponding LHCb result [35] (Fig. 77.2, top right panel), which confirmed the existence of the two states and reported a second measurement of the $B_c(2S)^\pm$ mass, $6872.1 \pm 1.3(\text{stat}) \pm 0.1(\text{syst}) \pm 0.8(B_c^+)$ MeV.

The "left peak" is interpreted as being the $B_c^*(2S)^\pm$ signal. It is observed at a mass lower than the real value because the experiments are unable to detect the low-energy photon emitted in the decay chain, $B_c^*(2S)^\pm \to B_c^{*\pm}\pi^+\pi^-$ followed by $B_c^{*\pm} \to B_c^\pm\gamma$ (Fig. 77.3). Its energy, expected to be in the range 40–80 MeV, leads to a very small probability that the photon converts into an e^+e^- pair and the two electrons are reconstructed. The relative ordering of the two peaks is based

Int. J. Mod. Phys. A 2026.41. Downloaded from www.worldscientific.com
UNIVERSITY OF CALIFORNIA @ BERKELEY on 09/16/26. Re-use and distribution is strictly not permitted, except for Open Access articles.

on a generally-agreed assumption: the $M(B_c^{*\pm}) - M(B_c^{\pm})$ mass difference is larger than the $M(B_c^*(2S)^{\pm}) - M(B_c(2S)^{\pm})$ difference. Naturally, these observations provide evidence for the existence of the $B_c^*(1S)^{\pm}$ state. They also provide measurements of two interesting mass differences, between the masses of the pseudoscalar mesons, $M(B_c(2S)^{\pm}) - M(B_c(1S)^{\pm}) = 596.1$ MeV, and of the vector mesons, $M(B_c^*(2S)^{\pm}) - M(B_c^*(1S)^{\pm}) = 567.0$ MeV (Fig. 77.3).

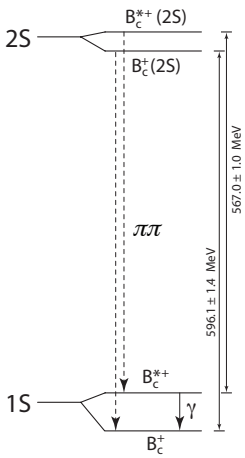

Figure 77.3: Diagram showing the decays mentioned in the text.

77.2 States Above Open-Flavor Threshold

Many states have been discovered both above and near the lowest open-flavor thresholds. They are displayed in Tables 77.2 and 77.3, respectively. With the exception of the $\psi_3(3842)$ and the tensor state located at 3930 MeV (now called $\chi_{c2}(3930)$), which have properties consistent with those expected for the $\psi_3(1^3D_3)$ and $\chi_{c2}(2^3P_2)$, respectively, none of these states can easily be assigned a place in the quark model spectrum of the charmonium or bottomonium families. The theoretical interpretation of these states remains under discussion.

77.2.1 *Charmonium*

Using proton-proton collisions, LHCb observed a narrow state, the $\psi_3(3842)$ resonance, in the decay modes $\psi_3(3842) \to D^0\bar{D}^0$ and D^+D^- [36]. The mass and width of this state are measured to be $3842.71 \pm 0.16 \pm 0.12$ MeV and $2.79 \pm 0.51 \pm 0.35$ MeV, respectively. The observed mass and narrow width are consistent with expectations for the spin-3 $\psi_3(1^3D_3)$ charmonium. Accordingly, the state is given the name $\psi_3(3842)$ in the listings, with the remark that the quantum numbers are fixed from the quark model and need to be confirmed.

The $\chi_{c2}(3930)$, which is a natural candidate for the $\chi_{c2}(2^3P_2)$ quark model state, was originally seen by Belle [37] and later confirmed by BaBar [38] in the $\gamma\gamma$ process $e^+e^- \to e^+e^-D\bar{D}$. This interpretation was strengthened by the more recent LHCb observation of the $\chi_{c2}(3930)$ alongside the $\psi_3(3842)$ in proton-proton collisions [36].

Unlike the $\chi_{c2}(2^3P_2)$, the identification of the $\chi_{c0}(2^3P_0)$ quark model state remains controversial. The original candidate was the $\chi_{c0}(3915)$, discovered by Belle in the $\gamma\gamma$ process $e^+e^- \to e^+e^-\omega J/\psi(1S)$ [39]. In a subsequent measurement by BaBar, its quantum numbers were determined to be $J^{PC} = 0^{++}$ [40]. However, its identification as the $\chi_{c0}(2^3P_0)$ quark model state was soon challenged [41, 42]. In addition, it was pointed out in Ref. [43] that if the assumption of helicity-2 dominance is abandoned and, instead, one allows for a sizeable helicity-0 component, a $J^{PC} = 2^{++}$ assignment is possible. This could imply that it is the same as the $\chi_{c2}(3930)$, but to explain the large helicity-0 component a sizable portion of non-$q\bar{q}$ is necessary [43]. A more recent LHCb amplitude analysis of the process $B^+ \to D^+D^-K^+$ finds distinct 0^{++} and 2^{++} components decaying to D^+D^- [44], which are currently identified in the listings as the $\chi_{c0}(3915)$ and $\chi_{c2}(3930)$, respectively.

An alternative candidate for the $\chi_{c0}(2^3P_0)$ (here referred to as the $\chi_{c0}(3860)$) was reported in Ref. [45] with properties more consistent with expectation: its mass is close to the potential model expectations, it decays to $D\bar{D}$, and the preferred quantum numbers are $J^{PC} = 0^{++}$ (this hypothesis is favored over the 2^{++} one with a 2.5σ significance).

In the excited vector charmonium spectrum, the $\psi(4040)$, $\psi(4160)$, and $\psi(4415)$ are prominent in the inclusive e^+e^- hadronic cross section and are naturally identified as the 3^3S_1, 2^3D_1, and 4^3S_1 $c\bar{c}$ quark model states, respectively. In addition to these long-established states, however, another set of peaks has been found in exclusive e^+e^- cross sections. Unlike conventional vector charmonia, they do not appear in the inclusive hadronic cross section and they apparently do not decay to $D^{(*)}\bar{D}^{(*)}$. The PDG summary table currently lists the $\psi(4230)$, $\psi(4360)$, and $\psi(4660)$ within this category. The first of these to be discovered was originally known as the $Y(4260)$ (now the $\psi(4230)$), seen by BaBar [46] and Belle [47, 48] in $e^+e^- \to \pi^+\pi^-J/\psi(1S)$ using initial state radiation. In a more recent high-statistics scan of $e^+e^- \to \pi^+\pi^-J/\psi(1S)$, BESIII demonstrated that the lineshape in this mass range is highly non-trivial [49]. The latter observation was interpreted by the authors as the presence of two states. This interpretation was supported by the coupled-channel analysis in Ref. [50]. However, this lineshape is also consistent with other possible interpretations, such as one assuming a molecular structure for the $\psi(4230)$ [51,52]. The data of Ref. [49] also called for a significant downward shift of the mass of what was originally called the $Y(4260)$, making it consistent with the masses (but not necessarily the widths) of peaks in other exclusive cross sections, such as $h_c(1P)\pi\pi$ [53]. We thus merged the original $Y(4260)$ (or, more formally, the $\psi(4260)$) with the $\psi(4230)$ in the listings.

BESIII observed the $\chi_{c1}(3872)$, also known as $X(3872)$, in $e^+e^- \to \gamma\chi_{c1}(3872)$ in the $\psi(4230)$ mass range [54], which could allow for additional insight into the structure of both states (see the review "Heavy non-$q\bar{q}$ mesons"). BESIII also performed a recent study of the process $e^+e^- \to \pi^+\pi^-\psi(2S)$ and found evidence for a lower mass state, possibly the $\psi(4230)$, in addition to the more dominant $\psi(4360)$ [55].

Another interesting question is whether a heavier $\pi^+\pi^-\psi(2S)$ state, the $\psi(4660)$, discovered by Belle [56, 57] and confirmed by BaBar [58], is identical to the $\Lambda_c^+\bar{\Lambda}_c^-$ resonance observed by Belle with a nearby mass and width [59]. Most probably it is, the $\Lambda_c^+\bar{\Lambda}_c^-$ being one more decay mode of the $\psi(4660)$ (see the review "Heavy non-$q\bar{q}$ mesons" for more details). Note that this is the interpretation adopted in the particle listings. In addition, Belle reported the first observation of a vector charmonium-like state decaying to $D_s^+D_{s1}(2536)$ with a significance of 5.9σ [60]. Its measured mass and width are $4625.9^{+6.2}_{-6.0} \pm 0.4$ MeV and $49.8^{+13.9}_{-11.5} \pm 4.0$ MeV, respectively, consistent with those of the $\psi(4660)$. Therefore, $D_s^+D_{s1}(2536)$ appears as an additional decay mode of the $\psi(4660)$ in the listings.

A series of isovector states[1] containing $c\bar{c}$ have been found in B decays to $K\pi(c\bar{c})$, where the isovector state decays to $\pi(c\bar{c})$ and $(c\bar{c})$ stands for $J/\psi(1S)$, $\psi(2S)$, or $\chi_{c1}(1P)$. They are manifestly non-$q\bar{q}$. The $T_{c\bar{c}1}(4430)$ (originally called the $Z_c(4430)$), decaying to $\pi\psi(2S)$, is the most well established state in this group. Based on a full amplitude analysis of $B^0 \to K^+\pi^-\psi(2S)$ decays, Belle determined the spin-parity of the $T_{c\bar{c}1}(4430)$ to be $J^P = 1^+$ [61]. From their study of $B^0 \to K^+\pi^-J/\psi(1S)$ decays, Belle also found evidence for the decay mode $T_{c\bar{c}1}(4430) \to \pi J/\psi(1S)$ [62], which has an order of magnitude lower branching fraction than the discovery mode $T_{c\bar{c}1}(4430) \to \pi\psi(2S)$. In the same analysis, Belle reported evidence for one more charged state, dubbed $T_{c\bar{c}1}(4200)$, decaying to $\pi J/\psi(1S)$. The observation of the $T_{c\bar{c}1}(4430)$ in $\pi\psi(2S)$, as well as its quantum number assignments, were confirmed by LHCb [63] with a much larger data sample, leading to improved mass and width values, consistent with earlier measurements; the experiment even reports a resonant behavior of the $T_{c\bar{c}1}(4430)$ amplitude. The $T_{c\bar{c}1}(4430)$ was not confirmed (or excluded) by BaBar [64].

[1] These isovector states were originally called Z_c. They are now referred

Int. J. Mod. Phys. A 2026.41. Downloaded from www.worldscientific.com
by UNIVERSITY OF CALIFORNIA @ BERKELEY on 09/16/26. Re-use and distribution is strictly not permitted, except for Open Access articles.

Table 77.2: As in Table 77.1, but for states above the first open-flavor thresholds in the $c\bar{c}$ and $b\bar{b}$ regions, ordered by mass.

PDG Name	Former Name(s)	m (MeV)	Γ (MeV)	$I^G(J^{PC})$	Production	Decay	Discovery Year	Summary Table
$\psi_3(3842)$		3842.71 ± 0.20	2.79 ± 0.62	$0^-(3^{--})^*$	$pp \to X...$	$D\bar{D}$	2019	YES
$\chi_{c0}(3860)$		3862^{+48}_{-35}	201^{+177}_{-106}	$0^+(0^{++})$	$e^+e^- \to J/\psi(1S)X$	$D\bar{D}$	2017	NO
$\chi_{c0}(3915)$	$X(3915)$, $Y(3940)$	3922.1 ± 1.8	20 ± 4	$0^+(0^{++})$	$B \to KX$ $e^+e^- \to e^+e^-X$	$\omega J/\psi(1S)$ $D\bar{D}$	2004	YES
$\chi_{c2}(3930)$	$\chi_{c2}(2P)$, $Z(3930)$	3922.5 ± 1.0	35.2 ± 2.2	$0^+(2^{++})$	$e^+e^- \to e^+e^-X$	$D\bar{D}$	2005	YES
$X(3940)$		3942 ± 9	43^{+28}_{-18}	$?^?(?^{??})$	$e^+e^- \to J/\psi(1S)X$ $B^+ \to K^+X$	$D\bar{D}^*$	2007	NO
$T_{c\bar{c}}(4050)$	$Z_1(4050)$ $X(4050)$	4051^{+24}_{-43}	82^{+51}_{-28}	$1^-(?^{?+})$	$\bar{B}^0 \to K^-X$	$\pi^+\chi_{c1}(1P)$	2008	NO
$T_{c\bar{c}}(4055)$	$Z_c(4055)$ $X(4055)$	4054 ± 3	45 ± 13	$1^+(?^{?-})$	$e^+e^- \to \pi^-X$	$\pi^+\psi(2S)$	2015	NO
$T_{c\bar{c}}(4100)$	$X(4100)$	4096^{+27}_{-30}	152^{+83}_{-68}	$1^-(?^{?+})$	$\bar{B}^0 \to K^-X$	$\pi^+\eta_c(1S)$	2018	NO
$\chi_{c1}(4140)$	$Y(4140)$	4146.5 ± 3.0	19^{+7}_{-5}	$0^+(1^{++})$	$B^+ \to K^+X$	$\phi J/\psi(1S)$	2009	YES
$X(4160)$		4153^{+23}_{-21}	136^{+60}_{-35}	$?^?(?^{??})$	$e^+e^- \to J/\psi(1S)X$ $B^+ \to K^+X$	$D^*\bar{D}^*$ $\phi J/\psi(1S)$	2007	NO
$T_{c\bar{c}1}(4200)$	$Z_c(4200)$	4242 ± 26	310 ± 40	$1^+(1^{+-})$	$\bar{B}^0 \to K^-X$	$J/\psi(1S)\pi^+$	2014	NO
$\psi(4230)$	$Y(4230)$ $Y(4260)$	4221.7 ± 2.5	51 ± 7	$0^-(1^{--})$	$e^+e^- \to X$	$\pi^+\pi^-J/\psi(1S)$ $\omega\chi_{c0}(1P)$ $\pi^+\pi^-h_c(1P)$ (see listings)	2015	YES
$T_{c\bar{c}0}(4240)$	$Z_c(4240)$ $R_{c0}(4240)$	4239^{+48}_{-21}	220^{+118}_{-88}	$1^+(0^{--})$	$\bar{B}^0 \to K^-X$	$\pi^+\psi(2S)$	2014	NO
$T_{c\bar{c}}(4250)$	$Z_2(4250)$ $X(4250)$	4248^{+185}_{-45}	177^{+321}_{-72}	$1^-(?^{?+})$	$\bar{B}^0 \to K^-X$	$\pi^+\chi_{c1}(1P)$	2008	NO
$\chi_{c1}(4274)$	$Y(4274)$	4290 ± 6	54 ± 8	$0^+(1^{++})$	$B^+ \to K^+X$ $pp \to ppX$	$\phi J/\psi(1S)$	2011	YES
$X(4350)$		$4350.6^{+4.7}_{-5.1}$	13^{+18}_{-10}	$0^+(?^{?+})$	$e^+e^- \to e^+e^-X$	$\phi J/\psi(1S)$	2009	NO
$\psi(4360)$	$Y(4360)$	4373 ± 7	124 ± 13	$0^-(1^{--})$	$e^+e^- \to X$	$\pi^+\pi^-\psi(2S)$ (see listings)	2007	YES
$T_{c\bar{c}1}(4430)$	$Z_c(4430)$	4478^{+15}_{-17}	189 ± 29	$1^+(1^{+-})$	$\bar{B}^0 \to K^-X$	$\pi^+\psi(2S)$ $\pi^+J/\psi(1S)$	2007	YES
$\chi_{c0}(4500)$	$X(4500)$	4484 ± 12	87^{+30}_{-24}	$0^+(0^{++})$	$B^+ \to K^+X$ $pp \to ppX$	$\phi J/\psi(1S)$	2017	YES
$X(4630)$		4636^{+29}_{-100}	350^{+140}_{-100}	$0^+(?^{?+})$	$B^+ \to K^+X$	$\phi J/\psi(1S)$	2021	NO
$\psi(4660)$	$Y(4660)$,	4623 ± 10	55 ± 9	$0^-(1^{--})$	$e^+e^- \to X$	$\pi^+\pi^-\psi(2S)$ $D_s^+D_{s1}(2536)$ (see listings)	2007	YES
$\chi_{c1}(4685)$		4677^{+13}_{-15}	180 ± 50	$0^+(1^{++})$	$B^+ \to K^+X$	$\phi J/\psi(1S)$	2021	NO
$\chi_{c0}(4700)$	$X(4700)$	4708^{+6}_{-4}	78^{+15}_{-11}	$0^+(0^{++})$	$B^+ \to K^+X$	$\phi J/\psi(1S)$	2017	NO
$T_{cc\bar{c}\bar{c}}(6600)$		6646^{+28}_{-25}	440 ± 70	$0^+(2^{++})$	$pp \to X...$	$J/\psi(1S)J/\psi(1S)$	2023	NO
$T_{cc\bar{c}\bar{c}}(6900)$	$X(6900)$	6898 ± 12	161 ± 26	$0^+(2^{++})$	$pp \to X...$	$J/\psi(1S)J/\psi(1S)$	2020	YES
$T_{cc\bar{c}\bar{c}}(7100)$		7134^{+63}_{-29}	97^{+49}_{-39}	$0^+(2^{++})$	$pp \to X...$	$J/\psi(1S)J/\psi(1S)$	2024	NO
$\Upsilon(10753)$		10756.6 ± 2.8	29 ± 9	$?^?(1^{--})$	$e^+e^- \to X$	$\pi\pi\Upsilon(1S, 2S, 3S)$	2019	NO

*Quantum numbers fixed from the quark model and need confirmation.

Belle also reported an observation of two charged states decaying to $\pi\chi_{c1}(1P)$ in an analysis of $B^0 \to K^+\pi^-\chi_{c1}(1P)$ decays [65]. These were originally called $Z_1(4050)^\pm$ and $Z_2(4250)^\pm$, but are referred to in Table 77.2 as $T_{c\bar{c}}(4050)$ and $T_{c\bar{c}}(4250)$. These states were not confirmed by BaBar [66]. Belle observes signals with 5.0σ significance for both the $T_{c\bar{c}}(4050)$ and $T_{c\bar{c}}(4250)$, whereas BaBar reports 1.1σ and 2.0σ effects, respectively, setting upper limits that are not inconsistent with Belle's measured rates. The situation remains unresolved.

The decay $B^+ \to K^+\phi J/\psi(1S)$ appears to be especially rich in resonant substructure. The $Y(4140)$ (now the $\chi_{c1}(4140)$), decaying to $\phi J/\psi(1S)$, was first observed in 2008 by CDF [67, 68], and confirmed by D0 and CMS [69, 70]. However, a second structure, the $Y(4274)$ (now the $\chi_{c1}(4274)$), could not be established unambiguously. Neither of the two states was seen in B decays at Belle [71], LHCb [72] and BaBar [73], or in $\gamma\gamma$ collisions at Belle [74]. The real breakthrough happened when LHCb performed a full amplitude analysis of $B^+ \to K^+\phi J/\psi(1S)$ with $J/\psi(1S) \to \mu^+\mu^-$, $\phi \to K^+K^-$ decays and showed that the data cannot be described in a model that contains only excited kaon states decaying into $K^+\phi$ [75, 76]. They observe two 1^{++} states with masses close to those originally reported by CDF (the $\chi_{c1}(4140)$ and $\chi_{c1}(4274)$), but the width of the one at 4140 MeV is much larger. In addition, they find two significant 0^{++} structures

to as $T_{c\bar{c}}$. See the "Naming scheme for hadrons" review.

Int. J. Mod. Phys. A 2026.41. Downloaded from www.worldscientific.com
UNIVERSITY OF CALIFORNIA @ BERKELEY on 09/16/26. Re-use and distribution is strictly not permitted, except for Open Access articles.

at 4500 and 4700 MeV (the $\chi_{c0}(4500)$ and $\chi_{c0}(4700)$). The LHCb analysis was extended even further in Ref. [77] with a factor of six increase in statistics: the $\chi_{c1}(4140)$, $\chi_{c1}(4274)$, $\chi_{c0}(4500)$, and $\chi_{c0}(4700)$ were confirmed, and two new states, the $X(4630)$ and $\chi_{c1}(4685)$ were reported, also decaying to $\phi J/\psi(1S)$. Note that the properties (or even the existence) of these states are sensitive to the parameterization of the amplitudes and, in particular, to the treatment of thresholds [78].

77.2.2 *Resonances in the $J/\psi(1S)$-pair mass spectrum*

Based on proton-proton event samples collected at $\sqrt{s} = 7$, 8 and 13 TeV, corresponding to an integrated luminosity of 9 fb^{-1}, the LHCb Collaboration reported the observation of a narrow structure in the invariant mass distribution of $J/\psi(1S)$ pairs [79]. The new resonance, denoted as $T_{cc\bar{c}\bar{c}}(6900)$ (also $X(6900)$), is clearly seen at a mass of 6.9 GeV in the bottom panel of Fig. 77.4, as indicated by the red curve. The ATLAS Collaboration has also

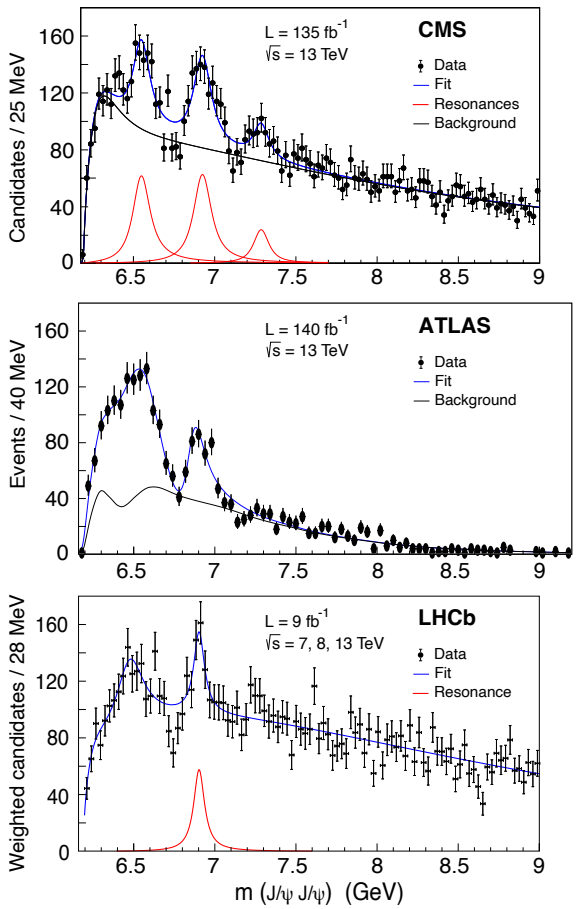

Figure 77.4: $J/\psi(1S)$-pair invariant mass distributions measured by the LHCb [79] (bottom), ATLAS [80] (middle), and CMS [81] (top) experiments.

observed the $T_{cc\bar{c}\bar{c}}(6900)$ resonance in the di-$J/\psi(1S)$ mass spectrum, using 140 fb^{-1} of pp collisions at $\sqrt{s} = 13$ TeV [80], as can be seen in the middle panel of Fig. 77.4. More recently, also the CMS Collaboration reported the observation of the $T_{cc\bar{c}\bar{c}}(6900)$ in the $J/\psi(1S)$-pair mass distribution, using 135 fb^{-1} of 13 TeV pp collisions [81]. Thanks to its good mass resolution and relatively large event yields, CMS determined the mass and width of the $T_{cc\bar{c}\bar{c}}(6900)$ with the best precision among the three measurements. Furthermore, another resonance is seen with a significance exceeding 5 standard deviations, at a mass of 6.55 GeV, as shown in the top panel of Fig. 77.4. The measured values of the masses and widths of the new states depend on whether the model used to fit the distributions includes interference effects between the resonances and the underlying continuum (and also among the resonances). In addition, fits that incorporate the scattering of vector charmonia to explain the structure in the $J/\psi(1S)$-pair mass distribution indicate the possible existence of a state very close to the di-$J/\psi(1S)$ threshold [82–85]. The larger event samples presently being collected by the LHC experiments will surely lead to significantly improved measurements, as well as to complementary results (including determinations of spin-parity quantum numbers), so that one can expect near-future progress in our understanding of the nature of these "narrow structures".

77.2.3 *Bottomonium*

In 2019, Belle reported a measurement of the $e^+e^- \to \Upsilon(nS)\pi^+\pi^-$ ($n = 1, 2, 3$) cross sections at energies from 10.52 to 11.02 GeV [86]. They observed, with a 5.2σ significance, a new structure with a mass near 10753 MeV in the energy dependence of the cross sections. The observation of the $\Upsilon(10753)$ was confirmed by Belle II using a dedicated energy scan with a total integrated luminosity of 19 fb^{-1} [87]. If the combined Belle and Belle II data is described by a Breit–Wigner function, the mass and width of the $\Upsilon(10753)$ are $10756.6 \pm 2.7 \pm 0.9$ MeV and $29.0 \pm 8.8 \pm 1.2$ MeV, respectively. The $\Upsilon(10753)$ was also seen by Belle II in the process $e^+e^- \to \omega\chi_{bJ}(1P)$ using data from the same energy scan [88]. The new structure could have a resonant origin and correspond to the not yet observed $\Upsilon(3D)$ state, provided $S-D$ mixing is enhanced, or an exotic state, e.g., a compact tetraquark or hadrobottomonium. It could also be a non-resonant effect due to rescattering. The $\Upsilon(10753)$ was confirmed in a global K-matrix fit to exclusive and inclusive $e^+e^- \to b\bar{b}$ cross sections in Ref. [89].

We no longer mention a hypothetical $Y_b(10888)$ state since a new analysis of the $\Upsilon(10860)$ energy range does not show evidence for an additional state with a mass different from that of the $\Upsilon(10860)$ [90]. After the mass of the $\eta_b(1S)$ was shifted upwards by about 10 MeV based on the Belle measurements [23,24], all of the bottomonium states mentioned above fit into their respective spectroscopies, roughly where expected. An independent experimental confirmation of the shifted masses came from the Belle observation of $\Upsilon(4S) \to \eta h_b(1P)$ decays [24]. This process turns out to be the strongest observed transition of the $\Upsilon(4S)$ to lower bottomonium states.

77.3 States Near Open-Flavor Threshold

A number of states, listed in Table 77.3, appear near open-flavor thresholds, which is likely an important factor in their theoretical interpretation [91].

77.3.1 *Charmonium*

The $\chi_{c1}(3872)$, also known as $X(3872)$, is widely studied and seen in many transitions — see Table 77.3. Yet its interpretation remains unsettled (see the review "Heavy non-$q\bar{q}$ mesons"). Its unique experimental features include: it has $J^{PC} = 1^{++}$ [92,93], yet it is too light to be the $\chi_{c1}(2^3P_1)$ quark model state; its mass is within 200 keV of the $D^0\bar{D}^{0*}$ threshold; it shows substantial isospin-breaking in its decays to $\rho J/\psi(1S)$ and $\pi^0\chi_{c1}(1P)$; and it is extremely narrow. Using a large sample of inclusively produced $\chi_{c1}(3872)$ decaying to $\pi^+\pi^- J/\psi(1S)$, LHCb recently determined the decay width of the $\chi_{c1}(3872)$ under two different assumptions [94]. Assuming a Flatté-inspired line shape and exploiting the strong coupling of the $\chi_{c1}(3872)$ to $D^0\bar{D}^{*0}$, LHCb performed the first exploration of the pole structure of the $\chi_{c1}(3872)$, finding a FWHM width of $0.22^{+0.06+0.25}_{-0.08-0.17}$ MeV. On the other hand, assuming a Breit–Wigner line shape, its width was found to be $1.39 \pm 0.24 \pm 0.10$ MeV. While the former analysis has a more firm theoretical foundation, the LHCb detector resolution did not allow for a distinction between the different line shapes. More recently, BESIII studied the line shape of the $\chi_{c1}(3872)$ by simultaneously fitting the $e^+e^- \to \gamma\chi_{c1}(3872) \to \gamma\left[D^0\bar{D}^0\pi^0\right]$ and $\gamma\left[J/\psi\pi^+\pi^-\right]$ reactions [95]. Two poles were found on the first and second Riemann sheets corresponding to the $D^{*0}\bar{D}^0$ channel, the most prominent being at $(3871.70 \pm 0.15^{+0.07}_{-0.08}) - i(0.19 \pm 0.08^{+0.14}_{-0.19})$ MeV on the first sheet, confirming the sub-MeV width found by LHCb.

In addition to the $T_{c\bar{c}}$ (also known as Z_c) states found in B decays, discussed above, several isovector states with masses near

Int. J. Mod. Phys. A 2026.41. Downloaded from www.worldscientific.com
by UNIVERSITY OF CALIFORNIA @ BERKELEY on 09/16/26. Re-use and distribution is strictly not permitted, except for Open Access articles.

Table 77.3: As in Table 77.1, but for states near the first open-flavor thresholds in the $c\bar{c}$ and $b\bar{b}$ regions, ordered by mass. Updated from Ref. [96] with kind permission, copyright (2011), Springer, and from Ref. [12] with kind permission from the authors.

PDG Name	Former Name(s)	m (MeV)	Γ (MeV)	$I^G(J^{PC})$	Production	Decay	Discovery Year	Summary Table
$\chi_{c1}(3872)$	$X(3872)$	3871.64 ± 0.06	1.19 ± 0.21	$0^+(1^{++})$	$B\to KX$ $p\bar{p}\to X...$ $pp\to X...$ $e^+e^-\to\gamma X$ $e^+e^-\to\omega X$	$\pi^+\pi^-J/\psi(1S)$ $3\pi J/\psi(1S)$ $D^{*0}\bar{D}^0$ $\gamma J/\psi(1S)$ $\gamma\psi(2S)$ $\pi^0\chi_{c1}(1P)$	2003	YES
$T_{cc}(3875)$		3874.74 ± 0.10	$0.048^{+0.002}_{-0.014}$	$?(?^?)$	$pp\to X...$	$D^0D^0\pi$	2022	NO
$T_{c\bar{c}1}(3900)$	$Z_c(3900)$	3886.7 ± 2.3	29.5 ± 2.4	$1^+(1^{+-})$	$\psi(4230)\to\pi^-X$ $\psi(4230)\to\pi^0X$	$\pi^+J/\psi(1S)$ $\pi^0J/\psi(1S)$ $(D\bar{D}^*)^+$ $(D\bar{D}^*)^0$	2013	YES
$T_{c\bar{c}\bar{s}1}(4000)$	$Z_{cs}(4000)$	$3980-4010$	$5-150$	$\frac{1}{2}(1^+)$	$e^+e^-\to KX$ $B^+\to\phi X$	$D_sD^*+D_s^*D$ $K^+J/\psi(1S)$	2021	NO
$T_{c\bar{c}}(4020)$	$Z_c(4020)$ $X(4020)$	4024.1 ± 1.9	13 ± 5	$1^+(?^{?-})$	$\psi(4230,4360)\to\pi^-X$ $\psi(4230,4360)\to\pi^0X$	$\pi^+h_c(1P)$ $\pi^0h_c(1P)$ $(D^*\bar{D}^*)^+$ $(D^*\bar{D}^*)^0$	2013	YES
$T_{c\bar{c}\bar{s}1}(4220)$	$Z_{cs}(4220)$	4216^{+49}_{-38}	233^{+110}_{-90}	$\frac{1}{2}(1^+)$	$B^+\to\phi X$	$K^+J/\psi(1S)$	2021	NO
$T_{b\bar{b}1}(10610)$	$Z_b(10610)$	10607.2 ± 2.0	18.4 ± 2.4	$1^+(1^{+-})$	$\Upsilon(10860)\to\pi^-X$ $\Upsilon(10860)\to\pi^0X$	$\pi^+\Upsilon(1S,2S,3S)$ $\pi^0\Upsilon(1S,2S,3S)$ $\pi^+h_b(1P,2P)$ $(B\bar{B}^*)^+$	2011	YES
$T_{b\bar{b}1}(10650)$	$Z_b(10650)$	10652.2 ± 1.5	11.5 ± 2.2	$1^+(1^{+-})$	$\Upsilon(10860)\to\pi^-X$	$\pi^+\Upsilon(1S,2S,3S)$ $\pi^+h_b(1P,2P)$ $(B^*\bar{B}^*)^+$	2011	YES

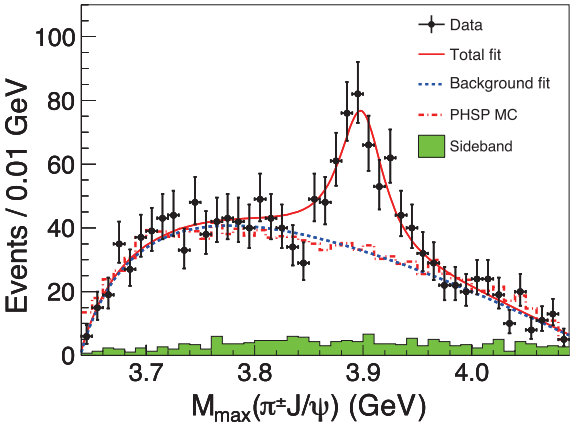

Figure 77.5: The $\pi^\pm J/\psi(1S)$ invariant mass distribution from BESIII [97] e^+e^- collision data taken at a center-of-mass energy near 4260 MeV.

$D\bar{D}^*$ and $D^*\bar{D}^*$ thresholds appear to be unique to e^+e^- annihilation. In 2013, a state named $T_{c\bar{c}1}(3900)$ (originally $Z_c(3900)$) was unearthed in the charmonium region at BESIII [97] and Belle [48] in the process $e^+e^-\to\pi^\mp T_{c\bar{c}1}(3900)^\pm$ with $T_{c\bar{c}1}(3900)^\pm\to\pi^\pm J/\psi(1S)$. The corresponding spectrum from BESIII is shown in Fig. 77.5. An analysis of CLEO data [98] confirmed this finding and also provided evidence for a neutral partner. A nearby signal was also seen in the $D\bar{D}^*$ channel [99] whose quantum numbers were fixed to 1^{+-}. BESIII reported its neutral partner in both $J/\psi(1S)\pi^0$ [100] and $D\bar{D}^*$ [101] decay modes. The masses extracted from these experiments in different decay modes agree within 2σ. However, since the extraction of the mass and width parameters did not allow for an interference with the background and Breit–Wigner line shapes are used, which is not justified near thresholds, there might be some additional systematic uncertainty in the mass values. Therefore, in the RPP listings as well as in Table 77.3 both structures appear under the name $T_{c\bar{c}1}(3900)$. BESIII also reported the observation of another charged state, the $T_{c\bar{c}}(4020)^\pm$ (originally called $Z_c(4020)^\pm$), in two decay modes: $h_c(1P)\pi^\pm$ [102] and $(D^*\bar{D}^*)^\pm$ [103]. The neutral partners have also been observed by BESIII in the $h_c(1P)\pi^0$ [104] and $(D^*\bar{D}^*)^0$ [105] final states. The $T_{c\bar{c}}$ states show some remarkable similarities to the $T_{b\bar{b}}$ states (discussed below), e.g. they decay dominantly to $D^{(*)}\bar{D}^*$ channels. However, current analyses suggest that the mass of the $T_{c\bar{c}1}(3900)$ might be somewhat above the $D\bar{D}^*$ threshold. If confirmed, this feature would challenge a possible $D\bar{D}^*$–molecular interpretation with S-wave interactions only — prominent D-waves can shift molecular poles above threshold (see the discussion in Sec. 77.3.3). Finally, 3.5σ evidence for one more charged charmonium-like state at 4055 MeV decaying into $\psi(2S)\pi^\pm$ was reported by Belle in their analysis of the process $e^+e^-\to\psi(2S)\pi^+\pi^-$ [57]. The same process was studied by BESIII, where there appears to be complications in the Dalitz plot requiring further investigation [55].

An isospin-1/2 state with open strangeness, the $T_{c\bar{c}\bar{s}1}(4000)$, has been reported near D_sD^* threshold by both BESIII [106,107] and LHCb [77]. BESIII observes the charged $T_{c\bar{c}\bar{s}1}(4000)$ in the process $e^+e^-\to K^+(D_s^-D^{*0}+D_s^{*-}D^0)$ [106] and the neutral $T_{c\bar{c}\bar{s}1}(4000)$ in the process $e^+e^-\to K_S(D_s^-D^{*+}+D_s^{*-}D^+)$ [107]. LHCb observes the charged version in $B^+\to\phi(K^+J/\psi(1S))$ [77], although with a much larger decay width. The same LHCb analysis also finds a higher mass $T_{c\bar{c}\bar{s}}$ candidate, the $T_{c\bar{c}\bar{s}1}(4220)$. A search by BESIII for a heavier partner $T'_{c\bar{c}\bar{s}}$ near $D_s^*D^*$ threshold was negative [108].

77.3.2 *Double Charm*

The most striking recent result, however, is due to the observation by LHCb [109, 110] of a doubly charmed state, the $T_{cc}(3875)^+$, in the inclusive cross section of $D^{*+}D^0\to D^0D^0\pi^+$ (see Fig. 77.6). The statistical significance is overwhelming, the minimal quark content is $cc\bar{u}\bar{d}$, and the width is approximately what would be expected for an isoscalar ground state having $J^P=1^+$. The integrated luminosity used in this study was 9 fb^{-1}. The larger integrated luminosity of the event sample to be collected by the end of the LHC Run 3, together with improved analysis techniques, might bring the T_{bc} states within reach.

Int. J. Mod. Phys. A 2026.41. Downloaded from www.worldscientific.com
UNIVERSITY OF CALIFORNIA @ BERKELEY on 09/16/26. Re-use and distribution is strictly not permitted, except for Open Access articles.

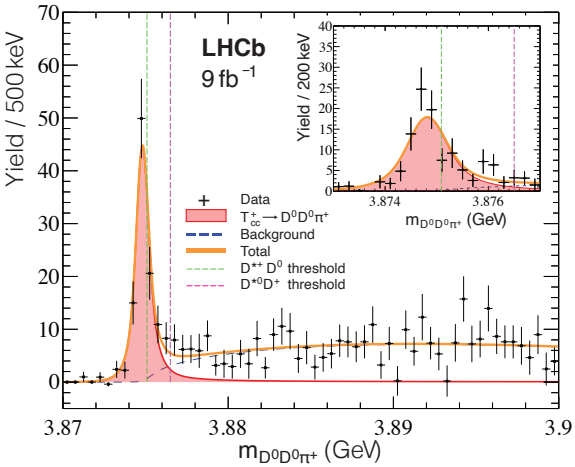

Figure 77.6: The $D^0D^0\pi^+$ invariant mass distribution from LHCb [109, 110].

77.3.3 *Bottomonium*

New results on the η_b, h_b, and $T_{b\bar{b}}$ mostly come from Belle [23,24,26,28,90,111–117], all from analyses of 121.4 fb^{-1} of e^+e^- collision data collected near the peak of the $\Upsilon(10860)$ resonance, as well as from an additional 25 fb^{-1} of data collected during the scans of the c.m. energy range 10.63–11.05 GeV. The η_b, h_b, and $T_{b\bar{b}}$ appear in the decay chains $\Upsilon(10860) \to \pi^- T_{b\bar{b}}^+$, $T_{b\bar{b}}^+ \to \pi^+(b\bar{b})$, and, when the $b\bar{b}$ forms an $h_b(1P)$, frequently decaying as $h_b(1P) \to \gamma\eta_b$.

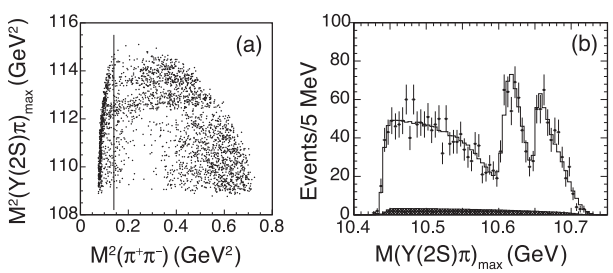

Figure 77.7: From Belle [111] e^+e^- collision data taken near the peak of the $\Upsilon(10860)$ for events with a $\pi^+\pi^-$-missing mass consistent with an $\Upsilon(2S) \to \mu^+\mu^-$, (a) the maximum of the two possible single $\pi^\pm$-missing-mass-squared combinations vs. the $\pi^+\pi^-$-mass-squared; and (b) projection of the maximum of the two possible single $\pi^\pm$-missing-mass combinations overlaid with a fit (*curve*). Events to the left of the vertical line in (a) are excluded from the amplitude analysis. The hatched histogram in (b) corresponds to the combinatorial background. The two horizontal stripes in (a) and two peaks in (b) correspond to the two $T_{b\bar{b}}$ states.

Belle soon noticed that, for events in the peaks of Fig. 77.1 corresponding to the processes $e^+e^- \to \pi^+\pi^-\Upsilon(1S, 2S, 3S)$ and $\pi^+\pi^- h_b(1P, 2P)$, there seemed to be two intermediate charged states in the $\pi^\pm\Upsilon$ and $\pi^\pm h_b$ channels, called the $T_{b\bar{b}}(10610)$ and the $T_{b\bar{b}}(10650)$. For example, Fig. 77.7 shows a Dalitz plot for events restricted to the $\Upsilon(2S)$ region of $\pi^+\pi^-$ recoil mass, with $\Upsilon(2S) \to \mu^+\mu^-$ [111]. The two bands observed in the maximum of the two $M[\pi^\pm\Upsilon(2S)]^2$ values also appear in the $\Upsilon(1S)$, $\Upsilon(3S)$, $h_b(1P)$, and $h_b(2P)$ samples. Belle fits all subsamples to resonant plus non-resonant amplitudes, allowing for interference (notably, between $\pi^- T_{b\bar{b}}^+$ and $\pi^+ T_{b\bar{b}}^-$), and finds consistent pairs of $T_{b\bar{b}}$ masses for all bottomonium transitions, and comparable strengths of the two states. A recent angular analysis assigned $J^P = 1^+$ for both $T_{b\bar{b}}$ states [112], which must also have negative G-parity. Transitions through $T_{b\bar{b}}$ to the $h_b(nP)$ saturate the observed $\pi^+\pi^- h_b(nP)$ cross sections. While the two masses of the $T_{b\bar{b}}$ states as extracted from Breit–Wigner fits for the various channels are just a few MeV above the $B^*\bar{B}$ and $B^*\bar{B}^*$ thresholds, more refined analyses using only S-waves find pole locations right below the corresponding thresholds either on the physical [118] or the unphysical [119] sheet. Once D-waves are included, the pole of the $T_{b\bar{b}}(10650)$ moves above the $B^*\bar{B}^*$ threshold [120]. Regardless of their proximity to the corresponding thresholds, both states predominantly decay into these open-flavor channels [114, 121] with branching fractions that exceed 80% and 70%, respectively, at 90% CL. This feature provides strong evidence for their molecular nature.

77.4 Concluding Remarks

The discovery of the $\chi_{c1}(3872)$ (also known as the $X(3872)$) in 2003 ushered in an era of tremendous progress in experimental heavy quark meson spectroscopy, even though many issues remain unsettled. As shown in Tables 77.1 to 77.3, more than 40 new states have been reported during this period, many of which were unanticipated. While the states below open-flavor thresholds (Table 77.1) appear to be well-explained by the conventional $q\bar{q}$ quark model, a thorough understanding of the suite of states above (Table 77.2) and near (Table 77.3) open-flavor thresholds remains elusive. After nearly two decades, experimental progress remains rapid with the continuation of BESIII, the commencement of the Belle II program, and the imminent accumulation of additional data at the LHC.

Acknowledgements

We thank Alexander Bondar and Christoph Hanhart for carefully reading the manuscript and for detailed and constructive suggestions.

References

[1] N. Brambilla *et al.*, Phys. Rept. **873**, 1 (2020), [arXiv:1907.07583].

[2] Y.-R. Liu *et al.*, Prog. Part. Nucl. Phys. **107**, 237 (2019), [arXiv:1903.11976].

[3] S. L. Olsen, T. Skwarnicki and D. Zieminska, Rev. Mod. Phys. **90**, 1, 015003 (2018), [arXiv:1708.04012].

[4] A. Ali, J. S. Lange and S. Stone, Prog. Part. Nucl. Phys. **97**, 123 (2017), [arXiv:1706.00610].

[5] F.-K. Guo *et al.*, Rev. Mod. Phys. **90**, 1, 015004 (2018), [arXiv:1705.00141].

[6] R. F. Lebed, R. E. Mitchell and E. S. Swanson, Prog. Part. Nucl. Phys. **93**, 143 (2017), [arXiv:1610.04528].

[7] A. E. Bondar, R. V. Mizuk and M. B. Voloshin, Mod. Phys. Lett. A **32**, 04, 1750025 (2017), [arXiv:1610.01102].

[8] H.-X. Chen *et al.*, Rept. Prog. Phys. **86**, 2, 026201 (2023), [arXiv:2204.02649].

[9] M. Mai, U.-G. Meißner and C. Urbach, Phys. Rept. **1001**, 1 (2023), [arXiv:2206.01477].

[10] N. Hüsken, E. S. Norella and I. Polyakov, Mod. Phys. Lett. A **40**, 17n18, 2530002 (2025), [arXiv:2410.06923].

[11] S. K. Choi *et al.* (Belle), Phys. Rev. Lett. **91**, 262001 (2003), [hep-ex/0309032].

[12] N. Brambilla *et al.*, Eur. Phys. J. **C74**, 10, 2981 (2014), [arXiv:1404.3723].

[13] J. L. Rosner *et al.* (CLEO), Phys. Rev. Lett. **95**, 102003 (2005), [hep-ex/0505073].

[14] M. Ablikim *et al.* (BESIII), Phys. Rev. D **99**, 7, 072008 (2019), [arXiv:1810.12023].

[15] M. Ablikim *et al.* (BESIII), Phys. Rev. D **102**, 112007 (2020), [arXiv:2010.12092].

[16] M. Ablikim *et al.* (BESIII), JHEP **05**, 108 (2022), [Erratum: JHEP 03, 022 (2023)], [arXiv:2203.10439].

[17] V. Bhardwaj *et al.* (Belle), Phys. Rev. Lett. **111**, 3, 032001 (2013), [arXiv:1304.3975].

[18] M. Ablikim *et al.* (BESIII), Phys. Rev. Lett. **115**, 1, 011803 (2015), [arXiv:1503.08203].

Int. J. Mod. Phys. A 2026.41. Downloaded from www.worldscientific.com
by UNIVERSITY OF CALIFORNIA @ BERKELEY on 09/16/26. Re-use and distribution is strictly not permitted, except for Open Access articles.

[19] M. Ablikim *et al.* (BESIII), Phys. Rev. Lett. **129**, 10, 102003 (2022), [arXiv:2203.05815].

[20] K. Chilikin *et al.* (Belle), JHEP **05**, 034 (2020), [arXiv:2003.08335].

[21] B. Aubert *et al.* (BaBar), Phys. Rev. Lett. **101**, 071801 (2008), [Erratum: Phys.Rev.Lett. 102, 029901 (2009)], [arXiv:0807.1086].

[22] B. Aubert *et al.* (BaBar), Phys. Rev. Lett. **103**, 161801 (2009), [arXiv:0903.1124].

[23] R. Mizuk *et al.* (Belle), Phys. Rev. Lett. **109**, 232002 (2012), [arXiv:1205.6351].

[24] U. Tamponi *et al.* (Belle), Phys. Rev. Lett. **115**, 14, 142001 (2015), [arXiv:1506.08914].

[25] B. G. Fulsom *et al.* (Belle), Phys. Rev. Lett. **121**, 23, 232001 (2018), [arXiv:1807.01201].

[26] I. Adachi *et al.* (Belle), Phys. Rev. Lett. **108**, 032001 (2012), [arXiv:1103.3419].

[27] T. K. Pedlar *et al.* (CLEO), Phys. Rev. Lett. **107**, 041803 (2011), [arXiv:1104.2025].

[28] I. Adachi (Belle), in "8th International Workshop On Heavy Quarkonium (QWG2011) Darmstadt, Germany, October 3-7, 2011," (2011), [arXiv:1110.3934].

[29] G. Aad *et al.* (ATLAS), Phys. Rev. Lett. **108**, 152001 (2012), [arXiv:1112.5154].

[30] V. M. Abazov *et al.* (D0), Phys. Rev. D **86**, 031103 (2012), [arXiv:1203.6034].

[31] R. Aaij *et al.* (LHCb), JHEP **10**, 088 (2014), [arXiv:1409.1408].

[32] A. M. Sirunyan *et al.* (CMS), Phys. Rev. Lett. **121**, 092002 (2018), [arXiv:1805.11192].

[33] G. Aad *et al.* (ATLAS), Phys. Rev. Lett. **113**, 212004 (2014), [arXiv:1407.1032].

[34] A. M. Sirunyan *et al.* (CMS), Phys. Rev. Lett. **122**, 132001 (2019), [arXiv:1902.00571].

[35] R. Aaij *et al.* (LHCb), Phys. Rev. Lett. **122**, 232001 (2019), [arXiv:1904.00081].

[36] R. Aaij *et al.* (LHCb), JHEP **07**, 035 (2019), [arXiv:1903.12240].

[37] S. Uehara *et al.* (Belle), Phys. Rev. Lett. **96**, 082003 (2006), [hep-ex/0512035].

[38] B. Aubert *et al.* (BaBar), Phys. Rev. D **81**, 092003 (2010), [arXiv:1002.0281].

[39] K. Abe *et al.* (Belle), Phys. Rev. Lett. **94**, 182002 (2005), [hep-ex/0408126].

[40] J. P. Lees *et al.* (BaBar), Phys. Rev. **D86**, 072002 (2012), [arXiv:1207.2651].

[41] F.-K. Guo and U.-G. Meissner, Phys. Rev. **D86**, 091501 (2012), [arXiv:1208.1134].

[42] S. L. Olsen, Phys. Rev. **D91**, 5, 057501 (2015), [arXiv:1410.6534].

[43] Z.-Y. Zhou, Z. Xiao and H.-Q. Zhou, Phys. Rev. Lett. **115**, 2, 022001 (2015), [arXiv:1501.00879].

[44] R. Aaij *et al.* (LHCb), Phys. Rev. D **102**, 112003 (2020), [arXiv:2009.00026].

[45] K. Chilikin *et al.* (Belle), Phys. Rev. **D95**, 112003 (2017), [arXiv:1704.01872].

[46] B. Aubert *et al.* (BaBar), Phys. Rev. Lett. **95**, 142001 (2005), [hep-ex/0506081].

[47] C. Z. Yuan *et al.* (Belle), Phys. Rev. Lett. **99**, 182004 (2007), [arXiv:0707.2541].

[48] Z. Q. Liu *et al.* (Belle), Phys. Rev. Lett. **110**, 252002 (2013), [arXiv:1304.0121].

[49] M. Ablikim *et al.* (BESIII), Phys. Rev. Lett. **118**, 9, 092001 (2017), [arXiv:1611.01317].

[50] S. X. Nakamura *et al.*, Phys. Rev. D **112**, 5, 054027 (2025), [arXiv:2312.17658].

[51] M. Cleven *et al.*, Phys. Rev. **D90**, 7, 074039 (2014), [arXiv:1310.2190].

[52] L. von Detten *et al.*, Phys. Rev. D **109**, 11, 116002 (2024), [arXiv:2402.03057].

[53] M. Ablikim *et al.* (BESIII), Phys. Rev. Lett. **118**, 9, 092002 (2017), [arXiv:1610.07044].

[54] M. Ablikim *et al.* (BESIII), Phys. Rev. Lett. **112**, 9, 092001 (2014), [arXiv:1310.4101].

[55] M. Ablikim *et al.* (BESIII), Phys. Rev. **D96**, 3, 032004 (2017), [erratum: Phys. Rev.D99,no.1,019903(2019)], [arXiv:1703.08787].

[56] X. L. Wang *et al.* (Belle), Phys. Rev. Lett. **99**, 142002 (2007), [arXiv:0707.3699].

[57] X. L. Wang *et al.* (Belle), Phys. Rev. **D91**, 112007 (2015), [arXiv:1410.7641].

[58] J. P. Lees *et al.* (BaBar), Phys. Rev. **D89**, 11, 111103 (2014), [arXiv:1211.6271].

[59] G. Pakhlova *et al.* (Belle), Phys. Rev. Lett. **101**, 172001 (2008), [arXiv:0807.4458].

[60] S. Jia *et al.* (Belle), Phys. Rev. **D100**, 11, 111103 (2019), [arXiv:1911.00671].

[61] K. Chilikin *et al.* (Belle), Phys. Rev. **D88**, 7, 074026 (2013), [arXiv:1306.4894].

[62] K. Chilikin *et al.* (Belle), Phys. Rev. **D90**, 11, 112009 (2014), [arXiv:1408.6457].

[63] R. Aaij *et al.* (LHCb), Phys. Rev. Lett. **112**, 22, 222002 (2014), [arXiv:1404.1903].

[64] B. Aubert *et al.* (BaBar), Phys. Rev. **D79**, 112001 (2009), [arXiv:0811.0564].

[65] R. Mizuk *et al.* (Belle), Phys. Rev. **D78**, 072004 (2008), [arXiv:0806.4098].

[66] J. P. Lees *et al.* (BaBar), Phys. Rev. **D85**, 052003 (2012), [arXiv:1111.5919].

[67] T. Aaltonen *et al.* (CDF), Phys. Rev. Lett. **102**, 242002 (2009), [arXiv:0903.2229].

[68] T. Aaltonen *et al.* (CDF), Mod. Phys. Lett. **A32**, 26, 1750139 (2017), [arXiv:1101.6058].

[69] V. M. Abazov *et al.* (D0), Phys. Rev. **D89**, 1, 012004 (2014), [arXiv:1309.6580].

[70] S. Chatrchyan *et al.* (CMS), Phys. Lett. **B734**, 261 (2014), [arXiv:1309.6920].

[71] J. Brodzicka, Conf. Proc. **C0908171**, 299 (2009).

[72] R. Aaij *et al.* (LHCb), Phys. Rev. **D85**, 091103 (2012), [arXiv:1202.5087].

[73] J. P. Lees *et al.* (BaBar), Phys. Rev. **D91**, 1, 012003 (2015), [arXiv:1407.7244].

[74] C. P. Shen *et al.* (Belle), Phys. Rev. Lett. **104**, 112004 (2010), [arXiv:0912.2383].

[75] R. Aaij *et al.* (LHCb), Phys. Rev. **D95**, 1, 012002 (2017), [arXiv:1606.07898].

[76] R. Aaij *et al.* (LHCb), Phys. Rev. Lett. **118**, 2, 022003 (2017), [arXiv:1606.07895].

[77] R. Aaij *et al.* (LHCb), Phys. Rev. Lett. **127**, 8, 082001 (2021), [arXiv:2103.01803].

[78] S. X. Nakamura, Phys. Lett. B **834**, 137486 (2022), [arXiv:2111.05115].

[79] R. Aaij *et al.* (LHCb), Sci. Bull. **65**, 1983 (2020), [arXiv:2006.16957].

[80] G. Aad *et al.* (ATLAS), Phys. Rev. Lett. **131**, 15, 151902 (2023), [arXiv:2304.08962].

[81] A. Hayrapetyan *et al.* (CMS), Phys. Rev. Lett. **132**, 11, 111901 (2024), [arXiv:2306.07164].

Int. J. Mod. Phys. A 2026.41. Downloaded from www.worldscientific.com
UNIVERSITY OF CALIFORNIA @ BERKELEY on 09/16/26. Re-use and distribution is strictly not permitted, except for Open Access articles.

[82] X.-K. Dong *et al.*, Phys. Rev. Lett. **126**, 13, 132001 (2021), [Erratum: Phys.Rev.Lett. 127, 119901 (2021)], [arXiv:2009.07795].

[83] C. Gong *et al.*, Phys. Lett. B **824**, 136794 (2022), [arXiv:2011.11374].

[84] Z.-R. Liang, X.-Y. Wu and D.-L. Yao, Phys. Rev. D **104**, 3, 034034 (2021), [arXiv:2104.08589].

[85] Y.-L. Song *et al.*, Phys. Rev. D **111**, 3, 034038 (2025), [arXiv:2411.12062].

[86] R. Mizuk *et al.* (Belle), JHEP **10**, 220 (2019), [arXiv:1905.05521].

[87] I. Adachi *et al.* (Belle-II), JHEP **07**, 116 (2024), [arXiv:2401.12021].

[88] I. Adachi *et al.* (Belle-II), Phys. Rev. Lett. **130**, 9, 091902 (2023), [arXiv:2208.13189].

[89] N. Hüsken, R. E. Mitchell and E. S. Swanson, Phys. Rev. D **106**, 9, 094013 (2022), [arXiv:2204.11915].

[90] D. Santel *et al.* (Belle), Phys. Rev. **D93**, 1, 011101 (2016), [arXiv:1501.01137].

[91] F.-K. Guo, X.-H. Liu and S. Sakai, Prog. Part. Nucl. Phys. **112**, 103757 (2020), [arXiv:1912.07030].

[92] R. Aaij *et al.* (LHCb), Phys. Rev. Lett. **110**, 222001 (2013), [arXiv:1302.6269].

[93] R. Aaij *et al.* (LHCb), Phys. Rev. **D92**, 1, 011102 (2015), [arXiv:1504.06339].

[94] R. Aaij *et al.* (LHCb), Phys. Rev. D **102**, 9, 092005 (2020), [arXiv:2005.13419].

[95] M. Ablikim *et al.* (BESIII), Phys. Rev. Lett. **132**, 15, 151903 (2024), [arXiv:2309.01502].

[96] N. Brambilla *et al.*, Eur. Phys. J. **C71**, 1534 (2011), [arXiv:1010.5827].

[97] M. Ablikim *et al.* (BESIII), Phys. Rev. Lett. **110**, 252001 (2013), [arXiv:1303.5949].

[98] T. Xiao *et al.*, Phys. Lett. **B727**, 366 (2013), [arXiv:1304.3036].

[99] M. Ablikim *et al.* (BESIII), Phys. Rev. Lett. **112**, 2, 022001 (2014), [arXiv:1310.1163].

[100] M. Ablikim *et al.* (BESIII), Phys. Rev. Lett. **115**, 11, 112003 (2015), [arXiv:1506.06018].

[101] M. Ablikim *et al.* (BESIII), Phys. Rev. Lett. **115**, 22, 222002 (2015), [arXiv:1509.05620].

[102] M. Ablikim *et al.* (BESIII), Phys. Rev. Lett. **111**, 24, 242001 (2013), [arXiv:1309.1896].

[103] M. Ablikim *et al.* (BESIII), Phys. Rev. Lett. **112**, 13, 132001 (2014), [arXiv:1308.2760].

[104] M. Ablikim *et al.* (BESIII), Phys. Rev. Lett. **113**, 21, 212002 (2014), [arXiv:1409.6577].

[105] M. Ablikim *et al.* (BESIII), Phys. Rev. Lett. **115**, 18, 182002 (2015), [arXiv:1507.02404].

[106] M. Ablikim *et al.* (BESIII), Phys. Rev. Lett. **126**, 10, 102001 (2021), [arXiv:2011.07855].

[107] M. Ablikim *et al.* (BESIII), Phys. Rev. Lett. **129**, 11, 112003 (2022), [arXiv:2204.13703].

[108] M. Ablikim *et al.* (BESIII), Chin. Phys. C **47**, 3, 033001 (2023), [arXiv:2211.12060].

[109] R. Aaij *et al.* (LHCb), Nature Phys. **18**, 7, 751 (2022), [arXiv:2109.01038].

[110] R. Aaij *et al.* (LHCb), Nature Commun. **13**, 1, 3351 (2022), [arXiv:2109.01056].

[111] A. Bondar *et al.* (Belle), Phys. Rev. Lett. **108**, 122001 (2012), [arXiv:1110.2251].

[112] A. Garmash *et al.* (Belle), Phys. Rev. **D91**, 7, 072003 (2015), [arXiv:1403.0992].

[113] P. Krokovny *et al.* (Belle), Phys. Rev. **D88**, 5, 052016 (2013), [arXiv:1308.2646].

[114] I. Adachi *et al.* (Belle) (2012), [arXiv:1209.6450].

[115] K. F. Chen *et al.* (Belle), Phys. Rev. Lett. **100**, 112001 (2008), [arXiv:0710.2577].

[116] P. Krokovny (Belle), Nuovo Cim. C **035**, 06, 223 (2012).

[117] A. Abdesselam *et al.* (Belle), Phys. Rev. Lett. **117**, 14, 142001 (2016), [arXiv:1508.06562].

[118] M. Cleven *et al.*, Eur. Phys. J. **A47**, 120 (2011), [arXiv:1107.0254].

[119] F. K. Guo *et al.*, Phys. Rev. **D93**, 7, 074031 (2016), [arXiv:1602.00940].

[120] Q. Wang *et al.*, Phys. Rev. D **98**, 7, 074023 (2018), [arXiv:1805.07453].

[121] A. Garmash *et al.* (Belle), Phys. Rev. Lett. **116**, 21, 212001 (2016), [arXiv:1512.07419].

Int. J. Mod. Phys. A 2026.41. Downloaded from www.worldscientific.com
by UNIVERSITY OF CALIFORNIA @ BERKELEY on 09/16/26. Re-use and distribution is strictly not permitted, except for Open Access articles.

78. Heavy Non-$q\bar{q}$ Mesons

Revised October 2025 by T. Gutsche (Tübingen U.), C. Hanhart (FZ Jülich) and R.E. Mitchell (Indiana U.).

The constituent quark model describes the observed meson spectrum as bound $q\bar{q}$ states grouped into SU(N) flavor multiplets (see the 'Quark Model' in this issue of the *Review of Particle Physics*). However, the self coupling of gluons in QCD suggests that additional mesons made of bound gluons (glueballs), or $q\bar{q}$-pairs with an excited gluon (hybrids), may exist. Furthermore, multiquark color singlet states such as $qq\overline{qq}$ (tetraquarks as compact diquark-antidiquark systems and 'molecular' bound states of two mesons) or $qqq\overline{qq}\overline{q}$ (six-quark, 'baryonium' or quasinuclear baryon-antibaryon bound states) have also been predicted—they were actually already mentioned in the pre-QCD works on the quark model in Refs. [1,2] . The focus of this review is on the current understanding of exotic states that apparently do not fit into the most simple realizations of the $q\bar{q}$ constituent quark model and contain at least one heavy quark (charm or bottom — the lifetime of the top quark is too short to provide the formation of hadrons with a sufficiently long life time that allows for spectroscopic investigations). Light non-$q\bar{q}$ candidates (made of u, d and s quarks) are discussed in 'Scalar Mesons below 1 GeV' and 'Spectroscopy of Light Meson Resonances' in this *Review*.

There are candidates for exotic states with both quantum numbers not allowed and quantum numbers allowed for $\bar{q}q$ states. For the latter class it is up to now unclear to what extend a mixing of conventional and unconventional states occurs. While Refs. [3–6] report a significant mixing, Refs. [7, 8] describe a scenario where the mixing especially between molecular structures and $\bar{q}q$ states is suppressed. Ref. [9] finds a mixing that depends strongly on the pole location of the state studied. A promising path to study mixing of different configurations is the use of few-body Bethe-Salpeter equation within the Dyson-Schwinger framework which is outlined in Refs. [10, 11] for open and hidden-flavor doubly heavy states, respectively.

Theoretically heavy non-$q\bar{q}$ mesons are studied using quark models, see, e.g., Refs. [12, 13], diquark-anti-diquark models, where (anti-)diquarks are treated as compact dynamical degrees of freedom within the hadron, see, e.g., Refs. [14–17], meson-exchange models, see, e.g., [18, 19], as well as different variants of effective field theories (EFTs). For mesons made of one heavy quark the proper non-relativistic EFT is called Heavy Quark Effective Theory (HQET), for reviews see [20, 21]. Doubly heavy systems are characterized by various scales. For $m_Q \gg m_Q v \gg m_Q v^2$, non-relativistic QCD (NRQCD) [22–24] can be employed at the scale $m_Q v$, obtained by integrating out QCD modes associated with the heavy scale m_Q, and potential NRQCD (pNRQCD) [25–27] at the scale $m_Q v^2$, obtained additionally integrating out modes associated with the energy scale $m_Q v$. The most modern development in this family of effective field theories is the Born-Oppenheimer EFT (BOEFT) [28–32] that can be applied to quarkonia, and all the exotics states discovered in the last decades that are all composed of two heavy quarks (or antiquarks): hybrids, tetraquarks, pentaquarks and doubly-heavy baryons.

To investigate the energy range around two-hadron thresholds, one can construct an NREFT with these hadrons as the effective degrees of freedom. In particular, in its most simple realisation for S-wave interactions, the LO interaction Lagrangian contains only constant contact terms, while higher-order terms involve derivatives of the hadron fields. The effective parameters that at the same time serve as counter terms in the renormalisation procedure are then adjusted by fits to experimental or lattice data. In this context the role of the one-pion exchange (OPE) is still under debate. There are three different approaches available in the literature, namely pionless EFT [33, 34], EFT with perturbative pions [35–40], and EFT with non-perturbative pions [41–48]. All those find their analogs in studies of the nucleon-nucleon interaction—see, e.g., Refs. [49–51] for reviews. Most of those were used to study the spectrum or line shapes of hadronic molecules [33, 35, 38, 41, 48, 52–56] (for a review, see Ref. [57]). Those are states that owe their existence to the QCD residual force between color–neutral hadrons and not to the gluon exchange between the colored quarks or diquarks. Here chiral symmetry and heavy quark spin symmetry typically guide the construction of the interactions.

QCD sum-rules are also employed to investigate QCD exotics. Here the analyticity of physical amplitudes is used in a dispersion integral to relate the integral over hadronic amplitudes to a sum over various perturbative QCD contributions as well as non-perturbative condensates. The proper choice of interpolating currents allows one to access certain configurations, although the construction is significantly more involved for multi-quark than for quark-antiquark systems [58]. For a recent review on the application of this technique to exotics see Ref. [59].

In recent years lattice QCD also became an important tool to investigate exotics in the light and heavy quark sectors. Lattice QCD, explained in detail in a dedicated section of this *Review*, is a numerical solution of QCD on a discretised space-time lattice, often employing unphysical quark masses, not only for numerical reasons but also to address certain physical phenomena as is detailed below. The applications and challenges of lattice QCD with regard to exotics are discussed in the review [60].

The review is split into 3 parts, discussing separately heavy–light systems, heavy–heavy systems, as well as systems with more than two heavy quarks. For a more detailed discussion of the experimental and/or theoretical status on exotic meson candidates in the doubly heavy meson sector we refer to Refs. [60–66]. Also see the "Spectroscopy of Mesons Containing Two Heavy Quarks" in this *Review*. Reviews with main focus on tetraquarks and molecular states are presented in Ref. [67] and in Ref. [57, 68], respectively. The latest reviews dealing with exotic hadrons are given by Refs. [59, 69, 70].

The naming scheme for hadrons has been updated by the Particle Data Group in 2023, and now covers the heavy "exotic" tetraquark ($qq\bar{q}\bar{q}$) and pentaquark ($qqqq\bar{q}$) candidates recently discovered. We use the new naming scheme in the following. See "Naming Scheme for Hadrons" in this *Review* for details and a table mapping old and new particle names.

78.1 Heavy-light systems

78.1.1 *Positive parity open charm ground states*

Two very narrow states, $D_{s0}^*(2317)^\pm$ and $D_{s1}(2460)^\pm$, were observed at B factories [71, 72]. They lie far below the predicted masses for the two expected broad P-wave $c\bar{s}$ mesons. However, strong cusp effects, due to the nearby DK (DK^*) thresholds, could shift their masses downwards and quench the observed widths, still allowing for a conventional explanation of these states [73]. Such an effect was also claimed for the $a_0(980)$ and $f_0(980)$ mesons, which lie just below the $K\overline{K}$ threshold. In contrast to this picture, many authors favor exotic explanations for these lightest positive parity charmed states, such as compact four-quark states with prominent diquark–anti-diquark structure [74–77] or DK (DK^*) molecules [78–83]. Both states are isoscalars, and thus strong decays are suppressed, since they are possible only to isovector channels $D_s^{(*)\pm}\pi^0$, leading to very small widths. For compact structures the hadronic decay is driven by η–π^0 mixing and one finds widths below 10 keV [73, 84]. In contrast to this, a hadronic width typically larger than 100 keV would be the unequivocal signature for a prominent molecular nature of $D_{s0}^*(2317)^\pm$ [80, 82, 83, 85, 86], since then meson loops generating enhanced isospin violation due to the energy difference between the $D^{(*)0}K^+$ and the $D^{(*)+}K^0$ thresholds would contribute significantly. The most refined analysis in the molecular scenario [85], where the parameters of the formalism are constrained by a large bulk of lattice QCD data on singly charmed systems, reports a prediction for the width in the range (104–116) keV. The currently measured upper bound for the width is 3.8 MeV.

It should be stressed that – akin to $q\bar{q}$ mesons – multiquark states also appear in multiplets. An important probe for the structure of hadrons is therefore the spectra, and in particular the SU(3) flavor multiplets within the different scenarios and associated mass splittings. For example, the tetraquark model advocated in Refs. [77, 87] finds that the $D_{s0}^*(2317)^\pm$ should be de-

Int. J. Mod. Phys. A 2026.41. Downloaded from www.worldscientific.com
UNIVERSITY OF CALIFORNIA @ BERKELEY on 09/16/26. Re-use and distribution is strictly not permitted, except for Open Access articles.

generate with its non-strange partner state $D_0^*(2300)$ in line with the currently available experimental analyses. However, Ref. [88] showed that the recent LHCb data for $B \to D\pi\pi$ [89, 90] call for a significantly lighter lightest non-strange scalar charmed meson as soon as constraints from the chiral symmetry of QCD are employed in the analysis. This claim is in line with the recent lattice QCD study of Ref. [91]. In fact, experimental as well as lattice data turn out to be consistent with the predictions from unitarised chiral perturbation theory pioneered for these systems in Ref. [79], where the lightest open flavor positive parity states appear as dynamically generated two-hadron states. For more recent calculations see Refs. [85, 92, 93]. Moreover, all the mentioned calculations that are consistent with chiral constraints predict that the interactions in the 15-plet should be repulsive while there should be in addition an about 300 MeV heavier flavor exotic state, formally a member of a flavor sixtet and absent for $c\bar{q}$ states. As shown in Ref. [93] there are indeed indications also for this state in the above mentioned LHCb data—why this state was not reported in the lattice study of Ref. [94] is explained in Ref. [95] by its being located on a hidden Riemann-sheet. The pattern described above—with the interactions in the flavor antitriplet most attractive, in the flavor sixtet attractive and in the 15-plet repulsive—was recently also observed in a lattice QCD analysis for πD scattering based on the Lüscher method at a pion mass of about 700 MeV [96]. Thus, in this picture the structure that appears as $D_0^*(2300)$ in the *Listings* originates from the interplay of two poles, similar to the $\Lambda(1405)$ in the baryon sector, see 'Pole structure of the $\Lambda(1405)$ region' in this *Review*. Two poles in the non-strange scalar sector are also generated in the tetraquark picture of Ref. [77], but in this work the real parts of the poles are located at 2308 MeV and 2666 MeV, in conflict with the data mentioned above. In the refined analysis of Ref. [87] it is shown, however, that the exact pole locations and even the ordering of the higher multiplets depend on the details of the model. In Ref. [97] it was argued that as soon as one restricts the diquark phenomenology to only scalar diquarks, as a consequence of the Pauli principle also the diquark–anti-diquark picture is consistent with a repulsion in the 15-plet. However, axial-vector diquarks, which would be needed for a consistent hadron phenomenology, if diquarks are indeed relevant degrees of freedom, also produce states in the 15-plet. In particular, while in the scalar D-meson sector those should be rather heavy, in the axial-vector spectrum, they should be even lighter than the states in the sixtet [98]. Contrary to this, in the two-hadron picture of unitarised chiral perturbation theory, the scalar and the axial-vector sectors should be equal (up to spin symmetry violations). In this sense the recent lattice study of Ref. [99] is in conflict with the predictions of the diquark-anti-diquark picture, while being consistent with a two-hadron structure for those states.

What is needed in addition to the above quoted strong, mostly theoretical, evidence for the unusual pattern of non-strange D-mesons, is a more direct experimental determination of the pole location of the lightest positive parity D-meson. This could be derived from a high quality measurement of the πD scattering parameters—analogously to the case of the $f_0(500)$, whose pole location was significantly constrained by high quality data on the $\pi\pi$ scattering length. One way to get access to the scattering parameters of unstable particles is to use the femtoscopy technique—here semi-inclusively, the correlations of two (or more) outgoing hadrons produced in a high-energy collision are measured—for reviews see Refs. [100, 101]. Recent studies using this technique find results for the DK and D^*K systems consistent with the above mentioned lattice and chiral effective field theory calculations, however, for $D\pi$ and $D^*\pi$ the extracted scattering parameters are below 0.03 fm and are thus inconsistent with the theoretical investigations [102][1]. It remains to be seen, if these latter values get confirmed by other investigations like in semi-leptonic B decays [104, 105].

Lattice QCD allows for predictions of the flavor partner states in the B-sector. The most recent analysis can be found in Ref. [106]. In this work also a comparison with theoretical predictions can be found. Unfortunately an experimental confirmation for those states is difficult with existing facilities. Radiative decays are predicted to be the most prominent decay channels [86], since the above mentioned isospin violation from meson loops is suppressed in the B sector as a consequence of the tiny $B^\pm - B^0$ mass difference.

78.1.2 *The $T^*_{cs0}(2870)$ and $T^*_{cs1}(2900)$*

Manifestly exotic candidates around 2.9 GeV were reported in Refs. [107–109] by LHCb in the $\bar{D}K$ system. Since the strong interaction preserves the quark flavor and the final state contains an $\bar{s}$ as well as a $\bar{c}$, color neutrality calls for a minimum quark content of $ud\bar{c}\bar{s}$. A resonant structure consistent with the $T^*_{cs0}(2870)$ is also observed in the $D^0K^0_s$ invariant-mass spectrum [110], although with no evidence for the $T^*_{cs1}(2900)$. Charged open-charm tetraquark structures were searched for in $B^0 \to D^+D^-K^0_s$ decays, but without any significant signal [111].

The explanation for those states include compact tetraquarks with a structure dominated by a diquark–anti-diquark pair [112–114], hadronic molecules with a prominent $D^*\bar{K}^*$ component [115–120], or kinematic effects such as cusps or triangle singularities (for an explanation of the latter terms we refer to the section 'Resonances' in this *Review*) without nearby poles [121, 122]. The different pictures are contrasted and observable differences between them are discussed in Ref. [123].

78.1.3 *The $T^*_{c\bar{s}0}(2900)^0$ and $T^*_{c\bar{s}0}(2900)^{++}$*

There is a recent report by LHCb [124] on the observation of a doubly charged open-charm tetraquark candidate together with a neutral partner in the $D_s\pi$ channel, with masses near 2.9 GeV. The results imply two states with $c\bar{s}\bar{u}d$ or $c\bar{s}u\bar{d}$ flavor structures. Although masses and widths are consistent with the T_{cs} states of Refs. [107, 108], the strangeness quantum numbers do not match. The first explanation for those states in coupled-channel studies is based on a kinematic effect such as a cusp [125]. In Ref. [126] a molecular structure with a dominant D^*K^* component is claimed to be excluded. However, since the $T^*_{c\bar{s}0}(2900)$ is situated near this threshold, some works [119,127–129] argue that this isospin triplet state should be interpreted as a D^*K^* hadronic molecule. Within this picture, in Ref. [129] predictions for states with other quantum numbers are given. A QCD sum rule study based on diquark–anti-diquark interpolating currents is presented in Ref. [130].

Recently LHCb reported an amplitude analysis on a resonant structure in $D_{s1}(2460)^+ \to D_s^+\pi^+\pi^-$ decays [131]. One of the analysis models calls for a new $T^{++}_{c\bar{s}}$ state and its isospin partner $T^0_{c\bar{s}}$ with mass and width of about 2327 MeV and 96 MeV. At first sight these $T_{c\bar{s}}$ states can be interpreted as two members of the isotriplet predicted in Ref. [97], although data could also be explained dynamically [132].

78.2 Heavy-heavy systems

With the discovery of the $\chi_{c1}(3872)$[2] in $B^\pm \to K^\pm X$ ($X \to J/\psi(1S)\,\pi^+\pi^-$) by Belle [133] in 2003, soon confirmed by BaBar [134], many searches for states beyond the standard $q\bar{q}$ quark model were initiated in the charm and bottom sectors. For an updated collection of the currently available experimental information on multiquark states we refer to 'Spectroscopy of mesons containing two heavy quarks' in this *Review*, and in particular to Table 77.2. Moreover, in the decay $\Lambda_b^0 \to J/\psi(1S)\,K^-p$ the LHCb collaboration has recently reported the observation of new baryons decaying into $J/\psi(1S)\,p$, which are candidates for heavy pentaquark states [135, 136]. They are discussed in some depth in 'Pentaquarks' in this *Review*.

In addition to the multiquark scenarios discussed for the heavy-light systems, in double heavy systems two more basic configurations are discussed in the literature. On the one hand there are the hadroquarkonia, which call for a compact quarkonium core surrounded by a light quark cloud [137]. On the other hand there are hybrid mesons, in which an excited gluon field, in combination with the valence quarks, contributes to the overall quantum numbers and properties of the meson.

[1] Ref. [103] shows that there is a systematic uncertainty in the femtoscopy method not yet accounted for.

[2] The $\chi_{c1}(3872)$ is also known as the $X(3872)$. According to the PDG naming scheme, the primary name for a meson expresses its quantum numbers.

Int. J. Mod. Phys. A 2026.41. Downloaded from www.worldscientific.com by UNIVERSITY OF CALIFORNIA @ BERKELEY on 09/16/26. Re-use and distribution is strictly not permitted, except for Open Access articles.

When restricting ourselves to confirmed states we are faced with several states that do not seem to fit into the mass and quantum number schemes of $q\bar{q}$ quark models. This is clear for the five established charged states ($T_{c\bar{c}1}(3900)^{\pm}$, $T_{c\bar{c}}(4020)^{\pm}$ and $T_{c\bar{c}1}(4430)^{\pm}$ in the charmonium sector, and $T_{b\bar{b}1}(10610)^{\pm}$ and $T_{b\bar{b}1}(10650)^{\pm}$ in the bottomonium sector[3]). The neutral states ($\chi_{c1}(3872)$, $\psi(4230)$, $\psi(4360)$, and $\psi(4660)$)[4] also challenge the quark model since their masses and decay properties are in conflict with expectations. Although so far seen just by a single experiment in a single channel [138,139], the $T_{cc}(3875)$ and its proposed heavy partner states are also discussed.

It should be stressed that mass parameters for resonances located not too far with respect to their width from a pertinent threshold extracted with Breit-Wigner methods should be considered with care, since the lineshape can very well be distorted by the threshold. An example for such a case is reported in Ref. [140], where it was demonstrated that the experimental data by Belle are consistent with a $\bar{D}D$ bound state at 3695 MeV in line with lattice QCD simulations for the same system [141], while from experiment a mass as high as 3860 MeV with a width of 200 MeV was extracted [142].

78.2.1 *The* $\chi_{c1}(3872)$

The quantum numbers of the $\chi_{c1}(3872)$ have been determined by LHCb to be $J^{PC} = 1^{++}$, first by assuming zero angular momentum between the $J/\psi(1S)$ and the dipion [143] and then by relaxing this constraint [144]. The $\chi_{c1}(3872)$ cannot be easily identified with the $\chi_{c1}(2^3P_1)$, since the latter is predicted to lie about 100 MeV higher in mass [145]. Instead, the $X(3940)$ reported by Belle in $e^+e^- \to J/\psi(1S)X$, decaying into $D^*\bar{D}$ but not into $D\bar{D}$ [146] could be the $\chi_{c1}(2^3P_1)$. The $\chi_{c2}(3930)$ 2^3P_2 tensor partner was reported by Belle at 3931 MeV in $\gamma\gamma$ interactions [147].

The $\chi_{c1}(3872)$ lies within 200 keV of the $D^0\bar{D}^{*0}$ threshold and its width is very small — recent Breit-Wigner analyses by LHCb [148, 149] result in an average value of $\Gamma = (1.19 \pm 0.21)$ MeV as indicated in the *Listings*. However, since the respective pole is located very close to an S-wave thresholds to which it couples strongly, the Breit-Wigner lineshape should not be used (see section 'Resonances' in this *Review*). Employing the more appropriate Flatté formalism of Ref. [150] under the constraint that the $D^*\bar{D}$ decay channel dominates, results in $\Gamma = 0.22^{+0.18}_{-0.19}$ MeV, where the standard convention is applied to use twice the imaginary part of the pole location as width. A recent determination of the $\chi_{c1}(3872)$ lineshape parameters and the resulting pole location based on BESIII data can be found in Ref. [151]. A combined analysis of the LHCb data and BESIII data is presented in Ref. [152], where the pole location of the $\chi_{c1}(3872)$ was determined with unprecedented accuracy. Moreover, further evidence was presented for the existence of an additional pole in the isovector channel, originally predicted in Ref. [153], which should show up more prominently in e.g. the decay $B^0 \to K^0 J/\psi\pi^+\pi^-$. In the future the mass parameters can be refined more by either a direct measurement of the width that should be possible at the planned PANDA experiment [154, 155] or by exploiting the interplay of a triangle singularity and the $\chi_{c1}(3872)$ pole [156–158].

The most natural explanation for the $\chi_{c1}(3872)$ is a 1^{++} $D\bar{D}^*$ molecule [159]. In this scenario a strong isospin breaking is predicted [159, 160], since the distance of the pole of the $\chi_{c1}(3872)$ to the $D^0\bar{D}^{*0}$ threshold is significantly smaller than to the D^+D^{*-} threshold. Indeed, the comparable rates for $\omega J/\psi(1S)$ and $\rho^0 J/\psi(1S)$ are consistent with an interpretation of $\chi_{c1}(3872)$ as an isoscalar $D\bar{D}^*$ molecule, when the different widths of the ρ and ω are taken into account [161]. A molecular component of above 99% was also found in Refs. [152, 162] in sophisticated analyzes that kept the full three-body dynamics of the intermediate state $D\bar{D}\pi$, first studied in Ref. [41].

A dominant molecular $D^0\bar{D}^{*0}$ structure in the $\chi_{c1}(3872)$ with further subleading more compact hadronic components is used to explain strong and radiative decays involving $J/\psi(1S)$ and $\psi(2S)$ in the final states [163, 164]—it should be mentioned that those rates are also consistent with a $c\bar{q}$ structure [165]. The most recent measurement of the ratio of radiative partial decay widths [166] indicates that the $\psi(2S)\gamma$ mode dominates over $J/\psi\gamma$. This observation is claimed to point to a sizable compact component in the $\chi_{c1}(3872)$ (for a compilation of various structure-dependent predictions see [166]). However, from an effective field theory point of view these radiative transitions are not well suited to quantify the molecular admixture in the $\chi_{c1}(3872)$, since there appears a counter term at leading order, diminishing the sensitivity to the long-ranged molecular component [167].

A diquark–anti-diquark structure $(cq)(\bar{c}\bar{q}')$ is another possible interpretation of the $\chi_{c1}(3872)$ [76]. Contrary to the two hadron structure discussed above, here diquark-anti-diquark substructures are assumed to be bound by QCD flux tubes—for a discussion of possible configurations see Ref. [168]. What speaks against this interpretation is that so far no near mass degenerate charged partner of the $\chi_{c1}(3872)$ has been observed (e.g. not in $B^- \to \bar{K}^0 X^-$ nor in $B^0 \to K^+X^-$, where $X^- \to J/\psi(1S)\,\pi^-\pi^0$ [169])—see [170] for a possible explanation of this non-observation within the tetraquark approach assuming specific diquark correlations and the more recent discussion in Ref. [171]. Note that the isovector partner state of the $\chi_{c1}(3872)$ discussed in [153] is not consistent with the proposed charged compact tetraquark state, since the pole is located on an unphysical sheet, clearly pointing at a molecular nature of the state [172], and its mass is close to the D^+D^{*-} threshold, 8 MeV above the mass of the $\chi_{c1}(3872)$.

The claim that $\chi_{c1}(3872)$ must be a compact (tetraquark) state, since it is also produced at very high p_T in $\bar{p}p$ collisions [173] and in high multiplicity final states [174], was challenged in [175] and [176], respectively, which in particular stress the importance of rescattering, see also Refs. [177, 178].

The high statistics measurement of the $\chi_{c1}(3872)$ lineshape of Ref. [148] also allowed for an extraction of the effective range for the $D^0\bar{D}^{*0}$ interaction. At face value, the values provided in this publication indicate a large and negative effective range [179], which could be interpreted as a signature of a prominent compact component in the $\chi_{c1}(3872)$ wave function — this follows from the famous Weinberg compositeness criterion [180]. The effect of the one-pion exchange on the effective range turns out to be small [40, 41, 181, 182] and should therefore not invalidate the Weinberg-type analysis. However, it was argued in Ref. [183] that once the effect of the large isospin violation as well as the strong correlations between the effective parameters appearing in Ref. [150] are subtracted, the effective range is consistent with a purely molecular $\chi_{c1}(3872)$. There is no consensus yet how to interpret the line shapes of $\chi_{c1}(3872)$.

78.2.2 *The* $\psi(4230)$ *and* $\psi(4360)$

A broad structure, originally called $Y(4260)$, decaying into $J/\psi(1S)\,\pi^+\pi^-$ was reported by BaBar in initial state radiation $e^+e^- \to (\gamma_{\rm ISR})Y(4260)$ [184]. A subsequent measurement with significantly improved precision was reported by BESIII [185], and revealed that the original $Y(4260)$ cannot be described with a simple resonant lineshape. Fitting the BESIII data with two Breit-Wigner distributions leads to a narrower and lighter structure (referred to in the *Listings* as the $\psi(4230)$), but also requires a second state at 4320 MeV. While the $D_1(2420)\bar{D}$ molecular model for the $\psi(4230)$ can describe the same data with just one single exotic pole [186, 187], the coupled channel analysis of Ref. [188] needs an additional exotic state near 4320 MeV. Both, Ref. [187] and Ref. [188] need the interference of the signal of the $\psi(4230)$ with the $\psi(4160)$ to get a good description of the large amount of available data. How many vector states are in the mass range between 4220 MeV and 4400 MeV is not yet settled, but knowing this is crucial to allow for further progress.

There are no charmonium states expected in this mass region with quantum numbers 1^{--} from quark models using the Cornell type of interaction, although this might not be true for some screened versions thereof—for a recent discussion we refer to Ref. [189]. In addition, a charmonium state at this mass is expected to have significant couplings to one or more of the $\bar{D}^{(*)}D^{(*)}$ channels [190, 191], a feature that is not observed for the $\psi(4230)$.

[3] In the literature those states are often labeled as Z_c and Z_b, respectively.

[4] The $\psi(4230)$, $\psi(4360)$, and $\psi(4660)$ are also known as the $Y(4230)$, $Y(4360)$, and $Y(4660)$, respectively. Before improved mass measurements, the $\psi(4230)$ was originally called the $\psi(4260)$ or $Y(4260)$.

Int. J. Mod. Phys. A 2026.41. Downloaded from www.worldscientific.com
UNIVERSITY OF CALIFORNIA @ BERKELEY on 09/16/26. Re-use and distribution is strictly not permitted, except for Open Access articles.

This state could be a hybrid charmonium with a spin-1 [28, 192] or a spin-0 [193, 194] $\bar{c}c$ core—for a recent review on this state see Ref. [195]. However, provided that the observation of $\psi(4230)$ decay into $h_c(1P)\pi\pi$ by BESIII [196] is confirmed, the hybrid hypothesis would be under pressure, since the spin of the heavy quarks (coupled to zero in the $h_c(1P)$) should be conserved in leading order in the expansion in $(\Lambda_{\rm QCD}/m_c)$. (The individual conservation of the heavy quark spin and the total angular momentum of the light quark cloud is a consequence of the heavy-quark spin symmetry, see 'Heavy-Quark and Soft-Collinear Effective Theory' in this issue of the *Review*.) The same criticism applies to the hadrocharmonium interpretation of the $\psi(4230)$. To circumvent the spin-symmetry argument, Ref. [197] suggests that $\psi(4230)$ and $\psi(4360)$ could be mixtures of two hadrocharmonia with spin-triplet and spin-singlet heavy quark pairs. The same kind of mixing could also be at work for hybrid structures. Hybrids can also be treated employing the Born-Oppenheimer EFT originally suggested in Ref. [30, 198]. Those studies revealed that while the $\psi(4230)$ is in principle a good candidate for a hybrid state [199], its decays are incompatible with this assignment [200].

A dominant $D_1(2420)\bar{D}$ component in the $\psi(4230)$ [201] explains naturally why the $T_{c\bar{c}1}(3900)^{\pm}$ (interpreted by the authors as a $\bar{D}D^*$ bound state) is seen in $\psi(4230) \to \pi^{\mp}T_{c\bar{c}1}(3900)^{\pm}$. A similar mechanism is also found in Ref. [202] linking in addition the $J/\psi(1S)\pi^+\pi^-$ and $\psi(2S)\pi^+\pi^-$ decays of the $\psi(4230)$. Furthermore, a copious production of $\chi_{c1}(3872)$ in $\psi(4230)$ radiative decays was predicted from the prominent $D_1\bar{D}$ component of the $\psi(4230)$ [203], which was confirmed by BESIII [204]. Possible charmonia components both in $\psi(4230)$ and $\chi_{c1}(3872)$ can influence the radiative transition but they are shown to be of subleading order [205]. It was proposed that $\psi(4360)$ as a $D_1\bar{D}^*$ bound state could be the spin partner of the $\psi(4230)$ [206, 207]. In Ref. [208] a dynamical model is presented that identifies the vector states $\psi(4230)$, $\psi(4360)$ and $\psi(4415)$ as $D\bar{D}_1$, $D^*\bar{D}_1$ and $D^*\bar{D}_2$ molecular states, respectively. Moreover, an exotic 0^{--} state is predicted as $D^*\bar{D}_1$ molecule with a mass of 4366 ± 18 MeV and a width of less than 10 MeV.

The tetraquark picture calls for four ground state vector states — once the parameters of the model are fixed from some candidate states in the negative and positive parity sector, states with other quantum numbers can be predicted. Possible scenarios are for instance discussed in Ref. [209] which builds on a tailor-made spin-spin interaction [16] to describe the $\chi_{c1}(3872)$, both $T_{c\bar{c}1}(3900)^{\pm,0}$ and $T_{c\bar{c}}(4020)^{\pm}$ and even the $T_{c\bar{c}1}(4430)^{\pm}$ confirmed by Belle [210] and LHCb [211]. This model also explains the copious production of $\chi_{c1}(3872)$ in $\psi(4230)$ radiative decays mentioned above [16, 212]. However, tetraquark models (in most cases based on diquark-antidiquark configurations) tend to predict many additional charged and neutral states which have not yet been discovered. In particular, as for the conventional $\bar{q}q$ structures one should expect nearly degenerate isoscalar and isovector states in analogy to the near degeneracy of $\rho(770)$ and $\omega(782)$. The problem and possible explanations are discussed in some detail in Refs. [170, 171].

Ref. [213] found a sizable SU(3) flavor octet contribution when analyzing the $\pi\pi$ final state from $\psi(4230) \to J/\psi(1S)\pi^+\pi^-$, which is consistent with both a molecular and a tetraquark interpretation of $\psi(4230)$, but is at odds with a hybrid or a $\bar{c}c$ interpretation.

78.2.3 *The* $\psi(4660)$

In the mass range above 4600 MeV, the number of poles is also not yet settled. Experimental signals are seen in the $\psi(2S)\pi\pi$, $\Lambda_c^+\bar{\Lambda}_c^-$, $D_s\bar{D}_{s1}$, $D_s\bar{D}^*_{s2}$, and $D^{*0}D^{*-}\pi^+$ final states. In the *Listings* these structures go into one node, $\psi(4660)$, due to their proximity in parameter values. Moreover, various theoretical works describe these states in a combined analysis [214–216]. The signal in the hidden strangeness mode around 4630 MeV still calls for confirmation and might be yet another realization of the same state, but there are already speculations about its nature. Ref. [217] finds a single state in this mass range and identifies it with the $\psi(5S)$. While Ref. [218] argues in favor of a $D_s^{(*)}\bar{D}_{s1}(2536)$ or $D_s^{(*)}\bar{D}_{s2}(2573)$ [219] molecular nature, Ref. [220] does not confirm these claims. Ref. [221] identifies the structure as P-wave $[cs][\bar{c}\bar{s}]$ tetraquark state. Other explanations of the $\psi(4660)$ include a $\psi(2S)f_0(980)$ molecule [222] and a $\Lambda_c^+\bar{\Lambda}_c^-$ baryonium [214]. Also in this mass range studies of the partner states, driven either by spin or flavor symmetry will be very valuable—see e.g. the predictions in Ref. [223].

78.2.4 *The* $T_{c\bar{c}1}(3900)$, $T_{c\bar{c}}(4020)$, $T_{b\bar{b}1}(10610)$, *and* $T_{b\bar{b}1}(10650)$

The isovector states $T_{c\bar{c}1}(3900)$ and $T_{c\bar{c}}(4020)$, first observed by BESIII [224, 225], decay predominantly into $\bar{D}D^*$ and $\bar{D}^*D^*$, respectively, while the $T_{b\bar{b}1}(10610)$ and $T_{b\bar{b}1}(10650)$, first observed by Belle [226, 227], decay predominantly into $\bar{B}B^*$ and $\bar{B}^*B^*$ [228], respectively, although all four were discovered in a decay into a heavy quarkonium plus a pion. This suggests that these states are close relatives and their interactions are connected via heavy quark flavor symmetry[5]. A molecular interpretation for the bottomonium states was proposed shortly after the discovery of the two $T_{b\bar{b}}$ states [230] and also shortly after that of the $T_{c\bar{c}1}(3900)$ [201]—the up-to-now most precise determination of the pole location of the latter state is reported in Ref. [231]. This picture is confirmed within the meson exchange model of Ref. [232]. Decay patterns of $T_{c\bar{c}1}(3900)$ and the two $T_{b\bar{b}}$ were also shown to be consistent with a molecular interpretation [233–235]. However, some of their properties also appear to be consistent with tetraquark structures [236]. If the molecular picture were correct for the $T_{b\bar{b}}$ states, spin symmetry would lead to the existence of spin partner states [37, 237, 238], which are still to be found. In Ref. [47] it was shown that the actual pole locations of these partner states would be good probes of one-pion exchange in the molecular potential, which makes the experimental search for those states even more interesting. A possible interpretation of $T_{c\bar{c}1}(3900)$ and $T_{c\bar{c}}(4020)$ as crossed channel effects is put forward in Ref. [239]. It remains to be seen, however, if this kind of explanation is also capable of explaining the observations of these lowest $T_{c\bar{c}}$ states, also at other total energies. A recent lattice QCD calculation suggests that the $T_{c\bar{c}1}(3900)$ can be reconciled with a two pole structure in the $J/\psi\pi - D\bar{D}^*$ coupled-channel [240]. In this study the coupling between $D\bar{D}^*$ and $J/\psi\pi$ is significant and plays a crucial role.

78.2.5 *The* $T_{c\bar{c}1}(4200)$ *and* $T_{c\bar{c}1}(4430)$

The heaviest confirmed charged state in the charmonium sector is the $T_{c\bar{c}1}(4430)^{\pm}$ observed by Belle [210]. It is interpreted as hadrocharmonium [137], $\bar{D}_1D^*$ molecule [241], as well as diquark–anti-diquark structure [16]. Alternatively, in [242, 243] the $T_{c\bar{c}1}(4430)^{\pm}$ is explained as a cross-channel effect enhanced by a triangle singularity from open charm states. These works were criticized in Ref. [244] where an alternative triangle consisting of a K^*, a π, and the $\psi(4230)$, is proposed to generate the $T_{c\bar{c}1}(4430)$. The Argand diagram shows an anticlockwise circle, in line with the experimental analysis [211], while the one of Ref. [243] shows a clockwise motion. By replacing the $\psi(4230)$ with the $\psi(3770)$, and changing the K^*, one can also interpret the $T_{c\bar{c}1}(4200)$ as a kinematic effect [244].

78.2.6 *The* $T_{c\bar{c}\bar{s}1}(4000)$

There is recent evidence for a charged charmonium-like state with strangeness, $T_{c\bar{c}\bar{s}1}(4000)$, from BESIII [245] and LHCb [246]. The possible existence of a strange partner to the $T_{c\bar{c}}$ near the $D_s\bar{D}^*$ thresholds has been predicted in molecular models [247, 248], for tetraquarks [249, 250], for hadrocharmonium structures [250, 251], and as a coupled-channel effect [252]. Later on this state is interpreted in Refs. [253, 254] as a member of the same multiquark octet and in Refs. [255–257] as a member of the same molecular one as the $T_{c\bar{c}1}(3900)$. Ref. [254] is also able to describe the recent LHCb data in the $J/\psi(1S)K^-$ system [246], although the extracted total width for their lowest $T_{c\bar{c}\bar{s}}$ state is an order of magnitude larger than that found by BESIII. Refs. [258, 259] claim that both the molecular components and the compact tetraquark core are relevant to describe the $T_{c\bar{c}1}(3900)$ and $T_{c\bar{c}\bar{s}1}(4000)$ resonances. Again, in [260] the $T_{c\bar{c}\bar{s}1}(4000)$ can

[5] For a critical examination of this claim from an effective field theory point of view see Ref. [229].

Int. J. Mod. Phys. A 2026.41. Downloaded from www.worldscientific.com by UNIVERSITY OF CALIFORNIA @ BERKELEY on 09/16/26. Re-use and distribution is strictly not permitted, except for Open Access articles.

be explained as a coupled-channel effect producing the enhancement close to threshold.

Ref. [255] comes to the conclusion that an understanding of the experimental data for the $T_{c\bar{c}\bar{s}1}(4000)$ calls for the inclusion of both triangle diagrams as well as a pole term. The authors conclude from their calculations that $T_{c\bar{c}\bar{s}1}(4000)$ and $T_{c\bar{c}1}(3900)$ are members of the same SU(3) multiplet. This conclusion was confirmed in Ref. [261] and the study extended to higher energies. The fit of the experimental data allowed for two solutions, one where the $T_{c\bar{c}}(4020)$ is a spin partner of the mentioned isovector states and one where it is not. Data e.g. for $e^+e^- \to K^+D^{*-}D^{*0}$ is claimed to be decisive which scenario is indeed realized.

It should be stressed that the various scenarios, while describing much of the available data, also make decisive predictions, *e.g.* for states with yet unobserved quantum numbers [209, 262]. The forthcoming data on heavy meson spectroscopy from various facilities should provide a much deeper understanding of how QCD forms matter out of quarks and gluons.

Note that for various states listed above it is still possible that they reflect the presence of cusps and not states—for recent studies see [263, 264].

78.2.7 *The $T_{cc}(3875)$*

There is a recent report and follow-up by LHCb [138, 139] on the observation of a narrow peak in the $D^0D^0\pi^+$ mass spectrum just below the $D^{*+}D^0$ threshold. The observed state is a candidate for an isoscalar double-charm T_{cc}^+ tetraquark configuration with a quark content of $cc\bar{u}\bar{d}$. Unsuccessful searches in $D^+D^0\pi^+$ and D^+D^+ mass spectra disfavour the isovector assignment. The $D^0\pi^+$ mass distribution indicates that the T_{cc}^+ proceeds through the formation of a D^* in the intermediate state. The additional proximity to the $D^{*+}D^0$ mass threshold favors the $J^P = 1^+$ assignment. The T_{cc}^+ has a remarkable narrow width and lies very close to the $D^{*+}D^0$ threshold [139], comparable to the properties of the $\chi_{c1}(3872)$. Indeed, employing a meson-exchange model [19] or the BOEFT [265] the two states can be described together in the same framework.

Evaluations in the context of QCD sum rules [266,267] result in mass and width values consistent with the assumption of a compact diquark-antidiquark structure of the T_{cc}^+. A pole analysis performed with $D^0D^0\pi^+ - D^{*+}D^0$ coupled-channels [268] suggests that the T_{cc}^+ has its origin in a $D^{*+}D^0$ virtual state resulting from the attraction in this channel and the coupling to $D^0D^0\pi^+$. The interpretation of the observed T_{cc}^+ as a D^*D molecular structure was pursued in [48,56] based on non-relativistic effective field theories without and with pion exchange, respectively, in [269,270] employing a combination of meson exchange and quark-gluon forces, and in [271] employing the Bethe-Salpeter framework. Predictions depend on fine model details and are usually accompanied by additional partner states, like an isovector molecule or higher radial excitations. A fit to the LHCb data on $T_{cc}(3875)$ [272] is also consistent with a molecular D^0D^{*+}, D^+D^{*0} interpretation in the isoscalar channel, while for the isovector case binding is prevented. A coupled-channel analysis of the $D^0D^0\pi^+$ mass spectrum within a meson-exchange model [19] also concludes the nature of T_{cc}^+ as an isoscalar DD^* hadronic molecule. As a consequence a double-charm isoscalar D^*D^* hadronic molecule candidate is predicted.

In analogy to the case of the $\chi_{c1}(3872)$ in Ref. [273] the production of T_{cc}^+ in high-energy proton-proton collisions at the LHC is studied. Effects of a charm-meson triangle singularity on the inclusive production of T_{cc}^+ from the rescattering of DD lead to a narrow peak in the $T_{cc}^+\pi^+$ invariant mass distribution. A spin 2 partner of the T_{cc}^+ is predicted in Refs. [48, 56], whose hadronic decays are studied in Ref. [274].

As for the $\chi_{c1}(3872)$ one can employ the effective range deduced from experiment for the effective range in the DD^*-channel as a measure of the nature of the $T_{cc}(3875)$. Also here isospin violations are significant. It turns out that in a calculation where the one-pion exchange is kept fully non-perturbative, its effect on the effective range is small and positive [48], while it is small and negative when being treated perturbatively [182, 275].

First lattice studies with fully dynamical quarks are also available for the $T_{cc}(3875)$ [276–278], all performed at pion masses slightly larger than physical such that the D^* and with this also the $T_{cc}(3875)$ are stable. They all find that at these pion masses the T_{cc} is a virtual state. In Ref. [279] it was stressed, however, that all those analyses should be redone, since the proximity of a left-hand cut invalidates the method used—analogously also the effective range expansion needs to be changed in the proximity of a left-hand cut [280, 281]. Possible modifications of the Lüscher method are proposed in Refs. [281–284]. Results point towards a resonance interpretation of the $T_{cc}(3875)$. Chiral extrapolations of lattice simulations for the isoscalar DD^* scattering with [285,286] and without left-hand cut [287] to the physical pion mass lead to a T_{cc} bound states with binding energies compatible with experiment, however, significantly different trajectories.

A first coupled channel isospin-0 DD^*, D^*D^* scattering calculation in lattice QCD [288] also indicates a pole below the DD^* threshold, a further pole corresponding to T_{cc}' is also found just below the D^*D^* threshold. A further lattice QCD study [289] in the doubly charm $cc\bar{q}\bar{q}$ isospin-1 channel concludes that no poles are found in the scattering amplitude near the DD^* threshold consistent with the current experimental status.

Not very long after the discovery of the charm quark it was stressed that, if the ratio of heavy (Q) to light quark (q) masses is well beyond 10, binding should occur for states of the kind $QQ\bar{q}\bar{q}$ [290–292]. These studies were performed within constituent quark models. Accordingly the quoted ratio refers to constituent masses, which are of the order of 300 MeV for the light quarks in contradistinction to the current quark masses of the order of a few MeV. Based on those studies one should expect binding for $bc\bar{q}\bar{q}$ systems and even more so for $bb\bar{q}\bar{q}$—the transition from a (predominantly) molecular structure to a diquark–anti-diquark structure as the masses of the heavy quarks are increased is discussed e.g. in the phenomenological models of Ref. [269, 270]. Nowadays many works investigate doubly heavy tetraquarks including phenomenological models [291–298], lattice QCD either employing static potentials [299–302] or NRQCD for the b-quarks [106, 303–307] as well as QCD sum rules [266, 308–310] . All those papers agree that a T_{bb} should be bound for the $I = 0$ and $J^P = 1^+$ channel, but there is no consensus about the binding energy relative to the lowest open bottom threshold (BB^*), which ranges from values near zero to 500 MeV. Since in contrast to the states that contain a heavy quark–anti-quark pair this family of states contains two heavy quarks, no strong decay channels are accessible for the heavier partner states of the $T_{cc}(3875)$ and they could only decay weakly. Accordingly, once found, they would provide an exciting laboratory not only to investigate the strong but also the weak interaction.

78.3 Systems containing four heavy quarks

78.3.1 *The $T_{cc\bar{c}\bar{c}}(6900)$*

LHCb reported the observation of pronounced structures in a double-$J/\psi(1S)$ invariant mass distribution [311] thus pointing at states with $cc\bar{c}\bar{c}$ quarks contents. First results on di-$J/\psi(1S)$ and $J/\psi(1S)\psi(2S)$ invariant mass distributions in proton-proton collision data by the CMS [312] and ATLAS [313] Collaborations confirm and extend the resonance structures seen by LHCb. In Ref. [314] the quantum numbers of the structures were determined to be $J^{PC} = 2^{++}$. Belle reported on a first search for a double-charmonium state with $e^+e^- \to \eta_c J/\psi(1S)$ near threshold via the ISR process. No significant signal of the double charmonium state is found in several bins of the invariant mass of $\eta_c J/\psi(1S)$ [315]. Recently the COMPASS [316] Collaboration also studied double $J/\psi(1S)$ production in pion scattering off nuclear targets. No significant signatures that could be associated with tetraquarks are found in the double $J/\psi(1S)$ mass spectrum in the relatively limited data set.

From quark models the possible existence of bound states like this was discussed already long ago [290]. There are now also many model calculations available in the literature. For discussions of those data from the compact tetraquark perspective see Refs. [317–323]. Most of these quark model calculations assign the reported structure to a $cc\bar{c}\bar{c}$ state in the $2S$ multiplet with near-degenerate $J^P = 0^+$, 1^+ and 2^+ configurations. The dominance of a compact tetraquark component in the apparently ex-

Int. J. Mod. Phys. A 2026.41. Downloaded from www.worldscientific.com
UNIVERSITY OF CALIFORNIA @ BERKELEY on 09/16/26. Re-use and distribution is strictly not permitted, except for Open Access articles.

otic structure is also supported by the coupled multichannel study of Ref. [324]. The extended coupled-channel study of Ref. [325], where two-meson states are coupled to a potential derived within a quark model, leads to a very rich spectrum of $c\bar{c}$-$c\bar{c}$ states where parts are candidates for the observed double $J/\psi(1S)$ structures. For direct analyses of the data within the tetraquark approach, see, e.g., Ref. [326]. Also QCD sum rule studies of the system were published, but do not give consistent results: For example Ref. [327] interprets the structure at 6900 MeV as a hybrid state, Ref. [328] as a tetraquark, and Ref. [329] states that both molecular and tetraquark interpretations are possible.

An alternative view on the double-$J/\psi(1S)$ data is provided in Refs. [330–332] where the analyses are performed using coupled channel T-matrices, involving vector-vector channels of quarkonia. In these works the structures in the data emerge from the interplay of thresholds and resonances. While the number of poles that appear above the double J/ψ threshold depends on the number of channels, there is the non-trivial prediction that there should exist, if this dynamical picture were correct, a state located very near the double-$J/\psi(1S)$ threshold. In Ref. [333] it was shown that a $J/\psi(1S)J/\psi(1S)$ scattering potential sufficiently strong to bind is in fact consistent with our current understanding of $\pi J/\psi(1S)$ scattering as well as the strength of the $\pi\pi$ interactions. In Ref. [334] it is shown that the above mentioned data by LHCb, CMS and ATLAS are consistent with the presence of the above mentioned pole, whose pole position could be determined with improved accuracy. In this work it is also stressed that the nature of this $X(6200)$ cannot be determined based on the data currently available.

In contrast, Ref. [335,336] explains the double-$J/\psi(1S)$ data as cusps without nearby poles. This claim can be tested experimentally: if this explanation were correct, there should not be any narrow near threshold structure in the channel that generates the cusp, for that would call for a non-perturbative interaction in that channel, as pointed out in Ref. [337].

Acknowledgements

We thank Jean-Marc Richard for carefully reading the manuscript and for detailed and constructive suggestions.

References

[1] M. Gell-Mann, Phys. Lett. **8**, 214 (1964).

[2] G. Zweig, CERN-TH-401 (1964).

[3] Y. S. Kalashnikova and A. V. Nefediev, Phys. Rev. D **80**, 074004 (2009), [arXiv:0907.4901].

[4] M. Takizawa and S. Takeuchi, PTEP **2013**, 093D01 (2013), [arXiv:1206.4877].

[5] P. G. Ortega, D. R. Entem and F. Fernandez, J. Phys. G **40**, 065107 (2013), [arXiv:1205.1699].

[6] S. Coito, G. Rupp and E. van Beveren, Eur. Phys. J. C **73**, 3, 2351 (2013), [arXiv:1212.0648].

[7] I. K. Hammer, C. Hanhart and A. V. Nefediev, Eur. Phys. J. A **52**, 11, 330 (2016), [arXiv:1607.06971].

[8] C. Hanhart and A. Nefediev, Phys. Rev. D **106**, 11, 114003 (2022), [arXiv:2209.10165].

[9] L. R. Dai, J. Song and E. Oset, Phys. Lett. B **846**, 138200 (2023), [arXiv:2306.01607].

[10] J. Hoffer, G. Eichmann and C. S. Fischer, Phys. Rev. D **111**, 5, 054028 (2025), [arXiv:2409.05779].

[11] J. Hoffer, G. Eichmann and C. S. Fischer, Phys. Rev. D **109**, 7, 074025 (2024), [arXiv:2402.12830].

[12] L. Meng *et al.*, Phys. Rev. D **108**, 11, 114016 (2023), [arXiv:2310.13354].

[13] P. G. Ortega *et al.*, Phys. Rev. D **110**, 5, 054038 (2024), [arXiv:2406.01697].

[14] M. Y. Barabanov *et al.*, Prog. Part. Nucl. Phys. **116**, 103835 (2021), [arXiv:2008.07630].

[15] L. Maiani and A. Pilloni (2022), [arXiv:2207.05141].

[16] L. Maiani *et al.*, Phys. Rev. D **89**, 114010 (2014), [arXiv:1405.1551].

[17] R. F. Lebed and S. R. Martinez, Phys. Rev. D **106**, 7, 074007 (2022), [arXiv:2207.01101].

[18] N. Li *et al.*, Phys. Rev. D **88**, 11, 114008 (2013), [arXiv:1211.5007].

[19] L. Qiu, C. Gong and Q. Zhao, Phys. Rev. D **109**, 7, 076016 (2024), [arXiv:2311.10067].

[20] M. Neubert, Phys. Rept. **245**, 259 (1994), [hep-ph/9306320].

[21] A. V. Manohar and M. B. Wise, *Heavy quark physics*, volume 10 (2000), ISBN 978-0-521-03757-0, 978-1-009-40212-5.

[22] W. E. Caswell and G. P. Lepage, Phys. Lett. B **167**, 437 (1986).

[23] G. P. Lepage *et al.*, Phys. Rev. D **46**, 4052 (1992), [hep-lat/9205007].

[24] G. T. Bodwin, E. Braaten and G. P. Lepage, Phys. Rev. D **51**, 1125 (1995), [Erratum: Phys.Rev.D 55, 5853 (1997)], [hep-ph/9407339].

[25] N. Brambilla *et al.*, Nucl. Phys. B **566**, 275 (2000), [hep-ph/9907240].

[26] N. Brambilla *et al.*, Rev. Mod. Phys. **77**, 1423 (2005), [hep-ph/0410047].

[27] A. Pineda and J. Soto, Nucl. Phys. B Proc. Suppl. **64**, 428 (1998), [hep-ph/9707481].

[28] M. Berwein *et al.*, Phys. Rev. **D92**, 11, 114019 (2015), [arXiv:1510.04299].

[29] M. Berwein *et al.*, Phys. Rev. D **110**, 9, 094040 (2024), [arXiv:2408.04719].

[30] N. Brambilla *et al.*, Phys. Rev. D **97**, 1, 016016 (2018), [arXiv:1707.09647].

[31] N. Brambilla *et al.*, Phys. Rev. D **99**, 1, 014017 (2019), [Erratum: Phys.Rev.D 101, 099902 (2020)], [arXiv:1805.07713].

[32] J. Soto and J. Tarrús Castellà, Phys. Rev. D **102**, 1, 014012 (2020), [Erratum: Phys.Rev.D 110, 099901 (2024)], [arXiv:2005.00552].

[33] M. T. AlFiky, F. Gabbiani and A. A. Petrov, Phys. Lett. B **640**, WSU-HEP-0502, 238 (2006), [hep-ph/0506141].

[34] M. Albaladejo *et al.*, Eur. Phys. J. C **75**, 11, 547 (2015), [arXiv:1504.00861].

[35] S. Fleming *et al.*, Phys. Rev. D **76**, 034006 (2007), [hep-ph/0703168].

[36] M. P. Valderrama, Phys. Rev. D **85**, 114037 (2012), [arXiv:1204.2400].

[37] T. Mehen and J. W. Powell, Phys. Rev. **D84**, 114013 (2011), [arXiv:1109.3479].

[38] L. Dai, F.-K. Guo and T. Mehen, Phys. Rev. D **101**, 5, 054024 (2020), [arXiv:1912.04317].

[39] L. Dai *et al.*, Phys. Rev. D **107**, 7, 076001 (2023), [arXiv:2301.11950].

[40] M. Jansen, H. W. Hammer and Y. Jia, Phys. Rev. D **89**, 1, 014033 (2014), [arXiv:1310.6937].

[41] V. Baru *et al.*, Phys. Rev. D **84**, 074029 (2011), [arXiv:1108.5644].

[42] V. Baru *et al.*, Phys. Lett. B **726**, 537 (2013), [arXiv:1306.4108].

[43] M. Schmidt, M. Jansen and H. W. Hammer, Phys. Rev. D **98**, 1, 014032 (2018), [arXiv:1804.00375].

[44] V. Baru *et al.*, Phys. Rev. D **92**, 11, 114016 (2015), [arXiv:1509.01789].

[45] V. Baru *et al.*, Phys. Lett. B **763**, 20 (2016), [arXiv:1605.09649].

[46] Q. Wang *et al.*, Phys. Rev. D **98**, 7, 074023 (2018), [arXiv:1805.07453].

[47] V. Baru *et al.*, Phys. Rev. **D99**, 9, 094013 (2019), [arXiv:1901.10319].

Int. J. Mod. Phys. A 2026.41. Downloaded from www.worldscientific.com
by UNIVERSITY OF CALIFORNIA @ BERKELEY on 09/16/26. Re-use and distribution is strictly not permitted, except for Open Access articles.

[48] M.-L. Du *et al.*, Phys. Rev. D **105**, 1, 014024 (2022), [arXiv:2110.13765].

[49] E. Epelbaum, H.-W. Hammer and U.-G. Meißner, Rev. Mod. Phys. **81**, 1773 (2009), [arXiv:0811.1338].

[50] H.-W. Hammer and S. König, Lect. Notes Phys. **936**, 93 (2017), [arXiv:1610.02961].

[51] U.-G. Meißner and A. Rusetsky, *Effective Field Theories*, Cambridge University Press (2022), ISBN 978-1-108-68903-8.

[52] E. Braaten, H. W. Hammer and T. Mehen, Phys. Rev. D **82**, INT-PUB-10-019, HISKP-TH-10-12, 034018 (2010), [arXiv:1005.1688].

[53] J. Nieves and M. P. Valderrama, Phys. Rev. D **86**, 056004 (2012), [arXiv:1204.2790].

[54] F.-K. Guo *et al.*, Phys. Rev. D **88**, 054007 (2013), [arXiv:1303.6608].

[55] J. B. Habashi *et al.*, Annals Phys. **422**, 168283 (2020), [arXiv:2007.07360].

[56] M. Albaladejo, Phys. Lett. B **829**, 137052 (2022), [arXiv:2110.02944].

[57] F.-K. Guo *et al.*, Rev. Mod. Phys. **90**, 1, 015004 (2018), [arXiv:1705.00141].

[58] W. Lucha, D. Melikhov and H. Sazdjian, Phys. Rev. D **100**, 1, 014010 (2019), [arXiv:1901.03881].

[59] Z.-G. Wang (2025), [arXiv:2502.11351].

[60] N. Brambilla *et al.*, Phys. Rept. **873**, 1 (2020), [arXiv:1907.07583].

[61] N. Brambilla *et al.*, Eur. Phys. J. **C71**, 1534 (2011), [arXiv:1010.5827].

[62] H.-X. Chen *et al.*, Phys. Rept. **639**, 1 (2016), [arXiv:1601.02092].

[63] A. Ali, J. S. Lange and S. Stone, Prog. Part. Nucl. Phys. **97**, 123 (2017), [arXiv:1706.00610].

[64] R. F. Lebed, R. E. Mitchell and E. S. Swanson, Prog. Part. Nucl. Phys. **93**, 143 (2017), [arXiv:1610.04528].

[65] S. L. Olsen, T. Skwarnicki and D. Zieminska, Rev. Mod. Phys. **90**, 1, 015003 (2018), [arXiv:1708.04012].

[66] Y.-R. Liu *et al.*, Prog. Part. Nucl. Phys. **107**, 237 (2019), [arXiv:1903.11976].

[67] A. Esposito, A. Pilloni and A. D. Polosa, Phys. Rept. **668**, 1 (2017), [arXiv:1611.07920].

[68] M.-Z. Liu *et al.*, Phys. Rept. **1108**, 1 (2025), [arXiv:2404.06399].

[69] D. Johnson *et al.*, Ann. Rev. Nucl. Part. Sci. **74**, 583 (2024), [arXiv:2403.04051].

[70] C. Hanhart (2025), [arXiv:2504.06043].

[71] B. Aubert *et al.* (BaBar), Phys. Rev. Lett. **90**, 242001 (2003), [hep-ex/0304021].

[72] D. Besson *et al.* (CLEO), Phys. Rev. **D68**, 032002 (2003), [Erratum: Phys. Rev.D75,119908(2007)], [hep-ex/0305100].

[73] S. Godfrey, Phys. Lett. **B568**, 254 (2003), [hep-ph/0305122].

[74] H.-Y. Cheng and W.-S. Hou, Phys. Lett. **B566**, 193 (2003), [hep-ph/0305038].

[75] K. Terasaki, Phys. Rev. **D68**, 011501 (2003), [hep-ph/0305213].

[76] L. Maiani *et al.*, Phys. Rev. **D71**, 014028 (2005), [hep-ph/0412098].

[77] V. Dmitrasinovic, Phys. Rev. Lett. **94**, 162002 (2005).

[78] T. Barnes, F. E. Close and H. J. Lipkin, Phys. Rev. **D68**, 054006 (2003), [hep-ph/0305025].

[79] E. E. Kolomeitsev and M. F. M. Lutz, Phys. Lett. **B582**, 39 (2004), [hep-ph/0307133].

[80] A. Faessler *et al.*, Phys. Rev. **D76**, 014005 (2007), [arXiv:0705.0254].

[81] A. Faessler *et al.*, Phys. Rev. D **76**, 114008 (2007), [arXiv:0709.3946].

[82] M. F. M. Lutz and M. Soyeur, Nucl. Phys. **A813**, 14 (2008), [arXiv:0710.1545].

[83] L. Liu *et al.*, Phys. Rev. **D87**, 1, 014508 (2013), [arXiv:1208.4535].

[84] P. Colangelo and F. De Fazio, Phys. Lett. **B570**, 180 (2003), [hep-ph/0305140].

[85] X.-Y. Guo, Y. Heo and M. F. M. Lutz, Phys. Rev. **D98**, 1, 014510 (2018), [arXiv:1801.10122].

[86] H.-L. Fu *et al.*, Eur. Phys. J. A **58**, 4, 70 (2022), [arXiv:2111.09481].

[87] V. Dmitrasinovic, Phys. Rev. D **86**, 016006 (2012).

[88] M.-L. Du *et al.*, Phys. Rev. Lett. **126**, 19, 192001 (2021), [arXiv:2012.04599].

[89] R. Aaij *et al.* (LHCb), Phys. Rev. **D94**, 7, 072001 (2016), [arXiv:1608.01289].

[90] R. Aaij *et al.* (LHCb), Phys. Rev. D **94**, 7, 072001 (2016), [arXiv:1608.01289].

[91] L. Gayer *et al.* (Hadron Spectrum), JHEP **07**, 123 (2021), [arXiv:2102.04973].

[92] M. Albaladejo *et al.*, Phys. Lett. **B767**, 465 (2017), [arXiv:1610.06727].

[93] M.-L. Du *et al.*, Phys. Rev. **D98**, 9, 094018 (2018), [arXiv:1712.07957].

[94] G. Moir *et al.*, JHEP **10**, 011 (2016), [arXiv:1607.07093].

[95] A. Asokan *et al.*, Eur. Phys. J. C **83**, 9, 850 (2023), [arXiv:2212.07856].

[96] J. D. E. Yeo, C. E. Thomas and D. J. Wilson (Hadron Spectrum), JHEP **07**, 012 (2024), [arXiv:2403.10498].

[97] L. Maiani, A. D. Polosa and V. Riquer, Phys. Rev. D **110**, 3, 034014 (2024), [arXiv:2405.08545].

[98] F.-K. Guo and C. Hanhart (2025), [arXiv:2503.05372].

[99] E. B. Gregory *et al.* (2025), [arXiv:2503.23954].

[100] S. Cho *et al.* (ExHIC), Prog. Part. Nucl. Phys. **95**, 279 (2017), [arXiv:1702.00486].

[101] L. Fabbietti, V. Mantovani Sarti and O. Vazquez Doce, Ann. Rev. Nucl. Part. Sci. **71**, 377 (2021), [arXiv:2012.09806].

[102] S. Acharya *et al.* (ALICE), Phys. Rev. D **110**, 3, 032004 (2024), [arXiv:2401.13541].

[103] E. Epelbaum *et al.* (2025), [arXiv:2504.08631].

[104] E. J. Gustafson *et al.*, Phys. Rev. D **110**, 9, L091502 (2024), [arXiv:2311.00864].

[105] M. L. Du *et al.* (2025), [arXiv:2509.12133].

[106] R. J. Hudspith and D. Mohler, Phys. Rev. D **107**, 11, 114510 (2023), [arXiv:2303.17295].

[107] R. Aaij *et al.* (LHCb), Phys. Rev. D **102**, 112003 (2020), [arXiv:2009.00026].

[108] R. Aaij *et al.* (LHCb), Phys. Rev. Lett. **125**, 242001 (2020), [arXiv:2009.00025].

[109] R. Aaij *et al.* (LHCb), Phys. Rev. Lett. **133**, 13, 131902 (2024), [arXiv:2406.03156].

[110] R. Aaij *et al.* (LHCb), Phys. Rev. Lett. **134**, 10, 101901 (2025), [arXiv:2411.19781].

[111] R. Aaij *et al.* (LHCb), JHEP **07**, 140 (2024), [arXiv:2403.03586].

[112] M. Karliner and J. L. Rosner, Phys. Rev. D **102**, 9, 094016 (2020), [arXiv:2008.05993].

[113] X.-G. He, W. Wang and R. Zhu, Eur. Phys. J. C **80**, 11, 1026 (2020), [arXiv:2008.07145].

Int. J. Mod. Phys. A 2026.41. Downloaded from www.worldscientific.com
UNIVERSITY OF CALIFORNIA @ BERKELEY on 09/16/26. Re-use and distribution is strictly not permitted, except for Open Access articles.

[114] Z.-G. Wang, Int. J. Mod. Phys. A **35**, 30, 2050187 (2020), [arXiv:2008.07833].

[115] R. Molina and E. Oset, Phys. Lett. B **811**, 135870 (2020), [arXiv:2008.11171].

[116] Y. Huang *et al.*, Eur. Phys. J. C **80**, 10, 973 (2020), [arXiv:2008.07959].

[117] M.-Z. Liu, J.-J. Xie and L.-S. Geng, Phys. Rev. D **102**, 9, 091502 (2020), [arXiv:2008.07389].

[118] B. Wang and S.-L. Zhu, Eur. Phys. J. C **82**, 5, 419 (2022), [arXiv:2107.09275].

[119] Z.-L. Yue, C.-J. Xiao and D.-Y. Chen, Phys. Rev. D **107**, 3, 034018 (2023), [arXiv:2212.03018].

[120] J.-Z. Wang *et al.*, Phys. Rev. D **110**, 11, 114003 (2024), [arXiv:2408.08965].

[121] T. J. Burns and E. S. Swanson, Phys. Lett. B **813**, 136057 (2021), [arXiv:2008.12838].

[122] X.-H. Liu *et al.*, Eur. Phys. J. C **80**, 12, 1178 (2020), [arXiv:2008.07190].

[123] T. J. Burns and E. S. Swanson, Phys. Rev. D **103**, 1, 014004 (2021), [arXiv:2009.05352].

[124] R. Aaij *et al.* (LHCb), Phys. Rev. D **108**, 1, 012017 (2023), [arXiv:2212.02717].

[125] R. Molina and E. Oset, Phys. Rev. D **107**, 5, 056015 (2023), [arXiv:2211.01302].

[126] H.-W. Ke *et al.*, Phys. Rev. D **106**, 11, 114032 (2022), [arXiv:2210.06215].

[127] S. S. Agaev, K. Azizi and H. Sundu, Phys. Rev. D **107**, 9, 094019 (2023), [arXiv:2212.12001].

[128] B. Wang *et al.*, Phys. Rev. D **109**, 3, 034027 (2024), [arXiv:2309.02191].

[129] M.-Y. Duan *et al.*, Phys. Rev. D **108**, 7, 074006 (2023), [arXiv:2307.04092].

[130] D.-K. Lian *et al.*, Eur. Phys. J. C **84**, 1, 1 (2024), [arXiv:2302.01167].

[131] R. Aaij *et al.* (LHCb), Sci. Bull. **70**, 1432 (2025), [arXiv:2411.03399].

[132] L. Roca, J. M. Dias and E. Oset (2025), [arXiv:2502.18401].

[133] S. K. Choi *et al.* (Belle), Phys. Rev. Lett. **91**, 262001 (2003), [hep-ex/0309032].

[134] B. Aubert *et al.* (BaBar), Phys. Rev. **D71**, 071103 (2005), [hep-ex/0406022].

[135] R. Aaij *et al.* (LHCb), Phys. Rev. Lett. **115**, 072001 (2015), [arXiv:1507.03414].

[136] R. Aaij *et al.* (LHCb), Phys. Rev. Lett. **122**, 22, 222001 (2019), [arXiv:1904.03947].

[137] M. B. Voloshin, Prog. Part. Nucl. Phys. **61**, 455 (2008), [arXiv:0711.4556].

[138] R. Aaij *et al.* (LHCb), Nature Phys. **18**, 7, 751 (2022), [arXiv:2109.01038].

[139] R. Aaij *et al.* (LHCb), Nature Commun. **13**, 1, 3351 (2022), [arXiv:2109.01056].

[140] O. Deineka, I. Danilkin and M. Vanderhaeghen, Phys. Lett. B **827**, 136982 (2022), [arXiv:2111.15033].

[141] S. Prelovsek *et al.*, JHEP **06**, 035 (2021), [arXiv:2011.02542].

[142] K. Chilikin *et al.* (Belle), Phys. Rev. D **95**, 112003 (2017), [arXiv:1704.01872].

[143] R. Aaij *et al.* (LHCb), Phys. Rev. Lett. **110**, 222001 (2013), [arXiv:1302.6269].

[144] R. Aaij *et al.* (LHCb), Phys. Rev. **D92**, 1, 011102 (2015), [arXiv:1504.06339].

[145] T. Barnes and S. Godfrey, Phys. Rev. **D69**, 054008 (2004), [hep-ph/0311162].

[146] K. Abe *et al.* (Belle), Phys. Rev. Lett. **98**, 082001 (2007), [hep-ex/0507019].

[147] S. Uehara *et al.* (Belle), Phys. Rev. Lett. **96**, 082003 (2006), [hep-ex/0512035].

[148] R. Aaij *et al.* (LHCb), Phys. Rev. D **102**, 9, 092005 (2020), [arXiv:2005.13419].

[149] R. Aaij *et al.* (LHCb), JHEP **08**, 123 (2020), [arXiv:2005.13422].

[150] C. Hanhart *et al.*, Phys. Rev. D **76**, 034007 (2007), [arXiv:0704.0605].

[151] M. Ablikim *et al.* (BESIII), Phys. Rev. Lett. **132**, 15, 151903 (2024), [arXiv:2309.01502].

[152] T. Ji *et al.* (2025), [arXiv:2502.04458].

[153] Z.-H. Zhang *et al.*, JHEP **08**, 130 (2024), [arXiv:2404.11215].

[154] G. Barucca *et al.* (PANDA), Eur. Phys. J. A **55**, 3, 42 (2019), [arXiv:1812.05132].

[155] G. Barucca *et al.* (PANDA), Eur. Phys. J. A **57**, 6, 184 (2021), [arXiv:2101.11877].

[156] F.-K. Guo, Phys. Rev. Lett. **122**, 20, 202002 (2019), [arXiv:1902.11221].

[157] E. Braaten, L.-P. He and K. Ingles, Phys. Rev. D **100**, 3, 031501 (2019), [arXiv:1904.12915].

[158] S. Sakai, H.-J. Jing and F.-K. Guo, Phys. Rev. D **102**, 11, 114041 (2020), [arXiv:2008.10829].

[159] N. A. Tornqvist, Phys. Lett. **B590**, 209 (2004), [hep-ph/0402237].

[160] E. S. Swanson, Phys. Lett. **B588**, 189 (2004), [hep-ph/0311229].

[161] D. Gamermann and E. Oset, Phys. Rev. **D80**, 014003 (2009), [arXiv:0905.0402].

[162] J.-Z. Wang *et al.*, Phys. Rev. D **111**, 11, L111502 (2025), [arXiv:2404.16575].

[163] Y.-b. Dong *et al.*, Phys. Rev. D **77**, 094013 (2008), [arXiv:0802.3610].

[164] Y. Dong *et al.*, Phys. Rev. D **79**, 094013 (2009), [arXiv:0903.5416].

[165] P. Colangelo, F. De Fazio and G. Roselli, Phys. Rev. D **111**, 7, 074014 (2025), [arXiv:2501.15888].

[166] R. Aaij *et al.* (LHCb), JHEP **11**, 121 (2024), [arXiv:2406.17006].

[167] F.-K. Guo *et al.*, Phys. Lett. B **742**, 394 (2015), [arXiv:1410.6712].

[168] O. Andreev, Phys. Rev. D **106**, 6, 066002 (2022), [arXiv:2205.12119].

[169] B. Aubert *et al.* (BaBar), Phys. Rev. **D71**, 031501 (2005), [hep-ex/0412051].

[170] L. Maiani, A. D. Polosa and V. Riquer, Phys. Lett. **B778**, 247 (2018), [arXiv:1712.05296].

[171] L. Maiani, A. D. Polosa and V. Riquer, Phys. Rev. D **102**, 3, 034017 (2020), [arXiv:2005.08764].

[172] I. Matuschek *et al.*, Eur. Phys. J. A **57**, 3, 101 (2021), [arXiv:2007.05329].

[173] C. Bignamini *et al.*, Phys. Rev. Lett. **103**, 162001 (2009), [arXiv:0906.0882].

[174] A. Esposito *et al.*, Eur. Phys. J. C **81**, 669 (2021), [arXiv:2006.15044].

[175] P. Artoisenet and E. Braaten, Phys. Rev. **D81**, 114018 (2010), [arXiv:0911.2016].

[176] E. Braaten *et al.*, Phys. Rev. D **103**, 7, L071901 (2021), [arXiv:2012.13499].

[177] F.-K. Guo *et al.*, JHEP **05**, 138 (2014), [arXiv:1403.4032].

[178] M. Albaladejo *et al.*, Chin. Phys. **C41**, 12, 121001 (2017), [arXiv:1709.09101].

Int. J. Mod. Phys. A 2026.41. Downloaded from www.worldscientific.com
by UNIVERSITY OF CALIFORNIA @ BERKELEY on 09/16/26. Re-use and distribution is strictly not permitted, except for Open Access articles.

[179] A. Esposito *et al.*, Phys. Rev. D **105**, 3, L031503 (2022), [arXiv:2108.11413].

[180] S. Weinberg, Phys. Rev. **137**, B672 (1965).

[181] E. Braaten, Phys. Rev. D **91**, 11, 114007 (2015), [arXiv:1503.04791].

[182] A. Esposito *et al.*, Phys. Lett. B **847**, 138285 (2023), [arXiv:2307.11400].

[183] V. Baru *et al.*, Phys. Lett. B **833**, 137290 (2022), [arXiv:2110.07484].

[184] B. Aubert *et al.* (BaBar), Phys. Rev. Lett. **95**, 142001 (2005), [hep-ex/0506081].

[185] M. Ablikim *et al.* (BESIII), Phys. Rev. Lett. **118**, 9, 092001 (2017), [arXiv:1611.01317].

[186] M. Cleven *et al.*, Phys. Rev. **D90**, 7, 074039 (2014), [arXiv:1310.2190].

[187] L. von Detten *et al.*, Phys. Rev. D **109**, 11, 116002 (2024), [arXiv:2402.03057].

[188] S. X. Nakamura *et al.* (2023), [arXiv:2312.17658].

[189] C. Hanhart and E. Klempt, Int. J. Mod. Phys. A **35**, 05, 2050019 (2020), [arXiv:1906.11971].

[190] T. Barnes, S. Godfrey and E. S. Swanson, Phys. Rev. D **72**, 054026 (2005), [hep-ph/0505002].

[191] L.-C. Gui *et al.*, Phys. Rev. D **98**, 1, 016010 (2018), [arXiv:1801.08791].

[192] F. E. Close and P. R. Page, Phys. Lett. **B628**, 215 (2005), [hep-ph/0507199].

[193] E. Kou and O. Pene, Phys. Lett. **B631**, 164 (2005), [hep-ph/0507119].

[194] Yu. S. Kalashnikova and A. V. Nefediev, Phys. Rev. **D77**, 054025 (2008), [arXiv:0801.2036].

[195] Q. Wang and Q. Zhao (2025), [arXiv:2508.05304].

[196] M. Ablikim *et al.* (BESIII), Phys. Rev. Lett. **111**, 24, 242001 (2013), [arXiv:1309.1896].

[197] X. Li and M. B. Voloshin, Mod. Phys. Lett. **A29**, 12, 1450060 (2014), [arXiv:1309.1681].

[198] E. Braaten, C. Langmack and D. H. Smith, Phys. Rev. D **90**, 1, 014044 (2014), [arXiv:1402.0438].

[199] N. Brambilla *et al.*, Phys. Rev. D **101**, 5, 054040 (2020), [arXiv:1908.11699].

[200] N. Brambilla *et al.*, Phys. Rev. D **107**, 5, 054034 (2023), [arXiv:2212.09187].

[201] Q. Wang, C. Hanhart and Q. Zhao, Phys. Rev. Lett. **111**, 13, 132003 (2013), [arXiv:1303.6355].

[202] Y. Dong *et al.*, Phys. Rev. D **89**, 3, 034018 (2014), [arXiv:1310.4373].

[203] F.-K. Guo *et al.*, Phys. Lett. **B725**, 127 (2013), [arXiv:1306.3096].

[204] M. Ablikim *et al.* (BESIII), Phys. Rev. Lett. **112**, 9, 092001 (2014), [arXiv:1310.4101].

[205] Y. Dong *et al.*, Phys. Rev. D **90**, 7, 074032 (2014), [arXiv:1404.6161].

[206] Q. Wang *et al.*, Phys. Rev. **D89**, 3, 034001 (2014), [arXiv:1309.4303].

[207] V. Baru *et al.*, Phys. Rev. **D91**, 3, 034002 (2015), [arXiv:1501.02924].

[208] T. Ji *et al.*, Phys. Rev. Lett. **129**, 10, 102002 (2022), [arXiv:2205.10994].

[209] A. Ali *et al.*, Eur. Phys. J. **C78**, 1, 29 (2018), [arXiv:1708.04650].

[210] K. Chilikin *et al.* (Belle), Phys. Rev. **D88**, 7, 074026 (2013), [arXiv:1306.4894].

[211] R. Aaij *et al.* (LHCb), Phys. Rev. Lett. **112**, 22, 222002 (2014), [arXiv:1404.1903].

[212] L. Maiani, A. D. Polosa and V. Riquer, Symmetry **13**, 5, 751 (2021), [arXiv:2103.14356].

[213] Y.-H. Chen *et al.*, Phys. Rev. **D99**, 7, 074016 (2019), [arXiv:1902.10957].

[214] G. Cotugno *et al.*, Phys. Rev. Lett. **104**, 132005 (2010), [arXiv:0911.2178].

[215] F.-K. Guo *et al.*, Phys. Rev. **D82**, 094008 (2010), [arXiv:1005.2055].

[216] L.-Y. Dai, J. Haidenbauer and U. G. Meissner, Phys. Rev. **D96**, 11, 116001 (2017), [arXiv:1710.03142].

[217] Z.-Y. Cui *et al.* (2025), [arXiv:2506.06652].

[218] J. He *et al.*, Eur. Phys. J. C **80**, 3, 246 (2020), [arXiv:1912.08420].

[219] F.-L. Wang and X. Liu, Phys. Rev. D **102**, 9, 094006 (2020), [arXiv:2008.13484].

[220] H.-W. Ke, X.-H. Liu and X.-Q. Li, Chin. Phys. C **44**, 9, 093104 (2020), [arXiv:2004.03167].

[221] J.-R. Zhang, Phys. Rev. D **102**, 5, 054006 (2020), [arXiv:2004.10985].

[222] F.-K. Guo, C. Hanhart and U.-G. Meiß ner, Phys. Lett. B **665**, 26 (2008), [arXiv:0803.1392].

[223] F.-K. Guo, C. Hanhart and U.-G. Meiß ner, Phys. Rev. Lett. **102**, 242004 (2009), [arXiv:0904.3338].

[224] M. Ablikim *et al.* (BESIII), Phys. Rev. Lett. **110**, 252001 (2013), [arXiv:1303.5949].

[225] M. Ablikim *et al.* (BESIII), Phys. Rev. Lett. **112**, 2, 022001 (2014), [arXiv:1310.1163].

[226] P. Krokovny *et al.* (Belle), Phys. Rev. **D88**, 5, 052016 (2013), [arXiv:1308.2646].

[227] A. Bondar *et al.* (Belle), Phys. Rev. Lett. **108**, 122001 (2012), [arXiv:1110.2251].

[228] A. Garmash *et al.* (Belle), Phys. Rev. Lett. **116**, 21, 212001 (2016), [arXiv:1512.07419].

[229] V. Baru *et al.*, Eur. Phys. J. C **79**, 1, 46 (2019), [arXiv:1810.06921].

[230] A. E. Bondar *et al.*, Phys. Rev. **D84**, 054010 (2011), [arXiv:1105.4473].

[231] Y.-H. Chen, M.-L. Du and F.-K. Guo, Sci. China Phys. Mech. Astron. **67**, 9, 291011 (2024), [arXiv:2310.15965].

[232] Z.-M. Ding, H.-Y. Jiang and J. He, Eur. Phys. J. C **80**, 12, 1179 (2020), [arXiv:2011.04980].

[233] Y. Dong *et al.*, Phys. Rev. D **88**, 1, 014030 (2013), [arXiv:1306.0824].

[234] F. Goerke *et al.*, Phys. Rev. D **94**, 9, 094017 (2016), [arXiv:1608.04656].

[235] F. Goerke *et al.*, Phys. Rev. D **96**, 5, 054028 (2017), [arXiv:1707.00539].

[236] A. Ali *et al.*, Phys. Rev. **D91**, 1, 017502 (2015), [arXiv:1412.2049].

[237] M. B. Voloshin, Phys. Rev. **D84**, 031502 (2011), [arXiv:1105.5829].

[238] V. Baru *et al.*, JHEP **06**, 158 (2017), [arXiv:1704.07332].

[239] J.-Z. Wang *et al.*, Eur. Phys. J. C **80**, 11, 1040 (2020), [arXiv:2007.02263].

[240] M. Sadl *et al.*, Phys. Rev. D **111**, 5, 054513 (2025), [arXiv:2406.09842].

[241] T. Branz, T. Gutsche and V. E. Lyubovitskij, Phys. Rev. **D82**, 054025 (2010), [arXiv:1005.3168].

[242] P. Pakhlov, Phys. Lett. **B702**, 139 (2011), [arXiv:1105.2945].

[243] P. Pakhlov and T. Uglov, Phys. Lett. **B748**, 183 (2015), [arXiv:1408.5295].

[244] S. X. Nakamura and K. Tsushima, Phys. Rev. **D100**, 5, 051502 (2019), [arXiv:1901.07385].

Int. J. Mod. Phys. A 2026.41. Downloaded from www.worldscientific.com
UNIVERSITY OF CALIFORNIA @ BERKELEY on 09/16/26. Re-use and distribution is strictly not permitted, except for Open Access articles.

[245] M. Ablikim *et al.* (BESIII), Phys. Rev. Lett. **126**, 10, 102001 (2021), [arXiv:2011.07855].

[246] R. Aaij *et al.* (LHCb), Phys. Rev. Lett. **127**, 8, 082001 (2021), [arXiv:2103.01803].

[247] S. H. Lee, M. Nielsen and U. Wiedner, J. Korean Phys. Soc. **55**, 424 (2009), [arXiv:0803.1168].

[248] J. M. Dias, X. Liu and M. Nielsen, Phys. Rev. D **88**, 9, 096014 (2013), [arXiv:1307.7100].

[249] D. Ebert, R. N. Faustov and V. O. Galkin, Eur. Phys. J. C **58**, 399 (2008), [arXiv:0808.3912].

[250] J. Ferretti and E. Santopinto, JHEP **04**, 119 (2020), [arXiv:2001.01067].

[251] M. B. Voloshin, Phys. Lett. B **798**, 135022 (2019), [arXiv:1901.01936].

[252] D.-Y. Chen, X. Liu and T. Matsuki, Phys. Rev. Lett. **110**, 23, 232001 (2013), [arXiv:1303.6842].

[253] L. Meng, B. Wang and S.-L. Zhu, Phys. Rev. D **102**, 11, 111502 (2020), [arXiv:2011.08656].

[254] P. G. Ortega, D. R. Entem and F. Fernandez, Phys. Lett. B **818**, 136382 (2021), [arXiv:2103.07871].

[255] Z. Yang *et al.*, Phys. Rev. D **103**, 7, 074029 (2021), [arXiv:2011.08725].

[256] B. Wang, L. Meng and S.-L. Zhu, Phys. Rev. D **103**, 2, L021501 (2021), [arXiv:2011.10922].

[257] M.-L. Du *et al.*, Phys. Rev. D **105**, 7, 074018 (2022), [arXiv:2201.08253].

[258] R. M. Albuquerque, S. Narison and D. Rabetiarivony, Phys. Rev. D **103**, 7, 074015 (2021), [arXiv:2101.07281].

[259] Z.-H. Guo and J. A. Oller, Phys. Rev. D **103**, 5, 054021 (2021), [arXiv:2012.11904].

[260] N. Ikeno, R. Molina and E. Oset, Phys. Lett. B **814**, 136120 (2021), [arXiv:2011.13425].

[261] V. Baru *et al.*, Phys. Rev. D **105**, 3, 034014 (2022), [arXiv:2110.00398].

[262] M. Cleven *et al.*, Phys. Rev. **D92**, 1, 014005 (2015), [arXiv:1505.01771].

[263] X. Luo and S. X. Nakamura, Phys. Rev. D **107**, L011504 (2023), [arXiv:2207.12875].

[264] S. X. Nakamura and X. Luo, Nuovo Cim. C **47**, 4, 189 (2024), [arXiv:2309.14694].

[265] N. Brambilla *et al.* (2024), [arXiv:2411.14306].

[266] R. Albuquerque, S. Narison and D. Rabetiarivony, Nucl. Phys. A **1034**, 122637 (2023), [arXiv:2301.08199].

[267] S. S. Agaev, K. Azizi and H. Sundu, Nucl. Phys. B **975**, 115650 (2022), [arXiv:2108.00188].

[268] L.-Y. Dai *et al.*, Phys. Rev. D **105**, 5, L051507 (2022), [arXiv:2108.06002].

[269] C. Deng and S.-L. Zhu, Phys. Rev. D **105**, 5, 054015 (2022), [arXiv:2112.12472].

[270] P. G. Ortega *et al.*, Phys. Lett. B **841**, 137918 (2023), [arXiv:2211.06118].

[271] H.-W. Ke, X.-H. Liu and X.-Q. Li, Eur. Phys. J. C **82**, 2, 144 (2022), [arXiv:2112.14142].

[272] L. R. Dai *et al.*, Eur. Phys. J. C **83**, 10, 983 (2023), [arXiv:2304.01870].

[273] E. Braaten *et al.*, Phys. Rev. D **106**, 3, 034033 (2022), [arXiv:2202.03900].

[274] Z.-S. Jia *et al.*, Phys. Rev. D **107**, 7, 074029 (2023), [arXiv:2211.02479].

[275] M. Mikhasenko (2022), [arXiv:2203.04622].

[276] M. Padmanath and S. Prelovsek, Phys. Rev. Lett. **129**, 3, 032002 (2022), [arXiv:2202.10110].

[277] S. Chen *et al.*, Phys. Lett. B **833**, 137391 (2022), [arXiv:2206.06185].

[278] Y. Lyu *et al.*, Phys. Rev. Lett. **131**, 16, 161901 (2023), [arXiv:2302.04505].

[279] M.-L. Du *et al.*, Phys. Rev. Lett. **131**, 13, 131903 (2023), [arXiv:2303.09441].

[280] M.-L. Du, F.-K. Guo and B. Wu, Phys. Rev. Lett. **135**, 1, 011903 (2025), [arXiv:2408.09375].

[281] R. Bubna *et al.* (2025), [arXiv:2507.18399].

[282] M. T. Hansen, F. Romero-López and S. R. Sharpe, JHEP **06**, 051 (2024), [arXiv:2401.06609].

[283] L. Meng *et al.*, Phys. Rev. D **109**, 7, L071506 (2024), [arXiv:2312.01930].

[284] R. Bubna *et al.*, JHEP **05**, 168 (2024), [arXiv:2402.12985].

[285] M. Abolnikov *et al.*, Phys. Lett. B **860**, 139188 (2025), [arXiv:2407.04649].

[286] S. Collins *et al.*, Phys. Rev. D **109**, 9, 094509 (2024), [arXiv:2402.14715].

[287] F. Gil-Domínguez, A. Giachino and R. Molina, Phys. Rev. D **111**, 1, 016029 (2025), [arXiv:2409.15141].

[288] T. Whyte, D. J. Wilson and C. E. Thomas (Hadron Spectrum), Phys. Rev. D **111**, 3, 034511 (2025), [arXiv:2405.15741].

[289] L. Meng *et al.*, Phys. Rev. D **111**, 3, 034509 (2025), [arXiv:2411.06266].

[290] J. P. Ader, J. M. Richard and P. Taxil, Phys. Rev. D **25**, 2370 (1982).

[291] J. l. Ballot and J. M. Richard, Phys. Lett. B **123**, 449 (1983).

[292] S. Zouzou *et al.*, Z. Phys. C **30**, 457 (1986).

[293] D. M. Brink and F. Stancu, Phys. Rev. D **57**, 6778 (1998).

[294] M. Karliner and J. L. Rosner, Phys. Rev. Lett. **119**, 20, 202001 (2017), [arXiv:1707.07666].

[295] E. J. Eichten and C. Quigg, Phys. Rev. Lett. **119**, 20, 202002 (2017), [arXiv:1707.09575].

[296] W. Park, S. Noh and S. H. Lee, Nucl. Phys. A **983**, 1 (2019), [arXiv:1809.05257].

[297] S. Noh, W. Park and S. H. Lee, Phys. Rev. D **103**, 114009 (2021), [arXiv:2102.09614].

[298] Y. Ma *et al.*, Phys. Rev. D **109**, 7, 074001 (2024), [arXiv:2309.17068].

[299] P. Bicudo and M. Wagner (European Twisted Mass), Phys. Rev. D **87**, 11, 114511 (2013), [arXiv:1209.6274].

[300] Z. S. Brown and K. Orginos, Phys. Rev. D **86**, 114506 (2012), [arXiv:1210.1953].

[301] P. Bicudo *et al.*, Phys. Rev. D **93**, 3, 034501 (2016), [arXiv:1510.03441].

[302] P. Bicudo, J. Scheunert and M. Wagner, Phys. Rev. D **95**, 3, 034502 (2017), [arXiv:1612.02758].

[303] A. Francis *et al.*, Phys. Rev. Lett. **118**, 14, 142001 (2017), [arXiv:1607.05214].

[304] P. Junnarkar, N. Mathur and M. Padmanath, Phys. Rev. D **99**, 3, 034507 (2019), [arXiv:1810.12285].

[305] S. Meinel, M. Pflaumer and M. Wagner, Phys. Rev. D **106**, 3, 034507 (2022), [arXiv:2205.13982].

[306] P. Mohanta and S. Basak, Phys. Rev. D **102**, 9, 094516 (2020), [arXiv:2008.11146].

[307] C. Alexandrou *et al.* (2024), [arXiv:2404.03588].

[308] F. S. Navarra, M. Nielsen and S. H. Lee, Phys. Lett. B **649**, 166 (2007), [hep-ph/0703071].

[309] M.-L. Du *et al.*, Phys. Rev. D **87**, 1, 014003 (2013), [arXiv:1209.5134].

[310] Z.-G. Wang, Acta Phys. Polon. B **49**, 1781 (2018), [arXiv:1708.04545].

[311] R. Aaij *et al.* (LHCb), Sci. Bull. **65**, 23, 1983 (2020), [arXiv:2006.16957].

[312] A. Hayrapetyan *et al.* (CMS) (2023), [arXiv:2306.07164].

[313] Y. Xu (ATLAS), Acta Phys. Polon. Supp. **16**, 3, 21 (2023), [arXiv:2209.12173].

[314] A. Hayrapetyan *et al.* (CMS) (2025), [arXiv:2506.07944].

[315] J. H. Yin *et al.* (Belle) (2023), [arXiv:2305.17947].

[316] G. D. Alexeev *et al.* (COMPASS), Phys. Lett. B **838**, 137702 (2023), [arXiv:2204.01817].

[317] L. Maiani, Sci. Bull. **65**, 1949 (2020), [arXiv:2008.01637].

[318] K.-T. Chao and S.-L. Zhu, Sci. Bull. **65**, 23, 1952 (2020), [arXiv:2008.07670].

[319] J.-M. Richard, Sci. Bull. **65**, 1954 (2020), [arXiv:2008.01962].

[320] R. N. Faustov, V. O. Galkin and E. M. Savchenko, Phys. Rev. D **102**, 11, 114030 (2020), [arXiv:2009.13237].

[321] J. F. Giron and R. F. Lebed, Phys. Rev. D **102**, 7, 074003 (2020), [arXiv:2008.01631].

[322] X. Jin *et al.*, Eur. Phys. J. C **80**, 11, 1083 (2020), [arXiv:2006.13745].

[323] Q.-F. Lü, D.-Y. Chen and Y.-B. Dong, Eur. Phys. J. C **80**, 9, 871 (2020), [arXiv:2006.14445].

[324] Z.-H. Guo and J. A. Oller, Phys. Rev. D **103**, 3, 034024 (2021), [arXiv:2011.00978].

[325] P. G. Ortega, D. R. Entem and F. Fernández, Phys. Rev. D **108**, 9, 094023 (2023), [arXiv:2307.00532].

[326] M. Karliner and J. L. Rosner, Phys. Rev. D **102**, 11, 114039 (2020), [arXiv:2009.04429].

[327] B.-D. Wan and C.-F. Qiao, Phys. Lett. B **817**, 136339 (2021), [arXiv:2012.00454].

[328] B.-C. Yang, L. Tang and C.-F. Qiao, Eur. Phys. J. C **81**, 4, 324 (2021), [arXiv:2012.04463].

[329] R. M. Albuquerque *et al.*, Phys. Rev. D **102**, 9, 094001 (2020), [arXiv:2008.01569].

[330] X.-K. Dong *et al.*, Phys. Rev. Lett. **126**, 13, 132001 (2021), [arXiv:2009.07795].

[331] C. Gong *et al.*, Phys. Lett. B **824**, 136794 (2022), [arXiv:2011.11374].

[332] Z.-R. Liang, X.-Y. Wu and D.-L. Yao, Phys. Rev. D **104**, 3, 034034 (2021), [arXiv:2104.08589].

[333] X.-K. Dong *et al.*, Sci. Bull. **66**, 24, 2462 (2021), [arXiv:2107.03946].

[334] Y.-L. Song *et al.*, Phys. Rev. D **111**, 3, 034038 (2025), [arXiv:2411.12062].

[335] J.-Z. Wang *et al.*, Phys. Rev. D **103**, 7, 071503 (2021), [arXiv:2008.07430].

[336] J.-Z. Wang, X. Liu and T. Matsuki, Phys. Lett. B **816**, 136209 (2021), [arXiv:2012.03281].

[337] F.-K. Guo *et al.*, Phys. Rev. D **91**, 5, 051504 (2015), [arXiv:1411.5584].

Int. J. Mod. Phys. A 2026.41. Downloaded from www.worldscientific.com
by UNIVERSITY OF CALIFORNIA @ BERKELEY on 09/16/26. Re-use and distribution is strictly not permitted, except for Open Access articles.

79. Baryon Decay Parameters

Revised August 2019 by E.D. Commins (UC Berkeley).

79.1 Baryon semileptonic decays

The typical spin-1/2 baryon semileptonic decay is described by a matrix element, the hadronic part of which may be written as:

$$\overline{B}_f \left[f_1(q^2)\gamma_\lambda + i\, f_2(q^2)\sigma_{\lambda\mu}q^\mu + g_1(q^2)\gamma_\lambda\gamma_5 + g_3(q^2)\gamma_5 q_\lambda \right] B_i \ . \tag{79.1}$$

Here B_i and $\overline{B}_f$ are spinors describing the initial and final baryons, and $q = p_i - p_f$, while the terms in f_1, f_2, g_1, and g_3 account for vector, induced tensor ("weak magnetism"), axial vector, and induced pseudoscalar contributions [1]. Second-class current contributions are ignored here. In the limit of zero momentum transfer, f_1 reduces to the vector coupling constant g_V, and g_1 reduces to the axial-vector coupling constant g_A. The latter coefficients are related by Cabibbo's theory [2], generalized to six quarks (and three mixing angles) by Kobayashi and Maskawa [3]. The g_3 term is negligible for transitions in which an $e^\pm$ is emitted, and gives a very small correction, which can be estimated by PCAC [4], for $\mu^\pm$ modes. Recoil effects include weak magnetism, and are taken into account adequately by considering terms of first order in

$$\delta = \frac{m_i - m_f}{m_i + m_f} \ , \tag{79.2}$$

where m_i and m_f are the masses of the initial and final baryons.

The experimental quantities of interest are the total decay rate, the lepton-neutrino angular correlation, the asymmetry coefficients in the decay of a polarized initial baryon, and the polarization of the decay baryon in its own rest frame for an unpolarized initial baryon. Formulae for these quantities are derived by standard means [5] and are analogous to formulae for nuclear beta decay [6]. We use the notation of Ref. [6] in the Listings for neutron beta decay. For comparison with experiments at higher q^2, it is necessary to modify the form factors at $q^2 = 0$ by a "dipole" q^2 dependence, and for high-precision comparisons to apply appropriate radiative corrections [7].

The ratio g_A/g_V may be written as

$$g_A/g_V = |\, g_A/g_V \,|\, e^{i\phi_{AV}} \ . \tag{79.3}$$

The presence of a "triple correlation" term in the transition probability, proportional to $\mathrm{Im}(g_A/g_V)$ and of the form

$$\boldsymbol{\sigma_i} \cdot (\boldsymbol{p_\ell} \times \boldsymbol{p_\nu}) \tag{79.4}$$

for initial baryon polarization or

$$\boldsymbol{\sigma_f} \cdot (\boldsymbol{p_\ell} \times \boldsymbol{p_\nu}) \tag{79.5}$$

for final baryon polarization, would indicate failure of time-reversal invariance. The phase angle ϕ has been measured precisely only in neutron decay (and in ^{19}Ne nuclear beta decay), and the results are consistent with T invariance.

79.2 Hyperon nonleptonic decays

The amplitude for a spin-1/2 hyperon decaying into a spin-1/2 baryon and a spin-0 meson may be written in the form

$$M = G_F\, m_\pi^2 \cdot \overline{B}_f\, (A - B\gamma_5)\, B_i \ , \tag{79.6}$$

where A and B are constants [1]. The transition rate is proportional to

$$\begin{aligned} R = 1 &+ \gamma\, \widehat{\boldsymbol{\omega}}_f \cdot \widehat{\boldsymbol{\omega}}_i + (1-\gamma)(\widehat{\boldsymbol{\omega}}_f \cdot \widehat{\mathbf{n}})(\widehat{\boldsymbol{\omega}}_i \cdot \widehat{\mathbf{n}}) \\ &+ \alpha(\widehat{\boldsymbol{\omega}}_f \cdot \widehat{\mathbf{n}} + \widehat{\boldsymbol{\omega}}_i \cdot \widehat{\mathbf{n}}) + \beta\widehat{\mathbf{n}} \cdot (\widehat{\boldsymbol{\omega}}_f \times \widehat{\boldsymbol{\omega}}_i) \ , \end{aligned} \tag{79.7}$$

where $\widehat{\mathbf{n}}$ is a unit vector in the direction of the final baryon momentum, and $\widehat{\boldsymbol{\omega}}_i$ and $\widehat{\boldsymbol{\omega}}_f$ are unit vectors in the directions of the initial and final baryon spins. (The sign of the last term in the above equation was incorrect in our 1988 and 1990 editions.) The parameters α, β, and γ are defined as

$$\begin{aligned} \alpha &= 2\,\mathrm{Re}(s^*p)/(\,|\,s\,|^2 + |\,p\,|^2) \ , \\ \beta &= 2\,\mathrm{Im}(s^*p)/(\,|\,s\,|^2 + |\,p\,|^2) \ , \\ \gamma &= (\,|\,s\,|^2 - |\,p\,|^2)/(\,|\,s\,|^2 + |\,p\,|^2) \ , \end{aligned} \tag{79.8}$$

where $s = A$ and $p = |\,\mathbf{p}_f\,|\,B/(E_f + m_f)$; here E_f and $\mathbf{p}_f$ are the energy and momentum of the final baryon. The parameters α, β, and γ satisfy

$$\alpha^2 + \beta^2 + \gamma^2 = 1 \tag{79.9}$$

If the hyperon polarization is $\mathbf{P}_Y$, the polarization $\mathbf{P}_B$ of the decay baryons is

$$\mathbf{P}_B = \frac{(\alpha + \mathbf{P}_Y \cdot \widehat{\mathbf{n}})\widehat{\mathbf{n}} + \beta(\mathbf{P}_Y \times \widehat{\mathbf{n}}) + \gamma\widehat{\mathbf{n}} \times (\mathbf{P}_Y \times \widehat{\mathbf{n}})}{1 + \alpha\mathbf{P}_Y \cdot \widehat{\mathbf{n}}} \ . \tag{79.10}$$

Here $\mathbf{P}_B$ is defined in the rest system of the baryon, obtained by a Lorentz transformation along $\widehat{\mathbf{n}}$ from the hyperon rest frame, in which $\widehat{\mathbf{n}}$ and $\mathbf{P}_Y$ are defined.

An additional useful parameter ϕ is defined by

$$\beta = (1 - \alpha^2)^{1/2}\, \sin\phi \ . \tag{79.11}$$

In the Listings, we compile α and ϕ for each decay, since these quantities are most closely related to experiment and are essentially uncorrelated. When necessary, we have changed the signs of reported values to agree with our sign conventions. In the Baryon Summary Table, we give α, ϕ, and Δ (defined below) with errors, and also give the value of γ without error.

Time-reversal invariance requires, in the absence of final-state interactions, that s and p be relatively real, and therefore that $\beta = 0$. However, for the decays discussed here, the final-state interaction is strong. Thus

$$s = |\,s\,|\,e^{i\delta_s} \text{ and } p = |\,p\,|\,e^{i\delta_p} \ , \tag{79.12}$$

where δ_s and δ_p are the pion-baryon s- and p-wave strong interaction phase shifts. We then have

$$\beta = \frac{-2\,|\,s\,|\,|\,p\,|}{|\,s\,|^2 + |\,p\,|^2}\, \sin(\delta_s - \delta_p) \ . \tag{79.13}$$

One also defines $\Delta = -\tan^{-1}(\beta/\alpha)$. If T invariance holds, $\Delta = \delta_s - \delta_p$. For $\Lambda \to p\pi^-$ decay, the value of Δ may be compared with the s- and p-wave phase shifts in low-energy $\pi^- p$ scattering, and the results are consistent with T invariance.

See also the note on "Radiative Hyperon Decays" in this *Review*.

References

[1] E. Commins and P. Bucksbaum, *Weak Interactions of Leptons and Quarks* (1983), ISBN 978-0-521-27370-1, (Cambridge, USA: University Press, 473p.).

[2] N. Cabibbo, Phys. Rev. Lett. **10**, 531 (1963).

[3] M. Kobayashi and T. Maskawa, Prog. Theor. Phys. **49**, 652 (1973).

[4] M. Goldberger and S. Treiman, Phys. Rev. **111**, 354 (1958).

[5] P. Frampton and W.-K. Tung, Phys. Rev. D **3**, 1114 (1971).

[6] J. Jackson, S. Treiman and H. Wyld, Nucl. Phys. **4**, 206 (1957).

[7] Y. Yokoo, S. Suzuki and M. Morita, Prog. Theor. Phys. **50**, 1894 (1973).

Int. J. Mod. Phys. A 2026.41. Downloaded from www.worldscientific.com
UNIVERSITY OF CALIFORNIA @ BERKELEY on 09/16/26. Re-use and distribution is strictly not permitted, except for Open Access articles.

Int. J. Mod. Phys. A 2026.41. Downloaded from www.worldscientific.com
by UNIVERSITY OF CALIFORNIA @ BERKELEY on 09/16/26. Re-use and distribution is strictly not permitted, except for Open Access articles.

80. N and Δ Resonances

Revised August 2019 by V. Crede (Florida State U.), U. Thoma (Bonn U.), L. Tiator (KPH, JGU Mainz) and R.L. Workman (George Washington U.).

80.1 Introduction

The excited states of the nucleon have been studied in a large number of formation and production experiments. Until recently, the Breit-Wigner masses and widths, the pole positions, and the elasticities of the N and Δ resonances in the Baryon Summary Table came largely from partial-wave analyses of πN total, elastic, and charge-exchange scattering data. The most comprehensive analyses were carried out by the Karlsruhe-Helsinki (KH80) [1], Carnegie Mellon-Berkeley (CMB80) [2], and George Washington U (GWU) [3] groups. Partial-wave analyses have also been performed on much smaller πN reaction data sets to get ηN, $K\Lambda$, and $K\Sigma$ branching fractions (see the Listings for references). Other branching fractions come from analyses of $\pi N \to \pi\pi N$ data.

In recent years, a large amount of data on photoproduction of many final states has been accumulated, and these data are beginning to tell us much about the properties of baryon resonances. A survey of data on photoproduction can be found in the proceedings of recent conferences [4] and workshops [5], and in recent reviews [6, 7].

80.2 Naming scheme for baryon resonances

In the past, when nearly all resonance information came from elastic πN scattering, it was common to label resonances with the incoming partial wave $L_{2I,2J}$, as in $\Delta(1232)P_{33}$ and $N(1680)F_{15}$. However, most recent information has come from γN experiments. Therefore, we have replaced $L_{2I,2J}$ with the spin-parity J^P of the state, as in $\Delta(1232)3/2^+$ and $N(1680)5/2^+$; this name gives intrinsic properties of the resonance that are independent of the specific particles and reactions used to study them. This applies equally to all baryons, including Ξ resonances and charm baryons that are not produced in formation experiments. We do not, however, attach the mass or spin-parity to the names of the ground-state ("stable") baryons $N, \Lambda, \Sigma, \Xi, \Omega, \Lambda_c, \cdots$.

80.3 Using the N and Δ listings

Tables 80.1 and 80.2 list all the N and Δ entries in the Baryon Listings and give our evaluation of the overall status and the status channel by channel. Only the established resonances (overall status 3 or 4 stars) are promoted to the Baryon Summary Table. We long ago omitted from the Listings information from old analyses, prior to KH80 and CMB80, which can be found in earlier editions. A rather complete survey of older results was given in our 1982 edition [8].

As a rule, we award an overall status **** or *** only to those resonances which are derived from analyses of data sets that include precision differential cross sections and polarization observables, and are confirmed by independent analyses. All other signals are given ** or * status. New results that are not accompanied by proper error evaluation are less valuable for evaluating star ratings. The following criteria are guidelines for future error analysis.

1. Uncertainties in resonance parameters: The publication should have a detailed discussion on how the uncertainties of parameters were estimated. This requires that the error estimates go beyond the simple fit error as e.g. given by MINUIT, and the robustness of the results should be demonstrated.

2. Fit quality: Concrete measures for the fit quality should be provided. The reduced global χ^2 value of the fit, while useful, is insufficient. Other possibilities include quoting variations of local χ^2 values in kinematic regions where evidence for new resonances, or significantly improved information on resonance parameters, is claimed.

3. Weight factors in observables: Analyses sometimes use weight factors for certain data sets to either increase or reduce their impact on the results. This has been particularly important when polarization observables are involved, which often are sensitive to resonance amplitudes through interferences, but usually have much poorer statistics than differential cross section data. To evaluate sensitivities, the resulting resonance parameters should be checked against variations of the specific weight factors.

Table 80.1: The status of the N resonances and their decays. Sub-threshold decay modes are omitted. Only resonances with an overall status of *** or **** are included in the main Baryon Summary Table.

			Status as seen in									
Particle	J^P	overall	$N\gamma$	$N\pi$	$\Delta\pi$	$N\sigma$	$N\eta$	ΛK	ΣK	$N\rho$	$N\omega$	$N\eta'$
N	$1/2^+$	****										
$N(1440)$	$1/2^+$	****	****	****	****	***						
$N(1520)$	$3/2^-$	****	****	****	****	**	****					
$N(1535)$	$1/2^-$	****	****	****	***	*	****					
$N(1650)$	$1/2^-$	****	****	****	***	*	****	*				
$N(1675)$	$5/2^-$	****	****	****	****	***	*	*	*			
$N(1680)$	$5/2^+$	****	****	****	****	***	*	*	*			
$N(1700)$	$3/2^-$	***	**	***	***	*	*			*		
$N(1710)$	$1/2^+$	****	****	****	*		***	**	*	*	*	
$N(1720)$	$3/2^+$	****	****	****	***	*	*	****	*	*	*	
$N(1860)$	$5/2^+$	**	*	**		*	*					
$N(1875)$	$3/2^-$	***	**	**	*	**	*	*	*	*	*	
$N(1880)$	$1/2^+$	***	**	*	**	*	*	**	**		**	
$N(1895)$	$1/2^-$	****	****	*	*	*	****	**	**	*	*	****
$N(1900)$	$3/2^+$	****	****	**	**	*	*	**	**		*	**
$N(1990)$	$7/2^+$	**	**	**			*	*	*			
$N(2000)$	$5/2^+$	**	**	*	**	*	*				*	
$N(2040)$	$3/2^+$	*		*								
$N(2060)$	$5/2^-$	***	***	**	*	*	*	*	*	*	*	
$N(2100)$	$1/2^+$	***	**	***	**	**	*	*		*	*	**
$N(2120)$	$3/2^-$	***	***	**	**	**		**	*		*	*
$N(2190)$	$7/2^-$	****	****	****	****	**	*	**	*	*	*	
$N(2220)$	$9/2^+$	****	**	****			*	*	*			
$N(2250)$	$9/2^-$	****	**	****			*	*	*			
$N(2300)$	$1/2^+$	**		**								
$N(2570)$	$5/2^-$	**		**								
$N(2600)$	$11/2^-$	***		***								
$N(2700)$	$13/2^+$	**		**								

**** Existence is certain.
*** Existence is very likely.
** Evidence of existence is fair.
* Evidence of existence is poor.

Table 80.2: The status of the Δ resonances and their decays. Sub-threshold decay modes are omitted. Only resonances with an overall status of *** or **** are included in the main Baryon Summary Table.

			Status as seen in					
Particle	J^P	overall	$N\gamma$	$N\pi$	$\Delta\pi$	ΣK	$N\rho$	$\Delta\eta$
$\Delta(1232)$	$3/2^+$	****	****	****				
$\Delta(1600)$	$3/2^+$	****	****	***	****			
$\Delta(1620)$	$1/2^-$	****	****	****	****			
$\Delta(1700)$	$3/2^-$	****	****	****	****	*	*	
$\Delta(1750)$	$1/2^+$	*	*	*		*		
$\Delta(1900)$	$1/2^-$	***	***	***	*	**	*	
$\Delta(1905)$	$5/2^+$	****	****	****	**	*	*	**
$\Delta(1910)$	$1/2^+$	****	***	****	**	**		*
$\Delta(1920)$	$3/2^+$	***	***	***	***	**		**
$\Delta(1930)$	$5/2^-$	***	*	***	*	*		
$\Delta(1940)$	$3/2^-$	**	*	**	*			*
$\Delta(1950)$	$7/2^+$	****	****	****	**	***		
$\Delta(2000)$	$5/2^+$	**	*	**	*		*	
$\Delta(2150)$	$1/2^-$	*		*				
$\Delta(2200)$	$7/2^-$	***	***	**	***	**		
$\Delta(2300)$	$9/2^+$	**		**				
$\Delta(2350)$	$5/2^-$	*		*				
$\Delta(2390)$	$7/2^+$	*		*				
$\Delta(2400)$	$9/2^-$	**	**	**				
$\Delta(2420)$	$11/2^+$	****	*	****				
$\Delta(2750)$	$13/2^-$	**		**				
$\Delta(2950)$	$15/2^+$	**		**				

**** Existence is certain.
*** Existence is very likely.
** Evidence of existence is fair.
* Evidence of existence is poor.

Claims of evidence for new baryon states must be based on a sufficiently complete set of partial waves in the fit. The robustness of signals must be demonstrated, e.g. by examining the effect of higher partial waves in the fit.

80.4 Properties of resonances

Resonances are defined by poles of the S-matrix, whether in scattering, production or decay matrix elements. These are poles

Int. J. Mod. Phys. A 2026.41. Downloaded from www.worldscientific.com
UNIVERSITY OF CALIFORNIA @ BERKELEY on 09/16/26. Re-use and distribution is strictly not permitted, except for Open Access articles.

in the complex plane in s, as discussed in the new review on *Resonances*. As is traditional, we quote here the pole positions in the complex energy $w = \sqrt{s}$ plane. Crucially, the position of the pole of the S-matrix is independent of the process, and the production and decay properties factorize. This is the rationale for listing the pole position first for each resonance. These key properties of the S-matrix pole are in contrast to other quantities related to resonance phenomena, such as Breit-Wigner parameters or any K-matrix pole. Breit-Wigner parameters depend on the formalism used, such as angular-momentum barrier factors, or cut-off parameters, and the assumed or modeled background. However, the accurate determination of pole parameters from the analysis of data on the real energy axis is not necessarily simple, or even straightforward. It requires the implementation of the correct analytic structure of the relevant (often coupled) channels.

In principle, there are two ways to extract pole parameters from experimental data: (i) analytic continuation of theoretical single- or multi-channel models into the complex energy plane or (ii) local expansions of the partial-wave T-matrix amplitudes in the complex energy plane in the vicinity of a pole.

At present, poles are usually extracted using the first method [9–14], but considerable effort has been put into the development of alternate approaches, such as the speed plot [15], time delay [16], N/D method [17], regularization procedure [18], or Padè approximation [19].

Methods of the second type are based on the idea to use first or higher-order derivatives in energy to reduce the importance of, or totally eliminate, the background contribution. One either has to model the background contribution and introduce model dependence, or one is faced with numerical derivatives of single-energy data. In both cases, one reaches almost unsurmountable difficulties.

An alternate way to extract pole parameters from partial waves has been proposed by introducing a Laurent+Pietarinen (L+P) expansion [20–22]

$$T(W) = \sum_{i=1}^{N} \frac{Res_i}{W - W_i} + \sum_{j=1}^{M} \sum_{n=0}^{n_{max}} c_n^j \left(\frac{\alpha_j - \sqrt{x_j - W}}{\alpha_j + \sqrt{x_j - W}}\right)^n , \quad (80.1)$$

where $T(W)$ is a given partial wave amplitude, W_i and Res_i are the N complex pole positions and residues. The background is parameterized with M Pietarinen functions, where α_j are positive range parameters and x_j are real or complex branch points; c_n^j are real expansion coefficients.

The main idea of this procedure is to find the simplest analytic function, with well-defined poles and cuts, regardless of whether they are generated by a theoretical model or some energy-independent procedure. Instead of searching for the function which reproduces the input amplitudes over the complete complex energy plane, on all Riemann sheets, a representation is searched only in a limited complex energy range, near the real axis, which is defined by the radius of convergence of the Laurent decomposition, and which contains the input amplitudes. All details are found in Ref. [21]. Applications of the method can be found in [20–27].

80.5 Photoproduction

A new approach to the nucleon excitation spectrum is provided by dedicated facilities at the Universities of Bonn, Grenoble, and Mainz, and at the national laboratories Jefferson Lab in the US and SPring-8 in Japan. High-precision cross sections and polarization observables for the photoproduction of pseudoscalar mesons provide a data set that is approaching a "complete experiment," one that fully constrains the four complex amplitudes describing the spin-structure of the reaction [28]. A large number of photoproduction reactions has been studied.

In pseudoscalar meson photoproduction, the four independent helicity amplitudes can be expressed in terms of the four CGLN [29] amplitudes allowed by Lorentz and gauge invariance. These amplitudes can be expanded in a series of electric and magnetic multipoles. Except for $J = 1/2$, one electric and one magnetic multipole contributes to each J^P combination.

For a given state, these two amplitudes determine the resonance photo-decay helicity amplitudes $A_{1/2}$ and $A_{3/2}$. As described below, this resonance extraction has been carried out either assuming a Breit-Wigner resonance or at the pole.

If a Breit-Wigner parametrization is used, the $N\gamma$ partial width, Γ_γ, is given in terms of the helicity amplitudes $A_{1/2}$ and $A_{3/2}$ by

$$\Gamma_\gamma = \frac{k_{\rm BW}^2}{\pi} \frac{2m_N}{(2J+1)m_{\rm BW}} \left(|A_{1/2}|^2 + |A_{3/2}|^2 \right) . \quad (80.2)$$

Here m_N and $m_{\rm BW}$ are the nucleon and resonance masses, J is the resonance spin, and $k_{\rm BW}$ is the photon c.m. decay momentum. Most earlier analyses have provided these real quantities $A_{1/2}$ and $A_{3/2}$.

More recent studies have quoted related complex quantities, evaluated at the T-matrix pole. These complex helicity amplitudes, $\tilde{A}_{1/2}$ and $\tilde{A}_{3/2}$, can be cast onto the form

$$\tilde{A}_h = \sqrt{\frac{\pi(2J+1)w_{\rm pole}}{m_N k_{\rm pole}^2}} \frac{Res(T_h(\gamma N \to N\, b))}{\sqrt{Res(T\,(N\, b \to N\, b))}} \quad (80.3)$$

where the residues (Res) are evaluated at the pole position, $w_{\rm pole}$, and $k_{\rm pole}^2 = (w_{\rm pole}^2 - m_N^2)^2/4w_{\rm pole}^2$ [30]. For Breit-Wigner amplitudes, $w_{\rm pole} = m_{\rm BW}$ and $\tilde{A}_h = A_h$. Similar relations for the photo and electro couplings at the pole position can be found in [31,32].

The determination of eight real numbers from four complex amplitudes (with one overall phase undetermined) requires at least seven independent measurements. At least one further measurement is required to resolve discrete ambiguities that result from the fact that data are proportional to squared amplitudes. Photon beams and nucleon targets can be polarized (with linear or circular polarization $P_\perp$, $P_\odot$ and $\vec{T}$, respectively); the recoil polarization of the outgoing baryon $\vec{R}$ can be measured. The experiments can be divided into three classes: (1) the beam and target are polarized (BT); (2) the beam is polarized and the recoil baryon polarization is measured (BR); (3) the target is polarized and the recoil polarization is measured (TR). Different sign conventions are used in the literature, as summarized in [33].

One of the best studied reactions is $\gamma p \to \Lambda K^+$. Published data include differential cross sections, the beam asymmetry Σ, the target asymmetry T, the recoil polarization P, and the BR double-polarization variables $C_{x'}, C_{z'}, O_{x'}$, and $O_{z'}$. For the photoproduction of pions and etas, off proton and neutron targets, differential cross sections, single- and double-polarization asymmetries have been measured, mainly for pions.

80.6 Electroproduction

Electroproduction of mesons provides information on the internal structure of resonances. The helicity amplitudes are functions of the (squared) momentum transfer $Q^2 = -(e-e')^2$, where e and e' are the 4-momenta of the incident and scattered electron, and a third amplitude, $S_{1/2}$, measures the resonance response to the longitudinal component of the virtual photon. Most data stem from the reactions $e^-p \to e^-\, n\pi^+$ and $e^-p \to e^-\, p\pi^0$ but also the reactions $e^-p \to e^-\, p\eta$, $e^-p \to e^-\, p\pi^+\pi^-$, and $e^-p \to e^-\, \Lambda(\Sigma^0)K^+$ have been studied. The data and their interpretation are reviewed in Refs. [34,35].

The transition to the $\Delta(1232)3/2^+$ is often quantified in terms of the magnetic dipole transition moment M_{1+} (or the magnetic transition form factor $G^*_{M,Ash}(Q^2)$) [36], and the electric and scalar quadrupole transition moments E_{1+} and S_{1+}. Figure 80.1 shows the strength of the $p \to \Delta^+$ transition plotted versus the photon virtuality Q^2. At $Q^2 = 0$, M_{1+} dominates the resonance transition strength. The two amplitudes E_{1+} and S_{1+} imply a quadrupole deformation of the transition to the lowest excited state. The magnitude of $R_{EM} = E_{1+}/M_{1+}$ remains nearly constant, while the magnitude of $R_{SM} = S_{1+}/M_{1+}$ increases rapidly up to 25% at the highest Q^2 value.

Figure 80.2 shows the transverse and scalar helicity amplitudes for the $N(1440)1/2^+$, $N(1520)3/2^-$, and $N(1535)1/2^-$ resonances from JLab [34]. Similar results have been achieved at

Int. J. Mod. Phys. A 2026.41. Downloaded from www.worldscientific.com
by UNIVERSITY OF CALIFORNIA @ BERKELEY on 09/16/26. Re-use and distribution is strictly not permitted, except for Open Access articles.

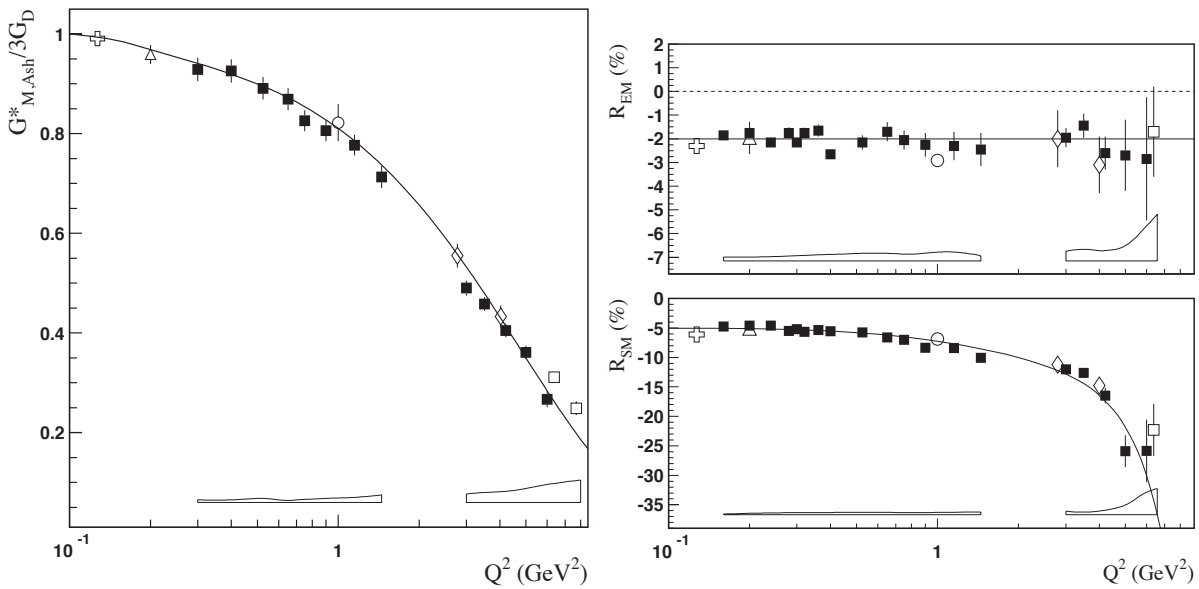

Figure 80.1: Left: The magnetic transition form factor for the $\gamma^* p \to \Delta^+(1232)$ transition versus the photon virtuality Q^2. Right: The electric and scalar quadrupole ratios R_{EM} and R_{SM}. The different symbols are results from different experiments at JLab (squares, diamonds, circle) and MAMI (triangle, cross). The boxes near the horizontal axis indicate model uncertainties of the squares. Curves to guide the eyes.

Mainz [35]. For the states $N(1440)1/2^+$ and $N(1520)3/2^-$, helicity amplitudes and $\pi\Delta$ and ρp decays were determined at JLab in an analysis of $\pi^+\pi^- p$ electroproduction [37]. The data show distinctly different Q^2 dependencies that indicate different internal structures.

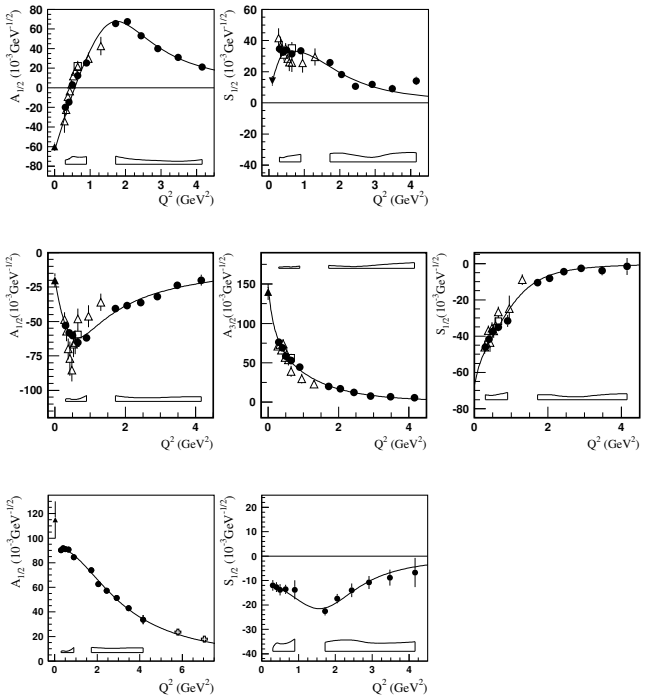

Figure 80.2: Transverse and scalar (longitudinal) helicity amplitudes for $\gamma p \to N(1440)1/2^+$ (top), $\gamma p \to N(1520)3/2^-$ (center), and $\gamma p \to N(1535)1/2^-$ (bottom) as extracted from the JLab/-CLAS data in $n\pi^+$ production (full circles), MAMI/A1 data in $p\pi^0$ production (full down triangle), in $p\pi^+\pi^-$ (open triangles), and combined single and double pion production (open squares). The solid triangle is the PDG 2014 value at $Q^2 = 0$. The open boxes are the model uncertainties of the full circles.

The $N(1520)3/2^-$ helicity amplitudes reveal the dominance of its three-quark nature: the $A_{3/2}$ amplitude is large at the photon point and decreases rapidly $\sim Q^{-5}$ with increasing Q^2; $A_{1/2}$ is small at the photon point, increases rapidly with Q^2 and then falls off with $\sim Q^{-3}$. Quantitative agreement with the data is, however, achieved only when meson cloud effects are included.

At high Q^2, both amplitudes for $N(1440)1/2^+$ are qualitatively described by light front quark models [38]: at short distances the resonance behaves as expected from a radial excitation of the nucleon. On the other hand, $A_{1/2}$ changes sign at about 0.6 GeV^2. This remarkable behavior has not been observed before for any nucleon form factor or transition amplitude. Obviously, an important change in the structure occurs when the resonance is probed as a function of Q^2.

The Q^2 dependence of $A_{1/2}$ of the $N(1535)1/2^-$ resonance exhibits the expected Q^{-3} dependence, except for small Q^2 values where meson cloud effects set in.

Figure 80.3 shows the transverse and scalar amplitudes for three states in the 3rd nucleon resonance region, the $\Delta(1620)1/2^-$, the $N(1675)5/2^-$ and $N(1680)5/2^+$. The latter two states have nearly degenerate masses and are parity partners. In the quark model picture, the transverse amplitudes for $N(1675)5/2^-$ on the proton are suppressed due to the Moorhouse selection rule, allowing for a quantitative evaluation of the meson-baryon contributions. The data show significant meson-baryon strength in the $A_{1/2}$ amplitude even at quite high Q^2, while $A_{3/2}$ drops much faster with Q^2. $N(1680)5/2^+$ shows qualitatively the features predicted in constituent quark models, a dominant $A_{3/2}$ at the real photon point that drops rapidly with increasing Q^2, while $A_{1/2}$ becomes the dominant contribution at high Q^2, indicating a switch of the helicity structure in the resonance transition at short distances.

80.7 Partial wave analyses

Several PWA groups are now actively involved in the analysis of the new data. The GWU group maintains a nearly complete database covering reactions from πN and KN elastic scattering to $\gamma N \to N\pi$, $N\eta$, and $N\eta'$. It is presently the only group determining πN elastic amplitudes from scattering data in sliced energy bins. Given the high-precision of photoproduction data already or soon to be collected, the spectrum of N and Δ resonances will in the near future be better known.

Fits to the data are performed by various groups with the aim

Int. J. Mod. Phys. A 2026.41. Downloaded from www.worldscientific.com
UNIVERSITY OF CALIFORNIA @ BERKELEY on 09/16/26. Re-use and distribution is strictly not permitted, except for Open Access articles.

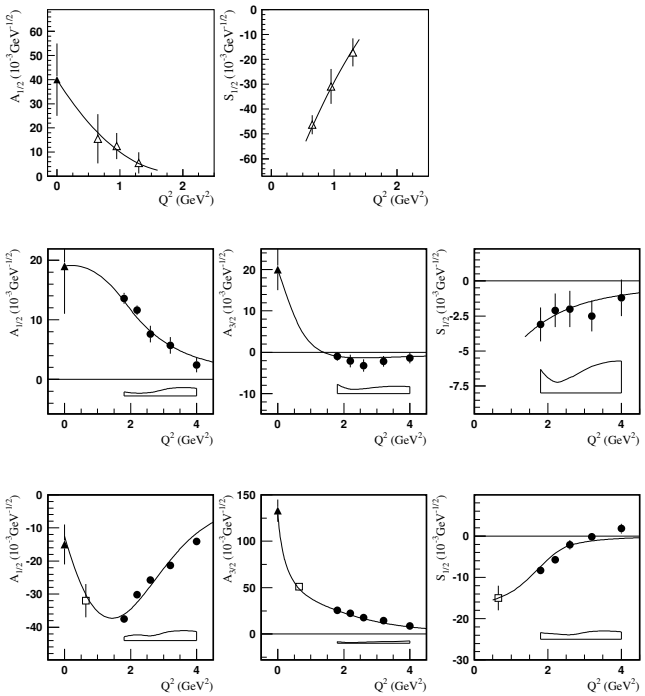

Figure 80.3: Transverse and scalar helicity amplitudes for $\gamma p \to \Delta(1620)1/2^-$ (top), $\gamma p \to N(1675)5/2^-$ (center), and $\gamma p \to N(1680)5/2^+$ (bottom) as extracted from the JLab/CLAS data in $n\pi^+$ production (full circles), $p\pi^+\pi^-$ (open triangles), combined single and double pion production (open square). The solid triangle is the 2014 PDG value at $Q^2 = 0$. The open boxes are the model uncertainties of the full circles. The curves are to guide the eye.

to understand the reaction dynamics and to identify N and Δ resonances. For practical reasons, approximations have to be made. We mention several analyses here: (1) The Mainz unitary isobar model [39] focuses on the correct treatment of the low-energy domain. Resonances are added to the unitary amplitude as a sum of Breit-Wigner amplitudes. This model also obtains resonance transition form factors and helicity amplitudes from electroproduction [35]. (2) For $N\pi$ electroproduction, the Yerevan/JLab group uses both the unitary isobar model and the dispersion relation approach developed in [38]. A phenomenological model was developed to extract resonance couplings and partial decay widths from exclusive $\pi^+\pi^-p$ electroproduction [37]. (3) Multichannel analyses using K-matrix parameterizations derive background terms from a chiral Lagrangian - providing a microscopical description of the background - (Giessen [40, 41]) or from phenomenology (KSU [42, 43], Bonn-Gatchina [44]). (4.) Several groups (EBAC-Jlab [45, 46], ANL-Osaka [47], Dubna-Mainz-Taipeh [48], Bonn-Jülich [49–51], Valencia [52]) use dynamical reaction models, driven by chiral Lagrangians, which take dispersive parts of intermediate states into account. Several other groups have made important contributions. The Giessen group pioneered multichannel analyses of large data sets on pion- and photo-induced reactions [40, 41]. The Bonn-Gatchina group included recent high-statistics data and reported systematic searches for new baryon resonances in all relevant partial waves. A summary of their results can be found in [44].

References

[1] G. Höhler, Pion-Nucleon Scattering, Landolt-Börnstein Vol. I/9b2 (1983), ed. H. Schopper, Springer Verlag.

[2] R. E. Cutkosky *et al.*, in "*VI International Conference on Baryon Resonances*," 19 (1980), Toronto, ed. N. Isgur.

[3] R. Arndt *et al.*, Phys. Rev. C **74**, 045205 (2006), [arXiv:nucl-th/0605082].

[4] "Hadron 2011: 14th International Conference on Hadron Spectroscopy", München, Germany, June, 13 - 17, 2011, published in eConf.

[5] "NSTAR 2013: 9th International Workshop on the Physics of Excited Nucleons", 27-30 May 2013, Peñíscola, Spain.

[6] E. Klempt and J.-M. Richard, Rev. Mod. Phys. **82**, 1095 (2010), [arXiv:0901.2055].

[7] V. Crede and W. Roberts, Rept. Prog. Phys. **76**, 076301 (2013), [arXiv:1302.7299].

[8] M. Roos *et al.* (Particle Data Group), Phys. Lett. B **111**, 1 (1982).

[9] M. Doring *et al.*, Nucl. Phys. A **829**, 170 (2009), [arXiv:0903.4337].

[10] N. Suzuki *et al.*, Phys. Rev. Lett. **104**, 042302 (2010), [arXiv:0909.1356].

[11] R. Cutkosky *et al.*, Phys. Rev. D **20**, 2839 (1979).

[12] R. Arndt *et al.*, Phys. Rev. C **69**, 035213 (2004), [arXiv:nucl-th/0311089].

[13] M. Batinic *et al.*, Phys. Rev. C **51**, 2310 (1995), [Erratum: Phys.Rev.C 57, 1004–1005 (1998)], [arXiv:nucl-th/9501011]; M. Batinić *et al.*, Phys. Scr. **58**, 15 (1998).

[14] A. Anisovich *et al.*, Eur. Phys. J. A **48**, 15 (2012), and references therein., [arXiv:1112.4937].

[15] G. Höhler, PiN Newslett. **1993**, 9, 1 (1993).

[16] N. Kelkar and M. Nowakowski, Phys. Rev. A **78**, 012709 (2008), and references therein., [arXiv:0805.0608].

[17] G. F. Chew and S. Mandelstam, Phys. Rev. **119**, 467 (1960).

[18] S. Ceci *et al.*, Phys. Rev. D **77**, 116007 (2008), [hep-ph/0609236].

[19] P. Masjuan and J. J. Sanz-Cillero, Eur. Phys. J. C **73**, 2594 (2013), [arXiv:1306.6308].

[20] A. Švarc *et al.*, Phys. Rev. C **88**, 3, 035206 (2013), [arXiv:1307.4613].

[21] A. Švarc *et al.*, Phys. Rev. C **89**, 4, 045205 (2014), [arXiv:1401.1947].

[22] A. Švarc *et al.*, Phys. Lett. B **755**, 452 (2016), [arXiv:1512.07403].

[23] A. Švarc *et al.*, Phys. Rev. C **89**, 6, 065208 (2014), [arXiv:1404.1544].

[24] A. Švarc *et al.*, Phys. Rev. C **91**, 1, 015207 (2015), [arXiv:1405.6474].

[25] L. Tiator *et al.*, Phys. Rev. C **94**, 6, 065204 (2016), [arXiv:1606.00371].

[26] A. Anisovich *et al.*, Eur. Phys. J. A **53**, 12, 242 (2017), [arXiv:1712.07537].

[27] A. Anisovich *et al.*, Phys. Rev. Lett. **119**, 6, 062004 (2017), [arXiv:1712.07549].

[28] C. Fasano, F. Tabakin and B. Saghai, Phys. Rev. C **46**, 2430 (1992).

[29] G. Chew *et al.*, Phys. Rev. **106**, 1345 (1957).

[30] R. Workman, L. Tiator and A. Sarantsev, Phys. Rev. C **87**, 6, 068201 (2013), [arXiv:1304.4029].

[31] N. Suzuki, T. Sato and T.-S. Lee, Phys. Rev. C **82**, 045206 (2010), [arXiv:1006.2196].

[32] H. Kamano, Phys. Rev. C **88**, 045203 (2013), [arXiv:1305.6678].

[33] A. Sandorfi *et al.*, AIP Conf. Proc. **1432**, 1, 219 (2012), [arXiv:1108.5411].

[34] I. Aznauryan and V. Burkert, Prog. Part. Nucl. Phys. **67**, 1 (2012), [arXiv:1109.1720].

[35] L. Tiator *et al.*, Eur. Phys. J. ST **198**, 141 (2011), [arXiv:1109.6745]; S. Štajner *et al.*, Phys. Rev. Lett. **119**, 2, 022001 (2017).

[36] W. Ash *et al.*, Phys. Lett. B **24**, 165 (1967).

[37] V. Mokeev *et al.* (CLAS), Phys. Rev. C **86**, 035203 (2012), [arXiv:1205.3948].

[38] I. Aznauryan, Phys. Rev. C **67**, 015209 (2003), [arXiv:nucl-th/0206033].

[39] D. Drechsel, S. Kamalov and L. Tiator, Eur. Phys. J. A **34**, 69 (2007), [arXiv:0710.0306].

[40] G. Penner and U. Mosel, Phys. Rev. C **66**, 055211 (2002), [arXiv:nucl-th/0207066].

[41] G. Penner and U. Mosel, Phys. Rev. C **66**, 055212 (2002), [arXiv:nucl-th/0207069].

[42] D. Manley and E. Saleski, Phys. Rev. D **45**, 4002 (1992).

[43] M. Shrestha and D. Manley, Phys. Rev. C **86**, 055203 (2012), [arXiv:1208.2710].

[44] A. Anisovich *et al.*, Eur. Phys. J. A **48**, 15 (2012), [arXiv:1112.4937].

[45] A. Matsuyama, T. Sato and T.-S. Lee, Phys. Rept. **439**, 193 (2007), [arXiv:nucl-th/0608051].

[46] T. Sato and T.-S. Lee, J. Phys. G **36**, 073001 (2009), [arXiv:0902.3653].

[47] H. Kamano *et al.*, Phys. Rev. C **88**, 3, 035209 (2013), [arXiv:1305.4351].

[48] G. Y. Chen *et al.*, Phys. Rev. C **76**, 035206 (2007), [arXiv:nucl-th/0703096].

[49] M. Doring *et al.*, Phys. Lett. B **681**, 26 (2009), [arXiv:0903.1781].

[50] M. Doring *et al.*, Nucl. Phys. A **829**, 170 (2009), [arXiv:0903.4337].

[51] D. Ronchen *et al.*, Eur. Phys. J. A **49**, 44 (2013), [arXiv:1211.6998].

[52] S. Sarkar, E. Oset and M. Vicente Vacas, Nucl. Phys. A **750**, 294 (2005), [Erratum: Nucl.Phys.A 780, 90–90 (2006)], [arXiv:nucl-th/0407025].

Int. J. Mod. Phys. A 2026.41. Downloaded from www.worldscientific.com
by UNIVERSITY OF CALIFORNIA @ BERKELEY on 09/16/26. Re-use and distribution is strictly not permitted, except for Open Access articles.

81. Λ and Σ Resonances

Revised August 2021 by V. Crede (Florida State U.), E. Klempt (Bonn U.), U. Thoma (Bonn U.), L. Tiator (KPH, JGU Mainz) and R.L. Workman (George Washington U.).

81.1 Introduction

For several decades, there has been very little new experimental data bearing on the properties of Λ and Σ resonances. An exception was the study at JLab of the reactions $\gamma p \to K^+\Sigma^\pm\pi^\mp$ and $\gamma p \to K^+\Sigma^0\pi^0$ [1], which established the spin and parity of the $\Lambda(1405)$ [2]. There was also from BNL new data on the very low energy region of K^-p scattering [3–7]. Otherwise, the field is starved for data. Recent analyses (see below) have improved what we know about the *properties* of the known Λ and Σ resonances, but the *established* resonances are the same ones that were listed in our 1984 edition [8] except for the $\Sigma(2250)$ which we consider 2-star only due to its unkown spin-parity. The 1990 Review [9] gave a full report of the status of Lambda and Sigma hyperons, and included Argand plots from the partial-wave analyses. The 2018 Review [10] has a short survey of the $\Sigma(1670)$-region.

In the last few years, four groups have re-analyzed K^-p reactions using more extensive collections of the old data. These analyses justify an update of the status of the Λ and Σ resonances. Although they have not established any new resonances, they have provided at least some evidence for new states and have given a better understanding of the old ones.

Table 81.1: The status of the Λ resonances. Only those with an overall status of *** or **** are included in the main Baryon Summary Table. Decay channels other than $N\overline{K}$ and $\Sigma\pi$ are only given for *** and **** resonances.

Particle	J^P	Overall status	Status as seen in — $N\overline{K}$	$\Sigma\pi$	Other channels
$\Lambda(1116)$	$1/2^+$	****			$N\pi$ (weak decay)
$\Lambda(1380)$	$1/2^-$	**	**	**	
$\Lambda(1405)$	$1/2^-$	****	****	****	
$\Lambda(1520)$	$3/2^-$	****	****	****	$\Lambda\pi\pi, \Lambda\gamma, \Sigma\pi\pi$
$\Lambda(1600)$	$1/2^+$	****	***	****	$\Lambda\pi\pi, \Sigma(1385)\pi$
$\Lambda(1670)$	$1/2^-$	****	****	****	$\Lambda\eta$
$\Lambda(1690)$	$3/2^-$	****	****	***	$\Lambda\pi\pi, \Sigma(1385)\pi$
$\Lambda(1710)$	$1/2^+$	*	*	*	
$\Lambda(1800)$	$1/2^-$	***	***	**	$\Lambda\pi\pi, N\overline{K}^*$
$\Lambda(1810)$	$1/2^+$	***	**	**	$N\overline{K}^*$
$\Lambda(1820)$	$5/2^+$	****	****	****	$\Sigma(1385)\pi$
$\Lambda(1830)$	$5/2^-$	****	****	****	$\Sigma(1385)\pi$
$\Lambda(1890)$	$3/2^+$	****	****	**	$\Sigma(1385)\pi, N\overline{K}^*$
$\Lambda(2000)$	$1/2^-$	*	*	*	
$\Lambda(2050)$	$3/2^-$	*	*	*	
$\Lambda(2070)$	$3/2^+$	*	*	*	
$\Lambda(2080)$	$5/2^-$	*	*	*	
$\Lambda(2085)$	$7/2^+$	**	**	*	
$\Lambda(2100)$	$7/2^-$	****	****	**	$N\overline{K}^*$
$\Lambda(2110)$	$5/2^+$	***	**	**	$N\overline{K}^*$
$\Lambda(2325)$	$3/2^-$	*	*		
$\Lambda(2350)$	$9/2^+$	***	***	*	
$\Lambda(2585)$		*	*		

Tables 81.1 and 81.2 give our evaluation of the status, both overall and channel by channel, of each Λ and Σ resonance in the Particle Listings. In making these evaluations, we considered, in addition to the four analyses [11–14], the ratings that predated them. The ratings use a 1- to 4-star system. For more details on the evaluation of the overall star ratings, see [15]. The main Summary Table includes only established states with an overall status of 3 or 4 stars; as has already been noted, these are the same fourteen Λ resonances (including $\Lambda(1116)$) and nine Σ resonances instead of the former ten (including $\Sigma(1193)3/2^+$, and $\Sigma(1385)3/2^+$) that had long been in the Table. In addition, there are seven 1-star and two 2-star Λ's, and fourteen 1-star and three 2-star Σ's in the Particle Listings.

Table 81.2: The status of the Σ resonances. Only those with an overall status of *** or **** are included in the main Baryon Summary Table. Decay channels other than $N\overline{K}$, $\Lambda\pi$ and $\Sigma\pi$ are only given for *** and **** resonances.

Particle	J^P	Overall status	Status as seen in — $N\overline{K}$	$\Lambda\pi$	$\Sigma\pi$	Other channels
$\Sigma(1193)$	$1/2^+$	****				$N\pi$ (weak decay)
$\Sigma(1385)$	$3/2^+$	****		****	****	$\Lambda\gamma$
$\Sigma(1580)$	$3/2^-$	*	*	*	*	
$\Sigma(1620)$	$1/2^-$	*	*	*	*	
$\Sigma(1660)$	$1/2^+$	***	***	***	***	
$\Sigma(1670)$	$3/2^-$	****	****	****	****	
$\Sigma(1750)$	$1/2^-$	***	***	**	***	$\Sigma\eta$
$\Sigma(1775)$	$5/2^-$	****	****	****	**	
$\Sigma(1780)$	$3/2^+$	*	*	*	*	
$\Sigma(1880)$	$1/2^+$	**	**	*		
$\Sigma(1900)$	$1/2^-$	**	**	*	**	
$\Sigma(1910)$	$3/2^-$	***	*	*	**	
$\Sigma(1915)$	$5/2^+$	****	***	***	***	
$\Sigma(1940)$	$3/2^+$	*	*		*	
$\Sigma(2010)$	$3/2^-$	*	*	*		
$\Sigma(2030)$	$7/2^+$	****	****	****	**	$\Delta(1232)\overline{K}, N\overline{K}^*$, $\Sigma(1385)\pi$
$\Sigma(2070)$	$5/2^+$	*	*		*	
$\Sigma(2080)$	$3/2^+$	*		*		
$\Sigma(2100)$	$7/2^-$	*	*	*	*	
$\Sigma(2110)$	$1/2^-$	*	*	*	*	
$\Sigma(2230)$	$3/2^+$	*	*	*	*	
$\Sigma(2250)$		**	**	*	*	
$\Sigma(2455)$		*	*			
$\Sigma(2620)$		*	*			
$\Sigma(3000)$		*	*	*		
$\Sigma(3170)$		*				

81.2 New analyses

The new analysis progress was pioneered by the Kent group which collected a large fraction of the available data and performed a comprehensive partial wave analysis [11,16]. K^-p scattering into a pseudoscalar meson and an octet baryon is governed by two complex amplitudes; hence four quantities need to be measured to fully construct the amplitudes (up to an arbitrary phase per energy and angular bin). Discussions of complete experiments also generally assume perfect data (no experimental uncertainties); realistic uncertainties further complicate the task of amplitude extraction. Here, the available data are limited to the differential cross section and the target or hyperon recoil polarization P; data on the polarization transfer do not exist. The authors of Ref. [16] overcame this difficulty by using start values for the partial wave amplitudes determined in [17] and/or from an energy-dependent fit and by freezing or releasing sets of amplitudes. The resulting amplitudes were fitted with a unitary multichannel parameterization [11].

The JPAC group presented a coupled-channel fit to the $\bar{K}N$ partial waves derived by the Kent group [13]. The JPAC approach was based on the K-matrix formalism. Special attention was paid to the analytical properties of the amplitudes determined by the square-root unitary branch points and the continuation to the complex angular momentum plane. The fit described the Kent partial waves reasonably well. However, when observables were calculated from their partial-wave amplitudes, significant discrepancies became apparent. The results were therefore not included in the RPP.

The ANL-Osaka group derived the energy-dependent amplitudes in fits to a large subset of the data collected in Ref. [16] and

Int. J. Mod. Phys. A 2026.41. Downloaded from www.worldscientific.com
UNIVERSITY OF CALIFORNIA @ BERKELEY on 09/16/26. Re-use and distribution is strictly not permitted, except for Open Access articles.

Int. J. Mod. Phys. A 2026.41. Downloaded from www.worldscientific.com
by UNIVERSITY OF CALIFORNIA @ BERKELEY on 09/16/26. Re-use and distribution is strictly not permitted, except for Open Access articles.

further data sets described in Ref. [18]. Their fits were based on a phenomenological SU(3) Lagrangian [18]. The two ANL-Osaka models agree on the leading contributions but differ significantly in cases with weaker candidates [12].

The Bonn-Gatchina (BnGa) group added further (old) data to those analyzed in Ref. [16]. The data set was fitted in a modified K-matrix approach and the resulting amplitudes were compared with those from Refs. [16, 18]. New resonances were found, other states, mostly one and two-star states could not be confirmed; all resonances were tested for their statistical significance. Additional states with any set of quantum numbers were tested and were found to produce only small improvements in the fit [14]. In Ref. [19], properties of the full set of contributing hyperons were reported.

The star ratings of Λ and Σ resonances given in our earlier editions, and the new results from the Kent, ANL-Osaka and BnGa groups were used to update the star rating of the hyperon resonances. In [19], the overall star rating is directly estimated, for [11] we estimate the star rating from the branching-ratio uncertainties. In [12], two solutions are given but no uncertainties for branching ratios. The overall star ratings are based on the evidence for the resonances in the new analyses as well as their consistency including also the results of earlier analyses given in [20]. For further details see also [15].

We decided to remove the three so-called *bumps* $\Sigma(1480)$, $\Sigma(1560)$, $\Sigma(1670)$, and $\Sigma(1690)$ as well as $\Sigma(1620)$ from production experiments. The entries from $\Sigma(1770)1/2^+$ are now listed under $\Sigma(1660)1/2^+$ and $\Sigma(1880)1/2^+$, the entries from $\Sigma(1730)3/2^+$ and $\Sigma(1840)3/2^+$ are now combined to one $\Sigma(1780)3/2^+$. The one-star $\Sigma(2000)1/2^-$ is combined with a new one-star $\Sigma(2160)1/2^-$ to a single one-star $\Sigma(2110)1/2^-$. Apart from $\Lambda(1380)1/2^-$, four further new resonances were included in the Listings: $\Lambda(2070)3/2^+$, $\Lambda(2080)5/2^-$, $\Sigma(2010)3/2^-$, and $\Sigma(2230)3/2^+$, all with one star.

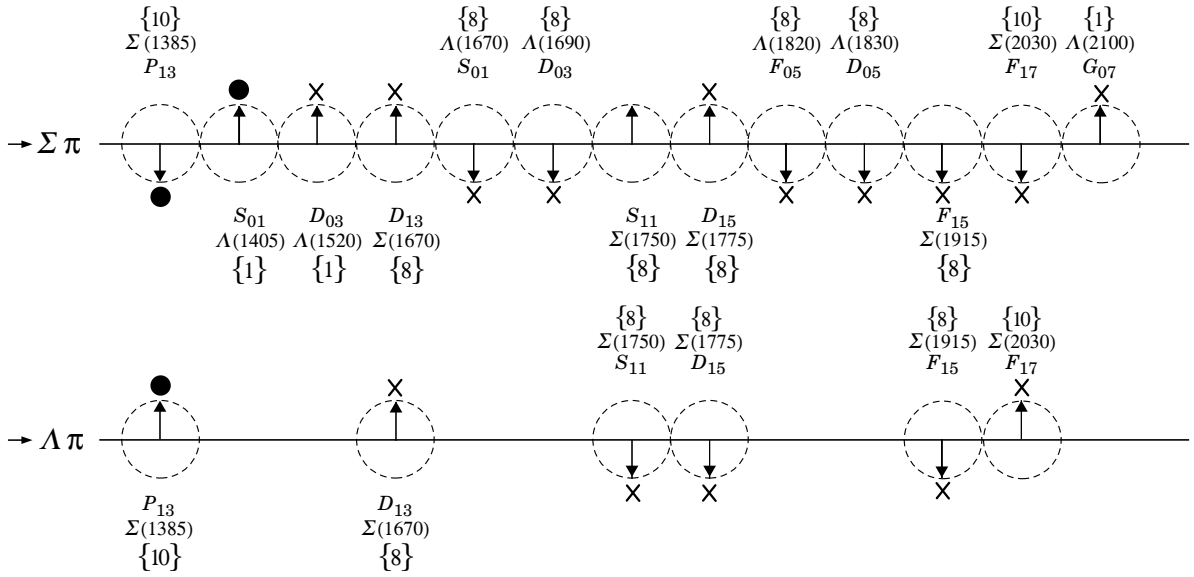

Figure 81.1: The signs of the imaginary parts of resonating amplitudes in the $\overline{K}N \to \Lambda\pi$ and $\Sigma\pi$ channels. The signs of the $\Sigma(1385)$ and $\Lambda(1405)$, marked with a •, are set by convention, and then the others are determined relative to them. The signs required by the SU(3) assignments of the resonances are shown with an arrow, and the experimentally determined signs are shown with an ×.

81.3 Sign conventions for resonance couplings

In terms of the isospin-0 and isospin-1 elastic scattering amplitudes A_0 and A_1, the amplitude for $K^-p \to \overline{K}^0 n$ scattering is $\pm(A_1 - A_0)/2$, where the sign depends on conventions used in conjunction with the Clebsch-Gordan coefficients (such as, is the baryon or the meson the "first" particle). If this reaction is partial-wave analyzed and if the overall phase is chosen so that, say, the $\Sigma(1775)5/2^-(D_{15})$ amplitude at resonance points along the positive imaginary axis (points "up"), then any Σ at resonance will point "up" and any Λ at resonance will point "down" (along the negative imaginary axis). Thus the phase at resonance determines the isospin. The above ignores background amplitudes in the resonating partial waves. That is the basic idea. In a similar but somewhat more complicated way, the phases of the $\overline{K}N \to \Lambda\pi$ and $\overline{K}N \to \Sigma\pi$ amplitudes for a resonating wave help determine the SU(3) multiplet to which the resonance belongs. Again, a convention has to be adopted for some overall arbitrary phases: which way is "up"? Our convention is that of Levi-Setti [21] and is shown in Fig. 81.1, which also compares experimental results with theoretical predictions for the signs of several resonances. In the Listings, a + or − sign in front of a measurement of an inelastic resonance coupling indicates the sign (the *absence* of a sign means that the sign is not determined, *not* that it is positive). Also other decay modes can be used to assign a hyperon to a SU(3) multiplet [22, 23]. Modern analyses determine properties of resonances at the pole position. In these analyses, the + or − sign is replaced by a phase. Background amplitudes can lead to significant phase shifts, and an additional phase shift due to rescattering is admitted in some analyses. In comparison to quark model predictions [19, 24], three Λ spin doublets can be identified as being mainly SU(3) singlets: the well-known ($\Lambda(1405)1/2^-$, $\Lambda(1520)3/2^-$), the ($\Lambda(2080)5/2^-$, $\Lambda(2100)7/2^-$), and ($\Lambda(2070)3/2^+$, $\Lambda(2110)5/2^+$).

81.4 The $\Lambda(1405)$

In coupled-channels calculations based on the chiral SU(3) effective field theory, the strongly attractive forces between $N\overline{K}$ and $\Sigma\pi$ generate five poles, one SU(3) singlet pole, two Λ octet poles and two (or one) octet Σ poles (see Section 82). In quark models, these five states are $\Lambda(1405)$, $\Lambda(1670)$, $\Lambda(1800)$, $\Sigma(1620)$, and $\Sigma(1750)$. The octet states are found 100 to 150 MeV above the corresponding nucleon resonances. In chiral SU(3) effective field theories, at least three of these states are seen in the 1300 to 1600 MeV mass range. The appearance of two Λ poles in this mass range, a narrow SU(3) octet at ∼1420 MeV and a wider SU(3) singlet at ∼1380 MeV, was unexpected. This approach has been pursued by a number of groups; for a summary of the results see our Review 82, "Pole Structure of the $\Lambda(1405)$ Region". In the Listings, we have introduced the $\Lambda(1380)$ as a new candidate reso-

nance (with two stars), named in accordance with its approximate pole position. The second SU(3) octet Λ state is the well-known $\Lambda(1670)$. The masses of the two associated Σ states are uncertain so far, and no new entries are introduced in the Listings.

In traditional approaches only one resonance was seen in this mass region, the narrow state at 1405 MeV. It was reported to be the SU(3) singlet state a long time ago in Ref. [25], in agreement with the quark-model expectations but in contrast to the findings based on coupled-channels calculations within chiral SU(3) effective field theories. In the Listings, the $\Lambda(1405)$ has been retained with its traditional name. In quark models, this state is identified with the SU(3) singlet state, the two Λ octet states with $\Lambda(1670)$ and $\Lambda(1800)$, and the two Σ states with $\Sigma(1620)$ and $\Sigma(1750)$.

81.5 Uncertainties on masses and widths

The uncertainties quoted on resonance parameters from partial-wave analyses are often only statistical, and the parameters can change beyond these uncertainties when a different parametrization of the waves is used. Furthermore, the different analyses use more or less the same data, so it is not really appropriate to treat the different determinations of the resonance parameters as independent or to average them. In any case, the spread of the masses, widths, and branching fractions from the different analyses is certainly a better indication of the uncertainties than are the quoted uncertainties. In the Listings, we usually give a range reflecting the spread of the values rather than a particular value with error.

81.6 Production experiments

Partial-wave analyses of course separate partial waves, whereas a peak in a cross section or an invariant mass distribution usually cannot be disentangled from background and analyzed for its quantum numbers; and more than one resonance may be contributing to the peak. The $\Sigma(1385)$ and $\Lambda(1405)$ lie below the $\overline{K}N$ threshold and nearly everything about $\Sigma(1385)$ is learned from production experiments. Our knowledge on $\Lambda(1405)$ benefits greatly from photoproduction of the three $\Sigma\pi$ charge states [1, 2] and from the precise measurement of the energy shift and width of the kaonic hydrogen atom [26].

Production and formation experiments agree quite well in the case of $\Lambda(1520)$ and results have been combined. Above this mass, no new results on peak hunting have been reported for about 40 years. For these early results, we refer the reader to our earlier editions. In photoproduction with energetic photons [27, 28] or at LHCb [29], hyperons are produced abundantly. So far, no attempt has been made to extract hyperon properties from these data. New data on hyperon spectroscopy can be expected from J-PARC [30], JLAB [31], and the forthcoming PANDA experiment [32].

References

[1] K. Moriya *et al.* (CLAS), Phys. Rev. **C87**, 3, 035206 (2013), [arXiv:1301.5000].

[2] K. Moriya *et al.* (CLAS), Phys. Rev. Lett. **112**, 8, 082004 (2014), [arXiv:1402.2296].

[3] A. Starostin *et al.* (Crystal Ball), Phys. Rev. **C64**, 055205 (2001).

[4] S. Prakhov *et al.*, Phys. Rev. **C69**, 042202 (2004).

[5] S. Prakhov *et al.* (Crystall Ball), Phys. Rev. **C70**, 034605 (2004).

[6] R. Manweiler *et al.*, Phys. Rev. **C77**, 015205 (2008).

[7] S. Prakhov *et al.*, Phys. Rev. **C80**, 025204 (2009), [arXiv:0812.1888].

[8] C. G. Wohl *et al.* (Particle Data Group), Rev. Mod. Phys. **56**, S1 (1984).

[9] J. J. Hernandez *et al.* (Particle Data Group), Phys. Lett. **B239**, 1 (1990), [Erratum: Phys. Lett.B253,524(1991)].

[10] M. Tanabashi *et al.* (Particle Data Group), Phys. Rev. **D98**, 3, 030001 (2018).

[11] H. Zhang *et al.*, Phys. Rev. **C88**, 3, 035205 (2013), [arXiv:1305.4575].

[12] H. Kamano *et al.*, Phys. Rev. **C92**, 2, 025205 (2015), [Erratum: Phys. Rev.C95,no.4,049903(2017)], [arXiv:1506.01768].

[13] C. Fernandez-Ramirez *et al.*, Phys. Rev. **D93**, 3, 034029 (2016), [arXiv:1510.07065].

[14] M. Matveev *et al.*, Eur. Phys. J. **A55**, 10, 179 (2019), [arXiv:1907.03645].

[15] E. Klempt *et al.* (Baryon@PDG Group), Eur. Phys. J. A **56**, 10, 261 (2020), [arXiv:2007.04232].

[16] H. Zhang *et al.*, Phys. Rev. **C88**, 3, 035204 (2013), [arXiv:1305.3598].

[17] J. Tulpan, PhD Disserstation, Kent State University (2007).

[18] H. Kamano *et al.*, Phys. Rev. **C90**, 6, 065204 (2014), [arXiv:1407.6839].

[19] A. V. Sarantsev *et al.*, Eur. Phys. J. **A55**, 10, 180 (2019), [arXiv:1907.13387].

[20] J. Beringer *et al.* (Particle Data Group), Phys. Rev. **D86**, 010001 (2012).

[21] R. Levi Setti, Conf. Proc. **C690625**, 339 (1969).

[22] V. Guzey and M. V. Polyakov, Annalen Phys. **13**, 673 (2004).

[23] V. Guzey and M. V. Polyakov (2005), [hep-ph/0512355].

[24] U. Loring, B. C. Metsch and H. R. Petry, Eur. Phys. J. **A10**, 447 (2001), [hep-ph/0103290].

[25] R. D. Tripp *et al.*, Phys. Rev. Lett. **21**, 1721 (1968).

[26] M. Bazzi *et al.* (SIDDHARTA), Phys. Lett. **B704**, 113 (2011), [arXiv:1105.3090].

[27] K. Moriya *et al.* (CLAS), Phys. Rev. **C88**, 045201 (2013), [Addendum: Phys. Rev.C88,no.4,049902(2013)], [arXiv:1305.6776].

[28] B. Dey *et al.* (CLAS), Phys. Rev. **C89**, 5, 055208 (2014), [Addendum: Phys. Rev.C90,no.1,019901(2014)], [arXiv:1403.2110].

[29] R. Aaij *et al.* (LHCb), Phys. Rev. Lett. **115**, 072001 (2015), [arXiv:1507.03414].

[30] K. Hicks and H. Sako, Proposal for J-PARC E45 .

[31] M. Amaryan *et al.* (KLF) (2020), [arXiv:2008.08215].

[32] F. Iazzi (PANDA), AIP Conf. Proc. **1743**, 1, 050006 (2016).

Int. J. Mod. Phys. A 2026.41. Downloaded from www.worldscientific.com
UNIVERSITY OF CALIFORNIA @ BERKELEY on 09/16/26. Re-use and distribution is strictly not permitted, except for Open Access articles.

82. Pole Structure of the $\Lambda(1405)$ Region

Revised Feb. 2025 by T. Hyodo (RCNP, Osaka U.; Tokyo Metropolitan U.) and U.-G. Meißner (Bonn U.; FZ Jülich).

The $\Lambda(1405)$ resonance emerges in the meson-baryon scattering amplitude with the strangeness $S = -1$ and isospin $I = 0$. It is the archetype of what is called a dynamically generated resonance, as pioneered by Dalitz and Tuan [1]. The most powerful and systematic approach for the low-energy regime of the strong interactions is chiral perturbation theory (ChPT), see e.g. Ref. [2]. A perturbative calculation is, however, not applicable to this sector because of the existence of the $\Lambda(1405)$ just below the $\bar{K}N$ threshold. In this case, ChPT has to be combined with a non-perturbative resummation technique, just as in the case of the nuclear forces. By solving the Lippmann-Schwinger equation with the interaction kernel determined by ChPT and using a particular regularization, in Ref. [3] a successful description of the low-energy K^-p scattering data as well as the mass distribution of the $\Lambda(1405)$ was achieved (for further developments, see Refs. [4–8] and references therein). As will be discussed below, lattice QCD calculations are also getting close to unraveling the complex structure of the scattering amplitude in this energy region.

The study of the pole structure was initiated by Ref. [9], which finds two poles of the scattering amplitude in the complex energy plane between the $\bar{K}N$ and $\pi\Sigma$ thresholds. The spectrum in experiments exhibits one effective resonance shape, while the existence of two poles results in reaction-dependent lineshapes [10]. The origin of this two-pole structure is attributed to the two attractive channels of the leading order interaction in the SU(3) basis (singlet and octet) [10] and in the isospin basis ($\bar{K}N$ and $\pi\Sigma$) [11]. It is remarkable that the sign and the strength of the leading order interaction is determined by a low-energy theorem of chiral symmetry, i.e. the so-called Weinberg-Tomozawa term. The two-pole nature of the $\Lambda(1405)$ is qualitatively different from the case of the N(1440) resonance. Two poles of the N(1440) appear on different Riemann sheets of the complex energy plane separated by the $\pi\Delta$ branch point. These poles reflect a single state, with a nearby pole and a more distant shadow pole. In contrast, the two poles in the $\Lambda(1405)$ region on the same Riemann sheet (where $\pi\Sigma$ channels are unphysical and all other channels physical, correspondingly to the one, connected to the real axis between the $\pi\Sigma$ and $\bar{K}N$ thresholds) are generated from two attractive forces mentioned above [10, 11].

There have been various experimental results related to the $\Lambda(1405)$ [4]. Among these, the most striking measurement is the precise determination of the energy shift and width of kaonic hydrogen by the SIDDHARTA collaboration [12, 13], which provides a quantitative and stringent constraint on the K^-p amplitude at threshold through the improved Deser formula [14]. Systematic studies with error analyses based on the next-to-leading order ChPT interaction including the SIDDHARTA constraint have been performed by various groups [15–20]. All these studies confirm that the new kaonic hydrogen data are compatible with the scattering data above threshold. Thanks to these developments, starting from the 2020 edition, the name $\Lambda(1405)$ is used to refer to the higher-energy pole, while the lower-energy pole is now called the $\Lambda(1380)$.

The results of the pole positions of the $\Lambda(1405)$ and $\Lambda(1380)$ in the various approaches are summarized in Table 82.1 and Fig. 82.1. We may regard the difference among the calculations as a systematic error, which stems from the various approximations of the Bethe-Salpeter equation, the fitting procedure, and also the inclusion of SU(3) breaking effects such as the choice of the various meson decay constants, and so on. A detailed comparison of the various approaches listed in the table is given in Ref. [21]. An analysis including also the $J^P = 1/2^+$ P-wave contribution (and also an explicit $\Sigma(1385)$ $3/2^+$ state) gives results consistent with the findings reported above, with the pole positions at $(1364 - i43)$ MeV and $(1430 - i15)$ MeV, respectively [22].

The main contribution in this energy region is provided by the $\Lambda(1405)$ pole, whose position converges within a relatively small region near the $\bar{K}N$ threshold. On the other hand, the position of the $\Lambda(1380)$ shows a sizeable scatter. Detailed studies of the $\pi\Sigma$ spectrum in various reaction processes, together with the precise experimental lineshape (see e.g. the recent precise photoproduction data from the LEPS collaboration [24] and from the CLAS collaboration [25, 26], electroproduction data from the CLAS collaboration [27], and proton-proton collision data from COSY [28] and the HADES collaboration [29]), will shed light on the position of the second pole. The $\pi\Sigma$ spectra from the CLAS data are analyzed in Ref. [30] and Ref. [19]. It was shown in Ref. [19] that

Table 82.1: Comparison of the pole positions of $\Lambda(1405)$ and $\Lambda(1380)$ in the complex energy plane from next-to-leading and next-to-next-to-leading order chiral unitary coupled-channel approaches including the SIDDHARTA constraint. The lower two results also include the CLAS photoproduction data.

approach	$\Lambda(1405)$ [MeV]	$\Lambda(1380)$ [MeV]
Ref. [16], NLO	$1424^{+7}_{-23} - i\,26^{+3}_{-14}$	$1381^{+18}_{-6} - i\,81^{+19}_{-8}$
Ref. [18], Fit II	$1421^{+3}_{-2} - i\,19^{+8}_{-5}$	$1388^{+9}_{-9} - i\,114^{+24}_{-25}$
Ref. [19], solution #2	$1434^{+2}_{-2} - i\,10^{+2}_{-1}$	$1330^{+4}_{-5} - i\,56^{+17}_{-11}$
Ref. [19], solution #4	$1429^{+8}_{-7} - i\,12^{+2}_{-3}$	$1325^{+15}_{-15} - i\,90^{+12}_{-18}$
Ref. [20]	$1420^{+15}_{-21} - i\,27^{+18}_{-11}$	$1419^{+16}_{-22} - i\,71^{+24}_{-31}$
Ref. [23], NNLO	$1425^{+1}_{-1} - i\,13^{+4}_{-4}$	$1392^{+8}_{-8} - i\,102^{+15}_{-15}$

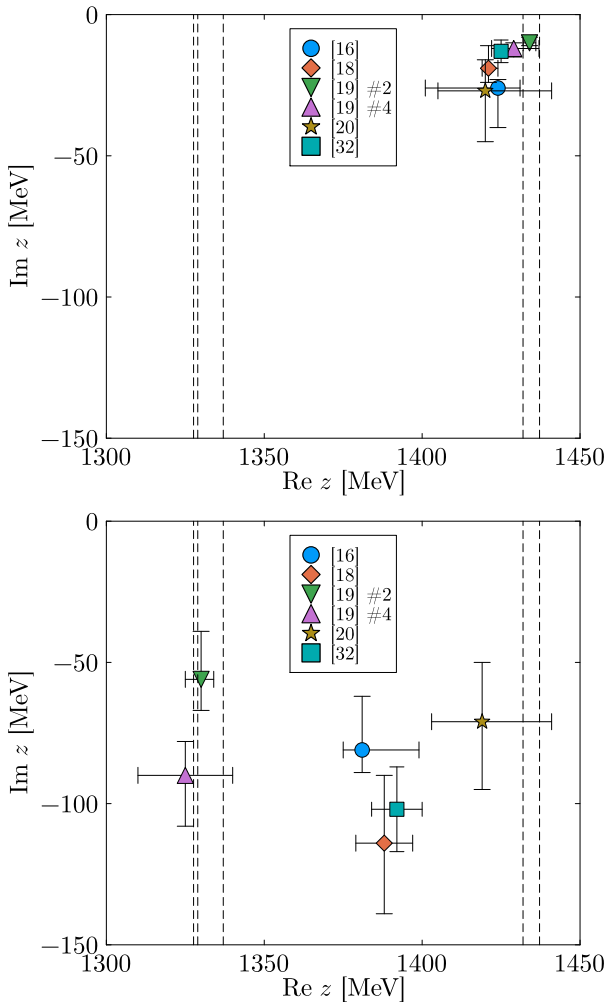

Figure 82.1: Pole positions of $\Lambda(1405)$ (top) and $\Lambda(1380)$ (bottom). Vertical dashed lines stand for the threshold energies of meson-baryon channels, $\pi^0\Sigma^0$, $\pi^-\Sigma^+$, $\pi^+\Sigma^-$, K^-p, $\bar{K}^0n$ (from left to right).

Int. J. Mod. Phys. A 2026.41. Downloaded from www.worldscientific.com by UNIVERSITY OF CALIFORNIA @ BERKELEY on 09/16/26. Re-use and distribution is strictly not permitted, except for Open Access articles.

several solutions, which agree with the scattering data, are ruled out if confronted with the recent CLAS data. The remaining solutions are collected as solution #2 and solution #4 in Table 82.1. The HADES data are analyzed in Ref. [31] and Ref. [32]. Although the result of the pole found in Ref. [31] is not compatible with other results, the authors of Ref. [32] invoke the anomalous triangle singularity mechanism to argue that the invariant mass distribution of the $\pi\Sigma$ system is found at lower masses than in other reactions. It is thus desirable to perform more comprehensive analyses of $\pi\Sigma$ spectra together with the systematic error analysis of the scattering data.

Recently, a next-to-next-to leading order (NNLO) analysis of the meson-baryon scattering was performed [23], by incorporating the constraints from the πN and KN scattering phase shifts, in addition to the $S = -1$ scattering. As tabulated in Table 82.1, the results are qualitatively consistent with the previous studies, reinforcing the existence of the two states, $\Lambda(1405)$ and $\Lambda(1380)$. It is also worth mentioning that the Baryon Scattering collaboration provides the lattice QCD calculation of the meson-baryon coupled-channel scattering [33, 34]. It is found that there appears a virtual state below the $\pi\Sigma$ threshold and a resonance pole just below the $\bar{K}N$ threshold at $M_\pi \approx 200$ MeV. Thus, the existence of $\Lambda(1405)$ and $\Lambda(1380)$ is also indicated by this first principles QCD calculation. These results have been critically assessed in Refs. [35, 36], where it is shown that the nature of the $\Lambda(1380)$ can not yet be definitively determined from these lattice data.

References

[1] R. Dalitz and S. Tuan, Phys. Rev. Lett. **2**, 425 (1959).

[2] V. Bernard, N. Kaiser and U.-G. Meißner, Int. J. Mod. Phys. E **4**, 193 (1995), [hep-ph/9501384].

[3] N. Kaiser, P. Siegel and W. Weise, Nucl. Phys. A **594**, 325 (1995), [arXiv:nucl-th/9505043].

[4] T. Hyodo and D. Jido, Prog. Part. Nucl. Phys. **67**, 55 (2012), [arXiv:1104.4474].

[5] U.-G. Meißner, Symmetry **12**, 6, 981 (2020), [arXiv:2005.06909].

[6] M. Mai, Eur. Phys. J. ST **230**, 6, 1593 (2021), [arXiv:2010.00056].

[7] T. Hyodo and M. Niiyama, Prog. Part. Nucl. Phys. **120**, 103868 (2021), [arXiv:2010.07592].

[8] D. Sadasivan *et al.*, Front. Phys. **11**, 1139236 (2023), [arXiv:2212.10415].

[9] J. Oller and U.-G. Meißner, Phys. Lett. B **500**, 263 (2001), [hep-ph/0011146].

[10] D. Jido *et al.*, Nucl. Phys. A **725**, 181 (2003), [arXiv:nucl-th/0303062].

[11] T. Hyodo and W. Weise, Phys. Rev. C **77**, 035204 (2008), [arXiv:0712.1613].

[12] M. Bazzi *et al.* (SIDDHARTA), Phys. Lett. B **704**, 113 (2011), [arXiv:1105.3090].

[13] M. Bazzi *et al.* (SIDDHARTA), Nucl. Phys. A **881**, 88 (2012), [arXiv:1201.4635].

[14] U.-G. Meißner, U. Raha and A. Rusetsky, Eur. Phys. J. C **35**, 349 (2004), [hep-ph/0402261].

[15] Y. Ikeda, T. Hyodo and W. Weise, Phys. Lett. B **706**, 63 (2011), [arXiv:1109.3005].

[16] Y. Ikeda, T. Hyodo and W. Weise, Nucl. Phys. A **881**, 98 (2012), [arXiv:1201.6549].

[17] M. Mai and U.-G. Meißner, Nucl. Phys. A **900**, 51 (2013), [arXiv:1202.2030].

[18] Z.-H. Guo and J. Oller, Phys. Rev. C **87**, 3, 035202 (2013), [arXiv:1210.3485].

[19] M. Mai and U.-G. Meißner, Eur. Phys. J. A **51**, 3, 30 (2015), [arXiv:1411.7884].

[20] A. Feijoo, V. Magas and A. Ramos, Phys. Rev. C **99**, 3, 035211 (2019), [arXiv:1810.07600].

[21] A. Cieplý *et al.*, Nucl. Phys. A **954**, 17 (2016), [arXiv:1603.02531].

[22] D. Sadasivan, M. Mai and M. Döring, Phys. Lett. B **789**, 329 (2019), [arXiv:1805.04534].

[23] J.-X. Lu *et al.*, Phys. Rev. Lett. **130**, 7, 071902 (2023), [arXiv:2209.02471].

[24] M. Niiyama *et al.*, Phys. Rev. C **78**, 035202 (2008), [arXiv:0805.4051].

[25] K. Moriya *et al.* (CLAS), Phys. Rev. C **87**, 3, 035206 (2013), [arXiv:1301.5000].

[26] K. Moriya *et al.* (CLAS), Phys. Rev. Lett. **112**, 8, 082004 (2014), [arXiv:1402.2296].

[27] H. Lu *et al.* (CLAS), Phys. Rev. C **88**, 045202 (2013), [arXiv:1307.4411].

[28] I. Zychor *et al.*, Phys. Lett. B **660**, 167 (2008), [arXiv:0705.1039].

[29] G. Agakishiev *et al.* (HADES), Phys. Rev. C **87**, 025201 (2013), [arXiv:1208.0205].

[30] L. Roca and E. Oset, Phys. Rev. C **87**, 5, 055201 (2013), [arXiv:1301.5741].

[31] M. Hassanvand *et al.*, Phys. Rev. C **87**, 5, 055202 (2013), [Addendum: Phys.Rev.C 88, 019905 (2013)], [arXiv:1210.7725].

[32] M. Bayar *et al.*, Phys. Rev. C **97**, 3, 035203 (2018), [arXiv:1710.03964].

[33] J. Bulava *et al.* (Baryon Scattering (BaSc)), Phys. Rev. Lett. **132**, 5, 051901 (2024), [arXiv:2307.10413].

[34] J. Bulava *et al.* (Baryon Scattering (BaSc)), Phys. Rev. D **109**, 1, 014511 (2024), [arXiv:2307.13471].

[35] F.-K. Guo *et al.*, Phys. Lett. B **846**, 138264 (2023), [arXiv:2308.07658].

[36] X.-L. Ren, Phys. Lett. B **855**, 138802 (2024), [arXiv:2404.02720].

Int. J. Mod. Phys. A 2026.41. Downloaded from www.worldscientific.com
UNIVERSITY OF CALIFORNIA @ BERKELEY on 09/16/26. Re-use and distribution is strictly not permitted, except for Open Access articles.

Int. J. Mod. Phys. A 2026.41. Downloaded from www.worldscientific.com
by UNIVERSITY OF CALIFORNIA @ BERKELEY on 09/16/26. Re-use and distribution is strictly not permitted, except for Open Access articles.

83. Pentaquarks

Revised November 2025 by M. Karliner (Tel Aviv U.) and T. Skwarnicki (Syracuse U.).

Experimental searches for pentaquark hadrons comprised of light flavors have a long and vivid history. No undisputed candidates had been found in 50 years. The first wave of claimed observations of pentaquark candidates containing a strange antiquark occurred in the early seventies, see e.g. a review in the 1976 edition of Particle Data Group listings for $Z_0(1780)$, $Z_0(1865)$ and $Z_1(1900)$ [1]. The last mention of these candidates can be found in the 1992 edition [2] with the perhaps prophetic comment "the results permit no definite conclusion - the same story for 20 years. [...] The skepticism about baryons not made of three quarks, and lack of any experimental activity in this area, make it likely that another 20 years will pass before the issue is decided." A decade later, a second wave of observations occurred, possibly motivated by specific theoretical predictions for their existence [3–5]. The evidence for pentaquarks was based on observations of peaks in the invariant mass distributions of their decay products. More data and subsequent more sensitive experiments did not confirm these claims [6]. In the last mention of the best known candidate from that period, $\Theta(1540)^+$, the 2006 Particle Data Group listing [7] included a statement: "The conclusion that pentaquarks in general, and that Θ^+, in particular, do not exist, appears compelling." which well reflected the prevailing mood in the particle physics community until a study of $\Lambda_b^0 \to J/\psi pK^-$ ($J/\psi \to \mu^+\mu^-$) decays by LHCb [8] (charge conjugate modes are implied). From an analysis of 3 fb^{-1} Run 1 data at 7 and 8 TeV at the LHC, the LHCb collaboration reported a significant $J/\psi p$ structure in $\Lambda_b^0 \to J/\psi pK^-$ decays [8]. The exotic character of this structure, with the minimal quark content of $uudc\bar{c}$, was demonstrated in a nearly model-independent way in Ref. [9], where it was shown that the $J/\psi p$ mass ($m_{J/\psi p}$) peak near 4450 MeV was too narrow to be accounted for by $\Lambda^* \to pK^-$ reflections (Λ^* denotes a generic Λ excitation), reinforcing the results from the earlier model-dependent six-dimensional amplitude analysis of invariant masses and decay angles describing the Λ_b^0 decay in the same data [8]. The LHCb 6 fb^{-1} Run 2 LHC data at 13 TeV, together with the improvements in the data selection for both runs, resulted in a nine-fold increase in the number of reconstructed $\Lambda_b^0 \to J/\psi pK^-$ decays (246,000 events) [10] and observation of new narrow $J/\psi p$ structures which were too faint to had been significant in the Run 1 data analysis. A second horizontal band is observed in the Dalitz plot (Fig. 83.1) near 4312 MeV in the $J/\psi p$ mass.

The 4450 MeV structure also appears to consist of two narrower peaks at 4440 and 4457 MeV. Performing a rigorous six-dimensional amplitude analysis of these faint $J/\psi p$ structures is challenging and has not been accomplished yet. Fortunately, the newly observed peaks are so narrow that it is not necessary to construct an amplitude model to prove that these states are not artifacts of interfering Λ^* resonances, as was previously demonstrated in Ref. [9]. Their masses and widths have been characterized by the LHCb (see Table 83.1) from one-dimensional fits to $J/\psi p$ mass distributions, with different levels of suppression of the Λ^* contributions, which peak at the lower pK^- masses (Fig. 83.1). Such analysis is not sensitive to any broad $J/\psi p$ contributions. The histograms analyzed by the LHCb are available in tabular form at https://www.hepdata.net/record/89271.

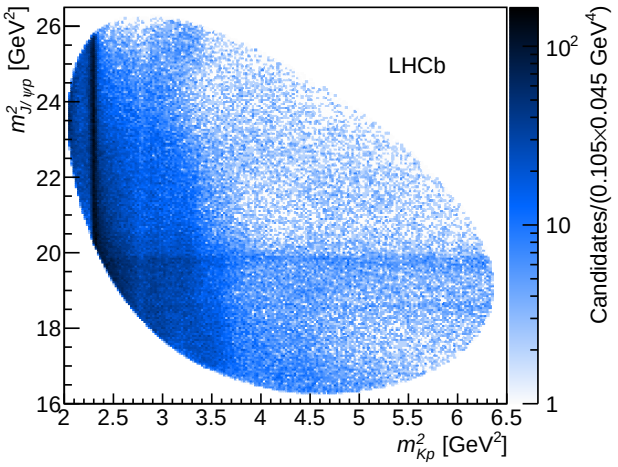

Figure 83.1: Dalitz plot distributions for $\Lambda_b^0 \to J/\psi pK^-$ decays as observed by LHCb.

The fit chosen by the LHCb for the central mass and width values is displayed in Fig. 83.2. The $P_{c\bar{c}}(4312)^+$ state (formerly known as $P_c(4312)^+$) peaks right below the $\Sigma_c^+\bar{D}^0$ threshold and has statistical significance over 7.6σ. The $P_{c\bar{c}}(4457)^+$ state peaks right below the $\Sigma_c^+\bar{D}^{*0}$ threshold, while the $P_{c\bar{c}}(4440)^+$ state peaks about 20 MeV below it. The significance of the two-peak versus one-peak hypothesis for the 4450 MeV structure is over 5.4σ, rendering the single peak interpretation of this region obsolete. The six-dimensional amplitude analysis reported in Ref. [8], which in addition to the structure near 4450 MeV, provided also evidence for the broad $P_{c\bar{c}}(4380)^+$ state, is obsolete since it used the single $P_{c\bar{c}}(4450)^+$ state and it lacked the $P_{c\bar{c}}(4312)^+$ state. Furthermore, it used the helicity formalism in which the half-integer spin of the proton was not aligned properly between the different Λ_b^0 decay chains [11, 12]. The newer one-dimensional analysis by LHCb [10] was not sensitive to wide $P_{c\bar{c}}^+$ states. The LHCb result from the six-dimensional amplitude analysis of the Cabibbo suppressed channel $\Lambda_b^0 \to J/\psi p\pi^-$ [13], which contains a statistically marginal evidence for the sum of the $P_{c\bar{c}}^+$ and the $T_{c\bar{c}1}^-$ (formerly known as $Z_c(4200)^-$) contributions, took extensive input from Ref. [8] and, like the $P_{c\bar{c}}(4380)^+$ state, should be treated with caution until the both amplitude analyses are completed on the enlarged data sets with the modified helicity formalism.

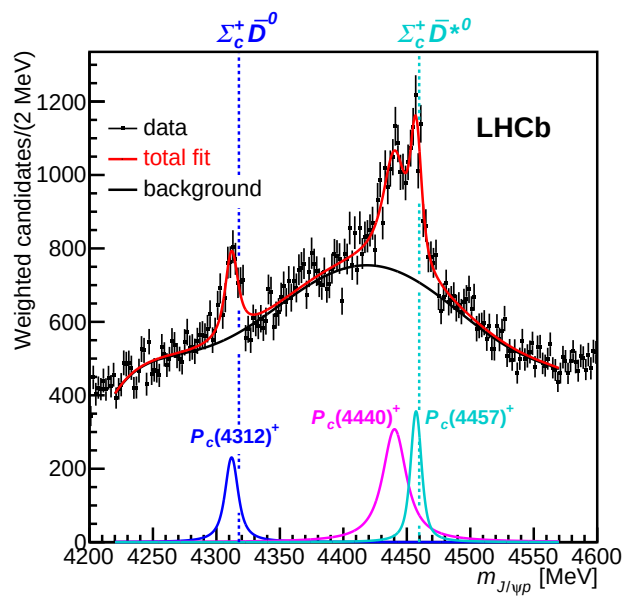

Figure 83.2: Fit to the $J/\psi p$ mass distribution, in which events were weighted to suppress $\Lambda^* \to pK^-$ backgrounds, of three Breit-Wigner functions and a sixth-order polynomial background. This fit was used to determine the central values of the masses and widths of the $P_{c\bar{c}}^+$ states (formerly known as P_c^+) reported by LHCb. The mass thresholds for the $\Sigma_c^+\bar{D}^0$ and $\Sigma_c^+\bar{D}^{*0}$ final states are superimposed.

While $\Sigma_c\bar{D}^{(*)}$ states had been predicted [14–17] before the first LHCb results [8], after these results became known, many theoretical groups interpreted the $P_{c\bar{c}}(4450)^+$ and $P_{c\bar{c}}(4380)^+$ states in terms of diquarks and triquarks as building blocks of a compact pentaquark [18–24]. In a different strategy, a tentative attempt has been made to treat the full 5-body dynamics, leading to states below the lowest threshold for spontaneous dissociation [25]. In the first implementation of the former approach [18], the pen-

Int. J. Mod. Phys. A 2026.41. Downloaded from www.worldscientific.com
UNIVERSITY OF CALIFORNIA @ BERKELEY on 09/16/26. Re-use and distribution is strictly not permitted, except for Open Access articles.

Table 83.1: Summary of the narrow $P_{c\bar{c}}^{+}$ (formerly known as P_c^{+}) properties, interpreted as Breit-Wigner resonances. The central values are based on the fit displayed in Fig. 83.2.

State	M [MeV]	Γ [MeV] (95% CL)	$\mathcal{R}$ [%]
$P_{c\bar{c}}(4312)^+$	$4311.9 \pm 0.7^{+6.8}_{-0.6}$	$9.8 \pm 2.7^{+\ 3.7}_{-\ 4.5}$ (< 27)	$0.30 \pm 0.07^{+0.34}_{-0.09}$
$P_{c\bar{c}}(4440)^+$	$4440.3 \pm 1.3^{+4.1}_{-4.7}$	$20.6 \pm 4.9^{+\ 8.7}_{-10.1}$ (< 49)	$1.11 \pm 0.33^{+0.22}_{-0.10}$
$P_{c\bar{c}}(4457)^+$	$4457.3 \pm 0.6^{+4.1}_{-1.7}$	$6.4 \pm 2.0^{+\ 5.7}_{-\ 1.9}$ (< 20)	$0.53 \pm 0.16^{+0.15}_{-0.13}$

taquark mass splitting was generated mostly by the change of angular momentum between the sub-components (L) from zero to one, which would also make the heavier state narrower and of opposite parity. Explicit modeling of multiquark systems [26] questions if centrifugal barrier factor provides enough width suppression via spatial separation of c and $\bar{c}$ quarks at these masses, as the phase space for $J/\psi p$ decay is very large (more than 400 MeV). Also, the observed mass splitting was too small to be only due to the mechanism proposed in Ref. [18] and required fine-tuning of such models. A variation of this model, in which the heavy (cu) diquark couples with heavy $\bar{c}$ to form colored triquark attracting the light diquark (ud), has been re-implemented for the narrow $P_{c\bar{c}}^{+}$ states [27]. In this model, the $P_{c\bar{c}}(4440)^+$ and $P_{c\bar{c}}(4457)^+$ states are accommodated via spin-orbit interactions for the $L = 1$ states, while the $P_{c\bar{c}}(4312)^+$ is one of the $L = 0$ states. However, the mass prediction for the latter is off by (-72 ± 29) MeV [27]. This work was later extended to $SU(3)_F$ [28]. The width dilemma becomes more severe in view of the narrow widths of the newly observed states (Table 83.1), especially for the $L = 0$ $P_{c\bar{c}}(4312)^+$ state, and requires a different origin of potential barrier between c and $\bar{c}$ than angular momentum [27, 29], which remains a subject of theoretical controversy. Measurement of spin-parity of $P_{c\bar{c}}(4312)^+$, $P_{c\bar{c}}(4440)^+$ and $P_{c\bar{c}}(4457)^+$ will be crucial for testing these and alternative theoretical ideas discussed in the following.

More effective width suppression mechanism is offered by a loosely bound charmed baryon-anticharmed meson molecular model, in which c and $\bar{c}$ can be separated by much larger distances, resulting in a smaller probability of them getting close enough to each other in order to make a J/ψ. Since molecular binding energy cannot be large, such molecules are in S-wave, so it has been realized early on that their masses must be near the sum of the baryon and meson masses and their spin and parity are inherited from their constituent hadrons, see e.g. discussion in [17]. The mass coincidence of the $P_{c\bar{c}}(4312)^+$ and of $P_{c\bar{c}}(4457)^+$ states, with the two related thresholds, $\Sigma_c^+\bar{D}^0$ and $\Sigma_c^+\bar{D}^{*0}$, provides very strong experimental evidence in favor of this interpretation. Given how close $P_{c\bar{c}}(4312)^+$ is to the $\Sigma_c^+\bar{D}^0$ threshold, it might be a virtual rather than a bound state [30]. Since the spins of Σ_c^+ and of $\bar{D}^{*0}$ can be combined in two different ways, the narrow $P_{c\bar{c}}(4440)^+$ peak also finds natural explanation in this physical picture. It cannot be a virtual state since it is sufficiently below the $\Sigma_c^+\bar{D}^{*0}$ threshold.

It is worth stressing that other baryon-meson combinations, $\Lambda_c^{(*)+}\bar{D}^{(*)0}$ and $\chi_{cJ}p$ are not expected to bind [14, 31]. Before the first pentaquark observation [8] heavy quark symmetry was used to show that, in addition to the three $\Sigma_c\bar{D}^{(*)0}$ states, one expects four $\Sigma_c^*\bar{D}^{(*)0}$ states, for a total of seven [32]. Indeed, additional states at, or below, the $\Sigma_c^{*+}\bar{D}$ and $\Sigma_c^{*+}\bar{D}^*$ thresholds, are expected [33–36]. Since Σ_c^{*+} width is likely around 15 MeV [37], more than the width of either $P_{c\bar{c}}(4312)^+$ or $P_{c\bar{c}}(4457)^+$, it is important to keep in mind that a molecule is typically as broad as the constituents[1] [38–40]. There is no significant evidence for $\Sigma_c^*\bar{D}^{(*)}$ states in the present LHCb data set [10, 41]. Larger data sets are expected from the Upgraded LHCb experiment. For a review on hadronic molecules, and a recent survey in a particular approach, see respectively Refs. [42, 43].

It is useful to consider the $P_{c\bar{c}}(4312)^+$, $P_{c\bar{c}}(4440)^+$ and $P_{c\bar{c}}(4457)^+$ narrow pentaquarks together with several analogous exotic states with hidden charm and bottom in the meson sector. This provides additional significant motivation for the molecular model. At least five exotic mesons are close to thresholds of two heavy-light mesons: $\chi_{c1}(3872)$ (formerly known as $X(3872)$) [44–47], $T_{b\bar{b}1}(10610)$ and $T_{b\bar{b}1}(10650)$ (formerly $Z_b(10610)$ and $Z_b(10650)$) in the bottomonium sector [48–52] and $T_{c\bar{c}1}(3900)$ (formerly $Z_c(3900)$) [53–57] and $T_{c\bar{c}1}(4020)$ (formerly $Z_c(4020)$) [58–60] in the charmonium sector (see Table II in Ref. [61]; for reviews of experimental information see Ref. [62, 63], as well as *Spectroscopy of Mesons Containing Two Heavy Quarks* and *Heavy Non-$q\bar{q}$ Mesons* in the current Review of Particle Properties. These states share several important features: a) their masses are near thresholds and their spin and parity correspond to S-wave combination of the two mesons; b) they are very narrow, despite very large phase space for decay into quarkonium + pion(s); c) the branching fractions for "fall apart" mode into two mesons are much larger than branching fractions for decay into quarkonium and pion(s). So far, there is no experimental evidence for states at two pseudoscalar thresholds ($D\bar{D}$ and $B\bar{B}$), suggesting that pseudoscalar exchange is essential for binding in meson-meson systems.

The above provide a strong hint that these states are deuteron-like loosely bound states of two heavy mesons [64–72]. It is then natural to conjecture that similar bound states might exist of two heavy baryons [73, 74], or a meson and a baryon or a baryon and an antibaryon, leading to a rather accurate prediction of the $P_{c\bar{c}}(4457)^+$ mass as $3/2^-$ $\Sigma_c\bar{D}^*$ molecule (the mass threshold is 4460 MeV for $\Sigma_c^+\bar{D}^{*0}$ and 4464 MeV for $\Sigma_c^{++}D^{*-}$) [17, 61], following similar predictions obtained in a wider framework of doubly heavy baryon-meson hadronic molecules, which might include mixtures of various two-hadron states [14–16, 31]. However, single pion exchange is not possible in $\Sigma_c^+\bar{D}^0$ system. Thus the existence of $P_{c\bar{c}}(4312)^+$ suggests a more general binding mechanism in baryon-meson molecules, e.g. vector or two-pion exchanges, and/or coupled-channel interactions. Two-pion exchange in $D\bar{D}$ system is highly suppressed, because the intermediate state is $D^*\bar{D}^*$, which is 282 MeV heavier than $D\bar{D}$. On the other hand, in the $\Sigma_c\bar{D}$ system the intermediate $\Lambda_c^+\bar{D}^*$ state is only 25 MeV lighter than $\Sigma_c\bar{D}$, and therefore does not have to suffer significant suppression, providing a possible binding mechanism [75]. In a generic hadronic molecule it is essential that the two hadrons are heavy, in order to minimize the repulsive kinetic energy [73, 74, 76].

Following the initial LHCb discovery [8], several groups carried out a detailed analysis of the $P_{c\bar{c}}^{+}$ states as hadronic molecules [77–86] followed by further analyses [35, 87–111] after the updated LHCb results [10]. Partial widths of all the allowed decay channels for the $P_{c\bar{c}}$ states have been estimated within a specific model in the molecular picture [112]. The most striking suggestion is that $P_{c\bar{c}}(4312)^+$ decays are totally dominated by the $\Lambda_c^+\bar{D}^{*0}$ channel. This channel is also suggested to be very prominent in decays of $P_{c\bar{c}}(4440)^+$ and $P_{c\bar{c}}(4457)^+$. But other scenarios are possible, as shown by a recent theoretical analysis, allowing for the most general scattering potential of the baryon-meson system consistent with QCD symmetries at leading order in a momentum counting [113]. They found that both large and vanishing transitions to $\Lambda_c^+\bar{D}^{(*)0}$ channels are allowed. Clearly, experimental determination of the branching fraction of these channels is of high priority.

The $P_{c\bar{c}}$ states have also been-interpreted as so called hadrocharmonium [114], a bound state of relatively compact charmonium states with light hadronic matter. It was proposed that $P_{c\bar{c}}(4440)^+$ and $P_{c\bar{c}}(4457)^+$ are spin-split $\psi(2S)p$ bound states with $J^P = \frac{1}{2}^-$ and $\frac{3}{2}^-$, while $P_{c\bar{c}}(4312)^+$ is a $\chi_{c0}p$ bound state with $J^P = \frac{1}{2}^+$ [115]. While very interesting from the theoretical point of view, it is not at all clear why the binding energies

[1] This feature gets changed if systems are more deeply bound.

Int. J. Mod. Phys. A 2026.41. Downloaded from www.worldscientific.com
by UNIVERSITY OF CALIFORNIA @ BERKELEY on 09/16/26. Re-use and distribution is strictly not permitted, except for Open Access articles.

between charmonia and the nucleon should conspire to produce states so close to the $\Sigma_c\bar{D}$ and $\Sigma_c\bar{D}^*$ thresholds. Moreover, the predicted widths of $P_{c\bar{c}}(4440)^+$ and $P_{c\bar{c}}(4457)^+$ are too big by a factor $\sim$ 2-3. One should also keep in mind that the molecular and hadro-charmonium pictures provide opposite predictions for the parity of $P_{c\bar{c}}(4312)^+$. In principle LHCb can check the spin and parity through partial wave analysis, but at present it is not known if systematic uncertainties can be sufficiently reduced to make such an analysis conclusive.

Shortly after the initial experimental discovery it was conjectured that the $P_{c\bar{c}}(4450)^+$ reflects the presence of a triangle singularity near the $\chi_{c1}p$ threshold [116–119]. These explanations are no longer viable, since the $P_{c\bar{c}}(4440)^+$ mass is not at any threshold and the $P_{c\bar{c}}(4312)^+$ and $P_{c\bar{c}}(4457)^+$ peak slightly below the $\Sigma_c^+\bar{D}^0$ and $\Sigma_c^+\bar{D}^{*0}$ thresholds. The $P_{c\bar{c}}(4457)^+$ mass is exactly at $\Lambda_c^{*+}\bar{D}^0$ threshold, but LHCb has demonstrated that the observed peaking is narrower in the data than expected from the triangle-diagram when a realistic width of the excited D_s^- state exchanged in the triangle is used (Supplemental Material in Ref. [10]).

More extensive pre-2019 reviews of some of the theoretical issues can be found in Refs. [120, 121]. Two recent relevant reviews are Refs. [122, 123].

So far the $P_{c\bar{c}}^+$ states have been observed by only one experiment in only one channel. It is essential to explore other possible experimental channels, such as $P_{c\bar{c}}^+ \to \Lambda_c^+\bar{D}^{(*)0}$, $\eta_c p$ [113]. These channels are however much more experimentally challenging than $P_{c\bar{c}}^+ \to J/\psi p$. The decays $\Lambda_b^0 \to \eta_c p K^-$ [124], $\Lambda_b^0 \to \Lambda_c^+\bar{D}^{(*)0}K^-$ [125] and $\Lambda_b^0 \to \Sigma_c^{(*)++}\bar{D}^{(*)-}K^-$ [126] have been observed by the LHCb, but larger data samples are needed to probe for $P_{c\bar{c}}^+$ signals. So far, search for prompt pp production of pentaquarks by the LHCb in charm hadron final states, including $\Lambda_c^+\bar{D}^0$ and $\Lambda_c^+\pi^+\bar{D}^-$, resulted in upper limits only [127]. Search for $P_{c\bar{c}}^+ \to pJ/\psi$ states in inclusive decays of $\Upsilon(1S)$ and $\Upsilon(2S)$ produced in e^+e^- annihilation by the Belle experiment also resulted in upper limits [128].

Proposals have also been made to search for heavy pentaquarks in photo-production [129–136]. Ref. [137] discusses photoproduction within the string-junction physical picture of the pentaquarks. Photoproduction is also related to recent work on $J/\psi(\eta_c)N$ scattering on the lattice [138] and on computation of $J/\psi(\eta_c)N$ and $\Upsilon(\eta_b)N$ cross sections [139]. In addition, pentaquark production has been discussed in the context of antiproton-deuterium collisions [140], of heavy ion collisions at LHC [141], in pA collisions [142] and in pion-induced processes [143–145]. The GlueX Collaboration reported negative search results for the $P_{c\bar{c}}^+$ states in photo-production at JLAB [146, 147], $\gamma p \to (J/\psi \to e^+e^-)p$. Within the large experimental errors and considerable theoretical model dependence these results do not contradict the molecular interpretations of the narrow $P_{c\bar{c}}^+$ states. In particular, vector-meson dominance often assumed in theoretical modelling may not hold for near-threshold J/ψ production, and $\Lambda_c\bar{D}^{(*)0}$ intermediate states may significantly contribute to the $J/\psi p$ production complicating probing for the $P_{c\bar{c}}^+$ states [148, 149].

As noted in e.g. [17], bottom analogues of the $P_{c\bar{c}}^+$ might well exist, but experimental search for such states involves very significant challenges. It is therefore hardly surprising that they have not been observed so far. A detailed discussion is beyond the scope of the current review.

The LHCb collaboration obtained a 3.1σ evidence for a $P_{c\bar{c}}^+ \to J/\psi p$ state in the four-dimensional amplitude analysis of about 800 $B_s^0 \to J/\psi p\bar{p}$ ($J/\psi \to \mu^+\mu^-$) decays [150]. The mass of the state, $4337^{+7}_{-4} \pm 2$ MeV, is not compatible with the the $P_{c\bar{c}}(4312)^+$ state at 3.1 standard deviations. The width is relatively small, $29^{+26}_{-12} \pm 14$ MeV. The present data do not provide sufficient discrimination between various J^P assignments. Its mass is about 19 MeV higher than the $\Sigma_c^+\bar{D}^0$ threshold and about 16 MeV lower than the $\chi_{c0}p$ threshold. At present, no specific explanation for this structure has been proposed, but some intriguing ideas have been raised in Ref. [151]. Since the statistical significance of this evidence is marginal, more data are required before this state is considered experimentally established.

Similarly inconclusive 3.1σ evidence for a $P_{c\bar{c}s}^0 \to J/\psi\Lambda$ structure was observed by the LHCb collaboration in the six-dimensional amplitude analysis of about 1750 $\Xi_b^- \to J/\psi\Lambda K^-$ ($J/\psi \to \mu^+\mu^-$, $\Lambda \to p\pi^-$ decays [12]. The strange counterparts of $P_{c\bar{c}}^+$ states have been predicted in both molecular and compact pentaquark models [15, 99, 101, 152–154]. When interpreted as a single peak, its mass, $4458.8 \pm 2.9^{+4.7}_{-1.1}$ MeV, is 15 MeV above the $\Xi_c'^0\bar{D}^0$ threshold and 18 MeV below the $\Xi_c^0\bar{D}^{*0}$ threshold. Its width, $17.3 \pm 6.5^{+8.0}_{-5.7}$ MeV, is relatively narrow, thus plausibly could be interpreted as a loosely bound $\Xi_c^0\bar{D}^{*0}$ state. However, in the latter model two states are expected with J^P equal to $1/2^-$ and $3/2^-$. In fact, the LHCb data are consistent with such hypothesis, under which 4454.9 ± 2.7 MeV ($\Gamma = 7.5 \pm 9.7$ MeV) and 4467.8 ± 3.7 MeV ($\Gamma = 5.2 \pm 5.3$ MeV) mass (width) estimates are obtained (statistical errors only). It is worth noting, that the $SU(3)$ flavor structure of $\Xi_c^0\bar{D}^{*0}$ states is different from that of $\Sigma_c^+\bar{D}^{*0}$ states, since Ξ_c^0 belongs to the charmed baryon triplet, together with Ξ_c^+ and Λ_c^+, where the two light quarks form a spin-zero diquark, unlike Σ_c^+, which together with $\Xi_c'^0$ and Ω_c^0 belongs to the charmed baryon sextet, where the two light quarks form a spin-1 diquark. More data are required to experimentally establish this structure, clarify its composition, and determine the related quantum numbers.

If the two states at 4455 MeV and 4468 MeV indeed correspond to a $\Xi_c^0\bar{D}^{*0}$ molecule, there perhaps exist two other states, corresponding to $\Xi_c'\bar{D}^*$ [15, 99, 101, 152–154], with a mass shifted upwards by approximately $\Xi_c' - \Xi_c$ mass difference [155, 156], i.e. about 108 MeV [37].

More recently, the LHCb experiment observed highly significant ($> 14\sigma$) pentaquark state $P_{c\bar{c}s}(4338)^0 \to J/\psi\Lambda$ (formerly known as $P_{cs}(4338)$) in the six-dimensional amplitude analysis of 4620 ± 70 $B^- \to J/\psi\Lambda\bar{p}$ decays [157]. Its mass $4338.2 \pm 0.7 \pm 0.4$ MeV is right at the $\Xi_c\bar{D}$ threshold (Fig. 83.3), its width is narrow $7.0 \pm 1.2 \pm 1.3$ MeV, and its spin is 1/2, with a preference for negative parity, which all fits the molecular model very well. This makes the $P_{c\bar{c}s}(4338)^0$ state a likely $\Xi_c^0\bar{D}^0$ analog of the $P_{c\bar{c}}(4312)^+$ state in $\Sigma_c^0\bar{D}^0$ system. In addition, as in the $P_{c\bar{c}s}(4459)^0$ case, a $\Xi_c'\bar{D}$ state is expected, for a total of three additional strange pentaquarks [156]. Experimental determination whether yet additional $\Xi_c^{(*,\prime)}\bar{D}^{(*)0}$ states actually exist will provide a useful testing ground for the various theoretical approaches which have been used to predict them.

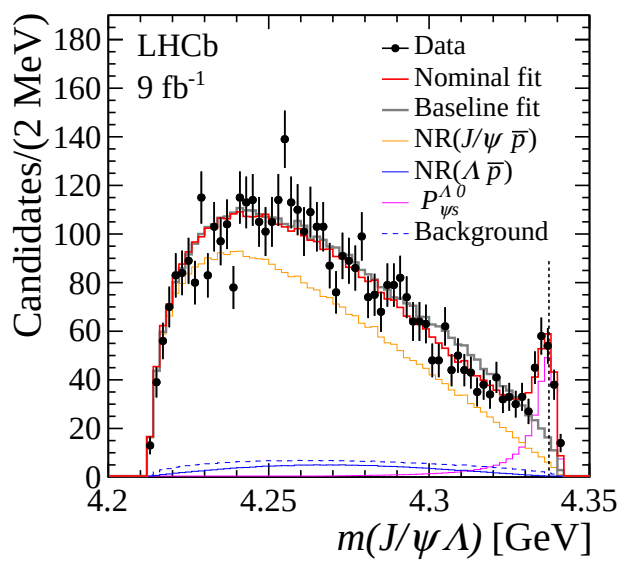

Figure 83.3: Distribution of invariant $J/\psi\Lambda$ mass, with the projection of the amplitude fit model superimposed. The model without the $P_{c\bar{c}s}(4338)^0$ state (labeled as $P_{\psi s}^{\Lambda\ 0}$) is also shown in grey. The $\Xi_c^+D^-$ baryon-meson threshold is indicated with a vertical dashed line.

Int. J. Mod. Phys. A 2026.41. Downloaded from www.worldscientific.com
UNIVERSITY OF CALIFORNIA @ BERKELEY on 09/16/26. Re-use and distribution is strictly not permitted, except for Open Access articles.

Search for the $P^0_{c\bar{c}s}$ states in decays to $\Lambda_c^+ D_s^-$ have been recently performed by the LHCb using a small sample of $\Lambda_b^0 \to \Lambda_c^+ D_s^- K^+ K^-$ decays [158]. Search by the Belle experiment for $P^+_{c\bar{c}s} \to J/\psi\,\Lambda$ states in inclusive decays of $\Upsilon(1S)$ and $\Upsilon(2S)$, produced in e^+e^- annihilation, yielded a hint of the $P_{c\bar{c}s}(4459)^0$ state and upper limits on production of the $P_{c\bar{c}s}(4338)^0$ state [159]. When combining the $\Upsilon(1S)$ and $\Upsilon(2S)$ samples together, a peak in $J/\psi\,\Lambda$ mass is observed at $4471.7 \pm 4.8 \pm 0.6$ MeV with a width of $22 \pm 13 \pm 3$ MeV, which are consistent with the LHCb results at 1.8σ and 0.3σ level, respectively. A local statistical significance of this peak is 3.8σ (not including systematic effects), which is an appropriate figure of merit if the mass and width are considered to be consistent between the LHCb and Belle results. A global signal significance, appropriate measure for stand-alone unbiased search, is 2.8σ (no systematic effects folded in). Imposing Gaussian constraints on the mass and width to the LHCb results, the $P_{c\bar{c}s}(4459)^0$ peak fitted to the Belle data is 3.3σ significant including systematic uncertainties. This result may be affected by the single-peak interpretation of the LHCb data, which has not been established as discussed above. More $\Upsilon(1S)$ and $\Upsilon(2S)$ data are highly desired to verify existence of this mass structure.

In hidden-charm exotics discussed above, the charmed and the anticharmed quarks can form a charmonium and thereby decouple from the light quarks. The molecular model provides an efficient mechanism to suppress such decays, thus making these states narrow. Compact direct color couplings between quarks, in diquark approach, are missing an obvious width suppression mechanism, thus could lead to broader states. In fact, there is plenty of evidence for them in form of broader tetraquark mass structures in $J/\psi\,\phi$ [160–166], $J/\psi\,J/\psi$ [167–169], $T_{c\bar{c}1}(4430)^+ \to \psi(2S)\pi^+$ (formerly $Z_c(4430)^+$) [170–172] and others, although alternative explanations of these structures have been also proposed. Analogous configurations may also exist for pentaquarks, but there is no firm evidence for them yet.

A relatively new theoretical approach to hidden-charm exotics is based on the recognition that heavy quarks move slowly compared to their light quark partners. This is analogous to atomic molecules, which have been successfully described as heavy nuclei vibrating slowly in Born-Oppenheimer (BO) potential, generated by fast-moving electrons. Unlike the hadro-charmonium picture, in which $c\bar{c}$ pair is assumed to be in a polarized color-singlet state, the BO approach assumes that the $c\bar{c}$ pair is in color-octet state [173–176]. Perturbative QCD predicts repulsive $1/r$ potential at short $c\bar{c}$ distances, while LQCD predicts a confining linear potential at large $c\bar{c}$ distances. The transition from octet to singlet charmonium requires hard gluon interaction. This suppresses decays to a charmonium and a light baryon, making the states narrow. To avoid the unobserved rich spectrum of bound states expected in the confining potential, it has been proposed that the potential transitions smoothly to a constant term at large distances, due to light quarks attaching themselves to the heavy quarks as they separate from each other, creating heavy-light charmed baryon – anticharmed meson pair. Thus, the hadronic molecule physical picture naturally emerges as the long-distance limit of the QCD-motivated BO approach. The baryon-meson threshold can be approached from below, creating a shallow potential well with few bound state(s) just below the threshold (e.g. $\Sigma_c^{(*)}\bar{D}^{(*)}$ case); smoothly from above, creating no bound states ($\Lambda_c\bar{D}^{(*)}$ case); or the intermediate potential raising to the confining part can overshoot the threshold somewhat, generating a bound state slightly above the threshold. This mechanism can accommodate the narrow tetraquark states observed just above the $D^*\bar{D}^{(*)}$ and $B^*\bar{B}^{(*)}$ thresholds. The non-relativistic Schrödinger equation can be used to solve the BO potential for bound state energies. The hyperfine structure is created by coupling the total angular momentum of the light quark (diquark) to heavy quark (antiquark) spins. If all combinations of the angular momenta of light quarks are allowed, the number of states and their spin-parity match the predictions of the molecular model [175]. However, in the BO approach the constituents are colored heavy quarks, rather than color-neutral heavy hadrons, providing for a different modelling approach and better prospects for a direct input from QCD via simulations of BO potentials on the lattice. Unlike in the naive molecular model, the short-range structure of the bound states is predictable. The BO approach predicts fewer states, with a different spin-parity pattern if not all values of total the angular momenta of light quarks are assumed to create bound states [176].

The hidden-charm exotic states, should not be confused with exotic hadrons containing two heavy quarks, rather than a heavy quark and a heavy antiquark. Decoupling from the light quarks is impossible in exotics which contain two heavy quarks. This has far-reaching consequences. The first tetraquark of the latter type, i.e. containing two heavy quarks, has been reported by LHCb [177, 178]. A comprehensive discussion of tetraquark candidates can be found in the "Heavy non-$Q\bar{Q}$ Mesons" review.

References

[1] T. G. Trippe *et al.* (Particle Data Group), Rev. Mod. Phys. **48**, S1 (1976), [Erratum: Rev. Mod. Phys.48,497(1976)].

[2] K. Hikasa *et al.* (Particle Data Group), Phys. Rev. **D45**, S1 (1992), [Erratum: Phys. Rev.D46,5210(1992)].

[3] M. Praszalowicz, *Skyrmions and Anomalies, p.112, M. Jezabek Ed.*, World Scientific Publishing (1987), ISBN 9971503506.

[4] D. Diakonov, V. Petrov and M. V. Polyakov, Z. Phys. **A359**, 305 (1997), [hep-ph/9703373].

[5] H. Weigel, Eur. Phys. J. **A2**, 391 (1998), [hep-ph/9804260].

[6] K. H. Hicks, Eur.Phys.J. **H37**, 1 (2012).

[7] W. M. Yao *et al.* (Particle Data Group), J. Phys. **G33**, 1 (2006).

[8] R. Aaij *et al.* (LHCb), Phys. Rev. Lett. **115**, 072001 (2015), [arXiv:1507.03414].

[9] R. Aaij *et al.* (LHCb), Phys. Rev. Lett. **117**, 8, 082002 (2016), [arXiv:1604.05708].

[10] R. Aaij *et al.* (LHCb), Phys. Rev. Lett. **122**, 22, 222001 (2019), [arXiv:1904.03947].

[11] M. Wang *et al.*, Chin. Phys. C **45**, 6, 063103 (2021), [arXiv:2012.03699].

[12] R. Aaij *et al.* (LHCb), Sci. Bull. **66**, 1391 (2021), [arXiv:2012.10380].

[13] R. Aaij *et al.* (LHCb), Phys. Rev. Lett. **117**, 8, 082003 (2016), [Addendum: Phys. Rev. Lett.118,119901(2017)], [arXiv:1606.06999].

[14] Z.-C. Yang *et al.*, Chin. Phys. **C36**, 6 (2012), [arXiv:1105.2901].

[15] J.-J. Wu *et al.*, Phys. Rev. Lett. **105**, 232001 (2010), [arXiv:1007.0573].

[16] J.-J. Wu, T. S. H. Lee and B. S. Zou, Phys. Rev. **C85**, 044002 (2012), [arXiv:1202.1036].

[17] M. Karliner and J. L. Rosner, Phys. Rev. Lett. **115**, 12, 122001 (2015), [arXiv:1506.06386].

[18] L. Maiani, A. D. Polosa and V. Riquer, Phys. Lett. **B749**, 289 (2015), [arXiv:1507.04980].

[19] R. F. Lebed, Phys. Lett. **B749**, 454 (2015), [arXiv:1507.05867].

[20] V. V. Anisovich *et al.* (2015), [arXiv:1507.07652].

[21] G.-N. Li, X.-G. He and M. He, JHEP **12**, 128 (2015), [arXiv:1507.08252].

[22] R. Ghosh, A. Bhattacharya and B. Chakrabarti, Phys. Part. Nucl. Lett. **14**, 4, 550 (2017), [arXiv:1508.00356].

[23] Z.-G. Wang, Eur. Phys. J. **C76**, 2, 70 (2016), [arXiv:1508.01468].

[24] R. Zhu and C.-F. Qiao, Phys. Lett. **B756**, 259 (2016), [arXiv:1510.08693].

[25] J. M. Richard, A. Valcarce and J. Vijande, Phys. Lett. **B774**, 710 (2017), [arXiv:1710.08239].

[26] E. Hiyama *et al.*, Phys. Rev. **C98**, 4, 045208 (2018), [arXiv:1803.11369].

Int. J. Mod. Phys. A 2026.41. Downloaded from www.worldscientific.com
by UNIVERSITY OF CALIFORNIA @ BERKELEY on 09/16/26. Re-use and distribution is strictly not permitted, except for Open Access articles.

[27] A. Ali and A. Y. Parkhomenko, Phys. Lett. **B793**, 365 (2019), [arXiv:1904.00446].

[28] A. Ali *et al.*, JHEP **10**, 256 (2019), [arXiv:1907.06507].

[29] L. Maiani, A. D. Polosa and V. Riquer, Phys. Lett. **B778**, 247 (2018), [arXiv:1712.05296].

[30] C. Fernandez-Ramirez *et al.* (JPAC), Phys. Rev. Lett. **123**, 9, 092001 (2019), [arXiv:1904.10021].

[31] W. L. Wang *et al.*, Phys. Rev. **C84**, 015203 (2011), [arXiv:1101.0453].

[32] J.-J. Wu *et al.*, Phys. Rev. C **84**, 015202 (2011), [arXiv:1011.2399].

[33] C. W. Xiao, J. Nieves and E. Oset, Phys. Rev. **D88**, 056012 (2013), [arXiv:1304.5368].

[34] C. W. Xiao, J. Nieves and E. Oset, Phys. Rev. **D100**, 1, 014021 (2019), [arXiv:1904.01296].

[35] M.-Z. Liu *et al.*, Phys. Rev. Lett. **122**, 24, 242001 (2019), [arXiv:1903.11560].

[36] G.-J. Wang *et al.*, Phys. Rev. D **102**, 3, 036012 (2020), [arXiv:1911.09613].

[37] P. A. Zyla *et al.* (Particle Data Group), PTEP **2020**, 8, 083C01 (2020).

[38] C. Hanhart, Yu. S. Kalashnikova and A. V. Nefediev, Phys. Rev. **D81**, 094028 (2010), [arXiv:1002.4097].

[39] A. A. Filin *et al.*, Phys. Rev. Lett. **105**, 019101 (2010), [arXiv:1004.4789].

[40] F.-K. Guo and U.-G. Meissner, Phys. Rev. **D84**, 014013 (2011), [arXiv:1102.3536].

[41] M.-L. Du *et al.*, Phys. Rev. Lett. **124**, 7, 072001 (2020), [arXiv:1910.11846].

[42] F.-K. Guo *et al.*, Rev. Mod. Phys. **90**, 1, 015004 (2018), [arXiv:1705.00141].

[43] X.-K. Dong, F.-K. Guo and B.-S. Zou, Progr. Phys. **41**, 65 (2021), [arXiv:2101.01021].

[44] S. K. Choi *et al.* (Belle), Phys. Rev. Lett. **91**, 262001 (2003), [hep-ex/0309032].

[45] D. Acosta *et al.* (CDF), Phys. Rev. Lett. **93**, 072001 (2004), [hep-ex/0312021].

[46] B. Aubert *et al.* (BaBar), Phys. Rev. **D71**, 071103 (2005), [hep-ex/0406022].

[47] V. M. Abazov *et al.* (D0), Phys. Rev. Lett. **93**, 162002 (2004), [hep-ex/0405004].

[48] M. Karliner and H. J. Lipkin (2008), [arXiv:0802.0649].

[49] K. F. Chen *et al.* (Belle), Phys. Rev. Lett. **100**, 112001 (2008), [arXiv:0710.2577].

[50] A. Bondar *et al.* (Belle), Phys. Rev. Lett. **108**, 122001 (2012), [arXiv:1110.2251].

[51] P. Krokovny *et al.* (Belle), Phys. Rev. **D88**, 5, 052016 (2013), [arXiv:1308.2646].

[52] A. Garmash *et al.* (Belle), Phys. Rev. **D91**, 7, 072003 (2015), [arXiv:1403.0992].

[53] M. Ablikim *et al.* (BESIII), Phys. Rev. Lett. **110**, 252001 (2013), [arXiv:1303.5949].

[54] Z. Q. Liu *et al.* (Belle), Phys. Rev. Lett. **110**, 252002 (2013), [arXiv:1304.0121].

[55] T. Xiao *et al.*, Phys. Lett. **B727**, 366 (2013), [arXiv:1304.3036].

[56] M. Ablikim *et al.* (BESIII), Phys. Rev. Lett. **112**, 2, 022001 (2014), [arXiv:1310.1163].

[57] M. Ablikim *et al.* (BESIII), Phys. Rev. Lett. **115**, 11, 112003 (2015), [arXiv:1506.06018].

[58] M. Ablikim *et al.* (BESIII), Phys. Rev. Lett. **111**, 24, 242001 (2013), [arXiv:1309.1896].

[59] M. Ablikim *et al.* (BESIII), Phys. Rev. Lett. **113**, 21, 212002 (2014), [arXiv:1409.6577].

[60] M. Ablikim *et al.* (BESIII), Phys. Rev. Lett. **112**, 13, 132001 (2014), [arXiv:1308.2760].

[61] M. Karliner, Acta Phys. Polon. **B47**, 117 (2016).

[62] M. Karliner, J. L. Rosner and T. Skwarnicki, Ann. Rev. Nucl. Part. Sci. **68**, 17 (2018), [arXiv:1711.10626].

[63] S. L. Olsen, T. Skwarnicki and D. Zieminska, Rev. Mod. Phys. **90**, 1, 015003 (2018), [arXiv:1708.04012].

[64] M. B. Voloshin and L. B. Okun, JETP Lett. **23**, 333 (1976), [Pisma Zh. Eksp. Teor. Fiz.23,369(1976)].

[65] A. De Rujula, H. Georgi and S. Glashow, Phys. Rev. Lett. **38**, 317 (1977).

[66] N. A. Tornqvist, Phys. Rev. Lett. **67**, 556 (1991).

[67] N. A. Tornqvist, Z. Phys. **C61**, 525 (1994), [hep-ph/9310247].

[68] N. A. Tornqvist, Phys. Lett. **B590**, 209 (2004), [hep-ph/0402237].

[69] C. E. Thomas and F. E. Close, Phys. Rev. **D78**, 034007 (2008), [arXiv:0805.3653].

[70] M. Suzuki, Phys. Rev. **D72**, 114013 (2005), [hep-ph/0508258].

[71] S. Fleming *et al.*, Phys. Rev. **D76**, 034006 (2007), [hep-ph/0703168].

[72] T. E. O. Ericson and G. Karl, Phys. Lett. **B309**, 426 (1993).

[73] M. Karliner, H. J. Lipkin and N. A. Tornqvist, in "Proceedings, 14th International Conference on Hadron spectroscopy (Hadron 2011)," (2011), [arXiv:1109.3472], URL `http://inspirehep.net/record/927616/files/arXiv:1109.3472.pdf`.

[74] M. Karliner, H. J. Lipkin and N. A. Tornqvist, Nucl. Phys. Proc. Suppl. **225-227**, 102 (2012).

[75] M. Karliner, Hidden Charm Molecular Pentaquarks: Some Open Questionsin Proc. Bled Mini-Workshop, Slovenia, July 15-19, 2019, B. Golli et al., Eds., p. 25, `http://www-f1.ijs.si/BledPub/bled2019.pdf` .

[76] X.-Q. Li and X. Liu, Eur. Phys. J. **C74**, 12, 3198 (2014), [arXiv:1409.3332].

[77] R. Chen *et al.*, Phys. Rev. Lett. **115**, 13, 132002 (2015), [arXiv:1507.03704].

[78] H.-X. Chen *et al.*, Phys. Rev. Lett. **115**, 17, 172001 (2015), [arXiv:1507.03717].

[79] L. Roca, J. Nieves and E. Oset, Phys. Rev. **D92**, 9, 094003 (2015), [arXiv:1507.04249].

[80] J. He, Phys. Lett. **B753**, 547 (2016), [arXiv:1507.05200].

[81] H. Huang *et al.*, Eur. Phys. J. **C76**, 11, 624 (2016), [arXiv:1510.04648].

[82] L. Roca and E. Oset, Eur. Phys. J. **C76**, 11, 591 (2016), [arXiv:1602.06791].

[83] Q.-F. Lü and Y.-B. Dong, Phys. Rev. **D93**, 7, 074020 (2016), [arXiv:1603.00559].

[84] Y. Shimizu, D. Suenaga and M. Harada, Phys. Rev. **D93**, 11, 114003 (2016), [arXiv:1603.02376].

[85] C.-W. Shen *et al.*, Nucl. Phys. **A954**, 393 (2016), [arXiv:1603.04672].

[86] Y. Yamaguchi *et al.*, Phys. Rev. **D96**, 11, 114031 (2017), [arXiv:1709.00819].

[87] J. F. Giron, R. F. Lebed and C. T. Peterson, JHEP **05**, 061 (2019), [arXiv:1903.04551].

[88] R. Chen *et al.*, Phys. Rev. **D100**, 1, 011502 (2019), [arXiv:1903.11013].

[89] F.-K. Guo *et al.*, Phys. Rev. **D99**, 9, 091501 (2019), [arXiv:1903.11503].

[90] J. He, Eur. Phys. J. **C79**, 5, 393 (2019), [arXiv:1903.11872].

[91] H. Huang, J. He and J. Ping (2019), [arXiv:1904.00221].

Int. J. Mod. Phys. A 2026.41. Downloaded from www.worldscientific.com
UNIVERSITY OF CALIFORNIA @ BERKELEY on 09/16/26. Re-use and distribution is strictly not permitted, except for Open Access articles.

[92] Y. Shimizu, Y. Yamaguchi and M. Harada (2019), [arXiv:1904.00587].

[93] Z.-H. Guo and J. A. Oller, Phys. Lett. **B793**, 144 (2019), [arXiv:1904.00851].

[94] C.-J. Xiao *et al.*, Phys. Rev. **D100**, 1, 014022 (2019), [arXiv:1904.00872].

[95] Z.-G. Wang, Int. J. Mod. Phys. A **35**, 01, 2050003 (2020), [arXiv:1905.02892].

[96] L. Meng *et al.*, Phys. Rev. **D100**, 1, 014031 (2019), [arXiv:1905.04113].

[97] F. Giannuzzi, Phys. Rev. **D99**, 9, 094006 (2019), [arXiv:1903.04430].

[98] Q. Wu and D.-Y. Chen, Phys. Rev. D **100**, 11, 114002 (2019), [arXiv:1906.02480].

[99] C.-W. Shen, J.-J. Wu and B.-S. Zou, Phys. Rev. **D100**, 5, 056006 (2019), [arXiv:1906.03896].

[100] F. Stancu, Eur. Phys. J. C **79**, 11, 957 (2019), [arXiv:1902.07101].

[101] C. W. Xiao, J. Nieves and E. Oset, Phys. Lett. B **799**, 135051 (2019), [arXiv:1906.09010].

[102] M. B. Voloshin, Phys. Rev. **D100**, 3, 034020 (2019), [arXiv:1907.01476].

[103] S. Sakai, H.-J. Jing and F.-K. Guo, Phys. Rev. D **100**, 7, 074007 (2019), [arXiv:1907.03414].

[104] Z.-G. Wang and X. Wang, Chin. Phys. C **44**, 103102 (2020), [arXiv:1907.04582].

[105] Y. Yamaguchi *et al.*, Phys. Rev. D **101**, 9, 091502 (2020), [arXiv:1907.04684].

[106] Y.-J. Xu *et al.*, Phys. Rev. D **102**, 3, 034028 (2020), [arXiv:1907.05097].

[107] M. Pavon Valderrama, Phys. Rev. D **100**, 9, 094028 (2019), [arXiv:1907.05294].

[108] F.-Z. Peng *et al.*, Nucl. Phys. B **983**, 115936 (2022), [arXiv:1907.05322].

[109] M.-Z. Liu *et al.*, Phys. Rev. D **103**, 5, 054004 (2021), [arXiv:1907.06093].

[110] Y.-W. Pan *et al.*, Phys. Rev. D **102**, 1, 011504 (2020), [arXiv:1907.11220].

[111] T. J. Burns and E. S. Swanson, Phys. Rev. D **100**, 11, 114033 (2019), [arXiv:1908.03528].

[112] Y.-H. Lin and B.-S. Zou, Phys. Rev. **D100**, 5, 056005 (2019), [arXiv:1908.05309].

[113] M.-L. Du *et al.*, JHEP **08**, 157 (2021), [arXiv:2102.07159].

[114] S. Dubynskiy and M. B. Voloshin, Phys. Lett. **B666**, 344 (2008), [arXiv:0803.2224].

[115] M. I. Eides, V. Y. Petrov and M. V. Polyakov, Mod. Phys. Lett. A **35**, 18, 2050151 (2020), [arXiv:1904.11616].

[116] F.-K. Guo *et al.*, Phys. Rev. **D92**, 7, 071502 (2015), [arXiv:1507.04950].

[117] U.-G. Meissner and J. A. Oller, Phys. Lett. **B751**, 59 (2015), [arXiv:1507.07478].

[118] X.-H. Liu, Q. Wang and Q. Zhao, Phys. Lett. **B757**, 231 (2016), [arXiv:1507.05359].

[119] M. Mikhasenko (2015), [arXiv:1507.06552].

[120] T. J. Burns, Eur. Phys. J. **A51**, 11, 152 (2015), [arXiv:1509.02460].

[121] H.-X. Chen *et al.*, Phys. Rept. **639**, 1 (2016), [arXiv:1601.02092].

[122] Y.-R. Liu *et al.*, Prog. Part. Nucl. Phys. **107**, 237 (2019), [arXiv:1903.11976].

[123] N. Brambilla *et al.*, Phys. Rept. **873**, 1 (2020), [arXiv:1907.07583].

[124] R. Aaij *et al.* (LHCb), Phys. Rev. D **102**, 11, 112012 (2020), [arXiv:2007.11292].

[125] R. Aaij *et al.* (LHCb), Eur. Phys. J. C **84**, 6, 575 (2024), [arXiv:2311.14088].

[126] R. Aaij *et al.* (LHCb), Phys. Rev. D **110**, 3, L031104 (2024), [arXiv:2404.19510].

[127] R. Aaij *et al.* (LHCb), Phys. Rev. D **110**, 3, 032001 (2024), [arXiv:2404.07131].

[128] X. Dong *et al.* (Belle) (2024), [arXiv:2403.04340].

[129] Y. Huang *et al.*, J. Phys. **G41**, 11, 115004 (2014), [arXiv:1305.4434].

[130] Q. Wang, X.-H. Liu and Q. Zhao, Phys. Rev. **D92**, 034022 (2015), [arXiv:1508.00339].

[131] V. Kubarovsky and M. B. Voloshin, Phys. Rev. **D92**, 3, 031502 (2015), [arXiv:1508.00888].

[132] M. Karliner and J. L. Rosner, Phys. Lett. **B752**, 329 (2016), [arXiv:1508.01496].

[133] A. N. Hiller Blin *et al.*, Phys. Rev. **D94**, 3, 034002 (2016), [arXiv:1606.08912].

[134] X. Cao and J.-p. Dai, Phys. Rev. **D100**, 5, 054033 (2019), [arXiv:1904.06015].

[135] X.-Y. Wang, X.-R. Chen and J. He, Phys. Rev. **D99**, 11, 114007 (2019), [arXiv:1904.11706].

[136] J.-J. Wu, T. S. H. Lee and B.-S. Zou, Phys. Rev. **C100**, 3, 035206 (2019), [arXiv:1906.05375].

[137] G. C. Rossi and G. Veneziano (2019), [arXiv:1909.01753].

[138] U. Skerbis and S. Prelovsek, Phys. Rev. **D99**, 9, 094505 (2019), [arXiv:1811.02285].

[139] C. W. Xiao and U. G. Meissner, Phys. Rev. **D92**, 11, 114002 (2015), [arXiv:1508.00924].

[140] M. B. Voloshin, Phys. Rev. **D99**, 9, 093003 (2019), [arXiv:1903.04422].

[141] R.-Q. Wang *et al.*, Phys. Rev. **C94**, 4, 044913 (2016), [arXiv:1601.02835].

[142] I. Schmidt and M. Siddikov, Phys. Rev. **D93**, 9, 094005 (2016), [arXiv:1601.05621].

[143] Q.-F. L"u *et al.*, Phys. Rev. **D93**, 3, 034009 (2016), [arXiv:1510.06271].

[144] X.-H. Liu and M. Oka, Nucl. Phys. **A954**, 352 (2016), [arXiv:1602.07069].

[145] X.-Y. Wang *et al.*, Phys. Lett. **B797**, 134862 (2019), [arXiv:1906.04044].

[146] A. Ali *et al.* (GlueX), Phys. Rev. Lett. **123**, 7, 072001 (2019), [arXiv:1905.10811].

[147] S. Adhikari *et al.* (GlueX), Phys. Rev. C **108**, 2, 025201 (2023), [arXiv:2304.03845].

[148] M.-L. Du *et al.*, Eur. Phys. J. C **80**, 11, 1053 (2020), [arXiv:2009.08345].

[149] D. Winney *et al.* (Joint Physics Analysis Center), Phys. Rev. D **108**, 5, 054018 (2023), [arXiv:2305.01449].

[150] R. Aaij *et al.* (LHCb), Phys. Rev. Lett. **128**, 062001 (2021), [arXiv:2108.04720].

[151] B. Wang, L. Meng and S.-L. Zhu, JHEP **11**, 108 (2019), [arXiv:1909.13054].

[152] R. Chen, J. He and X. Liu, Chin. Phys. C **41**, 10, 103105 (2017), [arXiv:1609.03235].

[153] E. Santopinto and A. Giachino, Phys. Rev. D **96**, 1, 014014 (2017), [arXiv:1604.03769].

[154] B. Wang, L. Meng and S.-L. Zhu, Phys. Rev. D **101**, 3, 034018 (2020), [arXiv:1912.12592].

[155] M. Karliner and J. L. Rosner, Sci. Bull. **66**, 13, 1256 (2021), [arXiv:2104.15077].

[156] M. Karliner and J. L. Rosner, Phys. Rev. D **106**, 3, 036024 (2022), [arXiv:2207.07581].

[157] R. Aaij *et al.* (LHCb), Phys. Rev. Lett. **131**, 3, 031901 (2023), [arXiv:2210.10346].

[158] R. Aaij *et al.* (LHCb), Phys. Rev. D **112**, 5, 052013 (2025), [arXiv:2507.10713].

[159] I. Adachi *et al.* (Belle, Belle-II), Phys. Rev. Lett. **135**, 4, 041901 (2025), [arXiv:2502.09951].

[160] T. Aaltonen *et al.* (CDF), Phys. Rev. Lett. **102**, 242002 (2009), [arXiv:0903.2229].

[161] T. Aaltonen *et al.* (CDF), Mod. Phys. Lett. A **32**, 26, 1750139 (2017), [arXiv:1101.6058].

[162] S. Chatrchyan *et al.* (CMS), Phys. Lett. B **734**, 261 (2014), [arXiv:1309.6920].

[163] R. Aaij *et al.* (LHCb), Phys. Rev. Lett. **118**, 2, 022003 (2017), [arXiv:1606.07895].

[164] R. Aaij *et al.* (LHCb), Phys. Rev. D **95**, 1, 012002 (2017), [arXiv:1606.07898].

[165] R. Aaij *et al.* (LHCb), Phys. Rev. Lett. **127**, 8, 082001 (2021), [arXiv:2103.01803].

[166] LHCb (LHCb), Phys. Rev. Lett. **131**, 13, 131901 (2023), [arXiv:2301.04899].

[167] R. Aaij *et al.* (LHCb), Sci. Bull. **65**, 23, 1983 (2020), [arXiv:2006.16957].

[168] A. Hayrapetyan *et al.* (CMS), Phys. Rev. Lett. **132**, 11, 111901 (2024), [arXiv:2306.07164].

[169] G. Aad *et al.* (ATLAS), Phys. Rev. Lett. **131**, 15, 151902 (2023), [arXiv:2304.08962].

[170] S. K. Choi *et al.* (Belle), Phys. Rev. Lett. **100**, 142001 (2008), [arXiv:0708.1790].

[171] K. Chilikin *et al.* (Belle), Phys. Rev. D **88**, 7, 074026 (2013), [arXiv:1306.4894].

[172] R. Aaij *et al.* (LHCb), Phys. Rev. Lett. **112**, 22, 222002 (2014), [arXiv:1404.1903].

[173] M. Berwein *et al.*, Phys. Rev. D **110**, 9, 094040 (2024), [arXiv:2408.04719].

[174] E. Braaten and R. Bruschini, Phys. Lett. B **863**, 139386 (2025), [arXiv:2409.08002].

[175] N. Brambilla, A. Mohapatra and A. Vairo (2025), [arXiv:2508.13050].

[176] F. Alasiri, E. Braaten and R. Bruschini (2025), [arXiv:2507.06991].

[177] R. Aaij *et al.* (LHCb), Nature Phys. **18**, 7, 751 (2022), [arXiv:2109.01038].

[178] R. Aaij *et al.* (LHCb), Nature Commun. **13**, 1, 3351 (2022), [arXiv:2109.01056].

Int. J. Mod. Phys. A 2026.41. Downloaded from www.worldscientific.com
by UNIVERSITY OF CALIFORNIA @ BERKELEY on 09/16/26. Re-use and distribution is strictly not permitted, except for Open Access articles.

Int. J. Mod. Phys. A 2026.41. Downloaded from www.worldscientific.com
UNIVERSITY OF CALIFORNIA @ BERKELEY on 09/16/26. Re-use and distribution is strictly not permitted, except for Open Access articles.

Hypothetical Particles and Concepts

84. Extra dimensions (rev.) 1067
85. W'-boson searches (rev.) 1076
86. Z'-boson searches (rev.) 1080
87. Supersymmetry: theory (rev.) 1086
88. Supersymmetry: experiment (rev.) 1108
89. Axions and other similar particles (rev.) 1130
90. Quark and lepton compositeness, searches for (rev.) . . . 1150
91. Dynamical electroweak symmetry breaking: implications of the H^0 (rev.) 1156
92. Grand unified theories (rev.) 1171
93. Leptoquarks (rev.) 1189
94. Magnetic monopoles (rev.) 1194

Int. J. Mod. Phys. A 2026.41. Downloaded from www.worldscientific.com
by UNIVERSITY OF CALIFORNIA @ BERKELEY on 09/16/26. Re-use and distribution is strictly not permitted, except for Open Access articles.

Int. J. Mod. Phys. A 2026.41. Downloaded from www.worldscientific.com
by UNIVERSITY OF CALIFORNIA @ BERKELEY on 09/16/26. Re-use and distribution is strictly not permitted, except for Open Access articles.

Int. J. Mod. Phys. A 2026.41. Downloaded from www.worldscientific.com
by UNIVERSITY OF CALIFORNIA @ BERKELEY on 09/16/26. Re-use and distribution is strictly not permitted, except for Open Access articles.

84. Extra Dimensions

Revised August 2025 by Z. Demiragli (Boston U.) and A. Pomarol (U. Autònoma de Barcelona; IFAE).

84.1 Introduction

Proposals for a spacetime with more than three spatial dimensions date back to the 1920s, mainly through the work of Kaluza and Klein, in an attempt to unify the forces of nature [1]. Although their initial idea failed, the formalism that they and others developed is still useful nowadays. Around 1980, string theory proposed again to enlarge the number of space dimensions, this time as a requirement for describing a consistent theory of quantum gravity. The extra dimensions were supposed to be compactified at a scale close to the Planck scale, and thus not testable experimentally in the near future.

A different approach was given by Arkani-Hamed, Dimopoulos, and Dvali (ADD) in their seminal paper in 1998 [2], where they showed that the weakness of gravity could be explained by postulating two or more flat extra dimensions in which only gravity could propagate. The size of these extra dimensions should range between roughly a millimeter and $\sim$1/TeV, leading to possible observable consequences in current and future experiments. A year later, Randall and Sundrum (RS) [3] found a new possibility using a warped geometry, postulating a five-dimensional Anti-de Sitter (AdS) spacetime with a compactification scale of order 1/TeV. The origin of the smallness of the electroweak scale versus the Planck scale was explained by the gravitational redshift factor present in the warped AdS metric. As in the ADD model, originally only gravity was assumed to propagate in the extra dimensions, although it was soon clear that this was not necessary in warped extra dimensions and also the SM gauge fields [4, 5] and SM fermions [6, 7] could propagate in the five-dimensional spacetime.

The physics of warped extra-dimensional models has an alternative interpretation by means of the AdS/Conformal Field Theory (CFT) correspondence [8–10]. Models with warped extra dimensions are related to four-dimensional strongly-interacting theories, allowing an understanding of the properties of five-dimensional fields as those of four-dimensional composite states [11]. This approach has opened new directions for tackling outstanding questions in particle physics, such as the flavor problem, grand unification, and the origin of electroweak symmetry breaking or supersymmetry breaking.

84.1.1 *Experimental Constraints*

Constraints on extra-dimensional models arise from astrophysical and cosmological considerations, tabletop experiments exploring gravity at sub-mm distances, and collider experiments. Collider limits on extra-dimensional models are dominated by LHC results, which can be found on the public WWW pages of ATLAS [12] and CMS [13]. This review includes the most recent limits, most of which are published results based on 140 fb^{-1}LHC data collected in 2015-18 at a center-of-mass energy of 13 TeV and legacy results from 20 fb^{-1}of 8 TeV data collected in Run 1. For most of the models, Run 2 results surpass the sensitivity of Run 1.

84.1.2 *Kaluza-Klein Theories*

Field theories with compact extra dimensions can be written as theories in ordinary four dimensions (4D) by performing a Kaluza-Klein (KK) reduction. As an illustration, consider a simple example, namely a field theory of a complex scalar in flat five-dimensional (5D) spacetime. The action will be given by [1]

$$S_5 = -\int d^4x\, dy\, M_5 \left[|\partial_\mu \phi|^2 + |\partial_y \phi|^2 + \lambda_5 |\phi|^4\right] , \qquad (84.1)$$

where y refers to the extra (fifth) dimension. A universal scale M_5 has been extracted in front of the action in order to keep the 5D field with the same mass-dimension as in 4D. This theory is perturbative for energies $E \lesssim \ell_5 M_5/\lambda_5$ where $\ell_5 = 24\pi^3$ [14].

Let us now consider that the fifth dimension is compact with the topology of a circle S^1 of radius R, which corresponds to the identification of y with $y + 2\pi R$. In such a case, the 5D complex scalar field can be expanded in a Fourier series:

$$\phi(x,y) = \frac{1}{\sqrt{2\pi R M_5}} \sum_{n=-\infty}^{\infty} e^{iny/R} \phi^{(n)}(x) , \qquad (84.2)$$

that, inserted in Eq. (84.1) and integrating over y, gives

$$S_5 = S_4^{(0)} + S_4^{(n)} , \qquad (84.3)$$

where

$$S_4^{(0)} = -\int d^4x \left[|\partial_\mu \phi^{(0)}|^2 + \lambda_4 |\phi^{(0)}|^4\right] , \qquad (84.4)$$

and,

$$S_4^{(n)} = -\int d^4x \sum_{n\neq 0} \left[|\partial_\mu \phi^{(n)}|^2 + \left(\frac{n}{R}\right)^2 |\phi^{(n)}|^2\right] + \text{quartic interactions} . \qquad (84.5)$$

The $n = 0$ mode self-coupling is given by

$$\lambda_4 = \frac{\lambda_5}{2\pi R M_5} . \qquad (84.6)$$

The above action corresponds to a 4D theory with a massless scalar $\phi^{(0)}$, referred to as the zero mode, and an infinite tower of massive modes $\phi^{(n)}$ with $n > 0$, known as KK modes. The KK reduction thus allows a treatment of 5D theories as 4D field theories with an infinite number of fields. At energies smaller than $1/R$, the KK modes can be neglected, leaving the zero-mode action of Eq. (84.4). The strength of the interaction of the zero-mode, given by Eq. (84.6), decreases as R increases. Thus, for a large extra dimension $R \gg 1/M_5$, the massless scalar is very weakly coupled.

84.2 Large Extra Dimensions for Gravity

84.2.1 *The ADD Scenario*

The ADD scenario [2, 15] (for a review see, for example, [16]) assumes a $D = 4 + \delta$ dimensional spacetime, with δ compactified spatial dimensions. The apparent weakness of gravity arises since it propagates in the higher-dimensional space. The SM is assumed to be localized in a 4D subspace, a 3-brane, as can be found in certain string theory constructions [17, 18]. Gravity is described by the Einstein-Hilbert action in $D = 4 + \delta$ spacetime dimensions

$$S_D = -\frac{\bar{M}_D^{2+\delta}}{2} \int d^4x d^\delta y \sqrt{-g}\, \mathcal{R} + \int d^4x \sqrt{-g_{\rm ind}}\, \mathcal{L}_{\rm SM} , \qquad (84.7)$$

where x labels the ordinary four coordinates, y the δ extra coordinates, g refers to the determinant of the D-dimensional metric whose Ricci scalar is defined by $\mathcal{R}$, and $\bar{M}_D$ is called the reduced Planck scale of the D-dimensional theory. In the second term of Eq. (84.7), which gives the gravitational interactions of SM fields, the D-dimensional metric reduces to the induced metric on the 3-brane where the SM fields propagate. The extra dimensions are assumed to be flat and compactified in a volume V_δ. As an example, consider a toroidal compactification of equal radii R and volume $V_\delta = (2\pi R)^\delta$. After a KK reduction, one finds that the fields that couple to the SM are the spin-2 gravitational field $G_{\mu\nu}(x,y)$ and a tower of spin-0 KK graviscalars [19]. The graviscalars, however, only couple to SM fields through the trace of the energy-momentum tensor, resulting in weaker couplings to the SM fields. The Fourier expansion of the spin-2 field is given by

$$G_{\mu\nu}(x,y) = G_{\mu\nu}^{(0)}(x) + \frac{1}{\sqrt{V_\delta}} \sum_{\vec{n}\neq 0} e^{i\vec{n}\cdot\vec{y}/R} G_{\mu\nu}^{(\vec{n})}(x) , \qquad (84.8)$$

where $\vec{y} = (y_1, y_2, ..., y_\delta)$ are the extra-dimensional coordinates and $\vec{n} = (n_1, n_2, ..., n_\delta)$. Eq. (84.8) contains a massless state, the 4D graviton $G_{\mu\nu}^{(0)}$, and its KK tower $G_{\mu\nu}^{(\vec{n})}$ with masses $m_{\vec{n}}^2 =$

[1] Our convention for the metric is $\eta_{MN} = \text{Diag}(-1, 1, 1, 1, 1)$.

Int. J. Mod. Phys. A 2026.41. Downloaded from www.worldscientific.com by UNIVERSITY OF CALIFORNIA @ BERKELEY on 09/16/26. Re-use and distribution is strictly not permitted, except for Open Access articles.

$|\vec{n}|^2/R^2$. At energies below $1/R$ the action is that of the zero mode

$$S_4^{(0)} = -\frac{\bar{M}_D^{2+\delta}}{2}\int d^4x\, V_\delta \sqrt{-g^{(0)}}\,\mathcal{R}^{(0)} + \int d^4x \sqrt{-g_{\rm ind}^{(0)}}\,\mathcal{L}_{\rm SM}\,, \tag{84.9}$$

where we can identify the 4D reduced Planck mass, $M_P \equiv 1/\sqrt{8\pi G_N} \simeq 2.4\times 10^{18}$ GeV, as a function of the D-dimensional parameters:

$$M_P^2 = V^\delta \bar{M}_D^{2+\delta} \equiv R^\delta M_D^{2+\delta}\,. \tag{84.10}$$

Fixing M_D at around the electroweak scale $M_D \sim$ TeV to avoid introducing a new mass scale in the model, Eq. (84.10) gives a prediction for R:

$$\delta = 1, 2, ..., 6 \;\rightarrow\; R \sim 10^9 \text{ km}\,, 0.5 \text{ mm}\,, ...\,, 0.1 \text{ MeV}^{-1}\,. \tag{84.11}$$

The option $\delta = 1$ is clearly ruled out, as it leads to modifications of Newton's law at solar system distances. However this is not the case for $\delta \geq 2$, and possible observable consequences can be sought in present and future experiments.

Consistency of the model requires a stabilization mechanism for the radii of the extra dimensions, to the values shown in Eq. (84.11). The fact that we need $R \gg 1/M_D$ leads to a new hierarchy problem, the solution of which might require imposing supersymmetry in the extra-dimensional bulk (for the case of two extra dimensions see for example [20]).

84.2.2 *Tests of the Gravitational Force Law at Sub-mm Distances*

The KK modes of the graviton give rise to deviations from Newton's law of gravitation for distances $\lesssim R$. Such deviations are usually parameterized by a modified Newtonian potential of the form

$$V(r) = -G_N \frac{m_1 m_2}{r}\left[1 + \alpha\, e^{-r/\lambda}\right]\,. \tag{84.12}$$

For a 2-torus compactification, $\alpha = 16/3$ and $\lambda = R$. Searches for deviations from Newton's law of gravitation have been performed in several experiments [21–24]. From Ref. [23] we have the constraint $R < 30\mu$m at 95% CL for $\delta = 2$, corresponding to $M_D > 4.0$ TeV. We see then that bounds from Newton's law deviations are already pushing the scale M_D beyond the TeV for two extra dimensions.

84.2.3 *Astrophysical and Cosmological Constraints*

The light KK gravitons could be copiously produced in stars, carrying away energy. Ensuring that the graviton luminosity is low enough to preserve the agreement of stellar models with observations provides powerful bounds on the scale M_D. The most stringent bound arises from supernova SN1987A, giving $M_D > 27$ (2.4) TeV for $\delta = 2$ (3) [25]. After a supernova explosion, most of the KK gravitons stay gravitationally trapped in the remnant neutron star. The requirement that neutron stars are not excessively heated by KK decays into photons leads to $M_D > 1700$ (76) TeV for $\delta = 2$ (3) [26].

Cosmological constraints are also quite stringent [27]. To avoid overclosure of the Universe by relic gravitons one needs $M_D > 7$ TeV for $\delta = 2$. Relic KK gravitons decaying into photons contribute to the cosmic diffuse gamma radiation, from which one can derive the bound $M_D > 100$ TeV for $\delta = 2$.

We must mention however that bounds coming from the decays of KK gravitons into photons can be reduced if we assume that KK gravitons decay mainly into other non-SM states. This could happen, for example, if there were other 3-branes with hidden sectors residing on them [15].

84.2.4 *Collider Signals*

84.2.4.1 *Graviton and Other Particle Production*

Although each KK graviton has a purely gravitational coupling, suppressed by $1/M_P$, inclusive processes in which one sums over the almost continuous spectrum of available gravitons have cross sections suppressed only by powers of M_D. Processes involving gravitons are therefore detectable in collider experiments if $M_D \sim$ TeV. A number of experimental searches for evidence of large extra dimensions have been performed at colliders, and interpreted in the context of the ADD model.

One signature arises from direct graviton emission. By making a derivative expansion of Einstein gravity, one can construct an effective theory, valid for energies much lower than M_D, and use it to make predictions for graviton-emission processes at colliders [19, 28, 29]. Gravitons produced in the final state would escape detection, giving rise to missing transverse momentum ($p_{\rm T}^{\rm miss}$). The results quoted below are 95% CL lower limits on M_D for a range of values of δ between 2 and 6, with more stringent limits corresponding to lower δ values.

At hadron colliders, experimentally sensitive channels include the jet $(j) + p_{\rm T}^{\rm miss}$ and $\gamma + p_{\rm T}^{\rm miss}$ final states. ATLAS (CMS) $j + p_{\rm T}^{\rm miss}$ results with 139 (137) fb^{-1} of 13 TeV data provide limits of $M_D > 5.9 - 11.2$ TeV [30] ($M_D > 5.5 - 10.7$ TeV [31]). For these analyses, both experiments are assuming leading order cross sections. Since the effective theory is only valid for energies much less than M_D, the results are quoted for the full space, and include the information that suppressing the graviton cross section by a factor $M_D^4/\hat{s}^2$ for $\sqrt{\hat{s}} > M_D$, where $\sqrt{\hat{s}}$ is the parton-level center-of-mass energy of the hard collision, weakens the limits on M_D by a negligible amount for $\delta = 2$ ($\sim$3% for $\delta = 6$). Less stringent limits are obtained by CMS [32] from analysis of 36 fb^{-1}of 13 TeV data in the $\gamma + p_{\rm T}^{\rm miss}$ final state ($M_D > 2.85 - 2.90$ TeV for $\delta = 3 - 6$). The analogous ATLAS search [33] uses full Run 2 statistics but does not quote ADD interpretation of the results.

In models in which the ADD scenario is embedded in a string theory at the TeV scale [18], we expect the string scale M_s to be smaller than M_D, and therefore expect production of string resonances at the LHC [34]. A result from CMS analyzing the dijet invariant mass distribution for 137 fb^{-1}of 13 TeV data excludes string resonances that decay predominantly to $q + g$ with masses below 7.9 TeV [35]. ATLAS dijet analysis [36] provides their results in the context of model-independent limits on the cross section times acceptance for generic resonances of a variety of possible widths, from which one can deduce similar lower mass limits ~ 8 TeV for string resonances decaying to $q + g$.

84.2.4.2 *Virtual graviton effects*

One can also search for virtual graviton effects, the calculation of which however depends on the ultraviolet cut-off of the theory and is therefore very model dependent. In the literature, several different formulations exist [19,29,37] for the dimension-eight operator for gravity exchange at tree level:

$$\mathcal{L}_8 = \pm\frac{4}{M_{TT}^4}\left(T_{\mu\nu}T^{\mu\nu} - \frac{1}{\delta+2}T^\mu_\mu T^\nu_\nu\right)\,, \tag{84.13}$$

where $T_{\mu\nu}$ is the energy-momentum tensor and M_{TT} is related to M_D by some model-dependent coefficient [38]. The relations with the parametrization of Refs. [37] and [19] are, respectively, $M_{TT} = M_S$ and $M_{TT} = (2/\pi)^{1/4}\Lambda_T$. The experimental results below are given as 95% CL lower limits on M_{TT}, including in some cases the possibility of both constructive or destructive interference, depending on the sign chosen in Eq. (9).

The most stringent limits arise from LHC analyses of the dijet angular distribution. Using 35.9 fb^{-1}of 13 TeV data, CMS [39] obtains results that correspond to an approximate limit of $M_{TT} \gtrsim 9$ TeV.

The next most restrictive results come from the analyses of diphoton ($M_{TT} > 6.1$ TeV from ATLAS [40] and $M_{TT} > 8.3$ TeV from CMS [41]) and dilepton ($M_{TT} > 6.5$ TeV from CMS [42]) mass spectra. The complete Run 2 (139 fb^{-1}) analysis of ATLAS di-lepton data [43] does not quote the limits on the ADD model.

At the one-loop level, gravitons can also generate dimension-six operators with coefficients that are also model dependent. Experimental bounds on these operators can also give stringent constraints on M_D [38].

84.2.4.3 *Black Hole Production*

The physics at energies $\sqrt{s} \sim M_D$ is sensitive to the details of the unknown quantum theory of gravity. Nevertheless, in the transplanckian regime, $\sqrt{s} \gg M_D$, one can rely on a semiclassical description of gravity to obtain predictions. An interesting feature of transplanckian physics is the creation of black holes [44,45] (for a review see, for example, [46]). A black hole is expected to be

Int. J. Mod. Phys. A 2026.41. Downloaded from www.worldscientific.com by UNIVERSITY OF CALIFORNIA @ BERKELEY on 09/16/26. Re-use and distribution is strictly not permitted, except for Open Access articles.

formed in a collision in which the impact parameter is smaller than the Schwarzschild radius [47]:

$$R_S = \frac{1}{M_D}\left[\frac{2^\delta \pi^{(\delta-3)/2}}{\delta+2}\Gamma\left(\frac{\delta+3}{2}\right)\frac{M_{BH}}{M_D}\right]^{1/(\delta+1)}, \quad (84.14)$$

where M_{BH} is the mass of the black hole, which would roughly correspond to the total energy in the collision. The cross section for black hole production can be estimated to be of the same order as the geometric area $\sigma \sim \pi R_S^2$. For $M_D \sim$ TeV, this gives a production of $\sim 10^7$ black holes at the $\sqrt{s} = 14$ TeV LHC with an integrated luminosity of 30 fb^{-1} [44,45]. A black hole would provide a striking experimental signature since it is expected to thermally radiate with a Hawking temperature $T_H = (\delta+1)/(4\pi R_S)$, and therefore would evaporate democratically into all SM states. Nevertheless, given the present constraints on M_D, the LHC will not be able to reach energies much above M_D. This implies that predictions based on the semiclassical approximation could receive sizable modifications from model-dependent quantum-gravity effects.

The most stringent limits on microscopic black holes arise from LHC searches which observed no excesses above the SM background in high-multiplicity final states. The results are usually quoted as model-independent limits on the cross section for new physics in the final state and kinematic region analyzed. These results can then be used to provide constraints of models of low-scale gravity and weakly-coupled string theory. In addition, limits are sometimes quoted on particular implementations of models, which are used as benchmarks to illustrate the sensitivity.

A CMS analysis [48] of multi-object final states using 36 fb^{-1}of 13 TeV data, excludes semiclassical black holes below masses of up to 10.1 TeV for $M_D = 2$ TeV and $\delta = 6$. Analogous Run 2 ATLAS analysis [49], using 3.0 fb^{-1}of 13 TeV data, excludes black hole masses up to $9.0 - 9.7$ TeV, depending on M_D, for $\delta = 6$. Another ATLAS search [50] for an excess of events with multiple high transverse momentum objects, including charged leptons and jets, using 3.2 fb^{-1}of 13 TeV data, excludes semiclassical black holes below masses of ~ 8.7 TeV for $M_D = 2$ TeV and $\delta = 6$.

A complementary approach is to look for jet extinction at high transverse momenta, as we expect hard short distance scattering processes to be highly suppressed at energies above M_D [51]. The CMS analysis [52] of inclusive jet p_T spectrum in 10.7 fb^{-1}of 8 TeV data set a lower limit of 3.3 TeV on the extinction mass scale.

For black hole masses near M_D, the semi-classical approximation is not valid, and one could instead expect quantum black holes (QBH) that decay primarily into two-body final states [53]. In the context of both ADD model with $\delta = 6$ the QBHs have been searched in few final state analysis (based on 2.3 fb^{-1} [54]), dijet [36,39,55], (same and different flavor) dilepton [56–60], photon+jet [61,62] and lepton+jet [63] channels by both ATLAS and CMS experiments. The Run 2 results at 13 TeV provide lower limits on QBH masses of up-to 9.4 TeV in an ADD model with $\delta = 6$. The strongest constraints are from dijet searches.

In weakly-coupled string models the semiclassical description of gravity fails in the energy range between M_s and M_s/g_s^2 where stringy effects are important. In this regime one expects, instead of black holes, the formation of string balls, made of highly excited long strings, that could be copiously produced at the LHC for $M_s \sim$ TeV [64], and would evaporate thermally at the Hagedorn temperature giving rise to high-multiplicity events. The same analyses used to search for black holes can be interpreted in the context of string balls. For example, for the case of $\delta = 6$ with $M_s = M_D/1.26 = 3$ TeV, the ATLAS multiple high transverse momentum object analysis [49] excludes string balls with masses below 6.5 to 9.0 TeV for values of $0.2 < g_s < 0.8$. The CMS multi-object analysis [48] studies string ball production in two scenarios, both assuming $\delta = 6$. For the constant $g_s = 0.2$ and $1 < M_s < 3.5$ TeV the string ball masses below 7.2 to 9.4 TeV are excluded, while at constant $M_s = 3.6$ TeV and $0.2 < g_s < 0.4$ masses below 7.2 to 8.1 TeV are excluded.

84.3 TeV-Scale Extra Dimensions

84.3.1 *Warped Extra Dimensions*

The RS model [3] is the most attractive setup of warped extra dimensions at the TeV scale, since it provides an alternative solution to the hierarchy problem. The RS model is based on a 5D theory with the extra dimension compactified in an orbifold, S^1/Z_2, a circle S^1 with the extra identification of y with $-y$. This corresponds to the segment $y \in [0, \pi R]$, a manifold with boundaries at $y = 0$ and $y = \pi R$. Let us now assume that this 5D theory has a cosmological constant in the bulk Λ, and on the two boundaries Λ_0 and $\Lambda_{\pi R}$. The action is given by

$$S_5 = -\int d^4x\, dy \Big\{ \sqrt{-g}\Big[\frac{1}{2}M_5^3\mathcal{R} + \Lambda\Big] + \sqrt{-g_0}\,\delta(y)\Lambda_0 + \sqrt{-g_{\pi R}}\,\delta(y-\pi R)\Lambda_{\pi R}\Big\}, \quad (84.15)$$

where g_0 and $g_{\pi R}$ are the values of the determinant of the induced metric on the two respective boundaries. Einstein's equations can be solved, giving in this case the metric

$$ds^2 = a(y)^2 dx^\mu dx^\nu \eta_{\mu\nu} + dy^2\,, \quad a(y) = e^{-ky}\,, \quad (84.16)$$

where $k = \sqrt{-\Lambda/6M_5^3}$. Consistency of the solution requires $\Lambda_0 = -\Lambda_{\pi R} = -\Lambda/k$. The metric in Eq. (84.16) corresponds to a 5D AdS space. The factor $a(y)$ is called the "warp" factor and determines how 4D scales change as a function of the position in the extra dimension. In particular, this implies that energy scales for 4D fields localized at the boundary at $y = \pi R$ are redshifted by a factor $e^{-k\pi R}$ with respect to those localized at $y = 0$. For this reason, the boundaries at $y = 0$ and $y = \pi R$ are usually referred to as the ultraviolet (UV) and infrared (IR) boundaries, respectively.

As in the ADD case, we can perform a KK reduction and obtain the low-energy effective theory of the 4D massless graviton. In this case we obtain

$$M_P^2 = \int_0^{\pi R} dy\, e^{-2ky} M_5^3 = \frac{M_5^3}{2k}\left(1 - e^{-2k\pi R}\right). \quad (84.17)$$

Taking $M_5 \sim k \sim M_P$, we can generate an IR-boundary scale of order $ke^{-k\pi R} \sim$ TeV for an extra dimension of radius $R \simeq 11/k$. Mechanisms to stabilize R to this value have been proposed [65,66] that, contrary to the ADD case, do not require introducing any new small or large parameter. Therefore a natural solution to the hierarchy problem can be achieved in this framework if the Higgs field, whose vacuum expectation value (VEV) is responsible for electroweak symmetry breaking, is localized at the IR-boundary where the effective mass scales are of order TeV. The radion field is generically heavy in models with a stabilized R. Nevertheless, it has been recently discussed that under some conditions a naturally light radion can arise [67–70]. In these cases the radion is identified with the dilaton, the Nambu-Goldstone boson associated to the spontaneous breaking of scale invariance, and its mass can be naturally below $ke^{-k\pi R} \sim$ TeV.

In the RS model [3], all the SM fields were assumed to be localized on the IR-boundary. Nevertheless, for the hierarchy problem, only the Higgs field has to be localized there. SM gauge bosons and fermions can propagate in the 5D bulk [4–7] (for a review see, for example, [71, 72]). By performing a KK reduction from the 5D action of a gauge boson, we find [4, 5]

$$\frac{1}{g_4^2} = \int_0^{\pi R} dy\, \frac{1}{g_5^2} = \frac{\pi R}{g_5^2}\,, \quad (84.18)$$

where g_D $(D = 4, 5)$ is the gauge coupling in D-dimensions. Therefore the 4D gauge couplings can be of order one, as is the case of the SM, if one demands $g_5^2 \sim \pi R$. Using $kR \sim 10$ and $g_4 \sim 0.5$, one obtains the 5D gauge coupling

$$g_5 \sim 4/\sqrt{k}\,. \quad (84.19)$$

Boundary kinetic terms for the gauge bosons can modify this relation, allowing for larger values of $g_5\sqrt{k}$.

Int. J. Mod. Phys. A 2026.41. Downloaded from www.worldscientific.com by UNIVERSITY OF CALIFORNIA @ BERKELEY on 09/16/26. Re-use and distribution is strictly not permitted, except for Open Access articles.

Fermions propagating in a warped extra dimension have 4D massless zero-modes with wavefunctions which vary as $f_0 \sim exp[(1/2-c_f)ky]$, where $c_f k$ is their 5D mass [7,73]. Depending on the free parameter $c_f k$, fermions can be localized either towards the UV-boundary ($c_f > 1/2$) or IR-boundary ($c_f < 1/2$). Since the Higgs boson is localized on the IR-boundary, one can generate exponentially suppressed Yukawa couplings by having the fermion zero-modes localized towards the UV-boundary, generating naturally the light SM fermion spectrum [7]. A large overlap with the wavefunction of the Higgs is needed for the top quark, in order to generate its large mass, thus requiring it to be localized towards the IR-boundary. In conclusion, the large mass hierarchies present in the SM fermion spectrum can be easily obtained in warped models via suitable choices of the order-one parameters c_f [74]. In these scenarios, deviations in flavor physics from the SM predictions are expected to arise from flavor-changing KK gluon couplings [75], putting certain constraints on the parameters of the models and predicting new physics effects to be observed in B-physics processes (see, for example, [76,77]).

The masses of the KK states can also be calculated. One finds [7]

$$m_n \simeq \left(n + \frac{\alpha}{2} - \frac{1}{4}\right) \pi k e^{-\pi k R}\,, \tag{84.20}$$

where $n = 1, 2, ...$ and $\alpha = \{|c_f - 1/2|, 0, 1\}$ for KK fermions, KK gauge bosons and KK gravitons, respectively. Their masses are of order $ke^{-\pi kR} \sim$ TeV (for this reason we refer to these scenarios as TeV-scale extra dimensions). The first KK state of the gauge bosons would be the lightest, while gravitons are expected to be the heaviest.

84.3.1.1 *Models of Electroweak Symmetry Breaking*

Theories in warped extra dimensions can be used to implement symmetry breaking at low energies by boundary conditions (for a review see, for example, [78]). For example, for a $U(1)$ gauge symmetry in the 5D bulk, this can be easily achieved by imposing a Dirichlet boundary condition on the IR-boundary for the gauge-boson field, $A_\mu|_{y=\pi R} = 0$. This makes the zero-mode gauge boson get a mass, given by $m_A = g_4\sqrt{2k/g_5^2}\, e^{-\pi kR}$. A very different situation occurs if the Dirichlet boundary condition is imposed on the UV-boundary, $A_\mu|_{y=0} = 0$. In this case the zero-mode gauge boson disappears from the spectrum. Finally, if a Dirichlet boundary condition is imposed on the two boundaries, one obtains a massless 4D scalar corresponding to the fifth component of the 5D gauge boson, A_5. Thus, different scenarios can be implemented by appropriately choosing the 5D bulk gauge symmetry, $\mathcal{G}_5$, and the symmetries to which it reduces on the UV and IR-boundary, $\mathcal{H}_{UV}$ and $\mathcal{H}_{IR}$, respectively. In all cases the KK spectrum comes in representations of the group $\mathcal{G}_5$.

Among the most interesting scenarios are those called gauge-Higgs unified models, where the Higgs boson appears as the fifth component of a 5D gauge boson, A_5. The Higgs mass is protected by the 5D gauge invariance and can only get a nonzero value from non-local one-loop effects [79]. To guarantee the relation $M_W^2 \simeq M_Z^2 \cos^2\theta_W$, a custodial $SU(2)_V$ symmetry is needed in the bulk and IR-boundary [80]. The simplest realization [81,82] has

$$\begin{aligned} \mathcal{G}_5 &= SU(3)_c \times SO(5) \times U(1)_X\,, \\ \mathcal{H}_{IR} &= SU(3)_c \times SO(4) \times U(1)_X\,, \\ \mathcal{H}_{UV} &= G_{SM}\,. \end{aligned}$$

The Higgs boson gets a potential at the one-loop level that triggers a VEV, breaking the electroweak symmetry. In these models there is a light Higgs boson whose mass can be around 125 GeV, as required by the discovered Higgs boson [83]. This state, as will be explained in Sec. 84.3.2, behaves as a composite pseudo-Nambu-Goldstone boson with couplings that deviate from the SM Higgs [84]. The present experimental determination of the Higgs couplings at the LHC, that agrees with the SM predictions, put important constraints on these scenarios [83]. The lightest KK modes of the model are color fermions with charges $Q = -1/3, 2/3$ and $5/3$ [85].

84.3.1.2 *Constraints from Electroweak Precision Tests*

Models in which the SM gauge bosons propagate in 1/TeV-sized extra dimensions give generically large corrections to electroweak observables. When the SM fermions are confined on a boundary these corrections are universal and can be parameterized by four quantities: $\widehat{S}$, $\widehat{T}$, W and Y, as defined in Ref. [86]. For warped models, where the 5D gauge coupling of Eq. (84.19) is large, the most relevant parameter is $\widehat{T}$, which gives the bound $m_{KK} \gtrsim$ 10 TeV [71]. When a custodial symmetry is imposed [80], the main constraint comes from the $\widehat{S}$ parameter, requiring $m_{KK} \gtrsim 3$ TeV, independent of the value of g_5. Corrections to the $Zb_L\bar{b}_L$ coupling can also be important [71], especially in warped models for electroweak symmetry breaking as the ones described above.

84.3.1.3 *Kaluza-Klein Searches*

The main prediction of 1/TeV-sized extra dimensions is the presence of a discretized KK spectrum, with masses around the TeV scale, associated with the SM fields that propagate in the extra dimension.

In the RS model [3], only gravity propagates in the 5D bulk. Experimental searches have been performed for the lightest KK graviton through its decay to a variety of SM particle-antiparticle pairs. The results are usually interpreted in the plane of the dimensionless coupling k/M_P versus m_1, where M_P is the reduced Planck mass defined previously and m_1 is the mass of the lightest KK excitation of the graviton. Since the AdS curvature $\sim k$ cannot exceed the cut-off scale of the model, which is estimated to be $\ell_5^{1/3} M_5$ [38], one must demand $k \ll \sqrt{2\ell_5} M_P \simeq 40 M_P$. The most stringent limits currently arise from LHC searches for resonances in the dilepton and diphoton final states, using 13 TeV collisions. Searches with the $\gamma\gamma$ final state are an especially powerful approach, given that these final states have a branching fraction twice that of any individual lepton flavor. The CMS analysis [41] of 138 fb^{-1}of 13 TeV data excludes KK gravitons below 2.2 to 5.6 TeV, depending on the value of the coupling k/M_P, which is varied between 0.01 and 0.2, while ATLAS [87] using 139 fb^{-1}and provides a lower limit on the KK graviton mass of 4.5 TeV for the coupling parameter 0.1. The CMS [42] dilepton analyses, combining results from the ee and $\mu\mu$ channels, exclude KK gravitons with masses 2.47–4.78 TeV for k/M_P values of 0.01–0.1. The ATLAS [88] analysis of 139 fb^{-1}of Run 2 data does not include a RS KK graviton interpretation of the results. Less stringent limits on the KK graviton mass can be derived from analyses of the dijet [35,36,89,90], HH [91–100], and VV [101–105] final states, where V can represent either a W or Z boson.

In addition, both ATLAS and CMS experiments directly search for heavy radions, with masses above 1 TeV where the dominant decay mode is to pairs of bosons. The main production mechanism is gluon fusion. ATLAS [103] (CMS [106]) excludes radion masses below 3.2 TeV (3.1 TeV) for a radion decaying into WW, ZZ. Radions are also searched in final states with pairs of Higgs bosons HH [91,94,96,97,99,107], and dijet final states [108] with additional gluons. Bounds for a light radion (1 keV–10 GeV mass range) can be found in [109].

In warped extra-dimensional models in which the SM fields propagate in the 5D bulk, the couplings of the KK graviton to $ee/\mu\mu/\gamma\gamma$ are suppressed [110], and the above bounds do not apply. Furthermore, the KK graviton is the heaviest KK state (see Eq. (84.20)), and therefore experimental searches for KK gauge bosons and fermions are more appropriate discovery channels in these scenarios. For the scenarios discussed above in which only the Higgs boson and the top quark decays are localized close to the IR-boundary, the KK gauge bosons mainly decay into top quarks, longitudinal W/Z bosons, and Higgs bosons. Couplings to light SM fermions are suppressed by a factor $g/\sqrt{g_5^2 k} \sim 0.2$ [7] for the value of Eq. (84.19) that is considered from now on. Searches have been made for evidence of the lightest KK excitation of the gluon, through its decay to $t\bar{t}$ pairs. The searches take into account the natural KK gluon width, which is typically $\sim 15\%$ of its mass. The decay of a heavy particle to $t\bar{t}$ would tend to produce highly boosted top (anti-)quarks in the final state. Products of the subsequent hadronic top quark decay would therefore tend to be close to each other in the detector. In the case of

Int. J. Mod. Phys. A 2026.41. Downloaded from www.worldscientific.com by UNIVERSITY OF CALIFORNIA @ BERKELEY on 09/16/26. Re-use and distribution is strictly not permitted, except for Open Access articles.

$t \to Wb \to jjb$ decays, the three jets could overlap with one another and not be individually reconstructed with the standard jet algorithms, while $t \to Wb \to \ell\nu b$ decays could result in the lepton failing standard isolation requirements due to its proximity to the b-jet; in both cases, the efficiency for properly reconstructing the final state would fall as the mass of the original particle increases. To avoid the loss in sensitivity which would result, a number of techniques, known generally as top quark tagging [111, 112], have been developed to reconstruct and identify highly boosted top quarks, for example by using a single wide jet to contain all the decay products of a hadronic top decay. The large backgrounds from QCD jets can then be reduced by requiring the jet mass be consistent with that of a top quark, and also by examining the substructure of the wide jet for indication that it resulted from the hadronic decay of a top quark. These techniques are key to extending to very high masses the range of accessible resonances decaying to $t\bar{t}$ pairs. While the ATLAS search in 139 fb^{-1}of Run 2 data [113] does not provide a KK interpretation, dedicated analysis from CMS [114] of 36 fb^{-1} of 13 TeV data combines di-lepton, lepton-plus-jet, and all-hadronic $t\bar{t}$ decays and excludes KK gluons with masses below 4.55 TeV. ATLAS uses all-hadronic [115] and lepton-plus-jet [116] final states to exclude KK gluons up to 3.4 and 3.8 TeV respectively with 36fb^{-1}of 13 TeV data. The results are not directly comparable between the two LHC experiments, since they employ in their respective analyses different implementations of the theoretical model. For masses between 3 and 5 TeV, the cross-section limits are around 20 fb for CMS analysis of 36 fb^{-1}and 30 fb (4 fb) for ATLAS analyses of 36 (139) fb^{-1}.

A gauge boson KK excitation could be also sought through its decay to longitudinal W/Z bosons. Recent analyses from ATLAS [117] (and CMS [118]) with 139 (137) fb^{-1}of 13 TeV data searching for heavy vector resonances decaying to a W or Z boson and a Higgs in the $q\bar{q}b\bar{b}$ final state have set a lower limit on the mass of these KK of 3.2 (3.7) TeV (warped models are equivalent to the Model B considered in the analyses with $g_V \sim g_5\sqrt{k}$). The decay to a pair of intermediate vector bosons has also been exploited to search for KK gravitons in models in which the SM fields propagate in the 5D bulk. The analyses typically reconstruct hadronic W/Z decays using variants of the boosted techniques mentioned previously. An ATLAS analysis [119] combines leptonic and hadronic final states from the KK graviton decay $G^* \to VV$, where V can represent either a W or Z boson, exclude KK gravitons with masses below 2.3 TeV, for a value of $k/M_P = 1$. CMS VV analyses [106, 120, 121] using 137 fb^{-1}of 13 TeV data also exclude KK gravitons with masses below 1.8 TeV in the context of bulk gravitons for a maximum value of $k/M_P = 0.5$.

Additionally, CMS has searched for the pair production of Standard Model Higgs bosons in the $HH \to b\bar{b}\,b\bar{b}$ final state from the decay of warped extra-dimensional resonances. This has excluded KK gravitons with $m_G < 1.2$ TeV under the narrow-width assumption. Similarly, for a radion, masses below 2.6 TeV (narrow) and 2.9 TeV (10% width) are excluded [122]. More generally the warped extra-dimensional interpretation in the CMS resonant-HH combination [123] sets a lower limit on $\Lambda_R \equiv \sqrt{6}e^{-\pi kR}M_P \approx$ 16 TeV for radion masses near 1.2 TeV, and excludes $k/M_P \gtrsim 0.3$ for KK graviton masses in the range $0.3 < m_G < 1.5$ TeV.

CMS has also probed the topology in which a KK gluon (g_{KK}) decays via an intermediate radion (R) to three gluons (ggg) [124]. The analysis reports upper limits on the model-independent quantity $\sigma \times \mathcal{B}(g_{KK} \to gR \to ggg) \times \mathcal{A}$ as a function of the KK-gluon mass $m_{g_{KK}}$ (and the mass ratio $\rho_m \equiv m_R/m_{g_{KK}}$). A closely related CMS analysis targets the cascade $g_{KK} \to gR \to gW^+W^-$ in the all-hadronic final state, using 138 fb^{-1} [125]. It sets model-independent upper limits on $\sigma \times \mathcal{B}(g_{KK} \to gR \to gWW) \times \mathcal{A}$ as functions of $m_{g_{KK}}$ and m_R; under the benchmark warped extra-dimensional couplings considered, exclusions extend up to $m_{g_{KK}} \sim 3.5$ TeV with $m_R \sim 2.2$ TeV.

The lightest KK states are, in certain models, the partners of the top quark. For example, in 5D composite Higgs models these are colored states with charges $Q = -1/3, 2/3$ and $5/3$ (arising from $SU(2)_L$ doublets with $Y = 7/6, 1/6$), and masses expected to be below the TeV [85]. They can be either singly or pair-produced, and mainly decay into a combination of W/Z with top/bottom quarks [126–129]. An exhaustive review of these searches can be found in Ref. [130]. Of particular note, the $Q = 5/3$ state decays mainly into $W^+t \to W^+W^+b$, giving a very clean signature of a pair of same-sign leptons in the final state. An analysis by ATLAS [131] searching in the lepton-plus-jets final state for evidence of pair production of the $Q = 5/3$ state provides a lower mass limit of 1.25 TeV. A CMS analysis [132] searching for pair production of the $Q = 5/3$ state using both lepton-plus-jets and same sign lepton final states excludes masses below 1.3 TeV. Similarly, searches for single production of the $Q = 5/3$ state [133], also excludes masses up to 0.9 to 1.5 TeV depending on the model parameters. Both LHC experiments have searched for pair production of vector-like quarks T and B of charges $Q = 2/3$ and $-1/3$ respectively, assuming the allowable decays are $T \to Wb/Zt/Ht$ and $B \to Wt/Zb/Hb$. In each case, it is assumed the branching fractions of the three decay modes sum to unity, but the individual branching fractions, which are model-dependent, are allowed to vary within this constraint. Both ATLAS [134–136] and CMS [137,138] obtain lower limits on the mass of the T and B vector-like quarks up to 1.5 TeV and 1.6 TeV respectively. A comprehensive review of such CMS searches can be found in Ref. [139].

Analyses from ATLAS [140–144] and CMS [133, 145–148] also search for a single top partner and single bottom partner production, the cross section for which is model-dependent [149] but does not carry the kinematic penalty for producing two heavy objects.

84.3.2 *Connection with Strongly Coupled Models via the AdS/CFT Correspondence*

The AdS/CFT correspondence [8] provides a connection between warped extra-dimensional models and strongly-coupled theories in ordinary 4D. Although the exact connection is only known for certain cases, the AdS/CFT techniques have been very useful to obtain, at the qualitative level, a 4D holographic description of the various phenomena in warped extra-dimensional models [11, 72].

The connection goes as follows. The physics of the bulk AdS$_5$ models can be interpreted as that of a 4D CFT which is strongly coupled. The extra-dimensional coordinate y plays the role of the renormalization scale μ of the CFT by means of the identification $\mu \equiv ke^{-ky}$. Therefore the UV-boundary corresponds in the CFT to a UV cut-off scale at $\Lambda_{UV} = k \sim M_P$, breaking explicitly conformal invariance, while the IR-boundary can be interpreted as a spontaneous breaking of the conformal symmetry at energies $ke^{-k\pi R} \sim$ TeV. Fields localized on the UV-boundary are elementary fields external to the CFT, while fields localized on the IR-boundary and KK states corresponds to composite resonances of the CFT. Furthermore, local gauge symmetries in the 5D models, $\mathcal{G}_5$, correspond to global symmetries of the CFT, while the UV-boundary symmetry can be interpreted as a gauging of the subgroup $\mathcal{H}_{UV}$ of $\mathcal{G}_5$ in the CFT. Breaking gauge symmetries by IR-boundary conditions corresponds to the spontaneous breaking $\mathcal{G}_5 \to \mathcal{H}_{IR}$ in the CFT at energies $\sim ke^{-k\pi R}$. Using this correspondence one can easily derive the 4D massless spectrum of the compactified AdS$_5$ models. One also has the identification $k^3/M_5^3 \approx 16\pi^2/N^2$ and $g_5^2 k \approx 16\pi^2/N^r$ ($r = 1$ or 2 for CFT fields in the fundamental or adjoint representation of the gauge group), where N plays the role of the number of colors of the CFT. Therefore the weak-coupling limit in AdS$_5$ corresponds to a large-N expansion in the CFT.

Following the above AdS/CFT dictionary one can understand the RS solution to the hierarchy problem from a 4D viewpoint. The equivalent 4D model is a CFT with a TeV mass gap and a Higgs boson emerging as a composite state. In the particular case where the Higgs is the fifth-component of the gauge-boson, A_5 [150], this corresponds to models, similar to those proposed in Ref. [151–154], where the Higgs is a composite pseudo-Nambu-Goldstone boson arising from the spontaneous breaking $\mathcal{G}_5 \to \mathcal{H}_{IR}$ in the CFT. The AdS/CFT dictionary tells us that KK states must behave as composite resonances. For example, if the SM gauge bosons propagate in the 5D bulk, the lowest KK $SU(2)_L$-gauge boson must have properties similar to those of the Technirho ρ_T [130] with a coupling to longitudinal W/Z bosons given by $g_5\sqrt{k} \approx g_{\rho_T}$, while the coupling to elementary fermions is

Int. J. Mod. Phys. A 2026.41. Downloaded from www.worldscientific.com by UNIVERSITY OF CALIFORNIA @ BERKELEY on 09/16/26. Re-use and distribution is strictly not permitted, except for Open Access articles.

$g^2/\sqrt{g_5^2 k} \approx g^2 F_{\rho_T}/M_{\rho_T}$.

Fermions in compactified AdS_5 also have a simple 4D holographic interpretation. The 4D massless mode described in Sec. 84.3.1 corresponds to an external fermion ψ_i linearly coupled to a fermionic CFT operator $\mathcal{O}_i$: $\mathcal{L}_{\rm int} = \lambda_i \bar{\psi}_i \mathcal{O}_i + h.c.$. The dimension of the operator $\mathcal{O}_i$ is related to the 5D fermion mass according to $\mathrm{Dim}[\mathcal{O}_i] = |c_f + 1/2| - 1$. Therefore, by varying c_f one varies $\mathrm{Dim}[\mathcal{O}_i]$, making the coupling λ_i irrelevant ($c_f > 1/2$), marginal ($c_f = 1/2$) or relevant ($c_f < 1/2$). When irrelevant, the coupling is exponentially suppressed at low energies, and then the coupling of ψ_i to the CFT (and eventually to the composite Higgs) is very small. When relevant, the coupling grows in the IR and become as large as g_5 (in units of k), meaning that the fermion is as strongly coupled as the CFT states [81]. In this latter case ψ_i behaves as a composite fermion.

84.3.3 *Linear dilaton geometry*

The warp factor $a(y)$ in Eq. (84.16) can be different from the exponential considered above, giving rise to a different KK mass spectrum. A particularly interesting case is the linear dilaton geometry [155] where the KK states become very narrowly-spaced. These scenarios can also be understood in 4D via the clockwork mechanism [156], and for this reason are usually referred to as Clockwork/Linear Dilaton (CW/LD) models. The collider phenomenology becomes different in these models since the decay of the narrowly-spaced KK spectrum appears as a periodic signal in the invariant mass of the decaying products. An excellent detector resolution is needed in order to resolve these KK modes which can be done by looking at 2 electrons or 2 photons in the final state. A search for this type of KK gravitons decaying into ee [157] and $\gamma\gamma$ [41,157,158] put bounds for M_5 in the range of 10 TeV to 1 TeV for values of the lightest KK graviton mass (referred as k in [157,158]) in the range of few TeVs.

84.3.4 *Flat Extra Dimensions*

Models with quantum gravity at the TeV scale, as in the ADD scenario, can have extra (flat) dimensions of 1/TeV size, as happens in string scenarios (see, for example, [159]). All SM fields may propagate in these extra dimensions, leading to the possibility of observing their corresponding KK states.

A simple example is to assume that the SM gauge bosons propagate in a flat five-dimensional orbifold S^1/Z_2 of radius R, with the fermions localized on a 4D boundary. The KK gauge bosons behave as sequential SM gauge bosons with a coupling to fermions enhanced by a factor $\sqrt{2}$ [159]. The experimental limits on such sequential gauge bosons could therefore be recast as limits on KK gauge bosons. Such an interpretation of the ATLAS 7 TeV dilepton analysis [160] yielded the bound $1/R > 4.16$ TeV, while a CMS 8 TeV search with a lepton and missing transverse energy in the final state [161] give $1/R > 3.4$ TeV. Indirect bounds from LEP2 require however $1/R \gtrsim 6$ TeV [86,162], a bound that can considerably improve in the future by high-energy measurements of the dilepton invariant mass spectrum from Drell-Yan processes at the LHC [163]. More recent LHC limits on leptonically decaying gauge bosons [88,164–168] are not interpreted as bounds on $1/R$ by the collaborations, but the published results allow for independent derivation of such bounds.

An alternative scenario, known as Universal Extra Dimensions (UED) [169] (for a review see, for example, [170]), assumes that all SM fields propagate universally in a flat orbifold S^1/Z_2 with an extra Z_2 parity, called KK-parity, that interchanges the two boundaries. In this case, the lowest KK state is stable and is a Dark Matter candidate. At colliders, the KK particles would have to be created in pairs, and would then cascade decay to the lightest KK particle, which would be stable and escape detection. The UED mass-spectrum depends not only on the extra-dimensional radius R, but also on the cut-off of the 5D theory Λ, since quantum corrections sensitive to ΛR induce mass-splittings between the KK states. Experimental signatures, such as jets or leptons and $p_{\rm T}^{\rm miss}$, would be similar to those of typical R-parity conserving SUSY searches. An interpretation of the recent LHC experimental SUSY searches for UED models has been presented in Refs. [171,172]. A lower bound $1/R > 1.4 - 1.5$ TeV was derived for ΛR in the range $5 - 35$ [171]. A recent analysis is given in Ref. [173] where it is shown that the minimal UED model is ruled out when LHC data is combined with Dark Matter relic density data. Extensions to the minimal UED model where boundary terms are included can however be compatible with experiments [173].

Finally, realistic models of electroweak symmetry breaking can also be constructed with flat extra spatial dimensions, similarly to those in the warped case, requiring, however, the presence of sizeable boundary kinetic terms [174]. There is also the possibility of breaking supersymmetry by boundary conditions [175]. Models of this type could explain naturally the presence of a Higgs boson lighter than $M_D \sim$ TeV (see, for example, [176–178]).

References

[1] For a comprehensive collection of the original papers see, "Modern Kaluza-Klein Theories", edited by T. Appelquist *et al.*, Addison-Wesley (1987).

[2] N. Arkani-Hamed, S. Dimopoulos and G. Dvali, Phys. Lett. **B429**, 263 (1998), [hep-ph/9803315].

[3] L. Randall and R. Sundrum, Phys. Rev. Lett. **83**, 3370 (1999), [hep-ph/9905221].

[4] H. Davoudiasl, J. L. Hewett and T. G. Rizzo, Phys. Lett. **B473**, 43 (2000), [hep-ph/9911262].

[5] A. Pomarol, Phys. Lett. **B486**, 153 (2000), [hep-ph/9911294].

[6] S. Chang *et al.*, Phys. Rev. **D62**, 084025 (2000), [hep-ph/9912498].

[7] T. Gherghetta and A. Pomarol, Nucl. Phys. **B586**, 141 (2000), [hep-ph/0003129].

[8] J. M. Maldacena, Int. J. Theor. Phys. **38**, 1113 (1999), [Adv. Theor. Math. Phys.2,231(1998)], [hep-th/9711200].

[9] E. Witten, Adv. Theor. Math. Phys. **2**, 253 (1998), [hep-th/9802150].

[10] S. S. Gubser, I. R. Klebanov and A. M. Polyakov, Phys. Lett. **B428**, 105 (1998), [hep-th/9802109].

[11] N. Arkani-Hamed, M. Porrati and L. Randall, JHEP **08**, 017 (2001), [hep-th/0012148].

[12] ATLAS public results are available on WWW at `https://twiki.cern.ch/twiki/bin/view/AtlasPublic`.

[13] CMS public results are available on WWW at `https://cms-results.web.cern.ch/cms-results/public-results/publications`.

[14] Z. Chacko, M. A. Luty and E. Ponton, JHEP **07**, 036 (2000), [hep-ph/9909248].

[15] N. Arkani-Hamed, S. Dimopoulos and G. R. Dvali, Phys. Rev. **D59**, 086004 (1999), [hep-ph/9807344].

[16] R. Rattazzi, `hep-ph/0607055 (2006)`; I. Antoniadis, Yellow report CERN-2002-002 (2002).

[17] J. D. Lykken, Phys. Rev. **D54**, R3693 (1996), [hep-th/9603133].

[18] I. Antoniadis *et al.*, Phys. Lett. **B436**, 257 (1998), [hep-ph/9804398].

[19] G. F. Giudice, R. Rattazzi and J. D. Wells, Nucl. Phys. **B544**, 3 (1999), [hep-ph/9811291].

[20] N. Arkani-Hamed *et al.*, Phys. Rev. **D62**, 105002 (2000), [hep-ph/9912453].

[21] E. G. Adelberger *et al.*, Prog. Part. Nucl. Phys. **62**, 102 (2009).

[22] J. Murata and S. Tanaka, Class. Quant. Grav. **32**, 3, 033001 (2015), [arXiv:1408.3588].

[23] W.-H. Tan *et al.*, Phys. Rev. Lett. **116**, 13, 131101 (2016).

[24] J. G. Lee *et al.*, Phys. Rev. Lett. **124**, 101101 (2020), [arXiv:2002.11761].

[25] C. Hanhart *et al.*, Phys. Lett. **B509**, 1 (2001), [arXiv:astro-ph/0102063].

[26] S. Hannestad and G. G. Raffelt, Phys. Rev. **D67**, 125008 (2003), [Erratum: Phys. Rev.D69,029901(2004)], [hep-ph/0304029].

Int. J. Mod. Phys. A 2026.41. Downloaded from www.worldscientific.com
by UNIVERSITY OF CALIFORNIA @ BERKELEY on 09/16/26. Re-use and distribution is strictly not permitted, except for Open Access articles.

[27] L. J. Hall and D. Tucker-Smith, Phys. Rev. **D60**, 085008 (1999), [hep-ph/9904267].

[28] E. A. Mirabelli, M. Perelstein and M. E. Peskin, Phys. Rev. Lett. **82**, 2236 (1999), [hep-ph/9811337].

[29] T. Han, J. D. Lykken and R.-J. Zhang, Phys. Rev. **D59**, 105006 (1999), [hep-ph/9811350].

[30] G. AaD *et al.* (ATLAS), Phys. Rev. D **103**, 112006 (2021), [arXiv:2102.10874].

[31] A. Tumasyan *et al.* (CMS), JHEP **11**, 153 (2021), [arXiv:2107.13021].

[32] A. M. Sirunyan *et al.* (CMS), JHEP **02**, 074 (2019), [arXiv:1810.00196].

[33] G. Aad *et al.* (ATLAS), JHEP **02**, 226 (2021), [arXiv:2011.05259].

[34] S. Cullen, M. Perelstein and M. E. Peskin, Phys. Rev. **D62**, 055012 (2000), [hep-ph/0001166].

[35] A. M. Sirunyan *et al.* (CMS), JHEP **05**, 033 (2020), [arXiv:1911.03947].

[36] G. Aad *et al.* (ATLAS), JHEP **03**, 145 (2020), [arXiv:1910.08447].

[37] J. L. Hewett, Phys. Rev. Lett. **82**, 4765 (1999), [hep-ph/9811356].

[38] G. F. Giudice and A. Strumia, Nucl. Phys. **B663**, 377 (2003), [hep-ph/0301232].

[39] A. M. Sirunyan *et al.* (CMS), Eur. Phys. J. **C78**, 9, 789 (2018), [arXiv:1803.08030].

[40] M. Aaboud *et al.* (ATLAS), Phys. Lett. **B775**, 105 (2017), [arXiv:1707.04147].

[41] A. Hayrapetyan *et al.* (CMS), JHEP **08**, 215 (2024), [arXiv:2405.09320].

[42] A. M. Sirunyan *et al.*, JHEP **07**, 7 (2021), [arXiv:2103.02708].

[43] G. Aad *et al.*, JHEP **11**, 005 (2020), [arXiv:2006.12946].

[44] S. B. Giddings and S. D. Thomas, Phys. Rev. **D65**, 056010 (2002), [hep-ph/0106219].

[45] S. Dimopoulos and G. L. Landsberg, Phys. Rev. Lett. **87**, 161602 (2001), [hep-ph/0106295].

[46] P. Kanti, Int. J. Mod. Phys. **A19**, 4899 (2004), [hep-ph/0402168].

[47] R. C. Myers and M. J. Perry, Annals Phys. **172**, 304 (1986).

[48] A. M. Sirunyan *et al.* (CMS), JHEP **11**, 042 (2018), [arXiv:1805.06013].

[49] G. Aad *et al.* (ATLAS), JHEP **03**, 026 (2016), [arXiv:1512.02586].

[50] M. Aaboud *et al.* (ATLAS), Phys. Lett. **B760**, 520 (2016), [arXiv:1606.02265].

[51] C. Kilic *et al.*, Phys. Rev. **D89**, 1, 016003 (2014), [arXiv:1207.3525].

[52] V. Khachatryan *et al.* (CMS), Phys. Rev. **D90**, 3, 032005 (2014), [arXiv:1405.7653].

[53] P. Meade and L. Randall, JHEP **05**, 003 (2008), [arXiv:0708.3017].

[54] A. M. Sirunyan *et al.* (CMS), Phys. Lett. **B774**, 279 (2017), [arXiv:1705.01403].

[55] G. Aad *et al.* (ATLAS), Phys. Lett. B **754**, 302 (2016), [arXiv:1512.01530].

[56] G. Aad *et al.* (ATLAS) (2023), [arXiv:2307.08567].

[57] M. Aaboud *et al.* (ATLAS), Eur. Phys. J. C **76**, 10, 541 (2016), [arXiv:1607.08079].

[58] M. Aaboud *et al.* (ATLAS), Phys. Rev. **D98**, 9, 092008 (2018), [arXiv:1807.06573].

[59] A. Tumasyan *et al.* (CMS), JHEP **05**, 227 (2023), [arXiv:2205.06709].

[60] A. M. Sirunyan *et al.* (CMS), JHEP **04**, 073 (2018), [arXiv:1802.01122].

[61] A. Tumasyan *et al.* (CMS) (2023), [arXiv:2305.07998].

[62] M. Aaboud *et al.* (ATLAS), Eur. Phys. J. C **78**, 2, 102 (2018), [arXiv:1709.10440].

[63] G. Aad *et al.* (ATLAS), Phys. Rev. D **109**, 3, 032010 (2024), [arXiv:2307.14967].

[64] S. Dimopoulos and R. Emparan, Phys. Lett. **B526**, 393 (2002), [hep-ph/0108060].

[65] W. D. Goldberger and M. B. Wise, Phys. Rev. Lett. **83**, 4922 (1999), [hep-ph/9907447].

[66] J. Garriga and A. Pomarol, Phys. Lett. **B560**, 91 (2003), [hep-th/0212227].

[67] See talk by R. Rattazzi at Planck 2010, CERN, `https://indico.cern.ch/event/75810/contributions/1250635/`.

[68] B. Bellazzini *et al.*, Eur. Phys. J. **C74**, 2790 (2014), [arXiv:1305.3919].

[69] F. Coradeschi *et al.*, JHEP **11**, 057 (2013), [arXiv:1306.4601].

[70] E. Megias and O. Pujolas, JHEP **08**, 081 (2014), [arXiv:1401.4998].

[71] E. P. H. Davoudiasl, S. Gopalakrishna and J. Santiago, New J. Phys. **12**, 075011 (2010), [arXiv:0908.1968].

[72] T. Gherghetta, in "Physics of the large and the small, TASI 09, proceedings of the Theoretical Advanced Study Institute in Elementary Particle Physics, Boulder, Colorado, USA, 1-26 June 2009," 165–232 (2011), [arXiv:1008.2570].

[73] Y. Grossman and M. Neubert, Phys. Lett. **B474**, 361 (2000), [hep-ph/9912408].

[74] S. J. Huber and Q. Shafi, Phys. Lett. **B498**, 256 (2001), [hep-ph/0010195].

[75] A. Delgado, A. Pomarol and M. Quiros, JHEP **01**, 030 (2000), [hep-ph/9911252].

[76] K. Agashe, G. Perez and A. Soni, Phys. Rev. **D71**, 016002 (2005), [hep-ph/0408134].

[77] M. Bauer *et al.*, JHEP **09**, 017 (2010), [arXiv:0912.1625].

[78] A. Pomarol, Int. J. Mod. Phys. **A24**, 61 (2009), [In *Kane, Gordon (ed.) et al.: Perspectives on LHC physics* ,259(2008)].

[79] Y. Hosotani, Phys. Lett. **126B**, 309 (1983).

[80] K. Agashe *et al.*, JHEP **08**, 050 (2003), [hep-ph/0308036].

[81] K. Agashe, R. Contino and A. Pomarol, Nucl. Phys. **B719**, 165 (2005), [hep-ph/0412089].

[82] For a review see, for example, R. Contino, `arXiv:1005.4269`.

[83] See, for example, PDG review of Higgs boson in this *Review*.

[84] G. F. Giudice *et al.*, JHEP **06**, 045 (2007), [hep-ph/0703164].

[85] R. Contino, L. Da Rold and A. Pomarol, Phys. Rev. **D75**, 055014 (2007), [hep-ph/0612048].

[86] R. Barbieri *et al.*, Nucl. Phys. **B703**, 127 (2004), [hep-ph/0405040].

[87] G. Aad *et al.* (ATLAS), Phys. Lett. B **822**, 136651 (2021), [arXiv:2102.13405].

[88] G. Aad *et al.* (ATLAS), Phys. Lett. **B796**, 68 (2019), [arXiv:1903.06248].

[89] A. M. Sirunyan *et al.* (CMS), JHEP **08**, 130 (2018), [arXiv:1806.00843].

[90] G. Aad *et al.* (ATLAS), Phys. Rev. Lett. **125**, 13, 131801 (2020), [arXiv:2005.02983].

[91] A. M. Sirunyan *et al.* (CMS), Phys. Rev. Lett. **122**, 12, 121803 (2019), [arXiv:1811.09689].

[92] M. Aaboud *et al.* (ATLAS), JHEP **01**, 030 (2019), [arXiv:1804.06174].

Int. J. Mod. Phys. A 2026.41. Downloaded from www.worldscientific.com
by UNIVERSITY OF CALIFORNIA @ BERKELEY on 09/16/26. Re-use and distribution is strictly not permitted, except for Open Access articles.

[93] G. Aad *et al.* (ATLAS), Phys. Lett. B **800**, 135103 (2020), [arXiv:1906.02025].

[94] G. Aad *et al.* (ATLAS), Phys. Rev. D **106**, 5, 052001 (2022), [arXiv:2112.11876].

[95] G. Aad *et al.* (ATLAS), JHEP **11**, 163 (2020), [arXiv:2007.14811].

[96] A. M. Sirunyan *et al.* (CMS), Phys. Rev. D **102**, 3, 032003 (2020), [arXiv:2006.06391].

[97] A. Tumasyan *et al.* (CMS), JHEP **05**, 005 (2022), [arXiv:2112.03161].

[98] A. Tumasyan *et al.* (CMS), JHEP **11**, 057 (2021), [arXiv:2106.10361].

[99] A. Tumasyan *et al.* (CMS), JHEP **07**, 095 (2023), [arXiv:2206.10268].

[100] A. Hayrapetyan *et al.* (CMS), JHEP **07**, 293 (2024), [arXiv:2403.09430].

[101] G. Aad *et al.* (ATLAS), JHEP **09**, 091 (2019), [Erratum: JHEP 06, 042 (2020)], [arXiv:1906.08589].

[102] A. M. Sirunyan *et al.* (CMS), Eur. Phys. J. C **80**, 3, 237 (2020), [arXiv:1906.05977].

[103] G. Aad *et al.* (ATLAS), Eur. Phys. J. C **80**, 12, 1165 (2020), [arXiv:2004.14636].

[104] G. Aad *et al.* (ATLAS), Eur. Phys. J. C **81**, 4, 332 (2021), [arXiv:2009.14791].

[105] A. Tumasyan *et al.* (CMS), Phys. Lett. B **844**, 137813 (2023), [arXiv:2210.00043].

[106] A. Tumasyan *et al.* (CMS), Phys. Rev. D **105**, 3, 032008 (2022), [arXiv:2109.06055].

[107] A. M. Sirunyan *et al.* (CMS), JHEP **01**, 051 (2019), [arXiv:1808.01365].

[108] A. Tumasyan *et al.* (CMS), Phys. Lett. B **832**, 137263 (2022), [arXiv:2201.02140].

[109] F. Abu-Ajamieh, J. S. Lee and J. Terning, JHEP **10**, 050 (2018), [arXiv:1711.02697].

[110] K. Agashe *et al.*, Phys. Rev. **D76**, 036006 (2007), [hep-ph/0701186].

[111] M. Aaboud *et al.* (ATLAS), Eur. Phys. J. C **79**, 5, 375 (2019), [arXiv:1808.07858].

[112] A. M. Sirunyan *et al.* (CMS), JINST **15**, 06, P06005 (2020), [arXiv:2004.08262].

[113] G. Aad *et al.* (ATLAS), JHEP **10**, 061 (2020), [arXiv:2005.05138].

[114] A. M. Sirunyan *et al.* (CMS), JHEP **04**, 031 (2019), [arXiv:1810.05905].

[115] M. Aaboud *et al.* (ATLAS), Phys. Rev. **D99**, 9, 092004 (2019), [arXiv:1902.10077].

[116] M. Aaboud *et al.* (ATLAS), Eur. Phys. J. **C78**, 7, 565 (2018), [arXiv:1804.10823].

[117] G. Aad *et al.* (ATLAS), Phys. Rev. D **102**, 11, 112008 (2020), [arXiv:2007.05293].

[118] A. M. Sirunyan *et al.* (CMS), Eur. Phys. J. C **81**, 8, 688 (2021), [arXiv:2102.08198].

[119] M. Aaboud *et al.* (ATLAS), Phys. Rev. **D98**, 5, 052008 (2018), [arXiv:1808.02380].

[120] A. Tumasyan *et al.* (CMS), Phys. Rev. D **106**, 1, 012004 (2022), [arXiv:2109.08268].

[121] A. Tumasyan *et al.* (CMS), JHEP **04**, 087 (2022), [arXiv:2111.13669].

[122] A. Tumasyan *et al.* (CMS), JHEP **02**, 040 (2025), [arXiv:2407.13872].

[123] A. Hayrapetyan *et al.* (CMS), Phys. Rept. **1115**, 368 (2025), [arXiv:2403.16926].

[124] A. Hayrapetyan *et al.* (CMS), Phys. Rev. Lett. **133**, 1, 011801 (2024), [arXiv:2310.14023].

[125] A. Hayrapetyan *et al.* (CMS), JHEP **02**, 199 (2025), [arXiv:2410.17303].

[126] R. Contino and G. Servant, JHEP **06**, 026 (2008), [arXiv:0801.1679].

[127] J. A. Aguilar-Saavedra, JHEP **11**, 030 (2009), [arXiv:0907.3155].

[128] J. Mrazek and A. Wulzer, Phys. Rev. **D81**, 075006 (2010), [arXiv:0909.3977].

[129] G. Dissertori *et al.*, JHEP **09**, 019 (2010), [arXiv:1005.4414].

[130] See, for example, PDG review of Technicolor searches in this volume.

[131] M. Aaboud *et al.* (ATLAS), JHEP **10**, 141 (2017), [arXiv:1707.03347].

[132] A. M. Sirunyan *et al.* (CMS), JHEP **03**, 082 (2019), [arXiv:1810.03188].

[133] A. M. Sirunyan *et al.* (CMS), Eur. Phys. J. C **79**, 90 (2019), [arXiv:1809.08597].

[134] G. Aad *et al.* (ATLAS), Eur. Phys. J. C **83**, 8, 719 (2023), [arXiv:2212.05263].

[135] G. Aad *et al.* (ATLAS), Phys. Lett. B **843**, 138019 (2023), [arXiv:2210.15413].

[136] M. Aaboud *et al.* (ATLAS), Phys. Rev. Lett. **121**, 21, 211801 (2018), [arXiv:1808.02343].

[137] A. Tumasyan *et al.* (CMS), JHEP **07**, 020 (2023), [arXiv:2209.07327].

[138] A. M. Sirunyan *et al.* (CMS), Phys. Rev. D **102**, 112004 (2020), [arXiv:2008.09835].

[139] A. Hayrapetyan *et al.* (CMS), Phys. Rept. **1115**, 570 (2025), [arXiv:2405.17605].

[140] G. Aad *et al.* (ATLAS), JHEP **11**, 168 (2023), [arXiv:2308.02595].

[141] G. Aad *et al.* (ATLAS), Phys. Rev. D **109**, 11, 112012 (2024), [arXiv:2307.07584].

[142] G. Aad *et al.* (ATLAS), JHEP **08**, 153 (2023), [arXiv:2305.03401].

[143] G. Aad *et al.* (ATLAS), Phys. Rev. D **105**, 9, 092012 (2022), [arXiv:2201.07045].

[144] M. Aaboud *et al.* (ATLAS), JHEP **05**, 164 (2019), [arXiv:1812.07343].

[145] A. Tumasyan *et al.* (CMS), JHEP **09**, 057 (2023), [arXiv:2302.12802].

[146] A. Tumasyan *et al.* (CMS), JHEP **05**, 093 (2022), [arXiv:2201.02227].

[147] A. M. Sirunyan *et al.* (CMS), JHEP **01**, 036 (2020), [arXiv:1909.04721].

[148] A. M. Sirunyan *et al.* (CMS), JHEP **06**, 031 (2018), [arXiv:1802.01486].

[149] A. De Simone *et al.*, JHEP **04**, 004 (2013), [arXiv:1211.5663].

[150] R. Contino, Y. Nomura and A. Pomarol, Nucl. Phys. **B671**, 148 (2003), [hep-ph/0306259].

[151] D. B. Kaplan and H. Georgi, Phys. Lett. **136B**, 183 (1984).

[152] D. B. Kaplan, H. Georgi and S. Dimopoulos, Phys. Lett. B **136**, 187 (1984).

[153] T. Banks, Nucl. Phys. B **243**, 125 (1984).

[154] H. Georgi, D. B. Kaplan and P. Galison, Phys. Lett. **143B**, 152 (1984).

[155] I. Antoniadis *et al.*, Phys. Rev. Lett. **108**, 081602 (2012), [arXiv:1102.4043].

[156] G. F. Giudice and M. McCullough, JHEP **02**, 036 (2017), [arXiv:1610.07962].

[157] G. Aad *et al.* (ATLAS), JHEP **10**, 079 (2023), [arXiv:2305.10894].

[158] A. M. Sirunyan *et al.* (CMS), Phys. Rev. D **98**, 9, 092001 (2018), [arXiv:1809.00327].

[159] I. Antoniadis and K. Benakli, Int. J. Mod. Phys. **A15**, 4237 (2000), [hep-ph/0007226].

[160] G. Aad *et al.* (ATLAS), JHEP **11**, 138 (2012), [arXiv:1209.2535].

[161] V. Khachatryan *et al.* (CMS), Phys. Rev. **D91**, 9, 092005 (2015), [arXiv:1408.2745].

[162] K. Cheung and G. L. Landsberg, Phys. Rev. **D65**, 076003 (2002), [hep-ph/0110346].

[163] M. Farina *et al.*, Phys. Lett. **B772**, 210 (2017), [arXiv:1609.08157].

[164] M. Aaboud *et al.* (ATLAS), Eur. Phys. J. C **78**, 5, 401 (2018), [arXiv:1706.04786].

[165] G. Aad *et al.* (ATLAS), Phys. Rev. D **100**, 5, 052013 (2019), [arXiv:1906.05609].

[166] A. M. Sirunyan *et al.* (CMS), JHEP **06**, 128 (2018), [arXiv:1803.11133].

[167] A. M. Sirunyan *et al.* (CMS), JHEP **06**, 120 (2018), [arXiv:1803.06292].

[168] A. Tumasyan *et al.* (CMS), JHEP **09**, 051 (2023), [arXiv:2212.12604].

[169] T. Appelquist, H.-C. Cheng and B. A. Dobrescu, Phys. Rev. **D64**, 035002 (2001), [hep-ph/0012100].

[170] A. Datta, K. Kong and K. T. Matchev, New J. Phys. **12**, 075017 (2010), [arXiv:1002.4624].

[171] N. Deutschmann, T. Flacke and J. S. Kim, Phys. Lett. **B771**, 515 (2017), [arXiv:1702.00410].

[172] J. Beuria *et al.*, Comput. Phys. Commun. **226**, 187 (2018), [arXiv:1702.00413].

[173] Avnish *et al.*, Phys. Rev. D **103**, 115011 (2021), [arXiv:2012.15137].

[174] G. Panico, M. Safari and M. Serone, JHEP **02**, 103 (2011), [arXiv:1012.2875].

[175] J. Scherk and J. H. Schwarz, Phys. Lett. **82B**, 60 (1979).

[176] A. Pomarol and M. Quiros, Phys. Lett. **B438**, 255 (1998), [hep-ph/9806263].

[177] I. Antoniadis *et al.*, Nucl. Phys. **B544**, 503 (1999), [hep-ph/9810410].

[178] R. Barbieri, L. J. Hall and Y. Nomura, Phys. Rev. **D63**, 105007 (2001), [hep-ph/0011311].

Int. J. Mod. Phys. A 2026.41. Downloaded from www.worldscientific.com
by UNIVERSITY OF CALIFORNIA @ BERKELEY on 09/16/26. Re-use and distribution is strictly not permitted, except for Open Access articles.

85. W'-Boson Searches

Revised October 2025 by B.A. Dobrescu (FNAL) and N. Saoulidou (Athens U.).

The W' boson is a massive hypothetical particle of spin 1 and electric charge ± 1, which is a color singlet and is predicted in various extensions of the Standard Model (SM).

85.1 W' couplings to quarks and leptons

The Lagrangian terms describing the couplings of a W'^+ boson to fermions are given by

$$\frac{W'^+_\mu}{\sqrt{2}}\left[\overline{u}_i\left(C^R_{q_{ij}}P_R+C^L_{q_{ij}}P_L\right)\gamma^\mu d_j+\overline{\nu}_i\left(C^R_{\ell_{ij}}P_R+C^L_{\ell_{ij}}P_L\right)\gamma^\mu e_j\right]. \tag{85.1}$$

Here, u, d, ν, and e are the SM fermions in the mass eigenstate basis, $i, j = 1, 2, 3$ label the fermion generation, and $P_{R,L} = (1 \pm \gamma_5)/2$. The coefficients $C^L_{q_{ij}}$, $C^R_{q_{ij}}$, $C^L_{\ell_{ij}}$, and $C^R_{\ell_{ij}}$ are complex dimensionless parameters. If $C^R_{\ell_{ij}} \neq 0$, then the ith generation includes a right-handed neutrino. Using this notation, the SM W couplings are $C^L_q = gV_{\rm CKM}$, $C^L_\ell = g \approx 0.63$ and $C^R_q = C^R_\ell = 0$.

Unitarity considerations imply that the W' boson is associated with a spontaneously-broken gauge symmetry. This is true even when it is a composite particle (*e.g.* $\rho^\pm$-like bound states [1]) if its mass is much smaller than the compositeness scale, or a Kaluza-Klein mode in theories where the W boson propagates in extra dimensions [2]. The simplest extension of the electroweak gauge group that includes a W' boson is $SU(2)_1 \times SU(2)_2 \times U(1)$, but larger groups are encountered in some theories. A generic property of these gauge theories is that they also include a Z' boson [3]; the W'-to-Z' mass ratio is often a free parameter.

A tree-level mass mixing may be induced between the electrically-charged gauge bosons. Upon diagonalization of their mass matrix, the W-to-Z mass ratio and the couplings of the observed W boson are shifted from the SM values. Their measurements imply that the mixing angle, θ_+, between the gauge eigenstates must be smaller than about 10^{-2} [4]. In certain theories the mixing is negligible (*e.g.*, due to a new parity [5]), even when the W' mass is near the electroweak scale. Note that $SU(2)$ gauge invariance suppresses the kinetic mixing between the W and W' bosons (in contrast to the case of a Z' boson [3]).

The W' coupling to WZ is fixed by Lorentz and gauge invariances, and to leading order in θ_+ is given by [6]

$$\frac{g\,\theta_+\,i}{\cos\theta_W}\left[W'^+_\mu\left(W^-_\nu Z^{\nu\mu}+Z_\nu W^{-\mu\nu}\right)+Z^\nu W^{-\mu}W'^+_{\nu\mu}\right]+\text{H.c.}, \tag{85.2}$$

where $W^{\mu\nu} \equiv \partial^\mu W^\nu - \partial^\nu W^\mu$, etc. The θ_W dependence shown here corrects the one given in Ref. [7], which has been referred to as the Extended Gauge Model by the experimental collaborations. The W' coupling to Wh^0, where h^0 is the SM Higgs boson, is

$$-\,\xi_h\, g_{W'}\, M_W\; W'^+_\mu\, W^{\mu-} h^0 + \text{H.c.}, \tag{85.3}$$

where $g_{W'}$ is the gauge coupling of the W' boson, and the coefficient ξ_h satisfies $\xi_h \leq 1$ in simple Higgs sectors [6].

In models based on the "left-right symmetric" gauge group [8], $SU(2)_L \times SU(2)_R \times U(1)_{B-L}$, the SM fermions that couple to the W boson transform as doublets under $SU(2)_L$ while the other fermions transform as doublets under $SU(2)_R$. Consequently, the W' boson couples primarily to right-handed fermions; its coupling to left-handed fermions arises due to the θ_+ mixing, so that C^L_q is proportional to the CKM matrix and its elements are much smaller than the diagonal elements of C^R_q. Generically, C^R_q does not need to be proportional to $V_{\rm CKM}$.

There are many other models based on the $SU(2)_1 \times SU(2)_2 \times U(1)$ gauge symmetry. In the "alternate left-right" model [9], all the couplings shown in Eq. (85.1) vanish, but there are some new fermions such that the W' boson couples to pairs involving a SM fermion and a new fermion. In the "ununified SM" [10], the left-handed quarks are doublets under one $SU(2)$, and the left-handed leptons are doublets under a different $SU(2)$, leading to a mostly leptophobic W' boson: $C^L_{\ell_{ij}} \ll C^L_{q_{ij}}$ and $C^R_{\ell_{ij}} = C^R_{q_{ij}} = 0$. Fermions of different generations may also transform as doublets under different $SU(2)$ gauge groups [11]. In particular, the couplings to third generation quarks may be enhanced [12].

It is also possible that the W' couplings to SM fermions are highly suppressed. For example, if the quarks and leptons are singlets under one $SU(2)$ [13], then the couplings are proportional to the tiny mixing angle θ_+. Similar suppressions may arise if some vectorlike fermions mix with the SM fermions [14].

Gauge groups that embed the electroweak symmetry, such as $SU(3)_W \times U(1)$ or $SU(4)_W \times U(1)$, also include one or more W' bosons [15].

85.2 Collider searches

At hadron colliders, W' bosons can be detected through resonant pair production of fermions (f and f') or electroweak bosons with a net electric charge equal to ± 1. When W' has a width much smaller than its mass ($\Gamma_{W'}/M_{W'} \lesssim 7\%$), the contribution of the s-channel W' exchange to the total rate for $pp \to f\bar{f}'X$, where X is any final state, may be approximated by the branching fraction $B(W' \to f\bar{f}')$ times the production cross section [16], which may be written as

$$\sigma\left(pp\to W'X\right) \simeq \frac{\pi}{6s}\sum_{i,j}\left[(C^L_{q_{ij}})^2+(C^R_{q_{ij}})^2\right] w_{ij}\left(M^2_{W'}/s, M_{W'}\right). \tag{85.4}$$

The functions w_{ij} include the information about proton structure, and are given to leading order in α_s by

$$w_{ij}(z,\mu) = \int_z^1 \frac{dx}{x}\left[u_i(x,\mu)\,\overline{d}_j\left(\frac{z}{x},\mu\right)+\overline{u}_i(x,\mu)\,d_j\left(\frac{z}{x},\mu\right)\right], \tag{85.5}$$

where $u_i(x,\mu)$ and $d_i(x,\mu)$ are the parton distributions inside the proton at the factorization scale μ and parton momentum fraction x for the up- and down-type quarks of the ith generation, respectively. QCD corrections to W' production are sizable (they also include quark-gluon initial states), but preserve the above factorization of couplings at next-to-leading order [17].

The most commonly studied W' signal consists of a high-momentum electron or muon and large missing transverse momentum. The signal transverse mass distribution forms a Jacobian peak with its endpoint at $M_{W'}$ (see Fig. 1 (top) of Ref. [18]). Given that the branching fractions for $W' \to e\nu$ and $W' \to \mu\nu$ could be very different, the results in these channels should be presented separately. Searches in these channels often implicitly assume that the left-handed couplings vanish (no interference between W and W'), and that the right-handed neutrino is light compared to the W' boson and escapes the detector. An example of parameter values that satisfy these assumptions is $C^R_q = gV_{\rm CKM}$, $C^R_\ell = g$, $C^L_q = C^L_\ell = 0$, which define a model that preserves lepton universality and predicts the same total cross section as the Sequential SM used in many W' searches. However, if a W' boson were discovered and the final state fermions have left-handed helicity, then the effects of $W - W'$ interference could be observed [22], providing information about the W' couplings. The effects of the W' width on interference are discussed in Ref. [23].

In the $e\nu$ channel, the ATLAS and CMS collaborations set limits on the W' production cross section times branching fraction $\sigma \times B$ (and thus indirectly on the W' couplings). These limits are set for $M_{W'}$ in the $0.15 - 7$ TeV range and are based on approximately 140 fb^{-1} at $\sqrt{s} = 13$ TeV [18,19], with the most stringent limits reproduced in Fig. 85.1. ATLAS sets the strongest mass limit $M_{W'} > 6.0$ TeV in the Sequential SM (all limits in this mini-review are at the 95% CL). The coupling limits are much weaker for $M_{W'} < 150$ GeV, a range last explored with the Tevatron at $\sqrt{s} = 1.8$ TeV [24].

In the $\mu\nu$ channel, ATLAS and CMS set rate limits for $M_{W'}$ in the $0.15-7$ TeV range [18,19], with the strongest mass lower limit of 5.6 TeV in the Sequential SM set by CMS [19] using 138 fb^{-1} of $\sqrt{s} = 13$ TeV data, as shown in Fig. 85.1. When combined with the $e\nu$ channel assuming lepton universality, the upper limit on the $\sqrt{s} = 13$ TeV cross section times branching fraction to $\ell\nu$ varies between 0.05 and 2.1 fb for $M_{W'}$ values between 1 and 6 TeV [18]. Only weak limits on $W' \to \mu\nu$ exist for $M_{W'} <$ 150 GeV [25]. Note that masses of the order of the electroweak

Int. J. Mod. Phys. A 2026.41. Downloaded from www.worldscientific.com by UNIVERSITY OF CALIFORNIA @ BERKELEY on 09/16/26. Re-use and distribution is strictly not permitted, except for Open Access articles.

Int. J. Mod. Phys. A 2026.41. Downloaded from www.worldscientific.com
by UNIVERSITY OF CALIFORNIA @ BERKELEY on 09/16/26. Re-use and distribution is strictly not permitted, except for Open Access articles.

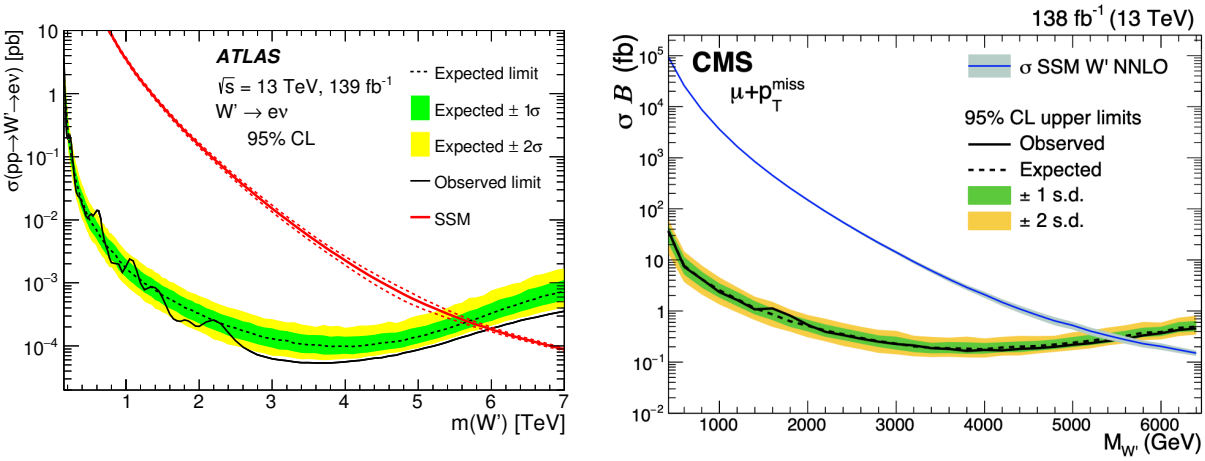

Figure 85.1: Upper limit on $\sigma(pp \to W'X) \times B(W' \to \ell\nu)$ in the $e\nu$ channel from ATLAS [18] (left) and the $\mu\nu$ channel from CMS [19] (right). The red (black) line shows the theoretical prediction in the Sequential SM in the $e\nu$ ($\mu\nu$) channel.

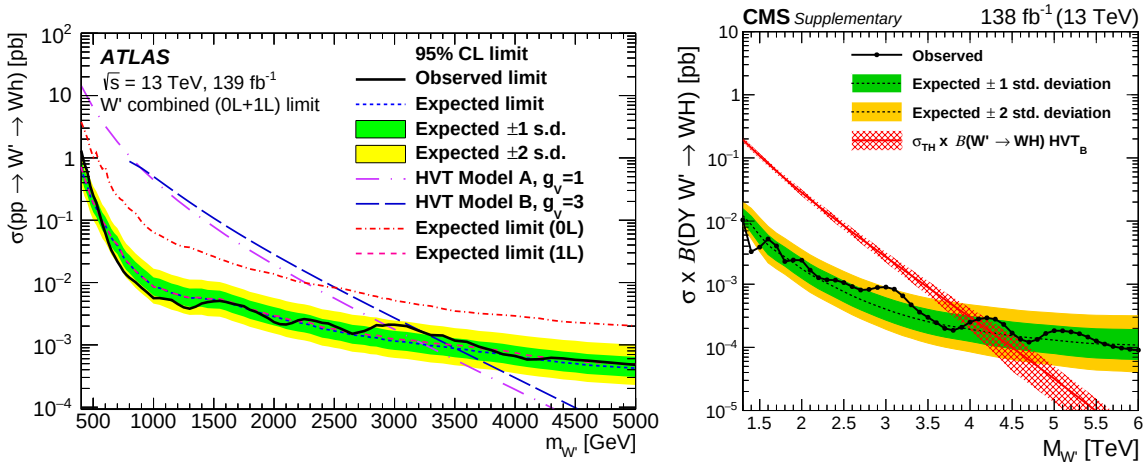

Figure 85.2: Upper limits on W' production cross section times branching fraction into a W and a SM Higgs boson decaying into heavy-flavor quarks, from ATLAS [20] (left) and CMS [21] (right).

scale are interesting from a theoretical point of view, while lepton universality does not necessarily apply to a W' boson.

Searches for $W' \to \tau\nu$ have been performed at 13 TeV by CMS with 138 fb^{-1} [26], and by ATLAS with 139 fb^{-1} [27]. Limits are set on $\sigma \times B$ for $M_{W'}$ between 0.5 and 6 TeV. A mass lower limit of 5.0 TeV is set in the Sequential SM, and the upper limit on the cross section times branching fraction to $\tau\nu$ at 13 TeV varies between 0.4 and 9 fb for $M_{W'}$ values between 1 and 5 TeV [27].

The W' decay into a charged lepton and a right-handed neutrino, ν_R, may also be followed by the ν_R decay through a virtual W' boson into a charged lepton and two quark jets. The CMS [28] and ATLAS [29] searches in the $eejj$ and $\mu\mu jj$ channels have set limits at $\sqrt{s} = 13$ TeV on the cross section times branching fractions as a function of the ν_R mass and of $M_{W'}$. No requirement is placed on the charge of the lepton pair. A related W' search in the $\tau\tau jj$ channel with hadronic τ decays was also performed by CMS [30].

The $t\bar{b}$ channel is particularly important because a W' boson that couples only to right-handed fermions cannot decay to leptons when the right-handed neutrinos are heavier than $M_{W'}$. Additional motivations are provided by a W' boson with enhanced couplings to the third generation [12], and by a leptophobic W' boson. The usual signature for $W' \to t\bar{b}$ consists of a leptonically-decaying W boson and two b-jets. Recent studies have also incorporated the fully hadronic decay channel for $M_{W'} \gg m_t$ with the use of jet substructure techniques to tag highly boosted top-jets. For a detailed discussion of this channel, see Ref. [31].

Searches for dijet resonances may be used to set limits on $W' \to q\bar{q}'$. ATLAS [32] and CMS [33] provide similar coverage in the $\sim$ 1.5−8 TeV mass range with 139 and 137 fb^{-1} of data, respectively, collected at $\sqrt{s} = 13$ TeV. Interpretation in terms of W' decays with 139 fb^{-1} of 13 TeV data yields a W' mass lower limit of 4.0 TeV in the Sequential SM [32]. For masses in the range $\sim 0.5 - 1.5$ TeV, analyses based on jets reconstructed online provide the best sensitivity because they circumvent trigger bandwidth limitations [34, 35]. For W' masses below ~ 0.5 TeV, the best limits are set in novel analyses exploiting boosted technologies and initial state radiation [36–39]. Cross-section limits for W' masses below ~ 1.5 TeV can be derived from the dijet limits on Z' bosons summarized in Ref. [3].

In some theories [5] the W' couplings to SM fermions are suppressed by discrete symmetries. W' production then occurs in pairs, through a photon or Z boson. The decay modes are model-dependent and often involve other new particles. The ensuing collider signals arise from cascade decays and often include missing transverse momentum or boosted multi-jet topologies. Even when single production of W' is large enough, it is possible that its main decay mode is into a new particle and a SM one. An example is a search performed by CMS [40] for W' decays into a vector-like quark and a top or a bottom quark. The final state studied in this analysis involves a boosted SM Higgs or Z boson, as well as a $t\bar{t}$ or $b\bar{b}$ pair, with all heavy particles decaying into jets. Another example is a search performed by ATLAS [41] for W' decays into a W boson and a Z' boson, the latter decaying

Int. J. Mod. Phys. A 2026.41. Downloaded from www.worldscientific.com
by UNIVERSITY OF CALIFORNIA @ BERKELEY on 09/16/26. Re-use and distribution is strictly not permitted, except for Open Access articles.

into a jet pair.

Searches for WZ resonances at the LHC have focused on the process $pp \to W' \to WZ$ with the production mainly from $u\bar{d} \to W'$, assuming SM-like couplings to quarks. ATLAS and CMS have set upper limits on the $W'WZ$ coupling for $M_{W'}$ in the $0.2 - 5.0$ TeV range with a combination of fully leptonic, semi-leptonic and fully hadronic channels with $\sim 36 - 139$ fb^{-1} at 13 TeV [42,43] (see also Ref. [31]). Constraints in individual channels of the same $pp \to W' \to WZ$ process were obtained based on the full Run 2 data sets by ATLAS [44–46] and CMS [21,47–49]. The strongest lower limit on the W' mass is set by ATLAS [45] in the semi-leptonic channel with a lower limit on $M_{W'}$ of 3.9 TeV [45] in the context of the Heavy Vector Triplet (HVT) weakly-coupled scenario A [50]. A similar result is obtained by CMS in the fully-hadronic channel [21]. A fermiophobic W' boson that couples to WZ may be produced at hadron colliders in association with a Z boson, or via WZ fusion. This would give rise to $(WZ)Z$ and $(WZ)jj$ final states [51]. Results of the search for the latter are reported in Refs. [21,45,47,49,52].

W' bosons have also been searched for in final states with a W boson and a SM Higgs boson in the channels $W \to \ell\nu$ or $W \to q\bar{q}'$ and $h^0 \to b\bar{b}$ by ATLAS [20,53] and CMS [21,49] with 138–139 fb^{-1} at $\sqrt{s} = 13$ TeV. CMS also searched for W' bosons in the $q\bar{q}'\tau\tau$ final state [54]. Cross-section limits are set for W' masses between 0.4 and 6.0 TeV. The most stringent upper limit on the cross section is set by the ATLAS analysis with $W \to \ell\nu$ at low $M_{W'}$ and the CMS analysis with $W \to q\bar{q}'$ at high $M_{W'}$, as shown in Fig. 85.2.

At lepton colliders, W' bosons may be produced in pairs via their photon coupling, which is model independent. At LEP-II, although dedicated searches for W' bosons have not been performed, the large cross section for $e^+e^- \to \gamma^* \to W'^+W'^-$ and small backgrounds suggest that any W' is ruled out up to the kinematic limit, $M_{W'} < \sqrt{s}/2 \approx 105$ GeV, for most decay modes. Sensitivity to $M_{W'}$ above $\sqrt{s}$ could be achieved [55] using the $e^+e^- \to \gamma\nu\bar{\nu}$ process via a t-channel W' exchange, if the W' coupling to $e\nu$ is large enough.

85.3 Low-energy constraints

The properties of W' bosons are also constrained by measurements of processes at energies much below $M_{W'}$. The bounds on $W - W'$ mixing [4] are mostly due to the change in W properties compared to the SM. Limits on deviations in the ZWW couplings provide a leading constraint for fermiophobic W' bosons [14].

Constraints arising from low-energy effects of W' exchange are strongly model-dependent. If the W' couplings to quarks are not suppressed, then box diagrams involving a W and a W' boson contribute to neutral meson-mixing. In the case of W' couplings to right-handed quarks as in the left-right symmetric model, the limit from $K_L - K_S$ mixing is severe: $M_{W'} > 2.9$ TeV for $C_q^R = gV_{\rm CKM}$ [56]. However, if no correlation between the W' and W couplings is assumed, then the limit on $M_{W'}$ may be significantly relaxed [57].

W' exchange also contributes at tree level to various low-energy processes. In particular, it would impact the measurement of the Fermi constant G_F in muon decay, which in turn would change the predictions of many other electroweak processes. A recent test of parity violation in polarized muon decay [58] has set limits of about 600 GeV on $M_{W'}$, assuming W' couplings to right-handed leptons as in left-right symmetric models and a light ν_R. There are also W' contributions to the neutron electric dipole moment, β decays, and other processes [4].

If right-handed neutrinos have Majorana masses, then there are tree-level contributions to neutrinoless double-beta decay, and a limit on $M_{W'}$ versus the ν_R mass may be derived [59]. For ν_R masses below a few GeV, the W' boson contributes to leptonic and semileptonic B meson decays, so that limits may be placed on various combinations of W' parameters [57]. For ν_R masses below $\sim$30 MeV, the most stringent constraints on $M_{W'}$ are due to the limits on ν_R emission from supernovae [60].

References

[1] M. Bando, T. Kugo and K. Yamawaki, Phys. Rept. **164**, 217 (1988).

[2] H.-C. Cheng *et al.*, Phys. Rev. D **64**, 065007 (2001), [hep-th/0104179].

[3] See the Section on "Z'-boson searches" in this *Review*.

[4] See the particle listings for W' in this *Review*.

[5] H.-C. Cheng and I. Low, JHEP **09**, 051 (2003), [hep-ph/0308199].

[6] B. A. Dobrescu and Z. Liu, JHEP **10**, 118 (2015), [arXiv:1507.01923].

[7] G. Altarelli, B. Mele and M. Ruiz-Altaba, Z. Phys. C **45**, 109 (1989), [Erratum: Z. Phys. C **47**, 676 (1990)].

[8] R. N. Mohapatra and J. C. Pati, Phys. Rev. D **11**, 566 (1975).

[9] K. S. Babu, X.-G. He and E. Ma, Phys. Rev. D **36**, 878 (1987).

[10] H. Georgi, E. E. Jenkins and E. H. Simmons, Nucl. Phys. B **331**, 541 (1990).

[11] X.-y. Li and E. Ma, J. Phys. G **19**, 1265 (1993), [hep-ph/9208210].

[12] D. J. Muller and S. Nandi, Phys. Lett. B **383**, 345 (1996), [hep-ph/9602390].

[13] A. Donini *et al.*, Nucl. Phys. B **507**, 51 (1997), [hep-ph/9705450].

[14] R. S. Chivukula *et al.*, Phys. Rev. D **74**, 075011 (2006), [hep-ph/0607124].

[15] F. Pisano and V. Pleitez, Phys. Rev. D **46**, 410 (1992), [hep-ph/9206242].

[16] V. D. Barger and R. J. N. Phillips, *Collider Physics* (1996), ISBN 978-0201149456.

[17] Z. Sullivan, Phys. Rev. D **66**, 075011 (2002), [hep-ph/0207290].

[18] G. Aad *et al.* (ATLAS), Phys. Rev. D **100**, 052013 (2019), [arXiv:1906.05609].

[19] A. Tumasyan *et al.* (CMS), JHEP **07**, 067 (2022), [arXiv:2202.06075].

[20] G. Aad *et al.* (ATLAS), JHEP **06**, 016 (2023), [arXiv:2207.00230].

[21] A. Tumasyan *et al.* (CMS), Phys. Lett. B **844**, 137813 (2023), [arXiv:2210.00043].

[22] T. G. Rizzo, JHEP **05**, 037 (2007), [arXiv:0704.0235].

[23] E. Accomando *et al.*, Phys. Rev. D **85**, 115017 (2012), [arXiv:1110.0713].

[24] F. Abe *et al.* (CDF), Phys. Rev. Lett. **74**, 2900 (1995).

[25] F. Abe *et al.* (CDF), Phys. Rev. Lett. **67**, 2609 (1991).

[26] A. Tumasyan *et al.* (CMS), JHEP **09**, 051 (2023), [arXiv:2212.12604].

[27] G. Aad *et al.* (ATLAS), Phys. Rev. D **109**, 11, 112008 (2024), [arXiv:2402.16576].

[28] A. Tumasyan *et al.* (CMS), JHEP **04**, 047 (2022), [arXiv:2112.03949].

[29] G. Aad *et al.* (ATLAS), Eur. Phys. J. C **83**, 12, 1164 (2023), [arXiv:2304.09553].

[30] A. M. Sirunyan *et al.* (CMS), JHEP **03**, 170 (2019), [arXiv:1811.00806].

[31] K.M. Black, R.S. Chivukula and A. Lister, "Dynamical electroweak symmetry breaking" in this *Review*.

[32] G. Aad *et al.* (ATLAS), JHEP **03**, 145 (2020), [arXiv:1910.08447].

[33] A. M. Sirunyan *et al.* (CMS), JHEP **05**, 033 (2020), [arXiv:1911.03947].

[34] M. Aaboud *et al.* (ATLAS), Phys. Rev. Lett. **121**, 081801 (2018), [arXiv:1804.03496].

[35] A. M. Sirunyan *et al.* (CMS), JHEP **08**, 130 (2018), [arXiv:1806.00843].

[36] M. Aaboud *et al.* (ATLAS), Phys. Lett. B **788**, 316 (2019), [arXiv:1801.08769].

[37] M. Aaboud *et al.* (ATLAS), Phys. Lett. B **795**, 56 (2019), [arXiv:1901.10917].

[38] A. M. Sirunyan *et al.* (CMS), Phys. Rev. D **100**, 112007 (2019), [arXiv:1909.04114].

[39] A. M. Sirunyan *et al.* (CMS), Phys. Rev. Lett. **123**, 231803 (2019), [arXiv:1905.10331].

[40] A. Tumasyan *et al.* (CMS), JHEP **09**, 088 (2022), [arXiv:2202.12988].

[41] G. Aad *et al.* (ATLAS), JHEP **07**, 202 (2023), [arXiv:2211.08945].

[42] G. Aad *et al.* (ATLAS), JHEP **04**, 118 (2024), [arXiv:2402.10607].

[43] A. M. Sirunyan *et al.* (CMS), Phys. Lett. B **798**, 134952 (2019), [arXiv:1906.00057].

[44] G. Aad *et al.* (ATLAS), JHEP **09**, 091 (2019), [Erratum: JHEP **06** (2020) 042], [arXiv:1906.08589].

[45] G. Aad *et al.* (ATLAS), Eur. Phys. J. C **80**, 1165 (2020), [arXiv:2004.14636].

[46] G. Aad *et al.* (ATLAS), Eur. Phys. J. C **83**, 633 (2023), [arXiv:2207.03925].

[47] A. Tumasyan *et al.* (CMS), Phys. Rev. D **106**, 012004 (2022), [arXiv:2109.08268].

[48] A. Tumasyan *et al.* (CMS), JHEP **04**, 087 (2022), [arXiv:2111.13669].

[49] A. Tumasyan *et al.* (CMS), Phys. Rev. D **105**, 032008 (2022), [arXiv:2109.06055].

[50] D. Pappadopulo *et al.*, JHEP **09**, 060 (2014), [arXiv:1402.4431].

[51] H.-J. He *et al.*, Phys. Rev. D **78**, 031701 (2008), [arXiv:0708.2588].

[52] M. Aaboud *et al.* (ATLAS), Phys. Rev. D **98**, 052008 (2018), [arXiv:1808.02380].

[53] G. Aad *et al.* (ATLAS), Phys. Rev. D **102**, 112008 (2020), [arXiv:2007.05293].

[54] A. M. Sirunyan *et al.* (CMS), JHEP **01**, 051 (2019), [arXiv:1808.01365].

[55] S. Godfrey *et al.*, Phys. Rev. D **61**, 113009 (2000), [hep-ph/0001074].

[56] Y. Zhang *et al.*, Phys. Rev. D **76**, 091301 (2007), [arXiv:0704.1662].

[57] P. Langacker and S. U. Sankar, Phys. Rev. D **40**, 1569 (1989).

[58] J. F. Bueno *et al.* (TWIST), Phys. Rev. D **84**, 032005 (2011), [arXiv:1104.3632].

[59] G. Prezeau, M. Ramsey-Musolf and P. Vogel, Phys. Rev. D **68**, 034016 (2003), [hep-ph/0303205].

[60] G. G. Raffelt, Ann. Rev. Nucl. Part. Sci. **49**, 163 (1999), [hep-ph/9903472].

Int. J. Mod. Phys. A 2026.41. Downloaded from www.worldscientific.com
by UNIVERSITY OF CALIFORNIA @ BERKELEY on 09/16/26. Re-use and distribution is strictly not permitted, except for Open Access articles.

86. Z'-Boson Searches

Revised October 2025 by B.A. Dobrescu (FNAL) and N. Saoulidou (Athens U.).

The Z' boson is a massive, electrically-neutral and color-singlet hypothetical particle of spin 1. This particle is predicted in many extensions of the Standard Model (SM) and has been the object of extensive phenomenological studies [1].

86.1 Z' boson couplings

The couplings of a Z' boson to the first-generation fermions are given by

$$Z'_\mu \left(g_u^L\, \overline{u}_L \gamma^\mu u_L + g_d^L\, \overline{d}_L \gamma^\mu d_L + g_u^R\, \overline{u}_R \gamma^\mu u_R + g_d^R\, \overline{d}_R \gamma^\mu d_R + g_\nu^L\, \overline{\nu}_L \gamma^\mu \nu_L + g_e^L\, \overline{e}_L \gamma^\mu e_L + g_e^R\, \overline{e}_R \gamma^\mu e_R \right), \tag{86.1}$$

where u, d, ν, e are the quark and lepton fields in the mass eigenstate basis, and the coefficients g_u^L, g_d^L, g_u^R, g_d^R, g_ν^L, g_e^L, g_e^R are real dimensionless parameters. If the Z' couplings to quarks and leptons are generation-independent, then these seven parameters describe the couplings of the Z' boson to all SM fermions. More generally, however, the Z' couplings to fermions are generation-dependent, in which case Eq. (86.1) may be written with generation indices i, $j = 1, 2, 3$ labeling the quark and lepton fields, and with the seven coefficients promoted to 3×3 Hermitian matrices (*e.g.*, $g_{e\,ij}^L\, \overline{e}_L^i \gamma^\mu e_L^j$, where e_L^2 is the left-handed muon, etc.).

The parameters describing the Z' boson interactions with quarks and leptons are subject to some theoretical constraints. Quantum field theories that include a heavy spin-1 particle are well behaved at high energies only if that particle is a gauge boson associated with a spontaneously broken gauge symmetry. Quantum effects preserve the gauge symmetry only if the couplings of the gauge boson to fermions satisfy the anomaly equations [2]. Furthermore, the fermion charges under the new gauge symmetry are constrained by the requirement that the quarks and leptons get masses from gauge-invariant interactions with the Higgs fields.

The relation between the couplings displayed in Eq. (86.1) and the gauge charges z_{fi}^L and z_{fi}^R of the fermions $f = u, d, \nu, e$ involves the unitary 3×3 matrices V_f^L and V_f^R that transform the gauge eigenstate fermions f_L^i and f_R^i, respectively, into the mass eigenstates. The Z' couplings also depend on the mixings of the new gauge boson in the gauge eigenstate basis ($\tilde{Z}'_\mu$). The main mixings are a kinetic mixing $(-\chi/2) B^{\mu\nu} \tilde{Z}'_{\mu\nu}$ with the hypercharge gauge boson B^μ (χ is a dimensionless parameter), and a mass mixing $\delta M^2\, \tilde{Z}^\mu \tilde{Z}'_\mu$ with the linear combination ($\tilde{Z}_\mu$) of neutral bosons identified as the SM Z boson [3]. Since both the kinetic and mass mixings shift the mass and couplings of the Z boson, electroweak measurements impose upper limits on χ and $\delta M^2/(M_{Z'}^2 - M_Z^2)$ of the order of 10^{-3} [4]. Keeping only linear terms in these two small quantities, the couplings of the mass-eigenstate Z' boson are given by

$$g_{f\,ij}^L = g_z V_{fii'}^L\, z_{f\,i'}^L \left(V_f^L\right)_{i'j}^\dagger + \frac{e}{c_W} \left(\frac{s_W \chi M_{Z'}^2 + \delta M^2}{2 s_W \left(M_{Z'}^2 - M_Z^2\right)} \sigma_f^3 - \epsilon\, Q_f \right), \tag{86.2}$$

$$g_{f\,ij}^R = g_z V_{fii'}^R\, z_{fi'}^R \left(V_f^R\right)_{i'j}^\dagger - \frac{e}{c_W}\, \epsilon\, Q_f, \tag{86.3}$$

where g_z is the new gauge coupling, Q_f is the electric charge of f, e is the electromagnetic gauge coupling, s_W and c_W are the sine and cosine of the weak mixing angle, $\sigma_f^3 = +1$ for $f = u, \nu$ and $\sigma_f^3 = -1$ for $f = d, e$, and

$$\epsilon = \frac{\chi \left(M_{Z'}^2 - c_W^2 M_Z^2\right) + s_W \delta M^2}{M_{Z'}^2 - M_Z^2}. \tag{86.4}$$

The interaction of the Z' boson with a pair of W bosons has the form

$$\left[i \left(W_\mu^- Z'_\nu - W_\nu^- Z'_\mu \right) \partial^\mu W^{+\nu} + \text{H.c.} \right] + i \left(W_\mu^+ W_\nu^- - W_\nu^+ W_\mu^- \right) \partial^\mu Z'^\nu \tag{86.5}$$

with a coefficient of order $M_W^2/M_{Z'}^2$ [5]. The Z' also couples to one SM Higgs boson and one Z boson, $Z'_\mu Z^\mu\, h^0$, with a coefficient of order M_Z.

86.2 Z' models

A simple origin of a Z' boson is a new $U(1)'$ gauge symmetry. In that case, the matricial equalities $z_u^L = z_d^L$ and $z_\nu^L = z_e^L$ are required by the SM $SU(2)_W$ gauge symmetry. Given that the $U(1)'$ interaction is not asymptotically free, the theory may be well-behaved at high energies (*e.g.*, by embedding $U(1)'$ in a non-Abelian gauge group) only if the charges are commensurate numbers, *i.e.* any ratio of charges is a rational number. Satisfying the anomaly equations [6] with rational numbers is highly nontrivial, and typically new fermions charged under $U(1)'$ are necessary.

If the couplings are generation-independent ($V_f^{L,R}$ are then unit matrices in Eq. (86.2)) and the mixings of $\tilde{Z}'$ are negligible, then there are five commensurate couplings: g_u^R, g_d^R, g_e^R, g_q^L ($q = u$ or d), g_l^L ($l = \nu$ or e). Four sets of charges are displayed in Table 86.1, each of them spanned by a free parameter x [6]. The first set, labeled $B - xL$, has charges proportional to the baryon number minus x times the lepton number. These charges allow all SM Yukawa couplings to the Higgs doublet which is neutral under $U(1)_{B-xL}$, so that there is no tree-level $\tilde{Z} - \tilde{Z}'$ mixing. For $x = 1$ one recovers the $U(1)_{B-L}$ group, which is non-anomalous in the presence of one "right-handed neutrino" (a chiral fermion that is a singlet under the SM gauge group) per generation. For $x \neq 1$, it is necessary to include some fermions that are vectorlike (*i.e.* their mass terms are gauge invariant) with respect to the electroweak gauge group and chiral with respect to $U(1)_{B-xL}$. In the particular cases $x = 0$ or $x \gg 1$, the Z' is leptophobic or quark-phobic, respectively.

The second set, $U(1)_{10+x\bar{5}}$, has charges that commute with the representations of the $SU(5)$ grand unified group. Here x is related to the mixing angle between the two $U(1)$ bosons encountered in the $E_6 \to SU(5) \times U(1) \times U(1)$ symmetry breaking patterns of grand unified theories [1,7]. With these charges, two Higgs doublets are typically required to generate masses for both up- and down- type fermions. This set leads to $\tilde{Z} - \tilde{Z}'$ mass mixing at tree level, such that for a Z' mass close to the electroweak scale, the measurements at the Z-pole require some fine tuning between the charges and VEVs of the two Higgs doublets. Vectorlike quarks charged under the electroweak gauge group are required (except for $x = -3$) to make this set anomaly free. The particular cases $x = -3, 1, -1/2$ are usually labeled $U(1)_\chi$, $U(1)_\psi$, and $U(1)_\eta$, respectively. Under the third set, $U(1)_{d-xu}$, the weak-doublet quarks are neutral, and the ratio of u_R and d_R charges is $-x$. For $x = 1$, this is the "right-handed" group $U(1)_R$. For $x = 0$, the charges are those of the E_6-inspired $U(1)_I$ group, which requires new quarks and leptons. Other generation-independent sets of $U(1)'$ charges are given in Ref. [8].

In the absence of new fermions charged under the SM group, the most general generation-independent charge assignment is $U(1)_{q+xu}$, which is a linear combination of hypercharge and $B-L$. Many other anomaly-free solutions exist if generation-dependent charges are allowed. An example is $B - xL_e - yL_\mu + (y-3)L_\tau$, with x, y free parameters. This allows all fermion masses to be generated by Yukawa couplings to a single Higgs doublet, without inducing tree-level flavor-changing neutral current (FCNC) processes. There are also lepton-flavor dependent charges that allow neutrino masses to arise only from operators of high dimensionality [9].

If the $SU(2)_W$-doublet quarks have generation-dependent $U(1)'$ charges, then the mass eigenstate quarks have flavor off-diagonal couplings to the Z' boson (see Eq. (86.1), and note that $V_u^L \left(V_d^L\right)^\dagger$

Int. J. Mod. Phys. A 2026.41. Downloaded from www.worldscientific.com by UNIVERSITY OF CALIFORNIA @ BERKELEY on 09/16/26. Re-use and distribution is strictly not permitted, except for Open Access articles.

Int. J. Mod. Phys. A 2026.41. Downloaded from www.worldscientific.com
by UNIVERSITY OF CALIFORNIA @ BERKELEY on 09/16/26. Re-use and distribution is strictly not permitted, except for Open Access articles.

Table 86.1: Examples of generation-independent $U(1)'$ charges for quarks and leptons. The parameter x is an arbitrary rational number. Gauge anomaly cancellation requires certain new fermions [6].

fermion	$U(1)_{B-xL}$	$U(1)_{10+x\bar{5}}$	$U(1)_{d-xu}$	$U(1)_{q+xu}$
(u_L, d_L)	$1/3$	$1/3$	0	$1/3$
u_R	$1/3$	$-1/3$	$-x/3$	$x/3$
d_R	$1/3$	$-x/3$	$1/3$	$(2-x)/3$
(ν_L, e_L)	$-x$	$x/3$	$(-1+x)/3$	-1
e_R	$-x$	$-1/3$	$x/3$	$-(2+x)/3$

is the CKM matrix). These are severely constrained by measurements of FCNC processes, which in this case are mediated at tree-level by Z' boson exchange [10]. The constraints are relaxed if the first and second generation charges are the same, although they are increasingly tightened by the measurements of B meson properties [11]. If only the $SU(2)_W$-singlet quarks have generation-dependent $U(1)'$ charges, there is more freedom in adjusting the flavor off-diagonal couplings because the $V^R_{u,d}$ matrices are not observable in the SM.

The anomaly equations for $U(1)'$ could be circumvented only if there is an axion with certain dimension-5 couplings to the gauge bosons. However, such a scenario violates unitarity unless the quantum field theory description breaks down at a scale near $M_{Z'}$ [12]. It is possible, though, that the SM fermions are not charged under the $U(1)'$, but have mass mixing with some vectorlike fermions which are charged under $U(1)'$, implying that the physical fermions have couplings to the Z' [13]. For example, if the only SM quarks that have large mixings with some vectorlike quarks are the b quarks, then the only currently known particles that couple to the Z' would be the physical b quarks.

Z' bosons may also arise from larger gauge groups. These may extend the electroweak group, as in $SU(2)\times SU(2)\times U(1)$, or may embed the electroweak group, as in $SU(3)_W \times U(1)$ [14]. If the larger group is spontaneously broken down to $SU(2)_W \times U(1)_Y \times U(1)'$ at a scale $v_\star \gg M_{Z'}/g_z$, then the above discussion applies up to corrections of order $M^2_{Z'}/(g_z v_\star)^2$. For $v_\star \sim M_{Z'}/g_z$, additional gauge bosons have masses comparable to $M_{Z'}$, including at least a W' boson [14]. If the larger gauge group breaks together with the electroweak symmetry directly to the electromagnetic $U(1)_{\rm em}$, then the left-handed fermion charges are no longer correlated ($z^L_u \neq z^L_d$, $z^L_\nu \neq z^L_e$) and a $Z'W^+W^-$ coupling is induced.

If the electroweak gauge bosons propagate in extra dimensions, then their Kaluza-Klein (KK) excitations include a series of Z' boson pairs. Each of these pairs can be associated with a different $SU(2)\times U(1)$ gauge group in four dimensions. The properties of the KK particles depend strongly on the extra dimensional theory [15]. For example, in universal extra dimensions there is a parity that forces all couplings of Eq. (86.1) to vanish in the case of the lightest KK bosons, while allowing couplings to pairs of fermions involving a SM and a heavy vectorlike fermion. There are also 4-dimensional gauge theories (*e.g.* little Higgs with T parity [16]) with Z' bosons exhibiting similar properties. By contrast, in a warped extra dimension, the couplings of Eq. (86.1) may be sizable even when SM fields propagate along the extra dimension.

Z' bosons may also be composite particles. For example, in confining gauge theories [17], the ρ-like bound state is a spin-1 boson that may be interpreted as arising from a spontaneously broken gauge symmetry [18].

86.3 Non-resonant Z' signatures at colliders

In the presence of the couplings shown in Eq. (86.1), the Z' boson may be produced in the s-channel at colliders, and would decay to pairs of fermions. The decay width into a pair of electrons is given by

$$\Gamma\left(Z' \to e^+e^-\right) \simeq \left[\left(g^L_e\right)^2 + \left(g^R_e\right)^2\right] \frac{M_{Z'}}{24\pi}, \tag{86.6}$$

where small corrections from electroweak loops are not included. The decay width into $q\bar{q}$ is similar, except for an additional color factor of 3, QCD radiative corrections, and fermion mass corrections. Thus, one may compute the Z' branching fractions in terms of the couplings of Eq. (86.1). However, other decay channels, such as WW or a pair of new particles, could have large widths and need to be added to the total decay width.

As mentioned above, there are theories in which the Z' couplings are controlled by a discrete symmetry that forbids decays into a pair of SM particles. Typically, such theories involve several new particles, which may be produced only in pairs and undergo cascade decays through Z' bosons, leading to signals involving missing transverse momentum. Given that the cascade decays depend on the properties of new particles other than the Z' boson (see, *e.g.* Ref. [19]), this case is not discussed further here.

The Z' contribution to the cross sections for $e^+e^- \to f\bar{f}$ proceeds through an s-channel Z' exchange (when $f = e$, there are also t- and u-channel exchanges). For $M_{Z'} < \sqrt{s}$, the Z' appears as an $f\bar{f}$ resonance in the radiative return process where photon emission tunes the effective center-of-mass energy to $M_{Z'}$. The agreement between the LEP-II measurements and the SM predictions implies that either the Z' couplings are smaller than or of order 10^{-2}, or else $M_{Z'}$ is above 209 GeV, the maximum energy of LEP-II. In the latter case, the Z' exchange may be approximated up to corrections of order $s/M^2_{Z'}$ by the contact interactions

$$\frac{g_z^2}{M^2_{Z'} - s}\left[\bar{e}\gamma_\mu\left(z^L_e P_L + z^R_e P_R\right)e\right]\left[\bar{f}\gamma^\mu\left(z^L_f P_L + z^R_f P_R\right)f\right], \tag{86.7}$$

where $P_{L,R}$ are chirality projection operators, and the relation between Z' couplings and charges (see Eq. (86.2) in the limit where the mass and kinetic mixings are neglected) is used, assuming generation-independent charges. The four LEP collaborations have set limits on the coefficients of such operators for all possible chiral structures and for various combinations of fermions [20]. Thus, one may derive bounds on $(M_{Z'}/g_z)|z^L_e z^L_f|^{-1/2}$ and the analogous combinations of LR, RL and RR charges, which are typically on the order of a few TeV. LEP-II limits were derived [6] on the four sets of charges shown in Table 86.1.

Somewhat stronger bounds can be set on $M_{Z'}/g_z$ for specific sets of Z' couplings if the effects of several operators (86.7) are combined. Dedicated analyses by the LEP collaborations have set limits on Z' bosons for particular values of the gauge coupling (see section 3.5 of Ref. [20]). For example, $M_{Z_{\rm SSM}} > 1.76$ TeV for a "sequential" Z' of same couplings as the SM Z boson, while $M_{Z_\chi} > 0.785$ TeV for the Z' associated with $U(1)_\chi$ assuming a unification condition for the gauge coupling.

86.4 Searches at hadron colliders

Z' bosons with couplings to quarks (see Eq. (86.1)) may be produced at hadron colliders in the s-channel and would show up as resonances in the invariant mass distribution of the decay products. The cross section for producing a Z' boson at the LHC, which then decays to some $f\bar{f}$ final state, takes the form [23]

$$\sigma\left(pp \to Z'X \to f\bar{f}X\right) \simeq \frac{\pi}{6\,s}\sum_q c^f_q\, w_q\left(s, M^2_{Z'}\right) \tag{86.8}$$

for flavor-diagonal couplings to quarks. Here, we have neglected the interference with the SM contribution to $f\bar{f}$ production, which is a good approximation for a narrow Z' resonance (deviations from the narrow width approximation are discussed in Ref. [24]). The coefficients

$$c^f_q = \left[\left(g^L_q\right)^2 + \left(g^R_q\right)^2\right] B(Z' \to f\bar{f}) \tag{86.9}$$

contain all the dependence on the Z' couplings, while the functions w_q include all the information about parton distributions and QCD corrections [6, 8]. This factorization holds exactly at next-to-leading order, and the deviations from it induced at NNLO are very small. Note that the w_u and w_d functions are substantially larger than the w_q functions for the other quarks.

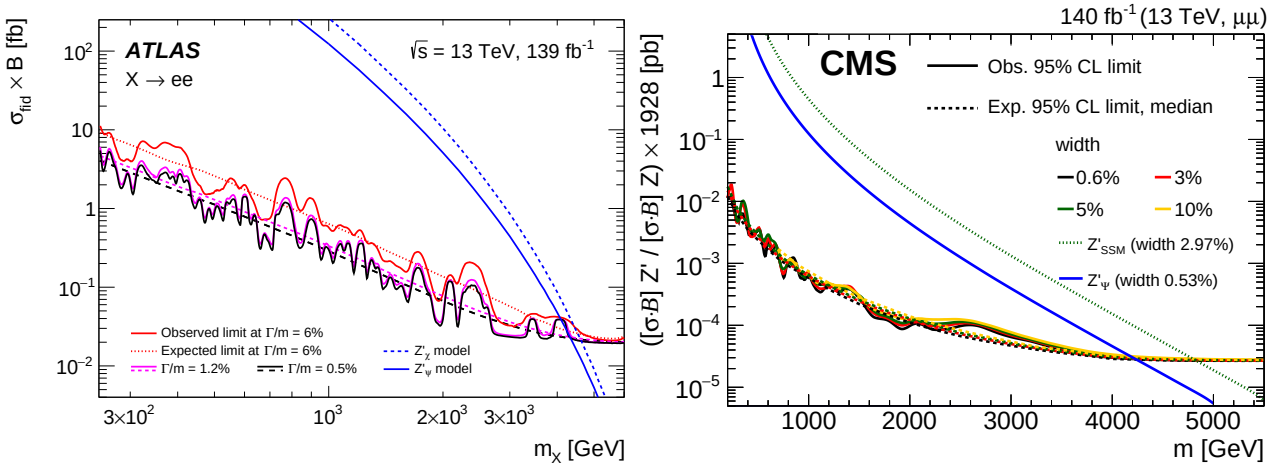

Figure 86.1: Upper limits on the cross section for Z' production times the branching fraction for $Z' \to e^+e^-$ (left panel, set by ATLAS [21]) or $Z' \to \mu^+\mu^-$ (right panel, set by CMS [22]) as a function of $M_{Z'}$. The lines labeled by Z'_ψ and Z'_χ are theoretical predictions for the $U(1)_{10+x\bar{5}}$ models in Table 86.1 with $x = -3$ and $x = +1$, respectively, for g_z fixed by an E_6 unification condition. The $Z'_{\rm SSM}$ line corresponds to Z' couplings equal to those of the Z boson.

Eq. (86.8) also applies to the Tevatron, except for changing the pp initial state to $p\bar{p}$, which implies that the $w_q(s, M^2_{Z'})$ functions are replaced by some other functions $\bar{w}_q((1.96\,\text{TeV})^2, M^2_{Z'})$.

It is common to present results of Z' searches as limits on the cross section versus $M_{Z'}$ (see for example Fig. 86.1). An alternative is to plot exclusion curves for fixed $M_{Z'}$ values in the $c_u^f - c_d^f$ planes, allowing a simple derivation of the mass limit within any Z' model. CMS upper limits in the $c_u^\ell - c_d^\ell$ plane ($\ell = e$ or μ) for different $M_{Z'}$ are shown in Ref. [22] (for Tevatron limits, see Refs. [8, 25]).

The discovery of a dilepton resonance at the LHC would determine the Z' mass and width. A measurement of the total cross section would define a band in the $c_u^\ell - c_d^\ell$ plane. Angular distributions can be used to measure several combinations of Z' parameters (angular distributions were used in Ref. [26] to improve the Tevatron sensitivity). Even though the original quark direction in a pp collider is unknown, the leptonic forward-backward asymmetry $A^\ell_{\rm FB}$ can be extracted from the kinematics of the dilepton system, and is sensitive to parity-violating couplings. A fit to the Z' rapidity distribution can distinguish between the couplings to up and down quarks. These measurements, combined with off-peak observables, have the potential to differentiate among various Z' models [27]. In some cases, $A^\ell_{\rm FB}$ may provide discovery sensitivity that is competitive with the mass distribution [28]. The spin of the Z' boson may be determined from angular distributions [29].

Searches for Z' decays into e^+e^- and $\mu^+\mu^-$ by the ATLAS and CMS collaborations [21, 22] have set 95% C.L. upper cross-section limits as low as 0.02 fb (see Fig. 86.1), with the mass lower limits in specific models as high as 4.9 TeV in a single channel. Cross section limits in the dimuon channel for low mass regions, below 200 GeV but not near the Z mass, have been set at the LHC by CMS [30, 31] and LHCb [32].

The $Z' \to \tau^+\tau^-$ decay has been searched for by CMS with 140 fb^{-1} of 13 TeV data [33], and a limit $M_{Z'} > 3.5$ TeV has been set in the case of a sequential Z'. Limits on heavy scalars in the $\tau^+\tau^-$ final state, set by ATLAS [34] and CMS [35] with the full Run 2 datasets, can be recast into limits on Z'. New searches of very low mass resonances decaying to $\tau^+\tau^-$ final states, in the ranges of 20 to 60 GeV have been published by the CMS experiment [36]. Limits in the flavor-violating leptonic final states have also been reported by ATLAS [37] and CMS [38, 39] at 13 TeV, for resonances in the $e^\pm\mu^\mp$, $e^\pm\tau^\mp$ and $\mu^\pm\tau^\mp$ channels.

Final states with higher background, jj, $b\bar{b}$ and $t\bar{t}$, are also important as they probe various combinations of Z' couplings to quarks. Besides the improved sensitivity at masses of several TeV, the LHC searches in the dijet channel have been also extended to masses as low as 10 GeV, through the use of new techniques involving boosted topologies and initial state radiation [40]. Such searches, utilizing now the full Run 2 ATLAS [41] and CMS [42] datasets, provide best limits in the low mass regime, below $\sim$300 GeV. In addition, new limits covering the intermediate mass range of $0.4-1.8$ TeV are published by CMS [43] and ATLAS [44], based on the full Run 2 datasets, using trigger-level data.

Given the large number of dijet resonance searches over almost three orders of magnitude in mass, it is convenient to compare all existing limits using a coupling-mass plot for a Z' that has flavor-universal vector couplings to quarks [45]. Limits from Z' searches performed by CMS [46] using hadronic final states are summarized in Fig. 86.2, for $g_d^L = g_d^R = g_u^L = g_u^R = g'_q$ in Eq. (86.1). A similar summary from ATLAS [47] uses axial couplings: $g_d^L = -g_d^R = g_u^L = -g_u^R = g_q$. Constraints from electroweak processes and from Z' mixing with the Υ meson are derived in Ref. [48] for the vector coupling as a function of mass.

Searches for the $Z' \to b\bar{b}$ decay have been performed for two production mechanisms. ATLAS [49] and CMS [50] searched for $b\bar{b}$ resonances using the full Run 2 datasets, setting limits under the assumption that the Z' boson couples to light quarks and thus is produced in the s-channel. The CMS upper limit on the cross-section times the $Z' \to b\bar{b}$ branching fraction decreases from 40 fb at $M_{Z'} = 1.8$ TeV to 0.4 fb at $M_{Z'} = 8$ TeV. The ATLAS search covered the 1.3 TeV – 5 TeV mass range, setting a lower mass limit of 2.7 TeV for the Z'_{SSM}. Independent of any other couplings, if the Z' couples to the b quark, then it can be produced in association with a $b\bar{b}$ pair, and it decays to a second $b\bar{b}$ pair, which forms a resonance. The cross-section limit for that process, set by ATLAS [51] with 103 fb^{-1} of 13 TeV data, is between 0.1 and 0.2 pb for $M_{Z'}$ in the 1.3 – 3 TeV range. For a vector coupling g_b of Z' to b quarks, *i.e*, $g^L_{d\,33} = g^R_{d\,33} = g_b$ using the notation of Eq. (86.1), the limit is $M_{Z'} > 1.45$ TeV when $g_b = 1$. Recently, the ATLAS Collaboration published a b-tagged version of a dijet resonance search [52] utilizing initial state radiation, which probes masses in the $200-600$ GeV range. Another search that depends on the Z' couplings to the b quark for production (more precisely, for a $b\bar{b}$, $s\bar{b}$ or $b\bar{s}$ initial state) was performed by CMS [53], under the assumption that the Z' boson decays into a muon pair. Searches for the $Z' \to t\bar{t}$ decay are discussed in Ref. [17].

Heavy resonances decaying into Zh^0 with $Z \to \ell^+\ell^-$, $\nu\bar{\nu}$ or $q\bar{q}$ and $h^0 \to b\bar{b}$ have been studied by ATLAS [54,55] and CMS [56,57] using the full 13 TeV dataset. CMS also searched for Z' bosons in the $q\bar{q}\tau\tau$ final state [58]. The most stringent constraint on Z' production in the context of the Heavy Vector Triplet (HVT) model weakly-coupled scenario A [59] is set in the semi-leptonic channel, with a mass lower limit of 3.5 TeV [56].

Int. J. Mod. Phys. A 2026.41. Downloaded from www.worldscientific.com by UNIVERSITY OF CALIFORNIA @ BERKELEY on 09/16/26. Re-use and distribution is strictly not permitted, except for Open Access articles.

Int. J. Mod. Phys. A 2026.41. Downloaded from www.worldscientific.com
by UNIVERSITY OF CALIFORNIA @ BERKELEY on 09/16/26. Re-use and distribution is strictly not permitted, except for Open Access articles.

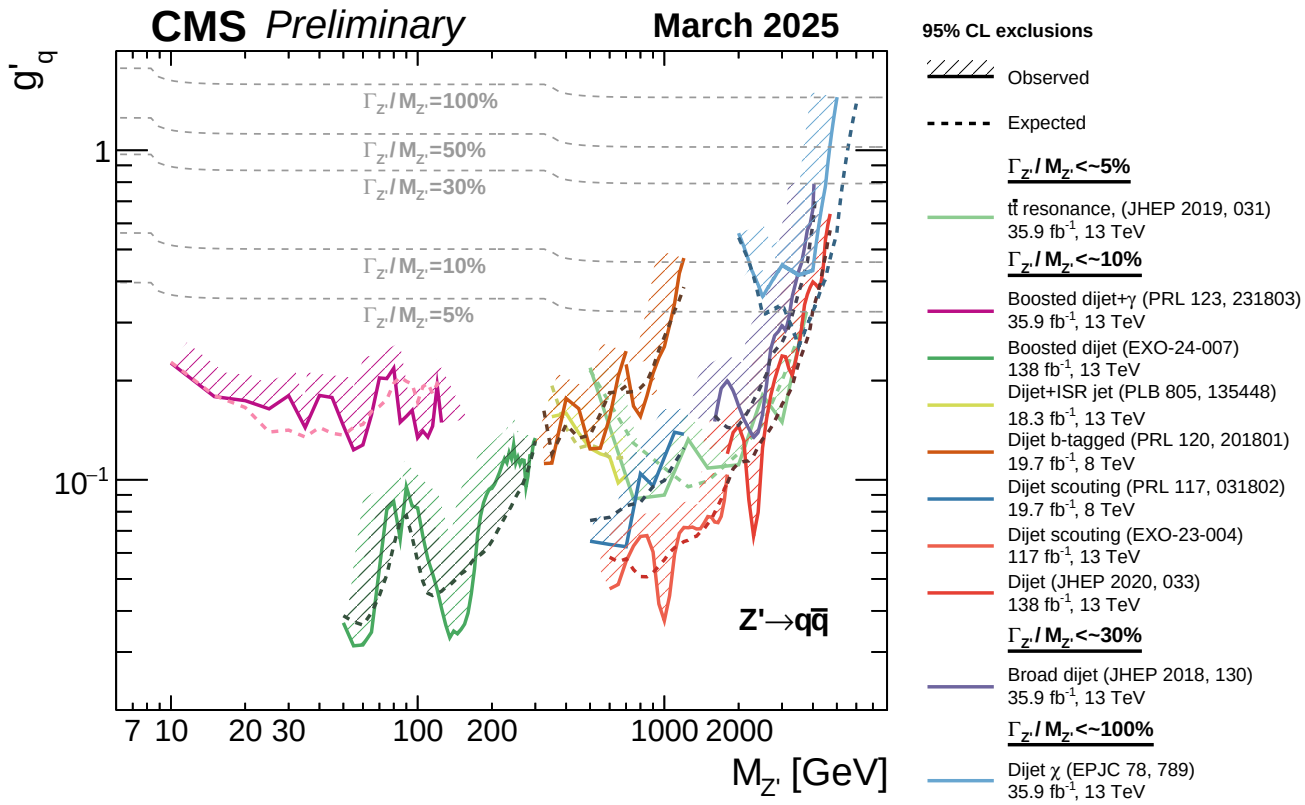

Figure 86.2: Upper limits on the Z' coupling to quarks as a function of $M_{Z'}$ based on various CMS searches [46], for a vector coupling $g_d^L = g_d^R = g_u^L = g_u^R = g'_q$ in Eq. (86.1). Constraints on the coupling due to electroweak and other processes are computed in [48]. Similar ATLAS limits [47] use an axial coupling: $g_d^L = -g_d^R = g_u^L = -g_u^R = g_q$.

Searches for a Z' boson lighter than the SM Z and which couples to leptons have been performed in the 4-lepton final state. ATLAS [60] and CMS [61] focused on the Z decays into a muon pair followed by the radiation of a narrow Z' boson which decays itself into a muon pair. A related CMS search [62] for Z decays into four leptons, but without requiring that a pair of leptons form a narrow resonance, was used to set limits on Z' couplings to electrons or muons as a function of mass, which are relevant for large widths. ATLAS [63] considered the $h^0 \to ZZ'$ and $h^0 \to Z'Z'$ processes followed by the leptonic decays of both spin-1 bosons.

The $pp \to Z'X \to W^+W^-X$ process has also been searched for at the LHC. The channel where the Z' boson is produced through its couplings to quarks, and the W bosons decay hadronically, has been explored using boosted techniques to analyze the 13 TeV data [57, 64–66] with a mass lower limit of 3.5 TeV in the HVT model A [65]. A search in the $e\nu\mu\nu$ final state sets cross-section limits at lower Z' mass [67]. The Z' boson may also be produced through its couplings to W bosons [68], which has been explored with the use of forward jets consistent with a vector boson fusion event topology [57, 65, 66]. The latter process provides a test of fermiophobic Z' models.

At the Tevatron, the CDF and DØ collaborations have searched for Z' bosons in the e^+e^- [69], $\mu^+\mu^-$ [70], $e^\pm\mu^\mp$ [71], $\tau^+\tau^-$ [72], $t\bar{t}$ [73], jj [74] and W^+W^- [75] final states. These limits have been mostly superseded by the LHC results.

86.5 Low-energy constraints

Z' boson properties are also constrained by a variety of low-energy experiments [76]. Polarized electron-nucleon scattering and atomic parity violation are sensitive to electron-quark contact interactions, which get contributions from Z' exchange that can be expressed in terms of the couplings introduced in Eq. (86.1) and M'_Z. Further corrections to the electron-quark contact interactions are induced in the presence of $\tilde{Z}-\tilde{Z}'$ mixing because of the shifts in the Z couplings to quarks and leptons [3]. Deep-inelastic neutrino-nucleon scattering is similarly affected by Z' bosons. Other low-energy observables are discussed in [4]. Viable models with Z' bosons much lighter than the Z boson have been constructed, despite many additional experimental constraints [77]. Limits on the Z' coupling to leptons in the mass range 0.02–10.2 GeV have been set in e^+e^- collisions by BaBar [78], assuming a dark photon, *i.e.*, a Z' boson whose couplings arise only from the kinetic mixing with the hypercharge gauge boson.

In some models, the lower limits on $M_{Z'}$ set by low-energy data are above 1 TeV. For example, $M_{Z_\chi} > 1.1$ TeV and $M_{Z_\eta} > 0.43$ TeV assuming that the Higgs sectors consist of electroweak doublets and singlets only [4], while the gauge coupling is fixed by an $SO(10)$ unification condition for $U(1)_\chi$ and $U(1)_\eta$. For more general models, see Refs. [1, 6, 79]. The mass bounds from direct searches at the LHC [21, 22] exceed the electroweak constraints by a factor of three or more for the models mentioned here. This conclusion could change if the collider bounds are weakened by exotic decay channels [80].

Although the LHC data are most constraining for many Z' models, one should be careful in assessing the relative reach of various experiments given the freedom in Z' couplings. For example, a Z' coupled to $B - yL_\mu + (y-3)L_\tau$ has implications for the muon $g-2$, neutrino oscillations or τ decays, and would be hard to see in processes involving first-generation fermions. Moreover, the combination of LHC searches and low-energy measurements could allow a precise determination of the Z' parameters [81].

References

[1] A. Leike, Phys. Rept. **317**, 143 (1999), [hep-ph/9805494].

[2] T. P. Cheng and L. F. Li, *Gauge Theory of Elementary Particle Physics* (1984), ISBN 9780198519614.

[3] K. S. Babu, C. F. Kolda and J. March-Russell, Phys. Rev. D **57**, 6788 (1998), [hep-ph/9710441].

[4] J. Erler *et al.*, JHEP **08**, 017 (2009), [arXiv:0906.2435].

Int. J. Mod. Phys. A 2026.41. Downloaded from www.worldscientific.com
by UNIVERSITY OF CALIFORNIA @ BERKELEY on 09/16/26. Re-use and distribution is strictly not permitted, except for Open Access articles.

[5] B. A. Dobrescu and P. J. Fox, JHEP **05**, 047 (2016), [arXiv:1511.02148].

[6] M. Carena *et al.*, Phys. Rev. D **70**, 093009 (2004), [hep-ph/0408098].

[7] F. Del Aguila, M. Cvetic and P. Langacker, Phys. Rev. D **52**, 37 (1995), [hep-ph/9501390].

[8] E. Accomando *et al.*, Phys. Rev. D **83**, 075012 (2011), [arXiv:1010.6058].

[9] M.-C. Chen, A. de Gouvea and B. A. Dobrescu, Phys. Rev. D **75**, 055009 (2007), [hep-ph/0612017].

[10] P. Langacker and M. Plumacher, Phys. Rev. D **62**, 013006 (2000), [hep-ph/0001204].

[11] A. J. Buras, F. De Fazio and J. Girrbach, JHEP **02**, 116 (2013), [arXiv:1211.1896].

[12] L. E. Ibanez and G. G. Ross, Phys. Lett. B **332**, 100 (1994), [hep-ph/9403338].

[13] P. J. Fox *et al.*, Phys. Rev. D **84**, 115006 (2011), [arXiv:1104.4127].

[14] See the Section on "W' searches" in this *Review*.

[15] Z. Demiragli and A. Pomarol, "Extra dimensions" in this *Review*.

[16] H.-C. Cheng and I. Low, JHEP **09**, 051 (2003), [hep-ph/0308199].

[17] K.M. Black, R.S. Chivukula and A. Lister, "Dynamical electroweak symmetry breaking" in this *Review*.

[18] M. Bando, T. Kugo and K. Yamawaki, Phys. Rept. **164**, 217 (1988).

[19] J. Y. Araz *et al.*, JHEP **02**, 092 (2018), [arXiv:1711.06302].

[20] S. Schael *et al.* (ALEPH, DELPHI, L3, OPAL, LEP Electroweak), Phys. Rept. **532**, 119 (2013), [arXiv:1302.3415].

[21] G. Aad *et al.* (ATLAS), Phys. Lett. B **796**, 68 (2019), [arXiv:1903.06248].

[22] A. M. Sirunyan *et al.* (CMS), JHEP **07**, 208 (2021), [arXiv:2103.02708].

[23] G. Paz and J. Roy, Phys. Rev. D **97**, 075025 (2018), [arXiv:1711.02655].

[24] E. Accomando *et al.*, JHEP **10**, 153 (2013), [arXiv:1304.6700].

[25] A. Abulencia *et al.* (CDF), Phys. Rev. Lett. **95**, 252001 (2005), [hep-ex/0507104].

[26] A. Abulencia *et al.* (CDF), Phys. Rev. Lett. **96**, 211801 (2006), [hep-ex/0602045].

[27] F. Petriello and S. Quackenbush, Phys. Rev. D **77**, 115004 (2008), [arXiv:0801.4389].

[28] E. Accomando *et al.*, JHEP **01**, 127 (2016), [arXiv:1503.02672].

[29] P. Osland *et al.*, Phys. Rev. D **79**, 115021 (2009), [arXiv:0904.4857].

[30] A. M. Sirunyan *et al.* (CMS), Phys. Rev. Lett. **124**, 13, 131802 (2020), [arXiv:1912.04776].

[31] A. Hayrapetyan *et al.* (CMS), JHEP **12**, 070 (2023), [arXiv:2309.16003].

[32] R. Aaij *et al.* (LHCb), JHEP **10**, 156 (2020), [arXiv:2007.03923].

[33] M. Aaboud *et al.* (ATLAS), JHEP **01**, 055 (2018), [arXiv:1709.07242].

[34] G. Aad *et al.* (ATLAS), Phys. Rev. Lett. **125**, 051801 (2020), [arXiv:2002.12223].

[35] A. Tumasyan *et al.* (CMS), JHEP **07**, 073 (2023), [arXiv:2208.02717].

[36] CMS Collab., PAS-EXO-24-012 (2025).

[37] G. Aad *et al.* (ATLAS), JHEP **23**, 082 (2020), [arXiv:2307.08567].

[38] A. Tumasyan *et al.* (CMS), JHEP **05**, 227 (2023), [arXiv:2205.06709].

[39] A. Hayrapetyan *et al.* (CMS) (2025), [arXiv:2508.07512].

[40] A. M. Sirunyan *et al.* (CMS), Phys. Rev. Lett. **123**, 231803 (2019), [arXiv:1905.10331].

[41] G. Aad *et al.* (ATLAS), JHEP **01**, 099 (2025), [arXiv:2408.00049].

[42] CMS Collab., PAS-EXO-24-007 (2024).

[43] CMS Collab., PAS-EXO-23-004 (2025).

[44] G. Aad *et al.* (ATLAS) (2025), [arXiv:2509.01219].

[45] B. A. Dobrescu and F. Yu, Phys. Rev. D **88**, 3, 035021 (2013), [arXiv:1306.2629].

[46] CMS Collab., `https://twiki.cern.ch/twiki/bin/view/CMSPublic/SummaryPlotsEXO13TeV#Dijet_Summary_Plot`.

[47] ATLAS Collab., https://atlas.web.cern.ch/ATL-PHYS-PUB-2024-010.

[48] B. A. Dobrescu and F. Yu, Phys. Rev. D **109**, 3, 035004 (2024), [arXiv:2112.05392].

[49] G. Aad *et al.* (ATLAS), JHEP **03**, 145 (2020), [arXiv:1910.08447].

[50] A. Tumasyan *et al.* (CMS), Phys. Rev. D **108**, 012009 (2023), [arXiv:2205.01835].

[51] G. Aad *et al.* (ATLAS), Phys. Rev. D **105**, 012001 (2022), [arXiv:2108.09059].

[52] G. Aad *et al.* (ATLAS), Phys. Rev. D **110**, 3, 032002 (2024), [arXiv:2403.08547].

[53] A. Hayrapetyan *et al.* (CMS), JHEP **10**, 043 (2023), [arXiv:2307.08708].

[54] G. Aad *et al.* (ATLAS), JHEP **06**, 016 (2023), [arXiv:2207.00230].

[55] G. Aad *et al.* (ATLAS), Phys. Rev. D **102**, 112008 (2020), [arXiv:2007.05293].

[56] A. M. Sirunyan *et al.* (CMS), Eur. Phys. J. C **81**, 688 (2021), [arXiv:2102.08198].

[57] A. Tumasyan *et al.* (CMS), Phys. Lett. B **844**, 137813 (2023), [arXiv:2210.00043].

[58] A. M. Sirunyan *et al.* (CMS), JHEP **01**, 051 (2019), [arXiv:1808.01365].

[59] D. Pappadopulo *et al.*, JHEP **09**, 060 (2014), [arXiv:1402.4431].

[60] G. Aad *et al.* (ATLAS), JHEP **07**, 090 (2023), [arXiv:2301.09342].

[61] A. M. Sirunyan *et al.* (CMS), Phys. Lett. B **792**, 345 (2019), [arXiv:1808.03684].

[62] CMS Collab., CMS PAS SMP-19-007, Aug. 2023.

[63] G. Aad *et al.* (ATLAS), JHEP **03**, 041 (2022), [arXiv:2110.13673].

[64] G. Aad *et al.* (ATLAS), JHEP **09**, 091 (2019), [arXiv:1906.08589].

[65] G. Aad *et al.* (ATLAS), Eur. Phys. J. C **80**, 1165 (2020), [arXiv:2004.14636].

[66] A. Tumasyan *et al.* (CMS), Phys. Rev. D **105**, 032008 (2022), [arXiv:2109.06055].

[67] ATLAS Collab., ATLAS-CONF-2022-066, Nov. 2022.

[68] H.-J. He *et al.*, Phys. Rev. D **78**, 031701 (2008), [arXiv:0708.2588].

[69] V. M. Abazov *et al.* (D0), Phys. Lett. B **695**, 88 (2011), [arXiv:1008.2023].

[70] T. Aaltonen *et al.* (CDF), Phys. Rev. Lett. **106**, 121801 (2011), [arXiv:1101.4578].

[71] A. Abulencia *et al.* (CDF), Phys. Rev. Lett. **96**, 211802 (2006), [hep-ex/0603006].

[72] D. Acosta *et al.* (CDF), Phys. Rev. Lett. **95**, 131801 (2005), [hep-ex/0506034].

[73] T. Aaltonen *et al.* (CDF), Phys. Rev. D **84**, 072004 (2011), [arXiv:1107.5063].

[74] T. Aaltonen *et al.* (CDF), Phys. Rev. D **79**, 112002 (2009), [arXiv:0812.4036].

[75] T. Aaltonen *et al.* (CDF), Phys. Rev. Lett. **104**, 241801 (2010), [arXiv:1004.4946].

[76] V. D. Barger *et al.*, Phys. Rev. D **57**, 391 (1998), [hep-ph/9707412].

[77] R. Harnik, J. Kopp and P. A. N. Machado, JCAP **1207**, 026 (2012), [arXiv:1202.6073].

[78] J. P. Lees *et al.* (BaBar), Phys. Rev. Lett. **113**, 201801 (2014), [arXiv:1406.2980].

[79] E. Rojas and J. Erler, JHEP **10**, 063 (2015), [arXiv:1505.03208].

[80] J. Kang and P. Langacker, Phys. Rev. D **71**, 035014 (2005), [hep-ph/0412190].

[81] Y. Li, F. Petriello and S. Quackenbush, Phys. Rev. D **80**, 055018 (2009), [arXiv:0906.4132].

Int. J. Mod. Phys. A 2026.41. Downloaded from www.worldscientific.com
by UNIVERSITY OF CALIFORNIA @ BERKELEY on 09/16/26. Re-use and distribution is strictly not permitted, except for Open Access articles.

87. Supersymmetry, Part I (Theory)

Revised August 2025 by B.C. Allanach (DAMTP, Cambridge U.) and H.E. Haber (UC Santa Cruz).

87.1 Introduction . . . 1086
87.2 Structure of the MSSM . . . 1086
87.2.1 R-parity and the lightest supersymmetric particle . . . 1087
87.2.2 The goldstino and gravitino . . . 1088
87.2.3 Hidden sectors and the structure of SUSY breaking . . . 1088
87.2.4 SUSY and extra dimensions . . . 1088
87.2.5 Split-SUSY . . . 1088
87.3 Parameters of the MSSM . . . 1089
87.3.1 The SUSY-conserving parameters . . . 1089
87.3.2 The SUSY-breaking parameters . . . 1089
87.3.3 MSSM-124 . . . 1090
87.4 The supersymmetric-particle spectrum . . . 1090
87.4.1 The charginos and neutralinos . . . 1090
87.4.2 The squarks and sleptons . . . 1091
87.5 The supersymmetric Higgs sector . . . 1091
87.5.1 The tree-level Higgs sector . . . 1091
87.5.2 The radiatively-corrected Higgs sector . . . 1092
87.5.3 The hMSSM approximation . . . 1093
87.5.4 The Higgs alignment limit and SUSY . . . 1093
87.6 Restricting the MSSM parameter freedom . . . 1094
87.6.1 Gaugino mass relations . . . 1094
87.6.2 Constrained versions of the MSSM: mSUGRA, CMSSM, etc. . . . 1095
87.6.3 Gauge-mediated SUSY breaking . . . 1095
87.6.4 The phenomenological MSSM . . . 1096
87.6.5 Simplified models . . . 1096
87.7 Experimental data confronts the MSSM . . . 1096
87.7.1 Naturalness constraints and the little hierarchy . . . 1097
87.7.2 Indirect constraints on supersymmetric models . . . 1098
87.7.3 Standard Model Effective Field Theory and SUSY . . . 1098
87.8 Massive neutrinos in weak-scale SUSY . . . 1099
87.8.1 The supersymmetric seesaw . . . 1099
87.8.2 R-parity-violating SUSY . . . 1099
87.9 Extensions beyond the MSSM . . . 1100
87.9.1 The origin of the μ parameter . . . 1100
87.9.2 Dirac gauginos . . . 1100

87.1 Introduction

Supersymmetry (SUSY) is a generalization of the space-time symmetries of quantum field theory that transforms fermions into bosons and vice versa [1]. The existence of such a non-trivial extension of the Poincaré symmetry of ordinary quantum field theory was initially surprising, and its form is highly constrained by theoretical principles [2]. For example, supersymmetry has been used as a theoretical laboratory for studying nonperturbative aspects of strongly-coupled quantum field theories (e.g., see Refs. [3, 4]).

SUSY also provides a framework for the unification of particle physics and gravity [5–7] at the Planck energy scale, $M_{\rm P} \sim 10^{19}$ GeV, where the gravitational interactions become comparable in strength to the gauge interactions. Moreover, supersymmetry can stabilize the hierarchy between the energy scale that characterizes electroweak symmetry breaking, $M_{\rm EW} \sim 100$ GeV, and the Planck scale [8–10] against large radiative corrections. The stability of this large gauge hierarchy with respect to radiative quantum corrections is not possible to maintain in the Standard Model (SM) without an unnatural fine-tuning of the parameters of the fundamental theory at the Planck scale. In contrast, in a supersymmetric extension of the SM, it is possible to maintain the gauge hierarchy while providing a natural framework for elementary scalar fields.

If supersymmetry were an exact symmetry of nature, then particles and their superpartners, which differ in spin by half a unit, would be degenerate in mass. Since superpartners have not (yet) been observed, supersymmetry must be a broken symmetry. Nevertheless, the stability of the gauge hierarchy can still be maintained if the SUSY breaking is soft [11,12], and the corresponding SUSY-breaking mass parameters are no larger than a few TeV. Whether this is still plausible in light of recent SUSY searches at the LHC (see Sec. 88) will be discussed in Sec. 87.7.

In particular, soft-SUSY-breaking terms of the Lagrangian involve combinations of fields with total mass dimension of three or less, with some restrictions on the dimension-three terms as elucidated in Ref. [11]. The impact of the soft terms becomes negligible at energy scales much larger than the size of the SUSY-breaking masses. Thus, a theory of weak-scale supersymmetry, where the effective scale of supersymmetry breaking is tied to the scale of electroweak symmetry breaking, provides a natural framework for the origin and stability of the gauge hierarchy [8–10].

At present, there is no unambiguous experimental evidence for the breakdown of the SM at or below the TeV scale. The expectations for new TeV-scale physics beyond the SM are based primarily on three theoretical arguments. First, in a theory with an elementary scalar field of mass m and interaction strength λ (*e.g.*, a quartic scalar self-coupling, the square of a gauge coupling or the square of a Yukawa coupling), the stability with respect to quantum corrections requires the existence of an energy cutoff roughly of order $(16\pi^2/\lambda)^{1/2}m$, beyond which new physics must enter [13]. A significantly larger energy cutoff would require an unnatural fine-tuning of parameters that govern the effective low-energy theory. Applying this argument to the SM leads to an expectation of new physics at the TeV scale [10].

Second, the unification of the three SM gauge couplings at a very high energy close to the Planck scale is possible if new physics beyond the SM (which modifies the running of the gauge couplings above the electroweak scale) is present. The minimal supersymmetric extension of the SM, where superpartner masses lie below a few TeV, provides an example of successful gauge coupling unification [14, 15].

Third, the existence of dark matter, which makes up approximately one quarter of the energy density of the universe, cannot be explained within the SM of particle physics [16]. Remarkably, a stable weakly-interacting massive particle (WIMP) whose mass and interaction rate are governed by new physics associated with the TeV-scale can be consistent with the observed density of dark matter (this is the so-called WIMP miracle, which is reviewed in Ref. [17]). The lightest supersymmetric particle (LSP), if stable, is a promising (although not the unique) candidate for dark matter [18–22]. Further aspects of dark matter can be found in Sec. 27.

87.2 Structure of the MSSM

The minimal supersymmetric extension of the SM (MSSM) consists of the fields of the two-Higgs-doublet extension of the SM and the corresponding superpartner fields [23–27]. A particle and its superpartner together form a supermultiplet. The corresponding field content of the supermultiplets of the MSSM and their gauge quantum numbers are shown in Table 87.1. The electric charge $Q = T_3 + \frac{1}{2}Y$ is determined in terms of the third component of the weak isospin (T_3) and the U(1) weak hypercharge (Y).

The gauge supermultiplets consist of the gluons and their gluino fermionic superpartners and the SU(2)×U(1) gauge bosons and their gaugino fermionic superpartners. The matter supermultiplets consist of three generations of left-handed quarks and leptons and their scalar superpartners (squarks and sleptons, collectively referred to as sfermions), and the corresponding antiparticles. The Higgs supermultiplets consist of two complex Higgs doublets, their higgsino fermionic superpartners, and the corresponding antiparticles. The enlarged Higgs sector of the MSSM constitutes the minimal structure needed to guarantee the cancellation of gauge anomalies [29] generated by the higgsino superpartners that can appear as internal lines in triangle diagrams with three external electroweak gauge bosons. Moreover, without a second Higgs doublet, one cannot generate mass for both "up"-type and "down"-type quarks (and charged leptons) in a way consistent with the underlying SUSY [30–32].

Int. J. Mod. Phys. A 2026.41. Downloaded from www.worldscientific.com by UNIVERSITY OF CALIFORNIA @ BERKELEY on 09/16/26. Re-use and distribution is strictly not permitted, except for Open Access articles.

Int. J. Mod. Phys. A 2026.41. Downloaded from www.worldscientific.com
by UNIVERSITY OF CALIFORNIA @ BERKELEY on 09/16/26. Re-use and distribution is strictly not permitted, except for Open Access articles.

Table 87.1: The fields of the MSSM and their representations under the SU(3)×SU(2)×U(1) gauge group are listed. For simplicity, only one generation of quarks and leptons is exhibited. For a given fermion f, we have defined $f_{L,R} \equiv P_{L,R} f$, where $P_{L,R} = \frac{1}{2}(1 \mp \gamma_5) f$, and the corresponding left-handed charge-conjugated fermion is given by $f_L^c \equiv P_L f^c = [f_R]^c$. For each lepton, quark, and Higgs supermultiplet (each denoted by a hatted upper-case letter), there is a corresponding antiparticle multiplet of charge-conjugated fermions and their associated scalar partners [28].

Field Content of the MSSM						
Super-multiplets	Super-field	Bosonic fields	Fermionic partners	SU(3)	SU(2)	U(1)
gluon/gluino	$\hat{V}_8$	g	$\widetilde{g}$	8	1	0
gauge boson/	$\hat{V}$	$W^\pm$, W^0	$\widetilde{W}^\pm$, $\widetilde{W}^0$	1	3	0
gaugino	$\hat{V}'$	B	$\widetilde{B}$	1	1	0
slepton/	$\hat{L}$	$(\widetilde{\nu}_L, \widetilde{e}_L^-)$	(ν_L, e_L^-)	1	2	-1
lepton	$\hat{E}^c$	$\widetilde{e}_R^+$	e_L^c	1	1	2
squark/	$\hat{Q}$	$(\widetilde{u}_L, \widetilde{d}_L)$	(u_L, d_L)	3	2	1/3
quark	$\hat{U}^c$	$\widetilde{u}_R^*$	u_L^c	$\bar{3}$	1	$-4/3$
	$\hat{D}^c$	$\widetilde{d}_R^*$	d_L^c	$\bar{3}$	1	2/3
Higgs boson/	$\hat{H}_d$	(H_d^0, H_d^-)	$(\widetilde{H}_d^0, \widetilde{H}_d^-)$	1	2	-1
higgsino	$\hat{H}_u$	(H_u^+, H_u^0)	$(\widetilde{H}_u^+, \widetilde{H}_u^0)$	1	2	1

In the most elegant treatment of SUSY, spacetime is extended to superspace which consists of the spacetime coordinates and new anticommuting fermionic coordinates θ and $\theta^\dagger$ [27, 33, 34]. Each supermultiplet is represented by a superfield that is a function of the superspace coordinates. The fields of a given supermultiplet (which are functions of the spacetime coordinates) are coefficients of the θ and $\theta^\dagger$ expansion of the corresponding superfield.

Vector superfields contain the gauge-boson fields and their gaugino partners. Chiral superfields contain the spin-0 and spin-1/2 fields of the matter or Higgs supermultiplets. A general supersymmetric Lagrangian is determined by three functions of the chiral superfields [6]: the superpotential, the Kähler potential, and the gauge kinetic function (which can be appropriately generalized to accommodate higher derivative terms [35]). Minimal forms for the Kähler potential and gauge kinetic function, which generate canonical kinetic energy terms for all the fields, are required for renormalizable globally supersymmetric theories. A renormalizable superpotential, which is at most cubic in the chiral superfields, yields supersymmetric Yukawa couplings and mass terms. A combination of gauge invariance and SUSY produces couplings of gaugino fields to matter (or Higgs) fields and their corresponding superpartners. The (renormalizable) MSSM Lagrangian is then constructed by including all possible supersymmetric interaction terms (of dimension four or less) that satisfy SU(3)×SU(2)×U(1) gauge invariance and B–L conservation (where B = baryon number and L = lepton number). Finally, the most general soft-supersymmetry-breaking terms consistent with these symmetries are added [11, 12, 36].

Although the MSSM is the focus of much of this review, there is some motivation for considering non-minimal supersymmetric extensions of the SM [37]. For example, extra structure is needed to generate non-zero neutrino masses as discussed in Sec. 87.8. In addition, in order to address some theoretical issues and tensions associated with the MSSM, it has been fruitful to introduce one additional singlet Higgs superfield. The resulting next-to-minimal supersymmetric extension of the Standard Model (NMSSM) [38] is briefly considered in Secs. 87.4–87.7 and 87.9.1. Finally, one is always free to add additional fields to the SM along with the corresponding superpartners, as noted in Sec. 87.9. For example, the motivation for adding a color octet chiral superfield [39, 40] to the MSSM is briefly discussed in Sec. 87.9.2. However, only certain choices for the new superfields (*e.g.*, the addition of complete SU(5) multiplets) will preserve the successful gauge coupling unification of the MSSM.

87.2.1 *R-parity and the lightest supersymmetric particle*

The (renormalizable) SM Lagrangian possesses an accidental global $B-L$ symmetry due to the fact that B and L-violating operators composed of SM fields must have dimension $d = 5$ or larger [41]. Consequently, B and L-violating effects are suppressed by $(M_{\rm EW}/M)^{d-4}$, where M is the characteristic mass scale of the physics that generates the corresponding higher-dimensional operators. Indeed, values of $M \gtrsim 10^{16}$ GeV, corresponding to the grand unification (GUT) scale or larger, may be responsible for the observed (approximate) stability of the proton and suppression of neutrino masses. Unfortunately, these results are not guaranteed in a generic supersymmetric extension of the SM. For example, it is possible to construct gauge-invariant supersymmetric dimension-four B and L-violating operators made up of fields of SM particles and their superpartners. Such operators, if simultaneously present in the theory, would typically yield a proton decay rate many orders of magnitude larger than the current experimental bound. It is for this reason that $B-L$ conservation is *imposed* on the supersymmetric Lagrangian when defining the MSSM, which is sufficient for eliminating all B and L-violating operators of dimension $d \leq 4$.

As a consequence of the $B-L$ symmetry, the MSSM possesses a multiplicative R-parity invariance, where $R = (-1)^{3(B-L)+2S}$ for a particle of spin S [42]. This implies that all the particles of the SM have even R-parity, whereas the corresponding superpartners have odd R-parity. The conservation of R-parity in scattering and decay processes has a critical impact on supersymmetric phenomenology. For example, any initial state in a scattering experiment will involve ordinary (R-even) particles. Consequently, it follows that supersymmetric particles must be produced in pairs. In general, these particles are highly unstable and decay into lighter states. Moreover, R-parity invariance also implies that the LSP is absolutely stable, and must eventually be produced at the end of a decay chain initiated by the decay of a heavy unstable supersymmetric particle. In order to be consistent with cosmological constraints, a stable LSP is almost certainly electrically and color neutral [20]. Consequently, the LSP in an R-parity-conserving theory is weakly interacting with ordinary matter, *i.e.*, it behaves like a stable heavy neutrino and will escape collider detectors without being directly observed. Thus, the canonical signature for conventional R-parity-conserving supersymmetric theories is missing (transverse) momentum, due to the escape of the LSP. Moreover, as noted in Sec. 87.1 and reviewed in Ref. [21, 22], the stability of the LSP in R-parity-conserving SUSY makes it a promising candidate for dark matter.

The possibility of relaxing the R-parity invariance of the MSSM (which would generate new B and/or L-violating interactions) will be addressed in Sec. 87.8.2. However, note that in R-parity violating (RPV) models, the LSP is no longer stable and thus would not be a viable candidate for the dark matter (unless its lifetime was significantly longer than the age of the universe). In such scenarios, one must look elsewhere to explain the origin of

Int. J. Mod. Phys. A 2026.41. Downloaded from www.worldscientific.com by UNIVERSITY OF CALIFORNIA @ BERKELEY on 09/16/26. Re-use and distribution is strictly not permitted, except for Open Access articles.

dark matter.

87.2.2 *The goldstino and gravitino*

In the MSSM, SUSY breaking is implemented by including the most general renormalizable soft-SUSY-breaking terms consistent with the SU(3)×SU(2)×U(1) gauge symmetry and R-parity invariance. These terms parameterize our ignorance of the fundamental mechanism of supersymmetry breaking. If supersymmetry breaking occurs spontaneously, then a massless Goldstone fermion called the goldstino ($\widetilde{G}_{1/2}$) must exist. The goldstino would then be the LSP, and could play an important role in supersymmetric phenomenology [43].

However, the goldstino degrees of freedom are physical only in models of spontaneously-broken global SUSY. If SUSY is a local symmetry, then the theory must incorporate gravity; the resulting theory is called supergravity [7, 44]. In models of spontaneously-broken supergravity, the goldstino is "absorbed" by the gravitino ($\widetilde{G}$), the spin-3/2 superpartner of the graviton, via the super-Higgs mechanism [45]. Consequently, the goldstino is removed from the physical spectrum and the gravitino acquires a mass (denoted by $m_{3/2}$). If $m_{3/2}$ is smaller than the mass of the lightest superpartner of the SM particles, then the gravitino is the LSP.

In processes with center-of-mass energy $E \gg m_{3/2}$, one can employ the goldstino–gravitino equivalence theorem [46], which implies that the interactions of the helicity $\pm\frac{1}{2}$ gravitino (whose properties approximate those of the goldstino) dominate those of the helicity $\pm\frac{3}{2}$ gravitino. The interactions of gravitinos with other light fields can be described by a low-energy effective Lagrangian that is determined by fundamental principles [47].

87.2.3 *Hidden sectors and the structure of SUSY breaking*

It is very difficult (perhaps impossible) to construct a realistic model of spontaneously-broken weak-scale supersymmetry where the supersymmetry breaking arises solely as a consequence of the interactions of the particles of the MSSM. A more successful scheme posits a theory with at least two distinct sectors: a visible sector consisting of the particles of the MSSM [36] and a sector where SUSY breaking is generated. It is often (but not always) assumed that particles of the hidden sector are neutral with respect to the SM gauge group. The effects of the hidden sector supersymmetry breaking are then transmitted to the MSSM by some mechanism (often involving the mediation by particles that comprise an additional messenger sector). Two theoretical scenarios that exhibit this structure are gravity-mediated and gauge-mediated SUSY breaking.

Supergravity models provide a natural mechanism for transmitting the SUSY breaking of the hidden sector to the particle spectrum of the MSSM. In models of gravity-mediated SUSY breaking, gravity is the messenger of supersymmetry breaking [48–52]. More precisely, supersymmetry breaking is mediated by effects of gravitational strength (*i.e.* suppressed by inverse powers of the Planck mass). The soft-SUSY-breaking parameters with dimensions of mass arise as model-dependent multiples of the gravitino mass $m_{3/2}$. In this scenario, $m_{3/2}$ is of order the electroweak-symmetry-breaking scale, while the gravitino couplings are roughly gravitational in strength [5, 53].[1]

Under certain theoretical assumptions that govern the structure of the Kähler potential (the so-called sequestered form introduced in Ref. [55]), SUSY breaking is due entirely to the super-conformal (super-Weyl) anomaly, which is common to all supergravity models [55]. In particular, gaugino masses are radiatively generated at one-loop, and squark and slepton squared-mass matrices are flavor-diagonal. In sequestered scenarios, sfermion squared-masses arise at two-loops, which implies that gluino and sfermion masses are of the same order of magnitude. This approach is called anomaly-mediated SUSY breaking (AMSB). Indeed, anomaly mediation is more generic than originally conceived, and provides a ubiquitous source of SUSY breaking [56]. However in the simplest formulation of AMSB as applied to the MSSM, the squared-masses of the sleptons are negative (known as the tachyonic slepton problem). It may be possible to cure this otherwise fatal flaw in non-minimal extensions of the MSSM [57]. Alternatively, one can assert that anomaly mediation is not the sole source of SUSY breaking in the sfermion sector. In non-sequestered scenarios, sfermion squared-masses can arise at tree-level, in which case squark masses would be parametrically larger than the loop-suppressed gaugino masses [58].

In gauge-mediated supersymmetry breaking, gauge forces transmit the supersymmetry breaking to the MSSM. A typical structure of such models involves a hidden sector where SUSY is broken, a messenger sector consisting of particles (messengers) with nontrivial SU(3)×SU(2)×U(1) quantum numbers, and the visible sector consisting of the fields of the MSSM [59–62]. The direct coupling of the messengers to the hidden sector generates a supersymmetry-breaking spectrum in the messenger sector. Supersymmetry breaking is then transmitted to the MSSM via the virtual exchange of the messenger fields. In models of direct gauge mediation, there is no separate hidden sector. In particular, the sector in which the SUSY breaking originates includes fields that carry nontrivial SM quantum numbers, which allows for the direct transmission of SUSY breaking to the MSSM [63].

In models of gauge-mediated SUSY breaking with a minimal Kähler potential, the gravitino is the LSP [18], as its mass can range from a few eV (in the case of low SUSY breaking scales) up to a few GeV (in the case of high SUSY breaking scales). In particular, the gravitino is a potential dark matter candidate (for a review and guide to the literature, see Ref. [22]). The couplings of the helicity $\pm\frac{1}{2}$ components of $\widetilde{G}$ to the particles of the MSSM (which approximate those of the goldstino as previously noted in Sec. 87.2.2) are significantly stronger than gravitational strength and amenable to experimental collider analyses.

The mass ranges of the gravitino in either gravity-mediated or gauge-mediated SUSY breaking are further constrained by cosmological considerations [64]. In particular, there is a danger of overabundance of gravitinos as the dark matter or modifications to the successful predictions of light element abundances if $\widetilde{G}$ decays before nucleosynthesis. Avoiding these cosmological gravitino problems imposes strong constraints on gravity-mediated and gauge-mediated SUSY breaking models.

The concept of a hidden sector is more general than SUSY. Hidden valley models [65] posit the existence of a hidden sector of new particles and interactions that are very weakly coupled to particles of the SM. The impact of a hidden valley on supersymmetric phenomenology at colliders can be significant if the LSP lies in the hidden sector [66].

87.2.4 *SUSY and extra dimensions*

Approaches to SUSY breaking have also been developed in the context of theories in which the number of spatial dimensions is greater than three. In particular, a number of SUSY-breaking mechanisms have been proposed that are inherently extra-dimensional [67]. The size of the extra dimensions can be significantly larger than $M_{\rm P}^{-1}$; in some cases of order $(\text{TeV})^{-1}$ or even larger (*e.g.*, see Sec. 84 and Ref. [68]).

For example, in one approach the fields of the MSSM live on some brane (a lower-dimensional manifold embedded in a higher-dimensional spacetime), while the sector of the theory that breaks SUSY lives on a second spatially-separated brane. Two examples of this approach are AMSB [55] and gaugino-mediated SUSY breaking [69]. In both cases, SUSY breaking is transmitted through fields that live in the bulk (the higher-dimensional space between the two branes). This setup has some features in common with both gravity-mediated and gauge-mediated SUSY breaking (*e.g.*, hidden and visible sectors and messengers).

Since a higher dimensional theory must be compactified to four spacetime dimensions, one can also generate a source of SUSY breaking by employing boundary conditions on the compactified space that distinguish between fermions and bosons. This is the so-called Scherk-Schwarz mechanism [70]. The phenomenology of such models can be strikingly different from that of the usual MSSM [71].

87.2.5 *Split-SUSY*

If SUSY is not connected with the origin of the electroweak scale, it may still be possible that some remnant of the superpar-

[1] However, such a gravitino typically plays no direct role in supersymmetric phenomenology at colliders (except perhaps indirectly in the case where the gravitino is the LSP [54]).

Int. J. Mod. Phys. A 2026.41. Downloaded from www.worldscientific.com
by UNIVERSITY OF CALIFORNIA @ BERKELEY on 09/16/26. Re-use and distribution is strictly not permitted, except for Open Access articles.

ticle spectrum survives down to the TeV-scale or below. This is the idea of split-SUSY [72,73], in which scalar superpartners of the quarks and leptons are significantly heavier than 1 TeV, whereas the fermionic superpartners of the gauge and Higgs bosons have masses on the order of 1 TeV or below. With the exception of a single light neutral scalar whose properties are practically indistinguishable from those of the SM Higgs boson, all other Higgs bosons are also assumed to be very heavy. Among the supersymmetric particles, only the fermionic superpartners may be kinematically accessible at the LHC.

In models of split SUSY, the top squark masses cannot be arbitrarily large, as these parameters enter in the radiative corrections to the mass of the observed Higgs boson [74–76]. In the MSSM, a Higgs boson mass of 125 GeV (see Sec. 11) implies an upper bound on the top squark mass scale in the range of 10 to 10^8 TeV [77], depending on the value of the ratio of the two neutral Higgs field vacuum expectation values (VEVs), although this mass range can be somewhat extended by varying other relevant MSSM parameters. In some approaches, gaugino masses are one-loop suppressed relative to the sfermion masses, corresponding to the so-called mini-split SUSY spectrum [75,78]. The higgsino mass scale may or may not be likewise suppressed depending on the details of the model [79].

The SUSY breaking required to produce such a split-SUSY spectrum would destabilize the gauge hierarchy, and thus would not provide an explanation for the scale of electroweak symmetry breaking. Nevertheless, models of split-SUSY can account for the dark matter (which is assumed to be the LSP gaugino or higgsino) and gauge coupling unification, thereby preserving two of the desirable features of weak-scale SUSY. Finally, as a consequence of the very large squark and slepton masses, neutral flavor changing and CP-violating effects, which can be problematic in models with TeV-scale SUSY-breaking masses, are sufficiently reduced to avoid conflict with experimental observations.

87.3 Parameters of the MSSM

The parameters of the MSSM are conveniently described by considering separately the supersymmetry-conserving and the supersymmetry-breaking sectors. A careful discussion of the conventions used here in defining the tree-level MSSM parameters can be found in Refs. [27, 80, 81]. For simplicity, consider first the case of one generation of quarks, leptons, and their scalar superpartners.

87.3.1 *The SUSY-conserving parameters*

The parameters of the supersymmetry-conserving sector consist of: (i) gauge couplings, g_s, g, and g', corresponding to the SM gauge group SU(3)×SU(2)×U(1) respectively; (ii) a supersymmetry-conserving higgsino mass parameter μ; and (iii) Higgs-fermion Yukawa couplings, y_u, y_d, and y_e, of one generation of left- and right-handed quarks and leptons, and their superpartners to the Higgs bosons and higgsinos. Because there is no right-handed neutrino/sneutrino in the MSSM as defined here, a Yukawa coupling y_ν is not included. The complex μ parameter and Yukawa couplings enter via the most general renormalizable R-parity-conserving superpotential,

$$W_{\rm MSSM} = y_d \hat{H}_d \hat{Q} \hat{D}^c - y_u \hat{H}_u \hat{Q} \hat{U}^c + y_e \hat{H}_d \hat{L} \hat{E}^c + \mu \hat{H}_u \hat{H}_d \,, \quad (87.1)$$

where the superfields are defined in Table 1 and the gauge group indices are suppressed. More explicitly, the so-called "μ-term" can be written out as $\mu\epsilon^{mn}(\hat{H}_u)_m(\hat{H}_d)_n$ with an implicit sum over repeated indices, where ϵ^{mn} is used to tie together the SU(2) weak isospin indices $m, n \in \{1, 2\}$ in a gauge-invariant way (where $\epsilon^{12} = -\epsilon^{21} = 1$ and $\epsilon^{11} = \epsilon^{22} = 0$). Likewise, the term $\hat{H}_u\hat{Q}\hat{U}^c$ can be written out as $\epsilon^{mn}(\hat{H}_u)_m\hat{Q}_{in}(\hat{U}^c)^i$, where there is an implicit sum over the SU(3) color index, $i \in \{1, 2, 3\}$. Finally, $\hat{H}_d\hat{Q}\hat{D}^c$ can be written out as $\epsilon^{mn}(\hat{H}_d)_m\hat{Q}_{in}(\hat{D}^c)^i$, with an analogous expression for $\hat{H}_d\hat{L}\hat{E}^c$. One can easily generalize Eq. (87.1) to a three generation model where y_u, y_d, and y_e are 3×3 matrices with the corresponding family indices suppressed.

87.3.2 *The SUSY-breaking parameters*

The supersymmetry-breaking sector contains the following sets of parameters: (i) three complex gaugino Majorana mass parameters, M_3, M_2, and M_1, associated with the SU(3), SU(2), and U(1) subgroups of the SM; (ii) five sfermion squared-mass parameters, $M^2_{\widetilde{Q}}$, $M^2_{\widetilde{U}}$, $M^2_{\widetilde{D}}$, $M^2_{\widetilde{L}}$, and $M^2_{\widetilde{E}}$, corresponding to the five electroweak gauge multiplets, *i.e.*, superpartners of the left-handed fields $(u, d)_L$, u^c_L, d^c_L, $(\nu, e^-)_L$, and e^c_L, where the superscript c indicates a charge-conjugated fermion field [28]; and (iii) three Higgs-squark-squark and Higgs-slepton-slepton trilinear interaction terms, with complex coefficients $T_U \equiv y_u A_U$, $T_D \equiv y_d A_D$, and $T_E \equiv y_e A_E$ (which define the "A-parameters"), following the notation employed in Ref. [81]. It is conventional to separate out the factors of the Yukawa couplings in defining the A-parameters [5,27] (originally motivated by a simple class of gravity-mediated SUSY-breaking models [5]). If the A-parameters are parametrically of the same order (or smaller) relative to other SUSY-breaking mass parameters, then in most cases only the third generation A-parameters will be phenomenologically relevant.

Finally, we have (iv) two real squared-mass parameters, $m^2_{H_d}$ and $m^2_{H_u}$ (also called m^2_1 and m^2_2, respectively, in the literature), and one complex squared-mass parameter, $m^2_{12} \equiv \mu B$ (the latter defines the "B-parameter"),[2] which appear in the MSSM tree-level scalar Higgs potential [27, 32],

$$\begin{aligned} V = {} & (m^2_{H_d} + |\mu|^2) H^\dagger_d H_d + (m^2_{H_u} + |\mu|^2) H^\dagger_u H_u \\ & + (m^2_{12} H_u H_d + \text{h.c.}) \\ & + \frac{1}{8}(g^2 + g'^2)(H^\dagger_d H_d - H^\dagger_u H_u)^2 + \frac{1}{2} g^2 |H^\dagger_d H_u|^2 \,, \end{aligned} \quad (87.2)$$

where the SU(2)-invariant combination of the complex doublet scalar fields H_u and H_d that appears in Eq. (87.2) is given by $H_u H_d \equiv \epsilon^{mn}(H_u)_m(H_d)_n = H^+_u H^-_d - H^0_u H^0_d$. Note that the quartic Higgs couplings are related to the gauge couplings g and g' as a consequence of SUSY. The breaking of the SU(2)×U(1) electroweak symmetry group to $\mathrm{U}(1)_{\rm EM}$ is only possible after incorporating the SUSY-breaking Higgs squared-mass parameters $m^2_{H_d}$, $m^2_{H_u}$ (which can be negative) and m^2_{12}. After minimizing the Higgs scalar potential, these three squared-mass parameters can be re-expressed in terms of the two Higgs VEVs, $\langle H^0_d \rangle \equiv v_d/\sqrt{2}$ and $\langle H^0_u \rangle \equiv v_u/\sqrt{2}$, and the CP-odd Higgs mass m_A [cf. Eqs. (87.4) and (87.5) below]. One is always free to rephase the Higgs doublet fields such that v_d and v_u (also called v_1 and v_2, respectively, in the literature) are both real and positive.

The quantity, $v^2 \equiv v^2_d + v^2_u = 4m^2_W/g^2 = (2G^2_F)^{-1/2} \simeq (246\ \text{GeV})^2$, is fixed by the Fermi constant, G_F, whereas the ratio

$$\tan\beta = v_u/v_d \quad (87.3)$$

is a free parameter such that $0 < \beta < \pi/2$. By employing the tree-level conditions resulting from the minimization of the scalar potential, one can eliminate the diagonal and off-diagonal Higgs squared-masses in favor of $m^2_Z = \frac{1}{4}(g^2 + g'^2)v^2$, the CP-odd Higgs mass m_A and the parameter $\tan\beta$,

$$\sin 2\beta = \frac{2m^2_{12}}{m^2_{H_d} + m^2_{H_u} + 2|\mu|^2} = \frac{2m^2_{12}}{m^2_A} \,, \quad (87.4)$$

$$\frac{1}{2} m^2_Z = -|\mu|^2 + \frac{m^2_{H_d} - m^2_{H_u} \tan^2\beta}{\tan^2\beta - 1} \,. \quad (87.5)$$

One must also guard against the existence of charge and/or color breaking global minima due to non-zero VEVs for the squark and charged slepton fields. This possibility can be avoided if the A-parameters are not unduly large [49,82,83]. Additional constraints must also be respected to avoid the possibility of directions in scalar field space in which the full tree-level scalar potential can become unbounded from below [83]. A computer program has been developed to calculate vacuum stability bounds in general

[2] Again, motivated by a simple class of gravity-mediated SUSY-breaking models, it is conventional to separate out the factor of μ in defining the B-parameter [5, 27]. In more general SUSY-breaking scenarios, it is possible to generate $m^2_{12} \neq 0$ even when $\mu = 0$.

Int. J. Mod. Phys. A 2026.41. Downloaded from www.worldscientific.com by UNIVERSITY OF CALIFORNIA @ BERKELEY on 09/16/26. Re-use and distribution is strictly not permitted, except for Open Access articles.

models at the one-loop level [84], and has been applied to the MSSM in Ref. [85].

Note that SUSY-breaking mass terms for the fermionic superpartners of the scalar fields and non-holomorphic trilinear scalar interactions (*i.e.*, interactions that mix scalar fields and their complex conjugates) have not been included above in the soft-SUSY-breaking sector. These terms can potentially destabilize the gauge hierarchy [11] in models with a gauge-singlet superfield. The latter is not present in the MSSM; hence as noted in Ref. [12], these so-called non-standard soft-SUSY-breaking terms are benign. The phenomenological impact of non-holomorphic soft SUSY-breaking terms has been reconsidered in Refs. [86–88]. However, in the most common approaches to constructing a fundamental theory of SUSY-breaking, the coefficients of these terms (which have dimensions of mass) are significantly suppressed compared to the TeV-scale [89]. Consequently, we follow the usual approach in the literature and omit these terms from further consideration.

87.3.3 *MSSM-124*

The total number of independent physical parameters that define the MSSM (in its most general form) is quite large, primarily due to the soft-supersymmetry-breaking sector. In particular, in the case of three generations of quarks, leptons, and their superpartners, $M^2_{\underset{\sim}{Q}}$, $M^2_{\underset{\sim}{U}}$, $M^2_{\underset{\sim}{D}}$, $M^2_{\underset{\sim}{L}}$, and $M^2_{\underset{\sim}{E}}$ are hermitian 3×3 matrices, and A_U, A_D, and A_E are complex 3×3 matrices. In addition, M_1, M_2, M_3, B, and μ are in general complex parameters. Finally, as in the SM, the Higgs-fermion Yukawa couplings, y_f ($f=u$, d, and e), are complex 3×3 matrices that are related to the quark and lepton mass matrices via: $M_f = y_f v_f/\sqrt{2}$, where $v_e = v_d$ [with v_u and v_d as defined above Eq. (87.3)].

However, not all these parameters are physical. Some of the MSSM parameters can be eliminated by expressing interaction eigenstates in terms of the mass eigenstates, with an appropriate redefinition of the MSSM fields to remove unphysical degrees of freedom. The analysis of Ref. [90] shows that the MSSM possesses 124 independent real degrees of freedom. Of these, 18 correspond to SM parameters (including the QCD vacuum angle $\theta_{\rm QCD}$), one corresponds to a Higgs sector parameter (the analogue of the SM Higgs mass), and 105 are genuinely new parameters of the model. The latter include: five real parameters and three CP-violating phases in the gaugino/higgsino sector, 21 squark and slepton (sfermion) masses, 36 real mixing angles to define the sfermion mass eigenstates, and 40 CP-violating phases that can appear in sfermion interactions. The most general parameterization of the R-parity-conserving MSSM (without additional theoretical assumptions) will be denoted henceforth as MSSM-124 [91].

87.4 The supersymmetric-particle spectrum

The supersymmetric particles (sparticles) differ in spin by half a unit from their SM partners. The superpartners of the gauge and Higgs bosons are fermions, whose names are obtained by appending "ino" to the end of the corresponding SM particle name. The gluino is the color-octet Majorana fermion partner of the gluon with mass $M_{\underset{\sim}{g}} = |M_3|$. The superpartners of the electroweak gauge and Higgs bosons (the gauginos and higgsinos) can mix due to SU(2)×U(1) breaking effects. As a result, the physical states of definite mass are parameter-dependent linear combinations of the charged or neutral gauginos and higgsinos, called charginos and neutralinos, respectively (sometimes collectively called electroweakinos). The neutralinos are Majorana fermions, which can lead to some distinctive phenomenological signatures [92,93]. The superpartners of the quarks and leptons are spin-zero bosons, with an "s" appended to the beginning of the corresponding SM particle name: the squarks, charged sleptons, and sneutrinos, respectively. A complete set of Feynman rules for the sparticles of the MSSM can be found in Ref. [94]. The MSSM Feynman rules are also implicitly contained in several amplitude generation and Feynman diagram software packages (*e.g.*, see Refs. [95–97]).

It should be noted that all mass formulae quoted below in this Section are tree-level results. Radiative loop corrections will modify these results and must be included in any precision study of supersymmetric phenomenology [98]. Beyond tree level, the definition of the supersymmetric parameters becomes convention-dependent. For example, one can define physical couplings or running couplings, which differ beyond the tree level. This provides a challenge to any effort that attempts to extract supersymmetric parameters from data. The SUSY Les Houches Accord (SLHA) [81,99] has been adopted, which establishes a set of conventions for specifying generic file structures for supersymmetric model specifications and input parameters, supersymmetric mass and coupling spectra, and decay tables. These provide a universal interface between spectrum calculation programs, decay packages, and high energy physics event generators.

87.4.1 *The charginos and neutralinos*

The mixing of the charged gauginos ($\widetilde{W}^\pm$) and charged higgsinos ($\widetilde{H}_u^+$ and $\widetilde{H}_d^-$) is described (at tree-level) by a 2×2 complex mass matrix [100,101],

$$M_C \equiv \begin{pmatrix} M_2 & \frac{1}{\sqrt{2}}gv_u \\ \frac{1}{\sqrt{2}}gv_d & \mu \end{pmatrix}. \tag{87.6}$$

To determine the physical chargino states and their masses, one must perform a singular value decomposition [102] of the complex matrix M_C [27,103]:

$$U^* M_C V^{-1} = \mathrm{diag}(M_{\tilde{\chi}_1^+}\,,\, M_{\tilde{\chi}_2^+})\,, \tag{87.7}$$

where U and V are unitary matrices, and the right-hand side of Eq. (87.7) is the diagonal matrix of (real non-negative) chargino masses. Explicit formulae for the singular value decomposition of M_C can be found in Ref. [104]. The physical chargino states are denoted by $\tilde{\chi}_1^\pm$ and $\tilde{\chi}_2^\pm$. These are linear combinations of the charged gaugino and higgsino states determined by the matrix elements of U and V [100,101] The chargino masses correspond to the singular values [102] of M_C, *i.e.*, the positive square roots of the eigenvalues of $M_C^\dagger M_C$:

$$\begin{aligned} M^2_{\tilde{\chi}_1^+,\tilde{\chi}_2^+} = \frac{1}{2}\Big\{ &|\mu|^2 + |M_2|^2 + 2m_W^2 \\ &\mp \sqrt{\left(|\mu|^2 + |M_2|^2 + 2m_W^2\right)^2 - 4|\mu M_2 - m_W^2 \sin 2\beta|^2}\,\Big\}, \end{aligned} \tag{87.8}$$

in a convention where v_u and v_d are real and positive, and where the states are ordered such that $M_{\tilde{\chi}_1^+} \le M_{\tilde{\chi}_2^+}$. The relative phase of μ^* and M_2 is physical and potentially observable [105].

The mixing of the neutral gauginos ($\widetilde{B}$ and $\widetilde{W}^0$) and neutral higgsinos ($\widetilde{H}_d^0$ and $\widetilde{H}_u^0$) is described (at tree-level) by a 4×4 complex symmetric mass matrix [100,101],

$$M_N \equiv \begin{pmatrix} M_1 & 0 & -\frac{1}{2}g'v_d & \frac{1}{2}g'v_u \\ 0 & M_2 & \frac{1}{2}gv_d & -\frac{1}{2}gv_u \\ -\frac{1}{2}g'v_d & \frac{1}{2}gv_d & 0 & -\mu \\ \frac{1}{2}g'v_u & -\frac{1}{2}gv_u & -\mu & 0 \end{pmatrix}. \tag{87.9}$$

To determine the physical neutralino states and their masses, one must perform an Autonne-Takagi factorization [102,106] (also called Takagi diagonalization in Refs. [27,103,107]) of the complex symmetric matrix M_N:

$$W^T M_N W = \mathrm{diag}(M_{\tilde{\chi}_1^0}\,,\, M_{\tilde{\chi}_2^0}\,,\, M_{\tilde{\chi}_3^0}\,,\, M_{\tilde{\chi}_4^0})\,, \tag{87.10}$$

where W is a unitary matrix (which is called N^{-1} in Refs. [23,32]) and the right-hand side of Eq. (87.10) is the diagonal matrix of (real non-negative) neutralino masses. The physical neutralino states are denoted by $\widetilde{\chi}_i^0$ (for $i=1,\ldots,4$), where the states are ordered such that $M_{\tilde{\chi}_1^0} \le M_{\tilde{\chi}_2^0} \le M_{\tilde{\chi}_3^0} \le M_{\tilde{\chi}_4^0}$. The $\widetilde{\chi}_i^0$ are the linear combinations of the neutral gaugino and higgsino states determined by the matrix elements of W. The neutralino masses correspond to the singular values of M_N, *i.e.*, the positive square roots of the eigenvalues of $M_N^\dagger M_N$. Exact formulae for these

Int. J. Mod. Phys. A 2026.41. Downloaded from www.worldscientific.com
by UNIVERSITY OF CALIFORNIA @ BERKELEY on 09/16/26. Re-use and distribution is strictly not permitted, except for Open Access articles.

masses can be found in Ref. [108]. A numerical algorithm for determining the mixing matrix W has been given in Ref. [109].

If a chargino or neutralino state approximates a particular gaugino or higgsino state, it is convenient to employ the corresponding nomenclature. Specifically, if $|M_1|$ and $|M_2|$ are small compared to m_Z and $|\mu|$, then the lightest neutralino $\widetilde{\chi}_1^0$ would be nearly a pure photino, $\widetilde{\gamma}$, the superpartner of the photon. If $|M_1|$ and m_Z are small compared to $|M_2|$ and $|\mu|$, then the lightest neutralino would be nearly a pure bino, $\widetilde{B}$, the superpartner of the weak hypercharge gauge boson. If $|M_2|$ and m_Z are small compared to $|M_1|$ and $|\mu|$, then the lightest chargino pair and neutralino would constitute a triplet of roughly mass-degenerate pure winos, $\widetilde{W}^\pm$, and $\widetilde{W}_3^0$, the superpartners of the weak SU(2) gauge bosons. Finally, if $|\mu|$ and m_Z are small compared to $|M_1|$ and $|M_2|$, then the lightest chargino pair and neutralino would be nearly pure higgsino states, the superpartners of the Higgs bosons. Each of the above cases leads to a strikingly different phenomenology.

In the NMSSM, an additional Higgs singlet superfield is added to the MSSM. This superfield comprises two real Higgs scalar degrees of freedom and an associated neutral higgsino degree of freedom. Consequently, there are five neutralino mass eigenstates that are obtained by a Takagi-diagonalization of the 5×5 neutralino mass matrix. In many cases, the fifth neutralino state is dominated by its SU(2)×U(1) singlet component, and thus is very weakly coupled to the SM particles and their superpartners.

87.4.2 *The squarks and sleptons*

For a given Dirac fermion f, there are two superpartners, $\widetilde{f}_L$ and $\widetilde{f}_R$, where the L and R subscripts simply identify the scalar partners that are related by SUSY to the left-handed and right-handed fermions, $f_{L,R}$, as indicated in Table 87.1. (Since right-handed neutrinos lie outside the SM, there is no corresponding $\widetilde{\nu}_R$ in the MSSM.) However, $\widetilde{f}_L$–$\widetilde{f}_R$ mixing is possible, in which case $\widetilde{f}_L$ and $\widetilde{f}_R$ are not mass eigenstates. For three generations of squarks, one must diagonalize 6×6 matrices corresponding to the basis $(\widetilde{q}_{iL}, \widetilde{q}_{iR})$, where $i = 1, 2, 3$ are the generation labels. For simplicity, only the one-generation case is illustrated in detail below.

Using the notation of the third family, the one-generation tree-level squark squared-mass matrix is given by [27, 110],

$$\mathcal{M}^2 = \begin{pmatrix} M^2_{\widetilde{Q}} + m_q^2 + L_q & m_q X_q^* \\ m_q X_q & M^2_{\widetilde{R}} + m_q^2 + R_q \end{pmatrix} , \tag{87.11}$$

where

$$X_q \equiv A_q - \mu^* (\cot\beta)^{2T_{3q}} , \tag{87.12}$$

and $T_{3q} = \frac{1}{2}$ $[-\frac{1}{2}]$ for $q = t$ $[b]$. The diagonal squared-masses are governed by soft-SUSY-breaking squared-masses $M^2_{\widetilde{Q}}$ and $M^2_{\widetilde{R}} \equiv M^2_{\widetilde{U}}$ $[M^2_{\widetilde{D}}]$ for $q = t$ $[b]$, the corresponding quark masses m_t $[m_b]$ and the electroweak correction terms:

$$\begin{aligned} L_q &\equiv (T_{3q} - e_q \sin^2\theta_W) m_Z^2 \cos 2\beta , \\ R_q &\equiv e_q \sin^2\theta_W \, m_Z^2 \cos 2\beta , \end{aligned} \tag{87.13}$$

where $e_q = \frac{2}{3}$ $[-\frac{1}{3}]$ for $q = t$ $[b]$. The off-diagonal squark squared-masses are proportional to the corresponding quark masses and depend on $\tan\beta$, the soft-SUSY-breaking A-parameters and the higgsino mass parameter μ. Assuming that the A-parameters are parametrically of the same order (or smaller) relative to other SUSY-breaking mass parameters, it then follows that the first and second generation $\widetilde{q}_L$–$\widetilde{q}_R$ mixing is smaller than that of the third generation where mixing can be enhanced by factors of m_t and $m_b \tan\beta$.

In the case of third generation $\widetilde{q}_L$–$\widetilde{q}_R$ mixing ($q = t$ or b), the top squark (also called *stop*) and bottom squark (also called *sbottom*) mass eigenstates, denoted by $\widetilde{q}_1$ and $\widetilde{q}_2$ (with $m_{\widetilde{q}_1} < m_{\widetilde{q}_2}$), are determined by diagonalizing the 2×2 matrix $\mathcal{M}^2$ given by Eq. (87.11). The corresponding squared-masses and mixing angle are given by [110]:

$$\begin{aligned} m^2_{\widetilde{q}_{1,2}} &= \frac{1}{2}\left[\mathrm{Tr}\,\mathcal{M}^2 \mp \sqrt{(\mathrm{Tr}\mathcal{M}^2)^2 - 4\det\mathcal{M}^2}\right] , \\ \sin 2\theta_{\widetilde{q}} &= \frac{2 m_q |X_q|}{m^2_{\widetilde{q}_2} - m^2_{\widetilde{q}_1}} . \end{aligned} \tag{87.14}$$

The above results also apply to the charged sleptons, with the obvious substitutions: $q \to \ell$ with $T_{3\ell} = -\frac{1}{2}$ and $e_\ell = -1$, and the replacement of the SUSY-breaking parameters: $M^2_{\widetilde{Q}} \to M^2_{\widetilde{L}}$, $M^2_{\widetilde{D}} \to M^2_{\widetilde{E}}$, and $A_q \to A_\ell$. For the neutral sleptons, $\widetilde{\nu}_R$ does not exist in the MSSM, so $\widetilde{\nu}_L$ is a mass eigenstate.

In the case of three generations, the SUSY-breaking scalar-squared masses $[M^2_{\widetilde{Q}}$, $M^2_{\widetilde{U}}$, $M^2_{\widetilde{D}}$, $M^2_{\widetilde{L}}$, and $M^2_{\widetilde{E}}]$ and the A-parameters $[A_U$, A_D, and $A_E]$ are now 3×3 matrices as noted in Sec. 87.3.3. The diagonalization of the 6×6 squark mass matrices yields $\widetilde{f}_{iL}$–$\widetilde{f}_{jR}$ mixing. In practice, since the $\widetilde{f}_L$–$\widetilde{f}_R$ mixing is appreciable only for the third generation, this additional complication can often be neglected (although see Ref. [111] for examples in which the mixing between the second and third generation squarks is relevant).

87.5 The supersymmetric Higgs sector

Consider first the Higgs sector of the MSSM [31, 32, 112, 113]. Despite the large number of possible CP-violating phases among the MSSM-124 parameters, the tree-level MSSM Higgs potential given by Eq. (87.2) is automatically CP-conserving. This follows from the fact that the only potentially complex parameter (m_{12}^2) of the MSSM Higgs potential can be chosen real and positive by rephasing the Higgs fields, in which case $\tan\beta$ is a real positive parameter. Consequently, in the tree-level approximation the physical neutral Higgs scalars are CP-eigenstates. The MSSM Higgs sector contains five physical spin-zero particles: a charged Higgs boson pair ($H^\pm$), two CP-even neutral Higgs bosons (denoted by h and H where $m_h < m_H$), and one CP-odd neutral Higgs boson (denoted by A). In principle, either h or H could be identified with the Higgs boson that was discovered at the LHC [114, 115]. Studies of the MSSM parameter space suggest [116] that it is unlikely that H is the LHC-observed Higgs boson (although this possibility is not yet completely ruled out). Henceforth, we shall identify h with the observed Higgs boson with $m_h \simeq 125$ GeV [117].

In the NMSSM [38], the scalar component of the singlet Higgs superfield adds two additional neutral states to the Higgs sector. In this model, the tree-level Higgs sector can exhibit explicit CP-violation. If CP is conserved, then the two extra neutral scalar states are CP-even and CP-odd, respectively. These states can potentially mix with the neutral Higgs states of the MSSM. If scalar states exist that are dominantly singlet, then they are weakly coupled to SM gauge bosons and fermions through their small mixing with the MSSM Higgs scalars. Consequently, it is possible that one (or both) of the singlet-dominated states is considerably lighter than the Higgs boson that was observed at the LHC.

87.5.1 *The tree-level Higgs sector*

The tree-level properties of the Higgs sector are determined by the Higgs potential given by Eq. (87.2) and the Yukawa Lagrangian discussed below. The quartic interaction terms are manifestly supersymmetric (although these are modified by SUSY-breaking effects at the loop level). In general, the quartic couplings arise from two sources: (i) the supersymmetric generalization of the scalar potential (the so-called "F-terms"), and (ii) interaction terms related by SUSY to the coupling of the scalar fields and the gauge fields, whose coefficients are proportional to the corresponding gauge couplings (the so-called "D-terms").

In the MSSM, F-term contributions to the quartic Higgs self-couplings are absent. As a result, the strengths of the MSSM quartic Higgs interactions are fixed in terms of the gauge couplings, as noted below Eq. (87.2). Consequently, all the tree-level MSSM Higgs-sector parameters depend only on two quantities: $\tan\beta$ [defined in Eq. (87.3)] and one Higgs mass usually taken to be m_A. For example, the tree-level squared mass of the charged

Int. J. Mod. Phys. A 2026.41. Downloaded from www.worldscientific.com by UNIVERSITY OF CALIFORNIA @ BERKELEY on 09/16/26. Re-use and distribution is strictly not permitted, except for Open Access articles.

Higgs boson is given by

$$m_{H^\pm}^2 = m_A^2 + m_W^2 \,, \tag{87.15}$$

where $m_A^2 = m_{H_d}^2 + m_{H_u}^2 + 2|\mu|^2$ [cf. Eq. (87.4)] and

$$H^\pm = H_d^\pm \sin\beta + H_u^\pm \cos\beta \,,\; A = \sqrt{2}\left(\mathrm{Im}\, H_d^0 \sin\beta + \mathrm{Im}\, H_u^0 \cos\beta\right) . \tag{87.16}$$

The CP-even scalar mass eigenstate fields h and H are identified by diagonalizing the 2×2 squared-mass matrix

$$\mathcal{M}^2 = \begin{pmatrix} m_A^2 \sin^2\beta + m_Z^2\cos^2\beta & -(m_A^2+m_Z^2)\sin\beta\cos\beta \\ -(m_A^2+m_Z^2)\sin\beta\cos\beta & m_A^2\cos^2\beta + m_Z^2\sin^2\beta \end{pmatrix} . \tag{87.17}$$

In particular,

$$h = -(\sqrt{2}\,\mathrm{Re}\, H_d^0 - v_d)\sin\alpha + (\sqrt{2}\,\mathrm{Re}\, H_u^0 - v_u)\cos\alpha \,, \tag{87.18}$$

$$H = (\sqrt{2}\,\mathrm{Re}\, H_d^0 - v_d)\cos\alpha + (\sqrt{2}\,\mathrm{Re}\, H_u^0 - v_u)\sin\alpha \,, \tag{87.19}$$

with corresponding tree-level squared masses,

$$m_{H,h}^2 = \frac{1}{2}\left(m_A^2 + m_Z^2 \pm \sqrt{(m_A^2+m_Z^2)^2 - 4m_Z^2 m_A^2\cos^2 2\beta}\right) , \tag{87.20}$$

and mixing angle α given by

$$\cos\alpha = \sqrt{\frac{m_A^2\sin^2\beta + m_Z^2\cos^2\beta - m_h^2}{m_H^2 - m_h^2}} \,, \tag{87.21}$$

in a convention where $|\alpha| \leq \pi/2$, where m_h^2 and m_H^2 are given by Eq. (87.20). However, because the off-diagonal elements of $\mathcal{M}^2$ are negative, it follows that $-\pi/2 \leq \alpha \leq 0$ [104]. In light of Eq. (87.20), the tree-level mass of the lighter CP-even Higgs boson is bounded [31, 32],

$$m_h \leq m_Z |\cos 2\beta| \leq m_Z \,. \tag{87.22}$$

This bound can be significantly modified when radiative corrections are included (see Sec. 87.5.2).

The tree-level Higgs couplings to gauge bosons and the Higgs boson self-couplings are governed by the electroweak gauge couplings and the parameter $\cos(\beta-\alpha)$. Explicitly,

$$\cos(\beta-\alpha) = \frac{m_Z^2 \sin 2\beta \cos 2\beta}{\sqrt{(m_H^2 - m_h^2)(m_H^2 - m_Z^2\cos^2 2\beta)}} \,. \tag{87.23}$$

Note that $\cos(\beta-\alpha) \to 0$ in the limit of $m_H \gg m_h, m_Z$. In this *decoupling limit* [118], the properties of h coincide with those of the SM Higgs boson (see Sec. 87.5.4).

The tree-level Higgs-quark and Higgs-lepton interactions of the MSSM are derived from the superpotential given in Eq. (87.1). The corresponding Higgs-fermion Yukawa couplings can be expressed in terms of the fermion masses and the separate parameters $\cos(\beta-\alpha)$ and $\tan\beta$. In particular, the Higgs sector of the MSSM is a Type-II two-Higgs doublet model [119], in which one Higgs doublet (H_d) couples exclusively to the right-handed down-type quark (or lepton) fields and the second Higgs doublet (H_u) couples exclusively to the right-handed up-type quark fields. For example, the Yukawa Lagrangian that governs the couplings of the Higgs bosons to the third generation of quarks is

$$-\mathcal{L}_Y = \epsilon^{mn}\left[y_b \bar{b}_R (H_d)_m (Q_{L3})_n - y_t \bar{t}_R (H_u)_m (Q_{L3})_n\right] + \text{h.c.}, \tag{87.24}$$

with an implicit sum over the $\mathrm{SU}(2)_L$ indices m and n, where $Q_{L3} \equiv (t_L\,, b_L)$, $y_b \equiv (y_d)_{33}$ and $y_t \equiv (y_u)_{33}$. Moreover, after generalizing Eq. (87.24) to three generations of quarks and charged leptons, the diagonalization of the up-type and down-type fermion mass matrices simultaneously diagonalizes the corresponding Yukawa coupling matrices, resulting in flavor-diagonal tree-level couplings of the neutral Higgs bosons h^0, H^0 and A^0 to quark and lepton pairs. As expected, in the decoupling limit where $\cos(\beta-\alpha) \to 0$, the couplings of h reduce to those of the SM.

In the NMSSM, we set $\mu = 0$ in Eq. (87.1) and add two additional terms to the superpotential,

$$W_{\mathrm{NMSSM}} \supset \lambda \hat{H}_u \hat{H}_d \hat{S} + \frac{1}{3}\kappa \hat{S}^3 \,, \tag{87.25}$$

where $\hat{S}$ is a singlet Higgs superfield. In the NMSSM as defined here, all terms in W_{NMSSM} are cubic in the superfields due to the presence of a discrete $\mathbb{Z}_3$ symmetry. An effective μ-term is generated, $\mu_{\mathrm{eff}} = \lambda\langle S\rangle$, where $\langle S\rangle$ is the VEV of the scalar field component of $\hat{S}$. Moreover, due to the term proportional to λ in Eq. (87.25), there is now an F-term contribution to the quartic Higgs self-couplings. Consequently, the tree-level bound for the mass of the lightest CP-even MSSM Higgs boson is modified [120],

$$m_h^2 \leq m_Z^2\cos^2 2\beta + \frac{1}{2}\lambda^2 v^2 \sin^2 2\beta \,, \tag{87.26}$$

where $v \equiv (v_u^2 + v_d^2)^{1/2} = 246$ GeV. By requiring that λ remain finite after renormalization-group evolution up to the Planck scale, one finds that λ is constrained to lie below about 0.7–0.8 at the electroweak scale [38] (although larger values of λ have also been considered in Ref. [121]).

87.5.2 *The radiatively-corrected Higgs sector*

When radiative corrections are incorporated, additional parameters of the supersymmetric model enter via virtual supersymmetric particles that appear in loops. The impact of these corrections can be significant [122]. The qualitative behavior of these radiative corrections can be most easily seen in the large top-squark mass limit. In addition, we shall assume that both the splitting of the two diagonal entries and the off-diagonal entries of the top-squark squared-mass matrix [Eq. (87.11)] are small in comparison to the geometric mean of the two top-squark squared-masses, $M_{\mathrm{S}}^2 \equiv M_{\tilde{t}_1} M_{\tilde{t}_2}$. In this case (assuming $m_A > m_Z$), the predicted upper bound for m_h is approximately given by [123]

$$m_h^2 \lesssim m_Z^2\cos^2 2\beta + \frac{3g^2 m_t^4}{8\pi^2 m_W^2}\left[\ln\left(\frac{M_{\mathrm{S}}^2}{m_t^2}\right) + \frac{X_t^2}{M_{\mathrm{S}}^2}\left(1 - \frac{X_t^2}{12 M_{\mathrm{S}}^2}\right)\right] , \tag{87.27}$$

where $X_t \equiv A_t - \mu\cot\beta$ [cf. Eq. (87.12)] is proportional to the off-diagonal entry of the top-squark squared-mass matrix (where for simplicity, A_t and μ are taken to be real). The Higgs mass upper limit specified by Eq. (87.27) is saturated when $\tan\beta$ is large (*i.e.*, $\cos^2 2\beta \sim 1$) and $X_t = \sqrt{6}\, M_S$, which defines the so-called maximal mixing scenario.

The set of approximations used to obtain Eq. (87.27) somewhat overestimates the value of m_h. A more complete treatment of the MSSM Higgs mass radiative corrections, which incorporate renormalization group improvement, two-loop and leading three-loop contributions [76, 124, 125], yields a predicted value of m_h shown in Fig. 87.1, as a function of X_t (assumed for simplicity to be real). Higher-order radiative corrections beyond those reviewed in Ref. [76] have recently been obtained in Ref. [126], although their impact on the results shown in Fig. 87.1 is quite small.

The predicted value of m_h can now be used to derive an upper bound for the lightest stop mass in light of the experimentally measured value of m_h. Using the m_h measurement along with the requirement of a valid electroweak minimum of the scalar potential, one obtains a rough upper bound of $m_{\tilde{t}_1} \lesssim 10^{11}$ GeV [127]. In contrast, since m_h receives radiative corrections from many MSSM fields, obtaining a nontrivial lower bound based on any single parameter such as $m_{\tilde{t}_1}$ would typically require additional assumptions regarding the other MSSM parameters.

The radiative corrections to the scalar squared masses discussed above derive from loop corrections to the tree-level neutral CP-even Higgs squared-mass matrix $\mathcal{M}^2$. A complete treatment of Higgs sector radiative corrections must also include radiatively generated vertex corrections to the Higgs-fermion Yukawa couplings. In addition to loop corrections to the Yukawa Lagrangian given in Eq. (87.24), new terms in the Yukawa Lagrangian [the so-called wrong-Higgs Yukawa terms [128],

$$-\Delta\mathcal{L}_Y = (\Delta y_b)\bar{b}_R (H_u^*)_m (Q_{L3})_m + (\Delta y_t)\bar{t}_R (H_d^*)_m (Q_{L3})_m + \text{h.c.}, \tag{87.28}$$

Int. J. Mod. Phys. A 2026.41. Downloaded from www.worldscientific.com
by UNIVERSITY OF CALIFORNIA @ BERKELEY on 09/16/26. Re-use and distribution is strictly not permitted, except for Open Access articles.

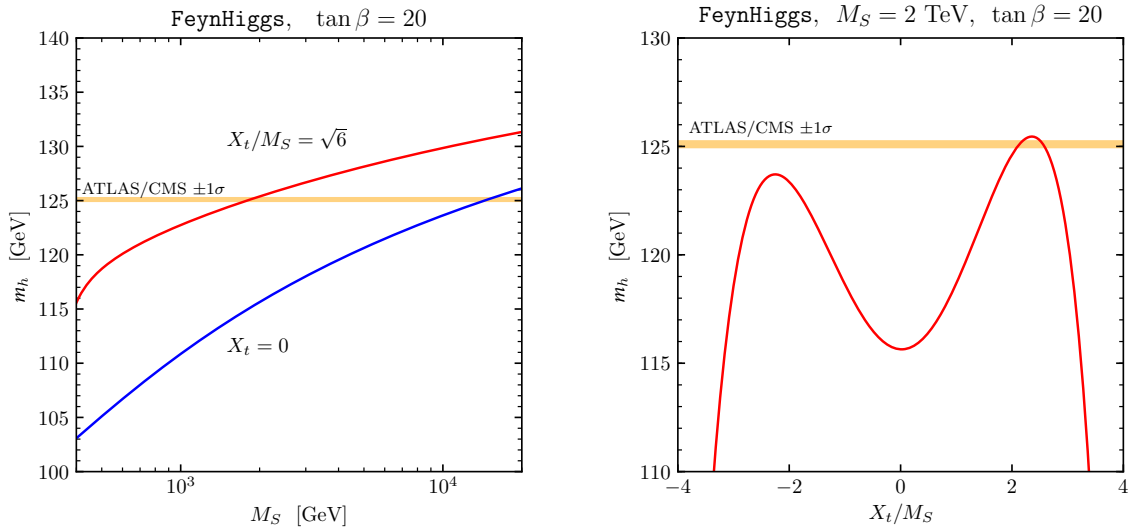

Figure 87.1: The radiatively-corrected value of the MSSM Higgs mass, m_h, as a function of a common SUSY mass parameter M_S and the stop mixing parameter X_t (normalized to M_S), for $\tan\beta = 20$. The value of the observed Higgs mass currently measured by the ATLAS and CMS collaborations [117] at the LHC is also shown. This figure has been adapted from Ref. [76].

are generated due to supersymmetry breaking effects. The most significant consequence of the wrong-Higgs Yukawa terms is to shift the relation between the bottom quark mass and its corresponding Yukawa coupling [129]

$$m_b = \frac{y_b v}{\sqrt{2}} \cos\beta (1 + \Delta_b)\,, \tag{87.29}$$

where $\Delta_b \simeq (\Delta y_b/y_b)\tan\beta$. That is, in parameter regimes where $\tan\beta \gg 1$, the impact of the Δ_b correction can be significantly enhanced, thereby modifying the couplings of the neutral Higgs bosons to b-quark pairs [113].

In obtaining Eqs. (87.27) and (87.29), the μ parameter and the potentially complex SUSY-breaking parameters were assumed to be real. In the so-called complex MSSM, where A_t, A_b, μ, and the gaugino mass parameters can be complex, there generically exist unremovable complex phases that provide new sources of CP violation. Thus, the radiatively-corrected Higgs sector, which now depends on these new CP-violating phases, is no longer CP conserving (*e.g.*, the neutral Higgs scalars are no longer CP-eigenstates). Further details on the complex MSSM Higgs sector can be found in Ref. [130].

In the NMSSM with $m_h \simeq 125$ GeV, the dominant radiative correction to Eq. (87.26) is the same as the one given in Eq. (87.27). However, in contrast to the MSSM, one does not need as large a boost from radiative corrections to achieve a Higgs mass of 125 GeV in certain regimes of the NMSSM parameter space (*e.g.*, $\tan\beta \sim 2$ and $\lambda \sim 0.7$ [131]).

87.5.3 *The hMSSM approximation*

As exhibited in Ref. [123], the dominant one-loop radiative correction to the value of m_h^2 in Eq. (87.27) that yields the term proportional to $m_t^4 \ln(M_S^2/m_t^2)$ is due entirely to the radiatively-corrected 22 element of the CP-even Higgs squared-mass matrix $\mathcal{M}_{22}^2$. Thus, the authors of Refs. [132, 133] suggested a simple recipe to account for the leading radiative corrections to the neutral CP-even Higgs sector of the MSSM without explicitly fixing the parameters of the top squark sector. In this recipe, the expressions for $\mathcal{M}_{11}^2$ and $\mathcal{M}_{12}^2$ given in Eq. (87.17) are retained, whereas $\mathcal{M}_{22}^2$ is left unspecified. After diagonalizing the resulting squared-mass matrix, expressions of the form are obtained

$$m_{h,H}^2 = f_\pm(m_A^2, m_Z^2, \tan\beta, \mathcal{M}_{22}^2)\,, \tag{87.30}$$

$$\cos\alpha = g(m_A^2, m_Z^2, \tan\beta, \mathcal{M}_{22}^2)\,, \tag{87.31}$$

where the functions $f_\pm$ and g are the result of the diagonalization procedure described above. One can use Eq. (87.30) to solve for $\mathcal{M}_{22}^2$ in terms of the experimentally measured Higgs mass, $m_h \simeq 125$ GeV. One then uses Eqs. (87.30) and (87.31) to obtain expressions for m_H^2 and $\cos\alpha$ that are functions of the *measured* mass m_h, which replace the tree-level results given in Eqs. (87.20) and (87.21). This framework was dubbed the hMSSM in Ref. [132]. Having fixed $m_h \simeq 125$ GeV, the Higgs phenomenology of the hMSSM is entirely governed by two MSSM input parameters, m_A and $\tan\beta$. For example, one must assume that the radiative corrections to the Yukawa Lagrangian [e.g., the Δ_b correction exhibited in Eq. (87.29)] are negligible.

Although the hMSSM can be readily applied to LHC data to constrain the neutral CP-even Higgs sector of the MSSM, it can lead to results that are not robust in a more general MSSM parameter scan. Indeed, a more complete treatment of the radiative corrections can yield results that cannot be accounted for in the hMSSM framework. Examples of benchmark points in the MSSM parameter space that cannot be reproduced by the hMSSM analysis are examined in Refs. [134–136]. Finally, we note that the hMSSM framework is not relevant for describing the shift in the properties of the charged Higgs boson due to radiative corrections.

87.5.4 *The Higgs alignment limit and SUSY*

In the Higgs alignment limit of an extended Higgs sector [118, 137], the tree-level properties of one of the neutral scalar states match those of the SM Higgs boson. In light of the LHC Higgs data (see Sec. 11), where the Higgs boson is observed to be SM-like [138, 139], any supersymmetric extension of the SM must account for a SM-like Higgs boson.

Starting from Eq. (87.2), we can define two linear combinations of the MSSM Higgs fields H_u and H_d:

$$\mathcal{H}_1 \equiv H_d \cos\beta + H_u \sin\beta\,, \qquad \mathcal{H}_2 \equiv -H_d \sin\beta + H_u \cos\beta\,. \tag{87.32}$$

Note that the corresponding VEVs of these fields are $\langle \mathcal{H}_1^0 \rangle = v/\sqrt{2}$ and $\langle \mathcal{H}_2^0 \rangle = 0$, respectively. If the neutral scalar field defined by $\varphi \equiv \sqrt{2}\,\mathrm{Re}\,\mathcal{H}_1^0 - v$ were an eigenstate of the CP-even neutral scalar squared-mass matrix (corresponding to the alignment in field space of φ with the direction of the VEV), then it would follow that $\cos(\beta - \alpha) = 0$, under the assumption that the observed Higgs boson is the lighter of the two CP-even scalars [114]. One can check that in the alignment limit described above, the tree-level properties of φ coincide with those of the SM Higgs boson.

Int. J. Mod. Phys. A 2026.41. Downloaded from www.worldscientific.com by UNIVERSITY OF CALIFORNIA @ BERKELEY on 09/16/26. Re-use and distribution is strictly not permitted, except for Open Access articles.

To achieve the Higgs alignment limit, one must suppress the mixing of the field φ and the second orthogonal CP-even scalar field. This can be achieved in two different scenarios. In the so-called decoupling limit of the extended Higgs sector, one neutral scalar mass eigenstate is identified with the SM-like Higgs boson, and all other Higgs scalar mass eigenstates are assumed to be much heavier. As previously noted below Eq. (87.23), $m_H \gg m_h$ yields $|\cos(\beta-\alpha)| \ll 1$, which is consistent with current LHC experimental bounds [140]. If the decoupling limit is realized in the MSSM, then H, A and $H^\pm$ must be significantly heavier (most likely with masses of order 500 GeV or larger [140]). Indeed, Higgs alignment via decoupling is generic and can be achieved in many extensions of the SM.

The Higgs alignment limit can also be realized without decoupling if the value of the off-diagonal element of the CP-even squared-mass matrix (expressed with respect to the $\mathcal{H}_1$–$\mathcal{H}_2$ field basis) is much smaller than the corresponding diagonal elements. This cannot be achieved at tree-level in a viable region of the MSSM parameter space (nor in the hMSSM framework discussed in Sec. 87.5.3). However, regions of the MSSM parameter space do exist, albeit quite fine-tuned, in which Higgs alignment without decoupling is achieved once radiative corrections are taken into account [135]. The NMSSM provides a more robust scenario for Higgs alignment without decoupling as shown in Ref. [131], where the discovery of additional Higgs scalar states at future runs at the LHC would be expected.

As recently reiterated in Ref. [141], the precise measurements of the Higgs boson properties, which would be sensitive to small departures from the Higgs alignment limit, offer a valuable and complementary probe of weak-scale SUSY models, due to the radiative effects of superpartners on Higgs couplings, even in scenarios where direct searches for superpartners are not effective.

87.6 Restricting the MSSM parameter freedom

In Sections 87.4 and 87.5, we surveyed the parameters that comprise the MSSM-124. However, the MSSM-124 is not a phenomenologically viable theory over much of its parameter space. In particular, a generic point of the MSSM-124 parameter space exhibits: (i) no conservation of the separate lepton numbers L_e, L_μ, and L_τ; (ii) unsuppressed flavor-changing neutral currents (FCNCs); and (iii) new sources of CP violation [142] that are inconsistent with the experimental bounds.

In addition, one-loop radiative corrections can introduce CP-violating effects in the Higgs sector that depend on some of the CP-violating phases among the MSSM-124 parameters [143]. This phenomenon is most easily understood in a scenario where $m_A \ll M_S$ (i.e., all five physical Higgs states are significantly lighter than the SUSY breaking scale). In this case, one can integrate out the heavy superpartners to obtain a low-energy effective theory with two Higgs doublets. The resulting effective two-Higgs doublet model will now contain all possible Higgs self-interaction terms (both CP-conserving and CP-violating) and Higgs-fermion interactions (beyond those of Type-II) that are consistent with electroweak gauge invariance [128].

As noted above, the MSSM contains new sources of CP violation. Indeed, for TeV-scale sfermion and gaugino masses, some combinations of the complex phases of the gaugino-mass parameters, the A-parameters, and μ must be less than about 10^{-2}–10^{-3} to avoid generating electric dipole moments for the neutron, electron, and atoms [144] in conflict with observed data [145]. The rarity of FCNCs [146, 147] places additional constraints on the off-diagonal matrix elements of the squark and slepton soft-SUSY-breaking squared-masses and A-parameters (see Sec. 87.3.3).

The MSSM-124 is also theoretically incomplete as it provides no explanation for the fundamental origin of the supersymmetry-breaking parameters. The successful unification of the MSSM gauge couplings at the GUT scale, $M_{\rm GUT} \sim 10^{16}$ GeV, close to the Planck scale [15, 73, 148, 149],

$$g_s(M_{\rm GUT}) = g(M_{\rm GUT}) = \sqrt{\frac{5}{3}}\, g'(M_{\rm GUT}), \tag{87.33}$$

suggests that the high-energy structure of the theory may be considerably simpler than its low-energy realization.[3] In a top-down approach, the dynamics that governs the theory at high energies is used to derive the effective broken-supersymmetric theory at the TeV scale.

In this Section, we examine a number of theoretical frameworks that potentially yield phenomenologically viable regions of the MSSM-124 parameter space. The resulting supersymmetric particle spectrum is then a function of a relatively small number of input parameters. This is accomplished by imposing a simple structure on the soft SUSY-breaking parameters at a common high-energy scale M_X (typically chosen to be the Planck scale, M_P, the GUT scale, $M_{\rm GUT}$, or the messenger scale, $M_{\rm mess}$). These serve as initial conditions for the MSSM renormalization group equations (RGEs), which are given in the two-loop approximation in Ref. [150]. An automated program to compute RGEs for the MSSM and other supersymmetric models of new physics has been developed in Ref. [151]. Solving these equations numerically, one can then derive the low-energy MSSM parameters relevant for phenomenology. A number of software packages exist that numerically calculate the spectrum of supersymmetric particles, consistent with theoretical conditions on SUSY breaking at high energies and some experimental data at low energies [76,152].

Examples of viable frameworks are provided by models of gravity-mediated, anomaly-mediated, and gauge-mediated SUSY breaking. In some of these approaches, one of the diagonal Higgs squared-mass parameters is driven negative by renormalization group evolution [153]. In such models, electroweak symmetry breaking is generated radiatively, and the resulting electroweak symmetry-breaking scale is intimately tied to the scale of low-energy SUSY breaking.

87.6.1 *Gaugino mass relations*

One prediction of many supersymmetric grand unified models is the unification of the (tree-level) gaugino mass parameters[4] at some high-energy scale, M_X,

$$M_1(M_X) = M_2(M_X) = M_3(M_X) = m_{1/2}\,. \tag{87.34}$$

Due to renormalization group running, in the one-loop approximation the effective low-energy gaugino mass parameters (at the electroweak scale) are related,

$$M_3 = (g_s^2/g^2)M_2 \simeq 3.5M_2\ , \qquad M_1 = (5{g'}^2/3g^2)M_2 \simeq 0.5M_2. \tag{87.35}$$

Eq. (87.35) can arise more generally in gauge-mediated SUSY-breaking models where the gaugino masses are generated at the messenger scale $M_{\rm mess}$ (which typically lies significantly below the unification scale where the gauge couplings unify). In this case, the gaugino mass parameters are proportional to the corresponding squared gauge couplings at the messenger scale.

When Eq. (87.35) is satisfied, the chargino and neutralino masses and mixing angles depend only on three unknown parameters: the gluino mass, μ, and $\tan\beta$. It then follows that the lightest neutralino must be heavier than 46 GeV due to the non-observation of charginos at LEP [155]. If in addition $|\mu| \gg |M_1| \gtrsim m_Z$, then the lightest neutralino is nearly a pure bino, an assumption often made in supersymmetric particle searches at colliders. Although Eq. (87.35) is often assumed in many phenomenological studies, a truly model-independent approach would take the gaugino mass parameters M_1, M_2, and M_3 to be independent parameters to be determined by experiment. Indeed, an approximately massless neutralino *cannot* be ruled out at present by a model-independent analysis [156].

It is possible that the tree-level masses of the gauginos are zero. In this case, the gaugino mass parameters arise at one-loop and do not satisfy Eq. (87.35). For example, the gaugino masses in

[3] Generically, the normalization of the U(1) hypercharges exhibited in Table 87.1 is a matter of convention. In particular, the U(1) hypercharges can be rescaled by absorbing the scaling factor into a redefinition of the hypercharge gauge coupling g'. However in a grand unified theory (GUT), the embedding of the hypercharge U(1) generator into the Lie algebra of a (unified) simple gauge group fixes the normalization of the U(1) hypercharges and results in the rescaled hypercharge gauge coupling shown in Eq. (87.33).

[4] Non-universal gaugino mass parameters can also be a viable option in grand unified models with non-minimal gauge kinetic functions [154].

Int. J. Mod. Phys. A 2026.41. Downloaded from www.worldscientific.com by UNIVERSITY OF CALIFORNIA @ BERKELEY on 09/16/26. Re-use and distribution is strictly not permitted, except for Open Access articles.

AMSB models arise entirely from a model-independent contribution derived from the super-conformal anomaly [55, 157]. In this case, Eq. (87.35) is replaced (in the one-loop approximation) by:

$$M_i \simeq \frac{b_i g_i^2}{16\pi^2} m_{3/2}\,, \tag{87.36}$$

where $m_{3/2}$ is the gravitino mass and the b_i are the coefficients of the MSSM gauge beta-functions corresponding to the corresponding U(1), SU(2), and SU(3) gauge groups, $(b_1, b_2, b_3) = (\frac{33}{5}, 1, -3)$. Eq. (87.36) yields $M_1 \simeq 2.8M_2$ and $M_3 \simeq -8.3M_2$, which implies that the lightest chargino pair and neutralino comprise a nearly mass-degenerate triplet of winos, $\widetilde{W}^\pm$, $\widetilde{W}^0$ (cf. Table 1), over most of the MSSM parameter space. For example, if $|\mu| \gg m_Z, |M_2|$, then Eq. (87.36) implies that $M_{\widetilde{\chi}^\pm} \simeq M_{\widetilde{\chi}_1^0} \simeq M_2$ [158]. Alternatively, one can construct an AMSB model where $|\mu|, m_Z \ll M_2$, which yields an LSP that is an approximate higgsino state [159]. In both cases, the corresponding supersymmetric phenomenology differs significantly from the standard phenomenology based on Eq. (87.35) [160, 161].

Finally, it should be noted that the unification of gaugino masses (and scalar masses) can be accidental. In particular, the energy scale where unification takes place may not be directly related to any physical scale. One version of this phenomenon has been called mirage unification and can occur in certain theories of fundamental SUSY breaking [162].

87.6.2 *Constrained versions of the MSSM: mSUGRA, CMSSM, etc.*

In the minimal supergravity (mSUGRA) framework [5–7,27,48–50], the minimal form of the Kähler potential is employed, which yields standard kinetic energy terms for the MSSM fields [52]. As a result, the soft supersymmetry-breaking parameters at the high-energy scale M_X take a particularly simple form in which the scalar squared-masses and the A-parameters are flavor-diagonal and universal [50]:

$$\begin{aligned}
&M^2_{\widetilde{Q}}(M_X) = M^2_{\widetilde{U}}(M_X) = M^2_{\widetilde{D}}(M_X) = m_0^2\mathbf{1}\,,\\
&M^2_{\widetilde{L}}(M_X) = M^2_{\widetilde{E}}(M_X) = m_0^2\mathbf{1}\,,\\
&m^2_{H_u}(M_X) = m^2_{H_d}(M_X) = m_0^2\,,\\
&A_U(M_X) = A_D(M_X) = A_E(M_X) = A_0\mathbf{1}\,,
\end{aligned} \tag{87.37}$$

where $\mathbf{1}$ is a 3×3 identity matrix in generation space. As in the SM, this approach exhibits minimal flavor violation (*e.g.*, see Ref. [163]), whose unique source is the nontrivial flavor structure of the Higgs-fermion Yukawa couplings. The gaugino masses are also unified according to Eq. (87.34).

Renormalization group evolution is then used to derive the values of the supersymmetric parameters at the low-energy (electroweak) scale. For example, to compute squark masses, one should use the low-energy values for $M^2_{\widetilde{Q}}$, $M^2_{\widetilde{U}}$, and $M^2_{\widetilde{D}}$ in Eq. (87.11). Through the renormalization group running with boundary conditions specified in Eq. (87.35) and Eq. (87.37), one can show that the low-energy values of $M^2_{\widetilde{Q}}$, $M^2_{\widetilde{U}}$, and $M^2_{\widetilde{D}}$ depend primarily on m_0^2 and $m^2_{1/2}$. A number of useful approximate analytic expressions for superpartner masses in terms of the mSUGRA parameters can be found in Ref. [164].

One can count the number of independent parameters in the mSUGRA framework. In addition to 18 SM parameters (excluding the Higgs mass), one must specify m_0, $m_{1/2}$, A_0, the Planck-scale values for μ and B-parameters (denoted by μ_0 and B_0), and the gravitino mass $m_{3/2}$. Without additional model assumptions, $m_{3/2}$ is independent of the parameters that govern the mass spectrum of the superpartners of the SM [50]. In principle, A_0, B_0, μ_0, and $m_{3/2}$ can be complex, although in the mSUGRA approach, these parameters are taken to be real for simplicity.

As previously noted, renormalization group evolution is used to compute the low-energy values of the mSUGRA parameters, which then fixes all the parameters of the low-energy MSSM. In particular, the two Higgs VEVs (or equivalently, m_Z and $\tan\beta$) can be expressed as a function of the Planck-scale supergravity parameters. In light of Eq. (87.4) and Eq. (87.5), a common procedure is to determine μ_0 and B_0 in terms of m_Z and $\tan\beta$ [the sign of μ_0, denoted $\mathrm{sgn}(\mu_0)$ below, is not fixed in this process]. In this case, the MSSM spectrum and its interaction strengths are fixed by five parameters:

$$m_0\,,\ A_0\,,\ m_{1/2}\,,\ \tan\beta\,,\ \text{and}\ \mathrm{sgn}(\mu_0)\,, \tag{87.38}$$

and an independent gravitino mass $m_{3/2}$ (in addition to the 18 parameters of the SM). In Ref. [165], this framework was dubbed the constrained minimal supersymmetric extension of the SM (CMSSM). Additional relations such as $B_0 = A_0 - m_0$ and $m_{3/2} = m_0$ comprise the original mSUGRA proposal [48, 52, 166].

One can also relax the universality of scalar masses by decoupling the squared-masses of the Higgs bosons and the squarks/sleptons. This leads to the non-universal Higgs mass models (NUHMs), thereby adding one or two new parameters to the CMSSM depending on whether the diagonal Higgs scalar squared-mass parameters ($m^2_{H_d}$ and $m^2_{H_u}$) are set equal (NUHM1 [167]) or taken to be independent (NUHM2 [168]) at the high energy scale M_X. Clearly, this modification preserves the minimal flavor violation of the mSUGRA approach. Nevertheless, the mSUGRA approach and its NUHM generalizations are probably too simplistic. Theoretical considerations suggest that the universality of Planck-scale soft SUSY-breaking parameters is not generic [169]. In particular, effective operators at the Planck scale exist that do not respect flavor universality, and it is difficult to find a theoretical principle that would forbid them.

In the framework of supergravity, if anomaly mediation is the sole source of SUSY breaking, then the gaugino mass parameters, diagonal scalar squared-mass parameters, and the SUSY-breaking trilinear scalar interaction terms (proportional to $\lambda_f A_F$) are determined in terms of the beta functions of the gauge and Yukawa couplings and the anomalous dimensions of the squark and slepton fields [55, 157, 161]. As noted in Sec. 87.2.3, this approach yields tachyonic sleptons in the MSSM unless additional sources of SUSY breaking are present. In the minimal AMSB (mAMSB) scenario, a universal squared-mass parameter, m_0^2, is added to the AMSB expressions for the diagonal scalar squared-masses [161]. Thus, the mAMSB spectrum and its interaction strengths are determined by four parameters, m_0^2, $m_{3/2}$, $\tan\beta$ and $\mathrm{sgn}(\mu_0)$.

The mAMSB scenario appears to be ruled out based on the observed value of the Higgs boson mass, assuming an upper limit on M_S of a few TeV, since the mAMSB constraint on A_F implies that the maximal mixing scenario cannot be achieved [cf. Eq. (87.27)]. Indeed, under the stated assumptions, the mAMSB Higgs mass upper bound lies below the observed Higgs mass value [170]. Thus within the mAMSB scenario, either an additional SUSY-breaking contribution to $\lambda_f A_F$, and/or new ingredients beyond the MSSM are required.

87.6.3 *Gauge-mediated SUSY breaking*

In contrast to models of gravity-mediated SUSY breaking, the flavor universality of the fundamental soft SUSY-breaking squark and slepton squared-mass parameters is guaranteed in gauge-mediated supersymmetry breaking (GMSB) because the supersymmetry breaking is communicated to the sector of MSSM fields via gauge interactions [60, 62]. In GMSB models, the mass scale of the messenger sector (or its equivalent) is sufficiently below the Planck scale such that the additional SUSY-breaking effects mediated by supergravity can be neglected.

In the minimal GMSB approach, there is one effective mass scale, Λ, that determines all low-energy scalar and gaugino mass parameters through loop effects, while the resulting A-parameters are suppressed. In addition, the minimal form of the Kähler potential is employed. Assuming that the superpartner masses are no larger than a few TeV, one must take $\Lambda \sim \mathcal{O}(100\ \text{TeV})$. The origin of the μ and B-parameters is model-dependent, and lies somewhat outside the purview of gauge-mediated SUSY breaking [171].

The simplest GMSB models appear to be ruled out based on the observed value of the Higgs boson mass. Due to suppressed A-parameters, it is difficult to boost the contributions of the radiative corrections in Eq. (87.27) to obtain a Higgs mass as large

Int. J. Mod. Phys. A 2026.41. Downloaded from www.worldscientific.com by UNIVERSITY OF CALIFORNIA @ BERKELEY on 09/16/26. Re-use and distribution is strictly not permitted, except for Open Access articles.

as 125 GeV, under the assumption that M_S is no larger than a few TeV. However, this conflict can be alleviated in more complicated GMSB models [172]. To analyze these generalized GMSB models, it has been especially fruitful to develop model-independent techniques that encompass all known GMSB models [173]. These techniques are well-suited for a comprehensive analysis [174] of the phenomenological profile of gauge-mediated SUSY breaking.

The gravitino is the LSP in minimal GMSB models, as noted in Sec. 87.2.3. As a result, the next-to-lightest supersymmetric particle (NLSP) now plays a crucial role in the phenomenology of supersymmetric particle production and decays. Note that unlike the LSP, the NLSP can be charged. In GMSB models, the most likely candidates for the NLSP are $\tilde{\chi}_1^0$ and $\widetilde{\tau}_R^{\pm}$. The NLSP will decay into its superpartner plus a gravitino (*e.g.*, $\tilde{\chi}_1^0 \to \gamma\widetilde{G}$, $\tilde{\chi}_1^0 \to Z\widetilde{G}$, $\tilde{\chi}_1^0 \to h^0\widetilde{G}$ or $\widetilde{\tau}_1^{\pm} \to \tau^{\pm}\widetilde{G}$), with lifetimes and branching ratios that depend on the model parameters. There are also GMSB scenarios in which there are several nearly degenerate co-NLSPs, any one of which can be produced at the penultimate step of a supersymmetric decay chain [175]. For example, in the slepton co-NLSP case, all three right-handed sleptons are close enough in mass and thus can each play the role of the NLSP.

Different choices for the identity of the NLSP and its decay rate lead to a variety of distinctive supersymmetric phenomenologies [62,176]. For example, a long-lived $\tilde{\chi}_1^0$-NLSP that decays outside collider detectors leads to supersymmetric decay chains with missing energy in association with leptons and/or hadronic jets (this case is indistinguishable from the standard phenomenology of the $\tilde{\chi}_1^0$-LSP). On the other hand, if $\tilde{\chi}_1^0 \to \gamma\widetilde{G}$ is the dominant decay mode, and the decay occurs inside the detector, then nearly *all* supersymmetric particle decay chains would produce a photon. In contrast, in the case of a $\widetilde{\tau}_1^{\pm}$-NLSP, the $\widetilde{\tau}_1^{\pm}$ would either be long-lived or would decay inside the detector into a τ-lepton plus missing energy.

A number of attempts have been made to address the origins of the μ and B-parameters in GMSB models based on the field content of the MSSM (*e.g.*, see Refs. [171, 177]). An alternative approach is to consider GMSB models based on the NMSSM [178]. The VEV of the additional singlet Higgs superfield can be used to generate effective μ and B-parameters [179]. Such models provide an alternative GMSB framework for achieving a Higgs mass of 125 GeV, while still being consistent with LHC bounds on supersymmetric particle masses.

87.6.4 *The phenomenological MSSM*

Any of the theoretical assumptions described in the previous three subsections must be tested experimentally and could turn out to be wrong. To facilitate the exploration of MSSM phenomena in a more model-independent way while respecting the constraints noted at the beginning of Sec. 87.6, the phenomenological MSSM (pMSSM) has been introduced [180].

The pMSSM is governed by 19 independent real supersymmetric parameters: the three gaugino mass parameters M_1, M_2 and M_3, the Higgs sector parameters m_A and $\tan\beta$, the Higgsino mass parameter μ, five sfermion squared-mass parameters for the degenerate first and second generations ($M^2_{\widetilde{Q}}$, $M^2_{\widetilde{U}}$, $M^2_{\widetilde{D}}$, $M^2_{\widetilde{L}}$ and $M^2_{\widetilde{E}}$), the five corresponding sfermion squared-mass parameters for the third generation, and three third-generation A-parameters (A_t, A_b and A_τ). The first and second generation A-parameters are typically neglected in pMSSM studies, as their phenomenological consequences are negligible in most applications. One counterexample arises when considering the A_μ dependence of the anomalous magnetic moment of the muon, which can be as significant as other contributions due to superpartner mediated radiative corrections [181]. Consequently, the original pMSSM approach has been extended to include a 20th parameter, A_μ [182]. Other pMSSM extensions that include CP-violating SUSY-breaking parameters have been considered in Ref. [183].

The 19-parameter pMSSM is often further constrained to expedite scans over the parameter space. For example, in Ref. [184], the number of pMSSM parameters is reduced to ten by assuming one common squark squared-mass parameter for the first two generations, a second common squark squared-mass parameter for the third generation, a common (charged) slepton squared-mass parameter and a common third generation Aparameter. In Ref. [185] an eleven parameter pMSSM is defined by allowing for a different stau squared-mass parameter from that of the first two generation charged sleptons. Other applications of the pMSSM approach (with a reduced pMSSM parameter space) to supersymmetric particle searches, and a discussion of the implications for past and future LHC and dark matter studies can be found in Refs. [184, 186].

87.6.5 *Simplified models*

As discussed in Sec. 88, the experimental collaborations present the results of their searches for supersymmetric particles primarily in terms of simplified models. Simplified models for supersymmetric particle searches [187] are defined mostly by the empirical objects and kinematic variables involved in the search. The interpretation of the experimental results usually involves only a small number of supersymmetric particles (often two or three). Other supersymmetric particles are assumed to play no role (this may happen by virtue of them being too heavy to be produced). Experimental bounds from the non-observation of a signal are usually presented in terms of the physical masses of the supersymmetric particles involved. Bounds on the relevant supersymmetric particle masses may be presented assuming values for the branching ratio of certain supersymmetric particle decays, or as an upper bound on the signal production cross section as a function of the relevant supersymmetric particle masses.

For example, consider a search for hadronic jets plus missing transverse momentum. One can match such a search to a simplified model of squark pair production followed by the subsequent decay of each squark into a quark (which appears as a jet) and a neutralino LSP that produces the missing transverse momentum, *i.e.* $\tilde{q}\tilde{q} \to (q\tilde{\chi}_1^0)(q\tilde{\chi}_1^0)$. Excluded cross sections resulting from the non-observation of a signal (which in this case could consist of some specified minimum value of missing transverse momentum and at least two hard jets) may be exhibited in the squark mass versus LSP mass plane.

The large number of free parameters that govern a typical supersymmetric model makes it difficult to present experimentally excluded regions in any generality. This is where simplified models have an apparent advantage in that they depend on far fewer free parameters than more complete supersymmetric models. However, if limits are quoted on supersymmetric particle masses without reference to the signal production cross section from a simplified model analysis, then there are several potential pitfalls. For example, chargino/neutralino mixing affect their production cross sections. Moreover, mass limits can differ from those obtained in full models because there may be contributions to the signal coming from processes involving supersymmetric particles other than those assumed. Indeed, in the $\tilde{q}\tilde{q} \to q\tilde{\chi}_1^0 q\tilde{\chi}_1^0$ process mentioned above, the simplified model analysis does not account for the interference with tree-level t-channel gluino contributions, nor does it account for other decay modes of the $\tilde{q}\tilde{q}$ pair. Nevertheless, simplified model bounds quoted purely in terms of supersymmetric particle masses may still approximately hold over sizable regions of parameter space of more complete models, within which the simplified model is embedded. When simplified model limits are phrased as bounds on signal cross sections, the aforementioned pitfalls are sidestepped.

Simplified models thus remain an efficient tool for organizing and presenting the results of supersymmetric particle searches. A comparison between supersymmetric particle search constraints in the context of simplified models and the corresponding constraints obtained in the more complete pMSSM can be found in Ref. [188].

87.7 Experimental data confronts the MSSM

At present, there is no significant evidence for weak-scale SUSY from the data analyzed by the LHC experiments [189]. Recent LHC data have been employed in ruling out the existence of colored supersymmetric particles (primarily the gluino and the first generation of squarks) with masses below about 2 TeV. Moreover, given that the mass of the observed Higgs boson is 125 GeV, the results exhibited in Fig. 87.1 tend to favor a mass scale of the top squarks somewhat above 2 TeV. However, the precise mass limits

Int. J. Mod. Phys. A 2026.41. Downloaded from www.worldscientific.com
by UNIVERSITY OF CALIFORNIA @ BERKELEY on 09/16/26. Re-use and distribution is strictly not permitted, except for Open Access articles.

are very model dependent. For example, as Fig. 88.13 demonstrates, regions of the pMSSM parameter space can be identified in which lighter squarks and gluinos below 1 TeV cannot be definitively ruled out. Under the assumption of gaugino mass unification [cf. Eq. (87.35)], LHC searches result in a lower bound on neutralino and chargino masses of roughly 200 GeV. It is also difficult to place general bounds on neutralino and chargino masses, since the limits in terms of masses from direct searches tend to be particularly model-dependent. It is therefore premature to rule out the entire framework of weak-scale supersymmetry based on current LHC searches for supersymmetric particles [141]. Nevertheless, one must confront the tension that exists between the theoretical expectations for the magnitude of the SUSY-breaking parameters and the non-observation of supersymmetric phenomena at colliders.

87.7.1 *Naturalness constraints and the little hierarchy*

In Sec. 87.1, weak-scale SUSY was motivated as a natural solution to the hierarchy problem, which could provide an understanding of the origin of the electroweak symmetry-breaking scale without a significant fine-tuning of the fundamental parameters that govern the MSSM. In this context, the weak-scale soft supersymmetry-breaking masses must be generally of the order of 1 TeV or below [190]. This requirement is most easily seen in the determination of m_Z by the scalar potential minimum condition. In light of Eq. (87.5), to avoid the fine-tuning of MSSM parameters, the soft SUSY-breaking squared-masses $m^2_{H_d}$ and $m^2_{H_u}$ and the higgsino squared-mass $|\mu|^2$ should all be roughly of $\mathcal{O}(m_Z^2)$. Many authors have proposed quantitative measures of fine-tuning [190–195]. One of the simplest measures is the one advocated by Barbieri and Giudice [190] (which was also introduced previously in Ref. [191]),

$$\Delta_i \equiv \left| \frac{\partial \ln m_Z^2}{\partial \ln p_i} \right| , \qquad \Delta \equiv \max\, \Delta_i \,, \tag{87.39}$$

where the p_i are the MSSM parameters at the high-energy scale M_X, which are set by the fundamental SUSY-breaking dynamics. The theory is more fine-tuned as Δ becomes larger. However, different measures of fine-tuning yield quantitatively different results [196]; in particular, calculating minimal fine-tuning based on the high-scale parameters [as defined in Eq. (87.39)] yields a difference by a factor of order 10 to fine-tuning based on TeV-scale parameters [197, 198].

One can apply the fine-tuning measure to any explicit model of SUSY breaking. For example, in the approaches discussed in Sec. 87.6, the p_i are parameters of the model at the energy scale M_X where the soft SUSY-breaking operators are generated by the dynamics of SUSY breaking. Renormalization group evolution then determines the values of the parameters appearing in Eq. (87.5) at the electroweak scale. In this way, Δ is sensitive to all the SUSY-breaking parameters of the model (see *e.g.* Ref. [199]). The computation of Δ is often based on Eq. (87.5), which is a tree-level condition. However, the fine-tuning measure obtained at tree level can be somewhat reduced in value when loop corrections are included while remaining consistent with all experimental constraints [88, 200].

One way of taking fine-tuning into account in fits to data using Bayesian statistics is to have a prior probability distribution proportional to $1/\Delta$ [201] so that fine-tuning is balanced against the fit to empirical data. In such a Bayesian approach, it is important to choose the prior probability distribution carefully, since prior probability densities that are flat in one set of variables may not be flat in another, more fundamental set. One can in fact derive a different measure of fine-tuning resulting from a Jacobian factor when transforming to other variables.[5] By comparing the results of several Bayesian fits with different (but reasonable) prior probability distributions, one can assess the robustness of the fit with respect to their variation, mitigating for subjectivity in the interpretation of the fine-tuning measure.

As anticipated, there is a tension between the present experimental lower limits on the masses of colored supersymmetric particles [203] and the expectation that supersymmetry-breaking is associated with the electroweak symmetry-breaking scale. Moreover, in light of the results exhibited in Fig. 87.1, this tension is exacerbated by the observed value of the Higgs mass ($m_h \simeq 125$ GeV), which is suggestive of a value of M_S in the multi-TeV range. Indeed, if M_S characterizes the scale of all supersymmetric particle masses, then one would crudely expect $\Delta \sim M_S^2/m_Z^2$. For example, if $M_S \sim 2$ TeV then one expects a fine-tuning of the MSSM parameters such that $\Delta^{-1} \sim 0.2\%$ to achieve the observed value of m_Z. This separation of the electroweak symmetry-breaking and SUSY-breaking scales is an example of the little hierarchy problem [204].

The fine-tuning parameter Δ can depend quite sensitively on the structure of the SUSY-breaking dynamics, such as the value of M_X and relations among SUSY-breaking parameters in the fundamental high energy theory [205]. For example, in so-called focus point SUSY models [194, 206], all squark masses can be as heavy as 5 TeV *without* significant fine-tuning. This can be attributed to a focusing behavior of the renormalization group evolution when certain relations hold among the high-energy values of the scalar squared-mass SUSY-breaking parameters. Although the focus point region of the CMSSM still yields an uncomfortably high value of Δ due to the observed Higgs mass of 125 GeV, one can achieve moderate values of Δ in models with NUHM2 boundary conditions for the scalar masses [207].

Among the colored superpartners, the third generation squarks typically have the most significant impact on the naturalness constraints [208], while their masses are the least constrained by the LHC data. Hence, in the absence of any relation between third generation squarks and those of the first two generations, the naturalness constraints due to present LHC data can be considerably weaker than those obtained in the CMSSM. Indeed, models with first and second generation squark masses in the multi-TeV range do not necessarily require significant fine tuning. Such models have the added benefit that undesirable FCNCs mediated by squark exchange are naturally suppressed [209]. Other MSSM mass spectra that are compatible with moderate fine tuning have been considered in Refs. [205, 210].

The lower bounds on squark and gluino masses may not be as large as suggested by the experimental analyses based on the CMSSM or simplified models. For example, mass bounds for the gluino and the first and second generation squarks based on the CMSSM can often be evaded in alternative or extended MSSM models, *e.g.*, compressed SUSY [211] and stealth SUSY [212]. Moreover, the experimental lower limits for the third generation squark masses (which have a more direct impact on the fine-tuning measure) are weaker than the corresponding mass limits for other colored supersymmetric states.

Among the uncolored superpartners, the higgsinos are typically the most impacted by the naturalness constraints. Eq. (87.5) suggests that the masses of the two neutral higgsinos and charged higgsino pair (which are governed by $|\mu|$) should not be significantly larger than m_Z to avoid an unnatural fine-tuning of the supersymmetric parameters, which would imply the existence of light higgsinos (whose masses are not well constrained, as they are difficult to detect directly at the LHC due to their soft decay products). However, it may be possible to avoid the conclusion that $\mu \sim \mathcal{O}(m_Z)$ if additional correlations among the SUSY breaking mass parameters and μ are present. Such a scenario can be realized in models in which the boundary conditions for SUSY breaking are generated by approximately conformal strong dynamics. For example, in the so-called scalar-sequestering model of Ref. [213], values of $|\mu| > 1$ TeV can be achieved while naturally maintaining the observed value of m_Z.

Finally, one can also consider extensions of the MSSM in which the degree of fine-tuning is relaxed. For example, it has already been noted in Sec. 87.5 that it is possible to accommodate the observed Higgs mass more easily in the NMSSM due to contributions to m_h^2 proportional to the parameter λ. This means that

[5] For example, one may consider the parameters μ and m_{12}^2 to be more fundamental than $\tan\beta$ and M_Z. In this case, one would choose a flat prior probability distribution in μ and m_{12}^2 rather than in $\tan\beta$ and M_Z [193, 202]. The Jacobian factor is then obtained from Eqs. (87.4) and (87.5).

Int. J. Mod. Phys. A 2026.41. Downloaded from www.worldscientific.com by UNIVERSITY OF CALIFORNIA @ BERKELEY on 09/16/26. Re-use and distribution is strictly not permitted, except for Open Access articles.

one does not have to rely on a large contribution from radiative corrections to boost the Higgs mass sufficiently above its tree-level bound. This allows for smaller top squark masses, which are more consistent with the demands of naturalness. The reduction of the fine-tuning in various NMSSM models was initially advocated in Ref. [214], and subsequently treated in more detail in Refs. [121, 215]. Naturalness can also be relaxed in extended supersymmetric models with vector-like quarks [216] and in gauge extensions of the MSSM [217].

The experimental absence of any new physics beyond the SM at the LHC suggests that the principle of naturalness is presently under significant stress [218]. Nevertheless, one must be very cautious when drawing conclusions about the viability of weak-scale SUSY to explain the origin of electroweak symmetry breaking, since different measures of fine-tuning noted above can lead to different assessments [196–198]. Moreover, the maximal value of Δ that determines whether weak-scale SUSY is a fine-tuned model (should it be $\Delta \sim 10$? 100? 1000?) is ultimately subjective. Thus, it is premature to conclude that weak-scale SUSY is on the verge of exclusion. It might be possible to sharpen the upper bounds on superpartner masses based on naturalness arguments, which ultimately will either confirm or refute the weak-scale SUSY hypothesis [219]. Of course, if evidence for supersymmetric phenomena in the multi-TeV regime were to be established at a future collider facility (with an energy reach beyond the LHC [220]), it would be viewed as a spectacularly successful explanation of the large gauge hierarchy between the (multi-)TeV scale and Planck scale. In this case, the remaining little hierarchy, characterized by the somewhat large value of the fine-tuning parameter Δ discussed above, would be regarded as a less pressing issue.

87.7.2 *Indirect constraints on supersymmetric models*

While direct empirical searches for supersymmetric particles provide various limits on their properties, indirect constraints can depend more sensitively on details of the whole model. The cold dark matter relic density inferred from cosmological fits to observational data is one such example of an indirect constraint. In supersymmetric models where the LSP is stable (and thus is a dark matter candidate), its thermally-produced relic density depends upon the scattering of various supersymmetric particles into dark matter particles and SM particles. The resulting relic density can depend sensitively on the masses of the non-LSP supersymmetric particles as well as on the mass of the LSP. In a typical model, an appreciable region of the parameter space is ruled out because it yields an overabundance of dark matter (see for example Ref. [221] for a fit to a seven parameter version of the pMSSM). However, subsequent tweaks to the supersymmetric model that yield an unstable LSP, such as the introduction of R-parity violating effects, can mean that the relic density no longer constrains the parameter space.

There are a number of indirect constraints based on low-energy measurements that are sensitive to the effects of new physics via supersymmetric loop effects. For example, the virtual exchange of supersymmetric particles can contribute to the muon anomalous magnetic moment, $a_\mu \equiv \frac{1}{2}(g-2)_\mu$, as reviewed in Ref. [222]. A current SM prediction for a_μ [223] uses conventional perturbative calculations, employing lattice QCD calculations for the hadronic vacuum polarisation contribution as well as dispersive methods *and* lattice QCD estimates of the hadronic light-by-light contribution. The resulting prediction displays no significant tension with the experimentally observed value [224]. This is in contrast to previous estimates that relied on dispersive methods for estimating the hadronic vacuum polarization contribution and found a significant deviation between the measured value and the SM prediction (see *e.g.* Ref. [225]).

The precision of the measured value of a_μ is not sensitive to the experimental error associated with the measured value of the fine structure constant, α. In contrast, the comparison of the SM prediction with the experimental measurement of the anomalous magnetic moment of the electron, a_e, depends critically on the value of α. Using the experimentally determined value of α given in Ref. [226] yields a SM prediction for a_e that is 2.4σ above its measured value [227]. However, this previous determination of α is in tension at the 5σ level with a more recent measurement of the fine structure constant [228]. The latter yields a SM prediction for a_e that is 1.6σ below its measured value [228]. Measurements of the fine structure constant, a_e and a_μ jointly constrain the pMSSM parameter space [229] due to shifts originating from supersymmetric loop effects.

Flavor transitions in radiative, leptonic and semi-leptonic b quark decays [230] provide a fertile ground for physics beyond the SM. For example, the rare inclusive decay $b \to s\gamma$ is a sensitive probe of the virtual effects of new physics beyond the SM. The experimental measurements of $B \to X_s + \gamma$ [231] are in agreement with the theoretical SM predictions of Ref. [232]. Since supersymmetric loop corrections can contribute an observable shift from the SM predictions, the absence of any significant deviation places useful constraints on the MSSM parameter space [233].

The rare decays $B_s \to \mu^+\mu^-$ and $B_d \to \mu^+\mu^-$ are especially sensitive to supersymmetric loop effects, with some loop contributions scaling as $\tan^6\beta$ when $\tan\beta \gg 1$ [234]. Since there are no significant deviations observed between the measurements of these rare decay modes [235] and the predicted SM rates [236], constraints on the parameter space of the MSSM can be derived [234].

Several tensions exist between SM predictions and measurements of some other experimental observables that probe $b \to s\mu^+\mu^-$ transitions, although the level of tension depends upon the theoretical treatment of the SM analysis. In a certain angular distribution parameter (denoted by P_5') extracted from $B^0 \to K^{*0}\mu^+\mu^-$ decays, the tension is around the 4σ level [237]. An even larger discrepancy is observed in a combination of angular distributions and rates derived from $B^\pm \to K^\pm\mu^+\mu^-$ and $B^0 \to K^0\mu^+\mu^-$ [238]. Moreover, there is a 3.6σ deviation in the branching ratio of $B_s \to \phi\mu^+\mu^-$ for di-muon invariant mass squared values between 1.1 GeV^2 and 6.0 GeV^2 [239]. Finally, a recent measurement of $B^+ \to K^+\nu\bar{\nu}$ by the Belle II Collaboration [240] obtained a branching fraction that is roughly four times larger than the SM prediction [241], corresponding to a 2.7σ deviation from the SM expectation. However, it is unlikely that this result can be attributed to new contributions from the MSSM [242], as the latter are expected to be negligible in comparison with the SM.

The decays $B^\pm \to \tau^\pm\nu_\tau$ and $\overline{B} \to D^{(*)}\tau^-\overline{\nu}_\tau$ are noteworthy, since in models with extended Higgs sectors such as the MSSM, these processes possess tree-level charged Higgs exchange contributions that can compete with the dominant W-exchange. As Sec. 71 shows, experimental measurements of $B^\pm \to \tau^\pm\nu_\tau$ are currently consistent with SM expectations [243]. The BaBar Collaboration measured values of the rates for $\overline{B} \to D\tau^-\overline{\nu}_\tau$ and $\overline{B} \to D^*\tau^-\overline{\nu}_\tau$ [244] which exhibited a combined 3.4σ discrepancy from the SM predictions, which was also not compatible with the Type-II Higgs Yukawa couplings employed by the MSSM. Subsequent measurements by the LHCb and Belle Collaborations were compatible with the BaBar measurements although they displayed less deviation from the SM expectations. The combined difference between the measured values of the $\overline{B} \to D\tau^-\overline{\nu}_\tau$ and $\overline{B} \to D^*\tau^-\overline{\nu}_\tau$ decay rates relative to the corresponding SM values has a significance of 3.1σ [245].

In summary, although there are a few hints of possible deviations from the SM in B decays, none of the discrepancies by themselves are significant enough to conclusively imply the existence of new physics beyond the SM. Moreover, the absence of evidence for sizable deviations in other B-physics observables from their SM predictions can place useful constraints on the MSSM parameter space [147, 203, 246].

87.7.3 *Standard Model Effective Field Theory and SUSY*

The SM effective field theory (SMEFT) [247] encodes the effects of fields beyond those of the SM under the assumption that the characteristic mass scale Λ associated with the new fields is much higher than the highest energy scale E of some set of experimentally probed observables. The total Lagrangian density is written

$$\mathcal{L} = \mathcal{L}_4 + \sum_{d=5}^{\infty}\sum_i \frac{C_i}{\Lambda^{d-4}}\mathcal{O}_i^{(d)}, \qquad (87.40)$$

Int. J. Mod. Phys. A 2026.41. Downloaded from www.worldscientific.com by UNIVERSITY OF CALIFORNIA @ BERKELEY on 09/16/26. Re-use and distribution is strictly not permitted, except for Open Access articles.

where $\mathcal{L}_4$ is the usual renormalizable Lagrangian density of the SM, $\mathcal{O}_i^{(d)}$ is an operator of mass dimension d composed of a product of SM fields (and their spacetime derivatives), and the C_i are dimensionless Wilson coefficients. The index i labels independent operators (for an example of an operator basis up to $d = 6$, see Ref. [248]). The summed term of Eq. (87.40) arises from integrating out fields with masses of order Λ (or larger) from the theory. The effects of successively higher-dimension operators on an observable are suppressed by a factor $(E/\Lambda)^{d-4}$. Thus, in a set of SMEFT operators that contribute to an observable, the dominant effects come from those operators with smallest dimension d. Experimental measurements can then be interpreted as bounds on the C_i, provided that no on-shell beyond-the-SM resonances affect the measurements. After electroweak symmetry breaking, the $d = 5$ operators describe neutrino mass terms and so $d = 6$ SMEFT operators are generically the most relevant for collider physics.

Measurements involving SM particles are often interpreted as constraints on the Wilson coefficients of $d = 6$ operators. The MSSM has been matched to the $d = 6$ SMEFT Lagrangian at the one-loop level in Ref. [249]. In principle, the bounds on the C_i obtained from experimental studies can be translated into constraints on the MSSM parameter space.

87.8 Massive neutrinos in weak-scale SUSY

In the minimal version of the SM and its supersymmetric extension, there are no right-handed neutrinos, and Majorana mass terms for the left-handed neutrinos are absent. However, given the overwhelming evidence for neutrino masses and mixing (see Sec. 14 and Ref. [250]), any viable model of the fundamental particles must provide a mechanism for generating neutrino masses [251]. In extended supersymmetric models, various mechanisms exist for producing massive neutrinos [252]. Although one can devise models for generating massive Dirac neutrinos [253], the most common approaches for incorporating neutrino masses are based on L-violating supersymmetric extensions of the MSSM, which generate massive Majorana neutrinos. Two classes of L-violating supersymmetric models will now be considered.

87.8.1 *The supersymmetric seesaw*

Neutrino masses can be incorporated into the SM by introducing SU(3)×SU(2)×U(1) singlet right-handed neutrinos (ν_R) whose mass parameters are very large, typically near the grand unification scale. In addition, one must also include a standard Yukawa couplings between the lepton doublets, the Higgs doublet, and ν_R. The Higgs VEV then induces an off-diagonal ν_L–ν_R mass on the order of the electroweak scale. Diagonalizing the neutrino mass matrix (in the three-generation model) yields three superheavy neutrino states, and three very light neutrino states that are identified with the light neutrinos observed in nature. This is the seesaw mechanism [254].

It is straightforward to construct a supersymmetric generalization of the seesaw model of neutrino masses [255, 256] by promoting the right-handed neutrino field to a superfield $\widehat{N}^c = (\widetilde{\nu}_R\,;\,\nu_R)$. Integrating out the heavy right-handed neutrino supermultiplet yields a new term in the superpotential [cf. Eq. (87.1)] of the form

$$W_{\rm seesaw} = \frac{f}{M_R}(\widehat{H}_U\widehat{L})(\widehat{H}_U\widehat{L})\,, \tag{87.41}$$

where M_R is the mass scale of the right-handed neutrino sector and f is a dimensionless constant. Note that lepton number is broken by two units by Eq. (87.41), which implies that R-parity invariance is preserved. The supersymmetric analogue of the Majorana neutrino mass term in the sneutrino sector leads to sneutrino–antisneutrino mixing phenomena [256, 257]. In addition, new Higgs-slepton interaction terms can probe the structure of the supersymmetric seesaw model [258]. The right-handed sneutrino that resides in $\widehat{N}^c$ also provides an intriguing dark matter candidate [259].

The SUSY Les Houches Accord [81,99], mentioned at the end of the introduction to Sec. 87.4, has been extended to the supersymmetric seesaw (and other extensions of the MSSM) in Ref. [260].

87.8.2 *R-parity-violating SUSY*

It is possible to incorporate massive neutrinos in renormalizable supersymmetric models while retaining the minimal particle content of the MSSM by relaxing the assumption of R-parity invariance. The most general R-parity-violating model involving the MSSM spectrum introduces many new parameters to both the SUSY-conserving and the SUSY-breaking sectors [81, 261]. Each new interaction term violates either B or L conservation. For example, starting from the MSSM superpotential given in Eq. (87.1) [suitably generalized to three generations of quarks, leptons and their superpartners], consider the effect of adding the following new terms:

$$\begin{aligned} W_{\rm RPV} =&(\lambda_L)_{pmn}\widehat{L}_p\widehat{L}_m\widehat{E}^c_n + (\lambda'_L)_{pmn}\widehat{L}_p\widehat{Q}_m\widehat{D}^c_n \\ &+ (\lambda_B)_{pmn}\widehat{U}^c_p\widehat{D}^c_m\widehat{D}^c_n + (\mu_L)_p\widehat{H}_u\widehat{L}_p\,, \end{aligned} \tag{87.42}$$

where p, m, and n are generation indices, and gauge group indices are suppressed. Eq. (87.42) yields new scalar-fermion Yukawa couplings consisting of all possible combinations involving two SM fermions and one scalar superpartner. Note that the term in Eq. (87.42) proportional to λ_B violates B, while the other three terms violate L. The L-violating term in Eq. (87.42) proportional to μ_L is the RPV analog of the $\mu\widehat{H}_u\widehat{H}_d$ term of the MSSM superpotential, in which the $Y = -1$ Higgs/higgsino supermultiplet $\widehat{H}_d$ is replaced by the slepton/lepton supermultiplet $\widehat{L}_p$.

Phenomenological constraints derived from data on various low-energy B- and L-violating processes can be used to establish limits on each of the coefficients $(\lambda_L)_{pmn}$, $(\lambda'_L)_{pmn}$, and $(\lambda_B)_{pmn}$ taken one at a time [261, 262]. If more than one coefficient is simultaneously non-zero, then the limits are in general more complicated [263]. All possible RPV terms cannot be simultaneously present and unsuppressed; otherwise the proton decay rate would be many orders of magnitude larger than the present experimental bound. One way to avoid proton decay is to impose B or L invariance (either one alone would suffice). Otherwise, one must accept the requirement that certain RPV coefficients must be extremely suppressed.

One particularly interesting class of RPV models is one in which B is conserved, but L is violated. It is possible to enforce baryon number conservation (and the stability of the proton), while allowing for lepton-number-violating interactions by imposing a discrete $\mathbb{Z}_3$ baryon triality symmetry on the low-energy theory [264], in place of the standard $\mathbb{Z}_2$ R-parity. Since the distinction between the Higgs and matter supermultiplets is lost in RPV models where L is violated, the mixing of sleptons and Higgs bosons, the mixing of neutrinos and neutralinos, and the mixing of charged leptons and charginos are now possible, leading to more complicated mass matrices and mass eigenstates than in the MSSM. The treatment of neutrino masses and mixing in this framework can be found, *e.g.*, in Ref. [265].

Alternatively, one can consider imposing a lepton parity such that all lepton superfields are odd [264, 266]. In this case, only the B-violating term in Eq. (87.42) survives, and L is conserved. Models of this type have been considered in Ref. [267]. Since L is conserved in these models, the mixing of the lepton and Higgs superfields is forbidden. Moreover, neutrino masses (and mixing) are not generated if lepton parity is an exact symmetry. However, one expects that lepton parity cannot be exact due to quantum gravity effects. Remarkably, the standard $\mathbb{Z}_2$ R-parity and the $\mathbb{Z}_3$ baryon triality are stable with respect to quantum gravity effects, as they can be identified as residual discrete symmetries that arise from spontaneously broken non-anomalous gauge symmetries [264]. The symmetries employed above to either remove or suppress R-parity violating operators were flavor independent. In contrast, there exist a number of motivated scenarios based on flavor symmetries that can also yield the suppression as required by the experimental data (*e.g.*, see Ref. [268]).

The supersymmetric phenomenology of the RPV models exhibits features that are distinct from that of the MSSM [261]. The LSP is no longer stable, which implies that not all supersymmetric decay chains must yield missing-energy events at colliders. A comprehensive examination of the phenomenology of the MSSM extended by a single R-parity violating coupling at the unifica-

Int. J. Mod. Phys. A 2026.41. Downloaded from www.worldscientific.com by UNIVERSITY OF CALIFORNIA @ BERKELEY on 09/16/26. Re-use and distribution is strictly not permitted, except for Open Access articles.

tion scale and its implications for LHC searches has been given in Ref. [269]. As an example, the sparticle mass bounds obtained in searches for R-parity-conserving SUSY can be considerably relaxed in certain RPV models due to the absence of large missing transverse momentum signatures [270]. This can alleviate some of the tension with naturalness (discussed in Sec. 87.7.1).

Nevertheless, the loss of the missing-energy signature is often compensated by other striking signals (which depend on which R-parity-violating terms are dominant). For example, supersymmetric particles in RPV models can be singly produced (in contrast to R-parity-conserving models where supersymmetric particles must be produced in pairs). The phenomenology of pair-produced supersymmetric particles is also modified in RPV models due to new decay chains not present in R-parity-conserving SUSY models [261].

In RPV models with lepton number violation (these include weak-scale SUSY models with baryon triality mentioned above), both $\Delta L = 1$ and $\Delta L = 2$ phenomena are allowed, leading to neutrino masses and mixing [271], neutrinoless double-beta decay [272], sneutrino-antisneutrino mixing [273], and resonant s-channel production of sneutrinos in e^+e^- collisions [274] and in charged sleptons in $p\bar{p}$ and pp collisions [275], respectively.

87.9 Extensions beyond the MSSM

In addition to possible extensions of the MSSM to incorporate massive neutrinos discussed in Sec. 87.8, there are numerous reasons for considering more general extensions of the MSSM [37]. Possible extensions include an enlarged electroweak gauge group beyond SU(2)×U(1) [107, 276, 277], the addition of new Higgs supermultiplets beyond the doublets and singlets of the MSSM/N-MSSM [278], and/or the addition of new (possibly exotic) matter supermultiplets [216, 279, 280] such as vector-like fermions and their superpartners or adjoint chiral superfields [281, 282].

In this final Section, we shall briefly focus on extensions of the MSSM that have been proposed to solve specific theoretical problems associated with the MSSM.

87.9.1 *The origin of the μ parameter*

In the MSSM, the parameter μ that appears in Eq. (87.1) is a SUSY-*preserving* parameter. However, its magnitude must be of order the effective SUSY-breaking scale of the MSSM to yield a consistent supersymmetric phenomenology [283]. Any natural solution to the so-called μ-problem must incorporate a symmetry that enforces $\mu = 0$ and a small symmetry-breaking parameter that generates a value of μ that is not parametrically larger than the effective SUSY-breaking scale [284]. A number of proposed mechanisms in the literature (*e.g.*, see Ref. [283–285]) provide concrete examples of a natural solution to the μ-problem of the MSSM.

In extensions of the MSSM, other compelling solutions to the μ-problem are possible. For example, one can replace μ by the VEV of a new SU(3)×SU(2)×U(1) singlet scalar field, as noted below Eq. (87.25). This is the NMSSM, which yields phenomena that were briefly discussed in Sections 87.4–87.7. The NMSSM superpotential consists only of trilinear terms whose coefficients are dimensionless. One can also extend the NMSSM further to the so-called USSM [107] by adding a new broken U(1) gauge symmetry [286], under which the singlet field is charged.

Alternatively, one can consider a generalized version of the NMSSM (called the GNMSSM in Ref. [215]), where all possible renormalizable terms in the superpotential are allowed, which yield new supersymmetric mass terms (analogous to the μ term of the MSSM). A discussion of the parameters of the GNMSSM can be found in Ref. [81]. Although the GNMSSM does not solve the μ-problem, it does exhibit regions of parameter space in which the degree of fine-tuning is relaxed, as mentioned in Sec. 87.7.1.

The generation of the μ-term may be connected with the solution to the strong CP problem [287]. Models of this type, which include new gauge singlet fields that are charged under the Peccei-Quinn (PQ) symmetry [288], were first proposed in Ref. [283]. The breaking of the PQ symmetry is thus intimately tied to SUSY breaking, while naturally yielding a value of μ that is of order the electroweak symmetry breaking scale [289].

87.9.2 *Dirac gauginos*

The MSSM and its extensions considered so far in this review contain self-conjugate fermions—the Majorana gluinos and neutralinos. The possibility of Dirac gluinos and neutralinos arises if the R-parity of the supersymmetric model is promoted to a continuous $\mathrm{U}(1)_R$ symmetry. In the MSSM, this could be (partially) achieved by setting the supersymmetry-conserving higgsino mass parameter μ and the supersymmetry-breaking gaugino Majorana mass parameters M_i $(i = 1, 2, 3)$ and A-parameters to zero. The resulting spectrum features a massless gluino and a pair of massive Dirac neutralinos whose masses are generated at the tree-level and at the one-loop level, respectively [40].

The mass spectrum of gluinos/neutralinos quoted above is not phenomenologically viable. Nevertheless, one can devise more realistic models by expanding the MSSM to include additional chiral superfields in the adjoint representation (*e.g.*, a color octet chiral superfield), while still respecting the $\mathrm{U}(1)_R$ symmetry. The spin-1/2 components of the adjoint chiral superfields can pair up with the gauginos to form Dirac gauginos [39, 40, 281, 282]. Such states appear in models of so-called supersoft SUSY breaking [290] and in some generalized GMSB models [281, 291]. Moreover, by introducing additional Higgs supermultiplets while maintaining the $\mathrm{U}(1)_R$ symmetry, the spin-1/2 components of these new superfields can pair up with the neutral higgsino states of the MSSM to form Dirac neutralinos [292]. Various scenarios, often referred to as constrained minimal Dirac gaugino supersymmetric models, have been proposed and analyzed in Refs. [292, 293].

The phenomenology of models with Dirac gauginos can be quite distinct from that of the MSSM, as noted in Ref. [294]. Moreover, such models can lead to significantly relaxed flavor constraints [292]. In particular, the higher mass scale of the gauginos and their Dirac nature lead to suppressed colored sparticle production at the LHC [295]. The implications of models of Dirac gauginos for the properties of the observed Higgs boson and possibilities for improved naturalness are addressed in Ref. [296].

References

[1] G. Kane and M. Shifman, editors, *The Supersymmetric World—The Beginnings of the Theory,* 2nd edition, World Scientific, Singapore (2025), contains an early history of supersymmetry and a guide to the original literature.

[2] R. Haag, J. T. Lopuszanski and M. Sohnius, Nucl. Phys. **B88**, 257 (1975); S. R. Coleman and J. Mandula, Phys. Rev. **159**, 1251 (1967).

[3] J. Terning, *Modern Supersymmetry: Dynamics and Duality* (Oxford Science Publications, Oxford, UK, 2006).

[4] M. Bertolini, *Supersymmetry: From the Basics to Exact Results in Gauge Theories* (World Scientific, Singapore, 2025).

[5] H. P. Nilles, Phys. Rept. **110**, 1 (1984).

[6] S. Weinberg, *The Quantum Theory of Fields, Volume III: Supersymmetry* (Cambridge University Press, Cambridge, UK, 2000).

[7] P. Nath, *Supersymmetry, Supergravity, and Unification* (Cambridge University Press, Cambridge, UK, 2017).

[8] E. Witten, Nucl. Phys. **B188**, 513 (1981).

[9] S. Dimopoulos and H. Georgi, Nucl. Phys. **B193**, 150 (1981); N. Sakai, Z. Phys. **C11**, 153 (1981).

[10] L. Susskind, Phys. Rept. **104**, 181 (1984).

[11] L. Girardello and M. T. Grisaru, Nucl. Phys. **B194**, 65 (1982).

[12] L. J. Hall and L. Randall, Phys. Rev. Lett. **65**, 2939 (1990); I. Jack and D. R. T. Jones, Phys. Lett. **B457**, 101 (1999), [hep-ph/9903365].

[13] V. F. Weisskopf, Phys. Rev. **56**, 72 (1939).

[14] M. B. Einhorn and D. R. T. Jones, Nucl. Phys. **B196**, 475 (1982); W. J. Marciano and G. Senjanovic, Phys. Rev. **D25**, 3092 (1982).

[15] N. Polonsky, *Supersymmetry: Structure and phenomena. Extensions of the standard model*, Lect. Notes Phys. Monogr. **68**, 1 (2001).

Int. J. Mod. Phys. A 2026.41. Downloaded from www.worldscientific.com
by UNIVERSITY OF CALIFORNIA @ BERKELEY on 09/16/26. Re-use and distribution is strictly not permitted, except for Open Access articles.

[16] G. Bertone, D. Hooper and J. Silk, Phys. Rept. **405**, 279 (2005), [hep-ph/0404175].

[17] D. Hooper, "TASI 2008 Lectures on Dark Matter," in *The Dawn of the LHC Era, Proceedings of the 2008 Theoretical and Advanced Study Institute in Elementary Particle Physics,* Boulder, Colorado, 2–27 June 2008, edited by Tao Han (World Scientific, Singapore, 2009).

[18] H. Pagels and J. R. Primack, Phys. Rev. Lett. **48**, 223 (1982).

[19] H. Goldberg, Phys. Rev. Lett. **50**, 1419 (1983).

[20] J. R. Ellis *et al.*, Nucl. Phys. **B238**, 453 (1984).

[21] G. Jungman, M. Kamionkowski, and K. Griest, Phys. Reports **267**, 195 (1996).

[22] F. D. Steffen, Eur. Phys. J. **C59**, 557 (2009), [arXiv:0811.3347].

[23] H. E. Haber and G. L. Kane, Phys. Rept. **117**, 75 (1985).

[24] S. P. Martin, *A Supersymmetry Primer*, [hep-ph/9709356].

[25] M. Drees, R. Godbole, and P. Roy, *Theory and Phenomenology of Sparticles* (World Scientific, Singapore, 2005).

[26] H. Baer and X. Tata, *Weak Scale Supersymmetry: from Superfields to Scattering Events* (Cambridge University Press, Cambridge, UK, 2006).

[27] H.K. Dreiner, H.E. Haber, and S.P. Martin, *From Spinors to Supersymmetry* (Cambridge University Press, Cambridge, UK, 2023).

[28] Our notation for the charge-conjugated fermion fields follows the conventions of Ref. [27].

[29] H. Georgi and S. L. Glashow, Phys. Rev. **D6**, 429 (1972).

[30] P. Fayet, Nucl. Phys. **B90**, 104 (1975).

[31] K. Inoue *et al.*, Prog. Theor. Phys. **67**, 1889 (1982).

[32] J. F. Gunion and H. E. Haber, Nucl. Phys. **B272**, 1 (1986), [Erratum: **B402**, 567 (1993)].

[33] A. Salam and J. A. Strathdee, Nucl. Phys. **B76**, 477 (1974).

[34] J. Wess and J. Bagger, *Supersymmetry and Supergravity* (Princeton University Press, Princeton, NJ, 1992).

[35] I. L. Buchbinder, S. Kuzenko and Z. Yarevskaya, Nucl. Phys. **B411**, 665 (1994); I. Antoniadis, E. Dudas and D. M. Ghilencea, JHEP **03**, 045 (2008), [arXiv:0708.0383]; E. Dudas and D. M. Ghilencea, JHEP **06**, 124 (2015), [arXiv:1503.08319].

[36] D. J. H. Chung *et al.*, Phys. Rept. **407**, 1 (2005), [hep-ph/0312378].

[37] S. Khalil and S. Moretti, *Supersymmetry Beyond Minimality: From Theory to Experiment* (CRC Press, Boca Raton, FL, 2018).

[38] J. R. Ellis *et al.*, Phys. Rev. **D39**, 844 (1989); U. Ellwanger and C. Hugonie, Eur. Phys. J. **C25**, 297 (2002), [hep-ph/9909260]; U. Ellwanger, C. Hugonie and A. M. Teixeira, Phys. Rept. **496**, 1 (2010), [arXiv:0910.1785]; M. Maniatis, Int. J. Mod. Phys. **A25**, 3505 (2010), [arXiv:0906.0777].

[39] P. Fayet, Phys. Lett. **78B**, 417 (1978).

[40] L. J. Hall and L. Randall, Nucl. Phys. B **352**, 289 (1991); L. Randall and N. Rius, Phys. Lett. B **286**, 299 (1992).

[41] S. Weinberg, Phys. Rev. Lett. **43**, 1566 (1979); S. Weinberg, Phys. Rev. **D22**, 1694 (1980); F. Wilczek and A. Zee, Phys. Rev. Lett. **43**, 1571 (1979); H. A. Weldon and A. Zee, Nucl. Phys. **B173**, 269 (1980).

[42] P. Fayet, Phys. Lett. **69B**, 489 (1977); G. R. Farrar and P. Fayet, Phys. Lett. **76B**, 575 (1978).

[43] P. Fayet, Phys. Lett. **84B**, 421 (1979); P. Fayet, Phys. Lett. **86B**, 272 (1979).

[44] D.Z. Freedman and A. Van Proeyen, *Supergravity* (Cambridge University Press, Cambridge, UK, 2012); M. Rausch de Traubenberg and M. Valenzuela, *A Supergravity Primer* (World Scientific, Singapore, 2020); H. Năstase, *Introduction to Supergravity and Its Applications* (Cambridge University Press, Cambridge, UK, 2025).

[45] S. Deser and B. Zumino, Phys. Rev. Lett. **38**, 1433 (1977); E. Cremmer *et al.*, Phys. Lett. **79B**, 231 (1978).

[46] R. Casalbuoni *et al.*, Phys. Lett. **B215**, 313 (1988); R. Casalbuoni *et al.*, Phys. Rev. **D39**, 2281 (1989); A. L. Maroto and J. R. Pelaez, Phys. Rev. **D62**, 023518 (2000), [hep-ph/9912212].

[47] Z. Komargodski and N. Seiberg, JHEP **09**, 066 (2009), [arXiv:0907.2441]; I. Antoniadis *et al.*, Nucl. Phys. B **841**, 157 (2010), [arXiv:1006.1662]; D. M. Ghilencea, Mod. Phys. Lett. A **31**, 1630011 (2016), [arXiv:1512.07484].

[48] A.H. Chamseddine, R. Arnowitt, and P. Nath, Phys. Rev. Lett. **49**, 970 (1982); R. Barbieri, S. Ferrara and C. A. Savoy, Phys. Lett. **119B**, 343 (1982); L. E. Ibanez, Nucl. Phys. **B218**, 514 (1983); H. P. Nilles, M. Srednicki and D. Wyler, Phys. Lett. **120B**, 346 (1983); H. P. Nilles, M. Srednicki and D. Wyler, Phys. Lett. **124B**, 337 (1983); E. Cremmer, P. Fayet and L. Girardello, Phys. Lett. **122B**, 41 (1983); N. Ohta, Prog. Theor. Phys. **70**, 542 (1983).

[49] L. Alvarez-Gaume, J. Polchinski and M. B. Wise, Nucl. Phys. B **221**, 495 (1983).

[50] L. J. Hall, J. D. Lykken and S. Weinberg, Phys. Rev. **D27**, 2359 (1983).

[51] S. K. Soni and H. A. Weldon, Phys. Lett. **126B**, 215 (1983); Y. Kawamura, H. Murayama and M. Yamaguchi, Phys. Rev. **D51**, 1337 (1995), [hep-ph/9406245].

[52] See *e.g.*, A. Brignole, L.E. Ibáñez, and C. Munoz, in *Perspectives on Supersymmetry II*, edited by G.L. Kane (World Scientific, Singapore, 2010) pp. 244–268.

[53] A. B. Lahanas and D. V. Nanopoulos, Phys. Rept. **145**, 1 (1987).

[54] J. L. Feng, A. Rajaraman and F. Takayama, Phys. Rev. Lett. **91**, 011302 (2003), [hep-ph/0302215]; J. L. Feng, A. Rajaraman and F. Takayama, Phys. Rev. **D68**, 063504 (2003), [hep-ph/0306024]; J. L. Feng, A. Rajaraman and F. Takayama, Int. J. Mod. Phys. **D13**, 2355 (2004), [hep-th/0405248].

[55] L. Randall and R. Sundrum, Nucl. Phys. **B557**, 79 (1999), [hep-th/9810155].

[56] F. D'Eramo, J. Thaler and Z. Thomas, JHEP **06**, 151 (2012), [arXiv:1202.1280]; F. D'Eramo, J. Thaler and Z. Thomas, JHEP **09**, 125 (2013), [arXiv:1307.3251]; S. P. de Alwis, Phys. Rev. **D77**, 105020 (2008), [arXiv:0801.0578]; S. P. de Alwis, JHEP **01**, 006 (2013), [arXiv:1206.6775]; K. Harigaya and M. Ibe, Phys. Rev. **D90**, 085028 (2014), [arXiv:1409.5029].

[57] I. Jack, D. R. T. Jones and R. Wild, Phys. Lett. **B535**, 193 (2002), [hep-ph/0202101]; B. Murakami and J. D. Wells, Phys. Rev. **D68**, 035006 (2003), [hep-ph/0302209]; R. Kitano, G. D. Kribs and H. Murayama, Phys. Rev. **D70**, 035001 (2004), [hep-ph/0402215]; R. Hodgson *et al.*, Nucl. Phys. **B728**, 192 (2005), [hep-ph/0507193]; D. R. T. Jones and G. G. Ross, Phys. Lett. **B642**, 540 (2006), [hep-ph/0609210].

[58] S. Asai *et al.*, Phys. Lett. **B653**, 81 (2007), [arXiv:0705.3086].

[59] M. Dine, W. Fischler and M. Srednicki, Nucl. Phys. **B189**, 575 (1981); S. Dimopoulos and S. Raby, Nucl. Phys. **B192**, 353 (1981); S. Dimopoulos and S. Raby, Nucl. Phys. **B219**, 479 (1983); M. Dine and W. Fischler, Phys. Lett. **110B**, 227 (1982); C. R. Nappi and B. A. Ovrut, Phys. Lett. **113B**, 175 (1982); L. Alvarez-Gaume, M. Claudson and M. B. Wise, Nucl. Phys. **B207**, 96 (1982).

Int. J. Mod. Phys. A 2026.41. Downloaded from www.worldscientific.com
by UNIVERSITY OF CALIFORNIA @ BERKELEY on 09/16/26. Re-use and distribution is strictly not permitted, except for Open Access articles.

[60] M. Dine and A. E. Nelson, Phys. Rev. **D48**, 1277 (1993), [hep-ph/9303230]; M. Dine, A. E. Nelson and Y. Shirman, Phys. Rev. **D51**, 1362 (1995), [hep-ph/9408384].

[61] M. Dine *et al.*, Phys. Rev. **D53**, 2658 (1996), [hep-ph/9507378].

[62] G. F. Giudice and R. Rattazzi, Phys. Rept. **322**, 419 (1999), [hep-ph/9801271].

[63] E. Poppitz and S. P. Trivedi, Phys. Rev. **D55**, 5508 (1997), [hep-ph/9609529]; H. Murayama, Phys. Rev. Lett. **79**, 18 (1997), [hep-ph/9705271]; M. A. Luty and J. Terning, Phys. Rev. **D57**, 6799 (1998), [hep-ph/9709306]; K. Agashe, Phys. Lett. **B435**, 83 (1998), [hep-ph/9804450]; N. Arkani-Hamed, J. March-Russell and H. Murayama, Nucl. Phys. **B509**, 3 (1998), [hep-ph/9701286]; C. Csaki, Y. Shirman and J. Terning, JHEP **05**, 099 (2007), [hep-ph/0612241]; M. Ibe and R. Kitano, Phys. Rev. **D77**, 075003 (2008), [arXiv:0711.0416].

[64] S. Weinberg, Phys. Rev. Lett. **48**, 1303 (1982); M. Kawasaki, F. Takahashi and T. T. Yanagida, Phys. Rev. D **74**, 043519 (2006), [hep-ph/0605297]; M. Kawasaki *et al.*, Phys. Rev. **D78**, 065011 (2008), [arXiv:0804.3745].

[65] M. J. Strassler and K. M. Zurek, Phys. Lett. **B651**, 374 (2007), [hep-ph/0604261]; T. Han *et al.*, JHEP **07**, 008 (2008), [arXiv:0712.2041].

[66] M. J. Strassler [hep-ph/0607160]; K. M. Zurek, Phys. Rev. **D79**, 115002 (2009), [arXiv:0811.4429].

[67] See *e.g.*, M. Quiros, in *Particle Physics and Cosmology: The Quest for Physics Beyond the Standard Model(s), Proceedings of the 2002 Theoretical Advanced Study Institute in Elementary Particle Physics (TASI 2002),* edited by H.E. Haber and A.E. Nelson (World Scientific, Singapore, 2004) pp. 549–601; C. Csaki, in *ibid.*, pp. 605–698.

[68] V.A. Rubakov, Sov. Phys. Usp. **44**, 871 (2001); J. L. Hewett and M. Spiropulu, Ann. Rev. Nucl. Part. Sci. **52**, 397 (2002), [hep-ph/0205106].

[69] Z. Chacko, M. A. Luty and E. Ponton, JHEP **07**, 036 (2000), [hep-ph/9909248]; D. E. Kaplan, G. D. Kribs and M. Schmaltz, Phys. Rev. **D62**, 035010 (2000), [hep-ph/9911293]; Z. Chacko *et al.*, JHEP **01**, 003 (2000), [hep-ph/9911323].

[70] J. Scherk and J. H. Schwarz, Phys. Lett. **82B**, 60 (1979); J. Scherk and J. H. Schwarz, Nucl. Phys. **B153**, 61 (1979).

[71] R. Barbieri, L. J. Hall and Y. Nomura, Phys. Rev. **D66**, 045025 (2002), [hep-ph/0106190]; R. Barbieri, L. J. Hall and Y. Nomura, Nucl. Phys. **B624**, 63 (2002), [hep-th/0107004]; I. Garcia Garcia, K. Howe and J. March-Russell, JHEP **12**, 005 (2015), [arXiv:1510.07045].

[72] J. D. Wells, Phys. Rev. **D71**, 015013 (2005), [hep-ph/0411041].

[73] N. Arkani-Hamed and S. Dimopoulos, JHEP **06**, 073 (2005), [hep-th/0405159]; G. F. Giudice and A. Romanino, Nucl. Phys. **B699**, 65 (2004), [Erratum: **B706**, 487 (2005)], [hep-ph/0406088].

[74] G. F. Giudice and A. Strumia, Nucl. Phys. **B858**, 63 (2012), [arXiv:1108.6077].

[75] A. Arvanitaki *et al.*, JHEP **02**, 126 (2013), [arXiv:1210.0555]; N. Arkani-Hamed *et al.* (2012), [arXiv:1212.6971].

[76] P. Slavich *et al.*, Eur. Phys. J. C **81**, 450 (2021), [arXiv:2012.15629].

[77] E. Bagnaschi *et al.*, JHEP **09**, 092 (2014), [arXiv:1407.4081]; J. Pardo Vega and G. Villadoro, JHEP **07**, 159 (2015), [arXiv:1504.05200].

[78] Y. Kahn, M. McCullough and J. Thaler, JHEP **11**, 161 (2013), [arXiv:1308.3490]; H. Baer *et al.*, Phys. Rev. D **111**, 095019 (2025), [arXiv:2412.15356].

[79] L. J. Hall and Y. Nomura, JHEP **01**, 082 (2012), [arXiv:1111.4519]; M. Ibe and T. T. Yanagida, Phys. Lett. **B709**, 374 (2012), [arXiv:1112.2462].

[80] H. E. Haber and L. Stephenson Haskins (2018), *Supersymmetric Theory and Models*, in *Anticipating the Next Discoveries in Particle Physics*, Proceedings of the 2016 Theoretical Advanced Study Institute in Elementary Particle Physics, edited by Rouven Essig and Ian Low (World Scientific, Singapore, 2018) pp. 355-499, [arXiv:1712.05926].

[81] B. C. Allanach *et al.*, Comput. Phys. Commun. **180**, 8 (2009), [arXiv:0801.0045].

[82] J. M. Frere, D. R. T. Jones and S. Raby, Nucl. Phys. **B222**, 11 (1983); J. P. Derendinger and C. A. Savoy, Nucl. Phys. **B237**, 307 (1984); J. F. Gunion, H. E. Haber and M. Sher, Nucl. Phys. **B306**, 1 (1988); D. Chowdhury *et al.*, JHEP **02**, 110 (2014), [Erratum: **03**, 149 (2018)], [arXiv:1310.1932]; W. G. Hollik, JHEP **08**, 126 (2016), [arXiv:1606.08356].

[83] J. A. Casas, A. Lleyda and C. Munoz, Nucl. Phys. **B471**, 3 (1996), [hep-ph/9507294].

[84] J. E. Camargo-Molina *et al.*, Eur. Phys. J. C **73**, 2588 (2013), [arXiv:1307.1477].

[85] N. Blinov and D. E. Morrissey, JHEP **03**, 106 (2014), [arXiv:1310.4174].

[86] C. S. Ün *et al.*, Phys. Rev. **D91**, 105033 (2015), [arXiv:1412.1440].

[87] G. G. Ross, K. Schmidt-Hoberg and F. Staub, Phys. Lett. **B759**, 110 (2016), [arXiv:1603.09347].

[88] G. G. Ross, K. Schmidt-Hoberg and F. Staub, JHEP **03**, 021 (2017), [arXiv:1701.03480].

[89] S. P. Martin, Phys. Rev. **D61**, 035004 (2000), [hep-ph/9907550].

[90] S. Dimopoulos and D. W. Sutter, Nucl. Phys. **B452**, 496 (1995), [hep-ph/9504415]; D. W. Sutter, Stanford Ph.D. thesis (1995), [hep-ph/9704390].

[91] H. E. Haber, Nucl. Phys. B Proc. Suppl. **62**, 469 (1998), [hep-ph/9709450].

[92] R. M. Barnett, J. F. Gunion and H. E. Haber, Phys. Lett. **B315**, 349 (1993), [hep-ph/9306204]; H. Baer, X. Tata and J. Woodside, Phys. Rev. **D41**, 906 (1990).

[93] S. M. Bilenky, N. P. Nedelcheva and E. K. Khristova, Phys. Lett. **161B**, 397 (1985); S. M. Bilenky, E. K. Khristova and N. P. Nedelcheva, Bulg. J. Phys. **13**, 283 (1986); G. A. Moortgat-Pick and H. Fraas, Eur. Phys. J. **C25**, 189 (2002), [hep-ph/0204333].

[94] J. Rosiek, Phys. Rev. **D41**, 3464 (1990), [Erratum: hep-ph/9511250]; M. Kuroda (1999), [hep-ph/9902340].

[95] J. Alwall *et al.*, JHEP **09**, 028 (2007), [arXiv:0706.2334].

[96] T. Hahn, Comput. Phys. Commun. **140**, 418 (2001), [hep-ph/0012260].

[97] A. Pukhov *et al.*, INP-MSU-98-41/542 (1998), [hep-ph/9908288]; E. Boos *et al.* (CompHEP Collaboration), Nucl. Instrum. Meth. A **534**, 250 (2004), [hep-ph/0403113]; The CompHEP homepage is `https://twiki.cern.ch/twiki/bin/view/Main/CompHep`.

[98] D. M. Pierce *et al.*, Nucl. Phys. **B491**, 3 (1997), [hep-ph/9606211].

[99] P. Z. Skands *et al.*, JHEP **07**, 036 (2004), [hep-ph/0311123].

[100] For further details, see *e.g.*, Appendix C of Ref. [23] and Appendix A of Ref. [32].

[101] J. L. Kneur and G. Moultaka, Phys. Rev. **D59**, 015005 (1999), [hep-ph/9807336].

[102] R.A. Horn and C.R. Johnson, *Matrix Analysis*, 2nd Edition (Cambridge University Press, Cambridge, UK, 2003).

[103] H. K. Dreiner, H. E. Haber and S. P. Martin, Phys. Rept. **494**, 1 (2010), [arXiv:0812.1594].

Int. J. Mod. Phys. A 2026.41. Downloaded from www.worldscientific.com
by UNIVERSITY OF CALIFORNIA @ BERKELEY on 09/16/26. Re-use and distribution is strictly not permitted, except for Open Access articles.

[104] H. E. Haber, Int. J. Mod. Phys. A **36**, 2130003 (2021), [arXiv:2009.03990].

[105] S. Pokorski, J. Rosiek and C. A. Savoy, Nucl. Phys. B **570**, 81 (2000), [hep-ph/9906206].

[106] L. Autonne, Annals de l'Université de Lyon, Nouvelle Série I, Fasc. **38**, 1 (1915); T. Takagi, Japan J. Math. **1**, 83 (1925).

[107] S. Y. Choi *et al.*, Nucl. Phys. **B778**, 85 (2007), [hep-ph/0612218].

[108] S. Y. Choi *et al.*, Eur. Phys. J. **C22**, 563 (2001), [Addendum: Eur. Phys. J. **C23**, 769 (2002)], [hep-ph/0108117]; M. M. El Kheishen, A. A. Aboshousha and A. A. Shafik, Phys. Rev. **D45**, 4345 (1992).

[109] T. Hahn (2006), [arXiv:physics/0607103].

[110] J. R. Ellis and S. Rudaz, Phys. Lett. **128B**, 248 (1983); F. Browning, D. Chang and W.-Y. Keung, Phys. Rev. **D64**, 015010 (2001), [hep-ph/0012258]; A. Bartl *et al.*, Phys. Lett. **B573**, 153 (2003), [hep-ph/0307317]; A. Bartl *et al.*, Phys. Rev. **D70**, 035003 (2004), [hep-ph/0311338].

[111] K.-i. Hikasa and M. Kobayashi, Phys. Rev. **D36**, 724 (1987); F. Gabbiani and A. Masiero, Nucl. Phys. **B322**, 235 (1989); P. Brax and C. A. Savoy, Nucl. Phys. **B447**, 227 (1995), [hep-ph/9503306].

[112] J.F. Gunion *et al.*, *The Higgs Hunter's Guide* (Westview Press, Boulder, CO, 2000); A. Djouadi, Phys. Rept. **459**, 1 (2008), [hep-ph/0503173].

[113] M. Carena and H. E. Haber, Prog. Part. Nucl. Phys. **50**, 63 (2003), [hep-ph/0208209].

[114] J. Bernon *et al.*, Phys. Rev. D **92**, 075004 (2015), [arXiv:1507.00933].

[115] J. Bernon *et al.*, Phys. Rev. D **93**, 035027 (2016), [arXiv:1511.03682].

[116] P. Bechtle *et al.*, Eur. Phys. J. **C77**, 67 (2017), [arXiv:1608.00638]; E. Bagnaschi *et al.*, Eur. Phys. J. **C79**, 617 (2019), [arXiv:1808.07542].

[117] G. Aad *et al.* (ATLAS Collaboration), Phys. Rept. **1116**, 4 (2025), [arXiv:2404.05498]; A. Hayrapetyan *et al.* (CMS Collaboration), Phys. Rev. D **111**, 092014 (2025), [arXiv:2409.13663].

[118] J. F. Gunion and H. E. Haber, Phys. Rev. D **67**, 075019 (2003), [hep-ph/0207010].

[119] L. J. Hall and M. B. Wise, Nucl. Phys. **B187**, 397 (1981).

[120] H. E. Haber and M. Sher, Phys. Rev. **D35**, 2206 (1987).

[121] L. J. Hall, D. Pinner and J. T. Ruderman, JHEP **04**, 131 (2012), [arXiv:1112.2703].

[122] H. E. Haber and R. Hempfling, Phys. Rev. Lett. **66**, 1815 (1991); Y. Okada, M. Yamaguchi and T. Yanagida, Prog. Theor. Phys. **85**, 1 (1991); J. R. Ellis, G. Ridolfi and F. Zwirner, Phys. Lett. **B257**, 83 (1991).

[123] H. E. Haber, R. Hempfling and A. H. Hoang, Z. Phys. C **75**, 539 (1997), [hep-ph/9609331].

[124] P. Draper and H. Rzehak, Phys. Rept. **619**, 1 (2016), [arXiv:1601.01890].

[125] E. Bagnaschi, J. Pardo Vega and P. Slavich, Eur. Phys. J. C **77**, 334 (2017), [arXiv:1703.08166].

[126] H. Bahl, D. Meuser and G. Weiglein, Eur. Phys. J. C **84**, 1017 (2024), [arXiv:2311.01889]; T. Kwasnitza *et al.*, Eur. Phys. J. C **86**, 590 (2026), [arXiv:2506.22208].

[127] B. C. Allanach and A. Voigt, Eur. Phys. J. C **78**, 573 (2018), [arXiv:1804.09410].

[128] H. E. Haber and J. D. Mason, Phys. Rev. **D77**, 115011 (2008), [arXiv:0711.2890].

[129] L. J. Hall, R. Rattazzi and U. Sarid, Phys. Rev. D **50**, 7048 (1994), [hep-ph/9306309]; R. Hempfling, Phys. Rev. D **49**, 6168 (1994); M. Carena *et al.*, Nucl. Phys. B **426**, 269 (1994), [hep-ph/9402253].

[130] A. Pilaftsis and C. E. M. Wagner, Nucl. Phys. B **553**, 3 (1999), [hep-ph/9902371]; M. Carena *et al.*, Nucl. Phys. B **586**, 92 (2000), [hep-ph/0003180]; S. Y. Choi, M. Drees and J. S. Lee, Phys. Lett. **B481**, 57 (2000), [hep-ph/0002287]; M. Carena *et al.*, Phys. Lett. **B495**, 155 (2000), [hep-ph/0009212]; S. Heinemeyer, Eur. Phys. J. C **22**, 521 (2001), [hep-ph/0108059]; M. Carena *et al.*, Nucl. Phys. **B625**, 345 (2002), [hep-ph/0111245]; M. Frank *et al.*, JHEP **02**, 047 (2007), [hep-ph/0611326]; S. Heinemeyer *et al.*, Phys. Lett. **B652**, 300 (2007), [arXiv:0705.0746].

[131] M. Carena *et al.*, Phys. Rev. **D93**, 035013 (2016), [arXiv:1510.09137].

[132] A. Djouadi *et al.*, Eur. Phys. J. C **73**, 2650 (2013), [arXiv:1307.5205].

[133] A. Djouadi *et al.*, JHEP **06**, 168 (2015), [arXiv:1502.05653].

[134] G. Lee and C. E. M. Wagner, Phys. Rev. D **92**, 075032 (2015), [arXiv:1508.00576].

[135] H. E. Haber, S. Heinemeyer and T. Stefaniak, Eur. Phys. J. C **77**, 742 (2017), [arXiv:1708.04416].

[136] H. Bahl, S. Liebler and T. Stefaniak, Eur. Phys. J. C **79**, 279 (2019), [arXiv:1901.05933].

[137] N. Craig and S. Thomas, JHEP **11**, 083 (2012), [arXiv:1207.4835]; N. Craig, J. Galloway and S. Thomas (2013), [arXiv:1305.2424]; M. Carena *et al.*, JHEP **04**, 015 (2014), [arXiv:1310.2248]; H. E. Haber, in "Proceedings of the 1st Toyama International Workshop on Higgs as a Probe of New Physics," (2013), [arXiv:1401.0152]; P. S. Bhupal Dev and A. Pilaftsis, JHEP **12**, 024 (2014), [Erratum: JHEP 11, 147 (2015)], [arXiv:1408.3405].

[138] G. Aad *et al.* (ATLAS Collaboration), Nature **607**, 52 (2022), [Erratum: Nature **612**, E24 (2022); *ibid.* **623**, E5 (2023)], [arXiv:2207.00092].

[139] A. Tumasyan *et al.* (CMS Collaboration), Nature **607**, 60 (2022), [Erratum: Nature **623**, E4 (2023)], [arXiv:2207.00043].

[140] G. Aad *et al.* (ATLAS Collaboration), JHEP **11**, 097 (2024), [arXiv:2402.05742].

[141] L. Constantin, S. Kraml and F. Mahmoudi, Nucl. Phys. B **1018**, 117012 (2025), [arXiv:2505.11251].

[142] S. Khalil, Int. J. Mod. Phys. **A18**, 1697 (2003), [hep-ph/0212050].

[143] D. A. Demir, Phys. Rev. **D60**, 055006 (1999), [hep-ph/9901389].

[144] W. Fischler, S. Paban and S. D. Thomas, Phys. Lett. **B289**, 373 (1992), [hep-ph/9205233]; A. Masiero and L. Silvestrini, in *Perspectives on Supersymmetry*, edited by G.L. Kane (World Scientific, Singapore, 1998) pp. 423–441; M. Pospelov and A. Ritz, Annals Phys. **318**, 119 (2005), [hep-ph/0504231].

[145] C. Abel *et al.*, Phys. Rev. Lett. **124**, 081803 (2020), [arXiv:2001.11966]; T. S. Roussy *et al.*, Science **381**, 46 (2023), [arXiv:2212.11841].

[146] F. Gabbiani *et al.*, Nucl. Phys. **B477**, 321 (1996), [hep-ph/9604387]; M. J. Ramsey-Musolf and S. Su, Phys. Rept. **456**, 1 (2008), [hep-ph/0612057].

[147] M. Carena, A. Menon and C. E. M. Wagner, Phys. Rev. **D79**, 075025 (2009), [arXiv:0812.3594].

[148] R.N. Mohapatra, *Unification and Supersymmetry*, Third Edition (Springer Science, New York, 2003).

[149] S. Raby, *Supersymmetric Grand Unified Theories* (Springer International Publishing AG, Cham, Switzerland, 2017).

[150] S. P. Martin and M. T. Vaughn, Phys. Rev. **D50**, 2282 (1994), [Erratum: **D78**, 039903 (2008)], [hep-ph/9311340]; R. M. Fonseca *et al.*, Nucl. Phys. **B854**, 28 (2012), [arXiv:1107.2670]; F. Staub, Comput. Phys. Commun. **182**, 808 (2011), [arXiv:1002.0840].

Int. J. Mod. Phys. A 2026.41. Downloaded from www.worldscientific.com
by UNIVERSITY OF CALIFORNIA @ BERKELEY on 09/16/26. Re-use and distribution is strictly not permitted, except for Open Access articles.

[151] F. Staub, Comput. Phys. Commun. **185**, 1773 (2014), [arXiv:1309.7223]; F. Staub, Adv. High Energy Phys. **2015**, 840780 (2015), [arXiv:1503.04200]; The SARAH homepage is `https://sarah.hepforge.org/`; R. M. Fonseca, Comput. Phys. Commun. **183**, 2298 (2012), [arXiv:1106.5016]; The Susyno homepage is `https://renatofonseca.net/susyno`.

[152] B. C. Allanach, Comput. Phys. Commun. **143**, 305 (2002), [hep-ph/0104145]; The SOFTSUSY homepage is `https://ballanach.github.io/softsusy/`; A. Djouadi, J.-L. Kneur and G. Moultaka, Comput. Phys. Commun. **176**, 426 (2007), [hep-ph/0211331]; The Suspect homepage is `http://suspect.in2p3.fr/`; F. E. Paige *et al.* (2003), [hep-ph/0312045]; Isajet may be obtained from `http://www.nhn.ou.edu/~isajet/`; W. Porod, Comput. Phys. Commun. **153**, 275 (2003), [hep-ph/0301101]; Spheno may be obtained from `https://spheno.hepforge.org/`; P. Athron *et al.*, Comput. Phys. Commun. **190**, 139 (2015), [arXiv:1406.2319]; The FlexibleSUSY homepage is `https://flexiblesusy.hepforge.org/`.

[153] L. E. Ibanez and G. G. Ross, Phys. Lett. **110B**, 215 (1982).

[154] M. Drees, Phys. Lett. B **158**, 409 (1985); J. R. Ellis *et al.*, Phys. Lett. B **155**, 381 (1985); S. P. Martin, Phys. Rev. D **79**, 095019 (2009), [arXiv:0903.3568].

[155] J. Abdallah *et al.* (DELPHI Collaboration), Eur. Phys. J. **C31**, 421 (2003), [hep-ex/0311019].

[156] H. K. Dreiner *et al.*, Eur. Phys. J. **C62**, 547 (2009), [arXiv:0901.3485].

[157] G. F. Giudice *et al.*, JHEP **12**, 027 (1998), [hep-ph/9810442]; A. Pomarol and R. Rattazzi, JHEP **05**, 013 (1999), [hep-ph/9903448]; D.-W. Jung and J. Y. Lee, JHEP **03**, 123 (2009), [arXiv:0902.0464].

[158] J. F. Gunion and H. E. Haber, Phys. Rev. **D37**, 2515 (1988); S. Y. Choi, M. Drees and B. Gaissmaier, Phys. Rev. **D70**, 014010 (2004), [hep-ph/0403054].

[159] H. Baer, V. Barger and D. Sengupta, Phys. Rev. **D98**, 015039 (2018), [arXiv:1801.09730].

[160] J. L. Feng *et al.*, Phys. Rev. Lett. **83**, 1731 (1999), [hep-ph/9904250]; J. F. Gunion and S. Mrenna, Phys. Rev. **D62**, 015002 (2000), [hep-ph/9906270].

[161] T. Gherghetta, G. F. Giudice and J. D. Wells, Nucl. Phys. **B559**, 27 (1999), [hep-ph/9904378].

[162] M. Endo, M. Yamaguchi and K. Yoshioka, Phys. Rev. **D72**, 015004 (2005), [hep-ph/0504036]; K. Choi, K. S. Jeong and K.-i. Okumura, JHEP **09**, 039 (2005), [hep-ph/0504037]; O. Loaiza-Brito *et al.*, AIP Conf. Proc. **805**, 198 (2005), [hep-th/0509158].

[163] G. D'Ambrosio *et al.*, Nucl. Phys. B **645**, 155 (2002), [hep-ph/0207036]; C. Smith, Acta Phys. Polon. Supp. **3**, 53 (2010), [arXiv:0909.4444].

[164] M. Drees and S.P. Martin, in *Electroweak Symmetry Breaking and New Physics at the TeV Scale*, edited by T. Barklow *et al.* (World Scientific, Singapore, 1996) pp. 146–215.

[165] G. L. Kane *et al.*, Phys. Rev. **D49**, 6173 (1994), [hep-ph/9312272].

[166] J. R. Ellis *et al.*, Phys. Lett. **B573**, 162 (2003), [hep-ph/0305212]; J. R. Ellis *et al.*, Phys. Rev. **D70**, 055005 (2004), [hep-ph/0405110].

[167] H. Baer *et al.*, Phys. Rev. **D71**, 095008 (2005), [hep-ph/0412059].

[168] V. Berezinsky *et al.*, Astropart. Phys. **5**, 1 (1996), [hep-ph/9508249]; J. R. Ellis *et al.*, Nucl. Phys. **B652**, 259 (2003), [hep-ph/0210205].

[169] L. E. Ibanez and D. Lust, Nucl. Phys. **B382**, 305 (1992), [hep-th/9202046]; B. de Carlos, J. A. Casas and C. Munoz, Phys. Lett. **B299**, 234 (1993), [hep-ph/9211266]; V. S. Kaplunovsky and J. Louis, Phys. Lett. **B306**, 269 (1993), [hep-th/9303040]; A. Brignole, L. E. Ibanez and C. Munoz, Nucl. Phys. **B422**, 125 (1994), [Erratum: **B436**, 747 (1995)], [hep-ph/9308271].

[170] A. Arbey *et al.*, Phys. Rev. **D87**, 115020 (2013), [arXiv:1304.0381].

[171] G. R. Dvali, G. F. Giudice and A. Pomarol, Nucl. Phys. **B478**, 31 (1996), [hep-ph/9603238].

[172] P. Draper *et al.*, Phys. Rev. **D85**, 095007 (2012), [arXiv:1112.3068].

[173] P. Meade, N. Seiberg and D. Shih, Prog. Theor. Phys. Suppl. **177**, 143 (2009), [arXiv:0801.3278]; M. Buican *et al.*, JHEP **03**, 016 (2009), [arXiv:0812.3668].

[174] A. Rajaraman *et al.*, Phys. Lett. **B678**, 367 (2009), [arXiv:0903.0668]; L. M. Carpenter *et al.*, Phys. Rev. **D79**, 035002 (2009), [arXiv:0805.2944].

[175] S. Ambrosanio, G. D. Kribs and S. P. Martin, Nucl. Phys. **B516**, 55 (1998), [hep-ph/9710217].

[176] For a review and guide to the literature, see J.F. Gunion and H.E. Haber, in *Perspectives on Supersymmetry II*, edited by G.L. Kane (World Scientific, Singapore, 2010) pp. 420–445.

[177] T. S. Roy and M. Schmaltz, Phys. Rev. **D77**, 095008 (2008), [arXiv:0708.3593].

[178] A. de Gouvea, A. Friedland and H. Murayama, Phys. Rev. **D57**, 5676 (1998), [hep-ph/9711264].

[179] T. Han, D. Marfatia and R.-J. Zhang, Phys. Rev. **D61**, 013007 (2000), [hep-ph/9906508]; Z. Chacko and E. Ponton, Phys. Rev. **D66**, 095004 (2002), [hep-ph/0112190]; A. Delgado, G. F. Giudice and P. Slavich, Phys. Lett. **B653**, 424 (2007), [arXiv:0706.3873]; T. Liu and C. E. M. Wagner, JHEP **06**, 073 (2008), [arXiv:0803.2895].

[180] A. Djouadi, J.L. Kneur, and G. Moultaka, Comp. Phys. Comm. **176**, 426 (2007); C. F. Berger *et al.*, JHEP **02**, 023 (2009), [arXiv:0812.0980]; B. Allanach *et al.*, Phys. Rev. **D92**, 015006 (2015), [arXiv:1502.05836].

[181] S. P. Martin and J. D. Wells, Phys. Rev. **D64**, 035003 (2001), [hep-ph/0103067].

[182] S. S. AbdusSalam *et al.*, Phys. Rev. D **81**, 095012 (2010), [arXiv:0904.2548].

[183] J. Berger *et al.*, Phys. Rev. **D93**, 035017 (2016), [arXiv:1510.08840].

[184] K. J. de Vries *et al.*, Eur. Phys. J. **C75**, 422 (2015), [arXiv:1504.03260].

[185] E. Bagnaschi *et al.*, Eur. Phys. J. **C78**, 256 (2018), [arXiv:1710.11091].

[186] M. Cahill-Rowley *et al.*, Phys. Rev. **D90**, 095017 (2014), [arXiv:1407.7021]; M. Cahill-Rowley *et al.*, Phys. Rev. **D91**, 055011 (2015), [arXiv:1405.6716]; G. Bertone *et al.*, JCAP **1604**, 037 (2016), [arXiv:1507.07008].

[187] N. Arkani-Hamed *et al.* (2007), [hep-ph/0703088]; J. Alwall *et al.*, Phys. Rev. **D79**, 015005 (2009), [arXiv:0809.3264]; J. Alwall, P. Schuster and N. Toro, Phys. Rev. **D79**, 075020 (2009), [arXiv:0810.3921]; D. S. M. Alves, E. Izaguirre and J. G. Wacker, Phys. Lett. **B702**, 64 (2011), [arXiv:1008.0407]; D. S. M. Alves, E. Izaguirre and J. G. Wacker, JHEP **10**, 012 (2011), [arXiv:1102.5338]; D. Alves (LHC New Physics Working Group), J. Phys. **G39**, 105005 (2012), [arXiv:1105.2838].

[188] F. Ambrogi *et al.*, Eur. Phys. J. **C78**, 215 (2018), [arXiv:1707.09036].

[189] G. Aad *et al.* (ATLAS Collaboration), Phys. Rept. **1116**, 261 (2025), [arXiv:2403.02455]; S. Sekmen, HiHEP **1**, 18 (2025), [arXiv:2510.17971].

[190] R. Barbieri and G. F. Giudice, Nucl. Phys. B **306**, 63 (1988).

[191] J. R. Ellis *et al.*, Mod. Phys. Lett. **A1**, 57 (1986).

[192] G. W. Anderson and D. J. Castano, Phys. Lett. **B347**, 300 (1995), [hep-ph/9409419]; G. W. Anderson and D. J. Castano, Phys. Rev. **D52**, 1693 (1995), [hep-ph/9412322]; G. W. Anderson and D. J. Castano, Phys. Rev. **D53**, 2403 (1996), [hep-ph/9509212]; P. Athron and D. J. Miller, Phys. Rev. **D76**, 075010 (2007), [arXiv:0705.2241].

Int. J. Mod. Phys. A 2026.41. Downloaded from www.worldscientific.com
by UNIVERSITY OF CALIFORNIA @ BERKELEY on 09/16/26. Re-use and distribution is strictly not permitted, except for Open Access articles.

[193] M. E. Cabrera, J. A. Casas and R. Ruiz de Austri, JHEP **03**, 075 (2009), [arXiv:0812.0536]; H. Baer *et al.*, Phys. Rev. Lett. **109**, 161802 (2012), [arXiv:1207.3343].

[194] J. L. Feng, K. T. Matchev and T. Moroi, Phys. Rev. **D61**, 075005 (2000), [hep-ph/9909334].

[195] D. M. Ghilencea and G. G. Ross, Nucl. Phys. **B868**, 65 (2013), [arXiv:1208.0837].

[196] H. Baer *et al.*, Phys. Rev. D **108**, 035050 (2023), [arXiv:2305.16125].

[197] H. Baer, V. Barger and D. Mickelson, Phys. Rev. **D88**, 095013 (2013), [arXiv:1309.2984].

[198] M. van Beekveld, S. Caron and R. Ruiz de Austri, JHEP **01**, 147 (2020), [arXiv:1906.10706].

[199] G. L. Kane and S. F. King, Phys. Lett. **B451**, 113 (1999), [hep-ph/9810374]; M. Bastero-Gil, G. L. Kane and S. F. King, Phys. Lett. **B474**, 103 (2000), [hep-ph/9910506]; J. A. Casas, J. R. Espinosa and I. Hidalgo, JHEP **01**, 008 (2004), [hep-ph/0310137]; H. Abe, T. Kobayashi and Y. Omura, Phys. Rev. **D76**, 015002 (2007), [hep-ph/0703044]; R. Essig and J.-F. Fortin, JHEP **04**, 073 (2008), [arXiv:0709.0980].

[200] B. de Carlos and J. A. Casas, Phys. Lett. **B309**, 320 (1993), [hep-ph/9303291]; S. Cassel, D. M. Ghilencea and G. G. Ross, Nucl. Phys. **B825**, 203 (2010), [arXiv:0903.1115]; S. Cassel, D. M. Ghilencea and G. G. Ross, Nucl. Phys. **B835**, 110 (2010), [arXiv:1001.3884]; D. M. Ghilencea, H. M. Lee and M. Park, JHEP **07**, 046 (2012), [arXiv:1203.0569].

[201] B. C. Allanach, Phys. Lett. B **635**, 123 (2006), [hep-ph/0601089].

[202] B. C. Allanach *et al.*, JHEP **08**, 023 (2007), [arXiv:0705.0487].

[203] O. Buchmueller *et al.*, Eur. Phys. J. **C74**, 2922 (2014), [arXiv:1312.5250]; P. Bechtle *et al.*, Eur. Phys. J. **C76**, 96 (2016), [arXiv:1508.05951]; C. Han *et al.*, Phys. Lett. B **769**, 470 (2017), [arXiv:1612.02296]; P. Athron *et al.* (GAMBIT Collaboration), Eur. Phys. J. C **77**, 824 (2017), [arXiv:1705.07935].

[204] R. Barbieri and A. Strumia, in "Proceedings of the 4th Rencontres du Vietnam: Physics at Extreme Energies (Particle Physics and Astrophysics) Hanoi, Vietnam, July 19-25, 2000," (2000), [hep-ph/0007265]; L. Giusti, A. Romanino and A. Strumia, Nucl. Phys. **B550**, 3 (1999), [hep-ph/9811386]; H.-C. Cheng and I. Low, JHEP **09**, 051 (2003), [hep-ph/0308199]; H.-C. Cheng and I. Low, JHEP **08**, 061 (2004), [hep-ph/0405243]; R. Harnik *et al.*, Phys. Rev. **D70**, 015002 (2004), [hep-ph/0311349].

[205] H. Baer *et al.*, Phys. Rev. **D87**, 035017 (2013), [arXiv:1210.3019]; H. Baer *et al.*, Phys. Rev. **D87**, 115028 (2013), [arXiv:1212.2655]; J. L. Feng, Ann. Rev. Nucl. Part. Sci. **63**, 351 (2013), [arXiv:1302.6587].

[206] J. L. Feng, K. T. Matchev and T. Moroi, Phys. Rev. Lett. **84**, 2322 (2000), [hep-ph/9908309]; J. L. Feng and F. Wilczek, Phys. Lett. **B631**, 170 (2005), [hep-ph/0507032]; D. Horton and G. G. Ross, Nucl. Phys. **B830**, 221 (2010), [arXiv:0908.0857].

[207] H. Baer *et al.*, Phys. Rev. **D89**, 115019 (2014), [arXiv:1404.2277].

[208] M. Drees, Phys. Rev. **D33**, 1468 (1986); S. Dimopoulos and G. F. Giudice, Phys. Lett. **B357**, 573 (1995), [hep-ph/9507282]; A. Pomarol and D. Tommasini, Nucl. Phys. **B466**, 3 (1996), [hep-ph/9507462].

[209] M. Dine, A. Kagan and S. Samuel, Phys. Lett. **B243**, 250 (1990); A. G. Cohen, D. B. Kaplan and A. E. Nelson, Phys. Lett. **B388**, 588 (1996), [hep-ph/9607394].

[210] C. Brust *et al.*, JHEP **03**, 103 (2012), [arXiv:1110.6670].

[211] S. P. Martin, Phys. Rev. **D75**, 115005 (2007), [hep-ph/0703097]; S. P. Martin, Phys. Rev. **D78**, 055019 (2008), [arXiv:0807.2820].

[212] J. Fan, M. Reece and J. T. Ruderman, JHEP **11**, 012 (2011), [arXiv:1105.5135]; J. Fan, M. Reece and J. T. Ruderman, JHEP **07**, 196 (2012), [arXiv:1201.4875].

[213] H. Murayama, Y. Nomura and D. Poland, Phys. Rev. **D77**, 015005 (2008), [arXiv:0709.0775]; G. Perez, T. S. Roy and M. Schmaltz, Phys. Rev. **D79**, 095016 (2009), [arXiv:0811.3206].

[214] R. Dermisek and J. F. Gunion, Phys. Rev. Lett. **95**, 041801 (2005), [hep-ph/0502105]; Phys. Rev. **D75**, 095019 (2007); R. Dermisek and J. F. Gunion, Phys. Rev. **D76**, 095006 (2007), [arXiv:0705.4387].

[215] G. G. Ross and K. Schmidt-Hoberg, Nucl. Phys. **B862**, 710 (2012), [arXiv:1108.1284]; G. G. Ross, K. Schmidt-Hoberg and F. Staub, JHEP **08**, 074 (2012), [arXiv:1205.1509]; A. Kaminska, G. G. Ross and K. Schmidt-Hoberg, JHEP **11**, 209 (2013), [arXiv:1308.4168].

[216] S. P. Martin and J. D. Wells, Phys. Rev. **D86**, 035017 (2012), [arXiv:1206.2956].

[217] B. Bellazzini *et al.*, Phys. Rev. **D79**, 095003 (2009), [arXiv:0902.0015].

[218] M. Dine, Ann. Rev. Nucl. Part. Sci. **65**, 43 (2015), [arXiv:1501.01035].

[219] H. Baer, V. Barger and M. Savoy, Phys. Rev. **D93**, 035016 (2016), [arXiv:1509.02929].

[220] M.L. Mangano, editor, *Physics at the FCC-hh, a 100 TeV pp collider*, CERN Yellow Report, CERN-2017-003-M (2017).

[221] P. Athron *et al.* (GAMBIT), Eur. Phys. J. C **77**, 879 (2017), [arXiv:1705.07917].

[222] P. Athron *et al.*, Prog. Part. Nucl. Phys. **148**, 104225 (2026), [arXiv:2507.09289].

[223] R. Aliberti *et al.*, Phys. Rept. **1143**, 1 (2025), [arXiv:2505.21476].

[224] D. P. Aguillard *et al.* (Muon $g-2$ Collaboration), Phys. Rev. Lett. **135**, 101802 (2025), [arXiv:2506.03069].

[225] T. Aoyama *et al.*, Phys. Rept. **887**, 1 (2020), [arXiv:2006.04822].

[226] D. Hanneke, S. Fogwell and G. Gabrielse, Phys. Rev. Lett. **100**, 120801 (2008), [arXiv:0801.1134].

[227] R. H. Parker *et al.*, Science **360**, 191 (2018), [arXiv:1812.04130].

[228] L. Morel *et al.*, Nature **588**, 61 (2020).

[229] B. Dutta and Y. Mimura, Phys. Lett. **B790**, 563 (2019), [arXiv:1811.10209]; M. Endo and W. Yin, JHEP **08**, 122 (2019), [arXiv:1906.08768]; M. Badziak and K. Sakurai, JHEP **10**, 024 (2019), [arXiv:1908.03607]; S. Li, Y. Xiao and J. M. Yang, Eur. Phys. J. C **82**, 276 (2022), [arXiv:2107.04962].

[230] J. Albrecht, D. van Dyk and C. Langenbruch, Prog. Part. Nucl. Phys. **120**, 103885 (2021), [arXiv:2107.04822].

[231] J. P. Lees *et al.* (BaBar Collaboration), Phys. Rev. Lett. **109**, 191801 (2012), [arXiv:1207.2690]; J. P. Lees *et al.* (BaBar Collaboration), Phys. Rev. **D86**, 112008 (2012), [arXiv:1207.5772]; T. Saito *et al.* (Belle Collaboration), Phys. Rev. D **91**, 052004 (2015), [arXiv:1411.7198].

[232] M. Misiak *et al.*, Phys. Rev. Lett. **114**, 221801 (2015), [arXiv:1503.01789]; M. Czakon *et al.*, JHEP **04**, 168 (2015), [arXiv:1503.01791]; M. Misiak, A. Rehman and M. Steinhauser, JHEP **06**, 175 (2020), [arXiv:2002.01548].

[233] H. Baer and M. Brhlik, Phys. Rev. **D55**, 3201 (1997), [hep-ph/9610224]; M. Ciuchini *et al.*, Phys. Rev. **D67**, 075016 (2003), [Erratum: **D68**, 079901 (2003)], [hep-ph/0212397]; T. Hurth, Rev. Mod. Phys. **75**, 1159 (2003), [hep-ph/0212304]; F. Mahmoudi, JHEP **12**, 026 (2007), [arXiv:0710.3791]; K. A. Olive and L. Velasco-Sevilla, JHEP **05**, 052 (2008), [arXiv:0801.0428].

Int. J. Mod. Phys. A 2026.41. Downloaded from www.worldscientific.com
by UNIVERSITY OF CALIFORNIA @ BERKELEY on 09/16/26. Re-use and distribution is strictly not permitted, except for Open Access articles.

[234] S. R. Choudhury and N. Gaur, Phys. Lett. **B451**, 86 (1999), [hep-ph/9810307]; K. S. Babu and C. F. Kolda, Phys. Rev. Lett. **84**, 228 (2000), [hep-ph/9909476]; G. Isidori and A. Retico, JHEP **11**, 001 (2001), [hep-ph/0110121]; G. Isidori and A. Retico, JHEP **09**, 063 (2002), [hep-ph/0208159].

[235] A. Tumasyan *et al.* (CMS Collaboration), Phys. Lett. B **842**, 137955 (2023), [arXiv:2212.10311]; M. Aaboud *et al.* (ATLAS Collaboration), JHEP **04**, 098 (2019), [arXiv:1812.03017]; R. Aaij *et al.* (LHCb Collaboration), Phys. Rev. D **105**, 012010 (2022), [arXiv:2108.09283].

[236] C. Bobeth *et al.*, Phys. Rev. Lett. **112**, 101801 (2014), [arXiv:1311.0903].

[237] R. Aaij *et al.* (LHCb Collaboration), Phys. Rev. Lett. **125**, 011802 (2020), [arXiv:2003.04831].

[238] N. Gubernari *et al.*, JHEP **09**, 133 (2022), [arXiv:2206.03797].

[239] R. Aaij *et al.* (LHCb Collaboration), Phys. Rev. Lett. **127**, 151801 (2021), [arXiv:2105.14007].

[240] I. Adachi *et al.* (Belle-II Collaboration), Phys. Rev. D **109**, 112006 (2024), [arXiv:2311.14647].

[241] W. G. Parrott, C. Bouchard and C. T. H. Davies (HPQCD Collaboration), Phys. Rev. D **107**, 014511 (2023), [Erratum: **D107**, 119903 (2023)], [arXiv:2207.13371].

[242] S. Bertolini *et al.*, Nucl. Phys. B **353**, 591 (1991); T. M. Aliev, G. Turan and O. Yilmaz, Nuovo Cim. A **106**, 1059 (1993).

[243] M. Bona *et al.* (UTfit Collaboration), Phys. Lett. **B687**, 61 (2010), [arXiv:0908.3470].

[244] J. P. Lees *et al.* (BaBar Collaboration), Phys. Rev. Lett. **109**, 101802 (2012), [arXiv:1205.5442]; J. P. Lees *et al.* (BaBar Collaboration), Phys. Rev. **D88**, 072012 (2013), [arXiv:1303.0571].

[245] S. Banerjee *et al.* (Heavy Flavor Averaging Group (HFLAV)), Phys. Rev. D **113**, 1, 012008 (2026), [arXiv:2411.18639].

[246] F. Mahmoudi, S. Neshatpour and J. Orloff, JHEP **08**, 092 (2012), [arXiv:1205.1845]; A. Arbey *et al.*, JHEP **11**, 132 (2017), [arXiv:1707.00426]; H. Eberl *et al.*, Phys. Rev. D **104**, 075025 (2021), [arXiv:2106.15228].

[247] G. Isidori, F. Wilsch and D. Wyler, Rev. Mod. Phys. **96**, 015006 (2024), [arXiv:2303.16922].

[248] B. Grzadkowski *et al.*, JHEP **10**, 085 (2010), [arXiv:1008.4884].

[249] S. Kraml *et al.*, JHEP **04**, 028 (2026), [arXiv:2506.05201].

[250] P. F. de Salas *et al.*, JHEP **02**, 071 (2021), [arXiv:2006.11237]; I. Esteban *et al.*, JHEP **09**, 178 (2020), [arXiv:2007.14792].

[251] K. Zuber, Phys. Rept. **305**, 295 (1998), [hep-ph/9811267]; S. F. King, J. Phys. **G42**, 123001 (2015), [arXiv:1510.02091]; S. F. King, Prog. Part. Nucl. Phys. **94**, 217 (2017), [arXiv:1701.04413].

[252] For a review of neutrino masses in supersymmetry, see *e.g.*, B. Mukhopadhyaya, *Proc. Indian National Science Academy* **A70**, 239 (2004); M. Hirsch and J. W. F. Valle, New J. Phys. **6**, 76 (2004), [hep-ph/0405015].

[253] F. Borzumati and Y. Nomura, Phys. Rev. **D64**, 053005 (2001), [hep-ph/0007018].

[254] P. Minkowski, Phys. Lett. **67B**, 421 (1977); M. Gell-Mann, P. Ramond, and R. Slansky, in *Supergravity*, edited by D. Freedman and P. van Nieuwenhuizen (North Holland, Amsterdam, 1979) p. 315; T. Yanagida, Prog. Theor. Phys. **64**, 1103 (1980); R. N. Mohapatra and G. Senjanovic, Phys. Rev. Lett. **44**, 912 (1980); R. N. Mohapatra and G. Senjanovic, Phys. Rev. **D23**, 165 (1981).

[255] J. Hisano *et al.*, Phys. Lett. **B357**, 579 (1995), [hep-ph/9501407]; J. Hisano *et al.*, Phys. Rev. **D53**, 2442 (1996), [hep-ph/9510309]; J. A. Casas and A. Ibarra, Nucl. Phys. **B618**, 171 (2001), [hep-ph/0103065]; J. R. Ellis *et al.*, Phys. Rev. **D66**, 115013 (2002), [hep-ph/0206110]; A. Masiero, S. K. Vempati and O. Vives, New J. Phys. **6**, 202 (2004), [hep-ph/0407325]; E. Arganda *et al.*, Phys. Rev. **D71**, 035011 (2005), [hep-ph/0407302]; F. R. Joaquim and A. Rossi, Phys. Rev. Lett. **97**, 181801 (2006), [hep-ph/0604083]; J. R. Ellis and O. Lebedev, Phys. Lett. **B653**, 411 (2007), [arXiv:0707.3419].

[256] Y. Grossman and H. E. Haber, Phys. Rev. Lett. **78**, 3438 (1997), [hep-ph/9702421]; A. Dedes, H. E. Haber and J. Rosiek, JHEP **11**, 059 (2007), [arXiv:0707.3718].

[257] M. Hirsch, H. V. Klapdor-Kleingrothaus and S. G. Kovalenko, Phys. Lett. **B398**, 311 (1997), [hep-ph/9701253]; L. J. Hall, T. Moroi and H. Murayama, Phys. Lett. **B424**, 305 (1998), [hep-ph/9712515]; K. Choi, K. Hwang and W. Y. Song, Phys. Rev. Lett. **88**, 141801 (2002), [hep-ph/0108028]; T. Honkavaara, K. Huitu and S. Roy, Phys. Rev. **D73**, 055011 (2006), [hep-ph/0512277].

[258] Y. Liu, S. Moretti and H. Waltari (2023), [arXiv:2307.05550].

[259] T. Faber *et al.*, Phys. Rev. D **101**, 055029 (2020), [arXiv:1909.11686].

[260] L. Basso *et al.*, Comput. Phys. Commun. **184**, 698 (2013), [arXiv:1206.4563].

[261] M. Chemtob, Prog. Part. Nucl. Phys. **54**, 71 (2005), [hep-ph/0406029]; R. Barbier *et al.*, Phys. Rept. **420**, 1 (2005), [hep-ph/0406039].

[262] H. Dreiner, in *Perspectives on Supersymmetry II*, edited by G.L. Kane (World Scientific, Singapore, 2010) pp. 565–583.

[263] B. C. Allanach, A. Dedes and H. K. Dreiner, Phys. Rev. **D60**, 075014 (1999), [hep-ph/9906209].

[264] L. E. Ibanez and G. G. Ross, Nucl. Phys. **B368**, 3 (1992); L. E. Ibanez, Nucl. Phys. **B398**, 301 (1993), [hep-ph/9210211].

[265] A. Dedes, S. Rimmer and J. Rosiek, JHEP **08**, 005 (2006), [hep-ph/0603225]; B. C. Allanach and C. H. Kom, JHEP **04**, 081 (2008), [arXiv:0712.0852]; H. K. Dreiner *et al.*, Phys. Rev. **D84**, 113005 (2011), [arXiv:1106.4338].

[266] H. K. Dreiner, C. Luhn and M. Thormeier, Phys. Rev. **D73**, 075007 (2006), [hep-ph/0512163].

[267] K. Tamvakis, Phys. Lett. **B382**, 251 (1996), [hep-ph/9604343]; G. Eyal and Y. Nir, JHEP **06**, 024 (1999), [hep-ph/9904473]; A. Florez *et al.*, Phys. Rev. **D87**, 095010 (2013), [arXiv:1303.0278].

[268] C. Csaki, Y. Grossman and B. Heidenreich, Phys. Rev. **D85**, 095009 (2012), [arXiv:1111.1239].

[269] D. Dercks *et al.*, Eur. Phys. J. **C77**, 856 (2017), [arXiv:1706.09418].

[270] B. C. Allanach and B. Gripaios, JHEP **05**, 062 (2012), [arXiv:1202.6616]; M. Asano, K. Rolbiecki and K. Sakurai, JHEP **01**, 128 (2013), [arXiv:1209.5778]; N. Chamoun *et al.*, JHEP **08**, 142 (2014), [arXiv:1407.2248].

[271] J. C. Romao, Nucl. Phys. Proc. Suppl. **81**, 231 (2000), [hep-ph/9907466]; Y. Grossman and S. Rakshit, Phys. Rev. **D69**, 093002 (2004), [hep-ph/0311310].

[272] R. N. Mohapatra, Phys. Rev. **D34**, 3457 (1986); K. S. Babu and R. N. Mohapatra, Phys. Rev. Lett. **75**, 2276 (1995), [hep-ph/9506354]; M. Hirsch, H. V. Klapdor-Kleingrothaus and S. G. Kovalenko, Phys. Rev. Lett. **75**, 17 (1995); M. Hirsch, H. V. Klapdor-Kleingrothaus and S. G. Kovalenko, Phys. Rev. **D53**, 1329 (1996), [hep-ph/9502385].

[273] Y. Grossman and H. E. Haber, Phys. Rev. **D59**, 093008 (1999), [hep-ph/9810536].

Int. J. Mod. Phys. A 2026.41. Downloaded from www.worldscientific.com
by UNIVERSITY OF CALIFORNIA @ BERKELEY on 09/16/26. Re-use and distribution is strictly not permitted, except for Open Access articles.

[274] S. Dimopoulos and L. J. Hall, Phys. Lett. **B207**, 210 (1988); J. Kalinowski *et al.*, Phys. Lett. **B406**, 314 (1997), [hep-ph/9703436]; J. Erler, J. L. Feng and N. Polonsky, Phys. Rev. Lett. **78**, 3063 (1997), [hep-ph/9612397].

[275] H. K. Dreiner, P. Richardson and M. H. Seymour, Phys. Rev. **D63**, 055008 (2001), [hep-ph/0007228].

[276] J. L. Hewett and T. G. Rizzo, Phys. Rept. **183**, 193 (1989).

[277] B. C. Allanach, M. Madigan and J. Tooby-Smith, JHEP **02**, 144 (2022), [arXiv:2107.07926].

[278] A. Delgado, G. Nardini and M. Quiros, Phys. Rev. **D86**, 115010 (2012), [arXiv:1207.6596].

[279] S. F. King, S. Moretti and R. Nevzorov, Phys. Lett. **B634**, 278 (2006), [hep-ph/0511256]; S. F. King, S. Moretti and R. Nevzorov, Phys. Rev. **D73**, 035009 (2006), [hep-ph/0510419].

[280] H. Kawase, JHEP **12**, 094 (2011), [arXiv:1110.3861]; N. Escudero, C. Munoz and A. M. Teixeira, Phys. Rev. D **73**, 055015 (2006), [hep-ph/0512046]; P. Fileviez Perez, Phys. Lett. B **711**, 353 (2012), [arXiv:1201.1501]; B. Dutta and Y. Mimura, Phys. Lett. B **790**, 589 (2019), [arXiv:1810.08413]; W. Altmannshofer *et al.*, JHEP **07**, 118 (2021), [arXiv:2104.08293].

[281] A. E. Nelson *et al.*, JHEP **08**, 039 (2002), [hep-ph/0206102].

[282] K. Benakli, M. D. Goodsell and A.-K. Maier, Nucl. Phys. B **851**, 445 (2011), [arXiv:1104.2695]; K. Benakli, Fortsch. Phys. **59**, 1079 (2011), [arXiv:1106.1649].

[283] J. E. Kim and H. P. Nilles, Phys. Lett. **138B**, 150 (1984).

[284] J. E. Kim and H. P. Nilles, Mod. Phys. Lett. **A9**, 3575 (1994), [hep-ph/9406296].

[285] G. F. Giudice and A. Masiero, Phys. Lett. **B206**, 480 (1988); J. A. Casas and C. Munoz, Phys. Lett. **B306**, 288 (1993), [hep-ph/9302227]; K. J. Bae *et al.*, Phys. Rev. **D99**, 115027 (2019), [arXiv:1902.10748].

[286] M. Cvetic *et al.*, Phys. Rev. **D56**, 2861 (1997), [Erratum: **D58**, 119905 (1998)], [hep-ph/9703317].

[287] R. D. Peccei, Lect. Notes Phys. **741**, 3 (2008), [hep-ph/0607268].

[288] R. D. Peccei and H. R. Quinn, Phys. Rev. Lett. **38**, 1440 (1977); R. D. Peccei and H. R. Quinn, Phys. Rev. **D16**, 1791 (1977).

[289] H. Murayama, H. Suzuki and T. Yanagida, Phys. Lett. **B291**, 418 (1992); T. Gherghetta and G. L. Kane, Phys. Lett. **B354**, 300 (1995), [hep-ph/9504420]; K. J. Bae, H. Baer and H. Serce, Phys. Rev. **D91**, 015003 (2015), [arXiv:1410.7500]; H. Baer, V. Barger and D. Sengupta, Phys. Lett. **B790**, 58 (2019), [arXiv:1810.03713].

[290] P. J. Fox, A. E. Nelson and N. Weiner, JHEP **08**, 035 (2002), [hep-ph/0206096].

[291] K. Benakli and M. D. Goodsell, Nucl. Phys. **B816**, 185 (2009), [arXiv:0811.4409]; K. Benakli and M. D. Goodsell, Nucl. Phys. **B840**, 1 (2010), [arXiv:1003.4957].

[292] G. D. Kribs, E. Poppitz and N. Weiner, Phys. Rev. **D78**, 055010 (2008), [arXiv:0712.2039].

[293] K. Benakli *et al.*, Phys. Rev. D **90**, 045017 (2014), [arXiv:1403.5122]; M. D. Goodsell *et al.*, SciPost Phys. **9**, 047 (2020), [arXiv:2007.08498]; K. Benakli *et al.*, Eur. Phys. J. C **83**, 43 (2023), [arXiv:2208.05867].

[294] G. Chalons *et al.*, JHEP **04**, 113 (2019), [arXiv:1812.09293].

[295] G. D. Kribs and A. Martin, Phys. Rev. D **85**, 115014 (2012), [arXiv:1203.4821].

[296] K. Benakli, M. D. Goodsell and F. Staub, JHEP **06**, 073 (2013), [arXiv:1211.0552]; E. Bertuzzo *et al.*, JHEP **04**, 089 (2015), [arXiv:1402.5432]; H. Nakano and M. Yoshikawa, PTEP **2016**, 033B01 (2016), [arXiv:1512.02377].

88. Supersymmetry, Part II (Experiment)

Revised August 2025 by M. D'Onofrio (Liverpool U.) and F. Moortgat (CERN; Ghent U.).

88.1 Introduction

Supersymmetry (SUSY), a transformation relating fermions to bosons and vice versa [1–9] is one of the most compelling possible extensions of the Standard Model of particle physics (SM).

On theoretical grounds SUSY is motivated as a generalization of space-time symmetries. A low-energy realization of SUSY, *i.e.*, SUSY at the TeV scale, is, however, not a necessary consequence. Instead, low-energy SUSY is motivated by the possible cancellation of quadratic divergences in radiative corrections to the Higgs boson mass [10–15]. Furthermore, it is intriguing that a weakly interacting, (meta)stable supersymmetric particle might make up some or all of the dark matter in the Universe [16–18]. In addition, SUSY GUTs predicts that gauge couplings, as measured experimentally at the electroweak scale, unify at an energy scale $\mathcal{O}(10^{16})$ GeV ("GUT scale") near the Planck scale [19–25].

In the minimal supersymmetric extension to the Standard Model, the so called MSSM [11, 26, 27], a supersymmetry transformation relates every chiral fermion and gauge boson in the SM to a supersymmetric partner with half a unit of spin difference, but otherwise with the same properties (such as mass) and quantum numbers. The MSSM Higgs sector contains two doublets, which give mass to the up-type and down-type quarks, respectively. After electroweak symmetry breaking, five Higgs bosons arise, of which two are charged. The supersymmetric partners of chiral fermions are squarks ($\tilde{q}$) and sleptons ($\tilde{\ell}$, $\tilde{\nu}$), and the "gauginos" for gauge bosons. The supersymmetric partners of the Higgs doublets are known as "higgsinos." The weak gauginos and higgsinos mix, giving rise to charged mass eigenstates called "charginos" ($\tilde{\chi}^{\pm}$), and neutral mass eigenstates called "neutralinos" ($\tilde{\chi}^0$). These are often collectively referred to as electroweakinos (EWkinos). The SUSY partners of the gluons are known as "gluinos" ($\tilde{g}$). The fact that such particles are not yet observed leads to the conclusion that, if supersymmetry is realized, it is a broken symmetry. A description of broken SUSY in the form of an effective Lagrangian with only "soft" SUSY breaking terms maintains the cancellation of quadratic divergences and furthermore if the SUSY particle masses are of order TeV, removes the need for large cancellations in the predicted Higgs vacuum expectation value.

The phenomenology of the MSSM is to a large extent defined by the interactions that bring SUSY breaking from the SUSY breaking sector to the MSSM, as well as the SUSY breaking scale. These determine the SUSY particle masses, the mass hierarchy, the field contents of physical particles, and their decay modes. In addition, phenomenology crucially depends on whether the multiplicative quantum number of R-parity [27], $R = (-1)^{3(B-L)+2S}$, where B and L are baryon and lepton numbers and S is the spin, is conserved or violated. If R-parity is conserved, SUSY particles (sparticles), which have odd R-parity, are produced in pairs and the decays of each SUSY particle must involve an odd number of lighter SUSY particles. The lightest SUSY particle (LSP) is then stable and often assumed to be a weakly interacting massive particle (WIMP). If R-parity is violated, new terms λ_{ijk}, λ'_{ijk} and λ''_{ijk} appear in the superpotential, where ijk are generation indices; λ-type couplings appear between lepton superfields only, λ''-type are between quark superfields only, and λ'-type couplings connect the two. R-parity violation implies lepton and/or baryon number violation. More details of the theoretical framework of SUSY are discussed elsewhere in this volume [28].

The discovery of a Higgs boson with a mass around 125 GeV imposes constraints on SUSY models, which are discussed in Section 87. Low-energy data from flavor physics experiments, high-precision electroweak observables as well as astrophysical data also impose strong constraints on the allowed SUSY parameter space. Recent examples of such data include measurements of the rare B-meson decay $B_s \to \mu^+\mu^-$ [29–31], measurements of the anomalous magnetic moment of the muon [32, 33], and accurate determinations of the cosmological dark matter relic density constraint [34, 35].

Indirect constraints can be more sensitive to higher SUSY mass scales than experiments searching for direct sparticle production at colliders, but the interpretation of these results is often strongly model dependent. In contrast, direct searches for sparticle production at collider experiments, which are the main topic of this review, are less subject to interpretation ambiguities and therefore they play a crucial role in the search for SUSY. Further discussion on indirect constraints can be found in 87.7.2.

88.2 Overview of the experimental search programme

The electron-positron collider LEP was operational at CERN between 1989 and 2000. In the initial phase, center-of-mass energies around the Z-peak were probed, but after 1995 the LEP experiments collected a significant amount of luminosity at higher center-of-mass energies, some 235 pb^{-1} per experiment at $\sqrt{s} \geq 204$ GeV, with a maximum $\sqrt{s}$ of 209 GeV. Searches for new physics at e^+e^- colliders benefit from the clean experimental environment and the fact that the initial state four-momentum is precisely known. This allows momentum balance to be exploited not only in the plane transverse to the beam but also along the beam direction (up to the small effects of beamstrahlung and the beam pipe holes). In contrast, at hadron colliders only the transverse momentum balance can be used, since the longitudinal momentum of the initial partons is not known on an event-by-event basis. Searches at LEP are dominated by the data samples taken at the highest center-of-mass energies.

The CDF and D0 experiments at the Tevatron, a proton-antiproton collider at a center-of-mass energy of up to 1.96 TeV, had an extensive search program for supersymmetric particles. CDF and D0 collected integrated luminosities between 10 and 11 fb^{-1} each up to the end of collider operations in 2011.

The electron-proton collider HERA provided collisions to the H1 and ZEUS experiments between 1992 and 2007, at a center-of-mass energy up to 318 GeV. A total integrated luminosity of approximately 0.5 fb^{-1} was collected by each experiment. At HERA, SUSY searches focused on R-parity violating processes mediated by λ' couplings, which allow resonant production of single squarks in electron–quark interactions.

The Large Hadron Collider (LHC) at CERN started proton-proton operation at a center-of-mass energy of 7 TeV in 2010. By the end of 2011 the ATLAS and CMS experiments had collected about 5 fb^{-1} of integrated luminosity each, and the LHCb experiment had collected approximately 1 fb^{-1}. In 2012, the LHC operated at a center-of-mass energy of 8 TeV, and ATLAS and CMS collected approximately 20 fb^{-1} each, whereas LHCb collected 2 fb^{-1}. In 2015, the LHC started Run 2, with a center-of-mass energy of 13 TeV. At the end of Run 2 in November 2018, ATLAS and CMS had both collected approximately 140 fb^{-1}, and LHCb had collected almost 6 fb^{-1}. The Run 3 of the LHC started in July 2022 with a center-of-mass energy of 13.6 TeV. Almost 240 fb^{-1} of data have been collected by ATLAS and CMS at the time of writing (August 2025), and LHCb collected around 90 fb^{-1}.

At the LHC, cross sections of QCD-mediated processes are the largest achievable at colliders, which is reflected in the higher sensitivity for SUSY particles carrying color charge, squarks and gluinos, with respect to LEP, Tevatron and HERA. In particular, proton-proton collisions at the LHC differ from proton-antiproton collisions at the Tevatron as there are no valence anti-quarks in the proton, and that gluon-initiated processes play a more dominant role. The increased center-of-mass energy of the LHC compared to the Tevatron significantly extends the kinematic reach for SUSY searches. This is reflected foremost in the sensitivity for squarks and gluinos, but also for SUSY particles produced via electroweak processes.

In this review we report results of direct searches for SUSY particles at colliders up to August 2023, mostly covering data analyses at the ATLAS and CMS experiments with reference to results from LEP, HERA and the Tevatron. For more details on LEP and Tevatron constraints, see earlier PDG reviews [36]. Analyses on the Run 3 datasets are still in progress hence the results reported for ATLAS and CMS are moslty based on Run 2 data. Results are categorized depending on the targeted SUSY

Int. J. Mod. Phys. A 2026.41. Downloaded from www.worldscientific.com by UNIVERSITY OF CALIFORNIA @ BERKELEY on 09/16/26. Re-use and distribution is strictly not permitted, except for Open Access articles.

Int. J. Mod. Phys. A 2026.41. Downloaded from www.worldscientific.com
by UNIVERSITY OF CALIFORNIA @ BERKELEY on 09/16/26. Re-use and distribution is strictly not permitted, except for Open Access articles.

particles, the nature of their production and decays, and the assumption on R-parity. Brief summaries of search techniques and approaches adopted for interpretation of the results are given in Section 88.3 and 88.4, respectively. Sections 88.5-88.8 focus on results for promptly-decaying gluinos and first and second generation squarks, top and bottom squarks, electroweakinos (charginos, neutralinos) and sleptons. Limits obtained for sparticle masses assuming R-parity violating models are also reported. Results of dedicated searches for long-lived (LL) SUSY particles are reported in Section 88.9. Finally, Section 88.10 provides examples of global reinterpretations of SUSY searches.

88.3 Experimental search techniques

Large background contributions from Standard Model processes pose challenges to the trigger and analysis. Such backgrounds are dominated by multijet production processes, including, particularly at the LHC, those of top quark production, as well as jet production in association with vector bosons. The proton's momentum is shared between its parton constituents, and in each collision only a fraction of the total center-of-mass energy is available in the hard parton-parton scattering. Since the parton momenta in the longitudinal direction are not known on an event-by-event basis, use of momentum conservation constraints in an analysis is restricted to the transverse plane, leading to the definition of transverse variables, such as the missing transverse momentum, and the transverse mass.

Under the assumption of R-parity conservation (RPC), the typical SUSY search signature for squarks and gluinos at hadron colliders contains high-p_{T} jets, which are produced in the decay chains of heavy squarks and gluinos, and significant missing transverse momentum originating from the two LSPs produced at the end of the decay chains, which escape experimental detection. Electroweakino decays are often characterised by the presence of leptons, for instance from W and Z bosons in the decay chain, plus missing transverse momentum. Standard Model backgrounds with missing transverse momentum include leptonic W/Z-boson decays, associated production of jets and a Z-boson decaying into neutrinos, semi-leptonic heavy-flavor decays to neutrinos, top-quark pair production with one or both W bosons decaying leptonically, and multijet events that may be affected by instrumental effects such as jet mis-measurement.

Selection variables designed to separate the SUSY signal from the Standard Model backgrounds include transverse variables such as H_{T}, $E_{\mathrm{T}}^{\mathrm{miss}}$, and m_{eff}. The quantities H_{T} and $E_{\mathrm{T}}^{\mathrm{miss}}$ refer to the measured transverse energy and the missing transverse momentum in the event, respectively. They are usually defined as the scalar sum of the transverse jet momenta or of the transverse energies of calorimeter clusters measured in the event (H_{T}), or the magnitude ($E_{\mathrm{T}}^{\mathrm{miss}}$) of the negative vector sum of transverse momenta of reconstructed objects like jets and leptons in the event ($\vec{p}_{\mathrm{T}}^{\mathrm{miss}}$). The quantity m_{eff} is referred to as the effective mass of the event and is defined as $m_{\mathrm{eff}} = H_{\mathrm{T}} + E_{\mathrm{T}}^{\mathrm{miss}}$. The peak of the m_{eff} distribution for SUSY signal events correlates with the SUSY mass scale, in particular with the produced sparticle masses and the mass difference between the primary produced SUSY particle and the LSP [37], whereas the Standard Model backgrounds dominate at low m_{eff}. An additional reduction of multijet backgrounds can be achieved by demanding isolated leptons or photons in the final states; in such events the lepton or photon transverse momentum may be added to H_{T} or m_{eff} for further signal-background separation. Other kinematic variables and approaches developed to increase the sensitivity to pair production of heavy sparticles with TeV-scale masses focusing on the kinematics of their decays are the α_{T} [38–42], *razor* [43], *stransverse mass* (m_{T2}) [44], and *contransverse mass* (m_{CT}) [45] variables. The *super-razor* [46] and *recursive jigsaw reconstruction* [47] techniques are topological event reconstruction methods also used in searches for sparticles with masses in the TeV-range. In case massive, unstable SM particles such as top quarks, vector bosons or the Higgs boson arise in the decay chain, dedicated procedures are employed for their reconstruction and identification. If these are produced with a significant boost, their decay products will typically overlap and become collimated (boosted) in the direction of the parent particle. Their hadronic decay products can be reconstructed as a single large-radius jet (see studies from ATLAS [48]), and *jet-substructure* [49] techniques can be adopted. Machine-learning (ML) approaches are also used to identify and classify hadronic decays of highly Lorentz-boosted bosons and top quarks, see as example recent studies from CMS [50].

Until recently, analyses used simple combinations of selections on kinematic variables (often referred to as *cut-and-count* analyses) and exploited multiple signal regions defined by categorizing events on the basis of several variables and their correlations. An example is provided in Fig. 88.1 from Ref. [51]: 39 signal regions are set to search for top squarks in events with one lepton, jets and missing transverse momentum. Regions depend on jet multiplicities, reconstructed top-quark candidates and thresholds applied to the most discriminant variables used for optimisation.

At present, shape analyses or analyses using more sophisticated techniques, e.g. machine learning, are being developed more and more often. ML techniques allow analyses to better capture the complexity of the events and achieve improved sensitivity with respect to counting experiments. For example, Boosted Decision Trees (BDTs) allow analyses to exploit simultaneously the discriminating power of multiple variables and that of correlations among objects in the events. Deep Neural Networks (NN) are also employed for object reconstruction and to use directly detector-recorded energies and momenta of produced particles instead of first deriving a restricted set of physical variables. Among others, currently in use are Convolutional NN for image classification techniques, Recurrent NN, parametric NN, Graph NN and Generative Adversarial Networks.

Variables and approaches reported above are also used in searches for R-parity violating (RPV) SUSY models where signal events are often characterised by the presence of multiple leptons and/or jets, and little or no missing transverse momentum. However, if R-parity violating couplings are small, sparticles might be long-lived and may travel macroscopic distances before decaying. Similarly, long lifetimes may be due to small mass splittings, as in the case of pure higgsino/wino scenarios, or to heavy mediators, as in Split SUSY models [52, 53]. The identification of long-lived particles requires dedicated tools and their signatures can be very diverse. At the LHC, customized techniques (also based on NN) have been developed, for example, to reconstruct significantly displaced decay vertices or short track segments, and to identify tracks with atypical properties or unusual ionization, small and localized deposits of energy inside of the calorimeters without associated tracks, or stopped particles that decay out of time with collisions. For an overview, see Ref. [54].

88.4 Interpretation of search results

Since the mechanism by which SUSY is broken is unknown, a general approach to SUSY via the most general soft SUSY breaking Lagrangian adds a significant number of new free parameters. For the minimal supersymmetric standard model, MSSM, *i.e.*, the model with the minimal particle content, these comprise 105 new real degrees of freedom. A phenomenological analysis of SUSY searches leaving all these parameters free is not feasible. For the practical interpretation of SUSY searches at colliders several approaches are taken to reduce the number of free parameters.

One approach is to assume a SUSY breaking mechanism and lower the number of free parameters through the assumption of additional constraints. Before the start of the LHC, interpretations of experimental results were often performed in constrained models of gravity mediated [55, 56], gauge-mediated [57–59], and anomaly mediated [60, 61] SUSY breaking. The most popular model was the constrained MSSM (CMSSM) [55, 62, 63], which in the literature is also referred to as minimal supergravity, or MSUGRA. These constrained SUSY models are theoretically well motivated and provide a rich spectrum of experimental signatures. However, with universality relations imposed on the soft SUSY breaking parameters, they do not cover all possible kinematic signatures and mass relations of SUSY. Furthermore, the Higgs mass measurement from LHC Run 1, together with other collider and non-collider measurements, substantially limits the allowed SUSY parameter space for these models. This indicates that very constrained models like the CMSSM are no longer good benchmark

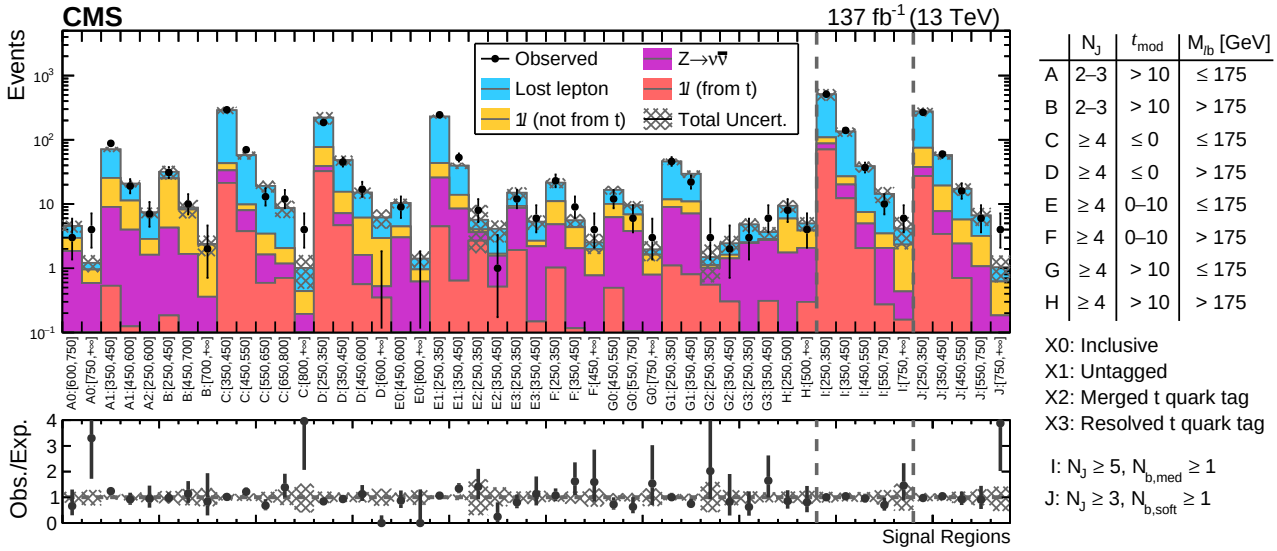

Figure 88.1: Example of multiple signal regions set for a typical SUSY search at the LHC. For definition of regions and acronyms specific for this search, see corresponding paper.

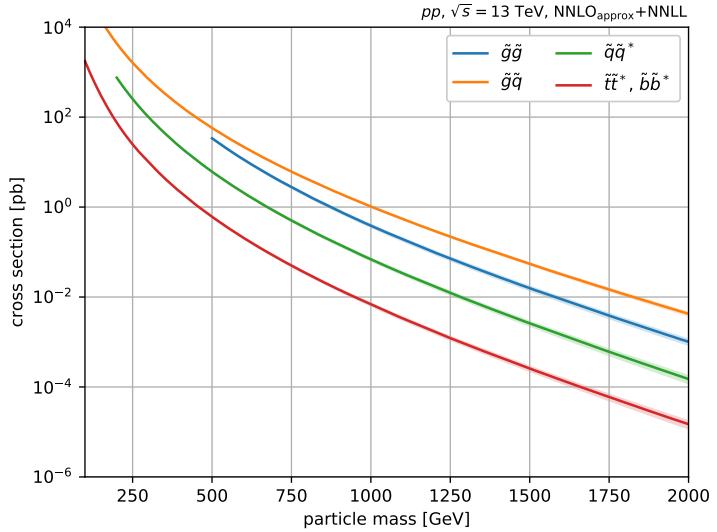

Figure 88.2: Cross sections for pair production of gluinos and squarks as a function of their mass at the LHC for a center-of-mass energy of 13 TeV. They are calculated at approximately next-to-next-to-leading-order (NNLO) including the resummation of soft gluon emission at the next-to-next-to-leading logarithmic accuracy.

scenarios to solely characterize the results of SUSY searches at the LHC and efforts have been made to complement them with more flexible approaches.

A broader and more comprehensive subset of the MSSM can be studied via the so-called phenomenological-MSSM, or pMSSM [64–67]. It is derived from the MSSM, using experimental data to eliminate parameters that are free in principle but have already been highly constrained by measurements of *e.g.*, flavor mixing and CP-violation. This effective approach reduces the number of free parameters in the MSSM to typically 19 or even less, making it a practical compromise between the full MSSM and highly constrained models such as the CMSSM.

Even less dependent on fundamental assumptions are interpretations in terms of so-called simplified models [68–71]. Such models assume a limited set of SUSY particle production and decay modes and leave open the possibility to vary masses and other parameters freely. Therefore, simplified models enable comprehensive studies of individual SUSY topologies, and are useful for optimization of the experimental searches over a wide parameter space without limitations on fundamental kinematic properties such as masses and decay modes.

As a consequence, ATLAS and CMS have adopted simplified models as the primary framework to provide interpretations of their searches. In addition to using simplified models that describe prompt decays of SUSY particles, the experiments are now also focusing more on the use of simplified models that allow for decays of long-lived SUSY particles as they can arise in different SUSY scenarios (see Section 88.9 for further discussion). Today, almost every individual search provides interpretations of their results in one or several simplified models that are characteristic of SUSY topologies probed by the analysis.

While simplified models are very convenient for the interpretation of individual SUSY production and decay topologies, care must be taken when applying these limits to more complex SUSY spectra. In particular, the branching ratio of SUSY particles into a specific final state is often assumed to be 100% and in many

Int. J. Mod. Phys. A 2026.41. Downloaded from www.worldscientific.com
by UNIVERSITY OF CALIFORNIA @ BERKELEY on 09/16/26. Re-use and distribution is strictly not permitted, except for Open Access articles.

Int. J. Mod. Phys. A 2026.41. Downloaded from www.worldscientific.com
by UNIVERSITY OF CALIFORNIA @ BERKELEY on 09/16/26. Re-use and distribution is strictly not permitted, except for Open Access articles.

of the quoted limits the LSP is assumed to be massless. Therefore, simplified model limits should be seen as an approximation of the constraints that can be placed on sparticle masses in more complex SUSY spectra. Only on a case-by-case basis can it be determined whether the limit of a given simplified model represents a good approximation of the true underlying constraint that can be applied on a sparticle mass in a complex SUSY spectrum. In the following, we will point out explicitly the assumptions that have entered the limits when quoting interpretations from simplified models.

Since none of the searches performed so far have shown significant excess above the SM background prediction, the interpretations of the presented results are exclusion limits on SUSY parameter space. Unless stated differently, all quoted exclusion limits are at the 95% confidence level. Finally, we note that many of the recent publications by ATLAS and CMS also present results in terms of model-independent limits such that their discovery potential is statistically quantified independently on a particular model.

88.5 Exclusion limits on gluino, first and second generation squark masses in RPC scenarios

Colored SUSY particles such as squarks and gluinos are produced via the strong interaction and have the highest cross sections at hadron colliders. Limits on squark masses of the order 100 GeV have been set by the LEP experiments [72], in the decay to quark plus neutralino, and for a mass difference between squark and quark plus neutralino of typically at least a few GeV. However, hadron collider experiments are able to set much more stringent mass limits.

The main production mechanisms at hadron colliders are squark-squark, squark-gluino and gluino-gluino production; when "squark" is used "antisquark" is also implied. Pair production usually involves both the s-channel and t-channel parton-parton interactions. However, since there is a negligible amount of bottom and top quark content in the proton, top and bottom squark production proceeds through s-channel diagrams only. Experimental analyses of squark and/or gluino production typically assume the first and second generation squarks to be approximately degenerate in mass. Cross section calculations at the center-of-mass energy of 13 TeV shown in Fig. 88.2 (from Ref. [73]) assume mass degeneracy of left- and right-handed u, d, s, c squarks. Other sparticle masses are considered decoupled, *i.e.* their masses are assumed to have a very high value (above or of the order of 10 TeV). The LHC experiments also provide simplified model limits on individual first or second generation squarks. Top and bottom squarks have the same production cross section, identical to that of a single light squark.

In this section, we focus on results assuming R-parity conservation. Limits set by the Tevatron experiments on the gluino mass assume the framework of the CMSSM, with $\tan\beta = 5$ (CDF) or $\tan\beta = 3$ (D0). Furthermore, the common trilinear term A_0 is set to 0 and the higgsino mass term μ is assumed to be less than 0. The resulting lower mass limits are about 310 GeV for all squark masses, or 390 GeV for the case $m_{\tilde{q}} = m_{\tilde{g}}$ [74, 75].

ATLAS and CMS limits on the gluino mass have been established in the framework of simplified models. Assuming only gluino pair production, three main primary decay chains of the gluino have been considered by the LHC experiments for interpretations of their search results. The first decay chain, $\tilde{g} \to q\bar{q}\tilde{\chi}_1^0$, assumes gluino mediated production of first and second generation squarks (on-shell or off-shell) which leads to four light flavor quarks in the final state. Therefore, inclusive all-hadronic analyses searching for multijet plus $E_{\mathrm{T}}^{\mathrm{miss}}$ final states are utilized to put limits on this simplified model. These limits are derived as a function of the gluino and neutralino (LSP) mass. As shown in Fig. 88.3 (left)the CMS collaboration [76] excludes in this simplified model gluino masses below approximately 2.1 TeV for a light neutralino mass below about 600 GeV. In scenarios where neutralinos are not very light, the efficiency of the analyses is reduced by the fact that jets are less energetic, and there is less missing transverse momentum in the event. This leads to weaker limits when the mass difference $\Delta m = m_{\tilde{g}} - m_{\tilde{\chi}_1^0}$ is reduced. For example, for neutralino masses above about 1.2 TeV no limit on the gluino mass can be set for this decay chain. Therefore, limits on gluino masses are strongly affected by the assumption of the neutralino mass. Similar results for this simplified model have been obtained by ATLAS [77]. A second simplified model postulates a decay chain where $\tilde{g} \to q\bar{q}W\tilde{\chi}_1^0$, assuming that the intermediate (on-shell or off-shell) squark is left-handed and decays to a chargino and a quark, with the chargino decaying to a W boson and the LSP. This leads to two W bosons and four light flavor quarks plus $E_{\mathrm{T}}^{\mathrm{miss}}$ in the final state. Both leptonic and hadronic decays of the W can be considered. In this scenario, the ATLAS collaboration [78, 79] excludes gluino masses below approximately 2.2 TeV for a sufficiently light neutralino and assuming the chargino mass is halfway between the gluino and neutralino mass, see Fig. 88.3 (right). Again, for neutralino masses above about 1.2 TeV, there exists no limit on the gluino mass for this decay chain. A similar reach has been obtained by the CMS collaboration [80, 80, 81], where the most recent results are obtained using novel algorithms based on deep neutral networks that identify hadronically decaying W bosons.

Gluino decays are not limited to first and second generation squarks: another important decay chain of the gluino considered for interpretation in simplified models is $\tilde{g} \to b\bar{b}\tilde{\chi}_1^0$. In this case the decay is mediated via bottom squarks and thus leads to four jets originating from b-quarks and $E_{\mathrm{T}}^{\mathrm{miss}}$ in the final state. For this topology as well, inclusive all-hadronic searches provide the highest sensitivity. In this case, the use of secondary vertex reconstruction for the identification of jets originating from the b-quarks in the event provides a powerful handle to reject SM background contributions. Therefore, in addition to a multijet plus $E_{\mathrm{T}}^{\mathrm{miss}}$ signature these searches also require between 1 and 4 jets to be tagged as b-jets. As shown in Fig. 88.4 (left), for this simplified model CMS [76] excludes gluino masses below ≈ 2.3 TeV for a sufficiently light neutralino, while for neutralino masses above ≈ 1.5 TeV no limit on the gluino mass can be set. Comparable limits for this simplified model are provided by searches from ATLAS [82, 83], with the most recent results pushing the boundary of gluino masses to 2.44 TeV in the case of a massless neutralino.

If kinematically allowed, decays of gluinos to top squarks via $\tilde{g} \to \tilde{t}t$ are also possible. This defines the next important simplified model characterizing gluino pair production, $\tilde{g} \to t\bar{t}\tilde{\chi}_1^0$, which leads to a "four tops" final state, $tttt\tilde{\chi}_1^0\tilde{\chi}_1^0$. The topology of this decay is very rich in different experimental signatures: as many as four isolated leptons, four b-jets, as many as eight light flavor quark jets, and significant missing transverse momentum from the neutrinos in the W decay and from the two neutralinos. As shown in Fig. 88.4 (right), the ATLAS search [82] rules out gluinos with masses below ≈ 2.4 TeV for light neutralinos in this model. For neutralino masses above ≈ 1.4 TeV, no limit can be placed on the gluino mass. Sensitivity is also achieved in case of gluino pairs with an off-shell top quark in the decay.

The CMS multiple b-jet search [84] and the search in full-hadronic events using identification techniques for boosted top-quarks in the final state [85] result in gluino mass limits of ≈ 2.3 TeV.

Assuming gluinos to be heavier than squarks, squarks will predominantly decay to a quark and a neutralino or chargino, if kinematically allowed. The decay may involve the lightest neutralino (typically the LSP) or chargino, but, depending on the masses and couplings of the gauginos and on the handedness of the squarks, may involve heavier neutralinos or charginos. For pair production of first and second generation squarks, the simplest decay modes involve two jets and missing transverse momentum, with potential extra jets stemming from initial state or final state radiation (ISR/FSR) or from decay modes with longer decay chains (cascades). In cascades, isolated photons or leptons may appear from the decays of sparticles such as neutralinos or charginos.

Limits on first and second generation squark masses set by the Tevatron experiments assume the CMSSM, and amount to lower limits of about 380 GeV for all gluino masses, or 390 GeV for the case $m_{\tilde{q}} = m_{\tilde{g}}$ [74, 75]. At the LHC, limits on squark masses have

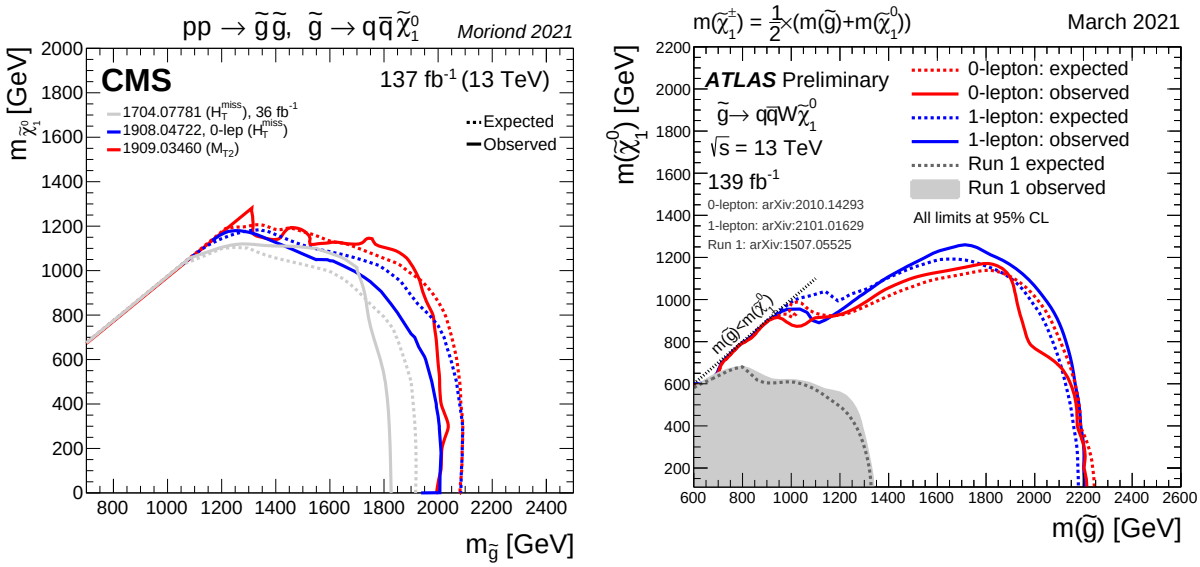

Figure 88.3: Lower mass limits, at 95% C.L., on gluino pair production for various decay chains in the framework of simplified models. Left: $\tilde{g} \to q\bar{q}\tilde{\chi}_1^0$, result of the CMS collaboration. Right: $\tilde{g} \to q\bar{q}W\tilde{\chi}_1^0$, result of the ATLAS collaboration.

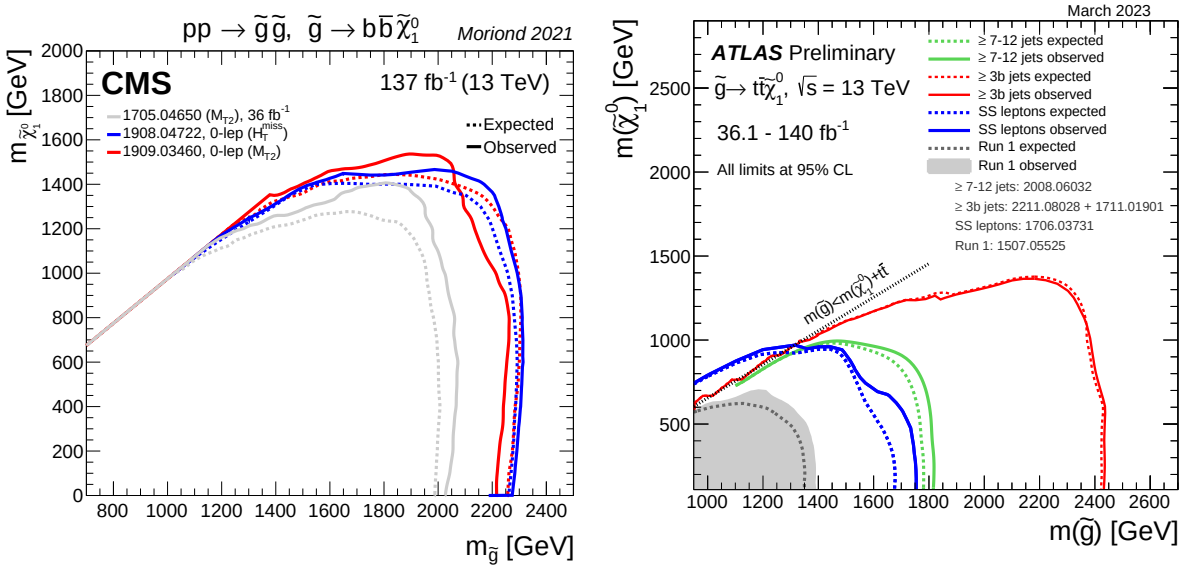

Figure 88.4: Lower mass limits, at 95% C.L., on gluino pair production for various decay chains in the framework of simplified models. Left: $\tilde{g} \to b\bar{b}\tilde{\chi}_1^0$. Right: $\tilde{g} \to t\bar{t}\tilde{\chi}_1^0$. Results from the CMS and ATLAS collaborations.

been set using up to approximately 140 fb^{-1} of data at 13 TeV. Interpretations in simplified models typically characterize squark pair production considering only one decay chain at the time for the squark, for instance $\tilde{q} \to q\tilde{\chi}_1^0$. It is usually assumed that the left and right-handed $\tilde{u}$, $\tilde{d}$, $\tilde{s}$ and $\tilde{c}$ squarks are degenerate in mass. Furthermore, it is assumed that the mass of the gluino is very high (above or order of 10 TeV) and thus contributions of the corresponding t-channel diagrams to squark pair production are negligible. Therefore, the total production cross section for this simplified model is eight times the production cross section of an individual squark (e.g. $\tilde{u}_L$). Under these assumptions, CMS obtains a lower squark mass limit of ≈ 1.75 TeV for light neutralinos [84], as shown in Fig. 88.5 (left). Only for neutralino masses below ≈ 800 GeV can any squark masses be excluded. Searches for new physics in monojet channels are sensitive to very compressed scenarios, and masses up to 900 GeV are excluded for $\Delta m = m_{\tilde{q}}, m_{\tilde{\chi}_1^0} \approx 5$ GeV [86].

If the assumption of mass degenerate first and second generation squarks is dropped and only the production of a single light squark is assumed, the limits weaken significantly. For example, the CMS limit on degenerate squarks of 1750 GeV for light neutralinos drops to ≈ 1300 GeV for pair production of a single light squark, and for neutralinos heavier than ≈ 600 GeV no squark mass limit can be placed. It should be noted that this limit is not a result of a simple scaling of the above mentioned mass limits assuming eight-fold mass degeneracy but it also takes into account that for an eight times lower production cross section the analyses must probe kinematic regions of phase space that are closer to the ones of SM background production.

A summary of results of the ATLAS searches also targeting more complicated decay chains, where e.g. intermediate bosons are produced as well, can be seen in Fig. 88.5 (right). Depending on the topology, the exclusion limit can reach up to ≈ 2 TeV (this value is only reached in gaugino-mediated simplified models [87]). Recent results include a search in two-opposite-sign, same-flavor dilepton final state events [88] targeting squarks decaying through the next-to-lightest neutralino via a slepton or a Z boson and exclude masses up to ≈ 1550 GeV for a massless

Int. J. Mod. Phys. A 2026.41. Downloaded from www.worldscientific.com
by UNIVERSITY OF CALIFORNIA @ BERKELEY on 09/16/26. Re-use and distribution is strictly not permitted, except for Open Access articles.

Int. J. Mod. Phys. A 2026.41. Downloaded from www.worldscientific.com
by UNIVERSITY OF CALIFORNIA @ BERKELEY on 09/16/26. Re-use and distribution is strictly not permitted, except for Open Access articles.

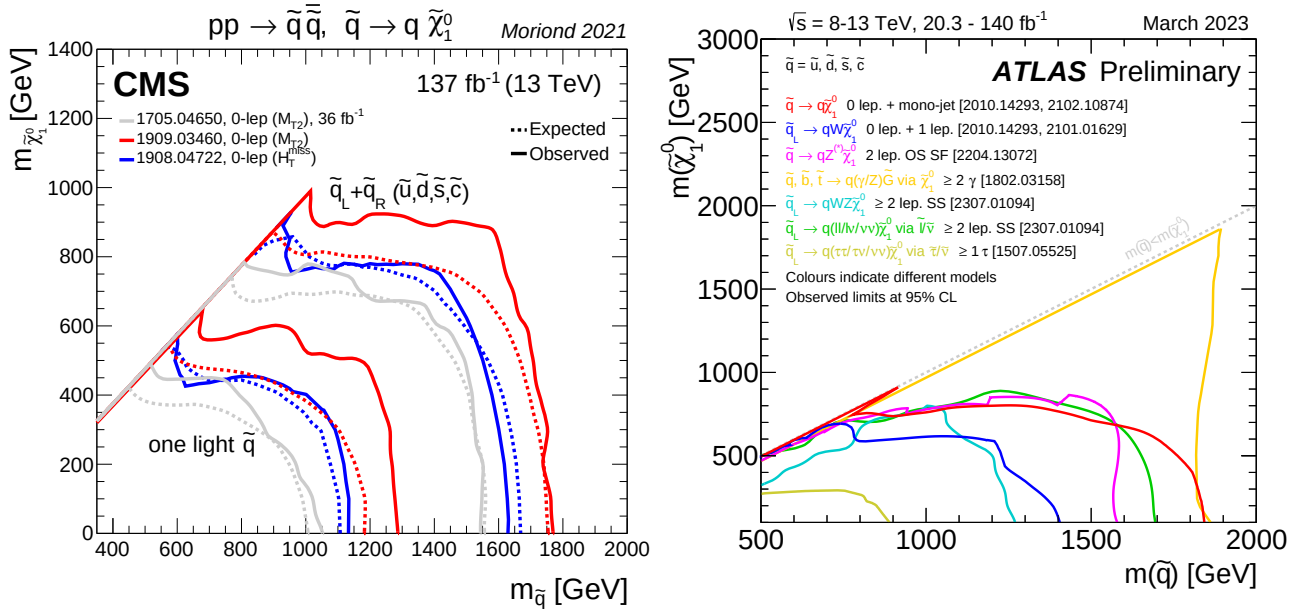

Figure 88.5: Left: 95% C.L. exclusion contours in the framework of simplified models assuming a single decay chain of $\tilde{q} \to q\tilde{\chi}_1^0$, obtained by the CMS collaboration. Right: Assuming more complicated decay chains including W or Z bosons, obtained by the ATLAS collaboration.

neutralino. Squarks decaying via charginos and next-to-lightest neutralinos in long decay chains including W and Z bosons are constrained with searches for same-sign dilepton or three-lepton final state events [89]: in this case, masses up to ≈ 1.7 TeV are excluded.

For single light squarks ATLAS also reports results of a dedicated search for pair production of scalar partners of charm quarks [90, 91]. Assuming that the scalar-charm state exclusively decays into a charm quark and a neutralino, scalar-charm masses up to 900 GeV are excluded for neutralino masses below 260 GeV.

Table 88.1: Summary of squark mass and gluino mass limits using different interpretation approaches assuming R-parity conservation. Masses in this table are provided in GeV. Further details about the assumptions and analyses from which these limits are obtained are discussed in the corresponding sections of the text.

Model	Assumption	$m_{\tilde{q}}$	$m_{\tilde{g}}$
Simplified models $\tilde{g}\tilde{g}$			
$\tilde{g} \to q\bar{q}\tilde{\chi}_1^0$	$m_{\tilde{\chi}_1^0} = 0$	-	≈ 2300
	$m_{\tilde{\chi}_1^0} > \approx 1200$	-	no limit
$\tilde{g} \to b\bar{b}\tilde{\chi}_1^0$	$m_{\tilde{\chi}_1^0} = 0$	-	≈ 2440
	$m_{\tilde{\chi}_1^0} > \approx 1600$	-	no limit
$\tilde{g} \to t\bar{t}\tilde{\chi}_1^0$	$m_{\tilde{\chi}_1^0} = 0$	-	≈ 2400
	$m_{\tilde{\chi}_1^0} > \approx 1400$	-	no limit
Simplified models $\tilde{q}\tilde{q}$			
$\tilde{q} \to q\tilde{\chi}_1^0$	$m_{\tilde{\chi}_1^0} = 0$	≈ 1900	-
	$m_{\tilde{\chi}_1^0} > \approx 800$	no limit	-
$\tilde{u}_L \to q\tilde{\chi}_1^0$	$m_{\tilde{\chi}_1^0} = 0$	≈ 1300	-
	$m_{\tilde{\chi}_1^0} > \approx 600$	no limit	-

A summary of the most important squark and gluino mass limits for different interpretation approaches assuming R-parity conservation is shown in Table 88.1. For gluino masses rather similar limits of about $2.3 - 2.4$ TeV are obtained from different model assumptions, indicating that the LHC is indeed probing direct gluino production at the TeV scale and beyond. However, for neutralino masses above approximately 1.2 to 1.6 TeV, even in the best case scenarios, ATLAS and CMS searches do not place any limits on the gluino mass. Limits on direct squark production, on the other hand, depend strongly on the chosen model. For neutralino masses above ≈ 600 GeV no limits on any direct squark pair production scenario are placed by the LHC.

88.6 Exclusion limits on bottom and top squarks masses in RPC scenarios

Besides placing stringent limits on first and second generation squark masses, the LHC experiments also search for the production of third generation squarks. SUSY at the TeV-scale is often motivated by naturalness arguments, most notably as a solution to cancel quadratic divergences in radiative corrections to the Higgs boson mass. In this context, the most relevant terms for SUSY phenomenology arise from the interplay between the masses of the third generation squarks and the Yukawa coupling of the top quark to the Higgs boson. This motivates a potential constraint on the masses of the top squarks and the left-handed bottom squark. Due to the large top quark mass, significant mixing between $\tilde{t}_{\rm L}$ and $\tilde{t}_{\rm R}$ is expected, leading to a lighter mass state $\tilde{t}_1$ and a heavier mass state $\tilde{t}_2$. In the MSSM, the lightest top squark ($\tilde{t}_1$) can be the lightest squark.

Bottom squarks are expected to decay predominantly to $b\tilde{\chi}_1^0$ giving rise to the characteristic multi b-jet and $E_{\rm T}^{\rm miss}$ signature. Direct production of bottom squark pairs has been searched for at the Tevatron and at the LHC. Limits from the Tevatron are $m_{\tilde{b}} > 247$ GeV for a massless neutralino [92, 93]. ATLAS has set a lower limit of $m_{\tilde{b}} > 1250$ GeV for massless neutralinos in this model [94] exploiting the two b-jets and missing transverse momentum analysis. For $m_{\tilde{\chi}_1^0} \approx 800$ GeV or higher no limit can be placed on direct bottom squark pair production in this simplified model. Limits from CMS are comparable [84]. Reinterpretations of the monojet analysis results can be used to constrain very compressed scenarios, with exclusion of masses up to 550 GeV in case of $\Delta m = m_{\tilde{b}} - m_{\tilde{\chi}_1^0} \approx 5$ GeV [86]. Further bottom squark decay modes have also been searched for by ATLAS [95–97] and CMS [76, 98, 99], for instance targeting more complex decay chains that include Higgs bosons in the cascade.

The top squark decay modes depend on the SUSY mass spectrum, and on the $\tilde{t}_{\rm L}$-$\tilde{t}_{\rm R}$ mixture of the top squark mass eigen-

Int. J. Mod. Phys. A 2026.41. Downloaded from www.worldscientific.com by UNIVERSITY OF CALIFORNIA @ BERKELEY on 09/16/26. Re-use and distribution is strictly not permitted, except for Open Access articles.

state. If kinematically allowed, the two-body decays $\tilde{t} \to t\tilde{\chi}_1^0$ (which requires $m_{\tilde{t}} - m_{\tilde{\chi}_1^0} > m_t$) and $\tilde{t} \to b\tilde{\chi}^{\pm}$ (which requires $m_{\tilde{t}} - m_{\tilde{\chi}^{\pm}} > m_b$) are expected to dominate, depending on L-R mixture. If not, the top squark decay may proceed either via the two-body decay $\tilde{t} \to c\tilde{\chi}_1^0$ or through $\tilde{t} \to bf\bar{f}'\tilde{\chi}_1^0$ (where f and $\bar{f}'$ denote a fermion-antifermion pair with appropriate quantum numbers). For $m_{\tilde{t}} - m_{\tilde{\chi}_1^0} > m_b$ the latter decay chain represents a four-body decay with a W boson, charged Higgs $H^{\pm}$, slepton $\tilde{\ell}$, or light flavor squark $\tilde{q}$, exchange. If the exchanged W boson and/or sleptons are kinematically allowed to be on-shell, the three-body decays $\tilde{t} \to Wb\tilde{\chi}_1^0$ and/or $\tilde{t} \to b\nu\tilde{\ell}(\tilde{\nu}\ell)$ will become dominant. For further discussion on top squark decays see for example Ref. [100].

Limits from LEP on the $\tilde{t}_1$ mass are $m_{\tilde{t}} > 96$ GeV in the charm plus neutralino final state, and > 93 GeV in the lepton, b-quark and sneutrino final state [72].

The Tevatron experiments have performed a number of searches for top squarks, often assuming direct pair production. In the $b\ell\tilde{\nu}$ decay channel, and assuming a 100% branching fraction, limits are set as $m_{\tilde{t}} > 210$ GeV for $m_{\tilde{\nu}} < 110$ GeV and $m_{\tilde{t}} - m_{\tilde{\nu}} > 30$ GeV, or $m_{\tilde{t}} > 235$ GeV for $m_{\tilde{\nu}} < 50$ GeV [101, 102]. In the $\tilde{t} \to c\tilde{\chi}_1^0$ decay mode, a top squark with a mass below 180 GeV is excluded for a neutralino lighter than 95 GeV [103, 104]. In both analyses, no limits on the top squark can be set for heavy sneutrinos or neutralinos. In the $\tilde{t} \to b\tilde{\chi}_1^{\pm}$ decay channel, searches for a relatively light top squark have been performed in the dilepton final state [105, 106]. The CDF experiment sets limits in the $\tilde{t} - \tilde{\chi}_1^0$ mass plane for various branching fractions of the chargino decay to leptons and for two values of $m_{\tilde{\chi}_1^{\pm}}$. For $m_{\tilde{\chi}_1^{\pm}} = 105.8$ GeV and $m_{\tilde{\chi}_1^0} = 47.6$ GeV, top squarks between 128 and 135 GeV are excluded for W-like leptonic branching fractions of the chargino.

The LHC experiments have improved these limits substantially and developed dedicated searches for all potential top-squark decay modes. This is well depicted in Fig. 88.6, where a summary of the limits on the top squark mass are reported for the single decay chain of $\tilde{t} \to t\tilde{\chi}_1^0$ as well as for the three-body and four-body decay modes. Interpretations are carried out in simplified models hence care must be taken when interpreting these limits in the context of more complete SUSY models.

The most important searches for the top squark decay topology are dedicated searches requiring zero or one isolated lepton, modest $E_{\mathrm{T}}^{\mathrm{miss}}$, and four or more jets out of which at least one jet must be reconstructed as a b-jet [51, 76, 84, 85, 107–109]. For example, using an all-hadronic analysis, CMS excludes top squarks with masses below about 1300 GeV in this model for light neutralinos, while for $m_{\tilde{\chi}_1^0} > 700$ GeV no limits can be provided [85]. Equivalent constraints are set by the ATLAS all-hadronic search [107]. Analyses targeting final state events characterised by the presence of one lepton (electron or muon) have similar albeit lower sensitivity in the $\tilde{t} \to t\tilde{\chi}_1^0$ decay mode, see for instance the recent ATLAS result [109] using NN methods.

Single and di-lepton analyses are most sensitive to models where the top squark decay exclusively proceeds via the chargino mediated decay chain $\tilde{t} \to b\tilde{\chi}_1^{\pm}$, $\tilde{\chi}_1^{\pm} \to W^{\pm(*)}\tilde{\chi}_1^0$. In this case, top squark mass exclusion limits vary strongly with the assumptions made on the $\tilde{t} - \tilde{\chi}_1^{\pm} - \tilde{\chi}_1^0$ mass hierarchy. For example, for $m_{\tilde{\chi}_1^{\pm}} = (m_{\tilde{t}} + m_{\tilde{\chi}_1^0})/2$, a stop mass below ≈ 1150 GeV for a light $\tilde{\chi}_1^0$ is excluded by CMS, while no limit can be placed for $m_{\tilde{\chi}_1^0} > 550$ GeV [51]. These limits, however, can weaken significantly when other assumptions about the mass hierarchy or the decay of the charginos are imposed [51, 110–112].

Other analyses with zero, one or two leptons target this kinematic region [113–119], also providing sensitivity in the case of alternative decay modes of the top squark, *i.e.* including tau sleptons [112, 120–122] or Higgs and Z bosons in the decay chain [123].

If the decays $\tilde{t} \to t\tilde{\chi}_1^0$ and $\tilde{t} \to b\tilde{\chi}_1^{\pm}$, $\tilde{\chi}_1^{\pm} \to W^{\pm(*)}\tilde{\chi}_1^0$ are kinematically forbidden, the decay chains $\tilde{t} \to Wb\tilde{\chi}_1^0$ and $\tilde{t} \to c\tilde{\chi}_1^0$ can become important. The one-lepton ATLAS search [108] provides for the kinematic region $m_{\tilde{t}} - m_{\tilde{\chi}^{\pm}} > m_b + m_W$ lower limits on the top squark mass of ≈ 700 GeV for a neutralino lighter than ≈ 570 GeV, as also shown in Fig. 88.6. For the kinematic region in which even the production of real W bosons is not allowed, ATLAS and CMS improve the Tevatron limit on $\tilde{t} \to c\tilde{\chi}_1^0$ substantially. Based on a monojet analysis [86] ATLAS excludes top squark masses below $m_{\tilde{\chi}_1^0} \approx 550$ GeV along the kinematic boundary for the $\tilde{t} \to c\tilde{\chi}_1^0$ decay. The ATLAS monojet analysis also places similar boundaries for the other decay chain relevant in this phase region, $\tilde{t} \to bf\bar{f}'\tilde{\chi}_1^0$. Other analyses, such as the search in events with one leptons and jets, are also sensitive to this decay mode: the ATLAS one-lepton analysis excludes up to ≈ 650 GeV for $\Delta m = m_{\tilde{t}}, m_{\tilde{\chi}_1^0} \approx 50$ GeV [108]. A recent dedicated analysis for $\tilde{t} \to c\tilde{\chi}_1^0$ exploiting c-tagging excludes stop masses below about 900 GeV for $m_{\tilde{\chi}_1^0}$ below 420 GeV [91]. Also a topology where one stop decays through $\tilde{t} \to c\tilde{\chi}_1^0$ and the other one through $\tilde{t} \to t\tilde{\chi}_1^0$ has been considered [91, 124] and limits have been placed, in the case of equal branching ratios, 800 GeV for light neutralinos and 600 GeV in the compressed region.

The CMS collaboration uses the hadronic searches [85, 114, 116] to place constraints on stop decay into charm-quark and excludes $m_{\tilde{t}} \approx 630$ GeV for $\Delta m = m_{\tilde{t}}, m_{\tilde{\chi}_1^0} \approx 50$ GeV [85]. Constraints are also set in case of $\tilde{t} \to bf\bar{f}'\tilde{\chi}_1^0$, with CMS excluding masses up to 480 and 700 GeV for $\Delta m = m_{\tilde{t}}, m_{\tilde{\chi}_1^0} \approx 10$ and 80 GeV, respectively [125].

In general, the variety of top squark decay chains in the phase space region where $\tilde{t} \to t\tilde{\chi}_1^0$ is kinematically forbidden represents a challenge for the experimental search program but more data and refined analyses in Run 2 have further improved the sensitivity in this difficult but important region of SUSY parameter space, and more is expected for future Runs of the LHC. Precision SM measurements can also provide important insights to such challenging regions. For instance, analyses of $t\bar{t}$ spin correlations can be used to set constraints on top squark masses close to the top-quark mass. ATLAS [126] excludes the mass region between 150 and 230 GeV for kinematically allowed values of the neutralino mass. CMS [119] results cover a similar mass range.

Table 88.2: Summary of bottom and top squark mass limits using different interpretation approaches assuming R-parity conservation. Masses in this table are provided in GeV. Further details about the assumptions and analyses from which these limits are obtained are discussed in the corresponding sections of the text.

Model	Assumption	$m_{\tilde{q}}$
$\tilde{b} \to b\tilde{\chi}_1^0$	$m_{\tilde{\chi}_1^0} = 0$	≈ 1250
	$m_{\tilde{\chi}_1^0} > \approx 700$	no limit
$\tilde{t} \to t\tilde{\chi}_1^0$	$m_{\tilde{\chi}_1^0} = 0$	≈ 1300
	$m_{\tilde{\chi}_1^0} > \approx 600$	no limit
$\tilde{t} \to b\tilde{\chi}_1^{\pm}$	$m_{\tilde{\chi}_1^0} = 0$	≈ 1150
$(m_{\tilde{\chi}_1^{\pm}} = (m_{\tilde{t}} - m_{\tilde{\chi}_1^0})/2)$	$m_{\tilde{\chi}_1^0} > \approx 550$	no limit
$\tilde{t} \to Wb\tilde{\chi}_1^0$	$m_{\tilde{\chi}_1^0} < \approx 570$	≈ 700
$(m_W < m_{\tilde{t}} - m_{\tilde{\chi}^0} < m_t)$		
$\tilde{t} \to c\tilde{\chi}_1^0$	$m_{\tilde{t}} - m_{\tilde{\chi}_1^0} \approx 50$	≈ 900
	$m_{\tilde{t}} \approx m_{\tilde{\chi}_1^0}$	≈ 550
$\tilde{t} \to bff'\tilde{\chi}_1^0$	$m_{\tilde{t}} - m_{\tilde{\chi}_1^0} \approx 50$	≈ 650
$(m_{\tilde{t}} - m_{\tilde{\chi}^0} < m_W)$	$m_{\tilde{t}} \approx m_{\tilde{\chi}_1^0}$	≈ 550

88.7 Exclusion limits on the masses of charginos, neutralinos and sleptons in RPC scenarios

Charginos, neutralinos and sleptons are produced through electroweak interactions and their cross sections depend on the assumptions made for mass and mixing parameters.

Charginos and neutralinos carry no color charge and the mixing of the charged wino and higgsino states (for charginos), and the

Int. J. Mod. Phys. A 2026.41. Downloaded from www.worldscientific.com
by UNIVERSITY OF CALIFORNIA @ BERKELEY on 09/16/26. Re-use and distribution is strictly not permitted, except for Open Access articles.

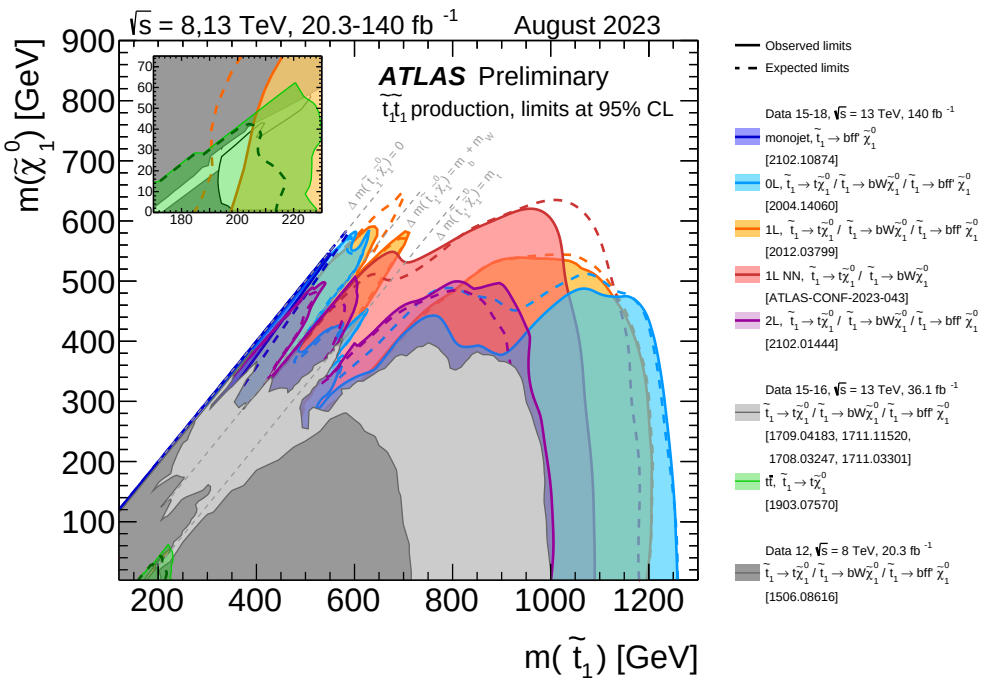

Figure 88.6: A summary of the 95% C.L. exclusion contours in the stop-neutralino mass plane for various possible decay chains, including two-, three- and four-body decays, as obtained in dedicated analyses by ATLAS.

neutral bino, wino and higgsino states (for neutralinos), is determined by a limited number of parameters. For charginos these are the wino mass parameter M_2, the higgsino mass parameter μ, and $\tan\beta$, and for neutralinos these are the same parameters plus the bino mass parameter M_1. If one of the parameters M_1, M_2 or μ is substantially smaller than the others, the chargino/neutralino composition would be dominated by specific states, which are referred to as bino-like ($M_1 \ll M_2, \mu$), wino-like ($M_2 \ll M_1, \mu$), or higgsino-like ($\mu \ll M_1, M_2$). If gaugino mass unification at the GUT scale is assumed, a relation between M_1 and M_2 at the electroweak scale follows: $M_1 = 5/3 \tan^2\theta_W M_2 \approx 0.5 M_2$, with θ_W the weak mixing angle. At hadron colliders the largest production rates arise when the lightest chargino and the next-to-lightest neutralino are wino-like and nearly mass-degenerate, forming an SU(2) triplet. In this case the LSP is typically bino-like. If instead the higgsino mass parameter is much smaller than the gaugino masses, the two lightest neutralinos and the lightest chargino form an approximately mass-degenerate SU(2) doublet; production rates are lower and the mass spectrum is compressed.

In models with slepton and gaugino mass unification at the GUT scale, the superpartner of the right-handed lepton, $\tilde{\ell}_{\rm R}$, is expected to be lighter than the left-handed one, $\tilde{\ell}_{\rm L}$. Cross sections depend on the L-R mixing which in turn depends on the mass of the fermion and other parameters. For tau sleptons there may be considerable mixing between the L and R states, leading to a significant mass difference between the lighter $\tilde{\tau}_1$ and the heavier $\tilde{\tau}_2$.

Fig. 88.7 [127, 128] (see also Ref. [73] for further details) shows typical production cross sections at hadron colliders for electroweakinos under various assumptions and considering a center-of-mass energy of 13 TeV. For masses of several hundreds of GeV, they are at least two orders of magnitude smaller than for colored SUSY particles. Thanks to the large data samples collected at the LHC, the sensitivity of LEP and Tevatron searches for direct chargino/neutralino or slepton production has been surpassed in several regions of SUSY parameter space.

88.7.1 *Exclusion limits on chargino masses*

The lightest chargino $\tilde{\chi}_1^\pm$ is searched for either considering pair production, or through associated production of $\tilde{\chi}_1^\pm$ and the next-to-lightest neutralino, $\tilde{\chi}_2^0$, if they are assumed to be degenerate in mass. If kinematically allowed, two body decay modes such as $\tilde{\chi}^\pm \to \tilde{f}\bar{f}'$ (including $\ell\tilde{\nu}$ and $\tilde{\ell}\nu$) are dominant. If not, three-body decays $\tilde{\chi}^\pm \to f\bar{f}'\tilde{\chi}_1^0$, mediated through virtual W bosons or sfermions, become dominant. If sfermions are heavy, the W mediation dominates, and $f\bar{f}'$ are distributed with branching fractions similar to W decay products (barring phase space effects for small mass gaps between $\tilde{\chi}^\pm$ and $\tilde{\chi}^0$). If, on the other hand, sleptons are light enough to play a significant role in the decay, leptonic final states will be enhanced.

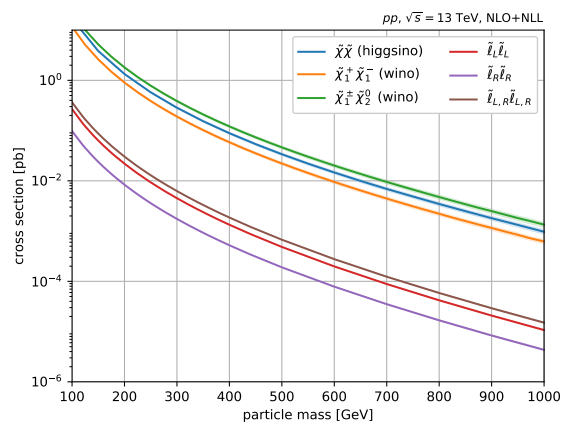

Figure 88.7: Cross sections for pair production of charginos, neutralinos and sleptons calculated for 13 TeV centre-of-mass energy at NLO plus next-to-leading-log (NLL) precision. Wino-like $\tilde{\chi}_1^\pm\tilde{\chi}_2^0$ and $\tilde{\chi}_1^+\tilde{\chi}_1^-$ productions are calculated in a limit of mass-degenerate $\tilde{\chi}_1^\pm$ and $\tilde{\chi}_2^0$, light bino $\tilde{\chi}_1^0$, and with all the other sparticles assumed to be heavy and decoupled. Higgsino-like cross sections assume mass-degenerate $\tilde{\chi}_1^\pm$, $\tilde{\chi}_2^0$ and $\tilde{\chi}_1^0$. For slepton pair cross sections, left(right)-handed only or 50% mixed states are considered.

Int. J. Mod. Phys. A 2026.41. Downloaded from www.worldscientific.com by UNIVERSITY OF CALIFORNIA @ BERKELEY on 09/16/26. Re-use and distribution is strictly not permitted, except for Open Access articles.

At LEP, $\tilde{\chi}_1^+\tilde{\chi}_1^-$ is the dominant production process. Charginos have been searched for in fully-hadronic, semi-leptonic and fully leptonic decay modes [129, 130]. A general lower limit on the lightest chargino mass of 103.5 GeV is derived, except in corners of phase space with low electron sneutrino mass, where destructive interference in chargino production, or two-body decay modes, play a role. The limit is also affected if the mass difference between $\tilde{\chi}_1^\pm$ and $\tilde{\chi}_1^0$ is small; dedicated searches for such scenarios set a lower limit of 92 GeV.

At the Tevatron, charginos have been searched for via associated production of $\tilde{\chi}_1^\pm\tilde{\chi}_2^0$ [131, 132]. Decay modes involving multilepton final states provide the best discrimination against the large multijet background. Analyses have looked for at least three charged isolated leptons, for two leptons with missing transverse momentum, or for two leptons with the same charge. Depending on the $(\tilde{\chi}_1^\pm - \tilde{\chi}_1^0)$ and/or $(\tilde{\chi}_2^0 - \tilde{\chi}_1^0)$ mass differences, leptons may have soft transverse momentum.

At the LHC, the search strategy is similar to that at the Tevatron but it also exploits the large datasets collected to target missing momentum and fully-hadronic final states and consider $\tilde{\chi}_1^+\tilde{\chi}_1^-$ production only i.e. releasing the assumption of $\tilde{\chi}_1^\pm, \tilde{\chi}_2^0$ mass degeneracy. Furthermore, compressed SUSY spectra are searched for considering low-momentum leptons recoiling against an ISR jet.

Chargino pair production is mainly searched for in the dilepton plus missing momentum final state. In a simplified model interpretation of the results where only the $\tilde{\chi}_1^+\tilde{\chi}_1^-$ process is considered and assuming mediation of the chargino decay by light sleptons ($\tilde{e}$ and $\tilde{\mu}$), ATLAS [133] and CMS [134] set limits on the chargino mass up to 1 TeV for massless LSPs, but no limits on the chargino mass can be set for $\tilde{\chi}_1^0$ heavier than 480 GeV. Limits are fairly robust against variation of the slepton mass, unless the mass gap between sparticles becomes small enough that the charged lepton has a too low-momentum to be reconstructed. For decays mediated through $\tilde{\tau}$ or $\tilde{\nu}_\tau$, recent results reach limits of 970 GeV as set by ATLAS [135] for LSPs not heavier than 440 GeV. The CMS experiment provides limits using Run 2 data [136].

In case slepton masses are higher than the mass of the chargino, searches are performed for charginos decaying via a W boson. Constraints on pair-produced pure-wino charginos using various decay channels have been recently summarized by ATLAS using statistical combinations of Run 2 searches [137]. The combination of the search results closes the gaps left by the individual searches in this simplified model, with chargino masses excluded up to 800 GeV for massless neutralinos. No limits are set for LSP masses above 170 GeV. Individual channels include 2-lepton final state events [133], resulting in masses below 420 GeV being excluded for massless LSPs. In the challenging case where the difference between chargino and LSP masses is close to that of the W boson, dedicated searches have been carried out by ATLAS [138], excluding chargino masses up to 140 GeV. Searches have also been carried out in the single lepton final state. ATLAS excludes chargino masses between 260 and 520 GeV for a massless LSP [139]. Further extension of the sensitivity in the high-mass region is achieved by ATLAS [140] and CMS [141] exploiting the large branching ratio of fully-hadronic final states and the identification of boosted W bosons through large-radius jets and jet substructure information. Considering only wino-like chargino pair production in case of a massless LSP, ATLAS excludes a region between 630 GeV and 760 GeV, while CMS excludes between 290 GeV and 670 GeV. No limits are set for LSP masses above 200 GeV.

Several final states characterized by the presence of missing transverse momentum are studied to set limits on the chargino mass through $\tilde{\chi}_1^\pm\tilde{\chi}_2^0$ associated production. Usually, wino-like $\tilde{\chi}_1^\pm$ and $\tilde{\chi}_2^0$ and bino-like $\tilde{\chi}_1^0$ are assumed with $m_{\tilde{\chi}_1^\pm} = m_{\tilde{\chi}_2^0}$, leaving $m_{\tilde{\chi}_1^\pm}$ and $m_{\tilde{\chi}_1^0}$ free. Higgsino models with small mass differences among the electroweakinos are targeted using low-momentum lepton signatures. Again, the branching fraction of leptonic final states is determined by the slepton masses. If the decay is predominantly mediated by a light $\tilde{\ell}_\mathrm{L}$, i.e. $\tilde{\ell}_\mathrm{R}$ is assumed to be heavy, the three charged-lepton flavors will be produced in equal amounts, and a multi-lepton signature is favored. For simplicity, $\tilde{\ell}_\mathrm{L}$ and $\tilde{\nu}$ are taken to be nearly mass-degenerate, and diagrams with sneutrinos are included.

In such a scenario, ATLAS [142] and CMS [143] exclude chargino masses below 1450 GeV for massless LSPs; no limits are set for LSP masses above 1 TeV. If the decay is dominated by a light $\tilde{\ell}_\mathrm{R}$, the chargino cannot be a pure wino but needs to have a large higgsino component, preferring the decays to tau leptons. Limits are set in various scenarios. If, like for $\tilde{\ell}_\mathrm{L}$, a flavor-democratic scenario is assumed (τ-enriched scenario), CMS sets limits of 1150 GeV on the chargino mass for massless LSPs, but under the assumption that both $\tilde{\chi}_1^\pm$ and $\tilde{\chi}_2^0$ decay leads to tau leptons in the final state (τ-dominated scenario), the chargino mass limit deteriorates to 970 GeV for massless LSPs [143]. ATLAS assumes a simplified model in which staus are significantly lighter than the other sleptons and search for a similar multi-tau final state, setting a lower limit on the chargino mass of 1160 GeV in this model [135].

If sleptons are heavy, the chargino is assumed to decay to a W boson plus LSP, and the $\tilde{\chi}_2^0$ into Z plus LSP (WZ searches) or H plus LSP (WH searches). Searches for the WZ channel exploit events with either two same-sign leptons or three leptons, a single lepton, or with no leptons (all-hadronic). If $\tilde{\chi}_2^0$ decays through a Higgs boson with $m_H = 125$ GeV, search strategies depend on the SM-like Higgs decay modes and branching fractions. Higgs bosons in the final state are identified by either two jets originating from bottom quarks ($h \to b\bar{b}$), two photons ($h \to \gamma\gamma$), or leptons from the WW, ZZ or $\tau\tau$ decay modes. Interpretations are also provided in scenarios where the $\tilde{\chi}_2^0$ does not decay exclusively into a Z or H boson and the LSP.

A combination of the results of several searches for the electroweak production of the supersymmetric partners of standard model bosons has been published by CMS [144]. In the case of wino-like $\tilde{\chi}_1^\pm\tilde{\chi}_2^0$ production, the combined CMS result gives an observed (expected) limit on the chargino mass of about 875 (950) GeV for the WZ topology. Limits on a higgsino-bino model where charginos decay to a W boson and the LSP up to 800 GeV are set in simplified models where it is degenerate with $\tilde{\chi}_2^0$ and $\tilde{\chi}_3^0$.

The recent ATLAS statistical combinations of Run 2 searches [137] excludes $\tilde{\chi}_1^\pm$ masses up to 1000 GeV, with no mass limits possible for LSP masses above 400 GeV. Searches for $\tilde{\chi}_1^\pm\tilde{\chi}_2^0$ production in events with three leptons and missing momentum allows to exclude wino-like chargino masses below 640 GeV for massless LSPs [145]. Results have also been reported for searches including same-sign lepton signal regions [146] and single lepton searches [139]. Limits are reduced in case of higgsino-like scenarios, with exclusion down to 210 GeV.

Additional constraints on the chargino mass are placed exploiting all-hadronic analyses. A wino-like (higgsino-like) chargino with mass up to 1060 (900) GeV is excluded by ATLAS [140] when the LSP mass is below 400 (240) GeV and the mass splitting is larger than 400 (450) GeV. This is also included in the Run 2 combination study. CMS [141] excludes wino-like charginos with mass up to 970 GeV for massless LSP.

Searches exploiting the presence of b-jets are most sensitive in the high-mass chargino region if $\tilde{\chi}_2^0$ decays through a Higgs boson, while analyses targeting photon pair or leptonic decays provide the best sensitivity in the region of low masses. CMS [147] sets lower limits on the chargino mass up to 820 GeV for massless LSPs, but vanish for LSP masses above 350 GeV using events with at least one lepton and missing transverse momentum in the final state. In the case of wino-like $\tilde{\chi}_1^\pm\tilde{\chi}_2^0$ production, the combined CMS result [144] gives an observed (expected) limit on the chargino mass of about 990 (1075) GeV for the WH topology, and 875 (1000) GeV for a mixed topology with WZ. Similar sensitivities are achieved by the ATLAS analyses [148–150], combined in [137].

In both the wino region (a characteristic of anomaly-mediated

Int. J. Mod. Phys. A 2026.41. Downloaded from www.worldscientific.com
by UNIVERSITY OF CALIFORNIA @ BERKELEY on 09/16/26. Re-use and distribution is strictly not permitted, except for Open Access articles.

SUSY breaking models) and the higgsino region of the MSSM, the mass splitting between $\tilde{\chi}_1^{\pm}$ and $\tilde{\chi}_1^0$ is small. The chargino decay products are very soft and may escape detection. These compressed spectra are hard to detect, and have triggered dedicated search strategies.

Studies from ATLAS [151] and CMS [152] for charginos and neutralinos in a compressed mass spectrum use initial state radiation and two or three low-momentum (soft) leptons. For wino-like charginos, assuming degenerate $\tilde{\chi}_1^{\pm}$ and $\tilde{\chi}_2^0$, exclusion contours in the chargino-mass versus $\Delta m(\tilde{\chi}_1^{\pm} - \tilde{\chi}_1^0)$ plane are derived. As an example, such charginos are excluded by CMS (ATLAS) below 280 (240) GeV for $\Delta m(\tilde{\chi}_1^{\pm} - \tilde{\chi}_1^0) = 10$ GeV. Considering the higgsino model, the masses probed by CMS reach up to 215 GeV for a mass difference of 7.5 GeV and 150 GeV in the highly compressed region with a mass difference of 3 GeV.

Recent ATLAS results [153] using vector boson fusion signatures and missing transverse momentum were interpreted in simplified RPC models in which the LSP is a bino-like neutralino with a mass similar to that of the lightest chargino and second-to-lightest neutralino, both of which are wino-like. Lower limits at 95% confidence level on the masses of NLSPs were established between 117 and 120 GeV when the LSP is within 1 GeV in mass. CMS has also searched for chargino-pair production through vector-boson-fusion [154], also targeting compressed mass spectra. Assuming degenerate $\tilde{\chi}_1^{\pm}$ and $\tilde{\chi}_2^0$, charginos with a mass below 112 GeV are excluded for $\Delta m(\tilde{\chi}_1^{\pm} - \tilde{\chi}_1^0) = 1$ GeV. CMS has published further searches for such compressed spectra with a soft tau lepton [155]. A combination of several searches for the electroweak production of winos, binos, higgsinos, and sleptons has also been recently been presented by CMS [144].

88.7.2 *Exclusion limits on neutralino masses*

In a considerable part of the MSSM parameter space, and in particular when demanding that the LSP carries no electric or color charge, the lightest neutralino $\tilde{\chi}_1^0$ is the LSP. If R-parity is conserved, such a $\tilde{\chi}_1^0$ is stable. Since it is weakly interacting, it will typically escape detectors unseen. Limits on the invisible width of the Z boson apply to neutralinos with a mass below 45.5 GeV, but depend on the Z-neutralino coupling. Such a coupling could be small or even absent; in such a scenario there is no general lower limit on the mass of the lightest neutralino [156]. In models with gaugino mass unification and sfermion mass unification at the GUT scale, a lower limit on the neutralino mass is derived from limits from direct searches, notably for charginos and sleptons, and amounts to 47 GeV [157]. Assuming a constrained model like the CMSSM, this limit increases to 50 GeV at LEP; however the strong constraints now set by the LHC increase such CMSSM-derived $\tilde{\chi}_1^0$ mass limits to well above a few hundred GeV (the latest reinterpretation only uses Run 1 data and indicates 200 GeV [158–160]).

In gauge-mediated SUSY breaking models (GMSB), the LSP is typically a gravitino, and the phenomenology is determined by the nature of the next-to-lightest supersymmetric particle (NLSP). A NLSP neutralino will decay to a gravitino and a SM particle whose nature is determined by the neutralino composition. Final states with two high p_{T} photons and missing momentum are searched for, and interpreted in gauge mediation models with bino-like neutralinos [161–167].

Assuming the production of at least two neutralinos per event, neutralinos with large non-bino components can also be searched for by their decay in final states with missing momentum plus any two bosons out of the collection γ, Z, H. A number of searches at the LHC have tried to cover the rich phenomenology predicted by the general gauge mediation model (GGM) where $\tilde{\chi}_1^0$ might decay with various BR in the Z and H decay modes [98, 149, 164, 168–178]. As an example, strong constraints for decay modes involving Z and H bosons arise from full-hadronic searches on higgsino-like scenarios: ATLAS [140] excludes higgsino production with decays into a massless gravitino LSP in a mass range between 450 (500) GeV and 940 (850) GeV assuming BR = 1 (0.5) for the Z plus gravitino decay mode. Assuming only H plus gravitino decays, CMS [179] excludes a higgsino mass range between 175 GeV and 1025 GeV. Assuming a mix of γ, Z, H decays, a CMS search [167] in the photonic final state excludes higgsinos up to 1.05 TeV.

Heavier neutralinos, in particular $\tilde{\chi}_2^0$, have been searched for in their decays to the lightest neutralino plus a γ, a Z boson or a Higgs boson. Limits on electroweak production of $\tilde{\chi}_2^0$ plus $\tilde{\chi}_1^{\pm}$ from all-hadronic, same-sign dilepton and trilepton analyses have been discussed in the section on charginos; the assumption of equal mass of $\tilde{\chi}_2^0$ and $\tilde{\chi}_1^{\pm}$ make the limits on chargino masses apply to $\tilde{\chi}_2^0$ as well. Multilepton analyses have also been used to set limits on $\tilde{\chi}_2^0\tilde{\chi}_3^0$ production; assuming equal mass and decay through light sleptons, limits are set up to 680 GeV for massless LSPs [180]. Again, compressed spectra with small mass differences between the heavier neutralinos and the LSP form the most challenging region.

Of particular relevance are supersymmetric models characterised by pure wino or pure higgsino states, with small mass splittings between $\tilde{\chi}_1^{\pm}$ and $\tilde{\chi}_1^0$, $\Delta m \sim 160$ MeV for winos and ~ 350 MeV for higgsinos. In this case, the $\tilde{\chi}_1^0$ is a natural candidate for dark matter (thermal relic), with pure winos predicted as $m_{\chi} \simeq 2.8 - 3.1$ TeV and pure higgsinos with thermal mass near 1.1 TeV. Winos feature a large annihilation cross section and predictions are currently in tension with reinterpretations of gamma-ray bounds. Higgsinos have lower annihilation rates and, under specific assumptions on the dark matter density, are constrained up to 270 GeV [181] (see also the Dark Matter Chapter in this review for references and further details).

In $\tilde{\chi}_2^0$ decays to $\tilde{\chi}_1^0$ and a lepton pair, the lepton pair invariant mass distribution may show a structure that can be used to measure the $\tilde{\chi}_2^0 - \tilde{\chi}_1^0$ mass difference in case of a signal [37]. This structure, however, can also be used in the search strategy itself, as demonstrated by ATLAS [182, 183] and CMS [98, 184].

Fig. 88.8 summarizes some of the most recent results from ATLAS and CMS for chargino pair or chargino and next-to-lightest neutralino pair productions comparing results obtained with various assumptions. The limits on weak gauginos in simplified models are also summarized in Table 88.3. Only results for promptly decaying charginos and neutralinos are included: limits from searches focusing on long-lived particle scenarios are reported in Section 88.9.

Interpretations of the search results outside simplified models, such as in the phenomenological MSSM (see [185–190] and, most recently, [191]), show that the simplified model limits can translate into accurate constraints but must also be interpreted with care. Electroweak gauginos in models that are compatible with the relic density of dark matter in the Universe, for example, have particularly tuned mixing parameters and mass spectra, which are not always captured by the simplified models used.

88.7.3 *Exclusion limits on slepton masses*

The most model-independent searches for selectrons, smuons and staus originate from the LEP experiments [192]. Smuon production only takes place via s-channel γ^*/Z exchange. Search results are often quoted for $\tilde{\mu}_{\mathrm{R}}$, since it is typically lighter than $\tilde{\mu}_{\mathrm{L}}$ and has a weaker coupling to the Z boson; limits are therefore conservative. Decays are expected to be dominated by $\tilde{\mu}_{\mathrm{R}} \to \mu\tilde{\chi}_1^0$, leading to two non-back-to-back muons and missing momentum. Slepton mass limits are calculated in the MSSM under the assumption of gaugino mass unification at the GUT scale, and depend on the mass difference between the smuon and $\tilde{\chi}_1^0$. A $\tilde{\mu}_{\mathrm{R}}$ with a mass below 94 GeV is excluded for $m_{\tilde{\mu}_{\mathrm{R}}} - m_{\tilde{\chi}_1^0} > 10$ GeV. The selectron case is similar to the smuon case, except that an additional production mechanism is provided by t-channel neutralino exchange. The $\tilde{e}_{\mathrm{R}}$ lower mass limit is 100 GeV for $m_{\tilde{\chi}_1^0} < 85$ GeV. Due to the t-channel neutralino exchange, $\tilde{e}_{\mathrm{R}}\tilde{e}_{\mathrm{L}}$ pair production was possible at LEP, and a lower limit of 73 GeV was set on the selectron mass regardless of the neutralino mass by scanning over MSSM parameter space [193]. The potentially large mixing between $\tilde{\tau}_{\mathrm{L}}$ and $\tilde{\tau}_{\mathrm{R}}$ not only makes the $\tilde{\tau}_1$ light, but can also make its coupling to the Z boson small. LEP lower limits on the $\tilde{\tau}$ mass range between 87 and 93 GeV depending on the $\tilde{\chi}_1^0$ mass, for $m_{\tilde{\tau}} - m_{\tilde{\chi}_1^0} > 7$ GeV [192].

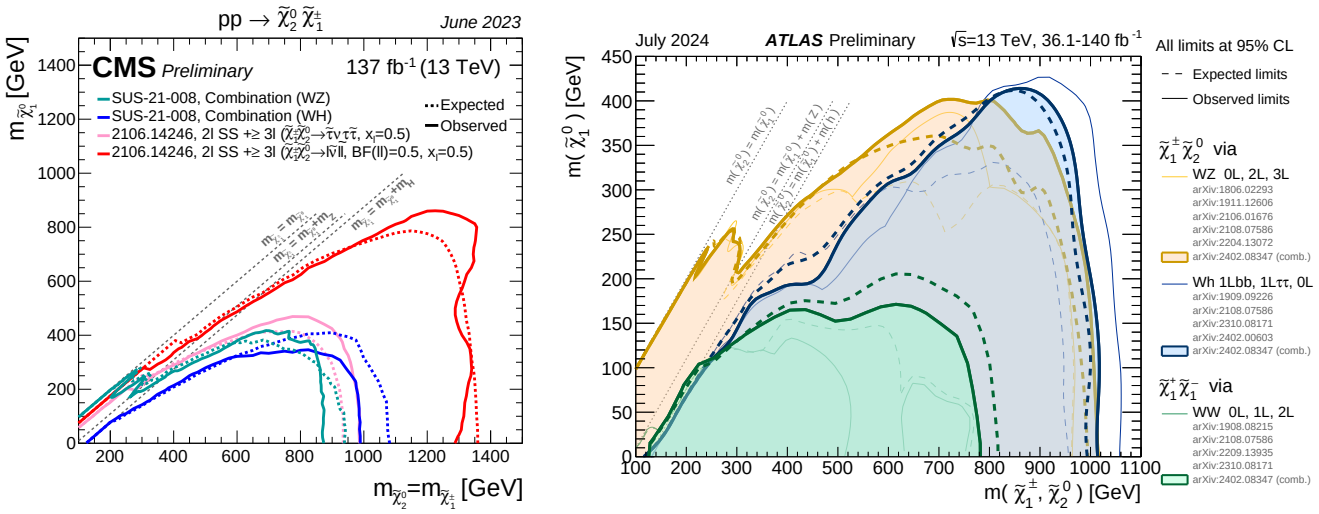

Figure 88.8: LHC exclusion limits on chargino and neutralino masses in a number of simplified models. Left: CMS limits on chargino and neutralino masses for pair production of charginos, pair production of heavier neutralinos, or pair production of chargino and neutralino, under a variety of assumptions including light sleptons mediating the decays. Right: ATLAS limits on chargino and neutralino masses for pair production of chargino and neutralino, under the assumption of decoupled sleptons, and chargino/neutralino decay through on- or off-shell W and Z or H.

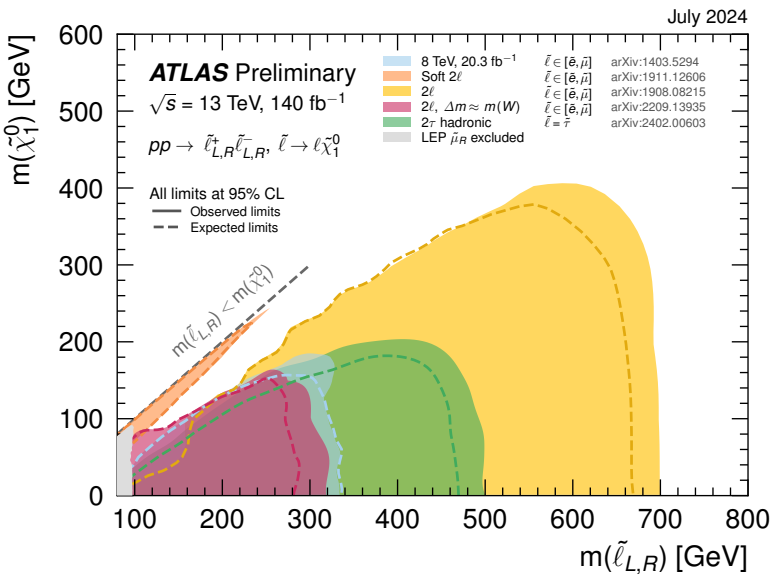

Figure 88.9: LHC exclusion limits on slepton (selectron, smuon and stau) masses, assuming equal masses of selectrons and smuons, degeneracy of $\tilde{\ell}_L$ and $\tilde{\ell}_R$, and a 100% branching fraction for $\tilde{\ell} \to \ell\tilde{\chi}_1^0$.

At the LHC, pair production of sleptons is not only heavily suppressed with respect to pair production of colored SUSY particles but the cross section is also almost two orders of magnitude smaller than the one of pair production of charginos and neutralinos. With the full data sets of Run 1 and Run 2, however, ATLAS and CMS have surpassed the sensitivity of the LEP analyses under certain assumptions.

ATLAS and CMS have searched for direct production of selectron pairs and smuon pairs at the LHC, with each slepton decaying to its corresponding SM partner lepton and the $\tilde{\chi}_1^0$ LSP. In simplified models, ATLAS [133] and CMS [184] set lower mass limits on sleptons of 700 GeV for degenerate $\tilde{\ell}_L$ and $\tilde{\ell}_R$, for a massless $\tilde{\chi}_1^0$ and assuming equal selectron and smuon masses, as shown in Fig. 88.9. The limits deteriorate with increasing $\tilde{\chi}_1^0$ mass due to decreasing missing momentum and lepton momentum. As a consequence, no limits are set for $\tilde{\chi}_1^0$ masses above 400 GeV. Limits are also derived without the assumption of slepton mass degeneracy [133, 194].

A recent combination of the results of several searches for electroweakly produced supersymmetric particles has been published by CMS [144], with improved analysis techniques employed to optimize sensitivity for the compressed spectra in the slepton pair production models, providing constraints up to 210 GeV for mass splitting of 5 GeV between slepton and LSP.

Dedicated searches for sleptons with small mass difference between $\tilde{\ell}$ and $\tilde{\chi}_1^0$ are also performed by ATLAS [151, 195] demanding the presence of ISR jets. The most recent analysis includes an event selection optimization carried out depending on Δm and with ML techniques. Selectrons (smuons) with masses up to 300 (350) GeV are excluded for Δm between 2 GeV and 100 GeV on simplified models of selectron and smuon pair production. A dedicated search [138] in the challenging regime where the mass difference between the slepton and the LSP is close to the W mass results in exclusion of sleptons with masses up to 150 GeV for a

Int. J. Mod. Phys. A 2026.41. Downloaded from www.worldscientific.com
by UNIVERSITY OF CALIFORNIA @ BERKELEY on 09/16/26. Re-use and distribution is strictly not permitted, except for Open Access articles.

Int. J. Mod. Phys. A 2026.41. Downloaded from www.worldscientific.com
by UNIVERSITY OF CALIFORNIA @ BERKELEY on 09/16/26. Re-use and distribution is strictly not permitted, except for Open Access articles.

Table 88.3: Summary of weak gaugino mass limits in simplified models, assuming R-parity conservation. Masses in the table are provided in GeV. Further details about assumptions and corresponding analyses are discussed in the text. Details on constraints for compressed scenarios from soft-lepton searches are not represented in the table.

Assumption	mass limit
$\tilde{\chi}_1^\pm$, all $\Delta m(\tilde{\chi}_1^\pm, \tilde{\chi}_1^0)$	> 92
$\tilde{\chi}_1^\pm$ $\Delta m > 5$, $m_{\tilde{\nu}} > 300$	> 103.5
$\tilde{\chi}_1^\pm$, $m_{(\tilde{\ell},\tilde{\nu})} = (m_{\tilde{\chi}_1^\pm} + m_{\tilde{\chi}_1^0})/2$	flavor-democratic
$m_{\tilde{\chi}_1^0} \approx 0$	> 1000
$\tilde{\chi}_1^\pm$, $m_{\tilde{\chi}_1^0} > 480$	no LHC limit
$\tilde{\chi}_1^\pm$, $m_{(\tilde{\tau},\tilde{\nu})} = (m_{\tilde{\chi}_1^\pm} + m_{\tilde{\chi}_1^0})/2$	$\tilde{\tau}$-dominated
$m_{\tilde{\chi}_1^0} \approx 0$	> 970
$\tilde{\chi}_1^\pm$, $m_{\tilde{\chi}_1^0} > 440$	no LHC limit
$\tilde{\chi}_1^\pm$, $m_{\tilde{\ell}} > m_{\tilde{\chi}_1^\pm}$	
$m_{\tilde{\chi}_1^0} \approx 0$	> 420 and $290 - 760$
$\tilde{\chi}_1^\pm$, $m_{\tilde{\chi}_1^0} > 120$	no LHC limit
$m_{\tilde{\chi}_1^\pm} = m_{\tilde{\chi}_2^0}$, $m_{\tilde{\ell}_\mathrm{L}} = (m_{\tilde{\chi}_1^\pm} + m_{\tilde{\chi}_1^0})/2$	
$m_{\tilde{\chi}_1^0} \approx 0$	> 1450
$m_{\tilde{\chi}_1^0} > 1000$	no LHC limit
$m_{\tilde{\chi}_1^\pm} = m_{\tilde{\chi}_2^0}$, $m_{\tilde{\ell}_\mathrm{R}} = (m_{\tilde{\chi}_1^\pm} + m_{\tilde{\chi}_1^0})/2$	flavor-democratic
$m_{\tilde{\chi}_1^0} \approx 0$	> 1150
$m_{\tilde{\chi}_1^0} > 700$	no LHC limit
$m_{\tilde{\chi}_1^\pm} = m_{\tilde{\chi}_2^0}$, $m_{\tilde{\tau}} = (m_{\tilde{\chi}_1^\pm} + m_{\tilde{\chi}_1^0})/2$	$\tilde{\tau}$-dominated
$m_{\tilde{\chi}_1^0} \approx 0$	> 1160
$m_{\tilde{\chi}_1^0} > 450$	no LHC limit
$m_{\tilde{\chi}_1^\pm} = m_{\tilde{\chi}_2^0}$, $m_{\tilde{\ell}} > m_{\tilde{\chi}_1^\pm}$, $\mathrm{BF}(WZ) = 1$	
$m_{\tilde{\chi}_1^0} \approx 0$	> 1000
$m_{\tilde{\chi}_1^0} > 400$	no LHC limit
$m_{\tilde{\chi}_1^\pm} = m_{\tilde{\chi}_2^0}$, $m_{\tilde{\ell}} > m_{\tilde{\chi}_1^\pm}$, $\mathrm{BF}(WH) = 1$	
$m_{\tilde{\chi}_1^0} \approx 0$, wino-like $\tilde{\chi}_1^\pm$	> 1060
$m_{\tilde{\chi}_1^0} \approx 0$, higgsino-like $\tilde{\chi}_1^\pm$	> 900
$m_{\tilde{\chi}_1^0} > 400(240)$	no LHC limit
$m_{\tilde{\chi}_1^0} > 300(270)$	wino(higgsino)-like indirect detection pure-wino(higgsino)

mass-splitting between the sleptons and the LSP of 50 GeV.

ATLAS and CMS have also searched for $\tilde{\tau}$-pair production. In simplified models, ATLAS excludes $\tilde{\tau}$ masses between 90 and 500 GeV assuming light $\tilde{\chi}_1^0$, combining the production of degenerate left- and right-handed $\tilde{\tau}$s [135]. Purely left-handed $\tilde{\tau}$s with masses up to 425 GeV and purely right-handed $\tilde{\tau}$s with masses up to 350 GeV are also excluded. The CMS analysis [196] covers lower masses also closing the mass gap with LEP. In a search for hadronic final states, CMS [197] excludes purely left-handed $\tilde{\tau}$s with masses between 115 and 340 GeV for massless LSP. The ATLAS search [135] for stau pair production in the fully hadronic final state excludes, for a massless LSP, degenerate left- and right-handed $\tilde{\tau}$s with masses up to 480 GeV.

In gauge-mediated SUSY breaking models, sleptons can be (co-)NLSPs, *i.e.*, the next-to-lightest SUSY particles and almost degenerate in mass, decaying to a lepton and a gravitino. This decay can either be prompt, or the slepton can have a non-zero lifetime. Combining several analyses, lower mass limits on $\tilde{\mu}_\mathrm{R}$ of 96.3 GeV and on $\tilde{e}_\mathrm{R}$ of 66 GeV are set for all slepton lifetimes at LEP [198]. In a considerable part of parameter space in these constrained models, the $\tilde{\tau}$ is the NLSP. The LEP experiments have set lower limits on the mass of such a $\tilde{\tau}$ between 87 and 97 GeV, depending on the $\tilde{\tau}$ lifetime. ATLAS and CMS have searched for final states with τs, jets and missing transverse momentum, and have interpreted the results in GMSB models setting limits on the model parameters [199, 200]. CMS has interpreted a multilepton analysis in terms of limits on gauge mediation models with slepton NLSP [201]. CDF has put limits on gauge mediation models at high $\tan\beta$ and slepton NLSP using an analysis searching for like-charge light leptons and taus [202].

The invisible width of the Z boson puts a lower limit on the sneutrino mass of about 45 GeV [203]. Tighter limits are derived from other searches, notably for gauginos and sleptons, under the assumption of gaugino and sfermion mass universality at the GUT scale, and amount to approximately 94 GeV in the MSSM [203].

The limits on sleptons in simplified models are summarized in Table 88.4.

Table 88.4: Summary of slepton mass limits from LEP and LHC, assuming R-parity conservation and 100% branching fraction for $\tilde{\ell} \to \ell\tilde{\chi}_1^0$. Masses in this table are provided in GeV.

Assumption	$m_{\tilde{\ell}}$
$\tilde{\mu}_\mathrm{R}$, $\Delta m(\tilde{\mu}_\mathrm{R}, \tilde{\chi}_1^0) > 10$	> 94
$\tilde{e}_\mathrm{R}$, $\Delta m(\tilde{e}_\mathrm{R}, \tilde{\chi}_1^0) > 10$	> 94
$\tilde{e}_\mathrm{R}$, any Δm	> 73
$\tilde{\tau}_\mathrm{R}$, $\Delta m(\tilde{\tau}_\mathrm{R}, \tilde{\chi}_1^0) > 7$	> 87
$\tilde{\nu}_e$, $\Delta m(\tilde{e}_\mathrm{R}, \tilde{\chi}_1^0) > 10$	> 94
$m_{\tilde{e}_\mathrm{L,R}} = m_{\tilde{\mu}_\mathrm{L,R}}$, $m_{\tilde{\chi}_1^0} \approx 0$	> 700
$m_{\tilde{\chi}_1^0} >\approx 400$	no LHC limit
$m_{\tilde{\tau}_\mathrm{L}} = m_{\tilde{\tau}_\mathrm{R}}$, $m_{\tilde{\chi}_1^0} \approx 0$	> 500
$m_{\tilde{\chi}_1^0} >\approx 200$	no LHC limit
$m_{\tilde{\tau}_\mathrm{L}}$, $m_{\tilde{\chi}_1^0} \approx 0$	> 425
$m_{\tilde{\chi}_1^0} >\approx 150$	no LHC limit
$m_{\tilde{\tau}_\mathrm{R}}$, $m_{\tilde{\chi}_1^0} \approx 0$	> 350
$m_{\tilde{\chi}_1^0} >\approx 100$	no LHC limit

88.8 Exclusion limits on promptly decaying sparticle masses in RPV scenarios

The large variety of possible configurations for non-zero λ, λ' and λ'' couplings in RPV SUSY scenarios leads to a huge number of potential signatures to be investigated in the strong and electroweak sectors. The lightest supersymmetric particle can be any particle, although most of the models considered at the LHC assume that to be the lightest neutralino, and can have a prompt or displaced decay. Cascade decays of sparticles down to the LSP can also be prompt or displaced depending on the strength of the couplings involved, although typically such cascades are dominated by gauge couplings which are prompt. In this section, we review dedicated searches for scenarios with small non-zero RPV couplings but still large enough to allow prompt decays of the sparticles involved (see Section 88.9 for examples of dedicated signatures searches for non-prompt decays).

Prompt RPV gluino and squark decays are searched for in final states generally characterised by the presence of multiple leptons or jets and moderate or no missing transverse momentum.

Searches in multilepton final states [89, 169, 204–208] set lower gluino mass limits between 1 and 2.5 TeV for decays mediated by λ and λ' couplings, with strong dependence on the couplings involved, the neutralino mass and the lepton flavor. Multijet final states have been used to search for fully hadronic gluino decays involving λ'' couplings, by CDF [209], ATLAS [96, 210–213] and CMS [214–216]. Lower gluino mass limits range between 600 and 2000 GeV depending on neutralino mass and flavor content of the final state. ATLAS [217] also searched in events characterised by high jet multiplicity, at least one isolated light lepton and either zero or at least three b-tagged jets, reaching as high as 2.4 TeV in gluino mass. If gluinos decay via top squarks into *tbd* final states through a non-zero λ''_{313} coupling, a search for same-sign/three-

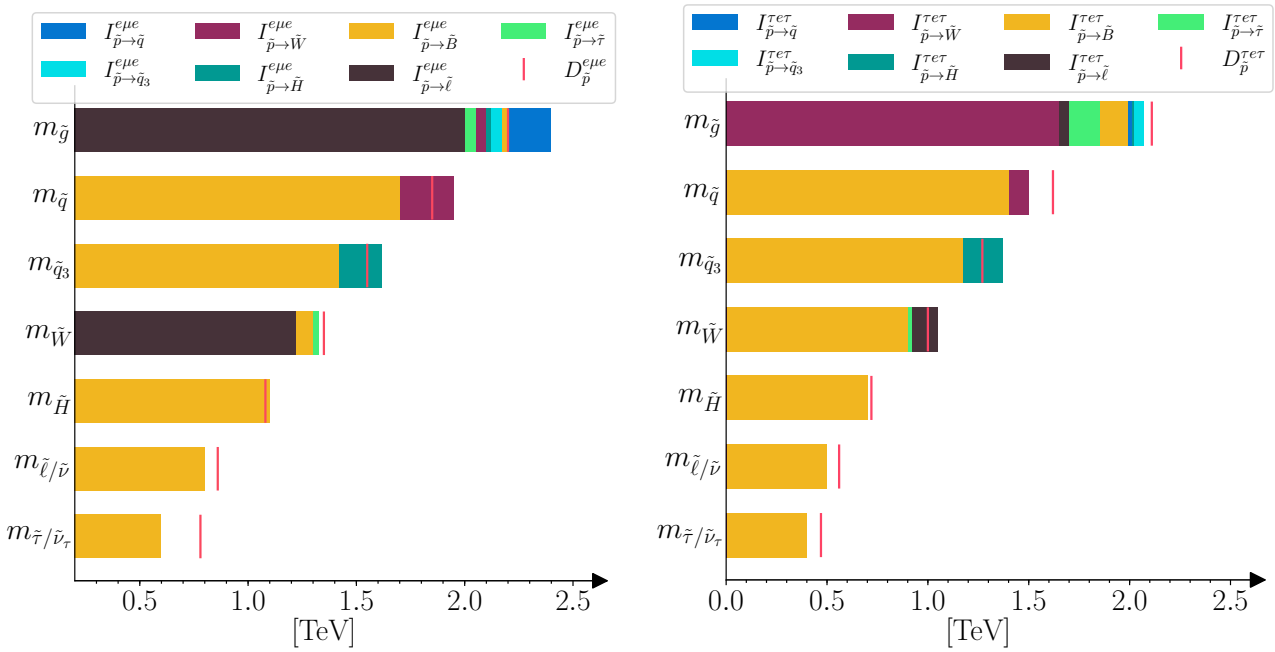

Figure 88.10: Summary of 95% C.L. limits on sparticle masses in RPV models, for λ_{121} (left), and for λ_{313} (right). The vertical red line represents the direct production mass bound when the sparticle under consideration is the LSP.

lepton events can be effective. ATLAS [89] sets a lower limit of 1.65 TeV for a top squark with a mass below 1.45 TeV.

RPV production of single squarks via a λ'-type coupling has been studied at HERA. In such models, a lower limit on the squark mass of the order of 275 GeV has been set for electromagnetic-strength-like couplings $\lambda' = 0.3$ [218]. At the LHC, prompt [205, 208, 219] R-parity violating squark decays have been searched for, with mass limits being very model-dependent.

Dedicated searches for RPV top squarks (at production and/or in decays) have been carried out in the past decades. Production of single top squarks has been searched for at LEP, HERA, and the Tevatron. For example, an analysis from the ZEUS collaboration [220] makes an interpretation of its search result assuming top squarks to be produced via a λ' coupling and decay either to $b\tilde{\chi}_1^{\pm}$ or R-parity-violating to a lepton and a jet. Limits are set on λ'_{131} as a function of the top squark mass in an MSSM framework with gaugino mass unification at the GUT scale. CMS and ATLAS have performed several searches for top squarks using a variety of multilepton and/or multijet final states and Run 2 data. The λ'-mediated top squark decay $\tilde{t} \to b\ell$ has been studied by ATLAS for prompt decays [221,222], and by ATLAS and CMS for non-prompt decays [223–225], setting limits up to $1.4 - 1.9$ TeV in simplified models for this mode. CMS also searched for the λ'-mediated decay $\tilde{t} \to b\ell qq$, setting lower stop mass limits of 890 GeV (e) or 1000 GeV (μ) [226]. The fully hadronic R-parity violating top squark decays $\tilde{t} \to bs$, $\tilde{t} \to ds$, and $\tilde{t} \to bd$, involving λ'', have been searched for by ATLAS [96,205,211,227,228], and CMS [229, 230]. Other recent searches target top squarks decaying through cascades into several $b-$ and light-quarks, for example as in [231]. The most recent results set limits up to 1.35 TeV in top-squark mass [217] if decays include top- and b-quarks [217]. Constraints on masses up to 700 GeV are found if the top squarks decays include top- and light-quarks [232, 233].

Various searches for multi-lepton and lepton plus jets events are interpreted in a model with RPV decays of charginos and neutralinos (including the LSP) involving a non-zero λ [169,204,208] or λ' [205,213,234,235] coupling. Neutralino decays involving non-zero λ'' lead to fully hadronic final states, and searches for multi-jet events and jet-pair resonances are used to set limits, typically on the production of colored particles like top squarks or gluinos, which are assumed to be the primary produced sparticles in these interpretations, as discussed earlier. For instance, the ATLAS search [217] in events with one lepton and high jet multiplicity excludes up to 320 (365) GeV in higgsino (wino) masses. If top quarks arise in the decay of the neutralino, lepton-enriched final state events are also relevant, see for example the results in [146]. The multilepton search in [236] set limits on the production of charginos and neutralinos for a minimal SUSY model with an approximate $B-L$ symmetry. In this case, charginos and neutralinos with masses between 100 GeV and 1.1 TeV are excluded depending on the assumed decay BR into a lepton plus a W, Z or H boson. Finally, recent results from ATLAS [146] set the first experimental constraints on bilinear RPV models (bRPV) with degenerate higgsino masses exploiting same-sign/three-lepton signatures, excluding masses smaller than 440 GeV.

Limits also exist on sleptons in RPV models, both from LEP and the Tevatron experiments. From LEP, lower limits on $\tilde{\mu}_{\rm R}$ and $\tilde{e}_{\rm R}$ masses in such models are 97 GeV, and the limits on the stau mass are very close: 96 GeV [237]. CMS has searched for resonant smuon production in a modified CMSSM scenario [238], putting limits on λ'_{211} as a function of $m_0, m_{1/2}$. Production of pairs of sneutrinos in R-parity violating models has been searched for at LEP [237]. Assuming fully leptonic decays via λ-type couplings, lower mass limits between 85 and 100 GeV are set. At the Tevatron [239, 240] and at the LHC [238, 241–243], searches have focused on scenarios with resonant production of a sneutrino decaying to $e\mu$, $\mu\tau$ and $e\tau$ final states. Limits have been set on sneutrino masses as a function of the value of relevant RPV couplings. As an example, the LHC experiments exclude a resonant tau sneutrino with a mass below 3.9 TeV for $\lambda_{312} = \lambda_{321} > 0.07$ and $\lambda'_{311} > 0.11$ [244].

Formulating a general assessment of the existing bounds on RPV SUSY models is becoming increasingly important in order to evaluate loopholes and potential new search directions. A classification of all potential RPV signatures at the LHC for small couplings has been recently published [245] to evaluate the coverage of the most general RPV-MSSM setup, without making any assumptions about the sparticle spectrum details. Small RPV couplings imply that sparticles are pair-produced at the LHC as in the RPC-MSSM case. Figure 88.10 shows a summary of the 95% C.L. limits on sparticle masses in RPV models for two types of λ couplings, compared to the direct production mass bound when the sparticle under consideration is the LSP. This is done to quantify the impact of possible assumptions made on the nature, mass and coupling choices for the LSP which in turn might lead to different leptons, jets and top-quark multiplicities. As under-

Int. J. Mod. Phys. A 2026.41. Downloaded from www.worldscientific.com by UNIVERSITY OF CALIFORNIA @ BERKELEY on 09/16/26. Re-use and distribution is strictly not permitted, except for Open Access articles.

Int. J. Mod. Phys. A 2026.41. Downloaded from www.worldscientific.com by UNIVERSITY OF CALIFORNIA @ BERKELEY on 09/16/26. Re-use and distribution is strictly not permitted, except for Open Access articles.

lined in [245], changes in exclusion limits on sparticle masses are at most around 20%.

Finally, RPV signatures are often similar to signatures of Stealth SUSY [246–248]. In these scenarios, squarks can decay to a quark and a chargino (neutralino), which can subsequently decay to a singlino $\tilde{S}$ and a $W^{\pm}$ (photon), with the $\tilde{S}$ decaying to two gluons and a soft gravitino $\tilde{G}$. Dedicated CMS searches [249, 250] exclude squark masses up to 1.85 TeV in the photon channel and up to 550 GeV in the charged lepton channel. Gluino masses up to 2.15 TeV are excluded in the di-photon channel [250]. Limits have also been placed on top squarks in stealth SUSY scenarios, where the top squark decays to a top quark, a gluon and a $\tilde{S}$, and the $\tilde{S}$ subsequently decays to a $\tilde{G}$ and two gluons. In such a scenario, top squark masses up to 930 GeV have been excluded by CMS [232, 233].

88.9 Exclusion limits on long-lived sparticles

Long-lived sparticles arise in many different SUSY models. In particular in co-annihilation scenarios, where the NLSP and LSP are nearly mass-degenerate, this is rather common in order to obtain the correct Dark Matter relic density. Prominent examples are scenarios featuring stau co-annihilation, or models of SUSY breaking, e.g. minimal anomaly-mediated SUSY breaking (AMSB), in which the appropriate Dark Matter density is obtained by co-annihilation of the LSP with an almost degenerate long-lived wino. R-parity violating SUSY models might also lead to non-prompt decays. Searches for events with a displaced hadronic vertex, with or without a matched lepton, are for instance interpreted in a model with RPV neutralino decays involving a non-zero λ' coupling [235]. However, in general, other sparticles can also be long-lived and it is desirable to establish a comprehensive search program for these special long-lived cases, which lead to distinct experimental search signatures. Past experiments have performed dedicated searches for long-lived SUSY signatures, but given the absence of any experimental evidence for SUSY so far, more effort and focus has gone into searches for long-lived sparticles at the LHC recently. Signatures interpreted in terms of SUSY models include disappearing tracks, identification of tracks with atypical properties or unusual ionization, small and localized deposits of energy inside of the calorimeters without associated tracks, or stopped particles that decay out of time with collisions. Some examples are reported below with interpretations provided for gluinos, squarks and electroweak SUSY particles in a variety of SUSY models.

If the decay of gluinos is suppressed, for example if squark masses are high, gluinos may live longer than typical hadronization times. It is expected that such gluinos will hadronize to long-living strongly interacting particles known as R-hadrons. In particular, if the suppression of the gluino decay is strong, as in the case that the squark masses are much higher than the TeV scale, these R-hadrons can be (semi-)stable in collider timescales. Searches for such R-hadrons exploit the typical signature of stable charged massive particles in the detector. R-hadrons decaying in the detector are searched for using dE/dx measurements and searches for displaced vertices. As shown in the left plot of Fig. 88.11, the ATLAS experiment excludes semi-stable gluino R-hadrons with masses below $1.9 - 2.3$ TeV for all lifetimes in a simplified model where such gluinos always form R-hadrons, and decay into jets and a light neutralino, by combining a number of analyses [211, 251–254]. A combination of CMS searches for long-lived particles, as shown in Fig. 88.12, reaches similar limits [255–259].

Alternatively, since such R-hadrons are strongly interacting, they may be stopped in the calorimeter or in other material, and decay later into energetic jets. These decays are searched for by identifying the jets [260–262] or muons [262] outside the time window associated with bunch-bunch collisions. As shown in Fig. 88.12, the CMS collaboration sets limits on such stopped R-hadrons over 13 orders of magnitude in gluino lifetime, up to masses of 1390 GeV [262]. Recent results from ATLAS [263] sets constraints on the mass of gluino R-hadrons using large out-of-time energy deposits in the calorimeters. Also in this case, masses of up to 1.4 TeV are excluded for gluino lifetimes of $10^{-5} - 10^{3}$ s.

Top squarks can also be long-lived and hadronize to a R-hadron, for example in the scenario where the top squark is the next-to-lightest SUSY particle, with a small mass difference to the LSP. Searches for massive stable charged particles are sensitive to such top squarks. Tevatron limits are approximately $m_{\tilde{t}} > 300$ GeV [264, 265]. ATLAS sets a limit of 1340 GeV on such top squarks [253], the CMS limits are comparable [257]. Intermediate lifetimes of top squarks decaying through RPV coupling into a quark and a lepton are also targeted by ATLAS and CMS. Limits on top squarks decaying into a quark and a muon are set by ATLAS [266] using events that pass a muon or missing-transverse-momentum trigger and contain a displaced muon track and a displaced vertex. Masses up to 1.7 TeV are excluded for a lifetime of 0.1 ns, and masses below 1.3 TeV are excluded for lifetimes between 0.01 ns and 30 ns. CMS [267] utilizes events with two leptons with transverse impact parameter values between 0.01 and 10 cm not required to form a common vertex to exclude top squarks with masses between 100 and at least 460 GeV for $0.01 < c\tau_0 < 1000$ cm, where $c\tau_0$ is the proper decay length.

In addition to colored sparticles, sparticles like charginos may also be long-lived, especially in scenarios with compressed mass spectra. Charginos decaying in the detectors away from the primary vertex could lead to signatures such as kinked-tracks, or apparently disappearing tracks, since, for example, the pion in $\tilde{\chi}_1^{\pm} \to \pi^{\pm}\tilde{\chi}_1^0$ might be too soft to be reconstructed. At the LHC, searches have been performed for such disappearing tracks, and interpreted within anomaly-mediated SUSY breaking models [268–271]. The right plot of Fig. 88.11 shows constraints for different ATLAS searches on the chargino mass-vs-lifetime plane for an AMSB model ($\tan\beta = 5$, $\mu > 0$) in which a wino-like $\tilde{\chi}^{\pm}$ decays to a soft pion and an almost mass-degenerated wino-like $\tilde{\chi}_1^0$ [253, 254, 269–272]. The disappearing track search [271] provides constraints also for higgsino-like models. Results from [272] exploiting anomalously large specific ionisation losses dE/dx are extrapolated to the stable regime. For a similar AMSB-like model, CMS excludes $c\tau$ values between 0.15 and 18 m for a chargino mass of 505 GeV [268], see Fig. 88.12. Their most recent results [273] expand and improve the constraints on masses of charginos as well as of colored sparticles (stop, sbottom, gluino) by making use of electron and muon plus disappearing track signatures, measurements of the dE/dx ionization energy loss of candidate tracks, and by re-analyzing the fully hadronic signatures using ML techniques. Bottom (top) squarks decaying to a long-lived chargino which results in a disappearing track signature are excluded below a mass of 900 – 1540 GeV (1100 – 1590 GeV), depending on the LSP mass and the chargino lifetime. Similarly, gluinos decaying to a long-lived chargino are excluded below a mass of 1450 - 2300 GeV, depending on LSP mass and chargino lifetime.

Charginos with a lifetime longer than the time needed to pass through the detector appear as charged stable massive particles. Limits have been derived by the LEP experiments [274], by D0 at the Tevatron [265], and by the LHC experiments [253, 275], and such charginos with mass below 1090 GeV are excluded.

In gauge mediation models, NLSP neutralino decays need not be prompt, and experiments have searched for late decays with photons in the final state. CDF has searched for delayed $\tilde{\chi}_1^0 \to \gamma\tilde{G}$ decays using the timing of photon signals in the calorimeter [276]. CMS has used the same technique at the LHC [277]. Results are given as exclusion contours in the neutralino mass versus lifetime plane, and for example in a GMSB model with a neutralino mass of 300 GeV, $c\tau$ values between 10 and 2000 cm are excluded [277]. D0 has looked at the direction of showers in the electromagnetic calorimeter with a similar goal [278], and ATLAS has searched for photon candidates that do not point back to the primary vertex, as well as for delayed photons [279].

Charged slepton decays may be kinematically suppressed, for example in the scenario of a NLSP slepton with a very small mass difference to the LSP. Such a slepton may appear to be a stable charged massive particle. Interpretation of searches at LEP for such signatures within GMSB models with a stau NLSP or slepton co-NLSP exclude masses up to 99 GeV [274]. Searches for stable charged particles at the Tevatron [264, 265] and at the LHC [253, 257] are also interpreted in terms of limits on stable

Int. J. Mod. Phys. A 2026.41. Downloaded from www.worldscientific.com
by UNIVERSITY OF CALIFORNIA @ BERKELEY on 09/16/26. Re-use and distribution is strictly not permitted, except for Open Access articles.

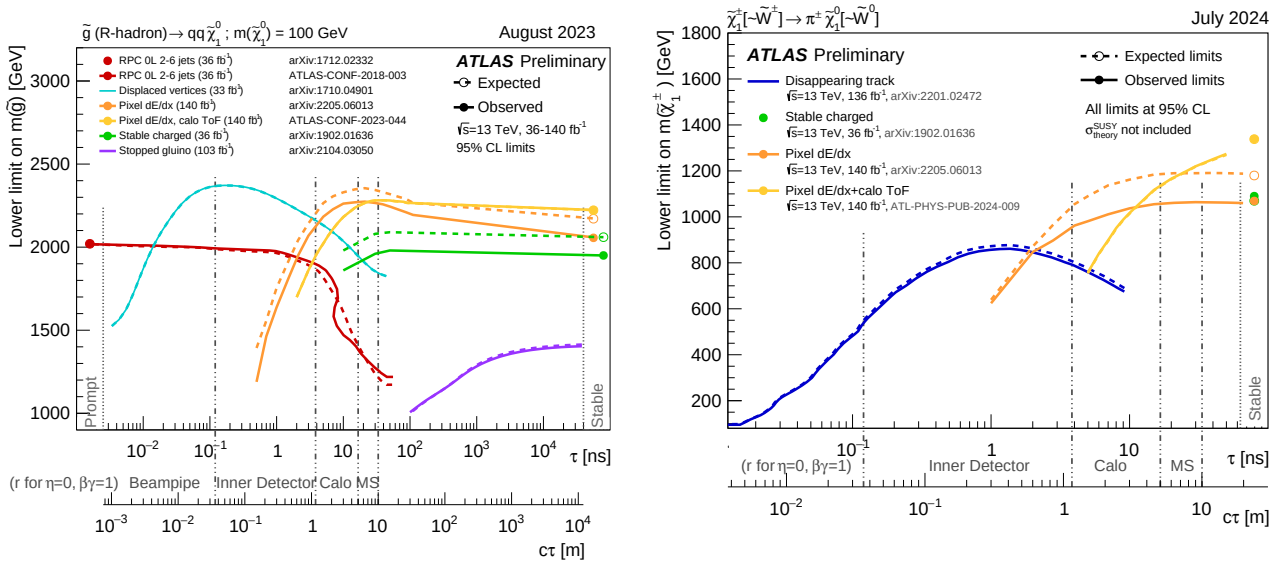

Figure 88.11: Limits at 95% C.L. on the gluino mass in R-hadron models (left), and on the chargino mass in a model where the wino-like chargino is almost degenerate with the LSP (right), as a function of gluino or chargino lifetime, as obtained by ATLAS.

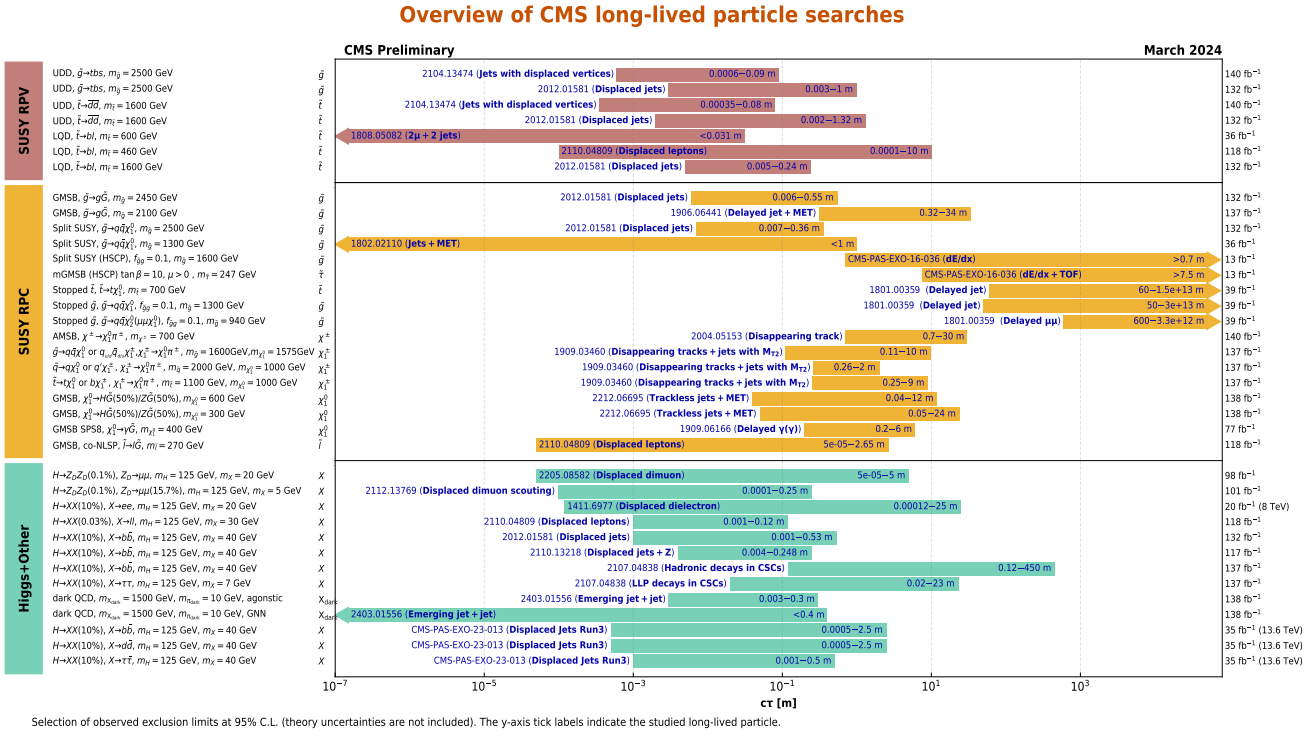

Selection of observed exclusion limits at 95% C.L. (theory uncertainties are not included). The y-axis tick labels indicate the studied long-lived particle.

Figure 88.12: Excluded regions, at 95% C.L., in the lifetimes of long-lived particles in several models, as obtained by CMS.

charged sleptons. The limits obtained at the LHC exclude stable staus with masses below 430 GeV when produced directly in pairs, and below 660 GeV when staus are produced both directly and indirectly in the decay of other particles in a GMSB model. Recent results from ATLAS and CMS set constraints on long-lived charged sleptons with intermediate lifetimes. ATLAS searches for charged leptons with large impact parameters and exclude selectron, smuon and stau masses up to 720 GeV, 680 GeV, and 340 GeV, respectively, in case of lifetimes of 0.1 ns. They also exclude smuons with lifetimes down to 1 ps for a smuon mass of 100 GeV, and smuon masses up to 520 GeV are excluded for a proper lifetime of 10 ps [280]. CMS [197] targets long-lived stau with $c\tau$ of about 0.1 mm excluding masses between 115 and 220 GeV for the case that the LSP is nearly massless.

88.10 Global interpretations

Apart from the interpretation of direct searches for sparticle production at colliders in terms of limits on masses of individual SUSY particles, model-dependent interpretations of allowed SUSY parameter space are derived from global SUSY fits. Typically these fits combine the results from collider experiments with indirect constraints on SUSY as obtained from low-energy experiments, flavor physics, high-precision electroweak results, and astrophysical data.

In the pre-LHC era these fits were mainly dominated by indirect constraints. Even for very constrained models like the CMSSM, the allowed parameter space, in terms of squark and

Int. J. Mod. Phys. A 2026.41. Downloaded from www.worldscientific.com
by UNIVERSITY OF CALIFORNIA @ BERKELEY on 09/16/26. Re-use and distribution is strictly not permitted, except for Open Access articles.

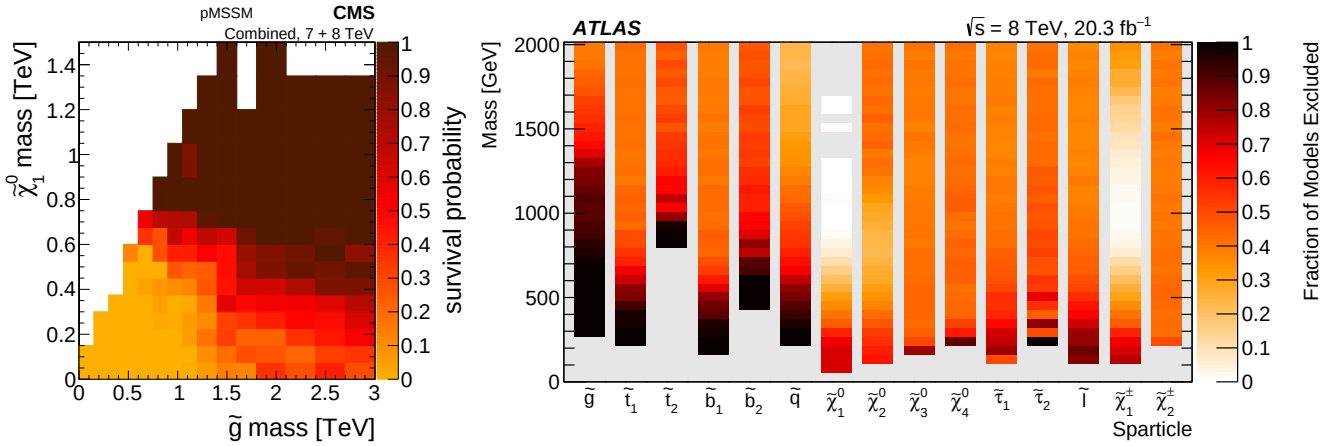

Figure 88.13: The plot on the left shows the survival probability of a pMSSM parameter space model in the gluino-neutralino mass plane after the application of the relevant CMS search results. The plot on the right shows a graphical representation of the ATLAS exclusion power in a pMSSM model. Each vertical bar is a one-dimensional projection of the fraction of models points excluded for each sparticle by ATLAS analyses. The experimental results are obtained from data taken at $\sqrt{s} = 7$ and 8 TeV.

gluino masses, ranged from several hundreds of GeV to a few TeV. Furthermore, these global fits indicated that squarks and gluino masses in the range of 500 to 1000 GeV were the preferred region of parameter space, although values as high as a few TeV were allowed with lower probabilities [281–288].

With ATLAS and CMS now probing mass scales around 1 TeV and beyond, the importance of the direct searches for global analyses of allowed SUSY parameter space has increased. For example, imposing the new experimental limits on constrained supergravity models pushes the most likely values of first generation squark and gluino masses significantly beyond 2 TeV, typically resulting in overall values of fit quality much worse than those in the pre-LHC era [158–160, 188, 289–296]. The measured value of m_h pushes the sparticle masses upwards. Although these constrained models are not yet ruled out, the extended experimental limits impose very tight constraints on the allowed parameter space.

For this reason, the emphasis of global SUSY fits has shifted towards less-constrained SUSY models. Interpretations in the pMSSM [186–190, 275, 289, 297] as well as in simplified models, have been useful to generalize SUSY searches, for example to redesign experimental analyses in order to increase their sensitivity for compressed spectra, where the mass of the LSP is much closer to squark and gluino masses than predicted by the CMSSM. As shown in Table 88.1, for neutralino LSP masses above $0.5-1$ TeV the current set of ATLAS and CMS searches, interpreted in simplified models, cannot exclude the existence of squarks or gluinos with masses only marginally above the neutralino mass. However, as these exclusion limits are defined in the context of simplified models, they are only valid for the assumptions in which these models are defined.

Fig. 88.13 shows graphically the LHC exclusion power in the pMSSM based on searches performed at $\sqrt{s} = 7$ and 8 TeV as reported by ATLAS [186] and CMS [187]. The plot on the left shows the survival probability in the gluino-neutralino mass plane, which is a measure of the parameter space that remains after inclusion of the relevant CMS search results. As can be seen, gluino masses below about 1.2 TeV are almost fully excluded. This result agrees well with the typical exclusion obtained at 8 TeV in simplified models for gluino production. However, as shown in the right plot of Fig. 88.13, when a similar analysis for other sparticles is performed it becomes apparent that exclusions on the pMSSM parameter can be significantly less stringent than simplified model limits might suggest.

More recently, the results of eight searches performed by ATLAS targeting the production of charginos and neutralinos, each using $\sqrt{s} = 13$ TeV data, have been interpreted in the context of the 19-parameter R-parity conserving pMSSM where the LSP is assumed to be the lightest neutralino [191]. Constraints from previous electroweak, flavor and dark matter related measurements are also considered. The results are presented in terms of constraints on supersymmetric particle masses and are compared with limits from simplified models. Example spectra for non-excluded supersymmetric models with light charginos and neutralinos are also reported. This again indicates that care must be taken when interpreting results from the LHC searches and there are still several scenarios where sparticles below the 1 TeV scale are not excluded, even when considering the most recent results at $\sqrt{s} = 13$ TeV.

Further interpretations in the pMSSM of searches performed on the full Run 2 dataset are in preparation and will offer further insights on the validity of constraints obtained with simplified models and, thus, guidance towards the future LHC runs and beyond.

Finally, the discovery of a Higgs boson with a mass around 125 GeV has triggered many studies regarding the compatibility of SUSY parameter space with this new particle (see for example [298, 299]). Much of it is still work in progress and it will be interesting to see how the interplay between the results from direct SUSY searches and more precise measurements of the properties of the Higgs boson will unfold in the future.

88.11 Summary and Outlook

The absence of any observation of new phenomena at the first run of the LHC at $\sqrt{s} = 7/8$ TeV, and after the second run at $\sqrt{s} = 13$ TeV, places significant constraints on SUSY parameter space. An overview of the current landscape of SUSY searches and limits at the LHC is shown in Figure 88.14, where a summary of results from the ATLAS experiment [300] (CMS results are similar [301]), is reported for illustration purposes. Inclusive searches probe production of gluinos at about 2.45 TeV, first and second generation squarks in the range of about 1 to 1.9 TeV, third generation squarks at scales around 600 GeV to 1.2 TeV, electroweak gauginos at scales around $400-1100$ GeV, and sleptons around 700 GeV. However, depending on the assumptions made on the underlying SUSY spectrum these limits can also weaken considerably.

With the LHC having reached almost its maximum energy of about $\sqrt{s} = 14$ TeV and analyses explored the full Run 2 dataset, future sensitivity improvements will have to originate from more data, the improvement of experimental analysis techniques and the focus on special signatures like the ones arising in long-lived sparticle decays. Therefore, it is expected that the current landscape of SUSY searches and corresponding exclusion limits at the LHC, especially for strongly produced sparticles in RPC scenarios, will not change as rapidly anymore as it did in the past, when the LHC underwent several successive increases of collision energy.

The interpretation of results at the LHC has moved away from constrained models like the CMSSM towards a large set of simplified models, or the pMSSM. Quoted limits in simplified models

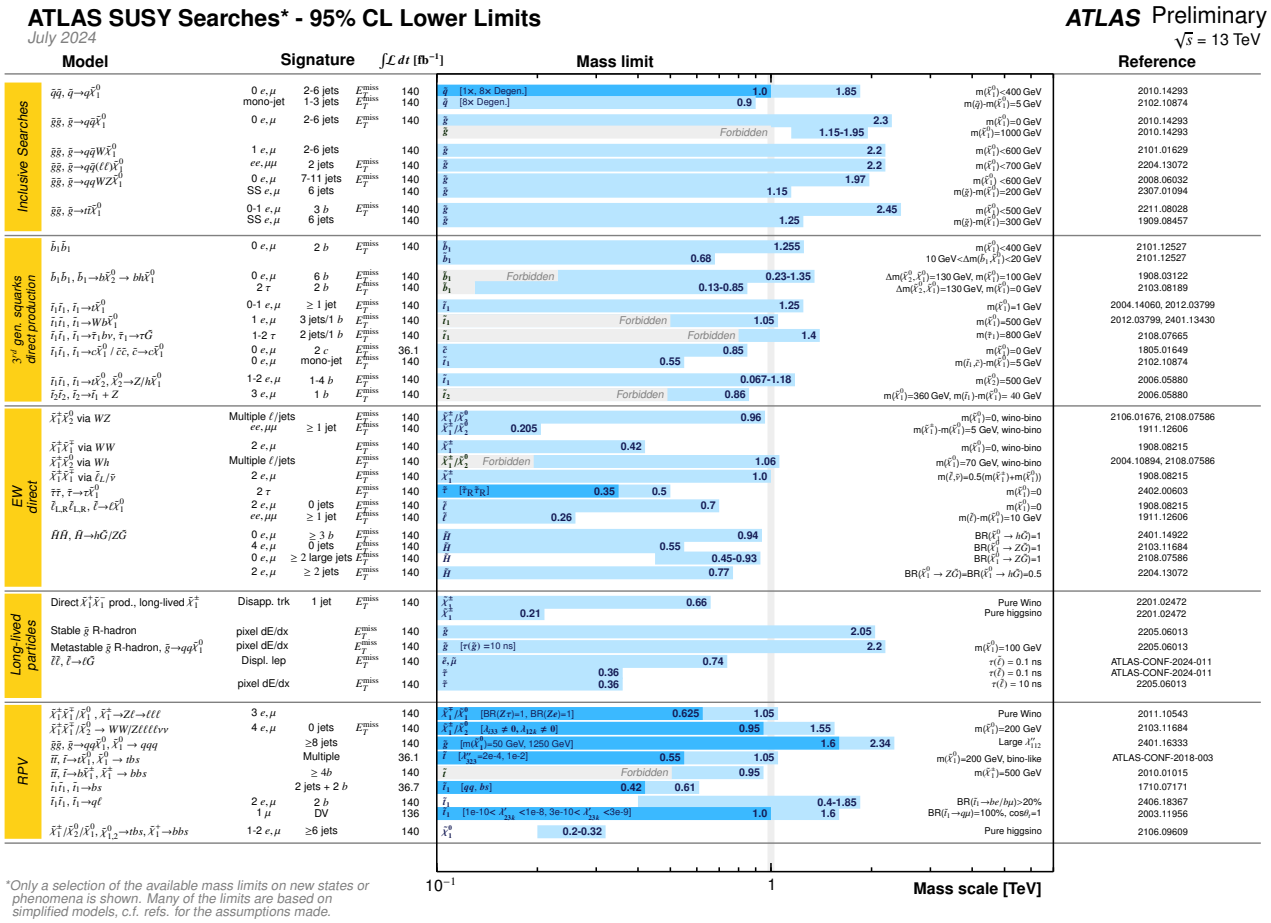

Figure 88.14: Overview of the current landscape of SUSY searches at the LHC (updated on August 2023). The plot shows exclusion mass limits of ATLAS for different searches and interpretation assumptions. The corresponding results of the CMS experiment are similar.

are only valid under the explicit assumptions made in these models. The addition of more comprehensive interpretations in the pMSSM complement those and therefore enable an even more refined understanding of the probed SUSY parameter space.

In this context, the limit range of $1.5 - 2.45$ TeV on generic colored SUSY particles only holds for light neutralinos, in the R-parity conserving MSSM. Limits on third generation squarks and electroweak gauginos also only hold for light neutralinos, and under specific assumptions for decay modes and slepton masses. Constraints in R-parity violating SUSY models strongly depend also on the assumed non-zero couplings.

The next LHC runs, with $\sqrt{s}$ between 13 and 14 TeV and significantly larger integrated luminosities (notably the High-Luminosity LHC), will provide a large data sample for future SUSY searches. As mentioned above, the improvement in sensitivity will largely have to come from a larger data set, and evolution of trigger and analysis techniques, since there will be no significant energy increase at the LHC anymore. Although the sensitivity for colored sparticles will increase somewhat as well, the expanded data set will be particularly beneficial for electroweak gaugino searches, and for the more difficult final states presented by compressed particle spectra, stealth SUSY, long-lived sparticles, or R-parity violating scenarios.

References

[1] H. Miyazawa, Prog. Theor. Phys. **36**, 6, 1266 (1966).

[2] Yu. A. Golfand and E. P. Likhtman, JETP Lett. **13**, 323 (1971), [Pisma Zh. Eksp. Teor. Fiz.13,452(1971)].

[3] J.-L. Gervais and B. Sakita, Nucl. Phys. **B34**, 632 (1971).

[4] D. V. Volkov and V. P. Akulov, Phys. Lett. **46B**, 109 (1973).

[5] J. Wess and B. Zumino, Phys. Lett. **49B**, 52 (1974).

[6] J. Wess and B. Zumino, Nucl. Phys. **B70**, 39 (1974).

[7] A. Salam and J. A. Strathdee, Nucl. Phys. **B76**, 477 (1974).

[8] H. P. Nilles, Phys. Rept. **110**, 1 (1984).

[9] H. E. Haber and G. L. Kane, Phys. Rept. **117**, 75 (1985).

[10] E. Witten, Nucl. Phys. **B188**, 513 (1981).

[11] S. Dimopoulos and H. Georgi, Nucl. Phys. **B193**, 150 (1981).

[12] M. Dine, W. Fischler and M. Srednicki, Nucl. Phys. **B189**, 575 (1981).

[13] S. Dimopoulos and S. Raby, Nucl. Phys. **B192**, 353 (1981).

[14] N. Sakai, Z. Phys. **C11**, 153 (1981).

[15] R. K. Kaul and P. Majumdar, Nucl. Phys. **B199**, 36 (1982).

[16] H. Goldberg, Phys. Rev. Lett. **50**, 1419 (1983).

[17] J. R. Ellis *et al.*, Nucl. Phys. **B238**, 453 (1984).

[18] G. Jungman, M. Kamionkowski and K. Griest, Phys. Rept. **267**, 195 (1996), [hep-ph/9506380].

[19] S. Dimopoulos, S. Raby and F. Wilczek, Phys. Rev. **D24**, 1681 (1981).

[20] W. J. Marciano and G. Senjanovic, Phys. Rev. **D25**, 3092 (1982).

[21] M. B. Einhorn and D. R. T. Jones, Nucl. Phys. **B196**, 475 (1982).

[22] L. E. Ibanez and G. G. Ross, Phys. Lett. **105B**, 439 (1981).

[23] U. Amaldi, W. de Boer and H. Furstenau, Phys. Lett. **B260**, 447 (1991).

Int. J. Mod. Phys. A 2026.41. Downloaded from www.worldscientific.com by UNIVERSITY OF CALIFORNIA @ BERKELEY on 09/16/26. Re-use and distribution is strictly not permitted, except for Open Access articles.

Int. J. Mod. Phys. A 2026.41. Downloaded from www.worldscientific.com
by UNIVERSITY OF CALIFORNIA @ BERKELEY on 09/16/26. Re-use and distribution is strictly not permitted, except for Open Access articles.

[24] P. Langacker and N. Polonsky, Phys. Rev. **D52**, 3081 (1995), [hep-ph/9503214].

[25] J. R. Ellis, S. Kelley and D. V. Nanopoulos, Phys. Lett. B **260**, 131 (1991).

[26] P. Fayet, Phys. Lett. **64B**, 159 (1976).

[27] G. R. Farrar and P. Fayet, Phys. Lett. **76B**, 575 (1978).

[28] B.C. Allanach and H.E. Haber, *Supersymmetry, Part I (Theory)*, in this *Review*.

[29] A. M. Sirunyan *et al.* (CMS), JHEP **04**, 188 (2020), [arXiv:1910.12127].

[30] M. Aaboud *et al.* (ATLAS), JHEP **04**, 098 (2019), [arXiv:1812.03017].

[31] R. Aaij *et al.* (LHCb), Phys. Rev. Lett. **118**, 19, 191801 (2017), [arXiv:1703.05747].

[32] A. Höcker and W.J. Marciano, *Muon Anomalous Magnetic Moment*, in this *Review*.

[33] D. P. Aguillard *et al.* (Muon g-2) (2025), [arXiv:2506.03069].

[34] G. Hinshaw *et al.* (WMAP), Astrophys. J. Suppl. **208**, 19 (2013), [arXiv:1212.5226].

[35] N. Aghanim *et al.* (Planck Collaboration), A&A **641**, A1 (2020).

[36] K. Nakamura *et al.* (Particle Data Group), J. Phys. **G37**, 075021 (2010).

[37] I. Hinchliffe *et al.*, Phys. Rev. **D55**, 5520 (1997), [hep-ph/9610544].

[38] L. Randall and D. Tucker-Smith, Phys. Rev. Lett. **101**, 221803 (2008), [arXiv:0806.1049].

[39] V. Khachatryan *et al.* (CMS), Phys. Lett. **B698**, 196 (2011), [arXiv:1101.1628].

[40] S. Chatrchyan *et al.* (CMS), Phys. Rev. Lett. **107**, 221804 (2011), [arXiv:1109.2352].

[41] S. Chatrchyan *et al.* (CMS), JHEP **01**, 077 (2013), [arXiv:1210.8115].

[42] S. Chatrchyan *et al.* (CMS), Eur. Phys. J. **C73**, 9, 2568 (2013), [arXiv:1303.2985].

[43] S. Chatrchyan *et al.* (CMS), Phys. Rev. **D85**, 012004 (2012), [arXiv:1107.1279].

[44] C. G. Lester and D. J. Summers, Phys. Lett. **B463**, 99 (1999), [hep-ph/9906349].

[45] D. R. Tovey, JHEP **04**, 034 (2008), [arXiv:0802.2879].

[46] M. R. Buckley *et al.*, Phys. Rev. **D89**, 5, 055020 (2014), [arXiv:1310.4827].

[47] P. Jackson, C. Rogan and M. Santoni, Phys. Rev. **D95**, 3, 035031 (2017), [arXiv:1607.08307].

[48] G. Aad *et al.* (ATLAS), Eur. Phys. J. C **81**, 4, 334 (2021), [arXiv:2009.04986].

[49] J. M. Butterworth *et al.*, Phys. Rev. Lett. **100**, 242001 (2008), [arXiv:0802.2470].

[50] A. M. Sirunyan *et al.* (CMS), JINST **15**, 06, P06005 (2020), [arXiv:2004.08262].

[51] A. M. Sirunyan *et al.* (CMS), JHEP **05**, 032 (2020), [arXiv:1912.08887].

[52] N. Arkani-Hamed and S. Dimopoulos, JHEP **06**, 073 (2005), [hep-th/0405159].

[53] G. F. Giudice and A. Romanino, Nucl. Phys. B **699**, 65 (2004), [Erratum: Nucl.Phys.B 706, 487–487 (2005)], [hep-ph/0406088].

[54] J. Alimena *et al.*, J. Phys. G **47**, 9, 090501 (2020), [arXiv:1903.04497].

[55] A.H. Chamseddine, R. Arnowitt, and P Nath, Phys. Rev. Lett. **49**, 970 (1982).

[56] E. Cremmer *et al.*, Nucl. Phys. **B212**, 413 (1983).

[57] P. Fayet, Phys. Lett. **70B**, 461 (1977).

[58] M. Dine, A. E. Nelson and Y. Shirman, Phys. Rev. **D51**, 1362 (1995), [hep-ph/9408384].

[59] P. Meade, N. Seiberg and D. Shih, Prog. Theor. Phys. Suppl. **177**, 143 (2009), [arXiv:0801.3278].

[60] G. F. Giudice *et al.*, JHEP **12**, 027 (1998), [hep-ph/9810442].

[61] L. Randall and R. Sundrum, Nucl. Phys. **B557**, 79 (1999), [hep-th/9810155].

[62] R. L. Arnowitt and P. Nath, Phys. Rev. Lett. **69**, 725 (1992).

[63] G. L. Kane *et al.*, Phys. Rev. **D49**, 6173 (1994), [hep-ph/9312272].

[64] A. Djouadi *et al.* (MSSM Working Group), in "GDR (Groupement De Recherche) - Supersymetrie," (1998), [hep-ph/9901246].

[65] A. Djouadi, J.-L. Kneur and G. Moultaka, Comput. Phys. Commun. **176**, 426 (2007), [hep-ph/0211331].

[66] C. F. Berger *et al.*, JHEP **02**, 023 (2009), [arXiv:0812.0980].

[67] H. Baer *et al.*, in "Workshop on Physics at Current Accelerators and the Supercollider Argonne, Illinois, June 2-5, 1993," 0703–720 (1993), [hep-ph/9305342], URL `http://lss.fnal.gov/cgi-bin/find_paper.pl?other/ssc/sscl-preprint-441`.

[68] R. M. Barnett, H. E. Haber and G. L. Kane, Nucl. Phys. **B267**, 625 (1986).

[69] H. Baer, D. Karatas and X. Tata, Phys. Lett. **B183**, 220 (1987).

[70] J. Alwall, P. Schuster and N. Toro, Phys. Rev. **D79**, 075020 (2009), [arXiv:0810.3921].

[71] J. Alwall *et al.*, Phys. Rev. **D79**, 015005 (2009), [arXiv:0809.3264].

[72] LEP2 SUSY Working Group, ALEPH, DELPHI, L3 and OPAL experiments, note LEPSUSYWG/04-02.1, `http://lepsusy.web.cern.ch/lepsusy`.

[73] LHC SUSY cross sections working group, `https://twiki.cern.ch/twiki/bin/view/LHCPhysics/SUSYCrossSections`.

[74] T. Aaltonen *et al.* (CDF), Phys. Rev. Lett. **102**, 121801 (2009), [arXiv:0811.2512].

[75] V. M. Abazov *et al.* (D0), Phys. Lett. **B660**, 449 (2008), [arXiv:0712.3805].

[76] A. M. Sirunyan *et al.* (CMS) (2019), [arXiv:1908.04722].

[77] ATLAS Collab., ATLAS-CONF-2019-040 (2019).

[78] G. Aad *et al.* (ATLAS), Eur. Phys. J. C **81**, 7, 600 (2021), [arXiv:2101.01629].

[79] G. Aad *et al.* (ATLAS), JHEP **02**, 143 (2021), [arXiv:2010.14293].

[80] A. Tumasyan *et al.* (CMS), JHEP **09**, 149 (2023), [arXiv:2211.08476].

[81] A. M. Sirunyan *et al.* (CMS), JHEP **10**, 244 (2019), [arXiv:1908.04722].

[82] G. Aad *et al.* (ATLAS), Eur. Phys. J. C **83**, 7, 561 (2023), [arXiv:2211.08028].

[83] ATLAS Collab., ATLAS-CONF-2018-041 (2018).

[84] A. M. Sirunyan *et al.* (CMS), Eur. Phys. J. C **80**, 1, 3 (2020), [arXiv:1909.03460].

[85] A. M. Sirunyan *et al.* (CMS), Phys. Rev. D **104**, 5, 052001 (2021), [arXiv:2103.01290].

[86] G. Aad *et al.* (ATLAS Collaboration), Phys. Rev. D **103**, 112006 (2021), URL `https://link.aps.org/doi/10.1103/PhysRevD.103.112006`.

[87] M. Aaboud *et al.* (ATLAS), Phys. Rev. D **97**, 9, 092006 (2018), [arXiv:1802.03158].

[88] G. Aad *et al.* (ATLAS), Eur. Phys. J. C **83**, 6, 515 (2023), [arXiv:2204.13072].

Int. J. Mod. Phys. A 2026.41. Downloaded from www.worldscientific.com
by UNIVERSITY OF CALIFORNIA @ BERKELEY on 09/16/26. Re-use and distribution is strictly not permitted, except for Open Access articles.

[89] G. Aad *et al.* (ATLAS), JHEP **02**, 107 (2024), [arXiv:2307.01094].

[90] M. Aaboud *et al.* (ATLAS), JHEP **09**, 050 (2018), [arXiv:1805.01649].

[91] G. Aad *et al.* (ATLAS), JHEP **02**, 193 (2025), [arXiv:2410.17824].

[92] T. Aaltonen *et al.* (CDF), Phys. Rev. Lett. **105**, 081802 (2010), [arXiv:1005.3600].

[93] V. M. Abazov *et al.* (D0), Phys. Lett. **B693**, 95 (2010), [arXiv:1005.2222].

[94] G. Aad *et al.* (ATLAS), JHEP **05**, 093 (2021), [arXiv:2101.12527].

[95] G. Aad *et al.* (ATLAS), JHEP **12**, 060 (2019), [arXiv:1908.03122].

[96] G. Aad *et al.* (ATLAS), JHEP **06**, 046 (2020), [arXiv:1909.08457].

[97] G. Aad *et al.* (ATLAS), Phys. Rev. D **104**, 3, 032014 (2021), [arXiv:2103.08189].

[98] A. M. Sirunyan *et al.* (CMS), JHEP **03**, 076 (2018), [arXiv:1709.08908].

[99] A. M. Sirunyan *et al.* (CMS), Eur. Phys. J. C **80**, 8, 752 (2020), [arXiv:2001.10086].

[100] C. Boehm, A. Djouadi and Y. Mambrini, Phys. Rev. **D61**, 095006 (2000), [hep-ph/9907428].

[101] T. Aaltonen *et al.* (CDF), Phys. Rev. **D82**, 092001 (2010), [arXiv:1009.0266].

[102] V. M. Abazov *et al.* (D0), Phys. Lett. **B696**, 321 (2011), [arXiv:1009.5950].

[103] T. Aaltonen *et al.* (CDF), JHEP **10**, 158 (2012), [arXiv:1203.4171].

[104] V. M. Abazov *et al.* (D0), Phys. Lett. **B665**, 1 (2008), [arXiv:0803.2263].

[105] T. Aaltonen *et al.* (CDF), Phys. Rev. Lett. **104**, 251801 (2010), [arXiv:0912.1308].

[106] V. M. Abazov *et al.* (D0), Phys. Lett. **B674**, 4 (2009), [arXiv:0901.1063].

[107] G. Aad *et al.* (ATLAS), Eur. Phys. J. C **80**, 8, 737 (2020), [arXiv:2004.14060].

[108] G. Aad *et al.* (ATLAS), JHEP **04**, 174 (2021), [arXiv:2012.03799].

[109] Technical report, CERN, Geneva (2023), all figures including auxiliary figures are available at `https://atlas.web.cern.ch/Atlas/GROUPS/PHYSICS/CONFNOTES/ATLAS-CONF-2023-043`, URL `https://cds.cern.ch/record/2869241`.

[110] M. Aaboud *et al.* (ATLAS), JHEP **06**, 108 (2018), [arXiv:1711.11520].

[111] M. Aaboud *et al.* (ATLAS), Phys. Rev. **D98**, 3, 032008 (2018), [arXiv:1803.10178].

[112] A. M. Sirunyan *et al.* (CMS), JHEP **02**, 015 (2020), [arXiv:1910.12932].

[113] G. Aad *et al.* (ATLAS), JHEP **04**, 165 (2021), [arXiv:2102.01444].

[114] A. M. Sirunyan *et al.* (CMS), Eur. Phys. J. **C77**, 10, 710 (2017), [arXiv:1705.04650].

[115] A. M. Sirunyan *et al.* (CMS), Phys. Rev. **D96**, 3, 032003 (2017), [arXiv:1704.07781].

[116] A. M. Sirunyan *et al.* (CMS), JHEP **10**, 005 (2017), [arXiv:1707.03316].

[117] A. M. Sirunyan *et al.* (CMS), JHEP **10**, 019 (2017), [arXiv:1706.04402].

[118] A. M. Sirunyan *et al.* (CMS), Eur. Phys. J. C **81**, 1, 3 (2021), [arXiv:2008.05936].

[119] A. M. Sirunyan *et al.* (CMS), JHEP **03**, 101 (2019), [arXiv:1901.01288].

[120] A. Tumasyan *et al.* (CMS), JHEP **07**, 110 (2023), [arXiv:2304.07174].

[121] M. Aaboud *et al.* (ATLAS), Phys. Rev. D **98**, 3, 032008 (2018), [arXiv:1803.10178].

[122] G. Aad *et al.* (ATLAS), Phys. Rev. D **104**, 11, 112005 (2021), [arXiv:2108.07665].

[123] G. Aad *et al.* (ATLAS), Eur. Phys. J. C **80**, 11, 1080 (2020), [arXiv:2006.05880].

[124] G. Aad *et al.* (ATLAS), JHEP **07**, 250 (2024), [arXiv:2402.12137].

[125] A. Tumasyan *et al.* (CMS), JHEP **06**, 060 (2023), [arXiv:2301.08096].

[126] M. Aaboud *et al.* (ATLAS), Eur. Phys. J. C **80**, 8, 754 (2020), [arXiv:1903.07570].

[127] B. Fuks *et al.*, JHEP **10**, 081 (2012), [arXiv:1207.2159].

[128] B. Fuks *et al.*, Eur. Phys. J. C **73**, 2480 (2013), [arXiv:1304.0790].

[129] LEP2 SUSY Working Group, ALEPH, DELPHI, L3 and OPAL experiments, note LEPSUSYWG/01-03.1, `http://lepsusy.web.cern.ch/lepsusy`.

[130] LEP2 SUSY Working Group, ALEPH, DELPHI, L3 and OPAL experiments, note LEPSUSYWG/02-04.1, `http://lepsusy.web.cern.ch/lepsusy`.

[131] CDF Collab., CDF Note 10636 (2011).

[132] V. M. Abazov *et al.* (D0), Phys. Lett. **B680**, 34 (2009), [arXiv:0901.0646].

[133] G. Aad *et al.* (ATLAS), Eur. Phys. J. C **80**, 2, 123 (2020), [arXiv:1908.08215].

[134] A. M. Sirunyan *et al.* (CMS), JHEP **11**, 079 (2018), [arXiv:1807.07799].

[135] G. Aad *et al.* (ATLAS), JHEP **05**, 150 (2024), [arXiv:2402.00603].

[136] A. M. Sirunyan *et al.* (CMS), JHEP **11**, 151 (2018), [arXiv:1807.02048].

[137] G. Aad *et al.* (ATLAS), Phys. Rev. Lett. **133**, 3, 031802 (2024), [arXiv:2402.08347].

[138] G. Aad *et al.* (ATLAS), JHEP **06**, 031 (2023), [arXiv:2209.13935].

[139] G. Aad *et al.* (ATLAS), JHEP **12**, 167 (2023), [arXiv:2310.08171].

[140] G. Aad *et al.* (ATLAS), Phys. Rev. D **104**, 11, 112010 (2021), [arXiv:2108.07586].

[141] A. Tumasyan *et al.* (CMS), Phys. Lett. B **842**, 137460 (2023), [arXiv:2205.09597].

[142] M. Aaboud *et al.* (ATLAS), Eur. Phys. J. **C78**, 12, 995 (2018), [arXiv:1803.02762].

[143] A. Tumasyan *et al.* (CMS), JHEP **04**, 147 (2022), [arXiv:2106.14246].

[144] A. Hayrapetyan *et al.* (CMS), Phys. Rev. D **109**, 11, 112001 (2024), [arXiv:2402.01888].

[145] G. Aad *et al.* (ATLAS), Eur. Phys. J. C **81**, 12, 1118 (2021), [arXiv:2106.01676].

[146] G. Aad *et al.* (ATLAS), JHEP **11**, 150 (2023), [arXiv:2305.09322].

[147] A. Tumasyan *et al.* (CMS), JHEP **10**, 045 (2021), [arXiv:2107.12553].

[148] M. Aaboud *et al.* (ATLAS), Phys. Rev. **D100**, 1, 012006 (2019), [arXiv:1812.09432].

[149] G. Aad *et al.* (ATLAS), JHEP **10**, 005 (2020), [arXiv:2004.10894].

[150] G. Aad *et al.* (ATLAS), Eur. Phys. J. C **80**, 8, 691 (2020), [arXiv:1909.09226].

[151] G. Aad *et al.* (ATLAS), Phys. Rev. D **101**, 5, 052005 (2020), [arXiv:1911.12606].

Int. J. Mod. Phys. A 2026.41. Downloaded from www.worldscientific.com
by UNIVERSITY OF CALIFORNIA @ BERKELEY on 09/16/26. Re-use and distribution is strictly not permitted, except for Open Access articles.

[152] A. Tumasyan *et al.* (CMS), JHEP **04**, 091 (2022), [arXiv:2111.06296].

[153] G. Aad *et al.* (ATLAS), JHEP **12**, 116 (2024), [arXiv:2409.18762].

[154] A. M. Sirunyan *et al.* (CMS), JHEP **08**, 150 (2019), [arXiv:1905.13059].

[155] A. M. Sirunyan *et al.* (CMS), Phys. Rev. Lett. **124**, 4, 041803 (2020), [arXiv:1910.01185].

[156] H. K. Dreiner *et al.*, Eur. Phys. J. **C62**, 547 (2009), [arXiv:0901.3485].

[157] LEP2 SUSY Working Group, ALEPH, DELPHI, L3 and OPAL experiments, note LEPSUSYWG/04-07.1, `http://lepsusy.web.cern.ch/lepsusy`.

[158] O. Buchmueller *et al.*, Eur. Phys. J. **C74**, 6, 2922 (2014), [arXiv:1312.5250].

[159] C. Strege *et al.*, JCAP **1304**, 013 (2013), [arXiv:1212.2636].

[160] A. Fowlie *et al.*, Phys. Rev. **D86**, 075010 (2012), [arXiv:1206.0264].

[161] LEP2 SUSY Working Group, ALEPH, DELPHI, L3 and OPAL experiments, note LEPSUSYWG/04-09.1, `http://lepsusy.web.cern.ch/lepsusy`.

[162] T. Aaltonen *et al.* (CDF), Phys. Rev. Lett. **104**, 011801 (2010), [arXiv:0910.3606].

[163] V. M. Abazov *et al.* (D0), Phys. Rev. Lett. **105**, 221802 (2010), [arXiv:1008.2133].

[164] M. Aaboud *et al.* (ATLAS), Phys. Rev. **D97**, 9, 092006 (2018), [arXiv:1802.03158].

[165] A. M. Sirunyan *et al.* (CMS), JHEP **06**, 143 (2019), [arXiv:1903.07070].

[166] A. M. Sirunyan *et al.* (CMS), Phys. Lett. B **801**, 135183 (2020), [arXiv:1907.00857].

[167] A. Hayrapetyan *et al.* (CMS), JHEP **10**, 046 (2023), [arXiv:2307.16216].

[168] M. Aaboud *et al.* (ATLAS), Phys. Rev. **D98**, 9, 092002 (2018), [arXiv:1806.04030].

[169] M. Aaboud *et al.* (ATLAS), Phys. Rev. **D98**, 3, 032009 (2018), [arXiv:1804.03602].

[170] M. Aaboud *et al.* (ATLAS), Phys. Rev. **D99**, 1, 012001 (2019), [arXiv:1808.03057].

[171] G. Aad *et al.* (ATLAS), Phys. Rev. D **104**, 11, 112010 (2021), [arXiv:2108.07586].

[172] A. M. Sirunyan *et al.* (CMS), JHEP **03**, 166 (2018), [arXiv:1709.05406].

[173] A. M. Sirunyan *et al.* (CMS), JHEP **03**, 160 (2018), [arXiv:1801.03957].

[174] A. M. Sirunyan *et al.* (CMS), Eur. Phys. J. **C79**, 5, 444 (2019), [arXiv:1901.06726].

[175] A. M. Sirunyan *et al.* (CMS), JHEP **01**, 154 (2019), [arXiv:1812.04066].

[176] A. M. Sirunyan *et al.* (CMS), Phys. Lett. **B780**, 118 (2018), [arXiv:1711.08008].

[177] A. M. Sirunyan *et al.* (CMS), Phys. Rev. **D97**, 3, 032007 (2018), [arXiv:1709.04896].

[178] A. M. Sirunyan *et al.* (CMS), Phys. Lett. **B779**, 166 (2018), [arXiv:1709.00384].

[179] A. Tumasyan *et al.* (CMS), JHEP **05**, 014 (2022), [arXiv:2201.04206].

[180] G. Aad *et al.* (ATLAS), Phys. Rev. **D93**, 5, 052002 (2016), [arXiv:1509.07152].

[181] N. L. Rodd, B. R. Safdi and W. L. Xu, Phys. Rev. D **110**, 4, 043003 (2024).

[182] M. Aaboud *et al.* (ATLAS), Eur. Phys. J. **C78**, 8, 625 (2018), [arXiv:1805.11381].

[183] M. Aaboud *et al.* (ATLAS), Eur. Phys. J. **C77**, 3, 144 (2017), [arXiv:1611.05791].

[184] A. M. Sirunyan *et al.* (CMS), JHEP **04**, 123 (2021), [arXiv:2012.08600].

[185] A. Arbey, M. Battaglia and F. Mahmoudi, Eur. Phys. J. C **72**, 1847 (2012), [arXiv:1110.3726].

[186] G. Aad *et al.* (ATLAS), JHEP **10**, 134 (2015), [arXiv:1508.06608].

[187] V. Khachatryan *et al.* (CMS), JHEP **10**, 129 (2016), [arXiv:1606.03577].

[188] P. Athron *et al.* (GAMBIT), Eur. Phys. J. **C77**, 12, 879 (2017), [arXiv:1705.07917].

[189] K. J. de Vries *et al.*, Eur. Phys. J. **C75**, 9, 422 (2015), [arXiv:1504.03260].

[190] C. Strege *et al.*, JHEP **09**, 081 (2014), [arXiv:1405.0622].

[191] G. Aad *et al.* (ATLAS), JHEP **05**, 106 (2024), [arXiv:2402.01392].

[192] LEP2 SUSY Working Group, ALEPH, DELPHI, L3 and OPAL experiments, note LEPSUSYWG/04-01.1, `http://lepsusy.web.cern.ch/lepsusy`.

[193] A. Heister *et al.* (ALEPH), Phys. Lett. **B544**, 73 (2002), [hep-ex/0207056].

[194] A. M. Sirunyan *et al.* (CMS), Phys. Lett. **B790**, 140 (2019), [arXiv:1806.05264].

[195] G. Aad *et al.* (ATLAS), JHEP **08**, 053 (2025), [arXiv:2503.17186].

[196] A. M. Sirunyan *et al.* (CMS), Eur. Phys. J. C **80**, 3, 189 (2020), [arXiv:1907.13179].

[197] A. Tumasyan *et al.* (CMS), Phys. Rev. D **108**, 1, 012011 (2023), [arXiv:2207.02254].

[198] LEP2 SUSY Working Group, ALEPH, DELPHI, L3 and OPAL experiments, note LEPSUSYWG/02-09.2, `http://lepsusy.web.cern.ch/lepsusy`.

[199] M. Aaboud *et al.* (ATLAS), Phys. Rev. **D99**, 1, 012009 (2019), [arXiv:1808.06358].

[200] S. Chatrchyan *et al.* (CMS), Eur. Phys. J. **C73**, 2493 (2013), [arXiv:1301.3792].

[201] S. Chatrchyan *et al.* (CMS), Phys. Rev. **D90**, 032006 (2014), [arXiv:1404.5801].

[202] T. Aaltonen *et al.* (CDF), Phys. Rev. Lett. **110**, 20, 201802 (2013), [arXiv:1302.4491].

[203] DELPHI Collab., Eur. Phys. J. **C31**, 412 (2003).

[204] G. Aad *et al.* (ATLAS), JHEP **07**, 167 (2021), [arXiv:2103.11684].

[205] M. Aaboud *et al.* (ATLAS), JHEP **09**, 084 (2017), [arXiv:1706.03731].

[206] CMS Collab., CMS-PAS-SUS-19-008 (2019).

[207] V. Khachatryan *et al.* (CMS), Phys. Rev. **D94**, 11, 112009 (2016), [arXiv:1606.08076].

[208] CMS Collab., CMS-PAS-SUS-13-010 (2013).

[209] T. Aaltonen *et al.* (CDF), Phys. Rev. Lett. **107**, 042001 (2011), [arXiv:1105.2815].

[210] M. Aaboud *et al.* (ATLAS), Phys. Lett. **B785**, 136 (2018), [arXiv:1804.03568].

[211] ATLAS Collab., ATLAS-CONF-2018-003 (2018).

[212] ATLAS Collab., ATLAS-CONF-2016-057 (2016).

[213] M. Aaboud *et al.* (ATLAS), JHEP **09**, 088 (2017), [arXiv:1704.08493].

[214] A. M. Sirunyan *et al.* (CMS), Phys. Lett. **B783**, 114 (2018), [arXiv:1712.08920].

[215] S. Chatrchyan *et al.* (CMS), Phys. Lett. **B730**, 193 (2014), [arXiv:1311.1799].

[216] V. Khachatryan *et al.* (CMS), Phys. Lett. **B770**, 257 (2017), [arXiv:1608.01224].

Int. J. Mod. Phys. A 2026.41. Downloaded from www.worldscientific.com
by UNIVERSITY OF CALIFORNIA @ BERKELEY on 09/16/26. Re-use and distribution is strictly not permitted, except for Open Access articles.

[217] G. Aad *et al.* (ATLAS), Eur. Phys. J. C **81**, 11, 1023 (2021), [arXiv:2106.09609].

[218] F. D. Aaron *et al.* (H1), Eur. Phys. J. **C71**, 1572 (2011), [arXiv:1011.6359].

[219] ATLAS Collab., ATLAS-CONF-2015-018 (2015).

[220] S. Chekanov *et al.* (ZEUS), Eur. Phys. J. **C50**, 269 (2007), [hep-ex/0611018].

[221] M. Aaboud *et al.* (ATLAS), Phys. Rev. **D97**, 3, 032003 (2018), [arXiv:1710.05544].

[222] G. Aad *et al.* (ATLAS), Phys. Rev. D **110**, 9, 092004 (2024), [arXiv:2406.18367].

[223] ATLAS Collab., ATLAS-CONF-2019-006 (2019).

[224] A. M. Sirunyan *et al.* (CMS), Phys. Rev. **D99**, 3, 032014 (2019), [arXiv:1808.05082].

[225] CMS Collab., CMS-PAS-EXO-16-022 (2016).

[226] V. Khachatryan *et al.* (CMS), Phys. Lett. **B760**, 178 (2016), [arXiv:1602.04334].

[227] M. Aaboud *et al.* (ATLAS), Eur. Phys. J. C **78**, 3, 250 (2018), [arXiv:1710.07171].

[228] M. Aaboud *et al.* (ATLAS), Eur. Phys. J. **C78**, 3, 250 (2018), [arXiv:1710.07171].

[229] V. Khachatryan *et al.* (CMS), Phys. Rev. **D95**, 1, 012009 (2017), [arXiv:1610.05133].

[230] V. Khachatryan *et al.* (CMS), Phys. Lett. **B747**, 98 (2015), [arXiv:1412.7706].

[231] G. Aad *et al.* (ATLAS), Eur. Phys. J. C **81**, 1, 11 (2021), [Erratum: Eur.Phys.J.C 81, 249 (2021)], [arXiv:2010.01015].

[232] A. M. Sirunyan *et al.* (CMS), Phys. Rev. D **104**, 3, 032006 (2021), [arXiv:2102.06976].

[233] V. Chekhovsky *et al.* (CMS) (2025), [arXiv:2506.08825].

[234] G. Aad *et al.* (ATLAS), Phys. Rev. **D92**, 7, 072004 (2015), [arXiv:1504.05162].

[235] V. Khachatryan *et al.* (CMS), Phys. Rev. **D91**, 1, 012007 (2015), [arXiv:1411.6530].

[236] G. Aad *et al.* (ATLAS), Phys. Rev. D **103**, 112003 (2021), [arXiv:2011.10543].

[237] LEP2 SUSY Working Group, ALEPH, DELPHI, L3 and OPAL experiments, note LEPSUSYWG/02-10.1, `http://lepsusy.web.cern.ch/lepsusy`.

[238] A. M. Sirunyan *et al.* (CMS), Eur. Phys. J. **C79**, 4, 305 (2019), [arXiv:1811.09760].

[239] T. Aaltonen *et al.* (CDF), Phys. Rev. Lett. **105**, 191801 (2010), [arXiv:1004.3042].

[240] V. M. Abazov *et al.* (D0), Phys. Rev. Lett. **105**, 191802 (2010), [arXiv:1007.4835].

[241] G. Aad *et al.* (ATLAS), Phys. Rev. Lett. **115**, 3, 031801 (2015), [arXiv:1503.04430].

[242] M. Aaboud *et al.* (ATLAS), Eur. Phys. J. **C76**, 10, 541 (2016), [arXiv:1607.08079].

[243] V. Khachatryan *et al.* (CMS), Eur. Phys. J. **C76**, 6, 317 (2016), [arXiv:1604.05239].

[244] G. Aad *et al.* (ATLAS), JHEP **23**, 082 (2020), [arXiv:2307.08567].

[245] H. K. Dreiner *et al.*, JHEP **07**, 215 (2023), [arXiv:2306.07317].

[246] J. Fan, M. Reece and J. T. Ruderman, JHEP **11**, 012 (2011), [arXiv:1105.5135].

[247] J. Fan, M. Reece and J. T. Ruderman, JHEP **07**, 196 (2012), [arXiv:1201.4875].

[248] J. Fan *et al.*, JHEP **07**, 016 (2016), [arXiv:1512.05781].

[249] V. Khachatryan *et al.* (CMS), Phys. Lett. B **743**, 503 (2015), [arXiv:1411.7255].

[250] A. Hayrapetyan *et al.* (CMS), Phys. Rev. D **109**, 11, 112009 (2024), [arXiv:2310.03154].

[251] Technical report, CERN, Geneva (2023), all figures including auxiliary figures are available at `https://atlas.web.cern.ch/Atlas/GROUPS/PHYSICS/CONFNOTES/ATLAS-CONF-2023-044`, URL `https://cds.cern.ch/record/2870112`.

[252] M. Aaboud *et al.* (ATLAS), Phys. Rev. **D97**, 5, 052012 (2018), [arXiv:1710.04901].

[253] M. Aaboud *et al.* (ATLAS), Phys. Rev. **D99**, 9, 092007 (2019), [arXiv:1902.01636].

[254] G. Aad *et al.* (ATLAS), Eur. Phys. J. **C75**, 9, 407 (2015), [arXiv:1506.05332].

[255] A. M. Sirunyan *et al.* (CMS), Phys. Lett. **B797**, 134876 (2019), [arXiv:1906.06441].

[256] A. M. Sirunyan *et al.* (CMS), JHEP **05**, 025 (2018), [arXiv:1802.02110].

[257] CMS Collab., CMS-PAS-EXO-16-036 (2016).

[258] A. M. Sirunyan *et al.* (CMS), Phys. Lett. B **806**, 135502 (2020), [arXiv:2004.05153].

[259] A. M. Sirunyan *et al.* (CMS), Phys. Rev. D **104**, 1, 012015 (2021), [arXiv:2012.01581].

[260] V. M. Abazov *et al.* (D0), Phys. Rev. Lett. **99**, 131801 (2007), [arXiv:0705.0306].

[261] G. Aad *et al.* (ATLAS), Phys. Rev. **D88**, 11, 112003 (2013), [arXiv:1310.6584].

[262] A. M. Sirunyan *et al.* (CMS), JHEP **05**, 127 (2018), [arXiv:1801.00359].

[263] G. Aad *et al.* (ATLAS), JHEP **07**, 173 (2021), [arXiv:2104.03050].

[264] T. Aaltonen *et al.* (CDF), Phys. Rev. Lett. **103**, 021802 (2009), [arXiv:0902.1266].

[265] V. M. Abazov *et al.* (D0), Phys. Rev. **D87**, 5, 052011 (2013), [arXiv:1211.2466].

[266] G. Aad *et al.* (ATLAS), Phys. Rev. D **102**, 3, 032006 (2020), [arXiv:2003.11956].

[267] A. Tumasyan *et al.* (CMS), Eur. Phys. J. C **82**, 2, 153 (2022), [arXiv:2110.04809].

[268] A. M. Sirunyan *et al.* (CMS), JHEP **08**, 016 (2018), [arXiv:1804.07321].

[269] M. Aaboud *et al.* (ATLAS), JHEP **06**, 022 (2018), [arXiv:1712.02118].

[270] G. Aad *et al.* (ATLAS), Phys. Rev. **D88**, 11, 112006 (2013), [arXiv:1310.3675].

[271] G. Aad *et al.* (ATLAS), Eur. Phys. J. C **82**, 7, 606 (2022), [arXiv:2201.02472].

[272] G. Aad *et al.* (ATLAS), JHEP **2306**, 158 (2023), [arXiv:2205.06013].

[273] A. Hayrapetyan *et al.* (CMS), Phys. Rev. D **109**, 7, 072007 (2024), [arXiv:2309.16823].

[274] LEP2 SUSY Working Group, ALEPH, DELPHI, L3 and OPAL experiments, note LEPSUSYWG/02-05.1, `http://lepsusy.web.cern.ch/lepsusy`.

[275] V. Khachatryan *et al.* (CMS), Eur. Phys. J. **C75**, 7, 325 (2015), [arXiv:1502.02522].

[276] T. Aaltonen *et al.* (CDF), Phys. Rev. **D88**, 3, 031103 (2013), [arXiv:1307.0474].

[277] A. M. Sirunyan *et al.* (CMS), Phys. Rev. D **100**, 11, 112003 (2019), [arXiv:1909.06166].

[278] V. M. Abazov *et al.* (D0), Phys. Rev. Lett. **101**, 111802 (2008), [arXiv:0806.2223].

[279] G. Aad *et al.* (ATLAS), Phys. Rev. **D90**, 11, 112005 (2014), [arXiv:1409.5542].

[280] G. Aad *et al.* (ATLAS), JHEP **12**, 081 (2023), [arXiv:2307.14759].

[281] O. Buchmueller *et al.*, Eur. Phys. J. **C71**, 1722 (2011), [arXiv:1106.2529].

[282] E. A. Baltz and P. Gondolo, JHEP **10**, 052 (2004), [hep-ph/0407039].

[283] B. C. Allanach and C. G. Lester, Phys. Rev. **D73**, 015013 (2006), [hep-ph/0507283].

[284] R. Ruiz de Austri, R. Trotta and L. Roszkowski, JHEP **05**, 002 (2006), [hep-ph/0602028].

[285] R. Lafaye *et al.*, Eur. Phys. J. **C54**, 617 (2008), [arXiv:0709.3985].

[286] M. Shaposhnikov, JHEP **08**, 008 (2008), [arXiv:0804.4542].

[287] R. Trotta *et al.*, JHEP **12**, 024 (2008), [arXiv:0809.3792].

[288] P. Bechtle *et al.*, Eur. Phys. J. **C66**, 215 (2010), [arXiv:0907.2589].

[289] E. Bagnaschi *et al.*, Eur. Phys. J. C **78**, 256, 1 (2018).

[290] J. Costa *et al.*, Eur. Phys. J. C **78**, 158, 1 (2018).

[291] E. Bagnaschi *et al.*, Eur. Phys. J. **C77**, 4, 268 (2017), [arXiv:1612.05210].

[292] E. Bagnaschi *et al.*, Eur. Phys. J. **C77**, 2, 104 (2017), [arXiv:1610.10084].

[293] L. A. Harland-Lang, V. A. Khoze and M. G. Ryskin, Eur. Phys. J. **C76**, 1, 9 (2016), [arXiv:1508.02718].

[294] E. A. Bagnaschi *et al.*, Eur. Phys. J. **C75**, 500 (2015), [arXiv:1508.01173].

[295] O. Buchmueller *et al.*, Eur. Phys. J. **C74**, 12, 3212 (2014), [arXiv:1408.4060].

[296] M. Citron *et al.*, Phys. Rev. **D87**, 3, 036012 (2013), [arXiv:1212.2886].

[297] F. Ambrogi *et al.*, Eur. Phys. J. C **78**, 3, 215 (2018), [arXiv:1707.09036].

[298] E. Bagnaschi *et al.*, Eur. Phys. J. C **79**, 2, 149 (2019), [arXiv:1810.10905].

[299] A. Arbey *et al.*, Phys. Rev. D **106**, 5, 055002 (2022), [arXiv:2201.00070].

[300] Supersymmetry Physics Results, ATLAS experiment, `http://twiki.cern.ch/twiki/bin/view/AtlasPublic/SupersymmetryPublicResults/`.

[301] Supersymmetry Physics Results, CMS experiment, `http://cms-results.web.cern.ch/cms-results/public-results/publications/SUS/index.html`.

Int. J. Mod. Phys. A 2026.41. Downloaded from www.worldscientific.com
by UNIVERSITY OF CALIFORNIA @ BERKELEY on 09/16/26. Re-use and distribution is strictly not permitted, except for Open Access articles.

89. Axions and Other Similar Particles

Revised August 2025 by C.A.J. O'Hare (Sydney U.), G. Rybka (U. Washington), B. Safdi (UC Berkeley) and L. Winslow (MIT).

89.1 Introduction

In this section, we list coupling-strength and mass limits for light axion-like particles (ALPs) and QCD axions [1–4]. Such bosons may arise from the spontaneous breaking of a global U(1) Peccei-Quinn (PQ) symmetry, resulting in a massless Nambu-Goldstone (NG) boson. If there is a small explicit symmetry breaking, either already in the Lagrangian or due to quantum effects such as anomalies, the boson acquires a mass and is called a pseudo-NG boson. Axions may also arise in extra dimension constructions as the zero-modes of higher-dimensional gauge fields compactified on internal manifolds; in this case, the absence of a local contribution to the axion mass is due to the higher-dimensional gauge symmetry [5,6].

A common feature of these light bosons a is that their coupling to Standard-Model particles is suppressed by the energy scale that characterizes the symmetry breaking, *i.e.*, the decay constant f_a. For example, in models where the axion arises as a Goldstone boson, the interaction Lagrangian at energy scales below f_a is

$$\mathcal{L} = f_a^{-1} J^\mu \partial_\mu a \,, \tag{89.1}$$

where J^μ is the Noether current of the spontaneously broken global symmetry. If f_a is very large, these new particles interact very weakly. Detecting them would provide a window to physics far beyond what can be probed at accelerators.

The QCD axions is of particular interest because it provides a compelling scheme to preserve CP-symmetry in QCD. Moreover, the cold dark matter (CDM) of the Universe may well consist of axions and they are searched for in dedicated experiments with a realistic chance of discovery.

Originally it was assumed that the PQ scale f_a was related to the electroweak symmetry-breaking scale $v_{\rm EW} = (\sqrt{2}G_{\rm F})^{-1/2} = 246.22$ GeV. However, the associated "standard" and "variant" axions were quickly excluded—we refer to the Listings for detailed limits. Here we focus on "invisible axions" with $f_a \gg v_{\rm EW}$ as the main possibility.

Axions have a characteristic two-photon vertex, inherited from their mixing with π^0 and η. This coupling allows for the main search strategy based on axion-photon conversion in external magnetic fields [7], an effect that also can be of astrophysical interest. While for axions the product "$a\gamma\gamma$ interaction strength $\times$ mass" is essentially fixed by the corresponding π^0 properties, one may consider a more general class of ALPs where the two parameters (coupling and mass) are independent. A number of experiments explore this more general ALP parameter space. ALPs populating the latter are predicted to arise generically, in addition to the axion, in low-energy effective field theories emerging from string theory [5,6,8–14].

89.2 Theory

89.2.1 *Peccei-Quinn mechanism and axions*

The QCD Lagrangian includes a CP-violating term $\mathcal{L}_\Theta = -\bar\Theta\,(\alpha_s/8\pi)\,G^{\mu\nu a}\tilde G^a_{\mu\nu}$, where $-\pi \le \bar\Theta \le +\pi$ is the effective Θ parameter after diagonalizing quark masses, $G^a_{\mu\nu}$ is the color field strength tensor, and $\tilde G^{a,\mu\nu} \equiv \epsilon^{\mu\nu\lambda\rho} G^a_{\lambda\rho}/2$, with $\varepsilon^{0123} = 1$, its dual. This term induces an electric dipole moment (EDM) of the neutron of strength $d_n = C_{\rm EDM}\, e\,\bar\Theta$. The coefficient $C_{\rm EDM}$ is calculated using QCD sum rules as $C_{\rm EDM} = 2.4(1.0) \times 10^{-16}$ cm [15], while lattice QCD computations find $C_{\rm EDM} = 1.48(14)(31) \times 10^{-16}$ cm [16] including statistical and systematic uncertainties. Experimental upper bounds on the latter, $|d_n| < 1.8 \times 10^{-26}\, e$ cm [17,18], imply $|\bar\Theta| \lesssim 10^{-10}$ even though $\bar\Theta = \mathcal{O}(1)$ is otherwise completely satisfactory. Note that the proton has a similar EDM as the neutron, but it is less strongly constrained at present; this could change in the future [19]. The proton EDM may be written as $d_p = C^p_{\rm EDM}\, e\,\bar\Theta$, with $C^p_{\rm EDM} = -3.8(11)(8)$ [16]. The opposite signs of the neutron and proton EDMs may be understood from the opposite signs of their magnetic moments. The spontaneously broken global PQ symmetry $\mathrm{U}(1)_{\rm PQ}$ was introduced to solve the "strong CP problem" [1,2] of small Θ , the axion being the pseudo-NG boson of $\mathrm{U}(1)_{\rm PQ}$ [3,4]. This symmetry is broken due to the axion's anomalous triangle coupling to gluons,

$$\mathcal{L} = \left(\frac{a}{f_a} - \bar\Theta\right) \frac{\alpha_s}{8\pi}\, G^{\mu\nu a} \tilde G^a_{\mu\nu} \,, \tag{89.2}$$

where a is the axion field and f_a the axion decay constant. Color anomaly factors have been absorbed in the normalization of f_a which is defined by this Lagrangian. Thus normalized, f_a is the quantity that enters all low-energy phenomena [20]. Non-perturbative topological fluctuations of the gluon fields in QCD induce a potential for a whose minimum is at $a = \bar\Theta\, f_a$, thereby canceling the $\bar\Theta$ term in the QCD Lagrangian and thus restoring CP symmetry.

The resulting axion mass, in units of the PQ scale f_a, is identical to the square root of the topological susceptibility in QCD, $m_a f_a = \sqrt{\chi}$. The latter can be evaluated further [21,22], exploiting the chiral limit (masses of up and down quarks much smaller than the scale of QCD), yielding $m_a f_a = \sqrt{\chi} \approx f_\pi m_\pi$, where $m_\pi \approx 135$ MeV and $f_\pi \approx 92$ MeV . In more detail one finds, by including $\mathcal{O}(\alpha)$ QED corrections and next-to-next-to-leading order (NNLO) corrections in chiral perturbation theory [23],

$$m_a = 5.691(51) \left(\frac{10^9\ \mathrm{GeV}}{f_a}\right) \mathrm{meV}\,. \tag{89.3}$$

A direct calculation of the topological susceptibility via QCD lattice simulations finds almost the same central value, albeit with an about five times larger error bar [24].

The QCD axion acquires a variety couplings to low-energy Standard Model observables, as we discuss in detail in this review. The most model-independent couplings are those of the axion to the neutron and proton EDM operators. While the axion removes the static neutron and proton EDMs, displacements of the axion field a from its vacuum expectation value induce field-dependent EDMs, which are characterized through the operator

$$\mathcal{L}_{aN\gamma} = -\frac{i}{2} g_{aN\gamma}\, a\, \overline{\Psi}_N \sigma_{\mu\nu}\gamma_5 \Psi_N F^{\mu\nu} \,, \tag{89.4}$$

with $N = n, p$ for neutrons or protons, respectively. The coupling $g_{an\gamma}$ is related to $C_{\rm EDM}$ by $g_{an\gamma} = eC_{\rm EDM}/f_a$ and similarly for $g_{ap\gamma}$. Direct probes of the axion-EDM operators are difficult, though by studying the thermal production of axions in the early universe one can broadly constrain, using Planck and Baryon Acoustic Oscillation (BAO) data, $m_a \lesssim 0.3$ eV [25]. In the presence of an oscillatory relic axion DM field, this operator induces an oscillating neutron EDM; this effect forms the basis of the CASPEr experiment [26,27] that is discussed more later in this review. Non-linearly realized discrete-symmetries may be used to suppress the QCD axion mass below the prediction in Eq. (89.3), in which case a variety of cosmological and terrestrial constraints on the operator in Eq. (89.4) are also relevant [28–35]

Axions with $f_a \gg v_{\rm EW}$ evade almost all current experimental limits. Given that the axion interacts with ordinary matter through higher-dimensional operators, it requires an ultraviolet (UV) completion at an energy scale of order f_a. Broadly speaking, there are two distinct classes of UV scenarios that give rise to axions in the infrared (IR) low-energy effective field theory (EFT) (see [36] for a review of UV axion models): (i) 4d field theory models that realize the axion as a Goldstone mode of a spontaneously broken but also anomalous abelian $U(1)_{\rm PQ}$ symmetry, (ii) extra-dimensional models where the axion arises as the zero-mode of a higher-dimensional gauge field. Within the first category, one generic class of models is that of "hadronic axions," where new heavy quarks carry $\mathrm{U}(1)_{\rm PQ}$ charges, leaving ordinary quarks and leptons without tree-level axion couplings. The archetype is the KSVZ model [37,38], where in addition the heavy new quarks are electrically neutral. Another generic class of field theory axion models requires at least two Higgs doublets and ordinary quarks and leptons carry PQ charges, the archetype being the DFSZ model [159,160]; in this case the quarks and leptons may have

Int. J. Mod. Phys. A 2026.41. Downloaded from www.worldscientific.com by UNIVERSITY OF CALIFORNIA @ BERKELEY on 09/16/26. Re-use and distribution is strictly not permitted, except for Open Access articles.

Int. J. Mod. Phys. A 2026.41. Downloaded from www.worldscientific.com
by UNIVERSITY OF CALIFORNIA @ BERKELEY on 09/16/26. Re-use and distribution is strictly not permitted, except for Open Access articles.

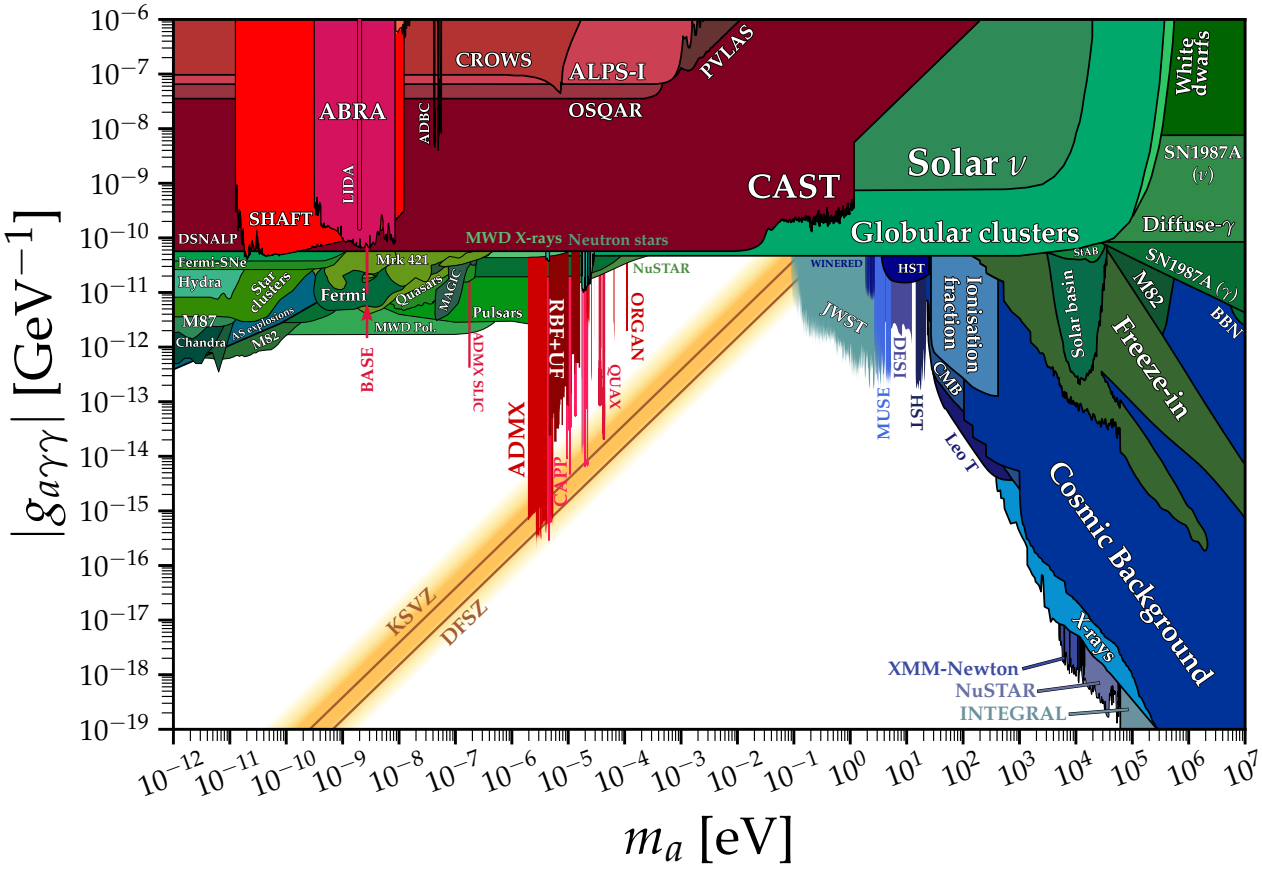

Figure 89.1: Exclusion plot for the ALP-photon coupling. Figure from [39], contains exclusions from refs. [40–158]. Constraints in red are from terrestrial experiments. Haloscope searches assume all local dark matter is axions. Those shown in green are astrophysical but make no assumption about axions being DM. See text for details regarding the diagonal yellow band expectation for the QCD axion and assumptions for blue high mass axion astrophysical limits.

tree-level axion couplings. All of these models contain at least one electroweak singlet scalar that acquires a vacuum expectation value and thereby breaks the PQ symmetry. The KSVZ and DFSZ models are frequently used as benchmark examples, but other field theory models exist where both heavy quarks and Higgs doublets carry PQ charges [36].

The field theory axion constructions, like KSVZ, DFSZ, and related variants, suffer from the so-called PQ quality problem [161–165]. The issue is that global symmetries are not expected to be respected in quantum gravity (see, *e.g.*, [166]); in particular, PQ-violating operators at the Planck scale spoil the quality of the $U(1)_{\rm PQ}$ symmetry, generating a neutron EDM in conflict with the experimental constraints. On the other hand, the axion quality is naturally exponentially better in the second class of UV completions mentioned in the previous paragraph, when the axion arises as the zero mode of an extra dimensional gauge field. In this case, the axion potential is protected by the gauge symmetry of the higher-dimensional theory, instead of a global symmetry. (More technically, the axion quality in extra dimensional constructions is best understood through the language of generalized global symmetries [167–169].) Contributions to the axion potential must be non-local and are thus naturally exponentially suppressed. Extra dimensional axions arise naturally in string theory constructions, as string theory has a plethora of higher-form gauge fields and lives most naturally in 10 or 11 dimensions, which requires some of those dimensions to be compactified. The presence of multiple distinct and non-trivial cycles in the compact manifold and higher-form gauge fields leads to a plethora of axions, which is known as the axiverse [6,10,12]—one of these axions can be the QCD axion. While field theory axions can have any $f_a \lesssim M_{\rm pl}$ and thus any mass larger than roughly 10^{-12} eV, axions in string theory most naturally have $m_a \lesssim 10^{-8}$ eV [6,170], though higher QCD axion masses are also possible in these constructions at the cost of fine tuning [171,172].

89.2.2 *Model-dependent axion couplings*

Although the generic axion interactions scale approximately with f_π/f_a from the corresponding π^0 couplings, there are non-negligible model-dependent factors and uncertainties. The axion's two-photon interaction plays a key role for many searches,

$$\mathcal{L}_{a\gamma\gamma} = -\frac{g_{a\gamma\gamma}}{4}\, a\, F_{\mu\nu}\tilde{F}^{\mu\nu} = g_{a\gamma\gamma}\, a\, \mathbf{E}\cdot\mathbf{B}\,, \tag{89.5}$$

where F is the electromagnetic field-strength tensor and $\tilde{F}^{\mu\nu} \equiv \epsilon^{\mu\nu\lambda\rho}F_{\lambda\rho}/2$, with $\varepsilon^{0123} = 1$, its dual. The coupling constant is [173]

$$g_{a\gamma\gamma} = \frac{\alpha}{2\pi f_a}\left(\frac{E}{N} - 1.92(4)\right) = \left(0.203(3)\frac{E}{N} - 0.39(1)\right)\frac{m_a}{\rm GeV^2}\,, \tag{89.6}$$

where E and N are the electromagnetic and color anomalies of the axial current associated with the axion, and α is the low-energy fine structure constant. In grand unified models, and notably for DFSZ [159,160], $E/N = 8/3$, whereas for KSVZ [37,38] $E/N = 0$ if the electric charge of the new heavy quark is taken to vanish. In general, a broad range of E/N values is possible [36,174–176], as indicated by the diagonal yellow band in Fig. 89.1, whose width is roughly determined by the boundary values $E/N = 44/3$ and $E/N = 5/3$, respectively. However, this band still does not exhaust all the possibilities. In fact, there exist classes of QCD axion models whose photon couplings populate the entire still-allowed region outside the yellow band in Fig. 89.1 [177–182], motivating axion search efforts over a wide range of masses and couplings.

Int. J. Mod. Phys. A 2026.41. Downloaded from www.worldscientific.com by UNIVERSITY OF CALIFORNIA @ BERKELEY on 09/16/26. Re-use and distribution is strictly not permitted, except for Open Access articles.

The two-photon decay width is

$$\Gamma_{a\to\gamma\gamma} = \frac{g^2_{a\gamma\gamma} m_a^3}{64\,\pi} \approx 1.1\times 10^{-24}\ \mathrm{s}^{-1}\left(\frac{m_a}{\mathrm{eV}}\right)^5 . \tag{89.7}$$

The second expression uses Eq. (89.6) with $E/N = 0$. Axions decay faster than the age of the Universe if $m_a \gtrsim 20$ eV.

The interaction with fermions f has derivative form and is invariant under a shift $a \to a + a_0$ as behooves a NG boson,

$$\mathcal{L}_{aff} = \frac{C_f}{2f_a}\,\partial_\mu a\,\bar{\Psi}_f\gamma^\mu\gamma_5\Psi_f\ . \tag{89.8}$$

Here, Ψ_f is the fermion field, m_f its mass, and C_f a model-dependent coefficient. The dimensionless combination $g_{aff} \equiv C_f m_f/f_a$ plays the role of a Yukawa coupling and $\alpha_{aff} \equiv g^2_{aff}/4\pi$ of a "fine-structure constant." The often-used pseudoscalar form $\mathcal{L}_{aff} = -\mathrm{i}\,(C_f m_f/f_a)\,a\,\bar{\Psi}_f\gamma_5\Psi_f$ need not be equivalent to the appropriate derivative structure, for example when two NG bosons are attached to one fermion line as in axion emission by nucleon bremsstrahlung [183–185].

In hadronic axion models, C_e vanishes at tree level, but is then generated radiatively at one loop [186, 187],

$$C_e \simeq \frac{3\alpha^2}{4\pi^2}\left[\frac{E}{N}\log\left(\frac{f_a}{m_e}\right) - 1.92\log\left(\frac{\Lambda_\chi}{m_e}\right)\right] , \tag{89.9}$$

where $\Lambda_\chi \simeq 1$ GeV is the chiral symmetry breaking scale. In the DFSZ model [159, 160], the tree-level coupling coefficient to electrons is [186]

$$C_e = \frac{\sin^2\beta}{3} , \tag{89.10}$$

where $\tan\beta$ is the ratio of the vacuum expectation values of the two Higgs doublets giving masses to the up- and down-type quarks, respectively: $\tan\beta = v_u/v_d$. As a cautionary note, many of the original axion references, such as [186], defined $\tan\beta = v_d/v_u$, but the choice $\tan\beta = v_u/v_d$ adopted here and in more modern axion works is a reflection of the choice taken in the two-Higgs-doublet literature [188]. The resulting prediction for the axion-electron coupling, as a function of the axion mass, for the KSVZ axion ($E/N = 0$), hadronic axions, with $5/3 \le E/N \le 44/3$, and the DFSZ axion is displayed in Fig. 89.2. For the DFSZ range we have taken into account the constraint $0.28 \lesssim \tan\beta \lesssim 140$ [189] arising from the requirement of perturbative unitarity of the Yukawa couplings of Standard Model fermions.

For nucleons, $C_{p,n}$ have been determined as [173]

$$\begin{aligned} C_p &= -0.47(3) + 0.88(3)C_u - 0.39(2)C_d - 0.038(5)C_s \\ &\qquad - 0.012(5)C_c - 0.009(2)C_b - 0.0035(4)C_t\ , \\ C_n &= -0.02(3) + 0.88(3)C_d - 0.39(2)C_u - 0.038(5)C_s \\ &\qquad - 0.012(5)C_c - 0.009(2)C_b - 0.0035(4)C_t\ , \end{aligned} \tag{89.11}$$

in terms of the corresponding model-dependent quark couplings C_q, $q = u, d, s, c, b, t$. For hadronic axions, the latter vanish at tree-level, which means that C_n is expected to be much smaller than C_p. In the DFSZ model, $C_u = C_c = C_t = \frac{1}{3}\cos^2\beta$ and $C_d = C_s = C_b = \frac{1}{3}\sin^2\beta$, and C_p and C_n, as functions of β,

$$\begin{aligned} C_p &= -0.435\sin^2\beta + (-0.182 \pm 0.025)\ , \\ C_n &= 0.414\sin^2\beta + (-0.160 \pm 0.025)\ . \end{aligned} \tag{89.12}$$

The resulting prediction for the axion-neutron coupling, as a function of the axion mass, for the KSVZ axion and the DFSZ axion is displayed in Fig. 89.3. Note, however, that these couplings receive in-medium corrections, which may be important when considering compact stars [190].

The axion-pion interaction is given by the Lagrangian [187, 191]

$$\mathcal{L}_{a\pi} = \frac{C_{a\pi}}{2f_\pi f_a}\,\partial_\mu a\left(\pi^0\pi^+\partial_\mu\pi^- + \pi^0\pi^-\partial_\mu\pi^+ - 2\pi^+\pi^-\partial_\mu\pi^0\right) , \tag{89.13}$$

where $C_{a\pi} = 2(C_p - C_n)/(3g_A)$ and $g_A = 1.2723(23)$ is the nucleon axial charge.

Additionally, there are axion-pion-nucleon interactions of the form

$$\mathcal{L}_{a\pi N} = \frac{C_{a\pi N}}{2f_\pi f_a}\partial_\mu a\left(i\pi^+\bar{p}\gamma^\mu n - i\pi^-\bar{n}\gamma^\mu p\right) , \tag{89.14}$$

where $C_{a\pi N} = (C_{ap} - C_{an})/(\sqrt{2}g_A)$. Axion-kaon interactions are also present.

89.3 Laboratory Searches

89.3.1 *Light shining through walls*

Searching for "invisible axions" is extremely challenging due to their extraordinarily feeble coupling to normal matter and radiation. Currently, the most promising approaches rely on the axion-two-photon interaction, allowing for axion-photon conversion in external electric or magnetic fields [7]. For the Coulomb field of a charged particle, the conversion can be viewed as a scattering process, $\gamma + Ze \leftrightarrow Ze + a$, called the Primakoff effect [192]. In the other extreme of a macroscopic field, usually a large-scale B-field, the momentum transfer is small, the interaction is coherent over a large distance, and the conversion can be viewed as an axion-photon oscillation phenomenon in analogy to neutrino flavor oscillations [193].

Photons propagating through a transverse magnetic field, with incident $\mathbf{E}_\gamma$ and magnetic field $\mathbf{B}$ parallel, may convert into axions. For $m_a^2 L/2\omega \ll 2\pi$, where L is the length of the B field region and ω the photon energy, the resultant axion beam is coherent with the incident photon beam and the conversion probability is $\Pi \sim (1/4)(g_{a\gamma\gamma}BL)^2$. One such realization uses a laser beam propagating down the bore of a superconducting dipole magnet (like, say, the bending magnets in high-energy accelerators). If another magnet is in line with the first, but shielded by an optical barrier, then photons may be regenerated from the pure axion beam [194, 195]. The overall probability is $P(\gamma \to A \to \gamma) = \Pi^2$.

The first such Light-Shining-through-Walls (LSW) experiment was performed by the BFRT (Brookhaven-Fermilab-Rochester-Trieste) collaboration. It utilized two magnets of length $L = 4.4$ m and $B = 3.7$ T and found $|g_{a\gamma\gamma}| < 6.7\times 10^{-7}$ GeV^{-1} at 95% CL for $m_a < 1$ meV [196, 197]. More recently, several such experiments were performed (see Listings) [75, 78, 198–202]. The current best limit, $|g_{a\gamma\gamma}| < 3.5\times 10^{-8}$ GeV^{-1} at 95% CL for $m_a \lesssim 0.3$ meV (see Fig. 89.1), has been achieved by the OSQAR (Optical Search for QED Vacuum Birefringence, Axions, and Photon Regeneration) experiment, which exploited two 9 T LHC dipole magnets and an 18.5 W continuous wave laser emitting at the wavelength of 532 nm [78]. The ALPS I (Any Light Particle Search I) experiment achieved a similar sensitivity [75], see Fig. 89.1. Some of these experiments have also reported limits for scalar bosons where the photon $\mathbf{E}_\gamma$ must be chosen perpendicular to the magnetic field $\mathbf{B}$.

The concept of resonantly enhanced photon regeneration may open unexplored regions of coupling strength [203–205]. In this scheme, both the production and detection magnets are within Fabry-Perot optical cavities and actively locked in frequency. The $\gamma \to a \to \gamma$ rate is enhanced by a factor $\mathcal{F}\mathcal{F}'/\pi^2$ relative to a single-pass experiment, where $\mathcal{F}$ and $\mathcal{F}'$ are the finesses of the two cavities. The resonant enhancement could be of order $10^{(10-12)}$, improving the $g_{a\gamma\gamma}$ sensitivity by $10^{(2.5-3)}$. The experiment ALPS II (Any Light Particle Search II) is based on this concept and aims at an improvement of the current laboratory bound on $g_{a\gamma\gamma}$ by a factor $\sim 10^3$ [206]. ALPS II began operations in 2023, the regeneration cavity has been characterized [207], and a result from the first data taking campaign is pending.

Resonantly enhanced photon regeneration has already been exploited in experiments searching for "radiowaves shining through a shielding" [208–211]. For $m_a \lesssim 10^{-5}$ eV, the upper bound on $g_{a\gamma\gamma}$ established by the CROWS (CERN Resonant Weakly Interacting sub-eV Particle Search) experiment [77] is slightly less stringent than the one set by OSQAR, see Fig. 89.1.

89.3.2 *Long-range forces*

New bosons would mediate new long-range forces, which are severely constrained by "fifth force" experiments [212]. Those

Int. J. Mod. Phys. A 2026.41. Downloaded from www.worldscientific.com
by UNIVERSITY OF CALIFORNIA @ BERKELEY on 09/16/26. Re-use and distribution is strictly not permitted, except for Open Access articles.

looking for new mass-spin couplings provide significant constraints on pseudoscalar bosons [213–218], see for example in Fig. 89.3 the limit on the axion-neutron coupling [219] from torsion balance tests of the gravitational inverse square law [220]. Presently, the most restrictive limits are obtained from combining long-range force measurements with stellar cooling arguments [221, 222]. For the moment, any of these limits are far from realistic values expected for the QCD axion. Still, these efforts provide constraints on more general low-mass bosons.

In Ref. [223], a method was proposed that can extend the search for axion-mediated spin-dependent forces by several orders of magnitude. By combining techniques used in nuclear magnetic resonance and short-distance tests of gravity, this method appears to be sensitive to the QCD axion in the μeV – meV mass range, independent of the cosmic axion abundance, if axions have a CP-violating interaction with nuclei as large as the current experimental bound on the electric dipole moment of the neutron allows. (Note that the CP-violation already present in the Standard Model is sufficient for generating an axion-mediated force, though in this case the signal appears too small to be detectable for the QCD axion in the foreseeable future [223].) The ARIADNE (Axion Resonant InterAction DetectioN Experiment) is under development and employs this approach to search for axion-mediated spin-dependent short-range interactions between a hyper-polarized ^{3}He sample and an unpolarized tungsten source mass [224]. The method relies on superconducting magnetic shielding to screen the sample from ordinary magnetic field noise. Experimental tests to demonstrate the requirements of ARIADNE, including characterization of the magnetic field backgrounds, are under way [225, 226].

89.4 Axions from Astrophysical Sources

89.4.1 *Stellar energy-loss limits*

Axions are produced in hot astrophysical plasmas, and can thus transport energy out of stars. The coupling strength of these particles with normal matter and radiation is bounded by the constraint that stellar lifetimes or energy-loss rates are not in conflict with observation [227, 228].

We begin this discussion with our Sun and concentrate first on the axion-photon coupling. In the Sun axions are produced by the Primakoff process $\gamma + Ze \to Ze + a$. Integrating this process over a standard solar model yields the axion luminosity [229]

$$L_a = g_{10}^2 \times 1.85 \times 10^{-3}\, L_\odot\,, \tag{89.15}$$

where $g_{10} = |g_{a\gamma\gamma}| \times 10^{10}$ GeV. The maximum of the spectrum is at 3.0 keV, the average at 4.2 keV, and the number flux at Earth is $g_{10}^2 \times 3.75 \times 10^{11}$ cm^{-2} s^{-1}. The solar photon luminosity is fixed, so energy losses due to the Primakoff process require enhanced nuclear energy production and thus enhanced neutrino fluxes. The all-flavor measurements by SNO (Sudbury Neutrino Observatory), together with a standard solar model, imply $L_a \lesssim 0.10\, L_\odot$, corresponding to $g_{10} \lesssim 7$ [230], mildly superseding a similar limit from helioseismology (sound speed, surface helium and convective radius) [231]. In Ref. [124], this limit was improved to $g_{10} < 4.1$ (at $3\,\sigma$), see Fig. 89.1, exploiting a new statistical analysis that combined helioseismology and solar neutrino observations, including theoretical and observational errors, and accounting for tensions between input parameters of solar models, in particular the solar element abundances. Going beyond the axion-photon coupling, Ref. [230] considered also a non-zero axion-electron coupling and obtained the bound on the latter displayed in Fig. 89.2.

A more restrictive limit derives from globular-cluster (GC) stars that allow for detailed tests of stellar-evolution theory. The stars on the horizontal branch (HB) in the color-magnitude diagram have reached helium burning with a core-averaged energy release of about 80 erg g^{-1} s^{-1}, compared to Primakoff axion losses of $g_{10}^2\, 30$ erg g^{-1} s^{-1}. The accelerated consumption of helium reduces the HB lifetime by about $80/(80 + 30\, g_{10}^2)$. In contrast, the red giant (RG) branch stars are not strongly affected by Primakoff losses, since unlike for the HB stars the plasma frequency in the RG stellar cores is below the temperature. Thus, Primakoff production reduces the R-parameter, which is the number of observed HB branch stars to RG branch stars in a GC. Measurements of

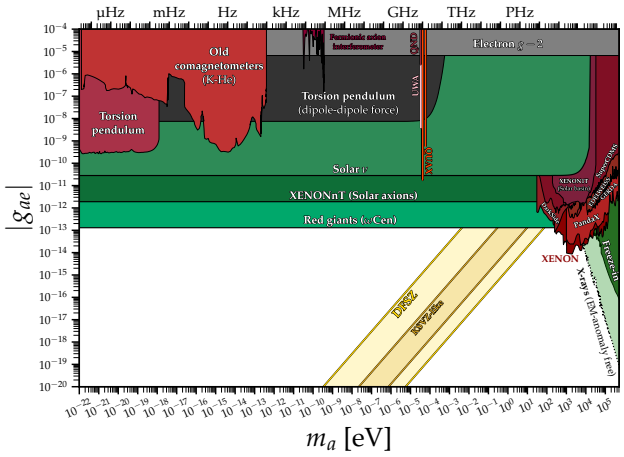

Figure 89.2: Exclusion plot for ALP-electron coupling as described in the text. Figure from [39], contains data from refs. [145, 230, 232–243]. The hadronic QCD axion-electron coupling arises at one loop and is given in Eq. (89.9); varying E/N between 5/3 and 44/3 gives the indicated hadronic axion band. The KSVZ axion has $E/N = 0$, while the DFSZ axion-electron coupling has the tree-level coupling given in Eq. (89.10) that depends on the unknown but bounded value of $\tan\beta$ (see text for details).

the R-parameter in a large sample of 39 Galactic GCs give a weak indication of non-standard losses which may be accounted by Primakoff-like axion emission, if the photon coupling is in the range $|g_{a\gamma\gamma}| = (2.9 \pm 1.8) \times 10^{-11}$ GeV^{-1} [99, 244]. Still, the upper bound found in this analysis,

$$|g_{a\gamma\gamma}| < 6.6 \times 10^{-11}\,\text{GeV}^{-1}\ (95\%\,\text{CL}), \tag{89.16}$$

represents one of the strongest limits on $g_{a\gamma\gamma}$ for a wide mass range. More recently, the R_2-parameter has emerged as a potentially more sensitive probe of axions; the R_2-parameter is defined as the ratio of the asymptotic giant branch (AGB) stars to the HB stars in a GC. AGB stars have more efficient Primakoff production than HB stars, meaning that R_2 is expected to decrease for increasing $|g_{a\gamma\gamma}|$. Ref. [100] used an R_2 measurement based off of 48 GCs as observed by the Hubble Space Telescope [245] to constrain

$$|g_{a\gamma\gamma}| < 4.7 \times 10^{-11}\,\text{GeV}^{-1}\ (95\%\,\text{CL})\,. \tag{89.17}$$

The constraint above on $g_{a\gamma\gamma}$ may be translated to $f_a > 4.8 \times 10^7$ GeV $(m_a < 0.12$ eV$)$, using $E/N = 0$ as in the KSVZ model, or to $f_a > 1.8 \times 10^7$ GeV $(m_a < 0.32$ eV$)$, for the DFSZ axion model, with $E/N = 8/3$, see Fig. 89.1.

If axions couple directly to electrons, the dominant emission processes are atomic axio-recombination and axio-deexcitation, axio-bremsstrahlung in electron-ion or electron-electron collisions, and Compton scattering [246]. Stars in the RG branch of the color-magnitude diagram of GCs are particularly sensitive to these processes: they would lead to an extension of the RG branch to larger brightness. In fact, the tip of the RG branch (TRGB) – the brightest point of the RG branch – provides the currently most sensitive method to test the axion coupling to electrons. The strongest bounds on it are derived from analyses of the TRGB in several GCs [247] and in the Galactic GC ω Centauri [239]. The two analyses lead to very similar results,

$$|g_{aee}| < 1.48{\times}10^{-13}\ (95\%\ \text{CL})\ \&\ |g_{aee}| < 1.3{\times}10^{-13}\ (95\%\ \text{CL}), \tag{89.18}$$

respectively, see Fig. 89.2. Reference [247] finds also a small hint for extra cooling, corresponding to $|g_{aee}| = 0.60^{+0..32}_{-0.58} \times 10^{-13}$, while Ref. [239] does not find any evidence for exotic cooling.

Bremsstrahlung is also efficient in white dwarfs (WDs), where the Primakoff and Compton processes are suppressed by the large plasma frequency. A comparison of the predicted and observed luminosity function of WDs can be used to put limits on $|g_{aee}|$

Int. J. Mod. Phys. A 2026.41. Downloaded from www.worldscientific.com
by UNIVERSITY OF CALIFORNIA @ BERKELEY on 09/16/26. Re-use and distribution is strictly not permitted, except for Open Access articles.

[248, 249]. An analysis based on detailed WD cooling treatment and data on the WD luminosity function (WDLF) of the Galactic disk found that electron couplings above $|g_{aee}| \gtrsim 3 \times 10^{-13}$ are disfavoured [250]. Lower couplings cannot be discarded from the current knowledge of the WDLF of the Galactic disk [250–252]. These probes may be improved by the Rubin Observatory Large Synoptic Survey Telescope (LSST), which is expected to increase the sample of WDs in the Galactic halo to hundreds of thousands [253]. For pulsationally unstable WDs (ZZ Ceti stars), the period decrease $\dot{P}/P$ is a measure of the cooling speed. The corresponding observations of a handful pulsating WDs imply additional cooling that can be interpreted in terms of axion energy losses [254–258], though with axion-electron coupling values likely incompatible with other constraints [259].

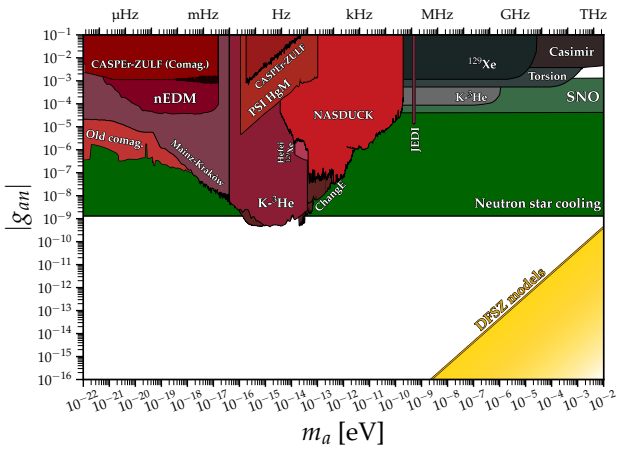

Figure 89.3: Exclusion plot for ALP-neutron coupling as described in the text. Figure from [39], includes data from refs. [31, 33, 219, 260–273]. The hadronic axion model prediction is given in Eq. (89.11) with vanishing quark couplings, while the DFSZ model prediction depends on $\tan\beta$ as is found in Eq. (89.12), giving the shaded yellow region above. Note that for a fine-tuned value of $\tan\beta$ g_{an} can be taken to zero. On the other hand, the neutron star cooling constraints [269] also probe the axion-proton coupling g_{ap} at a comparable level (not shown), and both g_{an} and g_{ap} cannot simultaneously be taken to zero in the DFSZ model.

Analogous constraints derive from neutron star (NS) cooling. Broadly speaking, there are two classes of NS cooling searches for axions. One approach uses the proto-NS formed after SN 1987A to constrain the axion luminosity produced during the first seconds of the proto-NS when the neutrino luminosity is measured with terrestrial experiments. The second class of NS cooling constraints consider older NSs, typically much older than ∼100 yr, and constrains the axion luminosity using the surface temperature as measured with photons versus the age of NS as measured through *e.g.* kinematic considerations. We begin with a discussion of the limits from SN 1987A.

Numerical simulations reveal that the energy-loss rate due to axions in a nuclear medium at the density 3×10^{14} g cm^{-3} and temperature 30 MeV should not exceed about 1×10^{19} erg g^{-1} s^{-1} to be consistent with the neutrino signal observed from SN 1987A [274]. The energy-loss rate from nucleon bremsstrahlung, $N + N \to N + N + a$, is $(C_N/2f_a)^2(T^4/\pi^2 m_N)\,F$. Here F is a numerical factor that represents an integral over the dynamical spin-density structure function because axions couple to the nucleon spin. For realistic conditions, even after considerable effort, one is limited to a heuristic estimate leading to $F \approx 1$ [228]. The SN 1987A limits are of particular interest for hadronic axions where the bounds on $|g_{aee}|$ are moot. Using a proton fraction of 0.3, $g_{ann} = 0$, $F = 1$, and $T = 30$ MeV, one finds $f_a > 4 \times 10^8$ GeV and $m_a < 16$ meV [228]. A more detailed numerical calculation [275] with state of the art SN models, again assuming $g_{ann} = 0$, found that a coupling larger than $|g_{app}| \gtrsim 6 \times 10^{-10}$, would shorten significantly the timescale of the neutrino emission. This result is, not surprisingly, rather close to the estimate in Ref. [228]. Improving the calculation of axion emission via nucleon-nucleon bremsstrahlung beyond the basic one-pion exchange approximation appears to loosen the bound [276, 277]. The latter analysis finds a reduction of the axion emissivity by an order of magnitude if one takes into account the non-vanishing mass of the exchanged pion, the contribution from two-pion exchange, effective in-medium nucleon masses and multiple nucleon scattering, leading to the result [277]

$$g_{ann}^2 + 0.61\, g_{app}^2 + 0.53\, g_{ann}\, g_{app} < 8.26 \times 10^{-19}\,, \qquad (89.19)$$

which is consistent with the original estimate in [228]. This analysis, however, still neglects another very efficient mechanism for axion production in a SN: the pion production process, $\pi^- + p \to a + n$, also induced by the axion coupling to nucleons. Pion production was recognized long ago as being competitive with nucleon bremsstrahlung [278–280]. However, only recently it was shown that the pion abundance in the early stages of a SN is much larger than previously expected [281]. It was shown in Ref. [282] that pion induced processes dominate over bremsstrahlung and so strengthen the bound on the axion-nucleon coupling. On the other hand, given the modeling uncertainties and the sparse data from SN 1987A, the constraint on the axion-nucleon couplings from SN 1987A should be considered more as indicative than as a sharp bound [275]. Furthermore, note that if axions interact sufficiently strongly they are trapped. Only about three orders of magnitude in g_{aNN}, where $N = n, p$, or m_a are excluded. For even larger couplings, the axion flux would have been negligible, yet it would have triggered additional events in the detectors, excluding a further range [283].

Further bounds on the axion-nucleon coupling can be derived from observations of the cooling of older NSs. Recently, strong constraints were obtained by modeling the cooling of the "Magnificent Seven" (M7) NSs in the presence of axions [269]. Axion emission would accelerate NS cooling. Thus, if the age and temperature of a NS are independently known, then by modeling axion-induced cooling in conjunction with the standard NS cooling mechanisms, in particular cooling via neutrino emission from the bulk of the NS and thermal emission from the NS surface, one is able to constrain the axion's coupling strength. Ref. [269] used a sample of four of the M7 along with PSR J0659 to constrain $m_a < 16$ meV for the KSVZ QCD axion at 95% CL and $m_a \lesssim 5$ meV ($m_a \lesssim 30$ meV) in the DFSZ scenario for asymptotically large (small) $\tan\beta$. For axions that couple exclusively to neutrons (protons) Ref. [269] constrains $|g_{ann}| < 1.3 \times 10^{-9}$ ($|g_{app}| < 1.5 \times 10^{-9}$), as illustrated in Fig. 89.3. The five NSs used in that work are unique in that their ages, all in the range $0.1 - 1$ Myr, are known by kinematic measurements (*e.g.*, tracing back to the SN remnant), while their surface temperatures are measured in the X-ray band. Beyond statistical uncertainties on these measurements, there are a number of confounding systematic uncertainties that must be accounted for in NS cooling analyses, including uncertainties related to the core-surface temperature relation, which involves the chemical composition of the NS envelope. The NS equation of state and the superfluid critical temperatures of the dense nuclear matter are also sources of uncertainty. Note that axions are predominantly produced by nuclear bremsstrahlung [284, 285] except for temperatures near the superfluid critical temperature, when Cooper pair breaking and formation (PBF) processes may efficiently produce axions [286, 287]. Given the large densities it is crucial to account for medium dependent couplings when computing the axion luminosities [288, 289].

The young NS in the supernova remnant Cassiopeia A (Cas A) was previously thought to strongly constrain axions, at a level similar to the NS cooling bound described above, due to PBF axion production [290]. This is because it was observed that Cas A was cooling rapidly, which may be explained by neutrino cooling with neutron superfluidity and proton superconductivity [291, 292]. However, it is possible that the excessive cooling of Cas A is at least in part instrumental in origin [293]. Fully accounting for uncertainties on both the NS properties and the data, constraints from young NSs such as Cas A and the NS in the supernova remnant HESS J1731-347 [294] appear to be sub-

Int. J. Mod. Phys. A 2026.41. Downloaded from www.worldscientific.com
by UNIVERSITY OF CALIFORNIA @ BERKELEY on 09/16/26. Re-use and distribution is strictly not permitted, except for Open Access articles.

dominant compared to the limits from SN 1987A and the M7 [269].

Finally, let us note that if $m_a \sim$meV, SNe would lose a large fraction of their energy as axions. This would lead to a diffuse SN axion background in the Universe with an energy density comparable to the extra-galactic background light [295]. However, there is no apparent way of detecting it or the axion burst from the next nearby SN. On the other hand, neutrino detectors such as IceCube, Super-Kamiokande or a future mega-ton water Cherenkov detector will probe exactly the mass region of interest by measuring the neutrino pulse duration of the next Galactic SN [275].

89.4.2 *Searches for solar axions and ALPs*

Instead of using stellar energy losses to derive axion limits, one can also search directly for these fluxes, notably from the Sun. The main focus has been on ALPs with a two-photon vertex. They are produced by the Primakoff process with a flux given by Eq. (89.15) and an average energy of 4.2 keV, and can be detected at Earth with the reverse process in a macroscopic B-field ("axion helioscope") [7]. In order to extend the sensitivity in mass towards larger values, one can endow the photon with an effective mass in a gas, $\omega_{\rm plas}$, and tune the mass to match the axion's dispersion relation ($\omega_{\rm plas} = m_a$) [296].

An early implementation of these ideas used a conventional dipole magnet, with a conversion volume of variable-pressure gas with a xenon proportional chamber as x-ray detector [297]. The conversion magnet was fixed in orientation and collected data for about 1000 s/day. Axions were excluded for $|g_{a\gamma\gamma}| < 3.6 \times 10^{-9}$ GeV^{-1} for $m_a < 0.03$ eV, and $|g_{a\gamma\gamma}| < 7.7 \times 10^{-9}$ GeV^{-1} for $0.03 < m_a < 0.11$ eV at 95% CL.

Later, the Tokyo axion helioscope used a superconducting magnet on a tracking mount, viewing the Sun continuously. They reported $|g_{a\gamma\gamma}| < 6 \times 10^{-10}$ GeV^{-1} for $m_a < 0.3$ eV [298,299]. This experiment was recommissioned and a similar limit for masses around 1 eV was reported [300].

The most recent helioscope CAST (CERN Axion Solar Telescope) uses a decommissioned LHC dipole magnet on a tracking mount. The hardware includes grazing-incidence x-ray optics with solid-state x-ray detectors, as well as x-ray Micromegas position-sensitive gaseous detectors. Exploiting an IAXO (see below) pathfinder system, CAST has established the limit

$$|g_{a\gamma\gamma}| < 5.8 \times 10^{-11}\ \text{GeV}^{-1} \quad (95\%\ \text{CL}), \tag{89.20}$$

for $m_a < 0.02$ eV [76, 158]. To cover larger masses, the magnet bores are filled with a gas at varying pressure. The runs with ^{4}He cover masses up to about 0.4 eV [301], providing the high-mass component of the CAST limits shown in Fig. 89.1. To cover yet larger masses, ^{3}He was used to achieve a larger pressure at cryogenic temperatures. Limits up to 1.17 eV allowed CAST to "cross the axion line" for the KSVZ model [302–304], see Fig. 89.1.

Sensitivity to significantly smaller values of $g_{a\gamma\gamma}$ can be achieved with a next-generation axion helioscope with a much larger magnetic-field cross section. Realistic design options for this "International Axion Observatory" (IAXO) have been studied in some detail [305], as well as its physics potential [306]. Such a next-generation axion helioscope may also push the sensitivity in the product of couplings to photons and to electrons, $g_{a\gamma\gamma} g_{aee}$, into a range beyond stellar energy-loss limits and test the hypothesis that WD, RG, and HB cooling is dominated by axion emission [307, 308]. As a first step towards IAXO, an intermediate experimental stage called BabyIAXO is currently under preparation at DESY [309].

Direct detection experiments searching for dark matter (DM) consisting of weakly interacting massive particles have also the capability to search for solar axions and ALPs. For low masses, $m_a \lesssim 100$ eV, the XENONnT experiment [310] has provided the most stringent bound among those experiments on the axion-electron coupling constant,

$$|g_{aee}| < 1.9 \times 10^{-12} \quad (90\%\ \text{CL}), \tag{89.21}$$

see Fig. 89.2, by exploiting the axio-electric effect in liquid xenon. Limits at approximately the same value have been set by PandaX-4T [311] and LZ [312]. However, this technique has not reached the sensitivity of energy-loss considerations in stars.

89.4.3 *Conversion of astrophysical axion fluxes*

Large-scale B fields exist in astrophysics that can induce axion-photon oscillations. In practical cases, the strength of B is much smaller than in the laboratory, whereas the conversion region L is much larger. Therefore, while the product BL can be large, realistic sensitivities are usually restricted to very low-mass particles, far away from the "QCD axion band" in a plot like Fig. 89.1.

One example of this is SN 1987A, which would have emitted a burst of ALPs due to the Primakoff production in its core. It was pointed out shortly after the SN that the ALPs could have partially converted into γ-rays in the Galactic B-field. The lack of a gamma-ray signal in the GRS instrument of the SMM satellite in coincidence with the observation of the neutrinos emitted from SN 1987A therefore provides a strong bound on their coupling to photons [313, 314]. This bound has been revisited and the underlying physics has been brought to the current state-of-the-art, as far as modeling of the supernova and the Milky-Way along with stellar magnetic field are concerned, resulting in the limit [128,129] $|g_{a\gamma\gamma}| < 5.2 \times 10^{-12}$ GeV^{-1} for $m_a \lesssim 5 \times 10^{-10}$ eV. More recently, it has been understood that the axions could convert to gamma-rays in the stellar magnetic fields of the progenitor star, extending the SN1987A limits to higher masses and potentially allowing gamma-ray observations of future SN to probe the QCD axion [315].

Reference [96] reports no evidence of a γ-ray burst in observations of extragalactic SNe with the Fermi Large Area Telescope (LAT). Under the assumption that at least one SN was contained within the LAT field of view, the authors derive an upper bound on the axion photon coupling which is about a factor of 5 weaker than the one from SN 1987A, see Fig. 89.1.

The cumulative emission of ALPs from all past core-collapse SNe would lead to a diffuse gamma-ray flux peaked at energies $\sim 50 - 100$ MeV which can convert in the Galactic magnetic field into photons. Using Fermi-LAT measurements of the diffuse γ-ray flux, Ref. [316] obtains a conservative bound on the photon coupling, $|g_{a\gamma\gamma}| < 5 \times 10^{-10}$ GeV^{-1}, for $m_a \lesssim 10^{-11}$ eV, see see Fig. 89.1, which can be decreased by nearly three orders of magnitude, if an ALP-nucleon coupling of maximal phenomenologically allowed strength, $|g_{aNN}| \sim 10^{-9}$, is allowed.

Hot, young stars, such as Wolf-Rayet stars, efficiently produce ALPs with energies $\sim 10 - 100$ keV via the Primakoff effect. Large numbers of those stars are hosted by the Galactic Quintuplet and Westerlund 1 super star clusters (SSCs). The non-observation of hard X-rays originating from axion-photon conversion in the Galactic magnetic field in archival NuSTAR (Nuclear Spectroscopic Telescope Array) data from these SSCs leads to a bound on the axion-photon coupling [136], $|g_{a\gamma\gamma}| < 3.6 \times 10^{-12}$ GeV^{-1}, for $m_a \lesssim 5 \times 10^{-11}$ eV, see Fig. 89.1. A somewhat weaker bound in the same mass range was established exploiting NuSTAR data on Betelgeuse [82]. Stronger constraints at low axion masses are found with NuSTAR data by considering axion production and conversion (or decay) in nearby galaxies, such as M82 and M87, accounting for production in all of the stellar members of the galaxies [317–319] (see Fig. 89.1).

A hard X-ray excess in data from the nearby M7 isolated NSs [320] may be explained by ALPs produced in the cores of those stars and converted in the surrounding magnetic fields, with $|g_{aNN} g_{a\gamma\gamma}| \in (2 \times 10^{-21}, 10^{-18})$ GeV^{-1}, for $m_a \lesssim 10^{-5}$ eV [321]. The non-observation of an X-ray excess from the magnetic WD RE J0317-853 [322] by Chandra yields the constraint $|g_{aee} g_{a\gamma\gamma}| \lesssim 1.3 \times 10^{-25}$ GeV^{-1}, for $m_a \ll 10^{-5}$ eV [105], which provides a non-trivial constraint on the ratio g_{aee}/g_{aNN} for axion models explaining the M7 X-ray excess.

In addition to being produced in NS cores, axions may also be produced in NS magnetospheres. In particular, it has recently been shown that axions could be copiously produced in the polar-cap regions of NS magnetospheres due to time-varying, un-screened electric fields [122]. Those axions could then convert to photons in the outer regions of the NS magnetosphere, leading to observable, broadband radio flux. The absence of such radio flux sets competitive constraints on ALPs, as indicated by the "pulsars" constraint in Fig. 89.1.

Int. J. Mod. Phys. A 2026.41. Downloaded from www.worldscientific.com by UNIVERSITY OF CALIFORNIA @ BERKELEY on 09/16/26. Re-use and distribution is strictly not permitted, except for Open Access articles.

89.4.4 *Conversion of astrophysical photon fluxes*

Magnetically induced oscillations between photons and ALPs can modify the photon fluxes from distant sources in various ways, featuring (i) frequency-dependent dimming, (ii) modified polarization, and (iii) avoiding absorption by propagation in the form of axions. For example, dimming of SNe Ia could influence the interpretation in terms of cosmic acceleration [323], although it has become clear that photon-ALP conversion could only be a subdominant effect [324].

Polarization measurements are particularly powerful probes of photon-to-axion conversion since only photons polarized parallel to astrophysical magnetic fields may convert into axions, meaning that in the presence of large-scale ordered magnetic fields axions tend to leave distinct polarization signatures in passing radiation. Searches for linear polarization from radio galaxies (see, *e.g.*, Ref. [325]) and quasars [326] may approach in sensitivity $|g_{a\gamma\gamma}| \sim$ few $\times\, 10^{-13}$ GeV^{-1}, albeit with uncertainties related to the underlying modeling assumptions. Recently, robust limits at the level $|g_{a\gamma\gamma}| \leq 1.7 \times 10^{-12}$ GeV^{-1} at 95% CL have been derived from optical polarization measurements of nearby magnetic WDs [106, 327] (see also [328]), see Fig. 89.1. The magnetic fields of magnetic WDs may be well-measured through the Zeeman splitting of bound-bound transitions in the WD atmospheres.

It appears that the Universe could be too transparent to TeV γ-rays that should be absorbed by pair production on the extragalactic background light [86, 329–332]. The situation is not conclusive at present [333–336], but the possibility of axions playing a role has been suggested [337–339]. On the other hand, much of this parameter space is excluded by the previously-discussed WD polarization probes. The region in ALP parameter space, $g_{a\gamma\gamma} \sim 10^{-12} - 10^{-10}$ GeV^{-1} for $m_a \lesssim 10^{-7}$ eV [340], required to explain the anomalous TeV transparency of the Universe, could be conceivably probed by the next generation of laboratory experiments (ALPS II) and helioscopes (IAXO) mentioned above.

This parameter region can also be probed by searching for an irregular behavior of the gamma ray spectrum of distant active galactic nuclei (AGN), expected to arise from photon-ALP mixing in a limited energy range. In these type of studies, the uncertainty in the magnetic field around the source needs to be taken into account. This typically leads to a range of limits on the ALP-photon coupling that depend on the modeling assumptions. The H.E.S.S. collaboration has set a limit of $|g_{a\gamma\gamma}| \lesssim 2.1 \times 10^{-11}$ GeV^{-1}, for 1.5×10^{-8} eV $\lesssim m_a \lesssim 6.0 \times 10^{-8}$ eV, from the non-observation of an irregular behavior of the spectrum of the AGN PKS 2155-304 [341]. The Fermi-LAT collaboration has put an even more stringent limit on the ALP-photon coupling [95] from observations of the gamma ray spectrum of NGC 1275, the central galaxy of the Perseus cluster, see Fig. 89.1. A similar analysis has been carried out in Ref. [342], using Fermi-LAT data of PKS 2155-304, and in Ref. [108], using ARGO-YBJ and Fermi-LAT data of Mrk 421, see Fig. 89.1. However, these constraints were obtained under certain theoretical assumptions about magnetic fields surrounding the sources, not confirmed yet by direct astronomical observations in these particular directions; this introduces large systematic uncertainties in the reported constraints [343].

Evidence for spectral irregularities has been reported in Galactic sources, such as pulsars and supernova remnants, and has been interpreted as hints for ALPs [344, 345] (see also discussion in Ref. [346] and references therein). However, the inferred ALP parameters, $|g_{a\gamma\gamma}| \sim 10^{-10}\,\mathrm{GeV}^{-1}$, $m_a \sim$neV, are in tension with the CAST helioscope bounds. Reference [346] updated the analysis of the pulsar signal region including astrophysical nuisance parameters and correctly deriving confidence intervals on ALP parameters by means of Monte Carlo simulations. The tension with the CAST bounds can be evaded if environmental effects in matter, which would suppress the ALP production in dense astrophysical plasmas like the solar interior, are invoked. If this explanation is correct, the claimed ALP signal would be in reach of the next-generation LSW experiment ALPS II. Other ways to make the CAST bound compatible with photon-ALP conversions in the low-density Galactic medium are invoking photon-ALP-dark photon oscillations [347] or the existence of a number of 'hidden' ALPs [348].

At smaller masses, $m_a \lesssim 10^{-12}$ eV, galaxy clusters become highly efficient at interconverting ALPs and photons at X-ray energies. Constraints on spectral irregularities in the spectra of luminous X-ray sources (Hydra A, M87, NGC 1275, NGC 3862, Seyfert galaxy 2E3140; taken by Chandra and XMM-Newton) located in or behind galaxy clusters then lead to stringent upper limits on the ALP-photon coupling [87–89, 349–351] (for the limits exploiting spectra from Hydra and M87 from Refs. [87] and [88], respectively, see Fig. 89.1). Reference [89] recently performed the most sensitive x-ray searches for ALPs to date by employing Chandra's High-Energy Transmission Gratings that allow for an unsurpassed spectral resolution. New observations of the AGN NGC 1275 then led to the bound $|g_{a\gamma\gamma}| < 8 \times 10^{-13}$ GeV^{-1} at 99.7% C.L. for ultra-light ALPs, as illustrated in Fig. 89.1. On the other hand, magnetic field modeling uncertainties in the clusters may not be fully accounted for in these analyses [343].

89.4.5 *Finite density effects for the QCD axion*

If the QCD axion sector has a discrete, $\mathbb{Z}_{\mathcal{N}}$, shift symmetry, its potential is much shallower, and its mass, in units of its decay constant, $m_a f_a \simeq (3\pi)^{-1/4}\,\mathcal{N}^{3/4}\,2^{-\mathcal{N}/2}\,m_\pi f_\pi$, is smaller than the one of the canonical QCD axion by an exponential factor $\propto 2^{-\mathcal{N}/2}$ [179, 180]. This opens up the parameter space over which one should search for a QCD axion towards the left of the yellow canonical QCD axion band in Fig. 89.1, Fig. 89.2, and Fig. 89.3. Novel bounds apply to this exceptionally light QCD axion due to finite density effects [352–354]. In fact, in dense stellar media, the minimum of the axion potential may be shifted to π. This has a number of phenomenological consequences that span from the modification of nuclear processes in stars due to $\theta = \mathcal{O}(\pi)$ to modifications in the orbital decay of binary systems (and subsequently in the emitted gravitational waves). Recently strong constraints have been set using the modification of the WD mass-radius relation due to such axions [355].

In fact, $\theta \sim 1$ in the solar core would lead to an increased proton-neutron mass difference, which would prohibit the neutrino line corresponding to the ^{7}Be-^{7}Li mass difference observed by Borexino [356].

Moreover, the fact that the position of the minimum of the axion potential depends on the nuclear density of the medium may also source a long-range force between dense stars [352]. This new long-range force sourced by the axion can be constrained by the measurement of the orbital decay of double pulsar or NS-pulsar binaries [352]. The gravitational wave signal of NS-NS mergers or black hole (BH) - NS mergers would also be modified by these axionic long-range forces [352, 353]. There is also a corresponding bound [354] exploiting the gravitational waves observation from the binary NS inspiral GW170817 detected by LIGO (Laser Interferometer Gravitational-Wave Observatory) and Virgo [357].

89.4.6 *Superradiance of black holes*

Light bosonic fields such as axions or ALPs can affect the dynamics and gravitational wave emission of rapidly rotating astrophysical BHs through the superradiance mechanism. When the boson's Compton wavelength is of order of the size of the BH's ergoregion, they form gravitational bound states around the BH. Their occupation number grows exponentially by extracting energy and angular momentum from the black hole, forming a coherent axion or ALP bound state emitting gravitational waves. When accretion cannot replenish the spin of the BH, superradiance dominates the BH spin evolution; this is true for both supermassive and stellar mass BHs. The existence of destabilizing light bosonic fields thus leads to exclusion regions in the mass versus spin plot of rotating BHs. Stellar BH spin measurements exploiting well-studied binaries and two independent techniques exclude a mass range – up to self-interaction caveats discussed below – $6 \times 10^{-13}\,\mathrm{eV} < m_a < 2 \times 10^{-11}\,\mathrm{eV}$ at $2\,\sigma$, which for the axion excludes $3 \times 10^{17}\,\mathrm{GeV} < f_a < 1 \times 10^{19}\,\mathrm{GeV}$ [10, 358, 359], see Fig. 89.4. These bounds apply when gravitational interactions dominate over the axion self-interaction, which is largely true for the QCD axion in this mass range. On the other hand, Refs. [360, 361] considered superradiance bounds for string theory ALPs with a quartic self-coupling (of either sign) given by $\lambda = m_a^2/f_a^2$, using the bosenova model of Ref. [359], and found

Int. J. Mod. Phys. A 2026.41. Downloaded from www.worldscientific.com
by UNIVERSITY OF CALIFORNIA @ BERKELEY on 09/16/26. Re-use and distribution is strictly not permitted, except for Open Access articles.

that for $m_a \sim 10^{-12}$ eV the superradiant cloud, and thus the constraints, are destroyed for $f_a \lesssim 10^{11} - 10^{12}$ GeV, depending precisely on the mass and the source.

Reference [362] used a more advanced model for the effect of self-interactions on superradiant evolution, and a different (frequentist) statistical methodology, leading to more conservative bounds from stellar mass BHs (region near 10^{-12} eV). In particular, Ref. [362] found that QCD axions are only excluded for $m_a \lesssim 6 \times 10^{-12}$ eV instead of the 2×10^{-11} eV, as claimed in [360,361]. Reference [362] also vetoed supermassive BHs (SMBHs) with spins measured at low significance, and thus found no ALP bounds in the SMBH region (near 10^{-18} eV); Ref. [360, 361, 363], in contrast, included SMBHs in a (quasi-)Bayesian analysis with a flat prior on the spin and found non-trivial constraints. In summary, it appears likely that the lower end of the QCD axion mass range is excluded by superradiance, with the requirement $m_a \gtrsim 10^{-11}$ eV, but the exact location of this limit is still debated. It is also too early to claim that ultra-light ALP parameter space is excluded by SMBHs, though this may change with future work.

Long lasting, monochromatic gravitational wave signals, which can be distinguished from ordinary astrophysical sources by their clustering in a narrow frequency range, are expected to be produced by axions or ALPs annihilating to gravitons. Gravitational waves could also be sourced by axions/ALPs transitioning between energy levels of the effective gravitational atom. Accordingly, the gravitational wave detector Advanced LIGO should be sensitive to the axion in the $m_a \lesssim 10^{-10}$ eV region. LIGO measurements of BH spins in binary merger events could also provide statistical evidence for the presence of an axion [364, 365]. Similar signatures could arise for supermassive and intermediate mass BHs for particles with masses $\lesssim 10^{-15}$ eV. Gravitational waves from such sources could be detected at lower-frequency observatories such as LISA (Laser Interferometer Space Antenna). First attempts to use LIGO/Virgo data to search for monochromatic signatures of axion superradiance were recently made in [366, 367].

89.5 Cosmic Axions

89.5.1 *Cosmic axion populations*

There are two distinct populations of cosmic relic axion populations: a non-thermal one behaving as CDM, and a thermal one comprising a hot DM (HDM) component, in analogy to massive neutrinos. For $m_a \lesssim 0.01$ eV, thermal axions are dominantly produced by processes involving quarks and gluons [368, 369], while, for larger masses, the dominant thermalization process is $\pi + \pi \leftrightarrow \pi + a$ [187,370,371]. A number of evaluations exploiting cosmological precision data have found restrictive constraints on a possible HDM fraction that translate into an upper bound on the axion mass, $m_a \lesssim 1$ eV, if a leading order (LO) axion-pion chiral effective field theory (EFT) analysis of the axion-pion thermalization rate is used [387–390]. Recently, it was found that the next leading order (NLO) contribution exceeds the LO contributions for masses below $m_a \lesssim 1.2\,(0.12/C_{a\pi})$ eV [391]. Therefore, in order to assess the reach in sensitivity of future cosmological data sets, one has to improve the EFT description or to compute axion-pion scattering via lattice QCD techniques. Alternatively, recently Ref. [392] used pion-pion scattering data to overcome the EFT description issues and found the constraint $m_a \lesssim 0.24$ eV, see Fig. 89.4.

For $m_a \gtrsim 10$ eV, axions may decay faster than the age of the Universe (see Eq. (89.7)), depending on the decay constant, which would remove the cosmic axion population while injecting photons. If the axions were in thermal equilibrium in the early Universe, which depends on the inflationary reheat temperature and assumptions about the pre-BBN cosmology [393, 394], this excess radiation provides additional limits on the axion- or ALP-photon coupling up to very large masses [393, 394]. Such photons could contribute to the extragalactic background light (EBL), could ionize primordial hydrogen and thus contribute to the optical depth after recombination, or could spoil the agreement of big bang nucleosynthesis (BBN) with observations. The corresponding up-to-date bounds from Refs. [143, 144] are displayed in Fig. 89.1. It has recently been shown that there is an *irreducible axion background* [145] that arises from axion freeze-in before BBN; decays of that axion population provide strong constraints on axions with masses above roughly 100 eV (see Fig. 89.1). For high enough decay constants, high-mass axions ($m_a \gtrsim 10$ eV) can account for the DM abundance through the misalignment mechanism, described in more detail below, though additional entropy dilution or fine-tuning is needed to avoid overproducing the DM abundance [395] (see also [396] for heavy axion production through lepton-flavor-violating decays). The decay of such high-mass axions to photon pairs could leave narrow spectral features in *e.g.* optical or X-ray backgrounds [103, 115–117, 138, 140, 397, 398] (see Fig. 89.1).

The main cosmological interest in axions at present derives from their possible role as CDM. In addition to thermal processes, axions are abundantly produced by the misalignment (MIS) mechanism [399–401]. The axion DM abundance crucially depends on the cosmological history. Let us first consider the so called *pre-inflationary PQ symmetry breaking scenario*, in which the PQ symmetry is broken before and during inflation and not restored afterwards. This is the cosmological scenario most naturally realized for string theory axions from the open-string sector [167,402]. After the breakdown of the PQ symmetry, the axion field relaxes somewhere in the bottom of the "wine-bottle-bottom" potential. Near the QCD epoch, topological fluctuations of the gluon fields such as instantons explicitly break the PQ symmetry. This tilting of the "wine-bottle-bottom" drives the axion field toward the CP-conserving minimum, thereby exciting coherent oscillations of the axion field that ultimately represent a condensate of CDM. The fractional cosmic mass density in this homogeneous field mode, created by the MIS mechanism, is [24, 403–405],

$$\begin{aligned} \Omega_a^{\rm MIS} h^2 &\approx 0.12 \left(\frac{f_a}{9\times 10^{11}\ \text{GeV}}\right)^{1.165} F\,\Theta_{\rm i}^2 \\ &\approx 0.12 \left(\frac{6\ \mu\text{eV}}{m_a}\right)^{1.165} F\,\Theta_{\rm i}^2\,, \end{aligned} \tag{89.22}$$

where h is the present-day Hubble expansion parameter in units of 100 km s^{-1} Mpc^{-1}, and $-\pi \le \Theta_{\rm i} \le \pi$ is the initial "misalignment angle" relative to the CP-conserving position attained in the causally connected region which evolved into today's observable Universe. $F = F(\Theta_{\rm i}, f_a)$ is a factor accounting for anharmonicities in the axion potential. For $F\Theta_{\rm i}^2 = \mathcal{O}(1)$, m_a should be above $\sim 6\,\mu$eV in order that the cosmic axion density does not exceed the observed CDM density, $\Omega_{\rm CDM} h^2 = 0.12$. However, much smaller axion masses (much higher PQ scales) are still possible if entropy is diluted for example by the late decay of a scalar condensate (see for example [406] and references therein) or the initial value $\Theta_{\rm i}$ just happens to be small enough in today's observable Universe ("anthropic axion window" [407]). In the latter cosmological scenario, however, quantum fluctuations of the axion field during inflation are expected to lead to isocurvature density fluctuations which get imprinted to the temperature fluctuations of the CMB [408,409]. Their non-observation puts severe constraints on the Hubble expansion rate H_I during inflation [410–415], which read, in the simplest cosmological inflationary scenario,

$$H_I \lesssim 5.7 \times 10^8\ \text{GeV} \left(\frac{5\ \text{neV}}{m_a}\right)^{0.4175}\,, \tag{89.23}$$

if axions represent all of DM. In Ref. [416] an alternative to the MIS mechanism was proposed: the so-called kinetic MIS mechanism. In this case, the axion field is assumed to have an initial velocity which may be generated, e.g., by a hypothesized explicit breaking of the axion shift symmetry in the early universe. The amount of QCD axion dark matter generated by the kinetic MIS mechanism can fit the observed dark matter abundance for any $f_a \lesssim 1.5 \times 10^{11}$ GeV, down to the minimum value allowed by the SN 1987A constraint.

In the above prediction of the fractional cosmic mass density in axions, the exponent, 1.165, arises from the non-trivial temperature dependence of the topological susceptibility $\chi(T) = m_A^2(T) f_A^2$ at temperatures slighty above the QCD quark-hadron phase transition. Lattice QCD calculations of this exponent [24, 375, 377, 417–419], but also Ref. [376], found it to be close

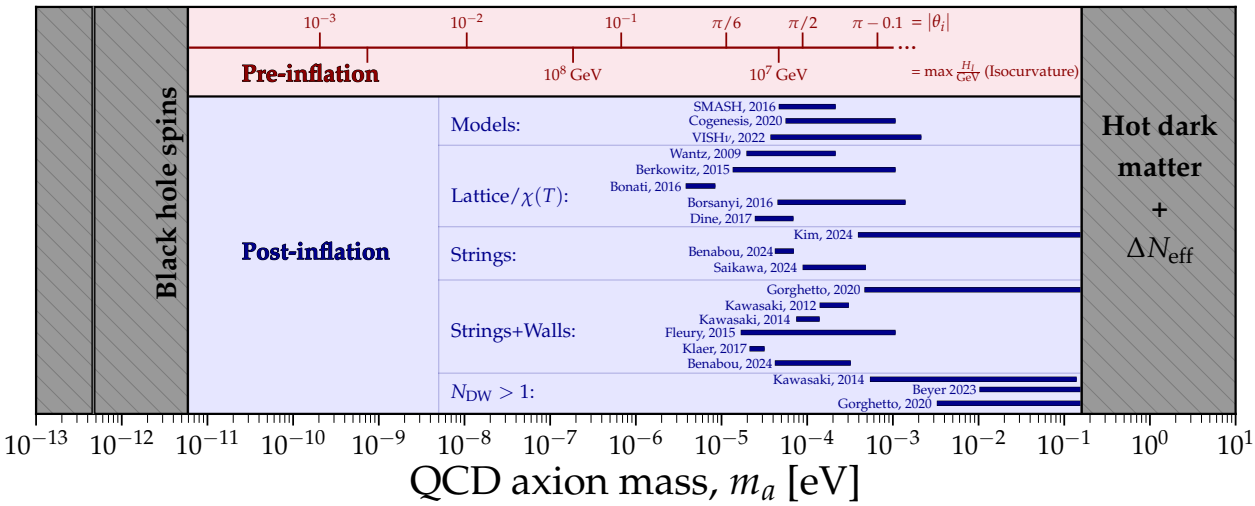

Figure 89.4: QCD axion mass predictions for obtaining the correct DM abundance assuming the PQ symmetry is and is not restored after inflation and, in the case the PQ symmetry is restored after inflation, depending on the domain wall number N. Figure from [39], includes data from refs. [24, 372–386]. The lower-end of the possible mass range is bounded by BH superradiance constraints and the theoretical requirement that f_a be below the Planck scale, while the upper end is bounded by the somewhat model-dependent NS cooling constraints (not shown), which exclude QCD axion masses above roughly ∼15-30 meV, depending on the UV completion. At even higher masses there are strong constraints from the production of DM in the early universe, which behaves as hot DM and contributes to $\Delta N_{\rm eff}$.

to the prediction of the dilute instanton gas approximation [420] which was previously exploited. Therefore, the state-of-the-art prediction of the axion mass relevant for DM for a fixed initial misalignment angle $\Theta_{\rm i}$ differs from the previous prediction by just a factor of order one.

In the *post-inflationary PQ symmetry breaking scenario*, on the other hand, $\Theta_{\rm i}$ will take on different values in different patches of the present Universe. The average contribution is [24, 403–405]

$$\Omega_a^{\rm MIS} h^2 \approx 0.12 \left(\frac{30\ \mu{\rm eV}}{m_a}\right)^{1.165} . \tag{89.24}$$

The decay of cosmic strings and domain walls gives rise to a further population of CDM axions, whose abundance suffers from significant uncertainties [373, 379–381, 404, 405, 421–432] which arise from the difficulty in understanding the energy loss process of topological defects and the generated axion spectrum in a quantitative way. In fact, in the present state-of-the-art it is still possible that the CDM contribution from the decay of topological defects is subdominant [379] or overwhelmingly large [380] in comparison to the one from the MIS mechanism. Correspondingly, the plausible range of axion masses providing all of CDM in scenarios with postinflationary PQ symmetry breaking is still rather large, namely [379, 380]

$$m_a \approx 26\ \mu{\rm eV} - 0.5\ {\rm meV}, \tag{89.25}$$

for models with short-lived (requiring unit color anomaly $N = 1$) domain walls, such as the KSVZ model. On the other hand, the most recent adaptive mesh refinement axion string simulations, which are able to evolve over larger dynamic ranges than static lattice simulations, suggest the mass range $m_a \approx 45 - 300\ \mu$eV, with domain wall decay providing the dominant contribution to DM on the upper end of the uncertainty range [432]. For models with long-lived ($N > 1$) domain walls, such as an accidental DFSZ model [433], where the PQ symmetry is broken by higher dimensional Planck suppressed operators, the mass is predicted to be significantly higher [306, 381, 433–435],

$$m_a \approx (0.58 - 130)\,{\rm meV}\,. \tag{89.26}$$

However, the upper part of the predicted range is in conflict with stellar energy-loss limits on the axion. The pre- and post-inflationary mass predictions are summarized in Fig. 89.4.

In this post-inflationary PQ symmetry breakdown scenario, the spatial axion density variations are large at the QCD transition, and they are not erased by free streaming. Gravitationally bound "axion miniclusters" form before and around matter-radiation equality [436–438]. A significant fraction of CDM axions can reside in these bound objects [426, 439]. The minicluster fraction can be bounded by gravitational lensing [440–442], although more simulations are required to understand whether miniclusters are dense enough and survive in sufficient quantities for lensing bounds to apply.

89.5.1.1 *Ultralight cosmological ALP relics*

The non-thermal production mechanisms attributed to axions are generic to light bosonic weakly interacting particles such as ALPs [384]. The relic abundance is set by the epoch when the axion mass becomes significant, $3H(t) \approx m_a(t)$, and ALP field oscillations begin. For ALPs to contribute to the DM density this epoch must precede that of matter radiation equality. For a temperature independent ALP mass this leads to the bound:

$$m_a \gtrsim 7 \times 10^{-28}\ {\rm eV} \left(\frac{\Omega_m\, h^2}{0.15}\right)^{1/2} \left(\frac{1+z_{\rm eq}}{3.4\times 10^3}\right)^{3/2} . \tag{89.27}$$

ALPs lighter than this bound are allowed if their cosmic energy density is small, but they are quite distinct from other forms of DM [443]. Ignoring anharmonicities in the ALP potential, and taking the ALP mass to be temperature independent, the relic density in DM ALPs due to the MIS mechanism is given by

$$\Omega_{\rm ALP}^{\rm MIS} h^2 = 0.12 \left(\frac{m_a}{4.7\times 10^{-19}\,{\rm eV}}\right)^{1/2} \left(\frac{f_a}{10^{16}\,{\rm GeV}}\right)^2 \times \left(\frac{\Omega_m h^2}{0.15}\right)^{3/4} \left(\frac{1+z_{\rm eq}}{3.4\times 10^3}\right)^{-3/4} \Theta_{\rm i}^2 . \tag{89.28}$$

An ALP decay constant near the GUT scale gives the correct relic abundance for *ultralight ALPs* (ULAs) with $m_{\rm ULA} \approx 10^{-19}$ eV [444, 445]. ULAs encompass the entire Earth in a single Compton wavelength, and for large occupation numbers are modelled as a coherent classical field. The coherence time is determined by the mass and virial velocity in the Milky Way, $\tau_{\rm coh} \sim 1/m_{\rm ULA} v_{\rm vir}^2$, with the detailed properties described by a stochastic model with an approximately Rayleigh Jeans distribution [446]. Natural models for ULAs can be found in string

Int. J. Mod. Phys. A 2026.41. Downloaded from www.worldscientific.com by UNIVERSITY OF CALIFORNIA @ BERKELEY on 09/16/26. Re-use and distribution is strictly not permitted, except for Open Access articles.

Int. J. Mod. Phys. A 2026.41. Downloaded from www.worldscientific.com
by UNIVERSITY OF CALIFORNIA @ BERKELEY on 09/16/26. Re-use and distribution is strictly not permitted, except for Open Access articles.

and M-theory compactifications [5, 6, 8–13], in field theory with accidental symmetries [447, 448], or new hidden strongly coupled sectors [449, 450].

In addition to the gravitational potential energy, the ULA field also carries gradient energy. On scales where the gradient energy is non-negligible, ULAs acquire an effective pressure and do not behave as CDM. The gradient energy opposes gravitational collapse, leading to a Jeans scale below which perturbations are stable [451]. The Jeans scale suppresses linear cosmological structure formation relative to CDM [452–454]. The Jeans scale at matter-radiation equality in the case that ULAs make up all of CDM is:

$$k_{\rm J,eq} = 8.7\,{\rm Mpc}^{-1}\left(\frac{1+z_{\rm eq}}{3.4\times10^3}\right)^{-1/4}\left(\frac{h^2\Omega_{\rm ALP}^{\rm MIS}}{0.12}\right)^{1/4}\times \left(\frac{m_{\rm ULA}}{10^{-22}\,{\rm eV}}\right)^{1/2}. \tag{89.29}$$

On non-linear scales the gradient energy leads to the existence of a class of pseudo-solitons known as oscillatons, or axion stars [455]. Axion stars are expected to form in all cosmological scenarios, and for all types of ALPs, including the QCD axion [456–458]. Some axion stars may explode into radio photons, heating the interstellar medium [81].

Cosmological and astrophysical observations are consistent with the CDM model, and departures from it are only allowed on the scales of the smallest observed DM structures with $M \sim 10^{6-8} M_\odot$. The CMB power spectrum and galaxy autocorrelation power spectrum limit the ULA mass to $m_{\rm ULA} \gtrsim \mathcal{O}(\text{few}) \times 10^{-24}$ eV from linear theory of structure formation [443, 459]. Analytic models [460] and N-body simulations [461] for non-linear structures show that halo formation is suppressed in ULA models relative to CDM. This leads to constraints on the ULA mass of $m_{\rm ULA} > 10^{-22}$ eV from observations of high-z galaxies [461–463], and $m_{\rm ULA} > 2\times10^{-20}$ eV from the Lyman-alpha forest flux power spectrum [464]. Including the effects of anharmonicities on structure formation with ALPs can weaken these bounds if the misalignment angle $\Theta_{\rm i} \approx \pi$ [465]. A comprehensive study of Milky Way satellites by the DES collaboration resulted in the bound $m_{\rm ULA} > 2.9\times10^{-21}$ eV [466].

Cosmological simulations that treat gradient energy in the ULA field beyond the N-body approximation have just recently become available [456, 467–469], and show, among other things, evidence for the formation of axion stars in the centres of ULA halos (various consequences of axion stars are considered in Refs. [470]). These central axion stars have been conjectured to play a role in the apparently cored density profiles of dwarf spheroidal galaxies, and other central galactic regions [104, 456, 471–475]. However, the relationship between the halo mass and the axion star mass [476] leads to problems with this scenario in some galaxies [477–479]. It should be emphasized that many of the conclusions about the role of ULA axion stars in galactic dynamics are based on use of simulation results that do not contain baryons and feedback could be important [480–482].

Inside DM halos the axion gradient energy causes coherence on the de Broglie wavelength and fluctuations on the coherence time [456, 483]. These fluctuations can be thought of as short-lived quasiparticles and lead to relaxation processes that can be described statistically [445, 484] (this relaxation processes also leads to the gravitational condensation of axion stars [457]). The typical relaxation time is:

$$t \sim 10^{10}\ \text{years}\left(\frac{m_{\rm ULA}}{10^{-22}\ {\rm eV}}\right)^3\left(\frac{v}{100\ {\rm km\ s^{-1}}}\right)^2\left(\frac{r}{5\ {\rm kpc}}\right)^4, \tag{89.30}$$

where v and r are the velocity and radius of the orbit in the host DM halo.

Relaxation processes such as these are not observed in galaxies, though there are some circumstances where they may be desirable [445]. An absence of observed relaxation can be used to set limits on the ULA mass. An absence of Milky Way disk thickening excludes $m_{\rm ULA} > 0.6\times10^{-22}$ eV [485], while stellar streams give the stronger bound $m_{\rm ULA} > 1.5\times10^{-22}$ eV [486]. The survival of the old star cluster in Eridanus II [487] excludes the range of masses 10^{-21} eV $\lesssim m_{\rm ULA} \lesssim 10^{-19}$ eV [488]. Recently Ref. [489] found that ULA DM is excluded for $m_{\rm ULA} \lesssim 3\times10^{-19}$ eV at 99% CL because such DM would kinematically heat the stars in the Segue I and Segue II ultra-faint dwarf galaxies to a level inconsistent with their observed dynamics.

Finally, one should note that the beyond-CDM physics of ULAs (Jeans scale, relaxation, axion star formation) of course also applies to the QCD axion on smaller length scales. This is of particular interest inside axion miniclusters [436, 437, 457, 458].

89.5.2 *Electron recoil searches*

In a DM direct detection experiment, a DM ALP featuring a coupling to the electron can be absorbed by the target material, leading to a mono-energetic electronic recoil signal peaked at m_a. This mechanism allowed the EDELWEISS [490], PandaX [234], SuperCDMS [235] and XENON1T [491] collaborations to put the bounds on the axion-electron coupling displayed in Fig. 89.2 in the keV mass range. As discussed in the last sub-section, additionally dynamics beyond the standard misalignment mechanism are needed to explain the axion DM abundance for keV-scale axion masses (*e.g.*, [395, 396]). Moreover, such models are subject to stringent constraints from axion decays to photons [395].

89.5.3 *Telescope searches*

The two-photon decay is extremely slow for axions with masses in the CDM regime, but could be detectable for eV masses. The signature would be a quasi-monochromatic emission line from galaxies and galaxy clusters. The expected optical line intensity for DFSZ axions is similar to the continuum night emission. A search for optical line emission in two Abell clusters using spectra from the VIMOS (Visible Multi-Object Spectrograph) integral field unit at the Very Large Telescope (VLT) excludes axions and ALPs with a two photon coupling bigger than $\sim 5\times10^{-12}\,{\rm GeV}^{-1}$ in the mass range between 4.5 and 5.5 eV [140], see Fig. 89.1. Spectral data on the dwarf spheroidal galaxy Leo T from the Multi Unit Spectroscopic Explorer (MUSE) at the VLT improve these constraints by more than an order of magnitude for ALP masses between 2.7 and 5.3 eV [139], see Fig. 89.1. More recently, as shown in Fig. 89.1, James Webb Space Telescope (JWST) data has been used to constrain axion decays in the mass range between roughly 0.1 - 4 eV [492, 493].

Very low-mass axions in halos produce a weak quasi-monochromatic radio line. Virial velocities in undisrupted dwarf galaxies are very low, and the axion decay line would therefore be extremely narrow. A search with the Haystack radio telescope on three nearby dwarf galaxies gave a limit $|g_{a\gamma\gamma}| < 1.0\times10^{-9}\ {\rm GeV}^{-1}$ at 96% CL for $298 < m_a < 363\ \mu$eV [138]. However, this combination of m_a and $g_{a\gamma\gamma}$ does not exclude plausible axion models.

A monochromatic signal is also produced in the conversion of DM axions in the background of slowly varying galactic B-fields [494]. The signal is, however, sensitive to magnetic field power on the scale of the axion mass [495]. Present and future radio telescopes appear to be able to probe ALP DM in the mass range $0.1 - 100\ \mu$eV for couplings $g_{a\gamma\gamma} \gtrsim 10^{-13}\ {\rm GeV}^{-1}$ [495] – several orders of magnitude above the KSVZ benchmark coupling for this mass range.

Resonant conversion of QCD axion or ALP DM in NS magnetospheres may give a detectable signal from individual NSs and populations of NSs for axion masses in the μeV range [496, 497]. Recent analyses of radio data in the frequency range 1-40 GHz from several NSs have found no evidence for a narrow peak predicted from this mechanism and therefore put bounds on the axion-photon coupling around $10^{-11}\,{\rm GeV}^{-2}$ for $m_a \sim 10\ \mu$eV [110–113], see Fig. 89.1. However, these limits may still suffer from uncertainties because the line intensity is difficult to predict in detail in the complicated environments of NSs [112, 498–501]. Still, next-generation radio telescopes such as the Square Kilometer Array (SKA) may reach sensitivity to QCD axion-strength couplings [113]. Stimulated ALP decays in high radiation environments may be detectable, by *e.g.* the future SKA, down to $g_{a\gamma\gamma} \gtrsim 10^{-11}\,{\rm GeV}^{-1}$, for masses between μeV and 0.1 meV [502]. Furthermore, in condensed ALP dark matter structures such as

Int. J. Mod. Phys. A 2026.41. Downloaded from www.worldscientific.com by UNIVERSITY OF CALIFORNIA @ BERKELEY on 09/16/26. Re-use and distribution is strictly not permitted, except for Open Access articles.

ALP stars, a parametric instability may lead to an exponential enhancement of the photon flux from ALP-photon conversion by a factor $\sim \exp\left[|g_{a\gamma\gamma}| \int ds \rho_a^{1/2}(s)\right]$, where the integral is along any photon trajectory through the ALP overdensity [503, 504].

Photon propagation on an ULA DM background can induce birefringence that can be compared with upper limits from the CMB [83, 118, 505] and may also be probed with other sources such as pulsars [506].

89.5.4 *Microwave cavity experiments*

Galactic halo axions in the 1-100 μeV mass range may be detected by their resonant conversion into a quasi-monochromatic microwave signal in a high-Q electromagnetic cavity permeated by a strong, static B field [7, 507, 508]. The signal should appear as excess electromagnetic power in the cavity at a frequency of the total axion energy, rest mass plus kinetic energy, $\nu = (m_a/2\pi)\,[1 + \mathcal{O}(10^{-6})]$, with a width representing the axions' virial distribution in the galaxy near Earth (though the frequency spectrum may also contain narrower components from *e.g.* DM streams or other substructure; cavity experiments have enhanced sensitivity to these narrow signals [509]). If the cavity resonant frequency is tuned to the axion frequency then the signal is enhanced by the Q of the cavity. Cavity experiments are thus tuning experiments, typically right circular cylindrical cavities in solenoidal magnets tuned through mechanical motion of conductive or dielectric rods in the hopes of aligning the resonant frequency with the unknown axion mass.

A number of cavity experiments have been executed, and have historically most successful for 1-100 μeV axion masses, where the length scale of the detected photons are at laboratory length scales. At present, the ADMX [45, 46, 510, 511] and CAPP [146,148] cavity experiments have explored CDM axions with sensitivity to the DFSZ benchmark model over much of the 2.7- 4.91 μeV mass range, with the expectation of continuing to scan upwards. A number of other cavity experiments with sensitivity at or near KSVZ coupling have been operated over narrow mass ranges, notably HAYSTAC [151], TASEH [70], QUAX aγ [66], and a higher-order mode of a DMAG (formerly CAPP) cavity [512]. Exclusions are shown in Fig. 89.5.

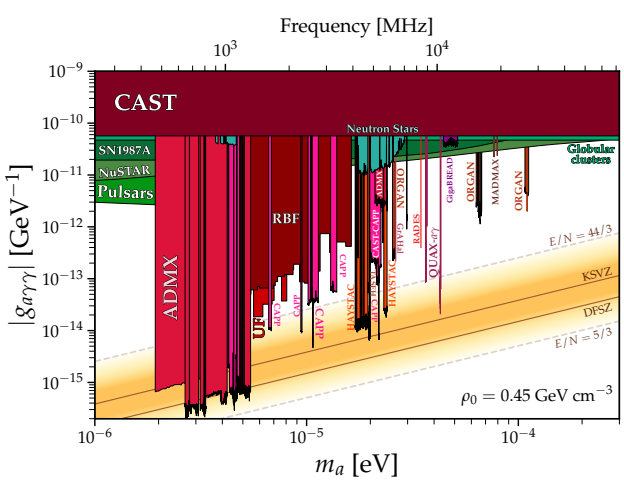

Figure 89.5: Exclusion plot for ALP-photon coupling with closeup on the parameter space of RF cavity experiments as described in the text. This is a zoom-in of Fig. 89.1 that highlights regions probed by axion DM direct detection experiments. In particular, note that all of the terrestrial experiments shaded in red, except that of CAST, assume that the axion is Figure from [39], including data from Refs. [34, 42, 44–46, 55, 58–61, 63, 64, 68, 70, 76, 99, 100, 122, 146, 146–156, 229, 513–518]

89.5.5 *Lower Mass Direct Axion Searches*

The mass range $m_a < 0.1\,\mu eV$ is increasingly of interest because of the strong theoretical motivations to prefer f_a near the GUT scale (see Sec. 89.2.1). As summarized in Fig. 89.1, there are currently no bounds in this region that reach the QCD axion parameter space. Compared to the cavity searches, the wavelength of these axions is much longer than the size of the experiments. When converted to electromagnetic fields in a strong laboratory magnetic field, the resulting signal can be modeled as currents in an equivalent "lumped" element or LC circuit [519–521]. A number of small-scale pathfinder experiments have implemented this approach focusing on the ∼neV region. Some examples are: ABRACADABRA-10cm [40, 41] used a broadband configuration in a toroidal magnet for a broadband search, ADMX-SLIC [48] used a resonant configuration in a solenoid magnet for a narrowband search, BASE [57] used the field of a penning trap for a similar search, and SHAFT [69] used a broadband configuration in a toroidal magnet enhanced with a ferromagnetic core. Future work in this direction is expected to have much more competitive sensitivity [522, 523]. There are several efforts using laser interferometry techniques to access the ∼neV parameter space: LIDA [62] and DANCE [524]. The ADBC experiment uses an optical bow-tie cavity to search for axion-induced birefringence [43].

89.5.6 *Higher Mass Direct Axion Searches*

For axion masses where the Compton wavelength is much smaller than the characteristic laboratory scale, the conversion volume becomes smaller, the characteristic resonator Q decreases, and the standard quantum noise limit increases. Techniques beyond the standard microwave cavity experiments are necessary to probe QCD axion dark matter. No experiment yet has explored a wide range of masses for high masses, beyond ∼25 μeV, at QCD axions couplings, but a number of promising techniques have been proposed and demonstrated. Only a small representative subset of these demonstrations and proposals can be cataloged here.

One path is to build a resonant structure with a characteristic dimension much longer than the converted photon wavelength. This has been proposed with subwavelength metamaterial-like conductive structure such as ALPHA [525], or VERA [526], and demonstrated with periodic dielectrics as in Orpheus [527], LAMPOST [528], and MADMAX [152]. Another option is to forgo resonance entirely and use a single conversion surface that is many wavelengths in dimension. [529] Experiments working on this concept include BRASS [530] and BREAD [150].

Due to the standard quantum limit readout for these higher-mass detectors to transition to quantum sensors and techniques beyond linear amplifiers [526,531]. Benefits of quantum squeezing have been demonstrated in HAYSTAC [60,532], and single photon counters have been shown to be beneficial in QUAX [533] and in dark photon searches using both qubit devices [534] and nanowire detectors [528], among others.

89.5.7 *Non-photon Coupling Axion Searches*

In Fig. 89.2 and Fig. 89.3, the status of the non-photon couplings are discussed in the context of the astrophysical ALP searches. These same non-photon couplings can also be used in direct searches for DM. Much of the recent focus is on the induced oscillating nuclear electric dipole moments (EDMs) [26]. An analysis of the ratio of spin-precession frequencies of stored ultracold neutrons and ^{199}Hg atoms measured by neutron EDM experiments excludes a sizeable region of parameter space in the mass region $10^{-24}\,\text{eV} \leq m_a \leq 10^{-17}\,\text{eV}$ [31], which surpass the limits on anomalous energy loss of SN 1987A by more than seven orders of magnitude and are competitive with the ones from the requirement of successful BBN established in [29].

The oscillating EDMs can also be studied with the precession of nuclear spins in a nucleon spin polarized sample in the presence of an electric field. The resulting transverse magnetization can be searched for by exploiting magnetic-resonance (MR) techniques, which are most sensitive to the low frequencies of the sub-neV axion masses. There are two interactions probed through MR: the electric dipole coupling as searched for by CASPEr-electric (with first result presented in [30]) and an interaction between the axion field gradient and the nuclear spin, which is aimed for by CASPEr-Gradient. The latter has been explored through comagnetometry between a variety of nuclei: H-^{12}C in CASPEr-ZULF [261, 262], Xe-Rb in NASDUCK [535], K-^{3}He [265–267] and K-^{3}He-Rb [273].

Int. J. Mod. Phys. A 2026.41. Downloaded from www.worldscientific.com
by UNIVERSITY OF CALIFORNIA @ BERKELEY on 09/16/26. Re-use and distribution is strictly not permitted, except for Open Access articles.

The exclusions from these searches are shown in Fig. 89.3.

Sub-μeV ALP masses can also be probed by using the storage ring EDM method proposed in Ref. [536] which exploits a combination of B and E-fields to produce a resonance between the $g-2$ spin precession frequency and the DM ALP field oscillation frequency. This method, however, does not reach the sensitivity to probe the QCD axion prediction for $g_{aN\gamma}$. An non-zero axion electron coupling g_{aee} will lead to an electron spin precession about the axion DM wind [537, 538]. The QUAX a-e experiment exploits MR inside a magnetized material [539]. Because of the higher Larmor frequency of the electron, it is sensitive to masses above 1μeV. Its first run established the bound in the mass range 42.4 to 43.2 μeV [240], slightly better than the solar ν bound, shown in Fig. 89.2. Updated sensitivity projections for MR techniques are detailed in [540], and examples of potential technological improvements in [541, 542].

89.6 Conclusions

There is a strengthening physics case for very weakly coupled light particles beyond the Standard Model. The elegant solution of the strong CP problem proposed by Peccei and Quinn yields a particularly strong motivation for the axion. In many theoretically appealing ultraviolet completions of the Standard Model axions and ALPs occur automatically. Moreover, they are natural CDM candidates. Interestingly, a significant portion of previously unexplored, but phenomenologically interesting and theoretically very well motivated, axion and ALP parameter space can be explored in the foreseeable future by a number of terrestrial experiments and astrophysical observations.

89.7 Acknowledgements

It is a pleasure to thank Masha Baryakhtar, Francesca Calore, Luca Di Luzio, Andrew Geraci, Maurizio Giannotti, Igor Irastorza, David J.E. Marsh, Alessandro Mirizzi, Georg Raffelt, Ken'ichi Saikawa, Yannis Semertzidis, Guenter Sigl, and Sergey Troitsky for discussions, suggestions, and comments on this review.

References

[1] R. D. Peccei and H. R. Quinn, Phys. Rev. Lett. **38**, 1440 (1977).

[2] R. D. Peccei and H. R. Quinn, Phys. Rev. **D16**, 1791 (1977).

[3] S. Weinberg, Phys. Rev. Lett. **40**, 223 (1978).

[4] F. Wilczek, Phys. Rev. Lett. **40**, 279 (1978).

[5] E. Witten, Phys. Lett. B **149**, 351 (1984).

[6] P. Svrcek and E. Witten, JHEP **06**, 051 (2006), [hep-th/0605206].

[7] P. Sikivie, Phys. Rev. Lett. **51**, 1415 (1983) and Erratum *ibid.*, **52**, 695 (1984).

[8] J. P. Conlon, JHEP **05**, 078 (2006), [hep-th/0602233].

[9] K.-S. Choi *et al.*, Phys. Lett. **B675**, 381 (2009), [arXiv:0902.3070].

[10] A. Arvanitaki *et al.*, Phys. Rev. **D81**, 123530 (2010), [arXiv:0905.4720].

[11] B. S. Acharya, K. Bobkov and P. Kumar, JHEP **11**, 105 (2010), [arXiv:1004.5138].

[12] M. Cicoli, M. Goodsell and A. Ringwald, JHEP **10**, 146 (2012), [arXiv:1206.0819].

[13] J. Halverson, C. Long and P. Nath, Phys. Rev. **D96**, 5, 056025 (2017), [arXiv:1703.07779].

[14] M. Demirtas *et al.*, JHEP **04**, 138 (2020), [arXiv:1808.01282].

[15] M. Pospelov and A. Ritz, Nucl. Phys. **B573**, 177 (2000), [hep-ph/9908508].

[16] J. Liang *et al.* (χQCD Collaboration), Phys. Rev. D **108**, 094512 (2023), URL `https://link.aps.org/doi/10.1103/PhysRevD.108.094512`.

[17] C. A. Baker *et al.*, Phys. Rev. Lett. **97**, 131801 (2006), [hep-ex/0602020].

[18] C. Abel *et al.* (nEDM), Phys. Rev. Lett. **124**, 8, 081803 (2020), [arXiv:2001.11966].

[19] J. Alexander *et al.* (2022), [arXiv:2205.00830].

[20] H. Georgi, D. B. Kaplan and L. Randall, Phys. Lett. **169B**, 73 (1986).

[21] R. J. Crewther, Phys. Lett. **70B**, 349 (1977).

[22] P. Di Vecchia and G. Veneziano, Nucl. Phys. **B171**, 253 (1980).

[23] M. Gorghetto and G. Villadoro, JHEP **03**, 033 (2019), [arXiv:1812.01008].

[24] S. Borsanyi *et al.*, Nature **539**, 7627, 69 (2016), [arXiv:1606.07494].

[25] L. Caloni *et al.*, JCAP **09**, 021 (2022), [arXiv:2205.01637].

[26] P. W. Graham and S. Rajendran, Phys. Rev. **D88**, 035023 (2013), [arXiv:1306.6088].

[27] D. Budker *et al.*, Phys. Rev. **X4**, 2, 021030 (2014), [arXiv:1306.6089].

[28] I. Schulthess *et al.*, Phys. Rev. Lett. **129**, 19, 191801 (2022), [arXiv:2204.01454].

[29] K. Blum *et al.*, Phys. Lett. B **737**, 30 (2014), [arXiv:1401.6460].

[30] D. Aybas *et al.*, Phys. Rev. Lett. **126**, 14, 141802 (2021), [arXiv:2101.01241].

[31] C. Abel *et al.*, Phys. Rev. **X7**, 4, 041034 (2017), [arXiv:1708.06367].

[32] T. S. Roussy *et al.*, Phys. Rev. Lett. **126**, 17, 171301 (2021), [arXiv:2006.15787].

[33] S. Karanth *et al.* (JEDI Collaboration), Phys. Rev. X **13**, 031004 (2023), URL `https://link.aps.org/doi/10.1103/PhysRevX.13.031004`.

[34] X. Zhang *et al.*, Phys. Rev. Lett. **130**, 251002 (2023), URL `https://link.aps.org/doi/10.1103/PhysRevLett.130.251002`.

[35] G. Lucente *et al.*, Phys. Rev. D **105**, 12, 123020 (2022), [arXiv:2203.15812].

[36] L. Di Luzio *et al.*, Phys. Rept. **870**, 1 (2020), [arXiv:2003.01100].

[37] J. E. Kim, Phys. Rev. Lett. **43**, 103 (1979).

[38] M. A. Shifman, A. I. Vainshtein and V. I. Zakharov, Nucl. Phys. **B166**, 493 (1980).

[39] C. O'Hare, cajohare/AxionLimits: AxionLimits (2023), URL `https://doi.org/10.5281/zenodo.3932430`.

[40] J. L. Ouellet *et al.* (ABRACADABRA), Phys. Rev. Lett. **122**, 12, 121802 (2019), [arXiv:1810.12257].

[41] C. P. Salemi *et al.*, Phys. Rev. Lett. **127**, 8, 081801 (2021), [arXiv:2102.06722].

[42] S. J. Asztalos *et al.* (ADMX), Phys. Rev. Lett. **104**, 041301 (2010), [arXiv:0910.5914].

[43] S. Pandey, E. D. Hall and M. Evans, Phys. Rev. Lett. **133**, 11, 111003 (2024), [arXiv:2404.12517].

[44] N. Du *et al.* (ADMX), Phys. Rev. Lett. **120**, 15, 151301 (2018), [arXiv:1804.05750].

[45] T. Braine *et al.* (ADMX), Phys. Rev. Lett. **124**, 10, 101303 (2020), [arXiv:1910.08638].

[46] C. Bartram *et al.* (ADMX Collaboration), Phys. Rev. Lett. **127**, 261803 (2021), URL `https://link.aps.org/doi/10.1103/PhysRevLett.127.261803`.

[47] C. Bartram *et al.*, Review of Scientific Instruments **94**, 4, 044703 (2023), ISSN 0034-6748, URL `https://doi.org/10.1063/5.0122907`.

[48] N. Crisosto *et al.*, Phys. Rev. Lett. **124**, 24, 241101 (2020), [arXiv:1911.05772].

[49] S. Lee *et al.*, Phys. Rev. Lett. **124**, 10, 101802 (2020), [arXiv:2001.05102].

Int. J. Mod. Phys. A 2026.41. Downloaded from www.worldscientific.com
by UNIVERSITY OF CALIFORNIA @ BERKELEY on 09/16/26. Re-use and distribution is strictly not permitted, except for Open Access articles.

[50] J. Jeong *et al.*, Phys. Rev. Lett. **125**, 22, 221302 (2020), [arXiv:2008.10141].

[51] O. Kwon *et al.* (CAPP), Phys. Rev. Lett. **126**, 19, 191802 (2021), [arXiv:2012.10764].

[52] Y. Lee *et al.*, Phys. Rev. Lett. **128**, 24, 241805 (2022), [arXiv:2206.08845].

[53] J. Kim *et al.*, Phys. Rev. Lett. **130**, 091602 (2023), URL `https://link.aps.org/doi/10.1103/PhysRevLett.130.091602`.

[54] B. Yang *et al.*, Phys. Rev. Lett. **131**, 081801 (2023), URL `https://link.aps.org/doi/10.1103/PhysRevLett.131.081801`.

[55] C. M. Adair *et al.*, Nature Commun. **13**, 1, 6180 (2022), [arXiv:2211.02902].

[56] Y. Oshima *et al.*, Phys. Rev. D **108**, 072005 (2023), URL `https://link.aps.org/doi/10.1103/PhysRevD.108.072005`.

[57] J. A. Devlin *et al.*, Phys. Rev. Lett. **126**, 4, 041301 (2021), [arXiv:2101.11290].

[58] T. Grenet *et al.* (2021), [arXiv:2110.14406].

[59] L. Zhong *et al.* (HAYSTAC), Phys. Rev. D **97**, 9, 092001 (2018), [arXiv:1803.03690].

[60] K. M. Backes *et al.* (HAYSTAC), Nature **590**, 7845, 238 (2021), [arXiv:2008.01853].

[61] M. J. Jewell *et al.* (HAYSTAC), Phys. Rev. D **107**, 7, 072007 (2023), [arXiv:2301.09721].

[62] J. Heinze *et al.*, Phys. Rev. Lett. **132**, 19, 191002 (2024), [arXiv:2307.01365].

[63] B. T. McAllister *et al.*, Phys. Dark Univ. **18**, 67 (2017), [arXiv:1706.00209].

[64] A. P. Quiskamp *et al.*, Sci. Adv. **8**, 27, abq3765 (2022), [arXiv:2203.12152].

[65] D. Alesini *et al.*, Phys. Rev. D **99**, 10, 101101 (2019), [arXiv:1903.06547].

[66] D. Alesini *et al.*, Phys. Rev. D **103**, 10, 102004 (2021), [arXiv:2012.09498].

[67] D. Alesini *et al.*, Phys. Rev. D **106**, 5, 052007 (2022), [arXiv:2208.12670].

[68] S. De Panfilis *et al.*, Phys. Rev. Lett. **59**, 839 (1987).

[69] A. V. Gramolin *et al.*, Nature Phys. **17**, 1, 79 (2021), [arXiv:2003.03348].

[70] H. Chang *et al.* (TASEH), Phys. Rev. Lett. **129**, 11, 111802 (2022), [arXiv:2205.05574].

[71] A. Arza *et al.*, Phys. Rev. D **105**, 9, 095007 (2022), [arXiv:2112.09620].

[72] C. Hagmann *et al.*, Phys. Rev. **D42**, 1297 (1990).

[73] C. A. Thomson *et al.*, Phys. Rev. Lett. **126**, 8, 081803 (2021), [Erratum: Phys.Rev.Lett. 127, 019901 (2021)], [arXiv:1912.07751].

[74] C. A. Thomson *et al.*, Phys. Rev. D **107**, 112003 (2023), URL `https://link.aps.org/doi/10.1103/PhysRevD.107.112003`.

[75] K. Ehret *et al.* (ALPS), Phys. Lett. **B689**, 149 (2010), [arXiv:1004.1313].

[76] V. Anastassopoulos *et al.* (CAST), Nature Phys. **13**, 584 (2017), [arXiv:1705.02290].

[77] M. Betz *et al.*, Phys. Rev. **D88**, 7, 075014 (2013), [arXiv:1310.8098].

[78] R. Ballou *et al.* (OSQAR), Phys. Rev. **D92**, 9, 092002 (2015), [arXiv:1506.08082].

[79] F. Della Valle *et al.*, Eur. Phys. J. **C76**, 1, 24 (2016), [arXiv:1510.08052].

[80] Y. Kirita *et al.* (SAPPHIRES), JHEP **10**, 176 (2022), [arXiv:2208.09880].

[81] M. Escudero *et al.*, Phys. Rev. D **109**, 4, 043018 (2024), [arXiv:2302.10206].

[82] M. Xiao *et al.*, Phys. Rev. Lett. **126**, 3, 031101 (2021), [arXiv:2009.09059].

[83] P. A. R. Ade *et al.* (BICEP/Keck Collaboration), Phys. Rev. D **105**, 022006 (2022), URL `https://link.aps.org/doi/10.1103/PhysRevD.105.022006`.

[84] A. Keller *et al.*, Astrophys. J. **927**, 1, 71 (2022), [arXiv:2112.03439].

[85] M. H. Chan, Sci. Rep. **11**, 20087 (2021), [arXiv:2109.11734].

[86] K. Kohri and H. Kodama, Phys. Rev. **D96**, 5, 051701 (2017), [arXiv:1704.05189].

[87] D. Wouters and P. Brun, Astrophys. J. **772**, 44 (2013), [arXiv:1304.0989].

[88] M. C. D. Marsh *et al.*, JCAP **1712**, 12, 036 (2017), [arXiv:1703.07354].

[89] C. S. Reynolds *et al.*, Astrophys. J. **890**, 1, 59 (2020), [arXiv:1907.05475].

[90] J. S. Reynés *et al.*, Mon. Not. Roy. Astron. Soc. **510**, 1, 1264 (2021), [arXiv:2109.03261].

[91] F. Capozzi *et al.*, Journal of Cosmology and Astroparticle Physics **2023**, 06, 060 (2023), URL `https://dx.doi.org/10.1088/1475-7516/2023/06/060`.

[92] H. Liu *et al.*, Phys. Rev. D **108**, 043531 (2023), URL `https://link.aps.org/doi/10.1103/PhysRevD.108.043531`.

[93] B. Bolliet, J. Chluba and R. Battye, Mon. Not. Roy. Astron. Soc. **507**, 3, 3148 (2021), [arXiv:2012.07292].

[94] M. A. Buen-Abad, J. Fan and C. Sun, Journal of High Energy Physics **2022**, 2, 103 (2022), ISSN 1029-8479, URL `https://doi.org/10.1007/JHEP02(2022)103`.

[95] M. Ajello *et al.* (Fermi-LAT), Phys. Rev. Lett. **116**, 16, 161101 (2016), [arXiv:1603.06978].

[96] M. Meyer and T. Petrushevska, Phys. Rev. Lett. **124**, 23, 231101 (2020), [Erratum: Phys.Rev.Lett. 125, 119901 (2020)], [arXiv:2006.06722].

[97] J. Davies, M. Meyer and G. Cotter, Phys. Rev. D **107**, 8, 083027 (2023), [arXiv:2211.03414].

[98] J. L. Bernal *et al.*, Phys. Rev. D **107**, 10, 103046 (2023), [arXiv:2208.13794].

[99] A. Ayala *et al.*, Phys. Rev. Lett. **113**, 19, 191302 (2014), [arXiv:1406.6053].

[100] M. J. Dolan, F. J. Hiskens and R. R. Volkas, JCAP **10**, 096 (2022), [arXiv:2207.03102].

[101] S. Jacobsen, T. Linden and K. Freese, JCAP **10**, 009 (2023), [arXiv:2203.04332].

[102] A. Abramowski *et al.* (H.E.S.S.), Phys. Rev. D **88**, 10, 102003 (2013), [arXiv:1311.3148].

[103] F. Calore *et al.*, Mon. Not. Roy. Astron. Soc. **520**, 3, 4167 (2023), [arXiv:2209.06299].

[104] D. Wadekar and G. R. Farrar, Phys. Rev. D **103**, 123028 (2021), URL `https://link.aps.org/doi/10.1103/PhysRevD.103.123028`.

[105] C. Dessert, A. J. Long and B. R. Safdi, Phys. Rev. Lett. **128**, 071102 (2022), URL `https://link.aps.org/doi/10.1103/PhysRevLett.128.071102`.

[106] C. Dessert, D. Dunsky and B. R. Safdi, Phys. Rev. D **105**, 10, 103034 (2022), [arXiv:2203.04319].

[107] M. M. Ivanov *et al.*, JCAP **02**, 059 (2019), [arXiv:1811.10997].

[108] H.-J. Li *et al.*, Phys. Rev. D **103**, 8, 083003 (2021), [arXiv:2008.09464].

[109] H.-J. Li, X.-J. Bi and P.-F. Yin, Chin. Phys. C **46**, 8, 085105 (2022), [arXiv:2110.13636].

[110] J. W. Foster *et al.*, Phys. Rev. Lett. **125**, 17, 171301 (2020), [arXiv:2004.00011].

Int. J. Mod. Phys. A 2026.41. Downloaded from www.worldscientific.com
by UNIVERSITY OF CALIFORNIA @ BERKELEY on 09/16/26. Re-use and distribution is strictly not permitted, except for Open Access articles.

[111] J. Darling, Astrophys. J. Lett. **900**, 2, L28 (2020), [arXiv:2008.11188].

[112] R. A. Battye *et al.*, Phys. Rev. D **105**, L021305 (2022), URL https://link.aps.org/doi/10.1103/PhysRevD.105.L021305.

[113] J. W. Foster *et al.*, Phys. Rev. Lett. **129**, 25, 251102 (2022), [arXiv:2202.08274].

[114] R. A. Battye *et al.*, Phys. Rev. D **108**, 063001 (2023), URL https://link.aps.org/doi/10.1103/PhysRevD.108.063001.

[115] K. Perez *et al.*, Phys. Rev. D **95**, 12, 123002 (2017), [arXiv:1609.00667].

[116] K. C. Y. Ng *et al.*, Phys. Rev. D **99**, 083005 (2019), [arXiv:1901.01262].

[117] B. M. Roach *et al.*, Phys. Rev. D **107**, 2, 023009 (2023), [arXiv:2207.04572].

[118] M. A. Fedderke, P. W. Graham and S. Rajendran, Phys. Rev. **D100**, 1, 015040 (2019), [arXiv:1903.02666].

[119] S. Adachi *et al.* (POLARBEAR Collaboration), Phys. Rev. D **108**, 043017 (2023), URL https://link.aps.org/doi/10.1103/PhysRevD.108.043017.

[120] A. Castillo *et al.*, JCAP **06**, 06, 014 (2022), [arXiv:2201.03422].

[121] T. Liu, X. Lou and J. Ren, Phys. Rev. Lett. **130**, 121401 (2023), URL https://link.aps.org/doi/10.1103/PhysRevLett.130.121401.

[122] D. Noordhuis *et al.*, Phys. Rev. Lett. **131**, 111004 (2023), URL https://link.aps.org/doi/10.1103/PhysRevLett.131.111004.

[123] C. Severino and I. Lopes, The Astrophysical Journal **943**, 2, 95 (2023), URL https://dx.doi.org/10.3847/1538-4357/aca897.

[124] N. Vinyoles *et al.*, JCAP **1510**, 10, 015 (2015), [arXiv:1501.01639].

[125] N. H. Nguyen, E. H. Tanin and M. Kamionkowski, Journal of Cosmology and Astroparticle Physics **2023**, 11, 091 (2023), URL https://dx.doi.org/10.1088/1475-7516/2023/11/091.

[126] J. Jaeckel, P. C. Malta and J. Redondo, Phys. Rev. D **98**, 5, 055032 (2018), [arXiv:1702.02964].

[127] E. Müller *et al.*, Journal of Cosmology and Astroparticle Physics **2023**, 07, 056 (2023), URL https://dx.doi.org/10.1088/1475-7516/2023/07/056.

[128] A. Payez *et al.*, JCAP **1502**, 02, 006 (2015), [arXiv:1410.3747].

[129] S. Hoof and L. Schulz, JCAP **03**, 054 (2023), [arXiv:2212.09764].

[130] G. Lucente *et al.*, JCAP **12**, 008 (2020), [arXiv:2008.04918].

[131] A. Caputo, G. Raffelt and E. Vitagliano, Phys. Rev. D **105**, 3, 035022 (2022), [arXiv:2109.03244].

[132] A. Caputo *et al.*, Phys. Rev. Lett. **128**, 22, 221103 (2022), [arXiv:2201.09890].

[133] M. Diamond *et al.*, Phys. Rev. D **107**, 10, 103029 (2023), [arXiv:2303.11395].

[134] W. DeRocco *et al.*, Phys. Rev. Lett. **129**, 10, 101101 (2022), [arXiv:2205.05700].

[135] C. Beaufort *et al.*, Phys. Rev. D **108**, L081302 (2023), URL https://link.aps.org/doi/10.1103/PhysRevD.108.L081302.

[136] C. Dessert, J. W. Foster and B. R. Safdi, Phys. Rev. Lett. **125**, 26, 261102 (2020), [arXiv:2008.03305].

[137] K. R. Ferguson *et al.* (SPT-3G), Phys. Rev. D **106**, 4, 042011 (2022), [arXiv:2203.16567].

[138] B. D. Blout *et al.*, Astrophys. J. **546**, 825 (2001), [arXiv:astro-ph/0006310].

[139] M. Regis *et al.*, Phys. Lett. B **814**, 136075 (2021), [arXiv:2009.01310].

[140] D. Grin *et al.*, Phys. Rev. D **75**, 105018 (2007), [arXiv:astro-ph/0611502].

[141] K. Nakayama and W. Yin, Phys. Rev. D **106**, 10, 103505 (2022), [arXiv:2205.01079].

[142] P. Carenza, G. Lucente and E. Vitagliano, Phys. Rev. D **107**, 8, 083032 (2023), [arXiv:2301.06560].

[143] D. Cadamuro and J. Redondo, JCAP **1202**, 032 (2012), [arXiv:1110.2895].

[144] P. F. Depta, M. Hufnagel and K. Schmidt-Hoberg, JCAP **05**, 009 (2020), [arXiv:2002.08370].

[145] K. Langhoff, N. J. Outmezguine and N. L. Rodd, Phys. Rev. Lett. **129**, 24, 241101 (2022), [arXiv:2209.06216].

[146] A. K. Yi *et al.*, Phys. Rev. Lett. **130**, 071002 (2023), URL https://link.aps.org/doi/10.1103/PhysRevLett.130.071002.

[147] S. Bae *et al.*, Phys. Rev. Lett. **133**, 21, 211803 (2024), [arXiv:2403.13390].

[148] S. Ahn *et al.*, Phys. Rev. X **14**, 031023 (2024), URL https://link.aps.org/doi/10.1103/PhysRevX.14.031023.

[149] Y. Kim *et al.*, Phys. Rev. Lett. **133**, 051802 (2024), URL https://link.aps.org/doi/10.1103/PhysRevLett.133.051802.

[150] G. Hoshino *et al.* (GigaBREAD Collaboration), Phys. Rev. Lett. **134**, 171002 (2025), URL https://link.aps.org/doi/10.1103/PhysRevLett.134.171002.

[151] X. Bai *et al.* (HAYSTAC Collaboration), Phys. Rev. Lett. **134**, 151006 (2025), URL https://link.aps.org/doi/10.1103/PhysRevLett.134.151006.

[152] B. Ary dos Santos Garcia *et al.* (MADMAX Collaboration), Phys. Rev. Lett. **135**, 041001 (2025), URL https://link.aps.org/doi/10.1103/c749-419q.

[153] A. P. Quiskamp *et al.*, Phys. Rev. D **111**, 095007 (2025), URL https://link.aps.org/doi/10.1103/PhysRevD.111.095007.

[154] A. Rettaroli *et al.* (QUAX), Phys. Rev. D **110**, 2, 022008 (2024), [arXiv:2402.19063].

[155] S. Ahyoune *et al.*, Journal of High Energy Physics **2025**, 4, 113 (2025), ISSN 1029-8479, URL https://doi.org/10.1007/JHEP04(2025)113.

[156] M. Friel *et al.*, Phys. Rev. D **110**, 115036 (2024), URL https://link.aps.org/doi/10.1103/PhysRevD.110.115036.

[157] Y. Kirita *et al.*, Journal of High Energy Physics **2025**, 6, 138 (2025), ISSN 1029-8479, URL https://doi.org/10.1007/JHEP06(2025)138.

[158] K. Altenmüller *et al.* (CAST Collaboration), Phys. Rev. Lett. **133**, 221005 (2024), URL https://link.aps.org/doi/10.1103/PhysRevLett.133.221005.

[159] M. Dine, W. Fischler and M. Srednicki, Phys. Lett. **104B**, 199 (1981).

[160] A. R. Zhitnitsky, Sov. J. Nucl. Phys. **31**, 260 (1980), [Yad. Fiz.31,497(1980)].

[161] H. M. Georgi, L. J. Hall and M. B. Wise, Nucl. Phys. B **192**, 409 (1981).

[162] M. Dine and N. Seiberg, Nucl. Phys. B **273**, 109 (1986).

[163] M. Kamionkowski and J. March-Russell, Phys. Lett. B **282**, 137 (1992), [hep-th/9202003].

[164] S. M. Barr and D. Seckel, Phys. Rev. D **46**, 539 (1992).

[165] R. Holman *et al.*, Phys. Lett. B **282**, 132 (1992), [hep-ph/9203206].

[166] D. Harlow and H. Ooguri, Commun. Math. Phys. **383**, 3, 1669 (2021), [arXiv:1810.05338].

[167] M. Reece, JHEP **07**, 130 (2025), [arXiv:2406.08543].

Int. J. Mod. Phys. A 2026.41. Downloaded from www.worldscientific.com
by UNIVERSITY OF CALIFORNIA @ BERKELEY on 09/16/26. Re-use and distribution is strictly not permitted, except for Open Access articles.

[168] N. Craig and M. Kongsore, Phys. Rev. D **111**, 1, 015047 (2025), [arXiv:2408.10295].

[169] P. Agrawal, M. Nee and M. Reig, JHEP **02**, 188 (2025), [arXiv:2410.03820].

[170] J. N. Benabou *et al.*, Phys. Rev. D **112**, 6, 066003 (2025), [arXiv:2505.15884].

[171] V. Loladze, A. Platschorre and M. Reig, JHEP **08**, 182 (2025), [arXiv:2503.18707].

[172] R. Petrossian-Byrne and G. Villadoro, JHEP **07**, 049 (2025), [arXiv:2503.16387].

[173] G. Grilli di Cortona *et al.*, JHEP **01**, 034 (2016), [arXiv:1511.02867].

[174] J. E. Kim, Phys. Rev. **D58**, 055006 (1998), [hep-ph/9802220].

[175] L. Di Luzio, F. Mescia and E. Nardi, Phys. Rev. Lett. **118**, 3, 031801 (2017), [arXiv:1610.07593].

[176] L. Di Luzio, F. Mescia and E. Nardi, Phys. Rev. D **96**, 7, 075003 (2017), [arXiv:1705.05370].

[177] M. Farina *et al.*, JHEP **01**, 095 (2017), [arXiv:1611.09855].

[178] P. Agrawal *et al.*, JHEP **02**, 006 (2018), [arXiv:1709.06085].

[179] A. Hook, Phys. Rev. Lett. **120**, 26, 261802 (2018), [arXiv:1802.10093].

[180] L. Di Luzio *et al.*, JHEP **05**, 184 (2021), [arXiv:2102.00012].

[181] A. V. Sokolov and A. Ringwald, JHEP **06**, 123 (2021), [arXiv:2104.02574].

[182] J. Diehl and E. Koutsangelas, Phys. Rev. D **107**, 9, 095020 (2023), [arXiv:2302.04667].

[183] G. Raffelt and D. Seckel, Phys. Rev. Lett. **60**, 1793 (1988).

[184] M. Carena and R. D. Peccei, Phys. Rev. **D40**, 652 (1989).

[185] K. Choi, K. Kang and J. E. Kim, Phys. Rev. Lett. **62**, 849 (1989).

[186] M. Srednicki, Nucl. Phys. **B260**, 689 (1985).

[187] S. Chang and K. Choi, Phys. Lett. **B316**, 51 (1993), [hep-ph/9306216].

[188] G. C. Branco *et al.*, Phys. Rept. **516**, 1 (2012), [arXiv:1106.0034].

[189] C.-Y. Chen and S. Dawson, Phys. Rev. **D87**, 055016 (2013), [arXiv:1301.0309].

[190] R. Balkin *et al.*, JHEP **07**, 221 (2020), [arXiv:2003.04903].

[191] K. Choi *et al.*, JHEP **02**, 143 (2022), [arXiv:2110.01972].

[192] D. A. Dicus *et al.*, Phys. Rev. **D18**, 1829 (1978).

[193] G. Raffelt and L. Stodolsky, Phys. Rev. **D37**, 1237 (1988).

[194] A. A. Anselm, Yad. Fiz. **42**, 1480 (1985).

[195] K. van Bibber *et al.*, Phys. Rev. Lett. **59**, 759 (1987).

[196] G. Ruoso *et al.*, Z. Phys. **C56**, 505 (1992).

[197] R. Cameron *et al.*, Phys. Rev. **D47**, 3707 (1993).

[198] M. Fouche *et al.*, Phys. Rev. **D78**, 032013 (2008), [arXiv:0808.2800].

[199] P. Pugnat *et al.* (OSQAR), Phys. Rev. **D78**, 092003 (2008), [arXiv:0712.3362].

[200] A. S. Chou *et al.* (GammeV (T-969)), Phys. Rev. Lett. **100**, 080402 (2008), [arXiv:0710.3783].

[201] A. Afanasev *et al.*, Phys. Rev. Lett. **101**, 120401 (2008), [arXiv:0806.2631].

[202] P. Pugnat *et al.* (OSQAR), Eur. Phys. J. **C74**, 8, 3027 (2014), [arXiv:1306.0443].

[203] F. Hoogeveen and T. Ziegenhagen, Nucl. Phys. **B358**, 3 (1991).

[204] P. Sikivie, D. B. Tanner and K. van Bibber, Phys. Rev. Lett. **98**, 172002 (2007), [hep-ph/0701198].

[205] G. Mueller *et al.*, Phys. Rev. **D80**, 072004 (2009), [arXiv:0907.5387].

[206] M. Diaz Ortiz *et al.*, Physics of the Dark Universe **35**, 100968 (2022), ISSN 2212-6864, URL `https://www.sciencedirect.com/science/article/pii/S2212686422000115`.

[207] T. Kozlowski *et al.*, Opt. Express **33**, 5, 11153 (2025), URL `https://opg.optica.org/oe/abstract.cfm?URI=oe-33-5-11153`.

[208] F. Hoogeveen, Phys. Lett. **B288**, 195 (1992).

[209] J. Jaeckel and A. Ringwald, Phys. Lett. **B659**, 509 (2008), [arXiv:0707.2063].

[210] F. Caspers, J. Jaeckel and A. Ringwald, JINST **4**, P11013 (2009), [arXiv:0908.0759].

[211] R. Povey, J. Hartnett and M. Tobar, Phys. Rev. **D82**, 052003 (2010), [arXiv:1003.0964].

[212] E. Fischbach and C. Talmadge, Nature **356**, 207 (1992).

[213] J. E. Moody and F. Wilczek, Phys. Rev. **D30**, 130 (1984).

[214] A. N. Youdin *et al.*, Phys. Rev. Lett. **77**, 2170 (1996).

[215] W.-T. Ni *et al.*, Phys. Rev. Lett. **82**, 2439 (1999).

[216] D. F. Phillips *et al.*, Phys. Rev. **D63**, 111101 (2001), [arXiv:physics/0008230].

[217] B. R. Heckel *et al.*, Phys. Rev. Lett. **97**, 021603 (2006), [hep-ph/0606218].

[218] S. A. Hoedl *et al.*, Phys. Rev. Lett. **106**, 041801 (2011).

[219] E. G. Adelberger *et al.*, Phys. Rev. Lett. **98**, 131104 (2007), [hep-ph/0611223].

[220] D. J. Kapner *et al.*, Phys. Rev. Lett. **98**, 021101 (2007), [hep-ph/0611184].

[221] G. Raffelt, Phys. Rev. **D86**, 015001 (2012), [arXiv:1205.1776].

[222] C. A. J. O'Hare and E. Vitagliano, Phys. Rev. D **102**, 11, 115026 (2020), [arXiv:2010.03889].

[223] A. Arvanitaki and A. A. Geraci, Phys. Rev. Lett. **113**, 16, 161801 (2014), [arXiv:1403.1290].

[224] A. A. Geraci *et al.* (ARIADNE), Springer Proc. Phys. **211**, 151 (2018), [arXiv:1710.05413].

[225] H. Fosbinder-Elkins *et al.* (2017), [arXiv:1710.08102].

[226] N. Aggarwal *et al.* (ARIADNE Collaboration), Phys. Rev. Res. **4**, 013090 (2022), URL `https://link.aps.org/doi/10.1103/PhysRevResearch.4.013090`.

[227] M. S. Turner, Phys. Rept. **197**, 67 (1990).

[228] G. G. Raffelt, Lect. Notes Phys. **741**, 51 (2008), [,51(2006)], [hep-ph/0611350].

[229] S. Andriamonje *et al.* (CAST), JCAP **0704**, 010 (2007), [hep-ex/0702006].

[230] P. Gondolo and G. G. Raffelt, Phys. Rev. **D79**, 107301 (2009), [arXiv:0807.2926].

[231] H. Schlattl, A. Weiss and G. Raffelt, Astropart. Phys. **10**, 353 (1999), [hep-ph/9807476].

[232] P. Agnes *et al.* (DarkSide), Phys. Rev. Lett. **130**, 10, 101002 (2023), [arXiv:2207.11968].

[233] M. Agostini *et al.* (GERDA), Phys. Rev. Lett. **125**, 1, 011801 (2020), [arXiv:2005.14184].

[234] C. Fu *et al.* (PandaX), Phys. Rev. Lett. **119**, 18, 181806 (2017), [arXiv:1707.07921].

[235] T. Aralis *et al.* (SuperCDMS), Phys. Rev. D **101**, 5, 052008 (2020), [Erratum: Phys.Rev.D 103, 039901 (2021)], [arXiv:1911.11905].

[236] E. Aprile *et al.* (XENON), Phys. Rev. D **102**, 7, 072004 (2020), [arXiv:2006.09721].

[237] E. Aprile *et al.* (XENON Collaboration), Phys. Rev. Lett. **129**, 161805 (2022), URL `https://link.aps.org/doi/10.1103/PhysRevLett.129.161805`.

[238] K. Van Tilburg, Phys. Rev. D **104**, 2, 023019 (2021), [arXiv:2006.12431].

Int. J. Mod. Phys. A 2026.41. Downloaded from www.worldscientific.com
by UNIVERSITY OF CALIFORNIA @ BERKELEY on 09/16/26. Re-use and distribution is strictly not permitted, except for Open Access articles.

[239] F. Capozzi and G. Raffelt, Phys. Rev. D **102**, 8, 083007 (2020), [arXiv:2007.03694].

[240] N. Crescini *et al.* (QUAX), Phys. Rev. Lett. **124**, 17, 171801 (2020), [arXiv:2001.08940].

[241] R. Z. Ferreira, M. C. D. Marsh and E. Müller, Phys. Rev. Lett. **128**, 22, 221302 (2022), [arXiv:2202.08858].

[242] T. Li *et al.* (PandaX), Phys. Rev. Lett. **134**, 7, 071004 (2025), [arXiv:2409.00773].

[243] A. Berlin *et al.*, Journal of High Energy Physics **2024**, 5, 314 (2024), ISSN 1029-8479, URL `https://doi.org/10.1007/JHEP05(2024)314`.

[244] O. Straniero *et al.*, in "Proceedings, 11th Patras Workshop on Axions, WIMPs and WISPs (Axion-WIMP 2015): Zaragoza, Spain, June 22-26, 2015," 77–81 (2015).

[245] T. Constantino *et al.* .

[246] J. Redondo, Journal of Cosmology and Astroparticle Physics **2013**, 12, 008 (2013).

[247] O. Straniero *et al.*, Astron. Astrophys. **644**, A166 (2020), [arXiv:2010.03833].

[248] G. G. Raffelt, Phys. Lett. **166B**, 402 (1986).

[249] S. I. Blinnikov and N. V. Dunina-Barkovskaya, Mon. Not. Roy. Astron. Soc. **266**, 289 (1994).

[250] M. M. Miller Bertolami *et al.*, JCAP **1410**, 10, 069 (2014), [arXiv:1406.7712].

[251] J. Isern *et al.*, Astrophys. J. **682**, L109 (2008), [arXiv:0806.2807].

[252] J. Isern *et al.*, J. Phys. Conf. Ser. **172**, 012005 (2009), [arXiv:0812.3043].

[253] A. Drlica-Wagner *et al.* (LSST Dark Matter Group) (2019), [arXiv:1902.01055].

[254] J. Isern *et al.*, Astron. & Astrophys. **512**, A86 (2010).

[255] A. H. Corsico *et al.*, Mon. Not. Roy. Astron. Soc. **424**, 2792 (2012), [arXiv:1205.6180].

[256] A. H. Corsico *et al.*, JCAP **1212**, 010 (2012), [arXiv:1211.3389].

[257] A. H. Córsico *et al.*, The Astronomy and Astrophysics Review **27**, 1, 7 (2019), URL `https://doi.org/10.1007/s00159-019-0118-4`.

[258] M. J. Dolan, F. J. Hiskens and R. R. Volkas, Journal of Cosmology and Astroparticle Physics **2021**, 09, 010 (2021), URL `https://doi.org/10.1088/1475-7516/2021/09/010`.

[259] J. Isern, S. Torres and A. Rebassa-Mansergas, Front. Astron. Space Sci. **9**, 815517 (2022), [arXiv:2202.02052].

[260] V. M. Mostepanenko and G. L. Klimchitskaya, Universe **6**, 9, 147 (2020), [arXiv:2009.04517].

[261] T. Wu *et al.*, Phys. Rev. Lett. **122**, 19, 191302 (2019), [arXiv:1901.10843].

[262] A. Garcon *et al.*, Sci. Adv. **5**, 10, eaax4539 (2019), [arXiv:1902.04644].

[263] K. Wei *et al.*, Reports on Progress in Physics **88**, 5, 057801 (2025), URL `https://dx.doi.org/10.1088/1361-6633/adca52`.

[264] M. Jiang *et al.*, Nature Phys. **17**, 12, 1402 (2021), [arXiv:2102.01448].

[265] I. M. Bloch *et al.*, Nature Communications **14**, 1, 5784 (2023), ISSN 2041-1723, URL `https://doi.org/10.1038/s41467-023-41162-4`.

[266] I. M. Bloch *et al.*, JHEP **01**, 167 (2020), [arXiv:1907.03767].

[267] G. Vasilakis *et al.*, Physical Review Letters **103**, 26 (2009), ISSN 1079-7114, URL `http://dx.doi.org/10.1103/PhysRevLett.103.261801`.

[268] J. Lee *et al.*, Phys. Rev. X **13**, 011050 (2023), URL `https://link.aps.org/doi/10.1103/PhysRevX.13.011050`.

[269] M. Buschmann *et al.*, Phys. Rev. Lett. **128**, 9, 091102 (2022), [arXiv:2111.09892].

[270] A. Bhusal, N. Houston and T. Li, Phys. Rev. Lett. **126**, 9, 091601 (2021), [arXiv:2004.02733].

[271] H. Su *et al.*, Phys. Rev. Lett. **133**, 191801 (2024), URL `https://link.aps.org/doi/10.1103/PhysRevLett.133.191801`.

[272] Z. Xu *et al.*, Communications Physics **7**, 1, 226 (2024), ISSN 2399-3650, URL `https://doi.org/10.1038/s42005-024-01713-7`.

[273] D. Gavilan-Martin *et al.*, Nature Commun. **16**, 1, 4953 (2025), [arXiv:2408.02668].

[274] G.G. Raffelt, *Stars as Laboratories for Fundamental Physics*, (Univ. of Chicago Press, Chicago, 1996).

[275] T. Fischer *et al.*, Phys. Rev. **D94**, 8, 085012 (2016), [arXiv:1605.08780].

[276] J. H. Chang, R. Essig and S. D. McDermott, JHEP **09**, 051 (2018), [arXiv:1803.00993].

[277] P. Carenza *et al.*, JCAP **10**, 10, 016 (2019), [Erratum: JCAP 05, E01 (2020)], [arXiv:1906.11844].

[278] M. S. Turner, Phys. Rev. D **45**, 1066 (1992).

[279] G. Raffelt and D. Seckel, Phys. Rev. D **52**, 1780 (1995), [arXiv:astro-ph/9312019].

[280] W. Keil *et al.*, Phys. Rev. D **56**, 2419 (1997), [arXiv:astro-ph/9612222].

[281] B. Fore and S. Reddy, Phys. Rev. C **101**, 3, 035809 (2020), [arXiv:1911.02632].

[282] P. Carenza *et al.*, Phys. Rev. Lett. **126**, 7, 071102 (2021), [arXiv:2010.02943].

[283] J. Engel, D. Seckel and A. C. Hayes, Phys. Rev. Lett. **65**, 960 (1990).

[284] N. Iwamoto, Phys. Rev. Lett. **53**, 1198 (1984).

[285] N. Iwamoto, Phys. Rev. D **64**, 043002 (2001).

[286] A. Sedrakian, Phys. Rev. **D93**, 6, 065044 (2016), [arXiv:1512.07828].

[287] J. Keller and A. Sedrakian, Nucl. Phys. **A897**, 62 (2013), [arXiv:1205.6940].

[288] T. Fischer, Astron. Astrophys. **593**, A103 (2016), [arXiv:1608.05004].

[289] K. Springmann *et al.*, JHEP **02**, 138 (2025), [arXiv:2410.10945].

[290] K. Hamaguchi *et al.*, Phys. Rev. **D98**, 10, 103015 (2018), [arXiv:1806.07151].

[291] D. Page *et al.*, Phys. Rev. Lett. **106**, 081101 (2011), [arXiv:1011.6142].

[292] P. S. Shternin *et al.*, Mon. Not. Roy. Astron. Soc. **412**, L108 (2011), [arXiv:1012.0045].

[293] B. Posselt and G. G. Pavlov, Astrophys. J. **864**, 2, 135 (2018), [arXiv:1808.00531].

[294] M. V. Beznogov *et al.*, Phys. Rev. **C98**, 3, 035802 (2018), [arXiv:1806.07991].

[295] G. G. Raffelt, J. Redondo and N. Viaux Maira, Phys. Rev. **D84**, 103008 (2011), [arXiv:1110.6397].

[296] K. van Bibber *et al.*, Phys. Rev. **D39**, 2089 (1989).

[297] D. M. Lazarus *et al.*, Phys. Rev. Lett. **69**, 2333 (1992).

[298] S. Moriyama *et al.*, Phys. Lett. **B434**, 147 (1998), [hep-ex/9805026].

[299] Y. Inoue *et al.*, Phys. Lett. **B536**, 18 (2002), [arXiv:astro-ph/0204388].

[300] Y. Inoue *et al.*, Phys. Lett. **B668**, 93 (2008), [arXiv:0806.2230].

[301] E. Arik *et al.* (CAST), JCAP **0902**, 008 (2009), [arXiv:0810.4482].

[302] S. Aune *et al.* (CAST), Phys. Rev. Lett. **107**, 261302 (2011), [arXiv:1106.3919].

Int. J. Mod. Phys. A 2026.41. Downloaded from www.worldscientific.com by UNIVERSITY OF CALIFORNIA @ BERKELEY on 09/16/26. Re-use and distribution is strictly not permitted, except for Open Access articles.

[303] M. Arik *et al.* (CAST), Phys. Rev. Lett. **112**, 9, 091302 (2014), [arXiv:1307.1985].

[304] M. Arik *et al.* (CAST), Phys. Rev. **D92**, 2, 021101 (2015), [arXiv:1503.00610].

[305] E. Armengaud *et al.*, JINST **9**, T05002 (2014), [arXiv:1401.3233].

[306] E. Armengaud *et al.* (IAXO), JCAP **1906**, 06, 047 (2019), [arXiv:1904.09155].

[307] M. Giannotti *et al.*, JCAP **1710**, 10, 010 (2017), [arXiv:1708.02111].

[308] K. Barth *et al.*, JCAP **1305**, 010 (2013), [arXiv:1302.6283].

[309] A. Abeln *et al.* (BabyIAXO), JCAP **2105**, 05, 137 (2021), [arXiv:2010.12076].

[310] E. Aprile *et al.* (XENON), Phys. Rev. Lett. **129**, 16, 161805 (2022), [arXiv:2207.11330].

[311] X. Zeng *et al.* (PandaX), Phys. Rev. Lett. **134**, 4, 041001 (2025), [arXiv:2408.07641].

[312] J. Aalbers *et al.* (LZ), Phys. Rev. D **108**, 7, 072006 (2023), [arXiv:2307.15753].

[313] J. W. Brockway, E. D. Carlson and G. G. Raffelt, Phys. Lett. **B383**, 439 (1996), [arXiv:astro-ph/9605197].

[314] J. A. Grifols, E. Masso and R. Toldra, Phys. Rev. Lett. **77**, 2372 (1996), [arXiv:astro-ph/9606028].

[315] C. A. Manzari *et al.*, Phys. Rev. Lett. **133**, 21, 211002 (2024), [arXiv:2405.19393].

[316] F. Calore *et al.*, Phys. Rev. D **102**, 12, 123005 (2020), [arXiv:2008.11741].

[317] O. Ning and B. R. Safdi (2025), [arXiv:2503.09682].

[318] O. Ning and B. R. Safdi, Phys. Rev. Lett. **134**, 17, 171003 (2025), [arXiv:2404.14476].

[319] F. R. Candón *et al.*, Phys. Rev. Lett. **134**, 17, 171004 (2025), [arXiv:2412.03660].

[320] C. Dessert, J. W. Foster and B. R. Safdi, Astrophys. J. **904**, 1, 42 (2020), [arXiv:1910.02956].

[321] M. Buschmann *et al.*, Phys. Rev. Lett. **126**, 2, 021102 (2021), [arXiv:1910.04164].

[322] C. Dessert, A. J. Long and B. R. Safdi, Phys. Rev. Lett. **123**, 6, 061104 (2019), [arXiv:1903.05088].

[323] C. Csaki, N. Kaloper and J. Terning, Phys. Rev. Lett. **88**, 161302 (2002), [hep-ph/0111311].

[324] A. Mirizzi, G.G. Raffelt, and P.D. Serpico, Lect. Notes Phys. **741**, 115 (2008).

[325] D. Horns *et al.*, Phys. Rev. **D85**, 085021 (2012), [arXiv:1203.2184].

[326] A. Payez, J. R. Cudell and D. Hutsemekers, JCAP **1207**, 041 (2012), [arXiv:1204.6187].

[327] J. N. Benabou *et al.* (2025), [arXiv:2504.12377].

[328] R. Gill and J. S. Heyl, Phys. Rev. **D84**, 085001 (2011), [arXiv:1105.2083].

[329] A. Dominguez, M. A. Sanchez-Conde and F. Prada, JCAP **1111**, 020 (2011), [arXiv:1106.1860].

[330] W. Essey and A. Kusenko, Astrophys. J. **751**, L11 (2012), [arXiv:1111.0815].

[331] D. Horns and M. Meyer, JCAP **1202**, 033 (2012), [arXiv:1201.4711].

[332] G. I. Rubtsov and S. V. Troitsky, JETP Lett. **100**, 6, 355 (2014), [Pisma Zh. Eksp. Teor. Fiz.100,no.6,397(2014)], [arXiv:1406.0239].

[333] D. A. Sanchez, S. Fegan and B. Giebels, Astron. Astrophys. **554**, A75 (2013), [arXiv:1303.5923].

[334] J. Biteau and D. A. Williams, Astrophys. J. **812**, 1, 60 (2015), [arXiv:1502.04166].

[335] A. Domínguez and M. Ajello, Astrophys. J. **813**, 2, L34 (2015), [arXiv:1510.07913].

[336] A. Korochkin, G. Rubtsov and S. Troitsky, JCAP **12**, 002 (2019), [arXiv:1810.03443].

[337] A. De Angelis, G. Galanti and M. Roncadelli, Phys. Rev. **D84**, 105030 (2011), [Erratum: Phys. Rev.D87,no.10,109903(2013)], [arXiv:1106.1132].

[338] M. Simet, D. Hooper and P. D. Serpico, Phys. Rev. **D77**, 063001 (2008), [arXiv:0712.2825].

[339] M. A. Sanchez-Conde *et al.*, Phys. Rev. **D79**, 123511 (2009), [arXiv:0905.3270].

[340] M. Meyer, D. Horns and M. Raue, Phys. Rev. **D87**, 3, 035027 (2013), [arXiv:1302.1208].

[341] A. Abramowski *et al.* (H.E.S.S.), Phys. Rev. **D88**, 10, 102003 (2013), [arXiv:1311.3148].

[342] C. Zhang *et al.*, Phys. Rev. **D97**, 6, 063009 (2018), [arXiv:1802.08420].

[343] M. Libanov and S. Troitsky, Phys. Lett. B **802**, 135252 (2020), [arXiv:1908.03084].

[344] Z.-Q. Xia *et al.*, Phys. Rev. **D97**, 6, 063003 (2018), [arXiv:1801.01646].

[345] J. Majumdar, F. Calore and D. Horns, JCAP **1804**, 04, 048 (2018), [arXiv:1801.08813].

[346] G. A. Pallathadka *et al.*, JCAP **11**, 036 (2021), [arXiv:2008.08100].

[347] K. Choi *et al.*, Phys. Rev. D **101**, 4, 043007 (2020), [arXiv:1806.09508].

[348] F. Chadha-Day, Journal of Cosmology and Astroparticle Physics **2022**, 01, 013 (2022), URL `https://dx.doi.org/10.1088/1475-7516/2022/01/013`.

[349] M. Berg *et al.*, Astrophys. J. **847**, 2, 101 (2017), [arXiv:1605.01043].

[350] J. P. Conlon *et al.*, JCAP **1707**, 07, 005 (2017), [arXiv:1704.05256].

[351] L. Chen and J. P. Conlon, Mon. Not. Roy. Astron. Soc. **479**, 2, 2243 (2018), [arXiv:1712.08313].

[352] A. Hook and J. Huang, JHEP **06**, 036 (2018), [arXiv:1708.08464].

[353] J. Huang *et al.*, Phys. Rev. D **99**, 6, 063013 (2019), [arXiv:1807.02133].

[354] J. Zhang *et al.*, Phys. Rev. Lett. **127**, 161101 (2021), URL `https://link.aps.org/doi/10.1103/PhysRevLett.127.161101`.

[355] R. Balkin *et al.*, Phys. Rev. D **109**, 095032 (2024), URL `https://link.aps.org/doi/10.1103/PhysRevD.109.095032`.

[356] G. Bellini *et al.* (Borexino), Phys. Rev. D **89**, 11, 112007 (2014), [arXiv:1308.0443].

[357] B. P. Abbott *et al.* (LIGO Scientific, Virgo), Phys. Rev. Lett. **119**, 16, 161101 (2017), [arXiv:1710.05832].

[358] A. Arvanitaki and S. Dubovsky, Phys. Rev. **D83**, 044026 (2011), [arXiv:1004.3558].

[359] A. Arvanitaki, M. Baryakhtar and X. Huang, Phys. Rev. **D91**, 8, 084011 (2015), [arXiv:1411.2263].

[360] V. M. Mehta *et al.* (2020), [arXiv:2011.08693].

[361] V. M. Mehta *et al.*, JCAP **07**, 033 (2021), [arXiv:2103.06812].

[362] M. Baryakhtar *et al.*, Phys. Rev. D **103**, 9, 095019 (2021), [arXiv:2011.11646].

[363] M. J. Stott (2020), [arXiv:2009.07206].

[364] A. Arvanitaki *et al.*, Phys. Rev. **D95**, 4, 043001 (2017), [arXiv:1604.03958].

[365] K. K. Y. Ng *et al.*, Phys. Rev. D **103**, 6, 063010 (2021), [arXiv:1908.02312].

[366] C. Palomba *et al.*, Phys. Rev. Lett. **123**, 171101 (2019), [arXiv:1909.08854].

Int. J. Mod. Phys. A 2026.41. Downloaded from www.worldscientific.com
by UNIVERSITY OF CALIFORNIA @ BERKELEY on 09/16/26. Re-use and distribution is strictly not permitted, except for Open Access articles.

[367] L. Sun, R. Brito and M. Isi, Phys. Rev. D **101**, 6, 063020 (2020), [Erratum: Phys.Rev.D 102, 089902 (2020)], [arXiv:1909.11267].

[368] E. Masso, F. Rota and G. Zsembinszki, Phys. Rev. D **66**, 023004 (2002), [hep-ph/0203221].

[369] P. Graf and F. D. Steffen, Phys. Rev. D **83**, 075011 (2011), [arXiv:1008.4528].

[370] Z. G. Berezhiani, A. S. Sakharov and M. Y. Khlopov, Sov. J. Nucl. Phys. **55**, 1063 (1992).

[371] S. Hannestad, A. Mirizzi and G. Raffelt, JCAP **07**, 002 (2005), [hep-ph/0504059].

[372] G. Ballesteros *et al.*, Phys. Rev. Lett. **118**, 071802 (2017), URL `https://link.aps.org/doi/10.1103/PhysRevLett.118.071802`.

[373] M. Buschmann *et al.*, Nature Commun. **13**, 1, 1049 (2022), [arXiv:2108.05368].

[374] C. Bonati *et al.*, JHEP **03**, 155 (2016), [arXiv:1512.06746].

[375] E. Berkowitz, M. I. Buchoff and E. Rinaldi, Phys. Rev. **D92**, 3, 034507 (2015), [arXiv:1505.07455].

[376] M. Dine *et al.*, Phys. Rev. **D96**, 9, 095001 (2017), [arXiv:1705.00676].

[377] P. Petreczky, H.-P. Schadler and S. Sharma, Phys. Lett. **B762**, 498 (2016), [arXiv:1606.03145].

[378] L. Fleury and G. D. Moore, Journal of Cosmology and Astroparticle Physics **2016**, 01, 004 (2016), URL `https://dx.doi.org/10.1088/1475-7516/2016/01/004`.

[379] V. B. Klaer and G. D. Moore, JCAP **1711**, 11, 049 (2017), [arXiv:1708.07521].

[380] M. Gorghetto, E. Hardy and G. Villadoro, SciPost Phys. **10**, 050 (2021), [arXiv:2007.04990].

[381] M. Kawasaki, K. Saikawa and T. Sekiguchi, Phys. Rev. **D91**, 6, 065014 (2015), [arXiv:1412.0789].

[382] R. T. Co, L. J. Hall and K. Harigaya, Journal of High Energy Physics **2021**, 1, 172 (2021), ISSN 1029-8479, URL `https://doi.org/10.1007/JHEP01(2021)172`.

[383] N. Blinov *et al.*, Phys. Rev. D **100**, 015049 (2019), URL `https://link.aps.org/doi/10.1103/PhysRevD.100.015049`.

[384] P. Arias *et al.*, JCAP **1206**, 013 (2012), [arXiv:1201.5902].

[385] C. A. J. O'Hare *et al.*, Phys. Rev. D **105**, 055025 (2022), URL `https://link.aps.org/doi/10.1103/PhysRevD.105.055025`.

[386] L. D. Luzio *et al.*, Journal of Cosmology and Astroparticle Physics **2021**, 10, 001 (2021), URL `https://dx.doi.org/10.1088/1475-7516/2021/10/001`.

[387] S. Hannestad *et al.*, JCAP **08**, 001 (2010), [arXiv:1004.0695].

[388] M. Archidiacono *et al.*, JCAP **10**, 020 (2013), [arXiv:1307.0615].

[389] E. Di Valentino *et al.*, Phys. Lett. B **752**, 182 (2016), [arXiv:1507.08665].

[390] W. Giarè *et al.*, Mon. Not. Roy. Astron. Soc. **505**, 2, 2703 (2021), [arXiv:2011.14704].

[391] L. Di Luzio, G. Martinelli and G. Piazza, Phys. Rev. Lett. **126**, 24, 241801 (2021), [arXiv:2101.10330].

[392] A. Notari, F. Rompineve and G. Villadoro, Phys. Rev. Lett. **131**, 1, 011004 (2023), [arXiv:2211.03799].

[393] E. Masso and R. Toldra, Phys. Rev. D **52**, 1755 (1995), [hep-ph/9503293].

[394] E. Masso and R. Toldra, Phys. Rev. **D55**, 7967 (1997), [hep-ph/9702275].

[395] J. W. Foster *et al.*, JHEP **12**, 119 (2022), [arXiv:2208.10504].

[396] P. Panci *et al.*, Phys. Lett. B **841**, 137919 (2023), [arXiv:2209.03371].

[397] M. Regis *et al.*, Physics Letters B **814**, 136075 (2021), ISSN 0370-2693, URL `https://www.sciencedirect.com/science/article/pii/S0370269321000150`.

[398] J. W. Foster *et al.*, Phys. Rev. Lett. **127**, 5, 051101 (2021), [arXiv:2102.02207].

[399] J. Preskill, M. B. Wise and F. Wilczek, Phys. Lett. **B120**, 127 (1983).

[400] L. F. Abbott and P. Sikivie, Phys. Lett. **B120**, 133 (1983).

[401] M. Dine and W. Fischler, Phys. Lett. **B120**, 137 (1983).

[402] J. N. Benabou *et al.*, Phys. Rev. D **110**, 3, 035021 (2024), [arXiv:2312.08425].

[403] K. J. Bae, J.-H. Huh and J. E. Kim, JCAP **0809**, 005 (2008), [arXiv:0806.0497].

[404] O. Wantz and E. P. S. Shellard, Phys. Rev. **D82**, 123508 (2010), [arXiv:0910.1066].

[405] G. Ballesteros *et al.*, JCAP **1708**, 08, 001 (2017), [arXiv:1610.01639].

[406] R. T. Co, F. D'Eramo and L. J. Hall, Phys. Rev. D **94**, 7, 075001 (2016), [arXiv:1603.04439].

[407] M. Tegmark *et al.*, Phys. Rev. **D73**, 023505 (2006), [arXiv:astro-ph/0511774].

[408] A. D. Linde, Phys. Lett. **158B**, 375 (1985).

[409] D. Seckel and M. S. Turner, Phys. Rev. **D32**, 3178 (1985).

[410] M. Beltran, J. Garcia-Bellido and J. Lesgourgues, Phys. Rev. **D75**, 103507 (2007), [hep-ph/0606107].

[411] M. P. Hertzberg, M. Tegmark and F. Wilczek, Phys. Rev. **D78**, 083507 (2008), [arXiv:0807.1726].

[412] J. Hamann *et al.*, JCAP **0906**, 022 (2009), [arXiv:0904.0647].

[413] P. A. R. Ade *et al.* (Planck), Astron. Astrophys. **571**, A22 (2014), [arXiv:1303.5082].

[414] P. A. R. Ade *et al.* (Planck), Astron. Astrophys. **594**, A20 (2016), [arXiv:1502.02114].

[415] B. Bolliet, J. Chluba and R. Battye, Monthly Notices of the Royal Astronomical Society **507**, 3, 3148 (2021), ISSN 0035-8711, URL `https://doi.org/10.1093/mnras/stab1997`.

[416] R. T. Co, L. J. Hall and K. Harigaya, Phys. Rev. Lett. **124**, 25, 251802 (2020), [arXiv:1910.14152].

[417] S. Borsanyi *et al.*, Phys. Lett. **B752**, 175 (2016), [arXiv:1508.06917].

[418] R. Kitano and N. Yamada, JHEP **10**, 136 (2015), [arXiv:1506.00370].

[419] Y. Taniguchi *et al.*, Phys. Rev. **D95**, 5, 054502 (2017), [arXiv:1611.02411].

[420] R. D. Pisarski and L. G. Yaffe, Phys. Lett. **97B**, 110 (1980).

[421] S. Chang, C. Hagmann and P. Sikivie, Phys. Rev. **D59**, 023505 (1999), [hep-ph/9807374].

[422] C. Hagmann, S. Chang and P. Sikivie, Phys. Rev. **D63**, 125018 (2001), [hep-ph/0012361].

[423] T. Hiramatsu *et al.*, Phys. Rev. **D83**, 123531 (2011), [arXiv:1012.5502].

[424] T. Hiramatsu *et al.*, Phys. Rev. **D85**, 105020 (2012), [Erratum: Phys. Rev.D86,089902(2012)], [arXiv:1202.5851].

[425] M. Gorghetto, E. Hardy and G. Villadoro, JHEP **07**, 151 (2018), [arXiv:1806.04677].

[426] M. Buschmann, J. W. Foster and B. R. Safdi, Phys. Rev. Lett. **124**, 16, 161103 (2020), [arXiv:1906.00967].

[427] M. Hindmarsh *et al.*, Phys. Rev. Lett. **124**, 2, 021301 (2020), [arXiv:1908.03522].

[428] M. Dine *et al.*, Journal of Cosmology and Astroparticle Physics **2021**, 11, 041 (2021), URL `https://dx.doi.org/10.1088/1475-7516/2021/11/041`.

[429] M. Hindmarsh *et al.*, Phys. Rev. D **103**, 10, 103534 (2021), [arXiv:2102.07723].

Int. J. Mod. Phys. A 2026.41. Downloaded from www.worldscientific.com
by UNIVERSITY OF CALIFORNIA @ BERKELEY on 09/16/26. Re-use and distribution is strictly not permitted, except for Open Access articles.

[430] K. Saikawa *et al.*, JCAP **10**, 043 (2024), [arXiv:2401.17253].

[431] H. Kim and M. Son, JHEP **07**, 052 (2025), [arXiv:2411.08455].

[432] J. N. Benabou *et al.*, Phys. Rev. Lett. **134**, 24, 241003 (2025), [arXiv:2412.08699].

[433] A. Ringwald and K. Saikawa, Phys. Rev. **D93**, 8, 085031 (2016), [Addendum: Phys. Rev.D94,no.4,049908(2016)], [arXiv:1512.06436].

[434] T. Hiramatsu *et al.*, JCAP **1301**, 001 (2013), [arXiv:1207.3166].

[435] K. A. Beyer and S. Sarkar, SciPost Phys. **15**, 003 (2023), [arXiv:2211.14635].

[436] C. J. Hogan and M. J. Rees, Phys. Lett. **B205**, 228 (1988).

[437] E. W. Kolb and I. I. Tkachev, Phys. Rev. Lett. **71**, 3051 (1993), [hep-ph/9303313].

[438] B. Eggemeier *et al.*, Phys. Rev. Lett. **125**, 4, 041301 (2020), [arXiv:1911.09417].

[439] A. Vaquero, J. Redondo and J. Stadler, Journal of Cosmology and Astroparticle Physics **2019**, 04, 012 (2019), URL `https://dx.doi.org/10.1088/1475-7516/2019/04/012`.

[440] E. W. Kolb and I. I. Tkachev, Astrophys. J. **460**, L25 (1996), [arXiv:astro-ph/9510043].

[441] M. Fairbairn, D. J. E. Marsh and J. Quevillon, Phys. Rev. Lett. **119**, 2, 021101 (2017), [arXiv:1701.04787].

[442] A. Katz *et al.*, JCAP **1812**, 005 (2018), [arXiv:1807.11495].

[443] R. Hlozek *et al.*, Phys. Rev. **D91**, 10, 103512 (2015), [arXiv:1410.2896].

[444] D. J. E. Marsh, Phys. Rept. **643**, 1 (2016), [arXiv:1510.07633].

[445] L. Hui *et al.*, Phys. Rev. **D95**, 4, 043541 (2017), [arXiv:1610.08297].

[446] G. P. Centers *et al.*, Nature Communications **12**, 1, 7321 (2021), ISSN 2041-1723, URL `https://doi.org/10.1038/s41467-021-27632-7`.

[447] A. G. Dias *et al.*, JHEP **06**, 037 (2014), [arXiv:1403.5760].

[448] J. E. Kim and D. J. E. Marsh, Phys. Rev. **D93**, 2, 025027 (2016), [arXiv:1510.01701].

[449] H. Davoudiasl and C. W. Murphy, Phys. Rev. Lett. **118**, 14, 141801 (2017), [arXiv:1701.01136].

[450] L. Di Luzio *et al.*, JCAP **10**, 001 (2021), [arXiv:2102.01082].

[451] M. Khlopov, B. A. Malomed and I. B. Zeldovich, Mon. Not. Roy. Astron. Soc. **215**, 575 (1985).

[452] W. Hu, R. Barkana and A. Gruzinov, Phys. Rev. Lett. **85**, 1158 (2000), [arXiv:astro-ph/0003365].

[453] L. Amendola and R. Barbieri, Phys. Lett. **B642**, 192 (2006), [hep-ph/0509257].

[454] D. J. E. Marsh and P. G. Ferreira, Phys. Rev. **D82**, 103528 (2010), [arXiv:1009.3501].

[455] E. Seidel and W. M. Suen, Phys. Rev. Lett. **66**, 1659 (1991).

[456] H.-Y. Schive, T. Chiueh and T. Broadhurst, Nature Phys. **10**, 496 (2014), [arXiv:1406.6586].

[457] D. G. Levkov, A. G. Panin and I. I. Tkachev, Phys. Rev. Lett. **121**, 15, 151301 (2018), [arXiv:1804.05857].

[458] B. Eggemeier and J. C. Niemeyer, Phys. Rev. D **100**, 6, 063528 (2019), [arXiv:1906.01348].

[459] R. Hlozek, D. J. E. Marsh and D. Grin, Mon. Not. Roy. Astron. Soc. **476**, 3, 3063 (2018), [arXiv:1708.05681].

[460] D. J. E. Marsh and J. Silk, Mon. Not. Roy. Astron. Soc. **437**, 3, 2652 (2014), [arXiv:1307.1705].

[461] H.-Y. Schive *et al.*, Astrophys. J. **818**, 1, 89 (2016), [arXiv:1508.04621].

[462] B. Bozek *et al.*, Mon. Not. Roy. Astron. Soc. **450**, 1, 209 (2015), [arXiv:1409.3544].

[463] P. S. Corasaniti *et al.*, Phys. Rev. **D95**, 8, 083512 (2017), [arXiv:1611.05892].

[464] K. K. Rogers and H. V. Peiris, Phys. Rev. Lett. **126**, 7, 071302 (2021), [arXiv:2007.12705].

[465] H.-Y. Schive and T. Chiueh, Mon. Not. Roy. Astron. Soc. **473**, 1, L36 (2018), [arXiv:1706.03723].

[466] E. O. Nadler *et al.* (DES), Phys. Rev. Lett. **126**, 091101 (2021), [arXiv:2008.00022].

[467] B. Schwabe, J. C. Niemeyer and J. F. Engels, Phys. Rev. **D94**, 4, 043513 (2016), [arXiv:1606.05151].

[468] J. Veltmaat and J. C. Niemeyer, Phys. Rev. **D94**, 12, 123523 (2016), [arXiv:1608.00802].

[469] P. Mocz *et al.*, Mon. Not. Roy. Astron. Soc. **471**, 4, 4559 (2017), [arXiv:1705.05845].

[470] D. G. Levkov, A. G. Panin and I. I. Tkachev, Phys. Rev. Lett. **118**, 011301 (2017); T. Helfer *et al.*, JCAP **1703**, 03, 055 (2017), [arXiv:1609.04724]; J. Eby *et al.*, Journal of High Energy Physics **2018**, 1, 66 (2018), ISSN 1029-8479, URL `https://doi.org/10.1007/JHEP01(2018)066`.

[471] D. J. E. Marsh and A.-R. Pop, Mon. Not. Roy. Astron. Soc. **451**, 3, 2479 (2015), [arXiv:1502.03456].

[472] S.-R. Chen, H.-Y. Schive and T. Chiueh, Mon. Not. Roy. Astron. Soc. **468**, 2, 1338 (2017), [arXiv:1606.09030].

[473] A. X. González-Morales *et al.*, Mon. Not. Roy. Astron. Soc. **472**, 2, 1346 (2017), [arXiv:1609.05856].

[474] I. De Martino *et al.*, Phys. Dark Univ. **28**, 100503 (2020), [arXiv:1807.08153].

[475] T. Broadhurst *et al.*, Phys. Rev. D **101**, 8, 083012 (2020), [arXiv:1902.10488].

[476] H.-Y. Schive *et al.*, Phys. Rev. Lett. **113**, 26, 261302 (2014), [arXiv:1407.7762].

[477] V. H. Robles, J. S. Bullock and M. Boylan-Kolchin, Mon. Not. Roy. Astron. Soc. **483**, 1, 289 (2019), [arXiv:1807.06018].

[478] V. Desjacques and A. Nusser, Monthly Notices of the Royal Astronomical Society **488**, 4, 4497 (2019), ISSN 0035-8711, URL `https://doi.org/10.1093/mnras/stz1978`.

[479] M. Safarzadeh and D. N. Spergel, The Astrophysical Journal **893**, 1, 21 (2020), URL `https://dx.doi.org/10.3847/1538-4357/ab7db2`.

[480] A. Pontzen and F. Governato, Nature **506**, 171 (2014), [arXiv:1402.1764].

[481] P. Mocz *et al.*, Phys. Rev. Lett. **123**, 14, 141301 (2019), [arXiv:1910.01653].

[482] J. Veltmaat, B. Schwabe and J. C. Niemeyer, Phys. Rev. D **101**, 8, 083518 (2020), [arXiv:1911.09614].

[483] J. Veltmaat, J. C. Niemeyer and B. Schwabe, Phys. Rev. **D98**, 4, 043509 (2018), [arXiv:1804.09647].

[484] B. Bar-Or, J.-B. Fouvry and S. Tremaine, Astrophys. J. **871**, 1, 28 (2019), [arXiv:1809.07673].

[485] B. V. Church, P. Mocz and J. P. Ostriker, MNRAS **485**, 2861 (2019), [arXiv:1809.04744].

[486] N. C. Amorisco and A. Loeb (2018), [arXiv:1808.00464].

[487] T. S. Li *et al.* (DES), Astrophys. J. **838**, 1, 8 (2017), [arXiv:1611.05052].

[488] D. J. E. Marsh and J. C. Niemeyer, Phys. Rev. Lett. **123**, 5, 051103 (2019), [arXiv:1810.08543].

[489] N. Dalal and A. Kravtsov, Phys. Rev. D **106**, 6, 063517 (2022), [arXiv:2203.05750].

[490] E. Armengaud *et al.* (EDELWEISS), Phys. Rev. D **98**, 8, 082004 (2018), [arXiv:1808.02340].

[491] E. Aprile *et al.* (XENON), Phys. Rev. Lett. **123**, 25, 251801 (2019), [arXiv:1907.11485].

[492] S. Roy *et al.*, Phys. Rev. Lett. **134**, 7, 071003 (2025), [arXiv:2311.04987].

Int. J. Mod. Phys. A 2026.41. Downloaded from www.worldscientific.com
by UNIVERSITY OF CALIFORNIA @ BERKELEY on 09/16/26. Re-use and distribution is strictly not permitted, except for Open Access articles.

[493] E. Pinetti (2025), [arXiv:2503.11753].

[494] K. Kelley and P. J. Quinn, Astrophys. J. **845**, 1, L4 (2017), [arXiv:1708.01399].

[495] G. Sigl, Phys. Rev. **D96**, 10, 103014 (2017), [arXiv:1708.08908].

[496] A. Hook *et al.*, Phys. Rev. Lett. **121**, 24, 241102 (2018), [arXiv:1804.03145].

[497] B. R. Safdi, Z. Sun and A. Y. Chen, Phys. Rev. D **99**, 12, 123021 (2019), [arXiv:1811.01020].

[498] S. J. Witte *et al.*, Phys. Rev. D **104**, 103030 (2021), URL `https://link.aps.org/doi/10.1103/PhysRevD.104.103030`.

[499] R. A. Battye *et al.*, Journal of High Energy Physics **2021**, 9, 105 (2021), ISSN 1029-8479, URL `https://doi.org/10.1007/JHEP09(2021)105`.

[500] A. J. Millar *et al.*, Journal of Cosmology and Astroparticle Physics **2021**, 11, 013 (2021), URL `https://dx.doi.org/10.1088/1475-7516/2021/11/013`.

[501] J. McDonald, B. Garbrecht and P. Millington, Journal of Cosmology and Astroparticle Physics **2023**, 12, 031 (2023), URL `https://dx.doi.org/10.1088/1475-7516/2023/12/031`.

[502] A. Caputo *et al.*, JCAP **1903**, 03, 027 (2019), [arXiv:1811.08436].

[503] P. Carenza, A. Mirizzi and G. Sigl, Phys. Rev. D **101**, 10, 103016 (2020), [arXiv:1911.07838].

[504] D. G. Levkov, A. G. Panin and I. I. Tkachev, Phys. Rev. D **102**, 2, 023501 (2020), [arXiv:2004.05179].

[505] T. Fujita *et al.*, Phys. Rev. D **103**, 4, 043509 (2021), [arXiv:2011.11894].

[506] T. Liu, G. Smoot and Y. Zhao, Phys. Rev. D **101**, 6, 063012 (2020), [arXiv:1901.10981].

[507] P. Sikivie, Phys. Rev. **D32**, 2988 (1985), [Erratum: Phys. Rev.D36,974(1987)].

[508] R. Bradley *et al.*, Rev. Mod. Phys. **75**, 777 (2003).

[509] C. Bartram *et al.* (ADMX Collaboration), Phys. Rev. D **109**, 083014 (2024), URL `https://link.aps.org/doi/10.1103/PhysRevD.109.083014`.

[510] C. Goodman *et al.* (ADMX Collaboration), Phys. Rev. Lett. **134**, 111002 (2025), URL `https://link.aps.org/doi/10.1103/PhysRevLett.134.111002`.

[511] G. C. e. al., Phys. Rev. Lett. – (2025), URL `https://link.aps.org/doi/10.1103/d7mg-6sqq`.

[512] S. Bae *et al.*, Phys. Rev. Lett. **135**, 091804 (2025), URL `https://link.aps.org/doi/10.1103/f11t-qy8z`.

[513] C. Boutan *et al.* (ADMX), Phys. Rev. Lett. **121**, 26, 261302 (2018), [arXiv:1901.00920].

[514] C. Bartram *et al.* (ADMX), Phys. Rev. D **103**, 3, 032002 (2021), [arXiv:2010.06183].

[515] R. Khatiwada *et al.*, Review of Scientific Instruments **92**, 12, 124502 (2021), ISSN 0034-6748, URL `https://doi.org/10.1063/5.0037857`.

[516] W. Wuensch *et al.*, Phys. Rev. **D40**, 3153 (1989).

[517] A. A. Melcón *et al.* (CAST), JHEP **21**, 075 (2020), [arXiv:2104.13798].

[518] B. T. McAllister *et al.*, Annalen der Physik **n/a**, n/a, 2200622 (2022), URL `https://onlinelibrary.wiley.com/doi/abs/10.1002/andp.202200622`.

[519] Unpulished work by P. Sikivie, N. Sullivan, and D. B. Tanner in the early 2000s and independent work by B. Cabrera and S. Thomas. presented in a talk at the Axions 2010 Conference in Gainesville, Florida, January 15–17., URL `http://www.physics.rutgers.edu/~scthomas/talks/Axion-LC-Florida.pdf`.

[520] P. Sikivie, N. Sullivan, and D. B. Tanner, Phys. Rev. Lett. **112**, 131301 (2014).

[521] Y. Kahn, B. R. Safdi and J. Thaler, Phys. Rev. Lett. **117**, 14, 141801 (2016), [arXiv:1602.01086].

[522] L. Brouwer *et al.* (DMRadio), Phys. Rev. D **106**, 10, 103008 (2022), [arXiv:2204.13781].

[523] L. Brouwer *et al.* (DMRadio), Phys. Rev. D **106**, 11, 112003 (2022), [arXiv:2203.11246].

[524] Y. Oshima *et al.*, Phys. Rev. D **108**, 072005 (2023), URL `https://link.aps.org/doi/10.1103/PhysRevD.108.072005`.

[525] A. J. Millar *et al.* (Endorsers), Phys. Rev. D **107**, 055013 (2023), URL `https://link.aps.org/doi/10.1103/PhysRevD.107.055013`.

[526] S. K. Lamoreaux *et al.*, Phys. Rev. D **88**, 035020 (2013), URL `https://link.aps.org/doi/10.1103/PhysRevD.88.035020`.

[527] R. Cervantes *et al.*, Phys. Rev. Lett. **129**, 201301 (2022), URL `https://link.aps.org/doi/10.1103/PhysRevLett.129.201301`.

[528] J. Chiles *et al.*, Phys. Rev. Lett. **128**, 231802 (2022), URL `https://link.aps.org/doi/10.1103/PhysRevLett.128.231802`.

[529] D. Horns *et al.*, JCAP **1304**, 016 (2013), [arXiv:1212.2970].

[530] F. Bajjali *et al.*, Journal of Cosmology and Astroparticle Physics **2023**, 08, 077 (2023), URL `https://dx.doi.org/10.1088/1475-7516/2023/08/077`.

[531] C.-L. Kuo *et al.*, Phys. Rev. D **111**, 123018 (2025), URL `https://link.aps.org/doi/10.1103/pgtg-3lhd`.

[532] M. J. Jewell *et al.* (HAYSTAC Collaboration), Phys. Rev. D **107**, 072007 (2023), URL `https://link.aps.org/doi/10.1103/PhysRevD.107.072007`.

[533] C. Braggio *et al.*, Phys. Rev. X **15**, 021031 (2025), URL `https://link.aps.org/doi/10.1103/PhysRevX.15.021031`.

[534] A. V. Dixit *et al.*, Phys. Rev. Lett. **126**, 141302 (2021), URL `https://link.aps.org/doi/10.1103/PhysRevLett.126.141302`.

[535] I. M. Bloch *et al.*, Sci. Adv. **8**, 5, abl8919 (2022), [arXiv:2105.04603].

[536] S. P. Chang *et al.*, Phys. Rev. **D99**, 8, 083002 (2019), [arXiv:1710.05271].

[537] L. Krauss *et al.*, Phys. Rev. Lett. **55**, 1797 (1985).

[538] R. Barbieri *et al.*, Phys. Lett. B **226**, 357 (1989).

[539] R. Barbieri *et al.*, Phys. Dark Univ. **15**, 135 (2017), [arXiv:1606.02201].

[540] J. A. Dror *et al.*, Phys. Rev. Lett. **130**, 181801 (2023), URL `https://link.aps.org/doi/10.1103/PhysRevLett.130.181801`.

[541] E. Boyers, G. Goldstein and A. O. Sushkov, Phys. Rev. D **111**, 052004 (2025), URL `https://link.aps.org/doi/10.1103/PhysRevD.111.052004`.

[542] M. Galanis *et al.*, Toward 48 dB Spin Squeezing and 96 dB Signal Magnification for Cosmic Relic Searches with Nuclear Spins (2025), [arXiv:2508.20520], URL `https://arxiv.org/abs/2508.20520`.

90. Searches for Quark and Lepton Compositeness

Revised August 2025 by K. Hikasa (Tohoku U.), M. Tanabashi (Nagoya U.; KMI, Nagoya U.), K. Terashi (ICEPP, Tokyo U.) and N. Varelas (U. of Illinois at Chicago).

90.1 Limits on contact interactions

If quarks and leptons are made of constituents, then at the scale of constituent binding energies (compositeness scale Λ) there should appear new interactions among them. At energies much below the compositeness scale, these interactions are suppressed by inverse powers of Λ. The dominant effect of the compositeness of fermion ψ should come from the lowest dimensional interactions with four fermions (contact terms), whose most general flavor-diagonal color-singlet chirally invariant form reads [1, 2]

$$\mathcal{L} = \mathcal{L}_{LL} + \mathcal{L}_{RR} + \mathcal{L}_{LR} + \mathcal{L}_{RL},$$

with

$$\mathcal{L}_{LL} = \frac{g^2_{\rm contact}}{2\Lambda^2} \sum_{i,j} \eta^{ij}_{LL} (\bar\psi^i_L \gamma_\mu \psi^i_L)(\bar\psi^j_L \gamma^\mu \psi^j_L),$$

$$\mathcal{L}_{RR} = \frac{g^2_{\rm contact}}{2\Lambda^2} \sum_{i,j} \eta^{ij}_{RR} (\bar\psi^i_R \gamma_\mu \psi^i_R)(\bar\psi^j_R \gamma^\mu \psi^j_R),$$

$$\mathcal{L}_{LR} = \frac{g^2_{\rm contact}}{2\Lambda^2} \sum_{i,j} \eta^{ij}_{LR} (\bar\psi^i_L \gamma_\mu \psi^i_L)(\bar\psi^j_R \gamma^\mu \psi^j_R),$$

$$\mathcal{L}_{RL} = \frac{g^2_{\rm contact}}{2\Lambda^2} \sum_{i,j} \eta^{ij}_{RL} (\bar\psi^i_R \gamma_\mu \psi^i_R)(\bar\psi^j_L \gamma^\mu \psi^j_L), \qquad (90.1)$$

where i, j are the indices of fermion species. Color and other indices are suppressed in Eq. (90.1). Such interactions can arise by interchanging constituents (when the fermions have common constituents), and/or by exchanging the binding quanta (whenever binding quanta couple to constituents of both particles). Chiral invariance provides a natural explanation why quark and lepton masses are much smaller than their inverse size (inverse radius) Λ. Note $\eta^{ij}_{\alpha\beta} = \eta^{ji}_{\beta\alpha}$, thus $\mathcal{L}_{LR}$ and $\mathcal{L}_{RL}$ are identical. Therefore, in order to specify the contact interaction among the same fermion species $i = j$, it is enough to use η_{LL}, η_{RR} and η_{LR}. We will suppress the indices of fermion species hereafter. We may determine the scale Λ unambiguously by using the above form of the effective interactions; the conventional method [1] is to fix its scale by setting $g^2_{\rm contact}/4\pi = g^2_{\rm contact}(\Lambda)/4\pi = 1$ for the new strong interaction coupling and by setting the largest magnitude of the coefficients $\eta_{\alpha\beta}$ to be unity. In the following, we denote

$$\Lambda = \Lambda^\pm_{LL}\,, \Lambda^\pm_{RR}\,, \Lambda^\pm_{VV}\,, \Lambda^\pm_{AA}\,, \Lambda^\pm_{V-A}\,, \qquad (90.2)$$

for $(\eta_{LL}, \eta_{RR}, \eta_{LR}) = (\pm1, 0, 0), (0, \pm1, 0), (\pm1, \pm1, \pm1), (\pm1, \pm1, \mp1), (0, 0, \pm1)$.

Fermion scattering amplitude induced from the contact interaction in Eq. (90.1) interferes with the Standard Model (SM) amplitude destructively or constructively [2]. The sign of interference depends on the sign of $\eta_{\alpha\beta}$ $(\alpha, \beta = L, R)$. For instance, in the parton level $qq \to qq$ scattering cross section in the $\Lambda^\pm_{LL}$ model, the contact interaction amplitude and the SM gluon exchange amplitude interfere destructively for $\eta_{LL} = +1$, while they interfere constructively for $\eta_{LL} = -1$. In models of quark compositeness, the quark scattering cross sections induced from the contact interactions receive sizable QCD radiative corrections. The exact next-to-leading order (NLO) QCD corrections to the quark scatterings cross sections induced by the contact interactions are given in [3].

Over the last three decades experiments at the CERN Sp$\bar{\rm p}$S [4, 5], the Fermilab Tevatron [6, 7], and the CERN LHC [8–12] have searched for quark contact interactions, characterized by the four-fermion effective Lagrangian in Eq. (90.1), using jet final states. These searches have been performed primarily by studying the angular distribution of the two highest transverse momentum, $p_{\rm T}$, jets (dijets), and the inclusive jet $p_{\rm T}$ spectrum. The variable $\chi = \exp(|(y_1 - y_2)|)$ is used to measure the dijet angular distribution, where y_1 and y_2 are the rapidities of the two jets with the highest transverse momenta. For collinear massless parton scattering, χ is related to the polar scattering angle θ^* in the partonic center-of-mass frame by $\chi = (1+|\cos\theta^*|)/(1-|\cos\theta^*|)$. The choice of χ is motivated by the fact that the angular distribution for Rutherford scattering, which is proportional to $1/(1-\cos\theta^*)^2$, is independent of χ. In perturbative QCD the χ distributions are relatively uniform and only mildly modified by higher-order QCD or electroweak corrections. Signatures of quark contact interactions exhibit more isotropic angular distribution than QCD and can be identified as an excess at low values of χ. In the inclusive jet cross section measurement, quark contact interaction effects are searched for as deviations from the predictions of perturbative QCD in the tails of the high-$p_{\rm T}$ jet spectrum [11].

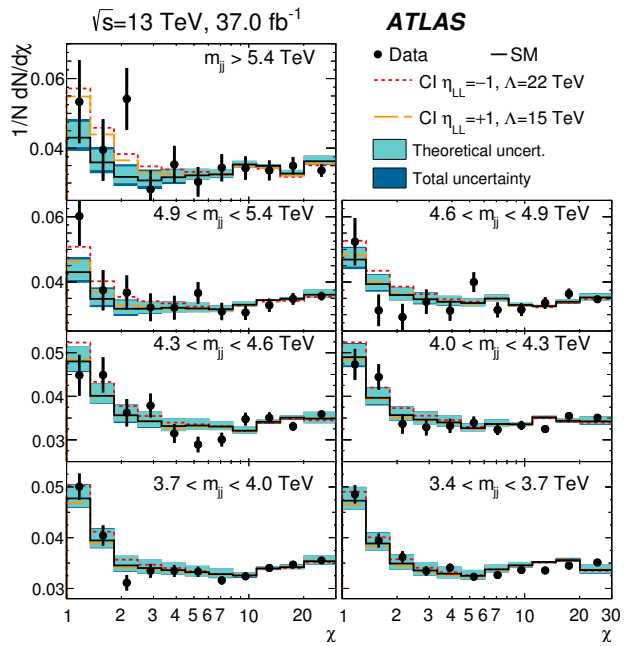

Figure 90.1: Normalized dijet angular distributions in several dijet mass (m_{jj}) ranges. The data distributions are compared to PYTHIA8 predictions with NLO and electroweak corrections applied (solid line) and with the predictions including a contact interaction (CI) term in which only left-handed quarks participate of compositeness scale $\Lambda^+_{LL} = 15$ TeV (dashed line) and $\Lambda^-_{LL} = 22$ TeV (dotted line). The theoretical uncertainties and the total theoretical and experimental uncertainties in the predictions are displayed as shaded bands around the SM prediction. Figure adopted from [9].

Recent results from the LHC, using data collected at proton-proton center-of-mass energy of $\sqrt{s} = 13$ TeV, extend previous limits on quark contact interactions. Figure 90.1 shows the normalized dijet angular distributions for several dijet mass ranges measured in ATLAS [9] at $\sqrt{s} = 13$ TeV. The data distributions are compared with SM predictions, estimated using PYTHIA8 [13] with GEANT4-based [14] ATLAS detector simulation and corrected to NLO QCD calculation provided by NLO Jet++ [15] including electroweak corrections [16]. Predictions including a contact interaction term in which only left-handed quarks participate at compositeness scale $\Lambda^+_{LL} = 15$ TeV ($\Lambda^-_{LL} = 22$ TeV) with destructive (constructive) interference are also shown. Over a wide range of χ and dijet mass the data are well described by the SM predictions. Using the dijet angular distributions measured at high dijet masses and $\sqrt{s} = 13$ TeV, the ATLAS [9] and CMS [12] Collaborations have set 95% confidence level (C.L.) lower limits on the contact interaction scale Λ, ranging from 9.2 to 29.5 TeV for different quark contact interaction models that correspond to various combinations of $(\eta_{LL}, \eta_{RR}, \eta_{LR})$, as summarized in Figure 90.2. The contact interaction scale limits extracted using the dijet angular distributions include the exact NLO QCD corrections to dijet production induced by contact interactions [3]. In proton-

Int. J. Mod. Phys. A 2026.41. Downloaded from www.worldscientific.com by UNIVERSITY OF CALIFORNIA @ BERKELEY on 09/16/26. Re-use and distribution is strictly not permitted, except for Open Access articles.

Int. J. Mod. Phys. A 2026.41. Downloaded from www.worldscientific.com
by UNIVERSITY OF CALIFORNIA @ BERKELEY on 09/16/26. Re-use and distribution is strictly not permitted, except for Open Access articles.

proton collisions, the $\Lambda^{\pm}_{LL}$ and $\Lambda^{\pm}_{RR}$ contact interaction models result in identical tree-level cross sections and NLO QCD corrections and yield the same exclusion limits. For $\Lambda^{\pm}_{VV}$ and $\Lambda^{\pm}_{AA}$, the contact interaction predictions are identical at tree level, but exhibit different NLO QCD corrections and yield different exclusion limits.

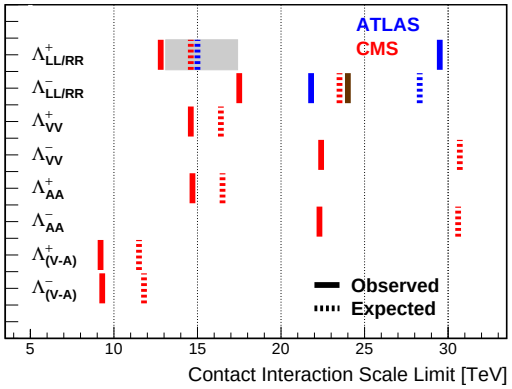

Figure 90.2: Observed (solid lines) and expected (dashed lines) 95% C.L. lower limits on the contact interaction scale Λ for different contact interaction models from ATLAS [9] and CMS [12] using the dijet angular distributions. The contact interaction models used for the dijet angular distributions include the exact NLO QCD corrections to dijet production. The shaded band for the $\Lambda^{+}_{LL/RR}$ model indicates the range of contact interaction scale that was not excluded in ATLAS [9], due to an observed excess in the data that produced a weaker limit. The observed 95% C.L. lower limit on the Λ^{-}_{LL} from CMS [17] is shown as the second solid line in brown.

If leptons (l) and quarks (q) are composite with common constituents, the interaction of these constituents will manifest itself in the form of a $llqq$-type four-fermion contact interaction Lagrangian at energies below the compositeness scale Λ. The $llqq$ terms in the contact interaction Lagrangian can be expressed as

$$\mathcal{L}_{LL} = \frac{g^2_{\text{contact}}}{\Lambda^2} \sum_{i,j} \eta^{ij}_{LL} (\bar{q}^i_L \gamma_\mu q^i_L)(\bar{l}^j_L \gamma^\mu l^j_L),$$

$$\mathcal{L}_{RR} = \frac{g^2_{\text{contact}}}{\Lambda^2} \sum_{i,j} \eta^{ij}_{RR} (\bar{q}^i_R \gamma_\mu q^i_R)(\bar{l}^j_R \gamma^\mu l^j_R),$$

$$\mathcal{L}_{LR} = \frac{g^2_{\text{contact}}}{\Lambda^2} \sum_{i,j} \eta^{ij}_{LR} (\bar{q}^i_L \gamma_\mu q^i_L)(\bar{l}^j_R \gamma^\mu l^j_R),$$

$$\mathcal{L}_{RL} = \frac{g^2_{\text{contact}}}{\Lambda^2} \sum_{i,j} \eta^{ij}_{RL} (\bar{q}^i_R \gamma_\mu q^i_R)(\bar{l}^j_L \gamma^\mu l^j_L). \qquad (90.3)$$

Searches on quark-lepton compositeness have been reported from experiments at LEP [18–21], HERA [22, 23], the Tevatron [24, 25], and recently from the ATLAS [26, 27] and CMS [28, 29] experiments at the LHC. The most stringent searches for $llqq$ contact interactions are performed by the LHC experiments using high-mass oppositely-charged lepton pairs produced through the $q\bar{q} \to l^+l^-$ Drell-Yan process. The contact interaction amplitude of the $u\bar{u} \to l^+l^-$ process ($l = e$ or μ) interferes with the corresponding SM amplitude constructively (destructively) for $\eta^{ul}_{\alpha\beta} = -1$ ($\eta^{ul}_{\alpha\beta} = +1$). The ATLAS Collaboration, using a 139 fb^{-1} dataset at $\sqrt{s} = 13$ TeV, has extracted limits on the $llqq$ contact interaction for the right-right ($\eta_{RR} = \pm 1$, $\eta_{LL} = \eta_{LR} = \eta_{RL} = 0$), left-left ($\eta_{LL} = \pm 1$, $\eta_{RR} = \eta_{LR} = \eta_{RL} = 0$), and left-right ($\eta_{LR} = \eta_{RL} = \pm 1$, $\eta_{RR} = \eta_{LL} = 0$) models. In Ref. [27], ATLAS used a background estimate directly obtained from data. Combining the dielectron and dimuon channels, the 95% C.L. lower limits on the $llqq$ contact interaction scale Λ are 35.5 TeV (26.5 TeV) for the right-right model, 35.8 TeV (26 TeV) for the left-left model, and 32.5 TeV (28.8 TeV) for the left-right model, each with constructive (destructive) interference [27]. The CMS Collaboration, using a 140 fb^{-1} dataset at 13 TeV, has set 95% C.L. exclusion limits on the $llqq$ contact interaction scale that range from $\Lambda_{LL} > 23.9$ TeV for the destructive interference to $\Lambda_{RR} > 36.4$ TeV for the constructive interference, for the left-left and the right-right models, respectively [29].

Note that the contact interactions arising from the compositeness of quarks and leptons in Eq. (90.1) can also be regarded as a part of more general dimension-six operators in the context of low-energy standard-model effective field theory (SMEFT). For a complete list of SM gauge-invariant dimension-six operators, see [30, 31]. A computation of the one-loop anomalous dimension matrix for SMEFT operators are found in Refs. [32–34]. See also Refs. [35–37] for recent reviews. Ref. [17] sets limits on the Wilson coefficients of the contact interaction operators in the SMEFT framework, using the CMS data of the inclusive jet production cross sections together with the deep inelastic scattering data from HERA and the CMS $t\bar{t}$ cross section data. The results are translated into a 95% C.L. exclusion limit on the quark compositeness $\Lambda^{-}_{LL} > 24$ TeV, which is shown as the second solid line in brown in Figure 90.2.

In models where the SM fermions get their masses though the mixing with the composite states, the top-quark is expected to show compositeness properties [38] resulting in the $t\bar{t}t\bar{t}$ contact interaction operators in the SMEFT context. An enhancement of the four-top-quark production cross section is expected at hadron colliders in these models [39]. The ATLAS Collaboration has extracted 95% C.L. observed (expected) limits on the $t\bar{t}t\bar{t}$ contact interaction operator $|C_{4t}|/\Lambda^2 < 1.9$ TeV^{-2} (1.6 TeV^{-2}) using their 36.1 fb^{-1} data at $\sqrt{s} = 13$ TeV [40]. Consistent SMEFT reinterpretations of top-quark data, and high energy non-resonant dijet and dilepton data are provided, e.g., in Refs. [41, 42].

Interactions of hypothetical dark matter candidate particles with SM particles through mediators can also be described as contact interactions at low energy. See *"Searches for WIMPs and Other Particles"* in this volume for limits on the interactions involving dark matter candidate particles.

90.2 Limits on excited fermions

Another typical consequence of compositeness is the appearance of excited leptons and quarks (l^* and q^*). Phenomenologically, an excited lepton is defined to be a heavy lepton which shares a leptonic quantum number with one of the existing leptons (an excited quark is defined similarly). For example, an excited electron e^* is characterized by a nonzero transition-magnetic coupling with electrons. The smallness of the lepton mass and the success of QED prediction for $g-2$ suggest chirality conservation, *i.e.,* an excited lepton should not couple to both left- and right-handed components of the corresponding lepton [43–45].

Excited leptons may be classified by $SU(2) \times U(1)$ quantum numbers. Typical examples are:

1. Sequential type

$$\begin{pmatrix} \nu^* \\ l^* \end{pmatrix}_L, \qquad [\nu^*_R], \qquad l^*_R.$$

   ν^*_R is necessary if we assume ν^* has a Dirac mass.

2. Mirror type

$$[\nu^*_L], \qquad l^*_L, \qquad \begin{pmatrix} \nu^* \\ l^* \end{pmatrix}_R.$$

3. Homodoublet type

$$\begin{pmatrix} \nu^* \\ l^* \end{pmatrix}_L, \qquad \begin{pmatrix} \nu^* \\ l^* \end{pmatrix}_R.$$

Similar classification can be made for excited quarks.

Excited fermions can be pair produced via their minimal gauge couplings. The couplings of excited leptons with Z are given by

$$\frac{e}{2\sin\theta_W \cos\theta_W} \left[(-1 + 2\sin^2\theta_W)\bar{l^*}\gamma^\mu l^* Z_\mu + \bar{\nu^*}\gamma^\mu \nu^* Z_\mu\right]$$

Int. J. Mod. Phys. A 2026.41. Downloaded from www.worldscientific.com by UNIVERSITY OF CALIFORNIA @ BERKELEY on 09/16/26. Re-use and distribution is strictly not permitted, except for Open Access articles.

in the homodoublet model. The corresponding couplings of excited quarks can be easily obtained. Although form factor effects can be present for the gauge couplings at $q^2 \neq 0$, they are usually neglected.

Excited fermions may also be produced via the contact interactions with ordinary quarks and leptons [46]

$$\mathcal{L} = \frac{g^2_{\rm contact}}{\Lambda^2}\left[\eta'_{LL}(\bar\psi_L\gamma_\mu\psi_L)(\bar\psi^*_L\gamma^\mu\psi^*_L) + (\eta''_{LL}(\bar\psi_L\gamma_\mu\psi_L)(\bar\psi^*_L\gamma^\mu\psi_L) + \text{h.c.}) + \cdots\right]. \tag{90.4}$$

Again, the coefficient is conventionally taken $g^2_{\rm contact} = 4\pi$. It is widely assumed $\eta'_{LL} = \eta''_{LL} = 1$, $\eta'_{LR} = \eta''_{LR} = \eta'_{RL} = \eta''_{RL} = \eta'_{RR} = \eta''_{RR} = 0$ in experimental analyses for simplicity.

In addition, transition-magnetic type couplings with a gauge boson are expected. These couplings can be generally parameterized as follows:

$$\begin{aligned}\mathcal{L} =& \frac{\lambda_\gamma^{(\psi^*)} e}{2m_{\psi^*}}\bar\psi^*\sigma^{\mu\nu}(\eta_L\frac{1-\gamma_5}{2} + \eta_R\frac{1+\gamma_5}{2})\psi F_{\mu\nu} \\ &+ \frac{\lambda_Z^{(\psi^*)} e}{2m_{\psi^*}}\bar\psi^*\sigma^{\mu\nu}(\eta_L\frac{1-\gamma_5}{2} + \eta_R\frac{1+\gamma_5}{2})\psi Z_{\mu\nu} \\ &+ \frac{\lambda_W^{(l^*)} g}{2m_{l^*}}\bar l^*\sigma^{\mu\nu}\frac{1-\gamma_5}{2}\nu W_{\mu\nu} \\ &+ \frac{\lambda_W^{(\nu^*)} g}{2m_{\nu^*}}\bar\nu^*\sigma^{\mu\nu}(\eta_L\frac{1-\gamma_5}{2} + \eta_R\frac{1+\gamma_5}{2})l W^\dagger_{\mu\nu} \\ &+ \text{h.c.},\end{aligned} \tag{90.5}$$

where $g = e/\sin\theta_W$, $\psi = \nu$ or l, $F_{\mu\nu} = \partial_\mu A_\nu - \partial_\nu A_\mu$ is the photon field strength, $Z_{\mu\nu} = \partial_\mu Z_\nu - \partial_\nu Z_\mu$, *etc.*. The normalization of the coupling is chosen such that

$$\max(|\eta_L|, |\eta_R|) = 1.$$

Chirality conservation requires

$$\eta_L\eta_R = 0. \tag{90.6}$$

These couplings in Eq. (90.5) can arise from $SU(2) \times U(1)$-invariant higher-dimensional interactions. A well-studied model is the interaction of homodoublet type l^* with the Lagrangian (see [47,48])

$$\mathcal{L} = \frac{1}{2\Lambda}\bar L^*\sigma^{\mu\nu}(gf\frac{\tau^a}{2}W^a_{\mu\nu} + g'f'YB_{\mu\nu})\frac{1-\gamma_5}{2}L + \text{h.c.}, \tag{90.7}$$

where L denotes the lepton doublet (ν, l), Λ is the compositeness scale, g, g' are $SU(2)$ and $U(1)_Y$ gauge couplings, and $W^a_{\mu\nu}$ and $B_{\mu\nu}$ are the field strengths for $SU(2)$ and $U(1)_Y$ gauge fields. These couplings satisfy the relation

$$\lambda_W = -\sqrt{2}\sin^2\theta_W(\lambda_Z\cot\theta_W + \lambda_\gamma), \tag{90.8}$$

with $\lambda_{W,Z,\gamma}$ being defined in Eq. (90.5) with $\lambda_{W,Z,\gamma} = \lambda^{(\ell^*)}_{W,Z,\gamma}$ or $\lambda_{W,Z,\gamma} = \lambda^{(\nu^*)}_{W,Z,\gamma}$. Here $(\eta_L, \eta_R) = (1, 0)$ is assumed. It should be noted that the electromagnetic radiative decay of l^* (ν^*) is forbidden if $f = -f'$ $(f = f')$.

Additional coupling with gluons is possible for excited quarks:

$$\mathcal{L} = \frac{1}{2\Lambda}\bar Q^*\sigma^{\mu\nu}\left(g_s f_s\frac{\lambda^a}{2}G^a_{\mu\nu} + gf\frac{\tau^a}{2}W^a_{\mu\nu} + g'f'YB_{\mu\nu}\right) \times \frac{1-\gamma_5}{2}Q + \text{h.c.}, \tag{90.9}$$

where Q denotes a quark doublet, g_s is the QCD gauge coupling, and $G^a_{\mu\nu}$ the gluon field strength.

If leptons are made of color triplet and antitriplet constituents, we may expect their color-octet partners. Transitions between the octet leptons (l_8) and the ordinary lepton (l) may take place via the dimension-five interactions

$$\mathcal{L} = \frac{1}{2\Lambda}\sum_l\left\{\bar l^\alpha_8 g_S F^\alpha_{\mu\nu}\sigma^{\mu\nu}(\eta_L l_L + \eta_R l_R) + \text{h.c.}\right\} \tag{90.10}$$

where the summation is over charged leptons and neutrinos. The leptonic chiral invariance implies $\eta_L\eta_R = 0$ as before.

Searches for the excited quarks and leptons have been performed over the last decades in experiments at the LEP [49–52], HERA [53, 54], Tevatron [55, 56], and LHC [57–91]. Most stringent constraints, which are described below at 95% confidence level, come from the LHC experiments.

The signature of excited quarks q^* at hadron colliders is characterized by a narrow resonant peak in the reconstructed invariant mass distribution of the q^* decay products. The decays via the transition-magnetic type operator in Eq. (90.9) are considered for excited quarks in LHC searches, and the final states to search for are dijet (qg) [57, 58, 70–73] or a jet in association with a photon $(q\gamma)$ [59,60,74,75,89] or a weak gauge boson (qW, qZ) [76,77]. All analyses consider only spin-1/2 excited states of first generation quarks (u^*, d^*) with degenerate masses, expected to be predominantly produced in proton-proton collisions except for the excited b quark searches described below. Only the minimal gauge interactions and the transition-magnetic couplings with the form given in Eq. (90.9) are considered in the production process, and hence the contact interactions in Eq. (90.4) are not considered. The compositeness scale Λ is taken to be the same as the excited quark mass m_{q^*}. The transition-magnetic coupling coefficients f_s, f and f' are assumed to be equal to 1 (denoted by f).

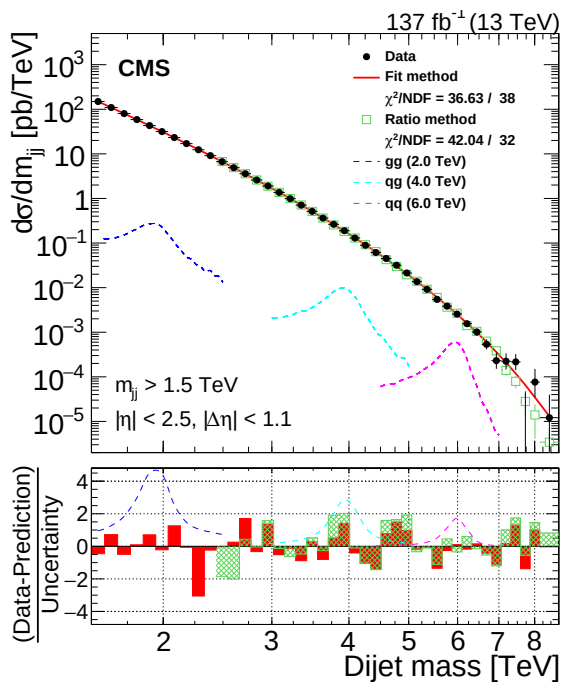

Figure 90.3: Dijet mass distribution measured by CMS using wide jets reconstructed from two highest transverse momentum jets by adding nearby jets within $\Delta R = \sqrt{\Delta\eta^2 + \Delta\phi^2} < 1.1$. The data distribution is compared to a fit representing a smooth background spectrum (solid curve) and the background prediction obtained from the $\Delta\eta_{\rm jj}$ control regions (open squares), denoted as Ratio method, at $m_{\rm jj} > 2.4$ TeV. The excited quark signal with mass of 4.0 TeV (labeled as qg) is shown together with other benchmark signals. Shown at the bottom panel is the difference between the data and the fitted parametrization from the fit method or the data and the background prediction from the Ratio method, divided by the statistical uncertainty of the data. Figure adopted from [73].

With proton-proton collision data recorded at $\sqrt{s} = 13$ TeV at the LHC, the excited quark masses are excluded in dijet resonance searches up to 6.7 TeV in ATLAS using 139 fb^{-1} [58] and 6.3 TeV in CMS using 137 fb^{-1} [73]. Figure 90.3 shows the dijet mass $(m_{\rm jj})$ distribution measured in CMS [73] by using the two highest $p_{\rm T}$ jets reconstructed with the anti-$k_{\rm T}$ algorithm [92] of

Int. J. Mod. Phys. A 2026.41. Downloaded from www.worldscientific.com
by UNIVERSITY OF CALIFORNIA @ BERKELEY on 09/16/26. Re-use and distribution is strictly not permitted, except for Open Access articles.

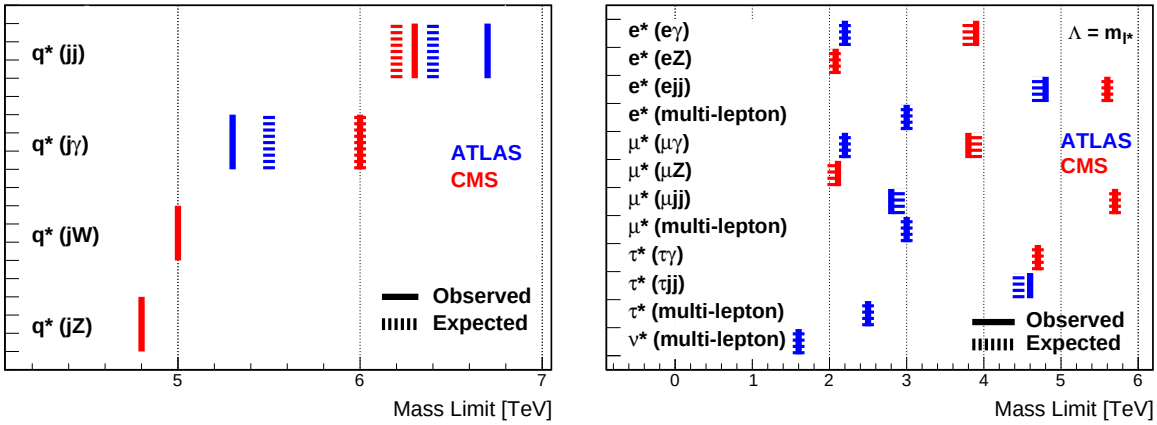

Figure 90.4: 95% C.L. lower mass limits for the excited quarks (left) and excited leptons (right) at ATLAS [58, 60, 66–68, 88] and CMS [73,75,77,80–82,89,90] experiments. Shown are the most stringent limits for each final state (denoted in parentheses) of the excited fermions from both experiments. Only first generation quarks (u, d) with transition-magnetic type interactions with $f_s = f = f' = 1$ are considered for the excited quarks. The excited lepton limits are given for the production via contact interactions with $\Lambda = m_{l^*}$.

a distance parameter of 0.4, and by combining nearby jets within $\Delta R = \sqrt{\Delta\eta^2 + \Delta\phi^2} < 1.1$ around the leading two jets. The measured dijet mass spectrum is compared to a fit with smoothly falling background shape (solid curve) at $m_{jj} > 1.5$ TeV and the background prediction obtained from $\Delta\eta_{jj}$ control regions (open squares), denoted as Ratio method, at $m_{jj} > 2.4$ TeV to look for a narrow resonance. Here $\Delta\eta_{jj}$ is the pseudorapidity separation between the two jets. An excited quark signal with mass of 4.0 TeV is shown in the figure (denoted by qg) as one of the benchmark signals considered in the analysis.

The photon + jet resonance searches, targeting excited quarks decaying into a quark and a photon ($q^* \to q + \gamma$), have excluded q^* masses up to 5.3 TeV in ATLAS [60] and 6.0 TeV in CMS [89] using collision data at $\sqrt{s} = 13$ TeV. The W/Z boson + jet final states are examined to look for the $q^* \to q + W$ and $q + Z$ signal in CMS [77], exploiting jet substructure technique designed to provide sensitivity for highly-boosted hadronically decaying W and Z bosons. The lower mass limit of 5.0 (4.8) TeV is obtained from the W + jet (Z + jet) search using dataset recorded at $\sqrt{s} = 13$ TeV.

The excited b quarks (b^*) are also considered in the present searches at the LHC. Assuming the similar production processes to the first-generation excited quarks, the b^* has been searched for in final states containing at least one jet identified as originating from a b quark (b-tagging). The searches using two jets including at least one b-tagged jet have been performed at 8 and 13 TeV [58, 61, 62, 71, 85], resulting in b^* lower mass limits of 3.2 TeV in ATLAS using 139 fb^{-1} at $\sqrt{s} = 13$ TeV [58] and 4.0 TeV in CMS using 138 fb^{-1} at $\sqrt{s} = 13$ TeV [85]. The CMS Collaboration also performed a search for $b^* \to b + \gamma$ in events with a b-tagged jet in association with a photon using data at $\sqrt{s} = 13$ TeV [89], and excluded b^* masses up to 2.2 TeV. The observed lower mass bounds on the excited bottom quarks extends to 3.8 TeV, when the production mode from contact interactions Eq. (90.4) is also considered. Excited b quarks with charged-current decay into a W-boson and a top quark ($b^* \to t + W$) were looked for in both ATLAS and CMS using the full 8 TeV data [63, 78] and in CMS using the full 13 TeV data [86, 87]. For the left(right)-handed couplings, CMS excluded the masses below 2.6(2.8) TeV in the fully hadronic final states [86] and 3.0(3.2) TeV in the lepton+jets final states [87].

The excited top quarks (t^*) have also been searched for at the LHC. The CMS Collaboration performed the search for pair-produced t^* quarks with the assumption of the t^* quark decay into a top quark and a gluon, in events with a charged lepton, missing transverse momentum and multiple jets including b-tagged jets at $\sqrt{s} = 8$ TeV [84] and 13 TeV [83, 91]. With 138 fb^{-1} data at 13 TeV, CMS excluded the t^* masses below 1.7 TeV and 1.05 TeV for spin 3/2 and 1/2 t^* quarks, respectively [91].

Searches for excited leptons l^* are also performed at the LHC using proton-proton collision data recorded at $\sqrt{s} = 7$ and 8 TeV [65–69,79,80] as well as at 13 TeV [81,90]. Considering single l^* production in contact interactions (Eq. (90.4)) and electromagnetic radiative decay to a SM lepton and a photon ($l^* \to l + \gamma$ where $l = e, \mu, \tau$), the excited electron and muon masses are excluded for $\Lambda = m_{l^*}$ up to 3.9 and 3.8 TeV, respectively, using 35.9 fb^{-1} at $\sqrt{s} = 13$ TeV in CMS [81] and 2.2 TeV using 13 fb^{-1} at $\sqrt{s} = 8$ TeV in ATLAS [66]. The CMS Collaboration performed the excited tau lepton search at $\sqrt{s} = 13$ TeV using 138 fb^{-1} [90], and excluded the excited tau lepton mass up to 4.7 TeV for $\Lambda = m_{\tau^*}$.

With the full 20.3 fb^{-1} data at $\sqrt{s} = 8$ TeV, the inclusive search on multi-lepton signatures with 3 or more charged leptons in ATLAS [67] further constrains the excited charged leptons and neutrinos. Considering both the transition-magnetic (Eq. (90.7)) and contact interaction (Eq. (90.4)) processes, the lower mass limits for the e^*, μ^*, τ^* and ν^* (for every excited neutrino flavor) are obtained to be 3.0, 3.0, 2.5 and 1.6 TeV, respectively, for $\Lambda = m_{e^*}$, m_{μ^*}, m_{τ^*} and m_{ν^*}. The rate of pair-produced excited leptons is independent of Λ for the minimal gauge interaction processes, and it allows to improve search sensitivity with multi-lepton signatures at high Λ, especially for excited neutrinos because the predominant $\nu_l^* \to l + W$ decays result in a higher acceptance for ≥ 3 charged lepton final states.

Both ATLAS and CMS Collaborations performed searches for singly produced excited leptons. The single excited leptons, both produced and decaying in contact interaction processes (Eq. (90.4)), were searched for in CMS with 77.4 fb^{-1} at 13 TeV [82] and in ATLAS with 20.3 fb^{-1} at 8 TeV [68] and 139 fb^{-1} at 13 TeV [88] using the final states with two leptons and two jets ($q\bar{q} \to ll^* \to llq\bar{q}$). The CMS search [82] considered both excited electrons and excited muons, using the invariant mass of the combination of the two leptons and two jets as a discriminating variable to separate signal from background. The ATLAS search considered excited muons [68] and excited τ leptons [88]. The single excited electrons, produced in contact interactions and decayed either in contact interaction or charged-current processes, were considered in ATLAS using 36.1 fb^{-1} at 13 TeV [69] in the final states with two electrons and two jets ($q\bar{q} \to ee^* \to eeq\bar{q}$) or an electron, missing transverse momentum and a hadronically decaying W-boson candidate ($q\bar{q} \to ee^* \to e\nu W$). The excited electron (muon) mass was excluded up to 5.6 (5.7) TeV in CMS [82] at $\Lambda = m_{e^*}$ ($\Lambda = m_{\mu^*}$), which is the best limit to date on the excited electrons (muons). The excited τ lepton mass was excluded up to 4.6 TeV in ATLAS [88] at $\Lambda = m_{\tau^*}$.

The CMS Collaboration also performed an excited lepton search

Int. J. Mod. Phys. A 2026.41. Downloaded from www.worldscientific.com by UNIVERSITY OF CALIFORNIA @ BERKELEY on 09/16/26. Re-use and distribution is strictly not permitted, except for Open Access articles.

in the final states containing a Z boson [80], probing the excited leptons produced in contact interactions and decayed in neutral-current processes ($l^* \to l + Z$) with $f = f' = 1$ or $f = -f' = 1$. The leptonic and hadronic decays of Z bosons have been considered in the search, and the most stringent limits are obtained from the hadronic Z decay to be 2.08 (2.34) TeV and 2.11 (2.37) TeV for the e^* and μ^*, respectively, with $f = f' = 1$ ($f = -f' = 1$) at $\Lambda = m_{l^*}$.

Figure 90.4 summarizes the most stringent 95% C.L. lower mass limits for excited quarks and leptons obtained from the LHC experiments.

References

[1] E. Eichten, K. D. Lane and M. E. Peskin, Phys. Rev. Lett. **50**, 811 (1983).

[2] E. Eichten *et al.*, Rev. Mod. Phys. **56**, 579 (1984), [Addendum: Rev.Mod.Phys. 58, 1065 (1986)].

[3] J. Gao *et al.*, Phys. Rev. Lett. **106**, 142001 (2011), [arXiv:1101.4611].

[4] G. Arnison *et al.* (UA1), Phys. Lett. B **177**, 244 (1986).

[5] J. Appel *et al.* (UA2), Phys. Lett. B **160**, 349 (1985).

[6] F. Abe *et al.* (CDF), Phys. Rev. Lett. **62**, 613 (1989); F. Abe *et al.* (CDF), Phys. Rev. Lett. **69**, 2896 (1992); F. Abe *et al.* (CDF), Phys. Rev. Lett. **77**, 5336 (1996), [Erratum: Phys.Rev.Lett. 78, 4307 (1997)], [hep-ex/9609011].

[7] B. Abbott *et al.* (D0), Phys. Rev. Lett. **80**, 666 (1998), [hep-ex/9707016]; B. Abbott *et al.* (D0), Phys. Rev. Lett. **82**, 2457 (1999), [hep-ex/9807014]; B. Abbott *et al.* (D0), Phys. Rev. D **62**, 031101 (2000), [hep-ex/9912023]; B. Abbott *et al.* (D0), Phys. Rev. D **64**, 032003 (2001), [hep-ex/0012046]; V. Abazov *et al.* (D0), Phys. Rev. Lett. **103**, 191803 (2009), [arXiv:0906.4819].

[8] G. Aad *et al.* (ATLAS), Phys. Lett. B **694**, 327 (2011), [arXiv:1009.5069]; G. Aad *et al.* (ATLAS), New J. Phys. **13**, 053044 (2011), [arXiv:1103.3864]; G. Aad *et al.* (ATLAS), JHEP **01**, 029 (2013), [arXiv:1210.1718]; G. Aad *et al.* (ATLAS), Phys. Rev. Lett. **114**, 22, 221802 (2015), [arXiv:1504.00357]; G. Aad *et al.* (ATLAS), Phys. Lett. B **754**, 302 (2016), [arXiv:1512.01530].

[9] M. Aaboud *et al.* (ATLAS), Phys. Rev. D **96**, 5, 052004 (2017), [arXiv:1703.09127].

[10] V. Khachatryan *et al.* (CMS), Phys. Rev. Lett. **105**, 262001 (2010), [arXiv:1010.4439]; V. Khachatryan *et al.* (CMS), Phys. Rev. Lett. **106**, 201804 (2011), [arXiv:1102.2020]; S. Chatrchyan *et al.* (CMS), JHEP **05**, 055 (2012), [arXiv:1202.5535]; V. Khachatryan *et al.* (CMS), Phys. Lett. B **746**, 79 (2015), [arXiv:1411.2646]; A. M. Sirunyan *et al.* (CMS), JHEP **07**, 013 (2017), [arXiv:1703.09986].

[11] S. Chatrchyan *et al.* (CMS), Phys. Rev. D **87**, 5, 052017 (2013), [arXiv:1301.5023].

[12] A. M. Sirunyan *et al.* (CMS), Eur. Phys. J. C **78**, 9, 789 (2018), [arXiv:1803.08030].

[13] T. Sjostrand, S. Mrenna and P. Z. Skands, Comput. Phys. Commun. **178**, 852 (2008), [arXiv:0710.3820].

[14] S. Agostinelli *et al.* (GEANT4), Nucl. Instrum. Meth. A **506**, 250 (2003), :GEANT4: a simulation toolkit.

[15] Z. Nagy, Phys. Rev. Lett. **88**, 122003 (2002), [hep-ph/0110315]; Z. Nagy, Phys. Rev. D **68**, 094002 (2003), [hep-ph/0307268].

[16] S. Dittmaier, A. Huss and C. Speckner, JHEP **11**, 095 (2012), [arXiv:1210.0438].

[17] A. Tumasyan *et al.* (CMS), JHEP **02**, 142 (2022), [Addendum: JHEP 12, 035 (2022)], [arXiv:2111.10431].

[18] S. Schael *et al.* (ALEPH), Eur. Phys. J. C **49**, 411 (2007), [hep-ex/0609051].

[19] J. Abdallah *et al.* (DELPHI), Eur. Phys. J. C **45**, 589 (2006), [hep-ex/0512012].

[20] M. Acciarri *et al.* (L3), Phys. Lett. B **489**, 81 (2000), [hep-ex/0005028].

[21] K. Ackerstaff *et al.* (OPAL), Phys. Lett. B **391**, 221 (1997); G. Abbiendi *et al.* (OPAL), Eur. Phys. J. C **33**, 173 (2004), [hep-ex/0309053].

[22] F. Aaron *et al.* (H1), Phys. Lett. B **705**, 52 (2011), [arXiv:1107.2478].

[23] S. Chekanov *et al.* (ZEUS), Phys. Lett. B **591**, 23 (2004), [hep-ex/0401009].

[24] F. Abe *et al.* (CDF), Phys. Rev. Lett. **68**, 1463 (1992); F. Abe *et al.* (CDF), Phys. Rev. Lett. **79**, 2198 (1997); T. Affolder *et al.* (CDF), Phys. Rev. Lett. **87**, 231803 (2001), [hep-ex/0107008]; A. Abulencia *et al.* (CDF), Phys. Rev. Lett. **96**, 211801 (2006), [hep-ex/0602045].

[25] B. Abbott *et al.* (D0), Phys. Rev. Lett. **82**, 4769 (1999), [hep-ex/9812010].

[26] G. Aad *et al.* (ATLAS), Phys. Rev. D **84**, 011101 (2011), [arXiv:1104.4398]; G. Aad *et al.* (ATLAS), Phys. Lett. B **712**, 40 (2012), [arXiv:1112.4462]; G. Aad *et al.* (ATLAS), Phys. Rev. D **87**, 1, 015010 (2013), [arXiv:1211.1150]; G. Aad *et al.* (ATLAS), Eur. Phys. J. C **74**, 12, 3134 (2014), [arXiv:1407.2410]; M. Aaboud *et al.* (ATLAS), Phys. Lett. B **761**, 372 (2016), [arXiv:1607.03669]; M. Aaboud *et al.* (ATLAS), JHEP **10**, 182 (2017), [arXiv:1707.02424].

[27] G. Aad *et al.* (ATLAS), JHEP **11**, 005 (2020), [Erratum: JHEP 04, 142 (2021)], [arXiv:2006.12946].

[28] S. Chatrchyan *et al.* (CMS), Phys. Rev. D **87**, 3, 032001 (2013), [arXiv:1212.4563]; V. Khachatryan *et al.* (CMS), JHEP **04**, 025 (2015), [arXiv:1412.6302]; A. M. Sirunyan *et al.* (CMS), JHEP **04**, 114 (2019), [arXiv:1812.10443].

[29] A. M. Sirunyan *et al.* (CMS), JHEP **07**, 208 (2021), [arXiv:2103.02708].

[30] W. Buchmuller and D. Wyler, Nucl. Phys. B **268**, 621 (1986).

[31] B. Grzadkowski *et al.*, JHEP **10**, 085 (2010), [arXiv:1008.4884].

[32] E. E. Jenkins, A. V. Manohar and M. Trott, JHEP **10**, 087 (2013), [arXiv:1308.2627].

[33] E. E. Jenkins, A. V. Manohar and M. Trott, JHEP **01**, 035 (2014), [arXiv:1310.4838].

[34] R. Alonso *et al.*, JHEP **04**, 159 (2014), [arXiv:1312.2014].

[35] I. Brivio and M. Trott, Phys. Rept. **793**, 1 (2019), [arXiv:1706.08945].

[36] A. V. Manohar (2018), [arXiv:1804.05863].

[37] A. Falkowski, Eur. Phys. J. C **83**, 7, 656 (2023).

[38] A. Pomarol and J. Serra, Phys. Rev. D **78**, 074026 (2008), [arXiv:0806.3247].

[39] C. Degrande *et al.*, JHEP **03**, 125 (2011), [arXiv:1010.6304].

[40] M. Aaboud *et al.* (ATLAS), Phys. Rev. D **99**, 5, 052009 (2019), [arXiv:1811.02305].

[41] D. Barducci *et al.* (2018), [arXiv:1802.07237]; S. Alte, M. König and W. Shepherd, JHEP **01**, 094 (2018), [arXiv:1711.07484]; S. Alte, M. König and W. Shepherd, JHEP **07**, 144 (2019), [arXiv:1812.07575]; J. Ellis *et al.*, JHEP **04**, 279 (2021), [arXiv:2012.02779].

[42] The ATLAS and CMS Collaborations (2022), updated results and plots available at `https://twiki.cern.ch/twiki/bin/view/LHCPhysics/LHCTopWGSummaryPlots`, URL `https://cds.cern.ch/record/2840588/files/ATL-PHYS-PUB-2022-048.pdf`.

[43] F. Renard, Phys. Lett. B **116**, 264 (1982).

[44] F. del Aguila, A. Mendez and R. Pascual, Phys. Lett. B **140**, 431 (1984).

[45] M. Suzuki, Phys. Lett. B **143**, 237 (1984).

[46] U. Baur, M. Spira and P. Zerwas, Phys. Rev. D **42**, 815 (1990).

[47] K. Hagiwara, D. Zeppenfeld and S. Komamiya, Z. Phys. C **29**, 115 (1985).

Int. J. Mod. Phys. A 2026.41. Downloaded from www.worldscientific.com
by UNIVERSITY OF CALIFORNIA @ BERKELEY on 09/16/26. Re-use and distribution is strictly not permitted, except for Open Access articles.

[48] N. Cabibbo, L. Maiani and Y. Srivastava, Phys. Lett. B **139**, 459 (1984).

[49] D. Decamp *et al.* (ALEPH), Phys. Rept. **216**, 253 (1992); R. Barate *et al.* (ALEPH), Eur. Phys. J. C **4**, 571 (1998).

[50] P. Abreu *et al.* (DELPHI), Nucl. Phys. B **367**, 511 (1991); J. Abdallah *et al.* (DELPHI), Eur. Phys. J. C **37**, 405 (2004), [hep-ex/0409058].

[51] O. Adriani *et al.* (L3), Phys. Rept. **236**, 1 (1993); P. Achard *et al.* (L3), Phys. Lett. B **531**, 28 (2002), [hep-ex/0202025]; P. Achard *et al.* (L3), Phys. Lett. B **568**, 23 (2003), [hep-ex/0306016].

[52] G. Abbiendi *et al.* (OPAL), Phys. Lett. B **544**, 57 (2002), [hep-ex/0206061]; G. Abbiendi *et al.* (OPAL), Phys. Lett. B **602**, 167 (2004), [hep-ex/0412011].

[53] C. Adloff *et al.* (H1), Phys. Lett. B **525**, 9 (2002), [hep-ex/0110037]; F. Aaron *et al.* (H1), Phys. Lett. B **663**, 382 (2008), [arXiv:0802.1858]; F. Aaron *et al.* (H1), Phys. Lett. B **666**, 131 (2008), [arXiv:0805.4530].

[54] S. Chekanov *et al.* (ZEUS), Phys. Lett. B **549**, 32 (2002), [hep-ex/0109018].

[55] D. Acosta *et al.* (CDF), Phys. Rev. Lett. **94**, 101802 (2005), [hep-ex/0410013]; A. Abulencia *et al.* (CDF), Phys. Rev. Lett. **97**, 191802 (2006), [hep-ex/0606043]; T. Aaltonen *et al.* (CDF), Phys. Rev. D **79**, 112002 (2009), [arXiv:0812.4036].

[56] V. Abazov *et al.* (D0), Phys. Rev. D **73**, 111102 (2006), [hep-ex/0604040]; V. Abazov *et al.* (D0), Phys. Rev. D **77**, 091102 (2008), [arXiv:0801.0877]; V. Abazov *et al.* (D0), Phys. Rev. Lett. **103**, 191803 (2009), [arXiv:0906.4819].

[57] G. Aad *et al.* (ATLAS), Phys. Lett. B **708**, 37 (2012), [arXiv:1108.6311]; G. Aad *et al.* (ATLAS), JHEP **01**, 029 (2013), [arXiv:1210.1718]; G. Aad *et al.* (ATLAS), Phys. Rev. D **91**, 5, 052007 (2015), [arXiv:1407.1376]; G. Aad *et al.* (ATLAS), Phys. Lett. B **754**, 302 (2016), [arXiv:1512.01530]; M. Aaboud *et al.* (ATLAS), Phys. Rev. D **96**, 5, 052004 (2017), [arXiv:1703.09127].

[58] G. Aad *et al.* (ATLAS), JHEP **03**, 145 (2020), [arXiv:1910.08447].

[59] G. Aad *et al.* (ATLAS), Phys. Rev. Lett. **108**, 211802 (2012), [arXiv:1112.3580]; G. Aad *et al.* (ATLAS), Phys. Lett. B **728**, 562 (2014), [arXiv:1309.3230]; G. Aad *et al.* (ATLAS), JHEP **03**, 041 (2016), [arXiv:1512.05910].

[60] M. Aaboud *et al.* (ATLAS), Eur. Phys. J. C **78**, 2, 102 (2018), [arXiv:1709.10440].

[61] M. Aaboud *et al.* (ATLAS), Phys. Rev. D **98**, 032016 (2018), [arXiv:1805.09299].

[62] M. Aaboud *et al.* (ATLAS), Phys. Lett. B **759**, 229 (2016), [arXiv:1603.08791].

[63] G. Aad *et al.* (ATLAS), JHEP **02**, 110 (2016), [arXiv:1510.02664].

[64] G. Aad *et al.* (ATLAS), Phys. Lett. B **721**, 171 (2013), [arXiv:1301.1583].

[65] G. Aad *et al.* (ATLAS), Phys. Rev. D **85**, 072003 (2012), [arXiv:1201.3293].

[66] G. Aad *et al.* (ATLAS), New J. Phys. **15**, 093011 (2013), [arXiv:1308.1364].

[67] G. Aad *et al.* (ATLAS), JHEP **08**, 138 (2015), [arXiv:1411.2921].

[68] G. Aad *et al.* (ATLAS), New J. Phys. **18**, 7, 073021 (2016), [Erratum: New J.Phys. 21, 109501 (2019)], [arXiv:1601.05627].

[69] M. Aaboud *et al.* (ATLAS), Eur. Phys. J. C **79**, 9, 803 (2019), [arXiv:1906.03204].

[70] S. Chatrchyan *et al.* (CMS), Phys. Lett. B **704**, 123 (2011), [arXiv:1107.4771]; S. Chatrchyan *et al.* (CMS), JHEP **01**, 013 (2013), [arXiv:1210.2387]; S. Chatrchyan *et al.* (CMS), Phys. Rev. D **87**, 11, 114015 (2013), [arXiv:1302.4794].

[71] V. Khachatryan *et al.* (CMS), Phys. Rev. D **91**, 5, 052009 (2015), [arXiv:1501.04198].

[72] V. Khachatryan *et al.* (CMS), Phys. Rev. Lett. **116**, 7, 071801 (2016), [arXiv:1512.01224]; V. Khachatryan *et al.* (CMS), Phys. Rev. Lett. **117**, 3, 031802 (2016), [arXiv:1604.08907]; A. M. Sirunyan *et al.* (CMS), Phys. Lett. B **769**, 520 (2017), [Erratum: Phys.Lett.B 772, 882–883 (2017)], [arXiv:1611.03568]; A. M. Sirunyan *et al.* (CMS), JHEP **08**, 130 (2018), [arXiv:1806.00843].

[73] A. M. Sirunyan *et al.* (CMS), JHEP **05**, 033 (2020), [arXiv:1911.03947].

[74] V. Khachatryan *et al.* (CMS), Phys. Lett. B **738**, 274 (2014), [arXiv:1406.5171].

[75] A. M. Sirunyan *et al.* (CMS), Phys. Lett. B **781**, 390 (2018), [arXiv:1711.04652].

[76] S. Chatrchyan *et al.* (CMS), Phys. Lett. B **722**, 28 (2013), [arXiv:1210.0867]; S. Chatrchyan *et al.* (CMS), Phys. Lett. B **723**, 280 (2013), [arXiv:1212.1910]; V. Khachatryan *et al.* (CMS), JHEP **08**, 173 (2014), [arXiv:1405.1994].

[77] A. M. Sirunyan *et al.* (CMS), Phys. Rev. D **97**, 7, 072006 (2018), [arXiv:1708.05379].

[78] V. Khachatryan *et al.* (CMS), JHEP **01**, 166 (2016), [arXiv:1509.08141].

[79] S. Chatrchyan *et al.* (CMS), Phys. Lett. B **704**, 143 (2011), [arXiv:1107.1773]; S. Chatrchyan *et al.* (CMS), Phys. Lett. B **720**, 309 (2013), [arXiv:1210.2422].

[80] V. Khachatryan *et al.* (CMS), JHEP **03**, 125 (2016), [arXiv:1511.01407].

[81] A. M. Sirunyan *et al.* (CMS), JHEP **04**, 015 (2019), [arXiv:1811.03052].

[82] A. M. Sirunyan *et al.* (CMS), JHEP **05**, 052 (2020), [arXiv:2001.04521].

[83] A. M. Sirunyan *et al.* (CMS), Phys. Lett. B **778**, 349 (2018), [arXiv:1711.10949].

[84] S. Chatrchyan *et al.* (CMS), JHEP **06**, 125 (2014), [arXiv:1311.5357].

[85] A. Tumasyan *et al.* (CMS), Phys. Rev. D **108**, 1, 012009 (2023), [arXiv:2205.01835].

[86] A. M. Sirunyan *et al.* (CMS), JHEP **12**, 106 (2021), [arXiv:2104.12853].

[87] A. Tumasyan *et al.* (CMS), JHEP **04**, 048 (2022), [arXiv:2111.10216].

[88] G. Aad *et al.* (ATLAS), JHEP **06**, 199 (2023), [arXiv:2303.09444].

[89] A. Tumasyan *et al.* (CMS), JHEP **12**, 189 (2023), [arXiv:2305.07998].

[90] A. Hayrapetyan *et al.* (CMS), JHEP **06**, 006 (2025), [arXiv:2410.21137].

[91] A. Hayrapetyan *et al.* (CMS), Eur. Phys. J. C **85**, 3, 342 (2025), [arXiv:2410.20601].

[92] M. Cacciari, G. P. Salam and G. Soyez, JHEP **04**, 063 (2008), [arXiv:0802.1189].

91. Dynamical Electroweak Symmetry Breaking: Implications of the H^0

Revised August 2025 by K.M. Black (Wisconsin U.), G. Cacciapaglia (LPTHE, Paris; CNRS) and A. Lister (U. of British Columbia).

91.1 Introduction and Phenomenology

In theories of dynamical symmetry breaking, the electroweak interactions are broken to electromagnetism by the vacuum expectation value of a composite operator. This is typically a bilinear operator made of fermions charged under a strongly-coupled extension of the standard model. In these theories, the longitudinal components of the massive weak bosons are identified with composite Nambu-Goldstone bosons. They arise from the spontaneous dynamical breaking of a global symmetry that envelops the electroweak gauge one. Viable theories must also explain (or at least accommodate) the presence of a composite scalar state to be identified with the 125 GeV H^0 scalar boson [1,2] – a state unlike any other observed previously.

Theories of dynamical electroweak symmetry breaking can be classified by the nature of the composite singlet state to be associated with H^0 and the corresponding dimensional scales f, the analog of the pion decay-constant in QCD, and Λ, the scale of the underlying strong dynamics.[1] Of particular importance is the ratio v/f, where $v^2 = 1/(\sqrt{2}G_F) \approx (246\,\text{GeV})^2$, since this ratio measures the expected size of deviations from typical standard model predictions – for instance, in some models, deviations of the composite Higgs couplings to other particles. In all models, new states are predicted below the scale Λ, and we describe the basic possibilities below.

91.1.1 *Technicolor-like models, $v/f \simeq 1$, $\Lambda \simeq 1$ TeV*

Technicolor models [8,9], based on a scaled-up version of two-flavor QCD, provided the first example of dynamical electroweak symmetry breaking. Models based on different dynamics have been proposed and studied, e.g. [10–14]. Such technicolor-like theories incorporate a new asymptotically free gauge interaction ("hypercolor") and charged massless fermions ("hyperfermions") transforming under a vectorial representation of the gauge group. The ensuing global chiral symmetry is spontaneously broken by the formation of a hyperfermion condensate, just as the approximate chiral symmetry in QCD is broken down to isospin by the formation of a quark condensate. The $\mathrm{SU}(2)_W \times \mathrm{U}(1)_Y$ interactions are embedded in the global hyperfermion chiral symmetries in such a way that the chiral condensate leaves only the electromagnetic $\mathrm{U}(1)_{em}$ unbroken.[2] The theories naturally provide the Nambu-Goldstone bosons "eaten" by the W and Z bosons. There would also typically be additional light states (scalars, analogous to pions) and heavy ones (e.g. vector mesons, analogous to the ρ and ω mesons in QCD) with masses in the TeV range [18,19]. The original technicolor was Higgsless, hence predicting the WW and ZZ scattering amplitudes to be strong at energies of order 1 TeV [20].

There are various possibilities for the scalar H^0 in technicolor-like models. First, the H^0 could be identified as an accidentally light singlet scalar resonance, analogous to the σ state expected in pion-scattering in QCD [21–23]. Alternatively, the H^0 could be identified as a dilaton, a pseudo-Nambu-Goldstone boson of scale invariance in theories of "walking technicolor" [24–29]. In both cases, the decay constant of the composite scalar requires tuning to obtain viable couplings to other standard model couplings, see e.g. [30].[3] Other possibilities exist, but are less viable in reproducing the standard model [31,32].

In all of these cases one expects large deviations in the Higgs self-couplings, while the measurements of the H^0 couplings to other particles, which match the standard model predictions at a few percent level [33], impose the most challenging constraints. Technicolor-like models would also predict new states at a few TeV, such as a ρ-like vector resonances below 4 TeV [34], and could accommodate for dark matter [14,35].

91.1.2 *The Higgs doublet as a pseudo-Nambu-Goldstone Boson, $v/f < 1$, $\Lambda > 1$ TeV*

The challenge with the Higgs couplings can be diminished by use of the vacuum misalignment mechanism [36,37] in models where the whole scalar quartet in the Higgs doublet arises as a set of (pseudo-)Nambu-Goldstone bosons [38,39]. Composite Goldstone Higgs models must, therefore, feature a chiral condensate that preserves the embedded electroweak symmetry. Its breaking occurs by misalignment of the vacuum due to external couplings, such as the electroweak gauging, top couplings and hyperfermion masses [40]. Hence, the electroweak scale v emerges as an "angle", $\sin\theta \equiv v/f$.[4] In this case, the underlying dynamics can occur at energies exceeding $f \geq 1$ TeV (hence, $\Lambda \gtrsim 10$ TeV), at the price of some fine-tuning in the Higgs potential [41] – closely related to the "Little Hierarchy Problem" [42]. Furthermore, the couplings of the composite Goldstone H^0 naturally equal those of the standard model Higgs boson, up to corrections of the order of $(v/f)^2$: the ones to weak gauge bosons are in fact universal [43,44], while the ones to fermions strongly depend on the fermion mass origin [45]. Hence, these theories feature a decoupling limit when $v/f \to 0$ at constant v, while also featuring a technicolor-like limit when $v/f \to 1$ [40].[5]

As the misalignment is due to gauge and top couplings, some model building efforts have been directed towards mitigating the fine tuning issue. For instance, "Little Higgs" theories [48–51] can be seen as realizations of a composite Goldstone Higgs, where misalignment occurs at higher loop order thanks to collective symmetry breaking. Another avenue involves the enlargement of the global symmetry, as in the case of "Maximal Symmetric Models" [52–54].

Composite Goldstone Higgs models typically require a larger global symmetry of the underlying theory than technicolor-like ones. Hence, additional relatively light (compared to Λ) scalar particles are present [55–57], some of which could play the role of dark matter [58–60]. In addition to these states, one would expect the underlying dynamics to yield additional scalar and vector resonances with masses of order Λ. Lighter resonances, with masses of order f, may play an important role in mitigating the little hierarchy problem in the Higgs potential [61], particularly spin-1 resonances of the weak gauge bosons [62] and fermionic top partners [63,64]. The presence of a custodial symmetry [65,66] constrains the couplings and quantum numbers of these light resonances, for instance requiring top partners of exotic charge $+5/3$ [66] or a charged vector resonance with similar branching ratios to WZ and WH. Colored top partners also provide additional contributions to Higgs production via gluon fusion [67] and to Higgs pair production [68,69]. A precise measurement of the Higgs properties at the LHC and future colliders, therefore, provides strong constraints on this class of models, together with electroweak precision (which currently yields the strongest bounds, $f \gtrsim 1$ TeV) and direct searches for light resonances.

The larger symmetry of the underlying composite Higgs theory also allows for more exotic states to appear (e.g. [70–72]), including colorless top partners in composite twin Higgs models [73,74]. The phenomenology of the additional scalar and fermionic states is rather different. Lacking color, the production of these particles at the LHC will be suppressed and their decays may lead to long-lived signatures.

91.1.3 *Top-Condensate, Top-Color, Top-Seesaw and related theories, $v/f < 1$, $\Lambda > 1$ TeV*

A third alternative is offered by strongly interacting theories where a fine-tuning in the coupling strength allows a hierarchy

[1] In a strongly interacting theory "Naive Dimensional Analysis" [3,4] implies that, in the absence of fine-tuning, $\Lambda \simeq g^* f$ where $g^* \lesssim 4\pi$ is the typical size of a strong coupling in the low-energy theory [5,6]. This estimate is modified in the presence of multiple flavors or colors [7] .

[2] For a review of technicolor models, see [15–17].

[3] For the dilaton, this would require that chiral and scale symmetries are broken by the same condensate.

[4] Equivalently, misalignment can be described as a vacuum expectation value of the pseudo-Nambu-Goldstone Higgs, whose potential is dynamically generated by loops of top quarks and weak gauge bosons, as well as the hyperfermion mass terms.

[5] For a review of composite Goldstone Higgs models, see [46,47].

Int. J. Mod. Phys. A 2026.41. Downloaded from www.worldscientific.com by UNIVERSITY OF CALIFORNIA @ BERKELEY on 09/16/26. Re-use and distribution is strictly not permitted, except for Open Access articles.

Int. J. Mod. Phys. A 2026.41. Downloaded from www.worldscientific.com
by UNIVERSITY OF CALIFORNIA @ BERKELEY on 09/16/26. Re-use and distribution is strictly not permitted, except for Open Access articles.

between the dynamical scale and the electroweak scale. This scenario is only possible if the electroweak (quantum) phase transition is continuous (second order) in the strength of the strong dynamics [75]. Similarly to the Goldstone Higgs scenario, the tuned underlying strong interactions generate a light composite Higgs bound state, whose couplings match those of the standard model Higgs boson up to corrections of order $(1\ \text{TeV}/\Lambda)^2$. Hence, a precise measurement of the H^0 couplings gives rise to lower bounds on the scale Λ. By construction, the theory has a decoupling limit $\Lambda \to \infty$, at the price of arbitrary fine adjustment of the interaction strength.

Concrete realizations often posit the top-quark itself as strongly interacting at high energies [76, 77], potentially through an extended color gauge sector [78–80]. In these theories, top-quark condensation (or the condensation of an admixture of the top with additional vector-like quarks) is responsible for electroweak symmetry breaking, and the H^0 is identified with a bound state involving the third generation of quarks. The mechanism of top condensation has also been combined to technicolor like theories to explain the large top mass [81]. Theories of top condensation typically include an extra set of massive color-octet vector bosons (top-gluons), and an extra $U(1)$ interaction (giving rise to a top-color Z') which couple preferentially to the third generation and whose masses define the scale Λ of the underlying physics.

91.1.4 *Extra-dimensions, CFTs and holography*

Theories with compact extra-dimensions [82] lead to low energy effective theories of "resonances", which are hard to distinguish from composite states. In these scenarios, the electroweak gauge symmetry can be broken by boundary conditions, leading to both technicolor-like scenarios [83, 84] and Goldstone Higgs ones [85, 86]. A dictionary between extra dimensions and composite models can be established for both the gauge [85] and fermion [87, 88] sector, motivated by the AdS/CFT correspondence [89] (dubbed holography).

A more formal application of holography would require the composite sector to behave as a strongly coupled conformal theory, where the gravity dual can be used as an analog computer to predict low energy properties of the composite resonances. This technique has been applied to technicolor-like models [34, 90, 91], composite Goldstone Higgs scenarios with top partners [92] and top-color models [90].

91.1.5 *Flavor*

In addition to the electroweak symmetry breaking dynamics described above, which gives rise to the masses of the W and Z bosons, additional interactions must be introduced to generate the masses of the standard model fermions. As they are typically induced by higher order terms (such as four-fermion interactions), small fermion masses are natural while a challenge is posed by the top mass, the only one which is close to the electroweak scale. Two broad classes have been suggested for these new interactions.

In "extended technicolor" (ETC) theories [93, 94], the gauge interactions in the underlying strongly interacting theory are extended to incorporate flavor. This extended gauge symmetry is broken down (possibly sequentially, at several different mass scales) to the residual hypercolor responsible for electroweak symmetry breaking. The massive gauge-bosons corresponding to the broken symmetries mediate interactions between mass operators for the quarks/leptons and the corresponding bilinears of hyperfermions, giving rise to the masses of the ordinary fermions via the electroweak symmetry breaking condensate.

In the "partial compositeness" class [95], the additional flavor-dependent interactions arise from mixing between the ordinary elementary quarks and leptons and (massive) composite operators in the strongly-interacting underlying theory. At low energies, fermionic resonances that couple largely to heavy fermions appear, with masses in the multi-TeV range. The main advantage of partial compositeness is that the coupling of the composite operators may be enhanced at low energy by large anomalous dimensions.[6]

Since the flavor interactions must give rise to quark and lepton mixing, a generic composite theory would give rise to large flavor-changing neutral-currents [94]. In ETC theories, these constraints are typically somewhat relaxed if the theory incorporates approximate generational flavor symmetries [97], the theory has a slowly running coupling constant or "walks" [24–28], or if $\Lambda > 1$ TeV [98]. In theories of partial compositeness, the masses of the ordinary fermions depend on the scaling-dimension of the operators corresponding to the composite fermions with which they mix. This leads to a new mechanism for generating the mass-hierarchy of the observed quarks and leptons that, potentially, ameliorates flavor-changing neutral current problems [99–103]. Alternatively, one can assume that the underlying flavor dynamics respect flavor symmetries ("minimal" [104, 105] or "next-to-minimal" [106] flavor violation) that suppress flavor-changing neutral currents in the two light generations [107]. Additional considerations apply when extending these arguments to potential explanation of neutrino masses (see, for example, [108]).

While most analyses of composite flavor rely on low energy effective theories, generating the necessary interactions in a complete model remains a challenge, often requiring multiple mechanisms at once (typically partial compositeness for the top, and bilinear ETC-like interactions for the light fermions). Theories of top partial compositeness have been defined in terms of hyperfermions [109], leading to possible ultra-violet completion which involve partial unification of the hypercolor interactions [110–112]. An alternative idea consists in adding Yukawa-like interactions with strongly interacting scalars, leading to "fundamental partial compositeness" for all fermions [113, 114]. Finally, one could assume that the theory flows to a conformal field theory above Λ, however no concrete and fully self-consistent model of this kind has been constructed yet.

91.1.6 *Theoretical Considerations*

Since the underlying low-energy dynamics in these theories is strongly coupled, there are no straightforward calculation techniques that can be applied to analyze their properties. Instead, most phenomenological studies depend on the construction of a "low-energy" effective theory describing additional scalar, fermion, or vector boson degrees of freedom, which incorporates the relevant symmetries and, when available, dynamical principles. In some cases, motivated by the AdS/CFT correspondence [89], the strongly-interacting theories described above have been investigated by analyzing a dual compactified five-dimensional gauge theory.

More recently, progress has been made in investigating strongly-coupled models using lattice gauge theory (see e.g. [115–120]). These calculations offer the prospect of establishing which strongly coupled theories of electroweak symmetry breaking have a particle with properties consistent with those observed for the H^0 – and for establishing concrete predictions for these theories at the LHC [121].

91.1.7 *Summary*

The theoretical ideas and models reviewed here motivate searches for a wide variety of new states. Heavy vector bound states decaying to dibosons and additional scalar states appear naturally in both technicolor-like (91.1.1) and Goldstone Higgs models (91.1.2). Light W' and Z' states are typically required in models featuring collective symmetry breaking, together with vector-like fermions that couple strongly to the top quark. The latter are also required by partial compositeness to generate a large mass for the top and address the flavor problem (91.1.5). Top-condensate and related models (91.1.3) predict the existence of colorons which preferentially couple to third-generation quarks. In all cases, realistic models that have a well-defined underlying model often predict the existence of more exotic states, such as exotic-color fermions and vectors, and colorless top partners. Finally, the new states discussed here also occur in extra-dimensional models (91.1.4)), which is understandable given that many strongly-coupled theories can be viewed as compactified five-dimensional gauge theories via duality. We turn now to a review the status of experimental searches related to dynamical electroweak symmetry breaking.

[6] For a review, see [47, 96].

Int. J. Mod. Phys. A 2026.41. Downloaded from www.worldscientific.com by UNIVERSITY OF CALIFORNIA @ BERKELEY on 09/16/26. Re-use and distribution is strictly not permitted, except for Open Access articles.

91.2 Experimental Searches

As discussed above, the extent to which the couplings of the H^0 conform to the expectations for a standard model Higgs boson constrains the viability of each of these models. Measurements of the H^0 couplings, and their interpretation in terms of effective field theory, are summarized in the H^0 review in this volume. In what follows, we will focus on searches for the additional particles that might be expected to accompany the singlet scalar: extra scalars, fermions, and vector bosons. In some cases, detailed model-specific searches have been made for the particles described above (though generally not yet taking account of the demonstrated existence of the H^0 boson).

In most cases, however, generic searches (e.g. for extra W' or Z' particles, extra scalars in the context of multi-Higgs models, or for fourth-generation quarks) are quoted that can be used – when appropriately translated – to derive bounds on a specific model of interest.

The mass scale of the new particles implied by the interpretations of the low mass of H^0 discussed above, and existing studies from the Tevatron and lower-energy colliders, suggests that only the Large Hadron Collider has any real sensitivity. A number of analyses already carried out by ATLAS and CMS use relevant final states and might have been expected to observe a deviation from standard model expectations – in no case so far has any such deviation been reported. The detailed implications of these searches in various model frameworks are described below.

Except where otherwise noted, all limits in this section are quoted at a confidence level of 95%. The searches at $\sqrt{s} = 8$ TeV (Run 1) are based on 20.3 fb^{-1} of data recorded by ATLAS, and an integrated luminosity of 19.7 fb^{-1} analyzed by CMS. The datasets collected at $\sqrt{s} = 13$ TeV during Run 2 of the LHC since 2015 are based on analyses with varied integrated luminosities ranging from ∼2-140 fb^{-1}.

91.2.1 *Searches for Z' or W' Bosons*

Massive vector bosons or particles with similar decay channels would be expected to arise in Little Higgs theories, in theories of Technicolor, or models involving a dilaton, adjusted to produce a light Higgs boson, consistent with the observed H^0. These particles would be expected to decay to pairs of vector bosons, or to third generation quarks, or to leptons. The generic searches for W' and Z' vector bosons listed below can, therefore, be used to constrain models incorporating a composite Higgs-like boson.

A general review of searches for Z' and W' bosons is also included in this volume [122, 123]. In the context of the dynamical electroweak symmetry breaking models, we emphasize their decays to third generation fermions by including a detailed overview, while also briefly summarizing the other searches.

$Z' \to \ell\ell$:

ATLAS [124] and CMS [125] have both searched for Z' production with $Z' \to ee$ or $\mu\mu$. No deviation from the standard model prediction was seen in the dielectron and dimuon invariant mass spectra, by either the ATLAS or the CMS analysis, and lower limits on possible Z' boson masses were set. A $Z'_{\rm SSM}$ with couplings equal to the standard model Z' (a "sequential standard model" Z') and a mass below 5.1 TeV was excluded by ATLAS, while CMS set a lower mass limit of 5.15 TeV. The experiments also place limits on the parameters of extra dimension models and in the case of ATLAS on the parameters of a minimal walking technicolor model [24–28], consistent with a 125 GeV Higgs boson [126]. For a general review of searches in these channels see the PDG review of Z prime in this volume [122].

In addition, both experiments have also searched for Z' decaying to a ditau final state [127,128]. An excess in $\tau^+\tau^-$ could have interesting implications for models in which lepton universality is not a requirement and enhanced couplings to the third generation are allowed. This analysis led to lower limits on the mass of a $Z'_{\rm SSM}$ of 2.4 and 2.1 TeV from ATLAS and CMS respectively.

$Z' \to q\bar{q}$:

The ability to relatively cleanly select $t\bar{t}$ pairs at the LHC together with the existence of enhanced couplings to the third generation in many models makes it worthwhile to search for new particles decaying in this channel. Both ATLAS [129] and CMS [130] have carried out searches for new particles decaying into $t\bar{t}$.

Both ATLAS and CMS searched for $t\bar{t}$ in the all hadronic mode [131] [132] in both the resolved and boosted regions. No evidence of resonance production were seen and limits were produced for various models including the Z' boson in topcolor-assisted technicolor which excludes masses less than 3.1 to 3.6 TeV (ATLAS) depending on the details of the model and 3.3, 5.25, and 6.65 TeV for widths of 1, 10 and 30 percent relative to the mass of the resonance .

ATLAS also presented results on the lepton plus jets final state, where the top quark pair decays as $t\bar{t} \to WbWb$ with one W boson decaying leptonically and the other hadronically; CMS used final states where both, one or neither W decays leptonically and then combined the results. The $t\bar{t}$ invariant mass spectrum was analyzed for any excess, and no evidence for any resonance was seen. ATLAS excluded a narrow ($\Gamma/m = 1.2\%$) leptophobic topcolor Z' boson with masses between 0.7 and 2.1 TeV and with $\Gamma/m = 3\%$ between 0.7 and 3.2 TeV. CMS set limits on leptophobic Z' bosons for three different assumed widths $\Gamma/m = 1.0\%$, $\Gamma/m = 10.0\%$, and $\Gamma/m = 30.0\%$ of 3.9 TeV to 4.0 TeV and exclude RS KK gluons up to 3.3 TeV.

Both ATLAS [133] and CMS [134] have also searched for resonances decaying into $q\bar{q}$, qg or gg using the dijet invariant mass spectrum. Excited quarks are excluded up to masses of 6.7 TeV and model-independent upper limits on cross sections with a Gaussian signal shape were set. CMS excluded string resonances with masses below 7.9 TeV, scalar diquarks below 7.5 TeV, axigluons and colorons below 6.6 TeV, excited quarks below 6.3 TeV, color-octet scalars below 3.7 TeV, W' bosons below 3.6 TeV, Z' bosons with SM-like couplings below 2.9 TeV and between 3.1 TeV and 3.3 TeV, Randall–Sundrum Gravitons below 2.6 TeV.

$W' \to \ell\nu$:

Both LHC experiments have also searched for massive charged vector bosons. In this section we include a summary of the results, with emphasis on final states with third generation fermions, while the details on other decays are discussed in the mini-review of W' [123]. ATLAS searched for a heavy W' decaying to $e\nu$ or $\mu\nu$ and found no excess over the standard model expectation. A sequential standard model (SSM) W' boson (assuming zero branching ratio to WZ) with mass less than 7 TeV was excluded [135] using the 139 fb^{-1} dataset at $\sqrt{s} = 13$ TeV. Model independent cross-section limits as a function of mass were also set. Based on a similar dataset, the CMS experiment excluded a SSM W' boson with mass up to 5.7 TeV [136] and presented upper limits on the production of generic W' bosons decaying into this final state using a model-independent approach.

CMS [137] has carried out a complementary search in the $\tau\nu$ final state. As noted above, such searches place limits on models with enhanced couplings to the third generation. No excess was observed and limits between 2.0 and 2.7 TeV were set on the mass of a W' decaying preferentially to the third generation; a W' with universal fermion couplings was also excluded for masses less than 2.7 TeV.

$W' \to t\bar{b}$:

Heavy new gauge bosons can couple to left-handed fermions like the SM W boson or to right-handed fermions. W' bosons that couple only to right-handed fermions (W'_R) may not have leptonic decay modes, depending on the mass of the right-handed neutrino. For these W' bosons, the tb ($t\bar{b} + \bar{t}b$) decay mode is especially important because in many models the W' boson is expected to have enhanced couplings to the third generation of quarks relative to those in the first and second generations. It is also the hadronic decay mode with the best signal-to-background. ATLAS and CMS have performed searches for W' bosons via the $W' \to tb$ decay channel in the lepton+jets and all-hadronic final state.

The CMS lepton+jets search [138–141], $W' \to tb \to Wbb \to \ell\nu bb$, proceeded via selecting events with an isolated lepton (electron or muon), and at least two jets, one of which is identified to originate from a b-quark. The mass of the W' boson (M_{tb}) was reconstructed using the four-momentum vectors of the final state objects ($bb\ell\nu$). The distribution of M_{tb} is used as the search dis-

Int. J. Mod. Phys. A 2026.41. Downloaded from www.worldscientific.com by UNIVERSITY OF CALIFORNIA @ BERKELEY on 09/16/26. Re-use and distribution is strictly not permitted, except for Open Access articles.

criminant. A search [141] using 35.9 fb^{-1} of data, collected at $\sqrt{s}$ = 13 TeV, led to an exclusion of W'_R bosons with masses below 3.4 TeV (3.6 TeV) if $M_{W'_R} >> M_{\nu_R}$ ($M_{W'_R} < M_{\nu_R}$), where M_{ν_R} is the mass of the right-handed neutrino.

The CMS search for $W' \to tb$ decays using the all-hadronic final state focused on W' masses above 1 TeV [140, 142]. In this region, the top quark gets a large Lorentz boost and hence the three hadronic products from its decay merge into a single large-radius jet. Deep neural network(DNN) algorithms are used to identify the jet initiated by the bottom quark. Techniques including DNN, which rely on substructure information of the jets [143] are employed to identify boosted all hadronic W boson and top quark [142] decays. The W' candidate mass was computed from back-to-back boosted top-tagged jet and a low mass b-tagged jet. From this all-hadronic search, W' bosons were excluded for masses up to 3.4 TeV [142].

ATLAS has searched for W'_R bosons in the $t\bar{b}$ final state both for lepton+jets [144] and all-hadronic [145] decays of the top. No significant deviations from the standard model were seen in either analysis and limits were set on the $W' \to t\bar{b}$ cross section times branching ratio and W' bosons with with both purely right and purely left-handed coupling and limits are set between 0.5 and 6 TeV for different values of the coupling strength.

In addition, the above studies also provided upper limits on the W' effective couplings to right- and left-handed fermions. In Fig. 91.1 (bottom) the upper limits on W' couplings normalized to the SM W boson couplings derived by ATLAS [145] are shown. The top panel of Fig. 91.1 shows the upper limits for arbitrary combinations of left- and right-handed couplings of the W' boson to fermions set using a model independent approach by CMS [141].

91.2.2 *Searches for Resonances decaying to Vector Bosons and/or Higgs Bosons*

Both ATLAS and CMS have used the data collected at $\sqrt{s}$ = 13 TeV to search for resonances decaying to pairs of bosons. Overall no significant excesses were seen in the full datasets that were analyzed and the results are interpreted in models with heavy vector triplets (HVT) [147], models with strong gravity and extra spatial dimensions, and model independent limits as a function of mass are set. For a full review of models including extra spatial dimensions and the interpretation of many of these results in that context please see the review of extra dimensions in this volume [82].

Utilizing data collected at $\sqrt{s}$ = 13 TeV, ATLAS [148] and CMS [149], have both looked for a resonant state decaying into VV (with $V = W$ or Z) , VH (with H representing the SM Higgs boson), and HH. ATLAS has searched in the $qqqq$, $\nu\nu qq$, $l\nu qq$, $llqq$, $l\nu l\nu$, $ll\nu\nu$, $l\nu ll$, $llll$, $qqbb$ $\nu\nu bb$, $l\nu bb$, and $llbb$ final states and combined the results . While CMS analyzed the $qqqq$, $\nu\nu qq$, $l\nu qq$, $llqq$, $ll\nu\nu$, $\nu\nu bb$, $l\nu bb$, $llbb$, $bbbb$, $\tau\tau bb$, and $qq\tau\tau$ final states.

The combined limits are expressed both as limits on the cross-section as a function resonance mass as well as constraints on the coupling of the heavy boson triplet to quarks, leptons, and the Higgs boson.

$X \to WZ$:

ATLAS searched for new heavy resonances decaying into WZ in the channels $WZ \to qqqq$ [150] , $l\nu qq$ [151], and $l\nu ll$ [152]. In the fully leptonic channel , the invariant mass of the W Z pair is obtained by considering all possible four lepton permutations in each event. The dominant background is Standard Model continuum WZ production, ZZ production where one lepton is not identified or falls outside the detector acceptance, and top quark plus vector boson production. No resonant production is seen in data and lower limits on the mass of a HVT decaying into WZ are set at 2260 (2460) GeV assuming a coupling constant of $g_V = 1$ ($g_V = 3$). In the $WZ \to l\nu qq$ mode, ATLAS searches in both the cases that the quarks are observed as individual jets (resolved) and where they merge into one jet in the detector (boosted) which probe the low and high p_T regime of the Z boson. No significant excess is seen in either channel and combined lower mass limits are placed at 2900 (3000) GeV for $g_V = 1$ ($g_V = 3$) in the HVT model. In the all hadronic decay mode, ATLAS searched for two high p_T hadronically decaying vector bosons looking for a resonant structure. No excess is seen and limits are placed exclude 1200-3000 (1200-3300) GeV for $g_V = 1$ ($g_V = 3$) in the HVT model.

CMS searched for new heavy resonances in the ZV final state using the semi-leptonic decay channels excluding W' masses up to 1800 GEV in HVT two models with $g_V = 1$ and 3 and in the ZZ channel excludes gravitons up to 1200 GeV. The CMS collaboration searched for $VV \to qqqq$ [153] in the large R dijet search. The W and Z boson are identified through the mass of the large R jet and substructure variables. No excess is seen and limits are set for charged HVT bosons with masses lower than 3200 (3800) GeV for $g_V = 1$ ($g_V = 3$). Cross-section limits as function of mass are reported for the charged spin-1 resonance interpretation and are placed at 44.4 fb at 1.4 TeV to 0.7 pb at 4 TeV. In the $\nu\nu qq$ final state [154], the CMS collaboration searched for a charged spin 1 resonance decaying into a VZ final state with a Z boson decaying into a pair of neutrinos and the other boson decaying into two collimated quarks reconstructed as a large R-jet. The transverse mass of the VZ candidate is reconstructed and utilized to search for evidence of resonant VZ production. No excess is seen and lower mass limits are placed on the charged resonance at 3100 (3400) GeV for $g_V = 1$ ($g_V = 3$) . In the $2l2q$ final state, the CMS collaboration searched for a heavy resonance decaying into ZV [155] looking for events with one large R-jet consistent with the hadronic decay of a vector boson and a Z boson reconstructed in the charged lepton decay channel (e or μ). Limits are set for a HVT W' with a lower mass of 2270 (2330) for $g_V = 1$ ($g_V = 3$) .

$X \to WW$:

ATLAS searched for a new heavy resonance decaying into WW in the channels $WW \to qqqq$ [150] , $l\nu qq$ [151], and $l\nu\nu$ [156]. In the case where both Ws decay leptonically, ATLAS utilized the transverse mass of the two lepton and two neutrino final state and searched for an excess in this distribution between 200 GeV and 5 TeV. No excess is seen and a HVT is excluded for masses below 1300 GeV. Vector boson fusion is also considered and cross-section limits as a function of mass are placed ranging from 1.3 pb to 0.006 pb at 200 GeV to 3 TeV, respectively. In the $l\nu qq$ mode , ATLAS completed a companion analysis to the $WZ \to$ analysis discussed above and places lower mass limits of 2850 (3150) GeV for $g_V = 1$ ($g_V = 3$) in the HVT model. ATLAS also interprets the all hadronic mode analysis in the hypothesis that $WW \to qqqq$ and places limits on a HVT boson decaying into WW in the all hadronic mode between 1200 and 2200 (1200 and 2800) GeV for $g_V = 1$ ($g_V = 3$).

The CMS collaboration searched for $VV \to qqqq$ [153] in the large R dijet search. The W and Z boson are identified through the mass of the large R jet and substructure variables. No excess is seen and limits are set for charged HVT bosons with masses lower than 2700 (2800) GeV for $g_V = 1$ ($g_V = 3$). Cross-section limits as function of mass are reported for the uncharged spin-1 resonance interpretation and are placed at 41.6 fb at 1.4 TeV to 0.6 pb at 4 TeV.

$X \to VH$:

ATLAS searched for a new heavy resonance decaying into WH and ZH in the $qqbb$ (WH and ZH) [157], $l\nu bb$ (WH), $\nu\nu bb$ (ZH), $llbb$(ZH) [158] modes. In the all hadronic mode, ATLAS searched for boosted VH production looking for two large R jets where the larger invariant mass large R jet is interpreted as the Higgs boson decay products while the lesser invariant mass jet is taken to be the hadronically decaying vector boson requiring b-tagging on the Higgs boson subjets. The invariant mass is reconstructed and a search is performed for resonant production of ZH. None is found and limits from 1100 to 2500 (1300 to 3800 GeV) are placed for $g_V = 1$ ($g_V = 3$). ATLAS also searched for XH where the W or Z boson decays into $\nu\nu$, $l\nu$, and ll . The analysis searched for both resolved and merged (boosted) b-jets from the decay of the Higgs boson and defines the signal regions based on the number of reconstructed charged leptons (0,1,or 2). In the dilepton channel the invariant mass is explicitly reconstructed of the entire diboson

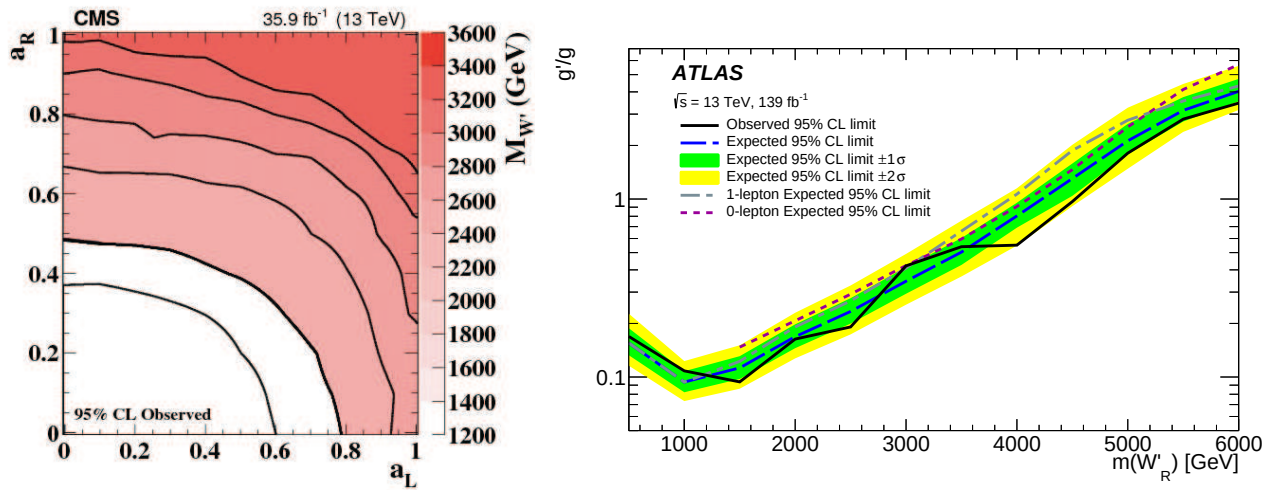

Figure 91.1: Left panel: Observed limits on the W' boson mass as function of the left-handed ($a_{\rm L}$) and right-handed ($a_{\rm R}$) couplings. Black lines represent contours of equal W' boson mass [141]. Right panel: Observed and expected regions, on the g$'$/g vs mass of the W' boson plane, that are excluded at 95% CL, for right-handed W' bosons [146] showing the exclusion of the values of a hypothetical right-handed coupling of a heavy W particle.

system, the single lepton channel reconstructs the diboson final state constraining the lepton and missing transverse momentum utilizing the known W boson mass, while the 0 charged lepton channel reconstructs the transverse mass of the diboson system. No excess is seen in any channel and limits on the production of a HVT are placed at 2800 GeV (2930) GeV for $g_V = 1$ ($g_V = 3$).

The CMS Collaboration searched for a heavy resonance decaying into VH [159] searching for a resonances decaying into a Higgs boson and a hadronically decaying W or Z boson. The search identifies events with two large-R jets using substructure variables and requires one large-R jets is tagged with a pair of b-hadrons clustered in a single jet. The invariant mass of the VH bosons is reconstructed and evidence for resonance production is sought. No excess is seen and limits are placed. With $g_V = 1$ (3) a narrow W' resonance with $m_{W'} < 2470(3150)$ GeV and $m_{Z'} < 1150(1190)$.

The CMS collaboration searched for a heavy resonance decaying into a pair of boosted Higgs boson with $HH \to b\bar{b}WW^*$ in the single and dilepton channel [160]. Events are categorized according to lepton flavor and multiplicity, along with discriminators that characterize the compatibility with having jets arising from the decay of boosted Higgs and W bosons. The reconstructed Higgs and diHiggs mass distributions are fit and used as the final discriminators. No significant deviations in the 12 sub-categories are seen and 95% confidence limits on spin-0 bosons are set from 24.5 fb at 0.8 TeV to 0.78 fb at 4.5 TeV and spin-2 bosons from 16.7 fb at 0.8 TeV to 0.67 fb at 4.5 TeV. A similar search in the four b-quark final state is used to set limits range 9.74 to 0.29 fb and 4.94 to 0.19 fb in the spin-0 bosons and spin-2 gravitons (respectively) interpretation with masses of 1-3 TeV [161].

$X \to H\gamma$ or $V\gamma$:

Both CMS and ATLAS search for heavy resonances decaying into either a vector boson and a photon or a Higgs boson or a photon. These searched are motivated generically by the fact that new heavy gauge bosons are generically predicted to decay to either a Higgs boson or a vector boson and a photon by one loop decays [162]. ATLAS searched for for a heavy resonances decaying into a Higgs boson and a photon and sets limits from 0.7 to 4 TeV from 11.6 fb to 0.11 fb [163]. ATLAS searched for a heavy resonance decaying into XH where $XH \to qqbb$ [164] and sets limits from 1 to 4 TeV. CMS searched for a heavy resonance decaying into a W boson and a photon [165] setting limits for narrow resonances range between 0.17 fb at 6.0 TeV and 55 fb at 0.7 TeV.

Summary of Searches with Diboson Final States:

Both ATLAS [148] and CMS [149] provide plots summarizing the various searched results and limits combining. The results are shown in the context of HVT models and models of strong gravity with extra spatial dimensions. No excess is seen in any search and limits on the 4.3 (4.5) TeV (ATLAS) and (CMS). Inclusion of decays directly to fermions increase these limits to 5.3 (5.5) TeV and 5.0 (5.2) TeV from the ATLAS and CMS combinations, respectively. Both collaborations also place varying limits on the coupling strength as a function of HVT boson mass as well.

Searches for Triboson Resonances:

The CMS collaboration presents the first search for massive triboson resonances in both the semi-leptonic [166] and fully hadronic final state [167]. Three boson final states can be produced via the decay of Kaluza-Klein (KK) states decaying via $W_{KK} \to WR$ with $R \to WW$ where R is a scalar radion. The search utilizes novel deep neural networks to perform optimal separation between signal and background and searched for evidence of resonance structure in the triboson invariant mass-spectrum. No excesses above SM backgrounds are seen and W_{KK} and radion masses are excluded up to $M_{W_{KK}} = 3.4$ TeV and $M_R = 1$ TeV and up to $M_{W_{KK}} = 3.6$ TeV and $M_R = 0.35$ TeV . $M_{W_{KK}}$ below 3 TeV are excluded for $0.6 < \frac{M_R}{M_{W_{KK}}} < 0.7$ in the semi-leptonic final state and up to $M_{W_{KK}} = 3.0$ TeV and $M_R = 200$ GeV and up to $M_{W_{KK}} = 1.5$ TeV and $M_R = 1.5$ TeV in the fully hadronic final state.

91.2.3 *Vector-like third generation quarks*

Vector-like quarks (VLQ) have non-chiral couplings to W bosons, i.e. their left- and right-handed components couple in the same way. They therefore have vectorial couplings to W bosons. Vector-like quarks arise in Little Higgs theories, top-coloron-models, and theories of a composite Higgs boson with partial compositeness. In the following, the notation T quark refers to a vector-like quark with charge 2/3 and the notation B quark refers to a vector-like quark with charge $-1/3$, the same charges as the SM top and b quarks respectively. The exotic vector-like quarks $X_{5/3}$ and $Y_{-4/3}$ have charges 5/3, and $-4/3$ respectively. Vector-like quarks couple with SM quarks with Yukawa interactions and may exist as SU(2) singlets (T, and B), doublets [$(X_{5/3}, T)$,(T, B),$(B, Y_{-4/3})$], or triplets [$(X_{5/3}, T, B)$, $(T, B, Y_{-4/3})$]. At the LHC, VLQs can be pair produced via the dominant gluon-gluon fusion process. VLQs can also be produced singly by their electroweak effective couplings to a weak boson and a standard model quark. The single production rate is expected to dominate over the rate of pair production at large VLQ masses. T quarks can decay to bW, tZ, or tH^0. Weak isospin singlets are expected to decay to all three final states with (asymptotic) branching fractions of 50%, 25%, 25%, respectively. Weak isospin doublets are expected to decay exclusively to tZ and to tH^0 [168]

Int. J. Mod. Phys. A 2026.41. Downloaded from www.worldscientific.com by UNIVERSITY OF CALIFORNIA @ BERKELEY on 09/16/26. Re-use and distribution is strictly not permitted, except for Open Access articles.

Int. J. Mod. Phys. A 2026.41. Downloaded from www.worldscientific.com
by UNIVERSITY OF CALIFORNIA @ BERKELEY on 09/16/26. Re-use and distribution is strictly not permitted, except for Open Access articles.

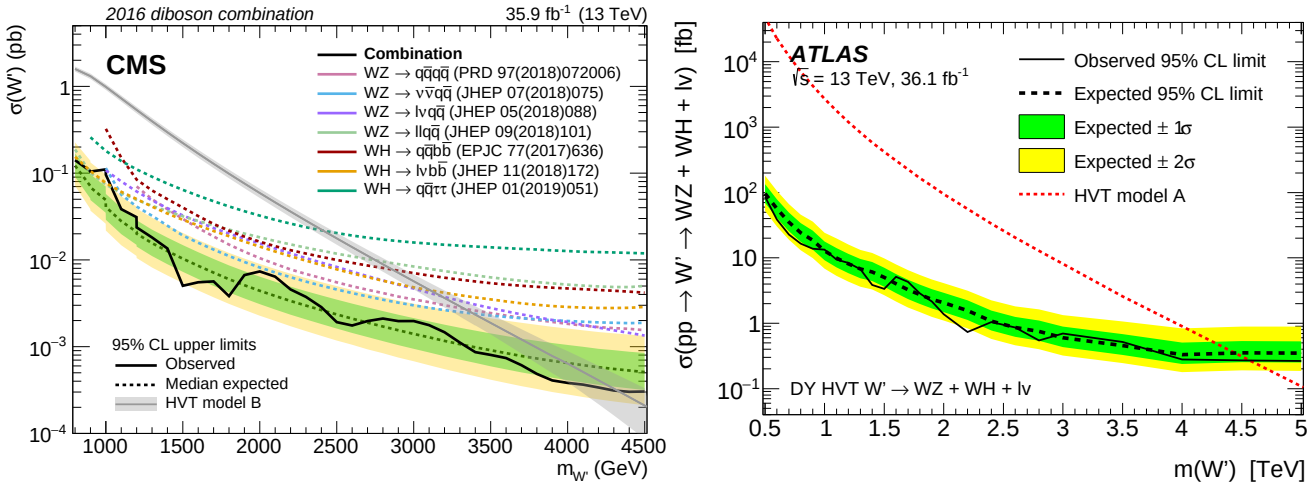

Figure 91.2: Left panel:Observed limits from W' to diboson from CMS [149]. Right panel: Observed limits from W' to diboson decays from ATLAS [148].

with equal branching ratios. Analogously, B quarks can decay to tW, bZ, or bH^0. The $Y_{-4/3}$ and $X_{5/3}$ quarks decay exclusively to bW and to tW. While these are taken as the benchmark scenarios, other representations and decays to exotic new particles are possible [169–171], and hence the final results are interpreted for many allowed branching fraction combinations.

Given the multiple decay modes of the VLQs, the final state signatures of both pair produced and the singly produced VLQs are fairly rich with leptons, jets, b-jets, and missing energy. Depending on the mass of the VLQ, the top quarks and $W/Z/H^0$ bosons may be Lorentz boosted and identified using jet substructure techniques. Thus the searches are performed using lepton+jets signatures, multi-lepton and all-hadronic decays. In addition, T or B quarks with their antiparticles can result in events with same-sign leptons, for example if the decay $T \to tH \to bWW^+W^-$ is present, followed by leptonic decays of two same-sign W bosons. In the following subsections, while we describe the searches for each of the decay modes of the VLQs, the same analysis can be re-interpreted to obtain the sensitivity to a combination with varied branching fractions to the different decay modes.

In the following sections, the results obtained for T (B) quarks assuming 100% branching ratio to Wb (Wt) are also applicable to heavy vector-like $Y_{-4/3}$ ($X_{5/3}$) with charge 4/3 (5/3).

91.2.3.1 *Searches for* $\boldsymbol{T}$ *quarks that decay to* $\boldsymbol{W}$, $\boldsymbol{Z}$ *and* $\boldsymbol{H^0}$ *bosons*

$T/Y \to qW$:

ATLAS has searched for pair production of heavy T quarks that decay to a W boson and a light quark q [172]. The search focuses on the channel where one W decays to a lepton (electron or muon) , and one W decays hadronically leading to a large R jet. Thus the final state is a charged lepton, missing transverse energy, a large radius jet, and multiple small radius jets. The analysis uses the scalar sum of all the final state objects S_T to discriminate against background and searches in hypothetical reconstructed heavy quark mass. The analysis excludes T masses below 1530 GeV.

$T/Y \to bW$:

CMS has searched for pair production of heavy T quarks that decay exclusively to bW [173–175]. The analysis selected events with exactly one charged lepton, assuming that the W boson from the second T quark decays hadronically. Under this hypothesis, a 2-constraint kinematic fit can be performed to reconstruct the mass of the T quark as a narrow mass peak with a mass resolution of around 7%. In Refs. [174] and [175], the two-dimensional distribution of reconstructed mass vs S_T was used to test for the signal, where S_T is the scalar sum of the missing p_T and the transverse momenta of the lepton and the leading four jets. This analysis, when combined with the search in the fully hadronic final state [176] excluded new quarks that decay 100% to bW for masses below 0.89 TeV [175]. At times the hadronically-decaying W boson is produced with a large Lorentz boost, leading to the W decay products merged into a large-radius jet. Algorithms such as jet pruning [177] were used to remove contributions from soft, wide angle radiation, from large-radius jets, leading to better discrimination between jets from multijet events and those arising from decays of the heavy particles. If the mass of the boosted jet was compatible with the W boson mass, then the W boson candidate jet and its subjets were used in the kinematic reconstruction of the T quark. No excess over standard model backgrounds was observed. Upper limits on the production cross section as a function of the mass of T quarks were measured. By comparing them with the predicted cross section for vector like quark pair production, the strong pair production of T quarks was excluded for masses below 1.30 TeV (1.28 TeV expected) [173].

Another "cut-based" search for pair produced T quarks in the all-hadronic final state targeting the Wb decay mode [178], relies on mass reconstruction of two highest p_T Wb combinations using boosted W boson candidates with $p_T > 200$ GeV and b-tagged jets. H_T is used as the signal discriminator, with selected events divided into nine categories based on the multiplicity of W and b-jets in the event. From this search T quarks with pure Wb decays are excluded for masses below 1.04 TeV (1.07 TeV expected).

An analogous search has been carried out by ATLAS [179,180] for the pair production of heavy T quarks. It used the lepton+jets final state with an isolated electron or muon and at least four jets, including a b-jet, and required reconstruction of the T quark mass. Given that the mass range for the T quark being explored was from a 0.4 TeV to a couple of TeV, the W boson from the T quark may fall in two categories: those with a high boost leading to merged decay products, and others where the two jets from the W boson were resolved. In addition, the selection was optimized to require large angular separation between the high p_T W bosons and the b-jets.

The $T \to Wb$ candidates were constructed from both the leptonically and hadronically decaying W bosons by pairing them with the two highest p_T b-tagged jets in the event. The pairing of b-jets with W bosons which minimizes the difference between the masses of leptonically decaying T ($m_{lep}(T)$) and the hadronic T ($m_{had}(T)$) was chosen. Finally, $m_{lep}(T)$ was used as the discriminating variable in a signal region defined by high S'_T (here S'_T is defined as the scalar sum of the missing p_T, the p_T of the lepton and jets), and the opening angle between the lepton and the neutrino ($\Delta R(e,\nu)$). With the 36.1 fb^{-1} data collected during Run 2 at $\sqrt{s} = 13$ TeV, assuming 100% branching ratio to the Wb decay, the observed lower limit on the T mass was 1.35 TeV, and in the SU(2) singlet scenario, the lower mass limit was obtained to be 1.17 TeV [179].

A targeted search for a T quark, produced singly in association with a light flavor quark and a b quark and decaying into

Int. J. Mod. Phys. A 2026.41. Downloaded from www.worldscientific.com
by UNIVERSITY OF CALIFORNIA @ BERKELEY on 09/16/26. Re-use and distribution is strictly not permitted, except for Open Access articles.

bW, was carried out by CMS at $\sqrt{s}$=13 TeV and a dataset corresponding to 2.3 fb^{-1} [181]. The analysis used lepton+jets events, with at least one b-tagged jet with large transverse momentum, and a jet in the forward η region. Selected events were required to have $S''_T > 500$ GeV, where S''_T is defined as the scalar sum of the transverse momenta of the lepton, the leading central jet, and the missing transverse momentum. The invariant mass of the T candidate was used as the discriminating variable and was reconstructed using the four-vectors of the leptonically decaying W boson and the leading central jet. No excess over the standard model prediction was observed. As the VLQ width is proportional to the square of the coupling, upper limits were set on the production cross section assuming a narrow width VLQ with coupling greater than 0.5. For Y/T quarks with a coupling of 0.5 and a 100% branching fraction for the decay to bW the excluded masses were in the range from 0.85 to 1.40 TeV [181]. A similar search [182, 183] was performed by ATLAS for a singly produced T or $Y_{-4/3}$ quark decaying to Wb using a dataset corresponding to 36.1 fb^{-1}. The search was performed using lepton+jets events with a high p_T b-tagged jet, and at least one forward jet. The reconstructed mass of the $T/Y_{-4/3}$ quark, was used as the discriminating variable and showed no excess above the expectation from SM. Interference effects with the SM background are included in the study. This search led to 95% CL upper limits on the mixing angle $|sin(\theta_L)|$ (C_L^{Wb}) in the range of 0.18–0.35 (0.25–0.49) for singlet T quark mass between 0.8–1.2 TeV. This search also provided limits as a function of the $Y_{-4/3}$ quark mass, on the coupling of the $Y_{-4/3}$ quark to bW, and the mixing parameter $|sin\theta_R|$ (C_R^{Wb}) for a (B,$Y_{-4/3}$) doublet model [182]. For VLQ masses between 0.08–1.8 TeV, the limits on $|sin(\theta_R)|$ (C_R^{Wb}) are in the range 0.17–0.55 (0.24–0.77), and for for $Y_{-4/3}$ quark mass between 0.9–1.25 TeV, the limits on $|sin\theta_R|$ are around 0.18–0.19 and below the constraints from electroweak precision observables. For $Y_{-4/3}$ quark in the triplets (T,B,$Y_{-4/3}$), limits on $|sin(\theta_L)|$ (C_L^{Wb}) are between 0.16–0.39 (0.31–0.78) for masses between 0.8 GeV–1.6 TeV [182].

$T \to tH^0$:

ATLAS has performed a search for $T\overline{T}$ production with $T \to tH^0$ [180, 184]. Given the dominant decay mode $H^0 \to b\bar{b}$, these events are characterized by a large number of jets, many of which are b-jets. Thus the event selection required one isolated electron or muon and high jet multiplicity (including b-tagged jets). The sample is categorized by the jet multiplicity (5 and $\geq$6 jets in the 1-lepton channel; 6 and $\geq$7 jets in the 0-lepton channel), b tag multiplicity (2, 3 and $\geq$4) and mass-tagged jet multiplicity (0, 1 and $\geq$2). The distributions of $m_{\rm eff}$, defined as the scalar sum of the lepton and jet p_T and the missing p_T, for each category were used as the discriminant for the final signal and background separation. No excess of events was found. Weak isospin doublet T quarks were excluded below 1.16 TeV.

A search by ATLAS for pair produced VLQs with an all-hadronic final state signature yields an exclusion of pure decays $T \to tH^0$ upto a T quark mass of 2.3 TeV [185].

The CMS search for $T\overline{T}$ production, with $T \to tH^0$ decays has been performed in lepton+jets, multilepton and all-hadronic final states. The lepton+jets analysis [186] emphasizes the presence of a large number of b-tagged jets, and combines it with other kinematic variables in a Boosted Decision Tree (BDT) to enhance signal to background discrimination. The multilepton analysis [186] was optimized for the presence of b-jets and the large hadronic activity. For $\mathcal{B}(T \to tH^0) = 1$, the combined lepton+jets and multilepton analyses led to a lower limit on T quark masses of 0.71 TeV. A search for $T \to tH^0$ in all-hadronic decays [187], optimized for a high mass T quark, and based on identifying boosted top quark jets has been carried out by CMS. This search aimed to resolve subjets within the jets arising from boosted top quark decays, including b tagging of the subjets. A likelihood discriminator was defined based on the distributions of H_T and the invariant mass of the two b-jets in the events for signal and background. No excess above background expectations was observed. Assuming 100% branching ratio for $T \to tH^0$, this analysis led to a lower limit of 0.75 TeV on the mass of the T quark.

Searches for T quarks at $\sqrt{s}$=13 TeV, based on a 2.6 fb^{-1} dataset [188] have been performed by CMS using the lepton+jets final state. This search has been optimized for high mass T quarks by exploiting techniques to identify W or Higgs bosons decaying hadronically with large transverse momenta. The boosted W channel excluded T quarks decaying only to bW with masses below 0.91 TeV, and the boosted tH channel excluded T quarks decaying only to tH for masses below 0.89 TeV.

A CMS search for $T \to tH^0$ with $H^0 \to \gamma\gamma$ decays has been performed [189] in pair production of T quarks. To identify the Higgs boson produced in the decay of the heavy T quark, and the subsequent $H^0 \to \gamma\gamma$ decay, the analysis focused on identification of two photons in events with one or more high p_T lepton+jets or events with no leptons and large hadronic activity. A search for a resonance in the invariant mass distribution of the two photons in events with large hadronic activity defined by the H_T variable showed no excess above the prediction from standard model processes. The analysis resulted in exclusion of T quark masses below 0.54 TeV. CMS also searches for a single vector like T decaying to either Z boson or a Higgs boson and a T quark [190] placing a limit of up to 1.4 TeV.

A search for single production of a vector-like quark either a singlet T with charge $\frac{2}{3}$ or a Y from a triplet (T,B,Y) with charge $-\frac{4}{3}$ decaying into W (l ν) and b-quark was performed by the ATLAS collaboration [191]. Limit on the coupling strength , κ ranges between 0.22 and 0.52 for masses from 1150 to 2300 GeV for the singlet interpretation while with the triplet assumption the limits on vary from 0.14 to 0.46 for masses from 1150 to 2600 GeV. A companion analysis [192] searches in the all hadronic final state for the same single production of a vector-like quark The observed lower limits on the masses of Y quarks with κ of 0.5 and κ of 0.7 and are 2.0 TeV and 2.4 TeV, respectively. For T quarks, the observed mass limits are 1.4 TeV for and 1.9 TeV for κ of 0.5 and κ of 0.7. The combination of these two analysis [193] results in a combined limit of κ 0.5 and m_T excluded for masses above 2.1 TeV, the most restrictive to date. ATLAS also searches for a a T quark decaying into Z t with the Z boson decaying leptonically into electron or muon pairs and the top quark resulting in a large-R top quark jet [194] which produces limits and excludes this decay up to 1.8 TeV.

A search for electroweak single production of T quarks decaying to tH^0 using boosted topologies in fully hadronic [195] and lepton+jets [196] in the final states has been performed by CMS. The electroweak couplings of the T quarks to the SM third generation quarks are highly model dependent, and hence these couplings determine the rates of the single T quark production. In both analyses, T quark invariant mass was reconstructed using the boosted Higgs boson jet and the top quark. Higgs boson jets were identified using jet substructure techniques and subjet b tagging. For the lepton+jets analysis, the top quark was reconstructed from the leptonically decaying W and the b jet, while in the all-hadronic analysis the top quark jet was tagged using substructure analysis. There was no excess of events observed above background. Exclusion limits on the product of the production cross section and the branching fraction ($\sigma(pp \to Tqt/b) \times \mathcal{B}(T \to tH^0)$ were derived for the T quark masses in the range 0.70-1.8 TeV. From the lepton+jets analysis, for a mass of 1.0 TeV, values of ($\sigma(pp \to Tqt/b) \times \mathcal{B}(T \to tH^0)$ greater than 0.8 and 0.7 pb were excluded assuming left- and right-handed coupling of the T quark to standard model fermions, respectively [196]. For the all-hadronic analysis, upper limits between 0.31 and 0.93 pb were obtained on ($\sigma(pp \to Tqt/b) \times \mathcal{B}(T \to tH^0)$ for T quark masses in the range 1.0-1.8 TeV [195]. ATLAS performs a similar search [197] for single production of vector-like T quarks decaying into a Higgs Boson and a top quark and places limits between 1 and 1.7 TeV depending on the coupling

$T \to tZ$:

Both ATLAS and CMS search for T quarks that decay exclusively into tZ in pp collisions at $\sqrt{s}$ = 13 TeV. No excesses were found in either search.

ATLAS performs a search [198] optimized for pair production of vector-like top quarks decaying into tZ where the Z boson subse-

Int. J. Mod. Phys. A 2026.41. Downloaded from www.worldscientific.com
by UNIVERSITY OF CALIFORNIA @ BERKELEY on 09/16/26. Re-use and distribution is strictly not permitted, except for Open Access articles.

quently decays into neutrino pairs, utilizing 139 fb^{-1} of data. The search selected events with one lepton, multiple jets, and significant missing transverse momentum. No significant excesses were found and lower limits on the mass of a vector like top quark were placed, excluding masses below 1.59 TeV (weak-isospin doublet) and 1.47 TeV (pure tZ mode).

Another search by ATLAS for pair produced T decaying to tZ has been carried out by reconstructing the high transverse momentum Z boson from a pair of opposite-sign same-flavor leptons, using events with two or three charged leptons [199]. The final analysis is based on three final state signatures. In the trilepton events, at least one b-tagged jet is required and H_T, formed from all hadronic jets and charged leptons, is used as the discriminating variable. In events with two leptons, at least 2 b-jets are requested and events with zero or one high p_T top-tagged jet, use H_T as the discriminator. The second dilepton analysis with two top-tagged high p_T jets focuses on hadronically decaying heavy resonances and the invariant mass of the Z boson and the highest p_T b-tagged jet is found to be a good discriminating variable. No excess was observed over the background expectations. Limits were placed at a heavy vector like top of 1.6 TeV.

ATLAS has subsequently carried out a search [200] for singly produced T quarks decaying to tZ where the Z boson decays into neutrino pairs. The search is carried out using 36.1 fb^{-1} of data in events with two different final state signatures: one with jets and significant missing p_T (0L) and the other with a single lepton, jets and missing p_T (1L). Events are divided into signal and dedicated W+jets and $t\bar{t}$ background control regions. The sensitivity to the T quark signal is extracted using distributions of missing p_T for the 1L and the distribution of T quark transverse mass constructed from missing p_T and the high p_T large-radius top-tagged jet, for 0L analysis. There is no excess found over the expected background and lower limits on the production of T singlets are obtained as a function of the left- and right-handed couplings $c_{L,W}$ and $c_{R,W}$ to top quarks and W bosons, where c_W above 0.7 is excluded for T quark mass of 1.4 TeV. The limits on c_W are also recasted into expected and observed 95% CL upper limits for the mixing angle (θ_L) of a singlet T with the top quark.

CMS searched [201] for single production of T quarks decaying into tZ with the Z boson decaying to pairs of charged leptons (electrons and muons) and the top quark decaying hadronically using 35.9 fb^{-1} of data. Limits were placed on T quarks with masses between 0.7 and 1.7 TeV excluding the product of cross section and branching fraction above values of 0.27 to 0.04 pb. Additionally, limits on the product of cross section and branching fractions for a Z' boson decaying into tZ were set between 0.13 and 0.06 pb for Z' boson masses in the range from 1.5 to 2.5 TeV.

Similar searches by ATLAS for singly produced T decaying to Zt have been performed in final state signatures with two or three charged leptons [202]. The analysis relies on tagging b-jets and high p_T large-radius jets originating from top-quarks. Additional selections are devised to reduce the contributions from pair production of T quarks. For events with dilepton analysis, the discriminating variable is the mass of the T quark formed using the invariant mass of the Z boson candidate and the highest p_T top-tagged jet, while for the trilepton analysis, the variable S_T is used to search for an excess of data over the expected SM background. No excess above the SM expectations is observed. The two final states (dilepton and trileptons) are combined to obtain the final results. For the coupling parameter κ_T between 0.1–1.6, the 95% CL upper limits on the production cross section times branching fraction into Zt is between 0.16–0.18 (0.03–0.05) pb at T quark mass of 0.7 (2) TeV.

The search by the ATLAS experiment for VLQ pair production optimized to search for $T \to tZ$ decays [203] in a dataset with 139 fb^{-1} of luminosity has been performed in final states with either two leptons or three or more leptons. A multi-class boosted object tagger based on DNN techniques for large-radius jets is used to categorize events according to the number of high p_T boosted H^0, Z/W, and top quark jets. The discriminant in the signal to evaluate the sensitivity depends on the number of leptons in the event. For the two lepton analysis, the discriminant is the mass of the T quark which is constructed from b and Z candidates, while for the three or more lepton analysis, H_T computed using the p_T of the jets and leptons is used as the discriminant. This analysis excludes T quark masses up to 1.27 GeV (1.46 GeV), for the singlet (doublet) configuration [203].

Combination of $T \to tZ/tH^0$:

The search performed by the ATLAS experiment for electroweak single production of T quark decaying to tH^0 and tZ uses a dataset corresponding to 139 fb^{-1} of integrated luminosity, and events with a single lepton with multiple jets and b-jets in the final state [204]. The single production channel for VLQs probes κ, the universal coupling constant, which also controls the production cross section and the resonance width of the VLQ. The analysis uses techniques to tag boosted jets, and categorizes events by numbers of jets and b-jets. The event discriminant is the "effective mass" (meff) observable, defined as the scalar sum of the p_T of all central jets, p_T of leptons and the missing p_T in the event. No significant excess is observed. Limits on the mass of T quark and universal coupling strength (κ) are obtained. For singlet T quarks, values of κ above 0.5 are excluded for all masses below 1.8 TeV. For T quark mass of 1.6 TeV, κ above 0.41 is excluded [204].

A CMS search published in 2020 concentrates on the electroweak production of the T quark with $T \to tH^0$, and $T \to tZ$ decays, where subsequently both H^0 and Z Bosons decay hadronically, leading to fully hadronic final states [205]. The search focuses on evidence of T quarks produced in association with a b quark ($qg \to T\bar{b}q'$) or a top quark ($qg \to T\bar{t}q$). The production cross sections are model dependent, as the electroweak production depends on the strength of the T quark coupling, TbW (TtZ), for the charged-current (neutral-current) process, at the production vertex. The searches are split into two domains depending on the mass of the T quark and consider a wide range of widths of the T quark from a few percent to about 30% of the T quark mass. The event selection relies primarily on the large number of jets and on efficient identification of jets from b-quarks, in addition to double-b jet decays of the H^0 and Z bosons. The final sensitivity is derived by the search for a resonant peak in the tH^0/Z invariant mass spectrum. For low mass T quark searches, three independent regions based on the b-tagged jet requirements are examined. For T quark masses above 1 TeV, which result in highly Lorentz-boosted top quarks and H^0 or Z boson, large-area jets are used to form the T quark. This search reports upper limits at 95% confidence level on $\sigma B(T \to tH)$ and $\sigma B(T \to tZ)$ between 2 pb and 20 fb for T masses between 0.6 to 2.6 TeV in the Tbq and Ttq production channels. The analysis also reports combined results for $T \to tH$ and $T \to tZ$ associated production with a bottom quark and provides constraints on T quarks in the T singlet model for masses below 1.00 TeV. For an expected fractional width of 30%, the expected sensitivity extends to 1.28 TeV, comparable to the most stringent results.

Another inclusive search for pair produced T in the all-hadronic final state [178] has been performed by CMS using the boosted event shape tagger (BEST NN) neural network technique to classify jets in six categories W, Z, H^0, t, b, and light. This search does not focus on a given VLQ mode, but on various combinations of the boson and quark jets in the final state. Anti-k_T jets with a distance parameter of 0.8 are used. The BEST NN algorithm simultaneously classifies jets according to heavy object type. For each of the six particle hypotheses, it boosts each jet constituent into corresponding frame along the jet momentum direction, and calculates event shape and angular variables in the boosted frame, with the expectation that when boosting to the correct rest frame, jet constituents will be isotropic and show the expected N-prong structure of the decaying object in its rest frame. A neural network is trained using the event shape and angular variables in the boosted frame to classify jets according to one of those six possibilities (W, Z, H, t, b, or light). The analysis bins the events into 126 categories depending on the number of W, Z, H, t, b, or light jets in the final state with a maximum of four such objects. For each category H_T^{AK8}, the scalar sum of p_T of all AK8 jets, is used as the signal discriminator. A scan over a combination of various branching fractions is also performed. This search excludes T quark masses in the range 0.74–1.37 TeV for the tH decay mode

Int. J. Mod. Phys. A 2026.41. Downloaded from www.worldscientific.com by UNIVERSITY OF CALIFORNIA @ BERKELEY on 09/16/26. Re-use and distribution is strictly not permitted, except for Open Access articles.

in the NN analysis.

An inclusive search for VLQs has been carried out by CMS targeted at heavy T quarks decaying to any combination of bW, tZ, or tH^0 as described in [186]. Selected events have at least one isolated charged lepton. Events were categorized according to number and flavor of the leptons, the number of jets, and the presence of hadronic vector boson and top quark decays that are merged into a single jet. The use of jet substructure to identify hadronic decays significantly increases the acceptance for high T quark masses. No excess above standard model backgrounds was observed. Limits on the pair production cross section of the new quarks are set, combining all event categories, for all combinations of branching fractions into the three final states. For T quarks that exclusively decay to $bW/tZ/tH^0$, masses below 0.70/0.78/0.71 TeV are excluded.

91.2.3.2 *Searches for* $\boldsymbol{B}$ *quarks that decay to* $\boldsymbol{W}$, $\boldsymbol{Z}$ *and* $\boldsymbol{H^0}$ *bosons*

ATLAS and CMS have performed searches for pair production of heavy B quarks which subsequently decay to Wt, bZ or bH^0. The searches have been carried out in final states with single leptons, dileptons (with same charge or opposite charge), multileptons, as well as in fully hadronic final states.

$B \to bH^0$:

A search for B pair-produced events has been performed by the CMS experiment [179] using 137 fb^{-1} of data where the B decays into a $b/\bar{b}$ quark and either a H^0 or a Z boson. This search concentrates on final states with fully hadronic signatures, and utilizes different jet multiplicity categories to account for two resolved jets or merged single jets from H^0 or Z boson to $b\bar{b}$ decays, depending on the p_T of the H^0 or Z bosons. Nine final state categories are used, depending on the number of observed jets and the reconstructed event mode. No significant excess over expected background is observed. For the case $\mathcal{B}(B \to bH) =$ 100%(50%), VLQs with masses below 1.57 (1.45) TeV are ruled out.

Using 36.1 fb^{-1} of data, ATLAS has performed a search for pair produced VLQs with all-hadronic final state signature [206]. While this analysis provides exclusion limits for all third generation VLQs, it provides the strongest results for the $B \to bH^0$ decay mode and excludes decays with $\mathcal{B}(\mathcal{B} \to \lfloor\mathcal{H}') = \infty.\prime$ scenario for B masses upto 1.01 TeV. The limits are also cast in a two-dimensional plane of branching ratio values of $B \to bH^0$ vs. $B \to Wb$. This analysis required the presence of high p_T jets and multiple b tags. It used a multi-class DNN to classify jets arising from W, Z, H^0 bosons and top-quarks. In addition, the matrix element method was used to compute the likelihood for the event to arise from a particular VLQ final state and to construct the final discriminator. To increase the sensitivity of the analysis, processes with the same number of top quarks, W/Z bosons, and H^0 Higgs bosons are combined into a single hypothesis.

ATLAS has performed a search for single production of a vector-like B quark decaying to a b-quark and a H^0 boson, with $H^0 \to b\bar{b}$ decay, using a dataset corresponding to an integrated luminosity of 139 fb^{-1} [207]. The all hadronic final state signature relies on identification of at least 3 b-jets, with an additional soft forward jet from the spectator quark. Large area jets are used to identify boosted H^0 decays. This analysis results in excluding the single production of a VLQ (B, Y) doublet with relative width larger than 5% between masses of 1.0 TeV and 2.0 TeV [208]. The CMS experiment has searched for a single vector-like quark decaying into tH or tZ in the all hadronic final state with 138 fb^{-1} of data in the all hadronic channel reconstructing both the boson invariant mass and the tH or tZ invariant mass and searching for a resonance. No significant excess is found and cross-section limits are placed between 600 GeV and 1200 GeV between 600 and 68 fb [209].

$B \to Wt$:

A search for $B \to tW$ in B pair produced events has been performed by ATLAS [179] using lepton+jets events with one hadronically decaying W and one leptonically decaying W utilizing 36.1 fb^{-1} of data at $\sqrt{s} = 13$ TeV. The search was optimized for T production decaying into Wb. Since the analysis was optimized for $T \to Wb$ rather than Wt decays the analysis does not reconstruct the full B mass. As discussed earlier, the hadronically and leptonically decaying heavy quarks were required to have similar reconstructed masses (within 300 GeV). The interpretation of the $T \to Wb$ in the context of $B \to tW$ production led to the exclusion of heavy B like VLQs for masses less than 1.25 TeV and 1.08 TeV, assuming a 100% branching fraction to tW or SU(2) singlet B scenario, respectively.

A similar search by CMS [210], using 19.8 fb^{-1} of $\sqrt{s} = 8$ TeV data, selected events with one lepton and four or more jets, with at least one b-tagged jet, significant missing p_T, and further categorized them based on the number of jets tagged as arising from the decay of boosted W, Z or H^0 bosons. The S_T distributions of the events in different categories showed no excess of events above the expected background and yielded a lower limit on the B quark mass of 0.73 TeV for $BR(B \to Wt) = 1$.

CMS [188] also searched for pair production of both TT and BB with collisions from 2.5 fb^{-1} of $\sqrt{s} = 13$ TeV data. The analysis searched for events with one high p_T lepton , multiple jets, and highly boosted W or Higgs bosons decaying hadronically. The analysis focused on pair production and selects events with either a boosted W or Higgs candidate and then proceeds to search for anomalous production in excess of standard model production. Seeing no significant excesses CMS then proceeded to set limits in many different interpretations. The strongest was from the $B \to Wt$ interpretation leading to excluding heavy vector-like B quarks with mass less than 0.73 TeV.

The all-hadronic inclusive analysis [178] performed by CMS using the BEST NN technique to classify $W/Z/H^0/t/b$/light jets also gives exclusion limits on B quark production for various combinations of branching fractions for decays to tW, bZ, bH^0. By considering categories based on various combinations of the boson and quark jets in the final state it excludes B quarks with masses up to 1230 GeV, for B decays to tW with a 100% branching fraction.

Electroweak production of single heavy B+b production has been studied by CMS in the decay to tW with the lepton+jets final state [211]. Single lepton events with hadronic jets, including a forward jet, and missing p_T are selected and divided into 10 different categories based on lepton flavor (e/μ), top-tagged, W-tagged, and 0/1/2 b-tagged jets. The B quark mass m_{reco} is fully reconstructed from lepton, jets, and missing p_T, where the neutrino four-momentum is computed using the missing p_T and the W mass constraint. For events within the top-tagged category, the high p_T top-tagged hadronic jet and the leptonically decaying W boson are used to compute m_{reco}. The m_{reco} distribution are used as the signal discriminator. In the absence of an excess over the expected SM background, the exclusion limits on the production cross section for B quark masses between 0.7-2 TeV varies between 0.3 to 0.03 pb. In addition, B quarks with left-handed couplings and a relative width of 10, 20, and 30% are excluded for masses below 1.49, 1.59, and 1.66 TeV respectively.

$B \to bZ$:

As mentioned above, a search for B pair produced events, with final states with fully hadronic signature, using 137 fb^{-1} of data, has been performed by the CMS experiment [179]. In this search, the B decays into a $b/\bar{b}$ quark and either a H^0 or a Z boson. For the case $\mathcal{B}(B \to bZ) = 100\%(50\%)$, VLQs with masses below 1.39 (1.45) TeV are ruled out by this analysis.

A search by CMS [212] for the pair-production of a heavy B quark and its antiparticle has been performed, where one of the heavy B quark decays to bZ. Events with a Z boson decaying to e^+e^- or $\mu^+\mu^-$ and at least one b jet are selected. The signal from $B \to bZ$ decays is expected to appear as a local enhancement in the bZ mass distribution. No such enhancement was found and B quarks that decay 100% into bZ are excluded below 0.70 TeV. This analysis also set upper limits on the branching fraction for $B \to bZ$ decays of 30-100% in the B quark mass range 0.45-0.70 TeV. A complementary search has been carried out by ATLAS for new heavy quarks decaying into a Z boson and a b-quark [213]. Selected dilepton events contain a high transverse momentum Z boson that decays leptonically, together with two b-jets. If the dilepton events have an extra lepton in addition to

Int. J. Mod. Phys. A 2026.41. Downloaded from www.worldscientific.com
by UNIVERSITY OF CALIFORNIA @ BERKELEY on 09/16/26. Re-use and distribution is strictly not permitted, except for Open Access articles.

those from the Z boson, then only one b-jet is required. No significant excess of events above the standard model expectation was observed, and mass limits were set depending on the assumed branching ratios. In a weak-isospin singlet scenario, a B quark with mass lower than 0.65 TeV was excluded, while for a particular weak-isospin doublet scenario, a B quark with mass lower than 0.73 TeV was ruled out.

The search by ATLAS for $B \to bZ$ decays [203] in final states with either two leptons or three or more leptons using a multi-class boosted object tagger to categorize events according to the number of high p_T boosted H^0, Z/W, and top quark jets excludes B quark masses up to 1.20 GeV (1.32 GeV), for the singlet (doublet) configuration [203].

In addition to pair production, ATLAS has also searched for the electroweak production of single B quarks, which is accompanied by a b-jet and a light jet [213]. The dilepton selection for double B production was modified for the single B production study by requiring the presence of an additional energetic jet in the forward region. An upper limit of 200 fb was obtained for the process $\sigma(pp \to B\bar{b}q) \times B(B \to Zb)$ with a heavy B quark mass at 0.70 TeV. This search indicated that the electroweak mixing parameter X_{Bb} below 0.5 is neither expected nor observed to be excluded for any values of B quark mass.

91.2.3.3 *Searches for top-partner quark* $\boldsymbol{X_{5/3}}$

Searches for a heavy top vector-like quark $X_{5/3}$, with exotic charge $\pm 5/3$, such as that proposed in Refs. [215, 216], have been performed by both ATLAS and CMS [179, 217].

The analyses assumed pair-production or single production of $X_{5/3}$ with $X_{5/3}$ decaying with 100% branching fraction to tW. Searches for $X_{5/3}$ have been performed using two final state signatures: same-sign leptons and lepton+jets.

The analysis based on searching for same-sign leptons, from the two W bosons from one of the $X_{5/3}$, has smaller backgrounds compared to the lepton+jets signature. Requiring same-sign leptons eliminates most of the standard model background processes, leaving those with smaller cross sections: $t\bar{t}W$, $t\bar{t}Z$, WWW, and same-sign WW. In addition, backgrounds from instrumental effects due to charge misidentification were considered. Assuming pair production of $X_{5/3}$, the analysis by CMS using H_T as the discriminating variable restrict the $X_{5/3}$ mass to be higher than 1.16 (1.10) TeV for a right (left) handed chirality particle [217–219]. The limits obtained by ATLAS, by classifying the signal region by number of b-jets, H_T, and missing p_T in the event, led to a lower mass limit on $X_{5/3}$ of 1.19 TeV [220, 221].

Searches for $X_{5/3}$ using leptons+jets final state signatures are based on either full or partial reconstruction of the T mass from the lepton, jets (including b-jets) and missing p_T. The CMS search [217, 222] also utilized jet substructure techniques to identify boosted $X_{5/3}$ topologies. The discriminating variable used was the mass constructed from the lepton and b-tagged jet, $M_{(\ell,b)}$, which corresponds to the visible mass of the leptonically decaying top quark. To optimize the search sensitivity, the events were further separated into categories based on lepton flavor (e, μ), the number of b-tagged jets, the number of W-tagged jets, and the number of t-tagged jets. In the absence of a signal, the CMS analysis excluded $X_{5/3}$ quark masses with right-handed (left-handed) couplings below 1.32 (1.30) TeV [222]. Combining the lepton+jets with the same-sign leptons analyses leads to a slight improvement and excludes $X_{5/3}$ quark masses with right-handed (left-handed) couplings below 1.33 (1.30) TeV.

The ATLAS lepton+jets search for $X_{5/3}$ utilized events with high p_T W bosons and b-jets. The search described earlier for T pair production, with $T \to Wb$ decays, can be reinterpreted as a search for $X \to tW$. This analysis excluded $X_{5/3}$ with masses below 1.25 TeV [179].

The single $X_{5/3}$ production cross section depends on the coupling constant λ of the tWX vertex. ATLAS has performed an analysis of same-sign dileptons which includes both the single and pair production. This analysis led to a lower limit on the mass of the $X_{5/3}$ of 0.75 TeV for both values of $\lambda = 0.5$ and 1.0 [223].

Single heavy $X_{5/3}$+t production has been studied by CMS in the decay to tW with the lepton+jets final state [211]. The description of the analysis is provided earlier in the discussion of $B \to WtX$ decays, where the reconstructed mass of $X_{5/3}$, m_{reco} distribution is used as the signal discriminator. In the absence of an excess over the expected SM background, the exclusion limits on the production cross section for $X_{5/3}$ quark masses between 0.7–2 TeV varies between 0.3 to 0.03 pb, depending on the width of $X_{5/3}$ between 1–10%. In addition, $X_{5/3}$ quarks with left-handed couplings and a relative width of 10, 20, and 30% are excluded for masses below 0.92, 1.3, and 1.45 TeV respectively.

91.2.4 *Heavy resonances decaying to VLQ*

CMS has performed search for VLQ production in the decay of massive resonances such as Z' and W' bosons.

$\underline{Z' \to tT}$: Specifically searches are presented by CMS in Refs. [224] and [225] for massive spin-1 Z' resonances decaying to a top quark and a heavy VLQ top quark partner T. The results of this search for a heavy spin-1 resonance are interpreted in the context of two different models. In the $G^\star$ model which predicts ten VLQs (T, $B, \tilde{T}, \tilde{B}, T_{5/3}, T_{2/3}, T', B', B_{-1/3}, B_{-4/3}$) with the mass relationship $M(T_{5/3}) = M(T_{2/3}) = M(T)\cos(\phi_L)$. For the benchmark scenario [226], $\cos(\phi_L)$=0.84 and the branching fractions $T \to tH^0, tZ, Wb$ are 0.25, 0.25 and 0.5 respectively. The ρ^0 model predicts a multiplet of four new VLQs $T, B, X_{2/3}, X_{5/3}$, and in the benchmark scenario [227], the branching fractions $T \to tH^0, tZ, Wb$ are 0.5, 0.5 and 0 respectively.

Two of the three decays of the $Z' \to tT$ with $T \to tH^0, tZ, Wb$ are characterized by the presence of two top quark decays and a boson (H^0/Z). A search [225] by CMS, optimized for $T \to tH/Zt$ decays was carried out in the lepton+jets final state using a dataset corresponding to an integrated luminosity of 35.9 fb^{-1}. Jet substructure techniques are used to identify (or tag) the high p_T large-radius jets originating from H^0, Z bosons and merged top quarks. The mass of the Z' boson is used as the signal discriminator and constructed using H^0 or Z-tagged dijet, the hadronic and leptonic top quark four vectors. For the leptonic top quark reconstruction ($t \to b\ell\nu_\ell$), the neutrino four vector is obtained from the event missing p_T using the W boson mass constraint. While the high p_T hadronic top quark jets from decays of massive Z' bosons are mostly merged and identified by top tagging techniques, those from T decays maybe resolved. The reconstructed Z' candidate events are classified into six different categories requiring the presence of either a H^0-tagged jet with 2 b-tagged subjets or one b-tagged subjet or a Z-tagged boson, each with either zero or one top-tagged jet. This search does not observe any significant deviation in data over the expectation from standard model backgrounds. Within the context of the $G^\star$ model, for a T mass of 1.2 (1.5) TeV, this search excludes $G^\star$ [226] resonances with masses between 1.5–2.3 (2.0–2.4) TeV.

The search in the all-hadronic final state is based on a 2.6 fb^{-1} dataset [224], and optimized for $T \to Wb$ decays. Jet substructure techniques are deployed for tagging jets from high p_T W boson and top quarks. Events are categorized into two groups based on the presence of b-tagged subjets in the top-tagged jet. The multijet background estimation is challenging and determined using side-bands defined by inverting the b-tagging requirement. Upper limits on the cross section for $Z' \to tT$ are obtained in the range of 0.13–10 pb.

$\underline{W' \to Tb/Bt}$: W' bosons are predicted to decay to VLQ third generation partners T, B quarks within composite Higgs and warped extra dimensional models [228]. In the benchmark scenarios of this framework, W' decays to Tb or Bt are equally distributed and the subsequent VLQ decays $T \to tH$ and $B \to bH^0$ each are assumed to have a branching fraction of 0.5. The search for $W' \to Tb/bH^0 \to tbH^0$ is performed using a sample of 35.9 fb^{-1} by CMS [229] in the final state with all-hadronic decays of both the Higgs boson ($H^0 \to b\bar{b}$) and the top quark. Both the H^0 boson and the top quark are expected to be boosted in the decay of a heavy W', and hence jet substructure techniques, including subjet b-tagging and double b-tagging are deployed to identify the H^0-tagged and the top-tagged jets. The three particle mass m_{tbH^0}, is used as the signal discriminant to observe the W' resonance. There is no excess observed in data above the expected SM background. This search excludes W' production cross section above 0.01–0.43 pb for masses between 1.5–4.0 TeV.

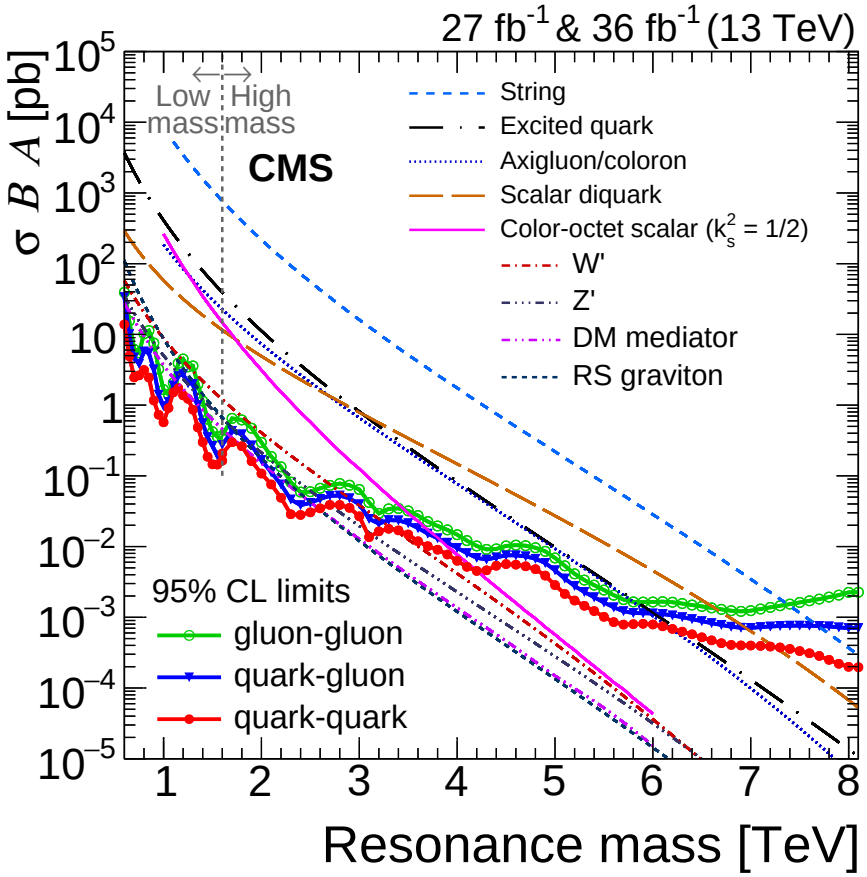

Figure 91.3: Observed 95% C.L. limits on $\sigma \times B \times A$ for string resonances, excited quarks, axigluons, colorons, E6 diquarks, s8 resonances, W' and Z' bosons, and Randall–Sundrum Gravitons g_{KK} from [214].

91.2.5 *Colorons and Colored Scalars*

These particles are associated with top-condensate and top-seesaw models, which involve an enlarged color gauge group. The new particles decay to dijets, $t\bar{t}$, and $b\bar{b}$.

Direct searches for colorons, color-octet scalars and other heavy objects decaying to $q\bar{q}$, qg, qq, or gg have been performed using LHC data from pp collisions at $\sqrt{s}$ =7, 8 and 13 TeV. Based on the analysis of dijet events from a data sample corresponding to a luminosity of 19.6 fb^{-1}, at $\sqrt{s}$ = 8 TeV, the CMS experiment excluded pair production of colorons with mass between 1.20−3.60 and 3.90 − 4.08 TeV [230]. Analyses of inclusive 8- and 10-jet final states with low missing transverse momentum by CMS [231], set limits in several benchmark models. Colorons (axigluons) with masses between 0.6 and 0.75 (up to 1.15) TeV were excluded, and gluinos in R-parity violating supersymmetric scenarios were ruled out from 0.6 up to 1.1 TeV.

A search for pair-produced colorons based on an integrated luminosity of 5.0 fb^{-1} at $\sqrt{s}$ = 7 TeV by CMS excluded colorons with masses between 0.25 TeV and 0.74 TeV, assuming colorons decay 100% into $q\bar{q}$ [232]. This analysis was based on events with at least four jets and two dijet combinations with similar dijet mass. Color-octet scalars (s8) with masses between 1.20−2.79 TeV were excluded by CMS [230], and below 2.7 TeV by ATLAS [233].

These studies have now been extended to take advantage of the increased center-of-mass energy during Run 2 of the LHC. Using 35.9 fb^{-1} of data collected at $\sqrt{s}$ =13 TeV, searches for narrow resonances have been performed by CMS. An analysis of the dijet invariant mass spectrum formed using wide jets [214, 234, 235], separated by $\Delta\eta_{jj} \leq 1.3$, led to limits on new particles decaying to parton pairs (qq, qg, gg). Specific exclusions on the masses of colorons and color-octet scalars were obtained and are shown in Fig. 91.3. Exclusions have been obtained for axigluons and colorons below 6.1 TeV, and color-octet scalars below 3.4 TeV.

Additional searches for dijet resonances have been performed by both ATLAS [236–238] and CMS [239, 240], though they have not been interpreted in the context of coloron production.

91.3 Conclusions

As the above analyses have demonstrated, there is already substantial sensitivity to possible new particles predicted to accompany the H^0 in dynamical frameworks of electroweak symmetry breaking. No significant hints of any deviations from the standard model have been observed, and limits typically at the scale of a few hundred GeV to a few TeV are set.

Given the need to better understand the H^0 and to determine in detail how it behaves, such analyses continue to be a major theme of Run 3 of the LHC, and we look forward to increased sensitivity as a result of the higher luminosity at the increased center of mass energy of collisions.

References

[1] G. Aad *et al.* (ATLAS), Phys. Lett. **B716**, 1 (2012), [arXiv:1207.7214].

[2] S. Chatrchyan *et al.* (CMS), Phys. Lett. **B716**, 30 (2012), [arXiv:1207.7235].

[3] S. Weinberg, Physica **A96**, 1-2, 327 (1979).

[4] A. Manohar and H. Georgi, Nucl. Phys. **B234**, 189 (1984).

[5] H. Georgi, Nucl. Phys. **B266**, 274 (1986).

[6] R. S. Chivukula, in "Flavor physics for the millennium. Proceedings, Theoretical Advanced Study Institute in elementary particle physics, TASI 2000, Boulder, USA, June 4-30, 2000," 731–772 (2000), [hep-ph/0011264].

[7] R. S. Chivukula, M. J. Dugan and M. Golden, Phys. Rev. **D47**, 2930 (1993), [hep-ph/9206222].

[8] S. Weinberg, Phys. Rev. **D13**, 974 (1976), [Addendum: Phys. Rev.D19,1277(1979)].

[9] L. Susskind, Phys. Rev. **D20**, 2619 (1979).

Int. J. Mod. Phys. A 2026.41. Downloaded from www.worldscientific.com by UNIVERSITY OF CALIFORNIA @ BERKELEY on 09/16/26. Re-use and distribution is strictly not permitted, except for Open Access articles.

Int. J. Mod. Phys. A 2026.41. Downloaded from www.worldscientific.com
by UNIVERSITY OF CALIFORNIA @ BERKELEY on 09/16/26. Re-use and distribution is strictly not permitted, except for Open Access articles.

[10] W. J. Marciano, Phys. Rev. D **21**, 2425 (1980).

[11] D. K. Hong, S. D. H. Hsu and F. Sannino, Phys. Lett. B **597**, 89 (2004), [hep-ph/0406200].

[12] D. D. Dietrich, F. Sannino and K. Tuominen, Phys. Rev. D **72**, 055001 (2005), [hep-ph/0505059].

[13] R. Foadi *et al.*, Phys. Rev. D **76**, 055005 (2007), [arXiv:0706.1696].

[14] T. A. Ryttov and F. Sannino, Phys. Rev. D **78**, 115010 (2008), [arXiv:0809.0713].

[15] K. Lane (2002), [hep-ph/0202255].

[16] C. T. Hill and E. H. Simmons, Phys. Rept. **381**, 235 (2003), [Erratum: Phys. Rept.390,553(2004)], [hep-ph/0203079].

[17] R. Shrock, in "The origin of mass and strong coupling gauge theories. Proceedings, 5th International Workshop, SCGT'06, Nagoya, Japan November 21-24, 2006," 227–241 (2007), [hep-ph/0703050].

[18] E. Eichten *et al.*, Rev. Mod. Phys. **56**, 579 (1984), [Addendum: Rev. Mod. Phys.58,1065(1986)].

[19] E. Eichten *et al.*, Phys. Rev. **D34**, 1547 (1986).

[20] R. F. Dashen and H. Neuberger, Phys. Rev. Lett. **50**, 1897 (1983).

[21] R. S. Chivukula and V. Koulovassilopoulos, Phys. Lett. **B309**, 371 (1993), [hep-ph/9304293].

[22] R. Foadi, M. T. Frandsen and F. Sannino, Phys. Rev. **D87**, 9, 095001 (2013), [arXiv:1211.1083].

[23] A. Belyaev *et al.*, Phys. Rev. D **90**, 035012 (2014), [arXiv:1309.2097].

[24] B. Holdom, Phys. Lett. **150B**, 301 (1985).

[25] K. Yamawaki, M. Bando, and K.-i. Matumoto, Phys. Rev. Lett. **56**, 1335 (1986).

[26] T. W. Appelquist, D. Karabali and L. C. R. Wijewardhana, Phys. Rev. Lett. **57**, 957 (1986).

[27] T. Appelquist and L. C. R. Wijewardhana, Phys. Rev. **D35**, 774 (1987).

[28] T. Appelquist and L. C. R. Wijewardhana, Phys. Rev. **D36**, 568 (1987).

[29] D. D. Dietrich and F. Sannino, Phys. Rev. D **75**, 085018 (2007), [hep-ph/0611341].

[30] F. Sannino, Phys. Rev. D **93**, 10, 105011 (2016), [arXiv:1508.07413].

[31] Z. Fodor *et al.*, Phys. Lett. B **718**, 657 (2012), [arXiv:1209.0391].

[32] E. Eichten, K. Lane and A. Martin (2012), [arXiv:1210.5462].

[33] See "Status of Higgs Boson Physics" review in this volume.

[34] A. Belyaev *et al.*, Phys. Rev. D **99**, 9, 095006 (2019), [arXiv:1812.09052].

[35] S. B. Gudnason, C. Kouvaris and F. Sannino, Phys. Rev. D **74**, 095008 (2006), [hep-ph/0608055].

[36] M. E. Peskin, Nucl. Phys. **B175**, 197 (1980).

[37] J. Preskill, Nucl. Phys. **B177**, 21 (1981).

[38] D. B. Kaplan and H. Georgi, Phys. Lett. **136B**, 183 (1984).

[39] D. B. Kaplan, H. Georgi and S. Dimopoulos, Phys. Lett. **136B**, 187 (1984).

[40] G. Cacciapaglia and F. Sannino, JHEP **04**, 111 (2014), [arXiv:1402.0233].

[41] G. Panico *et al.*, JHEP **03**, 051 (2013), [arXiv:1210.7114].

[42] R. Barbieri and A. Strumia, in "4th Rencontres du Vietnam: Physics at Extreme Energies (Particle Physics and Astrophysics) Hanoi, Vietnam, July 19-25, 2000," (2000), [hep-ph/0007265].

[43] D. Liu, I. Low and Z. Yin, JHEP **05**, 170 (2019), [arXiv:1809.09126].

[44] D. Liu, I. Low and Z. Yin, Phys. Rev. Lett. **121**, 26, 261802 (2018), [arXiv:1805.00489].

[45] M. Hashimoto, Phys. Rev. D **96**, 3, 035020 (2017), [arXiv:1704.02615].

[46] B. Bellazzini, C. Csáki and J. Serra, Eur. Phys. J. **C74**, 5, 2766 (2014), [arXiv:1401.2457].

[47] G. Cacciapaglia, C. Pica and F. Sannino, Phys. Rept. **877**, 1 (2020), [arXiv:2002.04914].

[48] N. Arkani-Hamed, A. G. Cohen and H. Georgi, Phys. Lett. **B513**, 232 (2001), [hep-ph/0105239].

[49] N. Arkani-Hamed *et al.*, JHEP **08**, 020 (2002), [hep-ph/0202089].

[50] N. Arkani-Hamed *et al.*, JHEP **07**, 034 (2002), [hep-ph/0206021].

[51] M. Schmaltz and D. Tucker-Smith, Ann. Rev. Nucl. Part. Sci. **55**, 229 (2005), [hep-ph/0502182].

[52] C. Csaki, T. Ma and J. Shu, Phys. Rev. Lett. **119**, 13, 131803 (2017), [arXiv:1702.00405].

[53] C. Csáki, T. Ma and J. Shu, Phys. Rev. Lett. **121**, 23, 231801 (2018), [arXiv:1709.08636].

[54] C. Csáki *et al.*, Phys. Rev. Lett. **124**, 24, 241801 (2020), [arXiv:1810.07704].

[55] M. J. Dugan, H. Georgi and D. B. Kaplan, Nucl. Phys. B **254**, 299 (1985).

[56] G. Ferretti, JHEP **06**, 107 (2016), [arXiv:1604.06467].

[57] A. Agugliaro *et al.*, JHEP **02**, 089 (2019), [arXiv:1808.10175].

[58] M. Frigerio *et al.*, JHEP **07**, 015 (2012), [arXiv:1204.2808].

[59] Y. Wu *et al.*, JHEP **11**, 058 (2017), [arXiv:1703.06903].

[60] C. Cai *et al.*, Phys. Rev. Lett. **125**, 2, 021801 (2020), [arXiv:1911.12130].

[61] R. Contino *et al.*, JHEP **10**, 081 (2011), [arXiv:1109.1570].

[62] R. Contino and M. Salvarezza, JHEP **07**, 065 (2015), [arXiv:1504.02750].

[63] R. Contino, L. Da Rold and A. Pomarol, Phys. Rev. D **75**, 055014 (2007), [hep-ph/0612048].

[64] O. Matsedonskyi, G. Panico and A. Wulzer, JHEP **01**, 164 (2013), [arXiv:1204.6333].

[65] P. Sikivie *et al.*, Nucl. Phys. **B173**, 189 (1980).

[66] K. Agashe *et al.*, Phys. Lett. **B641**, 62 (2006), [hep-ph/0605341].

[67] R. Essig *et al.*, JHEP **09**, 085 (2017), [arXiv:1707.03399].

[68] R. Grober and M. Muhlleitner, JHEP **06**, 020 (2011), [arXiv:1012.1562].

[69] A. Bharucha *et al.*, JHEP **09**, 069 (2021), [arXiv:2012.09470].

[70] A. Belyaev *et al.*, JHEP **01**, 094 (2017), [Erratum: JHEP 12, 088 (2017)], [arXiv:1610.06591].

[71] N. Bizot, G. Cacciapaglia and T. Flacke, JHEP **06**, 065 (2018), [arXiv:1803.00021].

[72] G. Cacciapaglia *et al.*, JHEP **02**, 208 (2022), [arXiv:2112.00019].

[73] Z. Chacko, H.-S. Goh and R. Harnik, Phys. Rev. Lett. **96**, 231802 (2006), [hep-ph/0506256].

[74] R. Barbieri *et al.*, JHEP **08**, 161 (2015), [arXiv:1501.07803].

[75] R. S. Chivukula, A. G. Cohen and K. D. Lane, Nucl. Phys. **B343**, 554 (1990).

[76] V. A. Miransky, M. Tanabashi and K. Yamawaki, Mod. Phys. Lett. **A4**, 1043 (1989).

[77] W. A. Bardeen, C. T. Hill and M. Lindner, Phys. Rev. **D41**, 1647 (1990).

[78] C. T. Hill, Phys. Lett. **B266**, 419 (1991).

Int. J. Mod. Phys. A 2026.41. Downloaded from www.worldscientific.com
by UNIVERSITY OF CALIFORNIA @ BERKELEY on 09/16/26. Re-use and distribution is strictly not permitted, except for Open Access articles.

[79] B. A. Dobrescu and C. T. Hill, Phys. Rev. Lett. **81**, 2634 (1998), [hep-ph/9712319].

[80] R. S. Chivukula *et al.*, Phys. Rev. **D59**, 075003 (1999), [hep-ph/9809470].

[81] C. T. Hill, Phys. Lett. B **345**, 483 (1995), [hep-ph/9411426].

[82] For a review, see C. Csaki, J. Hubisz, and P. Meade, `hep-ph/0510275` (2005), and "Extra Dimensions" review in this volume.

[83] Y. Hosotani, Phys. Lett. B **126**, 309 (1983).

[84] N. Haba *et al.*, Phys. Rev. D **70**, 015010 (2004), [hep-ph/0401183].

[85] R. Contino, Y. Nomura and A. Pomarol, Nucl. Phys. B **671**, 148 (2003), [hep-ph/0306259].

[86] K. Agashe, R. Contino and A. Pomarol, Nucl. Phys. **B719**, 165 (2005), [hep-ph/0412089].

[87] R. Contino and A. Pomarol, JHEP **11**, 058 (2004), [hep-th/0406257].

[88] G. Cacciapaglia, G. Marandella and J. Terning, JHEP **06**, 027 (2009), [arXiv:0802.2946].

[89] J. M. Maldacena, Int. J. Theor. Phys. **38**, 1113 (1999), [Adv. Theor. Math. Phys.2,231(1998)], [hep-th/9711200].

[90] W. Clemens, N. Evans and M. Scott, Phys. Rev. D **96**, 5, 055016 (2017), [arXiv:1703.08330].

[91] A. Belyaev *et al.*, Phys. Rev. D **101**, 8, 086013 (2020), [arXiv:1910.10928].

[92] N. Bizot *et al.*, Phys. Rev. D **95**, 7, 075006 (2017), [arXiv:1610.09293].

[93] S. Dimopoulos and L. Susskind, Nucl. Phys. **B155**, 237 (1979), [2,930(1979)].

[94] E. Eichten and K. D. Lane, Phys. Lett. **90B**, 125 (1980).

[95] D. B. Kaplan, Nucl. Phys. **B365**, 259 (1991).

[96] G. Panico and A. Wulzer, *The Composite Nambu-Goldstone Higgs*, volume 913, Springer (2016), [arXiv:1506.01961].

[97] T. Appelquist, M. Piai and R. Shrock, Phys. Rev. **D69**, 015002 (2004), [hep-ph/0308061].

[98] R.S. Chivukula, B.A. Dobrescu, and E.H. Simmons, Phys. Lett. **B401**, 74 (1997).

[99] G. F. Giudice *et al.*, JHEP **06**, 045 (2007), [hep-ph/0703164].

[100] C. Csaki, A. Falkowski and A. Weiler, JHEP **09**, 008 (2008), [arXiv:0804.1954].

[101] M. Redi and A. Weiler, JHEP **11**, 108 (2011), [arXiv:1106.6357].

[102] C. Hagedorn and M. Serone, JHEP **02**, 077 (2012), [arXiv:1110.4612].

[103] M. Frigerio *et al.*, JHEP **10**, 017 (2018), [arXiv:1807.04279].

[104] R. S. Chivukula and H. Georgi, Phys. Lett. **B188**, 99 (1987).

[105] G. D'Ambrosio *et al.*, Nucl. Phys. **B645**, 155 (2002), [hep-ph/0207036].

[106] K. Agashe *et al.* (2005), [hep-ph/0509117].

[107] A. Glioti *et al.*, SciPost Phys. **18**, 6, 201 (2025), [arXiv:2402.09503].

[108] T. Appelquist and R. Shrock, Phys. Lett. **B548**, 204 (2002), [hep-ph/0204141].

[109] G. Ferretti and D. Karateev, JHEP **03**, 077 (2014), [arXiv:1312.5330].

[110] G. Cacciapaglia and F. Sannino, Phys. Lett. B **755**, 328 (2016), [arXiv:1508.00016].

[111] G. Cacciapaglia, S. Vatani and C. Zhang, Phys. Lett. B **815**, 136177 (2021), [arXiv:1911.05454].

[112] G. Cacciapaglia, S. Vatani and C. Zhang, Phys. Rev. D **103**, 055001 (2021), [arXiv:2005.12302].

[113] F. Sannino *et al.*, JHEP **11**, 029 (2016), [arXiv:1607.01659].

[114] G. Cacciapaglia *et al.*, Phys. Rev. D **98**, 1, 015006 (2018), [arXiv:1704.07845].

[115] R. C. Brower *et al.*, Phys. Rev. D **93**, 7, 075028 (2016), [arXiv:1512.02576].

[116] R. Arthur *et al.*, Phys. Rev. D **94**, 9, 094507 (2016), [arXiv:1602.06559].

[117] C. Pica, PoS **LATTICE2016**, 015 (2016), [arXiv:1701.07782].

[118] B. Svetitsky, EPJ Web Conf. **175**, 01017 (2018), [arXiv:1708.04840].

[119] O. Witzel, PoS **LATTICE2018**, 006 (2019), [arXiv:1901.08216].

[120] V. Drach, PoS **LATTICE2019**, 242 (2020), [arXiv:2005.01002].

[121] T. Appelquist *et al.*, Phys. Rev. **D93**, 11, 114514 (2016), [arXiv:1601.04027].

[122] PDG review on "Z'-Boson Searches" in this volume.

[123] PDG review on "W'-Boson Searches" in this volume.

[124] M. Aaboud *et al.* (ATLAS), Phys. Lett. **B**, 68 (2019), [arXiv:1903.06248].

[125] CMS Collaboration, Technical Report CMS-PAS-EXO-19-019, CERN, Geneva (2019), URL `http://cds.cern.ch/record/2684757`.

[126] G. Aad *et al.* (ATLAS), Phys. Rev. **D90**, 5, 052005 (2014), [arXiv:1405.4123].

[127] M. Aaboud *et al.* (ATLAS), JHEP **01**, 055 (2018), [arXiv:1709.07242].

[128] CMS Collaboration, JHEP **0217**, 48 (2017).

[129] ATLAS Collaboration, ATLAS-CONF-2016-014 (2016).

[130] CMS Collaboration, JHEP **0717**, 001 (2016).

[131] M. Aaboud *et al.* (ATLAS), Phys. Rev. D. **99**, 092004 (2019), [arXiv:1902.10077].

[132] A. M. Sirunyan *et al.* (CMS), JHEP **04**, 031 (2019), [arXiv:1810.05905].

[133] ATLAS Collaboration, ATLAS-CONF-2019-007 (2019).

[134] CMS Collaboration, CMS-PAS-EXO-19-012 (2019).

[135] M. Aaboud *et al.* (ATLAS), Accepted by Phys. Rev. [arXiv:1906.05609].

[136] A. Tumasyan *et al.* (CMS), JHEP **07**, 067 (2022), [arXiv:2202.06075].

[137] V. Khachatryan *et al.* (CMS), Phys. Lett. **B755**, 196 (2016), [arXiv:1508.04308].

[138] S. Chatrchyan *et al.* (CMS), JHEP **05**, 108 (2014), [arXiv:1402.2176].

[139] V. Khachatryan *et al.* (CMS), JHEP **02**, 122 (2016), [arXiv:1509.06051].

[140] A. M. Sirunyan *et al.* (CMS), JHEP **08**, 029 (2017), [arXiv:1706.04260].

[141] A. M. Sirunyan *et al.* (CMS), Phys. Lett. **B777**, 39 (2018), [arXiv:1708.08539].

[142] A. M. Sirunyan *et al.* (CMS), Phys. Lett. B **820**, 136535 (2021), [arXiv:2104.04831].

[143] CMS Collaboration, Technical Report CMS-PAS-JME-15-002, CERN, Geneva (2016), URL `http://cds.cern.ch/record/2126325`.

[144] G. Aad *et al.* (ATLAS), Phys. Lett. **B788**, 347 (2019), [arXiv:1807.10473].

[145] G. Aad *et al.* (ATLAS) (2023), [arXiv:2308.08521].

[146] G. Aad *et al.* (ATLAS), Phys. Lett. **B743**, 235 (2015), [arXiv:1410.4103].

[147] D. Pappadopulo *et al.*, JHEP **09**, 060 (2014), [arXiv:1402.4431].

Int. J. Mod. Phys. A 2026.41. Downloaded from www.worldscientific.com
by UNIVERSITY OF CALIFORNIA @ BERKELEY on 09/16/26. Re-use and distribution is strictly not permitted, except for Open Access articles.

[148] M. Aaboud *et al.* (ATLAS), Phys. Rev. **D98**, 5, 052008 (2018), [arXiv:1601.04027].

[149] A. M. Sirunyan *et al.* (CMS), Phys. Lett. **B798**, 134952 (2019), [arXiv:1906.00057].

[150] M. Aaboud *et al.* (ATLAS), Phys. Lett. **B**, 91 (2017), [arXiv:1708.04445].

[151] M. Aaboud *et al.* (ATLAS), JHEP **03**, 042 (2018), [arXiv:1710.07235].

[152] M. Aaboud *et al.* (ATLAS), Phys. Lett. **B**, 68 (2018), [arXiv:1806.10532].

[153] A. M. Sirunyan *et al.* (CMS), Phys. Rev. **D97**, 072006, [arXiv:1708.05379].

[154] A. M. Sirunyan *et al.* (CMS), JHEP **07**, 075, [arXiv:1802.09407].

[155] A. M. Sirunyan *et al.* (CMS), JHEP **09**, 101, [arXiv:1803.10093].

[156] M. Aaboud *et al.* (ATLAS), Eur. Phys. J. **C**, 78 (2017), [arXiv:1710.01123].

[157] M. Aaboud *et al.* (ATLAS), Phys. Lett. **B**, 774 (2017), [arXiv:1707.06858].

[158] M. Aaboud *et al.* (ATLAS), JHEP **B**, 174 (2018), [arXiv:1712.06518].

[159] A. M. Sirunyan *et al.* (CMS), Eur. Phys. J. **C**, 636, [arXiv:1707.01303.].

[160] CMS Collaboration (CMS), Technical Report CMS-PAS-B2G-20-007 (2021).

[161] CMS Collaboration (CMS), Technical Report CMS-PAS-B2G-20-004 (2021).

[162] Eur. Phys. J. C **74**, 704 (2017).

[163] A. Collaboration, PRL **125**, 251802 (2020).

[164] A. Collaboration, Physics Letters B **779**, 24 (2018).

[165] A. Tumasyan *et al.* (CMS), Phys. Lett. B **826**, 136888 (2022), [arXiv:2106.10509].

[166] CMS Collaboration (CMS), Technical Report CMS-PAS-B2G-20-001 (2021).

[167] CMS Collaboration (CMS), Technical Report CMS-PAS-B2G-20-002 (2021).

[168] F. del Aguila *et al.*, Nucl. Phys. **B334**, 1 (1990).

[169] J. Serra, Journal of High Energy Physics **2015**, 9 (2015), ISSN 1029-8479, URL `http://dx.doi.org/10.1007/JHEP09(2015)176`.

[170] A. Anandakrishnan *et al.*, Physical Review D **93**, 7 (2016), ISSN 2470-0029, URL `http://dx.doi.org/10.1103/PhysRevD.93.075009`.

[171] M. Chala, Physical Review D **96**, 1 (2017), ISSN 2470-0029, URL `http://dx.doi.org/10.1103/PhysRevD.96.015028`.

[172] G. Aad *et al.* (ATLAS), Phys. Rev. D **110**, 5, 052009 (2024), [arXiv:2405.19862].

[173] A. M. Sirunyan *et al.* (CMS), Phys. Lett. **B779**, 82 (2018), [arXiv:1710.01539].

[174] CMS Collaboration, Technical Report CMS-PAS-B2G-12-017 (2014).

[175] V. Khachatryan *et al.* (CMS), Phys. Rev. **D93**, 1, 012003 (2016), [arXiv:1509.04177].

[176] CMS Collaboration, Technical Report CMS-PAS-B2G-12-013 (2012).

[177] S. D. Ellis, C. K. Vermilion and J. R. Walsh, Phys. Rev. **D80**, 051501 (2009), [arXiv:0903.5081].

[178] A. M. Sirunyan *et al.* (CMS), Phys. Rev. D **100**, 7, 072001 (2019), [arXiv:1906.11903].

[179] M. Aaboud *et al.* (ATLAS), JHEP **10**, 141 (2017), [arXiv:1707.03347].

[180] G. Aad *et al.* (ATLAS), JHEP **08**, 105 (2015), [arXiv:1505.04306].

[181] A. M. Sirunyan *et al.* (CMS), Phys. Lett. **B772**, 634 (2017), [arXiv:1701.08328].

[182] M. Aaboud *et al.* (ATLAS), JHEP **05**, 164 (2019), [arXiv:1812.07343].

[183] G. Aad *et al.* (ATLAS), Eur. Phys. J. **C76**, 8, 442 (2016), [arXiv:1602.05606].

[184] ATLAS Collaboration (ATLAS), Technical Report ATLAS-CONF-2016-104 (2016).

[185] J. H. Foo (ATLAS), PoS **LHCP2022**, 321 (2023).

[186] S. Chatrchyan *et al.* (CMS), Phys. Lett. **B729**, 149 (2014), [arXiv:1311.7667].

[187] V. Khachatryan *et al.* (CMS), JHEP **06**, 080 (2015), [arXiv:1503.01952].

[188] A. M. Sirunyan *et al.* (CMS), JHEP **11**, 085 (2017), [arXiv:1706.03408].

[189] CMS Collaboration, `cds.cern.ch/record/1709129` (2014).

[190] A. Hayrapetyan *et al.* (CMS), Phys. Rev. D **110**, 7, 072012 (2024), [arXiv:2405.05071].

[191] G. Aad *et al.* (ATLAS) (2025), [arXiv:2506.15515].

[192] G. Aad *et al.* (ATLAS), JHEP **02**, 075 (2025), [arXiv:2409.20273].

[193] G. Aad *et al.* (ATLAS), Phys. Rev. D **111**, 1, 012012 (2025), [arXiv:2408.08789].

[194] G. Aad *et al.* (ATLAS), JHEP **05**, 263 (2024), [arXiv:2402.16561].

[195] A. M. Sirunyan *et al.* (CMS), JHEP **04**, 136 (2017), [arXiv:1612.05336].

[196] V. Khachatryan *et al.* (CMS), Phys. Lett. **B771**, 80 (2017), [arXiv:1612.00999].

[197] G. Aad *et al.* (ATLAS), JHEP **08**, 153 (2023), [arXiv:2305.03401].

[198] G. Aad *et al.* (ATLAS), Eur. Phys. J. C **83**, 8, 719 (2023), [arXiv:2212.05263].

[199] G. Aad *et al.* (ATLAS), Phys. Lett. B **843**, 138019 (2023), [arXiv:2210.15413].

[200] M. Aaboud *et al.* (ATLAS), JHEP **05**, 041 (2019), [arXiv:1812.09743].

[201] A. M. Sirunyan *et al.* (CMS), Phys. Lett. **B781**, 574 (2018), [arXiv:1708.01062].

[202] M. Aaboud *et al.* (ATLAS), Phys. Rev. **D98**, 11, 112010 (2018), [arXiv:1806.10555].

[203] ATLAS Collaboration (ATLAS), Technical report, CERN, Geneva (2021), URL `https://cds.cern.ch/record/2773300`.

[204] ATLAS Collaboration (ATLAS), Technical report, CERN, Geneva (2021), URL `https://cds.cern.ch/record/2779174`.

[205] A. M. Sirunyan *et al.* (CMS), JHEP **01**, 036 (2020), [arXiv:1909.04721].

[206] M. Aaboud *et al.* (ATLAS), Phys. Rev. **D98**, 9, 092005 (2018), [arXiv:1808.01771].

[207] ATLAS Collaboration (ATLAS), Technical report, CERN, Geneva (2021), URL `https://cds.cern.ch/record/2760012`.

[208] G. Aad *et al.* (ATLAS) (2023), [arXiv:2308.02595].

[209] (2023).

[210] CMS Collaboration, Technical Report CMS-PAS-B2G-12-019 (2012).

[211] A. M. Sirunyan *et al.* (CMS), Eur. Phys. J. **C79**, 90 (2019), [arXiv:1809.08597].

[212] V. Khachatryan *et al.* (CMS), Phys. Rev. **D93**, 11, 112009 (2016), [arXiv:1507.07129].

[213] G. Aad *et al.* (ATLAS), JHEP **11**, 104 (2014), [arXiv:1409.5500].

[214] A. M. Sirunyan *et al.* (CMS), JHEP **08**, 130 (2018), [arXiv:1806.00843].

[215] R. Contino and G. Servant, JHEP **06**, 026 (2008), [arXiv:0801.1679].

[216] J. Mrazek and A. Wulzer, Phys. Rev. **D81**, 075006 (2010), [arXiv:0909.3977].

[217] A. M. Sirunyan *et al.* (CMS), JHEP **08**, 073 (2017), [arXiv:1705.10967].

[218] CMS Collaboration, Technical Report CMS-PAS-B2G-16-019 (2017).

[219] S. Chatrchyan *et al.* (CMS), Phys. Rev. Lett. **112**, 17, 171801 (2014), [arXiv:1312.2391].

[220] M. Aaboud *et al.* (ATLAS), JHEP **12**, 039 (2018), [arXiv:1807.11883].

[221] G. Aad *et al.* (ATLAS), Phys. Rev. **D91**, 11, 112011 (2015), [arXiv:1503.05425].

[222] A. M. Sirunyan *et al.* (CMS), JHEP **03**, 082 (2019), [arXiv:1810.03188].

[223] G. Aad *et al.* (ATLAS), JHEP **10**, 150 (2015), [arXiv:1504.04605].

[224] A. M. Sirunyan *et al.* (CMS), JHEP **09**, 053 (2017), [arXiv:1703.06352].

[225] A. M. Sirunyan *et al.* (CMS), Eur. Phys. J. **C79**, 3, 208 (2019), [arXiv:1812.06489].

[226] C. Bini, R. Contino and N. Vignaroli, JHEP **01**, 157 (2012), [arXiv:1110.6058].

[227] D. Greco and D. Liu, JHEP **12**, 126 (2014), [arXiv:1410.2883].

[228] N. Vignaroli, Phys. Rev. **D89**, 9, 095027 (2014), [arXiv:1404.5558].

[229] A. M. Sirunyan *et al.* (CMS), JHEP **03**, 127 (2019), [arXiv:1811.07010].

[230] V. Khachatryan *et al.* (CMS), Phys. Rev. **D91**, 5, 052009 (2015), [arXiv:1501.04198].

[231] V. Khachatryan *et al.* (CMS), Phys. Lett. **B770**, 257 (2017), [arXiv:1608.01224].

[232] S. Chatrchyan *et al.* (CMS), Phys. Rev. Lett. **110**, 14, 141802 (2013), [arXiv:1302.0531].

[233] G. Aad *et al.* (ATLAS), Phys. Rev. **D91**, 5, 052007 (2015), [arXiv:1407.1376].

[234] A. M. Sirunyan *et al.* (CMS), Phys. Lett. **B769**, 520 (2017), [Erratum: Phys. Lett.B772,882(2017)], [arXiv:1611.03568].

[235] CMS Collaboration, Technical Report CMS-PAS-EXO-15-001 (2015).

[236] G. Aad *et al.* (ATLAS), JHEP **06**, 151 (2020), [arXiv:2002.11325].

[237] G. Aad *et al.* (ATLAS), Phys. Rev. Lett. **125**, 13, 131801 (2020), [arXiv:2005.02983].

[238] M. Aaboud *et al.* (ATLAS), Phys. Rev. D **96**, 5, 052004 (2017), [arXiv:1703.09127].

[239] A. M. Sirunyan *et al.* (CMS), Phys. Lett. B **805**, 135448 (2020), [arXiv:1911.03761].

[240] A. M. Sirunyan *et al.* (CMS), JHEP **05**, 033 (2020), [arXiv:1911.03947].

Int. J. Mod. Phys. A 2026.41. Downloaded from www.worldscientific.com
by UNIVERSITY OF CALIFORNIA @ BERKELEY on 09/16/26. Re-use and distribution is strictly not permitted, except for Open Access articles.

Int. J. Mod. Phys. A 2026.41. Downloaded from www.worldscientific.com by UNIVERSITY OF CALIFORNIA @ BERKELEY on 09/16/26. Re-use and distribution is strictly not permitted, except for Open Access articles.

92. Grand Unified Theories

Revised August 2025 by N. Nagata (UTokyo); written with A. Hebecker (Heidelberg U.) and J. Hisano (Nagoya U.; KMI, Nagoya U).

92.1 The Standard Model

The Standard Model (SM) can be defined as a renormalizable quantum field theory with the gauge group $G_{\rm SM} = {\rm SU}(3)_C \times {\rm SU}(2)_L \times {\rm U}(1)_Y$ and three generations of fermions transforming under the representations

$$(\mathbf{3},\mathbf{2})_{1/3} + (\overline{\mathbf{3}},\mathbf{1})_{-4/3} + (\overline{\mathbf{3}},\mathbf{1})_{2/3} + (\mathbf{1},\mathbf{2})_{-1} + (\mathbf{1},\mathbf{1})_{2}\ , \quad (92.1)$$

along with a scalar Higgs doublet H transforming as $(\mathbf{1},\mathbf{2})_1$. Throughout this review, we use bold numbers to indicate the dimension of representations of non-Abelian gauge groups (fundamental and antifundamental in the present case), while the subscript denotes the ${\rm U}(1)_Y$ hypercharge.[1] The fermion fields in Eq. (92.1) correspond to the familiar set $[Q, u^c, d^c, L, e^c]$, where $Q = (u, d)$ and $L = (\nu, e)$ are the quark and lepton ${\rm SU}(2)_L$ doublets, and u^c, d^c, e^c are the charge-conjugate ${\rm SU}(2)_L$ singlets. Especially after the discovery of the Higgs boson, the SM stands out as a remarkably complete and experimentally consistent framework.

A notable exception to the success of the SM lies in the neutrino sector: although neutrino masses are now known to be non-zero, no such masses arise in the SM, even after the Higgs field acquires a vacuum expectation value (VEV). A minimal extension to account for these non-zero neutrino masses involves the inclusion of a dimension-five operator of the form $(HL)^2$ [1], which induces Majorana masses for neutrinos after electroweak symmetry breaking. This operator can be generated by integrating out heavy gauge-singlet fermions which couple to L and H—commonly referred to as right-handed neutrinos; this is known as the seesaw mechanism [2–8]. Alternatively, if light singlet neutrinos are introduced, neutrinos may instead acquire Dirac masses.

The SM also faces a variety of theoretical and phenomenological challenges. Among the most pressing is the electroweak hierarchy problem, which concerns the stability of the Higgs mass against large quantum corrections. Moreover, we still lack an understanding of the underlying dynamics responsible for spontaneous symmetry breaking in the electroweak sector. The SM also fails to provide a viable dark matter candidate, nor does it offer a mechanism for generating the observed baryon asymmetry of the Universe. In addition, the smallness of the QCD θ parameter, $\theta_{\rm QCD}$—the so-called strong CP problem—remains unexplained. The seemingly intricate pattern of quantum number assignments in Eq. (92.1) is also left without theoretical justification. Taken together with the large number of apparently arbitrary coupling constants, these shortcomings cast doubt on the plausibility of the SM as a truly fundamental theory, even leaving aside the issues expected to arise from quantum gravity at energies near the Planck scale, M_P.

To be precise, the SM contains 19 parameters that must be determined from experimental data. These include the three gauge couplings, g_3, g_2, and g_1;[2] 13 parameters associated with the Yukawa sector (comprising nine charged fermion masses, three mixing angles, and one CP phase in the CKM matrix); the Higgs mass and its quartic coupling; and $\theta_{\rm QCD}$. Majorana neutrinos add 3 mass parameters and 6 mixing and phase parameters. As we will see, grand unified theories (GUTs) can address the values of the three gauge couplings, in addition to the group-theoretic structure of Eq. (92.1). In many concrete realizations, GUTs can also shed light on other features of the SM, such as the family structure and the hierarchical values of fermion masses.

[1] We adopt the convention $Q = T_3 + Y/2$ for electric charge. All spinor fields are taken to be left-handed.

[2] Equivalently, the ${\rm SU}(2)_L$ and ${\rm U}(1)_Y$ gauge couplings are denoted by $g = g_2$ and $g' = \sqrt{3/5}\ g_1$. One often uses $\alpha_s = \alpha_3 = g_3^2/(4\pi)$ and $\alpha_{\rm EM} = e^2/(4\pi)$, with $e = g \sin\theta_W$ and $\sin^2\theta_W = (g')^2/(g^2 + (g')^2)$.

92.2 Basic group theory and charge quantization

92.2.1 ${\rm SU}(4)_C \times {\rm SU}(2)_L \times {\rm SU}(2)_R$

Historically, the first attempt at unification was the Pati–Salam model, based on the gauge group $G_{\rm PS} = {\rm SU}(4)_C \times {\rm SU}(2)_L \times {\rm SU}(2)_R$ [9].[3] In this framework, the SM fermions of one generation, together with an additional SM singlet, are embedded in the representations $(\mathbf{4},\mathbf{2},\mathbf{1})$ and $(\overline{\mathbf{4}},\mathbf{1},\mathbf{2})$ of $G_{\rm PS}$. The quantum numbers in Eq. (92.1) can be reproduced by considering the symmetry breaking pattern ${\rm SU}(4)_C \to {\rm SU}(3)_C \times {\rm U}(1)_{B-L}$, together with the identification of the SM hypercharge as a linear combination of $B-L$ (baryon minus lepton number) and the T_3 generator of ${\rm SU}(2)_R$: $Y/2 = T_{3R} + (B-L)/2$. The model naturally explains charge quantization—that is, why all electric charges in the SM are integer multiples of the smallest one. Specifically, the $\mathbf{4}$ and $\overline{\mathbf{4}}$ representations of ${\rm SU}(4)_C$ treat lepton number as a fourth color, and the traceless nature of the diagonal generator implies that quark charges are fixed as fractional multiples of lepton charges, proportional to $1/N_c$ with $N_c = 3$ the number of colors. However, since $G_{\rm PS}$ is not a simple group—it consists of three simple factors—it does not predict gauge coupling unification.

92.2.2 *SU(5)*

Since $G_{\rm SM}$ has rank four—two from ${\rm SU}(3)_C$, and one each from ${\rm SU}(2)_L$ and ${\rm U}(1)_Y$—the rank-four group SU(5) is the minimal choice for a simple group into which $G_{\rm SM}$ can be embedded [13]. In this framework, the three SM gauge couplings originate from a single unified coupling α_G at the grand unification scale M_G. The embedding of $G_{\rm SM}$ into SU(5) is straightforward. The ${\rm SU}(3)_C$ and ${\rm SU}(2)_L$ subgroups can be identified with the upper-left 3×3 and lower-right 2×2 blocks, respectively, within the traceless 5×5 matrices representing the generators of SU(5) in its fundamental representation. The ${\rm U}(1)_Y$ generator corresponds to the diagonal matrix ${\rm diag}(-2/3, -2/3, -2/3, 1, 1)$, which commutes with the generators of ${\rm SU}(3)_C \times {\rm SU}(2)_L \subset {\rm SU}(5)$. From this structure, one finds that a single generation of SM fermions is elegantly unified into the $\mathbf{10} \oplus \overline{\mathbf{5}}$ representations of SU(5), where the $\mathbf{10}$ denotes the rank-2 antisymmetric tensor representation:

$$\mathbf{10}: \begin{pmatrix} 0 & u_b^c & -u_g^c & u^r & d^r \\ -u_b^c & 0 & u_r^c & u^g & d^g \\ u_g^c & -u_r^c & 0 & u^b & d^b \\ -u^r & -u^g & -u^b & 0 & e^c \\ -d^r & -d^g & -d^b & -e^c & 0 \end{pmatrix} \quad \text{and} \quad \overline{\mathbf{5}}: \begin{pmatrix} d_r^c \\ d_g^c \\ d_b^c \\ e \\ -\nu_e \end{pmatrix}. \quad (92.2)$$

In addition to explaining charge quantization, this structure accounts for why the left-handed quark and lepton states form ${\rm SU}(2)_L$ doublets, while their right-handed counterparts are ${\rm SU}(2)_L$ singlets.

Since SU(5) has 24 generators, SU(5) GUTs predict 12 additional gauge bosons—known as X bosons (or X/Y bosons)—beyond those of the SM. These X bosons transform as an ${\rm SU}(3)_C$ triplet and an ${\rm SU}(2)_L$ doublet. Their interactions connect quarks and leptons, leading to the violation of both baryon and lepton number, and consequently predicting nucleon decay. Furthermore, the ${\rm U}(1)_Y$ hypercharge is automatically quantized, as it corresponds to a generator of SU(5).

In the minimal SU(5) model, the Higgs field is embedded in either a $\mathbf{5}_H$ or a $\overline{\mathbf{5}}_H$ representation. Each multiplet contains three extra states known as color-triplet Higgs bosons. These triplets couple to matter in a way that violates both baryon and lepton number, thereby inducing nucleon decay. To remain consistent with the experimental non-observation of such decay, the triplet mass must be $\gtrsim 10^{11}$ GeV [14–16].[4]

Supersymmetry (SUSY) is frequently invoked in the context of GUTs. It is a symmetry relating bosons and fermions, and it requires the existence of superpartners for all SM particles. SUSY was originally introduced as a solution to the electroweak hierarchy problem [18–21]. In addition, as discussed in Sec. 92.5, SUSY theories have the appealing feature that gauge coupling unification

[3] See also Refs. [10–12].

[4] This bound can be relaxed through a fine-tuned cancellation between the renormalizable Yukawa interactions and higher-dimensional operators involving the GUT-breaking Higgs field [17].

Int. J. Mod. Phys. A 2026.41. Downloaded from www.worldscientific.com by UNIVERSITY OF CALIFORNIA @ BERKELEY on 09/16/26. Re-use and distribution is strictly not permitted, except for Open Access articles.

is realized with high precision. In SUSY GUTs [22–27], both $\mathbf{5}_H$ and $\overline{\mathbf{5}}_H$ Higgs multiplets are required—not only to cancel gauge anomalies, but also to provide masses for both up- and down-type quarks. As we will discuss in Sec. 92.6, nucleon decay tends to be more severe in the minimal SUSY SU(5) model, since integrating out the color-triplet Higgs multiplets generates baryon-number-violating dimension-five operators [28, 29], whereas only dimension-six operators are generated in the non-SUSY case. The lower bound on the triplet mass from nucleon decay experiments depends on the SUSY scale but is typically above the unification scale M_G. The mass splitting between the Higgs doublet and triplet components arises from their interactions with the SU(5)-breaking sector, as discussed in Sec. 92.3.

92.2.3 *SO(10)*

While SU(5) provides the minimal framework for grand unification, it does not fully unify the matter content: each SM generation must be split across two distinct representations, **10** and $\overline{\mathbf{5}}$. To incorporate the right-handed neutrinos required for the seesaw mechanism, additional SU(5) singlets must be introduced. In this case, the right-handed neutrino masses are not necessarily tied to the grand unification scale.

By contrast, a single **16**-dimensional spinor representation of SO(10) accommodates an entire SM generation along with a singlet that naturally plays the role of a right-handed neutrino [30, 31]. This structure can be understood via the breaking pattern $\mathrm{SO}(10) \to \mathrm{SU}(5) \times \mathrm{U}(1)_X$ and the associated branching rule: $\mathbf{16} = \mathbf{10}_{-1} + \overline{\mathbf{5}}_3 + \mathbf{1}_{-5}$,[5] where the subscripts denote charges under the $\mathrm{U}(1)_X$ subgroup, which can be written as $2Y - 5(B-L)$. This $\mathrm{U}(1)_X$ is orthogonal to SU(5) and reflects the fact that SO(10) has rank five. Remarkably, all representations of SO(10) are anomaly-free in four dimensions (4d). As a result, the anomaly cancellation observed in SU(5) GUTs—or within each SM generation—can be viewed as a consequence of this broader property of SO(10).

We now describe in more detail how a single family of quarks and leptons is embedded in the **16**. To understand this, recall that the Γ-matrices of the 10-dimensional (10d) Clifford algebra give rise to five independent, anticommuting 'creation-annihilation' operators $\Gamma^{a\pm} = (\Gamma^{2a-1} \pm i\Gamma^{2a})/2$ for $a = 1, \ldots, 5$. These correspond to five fermionic harmonic oscillators, or "spin" 1/2 systems. The 32-dimensional spinor space, constructed as a tensor product of these five "spin" states, is reducible because the 10d rotation generators $M_{mn} = [\Gamma^m, \Gamma^n]/(4i)$ (for $m, n = 1, \ldots, 10$) always flip an even number of "spin" directions. This reducibility gives rise to the **16**-dimensional irreducible chiral spinor representation, as shown in Table 92.1. Next, one also recalls that the natural embedding of SU(5) in SO(10) relies on 'pairing up' the 10 real dimensions to produce 5 complex dimensions, $\mathbb{R}^{10} \equiv \mathbb{C}^5$, similarly to the paring up of Γ^ms used above. Specifically, each $|\pm\rangle$ system corresponds to a complex dimension of SU(5), as indicated by the labeling of the "spin" columns in Table 92.1: The first three and last two "spins" correspond to $\mathrm{SU}(3)_C$ and $\mathrm{SU}(2)_L$, respectively. An $\mathrm{SU}(3)_C$ rotation just raises one color index and lowers another, changing colors $\{r, g, b\}$, or changes relative phases between the three spin states. Similarly, an $\mathrm{SU}(2)_L$ rotation raises one weak index and lowers another, thereby flipping the weak isospin from up to down or vice versa, or changes the relative phase between the two spin states. In this representation $\mathrm{U}(1)_Y$ hypercharge is simply given by $Y = -2/3(\sum \text{color spins}) + (\sum \text{weak spins})$.[6] SU(5) rotations that are orthogonal to G_{SM} act by raising (or lowering) a color index while simultaneously lowering (or raising) a weak index. Such transformations can mix the states within the sets $\{Q, u^c, e^c\}$ and $\{d^c, L\}$, respectively, while ν^c remains a singlet under these rotations. Since SO(10) has 45 generators, it introduces 21 additional generators beyond those of SU(5), including $\mathrm{U}(1)_X$ mentioned above. The $\mathrm{U}(1)_X$ charge, associated with the SU(5)-invariant generator, is given by $X = 2\sum(\text{spins})$. The remaining 20 generators correspond to SO(10) transformations outside of SU(5), and can be realized as operations that simultaneously raise or lower two spin directions. These rotations relate **1** and $\overline{\mathbf{5}}$ to **10**.

Table 92.1: Quantum numbers in the **16** representation of SO(10)

State	$\mathrm{U}(1)_Y$	Color	Weak	SU(5)	$\mathrm{U}(1)_X$	SO(10)
ν^c	0	$---$	$--$	**1**	-5	
e^c	2	$---$	$++$			
u^r	1/3	$+--$	$-+$			
d^r	1/3	$+--$	$+-$			
u^g	1/3	$-+-$	$-+$			
d^g	1/3	$-+-$	$+-$	**10**	-1	
u^b	1/3	$--+$	$-+$			
d^b	1/3	$--+$	$+-$			**16**
u^c_r	$-4/3$	$-++$	$--$			
u^c_g	$-4/3$	$+-+$	$--$			
u^c_b	$-4/3$	$++-$	$--$			
d^c_r	2/3	$-++$	$++$			
d^c_g	2/3	$+-+$	$++$			
d^c_b	2/3	$++-$	$++$	$\overline{\mathbf{5}}$	3	
ν	-1	$+++$	$-+$			
e	-1	$+++$	$+-$			

SO(10) has two inequivalent maximal subgroups—and hence two distinct symmetry breaking patterns: $\mathrm{SO}(10) \to \mathrm{SU}(5) \times \mathrm{U}(1)_X$ and $\mathrm{SO}(10) \to \mathrm{SU}(4)_C \times \mathrm{SU}(2)_L \times \mathrm{SU}(2)_R$. In the first case, one can proceed with symmetry breaking down to $G_{\mathrm{SM}} \subset \mathrm{SU}(5)$ exactly as in the minimal SU(5). Alternatively, $\mathrm{U}(1)_Y$ can be identified as a linear combination of $\mathrm{U}(1)_X$ and the U(1) subgroup of SU(5), leading to the flipped SU(5) model [36–39] as an intermediate stage in the breaking of SO(10) to G_{SM}. The second path features the Pati–Salam model at the intermediate scale, with the decomposition $\mathbf{16} = (\mathbf{4}, \mathbf{2}, \mathbf{1}) \oplus (\overline{\mathbf{4}}, \mathbf{1}, \mathbf{2})$. Alternatively, SO(10) may break directly to the SM at M_G. In such "direct breaking" scenarios, as well as in those following the chain $\mathrm{SO}(10) \to \mathrm{SU}(5) \to G_{\mathrm{SM}}$ with SU(5) broken at M_G, gauge coupling unification remains intact. In contrast, gauge couplings need not unify at the intermediate scale in flipped SU(5) or Pati–Salam models.

In the minimal SO(10) model, the Higgs fields reside in the fundamental representation $\mathbf{10}_H$, which is decomposed as $\mathbf{10}_H = \mathbf{5}_H \oplus \overline{\mathbf{5}}_H$ in SU(5). Notably, SO(10) is unique among the discussed GUTs in that the representation itself distinguishes SM matter from Higgs fields (see Sec. 92.6).

92.2.4 *Beyond SO(10)*

Finally, one may consider larger symmetry groups. A notable example is the exceptional group E_6, which has a maximal subgroup $\mathrm{SO}(10) \times \mathrm{U}(1)$ [40]. Its fundamental representation decomposes as $\mathbf{27} = \mathbf{16}_1 + \mathbf{10}_{-2} + \mathbf{1}_4$. Another maximal subgroup is $\mathrm{SU}(3)_C \times \mathrm{SU}(3)_L \times \mathrm{SU}(3)_R \subset \mathrm{E}_6$, with the branching rule $\mathbf{27} = (\mathbf{3}, \mathbf{3}, \mathbf{1}) + (\overline{\mathbf{3}}, \mathbf{1}, \overline{\mathbf{3}}) + (\mathbf{1}, \overline{\mathbf{3}}, \mathbf{3})$. Even independently of an underlying E_6, the gauge group $[\mathrm{SU}(3)]^3$—augmented by a $\mathbb{Z}_3$ permutation symmetry that interchanges the three SU(3) factors—can be considered. This framework is known as "trinification" [41, 42], where the $\mathbb{Z}_3$ symmetry guarantees gauge coupling unification. The breaking pattern $\mathrm{E}_6 \to [\mathrm{SU}(3)]^3$ has been employed in phenomenological studies of heterotic string theory [43–46]. However, in models based on larger symmetry groups such as E_6, SU(6), etc., the presence of many additional states poses a challenge: these extra states must be decoupled from the low-energy EFT.

Intriguingly, the hierarchical embedding of gauge groups—where G_{SM} is a maximal subgroup of SU(5), which itself, together with $\mathrm{U}(1)_X$, forms a maximal subgroup of SO(10)—continues in a remarkably elegant and systematic fashion, culminating in the largest exceptional group. This leads to the well-known symmetry breaking chain $\mathrm{E}_8 \to \mathrm{E}_7 \to \mathrm{E}_6 \to \mathrm{SO}(10) \to \mathrm{SU}(5) \to G_{\mathrm{SM}}$ and,

[5] Useful references on group theory in this context include [32–35], and references therein.

[6] The spin sum is calculated as $(N_+ - N_-)/2$, where N_+ and N_- are the numbers of "+" and "−" entries in the color or weak column of Table 92.1.

Int. J. Mod. Phys. A 2026.41. Downloaded from www.worldscientific.com
by UNIVERSITY OF CALIFORNIA @ BERKELEY on 09/16/26. Re-use and distribution is strictly not permitted, except for Open Access articles.

together with the distinguished role of E_8 in both group theory and string theory, offers a tantalizing hint at a deeper unifying structure. However, since all representations of E_8 and E_7 are real and therefore incapable of accommodating chiral fermions in 4d, such constructions necessarily lie outside the scope of conventional 4d GUTs.

92.2.5 *Global structures of the Standard Model gauge group*

While our focus so far has been on the Lie algebra of the gauge symmetry, it is worth recalling that distinct Lie groups can share the same Lie algebra. In the case of the SM, it is known that there are four possible gauge groups that correspond to the same SM Lie algebra [47,48] (see also Ref. [49] for a recent discussion): $G_{\rm SM} = {\rm SU}(3)_C \times {\rm SU}(2)_L \times {\rm U}(1)_Y/\Gamma$ with $\Gamma = 1, \mathbb{Z}_2, \mathbb{Z}_3, \mathbb{Z}_6$.[7] While these gauge groups describe the same perturbative theory, they can differ in their non-perturbative properties, such as the types of topological defects or instanton effects they allow.

If the SM gauge symmetry originates from the spontaneous breaking of a GUT gauge symmetry, which of the above four gauge groups is realized depends on the choice of the GUT gauge group. For example, in the case of SU(5), the SM gauge group can be embedded as

$$\begin{pmatrix} U & 0 \\ 0 & V \end{pmatrix} \in {\rm SU}(5)\ , \tag{92.3}$$

where $U \in {\rm U}(3)$, $V \in {\rm U}(2)$, and $\det U \det V = 1$. Thus, the resulting subgroup is ${\rm S}({\rm U}(3) \times {\rm U}(2))$. Each element can be parametrized as $U = e^{i\theta/3}\widetilde{U}$ and $V = e^{-i\theta/2}\widetilde{V}$ with $\theta \in \mathbb{R}$, $\widetilde{U} \in {\rm SU}(3)$, and $\widetilde{V} \in {\rm SU}(2)$. Then, one finds that the parameters $\theta' = 2\pi n + \theta$, $\widetilde{U}' = e^{-2\pi i n/3}\widetilde{U}$, and $\widetilde{V}' = e^{2\pi i n/2}\widetilde{V}$ with $n = 0, 1, 2, 3, 4, 5$ all correspond to the same group element, indicating that the gauge group is equivalent to $G_{\rm SM} = {\rm SU}(3)_C \times {\rm SU}(2)_L \times {\rm U}(1)_Y/\mathbb{Z}_6$. Similarly, embeddings into other simple GUT groups such as SO(10) and E_6 lead to the same SM gauge group. In contrast, partial unification scenarios yield different global structures: the Pati–Salam group $G_{\rm PS}$ leads to $\Gamma = \mathbb{Z}_3$, whereas the trinification group ${\rm SU}(3)_C \times {\rm SU}(3)_L \times {\rm SU}(3)_R$ gives $\Gamma = \mathbb{Z}_2$.

92.3 GUT breaking and doublet-triplet splitting

In the standard 4d field-theoretic approach to GUTs, the unified gauge group is spontaneously broken by an appropriately chosen GUT Higgs sector. Scalar potentials (or superpotentials in the case of SUSY GUTs) can be constructed whose vacua break the GUT gauge group. While these potentials are somewhat ad hoc—much like the Higgs potential in the SM—the simplest expectation is that all dimensionful parameters in the theory are of $\mathcal{O}(M_G)$. In the minimal SU(5), the GUT-breaking Higgs field is the adjoint representation **24** and acquires a VEV along the $G_{\rm SM}$-singlet direction, $\langle\Phi\rangle \propto {\rm diag}(-2/3, -2/3, -2/3, 1, 1)$. For SO(10) to break to SU(5), a Higgs field in the **16** or **126** representation must acquire a VEV along a direction that is an SU(5) singlet but carries nonzero ${\rm U}(1)_X$ charge.

The masses of the doublet and triplet components in the $\mathbf{5}_H$ (and $\overline{\mathbf{5}}_H$) are generically split due to their couplings to the GUT-breaking Higgs field. In addition, both components receive an equal contribution from an SU(5)-invariant GUT-scale mass term. Without further structure, achieving a light doublet at the electroweak scale requires an extreme fine-tuning between two large contributions. SUSY helps stabilize the doublet mass against large radiative corrections, thanks to the non-renormalization theorem [50]. However, even in SUSY models, fine-tuning is still required at tree level. This constitutes the well-known doublet-triplet splitting problem, which is closely related—within the SUSY context—to the μ-problem, *i.e.*, the puzzle of why the coefficient of the superpotential term $\mu H_u H_d$ is much smaller than the GUT scale.

Several mechanisms for realizing natural doublet-triplet splitting have been proposed within the framework of SUSY. These include the sliding singlet mechanism [51], the missing partner mechanism [52, 53], the missing VEV mechanism [54, 55], and the pseudo-Nambu–Goldstone boson mechanism [56]. Concrete implementations of these ideas have been studied in various GUT models: the missing partner mechanism in SU(5) [57–61] and in the flipped SU(5) [38, 62], the missing VEV mechanism in SO(10) [63–75], and the pseudo-Nambu–Goldstone boson mechanism [76–84]. These models have been shown to be compatible with gauge coupling unification and nucleon decay constraints. Once a model with vanishing fundamental μ term has been realized, an *effective* μ term of order the SUSY breaking scale can then be induced by, for example, higher-mass-dimension terms in the Kähler potential [85] or superpotential [86]. For a review of the μ problem and some suggested solutions in SUSY GUTs and string theory, see Refs. [87–95] and references therein.

In general, GUT-breaking sectors that resolve the doublet-triplet splitting problem, stabilize all GUT-scale VEVs, and yield realistic neutrino masses and Yukawa couplings—including controlled violations of GUT relations in the latter—require a number of nontrivial ingredients. However, the introduction of large or numerous representations is constrained, as it can drive the theory to a Landau pole below the Planck scale. Moreover, in the 4d field-theoretic approach, GUTs are regarded as EFTs valid only below the Planck scale. Since the GUT scale M_G lies relatively close to this cutoff, the effects of higher-dimensional operators cannot be neglected in general. In particular, operators involving the GUT-breaking Higgs fields can influence low-energy observables, such as quark and lepton masses, and must therefore be taken into account in realistic model building.

Thus, especially in the context of GUT breaking and doublet-triplet splitting, models beyond 4d field theory appear attractive. While this is mainly the subject of the next section, some advantages can already be noted: In models with extra dimensions, in particular string constructions, GUT breaking may occur due to boundary conditions in the compactified dimensions [96–110]. No complicated GUT breaking sector is then required. Moreover, boundary conditions can give mass only to the triplet, leaving the doublet massless. This is similar to the missing partner mechanism since the effective mass term does not 'pair up' the triplets from $\mathbf{5}_H$ and $\overline{\mathbf{5}}_H$ but rather each of them with further fields which are automatically present in the higher-dimensional theory. This can eliminate dimension-five nucleon decay (cf. Sec. 92.6).

92.4 String-theoretic and higher-dimensional unified models

As noted earlier, the GUT scale is dangerously close to the scale of quantum gravity. It may hence be necessary to discuss unified models of particle physics in the latter, more ambitious context. Among the models of quantum gravity, superstring or M-theory stands out as the best-studied and technically most developed proposal, possessing in particular a high level of internal, mathematical consistency. For our purposes, it is sufficient to know that five 10d and one 11d low-energy effective supergravity theories arise in this setting (see Refs. [111–114] and references therein).

Grand unification is realized most naturally in the context of the two heterotic string theories with gauge groups $E_8 \times E_8$ and SO(32) [101, 115] (see Refs. [116–118] for some of the more recent results). Justified in part by the intriguing breaking path $E_8 \to \cdots \to G_{\rm SM}$ mentioned above, the focus has historically largely been on $E_8 \times E_8$. To describe particle physics, solutions of the 10d theory with geometry $\mathbb{R}^{1,3} \times M_6$ are considered, where M_6 is a Calabi–Yau (CY) 3-fold (with 6 real dimensions) [101]. The background solution involves expectation values of higher-dimensional components of the $E_8 \times E_8$ gauge fields. This includes both Wilson lines [96] and non-vanishing field-strength and leads, in general, to a reduced gauge symmetry and to chirality in the resulting 4d effective theory. The 4d fermions arise from 10d gauginos.

Given an appropriate embedding[8] of $G_{\rm SM}$ in $E_8 \times E_8$, gauge coupling unification is automatic at leading order. Corrections arise

[7] The cases with $\Gamma = \mathbb{Z}_2$, $\mathbb{Z}_3$, and $\mathbb{Z}_6$ are also referred to as ${\rm SU}(3) \times {\rm U}(2)$, ${\rm U}(3) \times {\rm SU}(2)$, and ${\rm S}({\rm U}(3) \times {\rm U}(2))$, respectively. The group ${\rm SU}(3) \times {\rm SU}(2) \times {\rm U}(1)$ serves as the covering group of these.

[8] All embeddings of $G_{\rm SM}$ in one E_8 factor which are consistent with a breaking-pattern $E_8 \to {\rm SU}(5) \to G_{\rm SM}$ are suitable. Other embeddings can change the ratios between the three resulting $G_{\rm SM}$ couplings at the GUT scale by group-theoretic factors. Crucially, due to the single 10d gauge coupling, no continuous tuning is possible.

Int. J. Mod. Phys. A 2026.41. Downloaded from www.worldscientific.com by UNIVERSITY OF CALIFORNIA @ BERKELEY on 09/16/26. Re-use and distribution is strictly not permitted, except for Open Access articles.

mainly through (string)-loop effects and are similar to the familiar field-theory thresholds of 4d GUTs [119] discussed in Sec. 92.5. Thus, one may say that coupling unification is a generic prediction in spite of the complete absence[9] of a 4d GUT at any energy scale. This absence is both an advantage and a weakness. On the up side, GUT breaking and doublet-triplet splitting [122] are more naturally realized and dimension-five nucleon decay is relatively easy to avoid. On the down side, there is no reason to expect full GUT representations in the matter sector and flavor model building is much less tied to the GUT structure than in 4d.

Let us pause to explain the beautiful idea behind the advertised solution of the doublet-triplet splitting problem: One starts with a simply connected CY X and mods out the action of a discrete group G (say $\mathbb{Z}_2$). In the absence of fixed points, X/G is smooth and has a non-contractible 1-cycle. Furthermore, let G also act on the gauge bundle, according to an embedding $G \to \mathrm{E}_8$. Now the parallel transport around the 1-cycle is tied to a gauge rotation (one says a non-trivial Wilson-line is present). Moreover, this Wilson line can not be continuously turned off since, *e.g.*, in the case of $\mathbb{Z}_2$, its square is the unit element of the group. The induced 'Wilson-line breaking', which comes on top of the breaking by non-zero field strengths, may remove certain sub-representations (*e.g.*, the triplet of $\mathrm{SU}(5) \to G_{\mathrm{SM}}$) while keeping others exactly massless. A simpler and, due to fixed points, singular version of this will appear below in the context of orbifold GUTs.

One technical problem of heterotic constructions is the dependence on the numerous size and shape parameters of M_6 (the so-called moduli), the stabilization of which is poorly understood (see Refs. [123–125] for recent developments). Another is the sheer mathematical complexity of the analysis, involving in particular the study of (non-Abelian) gauge-bundles on CY spaces [126] (see, however, Refs. [127, 128]).

An interesting aspect of heterotic string constructions is represented by orbifold models [97–100]. Here the internal space is given by a six-torus, modded out by a discrete symmetry group (*e.g.*, $T^6/\mathbb{Z}_n$). More recent progress is reported in Refs. [129–137], including in particular the systematic exploration of the phenomenological advantages of so-called 'non-prime' (referring to n) orbifolds. The symmetry breaking to G_{SM} as well as the survival of Higgs doublets without triplet partners is ensured by the appropriate embedding of the discrete orbifold group in $\mathrm{E}_8 \times \mathrm{E}_8$. String theory on such spaces, which are locally flat but include singularities, is much more calculable than in the CY case. The orbifold geometries can be viewed as singular limits of CYs.

An even simpler approach to unified model building—while still retaining many of the advantages of full-fledged string constructions—is offered by orbifold GUTs [102–110]. These are typically 5d or 6d SUSY field theories with a unified gauge group—such as SU(5) or SO(10)—that is broken through the compactification to 4d. To illustrate the idea with a simple example, consider SU(5) defined on the spacetime $\mathbb{R}^{1,3} \times S^1/(\mathbb{Z}_2 \times \mathbb{Z}_2')$. The compact space in this case is an interval of length $\pi R/2$, and the embedding of $\mathbb{Z}_2'$ in the hypercharge direction of SU(5) leads to the desired breaking to G_{SM}. Concretely, the 5d X bosons are assigned Dirichlet boundary conditions (BCs) at one end of the interval, eliminating their Kaluza–Klein (KK) zero modes. Their lightest modes have masses of $\sim 1/R$, setting the KK scale as the effective GUT scale. A key implication is that the boundary theory lacks full SU(5) invariance. Nevertheless, since the SU(5)-symmetric 5d bulk governs the running of the 4d gauge couplings, gauge coupling unification remains a prediction. Furthermore, many challenges inherent to conventional 4d GUTs can be avoided in this framework. In particular, the doublet-triplet splitting problem is resolved.

With the advent of the string-theory flux landscape [138, 139], which is best understood in 10d type-IIB supergravity, the focus in string model building has shifted to this framework. While type II string theories have no gauge group in 10d, brane-stacks support gauge dynamics. A particularly appealing setting (see, *e.g.*, Ref. [140]) is provided by type IIB models with D7 branes (defining 8d submanifolds). However, in the SO(10) context the **16** is not available and, for SU(5), the top-Yukawa coupling vanishes at leading order [141]. As a crucial insight, this can be overcome on the non-perturbative branch of type IIB, also known as F-theory [142–144]. This setting allows for more general branes, thus avoiding constraints of the Dp-brane framework. GUT breaking can be realized using hypercharge flux (the VEV of the $\mathrm{U}(1)_Y$ field strength), an option not available in heterotic models. The whole framework combines the advantages of the heterotic or higher-dimensional unification approach with the more recent progress in understanding moduli stabilization. It thus represents at this moment the most active and promising branch of theory-driven GUT model building (see, *e.g.*, Refs. [145–149] and references therein).

As a result of the flux-breaking, a characteristic 'type IIB' or 'F-theoretic' tree-level correction to gauge unification arises [150–154]. The fact that this correction can be rather significant numerically is occasionally held against the framework of F-theory GUTs. However, at a parametric level, this correction nevertheless behaves like a 4d threshold, *i.e.*, it provides $\mathcal{O}(1)$ additive contributions to the inverse 4d gauge couplings $\alpha_i^{-1}(M_G)$.

A final important issue in string GUTs is the so-called string-scale/GUT-scale problem [155]. It arises since, in heterotic compactifications, the Planck scale and the high-scale value of the gauge coupling unambiguously fix the string-scale to about 10^{18} GeV. As the compactification radius R is raised above the string length, the GUT scale (identified with $1/R$) goes down and the string coupling goes up. Within the domain of perturbative string theory, a gap of about a factor ~ 20 remains between the lowest GUT scale achievable in this way and the phenomenological goal of 2×10^{16} GeV. The situation can be improved by venturing into the non-perturbative regime [155], by considering 'anisotropic' geometries with hierarchically different radii R [155, 156] or by including GUT scale threshold corrections [157, 158].

In F-theory GUTs, the situation is dramatically improved since the gauge theory lives only in four out of the six compact dimensions. This allows for models with a 'decoupling limit', where the GUT scale is parametrically below the Planck scale [143, 144]. However, moduli stabilization may not be without problems in such constructions, in part due to a tension between the required large volume and the desirable low SUSY breaking scale.

92.5 Gauge coupling unification

The quantitative unification of the three SM gauge couplings at the energy scale M_G is one of the central pillars of the GUT paradigm, and it holds clear phenomenological significance. Gauge coupling unification is well understood within the framework of effective field theory (EFT) [159–161]. In the simplest scenario, the EFT at energy scales $\mu \gg M_G$ has a unified gauge symmetry and a single running gauge coupling $\alpha_G(\mu)$. At lower energies $\mu \ll M_G$, heavy states with masses around M_G—such as X bosons, GUT-breaking Higgs fields, and color-triplet Higgs fields—are integrated out. The resulting low-energy EFT then features three independent gauge couplings and the matter content of the SM or its SUSY extension. One-loop renormalization group equations (RGEs) provide a means of extrapolating the gauge couplings down to the electroweak scale,

$$\alpha_i^{-1}(m_Z) = \alpha_G^{-1}(M_G) + \frac{b_i}{2\pi} \log\left(\frac{M_G}{m_Z}\right) + \delta_i \ , \quad (i = 1, 2, 3) \ , \tag{92.4}$$

where b_i are the one-loop β-function coefficients (with $b_i^{\mathrm{SM}} = \{41/10, -19/6, -7\}$ in the SM and $b_i^{\mathrm{MSSM}} = \{33/5, 1, -3\}$ in the minimal SUSY SM (MSSM)), m_Z is the Z-boson mass, and δ_i encode all subleading effects. These include threshold corrections at or near the weak scale—such as those arising from superpartners and the extended Higgs sector in the MSSM—as well as threshold effects at the GUT scale and higher-order loop corrections.

When SUSY is invoked as a solution to the gauge hierarchy problem—that is, the issue of naturalness or fine-tuning associated with the electroweak scale [18–21]—it predicts that the superpartners of SM particles should lie near the weak scale. Assuming this, and adopting a minimal Higgs sector, gauge coupling unification is achieved with remarkable precision in the

[9] See, however, Refs. [120, 121].

Int. J. Mod. Phys. A 2026.41. Downloaded from www.worldscientific.com
by UNIVERSITY OF CALIFORNIA @ BERKELEY on 09/16/26. Re-use and distribution is strictly not permitted, except for Open Access articles.

MSSM [162–168], whereas it fails in the SM, as illustrated in Fig. 92.1.

The three equations contained in Eq. (92.4) can be used to determine the three 'unknowns' $\alpha_3(m_Z)$, $\alpha_G(M_G)$ and M_G, assuming that all other parameters entering the equations are given. Focusing on the SUSY case and using the $\overline{\rm MS}$ coupling constants $\alpha_{\rm EM}^{-1}(m_Z)$ and $\sin^2\theta_W(m_Z)$ taken from Ref. [170] as input, $\alpha_{\rm EM}^{-1}(m_Z) = 127.930 \pm 0.008$ and $\sin^2\theta_W(m_Z) = 0.23122 \pm 0.00004$, one determines $\alpha_{1,2}^{-1}(m_Z)$, which then gives

$$\alpha_G^{-1}(M_G) \simeq 24.3 \qquad \text{and} \qquad M_G \simeq 2\times 10^{16}\ \text{GeV}\ . \tag{92.5}$$

Here we have set $\delta_i = 0$ for simplicity. Crucially, one in addition obtains a prediction for the low-energy observable α_3,

$$\alpha_3^{-1}(m_Z) = -\frac{5}{7}\alpha_1^{-1}(m_Z) + \frac{12}{7}\alpha_2^{-1}(m_Z) + \Delta_3\ , \tag{92.6}$$

where

$$\Delta_3 = \frac{5}{7}\delta_1 - \frac{12}{7}\delta_2 + \delta_3\ . \tag{92.7}$$

Here we followed the elegant formulation in Ref. [171] of the classical analyses of Refs. [162–168]. Of course, it is a matter of convention which of the three low-energy gauge coupling parameters one 'predicts' and indeed, early works on the subject discussed the prediction of $\sin^2\theta_W$ in terms of $\alpha_{\rm EM}$ and α_3 [172–174]. Remarkably, the leading order result (*i.e.*, Eq. (92.6) with $\Delta_3 = 0$) is in excellent agreement with experiments [170]:

$$\alpha_3^{\rm LO}(m_Z) = 0.117 \quad \text{vs.} \quad \alpha_3^{\rm exp}(m_Z) = 0.1180 \pm 0.0009\ . \tag{92.8}$$

However, this near perfection is to some extent accidental. To see this, we now discuss the various contributions to the subleading corrections δ_i (and hence to Δ_3).

The two-loop running correction from the gauge sector $\Delta_3^{(2)}$ and the low-scale threshold correction $\Delta_3^{(l)}$ from superpartners can be summarized as [171]

$$\Delta_3^{(2)} \simeq -0.82 \qquad \text{and} \qquad \Delta_3^{(l)} \simeq \frac{19}{28\pi}\log\left(\frac{m_{\rm SUSY}}{m_Z}\right)\ . \tag{92.9}$$

The relevant scale $m_{\rm SUSY}$ can be estimated as [168]

$$m_{\rm SUSY} \simeq m_H^{3/19} m_{\widetilde{H}}^{12/19} m_{\widetilde{W}}^{4/19} \times \left(\frac{m_{\widetilde{W}}}{m_{\widetilde{g}}}\right)^{28/19} \left(\frac{m_{\widetilde{l}}}{m_{\widetilde{q}}}\right)^{3/19}\ , \tag{92.10}$$

where m_H stands for the masses of non-SM Higgs states and superpartner masses are given in self-evident notation. Detailed analyses including the above effects are best done using appropriate software packages, such as SOFTSUSY [169] (or alternatively SuSpect [175] or SPheno [176]). See also Ref. [169] for references for the underlying theoretical two-loop analyses.

To gain a rough estimate of these effects, let us assume that all superpartners are degenerate at $m_{\rm SUSY} = 1$ TeV except for gluino, with a mass ratio $m_{\widetilde{W}}/m_{\widetilde{g}} \simeq 1/3$. Under this assumption, one finds $\Delta_3^{(l)} \simeq -0.35 + 0.22\ln(m_{\rm SUSY}/m_Z) \simeq 0.18$. This leads to a predicted value of $\alpha_3(m_Z) \simeq 0.126$, which significantly deviates from the near-perfect one-loop unification observed earlier. Before exploring this discrepancy in more detail, it is useful to introduce another important class of corrections—those arising from high-scale (GUT-scale) thresholds.

To discuss high scale thresholds, let us set all other corrections to zero for the moment and write down a version of Eq. (92.4) that captures the running near and above the GUT scale more correctly. The threshold correction at one-loop level can be evaluated accurately by the simple step-function approximation for the β functions in the $\overline{\rm DR}$ scheme [26, 177],[10]

$$\alpha_i^{-1}(m_Z) = \alpha_G^{-1}(\mu) + \frac{1}{2\pi}\left[b_i \ln\frac{\mu}{m_Z} + b_i^C \ln\frac{\mu}{M_C} + b_i^X \ln\frac{\mu}{M_X} + b_i^\Phi \ln\frac{\mu}{M_\Phi}\right]\ . \tag{92.11}$$

We initiate the RG running at a scale $\mu \gg M_G$, considering the minimal set of states relevant for the transition from the SU(5) GUT to the MSSM. These include the color-triplet Higgs multiplets with mass M_C, the massive vector multiplets of the X-bosons with mass M_X (along with the associated GUT Higgs degrees of freedom), and the remaining GUT Higgs fields and superpartners with mass M_Φ. The corresponding β-function coefficients $b_i^{C,X,\Phi}$ are given in Refs. [182, 183]. Importantly, the combination of b_i coefficients in Eq. (92.11) is such that the RG evolution preserves GUT universality at high scales, rendering the prediction for α_3 independent of the choice of μ.

To relate this to our previous discussion, we can, for example, define $M_G \equiv M_X$ and then choose $\mu = M_G$ in Eq. (92.11). This gives the high-scale threshold corrections

$$\delta_i^{(h)} = \frac{1}{2\pi}\left[b_i^C \ln\frac{M_G}{M_C} + b_i^\Phi \ln\frac{M_G}{M_\Phi}\right]\ , \tag{92.12}$$

and a corresponding correction $\Delta_3^{(h)}$. To get some intuition for the magnitude, one can furthermore assume $M_\Phi = M_G$, finding (with $b_i^C = \{2/5, 0, 1\}$)

$$\Delta_3^{(h)} = \frac{9}{14\pi}\ln\left(\frac{M_G}{M_C}\right)\ . \tag{92.13}$$

To achieve the required effect of $-\Delta_3^{(2)} - \Delta_3^{(l)} \simeq +0.64$, the color-triplet Higgs would need to be roughly a factor of 20 lighter than the GUT scale. Although such a light triplet is excluded in the minimal model by current nucleon decay limits [184]—as will be discussed in Sec. 92.6—this example nonetheless illustrates that threshold corrections of this magnitude can, in principle, be realized through appropriate GUT-scale model building, for instance in specific SU(5) [57–61] or SO(10) [63–72] frameworks. In fact, much larger or even oppositely signed corrections can arise in models that involve extended field content, particularly those employing many higher-dimensional representations, as is often necessary in fully realistic 4d GUTs. Higher-dimensional operators suppressed by M_P^{-1}, involving the GUT gauge fields and the GUT-breaking Higgs field, can also induce threshold corrections of comparable magnitude [185–190]. These corrections can, in particular, be utilized to raise the mass of the color-triplet Higgs. Consequently, there exists substantial freedom in model building.

The analysis above implicitly assumes universal soft SUSY-breaking masses at the GUT scale, which directly affect the spectrum of SUSY particles at the weak scale; in the simplest scenario, motivated by SO(10) unification, one adopts a universal gaugino mass $M_{1/2}$, a common scalar mass m_{16} for squarks and sleptons, and a universal Higgs mass m_{10}. In some cases, threshold corrections to gauge couplings can be traded for threshold effects on the soft SUSY-breaking parameters (see Ref. [191] and references therein). For instance, if gaugino masses are not unified at M_G—in particular, if gluino is lighter than wino at the weak scale (cf. Eq. (92.10))—then weak-scale threshold corrections may allow for a significantly smaller or even slightly negative GUT-scale threshold correction to be consistent with successful gauge coupling unification [192, 193].

It is also noteworthy that precise gauge coupling unification can be achieved without significant GUT-scale threshold corrections simply by increasing $m_{\rm SUSY}$ in Eq. (92.10) [194–196]. This remains possible even if gauginos are kept at the TeV scale, by taking the masses of higgsinos and non-SM Higgs bosons to lie in the multi-TeV range. Such a setup is particularly attractive, as

[10] The $\overline{\rm DR}$ scheme is commonly employed for regularization in SUSY theories [178]. The transformation of gauge couplings from the $\overline{\rm MS}$ to the $\overline{\rm DR}$ scheme is provided in Ref. [177]. For an alternative approach based on holomorphic gauge couplings and the NSVZ β-functions, see, for example, Refs. [179–181].

Int. J. Mod. Phys. A 2026.41. Downloaded from www.worldscientific.com
by UNIVERSITY OF CALIFORNIA @ BERKELEY on 09/16/26. Re-use and distribution is strictly not permitted, except for Open Access articles.

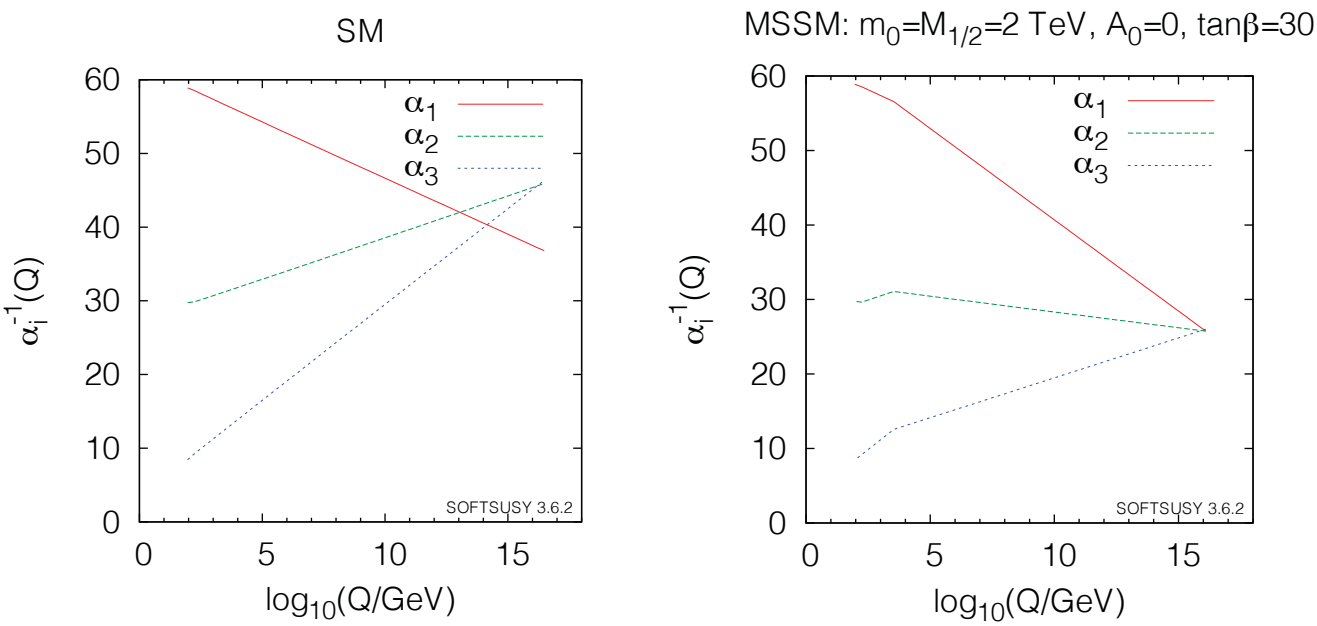

Figure 92.1: Running of the gauge couplings in the SM and MSSM, shown using two-loop RG evolution. The SUSY threshold, set at 2 TeV, is clearly visible on the MSSM side. (We thank Ben Allanach for providing the plots, which were generated using SOFTSUSY [169].)

it preserves a viable dark matter candidate—namely, the lightest neutralino. Hierarchical SUSY mass spectra of this type, often motivated by anomaly mediation [197,198], have been extensively studied in the literature [199–210]. This scenario has the additional merit of accommodating both the observed value of the SM-like Higgs boson mass[11] and the current null results from SUSY searches at the LHC, although it reintroduces a little hierarchy problem associated with the electroweak scale.

In non-SUSY GUTs or in SUSY GUTs with a very high SUSY breaking scale, achieving gauge coupling unification typically requires the presence of new light states in incomplete GUT multiplets or multiple symmetry-breaking scales. For example, in non-SUSY models with the breaking chain $\mathrm{SO}(10) \to \mathrm{SU}(4)_C \times \mathrm{SU}(2)_L \times \mathrm{SU}(2)_R \to G_{\mathrm{SM}}$, where the second stage of symmetry breaking occurs at an intermediate scale corresponding to the mass scale of right-handed neutrinos, gauge couplings can unify at the SO(10) breaking scale [219], while remaining consistent with current bounds on nucleon decay [220]. Similar unification can also be realized in alternative symmetry-breaking chains or in scenarios with extra light states—such as dark matter candidates—present at low energies [221, 222]. Alternatively, string-theoretic corrections discussed in Sec. 92.4 can be invoked to offset the effects of a high SUSY-breaking scale. This possibility has been explored concretely, for example, in the context of F-theory GUTs [223]. In principle, large threshold corrections arising from large GUT representations may also enable gauge coupling unification [224, 225].

In orbifold GUTs, certain "GUT scale" threshold corrections come from the KK modes between the compactification scale, $M_c \sim 1/R$, and the effective cutoff scale M_*, which is the string scale in string theory. Gauge coupling unification then constrains the values of M_c and M_*. It is interesting to note that a ratio $M_*/M_c \sim 100$, needed for gauge coupling unification to work in orbifold GUTs, is typically the maximum value for this ratio consistent with perturbativity [226]. Often, one finds M_c to be lower than the 4d GUT scale. Since the X-bosons, responsible for nucleon decay, get mass at the compactification scale, this has significant consequences for nucleon decay.

[11] In the MSSM, the tree-level Higgs boson mass is bounded from above by m_Z, but radiative corrections—particularly from heavy stop loops—can raise it to the observed value of ~ 125 GeV [211–218].

Finally, it has been shown that non-SUSY GUTs in warped 5d orbifolds can be consistent with gauge coupling unification. This assumes (in 4d language) that the right-handed top quark and the Higgs doublets are composite-like objects with a compositeness scale in the TeV range [227].

92.6 Nucleon decay

Quarks and leptons are indistinguishable in any 4d GUT, and both the baryon (B) and lepton number (L) are not conserved. This leads to baryon-number-violating nucleon decay. In addition to baryon-number violation, lepton-number violation is also required for nucleon decay since, in the SM, leptons are the only free fermions which are lighter than nucleons. In the SM, the lowest-dimension operators relevant for nucleon decay are $(B+L)$-violating dimension-six four-fermion terms, and all B-violating operators with dimension less than seven preserve $B-L$ [1, 228].

In SU(5) GUTs, the dimension-six baryon-number-violating operators are induced by X boson exchange. These operators are suppressed by $(1/M_X^2)$, where M_X is the X boson mass, and the nucleon lifetime is given by $\tau_N \propto M_X^4/(\alpha_G^2 m_N^5)$, with m_N the nucleon mass. The dominant proton decay mode, as well as the baryon-number-violating decay mode of the neutron, via the X-boson exchange is given by $p \to \pi^0 e^+$ and $n \to \pi^- e^+$, respectively.[12] The present experimental bound on $p \to \pi^0 e^+$ comes from Super-Kamiokande. With 450 kton-years of data they find $\tau_p/\mathrm{Br}(p \to \pi^0 e^+) > 2.4 \times 10^{34}$ years at 90% CL [233].[13] In addition, Hyper-Kamiokande [235] is planned to reach to $\tau_p/\mathrm{Br}(p \to \pi^0 e^+) \sim 10^{35}$ years. For a broader overview of planned experiments and historical developments, the reader is referred to Ref. [236]. The hadronic matrix elements relevant for baryon-number-violating operators are now reliably computed using lattice QCD simulations [237]. In SUSY SU(5) GUTs, the null results from nucleon decay searches place a lower bound on the X boson mass that is approaching 10^{16} GeV [238], which is remarkably close to the GUT scale inferred from gauge coupling unification. In contrast, predictions for nucleon decay rates in non-SUSY GUTs are more uncertain. This is because gauge cou-

[12] Other decay modes, such as $p \to \pi^+ \bar{\nu}$, $p \to \pi^0 \mu^+$, and $n \to \pi^0 \bar{\nu}$, can be dominant in extended GUT frameworks, including flipped SU(5) [229, 230], SO(10), and E_6 [231, 232] models.

[13] For $n \to \pi^- e^+$, the current limit is $\tau_p/\mathrm{Br}(n \to \pi^- e^+) > 5.3 \times 10^{33}$ years [234].

Int. J. Mod. Phys. A 2026.41. Downloaded from www.worldscientific.com
by UNIVERSITY OF CALIFORNIA @ BERKELEY on 09/16/26. Re-use and distribution is strictly not permitted, except for Open Access articles.

plings do not unify with the SM particle content alone. Once additional states or sizable threshold corrections are introduced to achieve precision unification, a broad range of possible unification scales becomes viable.

In SUSY GUTs, there exist additional sources of baryon- and/or lepton-number violation in the form of dimension-four/five operators [28, 29]. These arise because, in the SUSY SM, quarks and leptons are accompanied by scalar partners—squarks and sleptons. Note that in the SUSY context, fields are understood as chiral superfields, which include both fermionic and bosonic components. In this framework, baryon- and lepton-number-violating operators of dimension four and five appear as F-terms composed of chiral superfields. These operators involve two fermionic components, with the remaining fields being one or two scalar fields; in SU(5), they have the form:

$$\begin{aligned}(\mathbf{10}\,\overline{\mathbf{5}}\,\overline{\mathbf{5}}) &\supset (u^c\,d^c\,d^c) + (Q\,L\,d^c) + (e^c\,L\,L)\ ,\\ (\mathbf{10}\,\mathbf{10}\,\mathbf{10}\,\overline{\mathbf{5}}) &\supset (Q\,Q\,Q\,L) + (u^c\,u^c\,d^c\,e^c) + \\ &\qquad B\text{- and } L\text{-conserving terms}\ . \end{aligned} \tag{92.14}$$

The dimension-four operators in $(\mathbf{10}\,\overline{\mathbf{5}}\,\overline{\mathbf{5}})$ violate either B or L. The nucleon lifetime is extremely short if both types of dimension-four operators are present in the SUSY SM since squark or slepton exchange induces the dangerous dimension-six SM operators. Even in the case that they violate B or L only but not both, they are constrained by various phenomena [239, 240]. For example, the primordial baryon number in the Universe is washed out unless the dimensionless coupling constants are less than 10^{-7} [241–243]. Both types of operators can be eliminated by requiring R parity [244], which distinguishes Higgs multiplets from ordinary matter multiplets. R parity or its cousin, matter parity [22–27, 245, 246], act as $F \to -F$, $H \to H$ with $F = \{\mathbf{10}, \overline{\mathbf{5}}\}$, $H = \{\overline{\mathbf{5}}_H, \mathbf{5}_H\}$ in SU(5). This R parity forbids the dimension-four operator $(\mathbf{10}\,\overline{\mathbf{5}}\,\overline{\mathbf{5}})$, but allows the Yukawa couplings for quark and lepton masses of the form $(\mathbf{10}\,\overline{\mathbf{5}}\,\overline{\mathbf{5}}_H)$ and $(\mathbf{10}\,\mathbf{10}\,\mathbf{5}_H)$. It also forbids the dimension-three, L-violating operator $(\overline{\mathbf{5}}\,\mathbf{5}_H) \supset (L\,H_u)$ as well as the dimension-five, B-violating operator $(\mathbf{10}\,\mathbf{10}\,\mathbf{10}\,\overline{\mathbf{5}}_H) \supset (Q\,Q\,Q\,H_d) + \cdots$. In SU(5), the Higgs multiplet $\overline{\mathbf{5}}_H$ and the matter multiplets $\overline{\mathbf{5}}$ have identical gauge quantum numbers. In E_6, Higgs and matter multiplets could be unified within the fundamental **27** representation. Only in SO(10) are Higgs and matter multiplets distinguished by their gauge quantum numbers. The $\mathbb{Z}_4$ center of SO(10) distinguishes **10**s from **16**s and can be associated with R parity [247].

The baryon-number-violating dimension-five operators in SUSY GUTs arise with dimensionful couplings, typically suppressed by $1/M_G$, as they are generated by integrating out the color-triplet Higgs fields with GUT-scale masses. Both triplet higgsinos—due to their fermionic nature—and triplet Higgs scalars—via their mass-enhanced trilinear couplings to matter—contribute to the generation of these operators. Since the resulting operators involve squarks and/or sleptons, nucleon decay requires these scalar superpartners to be converted into light quarks or leptons through the exchange of a gaugino or higgsino in the SUSY SM. The corresponding nucleon lifetime scales as $M_G^2\,\widetilde{m}^2/m_N^5$, where $\widetilde{m}$ denotes the characteristic SUSY scalar mass. Consequently, dimension-five operators can induce nucleon decay rates significantly faster than those from dimension-six operators. In the absence of accidental cancellations, the dominant decay modes from these operators often include a kaon, such as $p \to K^+\bar{\nu}$ and $n \to K^0\bar{\nu}$. This can be understood from symmetry considerations. The relevant superpotential terms take the schematic form $(Q_i\,Q_j\,Q_k\,L_l)$ and $(u_i^c\,u_j^c\,d_k^c\,e_l^c)$, where $i, j, k, l = 1, 2, 3$ label generations, and color and weak indices are implicit. These operators must be invariant under both $SU(3)_C$ and $SU(2)_L$, implying that the color and weak indices must be antisymmetrized. However, as they arise from bosonic superfields, they must be totally symmetric under interchange of all flavor and gauge indices. This leads to the vanishing of the first operator when $i = j = k$, and of the second when $i = j$. As a result, contributions involving second- or third-generation fields dominate unless they are accidentally suppressed [245, 246].

The Super-Kamiokande experiment places stringent constraints on dimension-five proton decay operators. With an exposure of 306 kton · years, the current lower bound on the partial lifetime is $\tau_p/\mathrm{Br}(p \to K^+\bar{\nu}) > 6.61 \times 10^{33}$ years at 90% confidence level [248]. In the minimal SUSY SU(5) model, the predicted partial lifetime is less than about 10^{31} years if the color-triplet Higgs mass is 10^{16} GeV and the SUSY scale is $\widetilde{m} = 1$ TeV [249]. To evade this experimental limit, the color-triplet Higgs would need to be significantly heavier than the GUT scale, which, as discussed in Sec. 92.5, conflicts with the requirement for successful gauge coupling unification. As a result, the minimal SUSY SU(5) model is placed under significant tension by current proton decay constraints [184].

Since nucleon decay induced by the color-triplet Higgs is a serious issue in SUSY GUTs, a variety of mechanisms have been proposed to suppress it. One possibility is that an accidental symmetry or structural feature in non-minimal Higgs sectors suppresses the dimension-five operators [52,53,63–72,250,251]. A central idea behind such constructions is that nucleon decay can be suppressed if the Higgs triplets in the $\mathbf{5}_H$ and $\overline{\mathbf{5}}_H$ do not acquire a common mass term, but instead obtain their masses through couplings to additional SU(5) multiplets. Second, the SUSY-breaking scale may lie in the range $\mathcal{O}$(10–100) TeV, as discussed in Sec. 92.5. In such scenarios, nucleon decay is automatically suppressed due to the heavy sfermion masses, while the observed Higgs boson mass can be explained [252–258]. Third, accidental cancellations among contributing diagrams, arising from a finely tuned structure of squark and slepton flavor mixings, may also lead to suppressed decay rates [259]. The predicted upper bounds on the nucleon lifetime in some of these theories lie roughly an order of magnitude above current experimental limits, which may be within the reach of future experiments, such as JUNO [260, 261], Hyper-Kamiokande [235], and DUNE [262].

Orbifold GUTs and string theories contain grand unified symmetries realized in higher dimensions. In the process of compactification and GUT symmetry breaking, the triplet Higgs states may be removed (projected out of the massless sector of the theory). In such models, the nucleon decay due to dimension-five operators can be severely suppressed or eliminated completely. However, nucleon decay due to dimension-six operators may be enhanced, since the gauge-bosons mediating proton decay obtain mass at the compactification scale, M_c, which is typically less than the 4d GUT scale (cf. Sec. 92.5). Alternatively, the same projections which eliminate the triplet Higgs may rearrange the quark and lepton states such that the massless states of one family come from different higher-dimensional GUT multiplets. This can suppress or completely eliminate even dimension-six proton decay. Thus, enhancement or suppression of dimension-six proton decay is model-dependent. In some complete 5d orbifold GUT models [171, 263, 264] the lifetime for the decay $\tau_p/\mathrm{Br}(p \to \pi^0 e^+)$ can be near the bound of 1×10^{34} years with, however, large model-dependence and/or theoretical uncertainties. In other cases, the modes $p \to K^+\bar{\nu}$ and $p \to K^0\mu^+$ may be dominant [171].

In orbifold GUTs or string theory, new discrete symmetries consistent with SUSY GUTs can forbid all dimension-three and four baryon- and lepton-number-violating operators. Even the μ term and dimension-five baryon- and lepton-number-violating operators can be forbidden to all orders in perturbation theory [93–95]. The μ term and dimension-five baryon- and lepton-number-violating operators may then be generated, albeit sufficiently suppressed, via non-perturbative effects. The simplest example of this is a $\mathbb{Z}_4^R$ symmetry which is the unique discrete R symmetry consistent with SO(10) [93–95]. Even though it forbids the dimension-five proton decay operator to the desired level, it allows the required dimension-five neutrino mass term. In this case, proton decay is dominated by dimension-six operators, leading to decays such as $p \to \pi^0 e^+$.

92.7 Yukawa coupling unification

In the SM, the masses and mixings of quarks and leptons arise from their Yukawa couplings to the Higgs doublet; however, the origin and structure of these couplings remain unexplained. GUTs offer at least a partial explanation by embedding each generation into unified multiplets. In this framework, quarks and leptons are treated as components of the same representation, and the GUT

Int. J. Mod. Phys. A 2026.41. Downloaded from www.worldscientific.com by UNIVERSITY OF CALIFORNIA @ BERKELEY on 09/16/26. Re-use and distribution is strictly not permitted, except for Open Access articles.

symmetry imposes relations among their Yukawa couplings.

In SU(5), there are two types of independent renormalizable Yukawa interactions given by $\lambda_{ij}(\mathbf{10}_i\,\mathbf{10}_j\,\mathbf{5}_H) + \lambda'_{ij}(\mathbf{10}_i\,\overline{\mathbf{5}}_j\,\overline{\mathbf{5}}_H)$. These contain the SM interactions $\lambda_{ij}(Q_i\,u^c_j\,H_u)+\lambda'_{ij}(Q_i\,d^c_j\,H_d+ e^c_i\,L_j\,H_d)$, where $i,j = 1,2,3$ are family indices. At the GUT scale, this leads to tree-level relations among Yukawa couplings of the charged leptons and down-type quarks. For instance, one obtains $\lambda_b = \lambda_\tau$, where $\lambda_{b,\tau}$ denote the bottom quark and tau lepton Yukawa couplings, respectively [265–268]. In SO(10), there exists only one type of independent renormalizable Yukawa interaction, $\lambda_{ij}(\mathbf{16}_i\,\mathbf{16}_j\,\mathbf{10}_H)$, which implies unified relations among all Yukawa couplings within a single generation [269–282], such as $\lambda_t = \lambda_b = \lambda_\tau$, where λ_t denotes the top quark Yukawa coupling.

In addition to gauge coupling unification, the ratio of the b quark mass to the τ lepton mass has long been a key focus in GUT studies, ever since it was observed that this ratio, after accounting for QCD corrections, is remarkably consistent with experimental data [265, 266]. With the current high-precision determinations of quark masses and gauge couplings, this mass ratio has evolved into a target of detailed and quantitative analyses within the GUT framework, as discussed below.

92.7.1 *The third generation, b–τ or t–b–τ unification*

The third-generation Yukawa couplings are significantly larger than those of the first two generations. As a result, the fermion mass relations predicted by the renormalizable GUT interactions introduced above are expected to be more robust and reliable. To confront these predictions with experimental data, one must account for radiative corrections arising from RG evolution between the GUT scale and the fermion mass scale, as well as threshold corrections from integrating out heavy fields at the GUT and SUSY scales and from weak-scale physics.

Since the unification of Yukawa couplings can only be meaningfully tested in models that also achieve successful gauge coupling unification, we focus here on SUSY GUTs. In the MSSM, the masses of the top and bottom quarks and the τ lepton are related to their respective Yukawa couplings evaluated at the scale m_Z as

$$m_t(m_Z) = \lambda_t(m_Z)\,v_u\left(1+\frac{\delta m_t}{m_t}\right)\,,$$
$$m_{b,\tau}(m_Z) = \lambda_{b,\tau}(m_Z)\,v_d\left(1+\frac{\delta m_{b,\tau}}{m_{b,\tau}}\right)\,, \qquad (92.15)$$

where $v_u = \sin\beta\, v/\sqrt{2}$ and $v_d = \cos\beta\, v/\sqrt{2}$, with $v \simeq 246$ GeV, and $\delta m_f/m_f$ $(f = t, b, \tau)$ denotes the threshold correction arising from integrating out SUSY particles. For the b quark mass, it has been shown [283, 284] that the dominant corrections originate from gluino-sbottom and Higgsino-stop loop diagrams,

$$\left(\frac{\delta m_b}{m_b}\right)_{g_3} \simeq \frac{g_3^2}{6\pi^2}\,\frac{m_{\widetilde{g}}\,\mu}{\widetilde{m}^2}\tan\beta\,, \qquad \left(\frac{\delta m_b}{m_b}\right)_{\lambda_t} \simeq \frac{\lambda_t^2}{16\pi^2}\,\frac{A_t\mu}{\widetilde{m}^2}\tan\beta\,, \qquad (92.16)$$

where $m_{\widetilde{g}}$, μ, A_t, and $\widetilde{m}$ denote the gluino mass, higgsino mass, trilinear stop coupling, and the characteristic stop/sbottom mass scale, respectively. It should be noted that Eq. (92.16) captures only the schematic structure of the corrections; the full functional dependence on the soft SUSY-breaking parameters of order $\widetilde{m}$ has been omitted for clarity. For the complete one-loop expressions for the b quark mass corrections, see for example Ref. [285].

Note also that these corrections do not vanish even when SUSY particles are significantly heavier than the electroweak scale. For $\tan\beta = \mathcal{O}(10)$, they can alter the b quark mass by as much as $\mathcal{O}(10)\%$. The overall effect is sensitive to the relative phase between $m_{\widetilde{g}}$ and μ, especially because the infrared fixed-point behavior of the RGE for A_t tends to drive $A_t \simeq -m_{\widetilde{g}}$ [286] in scenarios where SUSY-breaking terms originate from Planck-scale physics, such as gravity mediation. Similar corrections affect the τ lepton mass, although typically only at the few-percent level. Corrections to the top quark mass are not enhanced by $\tan\beta$ and reach at most $\sim 10\%$ [287].

By including one-loop threshold corrections at the electroweak scale and performing the necessary RG evolution, one obtains the masses of the top quark, bottom quark, and τ lepton. In SUSY GUTs, b–τ Yukawa unification allows for two viable solutions corresponding to either small $\tan\beta \sim 1$ or large $\tan\beta = \mathcal{O}(10)$. The small $\tan\beta$ scenario can be realized in the MSSM if the superpartner masses lie at $\mathcal{O}(10)$ TeV [202]. On the other hand, large $\tan\beta$ values, such as $\tan\beta \sim 40$–50, are consistent with the SO(10) symmetry relation [287, 288]. In this regime, threshold corrections to down-type quark masses become significant, as discussed earlier. Consequently, successful Yukawa unification is only achieved within a restricted region of the SUSY parameter space, leading to important implications for SUSY searches [287, 289–293]. More recent studies of Yukawa unification in light of LHC results can be found in Refs. [294–297].

92.7.2 *Beyond leading order: three-family models*

Simple Yukawa unification does not work for the first two generations. In particular, the minimal implementation of SU(5) predicts the relations $\lambda_s = \lambda_\mu$ and $\lambda_d = \lambda_e$, which imply $\lambda_s/\lambda_d = \lambda_\mu/\lambda_e$. This relation is preserved under RG evolution and leads to the prediction $m_s/m_d = m_\mu/m_e$ at the weak scale, which is clearly incompatible with experimental observations, where $m_s/m_d \sim 20$ and $m_\mu/m_e \sim 200$. A compelling solution to this discrepancy was proposed by Georgi and Jarlskog [298]; for a more recent treatment in the context of SUSY, see Ref. [299].

More generally, it is important to recall that all previous discussions of Yukawa couplings were based on the assumption of renormalizable interactions and minimal matter and Higgs content. However, since the GUT scale lies close to the Planck scale, higher-dimensional operators involving GUT-breaking Higgs fields can lead to significant corrections, particularly for the first and second generations. A representative example is the dimension-five operator $\mathbf{10}\,\overline{\mathbf{5}}\,\overline{\mathbf{5}}_H\,\mathbf{24}_H$, where $\mathbf{24}_H$ denotes the SU(5) GUT-breaking Higgs field. Such operators can be used to fit the observed fermion masses, albeit at the cost of introducing some degree of fine-tuning. Moreover, the SM Higgs doublet itself may originate, at least in part, from higher-dimensional representations of the GUT group. For instance, the **45** representation of SU(5) contains an $\mathrm{SU}(2)_L$ doublet with the correct hypercharge to serve as a SM Higgs field [298]. This **45** can arise from larger representations such as the **120** or **126** of SO(10), once the symmetry is broken down to SU(5) [300–302]. These additional Higgs fields can also have renormalizable couplings to SM fermions, modifying the relations among the Yukawa couplings when the SM Higgs is a linear combination of doublets from different SU(5) multiplets. Finally, the embedding of SM fermions into GUT multiplets may not follow the minimal assignment. In minimal SO(10) models, all quarks and leptons reside in **16**-dimensional representations, but renormalizable Yukawa couplings with a single $\mathbf{10}_H$ cannot account for the observed CKM mixing angles. This issue can be alleviated by introducing additional matter multiplets, such as **10**s. After the breaking of $\mathrm{U}(1)_X$—which distinguishes the $\overline{\mathbf{5}}$ components originating from the **16** and **10** representations—the right-handed down-type quarks and left-handed leptons of the SM can be linear combinations of states from **16** and **10**. In this case, the two types of Yukawa couplings in SU(5) need not be identical [303].

To construct realistic three-family models, it is typically necessary to incorporate some or all of the effects discussed above. However, grand unification alone is generally insufficient to yield a predictive framework for fermion masses and mixing angles. Additional ingredients are required—most notably, global family symmetries. In particular, non-Abelian family symmetries can significantly reduce the number of free parameters by restricting the allowed structure of effective higher-dimensional operators that govern fermion masses. Moreover, the sequential breaking of family symmetries can naturally correlate with the observed fermion mass hierarchies [304]. A simple and widely studied approach is to assign each $\mathbf{10}_i$ representation a suppression factor ϵ^{3-i} in its Yukawa couplings, where ϵ is a small expansion parameter. This setup automatically generates a stronger hierarchy in the up-type quark Yukawa couplings compared to those of the down-

Int. J. Mod. Phys. A 2026.41. Downloaded from www.worldscientific.com by UNIVERSITY OF CALIFORNIA @ BERKELEY on 09/16/26. Re-use and distribution is strictly not permitted, except for Open Access articles.

type quarks and charged leptons, and no strong hierarchy in the neutrino sector—qualitatively consistent with observations. Fully realistic three-family models incorporating these ingredients have been constructed and are capable of reproducing the full spectrum of fermion masses and mixing parameters, including those in the neutrino sector [66–72, 305–313].

Finally, a particularly ambitious variant of unification is to require that the fermions of all three generations come from a single representation of a large gauge group. A somewhat weaker assumption is that the flavor group (*e.g.*, SU(3)) unifies with the SM gauge group in a simple gauge group at some energy scale $M \geq M_G$. Early work on such 'flavor-unified GUTs', see, *e.g.*, Refs. [303,314–320], has been reviewed in Refs. [321,322]. For a selection of more recent papers see Refs. [323–327]. In such settings, Yukawa couplings are generally determined by gauge couplings together with symmetry breaking VEVs. This is reminiscent of heterotic string GUTs, where all couplings come from the 10d gauge coupling. However, while the $\mathrm{E}_8 \to \mathrm{SU}(3) \times \mathrm{E}_6$ branching rule $\mathbf{248} = (\mathbf{8},\mathbf{1}) + (\mathbf{1},\mathbf{78}) + (\mathbf{3},\mathbf{27}) + (\overline{\mathbf{3}},\overline{\mathbf{27}})$ looks very suggestive in this context, the way in which most modern heterotic models arrive at three generations is actually more complicated.

92.8 Neutrino masses

Neutrino oscillation experiments have firmly established that neutrinos possess nonzero masses. By adding three "sterile" neutrinos ν_i^c with Yukawa couplings $\lambda_{\nu,ij}(\nu_i^c\, L_j\, H_u)$ $(i,j = 1,2,3)$, one obtains three massive Dirac neutrinos with mass $m_\nu^D = \lambda_\nu v_u$, analogously to quark and charged lepton masses. However, in order to obtain a τ neutrino with mass of order 0.1 eV, one requires the exceedingly small coupling ratio $\lambda_{\nu_\tau}/\lambda_\tau \lesssim 10^{-10}$. By contrast, in GUTs the seesaw mechanism *naturally* explains such tiny neutrino masses as follows [2–8]: The sterile neutrinos have no SM gauge quantum numbers so that there is no symmetry other than lepton number which forbids the Majorana mass term $\frac{1}{2}M_{ij}\nu_i^c\nu_j^c$. Note also that sterile neutrinos can be identified with the right-handed neutrinos necessarily contained in complete multiplets of SO(10), the flipped SU(5), or G_{PS}. Since the Majorana mass term violates these gauge symmetries, one might expect $M_{ij} \sim M_G$. The heavy sterile neutrinos can be integrated out, yielding an EFT with only light active neutrinos with the effective dimension-five operator

$$\mathcal{L}_{\mathrm{eff}} = -\frac{1}{2}c_{ij}(L_i\, H_u)(L_j\, H_u) + \mathrm{h.c.}\ , \qquad (92.17)$$

where $c = \lambda_\nu^T M^{-1}\lambda_\nu$. This leads to a 3×3 Majorana neutrino mass matrix $m_\nu = (m_\nu^D)^T M^{-1} m_\nu^D$ after the electroweak symmetry breaking. For example, if the neutrino Yukawa coupling λ_{ν_τ} is unified with the top quark Yukawa coupling at the GUT scale, $\lambda_{\nu_\tau} = \lambda_t$, as predicted in SO(10), flipped SU(5), or Pati–Salam models, then the observed value $m_{\nu_\tau} \sim 0.1$ eV implies a right-handed neutrino mass scale $M \sim 10^{14}$ GeV, intriguingly close to the GUT scale.

The seesaw mechanism implemented by right-handed neutrinos is sometimes called the type-I seesaw model. There are variant models in which the dimension-five operator for neutrino masses is induced in different ways: In the type-II model, an $\mathrm{SU}(2)_L$ triplet Higgs boson Σ is introduced to have couplings ΣL^2 and also ΣH_u^2 [300,328–331]. In the type-III model, an $\mathrm{SU}(2)_L$ triplet of fermions $\widetilde{\Sigma}$ with a Yukawa coupling $\widetilde{\Sigma} L H_u$ is introduced [332]. In these models, the dimension-five operator is generated by integrating out either the triplet Higgs bosons or fermions. Such mechanisms can be embedded into GUT frameworks by introducing, for example, Higgs bosons in the **15** or fermions in the **24** representations of SU(5), which can originate from the **126** representation of SO(10). It is important to note that the gauge non-singlet fields involved in type-II and type-III seesaw mechanisms typically acquire masses at an intermediate scale. As a result, gauge coupling unification is not automatically preserved when these mechanisms are implemented in SUSY GUTs.

The neutrino sector presents a challenge for GUTs: while the quark mixing angles in the CKM matrix are small, two of the lepton mixing angles in the PMNS matrix are large. Global fits to neutrino masses and mixing parameters can be found in Sec. 14. For reviews of SUSY GUT models that successfully reproduce quark and lepton masses, see Refs. [333, 334]. A compilation of the range of SUSY GUT predictions for neutrino mixing angles is provided in Ref. [335].

It is also worth noting that, both within and beyond the GUT framework, considerable effort has been devoted to constructing models of neutrino masses—and more broadly, flavor structure—based on discrete symmetries (see, *e.g.*, Refs. [334, 336, 337]). A particularly interesting recent development in this context is the application of the (non-linearly realized) modular group $\mathrm{SL}(2,\mathbb{Z})$ as a discrete flavor symmetry [338]. This group plays a central role in string theory as the group of large diffeomorphisms of the two-torus, which appears both as the string worldsheet and—as is especially relevant here—as part of the compactification space in torus orbifold models (cf. Sec. 92.4). For a selection of recent activity in this direction, see, *e.g.*, Refs. [339–342].

92.9 Selected topics

92.9.1 *Global symmetries*

As discussed above, global symmetries are often introduced in GUT models to control higher-dimensional operators. This is particularly crucial in the context of nucleon decay, but such symmetries also play important roles in solutions to the doublet-triplet splitting problem, GUT-based flavor model building, and cosmological applications such as baryogenesis and inflation. However, relying on global symmetries to suppress specific interactions is not always as straightforward. Broadly speaking, two possibilities exist: First, the relevant symmetry may be gauged at a high scale. In this case, the effects of the VEVs responsible for its spontaneous breaking can, in principle, induce dangerous operators, and their impact must be carefully assessed. Second, the symmetry may be truly global, as is necessarily the case for anomalous symmetries whose breaking arises through non-perturbative effects and may therefore be exponentially suppressed. Nonetheless, it is widely believed that exact global symmetries cannot be preserved in the presence of quantum gravity (see, *e.g.*, Refs. [343,344]). One must then determine the degree of suppression—whether polynomial or exponential—arising from Planck-scale physics. For instance, dimension-five baryon-number-violating operators suppressed by only a single power of the Planck or string scale are highly problematic in SUSY models [345].

In light of the above, it is worth recalling that in string-theoretic models, 4d global symmetries typically originate from higher-dimensional gauge symmetries [111–114, 346]. Here, the term 'global' refers to a symmetry whose gauge boson acquires a Stückelberg mass. This mass generation is necessary in the case of anomalous symmetries (via the Green–Schwarz mechanism [347]), but it can also occur for non-anomalous ones. In such scenarios, one generally expects no symmetry violation beyond well-understood non-perturbative effects. Discrete symmetries arise as subgroups of continuous gauge symmetries—for example, $\mathbb{Z}_N \subset \mathrm{U}(1)$. Notably, non-anomalous subgroups of Stückelberg-massive U(1)s correspond to unbroken discrete gauge symmetries, which are exact even non-perturbatively (see, *e.g.*, Refs. [348,349]). Such discrete gauge symmetries can also emerge as remnants of spontaneously broken continuous gauge symmetries in 4d.

92.9.2 *Anomaly constraints vs. GUT paradigm*

As emphasized at the very beginning, the fact that the SM fermions of one generation fill out the $\mathbf{10} + \overline{\mathbf{5}}$ of SU(5) appears to provide strong evidence for some form of GUT embedding. However, one should be aware that a counterargument can be made which is related to the issue of 'charge quantization by anomaly cancellation' (see Refs. [350–354] for some early papers and Ref. [355] for a more detailed reference list): Imagine we only knew that the low-energy gauge group were G_{SM} and the matter content included $(\mathbf{3},\mathbf{2})_Y$, *i.e.*, a 'quark doublet' with U(1)-charge Y. One can then ask which possibilities exist of adding further matter to ensure the cancellation of all triangle anomalies. It turns out that this problem has only three different, minimal[14]

[14] Adding extra vector-like sets of fields, *e.g.*, two fermions which only transform under U(1) and have charges Y and $-Y$, is considered to violate minimality.

Int. J. Mod. Phys. A 2026.41. Downloaded from www.worldscientific.com by UNIVERSITY OF CALIFORNIA @ BERKELEY on 09/16/26. Re-use and distribution is strictly not permitted, except for Open Access articles.

solutions [354]. One of those is precisely a single SM generation, with the apparent 'SU(5)-ness' emerging accidentally. Thus, if one randomly picks models from the set of consistent gauge theories, preconditioning on $G_{\rm SM}$ and $(\mathbf{3},\mathbf{2})_Y$, one may easily end up with '$\mathbf{10}+\overline{\mathbf{5}}$' of an SU(5) that is in no way dynamically present. This is precisely what happens in the context of non-GUT string model building [356–358].

92.9.3 *Topological defects and phase transitions*

Among the various topological defects that can arise in the broken phase of GUT models, magnetic monopoles are the most well-known. These are localized classical solutions carrying magnetic charge under an unbroken U(1) subgroup [359, 360]. Magnetic monopoles with masses of $\mathcal{O}(M_G/\alpha_G)$ can be produced during a GUT phase transition in the early Universe. Experimentally, the flux of such monopoles is constrained to be $\lesssim 10^{-16}$ cm$^{-2}\cdot$s$^{-1}\cdot$sr^{-1} [361–363]. It was also shown that GUT monopoles can catalyze nucleon decay [364–368], leading to significantly stronger constraints on the monopole flux when considering, for example, X-ray emission from radio pulsars induced by monopole capture and subsequent nucleon decay [369]. Nonetheless, GUTs typically predict a monopole abundance far exceeding these limits—this is the so-called monopole problem.

One of the original motivations for proposing inflation was to resolve the monopole problem by exponentially diluting their density after the GUT phase transition (for a review on inflation, see Sec. 23). Notably, the current upper bound on the inflationary vacuum energy scale is remarkably close to the GUT scale, given by $V_{\rm inf}^{1/4} = (1.88\times 10^{16}\ {\rm GeV})\times(r/0.10)^{1/4}$, where the scalar-to-tensor ratio is constrained to be $r < 0.036$ [370]. This ensures that reheating does not reach temperatures above the GUT scale M_G, thereby solving the monopole problem—provided M_G is not significantly lower than expected. Alternative mechanisms to address the monopole problem include sweeping monopoles away with domain walls [371], breaking the electromagnetic U(1) symmetry at high temperatures [372], or avoiding GUT symmetry restoration altogether [373].

Topological defects other than monopoles are also common, see, *e.g.*, Refs. [374–376]. They can be cosmologically relevant in GUT models based on a gauge group larger than SU(5), say, SO(10), where an intermediate gauge theory may appear. The breaking of this intermediate gauge symmetry can a priori occur anywhere between the GUT and the electroweak scales. Right-handed neutrino masses favor a value near $\mathcal{O}(10^{14})$ GeV and non-SUSY coupling unification may profit from such a two-step GUT breaking scheme (cf., Sec. 92.5). Crucially for the present context, the last breaking step may occur after inflation, generating topological defects (like cosmic strings) which are not diluted. Their signature can be probed through gravitational waves [377–381], with the metastable string case being of particular phenomenological interest [382–387]. Metastability arises because the nucleation of a monopole-anti-monopole pair, each of which serves as an endpoint for the string, allow the cosmic string to break. The lifetime becomes long and hence the string stable as the ratio between monopole mass and the square root of the string tension grows. This is related to the ratio of the two symmetry-breaking scales. It is of phenomenological interest that metastability allows the string network to evade the recent bound of $G\mu \lesssim 10^{-10}$ (or $\sqrt{\mu}\lesssim 10^{14}$ GeV) [387], where G is the gravitational constant and μ is the string tension. Moreover the spectrum is blue-tilted compared to the stable string case. Finally, we note that if the intermediate gauge symmetry breaking proceeds with a (strong) first order phase transition, this could also generate gravitational waves [387–391]. However, due to the relatively high energy scales involved, the peak frequency tends to be high, with signals hopefully to be explored in future gravitational wave experiments.

92.9.4 *Flavor violation*

Yukawa interactions involving GUT-scale particles and SM quarks and leptons can imprint flavor-violating structures onto the soft SUSY-breaking terms [392]. To illustrate this, consider the MSSM with flavor-universal soft terms given at the Planck scale. Working in a basis where the up-type quark and charged lepton Yukawa matrices are diagonal, one finds that the large top Yukawa coupling drives a radiative suppression of the third-generation left-handed squark mass squared via RG evolution. After CKM rotation, this leads to sizable off-diagonal entries in the left-handed down-type squark mass matrix. In GUTs, however, additional sources of flavor violation arise. For instance, in SU(5), the color-triplet Higgs radiatively generates flavor-violating right-handed slepton mass terms via the Yukawa interaction $\lambda_{ij}(\mathbf{10}_i\,\mathbf{10}_j\,\mathbf{5}_H)$ [393, 394]. In the SU(5) extension of the type-I seesaw mechanism—where right-handed neutrinos are introduced as SU(5) singlets with the interaction $\lambda''_{ij}(\mathbf{1}_i\,\overline{\mathbf{5}}_j\,\mathbf{5}_H)$—both the doublet and color-triplet Higgs bosons acquire additional Yukawa couplings. These give rise to radiatively induced flavor violation in the left-handed slepton sector [395–398] and in the right-handed down-type squark sector [399, 400]. Note that even if flavor-universal soft terms are assumed at the GUT scale, sizable flavor violation in the left-handed slepton masses can still be generated through the RG running from the GUT scale down to the right-handed neutrino mass scale, driven by the right-handed neutrino Yukawa couplings. These flavor-violating SUSY-breaking terms generate new contributions to flavor-changing neutral current (FCNC) processes in both the quark and lepton sectors, such as $\mu\to e\gamma$, K^0–$\bar{K}^0$ mixing, and B^0–$\bar{B}^0$ mixing. Flavor violation in the sfermion mass matrices can also enhance nucleon decay induced by the dimension-five baryon-number-violating operators, as not only higgsino and wino exchange but also gluino-mediated processes can contribute in this case [401]. Electric dipole moments (EDMs) may also arise when both left- and right-handed squarks or sleptons receive flavor-violating mass terms with relative complex phases. This has been discussed in the context of SO(10) [402] and SU(5) models with right-handed neutrinos [403]. Thus, low-energy flavor and CP-violating observables serve as important probes of GUT-scale interactions.

92.9.5 *From GUT baryogenesis to leptogenesis and B/L-violating transitions*

During inflation, any conserved quantum number is exponentially diluted. Consequently, the observed baryon asymmetry of the Universe must be generated during or after reheating. The situation, however, is somewhat more subtle: both B and L are classical global symmetries of the SM, but the combination $(B+L)$ is anomalous and violated by thermal fluctuations in the early Universe via sphaleron processes [404]. In addition, $(B+L)$ is also violated in GUTs, as evidenced by nucleon decay. By contrast, the combination $(B-L)$ is anomaly-free and remains conserved in both the SM and in gauge interactions of GUTs such as SU(5) and SO(10).

The classic idea of GUT baryogenesis [405–412] involves generating a $(B+L)$ asymmetry—and hence a baryon asymmetry—via the out-of-equilibrium decay of color-triplet Higgs bosons. However, such an asymmetry produced at the GUT scale is erased by sphaleron processes that become efficient at temperatures below $T\sim 10^{12}$ GeV.[15] This issue can be circumvented [413] by using lepton-number-violating interactions of neutrinos to convert part of the initial $(B+L)$ asymmetry into a $(B-L)$ asymmetry before sphaleron processes become active. The resulting $(B-L)$ asymmetry is preserved throughout the sphaleron era. However, this mechanism is not viable in the minimal SUSY GUT, where the triplet Higgs lies above the GUT scale. In such cases, achieving the required out-of-equilibrium decay would necessitate a reheating temperature exceeding the GUT scale, which—as discussed earlier—is disfavored by cosmological observations.

However, the most widely accepted resolution to this dilemma is to generate a net $(B-L)$ asymmetry dynamically in the early Universe, using right-handed neutrinos. If the decay of heavy right-handed neutrinos occurs out of equilibrium and violates both L and CP, it can produce a net lepton asymmetry. This lepton asymmetry is then partially converted into a baryon asymmetry through electroweak sphaleron processes. This mechanism is known as leptogenesis [414].

If the three heavy Majorana neutrinos have a hierarchical

[15] Strictly speaking, if lepton flavor asymmetries L_i $(i=1,2,3)$ are present with $(L_i-L_j)\neq 0$ for $i\neq j$, nonzero values of B and L may persist even when $(B-L)=0$ [243].

Int. J. Mod. Phys. A 2026.41. Downloaded from www.worldscientific.com by UNIVERSITY OF CALIFORNIA @ BERKELEY on 09/16/26. Re-use and distribution is strictly not permitted, except for Open Access articles.

mass spectrum, the net lepton asymmetry is primarily generated by the decay of the lightest one. The resulting asymmetry is proportional to the CP asymmetry in its decay. It is found that in order to account for the observed baryon asymmetry of the Universe, the mass of the lightest heavy neutrino must be $\gtrsim 10^9$ GeV [415, 416].[16] Consequently, the reheating temperature after inflation must also be $\gtrsim 10^9$ GeV to ensure thermal production of the heavy neutrinos. In SUSY models, however, there exists a potential tension between the thermal leptogenesis and Big Bang Nucleosynthesis (BBN), particularly if gravitinos are long-lived and decay during or after the BBN epoch. This so-called gravitino problem imposes an upper bound on the reheating temperature, typically in the range $\lesssim 10^{6-10}$ GeV, depending on the details of the SUSY breaking scenario [419]. This tension can be alleviated in the non-thermal leptogenesis scenario, in which right-handed neutrinos are produced non-thermally via the decay of inflaton [420–422]. For recent reviews of leptogenesis, see Refs. [423–425].

One of the key experimental probes of leptogenesis is the search for neutrinoless double-beta ($0\nu\beta\beta$) decay. In $0\nu\beta\beta$ decay, a nucleus emits two electrons without accompanying (anti)neutrinos, in contrast to the standard double-beta decay, where two antineutrinos are emitted alongside the electrons. This process violates lepton number by two units ($\Delta L = 2$). At the nucleon level, $0\nu\beta\beta$ decay is described by dimension-nine effective operators mediating the process $nn \to ppee$. These operators can originate from combinations of SM weak interactions and lower-dimensional L-violating operators. The leading contribution typically arises from the dimension-five Weinberg operator in Eq. (92.17). Thus, if lepton-number violation originates at energy scales much higher than the electroweak scale, the $0\nu\beta\beta$ decay rate is proportional to the Majorana neutrino masses. The current experimental status of $0\nu\beta\beta$ searches is reviewed in Ref. [170]. For recent studies incorporating all SM effective operators up to dimension nine, see Ref. [426] and references therein.

In addition to lepton-number violation, one can also consider processes that violate B or $(B - L)$. Such processes are of intrinsic theoretical interest and may also play a role in baryogenesis. The relevant operators typically have mass dimensions higher than the well-known dimension-six $(B + L)$-violating operators (cf., Sec. 92.6). Such higher-dimensional operators may arise in SO(10) GUTs featuring an intermediate scale at which baryogenesis is realized, as discussed in Refs. [427–429]. For instance, one may consider interactions that induce nucleon decay with $\Delta(B - L) = 2$, such as $n \to e^-\pi^+$. These processes are mediated by dimension-seven effective operators in the SM, suppressed by the Higgs VEV or derivative interactions. Another important class involves neutron-antineutron (n–$\bar{n}$) oscillations, which violate baryon number by two units ($\Delta B = 2$) and are described by dimension-nine effective operators. The current experimental lower bound on the n–$\bar{n}$ oscillation time is derived using free neutrons [430], while complementary constraints come from limits on the decay of bound neutrons in ^{16}O, obtained by Super-Kamiokande [431]. These bounds are of similar magnitude. Super-Kamiokande has also searched for dinucleon decay modes with $\Delta B = 2$, such as $pp \to \pi^+\pi^+$ and $nn \to \pi^\pm\pi^\mp$ [432].

92.9.6 *The QCD Axion*

The axion is a pseudo-Nambu–Goldstone boson arising from the spontaneous breaking of the Peccei–Quinn symmetry, which is capable of resolving the strong CP problem [433–436] and may potentially be related to GUT physics.[17] In particular, the strength of the direct coupling of the QCD axion to photons, relative to its coupling to gluons, may be seen as a phenomenological signature of grand unification. It is quantified by the predicted anomaly ratio $E/N = 8/3$ (see Sec. 89 and Refs. [443, 444]). This ratio follows from the GUT normalization of the relevant generators together with the completeness of GUT multiplets contributing to the anomaly.[18] It hence arises in both the DFSZ [445, 446] and KSVZ [447, 448] axion models as long as the Peccei-Quinn symmetry commutes with the GUT group (see, *e.g.*, [449, 450]). We, however, note that, in bottom-up approaches and in the presence of split GUT multiplets, other anomaly ratios can appear (cf., *e.g.*, Refs. [451, 452]). Their embedding in a UV GUT structure, possibly with explicit GUT symmetry breaking, requires case-by-case study. The ratio $E/N = 8/3$ also arises in string-theoretic GUTs [443, 453]. In this case, the axion does not come from the phase of a complex scalar but is a fundamental shift-symmetric real field, coupling through a higher-dimension operator directly to the product of the GUT field-strength and its dual.

92.10 Conclusion

In its most conservative form, grand unification assumes that some or all of the SM gauge interactions—$\mathrm{U}(1)_Y$, $\mathrm{SU}(2)_L$, and $\mathrm{SU}(3)_C$—are embedded within a larger gauge symmetry at high energies. In most models, particularly in the simplest and most compelling realizations based on SU(5) or SO(10), the unification hypothesis goes significantly further: one expects the SM gauge couplings to merge (up to small threshold corrections) at a single unification scale, M_G, the SM matter fields to be (partially) unified into larger multiplets, and the nucleon to become unstable due to exchange of GUT-scale fields. SUSY GUTs provide by far the most predictive and economical framework that achieves perturbative gauge coupling unification. Further details beyond the scope of this article can be found in reviews [321, 454–456] and textbooks [457–460]. See also Refs. [461, 462] for more recent overviews.

Thus, the three classical pillars of GUTs are: gauge coupling unification at $M_G \simeq 2 \times 10^{16}$ GeV, low-energy SUSY (with a large SUSY desert), and nucleon decay. Among these, gauge coupling unification remains robust even if the SUSY particle masses lie somewhat above the weak scale. However, from a conceptual standpoint, the steadily increasing experimental lower bound on the SUSY scale poses a challenge for the SUSY GUT framework. If the original motivation for low-energy SUSY—namely, the stabilization of the electroweak scale—is entirely discarded, then the SUSY scale becomes an arbitrary parameter, and the first two pillars lose their theoretical foundation. This highlights the importance of continuing to improve bounds on nucleon decay, which—though not a universal prediction of all GUT models—is arguably a more generic and robust feature of grand unification than low-energy SUSY.

Whether or not Yukawa couplings unify is highly model dependent. Nevertheless, regardless of the degree to which Yukawa unification is realized, there exists a rich and potentially fruitful interplay between flavor model building and grand unification. This interplay is particularly pronounced in the neutrino sector, where ongoing experimental developments continue to shape theoretical approaches.

It is probably fair to say that, due to limitations of the 4d approach, including especially remaining ambiguities (free parameters or ad hoc assumptions) in models of flavor and GUT breaking, the string theoretic approach has become more important in GUT model building. In this framework, challenges include learning how to deal with the many vacua of the 'landscape' as well as, for each vacuum, developing the tools for reliably calculating phenomenological observables. Finally, due to limitations of space, the present article has barely touched on the interesting cosmological implications of GUTs. They may become more important in the future, especially in the case that a high inflationary energy scale is established observationally.

References

[1] S. Weinberg, Phys. Rev. Lett. **43**, 1566 (1979).

[2] P. Minkowski, Phys. Lett. **67B**, 421 (1977).

[3] T. Yanagida, Conf. Proc. C **7902131**, 95 (1979).

[4] S. L. Glashow, NATO Sci. Ser. B **61**, 687 (1980).

[5] M. Gell-Mann, P. Ramond and R. Slansky, Conf. Proc. C **790927**, 315 (1979), [arXiv:1306.4669].

[6] F. Wilczek, eConf **C790823**, 437 (1979).

[7] E. Witten, Phys. Lett. **91B**, 81 (1980).

[16] This requirement can be circumvented in resonant leptogenesis [417, 418], where the heavy right-handed neutrinos are nearly degenerate in mass.

[17] For alternative approaches to addressing the strong CP problem within the context of GUTs, see Refs. [437–442].

[18] See, *e.g.*, Eq. (312) of Ref. [444].

Int. J. Mod. Phys. A 2026.41. Downloaded from www.worldscientific.com
by UNIVERSITY OF CALIFORNIA @ BERKELEY on 09/16/26. Re-use and distribution is strictly not permitted, except for Open Access articles.

[8] R. N. Mohapatra and G. Senjanovic, Phys. Rev. Lett. **44**, 912 (1980), [,231(1979)].

[9] J. C. Pati and A. Salam, Phys. Rev. **D8**, 1240 (1973).

[10] A. Davidson, Phys. Rev. D **20**, 776 (1979).

[11] R. E. Marshak and R. N. Mohapatra, Phys. Lett. B **91**, 222 (1980).

[12] J. C. Pati, Int. J. Mod. Phys. A **32**, 09, 1741013 (2017), [arXiv:1706.09531].

[13] H. Georgi and S. L. Glashow, Phys. Rev. Lett. **32**, 438 (1974).

[14] J. R. Ellis, M. K. Gaillard and D. V. Nanopoulos, Phys. Lett. **80B**, 360 (1979), [Erratum: Phys. Lett.82B,464(1979)].

[15] E. Golowich, Phys. Rev. **D24**, 2899 (1981).

[16] I. Dorsner, S. Fajfer and N. Kosnik, Phys. Rev. D **86**, 015013 (2012), [arXiv:1204.0674].

[17] I. Doršner and S. Saad, Phys. Rev. D **110**, 7, 075025 (2024), [arXiv:2404.09021].

[18] G. 't Hooft, NATO Sci. Ser. B **59**, 135 (1980).

[19] M. J. G. Veltman, Acta Phys. Polon. **B12**, 437 (1981).

[20] L. Maiani, Conf. Proc. C **7909031**, 1 (1979).

[21] E. Witten, Nucl. Phys. **B188**, 513 (1981).

[22] S. Dimopoulos, S. Raby and F. Wilczek, Phys. Rev. **D24**, 1681 (1981).

[23] S. Dimopoulos and H. Georgi, Nucl. Phys. **B193**, 150 (1981).

[24] L. E. Ibanez and G. G. Ross, Phys. Lett. **105B**, 439 (1981).

[25] N. Sakai, Z. Phys. **C11**, 153 (1981).

[26] M. B. Einhorn and D. R. T. Jones, Nucl. Phys. **B196**, 475 (1982).

[27] W. J. Marciano and G. Senjanovic, Phys. Rev. **D25**, 3092 (1982).

[28] S. Weinberg, Phys. Rev. **D26**, 287 (1982).

[29] N. Sakai and T. Yanagida, Nucl. Phys. **B197**, 533 (1982).

[30] H. Georgi, AIP Conf. Proc. **23**, 575 (1975).

[31] H. Fritzsch and P. Minkowski, Annals Phys. **93**, 193 (1975).

[32] R. Slansky, Phys. Rept. **79**, 1 (1981).

[33] H. Georgi, *Lie algebras in particle physics*, volume 54, Perseus Books, Reading, MA, 2nd ed. edition (1999).

[34] N. Yamatsu, PTEP **2016**, 4, 043B02 (2016), [arXiv:1512.05559].

[35] R. Feger, T. W. Kephart and R. J. Saskowski, Comput. Phys. Commun. **257**, 107490 (2020), [arXiv:1912.10969].

[36] S. M. Barr, Phys. Lett. **112B**, 219 (1982).

[37] J. P. Derendinger, J. E. Kim and D. V. Nanopoulos, Phys. Lett. **139B**, 170 (1984).

[38] I. Antoniadis *et al.*, Phys. Lett. **B194**, 231 (1987).

[39] I. Antoniadis *et al.*, Phys. Lett. **B231**, 65 (1989).

[40] F. Gursey, P. Ramond and P. Sikivie, Phys. Lett. **60B**, 177 (1976).

[41] Y. Achiman and B. Stech, NATO Sci. Ser. B 303–314 (1979).

[42] A. De Rujula, H. Georgi and S. L. Glashow, in "Fifth Workshop on Grand Unification," (1984).

[43] B. R. Greene *et al.*, Nucl. Phys. **B278**, 667 (1986).

[44] B. R. Greene *et al.*, Nucl. Phys. **B292**, 606 (1987).

[45] B. R. Greene, C. A. Lutken and G. G. Ross, Nucl. Phys. **B325**, 101 (1989).

[46] J. E. Kim, Phys. Lett. **B591**, 119 (2004), [hep-ph/0403196].

[47] L. O'Raifeartaigh, *GROUP STRUCTURE OF GAUGE THEORIES*, Cambridge Monographs on Mathematical Physics, Cambridge University Press (1988), ISBN 978-0-521-34785-3, 978-1-139-24180-9.

[48] J. Hucks, Phys. Rev. D **43**, 2709 (1991).

[49] D. Tong, JHEP **07**, 104 (2017), [arXiv:1705.01853].

[50] M. T. Grisaru, W. Siegel and M. Rocek, Nucl. Phys. B **159**, 429 (1979).

[51] E. Witten, Phys. Lett. **105B**, 267 (1981).

[52] A. Masiero *et al.*, Phys. Lett. **115B**, 380 (1982).

[53] B. Grinstein, Nucl. Phys. **B206**, 387 (1982).

[54] S. Dimopoulos and F. Wilczek (1981), print-81-0600 (SANTA BARBARA), NSF-ITP-82-07.

[55] M. Srednicki, Nucl. Phys. **B202**, 327 (1982).

[56] K. Inoue, A. Kakuto and H. Takano, Prog. Theor. Phys. **75**, 664 (1986).

[57] Y. Yamada, Z. Phys. **C60**, 83 (1993).

[58] J. Hisano *et al.*, Phys. Lett. **B342**, 138 (1995), [hep-ph/9406417].

[59] Z. Berezhiani and Z. Tavartkiladze, Phys. Lett. B **396**, 150 (1997), [hep-ph/9611277].

[60] G. Altarelli, F. Feruglio and I. Masina, JHEP **11**, 040 (2000), [hep-ph/0007254].

[61] J. Ellis *et al.*, Eur. Phys. J. C **81**, 6, 543 (2021), [arXiv:2103.15430].

[62] K. Hamaguchi, S. Hor and N. Nagata, JHEP **11**, 140 (2020), [arXiv:2008.08940].

[63] K. S. Babu and S. M. Barr, Phys. Rev. **D48**, 5354 (1993), [hep-ph/9306242].

[64] K. S. Babu and S. M. Barr, Phys. Rev. **D50**, 3529 (1994), [hep-ph/9402291].

[65] K. S. Babu, J. C. Pati and Z. Tavartkiladze, JHEP **06**, 084 (2010), [arXiv:1003.2625].

[66] K. S. Babu and R. N. Mohapatra, Phys. Rev. Lett. **74**, 2418 (1995), [hep-ph/9410326].

[67] V. Lucas and S. Raby, Phys. Rev. **D54**, 2261 (1996), [hep-ph/9601303].

[68] T. Blazek *et al.*, Phys. Rev. **D56**, 6919 (1997), [hep-ph/9611217].

[69] Z. Berezhiani and Z. Tavartkiladze, Phys. Lett. B **409**, 220 (1997), [hep-ph/9612232].

[70] S. M. Barr and S. Raby, Phys. Rev. Lett. **79**, 4748 (1997), [hep-ph/9705366].

[71] K. S. Babu, J. C. Pati and F. Wilczek, Nucl. Phys. **B566**, 33 (2000), [hep-ph/9812538].

[72] R. Dermisek, A. Mafi and S. Raby, Phys. Rev. **D63**, 035001 (2001), [hep-ph/0007213].

[73] N. Maekawa, Prog. Theor. Phys. **106**, 401 (2001), [hep-ph/0104200].

[74] N. Maekawa, Prog. Theor. Phys. **107**, 597 (2002), [hep-ph/0111205].

[75] N. Maekawa and T. Yamashita, Prog. Theor. Phys. **108**, 719 (2002), [hep-ph/0205185].

[76] A. A. Anselm and A. A. Johansen, Phys. Lett. B **200**, 331 (1988).

[77] A. A. Anselm, Sov. Phys. JETP **67**, 663 (1988).

[78] Z. G. Berezhiani and G. R. Dvali, Bull. Lebedev Phys. Inst. **5**, 55 (1989).

[79] R. Barbieri, G. R. Dvali and A. Strumia, Nucl. Phys. **B391**, 487 (1993).

[80] Z. Berezhiani, C. Csaki and L. Randall, Nucl. Phys. **B444**, 61 (1995), [hep-ph/9501336].

[81] G. R. Dvali and S. Pokorski, Phys. Rev. Lett. **78**, 807 (1997), [hep-ph/9610431].

[82] Q. Shafi and Z. Tavartkiladze, Phys. Lett. **B522**, 102 (2001), [hep-ph/0105140].

Int. J. Mod. Phys. A 2026.41. Downloaded from www.worldscientific.com
by UNIVERSITY OF CALIFORNIA @ BERKELEY on 09/16/26. Re-use and distribution is strictly not permitted, except for Open Access articles.

[83] M. Bando and T. Kugo, Prog. Theor. Phys. **109**, 87 (2003), [hep-ph/0209088].

[84] K. Hamaguchi, S. Hor and N. Nagata, Phys. Rev. D **107**, 3, 035016 (2023), [arXiv:2210.09333].

[85] G. F. Giudice and A. Masiero, Phys. Lett. **B206**, 480 (1988).

[86] J. E. Kim and H. P. Nilles, Mod. Phys. Lett. **A9**, 3575 (1994), [hep-ph/9406296].

[87] E. Witten, in "Supersymmetry and unification of fundamental interactions. Proceedings, 10th International Conference, SUSY'02, Hamburg, Germany, June 17-23, 2002," 472–491 (2001), [hep-ph/0201018], URL `http://www-library.desy.de/preparch/desy/proc/proc02-02/Proceedings/susy02/special/hertz_pr.ps`.

[88] L. Randall and C. Csaki, in "Supersymmetry and unification of fundamental interactions. Proceedings, International Workshop, SUSY 95, Palaiseau, France, May 15-19, 1995," 99–109 (1995), [,235(1995)], [hep-ph/9508208].

[89] M. Dine, Y. Nir and Y. Shadmi, Phys. Rev. **D66**, 115001 (2002), [hep-ph/0206268].

[90] A. Hebecker, J. March-Russell and R. Ziegler, JHEP **08**, 064 (2009), [arXiv:0801.4101].

[91] F. Brummer *et al.*, JHEP **08**, 011 (2009), [arXiv:0906.2957].

[92] F. Brummer *et al.*, JHEP **04**, 006 (2010), [arXiv:1003.0084].

[93] H. M. Lee *et al.*, Phys. Lett. **B694**, 491 (2011), [arXiv:1009.0905].

[94] R. Kappl *et al.*, Nucl. Phys. **B847**, 325 (2011), [arXiv:1012.4574].

[95] H. M. Lee *et al.*, Nucl. Phys. **B850**, 1 (2011), [arXiv:1102.3595].

[96] Y. Hosotani, Phys. Lett. **126B**, 309 (1983).

[97] L. J. Dixon *et al.*, Nucl. Phys. **B261**, 678 (1985), [,678(1985)].

[98] L. J. Dixon *et al.*, Nucl. Phys. **B274**, 285 (1986).

[99] L. E. Ibanez, H. P. Nilles and F. Quevedo, Phys. Lett. **B187**, 25 (1987).

[100] L. E. Ibanez *et al.*, Phys. Lett. **B191**, 282 (1987).

[101] P. Candelas *et al.*, Nucl. Phys. **B258**, 46 (1985).

[102] Y. Kawamura, Prog. Theor. Phys. **103**, 613 (2000), [hep-ph/9902423].

[103] Y. Kawamura, Prog. Theor. Phys. **105**, 999 (2001), [hep-ph/0012125].

[104] G. Altarelli and F. Feruglio, Phys. Lett. **B511**, 257 (2001), [hep-ph/0102301].

[105] L. J. Hall and Y. Nomura, Phys. Rev. **D64**, 055003 (2001), [hep-ph/0103125].

[106] A. Hebecker and J. March-Russell, Nucl. Phys. **B613**, 3 (2001), [hep-ph/0106166].

[107] T. Asaka, W. Buchmuller and L. Covi, Phys. Lett. **B523**, 199 (2001), [hep-ph/0108021].

[108] L. J. Hall *et al.*, Phys. Rev. **D65**, 035008 (2002), [hep-ph/0108071].

[109] R. Dermisek and A. Mafi, Phys. Rev. **D65**, 055002 (2002), [hep-ph/0108139].

[110] H. D. Kim and S. Raby, JHEP **01**, 056 (2003), [hep-ph/0212348].

[111] L. E. Ibanez and A. M. Uranga, *String theory and particle physics: An introduction to string phenomenology*, Cambridge University Press (2012), ISBN 978-0-521-51752-2, 978-1-139-22742-1.

[112] R. Blumenhagen *et al.*, Phys. Rept. **445**, 1 (2007), [hep-th/0610327].

[113] K.-S. Choi and J. E. Kim, Lect. Notes Phys. **954**, pp. (2020).

[114] A. Hebecker, *Naturalness, String Landscape and Multiverse: A Modern Introduction with Exercises*, volume 979 (2021), ISBN 978-3-030-65150-3, 978-3-030-65151-0, [arXiv:2008.10625].

[115] D. J. Gross *et al.*, Phys. Rev. Lett. **54**, 502 (1985).

[116] V. Braun *et al.*, JHEP **05**, 043 (2006), [hep-th/0512177].

[117] V. Bouchard and R. Donagi, Phys. Lett. **B633**, 783 (2006), [hep-th/0512149].

[118] L. B. Anderson *et al.*, Phys. Rev. **D84**, 106005 (2011), [arXiv:1106.4804].

[119] L. J. Dixon, V. Kaplunovsky and J. Louis, Nucl. Phys. **B355**, 649 (1991).

[120] G. Aldazabal *et al.*, Nucl. Phys. **B452**, 3 (1995), [hep-th/9410206].

[121] Z. Kakushadze *et al.*, Int. J. Mod. Phys. **A13**, 2551 (1998), [hep-th/9710149].

[122] E. Witten, Nucl. Phys. **B258**, 75 (1985).

[123] S. Gukov *et al.*, Phys. Rev. **D69**, 086008 (2004), [hep-th/0310159].

[124] G. Curio, A. Krause and D. Lust, Fortsch. Phys. **54**, 225 (2006), [hep-th/0502168].

[125] L. B. Anderson *et al.*, Phys. Rev. **D83**, 106011 (2011), [arXiv:1102.0011].

[126] R. Friedman, J. Morgan and E. Witten, Commun. Math. Phys. **187**, 679 (1997), [hep-th/9701162].

[127] R. Blumenhagen, G. Honecker and T. Weigand, JHEP **08**, 009 (2005), [hep-th/0507041].

[128] L. B. Anderson *et al.*, JHEP **01**, 047 (2014), [arXiv:1307.4787].

[129] T. Kobayashi, S. Raby and R.-J. Zhang, Phys. Lett. **B593**, 262 (2004), [hep-ph/0403065].

[130] S. Forste *et al.*, Phys. Rev. **D70**, 106008 (2004), [hep-th/0406208].

[131] T. Kobayashi, S. Raby and R.-J. Zhang, Nucl. Phys. **B704**, 3 (2005), [hep-ph/0409098].

[132] W. Buchmuller *et al.*, Nucl. Phys. **B712**, 139 (2005), [hep-ph/0412318].

[133] W. Buchmuller *et al.*, Phys. Rev. Lett. **96**, 121602 (2006), [hep-ph/0511035].

[134] W. Buchmuller *et al.*, Nucl. Phys. **B785**, 149 (2007), [hep-th/0606187].

[135] O. Lebedev *et al.*, Phys. Lett. **B645**, 88 (2007), [hep-th/0611095].

[136] J. E. Kim, J.-H. Kim and B. Kyae, JHEP **06**, 034 (2007), [hep-ph/0702278].

[137] O. Lebedev *et al.*, Phys. Rev. **D77**, 046013 (2008), [arXiv:0708.2691].

[138] S. B. Giddings, S. Kachru and J. Polchinski, Phys. Rev. **D66**, 106006 (2002), [hep-th/0105097].

[139] S. Kachru *et al.*, Phys. Rev. **D68**, 046005 (2003), [hep-th/0301240].

[140] R. Blumenhagen *et al.*, Nucl. Phys. **B815**, 1 (2009), [arXiv:0811.2936].

[141] R. Blumenhagen *et al.*, Nucl. Phys. **B616**, 3 (2001), [hep-th/0107138].

[142] R. Donagi and M. Wijnholt, Adv. Theor. Math. Phys. **15**, 5, 1237 (2011), [arXiv:0802.2969].

[143] C. Beasley, J. J. Heckman and C. Vafa, JHEP **01**, 058 (2009), [arXiv:0802.3391].

[144] C. Beasley, J. J. Heckman and C. Vafa, JHEP **01**, 059 (2009), [arXiv:0806.0102].

[145] T. Weigand, Class. Quant. Grav. **27**, 214004 (2010), [arXiv:1009.3497].

Int. J. Mod. Phys. A 2026.41. Downloaded from www.worldscientific.com
by UNIVERSITY OF CALIFORNIA @ BERKELEY on 09/16/26. Re-use and distribution is strictly not permitted, except for Open Access articles.

[146] J. J. Heckman, Ann. Rev. Nucl. Part. Sci. **60**, 237 (2010), [arXiv:1001.0577].

[147] M. Cvetic, I. Garcia-Etxebarria and J. Halverson, JHEP **01**, 073 (2011), [arXiv:1003.5337].

[148] A. Maharana and E. Palti, Int. J. Mod. Phys. **A28**, 1330005 (2013), [arXiv:1212.0555].

[149] S. Krippendorf, S. Schafer-Nameki and J.-M. Wong, JHEP **11**, 008 (2015), [arXiv:1507.05961].

[150] R. Donagi and M. Wijnholt, Adv. Theor. Math. Phys. **15**, 6, 1523 (2011), [arXiv:0808.2223].

[151] R. Blumenhagen, Phys. Rev. Lett. **102**, 071601 (2009), [arXiv:0812.0248].

[152] K.-S. Choi and J. E. Kim, Phys. Rev. **D83**, 065016 (2011), [arXiv:1012.0847].

[153] C. Mayrhofer, E. Palti and T. Weigand, JHEP **09**, 082 (2013), [arXiv:1303.3589].

[154] G. K. Leontaris and Q. Shafi, Phys. Rev. **D96**, 6, 066023 (2017), [arXiv:1706.08372].

[155] E. Witten, Nucl. Phys. **B471**, 135 (1996), [hep-th/9602070].

[156] A. Hebecker and M. Trapletti, Nucl. Phys. **B713**, 173 (2005), [hep-th/0411131].

[157] B. Dundee and S. Raby (2008), [arXiv:0808.0992].

[158] G. G. Ross (2004), [hep-ph/0411057].

[159] H. Georgi, H. R. Quinn and S. Weinberg, Phys. Rev. Lett. **33**, 451 (1974).

[160] S. Weinberg, Phys. Lett. **91B**, 51 (1980).

[161] L. J. Hall, Nucl. Phys. **B178**, 75 (1981).

[162] J. R. Ellis, S. Kelley and D. V. Nanopoulos, Phys. Lett. **B260**, 131 (1991).

[163] U. Amaldi, W. de Boer and H. Furstenau, Phys. Lett. **B260**, 447 (1991).

[164] P. Langacker and M.-x. Luo, Phys. Rev. **D44**, 817 (1991).

[165] C. Giunti, C. W. Kim and U. W. Lee, Mod. Phys. Lett. A **6**, 1745 (1991).

[166] S. Dimopoulos, S. A. Raby and F. Wilczek, Phys. Today **44N10**, 25 (1991).

[167] P. Langacker and N. Polonsky, Phys. Rev. **D47**, 4028 (1993), [hep-ph/9210235].

[168] M. Carena, S. Pokorski and C. E. M. Wagner, Nucl. Phys. **B406**, 59 (1993), [hep-ph/9303202].

[169] B. C. Allanach, Comput. Phys. Commun. **143**, 305 (2002), [hep-ph/0104145].

[170] S. Navas *et al.* (Particle Data Group), Phys. Rev. D **110**, 3, 030001 (2024).

[171] M. L. Alciati *et al.*, JHEP **03**, 054 (2005), [hep-ph/0501086].

[172] P. Langacker, in "2nd Workshop on Grand Unification," 131–150 (1981).

[173] W. J. Marciano and A. Sirlin, Conf. Proc. C **810424**, 151 (1981).

[174] W. J. Marciano, in "Eighth Workshop on Grand Unification," 185–199 (1987).

[175] A. Djouadi, J.-L. Kneur and G. Moultaka, Comput. Phys. Commun. **176**, 426 (2007), [hep-ph/0211331].

[176] W. Porod and F. Staub, Comput. Phys. Commun. **183**, 2458 (2012), [arXiv:1104.1573].

[177] I. Antoniadis, C. Kounnas and K. Tamvakis, Phys. Lett. B **119**, 377 (1982).

[178] W. Siegel, Phys. Lett. **94B**, 37 (1980).

[179] M. A. Shifman, Int. J. Mod. Phys. **A11**, 5761 (1996), [hep-ph/9606281].

[180] N. Arkani-Hamed and H. Murayama, JHEP **06**, 030 (2000), [hep-th/9707133].

[181] I. Jack, D. R. T. Jones and A. Pickering, Phys. Lett. **B435**, 61 (1998), [hep-ph/9805482].

[182] J. Hisano, H. Murayama and T. Yanagida, Phys. Rev. Lett. **69**, 1014 (1992).

[183] J. Hisano, H. Murayama and T. Yanagida, Nucl. Phys. B **402**, 46 (1993), [hep-ph/9207279].

[184] H. Murayama and A. Pierce, Phys. Rev. **D65**, 055009 (2002), [hep-ph/0108104].

[185] C. T. Hill, Phys. Lett. B **135**, 47 (1984).

[186] J. R. Ellis *et al.*, Phys. Lett. B **155**, 381 (1985).

[187] M. Drees, Phys. Lett. B **158**, 409 (1985).

[188] M. Drees, Phys. Rev. D **33**, 1468 (1986).

[189] K. Tobe and J. D. Wells, Phys. Lett. B **588**, 99 (2004), [hep-ph/0312159].

[190] J. Ellis *et al.*, Eur. Phys. J. C **76**, 11, 592 (2016), [arXiv:1608.05370].

[191] G. Anderson *et al.*, eConf **C960625**, SUP107 (1996), [hep-ph/9609457].

[192] L. Roszkowski and M. A. Shifman, Phys. Rev. **D53**, 404 (1996), [hep-ph/9503358].

[193] S. Raby, M. Ratz and K. Schmidt-Hoberg, Phys. Lett. **B687**, 342 (2010), [arXiv:0911.4249].

[194] J. Hisano, T. Kuwahara and N. Nagata, Phys. Lett. **B723**, 324 (2013), [arXiv:1304.0343].

[195] S. Pokorski, K. Rolbiecki and K. Sakurai, Phys. Rev. D **97**, 3, 035027 (2018), [arXiv:1707.06720].

[196] P. N. Bhattiprolu and J. D. Wells, Phys. Rev. D **109**, 1, L011704 (2024), [arXiv:2309.12954].

[197] L. Randall and R. Sundrum, Nucl. Phys. **B557**, 79 (1999), [hep-th/9810155].

[198] G. F. Giudice *et al.*, JHEP **12**, 027 (1998), [hep-ph/9810442].

[199] J. D. Wells, in "11th International Conference on Supersymmetry and the Unification of Fundamental Interactions," (2003), [hep-ph/0306127].

[200] J. D. Wells, Phys. Rev. D **71**, 015013 (2005), [hep-ph/0411041].

[201] N. Arkani-Hamed and S. Dimopoulos, JHEP **06**, 073 (2005), [hep-th/0405159].

[202] G. F. Giudice and A. Romanino, Nucl. Phys. **B699**, 65 (2004), [Erratum: Nucl. Phys.B706,487(2005)], [hep-ph/0406088].

[203] N. Arkani-Hamed *et al.*, Nucl. Phys. B **709**, 3 (2005), [hep-ph/0409232].

[204] L. J. Hall and Y. Nomura, JHEP **01**, 082 (2012), [arXiv:1111.4519].

[205] M. Ibe and T. T. Yanagida, Phys. Lett. B **709**, 374 (2012), [arXiv:1112.2462].

[206] M. Ibe, S. Matsumoto and T. T. Yanagida, Phys. Rev. D **85**, 095011 (2012), [arXiv:1202.2253].

[207] A. Arvanitaki *et al.*, JHEP **02**, 126 (2013), [arXiv:1210.0555].

[208] N. Arkani-Hamed *et al.* (2012), [arXiv:1212.6971].

[209] J. L. Evans *et al.*, Eur. Phys. J. C **73**, 2468 (2013), [arXiv:1302.5346].

[210] J. L. Evans *et al.*, Eur. Phys. J. C **73**, 10, 2611 (2013), [arXiv:1305.7461].

[211] Y. Okada, M. Yamaguchi and T. Yanagida, Prog. Theor. Phys. **85**, 1 (1991).

[212] Y. Okada, M. Yamaguchi and T. Yanagida, Phys. Lett. B **262**, 54 (1991).

[213] J. R. Ellis, G. Ridolfi and F. Zwirner, Phys. Lett. **B257**, 83 (1991).

Int. J. Mod. Phys. A 2026.41. Downloaded from www.worldscientific.com
by UNIVERSITY OF CALIFORNIA @ BERKELEY on 09/16/26. Re-use and distribution is strictly not permitted, except for Open Access articles.

[214] H. E. Haber and R. Hempfling, Phys. Rev. Lett. **66**, 1815 (1991).

[215] J. R. Ellis, G. Ridolfi and F. Zwirner, Phys. Lett. B **262**, 477 (1991).

[216] M. Carena *et al.*, Phys. Lett. **B355**, 209 (1995), [hep-ph/9504316].

[217] G. Degrassi *et al.*, Eur. Phys. J. **C28**, 133 (2003), [hep-ph/0212020].

[218] P. Kant *et al.*, JHEP **08**, 104 (2010), [arXiv:1005.5709].

[219] R. N. Mohapatra and M. K. Parida, Phys. Rev. **D47**, 264 (1993), [hep-ph/9204234].

[220] D.-G. Lee *et al.*, Phys. Rev. **D51**, 229 (1995), [hep-ph/9404238].

[221] Y. Mambrini *et al.*, Phys. Rev. D **91**, 9, 095010 (2015), [arXiv:1502.06929].

[222] N. Nagata, K. A. Olive and J. Zheng, JHEP **10**, 193 (2015), [arXiv:1509.00809].

[223] L. E. Ibanez *et al.*, JHEP **07**, 195 (2012), [arXiv:1206.2655].

[224] S. A. R. Ellis and J. D. Wells, Phys. Rev. D **91**, 7, 075016 (2015), [arXiv:1502.01362].

[225] J. Schwichtenberg, Eur. Phys. J. C **79**, 4, 351 (2019), [arXiv:1808.10329].

[226] K. R. Dienes, E. Dudas and T. Gherghetta, Phys. Rev. Lett. **91**, 061601 (2003), [hep-th/0210294].

[227] K. Agashe, R. Contino and R. Sundrum, Phys. Rev. Lett. **95**, 171804 (2005), [hep-ph/0502222].

[228] F. Wilczek and A. Zee, Phys. Rev. Lett. **43**, 1571 (1979).

[229] J. Ellis *et al.*, JHEP **05**, 021 (2020), [arXiv:2003.03285].

[230] K. Hamaguchi *et al.*, Universe **10**, 9, 379 (2024), [arXiv:2407.11892].

[231] N. Maekawa and Y. Muramatsu, Phys. Rev. D **88**, 9, 095008 (2013), [arXiv:1307.7529].

[232] N. Maekawa and Y. Muramatsu, Phys. Lett. B **767**, 398 (2017), [arXiv:1601.04789].

[233] A. Takenaka *et al.* (Super-Kamiokande), Phys. Rev. D **102**, 11, 112011 (2020), [arXiv:2010.16098].

[234] K. Abe *et al.* (Super-Kamiokande), Phys. Rev. D **96**, 1, 012003 (2017), [arXiv:1705.07221].

[235] K. Abe *et al.* (Hyper-Kamiokande) (2018), [arXiv:1805.04163].

[236] P. S. B. Dev *et al.* (2022), [arXiv:2203.08771].

[237] J.-S. Yoo *et al.*, Phys. Rev. D **105**, 7, 074501 (2022), [arXiv:2111.01608].

[238] J. Hisano, T. Kuwahara and Y. Omura, Nucl. Phys. **B898**, 1 (2015), [Erratum: Nucl. Phys.B907,476(2016)], [arXiv:1503.08561].

[239] R. Barbier *et al.*, Phys. Rept. **420**, 1 (2005), [hep-ph/0406039].

[240] F. Domingo *et al.*, JHEP **02**, 066 (2019), [arXiv:1810.08228].

[241] B. A. Campbell *et al.*, Phys. Lett. B **256**, 484 (1991).

[242] W. Fischler *et al.*, Phys. Lett. B **258**, 45 (1991).

[243] H. K. Dreiner and G. G. Ross, Nucl. Phys. **B410**, 188 (1993), [hep-ph/9207221].

[244] G. R. Farrar and P. Fayet, Phys. Lett. **76B**, 575 (1978).

[245] S. Dimopoulos, S. Raby and F. Wilczek, Phys. Lett. **112B**, 133 (1982).

[246] J. R. Ellis, D. V. Nanopoulos and S. Rudaz, Nucl. Phys. **B202**, 43 (1982).

[247] C. S. Aulakh *et al.*, Nucl. Phys. **B597**, 89 (2001), [hep-ph/0004031].

[248] S. Mine (Super Kamiokande), J. Phys. Conf. Ser. **718**, 6, 062044 (2016).

[249] T. Goto and T. Nihei, Phys. Rev. **D59**, 115009 (1999), [hep-ph/9808255].

[250] G. D. Coughlan *et al.*, Phys. Lett. **160B**, 249 (1985).

[251] J. L. Chkareuli and I. G. Gogoladze, Phys. Rev. **D58**, 055011 (1998), [hep-ph/9803335].

[252] D. McKeen, M. Pospelov and A. Ritz, Phys. Rev. D **87**, 11, 113002 (2013), [arXiv:1303.1172].

[253] M. Liu and P. Nath, Phys. Rev. D **87**, 9, 095012 (2013), [arXiv:1303.7472].

[254] J. Hisano *et al.*, JHEP **07**, 038 (2013), [arXiv:1304.3651].

[255] J. L. Evans, N. Nagata and K. A. Olive, Phys. Rev. D **91**, 055027 (2015), [arXiv:1502.00034].

[256] S. Pokorski *et al.*, JHEP **04**, 161 (2019), [arXiv:1902.06093].

[257] J. L. Evans, N. Nagata and K. A. Olive, Eur. Phys. J. C **79**, 6, 490 (2019), [arXiv:1902.09084].

[258] J. Ellis *et al.*, Eur. Phys. J. C **80**, 4, 332 (2020), [arXiv:1912.04888].

[259] B. Bajc, P. Fileviez Perez and G. Senjanovic, Phys. Rev. **D66**, 075005 (2002), [hep-ph/0204311].

[260] A. Abusleme *et al.* (JUNO), Prog. Part. Nucl. Phys. **123**, 103927 (2022), [arXiv:2104.02565].

[261] A. Abusleme *et al.* (JUNO), Chin. Phys. C **47**, 11, 113002 (2023), [arXiv:2212.08502].

[262] B. Abi *et al.* (DUNE), Eur. Phys. J. C **81**, 4, 322 (2021), [arXiv:2008.12769].

[263] L. J. Hall and Y. Nomura, Phys. Rev. **D66**, 075004 (2002), [hep-ph/0205067].

[264] H. D. Kim, S. Raby and L. Schradin, JHEP **05**, 036 (2005), [hep-ph/0411328].

[265] M. S. Chanowitz, J. R. Ellis and M. K. Gaillard, Nucl. Phys. B **128**, 506 (1977).

[266] A. J. Buras *et al.*, Nucl. Phys. **B135**, 66 (1978).

[267] K. Inoue *et al.*, Prog. Theor. Phys. **67**, 1889 (1982).

[268] L. E. Ibanez and C. Lopez, Nucl. Phys. **B233**, 511 (1984).

[269] H. Georgi and D. V. Nanopoulos, Nucl. Phys. **B159**, 16 (1979).

[270] J. A. Harvey, P. Ramond and D. B. Reiss, Phys. Lett. **92B**, 309 (1980).

[271] J. A. Harvey, D. B. Reiss and P. Ramond, Nucl. Phys. **B199**, 223 (1982).

[272] T. Banks, Nucl. Phys. **B303**, 172 (1988).

[273] M. Olechowski and S. Pokorski, Phys. Lett. **B214**, 393 (1988).

[274] S. Pokorski, Nucl. Phys. Proc. Suppl. **13**, 606 (1990).

[275] B. Ananthanarayan, G. Lazarides and Q. Shafi, Phys. Rev. **D44**, 1613 (1991).

[276] Q. Shafi and B. Ananthanarayan, in "Summer School in High-energy Physics and Cosmology," 233–244 (1991).

[277] S. Dimopoulos, L. J. Hall and S. Raby, Phys. Rev. Lett. **68**, 1984 (1992).

[278] S. Dimopoulos, L. J. Hall and S. Raby, Phys. Rev. **D45**, 4192 (1992).

[279] G. W. Anderson *et al.*, Phys. Rev. **D47**, R3702 (1993), [hep-ph/9209250].

[280] B. Ananthanarayan, G. Lazarides and Q. Shafi, Phys. Lett. **B300**, 245 (1993).

[281] G. Anderson *et al.*, Phys. Rev. **D49**, 3660 (1994), [hep-ph/9308333].

[282] B. Ananthanarayan, Q. Shafi and X. M. Wang, Phys. Rev. **D50**, 5980 (1994), [hep-ph/9311225].

[283] L. J. Hall, R. Rattazzi and U. Sarid, Phys. Rev. **D50**, 7048 (1994), [hep-ph/9306309].

Int. J. Mod. Phys. A 2026.41. Downloaded from www.worldscientific.com by UNIVERSITY OF CALIFORNIA @ BERKELEY on 09/16/26. Re-use and distribution is strictly not permitted, except for Open Access articles.

[284] M. Carena *et al.*, Nucl. Phys. **B426**, 269 (1994), [hep-ph/9402253].

[285] A. Anandakrishnan, B. C. Bryant and S. Raby, JHEP **05**, 088 (2015), [arXiv:1411.7035].

[286] M. Lanzagorta and G. G. Ross, Phys. Lett. **B364**, 163 (1995), [hep-ph/9507366].

[287] K. Tobe and J. D. Wells, Nucl. Phys. **B663**, 123 (2003), [hep-ph/0301015].

[288] G. Ross and M. Serna, Phys. Lett. **B664**, 97 (2008), [arXiv:0704.1248].

[289] T. Blazek, R. Dermisek and S. Raby, Phys. Rev. Lett. **88**, 111804 (2002), [hep-ph/0107097].

[290] T. Blazek, R. Dermisek and S. Raby, Phys. Rev. **D65**, 115004 (2002), [hep-ph/0201081].

[291] D. Auto *et al.*, JHEP **06**, 023 (2003), [hep-ph/0302155].

[292] R. Dermisek *et al.*, JHEP **04**, 037 (2003), [hep-ph/0304101].

[293] R. Dermisek *et al.*, JHEP **09**, 029 (2005), [hep-ph/0507233].

[294] A. Anandakrishnan, S. Raby and A. Wingerter, Phys. Rev. **D87**, 5, 055005 (2013), [arXiv:1212.0542].

[295] M. Adeel Ajaib *et al.*, JHEP **07**, 139 (2013), [arXiv:1303.6964].

[296] Z. Poh and S. Raby, Phys. Rev. **D92**, 1, 015017 (2015), [arXiv:1505.00264].

[297] M. Badziak, M. Olechowski and S. Pokorski, JHEP **10**, 088 (2013), [arXiv:1307.7999].

[298] H. Georgi and C. Jarlskog, Phys. Lett. **86B**, 297 (1979).

[299] S. Antusch and M. Spinrath, Phys. Rev. **D79**, 095004 (2009), [arXiv:0902.4644].

[300] G. Lazarides, Q. Shafi and C. Wetterich, Nucl. Phys. **B181**, 287 (1981).

[301] T. E. Clark, T.-K. Kuo and N. Nakagawa, Phys. Lett. **115B**, 26 (1982).

[302] K. S. Babu and R. N. Mohapatra, Phys. Rev. Lett. **70**, 2845 (1993), [hep-ph/9209215].

[303] R. Barbieri and D. V. Nanopoulos, Phys. Lett. **91B**, 369 (1980).

[304] C. D. Froggatt and H. B. Nielsen, Nucl. Phys. **B147**, 277 (1979).

[305] R. Barbieri *et al.*, Nucl. Phys. **B493**, 3 (1997), [hep-ph/9610449].

[306] T. Blazek, S. Raby and K. Tobe, Phys. Rev. **D60**, 113001 (1999), [hep-ph/9903340].

[307] T. Blazek, S. Raby and K. Tobe, Phys. Rev. **D62**, 055001 (2000), [hep-ph/9912482].

[308] Q. Shafi and Z. Tavartkiladze, Phys. Lett. **B487**, 145 (2000), [hep-ph/9910314].

[309] C. H. Albright and S. M. Barr, Phys. Rev. Lett. **85**, 244 (2000), [hep-ph/0002155].

[310] Z. Berezhiani and A. Rossi, Nucl. Phys. **B594**, 113 (2001), [hep-ph/0003084].

[311] C. H. Albright and S. M. Barr, Phys. Rev. **D64**, 073010 (2001), [hep-ph/0104294].

[312] M.-C. Chen and K. T. Mahanthappa, Int. J. Mod. Phys. **A18**, 5819 (2003), [hep-ph/0305088].

[313] R. Dermisek and S. Raby, Phys. Lett. **B622**, 327 (2005), [hep-ph/0507045].

[314] H. Georgi, Nucl. Phys. **B156**, 126 (1979).

[315] P. H. Frampton, Phys. Lett. **88B**, 299 (1979).

[316] P. Frampton and S. Nandi, Phys. Rev. Lett. **43**, 1460 (1979).

[317] J. E. Kim, Phys. Rev. Lett. **45**, 1916 (1980).

[318] J. E. Kim, Phys. Rev. D **23**, 2706 (1981).

[319] J. E. Kim, Phys. Rev. D **26**, 674 (1982).

[320] Y. Fujimoto, Phys. Rev. **D26**, 3183 (1982).

[321] P. Langacker, Phys. Rept. **72**, 185 (1981).

[322] H. Georgi, J. Phys. Colloq. **43**, C3, 705 (1982).

[323] S. M. Barr, Phys. Rev. **D78**, 055008 (2008), [arXiv:0805.4808].

[324] Y. Goto, Y. Kawamura and T. Miura, Phys. Rev. **D88**, 5, 055016 (2013), [arXiv:1307.2631].

[325] J. E. Kim, JHEP **06**, 114 (2015), [arXiv:1503.03104].

[326] C. H. Albright, R. P. Feger and T. W. Kephart, Phys. Rev. D **93**, 7, 075032 (2016), [arXiv:1601.07523].

[327] M. Reig *et al.*, Phys. Lett. B **774**, 667 (2017), [arXiv:1706.03116].

[328] M. Magg and C. Wetterich, Phys. Lett. **94B**, 61 (1980).

[329] J. Schechter and J. W. F. Valle, Phys. Rev. **D22**, 2227 (1980).

[330] R. N. Mohapatra and G. Senjanovic, Phys. Rev. **D23**, 165 (1981).

[331] G. B. Gelmini and M. Roncadelli, Phys. Lett. **99B**, 411 (1981).

[332] R. Foot *et al.*, Z. Phys. **C44**, 441 (1989).

[333] G. Altarelli, Soryushiron Kenkyu Electron. **116**, A29 (2008), [arXiv:0711.0161].

[334] S. F. King and C. Luhn, Rept. Prog. Phys. **76**, 056201 (2013), [arXiv:1301.1340].

[335] C. H. Albright and M.-C. Chen, Phys. Rev. **D74**, 113006 (2006), [hep-ph/0608137].

[336] G. Altarelli and F. Feruglio, Rev. Mod. Phys. **82**, 2701 (2010), [arXiv:1002.0211].

[337] H. Ishimori *et al.*, Prog. Theor. Phys. Suppl. **183**, 1 (2010), [arXiv:1003.3552].

[338] F. Feruglio, *Are neutrino masses modular forms?*, 227–266 (2019), [arXiv:1706.08749].

[339] T. Kobayashi, K. Tanaka and T. H. Tatsuishi, Phys. Rev. D **98**, 1, 016004 (2018), [arXiv:1803.10391].

[340] J. T. Penedo and S. T. Petcov, Nucl. Phys. B **939**, 292 (2019), [arXiv:1806.11040].

[341] Y. Almumin *et al.*, JHEP **05**, 078 (2021), [arXiv:2102.11286].

[342] H. P. Nilles, S. Ramos-Sánchez and P. K. S. Vaudrevange, JHEP **02**, 045 (2020), [arXiv:2001.01736].

[343] R. Kallosh *et al.*, Phys. Rev. **D52**, 912 (1995), [hep-th/9502069].

[344] T. Banks and N. Seiberg, Phys. Rev. D **83**, 084019 (2011), [arXiv:1011.5120].

[345] M. Dine, P. Draper and W. Shepherd, JHEP **02**, 027 (2014), [arXiv:1308.0274].

[346] H. Ruegg and M. Ruiz-Altaba, Int. J. Mod. Phys. **A19**, 3265 (2004), [hep-th/0304245].

[347] M. B. Green and J. H. Schwarz, Phys. Lett. **149B**, 117 (1984).

[348] L. E. Ibanez and G. G. Ross, Nucl. Phys. **B368**, 3 (1992).

[349] M. Berasaluce-Gonzalez *et al.*, JHEP **12**, 113 (2011), [arXiv:1106.4169].

[350] N. G. Deshpande (1979).

[351] C. Q. Geng and R. E. Marshak, Phys. Rev. **D39**, 693 (1989).

[352] A. Font, L. E. Ibanez and F. Quevedo, Phys. Lett. **B228**, 79 (1989).

[353] K. S. Babu and R. N. Mohapatra, Phys. Rev. Lett. **63**, 938 (1989).

[354] R. Foot *et al.*, Phys. Rev. **D39**, 3411 (1989).

[355] M. Nowakowski and A. Pilaftsis, Phys. Rev. **D48**, 259 (1993), [hep-ph/9304312].

[356] T. P. T. Dijkstra, L. R. Huiszoon and A. N. Schellekens, Phys. Lett. **B609**, 408 (2005), [hep-th/0403196].

Int. J. Mod. Phys. A 2026.41. Downloaded from www.worldscientific.com
by UNIVERSITY OF CALIFORNIA @ BERKELEY on 09/16/26. Re-use and distribution is strictly not permitted, except for Open Access articles.

[357] F. Gmeiner *et al.*, JHEP **01**, 004 (2006), [hep-th/0510170].

[358] B. Gato-Rivera and A. N. Schellekens, Nucl. Phys. **B883**, 529 (2014), [arXiv:1401.1782].

[359] G. 't Hooft, Nucl. Phys. B **79**, 276 (1974).

[360] A. M. Polyakov, JETP Lett. **20**, 194 (1974).

[361] M. Ambrosio *et al.* (MACRO), Eur. Phys. J. **C25**, 511 (2002), [hep-ex/0207020].

[362] S. Balestra *et al.* (2011), [arXiv:1105.5587].

[363] L. Patrizii and M. Spurio, Ann. Rev. Nucl. Part. Sci. **65**, 279 (2015), [arXiv:1510.07125].

[364] V. A. Rubakov (1981).

[365] V. A. Rubakov, Nucl. Phys. B **203**, 311 (1982).

[366] C. G. Callan, Jr., Phys. Rev. **D26**, 2058 (1982).

[367] F. Wilczek, Phys. Rev. Lett. **48**, 1146 (1982).

[368] S. Dawson and A. N. Schellekens, Phys. Rev. **D27**, 2119 (1983).

[369] K. Freese, M. S. Turner and D. N. Schramm, Phys. Rev. Lett. **51**, 1625 (1983).

[370] P. A. R. Ade *et al.* (BICEP, Keck), Phys. Rev. Lett. **127**, 15, 151301 (2021), [arXiv:2110.00483].

[371] G. R. Dvali, H. Liu and T. Vachaspati, Phys. Rev. Lett. **80**, 2281 (1998), [hep-ph/9710301].

[372] P. Langacker and S.-Y. Pi, Phys. Rev. Lett. **45**, 1 (1980).

[373] G. R. Dvali, A. Melfo and G. Senjanovic, Phys. Rev. Lett. **75**, 4559 (1995), [hep-ph/9507230].

[374] A. Vilenkin, Phys. Rept. **121**, 263 (1985).

[375] M. B. Hindmarsh and T. W. B. Kibble, Rept. Prog. Phys. **58**, 477 (1995), [hep-ph/9411342].

[376] R. Jeannerot, J. Rocher and M. Sakellariadou, Phys. Rev. D **68**, 103514 (2003), [hep-ph/0308134].

[377] B. P. Abbott *et al.* (LIGO Scientific, Virgo), Phys. Rev. D **97**, 10, 102002 (2018), [arXiv:1712.01168].

[378] S. F. King *et al.*, Phys. Rev. Lett. **126**, 2, 021802 (2021), [arXiv:2005.13549].

[379] S. Chigusa, Y. Nakai and J. Zheng, Phys. Rev. D **104**, 3, 035031 (2021), [arXiv:2011.04090].

[380] E. J. Chun and L. Velasco-Sevilla, Phys. Rev. D **106**, 3, 035008 (2022), [arXiv:2112.14483].

[381] R. Maji and Q. Shafi, JCAP **03**, 007 (2023), [arXiv:2208.08137].

[382] A. Vilenkin, Nucl. Phys. B **196**, 240 (1982).

[383] A. Monin and M. B. Voloshin, Phys. Rev. D **78**, 065048 (2008), [arXiv:0808.1693].

[384] W. Buchmuller *et al.*, Phys. Lett. B **809**, 135764 (2020), [arXiv:1912.03695].

[385] J. A. Dror *et al.*, Phys. Rev. Lett. **124**, 4, 041804 (2020), [arXiv:1908.03227].

[386] W. Buchmuller, V. Domcke and K. Schmitz, Phys. Lett. B **811**, 135914 (2020), [arXiv:2009.10649].

[387] A. Afzal *et al.* (NANOGrav), Astrophys. J. Lett. **951**, 1, L11 (2023), [arXiv:2306.16219].

[388] C. Caprini *et al.*, JCAP **04**, 001 (2016), [arXiv:1512.06239].

[389] A. Mazumdar and G. White, Rept. Prog. Phys. **82**, 7, 076901 (2019), [arXiv:1811.01948].

[390] C. Caprini *et al.*, JCAP **03**, 024 (2020), [arXiv:1910.13125].

[391] M. B. Hindmarsh *et al.*, SciPost Phys. Lect. Notes **24**, 1 (2021), [arXiv:2008.09136].

[392] L. J. Hall, V. A. Kostelecky and S. Raby, Nucl. Phys. **B267**, 415 (1986).

[393] R. Barbieri and L. J. Hall, Phys. Lett. **B338**, 212 (1994), [hep-ph/9408406].

[394] R. Barbieri, L. J. Hall and A. Strumia, Nucl. Phys. **B445**, 219 (1995), [hep-ph/9501334].

[395] F. Borzumati and A. Masiero, Phys. Rev. Lett. **57**, 961 (1986).

[396] J. Hisano *et al.*, Phys. Lett. **B357**, 579 (1995), [hep-ph/9501407].

[397] J. Hisano *et al.*, Phys. Rev. **D53**, 2442 (1996), [hep-ph/9510309].

[398] J. Hisano and D. Nomura, Phys. Rev. **D59**, 116005 (1999), [hep-ph/9810479].

[399] T. Moroi, JHEP **03**, 019 (2000), [hep-ph/0002208].

[400] D. Chang, A. Masiero and H. Murayama, Phys. Rev. **D67**, 075013 (2003), [hep-ph/0205111].

[401] N. Nagata and S. Shirai, JHEP **03**, 049 (2014), [arXiv:1312.7854].

[402] S. Dimopoulos and L. J. Hall, Phys. Lett. **B344**, 185 (1995), [hep-ph/9411273].

[403] J. Hisano *et al.*, Phys. Lett. **B604**, 216 (2004), [hep-ph/0407169].

[404] V. A. Kuzmin, V. A. Rubakov and M. E. Shaposhnikov, Phys. Lett. B **155**, 36 (1985).

[405] A. Yu. Ignatiev *et al.*, Phys. Lett. **76B**, 436 (1978).

[406] M. Yoshimura, Phys. Rev. Lett. **41**, 281 (1978), [Erratum: Phys. Rev. Lett.42,746(1979)].

[407] D. Toussaint *et al.*, Phys. Rev. **D19**, 1036 (1979).

[408] S. Weinberg, Phys. Rev. Lett. **42**, 850 (1979).

[409] M. Yoshimura, Phys. Lett. **88B**, 294 (1979).

[410] S. M. Barr, G. Segre and H. A. Weldon, Phys. Rev. **D20**, 2494 (1979).

[411] D. V. Nanopoulos and S. Weinberg, Phys. Rev. **D20**, 2484 (1979).

[412] A. Yildiz and P. H. Cox, Phys. Rev. **D21**, 906 (1980).

[413] M. Fukugita and T. Yanagida, Phys. Rev. Lett. **89**, 131602 (2002), [hep-ph/0203194].

[414] M. Fukugita and T. Yanagida, Phys. Lett. **B174**, 45 (1986).

[415] S. Davidson and A. Ibarra, Phys. Lett. **B535**, 25 (2002), [hep-ph/0202239].

[416] K. Hamaguchi, H. Murayama and T. Yanagida, Phys. Rev. **D65**, 043512 (2002), [hep-ph/0109030].

[417] A. Pilaftsis and T. E. J. Underwood, Nucl. Phys. B **692**, 303 (2004), [hep-ph/0309342].

[418] A. Pilaftsis and T. E. J. Underwood, Phys. Rev. **D72**, 113001 (2005), [hep-ph/0506107].

[419] M. Kawasaki *et al.*, Phys. Rev. **D78**, 065011 (2008), [arXiv:0804.3745].

[420] G. Lazarides and Q. Shafi, Phys. Lett. B **258**, 305 (1991).

[421] T. Asaka *et al.*, Phys. Lett. B **464**, 12 (1999), [hep-ph/9906366].

[422] T. Asaka *et al.*, Phys. Rev. D **61**, 083512 (2000), [hep-ph/9907559].

[423] W. Buchmuller, R. D. Peccei and T. Yanagida, Ann. Rev. Nucl. Part. Sci. **55**, 311 (2005), [hep-ph/0502169].

[424] S. Davidson, E. Nardi and Y. Nir, Phys. Rept. **466**, 105 (2008), [arXiv:0802.2962].

[425] C. S. Fong, E. Nardi and A. Riotto, Adv. High Energy Phys. **2012**, 158303 (2012), [arXiv:1301.3062].

[426] V. Cirigliano *et al.*, JHEP **12**, 097 (2018), [arXiv:1806.02780].

[427] K. S. Babu and R. N. Mohapatra, Phys. Rev. **D86**, 035018 (2012), [arXiv:1203.5544].

[428] K. S. Babu and R. N. Mohapatra, Phys. Lett. **B715**, 328 (2012), [arXiv:1206.5701].

[429] K. S. Babu and R. N. Mohapatra, Phys. Rev. Lett. **109**, 091803 (2012), [arXiv:1207.5771].

[430] M. Baldo-Ceolin *et al.*, Z. Phys. **C63**, 409 (1994).

[431] K. Abe *et al.* (Super-Kamiokande), Phys. Rev. D **103**, 1, 012008 (2021), [arXiv:2012.02607].

[432] J. Gustafson *et al.* (Super-Kamiokande), Phys. Rev. **D91**, 7, 072009 (2015), [arXiv:1504.01041].

[433] R. D. Peccei and H. R. Quinn, Phys. Rev. Lett. **38**, 1440 (1977).

[434] F. Wilczek, Phys. Rev. Lett. **40**, 279 (1978).

[435] S. Weinberg, Phys. Rev. Lett. **40**, 223 (1978).

[436] G. Grilli di Cortona *et al.*, JHEP **01**, 034 (2016), [arXiv:1511.02867].

[437] R. N. Mohapatra and D. Wyler, Phys. Lett. B **89**, 181 (1980).

[438] A. E. Nelson, Phys. Lett. B **136**, 387 (1984).

[439] S. M. Barr, Phys. Rev. Lett. **53**, 329 (1984).

[440] L. J. Hall and K. Harigaya, JHEP **10**, 130 (2018), [arXiv:1803.08119].

[441] Y. Mimura, R. N. Mohapatra and M. Severson, Phys. Rev. D **99**, 11, 115025 (2019), [arXiv:1903.07506].

[442] L. J. Hall and K. Harigaya, JHEP **11**, 033 (2019), [arXiv:1905.12722].

[443] P. Svrcek and E. Witten, JHEP **06**, 051 (2006), [hep-th/0605206].

[444] L. Di Luzio *et al.*, Phys. Rept. **870**, 1 (2020), [arXiv:2003.01100].

[445] M. Dine, W. Fischler and M. Srednicki, Phys. Lett. **104B**, 199 (1981).

[446] A. R. Zhitnitsky, Sov. J. Nucl. Phys. **31**, 260 (1980), [Yad. Fiz.31,497(1980)].

[447] J. E. Kim, Phys. Rev. Lett. **43**, 103 (1979).

[448] M. A. Shifman, A. I. Vainshtein and V. I. Zakharov, Nucl. Phys. B **166**, 493 (1980).

[449] J. Hisano, H. Murayama and T. Yanagida, Phys. Lett. B **291**, 263 (1992).

[450] R. T. Co, F. D'Eramo and L. J. Hall, Phys. Rev. D **94**, 7, 075001 (2016), [arXiv:1603.04439].

[451] G. F. Giudice, R. Rattazzi and A. Strumia, Phys. Lett. B **715**, 142 (2012), [arXiv:1204.5465].

[452] K. J. Bae, H. Baer and H. Serce, JCAP **06**, 024 (2017), [arXiv:1705.01134].

[453] J. P. Conlon, JHEP **05**, 078 (2006), [hep-th/0602233].

[454] K. R. Dienes, Phys. Rept. **287**, 447 (1997), [hep-th/9602045].

[455] P. Nath and P. Fileviez Perez, Phys. Rept. **441**, 191 (2007), [hep-ph/0601023].

[456] T. Fukuyama, Int. J. Mod. Phys. A **28**, 1330008 (2013), [arXiv:1212.3407].

[457] G. G. Ross, *GRAND UNIFIED THEORIES* (1985).

[458] R. N. Mohapatra, *Unification and Supersymmetry. The Frontiers of Quark-Lepton Physics*, Springer, Berlin (1986), ISBN 978-1-4757-1930-7, 978-1-4757-1928-4.

[459] P. Nath, *Supersymmetry, Supergravity, and Unification*, Cambridge Monographs on Mathematical Physics, Cambridge University Press (2016), ISBN 978-0-521-19702-1, 978-1-316-98396-6.

[460] S. Raby, Lect. Notes Phys. **939**, 1 (2017).

[461] P. Nath, Int. J. Mod. Phys. **A33**, 20, 1830017 (2018), [arXiv:1807.05302].

[462] D. Croon *et al.*, Front.in Phys. **7**, 76 (2019), [arXiv:1903.04977].

Int. J. Mod. Phys. A 2026.41. Downloaded from www.worldscientific.com
by UNIVERSITY OF CALIFORNIA @ BERKELEY on 09/16/26. Re-use and distribution is strictly not permitted, except for Open Access articles.

Int. J. Mod. Phys. A 2026.41. Downloaded from www.worldscientific.com
by UNIVERSITY OF CALIFORNIA @ BERKELEY on 09/16/26. Re-use and distribution is strictly not permitted, except for Open Access articles.

93. Leptoquarks

Revised October 2025 by S. Rolli (DOE) and M. Tanabashi (Nagoya U.; KMI, Nagoya U.).

Leptoquarks (LQs) are hypothetical particles carrying both baryon number (B) and lepton number (L). The possible quantum numbers of LQ states can be constrained by assuming that their direct interactions with the ordinary Standard Model (SM) fermions are dimensionless and invariant under the SM gauge group. Table 93.1 lists all possible quantum numbers under this assumption [1]. The columns labeled $SU(3)_C$, $SU(2)_W$, and $U(1)_Y$ in Table 93.1 indicate the QCD representation, the weak isospin representation, and the weak hypercharge, respectively. The spin of a LQ state is taken to be either 1 (vector LQ) or 0 (scalar LQ). If we do not require LQ states to couple directly with SM fermions, quantum number assignments beyond those listed in Table 93.1 become possible [2,3].

LQ states are predicted in various extensions of the SM. The Pati-Salam model [4] is one such example. LQs also apear in grand unified theories based on $SU(5)$ [5], $SO(10)$ [6] which includes Pati-Salam color $SU(4)$, and larger gauge groups. The presence of LQs at TeV-scale affect the renormalization group of the standard model gauge coupling strengths and may enable gauge coupling unification required by the grand unified theories [7]. Scalar quarks in supersymmetric models with R-parity violation may also exhibit LQ-like Yukawa couplings. Consequently, bounds on LQ states can constrain R-parity-violating supersymmetric models [8,9]. LQs are expected to exist at the TeV-scale in extended technicolor models [10,11] where they appear as bound states of techni-fermions. Models involving quark and lepton compositeness also predict light LQ states [12]. LQ-induced two-quark two-lepton interactions often lead to lepton-flavor non-universalities in heavy quark decays. The so called $R(D)$, $R(D^*)$ anomaly observed in the semi-leptonic B decays [13] may be explained by models with TeV-scale LQs.

Bounds on LQ states are obtained both directly and indirectly. Direct limits arise from production cross sections at colliders, while indirect limits are derived from constraints on LQ-induced two-quark two-lepton interactions. The quantum number assignments in Table 93.1 allow several LQ states to couple to both left- and right-handed quarks simultaneously. Such LQ states are termed non-chiral and give rise to low-energy interactions of the form:

$$(\bar{u}_R q_{Li})(\bar{e}_R \ell_{Lj})\epsilon^{ij} \qquad (\bar{d}_R q_{Li})(\bar{\ell}^i_L e_R)\,. \tag{93.1}$$

Here q_L and ℓ_L denote the left-handed quark and lepton $SU(2)_W$ doublets, while u_R, d_R and e_R are the right-handed up-type quark, down-type quark and charged lepton $SU(2)_W$ singlets. Indices i and j correspond to weak isospin, and ϵ^{ij} is the antisymmetric Levi-Civita tensor of $SU(2)_W$. These interactions affect the ratio $\Gamma(\pi \to e\nu)/\Gamma(\pi \to \mu\nu)$ [14]. Non-chiral scalar LQs also contribute to the anomalous magnetic moments of charged leptons [15,16]. On the other hand, chiral LQ exchanges induce effective two-quark two-lepton interactions below the LQ mass scale:

$$\begin{aligned}
&(\bar{q}^i_L\gamma^\mu q_{Li})(\bar{\ell}^j_L\gamma_\mu \ell_{Lj})\,, && (\bar{q}^i_L\gamma^\mu q_{Li})(\bar{e}_R\gamma_\mu e_R)\,, && (\bar{q}^i_L\gamma^\mu (\vec{\sigma})_i{}^j q_{Lj})\cdot(\bar{\ell}^k_L\gamma_\mu(\vec{\sigma})_k{}^l \ell_{Ll})\,,\\
&(\bar{u}_R\gamma^\mu u_R)(\bar{\ell}^j_L\gamma_\mu \ell_{Lj})\,, && (\bar{u}_R\gamma^\mu u_R)(\bar{e}_R\gamma_\mu e_R)\,, &&\\
&(\bar{d}_R\gamma^\mu d_R)(\bar{\ell}^j_L\gamma_\mu \ell_{Lj})\,, && (\bar{d}_R\gamma^\mu d_R)(\bar{e}_R\gamma_\mu e_R)\,. &&
\end{aligned} \tag{93.2}$$

Here $(\vec{\sigma})_i{}^j$ denotes the Pauli matrices of $SU(2)_W$. Generation labels for quarks and leptons are suppressed in (93.1) and (93.2). If a LQ couples to quarks and leptons from multiple generations in the mass eigenbasis, it can induce flavor-changing neutral currents and lepton-family-number violations. Indirect limits provide stringent constraints on non-chiral or flavor-violating LQs. Therefore, collider searches often assume that a LQ state couples only to a single generation of quarks and leptons in a chiral interaction, for which indirect limits are weaker. LQs that couple exclusively to the first, second, and third generation are referred to as first-, second-, and third-generation LQs, respectively. It is also possible to consider LQ states which couple dominantly with the i-th generation quarks and the j-th generation leptons ($i \neq j$) without conflicting with indirect constraints. Such couplings have recently gained renewed attention. See Ref. [17,18] and [19], and references therein for collider search strategies and limits on the pair-production cross sections of this class of LQ states.

Limits on the LQ induced two-quark two-lepton interactions can be derived from low-energy experiments and from collider experiments below threshold. Refs. [20–22] give extensive lists of such limits. For the isoscalar scalar and vector LQs, S_0 and V_0, for example, which couple with the first- (second-) generation left-handed quark, and the first-generation left-handed lepton, the bounds $\lambda^2 < 0.07 \times (M_{\rm LQ}/1\ {\rm TeV})^2$ for S_0, and $\lambda^2 < 0.4 \times (M_{\rm LQ}/1\ {\rm TeV})^2$ for V_0 ($\lambda^2 < 0.7 \times (M_{\rm LQ}/1\ {\rm TeV})^2$ for S_0, and $\lambda^2 < 0.5 \times (M_{\rm LQ}/1\ {\rm TeV})^2$ for V_0) can be derived from the limits listed in Ref. [22]. Here λ and $M_{\rm LQ}$ denote the LQ coupling strength and the LQ mass, respectively. See also Refs. [23,24] for earlier studies. The e^+e^- collider experiments are sensitive to the indirect effects coming from t- and u-channel exchanges of LQs in the $e^+e^- \to q\bar{q}$ process. The HERA experiments give bounds on the LQ-induced two-quark two-lepton interaction. It should also be stressed that the measurements of the high-mass Drell-Yan (DY) cross sections, $pp \to \ell\nu$ and $pp \to \ell^+\ell^-$, and low energy neutrino-nucleus coherent scattering measurements [25] are also sensitive to these LQ-induced interactions. NLO QCD corrections to the neutral DY process have been computed in the context of LQ models in Refs. [26,27]. For detailed bounds obtained in this way, see *e.g.,* Ref. [21], and the Heavy Boson Particle Listings under "Indirect Limits for Leptoquarks", and the references therein.

The two-quark two-lepton interactions arising from the LQ exchanges in Eq.(93.1) and Eq.(93.2) can also be interpreted as contributions to more general dimension-six operators within the framework of the SM Effective Field Theory (SMEFT). See *e.g.,* Refs. [28, 29] for reviews. A complete catalog of SM gauge-invariant dimension-six operators can be found in Refs. [30,31]. A computation of the one-loop anomalous dimension matrix for SMEFT operators are found in Refs. [32–34]. LQ-induced two-quark two-lepton interactions may cause the lepton flavor non-universality in the heavy quark decays. In particular, models with TeV-scale LQs may accommodate solutions to the $R(D)$ and $R(D^*)$ anomaly [13] observed in the semi-leptonic $b \to c$ decays.

Collider experiments provide direct limits on the LQ states through limits on the pair- and single-production cross sections. Among these, constraints on single-production often yield limits severer than those on pair-production. This is because, when particles colliding in the collider interact directly and strongly enough with heavy LQ particles, the energy required for the LQ production is lower in the single-production processes. Conversely, if the direct interaction between the colliding particles and LQs is weak, constraints from pair-production processes become more relevant.

LQs are produced singly in ep collisions through

$$e + q \to {\rm LQ}\,, \tag{93.3}$$

and at hadron colliders through [35],

$$g + q \to {\rm LQ} + \ell\,. \tag{93.4}$$

Depending on the LQ coupling with $q\ell$, the LQ single-production process (93.4) allows extending the mass reach higher than the

Int. J. Mod. Phys. A 2026.41. Downloaded from www.worldscientific.com
by UNIVERSITY OF CALIFORNIA @ BERKELEY on 09/16/26. Re-use and distribution is strictly not permitted, except for Open Access articles.

Table 93.1: Possible leptoquarks (LQs) and their quantum numbers.

Spin	$3B+L$	$SU(3)_C$	$SU(2)_W$	$U(1)_Y$	Allowed coupling
0	-2	3	1	1/3	$\bar{q}^c_L \ell_L$ or $\bar{u}^c_R e_R$
0	-2	$\bar{3}$	1	4/3	$\bar{d}^c_R e_R$
0	-2	$\bar{3}$	3	1/3	$\bar{q}^c_L \ell_L$
1	-2	$\bar{3}$	2	5/6	$\bar{q}^c_L \gamma^\mu e_R$ or $\bar{d}^c_R \gamma^\mu \ell_L$
1	-2	$\bar{3}$	2	$-1/6$	$\bar{u}^c_R \gamma^\mu \ell_L$
0	0	3	2	7/6	$\bar{q}_L e_R$ or $\bar{u}_R \ell_L$
0	0	3	2	1/6	$\bar{d}_R \ell_L$
1	0	3	1	2/3	$\bar{q}_L \gamma^\mu \ell_L$ or $\bar{d}_R \gamma^\mu e_R$
1	0	3	1	5/3	$\bar{u}_R \gamma^\mu e_R$
1	0	3	3	2/3	$\bar{q}_L \gamma^\mu \ell_L$

mass reach of the pair-production process [36]. The NLO computations for the single-production of the scalar LQ states at the LHC energies have been performed in Refs. [37–40]. Since protons contain leptons inside, it is possible to target lepton-induced processes (93.3) at high energy pp colliders. For a scalar LQ, the leading-order single-production cross section of the parton process (93.3) may be written as

$$\hat{\sigma}_{\rm LO}\left[eq \to {\rm LQ}\right] = \frac{\pi\lambda^2}{4}\delta(\hat{s} - M^2_{\rm LQ})\,. \tag{93.5}$$

The LQ Yukawa coupling is denoted by λ. The single LQ production cross sections induced from the lepton-quark collisions at the LHC have been computed at LO in Refs. [41–43] and at NLO in Ref. [44]. Ref. [45] performed searches for the LQ states produced in lepton-quark collisions at the LHC.

Pair-production of LQs has been studied at LHC, Tevatron and LEP. The LQ pair-production cross sections in e^+e^- collisions depend on the LQ $SU(2)_W \times U(1)_Y$ quantum numbers and Yukawa coupling with electron [46]. For a scalar LQ, the leading-order pair-production cross sections of the parton processes at hadron colliders

$$\begin{aligned} q + \bar{q} &\to {\rm LQ} + \overline{\rm LQ} \\ g + g &\to {\rm LQ} + \overline{\rm LQ} \end{aligned} \tag{93.6}$$

may be written as [47]

$$\begin{aligned} \hat{\sigma}_{\rm LO}\left[q\bar{q} \to {\rm LQ} + \overline{\rm LQ}\right] &= \frac{2\alpha_s^2\pi}{27\hat{s}}\beta^3, \\ \hat{\sigma}_{\rm LO}\left[gg \to {\rm LQ} + \overline{\rm LQ}\right] &= \frac{\alpha_s^2\pi}{96\hat{s}}\times \\ &\left[\beta(41 - 31\beta^2) + (18\beta^2 - \beta^4 - 17)\log\frac{1+\beta}{1-\beta}\right]. \end{aligned} \tag{93.7}$$

Here $\sqrt{\hat{s}}$ is the invariant energy of the parton subprocess, and $\beta \equiv \sqrt{1 - 4M^2_{\rm LQ}/\hat{s}}$. The QCD gauge coupling is given by

$$\alpha_s \equiv \frac{g_s^2}{4\pi}\,. \tag{93.8}$$

The cross sections of the pair-productions of scalar LQs in pp collisions at the LHC energies have been computed in Refs. [48,49] at the next-to-leading order (NLO) in QCD. The gauge couplings of a scalar LQ are determined uniquely according to its quantum numbers in Table 93.1. Since all of the LQ states belong to color-triplet representation, the QCD-induced scalar LQ pair-production cross section at the Tevatron and LHC can be determined solely as a function of the LQ mass without making further assumptions if we are able to neglect contributions from electroweak and Yukawa interactions in the parton cross sections. This is in contrast to the indirect or single-production limits, which give constraints in the LQ mass-coupling plane.

Vector LQ pair-production calculation often violate perturbative unitarity at high energies. Ultraviolet (UV) completion is required, either via extending gauge symmetries (treating vector LQs as gauge bosons) or compositeness (treating them as bound states). Additional heavy particles are typically introduced in both scenarios. Magnetic-dipole and electric-quadrupole interactions of vector LQs are not fixed by gauge quantum numbers [50]. LHC searches often assume gluon-mediated diagrams dominate near threshold, with two benchmark chromomagnetic dipole moments: Yang-Mills case ($\kappa = 1$) and minimal-coupling case ($\kappa = 0$).

Due to the typical decay of the LQ into charged and neutral leptons and quarks, the searches for the LQ states in collider experiments are carried on in signatures including high p_T charged leptons, high E_T jets and large missing transverse energy. Additionally, searches for pair-produced LQs are often organized by the decay mode of the pair of LQs, via the decay parameter β, which represents the branching fraction into a charged lepton vs a neutrino: $\beta = 1$ for LQs decaying into a charged lepton with 100% branching fraction, $\beta = 0.5$ for LQs decaying into a charged lepton with 50% branching fraction. It is worth noting that organizing LQs by flavor quantum number first before organizing them by gauge quantum number is becoming more common and advantageous because it relates more closely to some of the experimental searches being performed at the hadron colliders. See Ref. [21] for a comprehensive review on the LQ phenomenology in precision experiments and particle colliders.

Since the previous versions of this review, both ATLAS and CMS continue to update their results concerning searches for pair-productions of first, second, and third generation LQs and LQ states which couple only with the i-th generation quarks and the j-th generation leptons ($i \neq j$) without causing conflicts with severe indirect constraints. The datasets were almost all collected at center of mass energy of 13 TeV and corresponding to the latest integrated luminosity collected before the shutdown of the LHC occurring in 2019 and 2020. Older results from the Tevatron run can be found here: [51–54].

Current results extend previous mass limits for scalar LQs to $>$ 1435 GeV (first generation, CMS, $\beta = 1$, $\sqrt{s} = 13$ TeV) and $>$ 1270 GeV (first generation, CMS, $\beta = 0.5$, $\sqrt{s} = 13$ TeV) [55]; $>$ 1800 GeV (first generation, ATLAS, $\beta = 1$, $\sqrt{s} = 13$ TeV) [56] and $>$ 1290 GeV (first generation, ATLAS, $\beta = 0.5$, $\sqrt{s} = 13$ TeV) [57]; $>$ 1530 GeV (second generation, CMS, $\beta = 1$, $\sqrt{s} = 13$ TeV) and $>$ 1285 GeV (second generation, CMS, $\beta = 0.5$, $\sqrt{s} = 13$ TeV) [58]; and $>$ 1700 GeV (second generation, ATLAS, $\beta = 1$, $\sqrt{s} = 13$ TeV) [56] and $>$ 1230 GeV (second generation, ATLAS, $\beta = 0.5$, $\sqrt{s} = 13$ TeV) [57]. All limits are presented at 95% confidence level (C.L.).

As for third generation LQs, CMS results are the following: 1) assuming that all LQs decay to a top quark and a τ lepton, the existence of pair-produced, third-generation LQ up to a mass of 1120 GeV ($\beta = 1$, $\sqrt{s} = 13$ TeV) is excluded at 95% C.L. [59]; 2) assuming that all LQs decay to a bottom quark and a τ lepton, the existence of pair-produced, third-generation LQ up to a mass of 1020 GeV ($\beta = 1$, $\sqrt{s} = 13$ TeV) is excluded at 95% C.L. [60]; 3) assuming that all LQs decay to a bottom quark and a τ neutrino, the existence of pair-produced, third-generation LQ up to a mass of 1185 GeV ($\beta = 0$, $\sqrt{s} = 13$ TeV) is excluded at 95% C.L. [61]. In [62] signatures of $t\tau\nu b$ and $t\tau\nu$ were analyzed in the context of searches for scalar LQ of charge $(-1/3)e$ coupling to $t\tau$ or $b\nu$, or a vector particle of charge $(2/3)e$, coupling to $t\nu$ or $b\tau$. These choices are motivated by models that can explain a series

Int. J. Mod. Phys. A 2026.41. Downloaded from www.worldscientific.com
by UNIVERSITY OF CALIFORNIA @ BERKELEY on 09/16/26. Re-use and distribution is strictly not permitted, except for Open Access articles.

of anomalies observed in the measurement of B meson decays. The data are found to be in agreement with the SM prediction. Lower limits at 95% C.L. are set on the LQ mass in the range 0.98–1.73 TeV, depending on the LQ spin and its coupling λ to a lepton and a quark, and assuming equal couplings for the two LQ decay modes considered.

In [63] ATLAS present the result of searches for pair-production of third-generation scalar LQs decaying into a top quark and a τ-lepton, using 139 fb^{-1} of data collected at 13 TeV. Scalar LQs decaying exclusively into tτ are excluded up to masses of 1.43 TeV while, for a branching fraction of 50% into tτ , the lower mass limit is 1.22 TeV. In [64] and [65] ATLAS searched for pair-produced scalar or vector LQs decaying into a b-quark and a τ-lepton. Scalar LQ masses below 1.46 TeV are excluded assuming a 100% branching ratio, while for vector LQs the corresponding limit is 1.91 TeV (1.65 TeV) in the Yang–Mills $\kappa = 1$ (minimal-coupling $\kappa = 0$) scenario. Additionally, a search for pair-production of LQs with decays into third-generation leptons and quarks in final states with hadronically decaying τ leptons, b-jets, and missing transverse momentum was performed in [66]: depending on the branching fraction into charged leptons, LQs with masses up to around 1.25 TeV can be excluded at the 95% C.L. for the case of scalar LQs and up to 1.8 TeV (1.5 TeV) for vector LQs in a Yang–Mills (minimal-coupling) scenario.

As we explained before, the LQ models which couples only to quarks of the i-th generation and leptons of the j-th generation ($i \neq j$) are attracting attention. In this framework, in [67] and [59] CMS presents a search for pair-production of LQs coupled to a top quark and a leptons. As no deviation from the SM prediction was observed, scalar LQs decaying exclusively into top quark and lepton are excluded below $1.12 - 1.42$ TeV depending on the lepton flavor. In [68] ATLAS conducted a search for pair-production of LQs, each decaying into first and second generation leptons and a third generation quarks. This is part of LQ search using ATLAS data to investigate cross- generational couplings. All possible decays of the pair-produced LQs into quarks of the third generation and charged or neutral leptons of the first or second generation with exactly one electron or muon in the final state are investigated. No significant deviations from the SM expectation are observed. Upper limits on the production cross-section are provided for different models as a function of the LQ mass and the branching ratio of the LQ into the charged or neutral lepton. Some of these models have the goal of providing an explanation for the recent B-anomalies. In such models, a vector LQ decays into charged and neutral leptons of the second generation with a similar branching fraction. Lower limits of 1.98 TeV (1.71 TeV) are set on the vector leptoquark mass for Yang-Mills (minimal-coupling) scenario with $B(b\mu) = B(t\nu) = 0.5$. In [69] CMS search for pair-production of scalar and vector LQs decaying to μb. Assuming $B(\mu b) = 1$, Scalar LQs with $M_{\rm LQ} < 1.81$ TeV are excluded with 95% C.L.; Vector LQs with $M_{\rm LQ} < 2.46$ TeV (2.12 TeV) are excluded in the Yang-Mills (minimal) coupling scenario. CMS also set limits on the t-channel vector LQ exchange $\tau\tau$ production amplitude [70] and $\tau\nu$ production amplitude [71] in pp collisions at $\sqrt{s} = 13$ TeV. Their limits on the dimensionless vector LQ coupling to $q\tau$ and $q\nu$ range from 1 for $M_{\rm LQ} = 1$ TeV to 6 for $M_{\rm LQ} = 5$ TeV, depending on the scenario. ATLAS search result for pair-production of scalar and vector LQs decaying to te or $t\mu$ have been reported in [72]. Under the assumption of exclusive decays into te ($t\mu$), the lower limit on the scalar LQ mass is at 1.58 TeV (1.59 TeV), on the vector LQ mass with Yang-Mills coupling at 1.95 TeV (1.95 TeV), and on the vector LQ mass with minimal-coupling at 1.67 TeV (1.67 TeV). In [73] ATLAS have reported their results on searches for pair-production of scalar LQ decaying into $c\tau$. LQs with masses below 1.3 TeV are excluded at 95% C.L. when $B(c\tau) = 1$. A statistical combination of ATLAS searches for pair-produced LQs decaying into a third generation quark (t or b) and any charged or neutral lepton has been reported in [74]. The lower limits on the masses of scalar LQs range from 1.23 TeV to 1.73 TeV, depending on the branching ratio, LQ charge and flavor. Limits are also placed on benchmark vector LQ models. The mass limit on the charge $(2/3)e$ vector LQ ranges from 1.84 TeV to 1.98 TeV (from 1.58 TeV to 1.71 TeV) for 50% branching fraction, depending on LQ flavor in the Yang-Mills case $\kappa = 1$ (minimal-coupling case $\kappa = 0$).

Previous search results from CMS for squarks and gluinos have been reinterpreted to constrain models of LQ pair-production [75]. For a vector LQ decaying to $t\nu$ with 50% branching fraction, masses below 1.53 TeV are excluded assuming the Yang-Mills case $\kappa = 1$, or 1.115 TeV in the minimal-coupling case $\kappa = 0$. These results and the ones in [76] were updated in [61] where searches for phenomena beyond the standard model (BSM) were performed using events with hadronic jets and significant transverse momentum imbalance to constrain a range of BSM models including the pair-production of LQs each decaying to a neutrino and a top, bottom, or light-flavor quark.

Searches for first generation LQ singly produced were performed by the HERA experiments. Since the leptoquark single-production cross section depends on its Yukawa coupling, the LQ mass limits from HERA are usually displayed in the mass-coupling plane. For leptoquark Yukawa coupling $\lambda = 0.1$, early ZEUS Collaboration bounds on the first-generation LQ range from 248 to 290 GeV, depending on the LQ species [77]. The ZEUS Collaboration has released a paper [78] where data corresponding to a luminosity of around 1 fb^{-1} have been used in the framework of $eeqq$ contact interactions (CI) to set limits on possible high-energy contributions beyond the SM to electron-quark scattering. The analysis of the ep data has been based on simultaneous fits of parton distribution functions including contributions of Contact Interaction (CI) couplings to ep scattering. Several general CI models and scenarios with heavy leptoquarks were considered. As unambiguous deviations from the SM cannot be established, limits for CI compositeness scales and LQ mass scales were set that are in the TeV range. The H1 Collaboration has a comprehensive summary of searches for first generation LQs using the full data sample collected in ep collisions at HERA (446 pb^{-1}). No evidence of production of LQs was observed in final states with a large transverse momentum electron or large missing transverse momentum. For a coupling strength $\lambda = 0.3$, first generation leptoquarks with masses up to 800 GeV are excluded at 95% C.L. [79].

At the LHC, the CMS collaboration performed searches for single-production of first and second generation LQs [80], which is complementary to the HERA searches in the high λ region (for coupling strength $\lambda = 1.0$, first generation leptoquarks are excluded for masses up to 1.73 TeV and second generation leptoquark are excluded up to masses of 530 GeV). CMS also searched for third generation LQ decaying into τ and bottom in [81]. Assuming unit Yukawa coupling (λ), a third generation scalar LQ is excluded for masses below 740 GeV. Limits are also set on λ of the hypothesized LQ as a function of its mass. Above $\lambda = 1.4$, the results provide the best upper limit on the mass of a third-generation scalar LQ decaying to a τ lepton and a bottom quark. In [82] a CMS search is presented for a LQ coupled exclusively to $b\tau$. Events with τ and a varying number of jets originating from b are considered, targeting the single- and pair-production of LQs, as well as non-resonant t-channel LQ exchange. An excess is observed and for a benchmark LQ model with $M_{\rm LQ} = 2$ TeV and its coupling with $b\tau$ of 2.5, the excess reaches a local significance of 2.8σ. LQs are excluded below masses of 1.22–1.88 TeV for different LQ models and varying coupling strengths up to 2.5. In [64] and [65] ATLAS searched for single-production of vector LQ with electric charge of $(2/3)e$ and scalar LQ with an electric charge of $(4/3)e$ via bg fusion. For single vector LQ production Two models are considered: the Yang–Mills and Minimal-coupling models. Vector LQs with a mass below 1.58 TeV (1.35 TeV) are excluded in the Yang–Mills (minimal-coupling) scenario, for a LQ coupling of 1.0 and below 2.05 TeV (1.99 TeV) for a LQ coupling of 2.5. scalar LQ masses below 1.28 TeV (1.53 TeV) are excluded for a LQ Yukawa coupling of 1.0 (2.5). Single-production of a multigenerational scalar LQ has also been searched by ATLAS in [83] via charged-lepton-flavor-violating process. In [45] CMS search results for scalar LQ singly produced via quark-τ fusion have been reported.

Searches for LQ will continue with more LHC data, particularly in light of the renewed interest in this type of particle to explain violation of lepton flavor universality and other anomalies, which

point to explanations laying outside the Standard Model.

References

[1] W. Buchmuller, R. Ruckl and D. Wyler, Phys. Lett. B **191**, 442 (1987), [Erratum: Phys.Lett.B 448, 320–320 (1999)].

[2] K. Babu, C. F. Kolda and J. March-Russell, Phys. Lett. B **408**, 261 (1997), [hep-ph/9705414].

[3] J. L. Hewett and T. G. Rizzo, Phys. Rev. D **58**, 055005 (1998), [hep-ph/9708419].

[4] J. C. Pati and A. Salam, Phys. Rev. D **10**, 275 (1974), [Erratum: Phys.Rev.D 11, 703–703 (1975)].

[5] H. Georgi and S. Glashow, Phys. Rev. Lett. **32**, 438 (1974).

[6] H. Georgi, AIP Conf. Proc. **23**, 575 (1975); H. Fritzsch and P. Minkowski, Annals Phys. **93**, 193 (1975).

[7] H. Murayama and T. Yanagida, Mod. Phys. Lett. A **7**, 147 (1992).

[8] G. R. Farrar and P. Fayet, Phys. Lett. B **76**, 575 (1978).

[9] R. Barbier *et al.*, Phys. Rept. **420**, 1 (2005), [hep-ph/0406039].

[10] For a review, see, E. Farhi and L. Susskind, Phys. Rept. **74**, 277 (1981).

[11] K. D. Lane and M. Ramana, Phys. Rev. D **44**, 2678 (1991).

[12] See, for example, B. Schrempp and F. Schrempp, Phys. Lett. **153B**, 101 (1985).

[13] S. Banerjee *et al.* (Heavy Flavor Averaging Group (HFLAV)) (2024), updated results and plots available at `https://hflav.web.cern.ch/`, [arXiv:2411.18639].

[14] O. U. Shanker, Nucl. Phys. B **204**, 375 (1982).

[15] U. Mahanta, Eur. Phys. J. C **21**, 171 (2001), [hep-ph/0102176].

[16] K.-M. Cheung, Phys. Rev. D **64**, 033001 (2001), [hep-ph/0102238].

[17] B. Diaz, M. Schmaltz and Y.-M. Zhong, JHEP **10**, 097 (2017), [arXiv:1706.05033].

[18] M. Schmaltz and Y.-M. Zhong, JHEP **01**, 132 (2019), [arXiv:1810.10017].

[19] D. Müller, EPJ Web Conf. **179**, 01015 (2018), [arXiv:1801.03380].

[20] M. Carpentier and S. Davidson, Eur. Phys. J. C **70**, 1071 (2010), [arXiv:1008.0280].

[21] I. Doršner *et al.*, Phys. Rept. **641**, 1 (2016), [arXiv:1603.04993].

[22] S. Davidson and A. Saporta, Phys. Rev. D **99**, 1, 015032 (2019), [arXiv:1807.10288].

[23] S. Davidson, D. C. Bailey and B. A. Campbell, Z. Phys. C **61**, 613 (1994), [hep-ph/9309310].

[24] M. Leurer, Phys. Rev. D **49**, 333 (1994), [hep-ph/9309266]; M. Leurer, Phys. Rev. D **50**, 536 (1994), [hep-ph/9312341].

[25] R. Calabrese *et al.*, Phys. Rev. D **107**, 5, 055039 (2023), [arXiv:2212.11210].

[26] U. Haisch, L. Schnell and S. Schulte, JHEP **11**, 106 (2022), [arXiv:2207.00356].

[27] U. Haisch, L. Schnell and S. Schulte, JHEP **02**, 070 (2023), [arXiv:2209.12780].

[28] I. Brivio and M. Trott, Phys. Rept. **793**, 1 (2019), [arXiv:1706.08945].

[29] G. Isidori, F. Wilsch and D. Wyler, Rev. Mod. Phys. **96**, 1, 015006 (2024), [arXiv:2303.16922].

[30] W. Buchmuller and D. Wyler, Nucl. Phys. B **268**, 621 (1986).

[31] B. Grzadkowski *et al.*, JHEP **10**, 085 (2010), [arXiv:1008.4884].

[32] E. E. Jenkins, A. V. Manohar and M. Trott, JHEP **10**, 087 (2013), [arXiv:1308.2627].

[33] E. E. Jenkins, A. V. Manohar and M. Trott, JHEP **01**, 035 (2014), [arXiv:1310.4838].

[34] R. Alonso *et al.*, JHEP **04**, 159 (2014), [arXiv:1312.2014].

[35] J. Hewett and S. Pakvasa, Phys. Rev. D **37**, 3165 (1988); O. J. Eboli and A. V. Olinto, Phys. Rev. D **38**, 3461 (1988); A. Dobado, M. J. Herrero and C. Munoz, Phys. Lett. B **207**, 97 (1988); V. D. Barger *et al.*, Phys. Lett. B **220**, 464 (1989); M. De Montigny and L. Marleau, Phys. Rev. D **40**, 2869 (1989), [Erratum: Phys.Rev.D 56, 3156 (1997)].

[36] A. Belyaev *et al.*, JHEP **09**, 005 (2005), [hep-ph/0502067].

[37] A. Alves, O. Eboli and T. Plehn, Phys. Lett. B **558**, 165 (2003), [hep-ph/0211441].

[38] T. Mandal, S. Mitra and S. Seth, JHEP **07**, 028 (2015), [arXiv:1503.04689].

[39] J. B. Hammett and D. A. Ross, JHEP **07**, 148 (2015), [arXiv:1501.06719].

[40] I. Doršner and A. Greljo, JHEP **05**, 126 (2018), [arXiv:1801.07641].

[41] L. Buonocore *et al.*, Phys. Rev. Lett. **125**, 23, 231804 (2020), [arXiv:2005.06475].

[42] L. Buonocore *et al.*, JHEP **08**, 08, 019 (2020), [arXiv:2005.06477].

[43] A. Greljo and N. Selimovic, JHEP **03**, 279 (2021), [arXiv:2012.02092].

[44] L. Buonocore *et al.*, JHEP **11**, 129 (2022), [arXiv:2209.02599].

[45] A. Hayrapetyan *et al.* (CMS), Phys. Rev. Lett. **132**, 6, 061801 (2024), [arXiv:2308.06143].

[46] J. Blumlein and R. Ruckl, Phys. Lett. B **304**, 337 (1993).

[47] T. Plehn *et al.*, Z. Phys. C **74**, 611 (1997), [hep-ph/9703433]; M. Kramer *et al.*, Phys. Rev. Lett. **79**, 341 (1997), [hep-ph/9704322].

[48] M. Kramer *et al.*, Phys. Rev. D **71**, 057503 (2005), [hep-ph/0411038].

[49] T. Mandal, S. Mitra and S. Seth, Phys. Rev. D **93**, 3, 035018 (2016), [arXiv:1506.07369].

[50] J. Blumlein, E. Boos and A. Kryukov, Z. Phys. C **76**, 137 (1997), [hep-ph/9610408].

[51] V. Abazov *et al.* (D0), Phys. Lett. B **681**, 224 (2009), [arXiv:0907.1048].

[52] A. Abulencia *et al.* (CDF), Phys. Rev. D **73**, 051102 (2006), [hep-ex/0512055].

[53] V. Abazov *et al.* (D0), Phys. Lett. B **671**, 224 (2009), [arXiv:0808.4023].

[54] V. M. Abazov *et al.* (D0), Phys. Lett. B **693**, 95 (2010), [arXiv:1005.2222].

[55] A. M. Sirunyan *et al.* (CMS), Phys. Rev. D **99**, 5, 052002 (2019), [arXiv:1811.01197].

[56] G. Aad *et al.* (ATLAS), JHEP **10**, 112 (2020), [arXiv:2006.05872].

[57] M. Aaboud *et al.* (ATLAS), Eur. Phys. J. C **79**, 9, 733 (2019), [arXiv:1902.00377].

[58] A. M. Sirunyan *et al.* (CMS), Phys. Rev. D **99**, 3, 032014 (2019), [arXiv:1808.05082].

[59] A. Tumasyan *et al.* (CMS), Phys. Rev. D **105**, 11, 112007 (2022), [arXiv:2202.08676].

[60] A. M. Sirunyan *et al.* (CMS), JHEP **03**, 170 (2019), [arXiv:1811.00806].

[61] A. M. Sirunyan *et al.* (CMS), Eur. Phys. J. C **80**, 1, 3 (2020), [arXiv:1909.03460].

[62] A. M. Sirunyan *et al.* (CMS), Phys. Lett. B **819**, 136446 (2021), [arXiv:2012.04178].

[63] G. Aad *et al.* (ATLAS), JHEP **06**, 179 (2021), [arXiv:2101.11582].

[64] G. Aad *et al.* (ATLAS), Eur. Phys. J. C **83**, 11, 1075 (2023), [arXiv:2303.01294].

Int. J. Mod. Phys. A 2026.41. Downloaded from www.worldscientific.com by UNIVERSITY OF CALIFORNIA @ BERKELEY on 09/16/26. Re-use and distribution is strictly not permitted, except for Open Access articles.

[65] G. Aad *et al.* (ATLAS), JHEP **10**, 001 (2023), [arXiv:2305.15962].

[66] G. Aad *et al.* (ATLAS), Phys. Rev. D **104**, 11, 112005 (2021), [arXiv:2108.07665].

[67] A. M. Sirunyan *et al.* (CMS), Phys. Rev. Lett. **121**, 24, 241802 (2018), [arXiv:1809.05558].

[68] G. Aad *et al.* (ATLAS), JHEP **2306**, 188 (2023), [arXiv:2210.04517].

[69] A. Hayrapetyan *et al.* (CMS), Phys. Rev. D **109**, 11, 112003 (2024), [arXiv:2402.08668].

[70] A. Tumasyan *et al.* (CMS), JHEP **07**, 073 (2023), [arXiv:2208.02717].

[71] A. Tumasyan *et al.* (CMS), JHEP **09**, 051 (2023), [arXiv:2212.12604].

[72] G. Aad *et al.* (ATLAS), Eur. Phys. J. C **84**, 8, 818 (2024), [arXiv:2306.17642].

[73] G. Aad *et al.* (ATLAS), JHEP **06**, 199 (2023), [arXiv:2303.09444].

[74] G. Aad *et al.* (ATLAS), Phys. Lett. B **854**, 138736 (2024), [arXiv:2401.11928].

[75] A. M. Sirunyan *et al.* (CMS), Phys. Rev. D **98**, 3, 032005 (2018), [arXiv:1805.10228].

[76] S. Chatrchyan *et al.* (CMS), JHEP **12**, 055 (2012), [arXiv:1210.5627].

[77] S. Chekanov *et al.* (ZEUS), Phys. Rev. D **68**, 052004 (2003), [hep-ex/0304008].

[78] H. Abramowicz *et al.* (ZEUS), Phys. Rev. D **99**, 9, 092006 (2019), [arXiv:1902.03048].

[79] F. Aaron *et al.* (H1), Phys. Lett. B **704**, 388 (2011), [arXiv:1107.3716].

[80] V. Khachatryan *et al.* (CMS), Phys. Rev. D **93**, 3, 032005 (2016), [Erratum: Phys.Rev.D 95, 039906 (2017)], [arXiv:1509.03750].

[81] A. Sirunyan *et al.* (CMS), JHEP **07**, 115 (2018), [arXiv:1806.03472].

[82] A. Hayrapetyan *et al.* (CMS), JHEP **05**, 311 (2024), [arXiv:2308.07826].

[83] G. Aad *et al.* (ATLAS), Phys. Rev. D **110**, 1, 012014 (2024), [arXiv:2403.06742].

Int. J. Mod. Phys. A 2026.41. Downloaded from www.worldscientific.com
by UNIVERSITY OF CALIFORNIA @ BERKELEY on 09/16/26. Re-use and distribution is strictly not permitted, except for Open Access articles.

94. Magnetic Monopoles

Revised August 2025 by D. Milstead (Stockholm U.) and E.J. Weinberg (Columbia U.).

94.1 Theory of magnetic monopoles

The symmetry between electric and magnetic fields in the source-free Maxwell's equations naturally suggests that electric charges might have magnetic counterparts, known as magnetic monopoles. Although the greatest interest has been in the supermassive monopoles that are a firm prediction of all grand unified theories, one cannot exclude the possibility of lighter monopoles.

In either case, the magnetic charge is constrained by a quantization condition first found by Dirac [1]. Consider a monopole with magnetic charge Q_M and a Coulomb magnetic field

$$\mathbf{B} = \frac{Q_M}{4\pi}\frac{\hat{\mathbf{r}}}{r^2}\,. \tag{94.1}$$

Any vector potential $\mathbf{A}$ whose curl is equal to $\mathbf{B}$ must be singular along some line running from the origin to spatial infinity. This Dirac string singularity could potentially be detected through the extra phase that the wavefunction of a particle with electric charge Q_E would acquire if it moved along a loop encircling the string. For the string to be unobservable, this phase must be a multiple of 2π. Requiring that this be the case for any pair of electric and magnetic charges gives the condition that all charges be integer multiples of minimum charges $Q_E^{\rm min}$ and $Q_M^{\rm min}$ obeying

$$Q_E^{\rm min} Q_M^{\rm min} = 2\pi\,. \tag{94.2}$$

(For monopoles which also carry an electric charge, called dyons [2], the quantization conditions on their electric charges can be modified. However, the constraints on magnetic charges, as well as those on all purely electric particles, will be unchanged [3].)

Another way to understand this result is to note that the conserved orbital angular momentum of a point electric charge moving in the field of a magnetic monopole has an additional component, with

$$\mathbf{L} = m\mathbf{r}\times\mathbf{v} - \frac{1}{4\pi}Q_E Q_M \hat{\mathbf{r}} \tag{94.3}$$

Requiring the radial component of $\mathbf{L}$ to be quantized in half-integer units yields Eq. 94.2.

If there are unbroken gauge symmetries in addition to the U(1) of electromagnetism, the above analysis must be modified [4, 5]. The allowed color-magnetic charges are determined by the global structure of the gauge group, e.g., $SU(3)\times U(1)$ vs. $(SU(3)\times U(1))/\mathbb{Z}_3$. For example, in QCD the global structure of the gauge group could be $SU(3)\times U(1)$ or $(SU(3)\times U(1))/\mathbb{Z}_3$. In the latter case the magnetic monopole may carry a $\mathbb{Z}_3$-valued color-magnetic charge. While the color-magnetic charge does not lead to a long-range color magnetic field, its existence modifies the phase quantization underlying Eq. 94.2: the color and color-magnetic charges of a quark combine with the $U(1)$ magnetic charge to render the Dirac string unobservable; so that the U(1) charge could be the Dirac charge $Q_M^D \equiv 2\pi/e$, the result that would be obtained by substituting the electron charge into Eq. (94.2). On the other hand, for monopoles without color-magnetic charge, one would simply insert the quark electric charges into Eq. 94.2 and conclude that Q_M must be a multiple of $6\pi/e$. This is the minimal magnetic charge when the gauge group is not modded out by $\mathbb{Z}_3$.

The prediction of GUT monopoles arises from the work of 't Hooft [6] and Polyakov [7], who showed that certain spontaneously broken gauge theories have nonsingular classical solutions that lead to magnetic monopoles in the quantum theory. The simplest example occurs in a theory where the vacuum expectation value of a triplet Higgs field ϕ breaks an SU(2) gauge symmetry down to the U(1) of electromagnetism and gives a mass M_V to two of the gauge bosons. In order to have finite energy, ϕ must approach a vacuum value at infinity. However, there is a continuous family of possible vacua, since the scalar field potential determines only the magnitude v of $\langle\phi\rangle$, but not its orientation in the internal SU(2) space. In the monopole solution, the direction of ϕ in internal space is correlated with the position in physical space; *i.e.*, $\phi^a \sim v\hat{r}^a$. The stability of the solution follows from the fact that this twisting Higgs field cannot be smoothly deformed to a spatially uniform vacuum configuration. Reducing the energetic cost of the spatial variation of ϕ requires a nonzero gauge potential, which turns out to yield the magnetic field corresponding to a charge $Q_M = 4\pi/e$. Numerical solution of the classical field equations shows that the mass of this monopole is

$$M_{\rm mon} \sim \frac{4\pi M_V}{e^2}\,. \tag{94.4}$$

The essential ingredient here was the fact that the Higgs fields at spatial infinity could be arranged in a topologically nontrivial configuration. A discussion of the general conditions under which this is possible is beyond the scope of this review, so we restrict ourselves to the two phenomenologically most important cases.

The first is the standard electroweak theory, with $\mathrm{SU}(2)\times\mathrm{U}(1)$ broken to U(1). There are no topologically nontrivial configurations of the Higgs field, and hence no topologically stable monopole solutions. Although electroweak scale monopoles are thus not required, there have been claims that they might not be ruled out. For example, there have been a variety of proposals in this direction involving modifications of the Lagrangian.

The second case is when any simple Lie group is broken to a subgroup with a U(1) factor, a case that includes all grand unified theories. Here the spectrum of states must include a topologically stable monopole whose mass is determined by the mass scale of the symmetry breaking that allows nontrivial topology. For example, an SU(5) model with

$$\mathrm{SU}(5) \xrightarrow{M_X} (\mathrm{SU}(3)\times\mathrm{SU}(2)\times\mathrm{U}(1))/\mathbb{Z}_6 \xrightarrow{M_W} (\mathrm{SU}(3)\times\mathrm{U}(1))/\mathbb{Z}_6 \tag{94.5}$$

has a monopole [8] with $Q_M = 2\pi/e$ and mass

$$M_{\rm mon} \sim \frac{4\pi M_{\rm X}}{g^2}\,, \tag{94.6}$$

where g is the SU(5) gauge coupling. For a unification scale of 10^{16} GeV, these monopoles would have a mass $M_{\rm mon} \sim 10^{17}$ – 10^{18} GeV.

In theories with several stages of symmetry breaking, monopoles of different mass scales can arise. In an SO(10) theory with

$$\begin{aligned}\mathrm{SO}(10) &\xrightarrow{M_1} (\mathrm{SU}(4)\times\mathrm{SU}(2)\times\mathrm{SU}(2))/\mathbb{Z}_2\\ &\xrightarrow{M_2} (\mathrm{SU}(3)\times\mathrm{SU}(2)\times\mathrm{U}(1))/\mathbb{Z}_6\end{aligned} \tag{94.7}$$

there is monopole with $Q_M = 2\pi/e$ and mass $\sim 4\pi M_1/g^2$ and a much lighter monopole with $Q_M = 4\pi/e$ and mass $\sim 4\pi M_2/g^2$ [9].

The central core of a GUT monopole contains the fields of the superheavy gauge bosons that mediate baryon number violation, so one might expect that baryon number conservation could be violated in baryon–monopole scattering. The surprising feature, pointed out by Callan [10] and Rubakov [11], is that these processes are not suppressed by powers of the gauge boson mass. Instead, the cross-sections for catalysis processes such as $p + \text{monopole} \to e^+ + \pi^0 + \text{monopole}$ are essentially geometric; *i.e.*, $\sigma_{\Delta B}\beta \sim 10^{-27}$ cm^2, where $\beta = v/c$. Note, however, that this catalysis is model-dependent and is not even a universal property of all GUT monopoles.

94.2 Production and Annihilation

GUT monopoles are far too massive to be produced in any foreseeable accelerator. However, they could have been produced in the early Universe as topological defects arising via the Kibble mechanism [12] in a symmetry-breaking phase transition. Estimates of the initial monopole abundance, and of the degree to which it can be reduced by monopole-antimonopole annihilation, predict a present-day monopole abundance that exceeds by many orders of magnitude the astrophysical and experimental bounds described below [13]. Cosmological inflation and other proposed solutions to this primordial monopole problem generically lead to present-day abundances exponentially smaller than could be plausibly detected, although potentially observable abundances can be obtained in scenarios with carefully tuned parameters.

Int. J. Mod. Phys. A 2026.41. Downloaded from www.worldscientific.com by UNIVERSITY OF CALIFORNIA @ BERKELEY on 09/16/26. Re-use and distribution is strictly not permitted, except for Open Access articles.

Int. J. Mod. Phys. A 2026.41. Downloaded from www.worldscientific.com
by UNIVERSITY OF CALIFORNIA @ BERKELEY on 09/16/26. Re-use and distribution is strictly not permitted, except for Open Access articles.

Several theoretical models predict composite magnetic monopole solutions with masses of order of the electroweak scale (for a partial review see Ref. [14]). If monopoles light enough to be produced at colliders exist, one would expect that these could be produced by analogs of the electromagnetic processes that produce pairs of electrically charged particles. Because of the large size of the magnetic charge, this is a strong coupling problem for which perturbation theory cannot be trusted. The Schwinger production of monopole pairs mitigates the problem of the non-perturbative coupling due to the semi-classical calculation of production cross sections [15, 16]. Dyson-Schwinger resummation techniques have also been proposed as a solution to the non-perturbativity [17].

It should also be mentioned that bound monopole-antimonopole states may be formed (monopolium), the mass of which may be in reach at colliders [18, 19].

94.3 Astrophysical and Cosmological Bounds

If there were no galactic magnetic field, one would expect monopoles in the galaxy to have typical velocities of the order of $10^{-3}c$, comparable to the virial velocity in the galaxy (relevant if the monopoles cluster with the galaxy) and the peculiar velocity of the galaxy with respect to the CMB rest frame (relevant if the monopoles are not bound to the galaxy). This situation is modified by the existence of a galactic magnetic field $B \sim 3\mu$G. A monopole with the Dirac charge and mass M would be accelerated by this field to a velocity

$$v_{\rm mag} \sim \begin{cases} c, & M \lesssim 10^{11}{\rm GeV}\,, \\ 10^{-3}c\left(\frac{10^{17}\,{\rm GeV}}{M}\right)^{1/2}, & M \gtrsim 10^{11}{\rm GeV}\,. \end{cases} \tag{94.8}$$

Accelerating these monopoles drains energy from the magnetic field. Parker [20, 21] obtained an upper bound on the flux of monopoles in the galaxy by requiring that the rate of this energy loss be small compared to the time scale on which the galactic field can be regenerated. With reasonable choices for the astrophysical parameters (see Ref. [22] for details), this Parker bound is

$$F < \begin{cases} 10^{-15}\,{\rm cm}^{-2}\,{\rm sr}^{-1}\,{\rm sec}^{-1}\,, & M \lesssim 10^{17}\,{\rm GeV}\,, \\ 10^{-15}\left(\frac{M}{10^{17}\,{\rm GeV}}\right){\rm cm}^{-2}\,{\rm sr}^{-1}\,{\rm sec}^{-1}\,, & M \gtrsim 10^{17}\,{\rm GeV}\,. \end{cases} \tag{94.9}$$

Applying similar arguments to an earlier seed field that was the progenitor of the current galactic field leads to a tighter bound [23],

$$F < \left[\frac{M}{10^{17}{\rm GeV}} + (3\times 10^{-6})\right] 10^{-16}\,{\rm cm}^{-2}{\rm sr}^{-1}{\rm sec}^{-1}. \tag{94.10}$$

Considering magnetic fields in galactic clusters gives a bound [24] which, although less secure, is about three orders of magnitude lower than the Parker bound.

A flux bound can also be inferred from the total mass of monopoles in the Universe. If the monopole mass density is a fraction $\Omega_{\rm M}$ of the critical density, and the monopoles were uniformly distributed throughout the Universe, there would be a monopole flux

$$F_{\rm uniform} = 1.3\times 10^{-16}\Omega_{\rm M}\left(\frac{10^{17}\,{\rm GeV}}{M}\right)\left(\frac{v}{10^{-3}c}\right){\rm cm}^{-2}{\rm sr}^{-1}{\rm sec}^{-1}. \tag{94.11}$$

If we assume that $\Omega_{\rm M} \sim 0.1$, this gives a stronger constraint than the Parker bound for $M \sim 10^{15}$ GeV. However, monopoles with masses $\sim 10^{17}$ GeV are not ejected by the galactic field and can be gravitationally bound to the galaxy. In this case their flux within the galaxy is increased by about five orders of magnitude for a given value of $\Omega_{\rm M}$, and the mass density bound only becomes stronger than the Parker bound for $M \sim 10^{18}$ GeV.

A much more stringent flux bound applies to GUT monopoles that catalyze baryon number violation. The essential idea is that compact astrophysical objects would capture monopoles at a rate proportional to the galactic flux. These monopoles would then catalyze proton decay, with the energy released in the decay leading to an observable increase in the luminosity of the object. A variety of bounds, based on neutron stars [25–29] , white dwarfs [30], and Jovian planets [31] have been obtained. These depend in the obvious manner on the catalysis cross section, but also on the details of the astrophysical scenarios; *e.g.*, on how much the accumulated density is reduced by monopole-antimonopole annihilation, and on whether monopoles accumulated in the progenitor star survive its collapse to a white dwarf or neutron star. The bounds obtained in this manner lie in the range

$$F\left(\frac{\sigma_{\Delta B}\beta}{10^{-27}{\rm cm}^2}\right) \sim (10^{-18} - 10^{-29}){\rm cm}^{-2}{\rm sr}^{-1}{\rm sec}^{-1}. \tag{94.12}$$

It is important to remember that not all GUT monopoles catalyze baryon number nonconservation. In particular, the intermediate mass monopoles that arise in some GUTs at later stages of symmetry-breaking are examples of theoretically motivated monopoles that are exempt from the bound of the above equation.

94.4 Searches for Magnetic Monopoles

To date there have been no confirmed observations of exotic particles possessing magnetic charge. Precision measurements of the properties of known particles have led to tight limits on the values of magnetic charge they may possess. Using the induction method (see below), the electron's magnetic charge has been found to be $Q_e^m < 10^{-24}Q_M^D$ [32]. Furthermore, measurements of the anomalous magnetic moment of the muon have been used to place a model dependent lower limit of 120 GeV on the monopole mass [1] [33]. Nevertheless, guided mainly by Dirac's argument and the predicted existence of monopoles from spontaneous symmetry breaking mechanisms, searches have been routinely made for monopoles produced at accelerators, in cosmic rays, and bound in matter [34]. Although the resultant limits from such searches are usually made under the assumption of a particle possessing only magnetic charge, most of the searches are also sensitive to dyons.

94.5 Search Techniques

Search strategies are determined by the expected interactions of monopoles as they pass through matter. These would give rise to a number of striking characteristic signatures. Since a complete description of monopole search techniques falls outside of the scope of this minireview, only the most common methods are described below. More comprehensive descriptions of search techniques can be found in Refs. [14, 35, 36].

The induction method exploits the long-range electromagnetic interaction of the monopole with the quantum state of a superconducting ring which would lead to a monopole which passes through such a ring inducing a permanent current. The induction technique typically uses Superconducting Quantum Interference Devices (SQUID) technology for detection and is employed for searches for monopoles in cosmic rays and matter. Another approach is to exploit the electromagnetic energy loss of monopoles. Monopoles with Dirac charge would typically lose energy at a rate which is several thousand times larger than that expected from particles possessing the elementary electric charge. Consequently, scintillators, gas chambers and nuclear track detectors (NTDs) have been used in cosmic ray and collider experiments. A further approach, which has been used at colliders, is to search for particles describing a non-helical path in a uniform magnetic field.

94.5.1 *Searches for Monopoles Bound in Matter*

Monopoles have been sought in a range of bulk materials which it is assumed would have absorbed incident cosmic ray monopoles over a long exposure time of order million years. Materials which have been studied include moon rock, meteorites, manganese modules, and sea water [37, 38]. A stringent upper limit on the monopoles per nucleon ratio of $\sim 10^{-29}$ has been obtained [38].

[1] Where no ambiguity is likely to arise, a reference to a monopole implies a particle possessing Dirac charge.

Int. J. Mod. Phys. A 2026.41. Downloaded from www.worldscientific.com
by UNIVERSITY OF CALIFORNIA @ BERKELEY on 09/16/26. Re-use and distribution is strictly not permitted, except for Open Access articles.

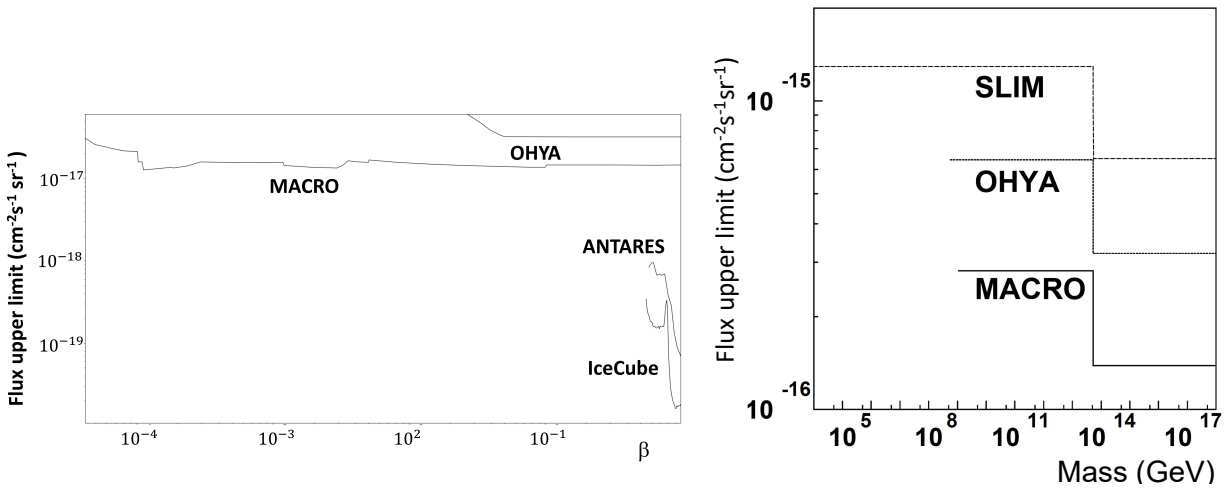

Figure 94.1: Left: upper flux limits for GUT monopoles as a function of β. Right: upper flux limits for monopoles as a function of monopole mass for $\beta > 0.05$.

94.5.2 *Searches in Cosmic Rays*

Direct searches for monopoles in cosmic rays refer to those experiments in which the passage of the monopole is measured by an active detector. Searches made assuming a catalysis processes in which GUT monopoles could induce nucleon decay are discussed in the next section. To interpret the results of the non-catalysis searches, the cross section for the catalysis process is typically either set to zero [39] or assigned a modest value (1mb) [40].

Although early cosmic ray searches using the induction technique [41] and NTDs [42] observed monopole candidates, none of these apparent observations have been confirmed. Recent experiments have typically employed large scale detectors. The MACRO experiment at the Gran Sasso underground laboratory comprised three different types of detector: liquid scintillator, limited stream tubes, and NTDs, which provided a total acceptance of $\sim 10000\text{m}^2$ for an isotropic flux. As shown in Fig. 94.1, this experiment has so far provided the most extensive β-dependent flux limits for GUT monopoles with Dirac charge [40]. Also shown are limits from an experiment at the OHYA mine in Japan [39], which used a 2000m^2 array of NTDs, and from the IceCube [43,44] and Antares [45] experiments which each employ the Cerenkov method.

In Fig. 94.1, upper flux limits are also shown as a function of monopole mass for monopole speed $\beta > 0.05$. In addition to MACRO and OYHA flux limits, results from the SLIM [46] high-altitude experiment are shown. The SLIM experiment provided a good sensitivity to intermediate mass monopoles ($10^5 \lesssim M \lesssim 10^{12}$ GeV).

In addition to the results shown in Fig. 94.1, the NoVA experiment [47] has recently set an upper limit on monopole flux of 2×10^{-14} $\text{cm}^{-2}\text{s}^{-1}\text{sr}^{-1}$ for speeds $6 \times 10^{-4} < \beta < 10^{-3}$ for masses greater thsan 5×10^8 GeV. Stringent constraints on the flux of ultra-relativistic monopoles have been obtained at the Pierre Auger Observatory [48] which was sensitive to monopoles with γ values ranging from 10^9 to 10^{12}, leading to flux limits in the range $10^{-15} - 2.5 \times 10^{-21}$ $\text{cm}^{-2}\text{s}^{-1}\text{sr}^{-1}$. The RICE [49] and ANITA-II experiments [50] at the South Pole have also sought ultra-relativistic monopoles with γ values of $10^7 \lesssim \gamma \lesssim 10^{12}$ and $10^9 \lesssim \gamma \lesssim 10^{13}$, respectively, and which produced flux limits as low as 2.5×10^{-21} $\text{cm}^{-2}\text{s}^{-1}\text{sr}^{-1}$.

94.5.3 *Searches via the Catalysis of Nucleon-Decay*

Searches have been performed for evidence of the catalysed decay of a nucleon by a monopole, as predicted by the Callan-Rubakov mechanism. The searches are thus sensitive to the assumed value of the catalysis decay cross section. Searches have been made with the Soudan [51] and Macro [52] experiments, using tracking detectors. Searches at IMB [53], the underwater Lake Baikal experiment [54,55] and the IceCube experiment [56] which exploit the Cerenkov effect have also been made. The resulting β-dependent flux limits from these experiments typically vary between $\sim 10^{-18}$ and $\sim 10^{-14}\text{cm}^{-2}\text{sr}^{-1}\text{s}^{-1}$. A search for low energy neutrinos (assumed to be produced from induced proton decay in the sun) was made at Super-Kamiokande [57]. A model- and β-dependent limit of $6.3 \times 10^{-24}(\frac{\beta}{10^{-3}})^2\text{cm}^{-2}\text{sr}^{-1}\text{s}^{-1}$ was obtained.

94.5.4 *Searches at Colliders*

Searches have been performed at hadron-hadron, electron-positron and lepton-hadron experiments. Collider searches can be broadly classed as being direct or indirect. In a direct search, evidence of the passage of a monopole through material, such as a charged particle track, is sought. In indirect searches, virtual monopole processes are assumed to influence the production rates of certain final states.

94.5.4.1 *Direct Searches at Colliders*

Collider experiments typically express their results in terms of upper limits on a production cross section and/or monopole mass. To calculate these limits, ansatzes are used to model the kinematics of monopole-antimonopole pair production processes since perturbative field theory cannot be used to calculate the rate and kinematic properties of produced monopoles. Limits therefore suffer from a degree of model-dependence, implying that a comparison between the results of different experiments can be problematic, in particular when this concerns excluded mass regions. A conservative approach with as little model-dependence as possible is thus to present representative values of the upper cross-section limits as a function of the centre-of-mass energy of the collisions, as shown in Fig. 94.2 for recent results from high energy colliders.

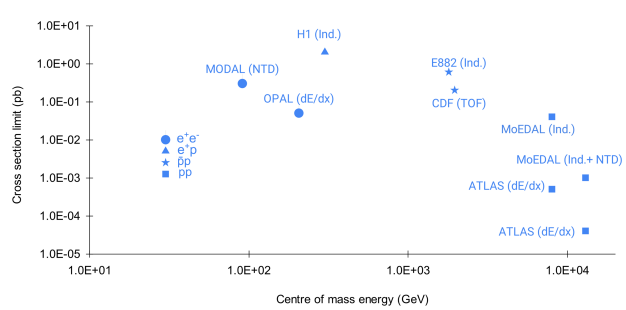

Figure 94.2: Upper limits on the production cross sections of monopoles from various collider-based experiments. Results from positron-proton, electron-positron, proton-antiproton, and proton-proton experiments are shown. The search techniques are also indicated: induction (Ind.), TOF, and $\frac{dE}{dx}$.

Int. J. Mod. Phys. A 2026.41. Downloaded from www.worldscientific.com
by UNIVERSITY OF CALIFORNIA @ BERKELEY on 09/16/26. Re-use and distribution is strictly not permitted, except for Open Access articles.

Searches for monopoles produced at the highest available energies in hadron-hadron collisions were made in *pp* collisions at the LHC by the ATLAS [58–60] and MoEDAL [61–67] experiments, with the latter including the first direct dyon search at the LHC [63]. ATLAS exploited the characteristic monopole energy loss behaviour ($\frac{dE}{dx}$) in the tracker and calorimeter. MoEDAL used a NTD to tag highly ionising particles and the induction method to search for stopped monopoles. The charge-dependent mass limits extend up to around 4 TeV. The ATLAS experiment has considered hypotheses of monopoles with charges between $0.5Q_M^D$ and $2Q_M^D$ while MoEDAL has quoted limits for monopoles in the charge range Q_M^D to $10Q_M^D$. Models considered include monopole-pair production via photon fusion along with, as is commonly used in hadron-hadron collisions, Drell-Yan processes [68]. MoEDAL has also looked for monopole produced via the Schwinger mechanism in the intense magnetic field created in PbPb collisions [65, 67]. A search has also been made by ATLAS with PbPb collisions which also considers the Schwinger mechanism [69]. Tevatron searches have also been carried out by the CDF [70] and E882 [71] experiments. The CDF experiment used a dedicated time-of-flight (TOF) system whereas the E882 experiment employed the induction technique to search for stopped monopoles in discarded detector material which had been part of the CDF and D0 detectors using periods of luminosity. Earlier searches at the Tevatron, such as [72], used NTDs and were based on comparatively modest amounts of integrated luminosity. Lower energy hadron-hadron experiments have employed a variety of search techniques including plastic track detectors [73] and searches for trapped monopoles [74].

The only LEP-2 search, based on the $\frac{dE}{dx}$ method, was made by OPAL [75] which quoted cross section limits for the production of monopoles possessing masses up to around 103 GeV. At LEP-1, searches were made with NTDs deployed around an interaction region. This allowed a range of charges to be sought for masses up to ~ 45 GeV. The MODAL detector [76] gave limits for monopoles with charges in the range $0.9Q_M^D$ and $3.6Q_M^D$, whilst an earlier search by the MODAL was sensitive to monopoles with charges as low as $0.1Q_M^D$ [77]. The deployment of NTDs around the beam interaction point was also used at earlier e^+e^- colliders such as KEK [78] and PETRA [79]. Searches at e^+e^- facilities have also been made for particles following non-helical trajectories [80, 81].

There has so far been one search for monopole production in lepton-hadron scattering. Using the induction method, monopoles were sought which could have stopped in the aluminium beampipe which had been used by the H1 experiment at HERA [82]. Cross section limits were set for monopoles with charges in the range $Q_M^D - 6Q_M^D$ for masses up to around 140 GeV.

94.5.4.2 *Indirect Searches at Colliders*

It has been proposed that virtual monopoles can mediate processes which give rise to multi-photon final-states [83,84]. Photon-based searches were made by the D0 [85] and L3 [86] experiments. The D0 work led to spin-dependent lower mass limits of between 610 and 1580 GeV, while L3 reported a lower mass limit of 510 GeV. Another indirect way to constrain monopoles is via the search for a monopolium (a bound state of a monopole and antimonopole) through multi-photon decays [87]. While there exist theoretical difficulties in estimating uncertainties related to these limits, stringent lower bounds of magnetic monopole masses in theoretical models can be derived (modulo the uncertainties arising due to the large coupling) by means of exploiting [88] the observed light-by-light scattering at the ATLAS [89, 90] and CMS [91, 92] experiments.

References

[1] P. A. M. Dirac, Proc. Roy. Soc. Lond. **A133**, 821, 60 (1931).

[2] J. S. Schwinger, Science **165**, 757 (1969).

[3] K. A. Milton, Rept. Prog. Phys. **69**, 1637 (2006), [hep-ex/0602040].

[4] F. Englert and P. Windey, Phys. Rev. **D14**, 2728 (1976).

[5] P. Goddard, J. Nuyts and D. I. Olive, Nucl. Phys. **B125**, 1 (1977).

[6] G. 't Hooft, Nucl. Phys. **B79**, 276 (1974).

[7] A. M. Polyakov, JETP Lett. **20**, 194 (1974).

[8] C. P. Dokos and T. N. Tomaras, Phys. Rev. **D21**, 2940 (1980).

[9] G. Lazarides and Q. Shafi, Phys. Lett. **94B**, 149 (1980).

[10] C. G. Callan, Jr., Phys. Rev. **D26**, 2058 (1982).

[11] V. A. Rubakov, Nucl. Phys. **B203**, 311 (1982).

[12] T. W. B. Kibble, J. Phys. **A9**, 1387 (1976).

[13] J. Preskill, Phys. Rev. Lett. **43**, 1365 (1979).

[14] N. E. Mavromatos and V. A. Mitsou, Int. J. Mod. Phys. A **35**, 23, 2030012 (2020), [arXiv:2005.05100].

[15] I. K. Affleck and N. S. Manton, Nucl. Phys. B **194**, 38 (1982).

[16] O. Gould and A. Rajantie, Phys. Rev. Lett. **119**, 24, 241601 (2017), [arXiv:1705.07052].

[17] J. Alexandre and N. E. Mavromatos, Phys. Rev. D **100**, 9, 096005 (2019), [arXiv:1906.08738].

[18] C. T. Hill, Nucl. Phys. B **224**, 469 (1983).

[19] L. N. Epele *et al.*, Eur. Phys. J. Plus **127**, 60 (2012), [arXiv:1205.6120].

[20] E. N. Parker, Astrophys. J. **160**, 383 (1970).

[21] D. Perri *et al.*, Phys. Dark Univ. **46**, 101704 (2024), [arXiv:2401.00560].

[22] M. S. Turner, E. N. Parker and T. J. Bogdan, Phys. Rev. **D26**, 1296 (1982).

[23] F. C. Adams *et al.*, Phys. Rev. Lett. **70**, 2511 (1993).

[24] Y. Rephaeli and M. S. Turner, Phys. Lett. **121B**, 115 (1983).

[25] E. W. Kolb, S. A. Colgate and J. A. Harvey, Phys. Rev. Lett. **49**, 1373 (1982).

[26] S. Dimopoulos, J. Preskill and F. Wilczek, Phys. Lett. **119B**, 320 (1982).

[27] K. Freese, M. S. Turner and D. N. Schramm, Phys. Rev. Lett. **51**, 1625 (1983).

[28] E. W. Kolb and M. S. Turner, Astrophys. J. **286**, 702 (1984).

[29] J. A. Harvey, Nucl. Phys. **B236**, 255 (1984).

[30] K. Freese and E. Krasteva, Phys. Rev. **D59**, 063007 (1999), [arXiv:astro-ph/9804148].

[31] J. Arafune, M. Fukugita and S. Yanagita, Phys. Rev. **D32**, 2586 (1985).

[32] L. L. Vant-Hull, Phys. Rev. **173**, 1412 (1968).

[33] S. Graf, A. Schaefer and W. Greiner, Phys. Lett. **B262**, 463 (1991).

[34] Review of Particle Physics 2024 (*this paper*), listing on *Searches for Magnetic Monopoles*.

[35] L. Patrizii and M. Spurio, Ann. Rev. Nucl. Part. Sci. **65**, 279 (2015), [arXiv:1510.07125].

[36] M. Fairbairn *et al.*, Phys. Rept. **438**, 1 (2007), [hep-ph/0611040].

[37] J. M. Kovalik and J. L. Kirschvink, Phys. Rev. **A33**, 1183 (1986).

[38] H. Jeon and M. J. Longo, Phys. Rev. Lett. **75**, 1443 (1995), [Erratum: Phys. Rev. Lett.76,159(1996)], [hep-ex/9508003].

[39] S. Orito *et al.*, Phys. Rev. Lett. **66**, 1951 (1991).

[40] M. Ambrosio *et al.* (MACRO), Eur. Phys. J. **C25**, 511 (2002), [hep-ex/0207020].

[41] B. Cabrera, Phys. Rev. Lett. **48**, 1378 (1982).

[42] P. B. Price *et al.*, Phys. Rev. Lett. **35**, 487 (1975).

[43] M. G. Aartsen *et al.* (IceCube), Eur. Phys. J. **C76**, 3, 133 (2016), [arXiv:1511.01350].

[44] R. Abbasi *et al.* (IceCube), Phys. Rev. Lett. **128**, 5, 051101 (2022), [arXiv:2109.13719].

[45] A. Albert *et al.* (ANTARES), JHEAp **34**, 1 (2022), [arXiv:2202.13786].

[46] S. Balestra *et al.*, Eur. Phys. J. **C55**, 57 (2008), [arXiv:0801.4913].

[47] M. A. Acero *et al.* (NOvA), Phys. Rev. D **103**, 1, 012007 (2021), [arXiv:2009.04867].

[48] A. Aab *et al.* (Pierre Auger), Phys. Rev. **D94**, 8, 082002 (2016), [arXiv:1609.04451].

[49] D. P. Hogan *et al.*, Phys. Rev. **D78**, 075031 (2008), [arXiv:0806.2129].

[50] M. Detrixhe *et al.* (ANITA-II), Phys. Rev. **D83**, 023513 (2011), [arXiv:1008.1282].

[51] J. E. Bartelt *et al.*, Phys. Rev. D **36**, 1990 (1987), [Erratum: Phys.Rev.D 40, 1701 (1989)].

[52] M. Ambrosio *et al.* (MACRO), Eur. Phys. J. **C26**, 163 (2002), [hep-ex/0207024].

[53] R. Becker-Szendy *et al.*, Phys. Rev. **D49**, 2169 (1994).

[54] V. A. Balkanov *et al.* (Baikal), Prog. Part. Nucl. Phys. **40**, 391 (1998), [arXiv:astro-ph/9801044].

[55] O. N. Gaponenko, Phys. At. Nucl. **84**, 3, 287 (2021).

[56] M. G. Aartsen *et al.* (IceCube), Eur. Phys. J. C **74**, 7, 2938 (2014), [Erratum: Eur.Phys.J.C 79, 124 (2019)], [arXiv:1402.3460].

[57] K. Ueno *et al.* (Super-Kamiokande), Astropart. Phys. **36**, 131 (2012), [arXiv:1203.0940].

[58] G. Aad *et al.* (ATLAS), Phys. Rev. **D93**, 5, 052009 (2016), [arXiv:1509.08059].

[59] G. Aad *et al.* (ATLAS), Phys. Rev. Lett. **124**, 3, 031802 (2020), [arXiv:1905.10130].

[60] G. Aad *et al.* (ATLAS), JHEP **11**, 112 (2023), [arXiv:2308.04835].

[61] B. Acharya *et al.* (MoEDAL), Phys. Rev. Lett. **118**, 6, 061801 (2017), [arXiv:1611.06817].

[62] B. Acharya *et al.* (MoEDAL), Phys. Rev. Lett. **123**, 2, 021802 (2019), [arXiv:1903.08491].

[63] B. Acharya *et al.* (MoEDAL), Phys. Rev. Lett. **126**, 7, 071801 (2021), [Erratum: Phys.Rev.Lett. 133, 239902 (2024)], [arXiv:2002.00861].

[64] B. Acharya *et al.* (MoEDAL), Eur. Phys. J. C **82**, 8, 694 (2022), [arXiv:2112.05806].

[65] B. Acharya *et al.* (MoEDAL), Nature **602**, 7895, 63 (2022), [arXiv:2106.11933].

[66] B. Acharya *et al.* (MoEDAL), Phys. Rev. Lett. **134**, 7, 071802 (2025), [arXiv:2311.06509].

[67] B. Acharya *et al.* (MoEDAL), Phys. Rev. Lett. **133**, 7, 071803 (2024), [arXiv:2402.15682].

[68] S. Baines *et al.*, Eur. Phys. J. **C78**, 11, 966 (2018), [Erratum: Eur. Phys. J.C79,no.2,166(2019)], [arXiv:1808.08942].

[69] G. Aad *et al.* (ATLAS), Phys. Rev. Lett. **134**, 6, 061803 (2025), [arXiv:2408.11035].

[70] A. Abulencia *et al.* (CDF), Phys. Rev. Lett. **96**, 201801 (2006), [hep-ex/0509015].

[71] G. R. Kalbfleisch *et al.*, Phys. Rev. **D69**, 052002 (2004), [hep-ex/0306045].

[72] P. B. Price, G.-X. Ren and K. Kinoshita, Phys. Rev. Lett. **59**, 2523 (1987).

[73] B. Aubert *et al.*, Phys. Lett. **120B**, 465 (1983).

[74] R. A. Carrigan, F. A. Nezrick and B. P. Strauss, Phys. Rev. **D8**, 3717 (1973).

[75] G. Abbiendi *et al.* (OPAL), Phys. Lett. **B663**, 37 (2008), [arXiv:0707.0404].

[76] J. L. Pinfold *et al.*, Phys. Lett. **B316**, 407 (1993).

[77] K. Kinoshita *et al.*, Phys. Rev. **D46**, R881 (1992).

[78] K. Kinoshita *et al.*, Phys. Lett. **B228**, 543 (1989).

[79] P. Musset, M. Price and E. Lohrmann, Phys. Lett. **128B**, 333 (1983).

[80] T. Gentile *et al.* (CLEO), Phys. Rev. **D35**, 1081 (1987).

[81] W. Braunschweig *et al.* (TASSO), Z. Phys. **C38**, 543 (1988).

[82] A. Aktas *et al.* (H1), Eur. Phys. J. **C41**, 133 (2005), [hep-ex/0501039].

[83] A. De Rujula, Nucl. Phys. **B435**, 257 (1995), [hep-th/9405191].

[84] I. F. Ginzburg and A. Schiller, Phys. Rev. **D60**, 075016 (1999), [hep-ph/9903314].

[85] B. Abbott *et al.* (D0), Phys. Rev. Lett. **81**, 524 (1998), [hep-ex/9803023].

[86] M. Acciarri *et al.* (L3), Phys. Lett. **B345**, 609 (1995).

[87] N. D. Barrie *et al.*, Nucl. Phys. B **972**, 115564 (2021), [arXiv:2104.06931].

[88] J. Ellis, N. E. Mavromatos and T. You, Phys. Rev. Lett. **118**, 26, 261802 (2017), [arXiv:1703.08450].

[89] G. Aad *et al.* (ATLAS), Phys. Rev. Lett. **123**, 5, 052001 (2019), [arXiv:1904.03536].

[90] G. Aad *et al.* (ATLAS), JHEP **03**, 243 (2021), [Erratum: JHEP 11, 050 (2021)], [arXiv:2008.05355].

[91] A. M. Sirunyan *et al.* (CMS), Phys. Lett. B **797**, 134826 (2019), [arXiv:1810.04602].

[92] A. Hayrapetyan *et al.* (CMS), JHEP **08**, 006 (2025), [arXiv:2412.15413].

Int. J. Mod. Phys. A 2026.41. Downloaded from www.worldscientific.com
by UNIVERSITY OF CALIFORNIA @ BERKELEY on 09/16/26. Re-use and distribution is strictly not permitted, except for Open Access articles.

INDEX

Int. J. Mod. Phys. A 2026.41. Downloaded from www.worldscientific.com
by UNIVERSITY OF CALIFORNIA @ BERKELEY on 09/16/26. Re-use and distribution is strictly not permitted, except for Open Access articles.

Int. J. Mod. Phys. A 2026.41. Downloaded from www.worldscientific.com
by UNIVERSITY OF CALIFORNIA @ BERKELEY on 09/16/26. Re-use and distribution is strictly not permitted, except for Open Access articles.

Index

a meson resonances
- $a_0(980)$ ... 36, 1526
- $a_0(1710)$ ... 1592
- $a_0(1450)$ ... 38, 1561
- $a_0(1950)$ ... 1604
- $a_1(1260)$ ... 37, 1537
- $a_1(1640)$ ... 39, 1577
- $a_2(1320)$ ... 37, 1547
- $a_2(1700)$ ... 40, 1591
- $a_4(1970)$ [*was* $a_4(2040)$] ... 41, 1606

A-parameter ... 1089
ABC, approximate Bayesian computation ... 740
Absolute monochromatic magnitude ... 146
Accelerating Universe evidence ... 491
Accelerator parameters ... 580
Accelerator parameters for neutrino beam lines ... 585
Accelerator-induced radioactivity ... 697
Acceptance-rejection method (Von Neumann) ... 768
Acoustic oscillations, baryon ... 499
Activation function ... 744
Active learning ... 739
Activity, unit of ... 695
AD, automatic differentiation ... 752
AdaBoost, adaptive boost ... 743
AdS, anti-de Sitter spacetime ... 1067
AdS/CFT
- correspondence ... 1067, 1157
- dictionary ... 1071

Advanced acceleration schemes ... 577
Age of the Universe ... 147, 452
AGN
- blazar ... 555
- radio galaxy ... 555
- active galactic nucleus ... 555

Air shower extensive, EAS ... 661
Aleatoric uncertainty ... 756
Algorithms for Monte Carlo ... 768, 769
Alignment limit ... 1093
α_s, QCD coupling constant ... 145
Amplitudes, Lorentz invariant ... 799
AMS, approximate median significance ... 755
AMSB, anomaly-mediated SUSY breaking ... 1088
Angular-diameter distance, d_A ... 452
Anisotropy of CMB ... 492, 531
Annihilating dark matter ... 539
Anomalous dimension quark mass ($\overline{\text{MS}}$) ... 861
Anomaly cancellation ... 1172
Anomaly detection ... 736, 758
Anomaly mediation ... 1176
Anomaly-mediated SUSY breaking, AMSB ... 1088
Anthropic approach ... 455
Anthropic axion window ... 1137
Anti-matter, primordial ... 544
Antineutrino flux from reactor ... 310
Antineutrinos, right-handed ... 969
Artificial intelligence ... 727
Astronomical unit ... 146
Astrophysics ... 505
Asymptotic freedom ... 161
Asymptotics, total hadronic cross sections behaviour ... 430
Atmospheric
- Cherenkov detectors ... 663
- fluorescence detector ... 661
  - Fly's Eye ... 661
  - HiRes (high resolution) Fly's Eye ... 661
  - Pierre Auger observatory ... 661
  - Telescope Array ... 661
- neutrino flux ... 305

Atmospheric pressure ... 145
Atomic
- and nuclear properties of materials, table ... 152
- mass unit ... 145

Atomic weights of elements ... 149
Attention ... 744, 749
Attenuation length for photons ... 594
Auger observatory ... 661, 1196
Authors and consultants ... 14
Autoencoder ... 732, 736
Averaging of data ... 18
Averaging, unconstrained ... 18
Avogadro constant ... 145
Axial-vector mesons
- K_{1A}-K_{1B} mixing ... 914, 919
- $\ell = 1$; 1^{++} or 1^{+-} ... 325
- $f_1(1285)$, $f_1(1420)$, $f_1(1510)$ ... 919, 920

Axion ... 1181
- as dark matter ... 1130
- DFSZ ... 1181
- KSVZ ... 1181
- searches ... 1130
- stars ... 1139

Axion as dark matter ... 508
Axion-like particles (ALP) ... 1130
Axion-photon mixing ... 539
Axions (A^0) and other very light bosons searches ... 29, 1338

$B\overline{B}$ mixing ... 996
$B\overline{B}$ oscillations
- effective tagging efficiency ... 997
- statistical significance ... 997

$b\bar{b}$ mesons ... 89, 2143
B decay, CP violation in ... 290, 993
B decays polarization, note ... 992
B mesons
- $B_{sJ}(6063)^0$ ... 1995
- $B_{sJ}(6114)^0$ ... 1995
- $B_c(1P)^{\pm}$ ... 2000
- B^* ... 74, 1961
- B^0 ... 65, 1849
- $B^{\pm}$ ... 58, 1776
- $B^{\pm}/B^0$ admixture ... 71, 1929
- $B^{\pm}/B^0/B_s^0/B$-baryon admixture ... 73, 1951
- $B_1(5721)$ ... 74, 1961
- $B_2^*(5747)$ ... 74, 1962
- $B_J^*(5732)$ [*was* B^{**}] ... 1962
- $B_J(5840)$ ... 1963
- $B_J(5970)$ ... 74, 1963
- B_c^+ ... 76, 1996
- $B_c(2S)^{\pm}$ ... 77, 2001
- $B_{s1}(5830)^0$ ... 76, 1994
- $B_{s2}^*(5840)^0$ ... 76, 1994
- $B_{sJ}^*(5850)$ ... 1995
- $B_{sJ}(6063)^0$ ... 1995
- $B_{sJ}(6114)^0$ ... 1995
- B_s^* ... 76, 1994
- B_s^0 ... 74, 1965

b' quark (4th generation), searches for ... 34, 1477
b-baryon admixture ... 118, 2421
b-flavored Hadrons, production and decay ... 980
b-quark fragmentation ... 404
$B^0_{(s)}$ effective lifetimes ... 998
$b_1(1235)$ meson ... 37, 1536
Background
- cosmic microwave, CMB ... 531
- cosmic ray radiation ... 696
- cosmology parameters ... 533
- relic cosmic neutrino ... 497
- relic light gravitons ... 1068

Backpropagation ... 740, 752
Bagging, bootstrap aggregating ... 743
Balitsky-Fadin-Kuraev-Lipatov (BFKL) limit ... 164
Barkas correcion ... 589
Baryogenesis ... 456, 1180
- GUT baryogenesis ... 1180
- leptogenesis ... 1180

Int. J. Mod. Phys. A 2026.41. Downloaded from www.worldscientific.com
by UNIVERSITY OF CALIFORNIA @ BERKELEY on 09/16/26. Re-use and distribution is strictly not permitted, except for Open Access articles.

Int. J. Mod. Phys. A 2026.41. Downloaded from www.worldscientific.com
by UNIVERSITY OF CALIFORNIA @ BERKELEY on 09/16/26. Re-use and distribution is strictly not permitted, except for Open Access articles.

Baryon
acoustic oscillations ... 468, 492, 499
decay parameters, note on ... 1046
density of the Universe ... 146
Hyperon nonleptonic decays ... 1046
magnetic moments ... 334, 339
oscillation spectroscopic survey ... 492
resonances, naming scheme ... 1047
resonances, SU(3) classification of ... 329
semileptonic decays ... 1046
Baryon quick reference table ... 98
Baryon-to-photon ratio ... 146, 482
Baryonia ... 914, 921
$\rho(1900)$ ... 919
$f_2(1565)$ ... 921
Baryons in quark model ... 329
Batch ... 751, 753
Bayes' theorem ... 472, 705
Bayesian
approach ... 714
intervals ... 721
method ... 710
statistics ... 721
Bayesian machine learning ... 756
Bayesian optimization ... 739, 743
BBN, Big-Bang nucleosynthesis ... 480
Beam collimation ... 571, 576
Beam cooling ... 571
Beam dynamics ... 569
Beam momentum, c.m. energy and momentum vs ... 799
Beam-beam interaction ... 572
Beamstrahlung ... 572, 574, 576
Becquerel, unit of radioactivity ... 695
BEPC ... 580
BEPC-II ... 580
β function of QCD ... 161
Beta distribution ... 708, 770
Beta function ... 570
β-rays, from radioactive sources ... 701
Betatron tune ... 570
Bethe equation ... 587
Beyond the general relativity physics ... 539
Beyond the SM physics, BSM ... 273, 484, 508, 775
Bhabha cross section ... 592
Bias of an estimator ... 711
Bias-variance tradeoff ... 730
Bidirectional RNN ... 747
Big-Bang cosmology ... 450, 463
Big-Bang nucleosynthesis (BBN) ... 480, 1181
Binary classification ... 729, 730, 742
Binary pulsars, strong-self-gravity ... 444
Bino ... 1091
Binomial distribution ... 708, 769
Biological damage from radiation ... 695
Birks' law ... 606
Black holes
binary ... 444
coalescing ... 441
horizon ... 439
microscopic, searches ... 1069
production ... 1068
strong gravitational fields ... 438
supermassive ... 444
Bloch correction ... 589
BMA, Bayesian model averaging ... 757
$B-L$ ... 1171, 1172, 1176, 1180
BN, batch normalization ... 745, 753
Bohr magneton ... 145
Bohr radius ... 145
Boiling points of cryogenic gases, table ... 152
Boltzmann constant k ... 145, 146
Bonding techniques ... 632
Booklet, Particle Physics, how to get ... 13
Boosting ... 743
Bose-Einstein correlations ... 425, 780, 839
Bosons, Nambu-Goldstone composite ... 1156
BOSS, baryon oscillation spectroscopic survey ... 492
Bottleneck ... 732, 733
Bottom baryons ... 114, 2398
Bottom mesons
experimental rate measurements ... 974
production and decay ... 980
theoretical decay-constant calculations ... 975
Bottom mesons (B, B^*) ... 58, 1776
Bottom, Charmed mesons (B_c, $B_c(2S)$) ... 76, 1996
Bottom, Strange mesons (B_s, B_s^*, X) ... 74, 1965
Bottomonium ... 89, 2143
Boundary condition, BC ... 1174
Dirichlet ... 1174
Bragg additivity ... 591
Brane ... 484, 1068, 1088
Dp ... 1174
D7 ... 1174
Breit-Wigner distribution ... 769
Bremsstrahlung
at very high energies ... 595
by $e^{\pm}$ ... 593
by muons ... 597
B_s^0 decay, CP violation in ... 290
BSM, beyond Standard Model ... 508
Bubble Universes ... 455

$c\bar{c}$ mesons (including possibly non-$q\bar{q}$ states) ... 77, 2002
c-quark fragmentation ... 404
Cabibbo angle ... 945
Calabi–Yau, CY ... 1173
Calorimeter
electromagnetic (ECAL) ... 642
hadronic (HCAL) ... 642
homogeneous ... 642
sampling ... 642
Categorical cross-entropy loss ... 729
CBR – Cosmic background radiation (see CMB) ... 531
CDM, cold dark matter ... 505
Central limit theorem ... 707
CEPC ... 574
Cepheid variable stars ... 491
CESR (Cornell) ... 581
CESR-C (Cornell) ... 581
CFT, 4d conformal field theory ... 1071
Chandrasekhar mass ... 146
Change of random variables ... 706
Channels ... 741, 745, 753
Characteristic functions ... 706
Charge conjugation of $q\bar{q}$ states ... 325
Charge quantization ... 1171, 1179
Charged Higgs bosons ($H^{\pm}$ and $H^{\pm\pm}$) searches ... 29, 1313
Chargino mass limits ... 1115
Charginos ... 1090
Charm decays, CP violation in ... 288
Charm mixing and CP violation ... 954
Charmed baryons (Λ_c^+, Σ_c, Ξ_c, Ω_c^+) ... 109, 2364
Charmed baryons, note on ... 109, 2364
Charmed mesons
experimental rate measurements ... 972
theoretical decay-constant calculations ... 973
Charmed mesons (D, D^*, D_J) ... 45, 1677
Charmed, Strange mesons (D_s, D_s^*, D_{sJ}, X) ... 54, 1749
Chemical potential ... 365, 453
Chemical potential, neutrino ... 539
Cherenkov detectors ... 610
at accelerators
differential ... 611
ring imaging ... 611
threshold ... 610
tracking ... 610

Int. J. Mod. Phys. A 2026.41. Downloaded from www.worldscientific.com
by UNIVERSITY OF CALIFORNIA @ BERKELEY on 09/16/26. Re-use and distribution is strictly not permitted, except for Open Access articles.

electromagnetic calorimeters 610
fast paticle counter 610
nonaccelerator
atmospheric 663
deep underground 665
particle identification PID 610
Cherenkov radiation 598
χ^2 distribution 708, 769
χ_b and χ_c mesons
$\chi_{b0}(1P)$ 91, 2151
$\chi_{b0}(2P)$ 92, 2163
$\chi_{b1}(1P)$ 91, 2153
$\chi_{b1}(2P)$ 92, 2165
$\chi_{b1}(3P)$ 93, 2174
$\chi_{b2}(1P)$ 91, 2155
$\chi_{b2}(2P)$ 93, 2168
$\chi_{b2}(3P)$ 93, 2174
$\chi_{c0}(1P)$ 80, 2042
$\chi_{c0}(3860)$ 2111
$\chi_{c0}(3915)$ [*was* $X(3915)$] 87, 2116
$\chi_{c0}(4500)$ [*was* $X(4500)$] 89, 2137
$\chi_{c0}(4700)$ [*was* $X(4700)$] 2141
$\chi_{c1}(1P)$ 81, 2054
$\chi_{c1}(3872)$ [*aka* $X(3872)$] 86, 2111
$\chi_{c1}(4140)$ [*was* $X(4140)$] 87, 2121
$\chi_{c1}(4274)$ [*was* $X(4274)$] 88, 2131
$\chi_{c1}(4685)$ 2140
$\chi_{c2}(1P)$ 82, 2067
$\chi_{c2}(3930)$ 87, 2117
Chiral perturbation theory 356, 864, 930, 937
Chiral superfields 1087, 1177
Chromaticity 571
Circular Colliders 569
Circular Higgs factories 574
CKM (Cabibbo-Kobayashi-Maskawa) quark mixing matrix 1021
CKM angles
α 1021
β 1021
γ 1023
from B hadrons determination, note 1021
CKM matrix elements 1021
CKM quark-mixing matrix, note on 273
CKM unitarity constraints 946
Classical electron radius 145
Classification 727, 729, 736, 741, 743, 745, 750, 757
Clebsch-Gordan coefficients 794, 795
Clifford algebra 1172
Clustering 732, 750
CMB
Planck satellite 468, 526, 534
anisotropy 459, 492
anisotropy power spectrum 531
COBE satellite 489, 531
Compton distortion 537
concordance with baryon density 483
cosmic microwave background 531
cosmic variance 532
detectors 680
dipole 531
lensing 500
LiteBIRD satellite 536
Lorentz-boosted temperature pattern 531
mean temperature, monopole 531
monopole 531
multipoles 531
non-Gaussianity 457, 473, 532
polarization 535
primordial perturbation 533
radiation density of Universe 146
scalar perturbations 533
Simons Observatory 495
sky map 531
Solar System motion 531
spectrum 531
tensor perturbations 533
Wilkinson Microwave Anisotropy Probe, *WMAP* ... 531
WMAP satellite 526
CMB–Cosmic microwave background 456, 492
CMSSM, Constrained MSSM 1095, 1109
CNN, convolutional neural network 730, 741, 745, 753
CNO cycle, solar neutrino 304
COBE – COsmic Background Explorer 531
Coherent radio Cherenkov radiation detectors 670
Cold dark matter (CDM) 458
Cold dark matter density 146
Collaboration databases 24
Collaborations
Planck 491
ALEPH 839
ALICE 419
ALPHA 363
ANITA 673
ARA 674
ARIANNA 674
ASTRI 663
ATLAS 419, 509, 839, 1026, 1076
B-factories 1026
BaBar 974, 980, 1026, 1098
Belle 974, 980, 1026, 1098
BERT 1132
BESIII 1026
CALICE 646
CDF 839, 980
CJ 387
CLEO 980
CLEO-c 1026
CMS 509, 839, 1026, 1076, 1082, 1121, 1191
COMPASS 912
COMPETE 420, 431
CTAO 663
D0 ..... 429, 839, 981, 1083
DAMIC-M 513
DELPHI 839
DRD1 619
DREAM/RD52 648
DSSV 379
ETM 976
Event Horizon Telescope 445
Fermi-LAT 1136
Fermilab-MILC 976
FLAG 976
FNAL/MILC 1004
GlueX 1059
GRAND 675
H.E.S.S. 663, 1136
H1 ..... 405, 1191
HERA 406, 1120
HFLAV 976
HPQCD 363, 976, 1004
JLQCD 1004
L3 839
Lattice QCD 865
LEP 839, 841, 1081, 1120
LHAASO/LACT 663
LHC 839, 1082
LHCb 839, 980, 993, 1026, 1036, 1082, 1098
LOFAR 674
MAGIC 663
MAMI 912
MILC 974
NEWS-G 514
NEWSdm 514
OPAL 839
PDG, Particle Data Group 2
PIBETA 911

Int. J. Mod. Phys. A 2026.41. Downloaded from www.worldscientific.com
by UNIVERSITY OF CALIFORNIA @ BERKELEY on 09/16/26. Re-use and distribution is strictly not permitted, except for Open Access articles.

PICO 514
Pierre Auger 674
PUEO 674
RBC/UKQCD 1010
RICE 674
RM123-Soton 970
RNO-G 674
SLD 844
Sp$\bar{p}$ 1150
Tevatron 839, 1083, 1120
TOTEM 417
Tunka-Rex 674
UA4 428
VERITAS 663
ZEUS 405, 1120, 1191
Collider parameters 580
Colliders 569
future 574
present 573
recent 572
Colliders based on Energy Recovery Linacs 576
Collinear and infrared safety 166, 170
Collinear factorization 163
Color confinement 1137
Color factor 161, 172
Color reconnection phenomenon 426, 781, 839
Color-triplet Higgs boson 1171, 1172, 1175, 1177, 1180
Colorons (axigluons) search 1166
Comments, e-mail address to contact 13
Compact Linear Collider (CLIC) 576
Compactification 1139
Compensation
intrinsic 647
software 648
Compton wavelength, electron 145
Concordance cosmology 489
Conditional probability density function 706
Confidence intervals 720
frequentist 721
Gaussian 18
Poisson 723
Confinement 365
-deconfinement quarks-hadrons transition 454
color 1137
harmonic 330
linear 330, 777
Conformal field theory, CFT 1071
Consistency of an estimator 711
Constancy of constants tests 443
Constrained fit 856
Constrained fits, procedures for 19
Constrained MSSM, CMSSM 1095, 1109
Constraints, parameter estimation with 713
Consultants 14
Contour-improved perturbation theory (CIPT) 177
Conversion constant 145
Conversion probability for photons to e^+e^- 594
Convolution kernel 745
Copernican Principle 450
Correlation coefficient, definition 706
Correlation matrices 856
Cosmic acceleration, dark energy 523
Cosmic background radiation temperature 531
Cosmic microwave background, CMB 456, 492, 531
Cosmic neutrino background, CνB 497
Cosmic ray(s)
air showers 546
anisotropies 546, 550
anti-nuclei 544
antimatter 546
detection techniques 548
diffusion 542
direct observations 544
electrons and positrons 545
origin 552
unstable nuclei 545
acceleration 542
background in counters 696
extra-galactic transport 544
fluorescence detectors FDs 661
galactic transport 542
hadronic interactions 552
indirect observations 546
origin 542
primaries 544
radio detection of air showers 674
secondaries 544
sources 542
ultra-high energy, UHE 672
Cosmic string 1180
Cosmic topology 491
Cosmological
constant Λ 146, 450, 463, 523, 533
density parameter, Ω 451
equation of state 451
mass density parameter 450
standard model 539
Cosmological probes
CMB 537
galaxy peculiar velocities 493
integrated Sachs-Wolfe effect 493
redshift 450
supernovae 491
Cosmology 488, 505
ΛCDM 505
Big-Bang 450, 463, 505
modern 505
outlook for the future 494
Robertson-Walker metric 463
scalar field 464
standard 508
standard early Universe 463
standard neutrino 497
Coupling between matter and gravity 443
Coupling constant in QCD 145, 161
Covariance matrix 713
Covariance, definition 706
Coverage 721
CP violation
and $D^0 - \overline{D}^0$ mixing 958
charm mixing 954
classification of effects 285
in $B\overline{B}$ mixing 999
in B and B_s^0 mixing and decay 290
in B decay 980
in K_L^0 decay 287
in K_L^0 decay, note on 949
in charm 288
in decays of Beauty to Charm 953
in the quark sector, note 283
induced by $B\overline{B}$ mixing 1000
interference between tree and penguin amplitudes 290
overview 283
the CKM matrix 286
the Kobayashi-Maskawa mechanism 286
CPT invariance tests in neutral kaon decay 943
Crab Nebula, flares 554
Crab Nebula, PeV Radiation 553
Critical density in cosmology 450
Critical density of the Universe 146
Critical energy
for electrons 594
for muons 597
Cross sections and related quantities, plots of 831
e^+e^- annihilation cross section near M_Z 834
Pseudorapidity distribution in pp and $\overline{p}p$ interactions 831

Average hadron multiplicities in e^+e^- annihilation events 832
nucleon structure functions ... 373
Cross sections, relations for ... 801, 815
Cross-entropy loss ... 729
Cross-validation ... 730
Cryogenic beam vacuum system ... 576
Cryogenic gases, boiling points, table ... 152
Crystal accelerator ... 577
Cumulative distribution function, definition ... 705
Curie, unit of radioactivity ... 695
Curvature ... 147

d functions ... 794
D mesons
$D^0, \overline{D}^0$ ... 48, 1698
$D^\pm$ ... 45, 1677
$D(3000)^0$ ... 1748
$D^*(2007)^0$ ... 53, 1738
$D^*(2010)^\pm$ ... 53, 1739
$D^*(2640)^\pm$ ... 1746
$D_0^*(2300)$ [*was* $D_0^*(2400)$] ... 53, 1741
$D_0(2550)^0$ ... 1745
$D_1^*(2600)^0$ [*was* $D_J^*(2600)$] ... 1745
$D_1^*(2760)^0$ ... 1747
$D_1(2420)$ ... 53, 1741
$D_1(2430)^0$ ... 53, 1743
$D_2^*(2460)$ ... 54, 1743
$D_2(2740)^0$ [*was* $D(2740)^0$] ... 1746
$D_3^*(2750)$ ... 54, 1747
$D_{s0}^*(2317)^\pm$ ... 56, 1769
$D_{s0}(2590)^+$ ... 1773
$D_{s1}^*(2700)^\pm$ ... 57, 1773
$D_{s1}^*(2860)^\pm$ ... 1774
$D_{s1}(2460)^\pm$ ... 57, 1769
$D_{s1}(2536)^\pm$ ... 57, 1771
$D_{s2}^*(2573)$ ... 57, 1772
$D_{s3}^*(2860)^\pm$ ... 57, 1774
$D_{sJ}(3040)^\pm$ ... 1774
$D_s^{*\pm}$ ... 56, 1768
$D_s^\pm$ ... 54, 1749
D^0-$\overline{D}^0$ mixing, note on ... 958
DAΦNE ... 580
$d_{\rm A}$, angular-diameter distance ... 492, 538
Dalitz plot, relations for ... 800
Damage, biological, from radiation ... 695
Dark energy ... 451, 490, 523
cosmic acceleration ... 523
density parameter ... 146
equation of state parameter w ... 147, 492, 523
Euclid satellite ... 477
experiments ... 526
observational probes
baryon acoustic oscillations, BAO ... 525
CMB anisotropies ... 525
Type Ia supernovae ... 525
weak gravitational lensing ... 525
parameter, $\Omega_{\rm N}$ ... 451
quintessence ... 460
repulsive gravity ... 524
Dark energy spectroscopic instrument (DESI) ... 492, 526
Dark matter ... 458, 490
annihilating ... 539
CDM cosmology ... 505
cusp-core problem ... 507
density distribution ... 506
detectors ... 680
Gaia satellite ... 507
Galactic halo shape ... 506
genesis, cannibalization ... 506
genesis, DM anti-DM asymmetry ... 506
genesis, freeze-in ... 506
genesis, freeze-out ... 505
genesis, non-thermal production ... 506
genesis, primordial black holes ... 506
laboratory detection ... 509
missing satellites problem ... 507
non-baryonic ... 505
Too-big-to-fail problem ... 507
velocity distribution ... 507
Dark matter astrophysical detection
cosmic-ray antimatter ... 516
cosmology ... 517
gamma rays ... 515
multi-wavelength ... 517
neutrinos ... 516
staller physics ... 517
Dark matter candidates
axions ... 508
dark photon ... 508
gaugino ... 1089
gravitino ... 1088
higgsino ... 1089
sterile neutrinos ... 508
WIMPs ... 508
Dark matter properties
darkness ... 505
mass lower and upper limits ... 505
self-interactions ... 505
stability ... 505
Dark matter, indirect detection ... 544
Data ... 24
Data augmentation ... 741, 755, 756
Data manifold ... 741
Data, averaging and fitting procedures ... 18
Data, selecting and treatment ... 17
Databases
availability online ... 22
conferences ... 23
experiments ... 23
high-energy physics ... 22
Insitutions ... 23
INSPIRE ... 22
Authors ... 23
Conferences ... 23
Experiments ... 23
Insitutions ... 23
Jobs ... 24
Journals ... 23
Literature ... 22
Seminars ... 23
institutions ... 23
journals ... 23
literature ... 22
ADS ... 22
arXiv.org ... 22
INSPIRE ... 22
MathSciNet ... 23
OSTI ... 23
ORCID ... 23
particle physics ... 22
PDG API ... 22
PDGLive, PDG web browser ... 22
Review of Particle Physics (RPP) ... 22
ROR ... 23
RPP computer-readable files ... 22
Day, sidereal ... 146
dE/dx ... 586
Decay parameters, Michel ... 859
Decays, kinematics and phase space for ... 799
Deceleration parameter, q_0 ... 451
Decision tree ... 727
Decoder ... 732, 733, 747, 749
Deep inelastic scattering, DIS ... 163, 373, 419
Deep learning ... 745

Int. J. Mod. Phys. A 2026.41. Downloaded from www.worldscientific.com
by UNIVERSITY OF CALIFORNIA @ BERKELEY on 09/16/26. Re-use and distribution is strictly not permitted, except for Open Access articles.

Int. J. Mod. Phys. A 2026.41. Downloaded from www.worldscientific.com
by UNIVERSITY OF CALIFORNIA @ BERKELEY on 09/16/26. Re-use and distribution is strictly not permitted, except for Open Access articles.

Deep set 741, 750
Degree of freedom, number of 713
Δ resonances
  $\Delta(1232)$ 103, 2263
  $\Delta(1600)$ 103, 2265
  $\Delta(1620)$ 103, 2267
  $\Delta(1700)$ 104, 2268
  $\Delta(1750)$ 2270
  $\Delta(1900)$ 104, 2271
  $\Delta(1905)$ 104, 2272
  $\Delta(1910)$ 104, 2274
  $\Delta(1920)$ 104, 2276
  $\Delta(1930)$ 104, 2278
  $\Delta(1940)$ 2279
  $\Delta(1950)$ 104, 2281
  $\Delta(2000)$ 2282
  $\Delta(2150)$ 2283
  $\Delta(2200)$ 105, 2284
  $\Delta(2300)$ 2285
  $\Delta(2350)$ 2285
  $\Delta(2390)$ 2285
  $\Delta(2400)$ 2286
  $\Delta(2420)$ 105, 2286
  $\Delta(2750)$ 2287
  $\Delta(2950)$ 2287
$\Delta(\sim 3000$ Region) Partial-Wave Analyses 2288
δ-rays 590
Density
  of CMB photons 146
  of Universe, critical 146
  parameter of the Universe Ω_0 146
Density effect in energy loss rate 587
Density estimation 732, 733, 740, 755, 757
Density of materials, table 152
DESI – dark energy spectroscopic instrument .. 476, 477, 492, 526
Detectors
  calorimeters
    electromagnetic 644
  Cherenkov 610, 663
  CMB detectors 680
  coherent radio Cherenkov radiation 670
  Dark matter 680
  fluorescence, atmospheric 661
  for rare events 675
  gas-filled 612
    drift chamber 615, 649
    high rate effects 616
    micro-pattern 616
    micro-strip chamber 619
    multi-wire proportional chambers, MWPC 615
    resitive plate chambers, RPC 623
    time-projection chambers, TPC 619
    transition radiation, TRD 621
  gravitation wave observatory, Virgo 441
  hadronic shower 602
  ice-based 673
  inorganic scintillator 607
  Kinetic Inductance Detectors (KIDs) 680
  LAr Time projection chambers 625
  laser interferometer gravitation observatory, LIGO .. 441
  liquid ionization chamber 650
  liquid scintillator 666
  Low Temperature Detectors (LTDs) 679
  low-noise readout 637
  low-radioactivitiy background techniques 684
  Magnetic Metallic Calorimeters (MMCs) 681
  Neutrino cryogenic detectors 680
  neutrino detectors 670
  neutrino telescopes 668
  neutrino, calibration of 701
  noble liquid 667
  organic scintillator 605
  proton decay 665
  radio-detection of cosmic ray air showers 674
  rare event search
    $0\nu\beta$ decay 678
    WIMPs 677
  semiconductor 629
    (D)MAPS 632
    3D-Si 632
    DEPFET 632
    hybrid pixels 632
    LGAD 634
    microstrip 632
    monolithic pixels 632
    radiation damage 635
    silicon drift chamber 632
    silicon drift diode (SDD) 632
  Semiconductor Thermistors 680
  showers 644
  superconducting solenoid magnets for 650
  superconducting toroidal magnets for 652
  Superconducting Tunnel Junctions (STJs) 680
  Transition Edge Sensors (TESs) 681
  water Cherenkov 667
  wire chambers 625
Deuterium abundance 480
Deuteron mass 145
Deuteron structure function 386
DIEHARD 768
Dielectric laser accelerator 577
Dielectric suppression of bremsstrahlung 593
Dielectric wakefield accelerators 577
Differential Cherenkov detectors 611
Diffraction and high energy soft QCD 413
Diffractive parton distribution 419
Diffractive processes 413
Diffuse gamma rays 552
Diffusion model 733, 736
Dinucleon decay 1181
Dirac gauginos 1100
Dirac neutrinos 298
Direct CP asymmetry in B decays 993
Directories, online, people, and organizations 22
DIS, deep inelastic scattering 373, 419
Discrete R symmetry 1177
Discrete symmetry 1179
Discriminative model 727, 729, 733
Disk density 146
Dispersion relation 928, 945
Distance ladders 491
Distance-redshift relation 450, 452, 488, 491, 524
Distribution shift 728
Dokshitzer-Gribov-Lipatov-Altarelli-Parisi (DGLAP) equations 163
Domain adaptation 754, 755
Domain shift 728, 754
Donnachie-Landshoff pp-scattering amplitude 414
Dose rate from γ ray sources 697
Dose, radioactivity, unit of absorbed 696
Double PDFs 378
Double-β decay 1416
Doubly charmed baryons 2396
Drell-Yan process 348, 381
Drift chambers 615
Drift velocities of electrons 649
Dropout 731, 745
Dual readout 648
DUNE 1177
Dynamic graph CNN 750
Dynamical electroweak symmetry breaking 1156

e (electron) 30, 1369
e (natural log base) 145
e^- Compton wavelength 145

Int. J. Mod. Phys. A 2026.41. Downloaded from www.worldscientific.com
by UNIVERSITY OF CALIFORNIA @ BERKELEY on 09/16/26. Re-use and distribution is strictly not permitted, except for Open Access articles.

E_6 1172
$E_8 \times E_8$ 1173
Early stopping 728, 731, 744, 751, 752
Early Universe 463, 480
Earth
  equatorial radius 146
  mass 146
Eddington luminosity 146
Edge 750
Education databases 24
Effective
  number of neutrinos 147
Effective dose of radioactivity 695
Effective field theories (EFTs) 343, 1174
Effective skin depth δ 153
Efficiency of an estimator 711
EFT – effective field theories 343
Elastic cross sections 419
Elastic scattering 413
ELBO, evidence lower bound objective 733, 734
Electric dipole moment, EDM 1180
Electromagnetic
  calorimeters 644
  cascades 596
  effects 339
  field equations 153
  relations 153
  showers, lateral distribution 597
  showers, longitudinal distribution 596
Electron
  charge magnitude e 145
  configuration of element, table 150
  critical energy 594
  cyclotron frequency/field e/m_e 145
  drift velocities 649
  mass 145
  radius, classical 145
  volt eV 145
Electron and photon interactions in matter 592
Electron-Ion Collider (EIC) 574
Electron-positron collider rings 573
Electron-positron colliders – future 575
Electronic energy loss by heavy particles 586
Electronic structure of the elements 150
Electroweak
  dynamical symmetry breaking 1156
  penguin decay 984, 993
Electroweak corrections 166, 175
Elements
  electronic structure of 150
  ionization energies of 150
Elements, periodic table of 149
Embedding 740
Emission probability 701
Emittance 570
Empirical risk 728
Encoder 732, 733, 745, 749
Encoder-decoder 747
Energy and momentum (c.m.) vs beam momentum 799
Energy density
  of CBR 146
  of dark energy 146
  of relativistic particles 146
Energy loss
  (fractional) for $e^{\pm}$ in lead 593
  at low energies 588
  by electrons 593
  by photons 594
  density effect 587
  higher order corrections 588
  rate for heavy charged particles 587
  rate for muons at high energies 597
  rate in compounds and mixtures 591
  rate, form factor corrections 587
  rate, most probable 590
  rate, restricted 587, 590
  scaling with mass 587
Energy per nucleon 542
Energy Recovery Linac 576
Energy resolution (calorimeter) 643
  constant term 643
  stochastic term 643
Energy-energy correlation 172
Ensemble methods 743
Entropy density 146, 453, 455
e^+e^- annihilation
  cross-section formulae 815
  two-photon process 816
Epistemic uncertainty 756
ϵ_0 (permittivity of free space) 145, 153
Equivalence principle, experimental tests of 443
Equivalence principle, GR 437
Error function 707
Error propagation 754
Errors, treatment of 18
Established nonets for the meson 326
Estimator 710
η mesons
  η 35, 1496
  $\eta_1(1855)$ 1602
  $\eta(1295)$ 37, 1546
  $\eta(1405)$ 38, 1554
  $\eta(1475)$ 38, 1565
  $\eta(1760)$ 1596
  $\eta(2225)$ 1618
  $\eta(2370)$ 1621
  $\eta'(958)$ 36, 1516
  $\eta_2(1645)$ 39, 1578
  $\eta_2(1870)$ 40, 1602
  $\eta_c(1S)$ 77, 2002
  $\eta_c(2S)$ 83, 2080
  $\eta_b(1S)$ 89, 2143
  $\eta_b(2S)$ 2157
Event pile up 576
Event shape 172
Excitation energy 587
Excited fermions searches 1151
Excited leptons searches 1151
Exotic quantum numbers 914
Expansion of the Universe 451
Expectation value, definition 705
Experiment databases 23
Experimental design optimization 738
Experimental rate measurements
  bottom mesons 974
  charmed mesons 972
  pions and kaons 970
Experimental sensitivity 724
Experimental tests of gravitational theory 437
Exploding gradient 744, 747, 752
Extensions to the cosmological standard model 490
Extensive air shower, EAS 661
Extra Dimensions 120, 1088, 1157, 2499
  note on 1067

f, F mesons
  $f_0(980)$ 36, 1523
  $f_0(1370)$ 38, 1551
  $f_0(1500)$ 39, 1566
  $f_0(1710)$ 40, 1593
  $f_0(2020)$ 41, 1608
  $f_0(2100)$ 1610
  $f_0(2200)$ 1616
  $f_0(2330)$ 1620
  $f_1(1285)$ 37, 1543
  $f_1(1420)$ 38, 1557

Int. J. Mod. Phys. A 2026.41. Downloaded from www.worldscientific.com
by UNIVERSITY OF CALIFORNIA @ BERKELEY on 09/16/26. Re-use and distribution is strictly not permitted, except for Open Access articles.

$f_1(1510)$ 1569
$f_2'(1525)$ 39, 1570
$f_2(1270)$ 37, 1539
$f_2(1430)$ 1560
$f_2(1565)$ 39, 1574
$f_2(1640)$ 1578
$f_2(1810)$ 1599
$f_2(1910)$ 1603
$f_2(1950)$ 41, 1605
$f_2(2010)$ 41, 1607
$f_2(2150)$ 41, 1611
$f_2(2300)$ 41, 1619
$f_2(2340)$ 41, 1620
$f_4(2050)$ 41, 1608
$f_4(2300)$ 1619
$f_6(2510)$ 1622
$f_J(2220)$ 1616
$f_0(600)$ [*was* $f_0(500)$ *was* σ] 35, 1502
$f_0(1810)$ 1597
$f_0(2470)$ 1622
F-theory 1174
F_2 structure function, plots 386
Factorization scale 163
Family symmetry 1178
FCC-ee (Future Circular Collider) 574
FCC-hh (Future Circular Collider) 576
Feature engineering 731
Feature map 745
Feature vector 727, 744
Fermi constant 1089
Fermi coupling constant $G_F/(\hbar c)^3$ 145
Fermi plateau 588
Fermions
left-handed 1158
right-handed 1158
Feynman's x variable 802
Field equations, electromagnetic 153
Filter 744
Fine-structure constant, α 145
Fine-structure constant, time variation 539
Fine-tuning 753, 1097
Fit to Z electroweak measurements 841
Fit, technical implementation 857
Fits to data 18
Fixed-order perturbation theory (FOPT) 177
Flat extra dimension 1072
Flatness of Universe 494
Flavor anomalies 1098
Flavor number scheme (FNS) 164
Flavor symmetric couplings 916
Flavor transitions (oscillations) in mesons 996
Flavor transitions (oscillations) neutrino 303
Flavor-changing neutral current, FCNC 1180
Flavour Lattice Averaging Group (FLAG) 176
Flow-matching model 733, 735
Fluctuation amplitude σ_8 146
Fluctuation amplitude at $8\,h^{-1}$ Mpc scale 147
Fluctuations in energy loss 590
Fluorescence detector, atmospheric 661
Flux conversion 146
Flux landscape 1174
Fly's Eye fluorescence detector 661
FM, foundation model 737
FODO cell 570
Forbidden states in quark model 155
Force, Lorentz 153
Form factors for radiative pion and kaon decays, note on .911
Foundation models 753
Four-quark states 329, 931
Fragmentation
functions 169
functions in e^+e^-, ep, and pp collisions, note on 396
functions, scaling violations in 397
heavy-quark 404
in e^+e^- annihilation 396
longitudinal 399
models 400
Free quark searches 34, 1482
Frequentist
approach 710
confidence intervals 721
statistics 721
Friedman equation 452
Friedmann constraint equation 463
Friedmann-Lemaître equations 450
Further states mesons 2194

g (gluon) 27, 1242
Galactic Diffuse Emission (GDE), origin 553
Galaxy clustering 477, 492
Galaxy power spectrum 492
γ (photon) 27, 1241
γ (Euler constant) 145
Gamma collider 576
Gamma distribution 708, 769
Gamma factory 577
Gamma ray source, Pulsars in TeV band 555
Gamma rays, astrophysical 552
Gamma rays, instruments 552
γ-rays, from radioactive sources 701
$\gamma\gamma$ collisions 916
GAN, generative adversarial network 733, 734, 755
Gas electron multiplier (GEM) 617
Gas-filled detectors
electron drift velocity 613, 649
gas properties 612
high rate effects 616
mobility of ions 614
Townsend coefficient 614
Gauge and Higgs bosons
H^0 Higgs 28, 1278
W 27, 1243
Z 27, 1258
γ (photon) 27, 1241
g (gluon) 27, 1242
Searches
graviton 27, 1242
Gauge and Higgs bosons searches
W', Z' 29, 1317
axion 29, 1338
charged Higgs $H^\pm, H^{\pm\pm}$ 29, 1313
Gauge coupling unification 1174
Gauge hierarchy 1086
Gauge kinetic function 1087
Gauge supermultiplet 1086
Gauge symmetry principle 297
Gauge-mediated supersymmetry breaking 1088, 1095
Gaugino 1087, 1090
Gaugino mass unification 1094
Gaussian
n-dimensional ellipsoid 707
(Normal) distribution 708
distribution, MC algorithm 769
distribution, Multivariate 707
General relativity predictions 437
equivalence principle 437
gravitational waves 438
isotropy of space 443
quasi-stationary, weak-field 438
radiative gravity tests 445
strong fields, neutron stars, black holes 438
universality of free fall tests 444
General relativity, GR 437
General-purpose Monte Carlo generators, (GPMC) 772
Generalization 728, 730
Generalized NMSSM, GNMSSM 1100

Int. J. Mod. Phys. A 2026.41. Downloaded from www.worldscientific.com
by UNIVERSITY OF CALIFORNIA @ BERKELEY on 09/16/26. Re-use and distribution is strictly not permitted, except for Open Access articles.

Generative model 727, 729, 733, 757
Generator of SU(3) transformation 795
Geometric deep learning 750
Glashow resonance 559
Global fit in SM 278
Glueballs 328, 914, 915
  $\eta(1405)$ 918
  $\eta(1760)$ 918
  $\eta(2370)$ 918
  $f_2(1950)$ 916
  $f_0(1500)$, $f_0(1710)$ 916
  lattice calculations 915
  scalar 916
  tensor 916
Gluino 1087
Gluino mass limits 1111
Gluon field, SU(3) valued 861
Gluon induced jets 172
GMSB 1095
GNMSSM, generalized NMSSM 1100
GNN, graph neural network 741, 750
Goldstino 1088
GP, Gaussian process 729, 739
GPMC generators
  General-purpose Monte Carlo generators 772
  HERWIG 772
  PHOTOS 775
  PYTHIA 772
  SHERPA 772
  uncertainties and tuning 781
GR, general relativity 437
Gradient boosting 743
Gradient clipping 752
Gradient descent 728, 731, 740, 744, 751
Grand unified theory, GUT 1171
  E_6 1172
  baryogenesis 1180
  baryon-number-violating nucleon decay 1176
  basic group theory 1171
  breaking 1173
  doublet-triplet splitting 1173
  flipped SU(5) 1172
  neutrino masses 1179
  orbifold 1174, 1177
  Pati-Salam model 1171, 1172
  scale 1171
  SO(10) 1172
  SU(5) 1171
  Yukawa coupling unification 1177
Graviscalar searches 1067
Gravitational
  constant G_N 145
  acceleration g_N 145
  lensing 457
  radiation 440
  theory, experimental tests of 437
  wave speed 441
  waves in GR 438
Gravitational lensing 493, 534, 536
Gravitational-wave source, GW170817 491
Gravitino 1088
Gravitino problem 1181
Graviton
  disperse 446
  mass 446
  Randall-Sundrum 1158
  searches 1068
Graviton searches 27, 1242
Gravity
  in extra dimensions 1067
  tests 442
Gravity mediation 1178
Gray, unit of absorbed dose of radiation 695
GRB, BOAT GRB221009A 557
GRB, burst of gamma-rays in TeV band 557
Green–Schwarz mechanism 1179
Group normalization 753
GRU, gated recurrent unit 747
GUT (grand unified theory) 1087, 1094
GUTs
  monopoles prediction 1194

h mesons
  $h_1(1170)$ 37, 1535
  $h_1(1415)$ [*was* $h_1(1380)$] 38, 1557
  $h_1(1595)$ 1575
  $h_b(1P)$ 91, 2155
  $h_b(2P)$ 93, 2168
  $h_c(1P)$ 82, 2064
H^0 (Higgs boson) 28, 1278
Hadron colliders 572
Hadron colliders – future 575
Hadron level 169
Hadronic
  calorimeters 602
  shower detectors 602
Hadronic Molecules 931
Hadronization corrections 170
Hadronization model 169
Half-lives of radioactive nuclides 701
Harrison–Zeldovich spectrum 488
h/e ratio 647
He initialization 753
Heavy baryons 332
Heavy charged lepton searches 32, 1403
Heavy neutral leptons searches 1440
Heavy Quark Expansion (HQE) 1007
Heavy quarks masses 866
Heavy vector-like quark B 1164
Heavy vector-like quark T 1161
Heavy-quark
  effective theory (HQET) 343
  expansion for inclusive decays 344
  fragmentation 404
  spin-flavor symmetry 343
Heavy-quark and soft-collinear effective theory, note on 343
Heavy-quarkonium spectroscopy 1026
Helium-3 abundance 481
Helium-4 abundance 481
HERA 572
HERA (DESY) collider parameters 583
Hessian 751
Heterotic string 1173
HFLAV charm mixing global fit 965
Hidden sector 1088
Hidden state 747
Hidden valley models 1088
Hierarchy problem 1068
Higgs alignment limit 1093
Higgs and electroweak factories 574
Higgs boson 226
  Couplings: κ framework and EFT approach 239
  Differential cross section measurements 238
  Electroweak symmetry breaking 227
  Higgs-boson decay channels 235
  Higgs-boson production channels 236
  Inclusive measurements 236
  Mass 246
  New physics models 251
  Self-coupling 245
  Spin and CP properties 249
  Width 247
Higgs production in e^+e^- annihilation 817
Higgsino 1087
High energy diffraction experiments 419
High energy diffraction, theoretical description 414

Int. J. Mod. Phys. A 2026.41. Downloaded from www.worldscientific.com
by UNIVERSITY OF CALIFORNIA @ BERKELEY on 09/16/26. Re-use and distribution is strictly not permitted, except for Open Access articles.

High energy soft QCD and diffraction, note on 413
High intensity beams 571
High-field accelerator magnets 576
High-frequency surface impedance 153
Highlights of this edition of the RPP 7
History of measurements, discussion 20
History plots 21
HL-LHC 573
HMSSM 1093
Holographic model 329, 916, 917
Holography 1157
Horizon scale 533
Hot Big-Bang cosmology 480
HQE parameters and V_{cb} 1007
HQET – Heavy-quark effective theory 343
HST, Hubble space telescope 491
Hubble
  constant H_0 ..... 488, 533, 538
  cosmic topology 491
  expansion 451
  expansion rate 146, 505
  flow 526
  length c/H_0 ..... 146, 452
  parameter $H(t)$ 450
  radius 533
  relativistic species 490
  scaling factor for expansion rate 146
  space telescope HST 491
  varying constants 491
Hubble tension 491
Hubble's law 450
Huber loss 729
Hybrid inflation model 465
Hybrid mesons 920
  $\eta_1(1855)$ 920
  $\pi(1800)$, $\pi_1(2015)$ 920
  $\pi_1(1600)$ 920
  $\rho(1450)$ 919
Hybrid states 329
Hyper-Kamiokande 1176, 1177
Hyperbolic tangent activation 744, 747
Hypercharge 324, 1080

Ice-based detectors 673
ID particle codes for MC 789
Ideal mixing 914
Ideal mixing in quark model 327
Ideograms, criteria for presentation 18
Image data 741, 745
Imaging Cherenkov detectors 611
Impedance of free space 153
Impedance, relations for 153
Importance sampling 770
Importance sampling in Monte Carlo calculations 768
Inception 745
Inclusive hadronic reactions 817
Inclusive reactions, kinematics for 801, 817
Inconsistent data, treatment of 18
Independence of random variables 706
Inductive bias 731, 741, 750
Inelastic cross sections 419
Inference 729, 755, 758
Inflation 1180
  CMB photons 463
  de Sitter limit $\epsilon \to 0$ 466
  effective field theory of 474
  Friedman equation 463
  future probes of 476
  motivation 463
  multi-field 474
  of early Universe 455, 463, 488
  quantum fluctuations 465
  reheating 464
  slow-roll 464, 532
Inflation models
  R^2 inflation 469
  axion monodromy 470
  chaotic with power-law potentials 469
  D-brane 469
  Higgs 470
  Hilltop 469
  natural 469
  pioneering 468
  supergravity 471
  supersymmetric 471
Inflation primordial perturbations 465
  density from single-field 466
  gravitational waves 465
  metric 465
  observational bounds 467
Inflaton
  field fluctuations 466
  Higgs scalar field as candidate 471
Inflaton scalar field 439, 455, 465
Information horizon 453
Infrared and collinear safety 166, 170
Initialization 744, 751–753
Inorganic scintillators 607
Input normalization 753
Instance normalization 753
Integer encoding 740
Integrated Sachs-Wolfe effect 460, 492, 523, 533
Inter-galactic medium clustering 493
Interaction length 642
International Linear Collider (ILC) 576
International System (SI) units 148
Interpretability 727, 747, 749
Introduction 13
Inverse problem 739
Inverse transform method in Monte Carlo 768
Invisible energy (calorimetry) 647
Ion colliders 574
Ionization
  energies of the elements 150
  energy loss at minimum, table 152
  history of the Universe 490
Ionization history 490
Ionization yields for charged particles 591
IoU, intersection over union 746
Isotropy of space tests 443

$J/\psi(1S)$ 77, 2012
Jansky 146
Jet algorithm
  cone 171
  sequential recombination 171
Jet definition 171
Jet shape 172
Jet substructure 172
J/ψ radiative decay 916, 917
JS, Jensen-Shannon divergence 734
JUNO 1177

K factor 170
K stable mesons
  K^0 ..... 43, 1638
  $K^\pm$ 42, 1623
  K^0_L 43, 1643
  K^0_L decay, CP violation in 949
  K^0_S 43, 1639
K, K^* meson resonances
  $K(1460)$ 45, 1669
  $K(1630)$ 1669
  $K(1830)$ 1673
  $K(3100)$ 1676
  $K_1(1270)$ 44, 1662

Int. J. Mod. Phys. A 2026.41. Downloaded from www.worldscientific.com
by UNIVERSITY OF CALIFORNIA @ BERKELEY on 09/16/26. Re-use and distribution is strictly not permitted, except for Open Access articles.

$K_1(1400)$ 44, 1664
$K_1(1650)$ 45, 1670
$K^*(892)$ 44, 1659
$K^*(1410)$ 44, 1665
$K^*(1680)$ 45, 1670
$K_0^*(1430)$ [*was* $\kappa(1350)$] 44, 1665
$K_0^*(1950)$ 45, 1673
$K_2^*(1430)$ 45, 1666
$K_2^*(1980)$ 45, 1674
$K_2(1580)$ 1669
$K_2(1770)$ 45, 1671
$K_2(1820)$ 45, 1672
$K_2(2250)$ 1675
$K_3^*(1780)$ 45, 1671
$K_3(2320)$ 1675
$K_4^*(2045)$ 45, 1674
$K_4(2500)$ 1676
$K_5^*(2380)$ 1676
k-means clustering 732
K_L^0 decay, *CP* violation in 287
Kähler potential 1087
Kaluza–Klein, KK
mode 1176
scale 1174
zero mode 1174
Kaluza-Klein
excitations 790, 1081
modes 1067, 1076
reduction 1067
searches 1070
theories 442, 1067
Kaon decay, *CPT* invariance tests in neutral 943
KEKB (KEK) collider parameters 581
Kernel machine 727
Kernel trick 742
Kinematic limits
sequential two-body decay 800
three-body decays 800
Kinematics, decays, and scattering 799
Kinetic Inductance Detectors (KIDs) 680
Kinetic Sunyaev-Zeldovich effect 460
KL, Kullback-Leibler divergence 730, 733–735
Knock-on electrons, energetic 590
Knowledge distillation 758
Kobayashi-Maskawa (Cabibbo-) mixing matrix 273

L1 loss 729
L1 regularization 730
L2 loss 729
L2 regularization 730
Label 727, 739
LAGEOS – laser geodynamics satellite 444
Lagged-Fibonacci-based random number generator 768
Lagrangian, QCD 161, 861
Λ QCD parameter 162
Λ and Σ resonances 1052, 1054
Λ baryons 105, 2289
$\Lambda_c(2910)^+$ 2377
Λ 105, 2289
$\Lambda(1405)$ 105, 2292
$\Lambda(1520)$ 105, 2294
$\Lambda(1600)$ 105, 2295
$\Lambda(1670)$ 105, 2297
$\Lambda(1690)$ 105, 2298
$\Lambda(1710)$ 2300
$\Lambda(1800)$ 106, 2300
$\Lambda(1810)$ 106, 2301
$\Lambda(1820)$ 106, 2303
$\Lambda(1830)$ 106, 2304
$\Lambda(1890)$ 106, 2306
$\Lambda(2000)$ 2308
$\Lambda(2050)$ 2308
$\Lambda(2070)$ 2308
$\Lambda(2085)$ 2310
$\Lambda(2100)$ 106, 2311
$\Lambda(2110)$ 106, 2312
$\Lambda(2325)$ 2313
$\Lambda(2350)$ 106, 2314
$\Lambda(2585)$ 2314
Λ_b^0 ..... 114, 2398
$\Lambda_b(5912)^0$ 115, 2408
$\Lambda_b(5920)^0$ 115, 2409
$\Lambda_b(6070)^0$ 115, 2409
$\Lambda_b(6146)^0$ 116, 2409
$\Lambda_b(6152)^0$ 116, 2410
Λ_c^+ 109, 2364
$\Lambda_c(2595)^+$ 111, 2375
$\Lambda_c(2625)^+$ 111, 2376
$\Lambda_c(2765)^+$ or $\Sigma_c(2765)$ 2376
$\Lambda_c(2860)^+$ 111, 2377
$\Lambda_c(2880)^+$ 111, 2377
$\Lambda_c(2940)^+$ 111, 2378
$\Lambda(1405)$ region, pole structure, note on 1055
Λ, cosmological constant 450
ΛCDM, minimal cosmological model 497
Landau distribution 590
Landau-Pomeranchuk-Migdal (LPM) effect 593
LAr Time projection chambers, detector 625
LARES – laser relativity satellite 444
Large extra dimensions 822, 1067
Large rapidity gap 413
Large-scale structure of the Universe 458
Last scattering surface, LSS 533
Lattice calculations of spectroscopy 336
Lattice for composite Higgs models 1157
Lattice QCD 352, 861, 998, 1137
Layer normalization 753
LBL, long baseline 301
Leaky ReLU 744
Learning rate 728, 751
Least squares 713
Left-handed
fermions 1158
neutrinos 969
Left-handedness of neutrinos 297
LEP 573
LEP (CERN) 581
Leptogenesis 1180
Lepton
mixing 299
Lepton flavour universality violation 1013
Lepton PDF 165
Leptonic decays of charged pseudoscalar mesons,
note on 969
phenomenological implications 975
Leptons
(see individual entries for e, μ, τ and ν) 30, 1369
Leptoproduction kinematics 815
Leptoquark review 1189
Leptoquark searches 1189
Lethal dose from penetrating ionizing radiation 696
LHC 573
LHC (CERN) collider parameters 583
LHC (CERN) heavy ion collider parameters 584
LHeC 576
Light
speed in vacuum of 145
year 146
Light meson spectrum 914
Light Quarks — u, d, s 1447
Light quarks masses 863
Light unflavored mesons 35, 1491
Lightest supersymmetric particle, LSP 1086
LIGO, Laser interferometer gravitational observatory 441
Likelihood-ratio trick 729, 740, 757
Limits 720

Int. J. Mod. Phys. A 2026.41. Downloaded from www.worldscientific.com
by UNIVERSITY OF CALIFORNIA @ BERKELEY on 09/16/26. Re-use and distribution is strictly not permitted, except for Open Access articles.

Linear colliders 572, 574
Linear confinement 330, 777
Linear Higgs factories 574
Linear regression 729
Linear-theory mass dispersion σ_8 489
Liquid ionization chambers 650
Lithium-7 abundance 483
Little hierarchy 1097
LIV, Lorentz Invariance Violation 557
Local dark matter density 146
Local disk density 146
Local Group velocity with respect to CMB 146
Log-normal distribution 708
Logistic activation 744
Logistic regression 728
Logits 744, 749
Lomonosov satellite. γ-ray burst,
high-energy cosmic rays 661
Long baseline neutrino sources (LBL) 301
Long-lived sparticles masses limits 1121
Longitudinal fragmentation 399
Longitudinal structure function, plots of 386
Lorentz force 153
Lorentz invariant amplitudes 799
Lorentz transformations of four-vectors 799
Loss 728
Low Temperature Detectors (LTDs) 679
Low-radioactivity background techniques 684
LQCD
heavy quark masses 356
heavy quarks 354
lattice quantum chromodynamics calculations 352
light quarks masses 356
Monte Carlo method 357
QED 355
scattering amplitudes and resonances 359
status of simulations 360
Wilson fermion action 353
Wilson gauge action 352
LSP, lightest supersymmetric particle 1086
LSTM, long short-term memory 747
Luminosity 569, 572
muon collider 577
circular collider 572
linear collider 576
Luminosity conversion 146
Luminosity distance d_L 452
Lund string model 777
Lyα forest 457

M-theory 1139, 1173
Machine learning 172, 727
MAE, mean-absolute error 729
MAF, masked autoregressive flow 735
Magnetic fields, primordial 539
Magnetic Metallic Calorimeters (MMCs) 681
Magnetic monopoles 1180
GUTs prediction 1194
note on 1194
Magnetic monopoles searches 119, 2429
Majorana neutrinos 298
mAMSB, minimal AMSB 1095
Mandelstam variables 801
MAP, maximum a posteriori 730, 757
Marginal probability density function 706
Markov chain 770
Mass attenuation coefficient for photons 594
Mass matrix
light quark 864
neutrino 298
Masses
heavy quarks 866
light quarks 863
Materials, atomic and nuclear properties of, table 152
Matter parity 1177
Matter supermultiplet 1086
Matter, passage of particles through 586
Maximal mixing scenario 1092
Maximum energy transfer to e^- in single collision 587
Maximum likelihood 711
Maxwell equations 153
MC – Monte Carlo 789
MDP, Markov decision process 738
Mean energy loss rate in H_2 liquid, He gas, C, Al, Fe, Sn 587
Mean excitation energy 586, 587
Mean range in H_2 liquid, He gas, C, Fe, Pb 587
Mean siderial day 146
Median, definition 705
Meson cloud 931, 1049
Meson electromagnetic radius 911
Meson multiplets in quark model 325
Meson nonets (established) 326
Meson quick reference table 97
Meson-meson bound states 931
Mesons
Further states 2194
axial vector $\ell = 1$; 1^{++} or 1^{+-} 325
bottomonium 1026
charmonium 1026
conventional 1026
pseudoscalar $\ell = 0$, 0^{-+} 325
scalar $\ell = 1$, 0^{++} 325, 928
tensor $\ell = 1$, 2^{++} 325
thresholds 1026
unconventional 1026
vector $\ell = 0$, 1^{--} 325
XYZ 1026
Messenger scale 1094
Metric prefixes, commonly used 148
Michel parameters 859
Micro-mesh gaseous structure (MicroMegas) 617
Micro-pattern gas detectors, MPGD 616
Micro-quasars, binary 555
Micro-quasars,Cygnus X-3 555
MicroMegas, micro-mesh gaseous structure 617
Microwave background 456
Mihheev-Smirnov-Wolfenstein effect for solar neutrinos .. 303
Minimal
7-parameter model, ΛCDM+$\sum m_\nu$ 501
cosmological model ΛCDM 497
Minimal AMSB, mAMSB 1095
Minimal supergravity, mSUGRA 1095, 1109
Minimal Supersymmetric SM, MSSM 1086, 1174
Minimum ionization 587
Minimum ionization loss, table 152
MIP (minimum ionizing particle) 587, 613
Missing partner mechanism 1173
Missing VEV mechanism 1173
Mixing angle, weak ($\sin^2\widehat{\theta}(M_Z)$) 145
Mixing, D^0-$\overline{D}^0$, note on 958
Mixing matrix 300
Mixing, singlet-octet in quark model 336
MLP, multilayer perceptron 740, 744, 750
Modified gravity 490
Modified minimal subtraction scheme ($\overline{\text{MS}}$) 161
Modular group 1179
Moduli 1174
stabilization 1174
Molar volume 145
Molecular states 914, 921
Molière radius 597
Momenta, measurement of, in a magnetic field 652
Monopole problem 1180
Monopoles
catalysis of nucleon decay 1196
Kibble mechanism 1194

Int. J. Mod. Phys. A 2026.41. Downloaded from www.worldscientific.com
by UNIVERSITY OF CALIFORNIA @ BERKELEY on 09/16/26. Re-use and distribution is strictly not permitted, except for Open Access articles.

Parker bound 1195
Monte Carlo
acceptance-rejection method 768
calculations, importance sampling in 768
codes for radiation protection studies 699
DIEHARD 768
inverse transform method 768
Lagged-Fibonacci-based generator 768
LQCD 357
neutrino event generators 784
particle numbering scheme 789
random number generators 768
RANLUX generator 768
techniques 768
Monte Carlo algorithm for
χ^2 distribution 769
beta distribution 770
binomial distribution 769
Breit-Wigner distribution 769
exponential decay 769
Gamma distribution 769
Gaussian distribution 769
Poisson distribution 769
sine and cosine of random angle 769
Student's t distribution 769
Monte Carlo dropout 757
Monte Carlo event generators 772
MPGD, micro-pattern gas detectors 619
MPNN, message-passing neural network 750
$\overline{\text{MS}}$ factorization scheme 163
$\overline{\text{MS}}$ mass 162
MSE, mean-squared error 729, 756
MSSM current experimental status 1096
MSSM parameters 1089
MSSM, minimal supersymmetric SM 1086
MSSM-124 1090
mSUGRA, minimal supergravity 1095, 1109
μ-term 1089, 1092, 1100
μ (muon) 30, 1370
μ_0 (permeability of free space) 145, 153
Multi-arm bandits 739
Multi-class classification 730, 744
Multi-head attention 749
Multi-wire proportional chamber, MWPC 615
Multibody charm analyses, review of 952
Multibody decay kinematics 801
Multinomial distributions 707
Multiple Coulomb scattering 591
Multiple parton-parton interactions, MPI 169, 418, 779
Multiplets, meson in quark model 325
Multiplets, SU(n) 796
Multiplexing 682
Multivariate Gaussian distribution 707
Multiverse 455, 476
Muon
critical energy 597
energy loss rate at high energies 597
Muon Anomalous Magnetic Moment 846
Muon collider 576
Muon collider, neutrino radiation hazard 577
Muon decay parameters 853
μ-problem 1173
MWPC, Multi-wire proportional chamber
maximum wire tension 615
wire stability 615
Møller cross section 592

n (neutron) 99, 2213
N and Δ Resonances 100, 2219
N and Δ Resonances, note on 1047
N baryons
$N(1440)$ 100, 2219
$N(1520)$ 100, 2221
$N(1535)$ 100, 2223
$N(1650)$ 100, 2225
$N(1675)$ 100, 2227
$N(1680)$ 101, 2230
$N(1700)$ 101, 2232
$N(1710)$ 101, 2234
$N(1720)$ 101, 2236
$N(1860)$ 2239
$N(1875)$ 101, 2240
$N(1880)$ 101, 2242
$N(1895)$ 102, 2244
$N(1900)$ 102, 2246
$N(1990)$ 2248
$N(2000)$ 2250
$N(2040)$ 2251
$N(2060)$ 102, 2251
$N(2100)$ 102, 2253
$N(2120)$ 102, 2255
$N(2190)$ 103, 2257
$N(2220)$ 103, 2259
$N(2250)$ 103, 2260
$N(2300)$ 2261
$N(2570)$ 2261
$N(2600)$ 103, 2262
$N(2700)$ 2262
N's and Δ's note 100, 2219
$N(\sim 3000$ Region) Partial-Wave Analyses 2262
n-body differencial cross sections 799
n-body phase space 799
Nambu-Goldstone bosons 1069, 1130
Nambu-Goldstone composite bosons 1156
Names, hadrons 17, 155
Naming scheme for baryon resonances 1047
Naturalness 1097
Neural network 727, 728, 730, 733, 744, 751, 752, 757
Neuron 744
Neutral Higgs bosons searches 29, 1300
Neutralinos 1090
Neutralinos mass limits 1117
Neutrino detectors (deep, large, enclosed volume)
heavy water 667
liquid scintillator 666
noble
time-projection chamber 667
table of detectors 665
water-filled 667
Neutrino detectors, cryogenic detectors 680
Neutrino oscillations 560
Neutrino telescopes
AMANDA, South Pole 669
ANTARES, Med. Sea 669
backgrounds 668
DUMAND, Pacific Ocean 669
effective area 668
GVD, Lake Baikal 669
HUNT, South China Sea or Lake Baikal 669
IceCube, South Pole 669
KM3NeT, Med. Sea 669
NEMO, Med. Sea 669
NEON, South China Sea 669
NESTOR, Med. Sea 669
NT-200, Lake Baikal 669
P-ONE, Pacific Ocean 669
technical realisation 669
TRIDENT, South China Sea 669
Neutrino(s)
astrophysical 668
atmospheric 557, 558
detectors 665
atmospheric flux 305
beam lines at high-energy proton synchrontrons 585
BSM physics 560
chemical potential 539

Int. J. Mod. Phys. A 2026.41. Downloaded from www.worldscientific.com
by UNIVERSITY OF CALIFORNIA @ BERKELEY on 09/16/26. Re-use and distribution is strictly not permitted, except for Open Access articles.

cosmic 557
cosmogenic 557, 559
cosmological constraints 497
current temperature 497
density of the Universe 147
diffuse extragalactic flux 559
diffuse fluxes 558
Dirac 298
flavor ratio 557
from astrophysical point sources 560
from Galactic Plane 560
in cosmology, note on 497
left-handed 297, 969
Majorana 298
mass density parameter, Ω_ν 488
mass hierarchy 668
mass matrix 298
mass, cosmological limit 493
masses 501
masses, mixing, and oscillations, note on 297
measurement methods 557
mixing 32, 1419
Monte Carlo event generators 784
neutrinoless double-β decay 319
non-standard 500
oscillation search 303
particle physics 560
production 557
prompt 558
properties 32, 1404
reactor
detectors 665
relic background 497
right-handed 297
see-saw mechanism 298
solar flux 304
solar, *pp* chain 304
solar, CNO cycle 304
sterile 297, 299, 316
supernova burst
detectors 665
Neutrinoless double-β decay searches 319
Neutrinoless double-beta ($0\nu\beta\beta$) deca 1181
Neutron 99, 2213
Neutron mass 145
Neutron-antineutron (n–$\bar{n}$) oscillation 1181
Neutrons at accelerators 696
Neutrons, from radioactive sources 701
New heavy bosons
(W', Z', leptoquarks, etc.) searches 29, 1317
New Physics (NP) beyond SM 299, 993
NEWS-G collaboration 514
NEWSdm collaboration 514
Newtonian gravitation constant G_N 146
Next-to-lightest supersymmetric particle, NLSP 1096
Next-to-minimal supersymmetric SM, NMSSM 1087
NF, normalizing flow 733, 735, 736, 740
NICA 574
NLSP, next-to-lightest supersymmetric particle 1096
NMS, non-maximum suppression 746
NMSSM, next-to-minimal supersymmetric SM 1087
Node 750
Noise
equivalent noise analysis 639
in analog signal processing 639
in digital signal processing 641
in timing measurements 641
noise origins 638
Nomenclature for hadrons 155
Non-Gaussianity CMB 457, 473, 532
Non-perturbative corrections 170
Non-standard neutrinos
interactions beyond weak force 500
sterile neutrinos 500
unstable neutrinos 500
Non$q\bar{q}$ candidates
$cc\bar{c}\bar{c}$ state 1039
Double-J/ψ(1S) invariant mass 1039
four heavy quarks 1039
heavy-heavy systems 1036
heavy-light systems 1035
Normal (Gaussian) distribution 708
Normal distribution 707
Nova, TeV Radiation 555
NP, new physics beyond SM 299
Neutrino properties 32, 1404
Nuclear
and atomic properties of materials, table 152
interaction length, table 152
magneton 145
Nuclear PDFs 378
Nucleon decay 1176
Nucleosynthesis 456
Nuclides, radioactive, commonly used 701
Number density of baryons 146
Number density of CMB photons 146
Number of degree of freedom 713
Number of neutrino types
and sum of neutrino masses 32, 1414
Numbering scheme for particles 789

Object detection 745
Observations, the light element abundance 480
Occupational radiation dose, U.S. maximum permissible . 696
Octet-singlet mixing in quark model 326
Odderon in soft QCD 428
Ω baryons
$\Omega_c(3185)^0$ 114, 2395
$\Omega_c(3327)^0$ 114, 2395
$\Omega(2109)^0$ 2363
Ω^- 109, 2361
$\Omega(2012)^-$ 109, 2362
$\Omega(2250)^-$ 109, 2363
$\Omega(2380)^-$ 2363
$\Omega(2470)^-$ 2363
Ω_b^- 117, 2420
$\Omega_b(6316)^-$ 117, 2420
$\Omega_b(6330)^-$ 117, 2420
$\Omega_b(6340)^-$ 117, 2420
$\Omega_b(6350)^-$ 117, 2420
Ω_c^0 ..... 113, 2391
$\Omega_c(2770)^0$ 114, 2393
$\Omega_c(3000)^0$ 114, 2393
$\Omega_c(3050)^0$ 114, 2394
$\Omega_c(3065)^0$ 114, 2394
$\Omega_c(3090)^0$ 114, 2394
$\Omega_c(3120)^0$ 114, 2395
$\Omega_{\rm dm}$, dark matter density 490
ω mesons
$\omega(2220)$ 1617
$\omega(782)$ 36, 1510
$\omega(1420)$ 38, 1559
$\omega(1650)$ 39, 1578
$\omega_3(1670)$ 39, 1580
Ω, cosmological density parameter 451
$\Omega_{\rm m}$, mass density parameter 451
Ω_Λ, scaled cosmological constant 451
Ω_ν, neutrino mass density parameter 488
$\Omega_{\rm tot}$, total energy density of Universe 494
$\Omega_{\rm v}$, vacuum energy parameter 451
One-hot encoding 740
OOD, out-of-distribution 736
Optimal control 738
Optimization 727
Orbifold GUT 1174, 1177
Organic scintillator 605

Int. J. Mod. Phys. A 2026.41. Downloaded from www.worldscientific.com
by UNIVERSITY OF CALIFORNIA @ BERKELEY on 09/16/26. Re-use and distribution is strictly not permitted, except for Open Access articles.

Other light mesons 2194
Other particle searches 2523
Overfitting 728, 730, 731, 733, 751, 752

p (proton) 99, 2203
PAE, probabilistic autoencoder 734
Parameter estimation 710
Parameter estimation with constraints 713
Parameterizing the Universe 488
Pardethadcal 646
Parity of $q\bar{q}$ states 325
Parsec 146
Partial Conserved Axial Current, PCAC 785, 911
Partial wave analyses, PWA 1049
Particle
  ID numbers for MC 789
  identification detectors, PID 610
  nomenclature 155
  symbol style conventions 155
Particle flow 644
Particle flow confusion 644
Particle level 169
Particle nomenclature 17
Particle Physics Booklet, how to get 13
Parton
  density functions 772
  distribution function, PDF 163, 419
  distributions 377
Parton level 170
Parton shower 169
Parton-shower formalism 774
Passage of particles through matter 586
Pati-Salam model 1171, 1172, 1189
$\bar{p}p$ annihilation 915
P_c, exotic baryons
  $P_{c\bar{c}s}(4338)^0$ 118, 2423
  $P_{c\bar{c}s}(4459)^0$ 2425
  $P_c(4312)^+$ 2423
  $P_c(4380)^+$ 2423
  $P_c(4440)$ 2424
  $P_c(4457)^+$ 2424
PCA, principle component analysis 731, 734
PCAC, Partial Conserved Axial Current 785, 911
PDF, parton distribution function 419
PdgLive, interactive access to RPP 13
PDGLive, PDG web presentation 22
Peccei–Quinn symmmetry 1181
Peccei-Quinn mechanism and axion 1130
Penguin decays, electroweak 984, 993
Penguin-dominated modes 277
Pentaquarks
  $P_{c\bar{c}}(4312)^+$ 1057
  $P_{c\bar{c}}(4440)^+$ 1057
  $P_{c\bar{c}}(4457)^+$ 1057
  search 1057
PEP-II (SLAC) collider parameters 581
Periodic table of the elements 149
Permeability μ_0 of free space 145, 153
Permittivity ϵ_0 of free space 145, 153
Permutation equivariance 741
Permutation invariance 741, 750
Perturbation of early Universe 488
Perturbation theory, chiral 930, 937
Phase space, Lorentz invariant 799
Phase space, relations for 799
Phenomenological MSSM, pMSSM 1096, 1110
ϕ mesons
  $\phi(1020)$ 36, 1527
  $\phi(1680)$ 40, 1582
  $\phi(2170)$ 41, 1614
  $\phi_3(1850)$ 40, 1601
Photon
  attenuation length 594
  cross section in carbon and lead, contributions to 594
  pair production cross section 594
  structure functions F_2^γ 403
  to e^+e^- conversion probability 594
  total cross sections (C and Pb) 594
  ultra-high energy 596
Photon and electron interactions with matter 592
Photon collider 576
Photon detectors 602
Photoproduction 165
Physical constants 145
Physics beyond general relativity 539
π mesons
  π^0 ..... 35, 1494
  $\pi^\pm$ 35, 1491
  $\pi(1300)$ 37, 1546
  $\pi_1(1400)$ 1553
  $\pi_1(1600)$ 39, 1575
  $\pi_2(1670)$ 39, 1580
  $\pi_2(1880)$ 41, 1602
  $\pi_2(2005)$ 1607
  $\pi_2(2100)$ 1610
  $\pi(1800)$ 40, 1596
π value 145
PID, particle identification detectors 610
Pions and kaons
  experimental rate measurements 970
  theoretical decay-constant calculations 971
Pixel detectors
  DEPFET pixels 632
  DMAPS 633
  hybrid pixels 632
  monolithic pixels 632
PixelCNN 735
Planck
  constant h 145
  constant, reduced 145
  length 146
  mass 146
Plasma acceleration 577
Plasma energy 586
pMSSM, phenomenological MSSM 1096
POEMMA – probe of extreme multi-mes. astrophys. 661
Point Net 750
Poisson distribution 708, 769
Polarization in B decays, note on 992
Polarization in penguin-dominated B decays 993
Pole mass 162
Pole structure of the $\Lambda(1405)$ region, note on 1055
Pomeron effective trajectory 423
Pomeron in soft QCD 422
Pontecorvo-Maki-Nakagawa-Sakata
  mixing matrix (PMNS) 300
Pooling 745
  average 745
  max 745
Potentials, electromagnetic 153
Power correction 162
pp-scattering amplitude by Donnachie-Landshoff 414
Pre-training 753
Preconfinement 777
Prefixes, metric, commonly used 148
PReLU, parametric ReLU 744
Present-day CMB
  dipole amplitude 146
  temperature 146
Pressureless matter parameter 146
Primordial
  element abundance 480
  helium fraction 146
  magnetic fields 539
Princeton Tritium Observatory for Light, Early universe,
  Massive-neutrino Yield (PTOLEMY) 502

Probability ... 705
density function, definition ... 705
Kolmagorovs definition ... 705
Production and Decay of b-flavored Hadrons ... 980
Propagation of errors ... 706
Properties (atomic and nuclear) of materials, table ... 152
Proton
cyclotron frequency/field e/m_p ... 145
mass ... 145
structure function ... 373
structure function, plots ... 386
structure functions ... 163
Proton (see p) ... 99, 2203
Proton decay detectors ... 665
Pruning ... 758
Pseudo-Nambu–Goldstone boson ... 1173, 1181
Pseudorapidity ... 413, 802
Pseudoscalar mesons ... 917
$\eta(1405)$, $\eta(1475)$ ... 917
$\ell = 0$, 0^{-+} ... 325
$\eta(1295)$ ... 917
$\eta(2370)$ ... 918
ψ mesons
$\psi_2(3823)$ [*was* $\psi(3823)$; *was* $X(3823)$] ... 86, 2110
$\psi_2(3842)$ ... 86, 2111
$\psi(2S)$ ... 84, 2083
$\psi(3770)$ ... 85, 2102
$\psi(4040)$ ... 87, 2118
$\psi(4160)$ ... 87, 2122
$\psi(4230)$ [*aka* $Y(4230)$; *was* $\psi(4260)$] ... 88, 2125
$\psi(4360)$ [*aka* $Y(4360)$; *was* $X(4360)$] ... 89, 2132
$\psi(4415)$ ... 89, 2135
$\psi(4660)$ [*aka* $Y(4660)$; *was* $X(4660)$] ... 89, 2138
PTOLEMY, neutrino background direct detection ... 502
PTQ, post-training quantization ... 758
Pulsars, binary ... 444

QAT, quantization-aware training ... 758
QCD
Λ parameter ... 781
$\overline{\text{MS}}$ renormalization scheme ... 161
β function ... 161
color factor ... 161, 172
coupling constant ... 161
jets ... 171
Lagrangian ... 161
lagrangian ... 861
Λ parameter ... 162
Lattice ... 352
lattice ... 861, 1137
photon structure functions ... 403
renormalization group equation (RGE) ... 161
running coupling ... 161, 180, 181
structure functions ... 375
Quality factor for biological damage due to radiation ... 695
Quantization ... 758
Quantum
fluctuations, inflation ... 465
gravity theory ... 1067
Quantum numbers in quark model ... 324
Quark
masses review ... 34, 1447
Quark induced jets ... 172
Quark model
baryon resonances in ... 329
ideal mixing in ... 327
meson multiplets in ... 325
mixing, singlet-octet in ... 336
quantum numbers in ... 324
Quark-antiquark annihilations $c\bar{d} \to W^+ \to \ell^+\nu$ ... 969
Quark-mixing CKM matrix ... 273
Quark-parton model ... 163
Quarks ... 34, 1447
and lepton compositeness searches ... 120, 1150, 2494
b ... 34, 1453
c ... 34, 1451
d ... 34, 1447
fragmentation in e^+e^- annihilation, heavy ... 404
masses, note on ... 861
model ... 324
model assignments ... 330
model, dynamical ingredients ... 335
properties of ... 324
s ... 34, 1447
t ... 34, 1455
u ... 34, 1447
Quasi-stationary general relativity ... 438

R-CNN, region convolutional neural network ... 745
R-parity ... 1087, 1108
R-parity conserving ... 1087
R-parity violation, RPV ... 1099
$\mathbb{R}^{1,3} \times S^1/(\mathbb{Z}_2 \times \mathbb{Z}_2')$ ... 1174
Rad, unit of absorbed dose of radiation ... 695
Radiation
-dominated epoch ... 454
Cherenkov ... 598
coherent radio Cherenkov radiation ... 599
gravitational ... 440
length ... 593
length of materials, table ... 152
length, approximate algorithm ... 593
protection ... 695
protection instrumentation ... 698
transition ... 599
weighting factor ... 695
Radiation damage
in silicon detectors ... 635
Radiation length ... 642
Radiative
gravity test, GR prediction ... 445
Radiative loss by muons ... 597
Radio-detection of cosmic ray air shower ... 674
Radioactive nuclides, half-lives of ... 701
Radioactive sources, commonly used ... 701
Radioactivity
accelerator-induced ... 697
accelerators prompt neutrons ... 696
ambient dose equivalent ... 695
and radiation protection ... 695
Becquerel, unit of ... 695
biological damage from chronic exposure ... 695
Cancer induction ... 696
cosmic ray background radiation ... 696
dose rate from γ ray sources ... 697
effective dose ... 695
effective dose limits ... 696
fluence, Φ ... 695
kerma, K ... 695
lethal dose from ... 696
long-term risk ... 695
natural annual background ... 696
personal dosimeters ... 699
rem, **r**oentgen **e**quivalent for **m**an ... 698
unit of absorbed dose, gray ... 695
unit of activity ... 695
weighting factor ... 695
Radion searches ... 1069
Randall-Sundrum
model ... 822, 1070
warped geometry ... 1067
Randall-Sundrum graviton ... 1158
Random angle, MC algorithm for sine and cosine of ... 769
Random forest ... 743
Random number generators ... 768
RANLUX Monte Carlo generator ... 768

Int. J. Mod. Phys. A 2026.41. Downloaded from www.worldscientific.com
by UNIVERSITY OF CALIFORNIA @ BERKELEY on 09/16/26. Re-use and distribution is strictly not permitted, except for Open Access articles.

Int. J. Mod. Phys. A 2026.41. Downloaded from www.worldscientific.com
by UNIVERSITY OF CALIFORNIA @ BERKELEY on 09/16/26. Re-use and distribution is strictly not permitted, except for Open Access articles.

Rapidity 801
Rare event search
  $0\nu\beta$ decay 678
  WIMPs 677
Rare kaon decay, constraints on CKM parameters 939
Reactor
  antineutrino flux 310
  antineutrino oscillation 310
Readout
  detector 637
  low-noise 637
Receptive field 745
Recombination scheme 171
Redshift 450
  $z \simeq 1100$, reionization 532
  age at half reionization 147
  age when acceleration was zero 147
  age when optical depth equals unity 147
  at half reionization 147
  at which optical depth equals unity 147
  comoving size of sound horizon at z_* 147
  matter-radiation equality 147
  when acceleration was zero 147
Redshift distortion 493
Refractive index of materials, table 152
Regge pole approach 413
Regge poles multiple exchange 414
Reggeon field theory 414
Regression 727, 728, 741, 743, 745, 750, 757
Regularization 727, 728, 730, 752, 757
Reionization of the Universe 491, 492
Reionization optical depth 146
Relativistic kinematics 799
Relativistic rise 587
Relativistic transformation of electromagnetic fields 153
ReLU, rectified linear unit 744, 752
Rem, **r**oentgen **e**quivalent for **m**an 695
Renormalization group
  quark mass 861
Renormalization group equation (RGE) 161, 1094, 1174
Renormalon 163, 866
Representation learning 731
Representations, SU(n) 796
Repulsive gravity, dark energy 524
Resistive plate chambers 623
Resistivity of metals 153
ResNet, residual network 746, 747
Resonances
  bound state 804
  branch points 804
  Breit–Wigner parameterization 808
  Chew-Mandelstam function 810
  effective-range expansion 810
  Flatte parameterization 809
  $\mathcal{K}$-matrix parameterization 809
  left-hand cut 804
  Mandelstam variables 803
  partial-wave decomposition 806
  physical sheet 804
  pole couplings 808
  pole residues 807
  properties of resonances 807
  resonance pole mass 807
  resonance pole position 807
  resonance pole width 807
  Riemann sheets 804
  right-hand cut 804
  $\mathcal{S}$-matrix properties 803
  scattering-length approximation 810
  triangle singularity 804
  unphysical sheet 804
  virtual state 804
  Watson theorem 807
Restricted energy loss rate 587, 590
Resummation 168
Review of multibody charm analyses 952
Review of Particle Physics overview 13
RG - renormalization group 347, 353
RGE, renormalization group equation 1094
RHIC 573
RHIC (Brookhaven) collider parameters 583
RHIC (Brookhaven) heavy ion collider parameters 584
ρ mesons
  $\rho(770)$ 35, 1504
  $\rho(1450)$ 38, 1562
  $\rho(1570)$ 1575
  $\rho(1700)$ 40, 1587
  $\rho(1900)$ 1603
  $\rho(2150)$ 1612
  $\rho_3(1690)$ 40, 1584
  $\rho_3(1990)$ 1607
  $\rho_3(2250)$ 1618
  $\rho_5(2350)$ 1621
Right-handed
  antineutrinos 969
  fermions 1158
  neutrinos 297
Right-handed neutrinos 1171
Rigidity 542
Risk 728, 756
Risk minimization 728
RL, reinforcement learning 727, 738, 739
RNN, recurrent neural network 741, 747
RNNSearch 749
Robertson-Walker metric 450, 463, 488
Robustness of an estimator 711
ROC, receiver operating characteristic 729
  curve 728
ROI, region of interest 746
Rotational invariance 741
Rounding errors, treatment of 19
Rounding, PDG rules 19
R parity 1177
RPC, resistive plate chambers 623
RPN, region proposal network 746
RPP authors and affiliations 2
RPP criteria for measured data 18
RPV, R-parity violation 1099
Running coupling in QCD 161, 180, 181
Running spectral index, $k_0 = 0.05\,\mathrm{Mpc}^{-1}$ 147
Rydberg energy 145

S-matrix
  approach to Z 842
  for two-body scattering 799
Sachs-Wolfe effect 459, 533
Sachs-Wolfe effect, integrated 460, 492, 523, 533
Satellite
  Planck, CMB 468, 526, 531, 534
  COBE, monopole 531
  Euclid, dark energy 477
  Gaia, density distribution 507
  LAGEOS, test of gravity 444
  LARES, test of gravity 444
  LiteBIRD, inflation, CMB 536
  Lomonosov, γ-ray bursts 661
  POEMMA, cosmic rays 661
  SMM, sun radiation 1135
  SPHEREx, inflation 477
  WMAP, CMB 526
Sbottom (bottom squark) 1091
Scalar field cosmology 464
Scalar mesons 915
  $a_0(1450)$ 915
  $a_0(980)$, $f_0(980)$, $f_0(500)$, $K_0^*(700)$ 921
  $f_0(1370)$, $f_0(1500)$, $f_0(1710)$ 915

Int. J. Mod. Phys. A 2026.41. Downloaded from www.worldscientific.com
by UNIVERSITY OF CALIFORNIA @ BERKELEY on 09/16/26. Re-use and distribution is strictly not permitted, except for Open Access articles.

$f_0(1770)$, $a_0(1710)$ 915
nonets 921
SU(3) couplings 916
Scalar mesons $\ell = 1$, 0^{++} 325, 928
Scalar mesons below 1 GeV, note on 928
Scalar spectral index 146
Scale dependence 162
Scale factor, definition of 18
Scaled cosmological constant, Ω_Λ 451
Scaled dot-product attention 749
Scaled Hubble constant 451
Scaling factor for Hubble expansion rate 146
Scaling for cosmological constant 146
Scaling violations in fragmentation functions 397
Scattering, relations for 815
SCET – soft-collinear effective theory 345
Scherk-Schwarz mechanism 1088
Schwarzschild
radius of a black hole 1068
radius of the Earth 146
radius of the Sun 146
Scintillator parameters 605
Score 736
Searches
W' bosons 1076, 1158
Z' bosons 1080, 1158
new light particles in rare K decay 938
axigluons 1158, 1166
axion like particles (ALP) 1135
axions (A^0) 508, 1130
colorons 1166
dark matter 120, 2505
dyons 1195
excited fermions 1151
excited leptons 1151
extra dimensions 508, 1067
graviscalar 1067
graviton 1068
heavy charged lepton 32, 1403
heavy neutral leptons 1440
heavy non-$q\bar{q}$ mesons 1035
leptoquark 1189
magnetic monopoles 119, 1194, 2429
neutrino oscillation or flavor transition 303
neutrinoless double-β decay 319
pentaquarks 1057
quark and lepton compositeness 120, 1150, 2494
radion 1069
rare events 675
SM explicit violations 937, 938
solar axions 1135
supersymmetric particle 119, 2432
technicolor 508, 1156
technifermions
spontaneously broken chiral symmetry 1156
WIMP 120, 2505
Seesaw mechanism 1171
type-I 1179
type-II 1179
type-III 1179
Selection and treatment of data 17
Self-attention 749
Self-supervised learning 737
Semantic segmentation 745
Semiconductor
detectors 629
materials 630, 636
radiation damage 635
type inversion 636
Semiconductor Thermistors 680
Semileptonic b-hadron decays,
determination of V_{cb}, V_{ub} 1003
Semitauonic decays 1013
Sequential data 741, 747
Sequential two-body decay, kinematic limits 800
sfermion 1086
SGD, stochastic gradient descent 751
Shape functions, SF 275, 345
Shared weights 745, 747
Shell correction 588
Shower detectors 644
Showers, electromagnetic
lateral distribution of 597
longitudinal distribution of 596
SI units, complete set 148
Sidereal day 146
Sievert, unit of radiation dose equivalent 695
σ 35, 1502
Σ baryons
Σ^+ 106, 2315
Σ^- 107, 2318
Σ^0 ..... 107, 2317
Σ_b^* 116, 2411
$\Sigma_b(6097)^+$ 116, 2411
$\Sigma_b(6097)^-$ 116, 2411
Σ_b 116, 2410
$\Sigma(1385)$ 107, 2320
$\Sigma(1580)$ 2323
$\Sigma(1620)$ 2324
$\Sigma(1660)$ 107, 2325
$\Sigma(1670)$ 107, 2326
$\Sigma(1750)$ 107, 2328
$\Sigma(1775)$ 107, 2330
$\Sigma(1780)$ 2332
$\Sigma(1880)$ 2333
$\Sigma(1900)$ 2333
$\Sigma(1910)$ 107, 2334
$\Sigma(1915)$ 108, 2335
$\Sigma(2010)$ 2338
$\Sigma(2030)$ 108, 2339
$\Sigma(2070)$ 2341
$\Sigma(2080)$ 2341
$\Sigma(2100)$ 2342
$\Sigma(2110)$ 2343
$\Sigma(2250)$ 2344
$\Sigma(2455)$ 2345
$\Sigma(2620)$ 2345
$\Sigma(3000)$ 2346
$\Sigma(3170)$ 2346
$\Sigma_c(2455)$ 111, 2378
$\Sigma_c(2520)$ 111, 2379
$\Sigma_c(2800)$ 111, 2380
Σ baryons ($S = -1$, $I = 1$) 106, 2315
σ_8 fluctuation amplitude at $8\,h^{-1}$ Mpc scale 146
Sign conventions for resonance couplings 1053
Silicon detector 629
radiation damage 635
timing measurement 634
Silk damping 534
Simplified models 1096
Simulation-based inference 729, 733, 735, 739, 757
Singlet-octet mixing in quark model 326
Skip connection 747, 749, 752
SL(2, $\mathbb{Z}$) 1179
SLC (SLAC) 573, 581
sleptons 1091
sleptons masses limits 1117
SLHA, SUSY Les Houches accord 1090
Sliding singlet mechanism 1173
Sloan Digital Sky Survey (SDSS) 493
Slow-roll inflation 532
SM effective field theory, SMEFT 1098
SMEFT, SM effective field theory 1098
SMM – solar maximum mission satellite 1135
SN1987A
light gravitons luminosity 1068

Int. J. Mod. Phys. A 2026.41. Downloaded from www.worldscientific.com
by UNIVERSITY OF CALIFORNIA @ BERKELEY on 09/16/26. Re-use and distribution is strictly not permitted, except for Open Access articles.

Sneutrino masses limits 1117
sneutrinos 1091
SNO - sudbury neutrino observatory 1133
SO(10) 1172
SO(32) 1173
Soft supersymmetry breaking 1086
Soft-collinear effective theory (SCET) 345
Softmax 744, 749
Software 24
Solar
  ν experiment 304
  ν fluxes 304
  ν problem 304
  constant, nominal 146
  distance from Galactic center 146
  equatorial radius, nominal 146
  escape velocity from the Galaxy 146
  luminosity, nominal 146
  mass 146
  photosphere temperature, nominal 146
  Schwarzschild radius of 146
  standard model 304
  velocity with respect to CMB 146
Solid angle 146
Sparticle 1090
Spectroscopy of mesons
  containing two heavy quarks, note on 1026
Speed of light in vacuum c 145
Sphaleron 1180
SPHEREx – spectro-photometer for history
  of epoch reionization, satellite 477
Spherical harmonics 794
Spin polarization 571
Spin-dependent structure functions 379
Spin-flavor symmetry 343
Split supersymmetry 1088
Splitting functions 163
SPPC 576
Squark mass limits 1111
squarks 1091
Sring theory 484
SSM, standard solar model 304
Stückelberg mass 1179
Standard
  gravitational acceleration 145
  neutrino cosmology 497
  particle numbering for MC 789
  Solar Model (SSM) 304
Standard cosmological model 489
Standard model of particle physics
  as EFT of more fundamental theory 343
Standard model, cosmological 539
Starobinsky model of gravity 460
Statistical procedures 18
Statistics, note on 710
Status of LQCD simulations 360
Stefan-Boltzmann constant 145
Sterile neutrinos 297, 316
Stop (top squark) 1091
Stopping power for heavy charged projectiles 586
String theory 1130
  flux landscape 1174
  type II 1174
Strong coupling constant 145, 172, 176
Strong CP problem 1171, 1181
Strong fields, neutron stars, black holes in GR 438
Structure functions 373
Student's t distribution 708, 769
SU(n) multiplets 796
SU(3)
  classification of baryon resonances 329
  isoscalar factors, note on 795
  multiplets 329
  representation matrices, note on 795
  transformation, generators of 795
SU(5) 334, 1171
SU(6) multiplets 329
Sudbury
  neutrino observatory, SNO 1133
Sum of neutrino masses 147
Sum rules 865
Summary tables, organization of 13
Sunyaev-Zeldovich effect 460, 492, 525, 537
Sunyaev-Zeldovich effect, kinetic 460
Super tau-charm factories 576
Super-conformal anomaly 1088
Super-Higgs mechanism 1088
Super-Kamiokande 1176, 1177, 1181
Superconducting Tunnel Junctions (STJs) 680
Supergravity
  10d type-IIB 1174
Supergravity 1088
SuperKEKB (KEK) collider parameters 581
Supermassive GUT monopoles 1194
Supermultiplet 1086
Supernova remnants 553
Supernovae
  as cosmological probes 491
  Type Ia 491
  Type II 491
Superpartners 1086
Superpotential 1087
Superspace 1087
Superstring 1173
Supersymmetric particle searches 119, 2432
Supersymmetric particle spectrum 1090
Supersymmetry breaking 1088
Supersymmetry, SUSY 1086, 1171
Supervised learning 727, 728, 733, 736, 741
Survival probability, relations for 799
SUSY Les Houches accord, SLHA 1090
SUSY, supersymmetry 1086
SVM, support vector machine 740, 741
Symbolic regression 758
Synchrotron oscillations 571
Synchrotron radiation 154, 571
Synchrotron tune 571
Systematic errors, treatment of 18
SZ, Sunyaev-Zeldovich effect 537

t (quark) 871
t' (4th Generation) Quark, Searches for 34, 1480
$T^6/\mathbb{Z}_n$ 1174
Tabular data 740
τ lepton 30, 1375
τ branching fractions, note on 856
τ decay parameters, note on 859
Technicolor 119, 2493
  electroweak symmetry breaking 1156
Technifermion condensate formation 1156
Telescope Array (TA) 661
Tensor mesons 916, 917
  $f_2(1910)$ 920
Tensor mesons $\ell = 1$, 2^{++} 325
Tensor-to-scalar field perturbations ratio, ... 147
Testing dataset 728, 733
Tests of Conservation Laws 121
  Baryon and lepton number 127
  Discrete space-time symmetries 121
  Electric charge 124
  Electric dipole moments 122
  Lepton family numbers 124
  Quantum number conservation laws 124
  Quark flavors 128
  Tests of CPT 124
  Violations of CP and T 121

Int. J. Mod. Phys. A 2026.41. Downloaded from www.worldscientific.com
by UNIVERSITY OF CALIFORNIA @ BERKELEY on 09/16/26. Re-use and distribution is strictly not permitted, except for Open Access articles.

Tests of conservation laws . . . 131
Tetraquark candidates
  $K_0^*(700)$ . . . 931
  $T_{c\bar{c}1}(4430)$ . . . 1038
  $X(3872)$ . . . 1037
  $\psi(4230)$ . . . 1038
  $a_0(980)$ . . . 931
  $f_0(500)$ . . . 931
  $f_0(980)$ . . . 931
Tetraquark states . . . 920
  $\phi(2170)$ . . . 921
  $a_0(980)$, $f_0(980)$ . . . 921
Tetraquarks . . . 328, 914
  $T^*_{c\bar{s}0}(2900)$ . . . 2184
  $T^*_{cs0}(2870)^0$ . . . 2183
  $T^*_{cs1}(2900)^0$ . . . 2183
  $T_{cc}(3875)^+$ . . . 2184
  $T_{b\bar{b}1}(10610)$ . . . 94, 2192
  $T_{b\bar{b}1}(10650)^+$ . . . 95, 2193
  $T_{b\bar{s}}(5568)^+$ . . . 2190
  $T_{c\bar{c}\bar{s}1}(4000)$ . . . 2186
  $T_{c\bar{c}\bar{s}1}(4220)^+$ . . . 2189
  $T_{c\bar{c}0}(4240)^+$ . . . 2189
  $T_{c\bar{c}1}(3900)$ . . . 94, 2184
  $T_{c\bar{c}1}(4200)^+$ . . . 2188
  $T_{c\bar{c}1}(4430)^+$ . . . 94, 2189
  $T_{c\bar{c}}(4020)$ . . . 94, 2186
  $T_{c\bar{c}}(4050)^+$ . . . 2187
  $T_{c\bar{c}}(4055)^+$ . . . 2188
  $T_{c\bar{c}}(4100)^+$ . . . 2188
  $T_{c\bar{c}}(4250)^+$ . . . 2189
  $T_{cc\bar{c}\bar{c}}(6900)^0$ . . . 94, 2191
  $T_{cc\bar{c}\bar{c}}(6600)$ . . . 2191
  $T_{cc\bar{c}\bar{c}}(7100)$ . . . 2191
TeV gamma ray detection sensitivity, Crab Unit . . . 552
TeV gamma ray instruments
  ARGO-YBJ . . . 552
  AS_γ . . . 552
  CTA-LST . . . 552
  H.E.E.S. . . . 552
  HAWC . . . 552
  LHAASO . . . 552
  MAGIC . . . 552
  VERITAS . . . 552
Tevatron . . . 572
Tevatron collider parameters . . . 583
Theoretical decay-constant calculations
  Bottom mesons . . . 975
  charmed mesons . . . 973
  pions and kaons . . . 971
Thermal
  history of the Universe . . . 453
θ_W, Weinberg angle . . . 297
Third generation vector-like quarks . . . 1160
Thomson cross section σ_T . . . 145
Three-body
  decay kinematics . . . 800
  decays, kinematic limits . . . 800
  phase space . . . 800
Threshold Cherenkov detectors . . . 610
Threshold correction . . . 1174
Thrust . . . 172
Time variation of the fine-structure constant . . . 539
Time-projection chambers, TPC . . . 619, 675
Timing measurement
  noise . . . 641
  silicon detectors . . . 634
Top quark t . . . 871
Top quark mass . . . 890
Top quark, note on . . . 871
Topological defect . . . 1180
Total cross sections . . . 419
Total energy density of Universe, $\Omega_{\rm tot}$ . . . 494
TPC, Time-projection chambers . . . 675
Track reconstruction . . . 839
Training . . . 727, 728, 731, 736, 744, 758
Training dataset . . . 727, 728, 730, 731, 733
Transfer learning . . . 753
Transformation of electromagnetic fields, relativistic . . . 153
Transformer . . . 741, 749
Transition Edge Sensors (TESs) . . . 681
Transition radiation . . . 599
Transition radiation detectors, TRD . . . 621
Translational invariance . . . 741, 745
Transposed convolution . . . 747
Transverse variables . . . 802
Tree . . . 740, 743
Triangle singularity . . . 328, 918, 920
Triangles, unitarity, note on . . . 273
Trilepton events . . . 1163
Trinification . . . 1172
Tropical year . . . 146
Two-body
  decay . . . 799
  differential cross sections . . . 801
  partial decay rate . . . 799
  reactions . . . 801
  scattering kinematics . . . 799
Two-photon processes in e^+e^- annihilation . . . 817
Type Ia supernovae . . . 491
Type II supernovae . . . 491

U-Net . . . 747
UHECRs, arrival directions . . . 550
UHECRs, dipolar anisotropy . . . 550
UHECRs, energy spectrum . . . 549
UHECRs, neutral particles . . . 551
UHECRs, primary composition . . . 550
ULA, ultralight axion-like particles . . . 1138
Ultra-high energy cosmic rays (UHECRs) . . . 542
Ultralight axion-like particles (ULAs) . . . 1138
Uncertainty quantification . . . 754, 757
Unconstrained averaging . . . 18
Underfitting . . . 728
Underlying event (UE) . . . 169
Unfolding . . . 740
Unified atomic mass unit . . . 145
Uniform distribution . . . 708
Units, electromagnetic . . . 153
Units, SI, complete set . . . 148
Universal approximation . . . 728, 730, 745
Universal Extra Dimension, UED . . . 821, 1072
Universality of free fall tests GR . . . 444
Universe
  accelerating evidence . . . 491
  age of . . . 452, 494
  as a particle detector . . . 502
  baryon density of . . . 146, 481
  bubble . . . 455
  composition . . . 450, 452
  cosmological structure . . . 454
  critical density of . . . 146
  curvature of . . . 451
  density fluctuations . . . 457
  density parameter of . . . 146
  entropy density . . . 455
  flatness . . . 494
  global description of . . . 488
  Hubble expansion of . . . 450, 488
  inflation . . . 488
  large-scale structure of . . . 452, 458
  matter-dominated . . . 456
  parameterizing . . . 488
  perturbation . . . 488
  phase transitions . . . 455
  radiation content at early times . . . 454

Int. J. Mod. Phys. A 2026.41. Downloaded from www.worldscientific.com
by UNIVERSITY OF CALIFORNIA @ BERKELEY on 09/16/26. Re-use and distribution is strictly not permitted, except for Open Access articles.

thermal history of 453, 463
thermodynamic equilibrium 454
Unsupervised learning 727, 731, 736
Υ ($b\bar{b}$) mesons
$\Upsilon(1S)$ 90, 2144
$\Upsilon(2S)$ 91, 2157
$\Upsilon_2(1D)$ [*was* $\Upsilon(1D)$] 92, 2163
$\Upsilon(3S)$ 93, 2170
$\Upsilon(4S)$ [*was* $\Upsilon(10580)$] 93, 2175
$\Upsilon(10753)$ 93, 2177
$\Upsilon(10860)$ 94, 2177
$\Upsilon(11020)$ 94, 2181

Vacuum energy parameter $\Omega_{\rm v}$ 451
Vacuum expectation value, VEV 1171
VAE, variational autoencoder 733
Validation dataset 728, 730, 731
Values of particle properties, historical perspective of 21
Vanishing gradient 744, 746, 747, 752
Variance, definition 705
Variational inference 733, 734, 757
Varying constants
gravitational $G_{\rm N}$, fine structure α 491
V_{cb} and V_{ub} CKM Matrix Elements 1959
V_{cb} and V_{ub} determination of, note on 1003
V_{cb} determination 1003
Vector mesons 918
ρ excitations 919
$\rho(1570) - C(1480)$ 919
$\rho(1900)$ 919
$\rho(770)$ 918
Vector mesons $\ell = 0$, 1^{--} 325
Vector superfields 1087
Vector-like quarks, VLQ 1160
VEPP-2000 580
VEPP-4M 580
Virgo, gravitational observatory 441
Virtual graviton process 822
VLQ, vector like quarks 1160
Von Neuman's acceptance-rejection method in MC 768
V_{ub} determination 1008
V_{ub}/V_{cb} determination 1012
V_{ud} determination 945
$V_{ud}, V_{us}, V_{ub}, V_{cd}, V_{cs}, V_{cb}, V_{td}, V_{ts}, V_{tb}$ 273
V_{us} determination 945

W and Z resonant production 816
W boson 27, 1243
mass 839
width 840
w, dark energy equation of state parameter 451
W-W' mixing 1078
Warped extra dimensions 1067
Wasserstein distance 733, 735, 736
Wasserstein GAN 734
Wavelength of 1 eV/c particle 145
WaveNet 735
Weak decay form factors 344
Weak gauge bosons pairs production 816
Weak-field general relativity 438
Weak-mixing angle ($\sin^2\widehat{\theta}(M_Z)$) 145
Weakly supervised learning 729
Weakly-interacting massive particle, WIMP 1086
Weight matrix 744
Weinberg angle θ_W 297
White-dwarf, weak-self-gravity 444
Wien displacement law constant $b = \lambda_m axT$ 145
WIMP 508
miracle 506, 1086
WIMP dark matter searches 120, 2505
WIMP, weakly-interacting massive particle 1086
Wino 1091
WMAP, Wilkinson Microwave Anisotropy Probe 492
Wolfenstein parameters 273, 945, 977
World average of $\alpha_s(m_Z^2)$ 177, 181
W'-boson searches 1076, 1165
Wraped extra dimension 822
Wrong-Higgs couplings 1092

X mesons
$X_0(2900)$ 2183
$X_1(2900)$ 2183
$X(1835)$ 1600
$X(3872)$ [*aka* $\chi_{c1}(3872)$] 86, 2111
$X(3940)$ 2117
$X(4020)^{\pm}$ 94, 2186
$X(4050)^{\pm}$ 2187
$X(4055)^{\pm}$ 2188
$X(4100)^{\pm}$ 2188
$X(4160)$ 2125
$X(4250)^{\pm}$ 2189
$X(4350)$ 2132
$X(4630)$ 2138
$X(5568)^{\pm}$ 2190
x variable (of Feynman's) 802
Xavier initialization 753
X boson 1171
xF_3 structure function, plots of 386
Ξ baryons
$\Xi_b(6087)^0$ 117, 2417
$\Xi_b(6095)^0$ 117, 2417
$\Xi_b(6227)^-$ 117, 2417
$\Xi_b(6327)^0$ 117, 2418
$\Xi_b(6333)^0$ 117, 2418
$\Xi_c(2882)$ 2388
Ξ^- 108, 2350
Ξ^0 ..... 108, 2347
Ξ_{bc}^0 2418
$\Xi(1530)$ 108, 2353
$\Xi(1620)$ 2354
$\Xi(1690)$ 108, 2355
$\Xi(1820)$ 109, 2356
$\Xi(1950)$ 109, 2357
$\Xi(2030)$ 109, 2358
$\Xi(2120)$ 2359
$\Xi(2250)$ 2359
$\Xi(2370)$ 2359
$\Xi(2500)$ 2360
Ξ_{cc}^{++} 114, 2396
Ξ_{cc}^{+} 2396
Ξ_b^- 116, 2412
Ξ_b^0 ..... 116, 2414
$\Xi_b(6100)^-$ 117, 2417
$\Xi_b(6227)^-$ 117, 2417
$\Xi_b(6227)^0$ 117, 2418
$\Xi_b^{'}(5935)^-$ 116, 2416
$\Xi_b(5945)^0$ 117, 2416
$\Xi_b(5955)^-$ 117, 2416
Ξ_c^+ 112, 2381
Ξ_c^0 ..... 112, 2383
$\Xi_c(2645)$ 113, 2386
$\Xi_c(2790)$ 113, 2386
$\Xi_c(2815)$ 113, 2387
$\Xi_c(2923)$ 2388
$\Xi_c(2930)$ 2388
$\Xi_c(2970)$ 113, 2389
$\Xi_c^{'+}$ 112, 2385
$\Xi_c(3055)$ 113, 2390
$\Xi_c(3080)$ 113, 2391
$\Xi_c(3123)$ 2391
$\Xi_c^{'0}$ 112, 2386

Year, sidereal 146
Year, tropical 146
Young diagrams (tableaux) 796

Young Massive star Cluster 554
Yukawa coupling
leptoquark-type 1189
Yukawa coupling unification 1177

Z boson 27, 1258
branching ratios 842
mass 841
note on 841
width 834, 841

Z'-boson searches, note on 1080
Z' or W' bosons, searches for 1158
$Z_c(4200)$ [*was* $X(4200)^{\pm}$] 2188
$\mathbb{Z}_4$ center 1177
$\mathbb{Z}_4^R$ symmetry 1177
$Z_b(10610)$ [*was* $X(10610)$] 94, 2192
$Z_b(10650)$ [*was* $X(10650)^{\pm}$] 95, 2193
$Z_c(3900)$ [*was* $X(3900)$] 94, 2184
$Z_c(4430)$ [*was* $X(4430)^{\pm}$] 94, 2189
Z'-boson searches 1165

Int. J. Mod. Phys. A 2026.41. Downloaded from www.worldscientific.com
by UNIVERSITY OF CALIFORNIA @ BERKELEY on 09/16/26. Re-use and distribution is strictly not permitted, except for Open Access articles.

VOLUME II: TABLE OF CONTENTS

PARTICLE LISTINGS*

Illustrative key and abbreviations 1227

Gauge and Higgs bosons
(γ, gluon, graviton, W, Z, Higgs, Axions) 1241

Leptons
(e, μ, τ, Heavy-charged lepton searches, Neutrino properties, Number of neutrino types Double-β decay, Neutrino mixing, Heavy-neutral lepton searches) 1369

Quarks
(u, d, s, c, b, t, b', t' (4th gen.), Free quarks) 1447

Mesons
Light unflavored (π, ρ, a, b) (η, ω, f, ϕ, h) 1491
Strange (K, K^*) 1623
Charmed (D, D^*) 1677
Charmed, strange (D_s, D_s^*, D_{sJ}) 1749
Bottom (B, V_{cb}/V_{ub}, B^*, B_J^*) 1775
Bottom, strange (B_s, B_s^*, B_{sJ}^*) 1965
Bottom, charmed (B_c) 1996
$c\overline{c}$ (η_c, $J/\psi(1S)$, χ_c, h_c, ψ) 2002
$b\overline{b}$ (η_b, Υ, χ_b, h_b) 2142
Other mesons (T_c, T_b tetraquarks) 2183

Baryons
N 2203
Δ 2263
Λ 2289
Σ 2315
Ξ 2347
Ω 2361
Charmed (Λ_c, Σ_c, Ξ_c, Ω_c) 2364
Doubly charmed (Ξ_{cc}) 2396
Bottom (Λ_b, Σ_b, Ξ_b, Ω_b, b-baryon admixture) 2398
Exotic baryons (P_c pentaquarks) 2423

Searches not in Other Sections
Magnetic monopole searches 2429
Supersymmetric particle searches 2432
Technicolor 2493
Searches for quark and lepton compositeness 2494
Extra dimensions 2499
WIMP and dark matter searches 2505
Other particle searches 2523

*The divider sheets give more detailed indices for each main section of the Particle Listings.

Int. J. Mod. Phys. A 2026.41. Downloaded from www.worldscientific.com
by UNIVERSITY OF CALIFORNIA @ BERKELEY on 09/16/26. Re-use and distribution is strictly not permitted, except for Open Access articles.

Int. J. Mod. Phys. A 2026.41. Downloaded from www.worldscientific.com
by UNIVERSITY OF CALIFORNIA @ BERKELEY on 09/16/26. Re-use and distribution is strictly not permitted, except for Open Access articles.

INTRODUCTION TO THE PARTICLE LISTINGS

Illustrative key 1227
Abbreviations 1228

Int. J. Mod. Phys. A 2026.41. Downloaded from www.worldscientific.com
by UNIVERSITY OF CALIFORNIA @ BERKELEY on 09/16/26. Re-use and distribution is strictly not permitted, except for Open Access articles.

Int. J. Mod. Phys. A 2026.41. Downloaded from www.w[redacted]
by UNIVERSITY OF CALIFORNIA @ BERKELEY on 09/16/26. Re-use and distribution is [redacted] except for Open Access articles.

Illustrative Key to the Particle Listings

Name of particle. "Old" name used before 1986 renaming scheme also given if different. See the section "Naming Scheme for Hadrons" for details.

$a_0(1200)$ $\quad I^G(J^{PC}) = 1^-(0^{++})$

Particle quantum numbers (where known).

OMITTED FROM SUMMARY TABLE

Indicates particle omitted from Particle Physics Summary Table, implying particle's existence is not confirmed.

Evidence not compelling, may be a kinematic effect.

General comments on particle.

Quantity tabulated below.

$a_0(1200)$ MASS

VALUE (MeV)	EVTS	DOCUMENT ID		TECN	CHG	COMMENT
1206± 7 OUR AVERAGE						
1210± 8±9	3000	FENNER	87	MMS	−	3.5 $\pi^- p$
1198±10		PIERCE	83	ASPK	+	2.1 $K^- p$
1216±11±9	1500	[1] MERRILL	81	HBC	0	3.2 $K^- p$
• • • We do not use the following data for averages, fits, limits, etc. • • •						
1192±16	200	LYNCH	81	HBC	±	2.7 $\pi^- p$

[1] Systematic error was added quadratically by us in our 1986 edition.

Top line gives our best value (and error) of quantity tabulated here, based on weighted average of measurements used. Could also be from fit, best limit, estimate, or other evaluation. See next page for details.

"Document id" for this result; full reference given below.

Footnote number linking measurement to text of footnote.

Measurement technique. (See abbreviations on next page.)

$a_0(1200)$ WIDTH

VALUE (MeV)	EVTS	DOCUMENT ID		TECN	CHG	COMMENT
41±11 OUR AVERAGE Error includes scale factor of 1.8. See the ideogram below.						
50± 8		PIERCE	83	ASPK	+	2.1 $K^- p$
70^{+30}_{-20}	200	LYNCH	81	HBC	±	2.7 $\pi^- p$
25± 5±7		MERRILL	81	HBC	0	3.2 $K^- p$
• • • We do not use the following data for averages, fits, limits, etc. • • •						
<60		FENNER	87	MMS	−	3.5 $\pi^- p$

Number of events *above background*.

Measured value used in averages, fits, limits, etc.

Scale factor > 1 indicates possibly inconsistent data.

Reaction producing particle, or general comments.

Error in measured value (often statistical only; followed by systematic if separately known; the two are combined in quadrature for averaging and fitting.)

"Change bar" indicates result added or changed since previous edition.

Measured value *not used* in averages, fits, limits, etc. See the Introductory Text for explanations.

Charge(s) of particle(s) detected.

Arrow points to weighted average.

Shaded pattern extends $\pm 1\sigma$ (scaled by "scale factor" S) from weighted average.

Ideogram to display possibly inconsistent data. Curve is sum of Gaussians, one for each experiment (area of Gaussian = 1/error; width of Gaussian = ±error). See Introductory Text for discussion.

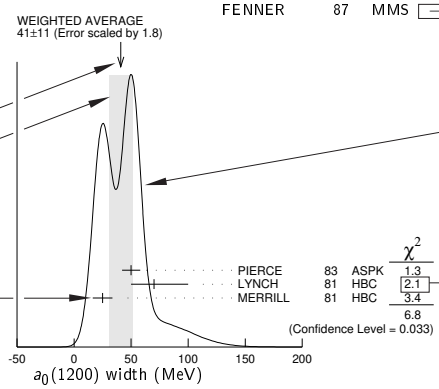

Value and error for each experiment.

Contribution of experiment to χ^2 (if no entry present, experiment not used in calculating χ^2 or scale factor because of very large error).

$a_0(1200)$ DECAY MODES

Mode	Fraction (Γ_i/Γ)	Scale factor/ Confidence level
Γ_1 3π	(65.2±1.3) %	S=1.7
Γ_2 $K\overline{K}$	(34.8±1.3) %	S=1.7
Γ_3 $\eta\pi^\pm$	< 5 $\times 10^{-4}$	CL=95%

Partial decay mode (labeled by Γ_i).

Our best value for branching fraction as determined from data averaging, fitting, evaluating, limit selection, etc. This list is basically a compact summary of results in the Branching Ratio section below.

$a_0(1200)$ BRANCHING RATIOS

Branching ratio.

$\Gamma(3\pi)/\Gamma_{total}$ $\quad \Gamma_1/\Gamma$

VALUE	DOCUMENT ID		TECN	CHG	COMMENT
0.652±0.013 OUR FIT Error includes scale factor of 1.7.					
0.643±0.010 OUR AVERAGE					
0.64 ±0.01	PIERCE	83	ASPK	+	2.1 $K^- p$
0.74 ±0.06	MERRILL	81	HBC	0	3.2 $K^- p$
• • • We do not use the following data for averages, fits, limits, etc. • • •					
0.48 ±0.15	[2] LYNCH	81	HBC	±	2.7 $\pi^- p$

[2] Data has questionable background subtraction.

Our best value (and error) of quantity tabulated, as determined from constrained fit (using *all significant* measured branching ratios for this particle).

Weighted average of measurements of this ratio only.

Footnote (referring to LYNCH 81).

$\Gamma(K\overline{K})/\Gamma_{total}$ $\quad \Gamma_2/\Gamma$

VALUE	DOCUMENT ID		TECN	CHG	COMMENT
0.348±0.013 OUR FIT Error includes scale factor of 1.7.					
0.35 ±0.05	PIERCE	83	ASPK	+	2.1 $K^- p$

Branching ratio in terms of partial decay mode(s) Γ_i above.

$\Gamma(K\overline{K})/\Gamma(3\pi)$ $\quad \Gamma_2/\Gamma_1$

VALUE	DOCUMENT ID		TECN	CHG	COMMENT
0.535±0.030 OUR FIT Error includes scale factor of 1.7.					
0.50 ±0.03	MERRILL	81	HBC	0	3.2 $K^- p$

$\Gamma(\eta(\text{neutral decay})\pi^\pm)/\Gamma_{total}$ $\quad 0.71\Gamma_3/\Gamma$

VALUE (units 10^{-4})	CL%	DOCUMENT ID		TECN	CHG	COMMENT
<3.5	95	PIERCE	83	ASPK	+	2.1 $K^- p$

Confidence level for measured upper limit.

$a_0(1200)$ REFERENCES

FENNER	87	PRL 55 14	H. Fenner *et al.*	(SLAC)	
PIERCE	83	PL 123B 230	J.H. Pierce	(FNAL)	JP
LYNCH	81	PR D24 610	G.R. Lynch *et al.*	(CLEO Collab.)	
MERRILL	81	PRL 47 143	D.W. Merrill *et al.*	(SACL, CERN)	

References, ordered inversely by year, then author.

Partial list of author(s) in addition to first author.

"Document id" used on data entries above.

Quantum number determinations in this reference.

Journal, report, preprint, etc. (See abbreviations on next page.)

Institution(s) of author(s). (See abbreviations on next page.)

Int. J. Mod. Phys. A 2026.41. Downloaded from www.worldscientific.com
by UNIVERSITY OF CALIFORNIA @ BERKELEY on 09/16/26. Re-use and distribution is strictly not permitted, except for Open Access articles.

Abbreviations Used in the Particle Listings

Int. J. Mod. Phys. A 2026.41. Downloaded from www.w[redacted] except for Open Access articles.
by UNIVERSITY OF CALIFORNIA @ BERKELEY on 09/16/26. Re-use and distribution is

Indicator of Procedure Used to Obtain Our Result

OUR AVERAGE	From a weighted average of selected data.
OUR FIT	From a constrained or overdetermined multiparameter fit of selected data.
OUR EVALUATION	Not from a direct measurement, but evaluated from measurements of other quantities.
OUR ESTIMATE	Based on the observed range of the data. Not from a formal statistical procedure.
OUR LIMIT	For special cases where the limit is evaluated by us from measured ratios or other data. Not from a direct measurement.

Measurement Techniques (i.e., Detectors and Methods of Analysis)

A1	A1 Collaboration at MAMI
A2MM	A2 spectrometer at the Mainz Microtron, MAMI
ABRA	ABRACADABRA QCD axion dark matter search
ACCM	ACCMOR Collaboration
ADMX	Axion Dark Matter Experiment
AEMS	Argonne effective mass spectrometer
ALCE	ALICE detector at CERN LHC
ALEP	ALEPH – CERN LEP detector
ALPS	Photon regeneration experiment
AMND	AMANDA South Pole neutrino detector
AMY	AMY detector at KEK-TRISTAN
ANAI	Direct DM detection exp. with NaI at Canfranc Underground Lab, Spain
ANIC	ANTARES and IceCube combined analysis
ANIT	Antarctic Impulsive Transient Antenna balloon mission
ANTR	ANTARES underwater neutrino telescope in the Western Mediterranean Sea
APEX	FNAL APEX Collab.
ARG	ARGUS detector at DORIS
ARGD	Fit to semicircular amplitude path on Argand diagram
ASP	Anomalous single-photon detector
ASPK	Automatic spark chambers
ASTE	ASTERIX detector at LEAR
ASTR	Astronomy
ATLS	ATLAS detector at CERN LHC
AUGE	Pierre Auger Observatory
AURG	Resonant-mass gravitational wave AURIGA detector
B787	BNL experiment 787 detector
B791	BNL experiment 791 detector
B845	BNL experiment 845 detector
B852	BNL E-852
B865	BNL E865 detector
B871	BNL experiment 871 detector
B949	BNL E949 detector at AGS
BABR	BaBar Collab.
BAIK	Lake Baikal neutrino telescope
BAKS	Baksan underground scintillation telescope
BC	Bubble chamber
BDMP	Beam dump
BEAT	CERN BEATRICE Collab.
BEBC	Big European bubble chamber at CERN
BEL2	Belle II Collab.
BELL	Belle Collab.
BES	BES Beijing Spectrometer at Beijing Electron-Positron Collider
BES2	BES Beijing Spectrometer at Beijing Electron-Positron Collider
BES3	BES Beijing Spectrometer at Beijing Electron-Positron Collider
BEST	Baksan Experiment on Sterile Transitions
BIS2	BIS-2 spectrometer at Serpukhov
BKEI	BENKEI spectrometer system at KEK Proton Synchroton
BOLO	Bolometer, a cryogenic thermal detector
BONA	Bonanza nonmagnetic detector at DORIS
BORX	BOREXINO
BPWA	Barrelet-zero partial-wave analysis
BRAS	BRASS: Broadband Radiometric Axion/ALPs Search Setup
BRED	GigaBREAD room-temperature dish antenna
C100	COSINE-100 experiment in South Korea
CALO	Calorimeter
CAPP	CAPP18T haloscope detector
CASK	CULTASK: CAPPs Ultra Low Temperature Axion Search in Korea
CASP	Cosmic Axion Spin Precession Experiments
CAST	CAST experiment at CERN
CBAL	Crystal Ball detector at SLAC-SPEAR or DORIS
CBAR	Crystal Barrel detector at CERN-LEAR
CBOX	Crystal Box at LAMPF
CBTP	CBELSA/TAPS Collaboration
CC	Cloud chamber
CCFR	Columbia-Chicago-Fermilab-Rochester detector
CCM	Coherent CAPTAIN-Mills 10-ton liquid Ar detector at Los Alamos
CDEX	China Dark Matter Experiment
CDF	Collider detector at Fermilab
CDF2	CDF-II Collab.
CDHS	CDHS neutrino detector at CERN
CDM2	CDMS II, Cryogenic Dark Matter Search at Soudan Underground Lab.
CDMS	CDMS Collaboration
CELL	CELLO detector at DESY
CGNT	CoGeNT dark matter search experiment
CHER	Cherenkov detector
CHM2	CHARM-II neutrino detector (glass) at CERN
CHOZ	Nuclear Power Station near Chooz, France
CHRM	CHARM neutrino detector (marble) at CERN
CHRS	CHORUS Collaboration – CERNS SPS
CIB	Cosmic Infrared Background
CIBS	CERN-IHEP boson spectrometer
CLAS	Jefferson CLAS Collab.
CLE2	CLEO II detector at CESR
CLE3	CLEO III detector at CESR
CLEC	CLEO-c detector at CESR
CLEO	Cornell magnetic detector at CESR
CMB	Cosmic Microwave Background
CMD	Cryogenic magnetic detector at VEPP-2M, Novosibirsk
CMD2	Cryogenic magnetic detector 2 at VEPP-2M, Novosibirsk
CMD3	Cryogenic magnetic detector 3 at VEPP-2000, Novosibirsk
CMS	CMS detector at CERN LHC
CNTR	Counters
COHR	COHERENT experiment at the SNS, Oak Ridge
COMB	Combined analysis of data from independent experiments.
COMP	COMPASS experiment at the CERN SPS
CONN	CONNIE: Coherent Neutrino-Nucleus Interaction Experiment
COSM	Cosmology and astrophysics
COSN	COSINUS Collab. undergroud searches
COSY	COSY-TOF Collaboration
COUP	COUPP (the Chicagoland Observatory for Underground Particle Physics) Collab.
CPLR	CPLEAR Collaboration
CRBT	Crystal Ball and TAPS detector at MAMI
CRES	CRESST cryogenic detector
CRYB	Crystal Ball at BNL
CRYM	Crystal Ball detector at Mainz Microtron MAMI
CSB2	Columbia U. - Stony Brook BGO calorimeter inserted in NaI array
CSME	COSME Collaboration
CUOR	CUORICINO experiment at Gran Sasso Laboratory.
CUSB	Columbia U. - Stony Brook segmented NaI detector at CESR
D0	D0 detector at Fermilab Tevatron Collider
DAMA	DAMA, dark matter detector at Gran Sasso National Lab.
DAMP	The DArk Matter Particle Explorer, DAMPE, detector
DANC	DANCE axion search experiment
DASP	DESY double-arm spectrometer
DAYA	Daya Bay Collaboration
DBC	Deuterium bubble chamber
DCHZ	Double Chooz Collaboration
DEAP	DEAP-3600 DM search with argon at SNOLAB
DISP	Graviton mass measurement based on dispersion measure
DLCO	DELCO detector at SLAC-SPEAR or SLAC-PEP
DLPH	DELPHI detector at LEP
DM1	Magnetic detector no. 1 at Orsay DCI collider
DM2	Magnetic detector no. 2 at Orsay DCI collider
DMIC	DAMIC Dark Matter in CCD experiment at Fermilab
DMTP	Dark Matter Time Projection Chamber (DMTPC) directional detection experiment
DONU	DONUT Collab.
DORR	DOSUE-RR Collab., dark photon dark matter search
DPWA	Energy-dependent partial-wave analysis
DRFT	Directional dark matter detector at Boulby Underground Science Facility
DS50	DarkSide-50 Liquid Argon TPC at Gran Sasso National Laboratory
E137	SLAC E137 beam-dump experiment
E621	Fermilab E621 detector
E653	Fermilab E653 detector

Int. J. Mod. Phys. A 2026.41. Downloaded from www.worldscientific.com
by UNIVERSITY OF CALIFORNIA @ BERKELEY on 09/16/26. Re-use and distribution is strictly not permitted, except for Open Access articles.

E665	Fermilab E665 detector
E687	Fermilab E687 detector
E691	Fermilab E691 detector
E705	Fermilab E705 Spectrometer-Calorimeter
E731	Fermilab E731 Spectrometer-Calorimeter
E756	Fermilab E756 detector
E760	Fermilab E760 detector
E761	Fermilab E761 detector
E771	Fermilab E771 detector
E773	Fermilab E773 Spectrometer-Calorimeter
E789	Fermilab E789 detector
E791	Fermilab E791 detector
E799	Fermilab E799 Spectrometer-Calorimeter
E835	Fermilab E835 detector
EDE2	EDELWEISS II dark matter search Collaboration
EDE3	EDELWEISS III dark matter search Collaboration
EDEL	EDELWEISS dark matter search Collaboration
EDGS	EDGES: Global EoR (Epoch of Reionization) Signature experiment
EHS	Four-pi detector at CERN
ELEC	Electronic combination
EMC	European muon collaboration detector at CERN
EMUL	Emulsions
EPTA	The European Pulsar Timing Array
ESR	Electron spin resonance spectroscopy
EXO2	Enriched Xenon Observatory 200-kg liquid Xe TPC
FASR	FASER light dark matter search at LHC
FAST	Fiber Active Scintillator Target detector at PSI
FBC	Freon bubble chamber
FENI	FENICE (at the ADONE collider of Frascati)
FIT	Fit to previously existing data
FLAT	Large Area Telescope onboard the Fermi Gamma-Ray Space Telescope (Fermi-LAT)
FMPS	Fermilab Multiparticle Spectrometer
FOCS	FNAL E831 FOCUS Collab.
FRAB	ADONE $B\overline{B}$ group detector
FRAG	ADONE $\gamma\gamma$ group detector
FRAM	ADONE MEA group detector
FREJ	FREJUS Collaboration – modular flash chamber detector (calorimeter)
FUNK	Finding U(1)'s of a Novel Kind experiment
GA24	Hodoscope Cherenkov γ calorimeter (IHEP GAMS-2000) (CERN GAMS-4000)
GALX	GALLEX solar neutrino detector in the Gran Sasso Underground Lab.
GAM2	IHEP hodoscope Cherenkov γ calorimeter GAMS-2000
GAM4	CERN hodoscope Cherenkov γ calorimeter GAMS-4000
GAMS	IHEP hodoscope Cherenkov γ calorimeter GAMS-4π
GLUX	GlueX exotic hybrid mesons search at JLAB
GNME	Global Network of Optical Magnetometers for Exotic searches (GNOME)
GNO	Gallium Neutrino Observatory in the Gran Sasso Underground Lab.
GOLI	CERN Goliath spectrometer
GRAL	GRAAL Collaboration
H1	H1 detector at DESY/HERA
HAWC	High Altitude Water Cherenkov Observatory experiment at Sierra Negra, Mexico
HBC	Hydrogen bubble chamber
HDBC	Hydrogen and deuterium bubble chambers
HDES	HADES Collaboration at GSI in Darmstadt
HDMO	Heidelberg-Moscow Experiment
HDMS	Heidelberg Dark Matter Search Experiment
HEBC	Helium bubble chamber
HEPT	Helium proportional tubes
HERA	H1 and ZEUS Collaborations at DESY/HERA
HERB	HERA-B detector at DESY/HERA
HERM	HERMES detector at DESY/HERA
HESS	High Energy Stereoscopic System gamma-ray instrument
HFR	HighFlow Reactor at the Institut Laue-Langevin
HFS	Hyperfine structure
HLBC	Heavy-liquid bubble chamber
HOME	Homestake underground scintillation detector
HPGE	High-purity Germanium detector
HPS	Heavy Photon Search experiment at JLAB
HPW	Harvard-Pennsylvania-Wisconsin detector
HRS	SLAC high-resolution spectrometer
HYBR	Hybrid: bubble chamber + electronics
HYCP	HyperCP Collab. (FNAL E-871)
HYST	HAYSTAC axion search experiment
IACT	Imaging Air Cherenkov Telescope
ICAR	ICARUS experiment at Gran Sasso Laboratory.
ICCB	IceCube neutrino detector at South Pole
IGEX	IGEX Collab.
IMB	Irvine-Michigan-Brookhaven underground Cherenkov detector
IMB3	Irvine-Michigan-Brookhaven underground Cherenkov detector
INDU	Magnetic induction
INDX	InDEx: Indian Dark matter search Experiment at Jaduguda
IPWA	Energy-independent partial-wave analysis
ISTR	IHEP ISTRA+ spectrometer-calorimeter
JADE	JADE detector at DESY
JPAC	Joint Physics Analysis Center (JPAC) Collaboration
JWST	James Webb Space Telescope
K246	KEK E246 detector with polarimeter
K2K	KEK to Super-Kamiokande
K391	KEK E391a detector
K470	KEK-E470 Stopping K detector
KAM2	KAMIOKANDE-II underground Cherenkov detector
KAMI	KAMIOKANDE underground Cherenkov detector
KAR2	KARMEN2 calorimeter at the ISIS neutron spallation source at Rutherford
KARM	KARMEN calorimeter at the ISIS neutron spallation source at Rutherford
KEDR	detector operating at VEPP-4M collider (Novosibirsk)
KIMS	Korea Invisible Mass Search experiment at YangYang, Korea
KLND	KamLand Collab. (Japan)
KLNZ	KamLAND-Zen Collaboration
KLOE	KLOE detector at DAFNE (the Frascati e+e- collider Italy)
KM3N	KM3NeT water Cherenkov ν detector in Mediterranean Sea
KOLR	Kolar Gold Field underground detector
KOTO	KOTO experiment with K_L^0 beam at J-PARC
KTEV	KTeV Collaboration
L3	L3 detector at LEP
LASR	Laser
LASS	Large-angle superconducting solenoid spectrometer at SLAC
LATT	Lattice calculations
LEBC	Little European bubble chamber at CERN
LEGS	BNL LEGS Collab.
LENA	Nonmagnetic lead-glass NaI detector at DORIS
LEP	From combination of all 4 LEP experiments: ALEPH, DELPHI, L3, OPAL
LEPS	Low-Energy Pion Spectrometer at the Paul Scherrer Institute
LGW	Lead Glass Wall collaboration at SPEAR/SLAC
LHAS	Large High Altitude Air Shower Observatory (LHAASO)
LHC	Combined analysis of LHC experiments
LHCB	LHCb detector at CERN LHC
LIDA	Laser-Interferometric Detector for Axions
L+P	Multichannel L + P model fit
LSD	Mont Blanc liquid scintillator detector
LSND	Liquid Scintillator Neutrino Detector
LSW	Light Shining through a Wall
LUX	Large Underground Xenon experiment at SURF
LZ	LUX-ZEPLIN dark matter Xe CPT detector at SURF
MAC	MAC detector at PEP/SLAC
MAJD	Majorana Demonstrator experiment at SURF
MBNE	Fermilab MiniBooNE neutrino experiment
MBR	Molecular beam resonance technique
MCBN	Fermilab MicroBooNE neutrino experiment
MCRO	MACRO detector in Gran Sasso
MD1	Magnetic detector at VEPP-4, Novosibirsk
MDHI	Multilayer Dielectric Haloscope Investigation
MDMX	Magnetized Disc and Mirror Axion eXperiment
MDRP	Millikan drop measurement
MEER	MeerKAT Galaxy Cluster Legacy Survey
MEG	Muon to electron conversion detector at PSI
MGFL	MAGIC and Fermi-LAT Collaborations
MGIC	MAGIC Telescopes gamma-ray observatory
MICA	Underground mica deposits
MICR	MICROSCOPE satellite test of weak equivalence principle
MINS	Fermilab MINOS experiment
MIRA	MIRABELLE Liquid-hydrogen bubble chamber
MLEV	Magnetic levitation
MLS	Modified Laurent Series
MMS	Missing mass spectrometer
MOED	MoEDAL magnetic monopoles search experiment at LHC

Int. J. Mod. Phys. A 2026.41. Downloaded from www.w
by UNIVERSITY OF CALIFORNIA @ BERKELEY on 09/16/26. Re-use and distribution is
except for Open Access articles.

MPS	Multiparticle spectrometer at BNL
MPS2	Multiparticle spectrometer upgrade at BNL
MPSF	Multiparticle spectrometer at Fermilab
MPWA	Model-dependent partial-wave analysis
MRK1	SLAC Mark-I detector
MRK2	SLAC Mark-II detector
MRK3	SLAC Mark-III detector
MRKJ	Mark-J detector at DESY
MRS	Magnetic resonance spectrometer
MUG2	Muon (g-2)
MWPC	Multi-Wire Proportional Chamber
NA14	CERN NA14
NA31	CERN NA31 Spectrometer-Calorimeter
NA32	CERN NA32 Spectrometer
NA48	CERN NA48 Collaboration
NA49	CERN NA49 Collaboration
NA60	CERN NA60 Collaboration
NA62	CERN NA62 Experiment
NA64	CERN SPS NA64 Experiment
NAGE	NEWAGE, New generation WIMP-search experiment with advanced gaseous tracking
NAIA	NAIAD (NaI Advanced Detector) dark matter search experiment
ND	NaI detector at VEPP-2M, Novosibirsk
NEOS	NEOS Collaboration
NEWS	NEWS-G direct dark matter search at LSM
NICE	Serpukhov nonmagnetic precision spectrometer
NIT	Nano-imaging technology
NMR	Nuclear magnetic resonance
NOMD	NOMAD Collaboration, CERN SPS
NOVA	NOvA experiment with Fermilab's NuMI neutrino beam
NTEV	NuTeV Collab. at Fermilab
nTRV	neutron Time-Reversal Violation
NUST	NuSTAR, Nuclear Spectroscopic Telescope Array X-ray observatory
NUSX	Mont Blanc NUSEX underground detector
OBLX	OBELIX detector at LEAR
OKA	OKA collaboration at U70 accelerator in Protvino, Russia
OLYA	Detector at VEPP-2M and VEPP-4, Novosibirsk
OMEG	CERN OMEGA spectrometer
OPAL	OPAL detector at LEP
OPER	OPERA experiment with emulsion tracking at Gran Sasso
ORGN	ORGAN (Oscillating Resonant Group AxioN) experiment
ORPH	ADMX-Orpheus Dark Matter Experiment
OSPK	Optical spark chamber
PIBE	The PIBETA detector at the Paul Scherrer Institute (PSI), Switzerland.
PICA	PICASSO dark matter search experiment
PICO	PICO bubble chamber experiment in SNOLAB underground laboratory
PIE3	πE3 beam-line of Paul Scherrer Institute
PLAS	Plastic detector
PLUT	DESY PLUTO detector
PMLA	PAMELA space spectrometer on Resurs-DK1 satellite
PNDX	PandaX dual-phase liquid xenon dark matter experiment at Jin-Ping
PPTA	Parkes Pulsar Timing Array
PRMX	The PRIMEX detector in Hall B at TJNAF
PTA	Pulsar timing array
PWA	Partial-wave analysis
QRDL	QROCODILE, Quantum Resolution-Optimized Cryogenic Observatory for DM
QUAX	QUAX axion search experiment
QULP	QUALIPHIDE, quantum limited photons in the dark exp.
RADE	CAST-RADES haloscope search for axions.
RDK2	NIST rare radioactive decay experiment
REDE	Resonance depolarization
RENO	RENO Collaboration
RICE	Radio Ice Cherenkov Experiment
RVUE	Review of previous data
SAGE	US - Russian Gallium Experiment
SAPH	SAPPHIRES collaboration search for sub-eV Axion LPs
SCDM	SuperCDMS experiment at Soudan Underground Lab.
SELX	FNAL SELEX Collab.
SENS	Sub-Electron-Noise Skipper CCD Experimental Instrument (SENSEI)
SFM	CERN split-field magnet
SHF	SLAC Hybrid Facility Photon Collaboration
SHFT	Search for Halo Axions with Ferromagnetic Toroids
SHNE	Superconducting cavity new hidden particles explorer
SHUK	SHUKET: search for U(1) dark matter with an electromagnetic telescope
SIGM	Serpukhov CERN-IHEP magnetic spectrometer (SIGMA)
SILI	Silicon detector
SIMP	SIMPLE, dark matter detector at Laboratori Nazionali del Sud
SKAM	Super-Kamiokande Collab.
SKT2	Super-Kamiokande and T2K Collaborations
SLAX	Solar Axion Experiment in Canfranc Underground Laboratory
SLD	SLC Large Detector for e^+e^- colliding beams at SLAC
SLIC	ADMX SLIC (Superconducting LC Circuit Investigating Cold Axions)
SMPL	SIMPLE, Superheated Instrument for Massive ParticLe Experiments
SND	Novosibirisk Spherical neutral detector at VEPP-2M
SNDR	SINDRUM spectrometer at PSI
SNO	SNO Collaboration (Sudbury Neutrino Observatory)
SNO+	SNO+ Collaboration (Sudbury Neutrino Observatory)
SNSP	SNSPD, Superconducting Nanowire Single-Photon Detectors
SOU2	Soudan 2 underground detector
SOUD	Soudan underground detector
SPEC	Spectrometer
SPED	From maximum of speed plot or resonant amplitude
SPHR	Bonn SAPHIR Collab.
SPNX	SPHINX spectrometer at IHEP accelerator
SPRK	Spark chamber
SQID	SQUID device
SRPH	SERAPH (SupERconducting Axion and Paraphoton Haloscope) experiment
STRC	Streamer chamber
SVD2	SVD-2 experiment at IHEP, Protvino
T2K	T2K Collaboration
TASE	Taiwan Axion Search Experiment with a Haloscope, TASEH, experiment
TASS	DESY TASSO detector
TESS	TESSERACT, DM search below the proton mass
TEVA	Combined analysis of CDF and DØ experiments
TEXO	TEXONO Collab., ultra low energy Ge detector at Kuo-Sheng Laboratory
THEO	Theoretical or heavily model-dependent result
TNF	TNF-IHEP facility at 70 GeV IHEP accelerator
TOF	Time-of-flight
TOPZ	TOPAZ detector at KEK-TRISTAN
TPC	TPC detector at PEP/SLAC
TPS	Tagged photon spectrometer at Fermilab
TRAP	Penning trap
TWST	TWIST spectrometer at TRIUMF
UA1	UA1 detector at CERN
UA2	UA2 detector at CERN
UA5	UA5 detector at CERN
UCNA	UCNA collaboration using polarizeed ultracold neutrons at LANSCE
UKDM	UK Dark Matter Collab.
UPLD	UPLOAD, upconversion low-noise oscillator axion detection experiment
VES	Vertex Spectrometer Facility at 70 GeV IHEP accelerator
VLBI	Very Long Baseline Interferometer
VNS	VENUS detector at KEK-TRISTAN
VRTS	Very Energetic Radiation Imaging Telescope Array System (VERITAS)
WA75	CERN WA75 experiment
WA82	CERN WA82 experiment
WA89	CERN WA89 experiment
WARP	Liquid argon detector for CDM searches at Gran Sasso
WASA	WASA detector at CELSIUS, Uppsala and at COSY, Juelich
WDMX	WISP Dark Matter eXperiment (WISPDMX) for direct hidden photon search
WIRE	Wire chamber
X100	XENON100 dark matter search experiment at Gran Sasso National Laboratory
XE10	XENON10 experiment at Gran Sasso National Laboratory
XE1T	XENON1T dark matter search experiment at Gran Sasso National Laboratory
XEBC	Xenon bubble chamber
XENT	XENONnT dark matter search experiment at Gran Sasso National Laboratory
XMAS	XMASS, liquid xenon scintillation detector at Kamioka Observatory

Int. J. Mod. Phys. A 2026.41. Downloaded from www.worldscientific.com
by UNIVERSITY OF CALIFORNIA @ BERKELEY on 09/16/26. Re-use and distribution is strictly not permitted, except for Open Access articles.

YUKA	Graviton mass measurement based on Yukawa potential
ZEP2	ZEPLIN-II dark matter detector
ZEP3	ZEPLIN-III dark matter detector at Palmer Underground Lab.
ZEPL	ZEPLIN-I galactic dark matter detector
ZEUS	ZEUS detector at DESY/HERA

Conferences

Conferences are generally referred to by the location at which they were held (e.g., HAMBURG, TORONTO, CORNELL, BRIGHTON, etc.).

Journals

AA	Astronomy and Astrophysics
ADVP	Advances in Physics
AFIS	Anales de Fisica
AJP	American Journal of Physics
AL	Astronomy Letters
ANP	Annals of Physics
ANPL	Annals of Physics (Leipzig)
ANYAS	Annals of the New York Academy of Sciences
AP	Atomic Physics
APAH	Acta Physica Academiae Scientiarum Hungaricae
APJ	Astrophysical Journal
APJS	Astrophysical Journal Suppl.
APP	Acta Physica Polonica
APS	Acta Physica Slovaca
ARNPS	Annual Review of Nuclear and Particle Science
ARNS	Annual Review of Nuclear Science
ASP	Astroparticle Physics
AST	American Statistician
BAPS	Bulletin of the American Physical Society
BASUP	Bulletin of the Academy of Science, USSR (Physics)
CJNP	Chinese Journal of Nuclear Physics
CJP	Canadian Journal of Physics
CNPP	Comments on Nuclear and Particle Physics
CP	Chinese Physics
CPC	Chinese Physics C
CPL	Chinese Physics Letters
CQG	Classical and Quantum Gravity
CTP	Communications in Theoretical Physics
CZJP	Czechoslovak Journal of Physics
DANS	Doklady Akademii nauk SSSR
DP	Doklady Physics (Magazine)
EPJ	The European Physical Journal
EPJA	The European Physical Journal A
EPJC	The European Physical Journal C
EPL	Europhysics Letters
FECAY	Fizika Elementarnykh Chastits i Atomnogo Yadra
HADJ	Hadronic Journal
IJMP	International Journal of Modern Physics
IJMPA	International Journal of Modern Physics A
JAP	Journal of Applied Physics
JCAP	Journal of Cosmology and Astroparticle Physics
JETP	English Translation of Soviet Physics ZETF
JETPL	English Translation of Soviet Physics ZETF Letters
JHEAP	Journal of High Energy Astrophysics
JHEP	Journal of High Energy Physics
JINR	Joint Inst. for Nuclear Research
JINRRC	JINR Rapid Communications
JP	Journal of Physics
JPA	Journal of Physics A
JPB	Journal of Physics B
JPCRD	Journal of Physical and Chemical Reference Data
JPCS	Journal of Physics: Conference Series
JPG	Journal of Physics G
JPSJ	Journal of the Physical Society of Japan
LHEP	Letters in High Energy Physics
LNC	Lettere Nuovo Cimento
MNRAS	Monthly Notices of the Royal Astronomical Society
MPL	Modern Physics Letters
MPLA	Modern Physics Letters A
NAST	New Astronomy
NAT	Nature
NATC	Nature Communications
NATP	Nature Physics
NC	Nuovo Cimento
NIM	Nuclear Instruments and Methods
NJP	New Journal of Physics
NP	Nuclear Physics
NPA	Nuclear Physics A
NPB	Nuclear Physics B
NPBPS	Nuclear Physics B Proceedings Supplement
NPPP	Nuclear and Particle Physics Proceedings
PAN	Physics of Atomic Nuclei (formerly SJNP)
PD	Physics Doklady (Magazine)
PDAT	Physik Daten
PDU	Physics of the Dark Universe
PL	Physics Letters
PLA	Physics Letters A
PLB	Physics Letters B
PN	Particles and Nuclei
PPCF	Plasma Physics and Controlled Fusion
PPN	Physics of Particles and Nuclei (formerly SJPN)
PPNL	Physics of Particles and Nuclei Letters
PPNP	Progress in Particles and Nuclear Physics
PPSL	Proc. of the Physical Society of London
PR	Physical Review
PRA	Physical Review A
PRAM	Pramana
PRC	Physical Review C
PRD	Physical Review D
PRL	Physical Review Letters
PRPL	Physics Reports (Physics Letters C)
PRSE	Proc. of the Royal Society of Edinburgh
PRSL	Proc. of the Royal Society of London, Section A
PRX	Physical Review X
PS	Physica Scripta
PTEP	Progress of Theoretical and Experimental Physics
PTP	Progress of Theoretical Physics
PTPS	Progress of Theoretical Physics Supplement
PTRSL	Phil. Trans. Royal Society of London
RA	Radiochimica Acta
RMP	Reviews of Modern Physics
RNC	La Rivista del Nuovo Cimento
RPP	Reports on Progress in Physics
RRP	Revue Roumaine de Physique
SADV	Science Advances
SCI	Science
SCIB	Science Bulletin
SCP	SciPost Physics
SCPMA	Science China Physics, Mechanics and Astronomy
SJNP	Soviet Journal of Nuclear Physics
SJPN	Soviet Journal of Particles and Nuclei
SPD	Soviet Physics Doklady (Magazine)
SPU	Soviet Physics - Uspekhi
SYM	Symmetry
UFN	Usp. Fiz. Nauk – Russian version of SPU
YAF	Yadernaya Fizika
ZETF	Zhurnal Eksperimental'noi i Teoreticheskoi Fiziki
ZETFP	Zhurnal Eksperimental'noi i Teoreticheskoi Fiziki, Pis'ma v Redakts
ZNAT	Zeitschrift fur Naturforschung
ZPHY	Zeitschrift fur Physik

Institutions

AACH	Phys. Inst. der Techn. Hochschule **Aachen** (Historical, use for general Inst. der Techn. Hochschule)	Aachen, Germany
AACH1	I Phys. Inst. B, RWTH **Aachen**	Aachen, Germany
AACH3	III Phys. Inst. A, RWTH **Aachen** Univ.	Aachen, Germany
AACHT	Inst. für Theoretische Teilchenphysik & Kosmologie, RWTH **Aachen**	Aachen, Germany
AARH	Univ. of **Aarhus**	Aarhus C, Denmark
ABO	**Åbo** Akademi Univ.	Turku, Finland
ADEL	**Adelphi** Univ.	Garden City, NY, USA
ADLD	The Univ. of **Adelaide**	Adelaide, SA, Australia
AERE	Atomic Energy Research Estab.	Didcot, United Kingdom
AFRR	**Armed Forces** Radiobiology Res. Inst.	Bethesda, MD, USA

Abbreviations Used in the Particle Listings

AHMED	Physical Research Lab.	**Ahmedabad**, Gujarat, India
AICH	**Aichi** Univ. of Education	Aichi, Japan
AKIT	**Akita** Univ.	Akita, Japan
ALAH	Univ. of **Alabama (Huntsville)**	Huntsville, AL, USA
ALAT	Univ. of **Alabama (Tuscaloosa)**	Tuscaloosa, AL, USA
ALBA	**SUNY at Albany**	Albany, NY, USA
ALBE	Univ. of **Alberta**	Edmonton, AB, Canada
AMES	**Ames Lab.**	Ames, IA, USA
AMHT	**Amherst** College	Amherst, MA, USA
AMST	Univ. van **Amsterdam**	GL Amsterdam, The Netherlands
ANIK	**NIKHEF**	**Amsterdam**, The Netherlands
ANKA	**Middle East** Technical Univ.; Dept. of Physics; Experimental HEP Lab	Ankara, Turkey
ANL	**Argonne** National Lab.; High Energy Physics Division, Bldg. 362; Physics Division, Bldg. 203	Argonne, IL, USA
ANSM	**St. Anselm** Coll.	Manchester, NH, USA
AQUI	Univ. di **LAquila**	**Aquila**, Italy
ARCBO	**Arecibo** Observatory	Arecibo, PR, USA
ARIZ	Univ. of **Arizona**	Tucson, AZ, USA
ARZS	**Arizona State** Univ.	Tempe, AZ, USA
ASCI	Russian Academy of Sciences	**Moscow**, Russian Federation
AST	**Academia Sinica**	Nankang, Taipei, Taiwan
ASTAR	Institute of Materials	Singapore, Singapore
ATEN	NCSR **"Demokritos"**	**Aghia** Paraskevi , Greece
ATHU	Univ. of **Athens**	Athens, Greece
AUCK	Univ. of **Auckland**	Auckland, New Zealand
BAKU	**Natl. Azerbaijan Academy of Sciences**, Inst. of Physics	**Baku**, Azerbaijan
BANG	Indian Inst. of Science	**Bangalore**, India
BANGB	**Bangabasi** College	Calcutta, India
BARC	Univ. Autónoma de **Barcelona**; Dept. de Fisica	Bellaterra (Barcelona), Spain
BARCE	Univ. Autónoma de **Barcelona**; Inst. de Física de Altas Energías	Bellaterra (Barcelona), Spain
BARI	Univ. e del Politecnico di **Bari**	Bari, Italy
BART	Univ. of **Delaware**; **Bartol** Research Inst.	Newark, DE, USA
BASL	Inst. für Physik der Univ. **Basel**	Basel, Switzerland
BAYR	Univ. **Bayreuth**	Bayreuth, Germany
BCEN	Centre d'Etudes Nucleaires de **Bordeaux-Gradignan**	Gradignan, France
BCIP	Natl. Inst. for Physics & Nuclear Eng. "Horia Hulubei" **(IFIN-HH)**	**Bucharest**-Magurele, Romania
BEIJ	**Beijing** Univ.	Beijing, China
BEIJT	**Inst. of Theoretical Physics**	**Beijing**, China
BELG	Inter-University Inst. for High Energies (ULB-VUB)	**Brussel**, Belgium
BELGV	Vrije Univ. Brussel **(VUB)**	**Brussel**, Belgium
BELL	AT & T **Bell** Labs	Murray Hill, NJ, USA
BERG	Univ. of **Bergen**	Bergen, Norway
BERL	**DESY**, Deutsches Elektronen-Synchrotron	**Zeuthen**, Germany
BERN	Univ. of **Berne**	Berne, Switzerland
BGNA	Univ. di **Bologna**, & **INFN**, Sezione di Bologna; Via Irnerio, 46, I-40126 Bologna; Viale C. Berti Pichat, n. 6/2	Bologna, Italy
BHAB	**Bhabha Atomic** Research Center	Trombay, Bombay, India
BHEP	**Inst. of High Energy Physics**	**Beijing**, China
BIEL	Univ. **Bielefeld**	Bielefeld, Germany
BING	**SUNY at Binghamton**	Binghamton, NY, USA
BIRK	**Birkbeck** College, Univ. of London	London, United Kingdom
BIRM	Univ. of **Birmingham**	Edgbaston, Birmingham, United Kingdom
BLSU	**Bloomsburg** Univ.	Bloomsburg, PA, USA
BNL	**Brookhaven National Lab.**	Upton, NY, USA
BNORM	**Beijing Normal** Univ.	Beijing, China
BOCH	**Ruhr** Univ. **Bochum**	Bochum, Germany
BOHR	**Niels Bohr Inst.**	Copenhagen Ø, Denmark
BOIS	**Boise** State Univ.	Boise, ID, USA
BOMB	Univ. of **Bombay**	Bombay, India
BONN	**Univ. of Bonn**	Bonn, Germany
BORD	Centre d'Etudes Nucléaires de **Bordeaux** Gradignan **(CENBG)**	Gradignan, France
BOSE	S.N. **Bose** National Centre for Basis Sciences	Calcutta, India
BOSK	**"Rudjer Bošković"** Inst.	Zagreb, Croatia
BOST	**Boston** Univ.	Boston, MA, USA
BRAN	**Brandeis** Univ.	Waltham, MA, USA
BRCO	Univ. of **British Columbia**	Vancouver, BC, Canada
BRIS	Univ. of **Bristol**	Bristol, United Kingdom
BROW	**Brown** Univ.	Providence, RI, USA
BRUN	**Brunel** Univ.	Uxbridge, Middlesex, United Kingdom
BRUX	Univ. Libre de **Bruxelles**; Physique des Particules Elémentaires	Bruxelles, Belgium
BRUXT	Univ. Libre de **Bruxelles**; Physique Théorique	Bruxelles, Belgium
BUCH	Univ. of **Bucharest**	Bucharest-Magurele, Romania
BUDA	**Wigner** Research Centre for Physics	**Budapest**, Hungary
BUFF	**SUNY at Buffalo**	Buffalo, NY, USA
BURE	Inst. des Hautes Etudes Scientifiques	**Bures-sur-Yvette**, France
CAEN	Lab. de Physique Corpusculaire, **ENSICAEN**	**Caen**, France
CAGL	Univ. degli Studi di **Cagliari**	Monserrato (CA), Italy
CAGLI	**INFN**, Sezione di **Cagliari**	Monserrato (CA), Italy
CAIR	**Cairo** University	Orman, Giza, Cairo, Egypt
CAIW	**Carnegie Inst.** of Washington	Washington, DC, USA
CALB	Univ. della **Calabria**	Cosenza, Italy
CALC	Univ. of **Calcutta**	Calcutta, India
CAMB	**DAMTP**	Cambridge, United Kingdom
CAMP	Univ. Estadual de **Campinas** (UNICAMP)	**Campinas**, SP, Brazil
CANB	**Australian National Univ.**	Canberra, ACT, Australia
CANTB	Inst. de Física de Cantabria (CSIC–Univ. **Cantabria**)	Santander, Spain
CAPE	University of **Cape Town**	Rondebosch, Cape Town, South Africa
CARA	Univ. Central de **Venezuela**	Caracas, Venezuela
CARL	**Carleton** Univ.	Ottawa, ON, Canada
CARLC	**Carleton** College	Northfield, MN, USA
CASE	**Case** Western Reserve Univ.	Cleveland, OH, USA
CAST	**China** Center of Advanced Science and Technology	Beijing, China
CATA	Univ. di **Catania**	Catania, Italy
CATH	**Catholic** Univ. of America	Washington, DC, USA
CAU	Chung-Ang Univ.	Seoul, Republic of Korea
CAVE	**Cavendish** Lab.	Cambridge, United Kingdom
CBNM	CBNM	**Geel**, Belgium
CBPF	Centro Brasileiro de Pesquisas Físicas – **BIB/CDI/CBPF**	**Rio de Janeiro**, RJ, Brazil
CCAC	**Allegheny** College	Meadville, PA, USA
CDEF	**Univ. Paris VII, Denis Diderot**	Paris, France
CEA	Cambridge Electron Accelerator (Historical in *Review*)	**Cambridge, MA**, USA
CEADE	Center for Apl. Studies for Nuclear Physics	Havana, Cuba
CEBAF	**Jefferson Lab—Thomas Jefferson National Accelerator Facility**	**Newport News**, VA, USA
CENG	Centre d'Etudes Nucleaires	**Grenoble**, France
CERN	**CERN**, European Organization for Nuclear Research	Genève, Switzerland
CFPA	Univ. of **California, (Berkeley)**	Berkeley, CA, USA
CHIC	Univ. of **Chicago**	Chicago, IL, USA
CIAE	**State Nuclear Power Research Inst.**	**Beijing**, China

Int. J. Mod. Phys. A 2026.41. Downloaded from www.w
by UNIVERSITY OF CALIFORNIA @ BERKELEY on 09/16/26. Re-use and distribution is
except for Open Access articles.

Abbreviations Used in the Particle Listings

CINC	Univ. of **Cincinnati**	Cincinnati, OH, USA
CINV	**CINVESTAV-IPN** Centro de Investigacion y de Estudios Avanzados del IPN	**México**, DF, Mexico
CIT	**California Inst. of Tech.**	Pasadena, CA, USA
CLEMS	**Clemson** University	Clemson, SC, USA
CLER	Univ. de **Clermont-Ferrand**	Aubière, France
CLEV	**Cleveland** State Univ.	Cleveland, OH, USA
CMNS	**Comenius** Univ. (FMFI UK)	**Bratislava**, Slovakia
CMU	**Carnegie Mellon** Univ.	Pittsburgh, PA, USA
CNEA	**Comisión Nacional de Energía Atómica**	Buenos Aires, Argentina
CNRC	Centre for Research in Particle Physics	Ottawa, ON, Canada
CNRS	National Center for Scientific Research	Paris, France
CNYIT	C. N. Yang Institute	New York, USA
COIM	Univ. de Coimbra	**Coimbra**, Portugal
COLO	Univ. of **Colorado**	Boulder, CO, USA
COLU	**Columbia** Univ.	New York, NY, USA
CONC	**Concordia** University	Montreal, PQ, Canada
CORN	**Cornell** Univ.	Ithaca, NY, USA
COSU	**Colorado State** Univ.	Fort Collins, CO, USA
CPPM	Centre National de la Recherche Scientifique, Luminy	**Marseille**, France
CRAC	Henryk Niewodnicza'nski Inst. of Nuclear Physics	**Kraków**, Poland
CRNL	**Chalk River** Labs.	Chalk River, ON, Canada
CSEB	California State University	Hayward, USA
CSOK	**Oklahoma** Central State Univ.	Edmond, OK, USA
CST	Univ. of **Science and Technology** of China	**Hefei**, Anhui 230026, China
CSULB	**California** State Univ.	Long Beach, CA, USA
CSUS	**California** State Univ.	Sacramento, CA, USA
CTUP	Czech Technical University	Prague, Czech Republic
CUHK	Chinese University of Hong Kong	Hong Kong, Hong Kong
CUNY	**City College** of **New York**	New York, NY, USA
CURCP	**Univ. Pierre et Marie Curie** (Paris VI), LCP	Paris, France
CURIN	**Univ. Pierre et Marie Curie** (Paris VI), LPNHE	Paris, France
CURIT	**Univ. Pierre et Marie Curie** (Paris VI), LPTHE	Paris, France
DALH	**Dalhousie** Univ.	Halifax, NS, Canada
DALI	**Dalian** Univ. of Tech.	Dalian, China
DARE	**Daresbury** Lab	Cheshire, United Kingdom
DARM	Tech. Hochschule **Darmstadt**	Darmstadt, Germany
DELA	Univ. of **Delaware**; Dept. of Physics & Astronomy	Newark, DE, USA
DELH	Univ. of **Delhi**	Delhi, India
DESY	**DESY**, Deutsches Elektronen-Synchrotron	**Hamburg**, Germany
DFAB	Escuela de Ingenieros	**Bilbao**, Spain
DOE	**Department of Energy**	Washington, DC, USA
DORT	Technische Univ. **Dortmund**	Dortmund, Germany
DREXL	**Drexel** Univ.	Philadelphia, PA, USA
DUKE	**Duke** Univ.	Durham, NC, USA
DURH	Univ. of **Durham**	Durham , United Kingdom
DUUC	**University College** Dublin	Dublin, Ireland
ECT	Europ. Cent. for Theor. Studies in Nucl. Phys.	Trento, Italy
EDIN	Univ. of **Edinburgh**	Edinburgh, United Kingdom
EFI	Univ. of Chicago, **The Enrico Fermi Inst.**	**Chicago**, IL, USA
ELMT	**Elmhurst** College	Elmhurst, IL, USA
ENSP	**l'Ecole Normale Supérieure**	**Paris**, France
EOTV	**Eötvös** University	Budapest, Hungary
EPOL	**École Polytechnique**	**Palaiseau**, France
ERLA	Univ. **Erlangen-Nurnberg**	Erlangen, Germany
ESAP	ESAP Territorial Meta	Villavicencio, Colombia
ETH	Eidg. Technische Hochschule	Zürich, Switzerland
FERR	Univ. di **Ferrara**	Ferrara, Italy
FIRZ	Univ. degli Studi di **Firenze**	Sesto Fiorentino, Italy
FISK	**Fisk** Univ.	Nashville, TN, USA
FLOR	Univ. of **Florida**	Gainesville, FL, USA
FNAL	**Fermilab**	Batavia, IL, USA
FOM	**FOM**, Stichting voor Fundamenteel Onderzoek der Materie	JP **Utrecht**, The Netherlands
FRAN	**Frankfurt Inst. for Advanced Studies (FIAS)**	Frankfurt am Main, Germany
FRAS	Lab. Nazionali di **Frascati** dell'**INFN**	Frascati (Roma), Italy
FREIB	**Albert-Ludwigs** Univ.	**Freiburg**, Germany
FREIE	**Freie Univ. Berlin**	Berlin, Germany
FRIB	Univ. de **Fribourg**	Fribourg, Switzerland
FSU	**Florida State** Univ.; High Energy Physics	Tallahassee, FL, USA
FSUSC	**Florida State** Univ.; SCS (School of Computational Science)	Tallahassee, FL, USA
FUKI	**Fukui** Univ.	Fukui, Japan
FUKU	**Fukushima** Univ.	Fukushima, Japan
GANIL	**GANIL** (Grand Accelerateur National d'Ions Lourds)	**Caen** CEDEX 5, France
GENO	Univ. di **Genova**	Genova, Italy
GEOR	**E. Andronikashvili Inst. of Physics**	Tbilisi, Republic of Georgia
GESC	**General Electric** Co.	Schenectady, NY, USA
GEVA	Univ. de **Genève**	Genève, Switzerland
GIES	Univ. **Giessen**	Giessen, Germany
GIFU	**Gifu** Univ.	Gifu, Japan
GLAS	Univ. of **Glasgow**	Glasgow, United Kingdom
GMAS	**George Mason** Univ.	Fairfax, VA, USA
GOET	Univ. **Göttingen**	Göttingen, Germany
GOML	**Gomel State** Univ.	Gomel, Belarus
GRAN	Univ. de **Granada**	Granada, Spain
GRAZ	Univ. **Graz**	Graz, Austria
GRON	Univ. of **Groningen**	Groningen, The Netherlands
GSCO	**Geological Survey of Canada**	Ottawa, ON, Canada
GSI	GSI Helmholtzzentrum für Schwerionenforschung GmbH	**Darmstadt**, Germany
GUAN	Univ. de **Guanajuato**	León, Gto., Mexico
GUEL	Univ. of **Guelph**	Guelph, ON, Canada
GWU	**George Washington** Univ.	Washington, DC, USA
GXU	Guangxi University	Guangxi, China
HAHN	**Hahn-Meitner** Inst. Berlin GmbH	Berlin, Germany
HAIF	**Technion** – Israel Inst. of Tech.	Technion, Haifa, Israel
HAMB	Univ. **Hamburg**	Hamburg, Germany
HANN	Univ. **Hannover**	Hannover, Germany
HARC	**Houston Advanced Research Ctr.**	The Woodlands, TX, USA
HARV	**Harvard** Univ.	Cambridge, MA, USA
HARV	**Harvard** Univ. (LPPC)	Cambridge, MA, USA
HAWA	Univ. of **Hawai'i**	Honolulu, HI, USA
HEBR	**Hebrew** Univ.	Jerusalem, Israel
HEID	Univ. **Heidelberg**; (unspecified division) (Historical in *Review*)	Heidelberg, Germany
HEIDH	Ruprecht-Karls Univ. **Heidelberg**	Heidelberg, Germany
HEIDP	Univ. **Heidelberg**; Physics Inst.	Heidelberg, Germany
HEIDT	Ruprecht-Karls-Univ. **Heidelberg**	Heidelberg, Germany
HELS	Univ. of **Helsinki**	University of Helsinki, Finland
HIAS	Hangzhou Inst. for Advanced Studies	Hangzhou, China
HINR	Inst. of Nuclear Research (**ATOMKI**)	**Debrecen**, Hungary
HIRO	**Hiroshima** Univ.	Higashi-Hiroshima, Japan
HOKK	**Hokkaido** Univ.	Sapporo, Japan
HOUS	Univ. of **Houston**	Houston, TX, USA
HPC	**Hewlett-Packard** Corp.	Cupertino, CA, USA
HSCA	**Harvard-Smithsonian** Center for Astrophysics	Cambridge, MA, USA
HYDER	Indian Inst. of Technology	Hyderabad, India
HZDR	Helmholtz-Zentrum Dresden-Rossendorf	Dresden, Germany

Int. J. Mod. Phys. A 2026.41. Downloaded from www.worldscientific.com
by UNIVERSITY OF CALIFORNIA @ BERKELEY on 09/16/26. Re-use and distribution is strictly not permitted, except for Open Access articles.

Int. J. Mod. Phys. A 2026.41. Downloaded from www.w
by UNIVERSITY OF CALIFORNIA @ BERKELEY on 09/16/26. Re-use and distribution is
except for Open Access articles.

IAC	Instituto de Astrofsica de Canarias	Tenerife, Spain
IACS	Indian Association for the Cultivation of Science	Kolkata, India
IAS	**Inst. for Advanced Study**	Princeton, NJ, USA
IASD	**Dublin** Inst. for Advanced Studies	Dublin, Ireland
IBAR	**Ibaraki** Univ.	Ibaraki, Japan
IBM	**IBM** Corp.	Palo Alto, CA, USA
IBMY	**IBM**	Yorktown Heights, NY, USA
IBS	Inst. for **Boson Studies**	Pasadena, CA, USA
IBSD	Inst. for Basic Science	Daejeon, Republic of Korea
ICC	Universitat de Barcelona	Balcelona, Spain
ICCUB	Institut Ciences del Cosmos, Universitat Barcelona	Barcelona, Spain
ICEPP	The Univ. of **Tokyo**	Tokyo, Japan
ICREA	Instituci Catalana de Recerca i Estudis Avanats	Barcelona, Spain
ICRR	Univ. of **Tokyo**	Chiba, Japan
ICTP	**Abdus Salam** International Centre for Theoretical Physics	**Trieste**, Italy
IFIC	**IFIC** (Instituto de Física Corpuscular)	**Paterna (Valencia)**, Spain
IFT	Instituto de Fisica Teorica	Madrid, Spain
IIT	**Illinois Inst. of Tech.**	Chicago, IL, USA
IITB	Indian Inst. of Tech. **IIT Bombay**	Powai, Mumbai, India
IITI	Indian Inst. of Tech. \ef IIT Indore	Simrol, Indore, India
IITJ	Indian Inst. of Tech. Jodhpur	Jodhpur, India
ILL	Univ. of **Illinois at Urbana-Champaign**	Urbana, IL, USA
ILLC	Univ. of **Illinois at Chicago**	Chicago, IL, USA
ILLG	Inst. **Laue-Langevin**	Grenoble, France
IND	**Indiana** Univ.	Bloomington, IN, USA
INEL	E G and G **Idaho**, Inc.	Idaho Falls, ID, USA
INFN	Ist. Nazionale di Fisica Nuclear (Generic INFN, unknown location)	Various places, Italy
INFNL	**INFN**, Sezione di **Lecce**	Lecce, Italy
INFNP	INFN, Sez. di Padova	Padova, Italy
INIT	Indian Inst. of Tech. Hyderabad	Hyderabad, India
INNS	Univ. of **Innsbruck**	**Innsbruck**, Austria
INPK	Henryk Niewodniczański Inst. of Nuclear Physics	**Kraków**, Poland
INRM	**INR**, Inst. for Nucl. Research	**Moscow**, Russian Federation
INUS	**KEK**, High Energy Accelerator Research Organization	Tokyo, Japan
IOAN	Univ. of **Ioannina**	Ioannina, Greece
IOFF	A.F. **Ioffe** Phys. Tech. Inst.	St. **Petersburg**, Russian Federation
IOWA	Univ. of **Iowa**	Iowa City, IA, USA
IPN	**IPN**, Inst. de Phys. Nucl.	**Orsay**, France
IPNP	Univ. Pierre et Marie Curie (**Paris** VI)	Paris, France
IRAD	Inst. du Radium (Historical)	**Paris**, France
ISNG	Lab. de Physique Subatomique et de Cosmologie **(LPSC)**	**Grenoble**, France
ISU	**Iowa State** Univ.	Ames, IA, USA
ISUT	Isfahan University of Technology	Isfahan, Iran
ITEP	**ITEP**, Inst. of Theor. and Exp. Physics	**Moscow**, Russian Federation
ITHA	**Ithaca** College	Ithaca, NY, USA
IUPU	**Indiana** Univ., **Purdue** Univ. **Indianapolis**	Indianapolis, IN, USA
JADA	**Jadavpur** Univ.	Calcutta, India
JAGL	**Jagiellonian** Univ.	Kraków, Poland
JHU	**Johns Hopkins** Univ.	Baltimore, MD, USA
JINR	**JINR**, Joint Inst. for Nucl. Research	**Dubna**, Russian Federation
JPL	Jet Propulsion Laboratory	Pasadena, USA
JULI	Forschungszentrum **Jülich**	Jülich, Germany
JYV	Univ. of **Jyväskylä**	Jyväskylä, Finland
KAGO	Univ. of **Kagoshima**	Kagoshima-shi, Japan
KAIST	**Korea** Advanced Inst. of Science and Technology	Yusung ku, Daejeon, Republic of Korea
KANP	Indian Inst. of Tech.	**Kanpur**, UT, India
KANS	Univ. of **Kansas**	Lawrence, KS, USA
KARAD	Karadeniz U.	Trabzon, Turkey
KARL	Univ. **Karlsruhe** (Historical in *Review*)	Karlsruhe, Germany
KARLE	**Karlsruhe** Inst. of Technology (KIT); Inst. for Experimental Nuclear Physics	Karlsruhe, Germany
KARLK	**Karlsruhe** Inst. of Technology (KIT)	Eggenstein-Leopoldshafen, Germany
KARLT	**Karlsruhe** Inst. of Technology (KIT); Inst. for Theoretical Physics	Karlsruhe, Germany
KAZA	**Kazakh** Inst. of High Energy Physics	Alma Ata, Kazakhstan
KEK	**KEK**, High Energy Accelerator Research Organization	Ibaraki-ken, Japan
KENT	Univ. of **Kent**	Canterbury, United Kingdom
KEYN	**Open** Univ.	Milton Keynes, United Kingdom
KFTI	**Kharkov** Inst. of Physics and Tech. (NSC KIPT)	Kharkov, Ukraine
KIAE	**Kurchatov** Inst.	**Moscow**, Russian Federation
KIAM	**Keldysh** Inst. of Applied Math., Acad. Sci., Russia	Moscow, Russian Federation
KIDR	**Vinča Inst. of Nuclear Sciences**	Belgrade, Serbia
KIEV	**Institute for Nuclear Research**	**Kyiv**, Ukraine
KINK	**Kinki** Univ.	Osaka, Japan
KIT	Karlsruhe Institute for Technology	Karlsruhe, Germany
KNTY	Univ. of **Kentucky**	Lexington, KY, USA
KOBE	**Kobe** Univ.	Kobe, Japan
KOMAB	Univ. of **Tokyo, Komaba**	Tokyo, Japan
KONAN	**Konan** Univ.	Kobe, Japan
KOSI	Inst. of Experimental Physics SAS	**Košice**, Slovakia
KYOT	**Kyoto** Univ.; Dept. of Physics, Graduate School of Science	Kyoto, Japan
KYOTU	**Kyoto** Univ.; **Yukawa** Inst. for Theor. Physics	Kyoto, Japan
KYUN	**Kyungpook** National Univ.	Daegu, Republic of Korea
KYUSH	**Kyushu** Univ.; Elementary ParticleTheory Group; Exp. Particle Physics Group; Research Center for Advanced Particle Physics	Fukuoka, Japan
LALO	**LAL**, Laboratoire de l'Accélérateur Linéaire	**Orsay**, France
LANC	**Lancaster** Univ.	Lancaster, United Kingdom
LANL	**Los Alamos National Lab.** (LANL)	Los Alamos, NM, USA
LAPL	Univ. Nacional de **La Plata**	La Plata, Argentina
LAPP	**LAPP**, Lab. d'Annecy-le-Vieux de Phys. des Particules	**Annecy-le-Vieux**, France
LAPTH	**LAPTh** Lab. d'Annecy-le-Vieux de Phys. Théorique	**Annecy-le-Vieux** CEDEX, France
LASL	U.C. **Los Alamos Scientific** Lab. (Old name for LANL)	Los Alamos, NM, USA
LATV	**Latvian** State Univ.	Riga, Latvia
LAUS	EPFL **Lausanne**	Lausanne, Switzerland
LAVL	Univ. **Laval**	Quebec, QC, Canada
LBL	**Lawrence Berkeley National Lab.**	Berkeley, CA, USA
LCGT	Univ. di **Torino**	Turin, Italy
LEBD	**Lebedev** Physical Inst.	**Moscow**, Russian Federation
LECE	Univ. di **Lecce**	Lecce, Italy
LEED	Univ. of **Leeds**	Leeds, United Kingdom
LEGN	Lab. Naz. di Legnaro	**Legnaro**, Italy
LEHI	**Lehigh** Univ.	Bethlehem, PA, USA
LEHM	**Lehman** College of CUNY	Bronx, NY, USA
LEID	Univ. **Leiden**	Leiden, The Netherlands
LEMO	**Le Moyne** Coll.	Syracuse, NY, USA
LENSU	**Saint-Petersburg** State Univ.	St. **Petersburg**, Russian Federation
LEUV	Katholieke Univ. **Leuven**	Leuven, Belgium
LIEG	Univ. de **Liège**	Liège, Belgium

LINZ	Univ. **Linz**	Linz, Austria
LISB	Inst. Nacional de Investigacion Cientifica	**Lisboa** CODEX, Portugal
LISBT	Centro de Física Teórica de Partículas **(CFTP)**	**Lisboa**, Portugal
LIVP	Univ. of **Liverpool**	Liverpool, United Kingdom
LJUB	Univerza v **Ljubljani**	Ljubljana, Slovenia
LLL	**Lawrence Livermore Lab.** (Old name for LLNL)	Livermore, CA, USA
LLNL	**Lawrence Livermore National Lab.**	Livermore, CA, USA
LNUDA	Liaoning Normal Univ.	Dalian, China
LOCK	**Lockheed** Palo Alto Res. Lab	Palo Alto, CA, USA
LOIC	**Imperial** College of Science Tech. & Medicine	London, United Kingdom
LOKC	**Univ. of London**, King's College	London, United Kingdom
LOQM	Queen Mary, **Univ. of London**	London, United Kingdom
LOUC	**University College** London	London, United Kingdom
LOUV	Univ. Catholique de **Louvain**	Louvain-la-Neuve, Belgium
LOWC	**Westfield** College (Historical, see LOQM (Queen Mary and Westfield joined))	London, United Kingdom
LRL	U.C. Lawrence Radiation Lab. (Old name for LBL)	**Berkeley**, CA, USA
LSU	**Louisiana** State Univ.	Baton Rouge, LA, USA
LUND	**Fysiska Institutionen**	**Lund**, Sweden
LUND	**Lund** Univ.	Lund, Sweden
LYON	Institute de Physique Nucléaire de **Lyon** (IPN)	Villeurbanne, France
MADE	**UAM/CSIC**, Inst. de Física Teórica	**Madrid**, Cantoblanco, Spain
MADR	**C.I.E.M.A.T**	**Madrid**, Spain
MADU	Univ. Autónoma de **Madrid**	Cantoblanco, Madrid, Spain
MAINZ	**Johannes-Gutenberg-Univ.**; Inst. für Kernphysik, J.-J.-Becher-Weg 45; Inst. für Physik, Staudingerweg 7	**Mainz**, Germany
MANI	Univ. of **Manitoba**	Winnipeg, MB, Canada
MARB	Univ. **Marburg**	Marburg, Germany
MARS	Centre de Physique des Particules de **Marseille**	Marseille, France
MASA	Univ. of **Massachusetts** Amherst	**Amherst**, MA, USA
MASB	Univ. of **Massachusetts** Boston	**Boston**, MA, USA
MASD	Univ. of **Massachusetts** Dartmouth	North **Dartmouth**, MA, USA
MCGI	**McGill** Univ.	Montreal, QC, Canada
MCHS	Univ. of **Manchester**	Manchester, United Kingdom
MCMS	**McMaster** Univ.	Hamilton, ON, Canada
MDRA	Univ. of **Madras**	Madras, India
MEHTA	**Harish-Chandra** Research Inst.	Allahabad, India
MEIS	**Meisei** Univ.	Tokyo, Japan
MELB	Univ. of **Melbourne**	Victoria, Australia
MEUD	Observatoire de **Meudon**	Meudon, France
MICH	Univ. of **Michigan**	Ann Arbor, MI, USA
MILA	Univ. di **Milano**	Milano, Italy
MILAI	**INFN**, Sez. di **Milano**	Milano, Italy
MINN	Univ. of **Minnesota**	Minneapolis, MN, USA
MIPT	Moscow Institute of Physics and Technology	Moscow, Russian Federation
MISS	Univ. of **Mississippi**	University, MS, USA
MISSR	Univ. of **Missouri**	Rolla, MO, USA
MIT	**MIT Massachusetts Inst. of Technology**	Cambridge, MA, USA
MIU	**Maharishi** International Univ.	Fairfield, IA, USA
MIYA	**Miyazaki** Univ.	Miyazaki-shi, Japan
MONP	Univ. de **Montpellier** II	Montpellier, France
MONS	Univ. of **Mons**	**Mons**, Belgium
MONT	Univ. de **Montréal**; Pavillon René-J.-A.-Lévesque	Montréal, PQ, Canada
MONTC	Univ. de **Montréal**; Centre de recherches mathématiques	Montréal, PQ, Canada
MOSU	**Skobeltsyn** Inst. of Nuclear Physics, Lomonosov Moscow State Univ.; Experimental HEP Division; Theoretical HEP Division	**Moscow**, Russian Federation
MPCM	Max Planck Inst. fur Chemie	**Mainz**, Germany
MPEI	**Moscow Physical Engineering** Inst.	Moscow, Russian Federation
MPIG	**Max-Planck**-Institute für Astrophysik	Garching, Germany
MPIK	**Max-Planck-Inst.** für Kernphysik	**Heidelberg**, Germany
MPIM	**Max-Planck-Inst.** für Physik	**München**, Germany
MPP	Max Planck Institute for Physics	Munich, Germany
MRION	Mirion Technologies Canberra	Meriden, CT, USA
MSST	Mississippi State University	Mississippi State, MS, USA
MSU	**Michigan State** Univ.	East Lansing, MI, USA
MTHO	**Mount Holyoke** College	South Hadley, MA, USA
MULH	Centre Univ. du **Haut-Rhin**	Mulhouse, France
MUNI	**Ludwig-Maximilians-Univ. München**	Garching, Germany
MURA	**Midwestern** Univ. Research Assoc. (Historical in *Review*)	Stroughton, WI, USA
MURC	Univ. of Murcia	Murcia, Spain
NAAS	North Americal Aviation Science Center (Historical in *Review*)	Thousand Oaks, CA, USA
NAGO	**Nagoya** Univ.	Nagoya, Japan
NANJ	**Nanjing** Univ.	Nanjing, China
NANKA	NanKai University	Tianjin, China
NAPL	Univ. di **Napoli** "Federico II"	Napoli, Italy
NAPLI	INFN, Sezione di Napoli	NAPOLI, Italy
NASA	**NASA**	Greenbelt, MD, USA
NBI	Niels Bohr Institut	Copenhagen, Denmark
NBS	U.S **National Bureau of Standards** (Old name for NIST)	Gaithersburg, MD, USA
NBSB	**National Inst. Standards Tech.**	Boulder, CO, USA
NCAR	**National Center for Atmospheric Research**	Boulder, CO, USA
NCBJ	NNational Centre for Nuclear Research	Otwock-Swieck, Poland
NCSU	**North Carolina** State Univ.	**Raleigh**, NC, USA
NDAM	Univ. of **Notre Dame**	Notre Dame, IN, USA
NEAS	**Northeastern** Univ.	Boston, MA, USA
NEBR	Univ. of **Nebraska**	Lincoln, NE, USA
NEUC	Univ. de **Neuchâtel**	Neuchâtel, Switzerland
NICEA	Univ. de **Nice**	Nice, France
NICEO	Observatoire de **Nice**	Nice, France
NIHO	**Nihon** Univ.	Tokyo, Japan
NIIG	**Niigata** Univ.	Niigata, Japan
NIJM	**Radboud** Univ. Nijmegen	AJ **Nijmegen**, The Netherlands
NIRS	Nat. Inst. Radiological Sciences	**Chiba**, Japan
NIST	**National Institute of Standards & Technology**	Gaithersburg, MD, USA
NIU	**Northern Illinois** Univ.	De Kalb, IL, USA
NJU	Nanjing University	Nanjing, China
NMSU	**New Mexico** State Univ.; Dept. of Physics, MSC 3D; Part. & Nucl. Phys. Group, Box 30001/Dept.	Las Cruces, NM, USA
NORD	**Nordita**	Stockholm, Sweden
NOTT	Univ. of **Nottingham**	Nottingham, United Kingdom
NOVM	Inst. of Mathematics	**Novosibirsk**, Russian Federation
NOVO	BINP, **Budker** Inst. of Nuclear Physics	**Novosibirsk**, Russian Federation
NOVOU	Novosibirsk State University	Novisibirsk, Russian Federation
NPLT	National Physical Laboratory	Teddington, United Kingdom
NPOL	Polytechnic of **North London**	London, United Kingdom
NRL	**Naval Research** Lab	Washington, DC, USA
NSF	**National Science Foundation**	Arlington, VA, USA
NTHU	**National Tsing Hua** Univ.	Hsinchu, Taiwan

Int. J. Mod. Phys. A 2026.41. Downloaded from www.worldscientific.com
by UNIVERSITY OF CALIFORNIA @ BERKELEY on 09/16/26. Re-use and distribution is strictly not permitted, except for Open Access articles.

NTUA	**National Tech. Univ. of Athens**	Athens, Greece
NWES	**Northwestern** Univ.	Evanston, IL, USA
NYU	**New York** Univ.	New York, NY, USA
OAKU	Oakland University	Rochester, USA
OBER	**Oberlin** College	Oberlin, OH, USA
OCH	**Ochanomizu** Univ.	Tokyo, Japan
OHIO	**Ohio** Univ.	Athens, OH, USA
OKAY	**Okayama** Univ.	Okayama, Japan
OKLA	Univ. of **Oklahoma**	Norman, OK, USA
OKSU	**Oklahoma State** Univ.	Stillwater, OK, USA
ONRJ	Observatorio Nacional, Rio de Janeiro	Rio de Janeiro, Brazil
OPAV	Silesian University	Opava, Czech Republic
OREG	Univ. of **Oregon**; Inst. of Theoretical Science; U.O. Center for High Energy Physics	Eugene, OR, USA
ORNL	**Oak Ridge** National Laboratory	Oak Ridge, TN, USA
ORSAY	Univ. de **Paris Sud** 11	**Orsay** CEDEX, France
ORST	**Oregon State** Univ.	Corvallis, OR, USA
OSAK	**Osaka** Univ.	Osaka, Japan
OSKC	**Osaka City** Univ.	Osaka, Japan
OSLO	Univ. of **Oslo**	Oslo, Norway
OSU	**Ohio State** Univ.	Columbus, OH, USA
OTTA	Univ. of **Ottawa**	Ottawa, ON, Canada
OXF	University of **Oxford**	Oxford, United Kingdom
OXFTP	Univ. of **Oxford**	Oxford, United Kingdom
PADO	Univ. degli Studi di **Padova**	Padova, Italy
PARIN	**LPNHE**, IN^2P^3/CNRS	Paris, France
PARIS	Univ. de Paris (Historical)	**Paris**, France
PARIT	**Univ. Paris VII**, LPTHE	Paris, France
PARM	**INFN**, Gruppo Collegato di **Parma**	Parma, Italy
PAST	Institut **Pasteur**	**Paris**, France
PATR	Univ. of **Patras**	Patras, Greece
PAVI	Univ. di **Pavia**	Pavia, Italy
PAVII	INFN, Sez. di **Pavia**	**Pavia**, Italy
PENN	Univ. of **Pennsylvania**	Philadelphia, PA, USA
PERIM	Perimeter Institute for Theoretical Physics	Ontario, Canada
PGIA	**INFN**, Sezione di **Perugia**	Perugia, Italy
PISA	Univ. di **Pisa**	Pisa, Italy
PISAI	**INFN**, Sez. di **Pisa**	Pisa, Italy
PITT	Univ. of **Pittsburgh**	Pittsburgh, PA, USA
PLAT	**SUNY at Plattsburgh**	Plattsburgh, NY, USA
PLRM	Univ. di **Palermo**	Palermo, Italy
PNL	**Battelle Memorial** Inst.	Richland, WA, USA
PNPI	**Petersburg** Nuclear Physics Inst. of Russian Academy of Sciences	Gatchina, Russian Federation
PPA	Princeton-Penn. Proton Accelerator (Historical in *Review*)	Princeton, NJ, USA
PRAG	Inst. of Physics, **ASCR**	**Prague**, Czech Republic
PRIN	**Princeton** Univ.	Princeton, NJ, USA
PSI	Paul Scherrer Institute	**Villigen**, Switzerland
PSLL	**Physical Science Lab**	Las Cruces, NM, USA
PSU	**Penn State** Univ.	University Park, PA, USA
PUCB	**Pontifícia Univ. Católica do Rio de Janeiro**	Rio de Janeiro, RJ, Brazil
PUEB	Univ. Autonoma de **Puebla**	**Puebla**, Pue, Mexico
PURD	**Purdue** Univ.	West Lafayette, IN, USA
QUKI	**Queen's** Univ.	Kingston, ON, Canada
RAL	**STFC Rutherford Appleton** Lab.	Chilton, Didcot, Oxfordshire, United Kingdom
REGE	Univ. **Regensburg**	Regensburg, Germany
REHO	**Weizmann** Inst. of Science	Rehovot, Israel
REZ	Nuclear Physics Inst. **AVČR**	**Řež**, Czech Republic
RGSUL	Univ. Federal do **Rio Grande do Sul** (UFRGS)	Porto Alegre, RS, Brazil
RHBL	**Royal Holloway, Univ. of London**	Egham, Surrey, United Kingdom
RHEL	**Rutherford** High Energy Lab (Old name for RAL)	Chilton, Didcot, Oxon., United Kingdom
RICE	**Rice** Univ.	Houston, TX, USA
RIKEN	**Riken** Nishina Center for Accelerator-Based Science	Saitama, Japan
RIKK	**Rikkyo** Univ.	Tokyo, Japan
RIS	**Rowland** Inst. for Science	Cambridge, MA, USA
RISC	**Rockwell** International	Thousand Oaks, CA, USA
RISL	**Universities Research Reactor**	**Risley**, Warrington, United Kingdom
RISO	**Riso** National Laboratory	Roskilde, Denmark
RITS	Royal Inst. of Technology (**KTH**)	**Stockholm**, Sweden
RL	**Rutherford** High Energy Lab (Old name for RAL)	Chilton, Didcot, Oxon., United Kingdom
RMCS	**Royal Military** Coll. of Science	Swindon, Wilts., United Kingdom
ROCH	Univ. of **Rochester**	Rochester, NY, USA
ROCK	**Rockefeller** Univ.	New York, NY, USA
ROMA	Univ. di **Roma** (Historical)	**Roma**, Italy
ROMA2	Univ. di **Roma**, "Tor Vergata"	Roma, Italy
ROMA3	**INFN, Sez. di Roma Tre**	**Roma**, Italy
ROMAI	**INFN, Sez. di Roma**	Roma, Italy
ROSE	**Rose-Hulman** Inst. of Technology	Terre Haute, IN, USA
RPI	**Rensselaer Polytechnic** Inst.	Troy, NY, USA
RUTG	**Rutgers**, the State Univ. of New Jersey	Piscataway, NJ, USA
S0GA	**Sogang** University	Seoul, Republic of Korea
SACL	**CEA Saclay**, IRFU	Gif-sur-Yvette, France
SACL5	**CEA Saclay** – IPhT	Gif-sur-Yvette, France
SACLD	**CEA Saclay** (Essonne)	Gif-sur-Yvette, France
SAGA	**Saga** Univ.	Saga-shi, Japan
SAHA	**Saha** Inst. of Nuclear Physics	Bidhan Nagar, Calcutta, India
SALEN	Universita del Salento	Lecce, Italy
SANG	**Kyoto Sangyo** Univ.	Kyoto-shi, Japan
SANI	Ist. Superiore di Sanità	**Roma**, Italy
SASK	Univ. of **Saskatchewan**	Saskatoon, SK, Canada
SASSO	Lab. Naz. **Gran Sasso** dell'INFN	**Assergi** (AQ), Italy
SAVO	Univ. de **Savoie**	Chambery, France
SBER	**California** State Univ.	**San Bernardino**, CA, USA
SCHAF	W.J. **Schafer** Assoc.	Livermore, DA, USA
SCIT	**Science** Univ. of **Tokyo**	Tokyo, Japan
SCOT	**Scottish** Univ. Research and Reactor Ctr.	Glasgow, United Kingdom
SCUC	Univ. of **South Carolina**	Columbia, SC, USA
SEAT	**Seattle Pacific** Coll.	Seattle, WA, USA
SEIB	Austrian Research Center, **Seibersdorf** LTD.	Seibersdorf, Austria
SEOU	**Korea** Univ.; Dept. of Physics; HEP Group	Seoul, Republic of Korea
SEOUL	**Seoul** National Univ.; Center for Theoretical Physics; Dept. of Physics & Astronomy, Coll. of Natural Sciences	Seoul, Republic of Korea
SERP	**IHEP**, Inst. for High Energy Physics	Protvino, Russian Federation
SETO	**Seton Hall** Univ.	South Orange, NJ, USA
SFLA	Univ. of **South Florida**	Tampa, FL, USA
SFRA	**Simon Fraser University**	Burnaby, BC, Canada
SFSU	**California** State Univ.	**San Francisco**, CA, USA
SHAMS	**Ain Shams** University	Abbassia, Cairo, Egypt
SHDN	**Shandong** Univ.	Jinan, Shandong, China
SHDNQ	Shandong Univ.	Qingdao, Shandong, China
SHEF	Univ. of **Sheffield**	Sheffield, United Kingdom
SHMP	Univ. of **Southampton**	Southampton, United Kingdom
SHRZ	**Shiraz** Univ.	Shiraz, Iran
SIEG	Univ. **Siegen**	Siegen, Germany
SILES	Univ. of **Silesia**	Katowice, Poland
SIN	Swiss Inst. of Nuclear Research (Old name for VILL)	**Villigen**, Switzerland
SING	**National Univ.** of Singapore	Kent Ridge, Singapore
SISSA	Scuola Internazionale Superiore di Studi Avanzati	**Trieste**, Italy
SLAC	**SLAC National Accelerator Laboratory**	Menlo Park, CA, USA
SLOV	Inst. of Physics, Slovak Acad. of Sciences	**Bratislava** 45, Slovakia
SMU	**Southern Methodist** Univ.	Dallas, TX, USA
SNSP	**Scuola Normale Superiore**	**Pisa**, Italy

Int. J. Mod. Phys. A 2026.41. Downloaded from www.w
by UNIVERSITY OF CALIFORNIA @ BERKELEY on 09/16/26. Re-use and distribution is
except for Open Access articles.

Abbreviations Used in the Particle Listings

SOFI	Inst. for Nuclear Research and Nuclear Energy	**Sofia**, Bulgaria
SOFU	Univ. of **Sofia** "St. Kliment Ohridski"	Sofia, Bulgaria
SORB	Sorbonne Université	Paris, France
SPIFT	Inst. de Física Teórica (**IFT**)	**São Paulo**, SP, Brazil
SSL	Univ. of **California (Berkeley)**	Berkeley, CA, USA
STAN	**Stanford** Univ.	Stanford, CA, USA
STEV	**Stevens** Inst. of Tech.	Hoboken, NJ, USA
STFN	**Jožef Stefan** Institute	**Ljubljana**, Slovenia
STLO	**St. Louis** Univ.	St. Louis, MO, USA
STOH	**Stockholm** Univ.	Stockholm, Sweden
STON	**SUNY at Stony Brook**	Stony Brook, NY, USA
STRB	Inst. Pluridisciplinaire Hubert Curien (**CNRS**)	**Strasbourg**, France
STUT	Univ. **Stuttgart**	Stuttgart, Germany
STUTM	Max-Planck-Inst.	**Stuttgart**, Germany
SUGI	**Sugiyama Jogakuen** Univ.	Aichi, Japan
SUNG	**Sungkyunkwan** Univ.	Suwon, Republic of Korea
SURR	Univ. of **Surrey**	Guildford, Surrey, United Kingdom
SUSS	Univ. of **Sussex**	Brighton, United Kingdom
SVR	**Savannah** River Labs.	Aiken, SC, USA
SYDN	Univ. of **Sydney**	Sydney, NSW, Australia
SYRA	**Syracuse** Univ.	Syracuse, NY, USA
TAJK	Acad. Sci., Tadzhik SSR	**Dushanbe**, Tadzhikstan
TAMU	**Texas A&M** Univ.	College Station, TX, USA
TATA	**Tata** Inst. of Fundamental Research	Bombay, India
TBIL	**Tbilisi State University**	Tbilisi, Republic of Georgia
TDLI	Tsung-Dao Lee Inst.	Shanghai, China
TELA	**Tel-Aviv** Univ.	Tel Aviv, Israel
TELE	**Teledyne Brown** Engineering	Huntsville, AL, USA
TEMP	**Temple** Univ.	Philadelphia, PA, USA
TENN	Univ. of **Tennessee**	Knoxville, TN, USA
TEXA	Univ. of **Texas** at **Austin**	Austin, TX, USA
TGAK	**Tokyo Gakugei** Univ.	Tokyo, Japan
TGU	**Tohoku Gakuin** Univ.	Miyagi, Japan
THES	Aristotle Univ. of **Thessaloniki** (AUTh)	Thessaloniki, Greece
TINT	**Tokyo Inst. of Technology**	Tokyo, Japan
TISA	**Sagamihara** Inst. of Space & Astronautical Sci.	Kanagawa, Japan
TMSK	**Tomsk** Polytechnic Univ.	**Tomsk**, Russian Federation
TMTC	**Tokyo Metropolitan** Coll. Tech.	Tokyo, Japan
TMU	**Tokyo Metropolitan Univ.**	Tokyo, Japan
TNTO	Univ. of **Toronto**	Toronto, ON, Canada
TOHO	**Toho** Univ.	Chiba, Japan
TOHOK	**Tohoku** Univ.	Sendai, Japan
TOKA	**Tokai** Univ.	Shimizu, Japan
TOKAH	**Tokai** Univ.	Hiratsuka, Japan
TOKMS	Univ. of **Tokyo**; Meson Science Laboratory	Tokyo, Japan
TOKU	Univ. of **Tokushima**	Tokushima-shi, Japan
TOKY	Univ. of **Tokyo**; High-Energy Physics Theory Group	Tokyo, Japan
TOKYC	Univ. of **Tokyo**; Dept. of Chemistry	Tokyo, Japan
TORI	Univ. degli Studi di **Torino**	Torino, Italy
TPTI	**Uzbek** Academy of Sciences	**Tashkent**, Republic of Uzbekistan
TRIN	Trinity College **Dublin**	Dublin, Ireland
TRIU	**TRIUMF**	Vancouver, BC, Canada
TRST	Univ. di **Trieste**	Trieste, Italy
TRSTI	**INFN**, Sez. di **Trieste**	Trieste, Italy
TRSTT	Univ. degli Studi di **Trieste**	**Trieste**, Italy
TSIN	**Tsinghua Univ.**	Beijing, China
TSUK	Univ. of **Tsukuba**	Ibaraki-ken, Japan
TTAM	**Tamagawa** Univ.	Tokyo, Japan
TUAT	**Tokyo** Univ. of Agriculture Tech.	Tokyo, Japan
TUBIN	Univ. **Tübingen**	Tübingen, Germany
TUFTS	**Tufts** Univ.	Medford, MA, USA
TUM	Tech. Univ. **München**	Garching, Germany
TURIN	Universita degli Studi di Torino	Turin, Italy
TUW	**Technische** Univ. **Wien**	Vienna, Austria
TUZL	**Tuzla** Univ.	Tuzla, Argentina
UBA	Univ. de **Buenos Aires**	Buenos Aires, Argentina
UCB	Univ. of **California (Berkeley)**	Berkeley, CA, USA
UCD	Univ. of **California (Davis)**	Davis, CA, USA
UCI	Univ. of **California (Irvine)**	Irvine, CA, USA
UCLA	Univ. of **California (Los Angeles)**	Los Angeles, CA, USA
UCND	**Union Carbide** Corp.	Oak Ridge, TN, USA
UCR	Univ. of **California (Riverside)**	Riverside, CA, USA
UCSB	Univ. of **California (Santa Barbara)**; Physics Dept., High Energy Physics Experiment	Santa Barbara, CA, USA
UCSBT	Univ. of **California (Santa Barbara)**; Kavli Inst. for Theoretical Physics	Santa Barbara, CA, USA
UCSC	Univ. of **California (Santa Cruz)**	Santa Cruz, CA, USA
UCSD	Univ. of **California (San Diego)**	La Jolla, CA, USA
UFABC	Univ. Federal do ABC	Santo Andre, Brazil
UFRJ	Univ. Federal do **Rio de Janeiro**	Rio de Janeiro, RJ, Brazil
UGAZ	Univ. of **Gaziantep**	Gaziantep, Turkey
ULL	Universidad de La Laguna	La Laguna, Spain
UMD	Univ. of **Maryland**	College Park, MD, USA
UNAM	Univ. Nac. Autónoma de México (**UNAM**)	**México**, DF, Mexico
UNAM	Univ. Nacional Autónoma de México (**UNAM**)	**México**, DF, Mexico
UNC	Univ. of **North Carolina**	Greensboro, NC, USA
UNCCH	Univ. of **North Carolina** at **Chapel Hill**	Chapel Hill, NC, USA
UNCS	**Union** College	Schenectady, NY, USA
UNESP	UNESP	Botucatu, Brazil
UNH	Univ. of **New Hampshire**	Durham, NH, USA
UNM	Univ. of **New Mexico**	Albuquerque, NM, USA
UOEH	Univ. of Occupational and Environmental Health	**Kitakyushu**, Japan
UPCIT	Univ. Paris Cite	Paris, France
UPNJ	**Upsala** College	East Orange, NJ, USA
UPPS	**Uppsala** Univ.	**Uppsala**, Sweden
UPR	Univ. of **Puerto Rico**	**San Juan**, PR, USA
URI	Univ. of **Rhode Island**	Kingston, RI, USA
USC	Univ. of **Southern California**	Los Angeles, CA, USA
USDC	Univ. Santiago de Cali	Cali, Colombia
USF	Univ. of **San Francisco**	San Francisco, CA, USA
USP	Univ. de **São Paulo**	São Paulo, SP, Brazil
USTA	Univ. Santo Toms	Bogota, Colombia
UTAH	Univ. of **Utah**	Salt Lake City, UT, USA
UTOL	Univ. del Tolima	Ibague, Colombia
UTRE	Univ. of **Utrecht**	Utrecht, The Netherlands
UTRO	**Norwegian Univ. of Science & Technology**	Trondheim, Norway
UVA	Univ. of **Virginia**	Charlottesville, VA, USA
UZINR	Acad. Sci., **Ukrainian** SSR	**Uzhgorod**, Ukraine
VALE	Univ. de **Valencia**	Burjassot, **Valencia**, Spain
VALP	**Valparaiso** Univ.	Valparaiso, IN, USA
VAND	**Vanderbilt** Univ.	Nashville, TN, USA
VASS	**Vassar** College	Poughkeepsie, NY, USA
VICT	Univ. of **Victoria**	Victoria, BC, Canada
VIEN	Inst. für Hochenergiephysik (HEPHY)	**Vienna**, Austria
VILL	Inst. for Part. Phys. and Astrophys. IPA at PSI	Villigen, Switzerland
VPI	**Virginia Tech.**	Blacksburg, VA, USA
VRIJ	**Vrije** Univ.	HV **Amsterdam**, The Netherlands
WABRN	Eidgenossisches Amt für Messwesen	**Waber**, Switzerland
WARS	Univ. of **Warsaw**	Warsaw, Poland
WASCR	**Waseda** Univ.; Cosmic Ray Division	Tokyo, Japan

Int. J. Mod. Phys. A 2026.41. Downloaded from www.worldscientific.com by UNIVERSITY OF CALIFORNIA @ BERKELEY on 09/16/26. Re-use and distribution is strictly not permitted, except for Open Access articles.

Abbreviations Used in the Particle Listings

WASH	Univ. of **Washington**; Elem. Particle Experiment (EPE); Particle Astrophysics (PA)	Seattle, WA, USA
WASU	**Waseda** Univ.; Dept. of Physics, High Energy Physics Group	Tokyo, Japan
WATER	Univ. of **Waterloo**	Waterloo, ON, Canada
WAUS	Univ. of **Western Australia**	Perth, WA, Australia
WAYN	**Wayne** State Univ.	Detroit, MI, USA
WESL	**Wesleyan** Univ.	Middletown, CT, USA
WIEN	Univ. **Wien**	Vienna, Austria
WILL	Coll. of **William and Mary**	Williamsburg, VA, USA
WILLC	Williams College	Williamstown, USA
WINR	National Centre for Nuclear Research	**Warsaw**, Poland
WISC	Univ. of **Wisconsin**	Madison, WI, USA
WITW	Univ. of the **Witwatersrand**	Wits, South Africa
WMIU	**Western Michigan** Univ.	Kalamazoo, MI, USA
WONT	The Univ. of **Western Ontario**	London, ON, Canada
WOOD	**Woodstock** College (No longer in existence)	Woodstock, MD, USA
WROC	University of Wroclaw	Wroclaw, Poland
WUPP	**Bergische** Univ. Wuppertal	**Wuppertal**, Germany
WURZ	Univ. **Würzburg**	Würzburg, Germany
WUSL	**Washington** Univ.	St. Louis, MO, USA
WYOM	Univ. of **Wyoming**	Laramie, WY, USA
YALE	**Yale** Univ.	New Haven, CT, USA
YARO	**Yaroslavl** State Univ.	Yaroslavl, Russian Federation
YCC	**Yokohama** Coll. of Commerce	Yokohama, Japan
YERE	**Yerevan** Physics Inst.	Yerevan, Armenia
YOKO	**Yokohama National** Univ.	Yokohama-shi, Japan
YORKC	**York** Univ.	Toronto, Canada
ZAGR	**Zagreb** Univ.	Zagreb, Croatia
ZARA	Univ. de **Zaragoza**	Zaragoza, Spain
ZEEM	Univ. van **Amsterdam**	TV Amsterdam, The Netherlands
ZHON	**Zhongshan** (Sun Yat-Sen) Univ.	Guangzhou, China
ZHZH	**Zhengzhou** Univ.	Zhengzhou, Henan, China
ZURI	Univ. **Zürich**	Zürich, Switzerland

Int. J. Mod. Phys. A 2026.41. Downloaded from www.w
by UNIVERSITY OF CALIFORNIA @ BERKELEY on 09/16/26. Re-use and distribution is
except for Open Access articles.

GAUGE AND HIGGS BOSONS

γ 1241
g (gluon) 1242
graviton 1242
W 1243
Z 1258
H 1278
Neutral Higgs Bosons, Searches for 1300
Charged Higgs Bosons ($H^{\pm}$ and $H^{\pm\pm}$), Searches for 1313
New Heavy Bosons 1317
Axions (A^0) and Other Very Light Bosons 1338

Notes in the Listings

Triple gauge couplings (TGC's) 1247
Anomalous $ZZ\gamma$, $Z\gamma\gamma$, and ZZV couplings 1274
Anomalous W/Z quartic couplings 1276

Related Reviews in Volume 1

54. Mass and width of the W boson (rev.) 839
55. Z boson (rev.) 841

Int. J. Mod. Phys. A 2026.41. Downloaded from www.worldscientific.com
by UNIVERSITY OF CALIFORNIA @ BERKELEY on 09/16/26. Re-use and distribution is strictly not permitted, except for Open Access articles.

Int. J. Mod. Phys. A 2026.41. Dov[redacted]orldscientific.com
by UNIVERSITY OF CALIFORNIA @ BERKELEY on 09/16/26. Re[redacted] strictly not permitted, except for Open Access articles.

Int. J. Mod. Phys. A 2026.41. Downloaded from www.worldscientific.com
by UNIVERSITY OF CALIFORNIA @ BERKELEY on 09/16/26. Re-use and distribution is strictly not permitted, except for Open Access articles.

GAUGE AND HIGGS BOSONS

γ (photon) $I(J^{PC}) = 0,1(1^{--})$

γ MASS

Results prior to 2008 are critiqued in GOLDHABER 10. All experimental results published prior to 2005 are summarized in detail by TU 05.

The following conversions are useful: 1 eV = 1.783×10^{-36} kg = 1.957×10^{-6} m_e; $\lambda\!\!\!^{-}_C = (1.973 \times 10^{-7}$ m$) \times (1$ eV$/m_\gamma)$.

VALUE (eV)	CL%	DOCUMENT ID		COMMENT
< 1 $\times 10^{-18}$		[1] RYUTOV	07	MHD of solar wind
• • • We do not use the following data for averages, fits, limits, etc. • • •				
< 3.0 $\times 10^{-9}$		[2] CHANG	25	Lensed fast radio burst time delay
$(16\ ^{+3}_{-9}) \times 10^{-15}$		[3] LEMOS	25	Fast Radio Bursts
< 4.9 $\times 10^{-7}$		[4] MALTA	24	Shapiro effect in solar system
< 2.5 $\times 10^{-18}$		[5] YAN	24A	Jovian magnetic field
< 2.1 $\times 10^{-15}$	68	[6] WANG	23B	Fast Radio Bursts
< 2.5 $\times 10^{-14}$		[7] MALTA	22	Schumann resonances in the Earth-ionosphere cavity
< 2.2 $\times 10^{-14}$		[8] BONETTI	17	Fast Radio Bursts, FRB 121102
< 1.8 $\times 10^{-14}$		[9] BONETTI	16	Fast Radio Bursts, FRB 150418
< 1.9 $\times 10^{-15}$		[10] RETINO	16	Ampere's Law in solar wind
< 2.3 $\times 10^{-9}$	95	[11] EGOROV	14	Lensed quasar position
		[12] ACCIOLY	10	Anomalous magn. mom.
< 1 $\times 10^{-26}$		[13] ADELBERGER	07A	Proca galactic field
no limit feasible		[13] ADELBERGER	07A	γ as Higgs particle
< 1 $\times 10^{-19}$		[14] TU	06	Torque on rotating magnetized toroid
< 1.4 $\times 10^{-7}$		ACCIOLY	04	Dispersion of GHz radio waves by sun
< 2 $\times 10^{-16}$		[15] FULLEKRUG	04	Speed of 5-50 Hz radiation in atmosphere
< 7 $\times 10^{-19}$		[16] LUO	03	Torque on rotating magnetized toroid
< 1 $\times 10^{-17}$		[17] LAKES	98	Torque on toroid balance
< 6 $\times 10^{-17}$		[18] RYUTOV	97	MHD of solar wind
< 8 $\times 10^{-16}$	90	[19] FISCHBACH	94	Earth magnetic field
< 5 $\times 10^{-13}$		[20] CHERNIKOV	92	Ampere's Law null test
< 1.5 $\times 10^{-9}$	90	[21] RYAN	85	Coulomb's Law null test
< 3 $\times 10^{-27}$		[22] CHIBISOV	76	Galactic magnetic field
< 4.5 $\times 10^{-16}$	99.7	[23] DAVIS	75	Jupiter's magnetic field
< 7.3 $\times 10^{-16}$		HOLLWEG	74	Alfven waves
< 6 $\times 10^{-17}$		[24] FRANKEN	71	Low freq. res. circuit
< 2.4 $\times 10^{-13}$		[25] KROLL	71A	Dispersion in atmosphere
< 1 $\times 10^{-14}$		[26] WILLIAMS	71	Tests Coulomb's Law
< 2.3 $\times 10^{-15}$		GOLDHABER	68	Satellite data

[1] RYUTOV 07 extends the method of RYUTOV 97 to the radius of Pluto's orbit.

[2] CHANG 25 sets upper limit on the photon mass using time delay between gravitationally lensed images of FRB 20190308C.

[3] LEMOS 25 gives constraints on the photon mass using, under several assumptions, data from Fast Radio Bursts and Supernovae. Do not present an upper limit.

[4] MALTA 24 gives an upper limit on the photon mass by analysing the gravitational time delay in a weak-field approximation using Doppler-tracking data from the Cassini mission.

[5] YAN 24A put constraints on the photon mass modelling non-zero-mass effects on the Jupiter magnetic field and using data of the JUNO Mission.

[6] WANG 23B use fast radio burst photon mass dependent dispersion relation to determine an upper limit of the photon mass.

[7] MALTA 22 consider the effect of a finite photon mass on Schumann resonances in the Earth-ionosphere cavity, improve limit by KROLL 71A by considering realistic conductivity profiles for the atmosphere.

[8] BONETTI 17 uses frequency-dependent time delays of repeating FRB with well-determined redshift, assuming the DM is caused by expected dispersion in IGM. There are several uncertainties, leading to mass limit 2.2×10^{-14} eV.

[9] BONETTI 16 uses frequency-dependent time delays of FRB, assuming the DM is caused by expected dispersion in IGM. There are several uncertainties, leading to mass limit 1.8×10^{-14} eV, if indeed the FRB is at the initially reported redshift.

[10] RETINO 16 looks for deviations from Ampere's law in the solar wind, using Cluster four spacecraft data. Authors quote a range of limits from 1.9×10^{-15} eV to 7.9×10^{-14} eV depending on the assumptions of the vector potential from the interplanetary magnetic field.

[11] EGOROV 14 studies chromatic dispersion of lensed quasar positions ("gravitational rainbows") that could be produced by any of several mechanisms, among them via photon mass. Limit not competitive but obtained on cosmological distance scales.

[12] ACCIOLY 10 limits come from possible alterations of anomalous magnetic moment of electron and gravitational deflection of electromagnetic radiation. Reported limits are not "claimed" by the authors and in any case are not competitive.

[13] When trying to measure m one must distinguish between measurements performed on large and small scales. If the photon acquires mass by the Higgs mechanism, the large-scale behavior of the photon might be effectively Maxwellian. If, on the other hand, one postulates the Proca regime for all scales, the very existence of the galactic field implies $m < 10^{-26}$ eV, as correctly calculated by YAMAGUCHI 59 and CHIBISOV 76.

[14] TU 06 continues the work of LUO 03, with extended LAKES 98 method, reporting the improved limit $\mu^2 A = (0.7 \pm 1.7) \times 10^{-13}$ T/m if $A = 0.2$ μG out to 4×10^{22} m. Reported result $\mu = (0.9 \pm 1.5) \times 10^{-52}$ g reduces to the frequentist mass limit 1.2×10^{-19} eV (FELDMAN 98). While the results of the torsion balance method give a value for the local limit on $\mu^2 A$, the deduced limit on the photon mass μ is open to question. See the discussions in TU 05 and GOLDHABER 03.

[15] FULLEKRUG 04 adopted KROLL 71A method with newer and better Schumann resonance data. Result questionable because assumed frequency shift with photon mass is assumed to be linear. It is quadratic according to theorem by GOLDHABER 71B, KROLL 71, and PARK 71.

[16] LUO 03 extends LAKES 98 technique to set a limit on $\mu^2 A$, where μ^{-1} is the Compton wavelength $\lambda\!\!\!^{-}_C$ of the massive photon and A is the ambient vector potential. The important departure is that the apparatus rotates, removing sensitivity to the direction of A. They take $A = 10^{12}$ Tm, due to "cluster level fields." But see comment of GOLDHABER 03 and reply by LUO 03B.

[17] LAKES 98 reports limits on torque on a toroid Cavendish balance, obtaining a limit on $\mu^2 A < 2 \times 10^{-9}$ Tm/m^2 via the Maxwell-Proca equations, where μ^{-1} is the characteristic length associated with the photon mass and A is the ambient vector potential in the Lorentz gauge. Assuming $A \approx 1 \times 10^{12}$ Tm due to cluster fields he obtains $\mu^{-1} > 2 \times 10^{10}$ m, corresponding to $\mu < 1 \times 10^{-17}$ eV. A more conservative limit, using $A \approx (1$ μG$) \times (600$ pc$)$ based on the galactic field, is $\mu^{-1} > 1 \times 10^9$ m or $\mu < 2 \times 10^{-16}$ eV.

[18] RYUTOV 97 uses a magnetohydrodynamics argument concerning survival of the Sun's field to the radius of the Earth's orbit. "To reconcile observations to theory, one has to reduce [the photon mass] by approximately an order of magnitude compared with" per DAVIS 75. "Secure limit, best by this method" (per GOLDHABER 10).

[19] FISCHBACH 94 analysis is based on terrestrial magnetic fields; approach analogous to DAVIS 75. Similar result based on a much smaller planet probably follows from more precise B field mapping. "Secure limit, best by this method" (per GOLDHABER 10).

[20] CHERNIKOV 92, motivated by possibility that photon exhibits mass only below some unknown critical temperature, searches for departure from Ampere's Law at 1.24 K. See also RYAN 85.

[21] RYAN 85, motivated by possibility that photon exhibits mass only below some unknown critical temperature, sets mass limit at $< (1.5 \pm 1.4) \times 10^{-42}$ g based on Coulomb's Law departure limit at 1.36 K. We report the result as frequentist 90% CL (FELDMAN 98).

[22] CHIBISOV 76 depends in critical way on assumptions such as applicability of virial theorem. Some of the arguments given only in unpublished references.

[23] DAVIS 75 analysis of Pioneer-10 data on Jupiter's magnetic field. "Secure limit, best by this method" (per GOLDHABER 10).

[24] FRANKEN 71 method is of dubious validity (KROLL 71A, JACKSON 99, GOLDHABER 10, and references therein).

[25] KROLL 71A used low frequency Schumann resonances in cavity between the conducting earth and resistive ionosphere, overcoming objections to resonant-cavity methods (JACKSON 99, GOLDHABER 10, and references therein). "Secure limit, best by this method" (per GOLDHABER 10).

[26] WILLIAMS 71 is landmark test of Coulomb's law. "Secure limit, best by this method" (per GOLDHABER 10).

γ CHARGE

OKUN 06 has argued that schemes in which all photons are charged are inconsistent. He says that if a neutral photon is also admitted to avoid this problem, then other problems emerge, such as those connected with the emission and absorption of charged photons by charged particles. He concludes that in the absence of a self-consistent phenomenological basis, interpretation of experimental data is at best difficult.

VALUE (e)	CHARGE	DOCUMENT ID		TECN	COMMENT
<1 $\times 10^{-46}$	**mixed**	[1] ALTSCHUL	07B	VLBI	Aharonov-Bohm effect
<1 $\times 10^{-35}$	**single**	[2] CAPRINI	05	CMB	Isotropy constraint
• • • We do not use the following data for averages, fits, limits, etc. • • •					
<1 $\times 10^{-32}$	single	[1] ALTSCHUL	07B	VLBI	Aharonov-Bohm effect
<3 $\times 10^{-33}$	mixed	[3] KOBYCHEV	05	VLBI	Smear as function of B·E$_\gamma$
<4 $\times 10^{-31}$	single	[3] KOBYCHEV	05	VLBI	Deflection as function of B·E$_\gamma$
<8.5 $\times 10^{-17}$		[4] SEMERTZIDIS	03		Laser light deflection in B-field
<3 $\times 10^{-28}$	single	[5] SIVARAM	95	CMB	For $\Omega_M = 0.3$, h$^2 = 0.5$
<5 $\times 10^{-30}$		[6] RAFFELT	94	TOF	Pulsar $f_1 - f_2$
<2 $\times 10^{-28}$		[7] COCCONI	92		VLBA radio telescope resolution
<2 $\times 10^{-32}$		COCCONI	88	TOF	Pulsar $f_1 - f_2$ TOF

[1] ALTSCHUL 07B looks for Aharonov-Bohm phase shift in addition to geometric phase shift in radio interference fringes (VSOP mission).

[2] CAPRINI 05 uses isotropy of the cosmic microwave background to place stringent limits on possible charge asymmetry of the Universe. Charge limits are set on the photon, neutrino, and dark matter particles. Valid if charge asymmetries produced by different particles are not anticorrelated.

[3] KOBYCHEV 05 considers a variety of observable effects of photon charge for extragalactic compact radio sources. Best limits if source observed through a foreground cluster of galaxies.

[4] SEMERTZIDIS 03 reports the first laboratory limit on the photon charge in the last 30 years. Straightforward improvements in the apparatus could attain a sensitivity of 10^{-20} e.

[5] SIVARAM 95 requires that CMB photon charge density not overwhelm gravity. Result scales as Ω_M h^2.

[6] RAFFELT 94 notes that COCCONI 88 neglects the fact that the time delay due to dispersion by free electrons in the interstellar medium has the same photon energy dependence as that due to bending of a charged photon in the magnetic field. His limit is based on the assumption that the entire observed dispersion is due to photon charge. It is a factor of 200 less stringent than the COCCONI 88 limit.

[7] See COCCONI 92 for less stringent limits in other frequency ranges. Also see RAFFELT 94 note.

Int. J. Mod. Phys. A 2026.41. Downloaded from www.worldscientific.com
by UNIVERSITY OF CALIFORNIA @ BERKELEY on 09/16/26. Reproduction is strictly not permitted, except for Open Access articles.

γ REFERENCES

CHANG	25	PR D111 L041304	C.-M. Chang *et al.*	
LEMOS	25	JCAP 2511 019	T. Lemos *et al.*	(ONRJ)
MALTA	24	PR D110 095017	P.C. Malta, C.A.D. Zarro	(UFRJ)
YAN	24A	JHEP 2406 028	S. Yan, L. Li, J.J. Fan	(BROW)
WANG	23B	JCAP 2309 025	B. Wang *et al.*	
MALTA	22	PR D106 116014	P.C. Malta, J.A. Helayel-Neto	
BONETTI	17	PL B768 326	L. Bonetti *et al.*	(ORLEANS, CERN)
BONETTI	16	PL B757 548	L. Bonetti *et al.*	
RETINO	16	ASP 82 49	A. Retino, A.D.A.M. Spallicci, A. Vaivads	(CURCP+)
EGOROV	14	MNRAS 437 L90	P. Egorov *et al.*	(MOSU, MIPT, INRM)
ACCIOLY	10	PR D82 065026	A. Acciolly, J. Helayel-Neto, E. Scatena	(LABEX+)
GOLDHABER	10	RMP 82 939	A.S. Goldhaber, M.M. Nieto	(STON, LANL)
ADELBERGER	07A	PRL 98 010402	E. Adelberger, G. Dvali, A. Gruzinov	(WASH, NYU)
ALTSCHUL	07B	PRL 98 261801	B. Altschul	(IND)
Also		ASP 29 290	B. Altschul	(SCUC)
RYUTOV	07	PPCF 49 B429	D.D. Ryutov	(LLNL)
OKUN	06	APP B37 565	L.B. Okun	(ITEP)
TU	06	PL A352 267	L.-C. Tu *et al.*	
CAPRINI	05	JCAP 0502 006	C. Caprini, P.G. Ferreira	(GEVA, OXFTP)
KOBYCHEV	05	AL 31 147	V.V. Kobychev, S.B. Popov	(KIEV, PADO)
TU	05	RPP 68 77	L.-C. Tu, J. Luo, G.T. Gillies	
ACCIOLY	04	PR D69 107501	A. Acciolly, R. Paszko	
FULLEKRUG	04	PRL 93 043901	M. Fullekrug	
GOLDHABER	03	PRL 91 149101	A.S. Goldhaber, M.M. Nieto	
LUO	03	PRL 90 081801	J. Luo *et al.*	
LUO	03B	PRL 91 149102	J. Luo *et al.*	
SEMERTZIDIS	03	PR D67 017701	Y.K. Semertzidis, G.T. Danby, D.M. Lazarus	
JACKSON	99	Classical Electrodynamics	J.D. Jackson (3rd ed., J. Wiley and Sons (1999))	
FELDMAN	98	PR D57 3873	G.J. Feldman, R.D. Cousins	
LAKES	98	PRL 80 1826	R. Lakes	(WISC)
RYUTOV	97	PPCF 39 A73	D.D. Ryutov	(LLNL)
SIVARAM	95	AJP 63 473	C. Sivaram	(BANG)
FISCHBACH	94	PRL 73 514	E. Fischbach *et al.*	(PURD, JHU+)
RAFFELT	94	PR D50 7729	G. Raffelt	(MPIM)
CHERNIKOV	92	PRL 68 3383	M.A. Chernikov *et al.*	(ETH)
Also		PRL 69 2999 (errat.)	M.A. Chernikov *et al.*	(ETH)
COCCONI	92	AJP 60 750	G. Cocconi	(CERN)
COCCONI	88	PL B206 705	G. Cocconi	(CERN)
RYAN	85	PR D32 802	J.J. Ryan, F. Accetta, R.H. Austin	(PRIN)
CHIBISOV	76	SPU 19 624	G.V. Chibisov	(LEBD)
		Translated from UFN 119 551.		
DAVIS	75	PRL 35 1402	L. Davis, A.S. Goldhaber, M.M. Nieto	(CIT, STON+)
HOLLWEG	74	PRL 32 961	J.V. Hollweg	(NCAR)
FRANKEN	71	PRL 26 115	P.A. Franken, G.W. Ampulski	(MICH)
GOLDHABER	71B	RMP 43 277	A.S. Goldhaber, M.M. Nieto	(STON, BOHR, UCSB)
KROLL	71	PRL 26 1395	N.M. Kroll	(SLAC)
KROLL	71A	PRL 27 340	N.M. Kroll	(SLAC)
PARK	71	PRL 26 1393	D. Park, E.R. Williams	(WILC)
WILLIAMS	71	PRL 26 721	E.R. Williams, J.E. Faller, H.A. Hill	(WESL)
GOLDHABER	68	PRL 21 567	A.S. Goldhaber, M.M. Nieto	(STON)
YAMAGUCHI	59	PTPS 11 37	Y. Yamaguchi	

g (gluon)

$I(J^P) = 0(1^-)$

SU(3) color octet

Mass $m = 0$. Theoretical value. A mass as large as a few MeV may not be precluded, see YNDURAIN 95.

gluon spin

VALUE	DOCUMENT ID		TECN	COMMENT
• • • We do not use the following data for averages, fits, limits, etc. • • •				
	ABREU	92E	DLPH	Spin 1, not 0
	ALEXANDER	91H	OPAL	Spin 1, not 0
	BEHREND	82D	CELL	Spin 1, not 0
	BERGER	80D	PLUT	Spin 1, not 0
	BRANDELIK	80C	TASS	Spin 1, not 0

gluon REFERENCES

YNDURAIN	95	PL B345 524	F.J. Yndurain	(MADU)
ABREU	92E	PL B274 498	P. Abreu *et al.*	(DELPHI Collab.)
ALEXANDER	91H	ZPHY C52 543	G. Alexander *et al.*	(OPAL Collab.)
BEHREND	82D	PL B110 329	H.J. Behrend *et al.*	(CELLO Collab.)
BERGER	80D	PL B97 459	C. Berger *et al.*	(PLUTO Collab.)
BRANDELIK	80C	PL B97 453	R. Brandelik *et al.*	(TASSO Collab.)

graviton

$J = 2$

graviton MASS

It is likely that the graviton is massless. More than fifty years ago Van Dam and Veltman (VANDAM 70), Iwasaki (IWASAKI 70), and Zakharov (ZAKHAROV 70) almost simultaneously showed that in the linear approximation a theory with a finite graviton mass does not approach GR as the mass approaches zero. Attempts have been made to evade this "vDVZ discontinuity" by invoking modified gravity or nonlinear theory by De Rahm (DE-RHAM 17) and others. More recently, the analysis of gravitational wave dispersion has led to bounds that are largely independent of the underlying model, even if not the strongest. We quote the best of these as our best limit.

Experimental limits have been set based on a Yukawa potential (YUKA), dispersion relation (DISP), or other modified gravity theories (MGRV).

The following conversions are useful: 1 eV $= 1.783 \times 10^{-36}$ kg $= 1.957 \times 10^{-6}$ m_e; $\lambda\!\!\!^{-}_C = (1.973 \times 10^{-7}$ m$) \times (1$ eV$/m_g)$.

VALUE (eV)	DOCUMENT ID		TECN	COMMENT
$<1.76 \times 10^{-23}$	[1] ABBOTT	21	DISP	LIGO Virgo catalog GWTC-2
• • • We do not use the following data for averages, fits, limits, etc. • • •				
$<6.6 \times 10^{-34}$	[2] DEFELICE	24	MGRV	Extended Minimal Theory of Massive Gravity
$<3.8 \times 10^{-23}$	[3] WANG	24	PTA	CPTA pulsar timing array
$<8.6 \times 10^{-24}$	[3] WANG	24	PTA	NANOgrav pulsar timing array
$<8 \times 10^{-34}$	[4] DEFELICE	21	MGRV	Normal branch Minimal Theory of Massive Gravity
$<3.2 \times 10^{-23}$	[5] BERNUS	20	YUKA	Planetary ephemeris INPOP19a
$<2 \times 10^{-28}$	[6] SHAO	20	DISP	Binary pulsar Galileon radiation
$<4.7 \times 10^{-23}$	[7] ABBOTT	19	DISP	LIGO Virgo catalog GWTC-1
$<7 \times 10^{-23}$	[8] BERNUS	19	YUKA	Planetary ephemeris INPOP17b
$<3.1 \times 10^{-20}$	[9] MIAO	19	DISP	Binary pulsar orbital decay rate
$<1.4 \times 10^{-29}$	[10] DESAI	18	YUKA	Gal cluster Abell 1689
$<5 \times 10^{-30}$	[11] GUPTA	18	YUKA	Using SPT-SZ
$<3 \times 10^{-30}$	[11] GUPTA	18	YUKA	Using Planck all-sky SZ
$<1.3 \times 10^{-29}$	[11] GUPTA	18	YUKA	Using redMaPPer SDSS-DR8
$<6 \times 10^{-30}$	[12] RANA	18	YUKA	Weak lensing in massive clusters
$<8 \times 10^{-30}$	[13] RANA	18	YUKA	SZ effect in massive clusters
$<1.0 \times 10^{-23}$	[14] WILL	18	YUKA	Perihelion advances of planets
$<7 \times 10^{-23}$	[7] ABBOTT	17	DISP	Combined dispersion limit from three BH mergers
$<1.2 \times 10^{-22}$	[7] ABBOTT	16	DISP	Combined dispersion limit from two BH mergers
$<2.9 \times 10^{-21}$	[15] ZAKHAROV	16	YUKA	S2 star orbit
$<5 \times 10^{-23}$	[16] BRITO	13	MGRV	Spinning black holes bounds
$<6 \times 10^{-32}$	[17] GRUZINOV	05	MGRV	Solar System observations
$<6 \times 10^{-32}$	[18] CHOUDHURY	04	YUKA	Weak gravitational lensing
$<9.0 \times 10^{-34}$	[19] GERSHTEIN	04	MGRV	From Ω_{tot} value assuming RTG
$<8 \times 10^{-20}$	[20,21] FINN	02	DISP	Binary pulsar orbital period decrease
$<7 \times 10^{-23}$	TALMADGE	88	YUKA	Solar system planetary astrometric data
$<1.3 \times 10^{-29}$	[22] GOLDHABER	74	YUKA	Rich clusters
$<7 \times 10^{-28}$	HARE	73	YUKA	Galaxy
$<8 \times 10^{4}$	HARE	73	YUKA	2γ decay

[1] ABBOTT 21 assumed modified gravitational-wave dispersion to establish a limit on graviton mass, using LIGO-Virgo O1-O3a binary black hole (BBH) events.

[2] DEFELICE 24 limits graviton mass in context of the "extended Minimal Theory of Massive Gravity" recently proposed by two of the authors, using constraints from Planck-CMB, BAO and SNe1a.

[3] WANG 24 investigates sensitivity to the graviton mass of overlap reduction functions due to stochastic gravitational wave background in the nano-Hertz band as observed in pulsar timing arrays.

[4] DEFELICE 21 studies the normal branch of the Minimal Theory of Massive Gravity (MTMG) to find that after five parameters are adjusted to obtain agreement with all presently available data, today's squared mass $m_g^2 = (2.5^{+4.5}_{-4.8}) \times 10^{-67}$ eV^2 or $m_g < 8.4 \times 10^{-33}$ eV, both at the 95% CL.

[5] BERNUS 20 use the latest solution of the ephemeris INPOP (19a) in order to improve the constraint in BERNUS 19 on the existence of a Yukawa suppression to the Newtonian potential, generically associated to a gravitons mass.

[6] SHAO 20 sets limit, 95% CL, based on non-observation of excess gravitational radiation in 14 well-timed binary pulsars in the context of the cubic Galileon model.

[7] ABBOTT 19, ABBOTT 17, and ABBOTT 16 assumed modified gravitational waves dispersion to establish limits on graviton mass.

[8] BERNUS 19 use the planetary ephemeris INPOP 17b to constraint the existence of a Yukawa suppression to the Newtonian potential, generically associated to a gravitons mass.

[9] MIAO 19 90% CL limit is based on orbital period decay rates of 9 binary pulsars using a Bayesian prior uniform in graviton mass. Limit becomes $< 5.2 \times 10^{-21}$ eV for a prior uniform in $\ln(m_g)$.

[10] DESAI 18 limit based on dynamical mass models of galaxy cluster Abell 1689.

[11] GUPTA 18 obtains graviton mass limits using stacked clusters from 3 disparate surveys.

[12] RANA 18 limit, 68% CL, obtained using weak lensing mass profiles out to the radius at which the cluster density falls to 200 times the critical density of the Universe. Limit is based on the fractional change between Newtonian and Yukawa accelerations for the 50 most massive galaxy clusters in the Local Cluster Substructure Survey. Limits for other CL's and other density cuts are also given.

[13] RANA 18 limit, 68% CL, obtained using mass measurements via the SZ effect out to the radius at which the cluster density falls to 500 times the critical density of the Universe for 182 optically confirmed galaxy clusters in an Altacama Cosmology Telescope survey. Limits for other CL's and other density cuts are also given.

[14] WILL 18 limit from perihelion advances of the planets, notably Earth, Mars, and Saturn. Alternate analysis yields $< 6 \times 10^{-24}$.

[15] ZAKHAROV 16 constrains range of Yukawa gravity interaction from S2 star orbit about black hole at Galactic center. The limit is $< 2.9 \times 10^{-21}$ eV for $\delta = 100$.

[16] BRITO 13 explore massive graviton (spin-2) fluctuations around rotating black holes.

[17] GRUZINOV 05 uses the DGP model (DVALI 00) showing that non-perturbative effects restore continuity with Einstein's equations as the gravition mass approaches zero, then bases his limit on Solar System observations.

[18] CHOUDHURY 04 concludes from a study of weak-lensing data that masses heavier than about the inverse of 100 Mpc seem to be ruled out if the gravitation field has the Yukawa form.

[19] GERSHTEIN 04 use non-Einstein field relativistic theory of gravity (RTG), with a massive graviton, to obtain the 95% CL mass limit implied by the value of $\Omega_{tot} = 1.02 \pm 0.02$ current at the time of publication.

[20] FINN 02 analyze the orbital decay rates of PSR B1913+16 and PSR B1534+12 with a possible graviton mass as a parameter. The combined frequentist mass limit is at 90%CL.

[21] As of 2020, limits on dP/dt are now about 0.1% (see T. Damour, "Experimental tests of gravitational theory," in this *Review*).

[22] GOLDHABER 74 establish this limit considering the binding of galactic clusters, corrected to Planck $h_0 = 0.67$.

Int. J. Mod. Phys. A 2026.41. Downloaded from www.worldscientific.com by UNIVERSITY OF CALIFORNIA @ BERKELEY on 09/16/26. Re-use and distribution is strictly not permitted, except for Open Access articles.

graviton REFERENCES

DEFELICE	24	JCAP 2404 013	A. De Felice *et al.*	
WANG	24	PR D109 L061502	S. Wang, Z-C. Zhao	
ABBOTT	21	PR D103 122002	R. Abbott *et al.*	(LIGO and Virgo Collabs.)
DEFELICE	21	JCAP 2112 011	A. De Felice, S. Mukohyama, M.C. Pookkillath	
BERNUS	20	PR D102 021501	L. Bernus *et al.*	
SHAO	20	PR D102 024069	L. Shao, N. Wex, S.-Y. Zhou	
ABBOTT	19	PR D100 104036	B.P. Abbott *et al.*	(LIGO and Virgo Collabs.)
BERNUS	19	PRL 123 161103	L. Bernus *et al.*	
MIAO	19	PR D99 123015	X. Miao, L. Shao, B.-Q. Ma	
DESAI	18	PL B778 325	S. Desai	(HYDER)
GUPTA	18	ANP 399 85	S. Gupta, S. Desai	
RANA	18	PL B781 220	A. Rana *et al.*	(DELHI)
WILL	18	CQG 35 17LT01	C.M. Will	
ABBOTT	17	PRL 118 221101	B.P. Abbott *et al.*	(LIGO and Virgo Collabs.)
DE-RHAM	17	RMP 89 025004	C. de Rham *et al.*	
ABBOTT	16	PRL 116 061102	B.P. Abbott *et al.*	(LIGO and Virgo Collabs.)
ZAKHAROV	16	JCAP 1605 045	A.F. Zakharov *et al.*	
BRITO	13	PR D88 023514	R. Brito, V. Cardoso, P. Pani	(LISB, MISS, HSCA+)
GRUZINOV	05	NAST 10 311	A. Gruzinov	(NYU)
CHOUDHURY	04	ASP 21 559	S.R. Choudhury *et al.*	(DELPH, MELB)
GERSHTEIN	04	PAN 67 1596	S.S. Gershtein *et al.*	(SERP)
		Translated from YAF 67 1618.		
FINN	02	PR D65 044022	L.S. Finn, P.J. Sutton	
DVALI	00	PL B485 208	G.R. Dvali, G. Gabadadze, M. Porrati	(NYU)
TALMADGE	88	PRL 61 1159	C. Talmadge *et al.*	(JPL)
GOLDHABER	74	PR D9 1119	A.S. Goldhaber, M.M. Nieto	(LANL, STON)
HARE	73	CJP 51 431	M.G. Hare	(SASK)
IWASAKI	70	PR D2 2255	Y. Iwasaki	
VANDAM	70	NP B22 397	H. van Dam, M. Veltman	(UTRE)
ZAKHAROV	70	JETPL 12 312	V.I. Zakharov *et al.*	

W

$J = 1$

See the related review(s):
Mass and Width of the W Boson

W MASS

The W-mass listed here corresponds to the mass parameter in a Breit-Wigner distribution with mass-dependent width. To obtain the world average of various measurements, common systematic uncertainties between experiments are evaluated and accounted for in combinations [SCHAEL 13A, AMOROSO 24]. Until 2022, the measurements of the W-boson mass at lepton and hadron colliders, LEP-2 (ALEPH, DELPHI, L3, and OPAL), Tevatron (CDF and D0), and LHC (ATLAS and LHCb), were in good agreement with each other [PDG 22]. However, with the 2022 CDF result [AALTONEN 22] based on their complete Run-II data set, this is no longer the case. The LHC-TeV MW Working Group, including W-mass experts from CDF, D0, ATLAS, CMS and LHCb, has examined this issue in depth [AMOROSO 24]. In May 2026 the LHC-TeV MW Working Group updated their combination [LHC-TeVatron M_W Working Group, Compatibility and combination of world W-boson mass measurements, 7 May 2026], including the improved ATLAS result [AAD 24CJ] and the new CMS result [CHEKHOVSKY 26]. They report that a combination of all W-mass measurements corrected to a common theory description and PDF set, has a probability of compatibility of 0.06% only. A 96.9% probability of compatibility is obtained when the CDF measurement [AALTONEN 22] is removed. The corresponding value of the W boson mass is 80362.5 ± 7.7 MeV, which we quote as the World Average. More information is given in [M. Grunewald, A. Gurtu, J.Kretzschmar, "Mass and Width of the W Boson" review, PDG 26] and references therein.

VALUE (GeV)	EVTS	DOCUMENT ID		TECN	COMMENT
80.3625 ± 0.0077 OUR EVALUATION		(LHC-TeVatron M_W Working Group)			
80.3602 ± 0.0024 ± 0.0096	117M	[1] CHEKHOVSKY	26	CMS	E^{pp}_{cm} = 13 TeV
80.3665 ± 0.0098 ± 0.0125	13.7M	[2] AAD	24CJ	ATLS	E^{pp}_{cm} = 7 TeV
80.354 ± 0.023 ± 0.022	2.4M	[3] AAIJ	22C	LHCB	E^{pp}_{cm} = 13 TeV
80.375 ± 0.011 ± 0.020	2177k	[4] ABAZOV	12F	D0	$E^{p\overline{p}}_{cm}$ = 1.96 TeV
80.336 ± 0.055 ± 0.039	10.3k	[5] ABDALLAH	08A	DLPH	E^{ee}_{cm} = 161–209 GeV
80.415 ± 0.042 ± 0.031	11830	[6] ABBIENDI	06	OPAL	E^{ee}_{cm} = 170–209 GeV
80.270 ± 0.046 ± 0.031	9909	[7] ACHARD	06	L3	E^{ee}_{cm} = 161–209 GeV
80.440 ± 0.043 ± 0.027	8692	[8] SCHAEL	06	ALEP	E^{ee}_{cm} = 161–209 GeV
80.483 ± 0.084	49247	[9] ABAZOV	02D	D0	$E^{p\overline{p}}_{cm}$ = 1.8 TeV
• • • We do not use the following data for averages, fits, limits, etc. • • •					
80.4335 ± 0.0064 ± 0.0069	4.2M	[10] AALTONEN	22	CDF	$E^{p\overline{p}}_{cm}$ = 1.96 TeV
80.370 ± 0.007 ± 0.017	13.7M	[11] AABOUD	18J	ATLS	E^{pp}_{cm} = 7 TeV
80.520 ± 0.070 ± 0.092		[12] ANDREEV	18A	H1	$e^{\pm}p$
80.387 ± 0.012 ± 0.015	1095k	[13] AALTONEN	12E	CDF	$E^{p\overline{p}}_{cm}$ = 1.96 TeV
80.367 ± 0.013 ± 0.022	1677k	[14] ABAZOV	12F	D0	$E^{p\overline{p}}_{cm}$ = 1.96 TeV
80.401 ± 0.021 ± 0.038	500k	[15] ABAZOV	09AB	D0	$E^{p\overline{p}}_{cm}$ = 1.96 TeV
80.413 ± 0.034 ± 0.034	115k	[16] AALTONEN	07F	CDF	$E^{p\overline{p}}_{cm}$ = 1.96 TeV
82.87 ± 1.82 $^{+0.30}_{-0.16}$	1500	[17] AKTAS	06	H1	$e^{\pm}p \to \overline{\nu}_e(\nu_e)X$, $\sqrt{s} \approx$ 300 GeV
80.3 ± 2.1 ± 1.2 ± 1.0	645	[18] CHEKANOV	02C	ZEUS	$e^-p \to \nu_e X$, $\sqrt{s}$= 318 GeV
80.433 ± 0.079	53841	[19] AFFOLDER	01E	CDF	$E^{p\overline{p}}_{cm}$ = 1.8 TeV
81.4 $^{+2.7}_{-2.6}$ ± 2.0 $^{+3.3}_{-3.0}$	1086	[20] BREITWEG	00D	ZEUS	$e^+p \to \overline{\nu}_e X$, $\sqrt{s} \approx$ 300 GeV
80.84 ± 0.22 ± 0.83	2065	[21] ALITTI	92B	UA2	see W/Z ratio below
80.79 ± 0.31 ± 0.84		[22] ALITTI	90B	UA2	$E^{p\overline{p}}_{cm}$ = 546,630 GeV
80.0 ± 3.3 ± 2.4	22	[23] ABE	89I	CDF	$E^{p\overline{p}}_{cm}$ = 1.8 TeV
82.7 ± 1.0 ± 2.7	149	[24] ALBAJAR	89	UA1	$E^{p\overline{p}}_{cm}$ = 546,630 GeV
81.8 $^{+6.0}_{-5.3}$ ± 2.6	46	[25] ALBAJAR	89	UA1	$E^{p\overline{p}}_{cm}$ = 546,630 GeV
89 ± 3 ± 6	32	[26] ALBAJAR	89	UA1	$E^{p\overline{p}}_{cm}$ = 546,630 GeV
81. ± 5.	6	ARNISON	83	UA1	E^{ee}_{cm} = 546 GeV
80. $^{+10.}_{-6.}$	4	BANNER	83B	UA2	Repl. by ALITTI 90B

[1] CHEKHOVSKY 26 analyse W-boson production and decay in the muon channel. The mass of the W boson is determined from analysing the differential distribution in muon transverse momentum (in the range from 26 GeV to 56 GeV) and muon pseudo rapidity (in the range from −2.4 to +2.4) separately for positively and negatively charged muons.

[2] AAD 24CJ provides an improved determination of the W boson mass using the same data as analysed for AABOUD 18J, thus superseding that W boson mass measurement. The distributions of the transverse lepton momentum and of the transverse mass are analysed to determine the W boson mass.

[3] AAIJ 22C analyse W production in the muon decay channel, with the transverse momentum of the muon required to be between 28 and 52 GeV. Analysing the distribution of the muon charge divided by the muon transverse momentum of approximately 2.4 million selected W candidates, a value of M_W = 80354 ± 23(stat.) ± 10(exp.) ± 17(theo.) ± 9(PDF) MeV is obtained; we combine the three systematic uncertainties in quadrature.

[4] Combination of results from ABAZOV 12F and ABAZOV 09AB as quoted in ABAZOV 12F.

[5] ABDALLAH 08A use direct reconstruction of the kinematics of $W^+W^- \to q\overline{q}\ell\nu$ and $W^+W^- \to q\overline{q}q\overline{q}$ events for energies 172 GeV and above. The W mass was also extracted from the dependence of the WW cross section close to the production threshold and combined appropriately to obtain the final result. The systematic error includes ±0.025 GeV due to final state interactions and ±0.009 GeV due to LEP energy uncertainty.

[6] ABBIENDI 06 use direct reconstruction of the kinematics of $W^+W^- \to q\overline{q}\ell\nu_\ell$ and $W^+W^- \to q\overline{q}q\overline{q}$ events. The result quoted here is obtained combining this mass value with the results using $W^+W^- \to \ell\nu_\ell\ell'\nu_{\ell'}$ events in the energy range 183–207 GeV (ABBIENDI 03C) and the dependence of the WW production cross-section on m_W at threshold. The systematic error includes ±0.009 GeV due to the uncertainty on the LEP beam energy.

[7] ACHARD 06 use direct reconstruction of the kinematics of $W^+W^- \to q\overline{q}\ell\nu_\ell$ and $W^+W^- \to q\overline{q}q\overline{q}$ events in the C.M. energy range 189–209 GeV. The result quoted here is obtained combining this mass value with the results obtained from a direct W mass reconstruction at 172 and 183 GeV and with those from the dependence of the WW production cross-section on m_W at 161 and 172 GeV (ACCIARRI 99).

[8] SCHAEL 06 use direct reconstruction of the kinematics of $W^+W^- \to q\overline{q}\ell\nu_\ell$ and $W^+W^- \to q\overline{q}q\overline{q}$ events in the C.M. energy range 183–209 GeV. The result quoted here is obtained combining this mass value with those obtained from the dependence of the W pair production cross-section on m_W at 161 and 172 GeV (BARATE 97 and BARATE 97S respectively). The systematic error includes ±0.009 GeV due to possible effects of final state interactions in the $q\overline{q}q\overline{q}$ channel and ±0.009 GeV due to the uncertainty on the LEP beam energy.

[9] ABAZOV 02D improve the measurement of the W-boson mass including $W \to e\nu_e$ events in which the electron is close to a boundary of a central electromagnetic calorimeter module. Properly combining the results obtained by fitting $m_T(W)$, $p_T(e)$, and $p_T(\nu)$, this sample provides a mass value of 80.574 ± 0.405 GeV. The value reported here is a combination of this measurement with all previous DØ W-boson mass measurements.

[10] AALTONEN 22 select a data sample of about 4 million W boson candidates in 8.8 fb^{-1} of Run-II data. The mass is determined using the transverse mass, transverse lepton momentum and transverse missing momentum distributions of W decays into electrons or muons, accounting for correlations. This measurement supersedes AALTONEN 12E, but is not used in OUR EVALUATION.

[11] AABOUD 18J select 4.61M $W^+ \to \mu^+\nu_\mu$, 3.40M $W^+ \to e^+\nu_e$, 3.23M $W^- \to \mu^-\overline{\nu}_\mu$ and 2.49M $W^- \to e^-\overline{\nu}_e$ events in 4.6 fb^{-1} pp data at 7 TeV. The W mass is determined using the transverse mass and transverse lepton momentum distributions, accounting for correlations. The systematic error includes 0.011 GeV experimental and 0.014 GeV modelling uncertainties.

[12] ANDREEV 18A obtain this result in a combined electroweak and QCD analysis using all deep-inelastic e^+p and e^-p neutral current and charged current scattering cross sections published by the H1 Collaboration, including data with longitudinally polarized lepton beams.

[13] AALTONEN 12E select 470k $W \to e\nu$ decays and 625k $W \to \mu\nu$ decays in 2.2 fb^{-1} of Run-II data. The mass is determined using the transverse mass, transverse lepton momentum and transverse missing energy distributions, accounting for correlations. This result supersedes AALTONEN 07F. AALTONEN 14D gives more details on the procedures followed by the authors. This measurement is superseded by AALTONEN 22.

[14] ABAZOV 12F select 1677k $W \to e\nu$ decays in 4.3 fb^{-1} of Run-II data. The mass is determined using the transverse mass and transverse lepton momentum distributions, accounting for correlations.

[15] ABAZOV 09AB study the transverse mass, transverse electron momentum, and transverse missing energy in a sample of 0.5 million $W \to e\nu$ decays selected in Run-II data. The quoted result combines all three methods, accounting for correlations.

[16] AALTONEN 07F obtain high purity $W \to e\nu_e$ and $W \to \mu\nu_\mu$ candidate samples totaling 63,964 and 51,128 events respectively. The W mass value quoted above is derived by simultaneously fitting the transverse mass and the lepton, and neutrino p_T distributions.

[17] AKTAS 06 fit the Q^2 dependence (300 < Q^2 < 30,000 GeV^2) of the charged-current differential cross section with a propagator mass. The first error is experimental and the second corresponds to uncertainties due to input parameters and model assumptions.

[18] CHEKANOV 02C fit the Q^2 dependence (200 < Q^2 < 60000 GeV^2) of the charged-current differential cross sections with a propagator mass fit. The last error is due to the uncertainty on the probability density functions.

[19] AFFOLDER 01E fit the transverse mass spectrum of 30115 $W \to e\nu_e$ events (M_W= 80.473 ± 0.065 ± 0.092 GeV) and of 14740 $W \to \mu\nu_\mu$ events (M_W= 80.465 ± 0.100 ± 0.103 GeV) obtained in the run IB (1994-95). Combining the electron and muon results, accounting for correlated uncertainties, yields M_W= 80.470 ± 0.089 GeV. They combine this value with their measurement of ABE 95P reported in run IA (1992-93) to obtain the quoted value.

[20] BREITWEG 00D fit the Q^2 dependence ($200 < Q^2 < 22500$ GeV^2) of the charged-current differential cross sections with a propagator mass fit. The last error is due to the uncertainty on the probability density functions.

[21] ALITTI 92B result has two contributions to the systematic error (±0.83); one (±0.81) cancels in m_W/m_Z and one (±0.17) is noncancelling. These were added in quadrature. We choose the ALITTI 92B value without using the LEP m_Z value, because we perform our own combined fit.

[22] There are two contributions to the systematic error (±0.84): one (±0.81) which cancels in m_W/m_Z and one (±0.21) which is non-cancelling. These were added in quadrature.

[23] ABE 89I systematic error dominated by the uncertainty in the absolute energy scale.

[24] ALBAJAR 89 result is from a total sample of 299 $W \to e\nu$ events.

[25] ALBAJAR 89 result is from a total sample of 67 $W \to \mu\nu$ events.

[26] ALBAJAR 89 result is from $W \to \tau\nu$ events.

W/*Z* MASS RATIO

VALUE	EVTS	DOCUMENT ID		TECN	COMMENT
0.88136±0.00015		[1] PDG	24		
• • • We do not use the following data for averages, fits, limits, etc. • • •					
0.8821 ±0.0011 ±0.0008	28323	[2] ABBOTT	98N	D0	$E^{p\overline{p}}_{cm}$= 1.8 TeV
0.88114±0.00154±0.00252	5982	[3] ABBOTT	98P	D0	$E^{p\overline{p}}_{cm}$= 1.8 TeV
0.8813 ±0.0036 ±0.0019	156	[4] ALITTI	92B	UA2	$E^{p\overline{p}}_{cm}$= 630 GeV

[1] This value was obtained using the world average values of m_Z and m_W as presented in these listings.

[2] ABBOTT 98N obtain this from a study of 28323 $W \to e\nu_e$ and 3294 $Z \to e^+e^-$ decays. Of this latter sample, 2179 events are used to calibrate the electron energy scale.

[3] ABBOTT 98P obtain this from a study of 5982 $W \to e\nu_e$ events. The systematic error includes an uncertainty of ±0.00175 due to the electron energy scale.

[4] Scale error cancels in this ratio.

$m_Z - m_W$

VALUE (GeV)	DOCUMENT ID		TECN	COMMENT
10.818±0.013	[1] PDG	24		
• • • We do not use the following data for averages, fits, limits, etc. • • •				
10.4 ±1.4 ±0.8	ALBAJAR	89	UA1	$E^{p\overline{p}}_{cm}$= 546,630 GeV
11.3 ±1.3 ±0.9	ANSARI	87	UA2	$E^{p\overline{p}}_{cm}$= 546,630 GeV

[1] This value was obtained using the world average values of m_Z and m_W as presented in these listings.

$m_{W^+} - m_{W^-}$

Test of *CPT* invariance.

VALUE (GeV)	EVTS	DOCUMENT ID		TECN	COMMENT
−0.029±0.028 OUR AVERAGE					
−0.029±0.013±0.025	13.7M	[1] AABOUD	18J	ATLS	E^{pp}_{cm} = 7 TeV
−0.19 ±0.58	1722	ABE	90G	CDF	$E^{p\overline{p}}_{cm}$= 1.8 TeV

[1] AABOUD 18J select 4.61M $W^+ \to \mu^+\nu_\mu$, 3.40M $W^+ \to e^+\nu_e$, 3.23M $W^- \to \mu^-\overline{\nu}_\mu$ and 2.49M $W^- \to e^-\overline{\nu}_e$ events in 4.6 fb^{-1} pp data at 7 TeV. The W mass is determined using the transverse mass and transverse lepton momentum distributions, accounting for correlations. The systematic error includes 0.007 GeV experimental and 0.024 GeV modelling uncertainties.

W WIDTH

The W width listed here corresponds to the width parameter in a Breit-Wigner distribution with mass-dependent width. To obtain the world average, common systematic uncertainties between experiments are properly taken into account. The LEP-2 average W width based on published results is 2.195 ± 0.083 GeV [SCHAEL 13A]. The combined Tevatron data yields an average W width of 2.046 ± 0.049 GeV [TEVEWWG 10]. OUR AVERAGE uses these average LEP and Tevatron width values and combines them together with the ATLAS result, assuming no correlations.

VALUE (GeV)	EVTS	DOCUMENT ID		TECN	COMMENT
2.14 ±0.05 OUR AVERAGE		Error includes scale factor of 1.7.			See the ideogram below.
2.202±0.032±0.034	13.7M	[1] AAD	24CJ	ATLS	E^{pp}_{cm} = 7 TeV
2.195±0.083		[2] SCHAEL	13A	LEP	E^{ee}_{cm}= 170–209 GeV
2.046±0.049		[3] TEVEWWG	10	TEVA	$E^{p\overline{p}}_{cm}$ = 1.8–1.96 TeV
• • • We do not use the following data for averages, fits, limits, etc. • • •					
2.028±0.072	5272	[4] ABAZOV	09AK	D0	$E^{p\overline{p}}_{cm}$ = 1.96 GeV
2.032±0.045±0.057	6055	[5] AALTONEN	08B	CDF	$E^{p\overline{p}}_{cm}$ = 1.96 TeV
2.404±0.140±0.101	10.3k	[6] ABDALLAH	08A	DLPH	E^{ee}_{cm}= 183–209 GeV
1.996±0.096±0.102	10729	[7] ABBIENDI	06	OPAL	E^{ee}_{cm}= 170–209 GeV
2.18 ±0.11 ±0.09	9795	[8] ACHARD	06	L3	E^{ee}_{cm}= 172–209 GeV
2.14 ±0.09 ±0.06	8717	[9] SCHAEL	06	ALEP	E^{ee}_{cm}= 183–209 GeV
$2.23\ ^{+0.15}_{-0.14}$ ±0.10	294	[10] ABAZOV	02E	D0	$E^{p\overline{p}}_{cm}$ = 1.8 TeV
2.152±0.066	79176	[11] ABBOTT	00B	D0	Extracted value
2.05 ±0.10 ±0.08	662	[12] AFFOLDER	00M	CDF	$E^{p\overline{p}}_{cm}$ = 1.8 TeV
2.064±0.060±0.059		[13] ABE	95W	CDF	Extracted value
$2.10\ ^{+0.14}_{-0.13}$ ±0.09	3559	[14] ALITTI	92	UA2	Extracted value
$2.18\ ^{+0.26}_{-0.24}$ ±0.04		[15] ALBAJAR	91	UA1	Extracted value

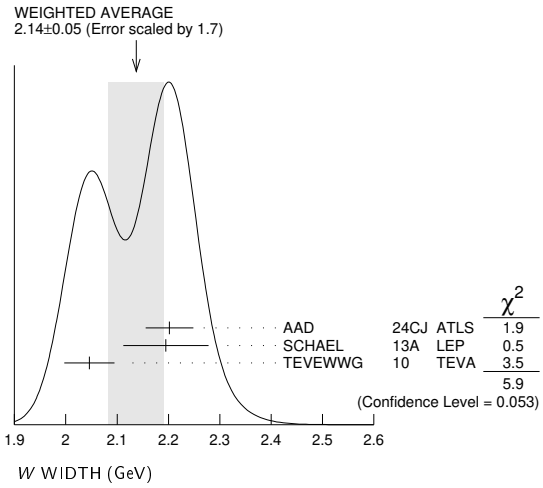

[1] AAD 24CJ provides an improved determination of the W boson mass using the same data as analysed for AABOUD 18J. In addition, the distributions of the transverse lepton momentum and of the transverse mass are analysed to determine the W boson width.

[2] SCHAEL 13A result combines the measurements from the LEP experiments ALEPH (SCHAEL 06), DELPHI(ABDALLAH 08A), L3 (ACHARD 06) and OPAL(ABBIENDI 06). The average of these four results takes correlations into account and has a χ^2 probability of 27%.

[3] TEVEWWG 10 result combines the measurements from the Tevtatron experiments CDF (ABE 95C, AFFOLDER 00M, AALTONEN 08B) and D0 (ABAZOV 02E, ABAZOV 09AK). The average of these five results takes correlations into account and has a χ^2 probability of 84%.

[4] ABAZOV 09AK obtain this result fitting the high-end tail (100-200 GeV) of the transverse mass spectrum in $W \to e\nu$ decays.

[5] AALTONEN 08B obtain this result fitting the high-end tail (90–200 GeV) of the transverse mass spectrum in semileptonic $W \to e\nu_e$ and $W \to \mu\nu_\mu$ decays.

[6] ABDALLAH 08A use direct reconstruction of the kinematics of $W^+W^- \to q\overline{q}\ell\nu$ and $W^+W^- \to q\overline{q}q\overline{q}$ events. The systematic error includes ±0.065 GeV due to final state interactions.

[7] ABBIENDI 06 use direct reconstruction of the kinematics of $W^+W^- \to q\overline{q}\ell\nu_\ell$ and $W^+W^- \to q\overline{q}q\overline{q}$ events. The systematic error includes ±0.003 GeV due to the uncertainty on the LEP beam energy.

[8] ACHARD 06 use direct reconstruction of the kinematics of $W^+W^- \to q\overline{q}\ell\nu_\ell$ and $W^+W^- \to q\overline{q}q\overline{q}$ events in the C.M. energy range 189–209 GeV. The result quoted here is obtained combining this value of the width with the result obtained from a direct W mass reconstruction at 172 and 183 GeV (ACCIARRI 99).

[9] SCHAEL 06 use direct reconstruction of the kinematics of $W^+W^- \to q\overline{q}\ell\nu_\ell$ and $W^+W^- \to q\overline{q}q\overline{q}$ events. The systematic error includes ±0.05 GeV due to possible effects of final state interactions in the $q\overline{q}q\overline{q}$ channel and ±0.01 GeV due to the uncertainty on the LEP beam energy.

[10] ABAZOV 02E obtain this result fitting the high-end tail (90–200 GeV) of the transverse-mass spectrum in semileptonic $W \to e\nu_e$ decays.

[11] ABBOTT 00B measure R = 10.43 ± 0.27 for the $W \to e\nu_e$ decay channel. They use the SM theoretical predictions for $\sigma(W)/\sigma(Z)$ and $\Gamma(W \to e\nu_e)$ and the world average for B($Z \to ee$). The value quoted here is obtained combining this result (2.169 ± 0.070 GeV) with that of ABBOTT 99H.

[12] AFFOLDER 00M fit the high transverse mass (100–200 GeV) $W \to e\nu_e$ and $W \to \mu\nu_\mu$ events to obtain $\Gamma(W)$= 2.04 ± 0.11(stat)±0.09(syst) GeV. This is combined with the earlier CDF measurement (ABE 95C) to obtain the quoted result.

[13] ABE 95W measured R = 10.90 ± 0.32 ± 0.29. They use m_W=80.23 ± 0.18 GeV, $\sigma(W)/\sigma(Z)$ = 3.35 ± 0.03, $\Gamma(W \to e\nu)$ = 225.9 ± 0.9 MeV, $\Gamma(Z \to e^+e^-)$ = 83.98 ± 0.18 MeV, and $\Gamma(Z)$ = 2.4969 ± 0.0038 GeV.

[14] ALITTI 92 measured $R = 10.4\ ^{+0.7}_{-0.6} \pm 0.3$. The values of $\sigma(Z)$ and $\sigma(W)$ come from $O(\alpha_s^2)$ calculations using m_W = 80.14 ± 0.27 GeV, and m_Z = 91.175 ± 0.021 GeV along with the corresponding value of $\sin^2\theta_W$ = 0.2274. They use $\sigma(W)/\sigma(Z)$ = 3.26 ± 0.07 ± 0.05 and $\Gamma(Z)$ = 2.487 ± 0.010 GeV.

[15] ALBAJAR 91 measured $R = 9.5\ ^{+1.1}_{-1.0}$ (stat. + syst.). $\sigma(W)/\sigma(Z)$ is calculated in QCD at the parton level using m_W = 80.18 ± 0.28 GeV and m_Z = 91.172 ± 0.031 GeV along with $\sin^2\theta_W$ = 0.2322 ± 0.0014. They use $\sigma(W)/\sigma(Z)$ = 3.23 ± 0.05 and $\Gamma(Z)$ = 2.498 ± 0.020 GeV. This measurement is obtained combining both the electron and muon channels.

Int. J. Mod. Phys. A 2026.41. Downloaded from www.worldscientific.com
by UNIVERSITY OF CALIFORNIA @ BERKELEY on 09/16/26. Reproduction strictly not permitted, except for Open Access articles.

Int. J. Mod. Phys. A 2026.41. Downloaded from www.worldscientific.com
by UNIVERSITY OF CALIFORNIA @ BERKELEY on 09/16/26. Re-use and distribution is strictly not permitted, except for Open Access articles.

W^+ DECAY MODES

W^- modes are charge conjugates of the modes below.

	Mode		Fraction (Γ_i/Γ)	Confidence level
Γ_1	$\ell^+\nu$	[a]	(10.86± 0.09) %	
Γ_2	$e^+\nu$		(10.71± 0.16) %	
Γ_3	$\mu^+\nu$		(10.63± 0.15) %	
Γ_4	$\tau^+\nu$		(11.38± 0.21) %	
Γ_5	hadrons		(67.41± 0.27) %	
Γ_6	$\pi^+\gamma$		$< 1.9 \times 10^{-6}$	95%
Γ_7	$\rho^+\gamma$		$< 5.2 \times 10^{-6}$	95%
Γ_8	$K^+\gamma$		$< 1.7 \times 10^{-6}$	95%
Γ_9	$D_s^+\gamma$		$< 6 \times 10^{-4}$	95%
Γ_{10}	cX		(33.0 ± 1.2) %	
Γ_{11}	$c\overline{s}$		$(31\ ^{+13}_{-11})$ %	
Γ_{12}	invisible	[b]	(1.4 ± 2.8) %	
Γ_{13}	$\pi^+\pi^+\pi^-$		$< 1.01 \times 10^{-6}$	95%

[a] ℓ indicates each type of lepton (e, μ, and τ), not sum over them.

[b] This represents the width for the decay of the W boson into a charged particle with momentum below detectability, p< 200 MeV.

W PARTIAL WIDTHS

Γ(invisible) — Γ_{12}

This represents the width for the decay of the W boson into a charged particle with momentum below detectability, p< 200 MeV.

VALUE (MeV)	DOCUMENT ID		TECN	COMMENT
$30^{+52}_{-48}\pm33$	[1] BARATE	99I	ALEP	E^{ee}_{cm}= 161+172+183 GeV
• • • We do not use the following data for averages, fits, limits, etc. • • •				
	[2] BARATE	99L	ALEP	E^{ee}_{cm}= 161+172+183 GeV

[1] BARATE 99I measure this quantity using the dependence of the total cross section σ_{WW} upon a change in the total width. The fit is performed to the WW measured cross sections at 161, 172, and 183 GeV. This partial width is < 139 MeV at 95%CL.

[2] BARATE 99L use W-pair production to search for effectively invisible W decays, tagging with the decay of the other W boson to Standard Model particles. The partial width for effectively invisible decay is < 27 MeV at 95%CL.

W BRANCHING RATIOS

Overall fits are performed to determine the branching ratios of the W boson. Averages on $W \to e\nu$, $W \to \mu\nu$, and $W \to \tau\nu$, and their correlations are obtained by combining results from the four LEP experiments properly taking into account the common systematic uncertainties and their correlations [SCHAEL 13A]. A first fit determines the three individual leptonic braching ratios B($W \to e\nu$), B($W \to \mu\nu$), and B($W \to \tau\nu$). This fit has a χ^2 = 6.3 for 9 degrees of freedom. The correlation coefficients between the branching fractions are 0.14 ($e-\mu$), −0.20 ($e-\tau$), −0.12 ($\mu-\tau$). A second fit assumes lepton universality and determines the leptonic branching ratio B($W \to \ell\nu$) and the hadronic branching ratio is derived as B($W \to$ hadrons) = 1 − 3 B($W \to \ell\nu$). This fit has a χ^2 = 15.4 for 11 degrees of freedom.

$\Gamma(\ell^+\nu)/\Gamma_{total}$ — Γ_1/Γ

ℓ indicates average over e, μ, and τ modes, not sum over modes.

VALUE (units 10^{-2})	EVTS	DOCUMENT ID		TECN	COMMENT
10.86±0.09 OUR FIT					
10.89±0.01±0.08		TUMASYAN	22F	CMS	E^{pp}_{cm} = 13 TeV
10.86±0.12±0.08	16438	ABBIENDI	07A	OPAL	E^{ee}_{cm}= 161–209 GeV
10.85±0.14±0.08	13600	ABDALLAH	04G	DLPH	E^{ee}_{cm}= 161–209 GeV
10.83±0.14±0.10	11246	ACHARD	04J	L3	E^{ee}_{cm}= 161–209 GeV
10.96±0.12±0.05	16116	SCHAEL	04A	ALEP	E^{ee}_{cm}= 183–209 GeV
• • • We do not use the following data for averages, fits, limits, etc. • • •					
11.02±0.52	11858	[1] ABBOTT	99H	D0	$E^{p\overline{p}}_{cm}$= 1.8 TeV
10.4 ±0.8	3642	[2] ABE	92I	CDF	$E^{p\overline{p}}_{cm}$= 1.8 TeV

[1] ABBOTT 99H measure $R \equiv [\sigma_W\ B(W \to \ell\nu_\ell)]/[\sigma_Z\ B(Z \to \ell\ell)]$ = 10.90 ± 0.52 combining electron and muon channels. They use M_W = 80.39 ± 0.06 GeV and the SM theoretical predictions for $\sigma(W)/\sigma(Z)$ and B($Z \to \ell\ell$).

[2] $1216 \pm 38^{+27}_{-31}$ $W \to \mu\nu$ events from ABE 92I and 2426 $W \to e\nu$ events of ABE 91C. ABE 92I give the inverse quantity as 9.6 ± 0.7 and we have inverted.

$\Gamma(e^+\nu)/\Gamma_{total}$ — Γ_2/Γ

VALUE (units 10^{-2})	EVTS	DOCUMENT ID		TECN	COMMENT
10.71±0.16 OUR FIT					
10.83±0.01±0.10		TUMASYAN	22F	CMS	E^{pp}_{cm} = 13 TeV
10.71±0.25±0.11	2374	ABBIENDI	07A	OPAL	E^{ee}_{cm}= 161–209 GeV
10.55±0.31±0.14	1804	ABDALLAH	04G	DLPH	E^{ee}_{cm}= 161–209 GeV
10.78±0.29±0.13	1576	ACHARD	04J	L3	E^{ee}_{cm}= 161–209 GeV
10.78±0.27±0.10	2142	SCHAEL	04A	ALEP	E^{ee}_{cm}= 183–209 GeV
• • • We do not use the following data for averages, fits, limits, etc. • • •					
10.61±0.28		[1] ABAZOV	04D	TEVA	$E^{p\overline{p}}_{cm}$= 1.8 TeV

[1] ABAZOV 04D take into account all correlations to properly combine the CDF (ABE 95W) and DØ (ABBOTT 00B) measurements of the ratio R in the electron channel. The ratio R is defined as $[\sigma_W \cdot B(W \to e\nu_e)]$ / $[\sigma_Z \cdot B(Z \to ee)]$. The combination gives $R^{Tevatron}$ = 10.59 ± 0.23. σ_W / σ_Z is calculated at next–to–next–to–leading order (3.360 ± 0.051). The branching fraction B($Z \to ee$) is taken from this *Review* as (3.363 ± 0.004)%.

$\Gamma(\mu^+\nu)/\Gamma_{total}$ — Γ_3/Γ

VALUE (units 10^{-2})	EVTS	DOCUMENT ID		TECN	COMMENT
10.63±0.15 OUR FIT					
10.94±0.01±0.08		TUMASYAN	22F	CMS	E^{pp}_{cm} = 13 TeV
10.78±0.24±0.10	2397	ABBIENDI	07A	OPAL	E^{ee}_{cm}= 161–209 GeV
10.65±0.26±0.08	1998	ABDALLAH	04G	DLPH	E^{ee}_{cm}= 161–209 GeV
10.03±0.29±0.12	1423	ACHARD	04J	L3	E^{ee}_{cm}= 161–209 GeV
10.87±0.25±0.08	2216	SCHAEL	04A	ALEP	E^{ee}_{cm}= 183–209 GeV

$\Gamma(\mu^+\nu)/\Gamma(e^+\nu)$ — Γ_3/Γ_2

VALUE	EVTS	DOCUMENT ID		TECN	COMMENT
1.000 ±0.004 OUR AVERAGE					
0.9995±0.0045		[1] AAD	24CG	ATLS	E^{pp}_{cm} = 13 TeV
1.009 ±0.009		TUMASYAN	22F	CMS	E^{pp}_{cm} = 13 TeV
1.003 ±0.010		[2] AABOUD	17Q	ATLS	E^{pp}_{cm}= 7 TeV
0.980 ±0.018		[3] AAIJ	16AJ	LHCB	E^{pp}_{cm}= 8 TeV
0.993 ±0.019		SCHAEL	13A	LEP	E^{ee}_{cm}= 130–209 GeV
0.89 ±0.10	13k	[4] ABACHI	95D	D0	$E^{p\overline{p}}_{cm}$= 1.8 TeV
1.02 ±0.08	1216	[5] ABE	92I	CDF	$E^{p\overline{p}}_{cm}$= 1.8 TeV
1.00 ±0.14 ±0.08	67	ALBAJAR	89	UA1	$E^{p\overline{p}}_{cm}$= 546,630 GeV
• • • We do not use the following data for averages, fits, limits, etc. • • •					
1.24 $^{+0.6}_{-0.4}$	14	ARNISON	84D	UA1	Repl. by ALBAJAR 89

[1] AAD 24CG analyse $t\overline{t}$ production rates in the ee, $e\mu$ and $\mu\mu$ dilepton final states. Using the ratio of B($Z \to \mu\mu$)/B($Z \to ee$) measured precisely at e^+e^- colliders, the ratio B($W \to \mu\nu$)/B($W \to e\nu$) is determined.

[2] AABOUD 17Q make a precise determination of $W \to e\nu$ and $W \to \mu\nu$ production in the follwoing fiducial phase space: lepton pseudo-rapidity range $|\eta| < 2.5$, lepton and neutrino transverse momenta larger than 25 GeV each, and W transverse mass larger than 25 GeV. They determine the ratio of the W branching fractions B($W \to e\nu$)/B($W \to \mu\nu$) = 0.9967 ± 0.0004 ± 0.0101 = 0.997 ± 0.010.

[3] AAIJ 16AJ make precise measurements of forward $W \to e\nu$ and $W \to \mu\nu$ production in proton-proton collisions at 8 TeV and determine the ratio of the W branching fractions B($W \to e\nu$)/B($W \to \mu\nu$) = 1.020 ± 0.002 ± 0.019.

[4] ABACHI 95D obtain this result from the measured σ_WB($W \to \mu\nu$)= 2.09 ± 0.23 ± 0.11 nb and σ_WB($W \to e\nu$)= 2.36 ± 0.07 ± 0.13 nb in which the first error is the combined statistical and systematic uncertainty, the second reflects the uncertainty in the luminosity.

[5] ABE 92I obtain σ_WB($W \to \mu\nu$)= 2.21 ± 0.07 ± 0.21 and combine with ABE 91C σ_W B(($W \to e\nu$)) to give a ratio of the couplings from which we derive this measurement.

$\Gamma(\tau^+\nu)/\Gamma_{total}$ — Γ_4/Γ

VALUE (units 10^{-2})	EVTS	DOCUMENT ID		TECN	COMMENT
11.38±0.21 OUR FIT					
10.77±0.05±0.21		TUMASYAN	22F	CMS	E^{pp}_{cm} = 13 TeV
11.14±0.31±0.17	2177	ABBIENDI	07A	OPAL	E^{ee}_{cm}= 161–209 GeV
11.46±0.39±0.19	2034	ABDALLAH	04G	DLPH	E^{ee}_{cm}= 161–209 GeV
11.89±0.40±0.20	1375	ACHARD	04J	L3	E^{ee}_{cm}= 161–209 GeV
11.25±0.32±0.20	2070	SCHAEL	04A	ALEP	E^{ee}_{cm}= 183–209 GeV

$\Gamma(\tau^+\nu)/\Gamma(e^+\nu)$ — Γ_4/Γ_2

VALUE	EVTS	DOCUMENT ID		TECN	COMMENT
1.003±0.020 OUR AVERAGE	Error includes scale factor of 1.5. See the ideogram below.				
0.975±0.023		[1] AAD	25Z	ATLS	E^{pp}_{cm} = 13 TeV
0.994±0.021		TUMASYAN	22F	CMS	E^{pp}_{cm} = 13 TeV
1.063±0.027		SCHAEL	13A	LEP	E^{ee}_{cm}= 130–209 GeV
0.961±0.061	980	[2] ABBOTT	00D	D0	$E^{p\overline{p}}_{cm}$= 1.8 TeV
0.94 ±0.14	179	[3] ABE	92E	CDF	$E^{p\overline{p}}_{cm}$= 1.8 TeV
1.04 ±0.08 ±0.08	754	[4] ALITTI	92F	UA2	$E^{p\overline{p}}_{cm}$= 630 GeV
1.02 ±0.20 ±0.12	32	ALBAJAR	89	UA1	$E^{p\overline{p}}_{cm}$= 546,630 GeV
• • • We do not use the following data for averages, fits, limits, etc. • • •					
0.995±0.112±0.083	198	ALITTI	91C	UA2	Repl. by ALITTI 92F
1.02 ±0.20 ±0.10	32	ALBAJAR	87	UA1	Repl. by ALBAJAR 89

[1] AAD 25Z use a sample of Ws produced from top quark decays, the Ws decaying leptonically as $W \to e\nu_e$ and $W \to \tau\nu_\tau$ with $\tau \to e\nu_e\nu_\tau$. These decay states are distinguished using differences in the impact parameter and transverse momentum spectra of the electrons to determine the ratio of branching fractions B($W \to \tau\nu$)/B($W \to e\nu$).

[2] ABBOTT 00D measure σ_W×B($W \to \tau\nu_\tau$) = 2.22 ± 0.09 ± 0.10 ± 0.10 nb. Using the ABBOTT 00B result σ_W×B($W \to e\nu_e$) = 2.31 ± 0.01 ± 0.05 ± 0.10 nb, they quote the ratio of the couplings from which we derive this measurement.

[3] ABE 92E use two procedures for selecting $W \to \tau\nu_\tau$ events. The missing E_T trigger leads to $132 \pm 14 \pm 8$ events and the τ trigger to $47 \pm 9 \pm 4$ events. Proper statistical and systematic correlations are taken into account to arrive at $\sigma B(W \to \tau\nu) = 2.05 \pm 0.27$ nb. Combined with ABE 91C result on $\sigma B(W \to e\nu)$, ABE 92E quote a ratio of the couplings from which we derive this measurement.

[4] This measurement is derived by us from the ratio of the couplings of ALITTI 92F.

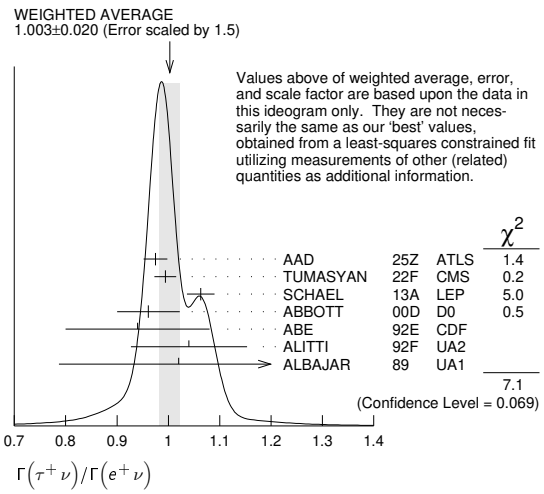

$\Gamma(\tau^+\nu)/\Gamma(\mu^+\nu)$ — Γ_4/Γ_3

VALUE	DOCUMENT ID		TECN	COMMENT
1.002±0.020 OUR AVERAGE	Error includes scale factor of 2.0.			See the ideogram below.
0.985±0.020	TUMASYAN	22F	CMS	E^{pp}_{cm} = 13 TeV
0.992±0.007±0.011	[1] AAD	21AN	ATLS	E^{pp}_{cm} = 13 TeV
1.070±0.026	SCHAEL	13A	LEP	E^{ee}_{cm} = 130–209 GeV

[1] AAD 21AN study $t\bar{t}$ production, with the W bosons in top-quark decay decaying to electrons or taus, with the tau decaying further into a muon. Analyzing the muon impact parameter and its transverse momentum, the contributions from prompt muons (arising from W decay) and non-prompt muons (arising from tau decay) are separated, allowing a measurement of the ratio of the W branching fractions into taus and muons, $R(\tau/\mu) = 0.992 \pm 0.007 \pm 0.011$ where the first error is statistical and the second systematic.

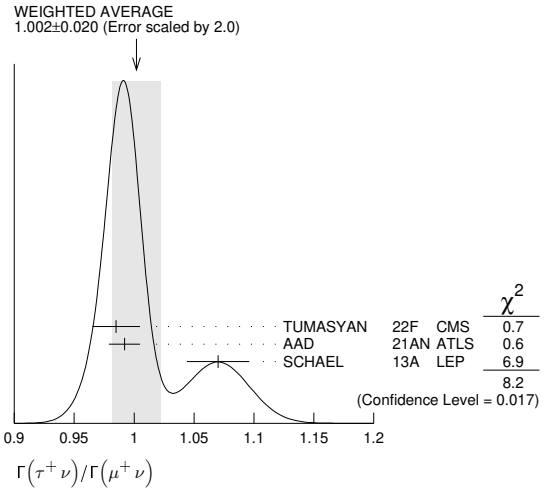

$\Gamma(\text{hadrons})/\Gamma_{total}$ — Γ_5/Γ

OUR FIT value is obtained by a fit to the lepton branching ratio data assuming lepton universality.

VALUE (units 10^{-2})	EVTS	DOCUMENT ID		TECN	COMMENT
67.41±0.27 OUR FIT					
67.32±0.02±0.23		TUMASYAN	22F	CMS	E^{pp}_{cm} = 13 TeV
67.41±0.37±0.23	16438	ABBIENDI	07A	OPAL	E^{ee}_{cm} = 161–209 GeV
67.45±0.41±0.24	13600	ABDALLAH	04G	DLPH	E^{ee}_{cm} = 161–209 GeV
67.50±0.42±0.30	11246	ACHARD	04J	L3	E^{ee}_{cm} = 161–209 GeV
67.13±0.37±0.15	16116	SCHAEL	04A	ALEP	E^{ee}_{cm} = 183–209 GeV

$\Gamma(\pi^+\gamma)/\Gamma_{total}$ — Γ_6/Γ

A stronger limit of $<1.9 \times 10^{-6}$ is obtained from $\Gamma(W^+ \to \pi^+\gamma)/\Gamma(W^+ \to e^+\nu)$ measurements.

VALUE	CL%	DOCUMENT ID		TECN	COMMENT
$<1.9 \times 10^{-6}$	95	[1] AAD	24BO	ATLS	E^{pp}_{cm} = 13 TeV
• • • We do not use the following data for averages, fits, limits, etc. • • •					
$<1.5 \times 10^{-5}$	95	[2] SIRUNYAN	21I	CMS	E^{pp}_{cm} = 13 TeV

[1] AAD 24BO search for exclusive hadronic decays of the W boson into a charged meson plus a photon, where the meson is a $\pi^\pm$, $K^\pm$ or $\rho^\pm$. The meson-photon invariant mass distribution is used to set the limit on the branching fraction.

[2] SIRUNYAN 21I search for the rare decay of a W boson into a charged pion accompanied by a photon. A signal is not observed, and an upper limit on the branching fraction $B(W \to \pi\gamma) < 1.50 \times 10^{-5}$ is obtained at 95% C.L.

$\Gamma(\rho^+\gamma)/\Gamma_{total}$ — Γ_7/Γ

VALUE	CL%	DOCUMENT ID		TECN	COMMENT
$<5.2 \times 10^{-6}$	95	[1] AAD	24BO	ATLS	E^{pp}_{cm} = 13 TeV

[1] AAD 24BO search for exclusive hadronic decays of the W boson into a charged meson plus a photon, where the meson is a $\pi^\pm$, $K^\pm$ or $\rho^\pm$. The meson-photon invariant mass distribution is used to set the limit on the branching fraction.

$\Gamma(K^+\gamma)/\Gamma_{total}$ — Γ_8/Γ

VALUE	CL%	DOCUMENT ID		TECN	COMMENT
$<1.7 \times 10^{-6}$	95	[1] AAD	24BO	ATLS	E^{pp}_{cm} = 13 TeV

[1] AAD 24BO search for exclusive hadronic decays of the W boson into a charged meson plus a photon, where the meson is a $\pi^\pm$, $K^\pm$ or $\rho^\pm$. The meson-photon invariant mass distribution is used to set the limit on the branching fraction.

$\Gamma(\pi^+\gamma)/\Gamma(e^+\nu)$ — Γ_6/Γ_2

VALUE	CL%	DOCUMENT ID		TECN	COMMENT
$< 6.4 \times 10^{-5}$	95	AALTONEN	12W	CDF	$E^{p\bar{p}}_{cm}$ = 1.96 Tev
• • • We do not use the following data for averages, fits, limits, etc. • • •					
$< 7 \times 10^{-4}$	95	ABE	98H	CDF	$E^{p\bar{p}}_{cm}$ = 1.8 TeV
$< 4.9 \times 10^{-3}$	95	[1] ALITTI	92D	UA2	$E^{p\bar{p}}_{cm}$ = 630 GeV
$<58 \times 10^{-3}$	95	[2] ALBAJAR	90	UA1	$E^{p\bar{p}}_{cm}$ = 546, 630 GeV

[1] ALITTI 92D limit is 3.8×10^{-3} at 90%CL.

[2] ALBAJAR 90 obtain < 0.048 at 90%CL.

$\Gamma(D_s^+\gamma)/\Gamma(e^+\nu)$ — Γ_9/Γ_2

VALUE	CL%	DOCUMENT ID		TECN	COMMENT
• • • We do not use the following data for averages, fits, limits, etc. • • •					
$<1.2 \times 10^{-2}$	95	ABE	98P	CDF	$E^{p\bar{p}}_{cm}$ = 1.8 TeV

$\Gamma(D_s^+\gamma)/\Gamma(\mu^+\nu)$ — Γ_9/Γ_3

VALUE	CL%	DOCUMENT ID		TECN	COMMENT
$<6.1 \times 10^{-3}$	95	[1] AAIJ	23AM	LHCB	E^{pp}_{cm} = 13 TeV

[1] AAIJ 23AM also quotes the branching fraction limit $B(W^+ \to D_s^+\gamma) < 6.5 \times 10^{-4}$, using the known $W \to \mu\nu$ branching fraction.

$\Gamma(cX)/\Gamma(\text{hadrons})$ — Γ_{10}/Γ_5

VALUE	EVTS	DOCUMENT ID		TECN	COMMENT
0.490±0.018 OUR AVERAGE					
0.489±0.020	917K	[1] HAYRAPETY...	25AI	CMS	E^{pp}_{cm} = 13 TeV
0.481±0.042±0.032	3005	[2] ABBIENDI	00V	OPAL	E^{ee}_{cm} = 183 + 189 GeV
0.51 ±0.05 ±0.03	746	[3] BARATE	99M	ALEP	E^{ee}_{cm} = 172 + 183 GeV

[1] HAYRAPETYAN 25AI analyse $t\bar{t}$ production and tag charm jets using the presence of a muon inside the jet. The error is composed of 0.005 statistical and 0.019 from systematics. Further constraints on CKM matrix elements are derived.

[2] ABBIENDI 00V tag $W \to cX$ decays using measured jet properties, lifetime information, and leptons produced in charm decays. From this result, and using the additional measurements of $\Gamma(W)$ and $B(W \to \text{hadrons})$, $|V_{cs}|$ is determined to be $0.969 \pm 0.045 \pm 0.036$.

[3] BARATE 99M tag c jets using a neural network algorithm. From this measurement $|V_{cs}|$ is determined to be $1.00 \pm 0.11 \pm 0.07$.

$R_{cs} = \Gamma(c\bar{s})/\Gamma(\text{hadrons})$ — Γ_{11}/Γ_5

VALUE	DOCUMENT ID		TECN	COMMENT
$0.46^{+0.18}_{-0.14} \pm 0.07$	[1] ABREU	98N	DLPH	E^{ee}_{cm} = 161+172 GeV

[1] ABREU 98N tag c and s jets by identifying a charged kaon as the highest momentum particle in a hadronic jet. They also use a lifetime tag to independently identify a c jet, based on the impact parameter distribution of charged particles in a jet. From this measurement $|V_{cs}|$ is determined to be $0.94^{+0.32}_{-0.26} \pm 0.13$.

$\Gamma(\pi^+\pi^+\pi^-)/\Gamma_{total}$ — Γ_{13}/Γ

VALUE (units 10^{-6})	CL%	DOCUMENT ID		TECN	COMMENT
<1.01	95	[1] SIRUNYAN	19BG	CMS	E^{pp}_{cm} = 13 TeV

[1] SIRUNYAN 19BG search for the rare decay of a W boson into three charged pions. Three pion candidates are required in each event, with transverse momentum larger than 35 GeV, 35 GeV, 18 GeV, respectively, while the transverse momentum of the three-pion system is required to be larger than 40 GeV. Analyzing the three-pion invariant mass, no excess is observed in the W mass region, leading to the 95% C.L. upper limit on the branching fraction.

Int. J. Mod. Phys. A 2026.41. Downloaded from www.worldscientific.com
by UNIVERSITY OF CALIFORNIA @ BERKELEY on 09/16/26. Reproduction is strictly not permitted, except for Open Access articles.

Int. J. Mod. Phys. A 2026.41. Downloaded from www.worldscientific.com by UNIVERSITY OF CALIFORNIA @ BERKELEY on 09/16/26. Re-use and distribution is strictly not permitted, except for Open Access articles.

AVERAGE PARTICLE MULTIPLICITIES IN HADRONIC *W* DECAY

Summed over particle and antiparticle, when appropriate.

$\langle N_{\pi^\pm} \rangle$

VALUE	DOCUMENT ID		TECN	COMMENT
15.70±0.35	[1] ABREU,P	00F	DLPH	E^{ee}_{cm}= 189 GeV

[1] ABREU,P 00F measure $\langle N_{\pi^\pm} \rangle$ = 31.65 ± 0.48 ± 0.76 and 15.51 ± 0.38 ± 0.40 in the fully hadronic and semileptonic final states respectively. The value quoted is a weighted average without assuming any correlations.

$\langle N_{K^\pm} \rangle$

VALUE	DOCUMENT ID		TECN	COMMENT
2.20±0.19	[1] ABREU,P	00F	DLPH	E^{ee}_{cm}= 189 GeV

[1] ABREU,P 00F measure $\langle N_{K^\pm} \rangle$ = 4.38 ± 0.42 ± 0.12 and 2.23 ± 0.32 ± 0.17 in the fully hadronic and semileptonic final states respectively. The value quoted is a weighted average without assuming any correlations.

$\langle N_p \rangle$

VALUE	DOCUMENT ID		TECN	COMMENT
0.92±0.14	[1] ABREU,P	00F	DLPH	E^{ee}_{cm}= 189 GeV

[1] ABREU,P 00F measure $\langle N_p \rangle$ = 1.82 ± 0.29 ± 0.16 and 0.94 ± 0.23 ± 0.06 in the fully hadronic and semileptonic final states respectively. The value quoted is a weighted average without assuming any correlations.

$\langle N_{\rm charged} \rangle$

VALUE	DOCUMENT ID		TECN	COMMENT
19.39±0.08 OUR AVERAGE				
19.38±0.05±0.08	[1] ABBIENDI	06A	OPAL	E^{ee}_{cm}= 189–209 GeV
19.44±0.17	[2] ABREU,P	00F	DLPH	E^{ee}_{cm}= 183+189 GeV
19.3 ±0.3 ±0.3	[3] ABBIENDI	99N	OPAL	E^{ee}_{cm}= 183 GeV
19.23±0.74	[4] ABREU	98C	DLPH	E^{ee}_{cm}= 172 GeV

[1] ABBIENDI 06A measure $\langle N_{\rm charged} \rangle$ = 38.74 ± 0.12 ± 0.26 when both *W* bosons decay hadronically and $\langle N_{\rm charged} \rangle$ = 19.39 ± 0.11 ± 0.09 when one *W* boson decays semileptonically. The value quoted here is obtained under the assumption that there is no color reconnection between *W* bosons; the value is a weighted average taking into account correlations in the systematic uncertainties.

[2] ABREU,P 00F measure $\langle N_{\rm charged} \rangle$ = 39.12 ± 0.33 ± 0.36 and 38.11 ± 0.57 ± 0.44 in the fully hadronic final states at 189 and 183 GeV respectively, and $\langle N_{\rm charged} \rangle$ = 19.49 ± 0.31 ± 0.27 and 19.78 ± 0.49 ± 0.43 in the semileptonic final states. The value quoted is a weighted average without assuming any correlations.

[3] ABBIENDI 99N use the final states $W^+W^- \rightarrow q\overline{q}\ell\overline{\nu}_\ell$ to derive this value.

[4] ABREU 98C combine results from both the fully hadronic as well semileptonic *W W* final states after demonstrating that the *W* decay charged multiplicity is independent of the topology within errors.

TRIPLE GAUGE COUPLINGS (TGC'S)

Revised April 2017 by M.W. Grünewald (U. College Dublin) and A. Gurtu (Formerly Tata Inst.).

Fourteen independent couplings, seven each for ZWW and γWW, completely describe the VWW vertices within the most general framework of the electroweak Standard Model (SM) consistent with Lorentz invariance and U(1) gauge invariance. Of each of the seven TGCs, three conserve C and P individually, three violate CP, and one violates C and P individually while conserving CP. Assumption of C and P conservation and electromagnetic gauge invariance reduces the number of independent VWW couplings to five: one common set [1,2] is $(\kappa_\gamma, \kappa_Z, \lambda_\gamma, \lambda_Z, g_1^Z)$, where $\kappa_\gamma = \kappa_Z = g_1^Z = 1$ and $\lambda_\gamma = \lambda_Z = 0$ in the Standard Model at tree level. The parameters κ_Z and λ_Z are related to the other three due to constraints of gauge invariance as follows: $\kappa_Z = g_1^Z - (\kappa_\gamma - 1)\tan^2\theta_W$ and $\lambda_Z = \lambda_\gamma$, where θ_W is the weak mixing angle. The W magnetic dipole moment, μ_W, and the W electric quadrupole moment, q_W, are expressed as $\mu_W = e\,(1+\kappa_\gamma+\lambda_\gamma)/2M_W$ and $q_W = -e\,(\kappa_\gamma - \lambda_\gamma)/M_W^2$.

Precision measurements of suitable observables at LEP1 has already led to an exploration of much of the TGC parameter space. At LEP2, the VWW coupling arises in W-pair production via s-channel exchange, or in single W production via the radiation of a virtual photon off the incident e^+ or e^-. At the Tevatron and the LHC, hard-photon bremsstrahlung off a produced W or Z signals the presence of a triple-gauge vertex. In order to extract the value of one TGC, the others are generally kept fixed to their SM values. While most analyses use the above gauge constraints in the extraction of TGCs, one analysis of W-pair events also determines the real and imaginary parts of all 14 couplings using unconstrained single-parameter fits [3]. The results are consistent. Some experiments have determined limits on the couplings under various non-LEP scenarios and assuming different values of the form factor Λ, where the coupling parameters are scaled by $1/(1+s/\Lambda^2)^2$. For practical reasons it is not possible to quote all such determinations in the listings. For that the individual papers may be consulted. Recently, EFT-inspired sets of couplings [4,5], such as $c_{WWW}/\Lambda^2, c_W/\Lambda^2, c_B/\Lambda^2$ which are linearly related to the couplings discussed above, are also determined by the LHC experiments.

References

1. K. Hagiwara *et al.*, Nucl. Phys. **B282**, 253 (1987).
2. G. Gounaris *et al.*, CERN 96-01 p. 525.
3. S. Schael *et al.* (ALEPH Collab.), Phys. Lett. **B614**, 7 (2005).
4. K. Hagiwara *et al.*, Phys. Rev. **D48**, 2182 (1993).
5. C. Degrande *et al.*, Annals Phys. 335 (2013) 21-32.

g_1^Z

OUR FIT below is taken from [SCHAEL 13A].

VALUE	EVTS	DOCUMENT ID		TECN	COMMENT
0.984 $^{+0.018}_{-0.020}$ OUR FIT					
0.975 $^{+0.033}_{-0.030}$	7872	[1] ABDALLAH	10	DLPH	E^{ee}_{cm} = 189–209 GeV
1.001±0.027±0.013	9310	[2] SCHAEL	05A	ALEP	E^{ee}_{cm} = 183–209 GeV
0.987 $^{+0.034}_{-0.033}$	9800	[3] ABBIENDI	04D	OPAL	E^{ee}_{cm} = 183–209 GeV
0.966 $^{+0.034}_{-0.032}$±0.015	8325	[4] ACHARD	04D	L3	E^{ee}_{cm} = 161–209 GeV
• • • We do not use the following data for averages, fits, limits, etc. • • •					
		[5] SIRUNYAN	20BA	CMS	E^{pp}_{cm} = 13 TeV
		[6] SIRUNYAN	19CL	CMS	E^{pp}_{cm} = 13 TeV
		[7] SIRUNYAN	18BZ	CMS	E^{pp}_{cm} = 13 TeV
		[8] AABOUD	17S	ATLS	E^{pp}_{cm} = 7+8 TeV
		[9] AABOUD	17U	ATLS	E^{pp}_{cm} = 8 TeV
		[10] KHACHATRY...	17O	CMS	E^{pp}_{cm} = 8 TeV
		[11] SIRUNYAN	17X	CMS	E^{pp}_{cm} = 8 TeV
		[12] AAD	16AR	ATLS	E^{pp}_{cm} = 8 TeV
		[13] AAD	16P	ATLS	E^{pp}_{cm} = 8 TeV
		[14] AAD	14Y	ATLS	E^{pp}_{cm} = 8 TeV
		[15] AAD	13AL	ATLS	E^{pp}_{cm} = 7 TeV
		[16] CHATRCHYAN	13BF	CMS	E^{pp}_{cm} = 7 TeV
		[17] AAD	12CD	ATLS	E^{pp}_{cm} = 7 TeV
		[18] AALTONEN	12AC	CDF	$E^{p\overline{p}}_{cm}$ = 1.96 TeV
		[19] ABAZOV	12AG	D0	$E^{p\overline{p}}_{cm}$ = 1.96 TeV
	34	[20] ABAZOV	11	D0	$E^{p\overline{p}}_{cm}$ = 1.96 TeV
	334	[21] AALTONEN	10K	CDF	$E^{p\overline{p}}_{cm}$ = 1.96 TeV
1.04 ±0.09		[22] ABAZOV	09AD	D0	$E^{p\overline{p}}_{cm}$ = 1.96 TeV
		[23] ABAZOV	09AJ	D0	$E^{p\overline{p}}_{cm}$ = 1.96 TeV
1.07 $^{+0.08}_{-0.12}$	1880	[24] ABDALLAH	08C	DLPH	Superseded by ABDALLAH 10
	13	[25] ABAZOV	07Z	D0	$E^{p\overline{p}}_{cm}$ = 1.96 TeV
	2.3	[26] ABAZOV	05S	D0	$E^{p\overline{p}}_{cm}$ = 1.96 TeV
0.98 ±0.07 ±0.01	2114	[27] ABREU	01I	DLPH	E^{ee}_{cm} = 183+189 GeV
	331	[28] ABBOTT	99I	D0	$E^{p\overline{p}}_{cm}$ = 1.8 TeV

[1] ABDALLAH 10 use data on the final states $e^+e^- \to jj\ell\nu$, $jjjj$, jjX, ℓX, at center-of-mass energies between 189–209 GeV at LEP2, where j = jet, ℓ = lepton, and X represents missing momentum. The fit is carried out keeping all other parameters fixed at their SM values.

[2] SCHAEL 05A study single–photon, single–W, and WW–pair production from 183 to 209 GeV. The result quoted here is derived from the WW–pair production sample. Each parameter is determined from a single–parameter fit in which the other parameters assume their Standard Model values.

[3] ABBIENDI 04D combine results from W^+W^- in all decay channels. Only *CP*-conserving couplings are considered and each parameter is determined from a single-parameter fit in which the other parameters assume their Standard Model values. The 95% confidence interval is $0.923 < g_1^Z < 1.054$.

[4] ACHARD 04D study WW–pair production, single–W production and single–photon production with missing energy from 189 to 209 GeV. The result quoted here is obtained from the WW–pair production sample including data from 161 to 183 GeV, ACCIARRI 99Q. Each parameter is determined from a single–parameter fit in which the other parameters assume their Standard Model values.

[5] SIRUNYAN 20BA study electroweak production of a W boson in association with two jets, using W decays in the electron or muon channel. The isolated muons (electrons) are required to have a transverse momentum larger than 25 (30) GeV, while the transverse momentum of the two jets has to be larger than 50 and 30 GeV. A total of 2.382 (1.051) million events are selected in the muon (electron) channel, with a Standard Model expectation of 2.39 ± 0.17 (1.054 ± 0.058) million events. Analyzing the transverse momentum distribution of the charged leptons from W decay, the following 95% C.L. limit is obtained: $0.971 < g_1^Z < 1.044$. Combining this result with that from the closely-related electroweak Z-jet-jet production SIRUNYAN 18BZ, the limit becomes: $0.979 < g_1^Z < 1.034$.

[6] SIRUNYAN 19CL study WW and WZ production in lepton + jet events, with one W boson decaying leptonically (electron or muon), and another W or Z boson decaying hadronically, reconstructed as a single massive large-radius jet. In the electron channel 2,456 (2,235) events are selected in the $WW(WZ)$ category, while in the muon channel 3,996 (3572) events are selected in the $WW(WZ)$ category. Analysing the di-boson invariant mass distribution, the following 95% C.L. limit is obtained: $0.9939 < g_1^Z < 1.0074$.

[7] SIRUNYAN 18BZ study $pp \to Z$ *jet jet* events at 13 TeV where $Z \to e^+e^-/\mu^+\mu^-$. Isolated electrons and muons are selected with p_T of the leading/sub-leading lepton > 30/20 GeV and $|\eta| < 2.4$, with the di-lepton invariant mass within 15 GeV of the Z mass. The two highest p_T jets are selected with p_T of the leading/sub-leading jet > 50/30 GeV respectively and dijet invariant mass > 200 GeV. Templates in the transverse momentum of the Z are utilized to set limits on the triple gauge couplings in the EFT and the LEP parametrizations. The following 95% C.L. limit is obtained: $0.965 < g_1^Z < 1.042$.

[8] AABOUD 17S analyze electroweak production of a W boson in association with two jets at high dijet invariant mass, with the W boson decaying to electron or muon plus neutrino. In the signal region of dijet mass larger than 1 TeV and leading-jet transverse momentum larger than 600 GeV, 30 events are observed in the data with 39 ± 4 events expected in the Standard Model, yielding the following limit at 95% CL for the form factor cut-off scale $\Lambda_{FF} \to \infty$: $0.87 < g_1^Z < 1.12$.

[9] AABOUD 17U analyze production of WW or WZ boson pairs with one W boson decaying to electron or muon plus neutrino, and the other W or Z boson decaying hadronically. The hadronic decay system is reconstructed as either a resolved two-jet system or as a single large jet. Analysing the transverse momentum distribution of the hadronic system above 100 GeV yields the following limit at 95% CL for the form factor cut-off scale $\Lambda_{FF} \to \infty$: $0.979 < g_1^Z < 1.024$.

[10] KHACHATRYAN 17O analyse WZ production where each boson decays into electrons or muons. Events are required to have a tri-lepton invariant mass larger than 100 GeV, with one of the lepton pairs having an invariant mass within 20 GeV of the Z boson mass. The Z transverse momentum spectrum is analyzed to set a 95% C.L. limit of: $0.982 < g_1^Z < 1.035$.

[11] SIRUNYAN 17X study $pp \to WW/WZ \to \ell\nu q\overline{q}$ production at 8 TeV where ℓ is an electron or muon with $p_T > 30$ or 25 GeV respectively. Suitable cuts are put on the p_T of the dijet system and the missing E_T of the event yielding a total of 285 and 204 WV events observed in the electron and muon channels. The following 95% C.L. limit is obtained: $0.9913 < g_1^Z < 1.024$.

[12] AAD 16AR study WW production in pp collisions and select 6636 WW candidates in decay modes with electrons or muons with an expected background of 1546 ± 157 events. Assuming the LEP formulation and setting the form-factor Λ to infinity, a fit to the transverse momentum distribution of the leading charged lepton, leads to a 95% C.L. range of $0.984 < g_1^Z < 1.027$.

[13] AAD 16P study WZ production in pp collisions and select 2091 WZ candidates in 4 decay modes with electrons and muons, with an expected background of 1825 ± 7 events. Analyzing the WZ transverse momentum distribution, the resulting 95% C.L. limit is: $0.981 < g_1^Z < 1.029$.

[14] AAD 14Y determine the electroweak Z-dijet cross section in 8 TeV pp collisions. $Z \to ee$ and $Z \to \mu\mu$ decays are selected with the di-lepton $p_T > 20$ GeV and mass in the 81–101 GeV range. Minimum two jets are required with $p_T > 55$ and 45 GeV and no additional jets with $p_T > 25$ GeV in the rapidity interval between them. The normalized p_T balance between the Z and the two jets is required to be < 0.15. This leads to a selection of 900 events with dijet mass > 1 TeV. The number of signal and background events expected is 261 and 592 respectively. A Poisson likelihood method is used on an event by event basis to obtain the 95% CL limit $0.5 < g_1^Z < 1.26$ for a form factor value $\Lambda = \infty$.

[15] AAD 13AL study WW production in pp collisions and select 1325 WW candidates in decay modes with electrons or muons with an expected background of 369 ± 61 events. Assuming the LEP formulation and setting the form-factor Λ = infinity, a fit to the transverse momentum distribution of the leading charged lepton, leads to a 95% C.L. range of $0.961 < g_1^Z < 1.052$. Supersedes AAD 12AC.

[16] CHATRCHYAN 13BF determine the W^+W^- production cross section using unlike sign di-lepton (e or μ) events with high $\not{p}_T$. The leptons have $p_T > 20$ GeV/c and are isolated. 1134 candidate events are observed with an expected SM background of 247 ± 34. The p_T distribution of the leading lepton is fitted to obtain 95% C.L. limits of $0.905 \le g_1^Z \le 1.095$.

[17] AAD 12CD study WZ production in pp collisions and select 317 WZ candidates in three $\ell\nu$ decay modes with an expected background of 68.0 ± 10.0 events. The resulting 95% C.L. range is: $0.943 < g_1^Z < 1.093$. Supersedes AAD 12V.

[18] AALTONEN 12AC study WZ production in $p\overline{p}$ collisions and select 63 WZ candidates in three $\ell\nu$ decay modes with an expected background of 7.9 ± 1.0 events. Based on the cross section and shape of the Z transverse momentum spectrum, the following 95% C.L. range is reported: $0.92 < g_1^Z < 1.20$ for a form factor of $\Lambda = 2$ TeV.

[19] ABAZOV 12AG combine new results with already published results on $W\gamma$, WW and WZ production in order to determine the couplings with increased precision, superseding ABAZOV 08R, ABAZOV 11AC, ABAZOV 09AJ, ABAZOV 09AD. The 68% C.L. result for a formfactor cutoff of $\Lambda = 2$ TeV is $g_1^Z = 1.022^{+0.032}_{-0.030}$.

[20] ABAZOV 11 study the $p\overline{p} \to 3\ell\nu$ process arising in WZ production. They observe 34 WZ candidates with an estimated background of 6 events. An analysis of the p_T spectrum of the Z boson leads to a 95% C.L. limit of $0.944 < g_1^Z < 1.154$, for a form factor $\Lambda = 2$ TeV.

[21] AALTONEN 10K study $p\overline{p} \to W^+W^-$ with $W \to e/\mu\nu$. The p_T of the leading (second) lepton is required to be > 20 (10) GeV. The final number of events selected is 654 of which 320 ± 47 are estimated to be background. The 95% C.L. interval is $0.76 < g_1^Z < 1.34$ for $\Lambda = 1.5$ TeV and $0.78 < g_1^Z < 1.30$ for $\Lambda = 2$ TeV.

[22] ABAZOV 09AD study the $p\overline{p} \to \ell\nu$ 2jet process arising in WW and WZ production. They select 12,473 (14,392) events in the electron (muon) channel with an expected di-boson signal of 436 (527) events. The results on the anomalous couplings are derived from an analysis of the p_T spectrum of the 2-jet system and quoted at 68% C.L. and for a form factor of 2 TeV. This measurement is not used for obtaining the mean as it is for a specific form factor. The 95% confidence interval is $0.88 < g_1^Z < 1.20$.

[23] ABAZOV 09AJ study the $p\overline{p} \to 2\ell 2\nu$ process arising in WW production. They select 100 events with an expected WW signal of 65 events. An analysis of the p_T spectrum of the two charged leptons leads to 95% C.L. limits of $0.86 < g_1^Z < 1.3$, for a form factor $\Lambda = 2$ TeV.

[24] ABDALLAH 08C determine this triple gauge coupling from the measurement of the spin density matrix elements in $e^+e^- \to W^+W^- \to (qq)(\ell\nu)$, where $\ell = e$ or μ. Values of all other couplings are fixed to their standard model values.

[25] ABAZOV 07Z set limits on anomalous TGCs using the measured cross section and $p_T(Z)$ distribution in WZ production with both the W and the Z decaying leptonically into electrons and muons. Setting the other couplings to their standard model values, the 95% C.L. limit for a form factor scale $\Lambda = 2$ TeV is $0.86 < g_1^Z < 1.35$.

[26] ABAZOV 05S study $\overline{p}p \to WZ$ production with a subsequent trilepton decay to $\ell\nu\ell'\overline{\ell}'$ (ℓ and $\ell' = e$ or μ). Three events (estimated background 0.71 ± 0.08 events) with WZ decay characteristics are observed from which they derive limits on the anomalous WWZ couplings. The 95% CL limit for a form factor scale $\Lambda = 1.5$ TeV is $0.51 < g_1^Z < 1.66$, fixing λ_Z and κ_Z to their Standard Model values.

[27] ABREU 01I combine results from e^+e^- interactions at 189 GeV leading to W^+W^- and $We\nu_e$ final states with results from ABREU 99L at 183 GeV. The 95% confidence interval is $0.84 < g_1^Z < 1.13$.

[28] ABBOTT 99I perform a simultaneous fit to the $W\gamma$, $WW \to$ dilepton, $WW/WZ \to e\nu jj$, $WW/WZ \to \mu\nu jj$, and $WZ \to$ trilepton data samples. For $\Lambda = 2.0$ TeV, the 95%CL limits are $0.63 < g_1^Z < 1.57$, fixing λ_Z and κ_Z to their Standard Model values, and assuming Standard Model values for the $WW\gamma$ couplings.

κ_γ

OUR FIT below is taken from [SCHAEL 13A].

VALUE	EVTS	DOCUMENT ID		TECN	COMMENT
0.982±0.042 OUR FIT					
$1.024^{+0.077}_{-0.081}$	7872	[1] ABDALLAH	10	DLPH	E_{cm}^{ee} = 189–209 GeV
$0.971 \pm 0.055 \pm 0.030$	10689	[2] SCHAEL	05A	ALEP	E_{cm}^{ee} = 183–209 GeV
$0.88\ ^{+0.09}_{-0.08}$	9800	[3] ABBIENDI	04D	OPAL	E_{cm}^{ee} = 183–209 GeV
$1.013^{+0.067}_{-0.064} \pm 0.026$	10575	[4] ACHARD	04D	L3	E_{cm}^{ee} = 161–209 GeV
• • • We do not use the following data for averages, fits, limits, etc. • • •					
		[5] AABOUD	17U	ATLS	E_{cm}^{pp} = 8 TeV
		[6] SIRUNYAN	17X	CMS	E_{cm}^{pp} = 8 TeV
		[7] CHATRCHYAN	14AB	CMS	E_{cm}^{pp} = 7 TeV
		[8] AAD	13AN	ATLS	E_{cm}^{pp} = 7 TeV
		[9] CHATRCHYAN	13BF	CMS	E_{cm}^{pp} = 7 TeV
		[10] ABAZOV	12AG	D0	$E_{cm}^{p\overline{p}}$ = 1.96 TeV
		[11] ABAZOV	11AC	D0	$E_{cm}^{p\overline{p}}$ = 1.96 TeV
		[12] CHATRCHYAN	11M	CMS	E_{cm}^{pp} = 7 TeV
	334	[13] AALTONEN	10K	CDF	$E_{cm}^{p\overline{p}}$ = 1.96 TeV
	53	[14] AARON	09B	H1	E_{cm}^{ep} = 0.3 TeV
$1.07\ ^{+0.26}_{-0.29}$		[15] ABAZOV	09AD	D0	$E_{cm}^{p\overline{p}}$ = 1.96 TeV
		[16] ABAZOV	09AJ	D0	$E_{cm}^{p\overline{p}}$ = 1.96 TeV
		[17] ABAZOV	08R	D0	$E_{cm}^{p\overline{p}}$ = 1.96 TeV
$0.68\ ^{+0.17}_{-0.15}$	1880	[18] ABDALLAH	08C	DLPH	Superseded by ABDALLAH 10
	1617	[19] AALTONEN	07L	CDF	$E_{cm}^{p\overline{p}}$ = 1.96 GeV
	17	[20] ABAZOV	06H	D0	$E_{cm}^{p\overline{p}}$ = 1.96 TeV
	141	[21] ABAZOV	05J	D0	$E_{cm}^{p\overline{p}}$ = 1.96 TeV
$1.25\ ^{+0.21}_{-0.20} \pm 0.06$	2298	[22] ABREU	01I	DLPH	E_{cm}^{ee} = 183+189 GeV
		[23] BREITWEG	00	ZEUS	$e^+p \to e^+W^\pm X$, $\sqrt{s} \approx$ 300 GeV
0.92 ± 0.34	331	[24] ABBOTT	99I	D0	$E_{cm}^{p\overline{p}}$ = 1.8 TeV

Int. J. Mod. Phys. A 2026.41. Downloaded from www.worldscientific.com
by UNIVERSITY OF CALIFORNIA @ BERKELEY on 09/16/26. Reproduction is strictly not permitted, except for Open Access articles.

Int. J. Mod. Phys. A 2026.41. Downloaded from www.worldscientific.com
by UNIVERSITY OF CALIFORNIA @ BERKELEY on 09/16/26. Re-use and distribution is strictly not permitted, except for Open Access articles.

[1] ABDALLAH 10 use data on the final states $e^+e^- \to jj\ell\nu$, $jjjj$, jjX, ℓX, at center-of-mass energies between 189–209 GeV at LEP2, where j = jet, ℓ = lepton, and X represents missing momentum. The fit is carried out keeping all other parameters fixed at their SM values.

[2] SCHAEL 05A study single–photon, single–W, and WW–pair production from 183 to 209 GeV. Each parameter is determined from a single–parameter fit in which the other parameters assume their Standard Model values.

[3] ABBIENDI 04D combine results from W^+W^- in all decay channels. Only *CP*-conserving couplings are considered and each parameter is determined from a single-parameter fit in which the other parameters assume their Standard Model values. The 95% confidence interval is $0.73 < \kappa_\gamma < 1.07$.

[4] ACHARD 04D study WW–pair production, single–W production and single–photon production with missing energy from 189 to 209 GeV. The result quoted here is obtained including data from 161 to 183 GeV, ACCIARRI 99Q. Each parameter is determined from a single–parameter fit in which the other parameters assume their Standard Model values.

[5] AABOUD 17U analyze production of WW or WZ boson pairs with one W boson decaying to electron or muon plus neutrino, and the other W or Z boson decaying hadronically. The hadronic decay system is reconstructed as either a resolved two-jet system or as a single large jet. Analysing the transverse momentum distribution of the hadronic system above 100 GeV yields the following limit at 95% CL for the form factor cut-off scale $\Lambda_{FF} \to \infty$: $0.939 < \kappa_\gamma < 1.064$.

[6] SIRUNYAN 17X study $pp \to WW/WZ \to \ell\nu q\overline{q}$ production at 8 TeV where ℓ is an electron or muon with p_T > 30 or 25 GeV respectively. Suitable cuts are put on the p_T of the dijet system and the missing E_T of the event yielding a total of 285 and 204 WV events observed in the electron and muon channels. The following 95% C.L. limit is obtained: $0.956 < \kappa_\gamma < 1.063$.

[7] CHATRCHYAN 14AB measure $W\gamma$ production cross section for $p_T^\gamma > 15$ GeV and R($\ell\gamma$) > 0.7, which is the separation between the γ and the final state charged lepton (e or μ) in the azimuthal angle-pseudorapidity ($\phi - \eta$) plane. After background subtraction the number of $e\nu\gamma$ and $\mu\nu\gamma$ events is determined to be 3200 ± 325 and 4970 ± 543 respectively, compatible with expectations from the SM. This leads to a 95% CL limit of $0.62 < \kappa_\gamma < 1.29$, assuming other parameters have SM values.

[8] AAD 13AN study $W\gamma$ production in pp collisions. In events with no additional jet, 4449 (6578) W decays to electron (muon) are selected, with an expected background of 1662 ± 262 (2538 ± 362) events. Analysing the photon p_T spectrum above 100 GeV yields a 95% C.L. limit of $0.59 < \kappa_\gamma < 1.46$. Supersedes AAD 12BX.

[9] CHATRCHYAN 13BF determine the W^+W^- production cross section using unlike sign di-lepton (e or μ) events with high $\not{p}_T$. The leptons have p_T > 20 GeV/c and are isolated. 1134 candidate events are observed with an expected SM background of 247 ± 34. The p_T distribution of the leading lepton is fitted to obtain 95% C.L. limits of $0.79 \le k_\gamma \le 1.22$.

[10] ABAZOV 12AG combine new results with already published results on $W\gamma$, WW and WZ production in order to determine the couplings with increased precision, superseding ABAZOV 08R, ABAZOV 11AC, ABAZOV 09AJ, ABAZOV 09AD. The 68% C.L. result for a formfactor cutoff of Λ = 2 TeV is $\kappa_\gamma = 1.048^{+0.106}_{-0.105}$.

[11] ABAZOV 11AC study $W\gamma$ production in $p\overline{p}$ collisions at 1.96 TeV, with the W decay products containing an electron or a muon. They select 196 (363) events in the electron (muon) mode, with a SM expectation of 190 (372) events. A likelihood fit to the photon E_T spectrum above 15 GeV yields at 95% C.L. the result: $0.6 < \kappa_\gamma < 1.4$ for a formfactor Λ = 2 TeV.

[12] CHATRCHYAN 11M study $W\gamma$ production in pp collisions at $\sqrt{s}$ = 7 TeV using 36 pb^{-1} pp data with the W decaying to electron and muon. The total cross section is measured for photon transverse energy E_T^γ > 10 GeV and spatial separation from charged leptons in the plane of pseudo rapidity and azimuthal angle $\Delta R(\ell,\gamma)$> 0.7. The number of candidate (background) events is 452 (228 ± 21) for the electron channel and 520 (277 ± 25) for the muon channel. Setting other couplings to their standard model value, they derive a 95% CL limit of $-0.11 < \kappa_\gamma < 2.04$.

[13] AALTONEN 10K study $p\overline{p} \to W^+W^-$ with $W \to e/\mu\nu$. The p_T of the leading (second) lepton is required to be > 20 (10) GeV. The final number of events selected is 654 of which 320 ± 47 are estimated to be background. The 95% C.L. interval is $0.37 < \kappa_\gamma < 1.72$ for Λ = 1.5 TeV and $0.43 < \kappa_\gamma < 1.65$ for Λ = 2 TeV.

[14] AARON 09B study single-W production in ep collisions at 0.3 TeV C.M. energy. They select 53 $W \to e/\mu$ events with a standard model expectation of 54.1 ± 7.4 events. Fitting the transverse momentum spectrum of the hadronic recoil system they obtain a 95% C.L. limit of $-3.7 < \kappa_\gamma < -1.5$ or $0.3 < \kappa_\gamma < 1.5$, where the ambiguity is due to the quadratic dependence of the cross section to the coupling parameter.

[15] ABAZOV 09AD study the $p\overline{p} \to \ell\nu$ 2jet process arising in WW and WZ production. They select 12,473 (14,392) events in the electron (muon) channel with an expected di-boson signal of 436 (527) events. The results on the anomalous couplings are derived from an analysis of the p_T spectrum of the 2-jet system and quoted at 68% C.L. and for a form factor of 2 TeV. This measurement is not used for obtaining the mean as it is for a specific form factor. The 95% confidence interval is $0.56 < \kappa_\gamma < 1.55$.

[16] ABAZOV 09AJ study the $p\overline{p} \to 2\ell 2\nu$ process arising in WW production. They select 100 events with an expected WW signal of 65 events. An analysis of the p_T spectrum of the two charged leptons leads to 95% C.L. limits of $0.46 < \kappa_\gamma < 1.83$, for a form factor Λ = 2 TeV.

[17] ABAZOV 08R use 0.7 fb^{-1} $p\overline{p}$ data at $\sqrt{s}$ = 1.96 TeV to select 263 $W\gamma + X$ events, of which 187 constitute signal, with the W decaying into an electron or a muon, which is required to be well separated from a photon with E_T > 9 GeV. A likelihood fit to the photon E_T spectrum yields a 95% CL limit $0.49 < \kappa_\gamma < 1.51$ with other couplings fixed to their Standard Model values.

[18] ABDALLAH 08C determine this triple gauge coupling from the measurement of the spin density matrix elements in $e^+e^- \to W^+W^- \to (qq)(\ell\nu)$, where $\ell = e$ or μ. Values of all other couplings are fixed to their standard model values.

[19] AALTONEN 07L set limits on anomalous TGCs using the $p_T(W)$ distribution in WW and WZ production with the W decaying to an electron or muon and the Z to 2 jets. Setting other couplings to their standard model value, the 95% C.L. limits are $0.54 < \kappa_\gamma < 1.39$ for a form factor scale Λ = 1.5 TeV.

[20] ABAZOV 06H study $\overline{p}p \to WW$ production with a subsequent decay $WW \to e^+\nu_e e^-\overline{\nu}_e$, $WW \to e^\pm\nu_e\mu^\mp\nu_\mu$ or $WW \to \mu^+\nu_\mu\mu^-\overline{\nu}_\mu$. The 95% C.L. limit for a form factor scale Λ = 1 TeV is $-0.05 < \kappa_\gamma < 2.29$, fixing λ_γ=0. With the assumption that the $WW\gamma$ and WWZ couplings are equal the 95% C.L. one-dimensional limit (Λ = 2 TeV) is $0.68 < \kappa < 1.45$.

[21] ABAZOV 05J perform a likelihood fit to the photon E_T spectrum of $W\gamma + X$ events, where the W decays to an electron or muon which is required to be well separated from the photon. For Λ = 2.0 TeV the 95% CL limits are $0.12 < \kappa_\gamma < 1.96$. In the fit λ_γ is kept fixed to its Standard Model value.

[22] ABREU 01I combine results from e^+e^- interactions at 189 GeV leading to W^+W^-, $We\nu_e$, and $\nu\overline{\nu}\gamma$ final states with results from ABREU 99L at 183 GeV. The 95% confidence interval is $0.87 < \kappa_\gamma < 1.68$.

[23] BREITWEG 00 search for W production in events with large hadronic p_T. For p_T >20 GeV, the upper limit on the cross section gives the 95%CL limit $-3.7 < \kappa_\gamma < 2.5$ (for λ_γ=0).

[24] ABBOTT 99I perform a simultaneous fit to the $W\gamma$, $WW \to$ dilepton, $WW/WZ \to e\nu jj$, $WW/WZ \to \mu\nu jj$, and $WZ \to$ trilepton data samples. For Λ = 2.0 TeV, the 95%CL limits are $0.75 < \kappa_\gamma < 1.39$.

λ_γ

OUR FIT below is taken from [SCHAEL 13A].

VALUE	EVTS	DOCUMENT ID		TECN	COMMENT
−0.022±0.019 OUR FIT					
0.002±0.035	7872	[1] ABDALLAH	10	DLPH	E_{cm}^{ee}= 189–209 GeV
−0.012±0.027±0.011	10689	[2] SCHAEL	05A	ALEP	E_{cm}^{ee}= 183–209 GeV
$-0.060^{+0.034}_{-0.033}$	9800	[3] ABBIENDI	04D	OPAL	E_{cm}^{ee}= 183–209 GeV
$-0.021^{+0.035}_{-0.034}$±0.017	10575	[4] ACHARD	04D	L3	E_{cm}^{ee}= 161–209 GeV
• • • We do not use the following data for averages, fits, limits, etc. • • •					
		[5] CHATRCHYAN	14AB	CMS	E_{cm}^{pp} = 7 TeV
		[6] AAD	13AN	ATLS	E_{cm}^{pp} = 7 TeV
		[7] ABAZOV	12AG	D0	$E_{cm}^{p\overline{p}}$ = 1.96 TeV
		[8] ABAZOV	11AC	D0	$E_{cm}^{p\overline{p}}$ = 1.96 TeV
		[9] CHATRCHYAN	11M	CMS	E_{cm}^{pp} = 7 TeV
	53	[10] AARON	09B	H1	E_{cm}^{ep} = 0.3 TeV
0.00 ±0.06		[11] ABAZOV	09AD	D0	$E_{cm}^{p\overline{p}}$ = 1.96 TeV
		[12] ABAZOV	09AJ	D0	$E_{cm}^{p\overline{p}}$ = 1.96 TeV
		[13] ABAZOV	08R	D0	$E_{cm}^{p\overline{p}}$ = 1.96 TeV
$0.16\ ^{+0.12}_{-0.13}$	1880	[14] ABDALLAH	08C	DLPH	Superseded by ABDALLAH 10
	1617	[15] AALTONEN	07L	CDF	$E_{cm}^{p\overline{p}}$ = 1.96 GeV
	17	[16] ABAZOV	06H	D0	$E_{cm}^{p\overline{p}}$ = 1.96 TeV
	141	[17] ABAZOV	05J	D0	$E_{cm}^{p\overline{p}}$ = 1.96 TeV
0.05 ±0.09 ±0.01	2298	[18] ABREU	01I	DLPH	E_{cm}^{ee}= 183+189 GeV
		[19] BREITWEG	00	ZEUS	$e^+p \to e^+W^\pm$X, $\sqrt{s} \approx$ 300 GeV
$0.00\ ^{+0.10}_{-0.09}$	331	[20] ABBOTT	99I	D0	$E_{cm}^{p\overline{p}}$= 1.8 TeV

[1] ABDALLAH 10 use data on the final states $e^+e^- \to jj\ell\nu$, $jjjj$, jjX, ℓX, at center-of-mass energies between 189–209 GeV at LEP2, where j = jet, ℓ = lepton, and X represents missing momentum. The fit is carried out keeping all other parameters fixed at their SM values.

[2] SCHAEL 05A study single–photon, single–W, and WW–pair production from 183 to 209 GeV. Each parameter is determined from a single–parameter fit in which the other parameters assume their Standard Model values.

[3] ABBIENDI 04D combine results from W^+W^- in all decay channels. Only *CP*-conserving couplings are considered and each parameter is determined from a single-parameter fit in which the other parameters assume their Standard Model values. The 95% confidence interval is $-0.13 < \lambda_\gamma < 0.01$.

[4] ACHARD 04D study WW–pair production, single–W production and single–photon production with missing energy from 189 to 209 GeV. The result quoted here is obtained including data from 161 to 183 GeV, ACCIARRI 99Q. Each parameter is determined from a single–parameter fit in which the other parameters assume their Standard Model values.

[5] CHATRCHYAN 14AB measure $W\gamma$ production cross section for p_T^γ > 15 GeV and R($\ell\gamma$) > 0.7, which is the separation between the γ and the final state charged lepton (e or μ) in the azimuthal angle-pseudorapidity ($\phi - \eta$) plane. After background subtraction the number of $e\nu\gamma$ and $\mu\nu\gamma$ events is determined to be 3200 ± 325 and 4970 ± 543 respectively, compatible with expectations from the SM. This leads to a 95% CL limit of $-0.050 < \lambda_\gamma < 0.037$, assuming all other parameters have SM values.

[6] AAD 13AN study $W\gamma$ production in pp collisions. In events with no additional jet, 4449 (6578) W decays to electron (muon) are selected, with an expected background of 1662 ± 262 (2538 ± 362) events. Analysing the photon p_T spectrum above 100 GeV yields a 95% C.L. limit of $-0.065 < \lambda_\gamma < 0.061$. Supersedes AAD 12BX.

[7] ABAZOV 12AG combine new results with already published results on $W\gamma$, WW and WZ production in order to determine the couplings with increased precision, superseding ABAZOV 08R, ABAZOV 11AC, ABAZOV 09AJ, ABAZOV 09AD. The 68% C.L. result for a formfactor cutoff of Λ = 2 TeV is $\lambda_\gamma = 0.007^{+0.021}_{-0.022}$.

[8] ABAZOV 11AC study $W\gamma$ production in $p\overline{p}$ collisions at 1.96 TeV, with the W decay products containing an electron or a muon. They select 196 (363) events in the electron (muon) mode, with a SM expectation of 190 (372) events. A likelihood fit to the photon E_T spectrum above 15 GeV yields at 95% C.L. the result: $-0.08 < \lambda_\gamma < 0.07$ for a formfactor Λ = 2 TeV.

[9] CHATRCHYAN 11M study $W\gamma$ production in pp collisions at $\sqrt{s}$ = 7 TeV using 36 pb^{-1} pp data with the W decaying to electron and muon. The total cross section is measured for photon transverse energy E_T^γ > 10 GeV and spatial separation from charged leptons in the plane of pseudo rapidity and azimuthal angle $\Delta R(\ell,\gamma)$> 0.7. The number of candidate (background) events is 452 (228 ± 21) for the electron channel and 520

Int. J. Mod. Phys. A 2026.41. Downloaded from www.worldscientific.com
by UNIVERSITY OF CALIFORNIA @ BERKELEY on 09/16/26. Reproduction is strictly not permitted, except for Open Access articles.

(277 ± 25) for the muon channel. Setting other couplings to their standard model value, they derive a 95% CL limit of $-0.18 < \lambda_\gamma < 0.17$.

[10] AARON 09B study single-W production in ep collisions at 0.3 TeV C.M. energy. They select 53 $W \to e/\mu$ events with a standard model expectation of 54.1 ± 7.4 events. Fitting the transverse momentum spectrum of the hadronic recoil system they obtain a 95% C.L. limit of $-2.5 < \lambda_\gamma < 2.5$.

[11] ABAZOV 09AD study the $p\overline{p} \to \ell\nu$ 2jet process arising in WW and WZ production. They select 12,473 (14,392) events in the electron (muon) channel with an expected di-boson signal of 436 (527) events. The results on the anomalous couplings are derived from an analysis of the p_T spectrum of the 2-jet system and quoted at 68% C.L. and for a form factor of 2 TeV. This measurement is not used for obtaining the mean as it is for a specific form factor. The 95% confidence interval is $-0.10 < \lambda_\gamma < 0.11$.

[12] ABAZOV 09AJ study the $p\overline{p} \to 2\ell 2\nu$ process arising in WW production. They select 100 events with an expected WW signal of 65 events. An analysis of the p_T spectrum of the two charged leptons leads to 95% C.L. limits of $-0.14 < \lambda_\gamma < 0.18$, for a form factor $\Lambda = 2$ TeV.

[13] ABAZOV 08R use 0.7 fb^{-1} $p\overline{p}$ data at $\sqrt{s} = 1.96$ TeV to select 263 $W\gamma + X$ events, of which 187 constitute signal, with the W decaying into an electron or a muon, which is required to be well separated from a photon with $E_T > 9$ GeV. A likelihood fit to the photon E_T spectrum yields a 95% CL limit $-0.12 < \lambda_\gamma < 0.13$ with other couplings fixed to their Standard Model values.

[14] ABDALLAH 08C determine this triple gauge coupling from the measurement of the spin density matrix elements in $e^+e^- \to W^+W^- \to (qq)(\ell\nu)$, where $\ell = e$ or μ. Values of all other couplings are fixed to their standard model values.

[15] AALTONEN 07L set limits on anomalous TGCs using the $p_T(W)$ distribution in WW and WZ production with the W decaying to an electron or muon and the Z to 2 jets. Setting other couplings to their standard model value, the 95% C.L. limits are $-0.18 < \lambda_\gamma < 0.17$ for a form factor scale $\Lambda = 1.5$ TeV.

[16] ABAZOV 06H study $p\overline{p} \to WW$ production with a subsequent decay $WW \to e^+\nu_e e^-\overline{\nu}_e$, $WW \to e^\pm\nu_e\mu^\mp\nu_\mu$ or $WW \to \mu^+\nu_\mu\mu^-\overline{\nu}_\mu$. The 95% C.L. limit for a form factor scale $\Lambda = 1$ TeV is $-0.97 < \lambda_\gamma < 1.04$, fixing κ_γ=1. With the assumption that the $WW\gamma$ and WWZ couplings are equal the 95% C.L. one-dimensional limit (Λ = 2 TeV) is $-0.29 < \lambda < 0.30$.

[17] ABAZOV 05J perform a likelihood fit to the photon E_T spectrum of $W\gamma$ + X events, where the W decays to an electron or muon which is required to be well separated from the photon. For $\Lambda = 2.0$ TeV the 95% CL limits are $-0.20 < \lambda_\gamma < 0.20$. In the fit κ_γ is kept fixed to its Standard Model value.

[18] ABREU 01I combine results from e^+e^- interactions at 189 GeV leading to W^+W^-, $We\nu_e$, and $\nu\overline{\nu}\gamma$ final states with results from ABREU 99L at 183 GeV. The 95% confidence interval is $-0.11 < \lambda_\gamma < 0.23$.

[19] BREITWEG 00 search for W production in events with large hadronic p_T. For p_T >20 GeV, the upper limit on the cross section gives the 95%CL limit $-3.2 < \lambda_\gamma < 3.2$ for κ_γ fixed to its Standard Model value.

[20] ABBOTT 99I perform a simultaneous fit to the $W\gamma$, $WW \to$ dilepton, $WW/WZ \to e\nu jj$, $WW/WZ \to \mu\nu jj$, and $WZ \to$ trilepton data samples. For $\Lambda = 2.0$ TeV, the 95%CL limits are $-0.18 < \lambda_\gamma < 0.19$.

κ_Z

This coupling is *CP*-conserving (*C*- and *P*- separately conserving).

VALUE	EVTS	DOCUMENT ID		TECN	COMMENT
$\mathbf{0.924^{+0.059}_{-0.056} \pm 0.024}$	7171	[1] ACHARD	04D	L3	E^{ee}_{cm} = 189–209 GeV
• • • We do not use the following data for averages, fits, limits, etc. • • •					
		[2] SIRUNYAN	20BA	CMS	E^{pp}_{cm} = 13 TeV
		[3] SIRUNYAN	19CL	CMS	E^{pp}_{cm} = 13 TeV
		[4] AABOUD	17S	ATLS	E^{pp}_{cm} = 7+8 TeV
		[5] KHACHATRY...	17O	CMS	E^{pp}_{cm} = 8 TeV
		[6] AAD	16AR	ATLS	E^{pp}_{cm} = 8 TeV
		[7] AAD	16P	ATLS	E^{pp}_{cm} = 8 TeV
		[8] AAD	13AL	ATLS	E^{pp}_{cm} = 7 TeV
		[9] AAD	12CD	ATLS	E^{pp}_{cm} = 7 TeV
		[10] AALTONEN	12AC	CDF	$E^{p\overline{p}}_{cm}$ = 1.96 TeV
	34	[11] ABAZOV	11	D0	$E^{p\overline{p}}_{cm}$ = 1.96 TeV
	17	[12] ABAZOV	06H	D0	$E^{p\overline{p}}_{cm}$ = 1.96 TeV
	2.3	[13] ABAZOV	05S	D0	$E^{p\overline{p}}_{cm}$ = 1.96 TeV

[1] ACHARD 04D study WW–pair production, single–W production and single–photon production with missing energy from 189 to 209 GeV. The result quoted here is obtained using the WW–pair production sample. Each parameter is determined from a single–parameter fit in which the other parameters assume their Standard Model values.

[2] SIRUNYAN 20BA study electroweak production of a W boson in association with two jets, using W decays in the electron or muon channel. The isolated muons (electrons) are required to have a transverse momentum larger than 25 (30) GeV, while the transverse momentum of the two jets has to be larger than 50 and 30 GeV. A total of 2.382 (1.051) million events are selected in the muon (electron) channel, with a Standard Model expectation of 2.39 ± 0.17 (1.054 ± 0.058) million events. Analysing the transverse momentum distribution of the charged leptons from W decay, the following 95% C.L. limit is obtained: $0.956 < \kappa_Z < 1.044$. Combining this result with that from the closely-related electroweak Z-jet-jet production SIRUNYAN 18BZ, the limit becomes: $0.957 < \kappa_Z < 1.042$.

[3] SIRUNYAN 19CL study WW and WZ production in lepton + jet events, with one W boson decaying leptonically (electron or muon), and another W or Z boson decaying hadronically, reconstructed as a single massive large-radius jet. In the electron channel 2,456 (2,235) events are selected in the $WW(WZ)$ category, while in the muon channel 3,996 (3572) events are selected in the $WW(WZ)$ category. Analysing the di-boson invariant mass distribution, the following 95% C.L. limit is obtained: $0.9921 < \kappa_Z < 1.0082$.

[4] AABOUD 17S analyze electroweak production of a W boson in association with two jets at high dijet invariant mass, with the W boson decaying to electron or muon plus neutrino. In the signal region of dijet mass larger than 1 TeV and leading-jet transverse momentum larger than 600 GeV, 30 events are observed in the data with 39 ± 4 events expected in the Standard Model, yielding the following limit at 95% CL for the form factor cut-off scale $\Lambda_{FF} \to \infty$: $0.85 < \kappa_Z < 1.16$.

[5] KHACHATRYAN 17O analyse WZ production where each boson decays into electrons or muons. Events are required to have a tri-lepton invariant mass larger than 100 GeV, with one of the lepton pairs having an invariant mass within 20 GeV of the Z boson mass. The Z transverse momentum spectrum is analyzed to set a 95% C.L. limit of: $0.79 < \kappa_Z < 1.25$.

[6] AAD 16AR study WW production in pp collisions and select 6636 WW candidates in decay modes with electrons or muons with an expected background of 1546 ± 157 events. Assuming the LEP formulation and setting the form-factor Λ to infinity, a fit to the transverse momentum distribution of the leading charged lepton, leads to a 95% C.L. range of $0.975 < \kappa_Z < 1.020$.

[7] AAD 16P study WZ production in pp collisions and select 2091 WZ candidates in 4 decay modes with electrons and muons, with an expected background of 1825 ± 7 events. Analyzing the WZ transverse momentum distribution, the resulting 95% C.L. limit is: $0.81 < \kappa_Z < 1.30$.

[8] AAD 13AL study WW production in pp collisions and select 1325 WW candidates in decay modes with electrons or muons with an expected background of 369 ± 61 events. Assuming the LEP formulation and setting the form-factor Λ = infinity, a fit to the transverse momentum distribution of the leading charged lepton, leads to a 95% C.L. range of $0.957 < \kappa_Z < 1.043$. Supersedes AAD 12AC.

[9] AAD 12CD study WZ production in pp collisions and select 317 WZ candidates in three $\ell\nu$ decay modes with an expected background of 68.0 ± 10.0 events. The resulting 95% C.L. range is: $0.63 < \kappa_Z < 1.57$. Supersedes AAD 12V.

[10] AALTONEN 12AC study WZ production in $p\overline{p}$ collisions and select 63 WZ candidates in three $\ell\nu$ decay modes with an expected background of 7.9 ± 1.0 events. Based on the cross section and shape of the Z transverse momentum spectrum, the following 95% C.L. range is reported: $0.61 < \kappa_Z < 1.90$ for a form factor of $\Lambda = 2$ TeV.

[11] ABAZOV 11 study the $p\overline{p} \to 3\ell\nu$ process arising in WZ production. They observe 34 WZ candidates with an estimated background of 6 events. An analysis of the p_T spectrum of the Z boson leads to a 95% C.L. limit of $0.600 < \kappa_Z < 1.675$, for a form factor $\Lambda = 2$ TeV.

[12] ABAZOV 06H study $\overline{p}p \to WW$ production with a subsequent decay $WW \to e^+\nu_e e^-\overline{\nu}_e$, $WW \to e^\pm\nu_e\mu^\mp\nu_\mu$ or $WW \to \mu^+\nu_\mu\mu^-\overline{\nu}_\mu$. The 95% C.L. limit for a form factor scale $\Lambda = 2$ TeV is $0.55 < \kappa_Z < 1.55$, fixing λ_Z=0. With the assumption that the $WW\gamma$ and WWZ couplings are equal the 95% C.L. one-dimensional limit (Λ = 2 TeV) is $0.68 < \kappa < 1.45$.

[13] ABAZOV 05S study $\overline{p}p \to WZ$ production with a subsequent trilepton decay to $\ell\nu\ell'\overline{\ell}'$ (ℓ and $\ell' = e$ or μ). Three events (estimated background 0.71 ± 0.08 events) with WZ decay characteristics are observed from which they derive limits on the anomalous WWZ couplings. The 95% CL limit for a form factor scale $\Lambda = 1$ TeV is $-1.0 < \kappa_Z < 3.4$, fixing λ_Z and g_1^Z to their Standard Model values.

λ_Z

This coupling is *CP*-conserving (*C*- and *P*- separately conserving).

VALUE	EVTS	DOCUMENT ID		TECN	COMMENT
$\mathbf{-0.088^{+0.060}_{-0.057} \pm 0.023}$	7171	[1] ACHARD	04D	L3	E^{ee}_{cm} = 189–209 GeV
• • • We do not use the following data for averages, fits, limits, etc. • • •					
		[2] SIRUNYAN	20BA	CMS	E^{pp}_{cm} = 13 TeV
		[3] SIRUNYAN	19CL	CMS	E^{pp}_{cm} = 13 TeV
		[4] SIRUNYAN	18BZ	CMS	E^{pp}_{cm} = 13 TeV
		[5] AABOUD	17S	ATLS	E^{pp}_{cm} = 7+8 TeV
		[6] AABOUD	17U	ATLS	E^{pp}_{cm} = 8 TeV
		[7] KHACHATRY...	17O	CMS	E^{pp}_{cm} = 8 TeV
		[8] SIRUNYAN	17X	CMS	E^{pp}_{cm} = 8 TeV
		[9] AAD	16AR	ATLS	E^{pp}_{cm} = 8 TeV
		[10] AAD	16P	ATLS	E^{pp}_{cm} = 8 TeV
		[11] AAD	14Y	ATLS	E^{pp}_{cm} = 8 TeV
		[12] AAD	13AL	ATLS	E^{pp}_{cm} = 7 TeV
		[13] CHATRCHYAN	13BF	CMS	E^{pp}_{cm} = 7 TeV
		[14] AAD	12CD	ATLS	E^{pp}_{cm} = 7 TeV
		[15] AALTONEN	12AC	CDF	$E^{p\overline{p}}_{cm}$ = 1.96 TeV
	34	[16] ABAZOV	11	D0	$E^{p\overline{p}}_{cm}$ = 1.96 TeV
	334	[17] AALTONEN	10K	CDF	$E^{p\overline{p}}_{cm}$ = 1.96 TeV
	13	[18] ABAZOV	07Z	D0	$E^{p\overline{p}}_{cm}$ = 1.96 TeV
	17	[19] ABAZOV	06H	D0	$E^{p\overline{p}}_{cm}$ = 1.96 TeV
	2.3	[20] ABAZOV	05S	D0	$E^{p\overline{p}}_{cm}$ = 1.96 TeV

[1] ACHARD 04D study WW–pair production, single–W production and single–photon production with missing energy from 189 to 209 GeV. The result quoted here is obtained using the WW–pair production sample. Each parameter is determined from a single–parameter fit in which the other parameters assume their Standard Model values.

[2] SIRUNYAN 20BA study electroweak production of a W boson in association with two jets, using W decays in the electron or muon channel. The isolated muons (electrons) are required to have a transverse momentum larger than 25 (30) GeV, while the transverse momentum of the two jets has to be larger than 50 and 30 GeV. A total of 2.382 (1.051) million events are selected in the muon (electron) channel, with a Standard Model expectation of 2.39 ± 0.17 (1.054 ± 0.058) million events. Analysing the transverse momentum distribution of the charged leptons from W decay, the following 95% C.L. limit is obtained: $-0.0088 < \lambda_Z < 0.0095$. Combining this result with that from the closely-related electroweak Z-jet-jet production SIRUNYAN 18BZ, the limit becomes: $-0.0071 < \lambda_Z < 0.0076$.

[3] SIRUNYAN 19CL study WW and WZ production in lepton + jet events, with one W boson decaying leptonically (electron or muon), and another W or Z boson decaying

Int. J. Mod. Phys. A 2026.41. Downloaded from www.worldscientific.com by UNIVERSITY OF CALIFORNIA @ BERKELEY on 09/16/26. Re-use and distribution is strictly not permitted, except for Open Access articles.

hadronically, reconstructed as a single massive large-radius jet. In the electron channel 2,456 (2,235) events are selected in the $WW(WZ)$ category, while in the muon channel 3,996 (3572) events are selected in the $WW(WZ)$ category. Analysing the di-boson invariant mass distribution, the following 95% C.L. limit is obtained: $-0.0065 < \lambda_Z < 0.0066$.

[4] SIRUNYAN 18BZ study $pp \to Z$ *jet jet* events at 13 TeV where $Z \to e^+e^-/\mu^+\mu^-$. Isolated electrons and muons are selected with p_T of the leading/sub-leading lepton > 30/20 GeV and $|\eta| < 2.4$, with the di-lepton invariant mass within 15 GeV of the Z mass. The two highest p_T jets are selected with p_T of the leading/sub-leading jet > 50/30 GeV respectively and dijet invariant mass > 200 GeV. Templates in the transverse momentum of the Z are utilized to set limits on the triple gauge couplings in the EFT and the LEP parametrizations. The following 95% C.L. limit is obtained $-0.010 < \lambda_Z < 0.010$.

[5] AABOUD 17S analyze electroweak production of a W boson in association with two jets at high dijet invariant mass, with the W boson decaying to electron or muon plus neutrino. In the signal region of dijet mass larger than 1 TeV and leading-jet transverse momentum larger than 600 GeV, 30 events are observed in the data with 39 ± 4 events expected in the Standard Model, yielding the following limit at 95% CL for the form factor cut-off scale $\Lambda_{FF} \to \infty$: $-0.053 < \lambda_Z < 0.042$.

[6] AABOUD 17U analyze production of WW or WZ boson pairs with one W boson decaying to electron or muon plus neutrino, and the other W or Z boson decaying hadronically. The hadronic decay system is reconstructed as either a resolved two-jet system or as a single large jet. Analysing the transverse momentum distribution of the hadronic system above 100 GeV yields the following limit at 95% CL for the form factor cut-off scale $\Lambda_{FF} \to \infty$: $-0.013 < \lambda_Z < 0.013$.

[7] KHACHATRYAN 17O analyse WZ production where each boson decays into electrons or muons. Events are required to have a tri-lepton invariant mass larger than 100 GeV, with one of the lepton pairs having an invariant mass within 20 GeV of the Z boson mass. The Z transverse momentum spectrum is analyzed to set a 95% C.L. limit of: $-0.018 < \lambda_Z < 0.016$.

[8] SIRUNYAN 17X study $pp \to WW/WZ \to \ell\nu q\overline{q}$ production at 8 TeV where ℓ is an electron or muon with $p_T > 30$ or 25 GeV respectively. Suitable cuts are put on the p_T of the dijet system and the missing E_T of the event yielding a total of 285 and 204 WV events observed in the electron and muon channels. The following 95% C.L. limit is obtained: $-0.011 < \lambda_Z < 0.011$.

[9] AAD 16AR study WW production in pp collisions and select 6636 WW candidates in decay modes with electrons or muons with an expected background of 1546 ± 157 events. Assuming the LEP formulation and setting the form-factor Λ to infinity, a fit to the transverse momentum distribution of the leading charged lepton, leads to a 95% C.L. range of $-0.019 < \lambda_Z < 0.019$.

[10] AAD 16P study WZ production in pp collisions and select 2091 WZ candidates in 4 decay modes with electrons and muons, with an expected background of 1825 ± 7 events. Analyzing the WZ transverse momentum distribution, the resulting 95% C.L. limit is: $-0.016 < \lambda_Z < 0.016$.

[11] AAD 14Y determine the electroweak Z-dijet cross section in 8 TeV pp collisions. $Z \to ee$ and $Z \to \mu\mu$ decays are selected with the di-lepton $p_T > 20$ GeV and mass in the 81–101 GeV range. Minimum two jets are required with $p_T > 55$ and 45 GeV and no additional jets with $p_T > 25$ GeV in the rapidity interval between them. The normalized p_T balance between the Z and the two jets is required to be < 0.15. This leads to a selection of 900 events with dijet mass > 1 TeV. The number of signal and background events expected is 261 and 592 respectively. A Poisson likelihood method is used on an event by event basis to obtain the 95% CL limit $-0.15 < \lambda_Z < 0.13$ for a form factor value $\Lambda = \infty$.

[12] AAD 13AL study WW production in pp collisions and select 1325 WW candidates in decay modes with electrons or muons with an expected background of 369 ± 61 events. Assuming the LEP formulation and setting the form-factor Λ = infinity, a fit to the transverse momentum distribution of the leading charged lepton, leads to a 95% C.L. range of $-0.062 < \lambda_Z < 0.059$. Supersedes AAD 12AC.

[13] CHATRCHYAN 13BF determine the W^+W^- production cross section using unlike sign di-lepton (e or μ) events with high $\not{p}_T$. The leptons have $p_T > 20$ GeV/c and are isolated. 1134 candidate events are observed with an expected SM background of 247 ± 34. The p_T distribution of the leading lepton is fitted to obtain 95% C.L. limits of $-0.048 \leq \lambda_Z \leq 0.048$.

[14] AAD 12CD study WZ production in pp collisions and select 317 WZ candidates in three $\ell\nu$ decay modes with an expected background of 68.0 ± 10.0 events. The resulting 95% C.L. range is: $-0.046 < \lambda_Z < 0.047$. Supersedes AAD 12V.

[15] AALTONEN 12AC study WZ production in $p\overline{p}$ collisions and select 63 WZ candidates in three $\ell\nu$ decay modes with an expected background of 7.9 ± 1.0 events. Based on the cross section and shape of the Z transverse momentum spectrum, the following 95% C.L. range is reported: $-0.08 < \lambda_Z < 0.10$ for a form factor of $\Lambda = 2$ TeV.

[16] ABAZOV 11 study the $p\overline{p} \to 3\ell\nu$ process arising in WZ production. They observe 34 WZ candidates with an estimated background of 6 events. An analysis of the p_T spectrum of the Z boson leads to a 95% C.L. limit of $-0.077 < \lambda_Z < 0.093$, for a form factor $\Lambda = 2$ TeV.

[17] AALTONEN 10K study $p\overline{p} \to W^+W^-$ with $W \to e/\mu\nu$. The p_T of the leading (second) lepton is required to be > 20 (10) GeV. The final number of events selected is 654 of which 320 ± 47 are estimated to be background. The 95% C.L. interval is $-0.16 < \lambda_Z < 0.16$ for $\Lambda = 1.5$ TeV and $-0.14 < \lambda_Z < 0.15$ for $\Lambda = 2$ TeV.

[18] ABAZOV 07Z set limits on anomalous TGCs using the measured cross section and $p_T(Z)$ distribution in WZ production with both the W and the Z decaying leptonically into electrons and muons. Setting the other couplings to their standard model values, the 95% C.L. limit for a form factor scale $\Lambda = 2$ TeV is $-0.17 < \lambda_Z < 0.21$.

[19] ABAZOV 06H study $\overline{p}p \to WW$ production with a subsequent decay $WW \to e^+\nu_e e^-\overline{\nu}_e$, $WW \to e^\pm\nu_e\mu^\mp\nu_\mu$ or $WW \to \mu^+\nu_\mu\mu^-\overline{\nu}_\mu$. The 95% C.L. limit for a form factor scale $\Lambda = 2$ TeV is $-0.39 < \lambda_Z < 0.39$, fixing κ_Z=1. With the assumption that the $WW\gamma$ and WWZ couplings are equal the 95% C.L. one-dimensional limit ($\Lambda = 2$ TeV) is $-0.29 < \lambda < 0.30$.

[20] ABAZOV 05S study $\overline{p}p \to WZ$ production with a subsequent trilepton decay to $\ell\nu\ell'\overline{\ell}'$ (ℓ and $\ell' = e$ or μ). Three events (estimated background 0.71 ± 0.08 events) with WZ decay characteristics are observed from which they derive limits on the anomalous WWZ couplings. The 95% CL limit for a form factor scale $\Lambda = 1.5$ TeV is $-0.48 < \lambda_Z < 0.48$, fixing g_1^Z and κ_Z to their Standard Model values.

g_5^Z

This coupling is CP-conserving but C- and P-violating.

VALUE	EVTS	DOCUMENT ID		TECN	COMMENT
-0.07 ± 0.09 OUR AVERAGE		Error includes scale factor of 1.1.			
$-0.04^{+0.13}_{-0.12}$	9800	[1] ABBIENDI	04D	OPAL	E^{ee}_{cm}= 183–209 GeV
$0.00 \pm 0.13 \pm 0.05$	7171	[2] ACHARD	04D	L3	E^{ee}_{cm}= 189–209 GeV
$-0.44^{+0.23}_{-0.22} \pm 0.12$	1154	[3] ACCIARRI	99Q	L3	E^{ee}_{cm}= 161+172+ 183 GeV
• • • We do not use the following data for averages, fits, limits, etc. • • •					
-0.31 ± 0.23		[4] EBOLI	00	THEO	LEP1, SLC+ Tevatron

[1] ABBIENDI 04D combine results from W^+W^- in all decay channels. Only CP-conserving couplings are considered and each parameter is determined from a single-parameter fit in which the other parameters assume their Standard Model values. The 95% confidence interval is $-0.28 < g_5^Z < +0.21$.

[2] ACHARD 04D study WW–pair production, single–W production and single–photon production with missing energy from 189 to 209 GeV. The result quoted here is obtained using the WW–pair production sample. Each parameter is determined from a single–parameter fit in which the other parameters assume their Standard Model values.

[3] ACCIARRI 99Q study W-pair, single-W, and single photon events.

[4] EBOLI 00 extract this indirect value of the coupling studying the non-universal one-loop contributions to the experimental value of the $Z \to b\overline{b}$ width (Λ=1 TeV is assumed).

g_4^Z

This coupling is CP-violating (C-violating and P-conserving).

VALUE	EVTS	DOCUMENT ID		TECN	COMMENT
-0.30 ± 0.17 OUR AVERAGE					
$-0.39^{+0.19}_{-0.20}$	1880	[1] ABDALLAH	08C	DLPH	E^{ee}_{cm}= 189–209 GeV
$-0.02^{+0.32}_{-0.33}$	1065	[2] ABBIENDI	01H	OPAL	E^{ee}_{cm}= 189 GeV

[1] ABDALLAH 08C determine this triple gauge coupling from the measurement of the spin density matrix elements in $e^+e^- \to W^+W^- \to (qq)(\ell\nu)$, where $\ell = e$ or μ. Values of all other couplings are fixed to their standard model values.

[2] ABBIENDI 01H study W-pair events, with one leptonically and one hadronically decaying W. The coupling is extracted using information from the W production angle together with decay angles from the leptonically decaying W.

$\tilde{\kappa}_Z$

This coupling is CP-violating (C-conserving and P-violating).

VALUE	EVTS	DOCUMENT ID		TECN	COMMENT
$-0.12^{+0.06}_{-0.04}$ OUR AVERAGE					
$-0.09^{+0.08}_{-0.05}$	1880	[1] ABDALLAH	08C	DLPH	E^{ee}_{cm}= 189–209 GeV
$-0.20^{+0.10}_{-0.07}$	1065	[2] ABBIENDI	01H	OPAL	E^{ee}_{cm}= 189 GeV
• • • We do not use the following data for averages, fits, limits, etc. • • •					
		[3] AABOUD	17S	ATLS	E^{pp}_{cm} = 7+8 TeV
		[4] BLINOV	11	LEP	E^{ee}_{cm}= 183–207 GeV

[1] ABDALLAH 08C determine this triple gauge coupling from the measurement of the spin density matrix elements in $e^+e^- \to W^+W^- \to (qq)(\ell\nu)$, where $\ell = e$ or μ. Values of all other couplings are fixed to their standard model values.

[2] ABBIENDI 01H study W-pair events, with one leptonically and one hadronically decaying W. The coupling is extracted using information from the W production angle together with decay angles from the leptonically decaying W.

[3] AABOUD 17S analyze electroweak production of a W boson in association with two jets at high dijet invariant mass, with the W boson decaying to electron or muon plus neutrino. In the signal region of dijet mass larger than 1 TeV and leading-jet transverse momentum larger than 600 GeV, 30 events are observed in the data with 39 ± 4 events expected in the Standard Model, yielding the following limit at 95% CL for the form factor cut-off scale $\Lambda_{FF} \to \infty$: $-0.56 < \tilde{\kappa}_Z < 0.56$.

[4] BLINOV 11 use the LEP-average $e^+e^- \to W^+W^-$ cross section data for $\sqrt{s}$ = 183–207 GeV to determine an upper limit on the TGC $\tilde{\kappa}_Z$. The average values of the cross sections as well as their correlation matrix, and standard model expectations of the cross sections are taken from the LEPEWWG note hep-ex/0612034. At 95% confidence level $|\tilde{\kappa}_Z| < 0.13$.

$\tilde{\lambda}_Z$

This coupling is CP-violating (C-conserving and P-violating).

VALUE	EVTS	DOCUMENT ID		TECN	COMMENT
-0.09 ± 0.07 OUR AVERAGE					
-0.08 ± 0.07	1880	[1] ABDALLAH	08C	DLPH	E^{ee}_{cm}= 189–209 GeV
$-0.18^{+0.24}_{-0.16}$	1065	[2] ABBIENDI	01H	OPAL	E^{ee}_{cm}= 189 GeV
• • • We do not use the following data for averages, fits, limits, etc. • • •					
		[3] AABOUD	17S	ATLS	E^{pp}_{cm} = 7+8 TeV
		[4] BLINOV	11	LEP	E^{ee}_{cm}= 183–207 GeV

[1] ABDALLAH 08C determine this triple gauge coupling from the measurement of the spin density matrix elements in $e^+e^- \to W^+W^- \to (qq)(\ell\nu)$, where $\ell = e$ or μ. Values of all other couplings are fixed to their standard model values.

[2] ABBIENDI 01H study W-pair events, with one leptonically and one hadronically decaying W. The coupling is extracted using information from the W production angle together with decay angles from the leptonically decaying W.

[3] AABOUD 17S analyze electroweak production of a W boson in association with two jets at high dijet invariant mass, with the W boson decaying to electron or muon plus neutrino. In the signal region of dijet mass larger than 1 TeV and leading-jet transverse momentum larger than 600 GeV, 30 events are observed in the data with 39 ± 4 events expected in the Standard Model, yielding the following limit at 95% CL for the form factor cut-off scale $\Lambda_{FF} \to \infty$: $-0.047 < \tilde{\lambda}_Z < 0.046$.

[4] BLINOV 11 use the LEP-average $e^+e^- \to W^+W^-$ cross section data for $\sqrt{s}$ = 183–207 GeV to determine an upper limit on the TGC $\tilde{\lambda}_Z$. The average values of the cross sections as well as their correlation matrix, and standard model expectations of the cross sections are taken from the LEPEWWG note hep-ex/0612034. At 95% confidence level $|\tilde{\lambda}_Z| < 0.31$.

Int. J. Mod. Phys. A 2026.41. Downloaded from www.worldscientific.com
by UNIVERSITY OF CALIFORNIA @ BERKELEY on 09/16/26. Re strictly not permitted, except for Open Access articles.

W ANOMALOUS MAGNETIC MOMENT

The full magnetic moment is given by $\mu_W = e(1+\kappa+\lambda)/2m_W$. In the Standard Model, at tree level, $\kappa = 1$ and $\lambda = 0$. Some papers have defined $\Delta\kappa = 1-\kappa$ and assume that $\lambda = 0$. Note that the electric quadrupole moment is given by $-e(\kappa-\lambda)/m_W^2$. A description of the parameterization of these moments and additional references can be found in HAGIWARA 87 and BAUR 88. The parameter Λ appearing in the theoretical limits below is a regularization cutoff which roughly corresponds to the energy scale where the structure of the *W* boson becomes manifest.

VALUE ($e/2m_W$)	EVTS	DOCUMENT ID		TECN	COMMENT
$\mathbf{2.22^{+0.20}_{-0.19}}$	2298	[1] ABREU	01I	DLPH	E^{ee}_{cm}= 183+189 GeV
• • • We do not use the following data for averages, fits, limits, etc. • • •					
		[2] ABE	95G	CDF	
		[3] ALITTI	92C	UA2	
		[4] SAMUEL	92	THEO	
		[5] SAMUEL	91	THEO	
		[6] GRIFOLS	88	THEO	
		[7] GROTCH	87	THEO	
		[8] VANDERBIJ	87	THEO	
		[9] GRAU	85	THEO	
		[10] SUZUKI	85	THEO	
		[11] HERZOG	84	THEO	

[1] ABREU 01I combine results from e^+e^- interactions at 189 GeV leading to W^+W^-, $We\nu_e$, and $\nu\overline{\nu}\gamma$ final states with results from ABREU 99L at 183 GeV to determine Δg_1^Z, $\Delta\kappa_\gamma$, and λ_γ. $\Delta\kappa_\gamma$ and λ_γ are simultaneously floated in the fit to determine μ_W.

[2] ABE 95G report $-1.3 < \kappa < 3.2$ for λ=0 and $-0.7 < \lambda < 0.7$ for κ=1 in $p\overline{p} \to e\nu_e\gamma X$ and $\mu\nu_\mu\gamma X$ at $\sqrt{s} = 1.8$ TeV.

[3] ALITTI 92C measure $\kappa = 1^{+2.6}_{-2.2}$ and $\lambda = 0^{+1.7}_{-1.8}$ in $p\overline{p} \to e\nu\gamma + X$ at $\sqrt{s} = 630$ GeV. At 95%CL they report $-3.5 < \kappa < 5.9$ and $-3.6 < \lambda < 3.5$.

[4] SAMUEL 92 use preliminary CDF and UA2 data and find $-2.4 < \kappa < 3.7$ at 96%CL and $-3.1 < \kappa < 4.2$ at 95%CL respectively. They use data for $W\gamma$ production and radiative *W* decay.

[5] SAMUEL 91 use preliminary CDF data for $p\overline{p} \to W\gamma X$ to obtain $-11.3 \leq \Delta\kappa \leq 10.9$. Note that their $\kappa = 1-\Delta\kappa$.

[6] GRIFOLS 88 uses deviation from ρ parameter to set limit $\Delta\kappa \lesssim 65\ (M_W^2/\Lambda^2)$.

[7] GROTCH 87 finds the limit $-37 < \Delta\kappa < 73.5$ (90% CL) from the experimental limits on $e^+e^- \to \nu\overline{\nu}\gamma$ assuming three neutrino generations and $-19.5 < \Delta\kappa < 56$ for four generations. Note their $\Delta\kappa$ has the opposite sign as our definition.

[8] VANDERBIJ 87 uses existing limits to the photon structure to obtain $|\Delta\kappa| < 33\ (m_W/\Lambda)$. In addition VANDERBIJ 87 discusses problems with using the ρ parameter of the Standard Model to determine $\Delta\kappa$.

[9] GRAU 85 uses the muon anomaly to derive a coupled limit on the anomalous magnetic dipole and electric quadrupole (λ) moments $1.05 > \Delta\kappa \ln(\Lambda/m_W) + \lambda/2 > -2.77$. In the Standard Model $\lambda = 0$.

[10] SUZUKI 85 uses partial-wave unitarity at high energies to obtain $|\Delta\kappa| \lesssim 190\ (m_W/\Lambda)^2$. From the anomalous magnetic moment of the muon, SUZUKI 85 obtains $|\Delta\kappa| \lesssim 2.2/\ln(\Lambda/m_W)$. Finally SUZUKI 85 uses deviations from the ρ parameter and obtains a very qualitative, order-of-magnitude limit $|\Delta\kappa| \lesssim 150\ (m_W/\Lambda)^4$ if $|\Delta\kappa| \ll 1$.

[11] HERZOG 84 consider the contribution of *W*-boson to muon magnetic moment including anomalous coupling of $WW\gamma$. Obtain a limit $-1 < \Delta\kappa < 3$ for $\Lambda \gtrsim 1$ TeV.

c_{WWW}/Λ^2, c_W/Λ^2, c_B/Λ^2

These couplings are used in EFT-based approaches to anomalous couplings. They are linearly related to the couplings discussed above.

VALUE	DOCUMENT ID		TECN	COMMENT
• • • We do not use the following data for averages, fits, limits, etc. • • •				
	[1] AAD	25AD	ATLS	E^{pp}_{cm} = 13 TeV
	[2] AAD	25BE	ATLS	E^{pp}_{cm} = 13 TeV
	[3] HAYRAPETY...	25AM	CMS	E^{pp}_{cm} = 13 TeV
	[4] TUMASYAN	22AB	CMS	E^{pp}_{cm} = 13 TeV
	[5] TUMASYAN	22E	CMS	E^{pp}_{cm} = 13 TeV
	[6] AAD	21AC	ATLS	E^{pp}_{cm} = 13 TeV
	[7] AAD	21W	ATLS	E^{pp}_{cm} = 13 TeV
	[8] SIRUNYAN	21G	CMS	E^{pp}_{cm} = 13 TeV
	[9] SIRUNYAN	20BA	CMS	E^{pp}_{cm} = 13 TeV
	[10] SIRUNYAN	20BF	CMS	E^{pp}_{cm} = 13 TeV
	[11] AABOUD	19BA	ATLS	E^{pp}_{cm} = 13 TeV
	[12] SIRUNYAN	19AD	CMS	E^{pp}_{cm} = 13 TeV
	[13] SIRUNYAN	19CL	CMS	E^{pp}_{cm} = 13 TeV
	[14] AABOUD	18Q	ATLS	E^{pp}_{cm} = 13 TeV
	[15] SIRUNYAN	18BZ	CMS	E^{pp}_{cm} = 13 TeV
	[16] AABOUD	17S	ATLS	E^{pp}_{cm} = 7+8 TeV
	[17] AABOUD	17U	ATLS	E^{pp}_{cm} = 8 TeV
	[18] KHACHATRY...	17O	CMS	E^{pp}_{cm} = 8 TeV
	[19] SIRUNYAN	17X	CMS	E^{pp}_{cm} = 8 TeV
	[20] AAD	16AR	ATLS	E^{pp}_{cm} = 8 TeV
	[21] AAD	16P	ATLS	E^{pp}_{cm} = 8 TeV
	[22] KHACHATRY...	16BI	CMS	E^{pp}_{cm} = 8 TeV

[1] AAD 25AD measures charged-current Drell-Yan production of *W* bosons decaying to electrons or muons. Analysing the transverse mass and lepton pseudo rapidity single and double differential distributions, the following 95% C.L. limits on EFT couplings are obtained: -0.0047 $< c^{(3)}_{\ell q}/\Lambda^2 < 0.0021$, -0.60 $< c^{(1)}_{\ell\ell}/\Lambda^2 < 1.15$, -1.14 $< c^{(3)}_{H\ell}/\Lambda^2 < 0.60$, -0.61 $< c^{(3)}_{Hq}/\Lambda^2 < 1.15$, in units of TeV^{-2}.

[2] AAD 25BE study *WZ* production, measuring cross sections and various distributions. Analysing the *WZ* transverse mass distribution without cutoff and considering linear and quadratic contributions, the following 95% C.L. limits on *CP*-conserving operators are derived in units of TeV^{-2}: $-0.093 < c_W/\Lambda^2 < 0.079$, $-0.458 < c_{HWB}/\Lambda^2 < 1.520$, $-5.840 < c_{HD}/\Lambda^2 < 1.680$, $-0.503 < c^{(1)}_{Hq}/\Lambda^2 < 2.550$, $-0.165 < c^{(3)}_{Hq}/\Lambda^2 < 0.015$. Limits on *CP*-violating operators are derived using the *WZ* transverse mass distribution and dedicated *CP*-sensitive observables at 95% C.L. in units of TeV^{-2}: $-1.505 < c_{H\widetilde{W}B}/\Lambda^2 < 1.263$, $-0.109 < c_{\widetilde{W}}/\Lambda^2 < 0.093$.

[3] HAYRAPETYAN 25AM study same-sign *WW* production, with one *W* boson decaying into electrons or muons and the other *W* boson decaying into a tau lepton, in association with at least two jets with large invariant mass and rapidity difference. Multivariate classifiers are used to extract the following 95% C.L. limits in units of TeV^{-2}: $-13.5 < c^{(1)}_{\ell\ell}/\Lambda^2 < 2.11$, $-0.605 < c^{(1)}_{qq}/\Lambda^2 < 0.681$, $-0.842 < c_W/\Lambda^2 < 0.818$, $-8.68 < c_{HW}/\Lambda^2 < 7.60$, $-49.7 < c_{HWB}/\Lambda^2 < 110$, $-20.9 < c_{Hbox}/\Lambda^2 < 22.7$, $-31.4 < c_{HD}/\Lambda^2 < 45.5$, $-69.3 < c^{(1)}_{H\ell}/\Lambda^2 < 68.3$, $-1.59 < c^{(3)}_{H\ell}/\Lambda^2 < 9.94$, $-5.55 < c^{(1)}_{Hq}/\Lambda^2 < 5.60$.

[4] TUMASYAN 22AB study *WZ* production, measuring cross sections and various distributions. Analysing the *WZ* invariant mass distribution, the following 95% C.L. limits are derived in units of TeV^{-2}: $-2.5 < c_W/\Lambda^2 < 0.3$, $-1.0 < c_{WWW}/\Lambda^2 < 1.2$, $-43 < c_b/\Lambda^2 < 113$, $-0.62 < \widetilde{c}_{WWW}/\Lambda^2 < 0.53$, $-32 < \widetilde{c}_W/\Lambda^2 < 32$.

[5] TUMASYAN 22E measure $W\gamma$ production where the *W* boson decays to electrons or muons. Analysing the photon transverse momentum distribution in bins of lepton azimuth, the following 95% C.L. limit is derived in units of TeV^{-2}: $-0.062 < c_{3W}/\Lambda^2 < 0.052$. This limit is derived including the non-SM, SM and their interference effects.

[6] AAD 21AC study the differential cross-section for the electroweak production of dijets in association with a *Z* boson, where the *Z* boson decays to electrons or muons. The number of events selected in the data is 10,870 (12,125) in the electron (muon) channel. Analyzing the distribution of the azimuthal separation of the two jets, the following 95% C.L. limits are derived in units of TeV^{-2}: $-2.7 < c_{WWW}/\Lambda^2 < 5.8$, $-1.6 < \widetilde{c}_{WWW}/\Lambda^2 < 2.0$, $-0.19 < c_W/\Lambda^2 < 0.41$, $-0.11 < \widetilde{c}_W/\Lambda^2 < 0.14$, $-6.31 < c_{HWB}/\Lambda^2 < 1.01$, $0.23 < \widetilde{c}_{HWB}/\Lambda^2 < 2.35$.

[7] AAD 21W analyze W^+W^- production in association with at least one jet. Events with exactly one oppositely-charged electron-muon pair and at least one hadronic jet of transverse momentum larger than 30 GeV (120 GeV) are selected. In the data, 89,239 (5,825) events are found, with a total Standard-Model expectation of 91600 ± 2500 (5980 ± 150). Analyzing the electron-muon invariant mass distribution, the following limit at 95% C.L. is obtained: $-0.33 < c_W/\Lambda^2 < 0.33$ ($-0.60 < c_W/\Lambda^2 < 0.58$), for a fixed choice of $\Lambda = 1$ TeV.

[8] SIRUNYAN 21G measure $W\gamma$ production where the *W* decays into electrons or muons. In the data, 385,224 (395,818) events are selected in the electron (muon) channel, with a total Standard-Model expectation of 396913±54686 (396257±22837) events. Analysing the photon transverse momentum distribution, the following 95% C.L. limits are derived in units of TeV^{-2}: $-0.90 < c_{WWW}/\Lambda^2 < 0.91$, $-40 < c_B/\Lambda^2 < 41$, $-0.45 < c_{\overline{W}WW}/\Lambda^2 < 0.45$, $-20 < c_{\overline{W}}/\Lambda^2 < 20$.

[9] SIRUNYAN 20BA study electroweak production of a *W* boson in association with two jets, using *W* decays in the electron or muon channel. The isolated muons (electrons) are required to have a transverse momentum larger than 25 (30) GeV, while the transverse momentum of the two jets has to be larger than 50 and 30 GeV. A total of 2.382 (1.051) million events are selected in the muon (electron) channel, with a Standard Model expectation of 2.39±0.17 (1.054±0.058) million events. Analysing the transverse momentum distribution of the charged leptons from *W* decay, the following 95% C.L. limits are obtained in units of TeV^{-2}: $-2.3 < c_{WWW}/\Lambda^2 < 2.5$, $-8.8 < c_W/\Lambda^2 < 16$, $-45 < c_B/\Lambda^2 < 46$. Combining these results with those from the closely-related electroweak *Z*-jet-jet production SIRUNYAN 18BZ, the limits become: $-1.8 < c_{WWW}/\Lambda^2 < 2.0$, $-5.8 < c_W/\Lambda^2 < 10$, $-43 < c_B/\Lambda^2 < 45$.

[10] SIRUNYAN 20BF study W^+W^- production with the *W* bosons decaying to electrons or muons. The leading (subleading) lepton is required to have a transverse momentum larger than 25 (20) GeV. Events with a same-flavor di-lepton invariant mass within 15 GeV of the *Z* mass are rejected, as are event with a third lepton of transverse momentum larger than 10 GeV. In the same- (different-) flavor category a total of 9,604 (20,270) events are selected while the number of expected events is 9640 ± 490 (20280 ± 430). Analyzing the different-flavor di-lepton invariant mass distribution, the following 95% C.L. limits are obtained in units of TeV^{-2}: $-1.8 < c_{WWW}/\Lambda^2 < 1.8$, $-3.6 < c_W/\Lambda^2 < 2.8$, $-9.4 < c_B/\Lambda^2 < 8.5$.

[11] AABOUD 19BA study *WW* production in decay modes with an electron and a muon. The charged leptons are each required to have a transverse momentum larger than 27 GeV and rapidity less than 2.5. The electron-muon system is required to have a mass larger than 55 GeV and a transverse momentum larger than 30 GeV. The missing transverse energy must be larger than 20 GeV. Events containing a jet with transverse momentum exceeding 35 GeV and rapidity smaller than 4.5 are rejected. A total of 12,659 events are selected in the data, with an expected background of 4240 ± 477 events. Analysing the transverse momentum spectrum of the leading charged lepton, the following 95% C.L. limits are derived in units of TeV^{-2}: $-3.4 < c_{WWW}/\Lambda^2 < 3.3$, $-7.4 < c_W/\Lambda^2 < 4.1$, $-21 < c_B/\Lambda^2 < 18$, $-1.6 < c_{\overline{W}WW}/\Lambda^2 < 1.6$, $-76 < c_{\overline{W}}/\Lambda^2 < 76$.

[12] SIRUNYAN 19AD study inclusive *WZ* production, with *W* and *Z* decaying to electrons or muons. The leading (subleading) charged lepton candidate from the *Z* boson decay is required to have a transverse momentum larger than 25 GeV (10 GeV). The charged lepton candidate from the *W* boson decay is required to have a transverse momentum larger than 25 GeV. The invariant mass of the two leptons from *Z* decay is required to be within 15 GeV of the *Z* mass, while the invariant mass of the tri-lepton system is required to exceed 100 GeV. A total of 3,831 tri-lepton events are observed, with a fitted SM *WZ* signal of 3166 ± 62 events and a fitted background of 666 ± 45 events.

Int. J. Mod. Phys. A 2026.41. Downloaded from www.worldscientific.com by UNIVERSITY OF CALIFORNIA @ BERKELEY on 09/16/26. Re-use and distribution is strictly not permitted, except for Open Access articles.

The approximated WZ invariant mass distribution is analyzed to set 95% C.L. limits as follows: $-4.1 < c_W/\Lambda^2 < 1.1$, $-2.0 < c_{WWW}/\Lambda^2 < 2.1$, $-100 < c_B/\Lambda^2 < 160$, in units of TeV^{-2}.

[13] SIRUNYAN 19CL study WW and WZ production in lepton + jet events, with one W boson decaying leptonically (electron or muon), and another W or Z boson decaying hadronically, reconstructed as a single massive large-radius jet. In the electron channel 2,456 (2,235) events are selected in the $WW(WZ)$ category, while in the muon channel 3,996 (3572) events are selected in the $WW(WZ)$ category. Analysing the di-boson invariant mass distribution, the following 95% C.L. limits are obtained in units of TeV^{-2}: $-1.58 < c_{WWW}/\Lambda^2 < 1.59$, $-2.00 < c_W/\Lambda^2 < 2.65$, $-8.78 < c_B/\Lambda^2 < 8.54$.

[14] AABOUD 18Q study $pp \to ZZ$ events at $\sqrt{s} = 13$ TeV with $Z \to e^+e^-$ or $Z \to \mu^+\mu^-$. The number of events observed in the $4e$, $2e\,2\mu$, and 4μ channels is 249, 465, and 303 respectively. Analysing the p_T spectrum of the leading Z boson, the following the following 95% C.L. limits are derived in units of TeV^{-4}: $-5.9 < c_{\widetilde{B}W}/\Lambda^4 < 5.9$, $-3.0 < c_{WW}/\Lambda^4 < 3.0$, $-3.3 < c_{BW}/\Lambda^4 < 3.3$, $-2.7 < c_{BB}/\Lambda^4 < 2.8$.

[15] SIRUNYAN 18BZ study $pp \to Z\,jet\,jet$ events at 13 TeV where $Z \to e^+e^-/\mu^+\mu^-$. Isolated electrons and muons are selected with p_T of the leading/sub-leading lepton > 30/20 GeV and $|\eta| < 2.4$, with the di-lepton invariant mass within 15 GeV of the Z mass. The two highest p_T jets are selected with p_T of the leading/sub-leading jet > 50/30 GeV respectively and dijet invariant mass > 200 GeV. Templates in the transverse momentum of the Z are utilized to set limits on the triple gauge couplings in the EFT and the LEP parametrizations. The following 95% C.L. limits are obtained in units of TeV^{-2}: $-2.6 < c_{WWW}/\Lambda^2 < 2.6$ and $-8.4 < c_W/\Lambda^2 < 10.1$.

[16] AABOUD 17S analyze electroweak production of a W boson in association with two jets at high dijet invariant mass, with the W boson decaying to electron or muon plus neutrino. In the signal region of dijet mass larger than 1 TeV and leading-jet transverse momentum larger than 600 GeV, 30 events are observed in the data with 39 ± 4 events expected in the Standard Model, yielding the following limits at 95% CL for the form factor cut-off scale $\Lambda_{FF} \to \infty$: $-33 < c_W/\Lambda^2 < 30$, $-170 < c_B/\Lambda^2 < 160$, $-13 < c_{WWW}/\Lambda^2 < 9$, $-580 < c_{\widetilde{W}}/\Lambda^2 < 580$, $-11 < c_{\widetilde{W}WW}/\Lambda^2 < 11$, in units of TeV^{-2}.

[17] AABOUD 17U analyze production of WW or WZ boson pairs with one W boson decaying to electron or muon plus neutrino, and the other W or Z boson decaying hadronically. The hadronic decay system is reconstructed as either a resolved two-jet system or as a single large jet. Analysing the transverse momentum distribution of the hadronic system above 100 GeV yields the following limits at 95% CL for the form factor cut-off scale $\Lambda_{FF} \to \infty$: $-3.1 < c_{WWW}/\Lambda^2 < 3.1$, $-19 < c_B/\Lambda^2 < 20$, $-5.1 < c_W/\Lambda^2 < 5.8$, in units of TeV^{-2}.

[18] KHACHATRYAN 17O analyse WZ production where each boson decays into electrons or muons. Events are required to have a tri-lepton invariant mass larger than 100 GeV, with one of the lepton pairs having an invariant mass within 20 GeV of the Z boson mass. The Z transverse momentum spectrum is analyzed to set 95% C.L. limits of: $-260 < c_B/\Lambda^2 < 210$, $-4.2 < c_W/\Lambda^2 < 8.0$, $-4.6 < c_{WWW}/\Lambda^2 < 4.2$, in units of TeV^{-2}.

[19] SIRUNYAN 17X study $pp \to WW/WZ \to \ell\nu q\bar{q}$ production at 8 TeV where ℓ is an electron or muon with $p_T > 30$ or 25 GeV respectively. Suitable cuts are put on the p_T of the dijet system and the missing E_T of the event yielding a total of 285 and 204 WV events observed in the electron and muon channels. The following 95% C.L. limits in units of TeV^{-2} are obtained: $-2.7 < c_{WWW}/\Lambda^2 < 2.7$, $-14 < c_B/\Lambda^2 < 17$, $-2.0 < c_W/\Lambda^2 < 5.7$.

[20] AAD 16AR study WW production in pp collisions and select 6636 WW candidates in decay modes with electrons or muons with an expected background of 1546 ± 157 events. Assuming an EFT formulation, a fit to the transverse momentum distribution of the leading charged lepton, leads to 95% C.L. ranges of: $-4.61 < c_{WWW}/\Lambda^2 < 4.60$, $-5.87 < c_W/\Lambda^2 < 10.54$ and $-20.9 < c_B/\Lambda^2 < 26.3$,in units of TeV^{-2}.

[21] AAD 16P study WZ production in pp collisions and select 2091 WZ candidates in 4 decay modes with electrons and muons, with an expected background of 1825 ± 7 events. Analyzing the WZ transverse momentum distribution, the resulting 95% C.L. limits are: $-3.9 < c_{WWW}/\Lambda^2 < 4.0$, $-4.3 < c_W/\Lambda^2 < 6.8$, and $-320 < c_B/\Lambda^2 < 210$, in units of TeV^{-2}.

[22] KHACHATRYAN 16BI determine the W^+W^- production cross section using unlike sign di-lepton (e or μ) events with high p_T. The leptons have $p_T > 20$ GeV/c and are isolated. Events are required to have no jets above p_T of 30 GeV/c. 4847 (2233) events are selected with different (same) flavor leptons, with an expected total background of 1179 ± 123 (643 ± 73) events. Analysing the di-lepton invariant mass spectrum, the following values are obtained: $c_{WWW}/\Lambda^2 = 0.1 \pm 3.2$, $c_W/\Lambda^2 = -3.6^{+5.0}_{-4.5}$ and $c_B/\Lambda^2 = -3.2^{+15.0}_{-14.5}$, in units of TeV^{-2}. The limits at 95% C.L. are: $-5.7 < c_{WWW}/\Lambda^2 < 5.9$, $-11.4 < c_W/\Lambda^2 < 5.4$ and $-29.2 < c_B/\Lambda^2 < 23.9$, in units of TeV^{-2}.

ANOMALOUS *W/Z* QUARTIC COUPLINGS

Revised March 2024 by M.W. Grünewald (U. College Dublin) and A. Gurtu (CERN; TIFR Mumbay).

Quartic couplings, $WWZZ$, $WWZ\gamma$, $WW\gamma\gamma$, and $ZZ\gamma\gamma$, were studied at LEP and Tevatron at energies at which the Standard Model predicts negligible contributions to multiboson production. Thus, to parametrize limits on these couplings, an effective theory approach is adopted which supplements the Standard Model Lagrangian with higher dimensional operators which include quartic couplings. The LEP collaborations chose the lowest dimensional representation of operators (dimension 6) which presumes the SU(2)×U(1) gauge symmetry is broken by means other than the conventional Higgs scalar doublet [1–3]. In this representation possible quartic couplings, a_0, a_c, a_n, are expressed in terms of the following dimension-6 operators [1,2];

$$L_6^0 = -\frac{e^2}{16\Lambda^2}\, a_0\, F^{\mu\nu}\, F_{\mu\nu}\vec{W}^{\alpha}\cdot\vec{W}_{\alpha}$$
$$L_6^c = -\frac{e^2}{16\Lambda^2}\, a_c\, F^{\mu\alpha}\, F_{\mu\beta}\vec{W}^{\beta}\cdot\vec{W}_{\alpha}$$
$$L_6^n = -i\frac{e^2}{16\Lambda^2}\, a_n\epsilon_{ijk}\, W^{(i)}_{\mu\alpha}\, W^{(j)}_{\nu}\, W^{(k)\alpha}F^{\mu\nu}$$
$$\widetilde{L}_6^0 = -\frac{e^2}{16\Lambda^2}\, \widetilde{a}_0\, F^{\mu\nu}\, \widetilde{F}_{\mu\nu}\vec{W}^{\alpha}\cdot\vec{W}_{\alpha}$$
$$\widetilde{L}_6^n = -i\frac{e^2}{16\Lambda^2}\, \widetilde{a}_n\epsilon_{ijk}\, W^{(i)}_{\mu\alpha}\, W^{(j)}_{\nu}\, W^{(k)\alpha}\widetilde{F}^{\mu\nu}$$

where F, W are photon and W fields, L_6^0 and L_6^c conserve C, P separately ($\widetilde{L}_6^0$ conserves only C) and generate anomalous $W^+W^-\gamma\gamma$ and $ZZ\gamma\gamma$ couplings, L_6^n violates CP ($\widetilde{L}_6^n$ violates both C and P) and generates an anomalous $W^+W^-Z\gamma$ coupling, and Λ is an energy scale for new physics. For the $ZZ\gamma\gamma$ coupling the CP-violating term represented by L_6^n does not contribute. These couplings are assumed to be real and to vanish at tree level in the Standard Model.

Within the same framework as above, a more recent description of the quartic couplings [3] treats the anomalous parts of the $WW\gamma\gamma$ and $ZZ\gamma\gamma$ couplings separately, leading to two sets parametrized as a_0^V/Λ^2 and a_c^V/Λ^2, where $V = W$ or Z.

With the discovery of a Higgs at the LHC in 2012, it is then useful to go to the next higher dimensional representation (dimension 8 operators) in which the gauge symmetry is broken by the conventional Higgs scalar doublet [3,4]. There are 14 operators which can contribute to the anomalous quartic coupling signal. Some of the operators have analogues in the dimension 6 scheme. The CMS collaboration, [5], have used this parametrization, in which the connections between the two schemes are also summarized:

$$\begin{aligned}\mathcal{L}_{AQGC} = &-\frac{e^2}{8}\frac{a_0^W}{\Lambda^2}F_{\mu\nu}F^{\mu\nu}W^{+a}W_a^- \\ &-\frac{e^2}{16}\frac{a_c^W}{\Lambda^2}F_{\mu\nu}F^{\mu a}(W^{+\nu}W_a^- + W^{-\nu}W_a^+) \\ &-e^2g^2\frac{\kappa_0^W}{\Lambda^2}F_{\mu\nu}Z^{\mu\nu}W^{+a}W_a^- \\ &-\frac{e^2g^2}{2}\frac{\kappa_c^W}{\Lambda^2}F_{\mu\nu}Z^{\mu a}(W^{+\nu}W_a^- + W^{-\nu}W_a^+) \\ &+\frac{f_{T,0}}{\Lambda^4}Tr[\widehat{W}_{\mu\nu}\widehat{W}^{\mu\nu}]\times Tr[\widehat{W}_{\alpha\beta}\widehat{W}^{\alpha\beta}]\end{aligned}$$

The energy scale of possible new physics is Λ, and $g = e/sin(\theta_W)$, e being the unit electric charge and θ_W the Weinberg angle. The field tensors are described in [3,4].

The two dimension 6 operators a_0^W/Λ^2 and a_c^W/Λ^2 are associated with the $WW\gamma\gamma$ vertex. Among dimension 8 operators, κ_0^W/Λ^2 and κ_c^W/Λ^2 are associated with the $WWZ\gamma$ vertex, whereas the parameter $f_{T,0}/\Lambda^4$ contributes to both vertices. There is a relationship between these two dimension 6 parameters and the dimension 8 parameters $f_{M,i}/\Lambda^4$ as follows [3]:

$$\frac{a_0^W}{\Lambda^2} = -\frac{4M_W^2}{g^2}\frac{f_{M,0}}{\Lambda^4} - \frac{8M_W^2}{g'^2}\frac{f_{M,2}}{\Lambda^4}$$

$$\frac{a_c^W}{\Lambda^2} = -\frac{4M_W^2}{g^2}\frac{f_{M,1}}{\Lambda^4} - \frac{8M_W^2}{g'^2}\frac{f_{M,3}}{\Lambda^4}$$

where $g' = e/cos(\theta_W)$ and M_W is the invariant mass of the W boson. This relation provides a translation between limits on dimension 6 operators $a_{0,c}^W$ and $f_{M,j}/\Lambda^4$. It is further required [4] that $f_{M,0} = 2f_{M,2}$ and $f_{M,1} = 2f_{M,3}$ which suppresses contributions to the $WWZ\gamma$ vertex. The complete set of Lagrangian contributions as presented in [4] corresponds to 19 anomalous couplings in total – $f_{S,i},\ i = 1, 2,\ f_{M,i},\ i = 0, \ldots, 8$ and $f_{T,i}, i = 0, \ldots, 9$ – each scaled by $1/\Lambda^4$.

Another approach to couplings is the so called K-matrix framework [7], in which the anomalous couplings can be expressed in terms of two parameters α_4 and α_5, which account for all BSM effects.

The LHC collaborations have published couplings results based on various theoretical frameworks. It is hoped that the collaborations will agree to use at least one common set of parameters to express these limits to enable the reader to make a comparison, and to allow for a possible LHC combination.

References

1. G. Belanger and F. Boudjema, Phys. Lett. **B288**, 201 (1992).
2. J.W. Stirling and A. Werthenbach, Eur. Phys. J. **C14**, 103 (2000);
   J.W. Stirling and A. Werthenbach, Phys. Lett. **B466**, 369 (1999);
   A. Denner *et al.*, Eur. Phys. J. **C20**, 201 (2001);
   G. Montagna *et al.*, Phys. Lett. **B515**, 197 (2001).
3. G. Belanger *et al.*, Eur. Phys. J. **C13**, 283 (2000).
4. O.J.P. Éboli, M.C. Gonzalez-Garcia, and S.M. Lietti, Phys. Rev. **D69**, 095005 (2004);
   O.J.P. Éboli, M.C. Gonzalez-Garcia, and J.K. Mizukoshi, Phys. Rev. **D77**, 073005 (2006).
5. S. Chatrchyan *et al.*, Phys. Rev. **D90**, 032008 (2014);
   S. Chatrchyan *et al.*, Phys. Rev. Lett. **114**, 051801 (2015).
6. G. Aad *et al.*, Phys. Rev. Lett. **113**, 141803 (2014).
7. A. Albateanu, W. Killian, and J. Reuter, JHEP **0811**, 010 (2008).

a_0/Λ^2, a_c/Λ^2, a_n/Λ^2, κ_0^W/Λ^2, κ_c^W/Λ^2, $f_{T,0}/\Lambda^4$, $f_{M,i}/\Lambda^4$, α_4, α_5, $F_{S,i}/\Lambda^4$, $F_{M,i}/\Lambda^4$, $F_{T,i}/\Lambda^4$

Anomalous W quartic couplings are measured by the experiments at LEP, the Tevatron, and the LHC. Some of the recent results from the Tevatron and LHC experiments individually surpass the combined LEP-2 results in precision (see below). As discussed in the review on the "Anomalous W/Z quartic couplings (QGCS)," the measurements are typically done using different operator expansions which then do not allow the results to be compared and averaged. At least one common framework should be agreed upon for the use in the future publications by the experiments.

Some publications from LHC experiments derive limits for various assumed values of the form-factor cutoff Λ_{FF}. The values quoted below are for $\Lambda_{FF} \rightarrow \infty$.

VALUE	DOCUMENT ID		TECN	COMMENT
• • • We do not use the following data for averages, fits, limits, etc. • • •				
	[1] AAD	25G	ATLS	E_{cm}^{pp} = 13 TeV
	[2] CHEKHOVSKY	25	CMS	E_{cm}^{pp} = 13 TeV
	[3] HAYRAPETY...	25AM	CMS	E_{cm}^{pp} = 13 TeV
	[4] AAD	24AD	ATLS	E_{cm}^{pp} = 13 TeV
	[5] AAD	24AM	ATLS	E_{cm}^{pp} = 13 TeV
	[6] AAD	24C	ATLS	E_{cm}^{pp} = 13 TeV
	[7] AAD	24CH	ATLS	E_{cm}^{pp} = 13 TeV
	[8] AAD	23BH	ATLS	E_{cm}^{pp} = 13 TeV
	[9] AAD	23K	ATLS	E_{cm}^{pp} = 13 TeV
	[10] TUMASYAN	23AK	CMS	E_{cm}^{pp} = 13 TeV
	[11] TUMASYAN	23AM	CMS	E_{cm}^{pp} = 13 TeV
	[12] SIRUNYAN	21	CMS	E_{cm}^{pp} = 13 TeV
	[13] TUMASYAN	21A	CMS	E_{cm}^{pp} = 13 TeV
	[14] TUMASYAN	21B	CMS	E_{cm}^{pp} = 13 TeV
	[15] SIRUNAYN	20	CMS	E_{cm}^{pp} = 13 TeV
	[16] SIRUNYAN	20AL	CMS	E_{cm}^{pp} = 13 TeV
	[17] SIRUNYAN	20BD	CMS	E_{cm}^{pp} = 13 TeV
	[18] SIRUNYAN	19BM	CMS	E_{cm}^{pp} = 13 TeV
	[19] SIRUNYAN	19BP	CMS	E_{cm}^{pp} = 13 TeV
	[20] SIRUNYAN	19CQ	CMS	E_{cm}^{pp} = 13 TeV
	[21] SIRUNYAN	18CC	CMS	E_{cm}^{pp} = 13 TeV
	[22] AABOUD	17AA	ATLS	E_{cm}^{pp} = 8 TeV
	[23] AABOUD	17AG	ATLS	E_{cm}^{pp} = 8 TeV
	[24] AABOUD	17D	ATLS	E_{cm}^{pp} = 8 TeV
	[25] AABOUD	17J	ATLS	E_{cm}^{pp} = 8 TeV
	[26] AABOUD	17M	ATLS	E_{cm}^{pp} = 8 TeV
	[27] KHACHATRY...	17AA	CMS	E_{cm}^{pp} = 8 TeV
	[28] KHACHATRY...	17M	CMS	E_{cm}^{pp} = 8 TeV
	[29] SIRUNYAN	17AD	CMS	E_{cm}^{pp} = 13 TeV
	[30] SIRUNYAN	17AR	CMS	E_{cm}^{pp} = 8 TeV
	[31] AABOUD	16E	ATLS	E_{cm}^{pp} = 8 TeV
	[32] AAD	16Q	ATLS	E_{cm}^{pp} = 8 TeV
	[33] KHACHATRY...	16AX	CMS	E_{cm}^{pp} = 8 TeV
	[34] AAD	15N	ATLS	E_{cm}^{pp} = 8 TeV
	[35] KHACHATRY...	15D	CMS	E_{cm}^{pp} = 8 TeV
	[36] AAD	14AM	ATLS	
	[37] CHATRCHYAN	14Q	CMS	
	[38] ABAZOV	13D	D0	
	[39] CHATRCHYAN	13AA	CMS	
	[40] ABBIENDI	04B	OPAL	
	[41] ABBIENDI	04L	OPAL	
	[42] HEISTER	04A	ALEP	
	[43] ABDALLAH	03I	DLPH	
	[44] ACHARD	02F	L3	

[1] AAD 25G analyse the production of three massive vector bosons VVZ ($V = W,\ Z$) using their decay modes into electrons or muons. Analysing the rates in terms of EFT couplings, the following 95% C.L. limits are set: $-19 < f_{M,2}/\Lambda^4 < 19$, $-28 < f_{M,3}/\Lambda^4 < 29$, $-12 < f_{M,4}/\Lambda^4 < 12$, $-9.1 < f_{M,5}/\Lambda^4 < 9.3$, in units of TeV^{-4}.

[2] CHEKHOVSKY 25 measure $WZ\gamma$ tri-boson producion where both W and Z decay to electrons or muons. 108 events are observed in the signal region whereas 109 $\pm$ 5 are predicted. The observed cross section is 5.48 $\pm$ 1.11 fb, compatible with the SM prediction. Analysing the $\ell\ell\ell\gamma$ invariant mass distribution, the following 95% C.L. limits are set: $-2.60 < f_{T,0}/\Lambda^4 < 2.60$, $-3.28 < f_{T,1}/\Lambda^4 < 3.24$, $-7.15 < f_{T,2}/\Lambda^4 < 7.05$, $-2.54 < f_{T,5}/\Lambda^4 < 2.56$, $-3.18 < f_{T,6}/\Lambda^4 < 3.22$, $-6.85 < f_{T,7}/\Lambda^4 < 7.05$, in units of TeV^{-4}.

[3] HAYRAPETYAN 25AM study same-sign WW production, with one W boson decaying into electrons or muons and the other W boson decaying into a tau lepton, in association with at least two jets with large invariant mass and rapidity difference. Multivariate classifiers are used to extract the following 95% C.L. limits in units of TeV^{-4}: $-1.32 < f_{T,0}/\Lambda^4 < 1.38$, $-0.552 < f_{T,1}/\Lambda^4 < 0.613$, $-1.51 < f_{T,2}/\Lambda^4 < 1.76$, $-13.1 < f_{M,0}/\Lambda^4 < 12.8$, $-16.4 < f_{M,1}/\Lambda^4 < 17.7$, $-27.6 < f_{M,7}/\Lambda^4 < 25.8$, $-15.9 < f_{S,0}/\Lambda^4 < 16.1$, $-60.9 < f_{S,1}/\Lambda^4 < 61.8$, $-60.9 < f_{S,2}/\Lambda^4 < 61.8$.

[4] AAD 24AD tag same-sign WW production, with the W bosons decaying into electrons or muons, in association with at least two jets with large invariant mass and rapidity difference. The di-lepton invariant mass distribution is used to extract the following 95% C.L. limits: $-4.1 < f_{M,0}/\Lambda^4 < 4.1$, $-6.8 < f_{M,1}/\Lambda^4 < 7.0$, $-9.8 < f_{M,7}/\Lambda^4 < 9.5$, $-5.9 < f_{S02}/\Lambda^4 < 5.9$, $-23.5 < f_{S,1}/\Lambda^4 < 23.6$, $-0.36 < f_{T,0}/\Lambda^4 < 0.36$, $-0.174 < f_{T,1}/\Lambda^4 < 0.186$, $-0.63 < f_{T,2}/\Lambda^4 < 0.74$, in units of TeV^{-4}.

[5] AAD 24AM tag WZ production, with the bosons decaying into electrons or muons, in association with two jets. The transverse mass of the WZ system is used to extract the following 95% C.L. limits: $-0.57 < f_{T,0}/\Lambda^4 < 0.56$, $-0.39 < f_{T,1}/\Lambda^4 < 0.35$, $-1.2 < f_{T,2}/\Lambda^4 < 1.0$, $-5.8 < f_{M,0}/\Lambda^4 < 5.6$, $-8.6 < f_{M,1}/\Lambda^4 < 8.5$, $-11.3 < f_{M,7}/\Lambda^4 < 11.3$, $-10.4 < f_{S02}/\Lambda^4 < 10.4$, $-30 < f_{S,1}/\Lambda^4 < 30$, in units of TeV^{-4}.

[6] AAD 24C study the production of four charged leptons (electrons or muons) in association with two jets. Analysing the 4-lepton invariant mass distribution and the di-jet invarinat mass distribution leads to the following 95% C.L. limits: $-0.98 < f_{T,0}/\Lambda^4 < 0.93$, $-1.2 < f_{T,1}/\Lambda^4 < 1.2$, $-2.5 < f_{T,2}/\Lambda^4 < 2.4$, $-2.5 < f_{T,5}/\Lambda^4 < 2.4$, $-3.9 < f_{T,6}/\Lambda^4 < 3.9$, $-8.5 < f_{T,7}/\Lambda^4 < 8.1$, $-2.1 < f_{T,8}/\Lambda^4 < 2.1$, $-4.5 < f_{T,9}/\Lambda^4 < 4.5$, in units of TeV^{-4}. The article also reports limits on these couplings by cutting the EFT expansion at various values of the cut-off scale.

Int. J. Mod. Phys. A 2026.41. Downloaded from www.worldscientific.com
by UNIVERSITY OF CALIFORNIA @ BERKELEY on 09/16/26. Reproduction is strictly not permitted, except for Open Access articles.

Int. J. Mod. Phys. A 2026.41. Downloaded from www.worldscientific.com
by UNIVERSITY OF CALIFORNIA @ BERKELEY on 09/16/26. Re-use and distribution is strictly not permitted, except for Open Access articles.

[7] AAD 24CH study electroweak $W\gamma$ production in association with two jets. The distribution of the transverse momentum of the two-jet system or of the lepton is analysed to set the following 95% C.L. limits: $-1.8 < f_{T,0}/\Lambda^4 < 1.8$, $-1.1 < f_{T,1}/\Lambda^4 < 1.2$, $-3.1 < f_{T,2}/\Lambda^4 < 3.5$, $-2.4 < f_{T,3}/\Lambda^4 < 2.6$, $-2.2 < f_{T,4}/\Lambda^4 < 2.2$, $-1.2 < f_{T,5}/\Lambda^4 < 1.3$, $-1.0 < f_{T,6}/\Lambda^4 < 1.1$, $-2.7 < f_{T,7}/\Lambda^4 < 2.8$, $-24 < f_{M,0}/\Lambda^4 < 24$, $-37 < f_{M,1}/\Lambda^4 < 38$, $-8.6 < f_{M,2}/\Lambda^4 < 8.5$, $-13 < f_{M,3}/\Lambda^4 < 14$, $-15 < f_{M,4}/\Lambda^4 < 15$, $-14 < f_{M,5}/\Lambda^4 < 12$, $-66 < f_{M,7}/\Lambda^4 < 65$, in units of TeV^{-4}.

[8] AAD 23BH study $pp \to Z\gamma\gamma$ events with the Z boson decaying to electron or muon pairs. The number of observed data events is 148 for the electron mode and 171 for the muon mode. The respective number of (data-background) events is 105.5 ± 12.2(stat)±8.1(syst) and 120.4 ± 13.1(stat)±9.4(syst). The corresponding number of predicted signal events is 91.5 ± 0.9 and 119.5 ± 1.0 using SHERPA (NLO), and 91.0 ± 1.0 and 118.1 ± 1.2 using MADGRAPH 5 AMC (NLO), where the error is statistical only. Analysing the transverse momentum distribution of the dilepton system, the following 95% C.L. limits are derived: $-9.87 < f_{T,0}/\Lambda^4 < 9.33$, $-9.88 < f_{T,1}/\Lambda^4 < 9.34$, $-20.31 < f_{T,2}/\Lambda^4 < 18.68$, $-4.64 < f_{T,5}/\Lambda^4 < 4.54$, $-7.04 < f_{T,6}/\Lambda^4 < 6.94$, $-15.55 < f_{T,7}/\Lambda^4 < 15.04$, $-1.64 < f_{T,8}/\Lambda^4 < 1.61$, $-3.26 < f_{T,9}/\Lambda^4 < 3.26$, in units of TeV^{-4}.

[9] AAD 23K measure Z production in association with a photon and two jets in proton-proton collisions at 13 TeV CM energy, where the Z boson decays into neutrinos. Within a sensitive fiducial phase-space region, 356 signal events are selected, with an expectation of 357 ± 30. Analysing the photon transverse energy distribution, the following 95% C.L. limits are derived in units of TeV^{-4}: $-0.094 < f_{T,0}/\Lambda^4 < 0.084$, $-0.088 < f_{T,5}/\Lambda^4 < 0.099$, $-0.059 < f_{T,8}/\Lambda^4 < 0.059$, $-0.13 < f_{T,9}/\Lambda^4 < 0.13$, $-4.6 < f_{M,0}/\Lambda^4 < 4.6$, $-7.7 < f_{M,1}/\Lambda^4 < 7.7$, $-1.9 < f_{M,2}/\Lambda^4 < 1.9$.

[10] TUMASYAN 23AK study electroweak $W\gamma$ production in association with 2 jets. The events selected for the couplings analysis are required to have a dijet invariant mass in excess of 800 GeV, jet-jet separation of at least 2.5 in rapidity, invariant mass of the $W\gamma$ system larger than 150 GeV and transverse photon momentum larger than 100 GeV. Analysing the $W\gamma$ invariant mass distribution, varying one coupling at a time while fixing the others to their Standard Model value, leads to the following 95% C.L. limits: $-5.6 < f_{M,0}/\Lambda^4 < 5.5$, $-7.8 < f_{M,1}/\Lambda^4 < 8.1$, $-1.9 < f_{M,2}/\Lambda^4 < 1.9$, $-2.7 < f_{M,3}/\Lambda^4 < 2.7$, $-3.7 < f_{M,4}/\Lambda^4 < 3.6$, $-3.9 < f_{M,5}/\Lambda^4 < 3.9$, $-14 < f_{M,7}/\Lambda^4 < 14$, $-0.47 < f_{T,0}/\Lambda^4 < 0.51$, $-0.31 < f_{T,1}/\Lambda^4 < 0.34$, $-0.85 < f_{T,2}/\Lambda^4 < 1.0$, $-0.31 < f_{T,5}/\Lambda^4 < 0.33$, $-0.25 < f_{T,6}/\Lambda^4 < 0.27$, $-0.67 < f_{T,7}/\Lambda^4 < 0.73$, in units of TeV^{-4}.

[11] TUMASYAN 23AM use the combined CMS-TOTEM detector system to study exclusive $\gamma\gamma \to WW$ and $\gamma\gamma \to ZZ$ production in pp collisions at 13 TeV. The W and Z are identified through their hadronic decays with the added requirements of the invariant mass of the di-boson pair to be larger than 1 TeV, and the relative beam proton momentum loss between 0.04 and 0.20. The following limits are obtained at 95% C.L.: (i) on the dimension-6 (LEP like) couplings, in units of GeV^{-2}: $|a_0^W/\Lambda^2| < 4.3 \times 10^{-6}$, $|a_C^W/\Lambda^2| < 1.6 \times 10^{-5}$, $|a_0^Z/\Lambda^2| < 0.9 \times 10^{-5}$, $|a_C^Z/\Lambda^2| < 4.0 \times 10^{-5}$. (ii) on the dimension-8 operators, in units of TeV^{-4}: $|f_{M,0}/\Lambda^4| < 66.0$, $|f_{M,1}/\Lambda^4| < 245.5$, $|f_{M,2}/\Lambda^4| < 9.8$, $|f_{M,3}/\Lambda^4| < 73.0$, $|f_{M,4}/\Lambda^4| < 36.0$, $|f_{M,5}/\Lambda^4| < 67.0$, $|f_{M,7}/\Lambda^4| < 490.9$.

[12] SIRUNYAN 21 study electroweak Z-pair production in association with two jets, with the Z bosons decaying to oppositely-charged electron or muon pairs. Leptons with high transverse momentum are selected, with the di-lepton invariant mass of the two Z boson candidates between 60 GeV and 120 GeV, and the four-lepton invariant mass larger than 180 GeV. A total of 365 events are selected in the data, while the number of expected events is 370 ± 48. Analyzing the four-lepton invariant mass distribution, the following 95% C.L. limits are derived: $-0.24 < f_{T,0}/\Lambda^4 < 0.22$, $-0.31 < f_{T,1}/\Lambda^4 < 0.31$, $-0.63 < f_{T,2}/\Lambda^4 < 0.59$, $-0.43 < f_{T,8}/\Lambda^4 < 0.43$, $-0.92 < f_{T,9}/\Lambda^4 < 0.92$, in units of TeV^{-4}.

[13] TUMASYAN 21A study electroweak $Z\gamma$ production in association with two jets, where the Z boson decays to electron or muon pairs and the pair of two jets has high invariant mass, superseeding SIRUNYAN 20AL. The number of observed (expected) electron events in the barrel and endcap regions are 375 (349 ± 9) and 174 (166 ± 6) events, respectively, while for muon events the respective numbers are 584 (612 ± 13) and 320 (303 ± 8). Analysing the $Z\gamma$ invariant mass distribution, the following 95% C.L. limits are derived: $-15.8 < f_{M,0}/\Lambda^4 < 16.0$, $-35.0 < f_{M,1}/\Lambda^4 < 34.7$, $-6.55 < f_{M,2}/\Lambda^4 < 6.49$, $-13.0 < f_{M,3}/\Lambda^4 < 13.0$, $-13.0 < f_{M,4}/\Lambda^4 < 12.7$, $-22.2 < f_{M,5}/\Lambda^4 < 21.3$, $-56.6 < f_{M,7}/\Lambda^4 < 55.9$, $-0.64 < f_{T,0}/\Lambda^4 < 0.57$, $-0.81 < f_{T,1}/\Lambda^4 < 0.90$, $-1.68 < f_{T,2}/\Lambda^4 < 1.54$, $-0.58 < f_{T,5}/\Lambda^4 < 0.64$, $-1.30 < f_{T,6}/\Lambda^4 < 1.33$, $-2.15 < f_{T,7}/\Lambda^4 < 2.43$, $-0.47 < f_{T,8}/\Lambda^4 < 0.47$, $-0.91 < f_{T,9}/\Lambda^4 < 0.91$, in units of TeV^{-4}.

[14] TUMASYAN 21B measure W or Z boson production in association with two photons, using the leptonic decays modes of W and Z with electrons or muons. The number of selected $W \to e(\mu)\nu$ events is 1987 (2384) and the number of selected $Z \to ee(\mu\mu)$ events is 110 (272) respectively. Analyzing the transverse momentum of the di-photon system, the following 95 % C.L. limits are derived in units of TeV^{-4}: In the W production channel, the observed limits are: $-39.9 < f_{M,2}/\Lambda^4 < 39.5$, $-63.8 < f_{M,3}/\Lambda^4 < 65.0$, $-1.30 < f_{T,0}/\Lambda^4 < 1.30$, $-1.70 < f_{T,1}/\Lambda^4 < 1.66$, $-3.64 < f_{T,2}/\Lambda^4 < 3.64$, $-0.52 < f_{T,5}/\Lambda^4 < 0.60$, $-0.60 < f_{T,6}/\Lambda^4 < 0.68$, $-1.16 < f_{T,7}/\Lambda^4 < 1.16$. In the Z production channel, the observed limits are: $-5.70 < f_{T,0}/\Lambda^4 < 5.46$, $-5.70 < f_{T,1}/\Lambda^4 < 5.46$, $-11.4 < f_{T,2}/\Lambda^4 < 10.9$, $-2.92 < f_{T,5}/\Lambda^4 < 2.92$, $-3.80 < f_{T,6}/\Lambda^4 < 3.88$, $-7.88 < f_{T,7}/\Lambda^4 < 7.72$, $-1.06 < f_{T,8}/\Lambda^4 < 1.10$, $-1.82 < f_{T,9}/\Lambda^4 < 1.82$, in units of TeV^{-4}.

[15] SIRUNAYN 20 study WZ and same-sign WW production in association with two jets, using the leptonic decays modes of the W and Z bosons with electrons or muons. Overall, 524 WW events and 229 WZ events are selected, with a Standard Model expectation of 535 ± 52 and 216 ± 21 events, respectively. Analyzing the transverse mass spectrum of the di-boson system and the di-jet invariant mass, the following 95% C.L. limits are derived, not using any unitarization procedure: $-0.25 < f_{T,0}/\Lambda^4 < 0.28$, $-0.12 < f_{T,1}/\Lambda^4 < 0.14$, $-0.35 < f_{T,2}/\Lambda^4 < 0.48$, $-2.7 < f_{M,0}/\Lambda^4 < 2.9$, $-4.1 < f_{M,1}/\Lambda^4 < 4.2$, $-5.4 < f_{M,6}/\Lambda^4 < 5.8$, $-5.7 < f_{M,7}/\Lambda^4 < 6.0$, $-5.7 < f_{S,0}/\Lambda^4 < 6.1$, $-16 < f_{S,1}/\Lambda^4 < 17$, in units of TeV^{-4}. The article also reports limits on these couplings by cutting the EFT expansion at the unitarity limit.

[16] SIRUNYAN 20AL study electroweak production of a Z boson and a photon in association with two jets in the electron and muon decay modes of the Z. A signal with a significance of 3.9 standard deviations is observed, compared to a Standard Model expectation of 5.2 standard deviations. Combining with KHACHATRYAN 17AA data at 8 TeV the final observed and expected signal significance is 4.7 and 5.5 standard deviations. Analyzing the Z-photon invariant mass distribution, the following 95% C.L. limits are derived: $-19.5 < f_{M,0}/\Lambda^4 < 20.3$, $-40.5 < f_{M,1}/\Lambda^4 < 39.5$, $-8.22 < f_{M,2}/\Lambda^4 < 8.10$, $-17.7 < f_{M,3}/\Lambda^4 < 17.9$, $-15.3 < f_{M,4}/\Lambda^4 < 15.8$, $-25.1 < f_{M,5}/\Lambda^4 < 24.5$, $-38.9 < f_{M,6}/\Lambda^4 < 40.6$, $-60.3 < f_{M,7}/\Lambda^4 < 62.5$, $-0.74 < f_{T,0}/\Lambda^4 < 0.69$, $-0.98 < f_{T,1}/\Lambda^4 < 0.96$, $-1.97 < f_{T,2}/\Lambda^4 < 1.86$, $-0.70 < f_{T,5}/\Lambda^4 < 0.75$, $-1.64 < f_{T,6}/\Lambda^4 < 1.68$, $-2.59 < f_{T,7}/\Lambda^4 < 2.82$, $-0.47 < f_{T,8}/\Lambda^4 < 0.47$, $-1.27 < f_{T,9}/\Lambda^4 < 1.27$, in units of TeV^{-4}.

[17] SIRUNYAN 20BD study electroweak $W\gamma$ production in association with two jets, where the W boson decays to electron or muon and the two jets have high invariant mass. The number of observed (expected) electron events with the photon in the barrel and endcap regions are 393 (397.1 ± 18.5) and 159 (145.2 ± 10.0) respectively, while for muon events the respective numbers are 565 (537.9 ± 21.4) and 201 (188.2 ± 10.5). Analyzing the $W\gamma$ invariant mass distribution, the following 95% C.L. limits are derived: $-8.1 < f_{M,0}/\Lambda^4 < 8.0$, $-12 < f_{M,1}/\Lambda^4 < 12$, $-2.8 < f_{M,2}/\Lambda^4 < 2.8$, $-4.4 < f_{M,3}/\Lambda^4 < 4.4$, $-5.0 < f_{M,4}/\Lambda^4 < 5.0$, $-8.3 < f_{M,5}/\Lambda^4 < 8.3$, $-16 < f_{M,6}/\Lambda^4 < 16$, $-21 < f_{M,7}/\Lambda^4 < 20$, $-0.6 < f_{T,0}/\Lambda^4 < 0.6$, $-0.4 < f_{T,1}/\Lambda^4 < 0.4$, $-1.0 < f_{T,2}/\Lambda^4 < 1.2$, $-0.5 < f_{T,5}/\Lambda^4 < 0.5$, $-0.4 < f_{T,6}/\Lambda^4 < 0.4$, $-0.9 < f_{T,7}/\Lambda^4 < 0.9$, in units of TeV^{-4}.

[18] SIRUNYAN 19BM search for the final state $W^+W^-W^\pm$ using W decays to electrons or muons. Two event samples are considered, events with three leptons, or events with two oppositely charged leptons accompanied by two jets. In a kinematic region selected to enhance the effect of anomalous couplings, no events are selected in the data, and 95% C.L. upper limits are obtained as follows: $-1.2 < f_{T,0}/\Lambda^4 < 1.2$, $-3.3 < f_{T,1}/\Lambda^4 < 3.3$, $-2.7 < f_{T,2}/\Lambda^4 < 2.6$, in units of TeV^{-4} and without application of a form factor.

[19] SIRUNYAN 19BP study WZ plus 2 jets production, using W and Z decay channels with electrons or muons. In the data, 75 events are selected, with a fitted SM signal of 15.1 ± 1.6 events and a fitted background of 62.4 ± 2.8 events. The transverse mass distribution of the WZ system is analyzed to set the following limits at 95% C.L., in units of TeV^{-4}: $-9.15 < f_{M,0}/\Lambda^4 < 9.15$, $-9.15 < f_{M,1}/\Lambda^4 < 9.45$, $-26.5 < f_{S,0}/\Lambda^4 < 27.5$, $-41.2 < f_{S,1}/\Lambda^4 < 42.8$, $-0.75 < f_{T,0}/\Lambda^4 < 0.81$, $-0.49 < f_{T,1}/\Lambda^4 < 0.55$, $-1.49 < f_{T,2}/\Lambda^4 < 1.85$.

[20] SIRUNYAN 19CQ search for anomalous electroweak production of vector boson pairs in association with two jets. Events are selected by requiring two jets with a large invariant mass and rapidity separation, one or two leptons (electrons or muons), and a W or Z boson decaying hadronically. In the WV (ZV) channel, 347 (47) events are selected in the data, with a total expected background of 352 ± 19 (50.3 ± 5.8) events. Analysing the mass distribution of the WV or ZV system, the following 95% C.L. limits are obtained: $-2.7 < f_{S,0}/\Lambda^4 < 2.7$, $-3.4 < f_{S,1}/\Lambda^4 < 3.4$, $-0.69 < f_{M,0}/\Lambda^4 < 0.70$, $-2.0 < f_{M,1}/\Lambda^4 < 2.1$, $-1.3 < f_{M,6}/\Lambda^4 < 1.3$, $-3.4 < f_{M,7}/\Lambda^4 < 3.4$, $-0.12 < f_{T,0}/\Lambda^4 < 0.11$, $-0.12 < f_{T,1}/\Lambda^4 < 0.13$, $-0.28 < f_{T,2}/\Lambda^4 < 0.28$, in units of TeV^{-4}.

[21] SIRUNYAN 18CC study pp collisions at $\sqrt{s} = 13$ TeV leading to a pair of same-sign W pairs decaying leptonically (e or μ) associated with a pair of jets. Isolated leptons with $p_T > 25$ (20) GeV for the leading (trailing) lepton, with $|\eta| < 2.5$ (2.4) for e (μ) and jets with $p_T > 30$ GeV, $|\eta| < 5.0$, $|\Delta\eta_{jj}| > 2.5$ and $m_{jj} > 500$ GeV is required. Further cuts are applied to minimize $Z \to ee$ events, non-prompt leptons and hadronically decaying taus. The number of selected events is 201, with an expected SM signal of 66.9 ± 2.4 and background of 138 ± 13 events. Analysing the dilepton invariant mass spectrum the following 95% C.L. limits are derived: $-7.7 < f_{S,0}/\Lambda^4 < 7.7$, $-21.6 < f_{S,1}/\Lambda^4 < 21.8$, $-6.0 < f_{M,0}/\Lambda^4 < 5.9$, $-8.7 < f_{M,1}/\Lambda^4 < 9.1$, $-11.9 < f_{M,6}/\Lambda^4 < 11.8$, $-13.3 < f_{M,7}/\Lambda^4 < 12.9$, $-0.62 < f_{T,0}/\Lambda^4 < 0.65$, $-0.28 < f_{T,1}/\Lambda^4 < 0.31$, $-0.89 < f_{T,2}/\Lambda^4 < 1.02$.

[22] AABOUD 17AA analyze $W^\pm W^\pm$ production in association with two jets and W decay modes with electrons or muons. In the kinematic region of VBS the effect of anomalous QGCs is enhanced by requiring the transverse mass of the WW system to be larger than 400 GeV. In the data, 8 events are selected with a total background expected from SM processes of 3.8 ± 0.6 events. Assuming the other QGC coupling to have the SM value of zero, the observed event yield is used to determine 95% CL limits on the QGCs: $-0.14 < \alpha_4 < 0.15$ and $-0.22 < \alpha_5 < 0.22$. Supersedes AAD 14AM.

[23] AABOUD 17AG determine the $WW\gamma$ and $WZ\gamma$ cross sections in 8 TeV pp interactions by studying the final states $e\nu\mu\nu\gamma$ and $e\nu jj\gamma$ or $\mu\nu jj\gamma$. Upper limits on the production cross sections are derived in a fiducial region optimized for BSM physics. These are used to derive the following 95% C.L. upper limits for quartic couplings assuming the form scale factor, $\Lambda_{FF} = \infty$ (all in units of 10^3 TeV^{-4}): $-0.3 < f_{M,0}/\Lambda^4 < 0.3$, $-0.5 < f_{M,1}/\Lambda^4 < 0.5$, $-1.8 < f_{M,2}/\Lambda^4 < 1.8$, $-1.1 < f_{M,4}/\Lambda^4 < 1.1$, $-1.7 < f_{M,5}/\Lambda^4 < 1.7$, $-0.6 < f_{M,6}/\Lambda^4 < 0.6$, $-1.1 < f_{M,7}/\Lambda^4 < 1.1$, $-0.1 < f_{T,0}/\Lambda^4 < 0.1$, $-0.2 < f_{T,1}/\Lambda^4 < 0.2$, $-0.4 < f_{T,4}/\Lambda^4 < 0.4$, $-1.5 < f_{T,5}/\Lambda^4 < 1.6$, $-1.9 < f_{T,6}/\Lambda^4 < 1.9$, $-4.3 < f_{T,7}/\Lambda^4 < 4.3$.

Int. J. Mod. Phys. A 2026.41. Downloaded from www.worldscientific.com
by UNIVERSITY OF CALIFORNIA @ BERKELEY on 09/16/26. Reproduction is strictly not permitted, except for Open Access articles.

[24] AABOUD 17D analyze electroweak diboson (WV, $V = W, Z$) production in association with a high-mass dijet system. In the data, 32 events are selected with an expected total background of 32 $\pm$ 12 events. Analysing the transverse mass distribution of the WV system, the following limits are set at 95% C.L.: $-0.024 < \alpha_4 < 0.030$ and $-0.028 < \alpha_5 < 0.033$.

[25] AABOUD 17J analyze the $Z\gamma$ production in association with a high-mass dijet system, with the Z boson decaying into a pair of electrons, muons, or neutrinos. In the charged lepton (neutrino) channel, events are selected with a dijet mass larger than 500 (600) GeV and a transverse photon energy larger than 250 (150) GeV, with 2 (4) events selected in the data and 0.30 $\pm$ 0.08 (1.6 $\pm$ 0.5) expected background events. The observed event yield is used to determine 95% CL limits as follows: $-4.1 \times 10^3 < f_{T,9}/\Lambda^4 < 4.2 \times 10^3$, $-1.9 \times 10^3 < f_{T,8}/\Lambda^4 < 2.1 \times 10^3$, $-1.9 \times 10^1 < f_{T,0}/\Lambda^4 < 1.6 \times 10^1$, $-1.6 \times 10^2 < f_{M,0}/\Lambda^4 < 1.8 \times 10^2$, $-3.5 \times 10^2 < f_{M,1}/\Lambda^4 < 3.4 \times 10^2$, $-8.9 \times 10^2 < f_{M,2}/\Lambda^4 < 8.9 \times 10^2$, $-1.7 \times 10^3 < f_{M,3}/\Lambda^4 < 1.7 \times 10^3$, in units of TeV^{-4} and without application of a form factor.

[26] AABOUD 17M analyze tri-boson $W^\pm W^\pm W^\mp$ production in decay channels with three charged leptons or two like-sign charged leptons with two jets, where the lepton can be an electron or muon. In the data, 24 tri-lepton events and 21 di-lepton plus jets events are selected, compared to a total event yield expected in the SM of 30.8 $\pm$ 3.0 and 21.9 $\pm$ 2.0, respectively. Analysing the tri-lepton transverse mass or the transverse momentum sum of the two leptons, two jets and the missing transverse energy, the following limits at 95% CL are derived for the form factor cut-off scale $\Lambda_{FF} \to \infty$: $-0.13 < f_{S,0}/\Lambda^4 < 0.18$, $-0.21 < f_{S,1}/\Lambda^4 < 0.27$, in units of 10^4 TeV^{-4}, which are converted into the following limits: $-0.49 < \alpha_4 < 0.75$ and $-0.48 < \alpha_5 < 0.62$.

[27] KHACHATRYAN 17AA analyse electroweak production of $Z\gamma$ in association with two hadronic jets, with the Z boson decaying to electron or muon pairs. Events with photon transverse momentum larger than 60 GeV and di-jet invariant mass larger than 400 GeV are selected. The $Z\gamma$ inavariant mass spectrum is analysed to set 95% C.L. limits as follows: $-71 < f_{M,0}/\Lambda^4 < 75$, $-190 < f_{M,1}/\Lambda^4 < 182$, $-32 < f_{M,2}/\Lambda^4 < 31$, $-58 < f_{M,3}/\Lambda^4 < 59$, $-3.8 < f_{T,0}/\Lambda^4 < 3.4$, $-4.4 < f_{T,1}/\Lambda^4 < 4.4$, $-9.9 < f_{T,2}/\Lambda^4 < 9.0$, $-1.8 < f_{T,8}/\Lambda^4 < 1.8$, $-4.0 < f_{T,9}/\Lambda^4 < 4.0$, in units of TeV^{-4} and without application of a form factor.

[28] KHACHATRYAN 17M analyse electroweak production of $W\gamma$ in association with two hadronic jets, with the W boson decaying to electrons or muons. Events with photon transverse momentum larger than 200 GeV and di-jet invariant mass larger than 200 GeV are selected. The W transverse momentum spectrum is analysed to set 95% C.L. limits as follows: $-77 < f_{M,0}/\Lambda^4 < 74$, $-125 < f_{M,1}/\Lambda^4 < 129$, $-26 < f_{M,2}/\Lambda^4 < 26$, $-43 < f_{M,3}/\Lambda^4 < 44$, $-40 < f_{M,4}/\Lambda^4 < 40$, $-65 < f_{M,5}/\Lambda^4 < 65$, $-129 < f_{M,6}/\Lambda^4 < 129$, $-164 < f_{M,7}/\Lambda^4 < 162$, $-5.4 < f_{T,0}/\Lambda^4 < 5.6$, $-3.7 < f_{T,1}/\Lambda^4 < 4.0$, $-11 < f_{T,2}/\Lambda^4 < 12$, $-3.8 < f_{T,5}/\Lambda^4 < 3.8$, $-2.8 < f_{T,6}/\Lambda^4 < 3.0$, $-7.3 < f_{T,7}/\Lambda^4 < 7.7$, in units of TeV^{-4} and without application of a form factor.

[29] SIRUNYAN 17AD study pp collisions at $\sqrt{s} = 13$ TeV to determine the cross section of $ZZjj$ with the Z decaying to ee or $\mu\mu$. The ZZ mass distribution is used to set upper limits on the anomalous quartic couplings. The 95% upper limits for the relevant quartic couplings in units of TeV^{-4} are: $-0.46 < f_{T,0}/\Lambda^4 < 0.44$, $-0.61 < f_{T,1}/\Lambda^4 < 0.61$, $-1.2 < f_{T,2}/\Lambda^4 < 1.2$, $-0.84 < f_{T,8}/\Lambda^4 < 0.84$, $-1.8 < f_{T,9}/\Lambda^4 < 1.8$.

[30] SIRUNYAN 17AR study pp collisions at $\sqrt{s} = 8$ TeV to determine the cross section of $pp \to W\gamma\gamma$ and $pp \to Z\gamma\gamma$ where $W \to \ell\nu$ and $Z \to \ell^+\ell^-$, ℓ being an electron or a muon. The number of W events in the e and μ channels is 63 and 108 respectively, and the number of Z events in the e and μ channels is 117 and 141. To increase sensitivity, the transverse momentum of the leading photon is required to be larger than 70 GeV. The 95% C.L. upper limits in units of TeV^{-4} are $-701 < f_{M,2}/\Lambda^4 < 683$, $-1170 < f_{M,3}/\Lambda^4 < 1220$, $-33.5 < f_{T,0}/\Lambda^4 < 34.0$, $-44.3 < f_{T,1}/\Lambda^4 < 44.8$, $-93.8 < f_{T,2}/\Lambda^4 < 93.2$.

[31] AABOUD 16E study WW production in two-photon mediated pp collisions at 8 TeV where the W boson decays into an electron or muon, probing the $\gamma\gamma WW$ vertex for anomalous quartic gauge couplings. The lepton p_T is required to be larger than 30 GeV. Limits on anomalous couplings are determined from events with p_T larger than 120 GeV where the aQGC effect is enhanced and the SM background reduced; in the data corresponding to an integrated luminosity of 20.2fb^{-1}, 1 event is selected with an expected SM background of 0.37 $\pm$ 0.13 events. The 95% C.L. limits without a form-factor cutoff ($\Lambda_{\rm cutoff} \to \infty$) are as follows: $-1.7 < a_0^W/\Lambda^2 < 1.7$ and $-6.4 < a_C^W/\Lambda^2 < 6.3$ in units of 10^{-6} GeV^{-2}. In terms of another set of variables: $-6.6 < f_{M,0}/\Lambda^4 < 6.6$ and $-24 < f_{M,1}/\Lambda^4 < 25$ in units of 10^{-11} GeV^{-4}.

[32] AAD 16Q study $Z\gamma\gamma$ production in pp collisions. In events with no additional jets, 29 (22) Z decays to electron (muon) pairs are selected, with an expected background of 3.3 $\pm$ 1.1 (6.5 $\pm$ 2.0) events, as well as 19 Z decays to netrino pairs with an expected background of 8.3 $\pm$ 4.4 events. Analysing the photon transverse momentum distribution for $m_{\gamma\gamma}$ above 200 GeV (300 GeV) for lepton (neutrino) events, yields the 95% C.L. limits: $-1.6 \times 10^4 < f_{M,2}/\Lambda^4 < 1.6 \times 10^4$, $-2.9 \times 10^4 < f_{M,3}/\Lambda^4 < 2.7 \times 10^4$, $-0.86 \times 10^2 < f_{T,0}/\Lambda^4 < 1.03 \times 10^2$, $-0.69 \times 10^3 < f_{T,5}/\Lambda^4 < 0.68 \times 10^3$, $-0.74 \times 10^4 < f_{T,9}/\Lambda^4 < 0.74 \times 10^4$ in units of TeV^{-4} and without application of a form factor $\Lambda_{\rm FF}$.

[33] KHACHATRYAN 16AX searches for anomalous $WW\gamma\gamma$ quartic gauge couplings in the two-photon-mediated process $pp \to ppWW$, assuming the $WW\gamma$ triple gauge boson couplings to be at their Standard Model values. 13 events containing an $e^\pm\mu^\mp$ pair with $p_T(e, \mu) > 30$ GeV are selected in a total luminosity of 19.7 fb^{-1}, with an expected $\gamma\gamma \to WW$ signal of 5.3 $\pm$ 0.1 events and an expected background of 3.9 $\pm$ 0.5 events. When combining with the data collected at 7 TeV (CHATRCHYAN 13AA), and not assuming a form factor, the following 1-parameter limits at 95% C.L. are obtained from the $p_T(e, \mu)$ spectrum: $|a_0^W/\Lambda^2| < 1.1 \times 10^{-6}$ GeV^{-2} ($a_C^W = 0$), and $|a_C^W/\Lambda^2| < 4.1 \times 10^{-6}$ GeV^{-2} ($a_0^W = 0$). In terms of another set of variables: $|f_{M,0}/\Lambda^4| < 4.2 \times 10^{-12}$ GeV^{-4}, $|f_{M,1}/\Lambda^4| < 16 \times 10^{-12}$ GeV^{-4}, $|f_{M,2}/\Lambda^4| < 2.1 \times 10^{-12}$ GeV^{-4}, $|f_{M,3}/\Lambda^4| < 7.8 \times 10^{-12}$ GeV^{-4}.

[34] AAD 15N study $W\gamma\gamma$ events in 8 TeV pp interactions, where the W decays into an electron or a muon. The events are characterized by an isolated lepton, a missing transverse energy due to the decay neutrino, and two isolated photons, with the p_T of the lepton and the photons being > 20 GeV. The number of candidate events observed in the electron channel for N(jet) $\geq$ 0 and N(jet) = 0 is 47 and 15, the corresponding numbers for the muon channel being 110 and 53. The backgrounds expected are 30.2 $\pm$ 7.4, 8.7 $\pm$ 3.0, 52.1 $\pm$ 12.2, and 24.4 $\pm$ 8.3 respectively. The 95% C.L. limits on the values of the parameters $f_{T,0}/\Lambda^4$, $f_{M,2}/\Lambda^4$ and $f_{M,3}/\Lambda^4$ are -0.9–0.9×10^2, -0.8–0.8×10^4, and -1.5–1.4×10^4 respectively, without application of a form factor $\Lambda_{\rm FF}$.

[35] KHACHATRYAN 15D study vector-boson-scattering tagged by two jets, requiring two same-sign charged leptons arising from $W^\pm W^\pm$ production and decay. The two jets must have a transverse momentum larger than 30 GeV, while the leptons, electrons or muons, must have a transverse momentum > 20 GeV. The dijet mass is required to be > 500 GeV, the dilepton mass > 50 GeV, with additional requirement of differing from the Z mass by > 15 GeV. In the two categories W^+W^+ and W^-W^-, 10 and 2 data events are observed in a data sample corresponding to an integrated luminosity of 19.4 fb^{-1}, with an expected background of 3.1 $\pm$ 0.6 and 2.6 $\pm$ 0.5 events. Analysing the distribution of the dilepton invariant mass, the following limits at 95% C.L. are obtained, in units of TeV^{-4}: $-38 < F_{S,0}/\Lambda^4 < 40$, $-118 < F_{S,1}/\Lambda^4 < 120$, $-33 < F_{M,0}/\Lambda^4 < 32$, $-44 < F_{M,1}/\Lambda^4 < 47$, $-65 < F_{M,6}/\Lambda^4 < 63$, $-70 < F_{M,7}/\Lambda^4 < 66$, $-4.2 < F_{T,0}/\Lambda^4 < 4.6$, $-1.9 < F_{T,1}/\Lambda^4 < 2.2$, $-5.2 < F_{T,2}/\Lambda^4 < 6.4$.

[36] AAD 14AM analyze electroweak production of WW jet jet same-charge diboson plus two jets production, with the W bosons decaying to electron or muon, to study the quartic $WWWW$ coupling. In a kinematic region enhancing the electroweak production over the strong production, 34 events are observed in the data while 29.8 $\pm$ 2.4 events are expected with a backgound of 15.9 $\pm$ 1.9 events. Assuming the other QGC coupling to have the SM value of zero, the observed event yield is used to determine 95% CL limits on the quartic gauge couplings: $-0.14 < \alpha_4 < 0.16$ and $-0.23 < \alpha_5 < 0.24$.

[37] CHATRCHYAN 14Q study $WV\gamma$ production in 8 TeV pp collisions, in the single lepton final state, with $W \to \ell\nu$, $Z \to$ dijet or $W \to \ell\nu$, $W \to$ dijet, the dijet mass resolution precluding differentiation between the W and Z. p_T and pseudo-rapidity cuts are put on the lepton, the photon and the two jets to minimize backgrounds. The dijet mass is required to be between 70–100 GeV and $|\Delta\eta_{jj}| < 1.4$. The selected number of muon (electron) events are 183 (139), with SM expectation being 194.2 $\pm$ 11.5 (147.9 $\pm$ 10.7) including signal and background. The photon E_T distribution is used to set limits on the anomalous quartic couplings. The following 95% CL limits are deduced (all in units of TeV^{-2} or TeV^{-4}): $-21 < a_0^W/\Lambda^2 < 20$, $-34 < a_c^W/\Lambda^2 < 32$, $-12 < \kappa_0^W/\Lambda^2 < 10$ and $-18 < \kappa_c^W/\Lambda^2 < 17$; and $-25 < f_{T,0}/\Lambda^4 < 24$ TeV^{-4}.

[38] ABAZOV 13D searches for anomalous $WW\gamma\gamma$ quartic gauge couplings in the two-photon-mediated process $pp \to ppWW$, assuming the $WW\gamma$ triple gauge boson couplings to be at their Standard Model values. 946 events containing an e^+e^- pair with missing energy are selected in a total luminosity of 9.7 fb^{-1}, with an expectation of 983 $\pm$ 108 events from Standard-Model processes. The following 1-parameter limits at 95% CL are otained: $|a_0^W/\Lambda^2| < 4.3 \times 10^{-4}$ GeV^{-2} ($a_c^W = 0$), $|a_c^W/\Lambda^2| < 1.5 \times 10^{-3}$ GeV^{-2} ($a_0^W = 0$).

[39] CHATRCHYAN 13AA searches for anomalous $WW\gamma\gamma$ quartic gauge couplings in the two-photon-mediated process $pp \to ppWW$, assuming the $WW\gamma$ triple gauge boson couplings to be at their Standard Model values. 2 events containing an $e^\pm\mu^\mp$ pair with $p_T(e, \mu) > 30$ GeV are selected in a total luminosity of 5.05 fb^{-1}, with an expected $ppWW$ signal of 2.2 $\pm$ 0.4 events and an expected background of 0.84 $\pm$ 0.15 events. The following 1-parameter limits at 95% CL are otained from the $p_T(e, \mu)$ spectrum: $|a_0^W/\Lambda^2| < 4.0 \times 10^{-6}$ GeV^{-2} ($a_c^W = 0$), $|a_c^W/\Lambda^2| < 1.5 \times 10^{-5}$ GeV^{-2} ($a_0^W = 0$).

[40] ABBIENDI 04B select 187 $e^+e^- \to W^+W^-\gamma$ events in the C.M. energy range 180–209 GeV, where E_γ >2.5 GeV, the photon has a polar angle $|\cos\theta_\gamma| < 0.975$ and is well isolated from the nearest jet and charged lepton, and the effective masses of both fermion-antifermion systems agree with the W mass within 3 Γ_W. The measured differential cross section as a function of the photon energy and photon polar angle is used to extract the 95% CL limits: -0.020 GeV^{-2} $< a_0/\Lambda^2 < 0.020$ GeV^{-2}, -0.053 GeV^{-2} $< a_c/\Lambda^2 < 0.037$ GeV^{-2} and -0.16 GeV^{-2} $< a_n/\Lambda^2 < 0.15$ GeV^{-2}.

[41] ABBIENDI 04L select 20 $e^+e^- \to \nu\overline{\nu}\gamma\gamma$ acoplanar events in the energy range 180–209 GeV and 176 $e^+e^- \to q\overline{q}\gamma\gamma$ events in the energy range 130–209 GeV. These samples are used to constrain possible anomalous $W^+W^-\gamma\gamma$ and $ZZ\gamma\gamma$ quartic couplings. Further combining with the $W^+W^-\gamma$ sample of ABBIENDI 04B the following one-parameter 95% CL limits are obtained: $-0.007 < a_0^Z/\Lambda^2 < 0.023$ GeV^{-2}, $-0.029 < a_c^Z/\Lambda^2 < 0.029$ GeV^{-2}, $-0.020 < a_0^W/\Lambda^2 < 0.020$ GeV^{-2}, $-0.052 < a_c^W/\Lambda^2 < 0.037$ GeV^{-2}.

[42] In the CM energy range 183 to 209 GeV HEISTER 04A select 30 $e^+e^- \to \nu\overline{\nu}\gamma\gamma$ events with two acoplanar, high energy and high transverse momentum photons. The photon–photon acoplanarity is required to be > 5°, $E_\gamma/\sqrt{s} > 0.025$ (the more energetic photon having energy > 0.2 $\sqrt{s}$), $p_{T_\gamma}/E_{\rm beam} > 0.05$ and $|\cos\theta_\gamma| < 0.94$. A likelihood fit to the photon energy and recoil missing mass yields the following one–parameter 95% CL limits: $-0.012 < a_0^Z/\Lambda^2 < 0.019$ GeV^{-2}, $-0.041 < a_c^Z/\Lambda^2 < 0.044$ GeV^{-2}, $-0.060 < a_0^W/\Lambda^2 < 0.055$ GeV^{-2}, $-0.099 < a_c^W/\Lambda^2 < 0.093$ GeV^{-2}.

[43] ABDALLAH 03I select 122 $e^+e^- \to W^+W^-\gamma$ events in the C.M. energy range 189–209 GeV, where E_γ >5 GeV, the photon has a polar angle $|\cos\theta_\gamma| < 0.95$ and is well isolated from the nearest charged fermion. A fit to the photon energy spectra yields $a_c/\Lambda^2 = 0.000^{+0.019}_{-0.040}$ GeV^{-2}, $a_0/\Lambda^2 = -0.004^{+0.018}_{-0.010}$ GeV^{-2}, $\bar{a}_0/\Lambda^2 = -0.007^{+0.019}_{-0.008}$ GeV^{-2}, $a_n/\Lambda^2 = -0.09^{+0.16}_{-0.05}$ GeV^{-2}, and $\bar{a}_n/\Lambda^2 = +0.05^{+0.07}_{-0.15}$ GeV^{-2}, keeping the other parameters fixed to their Standard Model values (0). The 95% CL limits are: -0.063 GeV^{-2} $< a_c/\Lambda^2 < +0.032$ GeV^{-2}, -0.020 GeV^{-2} $< a_0/\Lambda^2 < +0.020$ GeV^{-2}, -0.020 GeV^{-2} $< \bar{a}_0/\Lambda^2 < +0.020$ GeV^{-2}, -0.18 GeV^{-2} $< a_n/\Lambda^2 < +0.14$ GeV^{-2}, -0.16 GeV^{-2} $< \bar{a}_n/\Lambda^2 < +0.17$ GeV^{-2}.

[44] ACHARD 02F select 86 $e^+e^- \to W^+W^-\gamma$ events at 192–207 GeV, where E_γ >5 GeV and the photon is well isolated. They also select 43 acoplanar $e^+e^- \to \nu\overline{\nu}\gamma\gamma$ events in this energy range, where the photon energies are >5 GeV and >1 GeV and the

Int. J. Mod. Phys. A 2026.41. Downloaded from www.worldscientific.com
by UNIVERSITY OF CALIFORNIA @ BERKELEY on 09/16/26. Re-use and distribution is strictly not permitted, except for Open Access articles.

photon polar angles are between 14° and 166°. All these 43 events are in the recoil mass region corresponding to the Z (75–110 GeV). Using the shape and normalization of the photon spectra in the $W^+W^-\gamma$ events, and combining with the 42 event sample from 189 GeV data (ACCIARRI 00T), they obtain: $a_0/\Lambda^2 = 0.000 \pm 0.010$ GeV^{-2}, $a_c/\Lambda^2 = -0.013 \pm 0.023$ GeV^{-2}, and $a_n/\Lambda^2 = -0.002 \pm 0.076$ GeV^{-2}. Further combining the analyses of $W^+W^-\gamma$ events with the low recoil mass region of $\nu\overline{\nu}\gamma\gamma$ events (including samples collected at 183 + 189 GeV), they obtain the following one-parameter 95% CL limits: -0.015 GeV^{-2} $< a_0/\Lambda^2 < 0.015$ GeV^{-2}, -0.048 GeV^{-2} $< a_c/\Lambda^2 < 0.026$ GeV^{-2}, and -0.14 GeV^{-2} $< a_n/\Lambda^2 < 0.13$ GeV^{-2}.

W REFERENCES

CHEKHOVSKY	26	NAT 652 321	V. Chekhovsky *et al.*	(CMS Collab.)
PDG	26	IJMP A41 2630011	F. Takahashi *et al.*	(PDG Collab.)
AAD	25AD	JHEP 2507 026	G. Aad *et al.*	(ATLAS Collab.)
AAD	25BE	JHEP 2511 006	G. Aad *et al.*	(ATLAS Collab.)
AAD	25G	PL B866 139527	G. Aad *et al.*	(ATLAS Collab.)
AAD	25Z	JHEP 2505 038	G. Aad *et al.*	(ATLAS Collab.)
CHEKHOVSKY	25	PR D112 012009	V. Chekhovsky *et al.*	(CMS Collab.)
HAYRAPETY...	25AI	PL B868 139754	A. Hayrapetyan *et al.*	(CMS Collab.)
HAYRAPETY...	25AM	JHEP 2510 219	A. Hayrapetyan *et al.*	(CMS Collab.)
AAD	24AD	JHEP 2404 026	G. Aad *et al.*	(ATLAS Collab.)
AAD	24AM	JHEP 2406 192	G. Aad *et al.*	(ATLAS Collab.)
AAD	24BO	PRL 133 161804	G. Aad *et al.*	(ATLAS Collab.)
AAD	24C	JHEP 2401 004	G. Aad *et al.*	(ATLAS Collab.)
AAD	24CG	EPJ C84 993	G. Aad *et al.*	(ATLAS Collab.)
AAD	24CH	EPJ C84 1064	G. Aad *et al.*	(ATLAS Collab.)
AAD	24CJ	EPJ C84 1309	G. Aad *et al.*	(ATLAS Collab.)
AMOROSO	24	EPJ C84 451	S. Amoroso *et al.*	(DESY, SACL, EDIN+)
PDG	24	PR D110 030001	S. Navas *et al.*	(PDG Collab.)
AAD	23BH	EPJ C83 539	G. Aad *et al.*	(ATLAS Collab.)
AAD	23K	JHEP 2306 082	G. Aad *et al.*	(ATLAS Collab.)
AAIJ	23AM	CP C47 093002	R. Aaij *et al.*	(LHCb Collab.)
TUMASYAN	23AK	PR D108 032017	A. Tumasyan *et al.*	(CMS Collab.)
TUMASYAN	23AM	JHEP 2307 229	A. Tumasyan *et al.*	(CMS Collab.)
AAIJ	22C	JHEP 2201 036	R. Aaij *et al.*	(LHCb Collab.)
AALTONEN	22	SCI 376 170	T. Aaltonen *et al.*	(CDF Collab.)
PDG	22	PTEP 2022 083C01	R.L. Workman *et al.*	(PDG Collab.)
TUMASYAN	22AB	JHEP 2207 032	A. Tumasyan *et al.*	(CMS Collab.)
TUMASYAN	22E	PR D105 052003	A. Tumasyan *et al.*	(CMS Collab.)
TUMASYAN	22F	PR D105 072008	A. Tumasyan *et al.*	(CMS Collab.)
AAD	21AC	EPJ C81 163	G. Aad *et al.*	(ATLAS Collab.)
AAD	21AN	NATP 17 813	G. Aad *et al.*	(ATLAS Collab.)
AAD	21W	JHEP 2106 003	G. Aad *et al.*	(ATLAS Collab.)
SIRUNYAN	21	PL B812 135992	A.M. Sirunyan *et al.*	(CMS Collab.)
SIRUNYAN	21G	PRL 126 252002	A.M. Sirunyan *et al.*	(CMS Collab.)
SIRUNYAN	21I	PL B819 136409	A.M. Sirunyan *et al.*	(CMS Collab.)
TUMASYAN	21A	PR D104 072001	A. Tumasyan *et al.*	(CMS Collab.)
TUMASYAN	21B	JHEP 2110 174	A. Tumasyan *et al.*	(CMS Collab.)
SIRUNAYN	20	PL B809 135710	A.M. Sirunyan *et al.*	(CMS Collab.)
SIRUNYAN	20AL	JHEP 2006 076	A.M. Sirunyan *et al.*	(CMS Collab.)
SIRUNYAN	20BA	EPJ C80 43	A.M. Sirunyan *et al.*	(CMS Collab.)
SIRUNYAN	20BD	PL B811 135988	A.M. Sirunyan *et al.*	(CMS Collab.)
SIRUNYAN	20BF	PR D102 092001	A.M. Sirunyan *et al.*	(CMS Collab.)
AABOUD	19BA	EPJ C79 884	M. Aaboud *et al.*	(ATLAS Collab.)
SIRUNYAN	19AD	JHEP 1904 122	A.M. Sirunyan *et al.*	(CMS Collab.)
SIRUNYAN	19BG	PRL 122 151802	A.M. Sirunyan *et al.*	(CMS Collab.)
SIRUNYAN	19BM	PR D100 012004	A.M. Sirunyan *et al.*	(CMS Collab.)
SIRUNYAN	19BP	PL B795 281	A.M. Sirunyan *et al.*	(CMS Collab.)
SIRUNYAN	19CL	JHEP 1912 062	A.M. Sirunyan *et al.*	(CMS Collab.)
SIRUNYAN	19CQ	PL B798 134985	A.M. Sirunyan *et al.*	(CMS Collab.)
AABOUD	18J	EPJ C78 110	M. Aaboud *et al.*	(ATLAS Collab.)
Also		EPJ C78 898 (errat.)	M. Aaboud *et al.*	(ATLAS Collab.)
AABOUD	18Q	PR D97 032005	M. Aaboud *et al.*	(ATLAS Collab.)
ANDREEV	18A	EPJ C78 777	V. Andreev *et al.*	(H1 Collab.)
SIRUNYAN	18BZ	EPJ C78 589	A.M. Sirunyan *et al.*	(CMS Collab.)
SIRUNYAN	18CC	PRL 120 081801	A.M. Sirunyan *et al.*	(CMS Collab.)
AABOUD	17AA	PR D96 012007	M. Aaboud *et al.*	(ATLAS Collab.)
AABOUD	17AG	EPJ C77 646	M. Aaboud *et al.*	(ATLAS Collab.)
AABOUD	17D	PR D95 032001	M. Aaboud *et al.*	(ATLAS Collab.)
AABOUD	17J	JHEP 1707 107	M. Aaboud *et al.*	(ATLAS Collab.)
AABOUD	17M	EPJ C77 141	M. Aaboud *et al.*	(ATLAS Collab.)
AABOUD	17Q	EPJ C77 367	M. Aaboud *et al.*	(ATLAS Collab.)
AABOUD	17S	EPJ C77 474	M. Aaboud *et al.*	(ATLAS Collab.)
AABOUD	17U	EPJ C77 563	M. Aaboud *et al.*	(ATLAS Collab.)
KHACHATRY...	17AA	PL B770 380	V. Khachatryan *et al.*	(CMS Collab.)
KHACHATRY...	17M	JHEP 1706 106	V. Khachatryan *et al.*	(CMS Collab.)
KHACHATRY...	17O	EPJ C77 236	V. Khachatryan *et al.*	(CMS Collab.)
SIRUNYAN	17AD	PL B774 682	A.M. Sirunyan *et al.*	(CMS Collab.)
SIRUNYAN	17AR	JHEP 1710 072	A.M. Sirunyan *et al.*	(CMS Collab.)
SIRUNYAN	17X	PL B772 21	A.M. Sirunyan *et al.*	(CMS Collab.)
AABOUD	16E	PR D94 032011	M. Aaboud *et al.*	(ATLAS Collab.)
AAD	16AR	JHEP 1609 029	G. Aad *et al.*	(ATLAS Collab.)
AAD	16P	PR D93 092004	G. Aad *et al.*	(ATLAS Collab.)
AAD	16Q	PR D93 112002	G. Aad *et al.*	(ATLAS Collab.)
AAIJ	16AJ	JHEP 1610 030	R. Aaij *et al.*	(LHCb Collab.)
KHACHATRY...	16AX	JHEP 1608 119	V. Khachatryan *et al.*	(CMS Collab.)
KHACHATRY...	16BI	EPJ C76 401	V. Khachatryan *et al.*	(CMS Collab.)
AAD	15N	PRL 115 031802	G. Aad *et al.*	(ATLAS Collab.)
KHACHATRY...	15D	PRL 114 051801	V. Khachatryan *et al.*	(CMS Collab.)
AAD	14AM	PRL 113 141803	G. Aad *et al.*	(ATLAS Collab.)
AAD	14Y	JHEP 1404 031	G. Aad *et al.*	(ATLAS Collab.)
AALTONEN	14D	PR D89 072003	T. Aaltonen *et al.*	(CDF Collab.)
CHATRCHYAN	14AB	PR D89 092005	S. Chatrchyan *et al.*	(CMS Collab.)
CHATRCHYAN	14Q	PR D90 032008	S. Chatrchyan *et al.*	(CMS Collab.)
AAD	13AL	PR D87 112001	G. Aad *et al.*	(ATLAS Collab.)
Also		PR D88 079906 (errat.)	G. Aad *et al.*	(ATLAS Collab.)
AAD	13AN	PR D87 112003	G. Aad *et al.*	(ATLAS Collab.)
Also		PR D91 119901 (errat.)	G. Aad *et al.*	(ATLAS Collab.)
ABAZOV	13D	PR D88 012005	V.M. Abazov *et al.*	(D0 Collab.)
CHATRCHYAN	13AA	JHEP 1307 116	S. Chatrchyan *et al.*	(CMS Collab.)
CHATRCHYAN	13BF	EPJ C73 2610	S. Chatrchyan *et al.*	(CMS Collab.)
SCHAEL	13A	PRPL 532 119	S. Schael *et al.*	(ALEPH, DELPHI, L3, OPAL+)
AAD	12AC	PL B712 289	G. Aad *et al.*	(ATLAS Collab.)
AAD	12BX	PL B717 49	G. Aad *et al.*	(ATLAS Collab.)
AAD	12CD	EPJ C72 2173	G. Aad *et al.*	(ATLAS Collab.)
AAD	12V	PL B709 341	G. Aad *et al.*	(ATLAS Collab.)
AALTONEN	12AC	PR D86 031104	T. Aaltonen *et al.*	(CDF Collab.)
AALTONEN	12E	PRL 108 151803	T. Aaltonen *et al.*	(CDF Collab.)
AALTONEN	12W	PR D85 032001	T. Aaltonen *et al.*	(CDF Collab.)
ABAZOV	12AG	PL B718 451	V.M. Abazov *et al.*	(D0 Collab.)
ABAZOV	12F	PRL 108 151804	V.M. Abazov *et al.*	(D0 Collab.)
Also		PR D89 012005	V.M. Abazov *et al.*	(D0 Collab.)
ABAZOV	11	PL B695 67	V.M. Abazov *et al.*	(D0 Collab.)
ABAZOV	11AC	PRL 107 241803	V.M. Abazov *et al.*	(D0 Collab.)
BLINOV	11	PL B699 287	A.E. Blinov, A.S. Rudenko	(NOVO)
CHATRCHYAN	11M	PL B701 535	S. Chatrchyan *et al.*	(CMS Collab.)
AALTONEN	10K	PRL 104 201801	T. Aaltonen *et al.*	(CDF Collab.)
Also		PRL 105 019905(errat.)	T. Aaltonen *et al.*	(CDF Collab.)
ABDALLAH	10	EPJ C66 35	J. Abdallah *et al.*	(DELPHI Collab.)
TEVEWWG	10	arXiv: 1003.2826	TEVEWWG	(CDF, D0 Collab)
AARON	09B	EPJ C64 251	F.D. Aaron *et al.*	(H1 Collab.)
ABAZOV	09AB	PRL 103 141801	V.M. Abazov *et al.*	(D0 Collab.)
ABAZOV	09AD	PR D80 053012	V.M. Abazov *et al.*	(D0 Collab.)
ABAZOV	09AJ	PRL 103 191801	V.M. Abazov *et al.*	(D0 Collab.)
ABAZOV	09AK	PRL 103 231802	V.M. Abazov *et al.*	(D0 Collab.)
AALTONEN	08B	PRL 100 071801	T. Aaltonen *et al.*	(CDF Collab.)
ABAZOV	08R	PRL 100 241805	V.M. Abazov *et al.*	(D0 Collab.)
ABDALLAH	08A	EPJ C55 1	J. Abdallah *et al.*	(DELPHI Collab.)
ABDALLAH	08C	EPJ C54 345	J. Abdallah *et al.*	(DELPHI Collab.)
AALTONEN	07F	PRL 99 151801	T. Aaltonen *et al.*	(CDF Collab.)
Also		PR D77 112001	T. Aaltonen *et al.*	(CDF Collab.)
AALTONEN	07L	PR D76 111103	T. Aaltonen *et al.*	(CDF Collab.)
ABAZOV	07Z	PR D76 111104	V.M. Abazov *et al.*	(D0 Collab.)
ABBIENDI	07A	EPJ C52 767	G. Abbiendi *et al.*	(OPAL Collab.)
ABAZOV	06H	PR D74 057101	V.M. Abazov *et al.*	(D0 Collab.)
Also		PR D74 059904(errat.)	V.M. Abazov *et al.*	(D0 Collab.)
ABBIENDI	06	EPJ C45 307	G. Abbiendi *et al.*	(OPAL Collab.)
ABBIENDI	06A	EPJ C45 291	G. Abbiendi *et al.*	(OPAL Collab.)
ACHARD	06	EPJ C45 569	P. Achard *et al.*	(L3 Collab.)
AKTAS	06	PL B632 35	A. Aktas *et al.*	(H1 Collab.)
SCHAEL	06	EPJ C47 309	S. Schael *et al.*	(ALEPH Collab.)
ABAZOV	05J	PR D71 091108	V.M. Abazov *et al.*	(D0 Collab.)
ABAZOV	05S	PRL 95 141802	V.M. Abazov *et al.*	(D0 Collab.)
SCHAEL	05A	PL B614 7	S. Schael *et al.*	(ALEPH Collab.)
ABAZOV	04D	PR D70 092008	V.M. Abazov *et al.*	(D0 Collab.)
ABBIENDI	04B	PL B580 17	G. Abbiendi *et al.*	(OPAL Collab.)
ABBIENDI	04D	EPJ C33 463	G. Abbiendi *et al.*	(OPAL Collab.)
ABBIENDI	04L	PR D70 032005	G. Abbiendi *et al.*	(OPAL Collab.)
ABDALLAH	04G	EPJ C34 127	J. Abdallah *et al.*	(DELPHI Collab.)
ACHARD	04D	PL B586 151	P. Achard *et al.*	(L3 Collab.)
ACHARD	04J	PL B600 22	P. Achard *et al.*	(L3 Collab.)
HEISTER	04A	PL B602 31	A. Heister *et al.*	(ALEPH Collab.)
SCHAEL	04A	EPJ C38 147	S. Schael *et al.*	(ALEPH Collab.)
ABBIENDI	03C	EPJ C26 321	G. Abbiendi *et al.*	(OPAL Collab.)
ABDALLAH	03I	EPJ C31 139	J. Abdallah *et al.*	(DELPHI Collab.)
ABAZOV	02D	PR D66 012001	V.M. Abazov *et al.*	(D0 Collab.)
ABAZOV	02E	PR D66 032008	V.M. Abazov *et al.*	(D0 Collab.)
ACHARD	02F	PL B527 29	P. Achard *et al.*	(L3 Collab.)
CHEKANOV	02C	PL B539 197	S. Chekanov *et al.*	(ZEUS Collab.)
ABBIENDI	01H	EPJ C19 229	G. Abbiendi *et al.*	(OPAL Collab.)
ABREU	01I	PL B502 9	P. Abreu *et al.*	(DELPHI Collab.)
AFFOLDER	01E	PR D64 052001	T. Affolder *et al.*	(CDF Collab.)
ABBIENDI	00V	PL B490 71	G. Abbiendi *et al.*	(OPAL Collab.)
ABBOTT	00B	PR D61 072001	B. Abbott *et al.*	(D0 Collab.)
ABBOTT	00D	PRL 84 5710	B. Abbott *et al.*	(D0 Collab.)
ABREU,P	00F	EPJ C18 203	P. Abreu *et al.*	(DELPHI Collab.)
Also		EPJ C25 493 (errat.)	P. Abreu *et al.*	(DELPHI Collab.)
ACCIARRI	00T	PL B490 187	M. Acciarri *et al.*	(L3 Collab.)
AFFOLDER	00M	PRL 85 3347	T. Affolder *et al.*	(CDF Collab.)
BREITWEG	00	PL B471 411	J. Breitweg *et al.*	(ZEUS Collab.)
BREITWEG	00D	EPJ C12 411	J. Breitweg *et al.*	(ZEUS Collab.)
EBOLI	00	MPL A15 1	O. Eboli, M. Gonzalez-Garcia, S. Novaes	
ABBIENDI	99N	PL B453 153	G. Abbiendi *et al.*	(OPAL Collab.)
ABBOTT	99H	PR D60 052003	B. Abbott *et al.*	(D0 Collab.)
ABBOTT	99I	PR D60 072002	B. Abbott *et al.*	(D0 Collab.)
ABREU	99L	PL B459 382	P. Abreu *et al.*	(DELPHI Collab.)
ACCIARRI	99	PL B454 386	M. Acciarri *et al.*	(L3 Collab.)
ACCIARRI	99Q	PL B467 171	M. Acciarri *et al.*	(L3 Collab.)
BARATE	99I	PL B453 107	R. Barate *et al.*	(ALEPH Collab.)
BARATE	99L	PL B462 389	R. Barate *et al.*	(ALEPH Collab.)
BARATE	99M	PL B465 349	R. Barate *et al.*	(ALEPH Collab.)
ABBOTT	98N	PR D58 092003	B. Abbott *et al.*	(D0 Collab.)
ABBOTT	98P	PR D58 012002	B. Abbott *et al.*	(D0 Collab.)
ABE	98H	PR D58 031101	F. Abe *et al.*	(CDF Collab.)
ABE	98P	PR D58 091101	F. Abe *et al.*	(CDF Collab.)
ABREU	98C	PL B416 233	P. Abreu *et al.*	(DELPHI Collab.)
ABREU	98N	PL B439 209	P. Abreu *et al.*	(DELPHI Collab.)
BARATE	97	PL B401 347	R. Barate *et al.*	(ALEPH Collab.)
BARATE	97S	PL B415 435	R. Barate *et al.*	(ALEPH Collab.)
ABACHI	95D	PRL 75 1456	S. Abachi *et al.*	(D0 Collab.)
ABE	95C	PRL 74 341	F. Abe *et al.*	(CDF Collab.)
ABE	95G	PRL 74 1936	F. Abe *et al.*	(CDF Collab.)
ABE	95P	PRL 75 11	F. Abe *et al.*	(CDF Collab.)
Also		PR D52 4784	F. Abe *et al.*	(CDF Collab.)
ABE	95W	PR D52 2624	F. Abe *et al.*	(CDF Collab.)
Also		PRL 73 220	F. Abe *et al.*	(CDF Collab.)
ABE	92E	PRL 68 3398	F. Abe *et al.*	(CDF Collab.)
ABE	92I	PRL 69 28	F. Abe *et al.*	(CDF Collab.)
ALITTI	92	PL B276 365	J. Alitti *et al.*	(UA2 Collab.)
ALITTI	92B	PL B276 354	J. Alitti *et al.*	(UA2 Collab.)
ALITTI	92C	PL B277 194	J. Alitti *et al.*	(UA2 Collab.)
ALITTI	92D	PL B277 203	J. Alitti *et al.*	(UA2 Collab.)
ALITTI	92F	PL B280 137	J. Alitti *et al.*	(UA2 Collab.)
SAMUEL	92	PL B280 124	M.A. Samuel *et al.*	(OKSU, CARL)
ABE	91C	PR D44 29	F. Abe *et al.*	(CDF Collab.)
ALBAJAR	91	PL B253 503	C. Albajar *et al.*	(UA1 Collab.)
ALITTI	91C	ZPHY C52 209	J. Alitti *et al.*	(UA2 Collab.)
SAMUEL	91	PRL 67 9	M.A. Samuel *et al.*	(OKSU, CARL)
Also		PRL 67 2920 (errat.)	M.A. Samuel *et al.*	
ABE	90G	PRL 65 2243	F. Abe *et al.*	(CDF Collab.)
Also		PR D43 2070	F. Abe *et al.*	(CDF Collab.)
ALBAJAR	90	PL B241 283	C. Albajar *et al.*	(UA1 Collab.)
ALITTI	90B	PL B241 150	J. Alitti *et al.*	(UA2 Collab.)
ABE	89I	PRL 62 1005	F. Abe *et al.*	(CDF Collab.)
ALBAJAR	89	ZPHY C44 15	C. Albajar *et al.*	(UA1 Collab.)
BAUR	88	NP B308 127	U. Baur, D. Zeppenfeld	(FSU, WISC)
GRIFOLS	88	IJMP A3 225	J.A. Grifols, S. Peris, J. Sola	(BARC, DESY)
Also		PL B197 437	J.A. Grifols, S. Peris, J. Sola	(BARC, DESY)
ALBAJAR	87	PL B185 233	C. Albajar *et al.*	(UA1 Collab.)
ANSARI	87	PL B186 440	R. Ansari *et al.*	(UA2 Collab.)
GROTCH	87	PR D36 2153	H. Grotch, R.W. Robinett	(PSU)
HAGIWARA	87	NP B282 253	K. Hagiwara *et al.*	(KEK, UCLA, FSU)
VANDERBIJ	87	PR D35 1088	J.J. van der Bij	(FNAL)
GRAU	85	PL 154B 283	A. Grau, J.A. Grifols	(BARC)
SUZUKI	85	PL 153B 289	M. Suzuki	(LBL)
ARNISON	84D	PL 134B 469	G.T.J. Arnison *et al.*	(UA1 Collab.)
HERZOG	84	PL 148B 355	F. Herzog	(WISC)
Also		PL 155B 468 (errat.)	F. Herzog	(WISC)
ARNISON	83	PL 122B 103	G.T.J. Arnison *et al.*	(UA1 Collab.)
BANNER	83B	PL 122B 476	M. Banner *et al.*	(UA2 Collab.)

Int. J. Mod. Phys. A 2026.41. Downloaded from www.worldscientific.com
by UNIVERSITY OF CALIFORNIA @ BERKELEY on 09/16/26. Re-use and distribution is strictly not permitted, except for Open Access articles.

Z

$J = 1$

See the related review(s):
Z Boson

Z MASS

OUR AVERAGE is given by the weighted average of the combined CDF result and the combined LEP result, assuming no correlations between CDF and LEP. The combined LEP result, 91.1876 ± 0.0021 GeV, is obtained using the fit procedure and correlations as determined by the LEP Electroweak Working Group (see the note "The Z boson" and ref. LEP-SLC 06). The LEP fit is performed using the Z mass and width, the Z hadronic pole cross section, the ratios of hadronic to leptonic partial widths, and the Z pole forward-backward lepton asymmetries. This set is believed to be most free of correlations.

The Z-boson mass listed here corresponds to the mass parameter in a Breit-Wigner distribution with mass dependent width. The value is 34 MeV greater than the real part of the position of the pole (in the energy-squared plane) in the Z-boson propagator. Also the LEP experiments have generally assumed a fixed value of the $\gamma - Z$ interferences term based on the standard model. Keeping this term as free parameter leads to a somewhat larger error on the fitted Z mass. See ACCIARRI 00Q and ABBIENDI 04G for a detailed investigation of both these issues.

VALUE (GeV)	EVTS	DOCUMENT ID		TECN	COMMENT
91.1879±0.0020 OUR AVERAGE					
91.1857±0.0083±0.0039	174K	[1] AAIJ	25AH	LHCB	E_{cm}^{pp} = 13 TeV
91.1923±0.0071		[2] AALTONEN	22	CDF	$E_{cm}^{p\overline{p}}$ = 1.8 TeV
91.1876±0.0021		[3] LEP-SLC	06	LEP	E_{cm}^{ee} = 88–94 GeV
• • • We do not use the following data for averages, fits, limits, etc. • • •					
91.084 ±0.107		[4] ANDREEV	18A	H1	$e^{\pm}p$
91.1872±0.0033		[5] ABBIENDI	04G	OPAL	E_{cm}^{ee} = LEP1 + 130–209 GeV
91.272 ±0.032 ±0.033		[6] ACHARD	04C	L3	E_{cm}^{ee} = 183–209 GeV
91.1852±0.0030	4.57M	[7] ABBIENDI	01A	OPAL	E_{cm}^{ee} = 88–94 GeV
91.1863±0.0028	4.08M	[8] ABREU	00F	DLPH	E_{cm}^{ee} = 88–94 GeV
91.1898±0.0031	3.96M	[9] ACCIARRI	00C	L3	E_{cm}^{ee} = 88–94 GeV
91.1875±0.0039	3.97M	[10] ACCIARRI	00Q	L3	E_{cm}^{ee} = LEP1 + 130–189 GeV
91.1885±0.0031	4.57M	[11] BARATE	00C	ALEP	E_{cm}^{ee} = 88–94 GeV
91.151 ±0.008		[12] MIYABAYASHI	95	TOPZ	E_{cm}^{ee} = 57.8 GeV
91.74 ±0.28 ±0.93	156	[13] ALITTI	92B	UA2	$E_{cm}^{p\overline{p}}$ = 630 GeV
90.9 ±0.3 ±0.2	188	[14] ABE	89C	CDF	$E_{cm}^{p\overline{p}}$ = 1.8 TeV
91.14 ±0.12	480	[15] ABRAMS	89B	MRK2	E_{cm}^{ee} = 89–93 GeV
93.1 ±1.0 ±3.0	24	[16] ALBAJAR	89	UA1	$E_{cm}^{p\overline{p}}$ = 546,630 GeV

[1] AAIJ 25AH analyse Z production in the muon decay channel in their 2016 data, with the transverse momentum of the muon required to be above 20 GeV and the pseudorapidity of muons $2.2 < \eta < 4.4$. They obtain a Z mass measurement based on a template fit. The systematic error is dominated by 0.0036 GeV from momentum calibration.

[2] AALTONEN 22 analyse Z decays in the di-muon and di-electron channels using their full Run-II data set. They obtain Z mass values of 91192.0 ± 6.4(stat.) ± 4.0(syst.) MeV and 91194.3 ± 13.8(stat.) ± 7.6(syst.) MeV, respectively. Combining these results using the systematic uncertainty contributions and their correlations as given in AALTONEN 22, we obtain an average of 91192.3 ± 5.8(stat.) ± 4.1(syst.) MeV.

[3] This result combines ABBIENDI 01A, ABREU 00F, ACCIARRI 00C, BARATE 00C, taking correlated uncertainties into account.

[4] ANDREEV 18A obtain this result in a combined electroweak and QCD analysis using all deep-inelastic e^+p and e^-p neutral current and charged current scattering cross sections published by the H1 Collaboration, including data with longitudinally polarized lepton beams.

[5] ABBIENDI 04G obtain this result using the S–matrix formalism for a combined fit to their cross section and asymmetry data at the Z peak and their data at 130–209 GeV. The authors have corrected the measurement for the 34 MeV shift with respect to the Breit–Wigner fits.

[6] ACHARD 04C select $e^+e^- \to Z\gamma$ events with hard initial–state radiation. Z decays to $q\overline{q}$ and muon pairs are considered. The fit results obtained in the two samples are found consistent to each other and combined considering the uncertainty due to ISR modelling as fully correlated.

[7] ABBIENDI 01A error includes approximately 2.3 MeV due to statistics and 1.8 MeV due to LEP energy uncertainty. This result is included in the LEP average LEP-SLC 06.

[8] The error includes 1.6 MeV due to LEP energy uncertainty. This result is included in the LEP average LEP-SLC 06.

[9] The error includes 1.8 MeV due to LEP energy uncertainty. This result is included in the LEP average LEP-SLC 06.

[10] ACCIARRI 00Q interpret the s-dependence of the cross sections and lepton forward-backward asymmetries in the framework of the S-matrix formalism. They fit to their cross section and asymmetry data at high energies, using the results of S-matrix fits to Z-peak data (ACCIARRI 00C) as constraints. The 130–189 GeV data constrains the γ/Z interference term. The authors have corrected the measurement for the 34.1 MeV shift with respect to the Breit-Wigner fits. The error contains a contribution of ±2.3 MeV due to the uncertainty on the γZ interference.

[11] BARATE 00C error includes approximately 2.4 MeV due to statistics, 0.2 MeV due to experimental systematics, and 1.7 MeV due to LEP energy uncertainty. This result is included in the LEP average LEP-SLC 06.

[12] MIYABAYASHI 95 combine their low energy total hadronic cross-section measurement with the ACTON 93D data and perform a fit using an S-matrix formalism. As expected, this result is below the mass values obtained with the standard Breit-Wigner parametrization.

[13] Enters fit through W/Z mass ratio given in the W Particle Listings. The ALITTI 92B systematic error (±0.93) has two contributions: one (±0.92) cancels in m_W/m_Z and one (±0.12) is noncancelling. These were added in quadrature.

[14] First error of ABE 89 is combination of statistical and systematic contributions; second is mass scale uncertainty.

[15] ABRAMS 89B uncertainty includes 35 MeV due to the absolute energy measurement.

[16] ALBAJAR 89 result is from a total sample of 33 $Z \to e^+e^-$ events.

Z WIDTH

OUR EVALUATION is obtained using the fit procedure and correlations as determined by the LEP Electroweak Working Group (see the note "The Z boson" and ref. LEP-SLC 06). Corrections as discussed in VOUTSINAS 20 and JANOT 20 are also included.

VALUE (GeV)	EVTS	DOCUMENT ID		TECN	COMMENT
2.4955±0.0023 OUR EVALUATION					
2.4955±0.0023		[1] JANOT	20		
• • • We do not use the following data for averages, fits, limits, etc. • • •					
2.4955±0.0023		[2] VOUTSINAS	20		
2.4952±0.0023		[3] LEP-SLC	06		E_{cm}^{ee} = 88–94 GeV
2.4943±0.0041		[4] ABBIENDI	04G	OPAL	E_{cm}^{ee} = LEP1 + 130–209 GeV
2.4948±0.0041	4.57M	[5] ABBIENDI	01A	OPAL	E_{cm}^{ee} = 88–94 GeV
2.4876±0.0041	4.08M	[6] ABREU	00F	DLPH	E_{cm}^{ee} = 88–94 GeV
2.5024±0.0042	3.96M	[7] ACCIARRI	00C	L3	E_{cm}^{ee} = 88–94 GeV
2.5025±0.0041	3.97M	[8] ACCIARRI	00Q	L3	E_{cm}^{ee} = LEP1 + 130–189 GeV
2.4951±0.0043	4.57M	[9] BARATE	00C	ALEP	E_{cm}^{ee} = 88–94 GeV
2.50 ±0.21 ±0.06		[10] ABREU	96R	DLPH	E_{cm}^{ee} = 91.2 GeV
3.8 ±0.8 ±1.0	188	ABE	89C	CDF	$E_{cm}^{p\overline{p}}$ = 1.8 TeV
2.42 $^{+0.45}_{-0.35}$	480	[11] ABRAMS	89B	MRK2	E_{cm}^{ee} = 89–93 GeV
2.7 $^{+1.2}_{-1.0}$ ±1.3	24	[12] ALBAJAR	89	UA1	$E_{cm}^{p\overline{p}}$ = 546,630 GeV
2.7 ±2.0 ±1.0	25	[13] ANSARI	87	UA2	$E_{cm}^{p\overline{p}}$ = 546,630 GeV

[1] JANOT 20 applies a correction to LEP-SLC 06 using an updated Bhabha cross section calculation. This result also includes a correction to account for correlated luminosity bias as presented in VOUTSINAS 20.

[2] VOUTSINAS 20 applies a correction to LEP-SLC 06 to account for correlated luminosity bias.

[3] This result combines ABBIENDI 01A, ABREU 00F, ACCIARRI 00C, BARATE 00C, taking correlated uncertainties into account.

[4] ABBIENDI 04G obtain this result using the S–matrix formalism for a combined fit to their cross section and asymmetry data at the Z peak and their data at 130–209 GeV. The authors have corrected the measurement for the 1 MeV shift with respect to the Breit–Wigner fits.

[5] ABBIENDI 01A error includes approximately 3.6 MeV due to statistics, 1 MeV due to event selection systematics, and 1.3 MeV due to LEP energy uncertainty.

[6] The error includes 1.2 MeV due to LEP energy uncertainty.

[7] The error includes 1.3 MeV due to LEP energy uncertainty.

[8] ACCIARRI 00Q interpret the s-dependence of the cross sections and lepton forward-backward asymmetries in the framework of the S-matrix formalism. They fit to their cross section and asymmetry data at high energies, using the results of S-matrix fits to Z-peak data (ACCIARRI 00C) as constraints. The 130–189 GeV data constrains the γ/Z interference term. The authors have corrected the measurement for the 0.9 MeV shift with respect to the Breit-Wigner fits.

[9] BARATE 00C error includes approximately 3.8 MeV due to statistics, 0.9 MeV due to experimental systematics, and 1.3 MeV due to LEP energy uncertainty.

[10] ABREU 96R obtain this value from a study of the interference between initial and final state radiation in the process $e^+e^- \to Z \to \mu^+\mu^-$.

[11] ABRAMS 89B uncertainty includes 50 MeV due to the miniSAM background subtraction error.

[12] ALBAJAR 89 result is from a total sample of 33 $Z \to e^+e^-$ events.

[13] Quoted values of ANSARI 87 are from direct fit. Ratio of Z and W production gives either $\Gamma(Z) < (1.09 \pm 0.07) \times \Gamma(W)$, CL = 90% or $\Gamma(Z) = (0.82^{+0.19}_{-0.14} \pm 0.06) \times \Gamma(W)$. Assuming Standard-Model value $\Gamma(W) = 2.65$ GeV then gives $\Gamma(Z) < 2.89 \pm 0.19$ or $= 2.17^{+0.50}_{-0.37} \pm 0.16$.

Z DECAY MODES

	Mode		Fraction (Γ_i/Γ)	Scale factor/ Confidence level
Γ_1	e^+e^-		(3.3632±0.0042) %	
Γ_2	$\mu^+\mu^-$		(3.3662±0.0066) %	
Γ_3	$\tau^+\tau^-$		(3.3696±0.0083) %	
Γ_4	$\ell^+\ell^-$	[a]	(3.3658±0.0023) %	
Γ_5	$\mu^+\mu^-\mu^+\mu^-$			
Γ_6	$\ell^+\ell^-\ell^+\ell^-$	[b]	(4.55 ±0.17) $\times 10^{-6}$	
Γ_7	invisible		(20.000 ±0.055) %	
Γ_8	hadrons		(69.911 ±0.056) %	
Γ_9	$(u\overline{u}+c\overline{c})/2$		(11.6 ±0.6) %	
Γ_{10}	$(d\overline{d}+s\overline{s}+b\overline{b})/3$		(15.6 ±0.4) %	
Γ_{11}	$c\overline{c}$		(12.03 ±0.21) %	

Int. J. Mod. Phys. A 2026.41. Downloaded from www.worldscientific.com by UNIVERSITY OF CALIFORNIA @ BERKELEY on 09/16/26. Re-use and distribution is strictly not permitted, except for Open Access articles.

Γ_{12}	$b\overline{b}$			(15.12 ±0.05) %		
Γ_{13}	$b\overline{b}b\overline{b}$			(3.6 ±1.3) $\times 10^{-4}$		
Γ_{14}	ggg			< 1.1 %		CL=95%
Γ_{15}	$\pi^0\gamma$			< 2.01 $\times 10^{-5}$		CL=95%
Γ_{16}	$\eta\gamma$			< 5.1 $\times 10^{-5}$		CL=95%
Γ_{17}	$\rho^0\gamma$			< 4.0 $\times 10^{-6}$		CL=95%
Γ_{18}	$\omega\gamma$			< 3.9 $\times 10^{-6}$		CL=95%
Γ_{19}	$\eta'(958)\gamma$			< 4.2 $\times 10^{-5}$		CL=95%
Γ_{20}	$\phi\gamma$			< 7 $\times 10^{-7}$		CL=95%
Γ_{21}	$\gamma\gamma$			< 1.46 $\times 10^{-5}$		CL=95%
Γ_{22}	$\pi^0\pi^0$			< 1.52 $\times 10^{-5}$		CL=95%
Γ_{23}	$\gamma\gamma\gamma$			< 2.2 $\times 10^{-6}$		CL=95%
Γ_{24}	$\pi^\pm W^\mp$		[c]	< 7 $\times 10^{-5}$		CL=95%
Γ_{25}	$\rho^\pm W^\mp$		[c]	< 8.3 $\times 10^{-5}$		CL=95%
Γ_{26}	$J/\psi(1S)X$			(3.51 $^{+0.23}_{-0.25}$) $\times 10^{-3}$		S=1.1
Γ_{27}	$J/\psi(1S)\gamma$			< 6 $\times 10^{-7}$		CL=95%
Γ_{28}	$\psi(2S)X$			(1.60 ±0.29) $\times 10^{-3}$		
Γ_{29}	$\psi(2S)\gamma$			< 1.3 $\times 10^{-6}$		CL=95%
Γ_{30}	$J/\psi(1S)\ell^+\ell^-$					
Γ_{31}	$J/\psi(1S)J/\psi(1S)$			< 2.2 $\times 10^{-6}$		CL=95%
Γ_{32}	$\chi_{c1}(1P)X$			(2.9 ±0.7) $\times 10^{-3}$		
Γ_{33}	$\chi_{c2}(1P)X$			< 3.2 $\times 10^{-3}$		CL=90%
Γ_{34}	$\Upsilon(1S)X + \Upsilon(2S)X + \Upsilon(3S)X$			(1.0 ±0.5) $\times 10^{-4}$		
Γ_{35}	$\Upsilon(1S)X$			< 4.4 $\times 10^{-5}$		CL=95%
Γ_{36}	$\Upsilon(1S)\gamma$			< 1.1 $\times 10^{-6}$		CL=95%
Γ_{37}	$\Upsilon(2S)X$			< 1.39 $\times 10^{-4}$		CL=95%
Γ_{38}	$\Upsilon(2S)\gamma$			< 1.3 $\times 10^{-6}$		CL=95%
Γ_{39}	$\Upsilon(3S)X$			< 9.4 $\times 10^{-5}$		CL=95%
Γ_{40}	$\Upsilon(3S)\gamma$			< 2.4 $\times 10^{-6}$		CL=95%
Γ_{41}	$\Upsilon(1,2,3S)\Upsilon(1,2,3S)$			< 1.5 $\times 10^{-6}$		CL=95%
Γ_{42}	$K^0_S\gamma$			< 3.1 $\times 10^{-6}$		CL=95%
Γ_{43}	$D^0\gamma$			< 4.0 $\times 10^{-6}$		CL=95%
Γ_{44}	$(D^0/\overline{D}^0)X$			(20.7 ±2.0) %		
Γ_{45}	$D^\pm X$			(12.2 ±1.7) %		
Γ_{46}	$D^*(2010)^\pm X$		[c]	(11.4 ±1.3) %		
Γ_{47}	$D_{s1}(2536)^\pm X$			(3.6 ±0.8) $\times 10^{-3}$		
Γ_{48}	$D_{sJ}(2573)^\pm X$			(5.8 ±2.2) $\times 10^{-3}$		
Γ_{49}	$D^{*\prime}(2629)^\pm X$			searched for		
Γ_{50}	BX					
Γ_{51}	B^*X					
Γ_{52}	B^+X		[d]	(6.08 ±0.13) %		
Γ_{53}	B^0_sX		[d]	(1.59 ±0.13) %		
Γ_{54}	B^+_cX			searched for		
Γ_{55}	Λ^+_cX			(1.54 ±0.33) %		
Γ_{56}	Ξ^0_cX			seen		
Γ_{57}	Ξ_bX			seen		
Γ_{58}	b-baryon X		[d]	(1.38 ±0.22) %		
Γ_{59}	anomalous $\gamma+$ hadrons		[e]	< 3.2 $\times 10^{-3}$		CL=95%
Γ_{60}	$e^+e^-\gamma$		[e]	< 5.2 $\times 10^{-4}$		CL=95%
Γ_{61}	$\mu^+\mu^-\gamma$		[e]	< 5.6 $\times 10^{-4}$		CL=95%
Γ_{62}	$\tau^+\tau^-\gamma$		[e]	< 7.3 $\times 10^{-4}$		CL=95%
Γ_{63}	$\ell^+\ell^-\gamma\gamma$		[f]	< 6.8 $\times 10^{-6}$		CL=95%
Γ_{64}	$q\overline{q}\gamma\gamma$		[f]	< 5.5 $\times 10^{-6}$		CL=95%
Γ_{65}	$\nu\overline{\nu}\gamma\gamma$		[f]	< 3.1 $\times 10^{-6}$		CL=95%
Γ_{66}	$e^\pm\mu^\mp$	LF	[c]	< 1.9 $\times 10^{-7}$		CL=95%
Γ_{67}	$e^\pm\tau^\mp$	LF	[c]	< 5.0 $\times 10^{-6}$		CL=95%
Γ_{68}	$\mu^\pm\tau^\mp$	LF	[c]	< 6.5 $\times 10^{-6}$		CL=95%
Γ_{69}	pe	L,B		< 1.8 $\times 10^{-6}$		CL=95%
Γ_{70}	$p\mu$	L,B		< 1.8 $\times 10^{-6}$		CL=95%

[a] ℓ indicates each type of lepton (e, μ, and τ), not sum over them.

[b] Here ℓ indicates e or μ.

[c] The value is for the sum of the charge states or particle/antiparticle states indicated.

[d] This value is updated using the product of (i) the $Z \rightarrow b\overline{b}$ fraction from this listing and (ii) the b-hadron fraction in an unbiased sample of weakly decaying b-hadrons produced in Z-decays provided by the Heavy Flavor Averaging Group (HFLAV, http://www.slac.stanford.edu/xorg/hflav/osc/PDG_2009/#FRACZ).

[e] See the Particle Listings below for the γ energy range used in this measurement.

[f] For $m_{\gamma\gamma} = (60 \pm 5)$ GeV.

Z PARTIAL WIDTHS

$\Gamma(e^+e^-)$ — Γ_1

For the LEP experiments, this parameter is not directly used in the overall fit but is derived using the fit results; see the note "The Z boson" and ref. LEP-SLC 06.

VALUE (MeV)	EVTS	DOCUMENT ID		TECN	COMMENT
83.91±0.12 OUR FIT					
83.66±0.20	137.0k	ABBIENDI	01A	OPAL	E^{ee}_{cm}= 88–94 GeV
83.54±0.27	117.8k	ABREU	00F	DLPH	E^{ee}_{cm}= 88–94 GeV
84.16±0.22	124.4k	ACCIARRI	00C	L3	E^{ee}_{cm}= 88–94 GeV
83.88±0.19		BARATE	00C	ALEP	E^{ee}_{cm}= 88–94 GeV
82.89±1.20±0.89		[1] ABE	95J	SLD	E^{ee}_{cm}= 91.31 GeV

[1] ABE 95J obtain this measurement from Bhabha events in a restricted fiducial region to improve systematics. They use the values 91.187 and 2.489 GeV for the Z mass and total decay width to extract this partial width.

$\Gamma(\mu^+\mu^-)$ — Γ_2

This parameter is not directly used in the overall fit but is derived using the fit results; see the note "The Z boson" and ref. LEP-SLC 06.

VALUE (MeV)	EVTS	DOCUMENT ID		TECN	COMMENT
83.99±0.18 OUR FIT					
84.03±0.30	182.8k	ABBIENDI	01A	OPAL	E^{ee}_{cm}= 88–94 GeV
84.48±0.40	157.6k	ABREU	00F	DLPH	E^{ee}_{cm}= 88–94 GeV
83.95±0.44	113.4k	ACCIARRI	00C	L3	E^{ee}_{cm}= 88–94 GeV
84.02±0.28		BARATE	00C	ALEP	E^{ee}_{cm}= 88–94 GeV

$\Gamma(\tau^+\tau^-)$ — Γ_3

This parameter is not directly used in the overall fit but is derived using the fit results; see the note "The Z boson" and ref. LEP-SLC 06.

VALUE (MeV)	EVTS	DOCUMENT ID		TECN	COMMENT
84.08±0.22 OUR FIT					
83.94±0.41	151.5k	ABBIENDI	01A	OPAL	E^{ee}_{cm}= 88–94 GeV
83.71±0.58	104.0k	ABREU	00F	DLPH	E^{ee}_{cm}= 88–94 GeV
84.23±0.58	103.0k	ACCIARRI	00C	L3	E^{ee}_{cm}= 88–94 GeV
84.38±0.31		BARATE	00C	ALEP	E^{ee}_{cm}= 88–94 GeV

$\Gamma(\ell^+\ell^-)$ — Γ_4

ℓ indicates each type of lepton (e, μ, and τ), not sum over them.

In our fit $\Gamma(\ell^+\ell^-)$ is defined as the partial Z width for the decay into a pair of massless charged leptons. This parameter is not directly used in the 5-parameter fit assuming lepton universality but is derived using the fit results. See the note "The Z boson" and ref. LEP-SLC 06.

VALUE (MeV)	EVTS	DOCUMENT ID		TECN	COMMENT
83.984±0.086 OUR FIT					
83.82 ±0.15	471.3k	ABBIENDI	01A	OPAL	E^{ee}_{cm}= 88–94 GeV
83.85 ±0.17	379.4k	ABREU	00F	DLPH	E^{ee}_{cm}= 88–94 GeV
84.14 ±0.17	340.8k	ACCIARRI	00C	L3	E^{ee}_{cm}= 88–94 GeV
84.02 ±0.15	500k	BARATE	00C	ALEP	E^{ee}_{cm}= 88–94 GeV

Γ(invisible) — Γ_7

The Z boson also decays to final states invisible in any detector, for example, the decay to a neutrino pair as predicted in the Standard Model. Measurements of Γ(invisible) fall into two categories: direct or indirect. Direct measurements look for final states with missing energy, missing momentum, or missing mass, corresponding to the invisible decay of a produced Z boson, including single-photon final states which arise from initial-state radiation. The indirect determination is based on Z lineshape analyses performed at the LEP collider, where the invisible decay width is calculated by subtracting all visible partial decay widths from the total decay width of the Z boson. Within the framework of the Standard Model these two determinations should be identical, but not in non-SM scenarios.

VALUE (MeV)	EVTS	DOCUMENT ID		TECN	COMMENT
499.3± 1.5 OUR AVERAGE					
506 ± 2 ±12		[1] AAD	24L	ATLS	E^{pp}_{cm} = 13 TeV
523 ± 3 ±16		[2] TUMASYAN	23E	CMS	E^{pp}_{cm} = 13 TeV
499.0± 1.5		[3] LEP-SLC	06	LEP	E^{ee}_{cm}= 88–94 GeV
498 ±12 ±12	1791	[4] ACCIARRI	98G	L3	E^{ee}_{cm}= 88–94 GeV
539 ±26 ±17	410	[4] AKERS	95C	OPAL	E^{ee}_{cm}= 88–94 GeV
450 ±34 ±34	258	[4] BUSKULIC	93L	ALEP	E^{ee}_{cm}= 88–94 GeV
540 ±80 ±40	52	[4] ADEVA	92	L3	E^{ee}_{cm}= 88–94 GeV
• • • We do not use the following data for averages, fits, limits, etc. • • •					
498.1± 2.6		[5] ABBIENDI	01A	OPAL	E^{ee}_{cm}= 88–94 GeV
498.1± 3.2		[5] ABREU	00F	DLPH	E^{ee}_{cm}= 88–94 GeV
499.1± 2.9		[5] ACCIARRI	00C	L3	E^{ee}_{cm}= 88–94 GeV
499.1± 2.5		[5] BARATE	00C	ALEP	E^{ee}_{cm}= 88–94 GeV

[1] AAD 24L use the measured ratio of invisible Z decays and leptonic Z decays to derive the width of the Z decaying to invisible particles. Events with transverse momentum of the Z larger than 130 GeV and at least one central jet with transverse momentum larger than 110 GeV are selected.

[2] TUMASYAN 23E analyses leptonic Z decay modes, with the invisible Z decay identified by missing momentum.

[3] The LEP Collaborations perform a combined fit to their line-shape results and determine this quantity as a difference between the total width and the sum of all the visible widths, assuming lepton universality. This result combines ABBIENDI 01A, ABREU 00F, ACCIARRI 00C, BARATE 00C, taking correlated uncertainties into account.
[4] This analysis selects single-photon events arising from inital state radiation.
[5] This is an indirect determination of Γ(invisible) from a fit to the visible Z decay modes. It is included in the determination of the LEP average LEP-SLC 06 reported above.

Γ(hadrons) — Γ_8

This parameter is not directly used in the 5-parameter fit assuming lepton universality, but is derived using the fit results. See the note "The Z boson" and ref. LEP-SLC 06.

VALUE (MeV)	EVTS	DOCUMENT ID		TECN	COMMENT
1744.4±2.0 OUR FIT					
1745.4±3.5	4.10M	ABBIENDI	01A	OPAL	E^{ee}_{cm}= 88–94 GeV
1738.1±4.0	3.70M	ABREU	00F	DLPH	E^{ee}_{cm}= 88–94 GeV
1751.1±3.8	3.54M	ACCIARRI	00C	L3	E^{ee}_{cm}= 88–94 GeV
1744.0±3.4	4.07M	BARATE	00C	ALEP	E^{ee}_{cm}= 88–94 GeV

Z BRANCHING RATIOS

OUR FIT is obtained using the fit procedure and correlations as determined by the LEP Electroweak Working Group (see the note "The Z boson" and ref. LEP-SLC 06).

Γ(μ⁺μ⁻)/Γ(e⁺e⁻) — Γ_2/Γ_1

VALUE	DOCUMENT ID		TECN	COMMENT
1.0001±0.0024 OUR AVERAGE				
0.9974±0.0050	[1] AABOUD	17Q	ATLS	E^{pp}_{cm} = 7 TeV
1.0009±0.0028	[2] LEP-SLC	06		E^{ee}_{cm} = 88–94 GeV

[1] AABOUD 17Q make a precise determination of $Z \to ee$ and $Z \to \mu\mu$ production in the lepton pseudo-rapidity range $|\eta| < 2.5$ and determine the ratio of the Z branching fractions $B(Z \to ee)/B(Z \to \mu\mu) = 1.0026 \pm 0.0013 \pm 0.0048 = 1.0026 \pm 0.0050$.
[2] This parameter is not directly used in the overall fit but is derived using the fit results; see the note "The Z boson" and ref. LEP-SLC 06.

Γ(τ⁺τ⁻)/Γ(e⁺e⁻) — Γ_3/Γ_1

VALUE	DOCUMENT ID		TECN	COMMENT
1.0020±0.0032 OUR AVERAGE				
1.02 ±0.06	[1] AAIJ	18AR	LHCB	E^{pp}_{cm} = 8 TeV
1.0019±0.0032	[2] LEP-SLC	06		E^{ee}_{cm} = 88–94 GeV

[1] AAIJ 18AR obtain the result from the ratio of the measured $pp \to Z + X$ cross sections in the corresponding Z decay channels.
[2] This parameter is not directly used in the overall fit but is derived using the fit results; see the note "The Z boson" and ref. LEP-SLC 06.

Γ(τ⁺τ⁻)/Γ(μ⁺μ⁻) — Γ_3/Γ_2

VALUE	DOCUMENT ID		TECN	COMMENT
1.0010±0.0026 OUR AVERAGE				
1.01 ±0.05	[1] AAIJ	18AR	LHCB	E^{pp}_{cm} = 8 TeV
1.0010±0.0026	[2] LEP-SLC	06		E^{ee}_{cm} = 88–94 GeV

[1] AAIJ 18AR obtain the result from the ratio of the measured $pp \to Z + X$ cross sections in the corresponding Z decay channels.
[2] This parameter is not directly used in the overall fit but is derived using the fit results; see the note "The Z boson" and ref. LEP-SLC 06.

Γ(ℓ⁺ℓ⁻ℓ⁺ℓ⁻)/Γ_total — Γ_6/Γ

Here ℓ indicates either e or μ. The branching fractions in this node are given within the phase-space defined by the requirements that (i) the 4-lepton invariant mass is between 80 GeV and 100 GeV, and (ii) any opposite-sign same-flavor lepton pair has a di-lepton invariant mass larger than 4 GeV.

VALUE (units 10^{-6})	EVTS	DOCUMENT ID		TECN	COMMENT
4.55±0.17 OUR AVERAGE					
4.41±0.13±0.27		[1] AAD	21AQ	ATLS	E^{pp}_{cm} = 13 TeV
4.70±0.32±0.25		[2] AABOUD	19N	ATLS	E^{pp}_{cm} = 13 TeV
$4.83^{+0.23}_{-0.22}{}^{+0.35}_{-0.32}$	509	[3] SIRUNYAN	18BT	CMS	E^{pp}_{cm} = 13 TeV
$4.9\ ^{+0.8}_{-0.7}\ ^{+0.4}_{-0.2}$	39	[4] KHACHATRY...	16CC	CMS	E^{pp}_{cm} = 13 TeV
4.31±0.34±0.17	172	AAD	14N	ATLS	E^{pp}_{cm} = 7, 8 TeV
$4.6\ ^{+1.0}_{-0.9}$ ±0.2	28	[5] CHATRCHYAN	12BN	CMS	E^{pp}_{cm} = 7 TeV

[1] AAD 21AQ analyze differential cross-sections in four-lepton events. Based on the measured cross section in the $Z \to 4\ell$ channel, a branching fraction of $B(Z \to 4\ell) = (4.41 \pm 0.13 \pm 0.23 \pm 0.09 \pm 0.12) \times 10^{-6}$ is obtained, where the uncertainties are statistical, systematic, theory and luminosity, respectively.
[2] AABOUD 19N reports $(4.70 \pm 0.32 \pm 0.21 \pm 0.14) \times 10^{-6}$, where the uncertainties are statistical, systematic, and luminosity. We have combined the latter two in quadrature.
[3] SIRUNYAN 18BT report the $Z \to 4\ell$ branching fraction $= (4.83^{+0.23}_{-0.22}{}^{+0.32}_{-0.29} \pm 0.08 \pm 0.12) \times 10^{-6}$, where the uncertainties are statistical, systematic, due to theory, and luminosity. The last three have been added in quadrature to obtain the total systematic error.
[4] KHACHATRYAN 16CC reports $(4.9^{+0.8}_{-0.7}{}^{+0.3}_{-0.2}{}^{+0.2}_{-0.1}{}^{+0.1}_{-0.1}) \times 10^{-6}$ value, where the uncertainties are statistical, systematic, theory, and due to luminosity. We have combined uncertainties in quadrature.
[5] CHATRCHYAN 12BN reports $(4.2^{+0.9}_{-0.8} \pm 0.2) \times 10^{-6}$ value. Their result (both central value and uncertainties) is scaled up by 10% to account for the different phase-space definition used here (see RAINBOLT 19).

Γ(hadrons)/Γ(e⁺e⁻) — Γ_8/Γ_1

VALUE	EVTS	DOCUMENT ID		TECN	COMMENT
20.804± 0.050 OUR FIT					
20.902± 0.084	137.0k	[1] ABBIENDI	01A	OPAL	E^{ee}_{cm}= 88–94 GeV
20.88 ± 0.12	117.8k	ABREU	00F	DLPH	E^{ee}_{cm}= 88–94 GeV
20.816± 0.089	124.4k	ACCIARRI	00C	L3	E^{ee}_{cm}= 88–94 GeV
20.677± 0.075		[2] BARATE	00C	ALEP	E^{ee}_{cm}= 88–94 GeV
• • • We do not use the following data for averages, fits, limits, etc. • • •					
$27.0\ ^{+11.7}_{-8.8}$	12	[3] ABRAMS	89D	MRK2	E^{ee}_{cm}= 89–93 GeV

[1] ABBIENDI 01A error includes approximately 0.067 due to statistics, 0.040 due to event selection systematics, 0.027 due to the theoretical uncertainty in t-channel prediction, and 0.014 due to LEP energy uncertainty.
[2] BARATE 00C error includes approximately 0.062 due to statistics, 0.033 due to experimental systematics, and 0.026 due to the theoretical uncertainty in t-channel prediction.
[3] ABRAMS 89D have included both statistical and systematic uncertainties in their quoted errors.

Γ(hadrons)/Γ(μ⁺μ⁻) — Γ_8/Γ_2

OUR FIT is obtained using the fit procedure and correlations as determined by the LEP Electroweak Working Group (see the note "The Z boson" and ref. LEP-SLC 06).

VALUE	EVTS	DOCUMENT ID		TECN	COMMENT
20.785±0.033 OUR FIT					
20.811±0.058	182.8k	[1] ABBIENDI	01A	OPAL	E^{ee}_{cm}= 88–94 GeV
20.65 ±0.08	157.6k	ABREU	00F	DLPH	E^{ee}_{cm}= 88–94 GeV
20.861±0.097	113.4k	ACCIARRI	00C	L3	E^{ee}_{cm}= 88–94 GeV
20.799±0.056		[2] BARATE	00C	ALEP	E^{ee}_{cm}= 88–94 GeV
• • • We do not use the following data for averages, fits, limits, etc. • • •					
$18.9\ ^{+7.1}_{-5.3}$	13	[3] ABRAMS	89D	MRK2	E^{ee}_{cm}= 89–93 GeV

[1] ABBIENDI 01A error includes approximately 0.050 due to statistics and 0.027 due to event selection systematics.
[2] BARATE 00C error includes approximately 0.053 due to statistics and 0.021 due to experimental systematics.
[3] ABRAMS 89D have included both statistical and systematic uncertainties in their quoted errors.

Γ(hadrons)/Γ(τ⁺τ⁻) — Γ_8/Γ_3

OUR FIT is obtained using the fit procedure and correlations as determined by the LEP Electroweak Working Group (see the note "The Z boson" and ref. LEP-SLC 06).

VALUE	EVTS	DOCUMENT ID		TECN	COMMENT
20.764±0.045 OUR FIT					
20.832±0.091	151.5k	[1] ABBIENDI	01A	OPAL	E^{ee}_{cm}= 88–94 GeV
20.84 ±0.13	104.0k	ABREU	00F	DLPH	E^{ee}_{cm}= 88–94 GeV
20.792±0.133	103.0k	ACCIARRI	00C	L3	E^{ee}_{cm}= 88–94 GeV
20.707±0.062		[2] BARATE	00C	ALEP	E^{ee}_{cm}= 88–94 GeV
• • • We do not use the following data for averages, fits, limits, etc. • • •					
$15.2\ ^{+4.8}_{-3.9}$	21	[3] ABRAMS	89D	MRK2	E^{ee}_{cm}= 89–93 GeV

[1] ABBIENDI 01A error includes approximately 0.055 due to statistics and 0.071 due to event selection systematics.
[2] BARATE 00C error includes approximately 0.054 due to statistics and 0.033 due to experimental systematics.
[3] ABRAMS 89D have included both statistical and systematic uncertainties in their quoted errors.

Γ(hadrons)/Γ(ℓ⁺ℓ⁻) — Γ_8/Γ_4

ℓ indicates each type of lepton (e, μ, and τ), not sum over them.

Our fit result is obtained requiring lepton universality.

VALUE	EVTS	DOCUMENT ID		TECN	COMMENT
20.767±0.025 OUR FIT					
20.823±0.044	471.3k	[1] ABBIENDI	01A	OPAL	E^{ee}_{cm}= 88–94 GeV
20.730±0.060	379.4k	ABREU	00F	DLPH	E^{ee}_{cm}= 88–94 GeV
20.810±0.060	340.8k	ACCIARRI	00C	L3	E^{ee}_{cm}= 88–94 GeV
20.725±0.039	500k	[2] BARATE	00C	ALEP	E^{ee}_{cm}= 88–94 GeV
• • • We do not use the following data for averages, fits, limits, etc. • • •					
$18.9\ ^{+3.6}_{-3.2}$	46	ABRAMS	89B	MRK2	E^{ee}_{cm}= 89–93 GeV

[1] ABBIENDI 01A error includes approximately 0.034 due to statistics and 0.027 due to event selection systematics.
[2] BARATE 00C error includes approximately 0.033 due to statistics, 0.020 due to experimental systematics, and 0.005 due to the theoretical uncertainty in t-channel prediction.

Γ((uū+cc̄)/2)/Γ(hadrons) — Γ_9/Γ_8

This quantity is the branching ratio of $Z \to$ "up-type" quarks to $Z \to$ hadrons. Except ACKERSTAFF 97T the values of $Z \to$ "up-type" and $Z \to$ "down-type" branchings are extracted from measurements of Γ(hadrons), and $\Gamma(Z \to \gamma +$ jets) where γ is a high-energy (>5 or 7 GeV) isolated photon. As the experiments use different procedures and slightly different values of M_Z, Γ(hadrons) and α_s in their extraction procedures, our average has to be taken with caution.

VALUE	DOCUMENT ID		TECN	COMMENT
0.166±0.009 OUR AVERAGE				
$0.172^{+0.011}_{-0.010}$	[1] ABBIENDI	04E	OPAL	E^{ee}_{cm} = 91.2 GeV
0.160±0.019±0.019	[2] ACKERSTAFF	97T	OPAL	E^{ee}_{cm}= 88–94 GeV
$0.137^{+0.038}_{-0.054}$	[3] ABREU	95X	DLPH	E^{ee}_{cm}= 88–94 GeV
0.137±0.033	[4] ADRIANI	93	L3	E^{ee}_{cm}= 91.2 GeV

Int. J. Mod. Phys. A 2026.41. Downloaded from www.worldscientific.com
by UNIVERSITY OF CALIFORNIA @ BERKELEY on 09/16/26. Reproduction is strictly not permitted, except for Open Access articles.

Int. J. Mod. Phys. A 2026.41. Downloaded from www.worldscientific.com by UNIVERSITY OF CALIFORNIA @ BERKELEY on 09/16/26. Re-use and distribution is strictly not permitted, except for Open Access articles.

[1] ABBIENDI 04E select photons with energy > 7 GeV and use Γ(hadrons) = 1744.4 ± 2.0 MeV and α_s = 0.1172 ± 0.002 to obtain $\Gamma_u = 300^{+19}_{-18}$ MeV.

[2] ACKERSTAFF 97T measure $\Gamma_{u\overline{u}}/(\Gamma_{d\overline{d}}+\Gamma_{u\overline{u}}+\Gamma_{s\overline{s}})$ = 0.258 ± 0.031 ± 0.032. To obtain this branching ratio authors use R_c+R_b = 0.380 ± 0.010. This measurement is fully negatively correlated with the measurement of $\Gamma_{d\overline{d},s\overline{s}}/(\Gamma_{d\overline{d}}+\Gamma_{u\overline{u}}+\Gamma_{s\overline{s}})$ given in the next data block.

[3] ABREU 95X use M_Z = 91.187 ± 0.009 GeV, Γ(hadrons) = 1725 ± 12 MeV and α_s = 0.123 ± 0.005. To obtain this branching ratio we divide their value of $C_{2/3} = 91^{+0.25}_{-0.36}$ by their value of $(3C_{1/3} + 2C_{2/3})$ = 6.66 ± 0.05.

[4] ADRIANI 93 use M_Z = 91.181 ± 0.022 GeV, Γ(hadrons) = 1742 ± 19 MeV and α_s = 0.125 ± 0.009. To obtain this branching ratio we divide their value of $C_{2/3}$ = 0.92 ± 0.22 by their value of $(3C_{1/3} + 2C_{2/3})$ = 6.720 ± 0.076.

$\Gamma((d\overline{d}+s\overline{s}+b\overline{b})/3)/\Gamma$(hadrons) — Γ_{10}/Γ_8

This quantity is the branching ratio of $Z \to$ "down-type" quarks to $Z \to$ hadrons. Except ACKERSTAFF 97T the values of $Z \to$ "up-type" and $Z \to$ "down-type" branchings are extracted from measurements of Γ(hadrons), and $\Gamma(Z \to \gamma+$ jets) where γ is a high-energy (>5 or 7 GeV) isolated photon. As the experiments use different procedures and slightly different values of M_Z, Γ(hadrons) and α_s in their extraction procedures, our average has to be taken with caution.

VALUE	DOCUMENT ID		TECN	COMMENT
0.223±0.006 OUR AVERAGE				
0.218±0.007	[1] ABBIENDI	04E	OPAL	E^{ee}_{cm} = 91.2 GeV
0.230±0.010±0.010	[2] ACKERSTAFF	97T	OPAL	E^{ee}_{cm}= 88–94 GeV
$0.243^{+0.036}_{-0.026}$	[3] ABREU	95X	DLPH	E^{ee}_{cm}= 88–94 GeV
0.243±0.022	[4] ADRIANI	93	L3	E^{ee}_{cm}= 91.2 GeV

[1] ABBIENDI 04E select photons with energy > 7 GeV and use Γ(hadrons) = 1744.4 ± 2.0 MeV and α_s = 0.1172 ± 0.002 to obtain Γ_d = 381 ± 12 MeV.

[2] ACKERSTAFF 97T measure $\Gamma_{d\overline{d},s\overline{s}}/(\Gamma_{d\overline{d}}+\Gamma_{u\overline{u}}+\Gamma_{s\overline{s}})$ = 0.371 ± 0.016 ± 0.016. To obtain this branching ratio authors use R_c+R_b = 0.380 ± 0.010. This measurement is fully negatively correlated with the measurement of $\Gamma_{u\overline{u}}/(\Gamma_{d\overline{d}}+\Gamma_{u\overline{u}}+\Gamma_{s\overline{s}})$ presented in the previous data block.

[3] ABREU 95X use M_Z = 91.187 ± 0.009 GeV, Γ(hadrons) = 1725 ± 12 MeV and α_s = 0.123 ± 0.005. To obtain this branching ratio we divide their value of $C_{1/3} = 1.62^{+0.24}_{-0.17}$ by their value of $(3C_{1/3} + 2C_{2/3})$ = 6.66 ± 0.05.

[4] ADRIANI 93 use M_Z = 91.181 ± 0.022 GeV, Γ(hadrons) = 1742 ± 19 MeV and α_s = 0.125 ± 0.009. To obtain this branching ratio we divide their value of $C_{1/3}$ = 1.63 ± 0.15 by their value of $(3C_{1/3} + 2C_{2/3})$ = 6.720 ± 0.076.

$R_c = \Gamma(c\overline{c})/\Gamma$(hadrons) — Γ_{11}/Γ_8

OUR FIT is obtained by a simultaneous fit to several c- and b-quark measurements as explained in the note "The Z boson" and ref. LEP-SLC 06.

The Standard Model predicts R_c = 0.1723 for m_t = 174.3 GeV and M_H = 150 GeV.

VALUE	DOCUMENT ID		TECN	COMMENT
0.1721±0.0030 OUR FIT				
0.1744±0.0031±0.0021	[1] ABE	05F	SLD	E^{ee}_{cm}=91.28 GeV
0.1665±0.0051±0.0081	[2] ABREU	00	DLPH	E^{ee}_{cm}= 88–94 GeV
0.1698±0.0069	[3] BARATE	00B	ALEP	E^{ee}_{cm}= 88–94 GeV
0.180 ±0.011 ±0.013	[4] ACKERSTAFF	98E	OPAL	E^{ee}_{cm}= 88–94 GeV
0.167 ±0.011 ±0.012	[5] ALEXANDER	96R	OPAL	E^{ee}_{cm}= 88–94 GeV
• • • We do not use the following data for averages, fits, limits, etc. • • •				
0.1623±0.0085±0.0209	[6] ABREU	95D	DLPH	E^{ee}_{cm}= 88–94 GeV

[1] ABE 05F use hadronic Z decays collected during 1996–98 to obtain an enriched sample of $c\overline{c}$ events using a double tag method. The single c-tag is obtained with a neural network trained to perform flavor discrimination using as input several signatures (corrected secondary vertex mass, vertex decay length, multiplicity and total momentum of the hemisphere). A multitag approach is used, defining 4 regions of the output value of the neural network and R_c is extracted from a simultaneous fit to the count rates of the 4 different tags. The quoted systematic error includes an uncertainty of ±0.0006 due to the uncertainty on R_b.

[2] ABREU 00 obtain this result properly combining the measurement from the D^{*+} production rate (R_c= 0.1610 ± 0.0104 ± 0.0077 ± 0.0043 (BR)) with that from the overall charm counting (R_c= 0.1692 ± 0.0047 ± 0.0063 ± 0.0074 (BR)) in $c\overline{c}$ events. The systematic error includes an uncertainty of ±0.0054 due to the uncertainty on the charmed hadron branching fractions.

[3] BARATE 00B use exclusive decay modes to independently determine the quantities $R_c \times f(c \to X)$, X=D^0, D^+, D^+_s, and Λ_c. Estimating $R_c \times f(c \to \Xi_c/\Omega_c)$= 0.0034, they simply sum over all the charm decays to obtain R_c= 0.1738 ± 0.0047 ± 0.0088 ± 0.0075(BR). This is combined with all previous ALEPH measurements (BARATE 98T and BUSKULIC 94G, R_c= 0.1681 ± 0.0054 ± 0.0062) to obtain the quoted value.

[4] ACKERSTAFF 98E use an inclusive/exclusive double tag. In one jet $D^{*\pm}$ mesons are exclusively reconstructed in several decay channels and in the opposite jet a slow pion (opposite charge inclusive $D^{*\pm}$) tag is used. The b content of this sample is measured by the simultaneous detection of a lepton in one jet and an inclusively reconstructed $D^{*\pm}$ meson in the opposite jet. The systematic error includes an uncertainty of ±0.006 due to the external branching ratios.

[5] ALEXANDER 96R obtain this value via direct charm counting, summing the partial contributions from D^0, D^+, D^+_s, and Λ^+_c, and assuming that strange-charmed baryons account for the 15% of the Λ^+_c production. An uncertainty of ±0.005 due to the uncertainties in the charm hadron branching ratios is included in the overall systematics.

[6] ABREU 95D perform a maximum likelihood fit to the combined p and p_T distributions of single and dilepton samples. The second error includes an uncertainty of ±0.0124 due to models and branching ratios.

$R_b = \Gamma(b\overline{b})/\Gamma$(hadrons) — Γ_{12}/Γ_8

OUR FIT is obtained by a simultaneous fit to several c- and b-quark measurements as explained in the note "The Z boson" and ref. LEP-SLC 06.

The Standard Model predicts R_b=0.21581 for m_t=174.3 GeV and M_H=150 GeV.

VALUE	DOCUMENT ID		TECN	COMMENT
0.21629±0.00066 OUR FIT				
0.21594±0.00094±0.00075	[1] ABE	05F	SLD	E^{ee}_{cm}=91.28 GeV
0.2174 ±0.0015 ±0.0028	[2] ACCIARRI	00	L3	E^{ee}_{cm}= 89–93 GeV
0.2178 ±0.0011 ±0.0013	[3] ABBIENDI	99B	OPAL	E^{ee}_{cm}= 88–94 GeV
0.21634±0.00067±0.00060	[4] ABREU	99B	DLPH	E^{ee}_{cm}= 88–94 GeV
0.2159 ±0.0009 ±0.0011	[5] BARATE	97F	ALEP	E^{ee}_{cm}= 88–94 GeV
• • • We do not use the following data for averages, fits, limits, etc. • • •				
0.2145 ±0.0089 ±0.0067	[6] ABREU	95D	DLPH	E^{ee}_{cm}= 88–94 GeV
0.219 ±0.006 ±0.005	[7] BUSKULIC	94G	ALEP	E^{ee}_{cm}= 88–94 GeV
0.251 ±0.049 ±0.030	[8] JACOBSEN	91	MRK2	E^{ee}_{cm}= 91 GeV

[1] ABE 05F use hadronic Z decays collected during 1996–98 to obtain an enriched sample of $b\overline{b}$ events using a double tag method. The single b–tag is obtained with a neural network trained to perform flavor discrimination using as input several signatures (corrected secondary vertex mass, vertex decay length, multiplicity and total momentum of the hemisphere; the key tag is obtained requiring the secondary vertex corrected mass to be above the D–meson mass). ABE 05F obtain R_b =0.21604 ± 0.00098 ± 0.00074 where the systematic error includes an uncertainty of ±0.00012 due to the uncertainty on R_c. The value reported here is obtained properly combining with ABE 98D. The quoted systematic error includes an uncertainty of ±0.00012 due to the uncertainty on R_c.

[2] ACCIARRI 00 obtain this result using a double-tagging technique, with a high p_T lepton tag and an impact parameter tag in opposite hemispheres.

[3] ABBIENDI 99B tag $Z \to b\overline{b}$ decays using leptons and/or separated decay vertices. The b-tagging efficiency is measured directly from the data using a double-tagging technique.

[4] ABREU 99B obtain this result combining in a multivariate analysis several tagging methods (impact parameter and secondary vertex reconstruction, complemented by event shape variables). For R_c different from its Standard Model value of 0.172, R_b varies as $-0.024\times(R_c-0.172)$.

[5] BARATE 97F combine the lifetime-mass hemisphere tag (BARATE 97E) with event shape information and lepton tag to identify $Z \to b\overline{b}$ candidates. They further use c- and $u\,d\,s$-selection tags to identify the background. For R_c different from its Standard Model value of 0.172, R_b varies as $-0.019\times(R_c - 0.172)$.

[6] ABREU 95D perform a maximum likelihood fit to the combined p and p_T distributions of single and dilepton samples. The second error includes an uncertainty of ±0.0023 due to models and branching ratios.

[7] BUSKULIC 94G perform a simultaneous fit to the p and p_T spectra of both single and dilepton events.

[8] JACOBSEN 91 tagged $b\overline{b}$ events by requiring coincidence of ≥ 3 tracks with significant impact parameters using vertex detector. Systematic error includes lifetime and decay uncertainties (±0.014).

$\Gamma(b\overline{b}b\overline{b})/\Gamma$(hadrons) — Γ_{13}/Γ_8

VALUE (units 10^{-4})	DOCUMENT ID		TECN	COMMENT
5.2±1.9 OUR AVERAGE				
3.6±1.7±2.7	[1] ABBIENDI	01G	OPAL	E^{ee}_{cm}= 88–94 GeV
6.0±1.9±1.4	[2] ABREU	99U	DLPH	E^{ee}_{cm}= 88–94 GeV

[1] ABBIENDI 01G use a sample of four-jet events from hadronic Z decays. To enhance the $b\overline{b}b\overline{b}$ signal, at least three of the four jets are required to have a significantly detached secondary vertex.

[2] ABREU 99U force hadronic Z decays into 3 jets to use all the available phase space and require a b tag for every jet. This decay mode includes primary and secondary $4b$ production, *e.g*, from gluon splitting to $b\overline{b}$.

$\Gamma(ggg)/\Gamma$(hadrons) — Γ_{14}/Γ_8

VALUE	CL%	DOCUMENT ID		TECN	COMMENT
<1.6 × 10^{-2}	95	[1] ABREU	96S	DLPH	E^{ee}_{cm}= 88–94 GeV

[1] This branching ratio is slightly dependent on the jet-finder algorithm. The value we quote is obtained using the JADE algorithm, while using the DURHAM algorithm ABREU 96S obtain an upper limit of 1.5 × 10^{-2}.

$\Gamma(\pi^0\gamma)/\Gamma_{total}$ — Γ_{15}/Γ

VALUE	CL%	DOCUMENT ID		TECN	COMMENT
<2.01 × 10^{-5}	95	AALTONEN	14E	CDF	$E^{p\overline{p}}_{cm}$ = 1.96 TeV
<5.2 × 10^{-5}	95	[1] ACCIARRI	95G	L3	E^{ee}_{cm}= 88–94 GeV
<5.5 × 10^{-5}	95	ABREU	94B	DLPH	E^{ee}_{cm}= 88–94 GeV
<2.1 × 10^{-4}	95	DECAMP	92	ALEP	E^{ee}_{cm}= 88–94 GeV
<1.4 × 10^{-4}	95	AKRAWY	91F	OPAL	E^{ee}_{cm}= 88–94 GeV

[1] This limit is for both decay modes $Z \to \pi^0\gamma/\gamma\gamma$ which are indistinguishable in ACCIARRI 95G.

$\Gamma(\eta\gamma)/\Gamma_{total}$ — Γ_{16}/Γ

VALUE	CL%	DOCUMENT ID		TECN	COMMENT
<7.6 × 10^{-5}	95	ACCIARRI	95G	L3	E^{ee}_{cm}= 88–94 GeV
<8.0 × 10^{-5}	95	ABREU	94B	DLPH	E^{ee}_{cm}= 88–94 GeV
<5.1 × 10^{-5}	95	DECAMP	92	ALEP	E^{ee}_{cm}= 88–94 GeV
<2.0 × 10^{-4}	95	AKRAWY	91F	OPAL	E^{ee}_{cm}= 88–94 GeV

$\Gamma(\rho^0\gamma)/\Gamma_{total}$ — Γ_{17}/Γ

VALUE	CL%	EVTS	DOCUMENT ID		TECN	COMMENT
<4.0 × 10^{-6}	95	12.5k	[1] AABOUD	18AU	ATLS	E^{pp}_{cm} = 13 TeV

[1] AABOUD 18AU search for the $Z \to \rho\gamma$ decay mode where the ρ is identified through its decay $\rho \to \pi^+\pi^-$. In the data corresponding to 32.3 fb^{-1}, 12,583 events are selected for $635 < m(\pi^+\pi^-) < 915$ MeV. See erratum AABOUD 23A.

$\Gamma(\omega\gamma)/\Gamma_{total}$ — Γ_{18}/Γ

VALUE	CL%	DOCUMENT ID		TECN	COMMENT
$<3.9 \times 10^{-6}$	95	AAD	23BS	ATLAS	E^{pp}_{cm} = 13 TeV
• • • We do not use the following data for averages, fits, limits, etc. • • •					
$<6.5 \times 10^{-4}$	95	ABREU	94B	DLPH	E^{ee}_{cm} = 88–94 GeV

$\Gamma(\eta'(958)\gamma)/\Gamma_{total}$ — Γ_{19}/Γ

VALUE	CL%	DOCUMENT ID		TECN	COMMENT
$<4.2 \times 10^{-5}$	95	DECAMP	92	ALEP	E^{ee}_{cm} = 88–94 GeV

$\Gamma(\phi\gamma)/\Gamma_{total}$ — Γ_{20}/Γ

VALUE	CL%	EVTS	DOCUMENT ID		TECN	COMMENT
$<7 \times 10^{-7}$	95	3.3k	[1] AABOUD	18AU	ATLAS	E^{pp}_{cm} = 13 TeV
• • • We do not use the following data for averages, fits, limits, etc. • • •						
$<8.3 \times 10^{-6}$	95	1.0k	[2] AABOUD	16K	ATLAS	E^{pp}_{cm} = 13 TeV

[1] AABOUD 18AU search for the $Z \to \phi\gamma$ decay mode where the ϕ is identified through its decay $\phi \to K^+K^-$. In the data corresponding to 32.3 fb^{-1}, 3,364 events are selected for $1012 < m(K^+K^-) < 1028$ MeV. See erratum AABOUD 23A.

[2] AABOUD 16K search for the $Z \to \phi\gamma$ decay mode where the ϕ is identified through its decay into K^+K^-. In the data corresponding to a total luminosity of 2.7 fb^{-1}, 1065 events are selected and their $K^+K^-\gamma$ invariant mass spectrum is analyzed.

$\Gamma(\gamma\gamma)/\Gamma_{total}$ — Γ_{21}/Γ

This decay would violate the Landau-Yang theorem.

VALUE	CL%	DOCUMENT ID		TECN	COMMENT
$<1.46 \times 10^{-5}$	95	AALTONEN	14E	CDF	$E^{p\overline{p}}_{cm}$ = 1.96 TeV
$<5.2 \times 10^{-5}$	95	[1] ACCIARRI	95G	L3	E^{ee}_{cm} = 88–94 GeV
$<5.5 \times 10^{-5}$	95	ABREU	94B	DLPH	E^{ee}_{cm} = 88–94 GeV
$<1.4 \times 10^{-4}$	95	AKRAWY	91F	OPAL	E^{ee}_{cm} = 88–94 GeV

[1] This limit is for both decay modes $Z \to \pi^0\gamma/\gamma\gamma$ which are indistinguishable in ACCIARRI 95G.

$\Gamma(\pi^0\pi^0)/\Gamma_{total}$ — Γ_{22}/Γ

VALUE	CL%	DOCUMENT ID		TECN	COMMENT
$<1.52 \times 10^{-5}$	95	AALTONEN	14E	CDF	$E^{p\overline{p}}_{cm}$ = 1.96 TeV

$\Gamma(\gamma\gamma\gamma)/\Gamma_{total}$ — Γ_{23}/Γ

VALUE	CL%	DOCUMENT ID		TECN	COMMENT
$<2.2 \times 10^{-6}$	95	AAD	16L	ATLAS	E^{pp}_{cm} = 8 TeV
• • • We do not use the following data for averages, fits, limits, etc. • • •					
$<1.0 \times 10^{-5}$	95	[1] ACCIARRI	95C	L3	E^{ee}_{cm} = 88–94 GeV
$<1.7 \times 10^{-5}$	95	[1] ABREU	94B	DLPH	E^{ee}_{cm} = 88–94 GeV
$<6.6 \times 10^{-5}$	95	AKRAWY	91F	OPAL	E^{ee}_{cm} = 88–94 GeV

[1] Limit derived in the context of composite Z model.

$\Gamma(\pi^\pm W^\mp)/\Gamma_{total}$ — Γ_{24}/Γ

The value is for the sum of the charge states indicated.

VALUE	CL%	DOCUMENT ID		TECN	COMMENT
$<7 \times 10^{-5}$	95	DECAMP	92	ALEP	E^{ee}_{cm} = 88–94 GeV

$\Gamma(\rho^\pm W^\mp)/\Gamma_{total}$ — Γ_{25}/Γ

The value is for the sum of the charge states indicated.

VALUE	CL%	DOCUMENT ID		TECN	COMMENT
$<8.3 \times 10^{-5}$	95	DECAMP	92	ALEP	E^{ee}_{cm} = 88–94 GeV

$\Gamma(J/\psi(1S)X)/\Gamma_{total}$ — Γ_{26}/Γ

VALUE (units 10^{-3})	EVTS	DOCUMENT ID		TECN	COMMENT
$3.51^{+0.23}_{-0.25}$ OUR AVERAGE	Error includes scale factor of 1.1.				
$3.21 \pm 0.21^{+0.19}_{-0.28}$	553	[1] ACCIARRI	99F	L3	E^{ee}_{cm} = 88–94 GeV
$3.9 \pm 0.2 \pm 0.3$	511	[2] ALEXANDER	96B	OPAL	E^{ee}_{cm} = 88–94 GeV
$3.73 \pm 0.39 \pm 0.36$	153	[3] ABREU	94P	DLPH	E^{ee}_{cm} = 88–94 GeV

[1] ACCIARRI 99F combine $\mu^+\mu^-$ and e^+e^- $J/\psi(1S)$ decay channels. The branching ratio for prompt $J/\psi(1S)$ production is measured to be $(2.1 \pm 0.6 \pm 0.4^{+0.4}_{-0.2}(\text{theor.})) \times 10^{-4}$.

[2] ALEXANDER 96B identify $J/\psi(1S)$ from the decays into lepton pairs. (4.8 ± 2.4)% of this branching ratio is due to prompt $J/\psi(1S)$ production (ALEXANDER 96N).

[3] Combining $\mu^+\mu^-$ and e^+e^- channels and taking into account the common systematic errors. $(7.7^{+6.3}_{-5.4})$% of this branching ratio is due to prompt $J/\psi(1S)$ production.

$\Gamma(J/\psi(1S)\gamma)/\Gamma_{total}$ — Γ_{27}/Γ

VALUE	CL%	DOCUMENT ID		TECN	COMMENT
$<0.6 \times 10^{-6}$	95	HAYRAPETY...25H		CMS	E^{pp}_{cm} = 13 TeV
• • • We do not use the following data for averages, fits, limits, etc. • • •					
$<1.2 \times 10^{-6}$	95	AAD	23CD	ATLAS	E^{pp}_{cm} = 13 TeV
$<1.4 \times 10^{-6}$	95	[1] SIRUNYAN	19AJ	CMS	E^{pp}_{cm} = 13 TeV
$<2.3 \times 10^{-6}$	95	[2] AABOUD	18BL	ATLAS	E^{pp}_{cm} = 13 TeV
$<2.6 \times 10^{-6}$	95	[3] AAD	15I	ATLAS	E^{pp}_{cm} = 8 TeV

[1] SIRUNYAN 19AJ study $Z \to J/\psi\gamma$ with $J/\psi \to \mu^+\mu^-$. Candidate events are selected by requiring a pair of oppositely charged muons and a well isolated photon. The leading (subleading) muon is require to have a transverse momentum larger than 20 GeV (4 GeV), while the photon must have a transverse energy larger than 33 GeV. Requiring the invariant mass of the $\mu\mu$ ($\mu\mu\gamma$) system in the range 3.0 to 3.2 (81 to 101) GeV, selects 183 data events which is consistent with the expected background. The 95% C.L. limit on the Z branching fraction is obtained assuming the J/ψ to be unpolarized.

[2] AABOUD 18BL study $Z \to J/\psi\gamma$ in 13 TeV pp interactions. Two triggers were used: isolated photon of $p_T > 35(25)$ GeV and a muon with $p_T > 18(24)$ GeV. The J/ψ is detected via its dimuon decay and it is required that the azimuthal angle between the photon and the J/ψ in the plane transverse to the beam direction is $> \pi/2$. The number of observed/expected background events is $92/89 \pm 6$ in the dimuon mass range 2.9–3.3 GeV leading to the quoted 95% C.L. limit.

[3] AAD 15I use events with the highest p_T muon in the pair required to have $p_T > 20$ GeV, the dimuon mass required to be within 0.2 GeV of the $J/\psi(1S)$ mass and it's transverse momentum required to be > 36 GeV. The photon is also required to have it's $p_T > 36$ GeV.

$\Gamma(\psi(2S)X)/\Gamma_{total}$ — Γ_{28}/Γ

VALUE (units 10^{-3})	EVTS	DOCUMENT ID		TECN	COMMENT
1.60 ± 0.29 OUR AVERAGE					
$1.6 \pm 0.5 \pm 0.3$	39	[1] ACCIARRI	97J	L3	E^{ee}_{cm} = 88–94 GeV
$1.6 \pm 0.3 \pm 0.2$	46.9	[2] ALEXANDER	96B	OPAL	E^{ee}_{cm} = 88–94 GeV
$1.60 \pm 0.73 \pm 0.33$	5.4	[3] ABREU	94P	DLPH	E^{ee}_{cm} = 88–94 GeV

[1] ACCIARRI 97J measure this branching ratio via the decay channel $\psi(2S) \to \ell^+\ell^-$ ($\ell = \mu, e$).

[2] ALEXANDER 96B measure this branching ratio via the decay channel $\psi(2S) \to J/\psi\pi^+\pi^-$, with $J/\psi \to \ell^+\ell^-$.

[3] ABREU 94P measure this branching ratio via decay channel $\psi(2S) \to J/\psi\pi^+\pi^-$, with $J/\psi \to \mu^+\mu^-$.

$\Gamma(\psi(2S)\gamma)/\Gamma_{total}$ — Γ_{29}/Γ

VALUE	CL%	DOCUMENT ID		TECN	COMMENT
$<1.3 \times 10^{-6}$	95	HAYRAPETY...25H		CMS	E^{pp}_{cm} = 13 TeV
• • • We do not use the following data for averages, fits, limits, etc. • • •					
$<2.4 \times 10^{-6}$	95	AAD	23CD	ATLAS	E^{pp}_{cm} = 13 TeV
$<4.5 \times 10^{-6}$	95	[1] AABOUD	18BL	ATLAS	E^{pp}_{cm} = 13 TeV

[1] AABOUD 18BL study $Z \to \psi(2S)\gamma$ in 13 TeV pp interactions. Two triggers were used: isolated photon of $p_T > 35(25)$ GeV and a muon with $p_T > 18(24)$ GeV. The $\psi(2S)$ is detected via its dimuon decay and it is required that the azimuthal angle between the photon and the $\psi(2S)$ in the plane transverse to the beam direction is $> \pi/2$. The number of observed/expected background events is $43/42 \pm 5$ in the dimuon mass range 3.5–3.9 GeV leading to the quoted 95% C.L. limit.

$\Gamma(J/\psi(1S)\ell^+\ell^-)/\Gamma(\mu^+\mu^-\mu^+\mu^-)$ — Γ_{30}/Γ_5

VALUE	DOCUMENT ID		TECN	COMMENT
$0.67 \pm 0.18 \pm 0.05$	[1] SIRUNYAN	18DZ	CMS	pp at 13 TeV

[1] SIRUNYAN 18DZ observe the decay $Z \to \Psi\ell^+\ell^-$ in pp collisions at $\sqrt{s}$ = 13 TeV, where Ψ includes J/ψ as well as $\psi(2S) \to J/\psi X$, and $\ell^+\ell^-$ represents an electron or muon pair while the J/ψ is detected via its $\mu^+\mu^-$ decay channel. To reduce systematic errors they determine the ratio of the branching fraction of this decay to that of $Z \to \mu^+\mu^-\mu^+\mu^-$ within phase-space cuts imposed on lepton transverse momentum and pseudo rapidity, dilepton invariant mass, and J/ψ transverse momentum. The number of selected $\Psi\mu^+\mu^-$ (Ψe^+e^-) candidate events is 29 (18). Analyzing the $\mu^+\mu^-$ and $\mu^+\mu^-\ell^+\ell^-$ invariant mass distributions, a yield of 13.0 ± 3.9 (11.2 ± 3.4) events for the $\Psi\mu^+\mu^-$ (Ψe^+e^-) mode is obtained. The ratio of the branching fractions is determined as $0.67 \pm 0.18 \pm 0.05$ within the selected phase-space cuts. Assuming extrapolation to full phase space cancels in the ratio, and using their measured value of $B(Z \to \mu^+\mu^-\mu^+\mu^-) = (1.20 \pm 0.08) \times 10^{-6}$, they estimate $B(Z \to J/\psi\ell^+\ell^-) = 8 \times 10^{-7}$.

$\Gamma(J/\psi(1S)J/\psi(1S))/\Gamma_{total}$ — Γ_{31}/Γ

VALUE	CL%	EVTS	DOCUMENT ID		TECN	COMMENT
$<2.2 \times 10^{-6}$	95	189	[1] SIRUNYAN	19BR	CMS	E^{pp}_{cm} = 13 TeV

[1] SIRUNYAN 19BR search for Z decays to a pair of J/ψ mesons in the channel $J/\psi \to \mu^+\mu^-$. The invariant masses of the higher/lower-p_T J/ψ candidates have to be within 0.1/0.15 GeV of the nominal J/ψ mass. A total of 189 events are selected in the 40–140 GeV 4-muon invariant mass range. An un-binned extended maximum likelihood fit leads to the 95% C.L. upper limit, obtained assuming the J/ψ mesons to be unpolarised.

$\Gamma(\chi_{c1}(1P)X)/\Gamma_{total}$ — Γ_{32}/Γ

VALUE (units 10^{-3})	EVTS	DOCUMENT ID		TECN	COMMENT
2.9 ± 0.7 OUR AVERAGE					
$2.7 \pm 0.6 \pm 0.5$	33	[1] ACCIARRI	97J	L3	E^{ee}_{cm} = 88–94 GeV
$5.0 \pm 2.1^{+1.5}_{-0.9}$	6.4	[2] ABREU	94P	DLPH	E^{ee}_{cm} = 88–94 GeV

[1] ACCIARRI 97J measure this branching ratio via the decay channel $\chi_{c1} \to J/\psi + \gamma$, with $J/\psi \to \ell^+\ell^-$ ($\ell = \mu, e$). The $M(\ell^+\ell^-\gamma)$–$M(\ell^+\ell^-)$ mass difference spectrum is fitted with two gaussian shapes for χ_{c1} and χ_{c2}.

[2] This branching ratio is measured via the decay channel $\chi_{c1} \to J/\psi + \gamma$, with $J/\psi \to \mu^+\mu^-$.

Int. J. Mod. Phys. A 2026.41. Downloaded from www.worldscientific.com
by UNIVERSITY OF CALIFORNIA @ BERKELEY on 09/16/26. Reproduction is strictly not permitted, except for Open Access articles.

Int. J. Mod. Phys. A 2026.41. Downloaded from www.worldscientific.com by UNIVERSITY OF CALIFORNIA @ BERKELEY on 09/16/26. Re-use and distribution is strictly not permitted, except for Open Access articles.

$\Gamma(\chi_{c2}(1P)X)/\Gamma_{total}$ — Γ_{33}/Γ

VALUE	CL%	DOCUMENT ID		TECN	COMMENT
$<3.2\times10^{-3}$	90	[1] ACCIARRI	97J	L3	E^{ee}_{cm}= 88–94 GeV

[1] ACCIARRI 97J derive this limit via the decay channel $\chi_{c2} \to J/\psi + \gamma$, with $J/\psi \to \ell^+\ell^-$ ($\ell = \mu, e$). The $M(\ell^+\ell^-\gamma)$–$M(\ell^+\ell^-)$ mass difference spectrum is fitted with two gaussian shapes for χ_{c1} and χ_{c2}.

$\Gamma(\Upsilon(1S)X+\Upsilon(2S)X+\Upsilon(3S)X)/\Gamma_{total}$ — $\Gamma_{34}/\Gamma=(\Gamma_{35}+\Gamma_{37}+\Gamma_{39})/\Gamma$

VALUE (units 10^{-4})	EVTS	DOCUMENT ID		TECN	COMMENT
1.0±0.4±0.22	6.4	[1] ALEXANDER	96F	OPAL	E^{ee}_{cm}= 88–94 GeV

[1] ALEXANDER 96F identify the Υ (which refers to any of the three lowest bound states) through its decay into e^+e^- and $\mu^+\mu^-$. The systematic error includes an uncertainty of ±0.2 due to the production mechanism.

$\Gamma(\Upsilon(1S)X)/\Gamma_{total}$ — Γ_{35}/Γ

VALUE	CL%	DOCUMENT ID		TECN	COMMENT
$<4.4\times10^{-5}$	95	[1] ACCIARRI	99F	L3	E^{ee}_{cm}= 88–94 GeV

[1] ACCIARRI 99F search for $\Upsilon(1S)$ through its decay into $\ell^+\ell^-$ ($\ell = e$ or μ).

$\Gamma(\Upsilon(1S)\gamma)/\Gamma_{total}$ — Γ_{36}/Γ

VALUE	CL%	DOCUMENT ID		TECN	COMMENT
$<1.1\times10^{-6}$	95	AAD	23CD	ATLS	E^{pp}_{cm} = 13 TeV
• • • We do not use the following data for averages, fits, limits, etc. • • •					
$<2.8\times10^{-6}$	95	[1] AABOUD	18BL	ATLS	E^{pp}_{cm} = 13 TeV
$<3.4\times10^{-6}$	95	[2] AAD	15I	ATLS	E^{pp}_{cm} = 8 TeV

[1] AABOUD 18BL study $Z \to \Upsilon(1S)\gamma$ in 13 TeV pp interactions. Two triggers were used: isolated photon of $p_T > 35(25)$ GeV and a muon with $p_T > 18(24)$ GeV. The $\Upsilon(1S)$ is detected via its dimuon decay and it is required that the azimuthal angle between the photon and the $\Upsilon(1S)$ in the plane transverse to the beam direction is $> \pi/2$. The number of observed/expected background events is 115/126 ± 8 in the dimuon mass range 9.0–10.0 GeV leading to the quoted 95% C.L. limit.

[2] AAD 15I use events with the highest p_T muon in the pair required to have $p_T > 20$ GeV, the dimuon mass required to be in the range 8–12 GeV and it's transverse momentum required to be > 36 GeV. The photon is also required to have it's $p_T > 36$ GeV.

$\Gamma(\Upsilon(2S)X)/\Gamma_{total}$ — Γ_{37}/Γ

VALUE	CL%	DOCUMENT ID		TECN	COMMENT
$<13.9\times10^{-5}$	95	[1] ACCIARRI	97R	L3	E^{ee}_{cm}= 88–94 GeV

[1] ACCIARRI 97R search for $\Upsilon(2S)$ through its decay into $\ell^+\ell^-$ ($\ell = e$ or μ).

$\Gamma(\Upsilon(2S)\gamma)/\Gamma_{total}$ — Γ_{38}/Γ

VALUE	CL%	DOCUMENT ID		TECN	COMMENT
$<1.3\times10^{-6}$	95	AAD	23CD	ATLS	E^{pp}_{cm} = 13 TeV
• • • We do not use the following data for averages, fits, limits, etc. • • •					
$<1.7\times10^{-6}$	95	[1] AABOUD	18BL	ATLS	E^{pp}_{cm} = 13 TeV
$<6.5\times10^{-6}$	95	[2] AAD	15I	ATLS	E^{pp}_{cm} = 8 TeV

[1] AABOUD 18BL study $Z \to \Upsilon(2S)\gamma$ in 13 TeV pp interactions. Two triggers were used: isolated photon of $p_T > 35(25)$ GeV and a muon with $p_T > 18(24)$ GeV. The $\Upsilon(2S)$ is detected via its dimuon decay and it is required that the azimuthal angle between the photon and the $\Upsilon(2S)$ in the plane transverse to the beam direction is $> \pi/2$. The number of observed/expected background events is 106/121 ± 8 in the dimuon mass range 9.5–10.5 GeV leading to the quoted 95% C.L. limit.

[2] AAD 15I use events with the highest p_T muon in the pair required to have $p_T > 20$ GeV, the dimuon mass required to be in the range 8–12 GeV and it's transverse momentum required to be > 36 GeV. The photon is also required to have it's $p_T > 36$ GeV.

$\Gamma(\Upsilon(3S)X)/\Gamma_{total}$ — Γ_{39}/Γ

VALUE	CL%	DOCUMENT ID		TECN	COMMENT
$<9.4\times10^{-5}$	95	[1] ACCIARRI	97R	L3	E^{ee}_{cm}= 88–94 GeV

[1] ACCIARRI 97R search for $\Upsilon(3S)$ through its decay into $\ell^+\ell^-$ ($\ell = e$ or μ).

$\Gamma(\Upsilon(3S)\gamma)/\Gamma_{total}$ — Γ_{40}/Γ

VALUE	CL%	DOCUMENT ID		TECN	COMMENT
$<2.4\times10^{-6}$	95	AAD	23CD	ATLS	E^{pp}_{cm} = 13 TeV
• • • We do not use the following data for averages, fits, limits, etc. • • •					
$<4.8\times10^{-6}$	95	[1] AABOUD	18BL	ATLS	E^{pp}_{cm} = 13 TeV
$<5.4\times10^{-6}$	95	[2] AAD	15I	ATLS	E^{pp}_{cm} = 8 TeV

[1] AABOUD 18BL study $Z \to \Upsilon(3S)\gamma$ in 13 TeV pp interactions. Two triggers were used: isolated photon of $p_T > 35(25)$ GeV and a muon with $p_T > 18(24)$ GeV. The $\Upsilon(3S)$ is detected via its dimuon decay and it is required that the azimuthal angle between the photon and the $\Upsilon(3S)$ in the plane transverse to the beam direction is $> \pi/2$. The number of observed/expected background events is 112/113 ± 8 in the dimuon mass range 10.0–11.0 GeV leading to the quoted 95% C.L. limit.

[2] AAD 15I use events with the highest p_T muon in the pair required to have $p_T > 20$ GeV, the dimuon mass required to be in the range 8–12 GeV and it's transverse momentum required to be > 36 GeV. The photon is also required to have it's $p_T > 36$ GeV.

$\Gamma(\Upsilon(1,2,3S)\,\Upsilon(1,2,3S))/\Gamma_{total}$ — Γ_{41}/Γ

VALUE	CL%	EVTS	DOCUMENT ID		TECN	COMMENT
$<1.5\times10^{-6}$	95	106	[1] SIRUNYAN	19BR	CMS	E^{pp}_{cm} = 13 TeV

[1] SIRUNYAN 19BR search for Z decays to a pair of Υ mesons in the channel $\Upsilon \to \mu^+\mu^-$. The invariant mass of the Υ candidates has to be in the range of 8.5 to 11 GeV. A total of 106 events are selected in the 20–140 GeV 4-muon invariant mass range. An un-binned extended maximum likelihood fit leads to the 95% C.L. upper limit, obtained assuming the Υ mesons to be unpolarised.

$\Gamma(K^0_S\gamma)/\Gamma_{total}$ — Γ_{42}/Γ

VALUE	CL%	DOCUMENT ID		TECN	COMMENT
$<3.1\times10^{-6}$	95	[1] AAD	24R	ATLS	E^{pp}_{cm} = 13 TeV

[1] AAD 24R identify the K^0_S via its decay to $\pi^+\pi^-$. The transverse momentum of the photon is required to be larger than 25 GeV or 35 GeV for different periods of data taking.

$\Gamma(D^0\gamma)/\Gamma_{total}$ — Γ_{43}/Γ

VALUE	CL%	DOCUMENT ID		TECN	COMMENT
$<4.0\times10^{-6}$	95	[1] AAD	24R	ATLS	E^{pp}_{cm} = 13 TeV

[1] AAD 24R identify the D^0 via its decay to $K^-\pi^+$. The transverse momentum of the photon is required to be larger than 25 GeV or 35 GeV for different periods of data taking.

$\Gamma(D^0\gamma)/\Gamma(\mu^+\mu^-)$ — Γ_{43}/Γ_2

VALUE	CL%	DOCUMENT ID		TECN	COMMENT
$<6.4\times10^{-2}$	95	[1] AAIJ	23AM	LHCB	E^{pp}_{cm} = 13 TeV

[1] AAIJ 23AM also quotes the branching fraction limit $B(Z \to D^0\gamma) < 2.1\times10^{-3}$, using the known $Z \to \mu\mu$ branching fraction.

$\Gamma((D^0/\overline{D}^0)X)/\Gamma(\text{hadrons})$ — Γ_{44}/Γ_8

VALUE	EVTS	DOCUMENT ID		TECN	COMMENT
0.296±0.019±0.021	369	[1] ABREU	93I	DLPH	E^{ee}_{cm}= 88–94 GeV

[1] The $(D^0/\overline{D}^0)$ states in ABREU 93I are detected by the $K\pi$ decay mode. This is a corrected result (see the erratum of ABREU 93I).

$\Gamma(D^\pm X)/\Gamma(\text{hadrons})$ — Γ_{45}/Γ_8

VALUE	EVTS	DOCUMENT ID		TECN	COMMENT
0.174±0.016±0.018	539	[1] ABREU	93I	DLPH	E^{ee}_{cm}= 88–94 GeV

[1] The $D^\pm$ states in ABREU 93I are detected by the $K\pi\pi$ decay mode. This is a corrected result (see the erratum of ABREU 93I).

$\Gamma(D^*(2010)^\pm X)/\Gamma(\text{hadrons})$ — Γ_{46}/Γ_8

The value is for the sum of the charge states indicated.

VALUE	EVTS	DOCUMENT ID		TECN	COMMENT
0.163±0.019 OUR AVERAGE	Error includes scale factor of 1.3.				
0.155±0.010±0.013	358	[1] ABREU	93I	DLPH	E^{ee}_{cm}= 88–94 GeV
0.21 ±0.04	362	[2] DECAMP	91J	ALEP	E^{ee}_{cm}= 88–94 GeV

[1] $D^*(2010)^\pm$ in ABREU 93I are reconstructed from $D^0\pi^\pm$, with $D^0 \to K^-\pi^+$. The new CLEO II measurement of $B(D^{*\pm} \to D^0\pi^\pm) = (68.1 \pm 1.6)$ % is used. This is a corrected result (see the erratum of ABREU 93I).

[2] DECAMP 91J report $B(D^*(2010)^+ \to D^0\pi^+)\ B(D^0 \to K^-\pi^+)\ \Gamma(D^*(2010)^\pm X)\ /\ \Gamma(\text{hadrons}) = (5.11 \pm 0.34)\times10^{-3}$. They obtained the above number assuming $B(D^0 \to K^-\pi^+) = (3.62\pm0.34\pm0.44)$% and $B(D^*(2010)^+ \to D^0\pi^+) = (55\pm4)$%. We have rescaled their original result of 0.26 ± 0.05 taking into account the new CLEO II branching ratio $B(D^*(2010)^+ \to D^0\pi^+) = (68.1 \pm 1.6)$%.

$\Gamma(D_{s1}(2536)^\pm X)/\Gamma(\text{hadrons})$ — Γ_{47}/Γ_8

$D_{s1}(2536)^\pm$ is an expected orbitally-excited state of the D_s meson.

VALUE (%)	EVTS	DOCUMENT ID		TECN	COMMENT
0.52±0.09±0.06	92	[1] HEISTER	02B	ALEP	E^{ee}_{cm}= 88–94 GeV

[1] HEISTER 02B reconstruct this meson in the decay modes $D_{s1}(2536)^\pm \to D^{*\pm}K^0$ and $D_{s1}(2536)^\pm \to D^{*0}K^\pm$. The quoted branching ratio assumes that the decay width of the $D_{s1}(2536)$ is saturated by the two measured decay modes.

$\Gamma(D_{sJ}(2573)^\pm X)/\Gamma(\text{hadrons})$ — Γ_{48}/Γ_8

$D_{sJ}(2573)^\pm$ is an expected orbitally-excited state of the D_s meson.

VALUE (%)	EVTS	DOCUMENT ID		TECN	COMMENT
$0.83\pm0.29^{+0.07}_{-0.13}$	64	[1] HEISTER	02B	ALEP	E^{ee}_{cm}= 88–94 GeV

[1] HEISTER 02B reconstruct this meson in the decay mode $D^*_{s2}(2573)^\pm \to D^0K^\pm$. The quoted branching ratio assumes that the detected decay mode represents 45% of the full decay width.

$\Gamma(D^{*\prime}(2629)^\pm X)/\Gamma(\text{hadrons})$ — Γ_{49}/Γ_8

$D^{*\prime}(2629)^\pm$ is a predicted radial excitation of the $D^*(2010)^\pm$ meson.

VALUE	DOCUMENT ID		TECN	COMMENT
searched for	[1] ABBIENDI	01N	OPAL	E^{ee}_{cm}= 88–94 GeV

[1] ABBIENDI 01N searched for the decay mode $D^{*\prime}(2629)^\pm \to D^{*\pm}\pi^+\pi^-$ with $D^{*+} \to D^0\pi^+$, and $D^0 \to K^-\pi^+$. They quote a 95% CL limit for $Z \to D^{*\prime}(2629)^\pm \times B(D^{*\prime}(2629)^+ \to D^{*+}\pi^+\pi^-) < 3.1\times10^{-3}$.

Int. J. Mod. Phys. A 2026.41. Downloaded from worldscientific.com
by UNIVERSITY OF CALIFORNIA @ BERKELEY on 09/16/26. Reproduction is strictly not permitted, except for Open Access articles.

$\Gamma(B^*X)/[\Gamma(BX)+\Gamma(B^*X)]$ — $\Gamma_{51}/(\Gamma_{50}+\Gamma_{51})$

As the experiments assume different values of the b-baryon contribution, our average should be taken with caution.

VALUE	EVTS	DOCUMENT ID		TECN	COMMENT
0.75 ±0.04 OUR AVERAGE					
0.760±0.036±0.083		[1] ACKERSTAFF	97M	OPAL	E^{ee}_{cm}= 88–94 GeV
0.771±0.026±0.070		[2] BUSKULIC	96D	ALEP	E^{ee}_{cm}= 88–94 GeV
0.72 ±0.03 ±0.06		[3] ABREU	95R	DLPH	E^{ee}_{cm}= 88–94 GeV
0.76 ±0.08 ±0.06	1378	[4] ACCIARRI	95B	L3	E^{ee}_{cm}= 88–94 GeV

[1] ACKERSTAFF 97M use an inclusive B reconstruction method and assume a (13.2 ± 4.1)% b-baryon contribution. The value refers to a b-flavored meson mixture of B_u, B_d, and B_s.

[2] BUSKULIC 96D use an inclusive reconstruction of B hadrons and assume a (12.2 ± 4.3)% b-baryon contribution. The value refers to a b-flavored mixture of B_u, B_d, and B_s.

[3] ABREU 95R use an inclusive B-reconstruction method and assume a (10 ± 4)% b-baryon contribution. The value refers to a b-flavored meson mixture of B_u, B_d, and B_s.

[4] ACCIARRI 95B assume a 9.4% b-baryon contribution. The value refers to a b-flavored mixture of B_u, B_d, and B_s.

$\Gamma(B^+X)/\Gamma(\text{hadrons})$ — Γ_{52}/Γ_8

"OUR EVALUATION" is obtained using our current values for $f(\overline{b} \to B^+)$ and $R_b = \Gamma(b\overline{b})/\Gamma(\text{hadrons})$. We calculate $\Gamma(B^+ X)/\Gamma(\text{hadrons}) = R_b \times f(\overline{b} \to B^+)$.

VALUE	DOCUMENT ID		TECN	COMMENT
0.0869±0.0019 OUR EVALUATION	(Produced by HFLAV)			
0.0887±0.0030	[1] ABDALLAH	03K	DLPH	E^{ee}_{cm} = 88–94 GeV

[1] ABDALLAH 03K measure the production fraction of B^+ mesons in hadronic Z decays $f(B^+) = (40.99 \pm 0.82 \pm 1.11)\%$. The value quoted here is obtained multiplying this production fraction by our value of $R_b = \Gamma(\overline{b}b)/\Gamma(\text{hadrons})$.

$\Gamma(B^0_sX)/\Gamma(\text{hadrons})$ — Γ_{53}/Γ_8

"OUR EVALUATION" is obtained using our current values for $f(\overline{b} \to B^0_s)$ and $R_b = \Gamma(b\overline{b})/\Gamma(\text{hadrons})$. We calculate $\Gamma(B^0_s)/\Gamma(\text{hadrons}) = R_b \times f(\overline{b} \to B^0_s)$.

VALUE	DOCUMENT ID		TECN	COMMENT
0.0227±0.0019 OUR EVALUATION	(Produced by HFLAV)			
seen	[1] ABREU	92M	DLPH	E^{ee}_{cm}= 88–94 GeV
seen	[2] ACTON	92N	OPAL	E^{ee}_{cm}= 88–94 GeV
seen	[3] BUSKULIC	92E	ALEP	E^{ee}_{cm}= 88–94 GeV

[1] ABREU 92M reported value is $\Gamma(B^0_sX)*B(B^0_s \to D_s\mu\nu_\mu X)*B(D_s \to \phi\pi)/\Gamma(\text{hadrons}) = (18 \pm 8) \times 10^{-5}$.

[2] ACTON 92N find evidence for B^0_s production using D_s-ℓ correlations, with $D^+_s \to \phi\pi^+$ and $K^*(892)\,K^+$. Assuming R_b from the Standard Model and averaging over the e and μ channels, authors measure the product branching fraction to be $f(\overline{b} \to B^0_s)\times B(B^0_s \to D^-_s\ell^+\nu_\ell X)\times B(D^-_s \to \phi\pi^-) = (3.9 \pm 1.1 \pm 0.8) \times 10^{-4}$.

[3] BUSKULIC 92E find evidence for B^0_s production using D_s-ℓ correlations, with $D^+_s \to \phi\pi^+$ and $K^*(892)\,K^+$. Using $B(D^+_s \to \phi\pi^+) = (2.7 \pm 0.7)\%$ and summing up the e and μ channels, the weighted average product branching fraction is measured to be $B(\overline{b} \to B^0_s)\times B(B^0_s \to D^-_s\ell^+\nu_\ell X) = 0.040 \pm 0.011^{+0.010}_{-0.012}$.

$\Gamma(B^+_cX)/\Gamma(\text{hadrons})$ — Γ_{54}/Γ_8

VALUE	DOCUMENT ID		TECN	COMMENT
searched for	[1] ACKERSTAFF	98O	OPAL	E^{ee}_{cm}= 88–94 GeV
searched for	[2] ABREU	97E	DLPH	E^{ee}_{cm}= 88–94 GeV
searched for	[3] BARATE	97H	ALEP	E^{ee}_{cm}= 88–94 GeV

[1] ACKERSTAFF 98O searched for the decay modes $B_c \to J/\psi\pi^+$, $J/\psi a^+_1$, and $J/\psi\ell^+\nu_\ell$, with $J/\psi \to \ell^+\ell^-$, $\ell = e,\mu$. The number of candidates (background) for the three decay modes is 2 (0.63 ± 0.2), 0 (1.10 ± 0.22), and 1 (0.82 ± 0.19) respectively. Interpreting the 2 $B_c \to J/\psi\pi^+$ candidates as signal, they report $\Gamma(B^+_cX)\times B(B_c \to J/\psi\pi^+)/\Gamma(\text{hadrons}) = (3.8^{+5.0}_{-2.4} \pm 0.5)\times 10^{-5}$. Interpreted as background, the 90% CL bounds are $\Gamma(B^+_cX)*B(B_c \to J/\psi\pi^+)/\Gamma(\text{hadrons}) < 1.06\times 10^{-4}$, $\Gamma(B^+_cX)*B(B_c \to J/\psi a^+_1)/\Gamma(\text{hadrons}) < 5.29 \times 10^{-4}$, $\Gamma(B^+_cX)*B(B_c \to J/\psi\ell^+\nu_\ell)/\Gamma(\text{hadrons}) < 6.96 \times 10^{-5}$.

[2] ABREU 97E searched for the decay modes $B_c \to J/\psi\pi^+$, $J/\psi\ell^+\nu_\ell$, and $J/\psi(3\pi)^+$, with $J/\psi \to \ell^+\ell^-$, $\ell = e,\mu$. The number of candidates (background) for the three decay modes is 1 (1.7), 0 (0.3), and 1 (2.3) respectively. They report the following 90% CL limits: $\Gamma(B^+_cX)*B(B_c \to J/\psi\pi^+)/\Gamma(\text{hadrons}) <(1.05\text{–}0.84) \times 10^{-4}$, $\Gamma(B^+_cX)*B(B_c \to J/\psi\nu_\ell)/\Gamma(\text{hadrons}) <(5.8\text{–}5.0) \times 10^{-5}$, $\Gamma(B^+_cX)*B(B_c \to J/\psi(3\pi)^+)/\Gamma(\text{hadrons}) < 1.75 \times 10^{-4}$, where the ranges are due to the predicted B_c lifetime (0.4–1.4) ps.

[3] BARATE 97H searched for the decay modes $B_c \to J/\psi\pi^+$ and $J/\psi\ell^+\nu_\ell$ with $J/\psi \to \ell^+\ell^-$, $\ell = e,\mu$. The number of candidates (background) for the two decay modes is 0 (0.44) and 2 (0.81) respectively. They report the following 90% CL limits: $\Gamma(B^+_cX)*B(B_c \to J/\psi\pi^+)/\Gamma(\text{hadrons}) < 3.6 \times 10^{-5}$ and $\Gamma(B^+_cX)*B(B_c \to J/\psi\ell^+\nu_\ell)/\Gamma(\text{hadrons}) < 5.2 \times 10^{-5}$.

$\Gamma(\Lambda^+_cX)/\Gamma(\text{hadrons})$ — Γ_{55}/Γ_8

VALUE	DOCUMENT ID		TECN	COMMENT
0.022±0.005 OUR AVERAGE				
0.024±0.005±0.006	[1] ALEXANDER	96R	OPAL	E^{ee}_{cm} = 88–94 GeV
0.021±0.003±0.005	[2] BUSKULIC	96Y	ALEP	E^{ee}_{cm} = 88–94 GeV

[1] ALEXANDER 96R measure $R_b \times f(b \to \Lambda^+_c X) \times B(\Lambda^+_c \to pK^-\pi^+) = (0.122 \pm 0.023 \pm 0.010)\%$ in hadronic Z decays; the value quoted here is obtained using our best value $B(\Lambda^+_c \to pK^-\pi^+) = (5.0 \pm 1.3)\%$. The first error is the total experiment's error and the second error is the systematic error due to the branching fraction uncertainty.

[2] BUSKULIC 96Y obtain the production fraction of Λ^+_c baryons in hadronic Z decays $f(b \to \Lambda^+_c X) = 0.110 \pm 0.014 \pm 0.006$ using $B(\Lambda^+_c \to pK^-\pi^+) = (4.4 \pm 0.6)\%$; we have rescaled using our best value $B(\Lambda^+_c \to pK^-\pi^+) = (5.0 \pm 1.3)\%$ obtaining $f(b \to \Lambda^+_c X) = 0.097 \pm 0.013 \pm 0.025$ where the first error is their total experiment's error and the second error is the systematic error due to the branching fraction uncertainty. The value quoted here is obtained multiplying this production fraction by our value of $R_b = \Gamma(b\overline{b})/\Gamma(\text{hadrons})$.

$\Gamma(\Xi^0_cX)/\Gamma(\text{hadrons})$ — Γ_{56}/Γ_8

VALUE	DOCUMENT ID		TECN	COMMENT
• • • We do not use the following data for averages, fits, limits, etc. • • •				
seen	[1] ABDALLAH	05C	DLPH	E^{ee}_{cm} = 88–94 GeV

[1] ABDALLAH 05C searched for the charmed strange baryon Ξ^0_c in the decay channel $\Xi^0_c \to \Xi^-\pi^+$ ($\Xi^- \to \Lambda\pi^-$). The production rate is measured to be $f_{\Xi^0_c} \times B(\Xi^0_c \to \Xi^-\pi^+) = (4.7 \pm 1.4 \pm 1.1) \times 10^{-4}$ per hadronic Z decay.

$\Gamma(\Xi_bX)/\Gamma(\text{hadrons})$ — Γ_{57}/Γ_8

Here Ξ_b is used as a notation for the strange b-baryon states Ξ^-_b and Ξ^0_b.

VALUE	DOCUMENT ID		TECN	COMMENT
• • • We do not use the following data for averages, fits, limits, etc. • • •				
seen	[1] ABDALLAH	05C	DLPH	E^{ee}_{cm} = 88–94 GeV
seen	[2] BUSKULIC	96T	ALEP	E^{ee}_{cm} = 88–94 GeV
seen	[3] ABREU	95V	DLPH	E^{ee}_{cm} = 88–94 GeV

[1] ABDALLAH 05C searched for the beauty strange baryon Ξ_b in the inclusive semileptonic decay channel $\Xi_b \to \Xi^-\ell^-\overline{\nu}_\ell X$. Evidence for the Ξ_b production is seen from the observation of $\Xi^\mp$ production accompanied by a lepton of the same sign. From the excess of "right-sign" pairs $\Xi^\mp\ell^\mp$ compared to "wrong-sign" pairs $\Xi^\mp\ell^\pm$ the production rate is measured to be $B(b \to \Xi_b) \times B(\Xi_b \to \Xi^-\ell^-X) = (3.0 \pm 1.0 \pm 0.3) \times 10^{-4}$ per lepton species, averaged over electrons and muons.

[2] BUSKULIC 96T investigate Ξ-lepton correlations and find a significant excess of "right–sign" pairs $\Xi^\mp\ell^\mp$ compared to "wrong–sign" pairs $\Xi^\mp\ell^\pm$. This excess is interpreted as evidence for Ξ_b semileptonic decay. The measured product branching ratio is $B(b \to \Xi_b) \times B(\Xi_b \to X_cX\ell^-\overline{\nu}_\ell) \times B(X_c \to \Xi^-X') = (5.4 \pm 1.1 \pm 0.8) \times 10^{-4}$ per lepton species, averaged over electrons and muons, with X_c a charmed baryon.

[3] ABREU 95V observe an excess of "right-sign" pairs $\Xi^\mp\ell^\mp$ compared to "wrong-sign" pairs $\Xi^\mp\ell^\pm$ in jets: this excess is interpreted as evidence for the beauty strange baryon Ξ_b production, with $\Xi_b \to \Xi^-\ell^-\overline{\nu}_\ell X$. They find that the probability for this signal to come from non b-baryon decays is less than 5×10^{-4} and that Λ_b decays can account for less than 10% of these events. The Ξ_b production rate is then measured to be $B(b \to \Xi_b) \times B(\Xi_b \to \Xi^-\ell^-X) = (5.9 \pm 2.1 \pm 1.0) \times 10^{-4}$ per lepton species, averaged over electrons and muons.

$\Gamma(b\text{-baryon}\,X)/\Gamma(\text{hadrons})$ — Γ_{58}/Γ_8

"OUR EVALUATION" is obtained using our current values for $f(b \to b\text{-baryon})$ and $R_b = \Gamma(b\overline{b})/\Gamma(\text{hadrons})$. We calculate $\Gamma(b\text{-baryon}\ X)/\Gamma(\text{hadrons}) = R_b \times f(b \to b\text{-baryon})$.

VALUE	DOCUMENT ID		TECN	COMMENT
0.0197±0.0032 OUR EVALUATION	(Produced by HFLAV)			
0.0221±0.0015±0.0058	[1] BARATE	98V	ALEP	E^{ee}_{cm}= 88–94 GeV

[1] BARATE 98V use the overall number of identified protons in b-hadron decays to measure $f(b \to b\text{-baryon}) = 0.102 \pm 0.007 \pm 0.027$. They assume $BR(b\text{-baryon} \to pX) = (58 \pm 6)\%$ and $BR(B^0_s \to pX) = (8.0 \pm 4.0)\%$. The value quoted here is obtained multiplying this production fraction by our value of $R_b = \Gamma(b\overline{b})/\Gamma(\text{hadrons})$.

$\Gamma(\text{anomalous}\ \gamma + \text{hadrons})/\Gamma_{\text{total}}$ — Γ_{59}/Γ

Limits on additional sources of prompt photons beyond expectations for final-state bremsstrahlung.

VALUE	CL%	DOCUMENT ID		TECN	COMMENT
<3.2 × 10^{-3}	95	[1] AKRAWY	90J	OPAL	E^{ee}_{cm}= 88–94 GeV

[1] AKRAWY 90J report $\Gamma(\gamma X) < 8.2$ MeV at 95%CL. They assume a three-body $\gamma q\overline{q}$ distribution and use $E(\gamma) > 10$ GeV.

$\Gamma(e^+e^-\gamma)/\Gamma_{\text{total}}$ — Γ_{60}/Γ

VALUE	CL%	DOCUMENT ID		TECN	COMMENT
<5.2 × 10^{-4}	95	[1] ACTON	91B	OPAL	E^{ee}_{cm}= 91.2 GeV

[1] ACTON 91B looked for isolated photons with E>2% of beam energy (> 0.9 GeV).

$\Gamma(\mu^+\mu^-\gamma)/\Gamma_{\text{total}}$ — Γ_{61}/Γ

VALUE	CL%	DOCUMENT ID		TECN	COMMENT
<5.6 × 10^{-4}	95	[1] ACTON	91B	OPAL	E^{ee}_{cm}= 91.2 GeV

[1] ACTON 91B looked for isolated photons with E>2% of beam energy (> 0.9 GeV).

Int. J. Mod. Phys. A 2026.41. Downloaded from www.worldscientific.com by UNIVERSITY OF CALIFORNIA @ BERKELEY on 09/16/26. Re-use and distribution is strictly not permitted, except for Open Access articles.

$\Gamma(\tau^+\tau^-\gamma)/\Gamma_{total}$ — Γ_{62}/Γ

VALUE	CL%	DOCUMENT ID		TECN	COMMENT
$<7.3\times10^{-4}$	95	[1] ACTON	91B	OPAL	$E^{ee}_{cm}=$ 91.2 GeV

[1] ACTON 91B looked for isolated photons with $E>2\%$ of beam energy (>0.9 GeV).

$\Gamma(\ell^+\ell^-\gamma\gamma)/\Gamma_{total}$ — Γ_{63}/Γ

The value is the sum over $\ell = e, \mu, \tau$.

VALUE	CL%	DOCUMENT ID		TECN	COMMENT
$<6.8\times10^{-6}$	95	[1] ACTON	93E	OPAL	$E^{ee}_{cm}=$ 88–94 GeV

[1] For $m_{\gamma\gamma}=60\pm5$ GeV.

$\Gamma(q\overline{q}\gamma\gamma)/\Gamma_{total}$ — Γ_{64}/Γ

VALUE	CL%	DOCUMENT ID		TECN	COMMENT
$<5.5\times10^{-6}$	95	[1] ACTON	93E	OPAL	$E^{ee}_{cm}=$ 88–94 GeV

[1] For $m_{\gamma\gamma}=60\pm5$ GeV.

$\Gamma(\nu\overline{\nu}\gamma\gamma)/\Gamma_{total}$ — Γ_{65}/Γ

VALUE	CL%	DOCUMENT ID		TECN	COMMENT
$<3.1\times10^{-6}$	95	[1] ACTON	93E	OPAL	$E^{ee}_{cm}=$ 88–94 GeV

[1] For $m_{\gamma\gamma}=60\pm5$ GeV.

$\Gamma(e^\pm\mu^\mp)/\Gamma_{total}$ — Γ_{66}/Γ

Test of lepton family number conservation. The value is for the sum of the charge states indicated.

VALUE	CL%	DOCUMENT ID		TECN	COMMENT
$<1.9\times10^{-7}$	95	HAYRAPETY...	25AK	CMS	$E^{pp}_{cm}=$ 13 TeV
• • • We do not use the following data for averages, fits, limits, etc. • • •					
$<2.62\times10^{-7}$	95	AAD	23AQ	ATLS	$E^{pp}_{cm}=$ 13 TeV
$<7.5\times10^{-7}$	95	AAD	14AU	ATLS	$E^{pp}_{cm}=$ 8 TeV
$<2.5\times10^{-6}$	95	ABREU	97C	DLPH	$E^{ee}_{cm}=$ 88–94 GeV
$<1.7\times10^{-6}$	95	AKERS	95W	OPAL	$E^{ee}_{cm}=$ 88–94 GeV
$<0.6\times10^{-5}$	95	ADRIANI	93I	L3	$E^{ee}_{cm}=$ 88–94 GeV
$<2.6\times10^{-5}$	95	DECAMP	92	ALEP	$E^{ee}_{cm}=$ 88–94 GeV

$\Gamma(e^\pm\mu^\mp)/\Gamma(e^+e^-)$ — Γ_{66}/Γ_1

Test of lepton family number conservation. The value is for the sum of the charge states indicated.

VALUE	CL%	DOCUMENT ID		TECN	COMMENT
<0.07	90	ALBAJAR	89	UA1	$E^{p\overline{p}}_{cm}=$ 546,630 GeV

$\Gamma(e^\pm\tau^\mp)/\Gamma_{total}$ — Γ_{67}/Γ

Test of lepton family number conservation. The value is for the sum of the charge states indicated.

VALUE	CL%	DOCUMENT ID		TECN	COMMENT
$<5.0\times10^{-6}$	95	AAD	21AV	ATLS	$E^{pp}_{cm}=$ 13 TeV
• • • We do not use the following data for averages, fits, limits, etc. • • •					
$<13.8\times10^{-6}$	95	HAYRAPETY...	25AK	CMS	$E^{pp}_{cm}=$ 13 TeV
$<8.1\times10^{-6}$	95	AAD	21AO	ATLS	$E^{pp}_{cm}=$ 13 TeV
$<5.8\times10^{-5}$	95	AABOUD	18CN	ATLS	$E^{pp}_{cm}=$ 13 TeV
$<2.2\times10^{-5}$	95	ABREU	97C	DLPH	$E^{ee}_{cm}=$ 88–94 GeV
$<9.8\times10^{-6}$	95	AKERS	95W	OPAL	$E^{ee}_{cm}=$ 88–94 GeV
$<1.3\times10^{-5}$	95	ADRIANI	93I	L3	$E^{ee}_{cm}=$ 88–94 GeV
$<1.2\times10^{-4}$	95	DECAMP	92	ALEP	$E^{ee}_{cm}=$ 88–94 GeV

$\Gamma(\mu^\pm\tau^\mp)/\Gamma_{total}$ — Γ_{68}/Γ

Test of lepton family number conservation. The value is for the sum of the charge states indicated.

VALUE	CL%	DOCUMENT ID		TECN	COMMENT
$<6.5\times10^{-6}$	95	AAD	21AV	ATLS	$E^{pp}_{cm}=$ 13 TeV
• • • We do not use the following data for averages, fits, limits, etc. • • •					
$<12.0\times10^{-6}$	95	HAYRAPETY...	25AK	CMS	$E^{pp}_{cm}=$ 13 TeV
$<9.5\times10^{-6}$	95	AAD	21AO	ATLS	$E^{pp}_{cm}=$ 13 TeV
$<1.3\times10^{-5}$	95	AABOUD	18CN	ATLS	$E^{pp}_{cm}=$ 8, 13 TeV
$<1.2\times10^{-5}$	95	ABREU	97C	DLPH	$E^{ee}_{cm}=$ 88–94 GeV
$<1.7\times10^{-5}$	95	AKERS	95W	OPAL	$E^{ee}_{cm}=$ 88–94 GeV
$<1.9\times10^{-5}$	95	ADRIANI	93I	L3	$E^{ee}_{cm}=$ 88–94 GeV
$<1.0\times10^{-4}$	95	DECAMP	92	ALEP	$E^{ee}_{cm}=$ 88–94 GeV

$\Gamma(pe)/\Gamma_{total}$ — Γ_{69}/Γ

Test of baryon number and lepton number conservations. Charge conjugate states are implied.

VALUE	CL%	DOCUMENT ID		TECN	COMMENT
$<1.8\times10^{-6}$	95	[1] ABBIENDI	99I	OPAL	$E^{ee}_{cm}=$ 88–94 GeV

[1] ABBIENDI 99I give the 95%CL limit on the partial width $\Gamma(Z^0\to pe)<4.6$ KeV and we have transformed it into a branching ratio.

$\Gamma(p\mu)/\Gamma_{total}$ — Γ_{70}/Γ

Test of baryon number and lepton number conservations. Charge conjugate states are implied.

VALUE	CL%	DOCUMENT ID		TECN	COMMENT
$<1.8\times10^{-6}$	95	[1] ABBIENDI	99I	OPAL	$E^{ee}_{cm}=$ 88–94 GeV

[1] ABBIENDI 99I give the 95%CL limit on the partial width $\Gamma(Z^0\to p\mu)<4.4$ KeV and we have transformed it into a branching ratio.

AVERAGE PARTICLE MULTIPLICITIES IN HADRONIC Z DECAY

Summed over particle and antiparticle, when appropriate.

$\langle N_\gamma\rangle$

VALUE	DOCUMENT ID		TECN	COMMENT
20.97±0.02±1.15	ACKERSTAFF	98A	OPAL	$E^{ee}_{cm}=$ 91.2 GeV

$\langle N_{\pi^\pm}\rangle$

VALUE	DOCUMENT ID		TECN	COMMENT
17.03 ±0.16 OUR AVERAGE				
17.007±0.209	ABE	04C	SLD	$E^{ee}_{cm}=$ 91.2 GeV
17.26 ±0.10 ±0.88	ABREU	98L	DLPH	$E^{ee}_{cm}=$ 91.2 GeV
17.04 ±0.31	BARATE	98V	ALEP	$E^{ee}_{cm}=$ 91.2 GeV
17.05 ±0.43	AKERS	94P	OPAL	$E^{ee}_{cm}=$ 91.2 GeV

$\langle N_{\pi^0}\rangle$

VALUE	DOCUMENT ID		TECN	COMMENT
9.76±0.26 OUR AVERAGE				
9.55±0.06±0.75	ACKERSTAFF	98A	OPAL	$E^{ee}_{cm}=$ 91.2 GeV
9.63±0.13±0.63	BARATE	97J	ALEP	$E^{ee}_{cm}=$ 91.2 GeV
9.90±0.02±0.33	ACCIARRI	96	L3	$E^{ee}_{cm}=$ 91.2 GeV
9.2 ±0.2 ±1.0	ADAM	96	DLPH	$E^{ee}_{cm}=$ 91.2 GeV

$\langle N_\eta\rangle$

VALUE	DOCUMENT ID		TECN	COMMENT
1.01±0.08 OUR AVERAGE Error includes scale factor of 1.3. See the ideogram below.				
1.20±0.04±0.11	HEISTER	02C	ALEP	$E^{ee}_{cm}=$ 91.2 GeV
0.97±0.03±0.11	ACKERSTAFF	98A	OPAL	$E^{ee}_{cm}=$ 91.2 GeV
0.93±0.01±0.09	ACCIARRI	96	L3	$E^{ee}_{cm}=$ 91.2 GeV

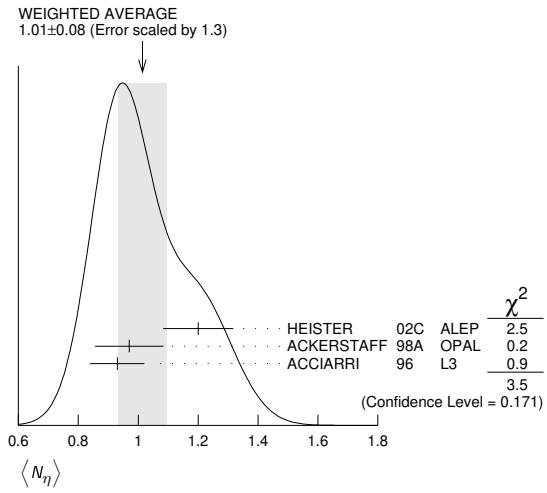

$\langle N_{\rho^\pm}\rangle$

VALUE	DOCUMENT ID		TECN	COMMENT
2.57±0.15 OUR AVERAGE				
2.59±0.03±0.16	[1] BEDDALL	09		ALEPH archive, $E^{ee}_{cm}=$ 91.2 GeV
2.40±0.06±0.43	ACKERSTAFF	98A	OPAL	$E^{ee}_{cm}=$ 91.2 GeV

[1] BEDDALL 09 analyse 3.2 million hadronic Z decays as archived by ALEPH collaboration and report a value of $2.59\pm0.03\pm0.15\pm0.04$. The first error is statistical, the second systematic, and the third arises from extrapolation to full phase space. We combine the systematic errors in quadrature.

$\langle N_{\rho^0}\rangle$

VALUE	DOCUMENT ID		TECN	COMMENT
1.24±0.10 OUR AVERAGE Error includes scale factor of 1.1.				
1.19±0.10	ABREU	99J	DLPH	$E^{ee}_{cm}=$ 91.2 GeV
1.45±0.06±0.20	BUSKULIC	96H	ALEP	$E^{ee}_{cm}=$ 91.2 GeV

$\langle N_\omega\rangle$

VALUE	DOCUMENT ID		TECN	COMMENT
1.02±0.06 OUR AVERAGE				
1.00±0.03±0.06	HEISTER	02C	ALEP	$E^{ee}_{cm}=$ 91.2 GeV
1.04±0.04±0.14	ACKERSTAFF	98A	OPAL	$E^{ee}_{cm}=$ 91.2 GeV
1.17±0.09±0.15	ACCIARRI	97D	L3	$E^{ee}_{cm}=$ 91.2 GeV

Int. J. Mod. Phys. A 2026.41. Downloaded from www.worldscientific.com
by UNIVERSITY OF CALIFORNIA @ BERKELEY on 09/16/26. Re strictly not permitted, except for Open Access articles.

$\langle N_{\eta'} \rangle$

VALUE	DOCUMENT ID		TECN	COMMENT
0.17 ±0.05 OUR AVERAGE	Error includes scale factor of 2.4.			
0.14 ±0.01 ±0.02	ACKERSTAFF	98A	OPAL	E^{ee}_{cm}= 91.2 GeV
0.25 ±0.04	[1] ACCIARRI	97D	L3	E^{ee}_{cm}= 91.2 GeV
• • • We do not use the following data for averages, fits, limits, etc. • • •				
0.068±0.018±0.016	[2] BUSKULIC	92D	ALEP	E^{ee}_{cm}= 91.2 GeV

[1] ACCIARRI 97D obtain this value averaging over the two decay channels $\eta' \to \pi^+\pi^-\eta$ and $\eta' \to \rho^0\gamma$.
[2] BUSKULIC 92D obtain this value for x> 0.1.

$\langle N_{f_0(980)} \rangle$

VALUE	DOCUMENT ID		TECN	COMMENT
0.147±0.011 OUR AVERAGE				
0.164±0.021	ABREU	99J	DLPH	E^{ee}_{cm}= 91.2 GeV
0.141±0.007±0.011	ACKERSTAFF	98Q	OPAL	E^{ee}_{cm}= 91.2 GeV

$\langle N_{a_0(980)^\pm} \rangle$

VALUE	DOCUMENT ID		TECN	COMMENT
0.27±0.04±0.10	ACKERSTAFF	98A	OPAL	E^{ee}_{cm}= 91.2 GeV

$\langle N_\phi \rangle$

VALUE	DOCUMENT ID		TECN	COMMENT
0.098±0.006 OUR AVERAGE	Error includes scale factor of 2.0.			See the ideogram below.
0.105±0.008	ABE	99E	SLD	E^{ee}_{cm}= 91.2 GeV
0.091±0.002±0.003	ACKERSTAFF	98Q	OPAL	E^{ee}_{cm}= 91.2 GeV
0.104±0.003±0.007	ABREU	96U	DLPH	E^{ee}_{cm}= 91.2 GeV
0.122±0.004±0.008	BUSKULIC	96H	ALEP	E^{ee}_{cm}= 91.2 GeV

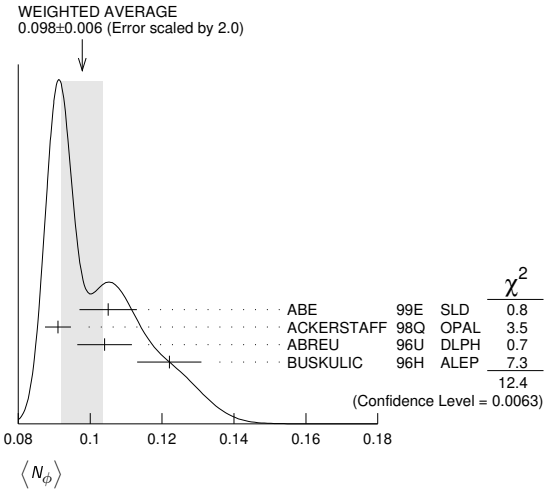

$\langle N_{f_2(1270)} \rangle$

VALUE	DOCUMENT ID		TECN	COMMENT
0.169±0.025 OUR AVERAGE	Error includes scale factor of 1.4.			
0.214±0.038	ABREU	99J	DLPH	E^{ee}_{cm}= 91.2 GeV
0.155±0.011±0.018	ACKERSTAFF	98Q	OPAL	E^{ee}_{cm}= 91.2 GeV

$\langle N_{f_1(1285)} \rangle$

VALUE	DOCUMENT ID		TECN	COMMENT
0.165±0.051	[1] ABDALLAH	03H	DLPH	E^{ee}_{cm}= 91.2 GeV

[1] ABDALLAH 03H assume a $K\overline{K}\pi$ branching ratio of (9.0 ± 0.4)%.

$\langle N_{f_1(1420)} \rangle$

VALUE	DOCUMENT ID		TECN	COMMENT
0.056±0.012	[1] ABDALLAH	03H	DLPH	E^{ee}_{cm}= 91.2 GeV

[1] ABDALLAH 03H assume a $K\overline{K}\pi$ branching ratio of 100%.

$\langle N_{f'_2(1525)} \rangle$

VALUE	DOCUMENT ID		TECN	COMMENT
0.012±0.006	ABREU	99J	DLPH	E^{ee}_{cm}= 91.2 GeV

$\langle N_{K^\pm} \rangle$

VALUE	DOCUMENT ID		TECN	COMMENT
2.24 ±0.04 OUR AVERAGE				
2.203±0.071	ABE	04C	SLD	E^{ee}_{cm}= 91.2 GeV
2.21 ±0.05 ±0.05	ABREU	98L	DLPH	E^{ee}_{cm}= 91.2 GeV
2.26 ±0.12	BARATE	98V	ALEP	E^{ee}_{cm}= 91.2 GeV
2.42 ±0.13	AKERS	94P	OPAL	E^{ee}_{cm}= 91.2 GeV

$\langle N_{K^0} \rangle$

VALUE	DOCUMENT ID		TECN	COMMENT
2.039±0.025 OUR AVERAGE	Error includes scale factor of 1.3.			See the ideogram below.
2.093±0.004±0.029	BARATE	00O	ALEP	E^{ee}_{cm}= 91.2 GeV
2.01 ±0.08	ABE	99E	SLD	E^{ee}_{cm}= 91.2 GeV
2.024±0.006±0.042	ACCIARRI	97L	L3	E^{ee}_{cm}= 91.2 GeV
1.962±0.022±0.056	ABREU	95L	DLPH	E^{ee}_{cm}= 91.2 GeV
1.99 ±0.01 ±0.04	AKERS	95U	OPAL	E^{ee}_{cm}= 91.2 GeV

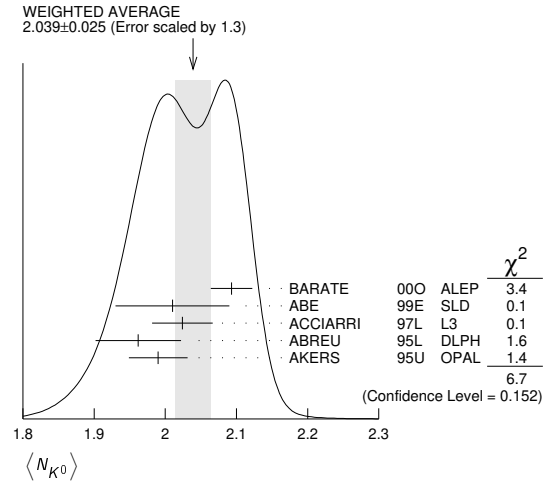

$\langle N_{K^*(892)^\pm} \rangle$

VALUE	DOCUMENT ID		TECN	COMMENT
0.72 ±0.05 OUR AVERAGE				
0.712±0.031±0.059	ABREU	95L	DLPH	E^{ee}_{cm}= 91.2 GeV
0.72 ±0.02 ±0.08	ACTON	93	OPAL	E^{ee}_{cm}= 91.2 GeV

$\langle N_{K^*(892)^0} \rangle$

VALUE	DOCUMENT ID		TECN	COMMENT
0.739±0.022 OUR AVERAGE				
0.707±0.041	ABE	99E	SLD	E^{ee}_{cm}= 91.2 GeV
0.74 ±0.02 ±0.02	ACKERSTAFF	97S	OPAL	E^{ee}_{cm}= 91.2 GeV
0.77 ±0.02 ±0.07	ABREU	96U	DLPH	E^{ee}_{cm}= 91.2 GeV
0.83 ±0.01 ±0.09	BUSKULIC	96H	ALEP	E^{ee}_{cm}= 91.2 GeV
0.97 ±0.18 ±0.31	ABREU	93	DLPH	E^{ee}_{cm}= 91.2 GeV

$\langle N_{K^*_2(1430)} \rangle$

VALUE	DOCUMENT ID		TECN	COMMENT
0.073±0.023	ABREU	99J	DLPH	E^{ee}_{cm}= 91.2 GeV
• • • We do not use the following data for averages, fits, limits, etc. • • •				
0.19 ±0.04 ±0.06	[1] AKERS	95X	OPAL	E^{ee}_{cm}= 91.2 GeV

[1] AKERS 95X obtain this value for x< 0.3.

$\langle N_{D^\pm} \rangle$

VALUE	DOCUMENT ID		TECN	COMMENT
0.187±0.020 OUR AVERAGE	Error includes scale factor of 1.5.			See the ideogram below.
0.170±0.009±0.014	ALEXANDER	96R	OPAL	E^{ee}_{cm}= 91.2 GeV
0.251±0.026±0.025	BUSKULIC	94J	ALEP	E^{ee}_{cm}= 91.2 GeV
0.199±0.019±0.024	[1] ABREU	93I	DLPH	E^{ee}_{cm}= 91.2 GeV

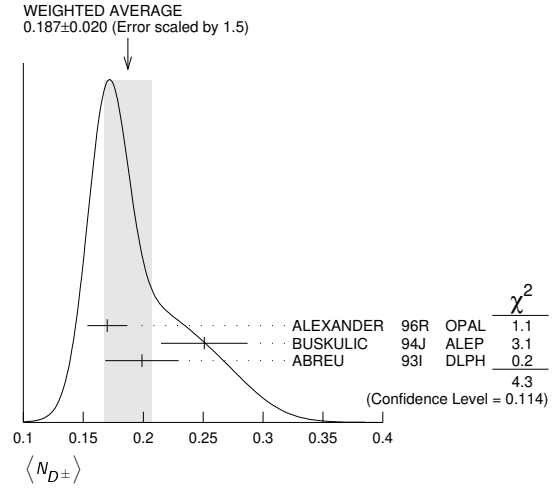

Int. J. Mod. Phys. A 2026.41. Downloaded from www.worldscientific.com
by UNIVERSITY OF CALIFORNIA @ BERKELEY on 09/16/26. Re-use and distribution is strictly not permitted, except for Open Access articles.

[1] See ABREU 95 (erratum).

$\langle N_{D^0} \rangle$

VALUE	DOCUMENT ID		TECN	COMMENT
0.462±0.026 OUR AVERAGE				
0.465±0.017±0.027	ALEXANDER	96R	OPAL	E^{ee}_{cm}= 91.2 GeV
0.518±0.052±0.035	BUSKULIC	94J	ALEP	E^{ee}_{cm}= 91.2 GeV
0.403±0.038±0.044	[1] ABREU	93I	DLPH	E^{ee}_{cm}= 91.2 GeV

[1] See ABREU 95 (erratum).

$\langle N_{D_s^\pm} \rangle$

VALUE	DOCUMENT ID		TECN	COMMENT
0.131±0.010±0.018	ALEXANDER	96R	OPAL	E^{ee}_{cm}= 91.2 GeV

$\langle N_{D^*(2010)^\pm} \rangle$

VALUE	DOCUMENT ID		TECN	COMMENT
0.183 ±0.008 OUR AVERAGE				
0.1854±0.0041±0.0091	[1] ACKERSTAFF	98E	OPAL	E^{ee}_{cm}= 91.2 GeV
0.187 ±0.015 ±0.013	BUSKULIC	94J	ALEP	E^{ee}_{cm}= 91.2 GeV
0.171 ±0.012 ±0.016	[2] ABREU	93I	DLPH	E^{ee}_{cm}= 91.2 GeV

[1] ACKERSTAFF 98E systematic error includes an uncertainty of ±0.0069 due to the branching ratios $B(D^{*+} \to D^0 \pi^+) = 0.683 \pm 0.014$ and $B(D^0 \to K^- \pi^+) = 0.0383 \pm 0.0012$.

[2] See ABREU 95 (erratum).

$\langle N_{D_{s1}(2536)^+} \rangle$

VALUE (units 10^{-3})	DOCUMENT ID		TECN	COMMENT
• • • We do not use the following data for averages, fits, limits, etc. • • •				
$2.9^{+0.7}_{-0.6}\pm0.2$	[1] ACKERSTAFF	97W	OPAL	E^{ee}_{cm}= 91.2 GeV

[1] ACKERSTAFF 97W obtain this value for $x > 0.6$ and with the assumption that its decay width is saturated by the $D^* K$ final states.

$\langle N_{B^*} \rangle$

VALUE	DOCUMENT ID		TECN	COMMENT
0.28±0.01±0.03	[1] ABREU	95R	DLPH	E^{ee}_{cm}= 91.2 GeV

[1] ABREU 95R quote this value for a flavor-averaged excited state.

$\langle N_{J/\psi(1S)} \rangle$

VALUE	DOCUMENT ID		TECN	COMMENT
0.0056±0.0003±0.0004	[1] ALEXANDER	96B	OPAL	E^{ee}_{cm}= 91.2 GeV

[1] ALEXANDER 96B identify $J/\psi(1S)$ from the decays into lepton pairs.

$\langle N_{\psi(2S)} \rangle$

VALUE	DOCUMENT ID		TECN	COMMENT
0.0023±0.0004±0.0003	ALEXANDER	96B	OPAL	E^{ee}_{cm}= 91.2 GeV

$\langle N_p \rangle$

VALUE	DOCUMENT ID		TECN	COMMENT
1.046±0.026 OUR AVERAGE				
1.054±0.035	ABE	04C	SLD	E^{ee}_{cm}= 91.2 GeV
1.08 ±0.04 ±0.03	ABREU	98L	DLPH	E^{ee}_{cm}= 91.2 GeV
1.00 ±0.07	BARATE	98V	ALEP	E^{ee}_{cm}= 91.2 GeV
0.92 ±0.11	AKERS	94P	OPAL	E^{ee}_{cm}= 91.2 GeV

$\langle N_{\Delta(1232)^{++}} \rangle$

VALUE	DOCUMENT ID		TECN	COMMENT
0.087±0.033 OUR AVERAGE	Error includes scale factor of 2.4.			
0.079±0.009±0.011	ABREU	95W	DLPH	E^{ee}_{cm}= 91.2 GeV
0.22 ±0.04 ±0.04	ALEXANDER	95D	OPAL	E^{ee}_{cm}= 91.2 GeV

$\langle N_\Lambda \rangle$

VALUE	DOCUMENT ID		TECN	COMMENT
0.388±0.009 OUR AVERAGE	Error includes scale factor of 1.7. See the ideogram below.			
0.404±0.002±0.007	BARATE	00O	ALEP	E^{ee}_{cm}= 91.2 GeV
0.395±0.022	ABE	99E	SLD	E^{ee}_{cm}= 91.2 GeV
0.364±0.004±0.017	ACCIARRI	97L	L3	E^{ee}_{cm}= 91.2 GeV
0.374±0.002±0.010	ALEXANDER	97D	OPAL	E^{ee}_{cm}= 91.2 GeV
0.357±0.003±0.017	ABREU	93L	DLPH	E^{ee}_{cm}= 91.2 GeV

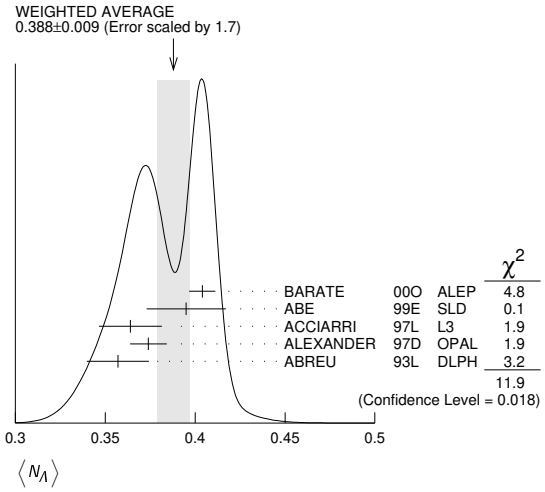

$\langle N_{\Lambda(1520)} \rangle$

VALUE	DOCUMENT ID		TECN	COMMENT
0.0224±0.0027 OUR AVERAGE				
0.029 ±0.005 ±0.005	ABREU	00P	DLPH	E^{ee}_{cm}= 91.2 GeV
0.0213±0.0021±0.0019	ALEXANDER	97D	OPAL	E^{ee}_{cm}= 91.2 GeV

$\langle N_{\Sigma^+} \rangle$

VALUE	DOCUMENT ID		TECN	COMMENT
0.107±0.010 OUR AVERAGE				
0.114±0.011±0.009	ACCIARRI	00J	L3	E^{ee}_{cm}= 91.2 GeV
0.099±0.008±0.013	ALEXANDER	97E	OPAL	E^{ee}_{cm}= 91.2 GeV

$\langle N_{\Sigma^-} \rangle$

VALUE	DOCUMENT ID		TECN	COMMENT
0.082±0.007 OUR AVERAGE				
0.081±0.002±0.010	ABREU	00P	DLPH	E^{ee}_{cm}= 91.2 GeV
0.083±0.006±0.009	ALEXANDER	97E	OPAL	E^{ee}_{cm}= 91.2 GeV

$\langle N_{\Sigma^+ + \Sigma^-} \rangle$

VALUE	DOCUMENT ID		TECN	COMMENT
0.181±0.018 OUR AVERAGE				
0.182±0.010±0.016	[1] ALEXANDER	97E	OPAL	E^{ee}_{cm}= 91.2 GeV
0.170±0.014±0.061	ABREU	95O	DLPH	E^{ee}_{cm}= 91.2 GeV

[1] We have combined the values of $\langle N_{\Sigma^+} \rangle$ and $\langle N_{\Sigma^-} \rangle$ from ALEXANDER 97E adding the statistical and systematic errors of the two final states separately in quadrature. If isospin symmetry is assumed this value becomes 0.174 ± 0.010 ± 0.015.

$\langle N_{\Sigma^0} \rangle$

VALUE	DOCUMENT ID		TECN	COMMENT
0.076±0.010 OUR AVERAGE				
0.095±0.015±0.013	ACCIARRI	00J	L3	E^{ee}_{cm}= 91.2 GeV
0.071±0.012±0.013	ALEXANDER	97E	OPAL	E^{ee}_{cm}= 91.2 GeV
0.070±0.010±0.010	ADAM	96B	DLPH	E^{ee}_{cm}= 91.2 GeV

$\langle N_{(\Sigma^+ + \Sigma^- + \Sigma^0)/3} \rangle$

VALUE	DOCUMENT ID		TECN	COMMENT
0.084±0.005±0.008	ALEXANDER	97E	OPAL	E^{ee}_{cm}= 91.2 GeV

$\langle N_{\Sigma(1385)^+} \rangle$

VALUE	DOCUMENT ID		TECN	COMMENT
0.0239±0.0009±0.0012	ALEXANDER	97D	OPAL	E^{ee}_{cm}= 91.2 GeV

$\langle N_{\Sigma(1385)^-} \rangle$

VALUE	DOCUMENT ID		TECN	COMMENT
0.0240±0.0010±0.0014	ALEXANDER	97D	OPAL	E^{ee}_{cm}= 91.2 GeV

$\langle N_{\Sigma(1385)^+ + \Sigma(1385)^-} \rangle$

VALUE	DOCUMENT ID		TECN	COMMENT
0.046 ±0.004 OUR AVERAGE	Error includes scale factor of 1.6.			
0.0479±0.0013±0.0026	ALEXANDER	97D	OPAL	E^{ee}_{cm}= 91.2 GeV
0.0382±0.0028±0.0045	ABREU	95O	DLPH	E^{ee}_{cm}= 91.2 GeV

$\langle N_{\Xi^-} \rangle$

VALUE	DOCUMENT ID		TECN	COMMENT
0.0258±0.0009 OUR AVERAGE				
0.0247±0.0009±0.0025	ABDALLAH	06E	DLPH	E^{ee}_{cm} = 91.2 GeV
0.0259±0.0004±0.0009	ALEXANDER	97D	OPAL	E^{ee}_{cm} = 91.2 GeV

Int. J. Mod. Phys. A 2026.41. Downloaded from www.worldscientific.com
by UNIVERSITY OF CALIFORNIA @ BERKELEY on 09/16/26. Re strictly not permitted, except for Open Access articles.

$\langle N_{\Xi(1530)^0} \rangle$

VALUE	DOCUMENT ID		TECN	COMMENT
0.0059±0.0011 OUR AVERAGE	Error includes scale factor of 2.3.			
0.0045±0.0005±0.0006	ABDALLAH	05C	DLPH	E^{ee}_{cm}= 91.2 GeV
0.0068±0.0005±0.0004	ALEXANDER	97D	OPAL	E^{ee}_{cm}= 91.2 GeV

$\langle N_{\Omega^-} \rangle$

VALUE	DOCUMENT ID		TECN	COMMENT
0.00164±0.00028 OUR AVERAGE				
0.0018 ±0.0003 ±0.0002	ALEXANDER	97D	OPAL	E^{ee}_{cm}= 91.2 GeV
0.0014 ±0.0002 ±0.0004	ADAM	96B	DLPH	E^{ee}_{cm}= 91.2 GeV

$\langle N_{\Lambda_c^+} \rangle$

VALUE	DOCUMENT ID		TECN	COMMENT
0.078±0.012±0.012	ALEXANDER	96R	OPAL	E^{ee}_{cm}= 91.2 GeV

$\langle N_{\overline{D}} \rangle$

VALUE (units 10^{-6})	DOCUMENT ID		TECN	COMMENT
• • • We do not use the following data for averages, fits, limits, etc. • • •				
5.9±1.8±0.5	[1] SCHAEL	06A	ALEP	E^{ee}_{cm} = 91.2 GeV

[1] SCHAEL 06A obtain this anti-deuteron production rate per hadronic Z decay in the anti-deuteron momentum range from 0.62 to 1.03 GeV/c.

$\langle N_{charged} \rangle$

VALUE	DOCUMENT ID		TECN	COMMENT
20.76±0.16 OUR AVERAGE	Error includes scale factor of 2.1. See the ideogram below.			
20.46±0.01±0.11	ACHARD	03G	L3	E^{ee}_{cm}= 91.2 GeV
21.21±0.01±0.20	ABREU	99	DLPH	E^{ee}_{cm}= 91.2 GeV
21.05±0.20	AKERS	95Z	OPAL	E^{ee}_{cm}= 91.2 GeV
20.91±0.03±0.22	BUSKULIC	95R	ALEP	E^{ee}_{cm}= 91.2 GeV
21.40±0.43	ACTON	92B	OPAL	E^{ee}_{cm}= 91.2 GeV
20.71±0.04±0.77	ABREU	91H	DLPH	E^{ee}_{cm}= 91.2 GeV
20.7 ±0.7	ADEVA	91I	L3	E^{ee}_{cm}= 91.2 GeV
20.1 ±1.0 ±0.9	ABRAMS	90	MRK2	E^{ee}_{cm}= 91.1 GeV

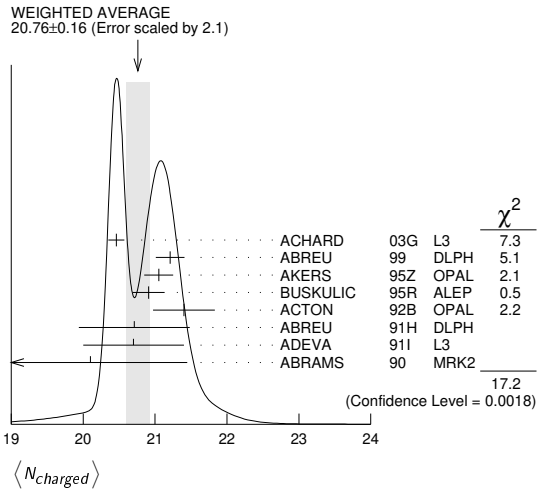

Z HADRONIC POLE CROSS SECTION

OUR EVALUATION is obtained using the fit procedure and correlations as determined by the LEP Electroweak Working Group (see the note "The Z boson" and ref. LEP-SLC 06). Corrections as discussed in VOUTSINAS 20 and JANOT 20 are also included. This quantity is defined as

$$\sigma^0_h = \frac{12\pi}{M_Z^2} \frac{\Gamma(e^+e^-)\Gamma(\text{hadrons})}{\Gamma_Z^2}$$

It is one of the parameters used in the Z lineshape fit.

VALUE (nb)	EVTS	DOCUMENT ID		TECN	COMMENT
41.4802±0.0325 OUR EVALUATION					
41.4802±0.0325		[1] JANOT	20		
• • • We do not use the following data for averages, fits, limits, etc. • • •					
41.500 ±0.037		[2] VOUTSINAS	20		
41.541 ±0.037		[3] LEP-SLC	06		E^{ee}_{cm} = 88–94 GeV
41.501 ±0.055	4.10M	[4] ABBIENDI	01A	OPAL	E^{ee}_{cm}= 88–94 GeV
41.578 ±0.069	3.70M	ABREU	00F	DLPH	E^{ee}_{cm}= 88–94 GeV
41.535 ±0.055	3.54M	ACCIARRI	00C	L3	E^{ee}_{cm}= 88–94 GeV
41.559 ±0.058	4.07M	[5] BARATE	00C	ALEP	E^{ee}_{cm}= 88–94 GeV
42 ±4	450	ABRAMS	89B	MRK2	E^{ee}_{cm}= 89.2–93.0 GeV

[1] JANOT 20 applies a correction to LEP-SLC 06 using an updated Bhabha cross section calculation. This result also includes a correction to account for correlated luminosity bias as presented in VOUTSINAS 20.
[2] VOUTSINAS 20 applies a correction to LEP-SLC 06 to account for correlated luminosity bias.
[3] This result combines ABBIENDI 01A, ABREU 00F, ACCIARRI 00C, BARATE 00C, taking correlated uncertainties into account.
[4] ABBIENDI 01A error includes approximately 0.031 due to statistics, 0.033 due to event selection systematics, 0.029 due to uncertainty in luminosity measurement, and 0.011 due to LEP energy uncertainty.
[5] BARATE 00C error includes approximately 0.030 due to statistics, 0.026 due to experimental systematics, and 0.025 due to uncertainty in luminosity measurement.

Z VECTOR COUPLINGS

These quantities are the effective vector couplings of the Z to charged leptons and quarks. Their magnitude is derived from a measurement of the Z lineshape and the forward-backward lepton asymmetries as a function of energy around the Z mass. The relative sign among the vector to axial-vector couplings is obtained from a measurement of the Z asymmetry parameters, A_e, A_μ, and A_τ. By convention the sign of g^e_A is fixed to be negative (and opposite to that of g^{ν_e} obtained using ν_e scattering measurements). For the light quarks, the sign of the couplings is assigned consistently with this assumption. The LEP/SLD-based fit values quoted below correspond to global nine- or five-parameter fits to lineshape, lepton forward-backward asymmetry, and A_e, A_μ, and A_τ measurements. See the note "The Z boson" and ref. LEP-SLC 06 for details. Where $p\overline{p}$ and ep data is quoted, OUR FIT value corresponds to a weighted average of this with the LEP/SLD fit result.

g^e_V

VALUE	EVTS	DOCUMENT ID		TECN	COMMENT
−0.03817±0.00047 OUR FIT					
−0.058 ±0.016 ±0.007	5026	[1] ACOSTA	05M	CDF	$E^{p\overline{p}}_{cm}$= 1.96 TeV
−0.0346 ±0.0023	137.0k	[2] ABBIENDI	01O	OPAL	E^{ee}_{cm}= 88–94 GeV
−0.0412 ±0.0027	124.4k	[3] ACCIARRI	00C	L3	E^{ee}_{cm}= 88–94 GeV
−0.0400 ±0.0037		BARATE	00C	ALEP	E^{ee}_{cm}= 88–94 GeV
−0.0414 ±0.0020		[4] ABE	95J	SLD	E^{ee}_{cm}= 91.31 GeV

[1] ACOSTA 05M determine the forward–backward asymmetry of e^+e^- pairs produced via $q\overline{q} \to Z/\gamma^* \to e^+e^-$ in 15 M(e^+e^-) effective mass bins ranging from 40 GeV to 600 GeV. These results are used to obtain the vector and axial–vector couplings of the Z to e^+e^-, assuming the quark couplings are as predicted by the standard model. Higher order radiative corrections have not been taken into account.
[2] ABBIENDI 01O use their measurement of the τ polarization in addition to the lineshape and forward-backward lepton asymmetries.
[3] ACCIARRI 00C use their measurement of the τ polarization in addition to forward-backward lepton asymmetries.
[4] ABE 95J obtain this result combining polarized Bhabha results with the A_{LR} measurement of ABE 94C. The Bhabha results alone give −0.0507 ± 0.0096 ± 0.0020.

g^μ_V

VALUE	EVTS	DOCUMENT ID		TECN	COMMENT
−0.0367±0.0023 OUR FIT					
$-0.0388^{+0.0060}_{-0.0064}$	182.8k	[1] ABBIENDI	01O	OPAL	E^{ee}_{cm}= 88–94 GeV
−0.0386±0.0073	113.4k	[2] ACCIARRI	00C	L3	E^{ee}_{cm}= 88–94 GeV
−0.0362±0.0061		BARATE	00C	ALEP	E^{ee}_{cm}= 88–94 GeV
• • • We do not use the following data for averages, fits, limits, etc. • • •					
−0.0413±0.0060	66143	[3] ABBIENDI	01K	OPAL	E^{ee}_{cm}= 89–93 GeV

[1] ABBIENDI 01O use their measurement of the τ polarization in addition to the lineshape and forward-backward lepton asymmetries.
[2] ACCIARRI 00C use their measurement of the τ polarization in addition to forward-backward lepton asymmetries.
[3] ABBIENDI 01K obtain this from an angular analysis of the muon pair asymmetry which takes into account effects of initial state radiation on an event by event basis and of initial-final state interference.

g^τ_V

VALUE	EVTS	DOCUMENT ID		TECN	COMMENT
−0.0366±0.0010 OUR FIT					
−0.0365±0.0023	151.5k	[1] ABBIENDI	01O	OPAL	E^{ee}_{cm}= 88–94 GeV
−0.0384±0.0026	103.0k	[2] ACCIARRI	00C	L3	E^{ee}_{cm}= 88–94 GeV
−0.0361±0.0068		BARATE	00C	ALEP	E^{ee}_{cm}= 88–94 GeV

[1] ABBIENDI 01O use their measurement of the τ polarization in addition to the lineshape and forward-backward lepton asymmetries.
[2] ACCIARRI 00C use their measurement of the τ polarization in addition to forward-backward lepton asymmetries.

g^ℓ_V

VALUE	EVTS	DOCUMENT ID		TECN	COMMENT
−0.03783±0.00041 OUR FIT					
−0.0358 ±0.0014	471.3k	[1] ABBIENDI	01O	OPAL	E^{ee}_{cm}= 88–94 GeV
−0.0397 ±0.0020	379.4k	[2] ABREU	00F	DLPH	E^{ee}_{cm}= 88–94 GeV
−0.0397 ±0.0017	340.8k	[3] ACCIARRI	00C	L3	E^{ee}_{cm}= 88–94 GeV
−0.0383 ±0.0018	500k	BARATE	00C	ALEP	E^{ee}_{cm}= 88–94 GeV

[1] ABBIENDI 01O use their measurement of the τ polarization in addition to the lineshape and forward-backward lepton asymmetries.
[2] Using forward-backward lepton asymmetries.
[3] ACCIARRI 00C use their measurement of the τ polarization in addition to forward-backward lepton asymmetries.

Int. J. Mod. Phys. A 2026.41. Downloaded from www.worldscientific.com by UNIVERSITY OF CALIFORNIA @ BERKELEY on 09/16/26. Re-use and distribution is strictly not permitted, except for Open Access articles.

g_V^u

VALUE	EVTS	DOCUMENT ID		TECN	COMMENT
0.266±0.034 OUR AVERAGE					
0.270±0.037		[1] ANDREEV	18A	H1	$e^\pm p$
0.201±0.112	156k	[2] ABAZOV	11D	D0	$E_{cm}^{p\overline{p}}$ = 1.97 TeV
$0.24\ ^{+0.28}_{-0.11}$		[3] LEP-SLC	06		E_{cm}^{ee} = 88–94 GeV
$0.399^{+0.152}_{-0.188}\pm0.066$	5026	[4] ACOSTA	05M	CDF	$E_{cm}^{p\overline{p}}$= 1.96 TeV
• • • We do not use the following data for averages, fits, limits, etc. • • •					
$0.14\ ^{+0.09}_{-0.09}$		[5] ABRAMOWICZ	16A	ZEUS	
$0.144^{+0.066}_{-0.058}$		[6] ABT	16		
0.27 ±0.13	1500	[7] AKTAS	06	H1	$e^\pm p \to \overline{\nu}_e(\nu_e)X$, $\sqrt{s}\approx$ 300 GeV

[1] ANDREEV 18A obtain this result in a combined electroweak and QCD analysis using all deep-inelastic e^+p and e^-p neutral current and charged current scattering cross sections published by the H1 Collaboration, including data with longitudinally polarized lepton beams.

[2] ABAZOV 11D study $p\overline{p} \to Z/\gamma^* e^+e^-$ events using 5 fb^{-1} data at $\sqrt{s}$ = 1.96 TeV. The candidate events are selected by requiring two isolated electromagnetic showers with E_T > 25 GeV, at least one electron in the central region and the di-electron mass in the range 50–1000 GeV. From the forward-backward asymmetry, determined as a function of the di-electron mass, they derive the axial and vector couplings of the u- and d- quarks and the value of $\sin^2\theta^\ell_{eff}$ = 0.2309 ± 0.0008(stat)±0.0006(syst).

[3] LEP-SLC 06 is a combination of the results from LEP and SLC experiments using light quark tagging. s- and d-quark couplings are assumed to be identical.

[4] ACOSTA 05M determine the forward-backward asymmetry of e^+e^- pairs produced via $q\overline{q} \to Z/\gamma^* \to e^+e^-$ in 15 M(e^+e^-) effective mass bins ranging from 40 GeV to 600 GeV. These results are used to obtain the vector and axial-vector couplings of the Z to the light quarks, assuming the electron couplings are as predicted by the Standard Model. Higher order radiative corrections have not been taken into account.

[5] ABRAMOWICZ 16A determine the Z^0 couplings to u- and d-quarks using the ZEUS polarised data from Run II together with the unpolarised data from both ZEUS and H1 Collaborations for Run I and unpolarised H1 data from Run II.

[6] ABT 16 determine the Z^0 couplings to u- and d-quarks using the same techniques and data as ABRAMOWICZ 16A but additionally use the published H1 polarised data.

[7] AKTAS 06 fit the neutral current (1.5 ≤ Q^2 ≤ 30,000 GeV^2) and charged current (1.5 ≤ Q^2 ≤ 15,000 GeV^2) differential cross sections. In the determination of the u-quark couplings the electron and d-quark couplings are fixed to their standard model values.

g_V^d

VALUE	EVTS	DOCUMENT ID		TECN	COMMENT
$-0.38\ ^{+0.04}_{-0.05}$ OUR AVERAGE					
−0.488±0.092		[1] ANDREEV	18A	H1	$e^\pm p$
−0.351±0.251	156k	[2] ABAZOV	11D	D0	$E_{cm}^{p\overline{p}}$ = 1.97 TeV
$-0.33\ ^{+0.05}_{-0.07}$		[3] LEP-SLC	06		E_{cm}^{ee} = 88–94 GeV
$-0.226^{+0.635}_{-0.290}\pm0.090$	5026	[4] ACOSTA	05M	CDF	$E_{cm}^{p\overline{p}}$= 1.96 TeV
• • • We do not use the following data for averages, fits, limits, etc. • • •					
$-0.41\ ^{+0.25}_{-0.20}$		[5] ABRAMOWICZ	16A	ZEUS	
$-0.503^{+0.171}_{-0.103}$		[6] ABT	16		
−0.33 ±0.33	1500	[7] AKTAS	06	H1	$e^\pm p \to \overline{\nu}_e(\nu_e)X$, $\sqrt{s}\approx$ 300 GeV

[1] ANDREEV 18A obtain this result in a combined electroweak and QCD analysis using all deep-inelastic e^+p and e^-p neutral current and charged current scattering cross sections published by the H1 Collaboration, including data with longitudinally polarized lepton beams.

[2] ABAZOV 11D study $p\overline{p} \to Z/\gamma^* e^+e^-$ events using 5 fb^{-1} data at $\sqrt{s}$ = 1.96 TeV. The candidate events are selected by requiring two isolated electromagnetic showers with E_T > 25 GeV, at least one electron in the central region and the di-electron mass in the range 50–1000 GeV. From the forward-backward asymmetry, determined as a function of the di-electron mass, they derive the axial and vector couplings of the u- and d- quarks and the value of $\sin^2\theta^\ell_{eff}$ = 0.2309 ± 0.0008(stat)±0.0006(syst).

[3] LEP-SLC 06 is a combination of the results from LEP and SLC experiments using light quark tagging. s- and d-quark couplings are assumed to be identical.

[4] ACOSTA 05M determine the forward-backward asymmetry of e^+e^- pairs produced via $q\overline{q} \to Z/\gamma^* \to e^+e^-$ in 15 M(e^+e^-) effective mass bins ranging from 40 GeV to 600 GeV. These results are used to obtain the vector and axial-vector couplings of the Z to the light quarks, assuming the electron couplings are as predicted by the Standard Model. Higher order radiative corrections have not been taken into account.

[5] ABRAMOWICZ 16A determine the Z^0 couplings to u- and d-quarks using the ZEUS polarised data from Run II together with the unpolarised data from both ZEUS and H1 Collaborations for Run I and unpolarised H1 data from Run II.

[6] ABT 16 determine the Z^0 couplings to u- and d-quarks using the same techniques and data as ABRAMOWICZ 16A but additionally use the published H1 polarised data.

[7] AKTAS 06 fit the neutral current (1.5 ≤ Q^2 ≤ 30,000 GeV^2) and charged current (1.5 ≤ Q^2 ≤ 15,000 GeV^2) differential cross sections. In the determination of the d-quark couplings the electron and u-quark couplings are fixed to their standard model values.

Z AXIAL-VECTOR COUPLINGS

These quantities are the effective axial-vector couplings of the Z to charged leptons and quarks. Their magnitude is derived from a measurement of the Z lineshape and the forward-backward lepton asymmetries as a function of energy around the Z mass. The relative sign among the vector to axial-vector couplings is obtained from a measurement of the Z asymmetry parameters, A_e, A_μ, and A_τ. By convention the sign of g_A^e is fixed to be negative (and opposite to that of $g_A^{\nu_e}$ obtained using ν_e scattering measurements). For the light quarks, the sign of the couplings is assigned consistently with this assumption. The LEP/SLD-based fit values quoted below correspond to global nine- or five-parameter fits to lineshape, lepton forward-backward asymmetry, and A_e, A_μ, and A_τ measurements. See the note "The Z boson" and ref. LEP-SLC 06 for details. Where $p\overline{p}$ and ep data is quoted, OUR FIT value corresponds to a weighted average of this with the LEP/SLD fit result.

g_A^e

VALUE	EVTS	DOCUMENT ID		TECN	COMMENT
−0.50111±0.00035 OUR FIT					
−0.528 ±0.123 ±0.059	5026	[1] ACOSTA	05M	CDF	$E_{cm}^{p\overline{p}}$= 1.96 TeV
−0.50062±0.00062	137.0k	[2] ABBIENDI	01O	OPAL	E_{cm}^{ee}= 88–94 GeV
−0.5015 ±0.0007	124.4k	[3] ACCIARRI	00C	L3	E_{cm}^{ee}= 88–94 GeV
−0.50166±0.00057		BARATE	00C	ALEP	E_{cm}^{ee}= 88–94 GeV
−0.4977 ±0.0045		[4] ABE	95J	SLD	E_{cm}^{ee}= 91.31 GeV

[1] ACOSTA 05M determine the forward–backward asymmetry of e^+e^- pairs produced via $q\overline{q} \to Z/\gamma^* \to e^+e^-$ in 15 M(e^+e^-) effective mass bins ranging from 40 GeV to 600 GeV. These results are used to obtain the vector and axial–vector couplings of the Z to e^+e^-, assuming the quark couplings are as predicted by the standard model. Higher order radiative corrections have not been taken into account.

[2] ABBIENDI 01O use their measurement of the τ polarization in addition to the lineshape and forward-backward lepton asymmetries.

[3] ACCIARRI 00C use their measurement of the τ polarization in addition to forward-backward lepton asymmetries.

[4] ABE 95J obtain this result combining polarized Bhabha results with the A_{LR} measurement of ABE 94C. The Bhabha results alone give −0.4968 ± 0.0039 ± 0.0027.

g_A^μ

VALUE	EVTS	DOCUMENT ID		TECN	COMMENT
−0.50120±0.00054 OUR FIT					
−0.50117±0.00099	182.8k	[1] ABBIENDI	01O	OPAL	E_{cm}^{ee}= 88–94 GeV
−0.5009 ±0.0014	113.4k	[2] ACCIARRI	00C	L3	E_{cm}^{ee}= 88–94 GeV
−0.50046±0.00093		BARATE	00C	ALEP	E_{cm}^{ee}= 88–94 GeV
• • • We do not use the following data for averages, fits, limits, etc. • • •					
−0.520 ±0.015	66143	[3] ABBIENDI	01K	OPAL	E_{cm}^{ee}= 89–93 GeV

[1] ABBIENDI 01O use their measurement of the τ polarization in addition to the lineshape and forward-backward lepton asymmetries.

[2] ACCIARRI 00C use their measurement of the τ polarization in addition to forward-backward lepton asymmetries.

[3] ABBIENDI 01K obtain this from an angular analysis of the muon pair asymmetry which takes into account effects of initial state radiation on an event by event basis and of initial-final state interference.

g_A^τ

VALUE	EVTS	DOCUMENT ID		TECN	COMMENT
−0.50204±0.00064 OUR FIT					
−0.50165±0.00124	151.5k	[1] ABBIENDI	01O	OPAL	E_{cm}^{ee}= 88–94 GeV
−0.5023 ±0.0017	103.0k	[2] ACCIARRI	00C	L3	E_{cm}^{ee}= 88–94 GeV
−0.50216±0.00100		BARATE	00C	ALEP	E_{cm}^{ee}= 88–94 GeV

[1] ABBIENDI 01O use their measurement of the τ polarization in addition to the lineshape and forward-backward lepton asymmetries.

[2] ACCIARRI 00C use their measurement of the τ polarization in addition to forward-backward lepton asymmetries.

g_A^ℓ

VALUE	EVTS	DOCUMENT ID		TECN	COMMENT
−0.50123±0.00026 OUR FIT					
−0.50089±0.00045	471.3k	[1] ABBIENDI	01O	OPAL	E_{cm}^{ee}= 88–94 GeV
−0.5007 ±0.0005	379.4k	ABREU	00F	DLPH	E_{cm}^{ee}= 88–94 GeV
−0.50153±0.00053	340.8k	[2] ACCIARRI	00C	L3	E_{cm}^{ee}= 88–94 GeV
−0.50150±0.00046	500k	BARATE	00C	ALEP	E_{cm}^{ee}= 88–94 GeV

[1] ABBIENDI 01O use their measurement of the τ polarization in addition to the lineshape and forward-backward lepton asymmetries.

[2] ACCIARRI 00C use their measurement of the τ polarization in addition to forward-backward lepton asymmetries.

g_A^u

VALUE	EVTS	DOCUMENT ID		TECN	COMMENT
$0.519^{+0.028}_{-0.033}$ OUR AVERAGE					
0.548±0.036		[1] ANDREEV	18A	H1	$e^\pm p$
0.501±0.110	156k	[2] ABAZOV	11D	D0	$E_{cm}^{p\overline{p}}$ = 1.97 TeV
$0.47\ ^{+0.05}_{-0.33}$		[3] LEP-SLC	06		E_{cm}^{ee} = 88–94 GeV
$0.441^{+0.207}_{-0.173}\pm0.067$	5026	[4] ACOSTA	05M	CDF	$E_{cm}^{p\overline{p}}$= 1.96 TeV

Int. J. Mod. Phys. A 2026.41. Downloaded from www.worldscientific.com by UNIVERSITY OF CALIFORNIA @ BERKELEY on 09/16/26. Re-use strictly not permitted, except for Open Access articles.

• • • We do not use the following data for averages, fits, limits, etc. • • •

$0.50\ ^{+0.12}_{-0.05}$		[5] ABRAMOWICZ 16A	ZEUS		
$0.532^{+0.107}_{-0.063}$		[6] ABT	16		
$0.57\ \pm0.08$	1500	[7] AKTAS	06	H1	$e^{\pm}p \to \overline{\nu}_e(\nu_e)X$, $\sqrt{s} \approx 300$ GeV

[1] ANDREEV 18A obtain this result in a combined electroweak and QCD analysis using all deep-inelastic e^+p and e^-p neutral current and charged current scattering cross sections published by the H1 Collaboration, including data with longitudinally polarized lepton beams.

[2] ABAZOV 11D study $p\overline{p} \to Z/\gamma^* e^+e^-$ events using 5 fb^{-1} data at $\sqrt{s} = 1.96$ TeV. The candidate events are selected by requiring two isolated electromagnetic showers with $E_T > 25$ GeV, at least one electron in the central region and the di-electron mass in the range 50–1000 GeV. From the forward-backward asymmetry, determined as a function of the di-electron mass, they derive the axial and vector couplings of the u- and d- quarks and the value of $\sin^2\theta^{\ell}_{eff} = 0.2309 \pm 0.0008(\text{stat}) \pm 0.0006(\text{syst})$.

[3] LEP-SLC 06 is a combination of the results from LEP and SLC experiments using light quark tagging. s- and d-quark couplings are assumed to be identical.

[4] ACOSTA 05M determine the forward-backward asymmetry of e^+e^- pairs produced via $q\overline{q} \to Z/\gamma^* \to e^+e^-$ in 15 M(e^+e^-) effective mass bins ranging from 40 GeV to 600 GeV. These results are used to obtain the vector and axial-vector couplings of the Z to the light quarks, assuming the electron couplings are as predicted by the Standard Model. Higher order radiative corrections have not been taken into account.

[5] ABRAMOWICZ 16A determine the Z^0 couplings to u- and d-quarks using the ZEUS polarised data from Run II together with the unpolarised data from both ZEUS and H1 Collaborations for Run I and unpolarised H1 data from Run II.

[6] ABT 16 determine the Z^0 couplings to u- and d-quarks using the same techniques and data as ABRAMOWICZ 16A but additionally use the published H1 polarised data.

[7] AKTAS 06 fit the neutral current ($1.5 \leq Q^2 \leq 30{,}000$ GeV^2) and charged current ($1.5 \leq Q^2 \leq 15{,}000$ GeV^2) differential cross sections. In the determination of the u-quark couplings the electron and d-quark couplings are fixed to their standard model values.

g_A^d

VALUE	EVTS	DOCUMENT ID		TECN	COMMENT
$-0.527^{+0.040}_{-0.028}$ OUR AVERAGE					
-0.619 ± 0.108		[1] ANDREEV	18A	H1	$e^{\pm}p$
-0.497 ± 0.165	156k	[2] ABAZOV	11D	D0	$E^{p\overline{p}}_{cm} = 1.97$ TeV
$-0.52\ ^{+0.05}_{-0.03}$		[3] LEP-SLC	06		$E^{ee}_{cm} = 88$–94 GeV
$-0.016^{+0.346}_{-0.536}\pm0.091$	5026	[4] ACOSTA	05M	CDF	$E^{p\overline{p}}_{cm} = 1.96$ TeV

• • • We do not use the following data for averages, fits, limits, etc. • • •

$-0.56\ ^{+0.41}_{-0.15}$		[5] ABRAMOWICZ 16A	ZEUS		
$-0.409^{+0.373}_{-0.213}$		[6] ABT	16		
$-0.80\ \pm0.24$	1500	[7] AKTAS	06	H1	$e^{\pm}p \to \overline{\nu}_e(\nu_e)X$, $\sqrt{s} \approx 300$ GeV

[1] ANDREEV 18A obtain this result in a combined electroweak and QCD analysis using all deep-inelastic e^+p and e^-p neutral current and charged current scattering cross sections published by the H1 Collaboration, including data with longitudinally polarized lepton beams.

[2] ABAZOV 11D study $p\overline{p} \to Z/\gamma^* e^+e^-$ events using 5 fb^{-1} data at $\sqrt{s} = 1.96$ TeV. The candidate events are selected by requiring two isolated electromagnetic showers with $E_T > 25$ GeV, at least one electron in the central region and the di-electron mass in the range 50–1000 GeV. From the forward-backward asymmetry, determined as a function of the di-electron mass, they derive the axial and vector couplings of the u- and d- quarks and the value of $\sin^2\theta^{\ell}_{eff} = 0.2309 \pm 0.0008(\text{stat}) \pm 0.0006(\text{syst})$.

[3] LEP-SLC 06 is a combination of the results from LEP and SLC experiments using light quark tagging. s- and d-quark couplings are assumed to be identical.

[4] ACOSTA 05M determine the forward-backward asymmetry of e^+e^- pairs produced via $q\overline{q} \to Z/\gamma^* \to e^+e^-$ in 15 M(e^+e^-) effective mass bins ranging from 40 GeV to 600 GeV. These results are used to obtain the vector and axial-vector couplings of the Z to the light quarks, assuming the electron couplings are as predicted by the Standard Model. Higher order radiative corrections have not been taken into account.

[5] ABRAMOWICZ 16A determine the Z^0 couplings to u- and d-quarks using the ZEUS polarised data from Run II together with the unpolarised data from both ZEUS and H1 Collaborations for Run I and unpolarised H1 data from Run II.

[6] ABT 16 determine the Z^0 couplings to u- and d-quarks using the same techniques and data as ABRAMOWICZ 16A but additionally use the published H1 polarised data.

[7] AKTAS 06 fit the neutral current ($1.5 \leq Q^2 \leq 30{,}000$ GeV^2) and charged current ($1.5 \leq Q^2 \leq 15{,}000$ GeV^2) differential cross sections. In the determination of the d-quark couplings the electron and u-quark couplings are fixed to their standard model values.

Z COUPLINGS TO NEUTRAL LEPTONS

Averaging over neutrino species, the invisible Z decay width determines the effective neutrino coupling g^{ν_ℓ}. For g^{ν_e} and g^{ν_μ}, $\nu_e e$ and $\nu_\mu e$ scattering results are combined with g_A^e and g_V^e measurements at the Z mass to obtain g^{ν_e} and g^{ν_μ} following NOVIKOV 93C.

g^{ν_ℓ}

VALUE	DOCUMENT ID		COMMENT
0.50076±0.00076	[1] LEP-SLC	06	$E^{ee}_{cm} = 88$–94 GeV

[1] From invisible Z-decay width.

g^{ν_e}

VALUE	DOCUMENT ID		TECN	COMMENT
0.528±0.085	[1] VILAIN	94	CHM2	From $\nu_\mu e$ and $\nu_e e$ scattering

[1] VILAIN 94 derive this value from their value of g^{ν_μ} and their ratio $g^{\nu_e}/g^{\nu_\mu} = 1.05^{+0.15}_{-0.18}$.

g^{ν_μ}

VALUE	DOCUMENT ID		TECN	COMMENT
0.502±0.017	[1] VILAIN	94	CHM2	From $\nu_\mu e$ scattering

[1] VILAIN 94 derive this value from their measurement of the couplings $g_A^{e\nu_\mu} = -0.503 \pm 0.017$ and $g_V^{e\nu_\mu} = -0.035 \pm 0.017$ obtained from $\nu_\mu e$ scattering. We have re-evaluated this value using the current PDG values for g_A^e and g_V^e.

Z ASYMMETRY PARAMETERS

For each fermion-antifermion pair coupling to the Z these quantities are defined as

$$A_f = \frac{2g_V^f g_A^f}{(g_V^f)^2 + (g_A^f)^2}$$

where g_V^f and g_A^f are the effective vector and axial-vector couplings. For their relation to the various lepton asymmetries see the note "The Z boson" and ref. LEP-SLC 06.

A_e

Using polarized beams, this quantity can also be measured as $(\sigma_L - \sigma_R)/(\sigma_L + \sigma_R)$, where σ_L and σ_R are the e^+e^- production cross sections for Z bosons produced with left-handed and right-handed electrons respectively.

VALUE	EVTS	DOCUMENT ID		TECN	COMMENT
0.1515±0.0019 OUR AVERAGE					
$0.1454\pm0.0108\pm0.0036$	144810	[1] ABBIENDI	01O	OPAL	$E^{ee}_{cm} = 88$–94 GeV
0.1516 ± 0.0021	559000	[2] ABE	01B	SLD	$E^{ee}_{cm} = 91.24$ GeV
$0.1504\pm0.0068\pm0.0008$		[3] HEISTER	01	ALEP	$E^{ee}_{cm} = 88$–94 GeV
$0.1382\pm0.0116\pm0.0005$	105000	[4] ABREU	00E	DLPH	$E^{ee}_{cm} = 88$–94 GeV
$0.1678\pm0.0127\pm0.0030$	137092	[5] ACCIARRI	98H	L3	$E^{ee}_{cm} = 88$–94 GeV
$0.162\ \pm0.041\ \pm0.014$	89838	[6] ABE	97	SLD	$E^{ee}_{cm} = 91.27$ GeV
$0.202\ \pm0.038\ \pm0.008$		[7] ABE	95J	SLD	$E^{ee}_{cm} = 91.31$ GeV

[1] ABBIENDI 01O fit for A_e and A_τ from measurements of the τ polarization at varying τ production angles. The correlation between A_e and A_τ is less than 0.03.

[2] ABE 01B use the left-right production and left-right forward-backward decay asymmetries in leptonic Z decays to obtain a value of 0.1544 ± 0.0060. This is combined with left-right production asymmetry measurement using hadronic Z decays (ABE 00B) to obtain the quoted value.

[3] HEISTER 01 obtain this result fitting the τ polarization as a function of the polar production angle of the τ.

[4] ABREU 00E obtain this result fitting the τ polarization as a function of the polar τ production angle. This measurement is a combination of different analyses (exclusive τ decay modes, inclusive hadronic 1-prong reconstruction, and a neural network analysis).

[5] Derived from the measurement of forward-backward τ polarization asymmetry.

[6] ABE 97 obtain this result from a measurement of the observed left-right charge asymmetry, $A_Q^{obs} = 0.225 \pm 0.056 \pm 0.019$, in hadronic Z decays. If they combine this value of A_Q^{obs} with their earlier measurement of A_{LR}^{obs} they determine A_e to be $0.1574 \pm 0.0197 \pm 0.0067$ independent of the beam polarization.

[7] ABE 95J obtain this result from polarized Bhabha scattering.

A_μ

This quantity is directly extracted from a measurement of the left-right forward-backward asymmetry in $\mu^+\mu^-$ production at SLC using a polarized electron beam. This double asymmetry eliminates the dependence on the Z-e-e coupling parameter A_e.

VALUE	EVTS	DOCUMENT ID		TECN	COMMENT
0.142±0.015	16844	[1] ABE	01B	SLD	$E^{ee}_{cm} = 91.24$ GeV

• • • We do not use the following data for averages, fits, limits, etc. • • •

0.153 ± 0.012	1.7M	[2] AAD	15BT	ATLS	$E^{pp}_{cm} = 7$ TeV

[1] ABE 01B obtain this direct measurement using the left-right production and left-right forward-backward polar angle asymmetries in $\mu^+\mu^-$ decays of the Z boson obtained with a polarized electron beam.

[2] AAD 15BT study $pp \to Z \to \ell^+\ell^-$ events where ℓ is an electron or a muon in the dilepton mass region 70–1000 GeV. The background in the Z peak region is estimated to be $< 1\%$ for the muon channel. The muon asymmetry parameter is derived from the measured forward-backward asymmetry assuming the value of the quark asymmetry parameter from the SM. For this reason it is not used in the average.

A_τ

The LEP and LHC Collaborations collaboration derive this quantity from the measurement of the τ polarization in $Z \to \tau^+\tau^-$. The SLD Collaboration directly extracts this quantity from its measured left-right forward-backward asymmetry in $Z \to \tau^+\tau^-$ produced using a polarized e^- beam. This double asymmetry eliminates the dependence on the Z-e-e coupling parameter A_e.

VALUE	EVTS	DOCUMENT ID		TECN	COMMENT
0.143 ±0.004 OUR AVERAGE					
$0.144\ \pm0.015$		[1] HAYRAPETY...24T		CMS	$E^{pp}_{cm} = 13$ TeV

Int. J. Mod. Phys. A 2026.41. Downloaded from www.worldscientific.com
by UNIVERSITY OF CALIFORNIA @ BERKELEY on 09/16/26. Re-use and distribution is strictly not permitted, except for Open Access articles.

$0.1456 \pm 0.0076 \pm 0.0057$	144810	[2] ABBIENDI	01O	OPAL	E^{ee}_{cm}= 88–94 GeV
0.136 ± 0.015	16083	[3] ABE	01B	SLD	E^{ee}_{cm}= 91.24 GeV
$0.1451 \pm 0.0052 \pm 0.0029$		[4] HEISTER	01	ALEP	E^{ee}_{cm}= 88–94 GeV
$0.1359 \pm 0.0079 \pm 0.0055$	105000	[5] ABREU	00E	DLPH	E^{ee}_{cm}= 88–94 GeV
$0.1476 \pm 0.0088 \pm 0.0062$	137092	ACCIARRI	98H	L3	E^{ee}_{cm}= 88–94 GeV

[1] HAYRAPETYAN 24T analyse the polarisation of tau leptons in Z bosons decaying to tau pairs.

[2] ABBIENDI 01O fit for A_e and A_τ from measurements of the τ polarization at varying τ production angles. The correlation between A_e and A_τ is less than 0.03.

[3] ABE 01B obtain this direct measurement using the left-right production and left-right forward-backward polar angle asymmetries in $\tau^+\tau^-$ decays of the Z boson obtained with a polarized electron beam.

[4] HEISTER 01 obtain this result fitting the τ polarization as a function of the polar production angle of the τ.

[5] ABREU 00E obtain this result fitting the τ polarization as a function of the polar τ production angle. This measurement is a combination of different analyses (exclusive τ decay modes, inclusive hadronic 1-prong reconstruction, and a neural network analysis).

A_s

The SLD Collaboration directly extracts this quantity by a simultaneous fit to four measured s-quark polar angle distributions corresponding to two states of e^- polarization (positive and negative) and to the K^+K^- and $K^\pm K^0_S$ strange particle tagging modes in the hadronic final states.

VALUE	EVTS	DOCUMENT ID		TECN	COMMENT
$0.895 \pm 0.066 \pm 0.062$	2870	[1] ABE	00D	SLD	E^{ee}_{cm}= 91.2 GeV

[1] ABE 00D tag $Z \to s\overline{s}$ events by an absence of B or D hadrons and the presence in each hemisphere of a high momentum $K^\pm$ or K^0_S.

A_c

This quantity is directly extracted from a measurement of the left-right forward-backward asymmetry in $c\overline{c}$ production at SLC using polarized electron beam. This double asymmetry eliminates the dependence on the Z-e-e coupling parameter A_e. OUR FIT is obtained by a simultaneous fit to several c- and b-quark measurements as explained in the note "The Z boson" and ref. LEP-SLC 06.

VALUE	DOCUMENT ID		TECN	COMMENT
0.670 ± 0.027 OUR FIT				
$0.6712 \pm 0.0224 \pm 0.0157$	[1] ABE	05	SLD	E^{ee}_{cm}= 91.24 GeV
• • • We do not use the following data for averages, fits, limits, etc. • • •				
$0.583 \pm 0.055 \pm 0.055$	[2] ABE	02G	SLD	E^{ee}_{cm}= 91.24 GeV
0.688 ± 0.041	[3] ABE	01C	SLD	E^{ee}_{cm}= 91.25 GeV

[1] ABE 05 use hadronic Z decays collected during 1996–98 to obtain an enriched sample of $c\overline{c}$ events tagging on the invariant mass of reconstructed secondary decay vertices. The charge of the underlying c–quark is obtained with an algorithm that takes into account the net charge of the vertex as well as the charge of tracks emanating from the vertex and identified as kaons. This yields (9970 events) $A_c = 0.6747 \pm 0.0290 \pm 0.0233$. Taking into account all correlations with earlier results reported in ABE 02G and ABE 01C, they obtain the quoted overall SLD result.

[2] ABE 02G tag b and c quarks through their semileptonic decays into electrons and muons. A maximum likelihood fit is performed to extract simultaneously A_b and A_c.

[3] ABE 01C tag $Z \to c\overline{c}$ events using two techniques: exclusive reconstruction of D^{*+}, D^+ and D^0 mesons and the soft pion tag for $D^{*+} \to D^0\pi^+$. The large background from D mesons produced in $b\overline{b}$ events is separated efficiently from the signal using precision vertex information. When combining the A_c values from these two samples, care is taken to avoid double counting of events common to the two samples, and common systematic errors are properly taken into account.

A_b

This quantity is directly extracted from a measurement of the left-right forward-backward asymmetry in $b\overline{b}$ production at SLC using polarized electron beam. This double asymmetry eliminates the dependence on the Z-e-e coupling parameter A_e. OUR FIT is obtained by a simultaneous fit to several c- and b-quark measurements as explained in the note "The Z boson" and ref. LEP-SLC 06.

VALUE	EVTS	DOCUMENT ID		TECN	COMMENT
0.923 ± 0.020 OUR FIT					
$0.9170 \pm 0.0147 \pm 0.0145$		[1] ABE	05	SLD	E^{ee}_{cm}= 91.24 GeV
• • • We do not use the following data for averages, fits, limits, etc. • • •					
$0.907 \pm 0.020 \pm 0.024$	48028	[2] ABE	03F	SLD	E^{ee}_{cm}= 91.24 GeV
$0.919 \pm 0.030 \pm 0.024$		[3] ABE	02G	SLD	E^{ee}_{cm}= 91.24 GeV
$0.855 \pm 0.088 \pm 0.102$	7473	[4] ABE	99L	SLD	E^{ee}_{cm}= 91.27 GeV

[1] ABE 05 use hadronic Z decays collected during 1996–98 to obtain an enriched sample of $b\overline{b}$ events tagging on the invariant mass of reconstructed secondary decay vertices. The charge of the underlying b–quark is obtained with an algorithm that takes into account the net charge of the vertex as well as the charge of tracks emanating from the vertex and identified as kaons. This yields (25917 events) $A_b = 0.9173 \pm 0.0184 \pm 0.0173$. Taking into account all correlations with earlier results reported in ABE 03F, ABE 02G and ABE 99L, they obtain the quoted overall SLD result.

[2] ABE 03F obtain an enriched sample of $b\overline{b}$ events tagging on the invariant mass of a 3-dimensional topologically reconstructed secondary decay. The charge of the underlying b quark is obtained using a self-calibrating track-charge method. For the 1996–1998 data sample they measure $A_b = 0.906 \pm 0.022 \pm 0.023$. The value quoted here is obtained combining the above with the result of ABE 98I (1993–1995 data sample).

[3] ABE 02G tag b and c quarks through their semileptonic decays into electrons and muons. A maximum likelihood fit is performed to extract simultaneously A_b and A_c.

[4] ABE 99L obtain an enriched sample of $b\overline{b}$ events tagging with an inclusive vertex mass cut. For distinguishing b and $\overline{b}$ quarks they use the charge of identified $K^\pm$.

TRANSVERSE SPIN CORRELATIONS IN $Z \to \tau^+\tau^-$

The correlations between the transverse spin components of $\tau^+\tau^-$ produced in Z decays may be expressed in terms of the vector and axial-vector couplings:

$$C_{TT} = \frac{|g^\tau_A|^2 - |g^\tau_V|^2}{|g^\tau_A|^2 + |g^\tau_V|^2}$$

$$C_{TN} = -2\frac{|g^\tau_A||g^\tau_V|}{|g^\tau_A|^2 + |g^\tau_V|^2}\sin(\Phi_{g^\tau_V} - \Phi_{g^\tau_A})$$

C_{TT} refers to the transverse-transverse (within the collision plane) spin correlation and C_{TN} refers to the transverse-normal (to the collision plane) spin correlation.

The longitudinal τ polarization P_τ $(= -A_\tau)$ is given by:

$$P_\tau = -2\frac{|g^\tau_A||g^\tau_V|}{|g^\tau_A|^2 + |g^\tau_V|^2}\cos(\Phi_{g^\tau_V} - \Phi_{g^\tau_A})$$

Here Φ is the phase and the phase difference $\Phi_{g^\tau_V} - \Phi_{g^\tau_A}$ can be obtained using both the measurements of C_{TN} and P_τ.

C_{TT}

VALUE	EVTS	DOCUMENT ID		TECN	COMMENT
1.01 ± 0.12 OUR AVERAGE					
$0.87 \pm 0.20^{+0.10}_{-0.12}$	9.1k	ABREU	97G	DLPH	E^{ee}_{cm}= 91.2 GeV
$1.06 \pm 0.13 \pm 0.05$	120k	BARATE	97D	ALEP	E^{ee}_{cm}= 91.2 GeV

C_{TN}

VALUE	EVTS	DOCUMENT ID		TECN	COMMENT
$0.08 \pm 0.13 \pm 0.04$	120k	[1] BARATE	97D	ALEP	E^{ee}_{cm}= 91.2 GeV

[1] BARATE 97D combine their value of C_{TN} with the world average $P_\tau = -0.140 \pm 0.007$ to obtain $\tan(\Phi_{g^\tau_V} - \Phi_{g^\tau_A}) = -0.57 \pm 0.97$.

FORWARD-BACKWARD $e^+e^- \to f\overline{f}$ CHARGE ASYMMETRIES

These asymmetries are experimentally determined by tagging the respective lepton or quark flavor in e^+e^- interactions. Details of heavy flavor (c- or b-quark) tagging at LEP are described in the note on "The Z boson" and ref. LEP-SLC 06. The Standard Model predictions for LEP data have been (re)computed using the ZFITTER package (version 6.36) with input parameters M_Z=91.187 GeV, M_{top}=174.3 GeV, M_{Higgs}=150 GeV, α_s=0.119, $\alpha^{(5)}$ (M_Z)= 1/128.877 and the Fermi constant G_F= 1.16637×10^{-5} GeV^{-2} (see the note on "The Z boson" for references). For non-LEP data the Standard Model predictions are as given by the authors of the respective publications.

$A^{(0,e)}_{FB}$ CHARGE ASYMMETRY IN $e^+e^- \to e^+e^-$

OUR FIT is obtained using the fit procedure and correlations as determined by the LEP Electroweak Working Group (see the note "The Z boson" and ref. LEP-SLC 06). For the Z peak, we report the pole asymmetry defined by $(3/4)A^2_e$ as determined by the nine-parameter fit to cross-section and lepton forward-backward asymmetry data.

ASYMMETRY (%)	STD. MODEL	$\sqrt{s}$ (GeV)	DOCUMENT ID		TECN
1.45 ± 0.25 OUR FIT					
0.89 ± 0.44	1.57	91.2	[1] ABBIENDI	01A	OPAL
1.71 ± 0.49	1.57	91.2	ABREU	00F	DLPH
1.06 ± 0.58	1.57	91.2	ACCIARRI	00C	L3
1.88 ± 0.34	1.57	91.2	[2] BARATE	00C	ALEP

[1] ABBIENDI 01A error includes approximately 0.38 due to statistics, 0.16 due to event selection systematics, and 0.18 due to the theoretical uncertainty in t-channel prediction.

[2] BARATE 00C error includes approximately 0.31 due to statistics, 0.06 due to experimental systematics, and 0.13 due to the theoretical uncertainty in t-channel prediction.

$A^{(0,\mu)}_{FB}$ CHARGE ASYMMETRY IN $e^+e^- \to \mu^+\mu^-$

OUR FIT is obtained using the fit procedure and correlations as determined by the LEP Electroweak Working Group (see the note "The Z boson" and ref. LEP-SLC 06). For the Z peak, we report the pole asymmetry defined by $(3/4)A_eA_\mu$ as determined by the nine-parameter fit to cross-section and lepton forward-backward asymmetry data.

ASYMMETRY (%)	STD. MODEL	$\sqrt{s}$ (GeV)	DOCUMENT ID		TECN
1.69 ± 0.13 OUR FIT					
1.59 ± 0.23	1.57	91.2	[1] ABBIENDI	01A	OPAL
1.65 ± 0.25	1.57	91.2	ABREU	00F	DLPH
1.88 ± 0.33	1.57	91.2	ACCIARRI	00C	L3
1.71 ± 0.24	1.57	91.2	[2] BARATE	00C	ALEP
• • • We do not use the following data for averages, fits, limits, etc. • • •					
9 ± 30	-1.3	20	[3] ABREU	95M	DLPH
7 ± 26	-8.3	40	[3] ABREU	95M	DLPH

−11 ±33	−24.1	57	[3] ABREU	95M	DLPH
−62 ±17	−44.6	69	[3] ABREU	95M	DLPH
−56 ±10	−63.5	79	[3] ABREU	95M	DLPH
−13 ± 5	−34.4	87.5	[3] ABREU	95M	DLPH
−29.0 $^{+5.0}_{-4.8}$ ±0.5	−32.1	56.9	[4] ABE	90I	VNS
− 9.9 ± 1.5 ±0.5	−9.2	35	HEGNER	90	JADE
0.05± 0.22	0.026	91.14	[5] ABRAMS	89D	MRK2
−43.4 ±17.0	−24.9	52.0	[6] BACALA	89	AMY
−11.0 ±16.5	−29.4	55.0	[6] BACALA	89	AMY
−30.0 ±12.4	−31.2	56.0	[6] BACALA	89	AMY
−46.2 ±14.9	−33.0	57.0	[6] BACALA	89	AMY
−29 ±13	−25.9	53.3	ADACHI	88C	TOPZ
+ 5.3 ± 5.0 ±0.5	−1.2	14.0	ADEVA	88	MRKJ
−10.4 ± 1.3 ±0.5	−8.6	34.8	ADEVA	88	MRKJ
−12.3 ± 5.3 ±0.5	−10.7	38.3	ADEVA	88	MRKJ
−15.6 ± 3.0 ±0.5	−14.9	43.8	ADEVA	88	MRKJ
− 1.0 ± 6.0	−1.2	13.9	BRAUNSCH...	88D	TASS
− 9.1 ± 2.3 ±0.5	−8.6	34.5	BRAUNSCH...	88D	TASS
−10.6 $^{+2.2}_{-2.3}$ ±0.5	−8.9	35.0	BRAUNSCH...	88D	TASS
−17.6 $^{+4.4}_{-4.3}$ ±0.5	−15.2	43.6	BRAUNSCH...	88D	TASS
− 4.8 ± 6.5 ±1.0	−11.5	39	BEHREND	87C	CELL
−18.8 ± 4.5 ±1.0	−15.5	44	BEHREND	87C	CELL
+ 2.7 ± 4.9	−1.2	13.9	BARTEL	86C	JADE
−11.1 ± 1.8 ±1.0	−8.6	34.4	BARTEL	86C	JADE
−17.3 ± 4.8 ±1.0	−13.7	41.5	BARTEL	86C	JADE
−22.8 ± 5.1 ±1.0	−16.6	44.8	BARTEL	86C	JADE
− 6.3 ± 0.8 ±0.2	−6.3	29	ASH	85	MAC
− 4.9 ± 1.5 ±0.5	−5.9	29	DERRICK	85	HRS
− 7.1 ± 1.7	−5.7	29	LEVI	83	MRK2
−16.1 ± 3.2	−9.2	34.2	BRANDELIK	82C	TASS

[1] ABBIENDI 01A error is almost entirely on account of statistics.
[2] BARATE 00C error is almost entirely on account of statistics.
[3] ABREU 95M perform this measurement using radiative muon-pair events associated with high-energy isolated photons.
[4] ABE 90I measurements in the range $50 \leq \sqrt{s} \leq 60.8$ GeV.
[5] ABRAMS 89D asymmetry includes both 9 $\mu^+\mu^-$ and 15 $\tau^+\tau^-$ events.
[6] BACALA 89 systematic error is about 5%.

$A_{FB}^{(0,\tau)}$ CHARGE ASYMMETRY IN $e^+e^- \rightarrow \tau^+\tau^-$

OUR FIT is obtained using the fit procedure and correlations as determined by the LEP Electroweak Working Group (see the note "The Z boson" and ref. LEP-SLC 06). For the Z peak, we report the pole asymmetry defined by $(3/4)A_eA_\tau$ as determined by the nine-parameter fit to cross-section and lepton forward-backward asymmetry data.

ASYMMETRY (%)	STD. MODEL	$\sqrt{s}$ (GeV)	DOCUMENT ID		TECN
1.88± 0.17 OUR FIT					
1.45± 0.30	1.57	91.2	[1] ABBIENDI	01A	OPAL
2.41± 0.37	1.57	91.2	ABREU	00F	DLPH
2.60± 0.47	1.57	91.2	ACCIARRI	00C	L3
1.70± 0.28	1.57	91.2	[2] BARATE	00C	ALEP
• • • We do not use the following data for averages, fits, limits, etc. • • •					
−32.8 $^{+6.4}_{-6.2}$ ±1.5	−32.1	56.9	[3] ABE	90I	VNS
− 8.1 ± 2.0 ±0.6	−9.2	35	HEGNER	90	JADE
−18.4 ±19.2	−24.9	52.0	[4] BACALA	89	AMY
−17.7 ±26.1	−29.4	55.0	[4] BACALA	89	AMY
−45.9 ±16.6	−31.2	56.0	[4] BACALA	89	AMY
−49.5 ±18.0	−33.0	57.0	[4] BACALA	89	AMY
−20 ±14	−25.9	53.3	ADACHI	88C	TOPZ
−10.6 ± 3.1 ±1.5	−8.5	34.7	ADEVA	88	MRKJ
− 8.5 ± 6.6 ±1.5	−15.4	43.8	ADEVA	88	MRKJ
− 6.0 ± 2.5 ±1.0	8.8	34.6	BARTEL	85F	JADE
−11.8 ± 4.6 ±1.0	14.8	43.0	BARTEL	85F	JADE
− 5.5 ± 1.2 ±0.5	−0.063	29.0	FERNANDEZ	85A	MAC
− 4.2 ± 2.0	0.057	29	LEVI	83	MRK2
−10.3 ± 5.2	−9.2	34.2	BEHREND	82	CELL
− 0.4 ± 6.6	−9.1	34.2	BRANDELIK	82C	TASS

[1] ABBIENDI 01A error includes approximately 0.26 due to statistics and 0.14 due to event selection systematics.
[2] BARATE 00C error includes approximately 0.26 due to statistics and 0.11 due to experimental systematics.
[3] ABE 90I measurements in the range $50 \leq \sqrt{s} \leq 60.8$ GeV.
[4] BACALA 89 systematic error is about 5%.

$A_{FB}^{(0,\ell)}$ CHARGE ASYMMETRY IN $e^+e^- \rightarrow \ell^+\ell^-$

For the Z peak, we report the pole asymmetry defined by $(3/4)A_\ell^2$ as determined by the five-parameter fit to cross-section and lepton forward-backward asymmetry data assuming lepton universality. For details see the note "The Z boson" and ref. LEP-SLC 06.

ASYMMETRY (%)	STD. MODEL	$\sqrt{s}$ (GeV)	DOCUMENT ID		TECN
1.71±0.10 OUR FIT					
1.45±0.17	1.57	91.2	[1] ABBIENDI	01A	OPAL
1.87±0.19	1.57	91.2	ABREU	00F	DLPH
1.92±0.24	1.57	91.2	ACCIARRI	00C	L3
1.73±0.16	1.57	91.2	[2] BARATE	00C	ALEP

[1] ABBIENDI 01A error includes approximately 0.15 due to statistics, 0.06 due to event selection systematics, and 0.03 due to the theoretical uncertainty in t-channel prediction.
[2] BARATE 00C error includes approximately 0.15 due to statistics, 0.04 due to experimental systematics, and 0.02 due to the theoretical uncertainty in t-channel prediction.

$A_{FB}^{(0,u)}$ CHARGE ASYMMETRY IN $e^+e^- \rightarrow u\overline{u}$

ASYMMETRY (%)	STD. MODEL	$\sqrt{s}$ (GeV)	DOCUMENT ID		TECN
4.0±6.7±2.8	**7.2**	**91.2**	[1] ACKERSTAFF	97T	OPAL

[1] ACKERSTAFF 97T measure the forward-backward asymmetry of various fast hadrons made of light quarks. Then using SU(2) isospin symmetry and flavor independence for down and strange quarks authors solve for the different quark types.

$A_{FB}^{(0,s)}$ CHARGE ASYMMETRY IN $e^+e^- \rightarrow s\overline{s}$

The s-quark asymmetry is derived from measurements of the forward-backward asymmetry of fast hadrons containing an s quark.

ASYMMETRY (%)	STD. MODEL	$\sqrt{s}$ (GeV)	DOCUMENT ID		TECN
9.8 ±1.1 OUR AVERAGE					
10.08±1.13±0.40	10.1	91.2	[1] ABREU	00B	DLPH
6.8 ±3.5 ±1.1	10.1	91.2	[2] ACKERSTAFF	97T	OPAL

[1] ABREU 00B tag the presence of an s quark requiring a high-momentum-identified charged kaon. The s-quark pole asymmetry is extracted from the charged-kaon asymmetry taking the expected d- and u-quark asymmetries from the Standard Model and using the measured values for the c- and b-quark asymmetries.
[2] ACKERSTAFF 97T measure the forward-backward asymmetry of various fast hadrons made of light quarks. Then using SU(2) isospin symmetry and flavor independence for down and strange quarks authors solve for the different quark types. The value reported here corresponds then to the forward-backward asymmetry for "down-type" quarks.

$A_{FB}^{(0,c)}$ CHARGE ASYMMETRY IN $e^+e^- \rightarrow c\overline{c}$

OUR FIT, which is obtained by a simultaneous fit to several c- and b-quark measurements as explained in the note "The Z boson" and ref. LEP-SLC 06, refers to the **Z pole** asymmetry. The experimental values, on the other hand, correspond to the measurements carried out at the respective energies.

ASYMMETRY (%)	STD. MODEL	$\sqrt{s}$ (GeV)	DOCUMENT ID		TECN
7.07± 0.35 OUR FIT					
6.31± 0.93±0.65	6.35	91.26	[1] ABDALLAH	04F	DLPH
5.68± 0.54±0.39	6.3	91.25	[2] ABBIENDI	03P	OPAL
6.45± 0.57±0.37	6.10	91.21	[3] HEISTER	02H	ALEP
6.59± 0.94±0.35	6.2	91.235	[4] ABREU	99Y	DLPH
6.3 ± 0.9 ±0.3	6.1	91.22	[5] BARATE	98O	ALEP
6.3 ± 1.2 ±0.6	6.1	91.22	[6] ALEXANDER	97C	OPAL
8.3 ± 3.8 ±2.7	6.2	91.24	[7] ADRIANI	92D	L3
• • • We do not use the following data for averages, fits, limits, etc. • • •					
3.1 ± 3.5 ±0.5	−3.5	89.43	[1] ABDALLAH	04F	DLPH
11.0 ± 2.8 ±0.7	12.3	92.99	[1] ABDALLAH	04F	DLPH
− 6.8 ± 2.5 ±0.9	−3.0	89.51	[2] ABBIENDI	03P	OPAL
14.6 ± 2.0 ±0.8	12.2	92.95	[2] ABBIENDI	03P	OPAL
−12.4 ±15.9 ±2.0	−9.6	88.38	[3] HEISTER	02H	ALEP
− 2.3 ± 2.6 ±0.2	−3.8	89.38	[3] HEISTER	02H	ALEP
− 0.3 ± 8.3 ±0.6	0.9	90.21	[3] HEISTER	02H	ALEP
10.6 ± 7.7 ±0.7	9.6	92.05	[3] HEISTER	02H	ALEP
11.9 ± 2.1 ±0.6	12.2	92.94	[3] HEISTER	02H	ALEP
12.1 ±11.0 ±1.0	14.2	93.90	[3] HEISTER	02H	ALEP
− 4.96± 3.68±0.53	−3.5	89.434	[4] ABREU	99Y	DLPH
11.80± 3.18±0.62	12.3	92.990	[4] ABREU	99Y	DLPH
− 1.0 ± 4.3 ±1.0	−3.9	89.37	[5] BARATE	98O	ALEP
11.0 ± 3.3 ±0.8	12.3	92.96	[5] BARATE	98O	ALEP
3.9 ± 5.1 ±0.9	−3.4	89.45	[6] ALEXANDER	97C	OPAL
15.8 ± 4.1 ±1.1	12.4	93.00	[6] ALEXANDER	97C	OPAL
−12.9 ± 7.8 ±5.5	−13.6	35	BEHREND	90D	CELL
7.7 ±13.4 ±5.0	−22.1	43	BEHREND	90D	CELL
−12.8 ± 4.4 ±4.1	−13.6	35	ELSEN	90	JADE
−10.9 ±12.9 ±4.6	−23.2	44	ELSEN	90	JADE
−14.9 ± 6.7	−13.3	35	OULD-SAADA	89	JADE

[1] ABDALLAH 04F tag b- and c-quarks using semileptonic decays combined with charge flow information from the hemisphere opposite to the lepton. Enriched samples of $c\overline{c}$ and $b\overline{b}$ events are obtained using lifetime information.
[2] ABBIENDI 03P tag heavy flavors using events with one or two identified leptons. This allows the simultaneous fitting of the b and c quark forward-backward asymmetries as well as the average B^0-$\overline{B}^0$ mixing.

Int. J. Mod. Phys. A 2026.41. Downloaded
by UNIVERSITY OF CALIFORNIA @ BERKELEY on 09/16/26. Re
orldscientific.com
strictly not permitted, except for Open Access articles.

Int. J. Mod. Phys. A 2026.41. Downloaded from www.worldscientific.com by UNIVERSITY OF CALIFORNIA @ BERKELEY on 09/16/26. Re-use and distribution is strictly not permitted, except for Open Access articles.

[3] HEISTER 02H measure simultaneously b and c quark forward-backward asymmetries using their semileptonic decays to tag the quark charge. The flavor separation is obtained with a discriminating multivariate analysis.

[4] ABREU 99Y tag $Z \to b\overline{b}$ and $Z \to c\overline{c}$ events by an exclusive reconstruction of several D meson decay modes (D^{*+}, D^0, and D^+ with their charge-conjugate states).

[5] BARATE 98O tag $Z \to c\overline{c}$ events requiring the presence of high-momentum reconstructed D^{*+}, D^+, or D^0 mesons.

[6] ALEXANDER 97C identify the b and c events using a D/D^* tag.

[7] ADRIANI 92D use both electron and muon semileptonic decays.

$A_{FB}^{(0,b)}$ CHARGE ASYMMETRY IN $e^+e^- \to b\overline{b}$

OUR FIT, which is obtained by a simultaneous fit to several c- and b-quark measurements as explained in the note "The Z boson" and ref. LEP-SLC 06, refers to the **Z pole** asymmetry. The experimental values, on the other hand, correspond to the measurements carried out at the respective energies.

ASYMMETRY (%)	STD. MODEL	$\sqrt{s}$ (GeV)	DOCUMENT ID		TECN
9.92± 0.16 OUR FIT					
9.58± 0.32± 0.14	9.68	91.231	[1] ABDALLAH	05	DLPH
10.04± 0.56± 0.25	9.69	91.26	[2] ABDALLAH	04F	DLPH
9.72± 0.42± 0.15	9.67	91.25	[3] ABBIENDI	03P	OPAL
9.77± 0.36± 0.18	9.69	91.26	[4] ABBIENDI	02I	OPAL
9.52± 0.41± 0.17	9.59	91.21	[5] HEISTER	02H	ALEP
10.00± 0.27± 0.11	9.63	91.232	[6] HEISTER	01D	ALEP
7.62± 1.94± 0.85	9.64	91.235	[7] ABREU	99Y	DLPH
9.60± 0.66± 0.33	9.69	91.26	[8] ACCIARRI	99D	L3
9.31± 1.01± 0.55	9.65	91.24	[9] ACCIARRI	98U	L3
9.4 ± 2.7 ± 2.2	9.61	91.22	[10] ALEXANDER	97C	OPAL
• • • We do not use the following data for averages, fits, limits, etc. • • •					
6.37± 1.43± 0.17	5.8	89.449	[1] ABDALLAH	05	DLPH
10.41± 1.15± 0.24	12.1	92.990	[1] ABDALLAH	05	DLPH
6.7 ± 2.2 ± 0.2	5.7	89.43	[2] ABDALLAH	04F	DLPH
11.2 ± 1.8 ± 0.2	12.1	92.99	[2] ABDALLAH	04F	DLPH
4.7 ± 1.8 ± 0.1	5.9	89.51	[3] ABBIENDI	03P	OPAL
10.3 ± 1.5 ± 0.2	12.0	92.95	[3] ABBIENDI	03P	OPAL
5.82± 1.53± 0.12	5.9	89.50	[4] ABBIENDI	02I	OPAL
12.21± 1.23± 0.25	12.0	92.91	[4] ABBIENDI	02I	OPAL
−13.1 ±13.5 ± 1.0	3.2	88.38	[5] HEISTER	02H	ALEP
5.5 ± 1.9 ± 0.1	5.6	89.38	[5] HEISTER	02H	ALEP
− 0.4 ± 6.7 ± 0.8	7.5	90.21	[5] HEISTER	02H	ALEP
11.1 ± 6.4 ± 0.5	11.0	92.05	[5] HEISTER	02H	ALEP
10.4 ± 1.5 ± 0.3	12.0	92.94	[5] HEISTER	02H	ALEP
13.8 ± 9.3 ± 1.1	12.9	93.90	[5] HEISTER	02H	ALEP
4.36± 1.19± 0.11	5.8	89.472	[6] HEISTER	01D	ALEP
11.72± 0.97± 0.11	12.0	92.950	[6] HEISTER	01D	ALEP
5.67± 7.56± 1.17	5.7	89.434	[7] ABREU	99Y	DLPH
8.82± 6.33± 1.22	12.1	92.990	[7] ABREU	99Y	DLPH
6.11± 2.93± 0.43	5.9	89.50	[8] ACCIARRI	99D	L3
13.71± 2.40± 0.44	12.2	93.10	[8] ACCIARRI	99D	L3
4.95± 5.23± 0.40	5.8	89.45	[9] ACCIARRI	98U	L3
11.37± 3.99± 0.65	12.1	92.99	[9] ACCIARRI	98U	L3
− 8.6 ±10.8 ± 2.9	5.8	89.45	[10] ALEXANDER	97C	OPAL
− 2.1 ± 9.0 ± 2.6	12.1	93.00	[10] ALEXANDER	97C	OPAL
−71 ±34 $^{+7}_{-8}$	−58	58.3	SHIMONAKA	91	TOPZ
−22.2 ± 7.7 ± 3.5	−26.0	35	BEHREND	90D	CELL
−49.1 ±16.0 ± 5.0	−39.7	43	BEHREND	90D	CELL
−28 ±11	−23	35	BRAUNSCH...	90	TASS
−16.6 ± 7.7 ± 4.8	−24.3	35	ELSEN	90	JADE
−33.6 ±22.2 ± 5.2	−39.9	44	ELSEN	90	JADE
3.4 ± 7.0 ± 3.5	−16.0	29.0	BAND	89	MAC
−72 ±28 ±13	−56	55.2	SAGAWA	89	AMY

[1] ABDALLAH 05 obtain an enriched samples of $b\overline{b}$ events using lifetime information. The quark (or antiquark) charge is determined with a neural network using the secondary vertex charge, the jet charge and particle identification.

[2] ABDALLAH 04F tag b– and c–quarks using semileptonic decays combined with charge flow information from the hemisphere opposite to the lepton. Enriched samples of $c\overline{c}$ and $b\overline{b}$ events are obtained using lifetime information.

[3] ABBIENDI 03P tag heavy flavors using events with one or two identified leptons. This allows the simultaneous fitting of the b and c quark forward-backward asymmetries as well as the average B^0-$\overline{B}^0$ mixing.

[4] ABBIENDI 02I tag $Z^0 \to b\overline{b}$ decays using a combination of secondary vertex and lepton tags. The sign of the b-quark charge is determined using an inclusive tag based on jet, vertex, and kaon charges.

[5] HEISTER 02H measure simultaneously b and c quark forward-backward asymmetries using their semileptonic decays to tag the quark charge. The flavor separation is obtained with a discriminating multivariate analysis.

[6] HEISTER 01D tag $Z \to b\overline{b}$ events using the impact parameters of charged tracks complemented with information from displaced vertices, event shape variables, and lepton identification. The b-quark direction and charge is determined using the hemisphere charge method along with information from fast kaon tagging and charge estimators of primary and secondary vertices. The change in the quoted value due to variation of A_{FB}^c and R_b is given as $+0.103\ (A_{FB}^c - 0.0651) - 0.440\ (R_b - 0.21585)$.

[7] ABREU 99Y tag $Z \to b\overline{b}$ and $Z \to c\overline{c}$ events by an exclusive reconstruction of several D meson decay modes (D^{*+}, D^0, and D^+ with their charge-conjugate states).

[8] ACCIARRI 99D tag $Z \to b\overline{b}$ events using high p and p_T leptons. The analysis determines simultaneously a mixing parameter $\chi_b = 0.1192 \pm 0.0068 \pm 0.0051$ which is used to correct the observed asymmetry.

[9] ACCIARRI 98U tag $Z \to b\overline{b}$ events using lifetime and measure the jet charge using the hemisphere charge.

[10] ALEXANDER 97C identify the b and c events using a D/D^* tag.

CHARGE ASYMMETRY IN $e^+e^- \to q\overline{q}$

Summed over five lighter flavors.

Experimental and Standard Model values are somewhat event-selection dependent. Standard Model expectations contain some assumptions on B^0-$\overline{B}^0$ mixing and on other electroweak parameters.

ASYMMETRY (%)	STD. MODEL	$\sqrt{s}$ (GeV)	DOCUMENT ID		TECN
• • • We do not use the following data for averages, fits, limits, etc. • • •					
− 0.76±0.12±0.15		91.2	[1] ABREU	92I	DLPH
4.0 ±0.4 ±0.63	4.0	91.3	[2] ACTON	92L	OPAL
9.1 ±1.4 ±1.6	9.0	57.9	ADACHI	91	TOPZ
− 0.84±0.15±0.04		91	DECAMP	91B	ALEP
8.3 ±2.9 ±1.9	8.7	56.6	STUART	90	AMY
11.4 ±2.2 ±2.1	8.7	57.6	ABE	89L	VNS
6.0 ±1.3	5.0	34.8	GREENSHAW	89	JADE
8.2 ±2.9	8.5	43.6	GREENSHAW	89	JADE

[1] ABREU 92I has 0.14 systematic error due to uncertainty of quark fragmentation.

[2] ACTON 92L use the weight function method on 259k selected $Z \to$ hadrons events. The systematic error includes a contribution of 0.2 due to B^0-$\overline{B}^0$ mixing effect, 0.4 due to Monte Carlo (MC) fragmentation uncertainties and 0.3 due to MC statistics. ACTON 92L derive a value of $\sin^2\theta_W^{\rm eff}$ to be $0.2321 \pm 0.0017 \pm 0.0028$.

CHARGE ASYMMETRY IN $p\overline{p} \to Z \to e^+e^-$

ASYMMETRY (%)	STD. MODEL	$\sqrt{s}$ (GeV)	DOCUMENT ID		TECN
• • • We do not use the following data for averages, fits, limits, etc. • • •					
5.2±5.9±0.4		91	ABE	91E	CDF

$\sin^2(\theta_{\rm eff})$

The leptonic effective electroweak mixing angle, $\sin^2\theta_{\rm eff}^{\rm lept}$, is given in terms of the ratio of leptonic vector and axial-vector coupling constants, $r = g_\ell^V/g_\ell^A$ for $\ell = e,\ \mu,\ \tau$, with $\sin^2\theta_{\rm eff}^{\rm lept} = (1-r)/4$. It can be extracted directly from the leptonic asymmetry parameter, $A_\ell = 2r/(1+r^2)$. See note "The Z boson" and ref. LEP-SLC 06.

VALUE	DOCUMENT ID		TECN	COMMENT
0.23148±0.00012 OUR AVERAGE				
0.23152±0.00031	[1] HAYRAPETY...	25AF	CMS	$E_{\rm cm}^{pp}$ = 13 TeV
0.23147±0.00050	[2] AAIJ	24AL	LHCB	$E_{\rm cm}^{pp}$ = 13 TeV
0.2319 ±0.0019	[3] HAYRAPETY...	24T	CMS	$E_{\rm cm}^{pp}$ = 13 TeV
0.23148±0.00033	[4] AALTONEN	18B	TEVA	$E_{\rm cm}^{p\overline{p}}$ = 1.96 TeV
0.23101±0.00053	[5] SIRUNYAN	18CY	CMS	$E_{\rm cm}^{pp}$ = 8 TeV
0.2308 ±0.0012	[6] AAD	15BT	ATLS	$E_{\rm cm}^{pp}$ = 7 TeV
0.2314 ±0.0011	[7] AAIJ	15BF	LHCB	$E_{\rm cm}^{pp}$ = 7+8 TeV
0.23153±0.00016	[8] LEP-SLC	06		$E_{\rm cm}^{ee}$ = 88–94 GeV
• • • We do not use the following data for averages, fits, limits, etc. • • •				
0.23016±0.00064	[9] ABAZOV	18	D0	$E_{\rm cm}^{p\overline{p}}$ = 1.96 TeV
0.23248±0.00053	[10] AALTONEN	16D	CDF2	$E_{\rm cm}^{p\overline{p}}$ = 1.96 TeV
0.23147±0.00047	[11] ABAZOV	15C	D0	$E_{\rm cm}^{p\overline{p}}$ = 1.96 TeV
0.2315 ±0.0010	[12] AALTONEN	14C	CDF2	$E_{\rm cm}^{p\overline{p}}$ = 1.96 TeV
0.23099±0.00053	[13] LEP-SLC	06	LEP	$E_{\rm cm}^{ee}$ = 88–94 GeV
0.23159±0.00041	[14] LEP-SLC	06	LEP	$E_{\rm cm}^{ee}$ = 88–94 GeV
0.23098±0.00026	[15] LEP-SLC	06	SLD	$E_{\rm cm}^{ee}$ = 88–94 GeV
0.23221±0.00029	[16] LEP-SLC	06		$E_{\rm cm}^{ee}$ = 88–94 GeV
0.23220±0.00081	[17] LEP-SLC	06		$E_{\rm cm}^{ee}$ = 88–94 GeV
0.2324 ±0.0012	[18] LEP-SLC	06	LEP	$E_{\rm cm}^{ee}$ = 88–94 GeV

[1] HAYRAPETYAN 25AF analyse the forward-backward asymmetry in Drell-Yan production of Z bosons decaying to electron and muon pairs.

[2] AAIJ 24AL analyse the forward-backward asymmetry in Drell-Yan production of Z bosons decaying to muon pairs.

[3] HAYRAPETYAN 24T analyse the polarisation of tau leptons in Z bosons decaying to tau pairs.

[4] AALTONEN 18B is a combination of the the results from the Tevatron experiments CDF and D0 in the electron and muon channels, AALTONEN 14C, AALTONEN 16D, ABAZOV 15C, ABAZOV 18, averaging the combined value from CDF and from D0 as also provided by the experiments in AALTONEN 16D and ABAZOV 18, respectively. The average of the two results takes correlations into account and has a χ^2 probability of 2.6%.

[5] SIRUNYAN 18CY analyse the forward-backward asymmetry in Drell-Yan production of Z bosons decaying to muon or electron pairs.

[6] AAD 15BT analyse the forward-backward asymmetry in Drell-Yan production of Z bosons decaying to muon or electron pairs.
[7] AAIJ 15BF analyse the forward-backward asymmetry in Drell-Yan production of Z bosons decaying to muon pairs.
[8] This result combines the six individual results from LEP and SLC. The average, described in LEP-SLC 06, has a χ^2 probability of 3.7%.
[9] ABAZOV 18 analyse the forward-backward asymmetry in Drell-Yan production of Z bosons decaying to muon pairs. Combining this result with the one from ABAZOV 15C, a value of 0.23095 ± 0.00040 is obtained.
[10] AALTONEN 16D analyse the forward-backward asymmetry in Drell-Yan production of Z bosons decaying to electron pairs. Combining this result with the one from AALTONEN 14C, a value of 0.23221 ± 0.00046 is obtained.
[11] ABAZOV 15C analyse the forward-backward asymmetry in Drell-Yan production of Z bosons decaying to electron pairs.
[12] AALTONEN 14C analyse the forward-backward asymmetry in Drell-Yan production of Z bosons decaying to muon pairs.
[13] The result is based on the forward-backward asymmetry measured in leptonic Z decays (electrons, muons, taus). It combines the results of the LEP experiments, ALEPH, DELPHI, L3 and OPAL, taking correlations into account, see LEP-SLC 06.
[14] The result is based on the polarisation of tau leptons measured in Z decays to tau-lepton pairs. It combines the results of the LEP experiments, ALEPH, DELPHI, L3 and OPAL, taking correlations into account, see LEP-SLC 06.
[15] The result is based on the left-right and forward-backward left-right asymmetry measured in leptonic Z decays (electrons, muons, taus). It combines the results of the SLC experiment, SLD, taking correlations into account, see LEP-SLC 06.
[16] The result is based on the forward-backward asymmetry measured at LEP and the forward-backward left-right asymmetry measured at SLC, in both cases using Z decays to b-quarks. It combines the results of the LEP and SLC experiments, ALEPH, DELPHI, L3, OPAL and SLD, taking correlations into account, see LEP-SLC 06.
[17] The result is based on the forward-backward asymmetry measured at LEP and the forward-backward left-right asymmetry measured at SLC, in both cases using Z decays to c-quarks. It combines the results of the LEP and SLC experiments ALEPH, DELPHI, L3, OPAL and SLD, taking correlations into account, see LEP-SLC 06.
[18] The result is based on the inclusive hadronic charge asymmetry measured in hadronic Z decays. It combines the results of the LEP experiments, ALEPH, DELPHI, L3 and OPAL, taking correlations into account, see LEP-SLC 06.

ANOMALOUS $ZZ\gamma$, $Z\gamma\gamma$, AND ZZV COUPLINGS

Revised September 2013 by M.W. Grünewald (U. College Dublin) and A. Gurtu (Formerly Tata Inst.).

In on-shell $Z\gamma$ production, deviations from the Standard Model for the $Z\gamma\gamma^*$ and $Z\gamma Z^*$ couplings may be described in terms of eight parameters, h_i^V $(i = 1, 4;\ V = \gamma, Z)$ [1]. The parameters h_i^γ describe the $Z\gamma\gamma^*$ couplings and the parameters h_i^Z the $Z\gamma Z^*$ couplings. In this formalism h_1^V and h_2^V lead to CP-violating and h_3^V and h_4^V to CP-conserving effects. All these anomalous contributions to the cross section increase rapidly with center-of-mass energy. In order to ensure unitarity, these parameters are usually described by a form-factor representation, $h_i^V(s) = h_{i0}^V/(1 + s/\Lambda^2)^n$, where Λ is the energy scale for the manifestation of a new phenomenon and n is a sufficiently large power. By convention one uses $n = 3$ for $h_{1,3}^V$ and $n = 4$ for $h_{2,4}^V$. Usually limits on h_i^V's are put assuming some value of Λ, sometimes ∞.

In on-shell ZZ production, deviations from the Standard Model for the $ZZ\gamma^*$ and ZZZ^* couplings may be described by means of four anomalous couplings f_i^V $(i = 4, 5; V = \gamma, Z)$ [2]. As above, the parameters f_i^γ describe the $ZZ\gamma^*$ couplings and the parameters f_i^Z the ZZZ^* couplings. The anomalous couplings f_5^V lead to violation of C and P symmetries while f_4^V introduces CP violation. Also here, formfactors depending on a scale Λ are used.

All these couplings h_i^V and f_i^V are zero at tree level in the Standard Model; they are measured in e^+e^-, $p\bar{p}$ and pp collisions at LEP, Tevatron and LHC.

References

1. U. Baur and E.L. Berger, Phys. Rev. **D47**, 4889 (1993).
2. K. Hagiwara *et al.*, Nucl. Phys. **B282**, 253 (1987).

h_i^V

Combining the LEP-2 results taking into account the correlations, the following 95% CL limits are derived [SCHAEL 13A]:

$$-0.12 < h_1^Z < +0.11, \qquad -0.07 < h_2^Z < +0.07,$$
$$-0.19 < h_3^Z < +0.06, \qquad -0.04 < h_4^Z < +0.13,$$
$$-0.05 < h_1^\gamma < +0.05, \qquad -0.04 < h_2^\gamma < +0.02,$$
$$-0.05 < h_3^\gamma < +0.00, \qquad +0.01 < h_4^\gamma < +0.05.$$

Some of the recent results from the Tevatron and LHC experiments individually surpass the combined LEP-2 results in precision (see below).

VALUE	DOCUMENT ID		TECN	COMMENT
• • • We do not use the following data for averages, fits, limits, etc. • • •				
	[1] AAD	16Q	ATLS	$E_{cm}^{pp} = 8$ TeV
	[2] KHACHATRY...	16AE	CMS	$E_{cm}^{pp} = 8$ TeV
	[3] KHACHATRY...	15AC	CMS	$E_{cm}^{pp} = 8$ TeV
	[4] CHATRCHYAN	14AB	CMS	$E_{cm}^{pp} = 7$ TeV
	[5] AAD	13AN	ATLS	$E_{cm}^{pp} = 7$ TeV
	[6] CHATRCHYAN	13BI	CMS	$E_{cm}^{pp} = 7$ TeV
	[7] ABAZOV	12S	D0	$E_{cm}^{p\bar{p}} = 1.96$ TeV
	[8] AALTONEN	11S	CDF	$E_{cm}^{p\bar{p}} = 1.96$ TeV
	[9] CHATRCHYAN	11M	CMS	$E_{cm}^{pp} = 7$ TeV
	[10] ABAZOV	09L	D0	$E_{cm}^{p\bar{p}} = 1.96$ TeV
	[11] ABAZOV	07M	D0	$E_{cm}^{p\bar{p}} = 1.96$ TeV
	[12] ABDALLAH	07C	DLPH	$E_{cm}^{ee} = 183$–208 GeV
	[13] ACHARD	04H	L3	$E_{cm}^{ee} = 183$–208 GeV
	[14] ABBIENDI,G	00C	OPAL	$E_{cm}^{ee} = 189$ GeV
	[15] ABBOTT	98M	D0	$E_{cm}^{p\bar{p}} = 1.8$ TeV
	[16] ABREU	98K	DLPH	$E_{cm}^{ee} = 161, 172$ GeV

[1] AAD 16Q study $Z\gamma$ production in pp collisions. In events with no additional jets, 10268 (12738) Z decays to electron (muon) pairs are selected, with an expected background of 1291 ± 340 (1537 ± 408) events, as well as 1039 Z decays to neutrino pairs with an expected background of 450 ± 96 events. Analyzing the photon transverse momentum distribution above 250 GeV (400 GeV) for lepton (neutrino) events, yields the 95% C.L. limits: $-7.8 \times 10^{-4} < h_3^Z < 8.6 \times 10^{-4}$, $-3.0 \times 10^{-6} < h_4^Z < 2.9 \times 10^{-6}$, $-9.5 \times 10^{-4} < h_3^\gamma < 9.9 \times 10^{-4}$, $-3.2 \times 10^{-6} < h_4^\gamma < 3.2 \times 10^{-6}$.

[2] KHACHATRYAN 16AE determine the $Z\gamma \to \nu\bar{\nu}\gamma$ cross section by selecting events with a photon of $E_T > 145$ GeV and $\not{E}_T > 140$ GeV. 630 candidate events are observed with an expected SM background of 269 ± 26. The E_T spectrum of the photon is used to set 95% C.L. limits as follows: $-1.5 \times 10^{-3} < h_3^Z < 1.6 \times 10^{-3}$, $-3.9 \times 10^{-6} < h_4^Z < 4.5 \times 10^{-6}$, $-1.1 \times 10^{-3} < h_3^\gamma < 0.9 \times 10^{-3}$, $-3.8 \times 10^{-6} < h_4^\gamma < 4.3 \times 10^{-6}$.

[3] KHACHATRYAN 15AC study $Z\gamma$ events in 8 TeV pp interactions, where the Z decays into 2 same-flavor, opposite sign leptons (e or μ) and a photon with $p_T > 15$ GeV. The p_T of a lepton is required to be > 20 GeV/c, their effective mass > 50 GeV, and the photon should have a separation $\Delta R > 0.7$ with each lepton. The observed p_T distribution of the photons is used to extract the 95% C.L. limits: $-3.8 \times 10^{-3} < h_3^Z < 3.7 \times 10^{-3}$, $-3.1 \times 10^{-5} < h_4^Z < 3.0 \times 10^{-5}$, $-4.6 \times 10^{-3} < h_3^\gamma < 4.6 \times 10^{-3}$, $-3.6 \times 10^{-5} < h_4^\gamma < 3.5 \times 10^{-5}$.

[4] CHATRCHYAN 14AB measure $Z\gamma$ production cross section for $p_T^\gamma > 15$ GeV and $R(\ell\gamma) > 0.7$, which is the separation between the γ and the final state charged lepton (e or μ) in the azimuthal angle-pseudorapidity ($\phi - \eta$) plane. The di-lepton mass is required to be > 50 GeV. After background subtraction the number of $ee\gamma$ and $\mu\mu\gamma$ events is determined to be 3160 ± 120 and 5030 ± 233 respectively, compatible with expectations from the SM. This leads to a 95% CL limits of $-1 \times 10^{-2} < h_3^\gamma < 1 \times 10^{-2}$, $-9 \times 10^{-5} < h_4^\gamma < 9 \times 10^{-5}$, $-9 \times 10^{-3} < h_3^Z < 9 \times 10^{-3}$, $-8 \times 10^{-5} < h_4^Z < 8 \times 10^{-5}$, assuming h_1^V and h_2^V have SM values, $V = \gamma$ or Z.

[5] AAD 13AN study $Z\gamma$ production in pp collisions. In events with no additional jet, 1417 (2031) Z decays to electron (muon) pairs are selected, with an expected background of 156 ± 54 (244 ± 64) events, as well as 662 Z decays to neutrino pairs with an expected background of 302 ± 42 events. Analysing the photon p_T spectrum above 100 GeV yields the 95% C.L. limts: $-0.013 < h_3^Z < 0.014$, $-8.7 \times 10^{-5} < h_4^Z < 8.7 \times 10^{-5}$, $-0.015 < h_3^\gamma < 0.016$, $-9.4 \times 10^{-5} < h_4^\gamma < 9.2 \times 10^{-5}$. Supersedes AAD 12BX.

[6] CHATRCHYAN 13BI determine the $Z\gamma \to \nu\bar{\nu}\gamma$ cross section by selecting events with a photon of $E_T > 145$ GeV and a $\not{E}_T > 130$ GeV. 73 candidate events are observed with an expected SM background of 30.2 ± 6.5. The E_T spectrum of the photon is used to set 95% C.L. limits as follows: $|h_3^Z| < 2.7 \times 10^{-3}$, $|h_4^Z| < 1.3 \times 10^{-5}$, $|h_3^\gamma| < 2.9 \times 10^{-3}$, $|h_4^\gamma| < 1.5 \times 10^{-5}$.

[7] ABAZOV 12S study $Z\gamma$ production in $p\bar{p}$ collisions at $\sqrt{s} = 1.96$ TeV using 6.2 fb^{-1} of data where the Z decays to electron (muon) pairs and the photon has at least 10 GeV of transverse momentum. In data, 304 (308) di-electron (di-muon) events are observed with an expected background of 255 ± 16 (285 ± 24) events. Based on the photon p_T spectrum, and including also earlier data and the $Z \to \nu\bar{\nu}$ decay mode (from ABAZOV 09L), the following 95% C.L. limits are reported: $|h_{03}^Z| < 0.026$, $|h_{04}^Z| < 0.0013$, $|h_{03}^\gamma| < 0.027$, $|h_{04}^\gamma| < 0.0014$ for a form factor scale of $\Lambda = 1.5$ TeV.

[8] AALTONEN 11S study $Z\gamma$ events in $p\bar{p}$ interactions at $\sqrt{s} = 1.96$ TeV with integrated luminosity 5.1 fb^{-1} for $Z \to e^+e^-/\mu^+\mu^-$ and 4.9 fb^{-1} for $Z \to \nu\bar{\nu}$. For the charged lepton case, the two leptons must be of the same flavor with the transverse

Int. J. Mod. Phys. A 2026.41. Downloaded from www.worldscientific.com
by UNIVERSITY OF CALIFORNIA @ BERKELEY on 09/16/26. Re strictly not permitted, except for Open Access articles.

Int. J. Mod. Phys. A 2026.41. Downloaded from www.worldscientific.com by UNIVERSITY OF CALIFORNIA @ BERKELEY on 09/16/26. Re-use and distribution is strictly not permitted, except for Open Access articles.

momentum/energy of one > 20 GeV and the other > 10 GeV. The isolated photon must have $E_T > 50$ GeV. They observe 91 events with 87.2 ± 7.8 events expected from standard model processes. For the $\nu\overline{\nu}$ case they require solitary photons with $E_T > 25$ GeV and missing $E_T > 25$ GeV and observe 85 events with standard model expectation of 85.9 ± 5.6 events. Taking the form factor $\Lambda = 1.5$ TeV they derive 95% C.L. limits as $|h_3^{\gamma,Z}| < 0.022$ and $|h_4^{\gamma,Z}| < 0.0009$.

[9] CHATRCHYAN 11M study $Z\gamma$ production in pp collisions at $\sqrt{s} = 7$ TeV using 36 pb^{-1} pp data, where the Z decays to e^+e^- or $\mu^+\mu^-$. The total cross sections are measured for photon transverse energy $E_T^\gamma > 10$ GeV and spatial separation from charged leptons in the plane of pseudo rapidity and azimuthal angle $\Delta R(\ell,\gamma) > 0.7$ with the dilepton invariant mass requirement of $M_{\ell\ell} > 50$ GeV. The number of $e^+e^-\gamma$ and $\mu^+\mu^-\gamma$ candidates is 81 and 90 with estimated backgrounds of 20.5 ± 2.5 and 27.3 ± 3.2 events respectively. The 95% CL limits for $ZZ\gamma$ couplings are $-0.05 < h_3^Z < 0.06$ and $-0.0005 < h_4^Z < 0.0005$, and for $Z\gamma\gamma$ couplings are $-0.07 < h_3^\gamma < 0.07$ and $-0.0005 < h_4^\gamma < 0.0006$.

[10] ABAZOV 09L study $Z\gamma$, $Z \to \nu\overline{\nu}$ production in $p\overline{p}$ collisions at 1.96 TeV C.M. energy. They select 51 events with a photon of transverse energy E_T larger than 90 GeV, with an expected background of 17 events. Based on the photon E_T spectrum and including also Z decays to charged leptons (from ABAZOV 07M), the following 95% CL limits are reported: $|h_{30}^\gamma| < 0.033$, $|h_{40}^\gamma| < 0.0017$, $|h_{30}^Z| < 0.033$, $|h_{40}^Z| < 0.0017$.

[11] ABAZOV 07M use 968 $p\overline{p} \to e^+e^-/\mu^+\mu^-\gamma X$ candidates, at 1.96 TeV center of mass energy, to tag $p\overline{p} \to Z\gamma$ events by requiring $E_T(\gamma) > 7$ GeV, lepton-gamma separation $\Delta R_{\ell\gamma} > 0.7$, and di-lepton invariant mass > 30 GeV. The cross section is in agreement with the SM prediction. Using these $Z\gamma$ events they obtain 95% C.L. limits on each h_i^V, keeping all others fixed at their SM values. They report: $-0.083 < h_{30}^Z < 0.082$, $-0.0053 < h_{40}^Z < 0.0054$, $-0.085 < h_{30}^\gamma < 0.084$, $-0.0053 < h_{40}^\gamma < 0.0054$, for the form factor scale $\Lambda = 1.2$ TeV.

[12] Using data collected at $\sqrt{s} = 183$–208, ABDALLAH 07C select 1,877 $e^+e^- \to Z\gamma$ events with $Z \to q\overline{q}$ or $\nu\overline{\nu}$, 171 $e^+e^- \to ZZ$ events with $Z \to q\overline{q}$ or lepton pair (except an explicit τ pair), and 74 $e^+e^- \to Z\gamma^*$ events with a $q\overline{q}\mu^+\mu^-$ or $q\overline{q}e^+e^-$ signature, to derive 95% CL limits on h_i^V. Each limit is derived with other parameters set to zero. They report: $-0.23 < h_1^Z < 0.23$, $-0.30 < h_3^Z < 0.16$, $-0.14 < h_1^\gamma < 0.14$, $-0.049 < h_3^\gamma < 0.044$.

[13] ACHARD 04H select 3515 $e^+e^- \to Z\gamma$ events with $Z \to q\overline{q}$ or $\nu\overline{\nu}$ at $\sqrt{s} = 189$–209 GeV to derive 95% CL limits on h_i^V. For deriving each limit the other parameters are fixed at zero. They report: $-0.153 < h_1^Z < 0.141$, $-0.087 < h_2^Z < 0.079$, $-0.220 < h_3^Z < 0.112$, $-0.068 < h_4^Z < 0.148$, $-0.057 < h_1^\gamma < 0.057$, $-0.050 < h_2^\gamma < 0.023$, $-0.059 < h_3^\gamma < 0.004$, $-0.004 < h_4^\gamma < 0.042$.

[14] ABBIENDI,G 00C study $e^+e^- \to Z\gamma$ events (with $Z \to q\overline{q}$ and $Z \to \nu\overline{\nu}$) at 189 GeV to obtain the central values (and 95% CL limits) of these couplings: $h_1^Z = 0.000 \pm 0.100$ $(-0.190, 0.190)$, $h_2^Z = 0.000 \pm 0.068$ $(-0.128, 0.128)$, $h_3^Z = -0.074^{+0.102}_{-0.103}$ $(-0.269, 0.119)$, $h_4^Z = 0.046 \pm 0.068$ $(-0.084, 0.175)$, $h_1^\gamma = 0.000 \pm 0.061$ $(-0.115, 0.115)$, $h_2^\gamma = 0.000 \pm 0.041$ $(-0.077, 0.077)$, $h_3^\gamma = -0.080^{+0.039}_{-0.041}$ $(-0.164, -0.006)$, $h_4^\gamma = 0.064^{+0.033}_{-0.030}$ $(+0.007, +0.134)$. The results are derived assuming that only one coupling at a time is different from zero.

[15] ABBOTT 98M study $p\overline{p} \to Z\gamma + X$, with $Z \to e^+e^-$, $\mu^+\mu^-$, $\overline{\nu}\nu$ at 1.8 TeV, to obtain 95% CL limits at $\Lambda = 750$ GeV: $|h_{30}^Z| < 0.36$, $|h_{40}^Z| < 0.05$ (keeping $h_i^\gamma = 0$), and $|h_{30}^\gamma| < 0.37$, $|h_{40}^\gamma| < 0.05$ (keeping $h_i^Z = 0$). Limits on the *CP*-violating couplings are $|h_{10}^Z| < 0.36$, $|h_{20}^Z| < 0.05$ (keeping $h_i^\gamma = 0$), and $|h_{10}^\gamma| < 0.37$, $|h_{20}^\gamma| < 0.05$ (keeping $h_i^Z = 0$).

[16] ABREU 98K determine a 95% CL upper limit on $\sigma(e^+e^- \to \gamma +$ invisible particles$) <$ 2.5 pb using 161 and 172 GeV data. This is used to set 95% CL limits on $|h_{30}^\gamma| < 0.8$ and $|h_{30}^Z| < 1.3$, derived at a scale Λ=1 TeV and with n=3 in the form factor representation.

f_i^V

Combining the LEP-2 results taking into account the correlations, the following 95% CL limits are derived [SCHAEL 13A]:

$$-0.28 < f_4^Z < +0.32, \qquad -0.34 < f_5^Z < +0.35,$$
$$-0.17 < f_4^\gamma < +0.19, \qquad -0.35 < f_5^\gamma < +0.32.$$

Some of the recent results from the Tevatron and LHC experiments individually surpass the combined LEP-2 results in precision (see below).

VALUE	DOCUMENT ID	TECN	COMMENT
• • • We do not use the following data for averages, fits, limits, etc. • • •			
	[1] AAD 23CH		$E_{cm}^{pp} = 13$ TeV
	[2] SIRUNYAN 21Q	CMS	$E_{cm}^{pp} = 13$ TeV
	[3] AABOUD 19AY	ATLS	$E_{cm}^{pp} = 13$ TeV
	[4] AABOUD 18Q	ATLS	$E_{cm}^{pp} = 13$ TeV
	[5] SIRUNYAN 18BT	CMS	$E_{cm}^{pp} = 13$ TeV
	[6] KHACHATRY...15B	CMS	$E_{cm}^{pp} = 8$ TeV
	[7] KHACHATRY...15BC	CMS	$E_{cm}^{pp} = 7, 8$ TeV
	[8] AAD 13Z	ATLS	$E_{cm}^{pp} = 7$ TeV
	[9] CHATRCHYAN 13B	CMS	$E_{cm}^{pp} = 7$ TeV
	[10] SCHAEL 09	ALEP	$E_{cm}^{ee} = 192$–209 GeV
	[11] ABAZOV 08K	D0	$E_{cm}^{p\overline{p}} = 1.96$ TeV
	[12] ABDALLAH 07C	DLPH	$E_{cm}^{ee} = 183$–208 GeV
	[13] ABBIENDI 04C	OPAL	
	[14] ACHARD 03D	L3	

[1] AAD 23CH measure ZZ production with the Z bosons decaying to electrons or muons. Analysing the angular information of the final-state four-lepton system, the following limits are derived at 95% C.L.: $-0.012 < f_4^Z < 0.012$, $-0.015 < f_4^\gamma < 0.015$.

[2] SIRUNYAN 21Q measure ZZ production where both Z bosons decay in the electron or muon channel. Analyzing the four-lepton invariant mass distribution, the following limits are derived at 95% C.L. in units of 10^{-4}: $-6.6 < f_4^Z < 6.0$, $-5.5 < f_5^Z < 7.5$, $-7.8 < f_4^\gamma < 7.1$, $-6.8 < f_5^\gamma < 7.5$. This set of parameters is linearly related to a set of EFT parameters, resulting in the following limits at 95% C.L. in units of TeV^{-4}: $-2.3 < c_{\widetilde{B}W}/\Lambda^4 < 2.5$, $-1.4 < c_{WW}/\Lambda^4 < 1.2$, $-1.4 < c_{BW}/\Lambda^4 < 1.3$, $-1.2 < c_{BB}/\Lambda^4 < 1.2$.

[3] AABOUD 19AY study ZZ production in the $\ell\ell\nu\nu$ decay channel. Events with a pair of isolated high-transverse momentum charged leptons (electron pairs or muon pairs), and with large missing energy, are selected. In the data, 371 (416) di-electron (di-muon) events are found, with a total expected background of 128 ± 8 (143 ± 8) events. Analysing the transverse momentum distribution of the charged dilepton system above 150 GeV, the following 95% C.L. limits are derived in units of 10^{-3}: $-1.2 < f_4^\gamma < 1.2$, $-1.0 < f_4^Z < 1.0$, $-1.2 < f_5^\gamma < 1.2$, $-1.0 < f_5^Z < 1.0$.

[4] AABOUD 18Q study $pp \to ZZ$ events at $\sqrt{s} = 13$ TeV with $Z \to e^+e^-$ or $Z \to \mu^+\mu^-$. The number of events observed in the $4e$, $2e\,2\mu$, and 4μ channels is 249, 465, and 303 respectively. Analysing the p_T spectrum of the leading Z boson, the following the following 95% C.L. limits are derived in units of 10^{-4}: $-1.8 < f_4^\gamma < 1.8$, $-1.5 < f_4^Z < 1.5$, $-1.8 < f_5^\gamma < 1.8$, $-1.5 < f_5^Z < 1.5$.

[5] SIRUNYAN 18BT study $ppZZ$ events at $\sqrt{s} = 13$ TeV with $Z \to e^+e^-$ or $Z \to \mu^+\mu^-$. The number of events observed in the $4e$, $2e2\mu$, and 4μ channels is 220, 543 and 335 respectively. Analysing the 4-lepton invariant mass spectrum, the following 95% C.L. limits are derived in units of 10^{-3}: $-1.2 < f_4^\gamma < 1.3$, $-1.2 < f_4^Z < 1.0$, $-1.2 < f_5^\gamma < 1.3$, $-1.0 < f_5^Z < 1.3$.

[6] KHACHATRYAN 15B study ZZ production in 8 TeV pp collisions. In the decay modes $ZZ \to 4e$, 4μ, $2e2\mu$, 54, 75, 148 events are observed, with an expected background of 2.2 ± 0.9, 1.2 ± 0.6, and 2.4 ± 1.0 events, respectively. Analysing the 4-lepton invariant mass spectrum in the range from 110 GeV to 1200 GeV, the following 95% C.L. limits are obtained: $|f_4^Z| < 0.004$, $|f_5^Z| < 0.004$, $|f_4^\gamma| < 0.005$, $|f_5^\gamma| < 0.005$.

[7] KHACHATRYAN 15BC use the cross section measurement of the final state $pp \to ZZ \to 2\ell 2\nu$, (ℓ being an electron or a muon) at 7 and 8 TeV to put limits on these triple gauge couplings. Effective mass of the charged lepton pair is required to be in the range 83.5–98.5 GeV and the dilepton $p_T > 45$ GeV. The reduced missing E_T is required to be > 65 GeV, which takes into account the fake missing E_T due to detector effects. The numbers of e^+e^- and $\mu^+\mu^-$ events selected are 35 and 40 at 7 TeV and 176 and 271 at 8 TeV respectively. The production cross sections so obtained are in agreement with SM predictions. The following 95% C.L. limits are set: $-0.0028 < f_4^Z < 0.0032$, $-0.0037 < f_4^\gamma < 0.0033$, $-0.0029 < f_5^Z < 0.0031$, $-0.0033 < f_5^\gamma < 0.0037$. Combining with previous results (KHACHATRYAN 15B and CHATRCHYAN 13B) which include 7 TeV and 8 TeV data on the final states $pp \to ZZ \to 2\ell 2\ell'$ where ℓ and ℓ' are an electron or a muon, the best limits are $-0.0022 < f_4^Z < 0.0026$, $-0.0029 < f_4^\gamma < 0.0026$, $-0.0023 < f_5^Z < 0.0023$, $-0.0026 < f_5^\gamma < 0.0027$.

[8] AAD 13Z study ZZ production in pp collisions at $\sqrt{s} = 7$ TeV. In the $ZZ \to \ell^+\ell^-\ell'^+\ell'^-$ final state they observe a total of 66 events with an expected background of 0.9 ± 1.3. In the $ZZ \to \ell^+\ell^-\nu\nu$ final state they observe a total of 87 events with an expected background of 46.9 ± 5.2. The limits on anomalous TGCs are determined using the observed and expected numbers of these ZZ events binned in p_T^Z. The 95% C.L. are as follows: for form factor scale $\Lambda = \infty$, $-0.015 < f_4^\gamma < 0.015$, $-0.013 < f_4^Z < 0.013$, $-0.016 < f_5^\gamma < 0.015$, $-0.013 < f_5^Z < 0.013$; for form factor scale $\Lambda =$ 3 TeV, $-0.022 < f_4^\gamma < 0.023$, $-0.019 < f_4^Z < 0.019$, $-0.023 < f_5^\gamma < 0.023$, $-0.020 < f_5^Z < 0.019$.

[9] CHATRCHYAN 13B study ZZ production in pp collisions and select 54 ZZ candidates in the Z decay channel with electrons or muons with an expected background of 1.4 ± 0.5 events. The resulting 95% C.L. ranges are: $-0.013 < f_4^\gamma < 0.015$, $-0.011 < f_4^Z < 0.012$, $-0.014 < f_5^\gamma < 0.014$, $-0.012 < f_5^Z < 0.012$.

[10] Using data collected in the center of mass energy range 192–209 GeV, SCHAEL 09 select 318 $e^+e^- \to ZZ$ events with 319.4 expected from the standard model. Using this data they derive the following 95% CL limits: $-0.321 < f_4^\gamma < 0.318$, $-0.534 < f_4^Z < 0.534$, $-0.724 < f_5^\gamma < 0.733$, $-1.194 < f_5^Z < 1.190$.

[11] ABAZOV 08K search for ZZ and $Z\gamma^*$ events with 1 fb^{-1} $p\overline{p}$ data at $\sqrt{s} = 1.96$ TeV in $(ee)(ee)$, $(\mu\mu)(\mu\mu)$, $(ee)(\mu\mu)$ final states requiring the lepton pair masses to be > 30 GeV. They observe 1 event, which is consistent with an expected signal of 1.71 ± 0.15 events and a background of 0.13 ± 0.03 events. From this they derive the following limits, for a form factor (Λ) value of 1.2 TeV: $-0.28 < f_{40}^Z < 0.28$, $-0.31 < f_{50}^Z < 0.29$, $-0.26 < f_{40}^\gamma < 0.26$, $-0.30 < f_{50}^\gamma < 0.28$.

[12] Using data collected at $\sqrt{s} = 183$–208 GeV, ABDALLAH 07C select 171 $e^+e^- \to ZZ$ events with $Z \to q\overline{q}$ or lepton pair (except an explicit τ pair), and 74 $e^+e^- \to Z\gamma^*$ events with a $q\overline{q}\mu^+\mu^-$ or $q\overline{q}e^+e^-$ signature, to derive 95% CL limits on f_i^V. Each

limit is derived with other parameters set to zero. They report: $-0.40 < f_4^Z < 0.42$, $-0.38 < f_5^Z < 0.62$, $-0.23 < f_4^\gamma < 0.25$, $-0.52 < f_5^\gamma < 0.48$.

[13] ABBIENDI 04C study ZZ production in e^+e^- collisions in the C.M. energy range 190–209 GeV. They select 340 events with an expected background of 180 events. Including the ABBIENDI 00N data at 183 and 189 GeV (118 events with an expected background of 65 events) they report the following 95% CL limits: $-0.45 < f_4^Z < 0.58$, $-0.94 < f_5^Z < 0.25$, $-0.32 < f_4^\gamma < 0.33$, and $-0.71 < f_5^\gamma < 0.59$.

[14] ACHARD 03D study Z-boson pair production in e^+e^- collisions in the C.M. energy range 200–209 GeV. They select 549 events with an expected background of 432 events. Including the ACCIARRI 99G and ACCIARRI 99O data (183 and 189 GeV respectively, 286 events with an expected background of 241 events) and the 192–202 GeV ACCIARRI 01I results (656 events, expected background of 512 events), they report the following 95% CL limits: $-0.48 \le f_4^Z \le 0.46$, $-0.36 \le f_5^Z \le 1.03$, $-0.28 \le f_4^\gamma \le 0.28$, and $-0.40 \le f_5^\gamma \le 0.47$.

ANOMALOUS W/Z QUARTIC COUPLINGS

Revised March 2024 by M.W. Grünewald (U. College Dublin) and A. Gurtu (CERN; TIFR Mumbay).

Quartic couplings, $WWZZ$, $WWZ\gamma$, $WW\gamma\gamma$, and $ZZ\gamma\gamma$, were studied at LEP and Tevatron at energies at which the Standard Model predicts negligible contributions to multiboson production. Thus, to parametrize limits on these couplings, an effective theory approach is adopted which supplements the Standard Model Lagrangian with higher dimensional operators which include quartic couplings. The LEP collaborations chose the lowest dimensional representation of operators (dimension 6) which presumes the SU(2)×U(1) gauge symmetry is broken by means other than the conventional Higgs scalar doublet [1–3]. In this representation possible quartic couplings, a_0, a_c, a_n, are expressed in terms of the following dimension-6 operators [1,2];

$$L_6^0 = -\frac{e^2}{16\Lambda^2}\, a_0\, F^{\mu\nu}\, F_{\mu\nu}\vec{W}^\alpha \cdot \vec{W}_\alpha$$
$$L_6^c = -\frac{e^2}{16\Lambda^2}\, a_c\, F^{\mu\alpha}\, F_{\mu\beta}\vec{W}^\beta \cdot \vec{W}_\alpha$$
$$L_6^n = -i\frac{e^2}{16\Lambda^2}\, a_n \epsilon_{ijk}\, W_{\mu\alpha}^{(i)}\, W_\nu^{(j)}\, W^{(k)\alpha} F^{\mu\nu}$$
$$\widetilde{L}_6^0 = -\frac{e^2}{16\Lambda^2}\, \widetilde{a}_0\, F^{\mu\nu}\, \widetilde{F}_{\mu\nu}\vec{W}^\alpha \cdot \vec{W}_\alpha$$
$$\widetilde{L}_6^n = -i\frac{e^2}{16\Lambda^2}\, \widetilde{a}_n \epsilon_{ijk}\, W_{\mu\alpha}^{(i)}\, W_\nu^{(j)}\, W^{(k)\alpha} \widetilde{F}^{\mu\nu}$$

where F, W are photon and W fields, L_6^0 and L_6^c conserve C, P separately ($\widetilde{L}_6^0$ conserves only C) and generate anomalous $W^+W^-\gamma\gamma$ and $ZZ\gamma\gamma$ couplings, L_6^n violates CP ($\widetilde{L}_6^n$ violates both C and P) and generates an anomalous $W^+W^-Z\gamma$ coupling, and Λ is an energy scale for new physics. For the $ZZ\gamma\gamma$ coupling the CP-violating term represented by L_6^n does not contribute. These couplings are assumed to be real and to vanish at tree level in the Standard Model.

Within the same framework as above, a more recent description of the quartic couplings [3] treats the anomalous parts of the $WW\gamma\gamma$ and $ZZ\gamma\gamma$ couplings separately, leading to two sets parametrized as a_0^V/Λ^2 and a_c^V/Λ^2, where $V = W$ or Z.

With the discovery of a Higgs at the LHC in 2012, it is then useful to go to the next higher dimensional representation (dimension 8 operators) in which the gauge symmetry is broken by the conventional Higgs scalar doublet [3,4]. There are 14 operators which can contribute to the anomalous quartic coupling signal. Some of the operators have analogues in the dimension 6 scheme. The CMS collaboration, [5], have used this parametrization, in which the connections between the two schemes are also summarized:

$$\begin{aligned}\mathcal{L}_{AQGC} = &-\frac{e^2}{8}\frac{a_0^W}{\Lambda^2}F_{\mu\nu}F^{\mu\nu}W^{+a}W_a^- \\ &-\frac{e^2}{16}\frac{a_c^W}{\Lambda^2}F_{\mu\nu}F^{\mu a}(W^{+\nu}W_a^- + W^{-\nu}W_a^+) \\ &-e^2g^2\frac{\kappa_0^W}{\Lambda^2}F_{\mu\nu}Z^{\mu\nu}W^{+a}W_a^- \\ &-\frac{e^2g^2}{2}\frac{\kappa_c^W}{\Lambda^2}F_{\mu\nu}Z^{\mu a}(W^{+\nu}W_a^- + W^{-\nu}W_a^+) \\ &+\frac{f_{T,0}}{\Lambda^4}Tr[\widehat{W}_{\mu\nu}\widehat{W}^{\mu\nu}] \times Tr[\widehat{W}_{\alpha\beta}\widehat{W}^{\alpha\beta}]\end{aligned}$$

The energy scale of possible new physics is Λ, and $g = e/sin(\theta_W)$, e being the unit electric charge and θ_W the Weinberg angle. The field tensors are described in [3,4].

The two dimension 6 operators a_0^W/Λ^2 and a_c^W/Λ^2 are associated with the $WW\gamma\gamma$ vertex. Among dimension 8 operators, κ_0^W/Λ^2 and κ_c^W/Λ^2 are associated with the $WWZ\gamma$ vertex, whereas the parameter $f_{T,0}/\Lambda^4$ contributes to both vertices. There is a relationship between these two dimension 6 parameters and the dimension 8 parameters $f_{M,i}/\Lambda^4$ as follows [3]:

$$\frac{a_0^W}{\Lambda^2} = -\frac{4M_W^2}{g^2}\frac{f_{M,0}}{\Lambda^4} - \frac{8M_W^2}{g'^2}\frac{f_{M,2}}{\Lambda^4}$$

$$\frac{a_c^W}{\Lambda^2} = -\frac{4M_W^2}{g^2}\frac{f_{M,1}}{\Lambda^4} - \frac{8M_W^2}{g'^2}\frac{f_{M,3}}{\Lambda^4}$$

where $g' = e/cos(\theta_W)$ and M_W is the invariant mass of the W boson. This relation provides a translation between limits on dimension 6 operators $a_{0,c}^W$ and $f_{M,j}/\Lambda^4$. It is further required [4] that $f_{M,0} = 2f_{M,2}$ and $f_{M,1} = 2f_{M,3}$ which suppresses contributions to the $WWZ\gamma$ vertex. The complete set of Lagrangian contributions as presented in [4] corresponds to 19 anomalous couplings in total – $f_{S,i},\ i = 1, 2,\ f_{M,i},\ i = 0, \ldots, 8$ and $f_{T,i}, i = 0, \ldots, 9$ – each scaled by $1/\Lambda^4$.

Another approach to couplings is the so called K-matrix framework [7], in which the anomalous couplings can be expressed in terms of two parameters α_4 and α_5, which account for all BSM effects.

The LHC collaborations have published couplings results based on various theoretical frameworks. It is hoped that the collaborations will agree to use at least one common set of parameters to express these limits to enable the reader to make a comparison, and to allow for a possible LHC combination.

References

1. G. Belanger and F. Boudjema, Phys. Lett. **B288**, 201 (1992).
2. J.W. Stirling and A. Werthenbach, Eur. Phys. J. **C14**, 103 (2000);
   J.W. Stirling and A. Werthenbach, Phys. Lett. **B466**, 369 (1999);
   A. Denner *et al.*, Eur. Phys. J. **C20**, 201 (2001);
   G. Montagna *et al.*, Phys. Lett. **B515**, 197 (2001).
3. G. Belanger *et al.*, Eur. Phys. J. **C13**, 283 (2000).
4. O.J.P. Éboli, M.C. Gonzalez-Garcia, and S.M. Lietti, Phys. Rev. **D69**, 095005 (2004);

Int. J. Mod. Phys. A 2026.41. Downloaded from www.worldscientific.com
by UNIVERSITY OF CALIFORNIA @ BERKELEY on 09/16/26. Reproduction strictly not permitted, except for Open Access articles.

Int. J. Mod. Phys. A 2026.41. Downloaded from www.worldscientific.com
by UNIVERSITY OF CALIFORNIA @ BERKELEY on 09/16/26. Re-use and distribution is strictly not permitted, except for Open Access articles.

O.J.P. Éboli, M.C. Gonzalez-Garcia, and J.K. Mizukoshi, Phys. Rev. **D77**, 073005 (2006).

5. S. Chatrchyan *et al.*, Phys. Rev. **D90**, 032008 (2014); S. Chatrchyan *et al.*, Phys. Rev. Lett. **114**, 051801 (2015).
6. G. Aad *et al.*, Phys. Rev. Lett. **113**, 141803 (2014).
7. A. Albateanu, W. Killian, and J. Reuter, JHEP **0811**, 010 (2008).

a_0/Λ^2, a_c/Λ^2

Combining published and unpublished preliminary LEP results the following 95% CL intervals for the QGCs associated with the $ZZ\gamma\gamma$ vertex are derived (CERN-PH-EP/2005-051 or hep-ex/0511027):

$$-0.008 < a_0^Z/\Lambda^2 < +0.021$$
$$-0.029 < a_c^Z/\Lambda^2 < +0.039$$

Anomalous Z quartic couplings have also been measured by the Tevatron and LHC experiments. As discussed in the review on "Anomalous W/Z quartic couplings," the coupling parameters in the Anomalous QGC Lagrangian may relate to processes involving only the W or only to the Z or to both. Thus, results on all other AQGCs are reported together in the W listings.

VALUE	DOCUMENT ID	TECN
• • • We do not use the following data for averages, fits, limits, etc. • • •		
	[1] ABBIENDI 04L	OPAL
	[2] HEISTER 04A	ALEP
	[3] ACHARD 02G	L3

[1] ABBIENDI 04L select 20 $e^+e^- \to \nu\overline{\nu}\gamma\gamma$ acoplanar events in the energy range 180–209 GeV and 176 $e^+e^- \to q\overline{q}\gamma\gamma$ events in the energy range 130–209 GeV. These samples are used to constrain possible anomalous $W^+W^-\gamma\gamma$ and $ZZ\gamma\gamma$ quartic couplings. Further combining with the $W^+W^-\gamma$ sample of ABBIENDI 04B the following one–parameter 95% CL limits are obtained: $-0.007 < a_0^Z/\Lambda^2 < 0.023$ GeV^{-2}, $-0.029 < a_c^Z/\Lambda^2 < 0.029$ GeV^{-2}, $-0.020 < a_0^W/\Lambda^2 < 0.020$ GeV^{-2}, $-0.052 < a_c^W/\Lambda^2 < 0.037$ GeV^{-2}.

[2] In the CM energy range 183 to 209 GeV HEISTER 04A select 30 $e^+e^- \to \nu\overline{\nu}\gamma\gamma$ events with two acoplanar, high energy and high transverse momentum photons. The photon–photon acoplanarity is required to be $> 5^\circ$, $E_\gamma/\sqrt{s} > 0.025$ (the more energetic photon having energy $> 0.2\sqrt{s}$), $p_{T_\gamma}/E_{beam} > 0.05$ and $|\cos\theta_\gamma| < 0.94$. A likelihood fit to the photon energy and recoil missing mass yields the following one–parameter 95% CL limits: $-0.012 < a_0^Z/\Lambda^2 < 0.019$ GeV^{-2}, $-0.041 < a_c^Z/\Lambda^2 < 0.044$ GeV^{-2}, $-0.060 < a_0^W/\Lambda^2 < 0.055$ GeV^{-2}, $-0.099 < a_c^W/\Lambda^2 < 0.093$ GeV^{-2}.

[3] ACHARD 02G study $e^+e^- \to Z\gamma\gamma \to q\overline{q}\gamma\gamma$ events using data at center-of-mass energies from 200 to 209 GeV. The photons are required to be isolated, each with energy >5 GeV and $|\cos\theta| < 0.97$, and the di-jet invariant mass to be compatible with that of the Z boson (74–111 GeV). Cuts on Z velocity ($\beta < 0.73$) and on the energy of the most energetic photon reduce the backgrounds due to non-resonant production of the $q\overline{q}\gamma\gamma$ state and due to ISR respectively, yielding a total of 40 candidate events of which 8.6 are expected to be due to background. The energy spectra of the least energetic photon are fitted for all ten center-of-mass energy values from 130 GeV to 209 GeV (as obtained adding to the present analysis 130–202 GeV data of ACCIARRI 01E, for a total of 137 events with an expected background of 34.1 events) to obtain the fitted values $a_0/\Lambda^2 = 0.00^{+0.02}_{-0.01}$ GeV^{-2} and $a_c/\Lambda^2 = 0.03^{+0.01}_{-0.02}$ GeV^{-2}, where the other parameter is kept fixed to its Standard Model value (0). A simultaneous fit to both parameters yields the 95% CL limits -0.02 GeV$^{-2} < a_0/\Lambda^2 < 0.03$ GeV^{-2} and -0.07 GeV$^{-2} < a_c/\Lambda^2 < 0.05$ GeV^{-2}.

Z REFERENCES

AAIJ	25AH	PRL 135 161802	R. Aaij *et al.*	(LHCb Collab.)
HAYRAPETY...	25AF	PL B866 139526	A. Hayrapetyan *et al.*	(CMS Collab.)
HAYRAPETY...	25AK	PR D112 112011	A. Hayrapetyan *et al.*	(CMS Collab.)
HAYRAPETY...	25H	PL B865 139462	A. Hayrapetyan *et al.*	(CMS Collab.)
AAD	24L	PL B854 138705	G. Aad *et al.*	(ATLAS Collab.)
AAD	24R	PL B855 138762	G. Aad *et al.*	(ATLAS Collab.)
AAIJ	24AL	JHEP 2412 026	R. Aaij *et al.*	(LHCb Collab.)
HAYRAPETY...	24T	JHEP 2401 101	A. Hayrapetyan *et al.*	(CMS Collab.)
AABOUD	23A	JHEP 2312 158 (errat.)	M. Aaboud *et al.*	(ATLAS Collab.)
AAD	23AQ	PR D108 032015	G. Aad *et al.*	(ATLAS Collab.)
AAD	23BS	PL B847 138292	G. Aad *et al.*	(ATLAS Collab.)
AAD	23CD	EPJ C83 781	G. Aad *et al.*	(ATLAS Collab.)
AAD	23CH	JHEP 2312 107	G. Aad *et al.*	(ATLAS Collab.)
AAIJ	23AM	CP C47 093002	R. Aaij *et al.*	(LHCb Collab.)
TUMASYAN	23E	PL B842 137563	A. Tumasyan *et al.*	(CMS Collab.)
AALTONEN	22	SCI 376 170	T. Aaltonen *et al.*	(CDF Collab.)
AAD	21AO	NATP 17 819	G. Aad *et al.*	(ATLAS Collab.)
AAD	21AQ	JHEP 2107 005	G. Aad *et al.*	(ATLAS Collab.)
AAD	21AV	PRL 127 271801	G. Aad *et al.*	(ATLAS Collab.)
SIRUNYAN	21Q	EPJ C81 200	A.M. Sirunyan *et al.*	(CMS Collab.)
JANOT	20	PL B803 135319	P. Janot, S. Jadach	(CERN, CRAC)
VOUTSINAS	20	PL B800 135068	G. Voutsinas *et al.*	(CERN, BOHR)
AABOUD	19AY	JHEP 1910 127	M. Aaboud *et al.*	(ATLAS Collab.)
AABOUD	19N	JHEP 1904 048	M. Aaboud *et al.*	(ATLAS Collab.)
RAINBOLT	19	PR D99 013004	J.L. Rainbolt, M. Schmitt	(NWES)
SIRUNYAN	19AJ	EPJ C79 94	A.M. Sirunyan *et al.*	(CMS Collab.)
SIRUNYAN	19BR	PL B797 134811	A.M. Sirunyan *et al.*	(CMS Collab.)
AABOUD	18AU	JHEP 1807 127	M. Aaboud *et al.*	(ATLAS Collab.)
Also		JHEP 2312 158 (errat.)	M. Aaboud *et al.*	(ATLAS Collab.)
AABOUD	18BL	PL B786 134	M. Aaboud *et al.*	(ATLAS Collab.)
AABOUD	18CN	PR D98 092010	M. Aaboud *et al.*	(ATLAS Collab.)
AABOUD	18Q	PR D97 032005	M. Aaboud *et al.*	(ATLAS Collab.)
AAIJ	18AR	JHEP 1809 159	R. Aaij *et al.*	(LHCb Collab.)
AALTONEN	18B	PR D97 112007	T. Aaltonen *et al.*	(CDF and D0 Collabs.)
ABAZOV	18	PRL 120 241802	V.M. Abazov *et al.*	(D0 Collab.)
ANDREEV	18A	EPJ C78 777	V. Andreev *et al.*	(H1 Collab.)
SIRUNYAN	18BT	EPJ C78 165	A.M. Sirunyan *et al.*	(CMS Collab.)
SIRUNYAN	18CY	EPJ C78 701	A.M. Sirunyan *et al.*	(CMS Collab.)
SIRUNYAN	18DZ	PRL 121 141801	A.M. Sirunyan *et al.*	(CMS Collab.)
AABOUD	17Q	EPJ C77 367	M. Aaboud *et al.*	(ATLAS Collab.)
AABOUD	16K	PRL 117 111802	M. Aaboud *et al.*	(ATLAS Collab.)
AAD	16L	EPJ C76 210	G. Aad *et al.*	(ATLAS Collab.)
AAD	16Q	PR D93 112002	G. Aad *et al.*	(ATLAS Collab.)
AALTONEN	16D	PR D93 112016	T. Aaltonen *et al.*	(CDF Collab.)
ABRAMOWICZ	16A	PR D93 092002	H. Abramowicz *et al.*	(ZEUS Collab.)
ABT	16	PR D94 052007	I. Abt *et al.*	(MPIM, OXF, HAMB, DESY)
KHACHATRY...	16AE	PL B760 448	V. Khachatryan *et al.*	(CMS Collab.)
KHACHATRY...	16CC	PL B763 280	V. Khachatryan *et al.*	(CMS Collab.)
AAD	15BT	JHEP 1509 049	G. Aad *et al.*	(ATLAS Collab.)
AAD	15I	PRL 114 121801	G. Aad *et al.*	(ATLAS Collab.)
AAIJ	15BF	JHEP 1511 190	R. Aaij *et al.*	(LHCb Collab.)
ABAZOV	15C	PRL 115 041801	V.M. Abazov *et al.*	(D0 Collab.)
KHACHATRY...	15AC	JHEP 1504 164	V. Khachatryan *et al.*	(CMS Collab.)
KHACHATRY...	15B	PL B740 250	V. Khachatryan *et al.*	(CMS Collab.)
KHACHATRY...	15BC	EPJ C75 511	V. Khachatryan *et al.*	(CMS Collab.)
AAD	14AU	PR D90 072010	G. Aad *et al.*	(ATLAS Collab.)
AAD	14N	PRL 112 231806	G. Aad *et al.*	(ATLAS Collab.)
AALTONEN	14C	PR D89 072005	T. Aaltonen *et al.*	(CDF Collab.)
AALTONEN	14E	PRL 112 111803	T. Aaltonen *et al.*	(CDF Collab.)
CHATRCHYAN	14AB	PR D89 092005	S. Chatrchyan *et al.*	(CMS Collab.)
AAD	13AN	PR D87 112003	G. Aad *et al.*	(ATLAS Collab.)
Also		PR D91 119901 (errat.)	G. Aad *et al.*	(ATLAS Collab.)
AAD	13Z	JHEP 1303 128	G. Aad *et al.*	(ATLAS Collab.)
CHATRCHYAN	13B	JHEP 1301 063	S. Chatrchyan *et al.*	(CMS Collab.)
CHATRCHYAN	13BI	JHEP 1310 164	S. Chatrchyan *et al.*	(CMS Collab.)
SCHAEL	13A	PRPL 532 119	S. Schael *et al.*	(ALEPH, DELPHI, L3, OPAL+)
AAD	12BX	PL B717 49	G. Aad *et al.*	(ATLAS Collab.)
ABAZOV	12S	PR D85 052001	V.M. Abazov *et al.*	(D0 Collab.)
CHATRCHYAN	12BN	JHEP 1212 034	S. Chatrchyan *et al.*	(CMS Collab.)
AALTONEN	11S	PRL 107 051802	T. Aaltonen *et al.*	(CDF Collab.)
ABAZOV	11D	PR D84 012007	V.M. Abazov *et al.*	(D0 Collab.)
CHATRCHYAN	11M	PL B701 535	S. Chatrchyan *et al.*	(CMS Collab.)
ABAZOV	09L	PRL 102 201802	V.M. Abazov *et al.*	(D0 Collab.)
BEDDALL	09	PL B670 300	A. Beddall, A. Beddall, A. Bingul	(UGAZ)
SCHAEL	09	JHEP 0904 124	S. Schael *et al.*	(ALEPH Collab.)
ABAZOV	08K	PRL 100 131801	V.M. Abazov *et al.*	(D0 Collab.)
ABAZOV	07M	PL B653 378	V.M. Abazov *et al.*	(D0 Collab.)
ABDALLAH	07C	EPJ C51 525	J. Abdallah *et al.*	(DELPHI Collab.)
ABDALLAH	06E	PL B639 179	J. Abdallah *et al.*	(DELPHI Collab.)
AKTAS	06	PL B632 35	A. Aktas *et al.*	(H1 Collab.)
LEP-SLC	06	PRPL 427 257	ALEPH, DELPHI, L3, OPAL, SLD and working groups	
SCHAEL	06A	PL B639 192	S. Schael *et al.*	(ALEPH Collab.)
ABDALLAH	05	EPJ C40 1	J. Abdallah *et al.*	(DELPHI Collab.)
ABDALLAH	05C	EPJ C44 299	J. Abdallah *et al.*	(DELPHI Collab.)
ABE	05	PRL 94 091801	K. Abe *et al.*	(SLD Collab.)
ABE	05F	PR D71 112004	K. Abe *et al.*	(SLD Collab.)
ACOSTA	05M	PR D71 052002	D. Acosta *et al.*	(CDF Collab.)
ABBIENDI	04B	PL B580 17	G. Abbiendi *et al.*	(OPAL Collab.)
ABBIENDI	04C	EPJ C32 303	G. Abbiendi *et al.*	(OPAL Collab.)
ABBIENDI	04E	PL B586 167	G. Abbiendi *et al.*	(OPAL Collab.)
ABBIENDI	04G	EPJ C33 173	G. Abbiendi *et al.*	(OPAL Collab.)
ABBIENDI	04L	PR D70 032005	G. Abbiendi *et al.*	(OPAL Collab.)
ABDALLAH	04F	EPJ C34 109	J. Abdallah *et al.*	(DELPHI Collab.)
ABE	04C	PR D69 072003	K. Abe *et al.*	(SLD Collab.)
ACHARD	04C	PL B585 42	P. Achard *et al.*	(L3 Collab.)
ACHARD	04H	PL B597 119	P. Achard *et al.*	(L3 Collab.)
HEISTER	04A	PL B602 31	A. Heister *et al.*	(ALEPH Collab.)
ABBIENDI	03P	PL B577 18	G. Abbiendi *et al.*	(OPAL Collab.)
ABDALLAH	03H	PL B569 129	J. Abdallah *et al.*	(DELPHI Collab.)
ABDALLAH	03K	PL B576 29	J. Abdallah *et al.*	(DELPHI Collab.)
ABE	03F	PRL 90 141804	K. Abe *et al.*	(SLD Collab.)
ACHARD	03D	PL B572 133	P. Achard *et al.*	(L3 Collab.)
ACHARD	03G	PL B577 109	P. Achard *et al.*	(L3 Collab.)
ABBIENDI	02I	PL B546 29	G. Abbiendi *et al.*	(OPAL Collab.)
ABE	02G	PRL 88 151801	K. Abe *et al.*	(SLD Collab.)
ACHARD	02G	PL B540 43	P. Achard *et al.*	(L3 Collab.)
HEISTER	02B	PL B526 34	A. Heister *et al.*	(ALEPH Collab.)
HEISTER	02C	PL B528 19	A. Heister *et al.*	(ALEPH Collab.)
HEISTER	02H	EPJ C24 177	A. Heister *et al.*	(ALEPH Collab.)
ABBIENDI	01A	EPJ C19 587	G. Abbiendi *et al.*	(OPAL Collab.)
ABBIENDI	01G	EPJ C18 447	G. Abbiendi *et al.*	(OPAL Collab.)
ABBIENDI	01K	PL B516 1	G. Abbiendi *et al.*	(OPAL Collab.)
ABBIENDI	01N	EPJ C20 445	G. Abbiendi *et al.*	(OPAL Collab.)
ABBIENDI	01O	EPJ C21 1	G. Abbiendi *et al.*	(OPAL Collab.)
ABE	01B	PRL 86 1162	K. Abe *et al.*	(SLD Collab.)
ABE	01C	PR D63 032005	K. Abe *et al.*	(SLD Collab.)
ACCIARRI	01E	PL B505 47	M. Acciarri *et al.*	(L3 Collab.)
ACCIARRI	01I	PL B497 23	M. Acciarri *et al.*	(L3 Collab.)
HEISTER	01	EPJ C20 401	A. Heister *et al.*	(ALEPH Collab.)
HEISTER	01D	EPJ C22 201	A. Heister *et al.*	(ALEPH Collab.)
ABBIENDI	00N	PL B476 256	G. Abbiendi *et al.*	(OPAL Collab.)
ABBIENDI,G	00C	EPJ C17 553	G. Abbiendi *et al.*	(OPAL Collab.)
ABE	00B	PRL 84 5945	K. Abe *et al.*	(SLD Collab.)
ABE	00D	PRL 85 5059	K. Abe *et al.*	(SLD Collab.)
ABREU	00	EPJ C12 225	P. Abreu *et al.*	(DELPHI Collab.)
ABREU	00B	EPJ C14 613	P. Abreu *et al.*	(DELPHI Collab.)
ABREU	00E	EPJ C14 585	P. Abreu *et al.*	(DELPHI Collab.)
ABREU	00F	EPJ C16 371	P. Abreu *et al.*	(DELPHI Collab.)
ABREU	00P	PL B475 429	P. Abreu *et al.*	(DELPHI Collab.)
ACCIARRI	00	EPJ C13 47	M. Acciarri *et al.*	(L3 Collab.)
ACCIARRI	00C	EPJ C16 1	M. Acciarri *et al.*	(L3 Collab.)
ACCIARRI	00J	PL B479 79	M. Acciarri *et al.*	(L3 Collab.)
ACCIARRI	00Q	PL B489 93	M. Acciarri *et al.*	(L3 Collab.)
BARATE	00B	EPJ C16 597	R. Barate *et al.*	(ALEPH Collab.)
BARATE	00C	EPJ C14 1	R. Barate *et al.*	(ALEPH Collab.)
BARATE	00O	EPJ C16 613	R. Barate *et al.*	(ALEPH Collab.)
ABBIENDI	99B	EPJ C8 217	G. Abbiendi *et al.*	(OPAL Collab.)
ABBIENDI	99I	PL B447 157	G. Abbiendi *et al.*	(OPAL Collab.)
ABE	99E	PR D59 052001	K. Abe *et al.*	(SLD Collab.)
ABE	99L	PRL 83 1902	K. Abe *et al.*	(SLD Collab.)
ABREU	99	EPJ C6 19	P. Abreu *et al.*	(DELPHI Collab.)
ABREU	99B	EPJ C10 415	P. Abreu *et al.*	(DELPHI Collab.)
ABREU	99J	PL B449 364	P. Abreu *et al.*	(DELPHI Collab.)
ABREU	99U	PL B462 425	P. Abreu *et al.*	(DELPHI Collab.)
ABREU	99Y	EPJ C10 219	P. Abreu *et al.*	(DELPHI Collab.)
ACCIARRI	99D	PL B448 152	M. Acciarri *et al.*	(L3 Collab.)
ACCIARRI	99F	PL B453 94	M. Acciarri *et al.*	(L3 Collab.)
ACCIARRI	99G	PL B450 281	M. Acciarri *et al.*	(L3 Collab.)
ACCIARRI	99O	PL B465 363	M. Acciarri *et al.*	(L3 Collab.)
ABBOTT	98M	PR D57 3817	B. Abbott *et al.*	(D0 Collab.)
ABE	98D	PRL 80 660	K. Abe *et al.*	(SLD Collab.)
ABE	98I	PRL 81 942	K. Abe *et al.*	(SLD Collab.)
ABREU	98K	PL B423 194	P. Abreu *et al.*	(DELPHI Collab.)
ABREU	98L	EPJ C5 585	P. Abreu *et al.*	(DELPHI Collab.)
ACCIARRI	98G	PL B431 199	M. Acciarri *et al.*	(L3 Collab.)
ACCIARRI	98H	PL B429 387	M. Acciarri *et al.*	(L3 Collab.)
ACCIARRI	98U	PL B439 225	M. Acciarri *et al.*	(L3 Collab.)
ACKERSTAFF	98A	EPJ C5 411	K. Ackerstaff *et al.*	(OPAL Collab.)

Int. J. Mod. Phys. A 2026.41. Downloaded from www.worldscientific.com
by UNIVERSITY OF CALIFORNIA @ BERKELEY on 09/16/26. Reproduction is strictly not permitted, except for Open Access articles.

ACKERSTAFF	98E	EPJ C1 439	K. Ackerstaff *et al.*	(OPAL Collab.)
ACKERSTAFF	98O	PL B420 157	K. Ackerstaff *et al.*	(OPAL Collab.)
ACKERSTAFF	98Q	EPJ C4 19	K. Ackerstaff *et al.*	(OPAL Collab.)
BARATE	98O	PL B434 415	R. Barate *et al.*	(ALEPH Collab.)
BARATE	98T	EPJ C4 557	R. Barate *et al.*	(ALEPH Collab.)
BARATE	98V	EPJ C5 205	R. Barate *et al.*	(ALEPH Collab.)
ABE	97	PRL 78 17	K. Abe *et al.*	(SLD Collab.)
ABREU	97C	ZPHY C73 243	P. Abreu *et al.*	(DELPHI Collab.)
ABREU	97E	PL B398 207	P. Abreu *et al.*	(DELPHI Collab.)
ABREU	97G	PL B404 194	P. Abreu *et al.*	(DELPHI Collab.)
ACCIARRI	97D	PL B393 465	M. Acciarri *et al.*	(L3 Collab.)
ACCIARRI	97J	PL B407 351	M. Acciarri *et al.*	(L3 Collab.)
ACCIARRI	97L	PL B407 389	M. Acciarri *et al.*	(L3 Collab.)
ACCIARRI	97R	PL B413 167	M. Acciarri *et al.*	(L3 Collab.)
ACKERSTAFF	97M	ZPHY C74 413	K. Ackerstaff *et al.*	(OPAL Collab.)
ACKERSTAFF	97S	PL B412 210	K. Ackerstaff *et al.*	(OPAL Collab.)
ACKERSTAFF	97T	ZPHY C76 387	K. Ackerstaff *et al.*	(OPAL Collab.)
ACKERSTAFF	97W	ZPHY C76 425	K. Ackerstaff *et al.*	(OPAL Collab.)
ALEXANDER	97C	ZPHY C73 379	G. Alexander *et al.*	(OPAL Collab.)
ALEXANDER	97D	ZPHY C73 569	G. Alexander *et al.*	(OPAL Collab.)
ALEXANDER	97E	ZPHY C73 587	G. Alexander *et al.*	(OPAL Collab.)
BARATE	97D	PL B405 191	R. Barate *et al.*	(ALEPH Collab.)
BARATE	97E	PL B401 150	R. Barate *et al.*	(ALEPH Collab.)
BARATE	97F	PL B401 163	R. Barate *et al.*	(ALEPH Collab.)
BARATE	97H	PL B402 213	R. Barate *et al.*	(ALEPH Collab.)
BARATE	97J	ZPHY C74 451	R. Barate *et al.*	(ALEPH Collab.)
ABREU	96R	ZPHY C72 31	P. Abreu *et al.*	(DELPHI Collab.)
ABREU	96S	PL B389 405	P. Abreu *et al.*	(DELPHI Collab.)
ABREU	96U	ZPHY C73 61	P. Abreu *et al.*	(DELPHI Collab.)
ACCIARRI	96	PL B371 126	M. Acciarri *et al.*	(L3 Collab.)
ADAM	96	ZPHY C69 561	W. Adam *et al.*	(DELPHI Collab.)
ADAM	96B	ZPHY C70 371	W. Adam *et al.*	(DELPHI Collab.)
ALEXANDER	96B	ZPHY C70 197	G. Alexander *et al.*	(OPAL Collab.)
ALEXANDER	96F	PL B370 185	G. Alexander *et al.*	(OPAL Collab.)
ALEXANDER	96N	PL B384 343	G. Alexander *et al.*	(OPAL Collab.)
ALEXANDER	96R	ZPHY C72 1	G. Alexander *et al.*	(OPAL Collab.)
BUSKULIC	96D	ZPHY C69 393	D. Buskulic *et al.*	(ALEPH Collab.)
BUSKULIC	96H	ZPHY C69 379	D. Buskulic *et al.*	(ALEPH Collab.)
BUSKULIC	96T	PL B384 449	D. Buskulic *et al.*	(ALEPH Collab.)
BUSKULIC	96Y	PL B388 648	D. Buskulic *et al.*	(ALEPH Collab.)
ABE	95J	PRL 74 2880	K. Abe *et al.*	(SLD Collab.)
ABREU	95	ZPHY C65 709 (errat.)	P. Abreu *et al.*	(DELPHI Collab.)
ABREU	95D	ZPHY C66 323	P. Abreu *et al.*	(DELPHI Collab.)
ABREU	95L	ZPHY C65 587	P. Abreu *et al.*	(DELPHI Collab.)
ABREU	95M	ZPHY C65 603	P. Abreu *et al.*	(DELPHI Collab.)
ABREU	95O	ZPHY C67 543	P. Abreu *et al.*	(DELPHI Collab.)
ABREU	95R	ZPHY C68 353	P. Abreu *et al.*	(DELPHI Collab.)
ABREU	95V	ZPHY C68 541	P. Abreu *et al.*	(DELPHI Collab.)
ABREU	95W	PL B361 207	P. Abreu *et al.*	(DELPHI Collab.)
ABREU	95X	ZPHY C69 1	P. Abreu *et al.*	(DELPHI Collab.)
ACCIARRI	95B	PL B345 589	M. Acciarri *et al.*	(L3 Collab.)
ACCIARRI	95C	PL B345 609	M. Acciarri *et al.*	(L3 Collab.)
ACCIARRI	95G	PL B353 136	M. Acciarri *et al.*	(L3 Collab.)
AKERS	95C	ZPHY C65 47	R. Akers *et al.*	(OPAL Collab.)
AKERS	95U	ZPHY C67 389	R. Akers *et al.*	(OPAL Collab.)
AKERS	95W	ZPHY C67 555	R. Akers *et al.*	(OPAL Collab.)
AKERS	95X	ZPHY C68 1	R. Akers *et al.*	(OPAL Collab.)
AKERS	95Z	ZPHY C68 203	R. Akers *et al.*	(OPAL Collab.)
ALEXANDER	95D	PL B358 162	G. Alexander *et al.*	(OPAL Collab.)
BUSKULIC	95R	ZPHY C69 15	D. Buskulic *et al.*	(ALEPH Collab.)
MIYABAYASHI	95	PL B347 171	K. Miyabayashi *et al.*	(TOPAZ Collab.)
ABE	94C	PRL 73 25	K. Abe *et al.*	(SLD Collab.)
ABREU	94B	PL B327 386	P. Abreu *et al.*	(DELPHI Collab.)
ABREU	94P	PL B341 109	P. Abreu *et al.*	(DELPHI Collab.)
AKERS	94P	ZPHY C63 181	R. Akers *et al.*	(OPAL Collab.)
BUSKULIC	94G	ZPHY C62 179	D. Buskulic *et al.*	(ALEPH Collab.)
BUSKULIC	94J	ZPHY C62 1	D. Buskulic *et al.*	(ALEPH Collab.)
VILAIN	94	PL B320 203	P. Vilain *et al.*	(CHARM II Collab.)
ABREU	93	PL B298 236	P. Abreu *et al.*	(DELPHI Collab.)
ABREU	93I	ZPHY C59 533	P. Abreu *et al.*	(DELPHI Collab.)
Also		ZPHY C65 709 (errat.)	P. Abreu *et al.*	(DELPHI Collab.)
ABREU	93L	PL B318 249	P. Abreu *et al.*	(DELPHI Collab.)
ACTON	93	PL B305 407	P.D. Acton *et al.*	(OPAL Collab.)
ACTON	93D	ZPHY C58 219	P.D. Acton *et al.*	(OPAL Collab.)
ACTON	93E	PL B311 391	P.D. Acton *et al.*	(OPAL Collab.)
ADRIANI	93	PL B301 136	O. Adriani *et al.*	(L3 Collab.)
ADRIANI	93I	PL B316 427	O. Adriani *et al.*	(L3 Collab.)
BUSKULIC	93L	PL B313 520	D. Buskulic *et al.*	(ALEPH Collab.)
NOVIKOV	93C	PL B298 453	V.A. Novikov, L.B. Okun, M.I. Vysotsky	(ITEP)
ABREU	92I	PL B277 371	P. Abreu *et al.*	(DELPHI Collab.)
ABREU	92M	PL B289 199	P. Abreu *et al.*	(DELPHI Collab.)
ACTON	92B	ZPHY C53 539	D.P. Acton *et al.*	(OPAL Collab.)
ACTON	92L	PL B294 436	P.D. Acton *et al.*	(OPAL Collab.)
ACTON	92N	PL B295 357	P.D. Acton *et al.*	(OPAL Collab.)
ADEVA	92	PL B275 209	B. Adeva *et al.*	(L3 Collab.)
ADRIANI	92D	PL B292 454	O. Adriani *et al.*	(L3 Collab.)
ALITTI	92B	PL B276 354	J. Alitti *et al.*	(UA2 Collab.)
BUSKULIC	92D	PL B292 210	D. Buskulic *et al.*	(ALEPH Collab.)
BUSKULIC	92E	PL B294 145	D. Buskulic *et al.*	(ALEPH Collab.)
DECAMP	92	PRPL 216 253	D. Decamp *et al.*	(ALEPH Collab.)
ABE	91E	PRL 67 1502	F. Abe *et al.*	(CDF Collab.)
ABREU	91H	ZPHY C50 185	P. Abreu *et al.*	(DELPHI Collab.)
ACTON	91B	PL B273 338	D.P. Acton *et al.*	(OPAL Collab.)
ADACHI	91	PL B255 613	I. Adachi *et al.*	(TOPAZ Collab.)
ADEVA	91I	PL B259 199	B. Adeva *et al.*	(L3 Collab.)
AKRAWY	91F	PL B257 531	M.Z. Akrawy *et al.*	(OPAL Collab.)
DECAMP	91B	PL B259 377	D. Decamp *et al.*	(ALEPH Collab.)
DECAMP	91J	PL B266 218	D. Decamp *et al.*	(ALEPH Collab.)
JACOBSEN	91	PRL 67 3347	R.G. Jacobsen *et al.*	(Mark II Collab.)
SHIMONAKA	91	PL B268 457	A. Shimonaka *et al.*	(TOPAZ Collab.)
ABE	90I	ZPHY C48 13	K. Abe *et al.*	(VENUS Collab.)
ABRAMS	90	PRL 64 1334	G.S. Abrams *et al.*	(Mark II Collab.)
AKRAWY	90J	PL B246 285	M.Z. Akrawy *et al.*	(OPAL Collab.)
BEHREND	90D	ZPHY C47 333	H.J. Behrend *et al.*	(CELLO Collab.)
BRAUNSCH...	90	ZPHY C48 433	W. Braunschweig *et al.*	(TASSO Collab.)
ELSEN	90	ZPHY C46 349	E. Elsen *et al.*	(JADE Collab.)
HEGNER	90	ZPHY C46 547	S. Hegner *et al.*	(JADE Collab.)
STUART	90	PRL 64 983	D. Stuart *et al.*	(AMY Collab.)
ABE	89	PRL 62 613	F. Abe *et al.*	(CDF Collab.)
ABE	89C	PRL 63 720	F. Abe *et al.*	(CDF Collab.)
ABE	89L	PL B232 425	K. Abe *et al.*	(VENUS Collab.)
ABRAMS	89B	PRL 63 2173	G.S. Abrams *et al.*	(Mark II Collab.)
ABRAMS	89D	PRL 63 2780	G.S. Abrams *et al.*	(Mark II Collab.)
ALBAJAR	89	ZPHY C44 15	C. Albajar *et al.*	(UA1 Collab.)
BACALA	89	PL B218 112	A. Bacala *et al.*	(AMY Collab.)
BAND	89	PL B218 369	H.R. Band *et al.*	(MAC Collab.)
GREENSHAW	89	ZPHY C42 1	T. Greenshaw *et al.*	(JADE Collab.)
OULD-SAADA	89	ZPHY C44 567	F. Ould-Saada *et al.*	(JADE Collab.)
SAGAWA	89	PRL 63 2341	H. Sagawa *et al.*	(AMY Collab.)
ADACHI	88C	PL B208 319	I. Adachi *et al.*	(TOPAZ Collab.)
ADEVA	88	PR D38 2665	B. Adeva *et al.*	(Mark-J Collab.)
BRAUNSCH...	88D	ZPHY C40 163	W. Braunschweig *et al.*	(TASSO Collab.)
ANSARI	87	PL B186 440	R. Ansari *et al.*	(UA2 Collab.)
BEHREND	87C	PL B191 209	H.J. Behrend *et al.*	(CELLO Collab.)
BARTEL	86C	ZPHY C30 371	W. Bartel *et al.*	(JADE Collab.)
Also		ZPHY C26 507	W. Bartel *et al.*	(JADE Collab.)
Also		PL 108B 140	W. Bartel *et al.*	(JADE Collab.)
ASH	85	PRL 55 1831	W.W. Ash *et al.*	(MAC Collab.)
BARTEL	85F	PL 161B 188	W. Bartel *et al.*	(JADE Collab.)
DERRICK	85	PR D31 2352	M. Derrick *et al.*	(HRS Collab.)
FERNANDEZ	85A	PRL 54 1620	E. Fernandez *et al.*	(MAC Collab.)
LEVI	83	PRL 51 1941	M.E. Levi *et al.*	(Mark II Collab.)
BEHREND	82	PL 114B 282	H.J. Behrend *et al.*	(CELLO Collab.)
BRANDELIK	82C	PL 110B 173	R. Brandelik *et al.*	(TASSO Collab.)

H

$J = 0$

was H^0

In the following H refers to the signal that has been discovered in the Higgs searches. Whereas the observed signal is labeled as a spin 0 particle and is called a Higgs Boson, the detailed properties of H and its role in the context of electroweak symmetry breaking need to be further clarified. These issues are addressed by the measurements listed below.

Concerning mass limits and cross section limits that have been obtained in the searches for neutral and charged Higgs bosons, see the sections "Searches for Neutral Higgs Bosons" and "Searches for Charged Higgs Bosons ($H^{\pm}$ and $H^{\pm\pm}$)", respectively.

H MASS

VALUE (GeV)	*DOCUMENT ID*		*TECN*	*COMMENT*
125.13±0.11 OUR AVERAGE	Error includes scale factor of 1.5. See the ideogram below.			
125.04±0.12	[1] HAYRAPETY...	25L	CMS	pp, 13 TeV, $ZZ^* \to 4\ell$
125.10±0.11	[2] AAD	23BP	ATLS	pp, 13 TeV, $\gamma\gamma$, $ZZ^* \to 4\ell$
125.78±0.26	[3] SIRUNYAN	20L	CMS	pp, 13 TeV, $\gamma\gamma$
125.09±0.21±0.11	[4,5] AAD	15B	LHC	pp, 7, 8 TeV
• • • We do not use the following data for averages, fits, limits, etc. • • •				
124.99±0.18±0.04	[6] AAD	23AU	ATLS	pp, 13 TeV, $ZZ^* \to 4\ell$
124.94±0.17±0.03	[7] AAD	23AU	ATLS	pp, 7, 8, 13 TeV, $ZZ^* \to 4\ell$
125.11±0.11	[8] AAD	23BP	ATLS	pp, 7, 8, 13 TeV, $\gamma\gamma$, $ZZ^* \to 4\ell$
125.17±0.11±0.09	[9] AAD	23BU	ATLS	pp, 13 TeV, $\gamma\gamma$
125.22±0.11±0.09	[10] AAD	23BU	ATLS	pp, 7, 8, 13 TeV, $\gamma\gamma$
125.46±0.16	[11] SIRUNYAN	20L	CMS	pp, 13 TeV, $\gamma\gamma$, $ZZ^* \to 4\ell$
125.38±0.14	[12] SIRUNYAN	20L	CMS	pp, 7, 8, 13 TeV, $\gamma\gamma$, $ZZ^* \to 4\ell$
124.79±0.37	[13] AABOUD	18BM	ATLS	pp, 13 TeV, $ZZ^* \to 4\ell$
124.93±0.40	[14] AABOUD	18BM	ATLS	pp, 13 TeV, $\gamma\gamma$
124.86±0.27	[4] AABOUD	18BM	ATLS	pp, 13 TeV, $\gamma\gamma$, $ZZ^* \to 4\ell$
124.97±0.24	[4,15] AABOUD	18BM	ATLS	pp, 7, 8, 13 TeV, $\gamma\gamma$, $ZZ^* \to 4\ell$
125.26±0.20±0.08	[16] SIRUNYAN	17AV	CMS	pp, 13 TeV, $ZZ^* \to 4\ell$
125.07±0.25±0.14	[5] AAD	15B	LHC	pp, 7, 8 TeV, $\gamma\gamma$
125.15±0.37±0.15	[5] AAD	15B	LHC	pp, 7, 8 TeV, $ZZ^* \to 4\ell$
126.02±0.43±0.27	AAD	15B	ATLS	pp, 7, 8 TeV, $\gamma\gamma$
124.51±0.52±0.04	AAD	15B	ATLS	pp, 7, 8 TeV, $ZZ^* \to 4\ell$
125.59±0.42±0.17	AAD	15B	CMS	pp, 7, 8 TeV, $ZZ^* \to 4\ell$
$125.02^{+0.26}_{-0.27}{}^{+0.14}_{-0.15}$	[17] KHACHATRY...	15AM	CMS	pp, 7, 8 TeV
125.36±0.37±0.18	[4,18] AAD	14W	ATLS	pp, 7, 8 TeV
125.98±0.42±0.28	[18] AAD	14W	ATLS	pp, 7, 8 TeV, $\gamma\gamma$
124.51±0.52±0.06	[18] AAD	14W	ATLS	pp, 7, 8 TeV, $ZZ^* \to 4\ell$
125.6 ±0.4 ±0.2	[19] CHATRCHYAN	14AA	CMS	pp, 7, 8 TeV, $ZZ^* \to 4\ell$
122 ±7	[20] CHATRCHYAN	14K	CMS	pp, 7, 8 TeV, $\tau\tau$
124.70±0.31±0.15	[21] KHACHATRY...	14P	CMS	pp, 7, 8 TeV, $\gamma\gamma$
$125.5 \pm 0.2\ ^{+0.5}_{-0.6}$	[4,22] AAD	13AK	ATLS	pp, 7, 8 TeV
126.8 ±0.2 ±0.7	[22] AAD	13AK	ATLS	pp, 7, 8 TeV, $\gamma\gamma$
$124.3\ ^{+0.6}_{-0.5} \pm 0.3$	[22] AAD	13AK	ATLS	pp, 7, 8 TeV, $ZZ^* \to 4\ell$
125.8 ±0.4 ±0.4	[4,23] CHATRCHYAN	13J	CMS	pp, 7, 8 TeV
126.2 ±0.6 ±0.2	[23] CHATRCHYAN	13J	CMS	pp, 7, 8 TeV, $ZZ^* \to 4\ell$
126.0 ±0.4 ±0.4	[4,24] AAD	12AI	ATLS	pp, 7, 8 TeV
125.3 ±0.4 ±0.5	[4,25] CHATRCHYAN	12N	CMS	pp, 7, 8 TeV

[1] HAYRAPETYAN 25L use 138 fb^{-1} of pp collisions at E_{cm} = 13 TeV with $H \to ZZ^* \to 4\ell$ where $\ell = e, \mu$.

[2] AAD 23BP combine 13 TeV results of $H \to \gamma\gamma$ (AAD 23BU) and $H \to ZZ^* \to 4\ell$ where $\ell = e, \mu$ (AAD 23AU) using 140 fb^{-1} of pp collision data. The result is 125.10 ± 0.09(stat)±0.07(syst) GeV.

[3] SIRUNYAN 20L use 35.9 fb^{-1} of pp collisions at E_{cm} = 13 TeV with $H \to \gamma\gamma$.

[4] Combined value from $\gamma\gamma$ and $ZZ^* \to 4\ell$ final states.

[5] ATLAS and CMS data are fitted simultaneously.

[6] AAD 23AU use 139 fb^{-1} of pp collisions at E_{cm} = 13 TeV with $H \to ZZ^* \to 4\ell$ where $\ell = e, \mu$.

[7] AAD 23AU combine 13 TeV results with 7 and 8 TeV results (AAD 14W).

[8] AAD 23BP combine 13 TeV results with 7 and 8 TeV results. The result is 125.11 ± 0.09(stat)±0.06(syst) GeV.

[9] AAD 23BU use 140 fb^{-1} of pp collisions at E_{cm} = 13 TeV with $H \to \gamma\gamma$.

Int. J. Mod. Phys. A 2026.41. Downloaded from www.worldscientific.com by UNIVERSITY OF CALIFORNIA @ BERKELEY on 09/16/26. Re-use and distribution is strictly not permitted, except for Open Access articles.

[10] AAD 23BU combine 13 TeV results with 7 and 8 TeV results (AAD 15B).

[11] SIRUNYAN 20L result of $H \to \gamma\gamma$ is combined with that of $H \to ZZ^* \to 4\ell$ where $\ell = e, \mu$ (SIRUNYAN 17AV).

[12] SIRUNYAN 20L combine 13 TeV results with 7 and 8 TeV results (KHACHATRYAN 15AM).

[13] AABOUD 18BM use 36.1 fb^{-1} of pp collisions at E_{cm} = 13 TeV with $H \to ZZ^* \to 4\ell$ where $\ell = e, \mu$.

[14] AABOUD 18BM use 36.1 fb^{-1} of pp collisions at E_{cm} = 13 TeV with $H \to \gamma\gamma$.

[15] AABOUD 18BM combine 13 TeV results with 7 and 8 TeV results. Other combined results are summarized in their Fig. 4.

[16] SIRUNYAN 17AV use 35.9 fb^{-1} of pp collisions at E_{cm} = 13 TeV with $H \to ZZ^* \to 4\ell$ where $\ell = e, \mu$.

[17] KHACHATRYAN 15AM use up to 5.1 fb^{-1} of pp collisions at E_{cm} = 7 TeV and up to 19.7 fb^{-1} at E_{cm} = 8 TeV.

[18] AAD 14W use 4.5 fb^{-1} of pp collisions at E_{cm} = 7 TeV and 20.3 fb^{-1} at 8 TeV.

[19] CHATRCHYAN 14AA use 5.1 fb^{-1} of pp collisions at E_{cm} = 7 TeV and 19.7 fb^{-1} at E_{cm} = 8 TeV.

[20] CHATRCHYAN 14K use 4.9 fb^{-1} of pp collisions at E_{cm} = 7 TeV and 19.7 fb^{-1} at E_{cm} = 8 TeV.

[21] KHACHATRYAN 14P use 5.1 fb^{-1} of pp collisions at E_{cm} = 7 TeV and 19.7 fb^{-1} at E_{cm} = 8 TeV.

[22] AAD 13AK use 4.7 fb^{-1} of pp collisions at E_{cm}=7 TeV and 20.7 fb^{-1} at E_{cm}=8 TeV. Superseded by AAD 14W.

[23] CHATRCHYAN 13J use 5.1 fb^{-1} of pp collisions at E_{cm} = 7 TeV and 12.2 fb^{-1} at E_{cm} = 8 TeV.

[24] AAD 12AI obtain results based on 4.6–4.8 fb^{-1} of pp collisions at E_{cm} = 7 TeV and 5.8–5.9 fb^{-1} at E_{cm} = 8 TeV. An excess of events over background with a local significance of 5.9 σ is observed at m_H = 126 GeV. See also AAD 12DA.

[25] CHATRCHYAN 12N obtain results based on 4.9–5.1 fb^{-1} of pp collisions at E_{cm} = 7 TeV and 5.1–5.3 fb^{-1} at E_{cm} = 8 TeV. An excess of events over background with a local significance of 5.0 σ is observed at about m_H = 125 GeV. See also CHATRCHYAN 12BY and CHATRCHYAN 13Y.

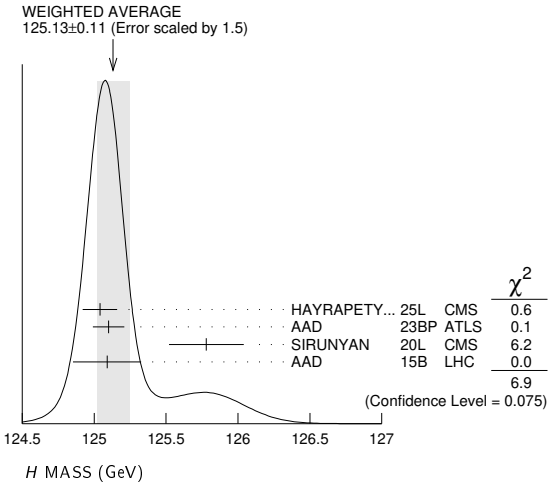

H SPIN AND *CP* PROPERTIES

The observation of the signal in the $\gamma\gamma$ final state rules out the possibility that the discovered particle has spin 1, as a consequence of the Landau-Yang theorem. This argument relies on the assumptions that the decaying particle is an on-shell resonance and that the decay products are indeed two photons rather than two pairs of boosted photons, which each could in principle be misidentified as a single photon.

Concerning distinguishing the spin 0 hypothesis from a spin 2 hypothesis, some care has to be taken in modelling the latter in order to ensure that the discriminating power is actually based on the spin properties rather than on unphysical behavior that may affect the model of the spin 2 state.

Under the assumption that the observed signal consists of a single state rather than an overlap of more than one resonance, it is sufficient to discriminate between distinct hypotheses in the spin analyses. On the other hand, the determination of the *CP* properties is in general much more difficult since in principle the observed state could consist of any admixture of *CP*-even and *CP*-odd components. As a first step, the compatibility of the data with distinct hypotheses of pure *CP*-even and pure *CP*-odd states with different spin assignments has been investigated. In order to treat the case of a possible mixing of different *CP* states, certain cross section ratios are considered. Those cross section ratios need to be distinguished from the amount of mixing between a *CP*-even and a *CP*-odd state, as the cross section ratios depend in addition also on the coupling strengths of the *CP*-even and *CP*-odd components to the involved particles. A small relative coupling implies a small sensitivity of the corresponding cross section ratio to effects of *CP* mixing.

VALUE	DOCUMENT ID		TECN	COMMENT
• • • We do not use the following data for averages, fits, limits, etc. • • •				
	[1] AAD	25BC	ATLS	$H \to \tau\tau$, VBF, 13 TeV
	[2] AAD	25BK	ATLS	WW^* ($\to \ell\nu\ell\nu$), ggF+VBF, 13 TeV
	[3] HAYRAPETY...	25R	CMS	$t\overline{t}H$, tH, $H \to b\overline{b}$, 13 TeV
	[4] AAD	24AG	ATLS	$H \to ZZ^* \to 4\ell$, VBF, 13 TeV
	[5] AAD	24J	ATLS	$t\overline{t}H$, tH, $H \to b\overline{b}$, 13 TeV
	[6] AAD	23AK	ATLS	$H \to \tau\tau$, 13 TeV
	[7] AAD	23AN	ATLS	$H \to \gamma\gamma$, VBF, 13 TeV
	[8] TUMASYAN	23AJ	CMS	$H \to \tau\tau$, 13 TeV
	[9] TUMASYAN	23P	CMS	$t\overline{t}H$, $H \to WW^*$, $\tau\tau$, 13 TeV
	[10] AAD	22V	ATLS	WW^* ($\to e\nu\mu\nu$)+2j, 13 TeV
	[11] TUMASYAN	22Y	CMS	$H \to \tau\tau$, 13 TeV
	[12] AAD	20N	ATLS	$H \to \tau\tau$, VBF, 13 TeV
	[13] AAD	20Z	ATLS	$t\overline{t}H$, $H \to \gamma\gamma$, 13 TeV
	[14] SIRUNYAN	20AS	CMS	$t\overline{t}H$, $H \to \gamma\gamma$, 13 TeV
	[15] SIRUNYAN	19BL	CMS	pp, 7, 8, 13 TeV, $ZZ^*/ZZ \to 4\ell$
	[16] SIRUNYAN	19BZ	CMS	$pp \to H$+2jets (VBF, ggF, VH), $H \to \tau\tau$, 13 TeV
	[17] AABOUD	18AJ	ATLS	$H \to ZZ^* \to 4\ell$ ($\ell = e, \mu$), 13TeV
	[18] SIRUNYAN	17AM	CMS	$pp \to H+ \geq 2j$, $H \to 4\ell$ ($\ell = e, \mu$)
	[19] AAD	16	ATLS	$H \to \gamma\gamma$
	[20] AAD	16BL	ATLS	$pp \to HjjX$ (VBF), $H \to \tau\tau$, 8 TeV
	[21] KHACHATRY...	16AB	CMS	$pp \to WH$, ZH, $H \to b\overline{b}$, 8 TeV
	[22] AAD	15AX	ATLS	$H \to WW^*$
	[23] AAD	15CI	ATLS	$H \to ZZ^*$, WW^*, $\gamma\gamma$
	[24] AALTONEN	15	TEVA	$p\overline{p} \to WH$, ZH, $H \to b\overline{b}$
	[25] AALTONEN	15B	CDF	$p\overline{p} \to WH$, ZH, $H \to b\overline{b}$
	[26] KHACHATRY...	15Y	CMS	$H \to 4\ell$, WW^*, $\gamma\gamma$
	[27] ABAZOV	14F	D0	$p\overline{p} \to WH$, ZH, $H \to b\overline{b}$
	[28] CHATRCHYAN	14AA	CMS	$H \to ZZ^*$
	[29] CHATRCHYAN	14G	CMS	$H \to WW^*$
	[30] KHACHATRY...	14P	CMS	$H \to \gamma\gamma$
	[31] AAD	13AJ	ATLS	$H \to \gamma\gamma$, $ZZ^* \to 4\ell$, $WW^* \to \ell\nu\ell\nu$
	[32] CHATRCHYAN	13J	CMS	$H \to ZZ^* \to 4\ell$

[1] AAD 25BC study *CP* properties in *H* production via VBF using $H \to \tau\tau$ decay channel with 140 fb^{-1} at E_{cm} = 13 TeV. By using the Optimal Observable method, the data constrain a parameter $\tilde{d}$, which is for the strength of *CP* violation in an effective field theory using the HISZ basis, and Wilson coefficient $c_{H\widetilde{W}}$ (Warsaw basis with Λ = 1 TeV) to be [−0.012, 0.044] and [−0.24, 0.83] at 95% CL, respectively, in both cases considering the linear and quadratic terms in the reweighting procedure. See their Fig. 6 and Table 9.

[2] AAD 25BK measure the *CP* properties using $H \to WW^* \to \ell\nu\ell\nu$ ($\ell = e, \mu$) with data of 140 fb^{-1} pp collisions at E_{cm} = 13 TeV. By adding the azimuthal angular difference between the forward and backward jets to the reduced stage-1.2 simplified template cross section framework (see their Fig. 4), the signal strengths are measured as shown in their Fig. 12, which is compatible with a *CP*-conserving scenario (*p*-value of 75%). EFT interpretations in *CP*-conserving and *CP*-violating scenarios are given as the five rotated-basis Wilson coefficients obtained from the 16 Warsaw-basis Wilson coefficients (see their Fig. 14) for the *CP*-conserving one and the 4 Warsaw-basis Wilson coefficients for the *CP*-violating one. The results are shown in their Figs. 15 and 16, respectively.

[3] HAYRAPETYAN 25R measure the $t\overline{t}H$ and tH productions with $H \to b\overline{b}$ decay channel using 138 fb^{-1} of data at E_{cm} = 13 TeV. Two-dimensional likelihood scan of (κ_t, $\tilde{\kappa}_t$) to measure the *CP* structure of the top Yukawa coupling is shown in their Fig. 16, where κ_V = 1. With other channels (SIRUNYAN 20AS, SIRUNYAN 21AE, TUMASYAN 23P), the *CP*-odd fraction f_{CP} and the *CP* mixing angle α are constrain to be $|f_{CP}| < 0.85$ and $\cos\alpha > 0.39$ at 95% CL.

[4] AAD 24AG search for *CP* violation in the decay kinematics and VBF production of the Higgs boson using $H \to ZZ^* \to 4\ell$ decay channel ($\ell = e, \mu$) with 139 fb^{-1} at E_{cm} = 13 TeV. By using the optimal observables, the data constrain six *CP*-odd Wilson coefficients in two effective field theory bases: the Warsaw basis and the Higgs basis. The result is given in their Table 5 and Figs. 7–11. The differential fiducial cross sections for the four optimal observables are measured as shown in their Fig. 13. The VBF fiducial cross sections are given in their Table 6.

[5] AAD 24J measure the *CP* structure of the top Yukawa coupling using 139 fb^{-1} of data at E_{cm} = 13 TeV. The *CP*-mixing angle α for top Yukawa coupling is measured to be $(11^{+52}_{-73})^\circ$ with the top Yukawa coupling strength modifier κ_t. See their Fig. 3. The data disfavour the pure *CP*-odd ($\alpha = 90^\circ$) at 1.2 σ.

[6] AAD 23AK measure the *CP* structure of the τ Yukawa coupling using 139 fb^{-1} of data at E_{cm} = 13 TeV. The *CP*-mixing angle α for τ Yukawa coupling is measured to be $9 \pm 16^\circ$. The data disfavour the pure *CP*-odd ($\alpha = 90^\circ$) at 3.4 σ.

[7] AAD 23AN test *CP* invariance in *H* production via VBF using $H \to \gamma\gamma$ decay channel with 139 fb^{-1} at E_{cm} = 13 TeV. By using the Optimal Observable method, the data constrain parameters describing the strength of the *CP*-odd component in the coupling between Higgs and W/Z in effective field theory bases: $\tilde{d}$ in the HISZ basis and $c_{H\widetilde{W}}$ in the Warsaw basis. The result is -0.010 $\leq \tilde{d} \leq$ 0.040 and -0.15 $\leq c_{H\widetilde{W}} \leq$ 0.67 at 68% CL. See their Table I, which shows the result combined with $H \to \tau\tau$ (AAD 20N): -0.012 $\leq \tilde{d} \leq$ 0.030 at 68% CL.

[8] TUMASYAN 23AJ constraint anomalous couplings of the Higgs to vector bosons and fermions using $pp \to H \to \tau\tau$ at E_{cm} = 13 TeV with 138 fb^{-1} data. The *CP*-violating parameter in gluon-fusion production f_{a3}^{ggH} and the effective mixing angle α^{Hff} are given in their Table VII with $H \to \tau\tau$ and f_{a3}^{ggH} in their Table X with $H \to \tau\tau$ and $H \to 4\ell$. Using the VBF production analysis, the *CP*-violating parameter f_{a3} and the *CP*-conserving parameters f_{a2}, $f_{\Lambda 1}$ and $f_{\Lambda 1}^{Z\gamma}$ are given in their Table VIII with $H \to$

Int. J. Mod. Phys. A 2026.41. Downloaded from www.worldscientific.com by UNIVERSITY OF CALIFORNIA @ BERKELEY on 09/16/26. Reproduction is strictly not permitted, except for Open Access articles.

$\tau\tau$ and Table IX with $H \to \tau\tau$ and $H \to 4\ell$. The *CP*-violating parameter f_{CP}^{Htt} is constrained to be $0.03^{+0.17}_{-0.03}$ using $H \to \tau\tau$, $H \to 4\ell$ and $H \to \gamma\gamma$.

[9] TUMASYAN 23P constrain $\widetilde{\kappa}_t$ from $t\overline{t}H$ and tH decaying $H \to WW^*$ and $H \to \tau\tau$ (multilepton decay mode) with 138 fb^{-1} pp collision data at E_{cm} = 13 TeV. The $\widetilde{\kappa}_t$ is constrained to be $|\widetilde{\kappa}_t| \leq 1.4$ at 95% CL by fixing $\kappa_t = 1$ and other couplings (κ_V etc.) to the SM values, see their Table 6 (see their Fig. 9 for 2-dim contours). The fractional contribution of the *CP*-odd component $|f_{CP}^{Htt}|$ is constrained to (0.24, 0.81) at 68% CL with a best fit value of 0.59. The combination with other $t\overline{t}H$ decaying $H \to \gamma\gamma$ (SIRUNYAN 20AS) and $H \to 4\ell$ (SIRUNYAN 21AE) constraints to be $|\widetilde{\kappa}_t| \leq 1.07$ at 95% CL and $|f_{CP}^{Htt}| < 0.55$ at 68% CL with a best fit value of 0.28.

[10] AAD 22V measure the *CP* properties of the effective Higgs-gluon interaction using gluon fusion $H \to WW^* \to e\nu\mu\nu$ plus two jets with 36.1 fb^{-1} of data at E_{cm} = 13 TeV. The measured tangent of the *CP*-mixing angle tanα is 0.0 ± 0.4 ± 0.3 assuming the standard model HVV couplings. See their Fig. 6.

[11] TUMASYAN 22Y measure the *CP* structure of the τ Yukawa coupling using 137 fb^{-1} of data at E_{cm} = 13 TeV. The *CP*-mixing angle α for τ Yukawa coupling is measured to be $-1 \pm 19^\circ$. The data disfavour the pure *CP*-odd ($\alpha = 90^\circ$) at 3.0 σ.

[12] AAD 20N test *CP* invariance in *H* production via VBF using $H \to \tau\tau$ decay channel with 36.1 fb^{-1} at E_{cm} = 13 TeV. By using the Optimal Observable method, the data constrain a parameter d, which is for the strength of *CP* violation in an effective field theory, to be $-0.090 \leq \widetilde{d} \leq 0.035$ at 68% CL (see their Fig. 6).

[13] AAD 20Z exclude a *CP*-mixing angle α, $|\alpha| > 43^\circ$ at 95% CL, where $\alpha = 0$ represents the Standard Model, in 139 fb^{-1} of data at E_{cm} = 13 TeV. The pure *CP*-odd structure of the top Yukawa coupling ($\alpha = 90^\circ$) is excluded at 3.9 σ.

[14] SIRUNYAN 20AS exclude the pure *CP*-odd structure of the top Yukawa coupling at 3.2 σ using $t\overline{t}H$, $H \to \gamma\gamma$ in 137 fb^{-1} of data at E_{cm} = 13 TeV. The fractional contribution of the *CP*-odd component $f_{CP}^{t\overline{t}H}$ is measured to be 0.00 ± 0.33.

[15] SIRUNYAN 19BL measure the anomalous HVV couplings from on-shell and off-shell production in the 4ℓ final state. Data of 80.2 fb^{-1} at 13 TeV, 19.7 fb^{-1} at 8 TeV, and 5.1 fb^{-1} at 7 TeV are used. See their Tables VI and VII for anomalous HVV couplings of *CP*-violating and *CP*-conserving parameters with on- and off-shells.

[16] SIRUNYAN 19BZ constrain anomalous HVV couplings of the Higgs boson with data of 35.9 fb^{-1} at E_{cm} = 13 TeV using Higgs boson candidates with two jets produced in VBF, ggF, and VH that decay to $\tau\tau$. See their Table 2 and Fig. 10, which show 68% CL and 95% CL intervals. Combining those with the $H \to 4\ell$ (SIRUNYAN 19BL, on-shell scenario), results shown in their Tables 3, 4, and Fig. 11 are obtained. A *CP*-violating parameter is set to be $f_{a3}\cos(\phi_{a3}) = (0.00 \pm 0.27) \times 10^{-3}$ and *CP*-conserving parameters are $f_{a2}\cos(\phi_{a2}) = (0.08^{+1.04}_{-0.21}) \times 10^{-3}$, $f_{\Lambda 1}\cos(\phi_{\Lambda 1}) = (0.00^{+0.53}_{-0.09}) \times 10^{-3}$, and $f_{\Lambda 1}^{Z\gamma}\cos(\phi_{\Lambda 1}^{Z\gamma}) = (0.0^{+1.1}_{-1.3}) \times 10^{-3}$.

[17] AABOUD 18AJ study the tensor structure of the Higgs boson couplings using an effective Lagrangian using 36.1 fb^{-1} of pp collision data at E_{cm} = 13 TeV. Constraints are set on the non-Standard-Model *CP*-even and *CP*-odd couplings to Z bosons and on the *CP*-odd coupling to gluons. See their Figs. 9 and 10, and Tables 10 and 11.

[18] SIRUNYAN 17AM constrain anomalous couplings of the Higgs boson with 5.1 fb^{-1} of pp collisions at E_{cm} = 7 TeV, 19.7 fb^{-1} at E_{cm} = 8 TeV, and 38.6 fb^{-1} at E_{cm} = 13 TeV. See their Table 3 and Fig. 3, which show 68% CL and 95% CL intervals. A *CP* violation parameter f_{a3} is set to be $f_{a3}\cos(\phi_{a3}) = [-0.38, 0.46]$ at 95% CL ($\phi_{a3} = 0$ or π).

[19] AAD 16 study $H \to \gamma\gamma$ with an effective Lagrangian including *CP* even and odd terms in 20.3 fb^{-1} of pp collisions at E_{cm} = 8 TeV. The data is consistent with the expectations for the Higgs boson of the Standard Model. Limits on anomalous couplings are also given.

[20] AAD 16BL study VBF $H \to \tau\tau$ with an effective Lagrangian including a *CP* odd term in 20.3 fb^{-1} of pp collisions at E_{cm} = 8 TeV. The measurement is consistent with the expectation of the Standard Model. The *CP*-mixing parameter $\widetilde{d}$ (a dimensionless coupling $\widetilde{d} = -(m_W^2/\Lambda^2) f_{\widetilde{W}W}$) is constrained to the interval of (−0.11, 0.05) at 68% CL under the assumption of $\widetilde{d} = \widetilde{d}_B$.

[21] KHACHATRYAN 16AB search for anomalous pseudoscalar couplings of the Higgs boson to W and Z with 18.9 fb^{-1} of pp collisions at E_{cm} = 8 TeV. See their Table 5 and Figs 5 and 6 for limits on possible anomalous pseudoscalar coupling parameters.

[22] AAD 15AX compare the $J^{CP} = 0^+$ Standard Model assignment with other J^{CP} hypotheses in 20.3 fb^{-1} of pp collisions at E_{cm} = 8 TeV, using the process $H \to WW^* \to e\nu\mu\nu$. 2^+ hypotheses are excluded at 84.5–99.4%CL, 0^- at 96.5%CL, 0^+ (field strength coupling) at 70.8%CL. See their Fig. 19 for limits on possible *CP* mixture parameters.

[23] AAD 15CI compare the $J^{CP} = 0^+$ Standard Model assignment with other J^{CP} hypotheses in 4.5 fb^{-1} of pp collisions at E_{cm} = 7 TeV and 20.3 fb^{-1} at E_{cm} = 8 TeV, using the processes $H \to ZZ^* \to 4\ell$. $H \to \gamma\gamma$ and combine with AAD 15AX data. 0^+ (field strength coupling), 0^- and several 2^+ hypotheses are excluded at more than 99.9% CL. See their Tables 7–9 for limits on possible *CP* mixture parameters.

[24] AALTONEN 15 combine AALTONEN 15B and ABAZOV 14F data. An upper limit of 0.36 of the Standard Model production rate at 95% CL is obtained both for a 0^- and a 2^+ state. Assuming the SM event rate, the $J^{CP} = 0^-$ (2^+) hypothesis is excluded at the 5.0σ (4.9σ) level.

[25] AALTONEN 15B compare the $J^{CP} = 0^+$ Standard Model assignment with other J^{CP} hypotheses in 9.45 fb^{-1} of $p\overline{p}$ collisions at E_{cm} = 1.96 TeV, using the processes $ZH \to \ell\ell b\overline{b}$, $WH \to \ell\nu b\overline{b}$, and $ZH \to \nu\nu b\overline{b}$. Bounds on the production rates of 0^- and 2^+ (graviton-like) states are set, see their tables II and III.

[26] KHACHATRYAN 15Y compare the $J^{CP} = 0^+$ Standard Model assignment with other J^{CP} hypotheses in up to 5.1 fb^{-1} of pp collisions at E_{cm} = 7 TeV and up to 19.7 fb^{-1} at E_{cm} = 8 TeV, using the processes $H \to 4\ell$, $H \to WW^*$, and $H \to \gamma\gamma$. 0^- is excluded at 99.98% CL, and several 2^+ hypotheses are excluded at more than 99% CL. Spin 1 models are excluded at more than 99.999% CL in ZZ^* and WW^* modes. Limits on anomalous couplings and several cross section fractions, treating the case of *CP*-mixed states, are also given.

[27] ABAZOV 14F compare the $J^{CP} = 0^+$ Standard Model assignment with $J^{CP} = 0^-$ and 2^+ (graviton-like coupling) hypotheses in up to 9.7 fb^{-1} of $p\overline{p}$ collisions at E_{cm} = 1.96 TeV. They use kinematic correlations between the decay products of the vector boson and the Higgs boson in the final states $ZH \to \ell\ell b\overline{b}$, $WH \to \ell\nu b\overline{b}$, and $ZH \to \nu\nu b\overline{b}$. The 0^- (2^+) hypothesis is excluded at 97.6% CL (99.0% CL). In order to treat the case of a possible mixture of a 0^+ state with another J^{CP} state, the cross section fractions $f_X = \sigma_X/(\sigma_{0^+} + \sigma_X)$ are considered, where $X = 0^-, 2^+$. Values for f_{0^-} (f_{2^+}) above 0.80 (0.67) are excluded at 95% CL under the assumption that the total cross section is that of the SM Higgs boson.

[28] CHATRCHYAN 14AA compare the $J^{CP} = 0^+$ Standard Model assignment with various J^{CP} hypotheses in 5.1 fb^{-1} of pp collisions at E_{cm} = 7 TeV and 19.7 fb^{-1} at E_{cm} = 8 TeV. $J^{CP} = 0^-$ and $1^\pm$ hypotheses are excluded at 99% CL, and several $J = 2$ hypotheses are excluded at 95% CL. In order to treat the case of a possible mixture of a 0^+ state with another J^{CP} state, the cross section fraction $f_{a3} = |a_3|^2 \sigma_3 / (|a_1|^2 \sigma_1 + |a_2|^2 \sigma_2 + |a_3|^2 \sigma_3)$ is considered, where the case $a_3 = 1$, $a_1 = a_2 = 0$ corresponds to a pure *CP*-odd state. Assuming $a_2 = 0$, a value for f_{a3} above 0.51 is excluded at 95% CL.

[29] CHATRCHYAN 14G compare the $J^{CP} = 0^+$ Standard Model assignment with $J^{CP} = 0^-$ and 2^+ (graviton-like coupling) hypotheses in 4.9 fb^{-1} of pp collisions at E_{cm} = 7 TeV and 19.4 fb^{-1} at E_{cm} = 8 TeV. Varying the fraction of the production of the 2^+ state via gg and $q\overline{q}$, 2^+ hypotheses are disfavored at CL between 83.7 and 99.8%. The 0^- hypothesis is disfavored against 0^+ at the 65.3% CL.

[30] KHACHATRYAN 14P compare the $J^{CP} = 0^+$ Standard Model assignment with a 2^+ (graviton-like coupling) hypothesis in 5.1 fb^{-1} of pp collisions at E_{cm} = 7 TeV and 19.7 fb^{-1} at E_{cm} = 8 TeV. Varying the fraction of the production of the 2^+ state via gg and $q\overline{q}$, 2^+ hypotheses are disfavored at CL between 71 and 94%.

[31] AAD 13AJ compare the spin 0, *CP*-even hypothesis with specific alternative hypotheses of spin 0, *CP*-odd, spin 1, *CP*-even and *CP*-odd, and spin 2, *CP*-even models using the Higgs boson decays $H \to \gamma\gamma$, $H \to ZZ^* \to 4\ell$ and $H \to WW^* \to \ell\nu\ell\nu$ and combinations thereof. The data are compatible with the spin 0, *CP*-even hypothesis, while all other tested hypotheses are excluded at confidence levels above 97.8%.

[32] CHATRCHYAN 13J study angular distributions of the lepton pairs in the ZZ^* channel where both Z bosons decay to e or μ pairs. Under the assumption that the observed particle has spin 0, the data are found to be consistent with the pure *CP*-even hypothesis, while the pure *CP*-odd hypothesis is disfavored.

H DECAY WIDTH

The total decay width for a light Higgs boson with a mass in the observed range is not expected to be directly observable at the LHC. For the case of the Standard Model the prediction for the total width is about 4 MeV, which is three orders of magnitude smaller than the experimental mass resolution. There is no indication from the results observed so far that the natural width is broadened by new physics effects to such an extent that it could be directly observable. Furthermore, as all LHC Higgs channels rely on the identification of Higgs decay products, the total Higgs width cannot be measured indirectly without additional assumptions. The different dependence of on-peak and off-peak contributions on the total width in Higgs decays to ZZ^* and interference effects between signal and background in Higgs decays to $\gamma\gamma$ can provide additional information in this context. Constraints on the total width from the combination of on-peak and off-peak contributions in Higgs decays to ZZ^* rely on the assumption of equal on- and off-shell effective couplings. Without an experimental determination of the total width or further theoretical assumptions, only ratios of couplings can be determined at the LHC rather than absolute values of couplings.

VALUE (MeV)	CL%	DOCUMENT ID		TECN	COMMENT
$3.0^{+1.5}_{-0.7}$ OUR AVERAGE					
$4.3^{+2.7}_{-1.9}$		[1] AAD	25AQ	ATLS	pp, 13 TeV, $ZZ^*/ZZ \to 4\ell$, $ZZ \to 2\ell 2\nu$
$0.9^{+3.4}_{-0.9}$		[2] AAD	25AV	ATLS	pp, 13 TeV, $WW^{(*)} \to 2\ell 2\nu$
$3.0^{+2.0}_{-1.5}$		[3] HAYRAPETY...	25L	CMS	pp, 13 TeV, $ZZ^*/ZZ \to 4\ell$, $ZZ \to 2\ell 2\nu$
• • • We do not use the following data for averages, fits, limits, etc. • • •					
< 160	95	[4] AAD	25E	ATLS	pp, 13 TeV, on-shell Higgs and $t\overline{t}t\overline{t}$
< 330	95	[5] HAYRAPETY...	25L	CMS	pp, 13 TeV, $ZZ^* \to 4\ell$
$2.9^{+2.3}_{-1.7}$		[6] HAYRAPETY...	25L	CMS	pp, 13 TeV, $ZZ^* \to 4\ell$
$4.4^{+3.0}_{-2.2}$		[7] AAD	23BR	ATLS	pp, 13 TeV, $ZZ^*/ZZ \to 4\ell$, $ZZ \to 2\ell 2\nu$
$3.2^{+2.4}_{-1.7}$		[8] TUMASYAN	22AM	CMS	pp, 13 TeV, $ZZ^*/ZZ \to 4\ell$, $ZZ \to 2\ell 2\nu$
$3.2^{+2.8}_{-2.2}$		[9] SIRUNYAN	19BL	CMS	pp, 7, 8, 13 TeV, $ZZ^*/ZZ \to 4\ell$
< 14.4	95	[10] AABOUD	18BP	ATLS	pp, 13 TeV, $ZZ \to 4\ell$, $2\ell 2\nu$
<1100	95	[11] SIRUNYAN	17AV	CMS	pp, 13 TeV, $ZZ^* \to 4\ell$
< 26	95	[12] KHACHATRY...	16BA	CMS	pp, 7, 8 TeV, $WW^{(*)}$
< 13	95	[13] KHACHATRY...	16BA	CMS	pp, 7, 8 TeV, $ZZ^{(*)}$, $WW^{(*)}$
< 22.7	95	[14] AAD	15BE	ATLS	pp, 8 TeV, $ZZ^{(*)}$, $WW^{(*)}$
<1700	95	[15] KHACHATRY...	15AM	CMS	pp, 7, 8 TeV
> 3.5×10^{-9}	95	[16] KHACHATRY...	15BA	CMS	pp, 7, 8 TeV, flight distance
< 46	95	[17] KHACHATRY...	15BA	CMS	pp, 7, 8 TeV, $ZZ^{(*)} \to 4\ell$

Int. J. Mod. Phys. A 2026.41. Downloaded from www.worldscientific.com by UNIVERSITY OF CALIFORNIA @ BERKELEY on 09/16/26. Re-use and distribution is strictly not permitted, except for Open Access articles.

<5000	95	[18] AAD	14W	ATLAS	pp, 7, 8 TeV, $\gamma\gamma$
<2600	95	[18] AAD	14W	ATLAS	pp, 7, 8 TeV, $ZZ^* \to 4\ell$
<3400	95	[19] CHATRCHYAN	14AA	CMS	pp, 7, 8 TeV, $ZZ^* \to 4\ell$
< 22	95	[20] KHACHATRY...	14D	CMS	pp, 7, 8 TeV, $ZZ^{(*)}$
<2400	95	[21] KHACHATRY...	14P	CMS	pp, 7, 8 TeV, $\gamma\gamma$

[1] AAD 25AQ use 140 fb^{-1} at E_{cm} = 13 TeV. The off-shell Higgs boson production in the $ZZ \to 4\ell$ ($\ell = e, \mu$) decay channel is combined with the on-shell production in the $ZZ^* \to 4\ell$ (AAD 20AQ) decay channel and the off-shell production in the $ZZ \to 2\ell 2\nu$ decay channel (AAD 23BR, AAD 25AP) to measure the total width assuming the same on-shell and off-shell coupling modifiers for gluon-fusion and for gauge-boson ($\kappa^2_{g,\text{on-shell}}\,\kappa^2_{V,\text{on-shell}} = \kappa^4_{V,\text{on-shell}} = \kappa^2_{g,\text{off-shell}}\,\kappa^2_{V,\text{off-shell}} = \kappa^4_{V,\text{off-shell}}$). $R_{gg} = \kappa^2_{g,\text{on-shell}}/\kappa^2_{g,\text{off-shell}}$ and $R_{VV} = \kappa^2_{V,\text{on-shell}}/\kappa^2_{V,\text{off-shell}}$ are measured to be $1.19^{+0.89}_{-0.66}$ and $0.95^{+0.44}_{-0.35}$, respectively. Using AAD 25AQ and AAD 23BR, $\kappa_{g,\text{off-shell}}$ and $\kappa_{V,\text{off-shell}}$ are measured to be $1.09^{+0.39}_{-0.35}$ and $0.99^{+0.16}_{-0.19}$, respectively. The quoted errors are values at 68%CL.

[2] AAD 25AV measure the total width Γ_H from off-shell $H^* \to WW \to 2\ell 2\nu$ and on-shell $H \to WW^* \to 2\ell 2\nu$ with data of 140 fb^{-1} pp collisions at E_{cm} = 13 TeV, assuming the off- and on-shell coupling modifiers are the same for both ggF and EW production modes. The quoted value corresponds to Γ_H < 13.1 MeV at 95% CL. The off-shell Higgs signal strength $\mu_{\text{off-shell}}$ is measured to be $0.3^{+0.9}_{-0.3}$ corresponding $\mu_{\text{off-shell}}$ < 3.4 at 95% CL. The two off-shell signal strengths for ggF and EW production modes ($\mu^{\text{ggF}}_{\text{off-shell}}$, $\mu^{\text{EW}}_{\text{off-shell}}$) are measured to be $\mu^{\text{ggF}}_{\text{off-shell}} = 0.2^{+1.3}_{-0.2}$ and $\mu^{\text{EW}}_{\text{off-shell}} = 0.4^{+3.4}_{-0.4}$.

[3] HAYRAPETYAN 25L use 138 fb^{-1} at E_{cm} = 13 TeV. The on- and off-shell Higgs boson production in the $ZZ \to 4\ell$ ($\ell = e, \mu$) decay channel is combined with the off-shell Higgs boson production in the $ZZ \to 2\ell 2\nu$ (TUMASYAN 22AM) decay channel to measure the total width. The off-shell Higgs signal strength is measured to be $0.67^{+0.42}_{-0.32}$. The scenario of no off-shell contribution is excluded at 3.8 σ.

[4] AAD 25E constrain the total width using on-shell Higgs measurements and the four top quarks production with 13 TeV data. The tree-level Higgs-top Yukawa coupling is assumed to be the same for on-shell and off-shell Higgs boson production processes. Another assumption is that no BSM contributions affect the $t\bar{t}t\bar{t}$ production. The quoted value is obtained by assuming the loop-induced ggF, $H \to \gamma\gamma$, and $H \to Z\gamma$ rates can be modeled as a function of κ_t and other SM couplings. Otherwise, Γ_H < 450 MeV is obtained at 95% CL. Two-dimensional likelihood scan of ($\Gamma_H/\Gamma_H^{\text{SM}}$, κ_t) is shown in their Fig. 3.

[5] HAYRAPETYAN 25L obtain an upper limit on the width from the on-shell $H \to ZZ^* \to 4\ell$ ($\ell = e, \mu$) decays. Data of 138 fb^{-1} pp collisions at E_{cm} = 13 TeV is used.

[6] HAYRAPETYAN 25L use 138 fb^{-1} at E_{cm} = 13 TeV. The on- and off-shell Higgs boson production in the $ZZ \to 4\ell$ ($\ell = e, \mu$) decay channel is used assuming that no new particles affect the gluon fusion production. The scenario of no off-shell contribution is excluded at 3.0 σ.

[7] AAD 23BR use 139 fb^{-1} at E_{cm} = 13 TeV. The off-shell Higgs boson production in the $ZZ \to 4\ell$ and $ZZ \to 2\ell 2\nu$ decay channels and the on-shell production in the $ZZ^* \to 4\ell$ ($\ell = e, \mu$, AAD 20AQ) decay channels are used to measure the total width. The off-shell Higgs signal strength is measured to be $1.1^{+0.7}_{-0.6}$ assuming the same on-shell and off-shell coupling modifiers are used individually for gluon-fusion and for gauge-boson modes. The scenario of no off-shell contribution is excluded at 3.3 σ. Combining with the on-shell signal strength measurement, the total width normalized to its SM expectation Γ_H/Γ_H^{SM} is measured to be $1.1^{+0.7}_{-0.5}$ assuming the same on-shell and off-shell coupling modifiers are used individually for gluon-fusion and for gauge-boson modes. The observed upper limit on the total width is 10.1 MeV at 95% CL. See their Fig. 7. See corrected width values in their erratum AAD 25AP.

[8] TUMASYAN 22AM use up to 140 fb^{-1} at E_{cm} = 13 TeV. The off-shell Higgs boson production in the $ZZ \to 4\ell$ and $ZZ \to 2\ell 2\nu$ decay channels and the on-shell production in the $ZZ^* \to 4\ell$ ($\ell = e, \mu$) decay channels are used to measure the total width. The off-shell Higgs signal strength is measured to be $0.62^{+0.68}_{-0.45}$ without the constraint on the ratio of the off-shell signal strengths for gluon-fusion and gauge-boson modes. The scenario of no off-shell contribution is excluded at 3.6 σ. The results are shown in their Table 1 with other constraint scenarios and the decay widths assuming the same coupling modifiers for on- and off-shell couplings (g_p and g_d in their notation). The measurement of anomalous HVV couplings is shown in their Extended Data Table 1 and Fig. 8.

[9] SIRUNYAN 19BL measure the width and anomalous HVV couplings from on-shell and off-shell production in the 4ℓ final state. Data of 80.2 fb^{-1} at 13 TeV, 19.7 fb^{-1} at 8 TeV, and 5.1 fb^{-1} at 7 TeV are used. The total width for the SM-like couplings is measured to be also [0.08, 9.16] MeV with 95% CL, assuming SM-like couplings for on- and off-shells (see their Table VIII). Constraints on the total width for anomalous HVV interaction cases are found in their Table IX. See their Table X for the Higgs boson signal strength in the off-shell region.

[10] AABOUD 18BP use 36.1 fb^{-1} at E_{cm} = 13 TeV. An observed upper limit on the off-shell Higgs signal strength of 3.8 is obtained at 95% CL using off-shell Higgs boson production in the $ZZ \to 4\ell$ and $ZZ \to 2\ell 2\nu$ decay channels ($\ell = e, \mu$). Combining with the on-shell signal strength measurements, the quoted upper limit on the Higgs boson total width is obtained, assuming the ratios of the relevant Higgs-boson couplings to the SM predictions are constant with energy from on-shell production to the high-mass range.

[11] SIRUNYAN 17AV obtain an upper limit on the width from the $m_{4\ell}$ distribution in $ZZ^* \to 4\ell$ ($\ell = e, \mu$) decays. Data of 35.9 fb^{-1} pp collisions at E_{cm} = 13 TeV is used. The expected limit is 1.60 GeV.

[12] KHACHATRYAN 16BA derive constraints on the total width from comparing $WW^{(*)}$ production via on-shell and off-shell H using 4.9 fb^{-1} of pp collisions at E_{cm} = 7 TeV and 19.4 fb^{-1} at 8 TeV.

[13] KHACHATRYAN 16BA combine the $WW^{(*)}$ result with $ZZ^{(*)}$ results of KHACHATRYAN 15BA and KHACHATRYAN 14D.

[14] AAD 15BE derive constraints on the total width from comparing $ZZ^{(*)}$ and $WW^{(*)}$ production via on-shell and off-shell H using 20.3 fb^{-1} of pp collisions at E_{cm} = 8 TeV. The K factor for the background processes is assumed to be equal to that for the signal.

[15] KHACHATRYAN 15AM combine $\gamma\gamma$ and $ZZ^* \to 4\ell$ results. The expected limit is 2.3 GeV.

[16] KHACHATRYAN 15BA derive a lower limit on the total width from an upper limit on the decay flight distance τ < 1.9×10^{-13} s. 5.1 fb^{-1} of pp collisions at E_{cm} = 7 TeV and 19.7 fb^{-1} at 8 TeV are used.

[17] KHACHATRYAN 15BA derive constraints on the total width from comparing $ZZ^{(*)}$ production via on-shell and off-shell H with an unconstrained anomalous coupling. 4ℓ final states in 5.1 fb^{-1} of pp collisions at E_{cm} = 7 TeV and 19.7 fb^{-1} at E_{cm} = 8 TeV are used.

[18] AAD 14W use 4.5 fb^{-1} of pp collisions at E_{cm} = 7 TeV and 20.3 fb^{-1} at 8 TeV. The expected limit is 6.2 GeV.

[19] CHATRCHYAN 14AA use 5.1 fb^{-1} of pp collisions at E_{cm} = 7 TeV and 19.7 fb^{-1} at E_{cm} = 8 TeV. The expected limit is 2.8 GeV.

[20] KHACHATRYAN 14D derive constraints on the total width from comparing $ZZ^{(*)}$ production via on-shell and off-shell H. 4ℓ and $\ell\ell\nu\nu$ final states in 5.1 fb^{-1} of pp collisions at E_{cm} = 7 TeV and 19.7 fb^{-1} at E_{cm} = 8 TeV are used.

[21] KHACHATRYAN 14P use 5.1 fb^{-1} of pp collisions at E_{cm} = 7 TeV and 19.7 fb^{-1} at E_{cm} = 8 TeV. The expected limit is 3.1 GeV.

H DECAY MODES

	Mode		Fraction (Γ_i/Γ)	Confidence level
Γ_1	WW^*		(25.7 ±2.5) %	
Γ_2	ZZ^*		(2.80±0.30) %	
Γ_3	$\gamma\gamma$		(2.50±0.20) $\times 10^{-3}$	
Γ_4	$b\bar{b}$		(53 ±8) %	
Γ_5	e^+e^-		< 3.0 $\times 10^{-4}$	95%
Γ_6	$\mu^+\mu^-$		(3.0 ±0.9) $\times 10^{-4}$	
Γ_7	$\tau^+\tau^-$		($6.0^{+0.8}_{-0.7}$) %	
Γ_8	$Z\gamma$		(3.4 ±1.1) $\times 10^{-3}$	
Γ_9	$Z\rho(770)$		< 1.21 %	95%
Γ_{10}	$Z\phi(1020)$		< 3.6 $\times 10^{-3}$	95%
Γ_{11}	$Z\eta_c$			
Γ_{12}	ZJ/ψ		< 1.9 $\times 10^{-3}$	95%
Γ_{13}	$Z\psi(2S)$		< 6.6 $\times 10^{-3}$	95%
Γ_{14}	$J/\psi\gamma$		< 2.0 $\times 10^{-4}$	95%
Γ_{15}	$J/\psi J/\psi$		< 3.8 $\times 10^{-4}$	95%
Γ_{16}	$\psi(2S)\gamma$		< 9.9 $\times 10^{-4}$	95%
Γ_{17}	$\psi(2S)J/\psi$		< 2.1 $\times 10^{-3}$	95%
Γ_{18}	$\psi(2S)\psi(2S)$		< 3.0 $\times 10^{-3}$	95%
Γ_{19}	$\Upsilon(1S)\gamma$		< 2.5 $\times 10^{-4}$	95%
Γ_{20}	$\Upsilon(1S)\Upsilon(1S)$		< 1.7 $\times 10^{-3}$	95%
Γ_{21}	$\Upsilon(2S)\gamma$		< 4.2 $\times 10^{-4}$	95%
Γ_{22}	$\Upsilon(3S)\gamma$		< 3.4 $\times 10^{-4}$	95%
Γ_{23}	$\Upsilon(nS)\Upsilon(mS)$		< 3.5 $\times 10^{-4}$	95%
Γ_{24}	$D^*\gamma$		< 1.0 $\times 10^{-3}$	95%
Γ_{25}	$\rho(770)\gamma$		< 3.7 $\times 10^{-4}$	95%
Γ_{26}	$\omega(782)\gamma$		< 5.5 $\times 10^{-4}$	95%
Γ_{27}	$K^*(892)\gamma$		< 2.2 $\times 10^{-4}$	95%
Γ_{28}	$\phi(1020)\gamma$		< 3.0 $\times 10^{-4}$	95%
Γ_{29}	$e\mu$	*LF*	< 4.4 $\times 10^{-5}$	95%
Γ_{30}	$e\tau$	*LF*	< 2.0 $\times 10^{-3}$	95%
Γ_{31}	$\mu\tau$	*LF*	< 1.5 $\times 10^{-3}$	95%
Γ_{32}	invisible		< 10.7 %	95%
Γ_{33}	γ invisible		< 1.3 %	95%

H BRANCHING RATIOS

$\Gamma(WW^*)/\Gamma_{\text{total}}$ — Γ_1/Γ

VALUE	DOCUMENT ID		TECN	COMMENT
$0.257^{+0.026}_{-0.024}$	[1] ATLAS	22	ATLS	pp, 13 TeV

[1] ATLAS 22 report combined results (see their Extended Data Table 1) using up to 139 fb^{-1} of data at E_{cm} = 13 TeV, assuming m_H = 125.09 GeV. SM values for the production cross-sections are assumed. See their Fig. 2b.

$\Gamma(ZZ^*)/\Gamma_{\text{total}}$ — Γ_2/Γ

VALUE	DOCUMENT ID		TECN	COMMENT
0.028±0.003	[1] ATLAS	22	ATLS	pp, 13 TeV

[1] ATLAS 22 report combined results (see their Extended Data Table 1) using up to 139 fb^{-1} of data at E_{cm} = 13 TeV, assuming m_H = 125.09 GeV. SM values for the production cross-sections are assumed. See their Fig. 2b.

$\Gamma(\gamma\gamma)/\Gamma_{\text{total}}$ — Γ_3/Γ

VALUE	DOCUMENT ID		TECN	COMMENT
0.0025±0.0002	[1] ATLAS	22	ATLS	pp, 13 TeV

[1] ATLAS 22 report combined results (see their Extended Data Table 1) using up to 139 fb^{-1} of data at E_{cm} = 13 TeV, assuming m_H = 125.09 GeV. SM values for the production cross-sections are assumed. See their Fig. 2b.

$\Gamma(b\bar{b})/\Gamma_{\text{total}}$ — Γ_4/Γ

VALUE	DOCUMENT ID		TECN	COMMENT
0.53±0.08	[1] ATLAS	22	ATLS	pp, 13 TeV

[1] ATLAS 22 report combined results (see their Extended Data Table 1) using up to 139 fb^{-1} of data at E_{cm} = 13 TeV, assuming m_H = 125.09 GeV. SM values for the production cross-sections are assumed. See their Fig. 2b.

$\Gamma(e^+e^-)/\Gamma_{total}$ — Γ_5/Γ

VALUE	CL%	DOCUMENT ID		TECN	COMMENT
<3.0 × 10^{-4}	95	[1] TUMASYAN	23AU	CMS	pp, 13 TeV
• • • We do not use the following data for averages, fits, limits, etc. • • •					
<3.6 × 10^{-4}	95	[2] AAD	20F	ATLS	pp, 13 TeV
<1.9 × 10^{-3}	95	[3] KHACHATRY...	15H	CMS	pp, 7, 8 TeV

[1] TUMASYAN 23AU use 138 fb^{-1} of pp collisions at E_{cm} = 13 TeV.
[2] AAD 20F use 139 fb^{-1} of pp collisions at E_{cm} = 13 TeV. The best-fit value of the $H \to ee$ branching fraction is (0.0 ± 1.7 ± 0.6) × 10^{-4} for m_H = 125 GeV.
[3] KHACHATRYAN 15H use 5.0 fb^{-1} of pp collisions at E_{cm} = 7 TeV and 19.7 fb^{-1} at 8 TeV.

$\Gamma(\mu^+\mu^-)/\Gamma_{total}$ — Γ_6/Γ

VALUE (units 10^{-4})	DOCUMENT ID		TECN	COMMENT
3.0±0.9	[1] AAD	25AR	ATLS	pp, 13, 13.6 TeV
• • • We do not use the following data for averages, fits, limits, etc. • • •				
2.6±1.3	[2] ATLAS	22	ATLS	pp, 13 TeV

[1] AAD 25AR report results using 140 fb^{-1} of data at E_{cm} = 13 TeV and 165 fb^{-1} of data at E_{cm} = 13.6 TeV assuming m_H = 125.09 GeV and SM values for the Higgs-boson production cross sections.
[2] ATLAS 22 report combined results (see their Extended Data Table 1) using up to 139 fb^{-1} of data at E_{cm} = 13 TeV, assuming m_H = 125.09 GeV. SM values for the production cross-sections are assumed. See their Fig. 2b.

$\Gamma(\tau^+\tau^-)/\Gamma_{total}$ — Γ_7/Γ

VALUE	DOCUMENT ID		TECN	COMMENT
0.060$^{+0.008}_{-0.007}$	[1] ATLAS	22	ATLS	pp, 13 TeV

[1] ATLAS 22 report combined results (see their Extended Data Table 1) using up to 139 fb^{-1} of data at E_{cm} = 13 TeV, assuming m_H = 125.09 GeV. SM values for the production cross-sections are assumed. See their Fig. 2b.

$\Gamma(Z\gamma)/\Gamma_{total}$ — Γ_8/Γ

VALUE (units 10^{-3})	DOCUMENT ID		TECN	COMMENT
3.4±1.1	[1] AAD	24D	LHC	pp, 13 TeV
• • • We do not use the following data for averages, fits, limits, etc. • • •				
3.2±1.5	[2] ATLAS	22	ATLS	pp, 13 TeV

[1] AAD 24D report combined results of ATLAS (AAD 20AG) and CMS (TUMASYAN 23F). SM values for the production cross-sections are assumed.
[2] ATLAS 22 report combined results (see their Extended Data Table 1) using up to 139 fb^{-1} of data at E_{cm} = 13 TeV, assuming m_H = 125.09 GeV. SM values for the production cross-sections are assumed. See their Fig. 2b.

$\Gamma(Z\rho(770))/\Gamma_{total}$ — Γ_9/Γ

VALUE	CL%	DOCUMENT ID		TECN	COMMENT
<1.21 × 10^{-2}	95	[1] SIRUNYAN	20BK	CMS	pp, 13 TeV

[1] SIRUNYAN 20BK search for $H \to Z\rho$, $Z \to e^+e^-/\mu^+\mu^-$, $\rho \to \pi^+\pi^-$ with 137 fb^{-1} of pp collision data at E_{cm} = 13 TeV. The quoted branching fraction is for the unpolarized decay. See their Table 3 for different polarizations.

$\Gamma(Z\phi(1020))/\Gamma_{total}$ — Γ_{10}/Γ

VALUE	CL%	DOCUMENT ID		TECN	COMMENT
<3.6 × 10^{-3}	95	[1] SIRUNYAN	20BK	CMS	pp, 13 TeV

[1] SIRUNYAN 20BK search for $H \to Z\phi$, $Z \to e^+e^-/\mu^+\mu^-$, $\phi \to K^+K^-$ with 137 fb^{-1} of pp collision data at E_{cm} = 13 TeV. The quoted branching fraction is for the unpolarized decay. See their Table 4 for different polarizations.

$\Gamma(Z\eta_c)/\Gamma_{total}$ — Γ_{11}/Γ

VALUE	DOCUMENT ID		TECN	COMMENT
• • • We do not use the following data for averages, fits, limits, etc. • • •				
	[1] AAD	25AT	ATLS	pp, 13 TeV
	[2] AAD	20AE	ATLS	pp, 13 TeV

[1] AAD 25AT search for $H \to Z\eta_c$ with two-leptons ($e^+e^-/\mu^+\mu^-$) plus jet events using 140 fb^{-1} of pp collision data at E_{cm} = 13 TeV. The branching fraction B($H \to Z\eta_c$) > 1.2 is excluded at 95% CL.
[2] AAD 20AE search for $H \to Z\eta_c$ with two-leptons ($e^+e^-/\mu^+\mu^-$) plus jet events using 139 fb^{-1} of pp collision data at E_{cm} = 13 TeV. The upper limit of $\sigma(pp \to H)$·B($H \to Z\eta_c$) is 110 pb at 95% CL.

$\Gamma(ZJ/\psi)/\Gamma_{total}$ — Γ_{12}/Γ

VALUE	CL%	DOCUMENT ID		TECN	COMMENT
<1.9 × 10^{-3}	95	[1] TUMASYAN	23C	CMS	pp, 13 TeV
• • • We do not use the following data for averages, fits, limits, etc. • • •					
		[2] AAD	25AT	ATLS	pp, 13 TeV
		[3] AAD	20AE	ATLS	pp, 13 TeV

[1] TUMASYAN 23C search for $H \to ZJ/\psi$, $Z \to e^+e^-$ or $\mu^+\mu^-$, $J/\psi \to \mu^+\mu^-$ with 138 fb^{-1} of pp collision data at E_{cm} = 13 TeV. The quoted value is for the Higgs decays for longitudinally polarized mesons. See their Table 1 for other cases.
[2] AAD 25AT search for $H \to ZJ/\psi$ with two-leptons ($e^+e^-/\mu^+\mu^-$) plus jet events using 140 fb^{-1} of pp collision data at E_{cm} = 13 TeV. The branching fraction B($H \to ZJ/\psi$) > 1.4 is excluded at 95% CL.
[3] AAD 20AE search for $H \to ZJ/\psi$ with two-leptons ($e^+e^-/\mu^+\mu^-$) plus jet events using 139 fb^{-1} of pp collision data at E_{cm} = 13 TeV. The upper limit of $\sigma(pp \to H)$·B($H \to ZJ/\psi$) is 100 pb at 95% CL.

$\Gamma(Z\psi(2S))/\Gamma_{total}$ — Γ_{13}/Γ

VALUE	CL%	DOCUMENT ID		TECN	COMMENT
<6.6 × 10^{-3}	95	[1] TUMASYAN	23C	CMS	pp, 13 TeV

[1] TUMASYAN 23C search for $H \to Z\psi(2S)$, $Z \to e^+e^-$ or $\mu^+\mu^-$, $\psi(2S) \to \mu^+\mu^-$ with 138 fb^{-1} of pp collision data at E_{cm} = 13 TeV. The quoted value is for the Higgs decays for longitudinally polarized mesons. See their Table 1 for other cases.

$\Gamma(J/\psi\gamma)/\Gamma_{total}$ — Γ_{14}/Γ

VALUE	CL%	DOCUMENT ID		TECN	COMMENT
<2.0 × 10^{-4}	95	[1] AAD	23CD	ATLS	13 TeV, 138 fb^{-1}
• • • We do not use the following data for averages, fits, limits, etc. • • •					
<2.6 × 10^{-4}	95	[2] HAYRAPETY...	25H	CMS	13 TeV, 123 fb^{-1}
<7.6 × 10^{-4}	95	[3] SIRUNYAN	19AJ	CMS	13 TeV, 35.9 fb^{-1}
<3.5 × 10^{-4}	95	[4] AABOUD	18BL	ATLS	13 TeV, 36.1 fb^{-1}
<1.5 × 10^{-3}	95	[5] KHACHATRY...	16B	CMS	8 TeV
<1.5 × 10^{-3}	95	[6] AAD	15I	ATLS	8 TeV

[1] AAD 23CD search for $H \to J/\psi\gamma$, $J/\psi \to \mu^+\mu^-$ with 138 fb^{-1} of pp collision data at E_{cm} = 13 TeV. SM values for the production cross-sections are assumed.
[2] HAYRAPETYAN 25H search for $H \to J/\psi\gamma$, $J/\psi \to \mu^+\mu^-$ with 123 fb^{-1} of pp collision data at E_{cm} = 13 TeV. SM values for the production cross-sections are assumed. See their Table 4 and Fig. 5.
[3] SIRUNYAN 19AJ search for $H \to J/\psi\gamma$, $J/\psi \to \mu^+\mu^-$ with 35.9 fb^{-1} of pp collision data at E_{cm} = 13 TeV. The upper limit corresponds to 260 times the SM prediction and by combining the KHACHATRYAN 16B, it is 220 times the SM prediction.
[4] AABOUD 18BL search for $H \to J/\psi\gamma$, $J/\psi \to \mu^+\mu^-$ with 36.1 fb^{-1} of pp collision data at E_{cm} = 13 TeV.
[5] KHACHATRYAN 16B use 19.7 fb^{-1} of pp collision data at 8 TeV.
[6] AAD 15I use 19.7 fb^{-1} of pp collision data at 8 TeV.

$\Gamma(J/\psi J/\psi)/\Gamma_{total}$ — Γ_{15}/Γ

VALUE	CL%	DOCUMENT ID		TECN	COMMENT
<3.8 × 10^{-4}	95	[1] TUMASYAN	23C	CMS	pp, 13 TeV
• • • We do not use the following data for averages, fits, limits, etc. • • •					
<1.8 × 10^{-3}	95	[2] SIRUNYAN	19BR	CMS	pp at 13 TeV

[1] TUMASYAN 23C search for $H \to J/\psi J/\psi$, $J/\psi \to \mu^+\mu^-$ with 138 fb^{-1} of pp collision data at E_{cm} = 13 TeV. The quoted value is for the Higgs decays for longitudinally polarized mesons. See their Table 1 for other cases.
[2] SIRUNYAN 19BR search for $H \to J/\psi J/\psi$, $J/\psi \to \mu^+\mu^-$ with 37.5 fb^{-1} of pp collision data at E_{cm} = 13 TeV. J/ψs from the Higgs decay are assumed to be unpolarized. For fully longitudinal (transverse) polarized J/ψs, limits change by −22% (+10%).

$\Gamma(\psi(2S)\gamma)/\Gamma_{total}$ — Γ_{16}/Γ

VALUE	CL%	DOCUMENT ID		TECN	COMMENT
<9.9 × 10^{-4}	95	[1] HAYRAPETY...	25H	CMS	13 TeV, 123 fb^{-1}
• • • We do not use the following data for averages, fits, limits, etc. • • •					
<1.05 × 10^{-3}	95	[2] AAD	23CD	ATLS	13 TeV, 138 fb^{-1}
<2.0 × 10^{-3}	95	[3] AABOUD	18BL	ATLS	13 TeV, 36.1 fb^{-1}

[1] HAYRAPETYAN 25H search for $H \to \psi(2S)\gamma$, $\psi(2S) \to \mu^+\mu^-$ with 123 fb^{-1} of pp collision data at E_{cm} = 13 TeV. SM values for the production cross-sections are assumed. See their Table 4 and Fig. 5.
[2] AAD 23CD search for $H \to \psi(2S)\gamma$, $\psi(2S) \to \mu^+\mu^-$ with 138 fb^{-1} of pp collision data at E_{cm} = 13 TeV. SM values for the production cross-sections are assumed.
[3] AABOUD 18BL search for $H \to \psi(2S)\gamma$, $\psi(2S) \to \mu^+\mu^-$ with 36.1 fb^{-1} of pp collision data at E_{cm} = 13 TeV.

$\Gamma(\psi(2S)J/\psi)/\Gamma_{total}$ — Γ_{17}/Γ

VALUE	CL%	DOCUMENT ID		TECN	COMMENT
<2.1 × 10^{-3}	95	[1] TUMASYAN	23C	CMS	pp, 13 TeV

[1] TUMASYAN 23C search for $H \to \psi(2S)J/\psi$, $\psi(2S) \to \mu^+\mu^-$, $J/\psi \to \mu^+\mu^-$ with 138 fb^{-1} of pp collision data at E_{cm} = 13 TeV. The quoted value is for the Higgs decays for longitudinally polarized mesons. See their Table 1 for other cases.

$\Gamma(\psi(2S)\psi(2S))/\Gamma_{total}$ — Γ_{18}/Γ

VALUE	CL%	DOCUMENT ID		TECN	COMMENT
<3.0 × 10^{-3}	95	[1] TUMASYAN	23C	CMS	pp, 13 TeV

[1] TUMASYAN 23C search for $H \to \psi(2S)\psi(2S)$, $\psi(2S) \to \mu^+\mu^-$ with 138 fb^{-1} of pp collision data at E_{cm} = 13 TeV. The quoted value is for the Higgs decays for longitudinally polarized mesons. See their Table 1 for other cases.

$\Gamma(\Upsilon(1S)\gamma)/\Gamma_{total}$ — Γ_{19}/Γ

VALUE	CL%	DOCUMENT ID		TECN	COMMENT
<2.5 × 10^{-4}	95	[1] AAD	23CD	ATLS	13 TeV, 138 fb^{-1}
• • • We do not use the following data for averages, fits, limits, etc. • • •					
<4.9 × 10^{-4}	95	[2] AABOUD	18BL	ATLS	13 TeV, 36.1 fb^{-1}
<1.3 × 10^{-3}	95	[3] AAD	15I	ATLS	8 TeV

[1] AAD 23CD search for $H \to \Upsilon(1S)\gamma$, $\Upsilon(1S) \to \mu^+\mu^-$ with 138 fb^{-1} of pp collision data at E_{cm} = 13 TeV. SM values for the production cross-sections are assumed.
[2] AABOUD 18BL search for $H \to \Upsilon(1S)\gamma$, $\Upsilon(1S) \to \mu^+\mu^-$ with 36.1 fb^{-1} of pp collision data at E_{cm} = 13 TeV.
[3] AAD 15I use 19.7 fb^{-1} of pp collision data at 8 TeV.

$\Gamma(\Upsilon(1S)\Upsilon(1S))/\Gamma_{total}$ — Γ_{20}/Γ

VALUE	CL%	DOCUMENT ID		TECN	COMMENT
<1.7 × 10^{-3}	95	[1] TUMASYAN	23C	CMS	pp, 13 TeV

[1] TUMASYAN 23C search for $H \to \Upsilon(1S)\Upsilon(1S)$, $\Upsilon(1S) \to \mu^+\mu^-$ with 138 fb^{-1} of pp collision data at E_{cm} = 13 TeV. The quoted value is for the Higgs decays for longitudinally polarized mesons. See their Table 1 for other cases.

Int. J. Mod. Phys. A 2026.41. Downloaded from www.worldscientific.com
by UNIVERSITY OF CALIFORNIA @ BERKELEY on 09/16/26. Reproduction is strictly not permitted, except for Open Access articles.

Int. J. Mod. Phys. A 2026.41. Downloaded from www.worldscientific.com by UNIVERSITY OF CALIFORNIA @ BERKELEY on 09/16/26. Re-use and distribution is strictly not permitted, except for Open Access articles.

$\Gamma(\Upsilon(2S)\gamma)/\Gamma_{total}$ — Γ_{21}/Γ

VALUE	CL%	DOCUMENT ID		TECN	COMMENT
$<4.2\times10^{-4}$	95	[1] AAD	23CD	ATLS	13 TeV, 138 fb^{-1}
• • • We do not use the following data for averages, fits, limits, etc. • • •					
$<5.9\times10^{-4}$	95	[2] AABOUD	18BL	ATLS	13 TeV, 36.1 fb^{-1}
$<1.9\times10^{-3}$	95	[3] AAD	15I	ATLS	8 TeV

[1] AAD 23CD search for $H\to\Upsilon(2S)\gamma$, $\Upsilon(2S)\to\mu^+\mu^-$ with 138 fb^{-1} of pp collision data at $E_{cm}=13$ TeV. SM values for the production cross-sections are assumed.
[2] AABOUD 18BL search for $H\to\Upsilon(2S)\gamma$, $\Upsilon(2S)\to\mu^+\mu^-$ with 36.1 fb^{-1} of pp collision data at $E_{cm}=13$ TeV.
[3] AAD 15I use 19.7 fb^{-1} of pp collision data at 8 TeV.

$\Gamma(\Upsilon(3S)\gamma)/\Gamma_{total}$ — Γ_{22}/Γ

VALUE	CL%	DOCUMENT ID		TECN	COMMENT
$<3.4\times10^{-4}$	95	[1] AAD	23CD	ATLS	13 TeV, 138 fb^{-1}
• • • We do not use the following data for averages, fits, limits, etc. • • •					
$<5.7\times10^{-4}$	95	[2] AABOUD	18BL	ATLS	13 TeV, 36.1 fb^{-1}
$<1.3\times10^{-3}$	95	[3] AAD	15I	ATLS	8 TeV

[1] AAD 23CD search for $H\to\Upsilon(3S)\gamma$, $\Upsilon(3S)\to\mu^+\mu^-$ with 138 fb^{-1} of pp collision data at $E_{cm}=13$ TeV. SM values for the production cross-sections are assumed.
[2] AABOUD 18BL search for $H\to\Upsilon(3S)\gamma$, $\Upsilon(3S)\to\mu^+\mu^-$ with 36.1 fb^{-1} of pp collision data at $E_{cm}=13$ TeV.
[3] AAD 15I use 19.7 fb^{-1} of pp collision data at 8 TeV.

$\Gamma(\Upsilon(nS)\,\Upsilon(mS))/\Gamma_{total}$ — Γ_{23}/Γ

VALUE	CL%	DOCUMENT ID		TECN	COMMENT
$<3.5\times10^{-4}$	95	[1] TUMASYAN	23C	CMS	pp, 13 TeV
• • • We do not use the following data for averages, fits, limits, etc. • • •					
$<1.4\times10^{-3}$	95	[2] SIRUNYAN	19BR	CMS	pp, 13 TeV

[1] TUMASYAN 23C search for $H\to\Upsilon(nS)\,\Upsilon(mS)$ with $\Upsilon(nS)$, $\Upsilon(mS)\to\mu^+\mu^-$ (n, m = 1, 2, 3) with 138 fb^{-1} of pp collision data at $E_{cm}=13$ TeV. The quoted value is for the Higgs decays for longitudinally polarized mesons. See their Table 1 for other cases.
[2] SIRUNYAN 19BR search for $H\to\Upsilon(nS)\,\Upsilon(mS)$ with $\Upsilon(nS),\Upsilon(mS)\to\mu^+\mu^-$ (n, m = 1, 2, 3) for 37.5 fb^{-1} of pp collision data at $E_{cm}=13$ TeV. Υs from the Higgs decay are assumed to be unpolarized. For fully longitudinal (transverse) polarized Υs, limits change by -22% ($+10\%$). The three Υ states selected in a mass range of 8.5–11 GeV are not distinguished.

$\Gamma(D^*\gamma)/\Gamma_{total}$ — Γ_{24}/Γ

VALUE	CL%	DOCUMENT ID		TECN	COMMENT
$<1.0\times10^{-3}$	95	[1] AAD	24R	ATLS	pp, 13 TeV

[1] AAD 24R use 136.3 fb^{-1} of pp collision data at 13 TeV. The 95% CL upper limit on the cross section times the branching ratio is 58 fb. The SM Higgs production cross section of $m_H=125.09$ GeV is assumed. See their Table 3.

$\Gamma(\rho(770)\gamma)/\Gamma_{total}$ — Γ_{25}/Γ

VALUE	CL%	DOCUMENT ID		TECN	COMMENT
$<3.7\times10^{-4}$	95	[1] HAYRAPETY...	25G	CMS	pp, 13 TeV
• • • We do not use the following data for averages, fits, limits, etc. • • •					
$<10.4\times10^{-4}$	95	[2] AABOUD	18AU	ATLS	pp, 13 TeV

[1] HAYRAPETYAN 25G search for $H\to\rho^0\gamma$, $\rho^0\to\pi^+\pi^-$ with up to 138 fb^{-1} of pp collision data at $E_{cm}=13$ TeV.
[2] AABOUD 18AU use 35.6 fb^{-1} of pp collision data at 13 TeV. See their erratum AABOUD 23A.

$\Gamma(\omega(782)\gamma)/\Gamma_{total}$ — Γ_{26}/Γ

VALUE	CL%	DOCUMENT ID		TECN	COMMENT
$<5.5\times10^{-4}$	95	[1] AAD	23BS	ATLS	pp, 13 TeV

[1] AAD 23BS use 89.5 fb^{-1} of pp collision data at 13 TeV.

$\Gamma(K^*(892)\gamma)/\Gamma_{total}$ — Γ_{27}/Γ

VALUE	CL%	DOCUMENT ID		TECN	COMMENT
$<2.2\times10^{-4}$	95	[1] AAD	23BS	ATLS	pp, 13 TeV
• • • We do not use the following data for averages, fits, limits, etc. • • •					
$<3.0\times10^{-4}$	95	[2] HAYRAPETY...	25G	CMS	pp, 13 TeV

[1] AAD 23BS use 134 fb^{-1} of pp collision data at 13 TeV.
[2] HAYRAPETYAN 25G search for $H\to K^{*0}\gamma$, $K^{*0}\to K^\pm\pi^\mp$ with up to 138 fb^{-1} of pp collision data at $E_{cm}=13$ TeV.

$\Gamma(\phi(1020)\gamma)/\Gamma_{total}$ — Γ_{28}/Γ

VALUE	CL%	DOCUMENT ID		TECN	COMMENT
$<3.0\times10^{-4}$	95	[1] HAYRAPETY...	25G	CMS	pp, 13 TeV
• • • We do not use the following data for averages, fits, limits, etc. • • •					
$<5.0\times10^{-4}$	95	[2] AABOUD	18AU	ATLS	pp, 13 TeV
$<1.4\times10^{-3}$	95	[3] AABOUD	16K	ATLS	pp, 13 TeV

[1] HAYRAPETYAN 25G search for $H\to\phi\gamma$, $\phi\to K^+K^-$ with up to 138 fb^{-1} of pp collision data at $E_{cm}=13$ TeV.
[2] AABOUD 18AU use 35.6 fb^{-1} of pp collision data at 13 TeV. See their erratum AABOUD 23A.
[3] AABOUD 16K use 2.7 fb^{-1} of pp collision data at 13 TeV.

$\Gamma(e\mu)/\Gamma_{total}$ — Γ_{29}/Γ

VALUE	CL%	DOCUMENT ID		TECN	COMMENT
$<4.4\times10^{-5}$	95	[1] HAYRAPETY...	23C	CMS	pp, 13 TeV
• • • We do not use the following data for averages, fits, limits, etc. • • •					
$<6.1\times10^{-5}$	95	[2] AAD	20F	ATLS	pp, 13 TeV
$<3.5\times10^{-4}$	95	[3] KHACHATRY...	16CD	CMS	pp, 8 TeV

[1] HAYRAPETYAN 23C use 138 fb^{-1} of pp collisions at $E_{cm}=13$ TeV. The limit constrains the $Y_{e\mu}$ Yukawa coupling to $\sqrt{|Y_{e\mu}|^2+|Y_{\mu e}|^2}<1.9\times10^{-4}$ at 95% CL (see their Fig. 6).
[2] AAD 20F use 139 fb^{-1} of pp collisions at $E_{cm}=13$ TeV. The best-fit value of the $H\to e\mu$ branching fraction is $(0.4\pm2.9\pm0.3)\times10^{-5}$ for $m_H=125$ GeV.
[3] KHACHATRYAN 16CD search for $H\to e\mu$ in 19.7 fb^{-1} of pp collisions at $E_{cm}=8$ TeV. The limit constrains the $Y_{e\mu}$ Yukawa coupling to $\sqrt{|Y_{e\mu}|^2+|Y_{\mu e}|^2}<5.4\times10^{-4}$ at 95% CL (see their Fig. 6).

$\Gamma(e\tau)/\Gamma_{total}$ — Γ_{30}/Γ

VALUE	CL%	DOCUMENT ID		TECN	COMMENT
$<2.0\times10^{-3}$	95	[1] AAD	23Q	ATLS	pp, 13 TeV
• • • We do not use the following data for averages, fits, limits, etc. • • •					
$<2.3\times10^{-3}$	95	[2] AAD	23Q	ATLS	pp, 13 TeV
$<2.2\times10^{-3}$	95	[3] SIRUNYAN	21Z	CMS	pp, 13 TeV
$<4.7\times10^{-3}$	95	[4] AAD	20A	ATLS	pp, 13 TeV
$<6.1\times10^{-3}$	95	[5] SIRUNYAN	18BH	CMS	pp, 13 TeV
$<10.4\times10^{-3}$	95	[6] AAD	17	ATLS	pp, 8 TeV
$<6.9\times10^{-3}$	95	[7] KHACHATRY...	16CD	CMS	pp, 8 TeV

[1] AAD 23Q search for $H\to e\tau$ in 138 fb^{-1} of pp collisions at $E_{cm}=13$ TeV. The result is obtained from a simultaneous fit of possible $H\to e\tau$ and $H\to\mu\tau$ signals (see their Figs. 13 and 14). The limit constrains the $Y_{e\tau}$ Yukawa coupling to $\sqrt{|Y_{e\tau}|^2+|Y_{\tau e}|^2}<1.3\times10^{-3}$ at 95% CL (see their Fig. 15).
[2] AAD 23Q search for $H\to e\tau$ in 138 fb^{-1} of pp collisions at $E_{cm}=13$ TeV. The limit constrains the $Y_{e\tau}$ Yukawa coupling to $\sqrt{|Y_{e\tau}|^2+|Y_{\tau e}|^2}<1.4\times10^{-3}$ at 95% CL (see their Fig. 12).
[3] SIRUNYAN 21Z search for $H\to e\tau$ in 137 fb^{-1} of pp collisions at $E_{cm}=13$ TeV. The limit constrains the $Y_{e\tau}$ Yukawa coupling to $\sqrt{|Y_{e\tau}|^2+|Y_{\tau e}|^2}<1.35\times10^{-3}$ at 95% CL (see their Fig. 8).
[4] AAD 20A search for $H\to e\tau$ in 36.1 fb^{-1} of pp collisions at $E_{cm}=13$ TeV. The limit constrains the $Y_{e\tau}$ Yukawa coupling to $\sqrt{|Y_{e\tau}|^2+|Y_{\tau e}|^2}<2.0\times10^{-3}$ at 95% CL (see their Fig. 5).
[5] SIRUNYAN 18BH search for $H\to e\tau$ in 35.9 fb^{-1} of pp collisions at $E_{cm}=13$ TeV. The limit constrains the $Y_{e\tau}$ Yukawa coupling to $\sqrt{|Y_{e\tau}|^2+|Y_{\tau e}|^2}<2.26\times10^{-3}$ at 95% CL (see their Fig. 10).
[6] AAD 17 search for $H\to e\tau$ in 20.3 fb^{-1} of pp collisions at $E_{cm}=8$ TeV.
[7] KHACHATRYAN 16CD search for $H\to e\tau$ in 19.7 fb^{-1} of pp collisions at $E_{cm}=8$ TeV. The limit constrains the $Y_{e\tau}$ Yukawa coupling to $\sqrt{|Y_{e\tau}|^2+|Y_{\tau e}|^2}<2.4\times10^{-3}$ at 95% CL (see their Fig. 6).

$\Gamma(\mu\tau)/\Gamma_{total}$ — Γ_{31}/Γ

VALUE	CL%	DOCUMENT ID		TECN	COMMENT
$<1.5\times10^{-3}$	95	[1] SIRUNYAN	21Z	CMS	pp, 13 TeV
• • • We do not use the following data for averages, fits, limits, etc. • • •					
$<1.8\times10^{-3}$	95	[2] AAD	23Q	ATLS	pp, 13 TeV
$<1.7\times10^{-3}$	95	[3] AAD	23Q	ATLS	pp, 13 TeV
$<2.8\times10^{-3}$	95	[4] AAD	20A	ATLS	pp, 13 TeV
$<26\times10^{-2}$	95	[5] AAIJ	18AM	LHCB	pp, 8 TeV
$<2.5\times10^{-3}$	95	[6] SIRUNYAN	18BH	CMS	pp, 13 TeV
$<1.43\times10^{-2}$	95	[7] AAD	17	ATLS	pp, 8 TeV
$<1.51\times10^{-2}$	95	[8] KHACHATRY...	15Q	CMS	pp, 8 TeV

[1] SIRUNYAN 21Z search for $H\to\mu\tau$ in 137 fb^{-1} of pp collisions at $E_{cm}=13$ TeV. The limit constrains the $Y_{\mu\tau}$ Yukawa coupling to $\sqrt{|Y_{\mu\tau}|^2+|Y_{\tau\mu}|^2}<1.11\times10^{-3}$ at 95% CL (see their Fig. 8).
[2] AAD 23Q search for $H\to\mu\tau$ in 138 fb^{-1} of pp collisions at $E_{cm}=13$ TeV. The result is obtained from a simultaneous fit of possible $H\to e\tau$ and $H\to\mu\tau$ signals (see their Figs. 13 and 14). The limit constrains the $Y_{\mu\tau}$ Yukawa coupling to $\sqrt{|Y_{\mu\tau}|^2+|Y_{\tau\mu}|^2}<1.2\times10^{-3}$ at 95% CL (see their Fig. 15).
[3] AAD 23Q search for $H\to\mu\tau$ in 138 fb^{-1} of pp collisions at $E_{cm}=13$ TeV. The limit constrains the $Y_{\mu\tau}$ Yukawa coupling to $\sqrt{|Y_{\mu\tau}|^2+|Y_{\tau\mu}|^2}<1.2\times10^{-3}$ at 95% CL (see their Fig. 12).
[4] AAD 20A search for $H\to\mu\tau$ in 36.1 fb^{-1} of pp collisions at $E_{cm}=13$ TeV. The limit constrains the $Y_{\mu\tau}$ Yukawa coupling to $\sqrt{|Y_{\mu\tau}|^2+|Y_{\tau\mu}|^2}<1.5\times10^{-3}$ at 95% CL (see their Fig. 5).
[5] AAIJ 18AM search for $H\to\mu\tau$ in 2.0 fb^{-1} of pp collisions at $E_{cm}=8$ TeV. The limit constrains the $Y_{\mu\tau}$ Yukawa coupling to $\sqrt{|Y_{\mu\tau}|^2+|Y_{\tau\mu}|^2}<1.7\times10^{-2}$ at 95% CL assuming SM production cross sections.
[6] SIRUNYAN 18BH search for $H\to\mu\tau$ in 35.9 fb^{-1} of pp collisions at $E_{cm}=13$ TeV. The limit constrains the $Y_{\mu\tau}$ Yukawa coupling to $\sqrt{|Y_{\mu\tau}|^2+|Y_{\tau\mu}|^2}<1.43\times10^{-3}$ at 95% CL (see their Fig. 10).
[7] AAD 17 search for $H\to\mu\tau$ in 20.3 fb^{-1} of pp collisions at $E_{cm}=8$ TeV.
[8] KHACHATRYAN 15Q search for $H\to\mu\tau$ with τ decaying electronically or hadronically in 19.7 fb^{-1} of pp collisions at $E_{cm}=8$ TeV. The fit gives $B(H\to\mu\tau)=(0.84^{+0.39}_{-0.37})\%$ with a significance of 2.4 σ.

Int. J. Mod. Phys. A 2026.41. Downloaded from www.worldscientific.com
by UNIVERSITY OF CALIFORNIA @ BERKELEY on 09/16/26. Re strictly not permitted, except for Open Access articles.

$\Gamma(\text{invisible})/\Gamma_{\text{total}}$ — Γ_{32}/Γ

Invisible final states.

VALUE	CL%	DOCUMENT ID		TECN	COMMENT
<0.107	95	[1] AAD	23A	ATLS	pp, 7, 8, 13 TeV
• • • We do not use the following data for averages, fits, limits, etc. • • •					
<0.113	95	[2] AAD	23A	ATLS	pp, 13 TeV
<0.38	95	[3] AAD	23AF	ATLS	$pp \to t\overline{t}H$, 13 TeV
<0.54	95	[4] TUMASYAN	23BA	CMS	$pp \to t\overline{t}H$, $V(\to q\overline{q})H$, 13 TeV
<0.15	95	[5] TUMASYAN	23BA	CMS	pp, 7, 8, 13 TeV
<0.19	95	[6] AAD	22D	ATLS	$pp \to ZH$, 13 TeV
<0.145	95	[7] AAD	22P	ATLS	$pp \to qqH$, 13 TeV
<0.37	95	[8] AAD	22S	ATLS	$pp \to qqH\gamma$, 13 TeV
<0.13	95	[9] ATLAS	22	ATLS	pp, 13 TeV
<0.16	95	[10] CMS	22	CMS	pp, 13 TeV
<0.18	95	[11] TUMASYAN	22G	CMS	$pp \to qqH$, 8, 13 TeV
<0.18	95	[12] TUMASYAN	22G	CMS	$pp \to qqH$, 13 TeV
<0.34	95	[13] AAD	21F	ATLS	pp, 13 TeV
<0.29	95	[14] SIRUNYAN	21A	CMS	$pp \to ZH$, 13 TeV
<0.278	95	[15] TUMASYAN	21D	CMS	pp, 13 TeV, jet or $V(\to q\overline{q})$
<0.37	95	[16] AABOUD	19AI	ATLS	$pp \to qqH$, 13 TeV
<0.38	95	[17] AABOUD	19AL	ATLS	pp, 13 TeV
<0.26	95	[18] AABOUD	19AL	ATLS	pp, 7, 8, 13 TeV
<0.22	95	[19] SIRUNYAN	19AT	CMS	pp, 13 TeV
<0.33	95	[20] SIRUNYAN	19BO	CMS	$pp \to qqH$, 13 TeV
<0.26	95	[21] SIRUNYAN	19BO	CMS	pp, 13 TeV
<0.19	95	[22] SIRUNYAN	19BO	CMS	pp, 7, 8, 13 TeV
<0.67	95	[23] AABOUD	18	ATLS	$pp \to ZH$, 13 TeV
<0.83	95	[24] AABOUD	18CA	ATLS	$pp \to WH/ZH$, $W/Z \to jj$, 13 TeV
<0.40	95	[25] SIRUNYAN	18BV	CMS	$pp \to ZH$, 13 TeV
<0.53	95	[26] SIRUNYAN	18S	CMS	pp, 13 TeV, jet or $V(\to q\overline{q})$
<0.46	95	[27] AABOUD	17BD	ATLS	$pp \to Hj$, qqH, 13 TeV
<0.24	95	[28] KHACHATRY...	17F	CMS	pp, 7, 8, 13 TeV
<0.28	95	[29] AAD	16AF	ATLS	$pp \to qqH$, 8 TeV
<0.34	95	[30] AAD	16AN	LHC	pp, 7, 8 TeV
<0.78	95	[31] AAD	15BD	ATLS	$pp \to WH/ZH$, 8 TeV
<0.25	95	[32] AAD	15CX	ATLS	pp, 7, 8 TeV
<0.75	95	[33] AAD	14O	ATLS	$pp \to ZH$, 7, 8 TeV
<0.58	95	[34] CHATRCHYAN	14B	CMS	$pp \to ZH$, qqH
<0.81	95	[35] CHATRCHYAN	14B	CMS	$pp \to ZH$, 7, 8 TeV
<0.65	95	[36] CHATRCHYAN	14B	CMS	$pp \to qqH$, 8 TeV

[1] AAD 23A report the combined results of 7, 8 (AAD 15CX) and 13 TeV assuming the Standard Model cross section ($m_H = 125$ GeV). See their Table 1 and Fig. 3.

[2] AAD 23A report the combined results using 139 fb^{-1} of data at $E_{\text{cm}} = 13$ TeV, where H decaying to invisible final states in VBF (AAD 22P), ZH, $Z \to ee$, $\mu\mu$ (AAD 22D), $pp \to t\overline{t}H$ (AAD 23AF), VBF+γ (AAD 22S) and gluon-fusion production with an energetic jet (AAD 21F) assuming the Standard Model cross section ($m_H = 125$ GeV). See their Table 1 and Fig. 3.

[3] AAD 23AF search for $pp \to t\overline{t}H$ with H decaying to invisible final states using 139 fb^{-1} of data. The quoted limit on the branching ratio is given for $m_H = 125$ GeV and assumes the Standard Model cross section. See their Table 3 for different decay topologies.

[4] TUMASYAN 23BA search for H decaying to invisible final states produced in association with a $t\overline{t}$ or a V, which decay to a fully hadronic final state. 138 fb^{-1} of data is used. The quoted limit on the branching ratio is given for $m_H = 125$ GeV and assumes the Standard Model cross section. See their Fig. 6 for the results of individual topologies.

[5] TUMASYAN 23BA report the combined results of 7, 8, and 13 TeV assuming the Standard Model cross section ($m_H = 125$ GeV). They combine results from TUMASYAN 22G, SIRUNYAN 21A, SIRUNYAN 21B, TUMASYAN 21D, SIRUNYAN 20AH, KHACHATRYAN 17F, CHATRCHYAN 14B as shown in their Table 8. See their Fig. 7 and Table 9 for the results of individual topologies.

[6] AAD 22D search for H decaying to invisible final states associated with a Z decaying $ee/\mu\mu$ using 139 fb^{-1} at 13 TeV. The limit is obtained for $m_H = 125$ GeV and assuming the SM ZH production cross section. The branching ratio is obtained to be (0.3 ± 9.0)%.

[7] AAD 22P search for $pp \to qqHX$ (VBF) with H decaying to invisible final states using 139 fb^{-1} of data. The quoted limit on the branching ratio is given for $m_H = 125$ GeV and assumes the Standard Model cross section.

[8] AAD 22S observe electroweak $Z(\to \nu\nu)\gamma$+2jets production process with 139 fb^{-1} of data. This result is applicable to search for $pp \to qqH\gamma X$ (VBF+γ) with H decaying to invisible final states. The quoted limit on the branching ratio is given for $m_H = 125$ GeV and assumes the Standard Model cross section.

[9] ATLAS 22 report the combined results using 139 fb^{-1} of data at $E_{\text{cm}} = 13$ TeV, where H decaying to invisible final states in VBF (AAD 22P), and ZH, $Z \to ee$, $\mu\mu$ (AAD 22D), assuming $\kappa_V \leq 1$ and $B_{undetected} \geq 0$.

[10] CMS 22 report the combined results using (a part of) 138 fb^{-1} of data at $E_{\text{cm}} = 13$ TeV, where H decaying to invisible final states in VBF (SIRUNYAN 19BO), associated with an energetic jet or a $V(\to q\overline{q})$ (TUMASYAN 21D), and ZH, $Z \to ee$, $\mu\mu$ (SIRUNYAN 21A) and assuming $\kappa_V \leq 1$ and $B_{undetected} \geq 0$.

[11] TUMASYAN 22G combine 13 TeV 101 fb^{-1} results with 8 TeV (KHACHATRYAN 17F) and other 13 TeV (KHACHATRYAN 17F for 2015 and SIRUNYAN 19BO for 2016) for H decaying to invisible final states with VBF topology. The quoted limit on the branching ratio is given for $m_H = 125.38$ GeV and assumes the Standard Model production rates. The branching ratio is obtained to be $0.086^{+0.054}_{-0.052}$. See their Figs. 11 and 12.

[12] TUMASYAN 22G search for $pp \to qqHX$ (VBF) with H decaying to invisible final states using 101 fb^{-1} of data (2017 and 2018). The quoted limit on the branching ratio is given for $m_H = 125.38$ GeV and assumes the Standard Model cross section. See their Figs. 11 and 12.

[13] AAD 21F search for an invisibly decaying Higgs boson with an energetic jet ($p_T > 150$ GeV) and missing transverse momentum (> 200 GeV) in 139 fb^{-1} at $E_{\text{cm}} = 13$ TeV. The quoted limit on the branching ratio is given for $m_H = 125$ GeV.

[14] SIRUNYAN 21A search for H decaying to invisible final states associated with a Z decaying $ee/\mu\mu$ using 137 fb^{-1} at 13 TeV. The limit is obtained for $m_H = 125$ GeV and assuming the SM ZH production cross section.

[15] TUMASYAN 21D search for H decaying to invisible final states associated with an energetic jet or a V, $V \to q\overline{q}$ using 101 fb^{-1} at 13 TeV and the result is combined with SIRUNYAN 18S.

[16] AABOUD 19AI search for $pp \to qqHX$ (VBF) with H decaying to invisible final states using 36.1 fb^{-1} of data. The quoted limit on the branching ratio is given for $m_H = 125$ GeV and assumes the Standard Model rates for VBF and gluon-fusion production.

[17] AABOUD 19AL combine results of H decaying to invisible final states with VBF(AABOUD 19AI), ZH, and WH productions (AABOUD 18, AABOUD 18CA), which use 36.1 fb^{-1} of data at 13 TeV. The quoted limit is given for $m_H = 125$ GeV and assumes the Standard Model rates for gluon fusion, VBF, ZH, and WH productions.

[18] AABOUD 19AL combine results of 7, 8 (AAD 15CX), and 13 TeV for H decaying to invisible final states.

[19] SIRUNYAN 19AT perform a combined fit with visible decay using 35.9 fb^{-1} of data at 13 TeV.

[20] SIRUNYAN 19BO search for $pp \to qqHX$ (VBF) with H decaying to invisible final states using 35.9 fb^{-1} of data. The quoted limit on the branching ratio is given for $m_H = 125.09$ GeV and assumes the Standard Model production rates.

[21] SIRUNYAN 19BO combine the VBF channel with results of other 13 TeV analyses: SIRUNYAN 18BV and SIRUNYAN 18S. The quoted limit on the branching ratio is given for $m_H = 125.09$ GeV and assumes the Standard Model production rates.

[22] SIRUNYAN 19BO combine 13 TeV 35.9 fb^{-1} results with 7, 8, 13 TeV (KHACHATRYAN 17F) for H decaying to invisible final states. The quoted limit on the branching ratio is given for $m_H = 125.09$ GeV and assumes the Standard Model production rates. The branching ratio is obtained to be 0.05 ± 0.03 (stat) ± 0.07(syst).

[23] AABOUD 18 search for $pp \to HZX$, $Z \to ee$, $\mu\mu$ with H decaying to invisible final states in 36.1 fb^{-1} at $E_{\text{cm}} = 13$ TeV. The quoted limit on the branching ratio is given for $m_H = 125$ GeV and assumes the Standard Model rate for HZ production.

[24] AABOUD 18CA search for H decaying to invisible final states using WH, and ZH productions, where W and Z hadronically decay. The data of 36.1 fb^{-1} at $E_{\text{cm}} = 13$ TeV is used. The quoted limit assumes SM production cross sections with combining the contributions from WH, ZH, ggF and VBF production modes.

[25] SIRUNYAN 18BV search for H decaying to invisible final states associated with a Z, $Z \to \ell\ell$ using 35.9 fb^{-1} at 13 TeV.The limit is obtained for $m_H = 125$ GeV and assuming the SM ZH production cross section.

[26] SIRUNYAN 18S search for H decaying to invisible final states associated with an energetic jet or a V, $V \to q\overline{q}$ using 35.9 fb^{-1} at 13 TeV.

[27] AABOUD 17BD search for H decaying to invisible final states with ≥ 1 jet and VBF events using 3.2 fb^{-1} of pp collisions at $E_{\text{cm}} = 13$ TeV. A cross-section ratio R^{miss} is used in the measurement. The quoted limit is given for $m_H = 125$ GeV.

[28] KHACHATRYAN 17F search for H decaying to invisible final states with gluon fusion, VBF, ZH, and WH productions using 2.3 fb^{-1} of pp collisions at $E_{\text{cm}} = 13$ TeV, 19.7 fb^{-1} at 8 TeV, and 5.1 fb^{-1} at 7 TeV. The quoted limit is given for $m_H = 125$ GeV and assumes the Standard Model rates for gluon fusion, VBF, ZH, and WH productions.

[29] AAD 16AF search for $pp \to qqHX$ (VBF) with H decaying to invisible final states in 20.3 fb^{-1} at $E_{\text{cm}} = 8$ TeV. The quoted limit on the branching ratio is given for $m_H = 125$ GeV and assumes the Standard Model rates for VBF and gluon-fusion production.

[30] AAD 16AN perform fits to the ATLAS and CMS data at $E_{\text{cm}} = 7$ and 8 TeV. The branching fraction of decays into BSM particles that are invisible or into undetected decay modes is measured for $m_0 = 125.09$ GeV.

[31] AAD 15BD search for $pp \to HWX$ and $pp \to HZX$ with W or Z decaying hadronically and H decaying to invisible final states using data at $E_{\text{cm}} = 8$ TeV. The quoted limit is given for $m_H = 125$ GeV, assumes the Standard Model rates for the production processes and is based on a combination of the contributions from HW, HZ and the gluon-fusion process.

[32] AAD 15CX search for H decaying to invisible final states with VBF, ZH, and WH productions using 20.3 fb^{-1} at 8 TeV, and 4.7 fb^{-1} at 7 TeV. The quoted limit is given for $m_H = 125.36$ GeV and assumes the Standard Model rates for gluon fusion, VBF, ZH, and WH productions. The upper limit is improved to 0.23 by adding the measured visible decay rates.

[33] AAD 14O search for $pp \to HZX$, $Z \to \ell\ell$, with H decaying to invisible final states in 4.5 fb^{-1} at $E_{\text{cm}} = 7$ TeV and 20.3 fb^{-1} at $E_{\text{cm}} = 8$ TeV. The quoted limit on the branching ratio is given for $m_H = 125.5$ GeV and assumes the Standard Model rate for HZ production.

[34] CHATRCHYAN 14B search for $pp \to HZX$, $Z \to \ell\ell$ and $Z \to b\overline{b}$, and also $pp \to qqHX$ with H decaying to invisible final states using data at $E_{\text{cm}} = 7$ and 8 TeV. The quoted limit on the branching ratio is obtained from a combination of the limits from HZ and qqH. It is given for $m_H = 125$ GeV and assumes the Standard Model rates for the two production processes.

[35] CHATRCHYAN 14B search for $pp \to HZX$ with H decaying to invisible final states and $Z \to \ell\ell$ in 4.9 fb^{-1} at $E_{\text{cm}} = 7$ TeV and 19.7 fb^{-1} at $E_{\text{cm}} = 8$ TeV, and also with $Z \to b\overline{b}$ in 18.9 fb^{-1} at $E_{\text{cm}} = 8$ TeV. The quoted limit on the branching ratio is given for $m_H = 125$ GeV and assumes the Standard Model rate for HZ production.

[36] CHATRCHYAN 14B search for $pp \to qqHX$ (vector boson fusion) with H decaying to invisible final states in 19.5 fb^{-1} at $E_{\text{cm}} = 8$ TeV. The quoted limit on the branching ratio is given for $m_H = 125$ GeV and assumes the Standard Model rate for qqH production.

$\Gamma(\gamma\text{invisible})/\Gamma_{\text{total}}$ — Γ_{33}/Γ

VALUE	CL%	DOCUMENT ID		TECN	COMMENT
<0.013	95	[1] AAD	24BH	ATLS	VBF, HZ, $H \to \gamma +$ invisible, 13 TeV
• • • We do not use the following data for averages, fits, limits, etc. • • •					
<0.035	95	[2] SIRUNYAN	21L	CMS	VBF, $H \to \gamma +$ invisible, 13 TeV
<0.029	95	[2,3] SIRUNYAN	21L	CMS	VBF, HZ, $H \to \gamma +$ invisible, 13 TeV
<0.046	95	[4] SIRUNYAN	19CG	CMS	$pp \to HZ$, $H \to \gamma +$ invisible, $Z \to \ell\ell$, 13 TeV

Int. J. Mod. Phys. A 2026.41. Downloaded from www.worldscientific.com by UNIVERSITY OF CALIFORNIA @ BERKELEY on 09/16/26. Re-use and distribution is strictly not permitted, except for Open Access articles.

[1] AAD 24BH search for H decaying to an invisible final state plus a γ in the VBF and HZ production using 139 fb^{-1} data at E_{cm} = 13 TeV. The invisible state is called a dark photon. The quoted limit on the branching ratio is given for m_H = 125 GeV assuming the Standard Model rates. The 95% CL upper limits on the branching ratio for the VBF and HZ production are 1.8% and 2.3%, respectively. See their Fig. 3(a).

[2] SIRUNYAN 21L search for H decaying to an invisible final state plus a γ in the VBF production using 130 fb^{-1} data at E_{cm} = 13 TeV. The invisible state is called a dark photon. The quoted limit on the branching ratio is given for m_H = 125 GeV assuming the Standard Model rates.

[3] The result of the VBF production is combined with the $pp \rightarrow HZ$ result (SIRUNYAN 19CG).

[4] SIRUNYAN 19CG search for $pp \rightarrow HZ$, $Z \rightarrow ee$, $\mu\mu$ with H decaying to invisible final states plus a γ in 137 fb^{-1} at E_{cm} = 13 TeV. The quoted limit on the branching ratio is given for m_H = 125 GeV assuming the Standard Model rate for HZ production and is obtained in the context of a theoretical model, where the undetected (invisible) particle is massless.

H SIGNAL STRENGTHS IN DIFFERENT CHANNELS

The H signal strength in a particular final state xx is given by the cross section times branching ratio in this channel normalized to the Standard Model (SM) value, $\sigma \cdot B(H \rightarrow xx) / (\sigma \cdot B(H \rightarrow xx))_{SM}$, for the specified mass value of H. For the SM predictions, see DITTMAIER 11, DITTMAIER 12, and HEINEMEYER 13A. Results for fiducial and differential cross sections are also listed below.

Combined final state

VALUE	DOCUMENT ID		TECN	COMMENT
1.03 ±0.04 OUR AVERAGE				
1.05 ±0.06	[1] ATLAS	22	ATLS	pp, 13 TeV
1.002±0.057	[2] CMS	22	CMS	pp, 13 TeV
1.09 ±0.07 $\pm 0.04^{+0.08}_{-0.07}$	[3,4] AAD	16AN	LHC	pp, 7, 8 TeV
1.44 $^{+0.59}_{-0.56}$	[5] AALTONEN	13M	TEVA	$p\overline{p} \rightarrow HX$, 1.96 TeV
• • • We do not use the following data for averages, fits, limits, etc. • • •				
1.11 $^{+0.09}_{-0.08}$	[6] AAD	20	ATLS	pp, 13 TeV
1.17 ±0.10	[7] SIRUNYAN	19AT	CMS	pp, 13 TeV
	[8] SIRUNYAN	19BA	CMS	pp, 13 TeV, diiferential cross sections
1.20 ±0.10 $\pm 0.06^{+0.09}_{-0.08}$	[4] AAD	16AN	ATLS	pp, 7, 8 TeV
0.97 ±0.09 $\pm 0.05^{+0.08}_{-0.07}$	[4] AAD	16AN	CMS	pp, 7, 8 TeV
1.18 ±0.10 $\pm 0.07^{+0.08}_{-0.07}$	[9] AAD	16K	ATLS	pp, 7, 8 TeV
0.75 $^{+0.28}_{-0.26}$ $^{+0.13}_{-0.11}$ $^{+0.08}_{-0.05}$	[9] AAD	16K	ATLS	pp, 7 TeV
1.28 ±0.11 $^{+0.08}_{-0.07}$ $^{+0.10}_{-0.08}$	[9] AAD	16K	ATLS	pp, 8 TeV
	[10] AAD	15P	ATLS	pp, 8 TeV, cross section
1.00 ±0.09 $\pm 0.07^{+0.08}_{-0.07}$	[11] KHACHATRY...	15AM	CMS	pp, 7, 8 TeV
1.33 $^{+0.14}_{-0.10}$ ±0.15	[12] AAD	13AK	ATLS	pp, 7 and 8 TeV
1.54 $^{+0.77}_{-0.73}$	[13] AALTONEN	13L	CDF	$p\overline{p} \rightarrow HX$, 1.96 TeV
1.40 $^{+0.92}_{-0.88}$	[14] ABAZOV	13L	D0	$p\overline{p} \rightarrow HX$, 1.96 TeV
1.4 ±0.3	[15] AAD	12AI	ATLS	$pp \rightarrow HX$, 7, 8 TeV
1.2 ±0.4	[15] AAD	12AI	ATLS	$pp \rightarrow HX$, 7 TeV
1.5 ±0.4	[15] AAD	12AI	ATLS	$pp \rightarrow HX$, 8 TeV
0.87 ±0.23	[16] CHATRCHYAN	12N	CMS	$pp \rightarrow HX$, 7, 8 TeV

[1] ATLAS 22 report combined results (see their Extended Data Table 1) using up to 139 fb^{-1} of data at E_{cm} = 13 TeV, assuming m_H = 125.09 GeV. The Higgs production cross-sections, branching fractions and several ratios are found in their Figs. 2 and 3.

[2] CMS 22 report combined results (see their Extended Data Table 2) using 138 fb^{-1} of data at E_{cm} = 13 TeV, assuming m_H = 125.38 GeV. Signal strengths for production modes and decay channels are found in their Fig. 2.

[3] AAD 16AN perform fits to the ATLAS and CMS data at E_{cm} = 7 and 8 TeV. The signal strengths for individual production processes are $1.03^{+0.16}_{-0.14}$ for gluon fusion, $1.18^{+0.25}_{-0.23}$ for vector boson fusion, $0.89^{+0.40}_{-0.38}$ for WH production, $0.79^{+0.38}_{-0.36}$ for ZH production, and $2.3^{+0.7}_{-0.6}$ for $t\overline{t}H$ production.

[4] AAD 16AN: The uncertainties represent statistics, experimental systematics, and added in quadrature theory systematics on the background and on the signal. The quoted signal strengths are given for m_H = 125.09 GeV. In the fit, relative branching ratios and relative production cross sections are fixed to those in the Standard Model.

[5] AALTONEN 13M combine all Tevatron data from the CDF and D0 Collaborations with up to 10.0 fb^{-1} and 9.7 fb^{-1}, respectively, of $p\overline{p}$ collisions at E_{cm} = 1.96 TeV. The quoted signal strength is given for m_H = 125 GeV.

[6] AAD 20 combine results of up to 79.8 fb^{-1} of data at E_{cm} = 13 TeV, assuming m_H = 125.09 GeV: $\gamma\gamma$, ZZ^*, WW^*, $\tau\tau$, $b\overline{b}$, $\mu\mu$, invisible, and off-shell analyses (see their Table I). The signal strengths for individual production processes are 1.04 ± 0.09 for gluon fusion, $1.21^{+0.24}_{-0.22}$ for vector boson fusion, $1.30^{+0.40}_{-0.38}$ for WH production, $1.05^{+0.31}_{-0.29}$ for ZH production, and $1.21^{+0.26}_{-0.24}$ for $t\overline{t}H+tH$ production (see their Fig. 2 and Table IV). Several results with the simplified template cross section and κ-frameworks are presented: see their Figs. 9–11, Figs 20, 21 and Table VIII for stage-1 simplified template cross sections, their Figs. 12–17 and Tables X–XII for the κ-framework.

[7] SIRUNYAN 19AT combine results of 35.9 fb^{-1} of data at E_{cm} = 13 TeV, assuming m_H = 125.09 GeV. The signal strengths for individual production processes are $1.22^{+0.14}_{-0.12}$ for gluon fusion, $0.73^{+0.30}_{-0.27}$ for vector boson fusion, $2.18^{+0.58}_{-0.55}$ for WH production, $0.87^{+0.44}_{-0.42}$ for ZH production, and $1.18^{+0.30}_{-0.27}$ for $t\overline{t}H$ production. Several results with the simplified template cross section and κ-frameworks are presented: see their Fig. 8 and Table 5 for stage-0 simplified template cross sections, their Figs. 9–18 and Tables 7–11 for the κ-framework.

[8] SIRUNYAN 19BA measure differential cross sections for the Higgs boson transverse momentum, the number of jets, the rapidity of the Higgs boson and the transverse momentum of the leading jet using 35.9 fb^{-1} of data at E_{cm} = 13 TeV with $H \rightarrow \gamma\gamma$, $H \rightarrow ZZ^*$, and $H \rightarrow b\overline{b}$. The total cross section for Higgs boson production is measured to be 61.1 ± 6.0 ± 3.7 pb using $H \rightarrow \gamma\gamma$ and $H \rightarrow ZZ^*$ channels. Several coupling measurements in the κ-framework are performed.

[9] AAD 16K use up to 4.7 fb^{-1} of pp collisions at E_{cm} = 7 TeV and up to 20.3 fb^{-1} at E_{cm} = 8 TeV. The third uncertainty in the measurement is theory systematics. The signal strengths for individual production modes are $1.23 \pm 0.14^{+0.09}_{-0.08}{}^{+0.16}_{-0.12}$ for gluon fusion, $1.23^{+0.28}_{-0.27}{}^{+0.13}_{-0.12}{}^{+0.11}_{-0.09}$ for vector boson fusion, $0.80^{+0.31}_{-0.30} \pm 0.17^{+0.10}_{-0.05}$ for W/ZH production, and $1.81^{+0.52}_{-0.50}{}^{+0.58}_{-0.55}{}^{+0.31}_{-0.12}$ for $t\overline{t}H$ production. The quoted signal strengths are given for m_H = 125.36 GeV.

[10] AAD 15P measure total and differential cross sections of the process $pp \rightarrow HX$ at E_{cm} = 8 TeV with 20.3 fb^{-1}. $\gamma\gamma$ and 4ℓ final states are used. $\sigma(pp \rightarrow HX)$ = 33.0 ± 5.3 ± 1.6 pb is given. See their Figs. 2 and 3 for data on differential cross sections.

[11] KHACHATRYAN 15AM use up to 5.1 fb^{-1} of pp collisions at E_{cm} = 7 TeV and up to 19.7 fb^{-1} at E_{cm} = 8 TeV. The third uncertainty in the measurement is theory systematics. Fits to each production mode give the value of $0.85^{+0.19}_{-0.16}$ for gluon fusion, $1.16^{+0.37}_{-0.34}$ for vector boson fusion, $0.92^{+0.38}_{-0.36}$ for WH, ZH production, and $2.90^{+1.08}_{-0.94}$ for $t\overline{t}H$ production.

[12] AAD 13AK use 4.7 fb^{-1} of pp collisions at E_{cm} = 7 TeV and 20.7 fb^{-1} at E_{cm} = 8 TeV. The combined signal strength is based on the $\gamma\gamma$, $ZZ^* \rightarrow 4\ell$, and $WW^* \rightarrow \ell\nu\ell\nu$ channels. The quoted signal strength is given for m_H = 125.5 GeV. Reported statistical error value modified following private communication with the experiment.

[13] AALTONEN 13L combine all CDF results with 9.45–10.0 fb^{-1} of $p\overline{p}$ collisions at E_{cm} = 1.96 TeV. The quoted signal strength is given for m_H = 125 GeV.

[14] ABAZOV 13L combine all D0 results with up to 9.7 fb^{-1} of $p\overline{p}$ collisions at E_{cm} = 1.96 TeV. The quoted signal strength is given for m_H = 125 GeV.

[15] AAD 12AI obtain results based on 4.6–4.8 fb^{-1} of pp collisions at E_{cm} = 7 TeV and 5.8–5.9 fb^{-1} at E_{cm} = 8 TeV. An excess of events over background with a local significance of 5.9 σ is observed at m_H = 126 GeV. The quoted signal strengths are given for m_H = 126 GeV. See also AAD 12DA.

[16] CHATRCHYAN 12N obtain results based on 4.9–5.1 fb^{-1} of pp collisions at E_{cm} = 7 TeV and 5.1–5.3 fb^{-1} at E_{cm} = 8 TeV. An excess of events over background with a local significance of 5.0 σ is observed at about m_H = 125 GeV. The combined signal strength is based on the $\gamma\gamma$, ZZ^*, WW^*, $\tau^+\tau^-$, and $b\overline{b}$ channels. The quoted signal strength is given for m_H = 125.5 GeV. See also CHATRCHYAN 13Y.

*WW** final state

VALUE	DOCUMENT ID		TECN	COMMENT
1.00±0.08 OUR AVERAGE				
0.97±0.09	[1] CMS	22	CMS	pp, 13 TeV
$1.09^{+0.18}_{-0.16}$	[2,3] AAD	16AN	LHC	pp, 7, 8 TeV
$0.94^{+0.85}_{-0.83}$	[4] AALTONEN	13M	TEVA	$p\overline{p} \rightarrow HX$, 1.96 TeV
• • • We do not use the following data for averages, fits, limits, etc. • • •				
$0.92^{+0.21}_{-0.20}{}^{+0.13}_{-0.12} \pm 0.02$	[5] AAD	25AG	CMS	$pp \rightarrow WH/ZH$, 13 TeV
	[6] AAD	25BK	ATLS	pp, 13 TeV, cross sections
1.20±0.50±0.11	[7] HAYRAPETY...	25AC	CMS	$pp \rightarrow ZH$, 13 TeV
	[8] HAYRAPETY...	24AG	CMS	pp, $H \rightarrow WW^*$ ($\rightarrow e\nu\mu\nu$), 13 TeV
	[9] AAD	23AP	ATLS	pp, 13 TeV, cross sections
	[10] AAD	23BV	ATLS	pp, 13 TeV, cross sections
$0.95^{+0.10}_{-0.09}$	[11,12] TUMASYAN	23W	CMS	pp, 13 TeV
$0.92^{+0.11}_{-0.10}$	[11,13,14] TUMASYAN	23W	CMS	pp, 13 TeV
$0.71^{+0.28}_{-0.25}$	[11,13,15] TUMASYAN	23W	CMS	pp, 13 TeV
2.2 ±0.6	[11,13,16] TUMASYAN	23W	CMS	pp, 13 TeV
2.0 ±0.7	[11,13,17] TUMASYAN	23W	CMS	pp, 13 TeV
	[11,18] TUMASYAN	23W	CMS	pp, 13 TeV
0.5 ±0.4 $^{+0.7}_{-0.6}$	[19] AAD	22V	ATLS	pp, WW^* ($\rightarrow e\nu\mu\nu$) +2j, 13 TeV
	[20] AAD	22V	ATLS	pp, WW^* ($\rightarrow e\nu\mu\nu$) +2j, 13 TeV
	[21] AABOUD	19F	ATLS	pp, 13 TeV, cross sections
2.5 $^{+0.9}_{-0.8}$	[22] AAD	19A	ATLS	$pp \rightarrow HW/HZ$, $H \rightarrow WW^*$, 13 TeV
$1.28^{+0.17}_{-0.16}$	[23] SIRUNYAN	19AT	CMS	pp, 13 TeV
$1.28^{+0.18}_{-0.17}$	[24] SIRUNYAN	19AX	CMS	pp, 13 TeV
$1.22^{+0.23}_{-0.21}$	[3] AAD	16AN	ATLS	pp, 7, 8 TeV
$0.90^{+0.23}_{-0.21}$	[3] AAD	16AN	CMS	pp, 7, 8 TeV
	[25] AAD	16AO	ATLS	pp, 8 TeV, cross sections
$1.18 \pm 0.16^{+0.17}_{-0.14}$	[26] AAD	16K	ATLS	pp, 7, 8 TeV
$1.09^{+0.16}_{-0.15}{}^{+0.17}_{-0.14}$	[27] AAD	15AA	ATLS	pp, 7, 8 TeV

$3.0\ ^{+1.3}_{-1.1}\ ^{+1.0}_{-0.7}$	[28] AAD	15AQ	ATLS	$pp \to HW/ZX$, 7, 8 TeV
$1.16^{+0.16}_{-0.15}{}^{+0.18}_{-0.15}$	[29] AAD	15AQ	ATLS	pp, 7, 8 TeV
$0.72 \pm 0.12 \pm 0.10^{+0.12}_{-0.10}$	[30] CHATRCHYAN	14G	CMS	pp, 7, 8 TeV
$0.99^{+0.31}_{-0.28}$	[31] AAD	13AK	ATLS	pp, 7 and 8 TeV
$0.00^{+1.78}_{-0.00}$	[32] AALTONEN	13L	CDF	$p\overline{p} \to HX$, 1.96 TeV
$1.90^{+1.63}_{-1.52}$	[33] ABAZOV	13L	D0	$p\overline{p} \to HX$, 1.96 TeV
1.3 ± 0.5	[34] AAD	12AI	ATLS	$pp \to HX$, 7, 8 TeV
0.5 ± 0.6	[34] AAD	12AI	ATLS	$pp \to HX$, 7 TeV
1.9 ± 0.7	[34] AAD	12AI	ATLS	$pp \to HX$, 8 TeV
$0.60^{+0.42}_{-0.37}$	[35] CHATRCHYAN	12N	CMS	$pp \to HX$, 7, 8 TeV

[1] CMS 22 report combined results (see their Extended Data Table 2) using up to 138 fb^{-1} of data at E_{cm} = 13 TeV, assuming m_H = 125.38 GeV. See their Fig. 2 right.

[2] AAD 16AN perform fits to the ATLAS and CMS data at E_{cm} = 7 and 8 TeV. The signal strengths for individual production processes are 0.84 ± 0.17 for gluon fusion, 1.2 ± 0.4 for vector boson fusion, $1.6^{+1.2}_{-1.0}$ for WH production, $5.9^{+2.6}_{-2.2}$ for ZH production, and $5.0^{+1.8}_{-1.7}$ for $t\overline{t}H$ production.

[3] AAD 16AN: In the fit, relative production cross sections are fixed to those in the Standard Model. The quoted signal strength is given for m_H = 125.09 GeV.

[4] AALTONEN 13M combine all Tevatron data from the CDF and D0 Collaborations with up to 10.0 fb^{-1} and 9.7 fb^{-1}, respectively, of $p\overline{p}$ collisions at E_{cm} = 1.96 TeV. The quoted signal strength is given for m_H = 125 GeV.

[5] AAD 25AG measure the signal strengths using $H \to WW^* \to \ell\nu\ell\nu$ and $H \to WW^* \to \ell\nu jj$ ($\ell = e, \mu$) with 140 fb^{-1} data at E_{cm} = 13 TeV. The last measurement uncertainty is due to the normalizing SM value. The signal strengths are summarized in their Table 9 and Fig. 12. The sum of WH and ZH cross sections times the $H \to WW^*$ branching ratio is measured to be $0.44^{+0.10}_{-0.09}{}^{+0.06}_{-0.05}$ pb and these two-dimensional likelihood scans are shown in their Fig. 14. Cross sections times the $H \to WW^*$ branching ratio and ratios to the SM values are given in their Tables 12, 13, 14 and Figs. 15 and 16, which are based on the simplified template cross section framework (reduced stage-1.2).

[6] AAD 25BK measure cross-sections times the $H \to WW^*$ branching fraction using $WW^* \to \ell\nu\ell\nu$ ($\ell = e, \mu$) with data of 140 fb^{-1} pp collisions at E_{cm} = 13 TeV: $\sigma_{ggF}\times$B($H \to WW^*$) = $12.4^{+1.3}_{-1.2}$ pb and $\sigma_{VBF}\times$B($H \to WW^*$) = $0.79^{+0.18}_{-0.16}$ pb. See their Fig. 11 for 2-dim contours. Measured cross sections and ratios to the SM predictions in the reduced stage-1.2 simplified template cross section framework (see their Fig. 2) are shown in their Fig. 10. The results are given for m_H = 125.09 GeV.

[7] HAYRAPETYAN 25AC measure the ZH production cross section to the SM prediction using $H \to WW^*$ decay channel with 138 fb^{-1} and 62 fb^{-1} of pp collision data at E_{cm} = 13 TeV and 13.6 TeV, respectively. Events with 4ℓ ($\ell = e, \mu$) are used. The cross section times the $H \to WW^*$ branching fraction and the signal strength for each center of mass energy are shown in their Table I. The corresponding significances are given in their Table II.

[8] HAYRAPETYAN 24AG search for the anomalous couplings of the Higgs boson to vector bosons, including CP violation effects using $H \to WW^* \to e\nu\mu\nu$ decay channel ($\ell = e, \mu$) with 138 fb^{-1} at E_{cm} = 13 TeV. The anomalous HVV and Hgg coupling parameters are given in their Table 7. The data constrain the SMEFT Higgs and Warsaw bases coupling parameters as shown in their Tables 8, 9 and Fig. 12.

[9] AAD 23AP measure cross-sections times the $H \to WW^*$ branching fraction in the $H \to WW^* \to e\nu\mu\nu$ channel using 139 fb^{-1} of pp collisions at E_{cm} = 13 TeV: $\sigma_{ggF}\times$B($H \to WW^*$) = 12.0 ± 1.4 pb, $\sigma_{VBF}\times$B($H \to WW^*$) = $0.75^{+0.19}_{-0.16}$ pb, and $\sigma_{ggF+VBF}\times$B($H \to WW^*$) = 12.3 ± 1.3 pb. The results are given for m_H = 125.09 GeV. Measured cross sections and ratios to the SM predictions in the reduced stage-1.2 (see their Fig. 5) simplified template cross section framework are shown in their Table VII and Fig. 15.

[10] AAD 23BV measure fiducial total and differential cross sections of VBF process at E_{cm} = 13 TeV with 139 fb^{-1} using $H \to WW^* \to e\nu\mu\nu$. The measured total fiducial cross section is 1.68 ± 0.33(stat) ± 0.23(syst) fb in their fiducial region (Table II and Section V). See their Fig. 9 for the comparison with theory predictions. The fiducial differential cross sections are shown in their Figs. 11, 12, and 13. Wilson coefficients in the Warsaw basis at 95% confidence interval are measured; see their Table V and Fig. 16.

[11] TUMASYAN 23W measure Higgs production rates with $H \to WW^*$ at E_{cm} = 13 TeV with 138 fb^{-1} data. The quoted results are given for m_H = 125.38 GeV.

[12] The quoted global signal strength is obtained assuming the relative ratios of different Higgs production modes fixed to the SM values.

[13] The 4 signal strengths for gluon-fusion (ggF), VBF, WH and ZH modes are fit assuming $t\overline{t}H$ and $b\overline{b}H$ fixed to the SM values.

[14] The quoted result is for ggF production mode.

[15] The quoted result is for VBF production mode.

[16] The quoted result is for WH production mode.

[17] The quoted result is for ZH production mode.

[18] Measured cross sections and ratios to the SM predictions in the reduced stage-1.2 (see their Fig. 17) simplified template cross section framework (6 ggF, 4 VBF, and 4 VH) are shown in their Table 18 and Fig. 26.

[19] AAD 22V measure the signal strength for ggF+2jets with 36.1 fb^{-1} data at 13 TeV.

[20] AAD 22V probe the Higgs couplings to longitudinally and transversely polarized W and Z using VBF ($H \to WW^* \to e\nu\mu\nu$ plus two jets) with 36.1 fb^{-1} of data at E_{cm} = 13 TeV. The ratios of the polarization-dependent couplings $g_{HV_LV_L}$ and $g_{HV_TV_T}$ to the Higgs-V coupling predicted by the SM, $a_L = g_{HV_LV_L}/g^{SM}_{HVV}$ and $a_T = g_{HV_TV_T}/g^{SM}_{HVV}$ are measured to be $0.91^{+0.10}_{-0.18}{}^{+0.09}_{-0.17}$ and $1.2 \pm 0.4^{+0.2}_{-0.3}$, respectively, assuming the standard Hgg coupling. These measurements are translated into pseudo-observables of κ_{VV} and ϵ_{VV}: $\kappa_{VV} = 0.91^{+0.10}_{-0.18}{}^{+0.09}_{-0.17}$ and $\epsilon_{VV} = 0.13^{+0.28}_{-0.20}{}^{+0.08}_{-0.10}$, where κ_{VV} = 1 and ϵ_{VV} = 0 for the SM. See their Tables 9 and 10.

[21] AABOUD 19F measure cross-sections times the $H \to WW^*$ branching fraction in the $H \to WW^* \to e\nu\mu\nu$ channel using 36.1 fb^{-1} of pp collisions at E_{cm} = 13 TeV: $\sigma_{ggF}\times$B($H \to WW^*$) = $11.4^{+1.2}_{-1.1}{}^{+1.8}_{-1.7}$ pb and $\sigma_{VBF}\times$B($H \to WW^*$) = $0.50^{+0.24}_{-0.22}$ ± 0.17 pb.

[22] AAD 19A use 36.1 fb^{-1} data at 13 TeV. The cross section times branching fraction values are measured to be $0.67^{+0.31}_{-0.27}{}^{+0.18}_{-0.14}$ pb for WH, $H \to WW^*$ and $0.54^{+0.31}_{-0.24}{}^{+0.15}_{-0.07}$ pb for ZH, $H \to WW^*$.

[23] SIRUNYAN 19AT perform a combine fit to 35.9 fb^{-1} of data at E_{cm} = 13 TeV.

[24] SIRUNYAN 19AX measure the signal strengths, cross sections and so on using gluon fusion, VBF and VH production processes with 35.9 fb^{-1} of data. The quoted signal strength is given for m_H = 125.09 GeV. Signal strengths for each production process is found in their Fig. 9. Measured cross sections and ratios to the SM predictions in the stage-0 simplified template cross section framework are shown in their Fig. 10. $\kappa_F = 1.52^{+0.48}_{-0.41}$ and κ_V = 1.10 ± 0.08 are obtained (see their Fig. 11 (right)).

[25] AAD 16AO measure fiducial total and differential cross sections of gluon fusion process at E_{cm} = 8 TeV with 20.3 fb^{-1} using $H \to WW^* \to e\nu\mu\nu$. The measured fiducial total cross section is 36.0 ± 9.7 fb in their fiducial region (Table 7). See their Fig. 6 for fiducial differential cross sections. The results are given for m_H = 125 GeV.

[26] AAD 16K use up to 4.7 fb^{-1} of pp collisions at E_{cm} = 7 TeV and up to 20.3 fb^{-1} at E_{cm} = 8 TeV. The quoted signal strength is given for m_H = 125.36 GeV.

[27] AAD 15AA use 4.5 fb^{-1} of pp collisions at E_{cm} = 7 TeV and 20.3 fb^{-1} at E_{cm} = 8 TeV. The signal strength for the gluon fusion and vector boson fusion mode is 1.02 ± $0.19^{+0.22}_{-0.18}$ and $1.27^{+0.44}_{-0.40}{}^{+0.30}_{-0.21}$, respectively. The quoted signal strengths are given for m_H = 125.36 GeV.

[28] AAD 15AQ use 4.5 fb^{-1} of pp collisions at E_{cm} = 7 TeV and 20.3 fb^{-1} at E_{cm} = 8 TeV. The quoted signal strength is given for m_H = 125.36 GeV.

[29] AAD 15AQ combine their result on W/ZH production with the results of AAD 15AA (gluon fusion and vector boson fusion, slightly updated). The quoted signal strength is given for m_H = 125.36 GeV.

[30] CHATRCHYAN 14G use 4.9 fb^{-1} of pp collisions at E_{cm} = 7 TeV and 19.4 fb^{-1} at E_{cm} = 8 TeV. The last uncertainty in the measurement is theory systematics. The quoted signal strength is given for m_H = 125.6 GeV.

[31] AAD 13AK use 4.7 fb^{-1} of pp collisions at E_{cm} = 7 TeV and 20.7 fb^{-1} at E_{cm} = 8 TeV. The quoted signal strength is given for m_H = 125.5 GeV. Superseded by AAD 15AA.

[32] AALTONEN 13L combine all CDF results with 9.45–10.0 fb^{-1} of $p\overline{p}$ collisions at E_{cm} = 1.96 TeV. The quoted signal strength is given for m_H = 125 GeV.

[33] ABAZOV 13L combine all D0 results with up to 9.7 fb^{-1} of $p\overline{p}$ collisions at E_{cm} = 1.96 TeV. The quoted signal strength is given for m_H = 125 GeV.

[34] AAD 12AI obtain results based on 4.7 fb^{-1} of pp collisions at E_{cm} = 7 TeV and 5.8 fb^{-1} at E_{cm} = 8 TeV. The quoted signal strengths are given for m_H = 126 GeV. See also AAD 12DA.

[35] CHATRCHYAN 12N obtain results based on 4.9 fb^{-1} of pp collisions at E_{cm} = 7 TeV and 5.1 fb^{-1} at E_{cm} = 8 TeV. The quoted signal strength is given for m_H = 125.5 GeV. See also CHATRCHYAN 13Y.

*ZZ** final state

VALUE	CL%	DOCUMENT ID		TECN	COMMENT
1.02±0.08 OUR AVERAGE					
$0.97^{+0.12}_{-0.11}$		[1] CMS	22	CMS	pp, 13 TeV
1.01 ± 0.11		[2,3] AAD	20AQ	ATLS	pp, 13 TeV
$1.29^{+0.26}_{-0.23}$		[4,5] AAD	16AN	LHC	pp, 7, 8 TeV
• • • We do not use the following data for averages, fits, limits, etc. • • •					
$1.06^{+0.61}_{-0.45}$		[6] AAD	25AQ	ATLS	pp, 13 TeV, off-shell
		[7] CHEKHOVSKY	25B	CMS	pp, 13.6 TeV, cross sections
		[8] AAD	24AQ	ATLS	pp, 13.6 TeV, cross sections
		[9] HAYRAPETY...	23	CMS	pp, 13 TeV cross sections
		[10] SIRUNYAN	21AE	CMS	pp, 13 TeV, couplings
$0.94 \pm 0.07^{+0.09}_{-0.08}$		[11] SIRUNYAN	21S	CMS	pp, 13 TeV
		[2,12] AAD	20AQ	ATLS	pp, 13 TeV
		[13] AAD	20BA	ATLS	pp, 13 TeV cross sections
<6.5	95	[14] AABOUD	19N	ATLS	pp, 13 TeV, off-shell
$1.06^{+0.19}_{-0.17}$		[15] SIRUNYAN	19AT	CMS	pp, 13 TeV
$1.28^{+0.21}_{-0.19}$		[16] AABOUD	18AJ	ATLS	pp, 13 TeV
<3.8	95	[17] AABOUD	18BP	ATLS	pp, 13 TeV, off-shell
$1.05^{+0.15}_{-0.14}{}^{+0.11}_{-0.09}$		[18] SIRUNYAN	17AV	CMS	pp, 13 TeV
$1.52^{+0.40}_{-0.34}$		[5] AAD	16AN	ATLS	pp, 7, 8 TeV
$1.04^{+0.32}_{-0.26}$		[5] AAD	16AN	CMS	pp, 7, 8 TeV
$1.46^{+0.35}_{-0.31}{}^{+0.19}_{-0.13}$		[19] AAD	16K	ATLS	pp, 7, 8 TeV
		[20] KHACHATRY...	16AR	CMS	pp, 7, 8 TeV cross sections
$1.44^{+0.34}_{-0.31}{}^{+0.21}_{-0.11}$		[21] AAD	15F	ATLS	$pp \to HX$, 7, 8 TeV
		[22] AAD	14AR	ATLS	pp, 8 TeV, cross sections
$0.93^{+0.26}_{-0.23}{}^{+0.13}_{-0.09}$		[23] CHATRCHYAN	14AA	CMS	pp, 7, 8 TeV

Int. J. Mod. Phys. A 2026.41. Downloaded from www.worldscientific.com
by UNIVERSITY OF CALIFORNIA @ BERKELEY on 09/16/26. Reproduction is strictly not permitted, except for Open Access articles.

Int. J. Mod. Phys. A 2026.41. Downloaded from www.worldscientific.com
by UNIVERSITY OF CALIFORNIA @ BERKELEY on 09/16/26. Re-use and distribution is strictly not permitted, except for Open Access articles.

$1.43^{+0.40}_{-0.35}$	[24] AAD	13AK	ATLS	pp, 7 and 8 TeV
$0.80^{+0.35}_{-0.28}$	[25] CHATRCHYAN	13J	CMS	$pp \to HX$, 7, 8 TeV
1.2 ± 0.6	[26] AAD	12AI	ATLS	$pp \to HX$, 7, 8 TeV
1.4 ± 1.1	[26] AAD	12AI	ATLS	$pp \to HX$, 7 TeV
1.1 ± 0.8	[26] AAD	12AI	ATLS	$pp \to HX$, 8 TeV
$0.73^{+0.45}_{-0.33}$	[27] CHATRCHYAN	12N	CMS	$pp \to HX$, 7, 8 TeV

[1] CMS 22 report combined results (see their Extended Data Table 2) using up to 138 fb^{-1} of data at E_{cm} = 13 TeV, assuming m_H = 125.38 GeV. See their Fig. 2 right.

[2] AAD 20AQ perform analyses using $H \to ZZ^* \to 4\ell$ ($\ell = e, \mu$) with data of 139 fb^{-1} at E_{cm} = 13 TeV. Results are given for m_H = 125 GeV.

[3] AAD 20AQ measured the inclusive cross section times branching ratio for $H \to ZZ^*$ decay ($|y(H)| < 2.5$) to be 1.34 ± 0.12 pb (with 1.33 ± 0.08 pb expected in the SM).

[4] AAD 16AN perform fits to the ATLAS and CMS data at E_{cm} = 7 and 8 TeV. The signal strengths for individual production processes are $1.13^{+0.34}_{-0.31}$ for gluon fusion and $0.1^{+1.1}_{-0.6}$ for vector boson fusion.

[5] AAD 16AN: In the fit, relative production cross sections are fixed to those in the Standard Model. The quoted signal strength is given for m_H = 125.09 GeV.

[6] AAD 25AQ measure the off-shell Higgs signal strength to be $0.87^{+0.75}_{-0.54}$ using $H^* \to ZZ \to 4\ell$ ($\ell = e, \mu$) with data of 140 fb^{-1} at E_{cm} = 13 TeV. This result is combined with $ZZ \to 2\ell 2\nu$ decay channel (AAD 23BR), which corresponds to a significance of 3.7 σ. The quoted errors are values at 68%CL.

[7] CHEKHOVSKY 25B measure the fiducial cross section using $H \to ZZ^* \to 4\ell$ ($\ell = e, \mu$) with data of 34.7 fb^{-1} at E_{cm} = 13.6 TeV. The inclusive fiducial cross section is $2.89^{+0.53}_{-0.49}{}^{+0.29}_{-0.21}$ fb with their defined fiducial region (see their Table 1), where $3.09^{+0.27}_{-0.24}$ fb is expected in the SM. Differential fiducial cross sections are shown in their Fig. 5. The quoted results are given for m_H = 125.38 GeV.

[8] AAD 24AQ measure fiducial and total cross sections at E_{cm} = 13.6 TeV with 29.0 fb^{-1} data. The quoted results are given for m_H = 125.09 GeV. The inclusive fiducial cross section is 2.80 ± 0.74 fb with their defined fiducial region (see their Table 5), where 3.67 ± 0.19 fb is expected in the SM. Assuming SM values for the acceptance and the branching fraction, the total cross section is 46 ± 12 pb, where 59.9 ± 2.6 pb is expected in the SM.

[9] HAYRAPETYAN 23 measure the cross sections for $pp \to H \to ZZ^* \to 4\ell$ ($\ell = e, \mu$) using 138 fb^{-1} at E_{cm} = 13 TeV. They give $\sigma = 2.73 \pm 0.22$(stat) ± 0.15(syst) fb in their fiducial region (see their Section5 and Table 2), where 2.86 ± 0.15 fb is expected in the Standard Model for m_H = 125.38 GeV. 26 differential and 6 double-differential cross sections are given; see their Figs. 6-23 and 24-25.

[10] SIRUNYAN 21AE obtains constraints on anomalous couplings to vector bosons (W, Z, and gluon) and top quark using $H \to ZZ^* \to 4\ell$ ($\ell = e, \mu$) with data of 137 fb^{-1} at E_{cm} = 13 TeV. Their Table 5 and Figs 14–17 show (effective) couplings to gluon and top with combining gluon fusion, $t\bar{t}H$ and tH production channels and the result of $t\bar{t}H$, $H \to \gamma\gamma$ (SIRUNYAN 20AS). Their Tables 6–9 and Figs 18–22 show couplings to W and Z for different assumptions and bases (Higgs and Warsaw).

[11] SIRUNYAN 21S measure cross sections with the $H \to ZZ^* \to 4\ell$ ($\ell = e, \mu$) channel using 137 fb^{-1} data at E_{cm} = 13 TeV. Results are given for m_H = 125.38 GeV. The signal strengths for individual production processes in their Table 4. Cross sections are given in their Table 6 and Fig. 14, which are based on the simplified template cross section framework (reduced stage-1.2).

[12] AAD 20AQ present several results for the channel $H \to ZZ^* \to 4\ell$ ($\ell = e, \mu$) with the simplified template cross section with κ-frameworks and the effective field theory (EFT) approach; see their Table 8 and Fig. 10 for simplified template cross sections. $\kappa_V = 1.02 \pm 0.06$ and $\kappa_F = 0.88 \pm 0.16$ are obtained, see their Fig. 12 for the κ-framework. See their Tables 9 and 10 and Figs. 16–18 for the EFT-framework.

[13] AAD 20BA measure the cross section for $pp \to H \to ZZ^* \to 4\ell$ ($\ell = e, \mu$) using 139 fb^{-1} at E_{cm} = 13 TeV. They give $\sigma \cdot B = 3.28 \pm 0.30 \pm 0.11$ fb in their fiducial region, where 3.41 ± 0.18 fb is expected in the Standard Model for m_H = 125 GeV. Various differential cross sections are also given; see their Figs. 19-39. Constraints on Yukawa couplings for bottom and charm quarks are given in their Table 9 and Fig. 41.

[14] AABOUD 19N measure the spectrum of the four-lepton invariant mass $m_{4\ell}$ ($\ell = e$ or μ) using 36.1 fb^{-1} of data at E_{cm} = 13 TeV. The quoted signal strength upper limit is obtained from 180 GeV $< m_{4\ell} <$ 1200 GeV.

[15] SIRUNYAN 19AT perform a combine fit to 35.9 fb^{-1} of data at E_{cm} = 13 TeV.

[16] AABOUD 18AJ perform analyses using $H \to ZZ^* \to 4\ell$ ($\ell = e, \mu$) with data of 36.1 fb^{-1} at E_{cm} = 13 TeV. Results are given for m_H = 125.09 GeV. The inclusive cross section times branching ratio for $H \to ZZ^*$ decay ($|\eta(H)| < 2.5$) is measured to be $1.73^{+0.26}_{-0.24}$ pb (with $1.34^{+0.09}_{-0.09}$ pb expected in the SM).

[17] AABOUD 18BP measure an off-shell Higgs boson production using $ZZ \to 4\ell$ and $ZZ \to 2\ell 2\nu$ ($\ell = e, \mu$) decay channels with 36.1 fb^{-1} of data at E_{cm} = 13 TeV. The quoted signal strength upper limit is obtained from a combination of these two channels, where 220 GeV $< m_{4\ell} <$ 2000 GeV for $ZZ \to 4\ell$ and 250 GeV $< m_T^{ZZ} <$ 2000 GeV for $ZZ \to 2\ell 2\nu$ (m_T^{ZZ} is defined in their Section 5). See their Table 2 for each measurement.

[18] SIRUNYAN 17AV use 35.9 fb^{-1} of pp collisions at E_{cm} = 13 TeV. The quoted signal strength, obtained from the analysis of $H \to ZZ^* \to 4\ell$ ($\ell = e, \mu$) decays, is given for m_H = 125.09 GeV. The signal strengths for different production modes are given in their Table 3. The fiducial and differential cross sections are shown in their Fig. 10.

[19] AAD 16K use up to 4.7 fb^{-1} of pp collisions at E_{cm} = 7 TeV and up to 20.3 fb^{-1} at E_{cm} = 8 TeV. The quoted signal strength is given for m_H = 125.36 GeV.

[20] KHACHATRYAN 16AR use data of 5.1 fb^{-1} at E_{cm} = 7 TeV and 19.7 fb^{-1} at 8 TeV. The fiducial cross sections for the production of 4 leptons via $H \to 4\ell$ decays are measured to be $0.56^{+0.67}_{-0.44}{}^{+0.21}_{-0.06}$ fb at 7 TeV and $1.11^{+0.41}_{-0.35}{}^{+0.14}_{-0.10}$ fb at 8 TeV in their fiducial region (Table 2). The differential cross sections at E_{cm} = 8 TeV are also shown in Figs. 4 and 5. The results are given for m_H = 125 GeV.

[21] AAD 15F use 4.5 fb^{-1} of pp collisions at E_{cm} = 7 TeV and 20.3 fb^{-1} at E_{cm} = 8 TeV. The quoted signal strength is given for m_H = 125.36 GeV. The signal strength for the gluon fusion production mode is $1.66^{+0.45}_{-0.41}{}^{+0.25}_{-0.15}$, while the signal strength for the vector boson fusion production mode is $0.26^{+1.60}_{-0.91}{}^{+0.36}_{-0.23}$.

[22] AAD 14AR measure the cross section for $pp \to H \to ZZ^* \to 4\ell$ ($\ell = e, \mu$) using 20.3fb^{-1} at E_{cm} = 8 TeV. They give $\sigma \cdot B = 2.11^{+0.53}_{-0.47} \pm 0.08$ fbin their fiducial region, where 1.30 ± 0.13 fb is expected in the Standard Model for m_H= 125.4 GeV. Various differential cross sections are also given; see their Fig. 2.

[23] CHATRCHYAN 14AA use 5.1 fb^{-1} of pp collisions at E_{cm} = 7 TeV and 19.7 fb^{-1} at E_{cm} = 8 TeV. The quoted signal strength is given for m_H = 125.6 GeV. The signal strength for the gluon fusion and $t\bar{t}H$ production mode is $0.80^{+0.46}_{-0.36}$, while the signal strength for the vector boson fusion and WH, ZH production mode is $1.7^{+2.2}_{-2.1}$.

[24] AAD 13AK use 4.7 fb^{-1} of pp collisions at E_{cm} = 7 TeV and 20.7 fb^{-1} at E_{cm} = 8 TeV. The quoted signal strength is given for m_H = 125.5 GeV.

[25] CHATRCHYAN 13J obtain results based on $ZZ \to 4\ell$ final states in 5.1 fb^{-1} of pp collisions at E_{cm} = 7 TeV and 12.2 fb^{-1} at E_{cm} = 8 TeV. The quoted signal strength is given for m_H = 125.8 GeV. Superseded by CHATRCHYAN 14AA.

[26] AAD 12AI obtain results based on 4.7–4.8 fb^{-1} of pp collisions at E_{cm} = 7 TeV and 5.8 fb^{-1} at E_{cm} = 8 TeV. The quoted signal strengths are given for m_H = 126 GeV. See also AAD 12DA.

[27] CHATRCHYAN 12N obtain results based on 4.9–5.1 fb^{-1} of pp collisions at E_{cm} = 7 TeV and 5.1–5.3 fb^{-1} at E_{cm} = 8 TeV. An excess of events over background with a local significance of 5.0 σ is observed at about m_H = 125 GeV. The quoted signal strengths are given for m_H = 125.5 GeV. See also CHATRCHYAN 12BY and CHATRCHYAN 13Y.

$\gamma\gamma$ final state

VALUE	DOCUMENT ID		TECN	COMMENT
1.10±0.06 OUR AVERAGE				
$1.04^{+0.10}_{-0.09}$	[1] AAD	23Y	ATLS	pp, 13 TeV
1.13 ± 0.09	[2] CMS	22	CMS	pp, 13 TeV
$1.14^{+0.19}_{-0.18}$	[3,4] AAD	16AN	LHC	pp, 7, 8 TeV
$5.97^{+3.39}_{-3.12}$	[5] AALTONEN	13M	TEVA	$p\bar{p} \to HX$, 1.96 TeV
• • • We do not use the following data for averages, fits, limits, etc. • • •				
	[6] HAYRAPETY...	25AL	CMS	pp, 13.6 TeV, diff. x-section
	[7] AAD	24AQ	ATLS	pp, 13.6 TeV, cross sections
	[8] TUMASYAN	23Q	CMS	pp, 13 TeV, cross sections
	[9] AAD	22N	ATLS	pp, 13 TeV, diff. x-sections
1.12 ± 0.09	[10] SIRUNYAN	21O	CMS	pp, 13 TeV
$1.20^{+0.18}_{-0.14}$	[11] SIRUNYAN	19AT	CMS	pp, 13 TeV
	[12] SIRUNYAN	19L	CMS	pp, 13 TeV, diff. x-section
$0.99^{+0.15}_{-0.14}$	[13] AABOUD	18BO	ATLS	pp, 13 TeV
$1.18^{+0.17}_{-0.14}$	[14] SIRUNYAN	18DS	CMS	pp, $H \to \gamma\gamma$, 13 TeV, floated m_H
$1.14^{+0.27}_{-0.25}$	[4] AAD	16AN	ATLS	pp, 7, 8 TeV
$1.11^{+0.25}_{-0.23}$	[4] AAD	16AN	CMS	pp, 7, 8 TeV
	[15] KHACHATRY...	16G	CMS	pp, 8 TeV, diff. x-section
$1.17 \pm 0.23^{+0.10}_{-0.08}{}^{+0.12}_{-0.08}$	[16] AAD	14BC	ATLS	$pp \to HX$, 7, 8 TeV
	[17] AAD	14BJ	ATLS	pp, 8 TeV, diff. x-section
$1.14 \pm 0.21^{+0.09}_{-0.05}{}^{+0.13}_{-0.09}$	[18] KHACHATRY...	14P	CMS	pp, 7, 8 TeV
$1.55^{+0.33}_{-0.28}$	[19] AAD	13AK	ATLS	pp, 7 and 8 TeV
$7.81^{+4.61}_{-4.42}$	[20] AALTONEN	13L	CDF	$p\bar{p} \to HX$, 1.96 TeV
$4.20^{+4.60}_{-4.20}$	[21] ABAZOV	13L	D0	$p\bar{p} \to HX$, 1.96 TeV
1.8 ± 0.5	[22] AAD	12AI	ATLS	$pp \to HX$, 7, 8 TeV
2.2 ± 0.7	[22] AAD	12AI	ATLS	$pp \to HX$, 7 TeV
1.5 ± 0.6	[22] AAD	12AI	ATLS	$pp \to HX$, 8 TeV
$1.54^{+0.46}_{-0.42}$	[23] CHATRCHYAN	12N	CMS	$pp \to HX$, 7, 8 TeV

[1] AAD 23Y use 139 fb^{-1} of pp collisions at E_{cm} = 13 TeV. The quoted results are given for m_H = 125.09 GeV and Γ_H = 4.07 MeV. Measured $\sigma \cdot B$ and ratios to the SM predictions for the different production modes are shown in their Table 9 and Fig. 9. Measured cross sections and ratios to the SM predictions in the reduced stage-1.2 (see their Fig. 11) simplified template cross section framework are shown in their Table 10 and Fig. 12. Wilson coefficients in the Warsaw basis (see their Table 11) at 95% CL are measured; see their Table 16 and Fig. 17.

[2] CMS 22 report combined results (see their Extended Data Table 2) using up to 138 fb^{-1} of data at E_{cm} = 13 TeV, assuming m_H = 125.38 GeV. See their Fig. 2 right.

[3] AAD 16AN perform fits to the ATLAS and CMS data at E_{cm} = 7 and 8 TeV. The signal strengths for individual production processes are $1.10^{+0.23}_{-0.22}$ for gluon fusion, 1.3 ± 0.5 for vector boson fusion, $0.5^{+1.3}_{-1.2}$ for WH production, $0.5^{+3.0}_{-2.5}$ for ZH production, and $2.2^{+1.6}_{-1.3}$ for $t\bar{t}H$ production.

[4] AAD 16AN: In the fit, relative production cross sections are fixed to those in the Standard Model. The quoted signal strength is given for m_H = 125.09 GeV.

[5] AALTONEN 13M combine all Tevatron data from the CDF and D0 Collaborations with up to 10.0 fb^{-1} and 9.7 fb^{-1}, respectively, of $p\bar{p}$ collisions at E_{cm} = 1.96 TeV. The quoted signal strength is given for m_H = 125 GeV.

[6] HAYRAPETYAN 25AL measure fiducial and differential cross sections of $pp \to H \to \gamma\gamma$ at E_{cm} = 13.6 TeV with 34.7 fb^{-1} data. The quoted results are given for m_H = 125.38 GeV. The inclusive fiducial cross section is $74 \pm 11^{+5}_{-4}$ fb with the fiducial region defined in their Section 6. Differential fiducial cross sections as a function of Higgs boson p_T, rapidity, the number of jets, leading jet p_T are shown in their Figs. 7–10.

[7] AAD 24AQ measure fiducial and total cross sections at E_{cm} = 13.6 TeV with 31.4 fb^{-1} data. The quoted results are given for m_H = 125.09 GeV. The inclusive fiducial cross section is 76^{+14}_{-13} fb with their defined fiducial region (see their Table 2), where 67.6 ± 3.7 fb is expected in the SM. Assuming SM values for the acceptance and the branching fraction, the total cross section is 67^{+12}_{-11} pb, where 59.9 ± 2.6 pb is expected in the SM.

[8] TUMASYAN 23Q measure fiducial and differential cross sections at E_{cm} = 13 TeV with 137 fb^{-1} data. The quoted results are given for m_H = 125.38 GeV. The inclusive fiducial $\sigma \cdot B$ is $73.4^{+5.4}_{-5.3}$(stat)$^{+2.4}_{-2.2}$(syst) fb with their defined fiducial region (see their Section 7 and Table 2), where 75.4 ± 4.1 fb is expected in the Standard Model. See their Fig. 8 including other fiducial $\sigma \cdot B$ defined in their Table 3. Differential $\sigma \cdot B$ are shown in their Figs. 10–15. Double-differential $\sigma \cdot B$ are in their Figs. 16 and 17.

[9] AAD 22N measure fiducial and differential cross sections of $pp \rightarrow H \rightarrow \gamma\gamma$ at E_{cm} = 13 TeV with 139 fb^{-1} data. The quoted results are given for m_H = 125.09 GeV. The inclusive fiducial $\sigma \cdot B$ is 67 ± 5 ± 4 fb with their defined fiducial region. Other fiducial $\sigma \cdot B$ are in their Table 3. Differential $\sigma \cdot B$ are shown in their Figs. 8–13, 15, 25–32, 35, 36. Double-differential $\sigma \cdot B$ are in their Figs. 14, 33, 34. Modifications of the *b*- and *c*-quark Yukawa couplings to *H*, κ_b and κ_c at 95% CL are in their Table 6 and Fig. 18. Wilson coefficients at 95% CL are in their Table 7 and Fig. 21.

[10] SIRUNYAN 21O measures cross sections and couplings with the $H \rightarrow \gamma\gamma$ channel using 137 fb^{-1} data at E_{cm} = 13 TeV. Results are given for m_H = 125.38 GeV. The signal strengths for individual production processes are given in their Fig. 16. Cross sections are given in their Tables 12 and 13 and Figs. 18 and 20, which are based on the simplified template cross section framework (reduced stage-1.2). Results in the κ-framework are given in their Fig. 22.

[11] SIRUNYAN 19AT perform a combine fit to 35.9 fb^{-1} of data at E_{cm} = 13 TeV.

[12] SIRUNYAN 19L measure fiducial and differential cross sections of the process $pp \rightarrow H \rightarrow \gamma\gamma$ at E_{cm} = 13 TeV with 35.9 fb^{-1}. See their Figs. 4–11.

[13] AABOUD 18BO use 36.1 fb^{-1} of pp collisions at E_{cm} = 13 TeV. The signal strengths for the individual production modes are: $0.81^{+0.19}_{-0.18}$ for gluon fusion, $2.0^{+0.6}_{-0.5}$ for vector boson fusion, $0.7^{+0.9}_{-0.8}$ for VH production ($V = W, Z$), and 0.5 ± 0.6 for $t\overline{t}H$ and tH production. Other measurements of cross sections and couplings are summarized in their Section 10. The quoted values are given for m_H = 125.09 GeV.

[14] SIRUNYAN 18DS use 35.9 fb^{-1} of $pp \rightarrow H$ collisions with $H \rightarrow \gamma\gamma$ at E_{cm} = 13 TeV. The Higgs mass is floated in the measurement of a signal strength. The result is $1.18^{+0.12}_{-0.11}$(stat.)$^{+0.09}_{-0.07}$(syst.)$^{+0.07}_{-0.06}$(theory), which is largely insensitive to the Higgs mass around 125 GeV.

[15] KHACHATRYAN 16G measure fiducial and differential cross sections of the process $pp \rightarrow HX$, $H \rightarrow \gamma\gamma$ at E_{cm} = 8 TeV with 19.7 fb^{-1}. See their Figs. 4–6 and Table 1 for data.

[16] AAD 14BC use 4.5 fb^{-1} of pp collisions at E_{cm} = 7 TeV and 20.3 fb^{-1} at E_{cm} = 8 TeV. The last uncertainty in the measurement is theory systematics. The quoted signal strength is given for m_H = 125.4 GeV. The signal strengths for the individual production modes are: 1.32 ± 0.38 for gluon fusion, 0.8 ± 0.7 for vector boson fusion, 1.0 ± 1.6 for WH production, $0.1^{+3.7}_{-0.1}$ for ZH production, and $1.6^{+2.7}_{-1.8}$ for $t\overline{t}H$ production.

[17] AAD 14BJ measure fiducial and differential cross sections of the process $pp \rightarrow HX$, $H \rightarrow \gamma\gamma$ at E_{cm} = 8 TeV with 20.3 fb^{-1}. See their Table 3 and Figs. 3–12 for data.

[18] KHACHATRYAN 14P use 5.1 fb^{-1} of pp collisions at E_{cm} = 7 TeV and 19.7 fb^{-1} at E_{cm} = 8 TeV. The last uncertainty in the measurement is theory systematics. The quoted signal strength is given for m_H = 124.7 GeV. The signal strength for the gluon fusion and $t\overline{t}H$ production mode is $1.13^{+0.37}_{-0.31}$, while the signal strength for the vector boson fusion and WH, ZH production mode is $1.16^{+0.63}_{-0.58}$.

[19] AAD 13AK use 4.7 fb^{-1} of pp collisions at E_{cm} = 7 TeV and 20.7 fb^{-1} at E_{cm} = 8 TeV. The quoted signal strength is given for m_H = 125.5 GeV.

[20] AALTONEN 13L combine all CDF results with 9.45–10.0 fb^{-1} of $p\overline{p}$ collisions at E_{cm} = 1.96 TeV. The quoted signal strength is given for m_H = 125 GeV.

[21] ABAZOV 13L combine all D0 results with up to 9.7 fb^{-1} of $p\overline{p}$ collisions at E_{cm} = 1.96 TeV. The quoted signal strength is given for m_H = 125 GeV.

[22] AAD 12AI obtain results based on 4.8 fb^{-1} of pp collisions at E_{cm} = 7 TeV and 5.9 fb^{-1} at E_{cm} = 8 TeV. The quoted signal strengths are given for m_H = 126 GeV. See also AAD 12DA.

[23] CHATRCHYAN 12N obtain results based on 5.1 fb^{-1} of pp collisions at E_{cm}=7 TeV and 5.3 fb^{-1} at E_{cm}=8 TeV. The quoted signal strength is given for m_H=125.5 GeV. See also CHATRCHYAN 13Y.

$c\overline{c}$ final state

VALUE	CL%	DOCUMENT ID		TECN	COMMENT
− 0.5 ± 3.4 OUR AVERAGE					
− 1.6 ± 4.5		[1] HAYRAPETY...	26	CMS	pp, $t\overline{t}H$, 13 TeV
$1.0^{+5.4}_{-5.2}$		[2] AAD	25Y	ATLS	$pp \rightarrow WH/ZH$, 13 TeV
• • • We do not use the following data for averages, fits, limits, etc. • • •					
< 7.8	95	[1] HAYRAPETY...	26	CMS	pp, $t\overline{t}H$, 13 TeV
< 11.5	95	[2] AAD	25Y	ATLS	$pp \rightarrow WH/ZH$, 13 TeV
$9.4^{+20.3}_{-19.9}$		[3] TUMASYAN	23AD	CMS	$pp \rightarrow WH/ZH$ (boosted), 13 TeV
< 47	95	[3] TUMASYAN	23AD	CMS	$pp \rightarrow WH/ZH$ (boosted), 13 TeV
< 14	95	[4] TUMASYAN	23AH	CMS	$pp \rightarrow WH/ZH$, 13 TeV
− 9 ± 10 ± 11		[5,6] AAD	22W	ATLS	$pp \rightarrow WH/ZH$, 13 TeV
− 9 ± 10 ± 12		[5,7] AAD	22W	ATLS	$pp \rightarrow WH/ZH$, 13 TeV
< 26	95	[5] AAD	22W	ATLS	$pp \rightarrow WH/ZH$, 13 TeV
37 ± 17 $^{+11}_{-9}$		[8] SIRUNYAN	20AE	CMS	pp, 13 TeV
< 110	95	[9] AABOUD	18M	ATLS	pp, 13 TeV

[1] HAYRAPETYAN 26 search for $t\overline{t}H$, $H \rightarrow c\overline{c}$ together with the $t\overline{t}H$, $H \rightarrow b\overline{b}$ measurement using 138 fb^{-1} of pp collision data at E_{cm} = 13 TeV. The quoted limit corresponds to $\sigma_{t\overline{t}H} \cdot B(H \rightarrow c\overline{c})$ < 0.11 pb at 95% CL.

[2] AAD 25Y present measurements of VH, $H \rightarrow b\overline{b}$ and $H \rightarrow c\overline{c}$ ($V = W, Z$) using 140 fb^{-1} of pp collision data at E_{cm} = 13 TeV. Two-dimensional likelihood scan of (μ^{bb}_{VH}, μ^{cc}_{VH}) is shown in their Fig. 11.

[3] TUMASYAN 23AD search for Higgs produced with transverse momenta greater than 450 GeV and decaying to $c\overline{c}$ using 138 fb^{-1} of pp collision data at E_{cm} = 13 TeV.

[4] TUMASYAN 23AH search for VH, $H \rightarrow c\overline{c}$ ($V = W, Z$) using 138 fb^{-1} of pp collision data at E_{cm} = 13 TeV. The upper limit on $\sigma(pp \rightarrow VH) \cdot B(H \rightarrow c\overline{c})$ is 0.94 pb at 95% CL. See their Fig. 4. The quoted values are given for m_H = 125.38 GeV.

[5] AAD 22W search for VH, $H \rightarrow c\overline{c}$ ($V = W, Z$) using 139 fb^{-1} of pp collision data at E_{cm} = 13 TeV. The results are given for m_H = 125 GeV.

[6] The analysis of VH, $H \rightarrow c\overline{c}$ is combined with VH, $H \rightarrow b\overline{b}$ (AAD 21AB). The ratio $|\kappa_c/\kappa_b|$ is constrained to be less than 4.5 at 95% CL. See their Fig. 7.

[7] The constraint on the charm Yukawa coupling modifier κ_c is measured to be $|\kappa_c|$ <8.5 at 95% CL. See their Fig. 4.

[8] SIRUNYAN 20AE use 35.9 fb^{-1} at of pp collisions at E_{cm} = 13 TeV. The measured best fit value of $\sigma(pp \rightarrow VH) \cdot B(H \rightarrow c\overline{c})$ is $2.40^{+1.12}_{-1.11}{}^{+0.65}_{-0.61}$ pb (equivalent to < 4.5 pb at 95% CL upper limit, i.e. 70 times the standard model), where V is $W \rightarrow \ell\nu$, $Z \rightarrow \ell\ell$, or $Z \rightarrow \nu\nu$ ($\ell = e, \mu$). The quoted values are given for m_H = 125 GeV.

[9] AABOUD 18M use 36.1 fb^{-1} at of pp collisions at E_{cm} = 13 TeV. The upper limit on $\sigma(pp \rightarrow ZH) \cdot B(H \rightarrow c\overline{c})$ is 2.7 pb at 95% CL. This corresponds to 110 times the standard model. The quoted values are given for m_H = 125 GeV.

$b\overline{b}$ final state

VALUE	DOCUMENT ID		TECN	COMMENT
0.94 ± 0.11 OUR AVERAGE				
$0.92^{+0.16}_{-0.15}$	[1] AAD	25Y	ATLS	$pp \rightarrow VH$, $H \rightarrow b\overline{b}$, 13 TeV
$1.05^{+0.22}_{-0.21}$	[2] CMS	22	CMS	pp, 13 TeV
$0.95 \pm 0.32^{+0.20}_{-0.17}$	[3] AAD	21AJ	ATLS	VBF, $H \rightarrow b\overline{b}$, pp, 13 TeV, 126 fb^{-1}
$0.70^{+0.29}_{-0.27}$	[4,5] AAD	16AN	LHC	pp, 7, 8 TeV
$1.59^{+0.69}_{-0.72}$	[6] AALTONEN	13M	TEVA	$p\overline{p} \rightarrow HX$, 1.96 TeV
• • • We do not use the following data for averages, fits, limits, etc. • • •				
$0.91^{+0.26}_{-0.22}$	[7] HAYRAPETY...	26	CMS	pp, $t\overline{t}H$, 13 TeV
	[8] CHEKHOVSKY	25A	CMS	VH, $H \rightarrow b\overline{b}$, pp, 13 TeV
$1.4\ ^{+1.0}_{-0.9}$	[9] AAD	24F	ATLS	VH, boosted $H \rightarrow b\overline{b}$, pp, 13 TeV
$2.2\ ^{+0.9}_{-0.8}$	[10] HAYRAPETY...	24AM	CMS	$pp \rightarrow ZH$, $Z/H \rightarrow b\overline{b}$, 13 TeV
$4.9\ ^{+1.9}_{-1.6}$	[11] HAYRAPETY...	24AY	CMS	ggF, VBF, boosted $H \rightarrow b\overline{b}$, pp, 13 TeV
$1.6\ ^{+1.7}_{-1.5}$	[12] HAYRAPETY...	24AY	CMS	ggF, VBF, boosted $H \rightarrow b\overline{b}$, pp, 13 TeV
$1.01^{+0.55}_{-0.46}$	[13] HAYRAPETY...	24U	CMS	VBF, $H \rightarrow b\overline{b}$, pp, 13 TeV, 90.8 fb^{-1}
$0.99^{+0.48}_{-0.41}$	[14] HAYRAPETY...	24U	CMS	ggF, VBF, $H \rightarrow b\overline{b}$, pp, 13 TeV, 90.8 fb^{-1}
$-2.7\ ^{+5.6}_{-2.1} \pm 3.5$	[15] HAYRAPETY...	24U	CMS	ggF, $H \rightarrow b\overline{b}$, pp, 13 TeV, 90.8 fb^{-1}
$1.59^{+0.63}_{-0.72} \pm 0.54$	[15] HAYRAPETY...	24U	CMS	VBF, $H \rightarrow b\overline{b}$, pp, 13 TeV, 90.8 fb^{-1}
$1.15^{+0.22}_{-0.20}$	[16] TUMASYAN	24	CMS	$pp \rightarrow WH/ZH$, $H \rightarrow b\overline{b}$, 13 TeV, 138 fb^{-1}
0.8 ± 3.2	[17] AAD	22X	ATLS	boosted $H \rightarrow b\overline{b}$, pp, 13 TeV
$1.02^{+0.12}_{-0.11}{}^{+0.14}_{-0.13}$	[18] AAD	21AB	ATLS	$pp \rightarrow VH$, $H \rightarrow b\overline{b}$, 13 TeV
$0.95 \pm 0.18^{+0.19}_{-0.18}$	[18] AAD	21AB	ATLS	$pp \rightarrow HW$, $H \rightarrow b\overline{b}$, 13 TeV, 139 fb^{-1}
$1.08 \pm 0.17^{+0.18}_{-0.15}$	[18] AAD	21AB	ATLS	$pp \rightarrow HZ$, $H \rightarrow b\overline{b}$, 13 TeV, 139 fb^{-1}
$0.72^{+0.29}_{-0.28}{}^{+0.26}_{-0.22}$	[19] AAD	21H	ATLS	$pp \rightarrow HW/HZ$, $H \rightarrow b\overline{b}$, boosted W/Z, 13 TeV, 139 fb^{-1}
1.3 ± 1.0	[20] AAD	21M	ATLS	VBF+γ, $H \rightarrow b\overline{b}$, pp, 13 TeV, 132 fb^{-1}
3.7 ± 1.2 $^{+0.11}_{-0.9}$	[21] SIRUNYAN	20BL	CMS	boosted $H \rightarrow b\overline{b}$, pp, 13 TeV
	[22] AABOUD	19U	ATLS	$pp \rightarrow VH$, $H \rightarrow b\overline{b}$, 13 TeV, cross sections
1.12 ± 0.29	[23] SIRUNYAN	19AT	CMS	pp, 13 TeV
$1.16^{+0.27}_{-0.25}$	[24] AABOUD	18BN	ATLS	$pp \rightarrow HW/HZ$, $H \rightarrow b\overline{b}$, 13 TeV, 79.8 fb^{-1}
$0.98^{+0.22}_{-0.21}$	[25] AABOUD	18BN	ATLS	$pp \rightarrow HW/HZ$, $H \rightarrow b\overline{b}$, 7, 8, 13 TeV
1.01 ± 0.20	[26] AABOUD	18BN	ATLS	$pp \rightarrow HX$, ggF, VBF, VH, $t\overline{t}H$ 7, 8, 13 TeV
$2.5\ ^{+1.4}_{-1.3}$	[27,28] AABOUD	18BQ	ATLS	$pp \rightarrow HX$, VBF, ggF, VH, $t\overline{t}H$, 13 TeV
$3.0\ ^{+1.7}_{-1.6}$	[27,29] AABOUD	18BQ	ATLS	$pp \rightarrow HX$, VBF, 13 TeV
	[30] AALTONEN	18C	CDF	$p\overline{p} \rightarrow HX$, 1.96 TeV
$1.19^{+0.40}_{-0.38}$	[31] SIRUNYAN	18AE	CMS	$pp \rightarrow HW/HZ$, $H \rightarrow b\overline{b}$, 13 TeV
$1.06^{+0.31}_{-0.29}$	[32] SIRUNYAN	18AE	CMS	$pp \rightarrow HW/HZ$, $H \rightarrow b\overline{b}$, 7, 8, 13 TeV

Int. J. Mod. Phys. A 2026.41. Downloaded from www.worldscientific.com
by UNIVERSITY OF CALIFORNIA @ BERKELEY on 09/16/26. Reproduction is strictly not permitted, except for Open Access articles.

Int. J. Mod. Phys. A 2026.41. Downloaded from www.worldscientific.com
by UNIVERSITY OF CALIFORNIA @ BERKELEY on 09/16/26. Re-use and distribution is strictly not permitted, except for Open Access articles.

1.06 ± 0.26	[33] SIRUNYAN	18DB	CMS	$pp \to HW/HZ$, $H \to b\overline{b}$, 13 TeV, 77.2 fb^{-1}
1.01 ± 0.22	[34] SIRUNYAN	18DB	CMS	$pp \to HW/HZ$, $H \to b\overline{b}$, 7, 8, 13 TeV
1.04 ± 0.20	[35] SIRUNYAN	18DB	CMS	$pp \to HX$, ggF, VBF, VH, $t\overline{t}H$ 7, 8, 13 TeV
$2.3\ ^{+1.8}_{-1.6}$	[36] SIRUNYAN	18E	CMS	$pp \to HX$, boosted, 13 TeV
$1.20^{+0.24}_{-0.23}{}^{+0.34}_{-0.28}$	[37] AABOUD	17BA	ATLS	$pp \to HW/ZX$, $H \to b\overline{b}$, 13 TeV, 36.1 fb^{-1}
$0.90 \pm 0.18^{+0.21}_{-0.19}$	[38] AABOUD	17BA	ATLS	$pp \to HW/ZX$, $H \to b\overline{b}$, 7, 8, 13 TeV
$-0.8\ \pm 1.3\ ^{+1.8}_{-1.9}$	[39] AABOUD	16X	ATLS	$pp \to HX$, VBF, 8 TeV
0.62 ± 0.37	[5] AAD	16AN	ATLS	pp, 7, 8 TeV
$0.81^{+0.45}_{-0.43}$	[5] AAD	16AN	CMS	pp, 7, 8 TeV
$0.63^{+0.31}_{-0.30}{}^{+0.24}_{-0.23}$	[40] AAD	16K	ATLS	pp, 7, 8 TeV
$0.52 \pm 0.32 \pm 0.24$	[41] AAD	15G	ATLS	$pp \to HW/ZX$, 7, 8 TeV
$2.8\ ^{+1.6}_{-1.4}$	[42] KHACHATRY...	15Z	CMS	$pp \to HX$, VBF, 8 TeV
$1.03^{+0.44}_{-0.42}$	[43] KHACHATRY...	15Z	CMS	pp, 8 TeV, combined
$1.0\ \pm 0.5$	[44] CHATRCHYAN	14AI	CMS	$pp \to HW/ZX$, 7, 8 TeV
$1.72^{+0.92}_{-0.87}$	[45] AALTONEN	13L	CDF	$p\overline{p} \to HX$, 1.96 TeV
$1.23^{+1.24}_{-1.17}$	[46] ABAZOV	13L	D0	$p\overline{p} \to HX$, 1.96 TeV
$0.5\ \pm 2.2$	[47] AAD	12AI	ATLS	$pp \to HW/ZX$, 7 TeV
	[48] AALTONEN	12T	TEVA	$p\overline{p} \to HW/ZX$, 1.96 TeV
$0.48^{+0.81}_{-0.70}$	[49] CHATRCHYAN	12N	CMS	$pp \to HW/ZX$, 7, 8 TeV

[1] AAD 25Y present measurements of VH, $H \to b\overline{b}$ ($V = W,\ Z$) using 140 fb^{-1} of pp collision data at $E_{cm} = 13$ TeV. The observed significance for WH and ZH are 5.3 and 4.9 σ, respectively. See their Fig. 12. Cross sections are given in their Table 8 and Figs. 15 and 16, which are based on the simplified template cross section framework (extended stage-1.2).

[2] CMS 22 report combined results (see their Extended Data Table 2) using up to 138 fb^{-1} of data at $E_{cm} = 13$ TeV, assuming $m_H = 125.38$ GeV. See their Fig. 2 right.

[3] AAD 21AJ present measurements of $H \to b\overline{b}$ in the VBF production mode. The inclusive VBF cross sections with and without the branching ratio of $H \to b\overline{b}$ are $2.07 \pm 0.70^{+0.46}_{-0.37}$ fb and $3.56 \pm 1.21^{+0.80}_{-0.64}$ fb, respectively. The latter is obtained assuming the SM value of B($H \to b\overline{b}$) = 0.5809 and $m_H = 125$ GeV.

[4] AAD 16AN perform fits to the ATLAS and CMS data at $E_{cm} = 7$ and 8 TeV. The signal strengths for individual production processes are 1.0 ± 0.5 for WH production, 0.4 ± 0.4 for ZH production, and 1.1 ± 1.0 for $t\overline{t}H$ production.

[5] AAD 16AN: In the fit, relative production cross sections are fixed to those in the Standard Model. The quoted signal strength is given for $m_H = 125.09$ GeV.

[6] AALTONEN 13M combine all Tevatron data from the CDF and D0 Collaborations with up to 10.0 fb^{-1} and 9.7 fb^{-1}, respectively, of $p\overline{p}$ collisions at $E_{cm} = 1.96$ TeV. The quoted signal strength is given for $m_H = 125$ GeV.

[7] HAYRAPETYAN 26 search for $t\overline{t}H$, $H \to c\overline{c}$ together with the $t\overline{t}H$, $H \to b\overline{b}$ measurement using 138 fb^{-1} of pp collision data at $E_{cm} = 13$ TeV.

[8] CHEKHOVSKY 25A constrain six Wilson coefficients in the Warsaw basis using 138 fb^{-1} of pp collision data at $E_{cm} = 13$ TeV. The results are shown in their Figs. 7 (for linear and quadratic), 9–13 (two-dimensional likelihood scan). The limits on the energy scale for three different assumptions for each Wilson coefficient are shown in their Fig. 8.

[9] AAD 24F present studies of the VH production mode in the boosted $V \to q\overline{q}$ and $H \to b\overline{b}$ ($p_T(H) > 250$ GeV) using 137 fb^{-1} of pp collision data at $E_{cm} = 13$ TeV. The quoted signal strength is given for $m_H = 125.09$ GeV and corresponds to a significance of 1.7 standard deviations. The corresponding inclusive cross section is $3.1 \pm 1.3^{+1.8}_{-1.4}$ pb. The signal strengths and cross sections are given in their Table I for three $p_T(H)$ regions: $250 < p_T(H) < 450$ GeV, $450 < p_T(H) < 650$ GeV, 650 GeV $< p_T(H)$ with $|y(H)| < 2$.

[10] HAYRAPETYAN 24AM search for ZH, $H \to b\overline{b}$, $Z \to b\overline{b}$ using 133 fb^{-1} of pp collision data at $E_{cm} = 13$ TeV. The upper limit at 95% CL on the ZH production is 5.0 times the SM prediction.

[11] HAYRAPETYAN 24AY present measurements of boosted $H \to b\overline{b}$ ($p_T > 450$ GeV) via VBF or gluon fusion productions using 138 fb^{-1} of pp collision data at $E_{cm} = 13$ TeV. The result is given for the VBF production. See their Table 3. The VH and $t\overline{t}H$ production rates are fixed to the SM values. The VBF signal strengths and the fiducial cross sections for two different m_{jj} regions and STXS stage 1.2 bins are shown in their Figs. 9 and 10, respectively.

[12] HAYRAPETYAN 24AY present measurements of boosted $H \to b\overline{b}$ ($p_T > 450$ GeV) via VBF or gluon fusion productions using 138 fb^{-1} of pp collision data at $E_{cm} = 13$ TeV. The result is given for the gluon fusion production. See their Table 3. The VH and $t\overline{t}H$ production rates are fixed to the SM values. The gluon fusion signal strengths and the fiducial cross sections for 6 different p_T regions and STXS stage 1.2 bins are shown in their Figs. 9 and 10, respectively.

[13] HAYRAPETYAN 24U present measurements of $H \to b\overline{b}$ in the VBF production mode using 90.8 fb^{-1} of data at $E_{cm} = 13$ TeV constraining the ggF production to be the SM expectation. The quoted signal strength corresponds to a significance of 2.4 standard deviations.

[14] HAYRAPETYAN 24U present measurements of $H \to b\overline{b}$ in the inclusive (ggF+VBF) production mode using 90.8 fb^{-1} of data at $E_{cm} = 13$ TeV. The quoted signal strength corresponds to a significance of 2.6 standard deviations.

[15] HAYRAPETYAN 24U present measurements of $H \to b\overline{b}$ in the ggF and VBF production modes using 90.8 fb^{-1} of data at $E_{cm} = 13$ TeV. The signal strengths for the ggF and VBF production modes are independently obtained. See their Fig. 11.

[16] TUMASYAN 24 report the measurement of VH, $H \to b\overline{b}$ ($V = W,\ Z$) using 138 fb^{-1} of pp collision data at $E_{cm} = 13$ TeV. The quoted signal strength corresponds to a significance of 6.3 standard deviations. Signal strengths for WH and ZH are given in their Fig. 7. Signal strengths and $\sigma \cdot B$ for 8 different bins defined based on the the simplified template cross section framework are given in their Figs. 8 and 9 and Table VII.

[17] AAD 22X measure cross sections using a boosted $H \to b\overline{b}$ with large-radius jets. The data is 136 fb^{-1} of pp collisions at $E_{cm} = 13$ TeV. All the results are given for $m_H = 125$ GeV. The inclusive signal strength is given using data with a H candidate jet $p_T > 250$ GeV. The fiducial H production cross section ($p_T(H) > 450$ GeV and $|y(H)| < 2$) is <115 fb (95% CL) and the upper limits for other four different p_T regions are shown in their Fig 12. The measured fiducial H production cross section ($p_T(H) > 1$ TeV) is $2.3 \pm 3.9(\text{stat}) \pm 1.3(\text{syst}) \pm 0.5(\text{theory})$ fb.

[18] AAD 21AB search for VH, $H \to b\overline{b}$ ($V = W,\ Z$) using 139 fb^{-1} of pp collision data at $E_{cm} = 13$ TeV. The results are given for $m_H = 125$ GeV. Cross sections are given in their Table 13 and Fig. 7, which are based on the simplified template cross section framework (reduced stage-1.2). Wilson coefficients of the Warsaw-basis operators are given in their Fig. 9.

[19] AAD 21H present measurements of $H \to b\overline{b}$ with a boosted vector boson ($p_T > 250$ GeV) using 139 fb^{-1} of pp collision data at $E_{cm} = 13$ TeV. Cross sections are given in their Table 6 and Fig. 4, which are based on the simplified template cross section framework (reduced stage-1.2). Wilson coefficients of the Warsaw-basis operators are given in their Fig. 5.

[20] AAD 21M search for VBF+γ, $H \to b\overline{b}$ using 132 fb^{-1} of pp collision data at $E_{cm} = 13$ TeV.

[21] SIRUNYAN 20BL search for boosted $H \to b\overline{b}$ (a H candidate jet $p_T > 450$ GeV) using 137 fb^{-1} of pp collision data at $E_{cm} = 13$ TeV. The quoted signal strength corresponds to a significance of 2.5 standard deviations and is given for $m_H = 125$ GeV. A differential fiducial cross section as a function of Higgs boson p_T for ggF is shown in their Fig. 7, assuming the other production modes occur at the expected SM rates. The reported value is $3.7 \pm 1.2^{+0.8}_{-0.7}{}^{+0.8}_{-0.5}$ where the last uncertainty comes from theoretical modeling. We have combined the systematic uncertainties in quadrature.

[22] AABOUD 19U measure cross sections of $pp \to VH$, $H \to b\overline{b}$ production as a function of the gauge boson transverse momentum using data of 79.8 fb^{-1}. The kinematic fiducial volumes used is based on the simplified template cross section framework (reduced stage-1). See their Table 3 and Fig. 3.

[23] SIRUNYAN 19AT perform a combine fit to 35.9 fb^{-1} of data at $E_{cm} = 13$ TeV.

[24] AABOUD 18BN search for VH, $H \to b\overline{b}$ ($V = W,\ Z$) using 79.8 fb^{-1} of pp collision data at $E_{cm} = 13$ TeV. The quoted signal strength corresponds to a significance of 4.9 standard deviations and is given for $m_H = 125$ GeV.

[25] AABOUD 18BN combine results of 79.8 fb^{-1} at $E_{cm} = 13$ TeV with results of VH at $E_{cm} = 7$ and 8 TeV.

[26] AABOUD 18BN combine results of VH at $E_{cm} = 7$, 8 and 13 TeV with results of VBF (+gluon fusion) and $t\overline{t}H$ at $E_{cm} = 7$, 8, and 13 TeV to perform a search for the $H \to b\overline{b}$ decay. The quoted signal strength assumes a SM production strength and corresponds to a significance of 5.4 standard deviations.

[27] AABOUD 18BQ search for $H \to b\overline{b}$ produced through vector-boson fusion (VBF) and VBF+γ with 30.6 fb^{-1} pp collision data at $E_{cm} = 13$ TeV. The quoted signal strength is given for $m_H = 125$ GeV.

[28] The signal strength is measured including all production modes (VBF, ggF, VH, $t\overline{t}H$).

[29] The signal strength is measured for VBF-only and others (ggF, VH, $t\overline{t}H$) are constrained to Standard Model expectations with uncertainties described in their Section VIII B.

[30] AALTONEN 18C use 5.4 fb^{-1} of $p\overline{p}$ collisions at $E_{cm} = 1.96$ TeV. The upper limit at 95% CL on $p\overline{p} \to H \to b\overline{b}$ is 33 times the SM prediction, which corresponds to a cross section of 40.6 pb.

[31] SIRUNYAN 18AE use 35.9 fb^{-1} of pp collision data at $E_{cm} = 13$ TeV. The quoted signal strength corresponds to 3.3 standard deviations and is given for $m_H = 125.09$ GeV.

[32] SIRUNYAN 18AE combine the result of 35.9 fb^{-1} at $E_{cm} = 13$ TeV with the results obtained from data of up to 5.1 fb^{-1} at $E_{cm} = 7$ TeV and up to 18.9 fb^{-1} at $E_{cm} = 8$ TeV (CHATRCHYAN 14AI and KHACHATRYAN 15Z). The quoted signal strength corresponds to 3.8 standard deviations and is given for $m_H = 125.09$ GeV.

[33] SIRUNYAN 18DB search for VH, $H \to b\overline{b}$ ($V = W,\ Z$) using 77.2 fb^{-1} of pp collision data at $E_{cm} = 13$ TeV. The quoted signal strength corresponds to a significance of 4.4 standard deviations and is given for $m_H = 125.09$ GeV.

[34] SIRUNYAN 18DB combine the result of 77.2 fb^{-1} at $E_{cm} = 13$ TeV with the results obtained from data of up to 5.1 fb^{-1} at $E_{cm} = 7$ TeV and up to 18.9 fb^{-1} at $E_{cm} = 8$ TeV. The quoted signal strength corresponds to a significance of 4.8 standard deviations and is given for $m_H = 125.09$ GeV.

[35] SIRUNYAN 18DB combine results of 77.2 fb^{-1} at $E_{cm} = 13$ TeV with results of gluon fusion (ggF), VBF and $t\overline{t}H$ at $E_{cm} = 7$ TeV, 8 TeV and 13 TeV to perform a search for the $H \to b\overline{b}$ decay. The quoted signal strength assumes a SM production strength and corresponds to a significance of 5.6 standard deviations and is given for $m_H = 125.09$ GeV.

[36] SIRUNYAN 18E use 35.9 fb^{-1} at $E_{cm} = 13$ TeV. The quoted signal strength is given for $m_H = 125$ GeV. They measure $\sigma \cdot B$ for gluon fusion production of $H \to b\overline{b}$ with $p_T > 450$ GeV, $|\eta| < 2.5$ to be $74 \pm 48^{+17}_{-10}$ fb.

[37] AABOUD 17BA use 36.1 fb^{-1} at $E_{cm} = 13$ TeV. The quoted signal strength is given for $m_H = 125$ GeV. They give $\sigma(\text{W H}) \cdot B(H \to b\overline{b}) = 1.08^{+0.54}_{-0.47}$ pb and $\sigma(\text{Z H}) \cdot B(H \to b\overline{b}) = 0.57^{+0.26}_{-0.23}$ pb.

[38] AABOUD 17BA combine 7, 8 and 13 TeV analyses. The quoted signal strength is given for $m_H = 125$ GeV.

[39] AABOUD 16X search for vector-boson fusion production of H decaying to $b\overline{b}$ in 20.2 fb^{-1} of pp collisions at $E_{cm} = 8$ TeV. The quoted signal strength is given for $m_H = 125$ GeV.

[40] AAD 16K use up to 4.7 fb^{-1} of pp collisions at $E_{cm} = 7$ TeV and up to 20.3 fb^{-1} at $E_{cm} = 8$ TeV. The quoted signal strength is given for $m_H = 125.36$ GeV.

[41] AAD 15G use 4.7 fb^{-1} of pp collisions at $E_{cm} = 7$ TeV and 20.3 fb^{-1} at $E_{cm} = 8$ TeV. The quoted signal strength is given for $m_H = 125.36$ GeV.

Int. J. Mod. Phys. A 2026.41. Downloaded from www.worldscientific.com
by UNIVERSITY OF CALIFORNIA @ BERKELEY on 09/16/26. Re strictly not permitted, except for Open Access articles.

[42] KHACHATRYAN 15Z search for vector-boson fusion production of H decaying to $b\overline{b}$ in up to 19.8 fb^{-1} of pp collisions at E_{cm} = 8 TeV. The quoted signal strength is given for m_H = 125 GeV.

[43] KHACHATRYAN 15Z combined vector boson fusion, WH, ZH production, and $t\overline{t}H$ production results. The quoted signal strength is given for m_H = 125 GeV.

[44] CHATRCHYAN 14AI use up to 5.1 fb^{-1} of pp collisions at E_{cm} = 7 TeV and up to 18.9 fb^{-1} at E_{cm} = 8 TeV. The quoted signal strength is given for m_H = 125 GeV. See also CHATRCHYAN 14AJ.

[45] AALTONEN 13L combine all CDF results with 9.45–10.0 fb^{-1} of $p\overline{p}$ collisions at E_{cm} = 1.96 TeV. The quoted signal strength is given for m_H = 125 GeV.

[46] ABAZOV 13L combine all D0 results with up to 9.7 fb^{-1} of $p\overline{p}$ collisions at E_{cm} = 1.96 TeV. The quoted signal strength is given for m_H = 125 GeV.

[47] AAD 12AI obtain results based on 4.6–4.8 fb^{-1} of pp collisions at E_{cm} = 7 TeV. The quoted signal strengths are given in their Fig. 10 for m_H = 126 GeV. See also Fig. 13 of AAD 12DA.

[48] AALTONEN 12T combine AALTONEN 12Q, AALTONEN 12R, AALTONEN 12S, ABAZOV 12O, ABAZOV 12P, and ABAZOV 12K. An excess of events over background is observed which is most significant in the region m_H = 120–135 GeV, with a local significance of up to 3.3 σ. The local significance at m_H = 125 GeV is 2.8 σ, which corresponds to $(\sigma(HW) + \sigma(HZ)) \cdot B(H \rightarrow b\overline{b}) = (0.23^{+0.09}_{-0.08})$ pb, compared to the Standard Model expectation at m_H = 125 GeV of 0.12 ± 0.01 pb. Superseded by AALTONEN 13M.

[49] CHATRCHYAN 12N obtain results based on 5.0 fb^{-1} of pp collisions at E_{cm}=7 TeV and 5.1 fb^{-1} at E_{cm}=8 TeV. The quoted signal strength is given for m_H=125.5 GeV. See also CHATRCHYAN 13Y.

$\mu^+\mu^-$ final state

VALUE	CL%	DOCUMENT ID		TECN	COMMENT
1.31±0.29 OUR AVERAGE					
1.4 ±0.4		[1] AAD	25AR	ATLS	pp, 13, 13.6 TeV
$1.21^{+0.45}_{-0.42}$		[2] CMS	22	CMS	pp, 13 TeV
• • • We do not use the following data for averages, fits, limits, etc. • • •					
1.6 ±0.6		[3] AAD	25AR	ATLS	pp, 13.6 TeV
1.2 ±0.6		[4] AAD	21	ATLS	pp, 13 TeV
$1.19^{+0.40}_{-0.39}{}^{+0.15}_{-0.14}$		[5] SIRUNYAN	21C	CMS	pp, 13 TeV
$0.68^{+1.25}_{-1.24}$		[6] SIRUNYAN	19AT	CMS	pp, 13 TeV
$0.7 \pm 1.0\ ^{+0.2}_{-0.1}$		[7] SIRUNYAN	19E	CMS	pp, 13 TeV, 35.9 fb^{-1}
1.0 ±1.0 ±0.1		[7] SIRUNYAN	19E	CMS	pp, 7, 8, 13 TeV
−0.1 ±1.4		[8] AABOUD	17Y	ATLS	pp, 7, 8, 13 TeV
−0.1 ±1.5		[8] AABOUD	17Y	ATLS	pp, 13 TeV
0.1 ±2.5		[9] AAD	16AN	LHC	pp, 7, 8 TeV
−0.6 ±3.6		[9] AAD	16AN	ATLS	pp, 7, 8 TeV
$0.9\ ^{+3.6}_{-3.5}$		[9] AAD	16AN	CMS	pp, 7, 8 TeV
< 7.4	95	[10] KHACHATRY...	15H	CMS	$pp \rightarrow HX$, 7, 8 TeV
< 7.0	95	[11] AAD	14AS	ATLS	$pp \rightarrow HX$, 7, 8 TeV

[1] AAD 25AR search for $H \rightarrow \mu^+\mu^-$ using 140 fb^{-1} of pp data at E_{cm} = 13 TeV and 165 fb^{-1} of pp data at E_{cm} = 13.6 TeV. The quoted signal strength corresponds to a significance of 3.4 standard deviations assuming m_H = 125.09 GeV.

[2] CMS 22 report combined results (see their Extended Data Table 2) using up to 138 fb^{-1} of data at E_{cm} = 13 TeV, assuming m_H = 125.38 GeV. See their Fig. 2 right.

[3] AAD 25AR search for $H \rightarrow \mu^+\mu^-$ using 165 fb^{-1} of pp collision data at E_{cm} = 13.6 TeV. The quoted signal strength corresponds to a significance of 2.8 standard deviations assuming m_H = 125.09 GeV.

[4] AAD 21 search for $H \rightarrow \mu^+\mu^-$ using 139 fb^{-1} of pp collision data at E_{cm} = 13 TeV. The quoted signal strength corresponds to a significance of 2.0 standard deviations and is given for m_H = 125.09 GeV. The upper limit on the cross section times branching fraction is 2.2 times the SM prediction at 95% CL, which corresponds to the branching fraction upper limit of 4.7×10^{-4} (assuming SM production cross sections).

[5] SIRUNYAN 21 search for $H \rightarrow \mu^+\mu^-$ using 137 fb^{-1} of pp collision data at E_{cm} = 13 TeV. The quoted signal strength corresponds to a significance of 3.0 standard deviations and is given for m_H = 125.38 GeV.

[6] SIRUNYAN 19AT perform a combine fit to 35.9 fb^{-1} of data at E_{cm} = 13 TeV.

[7] SIRUNYAN 19E search for $H \rightarrow \mu^+\mu^-$ using 35.9 fb^{-1} of pp collisions at E_{cm} = 13 TeV and combine with results of 7 TeV (5.0 fb^{-1}) and 8 TeV (19.7 fb^{-1}). The upper limit at 95% CL on the signal strength is 2.9, which corresponds to the SM Higgs boson branching fraction to a muon pair of 6.4×10^{-4}.

[8] AABOUD 17Y use 36.1 fb^{-1} of pp collisions at E_{cm} = 13 TeV, 20.3 fb^{-1} at 8 TeV and 4.5 fb^{-1} at 7 TeV. The quoted signal strength is given for m_H = 125 GeV.

[9] AAD 16AN: In the fit, relative production cross sections are fixed to those in the Standard Model. The quoted signal strength is given for m_H = 125.09 GeV.

[10] KHACHATRYAN 15H use 5.0 fb^{-1} of pp collisions at E_{cm} = 7 TeV and 19.7 fb^{-1} at 8 TeV. The quoted signal strength is given for m_H = 125 GeV.

[11] AAD 14AS search for $H \rightarrow \mu^+\mu^-$ in 4.5 fb^{-1} of pp collisions at E_{cm} = 7 TeV and 20.3 fb^{-1} at E_{cm} = 8 TeV. The quoted signal strength is given for m_H = 125.5 GeV.

$\tau^+\tau^-$ final state

VALUE	DOCUMENT ID		TECN	COMMENT
0.91±0.09 OUR AVERAGE				
0.85±0.10	[1] CMS	22	CMS	pp, 13 TeV
$1.09^{+0.18}_{-0.17}{}^{+0.26}_{-0.22}{}^{+0.16}_{-0.11}$	[2] AABOUD	19AQ	ATLS	pp, 13 TeV
$1.11^{+0.24}_{-0.22}$	[3,4] AAD	16AN	LHC	pp, 7, 8 TeV
$1.68^{+2.28}_{-1.68}$	[5] AALTONEN	13M	TEVA	$p\overline{p} \rightarrow HX$, 1.96 TeV
• • • We do not use the following data for averages, fits, limits, etc. • • •				
	[6] AAD	25W	ATLS	pp, 13 TeV
$1.28^{+0.30}_{-0.29}{}^{+0.25}_{-0.21}$	[7] AAD	24BE	ATLS	$pp \rightarrow WH/ZH$, $H \rightarrow \tau\tau$, 13 TeV
$1.64^{+0.68}_{-0.54}$	[8] HAYRAPETY...	24AT	CMS	pp, 13 TeV, boosted $H \rightarrow \tau\tau$
$0.82^{+0.11}_{-0.10}$	[9,10] TUMASYAN	23Y	CMS	pp, 13 TeV
$0.67^{+0.20}_{-0.18}$	[9,11] TUMASYAN	23Y	CMS	pp, 13 TeV
$0.81^{+0.17}_{-0.16}$	[9,12] TUMASYAN	23Y	CMS	pp, 13 TeV
$1.79^{+0.47}_{-0.42}$	[9,13] TUMASYAN	23Y	CMS	pp, 13 TeV
	[14] AAD	22Q	ATLS	pp, 13 TeV
	[15] TUMASYAN	22AJ	CMS	pp, 13 TeV
$2.5\ ^{+1.4}_{-1.3}$	[16] SIRUNYAN	19AF	CMS	$pp \rightarrow HW/HZ$, $H \rightarrow \tau\tau$, 13 TeV
$1.24^{+0.29}_{-0.27}$	[17] SIRUNYAN	19AF	CMS	pp, 13 TeV
$1.02^{+0.26}_{-0.24}$	[18] SIRUNYAN	19AT	CMS	pp, 13 TeV
$1.09^{+0.27}_{-0.26}$	[19] SIRUNYAN	18Y	CMS	pp, 13 TeV
0.98±0.18	[20] SIRUNYAN	18Y	CMS	pp, 7, 8, 13 TeV
2.3 ±1.6	[21] AAD	16AC	ATLS	$pp \rightarrow HW/ZX$, 8 TeV
$1.41^{+0.40}_{-0.36}$	[4] AAD	16AN	ATLS	pp, 7, 8 TeV
$0.88^{+0.30}_{-0.28}$	[4] AAD	16AN	CMS	pp, 7, 8 TeV
$1.44^{+0.30}_{-0.29}{}^{+0.29}_{-0.23}$	[22] AAD	16K	ATLS	pp, 7, 8 TeV
$1.43^{+0.27}_{-0.26}{}^{+0.32}_{-0.25}\pm0.09$	[23] AAD	15AH	ATLS	$pp \rightarrow HX$, 7, 8 TeV
0.78±0.27	[24] CHATRCHYAN	14K	CMS	$pp \rightarrow HX$, 7, 8 TeV
$0.00^{+8.44}_{-0.00}$	[25] AALTONEN	13L	CDF	$p\overline{p} \rightarrow HX$, 1.96 TeV
$3.96^{+4.11}_{-3.38}$	[26] ABAZOV	13L	D0	$p\overline{p} \rightarrow HX$, 1.96 TeV
$0.4\ ^{+1.6}_{-2.0}$	[27] AAD	12AI	ATLS	$pp \rightarrow HX$, 7 TeV
$0.09^{+0.76}_{-0.74}$	[28] CHATRCHYAN	12N	CMS	$pp \rightarrow HX$, 7, 8 TeV

[1] CMS 22 report combined results (see their Extended Data Table 2) using up to 138 fb^{-1} of data at E_{cm} = 13 TeV, assuming m_H = 125.38 GeV. See their Fig. 2 right.

[2] AABOUD 19AQ use 36.1 fb^{-1} of data. The first, second and third quoted errors are statistical, experimental systematic and theory systematic uncertainties, respectively. The quoted signal strength is given for m_H = 125 GeV and corresponds to 4.4 standard deviations. Combining with 7 TeV and 8 TeV results (AAD 15AH), the observed significance is 6.4 standard deviations. The cross sections in the $H \rightarrow \tau\tau$ decay channel (m_H = 125 GeV) are measured to $3.77^{+0.60}_{-0.59}$ (stat) $^{+0.87}_{-0.74}$ (syst) pb for the inclusive, $0.28 \pm 0.09^{+0.11}_{-0.09}$ pb for VBF, and $3.1 \pm 1.0^{+1.6}_{-1.3}$ pb for gluon-fusion production. See their Table XI for the cross sections in the framework of simplified template cross sections.

[3] AAD 16AN perform fits to the ATLAS and CMS data at E_{cm} = 7 and 8 TeV. The signal strengths for individual production processes are 1.0 ± 0.6 for gluon fusion, 1.3 ± 0.4 for vector boson fusion, −1.4 ± 1.4 for WH production, $2.2^{+2.2}_{-1.8}$ for ZH production, and $-1.9^{+3.7}_{-3.3}$ for $t\overline{t}H$ production.

[4] AAD 16AN: In the fit, relative production cross sections are fixed to those in the Standard Model. The quoted signal strength is given for m_H = 125.09 GeV.

[5] AALTONEN 13M combine all Tevatron data from the CDF and D0 Collaborations with up to 10.0 fb^{-1} and 9.7 fb^{-1}, respectively, of $p\overline{p}$ collisions at E_{cm} = 1.96 TeV. The quoted signal strength is given for m_H = 125 GeV.

[6] AAD 25W measure different types of cross sections with $pp \rightarrow H \rightarrow \tau\tau$ at E_{cm} = 13 TeV with 140 fb^{-1} data. Their Fig. 5 show $\sigma \cdot B$ relative to the SM expectations for the total and per-production-mode, and their Figs. 6 and 8 show those in the simplified template cross section framework. Their Table 7 show the measurements of $\sigma \cdot B$ for per-production-mode. The differential fiducial cross sections defined in their Table 8 are given in their Fig. 10. Six Wilson coefficients in the Warsaw basis are in their Figs. 12 and 13 at 95% CL. The constraints on the Wilson coefficients c_{HW} and $c_{H\widetilde{W}}$ are obtained to be [−1.90, +0.51] and [−0.31, +0.88] at 95% CL, respectively, for the interference term alone (the linear term) assuming only one of the Wilson coefficients is non-zero.

[7] AAD 24BE measure the VH Higgs production ($V = W, Z$) with $H \rightarrow \tau\tau$ at E_{cm} = 13 TeV with 140 fb^{-1} data. The quoted signal strength corresponds to 4.2 standard deviations. The signal strengths for individual WH and ZH productions are $1.48^{+0.56}_{-0.50}$ and $1.09^{+0.51}_{-0.44}$, respectively. The results are given for m_H = 125 GeV. See their Fig. 4.

[8] HAYRAPETYAN 24AT present measurements of the boosted $H \rightarrow \tau\tau$ (p_T > 250 GeV) using 138 fb^{-1} of pp collision data at E_{cm} = 13 TeV. The quoted signal strength corresponds to a significance of 3.5 standard deviations. The fiducial inclusive production cross section is measured to be $3.88^{+1.69}_{-1.35}$ fb. The differential fiducial cross sections as a function of Higgs boson and leading jet p_T are given in their Fig. 3.

[9] TUMASYAN 23Y measure Higgs production with $pp \rightarrow H \rightarrow \tau\tau$ at E_{cm} = 13 TeV with 138 fb^{-1} data. The quoted results are given for m_H = 125.38 GeV.

[10] The inclusive $\sigma \cdot B$ is 2800^{+356}_{-335} fb (see their Figs. 10 and 14). See their Fig. 15 for the 68 % and 95 % CL contours in the $\kappa_V - \kappa_F$ plane.

[11] The quoted result is for the stage-0 simplified template cross section (STXS) and the $\sigma_{ggF} \cdot B$ is 2030^{+598}_{-555} fb (see their Figs. 10 and 14). Measured cross sections and ratios to the SM predictions in the reduced stage-1.2 STXS (see their Fig. 1) are shown in their Table 9 and Figs. 12 and 14.

Int. J. Mod. Phys. A 2026.41. Downloaded from www.worldscientific.com by UNIVERSITY OF CALIFORNIA @ BERKELEY on 09/16/26. Re-use and distribution is strictly not permitted, except for Open Access articles.

[12] The quoted result is for the stage-0 STXS and the $\sigma_{VBF} \cdot B$ is $267^{+53.9}_{-52.6}$ fb (see their Figs. 10 and 14). Measured cross sections and ratios to the SM predictions in the reduced stage-1.2 STXS (see their Fig. 2) are shown in their Table 9 and Figs. 12, 14.

[13] The quoted result is for the stage-0 STXS and the $\sigma_{VH} \cdot B$ is $79.0^{+20.5}_{-18.6}$ fb (see their Figs. 10 and 14). Measured cross sections and ratios to the SM predictions in the reduced stage-1.2 STXS (see their Fig. 3) are shown in their Table 9 and Figs. 12, 14.

[14] AAD 22Q measure cross sections of $pp \rightarrow H \rightarrow \tau\tau$ at E_{cm} = 13 TeV with 139 fb^{-1} data. The quoted results are given for m_H = 125.09 GeV and $|y(H)|$ <2.5 is required. The inclusive fiducial $\sigma \cdot B$ is 2.94 ± $0.21^{+0.37}_{-0.32}$ pb. The fiducial $\sigma \cdot B$ for the four dominant production modes are 2.65 ± $0.41^{+0.91}_{-0.67}$ pb for ggF, 0.197 ± $0.028^{+0.032}_{-0.026}$ pb for VBF, 0.115 ± $0.058^{+0.042}_{-0.040}$ pb for VH, 0.033 ± $0.031^{+0.022}_{-0.017}$ pb for $t\bar{t}H$. The cross sections using simplified template cross section framework (STXS) are given in their Fig. 14(a) and Table 15. The STXS bins (a reduced stage 1.2) are defined in their Fig. 1.

[15] TUMASYAN 22AJ measure cross sections with $pp \rightarrow H \rightarrow \tau\tau$ at E_{cm} = 13 TeV with 138 fb^{-1} data. The fiducial inclusive $\sigma \cdot B$ is 426 ± 102 fb while 408 ± 27 fb is expected in the Standard Mode for m_H = 125.38 GeV. Three differential cross sections are given; see their Fig. 1.

[16] SIRUNYAN 19AF use 35.9 fb^{-1} of data. The quoted signal strength is given for m_H = 125 GeV and corresponds to 2.3 standard deviations.

[17] SIRUNYAN 19AF use 35.9 fb^{-1} of data. HW/Z channels are added with a few updates on gluon fusion and vector boson fusion with respect to SIRUNYAN 18Y. The quoted signal strength is given for m_H = 125 GeV and corresponds to 5.5 standard deviations. The signal strengths for the individual production modes are: $1.12^{+0.53}_{-0.50}$ for gluon fusion, $1.13^{+0.45}_{-0.42}$ for vector boson fusion, $3.39^{+1.68}_{-1.54}$ for WH and $1.23^{+1.62}_{-1.35}$ for ZH. See their Fig. 7 for other couplings (κ_V, κ_f).

[18] SIRUNYAN 19AT perform a combine fit to 35.9 fb^{-1} of data at E_{cm} = 13 TeV. This combination is based on SIRUNYAN 18Y.

[19] SIRUNYAN 18Y use 35.9 fb^{-1} of pp collisions at E_{cm} = 13 TeV. The quoted signal strength is given for m_H = 125.09 GeV and corresponds to 4.9 standard deviations.

[20] SIRUNYAN 18Y combine the result of 35.9 fb^{-1} at E_{cm} = 13 TeV with the results obtained from data of 4.9 fb^{-1} at E_{cm} = 7 TeV and 19.7 fb^{-1} at E_{cm} = 8 TeV (KHACHATRYAN 15AM). The quoted signal strength is given for m_H = 125.09 GeV and corresponds to 5.9 standard deviations.

[21] AAD 16AC measure the signal strength with $pp \rightarrow HW/ZX$ processes using 20.3 fb^{-1} of E_{cm} = 8 TeV. The quoted signal strength is given for m_H = 125 GeV.

[22] AAD 16K use up to 4.7 fb^{-1} of pp collisions at E_{cm} = 7 TeV and up to 20.3 fb^{-1} at E_{cm} = 8 TeV. The quoted signal strength is given for m_H = 125.36 GeV.

[23] AAD 15AH use 4.5 fb^{-1} of pp collisions at E_{cm} = 7 TeV and 20.3 fb^{-1} at E_{cm} = 8 TeV. The third uncertainty in the measurement is theory systematics. The signal strength for the gluon fusion mode is 2.0 ± $0.8^{+1.2}_{-0.8}$ ± 0.3 and that for vector boson fusion and W/ZH production modes is $1.24^{+0.49}_{-0.45}{}^{+0.31}_{-0.29}$ ± 0.08. The quoted signal strength is given for m_H = 125.36 GeV.

[24] CHATRCHYAN 14K use 4.9 fb^{-1} of pp collisions at E_{cm} = 7 TeV and 19.7 fb^{-1} at E_{cm} = 8 TeV. The quoted signal strength is given for m_H = 125 GeV. See also CHATRCHYAN 14AJ.

[25] AALTONEN 13L combine all CDF results with 9.45–10.0 fb^{-1} of $p\overline{p}$ collisions at E_{cm} = 1.96 TeV. The quoted signal strength is given for m_H = 125 GeV.

[26] ABAZOV 13L combine all D0 results with up to 9.7 fb^{-1} of $p\overline{p}$ collisions at E_{cm} = 1.96 TeV. The quoted signal strength is given for m_H = 125 GeV.

[27] AAD 12AI obtain results based on 4.7 fb^{-1} of pp collisions at E_{cm} = 7 TeV. The quoted signal strengths are given in their Fig. 10 for m_H = 126 GeV. See also Fig. 13 of AAD 12DA.

[28] CHATRCHYAN 12N obtain results based on 4.9 fb^{-1} of pp collisions at E_{cm}=7 TeV and 5.1 fb^{-1} at E_{cm}=8 TeV. The quoted signal strength is given for m_H=125.5 GeV. See also CHATRCHYAN 13Y .

$Z\gamma$ final state

VALUE	CL%	DOCUMENT ID		TECN	COMMENT
2.2 ±0.7		[1] AAD	24D	LHC	pp, 13 TeV
• • • We do not use the following data for averages, fits, limits, etc. • • •					
2.4 ±0.9		[2] TUMASYAN	23F	CMS	pp, 13 TeV
$2.59^{+1.07}_{-0.96}$		[3] CMS	22	CMS	pp, 13 TeV
< 3.6	95	[4] AAD	20AG	ATLS	pp, 13 TeV
< 7.4	95	[5] SIRUNYAN	18DQ	CMS	pp, 13 TeV
< 6.6	95	[6] AABOUD	17AW	ATLS	pp, 13 TeV
<11	95	[7] AAD	14J	ATLS	pp, 7, 8 TeV
< 9.5	95	[8] CHATRCHYAN	13BK	CMS	pp, 7, 8 TeV

[1] AAD 24D report combined results of ATLAS (AAD 20AG) and CMS (TUMASYAN 23F). The reported signal strength corresponds to a significance of 3.4 σ.

[2] TUMASYAN 23F search for $H \rightarrow Z\gamma$, $Z \rightarrow ee$, $\mu\mu$ in 138 fb^{-1} of pp collisions at E_{cm} = 13 TeV, assuming m_H = 125.38 GeV. $\sigma(pp \rightarrow H) \cdot B(H \rightarrow Z\gamma)$ is measured to be 0.21 ± 0.08 pb. The ratio of branching fractions $B(H \rightarrow Z\gamma)/B(H \rightarrow \gamma\gamma)$ is measured to be $1.5^{+0.7}_{-0.6}$.

[3] CMS 22 report combined results (see their Extended Data Table 2) using up to 138 fb^{-1} of data at E_{cm} = 13 TeV, assuming m_H = 125.38 GeV. See their Fig. 2 right.

[4] AAD 20AG search for $H \rightarrow Z\gamma$, $Z \rightarrow ee$, $\mu\mu$ in 139 fb^{-1} of pp collisions at E_{cm} = 13 TeV. The signal strength is 2.0 ± $0.9^{+0.4}_{-0.3}$ at m_H = 125.09 GeV, which corresponds to a significance of 2.2 σ. The upper limit of $\sigma(pp \rightarrow H) \cdot B(H \rightarrow Z\gamma)$ is 305 fb at 95% CL.

[5] SIRUNYAN 18DQ search for $H \rightarrow Z\gamma$, $Z \rightarrow ee$, $\mu\mu$ in 35.9 fb^{-1} of pp collisions at E_{cm} = 13 TeV. The quoted signal strength (see their Figs. 6 and 7) is given for m_H = 125 GeV.

[6] AABOUD 17AW search for $H \rightarrow Z\gamma$, $Z \rightarrow ee$, $\mu\mu$ in 36.1 fb^{-1} of pp collisions at E_{cm} = 13 TeV. The quoted signal strength is given for m_H = 125.09 GeV. The upper limit on the branching ratio of $H \rightarrow Z\gamma$ is 1.0% at 95% CL assuming the SM Higgs boson production.

[7] AAD 14J search for $H \rightarrow Z\gamma \rightarrow \ell\ell\gamma$ in 4.5 fb^{-1} of pp collisions at E_{cm} = 7 TeV and 20.3 fb^{-1} at E_{cm} = 8 TeV. The quoted signal strength is given for m_H = 125.5 GeV.

[8] CHATRCHYAN 13BK search for $H \rightarrow Z\gamma \rightarrow \ell\ell\gamma$ in 5.0 fb^{-1} of pp collisions at E_{cm} = 7 TeV and 19.6 fb^{-1} at E_{cm} = 8 TeV. A limit on cross section times branching ratio which corresponds to (4–25) times the expected Standard Model cross section is given in the range m_H = 120–160 GeV at 95% CL. The quoted limit is given for m_H = 125 GeV, where 10 is expected for no signal.

$\gamma^*\gamma$ final state

VALUE	CL%	DOCUMENT ID		TECN	COMMENT
$1.5 \pm 0.5^{+0.2}_{-0.1}$		[1] AAD	21I	ATLS	pp, 13 TeV, $H \rightarrow \ell\ell\gamma$, 139 fb^{-1}
• • • We do not use the following data for averages, fits, limits, etc. • • •					
<4.0	95	[2] SIRUNYAN	18DQ	CMS	$pp \rightarrow HX$, 13 TeV, $H \rightarrow \gamma^*\gamma$
<6.7	95	[3] KHACHATRY...	16B	CMS	pp, 8 TeV, $ee\gamma$, $\mu\mu\gamma$

[1] AAD 21I search for $H \rightarrow \ell\ell\gamma$ ($\ell = e, \mu$) in 139 fb^{-1} of pp collisions at E_{cm} = 13 TeV. The mass of dilepton $m_{\ell\ell}$ is smaller than 30 GeV. This region is dominated by the decay through γ^*. The quoted signal strength corresponds to a significance of 3.2 standard deviations and is given for m_H = 125.09 GeV. The cross section times the branching ratio of $H \rightarrow \ell\ell\gamma$ for $m_{\ell\ell}$ < 30 GeV is measured to be 8.7 ± $2.7^{+0.7}_{-0.6}$ fb.

[2] SIRUNYAN 18DQ search for $H \rightarrow \gamma^*\gamma$, $\gamma^* \rightarrow \mu\mu$ in 35.9 fb^{-1} of pp collisions at E_{cm} = 13 TeV. The mass of γ^* is smaller than 50 GeV except in J/ψ and Υ mass regions. The quoted signal strength (see their Figs. 6 and 7) is given for m_H = 125 GeV.

[3] KHACHATRYAN 16B search for $H \rightarrow \gamma^*\gamma \rightarrow e^+e^-\gamma$ and $\mu^+\mu^-\gamma$ (with $m(e^+e^-)$ < 3.5 GeV and $m(\mu^+\mu^-)$ < 20 GeV) in 19.7 fb^{-1} of pp collisions at E_{cm} = 8 TeV. See their Fig. 6 for limits on individual channels.

HIGGS COUPLINGS

Fermion coupling (κ_F)

VALUE	DOCUMENT ID		TECN	COMMENT
0.94 ±0.05 OUR AVERAGE				
$0.86^{+0.14}_{-0.11}$	[1] TUMASYAN	23W	CMS	pp, 13 TeV, $H \rightarrow WW^*$
0.95 ±0.05	[2] ATLAS	22	ATLS	pp, 13 TeV
• • • We do not use the following data for averages, fits, limits, etc. • • •				
$1.00^{+0.16}_{-0.13}$	[3] AAD	23Y	ATLS	pp, 13 TeV, $H \rightarrow \gamma\gamma$
0.906	[4] CMS	22	CMS	pp, 13 TeV

[1] TUMASYAN 23W measure Higgs production rates with $H \rightarrow WW^*$ at E_{cm} = 13 TeV with 138 fb^{-1} data, assuming m_H = 125.38 GeV. See their Fig. 25 for the 68% and 95% CL contours in the $\kappa_V - \kappa_f$ plane.

[2] ATLAS 22 report combined results (see their Extended Data Table 1) using up to 139 fb^{-1} of data at E_{cm} = 13 TeV, assuming m_H = 125.09 GeV, $\kappa_V \geq 0$, and $\kappa_F \geq 0$ ($B_{inv} = B_{undetected} = 0$). See their Fig. 4.

[3] AAD 23Y measure Higgs production rates with $H \rightarrow \gamma\gamma$ at E_{cm} = 13 TeV with 139 fb^{-1} data, assuming m_H = 125.09 GeV. See their Fig. 23 for the 68% and 95% CL contours in the $\kappa_V - \kappa_F$ plane, where $\kappa_F > 0$ is assumed.

[4] CMS 22 report combined results (see their Extended Data Table 2) using up to 138 fb^{-1} of data at E_{cm} = 13 TeV, assuming m_H = 125.38 GeV. No uncertainty is given while their Fig. 3 left shows 68% and 95% CL contours.

Gauge boson coupling (κ_V)

VALUE	CL%	DOCUMENT ID		TECN	COMMENT
1.023±0.026 OUR AVERAGE					
0.99 ±0.05		[1] TUMASYAN	23W	CMS	13 TeV, $H \rightarrow WW^*$
1.035±0.031		[2] ATLAS	22	ATLS	pp, 13 TeV
• • • We do not use the following data for averages, fits, limits, etc. • • •					
−3.7 to 3.8	95	[3] HAYRAPETY...	24AW	CMS	13 TeV, VHH, $HH \rightarrow b\bar{b}b\bar{b}$
$1.02^{+0.06}_{-0.05}$		[4] AAD	23Y	ATLS	13 TeV, $H \rightarrow \gamma\gamma$
1.014		[5] CMS	22	CMS	pp, 13 TeV

[1] TUMASYAN 23W measure Higgs production rates with $H \rightarrow WW^*$ at E_{cm} = 13 TeV with 138 fb^{-1} data, assuming m_H = 125.38 GeV. See their Fig. 25 for the 68% and 95% CL contours in the $\kappa_V - \kappa_f$ plane.

[2] ATLAS 22 report combined results (see their Extended Data Table 1) using up to 139 fb^{-1} of data at E_{cm} = 13 TeV, assuming m_H = 125.09 GeV, $\kappa_V \geq 0$, and $\kappa_F \geq 0$ ($B_{inv} = B_{undetected} = 0$). See their Fig. 4.

[3] HAYRAPETYAN 24AW search for non-resonant HH production in association with a vector boson using $HH \rightarrow b\bar{b}b\bar{b}$ with data of 138 fb^{-1} at E_{cm} = 13 TeV. The vector boson decays both leptonically ($W \rightarrow \ell\nu$, $Z \rightarrow \ell\ell$, $\nu\nu$, $\ell = e, \mu$) and hadronically. See their Fig. 19. All other Higgs couplings are fixed to the SM values.

[4] AAD 23Y measure Higgs production rates with $H \rightarrow \gamma\gamma$ at E_{cm} = 13 TeV with 139 fb^{-1} data, assuming m_H = 125.09 GeV. See their Fig. 23 for the 68% and 95% CL contours in the $\kappa_V - \kappa_F$ plane, where $\kappa_F > 0$ is assumed.

[5] CMS 22 report combined results (see their Extended Data Table 2) using up to 138 fb^{-1} of data at E_{cm} = 13 TeV, assuming m_H = 125.38 GeV. See their Fig. 3 left.

W boson coupling (κ_W)

VALUE	DOCUMENT ID		TECN	COMMENT
• • • We do not use the following data for averages, fits, limits, etc. • • •				
	[1] HAYRAPETY...	25B	CMS	pp, 13 TeV, VBF WH, coupling sign
	[2] AAD	24BM	ATLS	pp, 13 TeV, VBF WH, coupling sign

1.02 ± 0.05	[3,4] ATLAS	22	ATLS	pp, 13 TeV
1.05 ± 0.06	[3,5] ATLAS	22	ATLS	pp, 13 TeV
$1.00^{+0.00}_{-0.02}$	[3,6] ATLAS	22	ATLS	pp, 13 TeV
1.06 ± 0.07	[7,8] CMS	22	CMS	pp, 13 TeV
1.02 ± 0.08	[7,9] CMS	22	CMS	pp, 13 TeV

[1] HAYRAPETYAN 25B present the determination of the relative sign of κ_W and κ_Z with VBF WH, $H \rightarrow b\overline{b}$ using 138 fb^{-1} of data at E_{cm} = 13 TeV. The opposite-sign coupling hypothesis is excluded with a significance beyond 5σ.

[2] AAD 24BM present the determination of the relative sign of κ_W and κ_Z with VBF WH, $H \rightarrow b\overline{b}$ using 140 fb^{-1} of data at E_{cm} = 13 TeV. The opposite-sign coupling hypothesis is excluded with a significance beyond 5σ.

[3] ATLAS 22 report combined results (see their Extended Data Table 1) using up to 139 fb^{-1} of data at E_{cm} = 13 TeV, assuming m_H = 125.09 GeV.

[4] All modifiers(κ) > 0, and $\kappa_c = \kappa_t$ ($B_{inv} = B_{undetected} = 0$) are assumed. Only SM particles assume to contribute to the loop-induced processes.See their Fig. 5, which shows both $\kappa_c = \kappa_t$ andκ_c floating.

[5] $B_{inv} = B_{undetected} = 0$ is assumed. Coupling strength modifiers including effective photon, $Z\gamma$ and gluon are measured. See their Fig. 6.

[6] B_{inv} floating, $B_{undetected} \geq 0$, and $\kappa_V \leq 1$ are assumed. Coupling strength modifiers including effective photon, $Z\gamma$ and gluon are measured. See their Fig. 6.

[7] CMS 22 report combined results (see their Extended Data Table 2) using up to 138 fb^{-1} of data at E_{cm} = 13 TeV, assuming m_H = 125.38 GeV.

[8] Only SM particles assume to contribute to the loop-induced processes. See their Fig. 3 right.

[9] Coupling strength modifiers including effective photon, $Z\gamma$ and gluon are measured. See their Fig. 4 left.

Z boson coupling (κ_Z)

VALUE	DOCUMENT ID		TECN	COMMENT
• • • We do not use the following data for averages, fits, limits, etc. • • •				
	[1] HAYRAPETY...25B	CMS		pp, 13 TeV, VBF WH, coupling sign
	[2] AAD	24BM	ATLS	pp, 13 TeV, VBF WH, coupling sign
$0.99^{+0.06}_{-0.05}$	[3,4] ATLAS	22	ATLS	pp, 13 TeV
0.99 ± 0.06	[3,5] ATLAS	22	ATLS	pp, 13 TeV
$0.98^{+0.02}_{-0.05}$	[3,6] ATLAS	22	ATLS	pp, 13 TeV
1.04 ± 0.07	[7,8] CMS	22	CMS	pp, 13 TeV
1.04 ± 0.07	[7,9] CMS	22	CMS	pp, 13 TeV

[1] HAYRAPETYAN 25B present the determination of the relative sign of κ_W and κ_Z with VBF WH, $H \rightarrow b\overline{b}$ using 138 fb^{-1} of data at E_{cm} = 13 TeV. The opposite-sign coupling hypothesis is excluded with a significance beyond 5σ.

[2] AAD 24BM present the determination of the relative sign of κ_W and κ_Z with VBF WH, $H \rightarrow b\overline{b}$ using 140 fb^{-1} of data at E_{cm} = 13 TeV. The opposite-sign coupling hypothesis is excluded with a significance beyond 5σ.

[3] ATLAS 22 report combined results (see their Extended Data Table 1) using up to 139 fb^{-1} of data at E_{cm} = 13 TeV, assuming m_H = 125.09 GeV.

[4] All modifiers(κ) > 0, and $\kappa_c = \kappa_t$ ($B_{inv} = B_{undetected} = 0$) are assumed. Only SM particles assume to contribute to the loop-induced processes.See their Fig. 5, which shows both $\kappa_c = \kappa_t$ andκ_c floating.

[5] $B_{inv} = B_{undetected} = 0$ is assumed. Coupling strength modifiers including effective photon, $Z\gamma$ and gluon are measured. See their Fig. 6.

[6] B_{inv} floating, $B_{undetected} \geq 0$, and $\kappa_V \leq 1$ are assumed. Coupling strength modifiers including effective photon, $Z\gamma$ and gluon are measured. See their Fig. 6.

[7] CMS 22 report combined results (see their Extended Data Table 2) using up to 138 fb^{-1} of data at E_{cm} = 13 TeV, assuming m_H = 125.38 GeV.

[8] Only SM particles assume to contribute to the loop-induced processes. See their Fig. 3 right.

[9] Coupling strength modifiers including effective photon, $Z\gamma$ and gluon are measured. See their Fig. 4 left.

top Yukawa coupling (κ_t)

VALUE	CL%	DOCUMENT ID		TECN	COMMENT
• • • We do not use the following data for averages, fits, limits, etc. • • •					
		[1] HAYRAPETY...25R		CMS	$t\overline{t}H$, tH, $H \rightarrow b\overline{b}$, 13 TeV
$0.84^{+0.30}_{-0.46}$		[2] AAD	24J	ATLS	$t\overline{t}H$, tH, $H \rightarrow b\overline{b}$, 13 TeV
<1.9	95	[3] AAD	23BC	ATLS	pp, 13 TeV
0.87–1.20	95	[4] AAD	23Y	ATLS	pp, 13 TeV
0.65–1.25	95	[5] AAD	23Y	ATLS	pp, 13 TeV
−1.09− − 0.74 or 0.77–1.3	95	[6] TUMASYAN	23P	CMS	pp, 13 TeV
0.86–1.26		[6,7] TUMASYAN	23P	CMS	pp, 13 TeV
0.95 ± 0.07		[8,9] ATLAS	22	ATLS	pp, 13 TeV
0.94 ± 0.11		[8,10] ATLAS	22	ATLS	pp, 13 TeV
0.94 ± 0.11		[8,11] ATLAS	22	ATLS	pp, 13 TeV
$0.95^{+0.07}_{-0.08}$		[12,13] CMS	22	CMS	pp, 13 TeV
$1.01^{+0.11}_{-0.10}$		[12,14] CMS	22	CMS	pp, 13 TeV
−0.9− − 0.7 or 0.7–1.1	95	[15] SIRUNYAN	21R	CMS	pp, 13 TeV
<1.7	95	[16] SIRUNYAN	20C	CMS	pp, 13 TeV
<1.67	95	[17] SIRUNYAN	19BY	CMS	pp, 13 TeV
<2.1	95	[18] SIRUNYAN	18BU	CMS	pp, 13 TeV

[1] HAYRAPETYAN 25R measure the $t\overline{t}H$ and tH productions with $H \rightarrow b\overline{b}$ decay channel using 138 fb^{-1} of data at E_{cm} = 13 TeV. Two-dimensional likelihood scan of (κ_t, κ_V) is shown in their Fig. 15. Assuming $\kappa_V = 1$, κ_t is measured to be [−0.55, −0.24] and [0.20, 0.72] at 68% CL.

[2] AAD 24J measure the *CP* structure of the top Yukawa coupling using 139 fb^{-1} of data at E_{cm} = 13 TeV. The top Yukawa coupling strength modifier κ_t is measured with the *CP*-mixing angle α. See their Fig. 3.

[3] AAD 23BC measure the production of four top quarks with same-sign and multilepton final states with 140 fb^{-1} pp collision data at E_{cm} = 13 TeV. The results constraint the ratio of the top quark Yukawa coupling y_t to its Standard Model value, yielding $|y_t/y_t^{SM}| < 1.9$ (see their erratum) at 95% CL. See their Fig. 8 as a function of κ_t and *CP*-mixing angle.

[4] AAD 23Y constrain κ_t from Higgs production rates with $H \rightarrow \gamma\gamma$ with 139 fb^{-1} pp collision data at E_{cm} = 13 TeV. The quoted result is obtained assuming the SM loop structure in $gg \rightarrow H$ and $H \rightarrow \gamma\gamma$. See their Fig. 14.

[5] AAD 23Y constrain κ_t from Higgs production rates with $H \rightarrow \gamma\gamma$ with 139 fb^{-1} pp collision data at E_{cm} = 13 TeV. The quoted result is obtained assuming effective couplings κ_{gluon} and κ_γ for $gg \rightarrow H$ and $H \rightarrow \gamma\gamma$, respectively. See their Fig. 14.

[6] TUMASYAN 23P constrain κ_t from $t\overline{t}H$ and tH decaying $H \rightarrow WW^*$ and $H \rightarrow \tau\tau$ (multilepton decay mode) with 138 fb^{-1} pp collision data at E_{cm} = 13 TeV. The κ_t is obtained by fixing $\widetilde{\kappa}_t = 0$ and other couplings (κ_V etc.) to the SM values. See their Fig. 9 for 2-dim contours and Table 6.

[7] The quoted result is obtained by combining with other $t\overline{t}H$ decaying $H \rightarrow \gamma\gamma$ (SIRUNYAN 20AS) and $H \rightarrow 4\ell$ (SIRUNYAN 21AE) and $\widetilde{\kappa}_t = 0$. See their Fig. 12 for 2-dim contours and Table 7.

[8] ATLAS 22 report combined results (see their Extended Data Table 1) using up to 139 fb^{-1} of data at E_{cm} = 13 TeV, assuming m_H = 125.09 GeV.

[9] All modifiers(κ) > 0, and $\kappa_c = \kappa_t$ ($B_{inv} = B_{undetected} = 0$) are assumed. Only SM particles assume to contribute to the loop-induced processes.See their Fig. 5, which shows both $\kappa_c = \kappa_t$ andκ_c floating.

[10] $B_{inv} = B_{undetected} = 0$ is assumed. Coupling strength modifiers including effective photon, $Z\gamma$ and gluon are measured. See their Fig. 6.

[11] B_{inv} floating, $B_{undetected} \geq 0$, and $\kappa_V \leq 1$ are assumed. Coupling strength modifiers including effective photon, $Z\gamma$ and gluon are measured. See their Fig. 6.

[12] CMS 22 report combined results (see their Extended Data Table 2) using up to 138 fb^{-1} of data at E_{cm} = 13 TeV, assuming m_H = 125.38 GeV.

[13] Only SM particles assume to contribute to the loop-induced processes. See their Fig. 3 right.

[14] Coupling strength modifiers including effective photon, $Z\gamma$ and gluon are measured. See their Fig. 4 left.

[15] SIRUNYAN 21R constrain the ratio of the top quark Yukawa coupling y_t to its Standard Model value from $t\overline{t}H$ and tH production rates using 137 fb^{-1} pp collision data at E_{cm} = 13 TeV. Assuming a SM Higgs couplings to τ's, the joint interval $-0.9 < \kappa_t (= y_t/y_t^{SM}) < -0.7$ and $0.7 < \kappa_t < 1.1$ is obtained at 95% CL (see their Fig. 17).

[16] SIRUNYAN 20C search for the production of four top quarks with same-sign and multilepton final states with 137 fb^{-1} pp collision data at E_{cm} = 13 TeV. The results constraint the ratio of the top quark Yukawa coupling y_t to its Standard Model value by comparing to the central value of a theoretical prediction (see their Refs. [1-2]), yielding $|y_t/y_t^{SM}| < 1.7$ at 95% CL. See their Fig. 5.

[17] SIRUNYAN 19BY measure the top quark Yukawa coupling from $t\overline{t}$ kinematic distributions, the invariant mass of the top quark pair and the rapidity difference between t and $\overline{t}$, in the ℓ+jets final state with 35.8 fb^{-1} pp collision data at E_{cm} = 13 TeV. The results constraint the ratio of the top quark Yukawa coupling to its the Standard Model to be $1.07^{+0.34}_{-0.43}$ with an upper limit of 1.67 at 95% CL (see their Table III).

[18] SIRUNYAN 18BU search for the production of four top quarks with same-sign and multilepton final states with 35.9 fb^{-1} pp collision data at E_{cm} = 13 TeV. The results constraint the ratio of the top quark Yukawa coupling y_t to its the Standard Model by comparing to the central value of a theoretical prediction (see their Ref. [16]), yielding $|y_t/y_t^{SM}| < 2.1$ at 95% CL.

bottom quark Yukawa coupling (κ_b)

VALUE	CL%	DOCUMENT ID		TECN	COMMENT
• • • We do not use the following data for averages, fits, limits, etc. • • •					
$0.65 < \lvert\kappa_b\rvert < 1.37$	95	[1] AAD	25Y	ATLS	$pp \rightarrow VH$, $H \rightarrow b\overline{b}$, 13 TeV
-1.09 to -0.86 OR 0.81 to 1.09	95	[2] AAD	23C	ATLS	pp, 13 TeV, $\gamma\gamma$, $ZZ^* \rightarrow 4\ell$ cross sections
		[3] AAD	23CD	ATLS	pp, 13 TeV, $H \rightarrow \Upsilon(nS)\gamma$
−1.1 to 1.1	95	[4] HAYRAPETY...23		CMS	pp, 13 TeV, $ZZ^* \rightarrow 4\ell$ cross sections
0.90 ± 0.11		[5,6] ATLAS	22	ATLS	pp, 13 TeV
0.89 ± 0.11		[5,7] ATLAS	22	ATLS	pp, 13 TeV
$0.82^{+0.09}_{-0.08}$		[5,8] ATLAS	22	ATLS	pp, 13 TeV
$1.02^{+0.15}_{-0.17}$		[9,10] CMS	22	CMS	pp, 13 TeV
$0.99^{+0.17}_{-0.16}$		[9,11] CMS	22	CMS	pp, 13 TeV

[1] AAD 25Y present measurements of VH, $H \rightarrow b\overline{b}$ and $H \rightarrow c\overline{c}$ ($V = W, Z$) using 140 fb^{-1} of pp collision data at E_{cm} = 13 TeV. The quoted value is obtained assuming $\kappa_c = 1$, all other couplings to their SM predictions, and only SM decays.

[2] AAD 23C combine results of $H \rightarrow \gamma\gamma$ and $H \rightarrow ZZ^* \rightarrow 4\ell$ ($\ell = e, \mu$) using 139 fb^{-1} at E_{cm} = 13 TeV. The Higgs boson transverse momentum (p_T^H) distribution constrains κ_b and κ_c, assuming other couplings fixed to the SM values. The κ_b is obtained using the p_T^H shape and normalisation. Other cases are given in their Tables 6 and 7.

[3] AAD 23CD search for $H \rightarrow \Upsilon(nS)\gamma$, $\Upsilon(nS) \rightarrow \mu^+\mu^-$ (n=1,2,3) with 138 fb^{-1} of pp collision data at E_{cm} = 13 TeV. They interpret the $H \rightarrow \Upsilon(nS)\gamma$ search to constraint the bottom Yukawa coupling by comparing to $H \rightarrow \gamma\gamma$. An observed 95% CL interval of (-37, 40) is obtained for κ_b/κ_γ.

[4] HAYRAPETYAN 23 measure the cross sections for $pp \rightarrow H \rightarrow ZZ^* \rightarrow 4\ell$ ($\ell = e, \mu$) using 138 fb^{-1} at E_{cm} = 13 TeV. The κ_b is obtained from the p_T differential cross section of the ggF production employing the dependence of the branching fraction on κ_b and κ_c.

Int. J. Mod. Phys. A 2026.41. Downloaded from www.worldscientific.com
by UNIVERSITY OF CALIFORNIA @ BERKELEY on 09/16/26. Reproduction is strictly not permitted, except for Open Access articles.

Int. J. Mod. Phys. A 2026.41. Downloaded from www.worldscientific.com
by UNIVERSITY OF CALIFORNIA @ BERKELEY on 09/16/26. Re-use and distribution is strictly not permitted, except for Open Access articles.

[5] ATLAS 22 report combined results (see their Extended Data Table 1) using up to 139fb^{-1} of data at E_{cm} = 13 TeV, assuming m_H = 125.09 GeV.

[6] All modifiers (κ) > 0, and $\kappa_c = \kappa_t$ ($B_{inv} = B_{undetected}$ = 0) are assumed. Only SM particles assume to contribute to the loop-induced processes. See their Fig. 5, which shows both $\kappa_c = \kappa_t$ and κ_c floating.

[7] $B_{inv} = B_{undetected}$ = 0 is assumed. Coupling strength modifiers including effective photon, $Z\gamma$ and gluon are measured. See their Fig. 6.

[8] B_{inv} floating, $B_{undetected} \geq$ 0, and $\kappa_V \leq$ 1 are assumed. Coupling strength modifiers including effective photon, $Z\gamma$ and gluon are measured. See their Fig. 6.

[9] CMS 22 report combined results (see their Extended Data Table 2) using up to 138 fb^{-1} of data at E_{cm} = 13 TeV, assuming m_H = 125.38 GeV.

[10] Only SM particles assume to contribute to the loop-induced processes. See their Fig. 3 right.

[11] Coupling strength modifiers including effective photon, $Z\gamma$ and gluon are measured. See their Fig. 4 left.

charm quark Yukawa coupling (κ_c)

VALUE	CL%	DOCUMENT ID		TECN	COMMENT
• • • We do not use the following data for averages, fits, limits, etc. • • •					
$\lvert\kappa_c\rvert$ < 3.5	95	[1] HAYRAPETY...26		CMS	pp, $t\overline{t}H$, $H \to c\overline{c}$, 13 TeV
$\lvert\kappa_c\rvert$ < 4.2	95	[2] AAD	25Y	ATLS	$pp \to VH$, 13 TeV
$0.0^{+2.3}_{-2.8}$		[3] CHEKHOVSKY	25G	CMS	pp, 13 TeV, $H\gamma$, $H \to ZZ^* \to 4\ell$
$\lvert\kappa_c\rvert$ < 38.1	95	[4] CHEKHOVSKY	25L	CMS	pp, 13 TeV, $H \to \gamma\gamma$
−166 to 208	95	[5] HAYRAPETY...25H		CMS	pp, 13 TeV, $H \to J/\psi\gamma$
$\lvert\kappa_c\rvert$ < 190	95	[6] HAYRAPETY...24D		CMS	pp, 13 TeV, $H\gamma$, $H \to WW^* \to e\nu\mu\nu$
$\lvert\kappa_c\rvert$ < 2.27	95	[7] AAD	23C	ATLS	pp, 13 TeV, $\gamma\gamma$, $ZZ^* \to 4\ell$ cross sections
		[8] AAD	23CD	ATLS	pp, 13 TeV, $H \to J/\psi\gamma$
− 5.3 to 5.2	95	[9] HAYRAPETY...23		CMS	pp, 13 TeV, $ZZ^* \to 4\ell$ cross sections
1.1 < $\lvert\kappa_c\rvert$ < 5.5	95	[10] TUMASYAN	23AH	CMS	$pp \to WH/ZH$, 13 TeV
$0.03^{+3.02}_{-0.03}$		[11] ATLAS	22	ATLS	pp, 13 TeV

[1] HAYRAPETYAN 26 search for $t\overline{t}H$, $H \to c\overline{c}$ together with the $t\overline{t}H$, $H \to b\overline{b}$ measurement using 138 fb^{-1} of pp collision data at E_{cm} = 13 TeV. The quoted value is obtained by combining with the VH channel and assuming κ_b = 1.

[2] AAD 25Y present measurements of VH, $H \to b\overline{b}$ and $H \to c\overline{c}$ ($V = W, Z$) using 140 fb^{-1} of pp collision data at E_{cm} = 13 TeV. The quoted value is obtained assuming κ_b = 1, all other couplings to their SM predictions, and only SM decays. The ratio of κ_b and κ_c is measured to be $\lvert\kappa_c/\kappa_b\rvert$ < 3.6 at 95% CL.

[3] CHEKHOVSKY 25G search for the $H\gamma$ production with $H \to ZZ^* \to 4\ell$ ($\ell = e, \mu$) decay channel with data of 138 fb^{-1} at E_{cm} = 13 TeV. Coupling modifiers κ_u, κ_d, κ_s and κ_c are simultaneously obtained assuming the SM Yukawa couplings for the bottom and top quarks (κ_b = 1, κ_t =1) and constraining the HVV couplings ($\kappa^2_{ZZ} \leq$ 1, $\kappa^2_{WW} = \kappa^2_{ZZ}$). See their Tables III.

[4] CHEKHOVSKY 25L search for the production of a Higgs boson and one or more charm quarks (H+c) with $H \to \gamma\gamma$ using 138 fb^{-1} of data at E_{cm} = 13 TeV. The quoted value is obtained assuming the SM rates for all other Higgs production processes.

[5] HAYRAPETYAN 25H search for $H \to J/\psi\gamma$, $J/\psi \to \mu^+\mu^-$ with 123 fb^{-1} of pp collision data at E_{cm} = 13 TeV. They interpret the $H \to J/\psi\gamma$ search to constrain the charm Yukawa coupling by comparing to $H \to \gamma\gamma$. An observed 95% CL interval of (-157, 199) is obtained for κ_c/κ_γ. The quoted value is obtained assuming κ_γ = 1.

[6] HAYRAPETYAN 24D search for the $H\gamma$ production using $H \to WW^* \to e\nu\mu\nu$ with 138 fb^{-1} of pp collision data at E_{cm} = 13 TeV. They interpret the $H\gamma$ search to constraint the charm Yukawa coupling assuming that the charm quark and the Higgs interaction vertex shown in their Fig. 1 is the only parameter. See their Table II.

[7] AAD 23C combine results of $H \to \gamma\gamma$ and $H \to ZZ^* \to 4\ell$ ($\ell = e, \mu$) using 139 fb^{-1} at E_{cm} = 13 TeV. The Higgs boson transverse momentum (p^H_T) distribution constrains κ_b and κ_c, assuming other couplings fixed to the SM values. The κ_c is obtained using the p^H_T shape and normalisation. Other cases are given in their Tables 6 and 7. See their Table 8 for results combined with VH, $H \to b\overline{b}$ and $c\overline{c}$.

[8] AAD 23CD search for $H \to J/\psi\gamma$, $J/\psi \to \mu^+\mu^-$ with 138 fb^{-1} of pp collision data at E_{cm} = 13 TeV. They interpret the $H \to J/\psi\gamma$ search to constraint the charm Yukawa coupling by comparing to $H \to \gamma\gamma$. An observed 95% CL interval of (-133, 175) is obtained for κ_c/κ_γ.

[9] HAYRAPETYAN 23 measure the cross sections for $pp \to H \to ZZ^* \to 4\ell$ ($\ell = e, \mu$) using 138 fb^{-1} at E_{cm} = 13 TeV. The κ_c is obtained from the p_T differential cross section of the ggF production employing the dependence of the branching fraction of κ_b and κ_c.

[10] TUMASYAN 23AH search for VH, $H \to c\overline{c}$ ($V = W, Z$) using 138 fb^{-1} of pp collision data at E_{cm} = 13 TeV. The quoted values are obtained from the measured signal strength in the κ-framework, where only the Higgs decay width for $H \to c\overline{c}$ is changed while assuming all the other decay widths and the production cross section to be SM ones. The quoted values are given for m_H = 125.38 GeV.

[11] ATLAS 22 report combined results (see their Extended Data Table 1) using up to 139 fb^{-1} of data at E_{cm} = 13 TeV, assuming m_H = 125.09 GeV, and all modifiers (κ) > 0 ($B_{inv} = B_{undetected}$ = 0). Only SM particles assume to contribute to the loop-induced processes. See their Fig. 5, which shows both $\kappa_c = \kappa_t$ and κ_c floating.

strange quark Yukawa coupling (κ_s)

VALUE	CL%	DOCUMENT ID		TECN	COMMENT
• • • We do not use the following data for averages, fits, limits, etc. • • •					
0^{+30}_{-32}		[1] CHEKHOVSKY	25G	CMS	pp, 13 TeV, $H\gamma$, $H \to ZZ^* \to 4\ell$
$\lvert\kappa_s\rvert$ < 1700	95	[2] HAYRAPETY...24D		CMS	pp, 13 TeV, $H\gamma$, $H \to WW^* \to e\nu\mu\nu$

[1] CHEKHOVSKY 25G search for the $H\gamma$ production with $H \to ZZ^* \to 4\ell$ ($\ell = e, \mu$) decay channel with data of 138 fb^{-1} at E_{cm} = 13 TeV. Coupling modifiers κ_u, κ_d, κ_s and κ_c are simultaneously obtained assuming the SM Yukawa couplings for the bottom and top quarks (κ_b = 1, κ_t = 1) and constraining the HVV couplings ($\kappa^2_{ZZ} \leq$ 1, $\kappa^2_{WW} = \kappa^2_{ZZ}$). See their Tables III.

[2] HAYRAPETYAN 24D search for the $H\gamma$ production using $H \to WW^* \to e\nu\mu\nu$ with 138 fb^{-1} of pp collision data at E_{cm} = 13 TeV. They interpret the $H\gamma$ search to constraint the strange quark Yukawa coupling assuming that the strange quark and the Higgs interaction vertex shown in their Fig. 1 is the only parameter. See their Table II.

down quark Yukawa coupling (κ_d)

VALUE (units 10^2)	CL%	DOCUMENT ID		TECN	COMMENT
• • • We do not use the following data for averages, fits, limits, etc. • • •					
$0.0^{+6.7}_{-6.8}$		[1] CHEKHOVSKY	25G	CMS	pp, 13 TeV, $H\gamma$, $H \to ZZ^* \to 4\ell$
−170 to 170	95	[2] HAYRAPETY...24D		CMS	pp, 13 TeV, $H\gamma$, $H \to WW^* \to e\nu\mu\nu$

[1] CHEKHOVSKY 25G search for the $H\gamma$ production with $H \to ZZ^* \to 4\ell$ ($\ell = e, \mu$) decay channel with data of 138 fb^{-1} at E_{cm} = 13 TeV. Coupling modifiers κ_u, κ_d, κ_s and κ_c are simultaneously obtained assuming the SM Yukawa couplings for the bottom and top quarks (κ_b = 1, κ_t = 1) and constraining the HVV couplings ($\kappa^2_{ZZ} \leq$ 1, $\kappa^2_{WW} = \kappa^2_{ZZ}$). See their Tables III.

[2] HAYRAPETYAN 24D search for the $H\gamma$ production using $H \to WW^* \to e\nu\mu\nu$ with 138 fb^{-1} of pp collision data at E_{cm} = 13 TeV. They interpret the $H\gamma$ search to constraint the down quark Yukawa coupling assuming that the down quark and the Higgs interaction vertex shown in their Fig. 1 is the only parameter. See their Table II.

up quark Yukawa coupling (κ_u)

VALUE (units 10^3)	CL%	DOCUMENT ID		TECN	COMMENT
• • • We do not use the following data for averages, fits, limits, etc. • • •					
0.0±1.5		[1] CHEKHOVSKY	25G	CMS	pp, 13 TeV, $H\gamma$, $H \to ZZ^* \to 4\ell$
−16 to 16	95	[2] HAYRAPETY...24D		CMS	pp, 13 TeV, $H\gamma$, $H \to WW^* \to e\nu\mu\nu$

[1] CHEKHOVSKY 25G search for the $H\gamma$ production with $H \to ZZ^* \to 4\ell$ ($\ell = e, \mu$) decay channel with data of 138 fb^{-1} at E_{cm} = 13 TeV. Coupling modifiers κ_u, κ_d, κ_s and κ_c are simultaneously obtained assuming the SM Yukawa couplings for the bottom and top quarks (κ_b = 1 , κ_t = 1) and constraining the HVV couplings ($\kappa^2_{ZZ} \leq$ 1, $\kappa^2_{WW} = \kappa^2_{ZZ}$). See their Tables III.

[2] HAYRAPETYAN 24D search for the $H\gamma$ production using $H \to WW^* \to e\nu\mu\nu$ with 138 fb^{-1} of pp collision data at E_{cm} = 13 TeV. They interpret the $H\gamma$ search to constraint the up quark Yukawa coupling assuming that the up quark and the Higgs interaction vertex shown in their Fig. 1 is the only parameter. See their Table II.

tau Yukawa coupling (κ_τ)

VALUE	DOCUMENT ID		TECN	COMMENT
• • • We do not use the following data for averages, fits, limits, etc. • • •				
0.94±0.07	[1,2] ATLAS	22	ATLS	pp, 13 TeV
0.93±0.07	[1,3] ATLAS	22	ATLS	pp, 13 TeV
$0.91^{+0.07}_{-0.06}$	[1,4] ATLAS	22	ATLS	pp, 13 TeV
0.93±0.08	[5,6] CMS	22	CMS	pp, 13 TeV
0.92±0.08	[5,7] CMS	22	CMS	pp, 13 TeV

[1] ATLAS 22 report combined results (see their Extended Data Table 1) using up to 139 fb^{-1} of data at E_{cm} = 13 TeV, assuming m_H = 125.09 GeV.

[2] All modifiers(κ) > 0, and $\kappa_c = \kappa_t$ ($B_{inv} = B_{undetected}$ = 0) are assumed. Only SM particles assume to contribute to the loop-induced processes.See their Fig. 5, which shows both $\kappa_c = \kappa_t$ andκ_c floating.

[3] $B_{inv} = B_{undetected}$ = 0 is assumed. Coupling strength modifiers including effective photon, $Z\gamma$ and gluon are measured. See their Fig. 6.

[4] B_{inv} floating, $B_{undetected} \geq$ 0, and $\kappa_V \leq$ 1 are assumed. Coupling strength modifiers including effective photon, $Z\gamma$ and gluon are measured. See their Fig. 6.

[5] CMS 22 report combined results (see their Extended Data Table 2) using up to 138 fb^{-1} of data at E_{cm} = 13 TeV, assuming m_H = 125.38 GeV.

[6] Only SM particles assume to contribute to the loop-induced processes. See their Fig. 3 right.

[7] Coupling strength modifiers including effective photon, $Z\gamma$ and gluon are measured. See their Fig. 4 left.

muon Yukawa couping (κ_μ)

VALUE	DOCUMENT ID		TECN	COMMENT
• • • We do not use the following data for averages, fits, limits, etc. • • •				
$1.07^{+0.25}_{-0.31}$	[1,2] ATLAS	22	ATLS	pp, 13 TeV
$1.06^{+0.25}_{-0.30}$	[1,3] ATLAS	22	ATLS	pp, 13 TeV
$1.04^{+0.23}_{-0.30}$	[1,4] ATLAS	22	ATLS	pp, 13 TeV
1.12±0.20	[5,6] CMS	22	CMS	pp, 13 TeV
$1.12^{+0.21}_{-0.22}$	[5,7] CMS	22	CMS	pp, 13 TeV

[1] ATLAS 22 report combined results (see their Extended Data Table 1) using up to 139 fb^{-1} of data at E_{cm} = 13 TeV, assuming m_H = 125.09 GeV.

[2] All modifiers(κ) > 0, and $\kappa_c = \kappa_t$ ($B_{inv} = B_{undetected}$ = 0) are assumed. Only SM particles assume to contribute to the loop-induced processes.See their Fig. 5, which shows both $\kappa_c = \kappa_t$ andκ_c floating.

[3] $B_{inv} = B_{undetected} = 0$ is assumed. Coupling strength modifiers including effective photon, $Z\gamma$ and gluon are measured. See their Fig. 6.
[4] B_{inv} floating, $B_{undetected} \geq 0$, and $\kappa_V \leq 1$ are assumed. Coupling strength modifiers including effective photon, $Z\gamma$ and gluon are measured. See their Fig. 6.
[5] CMS 22 report combined results (see their Extended Data Table 2) using up to 138 fb^{-1} of data at E_{cm} = 13 TeV, assuming m_H = 125.38 GeV.
[6] Only SM particles assume to contribute to the loop-induced processes. See their Fig. 3 right.
[7] Coupling strength modifiers including effective photon, $Z\gamma$ and gluon are measured. See their Fig. 4 left.

photon effective coupling (κ_γ)

VALUE	DOCUMENT ID		TECN	COMMENT
• • • We do not use the following data for averages, fits, limits, etc. • • •				
$1.02^{+0.08}_{-0.07}$	[1] AAD	23Y	ATLS	pp, 13 TeV
1.01 ± 0.06	[2,3] ATLAS	22	ATLS	pp, 13 TeV
0.98 ± 0.05	[2,4] ATLAS	22	ATLS	pp, 13 TeV
1.10 ± 0.08	[5] CMS	22	CMS	pp, 13 TeV

[1] AAD 23Y constrain κ_γ from Higgs production rates with $H \to \gamma\gamma$ with 139 fb^{-1} pp collision data at E_{cm} = 13 TeV. The quoted result is obtained assuming effective couplings κ_{gluon} and κ_γ for $gg \to H$ and $H \to \gamma\gamma$, respectively and other couplings fixed to the SM values. See their Fig. 15.
[2] ATLAS 22 report combined results (see their Extended Data Table 1) using up to 139 fb^{-1} of data at E_{cm} = 13 TeV, assuming m_H = 125.09 GeV. Coupling strength modifiers including effective photon, $Z\gamma$ and gluon are measured. See their Fig. 6.
[3] $B_{inv} = B_{undetected} = 0$ is assumed.
[4] B_{inv} floating, $B_{undetected} \geq 0$, and $\kappa_V \leq 1$ are assumed.
[5] CMS 22 report combined results (see their Extended Data Table 2) using up to 138 fb^{-1} of data at E_{cm} = 13 TeV, assuming m_H = 125.38 GeV. Coupling strength modifiers including effective photon, $Z\gamma$ and gluon are measured. See their Fig. 4 left.

gluon effective coupling (κ_{gluon})

VALUE	DOCUMENT ID		TECN	COMMENT
• • • We do not use the following data for averages, fits, limits, etc. • • •				
$1.01^{+0.11}_{-0.09}$	[1] AAD	23Y	ATLS	pp, 13 TeV
0.95 ± 0.07	[2,3] ATLAS	22	ATLS	pp, 13 TeV
$0.94^{+0.07}_{-0.06}$	[2,4] ATLAS	22	ATLS	pp, 13 TeV
0.92 ± 0.08	[5] CMS	22	CMS	pp, 13 TeV

[1] AAD 23Y constrain κ_{gluon} from Higgs production rates with $H \to \gamma\gamma$ with 139 fb^{-1} pp collision data at E_{cm} = 13 TeV. The quoted result is obtained assuming effective couplings κ_{gluon} and κ_γ for $gg \to H$ and $H \to \gamma\gamma$, respectively and other couplings fixed to the SM values. See their Fig. 15.
[2] ATLAS 22 report combined results (see their Extended Data Table 1) using up to 139fb^{-1} of data at E_{cm} = 13 TeV, assuming m_H = 125.09 GeV. Coupling strength modifiers including effective photon, $Z\gamma$ andgluon are measured. See their Fig. 6.
[3] $B_{inv} = B_{undetected} = 0$ is assumed.
[4] B_{inv} floating, $B_{undetected} \geq 0$, and $\kappa_V \leq 1$ are assumed.
[5] CMS 22 report combined results (see their Extended Data Table 2) using up to 138 fb^{-1} of data at E_{cm} = 13 TeV, assuming m_H = 125.38 GeV. Coupling strength modifiers including effective photon, $Z\gamma$ and gluon are measured. See their Fig. 4 left.

$Z\gamma$ effective coupling ($\kappa_{Z\gamma}$)

VALUE	DOCUMENT ID		TECN	COMMENT
• • • We do not use the following data for averages, fits, limits, etc. • • •				
$1.38^{+0.31}_{-0.37}$	[1,2] ATLAS	22	ATLS	pp, 13 TeV
$1.35^{+0.29}_{-0.36}$	[1,3] ATLAS	22	ATLS	pp, 13 TeV
$1.65^{+0.34}_{-0.37}$	[4] CMS	22	CMS	pp, 13 TeV

[1] ATLAS 22 report combined results (see their Extended Data Table 1) using up to 139 fb^{-1} of data at E_{cm} = 13 TeV, assuming m_H = 125.09 GeV. Coupling strength modifiers including effective photon, $Z\gamma$ and gluon are measured. See their Fig. 6.
[2] $B_{inv} = B_{undetected} = 0$ is assumed.
[3] B_{inv} floating, $B_{undetected} \geq 0$, and $\kappa_V \leq 1$ are assumed.
[4] CMS 22 report combined results (see their Extended Data Table 2) using up to 138 fb^{-1} of data at E_{cm} = 13 TeV, assuming m_H = 125.38 GeV. Coupling strength modifiers including effective photon, $Z\gamma$ and gluon are measured. See their Fig. 4 left.

OTHER *H* PRODUCTION PROPERTIES

$t\bar{t}H$ production

Signal strength relative to the Standard Model cross section.

VALUE	DOCUMENT ID		TECN	COMMENT
$0.91^{+0.20}_{-0.18}$ OUR AVERAGE	Error includes scale factor of 1.6. See the ideogram below.			
$0.81^{+0.22}_{-0.19}$	[1] AAD	25AJ	ATLS	pp, 13 TeV, $H \to b\bar{b}$
0.33 ± 0.26	[2] HAYRAPETY...	25R	CMS	pp, 13 TeV, $H \to b\bar{b}$
$0.92 \pm 0.19^{+0.17}_{-0.13}$	[3] SIRUNYAN	21R	CMS	pp, 13 TeV, $H \to \tau\tau$, WW^*, ZZ^*
$1.43^{+0.33+0.21}_{-0.31-0.15}$	[4] AAD	20Z	ATLS	pp, 13 TeV, $H \to \gamma\gamma$
$1.6^{+0.5}_{-0.4}$	[5] AABOUD	18AC	ATLS	pp, 13 TeV, $H \to \tau\tau$, WW^*, ZZ^*
$1.9^{+0.8}_{-0.7}$	[6] AAD	16AN	ATLS	pp, 7, 8 TeV
• • • We do not use the following data for averages, fits, limits, etc. • • •				
-1.6 ± 4.5	[7] HAYRAPETY...	26	CMS	pp, 13 TeV, $H \to c\bar{c}$
$0.91^{+0.26}_{-0.22}$	[7] HAYRAPETY...	26	CMS	pp, 13 TeV, $H \to b\bar{b}$
$-0.27^{+0.86}_{-0.83}$	[8] TUMASYAN	23AI	ATLS	pp, 13 TeV, boosted $H \to b\bar{b}$
$0.35^{+0.36}_{-0.34}$	[9] AAD	22M	ATLS	pp, 13 TeV, $H \to b\bar{b}$
$1.38^{+0.36}_{-0.29}$	[10] SIRUNYAN	20AS	CMS	pp, 13 TeV, $H \to \gamma\gamma$
$0.72 \pm 0.24 \pm 0.38$	[11] SIRUNYAN	19R	CMS	pp, 13 TeV, $H \to b\bar{b}$
1.2 ± 0.3	[12] AABOUD	18AC	ATLS	pp, 13 TeV, $H \to b\bar{b}$ $\tau\tau$, $\gamma\gamma$, WW^*, ZZ^*
	[13] AABOUD	18BK	ATLS	pp, 13 TeV, $H \to b\bar{b}$ $\tau\tau$, $\gamma\gamma$, WW^*, ZZ^*
$0.84^{+0.64}_{-0.61}$	[14] AABOUD	18T	ATLS	pp, 13 TeV, $H \to b\bar{b}$
0.9 ± 1.5	[15] SIRUNYAN	18BD	CMS	pp, 13 TeV, $H \to b\bar{b}$
$1.23^{+0.45}_{-0.43}$	[16] SIRUNYAN	18BQ	CMS	pp, 13 TeV, $H \to \tau\tau$, WW^*, ZZ^*
$1.26^{+0.31}_{-0.26}$	[17] SIRUNYAN	18L	CMS	pp, 7, 8, 13 TeV, $H \to b\bar{b}$, $\tau\tau$, $\gamma\gamma$, WW^*, ZZ^*
1.7 ± 0.8	[18] AAD	16AL	ATLS	pp, 7, 8 TeV, $H \to b\bar{b}$, $\tau\tau$, $\gamma\gamma$, WW^*, and ZZ^*
$2.3^{+0.7}_{-0.6}$	[6,19] AAD	16AN	LHC	pp, 7, 8 TeV
$2.9^{+1.0}_{-0.9}$	[6] AAD	16AN	CMS	pp, 7, 8 TeV
$1.81^{+0.52+0.58+0.31}_{-0.50-0.55-0.12}$	[20] AAD	16K	ATLS	pp, 7, 8 TeV
$1.4^{+2.1}_{-1.4}{}^{+0.6}_{-0.3}$	[21] AAD	15	ATLS	pp, 7, 8 TeV
1.5 ± 1.1	[22] AAD	15BC	ATLS	pp, 8 TeV
$2.1^{+1.4}_{-1.2}$	[23] AAD	15T	ATLS	pp, 8 TeV
$1.2^{+1.6}_{-1.5}$	[24] KHACHATRY...	15AN	CMS	pp, 8 TeV
$2.8^{+1.0}_{-0.9}$	[25] KHACHATRY...	14H	CMS	pp, 7, 8 TeV
$9.49^{+6.60}_{-6.28}$	[26] AALTONEN	13L	CDF	$p\bar{p}$, 1.96 TeV
< 5.8 at 95% CL	[27] CHATRCHYAN	13X	CMS	pp, 7, 8 TeV, $H \to b\bar{b}$

[1] AAD 25AJ measure the $t\bar{t}H$ production with $H \to b\bar{b}$ decay channel using 140 fb^{-1} of data at E_{cm} = 13 TeV. The $t\bar{t}H$ cross section is measured to be 411^{+101}_{-92} fb for a Higgs boson mass of 125.09 GeV. The signal strengths with simplified template cross section bins are given in their Fig. 3.
[2] HAYRAPETYAN 25R measure the $t\bar{t}H$ and tH productions with $H \to b\bar{b}$ decay channel using 138 fb^{-1} of data at E_{cm} = 13 TeV. The quoted value is obtained assuming the tH contribution predicted in the SM. The signal strengths with simplified template cross section bins are given in their Fig. 12. Two-dimensional likelihood scan of (μ_{tH}, $\mu_{t\bar{t}H}$) is shown in their Fig. 14.
[3] SIRUNYAN 21R search for $t\bar{t}H$ in final states with electrons, muons and hadronically decaying τ leptons ($H \to WW^*$, ZZ^*, $\tau\tau$) with 137 fb^{-1} of pp collision data at E_{cm} = 13 TeV. The quoted signal strength corresponds to a significance of 4.7 standard deviations and is given for m_H = 125 GeV.
[4] AAD 20Z measure $\sigma_{t\bar{t}H} \cdot B(H \to \gamma\gamma)$ to be $1.64^{+0.38+0.17}_{-0.36-0.14}$ fb in 139 fb^{-1} of data at E_{cm} = 13 TeV.
[5] AABOUD 18AC search for $t\bar{t}H$ production with H decaying to $\tau\tau$, $WW^*(\to \ell\nu\ell\nu, \ell\nu q\bar{q})$, $ZZ^*(\to \ell\ell\nu\nu, \ell\ell q\bar{q})$ in 36.1 fb^{-1} of pp collisions at E_{cm} = 13 TeV. The quoted signal strength is given for m_H = 125 GeV. See their Table 13 and Fig. 13.
[6] AAD 16AN: In the fit, relative branching ratios are fixed to those in the Standard Model. The quoted signal strength is given for m_H = 125.09 GeV.
[7] HAYRAPETYAN 26 search for $t\bar{t}H$, $H \to c\bar{c}$ together with the $t\bar{t}H$, $H \to b\bar{b}$ measurement using 138 fb^{-1} of pp collision data at E_{cm} = 13 TeV.
[8] TUMASYAN 23AI measure boosted $H \to b\bar{b}$ (p_T > 200 GeV) in $t\bar{t}H$ production using 138 fb^{-1} of data at E_{cm} = 13 TeV. The differential cross section for the Higgs p_T is shown in their Fig. 8 and Table V. Limits on eight Wilson coefficients at 68% and 95% CL are shown in their Fig. 10 and Table VI.
[9] AAD 22M measure $H \to b\bar{b}$ in $t\bar{t}H$ production using 139 fb^{-1} of data at E_{cm} = 13 TeV. See their Fig. 14. The signal strengths and 95% CL cross section upper limits with simplified template cross section bins are given in their Figs. 18 and 19, respectively.
[10] SIRUNYAN 20AS measure $\sigma_{t\bar{t}H} \cdot B(H \to \gamma\gamma)$ to be $1.56^{+0.34}_{-0.32}$ fb in 137 fb^{-1} of data at E_{cm} = 13 TeV.
[11] SIRUNYAN 19R search for $t\bar{t}H$ production with H decaying to $b\bar{b}$ in 35.9 fb^{-1} of data at E_{cm} = 13 TeV. The quoted signal strength is given for m_H = 125 GeV.
[12] AABOUD 18AC combine results of $t\bar{t}H$, $H \to \tau\tau$, $WW^*(\to \ell\nu\ell\nu, \ell\nu q\bar{q})$, $ZZ^*(\to \ell\ell\nu\nu, \ell\ell q\bar{q})$ with results of $t\bar{t}H$, $H \to b\bar{b}$ (AABOUD 18T), $\gamma\gamma$ (AABOUD 18BO), $ZZ^*(\to 4\ell)$ (AABOUD 18AJ) in 36.1 fb^{-1} of pp collisions at E_{cm} = 13 TeV. The quoted signal strength is given for m_H = 125 GeV. See their Table 14.
[13] AABOUD 18BK use 79.8 fb^{-1} data for $t\bar{t}H$ production with $H \to \gamma\gamma$ and $ZZ^* \to 4\ell$ ($\ell = e, \mu$) and 36.1 fb^{-1} for other decay channels at E_{cm} = 13 TeV. A significance of 5.8 standard deviations is observed for m_H = 125.09 GeV and its signal strength without the uncertainty of the $t\bar{t}H$ cross section is $1.32^{+0.28}_{-0.26}$. Combining with results of 7 and 8 TeV (AAD 16K), the significance is 6.3 standard deviations. Assuming Standard Model branching fractions, the total $t\bar{t}H$ production cross section at 13 TeV is measured to be $670 \pm 90^{+110}_{-100}$ fb.
[14] AABOUD 18T search for $t\bar{t}H$ production with H decaying to $b\bar{b}$ in 36.1 fb^{-1} of pp collisions at E_{cm} = 13 TeV. The quoted signal strength is given for m_H = 125 GeV.

Int. J. Mod. Phys. A 2026.41. Downloaded from worldscientific.com
by UNIVERSITY OF CALIFORNIA @ BERKELEY on 09/16/26. Reproduction strictly not permitted, except for Open Access articles.

Int. J. Mod. Phys. A 2026.41. Downloaded from www.worldscientific.com
by UNIVERSITY OF CALIFORNIA @ BERKELEY on 09/16/26. Re-use and distribution is strictly not permitted, except for Open Access articles.

[15] SIRUNYAN 18BD search for $t\overline{t}H$, $H \to b\overline{b}$ in the all-jet final state with 35.9 fb^{-1} pp collision data at E_{cm} = 13 TeV. The quoted signal strength is given for m_H = 125 GeV.

[16] SIRUNYAN 18BQ search for $t\overline{t}H$ in final states with electrons, muons and hadronically decaying τ leptons ($H \to WW^*$, ZZ^*, $\tau\tau$) with 35.9 fb^{-1} of pp collision data at E_{cm} = 13 TeV. The quoted signal strength corresponds to a significance of 3.2 standard deviations and is given for m_H = 125 GeV.

[17] SIRUNYAN 18L use up to 5.1, 19.7 and 35.9 fb^{-1} of pp collisions at E_{cm} = 7, 8, and 13 TeV, respectively. The quoted signal strength corresponds to a significance of 5.2 standard deviations and is given for m_H = 125.09 GeV. H decay channels of WW^*, ZZ^*, $\gamma\gamma$, $\tau\tau$, and $b\overline{b}$ are used. See their Table 1 and Fig. 2 for results on individual channels.

[18] AAD 16AL search for $t\overline{t}H$ production with H decaying to $\gamma\gamma$ in 4.5 fb^{-1} of pp collisions at E_{cm} = 7 TeV and $b\overline{b}$, $\tau\tau$, $\gamma\gamma$, WW^*, and ZZ^* in 20.3 fb^{-1} at E_{cm} = 8 TeV. The quoted signal strength is given for m_H = 125 GeV. This paper combines the results of previous papers, and the new result of this paper only is: $\mu = 1.6 \pm 2.6$.

[19] AAD 16AN perform fits to the ATLAS and CMS data at E_{cm} = 7 and 8 TeV.

[20] AAD 16K use up to 4.7 fb^{-1} of pp collisions at E_{cm} = 7 TeV and up to 20.3 fb^{-1} at E_{cm} = 8 TeV. The third uncertainty in the measurement is theory systematics. The quoted signal strength is given for m_H = 125.36 GeV.

[21] AAD 15 search for $t\overline{t}H$ production with H decaying to $\gamma\gamma$ in 4.5 fb^{-1} of pp collisions at E_{cm} = 7 TeV and 20.3 fb^{-1} at E_{cm} = 8 TeV. The quoted result on the signal strength is equivalent to an upper limit of 6.7 at 95% CL and is given for m_H = 125.4 GeV.

[22] AAD 15BC search for $t\overline{t}H$ production with H decaying to $b\overline{b}$ in 20.3 fb^{-1} of pp collisions at E_{cm} = 8 TeV. The corresponding upper limit is 3.4 at 95% CL. The quoted signal strength is given for m_H = 125 GeV.

[23] AAD 15T search for $t\overline{t}H$ production with H resulting in multilepton final states (mainly from WW^*, $\tau\tau$, ZZ^*) in 20.3 fb^{-1} of pp collisions at E_{cm} = 8 TeV. The quoted result on the signal strength is given for m_H = 125 GeV and corresponds to an upper limit of 4.7 at 95% CL. The data sample is independent from AAD 15 and AAD 15BC.

[24] KHACHATRYAN 15AN search for $t\overline{t}H$ production with H decaying to $b\overline{b}$ in 19.5 fb^{-1} of pp collisions at E_{cm} = 8 TeV. The quoted result on the signal strength is equivalent to an upper limit of 4.2 at 95% CL and is given for m_H = 125 GeV.

[25] KHACHATRYAN 14H search for $t\overline{t}H$ production with H decaying to $b\overline{b}$, $\tau\tau$, $\gamma\gamma$, WW^*, and ZZ^*, in 5.1 fb^{-1} of pp collisions at E_{cm} = 7 TeV and 19.7 fb^{-1} at E_{cm} = 8 TeV. The quoted signal strength is given for m_H = 125.6 GeV.

[26] AALTONEN 13L combine all CDF results with 9.45–10.0 fb^{-1} of $p\overline{p}$ collisions at E_{cm} = 1.96 TeV. The quoted signal strength is given for m_H = 125 GeV.

[27] CHATRCHYAN 13X search for $t\overline{t}H$ production followed by $H \to b\overline{b}$, one top decaying to $\ell\nu$ and the other to either $\ell\nu$ or $q\overline{q}$ in 5.0 fb^{-1} and 5.1 fb^{-1} of pp collisions at E_{cm} = 7 and 8 TeV. A limit on cross section times branching ratio which corresponds to (4.0–8.6) times the expected Standard Model cross section is given for m_H = 110–140 GeV at 95% CL. The quoted limit is given for m_H = 125 GeV, where 5.2 is expected for no signal.

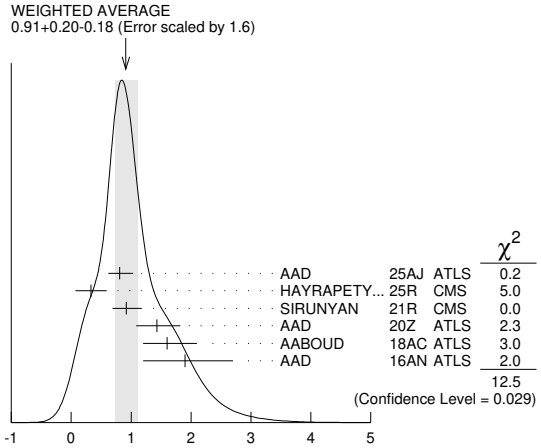

$t\overline{t}H$ production

$b\overline{b}H$ production

VALUE	CL%	DOCUMENT ID	TECN	COMMENT
<3.7	95	[1] HAYRAPETY...25	CMS	pp, 13 TeV, $H \to \tau\tau$, WW^*

[1] HAYRAPETYAN 25 search for $b\overline{b}H$ and bH in final states with leptons using 138 fb^{-1} of data at E_{cm} = 13 TeV. $H \to \tau\tau$ or $H \to WW^* \to \ell\nu\ell\nu$ are considered. Upper limits at 95% CL on the signal strength for each final state are found in their Fig. 3. Combing with TUMASYAN 23Y, two-dimensional exclusion regions as a function of the κ_b and κ_t parameters are shown in their Fig. 4. The best fit value is (κ_t, κ_b) = (-0.73, 1.58). All other Higgs couplings are fixed to the SM values.

tH production

VALUE	CL%	DOCUMENT ID	TECN	COMMENT
7.1±2.5 OUR AVERAGE				
8.1±2.6±2.0		[1] AAD 25BD	ATLS	pp, 13 TeV
5.7±2.7±3.0		[2] SIRUNYAN 21R	CMS	pp, 13 TeV
• • • We do not use the following data for averages, fits, limits, etc. • • •				
<13.9	95	[3] AAD 25BD	ATLS	pp, 13 TeV
<14.6	95	[4] HAYRAPETY...25R	CMS	pp, 13 TeV
<12	95	[5] AAD 20Z	ATLS	pp, 13 TeV
		[6] SIRUNYAN 19BK	CMS	pp, 13 TeV
		[7] KHACHATRY...16AU	CMS	pp, 8 TeV

[1] AAD 25BD search for tH in final states with leptons (electron or muon) ($H \to b\overline{b}$, WW^*, ZZ^*, $\tau\tau$) with 140 fb^{-1} of pp collision data at E_{cm} = 13 TeV. The quoted signal strength corresponds to the cross-section of $\sigma(tH)$ = 720 ± 270 fb and a significance of 2.8 standard deviations.

[2] SIRUNYAN 21R search for tH in final states with electrons, muons and hadronically decaying τ leptons ($H \to WW^*$, ZZ^*, $\tau\tau$) with 137 fb^{-1} of pp collision data at E_{cm} = 13 TeV. The quoted signal strength corresponds to a significance of 1.4 standard deviations and is given for m_H = 125 GeV.

[3] AAD 25BD search for tH in final states with leptons (electron or muon) ($H \to b\overline{b}$, WW^*, ZZ^*, $\tau\tau$) with 140 fb^{-1} of pp collision data at E_{cm} = 13 TeV.

[4] HAYRAPETYAN 25R measure the $t\overline{t}H$ and tH productions with $H \to b\overline{b}$ decay channel using 138 fb^{-1} of data at E_{cm} = 13 TeV. The quoted value is obtained assuming the $t\overline{t}H$ contribution predicted in the SM. Two-dimensional likelihood scan of (μ_{tH}, $\mu_{t\overline{t}H}$) is shown in their Fig. 14.

[5] AAD 20Z search for the tH associated production using $H \to \gamma\gamma$ in 139 fb^{-1} of data at E_{cm} = 13 TeV. An upper limit on its rate is set to be 12 times the Standard Model at 95% CL (m_H = 125.09 GeV).

[6] SIRUNYAN 19BK search for the tH associated production using multilepton signatures ($H \to WW^*$, $H \to \tau\tau$, $H \to ZZ^*$) and signatures with a single lepton and a $b\overline{b}$ pair ($H \to b\overline{b}$) using 35.9 fb^{-1} at E_{cm} = 13 TeV. Results are combined with $H \to \gamma\gamma$ (SIRUNYAN 18DS). The observed 95% CL upper limit on the tH production cross section times $H \to WW^* + \tau\tau + ZZ^* + b\overline{b} + \gamma\gamma$ branching fraction is 1.94 pb (assuming SM $t\overline{t}H$ production cross section). See their Table X and Fig. 14. The values outside the ranges of [−0.9, −0.5] and [1.0, 2.1] times the standard model top quark Yukawa coupling are excluded at 95% CL.

[7] KHACHATRYAN 16AU search for the tH associated production in 19.7 fb^{-1} at E_{cm} = 8 TeV. The 95% CL upper limits on the tH associated production cross section is measured to be 600–1000 fb depending on the assumed $\gamma\gamma$ branching ratios of the Higgs boson. The $\gamma\gamma$ branching ratio is varied to be by a factor of 0.5–3.0 of the Standard Model Higgs boson (m_H = 125 GeV). The results of the signal strengths for a negative Higgs-boson trilinear coupling are given. The results are given for m_H = 125 GeV.

cH production

VALUE	CL%	DOCUMENT ID	TECN	COMMENT
• • • We do not use the following data for averages, fits, limits, etc. • • •				
		[1] AAD 25R	ATLS	pp, 13 TeV, $H \to \gamma\gamma$
<243	95	[2] CHEKHOVSKY 25L	CMS	pp, 13 TeV, $H \to \gamma\gamma$

[1] AAD 25R search for the production of a Higgs boson and one or more charm quarks (H+c) with $H \to \gamma\gamma$ using 140 fb^{-1} of data at E_{cm} = 13 TeV. The observed H+c cross section is 5.3 ± 3.2 pb. The observed upper limit on the H+c cross section at 95% CL is 10.6 pb.

[2] CHEKHOVSKY 25L search for the production of a Higgs boson and one or more charm quarks (H+c) with $H \to \gamma\gamma$ using 138 fb^{-1} of data at E_{cm} = 13 TeV. The quoted value is obtained assuming the SM rates for all other Higgs production processes.

VBS/VBF WH production

WH production through vector boson scattering (VBS) or vector boson fusion (VBF). The VBS/VBF WH production cross section related to the SM prediction.

VALUE	CL%	DOCUMENT ID	TECN	COMMENT
• • • We do not use the following data for averages, fits, limits, etc. • • •				
<14.3	95	[1] HAYRAPETY...25B	CMS	pp, 13 TeV, VBF WH, coupling sign
< 9.0	95	[2] AAD 24BM	ATLS	pp, 13 TeV, VBF WH, coupling sign

[1] HAYRAPETYAN 25B present the determination of the relative sign of κ_W and κ_Z with VBF WH, $H \to b\overline{b}$ using 148 fb^{-1} of data at E_{cm} = 13 TeV. The upper limit at 95% CL on the cross section for VBF WH production is obtained. The signal strength is measured to be $2.2^{+6.1}_{-5.8}$.

[2] AAD 24BM present the determination of the relative sign of κ_W and κ_Z with VBF WH, $H \to b\overline{b}$ using 140 fb^{-1} of data at E_{cm} = 13 TeV. The upper limit at 95% CL on the cross section for VBF WH production is obtained. The signal strength is measured to be $0.9^{+4.0}_{-4.3}$.

γH production

VALUE	DOCUMENT ID	TECN	COMMENT
• • • We do not use the following data for averages, fits, limits, etc. • • •			
	[1] CHEKHOVSKY 25G	CMS	pp, 13 TeV, $H \to b\overline{b}$, $H \to ZZ^* \to 4\ell$

[1] CHEKHOVSKY 25G search for the γH production using a boosted Higgs boson recoiling against a high-energy photon with data of 138 fb^{-1} at E_{cm} = 13 TeV. The production cross section is constraint to be $\sigma_{\gamma H}$ < 16.4 fb at 95% CL. Constraints on four anomalous couplings involving $HZ\gamma$ and $H\gamma\gamma$ are shown in their Table I.

HH production

The HH production cross section relative to the SM prediction.

VALUE	CL%	DOCUMENT ID	TECN	COMMENT
< 2.4	95	[1] AAD 23AT	ATLS	13 TeV, $b\overline{b}b\overline{b}$, $b\overline{b}\tau\tau$, $b\overline{b}\gamma\gamma$
• • • We do not use the following data for averages, fits, limits, etc. • • •				
< 5.9	95	[2] AAD 24AZ	ATLS	13 TeV, $b\overline{b}\tau\tau$
< 17	95	[3] AAD 24BG	ATLS	13 TeV, $b\overline{b}ZZ^*$, VVVV, $VV\tau\tau$, $\tau\tau\tau\tau$, $\gamma\gamma VV$, $\gamma\gamma\tau\tau$
< 2.9	95	[4] AAD 24BL	ATLS	13 TeV, $b\overline{b}b\overline{b}$, $b\overline{b}\tau\tau$, $b\overline{b}\gamma\gamma$, multilepton , $b\overline{b}\ell\ell$
< 4.0	95	[5] AAD 24X	ATLS	13 TeV, $b\overline{b}\gamma\gamma$
< 9.7	95	[6] AAD 24Y	ATLS	13 TeV, $b\overline{b}WW^*$, $b\overline{b}ZZ^*$, $b\overline{b}\tau\tau$, multilepton
< 14	95	[7] HAYRAPETY...24AE	CMS	13 TeV, $b\overline{b}WW^*$
<294	95	[8] HAYRAPETY...24AW	CMS	13 TeV, VHH, $HH \to b\overline{b}b\overline{b}$

<183	95	[9] AAD	23AD	ATLAS	13 TeV, VHH, $HH \to b\overline{b}b\overline{b}$
< 5.4	95	[10] AAD	23BK	ATLAS	13 TeV, $b\overline{b}b\overline{b}$
< 4.7	95	[11] AAD	23Z	ATLAS	13 TeV, $b\overline{b}\tau\tau$
< 9.9	95	[12] TUMASYAN	23AE	CMS	13 TeV, $b\overline{b}b\overline{b}$
< 3.3	95	[13,14] TUMASYAN	23D	CMS	13 TeV, $b\overline{b}\tau\tau$
<124	95	[13,15] TUMASYAN	23D	CMS	13 TeV, $b\overline{b}\tau\tau$
< 32.4	95	[16] TUMASYAN	23I	CMS	13 TeV, $b\overline{b}ZZ^*$ ($ZZ^* \to 4\ell$)
< 21.3	95	[17] TUMASYAN	23O	CMS	13 TeV, WW^*WW^*, $WW^*\tau\tau$, $\tau\tau\tau\tau$
< 4.2	95	[18] AAD	22Y	ATLAS	13 TeV, $\gamma\gamma b\overline{b}$
< 3.4	95	[19] CMS	22	CMS	13 TeV, $b\overline{b}ZZ^*$, $b\overline{b}\gamma\gamma$, $b\overline{b}\tau\tau$, $b\overline{b}b\overline{b}$, multilepton
< 3.9	95	[20] TUMASYAN	22AN	CMS	13 TeV, $b\overline{b}b\overline{b}$
< 7.7	95	[21] SIRUNYAN	21K	CMS	13 TeV, $\gamma\gamma b\overline{b}$
< 6.9	95	[22] AAD	20C	ATLAS	13 TeV, $b\overline{b}\gamma\gamma$, $b\overline{b}\tau\tau$, $b\overline{b}b\overline{b}$, $b\overline{b}WW^*$, $WW^*\gamma\gamma$, WW^*WW^*
< 40	95	[23] AAD	20E	ATLAS	13 TeV, $HH \to b\overline{b}\ell\nu\ell\nu$
<840	95	[24] AAD	20X	ATLAS	13 TeV, VBF, $b\overline{b}b\overline{b}$
< 12.9	95	[25] AABOUD	19A	ATLAS	13 TeV, $b\overline{b}b\overline{b}$
<300	95	[26] AABOUD	19O	ATLAS	13 TeV, $b\overline{b}WW^*$
<160	95	[27] AABOUD	19T	ATLAS	13 TeV, WW^*WW^*
< 24	95	[28] SIRUNYAN	19	CMS	13 TeV, $\gamma\gamma b\overline{b}$
< 75	95	[29] SIRUNYAN	19AB	CMS	13 TeV, $b\overline{b}b\overline{b}$
< 22.2	95	[30] SIRUNYAN	19BE	CMS	13 TeV, $b\overline{b}\gamma\gamma$ $b\overline{b}\tau\tau$, $b\overline{b}b\overline{b}$, $b\overline{b}WW^*$, $b\overline{b}ZZ^*$
<179	95	[31] SIRUNYAN	19H	CMS	13 TeV, $b\overline{b}b\overline{b}$
<230	95	[32] AABOUD	18BU	ATLAS	13 TeV, $\gamma\gamma WW^*$
< 12.7	95	[33] AABOUD	18CQ	ATLAS	13 TeV, $b\overline{b}\tau\tau$
< 22	95	[34] AABOUD	18CW	ATLAS	13 TeV, $\gamma\gamma b\overline{b}$
< 30	95	[35] SIRUNYAN	18A	CMS	13 TeV, $b\overline{b}\tau\tau$
< 79	95	[36] SIRUNYAN	18F	CMS	13 TeV, $b\overline{b}\ell\nu\ell\nu$
< 43	95	[37] SIRUNYAN	17CN	CMS	8 TeV, $b\overline{b}\tau\tau$, $\gamma\gamma b\overline{b}$, $b\overline{b}b\overline{b}$
<108	95	[38] AABOUD	16I	ATLAS	13 TeV, $b\overline{b}b\overline{b}$
< 74	95	[39] KHACHATRY...	16BQ	CMS	8 TeV, $\gamma\gamma b\overline{b}$
< 70	95	[40] AAD	15CE	ATLAS	8 TeV, $b\overline{b}b\overline{b}$, $b\overline{b}\tau\tau$, $\gamma\gamma b\overline{b}$, $\gamma\gamma WW$

[1] AAD 23AT combine results from 126–139 fb^{-1} of data at E_{cm} = 13 TeV for $pp \to HH \to b\overline{b}b\overline{b}$ (AAD 23BK), $b\overline{b}\tau\tau$ (AAD 23Z), and $b\overline{b}\gamma\gamma$ (AAD 22Y).

[2] AAD 24AZ search for non-resonant HH production using $HH \to b\overline{b}\tau\tau$ with data of 140 fb^{-1} at E_{cm} = 13 TeV. The result is interpreted: limits on Wilson coefficients of the Higgs effective field theory (HEFT) and the SM effective field theory (SMEFT) are shown in their Table IV and Figs. 11 and 12; the ggF HH production cross sections (7 benchmark points) of HEFT are shown in their Fig. 10. In those interpretations the VBF HH production is neglected.

[3] AAD 24BG search for non-resonant HH production targeting the $b\overline{b}ZZ^*$, VVVV, $VV\tau\tau$, $\tau\tau\tau\tau$, $\gamma\gamma VV$, $\gamma\gamma\tau\tau$ decay channels with data of 140 fb^{-1} at E_{cm} = 13 TeV. Signal strengths for the 11 different signal regions are given in their Fig. 8.

[4] AAD 24BL combine results from 126–140 fb^{-1} of data at E_{cm} = 13 TeV for $pp \to HH \to b\overline{b}b\overline{b}$ (AAD 23BK, AAD 24BV), $b\overline{b}\tau\tau$ (AAD 24AZ), $b\overline{b}\gamma\gamma$ (AAD 24X), multilepton (AAD 24BG), and $b\overline{b}\ell\ell$ (AAD 24Y). See their Fig. 2. The signal strength is measured to be $0.5^{+1.2}_{-1.0}$. Constraints for three interaction parameters (c_{tthh}, c_{gghh}, c_{hhh}) in the Higgs effective field theory are set. See their Fig. 4.

[5] AAD 24X search for non-resonant HH production using $HH \to b\overline{b}\gamma\gamma$ with data of 140 fb^{-1} at E_{cm} = 13 TeV. The result is interpreted: limits on three Wilson coefficients and the ggF HH production cross sections (7 benchmark points shown in their Table 5) of the Higgs effective field theory are shown in their Table 4 and Fig. 8, respectively; limits on two Wilson coefficients of the SM effective field theory are shown in their Table 6 and Fig. 9. In those interpretations only the ggF HH production is considered instead of both ggF and VBF.

[6] AAD 24Y search for non-resonant HH production in $2b + 2\ell + \nu$s final state ($\ell = e$, μ) targeting $b\overline{b}WW^*$, $b\overline{b}ZZ^*$, and $b\overline{b}\tau\tau$ decay channels with data of 140 fb^{-1} at E_{cm} = 13 TeV. The signal strength is measured to be $-8.5^{+7.7}_{-8.4}$. See their Fig. 6.

[7] HAYRAPETYAN 24AE search for non-resonant HH production using $HH \to b\overline{b}WW^*$ with data of 138 fb^{-1} at E_{cm} = 13 TeV. The result is interpreted: the ggF HH production cross sections (20 benchmark points) of the Higgs effective field theory are shown in their Fig. 16; the coupling between two top quarks and two Higgs bosons is constrained between [-0.8, 1.3] at 95%CL (see their Fig. 17) with all other Higgs couplings fixed to the SM values.

[8] HAYRAPETYAN 24AW search for non-resonant HH production in association with a vector boson using $HH \to b\overline{b}b\overline{b}$ with data of 138 fb^{-1} at E_{cm} = 13 TeV. The vector boson decays both leptonically ($W \to \ell\nu$, $Z \to \ell\ell, \nu\nu$, $\ell = e, \mu$) and hadronically. The quoted value is the upper limit of the VHH cross section. See their Figs. 13 and 16 (left) for the best fit and the upper limit of the VHH cross section, respectively. In addition, upper limits at 95% CL on VHH and HH cross sections are shown as a function of κ_λ, κ_{2V}, and κ_V in their Figs. 17, 18, and 19.

[9] AAD 23AD search for non-resonant HH production in association with a vector boson using $HH \to b\overline{b}b\overline{b}$ with data of 139 fb^{-1} at E_{cm} = 13 TeV. The vector boson decays leptonically ($W \to \ell\nu$, $Z \to \ell\ell, \nu\nu$, $\ell = e, \mu$).

[10] AAD 23BK search for non-resonant HH production using $HH \to b\overline{b}b\overline{b}$ with data of 126 fb^{-1} at E_{cm} = 13 TeV.

[11] AAD 23Z search for non-resonant HH production using $HH \to b\overline{b}\tau\tau$ with data of 139 fb^{-1} at E_{cm} = 13 TeV. The upper limit on the $pp \to HH$ production cross section at 95% CL is measured to be 140 fb, which corresponds to 4.7 times the SM prediction (see their Table 6).

[12] TUMASYAN 23AE search for HH production using $HH \to b\overline{b}b\overline{b}$, where both $b\overline{b}$ pairs are highly boosted, with data of 138 fb^{-1} at E_{cm} = 13 TeV.

[13] TUMASYAN 23D search for non-resonant HH production using $HH \to b\overline{b}\tau\tau$ with data of 138 fb^{-1} at E_{cm} = 13 TeV.

[14] The upper limit on the $pp \to HH$ production cross section (gluon fusion and VBF) at 95% CL is measured to be 102 fb, which corresponds to 3.3 times the SM prediction (see their Table 2).

[15] The upper limit on the VBF $pp \to HH$ production cross section at 95% CL is measured to be 212 fb, which corresponds to 124 times the SM prediction (see their Table 3).

[16] TUMASYAN 23I search for non-resonant HH production using $HH \to b\overline{b}ZZ^*$ ($ZZ^* \to 4\ell$, $\ell = e, \mu$) with data of 138 fb^{-1} at E_{cm} = 13 TeV.

[17] TUMASYAN 23O search for non-resonant HH production using $HH \to WW^*WW^*$, $WW^*\tau\tau$, and $\tau\tau\tau\tau$ (multilepton) with data of 138 fb^{-1} at E_{cm} = 13 TeV. See their Fig. 9 for different final states and these combination.

[18] AAD 22Y search for non-resonant HH production using $HH \to \gamma\gamma b\overline{b}$ with data of 139 fb^{-1} at E_{cm} = 13 TeV. The upper limit on the $pp \to HH$ production cross section at 95% CL is measured to be 130 fb, which corresponds to 4.2 times the SM prediction.

[19] CMS 22 report combined results (see their Extended Data Table 2) using 138 fb^{-1} of data at E_{cm} = 13 TeV. See their Fig. 5 (left) for different final states and these combination.

[20] TUMASYAN 22AN search for non-resonant HH production using $HH \to b\overline{b}b\overline{b}$ with data of 138 fb^{-1} at E_{cm} = 13 TeV. The upper limit on the $pp \to HH$ production cross section at 95% CL is measured to be 120 fb, which corresponds to 3.9 times the SM prediction.

[21] SIRUNYAN 21K search for non-resonant HH production using $HH \to \gamma\gamma b\overline{b}$ with data of 137 fb^{-1} at E_{cm} = 13 TeV. The upper limit on the $pp \to HH \to \gamma\gamma b\overline{b}$ production cross section at 95% CL is measured to be 0.67 fb, which corresponds to about 7.7 times the SM prediction.

[22] AAD 20C combine results of up to 36.1 fb^{-1} data at E_{cm} = 13 TeV for $pp \to HH \to b\overline{b}\gamma\gamma$, $b\overline{b}\tau\tau$, $b\overline{b}b\overline{b}$, $b\overline{b}WW^*$, $WW^*\gamma\gamma$, WW^*WW^* (AABOUD 18CW, AABOUD 18CQ, AABOUD 19A, AABOUD 19O, AABOUD 18BU, and AABOUD 19T).

[23] AAD 20E search non-resonant for HH production using $HH \to b\overline{b}\ell\nu\ell\nu$, where one of the Higgs bosons decays to $b\overline{b}$ and the other decays to either WW^*, ZZ^*, or $\tau\tau$, with data of 139 fb^{-1} at E_{cm} = 13 TeV. The upper limit on the $pp \to HH$ production cross section at 95% CL is measured to be 1.2 pb, which corresponds to about 40 times the SM prediction.

[24] AAD 20X search for $HH \to b\overline{b}b\overline{b}$ process via VBF with data of 126 fb^{-1} at E_{cm} = 13 TeV. The upper limit on the SM non-resonant HH production cross section is 1460 fb at 95% CL, which corresponds to 840 times the SM prediction.

[25] AABOUD 19A search for HH production using $HH \to b\overline{b}b\overline{b}$ with data of 36.1 fb^{-1} at E_{cm} = 13 TeV. The upper limit on the $pp \to HH \to b\overline{b}b\overline{b}$ production cross section at 95% is measured to be 147 fb, which corresponds to about 12.9 times the SM prediction.

[26] AABOUD 19O search for HH production using $HH \to b\overline{b}WW^*$ with data of 36.1 fb^{-1} at E_{cm} = 13 TeV. The upper limit on the $pp \to HH$ production cross section at 95% CL is calculated to be 10 pb from the observed upper limit on the $pp \to HH \to b\overline{b}WW^*$ production cross section of 2.5 pb assuming the SM branching fractions. The former corresponds to about 300 times the SM prediction.

[27] AABOUD 19T search for HH production using $HH \to WW^*WW^*$ with data of 36.1 fb^{-1} at E_{cm} = 13 TeV. The upper limit on the $pp \to HH$ production cross section at 95% is measured to be 5.3 pb, which corresponds to about 160 times the SM prediction.

[28] SIRUNYAN 19 search for HH production using $HH \to \gamma\gamma b\overline{b}$ with data of 35.9 fb^{-1} at E_{cm} = 13 TeV. The upper limit on the $pp \to HH \to \gamma\gamma b\overline{b}$ production cross section at 95% CL is measured to be 2.0 fb, which corresponds to about 24 times the SM prediction.

[29] SIRUNYAN 19AB search for HH production using $HH \to b\overline{b}b\overline{b}$, where 4 heavy flavor jets from two Higgs bosons are resolved, with data of 35.9 fb^{-1} at E_{cm} = 13 TeV. The upper limit on the $pp \to HH \to b\overline{b}b\overline{b}$ production cross section at 95% is measured to be 847 fb, which corresponds to about 75 times the SM prediction.

[30] SIRUNYAN 19BE combine results of 13 TeV 35.9 fb^{-1} data: SIRUNYAN 19, SIRUNYAN 18A, SIRUNYAN 19AB, SIRUNYAN 19H, and SIRUNYAN 18F.

[31] SIRUNYAN 19H search for HH production using $HH \to b\overline{b}b\overline{b}$, where one of $b\overline{b}$ pairs is highly boosted and the other one is resolved, with data of 35.9 fb^{-1} at E_{cm} = 13 TeV. The upper limit on the $pp \to HH \to b\overline{b}b\overline{b}$ production cross section at 95% is measured to be 1980 fb, which corresponds to about 179 times the SM prediction.

[32] AABOUD 18BU search for HH production using $\gamma\gamma WW^*$ with the final state of $\gamma\gamma\ell\nu jj$ using data of 36.1 fb^{-1} at E_{cm} = 13 TeV. The upper limit on the $pp \to HH$ production cross section at 95% CL is measured to be 7.7 pb, which corresponds to about 230 times the SM prediction. The upper limit on the $pp \to HH \to \gamma\gamma WW^*$ at 95% CL is measured to be 7.5 fb (see thier Table 6).

[33] AABOUD 18CQ search for HH production using $HH \to b\overline{b}\tau\tau$ with data of 36.1 fb^{-1} at E_{cm} = 13 TeV. The upper limit on the $pp \to HH \to b\overline{b}\tau\tau$ production cross section at 95% is measured to be 30.9 fb, which corresponds to about 12.7 times the SM prediction.

[34] AABOUD 18CW search for HH production using $HH \to \gamma\gamma b\overline{b}$ with data of 36.1 fb^{-1} at E_{cm} = 13 TeV. The upper limit on the $pp \to HH$ production cross section at 95% is measured to be 0.73 pb, which corresponds to about 22 times the SM prediction.

[35] SIRUNYAN 18A search for HH production using $HH \to b\overline{b}\tau\tau$ with data of 35.9 fb^{-1} at E_{cm} = 13 TeV. The upper limit on the $gg \to HH \to b\overline{b}\tau\tau$ production cross section is measured to be 75.4 fb, which corresponds to about 30 times the SM prediction.

[36] SIRUNYAN 18F search non-resonant for HH production using $HH \to b\overline{b}\ell\nu\ell\nu$, where $\ell\nu\ell\nu$ is either $WW \to \ell\nu\ell\nu$ or $ZZ \to \ell\ell\nu\nu$ (ℓ is e, μ or a leptonically decaying τ), with data of 35.9 fb^{-1} at E_{cm} = 13 TeV. The upper limit on the $HH \to b\overline{b}\ell\nu\ell\nu$ production cross section at 95% CL is measured to be 72 fb, which corresponds to about 79 times the SM prediction.

[37] SIRUNYAN 17CN search for HH production using $HH \to b\overline{b}\tau\tau$ with data of 18.3 fb^{-1} at E_{cm} = 8 TeV. Results are then combined with the published results of the $HH \to \gamma\gamma b\overline{b}$ and $HH \to b\overline{b}b\overline{b}$, which use data of up to 19.7 fb^{-1} at E_{cm} = 8 TeV. The upper limit on the $gg \to HH$ production cross section is measured to be 0.59 pb from $b\overline{b}\tau\tau$, which corresponds to about 59 times the SM prediction (gluon fusion). The combined upper limit is 0.43 pb, which is about 43 times the SM prediction. The quoted values are given for m_H = 125 GeV.

[38] AABOUD 16I search for HH production using $HH \to b\overline{b}b\overline{b}$ with data of 3.2 fb^{-1} at E_{cm} = 13 TeV. The upper limit on the $pp \to HH \to b\overline{b}b\overline{b}$ production cross section is measured to be 1.22 pb. This result corresponds to about 108 times the SM prediction (gluon fusion), which is $11.3^{+0.9}_{-1.0}$ fb (NNLO+NNLL) including top quark mass effects. The quoted values are given for m_H = 125 GeV.

Int. J. Mod. Phys. A 2026.41. Downloaded
by UNIVERSITY OF CALIFORNIA @ BERKELEY on 09/16/26. Re
worldscientific.com
strictly not permitted, except for Open Access articles.

Int. J. Mod. Phys. A 2026.41. Downloaded from www.worldscientific.com by UNIVERSITY OF CALIFORNIA @ BERKELEY on 09/16/26. Re-use and distribution is strictly not permitted, except for Open Access articles.

[39] KHACHATRYAN 16BQ search for HH production using $HH \to \gamma\gamma b\overline{b}$ with data of 19.7 fb^{-1} at E_{cm} = 8 TeV. The upper limit on the $gg \to HH \to \gamma\gamma b\overline{b}$ production is measured to be 1.85 fb, which corresponds to about 74 times the SM prediction and is translated into 0.71 pb for $gg \to HH$ production cross section.

[40] AAD 15CE search for HH production using $HH \to b\overline{b}\tau\tau$ and $HH \to \gamma\gamma WW$ with data of 20.3 fb^{-1} at E_{cm} = 8 TeV. These results are then combined with the published results of the $HH \to \gamma\gamma b\overline{b}$ and $HH \to b\overline{b}b\overline{b}$, which use data of up to 20.3 fb^{-1} at E_{cm} = 8 TeV. The upper limits on the $gg \to HH$ production cross section are measured to be 1.6 pb, 11.4 pb, 2.2 pb and 0.62 pb from $b\overline{b}\tau\tau$, $\gamma\gamma WW$, $\gamma\gamma b\overline{b}$ and $b\overline{b}b\overline{b}$, respectively. The combined upper limit is 0.69 pb, which corresponds to about 70 times the SM prediction. The quoted results are given for m_H = 125.4 GeV. See their Table 4.

HHH production

The HHH production cross section relative to the SM prediction.

VALUE	CL%	DOCUMENT ID		TECN	COMMENT
<760	95	[1] AAD	25J	ATLS	13 TeV, $b\overline{b}b\overline{b}b\overline{b}$

[1] AAD 25J search for non-resonant HHH production using $HHH \to b\overline{b}b\overline{b}b\overline{b}$ with data of 126 fb^{-1} at E_{cm} = 13 TeV. The upper limit on the $pp \to HHH$ production cross section at 95% CL is measured to be 59 fb.

Higgs trilinear self coupling modifier κ_λ

Signal strength relative to the SM prediction, $\kappa_\lambda = \kappa_3 = \lambda_{HHH} / \lambda^{SM}_{HHH}$.

VALUE	CL%	DOCUMENT ID		TECN	COMMENT
3.8 $^{+2.1}_{-3.6}$		[1] AAD	24BL	ATLS	13 TeV, $b\overline{b}b\overline{b}$, $b\overline{b}\tau\tau$, $b\overline{b}\gamma\gamma$, multilepton , $b\overline{b}\ell\ell$
• • • We do not use the following data for averages, fits, limits, etc. • • •					
−11 to 17	95	[2] AAD	25J	ATLS	13 TeV, $b\overline{b}b\overline{b}b\overline{b}$
− 1.2 to 7.5	95	[3] HAYRAPETY...	25F	CMS	13 TeV, single and double Higgs production
− 3.1 to 9.0	95	[4] AAD	24AZ	ATLS	13 TeV, $b\overline{b}\tau\tau$
− 6.2 to 11.6	95	[5] AAD	24BG	ATLS	13 TeV, $b\overline{b}ZZ^*$, VVVV, $VV\tau\tau$, $\tau\tau\tau\tau$, $\gamma\gamma VV$, $\gamma\gamma\tau\tau$
− 1.2 to 7.2	95	[1] AAD	24BL	ATLS	13 TeV, $b\overline{b}b\overline{b}$, $b\overline{b}\tau\tau$, $b\overline{b}\gamma\gamma$, multilepton , $b\overline{b}\ell\ell$
− 1.4 to 6.9	95	[6] AAD	24X	ATLS	13 TeV, $b\overline{b}\gamma\gamma$
− 6.2 to 13.3	95	[7] AAD	24Y	ATLS	13 TeV, $b\overline{b}WW^*$, $b\overline{b}ZZ^*$, $b\overline{b}\tau\tau$, multilepton
− 7.2 to 13.8	95	[8] HAYRAPETY...	24AE	CMS	13 TeV, $b\overline{b}WW^*$
−37.7 to 37.2	95	[9] HAYRAPETY...	24AW	CMS	13 TeV, VHH, $HH \to b\overline{b}b\overline{b}$
−34.4 to 33.3	95	[10] AAD	23AD	ATLS	13 TeV, VHH, $HH \to b\overline{b}b\overline{b}$
− 0.6 to 6.6	95	[11] AAD	23AT	ATLS	13 TeV, $b\overline{b}b\overline{b}$, $b\overline{b}\tau\tau$, $b\overline{b}\gamma\gamma$
− 0.4 to 6.3	95	[12] AAD	23AT	ATLS	13 TeV, $b\overline{b}b\overline{b}$, $b\overline{b}\tau\tau$, $b\overline{b}\gamma\gamma$
− 3.5 to 11.3	95	[13] AAD	23BK	ATLS	13 TeV, $b\overline{b}b\overline{b}$
− 5.4 to 14.9	95	[14] HAYRAPETY...	23	CMS	13 TeV, $ZZ^* \to 4\ell$ cross sections
− 9.9 to 16.9	95	[15] TUMASYAN	23AE	CMS	13 TeV, $b\overline{b}b\overline{b}$
− 1.7 to 8.7	95	[16] TUMASYAN	23D	CMS	13 TeV, $b\overline{b}\tau\tau$
− 8.8 to 13.4	95	[17] TUMASYAN	23I	CMS	13 TeV, $b\overline{b}ZZ^*$ ($ZZ^* \to 4\ell$)
− 6.9 to 11.1	95	[18] TUMASYAN	23O	CMS	13 TeV, WW^*WW^*, $WW^*\tau\tau$, $\tau\tau\tau\tau$
− 1.5 to 6.7	95	[19] AAD	22Y	ATLS	13 TeV, $\gamma\gamma b\overline{b}$
− 1.24 to 6.49	95	[20] CMS	22	CMS	13 TeV, $b\overline{b}ZZ^*$, $b\overline{b}\gamma\gamma$, $b\overline{b}\tau\tau$, $b\overline{b}b\overline{b}$, multilepton
− 2.3 to 9.4	95	[21] TUMASYAN	22AN	CMS	13 TeV, $b\overline{b}b\overline{b}$
− 3.3 to 8.5	95	[22] SIRUNYAN	21K	CMS	13 TeV, $\gamma\gamma b\overline{b}$
− 5.0 to 12.0	95	[23] AAD	20C	ATLS	13 TeV, $b\overline{b}\gamma\gamma$, $b\overline{b}\tau\tau$, $b\overline{b}b\overline{b}$, $b\overline{b}WW^*$, $WW^*\gamma\gamma$, WW^*WW^*
−11 to 17	95	[24] SIRUNYAN	19	CMS	13 TeV, $\gamma\gamma b\overline{b}$
−11.8 to 18.8	95	[25] SIRUNYAN	19BE	CMS	13 TeV, $b\overline{b}\gamma\gamma$ $b\overline{b}\tau\tau$, $b\overline{b}b\overline{b}$, $b\overline{b}WW^*$, $b\overline{b}ZZ^*$
− 8.2 to 13.2	95	[26] AABOUD	18CW	ATLS	13 TeV, $\gamma\gamma b\overline{b}$
		[27] SIRUNYAN	18A	CMS	13 TeV, $b\overline{b}\tau\tau$
−17 to 22.5	95	[28] KHACHATRY...	16BQ	CMS	8 TeV, $\gamma\gamma b\overline{b}$

[1] AAD 24BL combine results from 126–140 fb^{-1} of data at E_{cm} = 13 TeV for $pp \to HH \to b\overline{b}b\overline{b}$ (AAD 23BK, AAD 24BV), $b\overline{b}\tau\tau$ (AAD 24AZ), $b\overline{b}\gamma\gamma$ (AAD 24X), multilepton (AAD 24BG), and $b\overline{b}\ell\ell$ (AAD 24Y). See their Fig. 3. All other Higgs couplings are fixed to the SM values.

[2] AAD 25J search for non-resonant HHH production using $HHH \to b\overline{b}b\overline{b}b\overline{b}$ with data of 126 fb^{-1} at E_{cm} = 13 TeV. Two-dimensional likelihood scan of (κ_3 (=κ_λ), κ_4) is shown in their Fig. 9. The quoted values are obtained by assuming κ_4 = 1. Note that the quoted values are calculated using the kappa framework, which outside the unitarity bounds requires additional modification to preserve unitarity for their results.

[3] HAYRAPETYAN 25F constrain the Higgs trilinear self-coupling using single and double Higgs production with data at E_{cm} = 13 TeV. The production modes and decay channels used are listed in their Tables 1 and 2 for single- and double-Higgs, respectively. Only single- and double-Higgs channels give $-1.8 < \kappa_\lambda < 12.0$ and $-1.7 < \kappa_\lambda < 7.0$, respectively. All the other Higgs boson couplings are fixed to their SM values. Their Table 3 shows results with some of the couplings are loosened. Two-dimensional likelihood scan of (κ_λ, κ_t) is shown in their Fig. 5.

[4] AAD 24AZ search for non-resonant HH production using $HH \to b\overline{b}\tau\tau$ with data of 140 fb^{-1} at E_{cm} = 13 TeV. Two-dimensional exclusion regions as a function of the κ_λ and κ_{2V} couplings are shown in their Fig. 9. All other Higgs couplings are fixed to the SM values.

[5] AAD 24BG search for non-resonant HH production targeting the $b\overline{b}ZZ^*$, VVVV, $VV\tau\tau$, $\tau\tau\tau\tau$, $\gamma\gamma VV$, $\gamma\gamma\tau\tau$ decay channels with data of 140 fb^{-1} at E_{cm} = 13 TeV. The limits are obtained with the values of all other couplings fixed to their SM value.

[6] AAD 24X search for non-resonant HH production using $HH \to b\overline{b}\gamma\gamma$ with data of 140 fb^{-1} at E_{cm} = 13 TeV. Two-dimensional exclusion regions as a function of the κ_λ and κ_{2V} couplings are shown in their Fig. 6. All other Higgs couplings are fixed to the SM values.

[7] AAD 24Y search for non-resonant HH production in $2b + 2\ell + \nu s$ final state ($\ell = e, \mu$) targeting $b\overline{b}WW^*$, $b\overline{b}ZZ^*$, and $b\overline{b}\tau\tau$ decay channels with data of 140 fb^{-1} at E_{cm} = 13 TeV. All other coupling modifiers are set to their SM values.

[8] HAYRAPETYAN 24AE search for non-resonant HH production using $HH \to b\overline{b}WW^*$ with data of 138 fb^{-1} at E_{cm} = 13 TeV. Two-dimensional exclusion regions as a function of the (κ_λ, κ_{2V}) and (κ_λ, κ_t) are shown in their Figs. 13 and 15. All other Higgs couplings are fixed to the SM values.

[9] HAYRAPETYAN 24AW search for non-resonant HH production in association with a vector boson using $HH \to b\overline{b}b\overline{b}$ with data of 138 fb^{-1} at E_{cm} = 13 TeV. The vector boson decays both leptonically ($W \to \ell\nu$, $Z \to \ell\ell$, $\nu\nu$, $\ell = e, \mu$) and hadronically. All other Higgs couplings are fixed to the SM values. Two-dimensional exclusion regions as a function of the κ_{2V} and κ_λ parameters are shown in their Fig. 14, with other couplings fixed to the SM values. The best fit value is (κ_λ, κ_{2V}) = (-2.6, 10.1).

[10] AAD 23AD search for non-resonant HH production in association with a vector boson using $HH \to b\overline{b}b\overline{b}$ with data of 139 fb^{-1} at E_{cm} = 13 TeV. The vector boson decays leptonically ($W \to \ell\nu$, $Z \to \ell\ell$, $\nu\nu$, $\ell = e, \mu$). The quoted κ_λ is measured assuming all other Higgs boson couplings are at their SM value.

[11] AAD 23AT combine results from 126–139 fb^{-1} of data at E_{cm} = 13 TeV for $pp \to HH \to b\overline{b}b\overline{b}$ (AAD 23BK), $b\overline{b}\tau\tau$ (AAD 23Z), and $b\overline{b}\gamma\gamma$ (AAD 22Y). The quoted values are obtained from the profile likelihood scan as a function of κ_λ as shown in their Fig. 5(a). All other coupling modifiers are assumed to have their SM values.

[12] AAD 23AT combine results from 126–139 fb^{-1} of data at E_{cm} = 13 TeV for $pp \to HH \to b\overline{b}b\overline{b}$ (AAD 23BK), $b\overline{b}\tau\tau$ (AAD 23Z), and $b\overline{b}\gamma\gamma$ (AAD 22Y) with single-Higgs boson analyses ($\gamma\gamma$, ZZ^*, WW^*, $\tau\tau$, $b\overline{b}$, see their Table 1). The quoted values are obtained from the profile likelihood scan as a function of κ_λ as shown in their Fig. 5(a), assuming that all other Higgs boson couplings are at their SM values. Results with other assumptions are shown in their Table 2.

[13] AAD 23BK search for non-resonant HH production using $HH \to b\overline{b}b\overline{b}$ with data of 126 fb^{-1} at E_{cm} = 13 TeV. The quoted values are obtained from the one-dimensional profile likelihood scan as a function of κ_λ. See their Fig. 12 (a). The $\mu_{ggF+VBF}$ measurement for different values of κ_λ constrains $-3.9 < \kappa_\lambda < 11.1$ at 95% CL as shown in their Fig. 10 (a). $\kappa_{2V} = \kappa_V = 1$ is assumed in both cases.

[14] HAYRAPETYAN 23 measure the cross sections for $pp \to H \to ZZ^* \to 4\ell$ ($\ell = e, \mu$) using 138 fb^{-1} at E_{cm} = 13 TeV.

[15] TUMASYAN 23AE search for HH production using $HH \to b\overline{b}b\overline{b}$, where both $b\overline{b}$ pairs are highly boosted, with data of 138 fb^{-1} at E_{cm} = 13 TeV. The quoted κ_λ is measured assuming all other Higgs boson couplings are at their SM values.

[16] TUMASYAN 23D search for non-resonant HH production using $HH \to b\overline{b}\tau\tau$ with data of 138 fb^{-1} at E_{cm} = 13 TeV. The quoted values are obtained from the upper limit on the HH production cross section times the $b\overline{b}\tau\tau$ branching fraction for different values of κ_λ. See their Fig. 8 (left). All other coupling modifiers are assumed to be 1. In addition, two-dimensional exclusion regions as a function of the κ_λ and κ_t couplings, with $\kappa_{2V} = \kappa_V = 1$, are shown in their Fig. 9 (left). The one-dimensional likelihood scan as a function of κ_λ is given in their Fig 10 (left), from which a 95% confidence interval of $-1.77 < \kappa_\lambda < 8.73$ is extracted.

[17] TUMASYAN 23AI search for non-resonant HH production using $HH \to b\overline{b}ZZ^*$ ($ZZ^* \to 4\ell$, ℓ=e,μ) with data of 138 fb^{-1} at E_{cm} = 13 TeV. See their Fig. 4.

[18] TUMASYAN 23O search for non-resonant HH production using $HH \to WW^*WW^*$, $WW^*\tau\tau$, and $\tau\tau\tau\tau$ (multilepton) with data of 138 fb^{-1} at E_{cm} = 13 TeV. See their Fig. 10 for different final states and these combination. Limits are set on a variety of new-physics models using an effective field theory approach. See their Figs. 11, 12, and 13.

[19] AAD 22Y search for non-resonant HH production using $HH \to \gamma\gamma b\overline{b}$ with data of 139 fb^{-1} at E_{cm} = 13 TeV. The quoted κ_λ is obtained from their Fig. 12 where the theory uncertainties are not included while a negative log-likelihood scan vs. $\kappa_\lambda$is shown in their Fig. 13 with the theory uncertainties, which provides $\kappa_\lambda = 2.8^{+2.0}_{-2.2}$ for the 1σ confidence interval.

[20] CMS 22 report combined results (see their Extended Data Table 2) using 138 fb^{-1} of data at E_{cm} = 13 TeV. See their Fig. 6 (left).

[21] TUMASYAN 22AN search for non-resonant HH production using $HH \to b\overline{b}b\overline{b}$ with data of 138 fb^{-1} at E_{cm} = 13 TeV. The upper limit on the $pp \to HH$ production cross section at 95% CL is shown as a function of κ_λ in their Fig. 2 (top).

[22] SIRUNYAN 21K search for non-resonant HH production using $HH \to \gamma\gamma b\overline{b}$ with data of 137 fb^{-1} at E_{cm} = 13 TeV.

[23] AAD 20C combine results of up to 36.1 fb^{-1} data at E_{cm} = 13 TeV for $pp \to HH \to b\overline{b}\gamma\gamma$, $b\overline{b}\tau\tau$, $b\overline{b}b\overline{b}$, $b\overline{b}WW^*$, $WW^*\gamma\gamma$, WW^*WW^* (AABOUD 18CW, AABOUD 18CQ, AABOUD 19A, AABOUD 19O, AABOUD 18BU, and AABOUD 19T).

[24] SIRUNYAN 19 search for HH production using $HH \to \gamma\gamma b\overline{b}$ with data of 35.9 fb^{-1} at E_{cm} = 13 TeV. The quoted κ_λ is measured assuming all other Higgs boson couplings are at their SM value.

[25] SIRUNYAN 19BE combine results of 13 TeV 35.9 fb^{-1} data: SIRUNYAN 19, SIRUNYAN 18A, SIRUNYAN 19AB, SIRUNYAN 19H, and SIRUNYAN 18F.

[26] AABOUD 18CW search for HH production using $HH \to \gamma\gamma b\overline{b}$ with data of 36.1 fb^{-1} at E_{cm} = 13 TeV. The quoted κ_λ is measured assuming all other Higgs boson couplings are at their SM value.

[27] SIRUNYAN 18A search for HH production using $HH \to b\overline{b}\tau\tau$ with data of 35.9 fb^{-1} at E_{cm} = 13 TeV. The upper limit on production cross section times branching fraction at 95% CL is shown as a function of κ_λ/κ_t in their Fig. 6 (top) where $\kappa_t = y_t / y_t^{SM}$ (top Yukawa coupling y_t).

[28] KHACHATRYAN 16BQ search for HH production using $HH \to \gamma\gamma b\overline{b}$ with data of 19.7 fb^{-1} at E_{cm} = 8 TeV.

Higgs quartic self coupling modifier κ_4

Signal strength relative to the SM prediction, $\kappa_4 = \lambda_{HHHH}/\lambda^{SM}_{HHHH}$.

VALUE	CL%	DOCUMENT ID		TECN	COMMENT
• • • We do not use the following data for averages, fits, limits, etc. • • •					
−230 to 240	95	[1] AAD	25J	ATLS	13 TeV, $b\overline{b}b\overline{b}b\overline{b}$

[1] AAD 25J search for non-resonant HHH production using $HHH \to b\bar{b}b\bar{b}b\bar{b}$ with data of 126 fb^{-1} at E_{cm} = 13 TeV. Two-dimensional likelihood scan of (κ_3 ($=\kappa_\lambda$), κ_4) is shown in their Fig. 9. The quoted values are obtained by assuming $\kappa_3 = 1$. Note that the quoted values are calculated using the kappa framework, which outside the unitarity bounds requires additional modification to preserve unitarity for their results.

Higgs-gauge boson quartic coupling modifier κ_{2V}

Signal strength relative to the SM prediction, $\kappa_{2V} = \lambda_{VVHH} / \lambda^{SM}_{VVHH}$, $V = W, Z$.

VALUE	CL%	DOCUMENT ID		TECN	COMMENT
$\mathbf{1.02^{+0.22}_{-0.23}}$		[1] AAD	24BL	ATLS	13 TeV, $b\bar{b}b\bar{b}$, $b\bar{b}\tau\tau$, $b\bar{b}\gamma\gamma$, multilepton , $b\bar{b}\ell\ell$
• • • We do not use the following data for averages, fits, limits, etc. • • •					
		[2] HAYRAPETY...	25F	CMS	13 TeV, single and double Higgs production
− 0.5 to 2.7	95	[3] AAD	24AZ	ATLS	13 TeV, $b\bar{b}\tau\tau$
− 2.5 to 4.6	95	[4] AAD	24BG	ATLS	13 TeV, $b\bar{b}ZZ^*$, VVVV, $VV\tau\tau$, $\tau\tau\tau\tau$, $\gamma\gamma VV$, $\gamma\gamma\tau\tau$
0.6 to 1.5	95	[1] AAD	24BL	ATLS	13 TeV, $b\bar{b}b\bar{b}$, $b\bar{b}\tau\tau$, $b\bar{b}\gamma\gamma$, multilepton , $b\bar{b}\ell\ell$
0.55 to 1.49	95	[5] AAD	24BV	ATLS	13 TeV, $b\bar{b}b\bar{b}$
0.52 to 1.52	95	[6] AAD	24BV	ATLS	13 TeV, $b\bar{b}b\bar{b}$
− 0.5 to 2.7	95	[7] AAD	24X	ATLS	13 TeV, $b\bar{b}\gamma\gamma$
− 0.17 to 2.4	95	[8] AAD	24Y	ATLS	13 TeV, $b\bar{b}WW^*$, $b\bar{b}ZZ^*$, $b\bar{b}\tau\tau$, multilepton
− 1.1 to 3.2	95	[9] HAYRAPETY...	24AE	CMS	13 TeV, $b\bar{b}WW^*$
−12.2 to 13.5	95	[10] HAYRAPETY...	24AW	CMS	13 TeV, VHH, $HH \to b\bar{b}b\bar{b}$
− 8.6 to 10.0	95	[11] AAD	23AD	ATLS	13 TeV, VHH, $HH \to b\bar{b}b\bar{b}$
0.1 to 2.0	95	[12] AAD	23AT	ATLS	13 TeV, $b\bar{b}b\bar{b}$, $b\bar{b}\tau\tau$, $b\bar{b}\gamma\gamma$
0.0 to 2.1	95	[13] AAD	23BK	ATLS	13 TeV, $b\bar{b}b\bar{b}$
0.62 to 1.41	95	[14] TUMASYAN	23AE	CMS	13 TeV, $b\bar{b}b\bar{b}$
− 0.4 to 2.6	95	[15] TUMASYAN	23D	CMS	13 TeV, $b\bar{b}\tau\tau$
0.67 to 1.38	95	[16] CMS	22	CMS	13 TeV, $b\bar{b}ZZ^*$, $b\bar{b}\gamma\gamma$, $b\bar{b}\tau\tau$, $b\bar{b}b\bar{b}$, multilepton
− 0.1 to 2.2	95	[17] TUMASYAN	22AN	CMS	13 TeV, $b\bar{b}b\bar{b}$
− 1.3 to 3.5	95	[18] SIRUNYAN	21K	CMS	13 TeV, $\gamma\gamma b\bar{b}$
− 0.43 to 2.56	95	[19] AAD	20X	ATLS	13 TeV, VBF, $b\bar{b}b\bar{b}$

[1] AAD 24BL combine results from 126–140 fb^{-1} of data at E_{cm} = 13 TeV for $pp \to HH \to b\bar{b}b\bar{b}$ (AAD 23BK, AAD 24BV), $b\bar{b}\tau\tau$ (AAD 24AZ), $b\bar{b}\gamma\gamma$ (AAD 24X), multilepton (AAD 24BG), and $b\bar{b}\ell\ell$ (AAD 24Y). See their Fig. 3. All other Higgs couplings are fixed to the SM values.

[2] HAYRAPETYAN 25F constrain the Higgs trilinear self-coupling using single and double Higgs production with data at E_{cm} = 13 TeV. The production modes and decay channels used are listed in their Tables 1 and 2 for single- and double-Higgs, respectively. Two-dimensional likelihood scan of (κ_V, κ_{2V}) is shown in their Fig. 6.

[3] AAD 24AZ search for non-resonant HH production using $HH \to b\bar{b}\tau\tau$ with data of 140 fb^{-1} at E_{cm} = 13 TeV. Two-dimensional exclusion regions as a function of the κ_λ and κ_{2V} couplings are shown in their Fig. 9. All other Higgs couplings are fixed to the SM values.

[4] AAD 24BG search for non-resonant HH production targeting the $b\bar{b}ZZ^*$, VVVV, $VV\tau\tau$, $\tau\tau\tau\tau$, $\gamma\gamma VV$, $\gamma\gamma\tau\tau$ decay channels with data of 140 fb^{-1} at E_{cm} = 13 TeV. The limits are obtained with the values of all other couplings fixed to their SM value.

[5] AAD 24BV search for non-resonant HH production via vector boson fusion in the $b\bar{b}b\bar{b}$ final state using two boosted Higgs (p_T > 250 GeV) with data of 140 fb^{-1} at E_{cm} = 13 TeV. The result is obtained by combining with the resolved result (AAD 23BK). The value $\kappa_{2V} = 0$ is excluded with a significance of 3.8 σ with other Higgs couplings fixed to their SM values. Two-dimensional exclusion regions as a function of the κ_λ and κ_{2V} parameters are shown in their Fig. 6. All other Higgs couplings are fixed to the SM values.

[6] AAD 24BV search for non-resonant HH production via vector boson fusion in the $b\bar{b}b\bar{b}$ final state using two boosted Higgs (p_T > 250 GeV) with data of 140 fb^{-1} at E_{cm} = 13 TeV. The value $\kappa_{2V} = 0$ is excluded with a significance of 3.4 σ with other Higgs couplings fixed to their SM values.

[7] AAD 24X search for non-resonant HH production using $HH \to b\bar{b}\gamma\gamma$ with data of 140 fb^{-1} at E_{cm} = 13 TeV. Two-dimensional exclusion regions as a function of the κ_λ and κ_{2V} couplings are shown in their Fig. 6. All other Higgs couplings are fixed to the SM values.

[8] AAD 24Y search for non-resonant HH production in $2b + 2\ell + \nu$s final state ($\ell = e, \mu$) targeting $b\bar{b}WW^*$, $b\bar{b}ZZ^*$, and $b\bar{b}\tau\tau$ decay channels with data of 140 fb^{-1} at E_{cm} = 13 TeV. All other coupling modifiers are set to their SM values.

[9] HAYRAPETYAN 24AE search for non-resonant HH production using $HH \to b\bar{b}WW^*$ with data of 138 fb^{-1} at E_{cm} = 13 TeV. Two-dimensional exclusion regions as a function of the (κ_λ, κ_{2V}) and (κ_V, κ_{2V}) are shown in their Figs. 13 and 14. All other Higgs couplings are fixed to the SM values.

[10] HAYRAPETYAN 24AW search for non-resonant HH production in association with a vector boson using $HH \to b\bar{b}b\bar{b}$ with data of 138 fb^{-1} at E_{cm} = 13 TeV. The vector boson decays both leptonically ($W \to \ell\nu$, $Z \to \ell\ell, \nu\nu$, $\ell = e, \mu$) and hadronically. All other Higgs couplings are fixed to the SM values. Two-dimensional exclusion regions as a function of the κ_{2V} and κ_λ parameters are shown in their Fig. 14, with other couplings fixed to the SM values. The best fit value is (κ_λ, κ_{2V}) = (-2.6, 10.1). The constraints on κ_{2W} and κ_{2Z} are separately measured to be -14.0 < κ_{2W} < 15.4 and -17.4 < κ_{2Z} < 18.5 (95% CL). The quoted κ_{2V} ($V = W, Z$) is measured assuming all other Higgs boson couplings are at their SM value. See their Table 7.

[11] AAD 23AD search for non-resonant HH production in association with a vector boson using $HH \to b\bar{b}b\bar{b}$ with data of 139 fb^{-1} at E_{cm} = 13 TeV. The vector boson decays leptonically ($W \to \ell\nu$, $Z \to \ell\ell, \nu\nu$, $\ell = e, \mu$). The constraints on κ_{2W} and κ_{2Z} are separately measured to be -12.3 < κ_{2W} < 13.5 and -9.9 < κ_{2Z} < 11.3 (95% CL). The quoted κ_{2V} ($V = W, Z$) is measured assuming all other Higgs boson couplings are at their SM value.

[12] AAD 23AT combine results from 126–139 fb^{-1} of data at E_{cm} = 13 TeV for $pp \to HH \to b\bar{b}b\bar{b}$ (AAD 23BK), $b\bar{b}\tau\tau$ (AAD 23Z), and $b\bar{b}\gamma\gamma$ (AAD 22Y). The quoted values are obtained from the 95% CL VBF HH cross-section upper limit as a function of κ_{2V} as shown in their Fig. 4(b). All other coupling modifiers are assumed to have their SM values.

[13] AAD 23BK search for non-resonant HH production using $HH \to b\bar{b}b\bar{b}$ with data of 126 fb^{-1} at E_{cm} = 13 TeV. The quoted values are obtained from the one-dimensional profile likelihood scan as a function of κ_{2V}. See their Fig. 12 (b). The μ_{VBF} measurement for different values of κ_{2V} constrains -0.03 < κ_{2V} < 2.11 at 95% CL as shown in their Fig. 10 (b). $\kappa_\lambda = \kappa_V = 1$ is assumed in both cases.

[14] TUMASYAN 23AE search for HH production using $HH \to b\bar{b}b\bar{b}$, where both $b\bar{b}$ pairs are highly boosted, with data of 138 fb^{-1} at E_{cm} = 13 TeV. The $\kappa_{2V} = 0$ is excluded at 6.3 σ assuming all other Higgs boson couplings are at their SM values.

[15] TUMASYAN 23D search for non-resonant HH production using $HH \to b\bar{b}\tau\tau$ with data of 138 fb^{-1} at E_{cm} = 13 TeV. The quoted values are obtained from the upper limits on the HH production cross section times the $b\bar{b}\tau\tau$ branching fraction for different values of κ_{2V}. See their Fig. 8 (right). All other coupling modifiers are assumed to be 1. In addition, two-dimensional exclusion regions as a function of the κ_{2V} and κ_V couplings, with $\kappa_\lambda = \kappa_t = 1$, are shown in their Fig. 9 (right). The one-dimensional likelihood scan as a function of κ_{2V} is given in their Fig. 10 (right), from which a 95% confidence interval of -0.34 < κ_{2V} < 2.49 is extracted.

[16] CMS 22 report combined results (see their Extended Data Table 2) using 138 fb^{-1} of data at E_{cm} = 13 TeV. See their Fig. 6 (right).

[17] TUMASYAN 22AN search for non-resonant HH production using $HH \to b\bar{b}b\bar{b}$ with data of 138 fb^{-1} at E_{cm} = 13 TeV. The upper limit on the $pp \to HH$ production cross section at 95% CL is shown as a function of κ_{2V} in their Fig. 2 (bottom).

[18] SIRUNYAN 21K search for non-resonant HH production using $HH \to \gamma\gamma b\bar{b}$ with data of 137 fb^{-1} at E_{cm} = 13 TeV.

[19] AAD 20X search for $HH \to b\bar{b}b\bar{b}$ process via VBF with data of 126 fb^{-1} at E_{cm} = 13 TeV.

H production cross section in *pp* collisions at $\sqrt{s}$ = 13 TeV

VALUE (pb)	DOCUMENT ID		TECN	COMMENT
56.8± 3.4 OUR AVERAGE				
$55.5^{+4.0}_{-3.8}$	[1] AAD	23C	ATLS	pp, 13 TeV, $\gamma\gamma$, $ZZ^* \to 4\ell$ ($\ell = e, \mu$)
61.1± 6.0±3.7	[2] SIRUNYAN	19BA	CMS	pp, 13 TeV, $\gamma\gamma$, $ZZ^* \to 4\ell$ ($\ell = e, \mu$)
• • • We do not use the following data for averages, fits, limits, etc. • • •				
58 ± 4 ±4	[3] AAD	22N	ATLS	pp, 13 TeV, $\gamma\gamma$
53.5± 4.9±2.1	[4] AAD	20BA	ATLS	pp, 13 TeV, $ZZ^* \to 4\ell$ ($\ell = e, \mu$)
$57.0^{+6.0+4.0}_{-5.9-3.3}$	[5] AABOUD	18CG	ATLS	pp, 13 TeV, $\gamma\gamma$, $ZZ^* \to 4\ell$ ($\ell = e, \mu$)
$47.9^{+9.1}_{-8.6}$	[5] AABOUD	18CG	ATLS	pp, 13 TeV, $\gamma\gamma$
68^{+11}_{-10}	[5] AABOUD	18CG	ATLS	pp, 13 TeV, $ZZ^* \to 4\ell$ ($\ell = e, \mu$)
69^{+10}_{-9} ±5	[6] AABOUD	17CO	ATLS	pp, 13 TeV, $ZZ^* \to 4\ell$

[1] AAD 23C combine AAD 22N and AAD 20BA, where both use 139 fb^{-1} of pp collisions at E_{cm} = 13 TeV. The Higgs production cross sections at E_{cm} = 7 and 8 TeV are obtained to be 34^{+11}_{-10} pb and $33.3^{+5.8}_{-5.4}$ pb, respectively. The quoted value is given for m_H = 125.09 GeV. The differential cross sections are given in their Figs. 3 and 4.

[2] SIRUNYAN 19BA use 35.9 fb^{-1} of pp collisions at E_{cm} = 13 TeV. The quoted value is given for m_H = 125.09 GeV.

[3] AAD 22N use 139 fb^{-1} of pp collisions at E_{cm} = 13 TeV. The quoted value is given for m_H = 125.09 GeV.

[4] AAD 20BA use 139 fb^{-1} of pp collisions at E_{cm} = 13 TeV with $H \to ZZ^* \to 4\ell$ where $\ell = e, \mu$. The quoted value is given for m_H = 125 GeV and assumes the Standard Model branching ratio.

[5] AABOUD 18CG use 36.1 fb^{-1} of pp collisions at E_{cm} = 13 TeV. All the quoted values are given for m_H = 125.09 GeV.

[6] AABOUD 17CO use 36.1 fb^{-1} of pp collisions at E_{cm} = 13 TeV with $H \to ZZ^* \to 4\ell$ where $\ell = e, \mu$ for m_H = 125 GeV. Differential cross sections for the Higgs boson transverse momentum, Higgs boson rapidity, and other related quantities are measured as shown in their Figs. 8 and 9.

H production cross section in *pp* collisions at $\sqrt{s}$ = 13.6 TeV

VALUE (pb)	DOCUMENT ID		TECN	COMMENT
58.2±8.7	[1] AAD	24AQ	ATLS	pp, 13.6 TeV, $\gamma\gamma$, $ZZ^* \to 4\ell$ ($\ell = e, \mu$)

[1] AAD 24AQ measure the total cross section to be 67^{+12}_{-11} pb and 46 ± 12 pb using $H \to \gamma\gamma$ and $H \to ZZ^* \to 4\ell$, respectively, with data of 31.4 fb^{-1} and 29.0 fb^{-1} of pp collisions at E_{cm} = 13.6 TeV. The SM expected value is 59.9 ± 2.6 pb. All the values are given for m_H = 125.09 GeV.

H REFERENCES

HAYRAPETY... 26 PRL 136 011801 A. Hayrapetyan *et al.* (CMS Collab.)
AAD 25AG JHEP 2508 034 G. Aad *et al.* (ATLAS Collab.)
AAD 25AJ EPJ C85 210 G. Aad *et al.* (ATLAS Collab.)
AAD 25AP PL B865 139449 (errat.) G. Aad *et al.* (ATLAS Collab.)
AAD 25AQ RPP 88 057803 G. Aad *et al.* (ATLAS Collab.)
AAD 25AR PRL 135 231802 G. Aad *et al.* (ATLAS Collab.)
AAD 25AT PL B868 139671 G. Aad *et al.* (ATLAS Collab.)
AAD 25AV PL B870 139898 G. Aad *et al.* (ATLAS Collab.)
AAD 25BC JHEP 2510 092 G. Aad *et al.* (ATLAS Collab.)
AAD 25BD JHEP 2510 093 G. Aad *et al.* (ATLAS Collab.)
AAD 25BK EPJ C85 1403 G. Aad *et al.* (ATLAS Collab.)
AAD 25E PL B861 139277 G. Aad *et al.* (ATLAS Collab.)
AAD 25J PR D111 032006 G. Aad *et al.* (ATLAS Collab.)
AAD 25R JHEP 2502 045 G. Aad *et al.* (ATLAS Collab.)

Int. J. Mod. Phys. A 2026.41. Downloaded from www.worldscientific.com
by UNIVERSITY OF CALIFORNIA @ BERKELEY on 09/16/26. Reproduction is strictly not permitted, except for Open Access articles.

Int. J. Mod. Phys. A 2026.41. Downloaded from www.worldscientific.com
by UNIVERSITY OF CALIFORNIA @ BERKELEY on 09/16/26. Re-use and distribution is strictly not permitted, except for Open Access articles.

AAD	25W	JHEP 2503 010	G. Aad *et al.*	(ATLAS Collab.)
AAD	25Y	JHEP 2504 075	G. Aad *et al.*	(ATLAS Collab.)
CHEKHOVSKY	25A	JHEP 2503 114	V. Chekhovsky *et al.*	(CMS Collab.)
CHEKHOVSKY	25B	JHEP 2505 079	V. Chekhovsky *et al.*	(CMS Collab.)
CHEKHOVSKY	25G	PR D112 112001	V. Chekhovsky *et al.*	(CMS Collab.)
CHEKHOVSKY	25L	JHEP 2511 060	V. Chekhovsky *et al.*	(CMS Collab.)
HAYRAPETY...	25	PL B860 139173	A. Hayrapetyan *et al.*	(CMS Collab.)
HAYRAPETY...	25AC	PRL 135 091802	A. Hayrapetyan *et al.*	(CMS Collab.)
HAYRAPETY...	25AL	JHEP 2509 070	A. Hayrapetyan *et al.*	(CMS Collab.)
HAYRAPETY...	25B	PL B860 139202	A. Hayrapetyan *et al.*	(CMS Collab.)
HAYRAPETY...	25F	PL B861 139210	A. Hayrapetyan *et al.*	(CMS Collab.)
HAYRAPETY...	25G	PL B862 139296	A. Hayrapetyan *et al.*	(CMS Collab.)
HAYRAPETY...	25H	PL B865 139462	A. Hayrapetyan *et al.*	(CMS Collab.)
HAYRAPETY...	25L	PR D111 092014	A. Hayrapetyan *et al.*	(CMS Collab.)
HAYRAPETY...	25R	JHEP 2502 097	A. Hayrapetyan *et al.*	(CMS Collab.)
AAD	24AG	JHEP 2405 105	G. Aad *et al.*	(ATLAS Collab.)
AAD	24AQ	EPJ C84 78	G. Aad *et al.*	(ATLAS Collab.)
AAD	24AZ	PR D110 032012	G. Aad *et al.*	(ATLAS Collab.)
AAD	24BE	PL B855 138817	G. Aad *et al.*	(ATLAS Collab.)
AAD	24BG	JHEP 2408 164	G. Aad *et al.*	(ATLAS Collab.)
AAD	24BH	JHEP 2408 153	G. Aad *et al.*	(ATLAS Collab.)
AAD	24BL	PRL 133 101801	G. Aad *et al.*	(ATLAS Collab.)
AAD	24BM	PRL 133 141801	G. Aad *et al.*	(ATLAS Collab.)
AAD	24BV	PL B858 139007	G. Aad *et al.*	(ATLAS Collab.)
AAD	24D	PRL 132 021803	G. Aad *et al.*	(ATLAS and CMS Collabs.)
AAD	24F	PRL 132 131802	G. Aad *et al.*	(ATLAS Collab.)
AAD	24J	PL B849 138469	G. Aad *et al.*	(ATLAS Collab.)
AAD	24R	PL B855 138762	G. Aad *et al.*	(ATLAS Collab.)
AAD	24X	JHEP 2401 066	G. Aad *et al.*	(ATLAS Collab.)
AAD	24Y	JHEP 2402 037	G. Aad *et al.*	(ATLAS Collab.)
HAYRAPETY...	24AE	JHEP 2407 293	A. Hayrapetyan *et al.*	(CMS Collab.)
HAYRAPETY...	24AG	EPJ C84 779	A. Hayrapetyan *et al.*	(CMS Collab.)
HAYRAPETY...	24AM	EPJ C84 712	A. Hayrapetyan *et al.*	(CMS Collab.)
HAYRAPETY...	24AT	PL B857 138964	A. Hayrapetyan *et al.*	(CMS Collab.)
HAYRAPETY...	24AW	JHEP 2410 061	A. Hayrapetyan *et al.*	(CMS Collab.)
HAYRAPETY...	24AY	JHEP 2412 035	A. Hayrapetyan *et al.*	(CMS Collab.)
HAYRAPETY...	24D	PRL 132 121901	A. Hayrapetyan *et al.*	(CMS Collab.)
HAYRAPETY...	24U	JHEP 2401 173	A. Hayrapetyan *et al.*	(CMS Collab.)
TUMASYAN	24	PR D109 092011	A. Tumasyan *et al.*	(CMS Collab.)
AABOUD	23A	JHEP 2312 158 (errat.)	M. Aaboud *et al.*	(ATLAS Collab.)
AAD	23A	PL B842 137963	G. Aad *et al.*	(ATLAS Collab.)
AAD	23AD	EPJ C83 519	G. Aad *et al.*	(ATLAS Collab.)
AAD	23AF	EPJ C83 503	G. Aad *et al.*	(ATLAS Collab.)
AAD	23AK	EPJ C83 563	G. Aad *et al.*	(ATLAS Collab.)
AAD	23AN	PRL 131 061802	G. Aad *et al.*	(ATLAS Collab.)
AAD	23AP	PR D108 032005	G. Aad *et al.*	(ATLAS Collab.)
AAD	23AT	PL B843 137745	G. Aad *et al.*	(ATLAS Collab.)
AAD	23AU	PL B843 137880	G. Aad *et al.*	(ATLAS Collab.)
AAD	23BC	EPJ C83 496	G. Aad *et al.*	(ATLAS Collab.)
Also		EPJ C84 156 (errat.)	G. Aad *et al.*	(ATLAS Collab.)
AAD	23BK	PR D108 052003	G. Aad *et al.*	(ATLAS Collab.)
AAD	23BP	PRL 131 251802	G. Aad *et al.*	(ATLAS Collab.)
AAD	23BR	PL B846 138223	G. Aad *et al.*	(ATLAS Collab.)
Also		PL B854 138734 (errat.)	G. Aad *et al.*	(ATLAS Collab.)
Also		PL B865 139449 (errat.)	G. Aad *et al.*	(ATLAS Collab.)
AAD	23BS	PL B847 138292	G. Aad *et al.*	(ATLAS Collab.)
AAD	23BU	PL B847 138315	G. Aad *et al.*	(ATLAS Collab.)
AAD	23BV	PR D108 072003	G. Aad *et al.*	(ATLAS Collab.)
AAD	23C	JHEP 2305 028	G. Aad *et al.*	(ATLAS Collab.)
AAD	23CD	EPJ C83 781	G. Aad *et al.*	(ATLAS Collab.)
AAD	23Q	JHEP 2307 166	G. Aad *et al.*	(ATLAS Collab.)
AAD	23Y	JHEP 2307 088	G. Aad *et al.*	(ATLAS Collab.)
AAD	23Z	JHEP 2307 040	G. Aad *et al.*	(ATLAS Collab.)
HAYRAPETY...	23	JHEP 2308 040	A. Hayrapetyan *et al.*	(CMS Collab.)
HAYRAPETY...	23C	PR D108 072004	A. Hayrapetyan *et al.*	(CMS Collab.)
TUMASYAN	23AD	PRL 131 041801	A. Tumasyan *et al.*	(CMS Collab.)
TUMASYAN	23AE	PRL 131 041803	A. Tumasyan *et al.*	(CMS Collab.)
TUMASYAN	23AH	PRL 131 061801	A. Tumasyan *et al.*	(CMS Collab.)
TUMASYAN	23AI	PR D108 032008	A. Tumasyan *et al.*	(CMS Collab.)
TUMASYAN	23AJ	PR D108 032013	A. Tumasyan *et al.*	(CMS Collab.)
TUMASYAN	23AU	PL B846 137783	A. Tumasyan *et al.*	(CMS Collab.)
TUMASYAN	23BA	EPJ C83 933	A. Tumasyan *et al.*	(CMS Collab.)
TUMASYAN	23C	PL B842 137534	A. Tumasyan *et al.*	(CMS Collab.)
TUMASYAN	23D	PL B842 137531	A. Tumasyan *et al.*	(CMS Collab.)
TUMASYAN	23F	JHEP 2305 233	A. Tumasyan *et al.*	(CMS Collab.)
TUMASYAN	23I	JHEP 2306 130	A. Tumasyan *et al.*	(CMS Collab.)
TUMASYAN	23O	JHEP 2307 095	A. Tumasyan *et al.*	(CMS Collab.)
TUMASYAN	23P	JHEP 2307 092	A. Tumasyan *et al.*	(CMS Collab.)
TUMASYAN	23Q	JHEP 2307 091	A. Tumasyan *et al.*	(CMS Collab.)
TUMASYAN	23W	EPJ C83 667	A. Tumasyan *et al.*	(CMS Collab.)
TUMASYAN	23Y	EPJ C83 562	A. Tumasyan *et al.*	(CMS Collab.)
AAD	22D	PL B829 137066	G. Aad *et al.*	(ATLAS Collab.)
AAD	22M	JHEP 2206 097	G. Aad *et al.*	(ATLAS Collab.)
AAD	22N	JHEP 2208 027	G. Aad *et al.*	(ATLAS Collab.)
AAD	22P	JHEP 2208 104	G. Aad *et al.*	(ATLAS Collab.)
AAD	22Q	JHEP 2208 175	G. Aad *et al.*	(ATLAS Collab.)
AAD	22S	EPJ C82 105	G. Aad *et al.*	(ATLAS Collab.)
AAD	22V	EPJ C82 622	G. Aad *et al.*	(ATLAS Collab.)
AAD	22W	EPJ C82 717	G. Aad *et al.*	(ATLAS Collab.)
AAD	22X	PR D105 092003	G. Aad *et al.*	(ATLAS Collab.)
AAD	22Y	PR D106 052001	G. Aad *et al.*	(ATLAS Collab.)
ATLAS	22	NAT 607 52	ATLAS Collaboration	(ATLAS Collab.)
Also		NAT 612 E24 (errat.)	ATLAS Collaboration	(ATLAS Collab.)
CMS	22	NAT 607 60	CMS Collaboration	(CMS Collab.)
TUMASYAN	22AJ	PRL 128 081805	A. Tumasyan *et al.*	(CMS Collab.)
TUMASYAN	22AM	NATP 18 1329	A. Tumasyan *et al.*	(CMS Collab.)
TUMASYAN	22AN	PRL 129 081802	A. Tumasyan *et al.*	(CMS Collab.)
TUMASYAN	22G	PR D105 092007	A. Tumasyan *et al.*	(CMS Collab.)
TUMASYAN	22Y	JHEP 2206 012	A. Tumasyan *et al.*	(CMS Collab.)
AAD	21	PL B812 135980	G. Aad *et al.*	(ATLAS Collab.)
AAD	21AB	EPJ C81 178	G. Aad *et al.*	(ATLAS Collab.)
AAD	21AJ	EPJ C81 537	G. Aad *et al.*	(ATLAS Collab.)
AAD	21F	PR D103 112006	G. Aad *et al.*	(ATLAS Collab.)
AAD	21H	PL B816 136204	G. Aad *et al.*	(ATLAS Collab.)
AAD	21I	PL B819 136412	G. Aad *et al.*	(ATLAS Collab.)
AAD	21M	JHEP 2103 268	G. Aad *et al.*	(ATLAS Collab.)
SIRUNYAN	21	PL B812 135992	A.M. Sirunyan *et al.*	(CMS Collab.)
SIRUNYAN	21A	EPJ C81 13	A.M. Sirunyan *et al.*	(CMS Collab.)
Also		EPJ C81 333 (errat.)	A.M. Sirunyan *et al.*	(CMS Collab.)
SIRUNYAN	21AE	PR D104 052004	A.M. Sirunyan *et al.*	(CMS Collab.)
SIRUNYAN	21B	EPJ C81 3	A.M. Sirunyan *et al.*	(CMS Collab.)
SIRUNYAN	21C	JHEP 2101 148	A.M. Sirunyan *et al.*	(CMS Collab.)
SIRUNYAN	21K	JHEP 2103 257	A.M. Sirunyan *et al.*	(CMS Collab.)
SIRUNYAN	21L	JHEP 2103 011	A.M. Sirunyan *et al.*	(CMS Collab.)
SIRUNYAN	21O	JHEP 2107 027	A.M. Sirunyan *et al.*	(CMS Collab.)
SIRUNYAN	21R	EPJ C81 378	A.M. Sirunyan *et al.*	(CMS Collab.)
SIRUNYAN	21S	EPJ C81 488	A.M. Sirunyan *et al.*	(CMS Collab.)
SIRUNYAN	21Z	PR D104 032013	A.M. Sirunyan *et al.*	(CMS Collab.)
TUMASYAN	21D	JHEP 2111 153	A. Tumasyan *et al.*	(CMS Collab.)
AAD	20	PR D101 012002	G. Aad *et al.*	(ATLAS Collab.)
AAD	20A	PL B800 135069	G. Aad *et al.*	(ATLAS Collab.)
AAD	20AE	PRL 125 221802	G. Aad *et al.*	(ATLAS Collab.)
AAD	20AG	PL B809 135754	G. Aad *et al.*	(ATLAS Collab.)
AAD	20AQ	EPJ C80 957	G. Aad *et al.*	(ATLAS Collab.)
Also		EPJ C81 29 (errat.)	G. Aad *et al.*	(ATLAS Collab.)
Also		EPJ C81 398 (errat.)	G. Aad *et al.*	(ATLAS Collab.)
AAD	20BA	EPJ C80 942	G. Aad *et al.*	(ATLAS Collab.)
AAD	20C	PL B800 135103	G. Aad *et al.*	(ATLAS Collab.)
AAD	20E	PL B801 135145	G. Aad *et al.*	(ATLAS Collab.)
AAD	20F	PL B801 135148	G. Aad *et al.*	(ATLAS Collab.)
AAD	20N	PL B805 135426	G. Aad *et al.*	(ATLAS Collab.)
AAD	20X	JHEP 2007 108	G. Aad *et al.*	(ATLAS Collab.)
Also		JHEP 2101 145 (errat.)	G. Aad *et al.*	(ATLAS Collab.)
Also		JHEP 2105 207 (errat.)	G. Aad *et al.*	(ATLAS Collab.)
AAD	20Z	PRL 125 061802	G. Aad *et al.*	(ATLAS Collab.)
SIRUNYAN	20AE	JHEP 2003 131	A.M. Sirunyan *et al.*	(CMS Collab.)
SIRUNYAN	20AH	JHEP 2005 032	A.M. Sirunyan *et al.*	(CMS Collab.)
SIRUNYAN	20AS	PRL 125 061801	A.M. Sirunyan *et al.*	(CMS Collab.)
SIRUNYAN	20BK	JHEP 2011 039	A.M. Sirunyan *et al.*	(CMS Collab.)
SIRUNYAN	20BL	JHEP 2012 085	A.M. Sirunyan *et al.*	(CMS Collab.)
SIRUNYAN	20C	EPJ C80 75	A.M. Sirunyan *et al.*	(CMS Collab.)
SIRUNYAN	20L	PL B805 135425	A.M. Sirunyan *et al.*	(CMS Collab.)
AABOUD	19A	JHEP 1901 030	M. Aaboud *et al.*	(ATLAS Collab.)
AABOUD	19AI	PL B793 499	M. Aaboud *et al.*	(ATLAS Collab.)
AABOUD	19AL	PRL 122 231801	M. Aaboud *et al.*	(ATLAS Collab.)
AABOUD	19AQ	PR D99 072001	M. Aaboud *et al.*	(ATLAS Collab.)
AABOUD	19F	PL B789 508	M. Aaboud *et al.*	(ATLAS Collab.)
AABOUD	19N	JHEP 1904 048	M. Aaboud *et al.*	(ATLAS Collab.)
AABOUD	19O	JHEP 1904 092	M. Aaboud *et al.*	(ATLAS Collab.)
AABOUD	19T	JHEP 1905 124	M. Aaboud *et al.*	(ATLAS Collab.)
AABOUD	19U	JHEP 1905 141	M. Aaboud *et al.*	(ATLAS Collab.)
AAD	19A	PL B798 134949	G. Aad *et al.*	(ATLAS Collab.)
SIRUNYAN	19	PL B788 7	A.M. Sirunyan *et al.*	(CMS Collab.)
SIRUNYAN	19AB	JHEP 1904 112	A.M. Sirunyan *et al.*	(CMS Collab.)
SIRUNYAN	19AF	JHEP 1906 093	A.M. Sirunyan *et al.*	(CMS Collab.)
SIRUNYAN	19AJ	EPJ C79 94	A.M. Sirunyan *et al.*	(CMS Collab.)
SIRUNYAN	19AT	EPJ C79 421	A.M. Sirunyan *et al.*	(CMS Collab.)
SIRUNYAN	19AX	PL B791 96	A.M. Sirunyan *et al.*	(CMS Collab.)
SIRUNYAN	19BA	PL B792 369	A.M. Sirunyan *et al.*	(CMS Collab.)
SIRUNYAN	19BE	PRL 122 121803	A.M. Sirunyan *et al.*	(CMS Collab.)
SIRUNYAN	19BK	PR D99 092005	A.M. Sirunyan *et al.*	(CMS Collab.)
SIRUNYAN	19BL	PR D99 112003	A.M. Sirunyan *et al.*	(CMS Collab.)
SIRUNYAN	19BO	PL B793 520	A.M. Sirunyan *et al.*	(CMS Collab.)
SIRUNYAN	19BR	PL B797 134811	A.M. Sirunyan *et al.*	(CMS Collab.)
SIRUNYAN	19BY	PR D100 072007	A.M. Sirunyan *et al.*	(CMS Collab.)
SIRUNYAN	19BZ	PR D100 112002	A.M. Sirunyan *et al.*	(CMS Collab.)
SIRUNYAN	19CG	JHEP 1910 139	A.M. Sirunyan *et al.*	(CMS Collab.)
SIRUNYAN	19E	PRL 122 021801	A.M. Sirunyan *et al.*	(CMS Collab.)
SIRUNYAN	19H	JHEP 1901 040	A.M. Sirunyan *et al.*	(CMS Collab.)
SIRUNYAN	19L	JHEP 1901 183	A.M. Sirunyan *et al.*	(CMS Collab.)
SIRUNYAN	19R	JHEP 1903 026	A.M. Sirunyan *et al.*	(CMS Collab.)
AABOUD	18	PL B776 318	M. Aaboud *et al.*	(ATLAS Collab.)
AABOUD	18AC	PR D97 072003	M. Aaboud *et al.*	(ATLAS Collab.)
AABOUD	18AJ	JHEP 1803 095	M. Aaboud *et al.*	(ATLAS Collab.)
AABOUD	18AU	JHEP 1807 127	M. Aaboud *et al.*	(ATLAS Collab.)
Also		JHEP 2312 158 (errat.)	M. Aaboud *et al.*	(ATLAS Collab.)
AABOUD	18BK	PL B784 173	M. Aaboud *et al.*	(ATLAS Collab.)
AABOUD	18BL	PL B786 134	M. Aaboud *et al.*	(ATLAS Collab.)
AABOUD	18BM	PL B784 345	M. Aaboud *et al.*	(ATLAS Collab.)
AABOUD	18BN	PL B786 59	M. Aaboud *et al.*	(ATLAS Collab.)
AABOUD	18BO	PR D98 052005	M. Aaboud *et al.*	(ATLAS Collab.)
AABOUD	18BP	PL B786 223	M. Aaboud *et al.*	(ATLAS Collab.)
AABOUD	18BQ	PR D98 052003	M. Aaboud *et al.*	(ATLAS Collab.)
AABOUD	18BU	EPJ C78 1007	M. Aaboud *et al.*	(ATLAS Collab.)
AABOUD	18CA	JHEP 1810 180	M. Aaboud *et al.*	(ATLAS Collab.)
AABOUD	18CG	PL B786 114	M. Aaboud *et al.*	(ATLAS Collab.)
AABOUD	18CQ	PRL 121 191801	M. Aaboud *et al.*	(ATLAS Collab.)
AABOUD	18CW	JHEP 1811 040	M. Aaboud *et al.*	(ATLAS Collab.)
AABOUD	18M	PRL 120 211802	M. Aaboud *et al.*	(ATLAS Collab.)
AABOUD	18T	PR D97 072016	M. Aaboud *et al.*	(ATLAS Collab.)
AAIJ	18AM	EPJ C78 1008	R. Aaij *et al.*	(LHCb Collab.)
AALTONEN	18C	PR D98 072002	T. Aaltonen *et al.*	(CDF Collab.)
SIRUNYAN	18A	PL B778 101	A.M. Sirunyan *et al.*	(CMS Collab.)
SIRUNYAN	18AE	PL B780 501	A.M. Sirunyan *et al.*	(CMS Collab.)
SIRUNYAN	18BD	JHEP 1806 101	A.M. Sirunyan *et al.*	(CMS Collab.)
SIRUNYAN	18BH	JHEP 1806 001	A.M. Sirunyan *et al.*	(CMS Collab.)
SIRUNYAN	18BQ	JHEP 1808 066	A.M. Sirunyan *et al.*	(CMS Collab.)
SIRUNYAN	18BU	EPJ C78 140	A.M. Sirunyan *et al.*	(CMS Collab.)
SIRUNYAN	18BV	EPJ C78 291	A.M. Sirunyan *et al.*	(CMS Collab.)
SIRUNYAN	18DB	PRL 121 121801	A.M. Sirunyan *et al.*	(CMS Collab.)
SIRUNYAN	18DQ	JHEP 1811 152	A.M. Sirunyan *et al.*	(CMS Collab.)
SIRUNYAN	18DS	JHEP 1811 185	A.M. Sirunyan *et al.*	(CMS Collab.)
SIRUNYAN	18E	PRL 120 071802	A.M. Sirunyan *et al.*	(CMS Collab.)
SIRUNYAN	18F	JHEP 1801 054	A.M. Sirunyan *et al.*	(CMS Collab.)
SIRUNYAN	18L	PRL 120 231801	A.M. Sirunyan *et al.*	(CMS Collab.)
SIRUNYAN	18S	PR D97 092005	A.M. Sirunyan *et al.*	(CMS Collab.)
SIRUNYAN	18Y	PL B779 283	A.M. Sirunyan *et al.*	(CMS Collab.)
AABOUD	17AW	JHEP 1710 112	M. Aaboud *et al.*	(ATLAS Collab.)
AABOUD	17BA	JHEP 1712 024	M. Aaboud *et al.*	(ATLAS Collab.)
AABOUD	17BD	EPJ C77 765	M. Aaboud *et al.*	(ATLAS Collab.)
AABOUD	17CO	JHEP 1710 132	M. Aaboud *et al.*	(ATLAS Collab.)
AABOUD	17Y	PRL 119 051802	M. Aaboud *et al.*	(ATLAS Collab.)
AAD	17	EPJ C77 70	G. Aad *et al.*	(ATLAS Collab.)
KHACHATRY...	17F	JHEP 1702 135	V. Khachatryan *et al.*	(CMS Collab.)
SIRUNYAN	17AM	PL B775 1	A.M. Sirunyan *et al.*	(CMS Collab.)
SIRUNYAN	17AV	JHEP 1711 047	A.M. Sirunyan *et al.*	(CMS Collab.)
SIRUNYAN	17CN	PR D96 072004	A.M. Sirunyan *et al.*	(CMS Collab.)
AABOUD	16I	PR D94 052002	M. Aaboud *et al.*	(ATLAS Collab.)
AABOUD	16K	PRL 117 111802	M. Aaboud *et al.*	(ATLAS Collab.)
AABOUD	16X	JHEP 1611 112	M. Aaboud *et al.*	(ATLAS Collab.)
AAD	16	PL B753 69	G. Aad *et al.*	(ATLAS Collab.)
AAD	16AC	PR D93 092005	G. Aad *et al.*	(ATLAS Collab.)
AAD	16AF	JHEP 1601 172	G. Aad *et al.*	(ATLAS Collab.)
AAD	16AL	JHEP 1605 160	G. Aad *et al.*	(ATLAS Collab.)
AAD	16AN	JHEP 1608 045	G. Aad *et al.*	(ATLAS and CMS Collabs.)
AAD	16AO	JHEP 1608 104	G. Aad *et al.*	(ATLAS Collab.)
AAD	16BL	EPJ C76 658	G. Aad *et al.*	(ATLAS Collab.)
AAD	16K	EPJ C76 6	G. Aad *et al.*	(ATLAS Collab.)
KHACHATRY...	16AB	PL B759 672	V. Khachatryan *et al.*	(CMS Collab.)
KHACHATRY...	16AR	JHEP 1604 005	V. Khachatryan *et al.*	(CMS Collab.)
KHACHATRY...	16AU	JHEP 1606 177	V. Khachatryan *et al.*	(CMS Collab.)
KHACHATRY...	16B	PL B753 341	V. Khachatryan *et al.*	(CMS Collab.)
KHACHATRY...	16BA	JHEP 1609 051	V. Khachatryan *et al.*	(CMS Collab.)
KHACHATRY...	16BQ	PR D94 052012	V. Khachatryan *et al.*	(CMS Collab.)
KHACHATRY...	16CD	PL B763 472	V. Khachatryan *et al.*	(CMS Collab.)
KHACHATRY...	16G	EPJ C76 13	V. Khachatryan *et al.*	(CMS Collab.)
AAD	15	PL B740 222	G. Aad *et al.*	(ATLAS Collab.)
AAD	15AA	PR D92 012006	G. Aad *et al.*	(ATLAS Collab.)
AAD	15AH	JHEP 1504 117	G. Aad *et al.*	(ATLAS Collab.)
AAD	15AQ	JHEP 1508 137	G. Aad *et al.*	(ATLAS Collab.)
AAD	15AX	EPJ C75 231	G. Aad *et al.*	(ATLAS Collab.)
AAD	15B	PRL 114 191803	G. Aad *et al.*	(ATLAS and CMS Collabs.)
AAD	15BC	EPJ C75 349	G. Aad *et al.*	(ATLAS Collab.)

AAD	15BD	EPJ C75 337	G. Aad *et al.*	(ATLAS Collab.)
AAD	15BE	EPJ C75 335	G. Aad *et al.*	(ATLAS Collab.)
AAD	15CE	PR D92 092004	G. Aad *et al.*	(ATLAS Collab.)
AAD	15CI	EPJ C75 476	G. Aad *et al.*	(ATLAS Collab.)
Also		EPJ C76 152 (errat.)	G. Aad *et al.*	(ATLAS Collab.)
AAD	15CX	JHEP 1511 206	G. Aad *et al.*	(ATLAS Collab.)
AAD	15F	PR D91 012006	G. Aad *et al.*	(ATLAS Collab.)
AAD	15G	JHEP 1501 069	G. Aad *et al.*	(ATLAS Collab.)
AAD	15I	PRL 114 121801	G. Aad *et al.*	(ATLAS Collab.)
AAD	15P	PRL 115 091801	G. Aad *et al.*	(ATLAS Collab.)
AAD	15T	PL B749 519	G. Aad *et al.*	(ATLAS Collab.)
AALTONEN	15	PRL 114 151802	T. Aaltonen *et al.*	(CDF and D0 Collabs.)
AALTONEN	15B	PRL 114 141802	T. Aaltonen *et al.*	(CDF Collab.)
KHACHATRY...	15AM	EPJ C75 212	V. Khachatryan *et al.*	(CMS Collab.)
KHACHATRY...	15AN	EPJ C75 251	V. Khachatryan *et al.*	(CMS Collab.)
KHACHATRY...	15BA	PR D92 072010	V. Khachatryan *et al.*	(CMS Collab.)
KHACHATRY...	15H	PL B744 184	V. Khachatryan *et al.*	(CMS Collab.)
KHACHATRY...	15Q	PL B749 337	V. Khachatryan *et al.*	(CMS Collab.)
KHACHATRY...	15Y	PR D92 012004	V. Khachatryan *et al.*	(CMS Collab.)
KHACHATRY...	15Z	PR D92 032008	V. Khachatryan *et al.*	(CMS Collab.)
AAD	14AR	PL B738 234	G. Aad *et al.*	(ATLAS Collab.)
AAD	14AS	PL B738 68	G. Aad *et al.*	(ATLAS Collab.)
AAD	14BC	PR D90 112015	G. Aad *et al.*	(ATLAS Collab.)
AAD	14BJ	JHEP 1409 112	G. Aad *et al.*	(ATLAS Collab.)
AAD	14J	PL B732 8	G. Aad *et al.*	(ATLAS Collab.)
AAD	14O	PRL 112 201802	G. Aad *et al.*	(ATLAS Collab.)
AAD	14W	PR D90 052004	G. Aad *et al.*	(ATLAS Collab.)
ABAZOV	14F	PRL 113 161802	V.M. Abazov *et al.*	(D0 Collab.)
CHATRCHYAN	14AA	PR D89 092007	S. Chatrchyan *et al.*	(CMS Collab.)
CHATRCHYAN	14AI	PR D89 012003	S. Chatrchyan *et al.*	(CMS Collab.)
CHATRCHYAN	14AJ	NATP 10 557	S. Chatrchyan *et al.*	(CMS Collab.)
CHATRCHYAN	14B	EPJ C74 2980	S. Chatrchyan *et al.*	(CMS Collab.)
CHATRCHYAN	14G	JHEP 1401 096	S. Chatrchyan *et al.*	(CMS Collab.)
CHATRCHYAN	14K	JHEP 1405 104	S. Chatrchyan *et al.*	(CMS Collab.)
KHACHATRY...	14D	PL B736 64	V. Khachatryan *et al.*	(CMS Collab.)
KHACHATRY...	14H	JHEP 1409 087	V. Khachartryan *et al.*	(CMS Collab.)
KHACHATRY...	14P	EPJ C74 3076	V. Khachatryan *et al.*	(CMS Collab.)
AAD	13AJ	PL B726 120	G. Aad *et al.*	(ATLAS Collab.)
AAD	13AK	PL B726 88	G. Aad *et al.*	(ATLAS Collab.)
Also		PL B734 406 (errat.)	G. Aad *et al.*	(ATLAS Collab.)
AALTONEN	13L	PR D88 052013	T. Aaltonen *et al.*	(CDF Collab.)
AALTONEN	13M	PR D88 052014	T. Aaltonen *et al.*	(CDF and D0 Collabs.)
ABAZOV	13L	PR D88 052011	V.M. Abazov *et al.*	(D0 Collab.)
CHATRCHYAN	13BK	PL B726 587	S. Chatrchyan *et al.*	(CMS Collab.)
CHATRCHYAN	13J	PRL 110 081803	S. Chatrchyan *et al.*	(CMS Collab.)
CHATRCHYAN	13X	JHEP 1305 145	S. Chatrchyan *et al.*	(CMS Collab.)
CHATRCHYAN	13Y	JHEP 1306 081	S. Chatrchyan *et al.*	(CMS Collab.)
HEINEMEYER	13A	arXiv:1307.1347	S. Heinemeyer *et al.*	(LHC Higgs CS Working Group)
AAD	12AI	PL B716 1	G. Aad *et al.*	(ATLAS Collab.)
AAD	12DA	SCI 338 1576	G. Aad *et al.*	(ATLAS Collab.)
AALTONEN	12Q	PRL 109 111803	T. Aaltonen *et al.*	(CDF Collab.)
AALTONEN	12R	PRL 109 111804	T. Aaltonen *et al.*	(CDF Collab.)
AALTONEN	12S	PRL 109 111805	T. Aaltonen *et al.*	(CDF Collab.)
AALTONEN	12T	PRL 109 071804	T. Aaltonen *et al.*	(CDF and D0 Collabs.)
ABAZOV	12K	PL B716 285	V.M. Abazov *et al.*	(D0 Collab.)
ABAZOV	12O	PRL 109 121803	V.M. Abazov *et al.*	(D0 Collab.)
ABAZOV	12P	PRL 109 121804	V.M. Abazov *et al.*	(D0 Collab.)
CHATRCHYAN	12BY	SCI 338 1569	S. Chatrchyan *et al.*	(CMS Collab.)
CHATRCHYAN	12N	PL B716 30	S. Chatrchyan *et al.*	(CMS Collab.)
DITTMAIER	12	arXiv:1201.3084	S. Dittmaier *et al.*	(LHC Higgs CS Working Group)
DITTMAIER	11	arXiv:1101.0593	S. Dittmaier *et al.*	(LHC Higgs CS Working Group)

Neutral Higgs Bosons, Searches for

CONTENTS:

Mass Limits for Neutral Higgs Bosons in Supersymmetric Models
- Mass Limits for heavy neutral Higgs bosons (H^0_2, A^0) in the MSSM
- Mass Limits for H^0_1 (Higgs Boson) in Supersymmetric Models

Mass Limits for Neutral Higgs Bosons in Extended Higgs Models
- Mass Limits in General two-Higgs-doublet Models
- Mass Limits for H^0 with Vanishing Yukawa Couplings
- Mass Limits for H^0 Decaying to Invisible Final States
- Mass Limits for Light A^0
- Other Mass Limits

Electroweak Constraints on the Standard Model Higgs Boson Mass

MASS LIMITS FOR NEUTRAL HIGGS BOSONS IN SUPERSYMMETRIC MODELS

The minimal supersymmetric model has two complex doublets of Higgs bosons. The resulting physical states are two scalars [H^0_1 and H^0_2, where we define $m_{H^0_1} < m_{H^0_2}$], a pseudoscalar (A^0), and a charged Higgs pair ($H^\pm$). H^0_1 and H^0_2 are also called h and H in the literature. There are two free parameters in the Higgs sector which can be chosen to be m_{A^0} and $\tan\beta = v_2/v_1$, the ratio of vacuum expectation values of the two Higgs doublets. Tree-level Higgs masses are constrained by the model to be $m_{H^0_1} \leq m_Z$, $m_{H^0_2} \geq m_Z$, $m_{A^0} \geq m_{H^0_1}$, and $m_{H^\pm} \geq m_W$. However, as described in the review on "Status of Higgs Boson Physics" in this Volume these relations are violated by radiative corrections.

The observed signal at about 125 GeV, see section "H", can be interpreted as one of the neutral Higgs bosons of supersymmetric models. Unless otherwise noted, we identify the lighter scalar H^0_1 with the Higgs discovered at 125 GeV at the LHC (AAD 12AI, CHATRCHYAN 12N).

Unless otherwise noted, the experiments in e^+e^- collisions search for the processes $e^+e^- \rightarrow H^0_1 Z^0$ in the channels used for the Standard Model Higgs searches and $e^+e^- \rightarrow H^0_1 A^0$ in the final states $b\overline{b}b\overline{b}$ and $b\overline{b}\tau^+\tau^-$. Unless otherwise stated, the following results assume no invisible H^0_1 or A^0 decays. Unless otherwise noted, the results are given in the m_h^{max} scenario, CARENA 13.

In $p\overline{p}$ and pp collisions the experiments search for a variety of processes, as explicitly specified for each entry. Limits on the A^0 mass arise from these direct searches, as well as from the relations valid in the minimal supersymmetric model between m_{A^0} and $m_{H^0_1}$. As discussed in the review on "Status of Higgs Boson Physics" in this Volume, these relations depend, via potentially large radiative corrections, on the mass of the t quark and on the supersymmetric parameters, in particular those of the stop sector. These indirect limits are weaker for larger t and $\tilde{t}$ masses. To include the radiative corrections to the Higgs masses, unless otherwise stated, the listed papers use theoretical predictions incorporating two-loop corrections and beyond (SLAVICH 21), and the results are given for the M_h^{125} benchmark scenario, see BAGNASCHI 19.

Mass Limits for heavy neutral Higgs bosons (H^0_2, A^0) in the MSSM

The limits rely on $pp \rightarrow H^0_2/A^0 \rightarrow \tau^+\tau^-$ and assume that H^0_2 and A^0 are (sufficiently) mass degenerate. The limits depend on $\tan\beta$.

VALUE (GeV)	CL%	DOCUMENT ID		TECN	COMMENT
$>$ 835	95	[1] TUMASYAN	23S	CMS	$\tan\beta = 10$ GeV
$>$1240	95	[1] TUMASYAN	23S	CMS	$\tan\beta = 20$ GeV
$>$1605	95	[1] TUMASYAN	23S	CMS	$\tan\beta = 30$ GeV
$>$1820	95	[1] TUMASYAN	23S	CMS	$\tan\beta = 40$ GeV
$>$1950	95	[1] TUMASYAN	23S	CMS	$\tan\beta = 50$ GeV
$>$2062	95	[1] TUMASYAN	23S	CMS	$\tan\beta = 60$ GeV
$>$1121	95	[2] AAD	20AA	ATLS	$\tan\beta = 10$ GeV
$>$1475	95	[2] AAD	20AA	ATLS	$\tan\beta = 20$ GeV
$>$1677	95	[2] AAD	20AA	ATLS	$\tan\beta = 30$ GeV
$>$1826	95	[2] AAD	20AA	ATLS	$\tan\beta = 40$ GeV
$>$1937	95	[2] AAD	20AA	ATLS	$\tan\beta = 50$ GeV
$>$2033	95	[2] AAD	20AA	ATLS	$\tan\beta = 60$ GeV
• • • We do not use the following data for averages, fits, limits, etc. • • •					
		[3] CHEKHOVSKY	25C	CMS	$H^0_2/A^0 \rightarrow b\overline{b}$
		[4] CHEKHOVSKY	25I	CMS	$A^0 \rightarrow ZH$
		[5] AAD	24AP	ATLS	$H^0_2, A^0 \rightarrow t\overline{t}$
		[6] AAD	24CB	ATLS	H properties
		[7] AAD	24H	ATLS	$H^0_2 \rightarrow HH$
		[8] AAD	20	ATLS	H properties
		[9] AAD	20C	ATLS	$H^0_2 \rightarrow HH$
		[10] AAD	20L	ATLS	$H^0_2 \rightarrow b\overline{b}$
		[11] SIRUNYAN	20AC	CMS	$A^0 \rightarrow ZH$
		[12] SIRUNYAN	20AF	CMS	$H^0_2/A^0 \rightarrow t\overline{t}$
		[13] SIRUNYAN	20Y	CMS	$H^0_2 \rightarrow W^+W^-$
		[14] SIRUNYAN	19CR	CMS	$H^0_2/A^0 \rightarrow \mu^+\mu^-$
$>$ 377	95	[15] AABOUD	18G	ATLS	$\tan\beta = 10$ GeV
$>$ 863	95	[15] AABOUD	18G	ATLS	$\tan\beta = 20$ GeV
$>$1157	95	[15] AABOUD	18G	ATLS	$\tan\beta = 30$ GeV
$>$1328	95	[15] AABOUD	18G	ATLS	$\tan\beta = 40$ GeV
$>$1483	95	[15] AABOUD	18G	ATLS	$\tan\beta = 50$ GeV
$>$1613	95	[15] AABOUD	18G	ATLS	$\tan\beta = 60$ GeV
		[16] SIRUNYAN	18A	CMS	$H^0_2 \rightarrow H^0H^0$
		[17] SIRUNYAN	18BP	CMS	$pp \rightarrow H^0_2/A^0 + b + X$, $H^0_2/A^0 \rightarrow b\overline{b}$
$>$ 389	95	[18] SIRUNYAN	18CX	CMS	$\tan\beta = 10$ GeV
$>$ 832	95	[18] SIRUNYAN	18CX	CMS	$\tan\beta = 20$ GeV
$>$1148	95	[18] SIRUNYAN	18CX	CMS	$\tan\beta = 30$ GeV
$>$1341	95	[18] SIRUNYAN	18CX	CMS	$\tan\beta = 40$ GeV
$>$1496	95	[18] SIRUNYAN	18CX	CMS	$\tan\beta = 50$ GeV
$>$1613	95	[18] SIRUNYAN	18CX	CMS	$\tan\beta = 60$ GeV
		[19] AABOUD	16AA	ATLS	$A^0 \rightarrow \tau^+\tau^-$
		[20] KHACHATRY...	16A	CMS	$H^0_{1,2}/A^0 \rightarrow \mu^+\mu^-$
		[21] KHACHATRY...	16P	CMS	$H^0_2 \rightarrow H^0H^0$, $A^0 \rightarrow ZH^0$
		[22] KHACHATRY...	15AY	CMS	$pp \rightarrow H^0_{1,2}/A^0 + b + X$, $H^0_{1,2}/A^0 \rightarrow b\overline{b}$
		[23] AAD	14AW	ATLS	$pp \rightarrow H^0_{1,2}/A^0 + X$, $H^0_{1,2}/A^0 \rightarrow \tau\tau$
		[24] KHACHATRY...	14M	CMS	$pp \rightarrow H^0_{1,2}/A^0 + X$, $H^0_{1,2}/A^0 \rightarrow \tau\tau$
		[25] AAD	13O	ATLS	$pp \rightarrow H^0_{1,2}/A^0 + X$, $H^0_{1,2}/A^0 \rightarrow \tau^+\tau^-$, $\mu^+\mu^-$
		[26] AAIJ	13T	LHCB	$pp \rightarrow H^0_{1,2}/A^0 + X$, $H^0_{1,2}/A^0 \rightarrow \tau^+\tau^-$
		[27] CHATRCHYAN	13AG	CMS	$pp \rightarrow H^0_{1,2}/A^0 + b + X$, $H^0_{1,2}/A^0 \rightarrow b\overline{b}$
		[28] AALTONEN	12AQ	TEVA	$p\overline{p} \rightarrow H^0_{1,2}/A^0 + b + X$, $H^0_{1,2}/A^0 \rightarrow b\overline{b}$

Int. J. Mod. Phys. A 2026.41. Downloaded from www.worldscientific.com
by UNIVERSITY OF CALIFORNIA @ BERKELEY on 09/16/26. Reproduction is strictly not permitted, except for Open Access articles.

Int. J. Mod. Phys. A 2026.41. Downloaded from www.worldscientific.com
by UNIVERSITY OF CALIFORNIA @ BERKELEY on 09/16/26. Re-use and distribution is strictly not permitted, except for Open Access articles.

		[29] AALTONEN	12X	CDF	$p\overline{p} \to H^0_{1,2}/A^0 + b + X$, $H^0_{1,2}/A^0 \to b\overline{b}$
		[30] ABAZOV	12G	D0	$p\overline{p} \to H^0_{1,2}/A^0 + X$, $H^0_{1,2}/A^0 \to \tau^+\tau^-$
		[31] CHATRCHYAN	12K	CMS	$pp \to H^0_{1,2}/A^0 + X$, $H^0_{1,2}/A^0 \to \tau^+\tau^-$
		[32] ABAZOV	11K	D0	$p\overline{p} \to H^0_{1,2}/A^0 + b + X$, $H^0_{1,2}/A^0 \to b\overline{b}$
		[33] ABAZOV	11W	D0	$p\overline{p} \to H^0_{1,2}/A^0 + b + X$, $H^0_{1,2}/A^0 \to \tau^+\tau^-$
		[34] AALTONEN	09AR	CDF	$p\overline{p} \to H^0_{1,2}/A^0 + X$, $H^0_{1,2}/A^0 \to \tau^+\tau^-$
> 90.4		[35] ABDALLAH	08B	DLPH	$E_{cm} \leq 209$ GeV
> 93.4	95	[36] SCHAEL	06B	LEP	$E_{cm} \leq 209$ GeV
		[37] ACOSTA	05Q	CDF	$p\overline{p} \to H^0_{1,2}/A^0 + X$
> 85.0	95	[38,39] ABBIENDI	04M	OPAL	$E_{cm} \leq 209$ GeV
		[40] ABBIENDI	03G	OPAL	$H^0_1 \to A^0 A^0$
> 86.5	95	[38,41] ACHARD	02H	L3	$E_{cm} \leq 209$ GeV, $\tan\beta > 0.4$
		[42] AKEROYD	02	RVUE	
> 90.1	95	[38,43] HEISTER	02	ALEP	$E_{cm} \leq 209$ GeV, $\tan\beta > 0.5$

[1] TUMASYAN 23S search for production of $H^0_2/A^0 \to \tau^+\tau^-$ by gluon fusion and b-associated prodution using 138 fb^{-1} of pp collisions at $E_{cm} = 13$ TeV. See their Fig. 13 for excluded regions in the m_{A^0}–$\tan\beta$ plane in M^{125}_h and M^{125}_{hEFT} MSSM scenarios. In both scenarios $m_{A^0} < 350$ GeV is excluded at 95% CL.

[2] AAD 20AA search for $H^0_2/A^0 \to \tau^+\tau^-$ produced by gluon fusion or b-associated production using 139 fb^{-1} of pp collisions at $E_{cm} = 13$ TeV. See their Fig. 2(c) for excluded region in the M^{125}_h scenario of MSSM. Values of $\tan\beta > 8$ (21) are excluded for $m_{A^0} = 1.0$ (1.5) TeV at 95%CL.

[3] CHEKHOVSKY 25C search for $H^0_2/A^0 \to b\overline{b}$ by b-associated prodution using 36.7–126.9 fb^{-1} of pp collisions at $E_{cm} = 13$ TeV. See their Figs. 16–18 for excluded regions in the m_{A^0}–$\tan\beta$ plane in various MSSM scenarios.

[4] CHEKHOVSKY 25I search for production of an A^0 in gluon-gluon fusion and in association with a $b\overline{b}$, decaying to ZH in the final states $\ell^+\ell^-\tau^+\tau^-$, assuming B($H \to \tau^+\tau^-$) of the SM, using 138 fb^{-1} of pp collisions at $E_{cm} = 13$ TeV. See their Fig. 7 for excluded parameter region in M^{125}_{hEFT} MSSM scenario.

[5] AAD 24AP search for production of a heavy H^0_2 and A^0 decaying to $t\overline{t}$ in 140 fb^{-1} of pp collisions at $E_{cm} = 13$ TeV. See their Fig. 13(b) for excluded parameter regions in hMSSM.

[6] AAD 24CB use ATLAS measurements from up to 139 fb^{-1} of H production cross sections and decays to constrain the MSSM Higgs sector. See their Figs. 22 and 23 for excluded regions in various MSSM scenarios.

[7] AAD 24H combine searches for a scalar resonance decaying to HH using up to 139 fb^{-1} of pp collisions at $E_{cm} = 13$ TeV from AAD 22F, AAD 23Z, and AAD 22Y. See their Fig. 3 for the excluded region in the MSSM $M^{125}_{h,EFT}$ and $M^{125}_{h,EFT}(\widetilde{\chi})$ benchmark scenarios (where only the resonant H-exchange contribution has been taken into account in the signal modelling).

[8] AAD 20 combine measurements on H production and decay using data taken in years 2015–2017 (up to 79.8 fb^{-1}) of pp collisions at $E_{cm} = 13$ TeV. See their Fig. 19 for excluded region in the hMSSM parameter space.

[9] AAD 20C combine searches for a scalar resonance decaying to HH in 36.1 fb^{-1} of pp collisions at $E_{cm} = 13$ TeV from AABOUD 19A, AABOUD 19O, AABOUD 18CQ, AABOUD 19T, AABOUD 18CW, and AABOUD 18BU. See their Fig. 7(b) for the excluded region in the hMSSM parameter space.

[10] AAD 20L search for b-associated production of H^0_2 decaying to $b\overline{b}$ in 27.8 fb^{-1} of pp collisions at $E_{cm} = 13$ TeV. See their Fig. 9 for excluded regions in hMSSM, m^{mod+}_h and m^{mod-}_h scenarios of MSSM.

[11] SIRUNYAN 20AC search for gluon-fusion and b-associated production of A^0 decaying to ZH in 35.9 fb^{-1} of pp collisions at $E_{cm} = 13$ TeV. See their Fig. 6 for excluded regions in the M^{125}_{hEFT} and hMSSM scenarios of the MSSM.

[12] SIRUNYAN 20AF search for $H^0_2/A^0 \to t\overline{t}$ with one or two charged leptons in the final state using kinematic variables in 35.9 fb^{-1} of pp collisions at $E_{cm} = 13$ TeV. See their Fig. 8 for excluded region in the hMSSM scenario of MSSM. Values of $\tan\beta$ below 1.0–1.5 are excluded for $m_{A^0} = 0.4$–0.75 TeV at 95%CL.

[13] SIRUNYAN 20Y search for gluon-fusion and vector-boson-fusion production of H^0_2 decaying to W^+W^- in the final states $\ell\nu\ell\nu$ and $\ell\nu qq$ in 35.9 fb^{-1} of pp collisions at $E_{cm} = 13$ TeV. See their Figs. 8 and 9 for excluded regions in various MSSM scenarios.

[14] SIRUNYAN 19CR search for production of H^0_2/A^0 in gluon fusion and in association with a $b\overline{b}$ pair, decaying to $\mu^+\mu^-$ in 35.9 fb^{-1} of pp collisions at $E_{cm} = 13$ TeV. See their Fig. 5 for the excluded region in the MSSM parameter space in the m^{mod+}_h and hMSSM scenarios.

[15] AABOUD 18G search for production of $H^0_2/A^0 \to \tau^+\tau^-$ by gluon fusion and b-associated prodution in 36.1 fb^{-1} of pp collisions at $E_{cm} = 13$ TeV. See their Fig. 10 for excluded regions in the m_{A^0}– $\tan\beta$ plane in several MSSM scenarios.

[16] SIRUNYAN 18A search for production of a scalar resonance decaying to $H^0H^0 \to b\overline{b}\tau^+\tau^-$ in 35.9 fb^{-1} of pp collisions at $E_{cm} = 13$ TeV. See their Fig. 5 (lower) for excluded regions in the $m_{A^0} - \tan\beta$ plane in the hMSSM scenario.

[17] SIRUNYAN 18BP search for production of $H^0_2/A^0 \to b\overline{b}$ by b-associated prodution in 35.7 fb^{-1} of pp collisions at $E_{cm} = 13$ TeV. See their Fig. 6 for the limits on cross section times branching ratio for $m_{H^0_2}$, $m_{A^0} = 0.3$–1.3 TeV, and Fig. 7 for excluded regions in the m_{A^0}– $\tan(\beta)$ plane in several MSSM scenarios.

[18] SIRUNYAN 18CX search for production of $H^0_{1,2}/A^0 \to \tau^+\tau^-$ by gluon fusion and b-associated prodution in 35.9 fb^{-1} of pp collisions at $E_{cm} = 13$ TeV. See their Fig. 9 for excluded regions in the m_{A^0}– $\tan(\beta)$ plane in several MSSM scenarios.

[19] AABOUD 16AA search for production of a Higgs boson in gluon fusion and in association with a $b\overline{b}$ pair followed by the decay $A^0 \to \tau^+\tau^-$ in 3.2 fb^{-1} of pp collisions at $E_{cm} = 13$ TeV. See their Fig. 5(a, b) for limits on cross section times branching ratio for $m_{A^0} = 200$–1200 GeV, and Fig. 5(c, d) for the excluded region in the MSSM parameter space in the m^{mod+}_h and hMSSM scenarios.

[20] KHACHATRYAN 16A search for production of a Higgs boson in gluon fusion and in association with a $b\overline{b}$ pair followed by the decay $H^0_{1,2}/A^0 \to \mu^+\mu^-$ in 5.1 fb^{-1} of pp collisions at $E_{cm} = 7$ TeV and 19.3 fb^{-1} at $E_{cm} = 8$ TeV. See their Fig. 7 for the excluded region in the MSSM parameter space in the m^{mod+}_h benchmark scenario and Fig. 9 for limits on cross section times branching ratio.

[21] KHACHATRYAN 16P search for gluon fusion production of an H^0_2 decaying to $H^0H^0 \to b\overline{b}\tau^+\tau^-$ and an A^0 decaying to $ZH^0 \to \ell^+\ell^-\tau^+\tau^-$ in 19.7 fb^{-1} of pp collisions at $E_{cm} = 8$ TeV. See their Fig. 12 for excluded region in the $\tan\beta - \cos(\beta - \alpha)$ plane for $m_{H^0_2} = m_{A^0} = 300$ GeV.

[22] KHACHATRYAN 15AY search for production of a Higgs boson in association with a b quark in the decay $H^0_{1,2}/A^0 \to b\overline{b}$ in 19.7 fb^{-1} of pp collisions at $E_{cm} = 8$ TeV and combine with CHATRCHYAN 13AG 7 TeV data. See their Fig. 6 for the limits on cross section times branching ratio for $m_{A^0} = 100$–900 GeV and Figs. 7–9 for the excluded region in the MSSM parameter space in various benchmark scenarios.

[23] AAD 14AW search for production of a Higgs boson followed by the decay $H^0_{1,2}/A^0 \to \tau^+\tau^-$ in 19.5–20.3 fb^{-1} of pp collisions at $E_{cm} = 8$ TeV. See their Fig. 11 for the limits on cross section times branching ratio and their Figs. 9 and 10 for the excluded region in the MSSM parameter space. For $m_{A^0} = 140$ GeV, the region $\tan\beta > 5.4$ is excluded at 95% CL in the m^{max}_h scenario.

[24] KHACHATRYAN 14M search for production of a Higgs boson in gluon fusion and in association with a b quark followed by the decay $H^0_{1,2}/A^0 \to \tau^+\tau^-$ in 4.9 fb^{-1} of pp collisions at $E_{cm} = 7$ TeV and 19.7 fb^{-1} at $E_{cm} = 8$ TeV. See their Figs. 7 and 8 for one- and two-dimensional limits on cross section times branching ratio and their Figs. 5 and 6 for the excluded region in the MSSM parameter space. For $m_{A^0} = 140$ GeV, the region $\tan\beta > 3.8$ is excluded at 95% CL in the m^{max}_h scenario.

[25] AAD 13O search for production of a Higgs boson in the decay $H^0_{1,2}/A^0 \to \tau^+\tau^-$ and $\mu^+\mu^-$ with 4.7–4.8 fb^{-1} of pp collisions at $E_{cm} = 7$ TeV. See their Fig. 6 for the excluded region in the MSSM parameter space and their Fig. 7 for the limits on cross section times branching ratio. For $m_{A^0} = 110$–170 GeV, $\tan\beta \gtrsim 10$ is excluded, and for $\tan\beta = 50$, m_{A^0} below 470 GeV is excluded at 95% CL in the m^{max}_h scenario.

[26] AAIJ 13T search for production of a Higgs boson in the forward region in the decay $H^0_{1,2}/A^0 \to \tau^+\tau^-$ in 1.0 fb^{-1} of pp collisions at $E_{cm} = 7$ TeV. See their Fig. 2 for the limits on cross section times branching ratio and the excluded region in the MSSM parameter space.

[27] CHATRCHYAN 13AG search for production of a Higgs boson in association with a b quark in the decay $H^0_{1,2}/A^0 \to b\overline{b}$ in 2.7–4.8 fb^{-1} of pp collisions at $E_{cm} = 7$ TeV. See their Fig. 6 for the excluded region in the MSSM parameter space and Fig. 5 for the limits on cross section times branching ratio. For $m_{A^0} = 90$–350 GeV, upper bounds on $\tan\beta$ of 18–42 at 95% CL are obtained in the m^{max}_h scenario with $\mu = +200$ GeV.

[28] AALTONEN 12AQ combine AALTONEN 12X and ABAZOV 11K. See their Table I and Fig. 1 for the limit on cross section times branching ratio and Fig. 2 for the excluded region in the MSSM parameter space.

[29] AALTONEN 12X search for associated production of a Higgs boson and a b quark in the decay $H^0_{1,2}/A^0 \to b\overline{b}$, with 2.6 fb^{-1} of $p\overline{p}$ collisions at $E_{cm} = 1.96$ TeV. See their Table III and Fig. 15 for the limit on cross section times branching ratio and Figs. 17, 18 for the excluded region in the MSSM parameter space.

[30] ABAZOV 12G search for production of a Higgs boson in the decay $H^0_{1,2}/A^0 \to \tau^+\tau^-$ with 7.3 fb^{-1} of $p\overline{p}$ collisions at $E_{cm} = 1.96$ TeV and combine with ABAZOV 11W and ABAZOV 11K. See their Figs. 4, 5, and 6 for the excluded region in the MSSM parameter space. For $m_{A^0} = 90$–180 GeV, $\tan\beta \gtrsim 30$ is excluded at 95% CL. in the m^{max}_h scenario.

[31] CHATRCHYAN 12K search for production of a Higgs boson in the decay $H^0_{1,2}/A^0 \to \tau^+\tau^-$ with 4.6 fb^{-1} of pp collisions at $E_{cm} = 7$ TeV. See their Fig. 3 and Table 4 for the excluded region in the MSSM parameter space. For $m_{A^0} = 160$ GeV, the region $\tan\beta > 7.1$ is excluded at 95% CL in the m^{max}_h scenario. Superseded by KHACHATRYAN 14M.

[32] ABAZOV 11K search for associated production of a Higgs boson and a b quark, followed by the decay $H^0_{1,2}/A^0 \to b\overline{b}$, in 5.2 fb^{-1} of $p\overline{p}$ collisions at $E_{cm} = 1.96$ TeV. See their Fig. 5/Table 2 for the limit on cross section times branching ratio and Fig. 6 for the excluded region in the MSSM parameter space for $\mu = -200$ GeV.

[33] ABAZOV 11W search for associated production of a Higgs boson and a b quark, followed by the decay $H^0_{1,2}/A^0 \to \tau\tau$, in 7.3 fb^{-1} of $p\overline{p}$ collisions at $E_{cm} = 1.96$ TeV. See their Fig. 2 for the limit on cross section times branching ratio and for the excluded region in the MSSM parameter space.

[34] AALTONEN 09AR search for Higgs bosons decaying to $\tau^+\tau^-$ in two doublet models in 1.8 fb^{-1} of $p\overline{p}$ collisions at $E_{cm} = 1.96$ TeV. See their Fig. 2 for the limit on $\sigma \cdot$ B($H^0_{1,2}/A^0 \to \tau^+\tau^-$) for different Higgs masses, and see their Fig. 3 for the excluded region in the MSSM parameter space.

Int. J. Mod. Phys. A 2026.41. Downloaded from www.worldscientific.com
by UNIVERSITY OF CALIFORNIA @ BERKELEY on 09/16/26. Re strictly not permitted, except for Open Access articles.

[35] ABDALLAH 08B give limits in eight *CP*-conserving benchmark scenarios and some *CP*-violating scenarios. See paper for excluded regions for each scenario. Supersedes ABDALLAH 04.

[36] SCHAEL 06B make a combined analysis of the LEP data. The quoted limit is for the m_h^{max} scenario with $m_t = 174.3$ GeV. In the *CP*-violating CPX scenario no lower bound on $m_{H_1^0}$ can be set at 95% CL. See paper for excluded regions in various scenarios. See Figs. 2–6 and Tabs. 14–21 for limits on $\sigma(ZH^0)\cdot B(H^0 \to b\overline{b}, \tau^+\tau^-)$ and $\sigma(H_1^0 H_2^0)\cdot B(H_1^0, H_2^0 \to b\overline{b}, \tau^+\tau^-)$.

[37] ACOSTA 05Q search for $H_{1,2}^0/A^0$ production in $p\overline{p}$ collisions at $E_{cm} = 1.8$ TeV with $H_{1,2}^0/A^0 \to \tau^+\tau^-$. At $m_{A^0} = 100$ GeV, the obtained cross section upper limit is above theoretical expectation.

[38] Search for $e^+e^- \to H_1^0 A^0$ in the final states $b\overline{b}b\overline{b}$ and $b\overline{b}\tau^+\tau^-$, and $e^+e^- \to H_1^0 Z$. Universal scalar mass of 1 TeV, SU(2) gaugino mass of 200 GeV, and $\mu = -200$ GeV are assumed, and two-loop radiative corrections incorporated. The limits hold for m_t=175 GeV, and for the m_h^{max} scenario.

[39] ABBIENDI 04M exclude $0.7 < \tan\beta < 1.9$, assuming $m_t = 174.3$ GeV. Limits for other MSSM benchmark scenarios, as well as for *CP* violating cases, are also given.

[40] ABBIENDI 03G search for $e^+e^- \to H_1^0 Z$ followed by $H_1^0 \to A^0 A^0$, $A^0 \to c\overline{c}, gg$, or $\tau^+\tau^-$. In the no-mixing scenario, the region $m_{H_1^0}$ = 45–85 GeV and m_{A^0} = 2–9.5 GeV is excluded at 95% CL.

[41] ACHARD 02H also search for the final state $H_1^0 Z \to 2A^0 q\overline{q}$, $A^0 \to q\overline{q}$. In addition, the MSSM parameter set in the "large-μ" and "no-mixing" scenarios are examined.

[42] AKEROYD 02 examine the possibility of a light A^0 with $\tan\beta$ <1. Electroweak measurements are found to be inconsistent with such a scenario.

[43] HEISTER 02 excludes the range 0.7 <$\tan\beta$ < 2.3. A wider range is excluded with different stop mixing assumptions. Updates BARATE 01C.

Mass Limits for H_1^0 (Higgs Boson) in Supersymmetric Models

VALUE (GeV)	CL%	DOCUMENT ID		TECN	COMMENT
>89.7		[1] ABDALLAH	08B	DLPH	$E_{cm} \leq 209$ GeV
>92.8	95	[2] SCHAEL	06B	LEP	$E_{cm} \leq 209$ GeV
>84.5	95	[3,4] ABBIENDI	04M	OPAL	$E_{cm} \leq 209$ GeV
>86.0	95	[3,5] ACHARD	02H	L3	$E_{cm} \leq 209$ GeV, $\tan\beta > 0.4$
>89.8	95	[3,6] HEISTER	02	ALEP	$E_{cm} \leq 209$ GeV, $\tan\beta > 0.5$
• • • We do not use the following data for averages, fits, limits, etc. • • •					
		[7] AALTONEN	12AQ	TEVA	$p\overline{p} \to H_{1,2}^0/A^0 + b + X$, $H_{1,2}^0/A^0 \to b\overline{b}$

[1] ABDALLAH 08B give limits in eight *CP*-conserving benchmark scenarios and some *CP*-violating scenarios. See paper for excluded regions for each scenario. Supersedes ABDALLAH 04.

[2] SCHAEL 06B make a combined analysis of the LEP data. The quoted limit is for the m_h^{max} scenario with $m_t = 174.3$ GeV. In the *CP*-violating CPX scenario no lower bound on $m_{H_1^0}$ can be set at 95% CL. See paper for excluded regions in various scenarios. See Figs. 2–6 and Tabs. 14–21 for limits on $\sigma(ZH^0)\cdot B(H^0 \to b\overline{b}, \tau^+\tau^-)$ and $\sigma(H_1^0 H_2^0)\cdot B(H_1^0, H_2^0 \to b\overline{b}, \tau^+\tau^-)$.

[3] Search for $e^+e^- \to H_1^0 A^0$ in the final states $b\overline{b}b\overline{b}$ and $b\overline{b}\tau^+\tau^-$, and $e^+e^- \to H_1^0 Z$. Universal scalar mass of 1 TeV, SU(2) gaugino mass of 200 GeV, and $\mu = -200$ GeV are assumed, and two-loop radiative corrections incorporated. The limits hold for m_t=175 GeV, and for the m_h^{max} scenario.

[4] ABBIENDI 04M exclude $0.7 < \tan\beta < 1.9$, assuming $m_t = 174.3$ GeV. Limits for other MSSM benchmark scenarios, as well as for *CP* violating cases, are also given.

[5] ACHARD 02H also search for the final state $H_1^0 Z \to 2A^0 q\overline{q}$, $A^0 \to q\overline{q}$. In addition, the MSSM parameter set in the "large-μ" and "no-mixing" scenarios are examined.

[6] HEISTER 02 excludes the range 0.7 <$\tan\beta$ < 2.3. A wider range is excluded with different stop mixing assumptions. Updates BARATE 01C.

[7] AALTONEN 12AQ combine AALTONEN 12X and ABAZOV 11K. See their Table I and Fig. 1 for the limit on cross section times branching ratio and Fig. 2 for the excluded region in the MSSM parameter space.

MASS LIMITS FOR NEUTRAL HIGGS BOSONS IN EXTENDED HIGGS MODELS

This Section covers models which do not fit into either the Standard Model or its simplest minimal Supersymmetric extension (MSSM), leading to anomalous production rates, or nonstandard final states and branching ratios. In particular, this Section covers limits which may apply to generic two-Higgs-doublet models (2HDM), or to special regions of the MSSM parameter space where decays to invisible particles or to photon pairs are dominant (see the review on "Status of Higgs Boson Physics"). Concerning the mass limits for H^0 and A^0 listed below, see the footnotes or the comment lines for details on the nature of the models to which the limits apply.

The observed signal at about 125 GeV, see section "*H*", can be interpreted as one of the neutral Higgs bosons of an extended Higgs sector.

Mass Limits in General two-Higgs-doublet Models

VALUE (GeV)	CL%	DOCUMENT ID		TECN	COMMENT
• • • We do not use the following data for averages, fits, limits, etc. • • •					
		[1] AAD	25AL	ATLS	$t\overline{t}H_2^0/A^0$
		[2] CHEKHOVSKY	25C	CMS	$H_2^0/A^0 \to b\overline{b}$
		[3] HAYRAPETY...	25I	CMS	$A^0 \to ZH_2^0$, $H_2^0 \to t\overline{t}$
		[4] AAD	24AB	ATLS	$A^0 \to ZH_2^0$
		[5] AAD	24AP	ATLS	$H_2^0, A^0 \to t\overline{t}$
		[6] AAD	24CB	ATLS	H properties
		[7] AAD	24H	ATLS	$H_2^0 \to HH$
		[8] HAYRAPETY...	24H	CMS	flavor changing H_2^0, A^0
		[9] AAD	23AD	ATLS	$A^0 \to ZH_2^0$, $H_2^0 \to HH$
		[10] AAD	23BG	ATLS	$t\overline{t}H_2^0/A^0$
		[11] AAD	23O	ATLS	$A^0 \to ZH$
		[12] AAD	21AF	ATLS	$H_2^0 \to ZZ$
		[13] AAD	21AI	ATLS	$A^0 \to ZH_2^0$
		[14] AAD	20	ATLS	H^0 properties
		[15] AAD	20L	ATLS	$H_2^0 \to b\overline{b}$
		[16] SIRUNYAN	20AA	CMS	$H_2^0 \to ZA^0$ or $A^0 \to ZH_2^0$
		[17] SIRUNYAN	20Y	CMS	$H_2^0 \to W^+W^-$
		[18] SIRUNYAN	19AE	CMS	$A^0 \to \tau^+\tau^-$
		[19] SIRUNYAN	19AV	CMS	$A^0 \to ZH^0$
		[20] AABOUD	18AH	ATLS	$A^0 \to ZH_2^0$
		[21] AABOUD	18AI	ATLS	$A^0 \to ZH^0$
		[22] AABOUD	18BF	ATLS	$H_2^0 \to ZZ$
		[23] AABOUD	18CE	ATLS	$pp \to H_2^0/A^0 t\overline{t}$, $H_2^0/A^0 \to t\overline{t}$
		[24] HALLER	18	RVUE	global fits
		[25] SIRUNYAN	18BP	CMS	$pp \to H_2^0/A^0 + b + X$, $H_2^0/A^0 \to b\overline{b}$
		[26] SIRUNYAN	18ED	CMS	$A^0 \to ZH^0$
		[27] AABOUD	17AN	ATLS	$H_2^0, A^0 \to t\overline{t}$
		[28] SIRUNYAN	17AX	CMS	$A^0 b\overline{b}$, $A^0 \to \mu^+\mu^-$
		[29] AAD	16AX	ATLS	$H_2^0 \to ZZ$
		[30] KHACHATRY...	16P	CMS	$H_2^0 \to H^0H^0$, $A^0 \to ZH^0$
		[31] KHACHATRY...	16W	CMS	$A^0 b\overline{b}$, $A^0 \to \tau^+\tau^-$
		[32] KHACHATRY...	16Z	CMS	$H_2^0 \to ZA^0$ or $A^0 \to ZH_2^0$
		[33] AAD	15BK	ATLS	$H_2^0 \to H^0H^0$
		[34] AAD	15S	ATLS	$A^0 \to ZH^0$
		[35] KHACHATRY...	15BB	CMS	$H_2^0, A^0 \to \gamma\gamma$
		[36] KHACHATRY...	15N	CMS	$A^0 \to ZH^0$
		[37] AAD	14M	ATLS	$H_2^0 \to H^\pm W^\mp \to H^0W^\pm W^\mp$, $H^0 \to b\overline{b}$
		[38] KHACHATRY...	14Q	CMS	$H_2^0 \to H^0H^0$, $A^0 \to ZH^0$
		[39] AALTONEN	09AR	CDF	$p\overline{p} \to H_{1,2}^0/A^0 + X$, $H_{1,2}^0/A^0 \to \tau^+\tau^-$
none 1–55	95	[40] ABBIENDI	05A	OPAL	H_1^0, Type II model
>110.6	95	[41] ABDALLAH	05D	DLPH	$H^0 \to$ 2 jets
		[42] ABDALLAH	04O	DLPH	$Z \to f\overline{f}H$
		[43] ABDALLAH	04O	DLPH	$e^+e^- \to H^0Z$, H^0A^0
		[44] ABBIENDI	02D	OPAL	$e^+e^- \to b\overline{b}H$
none 1–44	95	[45] ABBIENDI	01E	OPAL	H_1^0, Type-II model
> 68.0	95	[46] ABBIENDI	99E	OPAL	$\tan\beta > 1$
		[47] ABREU	95H	DLPH	$Z \to H^0Z^*$, H^0A^0
		[48] PICH	92	RVUE	Very light Higgs

[1] AAD 25AL search for production of H_2^0/A^0 in association with a $t\overline{t}$ pair, decaying to $t\overline{t}$, resulting in final states with one lepton or two opposite-sign leptons, using 139 fb^{-1} of pp collisions at E_{cm} = 13 TeV. See their Fig. 9 for excluded regions in the parameter space of the type II 2HDM. Combined limits with AAD 23BG are shown in Fig. 11.

[2] CHEKHOVSKY 25C search for $H_2^0/A^0 \to b\overline{b}$ by b-associated production using 36.7–126.9 fb^{-1} of pp collisions at E_{cm} = 13 TeV. See their Figs. 19 and 20 for excluded regions in the parameter space in Type II and flipped 2HDMs.

[3] HAYRAPETYAN 25I search for $A^0 \to ZH_2^0$ with $H_2^0 \to t\overline{t}$ using 138 fb^{-1} of pp collisions at E_{cm} = 13 TeV. See their Figs. 6 and 7 for excluded regions the 2HDM Type II.

[4] AAD 24AB search for gluon-fusion and $b\overline{b}$ associated production of A^0 decaying to $A^0 \to ZH_2^0$, in the final states $\ell^+\ell^- t\overline{t}$ and $\nu\overline{\nu}b\overline{b}$ using 140 fb^{-1} of pp collisions at E_{cm} = 13 TeV. See their Figs. 5 and 6 for limits on cross section times branching ratios in terms of two-Higgs-doublet models, and Fig. 7 for excluded model parameter space.

[5] AAD 24AP search for production of a heavy H_2^0 and A^0 decaying to $t\overline{t}$ in 140 fb^{-1} of pp collisions at E_{cm} = 13 TeV. See their Fig. 13(a) for excluded parameter regions in a Type II two-Higgs-doublet model.

[6] AAD 24CB use ATLAS measurements from up to 139 fb^{-1} of H production cross sections and decays to constrain two Higgs doublet models. See their Figs. 19–21 for excluded regions of 2HDM parameter space.

[7] AAD 24H combine searches for a scalar resonance decaying to HH using up to 139 fb^{-1} of pp collisions at E_{cm} = 13 TeV from AAD 22F, AAD 23Z, and AAD 22Y. See their Fig. 2 for the excluded region in the Type-I two-Higgs-doublet model parameter space (where only the resonant H-exchange contribution has been taken into account in the signal modelling).

[8] HAYRAPETYAN 24H search for H_2^0 and A^0 having flavor-violating couplings to tc or tu, produced in association with top quark(s), using 138 fb^{-1} of pp collisions at E_{cm} = 13 TeV. For the interpretation of the data in terms of flavor-violating two-Higgs-doublet models, given in the range m_{A^0} = 0.2–1.0 TeV, see their Figs. 4, 5, and 6.

[9] AAD 23AD search for associated production of W/ZH_2^0 and gluon fusion production of A^0 decaying to ZH_2^0, with the decay chain $H_2^0 \to HH \to b\overline{b}b\overline{b}$, using 139 fb^{-1} of

Int. J. Mod. Phys. A 2026.41. Downloaded from www.worldscientific.com
by UNIVERSITY OF CALIFORNIA @ BERKELEY on 09/16/26. Re-use and distribution is strictly not permitted, except for Open Access articles.

pp collisions at E_{cm} = 13 TeV. See their Figs. 12 and 13 for excluded regions in Type-I and lepton-specific 2HDMs.

[10] AAD 23BG search for production of H_2^0/A^0 in association with a $t\overline{t}$ pair, decaying to $t\overline{t}$, resulting in final states with two same-sign leptons or three or more leptons, using 139 fb^{-1} of pp collisions at E_{cm} = 13 TeV. See their Fig. 8 (corrected version in the erratum) for excluded regions in the parameter space of the type II 2HDM.

[11] AAD 23O search for production of an A^0 in gluon-gluon fusion and in association with a $b\overline{b}$, decaying to ZH in the final states $\nu\overline{\nu}b\overline{b}$ and $\ell^+\ell^-b\overline{b}$ using 139 fb^{-1} of pp collisions at E_{cm} = 13 TeV. See their Figs. 12 and 13 for excluded regions in the parameter space in various 2HDMs.

[12] AAD 21AF search for production of a heavy H_2^0 state decaying to ZZ in the final states $\ell^+\ell^-\ell'^+\ell'^-$ and $\ell^+\ell^-\nu\overline{\nu}$ in 139 fb^{-1} of pp collisions at E_{cm} = 13 TeV. See their Figs. 6 and 7 for excluded parameter regions of the 2HDM Type I and II.

[13] AAD 21AI search for production of an A^0 in gluon-gluon fusion and in association with a $b\overline{b}$, decaying to $ZH_2^0 \rightarrow \ell^+\ell^-b\overline{b}$ or $\ell^+\ell^-W^+W^-$ in 139 fb^{-1} of pp collisions at E_{cm} = 13 TeV. See their Figs. 10 and 14 for excluded regions in the parameter space of various 2HDMs.

[14] AAD 20 combine measurements on H^0 production and decay using data taken in years 2015–2017 (up to 79.8 fb^{-1}) of pp collisions at E_{cm} = 13 TeV. See their Fig. 18 for excluded regions in various 2HDMs.

[15] AAD 20L search for b-associated production of H_2^0 decaying to $b\overline{b}$ in 27.8 fb^{-1} of pp collisions at E_{cm} = 13 TeV. See their Figs. 10 and 11 for excluded regions in the flipped two Higgs doublet model.

[16] SIRUNYAN 20AA search for $H_2^0 \rightarrow ZA^0$, $A^0 \rightarrow b\overline{b}$ or $A^0 \rightarrow ZH_2^0$, $H_2^0 \rightarrow b\overline{b}$ in 35.9 fb^{-1} of pp collisions at E_{cm} = 13 TeV. See their Figs. 8 and 9 for excluded regions in the parameter space of Type-II two Higgs doublet model.

[17] SIRUNYAN 20Y search for gluon-fusion and vector-boson-fusion production of H_2^0 decaying to W^+W^- in the final states $\ell\nu\ell\nu$ and $\ell\nu qq$ in 35.9 fb^{-1} of pp collisions at E_{cm} = 13 TeV. See their Fig. 7 for excluded regions in Type I and II two Higgs doublet models.

[18] SIRUNYAN 19AE search for a pseudoscalar resonance produced in association with a $b\overline{b}$ pair, decaying to $\tau^+\tau^-$ in 35.9 fb^{-1} of pp collisions at E_{cm} = 13 TeV. See their Fig. 4 for cross section limits for m_{A^0} = 25–70 GeV and comparison with some representative 2HDMs.

[19] SIRUNYAN 19AV search for a scalar resonance produced by gluon fusion or b associated production, decaying to $ZH^0 \rightarrow \ell^+\ell^-b\overline{b}$ ($\ell = e, \mu$) or $\nu\overline{\nu}b\overline{b}$ in 35.9 fb^{-1} of pp collisions at E_{cm} = 13 TeV. See their Figs. 6 and 7 for excluded regions in the parameter space of various 2HDMs.

[20] AABOUD 18AH search for production of an A^0 in gluon-gluon fusion and in association with a $b\overline{b}$, decaying to $ZH_2^0 \rightarrow \ell^+\ell^-b\overline{b}$ in 36.1 fb^{-1} of pp collisions at E_{cm} = 13 TeV. See their Fig. 6 for excluded regions in the parameter space of various 2HDMs.

[21] AABOUD 18AI search for production of an A^0 in gluon-gluon fusion and in association with a $b\overline{b}$, decaying to ZH^0 in the final states $\nu\overline{\nu}b\overline{b}$ and $\ell^+\ell^-b\overline{b}$ in 36.1 fb^{-1} of pp collisions at E_{cm} = 13 TeV. See their Figs. 7 and 8 for excluded regions in the parameter space in various 2HDMs.

[22] AABOUD 18BF search for production of a heavy H_2^0 state decaying to ZZ in the final states $\ell^+\ell^-\ell^+\ell^-$ and $\ell^+\ell^-\nu\overline{\nu}$ in 36.1 fb^{-1} of pp collisions at E_{cm} = 13 TeV. See their Figs. 8 and 9 for excluded parameter regions in 2HDM Type I and II.

[23] AABOUD 18CE search for the process $pp \rightarrow H_2^0/A^0\,t\overline{t}$ followed by the decay $H_2^0/A^0 \rightarrow t\overline{t}$ in 36.1 fb^{-1} of pp collisions at E_{cm} = 13 TeV. See their Fig. 12 for limits on cross section times branching ratio, and for lower limits on tanβ for $m_{H_2^0}$, m_{A^0} = 0.4–1.0 TeV in the 2HDM type II.

[24] HALLER 18 perform global fits in the framework of two-Higgs-doublet models (type I, II, lepton specific, flipped). See their Fig. 8 for allowed parameter regions from fits to LHC H^0 measurements, Fig. 9 bottom and charm decays, Fig. 10 muon anomalous magnetic moment, Fig. 11 electroweak precision data, and Fig. 12 by combination of all data.

[25] SIRUNYAN 18BP search for production of $H_2^0/A^0 \rightarrow b\overline{b}$ by b-associated prodution in 35.7 fb^{-1} of pp collisions at E_{cm} = 13 TeV. See their Fig. 6 for the limits on cross section times branching ratio for $m_{H_2^0}$, m_{A^0} = 0.3–1.3 TeV, and Figs. 8 and 9 for excluded regions in the parameter space of type-II and flipped 2HDMs.

[26] SIRUNYAN 18ED search for production of an A^0 in gluon-gluon fusion and in association with a $b\overline{b}$, decaying to ZH^0 in the final states $\nu\overline{\nu}b\overline{b}$ or $\ell^+\ell^-b\overline{b}$ in 35.9 fb^{-1} of pp collisions at E_{cm} = 13 TeV. See their Fig. 9 for excluded regions in the parameter space in Type I and II 2HDMs.

[27] AABOUD 17AN search for production of a heavy H_2^0 and/or A^0 decaying to $t\overline{t}$ in 20.3 fb^{-1} of pp collisions at E_{cm} = 8 TeV. See their Fig. 3 and Table III for excluded parameter regions in Type II Two-Higgs-Doublet-Models.

[28] SIRUNYAN 17AX search for $A^0b\overline{b}$ production followed by the decay $A^0 \rightarrow \mu^+\mu^-$ in 19.7 fb^{-1} of pp collisions at E_{cm} = 8 TeV. Limits are set in the range m_{A^0} = 25–60 GeV. See their Fig. 5 for upper limits on $\sigma(A^0b\overline{b})\cdot$B$(A^0 \rightarrow \mu^+\mu^-)$.

[29] AAD 16AX search for production of a heavy H^0 state decaying to ZZ in the final states $\ell^+\ell^-\ell^+\ell^-$, $\ell^+\ell^-\nu\overline{\nu}$, $\ell^+\ell^-q\overline{q}$, and $\nu\overline{\nu}q\overline{q}$ in 20.3 fb^{-1} of pp collisions at E_{cm} = 8 TeV. See their Figs. 13 and 14 for excluded parameter regions in Type I and II models.

[30] KHACHATRYAN 16P search for gluon fusion production of an H_2^0 decaying to $H^0H^0 \rightarrow b\overline{b}\tau^+\tau^-$ and an A^0 decaying to $ZH^0 \rightarrow \ell^+\ell^-\tau^+\tau^-$ in 19.7 fb^{-1} of pp collisions at E_{cm} = 8 TeV. See their Fig. 11 for limits on tanβ for m_{A^0} = 230–350 GeV.

[31] KHACHATRYAN 16W search for $A^0b\overline{b}$ production followed by the decay $A^0 \rightarrow \tau^+\tau^-$ in 19.7 fb^{-1} of pp collisions at E_{cm} = 8 TeV. See their Fig. 3 for upper limits on $\sigma(A^0b\overline{b})\cdot$B$(A^0 \rightarrow \tau^+\tau^-)$.

[32] KHACHATRYAN 16Z search for $H_2^0 \rightarrow ZA^0$ followed by $A^0 \rightarrow b\overline{b}$ or $\tau^+\tau^-$, and $A^0 \rightarrow ZH_2^0$ followed by $H_2^0 \rightarrow b\overline{b}$ or $\tau^+\tau^-$, in 19.8 fb^{-1} of pp collisions at E_{cm} = 8 TeV. See their Fig. 4 for cross section limits and Fig. 5 for excluded region in the parameter space.

[33] AAD 15BK search for production of a heavy H_2^0 decaying to H^0H^0 in the final state $b\overline{b}b\overline{b}$ in 19.5 fb^{-1} of pp collisions at E_{cm} = 8 TeV. See their Figs. 15–18 for excluded regions in the parameter space.

[34] AAD 15S search for production of A^0 decaying to $ZH^0 \rightarrow \ell^+\ell^-b\overline{b}$, $\nu\overline{\nu}b\overline{b}$ and $\ell^+\ell^-\tau^+\tau^-$ in 20.3 fb^{-1} of pp collisions at E_{cm} = 8 TeV. See their Figs. 4 and 5 for excluded regions in the parameter space.

[35] KHACHATRYAN 15BB search for H_2^0, $A^0 \rightarrow \gamma\gamma$ in 19.7 fb^{-1} of pp collisions at E_{cm} = 8 TeV. See their Fig. 10 for excluded regions in the two-Higgs-doublet model parameter space.

[36] KHACHATRYAN 15N search for production of A^0 decaying to $ZH^0 \rightarrow \ell^+\ell^-b\overline{b}$ in 19.7 fb^{-1} of pp collisions at E_{cm} = 8 TeV. See their Fig. 5 for excluded regions in the tanβ − cos$(\beta-\alpha)$ plane for m_{A^0} = 300 GeV.

[37] AAD 14M search for the decay cascade $H_2^0 \rightarrow H^\pm W^\mp \rightarrow H^0W^\pm W^\mp$, H^0 decaying to $b\overline{b}$ in 20.3 fb^{-1} of pp collisions at E_{cm} = 8 TeV. See their Table IV for limits in a two-Higgs-doublet model for $m_{H_2^0}$= 325–1025 GeV and m_{H^+}= 225–825 GeV.

[38] KHACHATRYAN 14Q search for $H_2^0 \rightarrow H^0H^0$ and $A^0 \rightarrow ZH^0$ in 19.5 fb^{-1} of pp collisions at E_{cm} = 8 TeV. See their Figs. 4 and 5 for limits on cross section times branching ratio for m_{H_2,A^0}= 260–360 GeV and their Figs. 7–9 for limits in two-Higgs-doublet models.

[39] AALTONEN 09AR search for Higgs bosons decaying to $\tau^+\tau^-$ in two doublet models in 1.8 fb^{-1} of $p\overline{p}$ collisions at E_{cm} = 1.96 TeV. See their Fig. 2 for the limit on $\sigma\cdot$B$(H_{1,2}^0/A^0 \rightarrow \tau^+\tau^-)$ for different Higgs masses, and see their Fig. 3 for the excluded region in the MSSM parameter space.

[40] ABBIENDI 05A search for $e^+e^- \rightarrow H_1^0A^0$ in general Type-II two-doublet models, with decays H_1^0, $A^0 \rightarrow q\overline{q}, gg, \tau^+\tau^-$, and $H_1^0 \rightarrow A^0A^0$.

[41] ABDALLAH 05D search for $e^+e^- \rightarrow H^0Z$ and H^0A^0 with H^0, A^0 decaying to two jets of any flavor including gg. The limit is for SM H^0Z production cross section with B$(H^0 \rightarrow jj)$ = 1.

[42] ABDALLAH 04O search for $Z \rightarrow b\overline{b}H^0$, $b\overline{b}A^0$, $\tau^+\tau^-H^0$ and $\tau^+\tau^-A^0$ in the final states $4b$, $b\overline{b}\tau^+\tau^-$, and 4τ. See paper for limits on Yukawa couplings.

[43] ABDALLAH 04O search for $e^+e^- \rightarrow H^0Z$ and H^0A^0, with H^0, A^0 decaying to $b\overline{b}$, $\tau^+\tau^-$, or $H^0 \rightarrow A^0A^0$ at E_{cm} = 189–208 GeV. See paper for limits on couplings.

[44] ABBIENDI 02D search for $Z \rightarrow b\overline{b}H_1^0$ and $b\overline{b}A^0$ with $H_1^0/A^0 \rightarrow \tau^+\tau^-$, in the range 4<$m_H$ <12 GeV. See their Fig. 8 for limits on the Yukawa coupling.

[45] ABBIENDI 01E search for neutral Higgs bosons in general Type-II two-doublet models, at $E_{cm} \leq$ 189 GeV. In addition to usual final states, the decays H_1^0, $A^0 \rightarrow q\overline{q}, gg$ are searched for. See their Figs. 15,16 for excluded regions.

[46] ABBIENDI 99E search for $e^+e^- \rightarrow H^0A^0$ and H^0Z at E_{cm} = 183 GeV. The limit is with m_H=m_A in general two Higgs-doublet models. See their Fig. 18 for the exclusion limit in the m_H–m_A plane. Updates the results of ACKERSTAFF 98S.

[47] See Fig. 4 of ABREU 95H for the excluded region in the $m_{H^0} - m_{A^0}$ plane for general two-doublet models. For tanβ >1, the region $m_{H^0}+m_{A^0} \lesssim$ 87 GeV, m_{H^0} <47 GeV is excluded at 95% CL.

[48] PICH 92 analyse H^0 with $m_{H^0} < 2m_\mu$ in general two-doublet models. Excluded regions in the space of mass-mixing angles from LEP, beam dump, and $\pi^\pm$, η rare decays are shown in Figs. 3,4. The considered mass region is not totally excluded.

Mass Limits for H^0 with Vanishing Yukawa Couplings

These limits assume that H^0 couples to gauge bosons with the same strength as the Standard Model Higgs boson, but has no coupling to quarks and leptons (this is often referred to as "fermiophobic").

VALUE (GeV)	CL%	DOCUMENT ID		TECN	COMMENT
• • • We do not use the following data for averages, fits, limits, etc. • • •					
		[1] AALTONEN	13K	CDF	$H^0 \rightarrow WW^{(*)}$
none 100–113	95	[2] AALTONEN	13L	CDF	$H^0 \rightarrow \gamma\gamma$, WW^*, ZZ^*
none 100–116	95	[3] AALTONEN	13M	TEVA	$H^0 \rightarrow \gamma\gamma$, WW^*, ZZ^*
		[4] ABAZOV	13G	D0	$H^0 \rightarrow WW^{(*)}$
none 100–113	95	[5] ABAZOV	13H	D0	$H^0 \rightarrow \gamma\gamma$
		[6] ABAZOV	13I	D0	$H^0 \rightarrow WW^{(*)}$
		[7] ABAZOV	13J	D0	$H^0 \rightarrow WW^{(*)}$, $ZZ^{(*)}$
none 100–114	95	[8] ABAZOV	13L	D0	$H^0 \rightarrow \gamma\gamma$, WW^*, ZZ^*
none 110–147	95	[9] CHATRCHYAN	13AL	CMS	$H^0 \rightarrow \gamma\gamma$
none 110–118, 119.5–121	95	[10] AAD	12N	ATLS	$H^0 \rightarrow \gamma\gamma$
none 100–114	95	[11] AALTONEN	12AN	CDF	$H^0 \rightarrow \gamma\gamma$
none 110–194	95	[12] CHATRCHYAN	12AO	CMS	$H^0 \rightarrow \gamma\gamma$, $WW^{(*)}$, $ZZ^{(*)}$
none 70–106	95	[13] AALTONEN	09AB	CDF	$H^0 \rightarrow \gamma\gamma$
none 70–100	95	[14] ABAZOV	08U	D0	$H^0 \rightarrow \gamma\gamma$
>105.8	95	[15] SCHAEL	07	ALEP	$e^+e^- \rightarrow H^0Z$, $H^0 \rightarrow WW^*$
>104.1	95	[16,17] ABDALLAH	04L	DLPH	$e^+e^- \rightarrow H^0Z$, $H^0 \rightarrow \gamma\gamma$
>107	95	[18] ACHARD	03C	L3	$H^0 \rightarrow WW^*, ZZ^*, \gamma\gamma$
>105.5	95	[16,19] ABBIENDI	02F	OPAL	$H^0 \rightarrow \gamma\gamma$
>105.4	95	[20] ACHARD	02C	L3	$H^0 \rightarrow \gamma\gamma$
none 60–82	95	[21] AFFOLDER	01H	CDF	$p\overline{p} \rightarrow H^0W/Z$, $H^0 \rightarrow \gamma\gamma$
> 94.9	95	[22] ACCIARRI	00S	L3	$e^+e^- \rightarrow H^0Z$, $H^0 \rightarrow \gamma\gamma$
>100.7	95	[23] BARATE	00L	ALEP	$e^+e^- \rightarrow H^0Z$, $H^0 \rightarrow \gamma\gamma$
> 96.2	95	[24] ABBIENDI	99O	OPAL	$e^+e^- \rightarrow H^0Z$, $H^0 \rightarrow \gamma\gamma$
> 78.5	95	[25] ABBOTT	99B	D0	$p\overline{p} \rightarrow H^0W/Z$, $H^0 \rightarrow \gamma\gamma$
		[26] ABREU	99P	DLPH	$e^+e^- \rightarrow H^0\gamma$ and/or $H^0 \rightarrow \gamma\gamma$

[1] AALTONEN 13K search for $H^0 \rightarrow WW^{(*)}$ in 9.7 fb^{-1} of $p\overline{p}$ collisions at E_{cm} = 1.96 TeV. A limit on cross section times branching ratio which corresponds to (1.3–6.6) times the expected cross section is given in the range m_{H^0} = 110–200 GeV at 95% CL.

[2] AALTONEN 13L combine all CDF searches with 9.45–10.0 fb^{-1} of $p\overline{p}$ collisions at E_{cm} = 1.96 TeV.

[3] AALTONEN 13M combine all Tevatron data from the CDF and D0 Collaborations of $p\overline{p}$ collisions at E_{cm} = 1.96 TeV.

Int. J. Mod. Phys. A 2026.41. Downloaded from www.worldscientific.com by UNIVERSITY OF CALIFORNIA @ BERKELEY on 09/16/26. Reproduction is strictly not permitted, except for Open Access articles.

[4] ABAZOV 13G search for $H^0 \to WW^{(*)}$ in 9.7 fb^{-1} of $p\overline{p}$ collisions at E_{cm} = 1.96 TeV. A limit on cross section times branching ratio which corresponds to (2–9) times the expected cross section is given for m_{H^0} = 100–200 GeV at 95% CL.

[5] ABAZOV 13H search for $H^0 \to \gamma\gamma$ in 9.6 fb^{-1} of $p\overline{p}$ collisions at E_{cm} = 1.96 TeV.

[6] ABAZOV 13I search for H^0 production in the final state with one lepton and two or more jets plus missing E_T in 9.7 fb^{-1} of $p\overline{p}$ collisions at E_{cm} = 1.96 TeV. The search is sensitive to WH^0, ZH^0 and vector-boson fusion Higgs production with $H^0 \to WW^{(*)}$. A limit on cross section times branching ratio which corresponds to (8–30) times the expected cross section is given in the range m_{H^0} = 100–200 GeV at 95% CL.

[7] ABAZOV 13J search for H^0 production in the final states $ee\mu$, $e\mu\mu$, $\mu\tau\tau$, and $e^\pm\mu^\pm$ in 8.6–9.7 fb^{-1} of $p\overline{p}$ collisions at E_{cm} = 1.96 TeV. The search is sensitive to WH^0, ZH^0 production with $H^0 \to WW^{(*)}$, $ZZ^{(*)}$, decaying to leptonic final states. A limit on cross section times branching ratio which corresponds to (2.4–13.0) times the expected cross section is given in the range m_{H^0} = 100–200 GeV at 95% CL.

[8] ABAZOV 13L combine all D0 results with up to 9.7 fb^{-1} of $p\overline{p}$ collisions at E_{cm} = 1.96 TeV.

[9] CHATRCHYAN 13AL search for $H^0 \to \gamma\gamma$ in 5.1 fb^{-1} and 5.3 fb^{-1} of pp collisions at E_{cm} = 7 and 8 TeV.

[10] AAD 12N search for $H^0 \to \gamma\gamma$ with 4.9 fb^{-1} of pp collisions at E_{cm} = 7 TeV in the mass range m_{H^0} = 110–150 GeV.

[11] AALTONEN 12AN search for $H^0 \to \gamma\gamma$ with 10 fb^{-1} of $p\overline{p}$ collisions at E_{cm} = 1.96 TeV in the mass range m_{H^0} = 100–150 GeV.

[12] CHATRCHYAN 12AO use data from CHATRCHYAN 12G, CHATRCHYAN 12E, CHATRCHYAN 12H, CHATRCHYAN 12I, CHATRCHYAN 12D, and CHATRCHYAN 12C.

[13] AALTONEN 09AB search for $H^0 \to \gamma\gamma$ in 3.0 fb^{-1} of $p\overline{p}$ collisions at E_{cm} = 1.96 TeV in the mass range m_{H^0} = 70–150 GeV. Associated H^0W, H^0Z production and WW, ZZ fusion are considered.

[14] ABAZOV 08U search for $H^0 \to \gamma\gamma$ in $p\overline{p}$ collisions at E_{cm} = 1.96 TeV in the mass range m_{H^0} = 70–150 GeV. Associated H^0W, H^0Z production and WW, ZZ fusion are considered. See their Tab. 1 for the limit on $\sigma \cdot$ B($H^0 \to \gamma\gamma$), and see their Fig. 3 for the excluded region in the m_{H^0} — B($H^0 \to \gamma\gamma$) plane.

[15] SCHAEL 07 search for Higgs bosons in association with a fermion pair and decaying to WW^*. The limit is from this search and HEISTER 02L for a H^0 with SM production cross section.

[16] Search for associated production of a $\gamma\gamma$ resonance with a Z boson, followed by $Z \to q\overline{q}$, $\ell^+\ell^-$, or $\nu\overline{\nu}$, at $E_{cm} \leq$ 209 GeV. The limit is for a H^0 with SM production cross section.

[17] Updates ABREU 01F.

[18] ACHARD 03C search for $e^+e^- \to ZH^0$ followed by $H^0 \to WW^*$ or ZZ^* at E_{cm}= 200-209 GeV and combine with the ACHARD 02C result. The limit is for a H^0 with SM production cross section. For B($H^0 \to WW^*$) + B($H^0 \to ZZ^*$) = 1, m_{H^0} > 108.1 GeV is obtained. See fig. 6 for the limits under different BR assumptions.

[19] For B($H^0 \to \gamma\gamma$)=1, m_{H^0} >117 GeV is obtained.

[20] ACHARD 02C search for associated production of a $\gamma\gamma$ resonance with a Z boson, followed by $Z \to q\overline{q}$, $\ell^+\ell^-$, or $\nu\overline{\nu}$, at $E_{cm} \leq$ 209 GeV. The limit is for a H^0 with SM production cross section. For B($H^0 \to \gamma\gamma$)=1, m_{H^0} >114 GeV is obtained.

[21] AFFOLDER 01H search for associated production of a $\gamma\gamma$ resonance and a W or Z (tagged by two jets, an isolated lepton, or missing E_T). The limit assumes Standard Model values for the production cross section and for the couplings of the H^0 to W and Z bosons. See their Fig. 11 for limits with B($H^0 \to \gamma\gamma$)< 1.

[22] ACCIARRI 00S search for associated production of a $\gamma\gamma$ resonance with a $q\overline{q}$, $\nu\overline{\nu}$, or $\ell^+\ell^-$ pair in e^+e^- collisions at E_{cm}= 189 GeV. The limit is for a H^0 with SM production cross section. For B($H^0 \to \gamma\gamma$)=1, m_{H^0} > 98 GeV is obtained. See their Fig. 5 for limits on B($H \to \gamma\gamma$)$\cdot\sigma(e^+e^- \to Hf\overline{f})/\sigma(e^+e^- \to Hf\overline{f})$ (SM).

[23] BARATE 00L search for associated production of a $\gamma\gamma$ resonance with a $q\overline{q}$, $\nu\overline{\nu}$, or $\ell^+\ell^-$ pair in e^+e^- collisions at E_{cm}= 88–202 GeV. The limit is for a H^0 with SM production cross section. For B($H^0 \to \gamma\gamma$)=1, m_{H^0} > 109 GeV is obtained. See their Fig. 3 for limits on B($H \to \gamma\gamma$)$\cdot\sigma(e^+e^- \to Hf\overline{f})/\sigma(e^+e^- \to Hf\overline{f})$ (SM).

[24] ABBIENDI 99O search for associated production of a $\gamma\gamma$ resonance with a $q\overline{q}$, $\nu\overline{\nu}$, or $\ell^+\ell^-$ pair in e^+e^- collisions at 189 GeV. The limit is for a H^0 with SM production cross section. See their Fig. 4 for limits on $\sigma(e^+e^- \to H^0Z^0)\times$B($H^0 \to \gamma\gamma)\times$B($X^0 \to f\overline{f}$) for various masses. Updates the results of ACKERSTAFF 98Y.

[25] ABBOTT 99B search for associated production of a $\gamma\gamma$ resonance and a dijet pair. The limit assumes Standard Model values for the production cross section and for the couplings of the H^0 to W and Z bosons. Limits in the range of $\sigma(H^0 + Z/W)\cdot$B($H^0 \to \gamma\gamma$)= 0.80–0.34 pb are obtained in the mass range m_{H^0}= 65–150 GeV.

[26] ABREU 99P search for $e^+e^- \to H^0\gamma$ with $H^0 \to b\overline{b}$ or $\gamma\gamma$, and $e^+e^- \to H^0q\overline{q}$ with $H^0 \to \gamma\gamma$. See their Fig. 4 for limits on $\sigma\times$B. Explicit limits within an effective interaction framework are also given.

Mass Limits for H^0 Decaying to Invisible Final States

These limits are for a neutral scalar H^0 which predominantly decays to invisible final states. Standard Model values are assumed for the couplings of H^0 to ordinary particles unless otherwise stated.

VALUE (GeV)	CL%	DOCUMENT ID		TECN	COMMENT
• • • We do not use the following data for averages, fits, limits, etc. • • •					
		[1] AABOUD	19AI	ATLS	WW/ZZ fusion
		[2] AAD	15BD	ATLS	$pp \to H^0WX$, H^0ZX
		[3] AAD	15BH	ATLS	jet + missing E_T
		[4] AAD	14BA	ATLS	secondary vertex
		[5] AAD	14O	ATLS	$pp \to H^0ZX$
		[6] CHATRCHYAN	14B	CMS	$pp \to H^0ZX$, qqH^0X
		[7] AAD	13AG	ATLS	secondary vertex
		[8] AAD	13AT	ATLS	electron jets
		[9] CHATRCHYAN	13BJ	CMS	
		[10] AAD	12AQ	ATLS	secondary vertex
		[11] AALTONEN	12AB	CDF	secondary vertex
		[12] AALTONEN	12U	CDF	secondary vertex
>108.2	95	[13] ABBIENDI	10	OPAL	
		[14] ABBIENDI	07	OPAL	large width
>112.3	95	[15] ACHARD	05	L3	
>112.1	95	[15] ABDALLAH	04B	DLPH	
>114.1	95	[15] HEISTER	02	ALEP	$E_{cm} \leq$ 209 GeV
>106.4	95	[15] BARATE	01C	ALEP	$E_{cm} \leq$ 202 GeV
> 89.2	95	[16] ACCIARRI	00M	L3	

[1] AABOUD 19AI search for $H^0_{1,2}$ production by vector boson fusion and decay to invisible final states in 36.1 fb^{-1} of pp collisions at E_{cm} = 13 TeV. See their Fig. 6(b) for limits on cross section times branching ratios for $m_{H^0_{1,2}}$ = 0.1–3 TeV.

[2] AAD 15BD search for $pp \to H^0WX$ and $pp \to H^0ZX$ with W or Z decaying hadronically and H^0 decaying to invisible final states in 20.3 fb^{-1} at E_{cm} = 8TeV. See their Fig. 6 for a limit on the cross section times branching ratio for m_{H^0} = 115–300 GeV.

[3] AAD 15BH search for events with a jet and missing E_T in 20.3 fb^{-1} of pp collisions at E_{cm} = 8 TeV. Limits on $\sigma(H'^0)$ B($H'^0 \to$ invisible) < (44–10) pb (95%CL) is given for $m_{H'^0}$ = 115–300 GeV.

[4] AAD 14BA search for H^0 production in the decay mode $H^0 \to X^0X^0$, where X^0 is a long-lived particle which decays to collimated pairs of e^+e^-, $\mu^+\mu^-$, or $\pi^+\pi^-$ plus invisible particles, in 20.3 fb^{-1} of pp collisions at E_{cm} = 8 TeV. See their Figs. 15 and 16 for limits on cross section times branching ratio.

[5] AAD 14O search for $pp \to H^0ZX$, $Z \to \ell\ell$, with H^0 decaying to invisible final states in 4.5 fb^{-1} at E_{cm} = 7 TeV and 20.3 fb^{-1} at E_{cm} = 8 TeV. See their Fig. 3 for a limit on the cross section times branching ratio for m_{H^0} = 110–400 GeV.

[6] CHATRCHYAN 14B search for $pp \to H^0ZX$, $Z \to \ell\ell$ and $Z \to b\overline{b}$, and also $pp \to qqH^0X$ with H^0 decaying to invisible final states using data at E_{cm} = 7 and 8 TeV. See their Figs. 10, 11 for limits on the cross section times branching ratio for m_{H^0} = 100–400 GeV.

[7] AAD 13AG search for H^0 production in the decay mode $H^0 \to X^0X^0$, where X^0 is a long-lived particle which decays to $\mu^+\mu^-X'^0$, in 1.9 fb^{-1} of pp collisions at E_{cm} = 7 TeV. See their Fig. 7 for limits on cross section times branching ratio.

[8] AAD 13AT search for H^0 production in the decay $H^0 \to X^0X^0$, where X^0 eventually decays to clusters of collimated e^+e^- pairs, in 2.04 fb^{-1} of pp collisions at E_{cm} = 7 TeV. See their Fig. 3 for limits on cross section times branching ratio.

[9] CHATRCHYAN 13BJ search for H^0 production in the decay chain $H^0 \to X^0X^0$, $X^0 \to \mu^+\mu^-X'^0$ in 5.3 fb^{-1} of pp collisions at E_{cm} = 7 TeV. See their Fig. 2 for limits on cross section times branching ratio.

[10] AAD 12AQ search for H^0 production in the decay mode $H^0 \to X^0X^0$, where X^0 is a long-lived particle which decays mainly to $b\overline{b}$ in the muon detector, in 1.94 fb^{-1} of pp collisions at E_{cm} = 7 TeV. See their Fig. 3 for limits on cross section times branching ratio for m_{H^0} = 120, 140 GeV, m_{X^0} = 20, 40 GeV in the $c\tau$ range of 0.5–35 m.

[11] AALTONEN 12AB search for H^0 production in the decay $H^0 \to X^0X^0$, where X^0 eventually decays to clusters of collimated $\ell^+\ell^-$ pairs, in 5.1 fb^{-1} of $p\overline{p}$ collisions at E_{cm} = 1.96 TeV. Cross section limits are provided for a benchmark MSSM model incorporating the parameters given in Table VI.

[12] AALTONEN 12U search for H^0 production in the decay mode $H^0 \to X^0X^0$, where X^0 is a long-lived particle with $c\tau \approx$ 1 cm which decays mainly to $b\overline{b}$, in 3.2 fb^{-1} of $p\overline{p}$ collisions at E_{cm} = 1.96 TeV. See their Figs. 9 and 10 for limits on cross section times branching ratio for m_{H^0} = (130–170) GeV, m_{X^0} = 20, 40 GeV.

[13] ABBIENDI 10 search for $e^+e^- \to H^0Z$ with H^0 decaying invisibly. The limit assumes SM production cross section and B($H^0 \to$ invisible) = 1.

[14] ABBIENDI 07 search for $e^+e^- \to H^0Z$ with $Z \to q\overline{q}$ and H^0 decaying to invisible final states. The H^0 width is varied between 1 GeV and 3 TeV. A limit $\sigma\cdot$B($H^0 \to$ invisible) < (0.07–0.57) pb (95%CL) is obtained at E_{cm} = 206 GeV for m_{H^0} = 60–114 GeV.

[15] Search for $e^+e^- \to H^0Z$ with H^0 decaying invisibly. The limit assumes SM production cross section and B($H^0 \to$ invisible) = 1.

[16] ACCIARRI 00M search for $e^+e^- \to ZH^0$ with H^0 decaying invisibly at E_{cm}=183–189 GeV. The limit assumes SM production cross section and B($H^0 \to$ invisible)=1. See their Fig. 6 for limits for smaller branching ratios.

Mass Limits for Light A^0

These limits are for a pseudoscalar A^0 in the mass range below $\mathcal{O}(10)$ GeV.

VALUE (GeV)	DOCUMENT ID		TECN	COMMENT
• • • We do not use the following data for averages, fits, limits, etc. • • •				
	[1] AAD	25AT	ATLS	$H \to ZA^0$
	[2] ADACHI	23A	BEL2	$\tau \to eA^0$, $\tau \to \mu A^0$
	[3] TUMASYAN	23AR	CMS	$H \to A^0A^0 \to 4\gamma$
	[4] ABLIKIM	22H	BES3	$J/\psi \to A^0\gamma$
	[5] JIA	22	BELL	$\Upsilon(1S) \to A^0\gamma$
	[6] AAD	20AE	ATLS	$H^0 \to ZA^0$
	[7] AABOUD	18AP	ATLS	$H^0 \to A^0A^0$
	[8] KHACHATRY...	17AZ	CMS	$H^0 \to A^0A^0$
	[9] ABLIKIM	16E	BES3	$J/\psi \to A^0\gamma$
	[10] KHACHATRY...	16F	CMS	$H^0 \to A^0A^0$
	[11] LEES	15H	BABR	$\Upsilon(1S) \to A^0\gamma$
	[12] LEES	13C	BABR	$\Upsilon(1S) \to A^0\gamma$
	[13] LEES	13L	BABR	$\Upsilon(1S) \to A^0\gamma$
	[14] LEES	13R	BABR	$\Upsilon(1S) \to A^0\gamma$
	[15] ABLIKIM	12	BES3	$J/\psi \to A^0\gamma$
	[16] CHATRCHYAN	12V	CMS	$A^0 \to \mu^+\mu^-$
	[17] AALTONEN	11P	CDF	$t \to bH^+$, $H^+ \to W^+A^0$
	[18,19] ABOUZAID	11A	KTEV	$K_L \to \pi^0\pi^0A^0$, $A^0 \to \mu^+\mu^-$

Int. J. Mod. Phys. A 2026.41. Downloaded from www.worldscientific.com
by UNIVERSITY OF CALIFORNIA @ BERKELEY on 09/16/26. Re-use and distribution is strictly not permitted, except for Open Access articles.

[20] DEL-AMO-SA...11J	BABR	$\Upsilon(1S) \to A^0\gamma$
[21] LEES 11H	BABR	$\Upsilon(2S,3S) \to A^0\gamma$
[22] ANDREAS 10	RVUE	
[19,23] HYUN 10	BELL	$B^0 \to K^{*0}A^0$, $A^0 \to \mu^+\mu^-$
[19,24] HYUN 10	BELL	$B^0 \to \rho^0 A^0$, $A^0 \to \mu^+\mu^-$
[25] AUBERT 09P	BABR	$\Upsilon(3S) \to A^0\gamma$
[26] AUBERT 09Z	BABR	$\Upsilon(2S) \to A^0\gamma$
[27] AUBERT 09Z	BABR	$\Upsilon(3S) \to A^0\gamma$
[19,28] TUNG 09	K391	$K_L \to \pi^0\pi^0 A^0$, $A^0 \to \gamma\gamma$
[29] LOVE 08	CLEO	$\Upsilon(1S) \to A^0\gamma$
[30] BESSON 07	CLEO	$\Upsilon(1S) \to \eta_b\gamma$
[31] PARK 05	HYCP	$\Sigma^+ \to pA^0$, $A^0 \to \mu^+\mu^-$
[32] BALEST 95	CLE2	$\Upsilon(1S) \to A^0\gamma$
[33] ANTREASYAN 90C	CBAL	$\Upsilon(1S) \to A^0\gamma$

[1] AAD 25AT search for the decay $H \to ZA^0$, $Z \to \ell^+\ell^-$, A^0 decaying hadronically (gg or $q\overline{q}$), in 140 fb^{-1} of pp collisions at E_{cm} = 13 TeV. See their Fig. 4 for limits on B($H \to ZA^0$) with assumptions B($A^0 \to gg$) = 1 for m_{A^0} = 0.5–3.5 GeV, or B($A^0 \to q\overline{q}$) = 1 for m_{A^0} = 1.5–3.5 GeV. Supersedes AAD 20AE.

[2] ADACHI 23A search for flavor-changing τ decays $\tau \to eA^0$ and $\tau \to \mu A^0$, with A^0 invisible, using 62.8 fb^{-1} of e^+e^- collisions at E_{cm} = 10.58 GeV. Limits on B($\tau \to eA^0$)/B($\tau \to e\nu\nu$) in the range 1.1×10^{-3}–9.7×10^{-3} (95% CL) and B($\tau \to \mu A^0$)/B($\tau \to \mu\nu\nu$) in the range 0.7×10^{-3}–12.2×10^{-3} (95% CL) are given for m_{A^0} = 0–1.6 GeV. See their Fig. 2.

[3] TUMASYAN 23AR search for the decay $H \to A^0A^0$ with $A^0 \to \gamma\gamma$ (detected as a merged photonlike object) using 136 fb^{-1} of pp collisions at E_{cm} = 13 TeV. Limits on B($H \to A^0A^0$)·B^2($A^0 \to \gamma\gamma$) in the range 0.9×10^{-3}–3.3×10^{-3} (95% CL) are given for m_{A^0} = 0.1–1.2 GeV. See their Fig. 2.

[4] ABLIKIM 22H search for the process $J/\psi \to A^0\gamma$ with A^0 decaying to $\mu^+\mu^-$ in 9×10^9 J/ψ events and give limits on B($J/\psi \to A^0\gamma$)·B($A^0 \to \mu^+\mu^-$) in the range 1.2×10^{-9}–7.78×10^{-7} (90% CL) for 0.212 GeV $\le m_{A^0} \le$ 3.0 GeV. See their Fig. 4.

[5] JIA 22 search for the process $\Upsilon(2S) \to \Upsilon(1S)\pi^+\pi^- \to A^0\gamma\pi^+\pi^-$ with A^0 decaying to $\tau^+\tau^-$ or $\mu^+\mu^-$ in 158×10^6 $\Upsilon(2S)$ events and give limits on B($\Upsilon(1S) \to A^0\gamma$)·B($A^0 \to \tau^+\tau^-$) in the range 3.8×10^{-6}–1.5×10^{-4} (90% CL) for m_{A^0} = 3.6–9.2 GeV, and B($\Upsilon(1S) \to A^0\gamma$)·B($A^0 \to \mu^+\mu^-$) in the range 3.1×10^{-7}–1.6×10^{-5} (90% CL) for m_{A^0} = 0.21–9.2 GeV. See their Fig. 4.

[6] AAD 20AE search for the decay $H^0 \to ZA^0$, $Z \to \ell^+\ell^-$, A^0 decaying hadronically ($A^0 \to gg$ or $s\overline{s}$), in 139 fb^{-1} of pp collisions at E_{cm} = 13 TeV. Limit on the product of production cross section and the $H^0 \to ZA^0$ branching ratio in the range 17–340 pb (95% CL) is given for m_{A^0} = 0.5–4.0 GeV, see their Table I.

[7] AABOUD 18AP search for the decay $H^0 \to A^0A^0 \to \mu^+\mu^-\mu^+\mu^-$ in 36.1 fb^{-1} of pp collisions at E_{cm} = 13 TeV. See their Fig. 10(b) for limits on B($H^0 \to A^0A^0$) in the range m_{A^0} = 1–2.5, 4.5–8 GeV, assuming a type-II two-doublet plus singlet model with tan(β) = 5.

[8] KHACHATRYAN 17AZ search for the decay $H^0 \to A^0A^0 \to \tau^+\tau^-\tau^+\tau^-$, $\mu^+\mu^-b\overline{b}$, and $\mu^+\mu^-\tau^+\tau^-$ in 19.7 fb^{-1} of pp collisions at E_{cm} = 8 TeV. See their Figs. 4, 5, and 6 for cross section limits in the range m_{A^0} = 5–62.5 GeV. See also their Figs. 7, 8, and 9 for interpretation of the data in terms of models with two Higgs doublets and a singlet.

[9] ABLIKIM 16E search for the process $J/\psi \to A^0\gamma$ with A^0 decaying to $\mu^+\mu^-$ and give limits on B($J/\psi \to A^0\gamma$)·B($A^0 \to \mu^+\mu^-$) in the range 2.8×10^{-8}–5.0×10^{-6} (90% CL) for 0.212 $\le m_{A^0} \le$ 3.0 GeV. See their Fig. 5.

[10] KHACHATRYAN 16F search for the decay $H^0 \to A^0A^0 \to \tau^+\tau^-\tau^+\tau^-$ in 19.7 fb^{-1} of pp collisions at E_{cm} = 8 TeV. See their Fig. 8 for cross section limits for m_{A^0} = 4–8 GeV.

[11] LEES 15H search for the process $\Upsilon(2S) \to \Upsilon(1S)\pi^+\pi^- \to A^0\gamma\pi^+\pi^-$ with A^0 decaying to $c\overline{c}$ and give limits on B($\Upsilon(1S) \to A^0\gamma$)·B($A^0 \to c\overline{c}$) in the range 7.4×10^{-5}–2.4×10^{-3} (90% CL) for 4.00 $\le m_{A^0} \le$ 8.95 and 9.10 $\le m_{A^0} \le$ 9.25 GeV. See their Fig. 6.

[12] LEES 13C search for the process $\Upsilon(2S, 3S) \to \Upsilon(1S)\pi^+\pi^- \to A^0\gamma\pi^+\pi^-$ with A^0 decaying to $\mu^+\mu^-$ and give limits on B($\Upsilon(1S) \to A^0\gamma$)·B($A^0 \to \mu^+\mu^-$) in the range (0.3–9.7) $\times10^{-6}$ (90% CL) for 0.212 $\le m_{A^0} \le$ 9.20 GeV. See their Fig. 5(e) for limits on the $b-A^0$ Yukawa coupling derived by combining this result with AUBERT 09Z.

[13] LEES 13L search for the process $\Upsilon(2S) \to \Upsilon(1S)\pi^+\pi^- \to A^0\gamma\pi^+\pi^-$ with A^0 decaying to gg or $s\overline{s}$ and give limits on B($\Upsilon(1S) \to A^0\gamma$)·B($A^0 \to gg$) between 1×10^{-6} and 2×10^{-2} (90% CL) for 0.5 $\le m_{A^0} \le$ 9.0 GeV, and B($\Upsilon(1S) \to A^0\gamma$)·B($A^0 \to s\overline{s}$) between 4×10^{-6} and 1×10^{-3} (90%CL) for 1.5 $\le m_{A^0} \le$ 9.0 GeV. See their Fig. 4.

[14] LEES 13R search for the process $\Upsilon(2S) \to \Upsilon(1S)\pi^+\pi^- \to A^0\gamma\pi^+\pi^-$ with A^0 decaying to $\tau^+\tau^-$ and give limits on B($\Upsilon(1S) \to A^0\gamma$)·B($A^0 \to \tau^+\tau^-$) in the range 0.9–$13\times10^{-5}$ (90% CL) for 3.6 $\le m_{A^0} \le$ 9.2 GeV. See their Fig. 4 for limits on the $b-A^0$ Yukawa coupling derived by combining this result with AUBERT 09P.

[15] ABLIKIM 12 searches for the process $\psi(3686) \to \pi\pi J/\psi$, $J/\psi \to A^0\gamma$ with A^0 decaying to $\mu^+\mu^-$. It gives mass dependent limits on B($J/\psi \to A^0\gamma$)·B($A^0 \to \mu^+\mu^-$) in the range 4×10^{-7}–2.1×10^{-5} (90% C.L.) for 0.212 $\le m_{A^0} \le$ 3.0 GeV. See their Fig. 2.

[16] CHATRCHYAN 12V search for A^0 production in the decay $A^0 \to \mu^+\mu^-$ with 1.3 fb^{-1} of pp collisions at E_{cm} = 7 TeV. A limit on $\sigma(A^0)$·B($A^0 \to \mu^+\mu^-$) in the range (1.5–7.5) pb is given for m_{A^0} = (5.5–8.7) and (11.5–14) GeV at 95% CL.

[17] AALTONEN 11P search in 2.7 fb^{-1} of $p\overline{p}$ collisions at E_{cm} = 1.96 TeV for the decay chain $t \to bH^+$, $H^+ \to W^+A^0$, $A^0 \to \tau^+\tau^-$ with m_{A^0} between 4 and 9 GeV. See their Fig. 4 for limits on B($t \to bH^+$) for 90 < m_{H^+} < 160 GeV.

[18] ABOUZAID 11A search for the decay chain $K_L \to \pi^0\pi^0A^0$, $A^0 \to \mu^+\mu^-$ and give a limit B($K_L \to \pi^0\pi^0A^0$) · B($A^0 \to \mu^+\mu^-$) < 1.0×10^{-10} at 90% CL for m_{A^0} = 214.3 MeV.

[19] The search was motivated by PARK 05.

[20] DEL-AMO-SANCHEZ 11J search for the process $\Upsilon(2S) \to \Upsilon(1S)\pi^+\pi^- \to A^0\gamma\pi^+\pi^-$ with A^0 decaying to invisible final states. They give limits on B($\Upsilon(1S) \to A^0\gamma$)·B($A^0 \to$ invisible) in the range (1.9–4.5) $\times10^{-6}$ (90% CL) for 0 $\le m_{A^0} \le$ 8.0 GeV, and (2.7–37) $\times10^{-6}$ for 8.0 $\le m_{A^0} \le$ 9.2 GeV.

[21] LEES 11H search for the process $\Upsilon(2S, 3S) \to A^0\gamma$ with A^0 decaying hadronically and give limits on B($\Upsilon(2S, 3S) \to A^0\gamma$)·B($A^0 \to$ hadrons) in the range 1×10^{-6}–8×10^{-5} (90% CL) for 0.3 < m_{A^0} < 7 GeV. The decay rates for $\Upsilon(2S)$ and $\Upsilon(3S)$ are assumed to be equal up to the phase space factor. See their Fig. 5.

[22] ANDREAS 10 analyze constraints from rare decays and other processes on a light A^0 with $m_{A^0} < 2m_\mu$ and give limits on its coupling to fermions at the level of 10^{-4} times the Standard Model value.

[23] HYUN 10 search for the decay chain $B^0 \to K^{*0}A^0$, $A^0 \to \mu^+\mu^-$ and give a limit on B($B^0 \to K^{*0}A^0$) · B($A^0 \to \mu^+\mu^-$) in the range (2.26–5.53) $\times10^{-8}$ at 90%CL for m_{A^0} = 212–300 MeV. The limit for m_{A^0} = 214.3 MeV is 2.26×10^{-8}.

[24] HYUN 10 search for the decay chain $B^0 \to \rho^0A^0$, $A^0 \to \mu^+\mu^-$ and give a limit on B($B^0 \to \rho^0A^0$) · B($A^0 \to \mu^+\mu^-$) in the range (1.73–4.51) $\times10^{-8}$ at 90%CL for m_{A^0} = 212–300 MeV. The limit for m_{A^0} = 214.3 MeV is 1.73×10^{-8}.

[25] AUBERT 09P search for the process $\Upsilon(3S) \to A^0\gamma$ with $A^0 \to \tau^+\tau^-$ for 4.03 < m_{A^0} < 9.52 and 9.61 < m_{A^0} < 10.10 GeV, and give limits on B($\Upsilon(3S) \to A^0\gamma$)·B($A^0 \to \tau^+\tau^-$) in the range (1.5–16) $\times10^{-5}$ (90% CL).

[26] AUBERT 09Z search for the process $\Upsilon(2S) \to A^0\gamma$ with $A^0 \to \mu^+\mu^-$ for 0.212 < m_{A^0} < 9.3 GeV and give limits on B($\Upsilon(2S) \to A^0\gamma$)·B($A^0 \to \mu^+\mu^-$) in the range (0.3–8) $\times10^{-6}$ (90% CL).

[27] AUBERT 09Z search for the process $\Upsilon(3S) \to A^0\gamma$ with $A^0 \to \mu^+\mu^-$ for 0.212 < m_{A^0} < 9.3 GeV and give limits on B($\Upsilon(3S) \to A^0\gamma$)·B($A^0 \to \mu^+\mu^-$) in the range (0.3–5) $\times10^{-6}$ (90% CL).

[28] TUNG 09 search for the decay chain $K_L \to \pi^0\pi^0A^0$, $A^0 \to \gamma\gamma$ and give a limit on B($K_L \to \pi^0\pi^0A^0$) · B($A^0 \to \gamma\gamma$) in the range (2.4–10.7) $\times10^{-7}$ at 90%CL for m_{A^0} = 194.3–219.3 MeV. The limit for m_{A^0} = 214.3 MeV is 2.4×10^{-7}.

[29] LOVE 08 search for the process $\Upsilon(1S) \to A^0\gamma$ with $A^0 \to \mu^+\mu^-$ (for $m_{A^0} < 2m_\tau$) and $A^0 \to \tau^+\tau^-$. Limits on B($\Upsilon(1S) \to A^0\gamma$) · B($A^0 \to \ell^+\ell^-$) in the range 10^{-6}–10^{-4} (90% CL) are given.

[30] BESSON 07 give a limit B($\Upsilon(1S) \to \eta_b\gamma$) · B($\eta_b \to \tau^+\tau^-$) < 0.27% (95% CL), which constrains a possible A^0 exchange contribution to the η_b decay.

[31] PARK 05 found three candidate events for $\Sigma^+ \to p\mu^+\mu^-$ in the HyperCP experiment. Due to a narrow spread in dimuon mass, they hypothesize the events as a possible signal of a new boson. It can be interpreted as a neutral particle with $m_{A^0} = 214.3 \pm 0.5$ MeV and the branching fraction B($\Sigma^+ \to pA^0$)·B($A^0 \to \mu^+\mu^-$) = $(3.1^{+2.4}_{-1.9} \pm 1.5)\times10^{-8}$.

[32] BALEST 95 give limits B($\Upsilon(1S) \to A^0\gamma$) ¡ 1.5×10^{-5} at 90% CL for m_{A^0} < 5 GeV. The limit becomes < 10^{-4} for m_{A^0} < 7.7 GeV.

[33] ANTREASYAN 90C give limits B($\Upsilon(1S) \to A^0\gamma$) ¡ 5.6×10^{-5} at 90% CL for m_{A^0} < 7.2 GeV. A^0 is assumed not to decay in the detector.

Other Mass Limits

We use a symbol H_1^0 if mass < 125 GeV or H_2^0 if mass > 125 GeV. The notation H is reserved for the 125 GeV particle.

VALUE (GeV)	CL%	DOCUMENT ID		TECN	COMMENT
• • • We do not use the following data for averages, fits, limits, etc. • • •					
		[1] AAD	25AL	ATLS	$t\overline{t}H_2^0/A^0$
		[2] AAD	25AN	ATLS	$t\overline{t}A^0$, $A^0 \to b\overline{b}$
		[3] AAD	25AU	ATLS	$H \to A^0A^0$
		[4] AAD	25AW	ATLS	$H \to A^0A^0$
		[5] AAD	25AW	ATLS	$H \to A_1^0A_2^0$
		[6] AAD	25AY	ATLS	$H \to H_1^0H_1^0$
		[7] AAD	25F	ATLS	$H_{1/2}^0 \to Z'Z'$, $Z' \to \ell^+\ell^-$
		[8] AAD	25J	ATLS	$H_3^0 \to H_2^0H$, $H_2^0 \to HH$
		[9] AAD	25O	ATLS	$H_1^0 \to \gamma\gamma$
		[10] AAD	25X	ATLS	$H \to A^0A^0$
		[11] ADAN	25		$H \to A^0A^0$
		[12] CHEKHOVSKY	25C	CMS	$H_2^0/A^0 \to b\overline{b}$
		[13] CHEKHOVSKY	25D	CMS	$H_{1/2}^0/A^0 \to$ invisible
		[14] CHEKHOVSKY	25I	CMS	$A^0 \to ZH$
		[15] CHEKHOVSKY	25J	CMS	$A_2^0 \to HA_1^0$
		[16] CORTINA-GIL	25B	NA62	$K^+ \to \pi^+H_1^0$
		[17] HAYRAPETY...	25A	CMS	$H_1^0 \to \gamma\gamma$
		[18] HAYRAPETY...	25AP	CMS	$H_3^0 \to HH_{1/2}^0$
		[19] HAYRAPETY...	25C	CMS	$H_3^0 \to H_1^0H_1^0$
		[20] HAYRAPETY...	25I	CMS	$A^0 \to ZH_2^0$, $H_2^0 \to t\overline{t}$
		[21] HAYRAPETY...	25P	CMS	$b\overline{b}A^0$, $A^0 \to$ invisible
		[22] AAD	24A	ATLS	$H_2^0 \to Z\gamma$
		[23] AAD	24AP	ATLS	H_2^0, $A^0 \to t\overline{t}$
		[24] AAD	24BQ	ATLS	$H \to A^0A^0$
		[25] AAD	24BV	ATLS	$H_2^0 \to HH$

Int. J. Mod. Phys. A 2026.41. Downloaded from www.worldscientific.com
by UNIVERSITY OF CALIFORNIA @ BERKELEY on 09/16/26. Reproduction is strictly not permitted, except for Open Access articles.

[26] AAD	24BW	ATLS	$H^0_3 \to H^0_2 H$	
[27] AAD	24BX	ATLS	$H^0_4 \to H^0_2 H^0_3$	
[28] AAD	24BX	ATLS	$A^0 \to H^0_2 Z$	
[29] AAD	24CA	ATLS	$H^0_3 \to H^0_{1,2} H$	
[30] AAD	24CD	ATLS	$H^0_2 \to Z A$	
[31] AAD	24CF	ATLS	$A^0 \to \tau^+ \tau^-$	
[32] AAD	24CI	ATLS	$H^0_2, A^0 \to$ invisible	
[33] AAD	24CK	ATLS	two doublet + pseudoscalar + Dirac DM	
[34] AAD	24H	ATLS	$H^0_2 \to H H$	
[35] AAD	24K	ATLS	$H \to Z A^0$	
[36] ADACHI	24F	BEL2	$H^0_1 \to \mu^+ \mu^-$	
[37] HAYRAPETY...	24AA	CMS	$H \to A^0 A^0$	
[38] HAYRAPETY...	24AE	CMS	$H^0_2 \to H H$	
[39] HAYRAPETY...	24AF	CMS	$H \to A^0 A^0$	
[40] HAYRAPETY...	24AI	CMS	$H \to H^0_1 H^0_1$, long-lived	
[41] HAYRAPETY...	24AJ	CMS	$H^0_2 \to \gamma\gamma$	
[42] HAYRAPETY...	24AZ	CMS	$A^0 A^0$, $A^0 \to \mu^+ \mu^-$	
[43] HAYRAPETY...	24AZ	CMS	$H, H^0_{1,2} \to A^0 A^0$, $A^0 \to \mu^+ \mu^-$	
[44] HAYRAPETY...	24I	CMS	$H \to Z A^0$	
[45] TUMASYAN	24A	CMS	$H^0_{1,2} \to e^+ e^-, \mu^+ \mu^-, \tau^+ \tau^-$	
[46] TUMASYAN	24B	CMS	$H^0_2 \to H H$	
[47] TUMASYAN	24B	CMS	$H^0_3 \to H^0_{1,2} H$	
[48] AAD	23AD	ATLS	$H^0_2 \to H H$	
[49] AAD	23AD	ATLS	$A^0 \to Z H^0_2 \to Z H H$	
[50] AAD	23AJ	ATLS	$H^\pm \to W^\pm A^0$	
[51] AAD	23BD	ATLS	$t \to q H^0_{1,2}$	
[52] AAD	23BE	ATLS	$H^0_2 \to W^+ W^-$	
[53] AAD	23BG	ATLS	$t\bar{t} H^0_2 / A^0$	
[54] AAD	23BW	ATLS	$A^0 t\bar{t}$, $A^0 \to \mu^+ \mu^-$	
[55] AAD	23BX	ATLS	H + invisible A^0	
[56] AAD	23CA	ATLS	$H^0_3 \to H^0_2 H$	
[57] AAD	23CR	ATLS	flavor changing H^0_2	
[58] AAD	23O	ATLS	$A^0 \to Z H$	
[59] AAD	23R	ATLS	$A^0 \to \gamma\gamma$	
[60] AAD	23U	ATLS	$H^0_2 \to Z\gamma$	
[61] AAD	23Z	ATLS	$H^0_2 \to H H$	
[62] HAYRAPETY...	23C	CMS	$H^0_{1,2} \to e\mu$	
[63] HAYRAPETY...	23G	CMS	$A^0 \to \mu^+ \mu^-$	
[64] TUMASYAN	23	CMS	$H^0_3 \to H^0_{1,2} H$	
[65] TUMASYAN	23M	CMS	$H \to A^0 A^0$	
[66] TUMASYAN	23O	CMS	$H^0_2 \to H H$	
[67] TUMASYAN	23S	CMS	$H^0_{1,2} \to \tau^+ \tau^-$	
[68] AAD	22A	ATLS	$H \to A^0 A^0$	
[69] AAD	22D	ATLS	$Z A^0$, $A^0 \to$ invisible	
[70] AAD	22F	ATLS	$H^0_2 \to H H$	
[71] AAD	22I	ATLS	$H \to \tilde{\chi}^0_2 \tilde{\chi}^0_1$, $\tilde{\chi}^0_2 \to A^0 \tilde{\chi}^0_1$, $A^0 \to b\bar{b}$	
[72] AAD	22J	ATLS	$H \to Z A^0$	
[73] AAD	22J	ATLS	$H \to A^0 A^0$, $H^0_1 H^0_1$	
[74] AAD	22P	ATLS	H^0_1, $H^0_2 \to$ invisible	
[75] AAD	22Y	ATLS	$H^0_2 \to H H$	
[76] ABRATENKO	22A	MCBN	$K^+ \to H^0_1 \pi^+$	
[77] TUMASYAN	22AK	CMS	$H^0_3 \to H^0_1 H^0_1$	
[78] TUMASYAN	22D	CMS	$H^0_2 \to W^+ W^-$	
[79] AAD	21AF	ATLS	$H^0_2 \to Z Z$	
[80] AAD	21AI	ATLS	$A^0 \to Z H^0_2$	
[81] AAD	21AY	ATLS	$H^0_2 \to \gamma\gamma$	
[82] AAD	21AZ	ATLS	$A^0_2 \to H A^0_1$	
[83] AAD	21BB	ATLS	$A^0_2 \to H A^0_1$	
[84] AAD	21BE	ATLS	$A^0_1 \to$ invisible	
[85] ABRATENKO	21	MCBN	$K^+ \to H^0_1 \pi^+$	
[86] SIRUNYAN	21A	CMS	$H^0_2 \to Z A^0$, $A^0 \to$ invisible	
[87] TUMASYAN	21F	CMS	$H^0_3 \to H H^0_{1,2}$	
[88] AAD	20AA	ATLS	$H^0_2 / A^0 \to \tau^+ \tau^-$	
[89] AAD	20AI	ATLS	$H \to A^0 A^0$	
[90] AAD	20AO	ATLS	$H^0_2 \to H H$	
[91] AAD	20C	ATLS	$H^0_2 \to H H$	
[92] AAD	20L	ATLS	$H^0_2 \to b\bar{b}$	
[93] AAD	20X	ATLS	$H^0_2 \to H H$	
[94] AAIJ	20AL	LHCB	$A^0 \to \mu^+ \mu^-$	
[95] SIRUNYAN	20	CMS	$H \to A^0 A^0$	
[96] SIRUNYAN	20AA	CMS	$H^0_2 \to Z A^0$ or $A^0 \to Z H^0_2$	
[97] SIRUNYAN	20AC	CMS	$A^0 \to Z H$	
[98] SIRUNYAN	20AD	CMS	$H^0_2 \to \mu\tau$, $e\tau$	
[99] SIRUNYAN	20AF	CMS	$H^0_2 / A^0 \to t\bar{t}$	
[100] SIRUNYAN	20AP	CMS	$H, H^0_2 \to A^0 A^0$	
[101] SIRUNYAN	20Y	CMS	$H^0_2 \to W^+ W^-$	
[102] SIRUNYAN	20Z	CMS	$t\bar{t} H^0_{1,2}$ or $t\bar{t} A^0$, $H^0_{1,2} / A^0 \to e^+ e^-, \mu^+ \mu^-$	
[103] AABOUD	19A	ATLS	$H^0_2 \to H H$	
[104] AABOUD	19AG	ATLS	$H \to A^0 A^0$	
[105] AABOUD	19O	ATLS	$H^0_2 \to H H$	
[106] AABOUD	19T	ATLS	$H^0_2 \to H H$	
[107] AABOUD	19V	ATLS	two doublet + pseudoscalar model	
[108] AABOUD	19Y	ATLS	$H^0_2 \to \mu^+ \mu^-$	
[109] AALTONEN	19	CDF	$H^0_{1,2} \to b\bar{b}$	
[110] SIRUNYAN	19	CMS	$H^0_2 \to H H$	
[111] SIRUNYAN	19AE	CMS	$A^0 \to \tau^+ \tau^-$	
[112] SIRUNYAN	19AN	CMS	$A^0_2 \to H A^0_1$	
[113] SIRUNYAN	19AV	CMS	$A^0 \to Z H$	
[114] SIRUNYAN	19B	CMS	$H^0_{1,2} / A^0 \to b\bar{b}$	
[115] SIRUNYAN	19BB	CMS	$H^0_1 \to \gamma\gamma$	
[116] SIRUNYAN	19BD	CMS	$H \to A^0 A^0$	
[117] SIRUNYAN	19BE	CMS	$H^0_2 \to H H$	
[118] SIRUNYAN	19BQ	CMS	$H^0_{1,2} \to A^0 A^0$	
[119] SIRUNYAN	19CR	CMS	$H^0_2 / A^0 \to \mu^+ \mu^-$	
[120] SIRUNYAN	19H	CMS	$H^0_2 \to H H$	
[121] AABOUD	18AA	ATLS	$H^0_2 \to Z\gamma$	
[122] AABOUD	18AG	ATLS	$H \to A^0 A^0$	
[123] AABOUD	18AH	ATLS	$A^0 \to Z H^0_2$	
[124] AABOUD	18AI	ATLS	$A^0 \to Z H$	
[125] AABOUD	18BF	ATLS	$H^0_2 \to Z Z$	
[126] AABOUD	18BU	ATLS	$H^0_2 \to H H$	
[127] AABOUD	18BX	ATLS	$H \to A^0 A^0$	
[128] AABOUD	18CQ	ATLS	$H^0_2 \to H H$	
[129] AABOUD	18F	ATLS	$H^0_2 \to W^+ W^-, Z Z$	
[130] AAIJ	18AM	LHCB	$H^0_{1,2} \to \mu\tau$	
[131] AAIJ	18AQ	LHCB	$A^0 \to \mu^+ \mu^-$	
[132] AAIJ	18AQ	LHCB	$H \to A^0 A^0$, $A^0 \to \mu^+ \mu^-$	
[133] SIRUNYAN	18AF	CMS	$H^0_2 \to H H$	
[134] SIRUNYAN	18BA	CMS	$H^0_2 \to Z Z$	
[135] SIRUNYAN	18CW	CMS	$H^0_2 \to H H$	
[136] SIRUNYAN	18DK	CMS	$H^0_2 \to Z\gamma$	
[137] SIRUNYAN	18DT	CMS	$H \to A^0 A^0$	
[138] SIRUNYAN	18DU	CMS	$H^0_2 \to \gamma\gamma$	
[139] SIRUNYAN	18ED	CMS	$A^0 \to Z H$	
[140] SIRUNYAN	18EE	CMS	$H \to A^0 A^0$	
[141] SIRUNYAN	18F	CMS	pp, 13 TeV, $H^0_2 \to H H$	
[142] AABOUD	17	ATLS	$H^0_2 \to Z\gamma$	
[143] AABOUD	17AP	ATLS	$H^0_2 \to \gamma\gamma$	
[144] AABOUD	17AW	ATLS	$H^0_2 \to Z\gamma$	
[145] KHACHATRY...	17AZ	CMS	$H \to A^0 A^0$	
[146] KHACHATRY...	17D	CMS	pp, 8, 13 TeV, $H^0_2 \to Z\gamma$	
[147] KHACHATRY...	17R	CMS	$H^0_2 \to \gamma\gamma$	
[148] SIRUNYAN	17CN	CMS	pp, 8 TeV, $H^0_2 \to H H$	
[149] SIRUNYAN	17Y	CMS	pp, 8, 13 TeV, $H^0_2 \to Z\gamma$	
[150] AABOUD	16AB	ATLS	$H \to A^0 A^0$	
[151] AABOUD	16AE	ATLS	$H^0_2 \to W^+ W^-, Z Z$	
[152] AABOUD	16H	ATLS	$H^0_2 \to \gamma\gamma$	
[153] AABOUD	16I	ATLS	$H^0_2 \to H H$	
[154] AAD	16AX	ATLS	$H \to Z Z$	
[155] AAD	16C	ATLS	$H \to W^+ W^-$	
[156] AAD	16L	ATLS	$H \to A^0 A^0$	
[157] AAD	16L	ATLS	$H^0_2 \to A^0 A^0$	
[158] AALTONEN	16C	CDF	$H^0_1 H^\pm \to H^0_1 H^0_1 W^*$, $H^0_1 \to \gamma\gamma$	
[159] KHACHATRY...	16BG	CMS	$H^0_2 \to H H$	
[160] KHACHATRY...	16BQ	CMS	pp, 8 TeV, $H^0_2 \to H H$	
[161] KHACHATRY...	16F	CMS	$H \to H_1 H_1$	
[162] KHACHATRY...	16M	CMS	$H^0_2 \to \gamma\gamma$	
[163] KHACHATRY...	16P	CMS	$H^0_2 \to H H$	
[164] KHACHATRY...	16P	CMS	$A^0 \to Z H$	
[165] AAD	15BK	ATLS	$H^0_2 \to H H$	
[166] AAD	15BZ	ATLS	$H \to A^0 A^0$	
[167] AAD	15BZ	ATLS	$H^0_2 \to A^0 A^0$	
[168] AAD	15CE	ATLS	$H^0_2 \to H H$	
[169] AAD	15H	ATLS	$H^0_2 \to H H$	
[170] AAD	15S	ATLS	$A^0 \to Z H$	

Int. J. Mod. Phys. A 2026.41. Downloaded from www.worldscientific.com
by UNIVERSITY OF CALIFORNIA @ BERKELEY on 09/16/26. Re-use and distribution is strictly not permitted, except for Open Access articles.

		171 KHACHATRY...15AW	CMS	$H_2^0 \to W^+W^-, ZZ$
		172 KHACHATRY...15BB	CMS	$H \to \gamma\gamma$
		173 KHACHATRY...15N	CMS	$A^0 \to ZH$
		174 KHACHATRY...15O	CMS	$A^0 \to ZH$
		175 KHACHATRY...15R	CMS	$H_2^0 \to HH$
		176 AAD 14AP	ATLS	$H \to \gamma\gamma$
		177 AAD 14M	ATLS	$H_2^0 \to H^\pm W^\mp \to HW^\pm W^\mp$, $H \to b\overline{b}$
		178 CHATRCHYAN14G	CMS	$H \to WW^{(*)}$
		179 KHACHATRY...14P	CMS	$H \to \gamma\gamma$
		180 AALTONEN 13P	CDF	$H'^0 \to H^\pm W^\mp \to HW^+W^-$
		181 CHATRCHYAN13BJ	CMS	$H \to A^0A^0$
		182 AALTONEN 11P	CDF	$t \to bH^+$, $H^+ \to W^+A^0$
		183 ABBIENDI 10	OPAL	$H \to \tilde{\chi}_1^0\tilde{\chi}_2^0$
		184 SCHAEL 10	ALEP	$H \to A^0A^0$
		185 ABAZOV 09V	D0	$H \to A^0A^0$
none 3–63	95	186 ABBIENDI 05A	OPAL	A^0, Type II model
>104	95	187 ABBIENDI 04K	OPAL	$H \to$ 2 jets
		188 ABDALLAH 04	DLPH	HVV couplings
>110.3	95	189 ACHARD 04B	L3	$H \to$ 2 jets
		190 ACHARD 04F	L3	Anomalous coupling
		191 ABBIENDI 03F	OPAL	$e^+e^- \to HZ$, $H \to$ any
		192 ABBIENDI 03G	OPAL	$H_1^0 \to A^0A^0$
>105.4	95	193,194 HEISTER 02L	ALEP	$H_1^0 \to \gamma\gamma$
>109.1	95	195 HEISTER 02M	ALEP	$H \to$ 2 jets or $\tau^+\tau^-$
none 12–56	95	196 ABBIENDI 01E	OPAL	A^0, Type-II model
		197 ACCIARRI 00R	L3	$e^+e^- \to H\gamma$ and/or $H \to \gamma\gamma$
		198 ACCIARRI 00R	L3	$e^+e^- \to e^+e^-H$
		199 GONZALEZ... 98B	RVUE	Anomalous coupling
		200 KRAWCZYK 97	RVUE	$(g-2)_\mu$
		201 ALEXANDER 96H	OPAL	$Z \to H\gamma$

[1] AAD 25AL search for production of H_2^0/A^0 in association with a $t\overline{t}$ pair, decaying to $t\overline{t}$, resulting in final states with one lepton or two opposite-sign leptons, using 139 fb^{-1} of pp collisions at E_{cm} = 13 TeV. See their Fig. 8 for limits on cross section times branching ratios for $m_{H_2^0}$ and/or m_{A^0} = 0.4–1.0 TeV. Combined limits with AAD 23BG are shown in Fig. 10.

[2] AAD 25AN search for production of A^0 in association with a $t\overline{t}$ pair, in the decay $A^0 \to b\overline{b}$ using 140 fb^{-1} of pp collisions at E_{cm} = 13 TeV. See their Fig. 9 for limits on cross section times branching ratio for m_{A^0} = 12–100 GeV. If the top Yukawa coupling is as strong as the one of the Standard Model Higgs and B($A^0 \to b\overline{b}$) = 1, the whole mass range is excluded at 95%CL.

[3] AAD 25AU search for the decay $H \to A^0A^0 \to \tau^+\tau^-\tau^+\tau^-$, each tau pair decaying to hadrons + muon final states, in 140 fb^{-1} of pp collisions at E_{cm} = 13 TeV. See their Fig. 4 for limits on the product of production cross section (normalized to the SM) and branching ratios in the range m_{A^0} = 4–15 GeV, and Fig. 5 for the interpretation in terms of a model with two Higgs doublets plus a singlet.

[4] AAD 25AW search for the decay $H \to A^0A^0 \to b\overline{b}b\overline{b}$ in associated ZH production using 140 fb^{-1} of pp collisions at E_{cm} = 13 TeV. See their Fig. 14 for limits on the product of production cross section (normalized to the SM) and branching ratios in the range m_{A^0} = 12–60 GeV.

[5] AAD 25AW search for the decay $H \to A_1^0A_2^0 \to b\overline{b}b\overline{b}$ and $H \to A_1^0A_2^0 \to A_1^0A_1^0A_1^0 \to b\overline{b}b\overline{b}b\overline{b}$ in associated ZH production using 140 fb^{-1} of pp collisions at E_{cm} = 13 TeV. See their Fig. 15 for limits on the product of production cross section (normalized to the SM) and branching ratios for several combinations of $m_{A_1^0}$ and $m_{A_2^0}$.

[6] AAD 25AY search for $H \to H_1^0H_1^0$ with hadronically decaying H_1^0 having a long lifetime resulting in displaced vertex, using 140 fb^{-1} of pp collisions at E_{cm} = 13 TeV. The case the parent particle has a different mass $H_{2/3}^0 \to H_1^0H_1^0$) are also examined. See their Figs. 12 and 13 for limits with decay length in the range 0.01–1000 m.

[7] AAD 25F search for $H_{1/2}^0 \to Z'Z'$ with $Z' \to \ell^+\ell^-$ using 139 fb^{-1} of pp collisions at E_{cm} = 13 TeV. See their Fig. 5 for limits on production cross section times branching ratios for $m_{H_1^0}$ = 40–115 GeV, $m_{H_2^0}$ = 130–800 GeV, and $m_{Z'}$ = 15–300 GeV.

[8] AAD 25J search for production of H_3^0 decaying to H_2^0H, $H_2^0 \to HH$ in the $b\overline{b}b\overline{b}b\overline{b}$ final state, using 126 fb^{-1} of pp collisions at E_{cm} = 13 TeV. See their Figs. 7 and 8 for limits on production cross section times branching ratios in the ranges $m_{H_3^0}$ = 325–1500 GeV and $m_{H_2^0}$ = 250–1000 GeV.

[9] AAD 25O search for $H_1^0 \to \gamma\gamma$ in 140 fb^{-1} of pp collisions at E_{cm} = 13 TeV. See their Figs. 6(b), 8(b) and 9(b) for limits on cross section times branching ratio for $m_{H_1^0}$ = 66–110 GeV. Fig. 9(b) assumes Standard Model Higgs-like properties.

[10] AAD 25X search for the decay chain $H \to A^0A^0 \to \gamma\gamma\tau^+\tau^-$ in 140 fb^{-1} of pp collisions at E_{cm} = 13 TeV. See their Fig. 5(b) for limits on the product of branching ratios for m_{A^0} = 10–60 GeV, assuming SM-like production.

[11] ADAN 25 searches for $H \to A^0A^0 \to \mu^+\mu^-c\overline{c}$ using publicly available CMS data of 16.4 fb^{-1} of pp collisions at E_{cm} = 13 TeV. See his Fig. 7 for limits on the product of production cross section (normalized to the SM) and branching ratios in the range m_{A^0} = 4–11 GeV, and Fig. 8 for the interpretation in terms of a model with two Higgs doublets plus a singlet.

[12] CHEKHOVSKY 25C search for $H_2^0/A^0 \to b\overline{b}$ by b-associated prodution using 36.7–126.9 fb^{-1} of pp collisions at E_{cm} = 13 TeV. See their Figs. 11–14 for limits on cross section times branching ratio for $m_{H_2^0}$, m_{A^0} = 0.125–1.8 TeV.

[13] CHEKHOVSKY 25D search for invisibly decaying $H_1^0/H_2^0/A^0$ produced in association with t or $t\overline{t}$, using 138 fb^{-1} of pp collisions at E_{cm} = 13 TeV. See their Fig. 5 for limits on cross section times branching ratio for masses between 50 and 500 GeV.

[14] CHEKHOVSKY 25I search for production of an A^0 in gluon-gluon fusion and in association with a $b\overline{b}$, decaying to ZH in the final states $\ell^+\ell^-\tau^+\tau^-$, assuming B($H \to \tau^+\tau^-$) of the SM, using 138 fb^{-1} of pp collisions at E_{cm} = 13 TeV. See their Fig. 4 for limits on cross section times branching ratio for m_{A^0} = 0.225–1.0 TeV for the two production mechanisms, and Figs. 5, 6 for constraints on the combination of the two production mechanisms.

[15] CHEKHOVSKY 25J search for $A_2^0 \to HA_1^0$, A_1^0 escaping detection, using 101 fb^{-1} of pp collisions at E_{cm} = 13 TeV. In the framework of two Higgs doublet plus a singlet model, limits on signal strengths are given in their Figs. 3 and 4 with varying model parameters.

[16] CORTINA-GIL 25B search for the decay $K^+ \to \pi^+H_1^0$, with H_1^0 escaping detection or decaying to $\mu^+\mu^-$. See their Figs. 2, 3, and 6 for limits on the product of branching ratios for $m_{H_1^0}$ = 0–0.33 GeV, and Fig. 9 for limits on the mixing with the Standard Model Higgs boson.

[17] HAYRAPETYAN 25A search for the decay $H_1^0 \to \gamma\gamma$ in 132 fb^{-1} of pp collisions at E_{cm} = 13 TeV. See their Fig. 5 for limits on cross section times branching ratio for $m_{H_1^0}$ = 70–110 GeV.

[18] HAYRAPETYAN 25AP search for $H_3^0 \to HH_{1/2}^0$ with decays $H \to b\overline{b}$ and $H_{1/2}^0 \to \gamma\gamma$ using 132 fb^{-1} of pp collisions at E_{cm} = 13 TeV. See their Figs. 5 and 6 for limits on cross section times branching ratio for $m_{H_3^0}$ = 0.24–1.0 TeV and $m_{H_{1/2}^0}$ = 0.07–0.8 TeV.

[19] HAYRAPETYAN 25C search for production of H_3^0 in the decay chain $H_3^0 \to H_1^0H_1^0$, $H_1^0 \to \gamma\gamma$ using 138 fb^{-1} of pp collisions at E_{cm} = 13 TeV. See their Fig. 3 for limits on cross section times branching ratio for $m_{H_3^0}$ = 0.3–3 TeV, $m_{H_1^0}/m_{H_3^0}$ = 0.005–0.025.

[20] HAYRAPETYAN 25I search for $A^0 \to ZH_2^0$ with $H_2^0 \to t\overline{t}$ using 138 fb^{-1} of pp collisions at E_{cm} = 13 TeV. See their Fig. 5 for limits on production cross section times branching ratios for m_{A^0} = 0.45–2.1 TeV and $m_{H_2^0}$ = 0.35–2.0 TeV.

[21] HAYRAPETYAN 25P search for A^0 decaying to invisible final states, produced in association with a $b\overline{b}$ pair, using 138 fb^{-1} of pp collisions at E_{cm} = 13 TeV. See their Fig. 7 for limits on cross section times branching ratio for m_{A^0} = 50–500 GeV and Fig. 8 for excluded parameter space, both in the two-Higgs-doublet plus singlet pseudoscalar model.

[22] AAD 24A search for the decay $H_2^0 \to Z\gamma$ with Z decaying to e^+e^- or $\mu^+\mu^-$ using 140 fb^{-1} of pp collisions at E_{cm} = 13 TeV. See their Fig. 4 for limits on production cross section times branching ratios for $m_{H_2^0}$ = 0.22–3.4 TeV.

[23] AAD 24AP search for production of a heavy H_2^0 or A^0 decaying to $t\overline{t}$ in 140 fb^{-1} of pp collisions at E_{cm} = 13 TeV. See their Figs. 15 and 16 for limits on the Yukawa coupling for m_{A^0}, $m_{H_2^0}$ = 0.4–1.4 TeV for different assumptions on width over mass.

[24] AAD 24BQ search for the decay chain $H \to A^0A^0 \to b\overline{b}\tau^+\tau^-$, produced by gluon fusion, vector boson fusion, or in association with a weak vector boson, in 140 fb^{-1} of pp collisions at E_{cm} = 13 TeV. See their Fig. 10 for limits on the product of branching ratios in the range m_{A^0} = 12–60 GeV.

[25] AAD 24BV search for H_2^0 produced by vector-boson fusion, decaying to $HH \to b\overline{b}b\overline{b}$, using 140 fb^{-1} of pp collisions at E_{cm} = 13 TeV. See their Fig. 8 for limits on the product of production cross section times branching ratios for $m_{H_2^0}$ = 1–5 TeV.

[26] AAD 24BW search for production of H_3^0 decaying to H_2^0H, $H_2^0 \to W^+W^-$ or ZZ, and $H \to \gamma\gamma$ using 140 fb^{-1} of pp collisions at E_{cm} = 13 TeV. See their Figs. 6–8 for limits on production cross section times branching ratios in the ranges $m_{H_3^0}$ = 0.3–1.0 TeV and $m_{H_2^0}$ = 0.17–0.5 TeV.

[27] AAD 24BX search for production of H_4^0 decaying to $H_2^0H_3^0$, $H_2^0 \to$ invisible, and $H_3^0 \to ZZ \to 4\ell$, using 139 fb^{-1} of pp collisions at E_{cm} = 13 TeV. See their Fig. 8 (a), (b) for limits on production cross section times branching ratios in the ranges $m_{H_4^0}$ = 0.39–1.3 TeV, $m_{H_3^0}$ = 0.22–1.0 TeV, and $m_{H_2^0}$ = 160 GeV.

[28] AAD 24BX search for production of A^0 decaying to H_2^0Z, $H_2^0 \to ZZ$, resulting in 4ℓ final states, using 139 fb^{-1} of pp collisions at E_{cm} = 13 TeV. See their Fig. 8 (c), (d) for limits on production cross section times branching ratios in the ranges m_{A^0} = 0.32–1.3 TeV and $m_{H_2^0}$ = 0.22–1.0 TeV.

[29] AAD 24CA search for production of H_3^0 decaying to $H_{1,2}^0H$, $H_{1,2}^0 \to b\overline{b}$, and $H \to \gamma\gamma$ using 140 fb^{-1} of pp collisions at E_{cm} = 13 TeV. See their Fig. 4 for limits on production cross section times branching ratios in the ranges $m_{H_3^0}$ = 0.17–1.0 TeV and $m_{H_{1,2}^0}$ = 0.015–0.5 TeV.

[30] AAD 24CD search for production of H_2^0 decaying to ZA, $A \to$ invisible, using 140 fb^{-1} of pp collisions at E_{cm} = 13 TeV. See their Figs. 8–12 for excluded parameter regions in two-Higgs-doublet plus singlet pseudoscalar model.

[31] AAD 24CF search for gluon-fusion production of A^0 decaying to $\tau^+\tau^-$ in 140 fb^{-1} of pp collisions at E_{cm} = 13 TeV. See their Fig. 7 for limits on cross section times branching ratio in the range m_{A^0} = 20–90 GeV, and Fig. 8 for A^0 coupling with the top quark.

[32] AAD 24CI search for production of H_2^0, A^0 decaying to invisible final states, in various channels including $t\overline{t}$ + missing E_T and $t\overline{t}t\overline{t}$, using up to 140 fb^{-1} of pp collisions at E_{cm} = 13 TeV. See their Fig. 3 for cross section limits in a simplified model with fixed Dark Matter mass and couplings to quarks and Dark Matter.

[33] AAD 24CK combines published ATLAS data up to 139 fb^{-1} to constrain two-Higgs-doublet plus singlet pseudoscalar model with A_1^0 decaying to invisibly into Dirac Dark Matter final states. See their Figs. 4–9 for excluded parameter regions.

Int. J. Mod. Phys. A 2026.41. Downloaded from www.worldscientific.com by UNIVERSITY OF CALIFORNIA @ BERKELEY on 09/16/26. Reproduction is strictly not permitted, except for Open Access articles.

[34] AAD 24H combine searches for a scalar resonance decaying to HH using up to 139 fb^{-1} of pp collisions at E_{cm} = 13 TeV from AAD 22F, AAD 23Z, and AAD 22Y. See their Fig. 1 for limits on cross section times branching ratio for $m_{H_2^0}$ = 0.251–5.0 TeV.

[35] AAD 24K search for the decay $H \to ZA^0$ with $A^0 \to \gamma\gamma$ and $Z \to \ell^+\ell^-$ in 139 fb^{-1} of pp collisions at E_{cm} = 13 TeV. Merged $\gamma\gamma$ events as well as resolved ones are looked for. See their Fig. 3 for limits on the product of the branching ratios for m_{A^0} = 0.1–33 GeV.

[36] ADACHI 24F search for H_1^0, which couples preferentially to muon pairs, in the process $e^+e^- \to \mu^+\mu^- H_1^0 \to \mu^+\mu^-\mu^+\mu^-$ using 178 fb^{-1} of e^+e^- collisions at E_{cm} = 10.58 GeV. See their Fig. 13 (lower) for limits on cross section times branching ratio for $m_{H_1^0}$ = 0.212–9.0 GeV. Limits on the model parameter are given in Fig. 14 (lower).

[37] HAYRAPETYAN 24AA search for the decay chain $H \to A^0A^0 \to b\overline{b}b\overline{b}$, produced in association with $W^\pm$ or Z, in 138 fb^{-1} of pp collisions at E_{cm} = 13 TeV. See their Fig. 3 for limits on the product of branching ratios in the range m_{A^0} = 15–60 GeV.

[38] HAYRAPETYAN 24AE search for $H_2^0 \to HH$ in the final state $b\overline{b}W^+W^-$ using 138 fb^{-1} of pp collisions at E_{cm} = 13 TeV. See their Fig. 19 (upper) for limit on the product of production cross section times branching ratios for $m_{H_2^0}$ = 0.25–0.9 TeV.

[39] HAYRAPETYAN 24AF search for $H \to A^0A^0$ in the final state $b\overline{b}\mu^+\mu^-$ and $b\overline{b}\tau^+\tau^-$ in 138 fb^{-1} of pp collisions at E_{cm} = 13 TeV. See their Figs. 10, 11, and 12 for limits on the product of branching ratios in the range m_{A^0} = 12–60 GeV. Interpretation of the limits in terms of two Higgs doublet plus singlet models is given in their Figs. 13 and 14.

[40] HAYRAPETYAN 24AI search for $H \to H_1^0H_1^0$, with long-lived H_1^0 decaying in the muon detectors to $\gamma\gamma$, e^+e^-, $\pi^0\pi^0$, $\pi^+\pi^-$, K^+K^-, K^0K^0, $d\overline{d}$, $\tau^+\tau^-$, or $b\overline{b}$, using 138 fb^{-1} of pp collisions at E_{cm} = 13 TeV. See their Figs. 13–17 for limits on B($H \to H_1^0H_1^0$) in the mass range between 0.4 and 55 GeV for each of the decay modes.

[41] HAYRAPETYAN 24AJ search for production of a scalar resonance decaying to $\gamma\gamma$ in 138 fb^{-1} of pp collisions at E_{cm} = 13 TeV. See their Fig. 3 (right) for limits on production cross section times branching ratio for $m_{H_2^0}$ = 0.6–5.0 TeV, and Fig. 4 (lower) for their dependence on the width.

[42] HAYRAPETYAN 24AZ search for pair production of A^0 decaying to $\mu^+\mu^-$ using 101–137 fb^{-1} of pp collisions at E_{cm} = 13 TeV. See their Fig. 5 for limits on cross section times branching ratio for m_{A^0} = 0.21–60 GeV.

[43] HAYRAPETYAN 24AZ search for H or $H_{1,2}^0$ decaying to $A^0A^0 \to \mu^+\mu^-\mu^+\mu^-$ using 101–137 fb^{-1} of pp collisions at E_{cm} = 13 TeV. See their Fig. 8 for limits on cross section times branching ratio for m_{A^0} = 0.5–2.7 GeV and several choices of $m_{H_{1,2}^0}$ in a NMSSM scenario.

[44] HAYRAPETYAN 24I search for the decay $H \to ZA^0$ with $A^0 \to \gamma\gamma$ and $Z \to \ell^+\ell^-$ in 138 fb^{-1} of pp collisions at E_{cm} = 13 TeV. See their Fig. 7 for limits on the product of cross section times the branching ratios for m_{A^0} = 1–30 GeV.

[45] TUMASYAN 24A search for production of $H_{1,2}^0$ in association with W, Z, or $t\overline{t}$, decaying to e^+e^-, $\mu^+\mu^-$, or $\tau^+\tau^-$, using 138 fb^{-1} of pp collisions at E_{cm} = 13 TeV. See their Fig. 13 for limits on cross section times branching ratio for $m_{H_{1,2}^0}$ = 15–350 GeV. See also Figs. 16 and 17 for limits on the mixing with the Standard Model Higgs boson.

[46] TUMASYAN 24B search for $H_2^0 \to HH$ in the final state $\gamma\gamma b\overline{b}$ using 138 fb^{-1} of pp collisions at E_{cm} = 13 TeV. See their Fig. 6 (upper) for limit on the product of production cross section times branching ratios for $m_{H_2^0}$ = 0.26–1.0 TeV.

[47] TUMASYAN 24B search for production of H_3^0 decaying to $H_{1,2}^0H \to b\overline{b}\gamma\gamma$ using 138 fb^{-1} of pp collisions at E_{cm} = 13 TeV. See their Fig. 7 for limits on production cross section times branching ratios for $m_{H_3^0}$ = 0.3–1.0 TeV and $m_{H_{1,2}^0}$ = 0.09–0.8 TeV.

[48] AAD 23AD search for associated production of W/ZH_2^0 with the decay chain $H_2^0 \to HH \to b\overline{b}b\overline{b}$ using 139 fb^{-1} of pp collisions at E_{cm} = 13 TeV. See their Fig. 9 for limits on cross section times branching ratios for $m_{H_2^0}$ = 260–1000 GeV.

[49] AAD 23AD search for gluon fusion production of A^0 with the decay chain $A^0 \to ZH_2^0$, $H_2^0 \to HH \to b\overline{b}b\overline{b}$ using 139 fb^{-1} of pp collisions at E_{cm} = 13 TeV. See their Fig. 10 for limits on cross section times branching ratios for m_{A^0} = 350–800 GeV and $m_{H_2^0}$ = 260–400 GeV.

[50] AAD 23AJ search for production of $H^\pm$ in association with a top quark, followed by $H^\pm \to W^\pm A^0$, $A^0 \to$ invisible, using 139 fb^{-1} of pp collisions at E_{cm} = 13 TeV. See their Fig. 10 for excluded parameter regions of 2HDM + CP-odd singlet model.

[51] AAD 23BD search for a top quark decaying to $qH_{1,2}^0$ ($q = u, c$), $H_{1,2}^0 \to b\overline{b}$, using 139 fb^{-1} of pp collisions at E_{cm} = 13 TeV. See their Fig. 9 for limits on production cross section times branching ratios for $m_{H_{1,2}^0}$ = 20–160 GeV.

[52] AAD 23BE search for associated production of H_2^0W and decay $H_2^0 \to W^+W^-$ assuming the presence of higher dimensional $H_2^0W^+W^-$ interactions, using 139 fb^{-1} of pp collisions at E_{cm} = 13 TeV. See their Fig. 6 for excluded parameter region of higher dimensional operators, and Fig. 7 for limits on cross section times branching ratio for $m_{H_2^0}$ = 0.3–1.5 TeV.

[53] AAD 23BG search for production of H_2^0/A^0 in association with a $t\overline{t}$ pair, decaying to $t\overline{t}$, resulting in final states with two same-sign leptons or three or more leptons, using 139 fb^{-1} of pp collisions at E_{cm} = 13 TeV. See their Fig. 7 (corrected version in the erratum) for limits on cross section times branching ratios for $m_{H_2^0}$ and/or m_{A^0} = 0.4–1.0 TeV.

[54] AAD 23BW search for A^0 production in association with a $t\overline{t}$ pair, decaying to $\mu^+\mu^-$, using 139 fb^{-1} of pp collisions at E_{cm} = 13 TeV. See their Fig. 5(a) for limits on production cross section times branching ratio for m_{A^0} = 15–72 GeV.

[55] AAD 23BX search for production of $H \to \tau^+\tau^-$ with missing transverse momentum using 139 fb^{-1} of pp collisions at E_{cm} = 13 TeV. See their Fig. 8 for interpretation of the data in terms of 2HDM + a model.

[56] AAD 23CA search for production of H_3^0 decaying to H_2^0H, $H_2^0 \to W^+W^-$ or ZZ, and $H \to \tau^+\tau^-$ using 140 fb^{-1} of pp collisions at E_{cm} = 13 TeV. See their Figs. 4, 5 for limits on production cross section times branching ratios in the ranges $m_{H_3^0}$ = 0.5–1.5 TeV and $m_{H_2^0}$ = 0.2–0.5 TeV.

[57] AAD 23CR search for H_2^0 having flavor-violating couplings to tc or tu, produced in association with top quark(s), using 139 fb^{-1} of pp collisions at E_{cm} = 13 TeV. See their Fig. 14 for limits on production cross section times branching ratios for $m_{H_2^0}$ = 0.2–1.5 TeV with various assumptions on the flavor-changing couplings.

[58] AAD 23O search for production of an A^0 in gluon-gluon fusion and in association with a $b\overline{b}$, decaying to ZH in the final states $\nu\overline{\nu}b\overline{b}$ and $\ell^+\ell^-b\overline{b}$ using 139 fb^{-1} of pp collisions at E_{cm} = 13 TeV. See their Fig. 9 for limits on cross section times branching ratio for m_{A^0} = 0.22–2.0 TeV, and Fig. 11 for limits with both production components.

[59] AAD 23R search for the decay $A^0 \to \gamma\gamma$ in 138 fb^{-1} of pp collisions at E_{cm} = 13 TeV. See their Fig. 7 for limits on cross section times branching ratio for m_{A^0} = 10–70 GeV.

[60] AAD 23U search for the decay $H_2^0 \to Z\gamma$ with Z decaying hadronically in 139 fb^{-1} of pp collisions at E_{cm} = 13 TeV. See their Fig. 8(a) for limits on production cross section times branching ratios for $m_{H_2^0}$ = 1.0–6.8 TeV.

[61] AAD 23Z search for the decay chain $H_2^0 \to HH \to b\overline{b}\tau^+\tau^-$ using 139 fb^{-1} of pp collisions at E_{cm} = 13 TeV. See their Fig. 10 for limits on the product of production cross section times branching ratios for $m_{H_2^0}$ = 0.251–1.6 TeV.

[62] HAYRAPETYAN 23C search for $H_{1,2}^0 \to e\mu$ using 138 fb^{-1} of pp collisions at E_{cm} = 13 TeV. See their Fig. 7 for limits on production cross section times branching ratio for $m_{H_{1,2}^0}$ = 110–160 GeV.

[63] HAYRAPETYAN 23G search for dimuon resonance in the mass range 1.1–2.6 or 4.2–7.9 GeV in 96.6 fb^{-1} of pp collisions at E_{cm} = 13 TeV, in inclusive and high p_T selections. See their Fig. 5 for cross section times branching ratio limits and Fig. 7 for mixing angle limits in two Higgs doublet plus singlet model (at 90% CL).

[64] TUMASYAN 23 search for production of H_3^0 decaying to $H_{1,2}^0H \to b\overline{b}b\overline{b}$ using 138 fb^{-1} of pp collisions at E_{cm} = 13 TeV. See their Fig. 4 for limits on production cross section times branching ratios for $m_{H_3^0}$ = 0.9–4.0 TeV and $m_{H_{1,2}^0}$ = 60–600 GeV, and their interpretation in the NMSSM and the Two Real Singlet Model (TRSM).

[65] TUMASYAN 23M search for the decay chain $H \to A^0A^0 \to \gamma\gamma\gamma\gamma$ in 132 fb^{-1} of pp collisions at E_{cm} = 13 TeV. See their Fig. 6 for limits on cross section times branching ratio in the range m_{A^0} = 15–62 GeV.

[66] TUMASYAN 23O search for $H_2^0 \to HH$, each H decaying to either WW^* or $\tau^+\tau^-$ using 138 fb^{-1} of pp collisions at E_{cm} = 13 TeV. See their Fig. 14 (upper) for limit on the product of production cross section times branching ratios for $m_{H_2^0}$ = 0.25–1.0 TeV.

[67] TUMASYAN 23S search for gluon fusion and b-associated production of $H_{1,2}^0$ decaying to $\tau^+\tau^-$ using 138 fb^{-1} of pp collisions at E_{cm} = 13 TeV. See their Fig. 10 for limits on production cross section times branching ratios for $m_{H_{1,2}^0}$ = 0.06–3.5 TeV.

[68] AAD 22A search for the decay chain $H \to A^0A^0 \to \mu^+\mu^-b\overline{b}$ in 139 fb^{-1} of pp collisions at E_{cm} = 13 TeV. See their Fig. 9 for limits on the overall branching fraction in the range m_{A^0} = 16–62 GeV. See also Fig. 11 for limits without assuming A^0 is pseudoscalar.

[69] AAD 22D search for ZA^0 associate production with $Z \to \ell^+\ell^-$, A^0 decaying invisibly, in 139 fb^{-1} of pp collisions at E_{cm} = 13 TeV. See their Fig. 5 for excluded regions in the mass parameter space of two Higgs doublet plus singlet (2HDM+A^0) model with a certain choice of the model parameters.

[70] AAD 22F search for gluon fusion production of H_2^0 decaying to $HH \to b\overline{b}b\overline{b}$ using 126–139 fb^{-1} of pp collisions at E_{cm} = 13 TeV. B($H \to b\overline{b}$) = 0.582 is assumed. See their Fig. 14 for limit on the product of production cross section times branching ratios for $m_{H_2^0}$ = 0.251–5.0 TeV.

[71] AAD 22I search for ZH associate production with the decay chain $H \to \widetilde{\chi}_2^0\widetilde{\chi}_1^0$, $\widetilde{\chi}_2^0 \to A^0\widetilde{\chi}_1^0$, $A^0 \to b\overline{b}$, and $Z \to \ell^+\ell^-$, in 139 fb^{-1} of pp collisions at E_{cm} = 13 TeV. See their Figs. 3 and 4 for limits on the product of cross section times the branching ratios for m_{A^0} = 20–65 GeV with various choices of NMSSM model parameters.

[72] AAD 22J search for the decay $H \to ZA^0$ with $A^0 \to \mu^+\mu^-$ and $Z \to e^+e^-$, $\mu^+\mu^-$ in 139 fb^{-1} of pp collisions at E_{cm} = 13 TeV assuming SM gluon-gluon fusion production of the H. See their Fig. 17(b) for limits on the product of cross section times the branching ratios for m_{A^0} = 15–30 GeV.

[73] AAD 22J search for the decay $H \to A^0A^0$ with $A^0 \to \mu^+\mu^-$ in 139 fb^{-1} of pp collisions at E_{cm} = 13 TeV assuming SM gluon-gluon fusion production of the H in the range of m_{A^0} = 1–60 GeV . See their Fig. 14(b) for limits on the product of cross section times the branching ratios for m_{A^0} = 1.5–60 GeV (excluding ψ and Υ regions). The limit also applies to the decay $H \to H_1^0H_1^0$.

[74] AAD 22P search for invisibly decaying H_1^0, H_2^0 produced by vector boson fusion in 139 fb^{-1} of pp collisions at E_{cm} = 13 TeV. Limit on the product of cross section times branching ratio in the range 0.1–1 pb (95% CL) is given for the mass range 0.05–2 TeV. See their Fig. 14.

[75] AAD 22Y search for gluon fusion production of H_2^0 decaying to $HH \to b\overline{b}\gamma\gamma$ in 139 fb^{-1} of pp collisions at E_{cm} = 13 TeV. See their Fig. 15 for limit on the product of production cross section times branching ratios to HH for $m_{H_2^0}$ = 0.251–1.0 TeV.

[76] ABRATENKO 22A search for a singlet scalar boson H_1^0 having a small mixing with the SM Higgs boson in the decay chain $K^+ \to H_1^0\pi^+$, $H_1^0 \to \mu^+\mu^-$ from data corresponding to 7.01×10^{20} protons on NuMI target. See their Fig. 13 (right) and Table V for limits on the SM Higgs component of H_1^0 for $m_{H_1^0}$ = 212–279 MeV.

Int. J. Mod. Phys. A 2026.41. Downloaded from www.worldscientific.com
by UNIVERSITY OF CALIFORNIA @ BERKELEY on 09/16/26. Re-use and distribution is strictly not permitted, except for Open Access articles.

[77] TUMASYAN 22AK search for gluon-fusion production of H_3^0 decaying to $H_1^0 H_1^0 \rightarrow b\overline{b}b\overline{b}$ in 138 fb^{-1} of pp collisions at E_{cm} = 13 TeV. See their Fig. 5 for limits on cross section times branching ratio for $m_{H_3^0}$ = 1–3 TeV, $m_{H_1^0}$ = 25–100 GeV.

[78] TUMASYAN 22D search for production of an H_2^0 (denoted radion in the paper) in gluon fusion and vector boson fusion, decaying to W^+W^- in the final states $\ell\nu$ + hadrons, using 137 fb^{-1} of pp collisions at E_{cm} = 13 TeV. See their Fig. 7 for limits on cross section times branching ratio for $m_{H_2^0}$ = 1.0–4.5 TeV.

[79] AAD 21AF search for production of a heavy H_2^0 state decaying to ZZ in the final states $\ell^+\ell^-\ell'^+\ell'^-$ and $\ell^+\ell^-\nu\overline{\nu}$ in 139 fb^{-1} of pp collisions at E_{cm} = 13 TeV. See their Fig. 4 for upper limits on cross section times branching ratio for $m_{H_2^0}$ = 0.2–2.0 TeV assuming ggF or VBF with narrow width approximation, and Fig. 5 for upper limits on cross section times branching ratio for $m_{H_2^0}$ = 0.4–2.0 TeV assuming ggF, and with several assumptions on its width.

[80] AAD 21AI search for production of an A^0 in gluon-gluon fusion and in association with a $b\overline{b}$, decaying to $ZH_2^0 \rightarrow \ell^+\ell^-b\overline{b}$ or $\ell^+\ell^-W^+W^-$ in 139 fb^{-1} of pp collisions at E_{cm} = 13 TeV. See their Figs. 9 and 13 for cross section limits for m_{A^0} = 230–800 GeV and $m_{H_2^0}$ = 130–700 GeV.

[81] AAD 21AY search for production of a scalar resonance decaying to $\gamma\gamma$ in 139 fb^{-1} of pp collisions at E_{cm} = 13 TeV. See their Fig. 5(a) for limits on fiducial cross section times branching ratio for $m_{H_2^0}$ = 0.16–3 TeV with narrow width approximation, and Table 2 with several assumptions on the width.

[82] AAD 21AZ search for production of A_2^0 decaying to HA_1^0 followed by $H \rightarrow \gamma\gamma$, $A_1^0 \rightarrow$ invisible in 139 fb^{-1} of pp collisions at E_{cm} = 13 TeV. See their Figs. 10–12 for limits in terms of two-Higgs-doublet model plus singlet pseudoscalar and a fermionic Dark Matter particle.

[83] AAD 21BB search for production of A_2^0 by gluon fusion or associated $A_2^0 b\overline{b}$ production, decaying to HA_1^0 followed by $H \rightarrow b\overline{b}$, $A_1^0 \rightarrow$ invisible in 139 fb^{-1} of pp collisions at E_{cm} = 13 TeV. See their Fig. 8 for limits in terms of two-Higgs-doublet plus singlet pseudoscalar model.

[84] AAD 21BE search for production of A_1^0 associated with a single top quark and either a light quark or a W boson, decaying to invisible final states, in 139 fb^{-1} of pp collisions at E_{cm} = 13 TeV. See their Figs. 13–15 for limits in terms of two-Higgs-doublet model plus singlet pseudoscalar, which is assumed to decay to a pair of Dark Matter particles.

[85] ABRATENKO 21 search for a singlet scalar boson H_1^0 having a small mixing with the SM Higgs boson in the decay chain $K^+ \rightarrow H_1^0\pi^+$, $H_1^0 \rightarrow e^+e^-$ from data corresponding to 1.93×10^{20} protons on NuMI target. See their Fig. 2 for limits on the SM Higgs component of H_1^0 for $m_{H_1^0}$ = 3–210 MeV.

[86] SIRUNYAN 21A search for $H_2^0 \rightarrow ZA^0$ with $Z \rightarrow \ell^+\ell^-$, A^0 decaying invisibly, in 137 fb^{-1} of pp collisions at E_{cm} = 13 TeV. See their Fig. 8 for excluded regions in the mass parameter space of two Higgs doublet plus singlet model with a certain choice of the model parameters.

[87] TUMASYAN 21F search for gluon fusion production of H_3^0 decaying to $HH_{1,2}^0 \rightarrow \tau^+\tau^-b\overline{b}$ in 137 fb^{-1} of pp collisions at E_{cm} = 13 TeV. See their Figs. 5 and 6 for limits on cross section times branching ratios for $m_{H_{1,2}^0}$ = 0.06–2.8 TeV and $m_{H_3^0}$ = 0.24–3.0 TeV.

[88] AAD 20AA search for $H_2^0/A^0 \rightarrow \tau^+\tau^-$ produced by gluon fusion or b-associated production using 139 fb^{-1} of pp collisions at E_{cm} = 13 TeV. See their Fig. 2(a), 2(b) for limits on the product of cross section and branching ratio for $m_{H_2^0}$, m_{A^0} = 0.2–2.5 TeV.

[89] AAD 20AI search for ZH production followed by the decay $H \rightarrow A^0A^0 \rightarrow b\overline{b}b\overline{b}$ in 36 fb^{-1} of pp collisions at E_{cm} = 13 TeV. The search looks for collimated $A^0 \rightarrow b\overline{b}$ decays and is complementary to AABOUD 18BX. See their Fig. 10 for limits on the product of production cross section and branching ratios in the range m_{A^0} = 15–30 GeV.

[90] AAD 20AO search for gluon fusion production of H_2^0 decaying to $HH \rightarrow \tau^+\tau^-b\overline{b}$ (with hadronically decaying $\tau^+\tau^-$) using 139 fb^{-1} of pp collisions at E_{cm} = 13 TeV. Limit on the product of production cross section times branching ratios in the range 28–817 fb (95% CL) is given for m_{A^0} = 1.0–3.0 TeV, see their Fig. 13.

[91] AAD 20C combine searches for a scalar resonance decaying to HH in 36.1 fb^{-1} of pp collisions at E_{cm} = 13 TeV from AABOUD 19A, AABOUD 19O, AABOUD 18CQ, AABOUD 19T, AABOUD 18CW, and AABOUD 18BU. See their Fig. 5(a) for limits on cross section times branching ratio for $m_{H_2^0}$ = 0.26–3 TeV.

[92] AAD 20L search for b-associated production of H_2^0 decaying to $b\overline{b}$ in 27.8 fb^{-1} of pp collisions at E_{cm} = 13 TeV. See their Fig. 8 for limits on the product of cross section and branching ratio for $m_{H_2^0}$ = 0.45–1.4 TeV.

[93] AAD 20X search for vector-boson-fusion production of H_2^0 decaying to HH using 126 fb^{-1} of pp collisions at E_{cm} = 13 TeV. See their Fig. 5 for limits on the product of cross section and branching ratio for the assumptions of a narrow- and broad-width resonance.

[94] AAIJ 20AL search for dimuon resonance in the mass range 0.2–60 GeV in 5.1 fb^{-1} of pp collisions at E_{cm} = 13 TeV, in inclusive and b quark associated production. Displaced decays are searched for for masses below 3 GeV. See their Figs. 7–9 for cross section limits and Fig. 10 for limits for mixing angle in two Higgs doublet plus singlet model (at 90% CL).

[95] SIRUNYAN 20 search for the decay $H \rightarrow A^0A^0 \rightarrow \tau^+\tau^-\tau^+\tau^-$ or $\tau^+\tau^-\mu^+\mu^-$ in 35.9 fb^{-1} of pp collisions at E_{cm} = 13 TeV. See their Fig. 10 for limits on the product of production cross section (normalized to the SM) and branching ratios in the range m_{A^0} = 4–15 GeV.

[96] SIRUNYAN 20AA search for $H_2^0 \rightarrow ZA^0$, $A^0 \rightarrow b\overline{b}$ or $A^0 \rightarrow ZH_2^0$, $H_2^0 \rightarrow b\overline{b}$ in 35.9 fb^{-1} of pp collisions at E_{cm} = 13 TeV. See their Fig. 7 for limits on the product of cross section and branching ratio for $m_{H_2^0}$ = 0.12–1 TeV and m_{A^0} = 0.03–1 TeV.

[97] SIRUNYAN 20AC search for gluon-fusion production of A^0 decaying to ZH in 35.9 fb^{-1} of pp collisions at E_{cm} = 13 TeV. See their Fig. 5 for limits on the product of cross section and branching ratios for m_{A^0} = 220–400 GeV.

[98] SIRUNYAN 20AD search for lepton-flavor violating decays $H_2^0 \rightarrow \mu\tau$, $e\tau$ of gluon-fusion-produced H_2^0 in 35.9 fb^{-1} of pp collisions at E_{cm} = 13 TeV. See their Fig. 5 (9) and Table 5 (6) for limits on production cross section times branching ratio for $m_{H_2^0}$ = 0.2–0.9 TeV for the $\mu\tau$ ($e\tau$) final state.

[99] SIRUNYAN 20AF search for $H_2^0/A^0 \rightarrow t\overline{t}$ with one or two charged leptons in the final state using kinematic variables in 35.9 fb^{-1} of pp collisions at E_{cm} = 13 TeV. See their Figs. 5 and 6 for limits on top Yukawa coupling of H_2^0 and A^0 for $m_{H_2^0}$, m_{A^0} = 0.4–0.75 TeV for various width assumptions.

[100] SIRUNYAN 20AP search for the decay H or $H_2^0 \rightarrow A^0A^0 \rightarrow \mu^+\mu^-\tau^+\tau^-$ (for $m_{H_2^0}$ = 300 GeV) with boosted final-state topology in 35.9 fb^{-1} of pp collisions at E_{cm} = 13 TeV. See their Fig. 7 for limits on the product of production cross section (normalized to the SM) and branching ratios in the range m_{A^0} = 3.6–21 GeV, and Figs. 8 and 9 for its interpretation in terms of models with two Higgs doublets plus a singlet.

[101] SIRUNYAN 20Y search for gluon-fusion and vector-boson-fusion production of H_2^0 decaying to W^+W^- in the final states $\ell\nu\ell\nu$ and $\ell\nu qq$ in 35.9 fb^{-1} of pp collisions at E_{cm} = 13 TeV. See their Fig. 6 for limits on the product of cross section and branching ratio for $m_{H_2^0}$ = 0.2–3 TeV.

[102] SIRUNYAN 20Z search for $H_{1,2}^0$ or A^0 production in association with a $t\overline{t}$ pair, decaying to e^+e^- or $\mu^+\mu^-$, in 137 fb^{-1} of pp collisions at E_{cm} = 13 TeV. See their Fig. 12 for limits on production cross section times branching ratio for $m_{H_{1,2}^0}$, m_{A^0} = 15–75 GeV and 108–340 GeV.

[103] AABOUD 19A search for a narrow scalar resonance decaying to $HH \rightarrow b\overline{b}b\overline{b}$ in 27.5–36.1 fb^{-1} of pp collisions at E_{cm} = 13 TeV. See their Fig. 9(a) for limits on cross section times branching ratios for $m_{H_2^0}$ = 0.26–3 TeV.

[104] AABOUD 19AG search for the decay $H \rightarrow A^0A^0 \rightarrow \mu^+\mu^-b\overline{b}$ in 36.7 fb^{-1} of pp collisions at E_{cm} = 13 TeV. See their Fig. 6 (a) for limits on the product of production cross section (normalized to the SM) and branching ratios in the range m_{A^0} = 20–60 GeV.

[105] AABOUD 19O search for a scalar resonance decaying to $HH \rightarrow b\overline{b}WW^*$ in 36.1 fb^{-1} of pp collisions at E_{cm} = 13 TeV. See their Fig. 12 (left) for limits on cross section times branching ratio for $m_{H_2^0}$ = 0.5–3 TeV.

[106] AABOUD 19T search for a scalar resonance decaying to $HH \rightarrow WW^*WW^*$ in 36.1 fb^{-1} of pp collisions at E_{cm} = 13 TeV. See their Fig. 3 for limits on cross section times branching ratio for $m_{H_2^0}$ = 260–500 GeV, assuming SM decay rates for the H.

[107] AABOUD 19V combine published ATLAS data to constrain two-Higgs-doublet plus singlet pseudoscalar model with A_1^0 decaying to invisible final states. See their Fig. 19 for excluded parameter regions.

[108] AABOUD 19Y search for a narrow scalar resonance produced by gluon fusion or b associated production, decaying to $\mu^+\mu^-$ in 36.1 fb^{-1} of pp collisions at E_{cm} = 13 TeV. See their Figs. 4 and 5(a) for cross section limits for $m_{H_2^0}$ = 0.2–1.0 TeV.

[109] AALTONEN 19 search for b associated production of a scalar particle decaying to $b\overline{b}$ in 5.4 fb^{-1} of $p\overline{p}$ collisions at E_{cm} = 1.96 TeV. See their Fig. 3 for limits on cross section times branching ratio for $m_{H_{1,2}^0}$ = 100–300 GeV.

[110] SIRUNYAN 19 search for a narrow scalar resonance decaying to $HH \rightarrow \gamma\gamma b\overline{b}$ in 35.9 fb^{-1} of pp collisions at E_{cm} = 13 TeV. See their Fig. 9 (left) for limits on cross section times branching ratios for $m_{H_2^0}$ = 260–900 GeV.

[111] SIRUNYAN 19AE search for a scalar resonance produced in association with a $b\overline{b}$ pair, decaying to $\tau^+\tau^-$ in 35.9 fb^{-1} of pp collisions at E_{cm} = 13 TeV. See their Fig. 4 for cross section limits for m_{A^0} = 25–70 GeV.

[112] SIRUNYAN 19AN search for production of A_2^0 decaying to HA_1^0 followed by $H \rightarrow b\overline{b}$, $A_1^0 \rightarrow$ invisible in 35.9 fb^{-1} of pp collisions at E_{cm} = 13 TeV, in the mass range $m_{A_2^0}$ = 0.2–1.6 TeV, $m_{A_1^0}$ = 0.15–0.5 TeV. See their Fig. 6 for limits in terms of two-Higgs-doublet plus singlet pseudoscalar model.

[113] SIRUNYAN 19AV search for a scalar resonance produced by gluon fusion or b-associated production, decaying to $ZH \rightarrow \ell^+\ell^-b\overline{b}$ ($\ell = e, \mu$) or $\nu\overline{\nu}b\overline{b}$ in 35.9 fb^{-1} of pp collisions at E_{cm} = 13 TeV. See their Fig. 5 for cross section limits for m_{A^0} = 0.22–1.0 TeV.

[114] SIRUNYAN 19B search for gluon fusion production of narrow scalar resonance with large transverse momentum, decaying to $b\overline{b}$, in 35.9 fb^{-1} of pp collisions at E_{cm} = 13 TeV. See their Figs. 7 and 8 for limits on cross section times branching ratio for the resonance mass of 50–350 GeV.

[115] SIRUNYAN 19BB search for the decay $H_1^0 \rightarrow \gamma\gamma$ in 19.7 fb^{-1} of pp collisions at E_{cm} = 8 TeV and 35.9 fb^{-1} at E_{cm} = 13 TeV. See their Figs. 4–6 for limits on cross section times branching ratio for $m_{H_1^0}$ = 80–110 GeV (some results in Fig. 5 for $m_{H_1^0}$ = 70–110 GeV).

[116] SIRUNYAN 19BD search for the decay $H \rightarrow A^0A^0 \rightarrow \mu^+\mu^-b\overline{b}$ in 35.9 fb^{-1} of pp collisions at E_{cm} = 13 TeV. See their Fig. 5 for limits on the product of cross section times branching ratios in the range m_{A^0} = 20–62.5 GeV. See also their Figs. 6 and 7 for interpretation of the data in terms of models with two Higgs doublets and a singlet.

[117] SIRUNYAN 19BE combine searches for $H_2^0 \rightarrow HH$ in 35.9 fb^{-1} of pp collisions at E_{cm} = 13 TeV in various H decay modes, from SIRUNYAN 18A, SIRUNYAN 18AF, SIRUNYAN 18CW, SIRUNYAN 19, and SIRUNYAN 19H. See their Fig. 3 for limits on cross section times branching ratios for $m_{H_2^0}$ = 0.25–3 TeV.

[118] SIRUNYAN 19BQ search for production of $H_{1,2}^0$ decaying to $A^0A^0 \rightarrow \mu^+\mu^-\mu^+\mu^-$ in 35.9 fb^{-1} of pp collisions at E_{cm} = 13 TeV. See their Fig. 2 for limits on cross section times branching ratio for $m_{H_{1,2}^0}$ = 90–150 GeV, m_{A^0} = 0.25–3.55 GeV.

Int. J. Mod. Phys. A 2026.41. Downloaded from www.worldscientific.com
by UNIVERSITY OF CALIFORNIA @ BERKELEY on 09/16/26. Reproduction is strictly not permitted, except for Open Access articles.

[119] SIRUNYAN 19CR search for production of H_2^0/A^0 in gluon fusion and in association with a $b\overline{b}$ pair, decaying to $\mu^+\mu^-$ in 35.9 fb^{-1} of pp collisions at E_{cm} = 13 TeV. See their Fig. 6 for limits on cross section times branching ratio.

[120] SIRUNYAN 19H search for a narrow scalar resonance decaying to $HH \rightarrow b\overline{b}b\overline{b}$ in 35.9 fb^{-1} of pp collisions at E_{cm} = 13 TeV, where one $b\overline{b}$ pair is resolved and the other not. Limits on cross section times branching ratios for $m_{H_2^0}$ = 0.75–1.6 TeV are obtained and combined with data from SIRUNYAN 18AF. See their Fig. 5 (right).

[121] AABOUD 18AA search for production of a scalar resonance decaying to $Z\gamma$, with Z decaying hadronically, in 36.1 fb^{-1} of pp collisions at E_{cm} = 13 TeV. See their Fig. 8(a) for limits on cross section times branching ratio for $m_{H_2^0}$ = 1.0–6.8 TeV.

[122] AABOUD 18AG search for the decay $H \rightarrow A^0A^0 \rightarrow \gamma\gamma gg$ in 36.7 fb^{-1} of pp collisions at E_{cm} = 13 TeV. See their Fig. 2 and Table 6 for cross section limits in the range m_{A^0} = 20–60 GeV.

[123] AABOUD 18AH search for production of an A^0 in gluon-gluon fusion and in association with a $b\overline{b}$, decaying to $ZH_2^0 \rightarrow \ell^+\ell^-b\overline{b}$ in 36.1 fb^{-1} of pp collisions at E_{cm} = 13 TeV. See their Fig. 5 for cross section limits for m_{A^0} = 230–800 GeV and $m_{H_2^0}$ = 130–700 GeV.

[124] AABOUD 18AI search for production of an A^0 in gluon-gluon fusion and in association with a $b\overline{b}$, decaying to ZH in the final states $\nu\overline{\nu}b\overline{b}$ and $\ell^+\ell^-b\overline{b}$ in 36.1 fb^{-1} of pp collisions at E_{cm} = 13 TeV. See their Fig. 6 for cross section limits for m_{A^0} = 0.2–2 TeV. See also AABOUD 18CC.

[125] AABOUD 18BF search for production of a heavy H_2^0 state decaying to ZZ in the final states $\ell^+\ell^-\ell^+\ell^-$ and $\ell^+\ell^-\nu\overline{\nu}$ in 36.1 fb^{-1} of pp collisions at E_{cm} = 13 TeV. See their Fig. 6 for upper limits on cross section times branching ratio for $m_{H_2^0}$ = 0.2–1.2 TeV assuming ggF or VBF with the NWA. See their Fig. 7 for upper limits on cross section times branching ratio for $m_{H_2^0}$ = 0.4–1.0 TeV assuming ggF, and with several assumptions on its width.

[126] AABOUD 18BU search for a narrow scalar resonance decaying to $HH \rightarrow \gamma\gamma WW^*$ in 36.1 fb^{-1} of pp collisions at E_{cm} = 13 TeV. See their Fig. 4 for limits on cross section times branching ratios for $m_{H_2^0}$ = 260–500 GeV.

[127] AABOUD 18BX search for associated production of WH or ZH followed by the decay $H \rightarrow A^0A^0 \rightarrow b\overline{b}b\overline{b}$ in 36.1 fb^{-1} of pp collisions at E_{cm} = 13 TeV. See their Fig. 9 for limits on cross section times branching ratios for m_{A^0} = 20–60 GeV. See also their Fig. 10 for the dependence of the limit on A^0 lifetime.

[128] AABOUD 18CQ search for a narrow scalar resonance decaying to $HH \rightarrow b\overline{b}\tau^+\tau^-$ in 36.1 fb^{-1} of pp collisions at E_{cm} = 13 TeV. See their Fig. 2 (above) for limits on cross section times branching ratios for $m_{H_2^0}$ = 260–1000 GeV.

[129] AABOUD 18F search for production of a narrow scalar resonance decaying to W^+W^- and ZZ, followed by hadronic decays of W and Z, in 36.7 fb^{-1} of pp collisions at E_{cm} = 13 TeV. See their Fig. 5(c) for limits on cross section times branching ratio for $m_{H_2^0}$ = 1.2–3.0 TeV.

[130] AAIJ 18AM search for gluon-fusion production of $H_{1,2}^0$ decaying to $\mu\tau$ in 2 fb^{-1} of pp collisions at E_{cm} = 8 TeV. See their Fig. 2 for limits on cross section times branching ratio for $m_{H_{1,2}^0}$ = 45–195 GeV.

[131] AAIJ 18AQ search for gluon-fusion production of a scalar particle A^0 decaying to $\mu^+\mu^-$ in 1.99 fb^{-1} of pp collisions at E_{cm} = 8 TeV and 0.98 fb^{-1} at E_{cm} = 7 TeV. See their Fig. 4 for limits on cross section times branching ratio for m_{A^0} = 5.5–15 GeV (using the E_{cm} = 8 TeV data set).

[132] AAIJ 18AQ search for the decay $H \rightarrow A^0A^0$, with one of the A^0 decaying to $\mu^+\mu^-$, in 1.99 fb^{-1} of pp collisions at E_{cm} = 8 TeV and 0.98 fb^{-1} at E_{cm} = 7 TeV. See their Fig. 5 (right) for limits on the product of branching ratios for m_{A^0} = 5.5–15 GeV (using the E_{cm} = 8 TeV data set).

[133] SIRUNYAN 18AF search for a narrow scalar resonance decaying to $HH \rightarrow b\overline{b}b\overline{b}$ in 35.9 fb^{-1} of pp collisions at E_{cm} = 13 TeV, where both $b\overline{b}$ pairs are not resolved. See their Fig. 9 for limits on cross section times branching ratios for $m_{H_2^0}$ = 0.75–3 TeV.

[134] SIRUNYAN 18BA search for production of a heavy H_2^0 state decaying to ZZ in the final states $\ell^+\ell^-\ell^+\ell^-$, $\ell^+\ell^-q\overline{q}$, and $\ell^+\ell^-\nu\overline{\nu}$ in 35.9 fb^{-1} of pp collisions at E_{cm} = 13 TeV. See their Figs. 10 and 11 for upper limits on cross section times branching ratio for $m_{H_2^0}$ = 0.13–3 TeV with several assumptions on its width and on the fraction of Vector-Boson-Fusion of the total production cross section.

[135] SIRUNYAN 18CW search for a narrow scalar resonance decaying to $HH \rightarrow b\overline{b}b\overline{b}$ in 35.9 fb^{-1} of pp collisions at E_{cm} = 13 TeV, where both $b\overline{b}$ pairs are resolved. See their Fig. 9 for limits on cross section times branching ratios for $m_{H_2^0}$ = 260–1200 GeV.

[136] SIRUNYAN 18DK search for production of a scalar resonance decaying to $Z\gamma$, with Z decaying to $\ell^+\ell^-$ or hadronically, in 35.9 fb^{-1} of pp collisions at E_{cm} = 13 TeV. See their Fig. 7 for limits on cross section times branching ratio for $m_{H_2^0}$ = 0.35–4 TeV for different assumptions on the width of the resonance.

[137] SIRUNYAN 18DT search for the decay $H \rightarrow A^0A^0 \rightarrow \tau^+\tau^-b\overline{b}$ in 35.9 fb^{-1} of pp collisions at E_{cm} = 13 TeV. See their Fig. 7 for limits on the product of branching ratios in the range m_{A^0} = 15–60 GeV. See also their Fig. 8 for interpretation of the data in terms of models with two Higgs doublets and a singlet.

[138] SIRUNYAN 18DU search for production of a narrow scalar resonance decaying to $\gamma\gamma$ in 35.9 fb^{-1} (taken in 2016) of pp collisions at E_{cm} = 13 TeV. See their Fig. 3 (right) for limits on cross section times branching ratio for $m_{H_2^0}$ = 0.5–5 TeV for several values of its width-to-mass ratio.

[139] SIRUNYAN 18ED search for production of an A^0 in gluon-gluon fusion and in association with a $b\overline{b}$, decaying to ZH in the final states $\nu\overline{\nu}b\overline{b}$ or $\ell^+\ell^-b\overline{b}$ in 35.9 fb^{-1} of pp collisions at E_{cm} = 13 TeV. See their Fig. 8 for cross section limits for m_{A^0} = 0.8–2 TeV.

[140] SIRUNYAN 18EE search for the decay $H \rightarrow A^0A^0 \rightarrow \mu^+\mu^-\tau^+\tau^-$ in 35.9 fb^{-1} of pp collisions at E_{cm} = 13 TeV. See their Fig. 4 for limits on the product of branching ratios in the range m_{A^0} = 15–62.5 GeV, normalized to the SM production cross section. See also their Fig. 5 for interpretation of the data in terms of models with two Higgs doublets and a singlet.

[141] SIRUNYAN 18F search for a narrow scalar resonance decaying to $HH \rightarrow WWb\overline{b}$ or $ZZb\overline{b}$ in the final state $\ell\ell\nu\nu b\overline{b}$ in 35.9 fb^{-1} of pp collisions at E_{cm} = 13 TeV. See their Fig. 7 for limits on cross section times branching ratios for $m_{H_2^0}$ = 250–900 GeV.

[142] AABOUD 17 search for production of a scalar resonance decaying to $Z\gamma$ in 3.2 fb^{-1} of pp collisions at E_{cm} = 13 TeV. See their Fig. 4 for the limits on cross section times branching ratio for $m_{H_2^0}$ = 0.25–3.0 TeV.

[143] AABOUD 17AP search for production of a scalar resonance decaying to $\gamma\gamma$ in 36.7 fb^{-1} of pp collisions at E_{cm} = 13 TeV. See their Fig. 4(a) for limits on fiducial cross section times branching ratio for $m_{H_2^0}$ = 0.2–2.7 TeV with narrow width approximation.

[144] AABOUD 17AW search for production of a scalar resonance decaying to $Z\gamma$ in 36.1 fb^{-1} of pp collisions at E_{cm} = 13 TeV. See their Fig. 7 for limits on cross section times branching ratio for $m_{H_2^0}$ = 0.25–2.4 TeV.

[145] KHACHATRYAN 17AZ search for the decay $H \rightarrow A^0A^0 \rightarrow \tau^+\tau^-\tau^+\tau^-$, $\mu^+\mu^-b\overline{b}$, and $\mu^+\mu^-\tau^+\tau^-$ in 19.7 fb^{-1} of pp collisions at E_{cm} = 8 TeV. See their Figs. 4, 5, and 6 for cross section limits in the range m_{A^0} = 5–62.5 GeV. See also their Figs. 7, 8, and 9 for interpretation of the data in terms of models with two Higgs doublets and a singlet.

[146] KHACHATRYAN 17D search for production of a scalar resonance decaying to $Z\gamma$ in 19.7 fb^{-1} of pp collisions at E_{cm} = 8 TeV and 2.7 fb^{-1} at E_{cm} = 13 TeV. See their Figs. 3 and 4 for the limits on cross section times branching ratio for $m_{H_2^0}$ = 0.2–2.0 TeV.

[147] KHACHATRYAN 17R search for production of a narrow scalar resonance decaying to $\gamma\gamma$ in 12.9 fb^{-1} (taken in 2016) of pp collisions at E_{cm} = 13 TeV. See their Fig. 2 for limits on cross section times branching ratio for $m_{H_2^0}$ = 0.5–4.5 TeV for several values of its width-to-mass ratio. Limits from combination with KHACHATRYAN 16M are shown in their Figs. 4 and 6.

[148] SIRUNYAN 17CN search for a narrow scalar resonance decaying to $HH \rightarrow b\overline{b}\tau^+\tau^-$ in 18.3 fb^{-1} of pp collisions at E_{cm} = 8 TeV. See their Fig. 5 (above) and Table II for limits on the cross section times branching ratios for $m_{H_2^0}$ = 0.3–1 TeV, and Fig. 6 (above) and Table III for the corresponding limits by combining with data from KHACHATRYAN 16BQ and KHACHATRYAN 15R.

[149] SIRUNYAN 17Y search for production of a scalar resonance decaying to $Z\gamma$ in 19.7 fb^{-1} of pp collisions at E_{cm} = 8 TeV and 2.7 fb^{-1} at E_{cm} = 13 TeV. See their Figs. 3, 4 and Table 3 for limits on cross section times branching ratio for $m_{H_2^0}$ = 0.7–3.0 TeV, and Fig. 5 for the corresponding limits for $m_{H_2^0}$ = 0.2–3.0 TeV from combination with KHACHATRYAN 17D data.

[150] AABOUD 16AB search for associated production of WH with the decay $H \rightarrow A^0A^0 \rightarrow b\overline{b}b\overline{b}$ in 3.2 fb^{-1} of pp collisions at E_{cm} = 13 TeV. See their Fig. 8 for limits on cross section times branching ratios for m_{A^0} = 20–60 GeV.

[151] AABOUD 16AE search for production of a narrow scalar resonance decaying to W^+W^- and ZZ in 3.2 fb^{-1} of pp collisions at E_{cm} = 13 TeV. See their Fig. 4 for limits on cross section times branching ratio for $m_{H_2^0}$ = 0.5–3 TeV.

[152] AABOUD 16H search for production of a scalar resonance decaying to $\gamma\gamma$ in 3.2 fb^{-1} of pp collisions at E_{cm} = 13 TeV. See their Fig. 12 for limits on cross section times branching ratio for $m_{H_2^0}$ = 0.2–2 TeV with different assumptions on the width.

[153] AABOUD 16I search for a narrow scalar resonance decaying to $HH \rightarrow b\overline{b}b\overline{b}$ in 3.2 fb^{-1} of pp collisions at E_{cm} = 13 TeV. See their Fig. 10(c) for limits on cross section times branching ratios for $m_{H_2^0}$ = 0.5–3 TeV.

[154] AAD 16AX search for production of a heavy H state decaying to ZZ in the final states $\ell^+\ell^-\ell^+\ell^-$, $\ell^+\ell^-\nu\overline{\nu}$, $\ell^+\ell^-q\overline{q}$, and $\nu\overline{\nu}q\overline{q}$ in 20.3 fb^{-1} of pp collisions at E_{cm} = 8 TeV. See their Fig.12 for upper limits on $\sigma(H)$ B$(H \rightarrow ZZ)$ for m_H ranging from 140 GeV to 1000 GeV.

[155] AAD 16C search for production of a heavy H state decaying to W^+W^- in the final states $\ell\nu\ell\nu$ and $\ell\nu qq$ in 20.3 fb^{-1} of pp collisions at E_{cm} = 8 TeV. See their Figs. 12, 13, and 16 for upper limits on $\sigma(H)$ B$(H \rightarrow W^+W^-)$ for m_H ranging from 300 GeV to 1000 or 1500 GeV with various assumptions on the total width of H.

[156] AAD 16L search for the decay $H \rightarrow A^0A^0 \rightarrow \gamma\gamma\gamma\gamma$ in 20.3 fb^{-1} of pp collisions at E_{cm} = 8 TeV. See their Fig. 4 (upper right) for limits on cross section times branching ratios (normalized to the SM H cross section) for m_{A^0} = 10–60 GeV.

[157] AAD 16L search for the decay $H_2^0 \rightarrow A^0A^0 \rightarrow \gamma\gamma\gamma\gamma$ in 20.3 fb^{-1} of pp collisions at E_{cm} = 8 TeV. See their Fig. 4 (lower right) for limits on cross section times branching ratios for $m_{H_2^0}$ = 600 GeV and m_{A^0} = 10–245 GeV, and Table 5 for limits for $m_{H_2^0}$= 300 and 900 GeV.

[158] AALTONEN 16C search for electroweak associated production of $H_1^0H^\pm$ followed by the decays $H^\pm \rightarrow H_1^0W^*$, $H_1^0 \rightarrow \gamma\gamma$ for $m_{H_1^0}$ = 10–105 GeV and $m_{H^\pm}$ = 30–300 GeV. See their Fig. 3 for excluded parameter region in a two-doublet model in which H_1^0 has no direct decay to fermions.

[159] KHACHATRYAN 16BG search for a narrow scalar resonance decaying to $HH \rightarrow b\overline{b}b\overline{b}$ in 19.7 fb^{-1} of pp collisions at E_{cm} = 8 TeV. See their Fig. 6 for limits on the cross section times branching ratios for $m_{H_2^0}$ = 1.15–3 TeV.

[160] KHACHATRYAN 16BQ search for a resonance decaying to $HH \rightarrow \gamma\gamma b\overline{b}$ in 19.7 fb^{-1} of pp collisions at E_{cm} = 8 TeV. See their Fig. 9 for limits on the cross section times branching ratios for $m_{H_2^0}$ = 0.26–1.1 TeV.

[161] KHACHATRYAN 16F search for the decay $H \rightarrow H_1^0H_1^0 \rightarrow \tau^+\tau^-\tau^+\tau^-$ in 19.7 fb^{-1} of pp collisions at E_{cm} = 8 TeV. See their Fig. 8 for cross section limits for $m_{H_1^0}$ = 4–8 GeV.

[162] KHACHATRYAN 16M search for production of a narrow resonance decaying to $\gamma\gamma$ in 19.7 fb^{-1} of pp collisions at E_{cm} = 8 TeV and 3.3 fb^{-1} at E_{cm} = 13 TeV. See their Fig. 3 (top) for limits on cross section times branching ratio for $m_{H_2^0}$ = 0.5–4 TeV.

Int. J. Mod. Phys. A 2026.41. Downloaded from www.worldscientific.com by UNIVERSITY OF CALIFORNIA @ BERKELEY on 09/16/26. Re-use and distribution is strictly not permitted, except for Open Access articles.

[163] KHACHATRYAN 16P search for gluon fusion production of an H_2^0 decaying to $HH \to b\overline{b}\tau^+\tau^-$ in 19.7 fb^{-1} of pp collisions at E_{cm} = 8 TeV. See their Fig. 8 (lower right) for cross section limits for $m_{H_2^0}$ = 260–350 GeV.

[164] KHACHATRYAN 16P search for gluon fusion production of an A^0 decaying to $ZH \to \ell^+\ell^-\tau^+\tau^-$ in 19.7 fb^{-1} of pp collisions at E_{cm} = 8 TeV. See their Fig. 10 for cross section limits for $m_{H_2^0}$ = 220–350 GeV.

[165] AAD 15BK search for production of a heavy H_2^0 decaying to HH in the final state $b\overline{b}b\overline{b}$ in 19.5 fb^{-1} of pp collisions at E_{cm} = 8 TeV. See their Fig. 14(c) for $\sigma(H_2^0)$ B($H_2^0 \to HH$) for $m_{H_2^0}$ = 500–1500 GeV with $\Gamma_{H_2^0}$ = 1 GeV.

[166] AAD 15BZ search for the decay $H \to A^0A^0 \to \mu^+\mu^-\tau^+\tau^-$ (m_H = 125 GeV) in 20.3 fb^{-1} of pp collisions at E_{cm} = 8 TeV. See their Fig. 6 for limits on cross section times branching ratio for m_{A^0} = 3.7–50 GeV.

[167] AAD 15BZ search for a state H_2^0 via the decay $H_2^0 \to A^0A^0 \to \mu^+\mu^-\tau^+\tau^-$ in 20.3 fb^{-1} of pp collisions at E_{cm} = 8 TeV. See their Fig. 6 for limits on cross section times branching ratio for $m_{H_2^0}$ = 100–500 GeV and m_{A^0} = 5 GeV.

[168] AAD 15CE search for production of a heavy H_2^0 decaying to HH in the final states $b\overline{b}\tau^+\tau^-$ and $\gamma\gamma WW^*$ in 20.3 fb^{-1} of pp collisions at E_{cm} = 8 TeV and combine with data from AAD 15H and AAD 15BK. A limit $\sigma(H_2^0)$ B($H_2^0 \to HH$) < 2.1–0.011 pb (95% CL) is given for $m_{H_2^0}$ = 260–1000 GeV. See their Fig. 6.

[169] AAD 15H search for production of a heavy H_2^0 decaying to HH in the finalstate $\gamma\gamma b\overline{b}$ in 20.3 fb^{-1} of pp collisions at E_{cm} = 8 TeV.A limit of $\sigma(H_2^0)$ B($H_2^0 \to HH$) < 3.5–0.7 pb is given for $m_{H_2^0}$ = 260–500 GeV at 95% CL. See their Fig. 3.

[170] AAD 15S search for production of A^0 decaying to $ZH \to \ell^+\ell^-b\overline{b}$, $\nu\overline{\nu}b\overline{b}$ and $\ell^+\ell^-\tau^+\tau^-$ in 20.3 fb^{-1} of pp collisions at E_{cm} = 8 TeV. See their Fig. 3 for cross section limits for m_{A^0} = 200–1000 GeV.

[171] KHACHATRYAN 15AW search for production of a heavy state H_2^0 of an electroweak singlet extension of the Standard Model via the decays of H_2^0 to W^+W^- and ZZ in up to 5.1 fb^{-1} of pp collisions at E_{cm} = 7 TeV and up to 19.7 fb^{-1} at E_{cm} = 8 TeV in the range $m_{H_2^0}$ = 145–1000 GeV. See their Figs. 8 and 9 for limits in the parameter space of the model.

[172] KHACHATRYAN 15BB search for production of a resonance H decaying to $\gamma\gamma$ in 19.7 fb^{-1} of pp collisions at E_{cm} = 8 TeV. See their Fig. 7 for limits on cross section times branching ratio for m_H = 150–850 GeV.

[173] KHACHATRYAN 15N search for production of A^0 decaying to $ZH \to \ell^+\ell^-b\overline{b}$ in 19.7 fb^{-1} of pp collisions at E_{cm} = 8 TeV. See their Fig. 3 for limits on cross section times branching ratios for m_{A^0} = 225–600 GeV.

[174] KHACHATRYAN 15O search for production of a high-mass narrow resonance A^0 decaying to $ZH \to q\overline{q}\tau^+\tau^-$ in 19.7 fb^{-1} of pp collisions at E_{cm} = 8 TeV. See their Fig. 6 for limits on cross section times branching ratios for m_{A^0} = 800–2500 GeV.

[175] KHACHATRYAN 15R search for a narrow scalar resonance decaying to $HH \to b\overline{b}b\overline{b}$ in 17.9 fb^{-1} of pp collisions at E_{cm} = 8 TeV. See their Fig. 5 (top) for limits on cross section times branching ratios for $m_{H_2^0}$ = 0.27–1.1 TeV.

[176] AAD 14AP search for a second H state decaying to $\gamma\gamma$ in addition to the state at about 125 GeV in 20.3 fb^{-1} of pp collisions at E_{cm} = 8 TeV. See their Fig. 4 for limits on cross section times branching ratio for m_H = 65–600 GeV.

[177] AAD 14M search for the decay cascade $H_2^0 \to H^\pm W^\mp \to HW^\pm W^\mp$, H decaying to $b\overline{b}$ in 20.3 fb^{-1} of pp collisions at E_{cm} = 8 TeV. See their Table III for limits on cross section times branching ratio for $m_{H_2^0}$= 325–1025 GeV and m_{H^+}= 225–925 GeV.

[178] CHATRCHYAN 14G search for a second H state decaying to $WW^{(*)}$ in addition to the observed signal at about 125 GeV using 4.9 fb^{-1} of pp collisions at E_{cm} = 7 TeV and 19.4 fb^{-1} at E_{cm} = 8 TeV. See their Fig. 21 (right) for cross section limits in the mass range 110–600 GeV.

[179] KHACHATRYAN 14P search for a second H state decaying to $\gamma\gamma$ in addition to the observed signal at about 125 GeV using 5.1 fb^{-1} of pp collisions at E_{cm} = 7 TeV and 19.7 fb^{-1} at E_{cm} = 8 TeV. See their Figs. 27 and 28 for cross section limits in the mass range 110–150 GeV.

[180] AALTONEN 13P search for production of a heavy Higgs boson H'^0 that decays into a charged Higgs boson $H^\pm$ and a lighter Higgs boson H via the decay chain $H'^0 \to H^\pm W^\mp$, $H^\pm \to W^\pm H$, $H \to b\overline{b}$ in the final state $\ell\nu$ plus 4 jets in 8.7 fb^{-1} of $p\overline{p}$ collisions at E_{cm} = 1.96 TeV. See their Fig. 4 for limits on cross section times branching ratio in the $m_{H^\pm} - m_{H'^0}$ plane for m_H = 126 GeV.

[181] CHATRCHYAN 13BJ search for H production in the decay chain $H \to A^0A^0$, $A^0 \to \mu^+\mu^-$ in 5.3 fb^{-1} of pp collisions at E_{cm} = 7 TeV. See their Fig. 2 for limits on cross section times branching ratio.

[182] AALTONEN 11P search in 2.7 fb^{-1} of $p\overline{p}$ collisions at E_{cm} = 1.96 TeV for the decay chain $t \to bH^+$, $H^+ \to W^+A^0$, $A^0 \to \tau^+\tau^-$ with m_{A^0} between 4 and 9 GeV. See their Fig. 4 for limits on B($t \to bH^+$) for 90 < m_{H^+} < 160 GeV.

[183] ABBIENDI 10 search for $e^+e^- \to ZH$ with the decay chain $H \to \widetilde{\chi}_1^0\widetilde{\chi}_2^0$, $\widetilde{\chi}_2^0 \to \widetilde{\chi}_1^0$ + (γ or Z^*), when $\widetilde{\chi}_1^0$ and $\widetilde{\chi}_2^0$ are nearly degenerate. For a mass difference of 2 (4) GeV, a lower limit on m_H of 108.4 (107.0) GeV (95% CL) is obtained for SM ZH cross section and B($H \to \widetilde{\chi}_1^0\widetilde{\chi}_2^0$) = 1.

[184] SCHAEL 10 search for the process $e^+e^- \to HZ$ followed by the decay chain $H \to A^0A^0 \to \tau^+\tau^-\tau^+\tau^-$ with $Z \to \ell^+\ell^-$, $\nu\overline{\nu}$ at E_{cm} = 183–209 GeV. For a HZZ coupling equal to the SM value, B($H \to A^0A^0$) = B($A^0 \to \tau^+\tau^-$) = 1, and m_{A^0} = 4–10 GeV, m_H up to 107 GeV is excluded at 95% CL.

[185] ABAZOV 09V search for H production followed by the decay chain $H \to A^0A^0 \to \mu^+\mu^-\mu^+\mu^-$ or $\mu^+\mu^-\tau^+\tau^-$ in 4.2 fb^{-1} of $p\overline{p}$ collisions at E_{cm} = 1.96 TeV. See their Fig. 3 for limits on $\sigma(H)$·B($H \to A^0A^0$) for m_{A^0} = 3.6–19 GeV.

[186] ABBIENDI 05A search for $e^+e^- \to H_1^0A^0$ in general Type-II two-doublet models, with decays H_1^0, $A^0 \to q\overline{q}$, gg, $\tau^+\tau^-$, and $H_1^0 \to A^0A^0$.

[187] ABBIENDI 04K search for $e^+e^- \to HZ$ with H decaying to two jets of any flavor including gg. The limit is for SM production cross section with B($H \to jj$) = 1.

[188] ABDALLAH 04 consider the full combined LEP and LEP2 datasets to set limits on the Higgs coupling to W or Z bosons, assuming SM decays of the Higgs. Results in Fig. 26.

[189] ACHARD 04B search for $e^+e^- \to HZ$ with H decaying to $b\overline{b}$, $c\overline{c}$, or gg. The limit is for SM production cross section with B($H \to jj$) = 1.

[190] ACHARD 04F search for H with anomalous coupling to gauge boson pairs in the processes $e^+e^- \to H\gamma$, e^+e^-H, HZ with decays $H \to f\overline{f}$, $\gamma\gamma$, $Z\gamma$, and W^*W at E_{cm} = 189–209 GeV. See paper for limits.

[191] ABBIENDI 03F search for $H \to$ anything in $e^+e^- \to HZ$, using the recoil mass spectrum of $Z \to e^+e^-$ or $\mu^+\mu^-$. In addition, it searched for $Z \to \nu\overline{\nu}$ and $H \to e^+e^-$ or photons. Scenarios with large width or continuum H mass distribution are considered. See their Figs. 11–14 for the results.

[192] ABBIENDI 03G search for $e^+e^- \to H_1^0Z$ followed by $H_1^0 \to A^0A^0$, $A^0 \to c\overline{c}$, gg, or $\tau^+\tau^-$ in the region $m_{H_1^0}$ = 45-86 GeV and m_{A^0} = 2-11 GeV. See their Fig. 7 for the limits.

[193] Search for associated production of a $\gamma\gamma$ resonance with a Z boson, followed by $Z \to q\overline{q}$, $\ell^+\ell^-$, or $\nu\overline{\nu}$, at $E_{cm} \leq$ 209 GeV. The limit is for a H with SM production cross section and B($H \to f\overline{f}$)=0 for all fermions f.

[194] For B($H \to \gamma\gamma$)=1, m_H > 113.1 GeV is obtained.

[195] HEISTER 02M search for $e^+e^- \to HZ$, assuming that H decays to $q\overline{q}$, gg, or $\tau^+\tau^-$ only. The limit assumes SM production cross section.

[196] ABBIENDI 01E search for neutral Higgs bosons in general Type-II two-doublet models, at $E_{cm} \leq$ 189 GeV. In addition to usual final states, the decays H_1^0, $A^0 \to q\overline{q}$, gg are searched for. See their Figs. 15,16 for excluded regions.

[197] ACCIARRI 00R search for $e^+e^- \to H\gamma$ with $H \to b\overline{b}$, $Z\gamma$, or $\gamma\gamma$. See their Fig. 3 for limits on $\sigma \cdot$ B. Explicit limits within an effective interaction framework are also given, for which the Standard Model Higgs search results are used in addition.

[198] ACCIARRI 00R search for the two-photon type processes $e^+e^- \to e^+e^-H$ with $H \to b\overline{b}$ or $\gamma\gamma$. See their Fig. 4 for limits on $\Gamma(H \to \gamma\gamma)$·B($H \to \gamma\gamma$or $b\overline{b}$) for m_H=70–170 GeV.

[199] GONZALEZ-GARCIA 98B use DØ limit for $\gamma\gamma$ events with missing E_T in $p\overline{p}$ collisions (ABBOTT 98) to constrain possible ZH or WH production followed by unconventional $H \to \gamma\gamma$ decay which is induced by higher-dimensional operators. See their Figs. 1 and 2 for limits on the anomalous couplings.

[200] KRAWCZYK 97 analyse the muon anomalous magnetic moment in a two-doublet Higgs model (with type II Yukawa couplings) assuming no H_1^0ZZ coupling and obtain $m_{H_1^0} \gtrsim$ 5 GeV or $m_{A^0} \gtrsim$ 5 GeV for tanβ > 50. Other Higgs bosons are assumed to be much heavier.

[201] ALEXANDER 96H give B($Z \to H\gamma$)×B($H \to q\overline{q}$) < 1–4 × 10^{-5} (95%CL) and B($Z \to H\gamma$)×B($H \to b\overline{b}$) < 0.7–2 × 10^{-5} (95%CL) in the range 20 < m_H < 80 GeV.

Electroweak Constraints on the Standard Model Higgs Boson Mass

Here we list constraints on the mass of the Higgs boson derived from fits to precision electroweak observables, assuming the minimal Standard Model with a doublet Higgs field and three generations of fermions.

VALUE (GeV)	DOCUMENT ID		TECN
$\mathbf{90^{+21}_{-18}}$	[1] HALLER	18	RVUE
• • • We do not use the following data for averages, fits, limits, etc. • • •			
91^{+30}_{-23}	[2] BAAK	12	RVUE
94^{+25}_{-22}	[3] BAAK	12A	RVUE
91^{+31}_{-24}	[4] ERLER	10A	RVUE
129^{+74}_{-49}	[5] LEP-SLC	06	RVUE

[1] HALLER 18 make Standard Model fits to Z and neutral current parameters, m_t, m_W, and Γ_W measurements available in 2018. The direct mass measurement at the LHC is not used in the fit.

[2] BAAK 12 make Standard Model fits to Z and neutral current parameters, m_t, m_W, and Γ_W measurements available in 2010 (using also preliminary data). The quoted result is obtained from a fit that does not include the limit from the direct Higgs searches. The result including direct search data from LEP2, the Tevatron and the LHC is 120^{+12}_{-5} GeV.

[3] BAAK 12A make Standard Model fits to Z and neutral current parameters, m_t, m_W, and Γ_W measurements available in 2012 (using also preliminary data). The quoted result is obtained from a fit that does not include the measured mass value of the signal observed at the LHC and also no limits from direct Higgs searches.

[4] ERLER 10A makes Standard Model fits to Z and neutral current parameters, m_t, m_W measurements available in 2009 (using also preliminary data). The quoted result is obtained from a fit that does not include the limits from the direct Higgs searches. With direct search data from LEP2 and Tevatron added to the fit, the 90% CL (99% CL) interval is 115–148 (114–197) GeV.

[5] LEP-SLC 06 make Standard Model fits to Z parameters from LEP/SLC and m_t, m_W, and Γ_W measurements available in 2005 with $\Delta\alpha_{had}^{(5)}(m_Z)$ = 0.02758 ± 0.00035. The 95% CL limit is 285 GeV.

Int. J. Mod. Phys. A 2026.41. Downloaded from www.worldscientific.com
by UNIVERSITY OF CALIFORNIA @ BERKELEY on 09/16/26. Re[redacted] strictly not permitted, except for Open Access articles.

SEARCHES FOR NEUTRAL HIGGS BOSONS REFERENCES

AAD 25AL EPJ C85 573 G. Aad *et al.* (ATLAS Collab.)
AAD 25AN EPJ C85 886 G. Aad *et al.* (ATLAS Collab.)
AAD 25AT PL B868 139671 G. Aad *et al.* (ATLAS Collab.)
AAD 25AU PL B870 139843 G. Aad *et al.* (ATLAS Collab.)
AAD 25AW PR D112 072005 G. Aad *et al.* (ATLAS Collab.)
AAD 25AY PR D112 092001 G. Aad *et al.* (ATLAS Collab.)
AAD 25F PL B865 139472 G. Aad *et al.* (ATLAS Collab.)
AAD 25J PR D111 032006 G. Aad *et al.* (ATLAS Collab.)
AAD 25O JHEP 2501 053 G. Aad *et al.* (ATLAS Collab.)
AAD 25X JHEP 2503 190 G. Aad *et al.* (ATLAS Collab.)
ADAN 25 JHEP 2509 096 D.P. Adan (AACH1)
CHEKHOVSKY 25C JHEP 2506 144 V. Chekhovsky *et al.* (CMS Collab.)
CHEKHOVSKY 25D JHEP 2508 085 V. Chekhovsky *et al.* (CMS Collab.)
CHEKHOVSKY 25I JHEP 2510 074 V. Chekhovsky *et al.* (CMS Collab.)
CHEKHOVSKY 25J JHEP 2510 170 V. Chekhovsky *et al.* (CMS Collab.)
CORTINA-GIL 25B JHEP 2511 143 E. Cortina Gil *et al.* (NA62 Collab.)
HAYRAPETY... 25A PL B860 139067 A. Hayrapetyan *et al.* (CMS Collab.)
HAYRAPETY... 25AP JHEP 2512 178 A. Hayrapetyan *et al.* (CMS Collab.)
HAYRAPETY... 25C PRL 134 041801 A. Hayrapetyan *et al.* (CMS Collab.)
HAYRAPETY... 25I PL B866 139568 A. Hayrapetyan *et al.* (CMS Collab.)
HAYRAPETY... 25P JHEP 2502 050 A. Hayrapetyan *et al.* (CMS Collab.)
AAD 24A PL B848 138394 G. Aad *et al.* (ATLAS Collab.)
AAD 24AB JHEP 2402 197 G. Aad *et al.* (ATLAS Collab.)
AAD 24AP JHEP 2408 013 G. Aad *et al.* (ATLAS Collab.)
AAD 24BQ PR D110 052013 G. Aad *et al.* (ATLAS Collab.)
AAD 24BV PL B858 139007 G. Aad *et al.* (ATLAS Collab.)
AAD 24BW JHEP 2410 104 G. Aad *et al.* (ATLAS Collab.)
AAD 24BX JHEP 2410 130 G. Aad *et al.* (ATLAS Collab.)
AAD 24CA JHEP 2411 047 G. Aad *et al.* (ATLAS Collab.)
AAD 24CB JHEP 2411 097 G. Aad *et al.* (ATLAS Collab.)
AAD 24CD JHEP 2411 126 G. Aad *et al.* (ATLAS Collab.)
AAD 24CF JHEP 2412 126 G. Aad *et al.* (ATLAS Collab.)
AAD 24CI EPJ C84 1102 G. Aad *et al.* (ATLAS Collab.)
AAD 24CK SCIB 69 3005 G. Aad *et al.* (ATLAS Collab.)
AAD 24H PRL 132 231801 G. Aad *et al.* (ATLAS Collab.)
AAD 24K PL B850 138536 G. Aad *et al.* (ATLAS Collab.)
ADACHI 24F PR D109 112015 I. Adachi *et al.* (BELLE II Collab.)
HAYRAPETY... 24AA JHEP 2406 097 A. Hayrapetyan *et al.* (CMS Collab.)
HAYRAPETY... 24AE JHEP 2407 293 A. Hayrapetyan *et al.* (CMS Collab.)
HAYRAPETY... 24AF EPJ C84 493 A. Hayrapetyan *et al.* (CMS Collab.)
HAYRAPETY... 24AI PR D110 032007 A. Hayrapetyan *et al.* (CMS Collab.)
HAYRAPETY... 24AJ JHEP 2408 215 A. Hayrapetyan *et al.* (CMS Collab.)
HAYRAPETY... 24AZ JHEP 2412 172 A. Hayrapetyan *et al.* (CMS Collab.)
HAYRAPETY... 24H PL B850 138478 A. Hayrapetyan *et al.* (CMS Collab.)
HAYRAPETY... 24I PL B852 138582 A. Hayrapetyan *et al.* (CMS Collab.)
TUMASYAN 24A PR D110 012013 A. Tumasyan *et al.* (CMS Collab.)
TUMASYAN 24B JHEP 2405 316 A. Tumasyan *et al.* (CMS Collab.)
AAD 23AD EPJ C83 519 G. Aad *et al.* (ATLAS Collab.)
AAD 23AJ EPJ C83 603 G. Aad *et al.* (ATLAS Collab.)
AAD 23BD JHEP 2307 199 G. Aad *et al.* (ATLAS Collab.)
AAD 23BE JHEP 2307 200 G. Aad *et al.* (ATLAS Collab.)
AAD 23BG JHEP 2307 203 G. Aad *et al.* (ATLAS Collab.)
Also JHEP 2505 159 (errat.) G. Aad *et al.* (ATLAS Collab.)
AAD 23BW PR D108 092007 G. Aad *et al.* (ATLAS Collab.)
AAD 23BX JHEP 2309 189 G. Aad *et al.* (ATLAS Collab.)
AAD 23CA JHEP 2310 009 G. Aad *et al.* (ATLAS Collab.)
AAD 23CR JHEP 2312 081 G. Aad *et al.* (ATLAS Collab.)
AAD 23O JHEP 2306 016 G. Aad *et al.* (ATLAS Collab.)
AAD 23R JHEP 2307 155 G. Aad *et al.* (ATLAS Collab.)
AAD 23U JHEP 2307 125 G. Aad *et al.* (ATLAS Collab.)
AAD 23Z JHEP 2307 040 G. Aad *et al.* (ATLAS Collab.)
ADACHI 23A PRL 130 181803 I. Adachi *et al.* (BELLE II Collab.)
HAYRAPETY... 23C PR D108 072004 A. Hayrapetyan *et al.* (CMS Collab.)
HAYRAPETY... 23G JHEP 2312 070 A. Hayrapetyan *et al.* (CMS Collab.)
TUMASYAN 23 PL B842 137392 A. Tumasyan *et al.* (CMS Collab.)
TUMASYAN 23AR PRL 131 101801 A. Tumasyan *et al.* (CMS Collab.)
TUMASYAN 23M JHEP 2307 148 A. Tumasyan *et al.* (CMS Collab.)
TUMASYAN 23O JHEP 2307 095 A. Tumasyan *et al.* (CMS Collab.)
TUMASYAN 23S JHEP 2307 073 A. Tumasyan *et al.* (CMS Collab.)
AAD 22A PR D105 012006 G. Aad *et al.* (ATLAS Collab.)
AAD 22D PL B829 137066 G. Aad *et al.* (ATLAS Collab.)
AAD 22F PR D105 092002 G. Aad *et al.* (ATLAS Collab.)
AAD 22I JHEP 2201 063 G. Aad *et al.* (ATLAS Collab.)
AAD 22J JHEP 2203 041 G. Aad *et al.* (ATLAS Collab.)
AAD 22P JHEP 2208 104 G. Aad *et al.* (ATLAS Collab.)
AAD 22Y PR D106 052001 G. Aad *et al.* (ATLAS Collab.)
ABLIKIM 22H PR D105 012008 M. Ablikim *et al.* (BESIII Collab.)
ABRATENKO 22A PR D106 092006 P. Abratenko *et al.* (MicroBooNE Collab.)
JIA 22 PRL 128 081804 S. Jia *et al.* (BELLE Collab.)
TUMASYAN 22AK PL B835 137566 A. Tumasyan *et al.* (CMS Collab.)
TUMASYAN 22D PR D105 032008 A. Tumasyan *et al.* (CMS Collab.)
AAD 21AF EPJ C81 332 G. Aad *et al.* (ATLAS Collab.)
AAD 21AI EPJ C81 396 G. Aad *et al.* (ATLAS Collab.)
AAD 21AY PL B822 136651 G. Aad *et al.* (ATLAS Collab.)
AAD 21AZ JHEP 2110 013 G. Aad *et al.* (ATLAS Collab.)
AAD 21BB JHEP 2111 209 G. Aad *et al.* (ATLAS Collab.)
AAD 21BE EPJ C81 860 G. Aad *et al.* (ATLAS Collab.)
ABRATENKO 21 PRL 127 151803 P. Abratenko *et al.* (MicroBooNE Collab.)
SIRUNYAN 21A EPJ C81 13 A.M. Sirunyan *et al.* (CMS Collab.)
Also EPJ C81 333 (errat.) A.M. Sirunyan *et al.* (CMS Collab.)
SLAVICH 21 EPJ C81 450 P. Slavich *et al.*
TUMASYAN 21F JHEP 2111 057 A. Tumasyan *et al.* (CMS Collab.)
AAD 20 PR D101 012002 G. Aad *et al.* (ATLAS Collab.)
AAD 20AA PRL 125 051801 G. Aad *et al.* (ATLAS Collab.)
AAD 20AE PRL 125 221802 G. Aad *et al.* (ATLAS Collab.)
AAD 20AI PR D102 112006 G. Aad *et al.* (ATLAS Collab.)
AAD 20AO JHEP 2011 163 G. Aad *et al.* (ATLAS Collab.)
AAD 20C PL B800 135103 G. Aad *et al.* (ATLAS Collab.)
AAD 20L PR D102 032004 G. Aad *et al.* (ATLAS Collab.)
AAD 20X JHEP 2007 108 G. Aad *et al.* (ATLAS Collab.)
Also JHEP 2101 145 (errat.) G. Aad *et al.* (ATLAS Collab.)
Also JHEP 2105 207 (errat.) G. Aad *et al.* (ATLAS Collab.)
AAIJ 20AL JHEP 2010 156 R. Aaij *et al.* (LHCb Collab.)
SIRUNYAN 20 PL B800 135087 A.M. Sirunyan *et al.* (CMS Collab.)
SIRUNYAN 20AA JHEP 2003 055 A.M. Sirunyan *et al.* (CMS Collab.)
SIRUNYAN 20AC JHEP 2003 065 A.M. Sirunyan *et al.* (CMS Collab.)
SIRUNYAN 20AD JHEP 2003 103 A.M. Sirunyan *et al.* (CMS Collab.)
SIRUNYAN 20AF JHEP 2004 171 A.M. Sirunyan *et al.* (CMS Collab.)
SIRUNYAN 20AP JHEP 2008 139 A.M. Sirunyan *et al.* (CMS Collab.)
SIRUNYAN 20Y JHEP 2003 034 A.M. Sirunyan *et al.* (CMS Collab.)
SIRUNYAN 20Z JHEP 2003 051 A.M. Sirunyan *et al.* (CMS Collab.)
AABOUD 19A JHEP 1901 030 M. Aaboud *et al.* (ATLAS Collab.)
AABOUD 19AG PL B790 1 M. Aaboud *et al.* (ATLAS Collab.)
AABOUD 19AI PL B793 499 M. Aaboud *et al.* (ATLAS Collab.)
AABOUD 19O JHEP 1904 092 M. Aaboud *et al.* (ATLAS Collab.)
AABOUD 19T JHEP 1905 124 M. Aaboud *et al.* (ATLAS Collab.)
AABOUD 19V JHEP 1905 142 M. Aaboud *et al.* (ATLAS Collab.)
AABOUD 19Y JHEP 1907 117 M. Aaboud *et al.* (ATLAS Collab.)
AALTONEN 19 PR D99 052001 T. Aaltonen *et al.* (CDF Collab.)
BAGNASCHI 19 EPJ C79 617 E. Bagnaschi *et al.*
SIRUNYAN 19 PL B788 7 A.M. Sirunyan *et al.* (CMS Collab.)
SIRUNYAN 19AE JHEP 1905 210 A.M. Sirunyan *et al.* (CMS Collab.)
SIRUNYAN 19AN EPJ C79 280 A.M. Sirunyan *et al.* (CMS Collab.)
SIRUNYAN 19AV EPJ C79 564 A.M. Sirunyan *et al.* (CMS Collab.)
SIRUNYAN 19B PR D99 012005 A.M. Sirunyan *et al.* (CMS Collab.)
SIRUNYAN 19BB PL B793 320 A.M. Sirunyan *et al.* (CMS Collab.)
SIRUNYAN 19BD PL B795 398 A.M. Sirunyan *et al.* (CMS Collab.)
SIRUNYAN 19BE PRL 122 121803 A.M. Sirunyan *et al.* (CMS Collab.)
SIRUNYAN 19BQ PL B796 131 A.M. Sirunyan *et al.* (CMS Collab.)
SIRUNYAN 19CR PL B798 134992 A.M. Sirunyan *et al.* (CMS Collab.)
SIRUNYAN 19H JHEP 1901 040 A.M. Sirunyan *et al.* (CMS Collab.)
AABOUD 18AA PR D98 032015 M. Aaboud *et al.* (ATLAS Collab.)
AABOUD 18AG PL B782 750 M. Aaboud *et al.* (ATLAS Collab.)
AABOUD 18AH PL B783 392 M. Aaboud *et al.* (ATLAS Collab.)
AABOUD 18AI JHEP 1803 174 M. Aaboud *et al.* (ATLAS Collab.)
Also JHEP 1811 051 (errat.) M. Aaboud *et al.* (ATLAS Collab.)
AABOUD 18AP JHEP 1806 166 M. Aaboud *et al.* (ATLAS Collab.)
AABOUD 18BF EPJ C78 293 M. Aaboud *et al.* (ATLAS Collab.)
AABOUD 18BU EPJ C78 1007 M. Aaboud *et al.* (ATLAS Collab.)
AABOUD 18BX JHEP 1810 031 M. Aaboud *et al.* (ATLAS Collab.)
AABOUD 18CC JHEP 1811 051 (errat.) M. Aaboud *et al.* (ATLAS Collab.)
AABOUD 18CE JHEP 1812 039 M. Aaboud *et al.* (ATLAS Collab.)
AABOUD 18CQ PRL 121 191801 M. Aaboud *et al.* (ATLAS Collab.)
AABOUD 18CW JHEP 1811 040 M. Aaboud *et al.* (ATLAS Collab.)
AABOUD 18F PL B777 91 M. Aaboud *et al.* (ATLAS Collab.)
AABOUD 18G JHEP 1801 055 M. Aaboud *et al.* (ATLAS Collab.)
AAIJ 18AM EPJ C78 1008 R. Aaij *et al.* (LHCb Collab.)
AAIJ 18AQ JHEP 1809 147 R. Aaij *et al.* (LHCb Collab.)
HALLER 18 EPJ C78 675 J. Haller *et al.* (Gfitter Group)
SIRUNYAN 18A PL B778 101 A.M. Sirunyan *et al.* (CMS Collab.)
SIRUNYAN 18AF PL B781 244 A.M. Sirunyan *et al.* (CMS Collab.)
SIRUNYAN 18BA JHEP 1806 127 A.M. Sirunyan *et al.* (CMS Collab.)
Also JHEP 1903 128 (errat.) A.M. Sirunyan *et al.* (CMS Collab.)
SIRUNYAN 18BP JHEP 1808 113 A.M. Sirunyan *et al.* (CMS Collab.)
SIRUNYAN 18CW JHEP 1808 152 A.M. Sirunyan *et al.* (CMS Collab.)
SIRUNYAN 18CX JHEP 1809 007 A.M. Sirunyan *et al.* (CMS Collab.)
SIRUNYAN 18DK JHEP 1809 148 A.M. Sirunyan *et al.* (CMS Collab.)
SIRUNYAN 18DT PL B785 462 A.M. Sirunyan *et al.* (CMS Collab.)
SIRUNYAN 18DU PR D98 092001 A.M. Sirunyan *et al.* (CMS Collab.)
SIRUNYAN 18ED JHEP 1811 172 A.M. Sirunyan *et al.* (CMS Collab.)
SIRUNYAN 18EE JHEP 1811 018 A.M. Sirunyan *et al.* (CMS Collab.)
SIRUNYAN 18F JHEP 1801 054 A.M. Sirunyan *et al.* (CMS Collab.)
AABOUD 17 PL B764 11 M. Aaboud *et al.* (ATLAS Collab.)
AABOUD 17AN PRL 119 191803 M. Aaboud *et al.* (ATLAS Collab.)
AABOUD 17AP PL B775 105 M. Aaboud *et al.* (ATLAS Collab.)
AABOUD 17AW JHEP 1710 112 M. Aaboud *et al.* (ATLAS Collab.)
KHACHATRY... 17AZ JHEP 1710 076 V. Khachatryan *et al.* (CMS Collab.)
KHACHATRY... 17D JHEP 1701 076 V. Khachatryan *et al.* (CMS Collab.)
KHACHATRY... 17R PL B767 147 V. Khachatryan *et al.* (CMS Collab.)
SIRUNYAN 17AX JHEP 1711 010 A.M. Sirunyan *et al.* (CMS Collab.)
SIRUNYAN 17CN PR D96 072004 A.M. Sirunyan *et al.* (CMS Collab.)
SIRUNYAN 17Y PL B772 363 A.M. Sirunyan *et al.* (CMS Collab.)
AABOUD 16AA EPJ C76 585 M. Aaboud *et al.* (ATLAS Collab.)
AABOUD 16AB EPJ C76 605 M. Aaboud *et al.* (ATLAS Collab.)
AABOUD 16AE JHEP 1609 173 M. Aaboud *et al.* (ATLAS Collab.)
AABOUD 16H JHEP 1609 001 M. Aaboud *et al.* (ATLAS Collab.)
AABOUD 16I PR D94 052002 M. Aaboud *et al.* (ATLAS Collab.)
AAD 16AX EPJ C76 45 G. Aad *et al.* (ATLAS Collab.)
AAD 16C JHEP 1601 032 G. Aad *et al.* (ATLAS Collab.)
AAD 16L EPJ C76 210 G. Aad *et al.* (ATLAS Collab.)
AALTONEN 16C PR D93 112010 T. Aaltonen *et al.* (CDF Collab.)
ABLIKIM 16E PR D93 052005 M. Ablikim *et al.* (BESIII Collab.)
KHACHATRY... 16A PL B752 221 V. Khachatryan *et al.* (CMS Collab.)
KHACHATRY... 16BG EPJ C76 371 V. Khachatryan *et al.* (CMS Collab.)
KHACHATRY... 16BQ PR D94 052012 V. Khachatryan *et al.* (CMS Collab.)
KHACHATRY... 16F JHEP 1601 079 V. Khachatryan *et al.* (CMS Collab.)
KHACHATRY... 16M PRL 117 051802 V. Khachatryan *et al.* (CMS Collab.)
KHACHATRY... 16P PL B755 217 V. Khachatryan *et al.* (CMS Collab.)
KHACHATRY... 16W PL B758 296 V. Khachatryan *et al.* (CMS Collab.)
KHACHATRY... 16Z PL B759 369 V. Khachatryan *et al.* (CMS Collab.)
AAD 15BD EPJ C75 337 G. Aad *et al.* (ATLAS Collab.)
AAD 15BH EPJ C75 299 G. Aad *et al.* (ATLAS Collab.)
Also EPJ C75 408 (errat.) G. Aad *et al.* (ATLAS Collab.)
AAD 15BK EPJ C75 412 G. Aad *et al.* (ATLAS Collab.)
AAD 15BZ PR D92 052002 G. Aad *et al.* (ATLAS Collab.)
AAD 15CE PR D92 092004 G. Aad *et al.* (ATLAS Collab.)
AAD 15H PRL 114 081802 G. Aad *et al.* (ATLAS Collab.)
AAD 15S PL B744 163 G. Aad *et al.* (ATLAS Collab.)
KHACHATRY... 15AW JHEP 1510 144 V. Khachatryan *et al.* (CMS Collab.)
KHACHATRY... 15AY JHEP 1511 071 V. Khachatryan *et al.* (CMS Collab.)
KHACHATRY... 15BB PL B750 494 V. Khachatryan *et al.* (CMS Collab.)
KHACHATRY... 15N PL B748 221 V. Khachatryan *et al.* (CMS Collab.)
KHACHATRY... 15O PL B748 255 V. Khachatryan *et al.* (CMS Collab.)
KHACHATRY... 15R PL B749 560 V. Khachatryan *et al.* (CMS Collab.)
LEES 15H PR D91 071102 J.P. Lees *et al.* (BABAR Collab.)
AAD 14AP PRL 113 171801 G. Aad *et al.* (ATLAS Collab.)
AAD 14AW JHEP 1411 056 G. Aad *et al.* (ATLAS Collab.)
AAD 14BA JHEP 1411 088 G. Aad *et al.* (ATLAS Collab.)
AAD 14M PR D89 032002 G. Aad *et al.* (ATLAS Collab.)
AAD 14O PRL 112 201802 G. Aad *et al.* (ATLAS Collab.)
CHATRCHYAN 14B EPJ C74 2980 S. Chatrchyan *et al.* (CMS Collab.)
CHATRCHYAN 14G JHEP 1401 096 S. Chatrchyan *et al.* (CMS Collab.)
KHACHATRY... 14M JHEP 1410 160 V. Khachatryan *et al.* (CMS Collab.)
KHACHATRY... 14P EPJ C74 3076 V. Khachatryan *et al.* (CMS Collab.)
KHACHATRY... 14Q PR D90 112013 V. Khachatryan *et al.* (CMS Collab.)
AAD 13AG PL B721 32 G. Aad *et al.* (ATLAS Collab.)
AAD 13AT NJP 15 043009 G. Aad *et al.* (ATLAS Collab.)
AAD 13O JHEP 1302 095 G. Aad *et al.* (ATLAS Collab.)
AAIJ 13T JHEP 1305 132 R. Aaij *et al.* (LHCb Collab.)
AALTONEN 13K PR D88 052012 T. Aaltonen *et al.* (CDF Collab.)
AALTONEN 13L PR D88 052013 T. Aaltonen *et al.* (CDF Collab.)
AALTONEN 13M PR D88 052014 T. Aaltonen *et al.* (CDF and D0 Collabs.)
AALTONEN 13P PRL 110 121801 T. Aaltonen *et al.* (CDF Collab.)
ABAZOV 13G PR D88 052006 V.M. Abazov *et al.* (D0 Collab.)
ABAZOV 13H PR D88 052007 V.M. Abazov *et al.* (D0 Collab.)
ABAZOV 13I PR D88 052008 V.M. Abazov *et al.* (D0 Collab.)
ABAZOV 13J PR D88 052009 V.M. Abazov *et al.* (D0 Collab.)
ABAZOV 13L PR D88 052011 V.M. Abazov *et al.* (D0 Collab.)
CARENA 13 EPJ C73 2552 M. Carena *et al.*
CHATRCHYAN 13AG PL B722 207 S. Chatrchyan *et al.* (CMS Collab.)
CHATRCHYAN 13AL PL B725 36 S. Chatrchyan *et al.* (CMS Collab.)
CHATRCHYAN 13BJ PL B726 564 S. Chatrchyan *et al.* (CMS Collab.)
LEES 13C PR D87 031102 J.P. Lees *et al.* (BABAR Collab.)
LEES 13L PR D88 031701 J.P. Lees *et al.* (BABAR Collab.)
LEES 13R PR D88 071102 J.P. Lees *et al.* (BABAR Collab.)
AAD 12AI PL B716 1 G. Aad *et al.* (ATLAS Collab.)
AAD 12AQ PRL 108 251801 G. Aad *et al.* (ATLAS Collab.)
AAD 12N EPJ C72 2157 G. Aad *et al.* (ATLAS Collab.)
AALTONEN 12AB PR D85 092001 T. Aaltonen *et al.* (CDF Collab.)
AALTONEN 12AN PL B717 173 T. Aaltonen *et al.* (CDF Collab.)
AALTONEN 12AQ PR D86 091101 T. Aaltonen *et al.* (CDF and D0 Collabs.)
AALTONEN 12U PR D85 012007 T. Aaltonen *et al.* (CDF Collab.)

AALTONEN	12X	PR D85 032005	T. Aaltonen *et al.*	(CDF Collab.)
ABAZOV	12G	PL B710 569	V.M. Abazov *et al.*	(D0 Collab.)
ABLIKIM	12	PR D85 092012	M. Ablikim *et al.*	(BESIII Collab.)
BAAK	12	EPJ C72 2003	M. Baak *et al.*	(Gfitter Group)
BAAK	12A	EPJ C72 2205	M. Baak *et al.*	(Gfitter Group)
CHATRCHYAN	12AO	JHEP 1209 111	S. Chatrchyan *et al.*	(CMS Collab.)
CHATRCHYAN	12C	JHEP 1203 081	S. Chatrchyan *et al.*	(CMS Collab.)
CHATRCHYAN	12D	JHEP 1204 036	S. Chatrchyan *et al.*	(CMS Collab.)
CHATRCHYAN	12E	PL B710 91	S. Chatrchyan *et al.*	(CMS Collab.)
CHATRCHYAN	12G	PL B710 403	S. Chatrchyan *et al.*	(CMS Collab.)
CHATRCHYAN	12H	PRL 108 111804	S. Chatrchyan *et al.*	(CMS Collab.)
CHATRCHYAN	12I	JHEP 1203 040	S. Chatrchyan *et al.*	(CMS Collab.)
CHATRCHYAN	12K	PL B713 68	S. Chatrchyan *et al.*	(CMS Collab.)
CHATRCHYAN	12N	PL B716 30	S. Chatrchyan *et al.*	(CMS Collab.)
CHATRCHYAN	12V	PRL 109 121801	S. Chatrchyan *et al.*	(CMS Collab.)
AALTONEN	11P	PRL 107 031801	T. Aaltonen *et al.*	(CDF Collab.)
ABAZOV	11K	PL B698 97	V.M. Abazov *et al.*	(D0 Collab.)
ABAZOV	11W	PRL 107 121801	V.M. Abazov *et al.*	(D0 Collab.)
ABOUZAID	11A	PRL 107 201803	E. Abouzaid *et al.*	(KTeV Collab.)
DEL-AMO-SA...	11J	PRL 107 021804	P. del Amo Sanchez *et al.*	(BABAR Collab.)
LEES	11H	PRL 107 221803	J.P. Lees *et al.*	(BABAR Collab.)
ABBIENDI	10	PL B682 381	G. Abbiendi *et al.*	(OPAL Collab.)
ANDREAS	10	JHEP 1008 003	S. Andreas *et al.*	(DESY)
ERLER	10A	PR D81 051301	J. Erler	(UNAM)
HYUN	10	PRL 105 091801	H.J. Hyun *et al.*	(BELLE Collab.)
SCHAEL	10	JHEP 1005 049	S. Schael *et al.*	(ALEPH Collab.)
AALTONEN	09AB	PRL 103 061803	T. Aaltonen *et al.*	(CDF Collab.)
AALTONEN	09AR	PRL 103 201801	T. Aaltonen *et al.*	(CDF Collab.)
ABAZOV	09V	PRL 103 061801	V.M. Abazov *et al.*	(D0 Collab.)
AUBERT	09P	PRL 103 181801	B. Aubert *et al.*	(BABAR Collab.)
AUBERT	09Z	PRL 103 081803	B. Aubert *et al.*	(BABAR Collab.)
TUNG	09	PRL 102 051802	Y.C. Tung *et al.*	(KEK E391a Collab.)
ABAZOV	08U	PRL 101 051801	V.M. Abazov *et al.*	(D0 Collab.)
ABDALLAH	08B	EPJ C54 1	J. Abdallah *et al.*	(DELPHI Collab.)
Also		EPJ C56 165 (errat.)	J. Abdallah *et al.*	(DELPHI Collab.)
LOVE	08	PRL 101 151802	W. Love *et al.*	(CLEO Collab.)
ABBIENDI	07	EPJ C49 457	G. Abbiendi *et al.*	(OPAL Collab.)
BESSON	07	PRL 98 052002	D. Besson *et al.*	(CLEO Collab.)
SCHAEL	07	EPJ C49 439	S. Schael *et al.*	(ALEPH Collab.)
LEP-SLC	06	PRPL 427 257	ALEPH, DELPHI, L3, OPAL, SLD and working groups	
SCHAEL	06B	EPJ C47 547	S. Schael *et al.*	(LEP Collabs.)
ABBIENDI	05A	EPJ C40 317	G. Abbiendi *et al.*	(OPAL Collab.)
ABDALLAH	05D	EPJ C44 147	J. Abdallah *et al.*	(DELPHI Collab.)
ACHARD	05	PL B609 35	P. Achard *et al.*	(L3 Collab.)
ACOSTA	05Q	PR D72 072004	D. Acosta *et al.*	(CDF Collab.)
PARK	05	PRL 94 021801	H.K. Park *et al.*	(FNAL HyperCP Collab.)
ABBIENDI	04K	PL B597 11	G. Abbiendi *et al.*	(OPAL Collab.)
ABBIENDI	04M	EPJ C37 49	G. Abbiendi *et al.*	(OPAL Collab.)
ABDALLAH	04	EPJ C32 145	J. Abdallah *et al.*	(DELPHI Collab.)
ABDALLAH	04B	EPJ C32 475	J. Abdallah *et al.*	(DELPHI Collab.)
ABDALLAH	04L	EPJ C35 313	J. Abdallah *et al.*	(DELPHI Collab.)
ABDALLAH	04O	EPJ C38 1	J. Abdallah *et al.*	(DELPHI Collab.)
ACHARD	04B	PL B583 14	P. Achard *et al.*	(L3 Collab.)
ACHARD	04F	PL B589 89	P. Achard *et al.*	(L3 Collab.)
ABBIENDI	03F	EPJ C27 311	G. Abbiendi *et al.*	(OPAL Collab.)
ABBIENDI	03G	EPJ C27 483	G. Abbiendi *et al.*	(OPAL Collab.)
ACHARD	03C	PL B568 191	P. Achard *et al.*	(L3 Collab.)
ABBIENDI	02D	EPJ C23 397	G. Abbiendi *et al.*	(OPAL Collab.)
ABBIENDI	02F	PL B544 44	G. Abbiendi *et al.*	(OPAL Collab.)
ACHARD	02C	PL B534 28	P. Achard *et al.*	(L3 Collab.)
ACHARD	02H	PL B545 30	P. Achard *et al.*	(L3 Collab.)
AKEROYD	02	PR D66 037702	A.G. Akeroyd *et al.*	
HEISTER	02	PL B526 191	A. Heister *et al.*	(ALEPH Collab.)
HEISTER	02L	PL B544 16	A. Heister *et al.*	(ALEPH Collab.)
HEISTER	02M	PL B544 25	A. Heister *et al.*	(ALEPH Collab.)
ABBIENDI	01E	EPJ C18 425	G. Abbiendi *et al.*	(OPAL Collab.)
ABREU	01F	PL B507 89	P. Abreu *et al.*	(DELPHI Collab.)
AFFOLDER	01H	PR D64 092002	T. Affolder *et al.*	(CDF Collab.)
BARATE	01C	PL B499 53	R. Barate *et al.*	(ALEPH Collab.)
ACCIARRI	00M	PL B485 85	M. Acciarri *et al.*	(L3 Collab.)
ACCIARRI	00R	PL B489 102	M. Acciarri *et al.*	(L3 Collab.)
ACCIARRI	00S	PL B489 115	M. Acciarri *et al.*	(L3 Collab.)
BARATE	00L	PL B487 241	R. Barate *et al.*	(ALEPH Collab.)
ABBIENDI	99E	EPJ C7 407	G. Abbiendi *et al.*	(OPAL Collab.)
ABBIENDI	99O	PL B464 311	G. Abbiendi *et al.*	(OPAL Collab.)
ABBOTT	99B	PRL 82 2244	B. Abbott *et al.*	(D0 Collab.)
ABREU	99P	PL B458 431	P. Abreu *et al.*	(DELPHI Collab.)
ABBOTT	98	PRL 80 442	B. Abbott *et al.*	(D0 Collab.)
ACKERSTAFF	98S	EPJ C5 19	K. Ackerstaff *et al.*	(OPAL Collab.)
ACKERSTAFF	98Y	PL B437 218	K. Ackerstaff *et al.*	(OPAL Collab.)
GONZALEZ...	98B	PR D57 7045	M.C. Gonzalez-Garcia, S.M. Lietti, S.F. Novaes	
KRAWCZYK	97	PR D55 6968	M. Krawczyk, J. Zochowski	(WARS)
ALEXANDER	96H	ZPHY C71 1	G. Alexander *et al.*	(OPAL Collab.)
ABREU	95H	ZPHY C67 69	P. Abreu *et al.*	(DELPHI Collab.)
BALEST	95	PR D51 2053	R. Balest *et al.*	(CLEO Collab.)
PICH	92	NP B388 31	A. Pich, J. Prades, P. Yepes	(CERN, CPPM)
ANTREASYAN	90C	PL B251 204	D. Antreasyan *et al.*	(Crystal Ball Collab.)

Charged Higgs Bosons ($H^{\pm}$ and $H^{\pm\pm}$), Searches for

CONTENTS:

$H^{\pm}$ (charged Higgs) mass limits for $m_{H^+} < m(\text{top})$

$H^{\pm}$ (charged Higgs) mass limits for $m_{H^+} > m(\text{top})$

$H^{\pm\pm}$ (doubly-charged Higgs boson) mass limits

– Limits for $H^{\pm\pm}$ with $T_3 = \pm 1$

– Limits for $H^{\pm\pm}$ with $T_3 = 0$

$H^{\pm}$ (charged Higgs) mass limits for $m_{H^+} < m(\text{top})$

Unless otherwise stated, LEP limits assume $B(H^+ \to \tau^+\nu)+B(H^+ \to c\overline{s})=1$, and hold for all values of $B(H^+ \to \tau^+\nu_\tau)$, and assume H^+ weak isospin of $T_3=+1/2$. In the following, $\tan\beta$ is the ratio of the two vacuum expectation values in two-doublet models (2HDM).

The limits are also applicable to point-like technipions. For a discussion of techniparticles, see the Review of Dynamical Electroweak Symmetry Breaking in this Review.

Limits obtained at the LHC are given in the m_h^{mod-} benchmark scenario, see CARENA 13, and hold for all $\tan\beta$ values.

For limits obtained in hadronic collisions before the observation of the top quark, and based on the top mass values inconsistent with the current measurements, see the 1996 (Physical Review **D54** 1 (1996)) Edition of this Review.

Searches in e^+e^- collisions at and above the Z pole have conclusively ruled out the existence of a charged Higgs in the region $m_{H^+} \lesssim 45$ GeV, and are meanwhile superseded by the searches in higher energy e^+e^- collisions at LEP. Results that are by now obsolete are therefore not included in this compilation, and can be found in a previous Edition (The European Physical Journal **C15** 1 (2000)) of this Review.

In the following, and unless otherwise stated, results from the LEP experiments (ALEPH, DELPHI, L3, and OPAL) are assumed to derive from the study of the $e^+e^- \to H^+H^-$ process. Limits from $b \to s\gamma$ decays are usually stronger in generic 2HDM models than in Supersymmetric models.

VALUE (GeV)	*CL%*	*DOCUMENT ID*		*TECN*	*COMMENT*
none 80–140	95	[1] AAD	15AF	ATLS	$t \to bH^+$
none 90–155	95	[2] KHACHATRY...	15AX	CMS	$t \to bH^+$, $H^+ \to \tau^+\nu$
> 80	95	[3] LEP	13	LEP	$e^+e^- \to H^+H^-$, $E_{cm} \leq$ 209GeV
> 76.3	95	[4] ABBIENDI	12	OPAL	$e^+e^- \to H^+H^-$, $E_{cm} \leq$ 209GeV
> 74.4	95	ABDALLAH	04I	DLPH	$E_{cm} \leq 209$ GeV
> 76.5	95	ACHARD	03E	L3	$E_{cm} \leq 209$ GeV
> 79.3	95	HEISTER	02P	ALEP	$E_{cm} \leq 209$ GeV
• • • We do not use the following data for averages, fits, limits, etc. • • •					
		[5] AAD	25	ATLS	$H^{\pm} \to W^{\pm}Z$
		[6,7] AAD	25AI	ATLS	$t \to bH^+$, $H^+ \to c\overline{s}$
		[6,8] AAD	25K	ATLS	$t \to bH^+$, $H^+ \to \tau^+\nu$
		[6,9] AAD	25K	ATLS	$H^+ \to \tau^+\nu$
		[10] AAD	25U	ATLS	$H^+ \to W^+H$
		[11] HAYRAPETY...	24AV	CMS	$H^{\pm} \to W^{\pm}\gamma$
		[12] AAD	23AH	ATLS	$H^{\pm} \to W^{\pm}Z$
		[6,13] AAD	23BB	ATLS	$t \to bH^+$, $H^+ \to c\overline{b}$
		[6,14] AAD	23BW	ATLS	$t \to bH^+$, $H^+ \to W^+A^0$, $A^0 \to \mu^+\mu^-$
		[15] TUMASYAN	23AV	CMS	$H^{\pm} \to H_2^0 W^{\pm}$
		[16] TUMASYAN	22B	CMS	$H^{\pm} \to W^{\pm}\gamma$
		[17] AAD	21V	ATLS	$\overline{t}bH^+$, $H^+ \to t\overline{b}$
		[18] SIRUNYAN	21W	CMS	$H^+ \to W^+Z$
		[19] AAD	20W	ATLS	$H^+ \to t\overline{b}$
		[20] SIRUNYAN	20AO	CMS	$H^+ \to t\overline{b}$
		[21] SIRUNYAN	20AV	CMS	$H^+ \to t\overline{b}$
		[22] SIRUNYAN	20BE	CMS	$t \to bH^+$, $H^+ \to c\overline{s}$
		[23] SIRUNYAN	19AH	CMS	$H^+ \to \tau^+\nu$
		[24] SIRUNYAN	19BP	CMS	$H^+ \to W^+Z$
		[25] SIRUNYAN	19CC	CMS	$t \to bH^+$, $H^+ \to W^+A^0$, $A^0 \to \mu^+\mu^-$
		[26] SIRUNYAN	19CQ	CMS	$H^+ \to W^+Z$
		[27] AABOUD	18BW	ATLS	$\overline{t}bH^+$ or $t \to bH^+$, $H^+ \to \tau^+\nu$
		[28] AABOUD	18CD	ATLS	$\overline{t}bH^+$, $H^+ \to t\overline{b}$
		[29] AABOUD	18CH	ATLS	$H^{\pm} \to W^{\pm}Z$
		[30] HALLER	18	RVUE	$b \to s\gamma$
		[31] SIRUNYAN	18DO	CMS	$t \to bH^+$, $H^+ \to c\overline{b}$
		[32] MISIAK	17	RVUE	$b \to s(d)\gamma$
		[33] SIRUNYAN	17AE	CMS	$H^{\pm} \to W^{\pm}Z$
		[34] AABOUD	16A	ATLS	$t(b)$ H^+, $H^+ \to \tau^+\nu$
		[35] AAD	16AJ	ATLS	$t(b)$ H^+, $H^+ \to t\overline{b}$
		[36] AAD	16AJ	ATLS	$qq \to H^+$, $H^+ \to t\overline{b}$
		[37] AAD	15AF	ATLS	$tH^{\pm}$
		[38] AAD	15M	ATLS	$H^{\pm} \to W^{\pm}Z$
		[39] KHACHATRY...	15AX	CMS	tH^+, $H^+ \to t\overline{b}$
		[40] KHACHATRY...	15AX	CMS	$tH^{\pm}$, $H^{\pm} \to \tau^{\pm}\nu$
		[41] KHACHATRY...	15BF	CMS	$t \to bH^+$, $H^+ \to c\overline{s}$
		[42] AAD	14M	ATLS	$H_2^0 \to H^{\pm}W^{\mp} \to H^0W^{\pm}W^{\mp}$, $H^0 \to b\overline{b}$
		[43] AALTONEN	14A	CDF	$t \to b\tau\nu$
		[44] AAD	13AC	ATLS	$t \to bH^+$
		[45] AAD	13V	ATLS	$t \to bH^+$, lepton non-universality
		[46] AAD	12BH	ATLS	$t \to bH^+$
		[47] CHATRCHYAN	12AA	CMS	$t \to bH^+$
		[48] AALTONEN	11P	CDF	$t \to bH^+$, $H^+ \to W^+A^0$
>316	95	[49] DESCHAMPS	10	RVUE	Type II, flavor physics data
		[50] AALTONEN	09AJ	CDF	$t \to bH^+$
		[51] ABAZOV	09AC	D0	$t \to bH^+$
		[52] ABAZOV	09AG	D0	$t \to bH^+$
		[53] ABAZOV	09AI	D0	$t \to bH^+$
		[54] ABAZOV	09P	D0	$H^+ \to t\overline{b}$
		[55] ABULENCIA	06E	CDF	$t \to bH^+$
> 92.0	95	ABBIENDI	04	OPAL	$B(\tau\nu) = 1$

Int. J. Mod. Phys. A 2026.41. Downloaded from www.worldscientific.com
by UNIVERSITY OF CALIFORNIA @ BERKELEY on 09/16/26. Re-use and distribution is strictly not permitted, except for Open Access articles.

> 76.7	95	[56] ABDALLAH	04I	DLPH	Type I
		[57] ABBIENDI	03	OPAL	$\tau \to \mu\overline{\nu}\nu$, $e\overline{\nu}\nu$
		[58] ABAZOV	02B	D0	$t \to bH^+$, $H \to \tau\nu$
		[59] BORZUMATI	02	RVUE	
		[60] ABBIENDI	01Q	OPAL	$B \to \tau\nu_\tau X$
		[61] BARATE	01E	ALEP	$B \to \tau\nu_\tau$
>315	99	[62] GAMBINO	01	RVUE	$b \to s\gamma$
		[63] AFFOLDER	00I	CDF	$t \to bH^+$, $H \to \tau\nu$
> 59.5	95	ABBIENDI	99E	OPAL	$E_{cm} \leq 183$ GeV
		[64] ABBOTT	99E	D0	$t \to bH^+$
		[65] ACKERSTAFF	99D	OPAL	$\tau \to e\nu\nu$, $\mu\nu\nu$
		[66] ACCIARRI	97F	L3	$B \to \tau\nu_\tau$
		[67] AMMAR	97B	CLEO	$\tau \to \mu\nu\nu$
		[68] COARASA	97	RVUE	$B \to \tau\nu_\tau X$
		[69] GUCHAIT	97	RVUE	$t \to bH^+$, $H \to \tau\nu$
		[70] MANGANO	97	RVUE	$B_{u(c)} \to \tau\nu_\tau$
		[71] STAHL	97	RVUE	$\tau \to \mu\nu\nu$
>244	95	[72] ALAM	95	CLE2	$b \to s\gamma$
		[73] BUSKULIC	95	ALEP	$b \to \tau\nu_\tau X$

[1] AAD 15AF search for $t\overline{t}$ production followed by $t \to bH^+$, $H^+ \to \tau^+\nu$ in 19.5 fb^{-1} of pp collisions at E_{cm} = 8 TeV. Upper limits on B($t \to bH^+$) B($H^+ \to \tau\nu$) between 2.3×10^{-3} and 1.3×10^{-2} (95% CL) are given for m_{H^+} = 80–160 GeV. See their Fig. 8 for the excluded regions in different benchmark scenarios of the MSSM. The region m_{H^+} < 140 GeV is excluded for tanβ > 1 in the considered scenarios.

[2] KHACHATRYAN 15AX search for $t\overline{t}$ production followed by $t \to bH^+$, $H^+ \to \tau^+\nu$ in 19.7 fb^{-1} of pp collisions at E_{cm} = 8 TeV. Upper limits on B($t \to bH^+$) B($H^+ \to \tau\nu$) between 1.2×10^{-2} and 1.5×10^{-3} (95% CL) are given for m_{H^+} = 80–160 GeV. See their Fig. 11 for the excluded regions in different benchmark scenarios of the MSSM. The region m_{H^+} < 155 GeV is excluded for tanβ > 1 in the considered scenarios.

[3] LEP 13 give a limit that refers to the Type II scenario. The limit for B($H^+ \to \tau\nu$) = 1 is 94 GeV (95% CL), and for B($H^+ \to cs$) = 1 the region below 80.5 as well as the region 83–88 GeV is excluded (95% CL). LEP 13 also search for the decay mode $H^+ \to A^0 W^*$ with $A^0 \to b\overline{b}$, which is not negligible in Type I models. The limit in Type I models is 72.5 GeV (95% CL) if m_{A^0} > 12 GeV.

[4] ABBIENDI 12 also search for the decay mode $H^+ \to A^0 W^*$ with $A^0 \to b\overline{b}$.

[5] AAD 25 combine AAD 23AH and AAD 24AD and derive limits on the isotriplet contribution to the gauge boson masses in the Georgi-Machacek model. See their Fig. 5(c).

[6] Charge conjugated states are also implied.

[7] AAD 25AI search for $t\overline{t}$ production followed by $t \to bH^+$, $H^+ \to c\overline{s}$ using 140 fb^{-1} of pp collisions at E_{cm} = 13 TeV. See their Fig. 6 for limits on the product of branching ratios for m_{H^+} = 60–168 GeV.

[8] AAD 25K search for $t\overline{t}$ production followed by $t \to bH^+$, $H^+ \to \tau^+\nu$ using 140 fb^{-1} of pp collisions at E_{cm} = 13 TeV. See their Fig. 7(b) for limits on the product of branching ratios for m_{H^+} = 60–160 GeV.

[9] AAD 25K search for H^+ production in association with top quark, in the decay mode $H^+ \to \tau^+\nu$, using 140 fb^{-1} of pp collisions at E_{cm} = 13 TeV. See their Fig. 7(a) for limits on cross section times branching ratios for m_{H^+} = 80–3000 GeV, and Fig. 8 for excluded regions in m_{H^+}–tanβ plane in hMSSM and M_h^{125} MSSM scenarios.

[10] AAD 25U search for H^+ production in association with tb, in the decay mode $H^+ \to W^+H$, $H \to b\overline{b}$ in 140 fb^{-1} of pp collisions at E_{cm} = 13 TeV. See their Fig. 15 for limits on cross section times branching ratios for m_{H^+} = 0.25–3 TeV.

[11] HAYRAPETYAN 24AV search for production of scalar resonance decaying to $W^{\pm}\gamma$ with $W \to \ell\nu$ in 138 fb^{-1} of pp collisions at E_{cm} = 13 TeV. See their Fig. 7 for limits on cross section times branching ratio for the mass range 0.3–2.0 TeV for a narrow and a broad width. Combined limits with TUMASYAN 22B are shown in Fig. 8.

[12] AAD 23AH search for vector boson fusion production of $H^{\pm}$ decaying to $H^{\pm} \to W^{\pm}Z \to \ell^{\pm}\nu\ell^+\ell^-$ in 139 fb^{-1} of pp collisions at E_{cm} = 13 TeV. See their Fig. 9 for limits on cross section times branching ratio in the Georgi-Machacek model for $m_{H^{\pm}}$ = 0.2–1.0 TeV, and also for limits on the triplet vacuum expectation value fraction.

[13] AAD 23BB search for $t\overline{t}$ production followed by $t \to bH^+$, $H^+ \to c\overline{b}$ in 139 fb^{-1} of pp collisions at E_{cm} = 13 TeV. See their Fig. 8 for limits on the product of branching ratios for m_{H^+} = 60–160 GeV.

[14] AAD 23BW search for $t \to bH^+$ from pair produced top quarks, with the decay chain $H^+ \to W^+A^0$, $A^0 \to \mu^+\mu^-$ using 139 fb^{-1} of pp collisions at E_{cm} = 13 TeV. See their Fig. 5(b)-(d) for limits on the product of branching ratios for m_{H^+} = 120, 140, 160 GeV, and m_{A^0} = 15–72 GeV.

[15] TUMASYAN 23AV search for production of $H^{\pm}$ in association with a top quark, decaying to $H_2^0 W^{\pm}$, $H_2^0 \to \tau^+\tau^-$, using 138 fb^{-1} of pp collisions at E_{cm} = 13 TeV. See their Fig. 9 for limits on production cross section times branching ratios for $m_{H^{\pm}}$ = 0.3–0.7 TeV and $m_{H_2^0}$ = 0.2 TeV.

[16] TUMASYAN 22B search for production of scalar resonance decaying to $W^{\pm}\gamma \to qq\gamma$ in 137 fb^{-1} of pp collisions at E_{cm} = 13 TeV. See their Fig. 5 for limits on cross section times branching ratio for the mass range 0.7–6.0 TeV, assuming narrow width or Γ/M = 0.05.

[17] AAD 21V search for $\overline{t}bH^+$ associated production followed by $H^+ \to t\overline{b}$ in 139 fb^{-1} of pp collisions at E_{cm} = 13 TeV. See their Fig. 6 for upper limits on cross section times branching ratio for m_{H^+} = 0.2–2 TeV. See also their Fig. 7 for the excluded region in the parameter space of the hMSSM and the following MSSM benchmark scenarios: M_h^{125}, $M_h^{125}(\widetilde{\chi})$, $M_h^{125}(\widetilde{\tau})$, M_h^{125}(alignment), $M_{h_1}^{125}$(CPV).

[18] SIRUNYAN 21W search for vector boson fusion production of H^+ decaying to $H^+ \to W^+Z \to \ell^+\nu\ell^+\ell^-$ in 137 fb^{-1} of pp collisions at E_{cm} = 13 TeV. See their Fig. 8 for limits on cross section times branching ratio for m_{H^+} = 0.2–3.0 TeV, and also for limits on the fraction of the triplet vev contribution to the W mass in the Georgi-Machacek model.

[19] AAD 20W search for dijet resonances in events with isolated leptons using 139 fb^{-1} of pp collisions at E_{cm} = 13 TeV. As a byproduct, $H^+ \to t\overline{b}$ produced in association with $\overline{t}b$ is searched for. Limits on the product of cross section times branching ratio for m_{H^+} = 0.6–2 TeV are given in their Fig. 5(c).

[20] SIRUNYAN 20AO search for $H^+ \to t\overline{b}$ produced in association with $t(b)$ in all jet final states in 35.9 fb^{-1} of pp collisions at E_{cm} = 13 TeV. See their Fig. 6 for limits on the product of cross section times branching ratio for m_{H^+} = 0.2–3 TeV. Limits for s-channel production are also given for m_{H^+} = 0.8–3 TeV. See also Fig. 7 for the corresponding limits in scenarios in the minimal supersymmetric standard model. Cross section limits from combined results with SIRUNYAN 20AV are given in Fig. 8.

[21] SIRUNYAN 20AV search for $H^+ \to t\overline{b}$ produced in association with $t(b)$ in final states with one or two leptons, in 35.9 fb^{-1} of pp collisions at E_{cm} = 13 TeV. See their Fig. 5 for limits on the product of cross section times branching ratio for m_{H^+} = 0.2–3 TeV, and their Fig. 6 for the corresponding limits in scenarios in the minimal supersymmetric standard model.

[22] SIRUNYAN 20BE search for $t \to bH^+$ followed by the decay $H^+ \to c\overline{s}$ in pair produced top quark events using 35.9 fb^{-1} of pp collisions at E_{cm} = 13 TeV. Limits on the branching ratio in the range 1.68–0.25% (95%CL) are given for m_{H^+} = 80–160 GeV, see their Fig. 4.

[23] SIRUNYAN 19AH search for H^+ in the decay of a pair-produced t quark, or in associated tbH^+ or nonresonant $b\overline{b}H^+W^-$ production, followed by $H^+ \to \tau^+\nu$, in 35.9 fb^{-1} of pp collisions at E_{cm} = 13 TeV. Upper limits on cross section times branching ratio between 6 pb and 5 fb (95% CL) are given for m_{H^+} = 80–3000 GeV (including the non-resonant production near the top quark mass), see their Fig. 6 (left). See their Fig. 6 (right) for the excluded regions in the m_h^{mod-} scenario of the MSSM.

[24] SIRUNYAN 19BP search for vector boson fusion production of H^+ decaying to $H^+ \to W^+Z \to \ell^+\nu\ell^+\ell^-$ in 35.9 fb^{-1} of pp collisions at E_{cm} = 13 TeV. See their Fig. 7 for limits on cross section times branching ratio for m_{H^+} = 0.3–2.0 TeV, and also for limits on the fraction of the triplet vev contribution to the W mass in the Georgi-Machacek model.

[25] SIRUNYAN 19CC search for $t \to bH^+$ from pair produced top quarks, with the decay chain $H^+ \to W^+A^0$, $A^0 \to \mu^+\mu^-$ in 35.9 fb^{-1} of pp collisions at E_{cm} = 13 TeV. See their Fig. 2 for limits on the product of branching ratios for m_{A^0} = 15–75 GeV.

[26] SIRUNYAN 19CQ search for vector boson fusion production of H^+ decaying to $H^+ \to W^+Z \to \ell^+\nu q\overline{q}$ or $q\overline{q}\ell^+\ell^-$ in 35.9 fb^{-1} of pp collisions at E_{cm} = 13 TeV. See their Fig. 5 for limits on cross section times branching ratio for m_{H^+} = 0.6–2.0 TeV, and also for limits on the triplet vacuum expectation value fraction in the Georgi-Machacek model.

[27] AABOUD 18BW search for $\overline{t}bH^+$ associated production or the decay $t \to bH^+$, followed by $H^+ \to \tau^+\nu$, in 36.1 fb^{-1} of pp collisions at E_{cm} = 13 TeV. See their Fig. 8(a) for upper limits on cross section times branching ratio for m_{H^+} = 90–2000 GeV, and Fig. 8(b) for limits on B($t \to bH^+$) B($H^+ \to \tau^+\nu$) for m_{H^+} = 90–160 GeV. See also their Fig. 9 for the excluded region in the hMSSM parameter space.

[28] AABOUD 18CD search for $\overline{t}bH^+$ associated production followed by $H^+ \to t\overline{b}$ in 36.1 fb^{-1} of pp collisions at E_{cm} = 13 TeV. See their Fig. 8 for upper limits on cross section times branching ratio for m_{H^+} = 0.2–2 TeV. See also their Fig. 9 for the excluded region in the parameter space of the m_h^{mod-} and hMSSM scenarios of the MSSM. The theory predictions overlaid to the experimental limits to determine the excluded m_{H^+} range are shown without their respective uncertainty band.

[29] AABOUD 18CH search for vector boson fusion production of $H^{\pm}$ decaying to $H^{\pm} \to W^{\pm}Z \to \ell^{\pm}\nu\ell^+\ell^-$ in 36.1 fb^{-1} of pp collisions at E_{cm} = 13 TeV. See their Fig. 7 for limits on cross section times branching ratio for $m_{H^{\pm}}$ = 0.2–0.9 TeV, and also for limits on the triplet vacuum expectation value fraction in the Georgi-Machacek model.

[30] HALLER 18 give 95% CL lower limits on m_{H^+} of 590 GeV in type II two Higgs doublet model from combined data (including an unpublished BELLE result) for B($b \to s\gamma$).

[31] SIRUNYAN 18DO search for $t\overline{t}$ production followed by $t \to bH^+$, $H^+ \to c\overline{b}$ in 19.7 fb^{-1} of pp collisions at E_{cm} = 8 TeV. See their Fig. 3 for upper limits on B($t \to bH^+$) for m_{H^+} = 90–150 GeV assuming that B($H^+ \to c\overline{b}$) = 1 and B($t \to bH^+$) + B($t \to bW^+$) = 1.

[32] MISIAK 17 give 95% CL lower limits on m_{H^+} between 570 and 800 GeV in type II two Higgs doublet model from combined data (including an unpublished BELLE result) for B($b \to s(d)\gamma$).

[33] SIRUNYAN 17AE search for vector boson fusion production of $H^{\pm}$ decaying to $H^{\pm} \to W^{\pm}Z \to \ell^{\pm}\nu\ell^+\ell^-$ in 15.2 fb^{-1} of pp collisions at E_{cm} = 13 TeV. See their Fig. 3 for limits on cross section times branching ratio for $m_{H^{\pm}}$ = 0.2–2.0 TeV, and also for limits on the triplet vacuum expectation value fraction in the Georgi-Machacek model.

[34] AABOUD 16A search for $t(b)$ $H^{\pm}$ associated production followed by $H^+ \to \tau^+\nu$ in 3.2 fb^{-1} of pp collisions at E_{cm} = 13 TeV. Upper limits on $\sigma(t(b)\ H^{\pm})$ B($H^+ \to \tau\nu$) between 1.9 pb and 15 fb (95% CL) are given for m_{H^+} = 200–2000 GeV, see their Fig. 6. See their Fig. 7 for the excluded regions in the hMSSM scenario.

[35] AAD 16AJ search for $t(b)$ $H^{\pm}$ associated production followed by $H^{\pm} \to tb$ in 20.3 fb^{-1} of pp collisions at E_{cm} = 8 TeV. See their Fig. 6 for upper limits on $\sigma(t(b)\ H^{\pm})$ B($H^+ \to tb$) for m_{H^+} = 200–600 GeV.

[36] AAD 16AJ search for $H^{\pm}$ production from quark-antiquark annihilation, followed by $H^{\pm} \to tb$, in 20.3 fb^{-1} of pp collisions at E_{cm} = 8 TeV. See their Fig. 10 for upper limits on $\sigma(H^{\pm})$ B($H^+ \to tb$) for m_{H^+} = 400–3000 GeV.

[37] AAD 15AF search for $tH^{\pm}$ associated production followed by $H^{\pm} \to \tau^{\pm}\nu$ in 19.5 fb^{-1} of pp collisions at E_{cm} = 8 TeV. Upper limits on $\sigma(tH^{\pm})$ B($H^+ \to \tau\nu$) between 760 and 4.5 fb (95% CL) are given for m_{H^+} = 180–1000 GeV. See their Fig. 8 for the excluded regions in different benchmark scenarios of the MSSM.

[38] AAD 15M search for vector boson fusion production of $H^{\pm}$ decaying to $H^{\pm} \to W^{\pm}Z \to q\overline{q}\ell^+\ell^-$ in 20.3 fb^{-1} of pp collisions at E_{cm} = 8 TeV. See their Fig. 2 for limits on cross section times branching ratio for $m_{H^{\pm}}$ = 200–1000 GeV, and Fig. 3 for limits on thetriplet vacuum expectation value fraction in the Georgi-Machacek model.

[39] KHACHATRYAN 15AX search for $tH^{\pm}$ associated production followed by $H^{\pm} \to tb$ in 19.7 fb^{-1} of pp collisions at E_{cm} = 8 TeV. Upper limits on $\sigma(tH^{\pm})$ B($H^+ \to t\overline{b}$)

Int. J. Mod. Phys. A 2026.41. Downloaded from www.worldscientific.com
by UNIVERSITY OF CALIFORNIA @ BERKELEY on 09/16/26. Reproduction is strictly not permitted, except for Open Access articles.

Int. J. Mod. Phys. A 2026.41. Downloaded from www.worldscientific.com
by UNIVERSITY OF CALIFORNIA @ BERKELEY on 09/16/26. Re-use and distribution is strictly not permitted, except for Open Access articles.

between 2.0 and 0.13 pb (95% CL) are given for m_{H^+} = 180–600 GeV. See their Fig. 11 for the excluded regions in different benchmark scenarios of the MSSM.

[40] KHACHATRYAN 15AX search for $tH^\pm$ associated production followed by $H^\pm \to \tau^\pm\nu$ in 19.7 fb^{-1} of pp collisions at E_{cm} = 8 TeV. Upper limits on $\sigma(tH^\pm)$ B($H^+ \to \tau\nu$) between 380 and 25 fb (95% CL) are given for m_{H^+} = 180–600 GeV. See their Fig. 11 for the excluded regions in different benchmark scenarios of the MSSM.

[41] KHACHATRYAN 15BF search for $t\overline{t}$ production followed by $t \to bH^+$, $H^+ \to c\overline{s}$ in 19.7 fb^{-1} of pp collisions at E_{cm} = 8 TeV. Upper limits on B($t \to bH^+$) B($H^+ \to c\overline{s}$) between 1.2×10^{-2} and 6.5×10^{-2} (95% CL) are given for m_{H^+} = 90–160 GeV.

[42] AAD 14M search for the decay cascade $H_2^0 \to H^\pm W^\mp \to H^0 W^\pm W^\mp$, H^0 decaying to $b\overline{b}$ in 20.3 fb^{-1} of pp collisions at E_{cm} = 8 TeV. See their Table III for limits on cross section times branching ratio for $m_{H_2^0}$= 325–1025 GeV and m_{H^+}= 225–925 GeV.

[43] AALTONEN 14A measure B($t \to b\tau\nu$) = 0.096 ± 0.028 using 9 fb^{-1} of $p\overline{p}$ collisions at E_{cm} = 1.96 TeV. For m_{H^+}= 80–140 GeV, this measured value is translated to a limit B($t \to bH^+$) < 0.059 at 95% CL assuming B($H^+ \to \tau^+\nu$) = 1.

[44] AAD 13AC search for $t\overline{t}$ production followed by $t \to bH^+$, $H^+ \to c\overline{s}$ (flavor unidentified) in 4.7 fb^{-1} of pp collisions at E_{cm} = 7 TeV. Upper limits on B($t \to bH^+$) between 0.05 and 0.01 (95%CL) are given for m_{H^+}=90–150 GeV and B($H^+ \to c\overline{s}$)=1.

[45] AAD 13V search for $t\overline{t}$ production followed by $t \to bH^+$, $H^+ \to \tau^+\nu$ through violation of lepton universality with 4.6 fb^{-1} of pp collisions at E_{cm} = 7 TeV. Upper limits on B($t \to bH^+$) between 0.032 and 0.044 (95% CL) are given for m_{H^+} = 90–140 GeV and B($H^+ \to \tau^+\nu$) = 1. By combining with AAD 12BH, the limits improve to 0.008 to 0.034 for m_{H^+} = 90–160 GeV. See their Fig. 7 for the excluded region in the m_h^{max} scenario of the MSSM.

[46] AAD 12BH search for $t\overline{t}$ production followed by $t \to bH^+$, $H^+ \to \tau^+\nu$ with 4.6 fb^{-1} of pp collisions at E_{cm} = 7 TeV. Upper limits on B($t \to bH^+$) between 0.01 and 0.05 (95% CL) are given for m_{H^+} = 90–160 GeV and B($H^+ \to \tau^+\nu$) = 1. See their Fig. 8 for the excluded region in the m_h^{max} scenario of the MSSM.

[47] CHATRCHYAN 12AA search for $t\overline{t}$ production followed by $t \to bH^+$, $H^+ \to \tau^+\nu$ with 2 fb^{-1} of pp collisions at E_{cm} = 7 TeV. Upper limits on B($t \to bH^+$) between 0.019 and 0.041 (95% CL) are given for m_{H^+} = 80–160 GeV and B($H^+ \to \tau^+\nu$)=1.

[48] AALTONEN 11P search in 2.7 fb^{-1} of $p\overline{p}$ collisions at E_{cm} = 1.96 TeV for the decay chain $t \to bH^+$, $H^+ \to W^+A^0$, $A^0 \to \tau^+\tau^-$ with m_{A^0} between 4 and 9 GeV. See their Fig. 4 for limits on B($t \to bH^+$) for 90 < m_{H^+} < 160 GeV.

[49] DESCHAMPS 10 make Type II two Higgs doublet model fits to weak leptonic and semileptonic decays, $b \to s\gamma$, B, B_s mixings, and $Z \to b\overline{b}$. The limit holds irrespective of tanβ.

[50] AALTONEN 09AJ search for $t \to bH^+$, $H^+ \to c\overline{s}$ in $t\overline{t}$ events in 2.2 fb^{-1} of $p\overline{p}$ collisions at E_{cm} = 1.96 TeV. Upper limits on B($t \to bH^+$) between 0.08 and 0.32 (95% CL) are given for m_{H^+} = 60–150 GeV and B($H^+ \to c\overline{s}$) = 1.

[51] ABAZOV 09AC search for $t \to bH^+$, $H^+ \to \tau^+\nu$ in $t\overline{t}$ events in 0.9 fb^{-1} of $p\overline{p}$ collisions at E_{cm} = 1.96 TeV. Upper limits on B($t \to bH^+$) between 0.19 and 0.25 (95% CL) are given for m_{H^+} = 80–155 GeV and B($H^+ \to \tau^+\nu$) = 1. See their Fig. 4 for an excluded region in a MSSM scenario.

[52] ABAZOV 09AG measure $t\overline{t}$ cross sections in final states with ℓ + jets ($\ell = e, \mu$), $\ell\ell$, and $\tau\ell$ in 1 fb^{-1} of $p\overline{p}$ collisions at E_{cm} = 1.96 TeV, which constrains possible $t \to bH^+$ branching fractions. Upper limits (95% CL) on B($t \to bH^+$) between 0.15 and 0.40 (0.48 and 0.57) are given for B($H^+ \to \tau^+\nu$) = 1 (B($H^+ \to c\overline{s}$) = 1) for m_{H^+} = 80–155 GeV.

[53] ABAZOV 09AI search for $t \to bH^+$ in $t\overline{t}$ events in 1 fb^{-1} of $p\overline{p}$ collisions at E_{cm} = 1.96 TeV. Final states with ℓ + jets ($\ell = e, \mu$), $\ell\ell$, and $\tau\ell$ are examined. Upper limits on B($t \to bH^+$) (95% CL) between 0.15 and 0.19 (0.19 and 0.22) are given for B($H^+ \to \tau^+\nu$) = 1 (B($H^+ \to c\overline{s}$) = 1) for m_{H^+} = 80–155 GeV. For B($H^+ \to \tau^+\nu$) = 1 also a simultaneous extraction of B($t \to bH^+$) and the $t\overline{t}$ cross section is performed, yielding a limit on B($t \to bH^+$) between 0.12 and 0.26 for m_{H^+} = 80–155 GeV. See their Figs. 5–8 for excluded regions in several MSSM scenarios.

[54] ABAZOV 09P search for H^+ production by $q\overline{q}'$ annihilation followed by $H^+ \to t\overline{b}$ decay in 0.9 fb^{-1} of $p\overline{p}$ collisions at E_{cm} = 1.96 TeV. Cross section limits in several two-doublet models are given for m_{H^+} = 180–300 GeV. A region with 20 $\lesssim$ tanβ $\lesssim$ 70 is excluded (95% CL) for 180 GeV $\lesssim m_{H^+} \lesssim$ 184 GeV in type-I models.

[55] ABULENCIA 06E search for associated H^0W production in $p\overline{p}$ collisions at E_{cm} = 1.96 TeV. A fit is made for $t\overline{t}$ production processes in dilepton, lepton + jets, and lepton + τ final states, with the decays $t \to W^+b$ and $t \to H^+b$ followed by $H^+ \to \tau^+\nu$, $c\overline{s}$, $t^*\overline{b}$, or W^+H^0. Within the MSSM the search is sensitive to the region tanβ < 1 or > 30 in the mass range m_{H^+} = 80–160 GeV. See Fig. 2 for the excluded region in a certain MSSM scenario.

[56] ABDALLAH 04I search for $e^+e^- \to H^+H^-$ with $H^\pm$ decaying to $\tau\nu$, cs, or W^*A^0 in Type-I two-Higgs-doublet models.

[57] ABBIENDI 03 give a limit m_{H^+} > 1.28tanβ GeV (95%CL) in Type II two-doublet models.

[58] ABAZOV 02B search for a charged Higgs boson in top decays with $H^+ \to \tau^+\nu$ at E_{cm}=1.8 TeV. For m_{H^+}=75 GeV, the region tanβ > 32.0 is excluded at 95%CL. The excluded mass region extends to over 140 GeV for tanβ values above 100.

[59] BORZUMATI 02 point out that the decay modes such as $b\overline{b}W$, A^0W, and supersymmetric ones can have substantial branching fractions in the mass range explored at LEP II and Tevatron.

[60] ABBIENDI 01Q give a limit tanβ/m_{H^+} < 0.53 GeV^{-1} (95%CL) in Type II two-doublet models.

[61] BARATE 01E give a limit tanβ/m_{H^+} < 0.40 GeV^{-1} (90% CL) in Type II two-doublet models. An independent measurement of $B \to \tau\nu_\tau X$ gives tanβ/m_{H^+} < 0.49 GeV^{-1} (90% CL).

[62] GAMBINO 01 use the world average data in the summer of 2001 B($b \to s\gamma$) = (3.23 ± 0.42) × 10^{-4}. The limit applies for Type-II two-doublet models.

[63] AFFOLDER 00I search for a charged Higgs boson in top decays with $H^+ \to \tau^+\nu$ in $p\overline{p}$ collisions at E_{cm}=1.8 TeV. The excluded mass region extends to over 120 GeV for tanβ values above 100 and B($\tau\nu$) = 1. If B($t \to bH^+$) $\gtrsim$ 0.6, m_{H^+} up to 160 GeV is excluded. Updates ABE 97L.

[64] ABBOTT 99E search for a charged Higgs boson in top decays in $p\overline{p}$ collisions at E_{cm}=1.8 TeV, by comparing the observed $t\overline{t}$ cross section (extracted from the data assuming the dominant decay $t \to bW^+$) with theoretical expectation. The search is sensitive to regions of the domains tan$\beta \lesssim$1, 50 < m_{H^+}(GeV) $\lesssim$120 and tan$\beta \gtrsim$40, 50 < m_{H^+} (GeV) $\lesssim$160. See Fig. 3 for the details of the excluded region.

[65] ACKERSTAFF 99D measure the Michel parameters ρ, ξ, η, and $\xi\delta$ in leptonic τ decays from $Z \to \tau\tau$. Assuming e-μ universality, the limit m_{H^+} > 0.97 tanβ GeV (95%CL) is obtained for two-doublet models in which only one doublet couples to leptons.

[66] ACCIARRI 97F give a limit m_{H^+} > 2.6 tanβ GeV (90% CL) from their limit on the exclusive $B \to \tau\nu_\tau$ branching ratio.

[67] AMMAR 97B measure the Michel parameter ρ from $\tau \to e\nu\nu$ decays and assumes e/μ universality to extract the Michel η parameter from $\tau \to \mu\nu\nu$ decays. The measurement is translated to a lower limit on m_{H^+} in a two-doublet model m_{H^+} > 0.97 tanβ GeV (90% CL).

[68] COARASA 97 reanalyzed the constraint on the ($m_{H^\pm}$,tanβ) plane derived from the inclusive $B \to \tau\nu_\tau X$ branching ratio in GROSSMAN 95B and BUSKULIC 95. They show that the constraint is quite sensitive to supersymmetric one-loop effects.

[69] GUCHAIT 97 studies the constraints on m_{H^+} set by Tevatron data on $\ell\tau$ final states in $t\overline{t} \to (Wb)(Hb)$, $W \to \ell\nu$, $H \to \tau\nu_\tau$. See Fig. 2 for the excluded region.

[70] MANGANO 97 reconsiders the limit in ACCIARRI 97F including the effect of the potentially large $B_c \to \tau\nu_\tau$ background to $B_u \to \tau\nu_\tau$ decays. Stronger limits are obtained.

[71] STAHL 97 fit τ lifetime, leptonic branching ratios, and the Michel parameters and derive limit m_{H^+} > 1.5 tanβ GeV (90% CL) for a two-doublet model. See also STAHL 94.

[72] ALAM 95 measure the inclusive $b \to s\gamma$ branching ratio at $\Upsilon(4S)$ and give B($b \to s\gamma$)< 4.2 × 10^{-4} (95% CL), which translates to the limit m_{H^+} >[244 + 63/(tanβ)$^{1.3}$] GeV in the Type II two-doublet model. Light supersymmetric particles can invalidate this bound.

[73] BUSKULIC 95 give a limit m_{H^+} > 1.9 tanβ GeV (90% CL) for Type-II models from $b \to \tau\nu_\tau X$ branching ratio, as proposed in GROSSMAN 94.

$H^\pm$ (charged Higgs) mass limits for m_{H^+} > m(top)

Limits obtained at the LHC are given in the m_h^{mod-} benchmark scenario, see CARENA 13, and depend on the tanβ values.

VALUE (GeV)	CL%	DOCUMENT ID		TECN	COMMENT
> 181	95	[1] AABOUD	18BW	ATLS	tanβ = 10
> 249	95	[1] AABOUD	18BW	ATLS	tanβ = 20
> 390	95	[1] AABOUD	18BW	ATLS	tanβ = 30
> 894	95	[1] AABOUD	18BW	ATLS	tanβ = 40
>1017	95	[1] AABOUD	18BW	ATLS	tanβ = 50
>1103	95	[1] AABOUD	18BW	ATLS	tanβ = 60

[1] AABOUD 18BW search for $\overline{t}bH^+$ associated production in 36.1 fb^{-1} of pp collisions at E_{cm} = 13 TeV. See also their Fig. 9 for the excluded region in the hMSSM parameter space.

$H^{\pm\pm}$ (doubly-charged Higgs boson) mass limits

This section covers searches for a doubly-charged Higgs boson with couplings to lepton pairs. Its weak isospin T_3 is thus restricted to two possibilities depending on lepton chiralities: $T_3(H^{\pm\pm})$ = ±1, with the coupling $g_{\ell\ell}$ to $\ell_L^-\ell_L'^-$ and $\ell_R^+\ell_R'^+$ ("left-handed") and $T_3(H^{\pm\pm})$ = 0, with the coupling to $\ell_R^-\ell_R'^-$ and $\ell_L^+\ell_L'^+$ ("right-handed"). These Higgs bosons appear in some left-right symmetric models based on the gauge group SU(2)$_L$×SU(2)$_R$×U(1), the type-II seesaw model, and the Zee-Babu model. The two cases are listed separately in the following. Unless noted, one of the lepton flavor combinations is assumed to be dominant in the decay.

Limits for $H^{\pm\pm}$ with T_3 = ±1

VALUE (GeV)	CL%	DOCUMENT ID		TECN	COMMENT
>1020	95	[1] AAD	23AI	ATLS	$\ell\ell$
none 200–220	95	[2] AABOUD	19K	ATLS	$W^\pm W^\pm$
> 768	95	[3] AABOUD	18BC	ATLS	ee
> 846	95	[3] AABOUD	18BC	ATLS	$\mu\mu$
> 468	95	[4] AAD	15AG	ATLS	$e\mu$
> 400	95	[5] AAD	15AP	ATLS	$e\tau$
> 400	95	[5] AAD	15AP	ATLS	$\mu\tau$
> 169	95	[6] CHATRCHYAN	12AU	CMS	$\tau\tau$
> 300	95	[6] CHATRCHYAN	12AU	CMS	$\mu\tau$
> 293	95	[6] CHATRCHYAN	12AU	CMS	$e\tau$
> 395	95	[6] CHATRCHYAN	12AU	CMS	$\mu\mu$
> 391	95	[6] CHATRCHYAN	12AU	CMS	$e\mu$
> 382	95	[6] CHATRCHYAN	12AU	CMS	ee
> 98.1	95	[7] ABDALLAH	03	DLPH	$\tau\tau$
> 99.0	95	[8] ABBIENDI	02C	OPAL	$\tau\tau$
• • • We do not use the following data for averages, fits, limits, etc. • • •					
		[9] AAD	25	ATLS	$W^\pm W^\pm$
		[10] AAD	24AD	ATLS	$W^\pm W^\pm$
> 350	95	[11] AAD	21U	ATLS	$W^\pm W^\pm$

> 230	95	[12] AAD	21U	ATLS	$H^{\pm\pm}H^{\mp}$ associated production, $H^{\pm\pm} \to W^{\pm}W^{\pm}$, $H^{\pm} \to W^{\pm}Z$
		[13] SIRUNYAN	21W	CMS	$W^{\pm}W^{\pm}$
		[14] SIRUNYAN	19CQ	CMS	$W^{\pm}W^{\pm}$
		[15] SIRUNYAN	18CC	CMS	$W^{\pm}W^{\pm}$
> 551	95	[4] AAD	15AG	ATLS	ee
> 516	95	[4] AAD	15AG	ATLS	$\mu\mu$
		[16] KANEMURA	15	RVUE	$W^{(*)\pm}W^{(*)\pm}$
		[17] KHACHATRY...	15D	CMS	$W^{\pm}W^{\pm}$
		[18] KANEMURA	14	RVUE	$W^{(*)\pm}W^{(*)\pm}$
> 330	95	[19] AAD	13Y	ATLS	$\mu\mu$
> 237	95	[19] AAD	13Y	ATLS	$\mu\tau$
> 355	95	[20] AAD	12AY	ATLS	$\mu\mu$
> 398	95	[21] AAD	12CQ	ATLS	$\mu\mu$
> 375	95	[21] AAD	12CQ	ATLS	$e\mu$
> 409	95	[21] AAD	12CQ	ATLS	ee
> 128	95	[22] ABAZOV	12A	D0	$\tau\tau$
> 144	95	[22] ABAZOV	12A	D0	$\mu\tau$
> 245	95	[23] AALTONEN	11AF	CDF	$\mu\mu$
> 210	95	[23] AALTONEN	11AF	CDF	$e\mu$
> 225	95	[23] AALTONEN	11AF	CDF	ee
> 114	95	[24] AALTONEN	08AA	CDF	$e\tau$
> 112	95	[24] AALTONEN	08AA	CDF	$\mu\tau$
> 168	95	[25] ABAZOV	08V	D0	$\mu\mu$
		[26] AKTAS	06A	H1	single $H^{\pm\pm}$
> 133	95	[27] ACOSTA	05L	CDF	stable
> 118.4	95	[28] ABAZOV	04E	D0	$\mu\mu$
		[29] ABBIENDI	03Q	OPAL	$E_{cm} \leq 209$ GeV, single $H^{\pm\pm}$
		[30] GORDEEV	97	SPEC	muonium conversion
		[31] ASAKA	95	THEO	
> 45.6	95	[32] ACTON	92M	OPAL	
> 30.4	95	[33] ACTON	92M	OPAL	
none 6.5–36.6	95	[34] SWARTZ	90	MRK2	

[1] AAD 23AI search for $H^{++}H^{--}$ production using 139 fb^{-1} of pp collisions at E_{cm} = 13 TeV. Decay branching ratios B($H^{++} \to \ell^{+}\ell'^{+}$) for the six flavor combinations are assumed to be equal, adding up to unity. If the $T_3 = 0$ states are degenerate with the $T_3 = \pm 1$ states, the limit becomes 1080 GeV.

[2] AABOUD 19K search for pair production of $H^{++}H^{--}$ followed by the decay $H^{\pm\pm} \to W^{\pm}W^{\pm}$ in 36.1 fb^{-1} of pp collisions at E_{cm} = 13 TeV. The search is interpreted in a doublet-triplet extension of the scalar sector with a vev of 0.1 GeV, leading to B($H^{\pm\pm} \to W^{\pm}W^{\pm}$) = 1. See their Fig. 5 for limits on the cross section for $m_{H^{++}}$ between 200 and 700 GeV.

[3] See their Figs. 11(b) and 13 for limits with smaller branching ratios.

[4] AAD 15AG search for $H^{++}H^{--}$ production in 20.3 fb^{-1} of pp collisions at E_{cm} = 8 TeV. The limit assumes 100% branching ratio to the specified final state. See their Fig. 5 for limits for arbitrary branching ratios.

[5] AAD 15AP search for $H^{++}H^{--}$ production in 20.3 fb^{-1} of pp collisions at E_{cm} = 8 TeV. The limit assumes 100% branching ratio to the specified final state.

[6] CHATRCHYAN 12AU search for $H^{++}H^{--}$ production with 4.9 fb^{-1} of pp collisions at E_{cm} = 7 TeV. The limit assumes 100% branching ratio to the specified final state. See their Table 6 for limits including associated $H^{++}H^{-}$ production or assuming different scenarios.

[7] ABDALLAH 03 search for $H^{++}H^{--}$ pair production either followed by $H^{++} \to \tau^{+}\tau^{+}$, or decaying outside the detector.

[8] ABBIENDI 02C searches for pair production of $H^{++}H^{--}$, with $H^{\pm\pm} \to \ell^{\pm}\ell^{\pm}$ ($\ell,\ell' = e,\mu,\tau$). The limit holds for $\ell=\ell'=\tau$, and becomes stronger for other combinations of leptonic final states. To ensure the decay within the detector, the limit only applies for $g(H\ell\ell) \gtrsim 10^{-7}$.

[9] AAD 25 combine AAD 23AH and AAD 24AD and derive limits on the isotriplet contribution to the gauge boson masses in the Georgi-Machacek model. See their Fig. 5(c).

[10] AAD 24AD search for production of $H^{\pm\pm}$ by $W^{\pm}W^{\pm}$ fusion, in the decay to $W^{\pm}W^{\pm}$, using 139 fb^{-1} of pp collisions at E_{cm} = 13 TeV. See their Fig. 12 for limits on cross section times branching ratio for $m_{H^{\pm\pm}}$ between 0.2 and 3.0 TeV. Limits on the isotriplet contribution to the gauge-boson masses in the Georgi-Machacek model are also shown.

[11] AAD 21U search for pair production of $H^{++}H^{--}$ followed by the decay $H^{\pm\pm} \to W^{\pm}W^{\pm}$ in 139 fb^{-1} of pp collisions at E_{cm} = 13 TeV. The search is interpreted in a triplet extension of the SM Higgs sector with a triplet vev of 0.1 GeV, leading to B($H^{\pm\pm} \to W^{\pm}W^{\pm}$) = 1. See their Fig. 9(a) for limits on the cross section for $m_{H^{++}}$ between 200 and 600 GeV.

[12] AAD 21U search for associated production of $H^{\pm\pm}H^{\mp}$ followed by the decays $H^{\pm\pm} \to W^{\pm}W^{\pm}$, $H^{\pm} \to W^{\pm}Z$ in 139 fb^{-1} of pp collisions at E_{cm} = 13 TeV. $H^{\pm\pm}$ and $H^{\pm}$ are assumed to be degenerate in mass within 5 GeV. The search is interpreted in a triplet extension of the SM Higgs sector with a triplet vev of 0.1 GeV, leading to B($H^{\pm\pm} \to W^{\pm}W^{\pm}$) = 1. See their Fig. 9(b) for limits on the cross section for $m_{H^{++}}$ between 200 and 600 GeV.

[13] SIRUNYAN 21W search for vector boson fusion production of $H^{\pm\pm}$ decaying to $H^{\pm\pm} \to W^{\pm}W^{\pm} \to \ell^{\pm}\nu\ell^{\pm}\nu$ in 137 fb^{-1} of pp collisions at E_{cm} = 13 TeV. See their Fig. 8 for limits on cross section times branching ratio for $m_{H^{++}}$ = 0.2–3.0 TeV.

[14] SIRUNYAN 19CQ search for $H^{\pm\pm}$ production by vector boson fusion followed by the decay $H^{\pm\pm} \to W^{\pm}W^{\pm} \to qq\ell\nu$ in 35.9 fb^{-1} of pp collisions at E_{cm} = 13 TeV. See their Fig. 5 for limits on cross section times branching ratio for $m_{H^{\pm\pm}}$ between 0.6 and 2 TeV.

[15] SIRUNYAN 18CC search for $H^{\pm\pm}$ production by vector boson fusion followed by the decay $H^{\pm\pm} \to W^{\pm}W^{\pm}$ in 35.9 fb^{-1} of pp collisions at E_{cm} = 13 TeV. See their Fig. 3 for limits on cross section times branching ratio for $m_{H^{\pm\pm}}$ between 200 and 1000 GeV.

[16] KANEMURA 15 examine the case where H^{++} decays preferentially to $W^{(*)}W^{(*)}$ and estimate that a lower mass limit of ~ 84 GeV can be derived from the same-sign dilepton data of AAD 15AG if H^{++} decays with 100% branching ratio to $W^{(*)}W^{(*)}$.

[17] KHACHATRYAN 15D search for $H^{\pm\pm}$ production by vector boson fusion followed by the decay $H^{\pm\pm} \to W^{\pm}W^{\pm}$ in 19.4 fb^{-1} of pp collisions at E_{cm} = 8 TeV. See their Fig. 4 for limits on cross section times branching ratio for $m_{H^{++}}$ between 160 and 800 GeV.

[18] KANEMURA 14 examine the case where H^{++} decays preferentially to $W^{(*)}W^{(*)}$ and estimate that a lower mass limit of ~ 60 GeV can be derived from the same-sign dilepton data of AAD 12CY.

[19] AAD 13Y search for $H^{++}H^{--}$ production in a generic search of events with three charged leptons in 4.6 fb^{-1} of pp collisions at E_{cm} = 7 TeV. The limit assumes 100% branching ratio to the specified final state.

[20] AAD 12AY search for $H^{++}H^{--}$ production with 1.6 fb^{-1} of pp collisions at E_{cm} = 7 TeV. The limit assumes 100% branching ratio to the specified final state.

[21] AAD 12CQ search for $H^{++}H^{--}$ production with 4.7 fb^{-1} of pp collisions at E_{cm} = 7 TeV. The limit assumes 100% branching ratio to the specified final state. See their Table 1 for limits assuming smaller branching ratios.

[22] ABAZOV 12A search for $H^{++}H^{--}$ production in 7.0 fb^{-1} of $p\overline{p}$ collisions at E_{cm} = 1.96 TeV.

[23] AALTONEN 11AF search for $H^{++}H^{--}$ production in 6.1 fb^{-1} of $p\overline{p}$ collisions at E_{cm} = 1.96 TeV.

[24] AALTONEN 08AA search for $H^{++}H^{--}$ production in $p\overline{p}$ collisions at E_{cm} = 1.96 TeV. The limit assumes 100% branching ratio to the specified final state.

[25] ABAZOV 08V search for $H^{++}H^{--}$ production in $p\overline{p}$ collisions at E_{cm} = 1.96 TeV. The limit is for B($H \to \mu\mu$) = 1. The limit is updated in ABAZOV 12A.

[26] AKTAS 06A search for single $H^{\pm\pm}$ production in ep collisions at HERA. Assuming that H^{++} only couples to $e^{+}\mu^{+}$ with $g_{e\mu}$ = 0.3 (electromagnetic strength), a limit $m_{H^{++}} > 141$ GeV (95% CL) is derived. For the case where H^{++} couples to $e\tau$ only the limit is 112 GeV.

[27] ACOSTA 05L search for $H^{++}H^{--}$ pair production in $p\overline{p}$ collisions. The limit is valid for $g_{\ell\ell'} < 10^{-8}$ so that the Higgs decays outside the detector.

[28] ABAZOV 04E search for $H^{++}H^{--}$ pair production in $H^{\pm\pm} \to \mu^{\pm}\mu^{\pm}$. The limit is valid for $g_{\mu\mu} \gtrsim 10^{-7}$.

[29] ABBIENDI 03Q searches for single $H^{\pm\pm}$ via direct production in $e^{+}e^{-} \to e^{\mp}e^{\mp}H^{\pm\pm}$, and via t-channel exchange in $e^{+}e^{-} \to e^{+}e^{-}$. In the direct case, and assuming B($H^{\pm\pm} \to \ell^{\pm}\ell^{\pm}$) = 1, a 95% CL limit on $h_{ee} < 0.071$ is set for $m_{H^{\pm\pm}} < 160$ GeV (see Fig. 6). In the second case, indirect limits on h_{ee} are set for $m_{H^{\pm\pm}} < 2$ TeV (see Fig. 8).

[30] GORDEEV 97 search for muonium-antimuonium conversion and find $G_{M\overline{M}}/G_F < 0.14$ (90% CL), where $G_{M\overline{M}}$ is the lepton-flavor violating effective four-fermion coupling. This limit may be converted to $m_{H^{++}} > 210$ GeV if the Yukawa couplings of H^{++} to ee and $\mu\mu$ are as large as the weak gauge coupling. For similar limits on muonium-antimuonium conversion, see the muon Particle Listings.

[31] ASAKA 95 point out that H^{++} decays dominantly to four fermions in a large region of parameter space where the limit of ACTON 92M from the search of dilepton modes does not apply.

[32] ACTON 92M limit assumes $H^{\pm\pm} \to \ell^{\pm}\ell^{\pm}$ or $H^{\pm\pm}$ does not decay in the detector. Thus the region $g_{\ell\ell} \approx 10^{-7}$ is not excluded.

[33] ACTON 92M from $\Delta\Gamma_Z$ <40 MeV.

[34] SWARTZ 90 assume $H^{\pm\pm} \to \ell^{\pm}\ell^{\pm}$ (any flavor). The limits are valid for the Higgs-lepton coupling g($H\ell\ell$) $\gtrsim 7.4 \times 10^{-7}/[m_H/\text{GeV}]^{1/2}$. The limits improve somewhat for ee and $\mu\mu$ decay modes.

Limits for $H^{\pm\pm}$ with $T_3 = 0$

VALUE (GeV)	CL%	DOCUMENT ID		TECN	COMMENT
>900	95	[1] AAD	23AI	ATLS	$\ell\ell$
> 58	95	[2] AABOUD	18BC	ATLS	ee
>723	95	[2] AABOUD	18BC	ATLS	$\mu\mu$
>402	95	[3] AAD	15AG	ATLS	$e\mu$
>290	95	[4] AAD	15AP	ATLS	$e\tau$
>290	95	[4] AAD	15AP	ATLS	$\mu\tau$
> 97.3	95	[5] ABDALLAH	03	DLPH	$\tau\tau$
> 97.3	95	[6] ACHARD	03F	L3	$\tau\tau$
> 98.5	95	[7] ABBIENDI	02C	OPAL	$\tau\tau$
• • • We do not use the following data for averages, fits, limits, etc. • • •					
>374	95	[3] AAD	15AG	ATLS	ee
>438	95	[3] AAD	15AG	ATLS	$\mu\mu$
>251	95	[8] AAD	12AY	ATLS	$\mu\mu$
>306	95	[9] AAD	12CQ	ATLS	$\mu\mu$
>310	95	[9] AAD	12CQ	ATLS	$e\mu$
>322	95	[9] AAD	12CQ	ATLS	ee
>113	95	[10] ABAZOV	12A	D0	$\mu\tau$
>205	95	[11] AALTONEN	11AF	CDF	$\mu\mu$
>190	95	[11] AALTONEN	11AF	CDF	$e\mu$
>205	95	[11] AALTONEN	11AF	CDF	ee
>145	95	[12] ABAZOV	08V	D0	$\mu\mu$
		[13] AKTAS	06A	H1	single $H^{\pm\pm}$
>109	95	[14] ACOSTA	05L	CDF	stable
> 98.2	95	[15] ABAZOV	04E	D0	$\mu\mu$
		[16] ABBIENDI	03Q	OPAL	$E_{cm} \leq 209$ GeV, single $H^{\pm\pm}$
		[17] GORDEEV	97	SPEC	muonium conversion
> 45.6	95	[18] ACTON	92M	OPAL	
> 25.5	95	[19] ACTON	92M	OPAL	
none 7.3–34.3	95	[20] SWARTZ	90	MRK2	

Int. J. Mod. Phys. A 2026.41. Downloaded from worldscientific.com
by UNIVERSITY OF CALIFORNIA @ BERKELEY on 09/16/26. Reproduction is strictly not permitted, except for Open Access articles.

Int. J. Mod. Phys. A 2026.41. Downloaded from www.worldscientific.com
by UNIVERSITY OF CALIFORNIA @ BERKELEY on 09/16/26. Re-use and distribution is strictly not permitted, except for Open Access articles.

[1] AAD 23AI search for $H^{++}H^{--}$ production using 139 fb^{-1} of pp collisions at E_{cm} = 13 TeV. Decay branching ratios B($H^{++} \rightarrow \ell^+\ell'^+$) for the six flavor combinations are assumed to be equal, adding up to unity.

[2] See their Figs. 12(b) and 14 for limits with smaller branching ratios.

[3] AAD 15AG search for $H^{++}H^{--}$ production in 20.3 fb^{-1} of pp collisions at E_{cm} = 8 TeV. The limit assumes 100% branching ratio to the specified final state. See their Fig. 5 for limits for arbitrary branching ratios.

[4] AAD 15AP search for $H^{++}H^{--}$ production in 20.3 fb^{-1} of pp collisions at E_{cm} = 8 TeV. The limit assumes 100% branching ratio to the specified final state.

[5] ABDALLAH 03 search for $H^{++}H^{--}$ pair production either followed by $H^{++} \rightarrow \tau^+\tau^+$, or decaying outside the detector.

[6] ACHARD 03F search for $e^+e^- \rightarrow H^{++}H^{--}$ with $H^{\pm\pm} \rightarrow \ell^{\pm}\ell'^{\pm}$. The limit holds for $\ell = \ell' = \tau$, and slightly different limits apply for other flavor combinations. The limit is valid for $g_{\ell\ell'} \gtrsim 10^{-7}$.

[7] ABBIENDI 02C searches for pair production of $H^{++}H^{--}$, with $H^{\pm\pm} \rightarrow \ell^{\pm}\ell^{\pm}$ (ℓ,ℓ' = e,μ,τ). the limit holds for ℓ=ℓ'=τ, and becomes stronger for other combinations of leptonic final states. To ensure the decay within the detector, the limit only applies for $g(H\ell\ell) \gtrsim 10^{-7}$.

[8] AAD 12AY search for $H^{++}H^{--}$ production with 1.6 fb^{-1} of pp collisions at E_{cm} = 7 TeV. The limit assumes 100% branching ratio to the specified final state.

[9] AAD 12CQ search for $H^{++}H^{--}$ production with 4.7 fb^{-1} of pp collisions at E_{cm} = 7 TeV. The limit assumes 100% branching ratio to the specified final state. See their Table 1 for limits assuming smaller branching ratios.

[10] ABAZOV 12A search for $H^{++}H^{--}$ production in 7.0 fb^{-1} of $p\overline{p}$ collisions at E_{cm} = 1.96 TeV.

[11] AALTONEN 11AF search for $H^{++}H^{--}$ production in 6.1 fb^{-1} of $p\overline{p}$ collisions at E_{cm} = 1.96 TeV.

[12] ABAZOV 08V search for $H^{++}H^{--}$ production in $p\overline{p}$ collisions at E_{cm}= 1.96 TeV. The limit is for B($H \rightarrow \mu\mu$) = 1. The limit is updated in ABAZOV 12A.

[13] AKTAS 06A search for single $H^{\pm\pm}$ production in ep collisions at HERA. Assuming that H^{++} only couples to $e^+\mu^+$ with $g_{e\mu}$ = 0.3 (electromagnetic strength), a limit $m_{H^{++}}$ > 141 GeV (95% CL) is derived. For the case where H^{++} couples to $e\tau$ only the limit is 112 GeV.

[14] ACOSTA 05L search for $H^{++}H^{--}$ pair production in $p\overline{p}$ collisions. The limit is valid for $g_{\ell\ell'} < 10^{-8}$ so that the Higgs decays outside the detector.

[15] ABAZOV 04E search for $H^{++}H^{--}$ pair production in $H^{\pm\pm} \rightarrow \mu^{\pm}\mu^{\pm}$. The limit is valid for $g_{\mu\mu} \gtrsim 10^{-7}$.

[16] ABBIENDI 03Q searches for single $H^{\pm\pm}$ via direct production in $e^+e^- \rightarrow e^{\mp}e^{\mp}H^{\pm\pm}$, and via t-channel exchange in $e^+e^- \rightarrow e^+e^-$. In the direct case, and assuming B($H^{\pm\pm} \rightarrow \ell^{\pm}\ell^{\pm}$) = 1, a 95% CL limit on h_{ee} < 0.071 is set for $m_{H^{\pm\pm}}$ < 160 GeV (see Fig. 6). In the second case, indirect limits on h_{ee} are set for $m_{H^{\pm\pm}}$ < 2 TeV (see Fig. 8).

[17] GORDEEV 97 search for muonium-antimuonium conversion and find $G_{M\overline{M}}/G_F$ < 0.14 (90% CL), where $G_{M\overline{M}}$ is the lepton-flavor violating effective four-fermion coupling. This limit may be converted to $m_{H^{++}}$ > 210 GeV if the Yukawa couplings of H^{++} to ee and $\mu\mu$ are as large as the weak gauge coupling. For similar limits on muonium-antimuonium conversion, see the muon Particle Listings.

[18] ACTON 92M limit assumes $H^{\pm\pm} \rightarrow \ell^{\pm}\ell^{\pm}$ or $H^{\pm\pm}$ does not decay in the detector. Thus the region $g_{\ell\ell} \approx 10^{-7}$ is not excluded.

[19] ACTON 92M from $\Delta\Gamma_Z$ <40 MeV.

[20] SWARTZ 90 assume $H^{\pm\pm} \rightarrow \ell^{\pm}\ell^{\pm}$ (any flavor). The limits are valid for the Higgs-lepton coupling g($H\ell\ell$) $\gtrsim 7.4 \times 10^{-7}/[m_H/\text{GeV}]^{1/2}$. The limits improve somewhat for ee and $\mu\mu$ decay modes.

$H^{\pm}$ and $H^{\pm\pm}$ REFERENCES

AAD	25	PL B860 139137	G. Aad *et al.*	(ATLAS Collab.)
AAD	25AI	EPJ C85 153	G. Aad *et al.*	(ATLAS Collab.)
AAD	25K	PR D111 072006	G. Aad *et al.*	(ATLAS Collab.)
AAD	25U	JHEP 2502 143	G. Aad *et al.*	(ATLAS Collab.)
AAD	24AD	JHEP 2404 026	G. Aad *et al.*	(ATLAS Collab.)
HAYRAPETY...	24AV	JHEP 2409 186	A. Hayrapetyan *et al.*	(CMS Collab.)
AAD	23AH	EPJ C83 633	G. Aad *et al.*	(ATLAS Collab.)
AAD	23AI	EPJ C83 605	G. Aad *et al.*	(ATLAS Collab.)
AAD	23BB	JHEP 2309 004	G. Aad *et al.*	(ATLAS Collab.)
AAD	23BW	PR D108 092007	G. Aad *et al.*	(ATLAS Collab.)
TUMASYAN	23AV	JHEP 2309 032	A. Tumasyan *et al.*	(CMS Collab.)
TUMASYAN	22B	PL B826 136888	A. Tumasyan *et al.*	(CMS Collab.)
AAD	21U	JHEP 2106 146	G. Aad *et al.*	(ATLAS Collab.)
AAD	21V	JHEP 2106 145	G. Aad *et al.*	(ATLAS Collab.)
SIRUNYAN	21W	EPJ C81 723	A.M. Sirunyan *et al.*	(CMS Collab.)
AAD	20W	JHEP 2006 151	G. Aad *et al.*	(ATLAS Collab.)
SIRUNYAN	20AO	JHEP 2007 126	A.M. Sirunyan *et al.*	(CMS Collab.)
SIRUNYAN	20AV	JHEP 2001 096	A.M. Sirunyan *et al.*	(CMS Collab.)
SIRUNYAN	20BE	PR D102 072001	A.M. Sirunyan *et al.*	(CMS Collab.)
AABOUD	19K	EPJ C79 58	M. Aaboud *et al.*	(ATLAS Collab.)
SIRUNYAN	19AH	JHEP 1907 142	A.M. Sirunyan *et al.*	(CMS Collab.)
SIRUNYAN	19BP	PL B795 281	A.M. Sirunyan *et al.*	(CMS Collab.)
SIRUNYAN	19CC	PRL 123 131802	A.M. Sirunyan *et al.*	(CMS Collab.)
SIRUNYAN	19CQ	PL B798 134985	A.M. Sirunyan *et al.*	(CMS Collab.)
AABOUD	18BC	EPJ C78 199	M. Aaboud *et al.*	(ATLAS Collab.)
AABOUD	18BW	JHEP 1809 139	M. Aaboud *et al.*	(ATLAS Collab.)
AABOUD	18CD	JHEP 1811 085	M. Aaboud *et al.*	(ATLAS Collab.)
AABOUD	18CH	PL B787 68	M. Aaboud *et al.*	(ATLAS Collab.)
HALLER	18	EPJ C78 675	J. Haller *et al.*	(Gfitter Group)
SIRUNYAN	18CC	PRL 120 081801	A.M. Sirunyan *et al.*	(CMS Collab.)
SIRUNYAN	18DO	JHEP 1811 115	A.M. Sirunyan *et al.*	(CMS Collab.)
MISIAK	17	EPJ C77 201	M. Misiak, M. Steinhauser	
SIRUNYAN	17AE	PRL 119 141802	A.M. Sirunyan *et al.*	(CMS Collab.)
AABOUD	16A	PL B759 555	M. Aaboud *et al.*	(ATLAS Collab.)
AAD	16AJ	JHEP 1603 127	G. Aad *et al.*	(ATLAS Collab.)
AAD	15AF	JHEP 1503 088	G. Aad *et al.*	(ATLAS Collab.)
AAD	15AG	JHEP 1503 041	G. Aad *et al.*	(ATLAS Collab.)
AAD	15AP	JHEP 1508 138	G. Aad *et al.*	(ATLAS Collab.)
AAD	15M	PRL 114 231801	G. Aad *et al.*	(ATLAS Collab.)
KANEMURA	15	PTEP 2015 051B02	S. Kanemura *et al.*	
KHACHATRY...	15AX	JHEP 1511 018	V. Khachatryan *et al.*	(CMS Collab.)
KHACHATRY...	15BF	JHEP 1512 178	V. Khachatryan *et al.*	(CMS Collab.)
KHACHATRY...	15D	PRL 114 051801	V. Khachatryan *et al.*	(CMS Collab.)
AAD	14M	PR D89 032002	G. Aad *et al.*	(ATLAS Collab.)
AALTONEN	14A	PR D89 091101	T. Aaltonen *et al.*	(CDF Collab.)
KANEMURA	14	PR D90 115018	S. Kanemura *et al.*	
AAD	13AC	EPJ C73 2465	G. Aad *et al.*	(ATLAS Collab.)
AAD	13V	JHEP 1303 076	G. Aad *et al.*	(ATLAS Collab.)
AAD	13Y	PR D87 052002	G. Aad *et al.*	(ATLAS Collab.)
CARENA	13	EPJ C73 2552	M. Carena *et al.*	
LEP	13	EPJ C73 2463	LEP Collabs	(ALEPH, DELPHI, L3, OPAL, LEP)
AAD	12AY	PR D85 032004	G. Aad *et al.*	(ATLAS Collab.)
AAD	12BH	JHEP 1206 039	G. Aad *et al.*	(ATLAS Collab.)
AAD	12CQ	EPJ C72 2244	G. Aad *et al.*	(ATLAS Collab.)
AAD	12CY	JHEP 1212 007	G. Aad *et al.*	(ATLAS Collab.)
ABAZOV	12A	PRL 108 021801	V.M. Abazov *et al.*	(D0 Collab.)
ABBIENDI	12	EPJ C72 2076	G. Abbiendi *et al.*	(OPAL Collab.)
CHATRCHYAN	12AA	JHEP 1207 143	S. Chatrchyan *et al.*	(CMS Collab.)
CHATRCHYAN	12AU	EPJ C72 2189	S. Chatrchyan *et al.*	(CMS Collab.)
AALTONEN	11AF	PRL 107 181801	T. Aaltonen *et al.*	(CDF Collab.)
AALTONEN	11P	PRL 107 031801	T. Aaltonen *et al.*	(CDF Collab.)
DESCHAMPS	10	PR D82 073012	O. Deschamps *et al.*	(CLER, ORSAY, LAPP)
AALTONEN	09AJ	PRL 103 101803	T. Aaltonen *et al.*	(CDF Collab.)
ABAZOV	09AC	PR D80 051107	V.M. Abazov *et al.*	(D0 Collab.)
ABAZOV	09AG	PR D80 071102	V.M. Abazov *et al.*	(D0 Collab.)
ABAZOV	09AI	PL B682 278	V.M. Abazov *et al.*	(D0 Collab.)
ABAZOV	09P	PRL 102 191802	V.M. Abazov *et al.*	(D0 Collab.)
AALTONEN	08AA	PRL 101 121801	T. Aaltonen *et al.*	(CDF Collab.)
ABAZOV	08V	PRL 101 071803	V.M. Abazov *et al.*	(D0 Collab.)
ABULENCIA	06E	PRL 96 042003	A. Abulencia *et al.*	(CDF Collab.)
AKTAS	06A	PL B638 432	A. Aktas *et al.*	(H1 Collab.)
ACOSTA	05L	PRL 95 071801	D. Acosta *et al.*	(CDF Collab.)
ABAZOV	04E	PRL 93 141801	V.M. Abazov *et al.*	(D0 Collab.)
ABBIENDI	04	EPJ C32 453	G. Abbiendi *et al.*	(OPAL Collab.)
ABDALLAH	04I	EPJ C34 399	J. Abdallah *et al.*	(DELPHI Collab.)
ABBIENDI	03	PL B551 35	G. Abbiendi *et al.*	(OPAL Collab.)
ABBIENDI	03Q	PL B577 93	G. Abbiendi *et al.*	(OPAL Collab.)
ABDALLAH	03	PL B552 127	J. Abdallah *et al.*	(DELPHI Collab.)
ACHARD	03E	PL B575 208	P. Achard *et al.*	(L3 Collab.)
ACHARD	03F	PL B576 18	P. Achard *et al.*	(L3 Collab.)
ABAZOV	02B	PRL 88 151803	V.M. Abazov *et al.*	(D0 Collab.)
ABBIENDI	02C	PL B526 221	G. Abbiendi *et al.*	(OPAL Collab.)
BORZUMATI	02	PL B549 170	F.M. Borzumati, A. Djouadi	
HEISTER	02P	PL B543 1	A. Heister *et al.*	(ALEPH Collab.)
ABBIENDI	01Q	PL B520 1	G. Abbiendi *et al.*	(OPAL Collab.)
BARATE	01E	EPJ C19 213	R. Barate *et al.*	(ALEPH Collab.)
GAMBINO	01	NP B611 338	P. Gambino, M. Misiak	
AFFOLDER	00I	PR D62 012004	T. Affolder *et al.*	(CDF Collab.)
PDG	00	EPJ C15 1	D.E. Groom *et al.*	(PDG Collab.)
ABBIENDI	99E	EPJ C7 407	G. Abbiendi *et al.*	(OPAL Collab.)
ABBOTT	99E	PRL 82 4975	B. Abbott *et al.*	(D0 Collab.)
ACKERSTAFF	99D	EPJ C8 3	K. Ackerstaff *et al.*	(OPAL Collab.)
ABE	97L	PRL 79 357	F. Abe *et al.*	(CDF Collab.)
ACCIARRI	97F	PL B396 327	M. Acciarri *et al.*	(L3 Collab.)
AMMAR	97B	PRL 78 4686	R. Ammar *et al.*	(CLEO Collab.)
COARASA	97	PL B406 337	J.A. Coarasa, R.A. Jimenez, J. Sola	
GORDEEV	97	PAN 60 1164	V.A. Gordeev *et al.*	(PNPI)
		Translated from YAF 60 1291.		
GUCHAIT	97	PR D55 7263	M. Guchait, D.P. Roy	(TATA)
MANGANO	97	PL B410 299	M. Mangano, S. Slabospitsky	
STAHL	97	ZPHY C74 73	A. Stahl, H. Voss	(BONN)
PDG	96	PR D54 1	R. M. Barnett *et al.*	(PDG Collab.)
ALAM	95	PRL 74 2885	M.S. Alam *et al.*	(CLEO Collab.)
ASAKA	95	PL B345 36	T. Asaka, K.I. Hikasa	(TOHOK)
BUSKULIC	95	PL B343 444	D. Buskulic *et al.*	(ALEPH Collab.)
GROSSMAN	95B	PL B357 630	Y. Grossman, H. Haber, Y. Nir	
GROSSMAN	94	PL B332 373	Y. Grossman, Z. Ligeti	
STAHL	94	PL B324 121	A. Stahl	(BONN)
ACTON	92M	PL B295 347	P.D. Acton *et al.*	(OPAL Collab.)
SWARTZ	90	PRL 64 2877	M.L. Swartz *et al.*	(Mark II Collab.)

New Heavy Bosons (W', Z', leptoquarks, etc.), Searches for

We list here various limits on charged and neutral heavy vector bosons (other than W's and Z's), heavy scalar bosons (other than Higgs bosons), vector or scalar leptoquarks, and axigluons. The latest unpublished results are described in "W' Searches" and "Z' Searches" reviews. For recent searches on scalar bosons which could be identified as Higgs bosons, see the listings in the Higgs boson section.

CONTENTS:

Mass Limits for W' (Heavy Charged Vector Boson Other Than W) in Hadron Collider Experiments
W_R (Right-Handed W Boson) Mass Limits
Limit on W_L-W_R Mixing Angle ζ
Mass Limits for Z' (Heavy Neutral Vector Boson Other Than Z)
– Limits for Z'_{SM}
– Limits for Z_{LR}
– Limits for Z_χ
– Limits for Z_ψ
– Limits for Z_η
– Limits for other Z'
– Searches for Z' with Lepton-Flavor-Violating decays
Indirect Constraints on Kaluza-Klein Gauge Bosons
Mass Limits for Leptoquarks from Pair Production
Mass Limits for Leptoquarks from Single Production
Indirect Limits for Leptoquarks
Mass Limits for Diquarks
Mass Limits for g_A (axigluon) and Other Color-Octet Gauge Bosons
Mass Limits for Color-Octet Scalar Bosons
X^0 (Heavy Boson) Searches in Z Decays
Mass Limits for a Heavy Neutral Boson Coupling to e^+e^-
Search for X^0 Resonance in e^+e^- Collisions

Search for X^0 Resonance in ep Collisions
Search for X^0 Resonance in Two-Photon Process
Search for X^0 Resonance in $e^+e^- \to X^0\gamma$
Search for X^0 Resonance in $Z \to f\overline{f}X^0$
Search for X^0 Resonance in WX^0 final state
Search for X^0 Resonance in Quarkonium Decays

See the related review(s):

W'-Boson Searches

MASS LIMITS for W' (Heavy Charged Vector Boson Other Than W) in Hadron Collider Experiments

Couplings of W' to quarks and leptons are taken to be identical with those of W. The following limits are obtained from $p\overline{p}$ or $pp \to W'X$ with W' decaying to the mode indicated in the comments. New decay channels (*e.g.*, $W' \to WZ$) are assumed to be suppressed. The most recent preliminary results can be found in the "W'-boson searches" review above.

VALUE (GeV)	CL%	DOCUMENT ID		TECN	COMMENT
>6000 (CL = 95%) OUR LIMIT					
none 500–5000	95	[1] AAD	24T	ATLAS	$W' \to \tau\nu$
none 2000–4300	95	[2] HAYRAPETY...	24X	CMS	$W' \to tb$
>2500	95	[3] AAD	23AH	ATLAS	$W' \to WZ$
none 500–4600	95	[4] AAD	23CC	ATLAS	$W' \to tb$
>1200	95	[5] AAD	23L	ATLAS	$W' \to ZX$
none 400–3300	95	[6] AAD	23O	ATLAS	$W' \to WH$
>4400	95	[7] TUMASYAN	23AP	CMS	$W' \to WZ$
>4000	95	[8] TUMASYAN	23AP	CMS	$W' \to WH$
none 600–4800	95	[9] TUMASYAN	23AW	CMS	$W' \to \tau\nu$
>5700	95	[10] TUMASYAN	22AC	CMS	$W' \to e\nu,\ \mu\nu$
>3900	95	[11] TUMASYAN	22D	CMS	$W' \to WZ$
>4000	95	[11] TUMASYAN	22D	CMS	$W' \to WH$
none 1000–4000	95	[12] TUMASYAN	22J	CMS	$W' \to WZ$
none 500–2000	95	[13] TUMASYAN	22R	CMS	$W' \to WZ$
none 1000–3400	95	[14] SIRUNYAN	21Y	CMS	$W' \to tb$
>3200	95	[15] AAD	20AJ	ATLAS	$W' \to WH$
>4300	95	[16] AAD	20AT	ATLAS	$W' \to WZ$
none 1100–4000	95	[17] AAD	20T	ATLAS	$W' \to q\overline{q}$
none 1800–3600	95	[18] SIRUNYAN	20AI	CMS	$W' \to q\overline{q}$
none 1200–3800	95	[19] SIRUNYAN	20Q	CMS	$W' \to WZ$
none 500–3250	95	[20] AABOUD	19E	ATLAS	$W' \to tb$
>6000	95	[21] AAD	19C	ATLAS	$W' \to e\nu,\ \mu\nu$
none 1300–3600	95	[22] AAD	19D	ATLAS	$W' \to WZ$
none 400–4000	95	[23] SIRUNYAN	19AY	CMS	$W' \to \tau\nu$
>4300	95	[24] SIRUNYAN	19CP	CMS	$W' \to WZ,\ WH,\ \ell\nu$
>2600	95	[25] SIRUNYAN	19I	CMS	$W' \to WH$
none 1000–3000	95	[26] AABOUD	18AF	ATLAS	$W' \to tb$
none 500–2820	95	[27] AABOUD	18AI	ATLAS	$W' \to WH$
none 300–3000	95	[28] AABOUD	18AK	ATLAS	$W' \to WZ$
none 800–3200	95	[29] AABOUD	18AL	ATLAS	$W' \to WZ$
>5100	95	[30] AABOUD	18BG	ATLAS	$W' \to e\nu,\ \mu\nu$
none 250–2460	95	[31] AABOUD	18CH	ATLAS	$W' \to WZ$
none 1200–3300	95	[32] AABOUD	18F	ATLAS	$W' \to WZ$
none 500–3700	95	[33] AABOUD	18K	ATLAS	$W' \to \tau\nu$
none 1000–3600	95	[34] SIRUNYAN	18	CMS	$W' \to tb$
none 1000–3050	95	[35] SIRUNYAN	18AX	CMS	$W' \to WZ$
none 400–5200	95	[36] SIRUNYAN	18AZ	CMS	$W' \to e\nu,\ \mu\nu$
none 1000–3400	95	[37] SIRUNYAN	18BK	CMS	$W' \to WZ$
none 600–3300	95	[38] SIRUNYAN	18BO	CMS	$W' \to q\overline{q}$
none 800–2330	95	[39] SIRUNYAN	18DJ	CMS	$W' \to WZ$
>2800	95	[40] SIRUNYAN	18ED	CMS	$W' \to WH$
none 1200–3200, 3300–3600	95	[41] SIRUNYAN	18P	CMS	$W' \to WZ$
>3600	95	[42] AABOUD	17AK	ATLAS	$W' \to q\overline{q}$
none 1100–2500	95	[43] AABOUD	17AO	ATLAS	$W' \to WH$
>2220	95	[44] AABOUD	17B	ATLAS	$W' \to WH$
>2300	95	[45] KHACHATRY...	17J	CMS	$W' \to N_\tau\tau \to \tau\tau jj$
none 600–2700	95	[46] KHACHATRY...	17W	CMS	$W' \to q\overline{q}$
>4100	95	[47] KHACHATRY...	17Z	CMS	$W' \to e\nu,\ \mu\nu$
>2200	95	[48] SIRUNYAN	17A	CMS	$W' \to WZ$
>2300	95	[49] SIRUNYAN	17AK	CMS	$W' \to WZ,\ WH$
>2900	95	[50] SIRUNYAN	17H	CMS	$W' \to \tau N$
>2600	95	[51] SIRUNYAN	17I	CMS	$W' \to tb$
>2450	95	[52] SIRUNYAN	17R	CMS	$W' \to WH$
none 2780–3150	95	[52] SIRUNYAN	17R	CMS	$W' \to WH$
>2600	95	[53] AABOUD	16AE	ATLAS	$W' \to WZ$
>4070	95	[54] AABOUD	16V	ATLAS	$W' \to e\nu,\ \mu\nu$
>1810	95	[55] AAD	16R	ATLAS	$W' \to WZ$
>2600	95	[56] AAD	16S	ATLAS	$W' \to q\overline{q}$
>2150	95	[57] KHACHATRY...	16AO	CMS	$W' \to tb$
none 1000–1600	95	[58] KHACHATRY...	16AP	CMS	$W' \to WH$
none 800–1500	95	[59] KHACHATRY...	16BD	CMS	$W' \to WH \to b\overline{b}\ell\nu$
none 1500–2600	95	[60] KHACHATRY...	16K	CMS	$W' \to q\overline{q}$
none 500–1600	95	[61] KHACHATRY...	16L	CMS	$W' \to q\overline{q}$
none 300–2700	95	[62] KHACHATRY...	16O	CMS	$W' \to \tau\nu$
none 400–1590	95	[63] AAD	15AU	ATLAS	$W' \to WZ$
none 1500–1760	95	[64] AAD	15AV	ATLAS	$W' \to tb$
none 300–1490	95	[65] AAD	15AZ	ATLAS	$W' \to WZ$
none 1300–1500	95	[66] AAD	15CP	ATLAS	$W' \to WZ$
none 500–1920	95	[67] AAD	15R	ATLAS	$W' \to tb$
none 800–2450	95	[68] AAD	15V	ATLAS	$W' \to q\overline{q}$
>1470	95	[69] KHACHATRY...	15C	CMS	$W' \to WZ$
>3710	95	[70] KHACHATRY...	15T	CMS	$W' \to e\nu,\ \mu\nu$
none 1000–3010	95	[71] KHACHATRY...	14O	CMS	$W' \to N\ell \to \ell\ell jj$
• • • We do not use the following data for averages, fits, limits, etc. • • •					
		[72] AAD	25AX	ATLAS	$W' \to JJ$
>4400	95	[73] AAD	24AE	ATLAS	$M_{W'} = M_{Z'}$
		[74] AAD	24CM	ATLAS	Dark $\rho_D^\pm$
		[75] HAYRAPETY...	24AV	CMS	$X \to W\gamma$
		[76] AAD	23BF	ATLAS	$W' \to WZ' \to \ell\nu q\overline{q}$
		[77] AAD	23CG	ATLAS	$W' \to N\ell \to \ell\ell jj$
		[78] AAD	23CK	ATLAS	$W' \to XH$
		[79] AAD	23U	ATLAS	$W' \to W\gamma$
		[80] TUMASYAN	22	CMS	$W' \to WR \to WWW$
		[81] TUMASYAN	22AL	CMS	$W' \to tB,\ bT$
		[82] TUMASYAN	22B	CMS	$W' \to W\gamma$
		[83] TUMASYAN	22I	CMS	$W' \to WR \to WWW$
		[84] TUMASYAN	22P	CMS	$W' \to N\ell \to \ell\ell jj$
		[85] AAD	20AD	ATLAS	$W' \to JJ$
		[86] AAD	20W	ATLAS	$W' \to WZ' \to \ell\nu q\overline{q}$
		[87] AABOUD	19B	ATLAS	$W' \to N\ell \to \ell\ell jj$
		[88] AABOUD	19BB	ATLAS	$W' \to N\ell \to j\ell\ell$
		[89] SIRUNYAN	19V	CMS	$W' \to Bt,\ Tb$
		[90] AABOUD	18AA	ATLAS	$W' \to W\gamma$
		[91] AABOUD	18AD	ATLAS	$W' \to HX$
>4500	95	[92] AABOUD	18CJ	ATLAS	$W' \to WZ,\ WH,\ \ell\nu$
none 900–4400	95	[93] SIRUNYAN	18CV	CMS	$W' \to N\ell \to \ell\ell jj$
		[94] KHACHATRY...	17U	CMS	$W' \to WH$
		[95] AAD	15BB	ATLAS	$W' \to WH$
none 300–880	95	[96] AALTONEN	15C	CDF	$W' \to tb$
none 1200–1900 and 2000–2200	95	[97] KHACHATRY...	15V	CMS	$W' \to q\overline{q}$
>3240	95	AAD	14AI	ATLAS	$W' \to e\nu,\ \mu\nu$
		[98] AAD	14AT	ATLAS	$W' \to W\gamma$
none 200–1520	95	[99] AAD	14S	ATLAS	$W' \to WZ$
none 1000–1700	95	[100] KHACHATRY...	14	CMS	$W' \to WZ$
		[101] KHACHATRY...	14A	CMS	$W' \to WZ$
none 500–950	95	[102] AAD	13AO	ATLAS	$W' \to WZ$
none 1100–1680	95	AAD	13D	ATLAS	$W' \to q\overline{q}$
none 1000–1920	95	CHATRCHYAN	13A	CMS	$W' \to q\overline{q}$
		[103] CHATRCHYAN	13AJ	CMS	$W' \to WZ$
>2900	95	[104] CHATRCHYAN	13AQ	CMS	$W' \to e\nu,\ \mu\nu$
none 800–1510	95	[105] CHATRCHYAN	13E	CMS	$W' \to tb$
none 700–940	95	[106] CHATRCHYAN	13U	CMS	$W' \to WZ$
none 700–1130	95	[107] AAD	12AV	ATLAS	$W' \to tb$
none 200–760	95	[108] AAD	12BB	ATLAS	$W' \to WZ$
		[109] AAD	12CK	ATLAS	$W' \to \overline{t}q$
>2550	95	[110] AAD	12CR	ATLAS	$W' \to e\nu,\ \mu\nu$
		[111] AAD	12M	ATLAS	$W' \to N\ell \to \ell\ell jj$
		[112] AALTONEN	12N	CDF	$W' \to \overline{t}q$
none 200–1143	95	[108] CHATRCHYAN	12AF	CMS	$W' \to WZ$
		[113] CHATRCHYAN	12AR	CMS	$W' \to \overline{t}q$
		[114] CHATRCHYAN	12BG	CMS	$W' \to N\ell \to \ell\ell jj$
>1120	95	AALTONEN	11C	CDF	$W' \to e\nu$
none 180–690	95	[115] ABAZOV	11H	D0	$W' \to WZ$
none 600–863	95	[116] ABAZOV	11L	D0	$W' \to tb$
none 285–516	95	[117] AALTONEN	10N	CDF	$W' \to WZ$
none 280–840	95	[118] AALTONEN	09AC	CDF	$W' \to q\overline{q}$
>1000	95	ABAZOV	08C	D0	$W' \to e\nu$
none 300–800	95	ABAZOV	04C	D0	$W' \to q\overline{q}$
none 225–536	95	[119] ACOSTA	03B	CDF	$W' \to tb$
none 200–480	95	[120] AFFOLDER	02C	CDF	$W' \to WZ$
> 786	95	[121] AFFOLDER	01I	CDF	$W' \to e\nu,\ \mu\nu$
none 300–420	95	[122] ABE	97G	CDF	$W' \to q\overline{q}$
> 720	95	[123] ABACHI	96C	D0	$W' \to e\nu$
> 610	95	[124] ABACHI	95E	D0	$W' \to e\nu,\ \tau\nu$
none 260–600	95	[125] RIZZO	93	RVUE	$W' \to q\overline{q}$

[1] AAD 24T limit is for W' with SM-like coupling from pp collisions at $\sqrt{s}$ =1 3 TeV. Bosonic decays of W' and $W - W'$ interference are neglected. See their Fig. 7a for limits on $\sigma \cdot B$.

[2] HAYRAPETYAN 24X search for right-handed W' decaying to tb in pp collisions at $\sqrt{s}$ = 13 TeV. See their Fig. 7 for limits on $\sigma \cdot B$.

[3] AAD 23AH search for resonances produced through Drell-Yan and vector-boson-fusion processes in pp collisions at $\sqrt{s}$ = 13 TeV. See their Fig. 7 and Fig. 8 for limits on $\sigma \cdot B$. The quoted limit is for heavy-vector-triplet W' with $g_V = 3$ produced mainly via Drell-Yan.

[4] AAD 23CC search for resonances decaying to tb in pp collisions at $\sqrt{s}$ = 13 TeV. The limit quoted above is for right-handed W' assuming a W' coupling equal to the SM W

Int. J. Mod. Phys. A 2026.41. Downloaded from www.worldscientific.com
by UNIVERSITY OF CALIFORNIA @ BERKELEY on 09/16/26. Reuse and distribution is strictly not permitted, except for Open Access articles.

Int. J. Mod. Phys. A 2026.41. Downloaded from www.worldscientific.com
by UNIVERSITY OF CALIFORNIA @ BERKELEY on 09/16/26. Re-use and distribution is strictly not permitted, except for Open Access articles.

coupling. The limit becomes $M_{W'} > 4200$ GeV for left-handed W'. See their Figs. 12 and 13 for limits on $\sigma \cdot B$.

[5] AAD 23L perform a generic search for resonances with events containing a Z decaying into e^+e^- or $\mu^+\mu^-$ in pp collisions at $\sqrt{s} = 13$ TeV. See their Figs. 6, 7, 8 for model independent limits on $\sigma \cdot B$ for Gaussian-shaped resonances. The limit above is for heavy-vector-triplet W' decaying to WZ with $g_V = 3$ as well as with $g_V = 1$.

[6] AAD 23O search for resonances decaying to HW in pp collisions at $\sqrt{s} = 13$ TeV. The quoted limit is for heavy-vector-triplet W' with $g_V = 3$. The limit becomes $M_{W'} > 2950$ GeV for $g_V = 1$.

[7] TUMASYAN 23AP search for resonances decaying to WZ in pp collisions at $\sqrt{s} = 13$ TeV. The limit quoted above is for heavy-vector-triplet W' with $g_V = 3$. The limit becomes $M_{W'} > 4.8$ TeV assuming $M_{W'} = M_{Z'}$ and combining $W' \to WZ$, $W' \to WH$, $Z' \to WW$, $Z' \to ZH$ channels.

[8] TUMASYAN 23AP search for resonances decaying to WH in pp collisions at $\sqrt{s} = 13$ TeV. The limit quoted above is for heavy-vector-triplet W' with $g_V = 3$. The limit becomes $M_{W'} > 4.8$ TeV assuming $M_{W'} = M_{Z'}$ and combining $W' \to WZ$, $W' \to WH$, $Z' \to WW$, $Z' \to ZH$ channels.

[9] TUMASYAN 23AW search for SSM W' resonance decaying to $\tau\nu$ in pp collisions at $\sqrt{s} = 13$ TeV. W–W' intereference and bosonic decays of W' are not included. See their Fig. 6 for limits on $\sigma \cdot B$.

[10] TUMASYAN 22AC search for W' with SM-like couplings in pp collisions at $\sqrt{s} = 13$ TeV. The diboson decays of W' are assumed to be suppressed. See their Fig. 5 for limits on $\sigma \cdot B$.

[11] TUMASYAN 22D search for resonances produced through Drell-Yan and vector-boson-fusion processes in pp collisions at $\sqrt{s} = 13$ TeV. See their Fig. 8 for limits on $\sigma \cdot B$. The quoted limit is for heavy-vector-triplet W' with $g_V = 3$ produced mainly via Drell-Yan.

[12] TUMASYAN 22J search for resonances produced through Drell-Yan and vector-boson-fusion processes in pp collisions at $\sqrt{s} = 13$ TeV. The quoted limit is for heavy-vector-triplet W' with $g_V = 3$, produced mainly via Drell-Yan. See their Fig. 9 for limits on $\sigma \cdot B$.

[13] TUMASYAN 22R search for resonances decaying to WZ in pp collisions at $\sqrt{s} = 13$ TeV. The quoted limit is for heavy-vector-triplet W' produced mainly via Drell-Yan. See their Fig. 8 for limits on $\sigma \cdot B$.

[14] SIRUNYAN 21Y search for resonances decaying to tb in pp collisions at $\sqrt{s} = 13$ TeV. See their Fig. 2 for limits on $\sigma \cdot$ B($W' \to tb$).

[15] AAD 20AJ search for resonances decaying to HW in pp collisions at $\sqrt{s} = 13$ TeV. The quoted limit is for heavy-vector-triplet W' with $g_V = 3$. The limit becomes $M_{W'} > 2900$ GeV for $g_V = 1$. See their Fig. 6 for limits on $\sigma \cdot B$.

[16] AAD 20AT search for resonances decaying to WZ in pp collisions at $\sqrt{s} = 13$ TeV. The quoted limit is for heavy-vector-triplet W' with $g_V = 3$. The limit becomes $M_{W'} > 3900$ GeV for $g_V = 1$. See their Fig. 13 for limits on $\sigma \cdot B$.

[17] AAD 20T search for W' with SM-like couplings in pp collisions at $\sqrt{s} = 13$ TeV. See their Fig. 4(c) for limits on the product of the cross section, acceptance, and branching fraction.

[18] SIRUNYAN 20AI limit is for W' with SM-like coupling using pp collisions at $\sqrt{s} = 13$ TeV.

[19] SIRUNYAN 20Q search for resonances decaying to WZ in pp collisions at $\sqrt{s} = 13$ TeV. The quoted limit is for heavy-vector-triplet W' with $g_V = 3$.

[20] AABOUD 19E search for right-handed W' in pp collisions at $\sqrt{s} = 13$ TeV. See their Fig. 8 for limit on on $\sigma \cdot B$.

[21] AAD 19C search for W' with SM-like couplings in pp collisions at $\sqrt{s} = 13$ TeV. Bosonic decays and $W - W'$ interference are neglected. The limits on e and μ separately are 6.0 and 5.1 TeV respectively. See their Fig. 2 for limits on $\sigma \cdot B$.

[22] AAD 19D search for resonances decaying to WZ in pp collisions at $\sqrt{s} = 13$ TeV. The quoted limit is for heavy-vector-triplet W' with $g_V = 3$. The limit becomes $M_{W'} > 3400$ GeV for $g_V = 1$. If we assume $M_{W'} = M_{Z'}$, the limit increases $M_{W'} > 3800$ GeV and $M_{W'} > 3500$ GeV for $g_V = 3$ and $g_V = 1$, respectively. See their Fig. 9 for limits on $\sigma \cdot B$.

[23] SIRUNYAN 19AY limits shown for W' with SM-like coupling using pp collisions at $\sqrt{s} = 13$ TeV. $W - W'$ interference and bosonic decays of W' are not included. See their Fig. 5 for limits on $\sigma \cdot B$. Limits in the context of a nonuniversal gauge interaction are shown in Fig. 7. Model independent limits on $\sigma B A \epsilon$ can be seen in Fig. 8.

[24] SIRUNYAN 19CP present a statistical combinations of searches for W' decaying to pairs of bosons or leptons in pp collisions at $\sqrt{s} = 13$ TeV. The quoted limit is for heavy-vector-triplet W' with $g_V = 3$. If we assume $M_{W'} = M_{Z'}$, the limit becomes $M_{W'} > 4500$ GeV for $g_V = 3$ and $M_{W'} > 5000$ GeV for $g_V = 1$. See their Figs. 2 and 3 for limits on $\sigma \cdot B$.

[25] SIRUNYAN 19I search for resonances decaying to HW in pp collisions at $\sqrt{s} = 13$ TeV. The quoted limit is for heavy-vector-triplet W' with $g_V = 3$. The limit becomes $M_{W'} > 2800$ GeV if we assume $M_{W'} = M_{Z'}$.

[26] AABOUD 18AF give the limit above for right-handed W' using pp collisions at $\sqrt{s} = 13$ TeV. These limits also exclude W bosons with left-handed couplings with masses below 2.9 TeV, at the 95% confidence level. $W' \to \ell\nu_R$ is assumed to be forbidden. See their Fig.5 for limits on $\sigma \cdot B$ for both cases of left- and right-handed W'.

[27] AABOUD 18AI search for resonances decaying to HW in pp collisions at $\sqrt{s} = 13$ TeV. The quoted limit is for heavy-vector-triplet W' with $g_V = 3$. The limit becomes $M_{W'} > 2670$ GeV for $g_V = 1$. If we assume $M_{W'} = M_{Z'}$, the limit increases $M_{W'} > 2930$ GeV and $M_{W'} > 2800$ GeV for $g_V = 3$ and $g_V = 1$, respectively. See their Fig. 5 for limits on $\sigma \cdot B$.

[28] AABOUD 18AK search for resonances decaying to WZ in pp collisions at $\sqrt{s} = 13$ TeV. The limit quoted above is for heavy-vector-triplet W' with $g_V = 3$. The limit becomes $M_{W'} > 2800$ GeV for $g_V = 1$.

[29] AABOUD 18AL search for resonances decaying to WZ in pp collisions at $\sqrt{s} = 13$ TeV. The limit quoted above is for heavy-vector-triplet W' with $g_V = 3$. The limit becomes $M_{W'} > 2900$ GeV for $g_V = 1$.

[30] AABOUD 18BG limit is for W' with SM-like couplings using pp collisions at $\sqrt{s} = 13$ TeV. Bosonic decays of W' and $W - W'$ interference are neglected. See Fig. 2 for limits on $\sigma \cdot B$.

[31] AABOUD 18CH search for resonances decaying to WZ in pp collisions at $\sqrt{s} = 13$ TeV. The limit quoted above is for heavy-vector-triplet W' with $g_V = 3$. The limit becomes $M_{W'} > 2260$ GeV for $g_V = 1$.

[32] AABOUD 18F search for resonances decaying to WZ in pp collisions at $\sqrt{s} = 13$ TeV. The quoted limit is for heavy-vector-triplet W' with $g_V = 3$. The limit becomes $M_{W'} > 3000$ GeV for $g_V = 1$. If we assume $M_{Z'} = M_{W'}$, the limit increases $M_{W'} > 3500$ GeV and $M_{W'} > 3100$ GeV for $g_V = 3$ and $g_V = 1$, respectively. See their Fig.5 for limits on $\sigma \cdot B$.

[33] AABOUD 18K limit is for W' with SM-like coupling using pp collisions at $\sqrt{s} = 13$ TeV. $W - W'$ interference and bosonic decays of W' are not included. See their Fig. 4 for limit on $\sigma \cdot B$.

[34] SIRUNYAN 18 limit is for right-handed W' using pp collisions at $\sqrt{s} = 13$ TeV. $W' \to \ell\nu_R$ decay is assumed to be forbidden. The limit becomes $M_{W'} > 3.4$ TeV if $M_{\nu_R} \ll M_{W'}$. See their Fig. 5 for exclusion limits on W' models having both left- and right-handed couplings.

[35] SIRUNYAN 18AX search for resonances decaying to WZ in pp collisions at $\sqrt{s} = 13$ TeV. The quoted limit is for heavy-vector-triplet W' with $g_V = 3$. See their Fig.6 for limits on $\sigma \cdot$ B.

[36] SIRUNYAN 18AZ limit is derived for W' with SM-like coupling using pp collisions at $\sqrt{s} = 13$ TeV. No interference with SM W process is considered. The bosonic decays are assumed to be negligible. See their Fig.6 for limits on $\sigma \cdot B$.

[37] SIRUNYAN 18BK search for resonances decaying to WZ in pp collisions at $\sqrt{s} = 13$ TeV. The limit quoted above is for heavy-vector-triplet W' with $g_V = 3$. The limit becomes $M_{W'} > 3100$ GeV for $g_V = 1$.

[38] SIRUNYAN 18BO limit is for W' with SM-like coupling using pp collisions at $\sqrt{s} = 13$ TeV.

[39] SIRUNYAN 18DJ search for resonances decaying to WZ in pp collisions at $\sqrt{s} = 13$ TeV. The limit quoted above is for heavy-vector-triplet W' with $g_V = 3$. The limit becomes $M_{W'} > 2270$ GeV for $g_V = 1$.

[40] SIRUNYAN 18ED search for resonances decaying to HW in pp collisions at $\sqrt{s} = 13$ TeV. The limit above is for heavy-vector-triplet W' with $g_V = 3$. If we assume $M_{W'} = M_{Z'}$, the limit increases $M_{W'} > 2900$ GeV and $M_{W'} > 2800$ GeV for $g_V = 3$ and $g_V = 1$, respectively.

[41] SIRUNYAN 18P give this limit for a heavy-vector-triplet W' with $g_V = 3$. If they assume $M_{Z'} = M_{W'}$, the limit increases to $M_{W'} > 3800$ GeV.

[42] AABOUD 17AK search for a new resonance decaying to dijets in pp collisions at $\sqrt{s} = 13$ TeV. The limit above is for a W' boson having axial-vector SM couplings and decaying to quarks with 75% branching fraction.

[43] AABOUD 17AO search for resonances decaying to HW in pp collisions at $\sqrt{s} = 13$ TeV. The limit quoted above is for a W' in the heavy-vector-triplet model with $g_V = 3$. See their Fig.4 for limits on $\sigma \cdot B$.

[44] AABOUD 17B search for resonances decaying to HW ($H \to b\overline{b}, c\overline{c}$; $W \to \ell\nu$) in pp collisions at $\sqrt{s} = 13$ TeV. The quoted limit is for heavy-vector-triplet W' with $g_V = 3$. The limit becomes $M_{W'} > 1750$ GeV for $g_V = 1$. If we assume $M_{W'} = M_{Z'}$, the limit increases $M_{W'} > 2310$ GeV and $M_{W'} > 1730$ GeV for $g_V = 3$ and $g_V = 1$, respectively. See their Fig.3 for limits on $\sigma \cdot B$.

[45] KHACHATRYAN 17J search for right-handed W_R in pp collisions at $\sqrt{s} = 13$ TeV. W_R is assumed to decay into τ and hypothetical heavy neutrino N_τ, with N_τ decaying into τjj. The quoted limit is for $M_{N_\tau} = M_{W_R}/2$. The limit becomes $M_{W_R} > 2350$ GeV (1630 GeV) for $M_{W_R}/M_{N_\tau} = 0.8$ (0.2). See their Fig. 4 for excluded regions in the $M_{W_R} - M_{N_\tau}$ plane.

[46] KHACHATRYAN 17W search for resonances decaying to dijets in pp collisions at $\sqrt{s} = 13$ TeV.

[47] KHACHATRYAN 17Z limit is for W' with SM-like coupling using pp collisions at $\sqrt{s} = 13$ TeV. The bosonic decays of W' and the interference with SM W process are neglected.

[48] SIRUNYAN 17A search for resonances decaying to WZ with $WZ \to \ell\nu q\overline{q}$, $q\overline{q}q\overline{q}$ in pp collisions at $\sqrt{s} = 13$ TeV. The quoted limit is for heavy-vector-triplet W' with $g_V = 3$. The limit becomes $M_{W'} > 2000$ GeV for $g_V = 1$. If we assume $M_{Z'} = M_{W'}$, the limit increases $M_{W'} > 2400$ GeV and $M_{W'} > 2300$ GeV for $g_V = 3$ and $g_V = 1$, respectively. See their Fig.6 for limits on $\sigma \cdot B$.

[49] SIRUNYAN 17AK search for resonances decaying to WZ or HW in pp collisions at $\sqrt{s} = 8$ and 13 TeV. The quoted limit is for heavy-vector-triplet W' with $g_V = 3$. The limit becomes $M_{W'} > 2300$ GeV for $g_V = 1$. If we assume $M_{W'} = M_{Z'}$, the limit increases $M_{W'} > 2400$ GeV for both $g_V = 3$ and $g_V = 1$. See their Fig.1 and 2 for limits on $\sigma \cdot B$.

[50] SIRUNYAN 17H search for right-handed W' in pp collisions at $\sqrt{s} = 13$ TeV. W' is assumed to decay into τ and a heavy neutrino N, with N decaying to $\tau q\overline{q}$. The limit above assumes $M_N = M_{W'}/2$.

[51] SIRUNYAN 17I limit is for a right-handed W' using pp collisions at $\sqrt{s} = 13$ TeV. The limit becomes $M_{W'} > 2400$ GeV for $M_{\nu_R} \ll M_{W'}$.

[52] SIRUNYAN 17R search for resonances decaying to HW in pp collisions at $\sqrt{s} = 13$ TeV. The quoted limit is for heavy-vector-triplet W' with $g_V = 3$. Mass regions $M_{W'} < 2370$ GeV and $2870 < M_{W'} < 2970$ GeV are excluded for $g_V = 1$. If we assume $M_{Z'} = M_{W'}$, the excluded mass regions are $1000 < M_{W'} < 2500$ GeV and $2760 < M_{W'} < 3300$ GeV for $g_V = 3$; $1000 < M_{W'} < 2430$ GeV and $2810 < M_{W'} < 3130$ GeV for $g_V = 1$. See their Fig.5 for limits on $\sigma \cdot B$.

[53] AABOUD 16AE search for resonances decaying to VV ($V = W$ or Z) in pp collisions at $\sqrt{s} = 13$ TeV. Results from $\nu\nu qq$, $\nu\ell qq$, $\ell\ell qq$ and $qqqq$ final states are combined. The quoted limit is for a heavy-vector-triplet W' with $g_V = 3$ and $M_{W'} = M_{Z'}$.

[54] AABOUD 16V limit is for W' with SM-like coupling using pp collisions at $\sqrt{s} = 13$ TeV. The bosonic decays of W' and the interference with SM W process are neglected.

[55] AAD 16R search for $W' \to WZ$ in pp collisions at $\sqrt{s} = 8$ TeV. $\ell\nu\ell'\ell'$, $\ell\ell q\overline{q}$, $\ell\nu q\overline{q}$, and all hadronic channels are combined. The quoted limit assumes $g_{W'WZ}/g_{WWZ} = (M_W/M_{W'})^2$.

[56] AAD 16S search for a new resonance decaying to dijets in pp collisions at $\sqrt{s}$ = 13 TeV. The limit quoted above is for a W' having SM-like couplings to quarks.

[57] KHACHATRYAN 16AO limit is for a SM-like right-handed W' using pp collisions at $\sqrt{s}$ = 8 TeV. The quoted limit combines $t \to qqb$ and $t \to \ell\nu b$ events.

[58] KHACHATRYAN 16AP search for a resonance decaying to HW in pp collisions at $\sqrt{s}$ = 8 TeV. Both H and W are assumed to decay to fat jets. The quoted limit is for heavy-vector-triplet W' with $g_V = 3$.

[59] KHACHATRYAN 16BD search for resonance decaying to HW in pp collisions at $\sqrt{s}$ = 8 TeV. The quoted limit is for heavy-vector-triplet (HVT) W' with $g_V = 3$. The HVT model $m_{W'} = m_{Z'} > 1.8$ TeV is also obtained by combining $W'/Z' \to WH/ZH \to \ell\nu bb$, $qq\tau\tau$, $qqbb$, and $qqqqqq$ channels.

[60] KHACHATRYAN 16K search for resonances decaying to dijets in pp collisions at $\sqrt{s}$ = 13 TeV.

[61] KHACHATRYAN 16L search for resonances decaying to dijets in pp collisions at $\sqrt{s}$ = 8 TeV with the data scouting technique, increasing the sensitivity to the low mass resonances.

[62] KHACHATRYAN 16O limit is for W' having universal couplings. Interferences with the SM amplitudes are assumed to be absent.

[63] AAD 15AU search for W' decaying into the WZ final state with $W \to q\overline{q}'$, $Z \to \ell^+\ell^-$ using pp collisions at $\sqrt{s}$ = 8 TeV. The quoted limit assumes $g_{W'WZ}/g_{WWZ} = (M_W/M_{W'})^2$.

[64] AAD 15AV limit is for a SM like right-handed W' using pp collisions at $\sqrt{s}$ = 8 TeV. $W' \to \ell\nu$ decay is assumed to be forbidden.

[65] AAD 15AZ search for W' decaying into the WZ final state with $W \to \ell\nu$, $Z \to q\overline{q}$ using pp collisions at $\sqrt{s}$ = 8 TeV. The quoted limit assumes $g_{W'WZ}/g_{WWZ} = (M_W/M_{W'})^2$.

[66] AAD 15CP search for W' decaying into the WZ final state with $W \to q\overline{q}$, $Z \to q\overline{q}$ using pp collisions at $\sqrt{s}$ = 8 TeV. The quoted limit assumes $g_{W'WZ}/g_{WWZ} = (M_W/M_{W'})^2$.

[67] AAD 15R limit is for a SM like right-handed W' using pp collisions at $\sqrt{s}$ = 8 TeV. $W' \to \ell\nu$ decay is assumed to be forbidden.

[68] AAD 15V search for new resonance decaying to dijets in pp collisions at $\sqrt{s}$ = 8 TeV.

[69] KHACHATRYAN 15C search for W' decaying via WZ to fully leptonic final states using pp collisions at $\sqrt{s}$=8 TeV. The quoted limit assumes $g_{W'WZ}/g_{WWZ} = M_W M_Z/M^2_{W'}$.

[70] KHACHATRYAN 15T limit is for W' with SM-like coupling which interferes the SM W boson constructively using pp collisions at $\sqrt{s}$ = 8 TeV. For W' without interference, the limit becomes > 3280 GeV.

[71] KHACHATRYAN 14O search for right-handed W_R in pp collisions at $\sqrt{s}$ = 8 TeV. W_R is assumed to decay into ℓ and hypothetical heavy neutrino N, with N decaying into ℓjj. The quoted limit is for $M_{\nu_{eR}} = M_{\nu_{\mu R}} = M_{W_R}/2$. See their Fig. 3 and Fig. 5 for excluded regions in the $M_{W_R} - M_\nu$ plane.

[72] AAD 25AX search for a narrow resonance decaying to a pair of large-radius-jets using a machine-learning approach. See their Fig. 7 for limits on $\sigma \cdot B$ obtained with different classifier feature sets.

[73] AAD 24AE search for resonances decaying to qq, tt, tb, VV, VH, $\ell\ell$, $\ell\tau$, $\tau\nu$, $\tau\tau$ in pp collisions at $\sqrt{s}$ = 13 TeV. The quoted limit is for heavy-vector-triplet W' with g_V = 3. $M_{W'} = M_{Z'}$ is assumed. The limit becomes $M_{W'} > 5.8$ TeV for $g_V = 1$.

[74] AAD 24CM search for pair productions of dark pions $\pi_D^\pm \pi_D^0$ in $ttbb$ events of pp collisions at $\sqrt{s}$ = 13 TeV. $\pi_D^\pm \to tb$ and $\pi_D^0 \to tt$ decays are assumed. The production cross section is computed in a model with dark $\rho_D^\pm$ assuming dark isospin symmetry $m_{\rho_D^\pm} = m_{\rho_D^0}$, $m_{\pi_D^\pm} = m_{\pi_D^0}$. See their Fig. 12 for limits on the production cross sections.

[75] HAYRAPETYAN 24AV search for a spin-0 particle X decaying to $W\gamma$ in pp collisions at $\sqrt{s}$ = 13 TeV. See their Fig. 8 for limits on $\sigma \cdot B$.

[76] AAD 23BF search for W' decaying to WZ' in pp collisions at $\sqrt{s}$ = 13 TeV. The mass difference between W' and Z' is assumed to be 250 GeV. See their Fig. 9(a) for limits on $\sigma \cdot B$ as a function of $M_{W'}$.

[77] AAD 23CG search for right-handed W_R in pp collisions at $\sqrt{s}$ = 13 TeV. W_R is assumed to decay into ℓ and hypothetical heavy neutrino N, with N decaying into ℓjj. See their Fig. 9 for limits in m_N–m_{W_R} plane.

[78] AAD 23CK search for a new resonance decaying to HX ($H \to b\overline{b}$, $X \to q\overline{q}'$) in pp collisions at $\sqrt{s}$ = 13 TeV. See their Fig. 12 for limits on $\sigma \cdot B$.

[79] AAD 23U search for a narrow charged vector boson decaying to $W\gamma$. See their Fig. 8(d) for the exclusion limit in $m_{W'} - \sigma \cdot B$ plane.

[80] TUMASYAN 22 search for KK excited W decaying in cascade to three W via a scalar radion R. See their Fig. 4 for limits in $M_{W'} - M_R$ plane.

[81] TUMASYAN 22AL search for resonances decaying to tB or bT with vector-like quarks B (T) subsequently decaying to bH or bZ (tH or tZ). See their Fig. 7 for limits on $\sigma \cdot B$.

[82] TUMASYAN 22B search for a narrow charged vector boson decaying to $W\gamma$. See their Fig. 5 for limits on $\sigma \cdot B$.

[83] TUMASYAN 22I search for KK excited W decaying in cascade to three W via a scalar radion R. See their Fig. 10 for limits in $M_{W'} - M_R$ plane.

[84] TUMASYAN 22P search for right handed W_R in pp collisions at $\sqrt{s}$ = 13 TeV. W_R is assumed to decay into ℓ and hypothetical heavy neutrino N, with N decaying to ℓjj. See their Fig. 7 for excluded regions in $M_{W_R} - M_N$ plane.

[85] AAD 20AD search for a narrow resonance decaying to a pair of large-radius-jets J_1 and J_2 employing a machine-learning procedure. See their Fig. 3 for limits on $\sigma \cdot B$ depending on assumptions about invariant masses for J_1, J_2, and $J_1 J_2$.

[86] AAD 20W search for W' decaying to WZ' in pp collisions at $\sqrt{s}$ = 13 TeV. See their Fig. 5(b) for limits on $\sigma \cdot B$ as a function of $m_{Z'}$. The $W' \to WZ'$ branching fraction was chosen to be 0.5 and the mass difference between the W' and Z' was set to 250 GeV.

[87] AABOUD 19B search for right-handed W_R in pp collisions at $\sqrt{s}$ = 13 TeV. W_R is assumed to decay into ℓ and hypothetical heavy neutrino N, with N decaying to ℓjj. See their Figs. 7 and 8 for excluded regions in $M_{W_R} - M_N$ plane.

[88] AABOUD 19BB search for right handed W_R in pp collisions at $\sqrt{s}$ = 13 TeV. W_R is assumed to decay into ℓ and a boosted hypothetical heavy neutrino N, with N decaying to ℓ and a large radius jet $j = q\overline{q}$. See their Fig. 7 for excluded regions in $M_{W_R} - M_N$ plane.

[89] SIRUNYAN 19V search for a new resonance decaying to a top quark and a heavy vector-like bottom partner B decaying to Hb (or a bottom quark and a heavy vector-like top partner T decaying to Ht) in pp collisions at $\sqrt{s}$ = 13 TeV. See their Fig. 8 for limits on $\sigma \cdot B$.

[90] AABOUD 18AA search for a narrow charged vector boson decaying to $W\gamma$. See their Fig. 9 for the exclusion limit in $M_{W'} - \sigma B$ plane.

[91] AABOUD 18AD search for resonances decaying to HX ($H \to b\overline{b}$, $X \to q\overline{q}'$) in pp collisions at $\sqrt{s}$ = 13 TeV. See their Figs. 3–5 for limits on $\sigma \cdot B$.

[92] AABOUD 18CJ search for heavy-vector-triplet W' in pp collisions at $\sqrt{s}$ = 13 TeV. The limit quoted above is for model with $g_V = 3$ assuming $M_{W'} = M_{Z'}$. The limit becomes $M_{W'} > 5500$ GeV for model with $g_V = 1$.

[93] SIRUNYAN 18CV search for right-handed W_R in pp collisions at $\sqrt{s}$ = 13 TeV. W_R is assumed to decay into ℓ and hypothetical heavy neutrino N, with N decaying to ℓjj. The quoted limit is for $M_N = M_{W_R}/2$. See their Fig. 6 for excluded regions in the $M_{W_R} - M_N$ plane.

[94] KHACHATRYAN 17U search for resonances decaying to HW ($H \to b\overline{b}$; $W \to \ell\nu$) in pp collisions at $\sqrt{s}$ = 13 TeV. The limit on the heavy-vector-triplet model is $M_{Z'} = M_{W'} > 2$ TeV for $g_V = 3$, in which constraints from the $Z' \to HZ$ ($H \to b\overline{b}$; $Z \to \ell^+\ell^-$, $\nu\overline{\nu}$) are combined. See their Fig.3 and Fig.4 for limits on $\sigma \cdot B$.

[95] AAD 15BB search for W' decaying into WH with $W \to \ell\nu$, $H \to b\overline{b}$. See their Fig. 4 for the exclusion limits in the heavy vector triplet benchmark model parameter space.

[96] AALTONEN 15C limit is for a SM-like right-handed W' assuming $W' \to \ell\nu$ decays are forbidden, using $p\overline{p}$ collisions at $\sqrt{s}$=1.96 TeV. See their Fig. 3 for limit on $g_{W'}/g_W$.

[97] KHACHATRYAN 15V search new resonance decaying to dijets in pp collisions at $\sqrt{s}$ = 8 TeV.

[98] AAD 14AT search for a narrow charged vector boson decaying to $W\gamma$. See their Fig. 3a for the exclusion limit in $m_{W'} - \sigma B$ plane.

[99] AAD 14S search for W' decaying into the WZ final state with $W \to \ell\nu$, $Z \to \ell\ell$ using pp collisions at $\sqrt{s}$=8 TeV. The quoted limit assumes $g_{W'WZ}/g_{WWZ} = (M_W/M_{W'})^2$.

[100] KHACHATRYAN 14 search for W' decaying into WZ final state with $W \to q\overline{q}$, $Z \to q\overline{q}$ using pp collisions at $\sqrt{s}$=8 TeV. The quoted limit assumes $g_{W'WZ}/g_{WWZ} = (M_W/M_{W'})^2$.

[101] KHACHATRYAN 14A search for W' decaying into the WZ final state with $W \to \ell\nu$, $Z \to q\overline{q}$, or $W \to q\overline{q}$, $Z \to \ell\ell$. pp collisions data at $\sqrt{s}$=8 TeV are used for the search. See their Fig. 13 for the exclusion limit on the number of events in the mass−width plane.

[102] AAD 13AO search for W' decaying into the WZ final state with $W \to \ell\nu$, $Z \to 2j$ using pp collisions at $\sqrt{s}$=7 TeV. The quoted limit assumes $g_{W'WZ}/g_{WWZ} = (M_W/M_{W'})^2$.

[103] CHATRCHYAN 13AJ search for resonances decaying to WZ pair, using the hadronic decay modes of W and Z, in pp collisions at $\sqrt{s}$=7 TeV. See their Fig. 7 for the limit on the cross section.

[104] CHATRCHYAN 13AQ limit is for W' with SM-like coupling which interferes with the SM W boson using pp collisions at $\sqrt{s}$=7 TeV.

[105] CHATRCHYAN 13E limit is for W' with SM-like coupling which intereferes with the SM W boson using pp collisions at $\sqrt{s}$=7 TeV. For W' with right-handed coupling, the bound becomes >1850 GeV (>1910 GeV) if W' decays to both leptons and quarks (only to quarks). If both left- and right-handed couplings are present, the limit becomes >1640 GeV.

[106] CHATRCHYAN 13U search for W' decaying to the WZ final state, with W decaying into jets, in pp collisions at $\sqrt{s}$=7 TeV. The quoted limit assumes $g_{W'WZ}/g_{WWZ} = (M_W/M_{W'})^2$.

[107] The AAD 12AV quoted limit is for a SM-like right-handed W' using pp collisions at $\sqrt{s}$=7 TeV. $W' \to \ell\nu$ decay is assumed to be forbidden.

[108] AAD 12BB use pp collisions data at $\sqrt{s}$=7 TeV. The quoted limit assumes $g_{W'WZ}/g_{WWZ} = (M_W/M_{W'})^2$.

[109] AAD 12CK search for $pp \to tW'$, $W' \to \overline{t}q$ events in pp collisions. See their Fig. 5 for the limit on $\sigma \cdot B$.

[110] AAD 12CR use pp collisions at $\sqrt{s}$=7 TeV.

[111] AAD 12M search for right-handed W_R in pp collisions at $\sqrt{s}$ = 7 TeV. W_R is assumed to decay into ℓ and hypothetical heavy neutrino N, with N decaying into ℓjj. See their Fig. 4 for the limit in the m_N–$m_{W'}$ plane.

[112] AALTONEN 12N search for $p\overline{p} \to tW'$, $W' \to \overline{t}d$ events in $p\overline{p}$ collisions. See their Fig. 3 for the limit on $\sigma \cdot B$.

[113] CHATRCHYAN 12AR search for $pp \to tW'$, $W' \to \overline{t}d$ events in pp collisions. See their Fig. 2 for the limit on $\sigma \cdot B$.

[114] CHATRCHYAN 12BG search for right-handed W_R in pp collisions $\sqrt{s}$ = 7 TeV. W_R is assumed to decay into ℓ and hypothetical heavy neutrino N, with N decaying into ℓjj. See their Fig. 3 for the limit in the m_N–$m_{W'}$ plane.

[115] ABAZOV 11H use data from $p\overline{p}$ collisions at $\sqrt{s}$=1.96 TeV. The quoted limit is obtained assuming $W'WZ$ coupling strength is the same as the ordinary WWZ coupling strength in the Standard Model.

[116] ABAZOV 11L limit is for W' with SM-like coupling which interferes with the SM W boson, using $p\overline{p}$ collisions at $\sqrt{s}$=1.96 TeV. For W' with right-handed coupling, the bound becomes >885 GeV (>890 GeV) if W' decays to both leptons and quarks (only to quarks). If both left- and right-handed couplings present, the limit becomes >916 GeV.

[117] AALTONEN 10N use $p\overline{p}$ collision data at $\sqrt{s}$=1.96 TeV. The quoted limit assumes $g_{W'WZ}/g_{WWZ} = (M_W/M_{W'})^2$. See their Fig. 4 for limits in mass-coupling plane.

Int. J. Mod. Phys. A 2026.41. Downloaded from www.worldscientific.com
by UNIVERSITY OF CALIFORNIA @ BERKELEY on 09/16/26. Reproduction is strictly not permitted, except for Open Access articles.

Int. J. Mod. Phys. A 2026.41. Downloaded from www.worldscientific.com by UNIVERSITY OF CALIFORNIA @ BERKELEY on 09/16/26. Re-use and distribution is strictly not permitted, except for Open Access articles.

[118] AALTONEN 09AC search for new particle decaying to dijets using $p\overline{p}$ collisions at $\sqrt{s}$=1.96 TeV.

[119] The ACOSTA 03B quoted limit is for $M_{W'} \gg M_{\nu_R}$, using $p\overline{p}$ collisions at $\sqrt{s}$=1.8 TeV. For $M_{W'} < M_{\nu_R}$, $M_{W'}$ between 225 and 566 GeV is excluded.

[120] The quoted limit is obtained assuming $W'WZ$ coupling strength is the same as the ordinary WWZ coupling strength in the Standard Model, using $p\overline{p}$ collisions at $\sqrt{s}$=1.8 TeV. See their Fig. 2 for the limits on the production cross sections as a function of the W' width.

[121] AFFOLDER 01I combine a new bound on $W' \rightarrow e\nu$ of 754 GeV, using $p\overline{p}$ collisions at $\sqrt{s}$=1.8 TeV, with the bound of ABE 00 on $W' \rightarrow \mu\nu$ to obtain quoted bound.

[122] ABE 97G search for new particle decaying to dijets using $p\overline{p}$ collisions at $\sqrt{s}$=1.8 TeV.

[123] For bounds on W_R with nonzero right-handed mass, see Fig. 5 from ABACHI 96C.

[124] ABACHI 95E assume that the decay $W' \rightarrow WZ$ is suppressed and that the neutrino from W' decay is stable and has a mass significantly less $m_{W'}$.

[125] RIZZO 93 analyses CDF limit on possible two-jet resonances. The limit is sensitive to the inclusion of the assumed K factor.

W_R (Right-Handed W Boson) MASS LIMITS

Assuming a light right-handed neutrino, except for BEALL 82, LANGACKER 89B, and COLANGELO 91. $g_R = g_L$ assumed. [Limits in the section MASS LIMITS for W' below are also valid for W_R if $m_{\nu_R} \ll m_{W_R}$.] Some limits assume manifest left-right symmetry, *i.e.*, the equality of left- and right Cabibbo-Kobayashi-Maskawa matrices. For a comprehensive review, see LANGACKER 89B. Limits on the W_L-W_R mixing angle ζ are found in the next section. Values in brackets are from cosmological and astrophysical considerations and assume a light right-handed neutrino.

VALUE (GeV)	CL%	DOCUMENT ID		TECN	COMMENT
> 592	90	[1] BUENO	11	TWST	μ decay
> 715	90	[2] CZAKON	99	RVUE	Electroweak
• • • We do not use the following data for averages, fits, limits, etc. • • •					
>4000	95	[3] ALVES	24	RVUE	K and π decays
> 235	90	[4] PRIEELS	14	PIE3	μ decay
> 245	90	[5] WAUTERS	10	CNTR	^{60}Co β decay
>2500		[6] ZHANG	08	THEO	$m_{K^0_L} - m_{K^0_S}$
> 180	90	[7] MELCONIAN	07	CNTR	^{37}K β^+ decay
> 290.7	90	[8] SCHUMANN	07	CNTR	Polarized neutron decay
[> 3300]	95	[9] CYBURT	05	COSM	Nucleosynthesis; light ν_R
> 310	90	[10] THOMAS	01	CNTR	β^+ decay
> 137	95	[11] ACKERSTAFF	99D	OPAL	τ decay
>1400	68	[12] BARENBOIM	98	RVUE	Electroweak, Z-Z' mixing
> 549	68	[13] BARENBOIM	97	RVUE	μ decay
> 220	95	[14] STAHL	97	RVUE	τ decay
> 220	90	[15] ALLET	96	CNTR	β^+ decay
> 281	90	[16] KUZNETSOV	95	CNTR	Polarized neutron decay
> 282	90	[17] KUZNETSOV	94B	CNTR	Polarized neutron decay
> 439	90	[18] BHATTACH...	93	RVUE	Z-Z' mixing
> 250	90	[19] SEVERIJNS	93	CNTR	β^+ decay
		[20] IMAZATO	92	CNTR	K^+ decay
> 475	90	[21] POLAK	92B	RVUE	μ decay
> 240	90	[22] AQUINO	91	RVUE	Neutron decay
> 496	90	[22] AQUINO	91	RVUE	Neutron and muon decay
> 700		[23] COLANGELO	91	THEO	$m_{K^0_L} - m_{K^0_S}$
> 477	90	[24] POLAK	91	RVUE	μ decay
[none 540–23000]		[25] BARBIERI	89B	ASTR	SN 1987A; light ν_R
> 300	90	[26] LANGACKER	89B	RVUE	General
> 160	90	[27] BALKE	88	CNTR	$\mu \rightarrow e\nu\overline{\nu}$
> 406	90	[28] JODIDIO	86	ELEC	Any ζ
> 482	90	[28] JODIDIO	86	ELEC	$\zeta = 0$
> 800		MOHAPATRA	86	RVUE	SU(2)$_L$×SU(2)$_R$×U(1)
> 400	95	[29] STOKER	85	ELEC	Any ζ
> 475	95	[29] STOKER	85	ELEC	ζ <0.041
		[30] BERGSMA	83	CHRM	$\nu_\mu e \rightarrow \mu\nu_e$
> 380	90	[31] CARR	83	ELEC	μ^+ decay
>1600		[32] BEALL	82	THEO	$m_{K^0_L} - m_{K^0_S}$

[1] BUENO 11 limit is for manifest left-right symmetric model.

[2] CZAKON 99 perform a simultaneous fit to charged and neutral sectors.

[3] ALVES 24 limit quoted above is from B($\pi \rightarrow e\nu$)/B($\pi \rightarrow \mu\nu$) assuming $m_{\nu_R} = 50$ MeV in vanishing $W_L - W_R$ mixing limit. $g_L = g_R$ is assumed. See their Fig. 2 for limits in m_{ν_R}–m_{W_R} plane.

[4] PRIEELS 14 limit is from $\mu^+ \rightarrow e^+\nu\overline{\nu}$ decay parameter ξ'', which is determined by the positron polarization measurement.

[5] WAUTERS 10 limit is from a measurement of the asymmetry parameter of polarized ^{60}Co β decays. The listed limit assumes no mixing.

[6] ZHANG 08 limit uses a lattice QCD calculation of the relevant hadronic matrix elements, while BEALL 82 limit used the vacuum saturation approximation.

[7] MELCONIAN 07 measure the neutrino angular asymmetry in β^+-decays of polarized ^{37}K, stored in a magneto-optical trap. Result is consistent with SM prediction and does not constrain the $W_L - W_R$ mixing angle appreciably.

[8] SCHUMANN 07 limit is from measurements of the asymmetry $\langle \vec{p}_\nu \cdot \sigma_n \rangle$ in the β decay of polarized neutrons. Zero mixing is assumed.

[9] CYBURT 05 limit follows by requiring that three light ν_R's decouple when $T_{dec} > 140$ MeV. For different T_{dec}, the bound becomes $M_{W_R} > 3.3$ TeV $(T_{dec}$ / 140 MeV$)^{3/4}$.

[10] THOMAS 01 limit is from measurement of β^+ polarization in decay of polarized ^{12}N. The listed limit assumes no mixing.

[11] ACKERSTAFF 99D limit is from τ decay parameters. Limit increase to 145 GeV for zero mixing.

[12] BARENBOIM 98 assumes minimal left-right model with Higgs of SU(2)$_R$ in SU(2)$_L$ doublet. For Higgs in SU(2)$_L$ triplet, m_{W_R} >1100 GeV. Bound calculated from effect of corresponding Z_{LR} on electroweak data through Z–Z_{LR} mixing.

[13] The quoted limit is from μ decay parameters. BARENBOIM 97 also evaluate limit from K_L-K_S mass difference.

[14] STAHL 97 limit is from fit to τ-decay parameters.

[15] ALLET 96 measured polarization-asymmetry correlation in ^{12}Nβ^+ decay. The listed limit assumes zero L-R mixing.

[16] KUZNETSOV 95 limit is from measurements of the asymmetry $\langle \vec{p}_\nu \cdot \sigma_n \rangle$ in the β decay of polarized neutrons. Zero mixing assumed. See also KUZNETSOV 94B.

[17] KUZNETSOV 94B limit is from measurements of the asymmetry $\langle \vec{p}_\nu \cdot \sigma_n \rangle$ in the β decay of polarized neutrons. Zero mixing assumed.

[18] BHATTACHARYYA 93 uses Z-Z' mixing limit from LEP '90 data, assuming a specific Higgs sector of SU(2)$_L$×SU(2)$_R$×U(1) gauge model. The limit is for m_t=200 GeV and slightly improves for smaller m_t.

[19] SEVERIJNS 93 measured polarization-asymmetry correlation in ^{107}In β^+ decay. The listed limit assumes zero L-R mixing. Value quoted here is from SEVERIJNS 94 erratum.

[20] IMAZATO 92 measure positron asymmetry in $K^+ \rightarrow \mu^+\nu_\mu$ decay and obtain $\xi P_\mu > 0.990$ (90% CL). If W_R couples to $u\overline{s}$ with full weak strength (V^R_{us}=1), the result corresponds to m_{W_R} >653 GeV. See their Fig. 4 for m_{W_R} limits for general $|V^R_{us}|^2$=1−$|V^R_{ud}|^2$.

[21] POLAK 92B limit is from fit to muon decay parameters and is essentially determined by JODIDIO 86 data assuming ζ=0. Supersedes POLAK 91.

[22] AQUINO 91 limits obtained from neutron lifetime and asymmetries together with unitarity of the CKM matrix. Manifest left-right symmetry assumed. Stronger of the two limits also includes muon decay results.

[23] COLANGELO 91 limit uses hadronic matrix elements evaluated by QCD sum rule and is less restrictive than BEALL 82 limit which uses vacuum saturation approximation. Manifest left-right symmetry assumed.

[24] POLAK 91 limit is from fit to muon decay parameters and is essentially determined by JODIDIO 86 data assuming ζ=0. Superseded by POLAK 92B.

[25] BARBIERI 89B limit holds for $m_{\nu_R} \leq 10$ MeV.

[26] LANGACKER 89B limit is for any ν_R mass (either Dirac or Majorana) and for a general class of right-handed quark mixing matrices.

[27] BALKE 88 limit is for $m_{\nu_{eR}} = 0$ and $m_{\nu_{\mu R}} \leq 50$ MeV. Limits come from precise measurements of the muon decay asymmetry as a function of the positron energy.

[28] JODIDIO 86 is the same TRIUMF experiment as STOKER 85 (and CARR 83); however, it uses a different technique. The results given here are combined results of the two techniques. The technique here involves precise measurement of the end-point e^+ spectrum in the decay of the highly polarized μ^+.

[29] STOKER 85 is same TRIUMF experiment as CARR 83. Here they measure the decay e^+ spectrum asymmetry above 46 MeV/c using a muon-spin-rotation technique. Assumed a light right-handed neutrino. Quoted limits are from combining with CARR 83.

[30] BERGSMA 83 set limit m_{W_2}/m_{W_1} >1.9 at CL = 90%.

[31] CARR 83 is TRIUMF experiment with a highly polarized μ^+ beam. Looked for deviation from $V-A$ at the high momentum end of the decay e^+ energy spectrum. Limit from previous world-average muon polarization parameter is m_{W_R} >240 GeV. Assumes a light right-handed neutrino.

[32] BEALL 82 limit is obtained assuming that W_R contribution to K^0_L–K^0_S mass difference is smaller than the standard one, neglecting the top quark contributions. Manifest left-right symmetry assumed.

Limit on W_L-W_R Mixing Angle ζ

Lighter mass eigenstate $W_1 = W_L \cos\zeta - W_R \sin\zeta$. Light ν_R assumed unless noted. Values in brackets are from cosmological and astrophysical considerations.

VALUE	CL%	DOCUMENT ID		TECN	COMMENT
• • • We do not use the following data for averages, fits, limits, etc. • • •					
−0.020 to 0.017	90	BUENO	11	TWST	$\mu \rightarrow e\nu\overline{\nu}$
< 0.022	90	MACDONALD	08	TWST	$\mu \rightarrow e\nu\overline{\nu}$
< 0.12	95	[1] ACKERSTAFF	99D	OPAL	τ decay
< 0.013	90	[2] CZAKON	99	RVUE	Electroweak
< 0.0333		[3] BARENBOIM	97	RVUE	μ decay
< 0.04	90	[4] MISHRA	92	CCFR	νN scattering
−0.0006 to 0.0028	90	[5] AQUINO	91	RVUE	
[none 0.00001–0.02]		[6] BARBIERI	89B	ASTR	SN 1987A
< 0.040	90	[7] JODIDIO	86	ELEC	μ decay
−0.056 to 0.040	90	[7] JODIDIO	86	ELEC	μ decay

[1] ACKERSTAFF 99D limit is from τ decay parameters.

[2] CZAKON 99 perform a simultaneous fit to charged and neutral sectors.

[3] The quoted limit is from μ decay parameters. BARENBOIM 97 also evaluate limit from K_L-K_S mass difference.

[4] MISHRA 92 limit is from the absence of extra large-x, large-y $\overline{\nu}_\mu N \rightarrow \overline{\nu}_\mu X$ events at Tevatron, assuming left-handed ν and right-handed $\overline{\nu}$ in the neutrino beam. The result gives $\zeta^2(1-2m^2_{W_1}/m^2_{W_2})$< 0.0015. The limit is independent of ν_R mass.

[5] AQUINO 91 limits obtained from neutron lifetime and asymmetries together with unitarity of the CKM matrix. Manifest left-right asymmetry is assumed.

[6] BARBIERI 89B limit holds for $m_{\nu_R} \leq 10$ MeV.

[7] First JODIDIO 86 result assumes m_{W_R}=∞, second is for unconstrained m_{W_R}.

Int. J. Mod. Phys. A 2026.41. Downloaded from www.worldscientific.com
by UNIVERSITY OF CALIFORNIA @ BERKELEY on 09/16/26. Re-use and distribution is strictly not permitted, except for Open Access articles.

See the related review(s):

Z'-Boson Searches

MASS LIMITS for Z' (Heavy Neutral Vector Boson Other Than Z)

Limits for Z'_{SM}

Z'_{SM} is assumed to have couplings with quarks and leptons which are identical to those of Z, and decays only to known fermions. The most recent preliminary results can be found in the "Z'-boson searches" review above.

VALUE (GeV)	CL%	DOCUMENT ID		TECN	COMMENT
>5150 (CL = 95%) OUR LIMIT					
>3500	95	[1] HAYRAPETY...25M		CMS	pp; $Z'_{SM} \to \tau^+\tau^-$
none 1800–2400	95	[2] TUMASYAN	23AF	CMS	pp; $Z'_{SM} \to b\overline{b}$
>4400	95	[3] TUMASYAN	22AE	CMS	pp; $Z'_{SM} \to e^+e^-$, $\mu^+\mu^-$
>5150	95	[4] SIRUNYAN	21N	CMS	pp; $Z'_{SM} \to e^+e^-$, $\mu^+\mu^-$
none 1133–2700	95	[5] AAD	20T	ATLS	pp, $Z'_{SM} \to b\overline{b}$
none 1800–2900, 3100–3300	95	[6] SIRUNYAN	20AI	CMS	pp; $Z'_{SM} \to q\overline{q}$
none 250–5100	95	[7] AAD	19L	ATLS	pp; $Z'_{SM} \to e^+e^-$, $\mu^+\mu^-$
none 600–2000	95	[8] AABOUD	18AB	ATLS	pp; $Z'_{SM} \to b\overline{b}$
>2420	95	[9] AABOUD	18G	ATLS	pp; $Z'_{SM} \to \tau^+\tau^-$
none 200–4500	95	[10] SIRUNYAN	18BB	CMS	pp; $Z'_{SM} \to e^+e^-$, $\mu^+\mu^-$
none 600–2700	95	[11] SIRUNYAN	18BO	CMS	pp; $Z'_{SM} \to q\overline{q}$
>4500	95	[12] AABOUD	17AT	ATLS	pp; $Z'_{SM} \to e^+e^-$, $\mu^+\mu^-$
>2100	95	[13] KHACHATRY...17H		CMS	pp; $Z'_{SM} \to \tau^+\tau^-$
>3370	95	[14] KHACHATRY...17T		CMS	pp; $Z'_{SM} \to e^+e^-$, $\mu^+\mu^-$
none 600–2100, 2300–2600	95	[15] KHACHATRY...17W		CMS	pp; $Z'_{SM} \to q\overline{q}$
>3360	95	[16] AABOUD	16U	ATLS	pp; $Z'_{SM} \to e^+e^-$, $\mu^+\mu^-$
>2900	95	[17] KHACHATRY...15AE		CMS	pp; $Z'_{SM} \to e^+e^-$, $\mu^+\mu^-$
none 1200–1700	95	[18] KHACHATRY...15V		CMS	pp; $Z'_{SM} \to q\overline{q}$
>2900	95	[19] AAD	14V	ATLS	pp; $Z'_{SM} \to e^+e^-$, $\mu^+\mu^-$
• • • We do not use the following data for averages, fits, limits, etc. • • •					
		[20] BOBOVNIKOV 18		RVUE	pp, $Z'_{SM} \to W^+W^-$
>1900	95	[21] AABOUD	16AA	ATLS	pp; $Z'_{SM} \to \tau^+\tau^-$
>2020	95	[22] AAD	15AM	ATLS	pp; $Z'_{SM} \to \tau^+\tau^-$
>1400	95	[23] AAD	13S	ATLS	pp; $Z'_{SM} \to \tau^+\tau^-$
>1470	95	[24] CHATRCHYAN	13A	CMS	pp; $Z'_{SM} \to q\overline{q}$
>2590	95	[25] CHATRCHYAN	13AF	CMS	pp; $Z'_{SM} \to e^+e^-$, $\mu^+\mu^-$
>2220	95	[26] AAD	12CC	ATLS	pp; $Z'_{SM} \to e^+e^-$, $\mu^+\mu^-$
>1400	95	[27] CHATRCHYAN	12O	CMS	pp; $Z'_{SM} \to \tau^+\tau^-$
>1071	95	[28] AALTONEN	11I	CDF	$p\overline{p}$; $Z'_{SM} \to \mu^+\mu^-$
>1023	95	[29] ABAZOV	11A	D0	$p\overline{p}$, $Z'_{SM} \to e^+e^-$
none 247–544	95	[30] AALTONEN	10N	CDF	$Z' \to WW$
none 320–740	95	[31] AALTONEN	09AC	CDF	$Z' \to q\overline{q}$
> 963	95	[29] AALTONEN	09T	CDF	$p\overline{p}$, $Z'_{SM} \to e^+e^-$
>1403	95	[32] ERLER	09	RVUE	Electroweak
>1305	95	[33] ABDALLAH	06C	DLPH	e^+e^-
> 399	95	[34] ACOSTA	05R	CDF	$\overline{p}p$: $Z'_{SM} \to \tau^+\tau^-$
none 400–640	95	ABAZOV	04C	D0	$p\overline{p}$: $Z'_{SM} \to q\overline{q}$
>1018	95	[35] ABBIENDI	04G	OPAL	e^+e^-
> 670	95	[36] ABAZOV	01B	D0	$p\overline{p}$, $Z'_{SM} \to e^+e^-$
>1500	95	[37] CHEUNG	01B	RVUE	Electroweak
> 710	95	[38] ABREU	00S	DLPH	e^+e^-
> 898	95	[39] BARATE	00I	ALEP	e^+e^-
> 809	95	[40] ERLER	99	RVUE	Electroweak
> 690	95	[41] ABE	97S	CDF	$p\overline{p}$; $Z'_{SM} \to e^+e^-$, $\mu^+\mu^-$
> 398	95	[42] VILAIN	94B	CHM2	$\nu_\mu e \to \nu_\mu e$ and $\overline{\nu}_\mu e \to \overline{\nu}_\mu e$
> 237	90	[43] ALITTI	93	UA2	$p\overline{p}$; $Z'_{SM} \to q\overline{q}$
none 260–600	95	[44] RIZZO	93	RVUE	$p\overline{p}$; $Z'_{SM} \to q\overline{q}$
> 426	90	[45] ABE	90F	VNS	e^+e^-

[1] HAYRAPETYAN 25M search for resonances decaying to $\tau^+\tau^-$ in pp collisions at $\sqrt{s}$ = 13 TeV. See their Fig. 4 for limits on $\sigma \cdot B$.

[2] TUMASYAN 23AF search for resonance decaying to $b\overline{b}$ in pp collisions at $\sqrt{s}$ = 13 TeV. See their Fig. 4 for limits on $\sigma \cdot B$.

[3] TUMASYAN 22AE set limits on Z' from the measurements of the forward-backward asymmetry in e^+e^- and $\mu^+\mu^-$ events in pp collisions at $\sqrt{s}$ = 13 TeV. The quoted limit is for the sequential SM Z'. See their Fig. 6 for limits in mass-coupling plane.

[4] SIRUNYAN 21N search for resonance decaying to e^+e^-, $\mu^+\mu^-$ in pp collisions at $\sqrt{s}$ = 13 TeV.

[5] AAD 20T search for resonances decaying to $b\overline{b}$ in pp collisions at $\sqrt{s}$ = 13 TeV. See their Fig. 7(b) for limits on the product of the cross section, acceptance, b-tagging efficiency, and branching fraction.

[6] SIRUNYAN 20AI search for resonances decaying into dijets in pp collisions at $\sqrt{s}$ = 13 TeV.

[7] AAD 19L search for resonances decaying to $\ell^+\ell^-$ in pp collisions at $\sqrt{s}$ = 13 TeV.

[8] AABOUD 18AB search for resonances decaying to $b\overline{b}$ in pp collisions at $\sqrt{s}$ = 13 TeV.

[9] AABOUD 18G search for resonances decaying to $\tau^+\tau^-$ in pp collisions at $\sqrt{s}$ = 13 TeV.

[10] SIRUNYAN 18BB search for resonances decaying to $\ell^+\ell^-$ in pp collisions at $\sqrt{s}$ = 13 TeV. See their Fig.5 for limits on the Z' coupling strengths with light quarks.

[11] SIRUNYAN 18BO search for resonances decaying to dijets in pp collisions at $\sqrt{s}$ = 13 TeV.

[12] AABOUD 17AT search for resonances decaying to $\ell^+\ell^-$ in pp collisions at $\sqrt{s}$ = 13 TeV.

[13] KHACHATRYAN 17H search for resonances decaying to $\tau^+\tau^-$ in pp collisions at $\sqrt{s}$ = 13 TeV.

[14] KHACHATRYAN 17T search for resonances decaying to e^+e^-, $\mu^+\mu^-$ in pp collisions at $\sqrt{s}$ = 8, 13 TeV.

[15] KHACHATRYAN 17W search for resonances decaying to dijets in pp collisions at $\sqrt{s}$ = 13 TeV.

[16] AABOUD 16U search for resonances decaying to $\ell^+\ell^-$ in pp collisions at $\sqrt{s}$ = 13 TeV.

[17] KHACHATRYAN 15AE search for resonances decaying to e^+e^-, $\mu^+\mu^-$ in pp collisions at $\sqrt{s}$ = 8 TeV.

[18] KHACHATRYAN 15V search for resonances decaying to dijets in pp collisions at $\sqrt{s}$ = 8 TeV.

[19] AAD 14V search for resonances decaying to e^+e^-, $\mu^+\mu^-$ in pp collisions at $\sqrt{s}$ = 8 TeV.

[20] BOBOVNIKOV 18 use the ATLAS limits on $\sigma(pp \to Z')\cdot B(Z' \to W^+W^-)$ to constrain the Z-Z' mixing parameter ξ. See their Fig. 11 for limits in $M_{Z'} - \xi$ plane.

[21] AABOUD 16AA search for resonances decaying to $\tau^+\tau^-$ in pp collisions at $\sqrt{s}$ = 13 TeV.

[22] AAD 15AM search for resonances decaying to $\tau^+\tau^-$ in pp collisions at $\sqrt{s}$ = 8 TeV.

[23] AAD 13S search for resonances decaying to $\tau^+\tau^-$ in pp collisions at $\sqrt{s}$ = 7 TeV.

[24] CHATRCHYAN 13A use pp collisions at $\sqrt{s}$=7 TeV.

[25] CHATRCHYAN 13AF search for resonances decaying to e^+e^-, $\mu^+\mu^-$ in pp collisions at $\sqrt{s}$ = 7 TeV and 8 TeV.

[26] AAD 12CC search for resonances decaying to e^+e^-, $\mu^+\mu^-$ in pp collisions at $\sqrt{s}$ = 7 TeV.

[27] CHATRCHYAN 12O search for resonances decaying to $\tau^+\tau^-$ in pp collisions at $\sqrt{s}$ = 7 TeV.

[28] AALTONEN 11I search for resonances decaying to $\mu^+\mu^-$ in $p\overline{p}$ collisions at $\sqrt{s}$ = 1.96 TeV.

[29] ABAZOV 11A, AALTONEN 09T, AALTONEN 07H, and ABULENCIA 06L search for resonances decaying to e^+e^- in $p\overline{p}$ collisions at $\sqrt{s}$ = 1.96 TeV.

[30] The quoted limit assumes $g_{WWZ'}/g_{WWZ} = (M_W/M_{Z'})^2$. See their Fig. 4 for limits in mass-coupling plane.

[31] AALTONEN 09AC search for new particle decaying to dijets.

[32] ERLER 09 give 95% CL limit on the Z-Z' mixing $-0.0026 < \theta < 0.0006$.

[33] ABDALLAH 06C use data $\sqrt{s}$ = 130–207 GeV.

[34] ACOSTA 05R search for resonances decaying to tau lepton pairs in $\overline{p}p$ collisions at $\sqrt{s}$ = 1.96 TeV.

[35] ABBIENDI 04G give 95% CL limit on Z-Z' mixing $-0.00422 < \theta < 0.00091$. $\sqrt{s}$ = 91 to 207 GeV.

[36] ABAZOV 01B search for resonances in $p\overline{p} \to e^+e^-$ at $\sqrt{s}$=1.8 TeV. They find $\sigma \cdot B(Z' \to ee) < 0.06$ pb for $M_{Z'} > 500$ GeV.

[37] CHEUNG 01B limit is derived from bounds on contact interactions in a global electroweak analysis.

[38] ABREU 00S uses LEP data at $\sqrt{s}$=90 to 189 GeV.

[39] BARATE 00I search for deviations in cross section and asymmetries in $e^+e^- \to$ fermions at $\sqrt{s}$=90 to 183 GeV. Assume θ=0. Bounds in the mass-mixing plane are shown in their Figure 18.

[40] ERLER 99 give 90%CL limit on the Z-Z' mixing $-0.0041 < \theta < 0.0003$. ρ_0=1 is assumed.

[41] ABE 97S find $\sigma(Z') \times B(e^+e^-, \mu^+\mu^-) < 40$ fb for $m_{Z'} > 600$ GeV at $\sqrt{s}$= 1.8 TeV.

[42] VILAIN 94B assume m_t = 150 GeV.

[43] ALITTI 93 search for resonances in the two-jet invariant mass. The limit assumes $B(Z' \to q\overline{q})$=0.7. See their Fig. 5 for limits in the $m_{Z'}$–$B(q\overline{q})$ plane.

[44] RIZZO 93 analyses CDF limit on possible two-jet resonances.

[45] ABE 90F use data for R, $R_{\ell\ell}$, and $A_{\ell\ell}$. They fix m_W = 80.49 ± 0.43 ± 0.24 GeV and m_Z = 91.13 ± 0.03 GeV.

Limits for Z_{LR}

Z_{LR} is the extra neutral boson in left-right symmetric models. $g_L = g_R$ is assumed unless noted. Values in parentheses assume stronger constraint on the Higgs sector, usually motivated by specific left-right symmetric models (see the Note on the W'). Values in brackets are from cosmological and astrophysical considerations and assume a light right-handed neutrino. Direct search bounds assume decays to Standard Model fermions only, unless noted.

VALUE (GeV)	CL%	DOCUMENT ID		TECN	COMMENT
>1162	95	[1] DEL-AGUILA	10	RVUE	Electroweak
> 630	95	[2] ABE	97S	CDF	$p\overline{p}$; $Z'_{LR} \to e^+e^-$, $\mu^+\mu^-$
• • • We do not use the following data for averages, fits, limits, etc. • • •					
		[3] TUMASYAN	23BE	CMS	pp; $Z'_{LR} \to N\overline{N}$, $N \to \ell q\overline{q}'$
		[4] BOBOVNIKOV 18		RVUE	pp, $Z'_{LR} \to W^+W^-$
> 998	95	[5] ERLER	09	RVUE	Electroweak
> 600	95	SCHAEL	07A	ALEP	e^+e^-
> 455	95	[6] ABDALLAH	06C	DLPH	e^+e^-
> 518	95	[7] ABBIENDI	04G	OPAL	e^+e^-
> 860	95	[8] CHEUNG	01B	RVUE	Electroweak
> 380	95	[9] ABREU	00S	DLPH	e^+e^-
> 436	95	[10] BARATE	00I	ALEP	Repl. by SCHAEL 07A
> 550	95	[11] CHAY	00	RVUE	Electroweak
		[12] ERLER	00	RVUE	Cs
		[13] CASALBUONI	99	RVUE	Cs
(> 1205)	90	[14] CZAKON	99	RVUE	Electroweak

Int. J. Mod. Phys. A 2026.41. Downloaded from www.worldscientific.com
by UNIVERSITY OF CALIFORNIA @ BERKELEY on 09/16/26. Re-use and distribution is strictly not permitted, except for Open Access articles.

> 564	95	[15] ERLER	99	RVUE	Electroweak
(> 1673)	95	[16] ERLER	99	RVUE	Electroweak
(> 1700)	68	[17] BARENBOIM	98	RVUE	Electroweak
> 244	95	[18] CONRAD	98	RVUE	$\nu_\mu N$ scattering
> 253	95	[19] VILAIN	94B	CHM2	$\nu_\mu e \to \nu_\mu e$ and $\overline{\nu}_\mu e \to \overline{\nu}_\mu e$
none 200–600	95	[20] RIZZO	93	RVUE	$p\overline{p}$; $Z_{LR} \to q\overline{q}$
[> 2000]		WALKER	91	COSM	Nucleosynthesis; light ν_R
none 200–500		[21] GRIFOLS	90	ASTR	SN 1987A; light ν_R
none 350–2400		[22] BARBIERI	89B	ASTR	SN 1987A; light ν_R

[1] DEL-AGUILA 10 give 95% CL limit on the Z-Z' mixing $-0.0012 < \theta < 0.0004$.

[2] ABE 97S find $\sigma(Z')\times$B$(e^+e^-,\mu^+\mu^-)<$ 40 fb for $m_{Z'} >$ 600 GeV at $\sqrt{s}$= 1.8 TeV.

[3] TUMASYAN 23BE search for pair production of heavy Majorana neutrinos via the decay of a Z' boson in a final state with $\ell^+\ell^-$ and at least two jets. For cases with $m_N = M_{Z'}/4$, their 95% CL limits are $M_{Z'}$ > 3.59 TeV (> 4.10 TeV) in the dielectron (dimuon) channel. See their Fig. 5 for limits on $\sigma\cdot B$.

[4] BOBOVNIKOV 18 use the ATLAS limits on $\sigma(pp \to Z')\cdot$B$(Z' \to W^+W^-)$ to constrain the Z-Z' mixing parameter ξ. See their Fig. 10 for limits in $M_{Z'} - \xi$ plane.

[5] ERLER 09 give 95% CL limit on the Z-Z' mixing $-0.0013 < \theta < 0.0006$.

[6] ABDALLAH 06C give 95% CL limit $|\theta| < 0.0028$. See their Fig. 14 for limit contours in the mass-mixing plane.

[7] ABBIENDI 04G give 95% CL limit on Z-Z' mixing $-0.00098 < \theta < 0.00190$. See their Fig. 20 for the limit contour in the mass-mixing plane. $\sqrt{s}$ = 91 to 207 GeV.

[8] CHEUNG 01B limit is derived from bounds on contact interactions in a global electroweak analysis.

[9] ABREU 00S give 95% CL limit on Z-Z' mixing $|\theta| < 0.0018$. See their Fig. 6 for the limit contour in the mass-mixing plane. $\sqrt{s}$=90 to 189 GeV.

[10] BARATE 00I search for deviations in cross section and asymmetries in $e^+e^- \to$ fermions at $\sqrt{s}$=90 to 183 GeV. Assume θ=0. Bounds in the mass-mixing plane are shown in their Figure 18.

[11] CHAY 00 also find $-0.0003 < \theta < 0.0019$. For g_R free, $m_{Z'} >$ 430 GeV.

[12] ERLER 00 discuss the possibility that a discrepancy between the observed and predicted values of Q_W(Cs) is due to the exchange of Z'. The data are better described in a certain class of the Z' models including Z_{LR} and Z_χ.

[13] CASALBUONI 99 discuss the discrepancy between the observed and predicted values of Q_W(Cs). It is shown that the data are better described in a class of models including the Z_{LR} model.

[14] CZAKON 99 perform a simultaneous fit to charged and neutral sectors. Assumes manifest left-right symmetric model. Finds $|\theta| < 0.0042$.

[15] ERLER 99 give 90% CL limit on the Z-Z' mixing $-0.0009 < \theta < 0.0017$.

[16] ERLER 99 assumes 2 Higgs doublets, transforming as 10 of SO(10), embedded in E_6.

[17] BARENBOIM 98 also gives 68% CL limits on the Z-Z' mixing $-0.0005 < \theta < 0.0033$. Assumes Higgs sector of minimal left-right model.

[18] CONRAD 98 limit is from measurements at CCFR, assuming no Z-Z' mixing.

[19] VILAIN 94B assume m_t = 150 GeV and θ=0. See Fig. 2 for limit contours in the mass-mixing plane.

[20] RIZZO 93 analyses CDF limit on possible two-jet resonances.

[21] GRIFOLS 90 limit holds for $m_{\nu_R} \lesssim 1$ MeV. A specific Higgs sector is assumed. See also GRIFOLS 90D, RIZZO 91.

[22] BARBIERI 89B limit holds for $m_{\nu_R} \leq 10$ MeV. Bounds depend on assumed supernova core temperature.

Limits for Z_χ

Z_χ is the extra neutral boson in SO(10) $\to$ SU(5) $\times$ U(1)$_\chi$. $g_\chi = e/\cos\theta_W$ is assumed unless otherwise stated. We list limits with the assumption $\rho = 1$ but with no further constraints on the Higgs sector. Values in parentheses assume stronger constraint on the Higgs sector motivated by superstring models. Values in brackets are from cosmological and astrophysical considerations and assume a light right-handed neutrino.

VALUE (GeV)	CL%	DOCUMENT ID		TECN	COMMENT
>4800 (CL = 95%) OUR LIMIT					
none 250–4800	95	[1] AAD	19L	ATLS	pp; $Z'_\chi \to e^+e^-$, $\mu^+\mu^-$
>4100	95	[2] AABOUD	17AT	ATLS	pp; $Z'_\chi \to e^+e^-$, $\mu^+\mu^-$
• • • We do not use the following data for averages, fits, limits, etc. • • •					
		[3] HERBERMANN	25	COSM	$\Delta N_{\rm eff}$; light ν_R
		[4] BOBOVNIKOV	18	RVUE	pp, $Z'_\chi \to W^+W^-$
>3050	95	[5] AABOUD	16U	ATLS	pp; $Z'_\chi \to e^+e^-$, $\mu^+\mu^-$
>2620	95	[6] AAD	14V	ATLS	pp, $Z'_\chi \to e^+e^-$, $\mu^+\mu^-$
>1970	95	[7] AAD	12CC	ATLS	pp, $Z'_\chi \to e^+e^-$, $\mu^+\mu^-$
> 930	95	[8] AALTONEN	11I	CDF	$p\overline{p}$; $Z'_\chi \to \mu^+\mu^-$
> 903	95	[9] ABAZOV	11A	D0	$p\overline{p}$, $Z'_\chi \to e^+e^-$
>1022	95	[10] DEL-AGUILA	10	RVUE	Electroweak
> 862	95	[9] AALTONEN	09T	CDF	$p\overline{p}$, $Z'_\chi \to e^+e^-$
> 892	95	[11] AALTONEN	09V	CDF	Repl. by AALTONEN 11I
>1141	95	[12] ERLER	09	RVUE	Electroweak
> 822	95	[9] AALTONEN	07H	CDF	Repl. by AALTONEN 09T
> 680	95	SCHAEL	07A	ALEP	e^+e^-
> 545	95	[13] ABDALLAH	06C	DLPH	e^+e^-
> 740		[9] ABULENCIA	06L	CDF	Repl. by AALTONEN 07H
> 690	95	[14] ABULENCIA	05A	CDF	$p\overline{p}$; $Z'_\chi \to e^+e^-$, $\mu^+\mu^-$
> 781	95	[15] ABBIENDI	04G	OPAL	e^+e^-
>2100		[16] BARGER	03B	COSM	Nucleosynthesis; light ν_R
> 680	95	[17] CHEUNG	01B	RVUE	Electroweak
> 440	95	[18] ABREU	00S	DLPH	e^+e^-
> 533	95	[19] BARATE	00I	ALEP	Repl. by SCHAEL 07A
> 554	95	[20] CHO	00	RVUE	Electroweak
		[21] ERLER	00	RVUE	Cs
		[22] ROSNER	00	RVUE	Cs
> 545	95	[23] ERLER	99	RVUE	Electroweak
(> 1368)	95	[24] ERLER	99	RVUE	Electroweak
> 215	95	[25] CONRAD	98	RVUE	$\nu_\mu N$ scattering
> 595	95	[26] ABE	97S	CDF	$p\overline{p}$; $Z'_\chi \to e^+e^-$, $\mu^+\mu^-$
> 190	95	[27] ARIMA	97	VNS	Bhabha scattering
> 262	95	[28] VILAIN	94B	CHM2	$\nu_\mu e \to \nu_\mu e$; $\overline{\nu}_\mu e \to \overline{\nu}_\mu e$
[>1470]		[29] FARAGGI	91	COSM	Nucleosynthesis; light ν_R
> 231	90	[30] ABE	90F	VNS	e^+e^-
[> 1140]		[31] GONZALEZ...	90D	COSM	Nucleosynthesis; light ν_R
[> 2100]		[32] GRIFOLS	90	ASTR	SN 1987A; light ν_R

[1] AAD 19L search for resonances decaying to $\ell^+\ell^-$ in pp collisions at $\sqrt{s}$ = 13 TeV.

[2] AABOUD 17AT search for resonances decaying to $\ell^+\ell^-$ in pp collisions at $\sqrt{s}$ = 13 TeV.

[3] HERBERMANN 25 limit is from Atacama Cosmology Telescope (ACT) DR6 limit on effective number of light neutrino species $\Delta N_{\rm eff}$ < 0.17. See their Fig. 1 for limits in mass-coupling plane.

[4] BOBOVNIKOV 18 use the ATLAS limits on $\sigma(pp \to Z')\cdot$B$(Z' \to W^+W^-)$ to constrain the Z-Z' mixing parameter ξ. See their Fig. 9 for limits in $M_{Z'} - \xi$ plane.

[5] AABOUD 16U search for resonances decaying to $\ell^+\ell^-$ in pp collisions at $\sqrt{s}$ = 13 TeV.

[6] AAD 14V search for resonances decaying to e^+e^-, $\mu^+\mu^-$ in pp collisions at $\sqrt{s}$ = 8 TeV.

[7] AAD 12CC search for resonances decaying to e^+e^-, $\mu^+\mu^-$ in pp collisions at $\sqrt{s}$ = 7 TeV.

[8] AALTONEN 11I search for resonances decaying to $\mu^+\mu^-$ in $p\overline{p}$ collisions at $\sqrt{s}$ = 1.96 TeV.

[9] ABAZOV 11A, AALTONEN 09T, AALTONEN 07H, and ABULENCIA 06L search for resonances decaying to e^+e^- in $p\overline{p}$ collisions at $\sqrt{s}$ = 1.96 TeV.

[10] DEL-AGUILA 10 give 95% CL limit on the Z-Z' mixing $-0.0011 < \theta < 0.0007$.

[11] AALTONEN 09V search for resonances decaying to $\mu^+\mu^-$ in $p\overline{p}$ collisions at $\sqrt{s}$ = 1.96 TeV.

[12] ERLER 09 give 95% CL limit on the Z-Z' mixing $-0.0016 < \theta < 0.0006$.

[13] ABDALLAH 06C give 95% CL limit $|\theta| < 0.0031$. See their Fig. 14 for limit contours in the mass-mixing plane.

[14] ABULENCIA 05A search for resonances decaying to electron or muon pairs in $p\overline{p}$ collisions at $\sqrt{s}$ = 1.96 TeV.

[15] ABBIENDI 04G give 95% CL limit on Z-Z' mixing $-0.00099 < \theta < 0.00194$. See their Fig. 20 for the limit contour in the mass-mixing plane. $\sqrt{s}$ = 91 to 207 GeV.

[16] BARGER 03B limit is from the nucleosynthesis bound on the effective number of light neutrino δN_ν <1. The quark-hadron transition temperature T_c=150 MeV is assumed. The limit with T_c=400 MeV is >4300 GeV.

[17] CHEUNG 01B limit is derived from bounds on contact interactions in a global electroweak analysis.

[18] ABREU 00S give 95% CL limit on Z-Z' mixing $|\theta| < 0.0017$. See their Fig. 6 for the limit contour in the mass-mixing plane. $\sqrt{s}$=90 to 189 GeV.

[19] BARATE 00I search for deviations in cross section and asymmetries in $e^+e^- \to$ fermions at $\sqrt{s}$=90 to 183 GeV. Assume θ=0. Bounds in the mass-mixing plane are shown in their Figure 18.

[20] CHO 00 use various electroweak data to constrain Z' models assuming m_H=100 GeV. See Fig. 3 for limits in the mass-mixing plane.

[21] ERLER 00 discuss the possibility that a discrepancy between the observed and predicted values of Q_W(Cs) is due to the exchange of Z'. The data are better described in a certain class of the Z' models including Z_{LR} and Z_χ.

[22] ROSNER 00 discusses the possibility that a discrepancy between the observed and predicted values of Q_W(Cs) is due to the exchange of Z'. The data are better described in a certain class of the Z' models including Z_χ.

[23] ERLER 99 give 90% CL limit on the Z-Z' mixing $-0.0020 < \theta < 0.0015$.

[24] ERLER 99 assumes 2 Higgs doublets, transforming as 10 of SO(10), embedded in E_6.

[25] CONRAD 98 limit is from measurements at CCFR, assuming no Z-Z' mixing.

[26] ABE 97S find $\sigma(Z')\times$B$(e^+e^-,\mu^+\mu^-)<$ 40 fb for $m_{Z'} >$ 600 GeV at $\sqrt{s}$= 1.8 TeV.

[27] Z-Z' mixing is assumed to be zero. $\sqrt{s}$= 57.77 GeV.

[28] VILAIN 94B assume m_t = 150 GeV and θ=0. See Fig. 2 for limit contours in the mass-mixing plane.

[29] FARAGGI 91 limit assumes the nucleosynthesis bound on the effective number of neutrinos ΔN_ν < 0.5 and is valid for m_{ν_R} < 1 MeV.

[30] ABE 90F use data for R, $R_{\ell\ell}$, and $A_{\ell\ell}$. ABE 90F fix $m_W = 80.49 \pm 0.43 \pm 0.24$ GeV and $m_Z = 91.13 \pm 0.03$ GeV.

[31] Assumes the nucleosynthesis bound on the effective number of light neutrinos (δN_ν < 1) and that ν_R is light ($\lesssim$ 1 MeV).

[32] GRIFOLS 90 limit holds for $m_{\nu_R} \lesssim 1$ MeV. See also GRIFOLS 90D, RIZZO 91.

Limits for Z_ψ

Z_ψ is the extra neutral boson in E$_6$ $\to$ SO(10) $\times$ U(1)$_\psi$. $g_\psi = e/\cos\theta_W$ is assumed unless otherwise stated. We list limits with the assumption $\rho = 1$ but with no further constraints on the Higgs sector. Values in brackets are from cosmological and astrophysical considerations and assume a light right-handed neutrino.

VALUE (GeV)	CL%	DOCUMENT ID		TECN	COMMENT
>4560 (CL = 95%) OUR LIMIT					
>4560	95	[1] SIRUNYAN	21N	CMS	pp; $Z'_\psi \to e^+e^-$, $\mu^+\mu^-$
none 250–4500	95	[2] AAD	19L	ATLS	pp; $Z'_\psi \to e^+e^-$, $\mu^+\mu^-$
none 200–3900	95	[3] SIRUNYAN	18BB	CMS	pp; $Z'_\psi \to e^+e^-$, $\mu^+\mu^-$
>3800	95	[4] AABOUD	17AT	ATLS	pp; $Z'_\psi \to e^+e^-$, $\mu^+\mu^-$
>2820	95	[5] KHACHATRY...	17T	CMS	pp; $Z'_\psi \to e^+e^-$, $\mu^+\mu^-$
>1100	95	[6] CHATRCHYAN	12O	CMS	pp, $Z'_\psi \to \tau^+\tau^-$

Int. J. Mod. Phys. A 2026.41. Downloaded from www.worldscientific.com
by UNIVERSITY OF CALIFORNIA @ BERKELEY on 09/16/26. Reproduction is strictly not permitted, except for Open Access articles.

• • • We do not use the following data for averages, fits, limits, etc. • • •

		[7] BOBOVNIKOV	18	RVUE	pp, $Z'_\psi \to W^+W^-$
>2740	95	[8] AABOUD	16U	ATLS	pp; $Z'_\psi \to e^+e^-$, $\mu^+\mu^-$
>2570	95	[9] KHACHATRY...	15AE	CMS	pp; $Z'_\psi \to e^+e^-$, $\mu^+\mu^-$
>2510	95	[10] AAD	14V	ATLS	pp, $Z'_\psi \to e^+e^-$, $\mu^+\mu^-$
>2260	95	[11] CHATRCHYAN	13AF	CMS	pp, $Z'_\psi \to e^+e^-$, $\mu^+\mu^-$
>1790	95	[12] AAD	12CC	ATLS	pp, $Z'_\psi \to e^+e^-$, $\mu^+\mu^-$
>2000	95	[13] CHATRCHYAN	12M	CMS	Repl. by CHATRCHYAN 13AF
> 917	95	[14] AALTONEN	11I	CDF	$p\overline{p}$; $Z'_\psi \to \mu^+\mu^-$
> 891	95	[15] ABAZOV	11A	D0	$p\overline{p}$, $Z'_\psi \to e^+e^-$
> 476	95	[16] DEL-AGUILA	10	RVUE	Electroweak
> 851	95	[15] AALTONEN	09T	CDF	$p\overline{p}$, $Z'_\psi \to e^+e^-$
> 878	95	[17] AALTONEN	09V	CDF	Repl. by AALTONEN 11I
> 147	95	[18] ERLER	09	RVUE	Electroweak
> 822	95	[15] AALTONEN	07H	CDF	Repl. by AALTONEN 09T
> 410	95	SCHAEL	07A	ALEP	e^+e^-
> 475	95	[19] ABDALLAH	06C	DLPH	e^+e^-
> 725		[15] ABULENCIA	06L	CDF	Repl. by AALTONEN 07H
> 675	95	[20] ABULENCIA	05A	CDF	Repl. by AALTONEN 11I and AALTONEN 09T
> 366	95	[21] ABBIENDI	04G	OPAL	e^+e^-
> 600		[22] BARGER	03B	COSM	Nucleosynthesis; light ν_R
> 350	95	[23] ABREU	00S	DLPH	e^+e^-
> 294	95	[24] BARATE	00I	ALEP	Repl. by SCHAEL 07A
> 137	95	[25] CHO	00	RVUE	Electroweak
> 146	95	[26] ERLER	99	RVUE	Electroweak
> 54	95	[27] CONRAD	98	RVUE	$\nu_\mu N$ scattering
> 590	95	[28] ABE	97S	CDF	$p\overline{p}$; $Z'_\psi \to e^+e^-$, $\mu^+\mu^-$
> 135	95	[29] VILAIN	94B	CHM2	$\nu_\mu e \to \nu_\mu e$; $\overline{\nu}_\mu e \to \overline{\nu}_\mu e$
> 105	90	[30] ABE	90F	VNS	e^+e^-
[> 160]		[31] GONZALEZ...	90D	COSM	Nucleosynthesis; light ν_R
[> 2000]		[32] GRIFOLS	90D	ASTR	SN 1987A; light ν_R

[1] SIRUNYAN 21N search for resonance decaying to e^+e^-, $\mu^+\mu^-$ in pp collisions at $\sqrt{s}$ = 13 TeV.
[2] AAD 19L search for resonances decaying to $\ell^+\ell^-$ in pp collisions at $\sqrt{s}$ = 13 TeV.
[3] SIRUNYAN 18BB search for resonances decaying to $\ell^+\ell^-$ in pp collisions at $\sqrt{s}$ = 13 TeV.
[4] AABOUD 17AT search for resonances decaying to $\ell^+\ell^-$ in pp collisions at $\sqrt{s}$ = 13 TeV.
[5] KHACHATRYAN 17T search for resonances decaying to e^+e^-, $\mu^+\mu^-$ in pp collisions at $\sqrt{s}$ = 8, 13 TeV.
[6] CHATRCHYAN 12O search for resonances decaying to $\tau^+\tau^-$ in pp collisions at $\sqrt{s}$ = 7 TeV.
[7] BOBOVNIKOV 18 use the ATLAS limits on $\sigma(pp \to Z')\cdot B(Z' \to W^+W^-)$ to constrain the Z-Z' mixing parameter ξ. See their Fig. 10 for limits in $M_{Z'} - \xi$ plane.
[8] AABOUD 16U search for resonances decaying to $\ell^+\ell^-$ in pp collisions at $\sqrt{s}$ = 13 TeV.
[9] KHACHATRYAN 15AE search for resonances decaying to e^+e^-, $\mu^+\mu^-$ in pp collisions at $\sqrt{s}$ = 8 TeV.
[10] AAD 14V search for resonances decaying to e^+e^-, $\mu^+\mu^-$ in pp collisions at $\sqrt{s}$ = 8 TeV.
[11] CHATRCHYAN 13AF search for resonances decaying to e^+e^-, $\mu^+\mu^-$ in pp collisions at $\sqrt{s}$ = 7 TeV and 8 TeV.
[12] AAD 12CC search for resonances decaying to e^+e^-, $\mu^+\mu^-$ in pp collisions at $\sqrt{s}$ = 7 TeV.
[13] CHATRCHYAN 12M search for resonances decaying to e^+e^- or $\mu^+\mu^-$ in pp collisions at $\sqrt{s}$ = 7 TeV.
[14] AALTONEN 11I search for resonances decaying to $\mu^+\mu^-$ in $p\overline{p}$ collisions at $\sqrt{s}$ = 1.96 TeV.
[15] ABAZOV 11A, AALTONEN 09T, AALTONEN 07H, and ABULENCIA 06L search for resonances decaying to e^+e^- in $p\overline{p}$ collisions at $\sqrt{s}$ = 1.96 TeV.
[16] DEL-AGUILA 10 give 95% CL limit on the Z-Z' mixing $-0.0019 < \theta < 0.0007$.
[17] AALTONEN 09V search for resonances decaying to $\mu^+\mu^-$ in $p\overline{p}$ collisions at $\sqrt{s}$ = 1.96 TeV.
[18] ERLER 09 give 95% CL limit on the Z-Z' mixing $-0.0018 < \theta < 0.0009$.
[19] ABDALLAH 06C give 95% CL limit $|\theta| < 0.0027$. See their Fig. 14 for limit contours in the mass-mixing plane.
[20] ABULENCIA 05A search for resonances decaying to electron or muon pairs in $p\overline{p}$ collisions at $\sqrt{s}$ = 1.96 TeV.
[21] ABBIENDI 04G give 95% CL limit on Z-Z' mixing $-0.00129 < \theta < 0.00258$. See their Fig. 20 for the limit contour in the mass-mixing plane. $\sqrt{s}$ = 91 to 207 GeV.
[22] BARGER 03B limit is from the nucleosynthesis bound on the effective number of light neutrino δN_ν <1. The quark-hadron transition temperature T_c=150 MeV is assumed. The limit with T_c=400 MeV is >1100 GeV.
[23] ABREU 00S give 95% CL limit on Z-Z' mixing $|\theta| < 0.0018$. See their Fig. 6 for the limit contour in the mass-mixing plane. $\sqrt{s}$=90 to 189 GeV.
[24] BARATE 00I search for deviations in cross section and asymmetries in $e^+e^- \to$ fermions at $\sqrt{s}$=90 to 183 GeV. Assume θ=0. Bounds in the mass-mixing plane are shown in their Figure 18.
[25] CHO 00 use various electroweak data to constrain Z' models assuming m_H=100 GeV. See Fig. 3 for limits in the mass-mixing plane.
[26] ERLER 99 give 90% CL limit on the Z-Z' mixing $-0.0013 < \theta < 0.0024$.
[27] CONRAD 98 limit is from measurements at CCFR, assuming no Z-Z' mixing.
[28] ABE 97S find $\sigma(Z')\times B(e^+e^-,\mu^+\mu^-)$< 40 fb for $m_{Z'}$ > 600 GeV at $\sqrt{s}$= 1.8 TeV.
[29] VILAIN 94B assume m_t = 150 GeV and θ=0. See Fig. 2 for limit contours in the mass-mixing plane.
[30] ABE 90F use data for R, $R_{\ell\ell}$, and $A_{\ell\ell}$. ABE 90F fix $m_W = 80.49 \pm 0.43 \pm 0.24$ GeV and $m_Z = 91.13 \pm 0.03$ GeV.
[31] Assumes the nucleosynthesis bound on the effective number of light neutrinos ($\delta N_\nu < 1$) and that ν_R is light ($\lesssim$ 1 MeV).
[32] GRIFOLS 90D limit holds for $m_{\nu_R} \lesssim$ 1 MeV. See also RIZZO 91.

Limits for Z_η

Z_η is the extra neutral boson in E_6 models, corresponding to $Q_\eta = \sqrt{3/8}\ Q_\chi - \sqrt{5/8}\ Q_\psi$. $g_\eta = e/\cos\theta_W$ is assumed unless otherwise stated. We list limits with the assumption ρ=1 but with no further constraints on the Higgs sector. Values in parentheses assume stronger constraint on the Higgs sector motivated by superstring models. Values in brackets are from cosmological and astrophysical considerations and assume a light right-handed neutrino.

VALUE (GeV)	CL%	DOCUMENT ID		TECN	COMMENT
>3900	95	[1] AABOUD	17AT	ATLS	pp; $Z'_\eta \to e^+e^-$, $\mu^+\mu^-$

• • • We do not use the following data for averages, fits, limits, etc. • • •

		[2] BOBOVNIKOV	18	RVUE	pp, $Z'_\eta \to W^+W^-$
>2810	95	[3] AABOUD	16U	ATLS	pp; $Z'_\eta \to e^+e^-$, $\mu^+\mu^-$
>1870	95	[4] AAD	12CC	ATLS	pp, $Z'_\eta \to e^+e^-$, $\mu^+\mu^-$
> 938	95	[5] AALTONEN	11I	CDF	$p\overline{p}$; $Z'_\eta \to \mu^+\mu^-$
> 923	95	[6] ABAZOV	11A	D0	$p\overline{p}$, $Z'_\eta \to e^+e^-$
> 488	95	[7] DEL-AGUILA	10	RVUE	Electroweak
> 877	95	[6] AALTONEN	09T	CDF	$p\overline{p}$, $Z'_\eta \to e^+e^-$
> 904	95	[8] AALTONEN	09V	CDF	Repl. by AALTONEN 11I
> 427	95	[9] ERLER	09	RVUE	Electroweak
> 891	95	[6] AALTONEN	07H	CDF	Repl. by AALTONEN 09T
> 350	95	SCHAEL	07A	ALEP	e^+e^-
> 360	95	[10] ABDALLAH	06C	DLPH	e^+e^-
> 745		[6] ABULENCIA	06L	CDF	Repl. by AALTONEN 07H
> 720	95	[11] ABULENCIA	05A	CDF	Repl. by AALTONEN 11I and AALTONEN 09T
> 515	95	[12] ABBIENDI	04G	OPAL	e^+e^-
>1600		[13] BARGER	03B	COSM	Nucleosynthesis; light ν_R
> 310	95	[14] ABREU	00S	DLPH	e^+e^-
> 329	95	[15] BARATE	00I	ALEP	Repl. by SCHAEL 07A
> 619	95	[16] CHO	00	RVUE	Electroweak
> 365	95	[17] ERLER	99	RVUE	Electroweak
> 87	95	[18] CONRAD	98	RVUE	$\nu_\mu N$ scattering
> 620	95	[19] ABE	97S	CDF	$p\overline{p}$; $Z'_\eta \to e^+e^-$, $\mu^+\mu^-$
> 100	95	[20] VILAIN	94B	CHM2	$\nu_\mu e \to \nu_\mu e$; $\overline{\nu}_\mu e \to \overline{\nu}_\mu e$
> 125	90	[21] ABE	90F	VNS	e^+e^-
[> 820]		[22] GONZALEZ...	90D	COSM	Nucleosynthesis; light ν_R
[> 3300]		[23] GRIFOLS	90	ASTR	SN 1987A; light ν_R
[> 1040]		[22] LOPEZ	90	COSM	Nucleosynthesis; light ν_R

[1] AABOUD 17AT search for resonances decaying to $\ell^+\ell^-$ in pp collisions at $\sqrt{s}$ = 13 TeV.
[2] BOBOVNIKOV 18 use the ATLAS limits on $\sigma(pp \to Z')\cdot B(Z' \to W^+W^-)$ to constrain the Z-Z' mixing parameter ξ. See their Fig. 9 for limits in $M_{Z'} - \xi$ plane.
[3] AABOUD 16U search for resonances decaying to $\ell^+\ell^-$ in pp collisions at $\sqrt{s}$ = 13 TeV.
[4] AAD 12CC search for resonances decaying to e^+e^-, $\mu^+\mu^-$ in pp collisions at $\sqrt{s}$ = 7 TeV.
[5] AALTONEN 11I search for resonances decaying to $\mu^+\mu^-$ in $p\overline{p}$ collisions at $\sqrt{s}$ = 1.96 TeV.
[6] ABAZOV 11A, AALTONEN 09T, AALTONEN 07H, and ABULENCIA 06L search for resonances decaying to e^+e^- in $p\overline{p}$ collisions at $\sqrt{s}$ = 1.96 TeV.
[7] DEL-AGUILA 10 give 95% CL limit on the Z-Z' mixing $-0.0023 < \theta < 0.0027$.
[8] AALTONEN 09V search for resonances decaying to $\mu^+\mu^-$ in $p\overline{p}$ collisions at $\sqrt{s}$ = 1.96 TeV.
[9] ERLER 09 give 95% CL limit on the Z-Z' mixing $-0.0047 < \theta < 0.0021$.
[10] ABDALLAH 06C give 95% CL limit $|\theta| < 0.0092$. See their Fig. 14 for limit contours in the mass-mixing plane.
[11] ABULENCIA 05A search for resonances decaying to electron or muon pairs in $p\overline{p}$ collisions at $\sqrt{s}$ = 1.96 TeV.
[12] ABBIENDI 04G give 95% CL limit on Z-Z' mixing $-0.00447 < \theta <$0.00331. See their Fig. 20 for the limit contour in the mass-mixing plane. $\sqrt{s}$ = 91 to 207 GeV.
[13] BARGER 03B limit is from the nucleosynthesis bound on the effective number of light neutrino δN_ν <1. The quark-hadron transition temperature T_c=150 MeV is assumed. The limit with T_c=400 MeV is >3300 GeV.
[14] ABREU 00S give 95% CL limit on Z-Z' mixing $|\theta| < 0.0024$. See their Fig. 6 for the limit contour in the mass-mixing plane. $\sqrt{s}$=90 to 189 GeV.
[15] BARATE 00I search for deviations in cross section and asymmetries in $e^+e^- \to$ fermions at $\sqrt{s}$=90 to 183 GeV. Assume θ=0. Bounds in the mass-mixing plane are shown in their Figure 18.
[16] CHO 00 use various electroweak data to constrain Z' models assuming m_H=100 GeV. See Fig. 3 for limits in the mass-mixing plane.
[17] ERLER 99 give 90% CL limit on the Z-Z' mixing $-0.0062 < \theta < 0.0011$.
[18] CONRAD 98 limit is from measurements at CCFR, assuming no Z-Z' mixing.
[19] ABE 97S find $\sigma(Z')\times B(e^+e^-,\mu^+\mu^-)$< 40 fb for $m_{Z'}$ > 600 GeV at $\sqrt{s}$= 1.8 TeV.
[20] VILAIN 94B assume m_t = 150 GeV and θ=0. See Fig. 2 for limit contours in the mass-mixing plane.
[21] ABE 90F use data for R, $R_{\ell\ell}$, and $A_{\ell\ell}$. ABE 90F fix $m_W = 80.49 \pm 0.43 \pm 0.24$ GeV and $m_Z = 91.13 \pm 0.03$ GeV.
[22] These authors claim that the nucleosynthesis bound on the effective number of light neutrinos ($\delta N_\nu < 1$) constrains Z' masses if ν_R is light ($\lesssim$ 1 MeV).
[23] GRIFOLS 90 limit holds for $m_{\nu_R} \lesssim$ 1 MeV. See also GRIFOLS 90D, RIZZO 91.

Int. J. Mod. Phys. A 2026.41. Downloaded from www.worldscientific.com
by UNIVERSITY OF CALIFORNIA @ BERKELEY on 09/16/26. Re-use and distribution is strictly not permitted, except for Open Access articles.

Limits for other Z'

VALUE (GeV)	CL%	DOCUMENT ID		TECN	COMMENT
>2450	95	[1] HAYRAPETY...	25AB	CMS	VBF; $Z' \to \tau^+\tau^-, WW$
>3000	95	[2] HAYRAPETY...	25Q	CMS	$Z' \to ZH$
none 300–3200	95	[3] AAD	23O	ATLS	$Z' \to ZH$
none 1800–2400	95	[4] TUMASYAN	23AF	CMS	$Z' \to b\overline{b}$
none 1300–3100, 3300–3500	95	[5] TUMASYAN	23AP	CMS	$Z' \to WW$
>3900	95	[6] TUMASYAN	23AP	CMS	$Z' \to ZH$
>4000	95	[7] TUMASYAN	22D	CMS	$Z' \to WW$
none 800–3700	95	[8] SIRUNYAN	21X	CMS	$Z' \to HZ$
>2650	95	[9] AAD	20AJ	ATLS	$Z' \to HZ$
>3900	95	[10] AAD	20AM	ATLS	$Z' \to t\overline{t}$
>3900	95	[11] AAD	20AT	ATLS	$Z' \to WW$
none 1200–3500	95	[12] SIRUNYAN	20Q	CMS	$Z' \to WW$
none 580–3100	95	[13] AABOUD	19AS	ATLS	$Z' \to t\overline{t}$
none 1300–3100	95	[14] AAD	19D	ATLS	$Z' \to WW$
>3800	95	[15] SIRUNYAN	19AA	CMS	$Z' \to t\overline{t}$
>3700	95	[16] SIRUNYAN	19CP	CMS	$Z' \to WW, HZ, \ell^+\ell^-$
>1800	95	[17] SIRUNYAN	19I	CMS	$Z' \to HZ$
none 600–2100	95	[18] AABOUD	18AB	ATLS	$Z' \to b\overline{b}$
none 500–2830	95	[19] AABOUD	18AI	ATLS	$Z' \to HZ$
none 300–3000	95	[20] AABOUD	18AK	ATLS	$Z' \to WW$
>1300	95	[21] AABOUD	18B	ATLS	$Z' \to WW$
none 400–3000	95	[22] AABOUD	18BI	ATLS	$Z' \to t\overline{t}$
none 1200–2800	95	[23] AABOUD	18F	ATLS	$Z' \to WW$
>2300	95	[24] SIRUNYAN	18ED	CMS	$Z' \to HZ$
none 1200–2700	95	[25] SIRUNYAN	18P	CMS	$Z' \to WW$
>2900	95	[26] AABOUD	17AK	ATLS	$Z' \to q\overline{q}$
none 1100–2600	95	[27] AABOUD	17AO	ATLS	$Z' \to HZ$
>2300	95	[28] SIRUNYAN	17AK	CMS	$Z' \to WW,\ HZ$
>2500	95	[29] SIRUNYAN	17Q	CMS	$Z' \to t\overline{t}$
>1190	95	[30] SIRUNYAN	17R	CMS	$Z' \to HZ$
none 1210–2260	95	[30] SIRUNYAN	17R	CMS	$Z' \to HZ$
• • • We do not use the following data for averages, fits, limits, etc. • • •					
		[31] AAD	25AZ	ATLS	$Z' \to q\overline{q}$
		[32] AAD	25BA	ATLS	$Z' \to$ dark Higgs+ Z'
		[33] AAD	25BB	ATLS	$b\overline{b} \to Z' \to \tau^+\tau^-$
		[34] AAD	25C	ATLS	$Z' \to S\chi\chi \to b\overline{b}\chi\chi$
		[35] AAD	25F	ATLS	$pp;\ \ell^+\ell^-\ell^+\ell^-$
		[36] AAD	25N	ATLS	$Z' \to q_d\overline{q}_d$
		[37] AAD	25Q	ATLS	$Z' \to q\overline{q}$
>1050	95	[38] CHEKHOVSKY	25J	CMS	$Z' \to H\chi\chi$
>4030	95	[39] HAYRAPETY...	25V	CMS	$Z' \to \tau'\tau'$
		[40] AAD	24AA	ATLS	$Z' \to q_d\overline{q}_d$
>4400	95	[41] AAD	24AE	ATLS	$M_{Z'} = M_{W'}$
		[42] AAD	24AY	ATLS	$Z' \to q\overline{q}$
		[43] AAD	24BJ	ATLS	top-philic Z'
		[44] AAD	24BR	ATLS	$L_\mu - L_\tau$
		[45] AAD	24CD	ATLS	DM simplified Z'
		[46] AAD	24CI	ATLS	DM simplified Z'
		[47] AAD	24CM	ATLS	Dark ρ_D^0
		[48] ABLIKIM	24G	BES3	$J/\psi \to \mu^+\mu^- Z'$
		[49] ADACHI	24F	BEL2	$e^+e^- \to \mu^+\mu^- Z'$, $Z' \to \mu^+\mu^-$
		[50] AKITA	24	ASTR	SN1987A
		[51] ANDREEV	24	NA64	μ-nucleus scattering
		[52] ANDREEV	24B	NA64	e-nucleus scattering
		[53] ANDREEV	24E	NA64	μ-nucleus scattering
		[54] BISWAS	24	BELL	$e^+e^- \to \tau^+\tau^-\phi(\to e^+e^-,\ \mu^+\mu^-)$
		[55] HAYRAPETY...	24AZ	CMS	$Z' \to s_D\overline{s}_D \to 4\mu$
		[56] HAYRAPETY...	24G	CMS	$Z' \to ggg$
		[57] HAYRAPETY...	24W	CMS	$Z' \to \chi\chi S,\ S \to W^+W^-$
		[58] AAD	23BF	ATLS	DM simplified Z'
		[59] AAD	23W	ATLS	dark Higgs Z'
		[60] AAD	23X	ATLS	$L_\mu - L_\tau$
		[61] ADACHI	23B	BEL2	$L_\mu - L_\tau$
		[62] ADACHI	23F	BEL2	$L_\mu - L_\tau$
		[63] HAYRAPETY...	23D	CMS	$Z' \to \mu^+\mu^-$
		[64] HAYRAPETY...	23G	CMS	$Z' \to \mu^+\mu^-$
		[65] LI	23I	ASTR	Steller cooling
		[66] MANZARI	23	ASTR	DM mediator Z'
		[67] AAD	22	ATLS	$pp \to b\overline{b}Z' \to b\overline{b}b\overline{b}$
		[68] AAD	22D	ATLS	DM mediator Z'
		[69] ANDREEV	22	CALO	electron beam dump
		[70] BONET	22	HPGE	ν-nucleus scattring
		[71] COLOMA	22	RVUE	ν-nucleus scattering
		[72] COLOMA	22A	RVUE	ν-e scattering
		[73] CZANK	22	BELL	$e^+e^- \to \mu^+\mu^- Z'(\to \mu^+\mu^-)$
		[74] TUMASYAN	22AA	CMS	$Z' \to$ SVJs
		[75] AAD	21AQ	ATLS	$pp,\ \ell^+\ell^-\ell^+\ell^-$
		[76] AAD	21AZ	ATLS	DM mediator Z'
		[77] AAD	21BB	ATLS	$Z' \to AH$
		[78] AAD	21D	ATLS	dark Higgs Z'
		[79] AAD	21K	ATLS	$Z' \to \chi\chi$
		[80] BURAS	21	RVUE	leptophilic Z'
		[81] CADEDDU	21	RVUE	ν-nucleus scattering
		[82] COLARESI	21	HPGE	ν-nucleus scattering
		[83] KRIBS	21	RVUE	ep scattering
		[84] TUMASYAN	21D	CMS	$Z' \to \chi\chi$
		[85] AAD	20AF	ATLS	$Z' \to H\gamma$
		[86] AAD	20T	ATLS	DM simplified Z'
		[87] AAD	20W	ATLS	DM simplified Z'
		[88] AAIJ	20AL	LHCB	$Z' \to \mu^+\mu^-$
		[89] ADACHI	20	BEL2	$e^+e^- \to \mu^+\mu^- Z'$, $e^\pm\mu^\mp Z'$
		[90] SIRUNYAN	20AI	CMS	$Z' \to q\overline{q}$
		[91] SIRUNYAN	20AQ	CMS	$Z' \to \mu^+\mu^-$
		[92] SIRUNYAN	20M	CMS	$Z' \to q\overline{q}$
		[93] AABOUD	19AJ	ATLS	$Z' \to q\overline{q}$
		[94] AABOUD	19D	ATLS	$Z' \to q\overline{q}$
		[95] AABOUD	19V	ATLS	DM simplified Z'
		[96] AAD	19L	ATLS	$Z' \to e^+e^-,\ \mu^+\mu^-$
		[97] LONG	19	RVUE	Electroweak
		[98] PANDEY	19	RVUE	neutrino NSI
		[99] SIRUNYAN	19AL	CMS	$Z' \to tT,\ T \to Ht,\ Zt,\ Wb$
		[100] SIRUNYAN	19AN	CMS	DM simplified Z'
		[101] SIRUNYAN	19CB	CMS	$Z' \to q\overline{q}$
		[102] SIRUNYAN	19CD	CMS	$Z' \to q\overline{q}$
		[103] SIRUNYAN	19D	CMS	$Z' \to H\gamma$
		[104] AABOUD	18AA	ATLS	$Z' \to H\gamma$
>4500	95	[105] AABOUD	18CJ	ATLS	$Z' \to WW, HZ, \ell^+\ell^-$
		[106] AABOUD	18N	ATLS	$Z' \to q\overline{q}$
		[107] AAIJ	18AQ	LHCB	$Z' \to \mu^+\mu^-$
		[108] SIRUNYAN	18DR	CMS	$Z' \to \mu^+\mu^-$
		[109] SIRUNYAN	18G	CMS	$Z' \to q\overline{q}$
		[110] SIRUNYAN	18I	CMS	$Z' \to b\overline{b}$
>1580	95	[111] AABOUD	17B	ATLS	$Z' \to HZ$
		[112] KHACHATRY...	17AX	CMS	$Z' \to \ell\ell\ell\ell$
		[113] KHACHATRY...	17U	CMS	$Z' \to HZ$
>1700	95	[114] SIRUNYAN	17A	CMS	$Z' \to WW$
		[115] SIRUNYAN	17AP	CMS	$Z' \to HA$
		[116] SIRUNYAN	17T	CMS	$Z' \to q\overline{q}$
		[117] SIRUNYAN	17V	CMS	$Z' \to Tt$
none 1100–1500	95	[118] AABOUD	16	ATLS	$Z' \to b\overline{b}$
		[119] AAD	16L	ATLS	$Z' \to a\gamma,\ a \to \gamma\gamma$
none 1500–2600	95	[120] AAD	16S	ATLS	$Z' \to q\overline{q}$
none 1000–1100, none 1300–1500	95	[121] KHACHATRY...	16AP	CMS	$Z' \to HZ$
>2400	95	[122] KHACHATRY...	16E	CMS	$Z' \to t\overline{t}$
		[123] AAD	15AO	ATLS	$Z' \to t\overline{t}$
		[124] AAD	15AT	ATLS	monotop
		[125] AAD	15CD	ATLS	$H \to ZZ',\ Z'Z';\ Z' \to \ell^+\ell^-$
		[126] KHACHATRY...	15F	CMS	monotop
		[127] KHACHATRY...	15O	CMS	$Z' \to HZ$
		[128] AAD	14AT	ATLS	$Z' \to Z\gamma$
		[129] KHACHATRY...	14A	CMS	$Z' \to VV$
		[130] MARTINEZ	14	RVUE	Electroweak
none 500–1740	95	[131] AAD	13AQ	ATLS	$Z' \to t\overline{t}$
>1320 or 1000–1280	95	[132] AAD	13G	ATLS	$Z' \to t\overline{t}$
> 915	95	[132] AALTONEN	13A	CDF	$Z' \to t\overline{t}$
>1300	95	[133] CHATRCHYAN	13AP	CMS	$Z' \to t\overline{t}$
>2100	95	[132] CHATRCHYAN	13BM	CMS	$Z' \to t\overline{t}$
		[134] AAD	12BV	ATLS	$Z' \to t\overline{t}$
		[135] AAD	12K	ATLS	$Z' \to t\overline{t}$
		[136] AALTONEN	12AR	CDF	Chromophilic
		[137] AALTONEN	12N	CDF	$Z' \to \overline{t}u$
> 835	95	[138] ABAZOV	12R	D0	$Z' \to t\overline{t}$
		[139] CHATRCHYAN	12AI	CMS	$Z' \to t\overline{u}$
		[140] CHATRCHYAN	12AQ	CMS	$Z' \to t\overline{t}$
>1490	95	[132] CHATRCHYAN	12BL	CMS	$Z' \to t\overline{t}$
		[141] AALTONEN	11AD	CDF	$Z' \to t\overline{t}$
		[142] AALTONEN	11AE	CDF	$Z' \to t\overline{t}$
		[143] CHATRCHYAN	11O	CMS	$pp \to tt$
		[144] AALTONEN	08D	CDF	$Z' \to t\overline{t}$
		[144] AALTONEN	08Y	CDF	$Z' \to t\overline{t}$
		[144] ABAZOV	08AA	D0	$Z' \to t\overline{t}$
		[145] ABAZOV	04A	D0	Repl. by ABAZOV 08AA
		[146] BARGER	03B	COSM	Nucleosynthesis; light ν_R
		[147] CHO	00	RVUE	E_6-motivated
		[148] CHO	98	RVUE	E_6-motivated
		[149] ABE	97G	CDF	$Z' \to \overline{q}q$

Int. J. Mod. Phys. A 2026.41. Downloaded from www.worldscientific.com
by UNIVERSITY OF CALIFORNIA @ BERKELEY on 09/16/26. Reproduction is strictly not permitted, except for Open Access articles.

[1] HAYRAPETYAN 25AB search for Z' with nonuniversal fermion couplings produced via vector boson fusion (VBF) processes in pp collisions at $\sqrt{s}$ = 13 TeV. The limit quoted above assumes Z' couplings with first- and second-generation fermion are zero, and $g_{Z'WW} = (5.3 \times M_W/M_{Z'})^2$, $B(\tau^+\tau^-) = 0.5$. See their Fig. 2 for exclusion limits on $M_{Z'}$ under various model assumptions.

[2] HAYRAPETYAN 25Q search for resonances decaying to ZH in pp collisions at $\sqrt{s}$ = 13 TeV. The limit quoted above is for heavy-vector-triplet Z' with $g_V = 3$. See their Fig. 6 for limits on $\sigma \cdot B$.

[3] AAD 23O search for resonances decaying to HZ in pp collisions at $\sqrt{s}$ = 13 TeV. The quoted limit is for heavy-vector-triplet Z' with $g_V = 3$. The limit becomes $M_{Z'} >$ 2800 GeV for $g_V = 1$.

[4] TUMASYAN 23AF search for resonance decaying to $b\overline{b}$ in pp collisions at $\sqrt{s}$ = 13 TeV. The limit quoted above is for heavy-vector-triplet Z' with $g_V = 1$. See their Fig. 4 for limits on $\sigma \cdot B$.

[5] TUMASYAN 23AP search for resonances decaying to WW in pp collisions at $\sqrt{s}$ = 13 TeV. The limit quoted above is for heavy-vector-triplet Z' with $g_V = 3$. The limit becomes $M_{Z'} >$ 4.8 TeV assuming $M_{W'} = M_{Z'}$ and combining $W' \rightarrow WZ$, $W' \rightarrow WH$, $Z' \rightarrow WW$, $Z' \rightarrow ZH$ channels.

[6] TUMASYAN 23AP search for resonances decaying to ZH in pp collisions at $\sqrt{s}$ = 13 TeV. The limit quoted above is for heavy-vector-triplet Z' with $g_V = 3$. The limit becomes $M_{Z'} >$ 4.8 TeV assuming $M_{W'} = M_{Z'}$ and combining $W' \rightarrow WZ$, $W' \rightarrow WH$, $Z' \rightarrow WW$, $Z' \rightarrow ZH$ channels.

[7] TUMASYAN 22D search for resonances produced through Drell-Yan and vector-boson-fusion processes in pp collisions at $\sqrt{s}$ = 13 TeV. See their Fig. 8 for limits on $\sigma \cdot B$. The quoted limit is for heavy-vector-triplet W' with $g_V = 3$ produced mainly via Drell-Yan.

[8] SIRUNYAN 21X search for resonances decaying to HZ in pp collisions at $\sqrt{s}$ = 13 TeV. The limit quoted above is for heavy-vector-triplet Z' with $g_V = 3$. The limit becomes $M_{Z'} >$ 3500 GeV for $g_V = 1$.

[9] AAD 20AJ search for resonances decaying to HZ in pp collisions at $\sqrt{s}$ = 13 TeV. The quoted limit is for heavy-vector-triplet Z' with $g_V = 3$. The limit becomes $M_{Z'} >$ 2200 GeV for $g_V = 1$. See their Fig. 6 for limits on $\sigma \cdot B$.

[10] AAD 20AM search for a resonance decaying to $t\overline{t}$ in pp collisions at $\sqrt{s}$ = 13 TeV. The quoted limit is for a leptophobic top-color Z' with $\Gamma_{Z'}/M_{Z'} = 0.01$. The limit becomes $M_{Z'} >$ 4700 GeV for $\Gamma_{Z'}/M_{Z'} = 0.03$.

[11] AAD 20AT search for resonances decaying to WW in pp collisions at $\sqrt{s}$ = 13 TeV. The quoted limit is for heavy-vector-triplet Z' with $g_V = 3$. The limit becomes $M_{Z'} >$ 3500 GeV for $g_V = 1$. See their Fig. 14 for limits on $\sigma \cdot B$.

[12] SIRUNYAN 20Q search for resonances decaying to WW in pp collisions at $\sqrt{s}$ = 13 TeV. The quoted limit is for heavy-vector-triplet Z' with $g_V = 3$.

[13] AABOUD 19AS search for a resonance decaying to $t\overline{t}$ in pp collisions at $\sqrt{s}$ = 13 TeV. The quoted limit is for a top-color Z' with $\Gamma_{Z'}/M_{Z'} = 0.01$. Limits are also set on Z' masses in simplified Dark Matter models.

[14] AAD 19D search for resonances decaying to WW in pp collisions at $\sqrt{s}$ = 13 TeV. The quoted limit is for heavy-vector-triplet Z' with $g_V = 3$. The limit becomes $M_{Z'} >$ 2900 GeV for $g_V = 1$. If we assume $M_{Z'} = M_{W'}$, the limit increases $M_{Z'} >$ 3800 GeV and $M_{Z'} >$ 3500 GeV for $g_V = 3$ and $g_V = 1$, respectively. See their Fig. 9 for limits on $\sigma \cdot B$.

[15] SIRUNYAN 19AA search for a resonance decaying to $t\overline{t}$ in pp collisions at $\sqrt{s}$ = 13 TeV. The quoted limit is for a leptophobic top-color Z' with $\Gamma_{Z'}/M_{Z'} = 0.01$.

[16] SIRUNYAN 19CP present a statistical combinations of searches for Z' decaying to pairs of bosons or leptons in pp collisions at $\sqrt{s}$ = 13 TeV. The quoted limit is for heavy-vector-triplet Z' with $g_V = 3$. If we assume $M_{Z'} = M_{W'}$, the limit becomes $M_{Z'} >$ 4500 GeV for $g_V = 3$ and $M_{Z'} >$ 5000 GeV for $g_V = 1$. See their Figs. 2 and 3 for limits on $\sigma \cdot B$.

[17] SIRUNYAN 19I search for resonances decaying to ZW in pp collisions at $\sqrt{s}$ = 13 TeV. The quoted limit is for heavy-vector-triplet Z' with $g_V = 3$. The limit becomes $M_{Z'} >$ 2800 GeV if we assume $M_{Z'} = M_{W'}$.

[18] AABOUD 18AB search for resonances decaying to $b\overline{b}$ in pp collisions at $\sqrt{s}$ = 13 TeV. The limit quoted above is for a leptophobic Z' with SM-like couplings to quarks. See their Fig. 6 for limits on $\sigma \cdot B$. Additional limits on a Z' axial-vector mediator in a simplified dark-matter model are shown in Fig. 7.

[19] AABOUD 18AI search for resonances decaying to HZ in pp collisions at $\sqrt{s}$ = 13 TeV. The quoted limit is for heavy-vector-triplet Z' with $g_V = 3$. The limit becomes $M_{Z'} >$ 2650 GeV for $g_V = 1$. If we assume $M_{W'} = M_{Z'}$, the limit increases $M_{Z'} >$ 2930 GeV and $M_{Z'} >$ 2800 GeV for $g_V = 3$ and $g_V = 1$, respectively. See their Fig. 5 for limits on $\sigma \cdot B$.

[20] AABOUD 18AK search for resonances decaying to WW in pp collisions at $\sqrt{s}$ =1 3 TeV. The limit quoted above is for heavy-vector-triplet Z' with $g_V = 3$. The limit becomes $M_{Z'} >$ 2750 GeV for $g_V = 1$.

[21] AABOUD 18B search for resonances decaying to WW in pp collisions at $\sqrt{s}$ = 13 TeV. The quoted limit is for heavy-vector-triplet Z' with $g_V = 1$. See their Fig.11 for limits on $\sigma \cdot B$.

[22] AABOUD 18BI search for a resonance decaying to $t\overline{t}$ in pp collisions at $\sqrt{s}$ = 13 TeV. The quoted limit is for a top-color assisted TC Z' with $\Gamma_{Z'}/M_{Z'} = 0.01$. The limits for wider resonances are available. See their Fig. 14 for limits on $\sigma \cdot B$.

[23] AABOUD 18F search for resonances decaying to WW in pp collisions at $\sqrt{s}$ = 13 TeV. The quoted limit is for heavy-vector-triplet Z' with $g_V = 3$. The limit becomes $M_{Z'} >$ 2200 GeV for $g_V = 1$. If we assume $M_{Z'} = M_{W'}$, the limit increases $M_{Z'} >$3500 GeV and $M_{Z'} >$ 3100 GeV for $g_V = 3$ and $g_V = 1$, respectively. See their Fig.5 for limits on $\sigma \cdot B$.

[24] SIRUNYAN 18ED search for resonances decaying to HZ in pp collisions at $\sqrt{s}$ = 13 TeV. The limit above is for heavy-vector-triplet Z' with $g_V = 3$. If we assume $M_{Z'} = M_{W'}$, the limit increases $M_{Z'} >$ 2900 GeV and $M_{Z'} >$ 2800 GeV for $g_V = 3$ and $g_V = 1$, respectively.

[25] SIRUNYAN 18P give this limit for a heavy-vector-triplet Z' with $g_V = 3$. If they assume $M_{Z'} = M_{W'}$, the limit increases to $M_{Z'} >$ 3800 GeV.

[26] AABOUD 17AK search for a new resonance decaying to dijets in pp collisions at $\sqrt{s}$ = 13 TeV. The limit quoted above is for a leptophobic Z' boson having axial-vector coupling strength with quarks $g_q = 0.2$. The limit is 2100 GeV if $g_q = 0.1$.

[27] AABOUD 17AO search for resonances decaying to HZ in pp collisions at $\sqrt{s}$ = 13 TeV. The limit quoted above is for a Z' in the heavy-vector-triplet model with $g_V = 3$. See their Fig.4 for limits on $\sigma \cdot B$.

[28] SIRUNYAN 17AK search for resonances decaying to WW or HZ in pp collisions at $\sqrt{s}$ = 8 and 13 TeV. The quoted limit is for heavy-vector-triplet Z' with $g_V = 3$. The limit becomes $M_{Z'} >$ 2200 GeV for g_V =1. If we assume $M_{Z'} = M_{W'}$, the limit increases $M_{Z'} >$ 2400 GeV for both $g_V = 3$ and $g_V = 1$. See their Fig.1 and 2 for limits on $\sigma \cdot B$.

[29] SIRUNYAN 17Q search for a resonance decaying to $t\overline{t}$ in pp collisions at $\sqrt{s}$ = 13 TeV. The limit quoted above is for a resonance with relative width $\Gamma_{Z'}$ / $M_{Z'}$ = 0.01. Limits for wider resonances are available. See their Fig.6 for limits on $\sigma \cdot B$.

[30] SIRUNYAN 17R search for resonances decaying to HZ in pp collisions at $\sqrt{s}$ = 13 TeV. The quoted limit is for heavy-vector-triplet Z' with $g_V = 3$. Mass regions $M_{Z'} <$ 1150 GeV and 1250 GeV $< M_{Z'} <$ 1670 GeV are excluded for $g_V = 1$. If we assume $M_{Z'} = M_{W'}$, the excluded mass regions are 1000 $< M_{Z'} <$ 2500 GeV and 2760 $< M_{Z'} <$ 3300 GeV for $g_V = 3$; 1000 $< M_{Z'} <$ 2430 GeV and 2810 $< M_{Z'} <$ 3130 GeV for $g_V = 1$. See their Fig.5 for limits on $\sigma \cdot B$.

[31] AAD 25AZ search for a narrow resonance decaying to $q\overline{q}$ in pp collisions at $\sqrt{s}$ = 13 TeV, using trigger level analysis to enhance sensitivity in the low mass region. See their Fig. 9 for mass-coupling limits in the Z' mass range 375–1800 GeV.

[32] AAD 25BA set limits on Z' mediated dark Higgs scenarios with mass between 250–400 GeV and Z' masses $M_{Z'} <$ 2.3 TeV. Dark Higgs s is assumed to decay into HH. See their Fig. 7 for limits in $M_{Z'} - M_s$ plane.

[33] AAD 25BB search for $\tau^+\tau^-$ production from s-channel Z' exchange via $b\overline{b}$ annhilation in pp collisions at $\sqrt{s}$ = 13 TeV. See their Fig. 12 for limits in mass-coupling plane.

[34] AAD 25C search for a dark Higgs model spin-1 mediator Z' in pp collisions at $\sqrt{s}$ = 13 TeV using large $\not{E}_T$ and resonant $b\overline{b}$ production events. Z' decays to dark Higgs S and a pair of DM particles χ, and the dark Higgs S decays to $b\overline{b}$ subsequently. See their Fig. 3 for limits in $m_{Z'}$–m_S plane.

[35] AAD 25F search a new scalar particle S in pp collisions at $\sqrt{s}$ = 13 TeV. S decays to $Z'Z'$ with Z' subsequently decaying to $\ell^+\ell^-$. See their Fig. 5 for limits on $\sigma \cdot B$.

[36] AAD 25N search for Z' production in pp collisions at $\sqrt{s}$ = 13 TeV. Z' is assumed to decay into a pair of dark quarks $q_d\overline{q}_d$ with q_d generating semivisible jet topology upon decay. See their Fig. 8 for limits on $\sigma \cdot B$ as a function of $M_{Z'}$.

[37] AAD 25Q search for a low mass Z' produced in association with γ in pp collisions at $\sqrt{s}$ = 13 TeV. The decay products of $Z' \rightarrow q\overline{q}$ are reconstructed as a single large-radius jet. See their Fig. 5 for exclusion limits in the $m_{Z'} - g_q$ plane in the mass range 20 GeV $< m_{Z'} <$ 200 GeV.

[38] CHEKHOVSKY 25J search for "mono-Higgs" events produced from s-channel Z' exchange in pp collisions at $\sqrt{s}$ = 13 TeV, in which the SM Higgs H is reconstructed through $H \rightarrow \tau^+\tau^-$. The limit quoted above is for a baryonic Z' model with g_q = 0.25, $g_\chi = 1.0$, $m_\chi = 1$ GeV.

[39] HAYRAPETYAN 25V search for resonances decaying to a pair of heavy, stable (long-lived), charged particles (HSCPs) in pp collisions at $\sqrt{s}$ = 13 TeV. The limit quoted above assumes doubly-charged HSCP τ' with $m_{\tau'}$ = 600 GeV and Z'_ψ production cross section.

[40] AAD 24AA search for Z' production in pp collisions at $\sqrt{s}$ = 13 TeV. Z' is assumed to decay into a pair of dark quarks which hadronise into dark hadrons before promptly decaying back as SM particles. The dark pions are either assumed to decay directly to SM quarks or through dark photons. See their Fig. 7 for limits on $\sigma \cdot B$.

[41] AAD 24AE search for resonances decaying to qq, tt, tb, VV, VH, $\ell\ell$, $\ell\tau$, $\tau\nu$, $\tau\tau$ in pp collisions at $\sqrt{s}$ = 13 TeV. The quoted limit is for heavy-vector-triplet Z' with g_V = 3. $M_{Z'} = M_{W'}$ is assumed. The limit becomes $M_{Z'} >$ 5.8 TeV for $g_V = 1$.

[42] AAD 24AY search for a low-mass leptophobic Z' produced in association of high p_T ISR photon or jet in pp collisions at $\sqrt{s}$ = 13 TeV. The Z' coupling with quarks g_q is constrained below 0.07 for 250 $< M_{Z'} <$ 650 GeV. See their Fig. 8 for exclusion limit in the mass-coupling plane.

[43] AAD 24BJ search for top-philic Z' in pp collisions at $\sqrt{s}$ = 13 TeV. See their Fig. 9 for limits on $\sigma(pp \rightarrow t(\overline{t})Z') \cdot B(Z' \rightarrow t\overline{t})$.

[44] AAD 24BR search for $L_\mu - L_\tau$ Z' in 3μ final states in pp collisions at $\sqrt{s}$ = 13 TeV. Limits are combined with previous search results in the 4μ final states reported in AAD 23X. See their Fig. 4 for limits in mass-coupling plane.

[45] AAD 24CD search for a DM simplified Z' produced in association with W or Z in pp collisions at $\sqrt{s}$ = 13 TeV. Z' is assumed to decay invisibly. See their Fig. 13 for limits in $M_{Z'} - M_{DM}$ plane.

[46] AAD 24CI give a summary of searches for DM simplified Z' in pp collisions at $\sqrt{s}$ = 13 TeV. See their Figs. 6–11 for the limits.

[47] AAD 24CM search for pair productions of dark pions $\pi_D^+\pi_D^-$ in $ttbb$ events of pp collisions at $\sqrt{s}$ = 13 TeV. $\pi_D^\pm \rightarrow tb$ decay is assumed. The production cross section is computed in a model with dark ρ_D^0 assuming dark isospin symmetry $m_{\rho_D^\pm} = m_{\rho_D^0}$, $m_{\pi_D^\pm} = m_{\pi_D^0}$. See their Fig. 12 for limits on the production cross sections.

[48] ABLIKIM 24G search for a muonphilic Z' and a muonphilic scalar X_0 in decays of $J/\psi \rightarrow \mu^+\mu^-$ + invisible. See their Fig. 3 for limits in the mass coupling plane.

[49] ADACHI 24F for a muonphilic Z' and a muonphilic scalar X_0 in $\mu^+\mu^-\mu^+\mu^-$ events of e^+e^- collisions at $\sqrt{s}$ = 10.58 GeV. See their Fig. 14 for limits in mass-coupling plane.

[50] AKITA 24 limit is from no events of high-energy SN1987A neutrinos. The Z' coupling down to $g \sim 3 \times 10^{-10}$ is excluded for $M_{Z'} <$ 400 MeV in the $L_\mu - L_\tau$ Z' model. See their Fig. 3 and Fig. 4 for exclusion limits in mass-coupling plane.

Int. J. Mod. Phys. A 2026.41. Downloaded from www.worldscientific.com
by UNIVERSITY OF CALIFORNIA @ BERKELEY on 09/16/26. Re-use and distribution is strictly not permitted, except for Open Access articles.

[51] ANDREEV 24 search for Z' production in μ-nucleus scattering. Z' is assumed to decay invisibly. See their Fig. 4 for limits in mass-coupling plane.

[52] ANDREEV 24B search for Z' production in $e^{\pm}$-nucleus scattering. Z' is assumed to decay invisibly. See their Fig. 4 for limits in mass-coupling plane.

[53] ANDREEV 24E search for Z' production in μ-nucleus scattering. Invisible decays of Z' are assumed. See their Fig. 17 and Fig. 19 for limits in mass-coupling plane for Z' masses from 0.001 to 1 GeV.

[54] BISWAS 24 search for leptophilic scalar X_0 produced in association with $\tau^+\tau^-$ in e^+e^- collisions near $\sqrt{s} = 10.58$ GeV. X_0 is assumed to decay into e^+e^- or $\mu^+\mu^-$. See their Fig. 7 for limits in mass-coupling plane.

[55] HAYRAPETYAN 24AZ search for Z' resonances produced via kinetic mixing parameter ϵ and decaying to $s_D\overline{s}_D$ in pp collisions at $\sqrt{s} = 13$ TeV. Both s_D and $\overline{s}_D$ are assumed to decay into $\mu^+\mu^-$. See their Fig. 7 for limits on $\epsilon^2 B(Z' \to s_D\overline{s}_D)B^2(s_D \to \mu^+\mu^-)$.

[56] HAYRAPETYAN 24G search for singly produced narrow resonances decaying to jjj in pp collisions at $\sqrt{s} = 13$ TeV. See their Fig. 2 for limits on $\sigma \cdot B$.

[57] HAYRAPETYAN 24W search for $W^+W^- + \not{E}_T$ events in pp collisions at $\sqrt{s} = 13$ TeV. Z' is assumed to decay into dark Higgs S ($\to W^+W^-$) and DM particles $\chi\chi$. See their Fig. 5 for exclusion limits on the production cross section.

[58] AAD 23BF search for a Dark Matter (DM) simplified Z' produced in association with W in pp collisions at $\sqrt{s} = 13$ TeV. See their Fig. 9(c) for limits on $\sigma \cdot B$ as a function of $M_{Z'}$.

[59] AAD 23W set limits on a dark Higgs model with a spin-1 mediator Z' and a dark Higgs s. Dark Higgs s is assumed to decay into WW. See their Fig. 9 for limits in $M_{Z'} - M_s$ plane.

[60] AAD 23X set limits on $L_\mu - L_\tau$ of Z' using four-muon final states in pp collisions at $\sqrt{s} = 13$ TeV. See their Fig. 7 for limits in mass-coupling plane.

[61] ADACHI 23B search for Z' produced in association with $\mu^+\mu^-$ and decaying invisibly in e^+e^- collisions at $\sqrt{s} = 10.58$ GeV. See their Fig. 3 and Fig. 4 for limits in mass-coupling plane.

[62] ADACHI 23F search for resonances decaying to $\tau^+\tau^-$ in $\mu^+\mu^-\tau^+\tau^-$ events in e^+e^- collisions at $\sqrt{s} = 10.58$ GeV. See their Fig. 3 for limits on $\sigma \cdot B$.

[63] HAYRAPETYAN 23D search for $\mu^+\mu^-$ resonance produced in association with one or more b-jets in pp collisions at $\sqrt{s} = 13$ TeV. See their Fig. 8 for limits in the mass-coupling plane of the B_3–L_2 Z' model.

[64] HAYRAPETYAN 23G search for spin-0 and spin-1 resonances decaying to $\mu^+\mu^-$ in pp collisions at $\sqrt{s} = 13$ TeV in the mass ranges of 1.1–2.6 GeV and 4.2–7.9 GeV. See their Fig. 5 for limits on $\sigma \cdot B$.

[65] LI 23I limits on light Z' couplings are dervied from the steller cooling bounds in the mass range of 10^4–10^6 eV. See their Fig. 4 for limits on dark photon, B–L, L_μ-L_τ, and L_e-$L_{\mu(\tau)}$ models.

[66] MANZARI 23 study supernova cooling induced by the emission of light dark fermions χ assumed to couple with leptons via a new massive vector boson Z'. See their Figs. 4 and 5 for limits in mass-coupling plane.

[67] AAD 22 search for $b\overline{b}Z'$ productions in pp collisions at $\sqrt{s} = 13$ TeV. Z' is assumed to decay into $b\overline{b}$. See their Fig.4 for limits on $\sigma \cdot B$.

[68] AAD 22D search for DM mediator Z' produced in association with a Z boson in pp collisions at $\sqrt{s} = 13$ TeV. Z' is assumed to decay invisibly $Z' \to \chi\chi$. See their Fig. 4 for limits in $M_{Z'}$–M_χ plane.

[69] ANDREEV 22 search for missing energy in CERN NA64-e experiment. See their Fig. 7 for limits on couplings of $U(1)$ gauge $L_\mu - L_\tau$ Z' models, in the mass range of 1 MeV $< M_{Z'} <$ 600 MeV with the kinetic $Z' - \gamma$ mixing being determined by μ and τ loops.

[70] BONET 22 obtain limits on Z' coupling from ν-nucleus scattering data collected by the CONUS experiment at the nuclear power plant in Brokdorf. See their Fig. 5 for limits in mass-coupling plane.

[71] COLOMA 22 set limits on Z' coupling from ν-nucleus and ν-e scattering data collected by a Ge detector at the Dresden-II power reactor and the COHERENT experiment. See their Fig. 6 for limits in mass-coupling plane in the mass range of 1 keV $< M_{Z'} <$ 5 GeV.

[72] COLOMA 22A use Borexino Phase-II spectral data to constrain Z' couplings. See their Fig. 5 for limits in mass-coupling plane in the mass range of 10 keV $< M_{Z'} <$ 100 MeV.

[73] CZANK 22 search for Z' produced in association with $\mu^+\mu^-$ in e^+e^- collisions at and near Υ resonances. Z' is assumed to decay into $\mu^+\mu^-$. See their Fig. 8 for limits on $Z'\mu\mu$ couplings.

[74] TUMASYAN 22AA search for Z' production in pp collisions at $\sqrt{s} = 13$ TeV. Z' is assumed to decay into two "semivisible" jets (SVJ), i.e., collimated mixtures of visible and invisible particles. See their Fig. 7 and 8 for limits on $\sigma \cdot B$.

[75] AAD 21AQ limits are for a $B - L$ gauge boson model derived from their measurements on four-lepton differential cross sections. See their Fig. 13 for exclusion limits on the $B - L$ breaking Higgs boson mass.

[76] AAD 21AZ search for DM mediator Z' produced in association with a SM Higgs boson in pp collisions at $\sqrt{s} = 13$ TeV. Z' is assumed to decay invisibly $Z' \to \chi\chi$. See their Fig.7 for limits in $M_{Z'} - M_\chi$ plane.

[77] AAD 21BB search for Z' productions in pp collisions at $\sqrt{s} = 13$ TeV. Z' is assumed to decay into a SM Higgs boson H and an invisible particle A. See their Fig.7 for limits in $M_{Z'} - M_A$ plane.

[78] AAD 21D set limits on a dark Higgs model with a spin-1 mediator Z' and a scalar dark Higgs boson s. Dark Higgs s is assumed to decay into WW or ZZ. See their Fig.4 for limits in $M_{Z'} - M_s$ plane.

[79] AAD 21K search for $\gamma + \not{E}_T$ events in pp collision at $\sqrt{s} = 13$ TeV. See their Fig. 5 for limits on Z' particle invisibly decaying to $\chi\chi$.

[80] BURAS 21 performed global fit to leptophilic Z' models using a large number of observables.

[81] CADEDDU 21 obtain limits on Z' coupling $g_{Z'}$ from coherent ν-nucleus scattering data collected by COHERENT experiment. For limits in the $M_{Z'}$–$g_{Z'}$ plane, see their Figures 3 and 4 for the universal Z' model and Figures 5 and 6 for the $B - L$ model.

[82] COLARESI 21 obtain limits on Z' coupling from coherent ν-nucleus scattering data collected by a Ge detector at the Dresden-II power reactor. See their Fig.7 for limits in mass-coupling plane.

[83] KRIBS 21 set decay-agnostic limits on kinetic mixing parameter between $U(1)_Y$ field and new heavy abelian vector boson (dark photon) field using the HERA ep collision data. See their Fig. 3 for limits in mass-mixing plane.

[84] TUMASYAN 21D search for energetic jets + $\not{E}_T$ events in pp collisions at $\sqrt{s} = 13$ TeV. Z' is assumed to decay into a pair of invisible particles $\chi\chi$. See their Fig. 7 for limits on signal strength in $M_{Z'} - M_\chi$ plane, and Fig. 8 for limits on signal strength in quark and dark matter coupling vs mediator mass.

[85] AAD 20AF search for resonances decaying to $H\gamma$ in pp collisions at $\sqrt{s} = 13$ TeV. See their Fig. 1c for limits on $\sigma \cdot B$ for the mass range $0.7 < m_{Z'} < 4$ TeV.

[86] AAD 20T search for Dark Matter mediator Z' decaying invisibly or decaying to $q\overline{q}$ in pp collisions at $\sqrt{s} = 13$ TeV. See their Fig. 5 for limits in $M_{Z'} - g_q$ plane from the inclusive category. See their Fig. 7(a) for limits on the product of the cross section, acceptance, b-tagging efficiency, and branching fraction from the 2 b-tag category.

[87] AAD 20W search for a Dark Matter (DM) simplified model Z' produced in association with W in pp collisions at $\sqrt{s} = 13$ TeV. See their Fig. 5 for limits on Z' production cross section.

[88] AAIJ 20AL search for spin-0 and spin-1 resonances decaying to $\mu^+\mu^-$ in pp collisions at $\sqrt{s} = 13$ TeV in the mass regions $M_{Z'} < 60$ GeV, with non-negligible widths considered above 20 GeV. See their Figs. 7, 8, and 9 for limits on $\sigma \cdot B$.

[89] ADACHI 20 search for production of Z' in e^+e^- collisions. The Z' is assume to decay invisibly. See their Fig. 3 and Fig. 5 for limits on Z' coupling and $\sigma(e^+e^- \to e^{\pm}\mu^{\mp}Z')$.

[90] SIRUNYAN 20AI search for broad resonances decaying into dijets in pp collisions at $\sqrt{s} = 13$ TeV. See their Fig. 11 for exclusion limits in mass-coupling plane.

[91] SIRUNYAN 20AQ search for a narrow resonance lighter than 200 GeV decaying to $\mu^+\mu^-$ in pp collisions at $\sqrt{s} = 13$ TeV. See their Fig. 3 for limits on Z' kinetic mixing coefficient.

[92] SIRUNYAN 20M search for a narrow resonance with a mass between 350 and 700 GeV in pp collisions at $\sqrt{s} = 13$ TeV. See their Fig.3 for exclusion limits in mass-coupling plane.

[93] AABOUD 19AJ search in pp collisions at $\sqrt{s} = 13$ TeV for a new resonance decaying to $q\overline{q}$ and produced in association with a high p_T photon. For a leptophobic axial-vector Z' in the mass region 250 GeV $< M_{Z'} <$ 950 GeV, the Z' coupling with quarks g_q is constrained below 0.18. See their Fig.2 for limits in $M_{Z'} - g_q$ plane.

[94] AABOUD 19D search in pp collisions at $\sqrt{s} = 13$ TeV for a new resonance decaying to $q\overline{q}$ and produced in association with a high-p_T photon or jet. For a leptophobic axial-vector Z' in the mass region 100 GeV $< M_{Z'} <$ 220 GeV, the Z' coupling with quarks g_q is constrained below 0.23. See their Fig. 6 for limits in $M_{Z'} - g_q$ plane.

[95] AABOUD 19V search for Dark Matter simplified Z' decaying invisibly or decaying to fermion pair in pp collisions at $\sqrt{s} = 13$ TeV.

[96] AAD 19L search for resonances decaying to $\ell^+\ell^-$ in pp collisions at $\sqrt{s} = 13$ TeV. See their Fig. 4 for limits in the heavy vector triplet model couplings.

[97] LONG 19 uses the weak charge data of Cesium and proton to constrain mass of Z' in the 3-3-1 models.

[98] PANDEY 19 obtain limits on Z' induced neutrino non-standard interaction (NSI) parameter ϵ from LHC and IceCube data. See their Fig.2 for limits in $M_{Z'} - \epsilon$ plane, where $\epsilon = g_q\, g_\nu\, v^2 / (2\, M^2_{Z'})$.

[99] SIRUNYAN 19AL search for a new resonance decaying to a top quark and a heavy vector-like top partner in pp collisions at $\sqrt{s} = 13$ TeV. See their Fig. 8 for limits on Z' production cross section.

[100] SIRUNYAN 19AN search for a Dark Matter (DM) simplified model Z' decaying to H DM DM in pp collisions at $\sqrt{s} = 13$ TeV. See their Fig. 7 for limits on the signal strength modifiers.

[101] SIRUNYAN 19CB search in pp collisions at $\sqrt{s} = 13$ TeV for a new resonance decaying to $q\overline{q}$. For a leptophobic Z' in the mass region 50–300 GeV, the Z' coupling with quarks g'_q is constrained below 0.2. See their Figs. 4 and 5 for limits on g'_q in the mass range $50 < M_{Z'} < 450$ GeV.

[102] SIRUNYAN 19CD search in pp collisions at $\sqrt{s}$=13 TeV for a leptophobic Z' produced in association of high p_T ISR photon and decaying to $q\overline{q}$. See their Fig. 2 for limits on the Z' coupling strength g'_q to $q\overline{q}$ in the mass range between 10 and 125 GeV.

[103] SIRUNYAN 19D search for a narrow neutral vector resonance decaying to $H\gamma$. See their Fig. 3 for exclusion limit in $M_{Z'} - \sigma \cdot B$ plane. Upper limits on the production of $H\gamma$ resonances are set as a function of the resonance mass in the range of 720–3250 GeV.

[104] AABOUD 18AA search for a narrow neutral vector boson decaying to $H\gamma$. See their Fig. 10 for the exclusion limit in $M_{Z'} - \sigma B$ plane.

[105] AABOUD 18CJ search for heavy-vector-triplet Z' in pp collisions at $\sqrt{s} = 13$ TeV. The limit quoted above is for model with $g_V = 3$ assuming $M_{Z'} = M_{W'}$. The limit becomes $M_{Z'} > 5500$ GeV for model with $g_V = 1$.

[106] AABOUD 18N search for a narrow resonance decaying to $q\overline{q}$ in pp collisions at $\sqrt{s} =$ 13 TeV using trigger level analysis to improve the low mass region sensitivity. See their Fig. 5 for limits in the mass-coupling plane in the Z' mass range 450–1800 GeV.

[107] AAIJ 18AQ search for spin-0 and spin-1 resonances decaying to $\mu^+\mu^-$ in pp collisions at $\sqrt{s} = 7$ and 8 TeV in the mass region near 10 GeV. See their Figs. 4 and 5 for limits on $\sigma \cdot B$.

[108] SIRUNYAN 18DR searches for $\mu^+\mu^-$ resonances produced in association with b-jets in the pp collision data with $\sqrt{s} = 8$ TeV and 13 TeV. An excess of events near $m_{\mu\mu} =$ 28 GeV is observed in the 8 TeV data. See their Fig. 3 for the measured fiducial signal cross sections at $\sqrt{s} = 8$ TeV and the 95% CL upper limits at $\sqrt{s} = 13$ TeV.

[109] SIRUNYAN 18G search for a new resonance decaying to dijets in pp collisions at $\sqrt{s} =$ 13 TeV in the mass range 50–300 GeV. See their Fig.7 for limits in the mass-coupling plane.

[110] SIRUNYAN 18I search for a narrow resonance decaying to $b\overline{b}$ in pp collisions at $\sqrt{s} =$ 8 TeV using dedicated b-tagged dijet triggers to improve the sensitivity in the low mass region. See their Fig. 3 for limits on $\sigma \cdot B$ in the Z' mass range 325–1200 GeV.

[111] AABOUD 17B search for resonances decaying to HZ ($H \to b\overline{b}, c\overline{c}$; $Z \to \ell^+\ell^-, \nu\overline{\nu}$) in pp collisions at $\sqrt{s} = 13$ TeV. The quoted limit is for heavy-vector-triplet Z' with $g_V = 3$. The limit becomes $M_{Z'} > 1490$ GeV for $g_V = 1$. If we assume $M_{Z'} = M_{W'}$, the limit increases $M_{Z'} > 2310$ GeV and $M_{Z'} > 1730$ GeV for $g_V = 3$ and $g_V = 1$, respectively. See their Fig.3 for limits on $\sigma \cdot B$.

[112] KHACHATRYAN 17AX search for lepto-phobic resonances decaying to four leptons in pp collisions at $\sqrt{s}$ = 8 TeV.

[113] KHACHATRYAN 17U search for resonances decaying to HZ ($H \rightarrow b\overline{b}$; $Z \rightarrow \ell^+\ell^-$, $\nu\overline{\nu}$) in pp collisions at $\sqrt{s}$ = 13 TeV. The limit on the heavy-vector-triplet model is $M_{Z'} = M_{W'} > 2$ TeV for $g_V = 3$, in which constraints from the $W' \rightarrow HW$ ($H \rightarrow b\overline{b}$; $W \rightarrow \ell\nu$) are combined. See their Fig.3 and Fig.4 for limits on $\sigma \cdot B$.

[114] SIRUNYAN 17A search for resonances decaying to WW with $WW \rightarrow \ell\nu q\overline{q}$, $q\overline{q}q\overline{q}$ in pp collisions at $\sqrt{s}$ = 13 TeV. The quoted limit is for heavy-vector-triplet Z' with $g_V = 3$. The limit becomes $M_{Z'} > 1600$ GeV for $g_V = 1$. If we assume $M_{Z'} = M_{W'}$, the limit increases $M_{Z'} > 2400$ GeV and $M_{Z'} > 2300$ GeV for $g_V = 3$ and $g_V = 1$, respectively. See their Fig.6 for limits on $\sigma \cdot B$.

[115] SIRUNYAN 17AP search for resonances decaying into a SM-like Higgs scalar H and a light pseudo scalar A. A is assumed to decay invisibly. See their Fig.9 for limits on $\sigma \cdot B$.

[116] SIRUNYAN 17T search for a new resonance decaying to dijets in pp collisions at $\sqrt{s}$ = 13 TeV in the mass range 100–300 GeV. See their Fig.3 for limits in the mass-coupling plane.

[117] SIRUNYAN 17V search for a new resonance decaying to a top quark and a heavy vector-like top partner T in pp collisions at $\sqrt{s}$ = 13 TeV. See their table 5 for limits on the Z' production cross section for various values of $M_{Z'}$ and M_T in the range of $M_{Z'}$ = 1500–2500 GeV and M_T = 700–1500 GeV.

[118] AABOUD 16 search for a narrow resonance decaying into $b\overline{b}$ in pp collisions at $\sqrt{s}$ = 13 TeV. The limit quoted above is for a leptophobic Z' with SM-like couplings to quarks. See their Fig.6 for limits on $\sigma \cdot B$.

[119] AAD 16L search for $Z' \rightarrow a\gamma$, $a \rightarrow \gamma\gamma$ in pp collisions at $\sqrt{s}$ = 8 TeV. See their Table 6 for limits on $\sigma \cdot B$.

[120] AAD 16S search for a new resonance decaying to dijets in pp collisions at $\sqrt{s}$ = 13 TeV. The limit quoted above is for a leptophobic Z' having coupling strength with quark g_q = 0.3 and is taken from their Figure 3.

[121] KHACHATRYAN 16AP search for a resonance decaying to HZ in pp collisions at $\sqrt{s}$ = 8 TeV. Both H and Z are assumed to decay to fat jets. The quoted limit is for heavy-vector-triplet Z' with $g_V = 3$.

[122] KHACHATRYAN 16E search for a leptophobic top-color Z' decaying to $t\overline{t}$ using pp collisions at $\sqrt{s}$ = 8 TeV. The quoted limit assumes that $\Gamma_{Z'}/m_{Z'} = 0.012$. Also $m_{Z'} < 2.9$ TeV is excluded for wider topcolor Z' with $\Gamma_{Z'}/m_{Z'} = 0.1$.

[123] AAD 15AO search for narrow resonance decaying to $t\overline{t}$ using pp collisions at $\sqrt{s}$ = 8 TeV. See Fig. 11 for limit on σB.

[124] AAD 15AT search for monotop production plus large missing E_T events in pp collisions at $\sqrt{s}$ = 8 TeV and give constraints on a Z' model having $Z'u\overline{t}$ coupling. Z' is assumed to decay invisibly. See their Fig. 6 for limits on $\sigma \cdot B$.

[125] AAD 15CD search for decays of Higgs bosons to 4 ℓ states via Z' bosons, $H \rightarrow ZZ' \rightarrow 4\ell$ or $H \rightarrow Z'Z' \rightarrow 4\ell$. See Fig. 5 for the limit on the signal strength of the $H \rightarrow ZZ' \rightarrow 4\ell$ process and Fig. 16 for the limit on $H \rightarrow Z'Z' \rightarrow 4\ell$.

[126] KHACHATRYAN 15F search for monotop production plus large missing E_T events in pp collisions at $\sqrt{s}$ = 8 TeV and give constraints on a Z' model having $Z'u\overline{t}$ coupling. Z' is assumed to decay invisibly. See Fig. 3 for limits on σB.

[127] KHACHATRYAN 15O search for narrow Z' resonance decaying to ZH in pp collisions at $\sqrt{s}$ = 8 TeV. See their Fig. 6 for limit on σB.

[128] AAD 14AT search for a narrow neutral vector boson decaying to $Z\gamma$. See their Fig. 3b for the exclusion limit in $m_{Z'} - \sigma B$ plane.

[129] KHACHATRYAN 14A search for new resonance in the WW ($\ell\nu q\overline{q}$) and the ZZ ($\ell\ell q\overline{q}$) channels using pp collisions at $\sqrt{s}$=8 TeV. See their Fig.13 for the exclusion limit on the number of events in the mass-width plane.

[130] MARTINEZ 14 use various electroweak data to constrain the Z' boson in the 3-3-1 models.

[131] AAD 13AQ search for a leptophobic top-color Z' decaying to $t\overline{t}$. The quoted limit assumes that $\Gamma_{Z'}/m_{Z'} = 0.012$.

[132] CHATRCHYAN 13BM search for top-color Z' decaying to $t\overline{t}$ using pp collisions at $\sqrt{s}$=8 TeV. The quoted limit is for $\Gamma_{Z'}/m_{Z'} = 0.012$.

[133] CHATRCHYAN 13AP search for top-color leptophobic Z' decaying to $t\overline{t}$ using pp collisions at $\sqrt{s}$=7 TeV. The quoted limit is for $\Gamma_{Z'}/m_{Z'} = 0.012$.

[134] AAD 12BV search for narrow resonance decaying to $t\overline{t}$ using pp collisions at $\sqrt{s}$=7 TeV. See their Fig. 7 for limit on $\sigma \cdot$ B.

[135] AAD 12K search for narrow resonance decaying to $t\overline{t}$ using pp collisions at $\sqrt{s}$=7 TeV. See their Fig. 5 for limit on $\sigma \cdot$ B.

[136] AALTONEN 12AR search for chromophilic Z' in $p\overline{p}$ collisions at $\sqrt{s}$ = 1.96 TeV. See their Fig. 5 for limit on $\sigma \cdot$ B.

[137] AALTONEN 12N search for $p\overline{p} \rightarrow tZ'$, $Z' \rightarrow \overline{t}u$ events in $p\overline{p}$ collisions. See their Fig. 3 for the limit on $\sigma \cdot$ B.

[138] ABAZOV 12R search for top-color Z' boson decaying exclusively to $t\overline{t}$. The quoted limit is for $\Gamma_{Z'}/m_{Z'}$= 0.012.

[139] CHATRCHYAN 12AI search for $pp \rightarrow tt$ events and give constraints on a Z' model having $Z'\overline{u}t$ coupling. See their Fig. 4 for the limit in mass-coupling plane.

[140] Search for resonance decaying to $t\overline{t}$. See their Fig. 6 for limit on $\sigma \cdot$ B.

[141] Search for narrow resonance decaying to $t\overline{t}$. See their Fig. 4 for limit on $\sigma \cdot$ B.

[142] Search for narrow resonance decaying to $t\overline{t}$. See their Fig. 3 for limit on $\sigma \cdot$ B.

[143] CHATRCHYAN 11O search for same-sign top production in pp collisions induced by a hypothetical FCNC Z' at $\sqrt{s}$ = 7 TeV. See their Fig. 3 for limit in mass-coupling plane.

[144] Search for narrow resonance decaying to $t\overline{t}$. See their Fig. 3 for limit on $\sigma \cdot$ B.

[145] Search for narrow resonance decaying to $t\overline{t}$. See their Fig. 2 for limit on $\sigma \cdot$ B.

[146] BARGER 03B use the nucleosynthesis bound on the effective number of light neutrino δN_ν. See their Figs. 4–5 for limits in general E_6 motivated models.

[147] CHO 00 use various electroweak data to constrain Z' models assuming m_H=100 GeV. See Fig. 2 for limits in general E_6-motivated models.

[148] CHO 98 study constraints on four-Fermi contact interactions obtained from low-energy electroweak experiments, assuming no Z-Z' mixing.

[149] Search for Z' decaying to dijets at $\sqrt{s}$=1.8 TeV. For Z' with electromagnetic strength coupling, no bound is obtained.

Searches for Z' with Lepton-Flavor-Violating decays

The following limits are obtained from $p\overline{p}$ or $pp \rightarrow Z'X$ with Z' decaying to the mode indicated in the comments.

VALUE	DOCUMENT ID		TECN	COMMENT
• • • We do not use the following data for averages, fits, limits, etc. • • •				
	[1] HAYRAPETY...25AK		CMS	$Z' \rightarrow e\mu$
	[2] CABARCAS	24	RVUE	$Z' \rightarrow \mu\tau$
	[3] AAD	23CB	ATLS	$Z' \rightarrow e\mu$, $e\tau$, $\mu\tau$
	[4] TUMASYAN	23H	CMS	$Z' \rightarrow e\mu$, $e\tau$, $\mu\tau$
	[5] AABOUD	18CM	ATLS	$Z' \rightarrow e\mu$, $e\tau$, $\mu\tau$
	[6] SIRUNYAN	18AT	CMS	$Z' \rightarrow e\mu$
	[7] AABOUD	16P	ATLS	$Z' \rightarrow e\mu$, $e\tau$, $\mu\tau$
	[8] KHACHATRY...16BE		CMS	$Z' \rightarrow e\mu$
	[9] AAD	15O	ATLS	$Z' \rightarrow e\mu$, $e\tau$, $\mu\tau$
	[10] AAD	11H	ATLS	$Z' \rightarrow e\mu$
	[11] AAD	11Z	ATLS	$Z' \rightarrow e\mu$
	[12] ABULENCIA	06M	CDF	$Z' \rightarrow e\mu$

[1] HAYRAPETYAN 25AK search for a new particle with lepton-flavor violating decay in pp collisions at $\sqrt{s}$ = 13 TeV in the mass range 110 < $M_{Z'}$ < 500 GeV. See their Fig. 15 for limits on $\sigma \cdot B$.

[2] CABARCAS 24 use constraints on the non-standard neutrino interactions reported by ANTARES and IceCube expreriments to constrain Z' models with $\mu\tau$ coupling. See their Figs. 1 and 2 for limits in mass-coupling plane.

[3] AAD 23CB search for a new particle with lepton-flavor violating decay in pp collisions at $\sqrt{s}$ = 13 TeV. See their Figs.4, 5, and 6 for limits on $\sigma \cdot B$.

[4] TUMASYAN 23H search for a new particle with lepton-flavor violating decay in pp collisions at $\sqrt{s}$ = 13 TeV. See their Fig. 4 for limits on $\sigma \cdot B$.

[5] AABOUD 18CM search for a new particle with lepton-flavor violating decay in pp collisions at $\sqrt{s}$ = 13 TeV. See their Figs. 4, 5, and 6 for limits on $\sigma \cdot B$.

[6] SIRUNYAN 18AT search for a narrow resonance Z' decaying into $e\mu$ in pp collisions at $\sqrt{s}$ = 13 TeV. See their Fig.5 for limit on $\sigma \cdot B$ in the range of 600 GeV < $M_{Z'}$ < 5000 GeV.

[7] AABOUD 16P search for new particle with lepton flavor violating decay in pp collisions at $\sqrt{s}$ = 13 TeV. See their Figs.2, 3, and 4 for limits on $\sigma \cdot B$.

[8] KHACHATRYAN 16BE search for new particle Z' with lepton flavor violating decay in pp collisions at$\sqrt{s}$ = 8 TeV in the range of 200 GeV < $M_{Z'}$ < 2000 GeV. See their Fig.4 for limits on $\sigma \cdot B$ and their Table 5 for bounds on various masses.

[9] AAD 15O search for new particle Z' with lepton flavor violating decay in pp collisions at $\sqrt{s}$ = 8 TeV in the range of 500 GeV < $M_{Z'}$ < 3000 GeV. See their Fig. 2 for limits on σB.

[10] AAD 11H search for new particle Z' with lepton flavor violating decay in pp collisions at $\sqrt{s}$ = 7 TeV in the range of 700 GeV < $M_{Z'}$ < 1000 GeV. See their Fig. 3 for limits on $\sigma \cdot B$.

[11] AAD 11Z search for new particle Z' with lepton flavor violating decay in pp collisions at $\sqrt{s}$ = 7 TeV in the range 700 GeV < $M_{Z'}$ < 2000 GeV. See their Fig. 3 for limits on $\sigma \cdot B$.

[12] ABULENCIA 06M search for new particle Z' with lepton flavor violating decay in $p\overline{p}$ collisions at $\sqrt{s}$ = 1.96 TeV in the range of 100 GeV < $M_{Z'}$ < 800 GeV. See their Fig. 4 for limits in the mass-coupling plane.

Indirect Constraints on Kaluza-Klein Gauge Bosons

Bounds on a Kaluza-Klein excitation of the Z boson or photon in d=1 extra dimension. These bounds can also be interpreted as a lower bound on $1/R$, the size of the extra dimension. Unless otherwise stated, bounds assume all fermions live on a single brane and all gauge fields occupy the 4+d-dimensional bulk. See also the section on "Extra Dimensions" in the "Searches" Listings in this *Review*.

VALUE (TeV)	CL%	DOCUMENT ID		TECN	COMMENT
• • • We do not use the following data for averages, fits, limits, etc. • • •					
> 4.7		[1] MUECK	02	RVUE	Electroweak
> 3.3	95	[2] CORNET	00	RVUE	$e\nu qq'$
>5000		[3] DELGADO	00	RVUE	ϵ_K
> 2.6	95	[4] DELGADO	00	RVUE	Electroweak
> 3.3	95	[5] RIZZO	00	RVUE	Electroweak
> 2.9	95	[6] MARCIANO	99	RVUE	Electroweak
> 2.5	95	[7] MASIP	99	RVUE	Electroweak
> 1.6	90	[8] NATH	99	RVUE	Electroweak
> 3.4	95	[9] STRUMIA	99	RVUE	Electroweak

[1] MUECK 02 limit is 2σ and is from global electroweak fit ignoring correlations among observables. Higgs is assumed to be confined on the brane and its mass is fixed. For scenarios of bulk Higgs, of brane-SU(2)$_L$, bulk-U(1)$_Y$, and of bulk-SU(2)$_L$, brane-U(1)$_Y$, the corresponding limits are > 4.6 TeV, > 4.3 TeV and > 3.0 TeV, respectively.

[2] Bound is derived from limits on $e\nu qq'$ contact interaction, using data from HERA and the Tevatron.

[3] Bound holds only if first two generations of quarks lives on separate branes. If quark mixing is not complex, then bound lowers to 400 TeV from Δm_K.

[4] See Figs. 1 and 2 of DELGADO 00 for several model variations. Special boundary conditions can be found which permit KK states down to 950 GeV and that agree with the measurement of Q_W(Cs). Quoted bound assumes all Higgs bosons confined to brane; placing one Higgs doublet in the bulk lowers bound to 2.3 TeV.

[5] Bound is derived from global electroweak analysis assuming the Higgs field is trapped on the matter brane. If the Higgs propagates in the bulk, the bound increases to 3.8 TeV.

[6] Bound is derived from global electroweak analysis but considering only presence of the KK W bosons.

[7] Global electroweak analysis used to obtain bound independent of position of Higgs on brane or in bulk.

[8] Bounds from effect of KK states on G_F, α, M_W, and M_Z. Hard cutoff at string scale determined using gauge coupling unification. Limits for d=2,3,4 rise to 3.5, 5.7, and 7.8 TeV.

Int. J. Mod. Phys. A 2026.41. Downloaded from www.worldscientific.com
by UNIVERSITY OF CALIFORNIA @ BERKELEY on 09/16/26. Reproduction is strictly not permitted, except for Open Access articles.

[9] Bound obtained for Higgs confined to the matter brane with m_H=500 GeV. For Higgs in the bulk, the bound increases to 3.5 TeV.

See the related review(s):

Leptoquarks

MASS LIMITS for Leptoquarks from Pair Production

These limits rely only on the color or electroweak charge of the leptoquark.

VALUE (GeV)	CL%	DOCUMENT ID		TECN	COMMENT
> 900	95	[1] AAD	25V	ATLS	Scalar LQ. B($c\nu$) = 1
>1150	95	[2] AAD	25V	ATLS	Vector LQ. κ = 1, B($c\nu$)=0.5
>1580	95	[3] AAD	24AV	ATLS	Scalar LQ. B(te) = 1
>1590	95	[4] AAD	24AV	ATLS	Scalar LQ. B($t\mu$) = 1
>1950	95	[5] AAD	24AV	ATLS	Vector LQ. κ = 1. B(te) = 1
>1950	95	[6] AAD	24AV	ATLS	Vector LQ. κ = 1. B($t\mu$) = 1
>1230	95	[7] AAD	24O	ATLS	Scalar LQ. B($b\nu$) = 1
>1230	95	[8] AAD	24O	ATLS	Scalar LQ. B($t\nu$) = 1
>1480	95	[9] AAD	24O	ATLS	Scalar LQ. B($b\tau$) = 1
>1520	95	[10] AAD	24O	ATLS	Scalar LQ. B($t\tau$) = 1
>1710	95	[11] AAD	24O	ATLS	Scalar LQ. B($b\mu$) = 1
>1600	95	[12] AAD	24O	ATLS	Scalar LQ. B($t\mu$) = 1
>1730	95	[13] AAD	24O	ATLS	Scalar LQ. B(be) = 1
>1650	95	[14] AAD	24O	ATLS	Scalar LQ. B(te) = 1
>1840	95	[15] AAD	24O	ATLS	Vector LQ. κ = 1. $LQ \to t\nu,\ b\tau$
>1980	95	[16] AAD	24O	ATLS	Vector LQ. κ = 1. $LQ \to t\nu,\ b\mu$
>1900	95	[17] AAD	24O	ATLS	Vector LQ. κ = 1. $LQ \to t\nu,\ be$
>1810	95	[18] HAYRAPETY...	24O	CMS	Scalar LQ. B($b\mu$) = 1
>2460	95	[19] HAYRAPETY...	24O	CMS	Vector LQ. κ = 1. B($b\mu$) = 1
>1216	95	[20] HAYRAPETY...	24Z	CMS	Scalar LQ. B($b\tau$) = 1
>1820	95	[21] HAYRAPETY...	24Z	CMS	Vector LQ. κ = 1. B($b\tau$) = 1
>1300	95	[22] AAD	23BJ	ATLS	Scalar LQ. B($c\tau$) = 1
>1460	95	[23] AAD	23CF	ATLS	Scalar LQ. B($b\tau$) = 1
>1910	95	[24] AAD	23CF	ATLS	Vector LQ. κ = 1, B($b\tau$) = 1
>1460	95	[25] AAD	23F	ATLS	Scalar LQ. B($t\nu$)=B($b\mu$)=0.5
>1440	95	[26] AAD	23F	ATLS	Scalar LQ. B($t\nu$)=B(be)=0.5
>1370	95	[27] AAD	23F	ATLS	Scalar LQ. B($t\mu$)=B($b\nu$)=0.5
>1390	95	[28] AAD	23F	ATLS	Scalar LQ. B(te)=B($b\nu$)=0.5
>1980	95	[29] AAD	23F	ATLS	Vector LQ. κ = 1, B($t\nu$) = B($b\mu$) = 0.5
>1900	95	[30] AAD	23F	ATLS	Vector LQ. κ = 1, B($t\nu$) = B(be) = 0.5
>1340	95	[31] TUMASYAN	22H	CMS	Scalar LQ. B(te) = 1
>1420	95	[32] TUMASYAN	22H	CMS	Scalar LQ. B($t\mu$) = 1
>1120	95	[33] TUMASYAN	22H	CMS	Scalar LQ. B($t\tau$) = 1
>1480	95	[34] AAD	21AG	ATLS	Scalar LQ. B(te) = 1
>1470	95	[35] AAD	21AG	ATLS	Scalar LQ. B($t\mu$) = 1
>1190	95	[36] AAD	21AW	ATLS	Scalar LQ. B($b\tau$) = 1
>1030	95	[37] AAD	21AW	ATLS	Scalar LQ. B($t\tau$) = 1
>1760	95	[38] AAD	21AW	ATLS	Vector LQ. κ = 1. B($b\tau$) = 1
>1260	95	[39] AAD	21S	ATLS	Scalar LQ. B($b\nu$) = 1
>1430	95	[40] AAD	21T	ATLS	Scalar LQ. B($t\tau$) = 1
> 950	95	[41] SIRUNYAN	21J	CMS	Scalar LQ. B($t\tau$)=B($b\nu$)=0.5
>1650	95	[42] SIRUNYAN	21J	CMS	Vector LQ. κ=1, B($t\nu$) = B($b\tau$) = 0.5
>1800	95	[43] AAD	20AK	ATLS	Scalar LQ. B(eq) = 1
>1700	95	[44] AAD	20AK	ATLS	Scalar LQ. B(μq) = 1
>1240	95	[45] AAD	20S	ATLS	Scalar LQ. B($t\nu$) = 1
>1185	95	[46] SIRUNYAN	20A	CMS	Scalar LQ. B(νb) = 1
>1140	95	[47] SIRUNYAN	20A	CMS	Scalar LQ. B(νt) = 1
>1140	95	[48] SIRUNYAN	20A	CMS	Scalar LQ. B(νq) = 1 with q = u, d, s, c
>1925	95	[49] SIRUNYAN	20A	CMS	Vector LQ. κ = 1. B(νb) = 1
>1825	95	[50] SIRUNYAN	20A	CMS	Vector LQ. κ = 1. B(νt) = 1
>1980	95	[51] SIRUNYAN	20A	CMS	Vector LQ. κ = 1. B(νq) = 1 with q = u, d, s, c
>1400	95	[52] AABOUD	19AX	ATLS	Scalar LQ. B(eq) = 1
>1560	95	[53] AABOUD	19AX	ATLS	Scalar LQ. B(μq) = 1
>1000	95	[54] AABOUD	19X	ATLS	Scalar LQ. B($t\nu$) = 1
>1030	95	[55] AABOUD	19X	ATLS	Scalar LQ. B($b\tau$) = 1
> 970	95	[56] AABOUD	19X	ATLS	Scalar LQ. B($b\nu$) = 1
> 920	95	[57] AABOUD	19X	ATLS	Scalar LQ. B($t\tau$) = 1
>1530	95	[58] SIRUNYAN	19BI	CMS	Scalar LQ. B(μq)+B(νq) = 1
>1435	95	[59] SIRUNYAN	19BJ	CMS	Scalar LQ. B(eq)+B(νq) = 1
>1020	95	[60] SIRUNYAN	19Y	CMS	Scalar LQ. B(τb) = 1
none 300–900	95	[61] SIRUNYAN	18CZ	CMS	Scalar LQ. B(τt) = 1
>1420	95	[62] SIRUNYAN	18EC	CMS	Scalar LQ. B(μt) = 1
>1190	95	[63] SIRUNYAN	18EC	CMS	Vector LQ. μt, τt, νb
>1100	95	[64] SIRUNYAN	18U	CMS	Scalar LQ. B(νb) = 1
> 980	95	[65] SIRUNYAN	18U	CMS	Scalar LQ. B(νq) = 1 with q = u,d,s,c
>1020	95	[66] SIRUNYAN	18U	CMS	Scalar LQ. B(νt) = 1
>1810	95	[67] SIRUNYAN	18U	CMS	Vector LQ. κ=1. LQ$\to$ $b\nu$
>1790	95	[68] SIRUNYAN	18U	CMS	Vector LQ. κ=1. LQ$\to$ $q\nu$ with q = u,d,s,c
>1780	95	[69] SIRUNYAN	18U	CMS	Vector LQ. κ=1. LQ$\to$ $t\nu$
> 740	95	[70] KHACHATRY...	17J	CMS	Scalar LQ. B(τb) = 1
> 850	95	[71] SIRUNYAN	17H	CMS	Scalar LQ. B(τb) = 1
>1050	95	[72] AAD	16G	ATLS	Scalar LQ. B(eq) = 1
>1000	95	[73] AAD	16G	ATLS	Scalar LQ. B(μq) = 1
> 625	95	[74] AAD	16G	ATLS	Scalar LQ. B(νb) = 1
none 200–640	95	[75] AAD	16G	ATLS	Scalar LQ. B(νt) = 1
>1010	95	[76] KHACHATRY...	16AF	CMS	Scalar LQ. B(eq) = 1
>1080	95	[77] KHACHATRY...	16AF	CMS	Scalar LQ. B(μq) = 1
> 685	95	[78] KHACHATRY...	15AJ	CMS	Scalar LQ. B(τt) = 1
> 740	95	[79] KHACHATRY...	14T	CMS	Scalar LQ. B(τb) = 1
• • • We do not use the following data for averages, fits, limits, etc. • • •					
		[80] SIRUNYAN	19BC	CMS	Scalar LQ ($\to$ μq) LQ ($\to$ X + DM)
> 534	95	[81] AAD	13AE	ATLS	Third generation
> 525	95	[82] CHATRCHYAN	13M	CMS	Third generation
> 660	95	[83] AAD	12H	ATLS	First generation
> 685	95	[84] AAD	12O	ATLS	Second generation
> 830	95	[85] CHATRCHYAN	12AG	CMS	First generation
> 840	95	[86] CHATRCHYAN	12AG	CMS	Second generation
> 450	95	[87] CHATRCHYAN	12BO	CMS	Third generation
> 376	95	[88] AAD	11D	ATLS	Superseded by AAD 12H
> 422	95	[89] AAD	11D	ATLS	Superseded by AAD 12O
> 326	95	[90] ABAZOV	11V	D0	First generation
> 339	95	[91] CHATRCHYAN	11N	CMS	Superseded by CHATRCHYAN 12AG
> 384	95	[92] KHACHATRY...	11D	CMS	Superseded by CHATRCHYAN 12AG
> 394	95	[93] KHACHATRY...	11E	CMS	Superseded by CHATRCHYAN 12AG
> 247	95	[94] ABAZOV	10L	D0	Third generation
> 316	95	[95] ABAZOV	09	D0	Second generation
> 299	95	[96] ABAZOV	09AF	D0	Superseded by ABAZOV 11V
		[97] AALTONEN	08P	CDF	Third generation
> 153	95	[98] AALTONEN	08Z	CDF	Third generation
> 205	95	[99] ABAZOV	08AD	D0	All generations
> 210	95	[98] ABAZOV	08AN	D0	Third generation
> 229	95	[100] ABAZOV	07J	D0	Superseded by ABAZOV 10L
> 251	95	[101] ABAZOV	06A	D0	Superseded by ABAZOV 09
> 136	95	[102] ABAZOV	06L	D0	Superseded by ABAZOV 08AD
> 226	95	[103] ABULENCIA	06T	CDF	Second generation
> 256	95	[104] ABAZOV	05H	D0	First generation
> 117	95	[99] ACOSTA	05I	CDF	First generation
> 236	95	[105] ACOSTA	05P	CDF	First generation
> 99	95	[106] ABBIENDI	03R	OPAL	First generation
> 100	95	[106] ABBIENDI	03R	OPAL	Second generation
> 98	95	[106] ABBIENDI	03R	OPAL	Third generation
> 98	95	[107] ABAZOV	02	D0	All generations
> 225	95	[108] ABAZOV	01D	D0	First generation
> 85.8	95	[109] ABBIENDI	00M	OPAL	Superseded by ABBIENDI 03R
> 85.5	95	[109] ABBIENDI	00M	OPAL	Superseded by ABBIENDI 03R
> 82.7	95	[109] ABBIENDI	00M	OPAL	Superseded by ABBIENDI 03R
> 200	95	[110] ABBOTT	00C	D0	Second generation
> 123	95	[111] AFFOLDER	00K	CDF	Second generation
> 148	95	[112] AFFOLDER	00K	CDF	Third generation
> 160	95	[113] ABBOTT	99J	D0	Second generation
> 225	95	[114] ABBOTT	98E	D0	First generation
> 94	95	[115] ABBOTT	98J	D0	Third generation
> 202	95	[116] ABE	98S	CDF	Second generation
> 242	95	[117] GROSS-PILCH.	98		First generation
> 99	95	[118] ABE	97F	CDF	Third generation
> 213	95	[119] ABE	97X	CDF	First generation
> 45.5	95	[120,121] ABREU	93J	DLPH	First + second generation
> 44.4	95	[122] ADRIANI	93M	L3	First generation
> 44.5	95	[122] ADRIANI	93M	L3	Second generation
> 45	95	[122] DECAMP	92	ALEP	Third generation
none 8.9–22.6	95	[123] KIM	90	AMY	First generation
none 10.2–23.2	95	[123] KIM	90	AMY	Second generation
none 5–20.8	95	[124] BARTEL	87B	JADE	
none 7–20.5	95	[125] BEHREND	86B	CELL	

[1] AAD 25V search for scalar leptoquarks decaying to $c\nu$ in pp collisions at $\sqrt{s}$ = 13 TeV. See their Fig.10 for exclusion limits in M_{LQ}−B($c\nu$) plane.

[2] AAD 25V search for vector leptoquarks decaying to $c\nu$ in pp collisions at $\sqrt{s}$ = 13 TeV. See their Fig. 11 for exclusion limits on σ. The limit becomes M_{LQ} > 950 GeV for vector LQ with minimal coupling.

[3] AAD 24AV search for scalar leptoquarks decaying to te in pp collisions at $\sqrt{s}$ = 13 TeV. See their Fig. 9 for exclusion limit on σ.

[4] AAD 24AV search for scalar leptoquarks decaying to $t\mu$ in pp collisions at $\sqrt{s}$ = 13 TeV. See their Fig. 9 for exclusion limit on σ.

[5] AAD 24AV search for κ = 1 vector leptoquarks decaying to te in pp collisions at $\sqrt{s}$ = 13 TeV. See their Fig. 11 for exclusion limit on σ. The limit becomes M_{LQ} > 1.67 TeV for minimal coupling vector LQ with κ = 0.

[6] AAD 24AV search for κ = 1 vector leptoquarks decaying to $t\mu$ in pp collisions at $\sqrt{s}$ = 13 TeV. See their Fig. 11 for exclusion limit on σ. The limit becomes M_{LQ} > 1.67 TeV for minimal coupling vector LQ with κ = 0.

[7] AAD 24O search for scalar leptoquarks decaying to $b\nu$.

[8] AAD 24O search for scalar leptoquarks decaying to $t\nu$.

[9] AAD 24O search for scalar leptoquarks decaying to $b\tau$ or $t\nu$. See their Fig. 2a for exclusion limit on M_{LQ} as function of B($b\tau$).

[10] AAD 24O search for scalar leptoquarks decaying to $t\tau$ or $b\nu$. See their Fig. 2b for exclusion limit on M_{LQ} as function of B($t\tau$).

Int. J. Mod. Phys. A 2026.41. Downloaded from www.worldscientific.com
by UNIVERSITY OF CALIFORNIA @ BERKELEY on 09/16/26. Re-use and distribution is strictly not permitted, except for Open Access articles.

[11] AAD 24O search for scalar leptoquarks decaying to $b\mu$ or $t\nu$. See their Fig. 3a for exclusion limit on M_{LQ} as function of B($b\mu$).

[12] AAD 24O search for scalar leptoquarks decaying to $t\mu$ or $b\nu$. See their Fig.4 a for exclusion limit on M_{LQ} as function of B($t\mu$).

[13] AAD 24O search for scalar leptoquarks decaying to be or $t\nu$. See their Fig. 3b for exclusion limit on M_{LQ} as function of B(be).

[14] AAD 24O search for scalar leptoquarks decaying to te or $b\nu$. See their Fig. 4b for exclusion limit on M_{LQ} as function of B(te).

[15] AAD 24O search for vector leptoquarks decaying to $t\nu$ or $b\tau$ with $\kappa = 1$. The limit becomes > 1580 GeV for $\kappa = 0$.

[16] AAD 24O search for vector leptoquarks decaying to $t\nu$ or $b\mu$ with $\kappa = 1$. The limit becomes > 1710 GeV for $\kappa = 0$.

[17] AAD 24O search for vector leptoquarks decaying to $t\nu$ or be with $\kappa = 1$. The limit becomes > 1620 GeV for $\kappa = 0$.

[18] HAYRAPETYAN 24O search for scalar leptoquarks decaying to $b\mu$. See their Fig. 7 for exclusion limit on leptoquark pair production cross section as function of M_{LQ}.

[19] HAYRAPETYAN 24O search for $\kappa = 1$ vector leptoquarks decaying to $b\mu$. The limit becomes $M_{LQ} > 2120$ GeV for $\kappa = 0$.

[20] HAYRAPETYAN 24Z search for scalar and vector leptoquarks decaying to $b\tau$ and produced through single, pair, and nonresonantly in pp collisions at $\sqrt{s} = 13$ TeV. The limit quoted above assumes scalar leptoquarks with B($b\tau$) = 1 and leptoquark coupling strength $\lambda = 0$. See their Fig. 7 for limits in mass-coupling plane.

[21] HAYRAPETYAN 24Z search for scalar and vector leptoquarks decaying to $b\tau$ and produced through single, pair, and nonresonantly in pp collisions at $\sqrt{s} = 13$ TeV. The limit quoted above assumes $\kappa = 1$ vector leptoquarks with B($b\tau$) = 1 and leptoquark coupling strength $\lambda = 0$. See their Fig. 8 for limits in mass-coupling plane and for limits with $\kappa = 0$.

[22] AAD 23BJ search for scalar leptoquarks decaying to $c\tau$ in pp collisions at $\sqrt{s} = 13$ TeV. See their Fig. 8 for exclusion limit on σ as function of M_{LQ}.

[23] AAD 23CF search for scalar and vector leptoquarks decaying to $b\tau$. The limit quoted above is for scalar leptoquark. See their Fig. 9 for limits on leptoquark pair production cross sections.

[24] AAD 23CF search for scalar and vector leptoquarks decaying to $b\tau$. The limit quoted above is for vector leptoquark with $\kappa = 1$. The limit becomes $M_{LQ} > 1650$ for vector leptoquark with $\kappa = 0$. See their Fig. 9 for limits on leptoquark pair production cross sections.

[25] AAD 23F search for scalar leptoquarks decaying to $t\nu$ and $b\mu$ in pp collisions at $\sqrt{s} =$ 13 TeV. See their Fig. 9 for exclusion contour in B($b\mu$)$-M_{LQ}$ plane.

[26] AAD 23F search for scalar leptoquarks decaying to $t\nu$ and be in pp collisions at $\sqrt{s} =$ 13 TeV. See their Fig. 9 for exclusion contour in B(be)$-M_{LQ}$ plane.

[27] AAD 23F search for scalar leptoquarks decaying to $t\mu$ and $b\nu$ in pp collisions at $\sqrt{s} =$ 13 TeV. See their Fig. 9 for exclusion contour in B($t\mu$)$-M_{LQ}$ plane.

[28] AAD 23F search for scalar leptoquarks decaying to te and $b\nu$ in pp collisions at $\sqrt{s} =$ 13 TeV. See their Fig. 9 for exclusion contour in B(te)$-M_{LQ}$ plane.

[29] AAD 23F search for $\kappa = 1$ (YM coupling) vector leptoquarks decaying to $t\nu$ and $b\mu$ in pp collisions at $\sqrt{s} = 13$ TeV. If $\kappa = 0$ (minimal coupling) is assumed, the limit becomes $M_{LQ} > 1710$ GeV. See their Fig. 10 for exclusion contour in B($b\mu$)$-M_{LQ}$ plane.

[30] AAD 23F search for $\kappa = 1$ (YM coupling) vector leptoquarks decaying to $t\nu$ and be in pp collisions at $\sqrt{s} = 13$ TeV. If $\kappa = 0$ (minimal coupling) is assumed, the limit becomes $M_{LQ} > 1620$ GeV. See their Fig. 10 for exclusion contour in B(be)$-M_{LQ}$ plane.

[31] TUMASYAN 22H search for scalar leptoquarks decaying to te. See their Fig. 27 for exclusion limit on leptoquark pair production cross section as function of M_{LQ}.

[32] TUMASYAN 22H search for scalar leptoquarks decaying to $t\mu$. See their Fig. 27 for exclusion limit on leptoquark pair production cross section as function of M_{LQ}.

[33] TUMASYAN 22H search for scalar leptoquarks decaying to $t\tau$. See their Fig. 27 for exclusion limit on leptoquark pair production cross section as function of M_{LQ}.

[34] AAD 21AG search for scalar leptoquarks decaying to te. See their Fig. 6 for exclusion limit on B(te) as function of M_{LQ}.

[35] AAD 21AG search for scalar leptoquarks decaying to $t\mu$. See their Fig. 6 for exclusion limit on B($t\mu$) as function of M_{LQ}.

[36] AAD 21AW search for scalar leptoquarks decaying to $b\tau$. See their Fig. 9 for exclusion contour in B($b\tau$)$-M_{LQ}$ plane.

[37] AAD 21AW search for scalar leptoquarks decaying to $t\tau$. See their Fig. 9 for exclusion contour in B($t\tau$)$-M_{LQ}$ plane.

[38] AAD 21AW search for $\kappa = 1$ vector leptoquarks decaying to $b\tau$. See their Fig. 10 for exclusion contour in B($b\tau$)$-M_{LQ}$ plane and for limit on $\kappa = 0$ vector leptoquarks.

[39] AAD 21S search for scalar leptoquarks decaying to $b\nu$ in pp collisions at $\sqrt{s} = 13$ TeV. The limit above assumes B($b\nu$) = 1. For B($b\nu$) = 0.05, the limit becomes 400 GeV.

[40] AAD 21T search for scalar leptoquarks decaying to $t\tau$ in pp collisions at $\sqrt{s} = 13$ TeV. The limit above assumes B($t\tau$) = 1. For B($t\tau$) = 0.5, the limit becomes 1220 GeV. See their Fig. 15b for limits on B($t\tau$) as a function of leptoquark mass.

[41] SIRUNYAN 21J search for scalar leptoquarks decaying to $t\tau$ and $b\nu$ in pp collisions at $\sqrt{s} = 13$ TeV.

[42] SIRUNYAN 21J search for vector leptoquarks decaying to $t\nu$ and $b\tau$ in pp collisions at $\sqrt{s} = 13$ TeV. The limit quoted above assumes $\kappa = 1$. If we assume $\kappa = 0$, the limit becomes $M_{LQ} > 1290$ GeV.

[43] AAD 20AK search for scalar leptoquarks decaying to eq, eb, ec, μq, μb, μc. The quoted limit assumes B(eq) = 1. See their Fig. 9 for limits on B(eq), B(eb), B(ec), B(μq), B(μb), B(μc) as a function of leptoquark mass.

[44] AAD 20AK search for scalar leptoquarks decaying to eq, eb, ec, μq, μb, μc. The quoted limit assumes B(μq) = 1. See their Fig. 9 for limits on B(eq), B(eb), B(ec), B(μq), B(μb), B(μc) as a function of leptoquark mass.

[45] AAD 20S search for scalar leptoquarks decaying to $t\nu$ in pp collisions at $\sqrt{s} = 13$ TeV.

[46] SIRUNYAN 20A search for scalar and vector leptoquarks decaying to $t\nu$, $b\nu$, and $q\nu$ (q = u, d, s, c). The limit quoted above assumes scalar leptoquark with B(νb) = 1.

[47] SIRUNYAN 20A search for scalar and vector leptoquarks decaying to $t\nu$, $b\nu$, and $q\nu$ (q = u, d, s, c). The limit quoted above assumes scalar leptoquark with B(νt) = 1.

[48] SIRUNYAN 20A search for scalar and vector leptoquarks decaying to $t\nu$, $b\nu$, and $q\nu$ (q = u, d, s, c). The limit quoted above assumes scalar leptoquark with B(νq) = 1.

[49] SIRUNYAN 20A search for scalar and vector leptoquarks decaying to $t\nu$, $b\nu$, and $q\nu$ (q = u, d, s, c). The limit quoted above assumes vector leptoquark with B(νb) = 1 and $\kappa = 1$. If we assume $\kappa = 0$, the limit becomes $M_{LQ} > 1560$ GeV.

[50] SIRUNYAN 20A search for scalar and vector leptoquarks decaying to $t\nu$, $b\nu$, and $q\nu$ (q = u, d, s, c). The limit quoted above assumes vector leptoquark with B(νt) = 1 and $\kappa = 1$. If we assume $\kappa = 0$, the limit becomes $M_{LQ} > 1475$ GeV.

[51] SIRUNYAN 20A search for scalar and vector leptoquarks decaying to $t\nu$, $b\nu$, and $q\nu$ (q = u, d, s, c). The limit quoted above assumes vector leptoquark with B(νq) = 1 and $\kappa = 1$. If we assume $\kappa = 0$, the limit becomes $M_{LQ} > 1560$ GeV.

[52] AABOUD 19AX search for leptoquarks using $eejj$ events in pp collisions at $\sqrt{s} = 13$ TeV. The limit above assumes B(eq) = 1.

[53] AABOUD 19AX search for leptoquarks using $\mu\mu jj$ events in pp collisions at $\sqrt{s} = 13$ TeV. The limit above assumes B(μq) = 1.

[54] AABOUD 19X search for scalar leptoquarks decaying to $t\nu$ in pp collisions at $\sqrt{s} = 13$ TeV.

[55] AABOUD 19X search for scalar leptoquarks decaying to $b\tau$ in pp collisions at $\sqrt{s} = 13$ TeV.

[56] AABOUD 19X search for scalar leptoquarks decaying to $b\nu$ in pp collisions at $\sqrt{s} = 13$ TeV.

[57] AABOUD 19X search for scalar leptoquarks decaying to $t\tau$ in pp collisions at $\sqrt{s} = 13$ TeV.

[58] SIRUNYAN 19BI search for a pair of scalar leptoquarks decaying to $\mu\mu jj$ and to $\mu\nu jj$ final states in pp collisions at $\sqrt{s} = 13$ TeV. Limits are shown as a function of β where β is the branching fraction to a muon and a quark. For $\beta = 1.0$ (0.5) LQ masses up to 1530 (1285) GeV are excluded. See Fig. 9 for exclusion limits in the plane of β and LQ mass.

[59] SIRUNYAN 19BJ search for a pair of scalar leptoquarks decaying to $eejj$ and $e\nu jj$ final states in pp collisions at $\sqrt{s} = 13$ TeV. Limits are shown as a function of the branching fraction β to an electron and a quark. For $\beta = 1.0$ (0.5) LQ masses up to 1435 (1270) GeV are excluded. See Fig. 9 for exclusion limits in the plane of β and LQ mass.

[60] SIRUNYAN 19Y search for a pair of third generation scalar leptoquarks, each decaying to τ and a jet. Assuming B(τb) = 1, leptoquark masses below 1.02 TeV are excluded.

[61] SIRUNYAN 18CZ search for scalar leptoquarks decaying to τt in pp collisions at $\sqrt{s} =$ 13 TeV. The limit above assumes B(τt) = 1.

[62] SIRUNYAN 18EC set limits for scalar and vector leptoquarks decaying to μt, τt, and νb. The limit quoted above assumes scalar leptoquark with B(μt) = 1.

[63] SIRUNYAN 18EC set limits for scalar and vector leptoquarks decaying to μt, τt, and νb. The limit quoted above assumes vector leptoquark with all possible combinations of branching fractions to μt, τt, and νb.

[64] SIRUNYAN 18U set limits for scalar and vector leptoquarks decaying to $t\nu$, $b\nu$, and $q\nu$. The limit quoted above assumes scalar leptoquark with B($b\nu$) = 1. Vector leptoquarks with $\kappa = 1$ are excluded below masses of 1810 GeV.

[65] SIRUNYAN 18U set limits for scalar and vector leptoquarks decaying to $t\nu$, $b\nu$, and $q\nu$. The limit quoted above assumes scalar leptoquark with B($q\nu$) = 1. Vector leptoquarks with $\kappa = 1$ are excluded below masses of 1790 GeV.

[66] SIRUNYAN 18U set limits for scalar and vector leptoquarks decaying to $t\nu$, $b\nu$, and $q\nu$. The limit quoted above assumes scalar leptoquark with B(νt) = 1. Vector leptoquarks with $\kappa = 1$ are excluded below masses of 1780 GeV.

[67] SIRUNYAN 18U set limits for scalar and vector leptoquarks decaying to $t\nu$, $b\nu$, and $q\nu$. $\kappa = 1$ and LQ$\rightarrow$ $b\nu$ are assumed.

[68] SIRUNYAN 18U set limits for scalar and vector leptoquarks decaying to $t\nu$, $b\nu$, and $q\nu$. $\kappa = 1$ and LQ$\rightarrow$ $q\nu$ with $q = u,d,s,c$ are assumed.

[69] SIRUNYAN 18U set limits for scalar and vector leptoquarks decaying to $t\nu$, $b\nu$, and $q\nu$. $\kappa = 1$ and LQ$\rightarrow$ $t\nu$ are assumed.

[70] KHACHATRYAN 17J search for scalar leptoquarks decaying to τb using pp collisions at $\sqrt{s} = 13$ TeV. The limit above assumes B(τb) = 1.

[71] SIRUNYAN 17H search for scalar leptoquarks using $\tau\tau bb$ events in pp collisions at $\sqrt{s}$ = 8 TeV. The limit above assumes B(τb) = 1.

[72] AAD 16G search for scalar leptoquarks using $eejj$ events in collisions at $\sqrt{s} = 8$ TeV. The limit above assumes $B(eq) = 1$.

[73] AAD 16G search for scalar leptoquarks using $\mu\mu jj$ events in collisions at $\sqrt{s} = 8$ TeV. The limit above assumes $B(\mu q) = 1$.

[74] AAD 16G search for scalar leptoquarks decaying to $b\nu$. The limit above assumes $B(b\nu)$ = 1.

[75] AAD 16G search for scalar leptoquarks decaying to $t\nu$. The limit above assumes $B(t\nu)$ = 1.

[76] KHACHATRYAN 16AF search for scalar leptoquarks using $eejj$ and $e\nu jj$ events in pp collisions at $\sqrt{s} = 8$ TeV. The limit above assumes B(eq)= 1. For B(eq) = 0.5, the limit becomes 850 GeV.

[77] KHACHATRYAN 16AF search for scalar leptoquarks using $\mu\mu jj$ and $\mu\nu jj$ events in pp collisions at $\sqrt{s} = 8$ TeV. The limit above assumes B(μq) = 1. For B(μq) = 0.5, the limit becomes 760 GeV.

[78] KHACHATRYAN 15AJ search for scalar leptoquarks using $\tau\tau tt$ events in pp collisions at $\sqrt{s} = 8$ TeV. The limit above assumes $B(\tau t) = 1$.

[79] KHACHATRYAN 14T search for scalar leptoquarks decaying to τb using pp collisions at $\sqrt{s} = 8$ TeV. The limit above assumes B(τb) = 1. See their Fig. 5 for the exclusion limit as function of B(τb).

[80] SIRUNYAN 19BC search for scalar leptoquark (LQ) pair production in pp collisions at $\sqrt{s} = 13$ TeV. One LQ is assumed to decay to μq, while the other decays to dark matter pair and SM particles. See their Fig. 4 for limits in $M_{\rm LQ}$–$M_{\rm DM}$ plane.

[81] AAD 13AE search for scalar leptoquarks using $\tau\tau bb$ events in pp collisions at $E_{\rm cm}$ = 7 TeV. The limit above assumes B(τb) = 1.

[82] CHATRCHYAN 13M search for scalar and vector leptoquarks decaying to τb in pp collisions at $E_{\rm cm}$ = 7 TeV. The limit above is for scalar leptoquarks with B(τb) = 1.

[83] AAD 12H search for scalar leptoquarks using $eejj$ and $e\nu jj$ events in pp collisions at $E_{\rm cm}$ = 7 TeV. The limit above assumes B(eq) = 1. For B(eq) = 0.5, the limit becomes 607 GeV.

[84] AAD 12O search for scalar leptoquarks using $\mu\mu jj$ and $\mu\nu jj$ events in pp collisions at $E_{\rm cm}$ = 7 TeV. The limit above assumes B(μq) = 1. For B(μq) = 0.5, the limit becomes 594 GeV.

[85] CHATRCHYAN 12AG search for scalar leptoquarks using $eejj$ and $e\nu jj$ events in pp collisions at $E_{\rm cm}$ = 7 TeV. The limit above assumes B(eq) = 1. For B(eq) = 0.5, the limit becomes 640 GeV.

[86] CHATRCHYAN 12AG search for scalar leptoquarks using $\mu\mu jj$ and $\mu\nu jj$ events in pp collisions at $E_{\rm cm}$ = 7 TeV. The limit above assumes B(μq) = 1. For B(μq) = 0.5, the limit becomes 650 GeV.

Int. J. Mod. Phys. A 2026.41. Downloaded from worldscientific.com
by UNIVERSITY OF CALIFORNIA @ BERKELEY on 09/16/26. Reproduction strictly not permitted, except for Open Access articles.

Int. J. Mod. Phys. A 2026.41. Downloaded from www.worldscientific.com by UNIVERSITY OF CALIFORNIA @ BERKELEY on 09/16/26. Re-use and distribution is strictly not permitted, except for Open Access articles.

[87] CHATRCHYAN 12BO search for scalar leptoquarks decaying to νb in pp collisions at $\sqrt{s}$ = 7 TeV. The limit above assumes B(νb) = 1.

[88] AAD 11D search for scalar leptoquarks using $eejj$ and $e\nu jj$ events in pp collisions at E_{cm} = 7 TeV.The limit above assumes B(eq) = 1. For B(eq) = 0.5, the limit becomes 319 GeV.

[89] AAD 11D search for scalar leptoquarks using $\mu\mu jj$ and $\mu\nu jj$ events in pp collisions at E_{cm} = 7 TeV. The limit above assumes B(μq) = 1. For B(μq) = 0.5, the limit becomes 362 GeV.

[90] ABAZOV 11V search for scalar leptoquarks using $e\nu jj$ events in $p\overline{p}$ collisions at E_{cm} = 1.96 TeV. The limit above assumes B(eq) = 0.5.

[91] CHATRCHYAN 11N search for scalar leptoquarks using $e\nu jj$ events in pp collisions at E_{cm} = 7 TeV. The limit above assumes B(eq) = 0.5.

[92] KHACHATRYAN 11D search for scalar leptoquarks using $eejj$ events in pp collisions at E_{cm} = 7 TeV. The limit above assumes B(eq) = 1.

[93] KHACHATRYAN 11E search for scalar leptoquarks using $\mu\mu jj$ events in pp collisions at E_{cm} = 7 TeV. The limit above assumes B(μq) = 1.

[94] ABAZOV 10L search for pair productions of scalar leptoquark state decaying to νb in $p\overline{p}$ collisions at E_{cm} = 1.96 TeV. The limit above assumes B(νb) = 1.

[95] ABAZOV 09 search for scalar leptoquarks using $\mu\mu jj$ and $\mu\nu jj$ events in $p\overline{p}$ collisions at E_{cm} = 1.96 TeV. The limit above assumes B(μq) = 1. For B(μq) = 0.5, the limit becomes 270 GeV.

[96] ABAZOV 09AF search for scalar leptoquarks using $eejj$ and $e\nu jj$ events in $p\overline{p}$ collisions at E_{cm} = 1.96 TeV. The limit above assumes B(eq) = 1. For B(eq) = 0.5 the bound becomes 284 GeV.

[97] AALTONEN 08P search for vector leptoquarks using $\tau^+\tau^- b\overline{b}$ events in $p\overline{p}$ collisions at E_{cm} = 1.96 TeV. Assuming Yang-Mills (minimal) couplings, the mass limit is >317 GeV (251 GeV) at 95% CL for B(τb) = 1.

[98] Search for pair production of scalar leptoquark state decaying to τb in $p\overline{p}$ collisions at E_{cm}= 1.96 TeV. The limit above assumes B(τb) = 1.

[99] Search for scalar leptoquarks using $\nu\nu jj$ events in $\overline{p}p$ collisions at E_{cm} = 1.96 TeV. The limit above assumes B(νq) = 1.

[100] ABAZOV 07J search for pair productions of scalar leptoquark state decaying to νb in $p\overline{p}$ collisions at E_{cm} = 1.96 TeV. The limit above assumes B(νb) = 1.

[101] ABAZOV 06A search for scalar leptoquarks using $\mu\mu jj$ events in $p\overline{p}$ collisions at E_{cm} = 1.8 TeV and 1.96 TeV. The limit above assumes B(μq) = 1. For B(μq) = 0.5, the limit becomes 204 GeV.

[102] ABAZOV 06L search for scalar leptoquarks using $\nu\nu jj$ events in $p\overline{p}$ collisions at E_{cm} = 1.8 TeV and at 1.96 TeV. The limit above assumes B(νq) = 1.

[103] ABULENCIA 06T search for scalar leptoquarks using $\mu\mu jj$, $\mu\nu jj$, and $\nu\nu jj$ events in $p\overline{p}$ collisions at E_{cm} = 1.96 TeV. The quoted limit assumes B(μq) = 1. For B(μq) = 0.5 or 0.1, the bound becomes 208 GeV or 143 GeV, respectively. See their Fig. 4 for the exclusion limit as a function of B(μq).

[104] ABAZOV 05H search for scalar leptoquarks using $eejj$ and $e\nu jj$ events in $\overline{p}p$ collisions at E_{cm} = 1.8 TeV and 1.96 TeV. The limit above assumes B(eq) = 1. For B(eq) = 0.5 the bound becomes 234 GeV.

[105] ACOSTA 05P search for scalar leptoquarks using $eejj$, $e\nu jj$ events in $\overline{p}p$ collisions at E_{cm} = 1.96TeV. The limit above assumes B(eq) = 1. For B(eq) = 0.5 and 0.1, the bound becomes 205 GeV and 145 GeV, respectively.

[106] ABBIENDI 03R search for scalar/vector leptoquarks in e^+e^- collisions at $\sqrt{s}$ = 189–209 GeV. The quoted limits are for charge −4/3 isospin 0 scalar-leptoquark with B(ℓq) = 1. See their table 12 for other cases.

[107] ABAZOV 02 search for scalar leptoquarks using $\nu\nu jj$ events in $\overline{p}p$ collisions at E_{cm}=1.8 TeV. The bound holds for all leptoquark generations. Vector leptoquarks are likewise constrained to lie above 200 GeV.

[108] ABAZOV 01D search for scalar leptoquarks using $e\nu jj$, $eejj$, and $\nu\nu jj$ events in $p\overline{p}$ collisions at E_{cm}=1.8 TeV. The limit above assumes B(eq)=1. For B(eq)=0.5 and 0, the bound becomes 204 and 79 GeV, respectively. Bounds for vector leptoquarks are also given. Supersedes ABBOTT 98E.

[109] ABBIENDI 00M search for scalar/vector leptoquarks in e^+e^- collisions at $\sqrt{s}$=183 GeV. The quoted limits are for charge −4/3 isospin 0 scalar-leptoquarks with B(ℓq)=1. See their Table 8 and Figs. 6–9 for other cases.

[110] ABBOTT 00C search for scalar leptoquarks using $\mu\mu jj$, $\mu\nu jj$, and $\nu\nu jj$ events in $p\overline{p}$ collisions at E_{cm}=1.8 TeV. The limit above assumes B(μq)=1. For B(μq)=0.5 and 0, the bound becomes 180 and 79 GeV respectively. Bounds for vector leptoquarks are also given.

[111] AFFOLDER 00K search for scalar leptoquark using $\nu\nu cc$ events in $p\overline{p}$ collisions at E_{cm}=1.8 TeV. The quoted limit assumes B(νc)=1. Bounds for vector leptoquarks are also given.

[112] AFFOLDER 00K search for scalar leptoquark using $\nu\nu bb$ events in $p\overline{p}$ collisions at E_{cm}=1.8 TeV. The quoted limit assumes B(νb)=1. Bounds for vector leptoquarks are also given.

[113] ABBOTT 99J search for leptoquarks using $\mu\nu jj$ events in $p\overline{p}$ collisions at E_{cm}= 1.8TeV. The quoted limit is for a scalar leptoquark with B(μq) = B(νq) = 0.5. Limits on vector leptoquarks range from 240 to 290 GeV.

[114] ABBOTT 98E search for scalar leptoquarks using $e\nu jj$, $eejj$, and $\nu\nu jj$ events in $p\overline{p}$ collisions at E_{cm}=1.8 TeV. The limit above assumes B(eq)=1. For B(eq)=0.5 and 0, the bound becomes 204 and 79 GeV, respectively.

[115] ABBOTT 98J search for charge −1/3 third generation scalar and vector leptoquarks in $p\overline{p}$ collisions at E_{cm}= 1.8 TeV. The quoted limit is for scalar leptoquark with B(νb)=1.

[116] ABE 98S search for scalar leptoquarks using $\mu\mu jj$ events in $p\overline{p}$ collisions at E_{cm}= 1.8 TeV. The limit is for B(μq)= 1. For B(μq)=B(νq)=0.5, the limit is > 160 GeV.

[117] GROSS-PILCHER 98 is the combined limit of the CDF and DØ Collaborations as determined by a joint CDF/DØ working group and reported in this FNAL Technical Memo. Original data published in ABE 97X and ABBOTT 98E.

[118] ABE 97F search for third generation scalar and vector leptoquarks in $p\overline{p}$ collisions at E_{cm} = 1.8 TeV. The quoted limit is for scalar leptoquark with B(τb) = 1.

[119] ABE 97X search for scalar leptoquarks using $eejj$ events in $p\overline{p}$ collisions at E_{cm}=1.8 TeV. The limit is for B(eq)=1.

[120] Limit is for charge −1/3 isospin-0 leptoquark with B(ℓq) = 2/3.

[121] First and second generation leptoquarks are assumed to be degenerate. The limit is slightly lower for each generation.

[122] Limits are for charge −1/3, isospin-0 scalar leptoquarks decaying to $\ell^- q$ or νq with any branching ratio. See paper for limits for other charge-isospin assignments of leptoquarks.

[123] KIM 90 assume pair production of charge 2/3 scalar-leptoquark via photon exchange. The decay of the first (second) generation leptoquark is assumed to be any mixture of de^+ and $u\overline{\nu}$ ($s\mu^+$ and $c\overline{\nu}$). See paper for limits for specific branching ratios.

[124] BARTEL 87B limit is valid when a pair of charge 2/3 spinless leptoquarks X is produced with point coupling, and when they decay under the constraint B(X → $c\overline{\nu}_\mu$) + B(X → $s\mu^+$) = 1.

[125] BEHREND 86B assumed that a charge 2/3 spinless leptoquark, χ, decays either into $s\mu^+$ or $c\overline{\nu}$: B(χ → $s\mu^+$) + B(χ → $c\overline{\nu}$) = 1.

MASS LIMITS for Leptoquarks from Single Production

These limits depend on the q-ℓ-leptoquark coupling g_{LQ}. It is often assumed that $g^2_{LQ}/4\pi$=1/137. Limits shown are for a scalar, weak isoscalar, charge −1/3 leptoquark.

VALUE (GeV)	CL%	DOCUMENT ID		TECN	COMMENT
>3400	95	[1] AAD	25BN	ATLS	g_{de} = 1
>2050	95	[2] HAYRAPETY...	24C	CMS	B($u\tau$) = 1
>1800	95	[3] HAYRAPETY...	24C	CMS	B($d\tau$) = 1
> 780	95	[4] HAYRAPETY...	24Z	CMS	Third generation
>1280	95	[5] AAD	23BZ	ATLS	LQ → $b\tau$
> 550	95	[6] SIRUNYAN	21J	CMS	Third generation
none 150–740	95	[7] SIRUNYAN	18BJ	CMS	Third generation
>1755	95	[8] KHACHATRY...	16AG	CMS	First generation
> 660	95	[9] KHACHATRY...	16AG	CMS	Second generation
> 304	95	[10] ABRAMOWICZ	12A	ZEUS	First generation
> 73	95	[11] ABREU	93J	DLPH	Second generation
• • • We do not use the following data for averages, fits, limits, etc. • • •					
		[12] AAD	22E	ATLS	LQ → ue^-, $c\mu^-$
		[13] TUMASYAN	21D	CMS	First generation
		[14] DEY	16	ICCB	νq → LQ → νq
		[15] AARON	11A	H1	Lepton-flavor violation
> 300	95	[16] AARON	11B	H1	First generation
		[17] ABAZOV	07E	D0	Second generation
> 295	95	[18] AKTAS	05B	H1	First generation
		[19] CHEKANOV	05A	ZEUS	Lepton-flavor violation
> 298	95	[20] CHEKANOV	03B	ZEUS	First generation
> 197	95	[21] ABBIENDI	02B	OPAL	First generation
		[22] CHEKANOV	02	ZEUS	Repl. by CHEKANOV 05A
> 290	95	[23] ADLOFF	01C	H1	First generation
> 204	95	[24] BREITWEG	01	ZEUS	First generation
		[25] BREITWEG	00E	ZEUS	First generation
> 161	95	[26] ABREU	99G	DLPH	First generation
> 200	95	[27] ADLOFF	99	H1	First generation
		[28] DERRICK	97	ZEUS	Lepton-flavor violation
> 168	95	[29] DERRICK	93	ZEUS	First generation

[1] AAD 25BN search for single production of a scalar leptoquark in pp collisions at $\sqrt{s}$ = 13 TeV and at $\sqrt{s}$ = 13.6 TeV. The quoted limit assumes leptoquark production in de collisions with coupling strength g_{de} = 1. Masses below 3.1 TeV, 4.3 TeV, and 2.8 TeV are excluded at 95% CL for g_{be} = 3.5, $g_{s\mu}$ = 3.5 and $g_{b\mu}$ = 3.5, respectively. See their Figs. 14–17 for exclusion limits in mass-coupling plane.

[2] HAYRAPETYAN 24C search for single production of scalar leptoquarks decaying to $q\tau^+$ (q = u, d, s, b) in pp collisions at $\sqrt{s}$ = 13 TeV. The limit quoted above is for a leptoquark produced in τu collisions and the leptoquark coupling strength λ = 1. See their Fig. 4 for limits in mass-coupling plane.

[3] HAYRAPETYAN 24C search for single production of scalar leptoquarks decaying to $q\tau^+$ (q = u, d, s, b) in pp collisions at $\sqrt{s}$ = 13 TeV. The limit quoted above is for a leptoquark produced in τd collisions and the leptoquark coupling strength λ = 1. See their Fig. 4 for limits in mass-coupling plane.

[4] HAYRAPETYAN 24Z search for scalar and vector leptoquarks decaying to $b\tau$ and produced through single, pair, and nonresonantly in pp collisions at $\sqrt{s}$ = 13 TeV. The limit quoted above is derived solely from single production limit and assumes scalar leptoquark decaying to $b\tau$. The leptoquark coupling strength λ = 1 is assumed. See their Fig. 7 and Fig. 8 for combined limits in mass-coupling plane.

[5] AAD 23BZ search for single production of charge 4/3 scalar leptoquarks decaying to $b\tau^-$, and charge 2/3 vector leptoquarks decaying to $\overline{b}\tau^-$ in pp collisions at $\sqrt{s}$ = 13 TeV. The limit quoted above assumes a scalar leptoquark with B($b\tau$) = 1 and the leptoquark coupling strength λ = 1.0. The limit becomes M_{LQ} > 1530 GeV for λ = 2.5.

[6] SIRUNYAN 21J search for single production of charge −1/3 scalar leptoquarks decaying to $t\tau^-$ and $b\nu$, and charge 2/3 vector leptoquarks decaying to $t\nu$ and $b\tau^+$ in pp collisions at $\sqrt{s}$ = 13 TeV. The limit quoted above assumes a scalar leptoquark with B($t\tau$) = B($b\nu$) = 0.5 and the leptoquark coupling strength λ = 1.5. The limit becomes M_{LQ} > 750 GeV for λ = 2.5.

[7] SIRUNYAN 18BJ search for single production of charge 2/3 scalar leptoquarks decaying to τb in pp collisions at $\sqrt{s}$ = 13 TeV. The limit above assumes B(τb) = 1 and the leptoquark coupling strength λ = 1.

[8] KHACHATRYAN 16AG search for single production of charge ±1/3 scalar leptoquarks using eej events in pp collisions at $\sqrt{s}$ = 8 TeV. The limit above assumes B(eq) = 1 and the leptoquark coupling strength λ = 1.

[9] KHACHATRYAN 16AG search for single production of charge ±1/3 scalar leptoquarks using $\mu\mu j$ events in pp collisions at $\sqrt{s}$ = 8 TeV. The limit above assumes B(μq) = 1 and the leptoquark coupling strength λ = 1.

[10] ABRAMOWICZ 12A limit is for a scalar, weak isoscalar, charge −1/3 leptoquark coupled with e_R. See their Figs. 12–17 and Table 4 for states with different quantum numbers.

[11] Limit from single production in Z decay. The limit is for a leptoquark coupling of electromagnetic strength and assumes B(ℓq) = 2/3. The limit is 77 GeV if first and second leptoquarks are degenerate.

[12] AAD 22E leptoquarks decaying both to ue^- and $c\mu^-$ are constrained from the comparison of the production cross sections for $e^+\mu^-$ and $e^-\mu^+$ in pp collisions at $\sqrt{s}$ = 13 TeV. Scalar leptoquarks with M_{LQ} < 1880 GeV are excluded for $g^{eu} = g^{\mu c}$ = 1.

[13] TUMASYAN 21D search for energetic jets + $\not{E}_T$ events in pp collisions at $\sqrt{s}$ = 13 TeV. The branching fraction for the decay of the leptoquark into an electron neutrino

Int. J. Mod. Phys. A 2026.41. Downloaded from www.worldscientific.com
by UNIVERSITY OF CALIFORNIA @ BERKELEY on 09/16/26. Reproduction is strictly not permitted, except for Open Access articles.

and up quark is assumed to be 100% ($\beta = 0$). See their Fig. 12 for exclusion limits in mass-coupling plane.

[14] DEY 16 use the 2010-2012 IceCube PeV energy data set to constrain the leptoquark production cross section through the $\nu q \rightarrow$ LQ $\rightarrow \nu q$ process. See their Figure 4 for the exclusion limit in the mass-coupling plane.

[15] AARON 11A search for various leptoquarks with lepton-flavor violating couplings. See their Figs. 2–3 and Tables 1–4 for detailed limits.

[16] The quoted limit is for a scalar, weak isoscalar, charge $-1/3$ leptoquark coupled with e_R. See their Figs. 3–5 for limits on states with different quantum numbers.

[17] ABAZOV 07E search for leptoquark single production through qg fusion process in $p\overline{p}$ collisions. See their Fig. 4 for exclusion plot in mass-coupling plane.

[18] AKTAS 05B limit is for a scalar, weak isoscalar, charge $-1/3$ leptoquark coupled with e_R. See their Fig. 3 for limits on states with different quantum numbers.

[19] CHEKANOV 05 search for various leptoquarks with lepton-flavor violating couplings. See their Figs. 6–10 and Tables 1–8 for detailed limits.

[20] CHEKANOV 03B limit is for a scalar, weak isoscalar, charge $-1/3$ leptoquark coupled with e_R. See their Figs. 11–12 and Table 5 for limits on states with different quantum numbers.

[21] For limits on states with different quantum numbers and the limits in the mass-coupling plane, see their Fig. 4 and Fig. 5.

[22] CHEKANOV 02 search for various leptoquarks with lepton-flavor violating couplings. See their Figs. 6–7 and Tables 5–6 for detailed limits.

[23] For limits on states with different quantum numbers and the limits in the mass-coupling plane, see their Fig. 3.

[24] See their Fig. 14 for limits in the mass-coupling plane.

[25] BREITWEG 00E search for F=0 leptoquarks in e^+p collisions. For limits in mass-coupling plane, see their Fig. 11.

[26] ABREU 99G limit obtained from process $e\gamma \rightarrow LQ+q$. For limits on vector and scalar states with different quantum numbers and the limits in the coupling-mass plane, see their Fig. 4 and Table 2.

[27] For limits on states with different quantum numbers and the limits in the mass-coupling plane, see their Fig. 13 and Fig. 14. ADLOFF 99 also search for leptoquarks with lepton-flavor violating couplings. ADLOFF 99 supersedes AID 96B.

[28] DERRICK 97 search for various leptoquarks with lepton-flavor violating couplings. See their Figs. 5–8 and Table 1 for detailed limits.

[29] DERRICK 93 search for single leptoquark production in ep collisions with the decay eq and νq. The limit is for leptoquark coupling of electromagnetic strength and assumes B(eq) = B(νq) = 1/2. The limit for B(eq) = 1 is 176 GeV. For limits on states with different quantum numbers, see their Table 3.

Indirect Limits for Leptoquarks

VALUE (TeV)	CL%	DOCUMENT ID		TECN	COMMENT
• • • We do not use the following data for averages, fits, limits, etc. • • •					
		[1] AAD	25BB	ATLS	$b\overline{b} \rightarrow \tau^+\tau^-$, $g\,b \rightarrow \tau^+\tau^-\,b$
		[2] HAYRAPETY...	25AN	CMS	$pp \rightarrow e^+e^-$, $\mu^+\mu^-$
		[3] AAD	24W	ATLS	$\mu\tau q\,t$ ($q = u, c$)
		[4] CALABRESE	23	RVUE	ν-nucleus scattering
		[5] TUMASYAN	23AW	CMS	$q\overline{q}' \rightarrow \tau\nu$
		[6] TUMASYAN	23S	CMS	$pp \rightarrow \tau\tau$
		[7] CRIVELLIN	21A	RVUE	First generation
		[8] AEBISCHER	20	RVUE	B decays
		[9] DEPPISCH	20	RVUE	$K \rightarrow \pi\nu\nu$
> 3.1	95	[10] ABRAMOWICZ	19	ZEUS	First generation
		[11] MANDAL	19	RVUE	τ, μ, e, K
		[12] ZHANG	18A	RVUE	D decays
		[13] BARRANCO	16	RVUE	D decays
		[14] KUMAR	16	RVUE	neutral K mixing, rare K decays
		[15] BESSAA	15	RVUE	$q\overline{q} \rightarrow e^+e^-$
> 14	95	[16] SAHOO	15A	RVUE	$B_{s,d} \rightarrow \mu^+\mu^-$
		[17] SAKAKI	13	RVUE	$B \rightarrow D^{(*)}\tau\overline{\nu}$, $B \rightarrow X_s\nu\overline{\nu}$
		[18] KOSNIK	12	RVUE	$b \rightarrow s\ell^+\ell^-$
> 2.5	95	[19] AARON	11C	H1	First generation
		[20] DORSNER	11	RVUE	scalar, weak singlet, charge 4/3
		[21] AKTAS	07A	H1	Lepton-flavor violation
> 0.49	95	[22] SCHAEL	07A	ALEP	$e^+e^- \rightarrow q\overline{q}$
		[23] SMIRNOV	07	RVUE	$K \rightarrow e\mu$, $B \rightarrow e\tau$
		[24] CHEKANOV	05A	ZEUS	Lepton-flavor violation
> 1.7	96	[25] ADLOFF	03	H1	First generation
> 46	90	[26] CHANG	03	BELL	Pati-Salam type
		[27] CHEKANOV	02	ZEUS	Repl. by CHEKANOV 05A
> 1.7	95	[28] CHEUNG	01B	RVUE	First generation
> 0.39	95	[29] ACCIARRI	00P	L3	$e^+e^- \rightarrow q\,q$
> 1.5	95	[30] ADLOFF	00	H1	First generation
> 0.2	95	[31] BARATE	00I	ALEP	Repl. by SCHAEL 07A
		[32] BARGER	00	RVUE	Cs
		[33] GABRIELLI	00	RVUE	Lepton flavor violation
> 0.74	95	[34] ZARNECKI	00	RVUE	S_1 leptoquark
		[35] ABBIENDI	99	OPAL	
> 19.3	95	[36] ABE	98V	CDF	$B_s \rightarrow e^\pm\mu^\mp$, Pati-Salam type
		[37] ACCIARRI	98J	L3	$e^+e^- \rightarrow q\overline{q}$
		[38] ACKERSTAFF	98V	OPAL	$e^+e^- \rightarrow q\overline{q}$, $e^+e^- \rightarrow b\overline{b}$
> 0.76	95	[39] DEANDREA	97	RVUE	$\tilde{R}_2$ leptoquark
		[40] DERRICK	97	ZEUS	Lepton-flavor violation
		[41] GROSSMAN	97	RVUE	$B \rightarrow \tau^+\tau^-$(X)
		[42] JADACH	97	RVUE	$e^+e^- \rightarrow q\overline{q}$
>1200		[43] KUZNETSOV	95B	RVUE	Pati-Salam type
		[44] MIZUKOSHI	95	RVUE	Third generation scalar leptoquark
> 0.3	95	[45] BHATTACH...	94	RVUE	Spin-0 leptoquark coupled to $\overline{e}_R\,t_L$
		[46] DAVIDSON	94	RVUE	
> 18		[47] KUZNETSOV	94	RVUE	Pati-Salam type
> 0.43	95	[48] LEURER	94	RVUE	First generation spin-1 leptoquark
> 0.44	95	[48] LEURER	94B	RVUE	First generation spin-0 leptoquark
		[49] MAHANTA	94	RVUE	P and T violation
> 1		[50] SHANKER	82	RVUE	Nonchiral spin-0 leptoquark
> 125		[50] SHANKER	82	RVUE	Nonchiral spin-1 leptoquark

[1] AAD 25BB search for $\tau^+\tau^-$ production from t-channel LQ exchange in pp collisions at $\sqrt{s}$ = 13 TeV. See their Fig. 11 and Fig. 12 for limits in mass-coupling plane.

[2] HAYRAPETYAN 25AN use e^+e^- and $\mu^+\mu^-$ spectra in pp collisions at $\sqrt{s}$ = 13 TeV to set limits on t-channel LQ exchange amplitudes. See their Figs. 7–10 for limits in mass-coupling plane.

[3] AAD 24W search for leptoquark induced $\mu\tau q\,t$ ($q = u, c$) contact interaction in pp collisions at $\sqrt{s}$ = 13 TeV. See their Fig. 7b for limits in mass-coupling plane.

[4] CALABRESE 23 obtain limits on leptoquark coupling from coherent ν-nucleus scattering data collected by COHERENT experiment. See their Fig. 3 for limits in mass-coupling plane.

[5] TUMASYAN 23AW search for $\tau\nu$ events mediated by t-channel leptoquark exchange in pp collisions at $\sqrt{s}$ = 13 TeV. See their Fig. 10 for limits in mass-coupling plane.

[6] TUMASYAN 23S search for leptoquark induced $b\overline{b} \rightarrow \tau^+\tau^-$ process in pp collisions at $\sqrt{s}$ = 13 TeV. See their Fig. 12 for limits on a vector $b\tau$ leptoquark in mass-coupling plane.

[7] CRIVELLIN 21A set limits on coupling strengths of scalar and vector leptoquarks using $K \rightarrow \pi\nu\nu$, $K \rightarrow \pi e^+e^-$, $K^0 - \overline{K}^0$ and $D^0 - \overline{D}^0$ mixings, and weak neutral current measurements. See their Fig. 2 and Fig. 3 for the limits in mass-coupling plane.

[8] AEBISCHER 20 explain the B decay anomalies using four-fermion operator Wilson coefficients. See their Table 1. These Wilson coefficients may be generated by a U_1 vector leptoquark with U_1 transforming as $(3,1)_{2/3}$ under the SM gauge group. See their Figures 6, 7, 8 for the regions of the LQ parameter space which explains the B anomalies and avoids the indirect low energy constraints.

[9] DEPPISCH 20 limits on the lepton-number-violating higher-dimensional-operators are derived from $K \rightarrow \pi\nu\nu$ in the standard model effective field theory. These higher-dimensional-operators may be induced from leptoquark-exchange diagrams.

[10] ABRAMOWICZ 19 obtain a limit on $\lambda/M_{LQ} > 1.16$ TeV^{-1} for weak isotriplet spin-0 leptoquark S_1^L. We obtain the limit quoted above by converting the limit on λ/M_{LQ} for S_1^L assuming $\lambda = \sqrt{4\pi}$. See their Table 5 for the limits of leptoquarks with different quantum numbers. These limits are derived from bounds of eq contact interactions.

[11] MANDAL 19 give bounds on leptoquarks from τ-decays, leptonic dipole moments, lepton-flavor-violating processes, and K decays.

[12] ZHANG 18A give bounds on leptoquark induced four-fermion interactions from $D \rightarrow K\ell\nu$. The authors inform us that the shape parameter of the vector form factor in both the abstract and the conclusions of ZHANG 18A should be $r_{+1} = 2.16 \pm 0.07$ rather than ± 0.007. The numbers listed in their Table 7 are correct.

[13] BARRANCO 16 give bounds on leptoquark induced four-fermion interactions from $D \rightarrow K\ell\nu$ and $D_s \rightarrow \ell\nu$.

[14] KUMAR 16 gives bound on SU(2) singlet scalar leptoquark with chrge $-1/3$ from $K^0 - \overline{K}^0$ mixing, $K \rightarrow \pi\nu\overline{\nu}$, $K_L^0 \rightarrow \mu^+\mu^-$, and $K_L^0 \rightarrow \mu^\pm e^\mp$ decays.

[15] BESSAA 15 obtain limit on leptoquark induced four-fermion interactions from the ATLAS and CMS limit on the $\overline{q}q\overline{e}e$ contact interactions.

[16] SAHOO 15A obtain limit on leptoquark induced four-fermion interactions from $B_{s,d} \rightarrow \mu^+\mu^-$ for $\lambda \simeq O(1)$.

[17] SAKAKI 13 explain the $B \rightarrow D^{(*)}\tau\overline{\nu}$ anomaly using Wilson coefficients of leptoquark-induced four-fermion operators.

[18] KOSNIK 12 obtains limits on leptoquark induced four-fermion interactions from $b \rightarrow s\ell^+\ell^-$ decays.

[19] AARON 11C limit is for weak isotriplet spin-0 leptoquark at strong coupling $\lambda = \sqrt{4\pi}$. For the limits of leptoquarks with different quantum numbers, see their Table 3. Limits are derived from bounds of eq contact intereractions.

[20] DORSNER 11 give bounds on scalar, weak singlet, charge 4/3 leptoquark from K, B, τ decays, meson mixings, LFV, $g-2$ and $Z \rightarrow b\overline{b}$.

[21] AKTAS 07A search for lepton-flavor violation in ep collision. See their Tables 4–7 for limits on lepton-flavor violating four-fermion interactions induced by various leptoquarks.

[22] SCHAEL 07A limit is for the weak-isoscalar spin-0 left-handed leptoquark with the coupling of electromagnetic strength. For the limits of leptoquarks with different quantum numbers, see their Table 35.

[23] SMIRNOV 07 obtains mass limits for the vector and scalar chiral leptoquark states from $K \rightarrow e\mu$, $B \rightarrow e\tau$ decays.

[24] CHEKANOV 05 search for various leptoquarks with lepton-flavor violating couplings. See their Figs. 6–10 and Tables 1–8 for detailed limits.

[25] ADLOFF 03 limit is for the weak isotriplet spin-0 leptoquark at strong coupling $\lambda=\sqrt{4\pi}$. For the limits of leptoquarks with different quantum numbers, see their Table 3. Limits are derived from bounds on $e^\pm q$ contact interactions.

[26] The bound is derived from B($B^0 \rightarrow e^\pm\mu^\mp$) $< 1.7 \times 10^{-7}$.

[27] CHEKANOV 02 search for lepton-flavor violation in ep collisions. See their Tables 1–4 for limits on lepton-flavor violating and four-fermion interactions induced by various leptoquarks.

[28] CHEUNG 01B quoted limit is for a scalar, weak isoscalar, charge $-1/3$ leptoquark with a coupling of electromagnetic strength. The limit is derived from bounds on contact interactions in a global electroweak analysis. For the limits of leptoquarks with different quantum numbers, see Table 5.

[29] ACCIARRI 00P limit is for the weak isoscalar spin-0 leptoquark with the coupling of electromagnetic strength. For the limits of leptoquarks with different quantum numbers, see their Table 4.

[30] ADLOFF 00 limit is for the weak isotriplet spin-0 leptoquark at strong coupling, $\lambda=\sqrt{4\pi}$. For the limits of leptoquarks with different quantum numbers, see their Table 2. ADLOFF 00 limits are from the Q^2 spectrum measurement of $e^+p \rightarrow e^+$X.

[31] BARATE 00I search for deviations in cross section and jet-charge asymmetry in $e^+e^- \rightarrow \overline{q}q$ due to t-channel exchange of a leptoquark at $\sqrt{s}$=130 to 183 GeV. Limits for other scalar and vector leptoquarks are also given in their Table 22.

Int. J. Mod. Phys. A 2026.41. Downloaded from www.worldscientific.com by UNIVERSITY OF CALIFORNIA @ BERKELEY on 09/16/26. Re-use and distribution is strictly not permitted, except for Open Access articles.

[32] BARGER 00 explain the deviation of atomic parity violation in cesium atoms from prediction is explained by scalar leptoquark exchange.

[33] GABRIELLI 00 calculate various process with lepton flavor violation in leptoquark models.

[34] ZARNECKI 00 limit is derived from data of HERA, LEP, and Tevatron and from various low-energy data including atomic parity violation. Leptoquark coupling with electromagnetic strength is assumed.

[35] ABBIENDI 99 limits are from $e^+e^- \rightarrow q\overline{q}$ cross section at 130–136, 161–172, 183 GeV. See their Fig. 8 and Fig. 9 for limits in mass-coupling plane.

[36] ABE 98V quoted limit is from $B(B_s \rightarrow e^{\pm}\mu^{\mp}) < 8.2 \times 10^{-6}$. ABE 98V also obtain a similar limit on $M_{LQ} > 20.4$ TeV from $B(B_d \rightarrow e^{\pm}\mu^{\mp}) < 4.5 \times 10^{-6}$. Both bounds assume the non-canonical association of the b quark with electrons or muons under SU(4).

[37] ACCIARRI 98J limit is from $e^+e^- \rightarrow q\overline{q}$ cross section at $\sqrt{s}$= 130–172 GeV which can be affected by the t- and u-channel exchanges of leptoquarks. See their Fig. 4 and Fig. 5 for limits in the mass-coupling plane.

[38] ACKERSTAFF 98V limits are from $e^+e^- \rightarrow q\overline{q}$ and $e^+e^- \rightarrow b\overline{b}$ cross sections at $\sqrt{s}$ = 130–172 GeV, which can be affected by the t- and u-channel exchanges of leptoquarks. See their Fig. 21 and Fig. 22 for limits of leptoquarks in mass-coupling plane.

[39] DEANDREA 97 limit is for $\widetilde{R}_2$ leptoquark obtained from atomic parity violation (APV). The coupling of leptoquark is assumed to be electromagnetic strength. See Table 2 for limits of the four-fermion interactions induced by various scalar leptoquark exchange. DEANDREA 97 combines APV limit and limits from Tevatron and HERA. See Fig. 1–4 for combined limits of leptoquark in mass-coupling plane.

[40] DERRICK 97 search for lepton-flavor violation in ep collision. See their Tables 2–5 for limits on lepton-flavor violating four-fermion interactions induced by various leptoquarks.

[41] GROSSMAN 97 estimate the upper bounds on the branching fraction $B \rightarrow \tau^+\tau^-(X)$ from the absence of the B decay with large missing energy. These bounds can be used to constrain leptoquark induced four-fermion interactions.

[42] JADACH 97 limit is from $e^+e^- \rightarrow q\overline{q}$ cross section at $\sqrt{s}$=172.3 GeV which can be affected by the t- and u-channel exchanges of leptoquarks. See their Fig. 1 for limits on vector leptoquarks in mass-coupling plane.

[43] KUZNETSOV 95B use π, K, B, τ decays and μe conversion and give a list of bounds on the leptoquark mass and the fermion mixing matrix in the Pati-Salam model. The quoted limit is from $K_L \rightarrow \mu e$ decay assuming zero mixing.

[44] MIZUKOSHI 95 calculate the one-loop radiative correction to the Z-physics parameters in various scalar leptoquark models. See their Fig. 4 for the exclusion plot of third generation leptoquark models in mass-coupling plane.

[45] BHATTACHARYYA 94 limit is from one-loop radiative correction to the leptonic decay width of the Z. m_H=250 GeV, $\alpha_s(m_Z)$=0.12, m_t=180 GeV, and the electroweak strength of leptoquark coupling are assumed. For leptoquark coupled to $\overline{e}_L\, t_R$, $\overline{\mu}t$, and $\overline{\tau}t$, see Fig. 2 in BHATTACHARYYA 94B erratum and Fig. 3.

[46] DAVIDSON 94 gives an extensive list of the bounds on leptoquark-induced four-fermion interactions from π, K, D, B, μ, τ decays and meson mixings, *etc.* See Table 15 of DAVIDSON 94 for detail.

[47] KUZNETSOV 94 gives mixing independent bound of the Pati-Salam leptoquark from the cosmological limit on $\pi^0 \rightarrow \overline{\nu}\nu$.

[48] LEURER 94, LEURER 94B limits are obtained from atomic parity violation and apply to any chiral leptoquark which couples to the first generation with electromagnetic strength. For a nonchiral leptoquark, universality in $\pi_{\ell 2}$ decay provides a much more stringent bound.

[49] MAHANTA 94 gives bounds of P- and T-violating scalar-leptoquark couplings from atomic and molecular experiments.

[50] From $(\pi \rightarrow e\nu)/(\pi \rightarrow \mu\nu)$ ratio. SHANKER 82 assumes the leptoquark induced four-fermion coupling $4g^2/M^2\ (\overline{\nu}_{eL}\ u_R)\ (\overline{d}_L\, e_R)$with g=0.004 for spin-0 leptoquark and $g^2/M^2\ (\overline{\nu}_{eL}\ \gamma_\mu u_L)\ (\overline{d}_R\ \gamma^\mu e_R)$ with $g \simeq$ 0.6 for spin-1 leptoquark.

MASS LIMITS for Diquarks

VALUE (GeV)	CL%	DOCUMENT ID		TECN	COMMENT
>7200 (CL = 95%) OUR LIMIT					
none 600–7200	95	[1] SIRUNYAN	18BO	CMS	E_6 diquark
none 600–6900	95	[2] KHACHATRY...	17W	CMS	E_6 diquark
none 1500–6000	95	[3] KHACHATRY...	16K	CMS	E_6 diquark
none 500–1600	95	[4] KHACHATRY...	16L	CMS	E_6 diquark
none 1200–4700	95	[5] KHACHATRY...	15V	CMS	E_6 diquark
• • • We do not use the following data for averages, fits, limits, etc. • • •					
>3750	95	[6] CHATRCHYAN	13A	CMS	E_6 diquark
none 1000–4280	95	[7] CHATRCHYAN	13AS	CMS	Superseded by KHACHATRYAN 15V
>3520	95	[8] CHATRCHYAN	11Y	CMS	Superseded by CHATRCHYAN 13A
none 970–1080, 1450–1600	95	[9] KHACHATRY...	10	CMS	Superseded by CHATRCHYAN 13A
none 290–630	95	[10] AALTONEN	09AC	CDF	E_6 diquark
none 290–420	95	[11] ABE	97G	CDF	E_6 diquark
none 15–31.7	95	[12] ABREU	94O	DLPH	SUSY E_6 diquark

[1] SIRUNYAN 18BO search for resonances decaying into dijets in pp collisions at $\sqrt{s} = 13$ TeV.

[2] KHACHATRYAN 17W search for resonances decaying to dijets in pp collisions at $\sqrt{s} =$ 13 TeV.

[3] KHACHATRYAN 16K search for resonances decaying to dijets in pp collisions at $\sqrt{s} =$ 13 TeV.

[4] KHACHATRYAN 16L search for resonances decaying to dijets in pp collisions at $\sqrt{s}$ = 8 TeV with the data scouting technique, increasing the sensitivity to the low mass resonances.

[5] KHACHATRYAN 15V search for resonances decaying to dijets in pp collisions at $\sqrt{s} =$ 8 TeV.

[6] CHATRCHYAN 13A search for new resonance decaying to dijets in pp collisions at $\sqrt{s}$ = 7 TeV.

[7] CHATRCHYAN 13AS search for new resonance decaying to dijets in pp collisions at $\sqrt{s}$ = 8 TeV.

[8] CHATRCHYAN 11Y search for new resonance decaying to dijets in pp collisions at $\sqrt{s} = 7$ TeV.

[9] KHACHATRYAN 10 search for new resonance decaying to dijets in pp collisions at $\sqrt{s} = 7$ TeV.

[10] AALTONEN 09AC search for new narrow resonance decaying to dijets.

[11] ABE 97G search for new particle decaying to dijets.

[12] ABREU 94O limit is from $e^+e^- \rightarrow \overline{c}sc\,s$. Range extends up to 43 GeV if diquarks are degenerate in mass.

MASS LIMITS for g_A (axigluon) and Other Color-Octet Gauge Bosons

Axigluons are massive color-octet gauge bosons in chiral color models and have axial-vector coupling to quarks with the same coupling strength as gluons.

VALUE (GeV)	CL%	DOCUMENT ID		TECN	COMMENT
>6600 (CL = 95%) OUR LIMIT					
none 1800–6600	95	[1] SIRUNYAN	20AI	CMS	$pp \rightarrow g_A X$, $g_A \rightarrow 2j$
none 600–6100	95	[2] SIRUNYAN	18BO	CMS	$pp \rightarrow g_A X$, $g_A \rightarrow 2j$
none 600–5500	95	[3] KHACHATRY...	17W	CMS	$pp \rightarrow g_A X$, $g_A \rightarrow 2j$
none 1500–5100	95	[4] KHACHATRY...	16K	CMS	$pp \rightarrow g_A X$, $g_A \rightarrow 2j$
none 500–1600	95	[5] KHACHATRY...	16L	CMS	$pp \rightarrow g_A X$, $g_A \rightarrow 2j$
none 1300–3600	95	[6] KHACHATRY...	15V	CMS	$pp \rightarrow g_A X$, $g_A \rightarrow 2j$
• • • We do not use the following data for averages, fits, limits, etc. • • •					
		[7] KHACHATRY...	17Y	CMS	$pp \rightarrow g_A g_A \rightarrow 8j$
		[8] AAD	16W	ATLS	$pp \rightarrow g_A X$, $g_A \rightarrow b\overline{b}b\overline{b}$
>2800	95	[9] KHACHATRY...	16E	CMS	$pp \rightarrow g_{KK} X$, $g_{KK} \rightarrow t\overline{t}$
		[10] KHACHATRY...	15AV	CMS	$pp \rightarrow \Theta^0\Theta^0 \rightarrow b\overline{b}Zg$
		[11] AALTONEN	13R	CDF	$p\overline{p} \rightarrow g_A X$, $g_A \rightarrow \sigma\sigma$, $\sigma \rightarrow 2j$
>3360	95	[12] CHATRCHYAN	13A	CMS	$pp \rightarrow g_A X$, $g_A \rightarrow 2j$
none 1000–3270	95	[13] CHATRCHYAN	13AS	CMS	Superseded by KHACHATRYAN 15V
none 250–740	95	[14] CHATRCHYAN	13AU	CMS	$pp \rightarrow 2g_A X$,$g_A \rightarrow 2j$
> 775	95	[15] ABAZOV	12R	D0	$p\overline{p} \rightarrow g_A X$, $g_A \rightarrow t\overline{t}$
>2470	95	[16] CHATRCHYAN	11Y	CMS	Superseded by CHATRCHYAN 13A
		[17] AALTONEN	10L	CDF	$p\overline{p} \rightarrow g_A X$, $g_A \rightarrow t\overline{t}$
none 1470–1520	95	[18] KHACHATRY...	10	CMS	Superseded by CHATRCHYAN 13A
none 260–1250	95	[19] AALTONEN	09AC	CDF	$p\overline{p} \rightarrow g_A X$, $g_A \rightarrow 2j$
> 910	95	[20] CHOUDHURY	07	RVUE	$p\overline{p} \rightarrow t\overline{t}X$
> 365	95	[21] DONCHESKI	98	RVUE	$\Gamma(Z \rightarrow$ hadron)
none 200–980	95	[22] ABE	97G	CDF	$p\overline{p} \rightarrow g_A X$, $g_A \rightarrow 2j$
none 200–870	95	[23] ABE	95N	CDF	$p\overline{p} \rightarrow g_A X$, $g_A \rightarrow q\overline{q}$
none 240–640	95	[24] ABE	93G	CDF	$p\overline{p} \rightarrow g_A X$, $g_A \rightarrow 2j$
> 50	95	[25] CUYPERS	91	RVUE	$\sigma(e^+e^- \rightarrow$ hadrons)
none 120–210	95	[26] ABE	90H	CDF	$p\overline{p} \rightarrow g_A X$, $g_A \rightarrow 2j$
> 29		[27] ROBINETT	89	THEO	Partial-wave unitarity
none 150–310	95	[28] ALBAJAR	88B	UA1	$p\overline{p} \rightarrow g_A X$, $g_A \rightarrow 2j$
> 20		BERGSTROM	88	RVUE	$p\overline{p} \rightarrow \Upsilon X$ via $g_A g$
> 9		[29] CUYPERS	88	RVUE	Υ decay
> 25		[30] DONCHESKI	88B	RVUE	Υ decay

[1] SIRUNYAN 20AI search for resonances decaying into dijets in pp collisions at $\sqrt{s} = 13$ TeV.

[2] SIRUNYAN 18BO search for resonances decaying to dijets in pp collisions at $\sqrt{s} = 13$ TeV.

[3] KHACHATRYAN 17W search for resonances decaying to dijets in pp collisions at $\sqrt{s} =$ 13 TeV.

[4] KHACHATRYAN 16K search for resonances decaying to dijets in pp collisions at $\sqrt{s} =$ 13 TeV.

[5] KHACHATRYAN 16L search for resonances decaying to dijets in pp collisions at $\sqrt{s}$ = 8 TeV with the data scouting technique, increasing the sensitivity to the low mass resonances.

[6] KHACHATRYAN 15V search for resonances decaying to dijets in pp collisions at $\sqrt{s} =$ 8 TeV.

[7] KHACHATRYAN 17Y search for pair production of color-octet gauge boson g_A each decaying to $4j$ in pp collisions at $\sqrt{s} = 8$ TeV.

[8] AAD 16W search for a new resonance decaying to a pair of b and B_H in pp collisions at $\sqrt{s} = 8$ TeV. The vector-like quark B_H is assumed to decay to bH. See their Fig. 3 and Fig. 4 for limits on $\sigma \cdot B$.

[9] KHACHATRYAN 16E search for KK gluon decaying to $t\overline{t}$ in pp collisions at $\sqrt{s} = 8$ TeV.

[10] KHACHATRYAN 15AV search for pair productions of neutral color-octet weak-triplet scalar particles (Θ^0), decaying to $b\overline{b}$, Zg or γg, in pp collisions at $\sqrt{s} = 8$ TeV. The Θ^0 particle is often predicted in coloron (G', color-octet gauge boson) models and appear in the pp collisions through $G' \rightarrow \Theta^0\Theta^0$ decays. Assuming $B(\Theta^0 \rightarrow b\overline{b}) =$ 0.5, they give limits $m_{\Theta^0} > 623$ GeV (426 GeV) for $m_{G'} = 2.3\ m_{\Theta^0}$ ($m_{G'} = 5\ m_{\Theta^0}$).

[11] AALTONEN 13R search for new resonance decaying to $\sigma\sigma$, with hypothetical strongly interacting σ particle subsequently decaying to 2 jets, in $p\overline{p}$ collisions at $\sqrt{s} = 1.96$ TeV, using data corresponding to an integrated luminosity of 6.6 fb^{-1}. For 50 GeV $< m_\sigma <$ $m_{g_A}/2$, axigluons in mass range 150–400 GeV are excluded.

[12] CHATRCHYAN 13A search for new resonance decaying to dijets in pp collisions at $\sqrt{s}$ = 7 TeV.

[13] CHATRCHYAN 13AS search for new resonance decaying to dijets in pp collisions at $\sqrt{s}$ = 8 TeV.

[14] CHATRCHYAN 13AU search for the pair produced color-octet vector bosons decaying to $q\overline{q}$ pairs in pp collisions. The quoted limit is for $B(g_A \rightarrow q\overline{q}) = 1$.

[15] ABAZOV 12R search for massive color octet vector particle decaying to $t\overline{t}$. The quoted limit assumes g_A couplings with light quarks are suppressed by 0.2.

[16] CHATRCHYAN 11Y search for new resonance decaying to dijets in pp collisions at $\sqrt{s} = 7$ TeV.

Int. J. Mod. Phys. A 2026.41. Downloaded from www.worldscientific.com
by UNIVERSITY OF CALIFORNIA @ BERKELEY on 09/16/26. Reproduction is strictly not permitted, except for Open Access articles.

[17] AALTONEN 10L search for massive color octet non-chiral vector particle decaying into $t\overline{t}$ pair with mass in the range 400 GeV < M < 800 GeV. See their Fig. 6 for limit in the mass-coupling plane.
[18] KHACHATRYAN 10 search for new resonance decaying to dijets in pp collisions at $\sqrt{s} = 7$ TeV.
[19] AALTONEN 09AC search for new narrow resonance decaying to dijets.
[20] CHOUDHURY 07 limit is from the $t\overline{t}$ production cross section measured at CDF.
[21] DONCHESKI 98 compare α_s derived from low-energy data and that from $\Gamma(Z \to$ hadrons$)/\Gamma(Z \to$ leptons$)$.
[22] ABE 97G search for new particle decaying to dijets.
[23] ABE 95N assume axigluons decaying to quarks in the Standard Model only.
[24] ABE 93G assume $\Gamma(g_A) = N\alpha_s m_{g_A}/6$ with $N = 10$.
[25] CUYPERS 91 compare α_s measured in Υ decay and that from R at PEP/PETRA energies.
[26] ABE 90H assumes $\Gamma(g_A) = N\alpha_s m_{g_A}/6$ with $N = 5\,(\Gamma(g_A) = 0.09 m_{g_A})$. For $N = 10$, the excluded region is reduced to 120–150 GeV.
[27] ROBINETT 89 result demands partial-wave unitarity of $J = 0$ $t\overline{t} \to t\overline{t}$ scattering amplitude and derives a limit $m_{g_A} > 0.5\, m_t$. Assumes $m_t > 56$ GeV.
[28] ALBAJAR 88B result is from the nonobservation of a peak in two-jet invariant mass distribution. $\Gamma(g_A) < 0.4\, m_{g_A}$ assumed. See also BAGGER 88.
[29] CUYPERS 88 requires $\Gamma(\Upsilon \to g g_A) < \Gamma(\Upsilon \to g g g)$. A similar result is obtained by DONCHESKI 88.
[30] DONCHESKI 88B requires $\Gamma(\Upsilon \to g q\overline{q})/\Gamma(\Upsilon \to g g g) < 0.25$, where the former decay proceeds via axigluon exchange. A more conservative estimate of < 0.5 leads to $m_{g_A} > 21$ GeV.

MASS LIMITS for Color-Octet Scalar Bosons

VALUE (GeV)	CL%	DOCUMENT ID		TECN	COMMENT
• • • We do not use the following data for averages, fits, limits, etc. • • •					
none 400–1300	95	[1] AAD	25AL	ATLS	$pp \to S_8 S_8 X$, $S_8 \to t\overline{t}$
none 1800–3700	95	[2] SIRUNYAN	20AI	CMS	$pp \to S_8 X$, $S_8 \to g g$
none 600–3400	95	[3] SIRUNYAN	18BO	CMS	$pp \to S_8 X$, $S_8 \to g g$
		[4] KHACHATRY...	15AV	CMS	$pp \to \Theta^0 \Theta^0 \to b\overline{b} Z g$
none 150–287	95	[5] AAD	13K	ATLS	$pp \to S_8 S_8 X$, $S_8 \to 2$ jets

[1] AAD 25AL search for pair production of color-octet scalar particles in pp collisions at $\sqrt{s} = 13$ TeV. The limit quoted above assumes the $S_8\, t\overline{t}$ coupling parameter 0.1. See their Fig. 12 for limits on $\sigma \cdot B$.
[2] SIRUNYAN 20AI search for resonances decaying into dijets in pp collisions at $\sqrt{s} = 13$ TeV. The limit above assumes S_{8gg} coupling $k_s^2 = 1/2$.
[3] SIRUNYAN 18BO search for color octet scalar boson produced through gluon fusion process in pp collisions at $\sqrt{s} = 13$ TeV. The limit above assumes S_{8gg} coupling $k_s^2 = 1/2$.
[4] KHACHATRYAN 15AV search for pair productions of neutral color-octet weak-triplet scalar particles (Θ^0), decaying to $b\overline{b}$, Zg or γg, in pp collisions at $\sqrt{s} = 8$ TeV. The Θ^0 particle is often predicted in coloron (G', color-octet gauge boson) models and appear in the pp collisions through $G' \to \Theta^0 \Theta^0$ decays. Assuming $B(\Theta^0 \to b\overline{b}) = 0.5$, they give limits $m_{\Theta^0} > 623$ GeV (426 GeV) for $m_{G'} = 2.3\, m_{\Theta^0}$ ($m_{G'} = 5\, m_{\Theta^0}$).
[5] AAD 13K search for pair production of color-octet scalar particles in pp collisions at $\sqrt{s} = 7$ TeV. Cross section limits are interpreted as mass limits on scalar partners of a Dirac gluino.

X^0 (Heavy Boson) Searches in Z Decays

Searches for radiative transition of Z to a lighter spin-0 state X^0 decaying to hadrons, a lepton pair, a photon pair, or invisible particles as shown in the comments. The limits are for the product of branching ratios.

VALUE	CL%	DOCUMENT ID		TECN	COMMENT
• • • We do not use the following data for averages, fits, limits, etc. • • •					
		[1] RAINBOLT	19	RVUE	$X^0 \to \ell^+\ell^-$
		[2] SIRUNYAN	19AZ	CMS	$X^0 \to \mu^+\mu^-$
		[3] BARATE	98U	ALEP	$X^0 \to \ell\overline{\ell}$, $q\overline{q}$, gg, $\gamma\gamma$, $\nu\overline{\nu}$
		[4] ACCIARRI	97Q	L3	$X^0 \to$ invisible particle(s)
		[5] ACTON	93E	OPAL	$X^0 \to \gamma\gamma$
		[6] ABREU	92D	DLPH	$X^0 \to$ hadrons
		[7] ADRIANI	92F	L3	$X^0 \to$ hadrons
		[8] ACTON	91	OPAL	$X^0 \to$ anything
$<1.1 \times 10^{-4}$	95	[9] ACTON	91B	OPAL	$X^0 \to e^+e^-$
$<9 \times 10^{-5}$	95	[9] ACTON	91B	OPAL	$X^0 \to \mu^+\mu^-$
$<1.1 \times 10^{-4}$	95	[9] ACTON	91B	OPAL	$X^0 \to \tau^+\tau^-$
$<2.8 \times 10^{-4}$	95	[10] ADEVA	91D	L3	$X^0 \to e^+e^-$
$<2.3 \times 10^{-4}$	95	[10] ADEVA	91D	L3	$X^0 \to \mu^+\mu^-$
$<4.7 \times 10^{-4}$	95	[11] ADEVA	91D	L3	$X^0 \to$ hadrons
$<8 \times 10^{-4}$	95	[12] AKRAWY	90J	OPAL	$X^0 \to$ hadrons

[1] RAINBOLT 19 limits are from $B(Z \to \ell^+\ell^-\ell^+\ell^-)$. See their Figs. 5 and 6 for limits in mass-coupling plane.
[2] SIRUNYAN 19AZ search for $pp \to Z \to X^0\mu^+\mu^- \to \mu^+\mu^-\mu^+\mu^-$ events in pp collisions at $\sqrt{s} = 13$ TeV. See their Fig. 5 for limits on $\sigma(pp \to X^0\mu^+\mu^-) \cdot B(X^0 \to \mu^+\mu^-)$.
[3] BARATE 98U obtain limits on $B(Z \to \gamma X^0) B(X^0 \to \ell\overline{\ell}, q\overline{q}, gg, \gamma\gamma, \nu\overline{\nu})$. See their Fig. 17.
[4] See Fig. 4 of ACCIARRI 97Q for the upper limit on $B(Z \to \gamma X^0;\ E_\gamma > E_{\min})$ as a function of $E_{\min}$.
[5] ACTON 93E give $\sigma(e^+e^- \to X^0\gamma) \cdot B(X^0 \to \gamma\gamma) < 0.4$ pb (95%CL) for $m_{X^0} = 60 \pm 2.5$ GeV. If the process occurs via s-channel γ exchange, the limit translates to $\Gamma(X^0) \cdot B(X^0 \to \gamma\gamma)^2 < 20$ MeV for $m_{X^0} = 60 \pm 1$ GeV.
[6] ABREU 92D give $\sigma_Z \cdot B(Z \to \gamma X^0) \cdot B(X^0 \to$ hadrons$) <$(3–10) pb for $m_{X^0} =$ 10–78 GeV. A very similar limit is obtained for spin-1 X^0.
[7] ADRIANI 92F search for isolated γ in hadronic Z decays. The limit $\sigma_Z \cdot B(Z \to \gamma X^0) \cdot B(X^0 \to$ hadrons$) <$(2–10) pb (95%CL) is given for $m_{X^0} =$ 25–85 GeV.
[8] ACTON 91 searches for $Z \to Z^* X^0$, $Z^* \to e^+e^-$, $\mu^+\mu^-$, or $\nu\overline{\nu}$. Excludes any new scalar X^0 with $m_{X^0} < 9.5$ GeV/c if it has the same coupling to ZZ^* as the MSM Higgs boson.
[9] ACTON 91B limits are for $m_{X^0} =$ 60–85 GeV.
[10] ADEVA 91D limits are for $m_{X^0} =$ 30–89 GeV.
[11] ADEVA 91D limits are for $m_{X^0} =$ 30–86 GeV.
[12] AKRAWY 90J give $\Gamma(Z \to \gamma X^0) \cdot B(X^0 \to$ hadrons$) <$ 1.9 MeV (95%CL) for $m_{X^0} =$ 32–80 GeV. We divide by $\Gamma(Z) = 2.5$ GeV to get product of branching ratios. For nonresonant transitions, the limit is $B(Z \to \gamma q\overline{q}) < 8.2$ MeV assuming three-body phase space distribution.

MASS LIMITS for a Heavy Neutral Boson Coupling to e^+e^-

VALUE (GeV)	CL%	DOCUMENT ID		TECN	COMMENT
• • • We do not use the following data for averages, fits, limits, etc. • • •					
none 55–61		[1] ODAKA	89	VNS	$\Gamma(X^0 \to e^+e^-) \cdot B(X^0 \to$ had.$) \gtrsim 0.2$ MeV
>45	95	[2] DERRICK	86	HRS	$\Gamma(X^0 \to e^+e^-)=6$ MeV
>46.6	95	[3] ADEVA	85	MRKJ	$\Gamma(X^0 \to e^+e^-)=10$ keV
>48	95	[3] ADEVA	85	MRKJ	$\Gamma(X^0 \to e^+e^-)=4$ MeV
		[4] BERGER	85B	PLUT	
none 39.8–45.5		[5] ADEVA	84	MRKJ	$\Gamma(X^0 \to e^+e^-)=10$ keV
>47.8	95	[5] ADEVA	84	MRKJ	$\Gamma(X^0 \to e^+e^-)=4$ MeV
none 39.8–45.2		[5] BEHREND	84C	CELL	
>47	95	[5] BEHREND	84C	CELL	$\Gamma(X^0 \to e^+e^-)=4$ MeV

[1] ODAKA 89 looked for a narrow or wide scalar resonance in $e^+e^- \to$ hadrons at $E_{cm} =$ 55.0–60.8 GeV.
[2] DERRICK 86 found no deviation from the Standard Model Bhabha scattering at $E_{cm} =$ 29 GeV and set limits on the possible scalar boson e^+e^- coupling. See their figure 4 for excluded region in the $\Gamma(X^0 \to e^+e^-)$-m_{X^0} plane. Electronic chiral invariance requires a parity doublet of X^0, in which case the limit applies for $\Gamma(X^0 \to e^+e^-) =$ 3 MeV.
[3] ADEVA 85 first limit is from 2γ, $\mu^+\mu^-$, hadrons assuming X^0 is a scalar. Second limit is from e^+e^- channel. $E_{cm} =$ 40–47 GeV. Supersedes ADEVA 84.
[4] BERGER 85B looked for effect of spin-0 boson exchange in $e^+e^- \to e^+e^-$ and $\mu^+\mu^-$ at $E_{cm} = 34.7$ GeV. See Fig. 5 for excluded region in the $m_{X^0} - \Gamma(X^0)$ plane.
[5] ADEVA 84 and BEHREND 84C have $E_{cm} =$ 39.8–45.5 GeV. MARK-J searched X^0 in $e^+e^- \to$ hadrons, 2γ, $\mu^+\mu^-$, e^+e^- and CELLO in the same channels plus τ pair. No narrow or broad X^0 is found in the energy range. They also searched for the effect of X^0 with $m_X > E_{cm}$. The second limits are from Bhabha data and for spin-0 singlet. The same limits apply for $\Gamma(X^0 \to e^+e^-) = 2$ MeV if X^0 is a spin-0 doublet. The second limit of BEHREND 84C was read off from their figure 2. The original papers also list limits in other channels.

Search for X^0 Resonance in e^+e^- Collisions

The limit is for $\Gamma(X^0 \to e^+e^-) \cdot B(X^0 \to f)$, where f is the specified final state. Spin 0 is assumed for X^0.

VALUE (keV)	CL%	DOCUMENT ID		TECN	COMMENT
• • • We do not use the following data for averages, fits, limits, etc. • • •					
$<10^3$	95	[1] ABE	93C	VNS	$\Gamma(ee)$
<(0.4–10)	95	[2] ABE	93C	VNS	$f = \gamma\gamma$
<(0.3–5)	95	[3,4] ABE	93D	TOPZ	$f = \gamma\gamma$
<(2–12)	95	[3,4] ABE	93D	TOPZ	$f =$ hadrons
<(4–200)	95	[4,5] ABE	93D	TOPZ	$f = ee$
<(0.1–6)	95	[4,5] ABE	93D	TOPZ	$f = \mu\mu$
<(0.5–8)	90	[6] STERNER	93	AMY	$f = \gamma\gamma$

[1] Limit is for $\Gamma(X^0 \to e^+e^-)\ m_{X^0} =$ 56–63.5 GeV for $\Gamma(X^0) = 0.5$ GeV.
[2] Limit is for $m_{X^0} =$ 56–61.5 GeV and is valid for $\Gamma(X^0) \ll 100$ MeV. See their Fig. 5 for limits for $\Gamma =$ 1,2 GeV.
[3] Limit is for $m_{X^0} =$ 57.2–60 GeV.
[4] Limit is valid for $\Gamma(X^0) \ll 100$ MeV. See paper for limits for $\Gamma = 1$ GeV and those for $J = 2$ resonances.
[5] Limit is for $m_{X^0} =$ 56.6–60 GeV.
[6] STERNER 93 limit is for $m_{X^0} =$ 57–59.6 GeV and is valid for $\Gamma(X^0) <$100 MeV. See their Fig. 2 for limits for $\Gamma =$ 1,3 GeV.

Search for X^0 Resonance in ep Collisions

VALUE	DOCUMENT ID		TECN	COMMENT
• • • We do not use the following data for averages, fits, limits, etc. • • •				
	[1] CHEKANOV	02B	ZEUS	$X \to jj$

[1] CHEKANOV 02B search for photoproduction of X decaying into dijets in ep collisions. See their Fig. 5 for the limit on the photoproduction cross section.

Search for X^0 Resonance in $e^+e^- \to X^0\gamma$

VALUE (GeV)	DOCUMENT ID		TECN	COMMENT
• • • We do not use the following data for averages, fits, limits, etc. • • •				
	[1] ABBIENDI	03D	OPAL	$X^0 \to \gamma\gamma$

Int. J. Mod. Phys. A 2026.41. Downloaded from www.worldscientific.com
by UNIVERSITY OF CALIFORNIA @ BERKELEY on 09/16/26. Re-use and distribution is strictly not permitted, except for Open Access articles.

[2] ABREU 00Z DLPH X^0 decaying invisibly
[3] ADAM 96C DLPH X^0 decaying invisibly

[1] ABBIENDI 03D measure the $e^+e^- \to \gamma\gamma\gamma$ cross section at $\sqrt{s}$=181–209 GeV. The upper bound on the production cross section, $\sigma(e^+e^- \to X^0\gamma)$ times the branching ratio for $X^0 \to \gamma\gamma$, is less than 0.03 pb at 95%CL for X^0 masses between 20 and 180 GeV. See their Fig. 9b for the limits in the mass-cross section plane.

[2] ABREU 00Z is from the single photon cross section at $\sqrt{s}$=183, 189 GeV. The production cross section upper limit is less than 0.3 pb for X^0 mass between 40 and 160 GeV. See their Fig. 4 for the limit in mass-cross section plane.

[3] ADAM 96C is from the single photon production cross at $\sqrt{s}$=130, 136 GeV. The upper bound is less than 3 pb for X^0 masses between 60 and 130 GeV. See their Fig. 5 for the exact bound on the cross section $\sigma(e^+e^- \to \gamma X^0)$.

Search for X^0 Resonance in $Z \to f\overline{f}X^0$

The limit is for $B(Z \to f\overline{f}X^0) \cdot B(X^0 \to F)$ where f is a fermion and F is the specified final state. Spin 0 is assumed for X^0.

VALUE	CL%	DOCUMENT ID		TECN	COMMENT
• • • We do not use the following data for averages, fits, limits, etc. • • •					
		[1] ABREU	96T	DLPH	f=e,μ,τ; F=$\gamma\gamma$
$<3.7 \times 10^{-6}$	95	[2] ABREU	96T	DLPH	f=ν; F=$\gamma\gamma$
		[3] ABREU	96T	DLPH	f=q; F=$\gamma\gamma$
$<6.8 \times 10^{-6}$	95	[2] ACTON	93E	OPAL	f=e,μ,τ; F=$\gamma\gamma$
$<5.5 \times 10^{-6}$	95	[2] ACTON	93E	OPAL	f=q; F=$\gamma\gamma$
$<3.1 \times 10^{-6}$	95	[2] ACTON	93E	OPAL	f=ν; F=$\gamma\gamma$
$<6.5 \times 10^{-6}$	95	[2] ACTON	93E	OPAL	f=e,μ; F=$\ell\overline{\ell}$, $q\overline{q}$, $\nu\overline{\nu}$
$<7.1 \times 10^{-6}$	95	[2] BUSKULIC	93F	ALEP	f=e,μ; F=$\ell\overline{\ell}$, $q\overline{q}$, $\nu\overline{\nu}$
		[4] ADRIANI	92F	L3	f=q; F=$\gamma\gamma$

[1] ABREU 96T obtain limit as a function of m_{X^0}. See their Fig. 6.

[2] Limit is for m_{X^0} around 60 GeV.

[3] ABREU 96T obtain limit as a function of m_{X^0}. See their Fig. 15.

[4] ADRIANI 92F give $\sigma_Z \cdot B(Z \to q\overline{q}X^0) \cdot B(X^0 \to \gamma\gamma)$<(0.75–1.5) pb (95%CL) for m_{X^0} = 10–70 GeV. The limit is 1 pb at 60 GeV.

Search for X^0 Resonance in WX^0 final state

VALUE (MeV)	DOCUMENT ID		TECN	COMMENT
• • • We do not use the following data for averages, fits, limits, etc. • • •				
	[1] AALTONEN	13AA	CDF	$X^0 \to jj$
	[2] CHATRCHYAN	12BR	CMS	$X^0 \to jj$
	[3] ABAZOV	11I	D0	$X^0 \to jj$
	[4] ABE	97W	CDF	$X^0 \to b\overline{b}$

[1] AALTONEN 13AA search for X^0 production associated with W (or Z) in $p\overline{p}$ collisions at E_{cm} = 1.96 TeV. The upper limit on the cross section $\sigma(p\overline{p} \to WX^0)$ is 2.2 pb for M_{X^0} = 145 GeV.

[2] CHATRCHYAN 12BR search for X^0 production associated with W in pp collisions at E_{cm} = 7 TeV. The upper limit on the cross section is 5.0 pb at 95% CL for m_{X^0} = 150 GeV.

[3] ABAZOV 11I search for X^0 production associated with W in $p\overline{p}$ collisions at E_{cm} = 1.96 TeV. The 95% CL upper limit on the cross section ranges from 2.57 to 1.28 pb for X^0 mass between 110 and 170 GeV.

[4] ABE 97W search for X^0 production associated with W in $p\overline{p}$ collisions at E_{cm}=1.8 TeV. The 95%CL upper limit on the production cross section times the branching ratio for $X^0 \to b\overline{b}$ ranges from 14 to 19 pb for X^0 mass between 70 and 120 GeV. See their Fig. 3 for upper limits of the production cross section as a function of m_{X^0}.

Search for X^0 Resonance in Quarkonium Decays

Limits are for branching ratios to modes shown. Spin 1 is assumed for X^0.

VALUE	CL%	DOCUMENT ID		TECN	COMMENT
• • • We do not use the following data for averages, fits, limits, etc. • • •					
		[1] ABLIKIM	24G	BES3	$J/\psi \to \mu^+\mu^- X_{0,1}$
$< 3 \times 10^{-5}$–6×10^{-3}	90	[2] BALEST	95	CLE2	$\Upsilon(1S) \to X^0\overline{X}^0\gamma$, $m_{X^0} < 3.9$ GeV

[1] ABLIKIM 24G search for a muonphilic scalar X_0 or vector X_1 boson in decays of $J/\psi \to \mu^+\mu^-$ + invisible. See their Fig. 3 for limits in the mass coupling plane.

[2] BALEST 95 three-body limit is for phase-space photon energy distribution and angular distribution same as for $\Upsilon \to gg\gamma$.

Search for X^0 Resonance in $H(125)$ Decays

Spin 1 is assumed for X^0. See neutral Higgs search listing for pseudoscalar X^0.

VALUE	DOCUMENT ID		TECN	COMMENT
• • • We do not use the following data for averages, fits, limits, etc. • • •				
	[1] AAD	24BQ	ATLS	$H \to X^0X^0 \to b\overline{b}\tau^+\tau^-$
	[2] HAYRAPETY...	24AA	CMS	$H \to X^0X^0$, $X^0 \to b\overline{b}$
	[3] AAD	22J	ATLS	$X^0 \to \ell^+\ell^-$
	[4] AABOUD	18AP	ATLS	$H \to ZX^0$
	[5] AABOUD	18AP	ATLS	$H \to X^0X^0$

[1] AAD 24BQ search for X^0 production via $H \to X^0X^0 \to b\overline{b}\tau^+\tau^-$ in pp collisions at $\sqrt{s}$ = 13 TeV. See their Fig. 10 for limits on $\sigma \cdot B$.

[2] HAYRAPETYAN 24AA search for X^0 production via $H(125) \to X^0X^0 \to b\overline{b}b\overline{b}$ in pp collisions at $\sqrt{s}$ = 13 TeV. See their Fig. 3 for limits on $\sigma \cdot B$.

[3] AAD 22J search for X^0 production via $H(125) \to X^0X^0/ZX^0 \to 4\ell$ in pp collisions at $\sqrt{s}$ = 13 TeV. $X^0 \to \ell^+\ell^-$ decay is assumed. See their Fig. 13 and Fig. 17 for limits on $\sigma \cdot B$ in $H(125) \to X^0X^0$ and $H(125) \to ZX^0$ channels.

[4] AABOUD 18AP use pp collision data at $\sqrt{s}$ = 13 TeV. $X^0 \to \ell^+\ell^-$ decay is assumed. See their Fig. 9 for limits on $\sigma_{H(125)} \cdot B(ZX^0)$.

[5] AABOUD 18AP use pp collision data at $\sqrt{s}$ = 13 TeV. $X^0 \to \ell^+\ell^-$ decay is assumed. See their Fig. 10 for limits on $\sigma_{H(125)} \cdot B(X^0X^0)$.

REFERENCES FOR Searches for New Heavy Bosons (W', Z', leptoquarks, etc.)

AAD	25AL	EPJ C85 573	G. Aad et al.	(ATLAS Collab.)
AAD	25AX	PR D112 072009	G. Aad et al.	(ATLAS Collab.)
AAD	25AZ	PR D112 092015	G. Aad et al.	(ATLAS Collab.)
AAD	25BA	JHEP 2509 067	G. Aad et al.	(ATLAS Collab.)
AAD	25BB	JHEP 2510 054	G. Aad et al.	(ATLAS Collab.)
AAD	25BN	JHEP 2512 180	G. Aad et al.	(ATLAS Collab.)
AAD	25C	PRL 134 121801	G. Aad et al.	(ATLAS Collab.)
AAD	25F	PL B865 139472	G. Aad et al.	(ATLAS Collab.)
AAD	25N	PR D112 012021	G. Aad et al.	(ATLAS Collab.)
AAD	25Q	JHEP 2501 099	G. Aad et al.	(ATLAS Collab.)
AAD	25V	JHEP 2502 193	G.Aad et al.	(ATLAS Collab.)
CHEKHOVSKY	25J	JHEP 2510 170	V. Chekhovsky et al.	(CMS Collab.)
HAYRAPETY...	25AB	PRL 135 061803	A. Hayrapetyan et al.	(CMS Collab.)
HAYRAPETY...	25AK	PR D112 112011	A. Hayrapetyan et al.	(CMS Collab.)
HAYRAPETY...	25AN	JHEP 2512 052	A. Hayrapetyan et al.	(CMS Collab.)
HAYRAPETY...	25M	PR D111 112004	A. Hayrapetyan et al.	(CMS Collab.)
HAYRAPETY...	25Q	JHEP 2502 089	A. Hayrapetyan et al.	(CMS Collab.)
HAYRAPETY...	25V	JHEP 2504 109	A. Hayrapetyan et al.	(CMS Collab.)
HERBERMANN	25	JCAP 2509 078	T. Herbermann, M. Lindner	(MPIK)
AAD	24AA	JHEP 2402 128	G. Aad et al.	(ATLAS Collab.)
AAD	24AE	JHEP 2404 118	G. Aad et al.	(ATLAS Collab.)
AAD	24AV	EPJ C84 818	G. Aad et al.	(ATLAS Collab.)
AAD	24AY	PR D110 032002	G. Aad et al.	(ATLAS Collab.)
AAD	24BJ	EPJ C84 157	G. Aad et al.	(ATLAS Collab.)
AAD	24BQ	PR D110 052013	G. Aad et al.	(ATLAS Collab.)
AAD	24BR	PR D110 072008	G. Aad et al.	(ATLAS Collab.)
AAD	24CD	JHEP 2411 126	G. Aad et al.	(ATLAS Collab.)
AAD	24CI	EPJ C84 1102	G. Aad et al.	(ATLAS Collab.)
AAD	24CM	JHEP 2409 005	G. Aad et al.	(ATLAS Collab.)
AAD	24O	PL B854 138736	G. Aad et al.	(ATLAS Collab.)
AAD	24T	PR D109 112008	G. Aad et al.	(ATLAS Collab.)
AAD	24W	PR D110 012014	G. Aad et al.	(ATLAS Collab.)
ABLIKIM	24G	PR D109 L031102	M. Ablikim et al.	(BESIII Collab.)
ADACHI	24F	PR D109 112015	I. Adachi et al.	(BELLE II Collab.)
AKITA	24	JHEP 2407 057	K. Akita et al.	(IBSD, CAU)
ALVES	24	PRL 133 161802	G.F.S. Alves et al.	(USP, FNAL, UFABC)
ANDREEV	24	PRL 132 211803	Yu.M. Andreev et al.	(NA64 Collab.)
ANDREEV	24B	JHEP 2407 212	Yu.M. Andreev et al.	(NA64 Collab.)
ANDREEV	24E	PR D110 112015	Yu.M. Andreev et al.	(NA64 Collab.)
BISWAS	24	PR D109 032002	D. Biswas et al.	(BELLE Collab.)
CABARCAS	24	PL B848 138339	J.M. Cabarcas, A. Parada, N. Quinero-Poveda	(USTA+)
HAYRAPETY...	24AA	JHEP 2406 097	A. Hayrapetyan et al.	(CMS Collab.)
HAYRAPETY...	24AV	JHEP 2409 186	A. Hayrapetyan et al.	(CMS Collab.)
HAYRAPETY...	24AZ	JHEP 2412 172	A. Hayrapetyan et al.	(CMS Collab.)
HAYRAPETY...	24C	PRL 132 061801	A. Hayrapetyan et al.	(CMS Collab.)
HAYRAPETY...	24G	PRL 133 011801	A. Hayrapetyan et al.	(CMS Collab.)
HAYRAPETY...	24O	PR D109 112003	A. Hayrapetyan et al.	(CMS Collab.)
HAYRAPETY...	24W	JHEP 2403 134	A. Hayrapetyan et al.	(CMS Collab.)
HAYRAPETY...	24X	JHEP 2405 046	A. Hayrapetyan et al.	(CMS Collab.)
HAYRAPETY...	24Z	JHEP 2405 311	A. Hayrapetyan et al.	(CMS Collab.)
AAD	23AH	EPJ C83 633	G. Aad et al.	(ATLAS Collab.)
AAD	23BF	JHEP 2307 202	G. Aad et al.	(ATLAS Collab.)
AAD	23BJ	JHEP 2306 199	G. Aad et al.	(ATLAS Collab.)
AAD	23BZ	JHEP 2310 001	G. Aad et al.	(ATLAS Collab.)
AAD	23CB	JHEP 2310 082	G. Aad et al.	(ATLAS Collab.)
AAD	23CC	JHEP 2312 073	G. Aad et al.	(ATLAS Collab.)
AAD	23CF	EPJ C83 1075	G. Aad et al.	(ATLAS Collab.)
AAD	23CG	EPJ C83 1164	G. Aad et al.	(ATLAS Collab.)
AAD	23CK	PR D108 052009	G. Aad et al.	(ATLAS Collab.)
AAD	23F	JHEP 2306 188	G. Aad et al.	(ATLAS Collab.)
AAD	23L	JHEP 2306 036	G. Aad et al.	(ATLAS Collab.)
AAD	23O	JHEP 2306 016	G. Aad et al.	(ATLAS Collab.)
AAD	23U	JHEP 2307 125	G. Aad et al.	(ATLAS Collab.)
AAD	23W	JHEP 2307 116	G. Aad et al.	(ATLAS Collab.)
AAD	23X	JHEP 2307 090	G. Aad et al.	(ATLAS Collab.)
ADACHI	23B	PRL 130 231801	I. Adachi et al.	(BELLE II Collab.)
ADACHI	23F	PRL 131 121802	I. Adachi et al.	(BELLE II Collab.)
CALABRESE	23	PR D107 055039	R. Calabrese et al.	(NAPL, NAPLI)
HAYRAPETY...	23D	JHEP 2310 043	A. Hayrapetyan et al.	(CMS Collab.)
HAYRAPETY...	23G	JHEP 2312 070	A. Hayrapetyan et al.	(CMS Collab.)
LI	23I	JCAP 2309 009	S.-P. Li, X.-J. Xu	(BHEP)
MANZARI	23	PR D108 103020	C.A. Manzari et al.	(UCB, LBL, IAC+)
TUMASYAN	23AF	PR D108 012009	A. Tumasyan et al.	(CMS Collab.)
TUMASYAN	23AP	PL B844 137813	A. Tumasyan et al.	(CMS Collab.)
TUMASYAN	23AW	JHEP 2309 051	A. Tumasyan et al.	(CMS Collab.)
TUMASYAN	23BE	JHEP 2311 181	A. Tumasyan et al.	(CMS Collab.)
TUMASYAN	23H	JHEP 2305 227	A. Tumasyan et al.	(CMS Collab.)
TUMASYAN	23S	JHEP 2307 073	A. Tumasyan et al.	(CMS Collab.)
AAD	22	PR D105 012001	G. Aad et al.	(ATLAS Collab.)
AAD	22D	PL B829 137066	G. Aad et al.	(ATLAS Collab.)
AAD	22E	PL B830 137106	G. Aad et al.	(ATLAS Collab.)
AAD	22J	JHEP 2203 041	G. Aad et al.	(ATLAS Collab.)
ANDREEV	22	PR D106 032015	Yu.M. Andreev et al.	(NA64 Collab.)
BONET	22	JHEP 2205 085	H. Bonet et al.	(CONUS Collab.)
COLOMA	22	JHEP 2205 037	P. Coloma et al.	(IFT, OSU, STON, ICREA+)
COLOMA	22A	JHEP 2207 138	P. Coloma et al.	(IFT, CNYIT, ICC, ICREA+)
CZANK	22	PR D106 012003	T. Czank et al.	(BELLE Collab.)
TUMASYAN	22	PRL 129 021802	A. Tumasyan et al.	(CMS Collab.)
TUMASYAN	22AA	JHEP 2206 156	A. Tumasyan et al.	(CMS Collab.)
TUMASYAN	22AC	JHEP 2207 067	A. Tumasyan et al.	(CMS Collab.)
TUMASYAN	22AE	JHEP 2208 063	A. Tumasyan et al.	(CMS Collab.)
TUMASYAN	22AL	JHEP 2209 088	A. Tumasyan et al.	(CMS Collab.)
TUMASYAN	22B	PL B826 136888	A. Tumasyan et al.	(CMS Collab.)
TUMASYAN	22D	PR D105 032008	A. Tumasyan et al.	(CMS Collab.)
TUMASYAN	22H	PR D105 112007	A. Tumasyan et al.	(CMS Collab.)
TUMASYAN	22I	PR D106 012002	A. Tumasyan et al.	(CMS Collab.)
TUMASYAN	22J	PR D106 012004	A. Tumasyan et al.	(CMS Collab.)
TUMASYAN	22P	JHEP 2204 047	A. Tumasyan et al.	(CMS Collab.)
TUMASYAN	22R	JHEP 2204 087	A. Tumasyan et al.	(CMS Collab.)
AAD	21AG	EPJ C81 313	G. Aad et al.	(ATLAS Collab.)
AAD	21AQ	JHEP 2107 005	G. Aad et al.	(ATLAS Collab.)
AAD	21AW	PR D104 112005	G. Aad et al.	(ATLAS Collab.)
AAD	21AZ	JHEP 2110 013	G. Aad et al.	(ATLAS Collab.)
AAD	21BB	JHEP 2111 209	G. Aad et al.	(ATLAS Collab.)
AAD	21D	PRL 126 121802	G. Aad et al.	(ATLAS Collab.)
AAD	21K	JHEP 2102 226	G. Aad et al.	(ATLAS Collab.)

Int. J. Mod. Phys. A 2026.41. Downloaded
by UNIVERSITY OF CALIFORNIA @ BERKELEY on 09/16/26. Re
orldscientific.com
strictly not permitted, except for Open Access articles.

AAD	21S	JHEP 2105 093	G. Aad *et al.*	(ATLAS Collab.)
AAD	21T	JHEP 2106 179	G. Aad *et al.*	(ATLAS Collab.)
BURAS	21	JHEP 2106 068	A.J. Buras *et al.*	(TUM, CERN, ZURI+)
CADEDDU	21	JHEP 2101 116	M. Cadeddu *et al.*	(CAGLI, CAGL, INFN+)
COLARESI	21	PR D104 072003	J. Colaresi *et al.*	(MRION, FNAL, PNL+)
CRIVELLIN	21A	PR D103 115023	A. Crivellin, D. Mueller, L. Schnell	(CERN, ZURI+)
KRIBS	21	PRL 126 011801	G.D. Kribs, D. McKeen, N. Raj	(OREG, TRIU)
SIRUNYAN	21J	PL B819 136446	A.M. Sirunyan *et al.*	(CMS Collab.)
SIRUNYAN	21N	JHEP 2107 208	A.M. Sirunyan *et al.*	(CMS Collab.)
SIRUNYAN	21X	EPJ C81 688	A.M. Sirunyan *et al.*	(CMS Collab.)
SIRUNYAN	21Y	PL B820 136535	A.M. Sirunyan *et al.*	(CMS Collab.)
TUMASYAN	21D	JHEP 2111 153	A. Tumasyan *et al.*	(CMS Collab.)
AAD	20AD	PRL 125 131801	G. Aad *et al.*	(ATLAS Collab.)
AAD	20AF	PRL 125 251802	G. Aad *et al.*	(ATLAS Collab.)
AAD	20AJ	PR D102 112008	G. Aad *et al.*	(ATLAS Collab.)
AAD	20AK	JHEP 2010 112	G. Aad *et al.*	(ATLAS Collab.)
AAD	20AM	JHEP 2010 061	G. Aad *et al.*	(ATLAS Collab.)
AAD	20AT	EPJ C80 1165	G. Aad *et al.*	(ATLAS Collab.)
AAD	20S	EPJ C80 737	G. Aad *et al.*	(ATLAS Collab.)
AAD	20T	JHEP 2003 145	G. Aad *et al.*	(ATLAS Collab.)
AAD	20W	JHEP 2006 151	G. Aad *et al.*	(ATLAS Collab.)
AAIJ	20AL	JHEP 2010 156	R. Aaij *et al.*	(LHCb Collab.)
ADACHI	20	PRL 124 141801	I. Adachi *et al.*	(BELLE II Collab.)
AEBISCHER	20	EPJ C80 252	J. Aebischer *et al.*	(TUM, LAPTH, UCSC)
DEPPISCH	20	JHEP 2012 186	F.F. Deppisch, K. Fridell, J. Harz	(LOUC, TUM)
SIRUNYAN	20A	EPJ C80 3	A.M. Sirunyan *et al.*	(CMS Collab.)
SIRUNYAN	20AI	JHEP 2005 033	A.M. Sirunyan *et al.*	(CMS Collab.)
SIRUNYAN	20AQ	PRL 124 131802	A.M. Sirunyan *et al.*	(CMS Collab.)
SIRUNYAN	20M	PL B805 135448	A.M. Sirunyan *et al.*	(CMS Collab.)
SIRUNYAN	20Q	EPJ C80 237	A.M. Sirunyan *et al.*	(CMS Collab.)
AABOUD	19AJ	PL B795 56	M. Aaboud *et al.*	(ATLAS Collab.)
AABOUD	19AS	PR D99 092004	M. Aaboud *et al.*	(ATLAS Collab.)
AABOUD	19AX	EPJ C79 733	M. Aaboud *et al.*	(ATLAS Collab.)
AABOUD	19B	JHEP 1901 016	M. Aaboud *et al.*	(ATLAS Collab.)
AABOUD	19BB	PL B798 134942	M. Aaboud *et al.*	(ATLAS Collab.)
AABOUD	19D	PL B788 316	M. Aaboud *et al.*	(ATLAS Collab.)
AABOUD	19E	PL B788 347	M. Aaboud *et al.*	(ATLAS Collab.)
AABOUD	19V	JHEP 1905 142	M. Aaboud *et al.*	(ATLAS Collab.)
AABOUD	19X	JHEP 1906 144	M. Aaboud *et al.*	(ATLAS Collab.)
AAD	19C	PR D100 052013	G. Aad *et al.*	(ATLAS Collab.)
AAD	19D	JHEP 1909 091	G. Aad *et al.*	(ATLAS Collab.)
Also		JHEP 2006 042 (errat.)	G. Aad *et al.*	(ATLAS Collab.)
AAD	19L	PL B796 68	G. Aad *et al.*	(ATLAS Collab.)
ABRAMOWICZ	19	PR D99 092006	H. Abramowicz *et al.*	(ZEUS Collab.)
LONG	19	NP B943 114629	H.N. Long *et al.*	
MANDAL	19	JHEP 1912 089	R. Mandal, A. Pich	(VALE, SIEG)
PANDEY	19	JHEP 1911 046	S. Pandey, S. Karmakar, S. Rakshit	(IITI)
RAINBOLT	19	PR D99 013004	J.L. Rainbolt, M. Schmitt	(NWES)
SIRUNYAN	19AA	JHEP 1904 031	A.M. Sirunyan *et al.*	(CMS Collab.)
SIRUNYAN	19AL	EPJ C79 208	A.M. Sirunyan *et al.*	(CMS Collab.)
SIRUNYAN	19AN	EPJ C79 280	A.M. Sirunyan *et al.*	(CMS Collab.)
SIRUNYAN	19AY	PL B792 107	A.M. Sirunyan *et al.*	(CMS Collab.)
SIRUNYAN	19AZ	PL B792 345	A.M. Sirunyan *et al.*	(CMS Collab.)
SIRUNYAN	19BC	PL B795 76	A.M. Sirunyan *et al.*	(CMS Collab.)
SIRUNYAN	19BI	PR D99 032014	A.M. Sirunyan *et al.*	(CMS Collab.)
SIRUNYAN	19BJ	PR D99 052002	A.M. Sirunyan *et al.*	(CMS Collab.)
SIRUNYAN	19CB	PR D100 112007	A.M. Sirunyan *et al.*	(CMS Collab.)
SIRUNYAN	19CD	PRL 123 231803	A.M. Sirunyan *et al.*	(CMS Collab.)
SIRUNYAN	19CP	PL B798 134952	A.M. Sirunyan *et al.*	(CMS Collab.)
SIRUNYAN	19D	PRL 122 081804	A.M. Sirunyan *et al.*	(CMS Collab.)
SIRUNYAN	19I	JHEP 1901 051	A.M. Sirunyan *et al.*	(CMS Collab.)
SIRUNYAN	19V	JHEP 1903 127	A.M. Sirunyan *et al.*	(CMS Collab.)
SIRUNYAN	19Y	JHEP 1903 170	A.M. Sirunyan *et al.*	(CMS Collab.)
AABOUD	18AA	PR D98 032015	M. Aaboud *et al.*	(ATLAS Collab.)
AABOUD	18AB	PR D98 032016	M. Aaboud *et al.*	(ATLAS Collab.)
AABOUD	18AD	PL B779 24	M. Aaboud *et al.*	(ATLAS Collab.)
AABOUD	18AF	PL B781 327	M. Aaboud *et al.*	(ATLAS Collab.)
AABOUD	18AI	JHEP 1803 174	M. Aaboud *et al.*	(ATLAS Collab.)
Also		JHEP 1811 051 (errat.)	M. Aaboud *et al.*	(ATLAS Collab.)
AABOUD	18AK	JHEP 1803 042	M. Aaboud *et al.*	(ATLAS Collab.)
AABOUD	18AL	JHEP 1803 009	M. Aaboud *et al.*	(ATLAS Collab.)
AABOUD	18AP	JHEP 1806 166	M. Aaboud *et al.*	(ATLAS Collab.)
AABOUD	18B	EPJ C78 24	M. Aaboud *et al.*	(ATLAS Collab.)
AABOUD	18BG	EPJ C78 401	M. Aaboud *et al.*	(ATLAS Collab.)
AABOUD	18BI	EPJ C78 565	M. Aaboud *et al.*	(ATLAS Collab.)
AABOUD	18CH	PL B787 68	M. Aaboud *et al.*	(ATLAS Collab.)
AABOUD	18CJ	PR D98 052008	M. Aaboud *et al.*	(ATLAS Collab.)
AABOUD	18CM	PR D98 092008	M. Aaboud *et al.*	(ATLAS Collab.)
AABOUD	18F	PL B777 91	M. Aaboud *et al.*	(ATLAS Collab.)
AABOUD	18G	JHEP 1801 055	M. Aaboud *et al.*	(ATLAS Collab.)
AABOUD	18K	PRL 120 161802	M. Aaboud *et al.*	(ATLAS Collab.)
AABOUD	18N	PRL 121 081801	M. Aaboud *et al.*	(ATLAS Collab.)
AAIJ	18AQ	JHEP 1809 147	R. Aaij *et al.*	(LHCb Collab.)
BOBOVNIKOV	18	PR D98 095029	I.D. Bobovnikov, P. Osland, A.A. Pankov	(BERG+)
SIRUNYAN	18	PL B777 39	A.M. Sirunyan *et al.*	(CMS Collab.)
SIRUNYAN	18AT	JHEP 1804 073	A.M. Sirunyan *et al.*	(CMS Collab.)
SIRUNYAN	18AX	JHEP 1805 088	A.M. Sirunyan *et al.*	(CMS Collab.)
SIRUNYAN	18AZ	JHEP 1806 128	A.M. Sirunyan *et al.*	(CMS Collab.)
SIRUNYAN	18BB	JHEP 1806 120	A.M. Sirunyan *et al.*	(CMS Collab.)
SIRUNYAN	18BJ	JHEP 1807 115	A.M. Sirunyan *et al.*	(CMS Collab.)
SIRUNYAN	18BK	JHEP 1807 075	A.M. Sirunyan *et al.*	(CMS Collab.)
SIRUNYAN	18BO	JHEP 1808 130	A.M. Sirunyan *et al.*	(CMS Collab.)
SIRUNYAN	18CV	JHEP 1805 148	A.M. Sirunyan *et al.*	(CMS Collab.)
SIRUNYAN	18CZ	EPJ C78 707	A.M. Sirunyan *et al.*	(CMS Collab.)
SIRUNYAN	18DJ	JHEP 1809 101	A.M. Sirunyan *et al.*	(CMS Collab.)
SIRUNYAN	18DR	JHEP 1811 161	A.M. Sirunyan *et al.*	(CMS Collab.)
SIRUNYAN	18EC	PRL 121 241802	A.M. Sirunyan *et al.*	(CMS Collab.)
SIRUNYAN	18ED	JHEP 1811 172	A.M. Sirunyan *et al.*	(CMS Collab.)
SIRUNYAN	18G	JHEP 1801 097	A.M. Sirunyan *et al.*	(CMS Collab.)
SIRUNYAN	18I	PRL 120 201801	A.M. Sirunyan *et al.*	(CMS Collab.)
SIRUNYAN	18P	PR D97 072006	A.M. Sirunyan *et al.*	(CMS Collab.)
SIRUNYAN	18U	PR D98 032005	A.M. Sirunyan *et al.*	(CMS Collab.)
ZHANG	18A	EPJ C78 695	J. Zhang, C.-X. Yue, C.-H. Li	(LNUDA)
AABOUD	17AK	PR D96 052004	M. Aaboud *et al.*	(ATLAS Collab.)
AABOUD	17AO	PL B774 494	M. Aaboud *et al.*	(ATLAS Collab.)
AABOUD	17AT	JHEP 1710 182	M. Aaboud *et al.*	(ATLAS Collab.)
AABOUD	17B	PL B765 32	M. Aaboud *et al.*	(ATLAS Collab.)
KHACHATRY...	17AX	PL B773 563	V. Khachatryan *et al.*	(CMS Collab.)
KHACHATRY...	17H	JHEP 1702 048	V. Khachatryan *et al.*	(CMS Collab.)
KHACHATRY...	17J	JHEP 1703 077	V. Khachatryan *et al.*	(CMS Collab.)
KHACHATRY...	17T	PL B768 57	V. Khachatryan *et al.*	(CMS Collab.)
KHACHATRY...	17U	PL B768 137	V. Khachatryan *et al.*	(CMS Collab.)
KHACHATRY...	17W	PL B769 520	V. Khachatryan *et al.*	(CMS Collab.)
KHACHATRY...	17Y	PL B770 257	V. Khachatryan *et al.*	(CMS Collab.)
KHACHATRY...	17Z	PL B770 278	V. Khachatryan *et al.*	(CMS Collab.)
SIRUNYAN	17A	JHEP 1703 162	A.M. Sirunyan *et al.*	(CMS Collab.)
SIRUNYAN	17AK	PL B774 533	A.M. Sirunyan *et al.*	(CMS Collab.)
SIRUNYAN	17AP	JHEP 1710 180	A.M. Sirunyan *et al.*	(CMS Collab.)
SIRUNYAN	17H	JHEP 1707 121	A.M. Sirunyan *et al.*	(CMS Collab.)
SIRUNYAN	17I	JHEP 1708 029	A.M. Sirunyan *et al.*	(CMS Collab.)
SIRUNYAN	17Q	JHEP 1707 001	A.M. Sirunyan *et al.*	(CMS Collab.)
SIRUNYAN	17R	EPJ C77 636	A.M. Sirunyan *et al.*	(CMS Collab.)
SIRUNYAN	17T	PRL 119 111802	A.M. Sirunyan *et al.*	(CMS Collab.)
SIRUNYAN	17V	JHEP 1709 053	A.M. Sirunyan *et al.*	(CMS Collab.)
AABOUD	16	PL B759 229	M. Aaboud *et al.*	(ATLAS Collab.)
AABOUD	16AA	EPJ C76 585	M. Aaboud *et al.*	(ATLAS Collab.)
AABOUD	16AE	JHEP 1609 173	M. Aaboud *et al.*	(ATLAS Collab.)
AABOUD	16P	EPJ C76 541	M. Aaboud *et al.*	(ATLAS Collab.)
AABOUD	16U	PL B761 372	M. Aaboud *et al.*	(ATLAS Collab.)
AABOUD	16V	PL B762 334	M. Aaboud *et al.*	(ATLAS Collab.)
AAD	16G	EPJ C76 5	G. Aad *et al.*	(ATLAS Collab.)
AAD	16L	EPJ C76 210	G. Aad *et al.*	(ATLAS Collab.)
AAD	16R	PL B755 285	G. Aad *et al.*	(ATLAS Collab.)
AAD	16S	PL B754 302	G. Aad *et al.*	(ATLAS Collab.)
AAD	16W	PL B758 249	G. Aad *et al.*	(ATLAS Collab.)
BARRANCO	16	JP G43 115004	J. Barranco *et al.*	
DEY	16	JHEP 1604 187	U.K. Dey, S. Mohanty	
KHACHATRY...	16AF	PR D93 032004	V. Khachatryan *et al.*	(CMS Collab.)
KHACHATRY...	16AG	PR D93 032005	V. Khachatryan *et al.*	(CMS Collab.)
Also		PR D95 039906 (errat.)	V. Khachatryan *et al.*	(CMS Collab.)
KHACHATRY...	16AO	JHEP 1602 122	V. Khachatryan *et al.*	(CMS Collab.)
KHACHATRY...	16AP	JHEP 1602 145	V. Khachatryan *et al.*	(CMS Collab.)
KHACHATRY...	16BD	EPJ C76 237	V. Khachatryan *et al.*	(CMS Collab.)
KHACHATRY...	16BE	EPJ C76 317	V. Khachatryan *et al.*	(CMS Collab.)
KHACHATRY...	16E	PR D93 012001	V. Khachatryan *et al.*	(CMS Collab.)
KHACHATRY...	16K	PRL 116 071801	V. Khachatryan *et al.*	(CMS Collab.)
KHACHATRY...	16L	PRL 117 031802	V. Khachatryan *et al.*	(CMS Collab.)
KHACHATRY...	16O	PL B755 196	V. Khachatryan *et al.*	(CMS Collab.)
KUMAR	16	PR D94 014022	G. Kumar	
AAD	15AM	JHEP 1507 157	G. Aad *et al.*	(ATLAS Collab.)
AAD	15AO	JHEP 1508 148	G. Aad *et al.*	(ATLAS Collab.)
AAD	15AT	EPJ C75 79	G. Aad *et al.*	(ATLAS Collab.)
AAD	15AU	EPJ C75 69	G. Aad *et al.*	(ATLAS Collab.)
AAD	15AV	EPJ C75 165	G. Aad *et al.*	(ATLAS Collab.)
AAD	15AZ	EPJ C75 209	G. Aad *et al.*	(ATLAS Collab.)
Also		EPJ C75 370 (errat.)	G. Aad *et al.*	(ATLAS Collab.)
AAD	15BB	EPJ C75 263	G. Aad *et al.*	(ATLAS Collab.)
AAD	15CD	PR D92 092001	G. Aad *et al.*	(ATLAS Collab.)
AAD	15CP	JHEP 1512 055	G. Aad *et al.*	(ATLAS Collab.)
AAD	15O	PRL 115 031801	G. Aad *et al.*	(ATLAS Collab.)
AAD	15R	PL B743 235	G. Aad *et al.*	(ATLAS Collab.)
AAD	15V	PR D91 052007	G. Aad *et al.*	(ATLAS Collab.)
AALTONEN	15C	PRL 115 061801	T. Aaltonen *et al.*	(CDF Collab.)
BESSAA	15	EPJ C75 97	A. Bessaa, S. Davidson	
KHACHATRY...	15AE	JHEP 1504 025	V. Khachatryan *et al.*	(CMS Collab.)
KHACHATRY...	15AJ	JHEP 1507 042	V. Khachatryan *et al.*	(CMS Collab.)
KHACHATRY...	15AV	JHEP 1509 201	V. Khachatryan *et al.*	(CMS Collab.)
KHACHATRY...	15C	PL B740 83	V. Khachatryan *et al.*	(CMS Collab.)
KHACHATRY...	15F	PRL 114 101801	V. Khachatryan *et al.*	(CMS Collab.)
KHACHATRY...	15O	PL B748 255	V. Khachatryan *et al.*	(CMS Collab.)
KHACHATRY...	15T	PR D91 092005	V. Khachatryan *et al.*	(CMS Collab.)
KHACHATRY...	15V	PR D91 052009	V. Khachatryan *et al.*	(CMS Collab.)
SAHOO	15A	PR D91 094019	S. Sahoo, R. Mohanta	
AAD	14AI	JHEP 1409 037	G. Aad *et al.*	(ATLAS Collab.)
AAD	14AT	PL B738 428	G. Aad *et al.*	(ATLAS Collab.)
AAD	14S	PL B737 223	G. Aad *et al.*	(ATLAS Collab.)
AAD	14V	PR D90 052005	G. Aad *et al.*	(ATLAS Collab.)
KHACHATRY...	14	JHEP 1408 173	V. Khachatryan *et al.*	(CMS Collab.)
KHACHATRY...	14A	JHEP 1408 174	V. Khachatryan *et al.*	(CMS Collab.)
KHACHATRY...	14O	EPJ C74 3149	V. Khachatryan *et al.*	(CMS Collab.)
KHACHATRY...	14T	PL B739 229	V. Khachatryan *et al.*	(CMS Collab.)
MARTINEZ	14	PR D90 015028	R. Martinez, F. Ochoa	
PRIEELS	14	PR D90 112003	R. Prieels *et al.*	(LOUV, ETH, PSI+)
AAD	13AE	JHEP 1306 033	G. Aad *et al.*	(ATLAS Collab.)
AAD	13AO	PR D87 112006	G. Aad *et al.*	(ATLAS Collab.)
AAD	13AQ	PR D88 012004	G. Aad *et al.*	(ATLAS Collab.)
AAD	13D	JHEP 1301 029	G. Aad *et al.*	(ATLAS Collab.)
AAD	13G	JHEP 1301 116	G. Aad *et al.*	(ATLAS Collab.)
AAD	13K	EPJ C73 2263	G. Aad *et al.*	(ATLAS Collab.)
AAD	13S	PL B719 242	G. Aad *et al.*	(ATLAS Collab.)
AALTONEN	13A	PRL 110 121802	T. Aaltonen *et al.*	(CDF Collab.)
AALTONEN	13AA	PR D88 092004	T. Aaltonen *et al.*	(CDF Collab.)
AALTONEN	13R	PRL 111 031802	T. Aaltonen *et al.*	(CDF Collab.)
CHATRCHYAN	13A	JHEP 1301 013	S. Chatrchyan *et al.*	(CMS Collab.)
CHATRCHYAN	13AF	PL B720 63	S. Chatrchyan *et al.*	(CMS Collab.)
CHATRCHYAN	13AJ	PL B723 280	S. Chatrchyan *et al.*	(CMS Collab.)
CHATRCHYAN	13AP	PR D87 072002	S. Chatrchyan *et al.*	(CMS Collab.)
CHATRCHYAN	13AQ	PR D87 072005	S. Chatrchyan *et al.*	(CMS Collab.)
CHATRCHYAN	13AS	PR D87 114015	S. Chatrchyan *et al.*	(CMS Collab.)
CHATRCHYAN	13AU	PRL 110 141802	S. Chatrchyan *et al.*	(CMS Collab.)
CHATRCHYAN	13BM	PRL 111 211804	S. Chatrchyan *et al.*	(CMS Collab.)
Also		PRL 112 119903 (errat.)	S. Chatrchyan *et al.*	(CMS Collab.)
CHATRCHYAN	13E	PL B718 1229	S. Chatrchyan *et al.*	(CMS Collab.)
CHATRCHYAN	13M	PRL 110 081801	S. Chatrchyan *et al.*	(CMS Collab.)
CHATRCHYAN	13U	JHEP 1302 036	S. Chatrchyan *et al.*	(CMS Collab.)
SAKAKI	13	PR D88 094012	Y. Sakaki *et al.*	
AAD	12AV	PRL 109 081801	G. Aad *et al.*	(ATLAS Collab.)
AAD	12BB	PR D85 112012	G. Aad *et al.*	(ATLAS Collab.)
AAD	12BV	JHEP 1209 041	G. Aad *et al.*	(ATLAS Collab.)
AAD	12CC	JHEP 1211 138	G. Aad *et al.*	(ATLAS Collab.)
AAD	12CK	PR D86 091103	G. Aad *et al.*	(ATLAS Collab.)
AAD	12CR	EPJ C72 2241	G. Aad *et al.*	(ATLAS Collab.)
AAD	12H	PL B709 158	G. Aad *et al.*	(ATLAS Collab.)
Also		PL B711 442 (errat.)	G. Aad *et al.*	(ATLAS Collab.)
AAD	12K	EPJ C72 2083	G. Aad *et al.*	(ATLAS Collab.)
AAD	12M	EPJ C72 2056	G. Aad *et al.*	(ATLAS Collab.)
AAD	12O	EPJ C72 2151	G. Aad *et al.*	(ATLAS Collab.)
AALTONEN	12AR	PR D86 112002	T. Aaltonen *et al.*	(CDF Collab.)
AALTONEN	12N	PRL 108 211805	T. Aaltonen *et al.*	(CDF Collab.)
ABAZOV	12R	PR D85 051101	V.M. Abazov *et al.*	(D0 Collab.)
ABRAMOWICZ	12A	PR D86 012005	H. Abramowicz *et al.*	(ZEUS Collab.)
CHATRCHYAN	12AF	PRL 109 141801	S. Chatrchyan *et al.*	(CMS Collab.)
CHATRCHYAN	12AG	PR D86 052013	S. Chatrchyan *et al.*	(CMS Collab.)
CHATRCHYAN	12AI	JHEP 1208 110	S. Chatrchyan *et al.*	(CMS Collab.)
CHATRCHYAN	12AQ	JHEP 1209 029	S. Chatrchyan *et al.*	(CMS Collab.)
Also		JHEP 1403 132 (errat.)	S. Chatrchyan *et al.*	(CMS Collab.)
CHATRCHYAN	12AR	PL B717 351	S. Chatrchyan *et al.*	(CMS Collab.)
CHATRCHYAN	12BG	PRL 109 261802	S. Chatrchyan *et al.*	(CMS Collab.)
CHATRCHYAN	12BL	JHEP 1212 015	S. Chatrchyan *et al.*	(CMS Collab.)
CHATRCHYAN	12BO	JHEP 1212 055	S. Chatrchyan *et al.*	(CMS Collab.)
CHATRCHYAN	12BR	PRL 109 251801	S. Chatrchyan *et al.*	(CMS Collab.)
CHATRCHYAN	12M	PL B714 158	S. Chatrchyan *et al.*	(CMS Collab.)
CHATRCHYAN	12O	PL B716 82	S. Chatrchyan *et al.*	(CMS Collab.)
KOSNIK	12	PR D86 055004	N. Kosnik	(LALO, STFN)
AAD	11D	PR D83 112006	G. Aad *et al.*	(ATLAS Collab.)
AAD	11H	PRL 106 251801	G. Aad *et al.*	(ATLAS Collab.)
AAD	11Z	EPJ C71 1809	G. Aad *et al.*	(ATLAS Collab.)
AALTONEN	11AD	PR D84 072003	T. Aaltonen *et al.*	(CDF Collab.)
AALTONEN	11AE	PR D84 072004	T. Aaltonen *et al.*	(CDF Collab.)
AALTONEN	11C	PR D83 031102	T. Aaltonen *et al.*	(CDF Collab.)
AALTONEN	11I	PRL 106 121801	T. Aaltonen *et al.*	(CDF Collab.)
AARON	11A	PL B701 20	F. D. Aaron *et al.*	(H1 Collab.)
AARON	11B	PL B704 388	F. D. Aaron *et al.*	(H1 Collab.)
AARON	11C	PL B705 52	F. D. Aaron *et al.*	(H1 Collab.)

Int. J. Mod. Phys. A 2026.41. Downloaded from www.worldscientific.com
by UNIVERSITY OF CALIFORNIA @ BERKELEY on 09/16/26. Re-use and distribution is strictly not permitted, except for Open Access articles.

ABAZOV	11A	PL B695 88	V.M. Abazov *et al.*	(D0 Collab.)
ABAZOV	11H	PRL 107 011801	V.M. Abazov *et al.*	(D0 Collab.)
ABAZOV	11I	PRL 107 011804	V.M. Abazov *et al.*	(D0 Collab.)
ABAZOV	11L	PL B699 145	V.M. Abazov *et al.*	(D0 Collab.)
ABAZOV	11V	PR D84 071104	V.M. Abazov *et al.*	(D0 Collab.)
BUENO	11	PR D84 032005	J.F. Bueno *et al.*	(TWIST Collab.)
Also		PR D85 039908 (errat.)	J.F. Bueno *et al.*	(TWIST Collab.)
CHATRCHYAN	11N	PL B703 246	S. Chatrchyan *et al.*	(CMS Collab.)
CHATRCHYAN	11O	JHEP 1108 005	S. Chatrchyan *et al.*	(CMS Collab.)
CHATRCHYAN	11Y	PL B704 123	S. Chatrchyan *et al.*	(CMS Collab.)
DORSNER	11	JHEP 1111 002	I. Dorsner *et al.*	
KHACHATRY...	11D	PRL 106 201802	V. Khachatryan *et al.*	(CMS Collab.)
KHACHATRY...	11E	PRL 106 201803	V. Khachatryan *et al.*	(CMS Collab.)
AALTONEN	10L	PL B691 183	T. Aaltonen *et al.*	(CDF Collab.)
AALTONEN	10N	PRL 104 241801	T. Aaltonen *et al.*	(CDF Collab.)
ABAZOV	10L	PL B693 95	V.M. Abazov *et al.*	(D0 Collab.)
DEL-AGUILA	10	JHEP 1009 033	F. del Aguila, J. de Blas, M. Perez-Victoria	(GRAN)
KHACHATRY...	10	PRL 105 211801	V. Khachatryan *et al.*	(CMS Collab.)
Also		PRL 106 029902	V. Khachatryan *et al.*	(CMS Collab.)
WAUTERS	10	PR C82 055502	F. Wauters *et al.*	(REZ, TAMU)
AALTONEN	09AC	PR D79 112002	T. Aaltonen *et al.*	(CDF Collab.)
AALTONEN	09T	PRL 102 031801	T. Aaltonen *et al.*	(CDF Collab.)
AALTONEN	09V	PRL 102 091805	T. Aaltonen *et al.*	(CDF Collab.)
ABAZOV	09	PL B671 224	V.M. Abazov *et al.*	(D0 Collab.)
ABAZOV	09AF	PL B681 224	V.M. Abazov *et al.*	(D0 Collab.)
ERLER	09	JHEP 0908 017	J. Erler *et al.*	
AALTONEN	08D	PR D77 051102	T. Aaltonen *et al.*	(CDF Collab.)
AALTONEN	08P	PR D77 091105	T. Aaltonen *et al.*	(CDF Collab.)
AALTONEN	08Y	PRL 100 231801	T. Aaltonen *et al.*	(CDF Collab.)
AALTONEN	08Z	PRL 101 071802	T. Aaltonen *et al.*	(CDF Collab.)
ABAZOV	08AA	PL B668 98	V.M. Abazov *et al.*	(D0 Collab.)
ABAZOV	08AD	PL B668 357	V.M. Abazov *et al.*	(D0 Collab.)
ABAZOV	08AN	PRL 101 241802	V.M. Abazov *et al.*	(D0 Collab.)
ABAZOV	08C	PRL 100 031804	V.M. Abazov *et al.*	(D0 Collab.)
MACDONALD	08	PR D78 032010	R.P. MacDonald *et al.*	(TWIST Collab.)
ZHANG	08	NP B802 247	Y. Zhang *et al.*	(PKGU, UMD)
AALTONEN	07H	PRL 99 171802	T. Aaltonen *et al.*	(CDF Collab.)
ABAZOV	07E	PL B647 74	V.M. Abazov *et al.*	(D0 Collab.)
ABAZOV	07J	PRL 99 061801	V.M. Abazov *et al.*	(D0 Collab.)
AKTAS	07A	EPJ C52 833	A. Aktas *et al.*	(H1 Collab.)
CHOUDHURY	07	PL B657 69	D. Choudhury *et al.*	
MELCONIAN	07	PL B649 370	D. Melconian *et al.*	(TRIUMF)
SCHAEL	07A	EPJ C49 411	S. Schael *et al.*	(ALEPH Collab.)
SCHUMANN	07	PRL 99 191803	M. Schumann *et al.*	(HEID, ILLG, KARL+)
SMIRNOV	07	MPL A22 2353	A.D. Smirnov	
ABAZOV	06A	PL B636 183	V.M. Abazov *et al.*	(D0 Collab.)
ABAZOV	06L	PL B640 230	V.M. Abazov *et al.*	(D0 Collab.)
ABDALLAH	06C	EPJ C45 589	J. Abdallah *et al.*	(DELPHI Collab.)
ABULENCIA	06L	PRL 96 211801	A. Abulencia *et al.*	(CDF Collab.)
ABULENCIA	06M	PRL 96 211802	A. Abulencia *et al.*	(CDF Collab.)
ABULENCIA	06T	PR D73 051102	A. Abulencia *et al.*	(CDF Collab.)
ABAZOV	05H	PR D71 071104	V.M. Abazov *et al.*	(D0 Collab.)
ABULENCIA	05A	PRL 95 252001	A. Abulencia *et al.*	(CDF Collab.)
ACOSTA	05I	PR D71 112001	D. Acosta *et al.*	(CDF Collab.)
ACOSTA	05P	PR D72 051107	D. Acosta *et al.*	(CDF Collab.)
ACOSTA	05R	PRL 95 131801	D. Acosta *et al.*	(CDF Collab.)
AKTAS	05B	PL B629 9	A. Aktas *et al.*	(H1 Collab.)
CHEKANOV	05	PL B610 212	S. Chekanov *et al.*	(HERA ZEUS Collab.)
CHEKANOV	05A	EPJ C44 463	S. Chekanov *et al.*	(ZEUS Collab.)
CYBURT	05	ASP 23 313	R.H. Cyburt *et al.*	
ABAZOV	04A	PRL 92 221801	V.M. Abazov *et al.*	(D0 Collab.)
ABAZOV	04C	PR D69 111101	V.M. Abazov *et al.*	(D0 Collab.)
ABBIENDI	04G	EPJ C33 173	G. Abbiendi *et al.*	(OPAL Collab.)
ABBIENDI	03D	EPJ C26 331	G. Abbiendi *et al.*	(OPAL Collab.)
ABBIENDI	03R	EPJ C31 281	G. Abbiendi *et al.*	(OPAL)
ACOSTA	03B	PRL 90 081802	D. Acosta *et al.*	(CDF Collab.)
ADLOFF	03	PL B568 35	C. Adloff *et al.*	(H1 Collab.)
BARGER	03B	PR D67 075009	V. Barger, P. Langacker, H. Lee	
CHANG	03	PR D68 111101	M.-C. Chang *et al.*	(BELLE Collab.)
CHEKANOV	03B	PR D68 052004	S. Chekanov *et al.*	(ZEUS Collab.)
ABAZOV	02	PRL 88 191801	V.M. Abazov *et al.*	(D0 Collab.)
ABBIENDI	02B	PL B526 233	G. Abbiendi *et al.*	(OPAL Collab.)
AFFOLDER	02C	PRL 88 071806	T. Affolder *et al.*	(CDF Collab.)
CHEKANOV	02	PR D65 092004	S. Chekanov *et al.*	(ZEUS Collab.)
CHEKANOV	02B	PL B531 9	S. Chekanov *et al.*	(ZEUS Collab.)
MUECK	02	PR D65 085037	A. Mueck, A. Pilaftsis, R. Rueckl	
ABAZOV	01B	PRL 87 061802	V.M. Abazov *et al.*	(D0 Collab.)
ABAZOV	01D	PR D64 092004	V.M. Abazov *et al.*	(D0 Collab.)
ADLOFF	01C	PL B523 234	C. Adloff *et al.*	(H1 Collab.)
AFFOLDER	01I	PRL 87 231803	T. Affolder *et al.*	(CDF Collab.)
BREITWEG	01	PR D63 052002	J. Breitweg *et al.*	(ZEUS Collab.)
CHEUNG	01B	PL B517 167	K. Cheung	
THOMAS	01	NP A694 559	E. Thomas *et al.*	
ABBIENDI	00M	EPJ C13 15	G. Abbiendi *et al.*	(OPAL Collab.)
ABBOTT	00C	PRL 84 2088	B. Abbott *et al.*	(D0 Collab.)
ABE	00	PRL 84 5716	F. Abe *et al.*	(CDF Collab.)
ABREU	00S	PL B485 45	P. Abreu *et al.*	(DELPHI Collab.)
ABREU	00Z	EPJ C17 53	P. Abreu *et al.*	(DELPHI Collab.)
ACCIARRI	00P	PL B489 81	M. Acciarri *et al.*	(L3 Collab.)
ADLOFF	00	PL B479 358	C. Adloff *et al.*	(H1 Collab.)
AFFOLDER	00K	PRL 85 2056	T. Affolder *et al.*	(CDF Collab.)
BARATE	00I	EPJ C12 183	R. Barate *et al.*	(ALEPH Collab.)
BARGER	00	PL B480 149	V. Barger, K. Cheung	
BREITWEG	00E	EPJ C16 253	J. Breitweg *et al.*	(ZEUS Collab.)
CHAY	00	PR D61 035002	J. Chay, K.Y. Lee, S. Nam	
CHO	00	MPL A15 311	G. Cho	
CORNET	00	PR D61 037701	F. Cornet, M. Relano, J. Rico	
DELGADO	00	JHEP 0001 030	A. Delgado, A. Pomarol, M. Quiros	
ERLER	00	PRL 84 212	J. Erler, P. Langacker	
GABRIELLI	00	PR D62 055009	E. Gabrielli	
RIZZO	00	PR D61 016007	T.G. Rizzo, J.D. Wells	
ROSNER	00	PR D61 016006	J.L. Rosner	
ZARNECKI	00	EPJ C17 695	A. Zarnecki	
ABBIENDI	99	EPJ C6 1	G. Abbiendi *et al.*	(OPAL Collab.)
ABBOTT	99J	PRL 83 2896	B. Abbott *et al.*	(D0 Collab.)
ABREU	99G	PL B446 62	P. Abreu *et al.*	(DELPHI Collab.)
ACKERSTAFF	99D	EPJ C8 3	K. Ackerstaff *et al.*	(OPAL Collab.)
ADLOFF	99	EPJ C11 447	C. Adloff *et al.*	(H1 Collab.)
Also		EPJ C14 553 (errat.)	C. Adloff *et al.*	(H1 Collab.)
CASALBUONI	99	PL B460 135	R. Casalbuoni *et al.*	
CZAKON	99	PL B458 355	M. Czakon, J. Gluza, M. Zralek	
ERLER	99	PL B456 68	J. Erler, P. Langacker	
MARCIANO	99	PR D60 093006	W. Marciano	
MASIP	99	PR D60 096005	M. Masip, A. Pomarol	
NATH	99	PR D60 116004	P. Nath, M. Yamaguchi	
STRUMIA	99	PL B466 107	A. Strumia	
ABBOTT	98E	PRL 80 2051	B. Abbott *et al.*	(D0 Collab.)
ABBOTT	98J	PRL 81 38	B. Abbott *et al.*	(D0 Collab.)
ABE	98S	PRL 81 4806	F. Abe *et al.*	(CDF Collab.)
ABE	98V	PRL 81 5742	F. Abe *et al.*	(CDF Collab.)
ACCIARRI	98J	PL B433 163	M. Acciarri *et al.*	(L3 Collab.)
ACKERSTAFF	98V	EPJ C2 441	K. Ackerstaff *et al.*	(OPAL Collab.)
BARATE	98U	EPJ C4 571	R. Barate *et al.*	(ALEPH Collab.)
BARENBOIM	98	EPJ C1 369	G. Barenboim	
CHO	98	EPJ C5 155	G. Cho, K. Hagiwara, S. Matsumoto	
CONRAD	98	RMP 70 1341	J.M. Conrad, M.H. Shaevitz, T. Bolton	
DONCHESKI	98	PR D58 097702	M.A. Doncheski, R.W. Robinett	
GROSS-PILCH...	98	hep-ex/9810015	C. Grosso-Pilcher, G. Landsberg, M. Paterno	
ABE	97F	PRL 78 2906	F. Abe *et al.*	(CDF Collab.)
ABE	97G	PR D55 5263	F. Abe *et al.*	(CDF Collab.)
ABE	97S	PRL 79 2192	F. Abe *et al.*	(CDF Collab.)
ABE	97W	PRL 79 3819	F. Abe *et al.*	(CDF Collab.)
ABE	97X	PRL 79 4327	F. Abe *et al.*	(CDF Collab.)
ACCIARRI	97Q	PL B412 201	M. Acciarri *et al.*	(L3 Collab.)
ARIMA	97	PR D55 19	T. Arima *et al.*	(VENUS Collab.)
BARENBOIM	97	PR D55 4213	G. Barenboim *et al.*	(VALE, IFIC)
DEANDREA	97	PL B409 277	A. Deandrea	(MARS)
DERRICK	97	ZPHY C73 613	M. Derrick *et al.*	(ZEUS Collab.)
GROSSMAN	97	PR D55 2768	Y. Grossman, Z. Ligeti, E. Nardi	(REHO, CIT)
JADACH	97	PL B408 281	S. Jadach, B.F.L. Ward, Z. Was	(CERN, INPK+)
STAHL	97	ZPHY C74 73	A. Stahl, H. Voss	(BONN)
ABACHI	96C	PRL 76 3271	S. Abachi *et al.*	(D0 Collab.)
ABREU	96T	ZPHY C72 179	P. Abreu *et al.*	(DELPHI Collab.)
ADAM	96C	PL B380 471	W. Adam *et al.*	(DELPHI Collab.)
AID	96B	PL B369 173	S. Aid *et al.*	(H1 Collab.)
ALLET	96	PL B383 139	M. Allet *et al.*	(VILL, LEUV, LOUV, WISC)
ABACHI	95E	PL B358 405	S. Abachi *et al.*	(D0 Collab.)
ABE	95N	PRL 74 3538	F. Abe *et al.*	(CDF Collab.)
BALEST	95	PR D51 2053	R. Balest *et al.*	(CLEO Collab.)
KUZNETSOV	95	PRL 75 794	I.A. Kuznetsov *et al.*	(PNPI, KIAE, HARV+)
KUZNETSOV	95B	PAN 58 2113	A.V. Kuznetsov, N.V. Mikheev	(YARO)
		Translated from YAF 58 2228.		
MIZUKOSHI	95	NP B443 20	J.K. Mizukoshi, O.J.P. Eboli, M.C. Gonzalez-Garcia	
ABREU	94O	ZPHY C64 183	P. Abreu *et al.*	(DELPHI Collab.)
BHATTACH...	94	PL B336 100	G. Bhattacharyya, J. Ellis, K. Sridhar	(CERN)
Also		PL B338 522 (errat.)	G. Bhattacharyya, J. Ellis, K. Sridhar	(CERN)
BHATTACH...	94B	PL B338 522 (errat.)	G. Bhattacharyya, J. Ellis, K. Sridhar	(CERN)
DAVIDSON	94	ZPHY C61 613	S. Davidson, D. Bailey, B.A. Campbell	(CFPA+)
KUZNETSOV	94	PL B329 295	A.V. Kuznetsov, N.V. Mikheev	(YARO)
KUZNETSOV	94B	JETPL 60 315	I.A. Kuznetsov *et al.*	(PNPI, KIAE, HARV+)
		Translated from ZETFP 60 311.		
LEURER	94	PR D50 536	M. Leurer	(REHO)
LEURER	94B	PR D49 333	M. Leurer	(REHO)
Also		PRL 71 1324	M. Leurer	(REHO)
MAHANTA	94	PL B337 128	U. Mahanta	(MEHTA)
SEVERIJNS	94	PRL 73 611 (errat.)	N. Severijns *et al.*	(LOUV, WISC, LEUV+)
VILAIN	94B	PL B332 465	P. Vilain *et al.*	(CHARM II Collab.)
ABE	93C	PL B302 119	K. Abe *et al.*	(VENUS Collab.)
ABE	93D	PL B304 373	T. Abe *et al.*	(TOPAZ Collab.)
ABE	93G	PRL 71 2542	F. Abe *et al.*	(CDF Collab.)
ABREU	93J	PL B316 620	P. Abreu *et al.*	(DELPHI Collab.)
ACTON	93E	PL B311 391	P.D. Acton *et al.*	(OPAL Collab.)
ADRIANI	93M	PRPL 236 1	O. Adriani *et al.*	(L3 Collab.)
ALITTI	93	NP B400 3	J. Alitti *et al.*	(UA2 Collab.)
BHATTACH...	93	PR D47 3693	G. Bhattacharyya *et al.*	(CALC, JADA, ICTP+)
BUSKULIC	93F	PL B308 425	D. Buskulic *et al.*	(ALEPH Collab.)
DERRICK	93	PL B306 173	M. Derrick *et al.*	(ZEUS Collab.)
RIZZO	93	PR D48 4470	T.G. Rizzo	(ANL)
SEVERIJNS	93	PRL 70 4047	N. Severijns *et al.*	(LOUV, WISC, LEUV+)
Also		PRL 73 611 (errat.)	N. Severijns *et al.*	(LOUV, WISC, LEUV+)
STERNER	93	PL B303 385	K.L. Sterner *et al.*	(AMY Collab.)
ABREU	92D	ZPHY C53 555	P. Abreu *et al.*	(DELPHI Collab.)
ADRIANI	92F	PL B292 472	O. Adriani *et al.*	(L3 Collab.)
DECAMP	92	PRPL 216 253	D. Decamp *et al.*	(ALEPH Collab.)
IMAZATO	92	PRL 69 877	J. Imazato *et al.*	(KEK, INUS, TOKY+)
MISHRA	92	PRL 68 3499	S.R. Mishra *et al.*	(COLU, CHIC, FNAL+)
POLAK	92B	PR D46 3871	J. Polak, M. Zralek	(SILES)
ACTON	91	PL B268 122	D.P. Acton *et al.*	(OPAL Collab.)
ACTON	91B	PL B273 338	D.P. Acton *et al.*	(OPAL Collab.)
ADEVA	91D	PL B262 155	B. Adeva *et al.*	(L3 Collab.)
AQUINO	91	PL B261 280	M. Aquino, A. Fernandez, A. Garcia	(CINV, PUEB)
COLANGELO	91	PL B253 154	P. Colangelo, G. Nardulli	(BARI)
CUYPERS	91	PL B259 173	F. Cuypers, A.F. Falk, P.H. Frampton	(DURH, HARV+)
FARAGGI	91	MPL A6 61	A.E. Faraggi, D.V. Nanopoulos	(TAMU)
POLAK	91	NP B363 385	J. Polak, M. Zralek	(SILES)
RIZZO	91	PR D44 202	T.G. Rizzo	(WISC, ISU)
WALKER	91	APJ 376 51	T.P. Walker *et al.*	(HSCA, OSU, CHIC+)
ABE	90F	PL B246 297	K. Abe *et al.*	(VENUS Collab.)
ABE	90H	PR D41 1722	F. Abe *et al.*	(CDF Collab.)
AKRAWY	90J	PL B246 285	M.Z. Akrawy *et al.*	(OPAL Collab.)
GONZALEZ...	90D	PL B240 163	M.C. Gonzalez-Garcia, J.W.F. Valle	(VALE)
GRIFOLS	90	NP B331 244	J.A. Grifols, E. Masso	(BARC)
GRIFOLS	90D	PR D42 3293	J.A. Grifols, E. Masso, T.G. Rizzo	(BARC, CERN+)
KIM	90	PL B240 243	G.N. Kim *et al.*	(AMY Collab.)
LOPEZ	90	PL B241 392	J.L. Lopez, D.V. Nanopoulos	(TAMU)
BARBIERI	89B	PR D39 1229	R. Barbieri, R.N. Mohapatra	(PISA, UMD)
LANGACKER	89B	PR D40 1569	P. Langacker, S. Uma Sankar	(PENN)
ODAKA	89	JPSJ 58 3037	S. Odaka *et al.*	(VENUS Collab.)
ROBINETT	89	PR D39 834	R.W. Robinett	(PSU)
ALBAJAR	88B	PL B209 127	C. Albajar *et al.*	(UA1 Collab.)
BAGGER	88	PR D37 1188	J. Bagger, C. Schmidt, S. King	(HARV, BOST)
BALKE	88	PR D37 587	B. Balke *et al.*	(LBL, UCB, COLO, NWES+)
BERGSTROM	88	PL B212 386	L. Bergstrom	(STOH)
CUYPERS	88	PRL 60 1237	F. Cuypers, P.H. Frampton	(UNCCH)
DONCHESKI	88	PL B206 137	M.A. Doncheski, H. Grotch, R. Robinett	(PSU)
DONCHESKI	88B	PR D38 412	M.A. Doncheski, H. Grotch, R.W. Robinett	(PSU)
BARTEL	87B	ZPHY C36 15	W. Bartel *et al.*	(JADE Collab.)
BEHREND	86B	PL B178 452	H.J. Behrend *et al.*	(CELLO Collab.)
DERRICK	86	PL 166B 463	M. Derrick *et al.*	(HRS Collab.)
Also		PR D34 3286	M. Derrick *et al.*	(HRS Collab.)
JODIDIO	86	PR D34 1967	A. Jodidio *et al.*	(LBL, NWES, TRIU)
Also		PR D37 237 (errat.)	A. Jodidio *et al.*	(LBL, NWES, TRIU)
MOHAPATRA	86	PR D34 909	R.N. Mohapatra	(UMD)
ADEVA	85	PL 152B 439	B. Adeva *et al.*	(Mark-J Collab.)
BERGER	85B	ZPHY C27 341	C. Berger *et al.*	(PLUTO Collab.)
STOKER	85	PRL 54 1887	D.P. Stoker *et al.*	(LBL, NWES, TRIU)
ADEVA	84	PRL 53 134	B. Adeva *et al.*	(Mark-J Collab.)
BEHREND	84C	PL 140B 130	H.J. Behrend *et al.*	(CELLO Collab.)
BERGSMA	83	PL 122B 465	F. Bergsma *et al.*	(CHARM Collab.)
CARR	83	PRL 51 627	J. Carr *et al.*	(LBL, NWES, TRIU)
BEALL	82	PRL 48 848	G. Beall, M. Bander, A. Soni	(UCI, UCLA)
SHANKER	82	NP B204 375	O. Shanker	(TRIU)

Axions (A^0) and Other Very Light Bosons, Searches for

See the related review(s):

Axions and Other Similar Particles

A^0 (Axion) MASS LIMITS from Astrophysics and Cosmology

These bounds depend on model-dependent assumptions (i.e. — on a combination of axion parameters).

VALUE (MeV)	DOCUMENT ID		TECN	COMMENT
• • • We do not use the following data for averages, fits, limits, etc. • • •				
>0.2	BARROSO	82	ASTR	Standard Axion
>0.25	[1] RAFFELT	82	ASTR	Standard Axion
>0.2	[2] DICUS	78C	ASTR	Standard Axion
	MIKAELIAN	78	ASTR	Stellar emission
>0.3	[2] SATO	78	ASTR	Standard Axion
>0.2	VYSOTSKII	78	ASTR	Standard Axion

[1] Lower bound from 5.5 MeV γ-ray line from the sun.

[2] Lower bound from requiring the red giants' stellar evolution not be disrupted by axion emission.

A^0 (Axion) and Other Light Boson (X^0) Searches in Hadron Decays

Limits are for branching ratios.

VALUE	CL%	DOCUMENT ID		TECN	COMMENT
• • • We do not use the following data for averages, fits, limits, etc. • • •					
		[1] ABLIKIM	25AV	BES3	$\eta \to \pi^+\pi^- A^0$, $A^0 \to e^+e^-$
		[2] ADACHI	25AA	BEL2	$B \to K/K^* A^0$, $A^0 \to \gamma\gamma$
$<1 \times 10^{-12}$	90	[3] ALRAHMAN	25	ICRS	$K \to \pi A^0$, $A^0 \to \mu^+\mu^-$
$<5 \times 10^{-12}$	90	[4] CORTINA-GIL	25B	NA62	$K^+ \to \pi^+ X^0$
$<1 \times 10^{-4}$	90	[5] ABLIKIM	24AK	BES3	$\eta' \to \pi^+\pi^- A^0$, $A^0 \to e^+e^-$
		[6] ABLIKIM	24G	BES3	$J/\psi \to \mu^+\mu^- X^0$
$<0.5 \times 10^{-6}$	90	[7] ABLIKIM	24M	BES3	$\eta \to \gamma X^0$, $\eta' \to \gamma X^0$
$<2 \times 10^{-9}$	90	[8] CORTINA-GIL	24	NA62	$K^+ \to \pi^+ A^0$, $A^0 \to \gamma\gamma$
$<2 \times 10^{-7}$	90	[9] SADOVSKY	24	OKA	$K^+ \to \pi^+\pi^0 A^0$
$<4 \times 10^{-8}$	95	[10] ADACHI	23K	BEL2	$B^+ \to K^+ X^0$
$<9 \times 10^{-8}$	95	[11] ADACHI	23K	BEL2	$B^0 \to K^*(892)^0 X^0$ ($K^*(892)^0 \to K^+\pi^-$)
$<3.7 \times 10^{-10}$	95	[12] CORTINA-GIL	23B	NA62	$K^+ \to \pi^+ A^0 A^0$, $A^0 \to e^+e^-$
$<4.2 \times 10^{-8}$	90	[13] LEES	22B	BABR	$B^\pm \to K^\pm A^0$ ($A^0 \to \gamma\gamma$)
$<7 \times 10^{-13}$	95	[14] ABRATENKO	21	MCBN	$K^+ \to \pi^+ X^0$ ($X^0 \to e^+e^-$)
$<1.5 \times 10^{-7}$	90	[15] CORTINA-GIL	21	NA62	$K^+ \to \mu^+\nu X^0$
$<5 \times 10^{-11}$	90	[16] CORTINA-GIL	21A	NA62	$K^+ \to \pi^+ X^0$
$<9 \times 10^{-10}$	90	[17] CORTINA-GIL	21C	NA62	$K^+ \to \pi^+ X^0$
$<1.5 \times 10^{-8}$	90	[18] PARK	21	BELL	$B^0 \to X^0 X^0$ ($X^0 \to e^+e^-$, $\mu^+\mu^-$, $\pi^+\pi^-$)
$<2.4 \times 10^{-9}$	90	[19] AHN	19	KOTO	$K^0_L \to \pi^0 X^0$, $m_{X^0} = 135$ MeV
$<2 \times 10^{-10}$	95	[20] AAIJ	17AQ	LHCB	$B^+ \to K^+ X^0$ ($X^0 \to \mu^+\mu^-$)
$<3.7 \times 10^{-8}$	90	[21] AHN	17	KOTO	$K^0_L \to \pi^0 X^0$, $m_{X^0} = 135$ MeV
$<6 \times 10^{-11}$	90	[22] BATLEY	17	NA48	$K^\pm \to \pi^\pm X^0$($X^0 \to \mu^+\mu^-$)
		[23] WON	16	BELL	$\eta \to \gamma X^0$ ($X^0 \to \pi^+\pi^-$)
$<1 \times 10^{-9}$	95	[24] AAIJ	15AZ	LHCB	$B^0 \to K^{*0} X^0$ ($X^0 \to \mu^+\mu^-$)
$<1.5 \times 10^{-6}$	90	[25] ADLARSON	13	WASA	$\pi^0 \to \gamma X^0$ ($X^0 \to e^+e^-$), $m_{X^0} = 100$ MeV
$<2 \times 10^{-8}$	90	[26] BABUSCI	13B	KLOE	$\phi \to \eta X^0$ ($X^0 \to e^+e^-$)
		[27] ARCHILLI	12	KLOE	$\phi \to \eta X^0$, $X^0 \to e^+e^-$
$<2 \times 10^{-15}$	90	[28] GNINENKO	12A	BDMP	$\pi^0 \to \gamma X^0$ ($X^0 \to e^+e^-$)
$<3 \times 10^{-14}$	90	[29] GNINENKO	12B	BDMP	$\eta(\eta') \to \gamma X^0$ ($X^0 \to e^+e^-$)
$<7 \times 10^{-10}$	90	[30] ADLER	04	B787	$K^+ \to \pi^+ X^0$
$<7.3 \times 10^{-11}$	90	[31] ANISIMOVSK...	04	B949	$K^+ \to \pi^+ X^0$
$<4.5 \times 10^{-11}$	90	[32] ADLER	02C	B787	$K^+ \to \pi^+ X^0$
$<4 \times 10^{-5}$	90	[33] ADLER	01	B787	$K^+ \to \pi^+\pi^0 A^0$
$<4.9 \times 10^{-5}$	90	AMMAR	01B	CLEO	$B^\pm \to \pi^\pm(K^\pm)X^0$
$<5.3 \times 10^{-5}$	90	AMMAR	01B	CLEO	$B^0 \to K^0_S X^0$
$<3.3 \times 10^{-5}$	90	[34] ALTEGOER	98	NOMD	$\pi^0 \to \gamma X^0$, $m_{X^0} < 120$ MeV
$<5.0 \times 10^{-8}$	90	[35] KITCHING	97	B787	$K^+ \to \pi^+ X^0$ ($X^0 \to \gamma\gamma$)
$<5.2 \times 10^{-10}$	90	[36] ADLER	96	B787	$K^+ \to \pi^+ X^0$
$<2.8 \times 10^{-4}$	90	[37] AMSLER	96B	CBAR	$\pi^0 \to \gamma X^0$, $m_{X^0} < 65$ MeV
$<3 \times 10^{-4}$	90	[37] AMSLER	96B	CBAR	$\eta \to \gamma X^0$, m_{X^0}= 50–200 MeV
$<4 \times 10^{-5}$	90	[37] AMSLER	96B	CBAR	$\eta' \to \gamma X^0$, m_{X^0}= 50–925 MeV
$<6 \times 10^{-5}$	90	[37] AMSLER	94B	CBAR	$\pi^0 \to \gamma X^0$, m_{X^0}=65–125 MeV
$<6 \times 10^{-5}$	90	[37] AMSLER	94B	CBAR	$\eta \to \gamma X^0$, m_{X^0}=200–525 MeV
$<7 \times 10^{-3}$	90	[38] MEIJERDREES	94	CNTR	$\pi^0 \to \gamma X^0$, m_{X^0}=25 MeV
$<2 \times 10^{-3}$	90	[38] MEIJERDREES	94	CNTR	$\pi^0 \to \gamma X^0$, m_{X^0}=100 MeV
$<2 \times 10^{-7}$	90	[39] ATIYA	93B	B787	Sup. by ADLER 04
$<3 \times 10^{-13}$		[40] NG	93	COSM	$\pi^0 \to \gamma X^0$
$<1.1 \times 10^{-8}$	90	[41] ALLIEGRO	92	SPEC	$K^+ \to \pi^+ X^0$ ($X^0 \to e^+e^-$)
$<5 \times 10^{-4}$	90	[42] ATIYA	92	B787	$\pi^0 \to \gamma X^0$
$<1 \times 10^{-12}$	95	[43] BARABASH	92	BDMP	$\pi^\pm \to e^\pm\nu X^0$($X^0 \to e^+e^-$, $\gamma\gamma$), $m_{X^0} = 8$ MeV
$<1 \times 10^{-12}$	95	[44] BARABASH	92	BDMP	$K^\pm \to \pi^\pm X^0$($X^0 \to e^+e^-$, $\gamma\gamma$), $m_{X^0} = 10$ MeV
$<1 \times 10^{-11}$	95	[45] BARABASH	92	BDMP	$K^0_L \to \pi^0 X^0$($X^0 \to e^+e^-$, $\gamma\gamma$), $m_{X^0} = 10$ MeV
$<1 \times 10^{-14}$	95	[46] BARABASH	92	BDMP	$\eta' \to \eta X^0$($X^0 \to e^+e^-$, $\gamma\gamma$), $m_{X^0} = 10$ MeV
$<4 \times 10^{-6}$	90	[47] MEIJERDREES	92	SPEC	$\pi^0 \to \gamma X^0$ ($X^0 \to e^+e^-$), m_{X^0}= 100 MeV
$<1 \times 10^{-7}$	90	[48] ATIYA	90B	B787	Sup. by KITCHING 97
$<1.3 \times 10^{-8}$	90	[49] KORENCHE...	87	SPEC	$\pi^+ \to e^+\nu A^0$ ($A^0 \to e^+e^-$)
$<1 \times 10^{-9}$	90	[50] EICHLER	86	SPEC	Stopped $\pi^+ \to e^+\nu A^0$
$<2 \times 10^{-5}$	90	[51] YAMAZAKI	84	SPEC	For 160<m<260 MeV
$<(1.5–4) \times 10^{-6}$	90	[51] YAMAZAKI	84	SPEC	K decay, $m_{X^0} \ll 100$ MeV
		[52] ASANO	82	CNTR	Stopped $K^+ \to \pi^+ X^0$
		[53] ASANO	81B	CNTR	Stopped $K^+ \to \pi^+ X^0$
		[54] ZHITNITSKII	79		Heavy axion

[1] ABLIKIM 25AV search for η decays to A^0 subsequently decaying to an electron positron pair in the BESIII detector. They set limits down to 3×10^{-3} on the relative branching fraction for the decay process compared to $\eta \to \pi^+\pi^- e^+e^-$ for axion masses between 5 and 200 MeV - see their Fig. 7 for mass-dependent limits.

[2] ADACHI 25AA search for axion-like particles produced from decays of B to K or K^* mesons in the Belle detector, with the axion-like particle subsequently decaying to two photons. See their Fig. 5 for mass-dependent limits on the axion coupling to the W boson in the mass range 0.16–4.5 GeV.

[3] ALRAHMAN 25 present a search for scalars and axions produced from the kaon decays that then decay to two muons using the ICARUS detector at Fermilab. In their Fig. 2, they present a constraint on axions with masses up to 350 MeV for a particular choice of gauge field and muon couplings. The quoted value is from their model-independent branching ratio limit shown in Fig. 3 at $c\tau_{A^0} = 200$ m.

[4] CORTINA-GIL 25B report a search for an invisibly decaying X^0 produced in decays of K^+ in the NA62 detector, for masses up to 260 MeV. The quoted branching ratio limit is for $K^+ \to \pi^+ X^0$ for an invisibly decaying X^0. See their Fig. 2 for mass-dependent limits.

[5] ABLIKIM 24AK search for η' decays to axions in the mass range 0 to 500 MeV using the BESIII detector at the Beijing Electron-Positron Collider. See Fig. 9b for mass-dependent limits.

[6] ABLIKIM 24G search for muonphilic vector or scalar X^0 particles with masses between 1 and 1000 MeV in J/ψ decays at the BESIII detector. See their Fig. 3 for mass-dependent limits on the scalar/vector couplings under three different models.

[7] ABLIKIM 24M search for η and η' decays to dark photons in the mass range 0 to 0.7 GeV using the BESIII detector at the Beijing Electron-Positron Collider. The quoted limit is for $\eta' \to \gamma X^0$. See Fig. 7 a and b for mass-dependent limits.

[8] CORTINA-GIL 24 use $K^+ \to \pi^+\gamma\gamma$ events in NA62 to constrain 210 to 350 MeV-mass axions coupled to gluons, which promptly decay to $\gamma\gamma$. See their Fig. 8 for mass-dependent limits.

[9] SADOVSKY 24 report results from the OKA collaboration on a missing-mass search for invisible axions in K^+ decays to pions. The quoted limit applies at $m_{A^0} \simeq 200$ MeV. See their Fig. 6 for mass-dependent limits up to 200 MeV.

[10] ADACHI 23K quoted limit is for $m_{X^0} \simeq 3$ GeV, $c\tau_{X^0} = 1$ cm, and the decay channel $X^0 \to e^+e^-$. See their Fig. 2 for limits with different lifetimes and decay channels, $X^0 \to \mu^+\mu^-$, $\pi^+\pi^-$, K^+K^-.

[11] ADACHI 23K quoted limit is for $m_{X^0} \simeq 2$ GeV, $c\tau_{X^0} = 1$ cm, and the decay channel $X^0 \to e^+e^-$. See their Fig. 2 for limits with different lifetimes and decay channels, $X^0 \to \mu^+\mu^-$, $\pi^+\pi^-$, K^+K^-.

[12] CORTINA-GIL 23B limit extends over 10–170 MeV in mass. Quoted limit is at 155 MeV.

[13] LEES 22B quoted limit is for $m_{A^0} = 3.9$ GeV, assuming the promptly decaying axion. Limits of O(10^{-7}) are obtained for $m_{A^0} = 0.175$–4.78 GeV. See their Figs.3 and 4 for mass and lifetime dependent limits.

[14] ABRATENKO 21 quoted limit is for $m_{X^0} = 150$ MeV and the lifetime $c\tau_{X^0} = 80$ m. See their Fig. 4 for the limits in the range of $m_{X^0} = 10$–210 MeV.

[15] CORTINA-GIL 21 quoted limit is for $m_{X^0} = 370$ MeV. Limits from O(10^{-5}) and O(10^{-6}) are obtained for $m_{X^0} = 10$–370 MeV (see their Fig. 7).

[16] CORTINA-GIL 21A quoted limit is for $m_{X^0} = 160$–250 MeV. Limits between 5×10^{-11} and 2×10^{-10} are obtained in the range of $m_{X^0} = 0$–110 and 154–260 MeV, assuming stable or invisibly decaying X^0. See their Fig. 4 for mass- and lifetime-dependent limits.

[17] CORTINA-GIL 21C quoted limit is for $m_{X^0} = 130$–140 MeV, and limits of 9×10^{-10}–6×10^{-7} are obtained in the mass range of $m_{X^0} = 110$–155 MeV, assuming X^0 escapes detection. See their Fig. 6 for mass- and lifetime-dependent limits.

[18] PARK 21 look for dark photons produced by decays of B^0 through off-shell Higgs-dark Higgs mixing. See their Fig. 5 for limits in the range of $m_{X^0} = 0.01$–2.62 GeV.

[19] AHN 19 is an update of AHN 17 from a new data set. See their Fig. 4 for the limits in the range of $m_{X^0} = 0$–250 MeV.

[20] AAIJ 17AQ limit is for $\tau_{X^0} = 10$ ps. See their Fig. 4 for limits in the range of $m_{X^0} =$ 250–4700 MeV and $\tau_{X^0} = 0.1$–1000 ps.

[21] AHN 17 limit as a function of m_{X^0} from 0 to 250 MeV is provided in their Fig. 5.

[22] BATLEY 17 limit is for $m_{X^0} = 216$ MeV and $\tau_{X^0} \leq 10$ ps. See their Fig. 4(c) for limits in the range of $m_{X^0} = 211$–354 MeV and longer lifetimes.

[23] WON 16 look for a vector boson coupled to baryon number. Derived limits on $\alpha' < 10^{-3}$–10^{-2} for $m_{X^0} = 290$–520 MeV at 95% CL. See their Fig. 4 for mass-dependent limits.

[24] AAIJ 15AZ limit is for $\tau_{X^0} = 10$ ps and $m_{X^0} = 214$–4350 MeV. See their Fig. 4 for mass- and lifetime-dependent limits.

Int. J. Mod. Phys. A 2026.41. Downloaded from www.worldscientific.com
by UNIVERSITY OF CALIFORNIA @ BERKELEY on 09/16/26. Re-use and distribution is strictly not permitted, except for Open Access articles.

Int. J. Mod. Phys. A 2026.41. Downloaded from www.worldscientific.com
by UNIVERSITY OF CALIFORNIA @ BERKELEY on 09/16/26. Re-use and distribution is strictly not permitted, except for Open Access articles.

[25] ADLARSON 13 limits between 2.0×10^{-5} and 1.5×10^{-6} are obtained for m_{X^0} = 20–100 MeV (see their Fig. 8). Angular momentum conservation requires that X^0 has spin ≥ 1.

[26] BABUSCI 13B limit is for $B(\phi \to \eta X^0) \cdot B(X^0 \to e^+ e^-)$ and applies to $m_{X^0} = 410$ MeV. It is derived by analyzing $\eta \to \pi^0 \pi^0 \pi^0$ and $\pi^- \pi^+ \pi^0$. Limits between 1×10^{-6} and 2×10^{-8} are obtained for $m_{X^0} \leq 450$ MeV (see their Fig. 6).

[27] ARCHILLI 12 analyzed $\eta \to \pi^+ \pi^- \pi^0$ decays. Derived limits on $\alpha'/\alpha < 2 \times 10^{-5}$ for m_{X^0} = 50–420 MeV at 90% CL. See their Fig. 8 for mass-dependent limits.

[28] GNINENKO 12A limit is for $B(\pi^0 \to \gamma X^0) \cdot B(X^0 \to e^+ e^-)$ and applies for m_{X^0} = 90 MeV and $\tau_{X^0} \simeq 1 \times 10^{-8}$ sec. Limits between 10^{-8} and 2×10^{-15} are obtained for m_{X^0} = 3–120 MeV and $\tau_{X^0} = 1 \times 10^{-11}$–1 sec. See their Fig. 3 for limits at different masses and lifetimes.

[29] GNINENKO 12B limit is for $B(\eta \to \gamma X^0) \cdot B(X^0 \to e^+ e^-)$ and applies for m_{X^0} = 100 MeV and $\tau_{X^0} \simeq 6 \times 10^{-9}$ sec. Limits between 10^{-5} and 3×10^{-14} are obtained for $m_{X^0} \lesssim 550$ MeV and $\tau_{X^0} = 10^{-10}$–10 sec. See their Fig. 5 for limits at different mass and lifetime and for η' decays.

[30] ADLER 04 limit applies for a mass near 180 MeV. For other masses in the range m_{X^0} = 150–250 MeV the limit is less restrictive, but still improves ADLER 02C and ATIYA 93B.

[31] ANISIMOVSKY 04 bound is for m_{X^0}=0.

[32] ADLER 02C bound is for m_{X^0} <60 MeV. See Fig. 2 for limits at higher masses.

[33] The quoted limit is for m_{X^0} = 0–80 MeV. See their Fig. 5 for the limit at higher mass. The branching fraction limit assumes pure phase space decay distributions.

[34] ALTEGOER 98 looked for X^0 from π^0 decay which penetrate the shielding and convert to π^0 in the external Coulomb field of a nucleus.

[35] KITCHING 97 limit is for $B(K^+ \to \pi^+ X^0) \cdot B(X^0 \to \gamma\gamma)$ and applies for $m_{X^0} \simeq 50$ MeV, $\tau_{X^0} < 10^{-10}$ s. Limits are provided for $0 < m_{X^0} < 100$ MeV, $\tau_{X^0} < 10^{-8}$ s.

[36] ADLER 96 looked for a peak in missing-mass distribution. This work is an update of ATIYA 93. The limit is for massless stable X^0 particles and extends to m_{X^0}=80 MeV at the same level. See paper for dependence on finite lifetime.

[37] AMSLER 94B and AMSLER 96B looked for a peak in missing-mass distribution.

[38] MEIJERDREES 94 limit is based on inclusive photon spectrum and is independent of X^0 decay modes. It applies to $\tau(X^0) > 10^{-23}$ sec.

[39] ATIYA 93B looked for a peak in missing mass distribution. The bound applies for stable X^0 of m_{X^0}=150–250 MeV, and the limit becomes stronger (10^{-8}) for m_{X^0}=180–240 MeV.

[40] NG 93 studied the production of X^0 via $\gamma\gamma \to \pi^0 \to \gamma X^0$ in the early universe at $T \simeq 1$ MeV. The bound on extra neutrinos from nucleosynthesis $\Delta N_\nu < 0.3$ (WALKER 91) is employed. It applies to $m_{X^0} \ll 1$ MeV in order to be relativistic down to nucleosynthesis temperature. See paper for heavier X^0.

[41] ALLIEGRO 92 limit applies for m_{X^0}=150–340 MeV and is the branching ratio times the decay probability. Limit is $< 1.5 \times 10^{-8}$ at 99%CL.

[42] ATIYA 92 looked for a peak in missing mass distribution. The limit applies to m_{X^0}=0–130 MeV in the narrow resonance limit. See paper for the dependence on lifetime. Covariance requires X^0 to be a vector particle.

[43] BARABASH 92 is a beam dump experiment that searched for a light Higgs. Limits between 1×10^{-12} and 1×10^{-7} are obtained for $3 < m_{X^0} < 40$ MeV.

[44] Limits between 1×10^{-12} and 1 are obtained for $4 < m_{X^0} < 69$ MeV.

[45] Limits between 1×10^{-11} and 5×10^{-3} are obtained for $4 < m_{X^0} < 63$ MeV.

[46] Limits between 1×10^{-14} and 1 are obtained for $3 < m_{X^0} < 82$ MeV.

[47] MEIJERDREES 92 limit applies for $\tau_{X^0} = 10^{-23}$–10^{-11} sec. Limits between 2×10^{-4} and 4×10^{-6} are obtained for m_{X^0} = 25–120 MeV. Angular momentum conservation requires that X^0 has spin ≥ 1.

[48] ATIYA 90B limit is for $B(K^+ \to \pi^+ X^0) \cdot B(X^0 \to \gamma\gamma)$ and applies for $m_{X^0} = 50$ MeV, $\tau_{X^0} < 10^{-10}$ s. Limits are also provided for $0 < m_{X^0} < 100$ MeV, $\tau_{X^0} < 10^{-8}$ s.

[49] KORENCHENKO 87 limit assumes $m_{A^0} = 1.7$ MeV, $\tau_{A^0} \lesssim 10^{-12}$ s, and $B(A^0 \to e^+ e^-) = 1$.

[50] EICHLER 86 looked for $\pi^+ \to e^+ \nu A^0$ followed by $A^0 \to e^+ e^-$. Limits on the branching fraction depend on the mass and and lifetime of A^0. The quoted limits are valid when $\tau(A^0) \gtrsim 3. \times 10^{-10}$s if the decays are kinematically allowed.

[51] YAMAZAKI 84 looked for a discrete line in $K^+ \to \pi^+ X$. Sensitive to wide mass range (5–300 MeV), independent of whether X decays promptly or not.

[52] ASANO 82 at KEK set limits for $B(K^+ \to \pi^+ X^0)$ for m_{X^0} <100 MeV as BR $< 4. \times 10^{-8}$ for $\tau(X^0 \to n\gamma\text{'s}) > 1. \times 10^{-9}$ s, BR $< 1.4 \times 10^{-6}$ for $\tau < 1. \times 10^{-9}$s.

[53] ASANO 81B is KEK experiment. Set $B(K^+ \to \pi^+ X^0) < 3.8 \times 10^{-8}$ at CL = 90%.

[54] ZHITNITSKII 79 argue that a heavy axion predicted by YANG 78 ($3 < m < 40$ MeV) contradicts experimental muon anomalous magnetic moments.

A^0 (Axion) Searches in Quarkonium Decays

Decay or transition of quarkonium. Limits are for branching ratio.

VALUE	CL%	DOCUMENT ID		TECN	COMMENT
• • • We do not use the following data for averages, fits, limits, etc. • • •					
$<8.3 \times 10^{-8}$	95	[1] ABLIKIM	23E	BES3	$J/\psi \to A^0 \gamma (A^0 \to \gamma\gamma)$
$<3.1 \times 10^{-7}$	90	[2] JIA	22	BELL	$\Upsilon(1S) \to A^0 \gamma (A^0 \to \mu^+ \mu^-)$
$<2.8 \times 10^{-8}$	90	[3] ABLIKIM	16E	BES3	$J/\psi \to A^0 \gamma (A^0 \to \mu^+ \mu^-)$
$<4 \times 10^{-7}$	90	[4] ABLIKIM	12	BES3	$J/\psi \to A^0 \gamma (A^0 \to \mu^+ \mu^-)$
$<4.0 \times 10^{-5}$	90	[5] ANTREASYAN	90C	CBAL	$\Upsilon(1S) \to A^0 \gamma$
$<5 \times 10^{-5}$	90	[6] DRUZHININ	87	ND	$\phi \to A^0 \gamma (A^0 \to e^+ e^-)$
$<2 \times 10^{-3}$	90	[7] DRUZHININ	87	ND	$\phi \to A^0 \gamma (A^0 \to \gamma\gamma)$
$<7 \times 10^{-6}$	90	[8] DRUZHININ	87	ND	$\phi \to A^0 \gamma (A^0 \to$ missing)
$<1.4 \times 10^{-5}$	90	[9] EDWARDS	82	CBAL	$J/\psi \to A^0 \gamma$

[1] ABLIKIM 23E obtained limits in the range of 8.3×10^{-8}–1.8×10^{-6} for 0.165 GeV $\leq m_{A^0} \leq 2.84$ GeV. See their Fig. 5 for mass-dependent limits.

[2] JIA 22 limits between 3.1×10^{-7}–1.6×10^{-5} were obtained for 0.22 GeV $< m_{A^0} <$ 9.2 GeV. See their Fig. 4 for mass-dependent limits.

[3] ABLIKIM 16E limits between 2.8–495.3×10^{-8} were obtained for 0.212 GeV $< m_{A^0} <$ 3.0 GeV. See their Fig. 5 for mass-dependent limits.

[4] ABLIKIM 12 derived limits between 4×10^{-7}–2.1×10^{-5} for 0.212 GeV $< m_{A^0} <$ 3.0 GeV. See their Fig. 2(c) for mass-dependent limits.

[5] ANTREASYAN 90C assume that A^0 does not decay in the detector.

[6] The first DRUZHININ 87 limit is valid when $\tau_{A^0}/m_{A^0} < 3 \times 10^{-13}$ s/MeV and $m_{A^0} < 20$ MeV.

[7] The second DRUZHININ 87 limit is valid when $\tau_{A^0}/m_{A^0} < 5 \times 10^{-13}$ s/MeV and $m_{A^0} < 20$ MeV.

[8] The third DRUZHININ 87 limit is valid when $\tau_{A^0}/m_{A^0} > 7 \times 10^{-12}$ s/MeV and $m_{A^0} < 200$ MeV.

[9] EDWARDS 82 looked for $J/\psi \to \gamma A^0$ decays by looking for events with a single γ [of energy $\sim 1/2$ the $J/\psi(1S)$ mass], plus nothing else in the detector. The limit is inconsistent with the axion interpretation of the FAISSNER 81B result.

A^0 (Axion) Searches in Positronium Decays

Decay or transition of positronium. Limits are for branching ratio.

VALUE	CL%	DOCUMENT ID		TECN	COMMENT
• • • We do not use the following data for averages, fits, limits, etc. • • •					
$<4.4 \times 10^{-5}$	90	[1] BADERT...	02	CNTR	o-Ps $\to \gamma X_1 X_2$, $m_{X_1} + m_{X_2} \leq$ 900 keV
$<2 \times 10^{-4}$	90	MAENO	95	CNTR	o-Ps $\to A^0 \gamma$ m_{A^0}=850–1013 keV
$<3.0 \times 10^{-4}$	90	[2] ASAI	94	CNTR	o-Ps $\to A^0 \gamma$ m_{A^0}=30–500 keV
$<2.8 \times 10^{-5}$	90	[3] AKOPYAN	91	CNTR	o-Ps $\to A^0 \gamma (A^0 \to \gamma\gamma)$, $m_{A^0} < 30$ keV
$<1.1 \times 10^{-6}$	90	[4] ASAI	91	CNTR	o-Ps $\to A^0 \gamma$, $m_{A^0} < 800$ keV
$<3.8 \times 10^{-4}$	90	GNINENKO	90	CNTR	o-Ps $\to A^0 \gamma$, $m_{A^0} < 30$ keV
$<(1–5) \times 10^{-4}$	95	[5] TSUCHIAKI	90	CNTR	o-Ps $\to A^0 \gamma$, m_{A^0} = 300–900 keV
$<6.4 \times 10^{-5}$	90	[6] ORITO	89	CNTR	o-Ps $\to A^0 \gamma$, $m_{A^0} < 30$ keV
		[7] AMALDI	85	CNTR	Ortho-positronium
		[8] CARBONI	83	CNTR	Ortho-positronium

[1] BADERTSCHER 02 looked for a three-body decay of ortho-positronium into a photon and two penetrating (neutral or milli-charged) particles.

[2] The ASAI 94 limit is based on inclusive photon spectrum and is independent of A^0 decay modes.

[3] The AKOPYAN 91 limit applies for a short-lived A^0 with $\tau_{A^0} < 10^{-13}$ m_{A^0} [keV] s.

[4] ASAI 91 limit translates to $g^2_{A^0 e^+ e^-}/4\pi < 1.1 \times 10^{-11}$ (90% CL) for $m_{A^0} < 800$ keV.

[5] The TSUCHIAKI 90 limit is based on inclusive photon spectrum and is independent of A^0 decay modes.

[6] ORITO 89 limit translates to $g^2_{A^0 ee}/4\pi < 6.2 \times 10^{-10}$. Somewhat more sensitive limits are obtained for larger m_{A^0}: $B < 7.6 \times 10^{-6}$ at 100 keV.

[7] AMALDI 85 set limits $B(A^0\gamma)$ / $B(\gamma\gamma\gamma) < (1–5) \times 10^{-6}$ for m_{A^0} = 900–100 keV which are about 1/10 of the CARBONI 83 limits.

[8] CARBONI 83 looked for orthopositronium $\to A^0\gamma$. Set limit for A^0 electron coupling squared, $g(ee A^0)^2/(4\pi) < 6. \times 10^{-10}$–$7. \times 10^{-9}$ for m_{A^0} from 150–900 keV (CL = 99.7%). This is about 1/10 of the bound from $g-2$ experiments.

A^0 (Axion) Search in Photoproduction

VALUE	DOCUMENT ID		TECN	COMMENT
• • • We do not use the following data for averages, fits, limits, etc. • • •				
	[1] ADHIKARI	22C	GLUX	m_{A^0} = 180–480, 600–720 MeV
	[2] BASSOMPIE...	95		m_{A^0} = 1.8 ± 0.2 MeV

[1] ADHIKARI 22C search for $A^0 \to \gamma\gamma$ and $A^0 \to \pi^+ \pi^- \pi^0$ decays, and set limits of $f_{A^0} \lesssim$ 0.5–14 GeV at 90% CL. See their Fig. 4 for mass-dependent limits.

[2] BASSOMPIERRE 95 is an extension of BASSOMPIERRE 93. They looked for a peak in the invariant mass of $e^+ e^-$ pairs in the region $m_{e^+ e^-}$ = 1.8 ± 0.2 MeV. They obtained bounds on the production rate A^0 for $\tau(A^0) = 10^{-18}$–10^{-9} sec. They also found an excess of events in the range $m_{e^+ e^-}$ = 2.1–3.5 MeV.

A^0 (Axion) Production in Hadron Collisions

Limits are for $\sigma(A^0)$ / $\sigma(\pi^0)$.

VALUE	CL%	DOCUMENT ID		TECN	COMMENT
• • • We do not use the following data for averages, fits, limits, etc. • • •					
		[1] AAD	25AN	ATLS	$pp \to t\bar{t}A^0$, $A^0 \to b\bar{b}$
		[2] AAD	25AT	ATLS	$H \to ZA^0$, $A^0 \to gg$, $q\bar{q}$
		[3] AAD	25AY	ATLS	$Z^* \to ZA^0$, $A^0 \to gg$
		[4] CHEKHOVSKY	25	CMS	$q\bar{q} \to Wa$, $a \to Z\gamma$
		[5] AAD	24AT	ATLS	$H \to A^0 A^0 \to 4\gamma$
		[6] AAD	24BN	ATLS	$q\bar{q} \to VA^0$, $t \to A^0 q$, $A^0 \to gg$, $c\bar{c}$
		[7] AAD	24BZ	ATLS	$V \to VA^0$, $A^0 \to gg$
		[8] AAD	24CD	ATLS	$V \to VA^0$
		[9] AAD	24K	ATLS	$H \to ZA^0$

Int. J. Mod. Phys. A 2026.41. Downloaded from www.worldscientific.com
by UNIVERSITY OF CALIFORNIA @ BERKELEY on 09/16/26. Re[redacted]s strictly not permitted, except for Open Access articles.

	[10] HAYRAPETY...	24AZ	CMS	$H \to A^0 A^0$, $A^0 \to \mu^+\mu^-$
	[11] HAYRAPETY...	24I	CMS	$H \to A^0 Z \to \gamma\gamma\ell^+\ell^-$
	[12] TUMASYAN	24C	CMS	$\gamma\gamma \to A^0 \to \gamma\gamma$
	[13] ACCIARRI	23	ARNT	$A^0 \to \mu^+\mu^-$
	[14] BERTUZZO	23	ARNT	$A^0 \to \mu^+\mu^-$
	[15] AAD	22J	ATLS	$H \to A^0 A^0$, ZA^0 ($A^0 \to \mu^+\mu^-$)
	[16] TUMASYAN	22AH	CMS	$H \to A^0 A^0$, $A^0 \to e^+e^-$, $\mu^+\mu^-$
	[17] TUMASYAN	22R	CMS	$pp \to A^{*0} \to ZZ$, ZH
	[18] AAD	21F	ATLS	Monojet + missing p_T
	[19] AAD	21K	ATLS	Mono-γ + missing p_T
	[20] AAD	21N	ATLS	$\gamma\gamma$ scatt. in Pb+Pb
	[21] CARRA	21	ATLS	$pp \to A^{*0} \to WW$, $Z\gamma$
	[22] AAIJ	20AL	LHCB	$pp \to X^0 \to \mu^+\mu^-$
	[23] GAVELA	20	CMS	$pp \to A^{*0} \to \gamma\gamma$, ZZ
	[24] SIRUNYAN	19BQ	CMS	$X^0 \to \mu^+\mu^-$
	[25] JAIN	07	CNTR	$A^0 \to e^+e^-$
	[26] AHMAD	97	SPEC	e^+ production
	[27] LEINBERGER	97	SPEC	$A^0 \to e^+e^-$
	[28] GANZ	96	SPEC	$A^0 \to e^+e^-$
	[29] KAMEL	96	EMUL	^{32}S emulsion, $A^0 \to e^+e^-$
	[30] BLUEMLEIN	92	BDMP	$A^0 N_Z \to \ell^+\ell^- N_Z$
	[31] MEIJERDREES	92	SPEC	$\pi^- p \to nA^0$, $A^0 \to e^+e^-$
	[32] BLUEMLEIN	91	BDMP	$A^0 \to e^+e^-$, 2γ
	[33] FAISSNER	89	OSPK	Beam dump, $A^0 \to e^+e^-$
	[34] DEBOER	88	RVUE	$A^0 \to e^+e^-$
	[35] EL-NADI	88	EMUL	$A^0 \to e^+e^-$
	[36] FAISSNER	88	OSPK	Beam dump, $A^0 \to 2\gamma$
	[37] BADIER	86	BDMP	$A^0 \to e^+e^-$
$<2. \times 10^{-11}$	90	[38] BERGSMA	85	CHRM CERN beam dump
$<1. \times 10^{-13}$	90	[38] BERGSMA	85	CHRM CERN beam dump
		[39] FAISSNER	83	OSPK Beam dump, $A^0 \to 2\gamma$
		[40] FAISSNER	83B	RVUE LAMPF beam dump
		[41] FRANK	83B	RVUE LAMPF beam dump
		[42] HOFFMAN	83	CNTR $\pi p \to nA^0$ ($A^0 \to e^+e^-$)
		[43] FETSCHER	82	RVUE See FAISSNER 81B
		[44] FAISSNER	81	OSPK CERN PS ν wideband
		[45] FAISSNER	81B	OSPK Beam dump, $A^0 \to 2\gamma$
		[46] KIM	81	OSPK 26 GeV $pN \to A^0$X
		[47] FAISSNER	80	OSPK Beam dump, $A^0 \to e^+e^-$
$<1. \times 10^{-8}$	90	[48] JACQUES	80	HLBC 28 GeV protons
$<1. \times 10^{-14}$	90	[48] JACQUES	80	HLBC Beam dump
		[49] SOUKAS	80	CALO 28 GeV p beam dump
		[50] BECHIS	79	CNTR
$<1. \times 10^{-8}$	90	[51] COTEUS	79	OSPK Beam dump
$<1. \times 10^{-3}$	95	[52] DISHAW	79	CALO 400 GeV pp
$<1. \times 10^{-8}$	90	ALIBRAN	78	HYBR Beam dump
$<6. \times 10^{-9}$	95	ASRATYAN	78B	CALO Beam dump
$<1.5 \times 10^{-8}$	90	[53] BELLOTTI	78	HLBC Beam dump
$<5.4 \times 10^{-14}$	90	[53] BELLOTTI	78	HLBC m_{A^0}=1.5 MeV
$<4.1 \times 10^{-9}$	90	[53] BELLOTTI	78	HLBC m_{A^0}=1 MeV
$<1. \times 10^{-8}$	90	[54] BOSETTI	78B	HYBR Beam dump
		[55] DONNELLY	78	
$<0.5 \times 10^{-8}$	90	HANSL	78D	WIRE Beam dump
		[56] MICELMAC...	78	
		[57] VYSOTSKII	78	

[1] AAD 25AN search for axion-like particle production in proton-proton collisions in association with single top and a W or top quark pair, with the subsequent A^0 decaying to $b\bar{b}$. They search for axion-like particles with masses between 12 and 100 GeV as shown in the mass-dependent limits on the production cross section times branching fraction in their Fig. 9.

[2] AAD 25AT set limits on the branching fraction of Higgs boson decays to a Z boson and a 0.5–3.5 GeV-mass axion-like particle decaying to either a gluon or quark pair. See their Fig. 4 for detailed limits.

[3] AAD 25AY set limits on long-lived axion-like particles produced in proton-proton collisions via an intermediate off-shell Z boson, with the axion-like particle decaying to a gluon pair in association with a lepton pair in the final state. See their Fig. 15 for limits on the Z + axion cross section multiplied by the axion-to-2-gluon branching ratio as a function of the proper decay length for the axion. They search across axion masses 0.1–40 GeV.

[4] CHEKHOVSKY 25 constrain the production of heavy axion-like particles via a search for $WZ\gamma$ events in proton-proton collisions recorded by the CMS detector. They consider a process in which an ALP is produced alongside a W, and then decays to a Z and γ. See Fig. 3 for mass-dependent limits on the branching ratio multiplied by the cross section (or in terms of the ALP energy scale) across the 110 to 400 GeV ALP mass region.

[5] AAD 24AT search for Higgs decays to axions, constraining the effective coupling to photons between 100 MeV and 62 GeV axion mass. Limit strength is dependent on the effective axion-Higgs coupling and is strongest at the highest mass. See their Fig. 8 for full limits.

[6] AAD 24BN search for the production of long-lived axion-like particles produced in proton-proton collisions at the ATLAS detector. See their Fig. 2 for cross-section limits on benchmark ALP masses between 40 and 55 GeV, as a function of their proper decay length. Limits are presented for both ALP production from $q\bar{q}$ in association with the production of a vector boson, and ALP production from top decays.

[7] AAD 24BZ set limits on photo-phobic axion-like particles with masses between 0.1 and 40 GeV that are radiated from vector bosons and decay into gluons. See their Figs. 11 and 12 for limits on the ALP couplings to W, Z and gluons. An erratum for this publication can be found at AAD 25BF, which impacts the ALP branching ratio limit plots: Figures 9(a) and 10(a).

[8] AAD 24CD search for the production of axion-like particles in association with a hadronically decaying W or Z and large missing transverse energy in proton-proton collisions at the ATLAS detector. See their Fig. 7 for upper limits on the vector boson coupling for an ALP mass of 1 MeV as a function of f_{A^0}.

[9] AAD 24K search for Higgs decays to a Z and an axion-like particle in the mass range 0.1 to 33 GeV. They constrain the axion coupling to photons. See Fig. 3b for mass-dependent limits, which also depend on the coupling of the Higgs to ZA^0.

[10] HAYRAPETYAN 24AZ present results from CMS's search for axion-like particles produced from Higgs decays then promptly decaying to a dimuon. See their Fig. 6 for limits on the effective ALP coupling to the SM-like Higgs.

[11] HAYRAPETYAN 24I report a search by CMS for an exotic Higgs decay to an axion-like particle and a Z, which decay to two photons and two leptons respectively. See Fig. 7 and 8 for mass-dependent limits on the cross-section for the process and the effective axion coupling in the mass range 1 to 30 GeV.

[12] TUMASYAN 24C reports results from the CMS and TOTEM collaborations' search for photon-photon fusion events in proton collisions and the subsequent diphoton events which may occur via the production of axions. Constraints on the axion to two-photon coupling are presented at the 10^{-5} GeV^{-1} level for axion masses between 500 and 2000 GeV.

[13] ACCIARRI 23 search for axions in the NuMI neutrino beam target, which are produced through mixings with mesons due to the coupling with gluons, and exclude f_{A^0} around tens of TeV for m_{A^0} = 0.2–0.9 GeV. They assume a slightly suppressed axion coupling to muons. See their Fig. 4 for the limits.

[14] BERTUZZO 23 employs an analysis analogous to ACCIARRI 23. They search for leptophilic axions primarily produced via $\tau \to \mu A^0$ and $\tau \to e A^0$, and exclude f_{A^0} around 1×10^6–6×10^7 GeV for m_{A^0} = 0.2–1.7 GeV. See their Fig. 2 for the limits.

[15] AAD 22J set upper limits for the cross sections of $H \to A^0 A^0 \to 4\mu$ and $H \to ZA^0 \to 2\ell 2\mu$. See their Figs. 14 and 17 for the respective mass-dependent limits.

[16] TUMASYAN 22AH set the limits of $O(10^{-6})$ with respect to the product of the branching fractions of $H \to A^0 A^0$ and $A^0 \to e^+e^-$, $\mu^+\mu^-$. They also derive limits on the effective axion couplings contributing to $H \to A^0 A^0$ and $H \to ZA^0$. See their Figs. 5 and 7 for the limits.

[17] TUMASYAN 22R is analogous to GAVELA 20, and set a limit on the products of the axion couplings to gluons and Z bosons as $G_{AZZ}\, G_{Agg} < 6.64 \times 10^{-7}$ GeV^{-2} at 95% CL for f_{A^0} = 3 TeV and $m_{A^0} < 100$ GeV. Here we use $c_{\tilde{G}} = G_{Agg}\, f_{A^0}/4$ and $c_{\tilde{Z}} = G_{AZZ}\, f_{A^0}/4$ to translate their limits. They also set a limit on the product of the axion couplings to gluons and ZH. See their Fig. 9 for the f_{A^0}-dependent limits.

[18] AAD 21F look for axion production with an energetic jet and large missing p_T, and set a limit on the axion coupling to gluons, $c_{\tilde{G}}/f_{A^0} < 8 \times 10^{-6}$ GeV^{-1} at 95 % CL for m_{A^0} = 1 MeV. Using $c_{\tilde{G}} = \alpha_s/8\pi$, we interpret the limit as $f_{A^0} > 0.4$ TeV for $\alpha_s \simeq 0.08$.

[19] AAD 21K look for axion production with an energetic photon and large missing p_T, and set a limit on the axion coupling to a Z boson and photon, $G_{AZ\gamma} < 5.1 \times 10^{-4}$ GeV^{-1} at 95 % CL for m_{A^0} = 1 MeV and assuming $G_{A\gamma\gamma} = 0$.

[20] AAD 21N look for axion production using the measurement of light-by-light scattering based on Pb+Pb collision data. They set the limit on the axion-photon coupling, $G_{A\gamma\gamma} < 5.3 \times 10^{-5}$–$3.4 \times 10^{-4}$ GeV^{-1} at 95 % CL for m_{A^0} = 6–100 GeV. Here we use $\Lambda_a = {G_{A\gamma\gamma}}^{-1}$ to translate their limits. See their Fig. 9 for mass-dependent limits.

[21] CARRA 21 is analogous to GAVELA 20, and they use the differential cross sections for WW and $Z\gamma$ production measured with the ATLAS detector to set limits on the product of the axion couplings to gauge bosons as $G_{AWW}\, G_{Agg} < 6.2 \times 10^{-7}$ GeV^{-2} and $G_{AZ\gamma}\, G_{Agg} < 3.7 \times 10^{-7}$ GeV^{-2} at 95 % CL for $m_{A^0} \lesssim 100$ GeV.

[22] AAIJ 20AL look for a light new boson decaying into a pair of muons using the LHCb data with an integrated luminosity of 5.1 fb^{-1}, and set limits on the cross section over a range of m_{X^0} = 0.22–3 and 20–60 GeV. See Figs. 8 and 9 for mass-dependent limits.

[23] GAVELA 20 focus on the axion production as an s-channel off shell mediator, and use the Run 2 CMS public data to set limits on the product of the axion couplings to gluons and photons as well as Z bosons as $G_{A\gamma\gamma}\, G_{Agg} < 2.8 \times 10^{-7}$ GeV^{-2} and $G_{AZZ}\, G_{Agg} < 9.8 \times 10^{-7}$ GeV^{-2} for $m_{A^0} \lesssim 200$ GeV. See their Fig.3 for the limits.

[24] SIRUNYAN 19BQ look for the pair production of a new light boson decaying into a pair of muons, and set limits on the product of the production cross section times branching fraction to dimuons squared times acceptance over a range of m_{X^0} = 0.25–8.5 GeV. See the right panel of their Fig. 1 for mass-dependent limits.

[25] JAIN 07 claims evidence for $A^0 \to e^+e^-$ produced in ^{207}Pb collision on nuclear emulsion (Ag/Br) for $m(A^0) = 7 \pm 1$ or 19 ± 1 MeV and $\tau(A^0) \leq 10^{-13}$ s.

[26] AHMAD 97 reports a result of APEX Collaboration which studied positron production in ^{238}U+^{232}Ta and ^{238}U+^{181}Ta collisions, without requiring a coincident electron. No narrow lines were found for $250 < E_{e^+} < 750$ keV.

[27] LEINBERGER 97 (ORANGE Collaboration) at GSI looked for a narrow sum-energy e^+e^--line at $\sim$ 635 keV in ^{238}U+^{181}Ta collision. Limits on the production probability for a narrow sum-energy e^+e^- line are set. See their Table 2.

[28] GANZ 96 (EPos II Collaboration) has placed upper bounds on the production cross section of e^+e^- pairs from ^{238}U+^{181}Ta and ^{238}U+^{232}Th collisions at GSI. See Table 2 for limits both for back-to-back and isotropic configurations of e^+e^- pairs. These limits rule out the existence of peaks in the e^+e^- sum-energy distribution, reported by an earlier version of this experiment.

[29] KAMEL 96 looked for e^+e^- pairs from the collision of ^{32}S (200 GeV/nucleon) and emulsion. No evidence of mass peaks is found in the region of sensitivity $m_{ee} > 2$ MeV.

[30] BLUEMLEIN 92 is a proton beam dump experiment at Serpukhov with a secondary target to induce Bethe-Heitler production of e^+e^- or $\mu^+\mu^-$ from the produce A^0. See Fig. 5 for the excluded region in m_{A^0}-x plane. For the standard axion, $0.3 < x < 25$ is excluded at 95% CL. If combined with BLUEMLEIN 91, $0.008 < x < 32$ is excluded.

Int. J. Mod. Phys. A 2026.41. Downloaded from www.worldscientific.com by UNIVERSITY OF CALIFORNIA @ BERKELEY on 09/16/26. Re-use and distribution is strictly not permitted, except for Open Access articles.

[31] MEIJERDREES 92 give $\Gamma(\pi^- p \to nA^0)\cdot B(A^0 \to e^+e^-)/\Gamma(\pi^- p \to \text{all}) < 10^{-5}$ (90% CL) for $m_{A^0} = 100$ MeV, $\tau_{A^0} = 10^{-11}$–10^{-23} sec. Limits ranging from 2.5×10^{-3} to 10^{-7} are given for $m_{A^0} = 25$–136 MeV.

[32] BLUEMLEIN 91 is a proton beam dump experiment at Serpukhov. No candidate event for $A^0 \to e^+e^-$, 2γ are found. Fig. 6 gives the excluded region in m_{A^0}-x plane ($x = \tan\beta = v_2/v_1$). Standard axion is excluded for $0.2 < m_{A^0} < 3.2$ MeV for most $x > 1$, 0.2–11 MeV for most $x < 1$.

[33] FAISSNER 89 searched for $A^0 \to e^+e^-$ in a proton beam dump experiment at SIN. No excess of events was observed over the background. A standard axion with mass $2m_e$–20 MeV is excluded. Lower limit on f_{A^0} of $\simeq 10^4$ GeV is given for $m_{A^0} = 2m_e$–20 MeV.

[34] DEBOER 88 reanalyze EL-NADI 88 data and claim evidence for three distinct states with mass ~ 1.1, ~ 2.1, and ~ 9 MeV, lifetimes 10^{-16}–10^{-15} s decaying to e^+e^- and note the similarity of the data with those of a cosmic-ray experiment by Bristol group (B.M. Anand, Proc. of the Royal Society of London, Section A **A22** 183 (1953)). For a criticism see PERKINS 89, who suggests that the events are compatible with π^0 Dalitz decay. DEBOER 89B is a reply which contests the criticism.

[35] EL-NADI 88 claim the existence of a neutral particle decaying into e^+e^- with mass 1.60 ± 0.59 MeV, lifetime $(0.15 \pm 0.01) \times 10^{-14}$ s, which is produced in heavy ion interactions with emulsion nuclei at ~ 4 GeV/c/nucleon.

[36] FAISSNER 88 is a proton beam dump experiment at SIN. They found no candidate event for $A^0 \to \gamma\gamma$. A standard axion decaying to 2γ is excluded except for a region $x \simeq 1$. Lower limit on f_{A^0} of 10^2–10^3 GeV is given for $m_{A^0} = 0.1$–1 MeV.

[37] BADIER 86 did not find long-lived A^0 in 300 GeV π^- Beam Dump Experiment that decays into e^+e^- in the mass range $m_{A^0} = (20$–$200)$ MeV, which excludes the A^0 decay constant $f(A^0)$ in the interval (60–600) GeV. See their figure 6 for excluded region on $f(A^0)$-m_{A^0} plane.

[38] BERGSMA 85 look for $A^0 \to 2\gamma$, e^+e^-, $\mu^+\mu^-$. First limit above is for $m_{A^0} = 1$ MeV; second is for 200 MeV. See their figure 4 for excluded region on f_{A^0}–m_{A^0} plane, where f_{A^0} is A^0 decay constant. For Peccei-Quinn PECCEI 77 A^0, $m_{A^0} < 180$ keV and $\tau > 0.037$ s. (CL = 90%). For the axion of FAISSNER 81B at 250 keV, BERGSMA 85 expect 15 events but observe zero.

[39] FAISSNER 83 observed 19 1-γ and 12 2-γ events where a background of 4.8 and 2.3 respectively is expected. A small-angle peak is observed even if iron wall is set in front of the decay region.

[40] FAISSNER 83B extrapolate SIN γ signal to LAMPF ν experimental condition. Resulting 370 γ's are not at variance with LAMPF upper limit of 450 γ's. Derived from LAMPF limit that $[d\sigma(A^0)/d\omega$ at $90°]m_{A^0}/\tau_{A^0} < 14 \times 10^{-35}$ cm^2 sr^{-1} MeV ms^{-1}. See comment on FRANK 83B.

[41] FRANK 83B stress the importance of LAMPF data bins with negative net signal. By statistical analysis say that LAMPF and SIN-A0 are at variance when extrapolation by phase-space model is done. They find LAMPF upper limit is 248 not 450 γ's. See comment on FAISSNER 83B.

[42] HOFFMAN 83 set CL = 90% limit $d\sigma/dt\ B(e^+e^-) < 3.5 \times 10^{-32}$ cm^2/GeV^2 for $140 < m_{A^0} < 160$ MeV. Limit assumes $\tau(A^0) < 10^{-9}$ s.

[43] FETSCHER 82 reanalyzes SIN beam-dump data of FAISSNER 81. Claims no evidence for axion since 2-γ peak rate remarkably decreases if iron wall is set in front of the decay region.

[44] FAISSNER 81 see excess μe events. Suggest axion interactions.

[45] FAISSNER 81B is SIN 590 MeV proton beam dump. Observed 14.5 ± 5.0 events of 2γ decay of long-lived neutral penetrating particle with $m_{2\gamma} \lesssim 1$ MeV. Axion interpretation with η-A^0 mixing gives $m_{A^0} = 250 \pm 25$ keV, $\tau_{(2\gamma)} = (7.3 \pm 3.7) \times 10^{-3}$ s from above rate. See critical remarks below in comments of FETSCHER 82, FAISSNER 83, FAISSNER 83B, FRANK 83B, and BERGSMA 85. Also see in the next subsection ALEKSEEV 82B, CAVAIGNAC 83, and ANANEV 85.

[46] KIM 81 analyzed 8 candidates for $A^0 \to 2\gamma$ obtained by Aachen-Padova experiment at CERN with 26 GeV protons on Be. Estimated axion mass is about 300 keV and lifetime is $(0.86 \sim 5.6) \times 10^{-3}$ s depending on models. Faissner (private communication), says axion production underestimated and mass overestimated. Correct value around 200 keV.

[47] FAISSNER 80 is SIN beam dump experiment with 590 MeV protons looking for $A^0 \to e^+e^-$ decay. Assuming $A^0/\pi^0 = 5.5 \times 10^{-7}$, obtained decay rate limit $20/(A^0$ mass) MeV/s (CL = 90%), which is about 10^{-7} below theory and interpreted as upper limit to $m_{A^0} < 2m_{e^-}$.

[48] JACQUES 80 is a BNL beam dump experiment. First limit above comes from nonobservation of excess neutral-current-type events $[\sigma(\text{production})\sigma(\text{interaction}) < 7. \times 10^{-68}$ cm^4, CL = 90%$]$. Second limit is from nonobservation of axion decays into 2γ's or e^+e^-, and for axion mass a few MeV.

[49] SOUKAS 80 at BNL observed no excess of neutral-current-type events in beam dump.

[50] BECHIS 79 looked for the axion production in low energy electron Bremsstrahlung and the subsequent decay into either 2γ or e^+e^-. No signal found. CL = 90% limits for model parameter(s) are given.

[51] COTEUS 79 is a beam dump experiment at BNL.

[52] DISHAW 79 is a calorimetric experiment and looks for low energy tail of energy distributions due to energy lost to weakly interacting particles.

[53] BELLOTTI 78 first value comes from search for $A^0 \to e^+e^-$. Second value comes from search for $A^0 \to 2\gamma$, assuming mass $< 2m_{e^-}$. For any mass satisfying this, limit is above value$\times$(mass^{-4}). Third value uses data of PL 60B 401 and quotes $\sigma(\text{production})\sigma(\text{interaction}) < 10^{-67}$ cm^4.

[54] BOSETTI 78B quotes $\sigma(\text{production})\sigma(\text{interaction}) < 2. \times 10^{-67}$ cm^4.

[55] DONNELLY 78 examines data from reactor neutrino experiments of REINES 76 and GURR 74 as well as SLAC beam dump experiment. Evidence is negative.

[56] MICELMACHER 78 finds no evidence of axion existence in reactor experiments of REINES 76 and GURR 74. (See reference under DONNELLY 78 below).

[57] VYSOTSKII 78 derived lower limit for the axion mass 25 keV from luminosity of the sun and 200 keV from red supergiants.

A^0 (Axion) Searches in Reactor Experiments

VALUE	DOCUMENT ID		TECN	COMMENT
• • • We do not use the following data for averages, fits, limits, etc. • • •				
	[1] CHANG	07		Primakoff or Compton
	[2] ALTMANN	95	CNTR	Reactor; $A^0 \to e^+e^-$
	[3] KETOV	86	SPEC	Reactor, $A^0 \to \gamma\gamma$
	[4] KOCH	86	SPEC	Reactor; $A^0 \to \gamma\gamma$
	[5] DATAR	82	CNTR	Light water reactor
	[6] VUILLEUMIER	81	CNTR	Reactor, $A^0 \to 2\gamma$

[1] CHANG 07 looked for monochromatic photons from Primakoff or Compton conversion of axions from the Kuo-Sheng reactor due to axion coupling to photon or electron, respectively. The search places model-independent limits on the products $G_{A\gamma\gamma}G_{ANN}$ and $G_{Aee}G_{ANN}$ for $m(A^0)$ less than the MeV range.

[2] ALTMANN 95 looked for A^0 decaying into e^+e^- from the Bugey 5 nuclear reactor. They obtain an upper limit on the A^0 production rate of $\omega(A^0)/\omega(\gamma) \times B(A^0 \to e^+e^-) < 10^{-16}$ for $m_{A^0} = 1.5$ MeV at 90% CL. The limit is weaker for heavier A^0. In the case of a standard axion, this limit excludes a mass in the range $2m_e < m_{A^0} < 4.8$ MeV at 90% CL. See Fig. 5 of their paper for exclusion limits of axion-like resonances Z^0 in the (m_{X^0}, f_{X^0}) plane.

[3] KETOV 86 searched for A^0 at the Rovno nuclear power plant. They found an upper limit on the A^0 production probability of $0.8\ [100\ \text{keV}/m_{A^0}]^6 \times 10^{-6}$ per fission. In the standard axion model, this corresponds to $m_{A^0} > 150$ keV. Not valid for $m_{A^0} \gtrsim 1$ MeV.

[4] KOCH 86 searched for $A^0 \to \gamma\gamma$ at nuclear power reactor Biblis A. They found an upper limit on the A^0 production rate of $\omega(A^0)/\omega(\gamma(M1)) < 1.5 \times 10^{-10}$ (CL=95%). Standard axion with $m_{A^0} = 250$ keV gives 10^{-5} for the ratio. Not valid for $m_{A^0} > 1022$ keV.

[5] DATAR 82 looked for $A^0 \to 2\gamma$ in neutron capture ($np \to dA^0$) at Tarapur 500 MW reactor. Sensitive to sum of $l = 0$ and $l = 1$ amplitudes. With ZEHNDER 81 $[(l = 0) - (l = 1)]$ result, assert nonexistence of standard A^0.

[6] VUILLEUMIER 81 is at Grenoble reactor. Set limit $m_{A^0} < 280$ keV.

A^0 (Axion) and Other Light Boson (X^0) Searches in Nuclear Transitions

Limits are for branching ratio.

VALUE	CL%	DOCUMENT ID		TECN	COMMENT
• • • We do not use the following data for averages, fits, limits, etc. • • •					
$< 8.89 \times 10^{-6}$	90	[1] DERBIN	23	CNTR	M1 transition of ^{169}Tm
$< 8.5 \times 10^{-6}$	90	[2] DERBIN	02	CNTR	^{125m}Te decay
		[3] DEBOER	97C	RVUE	M1 transitions
$< 5.5 \times 10^{-10}$	95	[4] TSUNODA	95	CNTR	^{252}Cf fission, $A^0 \to ee$
$< 1.2 \times 10^{-6}$	95	[5] MINOWA	93	CNTR	^{139}La$^* \to {}^{139}$LaA^0
$< 2 \times 10^{-4}$	90	[6] HICKS	92	CNTR	^{35}S decay, $A^0 \to \gamma\gamma$
$< 1.5 \times 10^{-9}$	95	[7] ASANUMA	90	CNTR	^{241}Am decay
$< (0.4$–$10) \times 10^{-3}$	95	[8] DEBOER	90	CNTR	^{8}Be$^* \to {}^8$BeA^0, $A^0 \to e^+e^-$
$< (0.2$–$1) \times 10^{-3}$	90	[9] BINI	89	CNTR	^{16}O$^* \to {}^{16}$OX^0, $X^0 \to e^+e^-$
		[10] AVIGNONE	88	CNTR	Cu$^* \to$ CuA^0 ($A^0 \to 2\gamma$, $A^0 e \to \gamma e$, $A^0 Z \to \gamma Z$)
$< 1.5 \times 10^{-4}$	90	[11] DATAR	88	CNTR	^{12}C$^* \to {}^{12}$CA^0, $A^0 \to e^+e^-$
$< 5 \times 10^{-3}$	90	[12] DEBOER	88C	CNTR	^{16}O$^* \to {}^{16}$OX^0, $X^0 \to e^+e^-$
$< 3.4 \times 10^{-5}$	95	[13] DOEHNER	88	SPEC	^{2}H*, $A^0 \to e^+e^-$
$< 4 \times 10^{-4}$	95	[14] SAVAGE	88	CNTR	Nuclear decay (isovector)
$< 3 \times 10^{-3}$	95	[14] SAVAGE	88	CNTR	Nuclear decay (isoscalar)
$< 10.6 \times 10^{-2}$	90	[15] HALLIN	86	SPEC	^{6}Li isovector decay
< 10.8	90	[15] HALLIN	86	SPEC	^{10}B isoscalar decays
< 2.2	90	[15] HALLIN	86	SPEC	^{14}N isoscalar decays
$< 4 \times 10^{-4}$	90	[16] SAVAGE	86B	CNTR	^{14}N*
		[17] ANANEV	85	CNTR	Li*, deut* $A^0 \to 2\gamma$
		[18] CAVAIGNAC	83	CNTR	^{97}Nb*, deut* transition $A^0 \to 2\gamma$
		[19] ALEKSEEV	82B	CNTR	Li*, deut* transition $A^0 \to 2\gamma$
		[20] LEHMANN	82	CNTR	Cu$^* \to$ CuA^0 ($A^0 \to 2\gamma$)
		[21] ZEHNDER	82	CNTR	Li*, Nb* decay, n-capt.
		[22] ZEHNDER	81	CNTR	Ba$^* \to$ BaA^0 ($A^0 \to 2\gamma$)
		[23] CALAPRICE	79		Carbon

[1] DERBIN 23 use a thallium garnet bolometric detector to search for the 8.4 keV solar axion line emitted from the M1 nuclear transition of ^{169}Tm. Their limits are equivalent to an upper bound on the KSVZ and DFSZ axion masses of 141 eV and 244 eV, respectively.

[2] DERBIN 02 looked for the axion emission in an M1 transition in ^{125m}Te decay. They looked for a possible presence of a shifted energy spectrum in gamma rays due to the undetected axion.

[3] DEBOER 97C reanalyzed the existent data on Nuclear M1 transitions and find that a 9 MeV boson decaying into e^+e^- would explain the excess of events with large opening angles. See also DEBOER 01 for follow-up experiments.

[4] TSUNODA 95 looked for axion emission when ^{252}Cf undergoes a spontaneous fission, with the axion decaying into e^+e^-. The bound is for m_{A^0}=40 MeV. It improves to 2.5×10^{-5} for m_{A^0}=200 MeV.

[5] MINOWA 93 studied chain process, ^{139}Ce $\to {}^{139}$La* by electron capture and M1 transition of ^{139}La* to the ground state. It does not assume decay modes of A^0. The bound applies for $m_{A^0} < 166$ keV.

Int. J. Mod. Phys. A 2026.41. Downloaded from www.worldscientific.com
by UNIVERSITY OF CALIFORNIA @ BERKELEY on 09/16/26. Re[redacted]s strictly not permitted, except for Open Access articles.

[6] HICKS 92 bound is applicable for $\tau_{X^0} < 4 \times 10^{-11}$ sec.

[7] The ASANUMA 90 limit is for the branching fraction of X^0 emission per ^{241}Am α decay and valid for $\tau_{X^0} < 3 \times 10^{-11}$ s.

[8] The DEBOER 90 limit is for the branching ratio ^{8}Be* (18.15 MeV, 1^+) $\rightarrow$ ^{8}BeA^0, $A^0 \rightarrow e^+e^-$ for the mass range m_{A^0} = 4–15 MeV.

[9] The BINI 89 limit is for the branching fraction of ^{16}O*(6.05 MeV, 0^+) $\rightarrow$ ^{16}OX^0, $X^0 \rightarrow e^+e^-$ for m_X = 1.5–3.1 MeV. $\tau_{X^0} \lesssim 10^{-11}$ s is assumed. The spin-parity of X is restricted to 0^+ or 1^-.

[10] AVIGNONE 88 looked for the 1115 keV transition C* $\rightarrow$ CuA^0, either from $A^0 \rightarrow 2\gamma$ in-flight decay or from the secondary A^0 interactions by Compton and by Primakoff processes. Limits for axion parameters are obtained for $m_{A^0} < 1.1$ MeV.

[11] DATAR 88 rule out light pseudoscalar particle emission through its decay $A^0 \rightarrow e^+e^-$ in the mass range 1.02–2.5 MeV and lifetime range 10^{-13}–10^{-8} s. The above limit is for $\tau = 5 \times 10^{-13}$ s and m = 1.7 MeV; see the paper for the τ-m dependence of the limit.

[12] The limit is for the branching fraction of ^{16}O*(6.05 MeV, 0^+) $\rightarrow$ ^{16}OX^0, $X^0 \rightarrow e^+e^-$ against internal pair conversion for m_{X^0} = 1.7 MeV and $\tau_{X^0} < 10^{-11}$ s. Similar limits are obtained for m_{X^0} = 1.3–3.2 MeV. The spin parity of X^0 must be either 0^+ or 1^-. The limit at 1.7 MeV is translated into a limit for the X^0-nucleon coupling constant: $g^2_{X^0NN}/4\pi < 2.3 \times 10^{-9}$.

[13] The DOEHNER 88 limit is for m_{A^0} = 1.7 MeV, $\tau(A^0) < 10^{-10}$ s. Limits less than 10^{-4} are obtained for m_{A^0} = 1.2–2.2 MeV.

[14] SAVAGE 88 looked for A^0 that decays into e^+e^- in the decay of the 9.17 MeV $J^P = 2^+$ state in ^{14}N, 17.64 MeV state $J^P = 1^+$ in ^{8}Be, and the 18.15 MeV state $J^P = 1^+$ in ^{8}Be. This experiment constrains the isovector coupling of A^0 to hadrons, if m_{A^0} = (1.1 $\rightarrow$ 2.2) MeV and the isoscalar coupling of A^0 to hadrons, if m_{A^0} = (1.1 $\rightarrow$ 2.6) MeV. Both limits are valid only if $\tau(A^0) \lesssim 1 \times 10^{-11}$ s.

[15] Limits are for $\Gamma(A^0(1.8\ \text{MeV}))/\Gamma(\pi\text{M1})$; i.e., for 1.8 MeV axion emission normalized to the rate for internal emission of e^+e^- pairs. Valid for $\tau_{A^0} < 2 \times 10^{-11}$s. ^{6}Li isovector decay data strongly disfavor PECCEI 86 model I, whereas the ^{10}B and ^{14}N isoscalar decay data strongly reject PECCEI 86 model II and III.

[16] SAVAGE 86B looked for A^0 that decays into e^+e^- in the decay of the 9.17 MeV $J^P = 2^+$ state in ^{14}N. Limit on the branching fraction is valid if $\tau_{A^0} \lesssim 1. \times 10^{-11}$s for m_{A^0} = (1.1–1.7) MeV. This experiment constrains the iso-vector coupling of A^0 to hadrons.

[17] ANANEV 85 with IBR-2 pulsed reactor exclude standard A^0 at CL = 95% masses below 470 keV (Li* decay) and below $2m_e$ for deuteron* decay.

[18] CAVAIGNAC 83 at Bugey reactor exclude axion at any $m_{^{97}\text{Nb*decay}}$ and axion with m_{A^0} between 275 and 288 keV (deuteron* decay).

[19] ALEKSEEV 82 with IBR-2 pulsed reactor exclude standard A^0 at CL = 95% mass-ranges m_{A^0} <400 keV (Li* decay) and 330 keV <m_{A^0} <2.2 MeV. (deuteron* decay).

[20] LEHMANN 82 obtained $A^0 \rightarrow 2\gamma$ rate $< 6.2 \times 10^{-5}$/s (CL = 95%) excluding m_{A^0} between 100 and 1000 keV.

[21] ZEHNDER 82 used Gosgen 2.8GW light-water reactor to check A^0 production. No 2γ peak in Li*, Nb* decay (both single p transition) nor in n capture (combined with previous Ba* negative result) rules out standard A^0. Set limit m_{A^0} <60 keV for any A^0.

[22] ZEHNDER 81 looked for Ba* $\rightarrow$ A^0Ba transition with $A^0 \rightarrow 2\gamma$. Obtained 2γ coincidence rate $< 2.2 \times 10^{-5}$/s (CL = 95%) excluding m_{A^0} >160 keV (or 200 keV depending on Higgs mixing). However, see BARROSO 81.

[23] CALAPRICE 79 saw no axion emission from excited states of carbon. Sensitive to axion mass between 1 and 15 MeV.

A^0 (Axion) Limits from Its Electron Coupling

Limits are for $\tau(A^0 \rightarrow e^+e^-)$.

VALUE (s)	CL%	DOCUMENT ID		TECN	COMMENT
• • • We do not use the following data for averages, fits, limits, etc. • • •					
		[1] ANDREEV	21	NA64	$eN \rightarrow eA^0N$ ($A^0 \rightarrow$ invisibles)
		[2] ANDREEV	21B	NA64	$eN \rightarrow eA^0N$ ($A^0 \rightarrow ee$)
none 4×10^{-16}–4.5×10^{-12}	90	[3] BROSS	91	BDMP	$eN \rightarrow eA^0N$ ($A^0 \rightarrow ee$)
		[4] GUO	90	BDMP	$eN \rightarrow eA^0N$ ($A^0 \rightarrow ee$)
		[5] BJORKEN	88	CALO	$A \rightarrow e^+e^-$ or 2γ
		[6] BLINOV	88	MD1	$ee \rightarrow eeA^0$ ($A^0 \rightarrow ee$)
none 1×10^{-14}–1×10^{-10}	90	[7] RIORDAN	87	BDMP	$eN \rightarrow eA^0N$ ($A^0 \rightarrow ee$)
none 1×10^{-14}–1×10^{-11}	90	[8] BROWN	86	BDMP	$eN \rightarrow eA^0N$ ($A^0 \rightarrow ee$)
none 6×10^{-14}–9×10^{-11}	95	[9] DAVIER	86	BDMP	$eN \rightarrow eA^0N$ ($A^0 \rightarrow ee$)
none 3×10^{-13}–1×10^{-7}	90	[10] KONAKA	86	BDMP	$eN \rightarrow eA^0N$ ($A^0 \rightarrow ee$)

[1] ANDREEV 21 look for invisible decays of axions coupled to electrons, and set limits on $g_{Aee} < 4.6 \times 10^{-6}$–$3.1 \times 10^{-3}$ for $m_{A^0} = 10^{-3}$–1 GeV. This limits the axion contribution to the electron g−2 to an order of magnitude less than the current experimental uncertainty. See their Figs. 3 and 4 for mass-dependent limits.

[2] ANDREEV 21B set limits on g_{Aee} in the range of 6.3×10^{-6}–1.6×10^{-3} for m_{A^0} = 2–17 MeV at 90% CL. This excludes $6.6 \times 10^{-5} < g_{Aee} < 1 \times 10^{-4}$ at m_{A^0} = 16.7 MeV corresponding to the ATOMKI anomaly. See their Fig. 2 for mass-dependent limits.

[3] The listed BROSS 91 limit is for m_{A^0} = 1.14 MeV. B($A^0 \rightarrow e^+e^-$) = 1 assumed. Excluded domain in the τ_{A^0}–m_{A^0} plane extends up to $m_{A^0} \approx 7$ MeV (see Fig. 5). Combining with electron g−2 constraint, axions coupling only to e^+e^- ruled out for $m_{A^0} < 4.8$ MeV (90% CL).

[4] GUO 90 use the same apparatus as BROWN 86 and improve the previous limit in the shorter lifetime region. Combined with g−2 constraint, axions coupling only to e^+e^- are ruled out for $m_{A^0} < 2.7$ MeV (90% CL).

[5] BJORKEN 88 reports limits on axion parameters (f_A, m_A, τ_A) for $m_{A^0} < 200$ MeV from electron beam-dump experiment with production via Primakoff photoproduction, bremsstrahlung from electrons, and resonant annihilation of positrons on atomic electrons.

[6] BLINOV 88 assume zero spin, m = 1.8 MeV and lifetime $< 5 \times 10^{-12}$ s and find $\Gamma(A^0 \rightarrow \gamma\gamma)$B($A^0 \rightarrow e^+e^-$) < 2 eV (CL=90%).

[7] Assumes $A^0\gamma\gamma$ coupling is small and hence Primakoff production is small. Their figure 2 shows limits on axions for $m_{A^0} < 15$ MeV.

[8] Uses electrons in hadronic showers from an incident 800 GeV proton beam. Limits for $m_{A^0} < 15$ MeV are shown in their figure 3.

[9] m_{A^0} = 1.8 MeV assumed. The excluded domain in the τ_{A^0}–m_{A^0} plane extends up to $m_{A^0} \approx 14$ MeV, see their figure 4.

[10] The limits are obtained from their figure 3. Also given is the limit on the $A^0\gamma\gamma$–$A^0e^+e^-$ coupling plane by assuming Primakoff production.

Search for A^0 (Axion) Resonance in Bhabha Scattering

The limit is for $\Gamma(A^0)[\text{B}(A^0 \rightarrow e^+e^-)]^2$.

VALUE (10^{-3} eV)	CL%	DOCUMENT ID		TECN	COMMENT
• • • We do not use the following data for averages, fits, limits, etc. • • •					
< 1.3	97	[1] HALLIN	92	CNTR	m_{A^0} = 1.75–1.88 MeV
none 0.0016–0.47	90	[2] HENDERSON	92C	CNTR	m_{A^0}= 1.5–1.86 MeV
< 2.0	90	[3] WU	92	CNTR	m_{A^0}= 1.56–1.86 MeV
< 0.013	95	TSERTOS	91	CNTR	m_{A^0} = 1.832 MeV
none 0.19–3.3	95	[4] WIDMANN	91	CNTR	m_{A^0}= 1.78–1.92 MeV
< 5	97	BAUER	90	CNTR	m_{A^0} = 1.832 MeV
none 0.09–1.5	95	[5] JUDGE	90	CNTR	m_{A^0} = 1.832 MeV, elastic
< 1.9	97	[6] TSERTOS	89	CNTR	m_{A^0} = 1.82 MeV
<(10–40)	97	[6] TSERTOS	89	CNTR	m_{A^0} = 1.51–1.65 MeV
<(1–2.5)	97	[6] TSERTOS	89	CNTR	m_{A^0} = 1.80–1.86 MeV
< 31	95	LORENZ	88	CNTR	m_{A^0} = 1.646 MeV
< 94	95	LORENZ	88	CNTR	m_{A^0} = 1.726 MeV
< 23	95	LORENZ	88	CNTR	m_{A^0} = 1.782 MeV
< 19	95	LORENZ	88	CNTR	m_{A^0} = 1.837 MeV
< 3.8	97	[7] TSERTOS	88	CNTR	m_{A^0} = 1.832 MeV
		[8] VANKLINKEN	88	CNTR	
		[9] MAIER	87	CNTR	
<2500	90	MILLS	87	CNTR	m_{A^0} = 1.8 MeV
		[10] VONWIMMER..	87	CNTR	

[1] HALLIN 92 quote limits on lifetime, 8×10^{-14} – 5×10^{-13} sec depending on mass, assuming B($A^0 \rightarrow e^+e^-$) = 100%. They say that TSERTOS 91 overstated their sensitivity by a factor of 3.

[2] HENDERSON 92C exclude axion with lifetime τ_{A^0}=1.4×10^{-12} – 4.0×10^{-10} s, assuming B($A^0 \rightarrow e^+e^-$)=100%. HENDERSON 92C also exclude a vector boson with τ=1.4×10^{-12} – 6.0×10^{-10} s.

[3] WU 92 quote limits on lifetime $> 3.3 \times 10^{-13}$ s assuming B($A^0 \rightarrow e^+e^-$)=100%. They say that TSERTOS 89 overestimate the limit by a factor of $\pi/2$. WU 92 also quote a bound for vector boson, $\tau > 8.2 \times 10^{-13}$ s.

[4] WIDMANN 91 bound applies exclusively to the case B($A^0 \rightarrow e^+e^-$)=1, since the detection efficiency varies substantially as $\Gamma(A^0)_{\text{total}}$ changes. See their Fig. 6.

[5] JUDGE 90 excludes an elastic pseudoscalar e^+e^- resonance for 4.5×10^{-13} s < $\tau(A^0)$ < 7.5×10^{-12} s (95% CL) at m_{A^0} = 1.832 MeV. Comparable limits can be set for m_{A^0} = 1.776–1.856 MeV.

[6] See also TSERTOS 88B in references.

[7] The upper limit listed in TSERTOS 88 is too large by a factor of 4. See TSERTOS 88B, footnote 3.

[8] VANKLINKEN 88 looked for relatively long-lived resonance ($\tau = 10^{-10}$–10^{-12} s). The sensitivity is not sufficient to exclude such a narrow resonance.

[9] MAIER 87 obtained limits $R\Gamma \lesssim 60$ eV (100 eV) at $m_{A^0} \simeq 1.64$ MeV (1.83 MeV) for energy resolution $\Delta E_{\text{cm}} \simeq 3$ keV, where R is the resonance cross section normalized to that of Bhabha scattering, and $\Gamma = \Gamma^2_{ee}/\Gamma_{\text{total}}$. For a discussion implying that $\Delta E_{\text{cm}} \simeq 10$ keV, see TSERTOS 89.

[10] VONWIMMERSPERG 87 measured Bhabha scattering for E_{cm} = 1.37–1.86 MeV and found a possible peak at 1.73 with $\int \sigma dE_{\text{cm}} = 14.5 \pm 6.8$ keV·b. For a comment and a reply, see VANKLINKEN 88B and VONWIMMERSPERG 88. Also see CONNELL 88.

Search for A^0 (Axion) Resonance in $e^+e^- \rightarrow \gamma\gamma$

The limit is for $\Gamma(A^0 \rightarrow e^+e^-)\cdot\Gamma(A^0 \rightarrow \gamma\gamma)/\Gamma_{\text{total}}$

VALUE (10^{-3} eV)	CL%	DOCUMENT ID		TECN	COMMENT
• • • We do not use the following data for averages, fits, limits, etc. • • •					
< 0.18	95	VO	94	CNTR	m_{A^0}=1.1 MeV

Int. J. Mod. Phys. A 2026.41. Downloaded from www.worldscientific.com by UNIVERSITY OF CALIFORNIA @ BERKELEY on 09/16/26. Re-use and distribution is strictly not permitted, except for Open Access articles.

$<$ 1.5	95	VO	94	CNTR	m_{A^0}=1.4 MeV
$<$12	95	VO	94	CNTR	m_{A^0}=1.7 MeV
$<$ 6.6	95	[1] TRZASKA	91	CNTR	m_{A^0} = 1.8 MeV
$<$ 4.4	95	WIDMANN	91	CNTR	m_{A^0}= 1.78–1.92 MeV
		[2] FOX	89	CNTR	
$<$ 0.11	95	[3] MINOWA	89	CNTR	m_{A^0} = 1.062 MeV
$<$33	97	CONNELL	88	CNTR	m_{A^0} = 1.580 MeV
$<$42	97	CONNELL	88	CNTR	m_{A^0} = 1.642 MeV
$<$73	97	CONNELL	88	CNTR	m_{A^0} = 1.782 MeV
$<$79	97	CONNELL	88	CNTR	m_{A^0} = 1.832 MeV

[1] TRZASKA 91 also give limits in the range (6.6–30) $\times 10^{-3}$ eV (95%CL) for m_{A^0} = 1.6–2.0 MeV.

[2] FOX 89 measured positron annihilation with an electron in the source material into two photons and found no signal at 1.062 MeV ($< 9\times10^{-5}$ of two-photon annihilation at rest).

[3] Similar limits are obtained for m_{A^0} = 1.045–1.085 MeV.

Search for X^0 (Light Boson) Resonance in $e^+e^- \to \gamma\gamma\gamma$

The limit is for $\Gamma(X^0 \to e^+e^-)\cdot\Gamma(X^0 \to \gamma\gamma\gamma)/\Gamma_{\rm total}$. C invariance forbids spin-0 X^0 coupling to both e^+e^- and $\gamma\gamma\gamma$.

VALUE (10^{-3} eV)	CL%	DOCUMENT ID		TECN	COMMENT
• • • We do not use the following data for averages, fits, limits, etc. • • •					
$<$ 0.2	95	[1] VO	94	CNTR	m_{X^0}=1.1–1.9 MeV
$<$ 1.0	95	[2] VO	94	CNTR	m_{X^0}=1.1 MeV
$<$ 2.5	95	[2] VO	94	CNTR	m_{X^0}=1.4 MeV
$<$120	95	[2] VO	94	CNTR	m_{X^0}=1.7 MeV
$<$ 3.8	95	[3] SKALSEY	92	CNTR	m_{X^0}= 1.5 MeV

[1] VO 94 looked for $X^0 \to \gamma\gamma\gamma$ decaying at rest. The precise limits depend on m_{X^0}. See Fig. 2(b) in paper.

[2] VO 94 looked for $X^0 \to \gamma\gamma\gamma$ decaying in flight.

[3] SKALSEY 92 also give limits 4.3 for m_{X^0} = 1.54 and 7.5 for 1.64 MeV. The spin of X^0 is assumed to be one.

Light Boson (X^0) Search in Nonresonant e^+e^- Annihilation at Rest

Limits are for the ratio of $n\gamma + X^0$ production relative to $\gamma\gamma$.

VALUE (units 10^{-6})	CL%	DOCUMENT ID		TECN	COMMENT
• • • We do not use the following data for averages, fits, limits, etc. • • •					
$<$ 4.2	90	[1] MITSUI	96	CNTR	γX^0
$<$ 4	68	[2] SKALSEY	95	CNTR	γX^0
$<$40	68	[3] SKALSEY	95	RVUE	γX^0
$<$ 0.18	90	[4] ADACHI	94	CNTR	$\gamma\gamma X^0$, $X^0 \to \gamma\gamma$
$<$ 0.26	90	[5] ADACHI	94	CNTR	$\gamma\gamma X^0$, $X^0 \to \gamma\gamma$
$<$ 0.33	90	[6] ADACHI	94	CNTR	γX^0, $X^0 \to \gamma\gamma\gamma$

[1] MITSUI 96 looked for a monochromatic γ. The bound applies for a vector X^0 with C=-1 and m_{X^0} $<$200 keV. They derive an upper bound on $ee X^0$ coupling and hence on the branching ratio B(o-Ps $\to \gamma\gamma X^0$)$< 6.2\times10^{-6}$. The bounds weaken for heavier X^0.

[2] SKALSEY 95 looked for a monochromatic γ without an accompanying γ in e^+e^- annihilation. The bound applies for scalar and vector X^0 with $C = -1$ and m_{X^0} = 100–1000 keV.

[3] SKALSEY 95 reinterpreted the bound on γA^0 decay of o-Ps by ASAI 91 where 3% of delayed annihilations are not from $^3S_1$ states. The bound applies for scalar and vector X^0 with $C = -1$ and m_{X^0} = 0–800 keV.

[4] ADACHI 94 looked for a peak in the $\gamma\gamma$ invariant mass distribution in $\gamma\gamma\gamma\gamma$ production from e^+e^- annihilation. The bound applies for m_{X^0} = 70–800 keV.

[5] ADACHI 94 looked for a peak in the missing-mass mass distribution in $\gamma\gamma$ channel, using $\gamma\gamma\gamma\gamma$ production from e^+e^- annihilation. The bound applies for m_{X^0} $<$800 keV.

[6] ADACHI 94 looked for a peak in the missing mass distribution in $\gamma\gamma\gamma$ channel, using $\gamma\gamma\gamma\gamma$ production from e^+e^- annihilation. The bound applies for m_{X^0} = 200–900 keV.

Searches for Goldstone Bosons (X^0)

(Including Horizontal Bosons and Majorons.) Limits are for branching ratios.

VALUE	CL%	DOCUMENT ID		TECN	COMMENT
• • • We do not use the following data for averages, fits, limits, etc. • • •					
		[1] IVANEZ-BAL...	25	ASTR	Majoron, SN 1987A
$<0.2\times10^{-4}$	95	[2] UNO	25	BEL2	$\tau \to \mu X^0$, $\tau \to e X^0$
		[3] ADACHI	23A	BEL2	$\tau^- \to e^- X^0$, Familon
		[4] ADACHI	23A	BEL2	$\tau^- \to \mu^- X^0$, Familon
		[5] FIORILLO	23	ASTR	Majoron, SN 1987A
		[6] SANDNER	23	COSM	Majoron, CMB
		[7] COLOMA	22A	BORX	νe non-standard interactions
$<4.3\times10^{-6}$	90	[8] AGUILAR-AR...	21A	PIEN	$\pi \to \mu\nu X^0$, Majoron
$<5.2\times10^{-8}$	90	[9] AGUILAR-AR...	21A	PIEN	$\pi \to e\nu X^0$, Majoron
$<9 \times10^{-6}$	90	[10] AGUILAR-AR...	20	PIEN	$\mu^+ \to e^+ X^0$, Familon
$<7 \times10^{-12}$	90	[11] BALDINI	20	MEG	$\mu^+ \to e^+ X^0$ ($X^0 \to \gamma\gamma$), Familon
$<9 \times10^{-6}$	90	[12] BAYES	15	TWST	$\mu^+ \to e^+ X^0$, Familon
		[13] LATTANZI	13	COSM	Majoron dark matter decay
		[14] LESSA	07	RVUE	Meson, ℓ decays to Majoron
		[15] FARZAN	03	ASTR	Majoron, SN cooling
		[16] DIAZ	98	THEO	$H^0 \to X^0X^0$, $A^0 \to X^0X^0X^0$, Majoron
		[17] BOBRAKOV	91		Electron quasi-magnetic interaction
$<3.3\times10^{-2}$	95	[18] ALBRECHT	90E	ARG	$\tau \to \mu X^0$. Familon
$<1.8\times10^{-2}$	95	[18] ALBRECHT	90E	ARG	$\tau \to e X^0$. Familon
$<6.4\times10^{-9}$	90	[19] ATIYA	90	B787	$K^+ \to \pi^+ X^0$. Familon
$<1.4\times10^{-5}$	90	[20] BALKE	88	CNTR	$\mu^+ \to e^+ X^0$. Familon
$<1.1\times10^{-9}$	90	[21] BOLTON	88	CBOX	$\mu^+ \to e^+\gamma X^0$. Familon
		[22] CHANDA	88	ASTR	Sun, Majoron
		[23] CHOI	88	ASTR	Majoron, SN 1987A
$<5 \times10^{-6}$	90	[24] PICCIOTTO	88	CNTR	$\pi \to e\nu X^0$, Majoron
$<1.3\times10^{-9}$	90	[25] GOLDMAN	87	CNTR	$\mu \to e\gamma X^0$. Familon
$<3 \times10^{-4}$	90	[26] BRYMAN	86B	RVUE	$\mu \to e X^0$. Familon
$<1 \times10^{-10}$	90	[27] EICHLER	86	SPEC	$\mu^+ \to e^+ X^0$. Familon
$<2.6\times10^{-6}$	90	[28] JODIDIO	86	SPEC	$\mu^+ \to e^+ X^0$. Familon
		[29] BALTRUSAIT...	85	MRK3	$\tau \to \ell X^0$. Familon
		[30] DICUS	83	COSM	ν(hvy) $\to \nu$(light)X^0

[1] IVANEZ-BALLESTEROS 25 set new bounds on majorons coupled to neutrinos using the 24 neutrino events from SN 1987A, based on a three-neutrino likelihood analysis including nonradiative neutrino decay in matter and the resulting distortion of the neutrino energy spectrum. See their Figs. 1–3 for bounds on the majoron-neutrino coupling as a function of the lightest neutrino mass.

[2] UNO 25 search for the production of a 0–1.6 GeV mass spin-0 particle in lepton-flavour violating tau decays at Belle II. See Fig. 4 for mass-dependent limits on the branching ratio of tau decays to X^0 and electrons or muons.

[3] ADACHI 23A set limits in the range of 1.1×10^{-3}–9.7×10^{-3} for $0 < m_{X^0} < 1.6$ GeV on B($\tau^- \to e^- X^0$)/B($\tau^- \to e^-\overline{\nu}_e\nu_\tau$). See their Fig. 2 for mass-dependent limits.

[4] ADACHI 23A set limits in the range of 7×10^{-4}–1.22×10^{-2} for $0 < m_{X^0} < 1.6$ GeV on B($\tau^- \to \mu^- X^0$)/B($\tau^- \to \mu^-\overline{\nu}_\mu\nu_\tau$). See their Fig. 2 for mass-dependent limits.

[5] FIORILLO 23 used data from Kamiokande-II and IMB on the neutrino flux from SN1987A to constrain the universal neutrino Majoron Yukawa coupling, g. They set an upper limit of $g\, m_{X^0} \lesssim 10^{-9}$ MeV for Majoron masses 100 eV $\lesssim m_{X^0} \lesssim$ 100 MeV, using neutrino coalescence as production of Majorons which then decay back to neutrinos. See their Fig. 1 for the mass-dependent limits.

[6] SANDNER 23 study Majoron production via neutrino inverse decay and use Planck data to constrain the neutrino Majoron Yukawa coupling to $g \lesssim 2\times10^{-13}$–$1\times10^{-12}$ for Majoron masses m_{X^0} = 1–10 eV. See their Fig. 1 for mass-dependent limits.

[7] COLOMA 22A used the spectral data of Borexino Phase II to constrain the neutrino non-standard interaction with electrons mediated by a scalar or a pseudoscalar. Limits on the universal coupling to neutrinos and electrons between 2×10^{-6} and 10^{-4} are obtained for $m_{X^0} \lesssim$ 30–40 MeV. See their Fig. 6 for mass-dependent limits.

[8] AGUILAR-AREVALO 21A quoted limit applies to m_{X^0} = 33.9 MeV. Limits between 4.3×10^{-6} and 7.5×10^{-5} are obtained for $0 < m_{X^0} < 33.9$ MeV. The lifetime of X^0 is assumed to be long enough. See their Fig. 6 for mass-dependent limits.

[9] AGUILAR-AREVALO 21A quoted limit applies to m_{X^0} = 85 MeV. Limits between 5.2×10^{-8} and 1.4×10^{-6} are obtained for $0 < m_{X^0} < 120$ MeV, which improve the limits of PICCIOTTO 88 by an order of magnitude. The lifetime of X^0 is assumed to be long enough. See their Fig. 4 for mass-dependent limits.

[10] AGUILAR-AREVALO 20 obtained limits of order 10^{-5} for m_{X^0} = 47.8–95.1 MeV. The quoted limit applies to m_{X^0} = 75 MeV. See their Fig. 1 for mass-dependent limits.

[11] BALDINI 20 obtained limits for m_{X^0} = 20–45 MeV and $\tau_{X^0} < 40$ ps, and supersedes BOLTON 88 for m_{X^0} = 20–40 MeV. See their Fig. 17 for mass-dependent limits.

[12] BAYES 15 limits are the average over m_{X^0} = 13–80 MeV for the isotropic decay distribution of positrons. See their Fig. 4 and Table II for the mass-dependent limits as well as the dependence on the decay anisotropy. In particular, they find a limit $< 58\times10^{-6}$ at 90% CL for massless familons and for the same asymmetry as normal muon decay, a case not covered by JODIDIO 86.

[13] LATTANZI 13 use WMAP 9 year data as well as X-ray and γ-ray observations to derive limits on decaying majoron dark matter. A limit on the decay width $\Gamma(X^0 \to \nu\overline{\nu}) < 6.4\times10^{-19}$ s^{-1} at 95% CL is found if majorons make up all of the dark matter.

[14] LESSA 07 consider decays of the form Meson $\to \ell\nu$Majoron and $\ell \to \ell'\nu\overline{\nu}$Majoron and use existing data to derive limits on the neutrino-Majoron Yukawa couplings $g_{\alpha\beta}$ (α,β=e,μ,τ). Their best limits are $|g_{e\alpha}|^2 < 5.5\times10^{-6}$, $|g_{\mu\alpha}|^2 < 4.5\times10^{-5}$, $|g_{\tau\alpha}|^2 < 5.5\times10^{-2}$ at CL = 90%.

[15] FARZAN 03 set limits on the neutrino Majoron Yukawa coupling, $|g_{ee}| < 4\times10^{-7}$, by considering the SN cooling due to the massless Majoron emission via neutrino coalescence. They also exclude values around 10^{-5} for both $g_{e\mu}$ and $g_{\mu\mu}$ using the process $\nu\nu \to X^0X^0$. See also their Figs. 3 and 4 for mass-dependent limits.

[16] DIAZ 98 studied models of spontaneously broken lepton number with both singlet and triplet Higgses. They obtain limits on the parameter space from invisible decay $Z \to H^0A^0 \to X^0X^0X^0X^0X^0$ and $e^+e^- \to ZH^0$ with $H^0 \to X^0X^0$.

[17] BOBRAKOV 91 searched for anomalous magnetic interactions between polarized electrons expected from the exchange of a massless pseudoscalar boson (arion). A limit $x_e^2 < 2\times10^{-4}$ (95%CL) is found for the effective anomalous magneton parametrized as $x_e(G_F/8\pi\sqrt{2})^{1/2}$.

[18] ALBRECHT 90E limits are for B($\tau \to \ell X^0$)/B($\tau \to \ell\nu\overline{\nu}$). Valid for $m_{X^0} < 100$ MeV. The limits rise to 7.1% (for μ), 5.0% (for e) for m_{X^0} = 500 MeV.

[19] ATIYA 90 limit is for m_{X^0} = 0. The limit B $< 1\times10^{-8}$ holds for $m_{X^0} < 95$ MeV. For the reduction of the limit due to finite lifetime of X^0, see their Fig. 3.

[20] BALKE 88 limits are for $B(\mu^+ \to e^+ X^0)$. Valid for $m_{X^0} < 80$ MeV and $\tau_{X^0} > 10^{-8}$ sec.

[21] BOLTON 88 limit corresponds to $F > 3.1 \times 10^9$ GeV, which does not depend on the chirality property of the coupling.

[22] CHANDA 88 find $v_T < 10$ MeV for the weak-triplet Higgs vacuum expectation value in Gelmini-Roncadelli model, and $v_S > 5.8 \times 10^6$ GeV in the singlet Majoron model.

[23] CHOI 88 used the observed neutrino flux from the supernova SN 1987A to exclude the neutrino Majoron Yukawa coupling h in the range $2 \times 10^{-5} < h < 3 \times 10^{-4}$ for the interaction $L_{\rm int} = \frac{1}{2} i h \overline{\psi}^c_\nu \gamma_5 \psi_\nu \phi_X$. For several families of neutrinos, the limit applies for $(\Sigma h_i^4)^{1/4}$.

[24] PICCIOTTO 88 limit applies when $m_{X^0} < 55$ MeV and $\tau_{X^0} > 2$ns, and it decreases to 4×10^{-7} at $m_{X^0} = 125$ MeV, beyond which no limit is obtained.

[25] GOLDMAN 87 limit corresponds to $F > 2.9 \times 10^9$ GeV for the family symmetry breaking scale from the Lagrangian $L_{\rm int} = (1/F) \overline{\psi}_\mu \gamma^\mu (a + b\gamma_5) \psi_e \partial_\mu \phi_{X^0}$ with $a^2 + b^2 = 1$. This is not as sensitive as the limit $F > 9.9 \times 10^9$ GeV derived from the search for $\mu^+ \to e^+ X^0$ by JODIDIO 86, but does not depend on the chirality property of the coupling.

[26] Limits are for $\Gamma(\mu \to e X^0)/\Gamma(\mu \to e \nu \overline{\nu})$. Valid when $m_{X^0} = 0$–93.4, 98.1–103.5 MeV.

[27] EICHLER 86 looked for $\mu^+ \to e^+ X^0$ followed by $X^0 \to e^+ e^-$. Limits on the branching fraction depend on the mass and and lifetime of X^0. The quoted limits are valid when $\tau_{X^0} \lesssim 3. \times 10^{-10}$ s if the decays are kinematically allowed.

[28] JODIDIO 86 corresponds to $F > 9.9 \times 10^9$ GeV for the family symmetry breaking scale with the parity-conserving effective Lagrangian $L_{\rm int} = (1/F) \overline{\psi}_\mu \gamma^\mu \psi_e \partial^\mu \phi_{X^0}$.

[29] BALTRUSAITIS 85 search for light Goldstone boson(X^0) of broken U(1). CL = 95% limits are $B(\tau \to \mu^+ X^0)/B(\tau \to \mu^+ \nu\nu) < 0.125$ and $B(\tau \to e^+ X^0)/B(\tau \to e^+ \nu\nu) < 0.04$. Inferred limit for the symmetry breaking scale is $m > 3000$ TeV.

[30] The primordial heavy neutrino must decay into ν and familon, f_A, early so that the red-shifted decay products are below critical density, see their table. In addition, $K \to \pi f_A$ and $\mu \to e f_A$ are unseen. Combining these excludes $m_{{\rm heavy}\nu}$ between 5×10^{-5} and 5×10^{-4} MeV (μ decay) and $m_{{\rm heavy}\nu}$ between 5×10^{-5} and 0.1 MeV (K-decay).

Majoron Searches in Neutrinoless Double β Decay

Limits are for the half-life of neutrinoless $\beta\beta$ decay with a Majoron emission.

No experiment currently claims any such evidence. Only the best or comparable limits for each isotope are reported.

$t_{1/2}(10^{21}$ yr)	CL%	ISOTOPE	TRANSITION	METHOD	DOCUMENT ID	
>7200	**90**	**^{128}Te**		**CNTR**	[1] BERNATOW...	92
• • • We do not use the following data for averages, fits, limits, etc. • • •						
> 16–24	90	^{100}Mo	$0\nu1\chi$	CUPID-Mo	[2] AUGIER	24
> 120	90	^{82}Se	$0\nu1\chi$	CUPID-0	[3] AZZOLINI	23
> 640	90	^{76}Ge	$0\nu1\chi$	GERDA	[4] AGOSTINI	22
>4300	90	^{136}Xe	$0\nu1\chi$	EXO-200	[5] AL-KHARUSI	21
> 4.4	90	^{100}Mo	$0\nu1\chi$	NEMO-3	[6] ARNOLD	19
> 37	90	^{82}Se	$0\nu1\chi$	NEMO-3	[7] ARNOLD	18
> 420	90	^{76}Ge	$0\nu1\chi$	GERDA	[8] AGOSTINI	15A
> 400	90	^{100}Mo	$0\nu1\chi$	NEMO-3	[9] ARNOLD	15
>1200	90	^{136}Xe	$0\nu1\chi$	EXO-200	[10] ALBERT	14A
>2600	90	^{136}Xe	$0\nu1\chi$	KamLAND-Zen	[11] GANDO	12
> 16	90	^{130}Te	$0\nu1\chi$	NEMO-3	[12] ARNOLD	11
> 1.9	90	^{96}Zr	$2\nu1\chi$	NEMO-3	[13] ARGYRIADES	10
> 1.52	90	^{150}Nd	$0\nu1\chi$	NEMO-3	[14] ARGYRIADES	09
> 27	90	^{100}Mo	$0\nu1\chi$	NEMO-3	[15] ARNOLD	06
> 15	90	^{82}Se	$0\nu1\chi$	NEMO-3	[16] ARNOLD	06
> 14	90	^{100}Mo	$0\nu1\chi$	NEMO-3	[17] ARNOLD	04
> 12	90	^{82}Se	$0\nu1\chi$	NEMO-3	[18] ARNOLD	04
> 2.2	90	^{130}Te	$0\nu1\chi$	Cryog. det.	[19] ARNABOLDI	03
> 0.9	90	^{130}Te	$0\nu2\chi$	Cryog. det.	[20] ARNABOLDI	03
> 8	90	^{116}Cd	$0\nu1\chi$	$CdWO_4$ scint.	[21] DANEVICH	03
> 0.8	90	^{116}Cd	$0\nu2\chi$	$CdWO_4$ scint.	[22] DANEVICH	03
> 500	90	^{136}Xe	$0\nu1\chi$	Liquid Xe Scint.	[23] BERNABEI	02D
> 5.8	90	^{100}Mo	$0\nu1\chi$	ELEGANT V	[24] FUSHIMI	02
> 0.32	90	^{100}Mo	$0\nu1\chi$	Liq. Ar ioniz.	[25] ASHITKOV	01
> 0.0035	90	^{160}Gd	$0\nu1\chi$	$^{160}Gd_2SiO_5$:Ce	[26] DANEVICH	01
> 0.013	90	^{160}Gd	$0\nu2\chi$	$^{160}Gd_2SiO_5$:Ce	[27] DANEVICH	01
> 2.3	90	^{82}Se	$0\nu1\chi$	NEMO 2	[28] ARNOLD	00
> 0.31	90	^{96}Zr	$0\nu1\chi$	NEMO 2	[29] ARNOLD	00
> 0.63	90	^{82}Se	$0\nu2\chi$	NEMO 2	[30] ARNOLD	00
> 0.063	90	^{96}Zr	$0\nu2\chi$	NEMO 2	[30] ARNOLD	00
> 0.16	90	^{100}Mo	$0\nu2\chi$	NEMO 2	[30] ARNOLD	00
> 2.4	90	^{82}Se	$0\nu1\chi$	NEMO 2	[31] ARNOLD	98
> 7.2	90	^{136}Xe	$0\nu2\chi$	TPC	[32] LUESCHER	98
> 7.91	90	^{76}Ge		SPEC	[33] GUENTHER	96
> 17	90	^{76}Ge		CNTR	BECK	93

[1] BERNATOWICZ 92 studied double-β decays of ^{128}Te and ^{130}Te, and found the ratio $\tau(^{130}{\rm Te})/\tau(^{128}{\rm Te}) = (3.52 \pm 0.11) \times 10^{-4}$ in agreement with relatively stable theoretical predictions. The bound is based on the requirement that Majoron-emitting decay cannot be larger than the observed double-beta rate of ^{128}Te of $(7.7 \pm 0.4) \times 10^{24}$ year. We calculated 90% CL limit as $(7.7–1.28 \times 0.4 = 7.2) \times 10^{24}$.

[2] AUGIER 24 make use of 1.47 kg·yr of ^{100}Mo exposure of the CUPID-Mo scintillating cryogenic calorimeter, operated at the Laboratoire Souterrain de Modane to place a range of limits on the single Majoron mode of the $0\nu\beta\beta$ decay of ^{100}Mo. The range is due to the use of two different analysis strategies. Various limits on modes involving the emission of multiple Majorons are given too. The derived range of constraints on the Majoron-neutrino coupling constant is $g_{\nu\chi} < 4.0–8.5 \times 10^{-5}$, reflecting the variability of the used nuclear matrix elements and of the two data analysis strategies.

[3] AZZOLINI 23 use 9.95 kg·yr of data, collected by the CUPID-0 experiment, to place a limit on the single Majoron mode of the $0\nu\beta\beta$ decay of ^{82}Se. Various limits on modes involving the emission of multiple Majorons are given too. The resulting constraint on the Majoron-neutrino coupling constant is $g_{\nu\chi} < 1.8–4.4 \times 10^{-5}$. The range is due to the variability of the used nuclear matrix elements.

[4] AGOSTINI 22 use 32.8 kg·yr of GERDA phase 2 data to derive a limit of $g_{\nu\chi} < 1.8–4.4 \times 10^{-5}$ on the neutrino-Majoron coupling. The range reflects the author's evaluation of the spread of nuclear matrix elements.

[5] AL-KHARUSI 21 utilize the complete dataset of the EXO-200 experiment, corresponding to an exposure of 234 kg yr, to place a limit on the one Majoron mode of the neutrinoless double beta decay of ^{136}Xe. Several limits are reported, the one given here corresponds to a spectral index of 1, resulting in a limit of $g_{\nu\chi} < 0.4–0.9 \times 10^{-5}$ on the Majoron-neutrino coupling constant. The range reflects the spread of the nuclear matrix elements.

[6] ARNOLD 19 uses the NEMO-3 tracking calorimeter to determine limits for the Majoron emitting double beta decay, with spectral index n = 3. The limit corresponds to the range of the g_{ee} coupling of 0.013–0.035; dependimg on the nuclear matrix elements used.

[7] ARNOLD 18 use the NEMO-3 tracking detector. The limit corresponds to $\langle g_{ee} \rangle < 3.2–8.0 \times 10^{-5}$; the range corresponds to different nuclear matrix element calculations.

[8] AGOSTINI 15A analyze a 20.3 kg yr of data set of the GERDA calorimeter to determine $g_{\nu\chi} < 3.4–8.7 \times 10^{-5}$ on the Majoron-neutrino coupling constant. The range reflects the spread of the nuclear matrix elements.

[9] ARNOLD 15 use the NEMO-3 tracking calorimeter with 3.43 kg yr exposure to determine the limit on Majoron emission. The limit corresponds to $g_{\nu\chi} < 1.6–3.0 \times 10^{-4}$. The spread reflects different nuclear matrix elements. Supersedes ARNOLD 06.

[10] ALBERT 14A utilize 100 kg yr of exposure of the EXO-200 tracking calorimeter to place a limit on the $g_{\nu\chi} < 0.8–1.7 \times 10^{-5}$ on the Majoron-neutrino coupling constant. The range reflects the spread of the nuclear matrix elements.

[11] GANDO 12 use the KamLAND-Zen detector to obtain the limit on the $0\nu\chi$ decay with Majoron emission. It implies that the coupling constant $g_{\nu\chi} < 0.8–1.6 \times 10^{-5}$ depending on the nuclear matrix elements used.

[12] ARNOLD 11 use the NEMO-3 detector to obtain the reported limit on Majoron emission. It implies that the coupling constant $g_{\nu\chi} < 0.6–1.6 \times 10^{-4}$ depending on the nuclear matrix element used. Supercedes ARNABOLDI 03.

[13] ARGYRIADES 10 use the NEMO-3 tracking detector and ^{96}Zr to derive the reported limit. No limit for the Majoron electron coupling is given.

[14] ARGYRIADES 09 use ^{150}Nd data taken with the NEMO-3 tracking detector. The reported limit corresponds to $\langle g_{\nu\chi} \rangle < 1.7–3.0 \times 10^{-4}$ using a range of nuclear matrix elements that include the effect of nuclear deformation.

[15] ARNOLD 06 use ^{100}Mo data taken with the NEMO-3 tracking detector. The reported limit corresponds to $\langle g_{\nu\chi} \rangle < (0.4–1.8) \times 10^{-4}$ using a range of matrix element calculations. Superseded by ARNOLD 15.

[16] NEMO-3 tracking calorimeter is used in ARNOLD 06 . Reported half-life limit for ^{82}Se corresponds to $\langle g_{\nu\chi} \rangle < (0.66–1.9) \times 10^{-4}$ using a range of matrix element calculations. Supersedes ARNOLD 04.

[17] ARNOLD 04 use the NEMO-3 tracking detector. The limit corresponds to $\langle g_{\nu\chi} \rangle < (0.5–0.9)10^{-4}$ using the matrix elements of SIMKOVIC 99, STOICA 01 and CIVITARESE 03. Superseded by ARNOLD 06.

[18] ARNOLD 04 use the NEMO-3 tracking detector. The limit corresponds to $\langle g_{\nu\chi} \rangle < (0.7–1.6)10^{-4}$ using the matrix elements of SIMKOVIC 99, STOICA 01 and CIVITARESE 03.

[19] Supersedes ALESSANDRELLO 00. Array of TeO_2 crystals in high resolution cryogenic calorimeter. Some enriched in ^{130}Te. Derive $\langle g_{\nu\chi} \rangle < 17–33 \times 10^{-5}$ depending on matrix element.

[20] Supersedes ALESSANDRELLO 00. Cryogenic calorimeter search.

[21] Limit for the $0\nu\chi$ decay with Majoron emission of ^{116}Cd using enriched $CdWO_4$ scintillators. $\langle g_{\nu\chi} \rangle < 4.6–8.1 \times 10^{-5}$ depending on the matrix element. Supersedes DANEVICH 00.

[22] Limit for the $0\nu2\chi$ decay of ^{116}Cd. Supersedes DANEVICH 00.

[23] BERNABEI 02D obtain limit for $0\nu\chi$ decay with Majoron emission of ^{136}Xe using liquid Xe scintillation detector. They derive $\langle g_{\nu\chi} \rangle < 2.0–3.0 \times 10^{-5}$ with several nuclear matrix elements.

[24] Replaces TANAKA 93. FUSHIMI 02 derive half-life limit for the $0\nu\chi$ decay by means of tracking calorimeter ELEGANT V. Considering various matrix element calculations, a range of limits for the Majoron-neutrino coupling is given: $\langle g_{\nu\chi} \rangle < (6.3–360) \times 10^{-5}$.

[25] ASHITKOV 01 result for $0\nu\chi$ of ^{100}Mo is less stringent than ARNOLD 00.

[26] DANEVICH 01 obtain limit for the $0\nu\chi$ decay with Majoron emission of ^{160}Gd using Gd_2SiO_5:Ce crystal scintillators.

[27] DANEVICH 01 obtain limit for the $0\nu2\chi$ decay with 2 Majoron emission of ^{160}Gd.

[28] ARNOLD 00 reports limit for the $0\nu\chi$ decay with Majoron emission derived from tracking calorimeter NEMO 2. Using ^{82}Se source: $\langle g_{\nu\chi} \rangle < 1.6 \times 10^{-4}$. Matrix element from GUENTHER 96.

[29] Using ^{96}Zr source: $\langle g_{\nu\chi} \rangle < 2.6 \times 10^{-4}$. Matrix element from ARNOLD 99.

[30] ARNOLD 00 reports limit for the $0\nu2\chi$ decay with two Majoron emission derived from tracking calorimeter NEMO 2.

[31] ARNOLD 98 determine the limit for $0\nu_\chi$ decay with Majoron emission of ^{82}Se using the NEMO-2 tracking detector. They derive $\langle g_{\nu_\chi} \rangle < 2.3–4.3 \times 10^{-4}$ with several nuclear matrix elements.

[32] LUESCHER 98 report a limit for the 0ν decay with Majoron emission of ^{136}Xe using Xe TPC. This result is more stringent than BARABASH 89. Using the matrix elements of ENGEL 88, they obtain a limit on $\langle g_{\nu\chi} \rangle$ of 2.0×10^{-4}.

Int. J. Mod. Phys. A 2026.41. Downloaded from www.worldscientific.com
by UNIVERSITY OF CALIFORNIA @ BERKELEY on 09/16/26. Reproduction is strictly not permitted, except for Open Access articles.

[33] See Table 1 in GUENTHER 96 for limits on the Majoron coupling in different models.

Invisible A^0 (Axion) MASS LIMITS from Astrophysics and Cosmology

$v_1 = v_2$ is usually assumed (v_i = vacuum expectation values). For a review of these limits, see RAFFELT 91 and TURNER 90. In the comment lines below, D and K refer to DFSZ and KSVZ axion types, discussed in the above minireview.

VALUE (eV)	CL%	DOCUMENT ID		TECN	COMMENT
• • • We do not use the following data for averages, fits, limits, etc. • • •					
none 0.55–1.5 $\times 10^{-13}$, 2–5 $\times 10^{-13}$	90	[1] ASWATHI	25	ASTR	BH superradiance
> 2.2 $\times 10^{-21}$	95	[2] ZIMMER...	25	ASTR	Ultralight dark matter
< 0.16	95	[3] BIANCHINI	24	COSM	Hot dark matter
		[4] CHENG	23	ASTR	BH superradiance
> 3.2 $\times 10^{-19}$	95	[5] DELLA-MON...	23	ASTR	Ultralight DM soliton halo core
<141	90	[6] DERBIN	23	CNTR	K, solar axions
< 0.24	95	[7] NOTARI	23	COSM	K, Hot dark matter
		[8] ROGERS	23	COSM	Ultra-light axion DM
none 10^{-24}–5 $\times 10^{-23}$	95	[9] SMARRA	23	EPTA	Ultralight DM mass limit
		[10] XIA	23	ASTR	Fuzzy DM
		[11] LAGUE	22	COSM	Ultralight axion DM
none 0.15–1.5 $\times 10^{-12}$	95	[12] YUAN	22A	ASTR	BH superradiance
> 1.4 $\times 10^{-21}$	95	[13] BANIK	21	ASTR	Fuzzy DM
< 1.9 $\times 10^{4}$		[14] BAUMHOLZ...	21	COSM	warm dark matter
		[15] CROON	21	ASTR	SN 1987A, axion-muon coupling
		[16] FUJIKURA	21	ASTR	Microlensing
		[17] MARTINCAM...	21	ASTR	SN 1987A, Λ decay
none 1.3–2.7 $\times 10^{-13}$		[18] NG	21	ASTR	BH superradiance
> 2 $\times 10^{-20}$	95	[19] ROGERS	21	COSM	Lyman-α
none 0.8–6.5 $\times 10^{-13}$	95	[20] TSUKADA	21	ASTR	BH superradiance
> 2 $\times 10^{-17}$		[21] IRSIC	20	COSM	Isocurvature fluctuations
		[22] PODDAR	20	ASTR	Compact binary systems
> 2.1 $\times 10^{-21}$		[23] SCHUTZ	20	COSM	Fuzzy DM
none 6.4–8.0 $\times 10^{-13}$	95	[24] SUN	20	ASTR	BH superradiance
none 2.9–4.6 $\times 10^{-21}$		[25] DAVOUDIASL	19	ASTR	BH superradiance
none 10^{-21}–6 $\times 10^{-20}$		[26] MARSH	19	ASTR	Fuzzy DM
none 1.1–4 $\times 10^{-13}$	95	[27] PALOMBA	19	ASTR	BH superradiance
< 0.06		[28] CHANG	18	ASTR	K, SN 1987A
		[29] PORAYKO	18	PPTA	Fuzzy DM
< 0.67	95	[30] ARCHIDIACO...	13A	COSM	K, hot dark matter
none 0.7–3 $\times 10^{5}$		[31] CADAMURO	11	COSM	D abundance
<105	90	[32] DERBIN	11A	CNTR	D, solar axion
		[33] ANDRIAMON...	10	CAST	K, solar axions
< 0.72	95	[34] HANNESTAD	10	COSM	K, hot dark matter
		[35] ANDRIAMON...	09	CAST	K, solar axions
<191	90	[36] DERBIN	09A	CNTR	K, solar axions
<334	95	[37] KEKEZ	09	HPGE	K, solar axions
< 1.02	95	[38] HANNESTAD	08	COSM	K, hot dark matter
< 1.2	95	[39] HANNESTAD	07	COSM	K, hot dark matter
< 0.42	95	[40] MELCHIORRI	07A	COSM	K, hot dark matter
< 1.05	95	[41] HANNESTAD	05A	COSM	K, hot dark matter
3 to 20		[42] MOROI	98	COSM	K, hot dark matter
< 0.007		[43] BORISOV	97	ASTR	D, neutron star
< 4		[44] KACHELRIESS	97	ASTR	D, neutron star cooling
<(0.5–6) $\times 10^{-3}$		[45] KEIL	97	ASTR	SN 1987A
< 0.018		[46] RAFFELT	95	ASTR	D, red giant
< 0.010		[47] ALTHERR	94	ASTR	D, red giants, white dwarfs
		[48] CHANG	93	ASTR	K, SN 1987A
< 0.01		WANG	92	ASTR	D, white dwarf
< 0.03		WANG	92C	ASTR	D, C-O burning
none 3–8		[49] BERSHADY	91	ASTR	D, K, intergalactic light
< 10		[50] KIM	91C	COSM	D, K, mass density of the universe, supersymmetry
		[51] RAFFELT	91B	ASTR	D,K, SN 1987A
< 1 $\times 10^{-3}$		[52] RESSELL	91	ASTR	K, intergalactic light
none 10^{-3}–3		BURROWS	90	ASTR	D,K, SN 1987A
		[53] ENGEL	90	ASTR	D,K, SN 1987A
< 0.02		[54] RAFFELT	90D	ASTR	D, red giant
< 1 $\times 10^{-3}$		[55] BURROWS	89	ASTR	D,K, SN 1987A
<(1.4–10) $\times 10^{-3}$		[56] ERICSON	89	ASTR	D,K, SN 1987A
< 3.6 $\times 10^{-4}$		[57] MAYLE	89	ASTR	D,K, SN 1987A
< 12		CHANDA	88	ASTR	D, Sun
< 1 $\times 10^{-3}$		RAFFELT	88	ASTR	D,K, SN 1987A
		[58] RAFFELT	88B	ASTR	red giant
< 0.07		FRIEMAN	87	ASTR	D, red giant
< 0.7		[59] RAFFELT	87	ASTR	K, red giant
< 2–5		TURNER	87	COSM	K, thermal production
< 0.01		[60] DEARBORN	86	ASTR	D, red giant
< 0.06		RAFFELT	86	ASTR	D, red giant
< 0.7		[61] RAFFELT	86	ASTR	K, red giant
< 0.03		RAFFELT	86B	ASTR	D, white dwarf
< 1		[62] KAPLAN	85	ASTR	K, red giant
< 0.003–0.02		IWAMOTO	84	ASTR	D, K, neutron star
> 1 $\times 10^{-5}$		ABBOTT	83	COSM	D,K, mass density of the universe
> 1 $\times 10^{-5}$		DINE	83	COSM	D,K, mass density of the universe
< 0.04		ELLIS	83B	ASTR	D, red giant
> 1 $\times 10^{-5}$		PRESKILL	83	COSM	D,K, mass density of the universe
< 0.1		BARROSO	82	ASTR	D, red giant
< 1		[63] FUKUGITA	82	ASTR	D, stellar cooling
< 0.07		FUKUGITA	82B	ASTR	D, red giant

[1] ASWATHI 25 use LIGO-VIRGO-KAGRA data from the black hole binary merger events GW231123 and GW190517 to search for evidence of the superradiant build-up of a cloud of bosons, which could act to spin down the black holes. They rule out two windows of axion masses, and present limits in terms of the inverse energy scale for an attractive quartic scalar interaction in Fig. 2, e.g. the axion decay constant. The quoted limits are taken from Fig. 2 for the conservative spin-down timescale of 100,000 years.

[2] ZIMMERMANN 25 place a lower bound on the mass an ultralight boson assumed to be all of the dark matter, by ensuring it is possible to have a dynamically self-consistent dark matter halo density profile for the observed Leo II dwarf spheroidal galaxy.

[3] BIANCHINI 24 report a new limit on the axion mass, testing for the existence of a thermally produced hot dark matter population using current cosmic microwave background and baryon acoustic oscillation data. This analysis presents a stronger limit than previous bounds, e.g. NOTARI 23.

[4] CHENG 23 employ an improved approximation of the boson cloud eigenfrequency to calculate the superradiance rate. They find that sensitivity depends on initial spin distribution and the merger timescale, and identify two preferred ranges for boson mass centered at 1.78×10^{-12} and 7.94×10^{-13} eV.

[5] DELLA-MONICA 23 consider the solitonic core implied by ultralight scalar dark matter in the centre of the Milky Way and the effect its presence would have on the precisely tracked orbits of the stars orbiting our galaxy's central supermassive black hole, Sagittarius A*.

[6] DERBIN 23 employ a thulium garnet crystal bolometer to search for the 8.4 keV solar axion line emitted from the M1 nuclear transition of thulium-169, ^{169}Tm. Mass bound applies to KSVZ axions, value for DFSZ is 244 eV.

[7] NOTARI 23 improved the evaluation of axion production from pion scatterings by using pion-pion scattering data and incorporating the momentum dependence of the Boltzmann equation. The limit is based on the Planck 2018, BAO, and Pantheon SN Ia data.

[8] ROGERS 23 use the CMB and BOSS galaxy-clustering data to set limits on the abundance of ultralight axion DM. They obtained $\Omega_{A^0} < 0.002$ for $m_{A^0} = 10^{-30}$–10^{-28} eV and set upper limits ranging from 0.002 to 0.07 for $m_{A^0} = 10^{-32}$–10^{-25} eV. See their Fig. 22 for mass-dependent limits.

[9] SMARRA 23 is the European Pulsar Timing Array's constraint on the contribution of ultralight DM to the DM density in our local galactic neighbourhood. Ultralight DM cannot saturate the known DM density of 0.3 GeV/cc for masses inside this mass interval of 10^{-24}–5 $\times 10^{-23}$ eV.

[10] XIA 23 is analogous to PORAYKO 18 and use the Fermi-LAT pulsar timing array. They set a bound on the local density as $\rho_{A^0} \lesssim 8$ GeV/cm^3 for $m_{A^0} \lesssim 10^{-23}$ eV at 95% CL, with weaker constraints up to 10^{-22} eV. See their Fig. 1 for the mass-dependent limits.

[11] LAGUE 22 used the BOSS galaxy-clustering data to set limits on the abundance of ultralight axion dark matter. When combined with the CMB data, they obtained $\Omega_{A^0} h^2 < 0.004$ for $m_{A^0} = 10^{-31}$–10^{-26} eV. See their Figs. 1 and 15 for mass-dependent limits.

[12] YUAN 22A use the data of Advanced LIGO and Advanced Virgo's first three observing runs to search for stochastic GW background produced by scalar bosonic clouds formed by the BH superradiant instability. They set the limit, taking into account all the unstable modes.

[13] BANIK 21 use the subhalo mass function inferred from the analyses of the GD-1 and Pal 5 stellar streams. The limit is strengthened to 2.2×10^{-21} eV when adding dwarf satellite counts.

[14] BAUMHOLZER 21 study the freeze-in production of axion dark matter through couplings to photons, and set the limit using Lyman-α forest data and the observed number of Milky Way subhalos.

[15] CROON 21 study the supernova cooling effect of the axion-muon coupling, taking account of semi-Compton scattering and muon-proton bremsstrahlung, as well as the loop-induced axion-photon coupling, and exclude the range of $g_{A\mu\mu} \simeq 7\times10^{-3}$–$2\times10^{-10}$ for $m_{A^0} < 0.5$ GeV. See their Fig. 8 for mass-dependent limits.

[16] FUJIKURA 21 use the EROS-2 survey and the Subaru HSC observation to set limits on spherically symmetric axion clumps, taking account of the finite lens and source size effects. $f_{A^0} \gtrsim 10^{12}$ GeV can be constrained depending on the fraction of the axion dark matter collapsed into clumps, and the clump densities. See their Figs. 7–10 for the limits.

[17] MARTINCAMALICH 21 considered axion emission from a supernova core through the Λ hyperon decay, and set the limit on $B(\Lambda \to nA^0) \lesssim 8 \times 10^{-9}$, or equivalently, $f_{A^0}/C_{sd} \gtrsim 2.6 \times 10^9$ GeV in terms of the flavor-violating axion coupling to the down and strange quarks.

[18] NG 21 use the binary black holes reported by LIGO and Virgo to determine the black hole spin distribution at formation and the scalar boson mass simultaneously, neglecting the boson self-interaction.

[19] ROGERS 21 set the limit by using a framework involving Bayesian emulator optimization to accurately forward-model the Lyman-α flux power spectrum, and comparing this with small-scale data to constrain the predicted suppression of cosmic structure growth.

[20] TSUKADA 21 look for a stochastic GW background produced by extragalactic BH-hidden photon cloud systems through the superradiant instability. They assume a uniform spin distribution at birth of isolated BHs from 0 to 1.

[21] IRSIC 20 used the Lyman-α forest constraint on small-scale isocurvature perturbation to derive limits on the axion mass and decay constant, assuming that the axion makes up all dark matter in the post-inflationary scenario. See their Fig. 1 for other astrophysical limits as well as the limits on the case of the temperature-dependent axion mass.

[22] PODDAR 20 used the observed decay in orbital period of four compact binary systems to derive a limit on the emission of axions with $m_{A^0} < 1 \times 10^{-19}$ eV, assuming they couple to nucleons and the strong CP phase vanishes at the potential minimum. They exclude $f_{A^0} \lesssim 10^{11}$ GeV for such axions.

Int. J. Mod. Phys. A 2026.41. Downloaded from www.worldscientific.com
by UNIVERSITY OF CALIFORNIA @ BERKELEY on 09/16/26. Re-use and distribution is strictly not permitted, except for Open Access articles.

[23] SCHUTZ 20 set a limit on fuzzy dark matter based on the existing limits for warm dark matter derived from the inferred subhalo mass function.

[24] SUN 20 look for quasimonochromatic gravitational waves emitted from boson clouds around the Cygnus X-1 black hole. The quoted limit assume the black hole age of 5×10^6 years. A mass range of 9.6–15.5 $\times 10^{-13}$ eV is disfavored when repeated induction of bosenova for string axions with decay constant $f_{A^0} \simeq 10^{15}$ GeV prevents the superradiance from being saturated.

[25] DAVOUDIASL 19 used the observed data of M87* by the Event Horizon Telescope to set the limit. A mass range of 0.85–4.6 $\times 10^{-21}$ eV is disfavored for a spin-1 boson.

[26] MARSH 19 considered heating of star clusters due to the stochastic oscillations of the core and granular quasiparticles in the outer halo. The limit was derived by requiring the survival of the old star cluster in Eridanus II, where the lower end is set by the validity of diffusion approximation. The effect of tidal stripping is also discussed for lower masses.

[27] PALOMBA 19 used the LIGO O2 dataset to derive limits on nearly monochromatic gravitational waves emitted by boson clouds formed around a stellar-mass black hole. They exclude boson masses in a range of 1.1×10^{-13} and 4×10^{-13} eV for high initial black hole spin, and 1.2×10^{-13} and 1.8×10^{-13} eV for moderate spin. See their Figs. 2 and 3 for limits based on various values of black hole initial spin, boson cloud age, and distance.

[28] CHANG 18 update axion bremsstrahlung emission rates in nucleon-nucleon collisions, shifting the excluded mass range to higher values. They rule out the hadronic axion with mass up to a few hundred eV, closing the hadronic axion window. See their Fig. 11 for results based on several different choices of the temperature and density profile of the proto-neutron star.

[29] PORAYKO 18 look for time-dependent oscillations in the gravitational potential generated by ultralight scalar dark matter, and set a bound on its local density as $\rho_{A^0} \lesssim 6$ GeV/cm^3 for $m_{A^0} \lesssim 10^{-23}$ eV at 95% CL. See their Fig. 4 for the limits.

[30] ARCHIDIACONO 13A is analogous to HANNESTAD 05A. The limit is based on the CMB temperature power spectrum of the Planck data, the CMB polarization from the WMAP 9-yr data, the matter power spectrum from SDSS-DR7, and the local Hubble parameter measurement by the Carnegie Hubble program.

[31] CADAMURO 11 use the deuterium abundance to show that the m_{A^0} range 0.7 eV – 300 keV is excluded for axions, complementing HANNESTAD 10.

[32] DERBIN 11A look for solar axions produced by Compton and bremsstrahlung processes, in the resonant excitation of ^{169}Tm, constraining the axion-electron $\times$ axion nucleon couplings.

[33] ANDRIAMONJE 10 search for solar axions produced from ^{7}Li (478 keV) and D$(p,\gamma)^3$He (5.5 MeV) nuclear transitions. They show limits on the axion-photon coupling for two reference values of the axion-nucleon coupling for $m_A < 100$ eV.

[34] This is an update of HANNESTAD 08 including 7 years of WMAP data.

[35] ANDRIAMONJE 09 look for solar axions produced from the thermally excited 14.4 keV level of ^{57}Fe. They show limits on the axion-nucleon $\times$ axion-photon coupling assuming $m_A < 0.03$ eV.

[36] DERBIN 09A look for Primakoff-produced solar axions in the resonant excitation of ^{169}Tm, constraining the axion-photon $\times$ axion-nucleon couplings.

[37] KEKEZ 09 look at axio-electric effect of solar axions in HPGe detectors. The one-loop axion-electron coupling for hadronic axions is used.

[38] This is an update of HANNESTAD 07 including 5 years of WMAP data.

[39] This is an update of HANNESTAD 05A with new cosmological data, notably WMAP (3 years) and baryon acoustic oscillations (BAO). Lyman-α data are left out, in contrast to HANNESTAD 05A and MELCHIORRI 07A, because it is argued that systematic errors are large. It uses Bayesian statistics and marginalizes over a possible neutrino hot dark matter component.

[40] MELCHIORRI 07A is analogous to HANNESTAD 05A, with updated cosmological data, notably WMAP (3 years). Uses Bayesian statistics and marginalizes over a possible neutrino hot dark matter component. Leaving out Lyman-α data, a conservative limit is 1.4 eV.

[41] HANNESTAD 05A puts an upper limit on the mass of hadronic axion because in this mass range it would have been thermalized and contribute to the hot dark matter component of the universe. The limit is based on the CMB anisotropy from WMAP, SDSS large scale structure, Lyman α, and the prior Hubble parameter from HST Key Project. A χ^2 statistic is used. Neutrinos are assumed not to contribute to hot dark matter.

[42] MOROI 98 points out that a KSVZ axion of this mass range (see CHANG 93) can be a viable hot dark matter of Universe, as long as the model-dependent $g_{A\gamma}$ is accidentally small enough as originally emphasized by KAPLAN 85; see Fig. 1.

[43] BORISOV 97 bound is on the axion-electron coupling $g_{ae} < 1 \times 10^{-13}$ from the photo-production of axions off of magnetic fields in the outer layers of neutron stars.

[44] KACHELRIESS 97 bound is on the axion-electron coupling $g_{ae} < 1 \times 10^{-10}$ from the production of axions in strongly magnetized neutron stars. The authors also quote a stronger limit, $g_{ae} < 9 \times 10^{-13}$ which is strongly dependent on the strength of the magnetic field in white dwarfs.

[45] KEIL 97 uses new measurements of the axial-vector coupling strength of nucleons, as well as a reanalysis of many-body effects and pion-emission processes in the core of the neutron star, to update limits on the invisible-axion mass.

[46] RAFFELT 95 reexamined the constraints on axion emission from red giants due to the axion-electron coupling. They improve on DEARBORN 86 by taking into proper account degeneracy effects in the bremsstrahlung rate. The limit comes from requiring the red giant core mass at helium ignition not to exceed its standard value by more than 5% (0.025 solar masses).

[47] ALTHERR 94 bound is on the axion-electron coupling $g_{ae} < 1.5 \times 10^{-13}$, from energy loss via axion emission.

[48] CHANG 93 updates ENGEL 90 bound with the Kaplan-Manohar ambiguity in $z = m_u/m_d$ (see the Note on the Quark Masses in the Quark Particle Listings). It leaves the window $f_A = 3\times10^5$–3×10^6 GeV open. The constraint from Big-Bang Nucleosynthesis is satisfied in this window as well.

[49] BERSHADY 91 searched for a line at wave length from 3100–8300 Å expected from 2γ decays of relic thermal axions in intergalactic light of three rich clusters of galaxies.

[50] KIM 91C argues that the bound from the mass density of the universe will change drastically for the supersymmetric models due to the entropy production of saxion (scalar component in the axionic chiral multiplet) decay. Note that it is an *upperbound* rather than a lowerbound.

[51] RAFFELT 91B argue that previous SN 1987A bounds must be relaxed due to corrections to nucleon bremsstrahlung processes.

[52] RESSELL 91 uses absence of any intracluster line emission to set limit.

[53] ENGEL 90 rule out $10^{-10} \lesssim g_{AN} \lesssim 10^{-3}$, which for a hadronic axion with EMC motivated axion-nucleon couplings corresponds to 2.5×10^{-3} eV $\lesssim m_{A^0} \lesssim 2.5 \times 10^4$ eV. The constraint is loose in the middle of the range, i.e. for $g_{AN} \sim 10^{-6}$.

[54] RAFFELT 90D is a re-analysis of DEARBORN 86.

[55] The region $m_{A^0} \gtrsim 2$ eV is also allowed.

[56] ERICSON 89 considered various nuclear corrections to axion emission in a supernova core, and found a reduction of the previous limit (MAYLE 88) by a large factor.

[57] MAYLE 89 limit based on naive quark model couplings of axion to nucleons. Limit based on couplings motivated by EMC measurements is 2–4 times weaker. The limit from axion-electron coupling is weak: see HATSUDA 88B.

[58] RAFFELT 88B derives a limit for the energy generation rate by exotic processes in helium-burning stars $\epsilon < 100$ erg g^{-1} s^{-1}, which gives a firmer basis for the axion limits based on red giant cooling.

[59] RAFFELT 87 also gives a limit $g_{A\gamma} < 1 \times 10^{-10}$ GeV^{-1}.

[60] DEARBORN 86 also gives a limit $g_{A\gamma} < 1.4 \times 10^{-11}$ GeV^{-1}.

[61] RAFFELT 86 gives a limit $g_{A\gamma} < 1.1\times10^{-10}$ GeV^{-1} from red giants and $< 2.4\times10^{-9}$ GeV^{-1} from the sun.

[62] KAPLAN 85 says $m_{A^0} < 23$ eV is allowed for a special choice of model parameters.

[63] FUKUGITA 82 gives a limit $g_{A\gamma} < 2.3 \times 10^{-10}$ GeV^{-1}.

Search for Relic Invisible Axions

Limits are for the dimensionless quantity $[G_{A\gamma\gamma}/m_{A^0}]^2 \rho_A$ where $G_{A\gamma\gamma}$ denotes the axion two-photon coupling, $L_{\rm int} = -\frac{G_{A\gamma\gamma}}{4}\phi_A F_{\mu\nu}\tilde{F}^{\mu\nu} = G_{A\gamma\gamma}\phi_A \mathbf{E}\cdot\mathbf{B}$, and ρ_A is the axion energy density near the earth, unless otherwise stated. Notice that for QCD axions $G_{A\gamma\gamma}/m_{A^0}$ does not depend on m_{A^0}. For the reference values $m_{A^0} = 1$ μeV, $G_{A\gamma\gamma} = 3.9 \times 10^{-16}$ GeV^{-1} (that would apply to KSVZ axions at that mass), and $\rho_A = 300$ MeV/cm^3 one finds $[G_{A\gamma\gamma}/m_{A^0}]^2 \rho_A = 3.5 \times 10^{-43}$.

VALUE	CL%	DOCUMENT ID		TECN	COMMENT
• • • We do not use the following data for averages, fits, limits, etc. • • •					
$<6.5 \times 10^{-41}$	95	[1] AHYOUNE	25	RADS	$m_{A^0} = 36.5676$–36.5699 μeV
$<9.5 \times 10^{-43}$	90	[2] BAE	25	DMAG	$m_{A^0} = 20.95$–21.37 μeV
$<4.4 \times 10^{-42}$	90	[3] BAI	25	HYST	$m_{A^0} = 17.28$–19.46 μeV
$<1.8 \times 10^{-41}$	95	[4] BRAGGIO	25	QUAX	$m_{A^0} = 30.477$–30.479 μeV
$<2.3 \times 10^{-44}$	90	[5] CAROSI	25	ADMX	$m_{A^0} = 4.5$–5.44 μeV
$<2.9 \times 10^{-44}$	90	[6] GOODMAN	25	ADMX	$m_{A^0} = 3.27$–3.34 μeV
$<1.8 \times 10^{-36}$	90	[7] HOSHINO	25	BRED	$m_{A^0} = 44$–52 μeV
$<3 \times 10^{-4}$	95	[8] PORAYKO	25	EPTA	$m_{A^0} = 3 \times 10^{-24}$–$6 \times 10^{-21}$ eV
$<1.6 \times 10^{-37}$	95	[9] SANTOS-GAR..	25	MDMX	$m_{A^0} = 76.56$–76.82, 79.31–79.53 μeV
$<8.5 \times 10^{-43}$	90	[10] SARDO-INF...	25	QUAX	$m_{A^0} = 41.991$–42.234 μeV
$<1.0 \times 10^{-44}$	90	[11] AHN	24	CAPP	$m_{A^0} = 4.24$–4.91 μeV
$<7.3 \times 10^{-41}$	95	[12] BAE	24	CAPP	$m_{A^0} = 21.38$–21.79 μeV
$<1.0 \times 10^{-3}$	95	[13] DAVYDOV	24	ASTR	$m_{A^0} < 1 \times 10^{-20}$ eV
$<1.7 \times 10^{-26}$	95	[14] HEINZE	24	LIDA	$m_{A^0} = 1.97$–2.01 neV
$<3.5 \times 10^{-43}$	90	[15] KIM	24	CAPP	$m_{A^0} = 21.86$–22 μeV
$<3.3 \times 10^{-25}$	95	[16] PANDEY	24	ADBC	$m_{A^0} = 40.9$–43.3, 49.3–50.6, 54.4–56.7 neV
$<4.6 \times 10^{-39}$	95	[17] QUISKAMP	24	ORGN	$m_{A^0} = 107.42$–111.93 μeV
$<2 \times 10^{-41}$	90	[18] RETTAROLI	24	QUAX	$m_{A^0} = 36.52$–36.55 μeV
$<1.3 \times 10^{-3}$	95	[19] ADACHI	23D	CMB	$m_{A^0} = 0.096$–2.2×10^{-20} eV
$<7.5 \times 10^{-43}$	90	[20] DI-VORA	23	QUAX	$m_{A^0} = 42.8178$–42.8190 μeV
$<2.3 \times 10^{-42}$	90	[21] JEWELL	23	HYST	$m_{A^0} = 18.44$–18.71 μeV
$<2.0 \times 10^{-42}$	90	[22] JEWELL	23	HYST	$m_{A^0} = 16.96$–17.12, 17.14–17.28 μeV
$<2.5 \times 10^{-42}$	90	[23] KIM	23	CAPP	$m_{A^0} = 9.39$–9.51 μeV
$<3.0 \times 10^{-4}$	95	[24] OSHIMA	23	DANC	$m_{A^0} = 4.1 \times 10^{-16}$–$2.0 \times 10^{-12}$ eV
$<2.56 \times 10^{-24}$	95	[25] THOMSON	23	UPLD	$m_{A^0} = 1.12$–1.20 μeV
$<6.09 \times 10^{-43}$	90	[26] YANG	23	CAPP	$m_{A^0} = 19.883$–19.926 μeV
$<6.6 \times 10^{-44}$	90	[27] YI	23	CAPP	$m_{A^0} = 4.51$–4.59 μeV
$<2.6 \times 10^{-44}$	90	[28] YI	23A	CAPP	$m_{A^0} = 4.51$–4.59 μeV
$<4.7 \times 10^{-5}$	95	[29] ADE	22	CMB	$m_{A^0} = 0.16$–4.8×10^{-20} eV
$<1.0 \times 10^{-41}$	90	[30] ALESINI	22	QUAX	$m_{A^0} = 42.8210$–42.8223 μeV
$<7 \times 10^{-33}$	95	[31] BATTYE	22	ASTR	$m_{A^0} = 4.2$–60 μeV
$<5.8 \times 10^{-41}$	95	[32] CHANG	22	TASE	$m_{A^0} = 19.4687$–19.8436 μeV
$<3.2 \times 10^{-6}$	95	[33] FERGUSON	22	CMB	$m_{A^0} = 0.047$–4.7×10^{-20} eV
$<8.4 \times 10^{-43}$	90	[34] LEE	22	CAPP	$m_{A^0} = 19.764$–19.890 μeV
$<4.9 \times 10^{-39}$	95	[35] QUISKAMP	22	ORGN	$m_{A^0} = 63.2$–67.1 μeV
$<3.6 \times 10^{-43}$	90	[36] YOON	22	CAPP	$m_{A^0} = 19.764$–19.890 μeV
$<1.03 \times 10^{-35}$	95	[37] ZHOU	22	ASTR	$m_{A^0} = 3.18$–4.35 μeV
$<2.8 \times 10^{-4}$	95	[38] ADE	21	CMB	$m_{A^0} = 0.16$–4.8×10^{-20} eV
$<1.1 \times 10^{-41}$	90	[39] ALESINI	21	QUAX	$m_{A^0} = 43$ μeV
$<1 \times 10^{-44}$	90	[40] BARTRAM	21A	ADMX	$m_{A^0} = 3.3$–4.2 μeV
$<1.6 \times 10^{-29}$	95	[41] DEVLIN	21	TRAP	$m_{A^0} = 2.7906$–2.7914 neV
$<1.4 \times 10^{-23}$	95	[42] GRAMOLIN	21	SHFT	$m_{A^0} = 0.012$–12 neV

Int. J. Mod. Phys. A 2026.41. Downloaded from www.worldscientific.com
by UNIVERSITY OF CALIFORNIA @ BERKELEY on 09/16/26. Reproduction is strictly not permitted, except for Open Access articles.

See key on page 1227

Int. J. Mod. Phys. A 2026.41. Downloaded from www.worldscientific.com
by UNIVERSITY OF CALIFORNIA @ BERKELEY on 09/16/26. Re-use and distribution is strictly not permitted, except for Open Access articles.

$<7 \times 10^{-43}$	90	[43] KWON	21	CAPP	m_{A^0}	$= 10.7126$–10.7186 μeV
$<4.6 \times 10^{-40}$	95	[44] MELCON	21	RADE	m_{A^0}	$= 34.6738$–34.6771 μeV
$<3.5 \times 10^{-28}$	95	[45] SALEMI	21	ABRA	m_{A^0}	$= 0.41$–8.27 neV
$<3 \times 10^{-3}$	95	[46] THOMSON	21		m_{A^0}	$= 7.44$–19.38 neV
$<1 \times 10^{-2}$	95	[46] THOMSON	21		m_{A^0}	$= 74.4$–74.5 μeV
		[47] YUAN	21	ASTR	m_{A^0}	$= 10^{-20}$–10^{-17} eV
$<1.9 \times 10^{-44}$	90	[48] BRAINE	20	ADMX	m_{A^0}	$= 2.81$–3.31 μeV
$<2 \times 10^{-35}$	90	[49] CRISOSTO	20	SLIC	m_{A^0}	$= 180.07$–180.15 neV
$<4 \times 10^{-37}$	95	[50] DARLING	20A	ASTR	m_{A^0}	$= 4.2$–165.6 μeV
$<3.2 \times 10^{-36}$	95	[51] FOSTER	20	ASTR	m_{A^0}	$= 5$–7, 10–11 μeV
$<5.7 \times 10^{-41}$	90	[52] JEONG	20	CAPP	m_{A^0}	$= 13.0$–13.9 μeV
		[53] KENNEDY	20		m_{S^0}	$= 10^{-19}$–10^{-17} eV
$<4.8 \times 10^{-42}$	90	[54] LEE	20A	CAPP	m_{A^0}	$= 6.62$–6.82 μeV
$<2.6 \times 10^{-39}$	95	[55] ALESINI	19	QUAX	m_{A^0}	$= 37.5$ μeV
$<6 \times 10^{-5}$		[56] FUJITA	19	ASTR	m_{A^0}	$< 10^{-21}$ eV
$<2 \times 10^{-27}$	95	[57] OUELLET	19A	ABRA	m_{A^0}	$= 0.31$–8.3 neV
$<7.3 \times 10^{-40}$	90	[58] BOUTAN	18	ADMX	m_{A^0}	$= 17.38$–17.57 μeV
$<1.8 \times 10^{-39}$	90	[58] BOUTAN	18	ADMX	m_{A^0}	$= 21.03$–23.98 μeV
$<3.4 \times 10^{-39}$	90	[58] BOUTAN	18	ADMX	m_{A^0}	$= 29.67$–29.79 μeV
$<1.4 \times 10^{-44}$	90	[59] DU	18	ADMX	m_{A^0}	$=2.66$–2.81 μeV
$<2.87 \times 10^{-42}$	90	[60] ZHONG	18	HYST	m_{A^0}	$=23.15$–24 μeV
		[61] BRANCA	17	AURG	m_{S^0}	$= 3.5$–3.9 peV
$<3 \times 10^{-42}$	90	[62] BRUBAKER	17	HYST	m_{A^0}	$= 23.55$–24.0 μeV
$<1.0 \times 10^{-29}$	95	[63] CHOI	17	CAPP	m_{A^0}	$= 24.7$–29.1 μeV
$<5.9 \times 10^{-36}$	90	[64] MCALLISTER	17	ORGN	at m_{A^0}	$= 110$ μeV
$<8.6 \times 10^{-42}$	90	[65] HOSKINS	16	ADMX	m_{A^0}	$=3.36$–3.52 or 3.55–3.69 μeV
		[66] BECK	13		m_{A^0}	$= 0.11$ meV
$<3.5 \times 10^{-43}$		[67] HOSKINS	11	ADMX	m_{A^0}	$= 3.3$–3.69×10^{-6} eV
$<2.9 \times 10^{-43}$	90	[68] ASZTALOS	10	ADMX	m_{A^0}	$= 3.34$–3.53×10^{-6} eV
$<1.9 \times 10^{-43}$	97.7	[69] DUFFY	06	ADMX	m_{A^0}	$= 1.98$–2.17×10^{-6} eV
$<5.5 \times 10^{-43}$	90	[70] ASZTALOS	04	ADMX	m_{A^0}	$= 1.9$–3.3×10^{-6} eV
		[71] KIM	98	THEO		
$<2 \times 10^{-41}$		[72] HAGMANN	90	CNTR	m_{A^0}	$= (5.4$–$5.9)10^{-6}$ eV
$<6.3 \times 10^{-42}$	95	[73] WUENSCH	89	CNTR	m_{A^0}	$= (4.5$–$10.2)10^{-6}$ eV
$<5.4 \times 10^{-41}$	95	[73] WUENSCH	89	CNTR	m_{A^0}	$= (11.3$–$16.3)10^{-6}$ eV

[1] AHYOUNE 25 report results from the RADES collaboration, where a custom resonant cavity was used with an 11.7 T dipole magnet. See their Fig. 9 for mass-dependent limits.

[2] BAE 25 present first results from the IBS Dark Matter Axion Group (DMAG), using the TM020 mode of a cylindrical resonant cavity haloscope. See their Fig. 4 for mass-dependent limits.

[3] BAI 25 present results from Phase II of the HAYSTAC resonant cavity haloscope search for axion dark matter. See their Fig. 3 for mass-dependent limits together with previous results.

[4] BRAGGIO 25 presents limits from a cavity haloscope search for axion dark matter. This experiment employed a single-photon counter to circumvent the Standard Quantum Limit and enhance the search speed. See their Fig. 5 for mass-dependent limits.

[5] CAROSI 25 reports the latest results from the ADMX collaboration, extending the exclusion of relic QCD axions between 1.1 and 1.3 GHz down to the DFSZ model line using a near-quantum-limited amplifier. Quoted limit is for the strongest point in the exclusion limit just below 5.4 μeV.

[6] GOODMAN 25 present a limit on QCD axion dark matter from an ADMX resonant cavity haloscope with a sensitivity reaching the DFSZ model line. See their Fig. 4 for the mass-dependent limit.

[7] HOSHINO 25 present a first limit on axion dark matter from the GigaBREAD experiment. They used a coaxial dish antenna haloscope design placed inside a 3.9 T solenoidal magnet. See their Fig. 3 for mass-dependent limits.

[8] PORAYKO 25 use the European Pulsar Timing Array dataset to place constraints on ultralight axion-like particles making up the dark matter halo of the galaxy. They look for the effect of interactions between the local dark matter ALP field and the radio photons emitted by the pulsars, which would induce an oscillating rotation of the plane of linear polarisation. See their Fig. 7 for mass-dependent limits.

[9] SANTOS-GARCIA 25 present results for a prototype setup of the MADMAX dielectric haloscope searching for axion dark matter to photon conversion in a 1.6 T dipole magnet. See their Fig. 4 for mass-dependent limits.

[10] SARDO-INFIRRI 25 report a result from the QUAX haloscope around 10.2 GHz, using a quantum-limited detection chain to achieve sensitivity to axions down to close to the KSVZ model. See their Fig. 4 for mass-dependent limits.

[11] AHN 24 is from the CAPP-MAX experiment with sensitivity to DFSZ axions. See Fig. 22 for mass-dependent limits.

[12] BAE 24 search for dark matter axions using a microwave cavity with a tunable TM020 mode, scanning around 5 GHz. See their Fig. 6 for mass-dependent limits.

[13] DAVYDOV 24 constrain ultralight axion-like particle dark matter via the oscillating birefringence effect induced by the local ALP field. Their constraint is based on polarimetric measurements of the HL Tauri protoplanetary disk. Their constraint is $g_{a\gamma} < 2.111 \times 10^{-12}$ GeV$^{-1}(m_a/10^{-22})$ eV.

[14] HEINZE 24 search for ALP dark matter using the LIDA experiment - a laser interferometric haloscope that can detect the axion-induced polarisation rotation of light. Quoted limit assumes a dark matter density of 0.4 GeV/cm^3. See their Fig. 2 for mass-dependent limits.

[15] KIM 24 report results from the CAPP-12T experiment searching for dark matter axions around 22 μeV down to the KSVZ level. See their Fig. 5 for mass-dependent limits.

[16] PANDEY 24 report first search from the ADBC haloscope - an optical bow-tie laser cavity searching for the oscillating birefringence effect due to axion dark matter coupled to the photon. See their Fig. 3 for mass-dependent limits.

[17] QUISKAMP 24 present results from Phase 1b of the ORGAN experiment, a high-frequency resonant axion haloscope in the 15–50 GHz range. See their Fig. 5 for mass-dependent limits.

[18] RETTAROLI 24 report results from the QUAX resonant cavity haloscope at 8.8 GHz. This extends their previous search around this mass range reported in ALESINI 19. See their Fig. 7 for mass-dependent limits.

[19] ADACHI 23D is analogous to ADE 21. They used POLARBEAR data, and take account of a stochastic local axion field amplitude with the time-averaged local axion density $\rho_A = 0.3$ GeV/cm^3. Limits are set at $G_{A\gamma\gamma} < 2.4 \times 10^{-11}$ GeV^{-1} ($m_{A^0}/10^{-21}$ eV), which is 2.2 times larger than the deterministic case. See Fig. 5 for mass-dependent limits.

[20] DI-VORA 23 searches for axions in a narrow mass window using an 8T haloscope and a travelling wave parametric amplifier to achieve noise close to the quantum limit. This is an improvement on their previous scan at the same mass, ALESINI 21. See Fig. 7 for mass-dependent limits and a comparison.

[21] JEWELL 23 is an update of BRUBAKER 17. See their Fig. 11 for the mass-dependent limits.

[22] JEWELL 23 correct an underestimation of intermediate frequency noise in BACKES 21. See their Fig. 11 for the mass-dependent limits.

[23] KIM 23 is an update of KWON 21 on the CAPP-PACE experiment. See their Fig. 4 for mass-dependent limits.

[24] OSHIMA 23 report first limits from the DANCE experiment. This experiment is based on a novel bow-tie cavity design that searches for the oscillating rotation of polarised laser light driven by the DM axion-photon mixing at low frequencies. See their Fig. 6 for mass-dependent limits.

[25] THOMSON 23 used an AC microwave cavity to search for dark matter axions. The axion signal is resonantly enhanced when the axion mass matches the difference between a cavity which is pumped with power and another resonant mode close in frequency that is used to read out the signal. See their Fig. 7 for the mass-dependent limits.

[26] YANG 23 extends the first phase of CAPP 18T to KSVZ axions between 4.8077 and 4.8181 GHz. They used an 18T high-temperature superconducting magnet haloscope. See their Fig. 5 for mass-dependent limits. Quoted value is for their limit derived with a Bayesian method.

[27] YI 23 is analogous to LEE 20A, using the CAPP-12TB haloscope. See their Fig. 4 for mass-dependent limits.

[28] YI 23A used the same data as YI 23, but instead of the standard halo model, they searched for axion dark matter in the Sagittarius tidal stream with a velocity $v = 300$ km/sec and a velocity dispersion $\delta v = 20$ km/sec. See their Fig. 4 for mass-dependent limits.

[29] ADE 22 is an update of ADE 21 based on the expanded data of the 2012–2015 observing seasons. See their Fig. 3 for mass-dependent limits over the extended mass range 1×10^{-23}–6×10^{-19} eV.

[30] ALESINI 22 is an update of ALESINI 21, using the TM030 mode of the cylindrical dielectric cavity. See their Fig. 8 for mass-dependent limits.

[31] BATTYE 22 is analogous to DARLING 20A, and use plasma ray tracing technique to analyze the propagation of radio photons converted from axion dark matter in the magnetosphere of PSR J1745-2900. The quoted limit assumes $\rho_A = 6.5 \times 10^4$ GeV/cm^3 in the vicinity of the magnetar. See their Fig. 1 for mass-dependent limits.

[32] CHANG 22 used a microwave cavity detector to search for dark matter axions. See Fig. 3 for the mass-dependent limits.

[33] FERGUSON 22 is analogous to ADE 21. They use the data of the SPT-3G's 2019 observing season. See their Fig. 5 for mass-dependent limits over the extended mass range 0.047–9.5×10^{-20} eV.

[34] LEE 22 is analogous to LEE 20A. They used an 18T high-temperature superconducting magnet haloscope. See their Fig. 5 for mass-dependent limits.

[35] QUISKAMP 22 is a 15.28 to 16.23 GHz microwave cavity haloscope with 11.5 T B-field. See Fig. 4 for mass-dependent limits.

[36] YOON 22 analyzed the data from LEE 22 and changed from a frequentist to a Bayesian method to set limits. See their Fig. 27 for mass-dependent limits.

[37] ZHOU 22 is analogous to DARLING 20A, and they use the data from the MeerKAT radio telescope's observation of the neutron star J0806.4-4123, which is 250 pc from Earth. See their Fig.3 for mass-dependent limits.

[38] ADE 21 looks for a time-variable global rotation of the CMB polarization induced by the harmonic oscillations of local axion-like dark matter and uses data from the 2012 observing season of the Keck Array, part of the BICEP program. The limits get 25% weaker for $m_{A^0} = 4.8 \times 10^{-20}$–$5.7 \times 10^{-19}$ eV. See their Eq. (80) and Fig. 6 for mass-dependent limits.

[39] ALESINI 21 is an update of ALESINI 19. See their Figs. 5 and 6 for the mass-dependent limits.

[40] BARTRAM 21A is analogous to DU 18. See their Fig.4 for mass-dependent limits.

[41] DEVLIN 21 use the superconducting resonant detection circuit of a cryogenic Penning trap with a single antiproton. See their Fig. 3 for mass-dependent limits.

[42] GRAMOLIN 21 use two detection channels, each consisting of two stacked toroids to look for the axion-induced oscillating magnetic field. The quoted limit applies at $m_{A^0} = 0.02$ neV. See their Fig. 4 for mass-dependent limits.

[43] KWON 21 is analogous to LEE 20A. They also obtain weaker limits in the range of $m_{A^0} = 10.16$–11.37 μeV. See their Fig. 4 for mass-dependent limits.

[44] MELCON 21 use a radio frequency cavity consisting of 5 sub-cavities coupled by inductive irises installed inside the CAST dipole magnet to look for higher axion masses. See their Fig. 9 for mass-dependent limits.

[45] SALEMI 21 is an update of OUELLET 19A. See their Fig. 4 for mass-dependent limits.

[46] THOMSON 21 use a resonant cavity supporting two spatially overlapping microwave modes, which is sensitive to the axion mass corresponding to the sum or difference of the two resonant frequencies. The original limit was retracted due to a sign error. See their Fig. 2 in the erratum for the corrected limits.

[47] YUAN 21 use polarimetric observations of Sgr A* taken by the Event Horizon Telescope to search for periodic oscillation of the polarization induced by axion dark matter, assuming a solitonic core near the Galactic center. They obtained limits in the range of $G_{A\gamma\gamma} = 8 \times 10^{-13}$–$3 \times 10^{-11}$ GeV^{-1}.

[48] BRAINE 20 is analogous to DU 18. See Fig. 4 for their mass-dependent limits.

Int. J. Mod. Phys. A 2026.41. Downloaded from www.worldscientific.com
by UNIVERSITY OF CALIFORNIA @ BERKELEY on 09/16/26. Reproduction is strictly not permitted, except for Open Access articles.

[49] CRISOSTO 20 used a resonant LC circuit to look for lighter axion dark matter. They obtained a similar, slightly weaker limit for m_{A^0} = 174.98–175.19 and 177.34–177.38 neV. See their Fig. 4 for mass-dependent limits.

[50] DARLING 20A use VLA data to look for radio-frequency radiation converted from axion dark matter in the magnetosphere of the Galactic Center magnetar PSR J1745-2900. They extended the results of DARLING 20, which used only data with the highest angular resolution, by adding sub-optimal data. They use $\rho_A = 6.5\times10^4$ GeV/cm^3 in the vicinity of the magnetar. See their Fig. 2 for mass-dependent limits.

[51] FOSTER 20 look for radio-frequency radiation converted from axion dark matter in the magnetic field around neutron stars. They use the observed data of isolated local neutron stars and in the Galactic center. The quoted limit applies to $m_{A^0} \simeq 7$ μeV. See their Fig. 2 for mass-dependent limits.

[52] JEONG 20 is analogous to LEE 20A, and they use a double-cell cavity to look for axions with mass > 10 μeV. See their Fig. 5 for mass-dependent limits.

[53] KENNEDY 20 is analogous to BRANCA 17, and they compare the frequency ratios of the Si cavity measured by a Sr optical lattice clock and by a H maser. Assuming the local density of moduli dark matter, $\rho_S = 0.3$ GeV/cm^3, they obtain a limit $G_{S\gamma\gamma} < 5.8\times10^{-24}$ GeV^{-1} at $m_{S^0} = 2\times10^{-19}$ eV. See their Fig. 2 for mass-dependent limits as well as limits on the modulus coupling to electrons.

[54] LEE 20A used a microwave cavity detector at the IBS/CAPP to search for dark matter axions. See Fig. 3 for the mass-dependent limits.

[55] ALESINI 19 used a superconducting resonant cavity made of NbTi to increase the quality factor. The limit applies to a mass range of 0.2 neV around $m_{A^0} = 37.5$ μeV.

[56] FUJITA 19 look for photon birefringence under the oscillating axion background using the polarimetric imaging observation of a protoplanetary disk, AB Aur. See their Fig. 2 for a more conservative limit taking account of possible systematic effects.

[57] OUELLET 19A look for the axion-induced oscillating magnetic field generated by a toroidal magnetic field. The quoted limit applies at $m_{A^0} = 8$ neV. See their Fig. 3 for the mass-dependent limits.

[58] BOUTAN 18 use a small high frequency cavity installed above the main ADMX cavity to look for heavier axion dark matter. See their Fig. 4 for mass-dependent limits.

[59] DU 18 is analogous to DUFFY 06. They upgraded a dilution refrigerator to reduce the system noise. The quoted limit is around $m_{A^0} = 2.69$ μeV for the boosted Maxwellian axion line shape. See Fig. 4 for their mass-dependent limits.

[60] ZHONG 18 is analogous to BRUBAKER 17. The quoted limit applies at $m_{A^0} = 23.76$ μeV. See Fig. 4 for their mass-dependent limits.

[61] BRANCA 17 look for modulations of the fine-structure constant and the electron mass due to moduli dark matter by using the cryogenic resonant-mass AURIGA detector. The limit on the assumed dilatonic coupling implies $G_{S\gamma\gamma} < 1.5\times10^{-24}$ GeV^{-1} for the scalar to two-photon coupling. See Fig. 5 for the mass-dependent limits.

[62] BRUBAKER 17 used a microwave cavity detector at the Yale Wright Laboratory to search for dark matter axions. See Fig. 3 for the mass-dependent limits.

[63] CHOI 17 used a microwave cavity detector with toroidal geometry. See Fig. 4 for their mass-dependent limits.

[64] MCALLISTER 17 used a high-frequency microwave cavity haloscope at 26.6 GHz in a 7 T magnetic field. See Fig. 4 for mass-dependent limits.

[65] HOSKINS 16 is analogous to DUFFY 06. See Fig. 12 for mass-dependent limits in terms of the local dark matter density.

[66] BECK 13 argues that dark-matter axions passing through Earth may generate a small observable signal in resonant S/N/S Josephson junctions. A measurement by HOFFMANN 04 [Physical Review **B70** 180503 (2004)] is interpreted in terms of subdominant dark matter axions with $m_{A^0} = 0.11$ meV.

[67] HOSKINS 11 is analogous to DUFFY 06. See Fig. 4 for the mass-dependent limit in terms of the local density.

[68] ASZTALOS 10 used the upgraded detector of ASZTALOS 04 to search for halo axions. See their Fig. 5 for the m_{A^0} dependence of the limit.

[69] DUFFY 06 used the upgraded detector of ASZTALOS 04, while assuming a smaller velocity dispersion than the isothermal model as in Eq. (8) of their paper. See Fig. 10 of their paper on the axion mass dependence of the limit.

[70] ASZTALOS 04 looked for a conversion of halo axions to microwave photons in magnetic field. At 90% CL, the KSVZ axion cannot have a local halo density more than 0.45 GeV/cm^3 in the quoted mass range. See Fig. 7 of their paper on the axion mass dependence of the limit.

[71] KIM 98 calculated the axion-to-photon couplings for various axion models and compared them to the HAGMANN 90 bounds. This analysis demonstrates a strong model dependence of $G_{A\gamma\gamma}$ and hence the bound from relic axion search.

[72] HAGMANN 90 experiment is based on the proposal of SIKIVIE 83.

[73] WUENSCH 89 looks for condensed axions near the earth that could be converted to photons in the presence of an intense electromagnetic field via the Primakoff effect, following the proposal of SIKIVIE 83. The theoretical prediction with $[G_{A\gamma\gamma}/m_{A^0}]^2 = 2\times10^{-14}$ MeV^{-4} (the three generation DFSZ model) and $\rho_A = 300$ MeV/cm^3 that makes up galactic halos gives $(G_{A\gamma\gamma}/m_{A^0})^2\ \rho_A = 4\times10^{-44}$. Note that our definition of $G_{A\gamma\gamma}$ is $(1/4\pi)$ smaller than that of WUENSCH 89.

Invisible A^0 (Axion) Limits from Photon Coupling

Limits are for the modulus of the axion-two-photon coupling $G_{A\gamma\gamma}$ defined by $L = -G_{A\gamma\gamma}\phi_A \mathbf{E}\cdot\mathbf{B}$. For scalars S^0 the limit is on the coupling constant in $L = G_{S\gamma\gamma}\phi_S(\mathbf{E}^2-\mathbf{B}^2)$. The relation between $G_{A\gamma\gamma}$ and m_{A^0} is not used unless stated otherwise, i.e., many of these bounds apply to low-mass axion-like particles (ALPs), not to QCD axions.

VALUE (GeV^{-1})	CL%	DOCUMENT ID		TECN	COMMENT
• • • We do not use the following data for averages, fits, limits, etc. • • •					
$< 1\times10^{-4}$	90	[1] ABRAHAM	25	FASR	$m_{A^0} < 74$ MeV
$< 1\times10^{-10}$	80	[2] ADAMS	25C	ASTR	$m_{A^0} = 2\times10^{-7}$–4×10^{-7} eV
$< 9\times10^{-11}$	95	[3] ALTENMULL...	25	CAST	$m_{A^0} \lesssim 0.02$ eV
$< 6\times10^{-13}$	95	[4] CANDON	25	ASTR	$m_{A^0} = 10$–700 keV
$< 6.5\times10^{-13}$	95	[5] CHEN	25	ASTR	$m_{A^0} = 0.2$–10 keV
$< 4.33\times10^{-11}$	95	[6] CHEN	25A	ASTR	$m_{A^0} < 10^{-6}$ eV
$< 3.6\times10^{-11}$	95	[7] CHEN	25B	ASTR	$m_{A^0} = 4.4\times10^{-10}$ – 1.3×10^{-8} eV
$< 1\times10^{-18}$	95	[8] FONG	25	DM	$m_{A^0} = 1.78$–18.0 keV
$< 2\times10^{-12}$	95	[9] GOLDSTEIN	25	ASTR	$m_{A^0} = 2\times10^{-13}$–$3\times10^{-12}$ eV
$< 8\times10^{-5}$	95	[10] HAYRAPETY...	25Z	CMS	$m_{A^0} = 5$–100 GeV
$< 1.3\times10^{-11}$	95	[11] JANISH	25	DM	$m_{A^0} = 0.8$–2.5 eV
$< 3\times10^{-14}$	95	[12] KAR	25	DM	$m_{A^0} = 8$–20 eV
$< 4\times10^{-7}$	95	[13] KIRITA	25	SAPH	$m_{A^0} = 3\times10^{-3}$–0.5 eV
$< 1.1\times10^{-12}$	95	[14] LI	25D	ASTR	$m_{A^0} = 4\times10^{-10}$–$1\times10^{-8}$ eV
$< 1\times10^{-5}$	90	[15] MIRZAKHANI	25	MINR	$m_{A^0} < 10^7$ eV
$< 6\times10^{-13}$	95	[16] NING	25	ASTR	$m_{A^0} < 10^{-9}$ eV
$< 6.24\times10^{-6}$	95	[17] PARK	25	NEON	$m_{A^0} < 7$ MeV
$< 7.3\times10^{-12}$	95	[18] RUZ	25	ASTR	$m_{A^0} < 4\times10^{-7}$ eV
$< 2\times10^{-13}$	95	[19] TODARELLO	25	DM	$m_{A^0} = 14.4$–22.2 eV
$(6.5\ ^{+1.1}_{-1.3})\times10^{-11}$		[20] TROITSKY	25	ASTR	$m_{A^0} \lesssim 10$ keV
$< 2\times10^{-11}$	95	[21] YIN	25	DM	$m_{A^0} = 1.8$–2.7 eV
$< 5.6\times10^{-10}$	90	[22] ZENG	25	PNDX	$m_{A^0} \lesssim$ keV
$< 2.2\times10^{-4}$	95	[23] ABLIKIM	24AD	BES3	$m_{A^0} = 0.18$–2.85 GeV
$< 5.8\times10^{-11}$	95	[24] ALTENMULL...	24	CAST	$m_{A^0} < 0.02$ eV
$< 7\times10^{-12}$	95	[25] DEV	24	ASTR	$m_{A^0} = 0.01$–100 MeV
$< 5\times10^{-11}$		[26] DIAMOND	24	ASTR	$m_{A^0} = 1$–300 MeV
$< 1.38\times10^{-10}$	95	[27] FORDHAM	24	ASTR	$m_{A^0} <$ keV
$< 2\times10^{-11}$	95	[28] GAO	24	ASTR	$m_{A^0} = 10^{-9}$–10^{-7} eV
$< 2\times10^{-11}$	95	[29] GAO	24A	ASTR	$m_{A^0} = 10^{-10}$–2×10^{-7} eV
$< 4\times10^{-9}$	95	[30] GUO	24	DM	$m_{A^0} = 4.15$–6.06 or 8.3–12.2 μeV
$< 1.5\times10^{-11}$	95	[31] LI	24A	ASTR	$m_{A^0} = 5\times10^{-10}$–$1\times10^{-7}$ eV
$< 7.5\times10^{-11}$	95	[32] LI	24B	ASTR	$m_{A^0} = 2\times10^{-8}$–2×10^{-6} eV
$< 4\times10^{-12}$	99	[33] LI	24D	ASTR	$m_{A^0} = 10^{-9}$–10^{-8} eV
$< 3\times10^{-12}$	95	[34] MANZARI	24	ASTR	$m_{A^0} < 0.01$ eV
$< 3\times10^{-11}$	95	[35] PANT	24	ASTR	$m_{A^0} = 0.3$–1 neV
$< 8\times10^{-4}$	95	[36] PYBUS	24	GLUX	$m_{A^0} = 200$–450 MeV
$< 3\times10^{-11}$	95	[37] RAVENSBURG	24	ASTR	$m_{A^0} < 0.5$ MeV
$< 3\times10^{-13}$	95	[38] TODARELLO	24	DM	$m_{A^0} = 2.7$–5.3 eV
$< 1.1\times10^{-12}$		[39] WANG	24A	DM	$m_{A^0} = 2.8$–12.4 eV
$< 5.5\times10^{-11}$	95	[40] BATTYE	23	DM	$m_{A^0} = 3.9$–4.7 μeV
$< 2\times10^{-13}$	95	[41] BEAUFORT	23	ASTR	$m_{A^0} = 3$–38 keV
$< 2\times10^{-12}$	99	[42] BERNAL	23	COSM	$m_{A^0} = 8$–25 eV
$< 4\times10^{-14}$	99	[43] CAPOZZI	23	COSM	$m_{A^0} = 30$–800 eV
$< 1.3\times10^{-7}$	95	[44] CAPOZZI	23A	DUMP	$m_{A^0} = 10^3$–2×10^8 eV
$< 5\times10^{-12}$	95	[45] DAVIES	23	ASTR	$m_{A^0} = 5$–200 neV
$< 1.7\times10^{-10}$		[46] DIAMOND	23	ASTR	$m_{A^0} = 2$–56 MeV
$< 6\times10^{-29}$	95	[47] FILZINGER	23		Dilaton-like dark matter
$< 4.5\times10^{-12}$	95	[48] HOOF	23	ASTR	$m_{A^0} = 4\times10^{-10}$ eV
$< 3\times10^{-12}$	95	[49] HOOF	23	ASTR	$m_{A^0} = 60$ MeV
$< 2.7\times10^{-11}$	99.7	[50] JACOBSEN	23	ASTR	$m_{A^0} < 3\times10^{-7}$ eV
$< 2\times10^{-11}$	99	[51] LI	23H	ASTR	$m_{A^0} = 1$–100 neV
$< 3.0\times10^{-12}$	95	[52] NOORDHUIS	23	ASTR	$m_{A^0} = 10^{-9}$–10^{-5} eV
$< 5\times10^{-11}$	95	[53] PANT	23	ASTR	$m_{A^0} = 0.1$–1000 neV
$< 5\times10^{-26}$	95	[54] SHERRILL	23	DM	Dilaton-like dark matter
$< 8\times10^{-9}$	95	[55] SULAI	23	DM	$m_{A^0} = 0.25$–2×10^{-14} eV
$< 7.9\times10^{-12}$		[56] YAO	23	ASTR	$m_{A^0} \lesssim 10^{-13}$ eV
$< 3.8\times10^{-22}$	95	[57] ZHANG	23A		Dilaton-like dark matter
$< 5\times10^{-10}$	90	[58] APRILE	22B	XENT	Solar axions
$< 1.45\times10^{-9}$	95	[59] ARNQUIST	22	MAJD	$m_{A^0} < 100$ eV
$< 7\times10^{-11}$	95	[60] ARZA	22	DM	m_{A^0}=0.2–7×10^{-17}eV
3–6×10^{-11}	95	[61] BERNAL	22	COSM	$m_{A^0} = 8$–20 eV
$< 3.76\times10^{-11}$	95	[62] CALORE	22	ASTR	$m_{A^0} < 10^{-11}$ eV
$< 2\times10^{-10}$		[63] CAPUTO	22	ASTR	$m_{A^0} = 1$–500 MeV
$< 3\times10^{-14}$	95	[64] CASTILLO	22	ASTR	$m_{A^0} = 3\times10^{-23}$ eV
$< 6\times10^{-12}$	90	[65] DEROCCO	22	ASTR	$m_{A^0} = 5$–30 keV
$< 5.4\times10^{-12}$	95	[66] DESSERT	22A	ASTR	$m_{A^0} \lesssim 3\times10^{-7}$ eV
$< 2.1\times10^{-11}$	95	[67] ECKNER	22	ASTR	$m_{A^0} < 2\times10^{-7}$ eV
$< 1\times10^{-11}$	95	[68] FOSTER	22	ASTR	$m_{A^0} = 16.5$–32.5 μeV
$< 1.14\times10^{-5}$	95	[69] KIRITA	22	SAPH	$m_{A^0} = 0.5$–500 meV
$< 2\times10^{-16}$		[70] LANGHOFF	22	COSM	$m_{A^0} = 0.1$–3×10^4 keV
$< 6\times10^{-12}$	95	[71] LI	22	ASTR	$m_{A^0} = 0.2$–20 neV
$< 1.3\times10^{-11}$	95	[72] LI	22C	ASTR	$m_{A^0} = 8$–200 neV

Int. J. Mod. Phys. A 2026.41. Downloaded from www.worldscientific.com
by UNIVERSITY OF CALIFORNIA @ BERKELEY on 09/16/26. Re-use and distribution is strictly not permitted, except for Open Access articles.

< 1	$\times 10^{-5}$		[73] LUCENTE	22	ASTR	$m_{A^0} \lesssim 0.4$ MeV
< 9.2	$\times 10^{-11}$	95	[74] BASU	21	ASTR	$m_{A^0} = 3.6 \times 10^{-21}$ eV
< 1.8	$\times 10^{-10}$	95	[75] BI	21	ASTR	$m_{A^0} = 2$–6×10^{-7} eV
< 1.6	$\times 10^{-10}$	95	[76] DOLAN	21A	ASTR	$m_{A^0} = 1$–570 keV
< 5	$\times 10^{-11}$	95	[77] GUO	21	ASTR	$m_{A^0} = 8$–23 neV
< 1.2	$\times 10^{-4}$	95	[78] HOMMA	21	SAPH	$m_{A^0} = 0.4$–600 meV
< 1.2	$\times 10^{-11}$	95	[79] LI	21B	ASTR	$m_{A^0} = 0.5$–500 neV
			[80] LLOYD	21	ASTR	Magnetars
< 1	$\times 10^{-13}$	95	[81] REGIS	21	DM	$m_{A^0} = 2.7$–5.3 eV
< 1.8	$\times 10^{-11}$	95	[82] XIAO	21	ASTR	$m_{A^0} < 3.5 \times 10^{-11}$eV
< 7	$\times 10^{-4}$	95	[83] ABUDINEN	20	BEL2	$m_{A^0} = 0.2$–1 GeV
< 2	$\times 10^{-4}$	90	[84] BANERJEE	20A	NA64	$m_{A^0} < 55$ MeV
< 1.0	$\times 10^{-11}$	95	[85] BUEHLER	20	ASTR	$m_{A^0} < 3$ neV
< 5	$\times 10^{-10}$		[86] CALORE	20	ASTR	$m_{A^0} \lesssim 10^{-11}$ eV
			[87] CARENZA	20	ASTR	Globular clusters
2–4×10^{-10}		95	[88] DENT	20A	ASTR	Solar axions
			[89] DEPTA	20	COSM	Axion-like particles
< 3.6	$\times 10^{-12}$	95	[90] DESSERT	20A	ASTR	$m_{A^0} < 5 \times 10^{-11}$ eV
			[91] ESTEBAN	20	ANIT	Axion-like particles
4–6×10^{-10}		90	[92] GAO	20	ASTR	Solar axions
< 2.8	$\times 10^{-11}$	95	[93] KOROCHKIN	20	ASTR	$m_{A^0} = 25$ eV
none 6.0×10^{-9}–1.3×10^{-5}			[94] LUCENTE	20A	ASTR	$m_{A^0} < 270$ MeV
< 2.6	$\times 10^{-11}$	95	[95] MEYER	20	FLAT	$m_{A^0} < 3 \times 10^{-10}$ eV
< 8.4	$\times 10^{-8}$	99	[96] YAMAMOTO	20	COSM	$m_{A^0} < 4 \times 10^{-6}$ eV
< 1	$\times 10^{-3}$	95	[97] ALONI	19	PRMX	$m_{A^0} = 0.16$ GeV
< 1.4	$\times 10^{-14}$	95	[98] CAPUTO	19	ASTR	$m_{A^0} = 5 \times 10^{-24}$ eV
< 9.6	$\times 10^{-14}$	95	[99] FEDDERKE	19	CMB	$m_{A^0} = 10^{-22}$ eV
< 7	$\times 10^{-13}$	95	[100] IVANOV	19	ASTR	$m_{A^0} = 5 \times 10^{-23}$ eV
< 4	$\times 10^{-11}$	95	[101] LIANG	19	ASTR	$m_{A^0} = 1.2 \times 10^{-7}$ eV
			[102] FORTIN	18	ASTR	Axion-like particles
< 3	$\times 10^{-12}$		[103] JAECKEL	18	ASTR	$m_{A^0} = 30$–100 MeV
< 5.0	$\times 10^{-3}$	90	[104] YAMAJI	18	LSW	$m_{A^0} = 46$–1020 eV
< 1	$\times 10^{-11}$	99.9	[105] ZHANG	18	ASTR	$m_{A^0} = 0.6$–4 neV
			[106] ADE	17	CMB	Axion-like particles
< 6.6	$\times 10^{-11}$	95	[107] ANASTASSO...	17	CAST	$m_{A^0} < 0.02$ eV
			[108] DOLAN	17	RVUE	Axion-like particles
< 2.51	$\times 10^{-4}$	95	[109] INADA	17	LSW	$m_{A^0} < 0.1$ eV
> 1.5	$\times 10^{-11}$	95	[110] KOHRI	17	ASTR	$m_{A^0} = 0.7$–50 neV
< 2.6	$\times 10^{-12}$	95	[111] MARSH	17	ASTR	$m_{A^0} \leq 10^{-13}$ eV
< 6	$\times 10^{-13}$		[112] TIWARI	17	COSM	$m_{A^0} \leq 10^{-15}$ eV
< 5	$\times 10^{-12}$	95	[113] AJELLO	16	ASTR	$m_{A^0} = 0.5$–5 neV
< 1.2	$\times 10^{-7}$	95	[114] DELLA-VALLE	16	LASR	$m_{A^0} = 1.3$ meV
< 7.2	$\times 10^{-8}$	95	[115] DELLA-VALLE	16	LASR	$m_{A^0} < 0.5$ meV
< 8	$\times 10^{-4}$		[116] JAECKEL	16	ALPS	$m_{A^0} = 0.1$–100 GeV
< 6	$\times 10^{-21}$		[117] LEEFER	16		$m_{S^0} < 10^{-18}$ eV
			[118] ANASTASSO...	15	CAST	Chameleons
< 1.47	$\times 10^{-10}$	95	[119] ARIK	15	CAST	$m_{A^0} = 0.39$–0.42 eV
< 3.5	$\times 10^{-8}$	95	[120] BALLOU	15	LSW	$m_{A^0} < 2 \times 10^{-4}$ eV
			[121] BRAX	15	ASTR	$m_{S^0} < 4 \times 10^{-12}$ eV
< 5.42	$\times 10^{-4}$	95	[122] HASEBE	15	LASR	$m_{A^0} = 0.15$ eV
			[123] MILLEA	15	COSM	Axion-like particles
			[124] VANTILBURG	15		Dilaton-like dark matter
< 4.1	$\times 10^{-10}$	99.7	[125] VINYOLES	15	ASTR	$m_{A^0} = 0.6$–185 eV
< 3.3	$\times 10^{-10}$	95	[126] ARIK	14	CAST	$m_{A^0} = 0.64$–1.17 eV
< 6.6	$\times 10^{-11}$	95	[127] AYALA	14	ASTR	Globular clusters
< 1.4	$\times 10^{-7}$	95	[128] DELLA-VALLE	14	LASR	$m_{A^0} = 1$ meV
			[129] EJLLI	14	COSM	$m_{A^0} = 2.66$–48.8 μeV
< 8	$\times 10^{-8}$	95	[130] PUGNAT	14	LSW	$m_{A^0} < 0.3$ meV
< 1	$\times 10^{-11}$		[131] REESMAN	14	ASTR	$m_{A^0} < 1 \times 10^{-10}$ eV
< 2.1	$\times 10^{-11}$	95	[132] ABRAMOWSKI	13A	IACT	$m_{A^0} = 15$–60 neV
< 2.15	$\times 10^{-9}$	95	[133] ARMENGAUD	13	EDEL	$m_{A^0} < 200$ eV
< 4.5	$\times 10^{-8}$	95	[134] BETZ	13	LSW	$m_{A^0} = 7.2 \times 10^{-6}$ eV
< 8	$\times 10^{-11}$		[135] FRIEDLAND	13	ASTR	Red giants
> 2	$\times 10^{-11}$		[136] MEYER	13	ASTR	$m_{A^0} < 1 \times 10^{-7}$ eV
< 8.3	$\times 10^{-12}$	95	[137] WOUTERS	13	ASTR	$m_{A^0} < 7 \times 10^{-12}$ eV
			[138] CADAMURO	12	COSM	Axion-like particles
< 2.5	$\times 10^{-13}$	95	[139] PAYEZ	12	ASTR	$m_{A^0} < 4.2 \times 10^{-14}$ eV
< 2.3	$\times 10^{-10}$	95	[140] ARIK	11	CAST	$m_{A^0} = 0.39$–0.64 eV
< 6.5	$\times 10^{-8}$	95	[141] EHRET	10	ALPS	$m_{A^0} < 0.7$ meV
< 2.4	$\times 10^{-9}$	95	[142] AHMED	09A	CDMS	$m_{A^0} < 100$ eV
< 1.2–2.8×10^{-10}		95	[143] ARIK	09	CAST	$m_{A^0} = 0.02$–0.39 eV
			[144] CHOU	09		Chameleons
< 7	$\times 10^{-10}$		[145] GONDOLO	09	ASTR	$m_{A^0} <$ few keV
< 1.3	$\times 10^{-6}$	95	[146] AFANASEV	08		$m_{S^0} < 1$ meV
< 3.5	$\times 10^{-7}$	99.7	[147] CHOU	08		$m_{A^0} < 0.5$ meV
< 1.1	$\times 10^{-6}$	99.7	[148] FOUCHE	08		$m_{A^0} < 1$ meV
< 5.6–13.4×10^{-10}		95	[149] INOUE	08		$m_{A^0} = 0.84$–1.00 eV
< 5	$\times 10^{-7}$		[150] ZAVATTINI	08		$m_{A^0} < 1$ meV
< 8.8	$\times 10^{-11}$	95	[151] ANDRIAMON...	07	CAST	$m_{A^0} < 0.02$ eV
< 1.25	$\times 10^{-6}$	95	[152] ROBILLIARD	07		$m_{A^0} < 1$ meV
2–5×10^{-6}			[153] ZAVATTINI	06		$m_{A^0} = 1$–1.5 meV
< 1.1	$\times 10^{-9}$	95	[154] INOUE	02		$m_{A^0} = 0.05$–0.27 eV
< 2.78	$\times 10^{-9}$	95	[155] MORALES	02B		$m_{A^0} < 1$ keV
< 1.7	$\times 10^{-9}$	90	[156] BERNABEI	01B		$m_{A^0} < 100$ eV
< 1.5	$\times 10^{-4}$	90	[157] ASTIER	00B	NOMD	$m_{A^0} < 40$ eV
			[158] MASSO	00	THEO	induced γ coupling
< 2.7	$\times 10^{-9}$	95	[159] AVIGNONE	98	SLAX	$m_{A^0} < 1$ keV
< 6.0	$\times 10^{-10}$	95	[160] MORIYAMA	98		$m_{A^0} < 0.03$ eV
< 3.6	$\times 10^{-7}$	95	[161] CAMERON	93		$m_{A^0} < 10^{-3}$ eV, optical rotation
< 6.7	$\times 10^{-7}$	95	[162] CAMERON	93		$m_{A^0} < 10^{-3}$ eV, photon regeneration
< 3.6	$\times 10^{-9}$	99.7	[163] LAZARUS	92		$m_{A^0} < 0.03$ eV
< 7.7	$\times 10^{-9}$	99.7	[163] LAZARUS	92		$m_{A^0} = 0.03$–0.11 eV
< 7.7	$\times 10^{-7}$	99	[164] RUOSO	92		$m_{A^0} < 10^{-3}$ eV
< 2.5	$\times 10^{-6}$		[165] SEMERTZIDIS	90		$m_{A^0} < 7 \times 10^{-4}$ eV

[1] ABRAHAM 25 search for axions as a long-lived particle decaying into photons in the FASER detector at the LHC. They constrain models where the axion dominantly couples to W bosons. The quoted limit is from their Fig. 11, which shows the bound interpreted in terms of a coupling to photons, taking the value at a mass of 70 MeV where the constraint is strongest. Bounds on the axion-gluon coupling extend up to axion masses of up to 800 MeV.

[2] ADAMS 25C present a search for ALP-photon mixing imprinted on the gamma-ray spectrum of the flaring NGC 1275 radio galaxy at the centre of the Perseus cluster observed by the VERITAS observatory. They adopt the CLs method for reporting exclusion limits as shown in their Fig. 3. No point in the tested parameter space is excluded at or above 95% confidence. The quoted limit is reached at $m_{A^0} = 3.03 \times 10^{-7}$ eV.

[3] ALTENMULLER 25 primarily reports a new limit from the CAST helioscope on the product of the axion-photon and axion-electron coupling, but they also exploit the same analysis to set a new limit on the axion-photon coupling alone, although this is weaker than their previous limit in ALTENMULLER 24.

[4] CANDON 25 place bounds on heavy photon-coupled axion-like particles produced in the interiors of the stars in the starburst galaxy M82 and then decaying to two photons. This process would generate an X-ray flux peaking around 100 keV, which they search for using data from the NuSTAR space telescope. See their Fig. 2 for mass-dependent limits.

[5] CHEN 25 use data from X-ray satellites Chandra and eROSITA to search for the decays of axion-like particles produced by the Alpha Centauri binary system. Specifically, they consider the argument also used by BEAUFORT 23 in the case of the Sun, in which axions emitted with low speed from the star can build up in a gravitationally trapped 'basin' over the star's life. See their Fig. 3 for mass-dependent limits. The quoted value applies to the case where the axion-electron coupling is taken to be negligible.

[6] CHEN 25A constrain low-mass axion-like particles by searching for the imprints of axion-photon oscillations on the gamma-ray spectra of two active galactic nuclei measured by the Fermi and MAGIC gamma-ray telescopes. See their Fig. 11 for mass-dependent limits.

[7] CHEN 25B constrain low-mass axion-like particles by searching for the imprints of axion-photon oscillations on the gamma-ray spectra of several blazars observed by the Fermi gamma-ray telescope. See Figs. 2, 3 and 4 for mass-dependent limits.

[8] FONG 25 use early-release data from the eROSITA X-ray telescope's Final Equatorial Depth Survey to search for axion-like particle dark matter decaying to two photons in the Milky Way's dark matter halo. See their Fig. 7 for mass-dependent limits.

[9] GOLDSTEIN 25 place bounds on low mass axions mixing with photons over cosmological distances as they traverse large-scale structure, which would lead to an observable patchy screening effect in CMB anisotropy maps. See their Fig. 3 for mass-dependent limits. This bound is analogous to that placed on dark photons by MCCARTHY 24.

[10] HAYRAPETYAN 25Z places a bound on heavy axion-like particles coupled to photons via measurements of light-by-light scattering in ultraperipheral PbPb collisions at the CMS experiment. The bound is based on a search for diphoton events due to $\gamma\gamma \to a \to \gamma\gamma$ on top of the light-by-light scattering continuum. See Fig. 9 for mass-dependent limits on the axion-photon coupling.

[11] JANISH 25 use blank-sky observations of the James Webb Space Telescope to search for dark matter axions present in the galactic halo. eV-mass axions decaying into two photons would present an emission line in the infrared band. See their Fig. 2 for mass-dependent limits.

[12] KAR 25 use infrared to ultraviolet observations of the giant elliptical galaxy M87 to search for evidence of eV-scale axions decaying to two photons, assuming they make up the dark matter halo of the galaxy. See their Fig. 2, 3 and 4 for mass-dependent limits.

[13] KIRITA 25 presents a new result from the SAPPHIRES collaboration, namely a search for the production of axion-like particles in a quasi-parallel stimulated resonant photon-photon collider. See their Fig. 11 for mass-dependent limits.

[14] LI 25D search for evidence of axion-photon mixing imprinted on the gamma-ray spectrum of the flat-spectrum radio quasar Ton-599 detected by Fermi-LAT. See their Fig. 4 for mass-dependent limits.

[15] MIRZAKHANI 25 search for axion-like particles coupled to photons using the MINER reactor neutrino experiment. Their search assumes axions would be produced via Primakoff emission from the reactor photon flux, which can then decay to two photons or convert to a photon through the inverse Primakoff effect in the detector. See Fig. 10 for mass-dependent limits.

[16] NING 25 sets bounds on low-mass axion-like particle Primakoff emission by stars in the M87 and M82 starburst galaxies. They use data from the NuSTAR space telescope to search for evidence of the emitted axions converting into hard X-ray photons in the surrounding galactic magnetic fields. See Fig. 2 for mass-dependent limits.

Int. J. Mod. Phys. A 2026.41. Downloaded from www.worldscientific.com
by UNIVERSITY OF CALIFORNIA @ BERKELEY on 09/16/26. Re[redacted]s strictly not permitted, except for Open Access articles.

[17] PARK 25 present a search for axion-like particles from the NEON reactor neutrino experiment. Axions would be produced by the large MeV photon flux from the reactor and subsequently scatter or decay to a photon pair in the detector. The quoted limit is at $m_{A^0} = 3$ MeV. See their Fig. 3 for mass-dependent limits.

[18] RUZ 25 use data from the NuSTAR X-ray telescope to search for solar axions converting into photons as they traverse the Sun's atmospheric magnetic field. For larger m_{A^0}, the limit becomes weaker due to loss of coherence in the conversion. See their Fig. 1 for mass-dependent limits.

[19] TODARELLO 25 use observations of dwarf spheroidal galaxies and galaxy clusters made by the Hubble Space Telescope to constrain axions decaying to two photons at UV wavelengths, assuming axions make up the dark matter halos of those astrophysical objects. See their Fig. 3 for mass-dependent limits.

[20] TROITSKY 25 searches for evidence of any anomalous cooling due to axion emission from red giants and helium-burning stars in seven globular clusters observed by the Gaia survey. A 3.3σ hint for anomalous cooling is found, which could be explained by a non-zero axion-photon coupling.

[21] YIN 25 use the WINERED spectrograph on the Magellan Clay Telescope to search for evidence of dark matter axions decaying into photons in the halos of the Leo V and Tucana II dwarf spheroidal galaxies. See their Fig. 1 for mass-dependent limits and the dependence on the assumed dark matter halo models.

[22] ZENG 25 place a bound on axions emitted by the Sun due to a nonzero axion-photon coupling using electronic recoil data collected by the PandaX detector. Electron recoil events are generated via the axion-photon coupling by the inverse Primakoff effect. The limit is independent of the axion mass up to around the core temperature of the Sun.

[23] ABLIKIM 24AD constrain the axion-photon coupling through radiative J/ψ decays in the BESIII detector at the Beijing electron-positron collider. See their Fig. 5 for mass-dependent limits.

[24] ALTENMULLER 24 report an extended search for solar axions using the CAST experiment. The experiment employed a new xenon-based microMEGAS detector - a pathfinder for the future International Axion Observatory (IAXO). This limit improves upon ANASTASSOPOULOS 17. See Fig. 4 for mass-dependent limits.

[25] DEV 24 use Fermi gamma-ray observations of the neutron star merger GW170817 to constrain the production and subsequent decay of high-mass axion-like particles. Constraint extends diagonally in mass-coupling space, reaching 7×10^{-12} GeV^{-1} at 100 MeV. See Fig. 4 for mass-dependent limits.

[26] DIAMOND 24 use multi-messenger observations of the neutron star merger GW170817 to constrain the production and radiative decay of axions in the event. Limits shown in their Fig. 3 extend diagonally in mass-coupling space.

[27] FORDHAM 24 use asteroseismology observations of a solar-like star, KIC 6933899, to constrain axion emission from its interior via the photon coupling. Bound applies to all axion masses up to around the core temperature of the star $\sim$ keV.

[28] GAO 24 constrain ALP-photon oscillations via their imprint on the gamma-ray spectrum of the blazar Mrk 421, as observed by MAGIC and Fermi-LAT. See their Fig. 5 for mass-dependent limits.

[29] GAO 24A constrain ALP-photon oscillations using the high-energy gamma-ray spectrum observed by LHAASO of the brightest gamma-ray burst so far detected, GRB 221009A. See their Fig. 5 for mass-dependent limits. The strength of the limit depends on the magnetic field of the host galaxy.

[30] GUO 24 search for axion dark matter decaying or converting into photons in the Coma Berenices dwarf galaxy using the radio telescope FAST. The quoted limit is for the case of axions decaying, including stimulated emission. See their Fig. 2 for mass-dependent limits.

[31] LI 24A constrain the imprint of ALP-photon oscillations on the TeV gamma-ray spectrum of the BL Lac blazar 1ES 1215+303 using VERITAS and Fermi-LAT data. See their Fig. 4 for mass-dependent limits.

[32] LI 24B constrain the imprint of ALP-photon oscillations on the very-high-energy gamma-ray spectrum of various galactic sources detected by the LHAASO air-shower array. Best limits are obtained from the Crab Nebula after combining several observations from different gamma-ray observatories in addition to LHAASO. See their Fig. 5 for mass-dependent limits.

[33] LI 24D search for evidence of axion-photon oscillations imprinted on the gamma-ray spectrum of the nearby BL Lac blazar Markarian 421. They set upper limits using data from Fermi-LAT and HAWC. The quoted limit applies for $m_{A^0} \simeq 3 \times 10^{-9}$ eV. See their Fig. 3 for mass-dependent limits.

[34] MANZARI 24 search for evidence of axions produced in SN1987A converting into gamma-rays that would have been detectable by the Solar Maximum Mission. This analysis improves upon previous studies of axion-photon conversion after SN1987A (e.g. HOOF 23) by including the magnetic field of the progenitor star. Quoted limit applies for masses below 0.1 neV and rises towards larger masses. See their Fig. 1 for mass-dependent limits.

[35] PANT 24 searches for the imprint of axion-photon oscillations in the very-high-energy gamma-ray spectrum of the quasar QSO B1420+326 observed by the MAGIC telescope. Three small disconnected regions of mass-coupling parameter space below 1 neV are ruled out. See Fig. 4 for the limits.

[36] PYBUS 24 report results from the GlueX detector, which has searched for the two-photon decay of heavy axions produced through the nuclear Primakoff effect due to a beam of photons incident on a Carbon target. See their Fig. 8 for mass-dependent limits.

[37] RAVENSBURG 24 search for heavy axions decaying to two photons using the recent nearby type-II supernova SN 2023ixf. Constraint extends diagonally downwards in mass-coupling space, see their Fig. 2 for full limits. Quoted limit is the most constraining point for the most conservative choices for supernova parameters.

[38] TODARELLO 24 search for axions decaying to two photons in the halos of Milky Way dwarf galaxies observed in the MUSE-Faint survey. This study improves upon an earlier one presented in REGIS 21. See their Fig. 5 for compiled mass-dependent limits.

[39] WANG 24A search for axions decaying into two photons assuming that they make up the dark matter halos of galaxies. They use data from the Dark Energy Spectroscopic Instrument, searching for the axion decay line in optical wavelengths with their Bright Galaxy and Luminous Red Galaxy samples. See their Fig. 8 for mass-dependent limits on the axion to photon decay rate. Their constraint is quoted as a 5σ detection limit.

[40] BATTYE 23 look for dark-matter axions falling into pulsar magnetospheres and converting into narrow radio lines. Unlike the earlier FOSTER 22 they search for evidence of conversion in the time-domain signal of a single pulsar, using 1 hour of MeerKAT data on the pulsar PSR J2144-3933. The quoted limit applies to an assumed magnetic field of 2×10^{12} G and a dark matter density of 0.45 GeV/cm^3.

[41] BEAUFORT 23 extends DEROCCO 22 who searched for the X-ray decay of axions that build up in the gravitational well of the Sun over its lifetime, the 'solar basin'. They use data from NuSTAR and SphinX telescopes and extends the previous study by accounting for the axion production via photon coalescence.

[42] BERNAL 23 use gamma-ray data from 739 blazars observed by FermiLAT and 38 blazars by Cherenkov observatories. They estimate optical depth, subtract the astrophysical component, and attribute the residual to axion two-photon decay. The quoted limit is for $m_{A^0} \simeq 25$ eV. See their Fig. 3 for the mass-dependent limits.

[43] CAPOZZI 23 use Planck CMB and Lyman-α observations to set limits on early energy injection by decaying dark matter axions that would affect CMB anisotropies and the reionisation history of the Universe. The quoted limit applies to $m_{A^0} = 100$ eV and the reionization model of Fauchere-Giguere. See Fig. 4 for mass-dependent constraints from different reionization models.

[44] CAPOZZI 23A search for axions produced in electromagnetic showers in proton beam dumps and fixed target experiments. In this case, they reinterpret MiniBoone data. Quoted limit applies at 100 MeV but the limit does not extend to arbitrarily large couplings. See Fig. 7 for mass-dependent limits.

[45] DAVIES 23 is analogous to AJELLO 16, and use the Fermi-LAT data from three quasars (3C454.3, CTA 102, and 3C279), considering the blazer jets as the regions where the axion-photon oscillations occur. See Fig. 8 for the mass-dependent limits.

[46] DIAMOND 23 demonstrate that a window of decaying 10-MeV-mass ALP parameter space previously thought to be excluded by the lack of gamma-ray emission from the SN 1987A explosion is actually unconstrained because of the formation of a fireball that would prevent decay photons from escaping. They nevertheless re-exclude this window by considering the non-detection of the sub-MeV emission by the Pioneer Venus Orbiter. The quoted limit is at $m_{A^0} = 56$ MeV. See their Fig. 2 for mass-dependent limits.

[47] FILZINGER 23 searched for oscillations in the fine structure constant induced by dilaton-like dark matter by measuring the frequency ratio between the E3 and E2 transitions of ^{171}Yb$^+$. They assume the local dark matter density $\rho_S = 0.4$ GeV/cm^3. The quoted limit is set at $m_{S^0} \simeq 4 \times 10^{-23}$ eV. See their Fig. 4 for the limits over $m_{S^0} = 1 \times 10^{-24}$–$1 \times 10^{-17}$ eV.

[48] HOOF 23 consider axions emitted from SN1987A converting to gamma rays in Galactic magnetic fields, using temporal information of the Solar Maximum Mission data. They set a limit $G_{A\gamma\gamma} \lesssim 5 \times 10^{-12}$ for masses $m_{A^0} \lesssim 2 \times 10^{-10}$ eV. See left panel in Fig. 3 for mass-dependent limits.

[49] HOOF 23 look for gamma rays resulting from the decay of axions produced from SN1987A, using the Solar Maximum Mission data. See right panel in Fig. 3 for mass-dependent limits.

[50] JACOBSEN 23 search for the imprints of axion-photon mixing on the TeV spectra of several blazars using data from the HAWC air shower detector.

[51] LI 23H look for gamma-ray spectral irregularities induced by axion-photon oscillations from AGN VER J0521+211, using the Fermi-LAT and VERITAS data. See their Fig. 4 for mass-dependent limits.

[52] NOORDHUIS 23 places strong constraints on the axion-photon coupling over a broad mass window using the fact that the polar cap regions of pulsars can generate a population of axions, which would then convert into an observable outgoing radio flux in the presence of the neutron star's B-field. They search for this signal in 27 pulsars and set mass-dependent limits shown in their Fig. 2.

[53] PANT 23 study the effect of axion-photon oscillations on the gamma-ray spectrum from the extragalactic neutrino source, TXS 0506+056. The quoted limit is at $m_{A^0} \simeq 2.7 \times 10^{-7}$ eV. See their Fig. 2 for mass-dependent limits.

[54] SHERRILL 23 search for scalar dilaton-like dark matter via oscillations in the fundamental constants. Their most competitive constraint is on the scalar photon coupling (Fig. 6, upper panel) that affects the fine-structure constant, which they extract using an optical-to-optical clock comparison between ^{171}Yb$^+$ and ^{87}Sr. Quoted limit applies at the smallest mass in their search window for this case of 10^{-20} eV.

[55] SULAI 23 looked for ultralight axion dark matter using the "Earth as a transducer" concept over the 0.5 to 5 Hz frequency range. They situate several magnetometers at magnetically quiet places and search for spatially-correlated magnetic field patterns induced by axion dark matter interacting in the effective cavity formed between the Earth's surface and the ionosphere. See their Fig. 12 for mass-dependent limits in context. This limit extends to higher-frequencies than their previous limit using archival geomagnetic field data collected by the SuperMAG collaboration, see ARZA 22

[56] YAO 23 study an optical circular polarization in blazers induced by the axion-photon mixing. The quoted limit assumes the transverse magnetic field at the jet's emission site, with $B_T = 1$ G, and this limit inversely scales with B_T. See their Fig. 3 for the limits' dependence on B_T and electron density.

[57] ZHANG 23A searched for oscillations in the fine structure constant induced by dilaton-like dark matter by measuring the frequencies of a hyperfine-structure transition in ^{87}Rb and an electronic transition in ^{164}Dy, and by comparing them with that of a quartz oscillator. They assume the local dark matter density $\rho_S \simeq 0.4$ GeV/cm^3. The quoted limit is set at $m_{S^0} \simeq 1 \times 10^{-17}$ eV. See their Fig. 3 for the limits over $m_{S^0} = 1 \times 10^{-17}$–$8.3 \times 10^{-13}$ eV.

[58] APRILE 22B is an update of APRILE 20 based on a similar solar axion modeling to DENT 20A and GAO 20. They exclude the XENON1T excess found in APRILE 20. The quoted limit holds for small g_{Aee}. See Fig. 6 for correlation between $G_{A\gamma\gamma}$ and g_{Aee}.

[59] ARNQUIST 22 is analogous to AVIGNONE 98, and supersedes ANASTASSOPOULOS 17 for $m_{A^0} \gtrsim 1.2$ eV.

[60] ARZA 22 search for low-mass axions as dark matter using the Earth as a transducer for axion-photon conversion. The concept works because the region between the Earth and the ionosphere forms an insulating cavity that parametrically enhances the axion signal by the radius of the Earth. The result is an oscillating and spatially correlated magnetic field induced via the interaction between axion dark matter and the geomagnetic field, which they searched for using archival magnetometer field data over 20 years compiled by the SuperMAG collaboration. Quoted limit applies for masses 3–4 $\times 10^{-17}$ eV, see Fig. 1 for mass-dependent limits.

[61] BERNAL 22 explored the possibility that the excess in the cosmic optical background measured by New Horizonss Long Range Reconnaisance Imager was due to axion dark matter decaying into monoenergetic photons. See their Fig. 2 for the axion-photon coupling to explain the excess.

[62] CALORE 22 update CALORE 20 by evaluating axion fluxes from progenitors of various masses and performing a template-based analysis using 12 years of Fermi-LAT data in the energy range from 50 MeV to 500 GeV. See their Fig. 10 for mass-dependent limits.

[63] CAPUTO 22 study the effect of energy deposition by radiative decay of axions produced via the Primakoff process and photon coalescence in the supernova core, and set the

Int. J. Mod. Phys. A 2026.41. Downloaded from www.worldscientific.com by UNIVERSITY OF CALIFORNIA @ BERKELEY on 09/16/26. Re-use and distribution is strictly not permitted, except for Open Access articles.

limits by the radiative energy deposition $< 10^{50}$ erg and progenitor radius $= 5 \times 10^{13}$ cm. The quoted limit is at $m_{A^0} = 150$ MeV. See their Fig. 2 for mass-dependent limits.

[64] CASTILLO 22 update CAPUTO 19 using the polarization measurements of the Crab Pulsar by the QUIJOTE MFI instrument and 20 Galactic pulsars from the PPTA project. See their Table 1 for the assumed local axion energy density ρ_A for each pulsar and their Fig. 7 for the mass-dependent limits in the range of 3×10^{-23} eV $\leq m_{A^0} \leq 10^{-19}$ eV.

[65] DEROCCO 22 uses the NuSTAR data to search for monochromatic X-ray lines produced by the decay of solar axions trapped on bound orbits. The quoted limit applies to $m_{A^0} \simeq$ 9 keV. They also derive limits in the plane of g_{Aee} and $G_{A\gamma\gamma}$. See their Figs. 2 and 4 for mass-dependent limits.

[66] DESSERT 22A look for an axion-induced linear polarization using data from multiple magnetic white dwarf stars. See their Figs. 1 and 8 for the mass-dependent limits.

[67] ECKNER 22 set limits by using sub-PeV diffuse gamma-ray data from HAWC and Tibet ASγ by assuming that gamma rays produced simultaneously with high-energy neutrinos from extragalactic sources suggested by IceCube are converted to axions in the magnetic field at the source and reconverted to gamma rays in the Galactic magnetic field. See their Fig. 4 for mass-dependent limits.

[68] FOSTER 22 is an update of FOSTER 20 in the list of limits on relic invisible axions. They search for axion-photon transitions generated by neutron stars in the Galactic center region. They use improved population models of the Galactic center neutron stars and a Navarro-Frenk-White (NFW) model of the galactic dark matter distribution. The quoted limit applies to $m_{A^0} \simeq$ 17–25 μeV. See their Fig. 1 for mass-dependent limits.

[69] KIRITA 22 update HOMMA 21 by increasing the laser energy and developing a background discrimination method using the beam cross-section dependence of the background originated from optical elements. The quoted limits applies to $m_{A^0} = 0.18$ eV. See their Fig. 11 for mass-dependent limits.

[70] LANGHOFF 22 set limits by considering the freeze-in production of axions coupled only to photons. The quoted limit applies to $m_{A^0} = 2$ MeV for the reheating temperature equal to 5 MeV. See their Fig. 1 for mass-dependent limits.

[71] LI 22 is analogous to LI 21B, and use the spectra of the blazar FSRQ 4C+21.35 measured by MAGIC, VERITAS, and Fermi-LAT. The quoted limit applies to $m_{A^0} \simeq 8 \times 10^{-10}$ eV. See their Fig. 1 for mass-dependent limits.

[72] LI 22C is analogous to LI 21B, and use the spectra of the blazars Mrk 421 and PG 1553+113 measured by MAGIC and Fermi-LAT. The quoted limit applies to $m_{A^0} \simeq$ 1×10^{-8} eV. See their Fig. 4 for mass-dependent limits.

[73] LUCENTE 22 developed a method to correctly incorporate the effects of axions decaying into photons inside the core of horizontal-branch stars. They update CARENZA 20 by evaluating axion energy transfer in the range of axion mean free path where the diffusive energy transport and free streaming approximations are not applicable. See their Fig. 1 for the limits.

[74] BASU 21 searched for birefringence induced by axion dark matter using multiple images of the polarized source in the strongly gravitationally lensed system CLASS B1152+199. They assume the axion makes up all dark matter, and used the axion density in the emitting region, $\rho_A = 20$ GeV/cm^3. Limits between 9.2×10^{-11}–7.7×10^{-8} GeV^{-1} are obtained for $m_{A^0} = 3.6 \times 10^{-21}$–$4.6 \times 10^{-18}$eV. See their Fig. 2 for mass-dependent limits.

[75] BI 21 look for the gamma-ray spectral distortions induced by axion-photon oscillations in the presence of the Galactic magnetic field, using the measurements of sub-PeV gamma-rays from the Crab Nebula by the Tibet ASγ and HAWC experiments, together with MAGIC and HEGRA gamma-ray data. See their Fig. 3 for mass-dependent limits.

[76] DOLAN 21A study the effect of axion production on the evolution of asymptotic giant branch stars, and use the white-dwarf initial-final mass relation to set the limits. See their Fig. 1 for mass-dependent limits.

[77] GUO 21 is analogous to AJELLO 16, and use the Fermi-LAT and H.E.S.S. II measurements of PG 1553+113 and PKS 2155-304. See their Fig. 6 for mass-dependent limits.

[78] HOMMA 21 look for the production of axion resonance states and their subsequent stimulated decays by combining linearly polarized creation laser pulses and circularly polarized inducing laser pulses. The quoted limit is at $m_{A^0} \simeq 0.178$ eV. See their Fig. 14 for mass-dependent limits.

[79] LI 21B is analogous to AJELLO 16, and use the spectra of the blazar Mrk 421 measured by ARGO-YBJ and Fermi-LAT. They consider ALP-photon mixing in the magnetic fields of both the blazar jet and the Galaxy. The quoted limit applies to $m_{A^0} \simeq 1 \times 10^{-9}$ eV. See their Fig. 5 for mass-dependent limits.

[80] LLOYD 21 is analogous to FORTIN 18, and set limits on the product of the axion couplings to photons and nucleons as $g_{ANN}\, G_{A\gamma\gamma} \lesssim 4.6 \times 10^{-19}$ GeV^{-1} for $m_{A^0} \lesssim$ 10^{-5} eV by using the quiescent soft gamma-ray flux upper limits in five magnetars. We use $g_{ANN} = G_{AN}\, 2m_N$ to translate their limits. See their Table II and Fig. 3 for the limits.

[81] REGIS 21 look for monochromatic photons from axion decay, using the MUSE spectroscopic data on the Leo T dwarf spheroidal galaxy. They assume that axions make up all of dark matter and use the integrated dark matter density along the line of sight determined by observations.

[82] XIAO 21 use X-ray data from Betelgeuse to look for signals from axions produced in the stellar core that were converted to X-rays by the Galactic magnetic field. See their Fig. 1 for the mass-dependent limit.

[83] ABUDINEN 20 look for the process $e^+e^- \to \gamma A^0$ ($A^0 \to \gamma\gamma$) and set upper limits of around 10^{-3} over the mass range. The quoted limit is at $m_{A^0} = 0.3$ GeV. See their Fig. 5 for mass dependent limits.

[84] BANERJEE 20A look for axions produced from high-energy bremsstrahlung photons through the Primakoff effect with the electric field of the target nuclei. They exclude $G_{A\gamma\gamma} = 2 \times 10^{-4}$–$5 \times 10^{-2}$ GeV^{-1} for $m_{A^0} < 55$ MeV. See their Fig. 5 for mass-dependent limits.

[85] BUEHLER 20 look for the γ-ray transparency due to axion-photon oscillations using high-energy photon events from 79 sources in the Second Fermi-LAT Catalog of High-Energy Sources. The quoted limit is for the intergalactic magnetic field strength and coherence length of $B = 1$ nG and $s = 1$ Mpc. See their Figs. 4 and 5 for mass-dependent limits and for different magnetic-field parameters.

[86] CALORE 20 use the isotropic diffuse γ-ray background measured by the Fermi-LAT to constrain the γ-ray flux converted in the Galactic magnetic field from axions produced from past core-collapse supernovae. They also derive a limit on a heavier axion with $m_{A^0} \gtrsim$ keV decaying into two photons of $G_{A\gamma\gamma} \lesssim 5 \times 10^{-11}$ GeV^{-1} for m_{A^0} $= 5$ keV. See their Figs. 5 and 7 for the limits as well as limits in the presence of axion-nucleon couplings.

[87] CARENZA 20 extend the globular cluster bound of AYALA 14 to heavier masses ($m_{A^0} \leq$ a few 100 keV) by taking account of the coalescence process $\gamma + \gamma \to A^0$ as well as the decay of the ALP inside the stellar core. See their Fig.4 for mass-dependent limits.

[88] DENT 20A is analogous to GAO 20. The quoted limit is from their arXiv:2006.15118v3 (v2 is their published version), using the relativistic Hartree-Fock form factor. The limit is up to two times weaker than the published one. See Fig. 4 in their arXiv version 3 for the correlation between $G_{A\gamma\gamma}$ and g_{Aee} corresponding to the excess reported in APRILE 20.

[89] DEPTA 20 correct the underestimated D abundance in MILLEA 15, and derive robust cosmological bounds by allowing the reheating temperature, $N_{\rm eff}$, and neutrino chemical potential to vary. See their Fig. 6 for mass-dependent limits.

[90] DESSERT 20A use the NuSTAR data of the Quintuplet and Westerlund 1 super star clusters to look for X-rays converted in the Galactic magnetic field from the axions produced in stellar cores. See their Fig. 3 for the mass-dependent limits.

[91] ESTEBAN 20 show that the two anomalous ANITA events can be explained by the reflected radio pulses that are resonantly produced in the ionosphere via axion-photon conversion for $m_{A^0} \lesssim 1 \times 10^{-7}$ eV , if an axion clump passes the Earth about once a month. See their Fig.5 for the region consistent with this interpretation for different values of the axion density inside the clumps.

[92] GAO 20 correct the limit of APRILE 20 by including inverse Primakoff scattering in the XENON1T detector. The quoted limit is from their arXiv:2006.14598v4 (v3 is their published version), taking account of the atomic form factor of Xe as pointed out in ABE 20J. The limit is weaker by a factor of 1.5–2 than the published one. See Fig. 3 in their arXiv version 4 for correlation between $G_{A\gamma\gamma}$ and g_{Aee} corresponding to the excess reported in APRILE 20.

[93] KOROCHKIN 20 assume the axion makes up all dark matter, and look for a dip in the observed gamma-ray spectrum of the blazer 1ES 1218+304 by Fermi/LAT and VERITAS due to the extragalactic background light produced by the axion decay. Their analysis favors nonzero axion-induced absorption with $G_{A\gamma\gamma} = 3 \times 10^{-11}$–$2 \times 10^{-10}$ GeV^{-1} over a range of $m_{A^0} =$ 2–18 eV. See their Fig. 1 for mass-dependent limits between $0.25 < m_{A^0} < 25$ eV.

[94] LUCENTE 20A study the SN 1987A energy-loss argument on the axion-like particle production. In addition to the Primakoff process, they take account of photon coalescence as well as gravitational trapping that become relevant at $m_{A^0} > 100$ MeV. See their Fig. 12 for the mass-dependent limit.

[95] MEYER 20 look for prompt γ-rays converted in the Galactic magnetic fields from axions produced via the Primakoff process in a sample of 20 extragalactic core-collapse supernovae. The limits assume a progenitor mass of 10 times the solar mass and certain models for the optical emission and the galactic magnetic field. See their Figs. 2 and 6 in the erratum for mass- and model-dependent limits.

[96] YAMAMOTO 20 look for X-ray photons converted by the Earth's magnetic field from the axions produced by the two-body decay of dark matter, and set the limits by using the Suzaku data. The quoted limit is for the monochromatic X-ray line from the galactic dark matter with lifetime $\tau = 4.32 \times 10^{17}$ sec. They also derive limits on the continuum spectrum from the extragalactic component. See their Fig. 7 for the limits.

[97] ALONI 19 used the data collected by the PRIMEX experiment to derive a limit based on a data-driven method. See their Fig. 2 for mass-dependent limits.

[98] CAPUTO 19 look for an oscillating variation of the polarization angle of the pulsar J0437-4715, where they assume the local axion energy density $\rho_A = 0.3$ GeV/cm^3. See their Fig. 2 for mass-dependent limits for 5×10^{-24} eV $\leq m_{A^0} \leq 2 \times 10^{-19}$ eV.

[99] FEDDERKE 19 look for a uniform reduction of the CMB polarization at large scales, which is induced by the oscillating axion background during CMB decoupling. The quoted limit is based on the assumption that axions make up all of the dark matter. See their Fig. 3 for mass-dependent limits for $m_{A^0} = 10^{-22}$–10^{-19} eV.

[100] IVANOV 19 look for the axion-induced periodic changes in the polarization angle of parsec-scale jets in active galactic nuclei observed by the MOJAVE program, where they use the axion energy density $\rho_A = 20$ GeV/cm^3. See their Fig. 6 for mass-dependent limits for 5×10^{-23} eV $\leq m_{A^0} \leq 1.2 \times 10^{-21}$ eV.

[101] LIANG 19 look for spectral irregularities in the spectrum of 10 bright H.E.S.S. sources in the Galactic plane, assuming photon-ALP mixing in the Galactic magnetic fields. See their Fig. 2 for mass-dependent limits with different Galactic magnetic field models.

[102] FORTIN 18 studied the conversion of axion-like particles produced in the core of a magnetar to hard X-rays in the magnetosphere. See their Fig. 5 for mass-dependent limits with different values of the magnetar core temperature.

[103] JAECKEL 18 study axions produced through the Primakoff process from SN 1987A, which subsequently decay into photon pairs. See their Fig. 1 for the mass-dependent limits in the range of $m_{A^0} =$ 0.01–100 MeV.

[104] YAMAJI 18 search for axions with an x-ray LSW at Spring-8, using the Laue-case conversion in a silicon crystal. They also obtain $G_{A\gamma\gamma} < 4.2 \times 10^{-3}$ GeV^{-1} for $m_{A^0} <$ 10 eV. See their Fig. 5 for mass-dependent limits.

[105] ZHANG 18 look for spectral irregularities in the spectrum of PKS 2155-304 measured by Fermi LAT, assuming photon-ALP mixing in the intercluster and Galactic magnetic fields. See their Figs. 2 and 3 for mass-dependent limits with different values of the intercluster magnetic field parameters.

[106] ADE 17 look for cosmic birefringence from axion-like particles using CMB polarization data taken by the BICEP2 and Keck Array experiments. They set a limit $G_{A\gamma\gamma} H_I$ $< 7.2 \times 10^{-2}$ at 95 %CL for $m_{A^0} < 10^{-28}$ eV, where H_I is the Hubble parameter during inflation.

[107] ANASTASSOPOULOS 17 looked for solar axions by the CAST axion helioscope in the vacuum phase, and supersedes ANDRIAMONJE 07.

[108] DOLAN 17 update existing limits on $G_{A\gamma\gamma}$ for axion-like particles. The limits from the proton beam dump experiments in their Fig. 2 contained an error, and the corrected version is shown in Fig. 1 of DOLAN 21.

[109] INADA 17 search for axions with an x-ray LSW at Spring-8. See their Fig. 4 for mass-dependent limits.

[110] KOHRI 17 attributed to axion-photon oscillations the excess of cosmic infrared background observed by the CIBER experiment. See their Fig. 5 for the region preferred by their scenario.

[111] MARSH 17 is similar to WOUTERS 13, using Chandra observations of M87. See their Fig. 6 for mass-dependent limits.

Int. J. Mod. Phys. A 2026.41. Downloaded from www.worldscientific.com
by UNIVERSITY OF CALIFORNIA @ BERKELEY on 09/16/26. Re[redacted]s strictly not permitted, except for Open Access articles.

[112] TIWARI 17 use observed limits of the cosmic distance-duality relation to constrain the photon-ALP mixing based on 3D simulations of the magnetic field configuration. The quoted value is for the averaged magnetic field of 1nG with a coherent length of 1 Mpc. See their Fig. 5 for mass-dependent limits.

[113] AJELLO 16 look for irregularities in the energy spectrum of the NGC1275 measured by Fermi LAT, assuming photon-ALP mixing in the intra-cluster and Galactic magnetic fields. See their Fig. 2 for mass-dependent limits.

[114] DELLA-VALLE 16 look for the birefringence induced by axion-like particles. See their Fig. 14 for mass-dependent limits.

[115] DELLA-VALLE 16 look for the dichroism induced by axion-like particles. See their Fig. 14 for mass-dependent limits.

[116] JAECKEL 16 use the LEP data of $Z \to 2\gamma$ and $Z \to 3\gamma$ to constrain the ALP production via $e^+e^- \to Z \to A^0\gamma\,(A^0 \to \gamma\gamma)$, assuming the ALP coupling with two hypercharge bosons. See their Fig. 4 for mass-dependent limits.

[117] LEEFER 16 derived limits by using radio-frequency spectroscopy of dysprosium and atomic clock measurements. See their Fig. 1 for mass-dependent limits as well as limits on Yukawa-type couplings of the scalar to the electron and nucleons.

[118] ANASTASSOPOULOS 15 search for solar chameleons with CAST and derived limits on the chameleon coupling to photons and matter. See their Fig. 12 for the exclusion region.

[119] ARIK 15 is analogous to ARIK 09, and search for solar axions for m_{A^0} around 0.2 and 0.4 eV. See their Figs. 1 and 3 for the mass-dependent limits.

[120] Based on OSQAR photon regeneration experiment. See their Fig. 6 for mass-dependent limits on scalar and pseudoscalar bosons.

[121] BRAX 15 derived limits on conformal and disformal couplings of a scalar to photons by searching for a chaotic absorption pattern in the X-ray and UV bands of the Hydra A galaxy cluster and a BL lac object, respectively. See their Fig. 8.

[122] HASEBE 15 look for an axion via a four-wave mixing process at quasi-parallel colliding laser beams. They also derived limits on a scalar coupling to photons $G_{S\gamma\gamma} < 2.62 \times 10^{-4}$ GeV^{-1} at $m_{S^0} = 0.15$ eV. See their Figs. 11 and 12 for mass-dependent limits.

[123] MILLEA 15 is similar to CADAMURO 12, including the Planck data and the latest inferences of primordial deuterium abundance. See their Fig. 3 for mass-dependent limits.

[124] VANTILBURG 15 look for harmonic variations in the dyprosium transition frequency data, induced by coherent oscillations of the fine-structure constant due to dilaton-like dark matter, and set the limits, $G_{S\gamma\gamma} < 6 \times 10^{-27}$ GeV^{-1} at $m_{S^0} = 6 \times 10^{-23}$ eV. See their Fig. 4 for mass-dependent limits between $1 \times 10^{-24} < m_{S^0} < 1 \times 10^{-15}$ eV.

[125] VINYOLES 15 performed a global fit analysis based on helioseismology and solar neutrino observations. See their Fig. 9.

[126] ARIK 14 is similar to ARIK 11. See their Fig. 2 for mass-dependent limits.

[127] AYALA 14 derived the limit from the helium-burning lifetime of horizontal-branch stars based on number counts in globular clusters.

[128] DELLA-VALLE 14 use the new PVLAS apparatus to set a limit on vacuum magnetic birefringence induced by axion-like particles. See their Fig. 6 for the mass-dependent limits.

[129] EJLLI 14 set limits on a product of primordial magnetic field and the axion mass using CMB distortion induced by resonant axion production from CMB photons. See their Fig. 1 for limits applying specifically to the DFSZ and KSVZ axion models.

[130] PUGNAT 14 is analogous to EHRET 10. See their Fig. 5 for mass-dependent limits on scalar and pseudoscalar bosons.

[131] REESMAN 14 derive limits by requiring effects of axion-photon interconversion on gamma-ray spectra from distant blazars to be no larger than errors in the best-fit optical depth based on a certain extragalactic background light model. See their Fig. 5 for mass-dependent limits.

[132] ABRAMOWSKI 13A look for irregularities in the energy spectrum of the BL Lac object PKS 2155–304 measured by H.E.S.S. The limits depend on assumed magnetic field around the source. See their Fig. 7 for mass-dependent limits.

[133] ARMENGAUD 13 is analogous to AVIGNONE 98. See Fig. 6 for the limit.

[134] BETZ 13 performed a microwave-based light shining through the wall experiment. See their Fig. 13 for mass-dependent limits.

[135] FRIEDLAND 13 derived the limit by considering blue-loop suppression of the evolution of red giants with 7–12 solar masses.

[136] MEYER 13 attributed to axion-photon oscillations the observed excess of very high-energy γ-rays with respect to predictions based on extragalactic background light models. See their Fig.4 for mass-dependent lower limits for various magnetic field configurations.

[137] WOUTERS 13 look for irregularities in the X-ray spectrum of the Hydra cluster observed by Chandra. See their Fig. 4 for mass-dependent limits.

[138] CADAMURO 12 derived cosmological limits on $G_{A\gamma\gamma}$ for axion-like particles. See their Fig. 1 for mass-dependent limits.

[139] PAYEZ 12 derive limits from polarization measurements of quasar light (see their Fig. 3). The limits depend on assumed magnetic field strength in galaxy clusters. The limits depend on assumed magnetic field and electron density in the local galaxy supercluster.

[140] ARIK 11 search for solar axions using ^{3}He buffer gas in CAST, continuing from the ^{4}He version of ARIK 09. See Fig. 2 for the exact mass-dependent limits.

[141] ALPS is a photon regeneration experiment. See their Fig. 4 for mass-dependent limits on scalar and pseudoscalar bosons.

[142] AHMED 09A is analogous to AVIGNONE 98.

[143] ARIK 09 is the ^{4}He filling version of the CAST axion helioscope in analogy to INOUE 02 and INOUE 08. See their Fig. 7 for mass-dependent limits.

[144] CHOU 09 use the GammeV apparatus in the afterglow mode to search for chameleons, (pseudo)scalar bosons with a mass depending on the environment. For pseudoscalars they exclude at 3σ the range 2.6×10^{-7} GeV$^{-1} < G_{A\gamma\gamma} < 4.2 \times 10^{-6}$ GeV^{-1} for vacuum m_{A^0} roughly below 6 meV for density scaling index exceeding 0.8.

[145] GONDOLO 09 use the all-flavor measured solar neutrino flux to constrain solar interior temperature and thus energy losses.

[146] LIPSS photon regeneration experiment, assuming scalar particle S^0. See Fig. 4 for mass-dependent limits.

[147] CHOU 08 perform a variable-baseline photon regeneration experiment. See their Fig. 3 for mass-dependent limits. Excludes the PVLAS result of ZAVATTINI 06.

[148] FOUCHE 08 is an update of ROBILLIARD 07. See their Fig. 12 for mass-dependent limits.

[149] INOUE 08 is an extension of INOUE 02 to larger axion masses, using the Tokyo axion helioscope. See their Fig. 4 for mass-dependent limits.

[150] ZAVATTINI 08 is an upgrade of ZAVATTINI 06, see their Fig. 8 for mass-dependent limits. They now exclude the parameter range where ZAVATTINI 06 had seen a positive signature.

[151] ANDRIAMONJE 07 looked for Primakoff conversion of solar axions in 9T superconducting magnet into X-rays. Supersedes ZIOUTAS 05.

[152] ROBILLIARD 07 perform a photon regeneration experiment with a pulsed laser and pulsed magnetic field. See their Fig. 4 for mass-dependent limits. Excludes the PVLAS result of ZAVATTINI 06 with a CL exceeding 99.9%.

[153] ZAVATTINI 06 propagate a laser beam in a magnetic field and observe dichroism and birefringence effects that could be attributed to an axion-like particle. This result is now excluded by ROBILLIARD 07, ZAVATTINI 08, and CHOU 08.

[154] INOUE 02 looked for Primakoff conversion of solar axions in 4T superconducting magnet into X ray.

[155] MORALES 02B looked for the coherent conversion of solar axions to photons via the Primakoff effect in Germanium detector.

[156] BERNABEI 01B looked for Primakoff coherent conversion of solar axions into photons via Bragg scattering in NaI crystal in DAMA dark matter detector.

[157] ASTIER 00B looked for production of axions from the interaction of high-energy photons with the horn magnetic field and their subsequent re-conversion to photons via the interaction with the NOMAD dipole magnetic field.

[158] MASSO 00 studied limits on axion-proton coupling using the induced axion-photon coupling through the proton loop and CAMERON 93 bound on the axion-photon coupling using optical rotation. They obtained the bound $g_p^2/4\pi < 1.7 \times 10^{-9}$ for the coupling $g_p \overline{p}\gamma_5 p\phi_A$.

[159] AVIGNONE 98 result is based on the coherent conversion of solar axions to photons via the Primakoff effect in a single crystal germanium detector.

[160] Based on the conversion of solar axions to X-rays in a strong laboratory magnetic field.

[161] Experiment based on proposal by MAIANI 86.

[162] Experiment based on proposal by VANBIBBER 87.

[163] LAZARUS 92 experiment is based on proposal found in VANBIBBER 89.

[164] RUOSO 92 experiment is based on the proposal by VANBIBBER 87.

[165] SEMERTZIDIS 90 experiment is based on the proposal of MAIANI 86. The limit is obtained by taking the noise amplitude as the upper limit. Limits extend to $m_{A^0} = 4 \times 10^{-3}$ where $G_{A\gamma\gamma} < 1 \times 10^{-4}$ GeV^{-1}.

Limit on Invisible A^0 (Axion) Electron Coupling

The limit is for $g_{Aee}\,\phi_A\,\overline{e}(i\gamma_5)e$, or equivalently, the dipole-dipole potential $-\frac{g^2_{Aee}}{16\pi m^2_e}\left((\boldsymbol{\sigma}_1\cdot\boldsymbol{\sigma}_2) - 3(\boldsymbol{\sigma}_1\cdot\boldsymbol{n})\,(\boldsymbol{\sigma}_2\cdot\boldsymbol{n})\right)/r^3$ where $\boldsymbol{n}=\boldsymbol{r}/r$ and the sign of the potential was corrected based on DAIDO 17.

VALUE	CL%	DOCUMENT ID		TECN	COMMENT
• • • We do not use the following data for averages, fits, limits, etc. • • •					
$<4 \times 10^{-10}$	90	[1] ALBAKRY	25	CDMS	$m_{A^0} = 1.2$–23.3 eV
$<5 \times 10^{-13}$	90	[2] APRILE	25A	XENT	$m_{A^0} = 0.01$–0.4 keV
$<2.7 \times 10^{-13}$	90	[3] LI	25	PNDX	$m_{A^0} = 0.03$–1 MeV
$<4 \times 10^{-7}$	90	[4] MIRZAKHANI	25	MINR	$m_{A^0} < 2$ MeV
$<2 \times 10^{-19}$	95	[5] MONTEFAL...	25	CMB	$m_{A^0} = 10^2$–10^6 eV
$<4.95 \times 10^{-8}$	95	[6] PARK	25	NEON	$m_{A^0} < 1.6$ MeV
$<5.2 \times 10^{-14}$	95	[7] TROITSKY	25	ASTR	$m_{A^0} \lesssim 10$ keV
$<2.9 \times 10^{-12}$	90	[8] ZENG	25	PNDX	$m_{A^0} \lesssim$ keV
$<4 \times 10^{-14}$	90	[9] ZENG	25	PNDX	$m_{A^0} = 1$–30 keV
$<3.3 \times 10^{-12}$	90	[10] AGOSTINI	24A	GRDA	$m_{A^0} = 65$–1021 keV
$<1.5 \times 10^{-13}$	90	[11] ARNQUIST	24	MAJD	$m_{A^0} = 1$–100 keV
$<2.35 \times 10^{-12}$	90	[12] AALBERS	23A	LZ	Solar axions
$<1.3 \times 10^{-14}$	90	[13] AALBERS	23A	LZ	$m_{A^0} = 1$–17 keV
$<1.61 \times 10^{-11}$	90	[14] ADHIKARI	23	C100	Solar axions
$<6 \times 10^{-13}$	90	[15] ADHIKARI	23A	C100	$m_{A^0} = 10$–1000 keV
$<8 \times 10^{-14}$	90	[16] AGNES	23A	DS50	$m_{A^0} = 0.03$–20 keV
		[17] APRILE	23B	XE1T	Neutron star merger
$<3 \times 10^{-9}$	95	[18] CAPOZZI	23A	DUMP	$m_{A^0} = 10^4$–2×10^7 eV
$<6 \times 10^{-15}$		[19] WADEKAR	23	ASTR	$m_{A^0} = 100$ keV
$<4 \times 10^{-12}$	90	[20] APRILE	22	XE1T	$m_{A^0} = 0.01$–0.4 keV
$<9 \times 10^{-15}$	90	[21] APRILE	22B	XENT	$m_{A^0} = 1$–39, 44–140 keV
$<2 \times 10^{-12}$	90	[22] APRILE	22B	XENT	Solar axions
		[23] DESSERT	22	ASTR	Magnetic white dwarf
$<2.6 \times 10^{-6}$	95	[24] IKEDA	22		$m_{A^0} = 33.117$–33.130 μeV
$<2.5 \times 10^{-18}$		[25] LANGHOFF	22	COSM	$m_{A^0} = 20$–3×10^4 keV
		[26] WANG	22C		$m_{A^0} \leq 0.47$ meV
		[27] XIAO	22	ASTR	Betelgeuse
		[28] CALORE	21	ASTR	Core-collapse SNe
$<2 \times 10^{-9}$		[29] LUCENTE	21	ASTR	SN 1987A
$<5.1 \times 10^{-12}$	90	[30] AGOSTINI	20	HPGE	$m_{A^0} = 0.06$–1 MeV
$<1 \times 10^{-9}$	90	[31] AMARAL	20	SCDM	$m_{A^0} = 1.2$–50 eV
$<2 \times 10^{-14}$	90	[32] APRILE	20	XE1T	$m_{A^0} = 1$ keV
2.6–3.7×10^{-12}	90	[33] APRILE	20	XE1T	Solar axions
$<6 \times 10^{-13}$	90	[34] ARALIS	20	SCDM	$m_{A^0} = 0.04$–500 keV
$<1.3 \times 10^{-13}$	95	[35] CAPOZZI	20	ASTR	Tip of the Red Giant Branch
$<1.7 \times 10^{-11}$	95	[36] CRESCINI	20	QUAX	$m_{A^0} = 42.4$–43.1 μeV
$<1.8 \times 10^{-9}$		[37] GHOSH	20A	COSM	$m_{A^0} \lesssim 0.5$ MeV
$<1.48 \times 10^{-13}$	95	[38] STRANIERO	20	ASTR	Tip of the Red Giant Branch
$<2.48 \times 10^{-11}$	90	[39] WANG	20A	CDEX	Solar axions

$<4 \times 10^{-13}$	90	[40] WANG	20A	CDEX	$m_{A^0} = 1.5$ keV
$<1.7 \times 10^{-11}$	90	[41] ADHIKARI	19B	C100	Solar axions
$<2.3 \times 10^{-14}$	90	[42] APRILE	19D	XE1T	$m_{A^0} = 0.186$–1 keV
		[43] DESSERT	19	ASTR	Magnetic white dwarf
$<2.6 \times 10^{-10}$	95	[44] TERRANO	19		Torsion pendulum
$<1.5 \times 10^{-13}$	90	[45] ABE	18F	XMAS	$m_{A^0} = 40$–120 keV
$<1.1 \times 10^{-11}$	90	[46] ARMENGAUD	18	EDE3	Solar axions
$<4 \times 10^{-13}$	90	[47] ARMENGAUD	18	EDE3	$m_{A^0} = 0.8$–500 keV
$<4.9 \times 10^{-10}$	95	[48] CRESCINI	18	QUAX	$m_{A^0} = 58\ \mu$eV
		[49] FICEK	18	THEO	$m_{A^0} < 10$ keV
$<4.5 \times 10^{-13}$	90	[50] ABGRALL	17	HPGE	$m_{A^0} = 11.8$ keV
$<3.5 \times 10^{-12}$	90	[51] AKERIB	17B	LUX	Solar axions
$<4.2 \times 10^{-13}$	90	[52] AKERIB	17B	LUX	$m_{A^0} = 1$–16 keV
$<2.3 \times 10^{-13}$	90	[53] APRILE	17B	X100	$m_{A^0} = 6$ keV
$<4 \times 10^{-4}$	90	[54] FICEK	17	THEO	$m_{A^0} < 1$ keV
$<4.35 \times 10^{-12}$	90	[55] FU	17A	PNDX	Solar axions
$<4.3 \times 10^{-14}$	90	[56] FU	17A	PNDX	$m_{A^0} = 2$ keV
$<5 \times 10^{-13}$	90	[57] LIU	17A	CDEX	$m_{A^0} = 13$ keV
$<2.5 \times 10^{-11}$	90	[58] LIU	17A	CDEX	Solar axions
<0.15	95	[59] LUO	17		$m_{A^0} = 300$ eV
$<3.3 \times 10^{-13}$	68	[60] BATTICH	16	ASTR	White dwarf cooling
$<7 \times 10^{-13}$		[61] CORSICO	16	ASTR	White dwarf cooling
$<1.39 \times 10^{-11}$	90	[62] YOON	16	KIMS	Solar axions
$<7.4 \times 10^{-9}$	95	[63] TERRANO	15		$m_{A^0} < 30\ \mu$eV
$<8 \times 10^{-13}$	90	[64] ABE	14F	XMAS	$m_{A^0} = 60$ keV
$<7.7 \times 10^{-12}$	90	[65] APRILE	14B	X100	Solar axions
		[66] APRILE	14B	X100	$m_{A^0} = 5$–7 keV
< 0.96–8.2×10^{-8}	90	[67] DERBIN	14	CNTR	$m_{A^0} = 0.1$–1 MeV
$<2.8 \times 10^{-13}$	99	[68] MILLER-BER...	14	ASTR	White dwarf cooling
$<5.4 \times 10^{-11}$	90	[69] ABE	13D	XMAS	Solar axions
$<1.07 \times 10^{-12}$	90	[70] ARMENGAUD	13	EDEL	$m_{A^0} = 12.5$ keV
$<2.59 \times 10^{-11}$	90	[71] ARMENGAUD	13	EDEL	Solar axions
		[72] BARTH	13	CAST	Solar axions
< 1.4–9.7×10^{-7}	90	[73] DERBIN	13	CNTR	$m_{A^0} = 0.1$–1 MeV
$<1.5 \times 10^{-8}$	68	[74] HECKEL	13		$m_{A^0} \leq 0.1\ \mu$eV
$<4.3 \times 10^{-13}$	95	[75] VIAUX	13A	ASTR	Low-mass red giants
$<7 \times 10^{-13}$	95	[76] CORSICO	12	ASTR	White dwarf cooling
$<2.2 \times 10^{-10}$	90	[77] DERBIN	12	CNTR	Solar axions
< 0.02–1×10^{-10}	90	[78] AALSETH	11	CNTR	$m_{A^0} = 0.3$–8 keV
$<1.4 \times 10^{-12}$	90	[79] AHMED	09A	CDMS	$m_{A^0} = 2.5$ keV
$<4 \times 10^{-9}$		[80] DAVOUDIASL	09	ASTR	Earth cooling
$<2.7 \times 10^{-8}$	66	[81] NI	94		Induced magnetism
		[81] CHUI	93		Induced magnetism
$<3.6 \times 10^{-7}$	66	[82] PAN	92		Torsion pendulum
$<2.9 \times 10^{-8}$	95	[81] BOBRAKOV	91		Induced magnetism
$<1.9 \times 10^{-6}$	66	[83] WINELAND	91	NMR	
$<7 \times 10^{-7}$	66	[82] RITTER	90		Torsion pendulum
$<6.6 \times 10^{-8}$	95	[81] VOROBYOV	88		Induced magnetism

[1] ALBAKRY 25 report a search with the SuperCDMS detector for axion-like particle dark matter absorption on silicon. See their Fig. 4 for mass-dependent limits.

[2] APRILE 25A presents results from a search with XENONnT for axion-like particle dark matter absorption on electrons in liquid xenon. See their Fig. 5 for mass-dependent limits.

[3] LI 25 search for MeV-mass axion-like particles coupled to electrons making up the dark matter halo of the galaxy that could be absorbed by liquid xenon in the PandaX detector. The local density $\rho_A = 0.3$ GeV/cm^3 is assumed. The quoted limit is at $m_{A^0} = 150$ keV. See their Fig. 3 for mass-dependent limits.

[4] MIRZAKHANI 25 search for axion-like particles coupled to electrons using the MINER reactor neutrino experiment. Their search assumes the axions would be produced via Compton scattering of the reactor photon flux, which then either decay to an electron-positron pair or undergo inverse Compton scattering in the detector. See Fig. 10 for mass-dependent limits.

[5] MONTEFALCONE 25 place bounds on axion-like particle dark matter coupled to electrons using Planck CMB data. They search for the effects of anomalous energy injection on CMB anisotropies due to electron-loop induced ALP decays to two photons. See their Fig. 6 for mass-dependent limits.

[6] PARK 25 present a search for axion-like particles from the NEON reactor neutrino experiment. Axions would be produced through the Compton scattering of electrons with the large MeV photon flux from the reactor and then subsequently scatter or decay to an electron-positron pair in the detector. The quoted limit is at $m_{A^0} = 1.02$ MeV. See their Fig. 3 for mass-dependent limits.

[7] TROITSKY 25 sets a bound on axions coupled to electrons through their cooling effect on red giants and helium-burning stars in seven globular clusters observed by the Gaia survey. The bound is independent of the axion mass up to approximately values close to the stellar core temperatures.

[8] ZENG 25 place a bound on axions emitted by the Sun due to a nonzero axion-electron coupling using electronic recoil data collected by the PandaX detector. The limit is independent of the axion mass up to around the core temperature of the Sun.

[9] ZENG 25 place a bound on keV-scale axion-like particles making up the halo of the galaxy by searching for electron recoil events in the PandaX detector. See Fig. 3(e) for mass-dependent limits.

[10] AGOSTINI 24A report a search for axion-like particle dark matter absorption and dark Compton scattering on germanium, generating electron events in the GERDA experiment. The quoted limit is at $m_{A^0} = 150$ keV. See their Fig. 7 for mass-dependent limits.

[11] ARNQUIST 24 use the MAJORANA DEMONSTRATOR to search for high-mass axion-like particle dark matter absorption by Germanium. See Fig. 5 for mass-dependent limits.

[12] AALBERS 23A look for solar axions from the ABC processes. See their Fig. 6 for the limits.

[13] AALBERS 23A look for absorption of axion dark matter. The quoted limit is for $m_{A^0} \simeq 1.4$ keV. The local density $\rho_A = 0.3$ GeV/cm^3 is assumed. See their Fig. 7 for mass-dependent limits.

[14] ADHIKARI 23 is an update of ADHIKARI 19B.

[15] ADHIKARI 23A look for absorption and Compton-like processes of axion dark matter. The quoted limit is for $m_{A^0} \simeq 37$ keV. See their Fig. 4 for mass-dependent limits.

[16] AGNES 23A look for absorption of axion dark matter. The quoted limit is for $m_{A^0} \simeq 0.25$ keV. The local density $\rho_A = 0.3$ GeV/cm^3 is assumed. See their Fig. 2 for mass-dependent limits.

[17] APRILE 23B look for an absorption signal of axions within ± 500 seconds of the GW signals, including the neutron star merger GW170817. They set a 90% CL upper limit on the product of coincident fluence and cross section of axions to be less than 10^{-29} cm^2/cm^2 in the recoil energy range of 5.5–210 keV$_{ee}$.

[18] CAPOZZI 23A search for axions produced in electromagnetic showers in proton beam dumps and fixed target experiments. In this case, they reinterpret MiniBoone data. Quoted limit applies at 1 MeV. See Fig. 8 for mass-dependent limits.

[19] WADEKAR 23 use the Leo T dwarf galaxy's interstellar medium to derive limits, requiring the heating rate from axion dark matter absorption into hydrogen atoms and two-photon decay to be less than the astrophysical cooling rate. See Fig. 2 for limits over $m_{A^0} = 1$–100 keV, which loosen for lighter masses.

[20] APRILE 22 extend APRILE 19D to lower masses by removing the background of ionization signals correlated with high-energy events. The quoted limit applies to $m_{A^0} = 0.1$ keV. See their Fig. 15 for mass-dependent limits.

[21] APRILE 22B is an update of APRILE 20, and set the limit, $g_{Aee} \lesssim 9 \times 10^{-15}$–$3 \times 10^{-13}$. The quoted limit applies to $m_{A^0} = 2$ keV. They exclude the XENON1T excess found in APRILE 20. See their Fig. 6 for mass-dependent limits.

[22] APRILE 22B is an update of APRILE 20. They exclude the XENON1T excess found in APRILE 20. The quoted limit holds for small $G_{A\gamma\gamma}$. See their Fig. 6 for correlation between g_{Aee} and $G_{A\gamma\gamma}$.

[23] DESSERT 22 is an update of DESSERT 19. They used the Chandra observation of the magnetic white dwarf RE J0317-853 to look for converted X-rays in the magnetosphere from axions produced in the core through electron bremsstrahlung. They obtained the limit, $g_{Aee} \cdot G_{A\gamma\gamma} < 1.3 \times 10^{-25}$ GeV^{-1} at 95% CL for $m_{A^0} \lesssim 10^{-5}$ eV. See their Fig. 1 for mass-dependent limits.

[24] IKEDA 22 look for magnons excited by dark matter axions, using data taken with a hybrid quantum system consisting of a superconducting qubit and a spherical ferrimagnetic crystal. The quoted limit assumes the local dark matter density $\rho_A = 0.45$ GeV/cm^3 and the velocity $v = 220$ km/sec. See their Fig. 4 for the limits.

[25] LANGHOFF 22 set limits by considering the freeze-in production of axions coupled to electrons without anomalous coupling to photons. The quoted limit applies to $m_{A^0} = 15$ MeV for the reheating temperature equal to 5 MeV. See their Fig. 2 for mass-dependent limits.

[26] WANG 22C use the spin-amplifier based on hyperpolarized ^{129}Xe to set limits on the product of the axion couplings to electrons and nucleons as $g_{Aee}\, g_{Ann} < 4 \times 10^2$ (95 % CL) at $m_{A^0} = 0.1$ meV. Here g_{Ann} is the dimensionless axion-neutron coupling. See their Fig. 4 for the mass-dependent limits.

[27] XIAO 22 extend XIAO 21 in the list of photon coupling limits by including the production of axions from Compton and bremsstrahlung processes, and set limits on the product of the axion couplings to electrons and photons as $G_{A\gamma\gamma}\, g_{Aee} < 0.4$–$2.8 \times 10^{-24}$ GeV^{-1} (95 % CL) for $m_{A^0} < 3.5 \times 10^{-11}$eV. See their Fig. 5 for the limits. They are comparable to those of DESSERT 19 and more restrictive than the CAST bounds of BARTH 13.

[28] CALORE 21 consider the production of axions from Galactic and extragalactic SNe via nucleon-nucleon bremsstrahlung and their subsequent decay into electron-positron pairs, and exclude the range of $g_{Aee} \simeq 10^{-19}$–10^{-11} at $g_{App} = 10^{-9}$ for $m_{A^0} = 3$–30 MeV. See their Fig. 7 for the limits.

[29] LUCENTE 21 study the axion production in a supernova via electron-proton bremsstrahlung and electron-positron fusion, and exclude the range of $g_{Aee} \simeq 2 \times 10^{-9}$–$5.5 \times 10^{-7}$ for masses less than 1 MeV. See their Fig. 12 for the mass-dependent limits extending up to 150 MeV. This limit was corrected in the erratum.

[30] AGOSTINI 20 is analogous to AHMED 09A. The quoted limit applies to $m_{A^0} = 150$ keV. Their limits in their Fig. 3 were later found to be incorrect due to an error of their Eqs. (1) and (2). See Fig. 3 in AGOSTINI 22A for the corrected limits.

[31] AMARAL 20 use a second-generation SuperCDMS high-voltage eV-resolution detector to set limits on dark-matter axion absorption. The quoted limit is for $m_{A^0} \simeq 17$ eV. The local density $\rho_A = 0.3$ GeV/cm^3 is assumed. See their Fig. 3 for mass-dependent limits.

[32] APRILE 20 is an update of APRILE 17B where they look for an absorption signal of axion dark matter. They obtained the limit, $g_{Aee} \lesssim 2 \times 10^{-14}$–$1 \times 10^{-12}$ at 90%CL for $m_{A^0} = 1$–200 keV. They also found an excess over known backgrounds, which favors the mass $m_{A^0} = 2.3 \pm 0.2$ keV with a $3\,\sigma$ significance. See their Fig. 10 for mass-dependent limits.

[33] APRILE 20 look for solar axions from the ABC interactions, the Primakoff conversion, and the 14.4 keV M1 transition of ^{57}Fe, and set limits on g_{Aee}, $G_{A\gamma\gamma}$, g_{ANN}, and their products. An excess is observed at low energies between 2 and 3 keV. See their Fig.8 for correlation between the couplings. The quoted limit applies to the case of vanishing $G_{A\gamma\gamma}$ and g_{ANN}.

[34] ARALIS 20 is analogous to AHMED 09A. The quoted limit applies to $m_{A^0} = 0.3$ keV. The limits at masses above 3 keV in their Fig. 9 was later found to be incorrect due to an error in their analysis. See Fig. 2 in erratum for the corrected limits.

[35] CAPOZZI 20 obtains a limit on the axion-electron coupling from the brightness of the tip of the red-giant branch in ω Centauri. A similar limit of $< 1.6 \times 10^{-13}$ is obtained in NGC 4258.

[36] CRESCINI 20 is an update of CRESCINI 18. They assume a local axion dark matter density, $\rho_A = 0.3$ GeV/cm^3. See their Fig.4 for the limits.

Int. J. Mod. Phys. A 2026.41. Downloaded from www.worldscientific.com
by UNIVERSITY OF CALIFORNIA @ BERKELEY on 09/16/26. Re-use and distribution is strictly not permitted, except for Open Access articles.

[37] GHOSH 20A study thermal production of axion via coupling to leptons in the early universe and estimate its contribution to $\Delta N_{\rm eff}$. The quoted limit is for $\Delta N_{\rm eff} < 0.5$. See their Fig. 7 for their mass-dependent limits.

[38] STRANIERO 20 is analogous to CAPOZZI 20, with 22 galactic globular clusters used to derive the limit.

[39] WANG 20A is an update of LIU 17A. See their Fig. 9.

[40] WANG 20A is an update of LIU 17A. They assume a local axion dark matter density, $\rho_A = 0.3$ GeV/cm^3. See their Fig. 10 for limits between $0.185 < m_{A^0} < 10$ keV.

[41] ADHIKARI 19B is analogous to LIU 17A.

[42] APRILE 19D is analogous to APRILE 17B, but they use only ionization signals. The quoted limit applies to $m_{A^0} = 0.7$ keV. See their Fig. 5(e) for mass-dependent limits.

[43] DESSERT 19 used the Suzaku observations of a magnetic white dwarf (RE J0317-853) to look for X-ray signatures converted from axions in the surrounding magnetic fields. They obtained the limit, $g_{Aee} \cdot G_{A\gamma\gamma} < 1.6 \times 10^{-24}$ GeV^{-1} at 95%CL for $m_{A^0} \lesssim 10^{-5}$ eV. See their Fig. 2 for mass-dependent limits.

[44] TERRANO 19 look for the axion-induced oscillating magnetic field acting on the electron spin, using data taken with a rotating torsion pendulum containing polarized electrons. The quoted limit applies to $m_{A^0} = 10^{-23}$–10^{-18} eV and assumes a local axion dark matter density, $\rho_A = 0.45$ GeV/cm^3. See their Fig. 5 for mass-dependent limits.

[45] ABE 18F is an update of ABE 14F. The quoted limit applies to $m_{A^0} = 60$ keV. See their Fig. 5 for mass-dependent limits.

[46] ARMENGAUD 18 is analogous to LIU 17A.

[47] ARMENGAUD 18 is analogous to AHMED 09A. See the left panel of Fig. 5 for mass-dependent limits.

[48] CRESCINI 18 look for collective excitations of the electron spins caused by dark matter axions. The quoted limit assumes the local dark matter density, $\rho_A = 0.45$ GeV/cm^3.

[49] FICEK 18 use the measurements of the hyperfine structure of antiprotonic helium to constrain a dipole-dipole potential between electron and antiproton. See their Fig. 3 for limits on various spin- and velocity-dependent potentials.

[50] ABGRALL 17 is analogous to AHMED 09A using the MAJORANA DEMONSTRATOR. See their Fig. 2 for limits between 6 keV $< m_{A^0} <$ 97 keV.

[51] AKERIB 17B is analogous to LIU 17A.

[52] AKERIB 17B is analogous to AHMED 09A. See their Fig. 7 for mass-dependent limits.

[53] APRILE 17B is analogous to AHMED 09A. They found a bug in their code and needed to correct the limits in Fig. 7 of APRILE 14B. See their Fig. 1 for the corrected limits between 1 keV $< m_{A^0} <$ 40 keV.

[54] FICEK 17 look for spin-dependent interactions between electrons by comparing precision spectroscopic measurements in ^{4}He with theoretical calculations. See their Fig. 1 for limits up to $m_{A^0} = 10$ keV.

[55] FU 17A is analogous to LIU 17A. See their Fig. 3 for mass-dependent limits.

[56] FU 17A is analogous to AHMED 09A. See their Fig. 4 for mass-dependent limits.

[57] LIU 17A is analogous to AHMED 09A. See their Fig. 9 for limits between 0.25 keV $< m_{A^0} <$ 20 keV.

[58] LIU 17A look for solar axions produced from Compton, bremsstrahlung, atomic-recombination and deexcitation channels, and set a limit for $m_{A^0} < 1$ keV.

[59] LUO 17 use a recent measurement of the dipole-dipole interaction between two iron atoms at the nanometer scale and set a limit for $m_{A^0} < 1$ keV. See their Fig. 3 for mass-dependent limits.

[60] BATTICH 16 is analogous to CORSICO 16 and used the pulsating DB white dwarf PG 1351+489.

[61] CORSICO 16 studied the cooling rate of the pulsating DA white dwarf L19-2 based on an asteroseismic model.

[62] YOON 16 look for solar axions with the axio-electric effect in CsI(Tl) crystals and set a limit for $m_{A^0} < 1$ keV.

[63] TERRANO 15 used a torsion pendulum and rotating attractor with 20-pole electron-spin distributions. See their Fig. 4 for a mass-dependent limit up to $m_{A^0} = 500$ μeV.

[64] ABE 14F set limits on the axioelectric effect in the XMASS detector assuming the pseudoscalar constitutes all the local dark matter. See their Fig. 3 for limits between $m_{A^0} = 40$–120 keV.

[65] APRILE 14B look for solar axions using the XENON100 detector.

[66] APRILE 14B is analogous to AHMED 09A. Their Fig. 7 was later found to be incorrect due to a bug in their code. See Fig. 1 in APRILE 17B for the corrected limits.

[67] DERBIN 14 is an update of DERBIN 13 with a BGO scintillating bolometer. See their Fig. 3 for mass-dependent limits.

[68] MILLER-BERTOLAMI 14 studied the impact of axion emission on white dwarf cooling in a self-consistent way.

[69] ABE 13D is analogous to DERBIN 12, using the XMASS detector.

[70] ARMENGAUD 13 is similar to AALSETH 11. See their Fig. 10 for limits between 3 keV $< m_{A^0} <$ 100 keV.

[71] ARMENGAUD 13 is similar to DERBIN 12, and take account of axio-recombination and axio-deexcitation effects. See their Fig. 12 for mass-dependent limits.

[72] BARTH 13 search for solar axions produced by axion-electron coupling, and obtained the limit, $g_{Aee} \cdot G_{A\gamma\gamma} < 8.1 \times 10^{-23}$ GeV^{-1} at 95%CL.

[73] DERBIN 13 looked for 5.5 MeV solar axions produced in $pd \rightarrow {}^3$He A^0 in a BGO detector through the axioelectric effect. See their Fig. 4 for mass-dependent limits.

[74] HECKEL 13 studied the influence of 2 or 4 stationary sources each containing 6.0×10^{24} polarized electrons, on a rotating torsion pendulum containing 9.8×10^{24} polarized electrons. See their Fig. 4 for mass-dependent limits.

[75] VIAUX 13A constrain axion emission using the observed brightness of the tip of the red-giant branch in the globular cluster M5.

[76] CORSICO 12 attributed the excessive cooling rate of the pulsating white dwarf R548 to emission of axions with $g_{Aee} \simeq 4.8 \times 10^{-13}$.

[77] DERBIN 12 look for solar axions with the axio-electric effect in a Si(Li) detector. The solar production is based on Compton and bremsstrahlung processes.

[78] AALSETH 11 is analogous to AHMED 09A. See their Fig. 4 for mass-dependent limits.

[79] AHMED 09A assume keV-mass pseudoscalars are the local dark matter and constrain the axio-electric effect in the CDMS detector. See their Fig. 5 for mass-dependent limits.

[80] DAVOUDIASL 09 use geophysical constraints on Earth cooling by axion emission.

[81] These experiments measured induced magnetization of a bulk material by the spin-dependent potential generated from other bulk material with aligned electron spins, where the magnetic field is shielded with superconductor. The sign of the limit set by CHUI 93 is opposite to that of the axion-mediated dipole-dipole potential.

[82] These experiments used a torsion pendulum to measure the potential between two bulk matter objects where the spins are polarized but without a net magnetic field in either of them. The limits reflect the corrected sign of the dipole-dipole potential.

[83] WINELAND 91 looked for an effect of bulk matter with aligned electron spins on atomic hyperfine splitting using nuclear magnetic resonance.

Invisible A^0 (Axion) Limits from Nucleon Coupling

Limits are for the axion mass in eV.

VALUE (eV)	CL%	DOCUMENT ID		TECN	COMMENT
• • • We do not use the following data for averages, fits, limits, etc. • • •					
		[1] ALONSO-GON.	25	SK	Diffuse supernova axions
		[2] ARIAS-ARAG...	25	BORX	Solar axions
		[3] BASILICO	25	BORX	Solar axions
		[4] GENG	25		Solar axions
		[5] WALTER	25	CASP	Dark matter, NMR
		[6] ZHANG	25A	NMR	Ultralight dark matter
< 0.01	95	[7] LELLA	24	ASTR	SN1987A
		[8] SU	24	NMR	polarized ^{129}Xe
		[9] KARANTH	23		Deuteron EDM
		[10] LEE	23		Axion dark matter
< 0.016	95	[11] BUSCHMANN	22	ASTR	Neutron star cooling
<320	90	[12] GAVRILYUK	22	CNTR	Solar axion
		[13] SCHULTHESS	22		Neutron EDM
		[14] AYBAS	21	CASP	Nucleon EDM
		[15] BHUSAL	21		Solar axion
		[16] JIANG	21	NMR	Axion dark matter
		[17] ROUSSY	21		Molecular EDM
		[18] ZHANG	21B	ASTR	Neutron star inspiral
< 24	90	[19] ABDELHAME...	20	CNTR	Solar axion
		[20] ABDELHAME...	20	CNTR	Solar axion
		[21] APRILE	20	XE1T	Solar axion
		[22] KLIMCHITSK...	20		Casimir effect
< 7.3	90	[23] WANG	20A	CDEX	Solar axion
< 0.03		[24] LEINSON	19	ASTR	Neutron star cooling
$< 9.6 \times 10^{-3}$	95	[25] LLOYD	19	ASTR	γ-rays from NS
		[26] SMORRA	19		$\overline{p}$ g-factor
		[27] WU	19	NMR	Axion dark matter
< 65	95	[28] AKHMATOV	18	CNTR	Solar axion
< 6.6	90	[29] ARMENGAUD	18	EDE3	Solar axion
< 0.085	90	[30] BEZNOGOV	18	ASTR	Neutron star cooling
< 12.7	95	[31] GAVRILYUK	18	CNTR	Solar axion
< 0.01		[32] HAMAGUCHI	18	ASTR	Neutron star cooling
		[33] ABEL	17		Neutron EDM
< 93	90	[34] ABGRALL	17	HPGE	Solar axion
< 4	90	[35] FU	17A	PNDX	Solar axion
		[36] KLIMCHITSK...	17A		Casimir effect
<177	90	[37] LIU	17A	CDEX	Solar axion
< 0.079	95	[38] BERENJI	16	ASTR	γ-rays from NS
<100	95	[39] GAVRILYUK	15	CNTR	Solar axion
		[40] KLIMCHITSK...	15		Casimir-less
		[41] BEZERRA	14		Casimir effect
		[42] BEZERRA	14A		Casimir effect
		[43] BEZERRA	14B		Casimir effect
		[44] BEZERRA	14C		Casimir effect
		[45] BLUM	14	COSM	^{4}He abundance
		[46] LEINSON	14	ASTR	Neutron star cooling
<250	95	[47] ALESSANDRIA	13	CNTR	Solar axion
<155	90	[48] ARMENGAUD	13	EDEL	Solar axion
$< 8.6 \times 10^3$	90	[49] BELLI	12	CNTR	Solar axion
$< 1.4 \times 10^4$	90	[50] BELLINI	12B	BORX	Solar axion
<145	95	[51] DERBIN	11	CNTR	Solar axion
		[52] BELLINI	08	CNTR	Solar axion
		[53] ADELBERGER	07		Test of Newton's law

[1] ALONSO-GONZALEZ 25 use Super-Kamiokade data to search for the diffuse flux of axion-like particles produced in galactic core-collapse supernovae via the interaction with protons in the detector, $A^0 p \rightarrow p\gamma$. They set bounds on axion-proton couplings between a minimum and maximum of 2×10^{-5}–2×10^{-4} up to axion masses of 70 MeV, see their Fig. 4. ALONSO-GONZALEZ 25A details an erratum for this publication.

[2] ARIAS-ARAGON 25 use Borexino data to search for axion-induced pair production and inverse Compton scattering due to the flux of 5.5 MeV axions from proton-deuteron fusion in the Sun. They constrain the combination of axion-electron and axion-nucleon couplings for $m_{A^0} \lesssim 1$ MeV as shown in their Fig. 4.

[3] BASILICO 25 use Borexino data to search for the flux of 5.5 MeV axions produced through proton-deuteron fusion in the Sun, which can lead to detectable signals in the detector through axion decay to two photons, Primakoff and Compton conversion to photons, and the liberation of electrons through the axio-electric effect. They set bounds on the product of the axion-electron and axion-nucleon couplings, and the product of the axion-photon and axion-nucleon couplings, for $m_{A^0} < 1$ MeV.

[4] GENG 25 use a public electron recoil dataset from the XENONnT collaboration to search for events caused by the flux of 14.4 keV axions produced in M1 transitions of ^{57}Fe nuclei in the solar interior. They set limits on the product of the axion-photon and axion-nucleon couplings and the product of the axion-electron and axion-nucleon couplings for axion masses below 14.4 keV.

Int. J. Mod. Phys. A 2026.41. Downloaded from www.worldscientific.com
by UNIVERSITY OF CALIFORNIA @ BERKELEY on 09/16/26. Reproduction is strictly not permitted, except for Open Access articles.

Int. J. Mod. Phys. A 2026.41. Downloaded from www.worldscientific.com by UNIVERSITY OF CALIFORNIA @ BERKELEY on 09/16/26. Re-use and distribution is strictly not permitted, except for Open Access articles.

[5] WALTER 25 report results from a demonstrator for the CASPEr-Gradient experiment, which in this case used proton nuclear magnetic resonance spectroscopy of methanol to search for axion-like particle dark matter coupled to protons. They are sensitive in a narrow window around an ALP mass of 5.576741 neV. See their Fig. 3 for mass-dependent limits.

[6] ZHANG 25A set limits on dark matter axion-like particles coupled to nucleons in the 1×10^{-24}–5×10^{-21} eV mass range by reanalyzing data from a Helium-3/Xenon-129 comagnetometer experiment originally performed to test for Lorentz and CPT violations. See their Fig. 3 for mass-dependent limits.

[7] LELLA 24 update constraints on the axion-proton coupling from supernova 1987A based on the SN cooling argument (including a treatment of the trapping regime) as well as the non-observation of any coincident axion-induced events in the Kamiokande II neutrino detector. They exclude QCD axion models above 0.01 eV, and axion-like particles in a window that extends up to 300 MeV. See their Fig. 3 for mass-dependent limits.

[8] SU 24 search for an axion-mediated dipole-dipole force between two separated spin-polarized samples of ^{129}Xe gas. They set limits on the axion-neutron coupling for axion masses between 3.2 and 24.3 μeV. See their Fig. 4(b) for mass-dependent limits.

[9] KARANTH 23 utilized an in-plane polarized deuteron beam in a storage ring to constrain the axion-induced oscillating EDM of the deuteron for m_{A^0} = 0.496–0.502 neV. Assuming axions account for all dark matter with $\rho_A \simeq$ 0.55 GeV/cm^3, they derived constraints on axion couplings to the deuteron EDM operator, gluons, and the deuteron spin. For detailed limits, see their Figs. 19–21.

[10] LEE 23 analyzed data from a K–^{3}He comagnetometer, accounting for stochastic effects, to limit the axion-neutron coupling $g_{Ann} < 2.4\times10^{-10}$ GeV^{-1} at 95% CL for m_{A^0} = 0.4–4 feV. They assumed axions form all dark matter with a density of 0.3 GeV/cm^3. See their Fig. 5 for the limits.

[11] BUSCHMANN 22 studied the axion emission from five neutron stars with ages $\sim 10^5$–10^6 years, comparing the simulation with axions to age and luminosity measurements. The mass bound assumes the KSVZ axion model with $C_p = -0.47$ and $C_n = -0.02$. See their Fig. 3 for the limits on the DFSZ axion model.

[12] GAVRILYUK 22 look for solar axions from the ABC interactions with the experimental setup similar to GAVRILYUK 15. The mass bound assumes the KSVZ axion model, S = 0.5, and m_u/m_d = 0.56.

[13] SCHULTHESS 22 look for a time-oscillating neutron EDM caused by the coupling between axion dark matter and gluons, using a Ramsey-type apparatus for a cold neutron beam. See their Fig. 4 for limits in the range of $m_{A^0} = 10^{-19}$–4×10^{-12} eV.

[14] AYBAS 21 limits the axion couplings to the nucleon EDM and the nucleons as $g_{AN\gamma} < 9.5\times10^{-4}$ GeV^{-2} and $g_{ANN}/2m_N < 0.28$ GeV^{-1} (95 % CL) for m_{A^0} = 162–166 neV, based on a measurement of ^{207}Pb solid-state NMR in a polarized ferroelecrtric crystal. Here m_N is the nucleon mass and g_{ANN} is the dimensionless axion-nucleon coupling. They assume that axions make up all the dark matter with $\rho_A \simeq$ 0.46 GeV/cm^3. See their Fig. 3 for the limits.

[15] BHUSAL 21 looked for 5.5 MeV solar axions produced by $pd \to {}^3$He A^0 through the axion-induced dissociation of deuterons by using SNO data, and set a limit on the isovector axion-nucleon coupling, $|g^3_{aN}| < 2\times10^{-5}$ GeV^{-1}, which is equivalent to $|g_{Ann} - g_{App}| < 4\times10^{-5}$ in terms of the dimensionless axion-nucleon couplings.

[16] JIANG 21 use the spin-amplifier based on hyperpolarized ^{129}Xe gas to set limits on the axion couplings to nucleons as $g_{ANN}/2m_N < 3.2\times10^{-9}$ GeV^{-1} (95 % CL) at m_{A^0} = 52.94 feV, and comparable limits in the mass range of 8.3–744 feV. Here m_N is the nucleon mass and g_{ANN} is the dimensionless axion-nucleon coupling. They assume that axions make up all the dark matter with $\rho_A \simeq$ 0.4 GeV/cm^3. See their Fig. 4b for the limits.

[17] ROUSSY 21 look for a time-oscillating EDM of molecular ions HfF$^+$ induced by axion dark matter couplings to gluons. See their Fig. 3 for limits in the range of $m_{A^0} = 10^{-22}$–10^{-15} eV.

[18] ZHANG 21B use the gravitational waves from the binary neutron star inspiral GW170817 to look for a type of axion whose mass is suppressed due to cancellation with additional contributions. They exclude $1.6\times10^{16} < f_A < 10^{18}$ GeV at 3 σ for $m_{A^0} \lesssim 10^{-13}$ eV. See their Fig. 1 for mass-dependent limits.

[19] ABDELHAMEED 20 look for the resonant excitation of ^{169}Tm (8.41 keV) by solar axions produced via the Primakoff effect. The mass bound assumes the KSVZ axion model, S = 0.5, and m_u/m_d = 0.56. They set a limit on the product of axion couplings to photons and nucleons as $G_{A\gamma\gamma}\cdot g_{App} < 1.44\times10^{-14}$ GeV^{-1} (90 % CL).

[20] ABDELHAMEED 20 look for the resonant excitation of ^{169}Tm (8.41 keV) by solar axions produced via the axion-electron coupling. They set a limit on the product of axion couplings to electrons and nucleons as $g_{Aee}\cdot g_{App} < 2.81\times10^{-16}$ (90 % CL).

[21] APRILE 20 look for solar axions from the ABC interactions, the Primakoff conversion, and the 14.4 keV M1 transition of ^{57}Fe. An excess is observed at low energies between 2 and 3 keV. See their Fig.8 for correlation between the couplings.

[22] KLIMCHITSKAYA 20 use the measurement of the Casimir force between a Au-coated microsphere and a SiC plate to constrain the force due to two-axion exchange for 17.8 $< m_{A^0} <$ 100 eV. See their Fig. 2 for mass-dependent limits.

[23] WANG 20A is an update of LIU 17A. The limit assumes the DFSZ axion. See their Fig. 7 for the limit on product of axion couplings to electrons and nucleons.

[24] LEINSON 19 is analogous to BEZNOGOV 18, but estimating the axion luminosity based on the Tolman's analytic solution to the Einstein equations of spherical fluids in hydrostatic equilibrium. The dimensionless axion-neutron coupling is constrained as $g_{Ann} < 1.0\times10^{-10}$.

[25] LLOYD 19 is analogous to BERENJI 16. They highlight that the limit obtained with this technique strongly depends on the assumed NS core temperature.

[26] SMORRA 19 look for spin-precession effects from ultra-light axion dark matter in the $\overline{p}$ spin-flip resonance data. Assuming ρ_A = 0.4 GeV/cm^3, they constrain the dimensionless axion-antiproton coupling as $g_{A\overline{p}\overline{p}} <$ 2–9 at 95% CL for $m_{A^0} = 2\times10^{-23}$–$4\times10^{-17}$ eV. See the right panel of their Fig. 3.

[27] WU 19 look for axion-induced time-oscillating features of the NMR spectrum of acetonitrile-2-^{13}C. Assuming $C_p = C_n$ and ρ_A = 0.4 GeV/cm^3, they constrain the dimensionless axion-nucleon coupling as $g_{ANN} < 6\times10^{-5}$ for $m_{A^0} = 10^{-21}$–1.3×10^{-17} eV. Note that the limits for $m_{A^0} < 10^{-21}$ eV in their Fig. 3(a) should be weaker than those for heavier masses. See ADELBERGER 19 and WU 19C on this issue.

[28] AKHMATOV 18 is an update of GAVRILYUK 15.

[29] ARMENGAUD 18 is analogous to ALESSANDRIA 13. The quoted limit assumes the DFSZ axion model. See their Fig. 4 for the limit on product of axion couplings to electrons and nucleons.

[30] BEZNOGOV 18 constrain the axion-neutron coupling by assuming that thermal evolution of the hot neutron star HESS J1731-347 is dominated by the lowest possible neutrino emission. The quoted limit assumes the KSVZ axion with the effective Peccei-Quinn charge of the neutron $C_n = -0.02$. The dimensionless axion-neutron couling is constrained as $g_{Ann} < 2.8\times10^{-10}$.

[31] GAVRILYUK 18 look for the resonant excitation of ^{83}Kr (9.4 keV) by solar axions produced via the Primakoff effect. The mass bound assumes m_u/m_d = 0.56 and S = 0.5.

[32] HAMAGUCHI 18 studied the axion emission from the neutron star in Cassiopeia A based on the minimal cooling scenario which explains the observed rapid cooling rate. The quoted limit corresponds to $f_A > 5\times10^8$ GeV obtained for the KSVZ axion with $C_p = -0.47$ and $C_n = -0.02$.

[33] ABEL 17 look for a time-oscillating neutron EDM and an axion-wind spin-precession effect respectively induced by axion dark matter couplings to gluons and nucleons. See their Fig. 4 for limits in the range of $m_{A^0} = 10^{-24}$–10^{-17} eV.

[34] ABGRALL 17 limit assumes the hadronic axion model used in ALESSANDRIA 13. See their Fig. 4 for the limit on product of axion couplings to electrons and nucleons.

[35] FU 17A look for the 14.4 keV ^{57}Fe solar axions. The limit assumes the DFSZ axion model. See their Fig. 3 for mass-dependent limits on the axion-electron coupling. Notice that in this figure the DFSZ and KSVZ lines should be interchanged.

[36] KLIMCHITSKAYA 17A use the differential measurement of the Casimir force between a Ni-coated sphere and Au and Ni sectors of the structured disc to constrain the axion coupling to nucleons for 2.61 meV $< m_{A^0} <$ 0.9 eV. See their Figs. 1 and 2 for mass dependent limits.

[37] LIU 17 is analogous to ALESSANDRIA 13. The limit assumes the hadronic axion model. See their Fig. 6(b) for the limit on product of axion couplings to electrons and nucleons.

[38] BERENJI 16 used the Fermi LAT observations of neutron stars to look for photons from axion decay. They assume the effective Peccei-Quinn charge of the neutron C_n = 0.1 and a neutron-star core temperature of 20 MeV.

[39] GAVRILYUK 15 look for solar axions emitted by the M1 transition of ^{83}Kr (9.4 keV). The mass bound assumes m_u/m_d = 0.56 and S = 0.5.

[40] KLIMCHITSKAYA 15 use the measurement of differential forces between a test mass and rotating source masses of Au and Si to constrain the force due to two-axion exchange for $1.7\times10^{-3} < m_{A^0} <$ 0.9 eV. See their Figs. 1 and 2 for mass dependent limits.

[41] BEZERRA 14 use the measurement of the thermal Casimir-Polder force between a Bose-Einstein condensate of ^{87}Rb atoms and a SiO_2 plate to constrain the force mediated by exchange of two pseudoscalars for 0.1 meV $< m_{A^0} <$ 0.3 eV. See their Fig. 2 for the mass-dependent limit on pseudoscalar coupling to nucleons.

[42] BEZERRA 14A is analogous to BEZERRA 14. They use the measurement of the Casimir pressure between two Au-coated plates to constrain pseudoscalar coupling to nucleons for 1×10^{-3} eV $< m_{A^0} <$ 15 eV. See their Figs. 1 and 2 for the mass-dependent limit.

[43] BEZERRA 14B is analogous to BEZERRA 14. BEZERRA 14B use the measurement of the normal and lateral Casimir forces between sinusoidally corrugated surfaces of a sphere and a plate to constrain pseudoscalar coupling to nucleons for 1 eV $< m_{A^0} <$ 20 eV. See their Figs. 1–3 for mass-dependent limits.

[44] BEZERRA 14C is analogous to BEZERRA 14. They use the measurement of the gradient of the Casimir force between Au- and Ni-coated surfaces of a sphere and a plate to constrain pseudoscalar coupling to nucleons for 3×10^{-5} eV $< m_{A_0} <$ 1 eV. See their Figs. 1, 3, and 4 for the mass-dependent limits.

[45] BLUM 14 studied effects of an oscillating strong *CP* phase induced by axion dark matter on the primordial ^{4}He abundance. See their Fig. 1 for mass-dependent limits.

[46] LEINSON 14 attributes the excessive cooling rate of the neutron star in Cassiopeia A to axion emission from the superfluid core, and found $C_n^2\, m_{A^0}^2 \simeq 5.7\times10^{-6}$ eV^2, where C_n is the effective Peccei-Quinn charge of the neutron.

[47] ALESSANDRIA 13 used the CUORE experiment to look for 14.4 keV solar axions produced from the M1 transition of thermally excited ^{57}Fe nuclei in the solar core, using the axio-electric effect. The limit assumes the hadronic axion model. See their Fig. 4 for the limit on product of axion couplings to electrons and nucleons.

[48] ARMENGAUD 13 is analogous to ALESSANDRIA 13. The limit assumes the hadronic axion model. See their Fig. 8 for the limit on product of axion couplings to electrons and nucleons.

[49] BELLI 12 looked for solar axions emitted by the M1 transition of ^{7}Li* (478 keV) after the electron capture of ^{7}Be, using the resonant excitation ^{7}Li in the LiF crystal. The mass bound assumes m_u/m_d = 0.55, m_u/m_s = 0.029, and the flavor-singlet axial vector matrix element S = 0.4.

[50] BELLINI 12B looked for 5.5 MeV solar axions produced in the $pd \to {}^3$He A^0.The limit assumes the hadronic axion model. See their Figs. 6 and 7 for mass-dependent limits on productsof axion couplings to photons, electrons, and nucleons.

[51] DERBIN 11 looked for solar axions emitted by the M1 transition of thermally excited ^{57}Fe nuclei in the Sun, using their possible resonant capture on ^{57}Fe in the laboratory. The mass bound assumes m_u/m_d = 0.56 and the flavor-singlet axial vector matrix element $S = 3F - D \simeq 0.5$.

[52] BELLINI 08 consider solar axions emitted in the M1 transition of ^{7}Li* (478 keV) and look for a peak at 478 keV in the energy spectra of the Counting Test Facility (CTF), a Borexino prototype. For $m_{A^0} <$ 450 keV they find mass-dependent limits on products of axion couplings to photons, electrons, and nucleons.

[53] ADELBERGER 07 use precision tests of Newton's law to constrain a force contribution from the exchange of two pseudoscalars. See their Fig. 5 for limits on the pseudoscalar coupling to nucleons, relevant for m_{A^0} below about 1 meV.

Int. J. Mod. Phys. A 2026.41. Downloaded from www.worldscientific.com by UNIVERSITY OF CALIFORNIA @ BERKELEY on 09/16/26. Reproduction is strictly not permitted, except for Open Access articles.

Axion Limits from *T*-violating Medium-Range Forces

The limit is for the coupling $g = g_p\, g_s$ in a *T*-violating potential between nucleons, nucleon and electron, or electrons of the form $V = \frac{g\hbar^2}{8\pi m_p}(\boldsymbol{\sigma}\cdot\hat{\boldsymbol{r}})\,(\frac{1}{r^2} + \frac{1}{\lambda r})\, e^{-r/\lambda}$, where g_s and g_p are dimensionless scalar and pseudoscalar coupling constants, m_p is the fermion mass with the pseudoscalar coupling (whereas the mass m_s of the fermion with the scalar coupling does not explicitly appear), and $\lambda = \hbar/(m_A c)$ is the range of the force.

VALUE	DOCUMENT ID		TECN	COMMENT
• • • We do not use the following data for averages, fits, limits, etc. • • •				
	[1] AYRES	23	EDM	ultracold neutrons
	[2] PODDAR	23	ASTR	solar system
	[3] ZHANG	23	NMR	polarized ^{129}Xe and ^{131}Xe
	[4] CRESCINI	22	SQID	paramagnetic GSO crystal
	[5] FENG	22	NMR	polarized ^{129}Xe and ^{131}Xe
	[6] AFACH	21	GNME	Optical magnetometers
	[7] DZUBA	18	THEO	atomic EDM
	[8] STADNIK	18	THEO	atomic and molecular EDMs
	[9] CRESCINI	17	SQID	paramagnetic GSO crystal
	[10] AFACH	15		ultracold neutrons
	[11] STADNIK	15	THEO	nucleon spin contributions for nuclei
	[12] TERRANO	15		torsion pendulum
	[13] BULATOWICZ	13	NMR	polarized ^{129}Xe and ^{131}Xe
	[14] CHU	13		polarized ^{3}He
	[15] TULLNEY	13	SQID	polarized ^{3}He and ^{129}Xe
	[16] RAFFELT	12		stellar energy loss
	[17] HOEDL	11		torsion pendulum
	[18] PETUKHOV	10		polarized ^{3}He
	[19] SEREBROV	10		ultracold neutrons
	[20] IGNATOVICH	09	RVUE	ultracold neutrons
	[21] SEREBROV	09	RVUE	ultracold neutrons
	[22] BAESSLER	07		ultracold neutrons
	[23] HECKEL	06		torsion pendulum
	[24] NI	99		paramagnetic Tb F_3
	[25] POSPELOV	98	THEO	neutron EDM
	[26] YOUDIN	96		
	[27] RITTER	93		torsion pendulum
	[28] VENEMA	92		nuclear spin-precession frequencies
	[29] WINELAND	91	NMR	

[1] AYRES 23 at PSI use their neutron EDM setup to look for a mm to micron-range spin-dependent force between ultracold spin-polarized neutrons stored in vacuum and the unpolarised nucleons in the surrounding apparatus. They constrain a nucleon-neutron monopole-dipole interaction parameterised by the coupling $g_s^N g_p^n$. They set a limit of $g_s^N g_p^n < 10^{-20}$ (95% CL) for a 1 meV mass axion, see Fig. 6.

[2] PODDAR 23 search for long-range monopole-dipole forces between the polarized population of electrons inside the Earth and the unpolarised nucleons in the Sun, which would affect the precession of orbital perihelion. However, the most competitive limit is obtained by combining the monopole-monopole force constraints on g_s^N from planetary precession with the strongest stellar bound on the pseudoscalar electron coupling (g_p^e), shown in Fig. 5.

[3] ZHANG 23 look for changes of the ratio of precession frequencies between ^{129}Xe and ^{131}Xe as the bias field is flipped in Earth's gravitational field after Earth roation effect is subtracted. They find $g_p^n g_s^N < 1\times10^{-26}$–$3.7\times10^{-36}$ for $\lambda = 0.3$–1×10^{10} m. See their Fig. 4 for limits as a function of λ.

[4] CRESCINI 22 is an update of CRESCINI 17, and find $g_p^e g_s^N \leq 5.7\times10^{-32}$ and $g_p^e g_s^e \leq 1.6\times10^{-31}$ for $\lambda \gtrsim 10$ cm at 95% CL. See their Fig. 4 for limits as a function of λ.

[5] FENG 22 look for changes of the ratio of precession frequencies between ^{129}Xe and ^{131}Xe when a BGO crystal is positioned near the atomic cell. They find $g_p^n g_s^N < 2\times10^{-20}$–$3\times10^{-24}$ for $\lambda = 0.11$–0.55 mm. See their Fig. 4 for limits as a function of λ.

[6] AFACH 21 look for axion domain walls coupled to atomic spins by using the global network of optical magnetometers. Assuming that the axion domain walls make up all dark matter, they exclude the effective decay constant below 4×10^5 GeV for m_{A^0} in the range of 10^{-15}–10^{-11} eV. See their Fig. 4 for the mass-dependent limits.

[7] DZUBA 18 used atomic EDM measurements to derive limits on the product of the pseudoscalar coupling to nucleon and the scalar coupling to electron, which improved on the laboratory bounds for $m_{A^0} > 0.01$ eV. See their Fig. 1 for mass-dependent limits.

[8] STADNIK 18 used atomic and molecular EDM experiments to derive limits on the product of the pseudoscalar couplings to electron and the scalar coupling to nucleon and electron. See their Fig. 2 for mass-dependent limits, which improved on the laboratory bounds for $m_{A^0} > 0.01$ eV.

[9] CRESCINI 17 use the QUAX-$g_p g_s$ experiment to look for variation of a paramagnetic GSO crystal magnetization when rotating lead disks are positioned near the crystal, and find $g = g_p^e g_s^N < 4.3\times10^{-30}$ for $\lambda = 0.1$–0.2 m at 95% CL. See their Fig. 6 for limits as a function of λ.

[10] AFACH 15 look for a change of spin precession frequency of ultracold neutrons when a magnetic field with opposite directions is applied, and find $g < 2.2\times10^{-27}$ $(\mathrm{m}/\lambda)^2$ at 95% CL for 1 μm $< \lambda <$ 5 mm. See their Fig. 3 for their limits.

[11] STADNIK 15 studied proton and neutron spin contributions for nuclei and derive the limits $g < 10^{-28}$–10^{-23} for $\lambda > 3\times10^{-4}$ m using the data of TULLNEY 13. See their Figs. 1 and 2 for λ-dependent limits.

[12] TERRANO 15 used a torsion pendulum and rotating attractor, and derived a restrictive limit on the product of the pseudoscalar coupling to electron and the scalar coupling to nucleons, $g < 9\times10^{-29}$–5×10^{-26} for $m_{A^0} < 1.5$–400 μeV. See their Fig. 5 for mass-dependent limits.

[13] BULATOWICZ 13 looked for NMR frequency shifts in polarized ^{129}Xe and ^{131}Xe when a zirconia rod is positioned near the NMR cell, and find $g < 1\times10^{-19}$–1×10^{-24} for $\lambda = 0.01$–1 cm. See their Fig. 4 for their limits.

[14] CHU 13 look for a shift of the spin precession frequency of polarized ^{3}He in the presence of an unpolarized mass, in analogy to YOUDIN 96. See Fig. 3 for limits on g in the approximate m_{A^0} range 0.02–2 meV.

[15] TULLNEY 13 look for a shift of the precession frequency difference between the colocated ^{3}He and ^{129}Xe in the presence an unpolarized mass, and derive limits $g < 3\times10^{-29}$–2×10^{-22} for $\lambda > 3\times10^{-4}$ m. See their Fig. 3 for λ-dependent limits.

[16] RAFFELT 12 show that the pseudoscalar couplings to electron and nucleon and the scalar coupling to nucleon are individually constrained by stellar energy-loss arguments and searches for anomalous monopole-monopole forces, together providing restrictive constraints on g. See their Figs. 2 and 3 for results.

[17] HOEDL 11 use a novel torsion pendulum to study the force by the polarized electrons of an external magnet. In their Fig. 3 they show restrictive limits on g in the approximate m_{A^0} range 0.03–10 meV.

[18] PETUKHOV 10 use spin relaxation of polarized ^{3}He and find $g < 3\times10^{-23}$ $(\mathrm{cm}/\lambda)^2$ at 95% CL for the force range $\lambda = 10^{-4}$–1 cm.

[19] SEREBROV 10 use spin precession of ultracold neutrons close to bulk matter and find $g < 2\times10^{-21}$ $(\mathrm{cm}/\lambda)^2$ at 95% CL for the force range $\lambda = 10^{-4}$–1 cm.

[20] IGNATOVICH 09 use data on depolarization of ultracold neutrons in material traps. They show λ-dependent limits in their Fig. 1.

[21] SEREBROV 09 uses data on depolarization of ultracold neutrons stored in material traps and finds $g < 2.96\times10^{-21}$ $(\mathrm{cm}/\lambda)^2$ for the force range $\lambda = 10^{-3}$–1 cm and $g < 3.9\times10^{-22}$ $(\mathrm{cm}/\lambda)^2$ for $\lambda = 10^{-4}$–10^{-3} cm, each time at 95% CL, significantly improving on BAESSLER 07.

[22] BAESSLER 07 use the observation of quantum states of ultracold neutrons in the Earth's gravitational field to constrain g for an interaction range 1 μm–a few mm. See their Fig. 3 for results.

[23] HECKEL 06 studied the influence of unpolarized bulk matter, including the laboratory's surroundings or the Sun, on a torsion pendulum containing about 9×10^{22} polarized electrons. See their Fig. 4 for limits on g as a function of interaction range.

[24] NI 99 searched for a *T*-violating medium-range force acting on paramagnetic Tb F_3 salt. See their Fig. 1 for the result.

[25] POSPELOV 98 studied the possible contribution of *T*-violating Medium-Range Force to the neutron electric dipole moment, which is possible when axion interactions violate *CP*. The size of the force among nucleons must be smaller than gravity by a factor of 2×10^{-10} $(1\,\mathrm{cm}/\lambda_A)$, where $\lambda_A = \hbar/m_A c$.

[26] YOUDIN 96 compared the precession frequencies of atomic ^{199}Hg and Cs when a large mass is positioned near the cells, relative to an applied magnetic field. See Fig. 3 for their limits.

[27] RITTER 93 studied the influence of bulk mass with polarized electrons on an unpolarized torsion pendulum, providing limits in the interaction range from 1 to 100 cm.

[28] VENEMA 92 looked for an effect of Earth's gravity on nuclear spin-precession frequencies of ^{199}Hg and ^{201}Hg atoms.

[29] WINELAND 91 looked for an effect of bulk matter with aligned electron spins on atomic hyperfine resonances in stored ^{9}Be$^+$ ions using nuclear magnetic resonance.

Hidden Photons: Kinetic Mixing Parameter Limits

Limits are on the kinetic mixing parameter χ which is defined by the Lagrangian

$$L = -\frac{1}{4}F_{\mu\nu}F^{\mu\nu} - \frac{1}{4}F'_{\mu\nu}F'^{\mu\nu} - \frac{\chi}{2}F_{\mu\nu}F'^{\mu\nu} + \frac{m^2_{\gamma'}}{2}A'_\mu A'^\mu,$$

where A_μ and A'_μ are the photon and hidden-photon fields with field strengths $F_{\mu\nu}$ and $F'_{\mu\nu}$, respectively, and $m_{\gamma'}$ is the hidden-photon mass.

VALUE	CL%	DOCUMENT ID		TECN	COMMENT
• • • We do not use the following data for averages, fits, limits, etc. • • •					
$<3\times10^{-3}$	90	[1] ABLIKIM	25CL	BES3	$m_{\gamma'} = 1\times10^{-2}$–0.525 GeV
$<8\times10^{-15}$	90	[2] ALBAKRY	25	CDMS	$m_{\gamma'} = 1.2$–23.3 eV
$<1\times10^{-14}$	95	[3] AN	25	ASTR	$m_{\gamma'} = 1\times10^{-10}$–$8\times10^{-8}$ eV
$<4\times10^{-5}$	90	[4] ANDREEV	25	NA64	$m_{\gamma'} = 1\times10^{-3}$–0.4 GeV
$<2\times10^{-16}$	90	[5] APRILE	25A	XENT	$m_{\gamma'} = 0.01$–0.4 keV
$>5\times10^{-3}$	90	[6] ASWATHI	25	ASTR	$m_{\gamma'} = 1\times10^{-14}$–$1.8\times10^{-12}$ eV
$<1\times10^{-10}$	95	[7] BAUDIS	25	QRCD	$m_{\gamma'} = 0.1$–30 eV
$<4\times10^{-13}$	90	[8] BLOCH	25	SNSE	$m_{\gamma'} = 1$–8 eV
$<7\times10^{-10}$		[9] CAPUTO	25	ASTR	$m_{\gamma'} = 0.1$–0.4 MeV
$<1\times10^{-6}$	90	[10] CHOI	25	NEON	$m_{\gamma'} = 0.003$–3 MeV
$<4\times10^{-8}$	90	[11] CORTINA-GIL	25A	NA62	$m_{\gamma'} = 0.1$–1.5 GeV
$<1\times10^{-4}$	90	[12] CORTINA-GIL	25B	NA62	$m_{\gamma'} = 0.01$–0.26 GeV
$<1.1\times10^{-13}$	95	[13] EGGE	25	MDMX	$m_{\gamma'} = 78.62$–83.95 μeV
$<2.3\times10^{-13}$	90	[14] LI	25	PNDX	$m_{\gamma'} = 0.03$–1 MeV
$<3\times10^{-19}$	95	[15] LINDEN	25	ASTR	$m_{\gamma'} = 90$–1022 keV
<0.2	95	[16] MELO-GALIN...	25	ASTR	$m_{\gamma'} = 6\times10^{-8}$–$1\times10^{-5}$ eV
$<1\times10^{-9}$		[17] MIRASOLA	25	ASTR	$m_{\gamma'} = 2\times10^{-13}$–$1.4\times10^{-12}$ eV
$<3\times10^{-4}$		[18] ROMERO-JOR.	25	HION	$m_{\gamma'} = 0.01$–2 GeV
$<4\times10^{-15}$	95	[19] TROST	25	COSM	$m_{\gamma'} = 6\times10^{-14}$–$4\times10^{-13}$ eV

Int. J. Mod. Phys. A 2026.41. Downloaded from www.worldscientific.com
by UNIVERSITY OF CALIFORNIA @ BERKELEY on 09/16/26. Re-use and distribution is strictly not permitted, except for Open Access articles.

$<2 \times 10^{-16}$	90	[20] ZENG	25	PNDX $m_{\gamma'}$ = 1–30 keV
$<8.2 \times 10^{-15}$	95	[21] ZHAO	25	DM $m_{\gamma'}$ = 23.4575–23.5485 μeV
$<2.7 \times 10^{-9}$	95	[22] ZHAO	25A	DM $m_{\gamma'}$ = 2×10^{-17}–3×10^{-14} eV
$<3 \times 10^{-8}$	90	[23] AAD	24AS	ATLS $m_{\gamma'}$ = 0.01–10 GeV
$<3 \times 10^{-5}$	90	[24] ABRATENKO	24A	MBNE $m_{\gamma'}$ = 0.01–0.2 GeV
$<4 \times 10^{-6}$	90	[25] ABREU	24	FASR $m_{\gamma'} \simeq$ 50 MeV
$<0.5 \times 10^{-10}$	95	[26] ADACHI	24C	DORR $m_{\gamma'}$ = 41–74 μeV
$<3 \times 10^{-12}$	90	[27] AGOSTINI	24A	GRDA $m_{\gamma'}$ = 65–1021 keV
$<4.35 \times 10^{-13}$	90	[28] AGRAWAL	24	DM $m_{\gamma'}$ = 24.67 μeV
$<5 \times 10^{-6}$	90	[29] ANDREEV	24A	NA64 $m_{\gamma'}$ = 0.001–1 GeV
$<1.8 \times 10^{-3}$	90	[30] ANDREEV	24E	NA64 $m_{\gamma'}$ = 1×10^{-3}–1 GeV
$<8 \times 10^{-7}$	95	[31] ARAMBURO...	24	CMB $m_{\gamma'}$ = 3×10^{-15}–3×10^{-12} eV
$<1.4 \times 10^{-15}$	90	[32] ARNQUIST	24	MAJD $m_{\gamma'}$ = 1–100 keV
$<1.5 \times 10^{-16}$	90	[33] CERVANTES	24	SRPH $m_{\gamma'}$ = 5.35 μeV
$<5 \times 10^{-7}$	90	[34] CORTINA-GIL	24A	NA62 $m_{\gamma'}$ = 5–500 MeV
$<3 \times 10^{-16}$	90	[35] DOLAN	24	STAR $m_{\gamma'}$ = 0.5–16 keV
$<3.7 \times 10^{-13}$	90	[36] HE	24	DM $m_{\gamma'}$ = 29.5 μeV
$<1 \times 10^{-12}$	90	[37] KNIRCK	24	BRED $m_{\gamma'}$ = 44–52 μeV
$<6 \times 10^{-15}$	95	[38] LEVINE	24	DER $m_{\gamma'}$ = 0.21–1.24 μeV
$<1 \times 10^{-6}$	95	[39] LIU	24	DM $m_{\gamma'}$ = 2×10^{-2}–1×10^{4} eV
$<4.5 \times 10^{-8}$	95	[40] MCCARTHY	24	CMB $m_{\gamma'}$ = 10^{-13}–10^{-11} eV
$<2.2 \times 10^{-16}$	90	[41] TANG	24	SHNE $m_{\gamma'}$ = 5.367–5.373 μeV
$<3 \times 10^{-3}$	95	[42] YAN	24A	ASTR $m_{\gamma'}$ = 3×10^{-18}–3×10^{-14} eV
$<1 \times 10^{-3}$	90	[43] AAD	23BO	ATLS $m_{\gamma'}$ = 5–40 GeV
$<1.3 \times 10^{-8}$	90	[44] AAD	23I	ATLS $m_{\gamma'}$ = 0.017–15 GeV
		[45] AAD	23T	ATLS $m_{\gamma'} \lesssim$ 40 GeV
$<1 \times 10^{-16}$	90	[46] AALBERS	23A	LZ $m_{\gamma'}$ = 1–17 keV
$<1.6 \times 10^{-3}$	90	[47] ABLIKIM	23AF	BES3 $m_{\gamma'}$ = 1.5–2.9 GeV
		[48] ABUDINEN	23B	BEL2 $m_{\gamma'}$ = 4–9.7 GeV
$<1.61 \times 10^{-14}$	90	[49] ADHIKARI	23	C100 $m_{\gamma'}$ = 215 eV
$<6 \times 10^{-14}$	90	[50] ADHIKARI	23A	C100 $m_{\gamma'}$ = 10–1000 keV
$<2.1 \times 10^{-3}$	95	[51] ADRIAN	23	HPS $m_{\gamma'}$ = 19–81 MeV
$<1.1 \times 10^{-16}$	90	[52] AGNES	23A	DS50 $m_{\gamma'}$ = 0.03–20 keV
$<2 \times 10^{-12}$	95	[53] AN	23A	$m_{\gamma'}$ = 4.1–6.2 μeV
$<5 \times 10^{-6}$	90	[54] ANDREEV	23	NA64 $m_{\gamma'}$ = 10^{-3}–1.5 GeV
$<5.0 \times 10^{-14}$	68	[55] BAJJALI	23	BRAS $m_{\gamma'}$ = 49.63–74.44 μeV
$<2 \times 10^{-7}$	90	[56] CORTINA-GIL	23C	NA62 $m_{\gamma'}$ = 10–700 MeV
$<2.2 \times 10^{-3}$	90	[57] HAYRAPETY...	23G	CMS $m_{\gamma'}$ = 1.1–7.9 GeV
$<3 \times 10^{-11}$	95	[58] KOTAKA	23	DORR $m_{\gamma'}$ = 74–110 μeV
$<2 \times 10^{-15}$		[59] LI	23I	ASTR $m_{\gamma'}$ = 10^{-3}–10^{5} eV
$<7.9 \times 10^{-13}$	95	[60] RAMANATH...	23	QULP $m_{\gamma'}$ = 19.7–30.5 μeV
$<1.6 \times 10^{-9}$	95	[61] ROMANENKO	23	LSW $m_{\gamma'}$ = 0.21–5.7 μeV
		[62] XIA	23	ASTR $m_{\gamma'} \lesssim 10^{-23}$eV
		[63] AAD	22J	ATLS $m_{\gamma'}$ = 1–60 GeV
		[64] AAD	22S	ATLS $m_{\gamma'} \lesssim$ 10 GeV
$<2 \times 10^{-14}$	90	[65] APRILE	22	XE1T $m_{\gamma'}$ = 0.9 keV
$<2 \times 10^{-15}$	90	[66] APRILE	22	XE1T $m_{\gamma'}$ = 0.01–0.4 keV
$<5 \times 10^{-17}$	90	[67] APRILE	22B	XENT $m_{\gamma'}$= 1–39,44–140 keV
$<1 \times 10^{-2}$	90	[68] BATTAGLIERI	22	BDMP $m_{\gamma'}$ = 3–100 MeV
$(4.6^{+0.5}_{-0.4}) \times 10^{-15}$	68	[69] BOLTON	22	ASTR $m_{\gamma'}$ = $(8.4 \pm 0.6) \times 10^{-14}$ eV
$<1 \times 10^{-13}$	90	[70] CERVANTES	22	ORPH $m_{\gamma'}$ = 65.5–69.3 μeV
$<1 \times 10^{-12}$	90	[71] CHILES	22	$m_{\gamma'}$ = 0.7–0.8 eV
$<8.7 \times 10^{-11}$	90	[72] HOCHBERG	22	SNSP $m_{\gamma'}$ = 0.73–30 eV
		[73] LEES	22	BABR $m_{\gamma'}$ = 1×10^{-3}–3.16 GeV
$<7.97 \times 10^{-9}$	95	[74] LU	22	ASTR $m_{\gamma'} \lesssim 3\times10^{-5}$ eV
$<6.86 \times 10^{-11}$	90	[75] MANENTI	22	MDHI $m_{\gamma'}$ = 1.61 eV
$<3 \times 10^{-2}$	95	[76] THOMAS	22	$m_{\gamma'}$ = 1–80 GeV
		[77] TUMASYAN	22AH	CMS $m_{\gamma'}$ = 4–62.5 GeV
		[78] TUMASYAN	22N	CMS $m_{\gamma'}$ = 0.6–49 GeV
		[79] WU	22A	PPTA $m_{\gamma'} \lesssim 10^{-23}$eV
$<8 \times 10^{-6}$	90	[80] ANDREEV	21	NA64 $m_{\gamma'}$ = 1×10^{-3}–1 GeV
$<2.3 \times 10^{-4}$	90	[81] ANDREEV	21A	NA64 $m_{\gamma'}$ = 0.1–0.35 GeV
$<1.6 \times 10^{-4}$	95	[82] BI	21	ASTR $m_{\gamma'}$ = 0.03–0.06 eV
$<3 \times 10^{-5}$	90	[83] CAZZANIGA	21	NA64 $m_{\gamma'}$ = 10–390 MeV
$<1.68 \times 10^{-15}$	90	[84] DIXIT	21	CNTR $m_{\gamma'}$ = 24.86 μeV
$<2 \times 10^{-16}$	90	[85] GHOSH	21	RVUE $m_{\gamma'}$ = 2–30 μeV
$<1.8 \times 10^{-13}$		[86] GODFREY	21	DER $m_{\gamma'}$ = 0.2637–0.2648 μeV
$<3 \times 10^{-12}$	95	[87] KOPYLOV	21A	CNTR $m_{\gamma'}$ = 9–40 eV
$<2 \times 10^{-2}$	95	[88] KRIBS	21	$m_{\gamma'} \lesssim$ 10 GeV
		[89] SCHMIDT	21	THEO $m_{\gamma'}$ < 0.6 GeV
$<3 \times 10^{-8}$	90	[90] TSAI	21	BDMP $m_{\gamma'}$ = 0.78 GeV
$<1 \times 10^{-4}$	90	[91] AAIJ	20C	LHCB $m_{\gamma'}$ = 214 MeV
		[92] AAIJ	20C	LHCB $m_{\gamma'}$ = 218–315 MeV
		[93] ABLIKIM	20AB	BES3 $m_{\gamma'}$ = 0.2–2.1 GeV
$<4.1 \times 10^{-12}$	90	[94] AGOSTINI	20	HPGE $m_{\gamma'}$ = 60 keV – 1 MeV
$<3.3 \times 10^{-14}$	90	[95] AMARAL	20	SCDM $m_{\gamma'}$ = 1.2–50 eV
$<1.2 \times 10^{-14}$	90	[96] AN	20	XE1T $m_{\gamma'}$ = 200 eV
$<6.72 \times 10^{-13}$	95	[97] ANDRIANAV...	20	FUNK $m_{\gamma'}$ = 1.95–8.55 eV
$<1 \times 10^{-16}$	90	[98] APRILE	20	XE1T $m_{\gamma'}$ = 1–200 keV
$<9 \times 10^{-16}$	90	[99] ARALIS	20	SCDM $m_{\gamma'}$ = 0.04–500 keV
$<3 \times 10^{-5}$	90	[100] ARGUELLES	20	THEO $m_{\gamma'}$ = 0.01 GeV
$<7 \times 10^{-14}$	90	[101] ARNAUD	20	EDEL $m_{\gamma'}$ = 1–40 eV
$<8.2 \times 10^{-5}$	90	[102] BANERJEE	20	NA64 $m_{\gamma'}$ = 1.5–24 MeV
$<7 \times 10^{-15}$	90	[103] BARAK	20	SENS $m_{\gamma'}$ = 1.2–12.8 eV
		[104] KRASNIKOV	20	RVUE $m_{\gamma'}$ = 16.7 MeV
$<1.4 \times 10^{-14}$	90	[105] SHE	20	CDEX $m_{\gamma'}$ = 10–300 eV
$<1.3 \times 10^{-15}$	90	[106] SHE	20	CDEX $m_{\gamma'}$ = 0.1–4 keV
$<1 \times 10^{-3}$	90	[107] SIRUNYAN	20AQ	CMS $m_{\gamma'}$ = 11.5–75 GeV, 110–200 GeV
$<4.3 \times 10^{-10}$	95	[108] TOMITA	20	$m_{\gamma'}$ = 115.79–115.85 μeV
$<9 \times 10^{-16}$	90	[109] WANG	20A	CDEX $m_{\gamma'}$ = 0.185–10 keV
		[110] AABOUD	19G	ATLS $m_{\gamma'}$ = 20–60 GeV
$<6 \times 10^{-3}$	90	[111] ABLIKIM	19A	BES3 $m_{\gamma'}$ = 0.01–2.4 GeV
$<3.4 \times 10^{-3}$	90	[112] ABLIKIM	19H	BES3 $m_{\gamma'}$ = 0.1–2.1 GeV
$<8 \times 10^{-15}$	90	[113] AGUILAR-AR...	19A	DAMC $m_{\gamma'}$ = 1.2–30 eV
$<9 \times 10^{-17}$	90	[114] APRILE	19D	XE1T $m_{\gamma'}$ = 0.186–5 keV
$<7.5 \times 10^{-6}$	90	[115] BANERJEE	19	NA64 $m_{\gamma'}$ = 1–200 MeV
$<2 \times 10^{-11}$		[116] BHOONAH	19	ASTR $m_{\gamma'}$ = 10^{-22}–10^{-10} eV
$<5 \times 10^{-12}$	95	[117] BRUN	19	SHUK $m_{\gamma'}$ = 20.8–28.3 μeV
$<4.4 \times 10^{-4}$	90	[118] CORTINA-GIL	19	NA62 $m_{\gamma'}$ = 60–110 MeV
$<3 \times 10^{-5}$	95	[119] DANILOV	19	TEXO $m_{\gamma'}$ = 20 eV - 1 MeV
$<6 \times 10^{-9}$	95	[120] HOCHBERG	19	$m_{\gamma'}$ = 0.8–4 eV
$<1 \times 10^{-11}$	95	[121] KOPYLOV	19	CNTR $m_{\gamma'}$ = 9–40 eV
$<1.5 \times 10^{-9}$		[122] KOVETZ	19	COSM $m_{\gamma'}$ = 10^{-23}–10^{-13} eV
$<3 \times 10^{-14}$	95	[123] NGUYEN	19	WDMX $m_{\gamma'}$ = 6 neV – 2.07 μeV
$<4.5 \times 10^{-14}$	90	[124] ABE	18F	XMAS $m_{\gamma'}$ = 40–120 keV
$<2.5 \times 10^{-3}$	95	[125] ADRIAN	18	HPS $m_{\gamma'}$ = 19–81 MeV
$<4.4 \times 10^{-4}$	90	[126] ANASTASI	18B	KLOE $m_{\gamma'}$ = 519–987 MeV
$<4 \times 10^{-15}$	90	[127] ARMENGAUD	18	EDE3 $m_{\gamma'}$ = 0.8–500 keV
		[128] BANERJEE	18	NA64 $m_{\gamma'}$ = 1–23 MeV
$<1.8 \times 10^{-5}$	90	[129] BANERJEE	18A	NA64 $m_{\gamma'}$ = 1–100 MeV
$<1 \times 10^{-8}$	90	[130] KNIRCK	18	$m_{\gamma'}$ = 0.67–0.92 meV
$<3.1 \times 10^{-14}$	90	[131] ABGRALL	17	HPGE $m_{\gamma'}$ = 11.8 keV
$<6 \times 10^{-4}$	90	[132] ABLIKIM	17AA	BES3 $m_{\gamma'}$ = 1.5–3.4 GeV
$<7 \times 10^{-15}$	90	[133] ANGLOHER	17	CRES $m_{\gamma'}$ = 0.3–0.7 keV
$<1.2 \times 10^{-4}$	90	[134] BANERJEE	17	NA64 $m_{\gamma'}$ = 0.002–0.4 GeV
$<2 \times 10^{-11}$		[135] CHANG	17	ASTR $m_{\gamma'}$ = 15 MeV
$<4.5 \times 10^{-3}$	90	[136] DUBININA	17	EMUL $m_{\gamma'}$ = 1.1–24 MeV
$<4 \times 10^{-4}$	90	[137] LEES	17E	BABR $m_{\gamma'}$ = 4.7 GeV
		[138] AAD	16AG	ATLS $m_{\gamma'}$ = 0.1–2 GeV
$<4.4 \times 10^{-4}$	90	[139] ANASTASI	16	KLOE $m_{\gamma'}$ = 527–987 MeV
$<1.7 \times 10^{-6}$	95	[140] KHACHATRY...	16	CMS $m_{\gamma'}$ = 2 GeV
$<4 \times 10^{-2}$	95	[141] AAD	15CD	ATLS $m_{\gamma'}$ = 15–55 GeV
$<1.4 \times 10^{-3}$	90	[142] ADARE	15	$m_{\gamma'}$ = 30–90 MeV
		[143] AN	15A	$m_{\gamma'}$ = 12 eV - 40 keV
		[144] ANASTASI	15	KLOE $m_{\gamma'}$ = $2m_{\mu}$ - 1 GeV
$<1.7 \times 10^{-3}$	90	[145] ANASTASI	15A	KLOE $m_{\gamma'}$ = 5–320 MeV
$<4.2 \times 10^{-4}$	90	[146] BATLEY	15A	NA48 $m_{\gamma'}$ = 36 MeV
		[147] JAEGLE	15	BELL $m_{\gamma'}$ = 0.1–3.5 GeV

$<3 \times 10^{-13}$		[148] KAZANAS	15	ASTR	$m_{\gamma'} = 2m_e$ – 100 MeV
$<6 \times 10^{-12}$		[149] SUZUKI	15		$m_{\gamma'} = 1.9$–4.3 eV
$<2.3 \times 10^{-13}$	99.7	[150] VINYOLES	15	ASTR	$m_{\gamma'} = 8$ eV
$<2 \times 10^{-13}$		[151] ABE	14F	XMAS	$m_{\gamma'} = 40$–120 keV
$<1.8 \times 10^{-3}$	90	[152] AGAKISHIEV	14	HDES	$m_{\gamma'} = 63$ MeV
$<9.0 \times 10^{-4}$	90	[153] BABUSCI	14	KLOE	$m_{\gamma'} = 969$ MeV
		[154] BATELL	14	BDMP	$m_{\gamma'} = 10^{-3}$–1 GeV
$<1.3 \times 10^{-7}$	95	[155] BLUEMLEIN	14	BDMP	$m_{\gamma'} = 0.6$ GeV
$<3 \times 10^{-18}$		[156] FRADETTE	14	COSM	$m_{\gamma'} = 50$–300 MeV
$<3.5 \times 10^{-4}$	90	[157] LEES	14J	BABR	$m_{\gamma'} = 0.2$ GeV
$<9 \times 10^{-4}$	95	[158] MERKEL	14	A1	$m_{\gamma'} = 40$–300 MeV
$<3 \times 10^{-15}$		[159] AN	13B	ASTR	$m_{\gamma'} = 2$ keV
$<7 \times 10^{-14}$		[160] AN	13C	XE10	$m_{\gamma'} = 100$ eV
$<8 \times 10^{-4}$		[161] DIAMOND	13	BDMP	$m_{\gamma'} = 30$–250 MeV
$<2 \times 10^{-3}$	90	[162] GNINENKO	13	BDMP	$m_{\gamma'} = 25$–120 MeV
$<2.2 \times 10^{-13}$		[163] HORVAT	13	HPGE	$m_{\gamma'} = 230$ eV
$<8.06 \times 10^{-5}$	95	[164] INADA	13	LSW	$m_{\gamma'} = 0.04$ eV-26 keV
$<2 \times 10^{-10}$	95	[165] MIZUMOTO	13		$m_{\gamma'} = 1$ eV
$<1.7 \times 10^{-7}$		[166] PARKER	13	LSW	$m_{\gamma'} = 53$ μeV
$<5.32 \times 10^{-15}$		[167] PARKER	13		$m_{\gamma'} = 53$ μeV
$<1 \times 10^{-15}$		[168] REDONDO	13	ASTR	$m_{\gamma'} = 2$ keV
$<8 \times 10^{-8}$	90	[169] GNINENKO	12A	BDMP	$m_{\gamma'} = 1$–135 MeV
$<1 \times 10^{-7}$	90	[170] GNINENKO	12B	CHRM	$m_{\gamma'} = 1$–500 MeV
$<1 \times 10^{-3}$	90	[171] ABRAHAMY...	11		$m_{\gamma'} = 175$–250 MeV
$<9 \times 10^{-8}$	95	[172] BLUEMLEIN	11	BDMP	$m_{\gamma'} = 70$ MeV
$<1 \times 10^{-7}$		[173] BJORKEN	09	BDMP	$m_{\gamma'} = 2$–400 MeV
$<5 \times 10^{-9}$		[174] BJORKEN	09	ASTR	$m_{\gamma'} = 2$–50 MeV

[1] ABLIKIM 25CL search for kinetically mixed dark photons using the BESIII detector. They use the sample J/ψ events collected to measure the transition form factor of the η meson. Limits are derived on the branching ratio for $\eta \rightarrow \gamma\gamma'$, $\gamma' \rightarrow e^+e^-$ and presented in terms of mass-dependent limits on the kinetic mixing parameter in Fig. 7.

[2] ALBAKRY 25 report a search with the SuperCDMS detector for hidden photon dark matter absorption on silicon. See their Fig. 4 for mass-dependent limits.

[3] AN 25 search for dark photon dark matter resonantly converting into photons in the solar corona plasma, leading a signal detectable by the STEREO and Parker Solar Probe spacecraft. See their Fig. 2 for mass-dependent limits.

[4] ANDREEV 25 present the first hidden photon limits from the NA64e experiment using a 70 GeV positron beam. They set constraints on an invisibly decaying hidden photon that kinetically mixes with the photon. See Fig. 14 for various mass-dependent limits, noting the assumed parameter values for the dark gauge coupling and dark matter mass.

[5] APRILE 25A present results from a search with XENONnT for dark photon dark matter absorption on electrons in liquid xenon. See their Fig. 5 for mass-dependent limits.

[6] ASWATHI 25 use LIGO-VIRGO-KAGRA data from the black hole binary merger events GW231123 and GW190517 to search for evidence of the superradiant build-up of a cloud of vector bosons, which could act to spin down the black holes. They set lower limits on the dark photon kinetic mixing and present mass-dependent limits in Fig. 2.

[7] BAUDIS 25 presents results from the QROCODILE experiment which uses a superconducting nanowire single photon detector to search for low-mass dark matter. Fig. 2 shows mass-dependent constraints on hidden photon absorption.

[8] BLOCH 25 present results from a search for single-electron events in the SENSEI low-mass dark matter detector. See their Fig. 4 for mass-dependent limits on dark photon absorption.

[9] CAPUTO 25 present a new bound on dark photon emission from core-collapse supernovae. They consider the cooling effect of resonant dark photon production behind the shock wave which, if too excessive, can potentially prevent the explosion. In the case of SN1987A, this consideration supersedes the standard supernova cooling argument and leads to a bound that is strongest in the sub-MeV mass region. See their Fig. 2 for mass-dependent limits.

[10] CHOI 25 place bounds on a dark matter model using the NEON reactor neutrino experiment. They explore a scenario in which the high flux of photons from the nuclear reactor leads to a flux of dark photons; those dark photons can then decay into dark matter particles in the detector that scatter on electrons. See their Fig. 3 for mass-dependent bounds on the dark photon mediator, obtained for the dark matter mass $m_{\gamma'}/3$ and the hidden gauge coupling $\alpha_D = 0.1$.

[11] CORTINA-GIL 25A search for kinetically mixed hidden photons decaying to hadronic final states in the NA62 beam dump. Quoted limit applies around 0.8 GeV, but does not extend to arbitrarily large kinetic mixing. See their Fig. 7 for mass-dependent limits combining this hadronic analysis and the dilepton channel reported in CORTINA-GIL 24A.

[12] CORTINA-GIL 25B report limits on an invisibly decaying dark photon produced in the decays of K^+ and π^0 in the NA62 detector. See their Fig. 8 for mass-dependent limits.

[13] EGGE 25 search for dark photon dark matter using the prototype setup of the MADMAX dielectric disk haloscope. The local density $\rho_{\gamma'} = 0.3$ GeV/cm^3 is assumed. See their Fig. 4 for mass-dependent limits.

[14] LI 25 search for MeV-mass dark photons making up the dark matter halo of the galaxy that could be absorbed by liquid xenon in the PandaX detector. The local density $\rho_{\gamma'} = 0.3$ GeV/cm^3 is assumed. The quoted limit is at $m_{\gamma'} = 150$ keV. See their Fig. 3 for mass-dependent limits.

[15] LINDEN 25 extend limits on dark photons as a dark matter candidate at masses below the electron pair creation threshold. They search for evidence of dark photon-to-three-photon decays using data from the INTEGRAL space telescope. See their Fig. 4 for mass-dependent limits.

[16] MELO-GALINDO 25 search for evidence of mixing between standard model and dark photons imprinted on the TeV gamma-ray spectra of the Crab Nebula and gamma-ray source MGRO J1908+06, using data from HAWC and LHAASO. See their Figs. 3–6 for mass-dependent limits for both sources and under various model assumptions.

[17] MIRASOLA 25 search for evidence of superradiant clouds of dark photons surrounding black holes, which are expected to produce pulsating radio emissions, and continuous gravitational wave signals that could be observed by LIGO-Virgo-KAGRA. Their bound disfavours dark photons within a specific range of masses and kinetic mixing parameters between 10^{-9}–10^{-7}, subject to uncertainties about the black hole population and details about the cloud's radio emission. See their Fig. 5.

[18] ROMERO-JORGE 25 set limits on kinetically-mixed dark photons produced through various decays in heavy-ion collisions and then decaying to dileptons. They incorporate a range of heavy ion data from across the SIS, RHIC and LHC. They present various mass-dependent limits in their Fig. 7 for different choices for the dark photon "surplus" - the maximum permissible increase in a dilepton yield from dark photons compared to the Standard Model yield.

[19] TROST 25 use VLT/UVES observations of the quasar HE0940-1050 to search for resonant conversion of dark photon dark matter into photons, which would heat the intergalactic medium and imprint on the quasar's Lyman-alpha forest spectrum. See their Fig. 7 for mass-dependent limits.

[20] ZENG 25 place a bound on keV-scale dark photons making up the halo of the galaxy by searching for electron recoil events in the PandaX detector. See Fig. 3(f) for mass-dependent limits.

[21] ZHAO 25 use a flux-tunable resonant cavity to search for dark photon dark matter in a narrow frequency window around 5.69 GHz, performing microwave single photon detection using a transmon qubit. The quoted limit assumes a local dark matter density of $\rho_{\gamma'} = 0.45$ GeV/cm^3

[22] ZHAO 25A use a single-site, two-sensor array of commercial scalar optically pumped magnetometers to search for dark photon dark matter converting into photons. The relevant observable signal appears in this low-mass regime due to the action of the Earth's ionosphere as transducer. See their Fig. 4 for mass-dependent limits.

[23] AAD 24AS search for hidden photons resulting from Higgs decays in the Falkowski-Ruderman-Volansky-Zupan model. See Fig. 7 for mass-dependent limits, value shown taken from the most constraining point at 10 GeV mass. The limits do not extend to arbitrarily high values of the kinetic mixing, stopping between 10^{-4} and 10^{-7} at the lower and upper end of the mass range respectively. The limit is also dependent on the branching fraction for Higgs decays resulting in dark photons.

[24] ABRATENKO 24A search for dark trident scattering at a neutrino beam using the MicroBooNE detector. Events involve a pair of particles $\chi\overline{\chi}$ produced from π^0 or η decays mediated by a dark photon, these particles then scatter off Argon in the detector and can produce an additional dark photon which then decays. See Fig. 7 for mass-dependent limits under three possible scenarios for the χ particle.

[25] ABREU 24 look for hidden photons produced from the pp collision in the decay channel $\gamma' \rightarrow e^+e^-$, and exclude at 90% CL the region of $\chi = 4 \times 10^{-6}$–2×10^{-4} and $m_{\gamma'} = 10$–80 MeV, with the newly excluded region near the higher values of χ. See their Fig. 7 for mass-dependent limits.

[26] ADACHI 24C follows KOTAKA 23 of the DOSUE-RR collaboration, searching for hidden photon dark matter conversion using a millimetre-wave receiver and a radioshielding box. See Fig. 11 for mass dependent limits.

[27] AGOSTINI 24A report a search for dark photon dark matter absorption and dark Compton scattering on germanium, generating electron events in the GERDA experiment. The quoted limit is at $m_{A^0} = 150$ keV. See their Fig. 7 for mass-dependent limits.

[28] AGRAWAL 24 search for hidden photon dark matter via stimulated emission of a photon from a microwave cavity prepared in a non-classical state by a superconducting qubit.

[29] ANDREEV 24A perform a missing-energy search in the NA64 detector to look for an MeV-scale hidden photon mediator to a stable fermionic dark sector particle. See Fig. 3 for mass-dependent limits.

[30] ANDREEV 24E report results from the NA64μ beam dump experiment, employing a high-intensity muon beam. They set limits on the kinetic mixing parameter of an invisibly decaying hidden photon. See their Fig. 19 for mass-dependent limits.

[31] ARAMBURO-GARCIA 24 search for evidence of resonant conversion of regular photons into dark photons within the inter-galactic medium using the expected imprint on the CMB anisotropies. Quoted limit is for their "conservative" approach - see their Fig. 5 for mass-dependent limits.

[32] ARNQUIST 24 use the MAJORANA DEMONSTRATOR to search for keV-mass hidden photon dark matter absorption by Germanium. See Fig. 5 for mass-dependent limits.

[33] CERVANTES 24 use a superconducting radio frequency cavity at the SQMS Centre (Fermilab) to search for hidden photon dark matter at 1.3 GHz. See their Fig. 3 for limits in context.

[34] CORTINA-GIL 24A report results from the NA62 beam dump experiment, searching for production and decays of dark photons to lepton pairs. Quoted limit applies around 300 MeV, but does not extend to arbitrarily high kinetic mixing. See their Fig. 4 for mass-dependent limits

[35] DOLAN 24 constrain anomalous cooling of globular cluster stars due to the emission of hidden photons. Best limit is taken from the envelope of limits from the R parameter, R2 parameter and Tip of the Red Giant branch. This study includes hidden photon emission in stellar evolution simulation and so supersedes red giant bound in AN 20.

[36] HE 24 present results from the APEX collaboration. They look for hidden photon dark matter using a radio frequency cavity at 7.139 GHz. See their Fig. 4 for mass-dependent limits.

[37] KNIRCK 24 search for hidden photon dark matter using GigaBREAD, a broadband haloscope operating at room temperature that uses a parabolic reflector and a horn antenna. See their Fig. 4 for mass-dependent limits.

[38] LEVINE 24 search for hidden photon dark matter using Dark E-Field Radio, a broadband haloscope consisting of an E-field antenna inside a shielded room. This is a continuation of their experiment previously reported in GODFREY 21. See their Fig. 12 for mass-dependent limits.

[39] LIU 24 constrain hidden photon dark matter over a broad mass range using the very high-energy gamma-ray spectrum of blazars Mrk 501 and Mrk 421. See their Fig. 4 for mass-dependent limits which also depend on the density profiles of the host halos of the blazars. Quoted limit is for the case where the host halos have an NFW profile in Fig. 6.

[40] MCCARTHY 24 search for evidence of photons converting into hidden photons as they traverse large-scale structure, which would lead to a patchy-screening effect observable in CMB anisotropy maps. See their Fig. 3 for mass-dependent limits. This analysis improves upon a similar study by ARAMBURO-GARCIA 24 - see the note added in MCCARTHY 24.

Int. J. Mod. Phys. A 2026.41. Downloaded from www.worldscientific.com
by UNIVERSITY OF CALIFORNIA @ BERKELEY on 09/16/26. Re[redacted]s strictly not permitted, except for Open Access articles.

Int. J. Mod. Phys. A 2026.41. Downloaded from www.worldscientific.com by UNIVERSITY OF CALIFORNIA @ BERKELEY on 09/16/26. Re-use and distribution is strictly not permitted, except for Open Access articles.

[41] TANG 24 present results from a hidden photon dark matter search at 1.3 GHz with SHANHE, a tunable superconducting radio frequency cavity. See their Fig. 3 for mass-dependent limits.

[42] YAN 24A use data from the JUNO probe to constrain hidden photons via the way they would modify Jupiter's magnetic field. See their Fig. 7 for mass-dependent limits.

[43] AAD 23BO look for rare decays of the Z boson, $Z \rightarrow \gamma' + H'$, with dark Higgs decaying into a pair of hidden photons, assuming that at least two of the hidden photons decay into e^+e^- or $\mu^+\mu^-$. The quoted limit assumes the hidden fine structure constant $\alpha_D = 0.1$ and the dark Higgs mass ranging 20 to 70 GeV. See their Fig.5 for the mass-dependent limits.

[44] AAD 23I look for exotic decays of the SM-like Higgs boson, $H \rightarrow \gamma'\gamma'$ with hidden photons decaying into displaced lepton or light quark pairs, and set limits on the kinetic mixing within 1×10^{-4}–1×10^{-8} for the given mass range. The quoted limit is for $m_{A^0} \simeq 13$ GeV with a branching fraction of 0.1 for the Higgs decaying into hidden photon pairs. See their Fig. 13 for the mass-dependent limits.

[45] AAD 23T is analogous to AAD 22S, but using the ZH production mode, and set the upper limit on the branching ratio B($H \rightarrow \gamma\gamma'$) within 0.0219–0.0252 (95% CL).

[46] AALBERS 23A look for an absorption of hidden photon dark matter. The quoted limit is for $m_{\gamma'} = 1.4$ keV. The local density $\rho_{\gamma'} = 0.3$ GeV/cm^3 is assumed. See their Fig. 7 for mass-dependent limits.

[47] ABLIKIM 23AF look for invisible decays of hidden photons produced in the reaction $e^+e^- \rightarrow \gamma\gamma'$. They set limits within the 1.6×10^{-3}–5.7×10^{-3}. See their Fig. 3 for mass-dependent limits.

[48] ABUDINEN 23B look for hidden photons in the dark Higgsstrahlung process, $e^+e^- \rightarrow \gamma' H'$ ($\gamma' \rightarrow \mu^+\mu^-$) with H' being invisible. They set upper limits on the product of the kinetic mixing and the hidden gauge coupling, $\chi^2 \cdot \alpha_D$, in the range of 1.7×10^{-8}–2×10^{-6} at 90% CL for a 1 GeV dark Higgs mass. See their Fig. 3 for the mass-dependent limits.

[49] ADHIKARI 23 look for the annual modulation signal induced by solar flux of hidden photons. See their Fig. 10 for mass-dependent limits.

[50] ADHIKARI 23A look for absorption and Compton-like processes of hidden photon dark matter. The quoted limit is for $m_{\gamma'} \simeq 12$ keV. Limits between 6×10^{-14}–3×10^{-11} are obtained. See their Fig. 4 for mass-dependent limits.

[51] ADRIAN 23 is an update of ADRIAN 18, and use the data from the 2016 engineering run at 2.3 GeV. The quoted limit is at $m_{\gamma'} \simeq 74$ MeV. See their Fig. 28 for the mass-dependent limits.

[52] AGNES 23A look for an absorption of hidden photon dark matter. The quoted limit is for $m_{\gamma'} = 0.03$ keV. The local density $\rho_{\gamma'} = 0.3$ GeV/cm^3 is assumed. See their Fig. 2 for mass-dependent limits.

[53] AN 23A look for absorption of hidden photon dark matter at radio telescopes, setting limits based on data from the FAST telescope. The local density $\rho_{\gamma'} = 0.3$ GeV/cm^3 is assumed. See their Fig. 1 for mass-dependent limits.

[54] ANDREEV 23 is an update of ANDREEV 21 and ANDREEV 21A. The quoted limit applies to $m_{\gamma'} = 1$ MeV. See their Fig. 3 for mass-dependent limits.

[55] BAJJALI 23 look for hidden photon dark matter by using a 12–18 GHz dish antenna at U. Hamburg that is sensitive to vertically aligned hidden photon polarizations. They assume a local density of $\rho_{\gamma'} = 0.3$ GeV/cm^3. See their Figure 12 for mass-dependent limits in the range of $m_{\gamma'} = 50$–75 μeV under the assumption of randomly aligned hidden photon polarizations, defined as "1 sigma sensitivity". The run is labelled BRASS-p.

[56] CORTINA-GIL 23C NA62 beam dump experiment searches for hidden photons decaying to $\mu^+\mu^-$, extending their previous search CORTINA-GIL 19. The quoted limit applies at 300 MeV but does not extend to arbitrarily large kinetic mixing parameters. See Fig. 4 for mass-dependent limits.

[57] HAYRAPETYAN 23G search for kinetically mixed hidden photons in proton-proton collisions at the LHC that would generate a narrow peak in the mass spectrum of dimuon events. The mass window between 2.6 and 4.2 GeV is left unconstrained to avoid J/ψ and $\psi(2S)$ resonances. Mass dependent limits given in their Fig. 6.

[58] KOTAKA 23 is an update of TOMITA 20, and set limits $\chi < 0.3$–2×10^{-10} for the quoted mass range. The local density $\rho_{\gamma'} = 0.39$ GeV/cm^3 is assumed. See their Fig. 5 for mass-dependent limits.

[59] LI 23I set cooling bounds on the emission of hidden photons from the Sun, red giant, and horizontal branch stars, including emission of both the transverse and longitudinal modes. Cooling bounds are computed assuming a static model as opposed to considering the impact on stellar evolution. The result is comparable to earlier estimates of the same bound e.g. REDONDO 13. Limit applies at the most constraining mass around 200 eV for the solar bound.

[60] RAMANATHAN 23 look for hidden photon dark matter using a gold-plated copper dish antenna cooled to 20 mK. The local density $\rho_{\gamma'} = 0.45$ GeV/cm^3 is assumed. Limits between 7.9×10^{-13} and 3.81×10^{-12} are obtained. See their Fig. 5 for mass-dependent limits.

[61] ROMANENKO 23 employed two superconducting radio frequency cavities with a high quality factor, optimized for detecting the longitudinal polarization of the hidden photon. The quoted limit is set at $m_{\gamma'} \simeq 5\mu$eV. See their Fig. 4 for the mass-dependent limits.

[62] XIA 23 is analogous to WU 22A and use the Fermi-LAT pulsar timing array. They set a bound on the local density as $\rho_{\gamma'} \lesssim 7$ GeV/cm^3 for $m_{\gamma'} \lesssim 10^{-23}$ eV at 95% CL, with weaker constraints up to 10^{-22} eV. See their Fig. 1 for the mass-dependent limits.

[63] AAD 22J look for exotic decays of the SM-like Higgs boson, $H \rightarrow \gamma'\gamma' \rightarrow 4\ell$ and $H \rightarrow Z\gamma' \rightarrow 4\ell$, and set limits on the kinetic mixing and the Higgs portal coupling. See their Figs. 19 and 20 for the mass-dependent limits.

[64] AAD 22S look for decays of a Higgs boson into γ and γ' using the VBF production mode, and set the upper limit on the branching ratio at 0.018 (95% CL) for the 125 GeV Higgs boson. For the quoted mass range, the signal acceptance changes by less than 1%.

[65] APRILE 22 is analogous to AN 20, and their limit was corrected in the erratum to this paper: APRILE 24B. They set limits $\chi < 2\times10^{-12}$ (eV/$m_{\gamma'}$) for $m_{\gamma'} < 3$ eV (90% C.L.). For $m_{\gamma'} > 3$ eV, see Fig. 1 of APRILE 24B.

[66] APRILE 22 extend APRILE 19 to lower masses by removing the background of ionization signals correlated with high-energy events. The quoted limit applies to $m_{\gamma'} = 0.09$ keV. See their Fig. 15 for mass-dependent limits.

[67] APRILE 22B is an update of APRILE 20, and set limits $\chi \lesssim 5\times10^{-17}$–$2\times10^{-13}$. The quoted limit applies to $m_{\gamma'} = 1$ keV. They exclude the XENON1T excess found in APRILE 20. See their Fig. 6 for mass-dependent limits.

[68] BATTAGLIERI 22 is analogous to BATELL 14, and derived limits from the electron beam dump experiment at Jefferson Lab (BDX-MINI). Limits at the level of 7×10^{-5}–1×10^{-2} are obtained for the dark matter mass $m_{\gamma'}/3$ and the hidden gauge coupling $\alpha_D = 0.1$. See their Fig. 11.

[69] BOLTON 22 use the Ly-α forest at z $\simeq$ 0.1 as a calorimeter for heating in the intergalactic medium by the resonant conversion of hidden photon dark matter to photons, which is assumed to be responsible for the tension between the predicted and observed Ly-α absorption linewidths.

[70] CERVANTES 22 use a dielectrically loaded Fabry-Perot open cavity to look for hidden photon dark matter. The local density $\rho_{\gamma'} = 0.45$ GeV/cm^3 is assumed. See their Fig. 5 for mass-dependent limits.

[71] CHILES 22 look for hidden photon dark matter by using a layered dielectric target and a superconducting nanowire single-photon detector. The local density $\rho_{\gamma'} = 0.4$ GeV/cm^3 is assumed. See their Fig. 4 for mass-dependent limits.

[72] HOCHBERG 22 update HOCHBERG 19. The quoted limit applies to $m_{A^0} \simeq 11$ eV. See their Fig. 5 for mass-dependent limits.

[73] LEES 22 look for a hidden fermion-fermion bound state decaying into three hidden photons, which subsequently decay into e^+e^-, $\mu^+\mu^-$, or $\pi^+\pi^-$. For the bound-state mass in the range of 0.05–9.5 GeV, limits at the level of 5×10^{-5}–1×10^{-3} are obtained. See their Fig. 6 for mass-dependent limits.

[74] LU 22 derive the limit by studying the effect of photons oscillating into hidden photons on the surface luminosity of the neutron star RX J1856.6-3754.

[75] MANENTI 22 look for hidden photon dark matter by using a multilayer dielectric haloscope. Limits between 6.86×10^{-11} and 5×10^{-8} are obtained for $m_{\gamma'} \simeq 1.1$–3.1 eV. See their Fig. 11 for mass-dependent limits.

[76] THOMAS 22 improved KRIBS 21 by taking account of the changes in the parton distribution functions due to the inclusion of hidden photons. The quoted limit is at $m_{\gamma'} \simeq 4$ GeV. Limits in the range of 3×10^{-2}–9×10^{-2} are obtained for $m_{\gamma'} = 1$–80 GeV. See their Fig. 1 for the limits.

[77] TUMASYAN 22AH look for exotic decays of the SM-like Higgs boson, $H \rightarrow Z\gamma' \rightarrow 4\ell$, and set limits on the Higgs portal coupling. See their Fig. 6 for the limits.

[78] TUMASYAN 22N look for exotic decays of the SM-like Higgs boson, $H \rightarrow \gamma'\gamma'$ ($\gamma' \rightarrow \mu^+\mu^-$), and set limits on the branching fraction product. See their Fig. 7 for mass- and lifetime-dependent limits.

[79] WU 22A look for direction-dependent oscillations in the gravitational potential generated by ultralight hidden photon dark matter, and set a bound on its local density as $\rho_{\gamma'} \lesssim 5$ GeV/cm^3 for $m_{\gamma'} \lesssim 10^{-23}$ eV at 95% CL.

[80] ANDREEV 21 is analogous to BANERJEE 18A. The quoted limit applies to $m_{\gamma'} = 1$ MeV. See their Fig. 3 for mass-dependent limits.

[81] ANDREEV 21A extends the limits of BANERJEE 19 by taking account of production through the resonant annihilation of secondary positrons with atomic electrons. The quoted limit is at $m_{\gamma'} = 0.23$ GeV, assuming the fermion dark matter of mass $m_{\gamma'}/3$ and the hidden gauge coupling $\alpha_D = 0.1$. See their Fig.3 for mass-dependent limits.

[82] BI 21 look for the gamma-ray spectral attenuation due to scattering with hidden photons constituting all dark matter, using the measurements of sub-PeV gamma-rays from the Crab Nebula by the Tibet ASγ and HAWC experiments, together with MAGIC and HEGRA gamma-ray data. See their Fig. 4 for mass-dependent limits.

[83] CAZZANIGA 21 look for semi-visible decays of hidden photons, $\gamma' \rightarrow \chi_1\chi_2$ ($\chi_2 \rightarrow \chi_1 e^+e^-$), where χ_1 and χ_2 are hidden fermions. They exclude $3\times10^{-5} \lesssim \chi \lesssim 2\times10^{-2}$ assuming the hidden gauge coupling $\alpha_D = 0.1$, and the fermion masses $m_{\chi_1} = m_{\gamma'}/3$, $(m_{\chi_2} - m_{\chi_1})/m_{\chi_1} = 0.4$. See their Fig. 4 for mass-dependent limits.

[84] DIXIT 21 look for hidden photon dark matter by using a superconducting transmon qubit dispersively coupled to a high Q storage cavity. The local density $\rho_{\gamma'} = 0.4$ GeV/cm^3 is assumed. See their Fig.4 for mass-dependent limits.

[85] GHOSH 21 use existing haloscope axion search limits to set limits on hidden photon dark matter, considering the polarization of hidden photons. The quoted limit is at $m_{\gamma'} \simeq 3$ μeV. See their Fig. 1 for mass-dependent limits.

[86] GODFREY 21 look for hidden photon dark matter by using a wideband antenna, and set 5σ limits on χ. The local density $\rho_{\gamma'} = 0.38$ GeV/cm^3 is assumed. See their updated Fig. 12 in arXiv:2101.02805v4 for mass-dependent limits in the range of $m_{\gamma'} = 0.207$–1.24 μeV.

[87] KOPYLOV 21A is an update of KOPYLOV 19, but use Ne gas instead of Ar. The quoted limit applies to $m_{\gamma'} = 12$ eV. See their Fig. 4 for mass-dependent limits.

[88] KRIBS 21 used the HERA data on neutral current deep inelastic ep scattering to derive the limits, which become weaker for heavier masses. See their Fig. 3 for mass-dependent limits.

[89] SCHMIDT 21 use the microscopic Parton-Hadron-String Dynamics approach to extract limits by comparing the theoretically calculated dilepton spectra with the HADES data on the search for $\gamma' \rightarrow e^+e^-$. See their Fig. 5 for the mass-dependent limits for various allowed surplus of the hidden photon contribution over the standard model yield.

[90] TSAI 21 update the limits from the CHARM and NuCal experiments, taking account of additional production channels from proton bremsstrahlung and η meson decays, respectively. Limits between 3×10^{-8} and 1×10^{-4} are obtained for $0.01 < m_{\gamma'} < 0.8$ GeV (see their Fig. 1).

[91] AAIJ 20C look for hidden photons produced from the pp collision in the decay channel $\gamma' \rightarrow \mu^+\mu^-$. For prompt decaying hidden photons, limits at the level of 10^{-4}–10^{-3} are obtained for $m_{\gamma'} = 0.214$–30 GeV. See their Fig. 2 for mass-dependent limits.

[92] AAIJ 20C look for hidden photons produced from the pp collision in the decay channel $\gamma' \rightarrow \mu^+\mu^-$. For hidden photons with lifetimes of order ps, limits at the level of 10^{-5} are obtained for $m_{\gamma'} = 218$–315 MeV. See their Fig. 4 for mass-dependent limits.

[93] ABLIKIM 20AB search for $J/\psi \rightarrow \eta'\gamma'$ ($\gamma' \rightarrow \gamma\pi^0$), and set the upper limit on the product branching fraction of order 10^{-7}. See their Fig. 7 for mass-dependent limits.

Int. J. Mod. Phys. A 2026.41. Downloaded from www.worldscientific.com
by UNIVERSITY OF CALIFORNIA @ BERKELEY on 09/16/26. Reproduction is strictly not permitted, except for Open Access articles.

[94] AGOSTINI 20 is analogous to ABE 14F. The quoted limit applies to $m_{\gamma'} = 150$ keV. The local density $\rho_{\gamma'} = 0.3$ GeV/cm^3 is assumed. Their limits in their Fig. 3 were later found to be incorrect due to an error of their Eqs. (1) and (2). See Fig. 3 in AGOSTINI 22A for the corrected limits.

[95] AMARAL 20 use a second-generation SuperCDMS high-voltage eV-resolution detector to set limits on dark-matter hidden photon absorption. The quoted limit is for $m_{\gamma'} \simeq 17$ eV. The local density $\rho_{\gamma'} = 0.3$ GeV/cm^3 is assumed. See their Fig. 3 for mass-dependent limits.

[96] AN 20 updates the direct detection limit of AN 13C on solar flux of hidden photons; $\chi < 1.6 \times 10^{-12}$ (eV/$m_{\gamma'}$) for $m_{\gamma'} < 6$ eV (90% C.L.). For $m_{\gamma'} > 6$ eV, see their Fig. 1 for mass-dependent limits.

[97] ANDRIANAVALOMAHEFA 20 is analogous to SUZUKI 15, but uses a mirror that is about one order of magnitude larger than in similar studies in the past. Limits at the level of 10^{-12} are obtained for $m_{\gamma'} = 2.5$–7 eV. See their Fig.23 and Table III for mass-dependent limits.

[98] APRILE 20 is analogous to ABE 14F, and set limits $\chi \lesssim 10^{-16}$–10^{-12}. The quoted limit applies to $m_{\gamma'} = 1$ keV. They also found an excess over known backgrounds, which favors the mass $m_{\gamma'} = 2.3 \pm 0.2$ keV with a 3 σ significance. See their Fig. 10 for mass-dependent limits.

[99] ARALIS 20 is analogous to ABE 14F. The quoted limit applies to $m_{\gamma'} = 0.1$ keV. The local density $\rho_{\gamma'} = 0.3$ GeV/cm^3 is assumed. The limits at masses above 3 keV in their Fig. 10 was later found to be incorrect due to an error in their analysis. See Fig. 3 in erratum for the corrected limits.

[100] ARGUELLES 20 examine hidden-photon production in atmospheric cosmic-ray showers and its decay in IceCube and Super-Kamiokande. The quoted limit assumes a lifetime of $c\tau = 0.1$ km. See their Fig. 16 for mass- and lifetime-dependent limits.

[101] ARNAUD 20 look for the absorption signal of hidden photon dark matter in a Ge detector. The quoted limit applies to $m_{\gamma'} \simeq 9$ eV. The local density $\rho_{\gamma'} = 0.3$ GeV/cm^3 is assumed. See their Fig. 3 for mass-dependent limits.

[102] BANERJEE 20 is an update of BANERJEE 18. They exclude $8.2 \times 10^{-5} \lesssim \chi \lesssim 1 \times 10^{-2}$ for $m_{\gamma'} = 1.5$–24 MeV. In particular, they exclude $\chi = 1.2 \times 10^{-4}$–$6.8 \times 10^{-4}$ for the 16.7 MeV gauge boson. See their Fig. 5 for mass-dependent limits.

[103] BARAK 20 is analogous to AGUILAR-AREVALO 19A, and look for hidden photon dark matter by using the Skipper CCD. The quoted limit applies to $m_{\gamma'} = 12.8$ eV. See their Fig. 4 for mass-dependent limits.

[104] KRASNIKOV 20 showed that the limit of BANERJEE 20 combined with the measured anomalous magnetic moment of the electron exclude the 16.7 MeV gauge boson suggested by the ATOMKI (KRASZNAHORKAY 16) experiment if it has pure vector or axial-vector interactions.

[105] SHE 20 look for solar hidden photons. The quoted limit applies to $m_{\gamma'} = 180$ eV. See their Fig. 4 for mass-dependent limits.

[106] SHE 20 look for hidden photon dark matter and set limits $\chi < 1.3 \times 10^{-15}$–$2.8 \times 10^{-14}$ for the quoted mass range. The local density $\rho_{\gamma'} = 0.3$ GeV/cm^3 is assumed. See their Fig. 6 for mass-dependent limits.

[107] SIRUNYAN 20AQ look for a narrow resonance decaying into a pair of muons. For $m_{\gamma'} < 45$ GeV, they use dedicated high-rate dimuon triggers to reduce the muon transverse momentum thresholds. The quoted limit applies to $m_{\gamma'} = 50$ GeV, and limits of order 10^{-3} are obtained for the quoted mass range. See their Fig. 3 for mass-dependent limits.

[108] TOMITA 20 look for hidden photon dark matter using a planar metal plate and cryogenic receiver and set limits $\chi < 1.8$–4.3×10^{-10} for the quoted mass range. The local density $\rho_{\gamma'} = 0.39$ GeV/cm^3 is assumed. See their Fig. 7 for mass-dependent limits.

[109] WANG 20A is analogous to ABE 14F. The quoted limit applies to $m_{\gamma'} = 185$ eV. The local density $\rho_{\gamma'} = 0.3$ GeV/cm^3 is assumed. See their Fig. 11 for mass-dependent limits.

[110] AABOUD 19G look for $h \to \gamma'\gamma'$ ($\gamma' \to \mu^+\mu^-$) and exclude a kinetic mixing around 10^{-9}–10^{-8} for B($h \to \gamma'\gamma'$) = 0.01 and 0.1. See their Fig. 9 for mass-dependent limits.

[111] ABLIKIM 19A look for $J/\psi \to \gamma'\eta$ ($\gamma' \to e^+e^-$). Limits between 6×10^{-3} and 5×10^{-2} are obtained (see their Fig. 8).

[112] ABLIKIM 19H look for $J/\psi \to \gamma'\eta'$ ($\gamma' \to e^+e^-$). Limits between 3.4×10^{-3} and 2.6×10^{-2} are obtained. See their Fig. 5 for mass-dependent limits.

[113] AGUILAR-AREVALO 19A look for the absorption signal of hidden photon dark matter by using a CCD. The quoted limit applies to $m_{\gamma'} = 17$ eV. The local density $\rho_{\gamma'} = 0.3$ GeV/cm^3 is assumed. See their Fig. 4 for mass-dependent limits.

[114] APRILE 19D is analogous to ABE 14F. The quoted limit applies to $m_{\gamma'} = 0.7$ keV. See their Fig. 5(f) for mass-dependent limits.

[115] BANERJEE 19 is an update of BANERJEE 18A. The quoted limit is at $m_{\gamma'} = 1$ MeV. See their Fig. 3 for mass-dependent limits.

[116] BHOONAH 19 examine heating of Galactic Center gas clouds by hidden photon dark matter. The quoted limit applies to $m_{\gamma'} \simeq 10^{-12}$ eV. See their Fig. 2 for mass-dependent limits.

[117] BRUN 19 is analogous to SUZUKI 15. The limit is derived under an assumption that hidden photons constitute the local dark matter density $\rho_{\gamma'} = 0.3$ GeV/cm^3.

[118] CORTINA-GIL 19 look for an invisible hidden photon in the reaction $K^+ \to \pi^+\pi^0$ ($\pi^0 \to \gamma\gamma'$). The quoted limit applies to $m_{\gamma'} = 62.5$–65 MeV. See their Figs. 6 and 7 for mass-dependent limits.

[119] DANILOV 19 examined the hidden photon production in nuclear reactors, correctly taking account of the effective photon mass in the reactor and detector. The limit gets weaker for $m_{\gamma'}$ less than the effective photon mass in proportion to $1/m_{\gamma'}^2$. See their Fig. 1 for mass-dependent limits.

[120] HOCHBERG 19 look for the absorption signal of hidden photon dark matter by using superconducting-nanowire single-photon detectors. The quoted limit applies to $m_{\gamma'} \simeq 1$ eV. The local density $\rho_{\gamma'} = 0.3$ GeV/cm^3 is assumed. See their Fig. 4 for mass-dependent limits.

[121] KOPYLOV 19 look for hidden-photon dark matter using a counter with an aluminum cathode and derive limits assuming it constitute all the local dark matter. The quoted limit applies to $m_{\gamma'} = 12$ eV. See their Fig. 7 for mass-dependent limits.

[122] KOVETZ 19 examine heating of the early Universe plasma by hidden photon dark matter, and derive the limits by requiring that the cosmic mean 21 cm brightness temperature relative to the CMB temperature satisfy $T_{21} > -100$ mK. The quoted limit applies to $m_{\gamma'} \simeq 2 \times 10^{-14}$ eV. See their Fig. 3 for mass-dependent limits.

[123] NGUYEN 19 look for hidden photon dark matter with a resonant cavity, and set limits $\sim 10^{-12}$ for $m_{\gamma'} = 0.2$–2.07μeV. The quoted limit applies to $m_{\gamma'} = 1.3$ μeV. The local density $\rho_{\gamma'} = 0.3$ GeV/cm^3 is assumed. See their Fig. 19 for mass-dependent limits.

[124] ABE 18F is an update of ABE 14F. The quoted limit applies to $m_{\gamma'} \simeq 40$ keV. See their Fig. 5 for mass-dependent limits.

[125] ADRIAN 18 look for a hidden photon resonance in the reaction $e^-Z \to e^-Z\gamma'$ ($\gamma' \to e^+e^-$). The quoted limit applies to $m_{\gamma'} = 40$ MeV. See their Fig. 4 for mass-dependent limits.

[126] ANASTASI 18B look for a hidden photon resonance in the reaction $e^+e^- \to \gamma'\gamma$ ($\gamma' \to \mu^+\mu^-$). The quoted limit is obtained by combining the result of ANASTASI 16 and it applies to $m_{\gamma'} \simeq 519$–987 MeV. See their Fig. 9 for mass-dependent limits.

[127] ARMENGAUD 18 is analogous to ABE 14F. The quoted limits applies to $m_{\gamma'} = 1.6$ keV. See the right panel of Fig. 5 for mass-dependent limits.

[128] BANERJEE 18 look for hidden photons produced in the reaction $e^-Z \to e^-Z\gamma'$ ($\gamma' \to e^+e^-$), and exclude $9.2 \times 10^{-5} \lesssim \chi \lesssim 1 \times 10^{-2}$ for $m_{\gamma'} = 1$–23 MeV. They also set a limit on the electron coupling to a 16.7 MeV gauge boson suggested by the ATOMKI (KRASZNAHORKAY 16) experiment. See their Fig. 3 for mass-dependent limits.

[129] BANERJEE 18A look for invisible decays of hidden photons produced in the reaction $e^-Z \to e^-Z\gamma'$. The quoted limit is at $m_{\gamma'} = 1$ MeV. See their Fig. 15 for mass-dependent limits.

[130] KNIRCK 18 is analogous to SUZUKI 15. See their Fig. 5 for mass-dependent limits.

[131] ABGRALL 17 is analogous to ABE 14F using the MAJORANA DEMONSTRATOR. See their Fig. 3 for limits between 6 keV $< m_{\gamma'} <$ 97 keV.

[132] ABLIKIM 17AA look for $e^+e^- \to \gamma\gamma'$ ($\gamma' \to e^+e^-$ or $\mu^+\mu^-$). Limits between 10^{-3} and 10^{-4} are obtained (see their Fig. 3).

[133] ANGLOHER 17 is analogous to ABE 14F. The quoted limit is at $m_{\gamma'} = 0.7$ keV. See their Fig. 8 for mass-dependent limits.

[134] BANERJEE 17 look for invisible decays of hidden photons produced in the reaction $e^-Z \to e^-Z\gamma'$. The quoted limit applies to $m_{\gamma'} = 2$ MeV. See their Fig. 3 for mass-dependent limits.

[135] CHANG 17 examine the hidden photon emission from SN1987A, including the effects of finite temperature and density on χ and obtain limits χ ($m_{\gamma'}$/MeV) $\lesssim 3 \times 10^{-9}$ for $m_{\gamma'} < 15$ MeV and $\chi \lesssim 10^{-9}$ for $m_{\gamma'} = 15$–120 MeV.

[136] DUBININA 17 look for $\mu^+ \to e^+\overline{\nu}_\mu\nu_e\gamma'$ ($\gamma' \to e^+e^-$) in a nuclear photoemulsion. The quoted limit applies to $m_{\gamma'} = 1.1$ MeV. Limits between 4.5×10^{-3} and 10^{-2} are obtained (see their Fig. 3).

[137] LEES 17E look for invisible decays of hidden photons produced in the reaction $e^+e^- \to \gamma\gamma'$. See their Fig. 5 for limits in the mass range $m_{\gamma'} \leq 8$ GeV.

[138] AAD 16AG look for hidden photons promptly decaying into collimated electrons and/or muons, assuming that they are produced in the cascade decays of squarks or the Higgs boson. See their Fig. 10 and Fig.13 for their limits on the cross section times branching fractions.

[139] ANASTASI 16 look for the decay $\gamma' \to \pi^+\pi^-$ in the reaction $e^+e^- \to \gamma\gamma'$. Limits between 4.3×10^{-3} and 4.4×10^{-4} are obtained for 527 $< m_{\gamma'} <$ 987 MeV (see their Fig. 9).

[140] KHACHATRYAN 16 look for $\gamma' \to \mu^+\mu^-$ in a dark SUSY scenario where the SM-like Higgs boson decays into a pair of the visible lightest neutralinos with mass 10 GeV, both of which decay into γ' and a hidden neutralino with mass 1 GeV. See the right panel in their Fig. 2.

[141] AAD 15CD look for $H \to Z\gamma' \to 4\ell$ with the ATLAS detector at LHC and find $\chi < 4$–17×10^{-2} for $m_{\gamma'} = 15$–55 GeV. See their Fig. 6.

[142] ADARE 15 look for a hidden photon in $\pi^0, \eta^0 \to \gamma e^+e^-$ at the PHENIX experiment. See their Fig. 4 for mass-dependent limits.

[143] AN 15A derived limits from the absence of ionization signals in the XENON10 and XENON100 experiments, assuming hidden photons constitute all the local dark matter. Their best limit is $\chi < 1.3 \times 10^{-15}$ at $m_{\gamma'} = 18$ eV. See their Fig. 1 for mass-dependent limits.

[144] ANASTASI 15 look for a production of a hidden photon and a hidden Higgs boson with the KLOE detector at DAΦNE, where the hidden photon decays into a pair of muons and the hidden Higgs boson lighter than $m_{\gamma'}$ escape detection. See their Figs. 6 and 7 for mass-dependent limits on a product of the hidden fine structure constant and the kinetic mixing.

[145] ANASTASI 15A look for the decay $\gamma' \to e^+e^-$ in the reaction $e^+e^- \to e^+e^-\gamma$. Limits between 1.7×10^{-3} and 1×10^{-2} are obtained for $m_{\gamma'} = 5$–320 MeV (see their Fig. 7).

[146] BATLEY 15A look for $\pi^0 \to \gamma\gamma'$ ($\gamma' \to e^+e^-$) at the NA48/2 experiment. Limits between 4.2×10^{-4} and 8.8×10^{-3} are obtained for $m_{\gamma'} = 9$–120 MeV (see their Fig. 4).

[147] JAEGLE 15 look for the decay $\gamma' \to e^+e^-, \mu^+\mu^-$, or $\pi^+\pi^-$ in the dark Higgstrahlung channel, $e^+e^- \to \gamma' H'$ ($H' \to \gamma'\gamma'$) at the BELLE experiment. They set limits on a product of the branching fraction and the Born cross section as well as a product of the hidden fine structure constant and the kinetic mixing. See their Figs. 3 and 4.

[148] KAZANAS 15 set limits by studying the decay of hidden photons $\gamma' \to e^+e^-$ inside and near the progenitor star of SN1987A. See their Fig. 6 for mass-dependent limits.

Int. J. Mod. Phys. A 2026.41. Downloaded from www.worldscientific.com
by UNIVERSITY OF CALIFORNIA @ BERKELEY on 09/16/26. Re-use and distribution is strictly not permitted, except for Open Access articles.

[149] SUZUKI 15 looked for hidden-photon dark matter with a dish antenna and derived limits assuming they constitute all the local dark matter. Their limits are $\chi < 6 \times 10^{-12}$ for $m_{\gamma'} = 1.9$–4.3 eV. See their Fig. 7 for mass-dependent limits.

[150] VINYOLES 15 performed a global fit analysis based on helioseismology and solar neutrino observations, and set the limits $\chi m_{\gamma'} < 1.8 \times 10^{-12}$ eV for $m_{\gamma'} = 3 \times 10^{-5}$–8 eV. See their Fig. 11.

[151] ABE 14F look for the photoelectric-like interaction in the XMASS detector assuming the hidden photon constitutes all the local dark matter. Limits between 2×10^{-13} and 1×10^{-12} are obtained, where the relation $\chi^2 = \alpha'/\alpha$ is used to translate the original bound on the ratio of the hidden and EM fine-structure constants. See their Fig. 3 for mass-dependent limits.

[152] AGAKISHIEV 14 look for hidden photons $\gamma' \to e^+e^-$ at the HADES experiment, and set limits on χ for $m_{\gamma'} = 0.02$–0.6 GeV. See their Fig. 5 for mass-dependent limits.

[153] BABUSCI 14 look for the decay $\gamma' \to \mu^+\mu^-$ in the reaction $e^+e^- \to \mu^+\mu^-\gamma$. Limits between 4×10^{-3} and 9.0×10^{-4} are obtained for 520 MeV $< m_{\gamma'} <$ 980 MeV (see their Fig. 7).

[154] BATELL 14 derived limits from the electron beam dump experiment at SLAC (E-137) by searching for events with recoil electrons by sub-GeV dark matter produced from the decay of the hidden photon. Limits at the level of 10^{-4}–10^{-1} are obtained for $m_{\gamma'} = 10^{-3}$–1 GeV, depending on the dark matter mass and the hidden gauge coupling (see their Fig. 2).

[155] BLUEMLEIN 14 analyzed the beam dump data taken at the U-70 accelerator to look for γ'-bremsstrahlung and the subsequent decay into muon pairs and hadrons. See their Fig. 4 for mass-dependent excluded region.

[156] FRADETTE 14 studied effects of decay of relic hidden photons on BBN and CMB to set constraints on very small values of the kinetic mixing. See their Figs. 4 and 7 for mass-dependent excluded regions.

[157] LEES 14J look for hidden photons in the reaction $e^+e^- \to \gamma\gamma'$ ($\gamma' \to e^+e^-, \mu^+\mu^-$). Limits at the level of 10^{-4}–10^{-3} are obtained for 0.02 GeV $< m_{\gamma'} <$ 10.2 GeV. See their Fig. 4 for mass-dependent limits.

[158] MERKEL 14 look for $\gamma' \to e^+e^-$ at the A1 experiment at the Mainz Microtron (MAMI). See their Fig. 3 for mass-dependent limits.

[159] AN 13B examined the stellar production of hidden photons, correcting an important error of the production rate of the longitudinal mode which now dominates. See their Fig. 2 for mass-dependent limits based on solar energy loss.

[160] AN 13C use the solar flux of hidden photons to set a limit on the atomic ionization rate in the XENON10 experiment. They find $\chi\, m_{\gamma'} < 3 \times 10^{-12}$ eV for $m_{\gamma'} < 1$ eV. See their Fig. 2 for mass-dependent limits.

[161] DIAMOND 13 analyzed the beam dump data taken at the SLAC millicharge experiment to constrain a hidden photon invisibly decaying into lighter long-lived particles, which undergo elastic scattering off nuclei in the detector. Limits between 8×10^{-4}–2×10^{-2} are obtained. The quoted limit is applied when the dark gauge coupling is set equal to the electromagnetic coupling. See their Fig.4 for mass-dependent limits.

[162] GNINENKO 13 used the data taken at the SINDRUM experiment to constrain the decay, $\pi^0 \to \gamma\gamma'$ ($\gamma' \to e^+e^-$) to derive limits. See their Fig. 2 for their mass-dependent excluded region.

[163] HORVAT 13 look for hidden-photo-electric effect in HPGe detectors induced by solar hidden photons. See their Fig. 3 for mass-dependent limits.

[164] INADA 13 search for hidden photons using an intense X-ray beamline at SPring-8. See their Fig. 4 for mass-dependent limits.

[165] MIZUMOTO 13 look for solar hidden photons. See their Fig. 5 for mass-dependent limits.

[166] PARKER 13 look for hidden photons using a cryogenic resonant microwave cavity. See their Fig.5 for mass-dependent limits.

[167] PARKER 13 derived a limit for the hidden photon CDM with a randomly oriented hidden photon field.

[168] REDONDO 13 examined the solar emission of hidden photons including the enhancement factor for the longitudinal mode pointed out by AN 13B, and also updated stellar-energy loss arguments. See their Fig.3 for mass-dependent limits, including a review of the currently best limits from other arguments.

[169] GNINENKO 12A obtained bounds on $B(\pi^0 \to \gamma\gamma') \cdot B(\gamma' \to e^+e^-)$ from the NOMAD and PS191 neutrino experiments, and derived limits between 8×10^{-8}–2×10^{-4}. See their Fig.4 for mass-dependent excluded regions.

[170] GNINENKO 12B used the data taken at the CHARM experiment to constrain the decay, $\eta(\eta') \to \gamma\gamma'$ ($\gamma' \to e^+e^-$), and derived limits between 1×10^{-7}–1×10^{-4}. See their Fig.4 for mass-dependent excluded region.

[171] ABRAHAMYAN 11 look for $\gamma' \to e^+e^-$ in the electron-nucelon fixed-target experiment at the Jefferson Laboratory (APEX). See their Fig. 5 for mass-dependent limits.

[172] BLUEMLEIN 11 analyzed the beam dump data taken at the U-70 accelerator to look for $\pi^0 \to \gamma\gamma'$ ($\gamma' \to e^+e^-$). See their Fig. 5 for mass-dependent limits.

[173] BJORKEN 09 analyzed the beam dump data taken at E137, E141, and E774 to constrain a hidden photon produced by bremsstrahlung, subsequently decaying into e^+e^-, and derived limits between 10^{-7} and 10^{-2}. See their Fig. 1 for mass-dependent excluded region.

[174] BJORKEN 09 required the energy loss in the γ' emission from the core of SN1987A not to exceed 10^{53} erg/s, and derived limits between 5×10^{-9} and 2×10^{-6}. See their Fig. 1 for mass-dependent excluded region.

REFERENCES FOR Searches for Axions (A^0) and Other Very Light Bosons

AAD	25AN	EPJ C85 886	G. Aad *et al.*	(ATLAS Collab.)
AAD	25AT	PL B868 139671	G. Aad *et al.*	(ATLAS Collab.)
AAD	25AY	PR D112 092001	G. Aad *et al.*	(ATLAS Collab.)
AAD	25BF	JHEP 2511 061 (errat.)	G. Aad *et al.*	(ATLAS Collab.)
ABLIKIM	25AV	PR D111 072008	M. Ablikim *et al.*	(BESIII Collab.)
ABLIKIM	25CL	PR D112 052007	M. Ablikim *et al.*	(BESIII Collab.)
ABRAHAM	25	JHEP 2501 199	R. Abraham *et al.*	(FASER Collab.)
ADACHI	25AA	JHEP 2512 109	I. Adachi *et al.*	(BELLE II Collab.)
ADAMS	25C	PR D112 103044	C.B. Adams *et al.*	(VERITAS Collab.)
AHYOUNE	25	JHEP 2504 113	S. Ahyoune *et al.*	(RADES Collab.)
ALBAKRY	25	PR D111 012006	M.F. Albakry *et al.*	(SuperCDMS Collab.)
ALONSO-GON...	25	PR D111 083019	D. Alonso-Gonzalez *et al.*	(IFT, MADU)
Also		PR D112 029901 (errat.)	D. Alonso-Gonzalez *et al.*	(IFT, MADU)
ALONSO-GON...	25A	PR D112 029901 (errat.)	D. Alonso-Gonzalez *et al.*	(IFT, MADU)
ALRAHMAN	25	PRL 134 151801	F.A. Alrahman *et al.*	(ICARUS Collab.)
ALTENMULL...	25	JHEP 2512 009	K. Altenmueller *et al.*	(CAST Collab.)
AN	25	PRL 134 171001	H. An *et al.*	
ANDREEV	25	JHEP 2506 256	Yu.M. Andreev *et al.*	(NA64 Collab.)
APRILE	25A	PRL 134 161004	E. Aprile *et al.*	(XENONnT Collab.)
ARIAS-ARAG...	25	PR D111 043021	F. Arias-Aragon *et al.*	
ASWATHI	25	PR D112 123048	P.S. Aswathi *et al.*	
BAE	25	PRL 135 091804	S. Bae *et al.*	(DMAG Collab.)
BAI	25	PRL 134 151006	X. Bai *et al.*	(HAYSTAC Collab.)
BASILICO	25	EPJ C85 1182	D. Basilico *et al.*	(Borexino Collab.)
BAUDIS	25	PRL 135 081002	L. Baudis *et al.*	(QROCODILE Collab.)
BLOCH	25	PRL 134 161002	I. Bloch *et al.*	(SENSEI Collab.)
BRAGGIO	25	PR X15 021031	C. Braggio *et al.*	(QUAX Collab.)
CANDON	25	PRL 134 171004	F. Candon *et al.*	(ZARA, DESY, SLAC, PADO+)
CAPUTO	25	PRL 134 151002	A. Caputo *et al.*	(CERN, ROMA, MPIG, IBSD)
CAROSI	25	PRL 135 191001	G. Carosi *et al.*	(ADMX Collab.)
CHEKHOVSKY	25	PR D112 012009	V. Chekhovsky *et al.*	(CMS Collab.)
CHEN	25	PRL 134 241001	Y-X. Chen *et al.*	
CHEN	25A	PR D111 083002	Y-C. Chen *et al.*	
CHEN	25B	PR D111 123019	Y. Chen *et al.*	
CHOI	25	PRL 134 021802	J. Choi *et al.*	(NEON Collab.)
CORTINA-GIL	25A	EPJ C85 571	E. Cortina Gil *et al.*	(NA62 Collab.)
CORTINA-GIL	25B	JHEP 2511 143	E. Cortina Gil *et al.*	(NA62 Collab.)
EGGE	25	PRL 134 151004	J. Egge *et al.*	(MADMAX Collab.)
FONG	25	PR D112 083052	C. Fong, K.C.Y. Ng, Q. Liu	(CUHK)
GENG	25	JP G52 115004	X.P. Geng, B. Zhong, Z.H. Zhang	
GOLDSTEIN	25	PRL 134 081001	S. Goldstein *et al.*	(COLU, CAVE, WATER)
GOODMAN	25	PRL 134 111002	C. Goodman *et al.*	(ADMX Collab.)
HAYRAPETY...	25Z	JHEP 2508 006	A. Hayrapetyan *et al.*	(CMS Collab.)
HOSHINO	25	PRL 134 171002	G. Hoshino *et al.*	(BREAD Collab.)
IVANEZ-BAL...	25	PR D112 L101301	P. Ivanez-Ballesteros, M.C. Volpe	(UPCIT, CNRS)
JANISH	25	PRL 134 071002	R. Janish, E. Pinetti	(FNAL, CHIC)
KAR	25	JCAP 2505 100	A. Kar, S. Roy, P. Sarkar	(SORB, IACS)
KIRITA	25	JHEP 2506 138	Y. Kirita *et al.*	(SAPPHIRES Collab.)
LI	25	PRL 134 071004	T. Li *et al.*	(PandaX Collab.)
LI	25D	CP C49 105107	J. Li *et al.*	
LINDEN	25	PR D112 023026	T. Linden, T.T.Q. Nguyen, T.M.P. Tait	(STOH+)
MELO-GALIN...	25	PR D112 103049	A. Melo Galindo, S. Hernandez-Cadena, R. Alfaro Molina	
MIRASOLA	25	PR D111 084032	L. Mirasola *et al.*	(CAGL, PERIM, ROCK+)
MIRZAKHANI	25	PR D112 032013	M. Mirzakhani *et al.*	(MINER Collab.)
MONTEFAL...	25	PR D112 023506	G. Montefalcone *et al.*	(TEXA, INFNP)
NING	25	PRL 134 171003	O. Ning, B. Safdi	(UCB, LBL)
PARK	25	PRL 134 201002	B.J. Park *et al.*	(NEON Collab.)
PORAYKO	25	PR D111 062005	N.K. Porayko *et al.*	(EPTA Collab.)
ROMERO-JOR...	25	PR C112 054905	A.W. Romero Jorge *et al.*	(FRAN, GSI)
RUZ	25	PRL 135 141001	J. Ruz *et al.*	(ZARA, LLNL, DORT, TURIN+)
SANTOS-GAR...	25	PRL 135 041001	B.A. Dos Santos Garcia *et al.*	(MADMAX Collab.)
SARDO-INF...	25	PRL 135 211002	G. Sardo Infirri *et al.*	(QUAX Collab.)
TODARELLO	25	JCAP 2505 070	E. Todarello, M. Regis	(NOTT, TURIN, INFN)
TROITSKY	25	JETPL 121 159	S. Troitsky	(INRM, MOSU)
TROST	25	PR D111 083034	A. Trost *et al.*	(TRST, TRSTI, CERN, BOST+)
UNO	25	JHEP 2508 155	K. Uno *et al.*	(BELLE Collab.)
WALTER	25	PR D112 052008	J. Walter *et al.*	(CASPEr-gradient Collab.)
YIN	25	PRL 134 051004	W. Yin *et al.*	(WINERED Collab.)
ZENG	25	PRL 134 041001	X. Zeng *et al.*	(PandaX-4T Collab.)
ZHANG	25A	PRL 135 131001	K.Y. Zhang, L.Y. Wu, H. Yan	
ZHAO	25	PRL 135 201002	F. Zhao *et al.*	(SQUAD Collab.)
ZHAO	25A	PR D112 112016	P. Zhao *et al.*	(TUM)
ZIMMER...	25	PRL 134 151001	T. Zimmerman *et al.*	(OSLO, AMST, LOKC+)
AAD	24AS	EPJ C84 719	G. Aad *et al.*	(ATLAS Collab.)
AAD	24AT	EPJ C84 742	G. Aad *et al.*	(ATLAS Collab.)
AAD	24BN	PRL 133 161803	G. Aad *et al.*	(ATLAS Collab.)
AAD	24BZ	JHEP 2411 036	G. Aad *et al.*	(ATLAS Collab.)
Also		JHEP 2511 061 (errat.)	G. Aad *et al.*	(ATLAS Collab.)
AAD	24CD	JHEP 2411 126	G. Aad *et al.*	(ATLAS Collab.)
AAD	24K	PL B850 138536	G. Aad *et al.*	(ATLAS Collab.)
ABLIKIM	24AD	PR D110 L031101	M. Ablikim *et al.*	(BESIII Collab.)
ABLIKIM	24AK	JHEP 2407 135	M. Ablikim *et al.*	(BESIII Collab.)
ABLIKIM	24G	PR D109 L031102	M. Ablikim *et al.*	(BESIII Collab.)
ABLIKIM	24M	PR D109 072001	M. Ablikim *et al.*	(BESIII Collab.)
ABRATENKO	24A	PRL 132 241801	P. Abratenko *et al.*	(MicroBooNE Collab.)
ABREU	24	PL B848 138378	H. Abreu *et al.*	(FASER Collab.)
ADACHI	24C	PR D109 012008	S. Adachi *et al.*	(DOSUE-RR Collab.)
AGOSTINI	24A	EPJ C84 940	M. Agostini *et al.*	(GERDA Collab.)
AGRAWAL	24	PRL 132 140801	A. Agrawal *et al.*	(CHIC, RUTG, LBNL+)
AHN	24	PR X14 031023	S. Ahn *et al.*	(CAPP Collab.)
ALTENMULL...	24	PRL 133 221005	K. Altenmueller *et al.*	(CAST Collab.)
ANDREEV	24A	PR D109 L031103	Yu.M. Andreev *et al.*	(NA64 Collab.)
ANDREEV	24E	PR D110 112015	Yu.M. Andreev *et al.*	(NA64 Collab.)
APRILE	24B	PR D110 109903 (errat.)	E. Aprile *et al.*	(XENON1T Collab.)
ARAMBURO...	24	JCAP 2411 049	A. Aramburo-Garcia *et al.*	(LEID, NORD+)
ARNQUIST	24	PRL 132 041001	I.J. Arnquist *et al.*	(MAJORANA Collab.)
AUGIER	24	EPJ C84 925	C. Augier *et al.*	(CUPID-Mo Collab.)
BAE	24	PRL 133 211803	S. Bae *et al.*	(CAPP Collab.)
BIANCHINI	24	PR D110 123527	F. Bianchini, G. Grilli di Cortona, M. Valli	
CERVANTES	24	PR D110 043022	R. Cervantes *et al.*	(FNAL, NIST, PADO+)
CORTINA-GIL	24	PL B850 138513	E. Cortina Gil *et al.*	(NA62 Collab.)
CORTINA-GIL	24A	PRL 133 111802	E. Cortina-Gil *et al.*	(NA62 Collab.)
DAVYDOV	24	PR D110 103022	D. Davydov, A. Libanov	(ASCI, INRM)
DEV	24	PRL 132 101003	P.S.B. Dev *et al.*	(WUSL, LAVL, WASH+)
DIAMOND	24	PRL 132 101004	M. Diamond *et al.*	
DOLAN	24	JCAP 2405 099	M.J. Dolan, F.J. Hiskens, R.R. Volkas	(MELB)
FORDHAM	24	PR D109 123007	D. Fordham, I. Lopes	
GAO	24	PR D109 063003	L.-Q. Gao *et al.*	
GAO	24A	JCAP 2401 026	L.-Q. Gao *et al.*	
GUO	24	PL B852 138631	W.-Q. Guo, Z.-Q. Xia, X. Huang	
HAYRAPETY...	24AZ	JHEP 2412 172	A. Hayrapetyan *et al.*	(CMS Collab.)
HAYRAPETY...	24I	PL B852 138582	A. Hayrapetyan *et al.*	(CMS Collab.)
HE	24	PR D110 L021101	D. He *et al.*	(APEX Collab.)
HEINZE	24	PRL 132 191002	J. Heinze *et al.*	(LIDA Collab.)
KIM	24	PRL 133 051802	Y. Kim *et al.*	(CAPP Collab.)
KNIRCK	24	PRL 132 131004	S. Knirck *et al.*	(BREAD Collab.)
LELLA	24	PR D109 023001	A. Lella *et al.*	(BARI, STOH, INFNL, +)
LEVINE	24	PR D110 032010	J. Levine *et al.*	(Dark E-Field Radio Collab.)
LI	24A	PL B850 138531	H.-J. Li *et al.*	
LI	24B	CP C48 065107	J. Li *et al.*	
LI	24D	PL B858 139075	H.J. Li, W. Chao, Y.-F. Zhou	(BEIJ, HIAS)
LIU	24	EPJ C84 723	T.-C. Liu, M.-X. Lu, X.-S. Hu	(GXU)
MANZARI	24	PRL 133 211002	C.A. Manzari *et al.*	(UCB, LBL)
MCCARTHY	24	PRL 133 141003	F. McCarthy *et al.*	(CAMB, NYU, PERIM+)
PANDEY	24	PRL 133 111003	S. Pandey *et al.*	(MIT)
PANT	24	PR D109 023011	B.P. Pant	(IITJ)
PYBUS	24	PL B855 138790	J.R. Pybus *et al.*	(GLUEX Collab.)
QUISKAMP	24	PRL 132 031601	A. Quiskamp *et al.*	(ORGAN Collab.)
RAVENSBURG	24	PR D109 023018	E. Ravensberg *et al.*	(STOH, LAPTH, LAPP)
RETTAROLI	24	PR D110 022008	A. Rettaroli *et al.*	(QUAX Collab.)
SADOVSKY	24	EPJ C84 266	A.S. Sadovsky *et al.*	(OKA Collab.)
SU	24	PRL 133 191801	H. Su *et al.*	
TANG	24	PRL 133 021005	Z. Tang *et al.*	(SHANHE Collab.)

Int. J. Mod. Phys. A 2026.41. Downloaded from www.worldscientific.com
by UNIVERSITY OF CALIFORNIA @ BERKELEY on 09/16/26. Reproduction is strictly not permitted, except for Open Access articles.

TODARELLO	24	JCAP 2405 043	E. Todarello *et al.*	
TUMASYAN	24C	PR D110 012010	A. Tumasyan *et al.*	(CMS Collab.)
WANG	24A	PR D110 103007	H. Wang *et al.*	(HSCA, HARV, LBL, BOST+)
YAN	24A	JHEP 2406 028	S. Yan, L. Li, J.J. Fan	(BROW)
AAD	23BO	PRL 131 251801	G. Aad *et al.*	(ATLAS Collab.)
AAD	23I	JHEP 2306 153	G. Aad *et al.*	(ATLAS Collab.)
AAD	23T	JHEP 2307 133	G. Aad *et al.*	(ATLAS Collab.)
AALBERS	23A	PR D108 072006	J. Aalbers *et al.*	(LZ Collab.)
ABLIKIM	23AF	PL B839 137785	M. Ablikim *et al.*	(BESIII Collab.)
ABLIKIM	23E	PL B838 137698	M. Ablikim *et al.*	(BESIII Collab.)
ABUDINEN	23B	PRL 130 071804	F. Abudinen *et al.*	(BELLE II Collab.)
ACCIARRI	23	PRL 130 221802	R. Acciarri *et al.*	(ArgoNeuT Collab.)
ADACHI	23A	PRL 130 181803	I. Adachi *et al.*	(BELLE II Collab.)
ADACHI	23D	PR D108 043017	S. Adachi *et al.*	(POLARBEAR Collab.)
ADACHI	23K	PR D108 L111104	I. Adachi *et al.*	(BELLE II Collab.)
ADHIKARI	23	PR D107 122004	G. Adhikari *et al.*	(COSINE-100 Collab.)
ADHIKARI	23A	PR D108 L041301	G. Adhikari *et al.*	(COSINE-100 Collab.)
ADRIAN	23	PR D108 012015	P.H. Adrian *et al.*	(HPS Collab.)
AGNES	23A	PRL 130 101002	P. Agnes *et al.*	(DarkSide-50 Collab.)
AN	23A	PRL 130 181001	H. An *et al.*	
ANDREEV	23	PRL 131 161801	Yu.M. Andreev *et al.*	(NA64 Collab.)
APRILE	23B	PR D108 072015	E. Aprile *et al.*	(XENON Collab.)
AYRES	23	NJP 25 103012	N.J. Ayres *et al.*	
AZZOLINI	23	PR D107 032006	O. Azzolini *et al.*	(CUPID-0 Collab.)
BAJJALI	23	JCAP 2308 077	F. Bajjali *et al.*	(BRASS Collab.)
BATTYE	23	PR D108 063001	R. Battye *et al.*	
BEAUFORT	23	PR D108 L081302	C. Beaufort *et al.*	
BERNAL	23	PR D107 103046	J.L. Bernal *et al.*	(JHU, TELA, REHO+)
BERTUZZO	23	PRL 130 171801	E. Bertuzzo *et al.*	(USP)
CAPOZZI	23	JCAP 2306 060	F. Capozzi *et al.*	
CAPOZZI	23A	PR D108 075019	F. Capozzi *et al.*	
CHENG	23	PR D107 063021	L.-d. Cheng, H. Zhang, S.-s. Bao	(SHDNQ)
CORTINA-GIL	23B	PL B846 138193	E. Cortina-Gil *et al.*	(NA62 Collab.)
CORTINA-GIL	23C	JHEP 2309 035	E. Cortina Gil *et al.*	(NA62 Collab.)
DAVIES	23	PR D107 083027	J. Davies, M. Meyer, G. Cotter	(OXF, HAMB)
DELLA-MON...	23	PR D108 L101303	R. Della Monica, I. de Martino	
DERBIN	23	JETPL 118 160	A.V. Derbin *et al.*	(PNPI)
DIAMOND	23	PR D108 049902	M. Diamond *et al.*	
DI-VORA	23	PR D108 062005	R. Di Vora *et al.*	(QUAX Collab.)
FILZINGER	23	PRL 130 253001	M. Filzinger *et al.*	
FIORILLO	23	PRL 131 021001	D.F.G. Fiorillo, G.G. Raffelt, E. Vitagliano	(NBI+)
HAYRAPETY...	23G	JHEP 2312 070	A. Hayrapetyan *et al.*	(CMS Collab.)
HOOF	23	JCAP 2303 054	S. Hoof, L. Schulz	(KIT, GOET)
JACOBSEN	23	JCAP 2310 009	S. Jacobsen, T. Linden, K. Freese	(STOH, TEXA+)
JEWELL	23	PR D107 072007	M.J. Jewell *et al.*	(HAYSTAC Collab.)
KARANTH	23	PR X13 031004	S. Karanth *et al.*	(JEDI Collab.)
KIM	23	PRL 130 091602	J. Kim *et al.*	(KAIST, RIKEN, TOKY)
KOTAKA	23	PRL 130 071805	S. Kotaka *et al.*	(DOSUE-RR Collab.)
LEE	23	PR X13 011050	J. Lee *et al.*	(ASTAR, PRIN)
LI	23H	PR D107 063031	H.-J. Li, W. Chao	(BNORM)
LI	23I	JCAP 2309 009	S.-P. Li, X.-J. Xu	(BHEP)
NOORDHUIS	23	PRL 131 111004	D. Noordhuis *et al.*	(AMST, PRIN, STAN+)
NOTARI	23	PRL 131 011004	A. Notari, F. Rompineve, G. Villadoro	(ICCUB+)
OSHIMA	23	PR D108 072005	Y. Oshima *et al.*	(DANCE Collab.)
PANT	23	PR D108 023016	B.P. Pant *et al.*	(IITJ)
PODDAR	23	PR D108 103024	T.K. Poddar, D. Pachhar	
RAMANATH...	23	PRL 130 231001	K. Ramanathan *et al.*	(CIT, JPL)
ROGERS	23	JCAP 2306 023	K.K. Rogers *et al.*	
ROMANENKO	23	PRL 130 261801	A. Romanenko *et al.*	(FNAL)
SANDNER	23	EPJ C83 709	S. Sandner, M. Escudero, S.J. Witte	(VALE, CERN+)
SHERRILL	23	NJP 25 093012	N. Sherrill *et al.*	(SUSS, NPLT)
SMARRA	23	PRL 131 171001	C. Smarra *et al.*	(EPTA Collab.)
SULAI	23	PR D108 096026	I. Sulai *et al.*	(SNIPE Hunt Collab.)
THOMSON	23	PR D107 112003	C.A. Thomson *et al.*	(UPLOAD Collab.)
WADEKAR	23	PR D107 083011	D. Wadekar, Z. Wang	(IAS, NYU)
XIA	23	PR D107 L121302	Z.-Q. Xia *et al.*	
YANG	23	PRL 131 081801	B. Yang *et al.*	(CAPP Collab.)
YAO	23	PR D107 043031	R.-M. Yao *et al.*	
YI	23	PRL 130 071002	A.K. Yi *et al.*	(CAPP Collab.)
YI	23A	PR D108 L021304	A.K. Yi *et al.*	(CAPP Collab.)
ZHANG	23	PRL 130 201401	S.-B. Zhang *et al.*	(CST)
ZHANG	23A	PRL 130 251002	X. Zhang *et al.*	(MAINZ, REHO, UCB, +)
AAD	22J	JHEP 2203 041	G. Aad *et al.*	(ATLAS Collab.)
AAD	22S	EPJ C82 105	G. Aad *et al.*	(ATLAS Collab.)
ADE	22	PR D105 022006	P.A.R. Ade *et al.*	(BICEP/Keck Collab.)
ADHIKARI	22C	PR D105 052007	S. Adhikari *et al.*	(GLUEX Collab.)
AGOSTINI	22	JCAP 2212 012	M. Agostini *et al.*	(GERDA Collab.)
AGOSTINI	22A	PRL 129 089901	M. Agostini *et al.*	(GERDA Collab.)
ALESINI	22	PR D106 052007	D. Alesini *et al.*	(QUAX Collab.)
APRILE	22	PR D106 022001	E. Aprile *et al.*	(XENON1T Collab.)
Also		PR D110 109903 (errat.)	E. Aprile *et al.*	(XENON1T Collab.)
APRILE	22B	PRL 129 161805	E. Aprile *et al.*	(XENONnT Collab.)
ARNQUIST	22	PRL 129 081803	I.J. Arnquist *et al.*	(MAJORANA Collab.)
ARZA	22	PR D105 095007	A. Arza *et al.*	(ITEP, JHU, STAN, CSEB)
BATTAGLIERI	22	PR D106 072011	M. Battaglieri *et al.*	(BDX-MINI Collab.)
BATTYE	22	PR D105 L021305	R.A. Battye *et al.*	
BERNAL	22	PRL 129 231301	J.L. Bernal, G. Sato-Polito, M. Kamionkowski	(JHU)
BOLTON	22	PRL 129 211102	J.S. Bolton *et al.*	
BUSCHMANN	22	PRL 128 091102	M. Buschmann *et al.*	(PRIN, MICH, UCB+)
CALORE	22	PR D105 063028	F. Calore *et al.*	(LAPTH, STOH, BARI, WROC+)
CAPUTO	22	PRL 128 221103	A. Caputo *et al.*	
CASTILLO	22	JCAP 2206 014	A. Castillo *et al.*	
CERVANTES	22	PRL 129 201301	R. Cervantes *et al.*	(ADMX Collab.)
CHANG	22	PRL 129 111802	H. Chang *et al.*	(TASEH Collab.)
CHILES	22	PRL 128 231802	J. Chiles *et al.*	
COLOMA	22A	JHEP 2207 138	P. Coloma *et al.*	(IFT, CNYIT, ICC, ICREA+)
CRESCINI	22	PR D105 022007	N. Crescini *et al.*	
DEROCCO	22	PRL 129 101101	W. DeRocco *et al.*	
DESSERT	22	PRL 128 071102	C. Dessert, A.J. Long, B.R. Safdi	(MICH, UCB+)
DESSERT	22A	PR D105 103034	C. Dessert, D. Dunsky, B.R. Safdi	(UCB, LBL+)
ECKNER	22	PR D106 083020	C. Eckner, F. Calore	(LAPTH)
FENG	22	PRL 128 231803	Y.-K. Feng *et al.*	
FERGUSON	22	PR D106 042011	K.R. Ferguson *et al.*	(SPT-3G Collab.)
FOSTER	22	PRL 129 251102	J.W. Foster *et al.*	
GAVRILYUK	22	JETPL 116 11	Yu.M. Gavrilyuk *et al.*	
HOCHBERG	22	PR D106 112005	Y. Hochberg *et al.*	(SNSPD Collab.)
IKEDA	22	PR D105 102004	T. Ikeda *et al.*	
JIA	22	PRL 128 081804	S. Jia *et al.*	(BELLE Collab.)
KIRITA	22	JHEP 2210 176	Y. Kirita *et al.*	(SAPPHIRES Collab.)
LAGUE	22	JCAP 2201 049	A. Lague *et al.*	
LANGHOFF	22	PRL 129 241101	K. Langhoff, N.J. Outmezguine, N.L. Rodd	(UCB+)
LEE	22	PRL 128 241805	Y. Lee *et al.*	(CAPP Collab.)
LEES	22	PRL 128 021802	J.P. Lees *et al.*	(BABAR Collab.)
LEES	22B	PRL 128 131802	J.P. Lees *et al.*	(BABAR Collab.)
LI	22	PL B829 137047	H.-J. Li	(BNORM)
LI	22C	CP C46 085105	H.-J. Li, X.-J. Bi, P.-F. Yin	
LU	22	PR D105 123017	B.-Q. Lu, C.-W. Chiang	
LUCENTE	22	PRL 129 011101	G. Lucente *et al.*	
MANENTI	22	PR D105 052010	L. Manenti *et al.*	(MuDHI Collab.)
QUISKAMP	22	SADV 8 27	A. Quiskamp *et al.*	(ORGAN Collab.)
SCHULTHESS	22	PRL 129 191801	I. Schulthess *et al.*	(BERN, ILLG)
THOMAS	22	PR D105 L031901	A.W. Thomas, X.G. Wang, A.G. Williams	(ADLD)
TUMASYAN	22AH	EPJ C82 290	A. Tumasyan *et al.*	(CMS Collab.)
TUMASYAN	22N	JHEP 2204 062	A. Tumasyan *et al.*	(CMS Collab.)
TUMASYAN	22R	JHEP 2204 087	A. Tumasyan *et al.*	(CMS Collab.)
WANG	22C	PRL 129 051801	Y. Wang *et al.*	
WU	22A	PR D106 L081101	Y.M. Wu *et al.*	(PPTA Collab.)
XIAO	22	PR D106 123019	M. Xiao *et al.*	
YOON	22	PR D106 092007	H. Yoon *et al.*	
YUAN	22A	PR D106 023020	C. Yuan, Y. Jiang, Q.-G. Huang	
ZHOU	22	PR D106 083006	Y.-F. Zhou *et al.*	(MeerKAT-Axion Collab.)
AAD	21F	PR D103 112006	G. Aad *et al.*	(ATLAS Collab.)
AAD	21K	JHEP 2102 226	G. Aad *et al.*	(ATLAS Collab.)
AAD	21N	JHEP 2103 243	G. Aad *et al.*	(ATLAS Collab.)
Also		JHEP 2111 050 (errat.)	G. Aad *et al.*	(ATLAS Collab.)
ABRATENKO	21	PRL 127 151803	P. Abratenko *et al.*	(MicroBooNE Collab.)
ADE	21	PR D103 042002	P.A.R. Ade *et al.*	(BICEP/Keck Collab.)
AFACH	21	NATP 17 1396	S. Afach *et al.*	(GNOME Collab.)
AGUILAR-AR...	21A	PR D103 052006	A. Aguilar-Arevalo *et al.*	(PIENU Collab.)
ALESINI	21	PR D103 102004	D. Alesini *et al.*	(QUAX Collab.)
AL-KHARUSI	21	PR D104 112002	S. Al Kharusi *et al.*	(EXO-200 Collab.)
ANDREEV	21	PRL 126 211802	Yu.M. Andreev *et al.*	(NA64 Collab.)
ANDREEV	21A	PR D104 L091701	Yu.M. Andreev *et al.*	(NA64 Collab.)
ANDREEV	21B	PR D104 L111102	Yu.M. Andreev *et al.*	(NA64 Collab.)
AYBAS	21	PRL 126 141802	D. Aybas *et al.*	(CASPEr Collab.)
BACKES	21	NAT 590 238	K.M. Backes *et al.*	(HAYSTAC Collab.)
BANIK	21	JCAP 2110 043	N. Banik *et al.*	
BARTRAM	21A	PRL 127 261803	C. Bartram *et al.*	(ADMX Collab.)
BASU	21	PRL 126 191102	A. Basu *et al.*	(BIEL, NAGO)
BAUMHOLZ...	21	JCAP 2105 004	S. Baumholzer, V. Brdar, E. Morgante	(MAINZ, FNAL+)
BHUSAL	21	PRL 126 091601	A. Bhusal, N. Houston, T. Li	(BEIJ)
BI	21	PR D103 043018	X.-J. Bi *et al.*	(BHEP, TSIN)
CALORE	21	PR D104 043016	F. Calore *et al.*	(HEID)
CARRA	21	PR D104 092005	S. Carra *et al.*	
CAZZANIGA	21	EPJ C81 959	C. Cazzaniga *et al.*	(NA64 Collab.)
CORTINA-GIL	21	PL B816 136259	E. Cortina Gil *et al.*	(NA62 Collab.)
CORTINA-GIL	21A	JHEP 2103 058	E. Cortina Gil *et al.*	(NA62 Collab.)
CORTINA-GIL	21C	JHEP 2102 201	E. Cortina Gil *et al.*	(NA62 Collab.)
CROON	21	JHEP 2101 107	D. Croon *et al.*	(TRIU, WASH, MIT, FNAL)
DEVLIN	21	PRL 126 041301	J.A. Devlin *et al.*	(BASE Collab.)
DIXIT	21	PRL 126 141302	A.V. Dixit *et al.*	(CHIC, RUTG, UCB+)
DOLAN	21	JHEP 2103 190 (errat.)	M.J. Dolan *et al.*	(MELB, BRCO, DESY)
DOLAN	21A	JCAP 2109 010	M.J. Dolan, F.J. Hiskens, R.R. Volkas	(MELB)
FUJIKURA	21	PR D104 123012	K. Fujikura *et al.*	
GHOSH	21	PR D104 092016	S. Ghosh *et al.*	
GODFREY	21	PR D104 012013	B. Godfrey *et al.*	(UCD, CSUS, STAN)
GRAMOLIN	21	NATP 17 79	A.V. Gramolin *et al.*	(SHAFT Collab.)
GUO	21	CP C45 025105	J.-G. Guo *et al.*	(BHEP)
HOMMA	21	JHEP 2112 108	K. Homa *et al.*	(SAPPHIRES Collab.)
JIANG	21	NATP 17 1402	M. Jiang *et al.*	
KOPYLOV	21A	PPN 52 31	A.V. Kopylov, I.V. Orekhov, V.V. Petukhov	(INRM)
KRIBS	21	PRL 126 011801	G.D. Kribs, D. McKeen, N. Raj	(OREG, TRIU)
KWON	21	PRL 126 191802	O. Kwon *et al.*	(CAPP-ACTION Collab.)
LI	21B	PR D103 083003	H.-J. Li *et al.*	(BHEP)
LLOYD	21	PR D103 023010	S.J. Lloyd *et al.*	(DURH, OKLA)
LUCENTE	21	PR D104 103007	G. Lucente, P. Carenza	(BARI)
Also		PR D110 049901 (errat)	P. Carenza, G. Lucente	(BARI)
MARTINCAM...	21	PR D103 L121301	J.M. Camalich *et al.*	
MELCON	21	JHEP 2110 075	A.A. Melcon *et al.*	(CAST-RADES Collab.)
NG	21	PRL 126 151102	K.K.Y. Ng *et al.*	(MIT, ANIK, UTRE, LEUV)
PARK	21	JHEP 2104 191	S.-H. Park *et al.*	(BELLE Collab.)
REGIS	21	PL B814 136075	M. Regis *et al.*	(MUSE Collab.)
ROGERS	21	PRL 126 071302	K.K. Rogers, H.V. Peiris	(STOH, LOUC)
ROUSSY	21	PRL 126 171301	T.S. Roussy *et al.*	(COLO, MAINZ)
SALEMI	21	PRL 127 081801	C.P. Salemi *et al.*	(ABRACADABRA Collab.)
SCHMIDT	21	PR D104 015008	I. Schmidt *et al.*	(FRAN, GSI, +)
THOMSON	21	PRL 126 081803	C.A. Thomson *et al.*	(WAUS)
Also		PRL 127 019901 (errat.)	C.A. Thomson *et al.*	(WAUS)
TSAI	21	PRL 126 181801	Y.-D. Tsai, P. deNiverville, M.X. Liu	(FNAL+)
TSUKADA	21	PR D103 083005	L. Tsukada *et al.*	(ROMA, TOKY, WATER)
XIAO	21	PRL 126 031101	M. Xiao *et al.*	
YUAN	21	JCAP 2103 018	G.-W. Yuan *et al.*	(CST)
ZHANG	21B	PRL 127 161101	J. Zhang *et al.*	
AAIJ	20AL	JHEP 2010 156	R. Aaij *et al.*	(LHCb Collab.)
AAIJ	20C	PRL 124 041801	R. Aaij *et al.*	(LHCb Collab.)
ABDELHAME...	20	EPJ C80 376	A.H. Abdelhameed *et al.*	
ABE	20J	PL B815 136174	T. Abe, K. Hamaguchi, N. Nagata	(TOKY)
ABLIKIM	20AB	PR D102 052005	M. Ablikim *et al.*	(BESIII Collab.)
ABUDINEN	20	PRL 125 161806	F. Abudinen *et al.*	(BELLE II Collab.)
AGOSTINI	20	PRL 125 011801	M. Agostini *et al.*	(GERDA Collab.)
AGUILAR-AR...	20	PR D101 052014	A. Aguilar-Arevalo *et al.*	(PIENU Collab.)
AMARAL	20	PR D102 091101	D.W. Amaral *et al.*	(SuperCDMS Collab.)
AN	20	PR D102 115022	H. An *et al.*	(VIEN, MINN, VICT, TSIN)
ANDRIANAV...	20	PR D102 042001	A. Andrianavalomahefa *et al.*	(FUNK Collab.)
APRILE	20	PR D102 072004	E. Aprile *et al.*	(XENON Collab.)
ARALIS	20	PR D101 052008	T. Aralis *et al.*	(SuperCDMS Collab.)
Also		PR D103 039901 (errat.)	T. Aralis *et al.*	(SuperCDMS Collab.)
ARGUELLES	20	JHEP 2002 190	C. Arguelles *et al.*	(MIT, VALE)
ARNAUD	20	PRL 125 141301	Q. Arnaud *et al.*	(EDELWEISS Collab.)
BALDINI	20	EPJ C80 858	A.M. Baldini *et al.*	(MEG Collab.)
BANERJEE	20	PR D101 071101	D. Banerjee *et al.*	(NA64 Collab.)
BANERJEE	20A	PRL 125 081801	D. Banerjee *et al.*	(NA64 Collab.)
BARAK	20	PRL 125 171802	L. Barak *et al.*	(SENSEI Collab.)
BRAINE	20	PRL 124 101303	T. Braine *et al.*	(ADMX Collab.)
BUEHLER	20	JCAP 2009 027	R. Buehler *et al.*	(DESY, MADU)
CALORE	20	PR D102 123005	F. Calore *et al.*	(LAPP, BARI, HEID, +)
CAPOZZI	20	PR D102 083007	F. Capozzi, G. Raffelt	(MPIM)
CARENZA	20	PL B809 135709	P. Carenza *et al.*	
CRESCINI	20	PRL 124 171801	N. Crescini *et al.*	(QUAX Collab.)
CRISOSTO	20	PRL 124 241101	N. Crisosto *et al.*	(ADMX SLIC Collab.)
DARLING	20	PRL 125 121103	J. Darling	(COLO)
DARLING	20A	APJ 900 L28	J. Darling	(COLO)
DENT	20A	PRL 125 131805	J.B. Dent *et al.*	
DEPTA	20	JCAP 2005 009	P.F. Depta, M. Hufnagel, K. Schmidt-Hoberg	(DESY)
DESSERT	20A	PRL 125 261102	C. Dessert, J.W. Foster, B.R. Safdi	(MICH)
ESTEBAN	20	EPJ C80 259	I. Esteban *et al.*	
FOSTER	20	PRL 125 171301	J.W. Foster *et al.*	(MICH, ILL, TOKY+)
GAO	20	PRL 125 131806	C. Gao *et al.*	(FNAL, EFI, CHIC, ANL+)
GAVELA	20	PRL 124 051802	M.B. Gavela *et al.*	
GHOSH	20A	JCAP 2010 060	D. Ghosh, D. Sachdeva	
IRSIC	20	PR D101 123518	V. Irsic, H. Xiao, M. McQuinn	
JEONG	20	PRL 125 221302	J. Jeong *et al.*	
KENNEDY	20	PRL 125 201302	C.J. Kennedy *et al.*	(COLO, STAN)
KLIMCHITSK...	20	PR D101 056013	G.L. Klimchitskaya, P. Kuusk, V.M. Mostepanenko	
KOROCHKIN	20	JCAP 2003 064	A. Korochkin, A. Neronov, D. Semikoz	
KRASNIKOV	20	MPL A35 2050116	N.V. Krasnikov	
LEE	20A	PRL 124 101802	S. Lee *et al.*	(CULTASK Collab.)
LUCENTE	20A	JCAP 2012 008	G. Lucente *et al.*	
MEYER	20	PRL 124 231101	M. Meyer, T. Petrushevska	(Fermi-LAT Collab.)
Also		PRL 125 119901 (errat.)	M. Meyer, T. Petrushevska	(Fermi-LAT Collab.)
PODDAR	20	PR D101 083007	T.K. Poddar, S. Mohanty, S. Jana	
SCHUTZ	20	PR D101 123026	K. Schutz	(MIT)
SHE	20	PRL 124 111301	Z. She *et al.*	(CDEX Collab.)
SIRUNYAN	20AQ	PRL 124 131802	A.M. Sirunyan *et al.*	(CMS Collab.)

See key on page 1227

Int. J. Mod. Phys. A 2026.41. Downloaded from www.worldscientific.com
by UNIVERSITY OF CALIFORNIA @ BERKELEY on 09/16/26. Re-use and distribution is strictly not permitted, except for Open Access articles.

STRANIERO	20	AA 644 A166	O. Straniero *et al.*	(SASSO, BGNA, GRAN)
SUN	20	PR D101 063020	L. Sun, R. Brito, M. Isi	(CIT, ROMAI, MIT)
TOMITA	20	JCAP 2009 012	N. Tomita *et al.*	
WANG	20A	PR D101 052003	Y. Wang *et al.*	(CDEX Collab.)
YAMAMOTO	20	JCAP 2002 011	R. Yamamoto *et al.*	
AABOUD	19G	PR D99 012001	M. Aaboud *et al.*	(ATLAS Collab.)
ABLIKIM	19A	PR D99 012006	M. Ablikim *et al.*	(BESIII Collab.)
Also		PR D104 099901 (errat.)	M. Ablikim *et al.*	(BESIII Collab.)
ABLIKIM	19H	PR D99 012013	M. Ablikim *et al.*	(BESIII Collab.)
ADELBERGER	19	PRL 123 169001	E.G. Adelberger, W.A. Terrano	(WASH, PRIN)
ADHIKARI	19B	ASP 114 101	P. Adhikari *et al.*	(COSINE-100 Collab.)
AGUILAR-AR...	19A	PRL 123 181802	A. Aguilar-Arevalo *et al.*	(DAMIC Collab.)
AHN	19	PRL 122 021802	J.K. Ahn *et al.*	(KOTO Collab.)
ALESINI	19	PR D99 101101	D. Alesini *et al.*	(QUAX Collab.)
ALONI	19	PRL 123 071801	D. Aloni *et al.*	(REHO, MIT, CERN, HAIF)
APRILE	19	PRL 122 071301	E. Aprile *et al.*	(XENON1T Collab.)
APRILE	19D	PRL 123 251801	E. Aprile *et al.*	(XENON1T Collab.)
ARNOLD	19	EPJ C79 440	R. Arnold *et al.*	(NEMO-3 Collab.)
BANERJEE	19	PRL 123 121801	D. Banerjee *et al.*	(NA64 Collab.)
BHOONAH	19	PR D100 023001	A. Bhoonah *et al.*	
BRUN	19	PRL 122 201801	P. Brun, L. Chevalier, C. Flouzat	(SACL)
CAPUTO	19	PR D100 063515	A. Caputo *et al.*	
CORTINA-GIL	19	JHEP 1905 182	E. Cortina Gil *et al.*	(NA62 Collab.)
DANILOV	19	PRL 122 041801	M. Danilov, S. Demidov, D. Gorbunov	(LEBD, INRM+)
DAVOUDIASL	19	PRL 123 021102	H. Davoudiasl, P.B. Denton	(BNL)
DESSERT	19	PRL 123 061104	C. Dessert, A.J. Long, B.R. Safdi	(MICH)
FEDDERKE	19	PR D100 015040	M.A. Fedderke, P.W. Graham, S. Rajendran	(STAN+)
FUJITA	19	PRL 122 191101	T. Fujita, R. Tazaki, K. Toma	(KYOT, GEVA, TOHO)
HOCHBERG	19	PRL 123 151802	Y. Hochberg *et al.*	(HEBR, MIT, NIST)
IVANOV	19	JCAP 1902 059	M.M. Ivanov *et al.*	
KOPYLOV	19	JCAP 1907 008	A. Kopylov, I. Orekhov, V. Petukhov	(INRM)
KOVETZ	19	PR D99 123511	E.D. Kovetz, I. Cholis, D.E. Kaplan	(JHU)
LEINSON	19	JCAP 1911 031	L.B. Leinson	
LIANG	19	JCAP 1906 042	Y-F. Liang *et al.*	
LLOYD	19	PR D100 063005	S.J. Lloyd *et al.*	
MARSH	19	PRL 123 051103	D.J.E. Marsh, J.C. Niemeyer	(GOET)
NGUYEN	19	JCAP 1910 014	L.H. Nguyen, A. Lobanov, D. Horns	(WISPDMX Collab.)
OUELLET	19A	PRL 122 121802	J.L. Ouellet *et al.*	(ABRACADABRA Collab.)
PALOMBA	19	PRL 123 171101	C. Palomba *et al.*	
SIRUNYAN	19BQ	PL B796 131	A.M. Sirunyan *et al.*	(CMS Collab.)
SMORRA	19	NAT 575 310	C. Smorra *et al.*	
TERRANO	19	PRL 122 231301	W. Terrano *et al.*	(WASH)
WU	19	PRL 122 191302	T. Wu *et al.*	(CASPEr-ZULF Collab.)
WU	19C	PRL 123 169002	T. Wu *et al.*	(CASPEr-ZULF Collab.)
ABE	18F	PL B787 153	K. Abe *et al.*	(XMASS Collab.)
ADRIAN	18	PR D98 091101	P.H. Adrian *et al.*	(HPS Collab.)
AKHMATOV	18	PPN 49 599	Z.A. Akhmatov *et al.*	
ANASTASI	18B	PL B784 336	A. Anastasi *et al.*	(KLOE-2 Collab.)
ARMENGAUD	18	PR D98 082004	E. Armengaud *et al.*	(EDELWEISS-III Collab.)
ARNOLD	18	EPJ C78 821	R. Arnold *et al.*	(NEMO-3 Collab.)
BANERJEE	18	PRL 120 231802	D. Banerjee *et al.*	(NA64 Collab.)
BANERJEE	18A	PR D97 072002	D. Banerjee *et al.*	(NA64 Collab.)
BEZNOGOV	18	PR C98 035802	M.V. Beznogov *et al.*	
BOUTAN	18	PRL 121 261302	C. Boutan *et al.*	(ADMX Collab.)
CHANG	18	JHEP 1809 051	J.C. Chang, R. Essig, S.D. McDermott	
CRESCINI	18	EPJ C78 703	N. Crescini *et al.*	(QUAX Collab.)
DU	18	PRL 120 151301	N. Du *et al.*	(ADMX Collab.)
DZUBA	18	PR D98 035048	V.A. Dzuba *et al.*	
FICEK	18	PRL 120 183002	F. Ficek *et al.*	
FORTIN	18	JHEP 1806 048	J.-F. Fortin, K. Sinha	(LAVL, OKLA)
GAVRILYUK	18	JETPL 107 589	Yu.M. Gavrilyuk *et al.*	
HAMAGUCHI	18	PR D98 103015	K. Hamaguchi *et al.*	
JAECKEL	18	PR D98 055032	J. Jaeckel, P. C. Malta, J. Redondo	
KNIRCK	18	JCAP 1811 031	S. Knirck *et al.*	
PORAYKO	18	PR D98 102002	N.K. Porayako *et al.*	(PPTA Collab.)
STADNIK	18	PRL 120 013202	Y.V. Stadnik, V.A. Dzuba, V.V. Flambaum	
YAMAJI	18	PL B782 523	T. Yamaji *et al.*	(TOKY, RIKEN, KEK)
ZHANG	18	PR D97 063009	C. Zhang *et al.*	
ZHONG	18	PR D97 092001	L. Zhong *et al.*	(HAYSTAC Collab.)
AAIJ	17AQ	PR D95 071101	R. Aaij *et al.*	(LHCb Collab.)
ABEL	17	PR X7 041034	C. Abel *et al.*	(nEDM Collab.)
ABGRALL	17	PRL 118 161801	N. Abgrall *et al.*	(MAJORANA Collab.)
ABLIKIM	17AA	PL B774 252	M. Ablikim *et al.*	(BESIII Collab.)
ADE	17	PR D96 102003	P.A.R. Ade *et al.*	(BICEP2/Keck Array Collab.)
AHN	17	PTEP 2017 021C01	J.K. Ahn *et al.*	(KOTO Collab.)
AKERIB	17B	PRL 118 261301	D.S. Akerib *et al.*	(LUX Collab.)
ANASTASSO...	17	NATP 13 584	V. Anastassopoulos *et al.*	(CAST Collab.)
ANGLOHER	17	EPJ C77 299	G. Angloher *et al.*	(CRESST-II Collab.)
APRILE	17B	PR D95 029904	E. Aprile *et al.*	(XENON100 Collab.)
BANERJEE	17	PRL 118 011802	D. Banerjee *et al.*	(NA64 Collab.)
BATLEY	17	PL B769 67	J.R. Batley *et al.*	(NA48/2 Collab.)
BRANCA	17	PRL 118 021302	A. Branca *et al.*	(AURIGA Collab.)
BRUBAKER	17	PRL 118 061302	B.M. Brubaker *et al.*	(YALE, UCB, NIST+)
CHANG	17	JHEP 1701 107	J.H. Chang, R. Essig, S.D. McDermott	(STON)
CHOI	17	PR D96 061102	J. Choi *et al.*	(CAPP-ACTION Collab.)
CRESCINI	17	PL B773 677	N. Crescini *et al.*	(QUAX-gpgs Collab.)
DAIDO	17	PL B772 127	R. Daido, F. Takahashi	
DOLAN	17	JHEP 1712 094	M.J. Dolan *et al.*	
Also		JHEP 2103 190 (errat.)	M.J. Dolan *et al.*	(MELB, BRCO, DESY)
DUBININA	17	PAN 80 461	V.V. Dubinina *et al.*	
FICEK	17	PR A95 032505	F. Ficek *et al.*	
FU	17A	PRL 119 181806	C. Fu *et al.*	(PandaX-II Collab.)
INADA	17	PRL 118 071803	T. Inada *et al.*	
KLIMCHITSK...	17A	PR D95 123013	G.L. Klimchitskaya, V.M. Mostepanenko	
KOHRI	17	PR D96 051701	K. Kohri, H. Kodama	(KEK, KYOT)
LEES	17E	PRL 119 131804	J.P. Lees *et al.*	(BABAR Collab.)
LIU	17	PL B766 117	X.-H. Liu	(TINT)
LIU	17A	PR D95 052006	S.K. Liu *et al.*	(CDEX Collab.)
LUO	17	PR D96 055028	P. Luo *et al.*	
MARSH	17	JCAP 1712 036	M.C.D. Marsh *et al.*	
MCALLISTER	17	PDU 18 67	B.T. McAllister *et al.*	(WAUS)
TIWARI	17	PR D95 023005	P. Tiwari	(Technion)
AAD	16AG	JHEP 1602 062	G. Aad *et al.*	(ATLAS Collab.)
ABLIKIM	16E	PR D93 052005	M. Ablikim *et al.*	(BESIII Collab.)
AJELLO	16	PRL 116 161101	M. Ajello *et al.*	(Fermi-LAT Collab.)
ANASTASI	16	PL B757 356	A. Anastasi *et al.*	(KLOE-2 Collab.)
BATTICH	16	JCAP 1608 062	T. Battich *et al.*	
BERENJI	16	PR D93 045019	B. Berenji *et al.*	
CORSICO	16	JCAP 1607 036	A.H. Corsico *et al.*	
DELLA-VALLE	16	EPJ C76 24	F. Della Valle *et al.*	(PVLAS Collab.)
HOSKINS	16	PR D94 082001	J. Hoskins *et al.*	(ADMX Collab.)
JAECKEL	16	PL B753 482	J. Jaeckel, M. Spannowsky	(HEID, DURH)
KHACHATRY...	16	PL B752 146	V. Khachatryan *et al.*	(CMS Collab.)
KRASZNAHO...	16	PRL 116 042501	A.J. Krasznahorkay *et al.*	(HINR, ANIK+)
LEEFER	16	PRL 117 271601	N. Leefer *et al.*	(MAINZ, BONN, LBL, UCB+)
WON	16	PR D94 092006	E. Won *et al.*	(BELLE Collab.)
YOON	16	JHEP 1606 011	Y.S. Yoon *et al.*	(KIMS Collab.)
AAD	15CD	PR D92 092001	G. Aad *et al.*	(ATLAS Collab.)
AAIJ	15AZ	PRL 115 161802	R. Aaij *et al.*	(LHCb Collab.)
ADARE	15	PR C91 031901	A. Adare *et al.*	(PHENIX Collab.)
AFACH	15	PL B745 58	S. Afach *et al.*	(ETH, PSI, CAEN, +)
AGOSTINI	15A	EPJ C75 416	M. Agostini *et al.*	(GERDA Collab.)
AN	15A	PL B747 331	H. An *et al.*	(CIT, VICT, VIEN)
ANASTASI	15	PL B747 365	A. Anastasi *et al.*	(KLOE-2 Collab.)
ANASTASI	15A	PL B750 633	A. Anastasi *et al.*	(KLOE-2 Collab.)
ANASTASSO...	15	PL B749 172	V. Anastassopoulos *et al.*	(CAST Collab.)
ARIK	15	PR D92 021101	M. Arik *et al.*	(CAST Collab.)
ARNOLD	15	PR D92 072011	R. Arnold *et al.*	(NEMO-3 Collab.)
BALLOU	15	PR D92 092002	R. Ballou *et al.*	(OSQAR Collab.)
BATLEY	15A	PL B746 178	J.R. Batley *et al.*	(NA48/2 Collab.)
BAYES	15	PR D91 052020	R. Bayes *et al.*	(TWIST Collab.)
BRAX	15	PR D92 083501	P. Brax, P. Brun, D. Wouters	(SACL, SACL5)
GAVRILYUK	15	JETPL 101 664	Yu.M. Gavrilyuk *et al.*	
		Translated from ZETFP 101 739.		
HASEBE	15	PTEP 2015 073C01	T. Hasebe *et al.*	
JAEGLE	15	PRL 114 211801	I. Jaegle *et al.*	(BELLE Collab.)
KAZANAS	15	NP B890 17	D. Kazanas *et al.*	
KLIMCHITSK...	15	EPJ C75 164	G.L. Klimchitskaya, V.M. Mostepanenko	
MILLEA	15	PR D92 023010	M. Millea, L. Knox, B. Fields	(UCD, ILL)
STADNIK	15	EPJ C75 110	Y.V. Stadnik, V.V. Flambaum	(SYDN)
SUZUKI	15	JCAP 1509 042	J. Suzuki *et al.*	
TERRANO	15	PRL 115 201801	W.A. Terrano *et al.*	(WASH)
VANTILBURG	15	PRL 115 011802	K. Van Tilburg *et al.*	
VINYOLES	15	JCAP 1510 015	N. Vinyoles *et al.*	
ABE	14F	PRL 113 121301	K. Abe *et al.*	(XMASS Collab.)
AGAKISHIEV	14	PL B731 265	G. Agakishiev *et al.*	(HADES Collab.)
ALBERT	14A	PR D90 092004	J.B. Albert *et al.*	(EXO-200 Collab.)
APRILE	14B	PR D90 062009	E. Aprile *et al.*	(XENON100 Collab.)
ARIK	14	PRL 112 091302	M. Arik *et al.*	(CAST Collab.)
AYALA	14	PRL 113 191302	A. Ayala *et al.*	
BABUSCI	14	PL B736 459	D. Babusci *et al.*	(KLOE-2 Collab.)
BATELL	14	PRL 113 171802	B. Batell, R. Essig, Z. Surujon	(EFI, STON)
BEZERRA	14	PR D89 035010	V.B. Bezerra *et al.*	
BEZERRA	14A	EPJ C74 2859	V.B. Bezerra *et al.*	
BEZERRA	14B	PR D90 055013	V.B. Bezerra *et al.*	
BEZERRA	14C	PR D89 075002	V.B. Bezerra *et al.*	
BLUEMLEIN	14	PL B731 320	J. Bluemlein, J. Brunner	(CPPM, DESY)
BLUM	14	PL B737 30	K. Blum *et al.*	(IAS, PRIN)
DELLA-VALLE	14	PR D90 092003	F. Della Valle *et al.*	(PVLAS Collab.)
DERBIN	14	EPJ C74 3035	A.V. Derbin *et al.*	
EJLLI	14	PR D90 123527	D. Ejlli	
FRADETTE	14	PR D90 035022	A. Fradette *et al.*	
LEES	14J	PRL 113 201801	J.P. Lees *et al.*	(BABAR Collab.)
LEINSON	14	JCAP 1408 031	L. Leinson	
MERKEL	14	PRL 112 221802	H. Merkel *et al.*	(A1 at MAMI)
MILLER-BER...	14	JCAP 1410 069	M.M. Miller Bertolami *et al.*	
PUGNAT	14	EPJ C74 3027	P. Pugnat *et al.*	(OSQAR Collab.)
REESMAN	14	JCAP 1408 021	R. Reesman *et al.*	(OSU)
ABE	13D	PL B724 46	K. Abe *et al.*	(XMASS Collab.)
ABRAMOWSKI	13A	PR D88 102003	A. Abramowski *et al.*	(H.E.S.S. Collab.)
ADLARSON	13	PL B726 187	P. Adlarson *et al.*	(WASA-at-COSY Collab.)
ALESSANDRIA	13	JCAP 1305 007	F. Alessandria *et al.*	(CUORE Collab.)
AN	13B	PL B725 190	H. An, M. Pospelov, J. Pradler	
AN	13C	PRL 111 041302	H. An, M. Pospelov, J. Pradler	
ARCHIDIACO...	13A	JCAP 1310 020	M. Archidiacono *et al.*	
ARMENGAUD	13	JCAP 1311 067	E. Armengaud *et al.*	(EDELWEISS-II Collab.)
BABUSCI	13B	PL B720 111	D. Babusci *et al.*	(KLOE-2 Collab.)
BARTH	13	JCAP 1305 010	K. Barth *et al.*	(CAST Collab.)
BECK	13	PRL 111 231801	C. Beck	
BETZ	13	PR D88 075014	M. Betz *et al.*	(CROWS Collab.)
BULATOWICZ	13	PRL 111 102001	M. Bulatowicz *et al.*	
CHU	13	PR D87 011105	P.-H. Chu *et al.*	(DUKE, IND, SJTU)
DERBIN	13	EPJ C73 2490	A. V. Derbin *et al.*	
DIAMOND	13	PRL 111 221803	M.D. Diamond, P. Schuster	
FRIEDLAND	13	PRL 110 061101	A. Friedland, M. Giannotti, M. Wise	
GNINENKO	13	PR D87 035030	S.N. Gninenko	(INRM)
HECKEL	13	PRL 111 151802	B. R. Heckel *et al.*	
HORVAT	13	PL B721 220	R. Horvat *et al.*	
INADA	13	PL B722 301	T. Inada *et al.*	
LATTANZI	13	PR D88 063528	M. Lattanzi *et al.*	
MEYER	13	PR D87 035027	M. Meyer, D. Horns, M. Raue	
MIZUMOTO	13	JCAP 1307 013	T. Mizumoto *et al.*	
PARKER	13	PR D88 112004	S. Parker *et al.*	
REDONDO	13	JCAP 1308 034	J. Redondo, G. Raffelt	
TULLNEY	13	PRL 111 100801	K. Tullney *et al.*	
VIAUX	13A	PRL 111 231301	N. Viaux *et al.*	
WOUTERS	13	APJ 772 44	D. Wouters, P. Brun	(SACL)
ABLIKIM	12	PR D85 092012	M. Ablikim *et al.*	(BESIII Collab.)
ARCHILLI	12	PL B706 251	F. Archilli *et al.*	(KLOE-2 Collab.)
BELLI	12	PL B711 41	P. Belli *et al.*	(DAMA-KIEV)
BELLINI	12B	PR D85 092003	G. Bellini *et al.*	(Borexino Collab.)
CADAMURO	12	JCAP 1202 032	D. Cadamuro *et al.*	(MPIM)
CORSICO	12	JCAP 1212 010	A.H. Corsico *et al.*	(LAPL, RGSUL, WASH+)
DERBIN	12	JETPL 95 339	A.V. Derbin *et al.*	(PNPI)
		Translated from ZETFP 95 379.		
GANDO	12	PR C86 021601	A. Gando *et al.*	(KamLAND-Zen Collab.)
GNINENKO	12A	PR D85 055027	S.N. Gninenko	(INRM)
GNINENKO	12B	PL B713 244	S.N. Gninenko	(INRM)
PAYEZ	12	JCAP 1207 041	A. Payez *et al.*	(LIEG)
RAFFELT	12	PR D86 015001	G. Raffelt	(MPIM)
AALSETH	11	PRL 106 131301	C.E. Aalseth *et al.*	(CoGeNT Collab.)
ABRAHAMY...	11	PRL 107 191804	S. Abrahamyan *et al.*	
ARIK	11	PRL 107 261302	M. Arik *et al.*	(CAST Collab.)
ARNOLD	11	PRL 107 062504	R. Arnold *et al.*	(NEMO-3 Collab.)
BLUEMLEIN	11	PL B701 155	J. Bluemlein, J. Brunner	(DESY)
CADAMURO	11	JCAP 1102 003	D. Cadamuro *et al.*	(MPIM, AARHUS)
DERBIN	11	PAN 74 596	A.V. Derbin *et al.*	(PNPI)
		Translated from YAF 74 620.		
DERBIN	11A	PR D83 023505	A.V. Derbin *et al.*	(PNPI)
HOEDL	11	PRL 106 041801	S.A. Hoedl *et al.*	(WASH)
HOSKINS	11	PR D84 121302	J. Hoskins *et al.*	(ADMX Collab.)
ANDRIAMON...	10	JCAP 1003 032	S. Andriamonje *et al.*	(CAST Collab.)
ARGYRIADES	10	NP A847 168	J. Argyriades *et al.*	(NEMO-3 Collab.)
ASZTALOS	10	PRL 104 041301	S.J. Asztalos *et al.*	(ADMX Collab.)
EHRET	10	PL B689 149	K. Ehret *et al.*	(ALPS Collab.)
HANNESTAD	10	JCAP 1008 001	S. Hannestad *et al.*	
PETUKHOV	10	PRL 105 170401	A.K. Petukhov *et al.*	
SEREBROV	10	JETPL 91 6	A.P. Serebrov *et al.*	
		Translated from ZETFP 91 8.		
AHMED	09A	PRL 103 141802	Z. Ahmed *et al.*	(CDMS Collab.)
ANDRIAMON...	09	JCAP 0912 002	S. Andriamonje *et al.*	
ARGYRIADES	09	PR C80 032501	J. Argyriades *et al.*	(NEMO-3 Collab.)
ARIK	09	JCAP 0902 008	E. Arik *et al.*	(CAST Collab.)
BJORKEN	09	PR D80 075018	J. Bjorken *et al.*	
CHOU	09	PRL 102 030402	A.S. Chou *et al.*	(GammeV Collab.)
DAVOUDIASL	09	PR D79 095024	H. Davoudiasl, P. Huber	
DERBIN	09A	PL B678 181	A.V. Derbin *et al.*	
GONDOLO	09	PR D79 107301	P. Gondolo, G. Raffelt	(UTAH, MPIM)
IGNATOVICH	09	EPJ C64 19	V.K. Ignatovich, Y.N. Pokotilovski	(JINR)
KEKEZ	09	PL B671 345	D. Kekez *et al.*	
SEREBROV	09	PL B680 423	A.P. Serebrov	(PNPI)
AFANASEV	08	PRL 101 120401	A. Afanasev *et al.*	
BELLINI	08	EPJ C54 61	G. Bellini *et al.*	(Borexino Collab.)
CHOU	08	PRL 100 080402	A.S. Chou *et al.*	(GammeV Collab.)

Int. J. Mod. Phys. A 2026.41. Downloaded
by UNIVERSITY OF CALIFORNIA @ BERKELEY on 09/16/26. Re
worldscientific.com
s strictly not permitted, except for Open Access articles.

FOUCHE 08 PR D78 032013 M. Fouche *et al.*
HANNESTAD 08 JCAP 0804 019 S. Hannestad *et al.*
INOUE 08 PL B668 93 Y. Inoue *et al.*
ZAVATTINI 08 PR D77 032006 E. Zavattini *et al.* (PVLAS Collab.)
ADELBERGER 07 PRL 98 131104 E.G. Adelberger *et al.*
ANDRIAMON... 07 JCAP 0704 010 S. Andriamonje *et al.* (CAST Collab.)
BAESSLER 07 PR D75 075006 S. Baessler *et al.*
CHANG 07 PR D75 052004 H.M. Chang *et al.* (TEXONO Collab.)
HANNESTAD 07 JCAP 0708 015 S. Hannestad *et al.*
JAIN 07 JP G34 129 P.L. Jain, G. Singh
LESSA 07 PR D75 094001 A.P. Lessa, O.L.G. Peres
MELCHIORRI 07A PR D76 041303 A. Melchiorri, O. Mena, A. Slosar
ROBILLIARD 07 PRL 99 190403 C. Robilliard *et al.*
ARNOLD 06 NP A765 483 R. Arnold *et al.* (NEMO-3 Collab.)
DUFFY 06 PR D74 012006 L.D. Duffy *et al.*
HECKEL 06 PRL 97 021603 B.R. Heckel *et al.*
ZAVATTINI 06 PRL 96 110406 E. Zavattini *et al.* (PVLAS Collab.)
HANNESTAD 05A JCAP 0507 002 S. Hannestad, A. Mirizzi, G. Raffelt
ZIOUTAS 05 PRL 94 121301 K. Zioutas *et al.* (CAST Collab.)
ADLER 04 PR D70 037102 S. Adler *et al.* (BNL E787 Collab.)
ANISIMOVSK... 04 PRL 93 031801 V.V. Anisimovsky *et al.* (BNL E949 Collab.)
ARNOLD 04 JETPL 80 377 R. Arnold *et al.* (NEMO-3 Collab.)
Translated from ZETFP 80 429.
ASZTALOS 04 PR D69 011101 S.J. Asztalos *et al.*
HOFFMANN 04 PR B70 180503 C. Hoffmann *et al.*
ARNABOLDI 03 PL B557 167 C. Arnaboldi *et al.*
CIVITARESE 03 NP A729 867 O. Civitarese, J. Suhonen
DANEVICH 03 PR C68 035501 F.A. Danevich *et al.*
FARZAN 03 PR D67 073015 Y. Farzan (SLAC, SISSA)
ADLER 02C PL B537 211 S. Adler *et al.* (BNL E787 Collab.)
BADERT... 02 PL B542 29 A. Badertscher *et al.*
BERNABEI 02D PL B546 23 R. Bernabei *et al.* (DAMA Collab.)
DERBIN 02 PAN 65 1302 A.V. Derbin *et al.*
Translated from YAF 65 1335.
FUSHIMI 02 PL B531 190 K. Fushimi *et al.* (ELEGANT V Collab.)
INOUE 02 PL B536 18 Y. Inoue *et al.*
MORALES 02B ASP 16 325 A. Morales *et al.* (COSME Collab.)
ADLER 01 PR D63 032004 S. Adler *et al.* (BNL E787 Collab.)
AMMAR 01B PRL 87 271801 R. Ammar *et al.* (CLEO Collab.)
ASHITKOV 01 JETPL 74 529 V.D. Ashitkov *et al.*
Translated from ZETFP 74 601.
BERNABEI 01B PL B515 6 R. Bernabei *et al.* (DAMA Collab.)
DANEVICH 01 NP A694 375 F.A. Danevich *et al.*
DEBOER 01 JP G27 L29 F.W.N. de Boer *et al.*
STOICA 01 NP A694 269 S. Stoica, H.V. Klapdor-Kleingrothous
ALESSAND... 00 PL B486 13 A. Alessandrello *et al.*
ARNOLD 00 NP A678 341 R. Arnold *et al.*
ASTIER 00B PL B479 371 P. Astier *et al.* (NOMAD Collab.)
DANEVICH 00 PR C62 045501 F.A. Danevich *et al.*
MASSO 00 PR D61 011701 E. Masso
ARNOLD 99 NP A658 299 R. Arnold *et al.* (NEMO Collab.)
NI 99 PRL 82 2439 W.-T. Ni *et al.*
SIMKOVIC 99 PR C60 055502 F. Simkovic *et al.*
ALTEGOER 98 PL B428 197 J. Altegoer *et al.*
ARNOLD 98 NP A636 209 R. Arnold *et al.* (NEMO-2 Collab.)
AVIGNONE 98 PRL 81 5068 F.T. Avignone *et al.* (Solar Axion Experiment)
DIAZ 98 NP B527 44 M.A. Diaz *et al.*
KIM 98 PR D58 055006 J.E. Kim
LUESCHER 98 PL B434 407 R. Luescher *et al.*
MORIYAMA 98 PL B434 147 S. Moriyama *et al.*
MOROI 98 PL B440 69 T. Moroi, H. Murayama
POSPELOV 98 PR D58 097703 M. Pospelov
AHMAD 97 PRL 78 618 I. Ahmad *et al.* (APEX Collab.)
BORISOV 97 JETP 83 868 A.V. Borisov, V.Y. Grishinia (MOSU)
DEBOER 97C JP G23 L85 F.W.N. de Boer *et al.*
KACHELRIESS 97 PR D56 1313 M. Kachelriess, C. Wilke, G. Wunner (BOCH)
KEIL 97 PR D56 2419 W. Keil *et al.*
KITCHING 97 PRL 79 4079 P. Kitching *et al.* (BNL E787 Collab.)
LEINBERGER 97 PL B394 16 U. Leinberger *et al.* (ORANGE Collab.)
ADLER 96 PRL 76 1421 S. Adler *et al.* (BNL E787 Collab.)
AMSLER 96B ZPHY C70 219 C. Amsler *et al.* (Crystal Barrel Collab.)
GANZ 96 PL B389 4 R. Ganz *et al.* (GSI, HEID, FRAN, JAGL+)
GUENTHER 96 PR D54 3641 M. Gunther *et al.* (MPIK, SASSO)
KAMEL 96 PL B368 291 S. Kamel (SHAMS)
MITSUI 96 EPL 33 111 T. Mitsui *et al.* (TOKY)
YOUDIN 96 PRL 77 2170 A.N. Youdin *et al.* (AMHT, WASH)
ALTMANN 95 ZPHY C68 221 M. Altmann *et al.* (TUM, LAPP, CPPM)
BASSOMPIE... 95 PL B355 584 G. Bassompierre *et al.* (LAPP, LCGT, LYON)
MAENO 95 PL B351 574 T. Maeno *et al.* (TOKY)
RAFFELT 95 PR D51 1495 G. Raffelt, A. Weiss (MPIM, MPIG)
SKALSEY 95 PR D51 6292 M. Skalsey, R.S. Conti (MICH)
TSUNODA 95 EPL 30 273 T. Tsunoda *et al.* (TOKY)
ADACHI 94 PR A49 3201 S. Adachi *et al.* (TMU)
ALTHERR 94 ASP 2 175 T. Altherr, E. Petitgirard, T. del Rio Gaztelurrutia
AMSLER 94B PL B333 271 C. Amsler *et al.* (Crystal Barrel Collab.)
ASAI 94 PL B323 90 S. Asai *et al.* (TOKY)
MEIJERDREES 94 PR D49 4937 M.R. Drees *et al.* (BRCO, OREG, TRIU)
NI 94 Physica B194 153 W.T. Ni *et al.* (NTHU)
VO 94 PR C49 1551 D.T. Vo *et al.* (ISU, LBL, LLNL, UCD)
ATIYA 93 PRL 70 2521 M.S. Atiya *et al.* (BNL E787 Collab.)
Also PRL 71 305 (errat.) M.S. Atiya *et al.* (BNL E787 Collab.)
ATIYA 93B PR D48 1 M.S. Atiya *et al.* (BNL E787 Collab.)
BASSOMPIE... 93 EPL 22 239 G. Bassompierre *et al.* (LAPP, TORI, LYON)
BECK 93 PRL 70 2853 M. Beck *et al.* (MPIK, KIAE, SASSO)
CAMERON 93 PR D47 3707 R.E. Cameron *et al.* (ROCH, BNL, FNAL+)
CHANG 93 PL B316 51 S. Chang, K. Choi
CHUI 93 PRL 71 3247 T.C.P. Chui, W.T. Ni (NTHU)
MINOWA 93 PRL 71 4120 M. Minowa *et al.* (TOKY)
NG 93 PR D48 2941 K.W. Ng (AST)
RITTER 93 PRL 70 701 R.C. Ritter *et al.*
TANAKA 93 PR D48 5412 J. Tanaka, H. Ejiri (OSAK)
ALLIEGRO 92 PRL 68 278 C. Alliegro *et al.* (BNL, FNAL, PSI+)
ATIYA 92 PRL 69 733 M.S. Atiya *et al.* (BNL, LANL, PRIN+)
BARABASH 92 PL B295 154 L.S. Barabash *et al.* (JINR, CERN, SERP+)
BERNATOW... 92 PRL 69 2341 T. Bernatowicz *et al.* (WUSL, TATA)
BLUEMLEIN 92 IJMP A7 3835 J. Bluemlein *et al.* (BERL, BUDA, JINR+)
HALLIN 92 PR D45 3955 A.L. Hallin *et al.* (PRIN)
HENDERSON 92C PRL 69 1733 S.D. Henderson *et al.* (YALE, BNL)
HICKS 92 PL B276 423 K.H. Hicks, D.E. Alburger (OHIO, BNL)
LAZARUS 92 PRL 69 2333 D.M. Lazarus *et al.* (BNL, ROCH, FNAL)
MEIJERDREES 92 PRL 68 3845 R. Meijer Drees *et al.* (SINDRUM I Collab.)
PAN 92 MPL A7 1287 S.S. Pan, W.T. Ni, S.C. Chen (NTHU)
RUOSO 92 ZPHY C56 505 G. Ruoso *et al.* (ROCH, BNL, FNAL, TRST)
SKALSEY 92 PRL 68 456 M. Skalsey, J.J. Kolata (MICH, NDAM)
VENEMA 92 PRL 68 135 B.J. Venema *et al.*
WANG 92 MPL A7 1497 J. Wang (ILL)
WANG 92C PL B291 97 J. Wang (ILL)
WU 92 PRL 69 1729 X.Y. Wu *et al.* (BNL, YALE, CUNY)
AKOPYAN 91 PL B272 443 M.V. Akopyan *et al.* (INRM)
ASAI 91 PRL 66 2440 S. Asai *et al.* (ICEPP)
BERSHADY 91 PRL 66 1398 M.A. Bershady, M.T. Ressell, M.S. Turner (CHIC+)
BLUEMLEIN 91 ZPHY C51 341 J. Bluemlein *et al.* (BERL, BUDA, JINR+)
BOBRAKOV 91 JETPL 53 294 V.F. Bobrakov *et al.* (PNPI)
Translated from ZETFP 53 283.
BROSS 91 PRL 67 2942 A.D. Bross *et al.* (FNAL, ILL)
KIM 91C PRL 67 3465 J.E. Kim (SEOUL)
RAFFELT 91 PRPL 198 1 G.G. Raffelt (MPIM)
RAFFELT 91B PRL 67 2605 G. Raffelt, D. Seckel (MPIM, BART)
RESSELL 91 PR D44 3001 M.T. Ressell (CHIC, FNAL)
TRZASKA 91 PL B269 54 W.H. Trzaska *et al.* (TAMU)
TSERTOS 91 PL B266 259 H. Tsertos *et al.* (ILLG, GSI)
WALKER 91 APJ 376 51 T.P. Walker *et al.* (HSCA, OSU, CHIC+)
WIDMANN 91 ZPHY A340 209 E. Widmann *et al.* (STUT, GSI, STUTM)
WINELAND 91 PRL 67 1735 D.J. Wineland *et al.* (NBSB)
ALBRECHT 90E PL B246 278 H. Albrecht *et al.* (ARGUS Collab.)
ANTREASYAN 90C PL B251 204 D. Antreasyan *et al.* (Crystal Ball Collab.)
ASANUMA 90 PL B237 588 T. Asanuma *et al.* (TOKY)
ATIYA 90 PRL 64 21 M.S. Atiya *et al.* (BNL E787 Collab.)
ATIYA 90B PRL 65 1188 M.S. Atiya *et al.* (BNL E787 Collab.)
BAUER 90 NIM B50 300 W. Bauer *et al.* (STUT, VILL, GSI)
BURROWS 90 PR D42 3297 A. Burrows, M.T. Ressell, M.S. Turner (ARIZ+)
DEBOER 90 JP G16 L1 F.W.N. de Boer, J. Lehmann, J. Steyaert (LOUV)
ENGEL 90 PRL 65 960 J. Engel, D. Seckel, A.C. Hayes (BART, LANL)
GNINENKO 90 PL B237 287 S.N. Gninenko *et al.* (INRM)
GUO 90 PR D41 2924 R. Guo *et al.* (NIU, LANL, FNAL, CASE+)
HAGMANN 90 PR D42 1297 C. Hagmann *et al.* (FLOR)
JUDGE 90 PRL 65 972 S.M. Judge *et al.* (ILLG, GSI)
RAFFELT 90D PR D41 1324 G.G. Raffelt (MPIM)
RITTER 90 PR D42 977 R.C. Ritter *et al.* (UVA)
SEMERTZIDIS 90 PRL 64 2988 Y.K. Semertzidis *et al.* (ROCH, BNL, FNAL+)
TSUCHIAKI 90 PL B236 81 M. Tsuchiaki *et al.* (ICEPP)
TURNER 90 PRPL 197 67 M.S. Turner (FNAL)
BARABASH 89 PL B223 273 A.S. Barabash *et al.* (ITEP, INRM)
BINI 89 PL B221 99 M. Bini *et al.* (FIRZ, CERN, AARH)
BURROWS 89 PR D39 1020 A. Burrows, M.S. Turner, R.P. Brinkmann (ARIZ+)
Also PRL 60 1797 M.S. Turner (FNAL, EFI)
DEBOER 89B PRL 62 2639 F.W.N. de Boer, R. van Dantzig (ANIK)
ERICSON 89 PL B219 507 T.E.O. Ericson, J.F. Mathiot (CERN, IPN)
FAISSNER 89 ZPHY C44 557 H. Faissner *et al.* (AACH3, BERL, PSI)
FOX 89 PR C39 288 J.D. Fox *et al.* (FSU)
MAYLE 89 PL B219 515 R. Mayle *et al.* (LLL, CERN, MINN, FNAL+)
Also PL B203 188 R. Mayle *et al.* (LLL, CERN, MINN, FNAL+)
MINOWA 89 PRL 62 1091 H. Minowa *et al.* (ICEPP)
ORITO 89 PRL 63 597 S. Orito *et al.* (ICEPP)
PERKINS 89 PRL 62 2638 D.H. Perkins (OXF)
TSERTOS 89 PR D40 1397 H. Tsertos *et al.* (GSI, ILLG)
VANBIBBER 89 PR D39 2089 K. van Bibber *et al.* (LLL, TAMU, LBL)
WUENSCH 89 PR D40 3153 W.U. Wuensch *et al.* (ROCH, BNL, FNAL)
Also PRL 59 839 S. de Panfilis *et al.* (ROCH, BNL, FNAL)
AVIGNONE 88 PR D37 618 F.T. Avignone *et al.* (PRIN, SCUC, ORNL+)
BALKE 88 PR D37 587 B. Balke *et al.* (LBL, UCB, COLO, NWES+)
BJORKEN 88 PR D38 3375 J.D. Bjorken *et al.* (FNAL, SLAC, VPI)
BLINOV 88 SJNP 47 563 A.E. Blinov *et al.* (NOVO)
Translated from YAF 47 889.
BOLTON 88 PR D38 2077 R.D. Bolton *et al.* (LANL, STAN, CHIC+)
Also PRL 56 2461 R.D. Bolton *et al.* (LANL, STAN, CHIC+)
Also PRL 57 3241 D. Grosnick *et al.* (CHIC, LANL, STAN+)
CHANDA 88 PR D37 2714 R. Chanda, J.F. Nieves, P.B. Pal (UMD, UPR+)
CHOI 88 PR D37 3225 K. Choi *et al.* (JHU)
CONNELL 88 PRL 60 2242 S.H. Connell *et al.* (WITW)
DATAR 88 PR C37 250 V.M. Datar *et al.* (IPN)
DEBOER 88 PRL 61 1274 F.W.N. de Boer, R. van Dantzig (ANIK)
Also PRL 62 2644 (errat.) F.W.N. de Boer, R. van Dantzig (ANIK)
Also PRL 62 2638 D.H. Perkins (OXF)
Also PRL 62 2639 F.W.N. de Boer, R. van Dantzig (ANIK)
DEBOER 88C JP G14 L131 F.W.N. de Boer *et al.* (LOUV)
DOEHNER 88 PR D38 2722 J. Dohner *et al.* (HEIDP, ANL, ILLG)
EL-NADI 88 PRL 61 1271 M. el Nadi, O.E. Badawy (CAIR)
ENGEL 88 PR C37 731 J. Engel, P. Vogel, M.R. Zirnbauer
FAISSNER 88 ZPHY C37 231 H. Faissner *et al.* (AACH3, BERL, SIN)
HATSUDA 88B PL B203 469 T. Hatsuda, M. Yoshimura (KEK)
LORENZ 88 PL B214 10 E. Lorenz *et al.* (MPIM, PSI)
MAYLE 88 PL B203 188 R. Mayle *et al.* (LLL, CERN, MINN, FNAL+)
PICCIOTTO 88 PR D37 1131 C.E. Picciotto *et al.* (TRIU, CNRC)
RAFFELT 88 PRL 60 1793 G. Raffelt, D. Seckel (UCB, LLL, UCSC)
RAFFELT 88B PR D37 549 G.G. Raffelt, D.S.P. Dearborn (UCB, LLL)
SAVAGE 88 PR D37 1134 M.J. Savage, B.W. Filippone, L.W. Mitchell (CIT)
TSERTOS 88 PL B207 273 A. Tsertos *et al.* (GSI, ILLG)
TSERTOS 88B ZPHY A331 103 A. Tsertos *et al.* (GSI, ILLG)
VANKLINKEN 88 PL B205 223 J. van Klinken *et al.* (GRON, GSI)
VANKLINKEN 88B PRL 60 2442 J. van Klinken (GRON)
VONWIMMER... 88 PRL 60 2443 U. von Wimmersperg (BNL)
VOROBYOV 88 PL B208 146 P.V. Vorobiev, Y.I. Gitarts (NOVO)
DRUZHININ 87 ZPHY C37 1 V.P. Druzhinin *et al.* (NOVO)
FRIEMAN 87 PR D36 2201 J.A. Frieman, S. Dimopoulos, M.S. Turner (SLAC+)
GOLDMAN 87 PR D36 1543 T. Goldman *et al.* (LANL, CHIC, STAN+)
KORENCHE... 87 SJNP 46 192 S.M. Korenchenko *et al.* (JINR)
Translated from YAF 46 313.
MAIER 87 ZPHY A326 527 K. Maier *et al.* (STUT, GSI)
MILLS 87 PR D36 707 A.P. Mills, J. Levy (BELL)
RAFFELT 87 PR D36 2211 G.G. Raffelt, D.S.P. Dearborn (LLL, UCB)
RIORDAN 87 PRL 59 755 E.M. Riordan *et al.* (ROCH, CIT+)
TURNER 87 PRL 59 2489 M.S. Turner (FNAL, EFI)
VANBIBBER 87 PRL 59 759 K. van Bibber *et al.* (LLL, CIT, MIT+)
VONWIMMER... 87 PRL 59 266 U. von Wimmersperg *et al.* (WITW)
BADIER 86 ZPHY C31 21 J. Badier *et al.* (NA3 Collab.)
BROWN 86 PRL 57 2101 C.N. Brown *et al.* (FNAL, WASH, KYOT+)
BRYMAN 86B PRL 57 2787 D.A. Bryman, E.T.H. Clifford (TRIU)
DAVIER 86 PL B180 295 M. Davier, J. Jeanjean, H. Nguyen Ngoc (LALO)
DEARBORN 86 PRL 56 26 D.S.P. Dearborn, D.N. Schramm, G. Steigman (LLL+)
EICHLER 86 PL B175 101 R.A. Eichler *et al.* (SINDRUM Collab.)
HALLIN 86 PRL 57 2105 A.L. Hallin *et al.* (PRIN)
JODIDIO 86 PR D34 1967 A. Jodidio *et al.* (LBL, NWES, TRIU)
Also PR D37 237 (errat.) A. Jodidio *et al.* (LBL, NWES, TRIU)
KETOV 86 JETPL 44 146 S.N. Ketov *et al.* (KIAE)
Translated from ZETFP 44 114.
KOCH 86 NC 96A 182 H.R. Koch, O.W.B. Schult (JULI)
KONAKA 86 PRL 57 659 A. Konaka *et al.* (KYOT, KEK)
MAIANI 86 PL B175 359 L. Maiani, R. Petronzio, E. Zavattini (CERN)
PECCEI 86 PL B172 435 R.D. Peccei, T.T. Wu, T. Yanagida (DESY)
RAFFELT 86 PR D33 897 G.G. Raffelt (MPIM)
RAFFELT 86B PL 166B 402 G.G. Raffelt (MPIM)
SAVAGE 86B PRL 57 178 M.J. Savage *et al.* (CIT)
AMALDI 85 PL 153B 444 U. Amaldi *et al.* (CERN)
ANANEV 85 SJNP 41 585 V.D. Ananev *et al.* (JINR)
Translated from YAF 41 912.
BALTRUSAIT... 85 PRL 55 1842 R.M. Baltrusaitis *et al.* (Mark III Collab.)
BERGSMA 85 PL 157B 458 F. Bergsma *et al.* (CHARM Collab.)
KAPLAN 85 NP B260 215 D.B. Kaplan (HARV)
IWAMOTO 84 PRL 53 1198 N. Iwamoto (UCSB, WUSL)
YAMAZAKI 84 PRL 52 1089 T. Yamazaki *et al.* (INUS, KEK)
ABBOTT 83 PL 120B 133 L.F. Abbott, P. Sikivie (BRAN, FLOR)
CARBONI 83 PL 123B 349 G. Carboni, W. Dahme (CERN, MUNI)
CAVAIGNAC 83 PL 121B 193 J.F. Cavaignac *et al.* (ISNG, LAPP)
DICUS 83 PR D28 1778 D.A. Dicus, V.L. Teplitz (TEXA, UMD)

DINE	83	PL 120B 137	M. Dine, W. Fischler	(IAS, PENN)
ELLIS	83B	NP B223 252	J. Ellis, K.A. Olive	(CERN)
FAISSNER	83	PR D28 1198	H. Faissner *et al.*	(AACH)
FAISSNER	83B	PR D28 1787	H. Faissner *et al.*	(AACH3)
FRANK	83B	PR D28 1790	J.S. Frank *et al.*	(LANL, YALE, LBL+)
HOFFMAN	83	PR D28 660	C.M. Hoffman *et al.*	(LANL, ARZS)
PRESKILL	83	PL 120B 127	J. Preskill, M.B. Wise, F. Wilczek	(HARV, UCSBT)
SIKIVIE	83	PRL 51 1415	P. Sikivie	(FLOR)
Also		PRL 52 695 (errat.)	P. Sikivie	(FLOR)
ALEKSEEV	82	JETP 55 591	E.A. Alekseeva *et al.*	(KIAE)
		Translated from ZETF 82 1007.		
ALEKSEEV	82B	JETPL 36 116	G.D. Alekseev *et al.*	(MOSU, JINR)
		Translated from ZETFP 36 94.		
ASANO	82	PL 113B 195	Y. Asano *et al.*	(KEK, TOKY, INUS, OSAK)
BARROSO	82	PL 116B 247	A. Barroso, G.C. Branco	(LISB)
DATAR	82	PL 114B 63	V.M. Datar *et al.*	(BHAB)
EDWARDS	82	PRL 48 903	C. Edwards *et al.*	(Crystal Ball Collab.)
FETSCHER	82	JP G8 L147	W. Fetscher	(ETH)
FUKUGITA	82	PRL 48 1522	M. Fukugita, S. Watamura, M. Yoshimura	(KEK)
FUKUGITA	82B	PR D26 1840	M. Fukugita, S. Watamura, M. Yoshimura	(KEK)
LEHMANN	82	PL 115B 270	P. Lehmann *et al.*	(SACL)
RAFFELT	82	PL 119B 323	G. Raffelt, L. Stodolsky	(MPIM)
ZEHNDER	82	PL 110B 419	A. Zehnder, K. Gabathuler, J.L. Vuilleumier	(ETH+)
ASANO	81B	PL 107B 159	Y. Asano *et al.*	(KEK, TOKY, INUS, OSAK)
BARROSO	81	PL 106B 91	A. Barroso, N.C. Mukhopadhyay	(SIN)
FAISSNER	81	ZPHY C10 95	H. Faissner *et al.*	(AACH3)
FAISSNER	81B	PL 103B 234	H. Faissner *et al.*	(AACH3)
KIM	81	PL 105B 55	B.R. Kim, C. Stamm	(AACH3)
VUILLEUMIER	81	PL 101B 341	J.L. Vuilleumier *et al.*	(CIT, MUNI)
ZEHNDER	81	PL 104B 494	A. Zehnder	(ETH)
FAISSNER	80	PL 96B 201	H. Faissner *et al.*	(AACH3)
JACQUES	80	PR D21 1206	P.F. Jacques *et al.*	(RUTG, STEV, COLU)
SOUKAS	80	PRL 44 564	A. Soukas *et al.*	(BNL, HARV, ORNL, PENN)
BECHIS	79	PRL 42 1511	D.J. Bechis *et al.*	(UMD, COLU, AFRR)
CALAPRICE	79	PR D20 2708	F.P. Calaprice *et al.*	(PRIN)
COTEUS	79	PRL 42 1438	P. Coteus *et al.*	(COLU, ILL, BNL)
DISHAW	79	PL 85B 142	J.P. Dishaw *et al.*	(SLAC, CIT)
ZHITNITSKII	79	SJNP 29 517	A.R. Zhitnitsky, Y.I. Skovpen	(NOVO)
		Translated from YAF 29 1001.		
ALIBRAN	78	PL 74B 134	P. Alibran *et al.*	(Gargamelle Collab.)
ASRATYAN	78B	PL 79B 497	A.E. Asratyan *et al.*	(ITEP, SERP)
BELLOTTI	78	PL 76B 223	E. Bellotti, E. Fiorini, L. Zanotti	(MILA)
BOSETTI	78B	PL 74B 143	P.C. Bosetti *et al.*	(BEBC Collab.)
DICUS	78C	PR D18 1829	D.A. Dicus *et al.*	(TEXA, VPI, STAN)
DONNELLY	78	PR D18 1607	T.W. Donnelly *et al.*	(STAN)
Also		PRL 37 315	F. Reines, H.S. Gurr, H.W. Sobel	(UCI)
Also		PRL 33 179	H.S. Gurr, F. Reines, H.W. Sobel	(UCI)
HANSL	78D	PL 74B 139	T. Hansl *et al.*	(CDHS Collab.)
MICELMAC...	78	LNC 21 441	G.V. Mitselmakher, B. Pontecorvo	(JINR)
MIKAELIAN	78	PR D18 3605	K.O. Mikaelian	(FNAL, NWES)
SATO	78	PTP 60 1942	K. Sato	(KYOT)
VYSOTSKII	78	JETPL 27 502	M.I. Vysotsky *et al.*	(ASCI)
		Translated from ZETFP 27 533.		
YANG	78	PRL 41 523	T.C. Yang	(MASA)
PECCEI	77	PR D16 1791	R.D. Peccei, H.R. Quinn	(STAN, SLAC)
Also		PRL 38 1440	R.D. Peccei, H.R. Quinn	(STAN, SLAC)
REINES	76	PRL 37 315	F. Reines, H.S. Gurr, H.W. Sobel	(UCI)
GURR	74	PRL 33 179	H.S. Gurr, F. Reines, H.W. Sobel	(UCI)
ANAND	53	PRSL A22 183	B.M. Anand	

OTHER RELATED PAPERS

SREDNICKI	85	NP B260 689	M. Srednicki	(UCSB)
BARDEEN	78	PL 74B 229	W.A. Bardeen, S.-H.H. Tye	(FNAL)

Int. J. Mod. Phys. A 2026.41. Downloaded from www.worldscientific.com
by UNIVERSITY OF CALIFORNIA @ BERKELEY on 09/16/26. Re-use and distribution is strictly not permitted, except for Open Access articles.

Int. J. Mod. Phys. A 2026.41. Downloaded from www.worldscientific.com
by UNIVERSITY OF CALIFORNIA @ BERKELEY on 09/16/26. Reproduction is strictly not permitted, except for Open Access articles.

Int. J. Mod. Phys. A 2026.41. Downloaded from www.worldscientific.com
by UNIVERSITY OF CALIFORNIA @ BERKELEY on 09/16/26. Re-use and distribution is strictly not permitted, except for Open Access articles.

LEPTONS

e 1369
μ 1370
τ 1375
Heavy Charged Lepton Searches 1403
Neutrino Properties 1404
Number of Neutrino Types 1414
Double-β Decay 1416
Neutrino Mixing 1419
Heavy Neutral Leptons, Searches for 1440

Notes in the Listings

Neutrino properties 1404
Sum of neutrino masses (rev.) 1407
Number of light neutrino types from collider experiments . . . 1414

Related Reviews in Volume 1

56. Muon anomalous magnetic moment (rev.) 846
57. Muon decay parameters 853
58. τ branching fractions (rev.) 856
59. τ-lepton decay parameters 859

Int. J. Mod[redacted]wnloaded from www.worldscientific.com
by UNIVERSITY OF CALIFORNIA @ BERK[redacted]-use and distribution is strictly not permitted, except for Open Access articles.

Int. J. Mod. Phys. A 2026.41. Downloaded from www.worldscientific.com
by UNIVERSITY OF CALIFORNIA @ BERKELEY on 09/16/26. Re-use and distribution is strictly not permitted, except for Open Access articles.

LEPTONS

e $J = \frac{1}{2}$

e MASS (atomic mass units u)

The primary determination of an electron's mass comes from measuring the ratio of the mass to that of a nucleus, so that the result is obtained in u (atomic mass units). The conversion factor to MeV is more uncertain than the mass of the electron in u; indeed, the recent improvements in the mass determination are not evident when the result is given in MeV. In this datablock we give the result in u, and in the following datablock in MeV.

VALUE (10^{-6} u)		DOCUMENT ID		TECN	COMMENT
548.5799090441±0.0000000097		MOHR	25	RVUE	2022 CODATA value
• • • We do not use the following data for averages, fits, limits, etc. • • •					
548.579909065	±0.000000016	TIESINGA	21	RVUE	2018 CODATA value
548.579909070	±0.000000016	MOHR	16	RVUE	2014 CODATA value
548.57990946	±0.00000022	MOHR	12	RVUE	2010 CODATA value
548.57990943	±0.00000023	MOHR	08	RVUE	2006 CODATA value
548.57990945	±0.00000024	MOHR	05	RVUE	2002 CODATA value
548.5799092	±0.0000004	[1] BEIER	02	CNTR	Penning trap
548.5799110	±0.0000012	MOHR	99	RVUE	1998 CODATA value
548.5799111	±0.0000012	[2] FARNHAM	95	CNTR	Penning trap
548.579903	±0.000013	COHEN	87	RVUE	1986 CODATA value

[1] BEIER 02 compares Larmor frequency of the electron bound in a $^{12}C^{5+}$ ion with the cyclotron frequency of a single trapped $^{12}C^{5+}$ ion.
[2] FARNHAM 95 compares cyclotron frequency of trapped electrons with that of a single trapped $^{12}C^{6+}$ ion.

e MASS

The mass is known more precisely in u (atomic mass units) than in MeV. The conversion is: 1 u = 931.494 103 72(29) MeV/c^2 (2022 CODATA value, MOHR 25). The conversion error dominates the uncertainty of the masses given below.

VALUE (MeV)		DOCUMENT ID		TECN	COMMENT
0.51099895069±0.00000000016		MOHR	25	RVUE	2022 CODATA value
• • • We do not use the following data for averages, fits, limits, etc. • • •					
0.51099895000	±0.00000000015	TIESINGA	21	RVUE	2018 CODATA value
0.5109989461	±0.0000000031	MOHR	16	RVUE	2014 CODATA value
0.510998928	±0.000000011	MOHR	12	RVUE	2010 CODATA value
0.510998910	±0.000000013	MOHR	08	RVUE	2006 CODATA value
0.510998918	±0.000000044	MOHR	05	RVUE	2002 CODATA value
0.510998901	±0.000000020	[1,2] BEIER	02	CNTR	Penning trap
0.510998902	±0.000000021	MOHR	99	RVUE	1998 CODATA value
0.510998903	±0.000000020	[1,3] FARNHAM	95	CNTR	Penning trap
0.510998895	±0.000000024	[1] COHEN	87	RVUE	1986 CODATA value
0.5110034	±0.0000014	COHEN	73	RVUE	1973 CODATA value

[1] Converted to MeV using the 1998 CODATA value of the conversion constant, 931.494013 ± 0.000037 MeV/u.
[2] BEIER 02 compares Larmor frequency of the electron bound in a $^{12}C^{5+}$ ion with the cyclotron frequency of a single trapped $^{12}C^{5+}$ ion.
[3] FARNHAM 95 compares cyclotron frequency of trapped electrons with that of a single trapped $^{12}C^{6+}$ ion.

$(m_{e^+} - m_{e^-}) / m_{average}$

A test of CPT invariance.

VALUE	CL%	DOCUMENT ID		TECN	COMMENT
$<8 \times 10^{-9}$	90	[1] FEE	93	CNTR	Positronium spectroscopy
• • • We do not use the following data for averages, fits, limits, etc. • • •					
$<4 \times 10^{-23}$	90	[2] DOLGOV	14		From photon mass limit
$<4 \times 10^{-8}$	90	CHU	84	CNTR	Positronium spectroscopy

[1] FEE 93 value is obtained under the assumption that the positronium Rydberg constant is exactly half the hydrogen one.
[2] DOLGOV 14 result is obtained under the assumption that any mass difference between electron and positron would lead to a non-zero photon mass. The PDG 12 limit of 1×10^{-18} eV on the photon mass is in turn used to derive the value quoted here.

$|q_{e^+} + q_{e^-}|/e$

A test of CPT invariance. See also similar tests involving the proton.

VALUE	DOCUMENT ID		TECN	COMMENT
$<4 \times 10^{-8}$	[1] HUGHES	92	RVUE	
• • • We do not use the following data for averages, fits, limits, etc. • • •				
$<2 \times 10^{-18}$	[2] SCHAEFER	95	THEO	Vacuum polarization
$<1 \times 10^{-18}$	[3] MUELLER	92	THEO	Vacuum polarization

[1] HUGHES 92 uses recent measurements of Rydberg-energy and cyclotron-frequency ratios.
[2] SCHAEFER 95 removes model dependency of MUELLER 92.
[3] MUELLER 92 argues that an inequality of the charge magnitudes would, through higher-order vacuum polarization, contribute to the net charge of atoms.

e MAGNETIC MOMENT ANOMALY

$\mu_e/\mu_B - 1 = (g-2)/2$

VALUE (units 10^{-6})		DOCUMENT ID		TECN	CHG	COMMENT
1159.65218062±0.00000012 OUR AVERAGE						
1159.65218059	±0.00000013	[1] FAN	23	MRS		Single electron
1159.65218073	±0.00000028	HANNEKE	08	MRS		Single electron
1159.6521884	±0.0000043	VANDYCK	87	MRS	−	Single electron
• • • We do not use the following data for averages, fits, limits, etc. • • •						
1159.65218046	±0.00000018	MOHR	25	RVUE		2022 CODATA value
1159.65218128	±0.00000018	TIESINGA	21	RVUE		2018 CODATA value
1159.65218091	±0.00000026	MOHR	16	RVUE		2014 CODATA value
1159.65218076	±0.00000027	MOHR	12	RVUE		2010 CODATA value
1159.65218111	±0.00000074	[2] MOHR	08	RVUE		2006 CODATA value
1159.65218085	±0.00000076	[3] ODOM	06	MRS	−	Single electron
1159.6521859	±0.0000038	MOHR	05	RVUE		2002 CODATA value
1159.6521869	±0.0000041	MOHR	99	RVUE		1998 CODATA value
1159.652193	±0.000010	COHEN	87	RVUE		1986 CODATA value
1159.6521879	±0.0000043	[4] VANDYCK	87	MRS	+	Single positron

[1] FAN 23 report the most accurate measurement of the electron magnetic moment. A one-electron quantum cyclotron is used. We do not propagate at the moment this measurement to the fine structure and other physical constants. When discrepancies in the independent determinations of alpha are resolved, the new measurement uncertainty of 0.13 ppt is available for precise tests for BSM physics.
[2] MOHR 08 average is dominated by ODOM 06.
[3] Superseded by HANNEKE 08 per private communication with Gerald Gabrielse.
[4] This VANDYCK 87 reault is for a positron. We do not take it into account for the average to avoid the assumption of CPT invariance.

$(g_{e^+} - g_{e^-}) / g_{average}$

A test of CPT invariance.

VALUE (units 10^{-12})	CL%	DOCUMENT ID		TECN	COMMENT
− 0.5± 2.1		[1] VANDYCK	87	MRS	Penning trap
• • • We do not use the following data for averages, fits, limits, etc. • • •					
< 12	95	[2] VASSERMAN	87	CNTR	Assumes $m_{e^+} = m_{e^-}$
22 ±64		SCHWINBERG	81	MRS	Penning trap

[1] VANDYCK 87 measured $(g_-/g_+)-1$ and we converted it.
[2] VASSERMAN 87 measured $(g_+ - g_-)/(g-2)$. We multiplied by $(g-2)/g = 1.2 \times 10^{-3}$.

e ELECTRIC DIPOLE MOMENT (d)

A nonzero value is forbidden by both T invariance and P invariance.

VALUE (10^{-28} ecm)	CL%	DOCUMENT ID		TECN	COMMENT
< 0.041	90	[1] ROUSSY	23	ESR	electrons in intramolecular electric field
• • • We do not use the following data for averages, fits, limits, etc. • • •					
< 0.11	90	[2] ANDREEV	18	CNTR	ThO molecules
< 1.3	90	[3] CAIRNCROSS	17	ESR	$^{180}Hf^{19}F$ molecules
− 5570 ± 7980 ±120		KIM	15	CNTR	$Gd_3Ga_5O_{12}$ molecules
< 0.87	90	[4] BARON	14	CNTR	ThO molecules
< 6050	90	[5] ECKEL	12	CNTR	$Eu_{0.5}Ba_{0.5}TiO_3$ molecules
< 10.5	90	[6] HUDSON	11	NMR	YbF molecules
6.9 ± 7.4		REGAN	02	MRS	^{205}Tl beams
18 ± 12 ± 10		[7] COMMINS	94	MRS	^{205}Tl beams
− 27 ± 83		[7] ABDULLAH	90	MRS	^{205}Tl beams
− 1400 ± 2400		CHO	89	NMR	TlF molecules
− 150 ± 550 ±150		MURTHY	89		Cs, no B field
− 5000 ±11000		LAMOREAUX	87	NMR	^{199}Hg
19000 ±34000	90	SANDARS	75	MRS	Thallium
7000 ±22000	90	PLAYER	70	MRS	Xenon
< 30000	90	WEISSKOPF	68	MRS	Cesium

[1] ROUSSY 23 gives a measurement corresponding to this limit as $(-1.3 \pm 2.0 \pm 0.6) \times 10^{-30}$ ecm.
[2] ANDREEV 18 gives a measurement corresponding to this limit as $(4.3 \pm 3.1 \pm 2.6) \times 10^{-30}$ ecm.
[3] CAIRNCROSS 17 gives a measurement corresponding to this limit as $(0.09 \pm 0.77 \pm 0.17) \times 10^{-28}$ ecm.
[4] BARON 14 gives a measurement corresponding to this limit as $(-0.21 \pm 0.37 \pm 0.25) \times 10^{-28}$ ecm.
[5] ECKEL 12 gives a measurement corresponding to this limit as $(-1.07 \pm 3.06 \pm 1.74) \times 10^{-25}$ ecm.
[6] HUDSON 11 gives a measurement corresponding to this limit as $(-2.4 \pm 5.7 \pm 1.5) \times 10^{-28}$ ecm.
[7] ABDULLAH 90, COMMINS 94, and REGAN 02 use the relativistic enhancement of a valence electron's electric dipole moment in a high-Z atom.

Int. J. Mod
-use and distribution is strictly not permitted, except for Open Access articles.
by UNIVERSITY OF CALIFORNIA @ BERK
Downloaded from www.worldscientific.com

e^- MEAN LIFE / BRANCHING FRACTION

A test of charge conservation. See the "Note on Testing Charge Conservation and the Pauli Exclusion Principle" following this section in our 1992 edition (Physical Review **D45** S1 (1992), p. VI.10).

Most of these experiments are one of three kinds: Attempts to observe (a) the 255.5 keV gamma ray produced in $e^- \rightarrow \nu_e \gamma$, (b) the (K) shell x ray produced when an electron decays without additional energy deposit, e.g., $e^- \rightarrow \nu_e \overline{\nu}_e \nu_e$ ("disappearance" experiments), and (c) nuclear de-excitation gamma rays after the electron disappears from an atomic shell and the nucleus is left in an excited state. The last can include both weak boson and photon mediating processes. We use the best $e^- \rightarrow \nu_e \gamma$ limit for the Summary Tables.

Note that we use the mean life rather than the half life, which is often reported.

$e \rightarrow \nu_e \gamma$ and astrophysical limits

VALUE (yr)	CL%	DOCUMENT ID		TECN	COMMENT
$>6.6 \times 10^{28}$	90	AGOSTINI	15B	BORX	$e^- \rightarrow \nu\gamma$
• • • We do not use the following data for averages, fits, limits, etc. • • •					
$>5.4 \times 10^{25}$	90	[1] AGOSTINI	24A	HPGE	$e^- \rightarrow \nu\gamma$, ^{76}Ge detector
$>1.22 \times 10^{26}$	68	[2] KLAPDOR-K...	07	CNTR	$e^- \rightarrow \nu\gamma$
$>4.6 \times 10^{26}$	90	BACK	02	BORX	$e^- \rightarrow \nu\gamma$
$>3.4 \times 10^{26}$	68	BELLI	00B	DAMA	$e^- \rightarrow \nu\gamma$, liquid Xe
$>3.7 \times 10^{25}$	68	AHARONOV	95B	CNTR	$e^- \rightarrow \nu\gamma$
$>2.35 \times 10^{25}$	68	BALYSH	93	CNTR	$e^- \rightarrow \nu\gamma$, ^{76}Ge detector
$>1.5 \times 10^{25}$	68	AVIGNONE	86	CNTR	$e^- \rightarrow \nu\gamma$
$>1 \times 10^{39}$		[3] ORITO	85	ASTR	Astrophysical argument
$>3 \times 10^{23}$	68	BELLOTTI	83B	CNTR	$e^- \rightarrow \nu\gamma$

[1] AGOSTINI 24A search for coincident photons from the direct e-decay and from residual X-ray or Auger-e transitions.
[2] The authors of A. Derbin et al, arXiv:0704.2047v1 argue that this limit is overestimated by at least a factor of 5.
[3] ORITO 85 assumes that electromagnetic forces extend out to large enough distances and that the age of our galaxy is 10^{10} years.

Disappearance and nuclear-de-excitation experiments

VALUE (yr)	CL%	DOCUMENT ID		TECN	COMMENT
$>3.2 \times 10^{25}$	90	[1] ARNQUIST	24B	HPGE	Ge K-shell disappearance
• • • We do not use the following data for averages, fits, limits, etc. • • •					
$>1.2 \times 10^{24}$	90	ABGRALL	17	HPGE	Ge K-shell disappearance
$>4.2 \times 10^{24}$	68	BELLI	99	DAMA	Iodine L-shell disappearance
$>6.4 \times 10^{24}$	68	[2] BELLI	99B	DAMA	De-excitation of ^{129}Xe
$>2.4 \times 10^{23}$	90	[3] BELLI	99D	DAMA	De-excitation of ^{127}I (in NaI)
$>4.3 \times 10^{23}$	68	AHARONOV	95B	CNTR	Ge K-shell disappearance
$>2.7 \times 10^{23}$	68	REUSSER	91	CNTR	Ge K-shell disappearance
$>2 \times 10^{22}$	68	BELLOTTI	83B	CNTR	Ge K-shell disappearance

[1] ARNQUIST 24B limit on charge nonconserving e^- capture in 37.5 kg high-purity Ge implies limit on $e \rightarrow \nu\overline{\nu}\nu$ or more generally $e \rightarrow$ invisible.
[2] BELLI 99B limit on charge nonconserving e^- capture involving excitation of the 236.1 keV nuclear state of ^{129}Xe. The 90% CL limit is $>3.7 \times 10^{24}$ yr. Less stringent limits for other states are also given.
[3] BELLI 99D limit on charge nonconserving e^- capture involving excitation of the 57.6 keV nuclear state of ^{127}I. Less stringent limits for the other states and for the state of ^{23}Na are also given.

LIMITS ON LEPTON-FLAVOR VIOLATION IN PRODUCTION

Forbidden by lepton family number conservation.

This section was added for the 2008 edition of this *Review* and is not complete. For a list of further measurements see references in the papers listed below.

$\sigma(e^+e^- \rightarrow e^\pm\tau^\mp) / \sigma(e^+e^- \rightarrow \mu^+\mu^-)$

VALUE	CL%	DOCUMENT ID		TECN	COMMENT
$<8.9 \times 10^{-6}$	95	AUBERT	07P	BABR	e^+e^- at $E_{cm} = 10.58$ GeV
• • • We do not use the following data for averages, fits, limits, etc. • • •					
$<1.8 \times 10^{-3}$	95	GOMEZ-CAD...	91	MRK2	e^+e^- at $E_{cm} = 29$ GeV

$\sigma(e^+e^- \rightarrow \mu^\pm\tau^\mp) / \sigma(e^+e^- \rightarrow \mu^+\mu^-)$

VALUE	CL%	DOCUMENT ID		TECN	COMMENT
$<4.0 \times 10^{-6}$	95	AUBERT	07P	BABR	e^+e^- at $E_{cm} = 10.58$ GeV
• • • We do not use the following data for averages, fits, limits, etc. • • •					
$<6.1 \times 10^{-3}$	95	GOMEZ-CAD...	91	MRK2	e^+e^- at $E_{cm} = 29$ GeV

e REFERENCES

MOHR	25	RMP 97 025002	P.J. Mohr *et al.*	(NIST)
AGOSTINI	24A	EPJ C84 940	M. Agostini *et al.*	(GERDA Collab.)
ARNQUIST	24B	NATP 20 1078	I.J. Arnquist *et al.*	(MAJORANA Collab.)
FAN	23	PRL 130 071801	X. Fan *et al.*	(HARV, NWES)
ROUSSY	23	SCI 381 46	T.S. Roussy *et al.*	(COLO)
TIESINGA	21	RMP 93 025010	E. Tiesinga *et al.*	(NIST)
ANDREEV	18	NAT 562 355	V. Andreev *et al.*	(ACME Collab.)
ABGRALL	17	PRL 118 161801	N. Abgrall *et al.*	(MAJORANA Collab.)
CAIRNCROSS	17	PRL 119 153001	W.B. Cairncross *et al.*	(NIST,COLO)
MOHR	16	RMP 88 035009	P.J. Mohr, D.B. Newell, B.N. Taylor	(NIST)
AGOSTINI	15B	PRL 115 231802	M. Agostini *et al.*	(Borexino Collab.)
KIM	15	PR D91 102004	Y.J. Kim *et al.*	(IND, YALE, LANL)
BARON	14	SCI 343 269	J. Baron *et al.*	(ACME Collab.)
DOLGOV	14	PL B732 244	A.D. Dolgov, V.A. Novikov	
ECKEL	12	PRL 109 193003	S. Eckel, A.O. Sushkov, S.K. Lamoreaux	(YALE)
MOHR	12	RMP 84 1527	P.J. Mohr, B.N. Taylor, D.B. Newell	(NIST)
PDG	12	PR D86 010001	J. Beringer *et al.*	(PDG Collab.)
HUDSON	11	NAT 473 493	J.J. Hadson *et al.*	(LOIC)
HANNEKE	08	PRL 100 120801	D. Hanneke, S. Fogwell, G. Gabrielse	(HARV)
MOHR	08	RMP 80 633	P.J. Mohr, B.N. Taylor, D.B. Newell	(NIST)
AUBERT	07P	PR D75 031103	B. Aubert *et al.*	(BABAR Collab.)
KLAPDOR-K...	07	PL B644 109	H.V. Klapdor-Kleingrothaus, I.V. Krivosheina, I.V. Titkova	
ODOM	06	PRL 97 030801	B. Odom *et al.*	(HARV)
MOHR	05	RMP 77 1	P.J. Mohr, B.N. Taylor	(NIST)
BACK	02	PL B525 29	H.O. Back *et al.*	(Borexino/SASSO Collab.)
BEIER	02	PRL 88 011603	T. Beier *et al.*	
REGAN	02	PRL 88 071805	B.C. Regan *et al.*	
BELLI	00B	PR D61 117301	P. Belli *et al.*	(DAMA Collab.)
BELLI	99	PL B460 236	P. Belli *et al.*	(DAMA Collab.)
BELLI	99B	PL B465 315	P. Belli *et al.*	(DAMA Collab.)
BELLI	99D	PR C60 065501	P. Belli *et al.*	(DAMA Collab.)
MOHR	99	JPCRD 28 1713	P.J. Mohr, B.N. Taylor	(NIST)
Also		RMP 72 351	P.J. Mohr, B.N. Taylor	(NIST)
AHARONOV	95B	PR D52 3785	Y. Aharonov *et al.*	(SCUC, PNL, ZARA+)
Also		PL B353 168	Y. Aharonov *et al.*	(SCUC, PNL, ZARA+)
FARNHAM	95	PRL 75 3598	D.L. Farnham, R.S. van Dyck, P.B. Schwinberg	(WASH)
SCHAEFER	95	PR A51 838	A. Schaefer, J. Reinhardt	(FRAN)
COMMINS	94	PR A50 2960	E.D. Commins *et al.*	
BALYSH	93	PL B298 278	A. Balysh *et al.*	(KIAE, MPIK, SASSO)
FEE	93	PR A48 192	M.S. Fee *et al.*	
HUGHES	92	PRL 69 578	R.J. Hughes, B.I. Deutch	(LANL, AARH)
MUELLER	92	PRL 69 3432	B. Muller, M.H. Thoma	(DUKE)
PDG	92	PR D45 S1	K. Hikasa *et al.*	(KEK, LBL, BOST+)
GOMEZ-CAD...	91	PRL 66 1007	J.J. Gomez-Cadenas *et al.*	(SLAC MARK-2 Collab.)
REUSSER	91	PL B255 143	D. Reusser *et al.*	(NEUC, CIT, PSI)
ABDULLAH	90	PRL 65 2347	K. Abdullah *et al.*	(LBL, UCB)
CHO	89	PRL 63 2559	D. Cho, K. Sangster, E.A. Hinds	(YALE)
MURTHY	89	PRL 63 965	S.A. Murthy *et al.*	(AMHT)
COHEN	87	RMP 59 1121	E.R. Cohen, B.N. Taylor	(RISC, NBS)
LAMOREAUX	87	PRL 59 2275	S.K. Lamoreaux *et al.*	(WASH)
VANDYCK	87	PRL 59 26	R.S. van Dyck, P.B. Schwinberg, H.G. Dehmelt	(WASH)
VASSERMAN	87	PL B198 302	I.B. Vasserman *et al.*	(NOVO)
Also		PL B187 172	I.B. Vasserman *et al.*	(NOVO)
AVIGNONE	86	PR D34 97	F.T. Avignone *et al.*	(PNL, SCUC)
ORITO	85	PRL 54 2457	S. Orito, M. Yoshimura	(TOKY, KEK)
CHU	84	PRL 52 1689	S. Chu, A.P. Mills, J.L. Hall	(BELL, NBS, COLO)
BELLOTTI	83B	PL 124B 435	E. Bellotti *et al.*	(MILA)
SCHWINBERG	81	PRL 47 1679	P.B. Schwinberg, R.S. van Dyck, H.G. Dehmelt	(WASH)
SANDARS	75	PR A11 473	P.G.H. Sandars, D.M. Sternheimer	(OXF, BNL)
COHEN	73	JPCRD 2 664	E.R. Cohen, B.N. Taylor	(RISC, NBS)
PLAYER	70	JP B3 1620	M.A. Player, P.G.H. Sandars	(OXF)
WEISSKOPF	68	PRL 21 1645	M.C. Weisskopf *et al.*	(BRAN)

μ

$J = \frac{1}{2}$

μ MASS (atomic mass units u)

The muon's mass is obtained from the muon-electron mass ratio as determined from the measurement of Zeeman transition frequencies in muonium (μ^+e^- atom). Since the electron's mass is most accurately known in u, the muon's mass is also most accurately known in u. The conversion factor to MeV has approximately the same relative uncertainty as the mass of the muon in u. In this datablock we give the result in u, and in the following datablock in MeV.

VALUE (u)	DOCUMENT ID		TECN	COMMENT
0.1134289257 ± 0.0000000025	MOHR	25	RVUE	2022 CODATA value
• • • We do not use the following data for averages, fits, limits, etc. • • •				
0.1134289259 ± 0.0000000025	TIESINGA	21	RVUE	2018 CODATA value
0.1134289257 ± 0.0000000025	MOHR	16	RVUE	2014 CODATA value
0.1134289267 ± 0.0000000029	MOHR	12	RVUE	2010 CODATA value
0.1134289256 ± 0.0000000029	MOHR	08	RVUE	2006 CODATA value
0.1134289264 ± 0.0000000030	MOHR	05	RVUE	2002 CODATA value
0.1134289168 ± 0.0000000034	[1] MOHR	99	RVUE	1998 CODATA value
0.113428913 ± 0.000000017	[2] COHEN	87	RVUE	1986 CODATA value

[1] MOHR 99 make use of other 1998 CODATA entries below.
[2] COHEN 87 make use of other 1986 CODATA entries below.

μ MASS

The mass is known more precisely in u (atomic mass units) than in MeV. The conversion is: 1 u = 931.494 103 72(29) MeV/c^2 (2022 CODATA value, MOHR 25). The conversion error contributes significantly to the uncertainty of the masses given below.

VALUE (MeV)	DOCUMENT ID		TECN	CHG	COMMENT
105.6583755 ± 0.0000023	MOHR	25	RVUE		2022 CODATA value
• • • We do not use the following data for averages, fits, limits, etc. • • •					
105.6583755 ± 0.0000023	TIESINGA	21	RVUE		2018 CODATA value
105.6583745 ± 0.0000024	MOHR	16	RVUE		2014 CODATA value
105.6583715 ± 0.0000035	MOHR	12	RVUE		2010 CODATA value
105.6583668 ± 0.0000038	MOHR	08	RVUE		2006 CODATA value
105.6583692 ± 0.0000094	MOHR	05	RVUE		2002 CODATA value
105.6583568 ± 0.0000052	MOHR	99	RVUE		1998 CODATA value
105.658353 ± 0.000016	[1] COHEN	87	RVUE		1986 CODATA value
105.658386 ± 0.000044	[2] MARIAM	82	CNTR	+	
105.65836 ± 0.00026	[3] CROWE	72	CNTR		
105.65865 ± 0.00044	[4] CRANE	71	CNTR		

[1] Converted to MeV using the 1998 CODATA value of the conversion constant, 931.494013 ± 0.000037 MeV/u.

Int. J. Mod. Phys. A 2026.41. Downloaded from www.worldscientific.com
by UNIVERSITY OF CALIFORNIA @ BERKELEY on 09/16/26. Re-use and distribution is strictly not permitted, except for Open Access articles.

[2] MARIAM 82 give m_μ/m_e = 206.768259(62).
[3] CROWE 72 give m_μ/m_e = 206.7682(5).
[4] CRANE 71 give m_μ/m_e = 206.76878(85).

μ MEAN LIFE τ

Measurements with an error > 0.001×10^{-6} s have been omitted.

VALUE (10^{-6} s)	DOCUMENT ID		TECN	CHG	COMMENT
2.1969811±0.0000022 OUR AVERAGE					
2.1969803±0.0000021±0.0000007	[1] TISHCHENKO	13	CNTR	+	Surface μ^+ at PSI
2.197083 ±0.000032 ±0.000015	BARCZYK	08	CNTR	+	Muons from π^+ decay at rest
2.197013 ±0.000021 ±0.000011	CHITWOOD	07	CNTR	+	Surface μ^+ at PSI
2.197078 ±0.000073	BARDIN	84	CNTR	+	
2.197025 ±0.000155	BARDIN	84	CNTR	−	
2.19695 ±0.00006	GIOVANETTI	84	CNTR	+	
2.19711 ±0.00008	BALANDIN	74	CNTR	+	
2.1973 ±0.0003	DUCLOS	73	CNTR	+	
• • • We do not use the following data for averages, fits, limits, etc. • • •					
2.1969803±0.0000022	WEBBER	11	CNTR	+	Surface μ^+ at PSI

[1] TISHCHENKO 13 uses 1.6×10^{12} μ^+ events and supersedes WEBBER 11.

$\tau_{\mu^+}/\tau_{\mu^-}$ MEAN LIFE RATIO

A test of CPT invariance.

VALUE	DOCUMENT ID		TECN	COMMENT
1.000024±0.000078	BARDIN	84	CNTR	
• • • We do not use the following data for averages, fits, limits, etc. • • •				
1.0008 ±0.0010	BAILEY	79	CNTR	Storage ring
1.000 ±0.001	MEYER	63	CNTR	Mean life μ^+/μ^-

$(\tau_{\mu^+} - \tau_{\mu^-}) / \tau_{\text{average}}$

A test of CPT invariance. Calculated from the mean-life ratio, above.

VALUE	DOCUMENT ID
(2±8) × 10^{-5} OUR EVALUATION	

μ/p MAGNETIC MOMENT RATIO

This ratio is used to obtain a precise value of the muon mass and to reduce experimental muon Larmor frequency measurements to the muon magnetic moment anomaly. Measurements with an error > 0.00001 have been omitted. By convention, the minus sign on this ratio is omitted. CODATA values were fitted using their selection of data, plus other data from multiparameter fits.

VALUE	DOCUMENT ID		TECN	CHG	COMMENT
3.183345142±0.000000071	TIESINGA	21	RVUE		2018 CODATA value
• • • We do not use the following data for averages, fits, limits, etc. • • •					
3.183345142±0.000000071	MOHR	16	RVUE		2014 CODATA value
3.183345107±0.000000084	MOHR	12	RVUE		2010 CODATA value
3.183345137±0.000000085	MOHR	08	RVUE		2006 CODATA value
3.183345118±0.000000089	MOHR	05	RVUE		2002 CODATA value
3.18334513 ±0.00000039	LIU	99	CNTR	+	HFS in muonium
3.18334539 ±0.00000010	MOHR	99	RVUE		1998 CODATA value
3.18334547 ±0.00000047	COHEN	87	RVUE		1986 CODATA value
3.1833441 ±0.0000017	KLEMPT	82	CNTR	+	Precession strob
3.1833461 ±0.0000011	MARIAM	82	CNTR	+	HFS splitting
3.1833448 ±0.0000029	CAMANI	78	CNTR	+	See KLEMPT 82
3.1833403 ±0.0000044	CASPERSON	77	CNTR	+	HFS splitting
3.1833402 ±0.0000072	COHEN	73	RVUE		1973 CODATA value
3.1833467 ±0.0000082	CROWE	72	CNTR	+	Precession phase

See the related review(s):
Muon Anomalous Magnetic Moment

μ MAGNETIC MOMENT ANOMALY

The parity-violating decay of muons in a storage ring is observed. The difference frequency ω_a between the muon spin precession and the orbital angular frequency $(e/m_\mu c)\langle B\rangle$ is measured, as is the free proton NMR frequency ω_p, thus determining the ratio $R=\omega_a/\omega_p$. Given the magnetic moment ratio $\lambda=\mu_\mu/\mu_p$ (from hyperfine structure in muonium), $(g-2)/2 = R/(\lambda-R)$.

$\mu_\mu/(e\hbar/2m_\mu)-1 = (g_\mu-2)/2$

VALUE (units 10^{-10})	DOCUMENT ID		TECN	CHG	COMMENT
11659207.15 ± 1.45	[1] AGUILLARD	25	MUG2	±	Combined FNAL and BNL values
• • • We do not use the following data for averages, fits, limits, etc. • • •					
11659207.05 ± 1.48	[2] AGUILLARD	25	MUG2	+	Storage ring
11659205.5 ± 2.4	[3] AGUILLARD	23	MUG2	+	Storage ring
11659205.9 ± 2.2	[4] AGUILLARD	23	MUG2	±	Combined FNAL and BNL values
11659204.0 ± 5.4	ABI	21	MUG2	+	Storage ring
11659206.1 ± 4.1	[5] ABI	21	MUG2	±	Combined FNAL and BNL values
11659208.0 ± 5.4 ±3.3	BENNETT	06	MUG2	±	Average μ^+ and μ^-
11659208 ± 6	BENNETT	04	MUG2	±	Average μ^+ and μ^-
11659214 ± 8 ±3	BENNETT	04	MUG2	−	Storage ring
11659203 ± 6 ±5	BENNETT	04	MUG2	+	Storage ring
11659204 ± 7 ±5	BENNETT	02	MUG2	+	Storage ring
11659202 ± 14 ±6	BROWN	01	MUG2	+	Storage ring
11659191 ± 59	BROWN	00	MUG2	+	
11659100 ± 110	[6] BAILEY	79	CNTR	+	Storage ring
11659360 ± 120	[6] BAILEY	79	CNTR	−	Storage ring
11659230 ± 85	[6] BAILEY	79	CNTR	±	Storage ring
11620000 ±5000	CHARPAK	62	CNTR	+	

[1] AGUILLARD 25 combined their value with the previous independent BNL measurement of BENNETT 06.
[2] AGUILLARD 25 quote the combined value from all RUNS 1–6 (at 127 ppm precision). For the 2020–2023 data (Runs 4, 5, 6) alone AGUILLARD 25 measure a value of $(11659207.10 \pm 1.62) \times 10^{-10}$ (at precision of 139 ppb).
[3] This AGUILLARD 23 value is the combination of all 2018, 2019 and 2020 data, including the ABI 21 value. The new FNAL 2019 and 2020 data alone combined yield $(11659205.7 \pm 2.5) \times 10^{-10}$.
[4] AGUILLARD 23 combined their value with the previous independent BNL measurement of BENNETT 06.
[5] ABI 21 combined their value with the previous independent BNL measurement of BENNETT 06. ABI 21 also report that the difference of this combination with the standard model value of $(11659181.0 \pm 4.3) \times 10^{-10}$ (AOYAMA 20) has a significance of 4.2 σ.
[6] BAILEY 79 values recalculated by HUGHES 99 using the COHEN 87 μ/p magnetic moment. The improved MOHR 99 value does not change the result.

$(g_{\mu^+} - g_{\mu^-}) / g_{\text{average}}$

A test of CPT invariance.

VALUE (units 10^{-8})	DOCUMENT ID		TECN
−0.11±0.12	BENNETT	04	MUG2
• • • We do not use the following data for averages, fits, limits, etc. • • •			
−2.6 ±1.6	BAILEY	79	CNTR

μ ELECTRIC DIPOLE MOMENT (d)

A nonzero value is forbidden by both T invariance and P invariance.

VALUE (10^{-19} ecm)	CL%	DOCUMENT ID		TECN	CHG	COMMENT
< 1.8	95	[1] BENNETT	09	MUG2	±	Storage ring
• • • We do not use the following data for averages, fits, limits, etc. • • •						
< 0.19	90	[2] EMA	22			theory limit
−0.1 ±1.0		[3] BENNETT	09	MUG2	+	Storage ring
−0.1 ±0.7		[4] BENNETT	09	MUG2	−	Storage ring
−3.7 ±3.4		[5] BAILEY	78	CNTR	±	Storage ring
8.6 ±4.5		BAILEY	78	CNTR	+	Storage ring
0.8 ±4.3		BAILEY	78	CNTR	−	Storage ring

[1] This is the combination of the two BENNETT 09 measurements quoted here separately for μ^+ and μ^-. The result is also presented as a measurement of $(0.0 \pm 0.9) \times 10^{-19}$ e cm.
[2] EMA 22 determine indirect constraints on $|\mu_{EDM}|$ from EDM measurements performed on heavy atoms and molecules, based on the muon-loop induced light-by-light CP-odd amplitude.
[3] Also reported as the limit of $|d(\mu^+)| < 2.1 \times 10^{-19}$ e cm at 95% CL.
[4] Also reported as the limit of $|d(\mu^-)| < 1.5 \times 10^{-19}$ e cm at 95% CL.
[5] This is the combination of the two BAILEY 78 results quoted here separately for μ^+ and μ^-. BAILEY 78 uses the convention $d = 1/2 \cdot (d_{\mu^+} - d_{\mu^-})$ and reports 3.7 ± 3.4. We convert their result to use the same convention as BENNETT 09.

MUON-ELECTRON CHARGE RATIO ANOMALY $q_{\mu^+}/q_{e^-} + 1$

VALUE	DOCUMENT ID		TECN	CHG	COMMENT
(1.1±2.1) × 10^{-9}	[1] MEYER	00	CNTR	+	1s–2s muonium interval

[1] MEYER 00 measure the 1s–2s muonium interval, and then interpret the result in terms of muon-electron charge ratio q_{μ^+}/q_{e^-}.

μ^- DECAY MODES

μ^+ modes are charge conjugates of the modes below.

	Mode	Fraction (Γ_i/Γ)	Confidence level
Γ_1	$e^- \overline{\nu}_e \nu_\mu$	≈ 100%	
Γ_2	$e^- \overline{\nu}_e \nu_\mu \gamma$	[a] $(6.0 \pm 0.5) \times 10^{-8}$	
Γ_3	$e^- \overline{\nu}_e \nu_\mu e^+ e^-$	[b] $(3.4 \pm 0.4) \times 10^{-5}$	

Int. J. Mod
by UNIVERSITY OF CALIFORNIA @ BERK
wnloaded from www.worldscientific.com
-use and distribution is strictly not permitted, except for Open Access articles.

Lepton Family number (*LF*) violating modes

Γ_4	$e^- \nu_e \overline{\nu}_\mu$	*LF*	[c] < 1.2	%	90%
Γ_5	$e^- \gamma$	*LF*	< 1.5	$\times 10^{-13}$	90%
Γ_6	$e^- e^+ e^-$	*LF*	< 1.0	$\times 10^{-12}$	90%
Γ_7	$e^- 2\gamma$	*LF*	< 7.2	$\times 10^{-11}$	90%

[a] This only includes events with energy of $e > 45$ MeV and energy of $\gamma > 40$ MeV. Since the $e^- \overline{\nu}_e \nu_\mu$ and $e^- \overline{\nu}_e \nu_\mu \gamma$ modes cannot be clearly separated, we regard the latter mode as a subset of the former.

[b] See the Particle Listings below for the energy limits used in this measurement.

[c] A test of additive vs. multiplicative lepton family number conservation.

μ^- BRANCHING RATIOS

$\Gamma(e^- \overline{\nu}_e \nu_\mu \gamma)/\Gamma_{total}$ — Γ_2/Γ

VALUE	EVTS	DOCUMENT ID		TECN	COMMENT
$(6.03 \pm 0.14 \pm 0.53) \times 10^{-8}$	13k	[1] BALDINI	16A	SPEC	γ KE > 40 MeV
• • • We do not use the following data for averages, fits, limits, etc. • • •					
	862	BOGART	67	CNTR	γ KE > 14.5 MeV
$(3.3 \pm 1.3) \times 10^{-3}$		CRITTENDEN	61	CNTR	γ KE > 20 MeV
$(1.4 \pm 0.4) \times 10^{-2}$		CRITTENDEN	61	CNTR	γ KE > 10 MeV
	27	ASHKIN	59	CNTR	

[1] BALDINI 16 measurement refers to $\mu^+ \to e^+ \nu \overline{\nu} \gamma$ decay and requires energy of $e^+ > 45$ MeV and energy $\gamma > 40$ MeV.

$\Gamma(e^- \overline{\nu}_e \nu_\mu e^+ e^-)/\Gamma_{total}$ — Γ_3/Γ

VALUE (units 10^{-5})	EVTS	DOCUMENT ID		TECN	CHG	COMMENT
$3.4 \pm 0.2 \pm 0.3$	7443	[1] BERTL	85	SPEC	+	SINDRUM
• • • We do not use the following data for averages, fits, limits, etc. • • •						
2.2 ± 1.5	7	[2] CRITTENDEN	61	HLBC	+	$E(e^+e^-) > 10$ MeV
2	1	[3] GUREVICH	60	EMUL	+	
1.5 ± 1.0	3	[4] LEE	59	HBC	+	

[1] BERTL 85 has transverse momentum cut $p_T > 17$ MeV/c. Systematic error was increased by us.

[2] CRITTENDEN 61 count only those decays where total energy of either (e^+, e^-) combination is >10 MeV.

[3] GUREVICH 60 interpret their event as either virtual or real photon conversion. e^+ and e^- energies not measured.

[4] In the three LEE 59 events, the sum of energies $E(e^+) + E(e^-) + E(e^+)$ was 51 MeV, 55 MeV, and 33 MeV.

$\Gamma(e^- \nu_e \overline{\nu}_\mu)/\Gamma_{total}$ — Γ_4/Γ

Forbidden by the additive conservation law for lepton family number. A multiplicative law predicts this branching ratio to be 1/2. For a review see NEMETHY 81.

VALUE	CL%	DOCUMENT ID		TECN	CHG	COMMENT
< 0.012	90	[1] FREEDMAN	93	CNTR	+	ν oscillation search
• • • We do not use the following data for averages, fits, limits, etc. • • •						
< 0.018	90	KRAKAUER	91B	CALO	+	
< 0.05	90	[2] BERGSMA	83	CALO		$\overline{\nu}_\mu e \to \mu^- \overline{\nu}_e$
< 0.09	90	JONKER	80	CALO		See BERGSMA 83
-0.001 ± 0.061		WILLIS	80	CNTR	+	
0.13 ± 0.15		BLIETSCHAU	78	HLBC	$\pm$	Avg. of 4 values
< 0.25	90	EICHTEN	73	HLBC	+	

[1] FREEDMAN 93 limit on $\overline{\nu}_e$ observation is here interpreted as a limit on lepton family number violation.

[2] BERGSMA 83 gives a limit on the inverse muon decay cross-section ratio $\sigma(\overline{\nu}_\mu e^- \to \mu^- \overline{\nu}_e)/\sigma(\nu_\mu e^- \to \mu^- \nu_e)$, which is essentially equivalent to $\Gamma(e^- \nu_e \overline{\nu}_\mu)/\Gamma_{total}$ for small values like that quoted.

$\Gamma(e^- \gamma)/\Gamma_{total}$ — Γ_5/Γ

Forbidden by lepton family number conservation.

VALUE	CL%	DOCUMENT ID		TECN	CHG	COMMENT
$< 1.5 \times 10^{-13}$	90	[1] AFANACIEV	25A	SPEC	+	MEG II at PSI
• • • We do not use the following data for averages, fits, limits, etc. • • •						
$< 3.1 \times 10^{-13}$	90	[2] AFANACIEV	24	SPEC	+	MEG II at PSI
$< 4.2 \times 10^{-13}$	90	BALDINI	16	SPEC	+	MEG at PSI
$< 5.7 \times 10^{-13}$	90	ADAM	13B	SPEC	+	MEG at PSI
$< 2.4 \times 10^{-12}$	90	ADAM	11	SPEC	+	MEG at PSI
$< 2.8 \times 10^{-11}$	90	ADAM	10	SPEC	+	MEG at PSI
$< 1.2 \times 10^{-11}$	90	AHMED	02	SPEC	+	MEGA
$< 1.2 \times 10^{-11}$	90	BROOKS	99	SPEC	+	LAMPF
$< 4.9 \times 10^{-11}$	90	BOLTON	88	CBOX	+	LAMPF
$< 100 \times 10^{-11}$	90	AZUELOS	83	CNTR	+	TRIUMF
$< 17 \times 10^{-11}$	90	KINNISON	82	SPEC	+	LAMPF
$< 100 \times 10^{-11}$	90	SCHAAF	80	ELEC	+	SIN

[1] AFANACIEV 25A is based on all 2021-2022 data and supersedes previous results. A combination of MEG/MEG II would only improve the limit by a few % and thus is not reported separately by AFANACIEV 25A.

[2] AFANACIEV 24 reports results using data collected by MEGII in 2021 combined with the limit obtained by the MEG experiment. Supersedes BALDINI 16.

$\Gamma(e^- e^+ e^-)/\Gamma_{total}$ — Γ_6/Γ

Forbidden by lepton family number conservation.

VALUE (units 10^{-12})	CL%	DOCUMENT ID		TECN	CHG	COMMENT
< 1.0	90	[1] BELLGARDT	88	SPEC	+	SINDRUM
• • • We do not use the following data for averages, fits, limits, etc. • • •						
< 36	90	BARANOV	91	SPEC	+	ARES
< 35	90	BOLTON	88	CBOX	+	LAMPF
< 2.4	90	[1] BERTL	85	SPEC	+	SINDRUM
< 160	90	[1] BERTL	84	SPEC	+	SINDRUM
< 130	90	[1] BOLTON	84	CNTR		LAMPF

[1] These experiments assume a constant matrix element.

$\Gamma(e^- 2\gamma)/\Gamma_{total}$ — Γ_7/Γ

Forbidden by lepton family number conservation.

VALUE (units 10^{-11})	CL%	DOCUMENT ID		TECN	CHG	COMMENT
< 7.2	90	BOLTON	88	CBOX	+	LAMPF
• • • We do not use the following data for averages, fits, limits, etc. • • •						
< 1	90	[1] BALDINI	20	MEG		PSI
< 840	90	[2] AZUELOS	83	CNTR	+	TRIUMF
< 5000	90	[3] BOWMAN	78	CNTR		DEPOMMIER 77 data

[1] BALDINI 20 uses 7.5×10^{14} stopped muons to obtain limits on $\mu \to eX$ decay mediated by a new light particle X with lifetimes < 40 ps, which decays to $\gamma\gamma$ for X-mass ranges 20–45 MeV. The limit of the order $< 10^{-11}$ at 90% CL is for the mass range 20–30 MeV.

[2] AZUELOS 83 uses the phase space distribution of BOWMAN 78.

[3] BOWMAN 78 assumes an interaction Lagrangian local on the scale of the inverse μ mass.

LIMIT ON $\mu^- \to e^-$ CONVERSION

Forbidden by lepton family number conservation.

$\sigma(\mu^- {}^{32}S \to e^- {}^{32}S) / \sigma(\mu^- {}^{32}S \to \nu_\mu {}^{32}P^*)$

VALUE	CL%	DOCUMENT ID		TECN	COMMENT
$< 7 \times 10^{-11}$	90	BADERT...	80	STRC	SIN
• • • We do not use the following data for averages, fits, limits, etc. • • •					
$< 4 \times 10^{-10}$	90	BADERT...	77	STRC	SIN

$\sigma(\mu^- Cu \to e^- Cu) / \sigma(\mu^- Cu \to \text{capture})$

VALUE	CL%	DOCUMENT ID		TECN
• • • We do not use the following data for averages, fits, limits, etc. • • •				
$< 1.6 \times 10^{-8}$	90	BRYMAN	72	SPEC

$\sigma(\mu^- Ti \to e^- Ti) / \sigma(\mu^- Ti \to \text{capture})$

VALUE	CL%	DOCUMENT ID		TECN	COMMENT
$< 4.3 \times 10^{-12}$	90	[1] DOHMEN	93	SPEC	SINDRUM II
• • • We do not use the following data for averages, fits, limits, etc. • • •					
$< 4.6 \times 10^{-12}$	90	AHMAD	88	TPC	TRIUMF
$< 1.6 \times 10^{-11}$	90	BRYMAN	85	TPC	TRIUMF

[1] DOHMEN 93 assumes $\mu^- \to e^-$ conversion leaves the nucleus in its ground state, a process enhanced by coherence and expected to dominate.

$\sigma(\mu^- Pb \to e^- Pb) / \sigma(\mu^- Pb \to \text{capture})$

VALUE	CL%	DOCUMENT ID		TECN	COMMENT
$< 4.6 \times 10^{-11}$	90	HONECKER	96	SPEC	SINDRUM II
• • • We do not use the following data for averages, fits, limits, etc. • • •					
$< 4.9 \times 10^{-10}$	90	AHMAD	88	TPC	TRIUMF

$\sigma(\mu^- Au \to e^- Au) / \sigma(\mu^- Au \to \text{capture})$

VALUE	CL%	DOCUMENT ID		TECN	CHG	COMMENT
$< 7 \times 10^{-13}$	90	BERTL	06	SPEC	−	SINDRUM II

LIMIT ON $\mu^- \to e^+$ CONVERSION

Forbidden by total lepton number conservation.

$\sigma(\mu^- {}^{32}S \to e^+ {}^{32}Si^*) / \sigma(\mu^- {}^{32}S \to \nu_\mu {}^{32}P^*)$

VALUE	CL%	DOCUMENT ID		TECN	COMMENT
$< 9 \times 10^{-10}$	90	BADERT...	80	STRC	SIN
• • • We do not use the following data for averages, fits, limits, etc. • • •					
$< 1.5 \times 10^{-9}$	90	BADERT...	78	STRC	SIN

$\sigma(\mu^- {}^{127}I \to e^+ {}^{127}Sb^*) / \sigma(\mu^- {}^{127}I \to \text{anything})$

VALUE	CL%	DOCUMENT ID		TECN	COMMENT
$< 3 \times 10^{-10}$	90	[1] ABELA	80	CNTR	Radiochemical tech.

[1] ABELA 80 is upper limit for $\mu^- e^+$ conversion leading to particle-stable states of ${}^{127}Sb$. Limit for total conversion rate is higher by a factor less than 4 (G. Backenstoss, private communication).

$\sigma(\mu^- Cu \to e^+ Co) / \sigma(\mu^- Cu \to \nu_\mu Ni)$

VALUE	CL%	DOCUMENT ID		TECN
• • • We do not use the following data for averages, fits, limits, etc. • • •				
$< 2.6 \times 10^{-8}$	90	BRYMAN	72	SPEC
$< 2.2 \times 10^{-7}$	90	CONFORTO	62	OSPK

Int. J. Mod. Phys. A 2026.41. Downloaded from www.worldscientific.com
by UNIVERSITY OF CALIFORNIA @ BERKELEY on 09/16/26. Re-use and distribution is strictly not permitted, except for Open Access articles.

$\sigma(\mu^- \text{Ti} \rightarrow e^+ \text{Ca}) / \sigma(\mu^- \text{Ti} \rightarrow \text{capture})$

VALUE	CL%	EVTS	DOCUMENT ID		TECN	CHG	COMMENT
$<3.6 \times 10^{-11}$	90	1	[1,2] KAULARD	98	SPEC	−	SINDRUM II
• • • We do not use the following data for averages, fits, limits, etc. • • •							
$<1.7 \times 10^{-12}$	90	1	[2,3] KAULARD	98	SPEC	−	SINDRUM II
$<4.3 \times 10^{-12}$	90		[3] DOHMEN	93	SPEC		SINDRUM II
$<8.9 \times 10^{-11}$	90		[1] DOHMEN	93	SPEC		SINDRUM II
$<1.7 \times 10^{-10}$	90		[4] AHMAD	88	TPC		TRIUMF

[1] This limit assumes a giant resonance excitation of the daughter Ca nucleus (mean energy and width both 20 MeV).
[2] KAULARD 98 obtained these same limits using the unified classical analysis of FELDMAN 98.
[3] This limit assumes the daughter Ca nucleus is left in the ground state. However, the probability of this is unknown.
[4] Assuming a giant-resonance-excitation model.

LIMIT ON MUONIUM → ANTIMUONIUM CONVERSION

Forbidden by lepton family number conservation.

$R_g = G_C / G_F$

The effective Lagrangian for the $\mu^+ e^- \rightarrow \mu^- e^+$ conversion is assumed to be

$$\mathcal{L} = 2^{-1/2}\, G_C\, [\overline{\psi}_\mu \gamma_\lambda (1-\gamma_5)\, \psi_e]\, [\overline{\psi}_\mu \gamma_\lambda (1-\gamma_5)\, \psi_e] + \text{h.c.}$$

The experimental result is then an upper limit on G_C/G_F, where G_F is the Fermi coupling constant.

VALUE	CL%	EVTS	DOCUMENT ID		TECN	CHG	COMMENT
< 0.0030	90	1	[1] WILLMANN	99	SPEC	+	μ^+ at 26 GeV/c
• • • We do not use the following data for averages, fits, limits, etc. • • •							
< 0.14	90	1	[2] GORDEEV	97	SPEC	+	JINR phasotron
< 0.018	90	0	[3] ABELA	96	SPEC	+	μ^+ at 24 MeV
< 6.9	90		NI	93	CBOX		LAMPF
< 0.16	90		MATTHIAS	91	SPEC		LAMPF
< 0.29	90		HUBER	90B	CNTR		TRIUMF
<20	95		BEER	86	CNTR		TRIUMF
<42	95		MARSHALL	82	CNTR		

[1] WILLMANN 99 quote both probability $P_{M\overline{M}} < 8.3 \times 10^{-11}$ at 90%CL in a 0.1 T field and $R_g = G_C/G_F$.
[2] GORDEEV 97 quote limits on both $f = G_{MM}/GF$ and the probability $W_{MM} < 4.7 \times 10^{-7}$ (90% CL).
[3] ABELA 96 quote both probability $P_{M\overline{M}} < 8 \times 10^{-9}$ at 90% CL and $R_g = G_C/G_F$.

See the related review(s):
Muon Decay Parameters

μ DECAY PARAMETERS

ρ PARAMETER

($V-A$) theory predicts $\rho = 0.75$.

VALUE	EVTS	DOCUMENT ID		TECN	CHG	COMMENT
0.74979±0.00026 OUR AVERAGE						
0.74977±0.00012±0.00023		[1] BAYES	11	TWST	+	Surface μ^+
0.7518 ±0.0026		DERENZO	69	RVUE		
• • • We do not use the following data for averages, fits, limits, etc. • • •						
0.75014±0.00017±0.00045		[2] MACDONALD	08	TWST	+	Surface μ^+
0.75080±0.00032±0.00100	6G	[3] MUSSER	05	TWST	+	Surface μ^+
0.72 ±0.06 ±0.08		AMORUSO	04	ICAR		Liquid Ar TPC
0.762 ±0.008	170k	[4] FRYBERGER	68	ASPK	+	25–53 MeV e^+
0.760 ±0.009	280k	[4] SHERWOOD	67	ASPK	+	25–53 MeV e^+
0.7503 ±0.0026	800k	[4] PEOPLES	66	ASPK	+	20–53 MeV e^+

[1] The quoted systematic error includes a contribution of 0.00013 (added in quadrature) from uncertainties on radiative corrections and on the Michel parameter η.
[2] The quoted systematic error includes a contribution of 0.00011 (added in quadrature) from the dependence on the Michel parameter η.
[3] The quoted systematic error includes a contribution of 0.00023 (added in quadrature) from the dependence on the Michel parameter η.
[4] η constrained = 0. These values incorporated into a two parameter fit to ρ and η by DERENZO 69.

η PARAMETER

($V-A$) theory predicts $\eta = 0$.

VALUE	EVTS	DOCUMENT ID		TECN	CHG	COMMENT
0.057 ±0.034 OUR AVERAGE						
0.071 ±0.037 ±0.005	30M	DANNEBERG	05	CNTR	+	7–53 MeV e^+
0.011 ±0.081 ±0.026	5.3M	[1] BURKARD	85B	CNTR	+	9–53 MeV e^+
−0.12 ±0.21	6346	DERENZO	69	HBC	+	1.6–6.8 MeV e^+
• • • We do not use the following data for averages, fits, limits, etc. • • •						
−0.0021±0.0070±0.0010	30M	[2] DANNEBERG	05	CNTR	+	7–53 MeV e^+
−0.012 ±0.015 ±0.003	5.3M	[2] BURKARD	85B	CNTR	+	9–53 MeV e^+
−0.007 ±0.013	5.3M	[3] BURKARD	85B	FIT	+	9–53 MeV e^+
−0.7 ±0.5	170k	[4] FRYBERGER	68	ASPK	+	25–53 MeV e^+
−0.7 ±0.6	280k	[4] SHERWOOD	67	ASPK	+	25–53 MeV e^+
0.05 ±0.5	800k	[4] PEOPLES	66	ASPK	+	20–53 MeV e^+
−2.0 ±0.9	9213	[5] PLANO	60	HBC	+	Whole spectrum

[1] Previously we used the global fit result from BURKARD 85B in OUR AVERAGE, we now only include their actual measurement.
[2] $\alpha = \alpha' = 0$ assumed.
[3] Global fit to all measured parameters. The fit correlation coefficients are given in BURKARD 85B.
[4] ρ constrained = 0.75.
[5] Two parameter fit to ρ and η; PLANO 60 discounts value for η.

δ PARAMETER

($V-A$) theory predicts $\delta = 0.75$.

VALUE	EVTS	DOCUMENT ID		TECN	CHG	COMMENT
0.75047±0.00034 OUR AVERAGE						
0.75049±0.00021±0.00027		[1] BAYES	11	TWST	+	Surface μ^+
0.7486 ±0.0026 ±0.0028		[2] BALKE	88	SPEC	+	Surface μ^+
• • • We do not use the following data for averages, fits, limits, etc. • • •						
0.75067±0.00030±0.00067		MACDONALD	08	TWST	+	Surface μ^+
0.74964±0.00066±0.00112	6G	GAPONENKO	05	TWST	+	Surface μ^+
		[3] VOSSLER	69			
0.752 ±0.009	490k	FRYBERGER	68	ASPK	+	25–53 MeV e^+
0.782 ±0.031		KRUGER	61			
0.78 ±0.05	8354	PLANO	60	HBC	+	Whole spectrum

[1] The quoted systematic error includes a contribution of 0.00006 (added in quadrature) from uncertainties on radiative corrections and on the Michel parameter η.
[2] BALKE 88 uses $\rho = 0.752 \pm 0.003$.
[3] VOSSLER 69 has measured the asymmetry below 10 MeV. See comments about radiative corrections in VOSSLER 69.

|(ξ PARAMETER)×(μ LONGITUDINAL POLARIZATION)|

($V-A$) theory predicts $\xi = 1$, longitudinal polarization = 1.

VALUE	DOCUMENT ID		TECN	CHG	COMMENT
1.0009 $^{+0.0016}_{-0.0007}$ OUR AVERAGE					
1.00084±0.00029$^{+0.00165}_{-0.00063}$	BUENO	11	TWST		Surface μ^+ beam
1.0027 ±0.0079 ±0.0030	BELTRAMI	87	CNTR		SIN, π decay in flight
• • • We do not use the following data for averages, fits, limits, etc. • • •					
1.0003 ±0.0006 ±0.0038	JAMIESON	06	TWST	+	surface μ^+ beam
1.0013 ±0.0030 ±0.0053	[1] IMAZATO	92	SPEC	+	$K^+ \rightarrow \mu^+ \nu_\mu$
0.975 ±0.015	AKHMANOV	68	EMUL		140 kG
0.975 ±0.030	GUREVICH	64	EMUL		See AKHMANOV 68
0.903 ±0.027	[2] ALI-ZADE	61	EMUL	+	27 kG
0.93 ±0.06	PLANO	60	HBC	+	8.8 kG
0.97 ±0.05	BARDON	59	CNTR		Bromoform target

[1] The corresponding 90% confidence limit from IMAZATO 92 is $|\xi P_\mu| > 0.990$. This measurement is of K^+ decay, not π^+ decay, so we do not include it in an average, nor do we yet set up a separate data block for K results.
[2] Depolarization by medium not known sufficiently well.

ξ × (μ LONGITUDINAL POLARIZATION) × δ / ρ

VALUE	CL%	DOCUMENT ID		TECN	CHG	COMMENT
1.00179$^{+0.00156}_{-0.00071}$		[1] BAYES	11	TWST	+	Surface μ^+ beam
• • • We do not use the following data for averages, fits, limits, etc. • • •						
>0.99682	90	[2] JODIDIO	86	SPEC	+	TRIUMF
>0.9966	90	[3] STOKER	85	SPEC	+	μ-spin rotation
>0.9959	90	CARR	83	SPEC	+	11 kG

[1] BAYES 11 obtains the limit > 0.99909 (90% CL) with the constraint that $\xi\times(\mu$ LONGITUDINAL POLARIZATION$) \times \delta/\rho \leq 1.0$.
[2] JODIDIO 86 includes data from CARR 83 and STOKER 85. The value here is from the erratum.
[3] STOKER 85 find $(\xi P_\mu \delta/\rho) > 0.9955$ and > 0.9966, where the first limit is from new μ spin-rotation data and the second is from combination with CARR 83 data. In $V-A$ theory, $(\delta/\rho) = 1.0$.

ξ' = LONGITUDINAL POLARIZATION OF e^+

($V-A$) theory predicts the longitudinal polarization = ±1 for $e^\pm$, respectively. We have flipped the sign for e^- so our programs can average.

VALUE	EVTS	DOCUMENT ID		TECN	CHG	COMMENT
1.00 ±0.04 OUR AVERAGE						
0.998±0.045	1M	BURKARD	85	CNTR	+	Bhabha + annihil
0.89 ±0.28	29k	SCHWARTZ	67	OSPK	−	Moller scattering
0.94 ±0.38		BLOOM	64	CNTR	+	Brems. transmiss.
1.04 ±0.18		DUCLOS	64	CNTR	+	Bhabha scattering
1.05 ±0.30		BUHLER	63	CNTR	+	Annihilation

ξ'' PARAMETER

VALUE	EVTS	DOCUMENT ID		TECN	CHG	COMMENT
0.98 ±0.04 OUR AVERAGE						
0.981±0.045±0.003	3.87M	PRIEELS	14	CNTR	+	Bhabha + annihil
0.65 ±0.36	326k	[1] BURKARD	85	CNTR	+	Bhabha + annihil

[1] BURKARD 85 measure $(\xi''-\xi\xi')/\xi$ and ξ' and set $\xi = 1$.

TRANSVERSE e^+ POLARIZATION IN PLANE OF μ SPIN, e^+ MOMENTUM

VALUE (units 10^{-3})	EVTS	DOCUMENT ID		TECN	CHG	COMMENT
7 ± 8 OUR AVERAGE						
6.3± 7.7± 3.4	30M	DANNEBERG	05	CNTR	+	7–53 MeV e^+
16 ±21 ±10	5.3M	BURKARD	85B	CNTR	+	Annihil 9–53 MeV

Int. J. Mod
by UNIVERSITY OF CALIFORNIA @ BERK
wnloaded from www.worldscientific.com
-use and distribution is strictly not permitted, except for Open Access articles.

TRANSVERSE e^+ POLARIZATION NORMAL TO PLANE OF μ SPIN, e^+ MOMENTUM

Zero if T invariance holds.

VALUE (units 10^{-3})	EVTS	DOCUMENT ID		TECN	CHG	COMMENT
−2 ± 8 OUR AVERAGE						
−3.7± 7.7±3.4	30M	DANNEBERG	05	CNTR	+	7–53 MeV e^+
7 ±22 ±7	5.3M	BURKARD	85B	CNTR	+	Annihil 9–53 MeV

α/A

VALUE (units 10^{-3})	EVTS	DOCUMENT ID		TECN	CHG	COMMENT
0.4± 4.3		[1] BURKARD	85B	FIT		
• • • We do not use the following data for averages, fits, limits, etc. • • •						
15 ±50 ±14	5.3M	BURKARD	85B	CNTR	+	9–53 MeV e^+

[1] Global fit to all measured parameters. Correlation coefficients are given in BURKARD 85B.

α'/A

Zero if T invariance holds.

VALUE (units 10^{-3})	EVTS	DOCUMENT ID		TECN	CHG	COMMENT
−10 ±20 OUR AVERAGE						
− 3.4±21.3± 4.9	30M	DANNEBERG	05	CNTR	+	7–53 MeV e^+
−47 ±50 ±14	5.3M	[1] BURKARD	85B	CNTR	+	9–53 MeV e^+
• • • We do not use the following data for averages, fits, limits, etc. • • •						
− 0.2± 4.3		[2] BURKARD	85B	FIT		

[1] Previously we used the global fit result from BURKARD 85B in OUR AVERAGE, we now only include their actual measurement. BURKARD 85B measure e^+ polarizations P_{T_1} and P_{T_2} versus e^+ energy.

[2] Global fit to all measured parameters. The fit correlation coefficients are given in BURKARD 85B.

β/A

VALUE (units 10^{-3})	EVTS	DOCUMENT ID		TECN	CHG	COMMENT
3.9± 6.2		[1] BURKARD	85B	FIT		
• • • We do not use the following data for averages, fits, limits, etc. • • •						
2 ±17 ±6	5.3M	BURKARD	85B	CNTR	+	9–53 MeV e^+

[1] Global fit to all measured parameters. The fit correlation coefficients are given in BURKARD 85B.

β'/A

Zero if T invariance holds.

VALUE (units 10^{-3})	EVTS	DOCUMENT ID		TECN	CHG	COMMENT
2 ± 7 OUR AVERAGE						
− 0.5± 7.8±1.8	30M	DANNEBERG	05	CNTR	+	7–53 MeV e^+
17 ±17 ±6	5.3M	[1] BURKARD	85B	CNTR	+	9–53 MeV e^+
• • • We do not use the following data for averages, fits, limits, etc. • • •						
− 1.3± 3.5±0.6	30M	[2] DANNEBERG	05	CNTR	+	7–53 MeV e^+
1.5± 6.3		[3] BURKARD	85B	FIT		

[1] Previously we used the global fit result from BURKARD 85B in OUR AVERAGE, we now only include their actual measurement. BURKARD 85B measure e^+ polarizations P_{T_1} and P_{T_2} versus e^+ energy.

[2] $\alpha = \alpha' = 0$ assumed.

[3] Global fit to all measured parameters. The fit correlation coefficients are given in BURKARD 85B.

a/A

This comes from an alternative parameterization to that used in the Summary Table (see the "Note on Muon Decay Parameters" above).

VALUE (units 10^{-3})	CL%	DOCUMENT ID		TECN
• • • We do not use the following data for averages, fits, limits, etc. • • •				
<15.9	90	[1] BURKARD	85B	FIT

[1] Global fit to all measured parameters. Correlation coefficients are given in BURKARD 85B.

a'/A

This comes from an alternative parameterization to that used in the Summary Table (see the "Note on Muon Decay Parameters" above).

VALUE (units 10^{-3})	DOCUMENT ID		TECN
• • • We do not use the following data for averages, fits, limits, etc. • • •			
5.3±4.1	[1] BURKARD	85B	FIT

[1] Global fit to all measured parameters. Correlation coefficients are given in BURKARD 85B.

$(b'+b)/A$

This comes from an alternative parameterization to that used in the Summary Table (see the "Note on Muon Decay Parameters" above).

VALUE (units 10^{-3})	CL%	DOCUMENT ID		TECN
• • • We do not use the following data for averages, fits, limits, etc. • • •				
<1.04	90	[1] BURKARD	85B	FIT

[1] Global fit to all measured parameters. Correlation coefficients are given in BURKARD 85B.

c/A

This comes from an alternative parameterization to that used in the Summary Table (see the "Note on Muon Decay Parameters" above).

VALUE (units 10^{-3})	CL%	DOCUMENT ID		TECN
• • • We do not use the following data for averages, fits, limits, etc. • • •				
<6.4	90	[1] BURKARD	85B	FIT

[1] Global fit to all measured parameters. Correlation coefficients are given in BURKARD 85B.

c'/A

This comes from an alternative parameterization to that used in the Summary Table (see the "Note on Muon Decay Parameters" above).

VALUE (units 10^{-3})	DOCUMENT ID		TECN
• • • We do not use the following data for averages, fits, limits, etc. • • •			
3.5±2.0	[1] BURKARD	85B	FIT

[1] Global fit to all measured parameters. Correlation coefficients are given in BURKARD 85B.

$\overline{\eta}$ PARAMETER

$(V-A)$ theory predicts $\overline{\eta} = 0$. $\overline{\eta}$ affects spectrum of radiative muon decay.

VALUE	DOCUMENT ID		TECN	CHG	COMMENT
0.02 ±0.08 OUR AVERAGE					
−0.014±0.090	EICHENBER...	84	ELEC	+	ρ free
+0.09 ±0.14	BOGART	67	CNTR	+	
• • • We do not use the following data for averages, fits, limits, etc. • • •					
−0.035±0.098	EICHENBER...	84	ELEC	+	ρ=0.75 assumed

μ REFERENCES

AFANACIEV	25A	EPJ C85 1177	K. Afanaciev *et al.*	(MEG II Collab.)
Also		EPJ C85 1317 (errat.)	K. Afanaciev *et al.*	(MEG II Collab.)
AGUILLARD	25	PRL 135 101802	D.P. Aguillard *et al.*	(Muon g-2 Collab.)
MOHR	25	RMP 97 025002	P.J. Mohr *et al.*	(NIST)
AFANACIEV	24	EPJ C84 216	K. Afanaciev *et al.*	(MEG II Collab.)
AGUILLARD	23	PRL 131 161802	D.P. Aguillard *et al.*	(Muon g-2 Collab.)
EMA	22	PRL 128 131803	Y. Ema, T. Gao, M. Pospelov	(DESY, MINN)
ABI	21	PRL 126 141801	B. Abi *et al.*	(Muon g-2 Collab.)
TIESINGA	21	RMP 93 025010	E. Tiesinga *et al.*	(NIST)
AOYAMA	20	PRPL 887 1	T. Aoyama *et al.*	
BALDINI	20	EPJ C80 858	A.M. Baldini *et al.*	(MEG Collab.)
BALDINI	16	EPJ C76 434	A.M. Baldini *et al.*	(MEG Collab.)
BALDINI	16A	EPJ C76 108	A.M. Baldini *et al.*	(MEG Collab.)
MOHR	16	RMP 88 035009	P.J. Mohr, D.B. Newell, B.N. Taylor	(NIST)
PRIEELS	14	PR D90 112003	R. Prieels *et al.*	(LOUV, ETH, PSI+)
ADAM	13B	PRL 110 201801	J. Adam *et al.*	(MEG Collab.)
TISHCHENKO	13	PR D87 052003	V. Tishchenko *et al.*	(MuLan Collab.)
MOHR	12	RMP 84 1527	P.J. Mohr, B.N. Taylor, D.B. Newell	(NIST)
ADAM	11	PRL 107 171801	J. Adam *et al.*	(MEG Collab.)
BAYES	11	PRL 106 041804	R. Bayes *et al.*	(TWIST Collab.)
Also		PR D85 092013	A. Hillairet *et al.*	(TWIST Collab.)
BUENO	11	PR D84 032005	J.F. Bueno *et al.*	(TWIST Collab.)
Also		PR D85 039908 (errat.)	J.F. Bueno *et al.*	(TWIST Collab.)
WEBBER	11	PRL 106 041803	D.M. Webber *et al.*	(MuLan Collab.)
Also		PRL 106 079901 (errat.)	D.M. Webber *et al.*	(MuLan Collab.)
ADAM	10	NP B834 1	J. Adam *et al.*	(MEG Collab.)
BENNETT	09	PR D80 052008	G.W. Bennett *et al.*	(MUG-2 Collab.)
BARCZYK	08	PL B663 172	A. Barczyk *et al.*	(FAST Collab.)
MACDONALD	08	PR D78 032010	R.P. MacDonald *et al.*	(TWIST Collab.)
MOHR	08	RMP 80 633	P.J. Mohr, B.N. Taylor, D.B. Newell	(NIST)
CHITWOOD	07	PRL 99 032001	D.B. Chitwood *et al.*	(MULAN Collab.)
BENNETT	06	PR D73 072003	G.W. Bennett *et al.*	(MUG-2 Collab.)
BERTL	06	EPJ C47 337	W. Bertl *et al.*	(SINDRUM II Collab.)
JAMIESON	06	PR D74 072007	B. Jamieson *et al.*	(TWIST Collab.)
DANNEBERG	05	PRL 94 021802	N. Danneberg *et al.*	(ETH, JAGL, PSI+)
GAPONENKO	05	PR D71 071101	A. Gaponenko *et al.*	(TWIST Collab.)
MOHR	05	RMP 77 1	P.J. Mohr, B.N. Taylor	(NIST)
MUSSER	05	PRL 94 101805	J.R. Musser *et al.*	(TWIST Collab.)
AMORUSO	04	EPJ C33 233	S. Amoruso *et al.*	(ICARUS Collab.)
BENNETT	04	PRL 92 161802	G.W. Bennett *et al.*	(Muon g-2 Collab.)
AHMED	02	PR D65 112002	M. Ahmed *et al.*	(MEGA Collab.)
BENNETT	02	PRL 89 101804	G.W. Bennett *et al.*	(Muon g-2 Collab.)
BROWN	01	PRL 86 2227	H.N. Brown *et al.*	(Muon g-2 Collab.)
BROWN	00	PR D62 091101	H.N. Brown *et al.*	(BNL/G-2 Collab.)
MEYER	00	PRL 84 1136	V. Meyer *et al.*	
BROOKS	99	PRL 83 1521	M.L. Brooks *et al.*	(MEGA/LAMPF Collab.)
HUGHES	99	RMP 71 S133	V.W. Hughes, T. Kinoshita	
LIU	99	PRL 82 711	W. Liu *et al.*	(LAMPF Collab.)
MOHR	99	JPCRD 28 1713	P.J. Mohr, B.N. Taylor	(NIST)
Also		RMP 72 351	P.J. Mohr, B.N. Taylor	(NIST)
WILLMANN	99	PRL 82 49	L. Willmann *et al.*	
FELDMAN	98	PR D57 3873	G.J. Feldman, R.D. Cousins	
KAULARD	98	PL B422 334	J. Kaulard *et al.*	(SINDRUM-II Collab.)
GORDEEV	97	PAN 60 1164	V.A. Gordeev *et al.*	(PNPI)
		Translated from YAF 60 1291.		
ABELA	96	PRL 77 1950	R. Abela *et al.*	(PSI, ZURI, HEIDH, TBIL+)
HONECKER	96	PRL 76 200	W. Honecker *et al.*	(SINDRUM II Collab.)
DOHMEN	93	PL B317 631	C. Dohmen *et al.*	(PSI SINDRUM-II Collab.)
FREEDMAN	93	PR D47 811	S.J. Freedman *et al.*	(LAMPF E645 Collab.)
NI	93	PR D48 1976	B. Ni *et al.*	(LAMPF Crystal-Box Collab.)
IMAZATO	92	PRL 69 877	J. Imazato *et al.*	(KEK, INUS, TOKY+)
BARANOV	91	SJNP 53 802	V.A. Baranov *et al.*	(JINR)
		Translated from YAF 53 1302.		
KRAKAUER	91B	PL B263 534	D.A. Krakauer *et al.*	(UMD, UCI, LANL)
MATTHIAS	91	PRL 66 2716	B.E. Matthias *et al.*	(YALE, HEIDP, WILL+)
Also		PRL 67 932 (errat.)	B.E. Matthias *et al.*	(YALE, HEIDP, WILL+)
HUBER	90B	PR D41 2709	T.M. Huber *et al.*	(WYOM, VICT, ARIZ+)
AHMAD	88	PR D38 2102	S. Ahmad *et al.*	(TRIU, VICT, VPI, BRCO+)
Also		PRL 59 970	S. Ahmad *et al.*	(TRIU, VPI, VICT, BRCO+)
BALKE	88	PR D37 587	B. Balke *et al.*	(LBL, UCB, COLO, NWES+)
BELLGARDT	88	NP B299 1	U. Bellgardt *et al.*	(SINDRUM Collab.)
BOLTON	88	PR D38 2077	R.D. Bolton *et al.*	(LANL, STAN, CHIC+)
Also		PRL 56 2461	R.D. Bolton *et al.*	(LANL, STAN, CHIC+)
Also		PRL 57 3241	D. Grosnick *et al.*	(CHIC, LANL, STAN+)
BELTRAMI	87	PL B194 326	I. Beltrami *et al.*	(ETH, SIN, MAINZ)
COHEN	87	RMP 59 1121	E.R. Cohen, B.N. Taylor	(RISC, NBS)
BEER	86	PRL 57 671	G.A. Beer *et al.*	(VICT, TRIU, WYOM)
JODIDIO	86	PR D34 1967	A. Jodidio *et al.*	(LBL, NWES, TRIU)
Also		PR D37 237 (errat.)	A. Jodidio *et al.*	(LBL, NWES, TRIU)

Int. J. Mod. Phys. A 2026.41. Downloaded from www.worldscientific.com
by UNIVERSITY OF CALIFORNIA @ BERKELEY on 09/16/26. Re-use and distribution is strictly not permitted, except for Open Access articles.

BERTL	85	NP B260 1	W. Bertl *et al.*	(SINDRUM Collab.)
BRYMAN	85	PRL 55 465	D.A. Bryman *et al.*	(TRIU, CNRC, BRCO+)
BURKARD	85	PL 150B 242	H. Burkhardt *et al.*	(ETH, SIN, MAINZ)
BURKARD	85B	PL 160B 343	H. Burkhardt *et al.*	(ETH, SIN, MAINZ)
Also		PR D24 2004	F. Corriveau *et al.*	(ETH, SIN, MAINZ)
Also		PL 129B 260	F. Corriveau *et al.*	(ETH, SIN, MAINZ)
STOKER	85	PRL 54 1887	D.P. Stoker *et al.*	(LBL, NWES, TRIU)
BARDIN	84	PL 137B 135	G. Bardin *et al.*	(SACL, CERN, BGNA, FIRZ)
BERTL	84	PL 140B 299	W. Bertl *et al.*	(SINDRUM Collab.)
BOLTON	84	PRL 53 1415	R.D. Bolton *et al.*	(LANL, CHIC, STAN+)
EICHENBER...	84	NP A412 523	W. Eichenberger, R. Engfer, A. van der Schaff	
GIOVANETTI	84	PR D29 343	K.L. Giovanetti *et al.*	(WILL)
AZUELOS	83	PRL 51 164	G. Azuelos *et al.*	(MONT, TRIU, BRCO)
Also		PRL 39 1113	P. Depommier *et al.*	(MONT, BRCO, TRIU+)
BERGSMA	83	PL 122B 465	F. Bergsma *et al.*	(CHARM Collab.)
CARR	83	PRL 51 627	J. Carr *et al.*	(LBL, NWES, TRIU)
KINNISON	82	PR D25 2846	W.W. Kinnison *et al.*	(EFI, STAN, LANL)
Also		PRL 42 556	J.D. Bowman *et al.*	(LASL, EFI, STAN)
KLEMPT	82	PR D25 652	E. Klempt *et al.*	(MAINZ, ETH)
MARIAM	82	PRL 49 993	F.G. Mariam *et al.*	(YALE, HEIDH, BERN)
MARSHALL	82	PR D25 1174	G.M. Marshall *et al.*	(BRCO)
NEMETHY	81	CNPP 10 147	P. Nemethy, V.W. Hughes	(LBL, YALE)
ABELA	80	PL 95B 318	R. Abela *et al.*	(BASL, KARLK, KARLE)
BADERT...	80	LNC 28 401	A. Badertscher *et al.*	(BERN)
Also		NP A377 406	A. Badertscher *et al.*	(BERN)
JONKER	80	PL 93B 203	M. Jonker *et al.*	(CHARM Collab.)
SCHAAF	80	NP A340 249	A. van der Schaaf *et al.*	(ZURI, ETH+)
Also		PL 72B 183	H.P. Povel *et al.*	(ZURI, ETH, SIN)
WILLIS	80	PRL 44 522	S.E. Willis *et al.*	(YALE, LBL, LASL+)
Also		PRL 45 1370	S.E. Willis *et al.*	(YALE, LBL, LASL+)
BAILEY	79	NP B150 1	J.M. Bailey	(CERN, DARE, MAINZ)
BADERT...	78	PL 79B 371	A. Badertscher *et al.*	(BERN)
BAILEY	78	JP G4 345	J.M. Bailey	(DARE, BERN, SHEF, MAINZ, RMCS+)
Also		NP B150 1	J.M. Bailey	(CERN, DARE, MAINZ)
BLIETSCHAU	78	NP B133 205	J. Blietschau *et al.*	(Gargamelle Collab.)
BOWMAN	78	PRL 41 442	J.D. Bowman *et al.*	(LASL, IAS, CMU+)
CAMANI	78	PL 77B 326	M. Camani *et al.*	(ETH, MAINZ)
BADERT...	77	PRL 39 1385	A. Badertscher *et al.*	(BERN)
CASPERSON	77	PRL 38 956	D.E. Casperson *et al.*	(BERN, HEIDH, LASL+)
DEPOMMIER	77	PRL 39 1113	P. Depommier *et al.*	(MONT, BRCO, TRIU+)
BALANDIN	74	JETP 40 811	M.P. Balandin *et al.*	(JINR)
		Translated from ZETF 67 1631.		
COHEN	73	JPCRD 2 664	E.R. Cohen, B.N. Taylor	(RISC, NBS)
DUCLOS	73	PL 47B 491	J. Duclos, A. Magnon, J. Picard	(SACL)
EICHTEN	73	PL 46B 281	T. Eichten *et al.*	(Gargamelle Collab.)
BRYMAN	72	PRL 28 1469	D.A. Bryman *et al.*	(VPI)
CROWE	72	PR D5 2145	K.M. Crowe *et al.*	(LBL, WASH)
CRANE	71	PRL 27 474	T. Crane *et al.*	(YALE)
DERENZO	69	PR 181 1854	S.E. Derenzo	(EFI)
VOSSLER	69	NC 63A 423	C. Vossler	(EFI)
AKHMANOV	68	SJNP 6 230	V.V. Akhmanov *et al.*	(KIAE)
		Translated from YAF 6 316.		
FRYBERGER	68	PR 166 1379	D. Fryberger	(EFI)
BOGART	67	PR 156 1405	E. Bogart *et al.*	(COLU)
SCHWARTZ	67	PR 162 1306	D.M. Schwartz	(EFI)
SHERWOOD	67	PR 156 1475	B.A. Sherwood	(EFI)
PEOPLES	66	Nevis 147 unpub.	J. Peoples	(COLU)
BLOOM	64	PL 8 87	S. Bloom *et al.*	(CERN)
DUCLOS	64	PL 9 62	J. Duclos *et al.*	(CERN)
GUREVICH	64	PL 11 185	I.I. Gurevich *et al.*	(KIAE)
BUHLER	63	PL 7 368	A. Buhler-Broglin *et al.*	(CERN)
MEYER	63	PR 132 2693	S.L. Meyer *et al.*	(COLU)
CHARPAK	62	PL 1 16	G. Charpak *et al.*	(CERN)
CONFORTO	62	NC 26 261	G. Conforto *et al.*	(INFN, ROMA, CERN)
ALI-ZADE	61	JETP 13 313	S.A. Ali-Zade, I.I. Gurevich, B.A. Nikolsky	
		Translated from ZETF 40 452.		
CRITTENDEN	61	PR 121 1823	R.R. Crittenden, W.D. Walker, J. Ballam	(WISC+)
KRUGER	61	UCRL 9322 unpub.	H. Kruger	(LRL)
GUREVICH	60	JETP 10 225	I.I. Gurevich, B.A. Nikolsky, L.V. Surkova	(ITEP)
		Translated from ZETF 37 318.		
PLANO	60	PR 119 1400	R.J. Plano	(COLU)
ASHKIN	59	NC 14 1266	J. Ashkin *et al.*	(CERN)
BARDON	59	PRL 2 56	M. Bardon, D. Berley, L.M. Lederman	(COLU)
LEE	59	PRL 3 55	J. Lee, N.P. Samios	(COLU)

τ

$J = \frac{1}{2}$

τ discovery paper was PERL 75. $e^+e^- \to \tau^+\tau^-$ cross-section threshold behavior and magnitude are consistent with pointlike spin-1/2 Dirac particle. BRANDELIK 78 ruled out pointlike spin-0 or spin-1 particle. FELDMAN 78 ruled out $J = 3/2$. KIRKBY 79 also ruled out J=integer, $J = 3/2$.

τ MASS

VALUE (MeV)	EVTS	DOCUMENT ID		TECN	COMMENT
1776.93±0.09 OUR AVERAGE					
$1777.09 \pm 0.08 \pm 0.11$	175 M	[1] ADACHI	23C	BEL2	190 fb^{-1}, E^{ee}_{cm} = 10.6 GeV
$1776.69^{+0.17}_{-0.19} \pm 0.15$		[2] ANASHIN	23A	KEDR	(6.7+ 8.5) pb^{-1}, E^{ee}_{cm}= 3.54–3.78 GeV
$1776.91 \pm 0.12^{+0.10}_{-0.13}$	1171	[3] ABLIKIM	14D	BES3	23.3 pb^{-1}, E^{ee}_{cm}= 3.54–3.60 GeV
$1776.68 \pm 0.12 \pm 0.41$	682k	[1] AUBERT	09AK	BABR	423 fb^{-1}, E^{ee}_{cm}=10.6 GeV
$1776.61 \pm 0.13 \pm 0.35$		[1] BELOUS	07	BELL	414 fb^{-1} E^{ee}_{cm}=10.6 GeV
$1775.1 \pm 1.6 \pm 1.0$	13.3k	[4] ABBIENDI	00A	OPAL	1990–1995 LEP runs
$1778.2 \pm 0.8 \pm 1.2$		ANASTASSOV	97	CLEO	E^{ee}_{cm}= 10.6 GeV
$1776.96^{+0.18}_{-0.21}{}^{+0.25}_{-0.17}$	65	[5] BAI	96	BES	E^{ee}_{cm}= 3.54–3.57 GeV
$1776.3 \pm 2.4 \pm 1.4$	11k	[6] ALBRECHT	92M	ARG	E^{ee}_{cm}= 9.4–10.6 GeV
$1783\ ^{+3}_{-4}$	692	[7] BACINO	78B	DLCO	E^{ee}_{cm}= 3.1–7.4 GeV
• • • We do not use the following data for averages, fits, limits, etc. • • •					
$1776.81^{+0.25}_{-0.23} \pm 0.15$	81	ANASHIN	07	KEDR	6.7 pb^{-1}, E^{ee}_{cm}= 3.54–3.78 GeV
$1777.8 \pm 0.7 \pm 1.7$	35k	[8] BALEST	93	CLEO	Repl. by ANASTASSOV 97
$1776.9\ ^{+0.4}_{-0.5} \pm 0.2$	14	[9] BAI	92	BES	Repl. by BAI 96

[1] ADACHI 23C, AUBERT 09AK and BELOUS 07 fit τ pseudomass spectrum in $\tau \to \pi\pi^+\pi^-\nu_\tau$ decays. Result assumes $m_{\nu_\tau} = 0$.

[2] Previously also reported LEVICHEV 14. Superseedes ANASHIN 07.

[3] ABLIKIM 14D fit $\sigma(e^+e^- \to \tau^+\tau^-)$ at different energies near threshold.

[4] ABBIENDI 00A fit τ pseudomass spectrum in $\tau \to \pi^\pm \leq 2\pi^0\nu_\tau$ and $\tau \to \pi^\pm\pi^+\pi^- \leq 1\pi^0\nu_\tau$ decays. Result assumes m_{ν_τ}=0.

[5] BAI 96 fit $\sigma(e^+e^- \to \tau^+\tau^-)$ at different energies near threshold.

[6] ALBRECHT 92M fit τ pseudomass spectrum in $\tau^- \to 2\pi^-\pi^+\nu_\tau$ decays. Result assumes m_{ν_τ}=0.

[7] BACINO 78B value comes from $e^\pm X^\mp$ threshold. Published mass 1782 MeV increased by 1 MeV using the high precision $\psi(2S)$ mass measurement of ZHOLENTZ 80 to eliminate the absolute SPEAR energy calibration uncertainty.

[8] BALEST 93 fit spectra of minimum kinematically allowed τ mass in events of the type $e^+e^- \to \tau^+\tau^- \to (\pi^+ n\pi^0\nu_\tau)(\pi^- m\pi^0\nu_\tau)$ $n \leq 2$, $m \leq 2$, $1 \leq n+m \leq 3$. If $m_{\nu_\tau} \neq 0$, result increases by $(m^2_{\nu_\tau}/1100$ MeV).

[9] BAI 92 fit $\sigma(e^+e^- \to \tau^+\tau^-)$ near threshold using $e\mu$ events.

$(m_{\tau^+} - m_{\tau^-})/m_{\text{average}}$

A test of CPT invariance.

VALUE	CL%	DOCUMENT ID		TECN	COMMENT
$<2.8 \times 10^{-4}$	90	BELOUS	07	BELL	414 fb^{-1}, E^{ee}_{cm}=10.6 GeV
• • • We do not use the following data for averages, fits, limits, etc. • • •					
$<5.5 \times 10^{-4}$	90	[1] AUBERT	09AK	BABR	423 fb^{-1}, E^{ee}_{cm}=10.6 GeV
$<3.0 \times 10^{-3}$	90	ABBIENDI	00A	OPAL	1990–1995 LEP runs

[1] AUBERT 09AK quote both the listed upper limit and $(m_{\tau^+} - m_{\tau^-})/m_{\text{average}} = (-3.4 \pm 1.3 \pm 0.3) \times 10^{-4}$.

τ MEAN LIFE

VALUE (10^{-15} s)	EVTS	DOCUMENT ID		TECN	COMMENT
290.3 ± 0.5 OUR AVERAGE					
$290.17 \pm 0.53 \pm 0.33$	1.1M	BELOUS	14	BELL	711 fb^{-1} E^{ee}_{cm}=10.6 GeV
$290.9 \pm 1.4 \pm 1.0$		ABDALLAH	04T	DLPH	1991-1995 LEP runs
$293.2 \pm 2.0 \pm 1.5$		ACCIARRI	00B	L3	1991–1995 LEP runs
$290.1 \pm 1.5 \pm 1.1$		BARATE	97R	ALEP	1989–1994 LEP runs
$289.2 \pm 1.7 \pm 1.2$		ALEXANDER	96E	OPAL	1990–1994 LEP runs
$289.0 \pm 2.8 \pm 4.0$	57.4k	BALEST	96	CLEO	E^{ee}_{cm}= 10.6 GeV
• • • We do not use the following data for averages, fits, limits, etc. • • •					
$291.2 \pm 2.0 \pm 1.2$		BARATE	97I	ALEP	Repl. by BARATE 97R
291.4 ± 3.0		ABREU	96B	DLPH	Repl. by ABDALLAH 04T
290.1 ± 4.0	34k	ACCIARRI	96K	L3	Repl. by ACCIARRI 00B
$297 \pm 9 \pm 5$	1671	ABE	95Y	SLD	1992–1993 SLC runs
$304 \pm 14 \pm 7$	4100	BATTLE	92	CLEO	E^{ee}_{cm}= 10.6 GeV
301 ± 29	3780	KLEINWORT	89	JADE	E^{ee}_{cm}= 35–46 GeV
$288 \pm 16 \pm 17$	807	AMIDEI	88	MRK2	E^{ee}_{cm}= 29 GeV
$306 \pm 20 \pm 14$	695	BRAUNSCH...	88C	TASS	E^{ee}_{cm}= 36 GeV
$299 \pm 15 \pm 10$	1311	ABACHI	87C	HRS	E^{ee}_{cm}= 29 GeV
$295 \pm 14 \pm 11$	5696	ALBRECHT	87P	ARG	E^{ee}_{cm}= 9.3–10.6 GeV
$309 \pm 17 \pm 7$	3788	BAND	87B	MAC	E^{ee}_{cm}= 29 GeV
$325 \pm 14 \pm 18$	8470	BEBEK	87C	CLEO	E^{ee}_{cm}= 10.5 GeV
460 ± 190	102	FELDMAN	82	MRK2	E^{ee}_{cm}= 29 GeV

$(\tau_{\tau^+} - \tau_{\tau^-}) / \tau_{\text{average}}$

Test of CPT invariance.

VALUE	CL%	DOCUMENT ID		TECN	COMMENT
$<7.0 \times 10^{-3}$	90	[1] BELOUS	14	BELL	711 fb^{-1} E^{ee}_{cm} = 10.6 GeV

[1] BELOUS 14 quote limit on the absolute value of the relative lifetime difference.

τ MAGNETIC MOMENT ANOMALY

The q^2 dependence is expected to be small providing no thresholds are nearby.

$\mu_\tau/(e\hbar/2m_\tau) - 1 = (g_\tau - 2)/2$

For a theoretical calculation $[(g_\tau - 2)/2 = 117\,721(5) \times 10^{-8}]$, see EIDELMAN 07.

VALUE	CL%	DOCUMENT ID		TECN	COMMENT
−0.0024 to 0.0047	95	[1] AAD	25BB	ATLS	140 fb^{-1}, E^{pp}_{cm} = 13 TeV
• • • We do not use the following data for averages, fits, limits, etc. • • •					
$-0.041\ ^{+0.012}_{-0.009}$		[2,3] AAD	23BM	ATLS	$\gamma\gamma \to \tau^+\tau^-$, Pb–Pb
-0.057 to 0.024	95	[2] AAD	23BM	ATLS	$\gamma\gamma \to \tau^+\tau^-$, Pb–Pb
$0.001\ ^{+0.055}_{-0.089}$		[3,4] TUMASYAN	23AS	CMS	$\gamma\gamma \to \tau^+\tau^-$, Pb-Pb
-0.018 ± 0.017		[3,5] ABDALLAH	04K	DLPH	$e^+e^- \to e^+e^-\tau^+\tau^-$
< 0.107	95	[6] ACHARD	04G	L3	$e^+e^- \to e^+e^-\tau^+\tau^-$
-0.007 to 0.005	95	[7] GONZALEZ-S...00		RVUE	$e^+e^- \to \tau^+\tau^-$ and $W \to \tau\nu_\tau$

-0.052 to 0.058	95	[8] ACCIARRI	98E	L3	1991–1995 LEP runs
-0.068 to 0.065	95	[9] ACKERSTAFF	98N	OPAL	1990–1995 LEP runs
-0.004 to 0.006	95	[10] ESCRIBANO	97	RVUE	$Z \to \tau^+\tau^-$ at LEP
$<$ 0.01	95	[11] ESCRIBANO	93	RVUE	$Z \to \tau^+\tau^-$ at LEP
$<$ 0.12	90	GRIFOLS	91	RVUE	$Z \to \tau\tau\gamma$ at LEP
$<$ 0.023	95	[12] SILVERMAN	83	RVUE	$e^+e^- \to \tau^+\tau^-$ at PETRA

[1] AAD 25BB limits are obtained by comparing the inclusive $\tau^+\tau^-$ fiducial cross-section in pp collisions as a function of visible invariant mass at large masses to the Standard Model prediction.
[2] AAD 23BM measurement is derived from $\gamma\gamma \to \tau^+\tau^-$ total cross-section TeV. Authors report both the measured value and the corresponding 95% CL limit. from 1.44 nb^{-1} LHC Pb−Pb collisions at $\sqrt{S_{NN}} = 5.02$
[3] Measurement ill-suited for a standard average because its likelihood appears to be remarkably non-Gaussian and asymmetric according to the model-dependent extraction procedure and the reported 95% CL limits.
[4] TUMASYAN 23AS measurement is derived from $\gamma\gamma \to \tau^+\tau^-$ total cross-section from 404 μb^{-1} LHC Pb-Pb collisions at $\sqrt{S_{NN}} = 5.02$ TeV.
[5] ABDALLAH 04K measurement is derived from $e^+e^- \to e^+e^-\tau^+\tau^-$ total cross-section measurements at $\sqrt{s}$ between 183 and 208 GeV. In addition to the measurement, the authors also quote 95% CL limits of $>$ -0.052 and $<$ 0.013.
[6] ACHARD 04G limit is derived from $e^+e^- \to e^+e^-\tau^+\tau^-$ total cross-section measurements at $\sqrt{s}$ between 189 and 206 GeV, and is on the absolute value of the magnetic moment anomaly.
[7] GONZALEZ-SPRINBERG 00 use data on tau lepton production at LEP1, SLC, and LEP2, and data from colliders and LEP2 to determine limits. Assume imaginary component is zero.
[8] ACCIARRI 98E use $Z \to \tau^+\tau^-\gamma$ events. In addition to the limits, the authors also quote a value of 0.004 ± 0.027 ± 0.023.
[9] ACKERSTAFF 98N use $Z \to \tau^+\tau^-\gamma$ events. The limit applies to an average of the form factor for off-shell τ's having p^2 ranging from m_τ^2 to $(M_Z - m_\tau)^2$.
[10] ESCRIBANO 97 use preliminary experimental results.
[11] ESCRIBANO 93 limit derived from $\Gamma(Z \to \tau^+\tau^-)$, and is on the absolute value of the magnetic moment anomaly.
[12] SILVERMAN 83 limit is derived from $e^+e^- \to \tau^+\tau^-$ total cross-section measurements for q^2 up to (37 GeV)^2.

τ ELECTRIC DIPOLE MOMENT (d_τ)

A nonzero value is forbidden by both T invariance and P invariance.

The q^2 dependence is expected to be small providing no thresholds are nearby.

Re(d_τ)

VALUE (10^{-16} ecm)	CL%	DOCUMENT ID		TECN	COMMENT
− 0.185 to 0.061	95	[1] INAMI	22	BELL	$E^{ee}_{cm} = 10.6$ GeV
• • • We do not use the following data for averages, fits, limits, etc. • • •					
$<$ 2.3	90	[2] GROZIN	09A	RVUE	From e EDM limit
$<$ 3.7	95	[3] ABDALLAH	04K	DLPH	$e^+e^- \to e^+e^-\tau^+\tau^-$ at LEP2
$<$ 11.4	95	[4] ACHARD	04G	L3	$e^+e^- \to e^+e^-\tau^+\tau^-$ at LEP2
− 0.22 to 0.45	95	[5] INAMI	03	BELL	$E^{ee}_{cm} = 10.6$ GeV
$<$ 4.6	95	[6] ALBRECHT	00	ARG	$E^{ee}_{cm} = 10.4$ GeV
>-3.1 and <3.1	95	ACCIARRI	98E	L3	1991–1995 LEP runs
>-3.8 and <3.6	95	[7] ACKERSTAFF	98N	OPAL	1990–1995 LEP runs
$<$ 0.11	95	[8,9] ESCRIBANO	97	RVUE	$Z \to \tau^+\tau^-$ at LEP
$<$ 0.5	95	[10] ESCRIBANO	93	RVUE	$Z \to \tau^+\tau^-$ at LEP
$<$ 7	90	GRIFOLS	91	RVUE	$Z \to \tau\tau\gamma$ at LEP
$<$ 1.6	90	DELAGUILA	90	RVUE	$e^+e^- \to \tau^+\tau^-$ $E^{ee}_{cm} = 35$ GeV

[1] INAMI 22 use $e^+e^- \to \tau^+\tau^-$ events from 833 fb^{-1} of data. Also report a measurement of Re(d_τ) = $(-0.62 \pm 0.63) \times 10^{-17}$ ecm.
[2] GROZIN 09A calculate the contribution to the electron electric dipole moment from the τ electric dipole moment appearing in loops, which is $\Delta d_e = 6.9 \times 10^{-12}$ d_τ. Dividing the REGAN 02 upper limit $|d_e| \le 1.6 \times 10^{-27}$ e cm at CL=90% by 6.9×10^{-12} gives this limit.
[3] ABDALLAH 04K limit is derived from $e^+e^- \to e^+e^-\tau^+\tau^-$ total cross-section measurements at $\sqrt{s}$ between 183 and 208 GeV and is on the absolute value of d_τ.
[4] ACHARD 04G limit is derived from $e^+e^- \to e^+e^-\tau^+\tau^-$ total cross-section measurements at $\sqrt{s}$ between 189 and 206 GeV, and is on the absolute value of d_τ.
[5] INAMI 03 use $e^+e^- \to \tau^+\tau^-$ events.
[6] ALBRECHT 00 use $e^+e^- \to \tau^+\tau^-$ events. Limit is on the absolute value of Re(d_τ).
[7] ACKERSTAFF 98N use $Z \to \tau^+\tau^-\gamma$ events. The limit applies to an average of the form factor for off-shell τ's having p^2 ranging from m_τ^2 to $(M_Z - m_\tau)^2$.
[8] ESCRIBANO 97 derive the relationship $|d_\tau| = \cot\theta_W\, |d_\tau^W|$ using effective Lagrangian methods, and use a conference result $|d_\tau^W| < 5.8 \times 10^{-18}$ e cm at 95% CL (L. Silvestris, ICHEP96) to obtain this result.
[9] ESCRIBANO 97 use preliminary experimental results.
[10] ESCRIBANO 93 limit derived from $\Gamma(Z \to \tau^+\tau^-)$, and is on the absolute value of the electric dipole moment.

Im(d_τ)

VALUE (10^{-16} ecm)	CL%	DOCUMENT ID		TECN	COMMENT
−0.103 to 0.023	95	[1] INAMI	22	BELL	$E^{ee}_{cm} = 10.6$ GeV
• • • We do not use the following data for averages, fits, limits, etc. • • •					
−0.25 to 0.008	95	[2] INAMI	03	BELL	$E^{ee}_{cm} = 10.6$ GeV
$<$ 1.8	95	[3] ALBRECHT	00	ARG	$E^{ee}_{cm} = 10.4$ GeV

[1] INAMI 22 use $e^+e^- \to \tau^+\tau^-$ events from 833 fb^{-1} of data. Also report a measurement of Im(d_τ) = $(-0.40 \pm 0.32) \times 10^{-17}$ ecm.
[2] INAMI 03 use $e^+e^- \to \tau^+\tau^-$ events.
[3] ALBRECHT 00 use $e^+e^- \to \tau^+\tau^-$ events. Limit is on the absolute value of Im(d_τ).

τ WEAK DIPOLE MOMENT (d_τ^W)

A nonzero value is forbidden by CP invariance.

The q^2 dependence is expected to be small providing no thresholds are nearby.

Re(d_τ^W)

VALUE (10^{-17} ecm)	CL%	DOCUMENT ID		TECN	COMMENT
<0.50	95	[1] HEISTER	03F	ALEP	1990–1995 LEP runs
• • • We do not use the following data for averages, fits, limits, etc. • • •					
$<$3.0	90	[1] ACCIARRI	98C	L3	1991–1995 LEP runs
$<$0.56	95	ACKERSTAFF	97L	OPAL	1991–1995 LEP runs
$<$0.78	95	[2] AKERS	95F	OPAL	Repl. by ACKERSTAFF 97L
$<$1.5	95	[2] BUSKULIC	95C	ALEP	Repl. by HEISTER 03F
$<$7.0	95	[2] ACTON	92F	OPAL	$Z \to \tau^+\tau^-$ at LEP
$<$3.7	95	[2] BUSKULIC	92J	ALEP	Repl. by BUSKULIC 95C

[1] Limit is on the absolute value of the real part of the weak dipole moment.
[2] Limit is on the absolute value of the real part of the weak dipole moment, and applies for $q^2 = m_Z^2$.

Im(d_τ^W)

VALUE (10^{-17} ecm)	CL%	DOCUMENT ID		TECN	COMMENT
<1.1	95	[1] HEISTER	03F	ALEP	1990–1995 LEP runs
• • • We do not use the following data for averages, fits, limits, etc. • • •					
$<$1.5	95	ACKERSTAFF	97L	OPAL	1991–1995 LEP runs
$<$4.5	95	[2] AKERS	95F	OPAL	Repl. by ACKERSTAFF 97L

[1] HEISTER 03F limit is on the absolute value of the imaginary part of the weak dipole moment.
[2] Limit is on the absolute value of the imaginary part of the weak dipole moment, and applies for $q^2 = m_Z^2$.

τ WEAK ANOMALOUS MAGNETIC DIPOLE MOMENT (α_τ^W)

Electroweak radiative corrections are expected to contribute at the 10^{-6} level. See BERNABEU 95.

The q^2 dependence is expected to be small providing no thresholds are nearby.

Re(α_τ^W)

VALUE	CL%	DOCUMENT ID		TECN	COMMENT
<1.1 × 10^{-3}	95	[1] HEISTER	03F	ALEP	1990–1995 LEP runs
• • • We do not use the following data for averages, fits, limits, etc. • • •					
>-0.0024 and <0.0025	95	[2] GONZALEZ-S.	00	RVUE	$e^+e^- \to \tau^+\tau^-$ and $W \to \tau\nu_\tau$
$<4.5 \times 10^{-3}$	90	[1] ACCIARRI	98C	L3	1991–1995 LEP runs

[1] Limit is on the absolute value of the real part of the weak anomalous magnetic dipole moment.
[2] GONZALEZ-SPRINBERG 00 use data on tau lepton production at LEP1, SLC, and LEP2, and data from colliders and LEP2 to determine limits. Assume imaginary component is zero.

Im(α_τ^W)

VALUE	CL%	DOCUMENT ID		TECN	COMMENT
<2.7 × 10^{-3}	95	[1] HEISTER	03F	ALEP	1990–1995 LEP runs
• • • We do not use the following data for averages, fits, limits, etc. • • •					
$<9.9 \times 10^{-3}$	90	[1] ACCIARRI	98C	L3	1991–1995 LEP runs

[1] Limit is on the absolute value of the imaginary part of the weak anomalous magnetic dipole moment.

τ^- DECAY MODES

τ^+ modes are charge conjugates of the modes below. "$h^\pm$" stands for $\pi^\pm$ or $K^\pm$. "ℓ" stands for e or μ. "Neutrals" stands for γ's and/or π^0's.

	Mode		Fraction (Γ_i/Γ)	Scale factor/ Confidence level
	Modes with one charged particle			
Γ_1	particle$^- \ge 0$ neutrals $\ge 0 K^0 \nu_\tau$ ("1-prong")		(85.24 ± 0.06) %	
Γ_2	particle$^- \ge 0$ neutrals $\ge 0 K^0_L \nu_\tau$		(84.58 ± 0.06) %	
Γ_3	$\mu^- \overline{\nu}_\mu \nu_\tau$	[a]	(17.37 ± 0.04) %	
Γ_4	$\mu^- \overline{\nu}_\mu \nu_\tau \gamma$	[b]	(3.67 ± 0.08) $\times 10^{-3}$	
Γ_5	$e^- \overline{\nu}_e \nu_\tau$	[a]	(17.85 ± 0.04) %	
Γ_6	$e^- \overline{\nu}_e \nu_\tau \gamma$	[b]	(1.83 ± 0.05) %	
Γ_7	$h^- \ge 0 K^0_L \nu_\tau$		(12.03 ± 0.05) %	
Γ_8	$h^- \nu_\tau$		(11.51 ± 0.05) %	

Int. J. Mod
by UNIVERSITY OF CALIFORNIA @ BERK
wnloaded from www.worldscientific.com
-use and distribution is strictly not permitted, except for Open Access articles.

Int. J. Mod. Phys. A 2026.41. Downloaded from www.worldscientific.com
by UNIVERSITY OF CALIFORNIA @ BERKELEY on 09/16/26. Re-use and distribution is strictly not permitted, except for Open Access articles.

Γ_{9}	$\pi^- \nu_\tau$	[a]	(10.82 ± 0.05) %	
Γ_{10}	$K^- \nu_\tau$	[a]	$(6.97 \pm 0.10) \times 10^{-3}$	
Γ_{11}	$h^- \geq 1$ neutrals ν_τ		(37.00 ± 0.09) %	
Γ_{12}	$h^- \geq 1\pi^0 \nu_\tau$ (ex.K^0)		(36.50 ± 0.09) %	
Γ_{13}	$h^- \pi^0 \nu_\tau$		(25.93 ± 0.09) %	
Γ_{14}	$\pi^- \pi^0 \nu_\tau$	[a]	(25.49 ± 0.09) %	
Γ_{15}	$\pi^- \pi^0$ non-$\rho(770) \nu_\tau$		$(3.0 \pm 3.2) \times 10^{-3}$	
Γ_{16}	$K^- \pi^0 \nu_\tau$	[a]	$(4.33 \pm 0.15) \times 10^{-3}$	
Γ_{17}	$h^- \geq 2\pi^0 \nu_\tau$		(10.81 ± 0.09) %	
Γ_{18}	$h^- 2\pi^0 \nu_\tau$		(9.48 ± 0.10) %	
Γ_{19}	$h^- 2\pi^0 \nu_\tau$ (ex.K^0)		(9.32 ± 0.10) %	
Γ_{20}	$\pi^- 2\pi^0 \nu_\tau$ (ex.K^0)	[a]	(9.26 ± 0.10) %	
Γ_{21}	$\pi^- 2\pi^0 \nu_\tau$ (ex.K^0), scalar		$< 9 \times 10^{-3}$	CL=95%
Γ_{22}	$\pi^- 2\pi^0 \nu_\tau$ (ex.K^0), vector		$< 7 \times 10^{-3}$	CL=95%
Γ_{23}	$K^- 2\pi^0 \nu_\tau$ (ex.K^0)	[a]	$(6.5 \pm 2.2) \times 10^{-4}$	
Γ_{24}	$h^- \geq 3\pi^0 \nu_\tau$		(1.34 ± 0.07) %	
Γ_{25}	$h^- \geq 3\pi^0 \nu_\tau$ (ex. K^0)		(1.26 ± 0.07) %	
Γ_{26}	$h^- 3\pi^0 \nu_\tau$		(1.18 ± 0.07) %	
Γ_{27}	$\pi^- 3\pi^0 \nu_\tau$ (ex.K^0)	[a]	(1.04 ± 0.07) %	
Γ_{28}	$K^- 3\pi^0 \nu_\tau$ (ex.K^0, η)	[a]	$(4.8 \pm 2.1) \times 10^{-4}$	
Γ_{29}	$h^- 4\pi^0 \nu_\tau$ (ex.K^0)		$(1.6 \pm 0.4) \times 10^{-3}$	
Γ_{30}	$h^- 4\pi^0 \nu_\tau$ (ex.K^0,η)	[a]	$(1.1 \pm 0.4) \times 10^{-3}$	
Γ_{31}	$a_1(1260) \nu_\tau \rightarrow \pi^- \gamma \nu_\tau$		$(4.0 \pm 1.5) \times 10^{-4}$	
Γ_{32}	$K^- \geq 0\pi^0 \geq 0K^0 \geq 0\gamma \ \nu_\tau$		(1.552 ± 0.029) %	
Γ_{33}	$K^- \geq 1$ (π^0 or K^0 or γ) ν_τ		$(8.59 \pm 0.28) \times 10^{-3}$	

Modes with K^0's

Γ_{34}	K^0_S (particles)$^- \nu_\tau$		$(9.43 \pm 0.28) \times 10^{-3}$	
Γ_{35}	$h^- \overline{K}^0 \nu_\tau$		$(9.87 \pm 0.14) \times 10^{-3}$	
Γ_{36}	$\pi^- \overline{K}^0 \nu_\tau$	[a]	$(8.38 \pm 0.14) \times 10^{-3}$	
Γ_{37}	$\pi^- \overline{K}^0$ (non-$K^*(892)^-$) ν_τ		$(5.4 \pm 2.1) \times 10^{-4}$	
Γ_{38}	$K^- K^0 \nu_\tau$	[a]	$(1.486 \pm 0.034) \times 10^{-3}$	
Γ_{39}	$K^- K^0 \geq 0\pi^0 \nu_\tau$		$(2.99 \pm 0.07) \times 10^{-3}$	
Γ_{40}	$h^- \overline{K}^0 \pi^0 \nu_\tau$		$(5.32 \pm 0.13) \times 10^{-3}$	
Γ_{41}	$\pi^- \overline{K}^0 \pi^0 \nu_\tau$	[a]	$(3.82 \pm 0.13) \times 10^{-3}$	
Γ_{42}	$\overline{K}^0 \rho^- \nu_\tau$		$(2.2 \pm 0.5) \times 10^{-3}$	
Γ_{43}	$K^- K^0 \pi^0 \nu_\tau$	[a]	$(1.50 \pm 0.07) \times 10^{-3}$	
Γ_{44}	$\pi^- \overline{K}^0 \geq 1\pi^0 \nu_\tau$		$(4.08 \pm 0.25) \times 10^{-3}$	
Γ_{45}	$\pi^- \overline{K}^0 \pi^0 \pi^0 \nu_\tau$ (ex.K^0)	[a]	$(2.6 \pm 2.3) \times 10^{-4}$	
Γ_{46}	$K^- K^0 \pi^0 \pi^0 \nu_\tau$		$< 1.6 \times 10^{-4}$	CL=95%
Γ_{47}	$\pi^- K^0 \overline{K}^0 \nu_\tau$		$(1.55 \pm 0.24) \times 10^{-3}$	
Γ_{48}	$\pi^- K^0_S K^0_S \nu_\tau$	[a]	$(2.35 \pm 0.06) \times 10^{-4}$	
Γ_{49}	$\pi^- K^0_S K^0_L \nu_\tau$	[a]	$(1.08 \pm 0.24) \times 10^{-3}$	
Γ_{50}	$\pi^- K^0_L K^0_L \nu_\tau$		$(2.35 \pm 0.06) \times 10^{-4}$	
Γ_{51}	$\pi^- K^0 \overline{K}^0 \pi^0 \nu_\tau$		$(3.6 \pm 1.2) \times 10^{-4}$	
Γ_{52}	$\pi^- K^0_S K^0_S \pi^0 \nu_\tau$	[a]	$(1.82 \pm 0.21) \times 10^{-5}$	
Γ_{53}	$K^{*-} K^0 \pi^0 \nu_\tau \rightarrow \pi^- K^0_S K^0_S \pi^0 \nu_\tau$		$(1.08 \pm 0.21) \times 10^{-5}$	
Γ_{54}	$f_1(1285) \pi^- \nu_\tau \rightarrow \pi^- K^0_S K^0_S \pi^0 \nu_\tau$		$(6.8 \pm 1.5) \times 10^{-6}$	
Γ_{55}	$f_1(1420) \pi^- \nu_\tau \rightarrow \pi^- K^0_S K^0_S \pi^0 \nu_\tau$		$(2.4 \pm 0.8) \times 10^{-6}$	
Γ_{56}	$\pi^- K^0_S K^0_S \pi^0 \nu_\tau$	[a]	$(3.2 \pm 1.2) \times 10^{-4}$	
Γ_{57}	$\pi^- K^0_L K^0_L \pi^0 \nu_\tau$		$(1.82 \pm 0.21) \times 10^{-5}$	
Γ_{58}	$K^- K^0_S K^0_S \nu_\tau$		$< 6.3 \times 10^{-7}$	CL=90%
Γ_{59}	$K^- K^0_S K^0_S \pi^0 \nu_\tau$		$< 4.0 \times 10^{-7}$	CL=90%
Γ_{60}	$K^0 h^+ h^- h^- \geq 0$ neutrals ν_τ		$< 1.7 \times 10^{-3}$	CL=95%
Γ_{61}	$K^0 h^+ h^- h^- \nu_\tau$	[a]	$(2.5 \pm 2.0) \times 10^{-4}$	

Modes with three charged particles

Γ_{62}	$h^- h^- h^+ \geq 0$ neutrals $\geq 0K^0_L \nu_\tau$		(15.20 ± 0.06) %	
Γ_{63}	$h^- h^- h^+ \geq 0$ neutrals ν_τ (ex. $K^0_S \rightarrow \pi^+ \pi^-$) ("3-prong")		(14.55 ± 0.06) %	
Γ_{64}	$h^- h^- h^+ \nu_\tau$		(9.80 ± 0.05) %	
Γ_{65}	$h^- h^- h^+ \nu_\tau$ (ex.K^0)		(9.45 ± 0.05) %	
Γ_{66}	$h^- h^- h^+ \nu_\tau$ (ex.K^0,ω)		(9.42 ± 0.05) %	
Γ_{67}	$\pi^- \pi^+ \pi^- \nu_\tau$		(9.31 ± 0.05) %	
Γ_{68}	$\pi^- \pi^+ \pi^- \nu_\tau$ (ex.K^0)		(9.02 ± 0.05) %	
Γ_{69}	$\pi^- \pi^+ \pi^- \nu_\tau$ (ex.K^0), non-axial vector		< 2.4 %	CL=95%
Γ_{70}	$\pi^- \pi^+ \pi^- \nu_\tau$ (ex.K^0,ω)	[a]	(8.99 ± 0.05) %	
Γ_{71}	$h^- h^- h^+ \geq 1$ neutrals ν_τ		(5.29 ± 0.05) %	
Γ_{72}	$h^- h^- h^+ \geq 1\pi^0 \nu_\tau$ (ex. K^0)		(5.09 ± 0.05) %	
Γ_{73}	$h^- h^- h^+ \pi^0 \nu_\tau$		(4.76 ± 0.05) %	
Γ_{74}	$h^- h^- h^+ \pi^0 \nu_\tau$ (ex.K^0)		(4.57 ± 0.05) %	
Γ_{75}	$h^- h^- h^+ \pi^0 \nu_\tau$ (ex. K^0, ω)		(2.79 ± 0.07) %	
Γ_{76}	$\pi^- \pi^+ \pi^- \pi^0 \nu_\tau$		(4.62 ± 0.05) %	
Γ_{77}	$\pi^- \pi^+ \pi^- \pi^0 \nu_\tau$ (ex.K^0)		(4.49 ± 0.05) %	
Γ_{78}	$\pi^- \pi^+ \pi^- \pi^0 \nu_\tau$ (ex.K^0,ω)	[a]	(2.74 ± 0.07) %	
Γ_{79}	$h^- \rho \pi^0 \nu_\tau$			
Γ_{80}	$h^- \rho^+ h^- \nu_\tau$			
Γ_{81}	$h^- \rho^- h^+ \nu_\tau$			
Γ_{82}	$h^- h^- h^+ \geq 2\pi^0 \nu_\tau$ (ex. K^0)		$(5.17 \pm 0.31) \times 10^{-3}$	
Γ_{83}	$h^- h^- h^+ 2\pi^0 \nu_\tau$		$(5.05 \pm 0.31) \times 10^{-3}$	
Γ_{84}	$h^- h^- h^+ 2\pi^0 \nu_\tau$ (ex.K^0)		$(4.95 \pm 0.31) \times 10^{-3}$	
Γ_{85}	$h^- h^- h^+ 2\pi^0 \nu_\tau$ (ex.K^0,ω,η)	[a]	$(10 \pm 4) \times 10^{-4}$	
Γ_{86}	$h^- h^- h^+ 3\pi^0 \nu_\tau$		$(2.13 \pm 0.30) \times 10^{-4}$	
Γ_{87}	$2\pi^- \pi^+ 3\pi^0 \nu_\tau$ (ex.K^0)		$(1.94 \pm 0.30) \times 10^{-4}$	
Γ_{88}	$2\pi^- \pi^+ 3\pi^0 \nu_\tau$ (ex.K^0, η, $f_1(1285)$)		$(1.7 \pm 0.4) \times 10^{-4}$	
Γ_{89}	$2\pi^- \pi^+ 3\pi^0 \nu_\tau$ (ex.K^0, η, ω, $f_1(1285)$)	[a]	$(1.4 \pm 2.7) \times 10^{-5}$	
Γ_{90}	$K^- h^+ h^- \geq 0$ neutrals ν_τ		$(6.29 \pm 0.14) \times 10^{-3}$	
Γ_{91}	$K^- h^+ \pi^- \nu_\tau$ (ex.K^0)		$(4.37 \pm 0.07) \times 10^{-3}$	
Γ_{92}	$K^- h^+ \pi^- \pi^0 \nu_\tau$ (ex.K^0)		$(8.6 \pm 1.2) \times 10^{-4}$	
Γ_{93}	$K^- \pi^+ \pi^- \geq 0$ neutrals ν_τ		$(4.77 \pm 0.14) \times 10^{-3}$	
Γ_{94}	$K^- \pi^+ \pi^- \geq 0\pi^0 \nu_\tau$ (ex.K^0)		$(3.73 \pm 0.13) \times 10^{-3}$	
Γ_{95}	$K^- \pi^+ \pi^- \nu_\tau$		$(3.45 \pm 0.07) \times 10^{-3}$	
Γ_{96}	$K^- \pi^+ \pi^- \nu_\tau$ (ex.K^0)		$(2.93 \pm 0.07) \times 10^{-3}$	
Γ_{97}	$K^- \pi^+ \pi^- \nu_\tau$ (ex.K^0,ω)	[a]	$(2.93 \pm 0.07) \times 10^{-3}$	
Γ_{98}	$K^- \rho^0 \nu_\tau \rightarrow K^- \pi^+ \pi^- \nu_\tau$		$(1.4 \pm 0.5) \times 10^{-3}$	
Γ_{99}	$K^- \pi^+ \pi^- \pi^0 \nu_\tau$		$(1.31 \pm 0.12) \times 10^{-3}$	
Γ_{100}	$K^- \pi^+ \pi^- \pi^0 \nu_\tau$ (ex.K^0)		$(8.0 \pm 1.2) \times 10^{-4}$	
Γ_{101}	$K^- \pi^+ \pi^- \pi^0 \nu_\tau$ (ex.K^0,η)		$(7.6 \pm 1.2) \times 10^{-4}$	
Γ_{102}	$K^- \pi^+ \pi^- \pi^0 \nu_\tau$ (ex.K^0,ω)		$(3.7 \pm 0.9) \times 10^{-4}$	
Γ_{103}	$K^- \pi^+ \pi^- \pi^0 \nu_\tau$ (ex.K^0,ω,η)	[a]	$(3.9 \pm 1.4) \times 10^{-4}$	
Γ_{104}	$K^- \pi^+ K^- \geq 0$ neut. ν_τ		$< 9 \times 10^{-4}$	CL=95%
Γ_{105}	$K^- K^+ \pi^- \geq 0$ neut. ν_τ		$(1.496 \pm 0.033) \times 10^{-3}$	
Γ_{106}	$K^- K^+ \pi^- \nu_\tau$	[a]	$(1.435 \pm 0.027) \times 10^{-3}$	
Γ_{107}	$K^- K^+ \pi^- \pi^0 \nu_\tau$	[a]	$(6.1 \pm 1.8) \times 10^{-5}$	
Γ_{108}	$K^- K^+ K^- \nu_\tau$		$(2.2 \pm 0.8) \times 10^{-5}$	S=5.4
Γ_{109}	$K^- K^+ K^- \nu_\tau$ (ex. ϕ)		$< 2.5 \times 10^{-6}$	CL=90%
Γ_{110}	$K^- K^+ K^- \pi^0 \nu_\tau$		$< 4.8 \times 10^{-6}$	CL=90%
Γ_{111}	$\pi^- K^+ \pi^- \geq 0$ neut. ν_τ		$< 2.5 \times 10^{-3}$	CL=95%
Γ_{112}	$e^- e^- e^+ \overline{\nu}_e \nu_\tau$		$(2.8 \pm 1.5) \times 10^{-5}$	
Γ_{113}	$\mu^- e^- e^+ \overline{\nu}_\mu \nu_\tau$		$< 3.2 \times 10^{-5}$	CL=90%
Γ_{114}	$\pi^- e^- e^+ \nu_\tau$		seen	
Γ_{115}	$\pi^- \mu^- \mu^+ \nu_\tau$		$< 1.14 \times 10^{-5}$	CL=90%

Modes with five charged particles

Γ_{116}	$3h^- 2h^+ \geq 0$ neutrals ν_τ (ex. $K^0_S \rightarrow \pi^+ \pi^-$) ("5-prong")		$(9.9 \pm 0.4) \times 10^{-4}$	
Γ_{117}	$3h^- 2h^+ \nu_\tau$ (ex.K^0)		$(8.29 \pm 0.31) \times 10^{-4}$	
Γ_{118}	$3\pi^- 2\pi^+ \nu_\tau$ (ex.K^0, ω)		$(8.27 \pm 0.31) \times 10^{-4}$	
Γ_{119}	$3\pi^- 2\pi^+ \nu_\tau$ (ex.K^0, ω, $f_1(1285)$)	[a]	$(7.75 \pm 0.30) \times 10^{-4}$	
Γ_{120}	$K^- 2\pi^- 2\pi^+ \nu_\tau$ (ex.K^0)	[a]	$(6 \pm 12) \times 10^{-7}$	
Γ_{121}	$K^+ 3\pi^- \pi^+ \nu_\tau$		$< 5.0 \times 10^{-6}$	CL=90%
Γ_{122}	$K^+ K^- 2\pi^- \pi^+ \nu_\tau$		$< 4.5 \times 10^{-7}$	CL=90%
Γ_{123}	$3h^- 2h^+ \pi^0 \nu_\tau$ (ex.K^0)		$(1.65 \pm 0.11) \times 10^{-4}$	
Γ_{124}	$3\pi^- 2\pi^+ \pi^0 \nu_\tau$ (ex.K^0)		$(1.64 \pm 0.11) \times 10^{-4}$	
Γ_{125}	$3\pi^- 2\pi^+ \pi^0 \nu_\tau$ (ex.K^0, η, $f_1(1285)$)		$(1.11 \pm 0.10) \times 10^{-4}$	
Γ_{126}	$3\pi^- 2\pi^+ \pi^0 \nu_\tau$ (ex.K^0, η, ω, $f_1(1285)$)	[a]	$(3.8 \pm 0.9) \times 10^{-5}$	
Γ_{127}	$K^- 2\pi^- 2\pi^+ \pi^0 \nu_\tau$ (ex.K^0)	[a]	$(1.1 \pm 0.6) \times 10^{-6}$	
Γ_{128}	$K^+ 3\pi^- \pi^+ \pi^0 \nu_\tau$		$< 8 \times 10^{-7}$	CL=90%
Γ_{129}	$3h^- 2h^+ 2\pi^0 \nu_\tau$		$< 3.4 \times 10^{-6}$	CL=90%

Miscellaneous other allowed modes

Γ_{130}	$(5\pi)^- \nu_\tau$		$(7.8 \pm 0.5) \times 10^{-3}$	
Γ_{131}	$4h^- 3h^+ \geq 0$ neutrals ν_τ ("7-prong")		$< 3.0 \times 10^{-7}$	CL=90%
Γ_{132}	$4h^- 3h^+ \nu_\tau$		$< 4.3 \times 10^{-7}$	CL=90%
Γ_{133}	$4h^- 3h^+ \pi^0 \nu_\tau$		$< 2.5 \times 10^{-7}$	CL=90%
Γ_{134}	$X^- (S=-1) \nu_\tau$		(2.92 ± 0.04) %	

Γ_{135}	$K^*(892)^- \geq 0$ neutrals $\geq 0 K^0_L \nu_\tau$		(1.42 ± 0.18) %	S=1.4
Γ_{136}	$K^*(892)^- \nu_\tau$		(1.20 ± 0.07) %	S=1.8
Γ_{137}	$K^*(892)^- \nu_\tau \to \pi^- \overline{K}^0 \nu_\tau$		$(7.82 \pm 0.26) \times 10^{-3}$	
Γ_{138}	$K^*(892)^0 K^- \geq 0$ neutrals ν_τ		$(3.2 \pm 1.4) \times 10^{-3}$	
Γ_{139}	$K^*(892)^0 K^- \nu_\tau$		$(2.1 \pm 0.4) \times 10^{-3}$	
Γ_{140}	$\overline{K}^*(892)^0 \pi^- \geq 0$ neutrals ν_τ		$(3.8 \pm 1.7) \times 10^{-3}$	
Γ_{141}	$\overline{K}^*(892)^0 \pi^- \nu_\tau$		$(2.2 \pm 0.5) \times 10^{-3}$	
Γ_{142}	$(\overline{K}^*(892)\pi)^- \nu_\tau \to \pi^- \overline{K}^0 \pi^0 \nu_\tau$		$(1.0 \pm 0.4) \times 10^{-3}$	
Γ_{143}	$K_1(1270)^- \nu_\tau$		$(4.7 \pm 1.1) \times 10^{-3}$	
Γ_{144}	$K_1(1400)^- \nu_\tau$		$(1.7 \pm 2.6) \times 10^{-3}$	S=1.7
Γ_{145}	$K^*(1410)^- \nu_\tau$		$(1.5 {}^{+1.4}_{-1.0}) \times 10^{-3}$	
Γ_{146}	$K^*_0(1430)^- \nu_\tau$		$< 5 \times 10^{-4}$	CL=95%
Γ_{147}	$K^*_2(1430)^- \nu_\tau$		$< 3 \times 10^{-3}$	CL=95%
Γ_{148}	$a_0(980)^- \geq 0$ neutrals ν_τ			
Γ_{149}	$\eta \pi^- \nu_\tau$		$< 9.9 \times 10^{-5}$	CL=95%
Γ_{150}	$\eta \pi^- \pi^0 \nu_\tau$	[a]	$(1.39 \pm 0.07) \times 10^{-3}$	
Γ_{151}	$\eta \pi^- \pi^0 \pi^0 \nu_\tau$	[a]	$(1.9 \pm 0.4) \times 10^{-4}$	
Γ_{152}	$\eta K^- \nu_\tau$	[a]	$(1.55 \pm 0.08) \times 10^{-4}$	
Γ_{153}	$\eta K^*(892)^- \nu_\tau$		$(1.38 \pm 0.15) \times 10^{-4}$	
Γ_{154}	$\eta K^- \pi^0 \nu_\tau$	[a]	$(4.8 \pm 1.2) \times 10^{-5}$	
Γ_{155}	$\eta K^- \pi^0 (\text{non-}K^*(892)) \nu_\tau$		$< 3.5 \times 10^{-5}$	CL=90%
Γ_{156}	$\eta \overline{K}^0 \pi^- \nu_\tau$	[a]	$(9.4 \pm 1.5) \times 10^{-5}$	
Γ_{157}	$\eta \overline{K}^0 \pi^- \pi^0 \nu_\tau$		$< 5.0 \times 10^{-5}$	CL=90%
Γ_{158}	$\eta K^- K^0 \nu_\tau$		$< 9.0 \times 10^{-6}$	CL=90%
Γ_{159}	$\eta \pi^+ \pi^- \pi^- \geq 0$ neutrals ν_τ		$< 3 \times 10^{-3}$	CL=90%
Γ_{160}	$\eta \pi^- \pi^+ \pi^- \nu_\tau (\text{ex.}K^0)$	[a]	$(2.20 \pm 0.13) \times 10^{-4}$	
Γ_{161}	$\eta \pi^- \pi^+ \pi^- \nu_\tau (\text{ex.}K^0, f_1(1285))$		$(9.9 \pm 1.6) \times 10^{-5}$	
Γ_{162}	$\eta a_1(1260)^- \nu_\tau \to \eta \pi^- \rho^0 \nu_\tau$		$< 3.9 \times 10^{-4}$	CL=90%
Γ_{163}	$\eta \eta \pi^- \nu_\tau$		$< 7.4 \times 10^{-6}$	CL=90%
Γ_{164}	$\eta \eta \pi^- \pi^0 \nu_\tau$		$< 2.0 \times 10^{-4}$	CL=95%
Γ_{165}	$\eta \eta K^- \nu_\tau$		$< 3.0 \times 10^{-6}$	CL=90%
Γ_{166}	$\eta'(958) \pi^- \nu_\tau$		$< 4.0 \times 10^{-6}$	CL=90%
Γ_{167}	$\eta'(958) \pi^- \pi^0 \nu_\tau$		$< 1.2 \times 10^{-5}$	CL=90%
Γ_{168}	$\eta'(958) K^- \nu_\tau$		$< 2.4 \times 10^{-6}$	CL=90%
Γ_{169}	$\phi \pi^- \nu_\tau$		$(3.4 \pm 0.6) \times 10^{-5}$	
Γ_{170}	$\phi K^- \nu_\tau$	[a]	$(4.4 \pm 1.6) \times 10^{-5}$	
Γ_{171}	$f_1(1285) \pi^- \nu_\tau$		$(3.9 \pm 0.5) \times 10^{-4}$	S=1.9
Γ_{172}	$f_1(1285) \pi^- \nu_\tau \to \eta \pi^- \pi^+ \pi^- \nu_\tau$		$(1.18 \pm 0.07) \times 10^{-4}$	S=1.3
Γ_{173}	$f_1(1285) \pi^- \nu_\tau \to 3\pi^- 2\pi^+ \nu_\tau$	[a]	$(5.2 \pm 0.4) \times 10^{-5}$	
Γ_{174}	$\pi(1300)^- \nu_\tau \to (\rho\pi)^- \nu_\tau \to (3\pi)^- \nu_\tau$		$< 1.0 \times 10^{-4}$	CL=90%
Γ_{175}	$\pi(1300)^- \nu_\tau \to ((\pi\pi)_{S-\text{wave}} \pi)^- \nu_\tau \to (3\pi)^- \nu_\tau$		$< 1.9 \times 10^{-4}$	CL=90%
Γ_{176}	$h^- \omega \geq 0$ neutrals ν_τ		(2.40 ± 0.08) %	
Γ_{177}	$h^- \omega \nu_\tau$		(1.99 ± 0.06) %	
Γ_{178}	$\pi^- \omega \nu_\tau$	[a]	(1.95 ± 0.06) %	
Γ_{179}	$K^- \omega \nu_\tau$	[a]	$(4.1 \pm 0.9) \times 10^{-4}$	
Γ_{180}	$h^- \omega \pi^0 \nu_\tau$	[a]	$(4.1 \pm 0.4) \times 10^{-3}$	
Γ_{181}	$h^- \omega 2\pi^0 \nu_\tau$		$(1.4 \pm 0.5) \times 10^{-4}$	
Γ_{182}	$\pi^- \omega 2\pi^0 \nu_\tau$	[a]	$(7.2 \pm 1.6) \times 10^{-5}$	
Γ_{183}	$h^- 2\omega \nu_\tau$		$< 5.4 \times 10^{-7}$	CL=90%
Γ_{184}	$2h^- h^+ \omega \nu_\tau$		$(1.20 \pm 0.22) \times 10^{-4}$	
Γ_{185}	$2\pi^- \pi^+ \omega \nu_\tau (\text{ex.}K^0)$	[a]	$(8.4 \pm 0.6) \times 10^{-5}$	

Lepton Family number (*LF*), Lepton number (*L*), or Baryon number (*B*) violating modes

L means lepton number violation (*e.g.* $\tau^- \to e^+ \pi^- \pi^-$). Following common usage, *LF* means lepton family violation *and not* lepton number violation (*e.g.* $\tau^- \to e^- \pi^+ \pi^-$). *B* means baryon number violation.

Γ_{186}	$e^- \gamma$	*LF*	$< 3.3 \times 10^{-8}$	CL=90%
Γ_{187}	$e^- \gamma\gamma$	*LF*	$< 2.5 \times 10^{-4}$	CL=90%
Γ_{188}	$\mu^- \gamma$	*LF*	$< 4.2 \times 10^{-8}$	CL=90%
Γ_{189}	$\mu^- \gamma\gamma$	*LF*	$< 5.8 \times 10^{-4}$	CL=90%
Γ_{190}	$e^- \pi^0$	*LF*	$< 8.0 \times 10^{-8}$	CL=90%
Γ_{191}	$\mu^- \pi^0$	*LF*	$< 1.1 \times 10^{-7}$	CL=90%
Γ_{192}	$e^- K^0_S$	*LF*	$< 8 \times 10^{-9}$	CL=90%
Γ_{193}	$\mu^- K^0_S$	*LF*	$< 1.2 \times 10^{-8}$	CL=90%
Γ_{194}	$e^- \eta$	*LF*	$< 9.2 \times 10^{-8}$	CL=90%
Γ_{195}	$\mu^- \eta$	*LF*	$< 6.5 \times 10^{-8}$	CL=90%
Γ_{196}	$e^- \rho^0$	*LF*	$< 2.2 \times 10^{-8}$	CL=90%
Γ_{197}	$\mu^- \rho^0$	*LF*	$< 1.7 \times 10^{-8}$	CL=90%
Γ_{198}	$e^- \omega$	*LF*	$< 2.4 \times 10^{-8}$	CL=90%
Γ_{199}	$\mu^- \omega$	*LF*	$< 3.9 \times 10^{-8}$	CL=90%
Γ_{200}	$e^- K^*(892)^0$	*LF*	$< 1.9 \times 10^{-8}$	CL=90%
Γ_{201}	$\mu^- K^*(892)^0$	*LF*	$< 2.9 \times 10^{-8}$	CL=90%
Γ_{202}	$e^- \overline{K}^*(892)^0$	*LF*	$< 1.7 \times 10^{-8}$	CL=90%
Γ_{203}	$\mu^- \overline{K}^*(892)^0$	*LF*	$< 4.3 \times 10^{-8}$	CL=90%
Γ_{204}	$e^- \eta'(958)$	*LF*	$< 1.6 \times 10^{-7}$	CL=90%
Γ_{205}	$\mu^- \eta'(958)$	*LF*	$< 1.3 \times 10^{-7}$	CL=90%
Γ_{206}	$e^- f_0(980) \to e^- \pi^+ \pi^-$	*LF*	$< 3.2 \times 10^{-8}$	CL=90%
Γ_{207}	$\mu^- f_0(980) \to \mu^- \pi^+ \pi^-$	*LF*	$< 3.4 \times 10^{-8}$	CL=90%
Γ_{208}	$e^- \phi$	*LF*	$< 2.0 \times 10^{-8}$	CL=90%
Γ_{209}	$\mu^- \phi$	*LF*	$< 2.3 \times 10^{-8}$	CL=90%
Γ_{210}	$e^- e^+ e^-$	*LF*	$< 2.5 \times 10^{-8}$	CL=90%
Γ_{211}	$e^- \mu^+ \mu^-$	*LF*	$< 2.4 \times 10^{-8}$	CL=90%
Γ_{212}	$e^+ \mu^- \mu^-$	*LF*	$< 1.3 \times 10^{-8}$	CL=90%
Γ_{213}	$\mu^- e^+ e^-$	*LF*	$< 1.6 \times 10^{-8}$	CL=90%
Γ_{214}	$\mu^+ e^- e^-$	*LF*	$< 1.5 \times 10^{-8}$	CL=90%
Γ_{215}	$\mu^- \mu^+ \mu^-$	*LF*	$< 1.9 \times 10^{-8}$	CL=90%
Γ_{216}	$e^- \pi^+ \pi^-$	*LF*	$< 2.3 \times 10^{-8}$	CL=90%
Γ_{217}	$e^+ \pi^- \pi^-$	*L*	$< 2.0 \times 10^{-8}$	CL=90%
Γ_{218}	$\mu^- \pi^+ \pi^-$	*LF*	$< 2.1 \times 10^{-8}$	CL=90%
Γ_{219}	$\mu^+ \pi^- \pi^-$	*L*	$< 3.9 \times 10^{-8}$	CL=90%
Γ_{220}	$e^- \pi^+ K^-$	*LF*	$< 3.7 \times 10^{-8}$	CL=90%
Γ_{221}	$e^- \pi^- K^+$	*LF*	$< 3.1 \times 10^{-8}$	CL=90%
Γ_{222}	$e^+ \pi^- K^-$	*L*	$< 3.2 \times 10^{-8}$	CL=90%
Γ_{223}	$e^- K^0_S K^0_S$	*LF*	$< 7.1 \times 10^{-8}$	CL=90%
Γ_{224}	$e^- K^+ K^-$	*LF*	$< 3.4 \times 10^{-8}$	CL=90%
Γ_{225}	$e^+ K^- K^-$	*L*	$< 3.3 \times 10^{-8}$	CL=90%
Γ_{226}	$\mu^- \pi^+ K^-$	*LF*	$< 8.6 \times 10^{-8}$	CL=90%
Γ_{227}	$\mu^- \pi^- K^+$	*LF*	$< 4.5 \times 10^{-8}$	CL=90%
Γ_{228}	$\mu^+ \pi^- K^-$	*L*	$< 4.8 \times 10^{-8}$	CL=90%
Γ_{229}	$\mu^- K^0_S K^0_S$	*LF*	$< 8.0 \times 10^{-8}$	CL=90%
Γ_{230}	$\mu^- K^+ K^-$	*LF*	$< 4.4 \times 10^{-8}$	CL=90%
Γ_{231}	$\mu^+ K^- K^-$	*L*	$< 4.7 \times 10^{-8}$	CL=90%
Γ_{232}	$e^- \pi^0 \pi^0$	*LF*	$< 6.5 \times 10^{-6}$	CL=90%
Γ_{233}	$\mu^- \pi^0 \pi^0$	*LF*	$< 1.4 \times 10^{-5}$	CL=90%
Γ_{234}	$e^- \eta\eta$	*LF*	$< 3.5 \times 10^{-5}$	CL=90%
Γ_{235}	$\mu^- \eta\eta$	*LF*	$< 6.0 \times 10^{-5}$	CL=90%
Γ_{236}	$e^- \pi^0 \eta$	*LF*	$< 2.4 \times 10^{-5}$	CL=90%
Γ_{237}	$\mu^- \pi^0 \eta$	*LF*	$< 2.2 \times 10^{-5}$	CL=90%
Γ_{238}	$p e^- e^-$	*L,B*	$< 3.0 \times 10^{-8}$	CL=90%
Γ_{239}	$\overline{p} e^+ e^-$	*L,B*	$< 3.0 \times 10^{-8}$	CL=90%
Γ_{240}	$\overline{p} e^+ \mu^-$	*L,B*	$< 2.0 \times 10^{-8}$	CL=90%
Γ_{241}	$\overline{p} e^- \mu^+$	*L,B*	$< 1.8 \times 10^{-8}$	CL=90%
Γ_{242}	$p \mu^- \mu^-$	*L,B*	$< 4.0 \times 10^{-8}$	CL=90%
Γ_{243}	$\overline{p} \mu^+ \mu^-$	*L,B*	$< 1.8 \times 10^{-8}$	CL=90%
Γ_{244}	$\overline{p} \gamma$	*L,B*	$< 3.5 \times 10^{-6}$	CL=90%
Γ_{245}	$\overline{p} \pi^0$	*L,B*	$< 1.5 \times 10^{-5}$	CL=90%
Γ_{246}	$\overline{p} 2\pi^0$	*L,B*	$< 3.3 \times 10^{-5}$	CL=90%
Γ_{247}	$\overline{p} \eta$	*L,B*	$< 8.9 \times 10^{-6}$	CL=90%
Γ_{248}	$\overline{p} \pi^0 \eta$	*L,B*	$< 2.7 \times 10^{-5}$	CL=90%
Γ_{249}	$\Lambda \pi^-$	*L,B*	$< 4.7 \times 10^{-8}$	CL=90%
Γ_{250}	$\overline{\Lambda} \pi^-$	*L,B*	$< 4.3 \times 10^{-8}$	CL=90%
Γ_{251}	e^- light boson	*LF*	$< 4.5 \times 10^{-4}$	CL=90%
Γ_{252}	μ^- light boson	*LF*	$< 2.8 \times 10^{-4}$	CL=90%

[a] Basis mode for the τ.

[b] See the Particle Listings below for the energy limits used in this measurement.

Int. J. Mod
by UNIVERSITY OF CALIFORNIA @ BERK
wnloaded from www.worldscientific.com
-use and distribution is strictly not permitted, except for Open Access articles.

Int. J. Mod. Phys. A 2026.41. Downloaded from www.worldscientific.com
by UNIVERSITY OF CALIFORNIA @ BERKELEY on 09/16/26. Re-use and distribution is strictly not permitted, except for Open Access articles.

CONSTRAINED FIT INFORMATION

An overall fit to 85 branching ratios uses 170 measurements and one constraint to determine 46 parameters. The overall fit has a $\chi^2 = 135.0$ for 125 degrees of freedom.

The following *off-diagonal* array elements are the correlation coefficients $\langle \delta x_i \delta x_j \rangle / (\delta x_i \cdot \delta x_j)$, in percent, from the fit to the branching fractions, $x_i \equiv \Gamma_i/\Gamma_{\text{total}}$. The fit constrains the x_i whose labels appear in this array to sum to one.

	x_3	x_5	x_9	x_{10}	x_{14}	x_{16}	x_{20}	x_{23}	x_{27}	x_{28}
x_5	39									
x_9	2	0								
x_{10}	3	4	5							
x_{14}	−20	−20	−17	−5						
x_{16}	−1	−1	0	−2	−9					
x_{20}	−12	−12	−14	−4	−46	−1				
x_{23}	−1	0	−2	−3	−1	−14	−10			
x_{27}	−7	−6	−10	−1	0	1	−39	1		
x_{28}	−1	−1	−1	−2	0	−13	−3	−23	−11	
x_{30}	−5	−4	−11	−1	−9	0	7	−2	−44	2
x_{36}	−3	−3	−3	−1	−1	−1	−2	0	−1	0
x_{38}	−1	−1	1	0	0	0	0	−2	0	−2
x_{41}	−2	−2	−2	−1	−1	0	−2	0	−1	0
x_{43}	−1	−1	−1	−1	0	−3	0	−5	0	−5
x_{45}	−5	−5	−5	−2	−3	−1	−4	−2	−1	−2
x_{48}	−1	−1	2	0	−1	2	−1	−1	0	−1
x_{49}	−5	−5	−5	−2	−3	−1	−5	−2	−1	−2
x_{52}	0	0	0	0	0	0	0	−1	0	−1
x_{56}	−2	−2	−2	−1	−1	−1	−2	−1	−1	−1
x_{61}	−5	−5	−5	−2	−3	−1	−4	−2	−1	−2
x_{70}	−8	−9	4	−2	−6	3	−12	−2	−7	−1
x_{78}	−4	−4	−5	0	−9	0	1	1	−1	1
x_{85}	0	0	−2	0	−2	0	0	0	2	0
x_{89}	0	0	0	0	0	0	0	0	0	0
x_{97}	−2	−2	−1	−1	−1	−1	−3	−1	−2	−1
x_{103}	1	1	0	−1	1	−1	−1	−1	0	−1
x_{106}	−2	−2	2	−1	−1	1	−2	−1	−1	−1
x_{107}	0	0	0	0	0	0	0	0	0	0
x_{119}	−1	−1	1	0	−1	1	−2	−1	−1	0
x_{120}	0	0	0	0	0	0	0	0	0	0
x_{126}	0	0	0	0	0	0	0	0	0	0
x_{127}	0	0	0	0	0	0	0	0	0	0
x_{150}	−1	−1	−1	0	−1	0	−2	−1	0	−1
x_{151}	−1	−1	0	0	−1	0	−1	0	0	0
x_{152}	0	0	0	0	0	0	0	−1	0	−1
x_{154}	0	0	0	0	0	0	0	0	0	0
x_{156}	0	0	0	0	0	0	0	0	0	0
x_{160}	−1	−1	1	0	−1	1	−1	0	−1	0
x_{170}	0	0	0	0	0	0	0	0	0	0
x_{173}	−1	−1	1	0	0	1	−1	0	0	0
x_{178}	−3	−3	−3	−1	−4	0	−1	0	−1	0
x_{179}	0	0	0	0	0	0	0	0	0	0
x_{180}	−2	−2	−5	−1	−3	0	−2	−1	2	−1
x_{182}	0	0	0	0	0	0	0	0	0	0
x_{185}	−1	−1	0	0	−1	1	−1	0	0	0

	x_{30}	x_{36}	x_{38}	x_{41}	x_{43}	x_{45}	x_{48}	x_{49}	x_{52}	x_{56}
x_{36}	0									
x_{38}	0	−15								
x_{41}	0	−13	2							
x_{43}	0	−1	−14	−20						
x_{45}	0	−3	0	−6	0					
x_{48}	0	−2	3	−4	1	0				
x_{49}	0	−5	0	−4	−1	−10	−1			
x_{52}	0	1	5	−1	6	0	−7	0		
x_{56}	0	−2	0	−2	−1	−4	0	−8	0	
x_{61}	0	−2	0	−2	0	−4	0	−4	0	−2
x_{70}	−5	−2	3	−2	−1	−4	5	−4	0	−2
x_{78}	3	1	−1	1	0	2	−1	2	0	1
x_{85}	2	0	0	0	0	0	0	0	0	0
x_{89}	0	0	0	0	0	0	0	0	−1	0
x_{97}	−1	−1	0	−1	0	−2	0	−2	0	−1
x_{103}	−1	−1	0	−1	0	−1	0	−1	0	−1
x_{106}	−1	−1	1	0	0	−1	2	−1	0	0
x_{107}	0	0	0	0	0	0	0	0	0	0
x_{119}	−1	−1	1	0	0	−1	2	−1	0	0
x_{120}	0	0	0	0	0	0	0	0	0	0
x_{126}	0	0	0	0	0	0	0	0	0	0
x_{127}	0	0	0	0	0	0	0	0	0	0
x_{150}	−2	−1	0	0	0	−1	0	−1	0	0
x_{151}	0	0	0	0	0	−1	0	−1	0	0
x_{152}	0	0	1	0	0	0	1	0	0	0
x_{154}	0	0	0	0	0	0	0	0	0	0
x_{156}	0	0	0	0	0	0	0	−1	0	0
x_{160}	−1	0	1	0	0	−1	1	−1	0	0
x_{170}	0	0	0	0	0	0	0	0	0	0
x_{173}	−1	0	1	0	0	0	1	0	0	0
x_{178}	1	0	0	0	0	−1	0	−1	0	0
x_{179}	0	0	0	0	0	0	0	0	0	0
x_{180}	2	−1	0	0	0	−1	0	−1	0	0
x_{182}	0	0	0	0	0	0	0	0	0	0
x_{185}	−1	0	1	0	0	0	1	−1	0	0

	x_{61}	x_{70}	x_{78}	x_{85}	x_{89}	x_{97}	x_{103}	x_{106}	x_{107}	x_{119}
x_{70}	−4									
x_{78}	2	−19								
x_{85}	0	−1	−8							
x_{89}	0	−1	−1	0						
x_{97}	−2	19	−6	0	0					
x_{103}	−1	−4	−14	−1	0	−1				
x_{106}	−1	15	−4	0	0	0	−1			
x_{107}	0	−1	−1	0	0	0	−3	0		
x_{119}	−1	3	−1	0	−4	−1	0	1	0	
x_{120}	0	0	0	0	0	0	0	0	0	−1
x_{126}	0	0	0	0	0	0	0	0	0	3
x_{127}	0	0	0	0	0	0	0	0	0	−1
x_{150}	−1	0	0	−5	0	0	0	0	0	0
x_{151}	−1	0	0	0	−11	0	0	0	0	9
x_{152}	0	2	0	0	0	0	−1	1	0	1
x_{154}	0	0	0	−1	0	0	0	0	0	0
x_{156}	0	0	0	0	−2	0	0	0	0	0
x_{160}	−1	1	−1	0	−8	−1	0	1	0	46
x_{170}	0	−1	0	0	0	1	0	1	0	0
x_{173}	0	1	0	0	−2	0	0	1	0	34
x_{178}	−1	−9	−67	−3	0	−2	10	−2	0	−1
x_{179}	0	0	12	0	0	−2	−58	0	0	0
x_{180}	−1	−2	−11	−64	−1	−1	−1	−1	0	0
x_{182}	0	0	0	0	−16	0	0	0	0	7
x_{185}	0	1	−1	0	−4	0	0	1	0	39

	x_{120}	x_{126}	x_{127}	x_{150}	x_{151}	x_{152}	x_{154}	x_{156}	x_{160}	x_{170}
x_{126}	0									
x_{127}	0	−1								
x_{150}	0	0	0							
x_{151}	0	2	0	0						
x_{152}	0	0	0	4	0					
x_{154}	0	0	0	1	0	1				
x_{156}	0	0	0	2	−1	1	0			
x_{160}	−1	3	−1	0	25	0	0	0		
x_{170}	0	0	0	0	0	0	0	0	0	
x_{173}	−1	1	0	0	4	0	0	0	20	0
x_{178}	0	0	0	0	0	0	0	0	0	0
x_{179}	0	0	0	0	0	0	0	0	0	0
x_{180}	0	0	0	0	0	0	0	0	0	0
x_{182}	0	2	0	0	10	0	0	−1	20	0
x_{185}	−1	−2	−1	0	17	0	0	0	38	0

	x_{173}	x_{178}	x_{179}	x_{180}	x_{182}
x_{178}	0				
x_{179}	0	−14			
x_{180}	0	−4	0		
x_{182}	3	0	0	0	
x_{185}	17	0	0	0	14

See the related review(s):
τ Branching Fractions

$(\Gamma(\tau^+) - \Gamma(\tau^-)) / (\Gamma(\tau^+) + \Gamma(\tau^-))$

$\tau^\pm \to \pi^\pm K^0_S \nu_\tau$ (RATE DIFFERENCE) / (RATE SUM)

VALUE (%)	DOCUMENT ID		TECN	COMMENT
−0.36±0.23±0.11	LEES	12M	BABR	476 fb^{-1} E^{ee}_{cm} = 10.6 GeV

τ^- BRANCHING RATIOS

$\Gamma(\text{particle}^- \geq 0 \text{ neutrals } \geq 0K^0 \nu_\tau(\text{"1-prong"}))/\Gamma_{total}$ — Γ_1/Γ

$\Gamma_1/\Gamma = (\Gamma_3+\Gamma_5+\Gamma_9+\Gamma_{10}+\Gamma_{14}+\Gamma_{16}+\Gamma_{20}+\Gamma_{23}+\Gamma_{27}+\Gamma_{28}+\Gamma_{30}+\Gamma_{36}+\Gamma_{38}+\Gamma_{41}+\Gamma_{43}+\Gamma_{45}+\Gamma_{48}+\Gamma_{49}+\Gamma_{50}+\Gamma_{52}+\Gamma_{56}+\Gamma_{57}+0.7195\Gamma_{150}+0.7195\Gamma_{152}+0.7195\Gamma_{154}+0.7195\Gamma_{156}+0.336\Gamma_{170}+0.0833\Gamma_{178}+0.0833\Gamma_{179}+0.0833\Gamma_{180})/\Gamma$

The charged particle here can be e, μ, or hadron. In many analyses, the sum of the topological branching fractions (1, 3, and 5 prongs) is constrained to be unity. Since the 5-prong fraction is very small, the measured 1-prong and 3-prong fractions are highly correlated and cannot be treated as independent quantities in our overall fit. We arbitrarily choose to use the 3-prong fraction in our fit, and leave the 1-prong fraction out. We do, however, use these 1-prong measurements in our average below.

VALUE (%)	EVTS	DOCUMENT ID		TECN	COMMENT
85.24 ±0.06 OUR FIT (Produced by HFLAV)					
85.26 ±0.13 OUR AVERAGE Error includes scale factor of 1.6. See the ideogram below.					
• • • We use the following data for averages but not for fits. • • •					
85.316±0.093±0.049	78k	[1] ABREU	01M	DLPH	1992–1995 LEP runs
85.274±0.105±0.073		[2] ACHARD	01D	L3	1992–1995 LEP runs
84.48 ±0.27 ±0.23		ACTON	92H	OPAL	1990–1991 LEP runs
• • • We do not use the following data for averages, fits, limits, etc. • • •					
85.45 $^{+0.69}_{-0.73}$ ±0.65		DECAMP	92C	ALEP	Repl. by SCHAEL 05C

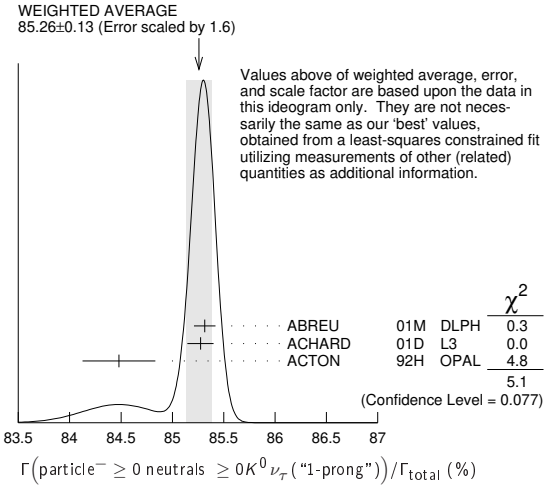

[1] The correlation coefficients between this measurement and the ABREU 01M measurements of B($\tau \to$ 3-prong) and B($\tau \to$ 5-prong) are −0.98 and −0.08 respectively.
[2] The correlation coefficients between this measurement and the ACHARD 01D measurements of B($\tau \to$ "3-prong") and B($\tau \to$ "5-prong") are −0.978 and −0.082 respectively.

$\Gamma(\text{particle}^- \geq 0 \text{ neutrals } \geq 0K^0_L \nu_\tau)/\Gamma_{total}$ — Γ_2/Γ

$\Gamma_2/\Gamma = (\Gamma_3+\Gamma_5+\Gamma_9+\Gamma_{10}+\Gamma_{14}+\Gamma_{16}+\Gamma_{20}+\Gamma_{23}+\Gamma_{27}+\Gamma_{28}+\Gamma_{30}+0.6534\Gamma_{36}+0.6534\Gamma_{38}+0.6534\Gamma_{41}+0.6534\Gamma_{43}+0.6534\Gamma_{45}+0.0942\Gamma_{48}+0.3069\Gamma_{49}+\Gamma_{50}+0.0942\Gamma_{52}+0.3069\Gamma_{56}+\Gamma_{57}+0.7195\Gamma_{150}+0.7195\Gamma_{152}+0.7195\Gamma_{154}+0.4701\Gamma_{156}+0.1049\Gamma_{170}+0.0833\Gamma_{178}+0.0833\Gamma_{179}+0.0833\Gamma_{180})/\Gamma$

VALUE (%)	EVTS	DOCUMENT ID		TECN	COMMENT
84.58±0.06 OUR FIT (Produced by HFLAV)					
85.1 ±0.4 OUR AVERAGE					
• • • We use the following data for averages but not for fits. • • •					
85.6 ±0.6 ±0.3	3300	[1] ADEVA	91F	L3	E^{ee}_{cm} = 88.3–94.3 GeV
84.9 ±0.4 ±0.3		BEHREND	89B	CELL	E^{ee}_{cm} = 14–47 GeV
84.7 ±0.8 ±0.6		[2] AIHARA	87B	TPC	E^{ee}_{cm} = 29 GeV
• • • We do not use the following data for averages, fits, limits, etc. • • •					
86.4 ±0.3 ±0.3		ABACHI	89B	HRS	E^{ee}_{cm} = 29 GeV
87.1 ±1.0 ±0.7		[3] BURCHAT	87	MRK2	E^{ee}_{cm} = 29 GeV
87.2 ±0.5 ±0.8		SCHMIDKE	86	MRK2	E^{ee}_{cm} = 29 GeV
84.7 ±1.1 $^{+1.6}_{-1.3}$	169	[4] ALTHOFF	85	TASS	E^{ee}_{cm} = 34.5 GeV
86.1 ±0.5 ±0.9		BARTEL	85F	JADE	E^{ee}_{cm} = 34.6 GeV
87.8 ±1.3 ±3.9		[5] BERGER	85	PLUT	E^{ee}_{cm} = 34.6 GeV
86.7 ±0.3 ±0.6		FERNANDEZ	85	MAC	E^{ee}_{cm} = 29 GeV

[1] Not independent of ADEVA 91F $\Gamma(h^- h^- h^+ \geq 0 \text{ neutrals } \geq 0K^0_L \nu_\tau)/\Gamma_{total}$ value.
[2] Not independent of AIHARA 87B $\Gamma(\mu^- \overline{\nu}_\mu \nu_\tau)/\Gamma_{total}$, $\Gamma(e^- \overline{\nu}_e \nu_\tau)/\Gamma_{total}$, and $\Gamma(h^- \geq 0 \text{ neutrals } \geq 0K^0_L \nu_\tau)/\Gamma_{total}$ values.
[3] Not independent of SCHMIDKE 86 value (also not independent of BURCHAT 87 value for $\Gamma(h^- h^- h^+ \geq 0 \text{ neutrals } \geq 0K^0_L \nu_\tau)/\Gamma_{total}$.
[4] Not independent of ALTHOFF 85 $\Gamma(\mu^- \overline{\nu}_\mu \nu_\tau)/\Gamma_{total}$, $\Gamma(e^- \overline{\nu}_e \nu_\tau)/\Gamma_{total}$, $\Gamma(h^- \geq 0 \text{ neutrals } \geq 0K^0_L \nu_\tau)/\Gamma_{total}$, and $\Gamma(h^- h^- h^+ \geq 0 \text{ neutrals } \geq 0K^0_L \nu_\tau)/\Gamma_{total}$ values.
[5] Not independent of (1-prong + $0\pi^0$) and (1-prong + $\geq 1\pi^0$) values.

$\Gamma(\mu^- \overline{\nu}_\mu \nu_\tau)/\Gamma_{total}$ — Γ_3/Γ

To minimize the effect of experiments with large systematic errors, we exclude experiments which together would contribute 5% of the weight in the average.

VALUE (%)	EVTS	DOCUMENT ID		TECN	COMMENT
17.37 ±0.04 OUR FIT (Produced by HFLAV)					
17.33 ±0.05 OUR AVERAGE					
17.319±0.070±0.032	54k	[1] SCHAEL	05C	ALEP	1991–1995 LEP runs
17.34 ±0.09 ±0.06	31.4k	ABBIENDI	03	OPAL	1990–1995 LEP runs
17.342±0.110±0.067	21.5k	[2] ACCIARRI	01F	L3	1991–1995 LEP runs
17.325±0.095±0.077	27.7k	ABREU	99X	DLPH	1991–1995 LEP runs
• • • We use the following data for averages but not for fits. • • •					
17.37 ±0.08 ±0.18		[3] ANASTASSOV	97	CLEO	E^{ee}_{cm} = 10.6 GeV
• • • We do not use the following data for averages, fits, limits, etc. • • •					
17.31 ±0.11 ±0.05	20.7k	BUSKULIC	96C	ALEP	Repl. by SCHAEL 05C
17.02 ±0.19 ±0.24	6586	ABREU	95T	DLPH	Repl. by ABREU 99X
17.36 ±0.27	7941	AKERS	95I	OPAL	Repl. by ABBIENDI 03
17.6 ±0.4 ±0.4	2148	ADRIANI	93M	L3	Repl. by ACCIARRI 01F
17.4 ±0.3 ±0.5		[4] ALBRECHT	93G	ARG	E^{ee}_{cm} = 9.4–10.6 GeV
17.35 ±0.41 ±0.37		DECAMP	92C	ALEP	1989–1990 LEP runs
17.7 ±0.8 ±0.4	568	BEHREND	90	CELL	E^{ee}_{cm} = 35 GeV
17.4 ±1.0	2197	ADEVA	88	MRKJ	E^{ee}_{cm} = 14–16 GeV
17.7 ±1.2 ±0.7		AIHARA	87B	TPC	E^{ee}_{cm} = 29 GeV
18.3 ±0.9 ±0.8		BURCHAT	87	MRK2	E^{ee}_{cm} = 29 GeV
18.6 ±0.8 ±0.7	558	[5] BARTEL	86D	JADE	E^{ee}_{cm} = 34.6 GeV
12.9 ±1.7 $^{+0.7}_{-0.5}$		ALTHOFF	85	TASS	E^{ee}_{cm} = 34.5 GeV
18.0 ±0.9 ±0.5	473	[5] ASH	85B	MAC	E^{ee}_{cm} = 29 GeV
18.0 ±1.0 ±0.6		[6] BALTRUSAIT...85		MRK3	E^{ee}_{cm} = 3.77 GeV
19.4 ±1.6 ±1.7	153	BERGER	85	PLUT	E^{ee}_{cm} = 34.6 GeV
17.6 ±2.6 ±2.1	47	BEHREND	83C	CELL	E^{ee}_{cm} = 34 GeV
17.8 ±2.0 ±1.8		BERGER	81B	PLUT	E^{ee}_{cm} = 9–32 GeV

[1] See footnote to SCHAEL 05C $\Gamma(\tau^- \to e^- \overline{\nu}_e \nu_\tau)/\Gamma_{total}$ measurement for correlations with other measurements.
[2] The correlation coefficient between this measurement and the ACCIARRI 01F measurement of B($\tau^- \to e^- \overline{\nu}_e \nu_\tau$) is 0.08.
[3] The correlation coefficients between this measurement and the ANASTASSOV 97 measurements of B($e\overline{\nu}_e \nu_\tau$), B($\mu\overline{\nu}_\mu \nu_\tau$)/B($e\overline{\nu}_e \nu_\tau$), B($h^- \nu_\tau$), and B($h^- \nu_\tau$)/B($e\overline{\nu}_e \nu_\tau$) are 0.50, 0.58, 0.50, and 0.08 respectively.
[4] Not independent of ALBRECHT 92D $\Gamma(\mu^- \overline{\nu}_\mu \nu_\tau)/\Gamma(e^- \overline{\nu}_e \nu_\tau)$ and ALBRECHT 93G $\Gamma(\mu^- \overline{\nu}_\mu \nu_\tau) \times \Gamma(e^- \overline{\nu}_e \nu_\tau)/\Gamma^2_{total}$ values.
[5] Modified using B($e^- \overline{\nu}_e \nu_\tau$)/B("1 prong") and B("1 prong") ,= 0.855.
[6] Error correlated with BALTRUSAITIS 85 $e\nu\overline{\nu}$ value.

Int. J. Mod. Phys. A 2026.41. Downloaded from www.worldscientific.com
by UNIVERSITY OF CALIFORNIA @ BERKELEY on 09/16/26. Re-use and distribution is strictly not permitted, except for Open Access articles.

Int. J. Mod. Phys. A 2026.41. Downloaded from www.worldscientific.com
by UNIVERSITY OF CALIFORNIA @ BERKELEY on 09/16/26. Re-use and distribution is strictly not permitted, except for Open Access articles.

$\Gamma(\mu^- \overline{\nu}_\mu \nu_\tau \gamma)/\Gamma_{total}$ — Γ_4/Γ

VALUE (%)	EVTS	DOCUMENT ID		TECN	COMMENT
0.367±0.008 OUR AVERAGE					
0.363±0.002±0.015	22k	[1] SHIMIZU	18A	BELL	711 fb^{-1} E^{ee}_{cm}=10.6 GeV
0.369±0.003±0.010	16k	[2] LEES	15G	BABR	431 fb^{-1} E^{ee}_{cm}=10.6 GeV
0.361±0.016±0.035		[3] BERGFELD	00	CLEO	E^{ee}_{cm}= 10.6 GeV
• • • We do not use the following data for averages, fits, limits, etc. • • •					
0.30 ±0.04 ±0.05	116	[4] ALEXANDER	96S	OPAL	1991–1994 LEP runs
0.23 ±0.10	10	[5] WU	90	MRK2	E^{ee}_{cm}= 29 GeV

[1] SHIMIZU 18A impose requirements on detected γ's corresponding to a τ-rest-frame energy cutoff $E^*_\gamma > 10$ MeV.

[2] LEES 15G impose requirements on detected γ's corresponding to a τ-rest-frame energy cutoff $E^*_\gamma > 10$ MeV.

[3] BERGFELD 00 impose requirements on detected γ's corresponding to a τ-rest-frame energy cutoff $E^*_\gamma > 10$ MeV. For $E^*_\gamma > 20$ MeV, they quote $(3.04 \pm 0.14 \pm 0.30) \times 10^{-3}$.

[4] ALEXANDER 96S impose requirements on detected γ's corresponding to a τ-rest-frame energy cutoff E_γ >20 MeV.

[5] WU 90 reports $\Gamma(\mu^- \overline{\nu}_\mu \nu_\tau \gamma)/\Gamma(\mu^- \overline{\nu}_\mu \nu_\tau) = 0.013 \pm 0.006$, which is converted to $\Gamma(\mu^- \overline{\nu}_\mu \nu_\tau \gamma)/\Gamma_{total}$ using $\Gamma(\mu^- \overline{\nu}_\mu \nu_\tau \gamma)/\Gamma_{total} = 17.35\%$. Requirements on detected γ's correspond to a τ rest frame energy cutoff $E_\gamma > 37$ MeV.

$\Gamma(e^- \overline{\nu}_e \nu_\tau)/\Gamma_{total}$ — Γ_5/Γ

To minimize the effect of experiments with large systematic errors, we exclude experiments which together would contribute 5% of the weight in the average.

VALUE (%)	EVTS	DOCUMENT ID		TECN	COMMENT
17.85 ±0.04 OUR FIT (Produced by HFLAV)					
17.82 ±0.05 OUR AVERAGE					
17.837±0.072±0.036	56k	[1] SCHAEL	05C	ALEP	1991-1995 LEP runs
17.806±0.104±0.076	24.7k	[2] ACCIARRI	01F	L3	1991–1995 LEP runs
17.81 ±0.09 ±0.06	33.1k	ABBIENDI	99H	OPAL	1991–1995 LEP runs
17.877±0.109±0.110	23.3k	ABREU	99X	DLPH	1991–1995 LEP runs
17.76 ±0.06 ±0.17		[3] ANASTASSOV	97	CLEO	E^{ee}_{cm}= 10.6 GeV
• • • We do not use the following data for averages, fits, limits, etc. • • •					
17.78 ±0.10 ±0.09	25.3k	ALEXANDER	96D	OPAL	Repl. by ABBIENDI 99H
17.79 ±0.12 ±0.06	20.6k	BUSKULIC	96C	ALEP	Repl. by SCHAEL 05C
17.51 ±0.23 ±0.31	5059	ABREU	95T	DLPH	Repl.. by ABREU 99X
17.9 ±0.4 ±0.4	2892	ADRIANI	93M	L3	Repl. by ACCIARRI 01F
17.5 ±0.3 ±0.5		[4] ALBRECHT	93G	ARG	E^{ee}_{cm}= 9.4–10.6 GeV
17.97 ±0.14 ±0.23	3970	AKERIB	92	CLEO	Repl. by ANASTASSOV 97
19.1 ±0.4 ±0.6	2960	[5] AMMAR	92	CLEO	E^{ee}_{cm}= 10.5–10.9 GeV
18.09 ±0.45 ±0.45		DECAMP	92C	ALEP	Repl. by SCHAEL 05C
17.0 ±0.5 ±0.6	1.7k	ABACHI	90	HRS	E^{ee}_{cm}= 29 GeV
18.4 ±0.8 ±0.4	644	BEHREND	90	CELL	E^{ee}_{cm}= 35 GeV
16.3 ±0.3 ±3.2		JANSSEN	89	CBAL	E^{ee}_{cm}= 9.4–10.6 GeV
18.4 ±1.2 ±1.0		AIHARA	87B	TPC	E^{ee}_{cm}= 29 GeV
19.1 ±0.8 ±1.1		BURCHAT	87	MRK2	E^{ee}_{cm}= 29 GeV
16.8 ±0.7 ±0.9	515	[5] BARTEL	86D	JADE	E^{ee}_{cm}= 34.6 GeV
20.4 ±3.0 $^{+1.4}_{-0.9}$		ALTHOFF	85	TASS	E^{ee}_{cm}= 34.5 GeV
17.8 ±0.9 ±0.6	390	[5] ASH	85B	MAC	E^{ee}_{cm}= 29 GeV
18.2 ±0.7 ±0.5		[6] BALTRUSAIT...	85	MRK3	E^{ee}_{cm}= 3.77 GeV
13.0 ±1.9 ±2.9		BERGER	85	PLUT	E^{ee}_{cm}= 34.6 GeV
18.3 ±2.4 ±1.9	60	BEHREND	83C	CELL	E^{ee}_{cm}= 34 GeV
16.0 ±1.3	459	[7] BACINO	78B	DLCO	E^{ee}_{cm}= 3.1–7.4 GeV

[1] Correlation matrix for SCHAEL 05C branching fractions, in percent:

(1) $\Gamma(\tau^- \to e^- \overline{\nu}_e \nu_\tau)/\Gamma_{total}$
(2) $\Gamma(\tau^- \to \mu^- \overline{\nu}_\mu \nu_\tau)/\Gamma_{total}$
(3) $\Gamma(\tau^- \to \pi^- \nu_\tau)/\Gamma_{total}$
(4) $\Gamma(\tau^- \to \pi^- \pi^0 \nu_\tau)/\Gamma_{total}$
(5) $\Gamma(\tau^- \to \pi^- 2\pi^0 \nu_\tau (\text{ex.}K^0))/\Gamma_{total}$
(6) $\Gamma(\tau^- \to \pi^- 3\pi^0 \nu_\tau (\text{ex.}K^0))/\Gamma_{total}$
(7) $\Gamma(\tau^- \to h^- 4\pi^0 \nu_\tau (\text{ex.}K^0,\eta))/\Gamma_{total}$
(8) $\Gamma(\tau^- \to \pi^- \pi^+ \pi^- \nu_\tau (\text{ex.}K^0,\omega))/\Gamma_{total}$
(9) $\Gamma(\tau^- \to \pi^- \pi^+ \pi^- \pi^0 \nu_\tau (\text{ex.}K^0))/\Gamma_{total}$
(10) $\Gamma(\tau^- \to h^- h^- h^+ 2\pi^0 \nu_\tau (\text{ex.}K^0))/\Gamma_{total}$
(11) $\Gamma(\tau^- \to h^- h^- h^+ 3\pi^0 \nu_\tau)/\Gamma_{total}$
(12) $\Gamma(\tau^- \to 3h^- 2h^+ \nu_\tau (\text{ex.}K^0))/\Gamma_{total}$
(13) $\Gamma(\tau^- \to 3h^- 2h^+ \pi^0 \nu_\tau (\text{ex.}K^0))/\Gamma_{total}$

	(1)	(2)	(3)	(4)	(5)	(6)	(7)	(8)	(9)	(10)	(11)	(12)
(2)	-20											
(3)	-9	-6										
(4)	-16	-12	2									
(5)	-5	-5	-17	-37								
(6)	0	-4	-15	2	-27							
(7)	-2	-4	-24	-15	20	-47						
(8)	-14	-9	15	-5	-17	-14	-8					
(9)	-13	-12	-25	-30	4	-2	16	-15				
(10)	0	-2	-23	-14	4	10	13	-6	-17			
(11)	1	0	-5	1	4	6	0	-9	-2	-11		
(12)	0	1	9	4	-8	-4	-6	9	-5	-4	-2	
(13)	1	-4	-3	-5	3	2	-4	-3	-1	4	1	-24

[2] The correlation coefficient between this measurement and the ACCIARRI 01F measurement of $B(\tau^- \to \mu^- \overline{\nu}_\mu \nu_\tau)$ is 0.08.

[3] The correlation coefficients between this measurement and the ANASTASSOV 97 measurements of $B(\mu \overline{\nu}_\mu \nu_\tau)$, $B(\mu \overline{\nu}_\mu \nu_\tau)/B(e \overline{\nu}_e \nu_\tau)$, $B(h^- \nu_\tau)$, and $B(h^- \nu_\tau)/B(e \overline{\nu}_e \nu_\tau)$ are 0.50, −0.42, 0.48, and −0.39 respectively.

[4] Not independent of ALBRECHT 92D $\Gamma(\mu^- \overline{\nu}_\mu \nu_\tau)/\Gamma(e^- \overline{\nu}_e \nu_\tau)$ and ALBRECHT 93G $\Gamma(\mu^- \overline{\nu}_\mu \nu_\tau) \times \Gamma(e^- \overline{\nu}_e \nu_\tau)/\Gamma^2_{total}$ values.

[5] Modified using $B(e^- \overline{\nu}_e \nu_\tau)/B(\text{"1 prong"})$ and B("1 prong") ,= 0.855.

[6] Error correlated with BALTRUSAITIS 85 $\Gamma(\mu^- \overline{\nu}_\mu \nu_\tau)/\Gamma_{total}$.

[7] BACINO 78B value comes from fit to events with $e^\pm$ and one other nonelectron charged prong.

$\Gamma(\mu^- \overline{\nu}_\mu \nu_\tau)/\Gamma(e^- \overline{\nu}_e \nu_\tau)$ — Γ_3/Γ_5

Standard Model prediction including mass effects is 0.9726.

VALUE (units 10^{-2})	EVTS	DOCUMENT ID		TECN	COMMENT
97.30±0.22 OUR FIT (Produced by HFLAV)					
97.3 ±0.4 OUR AVERAGE Error includes scale factor of 1.6. See the ideogram below.					
96.75±0.07±0.36	333E6	ADACHI	24K	BELL	
97.96±0.16±0.36	731k	[1] AUBERT	10F	BABR	467 fb^{-1} E^{ee}_{cm}= 10.6 GeV
97.77±0.63±0.87		[2] ANASTASSOV	97	CLEO	E^{ee}_{cm}= 10.6 GeV
99.7 ±3.5 ±4.0		ALBRECHT	92D	ARG	E^{ee}_{cm}= 9.4–10.6 GeV

[1] Correlation matrix for AUBERT 10F branching fractions:

(1) $\Gamma(\tau^- \to \mu^- \overline{\nu}_\mu \nu_\tau) / \Gamma(\tau^- \to e^- \overline{\nu}_e \nu_\tau)$
(2) $\Gamma(\tau^- \to \pi^- \nu_\tau) / \Gamma(\tau^- \to e^- \overline{\nu}_e \nu_\tau)$
(3) $\Gamma(\tau^- \to K^- \nu_\tau) / \Gamma(\tau^- \to e^- \overline{\nu}_e \nu_\tau)$

	(1)	(2)
(2)	0.25	
(3)	0.12	0.33

[2] The correlation coefficients between this measurement and the ANASTASSOV 97 measurements of $B(\mu \overline{\nu}_\mu \nu_\tau)$, $B(e \overline{\nu}_e \nu_\tau)$, $B(h^- \nu_\tau)$, and $B(h^- \nu_\tau)/B(e \overline{\nu}_e \nu_\tau)$ are 0.58, −0.42, 0.07, and 0.45 respectively.

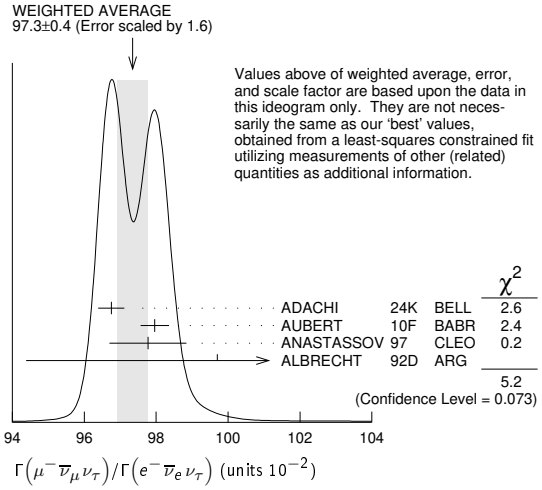

$\Gamma(e^- \overline{\nu}_e \nu_\tau \gamma)/\Gamma_{total}$ — Γ_6/Γ

VALUE (%)	EVTS	DOCUMENT ID		TECN	COMMENT
1.83 ±0.05 OUR AVERAGE					
1.79 ±0.02 ±0.10	12k	[1] SHIMIZU	18A	BELL	711 fb^{-1} E^{ee}_{cm}=10.6 GeV
1.847±0.015±0.052	18k	[2] LEES	15G	BABR	431 fb^{-1} E^{ee}_{cm}=10.6 GeV
1.75 ±0.06 ±0.17		[3] BERGFELD	00	CLEO	E^{ee}_{cm}= 10.6 GeV

[1] SHIMIZU 18A impose requirements on detected γ's corresponding to a τ-rest-frame energy cutoff $E^*_\gamma > 10$ MeV.

[2] LEES 15G impose requirements on detected γ's corresponding to a τ-rest-frame energy cutoff $E^*_\gamma > 10$ MeV.

[3] BERGFELD 00 impose requirements on detected γ's corresponding to a τ-rest-frame energy cutoff $E^*_\gamma > 10$ MeV.

$\Gamma(h^- \geq 0 K^0_L \nu_\tau)/\Gamma_{total}$ — Γ_7/Γ

$\Gamma_7/\Gamma = (\Gamma_9 + \Gamma_{10} + \frac{1}{2}\Gamma_{36} + \frac{1}{2}\Gamma_{38} + \Gamma_{50})/\Gamma$

VALUE (%)	EVTS	DOCUMENT ID		TECN	COMMENT
12.03±0.05 OUR FIT (Produced by HFLAV)					
12.2 ±0.4 OUR AVERAGE					
12.47±0.26±0.43	2967	[1] ACCIARRI	95	L3	1992 LEP run
12.4 ±0.7 ±0.7	283	[2] ABREU	92N	DLPH	1990 LEP run
12.1 ±0.7 ±0.5	309	ALEXANDER	91D	OPAL	1990 LEP run

Int. J. Mod
by UNIVERSITY OF CALIFORNIA @ BERK
Downloaded from www.worldscientific.com
-use and distribution is strictly not permitted, except for Open Access articles.

• • • We use the following data for averages but not for fits. • • •

11.3 ±0.5 ±0.8	798	[3] FORD	87	MAC	E^{ee}_{cm}= 29 GeV

• • • We do not use the following data for averages, fits, limits, etc. • • •

12.44±0.11±0.11	15k	[4] BUSKULIC	96	ALEP	Repl. by SCHAEL 05C
11.7 ±0.6 ±0.8		[5] ALBRECHT	92D	ARG	E^{ee}_{cm}= 9.4–10.6 GeV
12.98±0.44±0.33		[6] DECAMP	92C	ALEP	Repl. by SCHAEL 05C
12.3 ±0.9 ±0.5	1338	BEHREND	90	CELL	E^{ee}_{cm}= 35 GeV
11.1 ±1.1 ±1.4		[7] BURCHAT	87	MRK2	E^{ee}_{cm}= 29 GeV
12.3 ±0.6 ±1.1	328	[8] BARTEL	86D	JADE	E^{ee}_{cm}= 34.6 GeV
13.0 ±2.0 ±4.0		BERGER	85	PLUT	E^{ee}_{cm}= 34.6 GeV
11.2 ±1.7 ±1.2	34	[9] BEHREND	83C	CELL	E^{ee}_{cm}= 34 GeV

[1] ACCIARRI 95 with 0.65% added to remove their correction for $\pi^- K^0_L$ backgrounds.
[2] ABREU 92N with 0.5% added to remove their correction for $K^*(892)^-$ backgrounds.
[3] FORD 87 result for $B(\pi^-\nu_\tau)$ with 0.67% added to remove their K^- correction and adjusted for 1992 B("1 prong").
[4] BUSKULIC 96 quote 11.78 ± 0.11 ± 0.13 We add 0.66 to undo their correction for unseen K^0_L and modify the systematic error accordingly.
[5] Not independent of ALBRECHT 92D $\Gamma(\mu^-\overline{\nu}_\mu\nu_\tau)/\Gamma(e^-\overline{\nu}_e\nu_\tau)$, $\Gamma(\mu^-\overline{\nu}_\mu\nu_\tau)\times\Gamma(e^-\overline{\nu}_e\nu_\tau)$, and $\Gamma(h^-\geq 0K^0_L\nu_\tau)/\Gamma(e^-\overline{\nu}_e\nu_\tau)$ values.
[6] DECAMP 92C quote $B(h^-\geq 0K^0_L\geq 0(K^0_S\to\pi^+\pi^-)\nu_\tau)=13.32\pm0.44\pm0.33$. We subtract 0.35 to correct for their inclusion of the K^0_S decays.
[7] BURCHAT 87 with 1.1% added to remove their correction for K^- and $K^*(892)^-$ backgrounds.
[8] BARTEL 86D result for $B(\pi^-\nu_\tau)$ with 0.59% added to remove their K^- correction and adjusted for 1992 B("1 prong").
[9] BEHREND 83C quote $B(\pi^-\nu_\tau)=9.9\pm1.7\pm1.3$ after subtracting 1.3 ± 0.5 to correct for $B(K^-\nu_\tau)$.

$\Gamma(h^-\nu_\tau)/\Gamma_{total}$ — $\Gamma_8/\Gamma=(\Gamma_9+\Gamma_{10})/\Gamma$

VALUE (%)	EVTS	DOCUMENT ID		TECN	COMMENT
11.51 ±0.05 OUR FIT (Produced by HFLAV)					
11.63 ±0.12 OUR AVERAGE Error includes scale factor of 1.4. See the ideogram below.					
11.571±0.120±0.114	19k	[1] ABDALLAH	06A	DLPH	1992–1995 LEP runs
11.98 ±0.13 ±0.16		ACKERSTAFF	98M	OPAL	1991–1995 LEP runs
11.52 ±0.05 ±0.12		[2] ANASTASSOV	97	CLEO	E^{ee}_{cm}= 10.6 GeV

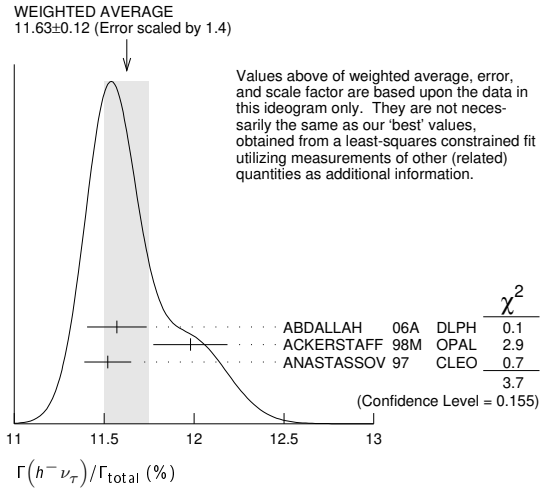

[1] Correlation matrix for ABDALLAH 06A branching fractions, in percent:

(1) $\Gamma(\tau^-\to h^-\nu_\tau)/\Gamma_{total}$
(2) $\Gamma(\tau^-\to h^-\pi^0\nu_\tau)/\Gamma_{total}$
(3) $\Gamma(\tau^-\to h^-\geq1\pi^0\nu_\tau(\text{ex.}K^0))/\Gamma_{total}$
(4) $\Gamma(\tau^-\to h^-2\pi^0\nu_\tau(\text{ex.}K^0))/\Gamma_{total}$
(5) $\Gamma(\tau^-\to h^-\geq3\pi^0\nu_\tau(\text{ex. }K^0))/\Gamma_{total}$
(6) $\Gamma(\tau^-\to h^-h^-h^+\nu_\tau(\text{ex.}K^0))/\Gamma_{total}$
(7) $\Gamma(\tau^-\to h^-h^-h^+\pi^0\nu_\tau(\text{ex.}K^0))/\Gamma_{total}$
(8) $\Gamma(\tau^-\to h^-h^-h^+\geq1\pi^0\nu_\tau(\text{ex. }K^0))/\Gamma_{total}$
(9) $\Gamma(\tau^-\to h^-h^-h^+\geq2\pi^0\nu_\tau(\text{ex. }K^0))/\Gamma_{total}$
(10) $\Gamma(\tau^-\to 3h^-2h^+\nu_\tau(\text{ex.}K^0))/\Gamma_{total}$
(11) $\Gamma(\tau^-\to 3h^-2h^+\pi^0\nu_\tau(\text{ex.}K^0))/\Gamma_{total}$

	(1)	(2)	(3)	(4)	(5)	(6)	(7)	(8)	(9)	(10)
(2)	-34									
(3)	-47	56								
(4)	6	-66	15							
(5)	-6	38	11	-86						
(6)	-7	-8	15	0	-2					
(7)	-2	-1	-5	-3	3	-53				
(8)	-4	-4	-13	-4	-2	-56	75			
(9)	-1	-1	-4	3	-6	26	-78	-16		
(10)	-1	-1	1	0	0	-2	-3	-1	3	
(11)	0	0	0	0	0	1	0	-5	5	-57

[2] The correlation coefficients between this measurement and the ANASTASSOV 97 measurements of $B(\mu\overline{\nu}_\mu\nu_\tau)$, $B(e\overline{\nu}_e\nu_\tau)$, $B(\mu\overline{\nu}_\mu\nu_\tau)/B(e\overline{\nu}_e\nu_\tau)$, and $B(h^-\nu_\tau)/B(e\overline{\nu}_e\nu_\tau)$ are 0.50, 0.48, 0.07, and 0.63 respectively.

$\Gamma(h^-\nu_\tau)/\Gamma(e^-\overline{\nu}_e\nu_\tau)$ — $\Gamma_8/\Gamma_5=(\Gamma_9+\Gamma_{10})/\Gamma_5$

VALUE (units 10^{-2})	EVTS	DOCUMENT ID		TECN	COMMENT
64.50±0.32 OUR FIT (Produced by HFLAV)					
64.0 ±0.7 OUR AVERAGE Error includes scale factor of 1.6.					
• • • We use the following data for averages but not for fits. • • •					
63.33±0.14±0.61	394k	[1] AUBERT	10F	BABR	467 fb^{-1} E^{ee}_{cm}=10.6 GeV
64.84±0.41±0.60		[2] ANASTASSOV	97	CLEO	E^{ee}_{cm}= 10.6 GeV

[1] Not independent of AUBERT 10F $\Gamma(\tau^-\to\pi^-\nu_\tau)/\Gamma(\tau^-\to e^-\overline{\nu}_e\nu_\tau)$ and $\Gamma(\tau^-\to K^-\nu_\tau)/\Gamma(\tau^-\to e^-\overline{\nu}_e\nu_\tau)$.
[2] The correlation coefficients between this measurement and the ANASTASSOV 97 measurements of $B(\mu\overline{\nu}_\mu\nu_\tau)$, $B(e\overline{\nu}_e\nu_\tau)$, $B(\mu\overline{\nu}_\mu\nu_\tau)/B(e\overline{\nu}_e\nu_\tau)$, and $B(h^-\nu_\tau)$ are 0.08, −0.39, 0.45, and 0.63 respectively.

$\Gamma(\pi^-\nu_\tau)/\Gamma_{total}$ — Γ_9/Γ

VALUE (%)	EVTS	DOCUMENT ID		TECN	COMMENT
10.82 ±0.05 OUR FIT (Produced by HFLAV)					
10.828±0.070±0.078	38k	[1] SCHAEL	05C	ALEP	1991–1995 LEP runs
• • • We do not use the following data for averages, fits, limits, etc. • • •					
11.06 ±0.11 ±0.14		[2] BUSKULIC	96	ALEP	Repl. by SCHAEL 05C
11.7 ±0.4 ±1.8	1138	BLOCKER	82D	MRK2	E^{ee}_{cm}= 3.5–6.7 GeV

[1] See footnote to SCHAEL 05C $\Gamma(\tau^-\to e^-\overline{\nu}_e\nu_\tau)/\Gamma_{total}$ measurement for correlations with other measurements.
[2] Not independent of BUSKULIC 96 $B(h^-\nu_\tau)$ and $B(K^-\nu_\tau)$ values.

$\Gamma(\pi^-\nu_\tau)/\Gamma(e^-\overline{\nu}_e\nu_\tau)$ — Γ_9/Γ_5

VALUE (units 10^{-2})	EVTS	DOCUMENT ID		TECN	COMMENT
60.60±0.31 OUR FIT (Produced by HFLAV)					
59.45±0.14±0.61	369k	[1] AUBERT	10F	BABR	467 fb^{-1} E^{ee}_{cm}= 10.6 GeV

[1] See footnote to AUBERT 10F $\Gamma(\tau^-\to\mu^-\overline{\nu}_\mu\nu_\tau)/\Gamma(\tau^-\to e^-\overline{\nu}_e\nu_\tau)$ for correlations with other measurements.

$\Gamma(K^-\nu_\tau)/\Gamma_{total}$ — Γ_{10}/Γ

VALUE (%)	EVTS	DOCUMENT ID		TECN	COMMENT
0.697±0.010 OUR FIT (Produced by HFLAV)					
0.685±0.023 OUR AVERAGE					
0.658±0.027±0.029		[1] ABBIENDI	01J	OPAL	1990–1995 LEP runs
0.696±0.025±0.014	2032	BARATE	99K	ALEP	1991–1995 LEP runs
0.85 ±0.18	27	ABREU	94K	DLPH	LEP 1992 Z data
0.66 ±0.07 ±0.09	99	BATTLE	94	CLEO	$E^{ee}_{cm}\approx$ 10.6 GeV
• • • We do not use the following data for averages, fits, limits, etc. • • •					
0.72 ±0.04 ±0.04	728	BUSKULIC	96	ALEP	Repl. by BARATE 99K
0.59 ±0.18	16	MILLS	84	DLCO	E^{ee}_{cm}= 29 GeV
1.3 ±0.5	15	BLOCKER	82B	MRK2	E^{ee}_{cm}= 3.9–6.7 GeV

[1] The correlation coefficient between this measurement and the ABBIENDI 01J $B(\tau^-\to K^-\geq0\pi^0\geq0K^0\geq0\gamma\nu_\tau)$ is 0.60.

$\Gamma(K^-\nu_\tau)/\Gamma(e^-\overline{\nu}_e\nu_\tau)$ — Γ_{10}/Γ_5

VALUE (units 10^{-2})	EVTS	DOCUMENT ID		TECN	COMMENT
3.90 ±0.05 OUR FIT (Produced by HFLAV)					
3.882±0.032±0.057	25k	[1] AUBERT	10F	BABR	467 fb^{-1} E^{ee}_{cm}= 10.6 GeV

[1] See footnote to AUBERT 10F $\Gamma(\tau^-\to\mu^-\overline{\nu}_\mu\nu_\tau)/\Gamma(\tau^-\to e^-\overline{\nu}_e\nu_\tau)$ for correlations with other measurements.

$\Gamma(K^-\nu_\tau)/\Gamma(\pi^-\nu_\tau)$ — Γ_{10}/Γ_9

VALUE (units 10^{-2})	DOCUMENT ID		TECN	COMMENT
6.44 ±0.09 OUR FIT (Produced by HFLAV)				
• • • We use the following data for averages but not for fits. • • •				
6.531±0.056±0.093	[1] AUBERT	10F	BABR	467 fb^{-1} E^{ee}_{cm}= 10.6 GeV

[1] Not independent of AUBERT 10F $\Gamma(\tau^-\to\pi^-\nu_\tau)/\Gamma(\tau^-\to e^-\overline{\nu}_e\nu_\tau)$ and $\Gamma(\tau^-\to K^-\nu_\tau)/\Gamma(\tau^-\to e^-\overline{\nu}_e\nu_\tau)$.

$\Gamma(h^-\geq1\text{ neutrals}\nu_\tau)/\Gamma_{total}$ — Γ_{11}/Γ

$\Gamma_{11}/\Gamma=(\Gamma_{14}+\Gamma_{16}+\Gamma_{20}+\Gamma_{23}+\Gamma_{27}+\Gamma_{28}+\Gamma_{30}+0.15344\Gamma_{36}+0.15344\Gamma_{38}+0.15344\Gamma_{41}+0.15344\Gamma_{43}+0.0942\Gamma_{48}+0.0942\Gamma_{52}+0.7195\Gamma_{150}+0.7195\Gamma_{152}+0.7195\Gamma_{154}+0.1107\Gamma_{156}+0.0833\Gamma_{178}+0.0833\Gamma_{179}+0.0833\Gamma_{180})/\Gamma$

VALUE (%)	DOCUMENT ID		TECN	COMMENT
37.00±0.09 OUR FIT (Produced by HFLAV)				
• • • We do not use the following data for averages, fits, limits, etc. • • •				
36.14±0.33±0.58	[1] AKERS	94E	OPAL	1991–1992 LEP runs
38.4 ±1.2 ±1.0	[2] BURCHAT	87	MRK2	E^{ee}_{cm}= 29 GeV
42.7 ±2.0 ±2.9	BERGER	85	PLUT	E^{ee}_{cm}= 34.6 GeV

[1] Not independent of ACKERSTAFF 98M $B(h^-\pi^0\nu_\tau)$ and $B(h^-\geq2\pi^0\nu_\tau)$ values.
[2] BURCHAT 87 quote for $B(\pi^\pm\geq1\text{ neutral}\nu_\tau)=0.378\pm0.012\pm0.010$. We add 0.006 to account for contribution from $(K^{*-}\nu_\tau)$ which they fixed at BR = 0.013.

Int. J. Mod. Phys. A 2026.41. Downloaded from www.worldscientific.com
by UNIVERSITY OF CALIFORNIA @ BERKELEY on 09/16/26. Re-use and distribution is strictly not permitted, except for Open Access articles.

$\Gamma(h^- \geq 1\pi^0\nu_\tau(\text{ex.}K^0))/\Gamma_{\text{total}}$ — Γ_{12}/Γ

$\Gamma_{12}/\Gamma = (\Gamma_{14}+\Gamma_{16}+\Gamma_{20}+\Gamma_{23}+\Gamma_{27}+\Gamma_{28}+\Gamma_{30}+0.3256\Gamma_{150}+0.3256\Gamma_{152}+0.3256\Gamma_{154})/\Gamma$

VALUE (%)	EVTS	DOCUMENT ID		TECN	COMMENT
36.50 ±0.09 OUR FIT		(Produced by HFLAV)			
• • • We use the following data for averages but not for fits. • • •					
36.641±0.155±0.127	45k	[1] ABDALLAH	06A	DLPH	1992–1995 LEP runs

[1] See footnote to ABDALLAH 06A $\Gamma(\tau^- \to h^-\nu_\tau)/\Gamma_{\text{total}}$ measurement for correlations with other measurements.

$\Gamma(h^-\pi^0\nu_\tau)/\Gamma_{\text{total}}$ — $\Gamma_{13}/\Gamma = (\Gamma_{14}+\Gamma_{16})/\Gamma$

VALUE (%)	EVTS	DOCUMENT ID		TECN	COMMENT
25.93 ±0.09 OUR FIT		(Produced by HFLAV)			
25.73 ±0.16 OUR AVERAGE					
25.67 ±0.01 ±0.39	5.4M	FUJIKAWA	08	BELL	72 fb^{-1} E^{ee}_{cm}=10.6GeV
25.740±0.201±0.138	35k	[1] ABDALLAH	06A	DLPH	1992–1995 LEP runs
25.89 ±0.17 ±0.29		ACKERSTAFF	98M	OPAL	1991–1995 LEP runs
25.05 ±0.35 ±0.50	6613	ACCIARRI	95	L3	1992 LEP run
25.87 ±0.12 ±0.42	51k	[2] ARTUSO	94	CLEO	E^{ee}_{cm}= 10.6 GeV
• • • We do not use the following data for averages, fits, limits, etc. • • •					
25.76 ±0.15 ±0.13	31k	BUSKULIC	96	ALEP	Repl. by SCHAEL 05C
25.98 ±0.36 ±0.52		[3] AKERS	94E	OPAL	Repl. by ACKERSTAFF 98M
22.9 ±0.8 ±1.3	283	[4] ABREU	92N	DLPH	E^{ee}_{cm}= 88.2–94.2 GeV
23.1 ±0.4 ±0.9	1249	[5] ALBRECHT	92Q	ARG	E^{ee}_{cm}= 10 GeV
25.02 ±0.64 ±0.88	1849	DECAMP	92C	ALEP	1989–1990 LEP runs
22.0 ±0.8 ±1.9	779	ANTREASYAN	91	CBAL	E^{ee}_{cm}= 9.4–10.6 GeV
22.6 ±1.5 ±0.7	1101	BEHREND	90	CELL	E^{ee}_{cm}= 35 GeV
23.1 ±1.9 ±1.6		BEHREND	84	CELL	E^{ee}_{cm}= 14,22 GeV

[1] See footnote to ABDALLAH 06A $\Gamma(\tau^- \to h^-\nu_\tau)/\Gamma_{\text{total}}$ measurement for correlations with other measurements.
[2] ARTUSO 94 reports the combined result from three independent methods, one of which (23% of the $\tau^- \to h^-\pi^0\nu_\tau$) is normalized to the inclusive one-prong branching fraction, taken as 0.854 ± 0.004. Renormalization to the present value causes negligible change.
[3] AKERS 94E quote $(26.25 \pm 0.36 \pm 0.52)\times 10^{-2}$; we subtract 0.27% from their number to correct for $\tau^- \to h^- K^0_L \nu_\tau$.
[4] ABREU 92N with 0.5% added to remove their correction for $K^*(892)^-$ backgrounds.
[5] ALBRECHT 92Q with 0.5% added to remove their correction for $\tau^- \to K^*(892)^-\nu_\tau$ background.

$\Gamma(\pi^-\pi^0\nu_\tau)/\Gamma_{\text{total}}$ — Γ_{14}/Γ

VALUE (%)	EVTS	DOCUMENT ID		TECN	COMMENT
25.49 ±0.09 OUR FIT		(Produced by HFLAV)			
25.46 ±0.12 OUR AVERAGE					
25.471±0.097±0.085	81k	[1] SCHAEL	05C	ALEP	1991-1995 LEP runs
• • • We use the following data for averages but not for fits. • • •					
25.36 ±0.44		[2] ARTUSO	94	CLEO	E^{ee}_{cm}= 10.6 GeV
• • • We do not use the following data for averages, fits, limits, etc. • • •					
25.30 ±0.15 ±0.13		[3] BUSKULIC	96	ALEP	Repl. by SCHAEL 05C
21.5 ±0.4 ±1.9	4400	[4,5] ALBRECHT	88L	ARG	E^{ee}_{cm}= 10 GeV
23.0 ±1.3 ±1.7	582	ADLER	87B	MRK3	E^{ee}_{cm}= 3.77 GeV
25.8 ±1.7 ±2.5		[6] BURCHAT	87	MRK2	E^{ee}_{cm}= 29 GeV
22.3 ±0.6 ±1.4	629	[5] YELTON	86	MRK2	E^{ee}_{cm}= 29 GeV

[1] See footnote to SCHAEL 05C $\Gamma(\tau^- \to e^-\overline{\nu}_e\nu_\tau)/\Gamma_{\text{total}}$ measurement for correlations with other measurements.
[2] Not independent of ARTUSO 94 $B(h^-\pi^0\nu_\tau)$ and BATTLE 94 $B(K^-\pi^0\nu_\tau)$ values.
[3] Not independent of BUSKULIC 96 $B(h^-\pi^0\nu_\tau)$ and $B(K^-\pi^0\nu_\tau)$ values.
[4] The authors divide by $(\Gamma_3+\Gamma_5+\Gamma_9+\Gamma_{10})/\Gamma = 0.467$ to obtain this result.
[5] Experiment had no hadron identification. Kaon corrections were made, but insufficient information is given to permit their removal.
[6] BURCHAT 87 value is not independent of YELTON 86 value. Nonresonant decays included.

$\Gamma(\pi^-\pi^0\,\text{non-}\rho(770)\nu_\tau)/\Gamma_{\text{total}}$ — Γ_{15}/Γ

VALUE (%)	DOCUMENT ID		TECN	COMMENT
0.3±0.1±0.3	[1] BEHREND	84	CELL	E^{ee}_{cm}= 14,22 GeV

[1] BEHREND 84 assume a flat nonresonant mass distribution down to the $\rho(770)$ mass, using events with mass above 1300 to set the level.

$\Gamma(K^-\pi^0\nu_\tau)/\Gamma_{\text{total}}$ — Γ_{16}/Γ

VALUE (%)	EVTS	DOCUMENT ID		TECN	COMMENT
0.433±0.015 OUR FIT		(Produced by HFLAV)			
0.426±0.016 OUR AVERAGE					
0.416±0.003±0.018	78k	AUBERT	07AP	BABR	230 fb^{-1} E^{ee}_{cm}= 10.6 GeV
0.471±0.059±0.023	360	ABBIENDI	04J	OPAL	1991-1995 LEP runs
0.444±0.026±0.024	923	BARATE	99K	ALEP	1991-1995 LEP runs
0.51 ±0.10 ±0.07	37	BATTLE	94	CLEO	E^{ee}_{cm} ≈ 10.6 GeV
• • • We do not use the following data for averages, fits, limits, etc. • • •					
0.52 ±0.04 ±0.05	395	BUSKULIC	96	ALEP	Repl. by BARATE 99K

$\Gamma(h^- \geq 2\pi^0\nu_\tau)/\Gamma_{\text{total}}$ — Γ_{17}/Γ

$\Gamma_{17}/\Gamma = (\Gamma_{20}+\Gamma_{23}+\Gamma_{27}+\Gamma_{28}+\Gamma_{30}+0.15344\Gamma_{36}+0.15344\Gamma_{38}+0.15344\Gamma_{41}+0.15344\Gamma_{43}+0.09419\Gamma_{48}+0.0942\Gamma_{52}+0.3256\Gamma_{150}+0.3256\Gamma_{152}+0.3256\Gamma_{154})/\Gamma$

VALUE (%)	EVTS	DOCUMENT ID		TECN	COMMENT
10.81±0.09 OUR FIT		(Produced by HFLAV)			
9.91±0.31±0.27		ACKERSTAFF	98M	OPAL	1991–1995 LEP runs
• • • We do not use the following data for averages, fits, limits, etc. • • •					
9.89±0.34±0.55		[1] AKERS	94E	OPAL	Repl. by ACKERSTAFF 98M
14.0 ±1.2 ±0.6	938	[2] BEHREND	90	CELL	E^{ee}_{cm}= 35 GeV
12.0 ±1.4 ±2.5		[3] BURCHAT	87	MRK2	E^{ee}_{cm}= 29 GeV
13.9 ±2.0 $^{+1.9}_{-2.2}$		[4] AIHARA	86E	TPC	E^{ee}_{cm}= 29 GeV

[1] AKERS 94E not independent of AKERS 94E $B(h^- \geq 1\pi^0\nu_\tau)$ and $B(h^-\pi^0\nu_\tau)$ measurements.
[2] No independent of BEHREND 90 $\Gamma(h^-2\pi^0\nu_\tau(\text{exp. } K^0))$ and $\Gamma(h^- \geq 3\pi^0\nu_\tau)$.
[3] Error correlated with BURCHAT 87 $\Gamma(\rho^-\nu_e)/\Gamma(\text{total})$ value.
[4] AIHARA 86E (TPC) quote $B(2\pi^0\pi^-\nu_\tau) + 1.6B(3\pi^0\pi^-\nu_\tau) + 1.1B(\pi^0\eta\pi^-\nu_\tau)$.

$\Gamma(h^-2\pi^0\nu_\tau)/\Gamma_{\text{total}}$ — Γ_{18}/Γ

$\Gamma_{18}/\Gamma = (\Gamma_{20}+\Gamma_{23}+0.15344\Gamma_{36}+0.15344\Gamma_{38})/\Gamma$

VALUE (%)	EVTS	DOCUMENT ID		TECN	COMMENT
9.48±0.10 OUR FIT		(Produced by HFLAV)			
• • • We do not use the following data for averages, fits, limits, etc. • • •					
9.48±0.13±0.10	12k	[1] BUSKULIC	96	ALEP	Repl. by SCHAEL 05C

[1] BUSKULIC 96 quote 9.29 ± 0.13 ± 0.10. We add 0.19 to undo their correction for $\tau^- \to h^- K^0\nu_\tau$.

$\Gamma(h^-2\pi^0\nu_\tau(\text{ex.}K^0))/\Gamma_{\text{total}}$ — Γ_{19}/Γ

$\Gamma_{19}/\Gamma = (\Gamma_{20}+\Gamma_{23})/\Gamma$

VALUE (%)	EVTS	DOCUMENT ID		TECN	COMMENT
9.32 ±0.10 OUR FIT		(Produced by HFLAV)			
9.17 ±0.27 OUR AVERAGE					
9.498±0.320±0.275	9.5k	[1] ABDALLAH	06A	DLPH	1992–1995 LEP runs
8.88 ±0.37 ±0.42	1060	ACCIARRI	95	L3	1992 LEP run
• • • We use the following data for averages but not for fits. • • •					
8.96 ±0.16 ±0.44		[2] PROCARIO	93	CLEO	E^{ee}_{cm} ≈ 10.6 GeV
• • • We do not use the following data for averages, fits, limits, etc. • • •					
10.38 ±0.66 ±0.82	809	[3] DECAMP	92C	ALEP	Repl. by SCHAEL 05C
5.7 ±0.5 $^{+1.7}_{-1.0}$	133	[4] ANTREASYAN	91	CBAL	E^{ee}_{cm}= 9.4–10.6 GeV
10.0 ±1.5 ±1.1	333	[5] BEHREND	90	CELL	E^{ee}_{cm}= 35 GeV
8.7 ±0.4 ±1.1	815	[6] BAND	87	MAC	E^{ee}_{cm}= 29 GeV
6.2 ±0.6 ±1.2		[7] GAN	87	MRK2	E^{ee}_{cm}= 29 GeV
6.0 ±3.0 ±1.8		BEHREND	84	CELL	E^{ee}_{cm}= 14,22 GeV

[1] See footnote to ABDALLAH 06A $\Gamma(\tau^- \to h^-\nu_\tau)/\Gamma_{\text{total}}$ measurement for correlations with other measurements.
[2] PROCARIO 93 entry is obtained from $B(h^-2\pi^0\nu_\tau)/B(h^-\pi^0\nu_\tau)$ using ARTUSO 94 result for $B(h^-\pi^0\nu_\tau)$.
[3] We subtract 0.0015 to account for $\tau^- \to K^*(892)^-\nu_\tau$ contribution.
[4] ANTREASYAN 91 subtract 0.001 to account for the $\tau^- \to K^*(892)^-\nu_\tau$ contribution.
[5] BEHREND 90 subtract 0.002 to account for the $\tau^- \to K^*(892)^-\nu_\tau$ contribution.
[6] BAND 87 assume $B(\pi^-3\pi^0\nu_\tau) = 0.01$ and $B(\pi^-\pi^0\eta\nu_\tau) = 0.005$.
[7] GAN 87 analysis use photon multiplicity distribution.

$\Gamma(h^-2\pi^0\nu_\tau(\text{ex.}K^0))/\Gamma(h^-\pi^0\nu_\tau)$ — Γ_{19}/Γ_{13}

$\Gamma_{19}/\Gamma_{13} = (\Gamma_{20}+\Gamma_{23})/(\Gamma_{14}+\Gamma_{16})$

VALUE (units 10^{-2})	DOCUMENT ID		TECN	COMMENT
36.0±0.4 OUR FIT	(Produced by HFLAV)			
34.2±0.6±1.6	[1] PROCARIO	93	CLEO	E^{ee}_{cm} ≈ 10.6 GeV

[1] PROCARIO 93 quote 0.345 ± 0.006 ± 0.016 after correction for 2 kaon backgrounds assuming $B(K^{*-}\nu_\tau)$=1.42 ± 0.18% and $B(h^-K^0\pi^0\nu_\tau)$=0.48 ± 0.48%. We multiply by 0.990 ± 0.010 to remove these corrections to $B(h^-\pi^0\nu_\tau)$.

$\Gamma(\pi^-2\pi^0\nu_\tau(\text{ex.}K^0))/\Gamma_{\text{total}}$ — Γ_{20}/Γ

VALUE (%)	EVTS	DOCUMENT ID		TECN	COMMENT
9.26 ±0.10 OUR FIT		(Produced by HFLAV)			
9.239±0.086±0.090	31k	[1] SCHAEL	05C	ALEP	1991-1995 LEP runs
• • • We do not use the following data for averages, fits, limits, etc. • • •					
9.21 ±0.13 ±0.11		[2] BUSKULIC	96	ALEP	Repl. by SCHAEL 05C

[1] See footnote to SCHAEL 05C $\Gamma(\tau^- \to e^-\overline{\nu}_e\nu_\tau)/\Gamma_{\text{total}}$ measurement for correlations with other measurements.
[2] Not independent of BUSKULIC 96 $B(h^-2\pi^0\nu_\tau(\text{ex. } K^0))$ and $B(K^-2\pi^0\nu_\tau(\text{ex. } K^0))$ values.

$\Gamma(\pi^-2\pi^0\nu_\tau(\text{ex.}K^0),\text{scalar})/\Gamma(\pi^-2\pi^0\nu_\tau(\text{ex.}K^0))$ — Γ_{21}/Γ_{20}

VALUE	CL%	DOCUMENT ID		TECN	COMMENT
<0.094	95	[1] BROWDER	00	CLEO	4.7 fb^{-1} E^{ee}_{cm}= 10.6 GeV

[1] Model-independent limit from structure function analysis on contribution to $B(\tau^- \to \pi^-2\pi^0\nu_\tau(\text{ex. } K^0))$ from scalars.

Int. J. Mod
by UNIVERSITY OF CALIFORNIA @ BERK
Downloaded from www.worldscientific.com
-use and distribution is strictly not permitted, except for Open Access articles.

$\Gamma(\pi^- 2\pi^0 \nu_\tau (\text{ex.}K^0), \text{vector})/\Gamma(\pi^- 2\pi^0 \nu_\tau (\text{ex.}K^0))$ — Γ_{22}/Γ_{20}

VALUE	CL%	DOCUMENT ID		TECN	COMMENT
<0.073	95	[1] BROWDER	00	CLEO	4.7 fb^{-1} $E^{ee}_{\rm cm}$ = 10.6 GeV

[1] Model-independent limit from structure function analysis on contribution to $B(\tau^- \to \pi^- 2\pi^0 \nu_\tau (\text{ex. } K^0))$ from vectors.

$\Gamma(K^- 2\pi^0 \nu_\tau (\text{ex.}K^0))/\Gamma_{\rm total}$ — Γ_{23}/Γ

VALUE (units 10^{-4})	EVTS	DOCUMENT ID		TECN	COMMENT
6.5± 2.2 OUR FIT (Produced by HFLAV)					
5.8± 2.4 OUR AVERAGE					
5.6± 2.0±1.5	131	BARATE	99K	ALEP	1991–1995 LEP runs
9 ±10 ±3	3	[1] BATTLE	94	CLEO	$E^{ee}_{\rm cm} \approx$ 10.6 GeV
• • • We do not use the following data for averages, fits, limits, etc. • • •					
8 ± 2 ±2	59	BUSKULIC	96	ALEP	Repl. by BARATE 99K

[1] BATTLE 94 quote $(14 \pm 10 \pm 3) \times 10^{-4}$ or $< 30 \times 10^{-4}$ at 90% CL. We subtract $(5 \pm 2) \times 10^{-4}$ to account for $\tau^- \to K^-(K^0 \to \pi^0\pi^0)\nu_\tau$ background.

$\Gamma(h^- \geq 3\pi^0 \nu_\tau)/\Gamma_{\rm total}$ — Γ_{24}/Γ

$\Gamma_{24}/\Gamma = (\Gamma_{27}+\Gamma_{28}+\Gamma_{30}+0.15344\Gamma_{41}+0.15344\Gamma_{43}+0.0942\Gamma_{48}+0.0942\Gamma_{52}+0.3256\Gamma_{150}+0.3256\Gamma_{152}+0.3256\Gamma_{154}+0.0501\Gamma_{156})/\Gamma$

VALUE (%)	EVTS	DOCUMENT ID		TECN	COMMENT
1.34±0.07 OUR FIT (Produced by HFLAV)					
• • • We do not use the following data for averages, fits, limits, etc. • • •					
1.53±0.40±0.46	186	DECAMP	92C	ALEP	Repl. by SCHAEL 05C
3.2 ±1.0 ±1.0		BEHREND	90	CELL	$E^{ee}_{\rm cm}$ = 35 GeV

$\Gamma(h^- \geq 3\pi^0 \nu_\tau (\text{ex. } K^0))/\Gamma_{\rm total}$ — Γ_{25}/Γ

$\Gamma_{25}/\Gamma = (\Gamma_{27}+\Gamma_{28}+\Gamma_{30}+0.3256\Gamma_{150}+0.3256\Gamma_{152}+0.3256\Gamma_{154})/\Gamma$

VALUE (%)	EVTS	DOCUMENT ID		TECN	COMMENT
1.26 ±0.07 OUR FIT (Produced by HFLAV)					
1.403±0.214±0.224	1.1k	[1] ABDALLAH	06A	DLPH	1992–1995 LEP runs

[1] See footnote to ABDALLAH 06A $\Gamma(\tau^- \to h^- \nu_\tau)/\Gamma_{\rm total}$ measurement for correlations with other measurements.

$\Gamma(h^- 3\pi^0 \nu_\tau)/\Gamma_{\rm total}$ — Γ_{26}/Γ

$\Gamma_{26}/\Gamma = (\Gamma_{27}+\Gamma_{28}+0.15344\Gamma_{41}+0.15344\Gamma_{43}+0.3256\Gamma_{152})/\Gamma$

VALUE (%)	EVTS	DOCUMENT ID		TECN	COMMENT
1.18±0.07 OUR FIT (Produced by HFLAV)					
1.21±0.17 OUR AVERAGE Error includes scale factor of 1.2.					
1.70±0.24±0.38	293	ACCIARRI	95	L3	1992 LEP run
• • • We use the following data for averages but not for fits. • • •					
1.15±0.08±0.13		[1] PROCARIO	93	CLEO	$E^{ee}_{\rm cm} \approx$ 10.6 GeV
• • • We do not use the following data for averages, fits, limits, etc. • • •					
1.24±0.09±0.11	2.3k	[2] BUSKULIC	96	ALEP	Repl. by SCHAEL 05C
$0.0 \; ^{+1.4}_{-0.1} \; ^{+1.1}_{-0.1}$		[3] GAN	87	MRK2	$E^{ee}_{\rm cm}$ = 29 GeV

[1] PROCARIO 93 entry is obtained from $B(h^- 3\pi^0 \nu_\tau)/B(h^- \pi^0 \nu_\tau)$ using ARTUSO 94 result for $B(h^- \pi^0 \nu_\tau)$.

[2] BUSKULIC 96 quote $B(h^- 3\pi^0 \nu_\tau (\text{ex. } K^0)) = 1.17 \pm 0.09 \pm 0.11$. We add 0.07 to remove their correction for K^0 backgrounds.

[3] Highly correlated with GAN 87 $\Gamma(\eta\pi^-\pi^0\nu_\tau)/\Gamma_{\rm total}$ value. Authors quote $B(\pi^\pm 3\pi^0 \nu_\tau) + 0.67B(\pi^\pm \eta\pi^0 \nu_\tau) = 0.047 \pm 0.010 \pm 0.011$.

$\Gamma(h^- 3\pi^0 \nu_\tau)/\Gamma(h^- \pi^0 \nu_\tau)$ — Γ_{26}/Γ_{13}

$\Gamma_{26}/\Gamma_{13} = (\Gamma_{27}+\Gamma_{28}+0.15344\Gamma_{41}+0.15344\Gamma_{43}+0.3256\Gamma_{152})/(\Gamma_{14}+\Gamma_{16})$

VALUE (units 10^{-2})	DOCUMENT ID		TECN	COMMENT
4.54±0.28 OUR FIT (Produced by HFLAV)				
4.4 ±0.3 ±0.5	[1] PROCARIO	93	CLEO	$E^{ee}_{\rm cm} \approx$ 10.6 GeV

[1] PROCARIO 93 quote $0.041 \pm 0.003 \pm 0.005$ after correction for 2 kaon backgrounds assuming $B(K^{*-}\nu_\tau)$=1.42 ± 0.18% and $B(h^- K^0 \pi^0 \nu_\tau)$=0.48 ± 0.48%. We add 0.003 ± 0.003 and multiply the sum by 0.990 ± 0.010 to remove these corrections.

$\Gamma(\pi^- 3\pi^0 \nu_\tau (\text{ex.}K^0))/\Gamma_{\rm total}$ — Γ_{27}/Γ

VALUE (%)	EVTS	DOCUMENT ID		TECN	COMMENT
1.04 ±0.07 OUR FIT (Produced by HFLAV)					
0.977±0.069±0.058	6.1k	[1] SCHAEL	05C	ALEP	1991-1995 LEP runs

[1] See footnote to SCHAEL 05C $\Gamma(\tau^- \to e^- \overline{\nu}_e \nu_\tau)/\Gamma_{\rm total}$ measurement for correlations with other measurements.

$\Gamma(K^- 3\pi^0 \nu_\tau (\text{ex.}K^0, \eta))/\Gamma_{\rm total}$ — Γ_{28}/Γ

VALUE (units 10^{-4})	EVTS	DOCUMENT ID		TECN	COMMENT
4.8± 2.1 OUR FIT (Produced by HFLAV)					
3.7± 2.1±1.1	22	BARATE	99K	ALEP	1991–1995 LEP runs
• • • We do not use the following data for averages, fits, limits, etc. • • •					
5 ±13		[1] BUSKULIC	94E	ALEP	Repl. by BARATE 99K

[1] BUSKULIC 94E quote $B(K^- \geq 0\pi^0 \geq 0K^0\nu_\tau) - [B(K^-\nu_\tau) + B(K^-\pi^0\nu_\tau) + B(K^-K^0\nu_\tau) + B(K^-\pi^0\pi^0\nu_\tau) + B(K^-\pi^0K^0\nu_\tau)] = (5 \pm 13) \times 10^{-4}$ accounting for common systematic errors in BUSKULIC 94E and BUSKULIC 94F measurements of these modes. We assume $B(K^- \geq 2K^0\nu_\tau)$ and $B(K^- \geq 4\pi^0\nu_\tau)$ are negligible.

$\Gamma(h^- 4\pi^0 \nu_\tau (\text{ex.}K^0))/\Gamma_{\rm total}$ — Γ_{29}/Γ

$\Gamma_{29}/\Gamma = (\Gamma_{30}+0.3256\Gamma_{150}+0.3256\Gamma_{154})/\Gamma$

VALUE (%)	EVTS	DOCUMENT ID		TECN	COMMENT
0.16±0.04 OUR FIT (Produced by HFLAV)					
0.16±0.05±0.05		[1] PROCARIO	93	CLEO	$E^{ee}_{\rm cm} \approx$ 10.6 GeV
• • • We do not use the following data for averages, fits, limits, etc. • • •					
0.16±0.04±0.09	232	[2] BUSKULIC	96	ALEP	Repl. by SCHAEL 05C

[1] PROCARIO 93 quotes $B(h^- 4\pi^0 \nu_\tau)/B(h^- \pi^0 \nu_\tau) = 0.006 \pm 0.002 \pm 0.002$. We multiply by the ARTUSO 94 result for $B(h^- \pi^0 \nu_\tau)$ to obtain $B(h^- 4\pi^0 \nu_\tau)$. PROCARIO 93 assume $B(h^- \geq 5\pi^0 \nu_\tau)$ is small and do not correct for it.

[2] BUSKULIC 96 quote result for $\tau^- \to h^- \geq 4\pi^0 \nu_\tau$. We assume $B(h^- \geq 5\pi^0 \nu_\tau)$ is negligible.

$\Gamma(h^- 4\pi^0 \nu_\tau (\text{ex.}K^0, \eta))/\Gamma_{\rm total}$ — Γ_{30}/Γ

VALUE (%)	EVTS	DOCUMENT ID		TECN	COMMENT
0.11 ±0.04 OUR FIT (Produced by HFLAV)					
0.112±0.037±0.035	957	[1] SCHAEL	05C	ALEP	1991-1995 LEP runs

[1] See footnote to SCHAEL 05C $\Gamma(\tau^- \to e^- \overline{\nu}_e \nu_\tau)/\Gamma_{\rm total}$ measurement for correlations with other measurements.

$\Gamma(a_1(1260)\nu_\tau \to \pi^- \gamma \nu_\tau)/\Gamma_{\rm total}$ — $\Gamma_{31}/\Gamma = (0.0022\Gamma_{20}+0.0022\Gamma_{70})/\Gamma$

In the fit, $\Gamma(\tau^- \to a_1(1260)\nu_\tau \to \pi^-\gamma\nu_\tau)/\Gamma_{\rm total}$ is set equal to $(\Gamma(\tau^- \to \pi^- 2\pi^0 \nu_\tau (\text{ex.}K^0)) + \Gamma(\tau^- \to \pi^-\pi^+\pi^-\nu_\tau (\text{ex.}K^0, \omega))/\Gamma_{\rm total} \times B(a_1(1260) \to \pi\gamma)/(1 - B(a_1(1260) \to \pi\gamma))$ and $B(a_1(1260) \to \pi\gamma) = \Gamma(a_1(1260) \to \pi\gamma)/\Gamma^{a_1(1260)}_{\rm total}$ is a nuisance fit variable with a χ^2 term corresponding to its estimate in reference SCHAEL 05C.

VALUE (units 10^{-4})	DOCUMENT ID
4.0±1.5 OUR FIT (Produced by HFLAV)	

$\Gamma(K^- \geq 0\pi^0 \geq 0K^0 \geq 0\gamma \nu_\tau)/\Gamma_{\rm total}$ — Γ_{32}/Γ

$\Gamma_{32}/\Gamma = (\Gamma_{10}+\Gamma_{16}+\Gamma_{23}+\Gamma_{28}+\Gamma_{38}+\Gamma_{43}+0.7195\Gamma_{152}+0.1049\Gamma_{170})/\Gamma$

VALUE (%)	EVTS	DOCUMENT ID		TECN	COMMENT
1.552±0.029 OUR FIT (Produced by HFLAV)					
1.53 ±0.04 OUR AVERAGE					
1.528±0.039±0.040		[1] ABBIENDI	01J	OPAL	1990–1995 LEP runs
1.54 ±0.24		ABREU	94K	DLPH	LEP 1992 Z data
1.70 ±0.12 ±0.19	202	[2] BATTLE	94	CLEO	$E^{ee}_{\rm cm} \approx$ 10.6 GeV
• • • We use the following data for averages but not for fits. • • •					
1.520±0.040±0.041	4006	[3] BARATE	99K	ALEP	1991–1995 LEP runs
• • • We do not use the following data for averages, fits, limits, etc. • • •					
1.70 ±0.05 ±0.06	1610	[4] BUSKULIC	96	ALEP	Repl. by BARATE 99K
1.6 ±0.4 ±0.2	35	AIHARA	87B	TPC	$E^{ee}_{\rm cm}$ = 29 GeV
1.71 ±0.29	53	MILLS	84	DLCO	$E^{ee}_{\rm cm}$ = 29 GeV

[1] The correlation coefficient between this measurement and the ABBIENDI 01J $B(\tau^- \to K^-\nu_\tau)$ is 0.60.

[2] BATTLE 94 quote $1.60 \pm 0.12 \pm 0.19$. We add 0.10 ± 0.02 to correct for their rejection of $K^0_S \to \pi^+\pi^-$ decays.

[3] Not independent of BARATE 99K $B(K^-\nu_\tau)$, $B(K^-\pi^0\nu_\tau)$, $B(K^-2\pi^0\nu_\tau (\text{ex. } K^0))$, $B(K^-3\pi^0\nu_\tau (\text{ex. } K^0))$, $B(K^-K^0\nu_\tau)$, and $B(K^-K^0\pi^0\nu_\tau)$ values.

[4] Not independent of BUSKULIC 96 $B(K^-\nu_\tau)$, $B(K^-\pi^0\nu_\tau)$, $B(K^-2\pi^0\nu_\tau)$, $B(K^-K^0\nu_\tau)$, and $B(K^-K^0\pi^0\nu_\tau)$ values.

$\Gamma(K^- \geq 1(\pi^0 \text{ or } K^0 \text{ or } \gamma)\nu_\tau)/\Gamma_{\rm total}$ — Γ_{33}/Γ

$\Gamma_{33}/\Gamma = (\Gamma_{16}+\Gamma_{23}+\Gamma_{28}+\Gamma_{38}+\Gamma_{43}+0.7195\Gamma_{152}+0.7195\Gamma_{154}+0.1049\Gamma_{170})/\Gamma$

VALUE (%)	EVTS	DOCUMENT ID		TECN	COMMENT
0.859±0.028 OUR FIT (Produced by HFLAV)					
0.86 ±0.05 OUR AVERAGE					
• • • We use the following data for averages but not for fits. • • •					
0.869±0.031±0.034		[1] ABBIENDI	01J	OPAL	1990–1995 LEP runs
0.69 ±0.25		[2] ABREU	94K	DLPH	LEP 1992 Z data
• • • We do not use the following data for averages, fits, limits, etc. • • •					
$1.2 \pm 0.5 \; ^{+0.2}_{-0.4}$	9	AIHARA	87B	TPC	$E^{ee}_{\rm cm}$ = 29 GeV

[1] Not independent of ABBIENDI 01J $B(\tau^- \to K^-\nu_\tau)$ and $B(\tau^- \to K^- \geq 0\pi^0 \geq 0K^0 \geq 0\gamma\nu_\tau)$ values.

[2] Not independent of ABREU 94K $B(K^-\nu_\tau)$ and $B(K^- \geq 0 \text{ neutrals}\nu_\tau)$ measurements.

$\Gamma(K^0_S(\text{particles})^-\nu_\tau)/\Gamma_{\rm total}$ — Γ_{34}/Γ

$\Gamma_{34}/\Gamma = (\frac{1}{2}\Gamma_{36}+\frac{1}{2}\Gamma_{38}+\frac{1}{2}\Gamma_{41}+\frac{1}{2}\Gamma_{43}+\frac{1}{2}\Gamma_{45}+\Gamma_{48}+\Gamma_{49}+\Gamma_{52}+\Gamma_{56}+0.3598\Gamma_{156}+0.336\Gamma_{170})/\Gamma$

VALUE (%)	EVTS	DOCUMENT ID		TECN	COMMENT
0.943±0.028 OUR FIT (Produced by HFLAV)					
0.918±0.015 OUR AVERAGE					
0.970±0.058±0.062	929	BARATE	98E	ALEP	1991–1995 LEP runs
0.97 ±0.09 ±0.06	141	AKERS	94G	OPAL	$E^{ee}_{\rm cm}$ = 88–94 GeV
• • • We use the following data for averages but not for fits. • • •					
0.915±0.001±0.015	398k	[1] RYU	14	BELL	669 fb^{-1} $E^{ee}_{\rm cm}$=10.6 GeV

[1] Not independent of RYU 14 measurements of $B(\tau^- \to \pi^-\overline{K}^0\nu_\tau)$, $B(\tau^- \to K^-K^0\nu_\tau)$, $B(\tau^- \to \pi^-\overline{K}^0\pi^0\nu_\tau)$, $B(\tau^- \to K^-K^0\pi^0\nu_\tau)$, $B(\tau^- \to \pi^-K^0_SK^0_S\nu_\tau)$, and $B(\tau^- \to \pi^-K^0_SK^0_S\pi^0\nu_\tau)$.

Int. J. Mod. Phys. A 2026.41. Downloaded from www.worldscientific.com
by UNIVERSITY OF CALIFORNIA @ BERKELEY on 09/16/26. Re-use and distribution is strictly not permitted, except for Open Access articles.

$\Gamma(h^- \overline{K}^0 \nu_\tau)/\Gamma_{total}$ — $\Gamma_{35}/\Gamma = (\Gamma_{36}+\Gamma_{38})/\Gamma$

VALUE (%)	EVTS	DOCUMENT ID		TECN	COMMENT
0.987±0.014 OUR FIT (Produced by HFLAV)					
0.90 ±0.07 OUR AVERAGE					
0.855±0.036±0.073	1242	COAN	96	CLEO	$E^{ee}_{cm} \approx$ 10.6 GeV
• • • We use the following data for averages but not for fits. • • •					
1.01 ±0.11 ±0.07	555	[1] BARATE	98E	ALEP	1991–1995 LEP runs

[1] Not independent of BARATE 98E B($\tau^- \to \pi^- \overline{K}^0 \nu_\tau$) and B($\tau^- \to K^- K^0 \nu_\tau$) values.

$\Gamma(\pi^- \overline{K}^0 \nu_\tau)/\Gamma_{total}$ — Γ_{36}/Γ

VALUE (units 10^{-3})	EVTS	DOCUMENT ID		TECN	COMMENT
8.38±0.14 OUR FIT (Produced by HFLAV)					
8.39±0.22 OUR AVERAGE Error includes scale factor of 1.5. See the ideogram below.					
8.32±0.02±0.16	158k	[1] RYU	14	BELL	669 fb^{-1} E^{ee}_{cm}=10.6 GeV
9.33±0.68±0.49	377	ABBIENDI	00C	OPAL	1991–1995 LEP runs
9.28±0.45±0.34	937	[2] BARATE	99K	ALEP	1991–1995 LEP runs
9.5 ±1.5 ±0.6		[3] ACCIARRI	95F	L3	1991–1993 LEP runs
• • • We use the following data for averages but not for fits. • • •					
8.55±1.17±0.66	509	[4] BARATE	98E	ALEP	1991–1995 LEP runs
7.04±0.41±0.72		[5] COAN	96	CLEO	$E^{ee}_{cm} \approx$ 10.6 GeV
• • • We do not use the following data for averages, fits, limits, etc. • • •					
8.08±0.04±0.26	53k	EPIFANOV	07	BELL	Repl. by RYU 14
7.9 ±1.0 ±0.9	98	[6] BUSKULIC	96	ALEP	Repl. by BARATE 99K

[1] RYU 14 reconstruct K^0's using $K^0_S \to \pi^+\pi^-$ decays.
[2] BARATE 99K measure K^0's by detecting K^0_L's in their hadron calorimeter.
[3] ACCIARRI 95F do not identify π^-/K^- and assume B($K^- K^0 \nu_\tau$) = (0.29 ± 0.12)%.
[4] BARATE 98E reconstruct K^0's using $K^0_S \to \pi^+\pi^-$ decays. Not independent of BARATE 98E B(K^0particles$^- \nu_\tau$) value.
[5] Not independent of COAN 96 B($h^- K^0 \nu_\tau$) and B($K^- K^0 \nu_\tau$) measurements.
[6] BUSKULIC 96 measure K^0's by detecting K^0_L's in their hadron calorimeter.

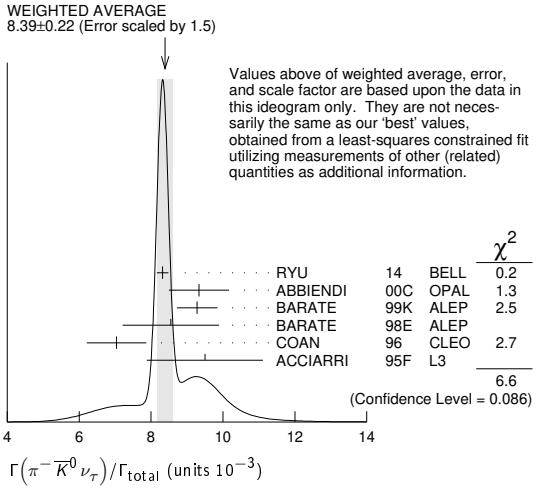

$\Gamma(\pi^- \overline{K}^0 (\text{non-}K^*(892)^-) \nu_\tau)/\Gamma_{total}$ — Γ_{37}/Γ

VALUE (units 10^{-4})	CL%	DOCUMENT ID		TECN	COMMENT
5.4±2.1		[1] EPIFANOV	07	BELL	351 fb^{-1} E^{ee}_{cm}= 10.6 GeV
• • • We do not use the following data for averages, fits, limits, etc. • • •					
<17	95	ACCIARRI	95F	L3	1991–1993 LEP runs

[1] EPIFANOV 07 quote B($\tau^- \to K^*(892)^- \nu_\tau$) B($K^*(892)^- \to K^0_S \pi^-$) / B($\tau^- \to K^0_S \pi^- \nu_\tau$) = 0.933 ± 0.027. We multiply their B($\tau^- \to \overline{K}^0 \pi^- \nu_\tau$) by [1−(0.933 ± 0.027)] to obtain this result.

$\Gamma(K^- K^0 \nu_\tau)/\Gamma_{total}$ — Γ_{38}/Γ

VALUE (units 10^{-4})	EVTS	DOCUMENT ID		TECN	COMMENT
14.86±0.34 OUR FIT (Produced by HFLAV)					
14.83±0.35 OUR AVERAGE					
14.78±0.22±0.40	29k	[1] LEES	18B	BABR	468 fb^{-1} E^{ee}_{cm}=10.6 GeV
14.80±0.14±0.54	33k	[2] RYU	14	BELL	669 fb^{-1} E^{ee}_{cm}=10.6 GeV
16.2 ±2.1 ±1.1	150	[3] BARATE	99K	ALEP	1991–1995 LEP runs
15.8 ±4.2 ±1.7	46	[4] BARATE	98E	ALEP	1991–1995 LEP runs
15.1 ±2.1 ±2.2	111	COAN	96	CLEO	$E^{ee}_{cm} \approx$ 10.6 GeV
• • • We do not use the following data for averages, fits, limits, etc. • • •					
26 ±9 ±2	13	[5] BUSKULIC	96	ALEP	Repl. by BARATE 99K

[1] LEES 18B reconstructs K^0_S's using $K^0_S \to \pi^+\pi^-$ decays.
[2] RYU 14 reconstruct K^0's using $K^0_S \to \pi^+\pi^-$ decays.
[3] BARATE 99K measure K^0's by detecting K^0_L's in their hadron calorimeter.
[4] BARATE 98E reconstruct K^0's using $K^0_S \to \pi^+\pi^-$ decays.
[5] BUSKULIC 96 measure K^0's by detecting K^0_L's in their hadron calorimeter.

$\Gamma(K^- K^0 \geq 0\pi^0 \nu_\tau)/\Gamma_{total}$ — $\Gamma_{39}/\Gamma = (\Gamma_{38}+\Gamma_{43})/\Gamma$

VALUE (%)	EVTS	DOCUMENT ID		TECN	COMMENT
0.299±0.007 OUR FIT (Produced by HFLAV)					
0.330±0.055±0.039	124	ABBIENDI	00C	OPAL	1991–1995 LEP runs

$\Gamma(h^- \overline{K}^0 \pi^0 \nu_\tau)/\Gamma_{total}$ — $\Gamma_{40}/\Gamma = (\Gamma_{41}+\Gamma_{43})/\Gamma$

VALUE (%)	EVTS	DOCUMENT ID		TECN	COMMENT
0.532±0.013 OUR FIT (Produced by HFLAV)					
0.50 ±0.06 OUR AVERAGE Error includes scale factor of 1.2.					
0.562±0.050±0.048	264	COAN	96	CLEO	$E^{ee}_{cm} \approx$ 10.6 GeV
• • • We use the following data for averages but not for fits. • • •					
0.446±0.052±0.046	157	[1] BARATE	98E	ALEP	1991–1995 LEP runs

[1] Not independent of BARATE 98E B($\tau^- \to \pi^- \overline{K}^0 \pi^0 \tau$) and B($\tau^- \to K^- K^0 \pi^0 \nu_\tau$) values.

$\Gamma(\pi^- \overline{K}^0 \pi^0 \nu_\tau)/\Gamma_{total}$ — Γ_{41}/Γ

VALUE (%)	EVTS	DOCUMENT ID		TECN	COMMENT
0.382±0.013 OUR FIT (Produced by HFLAV)					
0.383±0.014 OUR AVERAGE					
0.386±0.004±0.014	27k	[1] RYU	14	BELL	669 fb^{-1} E^{ee}_{cm}=10.6 GeV
0.347±0.053±0.037	299	[2] BARATE	99K	ALEP	1991–1995 LEP runs
0.294±0.073±0.037	142	[3] BARATE	98E	ALEP	1991–1995 LEP runs
0.41 ±0.12 ±0.03		[4] ACCIARRI	95F	L3	1991–1993 LEP runs
• • • We use the following data for averages but not for fits. • • •					
0.417±0.058±0.044		[5] COAN	96	CLEO	$E^{ee}_{cm} \approx$ 10.6 GeV
• • • We do not use the following data for averages, fits, limits, etc. • • •					
0.32 ±0.11 ±0.05	23	[6] BUSKULIC	96	ALEP	Repl. by BARATE 99K

[1] RYU 14 reconstruct K^0's using $K^0_S \to \pi^+\pi^-$ decays.
[2] BARATE 99K measure K^0's by detecting K^0_L's in their hadron calorimeter.
[3] BARATE 98E reconstruct K^0's using $K^0_S \to \pi^+\pi^-$ decays.
[4] ACCIARRI 95F do not identify π^-/K^- and assume B($K^- K^0 \pi^0 \nu_\tau$) = (0.05 ± 0.05)%.
[5] Not independent of COAN 96 B($h^- K^0 \pi^0 \nu_\tau$) and B($K^- K^0 \pi^0 \nu_\tau$) measurements.
[6] BUSKULIC 96 measure K^0's by detecting K^0_L's in their hadron calorimeter.

$\Gamma(\overline{K}^0 \rho^- \nu_\tau)/\Gamma_{total}$ — Γ_{42}/Γ

VALUE (%)	DOCUMENT ID		TECN	COMMENT
0.22 ±0.05 OUR AVERAGE				
0.250±0.057±0.044	[1] BARATE	99K	ALEP	1991–1995 LEP runs
0.188±0.054±0.038	[2] BARATE	98E	ALEP	1991–1995 LEP runs

[1] BARATE 99K measure K^0's by detecting K^0_L's in hadron calorimeter. They determine the $\overline{K}^0 \rho^-$ fraction in $\tau^- \to \pi^- \overline{K}^0 \pi^0 \nu_\tau$ decays to be (0.72 ± 0.12 ± 0.10) and multiply their B($\pi^- \overline{K}^0 \pi^0 \nu_\tau$) measurement by this fraction to obtain the quoted result.
[2] BARATE 98E reconstruct K^0's using $K^0_S \to \pi^+\pi^-$ decays. They determine the $\overline{K}^0 \rho^-$ fraction in $\tau^- \to \pi^- \overline{K}^0 \pi^0 \nu_\tau$ decays to be (0.64 ± 0.09 ± 0.10) and multiply their B($\pi^- \overline{K}^0 \pi^0 \nu_\tau$) measurement by this fraction to obtain the quoted result.

$\Gamma(K^- K^0 \pi^0 \nu_\tau)/\Gamma_{total}$ — Γ_{43}/Γ

VALUE (units 10^{-4})	EVTS	DOCUMENT ID		TECN	COMMENT
15.0 ±0.7 OUR FIT (Produced by HFLAV)					
14.9 ±0.7 OUR AVERAGE					
14.96±0.20±0.74	8.3k	[1] RYU	14	BELL	669 fb^{-1} E^{ee}_{cm}=10.6 GeV
14.3 ±2.5 ±1.5	78	[2] BARATE	99K	ALEP	1991–1995 LEP runs
15.2 ±7.6 ±2.1	15	[3] BARATE	98E	ALEP	1991–1995 LEP runs
14.5 ±3.6 ±2.0	32	COAN	96	CLEO	$E^{ee}_{cm} \approx$ 10.6 GeV
• • • We do not use the following data for averages, fits, limits, etc. • • •					
10 ±5 ±3	5	[4] BUSKULIC	96	ALEP	Repl. by BARATE 99K

[1] RYU 14 reconstruct K^0's using $K^0_S \to \pi^+\pi^-$ decays.
[2] BARATE 99K measure K^0's by detecting K^0_L's in their hadron calorimeter.
[3] BARATE 98E reconstruct K^0's using $K^0_S \to \pi^+\pi^-$ decays.
[4] BUSKULIC 96 measure K^0's by detecting K^0_L's in their hadron calorimeter.

$\Gamma(\pi^- \overline{K}^0 \geq 1\pi^0 \nu_\tau)/\Gamma_{total}$ — $\Gamma_{44}/\Gamma = (\Gamma_{41}+\Gamma_{45})/\Gamma$

VALUE (%)	EVTS	DOCUMENT ID		TECN	COMMENT
0.408±0.025 OUR FIT (Produced by HFLAV)					
0.324±0.074±0.066	148	ABBIENDI	00C	OPAL	1991–1995 LEP runs

$\Gamma(\pi^- \overline{K}^0 \pi^0 \pi^0 \nu_\tau (\text{ex.}K^0))/\Gamma_{total}$ — Γ_{45}/Γ

VALUE (units 10^{-3})	CL%	EVTS	DOCUMENT ID		TECN	COMMENT
0.26±0.23 OUR FIT (Produced by HFLAV)						
0.26±0.24			[1] BARATE	99R	ALEP	1991–1995 LEP runs
• • • We do not use the following data for averages, fits, limits, etc. • • •						
<0.66	95	17	[2] BARATE	99K	ALEP	1991–1995 LEP runs
0.58±0.33±0.14		5	[3] BARATE	98E	ALEP	1991–1995 LEP runs

[1] BARATE 99R combine the BARATE 98E and BARATE 99K measurements to obtain this value.
[2] BARATE 99K measure K^0's by detecting K^0_L's in their hadron calorimeter.
[3] BARATE 98E reconstruct K^0's using $K^0_S \to \pi^+\pi^-$ decays.

Int. J. Mod
by UNIVERSITY OF CALIFORNIA @ BERK
wnloaded from www.worldscientific.com
-use and distribution is strictly not permitted, except for Open Access articles.

$\Gamma(K^- K^0 \pi^0 \pi^0 \nu_\tau)/\Gamma_{total}$ — Γ_{46}/Γ

VALUE	CL%	DOCUMENT ID		TECN	COMMENT
$<0.16 \times 10^{-3}$	95	[1] BARATE	99R	ALEP	1991–1995 LEP runs
• • • We do not use the following data for averages, fits, limits, etc. • • •					
$<0.18 \times 10^{-3}$	95	[2] BARATE	99K	ALEP	1991–1995 LEP runs
$<0.39 \times 10^{-3}$	95	[3] BARATE	98E	ALEP	1991–1995 LEP runs

[1] BARATE 99R combine the BARATE 98E and BARATE 99K bounds to obtain this value.
[2] BARATE 99K measure K^0's by detecting K^0_L's in hadron calorimeter.
[3] BARATE 98E reconstruct K^0's by using $K^0_S \to \pi^+\pi^-$ decays.

$\Gamma(\pi^- K^0 \overline{K}^0 \nu_\tau)/\Gamma_{total}$ — $\Gamma_{47}/\Gamma = (\Gamma_{48}+\Gamma_{49}+\Gamma_{50})/\Gamma$

VALUE (%)	EVTS	DOCUMENT ID		TECN	COMMENT
0.155±0.024 OUR FIT (Produced by HFLAV)					
• • • We use the following data for averages but not for fits. • • •					
0.153±0.030±0.016	74	[1] BARATE	98E	ALEP	1991–1995 LEP runs
• • • We do not use the following data for averages, fits, limits, etc. • • •					
0.31 ±0.12 ±0.04		[2] ACCIARRI	95F	L3	1991–1993 LEP runs

[1] BARATE 98E obtain this value by adding twice their $B(\pi^- K^0_S K^0_S \nu_\tau)$ value to their $B(\pi^- K^0_S K^0_L \nu_\tau)$ value.
[2] ACCIARRI 95F assume $B(\pi^- K^0_S K^0_S \nu) = B(\pi^- K^0_S K^0_L \nu) = 1/2 B(\pi^- K^0_S K^0_L \nu)$.

$\Gamma(\pi^- K^0_S K^0_S \nu_\tau)/\Gamma_{total}$ — Γ_{48}/Γ

Bose-Einstein correlations might make the mixing fraction different than 1/4.

VALUE (units 10^{-4})	EVTS	DOCUMENT ID		TECN	COMMENT
2.35±0.06 OUR FIT (Produced by HFLAV)					
2.32±0.06 OUR AVERAGE					
2.33±0.03±0.09	6.7k	RYU	14	BELL	669 fb^{-1} E^{ee}_{cm}=10.6 GeV
2.31±0.04±0.08	5.0k	[1] LEES	12Y	BABR	468 fb^{-1} E^{ee}_{cm}=10.6 GeV
2.6 ±1.0 ±0.5	6	BARATE	98E	ALEP	1991–1995 LEP runs
2.3 ±0.5 ±0.3	42	COAN	96	CLEO	$E^{ee}_{cm} \approx$ 10.6 GeV

[1] The correlation coefficient between this measurement and the LEES 12Y $\Gamma(\tau^- \to \pi^- K^0_S K^0_S \pi^0 \nu_\tau)/\Gamma_{total}$ one is 0.0828.

$\Gamma(\pi^- K^0_S K^0_L \nu_\tau)/\Gamma_{total}$ — Γ_{49}/Γ

VALUE (units 10^{-4})	EVTS	DOCUMENT ID		TECN	COMMENT
10.8±2.4 OUR FIT (Produced by HFLAV)					
10.1±2.3±1.3	68	BARATE	98E	ALEP	1991–1995 LEP runs

$\Gamma(\pi^- K^0_L K^0_L \nu_\tau)/\Gamma_{total}$ — $\Gamma_{50}/\Gamma = \Gamma_{48}/\Gamma$

VALUE (units 10^{-4})	DOCUMENT ID
2.35±0.06 OUR FIT (Produced by HFLAV)	

$\Gamma(\pi^- K^0 \overline{K}^0 \pi^0 \nu_\tau)/\Gamma_{total}$ — $\Gamma_{51}/\Gamma = (\Gamma_{52}+\Gamma_{56}+\Gamma_{57})/\Gamma$

VALUE (units 10^{-4})	DOCUMENT ID		TECN	COMMENT
3.6±1.2 OUR FIT (Produced by HFLAV)				
• • • We use the following data for averages but not for fits. • • •				
3.1±2.3	[1] BARATE	99R	ALEP	1991–1995 LEP runs

[1] BARATE 99R combine BARATE 98E $\Gamma(\pi^- K^0_S K^0_S \pi^0 \nu_\tau)/\Gamma_{total}$ and $\Gamma(\pi^- K^0_S K^0_L \pi^0 \nu_\tau)/\Gamma_{total}$ measurements to obtain this value.

$\Gamma(\pi^- K^0_S K^0_S \pi^0 \nu_\tau)/\Gamma_{total}$ — Γ_{52}/Γ

VALUE (units 10^{-5})	CL%	EVTS	DOCUMENT ID		TECN	COMMENT
1.82±0.21 OUR FIT (Produced by HFLAV)						
1.80±0.21 OUR AVERAGE						
2.00±0.22±0.20		303	RYU	14	BELL	669 fb^{-1} E^{ee}_{cm}=10.6 GeV
1.60±0.20±0.22		409	[1] LEES	12Y	BABR	468 fb^{-1} E^{ee}_{cm}=10.6 GeV
• • • We do not use the following data for averages, fits, limits, etc. • • •						
<20	95		BARATE	98E	ALEP	1991–1995 LEP runs

[1] The correlation coefficient between this measurement and the LEES 12Y $\Gamma(\tau^- \to \pi^- K^0_S K^0_S \nu_\tau)/\Gamma_{total}$ one is 0.0828.

$\Gamma(K^{*-} K^0 \pi^0 \nu_\tau \to \pi^- K^0_S K^0_S \pi^0 \nu_\tau)/\Gamma_{total}$ — Γ_{53}/Γ

VALUE (units 10^{-6})	DOCUMENT ID		TECN	COMMENT
10.8±1.4±1.5	RYU	14	BELL	669 fb^{-1} E^{ee}_{cm}=10.6 GeV

$\Gamma(f_1(1285) \pi^- \nu_\tau \to \pi^- K^0_S K^0_S \pi^0 \nu_\tau)/\Gamma_{total}$ — Γ_{54}/Γ

VALUE (units 10^{-6})	DOCUMENT ID		TECN	COMMENT
6.8±1.3±0.7	RYU	14	BELL	669 fb^{-1} E^{ee}_{cm}=10.6 GeV

$\Gamma(f_1(1420) \pi^- \nu_\tau \to \pi^- K^0_S K^0_S \pi^0 \nu_\tau)/\Gamma_{total}$ — Γ_{55}/Γ

VALUE (units 10^{-6})	DOCUMENT ID		TECN	COMMENT
2.4±0.5±0.6	RYU	14	BELL	669 fb^{-1} E^{ee}_{cm}=10.6 GeV

$\Gamma(\pi^- K^0_S K^0_L \pi^0 \nu_\tau)/\Gamma_{total}$ — Γ_{56}/Γ

VALUE (units 10^{-4})	EVTS	DOCUMENT ID		TECN	COMMENT
3.2±1.2 OUR FIT (Produced by HFLAV)					
3.1±1.1±0.5	11	BARATE	98E	ALEP	1991–1995 LEP runs

$\Gamma(\pi^- K^0_L K^0_L \pi^0 \nu_\tau)/\Gamma_{total}$ — $\Gamma_{57}/\Gamma = \Gamma_{52}/\Gamma$

VALUE (units 10^{-5})	DOCUMENT ID
1.82±0.21 OUR FIT (Produced by HFLAV)	

$\Gamma(K^- K^0_S K^0_S \nu_\tau)/\Gamma_{total}$ — Γ_{58}/Γ

VALUE	CL%	DOCUMENT ID		TECN	COMMENT
$<6.3 \times 10^{-7}$	90	LEES	12Y	BABR	468 fb^{-1} E^{ee}_{cm}=10.6 GeV

$\Gamma(K^- K^0_S K^0_S \pi^0 \nu_\tau)/\Gamma_{total}$ — Γ_{59}/Γ

VALUE	CL%	DOCUMENT ID		TECN	COMMENT
$<4.0 \times 10^{-7}$	90	LEES	12Y	BABR	468 fb^{-1} E^{ee}_{cm}=10.6 GeV

$\Gamma(K^0 h^+ h^- h^- \geq 0 \text{ neutrals } \nu_\tau)/\Gamma_{total}$ — Γ_{60}/Γ

VALUE (%)	CL%	DOCUMENT ID		TECN	COMMENT
<0.17	95	TSCHIRHART	88	HRS	E^{ee}_{cm}= 29 GeV
• • • We do not use the following data for averages, fits, limits, etc. • • •					
<0.27	90	BELTRAMI	85	HRS	E^{ee}_{cm}= 29 GeV

$\Gamma(K^0 h^+ h^- h^- \nu_\tau)/\Gamma_{total}$ — Γ_{61}/Γ

VALUE (units 10^{-4})	EVTS	DOCUMENT ID		TECN	COMMENT
2.5±2.0 OUR FIT (Produced by HFLAV)					
2.3±1.9±0.7	6	[1] BARATE	98E	ALEP	1991–1995 LEP runs

[1] BARATE 98E reconstruct K^0's using $K^0_S \to \pi^+\pi^-$ decays.

$\Gamma(h^- h^- h^+ \geq 0 \text{ neutrals } \geq 0 K^0_L \nu_\tau)/\Gamma_{total}$ — Γ_{62}/Γ

$\Gamma_{62}/\Gamma = (0.34598\Gamma_{36}+0.34598\Gamma_{38}+0.34598\Gamma_{41}+0.34598\Gamma_{43}+0.4247\Gamma_{48}+0.6920\Gamma_{49}+0.4247\Gamma_{52}+0.6920\Gamma_{56}+0.6534\Gamma_{61}+\Gamma_{70}+\Gamma_{78}+\Gamma_{85}+\Gamma_{86}+\Gamma_{97}+\Gamma_{103}+\Gamma_{106}+\Gamma_{107}+0.2805\Gamma_{150}+0.2805\Gamma_{152}+0.2805\Gamma_{154}+0.2628\Gamma_{156}+0.7259\Gamma_{170}+0.9078\Gamma_{178}+0.9078\Gamma_{179}+0.9078\Gamma_{180})/\Gamma$

VALUE (%)	EVTS	DOCUMENT ID		TECN	COMMENT
15.20± 0.06 OUR FIT (Produced by HFLAV)					
14.8 ± 0.4 OUR AVERAGE					
14.4 ± 0.6 ±0.3		ADEVA	91F	L3	E^{ee}_{cm}= 88.3–94.3 GeV
15.0 ± 0.4 ±0.3		BEHREND	89B	CELL	E^{ee}_{cm}= 14–47 GeV
15.1 ± 0.8 ±0.6		AIHARA	87B	TPC	E^{ee}_{cm}= 29 GeV
• • • We do not use the following data for averages, fits, limits, etc. • • •					
13.5 ± 0.3 ±0.3		ABACHI	89B	HRS	E^{ee}_{cm}= 29 GeV
12.8 ± 1.0 ±0.7		[1] BURCHAT	87	MRK2	E^{ee}_{cm}= 29 GeV
12.1 ± 0.5 ±1.2		RUCKSTUHL	86	DLCO	E^{ee}_{cm}= 29 GeV
12.8 ± 0.5 ±0.8	1420	SCHMIDKE	86	MRK2	E^{ee}_{cm}= 29 GeV
15.3 ± 1.1 $^{+1.3}_{-1.6}$	367	ALTHOFF	85	TASS	E^{ee}_{cm}= 34.5 GeV
13.6 ± 0.5 ±0.8		BARTEL	85F	JADE	E^{ee}_{cm}= 34.6 GeV
12.2 ± 1.3 ±3.9		[2] BERGER	85	PLUT	E^{ee}_{cm}= 34.6 GeV
13.3 ± 0.3 ±0.6		FERNANDEZ	85	MAC	E^{ee}_{cm}= 29 GeV
24 ± 6	35	BRANDELIK	80	TASS	E^{ee}_{cm}= 30 GeV
32 ± 5	692	[3] BACINO	78B	DLCO	E^{ee}_{cm}= 3.1–7.4 GeV
35 ±11		[3] BRANDELIK	78	DASP	Assumes $V-A$ decay
18 ± 6.5	33	[3] JAROS	78	LGW	E^{ee}_{cm} > 6 GeV

[1] BURCHAT 87 value is not independent of SCHMIDKE 86 value.
[2] Not independent of BERGER 85 $\Gamma(\mu^- \overline{\nu}_\mu \nu_\tau)/\Gamma_{total}$, $\Gamma(e^- \overline{\nu}_e \nu_\tau)/\Gamma_{total}$, $\Gamma(h^- \geq 1 \text{ neutrals} \nu_\tau)/\Gamma_{total}$, and $\Gamma(h^- \geq 0 K^0_L \nu_\tau)/\Gamma_{total}$, and therefore not used in the fit.
[3] Low energy experiments are not in average or fit because the systematic errors in background subtraction are judged to be large.

$\Gamma(h^- h^- h^+ \geq 0 \text{ neutrals } \nu_\tau (\text{ex. } K^0_S \to \pi^+\pi^-)(\text{"3-prong"}))/\Gamma_{total}$ — Γ_{63}/Γ

$\Gamma_{63}/\Gamma = (\Gamma_{70}+\Gamma_{78}+\Gamma_{85}+\Gamma_{86}+\Gamma_{97}+\Gamma_{103}+\Gamma_{106}+\Gamma_{107}+0.2805\Gamma_{150}+0.2805\Gamma_{152}+0.2805\Gamma_{154}+0.501\Gamma_{170}+0.9078\Gamma_{178}+0.9078\Gamma_{179}+0.9078\Gamma_{180})/\Gamma$

VALUE (%)	EVTS	DOCUMENT ID		TECN	COMMENT
14.55 ±0.06 OUR FIT (Produced by HFLAV)					
14.61 ±0.06 OUR AVERAGE					
14.556±0.105±0.076		[1] ACHARD	01D	L3	1992–1995 LEP runs
14.96 ±0.09 ±0.22	10.4k	AKERS	95Y	OPAL	1991–1994 LEP runs
• • • We use the following data for averages but not for fits. • • •					
14.652±0.067±0.086		SCHAEL	05C	ALEP	1991–1995 LEP runs
14.569±0.093±0.048	23k	[2] ABREU	01M	DLPH	1992–1995 LEP runs
14.22 ±0.10 ±0.37		[3] BALEST	95C	CLEO	$E^{ee}_{cm} \approx$ 10.6 GeV
• • • We do not use the following data for averages, fits, limits, etc. • • •					
15.26 ±0.26 ±0.22		ACTON	92H	OPAL	Repl. by AKERS 95Y
13.3 ±0.3 ±0.8		[4] ALBRECHT	92D	ARG	E^{ee}_{cm}= 9.4–10.6 GeV
14.35 $^{+0.40}_{-0.45}$ ±0.24		DECAMP	92C	ALEP	1989–1990 LEP runs

[1] The correlation coefficients between this measurement and the ACHARD 01D measurements of $B(\tau \to$ "1-prong") and $B(\tau \to$ "5-prong") are -0.978 and -0.19 respectively.
[2] The correlation coefficients between this measurement and the ABREU 01M measurements of $B(\tau \to$ 1-prong) and $B(\tau \to$ 5-prong) are -0.98 and -0.08 respectively.
[3] Not independent of BALEST 95C $B(h^- h^- h^+ \nu_\tau)$ and $B(h^- h^- h^+ \pi^0 \nu_\tau)$ values, and BORTOLETTO 93 $B(h^- h^- h^+ 2\pi^0 \nu_\tau)/B(h^- h^- h^+ \geq 0 \text{ neutrals } \nu_\tau)$ value.
[4] This ALBRECHT 92D value is not independent of their $\Gamma(\mu^- \overline{\nu}_\mu \nu_\tau)\Gamma(e^- \overline{\nu}_e \nu_\tau)/\Gamma^2_{total}$ value.

Int. J. Mod. Phys. A 2026.41. Downloaded from www.worldscientific.com
by UNIVERSITY OF CALIFORNIA @ BERKELEY on 09/16/26. Re-use and distribution is strictly not permitted, except for Open Access articles.

$\Gamma(h^- h^- h^+ \nu_\tau)/\Gamma_{total}$ — Γ_{64}/Γ

$\Gamma_{64}/\Gamma = (0.34598\Gamma_{36}+0.34598\Gamma_{38}+\Gamma_{70}+\Gamma_{97}+\Gamma_{106}+0.501\Gamma_{170}+0.0153\Gamma_{178}+0.0153\Gamma_{179})/\Gamma$

VALUE (%)	EVTS	DOCUMENT ID		TECN	COMMENT
9.80±0.05 OUR FIT	(Produced by HFLAV)				
• • • We use the following data for averages but not for fits. • • •					
7.6 ±0.1 ±0.5	7.5k	[1] ALBRECHT	96E	ARG	E^{ee}_{cm}= 9.4–10.6 GeV
• • • We do not use the following data for averages, fits, limits, etc. • • •					
9.92±0.10±0.09	11.2k	[2] BUSKULIC	96	ALEP	Repl. by SCHAEL 05C
9.49±0.36±0.63		DECAMP	92C	ALEP	Repl. by SCHAEL 05C
8.7 ±0.7 ±0.3	694	[3] BEHREND	90	CELL	E^{ee}_{cm}= 35 GeV
7.0 ±0.3 ±0.7	1566	[4] BAND	87	MAC	E^{ee}_{cm}= 29 GeV
6.7 ±0.8 ±0.9		[5] BURCHAT	87	MRK2	E^{ee}_{cm}= 29 GeV
6.4 ±0.4 ±0.9		[6] RUCKSTUHL	86	DLCO	E^{ee}_{cm}= 29 GeV
7.8 ±0.5 ±0.8	890	SCHMIDKE	86	MRK2	E^{ee}_{cm}= 29 GeV
8.4 ±0.4 ±0.7	1255	[6] FERNANDEZ	85	MAC	E^{ee}_{cm}= 29 GeV
9.7 ±2.0 ±1.3		BEHREND	84	CELL	E^{ee}_{cm}= 14,22 GeV

[1] ALBRECHT 96E not independent of ALBRECHT 93C $\Gamma(h^- h^- h^+ \nu_\tau(\text{ex. } K^0)) \times \Gamma(\text{particle}^- \geq 0 \text{ neutrals } \geq 0 K^0_L \nu_\tau)/\Gamma^2_{total}$ value.

[2] BUSKULIC 96 quote $B(h^- h^- h^+ \nu_\tau(\text{ex. } K^0)) = 9.50 \pm 0.10 \pm 0.11$. We add 0.42 to remove their K^0 correction and reduce the systematic error accordingly.

[3] BEHREND 90 subtract 0.3% to account for the $\tau^- \to K^*(892)^- \nu_\tau$ contribution to measured events.

[4] BAND 87 subtract for charged kaon modes; not independent of FERNANDEZ 85 value.

[5] BURCHAT 87 value is not independent of SCHMIDKE 86 value.

[6] Value obtained by multiplying paper's $R = B(h^- h^- h^+ \nu_\tau)/B(\text{3-prong})$ by B(3-prong) = 0.143 and subtracting 0.3% for $K^*(892)$ background.

$\Gamma(h^- h^- h^+ \nu_\tau(\text{ex.}K^0))/\Gamma_{total}$ — Γ_{65}/Γ

$\Gamma_{65}/\Gamma = (\Gamma_{70}+\Gamma_{97}+\Gamma_{106}+0.501\Gamma_{170}+0.0153\Gamma_{178}+0.0153\Gamma_{179})/\Gamma$

VALUE (%)	EVTS	DOCUMENT ID		TECN	COMMENT
9.45 ±0.05 OUR FIT	(Produced by HFLAV)				
9.44 ±0.14 OUR AVERAGE	Error includes scale factor of 1.4. See the ideogram below.				
9.317±0.090±0.082	12.2k	[1] ABDALLAH	06A	DLPH	1992–1995 LEP runs
9.51 ±0.07 ±0.20	37.7k	BALEST	95C	CLEO	$E^{ee}_{cm} \approx$ 10.6 GeV
• • • We use the following data for averages but not for fits. • • •					
9.87 ±0.10 ±0.24		[2] AKERS	95Y	OPAL	1991–1994 LEP runs
• • • We do not use the following data for averages, fits, limits, etc. • • •					
9.50 ±0.10 ±0.11	11.2k	[3] BUSKULIC	96	ALEP	Repl. by SCHAEL 05C

[1] See footnote to ABDALLAH 06A $\Gamma(\tau^- \to h^- \nu_\tau)/\Gamma_{total}$ measurement for correlations with other measurements.

[2] Not independent of AKERS 95Y $B(h^- h^- h^+ \geq 0 \text{ neutrals} \nu_\tau(\text{ex. } K^0_S \to \pi^+\pi^-))$ and $B(h^- h^- h^+ \nu_\tau(\text{ex. } K^0))/B(h^- h^- h^+ \geq 0 \text{ neutrals} \nu_\tau(\text{ex. } K^0_S \to \pi^+\pi^-))$ values.

[3] Not independent of BUSKULIC 96 $B(h^- h^- h^+ \nu_\tau)$ value.

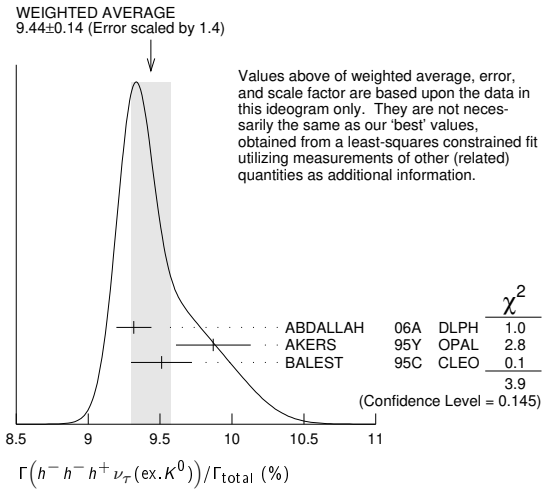

$\Gamma(h^- h^- h^+ \nu_\tau(\text{ex.}K^0))/\Gamma(h^- h^- h^+ \geq 0 \text{ neutrals } \nu_\tau(\text{ex. } K^0_S \to \pi^+\pi^-)$ ("3-prong")) — Γ_{65}/Γ_{63}

$\Gamma_{65}/\Gamma_{63} = (\Gamma_{70}+\Gamma_{97}+\Gamma_{106}+0.501\Gamma_{170}+0.0153\Gamma_{178}+0.0153\Gamma_{179})/(0.4247\Gamma_{52}+\Gamma_{70}+\Gamma_{78}+\Gamma_{85}+\Gamma_{89}+\Gamma_{97}+\Gamma_{103}+\Gamma_{106}+\Gamma_{107}+0.2805\Gamma_{150}+0.2302\Gamma_{151}+0.2805\Gamma_{152}+0.2805\Gamma_{154}+0.1131\Gamma_{156}+0.3256\Gamma_{160}+0.501\Gamma_{170}+0.9078\Gamma_{178}+0.9078\Gamma_{179}+0.9078\Gamma_{180}+0.892\Gamma_{182})$

VALUE (units 10^{-2})	DOCUMENT ID		TECN	COMMENT
64.98±0.31 OUR FIT	(Produced by HFLAV)			
66.0 ±0.4 ±1.4	AKERS	95Y	OPAL	1991–1994 LEP runs

$\Gamma(h^- h^- h^+ \nu_\tau(\text{ex.}K^0,\omega))/\Gamma_{total}$ — Γ_{66}/Γ

$\Gamma_{66}/\Gamma = (\Gamma_{70}+\Gamma_{97}+\Gamma_{106}+0.501\Gamma_{170})/\Gamma$

VALUE (%)	DOCUMENT ID
9.42±0.05 OUR FIT	(Produced by HFLAV)

$\Gamma(\pi^-\pi^+\pi^-\nu_\tau)/\Gamma_{total}$ — $\Gamma_{67}/\Gamma = (0.34598\Gamma_{36}+\Gamma_{70}+0.0153\Gamma_{178})/\Gamma$

VALUE (%)	DOCUMENT ID
9.31±0.05 OUR FIT	(Produced by HFLAV)

$\Gamma(\pi^-\pi^+\pi^-\nu_\tau(\text{ex.}K^0))/\Gamma_{total}$ — $\Gamma_{68}/\Gamma = (\Gamma_{70}+0.0153\Gamma_{178})/\Gamma$

VALUE (%)	EVTS	DOCUMENT ID		TECN	COMMENT
9.02±0.05 OUR FIT	(Produced by HFLAV)				
8.77±0.13 OUR AVERAGE	Error includes scale factor of 1.1.				
$8.42\pm0.00^{+0.26}_{-0.25}$	8.9M	[1] LEE	10	BELL	666 fb^{-1} E^{ee}_{cm} = 10.6 GeV
8.83±0.01±0.13	1.6M	[2] AUBERT	08	BABR	342 fb^{-1} E^{ee}_{cm} = 10.6 GeV
9.13±0.05±0.46	43k	[3] BRIERE	03	CLE3	E^{ee}_{cm} = 10.6 GeV

[1] Quoted statistical error is 0.003%. Correlation matrix for LEE 10 branching fractions:

(1) $\Gamma(\tau^- \to \pi^-\pi^+\pi^-\nu_\tau(\text{ex.}K^0))/\Gamma_{total}$
(2) $\Gamma(\tau^- \to K^-\pi^+\pi^-\nu_\tau(\text{ex.}K^0))/\Gamma_{total}$
(3) $\Gamma(\tau^- \to K^-K^+\pi^-\nu_\tau)/\Gamma_{total}$
(4) $\Gamma(\tau^- \to K^-K^+K^-\nu_\tau)/\Gamma_{total}$

	(1)	(2)	(3)
(2)	0.175		
(3)	0.049	0.080	
(4)	−0.053	0.035	−0.008

[2] Correlation matrix for AUBERT 08 branching fractions:

(1) $\Gamma(\tau^- \to \pi^-\pi^+\pi^-\nu_\tau(\text{ex.}K^0))/\Gamma_{total}$
(2) $\Gamma(\tau^- \to K^-\pi^+\pi^-\nu_\tau(\text{ex.}K^0))/\Gamma_{total}$
(3) $\Gamma(\tau^- \to K^-K^+\pi^-\nu_\tau)/\Gamma_{total}$
(4) $\Gamma(\tau^- \to K^-K^+K^-\nu_\tau)/\Gamma_{total}$

	(1)	(2)	(3)
(2)	0.544		
(3)	0.390	0.177	
(4)	0.031	0.093	0.087

[3] 47% correlated with BRIERE 03 $\tau^- \to K^-\pi^+\pi^-\nu_\tau$ and 71% correlated with $\tau^- \to K^-K^+\pi^-\nu_\tau$ because of a common 5% normalization error.

$\Gamma(\pi^-\pi^+\pi^-\nu_\tau(\text{ex.}K^0),\text{non-axial vector})/\Gamma(\pi^-\pi^+\pi^-\nu_\tau(\text{ex.}K^0))$ — Γ_{69}/Γ_{68}

$\Gamma_{69}/\Gamma_{68} = \Gamma_{69}/(\Gamma_{70}+0.0153\Gamma_{177})$

VALUE	CL%	DOCUMENT ID		TECN	COMMENT
<0.261	95	[1] ACKERSTAFF	97R	OPAL	1992–1994 LEP runs

[1] Model-independent limit from structure function analysis on contribution to $B(\tau^- \to \pi^-\pi^+\pi^-\nu_\tau(\text{ex. } K^0))$ from non-axial vectors.

$\Gamma(\pi^-\pi^+\pi^-\nu_\tau(\text{ex.}K^0,\omega))/\Gamma_{total}$ — Γ_{70}/Γ

VALUE (%)	EVTS	DOCUMENT ID		TECN	COMMENT
8.99 ±0.05 OUR FIT	(Produced by HFLAV)				
9.041±0.060±0.076	29k	[1] SCHAEL	05C	ALEP	1991-1995 LEP runs

[1] See footnote to SCHAEL 05C $\Gamma(\tau^- \to e^-\overline{\nu}_e\nu_\tau)/\Gamma_{total}$ measurement for correlations with other measurements.

$\Gamma(h^- h^- h^+ \geq 1 \text{ neutrals } \nu_\tau)/\Gamma_{total}$ — Γ_{71}/Γ

$\Gamma_{71}/\Gamma = (0.34598\Gamma_{41}+0.34598\Gamma_{43}+0.4247\Gamma_{48}+0.4247\Gamma_{52}+\Gamma_{78}+\Gamma_{85}+\Gamma_{86}+\Gamma_{103}+\Gamma_{107}+0.2805\Gamma_{150}+0.2805\Gamma_{152}+0.2805\Gamma_{154}+0.2926\Gamma_{156}+0.892\Gamma_{178}+0.892\Gamma_{179}+0.9078\Gamma_{180})/\Gamma$

VALUE (%)	EVTS	DOCUMENT ID		TECN	COMMENT
5.29±0.05 OUR FIT	(Produced by HFLAV)				
• • • We do not use the following data for averages, fits, limits, etc. • • •					
5.6 ±0.7 ±0.3	352	[1] BEHREND	90	CELL	E^{ee}_{cm}= 35 GeV
4.2 ±0.5 ±0.9	203	[2] ALBRECHT	87L	ARG	E^{ee}_{cm}= 10 GeV
6.1 ±0.8 ±0.9		[3] BURCHAT	87	MRK2	E^{ee}_{cm}= 29 GeV
7.6 ±0.4 ±0.9		[4,5] RUCKSTUHL	86	DLCO	E^{ee}_{cm}= 29 GeV
4.7 ±0.5 ±0.8	530	[6] SCHMIDKE	86	MRK2	E^{ee}_{cm}= 29 GeV
5.6 ±0.4 ±0.7		[5] FERNANDEZ	85	MAC	E^{ee}_{cm}= 29 GeV
6.2 ±2.3 ±1.7		BEHREND	84	CELL	E^{ee}_{cm}= 14,22 GeV

[1] BEHREND 90 value is not independent of BEHREND 90 $B(3h\nu_\tau \geq 1 \text{ neutrals}) + B(\text{5-prong})$.

[2] ALBRECHT 87L measure the product of branching ratios $B(3\pi^\pm\pi^0\nu_\tau)\ B((e\overline{\nu} \text{or} \mu\overline{\nu} \text{or} \pi \text{or} K \text{or} \rho)\nu_\tau) = 0.029$ and use the PDG 86 values for the second branching ratio which sum to 0.69 ± 0.03 to get the quoted value.

[3] BURCHAT 87 value is not independent of SCHMIDKE 86 value.

[4] Contributions from kaons and from $>1\pi^0$ are subtracted. Not independent of (3-prong + $0\pi^0$) and (3-prong + $\geq 0\pi^0$) values.

[5] Value obtained using paper's $R = B(h^- h^- h^+ \nu_\tau)/B(\text{3-prong})$ and current B(3-prong) = 0.143.

[6] Not independent of SCHMIDKE 86 $h^- h^- h^+ \nu_\tau$ and $h^- h^- h^+(\geq 0\pi^0)\nu_\tau$ values.

Int. J. Mod
by UNIVERSITY OF CALIFORNIA @ BERK
wnloaded from www.worldscientific.com
-use and distribution is strictly not permitted, except for Open Access articles.

$\Gamma(h^- h^- h^+ \geq 1\pi^0 \nu_\tau (\text{ex. } K^0))/\Gamma_{total}$ — Γ_{72}/Γ

$\Gamma_{72}/\Gamma = (\Gamma_{78}+\Gamma_{85}+\Gamma_{86}+\Gamma_{103}+\Gamma_{107}+0.2302\Gamma_{150}+0.2302\Gamma_{152}+0.2302\Gamma_{154}+0.892\Gamma_{178}+0.892\Gamma_{179}+0.9078\Gamma_{180})/\Gamma$

VALUE (%)	EVTS	DOCUMENT ID		TECN	COMMENT
5.09 ±0.05 OUR FIT		(Produced by HFLAV)			
5.10 ±0.12 OUR AVERAGE					
• • • We use the following data for averages but not for fits. • • •					
5.106±0.083±0.103	10.1k	[1] ABDALLAH	06A	DLPH	1992–1995 LEP runs
5.09 ±0.10 ±0.23		[2] AKERS	95Y	OPAL	1991–1994 LEP runs
• • • We do not use the following data for averages, fits, limits, etc. • • •					
4.95 ±0.29 ±0.65	570	DECAMP	92C	ALEP	Repl. by SCHAEL 05C

[1] See footnote to ABDALLAH 06A $\Gamma(\tau^- \to h^- \nu_\tau)/\Gamma_{total}$ measurement for correlations with other measurements.
[2] Not independent of AKERS 95Y $B(h^- h^- h^+ \geq 0 \text{ neutrals} \nu_\tau(\text{ex. } K^0_S \to \pi^+\pi^-))$ and $B(h^- h^- h^+ \geq 0 \text{ neutrals} \nu_\tau(\text{ex. } K^0))/B(h^- h^- h^+ \geq 0 \text{ neutrals} \nu_\tau(\text{ex. } K^0_S \to \pi^+\pi^-))$ values.

$\Gamma(h^- h^- h^+ \pi^0 \nu_\tau)/\Gamma_{total}$ — Γ_{73}/Γ

$\Gamma_{73}/\Gamma = (0.34598\Gamma_{41}+0.34598\Gamma_{43}+\Gamma_{78}+\Gamma_{103}+\Gamma_{107}+0.2302\Gamma_{152}+0.892\Gamma_{178}+0.892\Gamma_{179}+0.0153\Gamma_{180})/\Gamma$

VALUE (%)	EVTS	DOCUMENT ID		TECN	COMMENT
4.76±0.05 OUR FIT		(Produced by HFLAV)			
• • • We do not use the following data for averages, fits, limits, etc. • • •					
4.45±0.09±0.07	6.1k	[1] BUSKULIC	96	ALEP	Repl. by SCHAEL 05C

[1] BUSKULIC 96 quote $B(h^- h^- h^+ \pi^0 \nu_\tau(\text{ex. } K^0)) = 4.30 \pm 0.09 \pm 0.09$. We add 0.15 to remove their K^0 correction and reduce the systematic error accordingly.

$\Gamma(h^- h^- h^+ \pi^0 \nu_\tau (\text{ex.} K^0))/\Gamma_{total}$ — Γ_{74}/Γ

$\Gamma_{74}/\Gamma = (\Gamma_{78}+\Gamma_{103}+\Gamma_{107}+0.2302\Gamma_{152}+0.892\Gamma_{178}+0.892\Gamma_{179}+0.0153\Gamma_{180})/\Gamma$

VALUE (%)	EVTS	DOCUMENT ID		TECN	COMMENT
4.57 ±0.05 OUR FIT		(Produced by HFLAV)			
4.45 ±0.14 OUR AVERAGE		Error includes scale factor of 1.2.			
4.545±0.106±0.103	8.9k	[1] ABDALLAH	06A	DLPH	1992–1995 LEP runs
4.23 ±0.06 ±0.22	7.2k	BALEST	95C	CLEO	$E^{ee}_{cm} \approx 10.6$ GeV

[1] See footnote to ABDALLAH 06A $\Gamma(\tau^- \to h^- \nu_\tau)/\Gamma_{total}$ measurement for correlations with other measurements.

$\Gamma(h^- h^- h^+ \pi^0 \nu_\tau (\text{ex. } K^0, \omega))/\Gamma_{total}$

$\Gamma_{75}/\Gamma = (\Gamma_{78}+\Gamma_{103}+\Gamma_{107}+0.2302\Gamma_{152})/\Gamma$

VALUE (%)	DOCUMENT ID
2.79±0.07 OUR FIT	(Produced by HFLAV)

$\Gamma(\pi^- \pi^+ \pi^- \pi^0 \nu_\tau)/\Gamma_{total}$ — Γ_{76}/Γ

$\Gamma_{76}/\Gamma = (0.34598\Gamma_{41}+\Gamma_{78}+0.892\Gamma_{178}+0.0153\Gamma_{180})/\Gamma$

VALUE (%)	DOCUMENT ID
4.62±0.05 OUR FIT	(Produced by HFLAV)

$\Gamma(\pi^- \pi^+ \pi^- \pi^0 \nu_\tau (\text{ex.} K^0))/\Gamma_{total}$ — Γ_{77}/Γ

$\Gamma_{77}/\Gamma = (\Gamma_{78}+0.892\Gamma_{178}+0.0153\Gamma_{180})/\Gamma$

VALUE (%)	EVTS	DOCUMENT ID		TECN	COMMENT
4.49 ±0.05 OUR FIT		(Produced by HFLAV)			
4.55 ±0.13 OUR AVERAGE		Error includes scale factor of 1.6.			
4.598±0.057±0.064	16k	[1] SCHAEL	05C	ALEP	1991-1995 LEP runs
4.19 ±0.10 ±0.21		[2] EDWARDS	00A	CLEO	4.7 fb^{-1} $E^{ee}_{cm} = 10.6$ GeV

[1] SCHAEL 05C quote $(4.590 \pm 0.057 \pm 0.064)\%$. We add 0.008% to remove their correction for $\tau^- \to \pi^-\pi^0\omega\nu_\tau \to \pi^-\pi^0\pi^+\pi^-\nu_\tau$ decays. See footnote to SCHAEL 05C $\Gamma(\tau^- \to e^-\overline{\nu}_e\nu_\tau)/\Gamma_{total}$ measurement for correlations with other measurements.
[2] EDWARDS 00A quote $(4.19 \pm 0.10) \times 10^{-2}$ with a 5% systematic error.

$\Gamma(\pi^- \pi^+ \pi^- \pi^0 \nu_\tau (\text{ex.} K^0, \omega))/\Gamma_{total}$ — Γ_{78}/Γ

VALUE (%)	DOCUMENT ID
2.74±0.07 OUR FIT	(Produced by HFLAV)

$\Gamma(h^- \rho\pi^0 \nu_\tau)/\Gamma(h^- h^- h^+ \pi^0 \nu_\tau)$ — Γ_{79}/Γ_{73}

VALUE	EVTS	DOCUMENT ID		TECN	COMMENT
• • • We do not use the following data for averages, fits, limits, etc. • • •					
0.30±0.04±0.02	393	ALBRECHT	91D	ARG	$E^{ee}_{cm} = 9.4$–10.6 GeV

$\Gamma(h^- \rho^+ h^- \nu_\tau)/\Gamma(h^- h^- h^+ \pi^0 \nu_\tau)$ — Γ_{80}/Γ_{73}

VALUE	EVTS	DOCUMENT ID		TECN	COMMENT
• • • We do not use the following data for averages, fits, limits, etc. • • •					
0.10±0.03±0.04	142	ALBRECHT	91D	ARG	$E^{ee}_{cm} = 9.4$–10.6 GeV

$\Gamma(h^- \rho^- h^+ \nu_\tau)/\Gamma(h^- h^- h^+ \pi^0 \nu_\tau)$ — Γ_{81}/Γ_{73}

VALUE	EVTS	DOCUMENT ID		TECN	COMMENT
• • • We do not use the following data for averages, fits, limits, etc. • • •					
0.26±0.05±0.01	370	ALBRECHT	91D	ARG	$E^{ee}_{cm} = 9.4$–10.6 GeV

$\Gamma(h^- h^- h^+ \geq 2\pi^0 \nu_\tau (\text{ex. } K^0))/\Gamma_{total}$ — Γ_{82}/Γ

$\Gamma_{82}/\Gamma = (\Gamma_{85}+\Gamma_{86}+0.2302\Gamma_{150}+0.2302\Gamma_{154}+0.892\Gamma_{180})/\Gamma$

VALUE (%)	EVTS	DOCUMENT ID		TECN	COMMENT
0.517±0.031 OUR FIT		(Produced by HFLAV)			
0.561±0.068±0.095	1.3k	[1] ABDALLAH	06A	DLPH	1992–1995 LEP runs

[1] See footnote to ABDALLAH 06A $\Gamma(\tau^- \to h^- \nu_\tau)/\Gamma_{total}$ measurement for correlations with other measurements.

$\Gamma(h^- h^- h^+ 2\pi^0 \nu_\tau)/\Gamma_{total}$ — Γ_{83}/Γ

$\Gamma_{83}/\Gamma = (0.4247\Gamma_{48}+\Gamma_{85}+0.2302\Gamma_{150}+0.2302\Gamma_{154}+0.892\Gamma_{180})/\Gamma$

VALUE (%)	DOCUMENT ID
0.505±0.031 OUR FIT	(Produced by HFLAV)

$\Gamma(h^- h^- h^+ 2\pi^0 \nu_\tau (\text{ex.} K^0))/\Gamma_{total}$ — Γ_{84}/Γ

$\Gamma_{84}/\Gamma = (\Gamma_{85}+0.2302\Gamma_{150}+0.2302\Gamma_{154}+0.892\Gamma_{180})/\Gamma$

VALUE (%)	EVTS	DOCUMENT ID		TECN	COMMENT
0.495±0.031 OUR FIT		(Produced by HFLAV)			
0.435±0.030±0.035	2.6k	[1] SCHAEL	05C	ALEP	1991-1995 LEP runs
• • • We do not use the following data for averages, fits, limits, etc. • • •					
0.50 ±0.07 ±0.07	1.8k	BUSKULIC	96	ALEP	Repl. by SCHAEL 05C

[1] SCHAEL 05C quote $(0.392 \pm 0.030 \pm 0.035)\%$. We add 0.043% to remove their correction for $\tau^- \to \pi^-\eta\pi^0\nu_\tau \to \pi^-\pi^+\pi^-2\pi^0\nu_\tau$ and $\tau^- \to K^*(892)^-\eta\nu_\tau \to K^-\pi^+\pi^-2\pi^0\nu_\tau$ decays. See footnote to SCHAEL 05C $\Gamma(\tau^- \to e^-\overline{\nu}_e\nu_\tau)/\Gamma_{total}$ measurement for correlations with other measurements.

$\Gamma(h^- h^- h^+ 2\pi^0 \nu_\tau (\text{ex.} K^0))/\Gamma(h^- h^- h^+ \geq 0 \text{ neutrals} \geq 0 K^0_L \nu_\tau)$ — Γ_{84}/Γ_{62}

$\Gamma_{84}/\Gamma_{62} = (\Gamma_{85}+0.2302\Gamma_{150}+0.2302\Gamma_{154}+0.892\Gamma_{180})/(0.34598\Gamma_{36}+0.34598\Gamma_{38}+0.34598\Gamma_{41}+0.34598\Gamma_{43}+0.4247\Gamma_{48}+0.6920\Gamma_{49}+0.8494\Gamma_{52}+0.6920\Gamma_{56}+0.6534\Gamma_{61}+\Gamma_{70}+\Gamma_{78}+\Gamma_{85}+\Gamma_{89}+\Gamma_{97}+\Gamma_{103}+\Gamma_{106}+\Gamma_{107}+0.2805\Gamma_{150}+0.2302\Gamma_{151}+0.2805\Gamma_{152}+0.2805\Gamma_{154}+0.3759\Gamma_{156}+0.3256\Gamma_{160}+0.7259\Gamma_{170}+0.9078\Gamma_{178}+0.9078\Gamma_{179}+0.9078\Gamma_{180}+0.892\Gamma_{182})$

VALUE (units 10^{-2})	EVTS	DOCUMENT ID		TECN	COMMENT
3.26±0.20 OUR FIT		(Produced by HFLAV)			
3.4 ±0.2 ±0.3	668	BORTOLETTO	93	CLEO	$E^{ee}_{cm} \approx 10.6$ GeV

$\Gamma(h^- h^- h^+ 2\pi^0 \nu_\tau (\text{ex.} K^0, \omega, \eta))/\Gamma_{total}$ — Γ_{85}/Γ

VALUE (units 10^{-4})	DOCUMENT ID
10±4 OUR FIT	(Produced by HFLAV)

$\Gamma(h^- h^- h^+ 3\pi^0 \nu_\tau)/\Gamma_{total}$ — $\Gamma_{86}/\Gamma = (0.4247\Gamma_{52}+\Gamma_{87}+0.1131\Gamma_{156})/\Gamma$

VALUE (units 10^{-4})	CL%	EVTS	DOCUMENT ID		TECN	COMMENT
2.13±0.30 OUR FIT			(Produced by HFLAV)			
2.2 ±0.3 ±0.4		139	ANASTASSOV	01	CLEO	$E^{ee}_{cm} = 10.6$ GeV
• • • We do not use the following data for averages, fits, limits, etc. • • •						
< 4.9		95	SCHAEL	05C	ALEP	1991-1995 LEP runs
2.85±0.56±0.51		57	ANDERSON	97	CLEO	Repl. by ANASTASSOV 01
11 ±4 ±5		440	[1] BUSKULIC	96	ALEP	Repl. by SCHAEL 05C

[1] BUSKULIC 96 state their measurement is for $B(h^- h^- h^+ \geq 3\pi^0 \nu_\tau)$. We assume that $B(h^- h^- h^+ \geq 4\pi^0 \nu_\tau)$ is very small.

$\Gamma(2\pi^- \pi^+ 3\pi^0 \nu_\tau (\text{ex.} K^0))/\Gamma_{total}$ — Γ_{87}/Γ

$\Gamma_{87}/\Gamma = (\Gamma_{89}+0.2302\Gamma_{151}+0.3256\Gamma_{160}+0.892\Gamma_{182})/\Gamma$

VALUE (units 10^{-4})	DOCUMENT ID		TECN	COMMENT
1.94±0.30 OUR FIT	(Produced by HFLAV)			
• • • We use the following data for averages but not for fits. • • •				
2.07±0.18±0.37	[1] LEES	12X	BABR	468 fb^{-1} $E^{ee}_{cm} = 10.6$ GeV

[1] Not independent of LEES 12X $\Gamma(\tau^- \to \eta\pi^-\pi^+\pi^-\nu_\tau(\text{ex.} K^0))/\Gamma$, $\Gamma(\tau^- \to \eta\pi^-\pi^0\pi^0\nu_\tau)/\Gamma$, $\Gamma(\tau^- \to \pi^-\omega 2\pi^0\nu_\tau)/\Gamma$, and $\Gamma(\tau^- \to f_1(1285)\pi^-\nu_\tau \to \eta\pi^-\pi^+\pi^-\nu_\tau)/\Gamma$ values.

$\Gamma(2\pi^- \pi^+ 3\pi^0 \nu_\tau (\text{ex.} K^0, \eta, f_1(1285)))/\Gamma_{total}$ — Γ_{88}/Γ

VALUE (units 10^{-4})	DOCUMENT ID		TECN	COMMENT
1.69±0.08±0.43	LEES	12X	BABR	468 fb^{-1} $E^{ee}_{cm} = 10.6$ GeV

$\Gamma(2\pi^- \pi^+ 3\pi^0 \nu_\tau (\text{ex.} K^0, \eta, \omega, f_1(1285)))/\Gamma_{total}$ — Γ_{89}/Γ

VALUE (units 10^{-5})	DOCUMENT ID		TECN	COMMENT
1.4±2.7 OUR FIT	(Produced by HFLAV)			
1.0±0.8±3.0	[1] LEES	12X	BABR	468 fb^{-1} $E^{ee}_{cm} = 10.6$ GeV

[1] LEES 12X meaurement corresponds to the lower limit of $< 5.8 \times 10^{-5}$ at 90% CL.

$\Gamma(K^- h^+ h^- \geq 0 \text{ neutrals} \nu_\tau)/\Gamma_{total}$ — Γ_{90}/Γ

$\Gamma_{90}/\Gamma = (0.34598\Gamma_{38}+0.34598\Gamma_{43}+\Gamma_{97}+\Gamma_{103}+\Gamma_{106}+\Gamma_{107}+0.2805\Gamma_{152}+0.501\Gamma_{170}+0.9078\Gamma_{179})/\Gamma$

VALUE (%)	CL%	DOCUMENT ID		TECN	COMMENT
0.629±0.014 OUR FIT		(Produced by HFLAV)			
<0.6	90	AIHARA	84C	TPC	$E^{ee}_{cm} = 29$ GeV

Int. J. Mod. Phys. A 2026.41. Downloaded from www.worldscientific.com
by UNIVERSITY OF CALIFORNIA @ BERKELEY on 09/16/26. Re-use and distribution is strictly not permitted, except for Open Access articles.

$\Gamma(K^- h^+ \pi^- \nu_\tau (\text{ex.}K^0))/\Gamma_{\text{total}}$ — $\Gamma_{91}/\Gamma = (\Gamma_{97}+\Gamma_{106}+0.0153\Gamma_{179})/\Gamma$

VALUE (%)	DOCUMENT ID
0.437±0.007 OUR FIT (Produced by HFLAV)	

$\Gamma(K^- h^+ \pi^- \nu_\tau (\text{ex.}K^0))/\Gamma(\pi^- \pi^+ \pi^- \nu_\tau (\text{ex.}K^0))$ — Γ_{91}/Γ_{68}

$\Gamma_{91}/\Gamma_{68} = (\Gamma_{97}+\Gamma_{106}+0.0153\Gamma_{179})/(\Gamma_{70}+0.0153\Gamma_{178})$

VALUE (%)	EVTS	DOCUMENT ID		TECN	COMMENT
4.85±0.08 OUR FIT (Produced by HFLAV)					
5.44±0.21±0.53	7.9k	RICHICHI	99	CLEO	E^{ee}_{cm}= 10.6 GeV

$\Gamma(K^- h^+ \pi^- \pi^0 \nu_\tau (\text{ex.}K^0))/\Gamma_{\text{total}}$ — Γ_{92}/Γ

$\Gamma_{92}/\Gamma = (\Gamma_{103}+\Gamma_{107}+0.2302\Gamma_{152}+0.892\Gamma_{179})/\Gamma$

VALUE (units 10^{-4})	DOCUMENT ID
8.6±1.2 OUR FIT (Produced by HFLAV)	

$\Gamma(K^- h^+ \pi^- \pi^0 \nu_\tau (\text{ex.}K^0))/\Gamma(\pi^- \pi^+ \pi^- \pi^0 \nu_\tau (\text{ex.}K^0))$ — Γ_{92}/Γ_{77}

$\Gamma_{92}/\Gamma_{77} = (\Gamma_{103}+\Gamma_{107}+0.2302\Gamma_{152}+0.892\Gamma_{179})/(\Gamma_{78}+0.892\Gamma_{178}+0.0153\Gamma_{180})$

VALUE (%)	EVTS	DOCUMENT ID		TECN	COMMENT
1.91±0.26 OUR FIT (Produced by HFLAV)					
2.61±0.45±0.42	719	RICHICHI	99	CLEO	E^{ee}_{cm}= 10.6 GeV

$\Gamma(K^- \pi^+ \pi^- \geq 0 \text{ neutrals } \nu_\tau)/\Gamma_{\text{total}}$ — Γ_{93}/Γ

$\Gamma_{93}/\Gamma = (0.34598\Gamma_{38}+0.34598\Gamma_{43}+\Gamma_{97}+\Gamma_{103}+0.2805\Gamma_{152}+0.9078\Gamma_{179})/\Gamma$

VALUE (%)	EVTS	DOCUMENT ID		TECN	COMMENT
0.477±0.014 OUR FIT (Produced by HFLAV)					
0.58 $^{+0.15}_{-0.13}$ ±0.12	20	[1] BAUER	94	TPC	E^{ee}_{cm}= 29 GeV
• • • We do not use the following data for averages, fits, limits, etc. • • •					
0.22 $^{+0.16}_{-0.13}$ ±0.05	9	[2] MILLS	85	DLCO	E^{ee}_{cm}= 29 GeV

[1] We multiply 0.58% by 0.20, the relative systematic error quoted by BAUER 94, to obtain the systematic error.

[2] Error correlated with MILLS 85 ($K K \pi \nu$) value. We multiply 0.22% by 0.23, the relative systematic error quoted by MILLS 85, to obtain the systematic error.

$\Gamma(K^- \pi^+ \pi^- \geq 0\pi^0 \nu_\tau (\text{ex.}K^0))/\Gamma_{\text{total}}$ — Γ_{94}/Γ

$\Gamma_{94}/\Gamma = (\Gamma_{97}+\Gamma_{103}+0.2302\Gamma_{152}+0.9078\Gamma_{179})/\Gamma$

VALUE (%)	DOCUMENT ID		TECN	COMMENT
0.373±0.013 OUR FIT (Produced by HFLAV)				
0.30 ±0.05 OUR AVERAGE				
• • • We use the following data for averages but not for fits. • • •				
0.343±0.073±0.031	ABBIENDI	00D	OPAL	1990–1995 LEP runs
0.275±0.064	[1] BARATE	98	ALEP	1991–1995 LEP runs

[1] Not independent of BARATE 98 $\Gamma(\tau^- \to K^- \pi^+ \pi^- \nu_\tau)/\Gamma_{\text{total}}$ and $\Gamma(\tau^- \to K^- \pi^+ \pi^- \pi^0 \nu_\tau)/\Gamma_{\text{total}}$ values.

$\Gamma(K^- \pi^+ \pi^- \nu_\tau)/\Gamma_{\text{total}}$ — $\Gamma_{95}/\Gamma = (0.34598\Gamma_{38}+\Gamma_{97}+0.0153\Gamma_{179})/\Gamma$

VALUE (%)	DOCUMENT ID
0.345±0.007 OUR FIT (Produced by HFLAV)	

$\Gamma(K^- \pi^+ \pi^- \nu_\tau (\text{ex.}K^0))/\Gamma_{\text{total}}$ — $\Gamma_{96}/\Gamma = (\Gamma_{97}+0.0153\Gamma_{179})/\Gamma$

VALUE (%)	EVTS	DOCUMENT ID		TECN	COMMENT
0.293±0.007 OUR FIT (Produced by HFLAV)					
0.290±0.018 OUR AVERAGE Error includes scale factor of 2.4. See the ideogram below.					
0.330±0.001 $^{+0.016}_{-0.017}$	794k	[1] LEE	10	BELL	666 fb^{-1} E^{ee}_{cm}=10.6 GeV
0.273±0.002±0.009	70k	[2] AUBERT	08	BABR	342 fb^{-1} E^{ee}_{cm}=10.6 GeV
0.415±0.053±0.040	269	ABBIENDI	04J	OPAL	1991–1995 LEP runs
0.384±0.014±0.038	3.5k	[3] BRIERE	03	CLE3	E^{ee}_{cm}= 10.6 GeV
0.214±0.037±0.029		BARATE	98	ALEP	1991–1995 LEP runs
• • • We use the following data for averages but not for fits. • • •					
0.346±0.023±0.056	158	[4] RICHICHI	99	CLEO	E^{ee}_{cm}= 10.6 GeV
• • • We do not use the following data for averages, fits, limits, etc. • • •					
0.360±0.082±0.048		ABBIENDI	00D	OPAL	1990–1995 LEP runs

[1] See footnote to LEE 10 $\Gamma(\tau^- \to \pi^- \pi^+ \pi^- \nu_\tau(\text{ex.}K^0))/\Gamma_{\text{total}}$ measurement for correlations with other measurements. Not independent of LEE 10 $\Gamma(\tau^- \to K^- \pi^+ \pi^- \nu_\tau(\text{ex.}K^0))/\Gamma(\tau^- \to \pi^- \pi^+ \pi^- \nu_\tau(\text{ex.}K^0))$ value.

[2] See footnote to AUBERT 08 $\Gamma(\tau^- \to \pi^- \pi^+ \pi^- \nu_\tau(\text{ex.}K^0))/\Gamma_{\text{total}}$ measurement for correlations with other measurements.

[3] 47% correlated with BRIERE 03 $\tau^- \to \pi^- \pi^+ \pi^- \nu_\tau$ and 34% correlated with $\tau^- \to K^- K^+ \pi^- \nu_\tau$ because of a common 5% normalization error.

[4] Not independent of RICHICHI 99 $\Gamma(\tau^- \to K^- h^+ \pi^- \nu_\tau(\text{ex.}K^0))/\Gamma(\tau^- \to \pi^- \pi^+ \pi^- \nu_\tau(\text{ex.}K^0))$, $\Gamma(\tau^- \to K^- K^+ \pi^- \nu_\tau)/\Gamma(\tau^- \to \pi^- \pi^+ \pi^- \nu_\tau(\text{ex.}K^0))$ and BALEST 95C $\Gamma(\tau^- \to h^- h^- h^+ \nu_\tau(\text{ex.}K^0))/\Gamma_{\text{total}}$ values.

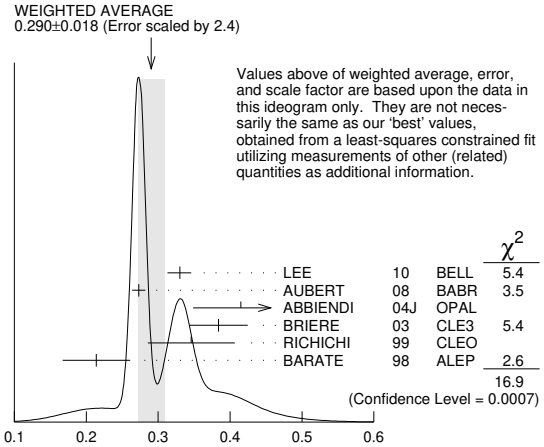

$\Gamma(K^- \pi^+ \pi^- \nu_\tau (\text{ex.}K^0))/\Gamma(\pi^- \pi^+ \pi^- \nu_\tau (\text{ex.}K^0))$ — Γ_{96}/Γ_{68}

$\Gamma_{96}/\Gamma_{68} = (\Gamma_{97}+0.0153\Gamma_{179})/(\Gamma_{70}+0.0153\Gamma_{178})$

VALUE (units 10^{-2})	EVTS	DOCUMENT ID		TECN	COMMENT
3.25±0.07 OUR FIT (Produced by HFLAV)					
• • • We use the following data for averages but not for fits. • • •					
3.92±0.02 $^{+0.15}_{-0.16}$	794k	[1] LEE	10	BELL	666 fb^{-1} E^{ee}_{cm} = 10.6 GeV

[1] Not independent of LEE 10 $\Gamma(\tau^- \to K^- \pi^+ \pi^- \nu_\tau(\text{ex.}K^0))/\Gamma_{\text{total}}$ and $\Gamma(\tau^- \to \pi^- \pi^+ \pi^- \nu_\tau(\text{ex.}K^0))/\Gamma_{\text{total}}$ values.

$\Gamma(K^- \pi^+ \pi^- \nu_\tau (\text{ex.}K^0,\omega))/\Gamma_{\text{total}}$ — Γ_{97}/Γ

VALUE (units 10^{-3})	DOCUMENT ID
2.93±0.07 OUR FIT (Produced by HFLAV)	

$\Gamma(K^- \rho^0 \nu_\tau \to K^- \pi^+ \pi^- \nu_\tau)/\Gamma(K^- \pi^+ \pi^- \nu_\tau (\text{ex.}K^0))$ — Γ_{98}/Γ_{96}

VALUE	DOCUMENT ID		TECN	COMMENT
0.48±0.14±0.10	[1] ASNER	00B	CLEO	E^{ee}_{cm}= 10.6 GeV
• • • We do not use the following data for averages, fits, limits, etc. • • •				
0.39±0.14	[2] BARATE	99R	ALEP	1991–1995 LEP runs

[1] ASNER 00B assume $\tau^- \to K^- \pi^+ \pi^- \nu_\tau$ (ex. K^0) decays proceed only through $K\rho$ and $K^*\pi$ intermediate states. They assume the resonance structure of $\tau^- \to K^- \pi^+ \pi^- \nu_\tau$ (ex. K^0) decays is dominated by $K_1(1270)^-$ and $K_1(1400)^-$ resonances, and assume $B(K_1(1270) \to K^*(892)\pi) = (16 \pm 5)\%$, $B(K_1(1270) \to K\rho) = (42 \pm 6)\%$, and $B(K_1(1400) \to K\rho) = 0$.

[2] BARATE 99R assume $\tau^- \to K^- \pi^+ \pi^- \nu_\tau$ (ex. K^0) decays proceed only through $K\rho$ and $K^*\pi$ intermediate states. The quoted error is statistical only.

$\Gamma(K^- \pi^+ \pi^- \pi^0 \nu_\tau)/\Gamma_{\text{total}}$ — Γ_{99}/Γ

$\Gamma_{99}/\Gamma = (0.34598\Gamma_{43}+\Gamma_{103}+0.2302\Gamma_{152}+0.892\Gamma_{179})/\Gamma$

VALUE (units 10^{-4})	DOCUMENT ID
13.1±1.2 OUR FIT (Produced by HFLAV)	

$\Gamma(K^- \pi^+ \pi^- \pi^0 \nu_\tau (\text{ex.}K^0))/\Gamma_{\text{total}}$ — Γ_{100}/Γ

$\Gamma_{100}/\Gamma = (\Gamma_{103}+0.2302\Gamma_{152}+0.892\Gamma_{179})/\Gamma$

VALUE (units 10^{-4})	CL%	DOCUMENT ID		TECN	COMMENT
8.0±1.2 OUR FIT (Produced by HFLAV)					
7.3±1.2 OUR AVERAGE					
7.4±0.8±1.1		[1] ARMS	05	CLE3	7.6 fb^{-1}, E^{ee}_{cm}= 10.6 GeV
6.1±3.9±1.8		BARATE	98	ALEP	1991–1995 LEP runs
• • • We use the following data for averages but not for fits. • • •					
7.5±2.6±1.8		[2] RICHICHI	99	CLEO	E^{ee}_{cm}= 10.6 GeV
• • • We do not use the following data for averages, fits, limits, etc. • • •					
<17	95	ABBIENDI	00D	OPAL	1990–1995 LEP runs

[1] Not independent of ARMS 05 $\Gamma(\tau^- \to K^- \pi^+ \pi^- \pi^0 \nu_\tau(\text{ex.}K^0,\omega))$ / Γ_{total} and $\Gamma(\tau^- \to K^- \omega \nu_\tau)$ / Γ_{total} values.

[2] Not independent of RICHICHI 99 $\Gamma(\tau^- \to K^- h^+ \pi^- \nu_\tau(\text{ex.}K^0))/\Gamma(\tau^- \to \pi^- \pi^+ \pi^- \nu_\tau(\text{ex.}K^0))$, $\Gamma(\tau^- \to K^- K^+ \pi^- \nu_\tau)/\Gamma(\tau^- \to \pi^- \pi^+ \pi^- \nu_\tau(\text{ex.}K^0))$ and BALEST 95C $\Gamma(\tau^- \to h^- h^- h^+ \nu_\tau(\text{ex.}K^0))/\Gamma_{\text{total}}$ values.

$\Gamma(K^- \pi^+ \pi^- \pi^0 \nu_\tau (\text{ex.}K^0,\eta))/\Gamma_{\text{total}}$ — $\Gamma_{101}/\Gamma = (\Gamma_{103}+0.892\Gamma_{179})/\Gamma$

VALUE (units 10^{-4})	DOCUMENT ID
7.6±1.2 OUR FIT (Produced by HFLAV)	

Int. J. Mod
by UNIVERSITY OF CALIFORNIA @ BERK
wnloaded from www.worldscientific.com
-use and distribution is strictly not permitted, except for Open Access articles.

$\Gamma(K^-\pi^+\pi^-\pi^0\nu_\tau(\text{ex.}K^0,\omega))/\Gamma_{\text{total}}$ — Γ_{102}/Γ

VALUE (units 10^{-4})	EVTS	DOCUMENT ID		TECN	COMMENT
3.7±0.5±0.8	833	ARMS	05	CLE3	7.6 fb^{-1}, E^{ee}_{cm}= 10.6 GeV

$\Gamma(K^-\pi^+\pi^-\pi^0\nu_\tau(\text{ex.}K^0,\omega,\eta))/\Gamma_{\text{total}}$ — Γ_{103}/Γ

VALUE (units 10^{-4})	DOCUMENT ID
3.9±1.4 OUR FIT (Produced by HFLAV)	

$\Gamma(K^-\pi^+K^- \geq 0 \text{ neut. } \nu_\tau)/\Gamma_{\text{total}}$ — Γ_{104}/Γ

VALUE (%)	CL%	DOCUMENT ID		TECN	COMMENT
<0.09	95	BAUER	94	TPC	E^{ee}_{cm}= 29 GeV

$\Gamma(K^-K^+\pi^- \geq 0 \text{ neut. } \nu_\tau)/\Gamma_{\text{total}}$ — $\Gamma_{105}/\Gamma = (\Gamma_{106}+\Gamma_{107})/\Gamma$

VALUE (%)	EVTS	DOCUMENT ID		TECN	COMMENT
0.1496±0.0033 OUR FIT (Produced by HFLAV)					
0.203 ±0.031 OUR AVERAGE					
0.159 ±0.053 ±0.020		ABBIENDI	00D	OPAL	1990–1995 LEP runs
0.15 $^{+0.09}_{-0.07}$ ±0.03	4	[1] BAUER	94	TPC	E^{ee}_{cm}= 29 GeV
• • • We use the following data for averages but not for fits. • • •					
0.238 ±0.042		[2] BARATE	98	ALEP	1991–1995 LEP runs

[1] We multiply 0.15% by 0.20, the relative systematic error quoted by BAUER 94, to obtain the systematic error.
[2] Not independent of BARATE 98 $\Gamma(\tau^- \to K^-K^+\pi^-\nu_\tau)/\Gamma_{\text{total}}$ and $\Gamma(\tau^- \to K^-K^+\pi^-\pi^0\nu_\tau)/\Gamma_{\text{total}}$ values.

$\Gamma(K^-K^+\pi^-\nu_\tau)/\Gamma_{\text{total}}$ — Γ_{106}/Γ

VALUE (units 10^{-3})	EVTS	DOCUMENT ID		TECN	COMMENT
1.435±0.027 OUR FIT (Produced by HFLAV)					
1.43 ±0.07 OUR AVERAGE Error includes scale factor of 2.4. See the ideogram below.					
1.55 ±0.01 $^{+0.06}_{-0.05}$	108k	[1] LEE	10	BELL	666 fb^{-1} E^{ee}_{cm}=10.6 GeV
1.346±0.010±0.036	18k	[2] AUBERT	08	BABR	342 fb^{-1} E^{ee}_{cm}= 10.6 GeV
1.55 ±0.06 ±0.09	932	[3] BRIERE	03	CLE3	E^{ee}_{cm}= 10.6 GeV
1.63 ±0.21 ±0.17		BARATE	98	ALEP	1991–1995 LEP runs
• • • We use the following data for averages but not for fits. • • •					
0.87 ±0.56 ±0.40		ABBIENDI	00D	OPAL	1990–1995 LEP runs
1.45 ±0.13 ±0.28	2.3k	[4] RICHICHI	99	CLEO	E^{ee}_{cm}= 10.6 GeV
• • • We do not use the following data for averages, fits, limits, etc. • • •					
2.2 $^{+1.7}_{-1.1}$ ±0.5	9	[5] MILLS	85	DLCO	E^{ee}_{cm}= 29 GeV

[1] See footnote to LEE 10 $\Gamma(\tau^- \to \pi^-\pi^+\pi^-\nu_\tau(\text{ex.}K^0))/\Gamma_{\text{total}}$ measurement for correlations with other measurements. Not independent of LEE 10 $\Gamma(\tau^- \to K^-K^+\pi^-\nu_\tau)/\Gamma(\tau^- \to \pi^-\pi^+\pi^-\nu_\tau(\text{ex.}K^0))$ value.
[2] See footnote to AUBERT 08 $\Gamma(\tau^- \to \pi^-\pi^+\pi^-\nu_\tau(\text{ex.}K^0))/\Gamma_{\text{total}}$ measurement for correlations with other measurements.
[3] 71% correlated with BRIERE 03 $\tau^- \to \pi^-\pi^+\pi^-\nu_\tau$ and 34% correlated with $\tau \to K^-\pi^+\pi^-\nu_\tau$ because of a common 5% normalization error.
[4] Not independent of RICHICHI 99 $\Gamma(\tau^- \to K^-K^+\pi^-\nu_\tau)/\Gamma(\tau^- \to \pi^-\pi^+\pi^-\nu_\tau(\text{ex.}K^0))$ and BALEST 95C $\Gamma(\tau^- \to h^-h^-h^+\nu_\tau(\text{ex.}K^0))/\Gamma_{\text{total}}$ values.
[5] Error correlated with MILLS 85 ($K\pi\pi\pi^0\nu$) value. We multiply 0.22% by 0.23, the relative systematic error quoted by MILLS 85, to obtain the systematic error.

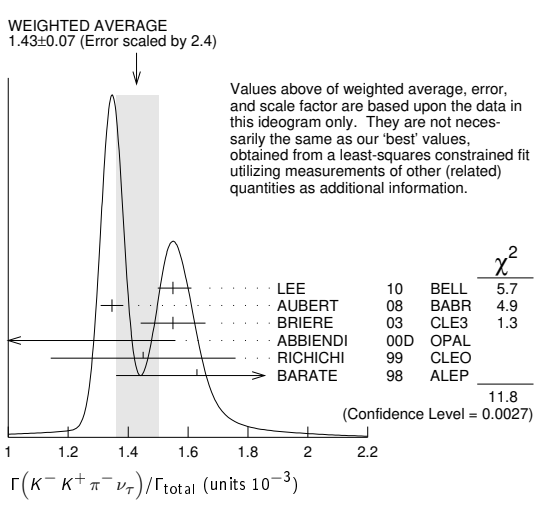

$\Gamma(K^-K^+\pi^-\nu_\tau)/\Gamma(\pi^-\pi^+\pi^-\nu_\tau(\text{ex.}K^0))$ — Γ_{106}/Γ_{68}

$\Gamma_{106}/\Gamma_{68} = \Gamma_{106}/(\Gamma_{70}+0.0153\Gamma_{178})$

VALUE (%)	EVTS	DOCUMENT ID		TECN	COMMENT
1.592±0.030 OUR FIT (Produced by HFLAV)					
1.83 ±0.05 OUR AVERAGE					
1.60 ±0.15 ±0.30	2.3k	RICHICHI	99	CLEO	E^{ee}_{cm}= 10.6 GeV
• • • We use the following data for averages but not for fits. • • •					
1.84 ±0.01 ±0.05	108k	[1] LEE	10	BELL	666 fb^{-1} E^{ee}_{cm}= 10.6 GeV

[1] Not independent of LEE 10 $\Gamma(\tau^- \to K^-K^+\pi^-\nu_\tau)/\Gamma_{\text{total}}$ and $\Gamma(\tau^- \to \pi^-\pi^+\pi^-\nu_\tau(\text{ex.}K^0))/\Gamma_{\text{total}}$ values.

$\Gamma(K^-K^+\pi^-\pi^0\nu_\tau)/\Gamma_{\text{total}}$ — Γ_{107}/Γ

VALUE (units 10^{-4})	CL%	EVTS	DOCUMENT ID		TECN	COMMENT
0.61±0.18 OUR FIT (Produced by HFLAV)						
0.60±0.18 OUR AVERAGE						
0.55±0.14±0.12		48	ARMS	05	CLE3	7.6 fb^{-1},E^{ee}_{cm}=10.6 GeV
7.5 ±2.9 ±1.5			BARATE	98	ALEP	1991–1995 LEP runs
• • • We use the following data for averages but not for fits. • • •						
3.3 ±1.8 ±0.7		158	[1] RICHICHI	99	CLEO	E^{ee}_{cm}= 10.6 GeV
• • • We do not use the following data for averages, fits, limits, etc. • • •						
<27	95		ABBIENDI	00D	OPAL	1990–1995 LEP runs

[1] Not independent of RICHICHI 99 $\Gamma(\tau^- \to K^-K^+\pi^-\nu_\tau)/\Gamma(\tau^- \to \pi^-\pi^+\pi^-\nu_\tau(\text{ex.}K^0))$ and BALEST 95C $\Gamma(\tau^- \to h^-h^-h^+\nu_\tau(\text{ex.}K^0))/\Gamma_{\text{total}}$ values.

$\Gamma(K^-K^+\pi^-\pi^0\nu_\tau)/\Gamma(\pi^-\pi^+\pi^-\pi^0\nu_\tau(\text{ex.}K^0))$ — Γ_{107}/Γ_{77}

$\Gamma_{107}/\Gamma_{77} = \Gamma_{107}/(\Gamma_{78}+0.892\Gamma_{178}+0.0153\Gamma_{180})$

VALUE (%)	EVTS	DOCUMENT ID		TECN	COMMENT
0.14±0.04 OUR FIT (Produced by HFLAV)					
0.79±0.44±0.16	158	[1] RICHICHI	99	CLEO	E^{ee}_{cm}= 10.6 GeV

[1] RICHICHI 99 also quote a 95%CL upper limit of 0.0157 for this measurement.

$\Gamma(K^-K^+K^-\nu_\tau)/\Gamma_{\text{total}}$ — $\Gamma_{108}/\Gamma = 0.501\Gamma_{170}/\Gamma$

VALUE (units 10^{-5})	CL%	EVTS	DOCUMENT ID		TECN	COMMENT
2.2 ±0.8 OUR FIT Error includes scale factor of 5.4. (Produced by HFLAV)						
2.1 ±0.8 OUR AVERAGE Error includes scale factor of 5.4.						
3.29±0.17 $^{+0.19}_{-0.20}$		3.2k	[1] LEE	10	BELL	666 fb^{-1} E^{ee}_{cm} = 10.6 GeV
1.58±0.13±0.12		275	[2] AUBERT	08	BABR	342 fb^{-1} E^{ee}_{cm}= 10.6 GeV
• • • We do not use the following data for averages, fits, limits, etc. • • •						
< 3.7	90		BRIERE	03	CLE3	E^{ee}_{cm}= 10.6 GeV
< 19	90		BARATE	98	ALEP	1991–1995 LEP runs

[1] See footnote to LEE 10 $\Gamma(\tau^- \to \pi^-\pi^+\pi^-\nu_\tau(\text{ex.}K^0))/\Gamma_{\text{total}}$ measurement for correlations with other measurements. Not independent of LEE 10 $\Gamma(\tau^- \to K^-K^+K^-\nu_\tau)/\Gamma(\tau^- \to \pi^-\pi^+\pi^-\nu_\tau(\text{ex.}K^0))$ value.
[2] See footnote to AUBERT 08 $\Gamma(\tau^- \to \pi^-\pi^+\pi^-\nu_\tau(\text{ex.}K^0))/\Gamma_{\text{total}}$ measurement for correlations with other measurements.

$\Gamma(K^-K^+K^-\nu_\tau)/\Gamma(\pi^-\pi^+\pi^-\nu_\tau(\text{ex.}K^0))$ — Γ_{108}/Γ_{68}

VALUE (units 10^{-4})	EVTS	DOCUMENT ID		TECN	COMMENT
• • • We do not use the following data for averages, fits, limits, etc. • • •					
3.90±0.02 $^{+0.22}_{-0.23}$	3.2k	[1] LEE	10	BELL	666 fb^{-1} E^{ee}_{cm} = 10.6 GeV

[1] Not independent of LEE 10 $\Gamma(\tau^- \to K^-K^+K^-\nu_\tau)/\Gamma_{\text{total}}$ and $\Gamma(\tau^- \to \pi^-\pi^+\pi^-\nu_\tau(\text{ex.}K^0))/\Gamma_{\text{total}}$ values.

$\Gamma(K^-K^+K^-\nu_\tau(\text{ex. }\phi))/\Gamma_{\text{total}}$ — Γ_{109}/Γ

VALUE	CL%	DOCUMENT ID		TECN	COMMENT
<2.5 × 10^{-6}	90	AUBERT	08	BABR	342 fb^{-1} E^{ee}_{cm} = 10.6 GeV

$\Gamma(K^-K^+K^-\pi^0\nu_\tau)/\Gamma_{\text{total}}$ — Γ_{110}/Γ

VALUE	CL%	DOCUMENT ID		TECN	COMMENT
<4.8 × 10^{-6}	90	ARMS	05	CLE3	7.6 fb^{-1}, E^{ee}_{cm}= 10.6 GeV

$\Gamma(\pi^-K^+\pi^- \geq 0 \text{ neut. } \nu_\tau)/\Gamma_{\text{total}}$ — Γ_{111}/Γ

VALUE (%)	CL%	DOCUMENT ID		TECN	COMMENT
<0.25	95	BAUER	94	TPC	E^{ee}_{cm}= 29 GeV

$\Gamma(e^-e^-e^+\overline{\nu}_e\nu_\tau)/\Gamma_{\text{total}}$ — Γ_{112}/Γ

VALUE (units 10^{-5})	EVTS	DOCUMENT ID		TECN	COMMENT
2.8±1.4±0.4	5	ALAM	96	CLEO	E^{ee}_{cm}= 10.6 GeV

$\Gamma(\mu^-e^-e^+\overline{\nu}_\mu\nu_\tau)/\Gamma_{\text{total}}$ — Γ_{113}/Γ

VALUE (units 10^{-5})	CL%	DOCUMENT ID		TECN	COMMENT
<3.2	90	ALAM	96	CLEO	E^{ee}_{cm}= 10.6 GeV

$\Gamma(\pi^-e^-e^+\nu_\tau)/\Gamma_{\text{total}}$ — Γ_{114}/Γ

VALUE (units 10^{-5})	EVTS	DOCUMENT ID		TECN	COMMENT
seen	400	[1] JIN	19	BELL	562 fb^{-1}, E^{ee}_{cm} = 10.6 GeV
• • • We do not use the following data for averages, fits, limits, etc. • • •					
1.46±0.13±0.21	400	[1] JIN	19	BELL	axial-vector, 562 fb^{-1}, E^{ee}_{cm} = 10.6 GeV
3.01±0.27±0.43	400	[1] JIN	19	BELL	vector, 562 fb^{-1}, E^{ee}_{cm} = 10.6 GeV

[1] JIN 19 measures $B(\tau^- \to \pi^-e^-e^+\nu_\tau(\ m_{\pi^-e^-e^+} > 1.05\,\text{GeV}/c^2)) = (5.90 \pm 0.53 \pm 0.86) \times 10^{-6}$, which is only sensitive to the structure-dependent contribution, and assumes that the decay proceeds with either a pure axial-vector current or a pure vector current to obtain the two respective branching fraction measurements for this mode, which are 100% correlated.

Int. J. Mod. Phys. A 2026.41. Downloaded from www.worldscientific.com
by UNIVERSITY OF CALIFORNIA @ BERKELEY on 09/16/26. Re-use and distribution is strictly not permitted, except for Open Access articles.

$\Gamma(\pi^- \mu^- \mu^+ \nu_\tau)/\Gamma_{total}$ — Γ_{115}/Γ

VALUE	CL%	DOCUMENT ID		TECN	COMMENT
$<1.14 \times 10^{-5}$	90	JIN	19	BELL	562 fb^{-1}, E^{ee}_{cm} = 10.6 GeV

$\Gamma(3h^- 2h^+ \geq 0$ neutrals ν_τ (ex. $K^0_S \to \pi^- \pi^+$)("5-prong"))$/\Gamma_{total}$ — Γ_{116}/Γ

$\Gamma_{116}/\Gamma = (\Gamma_{117}+\Gamma_{123})/\Gamma$

VALUE (%)	EVTS	DOCUMENT ID		TECN	COMMENT
0.099±0.004 OUR FIT (Produced by HFLAV)					
0.107±0.007 OUR AVERAGE Error includes scale factor of 1.1.					
0.170±0.022±0.026		[1] ACHARD	01D	L3	1992–1995 LEP runs
0.097±0.005±0.011	419	GIBAUT	94B	CLEO	E^{ee}_{cm} = 10.6 GeV
0.102±0.029	13	BYLSMA	87	HRS	E^{ee}_{cm} = 29 GeV
• • • We use the following data for averages but not for fits. • • •					
0.093±0.009±0.012		SCHAEL	05C	ALEP	1991–1995 LEP runs
0.115±0.013±0.006	112	[2] ABREU	01M	DLPH	1992–1995 LEP runs
0.119±0.013±0.008	119	[3] ACKERSTAFF	99E	OPAL	1991–1995 LEP runs
• • • We do not use the following data for averages, fits, limits, etc. • • •					
0.26 ±0.06 ±0.05		ACTON	92H	OPAL	E^{ee}_{cm} = 88.2–94.2 GeV
0.10 $^{+0.05}_{-0.04}$ ±0.03		DECAMP	92C	ALEP	1989–1990 LEP runs
0.16 ±0.13 ±0.04		BEHREND	89B	CELL	E^{ee}_{cm} = 14–47 GeV
0.3 ±0.1 ±0.2		BARTEL	85F	JADE	E^{ee}_{cm} = 34.6 GeV
0.13 ±0.04	10	BELTRAMI	85	HRS	Repl. by BYLSMA 87
0.16 ±0.08 ±0.04	4	BURCHAT	85	MRK2	E^{ee}_{cm} = 29 GeV
1.0 ±0.4	10	BEHREND	82	CELL	Repl. by BEHREND 89B

[1] The correlation coefficients between this measurement and the ACHARD 01D measurements of B($\tau \to$ "1-prong") and B($\tau \to$ "3-prong") are −0.082 and −0.19 respectively.
[2] The correlation coefficients between this measurement and the ABREU 01M measurements of B($\tau \to$ 1-prong) and B($\tau \to$ 3-prong) are −0.08 and −0.08 respectively.
[3] Not independent of ACKERSTAFF 99E B($\tau^- \to 3h^- 2h^+ \nu_\tau$(ex. K^0)) and B($\tau^- \to 3h^- 2h^+ \pi^0 \nu_\tau$(ex. K^0)) measurements.

$\Gamma(3h^- 2h^+ \nu_\tau$(ex.$K^0$))$/\Gamma_{total}$ — $\Gamma_{117}/\Gamma = (\Gamma_{118}+\Gamma_{120}+0.0153\Gamma_{185})/\Gamma$

VALUE (units 10^{-4})	EVTS	DOCUMENT ID		TECN	COMMENT
8.29±0.31 OUR FIT (Produced by HFLAV)					
8.32±0.35 OUR AVERAGE					
9.7 ±1.5 ±0.5	96	[1] ABDALLAH	06A	DLPH	1992–1995 LEP runs
7.2 ±0.9 ±1.2	165	[2] SCHAEL	05C	ALEP	1991–1995 LEP runs
9.1 ±1.4 ±0.6	97	ACKERSTAFF	99E	OPAL	1991–1995 LEP runs
7.7 ±0.5 ±0.9	295	GIBAUT	94B	CLEO	E^{ee}_{cm} = 10.6 GeV
6.4 ±2.3 ±1.0	12	ALBRECHT	88B	ARG	E^{ee}_{cm} = 10 GeV
5.1 ±2.0	7	BYLSMA	87	HRS	E^{ee}_{cm} = 29 GeV
• • • We use the following data for averages but not for fits. • • •					
8.56±0.05±0.42	34k	AUBERT,B	05W	BABR	232 fb^{-1}, E^{ee}_{cm} = 10.6 GeV
• • • We do not use the following data for averages, fits, limits, etc. • • •					
8.0 ±1.1 ±1.3	58	BUSKULIC	96	ALEP	Repl. by SCHAEL 05C
6.7 ±3.0	5	[3] BELTRAMI	85	HRS	Repl. by BYLSMA 87

[1] See footnote to ABDALLAH 06A $\Gamma(\tau^- \to h^- \nu_\tau)/\Gamma_{total}$ measurement for correlations with other measurements.
[2] See footnote to SCHAEL 05C $\Gamma(\tau^- \to e^- \overline{\nu}_e \nu_\tau)/\Gamma_{total}$ measurement for correlations with other measurements.
[3] The error quoted is statistical only.

$\Gamma(3\pi^- 2\pi^+ \nu_\tau$(ex.$K^0, \omega$))$/\Gamma_{total}$ — $\Gamma_{118}/\Gamma = (\Gamma_{119}+\Gamma_{173})/\Gamma$

VALUE (units 10^{-4})	DOCUMENT ID		TECN	COMMENT
8.27±0.31 OUR FIT (Produced by HFLAV)				
• • • We use the following data for averages but not for fits. • • •				
8.33±0.04±0.43	[1] LEES	12X	BABR	468 fb^{-1} E^{ee}_{cm} = 10.6 GeV

[1] Not independent of LEES 12X $\Gamma(\tau^- \to f_1(1285)\pi^- \nu_\tau \to 3\pi^- 2\pi^+ \nu_\tau)/\Gamma$ and $\Gamma(\tau^- \to 3\pi^- 2\pi^+ \nu_\tau$(ex.$K^0, \omega, f_1(1285)$))$/\Gamma$ values.

$\Gamma(3\pi^- 2\pi^+ \nu_\tau$(ex.$K^0, \omega, f_1(1285)$))$/\Gamma_{total}$ — Γ_{119}/Γ

VALUE (units 10^{-4})	EVTS	DOCUMENT ID		TECN	COMMENT
7.75±0.30 OUR FIT (Produced by HFLAV)					
7.68±0.04±0.40	69k	LEES	12X	BABR	468 fb^{-1} E^{ee}_{cm} = 10.6 GeV

$\Gamma(K^- 2\pi^- 2\pi^+ \nu_\tau$(ex.$K^0$))$/\Gamma_{total}$ — Γ_{120}/Γ

VALUE (units 10^{-6})	DOCUMENT ID		TECN	COMMENT
0.6±1.2 OUR FIT (Produced by HFLAV)				
0.6±0.5±1.1	[1] LEES	12X	BABR	468 fb^{-1} E^{ee}_{cm} = 10.6 GeV

[1] LEES 12X meaurement corresponds to the lower limit of $< 2.4 \times 10^{-6}$ at 90% CL.

$\Gamma(K^+ 3\pi^- \pi^+ \nu_\tau)/\Gamma_{total}$ — Γ_{121}/Γ

VALUE	CL%	DOCUMENT ID		TECN	COMMENT
$<5.0 \times 10^{-6}$	90	LEES	12X	BABR	468 fb^{-1} E^{ee}_{cm} = 10.6 GeV

$\Gamma(K^+ K^- 2\pi^- \pi^+ \nu_\tau)/\Gamma_{total}$ — Γ_{122}/Γ

VALUE	CL%	DOCUMENT ID		TECN	COMMENT
$<4.5 \times 10^{-7}$	90	LEES	12X	BABR	468 fb^{-1} E^{ee}_{cm} = 10.6 GeV

$\Gamma(3h^- 2h^+ \pi^0 \nu_\tau$(ex.$K^0$))$/\Gamma_{total}$ — $\Gamma_{123}/\Gamma = (\Gamma_{124}+\Gamma_{127})/\Gamma$

VALUE (units 10^{-4})	EVTS	DOCUMENT ID		TECN	COMMENT
1.65±0.11 OUR FIT (Produced by HFLAV)					
1.74±0.27 OUR AVERAGE					
1.6 ±1.2 ±0.6	13	[1] ABDALLAH	06A	DLPH	1992–1995 LEP runs
2.1 ±0.7 ±0.9	95	[2] SCHAEL	05C	ALEP	1991–1995 LEP runs
1.7 ±0.2 ±0.2	231	ANASTASSOV	01	CLEO	E^{ee}_{cm} = 10.6 GeV
2.7 ±1.8 ±0.9	23	ACKERSTAFF	99E	OPAL	1991–1995 LEP runs
• • • We do not use the following data for averages, fits, limits, etc. • • •					
1.8 ±0.7 ±1.2	18	BUSKULIC	96	ALEP	Repl. by SCHAEL 05C
1.9 ±0.4 ±0.4	31	GIBAUT	94B	CLEO	Repl. by ANASTASSOV 01
5.1 ±2.2	6	BYLSMA	87	HRS	E^{ee}_{cm} = 29 GeV
6.7 ±3.0	5	[3] BELTRAMI	85	HRS	Repl. by BYLSMA 87

[1] See footnote to ABDALLAH 06A $\Gamma(\tau^- \to h^- \nu_\tau)/\Gamma_{total}$ measurement for correlations with other measurements.
[2] SCHAEL 05C quote $(1.4 \pm 0.7 \pm 0.9) \times 10^{-4}$. We add 0.7×10^{-4} to remove their correction for $\tau^- \to \eta\pi^-\pi^+\pi^-\nu_\tau \to 3\pi^- 2\pi^+ \pi^0 \nu_\tau$ and $\tau^- \to K^*(892)^- \eta \nu_\tau \to 3\pi^- 2\pi^+ \pi^0 \nu_\tau$ decays. See footnote to SCHAEL 05C $\Gamma(\tau^- \to e^- \overline{\nu}_e \nu_\tau)/\Gamma_{total}$ measurement for correlations with other measurements.
[3] The error quoted is statistical only.

$\Gamma(3\pi^- 2\pi^+ \pi^0 \nu_\tau$(ex.$K^0$))$/\Gamma_{total}$ — Γ_{124}/Γ

$\Gamma_{124}/\Gamma = (\Gamma_{126}+0.2302\Gamma_{160}+0.892\Gamma_{185})/\Gamma$

VALUE (units 10^{-4})	DOCUMENT ID		TECN	COMMENT
1.64±0.11 OUR FIT (Produced by HFLAV)				
• • • We use the following data for averages but not for fits. • • •				
1.65±0.05±0.09	[1] LEES	12X	BABR	468 fb^{-1} E^{ee}_{cm} = 10.6 GeV

[1] Not independent of LEES 12X measurements of $\Gamma(\tau^- \to 2\pi^-\pi^+\omega\nu_\tau$(ex.$K^0$))$/\Gamma$, $\Gamma(\tau^- \to \eta\pi^-\pi^+\pi^-\nu_\tau$(ex.$K^0$))$/\Gamma$, and $\Gamma(\tau^- \to 3\pi^- 2\pi^+ \pi^0 \nu_\tau$(ex.$K^0, \eta, \omega, f_1(1285)$))$/\Gamma$.

$\Gamma(3\pi^- 2\pi^+ \pi^0 \nu_\tau$(ex.$K^0, \eta, f_1(1285)$))$/\Gamma_{total}$ — Γ_{125}/Γ

VALUE (units 10^{-4})	DOCUMENT ID		TECN	COMMENT
1.11±0.04±0.09	[1] LEES	12X	BABR	468 fb^{-1} E^{ee}_{cm} = 10.6 GeV

[1] Not independent of LEES 12X $\Gamma(\tau^- \to 2\pi^-\pi^+\omega\nu_\tau$(ex.$K^0$))$/\Gamma$ and $\Gamma(\tau^- \to 3\pi^- 2\pi^+ \pi^0 \nu_\tau$(ex.$K^0, \eta, \omega, f_1(1285)$))$/\Gamma$ values.

$\Gamma(3\pi^- 2\pi^+ \pi^0 \nu_\tau$(ex.$K^0, \eta, \omega, f_1(1285)$))$/\Gamma_{total}$ — Γ_{126}/Γ

VALUE (units 10^{-4})	EVTS	DOCUMENT ID		TECN	COMMENT
0.38±0.09 OUR FIT (Produced by HFLAV)					
0.36±0.03±0.09	7.3k	LEES	12X	BABR	468 fb^{-1} E^{ee}_{cm} = 10.6 GeV

$\Gamma(K^- 2\pi^- 2\pi^+ \pi^0 \nu_\tau$(ex.$K^0$))$/\Gamma_{total}$ — Γ_{127}/Γ

VALUE (units 10^{-6})	DOCUMENT ID		TECN	COMMENT
1.1±0.6 OUR FIT (Produced by HFLAV)				
1.1±0.4±0.4	[1] LEES	12X	BABR	468 fb^{-1} E^{ee}_{cm} = 10.6 GeV

[1] LEES 12X meaurement corresponds to the lower limit of $< 1.9 \times 10^{-6}$ at 90% CL.

$\Gamma(K^+ 3\pi^- \pi^+ \pi^0 \nu_\tau)/\Gamma_{total}$ — Γ_{128}/Γ

VALUE	CL%	DOCUMENT ID		TECN	COMMENT
$<8 \times 10^{-7}$	90	LEES	12X	BABR	468 fb^{-1} E^{ee}_{cm} = 10.6 GeV

$\Gamma(3h^- 2h^+ 2\pi^0 \nu_\tau)/\Gamma_{total}$ — Γ_{129}/Γ

VALUE	CL%	DOCUMENT ID		TECN	COMMENT
$<3.4 \times 10^{-6}$	90	AUBERT,B	06	BABR	232 fb^{-1} E^{ee}_{cm} = 10.6 GeV
• • • We do not use the following data for averages, fits, limits, etc. • • •					
$<1.1 \times 10^{-4}$	90	GIBAUT	94B	CLEO	E^{ee}_{cm} = 10.6 GeV

$\Gamma((5\pi)^- \nu_\tau)/\Gamma_{total}$ — Γ_{130}/Γ

$\Gamma_{130}/\Gamma = (\Gamma_{30}+\frac{1}{2}\Gamma_{45}+\Gamma_{48}+\frac{1}{2}\Gamma_{61}+\Gamma_{85}+\Gamma_{117}+0.5559\Gamma_{150}+0.892\Gamma_{180})/\Gamma$

VALUE (%)	DOCUMENT ID		TECN	COMMENT
0.78±0.05 OUR FIT (Produced by HFLAV)				
• • • We use the following data for averages but not for fits. • • •				
0.61±0.06±0.08	[1] GIBAUT	94B	CLEO	E^{ee}_{cm} = 10.6 GeV

[1] Not independent of GIBAUT 94B B($3h^- 2h^+ \nu_\tau$), PROCARIO 93 B($h^- 4\pi^0 \nu_\tau$), and BORTOLETTO 93 B($2h^- h^+ 2\pi^0 \nu_\tau$)/B("3prong") measurements. Result is corrected for η contributions.

$\Gamma(4h^- 3h^+ \geq 0$ neutrals ν_τ ("7-prong"))$/\Gamma_{total}$ — Γ_{131}/Γ

VALUE	CL%	DOCUMENT ID		TECN	COMMENT
$<3.0 \times 10^{-7}$	90	AUBERT,B	05F	BABR	232 fb^{-1}, E^{ee}_{cm} = 10.6 GeV
• • • We do not use the following data for averages, fits, limits, etc. • • •					
$<1.8 \times 10^{-5}$	95	ACKERSTAFF	97J	OPAL	1990–1995 LEP runs
$<2.4 \times 10^{-6}$	90	EDWARDS	97B	CLEO	E^{ee}_{cm} = 10.6 GeV
$<2.9 \times 10^{-4}$	90	BYLSMA	87	HRS	E^{ee}_{cm} = 29 GeV

$\Gamma(4h^- 3h^+ \nu_\tau)/\Gamma_{total}$ — Γ_{132}/Γ

VALUE	CL%	DOCUMENT ID		TECN	COMMENT
$<4.3 \times 10^{-7}$	90	AUBERT,B	05F	BABR	232 fb^{-1}, E^{ee}_{cm} = 10.6 GeV

Int. J. Mod
by UNIVERSITY OF CALIFORNIA @ BERK
wnloaded from www.worldscientific.com
-use and distribution is strictly not permitted, except for Open Access articles.

$\Gamma(4h^- 3h^+ \pi^0 \nu_\tau)/\Gamma_{total}$ — Γ_{133}/Γ

VALUE	CL%	DOCUMENT ID		TECN	COMMENT
$<2.5 \times 10^{-7}$	90	AUBERT,B	05F	BABR	232 fb^{-1}, E^{ee}_{cm} = 10.6 GeV

$\Gamma(X^-(S=-1)\nu_\tau)/\Gamma_{total}$ — Γ_{134}/Γ

$\Gamma_{134}/\Gamma = (\Gamma_{10}+\Gamma_{16}+\Gamma_{23}+\Gamma_{28}+\Gamma_{36}+\Gamma_{41}+\Gamma_{45}+\Gamma_{61}+\Gamma_{97}+\Gamma_{103}+\Gamma_{120}+\Gamma_{127}+\Gamma_{152}+\Gamma_{154}+\Gamma_{156}+0.8312\Gamma_{170}+\Gamma_{179})/\Gamma$

VALUE (%)	DOCUMENT ID		TECN	COMMENT
2.92±0.04 OUR FIT (Produced by HFLAV)				
• • • We use the following data for averages but not for fits. • • •				
2.87±0.12	[1] BARATE	99R	ALEP	1991–1995 LEP runs

[1] BARATE 99R perform a combined analysis of all ALEPH LEP 1 data on τ branching fraction measurements for decay modes having total strangeness equal to -1.

$\Gamma(K^*(892)^- \geq 0 \text{ neutrals } \geq 0 K^0_L \nu_\tau)/\Gamma_{total}$ — Γ_{135}/Γ

VALUE (%)	EVTS	DOCUMENT ID		TECN	COMMENT
1.42±0.18 OUR AVERAGE		Error includes scale factor of 1.4. See the ideogram below.			
$1.19 \pm 0.15^{+0.13}_{-0.18}$	104	ALBRECHT	95H	ARG	E^{ee}_{cm} = 9.4–10.6 GeV
$1.94 \pm 0.27 \pm 0.15$	74	[1] AKERS	94G	OPAL	E^{ee}_{cm} = 88–94 GeV
$1.43 \pm 0.11 \pm 0.13$	475	[2] GOLDBERG	90	CLEO	E^{ee}_{cm} = 9.4–10.9 GeV

[1] AKERS 94G reject events in which a K^0_S accompanies the $K^*(892)^-$. We do not correct for them.
[2] GOLDBERG 90 estimates that 10% of observed $K^*(892)$ are accompanied by a π^0.

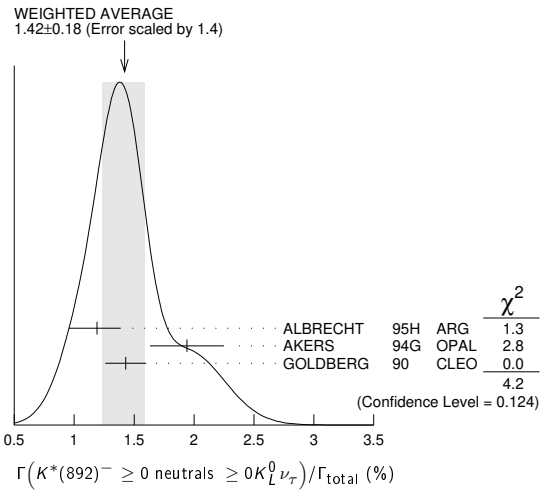

$\Gamma(K^*(892)^- \nu_\tau)/\Gamma_{total}$ — Γ_{136}/Γ

VALUE (%)	EVTS	DOCUMENT ID		TECN	COMMENT
1.20 ±0.07 OUR AVERAGE		Error includes scale factor of 1.8. See the ideogram below.			
$1.131 \pm 0.006 \pm 0.051$	49k	[1] EPIFANOV	07	BELL	351 fb^{-1} E^{ee}_{cm}=10.6 GeV
1.326 ± 0.063		BARATE	99R	ALEP	1991–1995 LEP runs
1.11 ± 0.12		[2] COAN	96	CLEO	$E^{ee}_{cm} \approx$ 10.6 GeV
$1.42 \pm 0.22 \pm 0.09$		[3] ACCIARRI	95F	L3	1991–1993 LEP runs
• • • We do not use the following data for averages, fits, limits, etc. • • •					
$1.39 \pm 0.09 \pm 0.10$		[4] BUSKULIC	96	ALEP	Repl. by BARATE 99R
$1.45 \pm 0.13 \pm 0.11$	273	[5] BUSKULIC	94F	ALEP	Repl. by BUSKULIC 96
$1.23 \pm 0.21 \; {}^{+0.11}_{-0.21}$	54	[6] ALBRECHT	88L	ARG	E^{ee}_{cm} = 10 GeV
$1.9 \pm 0.3 \pm 0.4$	44	[7] TSCHIRHART	88	HRS	E^{ee}_{cm} = 29 GeV
$1.5 \pm 0.4 \pm 0.4$	15	[8] AIHARA	87C	TPC	E^{ee}_{cm} = 29 GeV
$1.3 \pm 0.3 \pm 0.3$	31	YELTON	86	MRK2	E^{ee}_{cm} = 29 GeV
1.7 ± 0.7	11	DORFAN	81	MRK2	E^{ee}_{cm} = 4.2–6.7 GeV

[1] EPIFANOV 07 quote $B(\tau^- \to K^*(892)^- \nu_\tau)\, B(K^*(892)^- \to K^0_S \pi^-) = (3.77 \pm 0.02(\text{stat}) \pm 0.12(\text{syst}) \pm 0.12(\text{mod})) \times 10^{-3}$. We add the systematic and model uncertainties in quadrature and divide by $B(K^*(892)^- \to K^0_S \pi^-) = 0.3333$.
[2] Not independent of COAN 96 $B(\pi^- \overline{K}^0 \nu_\tau)$ and BATTLE 94 $B(K^- \pi^0 \nu_\tau)$ measurements. $K\pi$ final states are consistent with and assumed to originate from $K^*(892)^-$ production.
[3] This result is obtained from their $B(\pi^- \overline{K}^0 \nu_\tau)$ assuming all those decays originate in $K^*(892)^-$ decays.
[4] Not independent of BUSKULIC 96 $B(\pi^- \overline{K}^0 \nu_\tau)$ and $B(K^- \pi^0 \nu_\tau)$ measurements.
[5] BUSKULIC 94F obtain this result from BUSKULIC 94F $B(\overline{K}^0 \pi^- \nu_\tau)$ and BUSKULIC 94E $B(K^- \pi^0 \nu_\tau)$ assuming all of those decays originate in $K^*(892)^-$ decays.
[6] The authors divide by $\Gamma_2/\Gamma = 0.865$ to obtain this result.
[7] Not independent of TSCHIRHART 88 $\Gamma(\tau^- \to h^- \overline{K}^0 \geq 0 \text{ neutrals } \geq 0 K^0_L \nu_\tau) / \Gamma$.
[8] Decay π^- identified in this experiment, is assumed in the others.

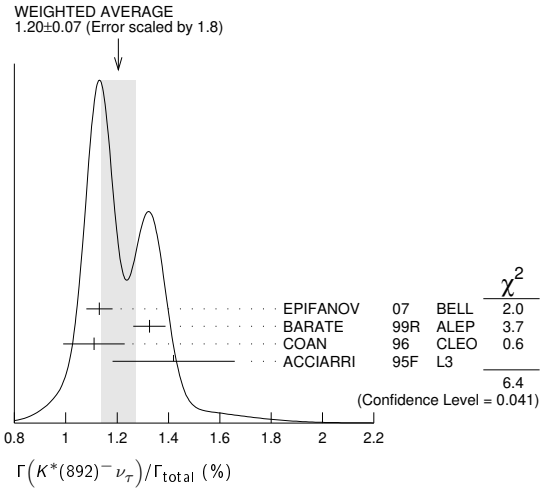

$\Gamma(K^*(892)^- \nu_\tau)/\Gamma(\pi^- \pi^0 \nu_\tau)$ — Γ_{136}/Γ_{14}

VALUE	DOCUMENT ID		TECN	COMMENT
0.075±0.027	[1] ABREU	94K	DLPH	LEP 1992 Z data

[1] ABREU 94K quote $B(\tau^- \to K^*(892)^- \nu_\tau) B(K^*(892)^- \to K^- \pi^0)/B(\tau^- \to \rho^- \nu_\tau) = 0.025 \pm 0.009$. We divide by $B(K^*(892)^- \to K^- \pi^0) = 0.333$ to obtain this result.

$\Gamma(K^*(892)^- \nu_\tau \to \pi^- \overline{K}^0 \nu_\tau)/\Gamma(\pi^- \overline{K}^0 \nu_\tau)$ — Γ_{137}/Γ_{36}

VALUE	EVTS	DOCUMENT ID		TECN	COMMENT
0.933±0.027	49k	EPIFANOV	07	BELL	351 fb^{-1} E^{ee}_{cm} = 10.6 GeV

$\Gamma(K^*(892)^0 K^- \geq 0 \text{ neutrals } \nu_\tau)/\Gamma_{total}$ — Γ_{138}/Γ

VALUE (%)	EVTS	DOCUMENT ID		TECN	COMMENT
0.32±0.08±0.12	119	GOLDBERG	90	CLEO	E^{ee}_{cm} = 9.4–10.9 GeV

$\Gamma(K^*(892)^0 K^- \nu_\tau)/\Gamma_{total}$ — Γ_{139}/Γ

VALUE (%)	EVTS	DOCUMENT ID		TECN	COMMENT
0.21 ±0.04 OUR AVERAGE					
0.213 ± 0.048		[1] BARATE	98	ALEP	1991–1995 LEP runs
$0.20 \pm 0.05 \pm 0.04$	47	ALBRECHT	95H	ARG	E^{ee}_{cm} = 9.4–10.6 GeV

[1] BARATE 98 measure the K^- ($\rho^0 \to \pi^+ \pi^-$) fraction in $\tau^- \to K^- \pi^+ \pi^- \nu_\tau$ decays to be (35 ± 11)% and derive this result from their measurement of $\Gamma(\tau^- \to K^- \pi^+ \pi^- \nu_\tau)/\Gamma_{total}$ assuming the intermediate states are all $K^- \rho$ and $K^- K^*(892)^0$.

$\Gamma(\overline{K}^*(892)^0 \pi^- \geq 0 \text{ neutrals } \nu_\tau)/\Gamma_{total}$ — Γ_{140}/Γ

VALUE (%)	EVTS	DOCUMENT ID		TECN	COMMENT
0.38±0.11±0.13	105	GOLDBERG	90	CLEO	E^{ee}_{cm} = 9.4–10.9 GeV

$\Gamma(\overline{K}^*(892)^0 \pi^- \nu_\tau)/\Gamma_{total}$ — Γ_{141}/Γ

VALUE (%)	EVTS	DOCUMENT ID		TECN	COMMENT
0.22 ±0.05 OUR AVERAGE					
0.209 ± 0.058		[1] BARATE	98	ALEP	1991–1995 LEP runs
$0.25 \pm 0.10 \pm 0.05$	27	ALBRECHT	95H	ARG	E^{ee}_{cm} = 9.4–10.6 GeV

[1] BARATE 98 measure the $K^- K^*(892)^0$ fraction in $\tau^- \to K^- K^+ \pi^- \nu_\tau$ decays to be (87 ± 13)% and derive this result from their measurement of $\Gamma(\tau^- \to K^- K^+ \pi^- \nu_\tau)/\Gamma_{total}$.

$\Gamma((\overline{K}^*(892)\pi)^- \nu_\tau \to \pi^- \overline{K}^0 \pi^0 \nu_\tau)/\Gamma_{total}$ — Γ_{142}/Γ

VALUE (%)	DOCUMENT ID		TECN	COMMENT
0.10 ±0.04 OUR AVERAGE				
$0.097 \pm 0.044 \pm 0.036$	[1] BARATE	99K	ALEP	1991–1995 LEP runs
$0.106 \pm 0.037 \pm 0.032$	[2] BARATE	98E	ALEP	1991–1995 LEP runs

[1] BARATE 99K measure K^0's by detecting K^0_L's in their hadron calorimeter. They determine the $\overline{K}^0 \rho^-$ fraction in $\tau^- \to \pi^- \overline{K}^0 \pi^0 \nu_\tau$ decays to be (0.72 ± 0.12 ± 0.10) and multiply their $B(\pi^- \overline{K}^0 \pi^0 \nu_\tau)$ measurement by one minus this fraction to obtain the quoted result.
[2] BARATE 98E reconstruct K^0's using $K^0_S \to \pi^+ \pi^-$ decays. They determine the $\overline{K}^0 \rho^-$ fraction in $\tau^- \to \pi^- \overline{K}^0 \pi^0 \nu_\tau$ decays to be (0.64 ± 0.09 ± 0.10) and multiply their $B(\pi^- \overline{K}^0 \pi^0 \nu_\tau)$ measurement by one minus this fraction to obtain the quoted result.

$\Gamma(K_1(1270)^- \nu_\tau)/\Gamma_{total}$ — Γ_{143}/Γ

VALUE (%)	EVTS	DOCUMENT ID		TECN	COMMENT
0.47±0.11 OUR AVERAGE					
0.48 ± 0.11		BARATE	99R	ALEP	1991–1995 LEP runs
$0.41 \; {}^{+0.41}_{-0.35} \pm 0.10$	5	[1] BAUER	94	TPC	E^{ee}_{cm} = 29 GeV

[1] We multiply 0.41% by 0.25, the relative systematic error quoted by BAUER 94, to obtain the systematic error.

Int. J. Mod. Phys. A 2026.41. Downloaded from www.worldscientific.com
by UNIVERSITY OF CALIFORNIA @ BERKELEY on 09/16/26. Re-use and distribution is strictly not permitted, except for Open Access articles.

$\Gamma(K_1(1400)^-\nu_\tau)/\Gamma_{total}$ — Γ_{144}/Γ

VALUE (%)	EVTS	DOCUMENT ID		TECN	COMMENT
0.17±0.26 OUR AVERAGE Error includes scale factor of 1.7.					
0.05±0.17		BARATE	99R	ALEP	1991–1995 LEP runs
$0.76^{+0.40}_{-0.33}\pm0.20$	11	[1] BAUER	94	TPC	E^{ee}_{cm}= 29 GeV

[1] We multiply 0.76% by 0.25, the relative systematic error quoted by BAUER 94, to obtain the systematic error.

$[\Gamma(K_1(1270)^-\nu_\tau)+\Gamma(K_1(1400)^-\nu_\tau)]/\Gamma_{total}$ — $(\Gamma_{143}+\Gamma_{144})/\Gamma$

VALUE (%)	EVTS	DOCUMENT ID		TECN	COMMENT
$\mathbf{1.17^{+0.41}_{-0.37}\pm0.29}$	16	[1] BAUER	94	TPC	E^{ee}_{cm}= 29 GeV

[1] We multiply 1.17% by 0.25, the relative systematic error quoted by BAUER 94, to obtain the systematic error. Not independent of BAUER 94 $B(K_1(1270)^-\nu_\tau)$ and BAUER 94 $B(K_1(1400)^-\nu_\tau)$ measurements.

$\Gamma(K_1(1270)^-\nu_\tau)/[\Gamma(K_1(1270)^-\nu_\tau)+\Gamma(K_1(1400)^-\nu_\tau)]$ — $\Gamma_{143}/(\Gamma_{143}+\Gamma_{144})$

VALUE	DOCUMENT ID		TECN	COMMENT
0.69±0.15 OUR AVERAGE				
0.71±0.16±0.11	[1] ABBIENDI	00D	OPAL	1990–1995 LEP runs
0.66±0.19±0.13	[2] ASNER	00B	CLEO	E^{ee}_{cm}= 10.6 GeV

[1] ABBIENDI 00D assume the resonance structure of $\tau^- \to K^-\pi^+\pi^-\nu_\tau$ decays is dominated by the $K_1(1270)^-$ and $K_1(1400)^-$ resonances.
[2] ASNER 00B assume the resonance structure of $\tau^- \to K^-\pi^+\pi^-\nu_\tau$ (ex. K^0) decays is dominated by $K_1(1270)^-$ and $K_1(1400)^-$ resonances.

$\Gamma(K^*(1410)^-\nu_\tau)/\Gamma_{total}$ — Γ_{145}/Γ

VALUE (units 10^{-3})	DOCUMENT ID		TECN	COMMENT
$\mathbf{1.5^{+1.4}_{-1.0}}$	BARATE	99R	ALEP	1991–1995 LEP runs

$\Gamma(K_0^*(1430)^-\nu_\tau)/\Gamma_{total}$ — Γ_{146}/Γ

VALUE (units 10^{-3})	CL%	DOCUMENT ID		TECN	COMMENT
<0.5	95	BARATE	99R	ALEP	1991–1995 LEP runs

$\Gamma(K_2^*(1430)^-\nu_\tau)/\Gamma_{total}$ — Γ_{147}/Γ

VALUE (%)	CL%	EVTS	DOCUMENT ID		TECN	COMMENT
<0.3	95		TSCHIRHART	88	HRS	E^{ee}_{cm}= 29 GeV
• • • We do not use the following data for averages, fits, limits, etc. • • •						
<0.33	95		[1] ACCIARRI	95F	L3	1991–1993 LEP runs
<0.9	95	0	DORFAN	81	MRK2	E^{ee}_{cm}= 4.2–6.7 GeV

[1] ACCIARRI 95F quote $B(\tau^- \to K^*(1430)^- \to \pi^-\overline{K}^0\nu_\tau) < 0.11\%$. We divide by $B(K^*(1430)^- \to \pi^-\overline{K}^0) = 0.33$ to obtain the limit shown.

$\Gamma(a_0(980)^- \geq 0 \text{ neutrals } \nu_\tau)/\Gamma_{total} \times B(a_0(980) \to K^0K^-)$ — $\Gamma_{148}/\Gamma \times B$

VALUE (10^{-4})	CL%	DOCUMENT ID		TECN	COMMENT
<2.8	90	GOLDBERG	90	CLEO	E^{ee}_{cm}= 9.4–10.9 GeV

$\Gamma(\eta\pi^-\nu_\tau)/\Gamma_{total}$ — Γ_{149}/Γ

VALUE (units 10^{-4})	CL%	EVTS	DOCUMENT ID		TECN	COMMENT
< 0.99	95		[1] DEL-AMO-SA...	11E	BABR	470 fb^{-1} E^{ee}_{cm}= 10.6 GeV
• • • We do not use the following data for averages, fits, limits, etc. • • •						
< 6.2	95		BUSKULIC	97C	ALEP	1991–1994 LEP runs
< 1.4	95	0	BARTELT	96	CLEO	$E^{ee}_{cm}\approx$ 10.6 GeV
< 3.4	95		ARTUSO	92	CLEO	$E^{ee}_{cm}\approx$ 10.6 GeV
< 90	95		ALBRECHT	88M	ARG	$E^{ee}_{cm}\approx$ 10 GeV
<140	90		BEHREND	88	CELL	E^{ee}_{cm}= 14–46.8 GeV
<180	95		BARINGER	87	CLEO	E^{ee}_{cm}= 10.5 GeV
<250	90	0	COFFMAN	87	MRK3	E^{ee}_{cm}= 3.77 GeV
510 ±100±120		65	DERRICK	87	HRS	E^{ee}_{cm}= 29 GeV
<100	95		GAN	87B	MRK2	E^{ee}_{cm}= 29 GeV

[1] DEL-AMO-SANCHEZ 11E also quote $B(\tau^- \to \eta\pi^-\nu_\tau) = (3.4 \pm 3.4 \pm 2.1)\times10^{-5}$.

$\Gamma(\eta\pi^-\pi^0\nu_\tau)/\Gamma_{total}$ — Γ_{150}/Γ

VALUE (units 10^{-3})	CL%	EVTS	DOCUMENT ID		TECN	COMMENT
1.39± 0.07 OUR FIT (Produced by HFLAV)						
1.38± 0.09 OUR AVERAGE Error includes scale factor of 1.2.						
1.35± 0.03± 0.07		6.0k	INAMI	09	BELL	490 fb^{-1} E^{ee}_{cm}= 10.6 GeV
1.8 ± 0.4 ± 0.2			BUSKULIC	97C	ALEP	1991–1994 LEP runs
1.7 ± 0.2 ± 0.2		125	ARTUSO	92	CLEO	$E^{ee}_{cm}\approx$ 10.6 GeV
• • • We do not use the following data for averages, fits, limits, etc. • • •						
< 11.0	95		ALBRECHT	88M	ARG	$E^{ee}_{cm}\approx$ 10 GeV
< 21.0	95		BARINGER	87	CLEO	E^{ee}_{cm}= 10.5 GeV
$42.0^{+7.0}_{-12.0}\pm16.0$			[1] GAN	87	MRK2	E^{ee}_{cm}= 29 GeV

[1] Highly correlated with GAN 87 $\Gamma(\pi^-3\pi^0\nu_\tau)/\Gamma(\text{total})$ value.

$\Gamma(\eta\pi^-\pi^0\pi^0\nu_\tau)/\Gamma_{total}$ — Γ_{151}/Γ

VALUE (units 10^{-4})	CL%	EVTS	DOCUMENT ID		TECN	COMMENT
1.9 ±0.4 OUR FIT (Produced by HFLAV)						
1.81±0.31 OUR AVERAGE						
2.01±0.34±0.22		381	LEES	12X	BABR	468 fb^{-1} E^{ee}_{cm}= 10.6 GeV
• • • We use the following data for averages but not for fits. • • •						
1.5 ±0.5		30	[1] ANASTASSOV 01		CLEO	E^{ee}_{cm}= 10.6 GeV
• • • We do not use the following data for averages, fits, limits, etc. • • •						
1.4 ±0.6 ±0.3		15	[2] BERGFELD	97	CLEO	Repl. by ANASTASSOV 01
< 4.3	95		ARTUSO	92	CLEO	$E^{ee}_{cm}\approx$ 10.6 GeV
<120	95		ALBRECHT	88M	ARG	$E^{ee}_{cm}\approx$ 10 GeV

[1] Weighted average of BERGFELD 97 and ANASTASSOV 01 value of $(1.5 \pm 0.6 \pm 0.3)\times10^{-4}$ obtained using η's reconstructed from $\eta \to \pi^+\pi^-\pi^0$ decays.
[2] BERGFELD 97 reconstruct η's using $\eta \to \gamma\gamma$ decays.

$\Gamma(\eta K^-\nu_\tau)/\Gamma_{total}$ — Γ_{152}/Γ

VALUE (units 10^{-4})	CL%	EVTS	DOCUMENT ID		TECN	COMMENT
1.55±0.08 OUR FIT (Produced by HFLAV)						
1.54±0.08 OUR AVERAGE						
1.42±0.11±0.07		690	DEL-AMO-SA...	11E	BABR	470 fb^{-1} E^{ee}_{cm}= 10.6 GeV
1.58±0.05±0.09		1.6k	INAMI	09	BELL	490 fb^{-1} E^{ee}_{cm}= 10.6 GeV
$2.9^{+1.3}_{-1.2}\pm0.7$			BUSKULIC	97C	ALEP	1991–1994 LEP runs
2.6 ±0.5 ±0.5		85	BARTELT	96	CLEO	$E^{ee}_{cm}\approx$ 10.6 GeV
• • • We do not use the following data for averages, fits, limits, etc. • • •						
< 4.7	95		ARTUSO	92	CLEO	$E^{ee}_{cm}\approx$ 10.6 GeV

$\Gamma(\eta K^*(892)^-\nu_\tau)/\Gamma_{total}$ — Γ_{153}/Γ

VALUE (units 10^{-4})	EVTS	DOCUMENT ID		TECN	COMMENT
1.38±0.15 OUR AVERAGE					
1.34±0.12±0.09	245	[1] INAMI	09	BELL	490 fb^{-1} E^{ee}_{cm}= 10.6 GeV
2.90±0.80±0.42	25	BISHAI	99	CLEO	E^{ee}_{cm}= 10.6 GeV

[1] Not independent of INAMI 09 $B(\tau^- \to \eta K^-\pi^0\nu_\tau)$ and $B(\tau^- \to \eta\overline{K}^0\pi^-\nu_\tau)$ values.

$\Gamma(\eta K^-\pi^0\nu_\tau)/\Gamma_{total}$ — Γ_{154}/Γ

VALUE (units 10^{-4})	EVTS	DOCUMENT ID		TECN	COMMENT
0.48±0.12 OUR FIT (Produced by HFLAV)					
0.48±0.12 OUR AVERAGE					
0.46±0.11±0.04	270	INAMI	09	BELL	490 fb^{-1} E^{ee}_{cm}= 10.6 GeV
1.77±0.56±0.71	36	BISHAI	99	CLEO	E^{ee}_{cm}= 10.6 GeV

$\Gamma(\eta K^-\pi^0(\text{non-}K^*(892))\nu_\tau)/\Gamma_{total}$ — Γ_{155}/Γ

VALUE	CL%	DOCUMENT ID		TECN	COMMENT
$\mathbf{<3.5\times10^{-5}}$	90	INAMI	09	BELL	490 fb^{-1} E^{ee}_{cm}= 10.6 GeV

$\Gamma(\eta\overline{K}^0\pi^-\nu_\tau)/\Gamma_{total}$ — Γ_{156}/Γ

VALUE (units 10^{-4})	EVTS	DOCUMENT ID		TECN	COMMENT
0.94±0.15 OUR FIT (Produced by HFLAV)					
0.93±0.15 OUR AVERAGE					
0.88±0.14±0.06	161	[1] INAMI	09	BELL	490 fb^{-1} E^{ee}_{cm}= 10.6 GeV
2.20±0.70±0.22	15	[2] BISHAI	99	CLEO	E^{ee}_{cm}= 10.6 GeV

[1] We multiply the INAMI 09 measurement $B(\tau^- \to \eta K^0_S\pi^-\nu_\tau) = (0.44 \pm 0.07 \pm 0.03)\times10^{-4}$ by 2 to obtain the listed value.
[2] We multiply the BISHAI 99 measurement $B(\tau^- \to \eta K^0_S\pi^-\nu_\tau) = (1.10 \pm 0.35 \pm 0.11)\times10^{-4}$ by 2 to obtain the listed value.

$\Gamma(\eta\overline{K}^0\pi^-\pi^0\nu_\tau)/\Gamma_{total}$ — Γ_{157}/Γ

VALUE	CL%	DOCUMENT ID		TECN	COMMENT
$\mathbf{<5.0\times10^{-5}}$	90	[1] INAMI	09	BELL	490 fb^{-1} E^{ee}_{cm}= 10.6 GeV

[1] We multiply the INAMI 09 measurement $B(\tau^- \to \eta K^0_S\pi^-\pi^0\nu_\tau) < 2.5\times10^{-5}$ by 2 to obtain the listed value.

$\Gamma(\eta K^-K^0\nu_\tau)/\Gamma_{total}$ — Γ_{158}/Γ

VALUE	CL%	DOCUMENT ID		TECN	COMMENT
$\mathbf{<9.0\times10^{-6}}$	90	[1] INAMI	09	BELL	490 fb^{-1} E^{ee}_{cm}= 10.6 GeV

[1] We multiply the INAMI 09 measurement $B(\tau^- \to \eta K^-K^0_S\nu_\tau) < 4.5\times10^{-6}$ by 2 to obtain the listed value.

$\Gamma(\eta\pi^+\pi^-\pi^- \geq 0 \text{ neutrals } \nu_\tau)/\Gamma_{total}$ — Γ_{159}/Γ

VALUE (%)	CL%	DOCUMENT ID		TECN	COMMENT
<0.3	90	ABACHI	87B	HRS	E^{ee}_{cm}= 29 GeV

$\Gamma(\eta\pi^-\pi^+\pi^-\nu_\tau(\text{ex.}K^0))/\Gamma_{total}$ — Γ_{160}/Γ

VALUE (units 10^{-4})	EVTS	DOCUMENT ID		TECN	COMMENT
2.20±0.13 OUR FIT (Produced by HFLAV)					
2.23±0.12 OUR AVERAGE					
2.10±0.09±0.13	2.9k	[1] LEES	12X	BABR	$\eta \to \gamma\gamma$
2.37±0.12±0.18	1.4k	[1] LEES	12X	BABR	$\eta \to \pi^+\pi^-\pi^0$
2.54±0.27±0.25	315	[1] LEES	12X	BABR	$\eta \to 3\pi^0$

Int. J. Mod
by UNIVERSITY OF CALIFORNIA @ BERK
Downloaded from www.worldscientific.com
-use and distribution is strictly not permitted, except for Open Access articles.

• • • We use the following data for averages but not for fits. • • •

2.3 ±0.5	170	[2] ANASTASSOV 01	CLEO	E^{ee}_{cm}= 10.6 GeV	

• • • We do not use the following data for averages, fits, limits, etc. • • •

1.60±0.05±0.11	1.8 k	AUBERT	08AE	BABR	Repl. by LEES 12X
3.4 $^{+0.6}_{-0.5}$ ±0.6	89	[3] BERGFELD	97	CLEO	Repl. by ANASTASSOV 01

[1] LEES 12X uses 468 fb^{-1} of data taken at E^{ee}_{cm} = 10.6 GeV. It gives the average of the three measurements listed here as (2.25 ± 0.07 ± 0.12) × 10^{-4}.

[2] Weighted average of BERGFELD 97 and ANASTASSOV 01 measurements using η's reconstructed from $\eta \to \pi^+\pi^-\pi^0$ and $\eta \to 3\pi^0$ decays.

[3] BERGFELD 97 reconstruct η's using $\eta \to \gamma\gamma$ and $\eta \to 3\pi^0$ decays.

$\Gamma(\eta\pi^-\pi^+\pi^-\nu_\tau(\text{ex.}K^0,f_1(1285)))/\Gamma_{total}$ — Γ_{161}/Γ

VALUE (units 10^{-4})	DOCUMENT ID		TECN	COMMENT
0.99±0.09±0.13	[1] LEES	12X	BABR	468 fb^{-1} E^{ee}_{cm} = 10.6 GeV

[1] LEES 12X obtain this result by subtracting their B($\tau^- \to f_1(1285)\pi^-\nu_\tau \to \eta\pi^-\pi^+\pi^-\nu_\tau$) measurement from their B($\tau^- \to \eta\pi^-\pi^+\pi^-\nu_\tau$(ex.$K^0$)) measurement.

$\Gamma(\eta a_1(1260)^-\nu_\tau \to \eta\pi^-\rho^0\nu_\tau)/\Gamma_{total}$ — Γ_{162}/Γ

VALUE	CL%	DOCUMENT ID		TECN	COMMENT
<3.9 × 10^{-4}	90	BERGFELD	97	CLEO	E^{ee}_{cm}= 10.6 GeV

$\Gamma(\eta\eta\pi^-\nu_\tau)/\Gamma_{total}$ — Γ_{163}/Γ

VALUE	CL%	DOCUMENT ID		TECN	COMMENT
<7.4 × 10^{-6}	90	INAMI	09	BELL	490 fb^{-1} E^{ee}_{cm}= 10.6 GeV

• • • We do not use the following data for averages, fits, limits, etc. • • •

<1.1 × 10^{-4}	95	ARTUSO	92	CLEO	E^{ee}_{cm} ≈ 10.6 GeV
<8.3 × 10^{-3}	95	ALBRECHT	88M	ARG	E^{ee}_{cm} ≈ 10 GeV

$\Gamma(\eta\eta\pi^-\pi^0\nu_\tau)/\Gamma_{total}$ — Γ_{164}/Γ

VALUE (units 10^{-4})	CL%	DOCUMENT ID		TECN	COMMENT
< 2.0	95	ARTUSO	92	CLEO	E^{ee}_{cm} ≈ 10.6 GeV

• • • We do not use the following data for averages, fits, limits, etc. • • •

<90	95	ALBRECHT	88M	ARG	E^{ee}_{cm} ≈ 10 GeV

$\Gamma(\eta\eta K^-\nu_\tau)/\Gamma_{total}$ — Γ_{165}/Γ

VALUE	CL%	DOCUMENT ID		TECN	COMMENT
<3.0 × 10^{-6}	90	INAMI	09	BELL	490 fb^{-1} E^{ee}_{cm}= 10.6 GeV

$\Gamma(\eta'(958)\pi^-\nu_\tau)/\Gamma_{total}$ — Γ_{166}/Γ

VALUE	CL%	DOCUMENT ID		TECN	COMMENT
<4.0 × 10^{-6}	90	LEES	12X	BABR	468 fb^{-1} E^{ee}_{cm} = 10.6 GeV

• • • We do not use the following data for averages, fits, limits, etc. • • •

<7.2 × 10^{-6}	90	AUBERT	08AE	BABR	384 fb^{-1}, E^{ee}_{cm}= 10.6 GeV
<7.4 × 10^{-5}	90	BERGFELD	97	CLEO	E^{ee}_{cm}= 10.6 GeV

$\Gamma(\eta'(958)\pi^-\pi^0\nu_\tau)/\Gamma_{total}$ — Γ_{167}/Γ

VALUE	CL%	DOCUMENT ID		TECN	COMMENT
<1.2 × 10^{-5}	90	LEES	12X	BABR	468 fb^{-1} E^{ee}_{cm} = 10.6 GeV

• • • We do not use the following data for averages, fits, limits, etc. • • •

<8.0 × 10^{-5}	90	BERGFELD	97	CLEO	E^{ee}_{cm}= 10.6 GeV

$\Gamma(\eta'(958)K^-\nu_\tau)/\Gamma_{total}$ — Γ_{168}/Γ

VALUE	CL%	DOCUMENT ID		TECN	COMMENT
<2.4 × 10^{-6}	90	LEES	12X	BABR	468 fb^{-1} E^{ee}_{cm} = 10.6 GeV

$\Gamma(\phi\pi^-\nu_\tau)/\Gamma_{total}$ — Γ_{169}/Γ

VALUE (units 10^{-5})	CL%	EVTS	DOCUMENT ID		TECN	COMMENT
3.42±0.55±0.25		344	AUBERT	08	BABR	342 fb^{-1} E^{ee}_{cm} = 10.6 GeV

• • • We do not use the following data for averages, fits, limits, etc. • • •

< 20	90	[1] AVERY	97	CLEO	E^{ee}_{cm}= 10.6 GeV
< 35	90	ALBRECHT	95H	ARG	E^{ee}_{cm}= 9.4–10.6 GeV

[1] AVERY 97 limit varies from (1.2–2.0) × 10^{-4} depending on decay model assumptions.

$\Gamma(\phi K^-\nu_\tau)/\Gamma_{total}$ — Γ_{170}/Γ

VALUE (units 10^{-5})	CL%	EVTS	DOCUMENT ID		TECN	COMMENT
4.4 ±1.6 OUR FIT			(Produced by HFLAV)			
3.70±0.33 OUR AVERAGE			Error includes scale factor of 1.3.			

• • • We use the following data for averages but not for fits. • • •

3.39±0.20±0.28		274	AUBERT	08	BABR	342 fb^{-1} E^{ee}_{cm} = 10.6 GeV
4.05±0.25±0.26		551	INAMI	06	BELL	401 fb^{-1} E^{ee}_{cm}=10.6 GeV

• • • We do not use the following data for averages, fits, limits, etc. • • •

<6.7	90	[1] AVERY	97	CLEO	E^{ee}_{cm}= 10.6 GeV

[1] AVERY 97 limit varies from (5.4–6.7) × 10^{-5} depending on decay model assumptions.

$\Gamma(f_1(1285)\pi^-\nu_\tau)/\Gamma_{total}$ — Γ_{171}/Γ

VALUE (units 10^{-4})	EVTS	DOCUMENT ID		TECN	COMMENT
3.9 ±0.5 OUR AVERAGE		Error includes scale factor of 1.9.			
4.73±0.28±0.45	3.7k	[1] LEES	12X	BABR	468 fb^{-1} E^{ee}_{cm} = 10.6 GeV
3.60±0.18±0.23	2.5k	[2] LEES	12X	BABR	468 fb^{-1} E^{ee}_{cm} = 10.6 GeV

• • • We do not use the following data for averages, fits, limits, etc. • • •

3.19±0.18±1.00	1.3 k	[3] AUBERT	08AE	BABR	Repl. by LEES 12X
3.9 ±0.7 ±0.5	1.4 k	[4] AUBERT,B	05W	BABR	Repl. by LEES 12X
5.8 $^{+1.4}_{-1.3}$ ±1.8	54	[5] BERGFELD	97	CLEO	E^{ee}_{cm}= 10.6 GeV

[1] LEES 12X obtain this value by dividing their B($\tau^- \to f_1(1285)\pi^-\nu_\tau \to 3\pi^-2\pi^+\nu_\tau$) measurement by the PDG 12 value of B($f_1(1285) \to 2\pi^+2\pi^-$) = 0.111$^{+0.007}_{-0.006}$.

[2] LEES 12X obtain this value by dividing their B($\tau^- \to f_1(1285)\pi^-\nu_\tau \to \eta\pi^-\pi^+\pi^-\nu_\tau$) measurement by 2/3 of the PDG 12 value of B($f_1(1285) \to \eta\pi\pi$) = 0.524$^{+0.019}_{-0.021}$.

[3] AUBERT 08AE obtain this value by dividing their B($\tau^- \to f_1(1285)\pi^-\nu_\tau \to \eta\pi^-\pi^+\pi^-\nu_\tau$) measurement by the PDG 06 value of B($f_1(1285) \to \eta\pi^-\pi^+$) = 0.35 ± 0.11. The quote (3.19 ± 0.18 ± 0.16 ± 0.99) × 10^{-4} where the final error is due to the uncertainty on B($f_1(1285) \to \eta\pi^-\pi^+$). We combine the two systematic errors in quadrature.

[4] AUBERT,B 05W use the $f_1(1285) \to 2\pi^+2\pi^-$ decay mode and the PDG 04 value of B($f_1(1285) \to 2\pi^+2\pi^-$) = 0.110$^{+0.007}_{-0.006}$.

[5] BERGFELD 97 use the $f_1(1285) \to \eta\pi^+\pi^-$ decay mode.

$\Gamma(f_1(1285)\pi^-\nu_\tau \to \eta\pi^-\pi^+\pi^-\nu_\tau)/\Gamma_{total}$ — Γ_{172}/Γ

VALUE (units 10^{-4})	EVTS	DOCUMENT ID		TECN	COMMENT
1.18±0.07 OUR AVERAGE		Error includes scale factor of 1.3.			
1.26±0.06±0.06	2.5k	LEES	12X	BABR	468 fb^{-1} E^{ee}_{cm} = 10.6 GeV
1.11±0.06±0.05	1.3 k	AUBERT	08AE	BABR	384 fb^{-1}, E^{ee}_{cm}= 10.6 GeV

$\Gamma(f_1(1285)\pi^-\nu_\tau \to \eta\pi^-\pi^+\pi^-\nu_\tau)/\Gamma(\eta\pi^-\pi^+\pi^-\nu_\tau(\text{ex.}K^0))$ — $\Gamma_{172}/\Gamma_{160}$

VALUE	DOCUMENT ID		TECN	COMMENT
0.69±0.01±0.05	[1] AUBERT	08AE	BABR	384 fb^{-1}, E^{ee}_{cm}= 10.6 GeV

• • • We do not use the following data for averages, fits, limits, etc. • • •

0.55±0.14	BERGFELD	97	CLEO	E^{ee}_{cm}= 10.6 GeV

[1] Not independent of AUBERT 08AE B($\tau^- \to f_1(1285)\pi^-\nu_\tau \to \eta\pi^-\pi^+\pi^-\nu_\tau$) and B($\tau^- \to \eta\pi^-\pi^+\pi^-\nu_\tau$(ex.$K^0$)) values.

$\Gamma(f_1(1285)\pi^-\nu_\tau \to 3\pi^-2\pi^+\nu_\tau)/\Gamma_{total}$ — Γ_{173}/Γ

VALUE (units 10^{-4})	EVTS	DOCUMENT ID		TECN	COMMENT
0.52 ±0.04 OUR FIT		(Produced by HFLAV)			
0.520±0.031±0.037	3.7k	LEES	12X	BABR	468 fb^{-1} E^{ee}_{cm}=10.6 GeV

$\Gamma(\pi(1300)^-\nu_\tau \to (\rho\pi)^-\nu_\tau \to (3\pi)^-\nu_\tau)/\Gamma_{total}$ — Γ_{174}/Γ

VALUE	CL%	DOCUMENT ID		TECN	COMMENT
<1.0 × 10^{-4}	90	ASNER	00	CLEO	E^{ee}_{cm}= 10.6 GeV

$\Gamma(\pi(1300)^-\nu_\tau \to ((\pi\pi)_{S-wave}\pi)^-\nu_\tau \to (3\pi)^-\nu_\tau)/\Gamma_{total}$ — Γ_{175}/Γ

VALUE	CL%	DOCUMENT ID		TECN	COMMENT
<1.9 × 10^{-4}	90	ASNER	00	CLEO	E^{ee}_{cm}= 10.6 GeV

$\Gamma(h^-\omega \geq 0 \text{ neutrals } \nu_\tau)/\Gamma_{total}$ — Γ_{176}/Γ

$\Gamma_{176}/\Gamma = (\Gamma_{178}+\Gamma_{179}+\Gamma_{180})/\Gamma$

VALUE (%)	EVTS	DOCUMENT ID		TECN	COMMENT
2.40±0.08 OUR FIT		(Produced by HFLAV)			

• • • We use the following data for averages but not for fits. • • •

1.65±0.3 ±0.2	1513	ALBRECHT	88M	ARG	E^{ee}_{cm} ≈ 10 GeV

$\Gamma(h^-\omega\nu_\tau)/\Gamma_{total}$ — $\Gamma_{177}/\Gamma = (\Gamma_{178}+\Gamma_{179})/\Gamma$

VALUE (%)	EVTS	DOCUMENT ID		TECN	COMMENT
1.99±0.06 OUR FIT		(Produced by HFLAV)			
1.92±0.07 OUR AVERAGE					
1.91±0.07±0.06	5803	BUSKULIC	97C	ALEP	1991–1994 LEP runs
1.60±0.27±0.41	139	BARINGER	87	CLEO	E^{ee}_{cm}= 10.5 GeV

• • • We use the following data for averages but not for fits. • • •

1.95±0.07±0.11	2223	[1] BALEST	95C	CLEO	E^{ee}_{cm} ≈ 10.6 GeV

[1] Not independent of BALEST 95C B($\tau^- \to h^-\omega\nu_\tau$)/B($\tau^- \to h^-h^-h^+\pi^0\nu_\tau$) value.

$[\Gamma(\pi^-\omega\nu_\tau)+\Gamma(K^-\omega\nu_\tau)]/\Gamma(h^-h^-h^+\pi^0\nu_\tau(\text{ex.}K^0))$ — $(\Gamma_{178}+\Gamma_{179})/\Gamma_{74}$

$(\Gamma_{178}+\Gamma_{179})/\Gamma_{74} = (\Gamma_{178}+\Gamma_{179})/(\Gamma_{78}+\Gamma_{103}+\Gamma_{107}+0.2302\Gamma_{152}+0.892\Gamma_{178}+0.892\Gamma_{179}+0.0153\Gamma_{180})$

VALUE (units 10^{-2})	EVTS	DOCUMENT ID		TECN	COMMENT
43.5±1.4 OUR FIT		(Produced by HFLAV)			
45.3±1.9 OUR AVERAGE					
43.1±3.3	2350	[1] BUSKULIC	96	ALEP	LEP 1991–1993 data
46.4±1.6±1.7	2223	[2] BALEST	95C	CLEO	E^{ee}_{cm} ≈ 10.6 GeV

• • • We do not use the following data for averages, fits, limits, etc. • • •

37 ±5 ±2	458	[3] ALBRECHT	91D	ARG	E^{ee}_{cm}= 9.4–10.6 GeV

Int. J. Mod. Phys. A 2026.41. Downloaded from www.worldscientific.com
by UNIVERSITY OF CALIFORNIA @ BERKELEY on 09/16/26. Re-use and distribution is strictly not permitted, except for Open Access articles.

[1] BUSKULIC 96 quote the fraction of $\tau \to h^- h^- h^+ \pi^0 \nu_\tau$ (ex. K^0) decays which originate in a $h^- \omega$ final state = 0.383 ± 0.029. We divide this by the $\omega(782) \to \pi^+ \pi^- \pi^0$ branching fraction (0.888).

[2] BALEST 95C quote the fraction of $\tau^- \to h^- h^- h^+ \pi^0 \nu_\tau$ (ex. K^0) decays which originate in a $h^- \omega$ final state equals 0.412 ± 0.014 ± 0.015. We divide this by the $\omega(782) \to \pi^+ \pi^- \pi^0$ branching fraction (0.888).

[3] ALBRECHT 91D quote the fraction of $\tau^- \to h^- h^- h^+ \pi^0 \nu_\tau$ decays which originate in a $\pi^- \omega$ final state equals 0.33 ± 0.04 ± 0.02. We divide this by the $\omega(782) \to \pi^+ \pi^- \pi^0$ branching fraction (0.888).

$\Gamma(\pi^- \omega \nu_\tau)/\Gamma_{total}$ — Γ_{178}/Γ

VALUE (%)	DOCUMENT ID
1.95±0.06 OUR FIT (Produced by HFLAV)	

$\Gamma(K^- \omega \nu_\tau)/\Gamma_{total}$ — Γ_{179}/Γ

VALUE (units 10^{-4})	EVTS	DOCUMENT ID		TECN	COMMENT
4.1±0.9 OUR FIT (Produced by HFLAV)					
4.1±0.6±0.7	500	ARMS	05	CLE3	7.6 fb^{-1}, E^{ee}_{cm} = 10.6 GeV

$\Gamma(h^- \omega \pi^0 \nu_\tau)/\Gamma_{total}$ — Γ_{180}/Γ

VALUE (%)	EVTS	DOCUMENT ID		TECN	COMMENT
0.41±0.04 OUR FIT (Produced by HFLAV)					
0.43±0.06±0.05	7283	BUSKULIC	97C	ALEP	1991–1994 LEP runs

$\Gamma(h^- \omega \pi^0 \nu_\tau)/\Gamma(h^- h^- h^+ \geq 0 \text{ neutrals} \geq 0 K^0_L \nu_\tau)$ — Γ_{180}/Γ_{62}

$\Gamma_{180}/\Gamma_{62} = \Gamma_{180}/(0.34598\Gamma_{36} + 0.34598\Gamma_{38} + 0.34598\Gamma_{41} + 0.34598\Gamma_{43} + 0.4247\Gamma_{48} + 0.6920\Gamma_{49} + 0.8494\Gamma_{52} + 0.6920\Gamma_{56} + 0.6534\Gamma_{61} + \Gamma_{70} + \Gamma_{78} + \Gamma_{85} + \Gamma_{89} + \Gamma_{97} + \Gamma_{103} + \Gamma_{106} + \Gamma_{107} + 0.2805\Gamma_{150} + 0.2302\Gamma_{151} + 0.2805\Gamma_{152} + 0.2805\Gamma_{154} + 0.3759\Gamma_{156} + 0.3256\Gamma_{160} + 0.7259\Gamma_{170} + 0.9078\Gamma_{178} + 0.9078\Gamma_{179} + 0.9078\Gamma_{180} + 0.892\Gamma_{182})$

VALUE	EVTS	DOCUMENT ID		TECN	COMMENT
(2.69 ±0.28) × 10^{-2} OUR FIT (Produced by HFLAV)					
• • • We use the following data for averages but not for fits. • • •					
0.028±0.003±0.003	430	[1] BORTOLETTO	93	CLEO	$E^{ee}_{cm} \approx 10.6$ GeV

[1] Not independent of BORTOLETTO 93 $\Gamma(\tau^- \to h^- \omega \pi^0 \nu_\tau)/\Gamma(\tau^- \to h^- h^- h^+ 2\pi^0 \nu_\tau$ (ex. K^0)) value.

$\Gamma(h^- \omega \pi^0 \nu_\tau)/\Gamma(h^- h^- h^+ 2\pi^0 \nu_\tau$ (ex. K^0)) — Γ_{180}/Γ_{84}

$\Gamma_{180}/\Gamma_{84} = \Gamma_{180}/(\Gamma_{85} + 0.2302\Gamma_{150} + 0.2302\Gamma_{154} + 0.892\Gamma_{180})$

VALUE (units 10^{-2})	DOCUMENT ID		TECN	COMMENT
82±8 OUR FIT (Produced by HFLAV)				
81±6±6	BORTOLETTO	93	CLEO	$E^{ee}_{cm} \approx 10.6$ GeV

$\Gamma(h^- \omega 2\pi^0 \nu_\tau)/\Gamma_{total}$ — Γ_{181}/Γ

VALUE (units 10^{-4})	EVTS	DOCUMENT ID		TECN	COMMENT
1.4 ±0.4 ±0.3	53	ANASTASSOV	01	CLEO	E^{ee}_{cm} = 10.6 GeV
• • • We do not use the following data for averages, fits, limits, etc. • • •					
$1.89^{+0.74}_{-0.67} \pm 0.40$	19	ANDERSON	97	CLEO	Repl. by ANASTASSOV 01

$\Gamma(\pi^- \omega 2\pi^0 \nu_\tau)/\Gamma_{total}$ — Γ_{182}/Γ

VALUE (units 10^{-4})	EVTS	DOCUMENT ID		TECN	COMMENT
0.72±0.16 OUR FIT (Produced by HFLAV)					
0.73±0.12±0.12	1.1k	LEES	12X	BABR	468 fb^{-1} E^{ee}_{cm} = 10.6 GeV

$\Gamma(h^- 2\omega \nu_\tau)/\Gamma_{total}$ — Γ_{183}/Γ

VALUE	CL%	DOCUMENT ID		TECN	COMMENT
<5.4 × 10^{-7}	90	AUBERT,B	06	BABR	232 fb^{-1} E^{ee}_{cm} = 10.6 GeV

$\Gamma(2h^- h^+ \omega \nu_\tau)/\Gamma_{total}$ — Γ_{184}/Γ

VALUE (units 10^{-4})	EVTS	DOCUMENT ID		TECN	COMMENT
1.2±0.2±0.1	110	ANASTASSOV	01	CLEO	E^{ee}_{cm} = 10.6 GeV

$\Gamma(2\pi^- \pi^+ \omega \nu_\tau$ (ex. K^0))$/\Gamma_{total}$ — Γ_{185}/Γ

VALUE (units 10^{-4})	EVTS	DOCUMENT ID		TECN	COMMENT
0.84±0.06 OUR FIT (Produced by HFLAV)					
0.84±0.04±0.06	2.4k	LEES	12X	BABR	468 fb^{-1} E^{ee}_{cm} = 10.6 GeV

$\Gamma(e^- \gamma)/\Gamma_{total}$ — Γ_{186}/Γ

Test of lepton family number conservation.

VALUE	CL%	DOCUMENT ID		TECN	COMMENT
<3.3 × 10^{-8}	90	AUBERT	10B	BABR	516 fb^{-1}, E^{ee}_{cm} = 10.6 GeV
• • • We do not use the following data for averages, fits, limits, etc. • • •					
<5.6 × 10^{-8}	90	UNO	21	BELL	988 fb^{-1}, E^{ee}_{cm} = 10.6 GeV
<1.2 × 10^{-7}	90	HAYASAKA	08	BELL	535 fb^{-1}, E^{ee}_{cm} = 10.6 GeV
<1.1 × 10^{-7}	90	AUBERT	06C	BABR	232 fb^{-1}, E^{ee}_{cm} = 10.6 GeV
<3.9 × 10^{-7}	90	HAYASAKA	05	BELL	86.7 fb^{-1}, E^{ee}_{cm} = 10.6 GeV
<2.7 × 10^{-6}	90	EDWARDS	97	CLEO	
<1.1 × 10^{-4}	90	ABREU	95U	DLPH	1990–1993 LEP runs
<1.2 × 10^{-4}	90	ALBRECHT	92K	ARG	E^{ee}_{cm} = 10 GeV
<2.0 × 10^{-4}	90	KEH	88	CBAL	E^{ee}_{cm} = 10 GeV
<6.4 × 10^{-4}	90	HAYES	82	MRK2	E^{ee}_{cm} = 3.8–6.8 GeV

$\Gamma(e^- \gamma\gamma)/\Gamma_{total}$ — Γ_{187}/Γ

VALUE	CL%	DOCUMENT ID		TECN	COMMENT
<2.5 × 10^{-4}	90	[1] BRYMAN	21	RVUE	516 fb^{-1}, E^{ee}_{cm} = 10.6 GeV

[1] BRYMAN 21 reinterprets the upper limit result on B($\tau^- \to e^- \gamma$) and B($\tau^- \to \mu^- \gamma$) by AUBERT 10B, estimating with a simulation the efficiency for this decay mode to be detected as the corresponding AUBERT 10B decay mode.

$\Gamma(\mu^- \gamma)/\Gamma_{total}$ — Γ_{188}/Γ

Test of lepton family number conservation.

VALUE	CL%	DOCUMENT ID		TECN	COMMENT
< 4.2 × 10^{-8}	90	UNO	21	BELL	988 fb^{-1}, E^{ee}_{cm} = 10.6 GeV
• • • We do not use the following data for averages, fits, limits, etc. • • •					
< 4.4 × 10^{-8}	90	AUBERT	10B	BABR	516 fb^{-1}, E^{ee}_{cm} = 10.6 GeV
< 4.5 × 10^{-8}	90	HAYASAKA	08	BELL	535 fb^{-1}, E^{ee}_{cm} = 10.6 GeV
< 6.8 × 10^{-8}	90	AUBERT,B	05A	BABR	232 fb^{-1}, E^{ee}_{cm} = 10.6 GeV
< 3.1 × 10^{-7}	90	ABE	04B	BELL	86.3 fb^{-1}, E^{ee}_{cm} = 10.6 GeV
< 1.1 × 10^{-6}	90	AHMED	00	CLEO	E^{ee}_{cm} = 10.6 GeV
< 3.0 × 10^{-6}	90	EDWARDS	97	CLEO	
< 6.2 × 10^{-5}	90	ABREU	95U	DLPH	1990–1993 LEP runs
< 0.42 × 10^{-5}	90	BEAN	93	CLEO	E^{ee}_{cm} = 10.6 GeV
< 3.4 × 10^{-5}	90	ALBRECHT	92K	ARG	E^{ee}_{cm} = 10 GeV
<55 × 10^{-5}	90	HAYES	82	MRK2	E^{ee}_{cm} = 3.8–6.8 GeV

$\Gamma(\mu^- \gamma\gamma)/\Gamma_{total}$ — Γ_{189}/Γ

VALUE	CL%	DOCUMENT ID		TECN	COMMENT
<5.8 × 10^{-4}	90	[1] BRYMAN	21	RVUE	516 fb^{-1}, E^{ee}_{cm} = 10.6 GeV

[1] BRYMAN 21 reinterprets the upper limit result on B($\tau^- \to e^- \gamma$) and B($\tau^- \to \mu^- \gamma$) by AUBERT 10B, estimating with a simulation the efficiency for this decay mode to be detected as the corresponding AUBERT 10B decay mode.

$\Gamma(e^- \pi^0)/\Gamma_{total}$ — Γ_{190}/Γ

Test of lepton family number conservation.

VALUE	CL%	DOCUMENT ID		TECN	COMMENT
< 8.0 × 10^{-8}	90	MIYAZAKI	07	BELL	401 fb^{-1}, E^{ee}_{cm}=10.6 GeV
• • • We do not use the following data for averages, fits, limits, etc. • • •					
< 1.3 × 10^{-7}	90	AUBERT	07I	BABR	339 fb^{-1}, E^{ee}_{cm}=10.6 GeV
< 1.9 × 10^{-7}	90	ENARI	05	BELL	154 fb^{-1}, E^{ee}_{cm}= 10.6 GeV
< 3.7 × 10^{-6}	90	BONVICINI	97	CLEO	E^{ee}_{cm} = 10.6 GeV
< 17 × 10^{-5}	90	ALBRECHT	92K	ARG	E^{ee}_{cm} = 10 GeV
< 14 × 10^{-5}	90	KEH	88	CBAL	E^{ee}_{cm} = 10 GeV
<210 × 10^{-5}	90	HAYES	82	MRK2	E^{ee}_{cm} = 3.8–6.8 GeV

$\Gamma(\mu^- \pi^0)/\Gamma_{total}$ — Γ_{191}/Γ

Test of lepton family number conservation.

VALUE	CL%	DOCUMENT ID		TECN	COMMENT
< 1.1 × 10^{-7}	90	AUBERT	07I	BABR	339 fb^{-1}, E^{ee}_{cm}=10.6 GeV
• • • We do not use the following data for averages, fits, limits, etc. • • •					
< 1.2 × 10^{-7}	90	MIYAZAKI	07	BELL	401 fb^{-1}, E^{ee}_{cm}=10.6 GeV
< 4.1 × 10^{-7}	90	ENARI	05	BELL	154 fb^{-1}, E^{ee}_{cm}= 10.6 GeV
< 4.0 × 10^{-6}	90	BONVICINI	97	CLEO	E^{ee}_{cm} = 10.6 GeV
< 4.4 × 10^{-5}	90	ALBRECHT	92K	ARG	E^{ee}_{cm} = 10 GeV
<82 × 10^{-5}	90	HAYES	82	MRK2	E^{ee}_{cm} = 3.8–6.8 GeV

$\Gamma(e^- K^0_S)/\Gamma_{total}$ — Γ_{192}/Γ

Test of lepton family number conservation.

VALUE	CL%	DOCUMENT ID		TECN	COMMENT
<0.8 × 10^{-8}	90	[1] ADACHI	25P	BELL	E^{ee}_{cm} = 10.6 GeV
• • • We do not use the following data for averages, fits, limits, etc. • • •					
<2.6 × 10^{-8}	90	MIYAZAKI	10A	BELL	671 fb^{-1} E^{ee}_{cm} = 10.6 GeV
<3.3 × 10^{-8}	90	AUBERT	09D	BABR	469 fb^{-1} E^{ee}_{cm} = 10.6 GeV
<5.6 × 10^{-8}	90	MIYAZAKI	06A	BELL	281 fb^{-1} E^{ee}_{cm} = 10.6 GeV
<9.1 × 10^{-7}	90	CHEN	02C	CLEO	E^{ee}_{cm}= 10.6 GeV
<1.3 × 10^{-3}	90	HAYES	82	MRK2	E^{ee}_{cm}= 3.8–6.8 GeV

[1] ADACHI 25P limit based on 428 fb^{-1} (Belle II) + 980 fb^{-1} (Belle) data.

$\Gamma(\mu^- K^0_S)/\Gamma_{total}$ — Γ_{193}/Γ

Test of lepton family number conservation.

VALUE	CL%	DOCUMENT ID		TECN	COMMENT
<1.2 × 10^{-8}	90	[1] ADACHI	25P	BELL	E^{ee}_{cm} = 10.6 GeV
• • • We do not use the following data for averages, fits, limits, etc. • • •					
<2.3 × 10^{-8}	90	MIYAZAKI	10A	BELL	671 fb^{-1} E^{ee}_{cm} = 10.6 GeV
<4.0 × 10^{-8}	90	AUBERT	09D	BABR	469 fb^{-1} E^{ee}_{cm} = 10.6 GeV
<4.9 × 10^{-8}	90	MIYAZAKI	06A	BELL	281 fb^{-1} E^{ee}_{cm} = 10.6 GeV
<9.5 × 10^{-7}	90	CHEN	02C	CLEO	E^{ee}_{cm}= 10.6 GeV
<1.0 × 10^{-3}	90	HAYES	82	MRK2	E^{ee}_{cm}= 3.8–6.8 GeV

[1] ADACHI 25P limit based on 428 fb^{-1} (Belle II) + 980 fb^{-1} (Belle) data.

$\Gamma(e^-\eta)/\Gamma_{total}$ — Γ_{194}/Γ

Test of lepton family number conservation.

VALUE	CL%	DOCUMENT ID		TECN	COMMENT
$< 9.2 \times 10^{-8}$	90	MIYAZAKI	07	BELL	401 fb^{-1}, E^{ee}_{cm}=10.6 GeV
• • • We do not use the following data for averages, fits, limits, etc. • • •					
$< 1.6 \times 10^{-7}$	90	AUBERT	07I	BABR	339 fb^{-1}, E^{ee}_{cm}=10.6 GeV
$< 2.4 \times 10^{-7}$	90	ENARI	05	BELL	154 fb^{-1}, E^{ee}_{cm}= 10.6 GeV
$< 8.2 \times 10^{-6}$	90	BONVICINI	97	CLEO	E^{ee}_{cm}= 10.6 GeV
$< 6.3 \times 10^{-5}$	90	ALBRECHT	92K	ARG	E^{ee}_{cm}= 10 GeV
$<24 \times 10^{-5}$	90	KEH	88	CBAL	E^{ee}_{cm}= 10 GeV

$\Gamma(\mu^-\eta)/\Gamma_{total}$ — Γ_{195}/Γ

Test of lepton family number conservation.

VALUE	CL%	DOCUMENT ID		TECN	COMMENT
$<6.5 \times 10^{-8}$	90	MIYAZAKI	07	BELL	401 fb^{-1}, E^{ee}_{cm}=10.6 GeV
• • • We do not use the following data for averages, fits, limits, etc. • • •					
$<1.5 \times 10^{-7}$	90	AUBERT	07I	BABR	339 fb^{-1}, E^{ee}_{cm}=10.6 GeV
$<1.5 \times 10^{-7}$	90	ENARI	05	BELL	154 fb^{-1}, E^{ee}_{cm}= 10.6 GeV
$<3.4 \times 10^{-7}$	90	ENARI	04	BELL	84.3 fb^{-1}, E^{ee}_{cm}=10.6 GeV
$<9.6 \times 10^{-6}$	90	BONVICINI	97	CLEO	E^{ee}_{cm}= 10.6 GeV
$<7.3 \times 10^{-5}$	90	ALBRECHT	92K	ARG	E^{ee}_{cm}= 10 GeV

$\Gamma(e^-\rho^0)/\Gamma_{total}$ — Γ_{196}/Γ

Test of lepton family number conservation.

VALUE	CL%	DOCUMENT ID		TECN	COMMENT
$< 2.2 \times 10^{-8}$	90	[1] TSUZUKI	23	BELL	980 fb^{-1} E^{ee}_{cm} = 10.6 GeV
• • • We do not use the following data for averages, fits, limits, etc. • • •					
$< 1.8 \times 10^{-8}$	90	MIYAZAKI	11	BELL	854 fb^{-1} E^{ee}_{cm} = 10.6 GeV
$< 4.6 \times 10^{-8}$	90	AUBERT	09W	BABR	451 fb^{-1} E^{ee}_{cm} = 10.6 GeV
$< 6.3 \times 10^{-8}$	90	NISHIO	08	BELL	543 fb^{-1} E^{ee}_{cm} = 10.6 GeV
$< 6.5 \times 10^{-7}$	90	YUSA	06	BELL	158 fb^{-1} E^{ee}_{cm} = 10.6 GeV
$< 2.0 \times 10^{-6}$	90	BLISS	98	CLEO	E^{ee}_{cm}= 10.6 GeV
$< 4.2 \times 10^{-6}$	90	[2] BARTELT	94	CLEO	Repl. by BLISS 98
$< 1.9 \times 10^{-5}$	90	ALBRECHT	92K	ARG	E^{ee}_{cm}= 10 GeV
$<37 \times 10^{-5}$	90	HAYES	82	MRK2	E^{ee}_{cm}= 3.8–6.8 GeV

[1] Supersedes MIYAZAKI 11.
[2] BARTELT 94 assume phase space decays.

$\Gamma(\mu^-\rho^0)/\Gamma_{total}$ — Γ_{197}/Γ

Test of lepton family number conservation.

VALUE	CL%	DOCUMENT ID		TECN	COMMENT
$< 1.7 \times 10^{-8}$	90	[1] TSUZUKI	23	BELL	980 fb^{-1} E^{ee}_{cm} = 10.6 GeV
• • • We do not use the following data for averages, fits, limits, etc. • • •					
$< 1.2 \times 10^{-8}$	90	MIYAZAKI	11	BELL	854 fb^{-1} E^{ee}_{cm} = 10.6 GeV
$< 2.6 \times 10^{-8}$	90	AUBERT	09W	BABR	451 fb^{-1} E^{ee}_{cm} = 10.6 GeV
$< 6.8 \times 10^{-8}$	90	NISHIO	08	BELL	543 fb^{-1} E^{ee}_{cm} = 10.6 GeV
$< 2.0 \times 10^{-7}$	90	YUSA	06	BELL	158 fb^{-1} E^{ee}_{cm} = 10.6 GeV
$< 6.3 \times 10^{-6}$	90	BLISS	98	CLEO	E^{ee}_{cm}= 10.6 GeV
$< 5.7 \times 10^{-6}$	90	[2] BARTELT	94	CLEO	Repl. by BLISS 98
$< 2.9 \times 10^{-5}$	90	ALBRECHT	92K	ARG	E^{ee}_{cm}= 10 GeV
$<44 \times 10^{-5}$	90	HAYES	82	MRK2	E^{ee}_{cm}= 3.8–6.8 GeV

[1] Supersedes MIYAZAKI 11.
[2] BARTELT 94 assume phase space decays.

$\Gamma(e^-\omega)/\Gamma_{total}$ — Γ_{198}/Γ

VALUE	CL%	DOCUMENT ID		TECN	COMMENT
$<2.4 \times 10^{-8}$	90	[1] TSUZUKI	23	BELL	980 fb^{-1} E^{ee}_{cm} = 10.6 GeV
• • • We do not use the following data for averages, fits, limits, etc. • • •					
$<4.8 \times 10^{-8}$	90	MIYAZAKI	11	BELL	854 fb^{-1} E^{ee}_{cm} = 10.6 GeV
$<1.1 \times 10^{-7}$	90	AUBERT	08K	BABR	384 fb^{-1} E^{ee}_{cm} = 10.6 GeV
$<1.8 \times 10^{-7}$	90	NISHIO	08	BELL	543 fb^{-1} E^{ee}_{cm} = 10.6 GeV

[1] Supersedes MIYAZAKI 11.

$\Gamma(\mu^-\omega)/\Gamma_{total}$ — Γ_{199}/Γ

VALUE	CL%	DOCUMENT ID		TECN	COMMENT
$<3.9 \times 10^{-8}$	90	[1] TSUZUKI	23	BELL	980 fb^{-1} E^{ee}_{cm} = 10.6 GeV
• • • We do not use the following data for averages, fits, limits, etc. • • •					
$<4.7 \times 10^{-8}$	90	MIYAZAKI	11	BELL	854 fb^{-1} E^{ee}_{cm} = 10.6 GeV
$<1.0 \times 10^{-7}$	90	AUBERT	08K	BABR	384 fb^{-1} E^{ee}_{cm} = 10.6 GeV
$<8.9 \times 10^{-8}$	90	NISHIO	08	BELL	543 fb^{-1} E^{ee}_{cm} = 10.6 GeV

[1] Supersedes MIYAZAKI 11.

$\Gamma(e^- K^*(892)^0)/\Gamma_{total}$ — Γ_{200}/Γ

Test of lepton family number conservation.

VALUE	CL%	DOCUMENT ID		TECN	COMMENT
$<1.9 \times 10^{-8}$	90	[1] TSUZUKI	23	BELL	980 fb^{-1} E^{ee}_{cm} = 10.6 GeV
• • • We do not use the following data for averages, fits, limits, etc. • • •					
$<3.2 \times 10^{-8}$	90	MIYAZAKI	11	BELL	854 fb^{-1} E^{ee}_{cm} = 10.6 GeV
$<5.9 \times 10^{-8}$	90	AUBERT	09W	BABR	451 fb^{-1} E^{ee}_{cm} = 10.6 GeV
$<7.8 \times 10^{-8}$	90	NISHIO	08	BELL	543 fb^{-1} E^{ee}_{cm} = 10.6 GeV
$<3.0 \times 10^{-7}$	90	YUSA	06	BELL	158 fb^{-1} E^{ee}_{cm} = 10.6 GeV
$<5.1 \times 10^{-6}$	90	BLISS	98	CLEO	E^{ee}_{cm}= 10.6 GeV
$<6.3 \times 10^{-6}$	90	[2] BARTELT	94	CLEO	Repl. by BLISS 98
$<3.8 \times 10^{-5}$	90	ALBRECHT	92K	ARG	E^{ee}_{cm}= 10 GeV

[1] Supersedes MIYAZAKI 11.
[2] BARTELT 94 assume phase space decays.

$\Gamma(\mu^- K^*(892)^0)/\Gamma_{total}$ — Γ_{201}/Γ

Test of lepton family number conservation.

VALUE	CL%	DOCUMENT ID		TECN	COMMENT
$<2.9 \times 10^{-8}$	90	[1] TSUZUKI	23	BELL	980 fb^{-1} E^{ee}_{cm} = 10.6 GeV
• • • We do not use the following data for averages, fits, limits, etc. • • •					
$<7.2 \times 10^{-8}$	90	MIYAZAKI	11	BELL	854 fb^{-1} E^{ee}_{cm} = 10.6 GeV
$<1.7 \times 10^{-7}$	90	AUBERT	09W	BABR	451 fb^{-1} E^{ee}_{cm} = 10.6 GeV
$<5.9 \times 10^{-8}$	90	NISHIO	08	BELL	543 fb^{-1} E^{ee}_{cm} = 10.6 GeV
$<3.9 \times 10^{-7}$	90	YUSA	06	BELL	158 fb^{-1} E^{ee}_{cm} = 10.6 GeV
$<7.5 \times 10^{-6}$	90	BLISS	98	CLEO	E^{ee}_{cm}= 10.6 GeV
$<9.4 \times 10^{-6}$	90	[2] BARTELT	94	CLEO	Repl. by BLISS 98
$<4.5 \times 10^{-5}$	90	ALBRECHT	92K	ARG	E^{ee}_{cm}= 10 GeV

[1] Supersedes MIYAZAKI 11.
[2] BARTELT 94 assume phase space decays.

$\Gamma(e^-\overline{K}^*(892)^0)/\Gamma_{total}$ — Γ_{202}/Γ

Test of lepton family number conservation.

VALUE	CL%	DOCUMENT ID		TECN	COMMENT
$<1.7 \times 10^{-8}$	90	[1] TSUZUKI	23	BELL	980 fb^{-1} E^{ee}_{cm} = 10.6 GeV
• • • We do not use the following data for averages, fits, limits, etc. • • •					
$<3.4 \times 10^{-8}$	90	MIYAZAKI	11	BELL	854 fb^{-1} E^{ee}_{cm} = 10.6 GeV
$<4.6 \times 10^{-8}$	90	AUBERT	09W	BABR	451 fb^{-1} E^{ee}_{cm} = 10.6 GeV
$<7.7 \times 10^{-8}$	90	NISHIO	08	BELL	543 fb^{-1} E^{ee}_{cm} = 10.6 GeV
$<4.0 \times 10^{-7}$	90	YUSA	06	BELL	158 fb^{-1} E^{ee}_{cm} = 10.6 GeV
$<7.4 \times 10^{-6}$	90	BLISS	98	CLEO	E^{ee}_{cm}= 10.6 GeV
$<1.1 \times 10^{-5}$	90	[2] BARTELT	94	CLEO	Repl. by BLISS 98

[1] Supersedes MIYAZAKI 11.
[2] BARTELT 94 assume phase space decays.

$\Gamma(\mu^-\overline{K}^*(892)^0)/\Gamma_{total}$ — Γ_{203}/Γ

Test of lepton family number conservation.

VALUE	CL%	DOCUMENT ID		TECN	COMMENT
$<4.3 \times 10^{-8}$	90	[1] TSUZUKI	23	BELL	980 fb^{-1} E^{ee}_{cm} = 10.6 GeV
• • • We do not use the following data for averages, fits, limits, etc. • • •					
$<7.0 \times 10^{-8}$	90	MIYAZAKI	11	BELL	854 fb^{-1} E^{ee}_{cm} = 10.6 GeV
$<7.3 \times 10^{-8}$	90	AUBERT	09W	BABR	451 fb^{-1} E^{ee}_{cm} = 10.6 GeV
$<1.0 \times 10^{-7}$	90	NISHIO	08	BELL	543 fb^{-1} E^{ee}_{cm} = 10.6 GeV
$<4.0 \times 10^{-7}$	90	YUSA	06	BELL	158 fb^{-1} E^{ee}_{cm} = 10.6 GeV
$<7.5 \times 10^{-6}$	90	BLISS	98	CLEO	E^{ee}_{cm}= 10.6 GeV
$<8.7 \times 10^{-6}$	90	[2] BARTELT	94	CLEO	Repl. by BLISS 98

[1] Supersedes MIYAZAKI 11.
[2] BARTELT 94 assume phase space decays.

$\Gamma(e^-\eta'(958))/\Gamma_{total}$ — Γ_{204}/Γ

VALUE	CL%	DOCUMENT ID		TECN	COMMENT
$< 1.6 \times 10^{-7}$	90	MIYAZAKI	07	BELL	401 fb^{-1}, E^{ee}_{cm}=10.6 GeV
• • • We do not use the following data for averages, fits, limits, etc. • • •					
$< 2.4 \times 10^{-7}$	90	AUBERT	07I	BABR	339 fb^{-1}, E^{ee}_{cm}=10.6 GeV
$<10. \times 10^{-7}$	90	ENARI	05	BELL	154 fb^{-1}, E^{ee}_{cm}= 10.6 GeV

$\Gamma(\mu^-\eta'(958))/\Gamma_{total}$ — Γ_{205}/Γ

VALUE	CL%	DOCUMENT ID		TECN	COMMENT
$<1.3 \times 10^{-7}$	90	MIYAZAKI	07	BELL	401 fb^{-1}, E^{ee}_{cm}=10.6 GeV
• • • We do not use the following data for averages, fits, limits, etc. • • •					
$<1.4 \times 10^{-7}$	90	AUBERT	07I	BABR	339 fb^{-1}, E^{ee}_{cm}=10.6 GeV
$<4.7 \times 10^{-7}$	90	ENARI	05	BELL	154 fb^{-1}, E^{ee}_{cm}= 10.6 GeV

$\Gamma(e^- f_0(980) \to e^-\pi^+\pi^-)/\Gamma_{total}$ — Γ_{206}/Γ

VALUE	CL%	DOCUMENT ID		TECN	COMMENT
$<3.2 \times 10^{-8}$	90	MIYAZAKI	09	BELL	671 fb^{-1} E^{ee}_{cm}= 10.6 GeV

$\Gamma(\mu^- f_0(980) \to \mu^-\pi^+\pi^-)/\Gamma_{total}$ — Γ_{207}/Γ

VALUE	CL%	DOCUMENT ID		TECN	COMMENT
$<3.4 \times 10^{-8}$	90	MIYAZAKI	09	BELL	671 fb^{-1} E^{ee}_{cm}= 10.6 GeV

$\Gamma(e^-\phi)/\Gamma_{total}$ — Γ_{208}/Γ

Test of lepton family number conservation.

VALUE	CL%	DOCUMENT ID		TECN	COMMENT
$<2.0 \times 10^{-8}$	90	[1] TSUZUKI	23	BELL	980 fb^{-1} E^{ee}_{cm} = 10.6 GeV

Int. J. Mod
by UNIVERSITY OF CALIFORNIA @ BERK
wnloaded from www.worldscientific.com
-use and distribution is strictly not permitted, except for Open Access articles.

Int. J. Mod. Phys. A 2026.41. Downloaded from www.worldscientific.com
by UNIVERSITY OF CALIFORNIA @ BERKELEY on 09/16/26. Re-use and distribution is strictly not permitted, except for Open Access articles.

• • • We do not use the following data for averages, fits, limits, etc. • • •

$<3.1 \times 10^{-8}$	90	MIYAZAKI	11	BELL	854 fb^{-1} E^{ee}_{cm} = 10.6 GeV
$<3.1 \times 10^{-8}$	90	AUBERT	09W	BABR	451 fb^{-1} E^{ee}_{cm} = 10.6 GeV
$<7.3 \times 10^{-8}$	90	NISHIO	08	BELL	543 fb^{-1} E^{ee}_{cm} = 10.6 GeV
$<7.3 \times 10^{-7}$	90	YUSA	06	BELL	158 fb^{-1} E^{ee}_{cm} = 10.6 GeV
$<6.9 \times 10^{-6}$	90	BLISS	98	CLEO	E^{ee}_{cm} = 10.6 GeV

[1] Supersedes MIYAZAKI 11.

$\Gamma(\mu^- \phi)/\Gamma_{total}$ — Γ_{209}/Γ

Test of lepton family number conservation.

VALUE	CL%	DOCUMENT ID		TECN	COMMENT
$<2.3 \times 10^{-8}$	90	[1] TSUZUKI	23	BELL	980 fb^{-1} E^{ee}_{cm} = 10.6 GeV

• • • We do not use the following data for averages, fits, limits, etc. • • •

$<8.4 \times 10^{-8}$	90	MIYAZAKI	11	BELL	854 fb^{-1} E^{ee}_{cm} = 10.6 GeV
$<1.9 \times 10^{-7}$	90	AUBERT	09W	BABR	451 fb^{-1} E^{ee}_{cm} = 10.6 GeV
$<1.3 \times 10^{-7}$	90	NISHIO	08	BELL	543 fb^{-1} E^{ee}_{cm} = 10.6 GeV
$<7.7 \times 10^{-7}$	90	YUSA	06	BELL	158 fb^{-1} E^{ee}_{cm} = 10.6 GeV
$<7.0 \times 10^{-6}$	90	BLISS	98	CLEO	E^{ee}_{cm} = 10.6 GeV

[1] Supersedes MIYAZAKI 11.

$\Gamma(e^- e^+ e^-)/\Gamma_{total}$ — Γ_{210}/Γ

Test of lepton family number conservation.

VALUE	CL%	DOCUMENT ID		TECN	COMMENT
$< 2.5 \times 10^{-8}$	90	ADACHI	25AB	BEL2	428 fb^{-1} E^{ee}_{cm} = 10.5–10.8 GeV

• • • We do not use the following data for averages, fits, limits, etc. • • •

$< 2.7 \times 10^{-8}$	90	HAYASAKA	10	BELL	782 fb^{-1} E^{ee}_{cm} = 10.6 GeV
$< 2.9 \times 10^{-8}$	90	LEES	10A	BABR	468 fb^{-1} E^{ee}_{cm} = 10.6 GeV
$< 3.6 \times 10^{-8}$	90	MIYAZAKI	08	BELL	535 fb^{-1} E^{ee}_{cm} = 10.6 GeV
$< 4.3 \times 10^{-8}$	90	AUBERT	07BK	BABR	376 fb^{-1} E^{ee}_{cm} = 10.6 GeV
$< 2.0 \times 10^{-7}$	90	AUBERT	04J	BABR	91.5 fb^{-1} E^{ee}_{cm} = 10.6 GeV
$< 3.5 \times 10^{-7}$	90	YUSA	04	BELL	87.1 fb^{-1} E^{ee}_{cm} = 10.6 GeV
$< 2.9 \times 10^{-6}$	90	BLISS	98	CLEO	E^{ee}_{cm} = 10.6 GeV
$< 0.33 \times 10^{-5}$	90	[1] BARTELT	94	CLEO	Repl. by BLISS 98
$< 1.3 \times 10^{-5}$	90	ALBRECHT	92K	ARG	E^{ee}_{cm} = 10 GeV
$< 2.7 \times 10^{-5}$	90	BOWCOCK	90	CLEO	E^{ee}_{cm} = 10.4–10.9
$<40 \times 10^{-5}$	90	HAYES	82	MRK2	E^{ee}_{cm} = 3.8–6.8 GeV

[1] BARTELT 94 assume phase space decays.

$\Gamma(e^- \mu^+ \mu^-)/\Gamma_{total}$ — Γ_{211}/Γ

Test of lepton family number conservation.

VALUE	CL%	DOCUMENT ID		TECN	COMMENT
$< 2.4 \times 10^{-8}$	90	ADACHI	25AB	BEL2	428 fb^{-1} E^{ee}_{cm} = 10.5–10.8 GeV

• • • We do not use the following data for averages, fits, limits, etc. • • •

$< 2.7 \times 10^{-8}$	90	HAYASAKA	10	BELL	782 fb^{-1} E^{ee}_{cm} = 10.6 GeV
$< 3.2 \times 10^{-8}$	90	LEES	10A	BABR	468 fb^{-1} E^{ee}_{cm} = 10.6 GeV
$< 4.1 \times 10^{-8}$	90	MIYAZAKI	08	BELL	535 fb^{-1} E^{ee}_{cm} = 10.6 GeV
$< 3.7 \times 10^{-8}$	90	AUBERT	07BK	BABR	376 fb^{-1} E^{ee}_{cm} = 10.6 GeV
$< 3.3 \times 10^{-7}$	90	AUBERT	04J	BABR	91.5 fb^{-1} E^{ee}_{cm} = 10.6 GeV
$< 2.0 \times 10^{-7}$	90	YUSA	04	BELL	87.1 fb^{-1} E^{ee}_{cm} = 10.6 GeV
$< 1.8 \times 10^{-6}$	90	BLISS	98	CLEO	E^{ee}_{cm} = 10.6 GeV
$< 0.36 \times 10^{-5}$	90	[1] BARTELT	94	CLEO	Repl. by BLISS 98
$< 1.9 \times 10^{-5}$	90	ALBRECHT	92K	ARG	E^{ee}_{cm} = 10 GeV
$< 2.7 \times 10^{-5}$	90	BOWCOCK	90	CLEO	E^{ee}_{cm} = 10.4–10.9
$<33 \times 10^{-5}$	90	HAYES	82	MRK2	E^{ee}_{cm} = 3.8–6.8 GeV

[1] BARTELT 94 assume phase space decays.

$\Gamma(e^+ \mu^- \mu^-)/\Gamma_{total}$ — Γ_{212}/Γ

Test of lepton family number conservation.

VALUE	CL%	DOCUMENT ID		TECN	COMMENT
$<1.3 \times 10^{-8}$	90	ADACHI	25AB	BEL2	428 fb^{-1} E^{ee}_{cm} = 10.5–10.8 GeV

• • • We do not use the following data for averages, fits, limits, etc. • • •

$<1.7 \times 10^{-8}$	90	HAYASAKA	10	BELL	782 fb^{-1} E^{ee}_{cm} = 10.6 GeV
$<2.6 \times 10^{-8}$	90	LEES	10A	BABR	468 fb^{-1} E^{ee}_{cm} = 10.6 GeV
$<2.3 \times 10^{-8}$	90	MIYAZAKI	08	BELL	535 fb^{-1} E^{ee}_{cm} = 10.6 GeV
$<5.6 \times 10^{-8}$	90	AUBERT	07BK	BABR	376 fb^{-1} E^{ee}_{cm} = 10.6 GeV
$<1.3 \times 10^{-7}$	90	AUBERT	04J	BABR	91.5 fb^{-1} E^{ee}_{cm} = 10.6 GeV
$<2.0 \times 10^{-7}$	90	YUSA	04	BELL	87.1 fb^{-1} E^{ee}_{cm} = 10.6 GeV
$<1.5 \times 10^{-6}$	90	BLISS	98	CLEO	E^{ee}_{cm} = 10.6 GeV
$<0.35 \times 10^{-5}$	90	[1] BARTELT	94	CLEO	Repl. by BLISS 98
$<1.8 \times 10^{-5}$	90	ALBRECHT	92K	ARG	E^{ee}_{cm} = 10 GeV
$<1.6 \times 10^{-5}$	90	BOWCOCK	90	CLEO	E^{ee}_{cm} = 10.4–10.9

[1] BARTELT 94 assume phase space decays.

$\Gamma(\mu^- e^+ e^-)/\Gamma_{total}$ — Γ_{213}/Γ

Test of lepton family number conservation.

VALUE	CL%	DOCUMENT ID		TECN	COMMENT
$< 1.6 \times 10^{-8}$	90	ADACHI	25AB	BEL2	428 fb^{-1} E^{ee}_{cm} = 10.5–10.8 GeV

• • • We do not use the following data for averages, fits, limits, etc. • • •

$< 1.8 \times 10^{-8}$	90	HAYASAKA	10	BELL	782 fb^{-1} E^{ee}_{cm} = 10.6 GeV
$< 2.2 \times 10^{-8}$	90	LEES	10A	BABR	468 fb^{-1} E^{ee}_{cm} = 10.6 GeV
$< 2.7 \times 10^{-8}$	90	MIYAZAKI	08	BELL	535 fb^{-1} E^{ee}_{cm} = 10.6 GeV
$< 8.0 \times 10^{-8}$	90	AUBERT	07BK	BABR	376 fb^{-1} E^{ee}_{cm} = 10.6 GeV
$< 2.7 \times 10^{-7}$	90	AUBERT	04J	BABR	91.5 fb^{-1} E^{ee}_{cm} = 10.6 GeV
$< 1.9 \times 10^{-7}$	90	YUSA	04	BELL	87.1 fb^{-1} E^{ee}_{cm} = 10.6 GeV
$< 1.7 \times 10^{-6}$	90	BLISS	98	CLEO	E^{ee}_{cm} = 10.6 GeV
$< 0.34 \times 10^{-5}$	90	[1] BARTELT	94	CLEO	Repl. by BLISS 98
$< 1.4 \times 10^{-5}$	90	ALBRECHT	92K	ARG	E^{ee}_{cm} = 10 GeV
$< 2.7 \times 10^{-5}$	90	BOWCOCK	90	CLEO	E^{ee}_{cm} = 10.4–10.9
$<44 \times 10^{-5}$	90	HAYES	82	MRK2	E^{ee}_{cm} = 3.8–6.8 GeV

[1] BARTELT 94 assume phase space decays.

$\Gamma(\mu^+ e^- e^-)/\Gamma_{total}$ — Γ_{214}/Γ

Test of lepton family number conservation.

VALUE	CL%	DOCUMENT ID		TECN	COMMENT
$<1.5 \times 10^{-8}$	90	HAYASAKA	10	BELL	782 fb^{-1} E^{ee}_{cm} = 10.6 GeV

• • • We do not use the following data for averages, fits, limits, etc. • • •

$<1.6 \times 10^{-8}$	90	ADACHI	25AB	BEL2	428 fb^{-1} E^{ee}_{cm} = 10.5–10.8 GeV
$<1.8 \times 10^{-8}$	90	LEES	10A	BABR	468 fb^{-1} E^{ee}_{cm} = 10.6 GeV
$<2.0 \times 10^{-8}$	90	MIYAZAKI	08	BELL	535 fb^{-1} E^{ee}_{cm} = 10.6 GeV
$<5.8 \times 10^{-8}$	90	AUBERT	07BK	BABR	376 fb^{-1} E^{ee}_{cm} = 10.6 GeV
$<1.1 \times 10^{-7}$	90	AUBERT	04J	BABR	91.5 fb^{-1} E^{ee}_{cm} = 10.6 GeV
$<2.0 \times 10^{-7}$	90	YUSA	04	BELL	87.1 fb^{-1} E^{ee}_{cm} = 10.6 GeV
$<1.5 \times 10^{-6}$	90	BLISS	98	CLEO	E^{ee}_{cm} = 10.6 GeV
$<0.34 \times 10^{-5}$	90	[1] BARTELT	94	CLEO	Repl. by BLISS 98
$<1.4 \times 10^{-5}$	90	ALBRECHT	92K	ARG	E^{ee}_{cm} = 10 GeV
$<1.6 \times 10^{-5}$	90	BOWCOCK	90	CLEO	E^{ee}_{cm} = 10.4–10.9

[1] BARTELT 94 assume phase space decays.

$\Gamma(\mu^- \mu^+ \mu^-)/\Gamma_{total}$ — Γ_{215}/Γ

Test of lepton family number conservation.

VALUE	CL%	DOCUMENT ID		TECN	COMMENT
$< 1.9 \times 10^{-8}$	90	ADACHI	24R	BELL	424 fb^{-1}, E^{ee}_{cm} = 10.6 GeV

• • • We do not use the following data for averages, fits, limits, etc. • • •

$< 2.9 \times 10^{-8}$	90	[1] HAYRAPETY...24J		CMS	131 fb^{-1}, pp at 13 TeV
$< 8.0 \times 10^{-8}$	90	[2] SIRUNYAN	21D	CMS	33.2 fb^{-1}, pp at 13 TeV
$< 3.8 \times 10^{-7}$	90	AAD	16BA	ATLS	20.3 fb^{-1}, pp at 8 TeV
$< 4.6 \times 10^{-8}$	90	AAIJ	15AI	LHCB	3.0 fb^{-1}, pp at 7, 8 TeV
$< 8.0 \times 10^{-8}$	90	[3] AAIJ	13AH	LHCB	1.0 fb^{-1}, pp at 7 TeV
$< 2.1 \times 10^{-8}$	90	HAYASAKA	10	BELL	782 fb^{-1} E^{ee}_{cm} = 10.6 GeV
$< 3.3 \times 10^{-8}$	90	LEES	10A	BABR	468 fb^{-1} E^{ee}_{cm} = 10.6 GeV
$< 3.2 \times 10^{-8}$	90	MIYAZAKI	08	BELL	535 fb^{-1} E^{ee}_{cm} = 10.6 GeV
$< 5.3 \times 10^{-8}$	90	AUBERT	07BK	BABR	376 fb^{-1} E^{ee}_{cm} = 10.6 GeV
$< 1.9 \times 10^{-7}$	90	AUBERT	04J	BABR	91.5 fb^{-1} E^{ee}_{cm} = 10.6 GeV
$< 2.0 \times 10^{-7}$	90	YUSA	04	BELL	87.1 fb^{-1} E^{ee}_{cm} = 10.6 GeV
$< 1.9 \times 10^{-6}$	90	BLISS	98	CLEO	E^{ee}_{cm} = 10.6 GeV
$< 0.43 \times 10^{-5}$	90	[4] BARTELT	94	CLEO	Repl. by BLISS 98
$< 1.9 \times 10^{-5}$	90	ALBRECHT	92K	ARG	E^{ee}_{cm} = 10 GeV
$< 1.7 \times 10^{-5}$	90	BOWCOCK	90	CLEO	E^{ee}_{cm} = 10.4–10.9
$<49 \times 10^{-5}$	90	HAYES	82	MRK2	E^{ee}_{cm} = 3.8–6.8 GeV

[1] HAYRAPETYAN 24J use 33.2 fb^{-1} of data taken in 2016 and used for the same search in SIRUNYAN 21D and 97.7 fb^{-1} of data taken in 2017-2018.
[2] Superseded by HAYRAPETYAN 24J.
[3] Repl. by AAIJ 15AI.
[4] BARTELT 94 assume phase space decays.

$\Gamma(e^- \pi^+ \pi^-)/\Gamma_{total}$ — Γ_{216}/Γ

Test of lepton family number conservation.

VALUE	CL%	DOCUMENT ID		TECN	COMMENT
$<2.3 \times 10^{-8}$	90	MIYAZAKI	13	BELL	854 fb^{-1} E^{ee}_{cm} = 10.6 GeV

• • • We do not use the following data for averages, fits, limits, etc. • • •

$<4.4 \times 10^{-8}$	90	MIYAZAKI	10	BELL	Repl. by MIYAZAKI 13
$<7.3 \times 10^{-7}$	90	YUSA	06	BELL	158 fb^{-1} E^{ee}_{cm} = 10.6 GeV
$<1.2 \times 10^{-7}$	90	AUBERT,BE	05D	BABR	221 fb^{-1}, E^{ee}_{cm} = 10.6 GeV
$<2.2 \times 10^{-6}$	90	BLISS	98	CLEO	E^{ee}_{cm} = 10.6 GeV
$<4.4 \times 10^{-6}$	90	[1] BARTELT	94	CLEO	Repl. by BLISS 98
$<2.7 \times 10^{-5}$	90	ALBRECHT	92K	ARG	E^{ee}_{cm} = 10 GeV
$<6.0 \times 10^{-5}$	90	BOWCOCK	90	CLEO	E^{ee}_{cm} = 10.4–10.9

[1] BARTELT 94 assume phase space decays.

$\Gamma(e^+ \pi^- \pi^-)/\Gamma_{total}$ — Γ_{217}/Γ

Test of lepton number conservation.

VALUE	CL%	DOCUMENT ID		TECN	COMMENT
$<2.0 \times 10^{-8}$	90	MIYAZAKI	13	BELL	854 fb^{-1} E^{ee}_{cm} = 10.6 GeV

• • • We do not use the following data for averages, fits, limits, etc. • • •

$<8.8 \times 10^{-8}$	90	MIYAZAKI	10	BELL	Repl. by MIYAZAKI 13

$<2.0\times10^{-7}$	90	YUSA	06	BELL	158 fb^{-1} E^{ee}_{cm} = 10.6 GeV
$<2.7\times10^{-7}$	90	AUBERT,BE	05D	BABR	221 fb^{-1}, E^{ee}_{cm} = 10.6 GeV
$<1.9\times10^{-6}$	90	BLISS	98	CLEO	E^{ee}_{cm} = 10.6 GeV
$<4.4\times10^{-6}$	90	[1] BARTELT	94	CLEO	Repl. by BLISS 98
$<1.8\times10^{-5}$	90	ALBRECHT	92K	ARG	E^{ee}_{cm} = 10 GeV
$<1.7\times10^{-5}$	90	BOWCOCK	90	CLEO	E^{ee}_{cm} = 10.4–10.9

[1] BARTELT 94 assume phase space decays.

$\Gamma(\mu^-\pi^+\pi^-)/\Gamma_{total}$ — Γ_{218}/Γ

Test of lepton family number conservation.

VALUE	CL%	DOCUMENT ID		TECN	COMMENT
$<2.1\times10^{-8}$	90	MIYAZAKI	13	BELL	854 fb^{-1} E^{ee}_{cm} = 10.6 GeV
• • • We do not use the following data for averages, fits, limits, etc. • • •					
$<3.3\times10^{-8}$	90	MIYAZAKI	10	BELL	Repl. by MIYAZAKI 13
$<4.8\times10^{-7}$	90	YUSA	06	BELL	158 fb^{-1} E^{ee}_{cm} = 10.6 GeV
$<2.9\times10^{-7}$	90	AUBERT,BE	05D	BABR	221 fb^{-1}, E^{ee}_{cm} = 10.6 GeV
$<8.2\times10^{-6}$	90	BLISS	98	CLEO	E^{ee}_{cm} = 10.6 GeV
$<7.4\times10^{-6}$	90	[1] BARTELT	94	CLEO	Repl. by BLISS 98
$<3.6\times10^{-5}$	90	ALBRECHT	92K	ARG	E^{ee}_{cm} = 10 GeV
$<3.9\times10^{-5}$	90	BOWCOCK	90	CLEO	E^{ee}_{cm} = 10.4–10.9

[1] BARTELT 94 assume phase space decays.

$\Gamma(\mu^+\pi^-\pi^-)/\Gamma_{total}$ — Γ_{219}/Γ

Test of lepton number conservation.

VALUE	CL%	DOCUMENT ID		TECN	COMMENT
$<3.9\times10^{-8}$	90	MIYAZAKI	13	BELL	854 fb^{-1} E^{ee}_{cm} = 10.6 GeV
• • • We do not use the following data for averages, fits, limits, etc. • • •					
$<3.7\times10^{-8}$	90	MIYAZAKI	10	BELL	Repl. by MIYAZAKI 13
$<3.4\times10^{-7}$	90	YUSA	06	BELL	158 fb^{-1} E^{ee}_{cm} = 10.6 GeV
$<7\times10^{-8}$	90	AUBERT,BE	05D	BABR	221 fb^{-1}, E^{ee}_{cm} = 10.6 GeV
$<3.4\times10^{-6}$	90	BLISS	98	CLEO	E^{ee}_{cm} = 10.6 GeV
$<6.9\times10^{-6}$	90	[1] BARTELT	94	CLEO	Repl. by BLISS 98
$<6.3\times10^{-5}$	90	ALBRECHT	92K	ARG	E^{ee}_{cm} = 10 GeV
$<3.9\times10^{-5}$	90	BOWCOCK	90	CLEO	E^{ee}_{cm} = 10.4–10.9

[1] BARTELT 94 assume phase space decays.

$\Gamma(e^-\pi^+K^-)/\Gamma_{total}$ — Γ_{220}/Γ

Test of lepton family number conservation.

VALUE	CL%	DOCUMENT ID		TECN	COMMENT
$<3.7\times10^{-8}$	90	MIYAZAKI	13	BELL	854 fb^{-1} E^{ee}_{cm} = 10.6 GeV
• • • We do not use the following data for averages, fits, limits, etc. • • •					
$<5.8\times10^{-8}$	90	MIYAZAKI	10	BELL	Repl. by MIYAZAKI 13
$<7.2\times10^{-7}$	90	YUSA	06	BELL	158 fb^{-1} E^{ee}_{cm} = 10.6 GeV
$<3.2\times10^{-7}$	90	AUBERT,BE	05D	BABR	221 fb^{-1}, E^{ee}_{cm} = 10.6 GeV
$<6.4\times10^{-6}$	90	BLISS	98	CLEO	E^{ee}_{cm} = 10.6 GeV
$<7.7\times10^{-6}$	90	[1] BARTELT	94	CLEO	Repl. by BLISS 98
$<2.9\times10^{-5}$	90	ALBRECHT	92K	ARG	E^{ee}_{cm} = 10 GeV
$<5.8\times10^{-5}$	90	BOWCOCK	90	CLEO	E^{ee}_{cm} = 10.4–10.9

[1] BARTELT 94 assume phase space decays.

$\Gamma(e^-\pi^-K^+)/\Gamma_{total}$ — Γ_{221}/Γ

Test of lepton family number conservation.

VALUE	CL%	DOCUMENT ID		TECN	COMMENT
$<3.1\times10^{-8}$	90	MIYAZAKI	13	BELL	854 fb^{-1} E^{ee}_{cm} = 10.6 GeV
• • • We do not use the following data for averages, fits, limits, etc. • • •					
$<5.2\times10^{-8}$	90	MIYAZAKI	10	BELL	Repl. by MIYAZAKI 13
$<1.6\times10^{-7}$	90	YUSA	06	BELL	158 fb^{-1} E^{ee}_{cm} = 10.6 GeV
$<1.7\times10^{-7}$	90	AUBERT,BE	05D	BABR	221 fb^{-1}, E^{ee}_{cm} = 10.6 GeV
$<3.8\times10^{-6}$	90	BLISS	98	CLEO	E^{ee}_{cm} = 10.6 GeV
$<4.6\times10^{-6}$	90	[1] BARTELT	94	CLEO	Repl. by BLISS 98
$<5.8\times10^{-5}$	90	BOWCOCK	90	CLEO	E^{ee}_{cm} = 10.4–10.9

[1] BARTELT 94 assume phase space decays.

$\Gamma(e^+\pi^-K^-)/\Gamma_{total}$ — Γ_{222}/Γ

Test of lepton number conservation.

VALUE	CL%	DOCUMENT ID		TECN	COMMENT
$<3.2\times10^{-8}$	90	MIYAZAKI	13	BELL	854 fb^{-1} E^{ee}_{cm} = 10.6 GeV
• • • We do not use the following data for averages, fits, limits, etc. • • •					
$<6.7\times10^{-8}$	90	MIYAZAKI	10	BELL	Repl. by MIYAZAKI 13
$<1.9\times10^{-7}$	90	YUSA	06	BELL	158 fb^{-1} E^{ee}_{cm} = 10.6 GeV
$<1.8\times10^{-7}$	90	AUBERT,BE	05D	BABR	221 fb^{-1}, E^{ee}_{cm} = 10.6 GeV
$<2.1\times10^{-6}$	90	BLISS	98	CLEO	E^{ee}_{cm} = 10.6 GeV
$<4.5\times10^{-6}$	90	[1] BARTELT	94	CLEO	Repl. by BLISS 98
$<2.0\times10^{-5}$	90	ALBRECHT	92K	ARG	E^{ee}_{cm} = 10 GeV
$<4.9\times10^{-5}$	90	BOWCOCK	90	CLEO	E^{ee}_{cm} = 10.4–10.9

[1] BARTELT 94 assume phase space decays.

$\Gamma(e^-K^0_SK^0_S)/\Gamma_{total}$ — Γ_{223}/Γ

Test of lepton family number conservation.

VALUE	CL%	DOCUMENT ID		TECN	COMMENT
$<7.1\times10^{-8}$	90	MIYAZAKI	10A	BELL	671 fb^{-1} E^{ee}_{cm} = 10.6 GeV
• • • We do not use the following data for averages, fits, limits, etc. • • •					
$<2.2\times10^{-6}$	90	CHEN	02C	CLEO	E^{ee}_{cm} = 10.6 GeV

$\Gamma(e^-K^+K^-)/\Gamma_{total}$ — Γ_{224}/Γ

Test of lepton family number conservation.

VALUE	CL%	DOCUMENT ID		TECN	COMMENT
$<3.4\times10^{-8}$	90	MIYAZAKI	13	BELL	854 fb^{-1} E^{ee}_{cm} = 10.6 GeV
• • • We do not use the following data for averages, fits, limits, etc. • • •					
$<5.4\times10^{-8}$	90	MIYAZAKI	10	BELL	Repl. by MIYAZAKI 13
$<3.0\times10^{-7}$	90	YUSA	06	BELL	158 fb^{-1} E^{ee}_{cm} = 10.6 GeV
$<1.4\times10^{-7}$	90	AUBERT,BE	05D	BABR	221 fb^{-1}, E^{ee}_{cm} = 10.6 GeV
$<6.0\times10^{-6}$	90	BLISS	98	CLEO	E^{ee}_{cm} = 10.6 GeV

$\Gamma(e^+K^-K^-)/\Gamma_{total}$ — Γ_{225}/Γ

Test of lepton number conservation.

VALUE	CL%	DOCUMENT ID		TECN	COMMENT
$<3.3\times10^{-8}$	90	MIYAZAKI	13	BELL	854 fb^{-1} E^{ee}_{cm} = 10.6 GeV
• • • We do not use the following data for averages, fits, limits, etc. • • •					
$<6.0\times10^{-8}$	90	MIYAZAKI	10	BELL	Repl. by MIYAZAKI 13
$<3.1\times10^{-7}$	90	YUSA	06	BELL	158 fb^{-1} E^{ee}_{cm} = 10.6 GeV
$<1.5\times10^{-7}$	90	AUBERT,BE	05D	BABR	221 fb^{-1}, E^{ee}_{cm} = 10.6 GeV
$<3.8\times10^{-6}$	90	BLISS	98	CLEO	E^{ee}_{cm} = 10.6 GeV

$\Gamma(\mu^-\pi^+K^-)/\Gamma_{total}$ — Γ_{226}/Γ

Test of lepton family number conservation.

VALUE	CL%	DOCUMENT ID		TECN	COMMENT
$<8.6\times10^{-8}$	90	MIYAZAKI	13	BELL	854 fb^{-1} E^{ee}_{cm} = 10.6 GeV
• • • We do not use the following data for averages, fits, limits, etc. • • •					
$<1.6\times10^{-7}$	90	MIYAZAKI	10	BELL	Repl. by MIYAZAKI 13
$<2.7\times10^{-7}$	90	YUSA	06	BELL	158 fb^{-1} E^{ee}_{cm} = 10.6 GeV
$<2.6\times10^{-7}$	90	AUBERT,BE	05D	BABR	221 fb^{-1}, E^{ee}_{cm} = 10.6 GeV
$<7.5\times10^{-6}$	90	BLISS	98	CLEO	E^{ee}_{cm} = 10.6 GeV
$<8.7\times10^{-6}$	90	[1] BARTELT	94	CLEO	Repl. by BLISS 98
$<11\times10^{-5}$	90	ALBRECHT	92K	ARG	E^{ee}_{cm} = 10 GeV
$<7.7\times10^{-5}$	90	BOWCOCK	90	CLEO	E^{ee}_{cm} = 10.4–10.9

[1] BARTELT 94 assume phase space decays.

$\Gamma(\mu^-\pi^-K^+)/\Gamma_{total}$ — Γ_{227}/Γ

Test of lepton family number conservation.

VALUE	CL%	DOCUMENT ID		TECN	COMMENT
$<4.5\times10^{-8}$	90	MIYAZAKI	13	BELL	854 fb^{-1} E^{ee}_{cm} = 10.6 GeV
• • • We do not use the following data for averages, fits, limits, etc. • • •					
$<1.0\times10^{-7}$	90	MIYAZAKI	10	BELL	Repl. by MIYAZAKI 13
$<7.3\times10^{-7}$	90	YUSA	06	BELL	158 fb^{-1} E^{ee}_{cm} = 10.6 GeV
$<3.2\times10^{-7}$	90	AUBERT,BE	05D	BABR	221 fb^{-1}, E^{ee}_{cm} = 10.6 GeV
$<7.4\times10^{-6}$	90	BLISS	98	CLEO	E^{ee}_{cm} = 10.6 GeV
$<1.5\times10^{-5}$	90	[1] BARTELT	94	CLEO	Repl. by BLISS 98
$<7.7\times10^{-5}$	90	BOWCOCK	90	CLEO	E^{ee}_{cm} = 10.4–10.9

[1] BARTELT 94 assume phase space decays.

$\Gamma(\mu^+\pi^-K^-)/\Gamma_{total}$ — Γ_{228}/Γ

Test of lepton number conservation.

VALUE	CL%	DOCUMENT ID		TECN	COMMENT
$<4.8\times10^{-8}$	90	MIYAZAKI	13	BELL	854 fb^{-1} E^{ee}_{cm} = 10.6 GeV
• • • We do not use the following data for averages, fits, limits, etc. • • •					
$<9.4\times10^{-8}$	90	MIYAZAKI	10	BELL	Repl. by MIYAZAKI 13
$<2.9\times10^{-7}$	90	YUSA	06	BELL	158 fb^{-1} E^{ee}_{cm} = 10.6 GeV
$<2.2\times10^{-7}$	90	AUBERT,BE	05D	BABR	221 fb^{-1}, E^{ee}_{cm} = 10.6 GeV
$<7.0\times10^{-6}$	90	BLISS	98	CLEO	E^{ee}_{cm} = 10.6 GeV
$<2.0\times10^{-5}$	90	[1] BARTELT	94	CLEO	Repl. by BLISS 98
$<5.8\times10^{-5}$	90	ALBRECHT	92K	ARG	E^{ee}_{cm} = 10 GeV
$<4.0\times10^{-5}$	90	BOWCOCK	90	CLEO	E^{ee}_{cm} = 10.4–10.9

[1] BARTELT 94 assume phase space decays.

$\Gamma(\mu^-K^0_SK^0_S)/\Gamma_{total}$ — Γ_{229}/Γ

VALUE	CL%	DOCUMENT ID		TECN	COMMENT
$<8.0\times10^{-8}$	90	MIYAZAKI	10A	BELL	671 fb^{-1} E^{ee}_{cm} = 10.6 GeV
• • • We do not use the following data for averages, fits, limits, etc. • • •					
$<3.4\times10^{-6}$	90	CHEN	02C	CLEO	E^{ee}_{cm} = 10.6 GeV

$\Gamma(\mu^-K^+K^-)/\Gamma_{total}$ — Γ_{230}/Γ

Test of lepton family number conservation.

VALUE	CL%	DOCUMENT ID		TECN	COMMENT
$<4.4\times10^{-8}$	90	MIYAZAKI	13	BELL	854 fb^{-1} E^{ee}_{cm} = 10.6 GeV

Int. J. Mod
by UNIVERSITY OF CALIFORNIA @ BERK
wnloaded from www.worldscientific.com
-use and distribution is strictly not permitted, except for Open Access articles.

Int. J. Mod. Phys. A 2026.41. Downloaded from www.worldscientific.com
by UNIVERSITY OF CALIFORNIA @ BERKELEY on 09/16/26. Re-use and distribution is strictly not permitted, except for Open Access articles.

• • • We do not use the following data for averages, fits, limits, etc. • • •

$< 6.8 \times 10^{-8}$	90	MIYAZAKI	10	BELL	Repl. by MIYAZAKI 13
$< 8.0 \times 10^{-7}$	90	YUSA	06	BELL	158 fb^{-1} $E^{ee}_{cm} = 10.6$ GeV
$< 2.5 \times 10^{-7}$	90	AUBERT,BE	05D	BABR	221 fb^{-1}, $E^{ee}_{cm} = 10.6$ GeV
$<15 \times 10^{-6}$	90	BLISS	98	CLEO	$E^{ee}_{cm} = 10.6$ GeV

$\Gamma(\mu^+ K^- K^-)/\Gamma_{total}$ — Γ_{231}/Γ

Test of lepton number conservation.

VALUE	CL%	DOCUMENT ID		TECN	COMMENT
$<4.7 \times 10^{-8}$	90	MIYAZAKI	13	BELL	854 fb^{-1} $E^{ee}_{cm} = 10.6$ GeV

• • • We do not use the following data for averages, fits, limits, etc. • • •

$<9.6 \times 10^{-8}$	90	MIYAZAKI	10	BELL	Repl. by MIYAZAKI 13
$<4.4 \times 10^{-7}$	90	YUSA	06	BELL	158 fb^{-1} $E^{ee}_{cm} = 10.6$ GeV
$<4.8 \times 10^{-7}$	90	AUBERT,BE	05D	BABR	221 fb^{-1}, $E^{ee}_{cm} = 10.6$ GeV
$<6.0 \times 10^{-6}$	90	BLISS	98	CLEO	$E^{ee}_{cm} = 10.6$ GeV

$\Gamma(e^- \pi^0 \pi^0)/\Gamma_{total}$ — Γ_{232}/Γ

Test of lepton family number conservation.

VALUE	CL%	DOCUMENT ID		TECN	COMMENT
$<6.5 \times 10^{-6}$	90	BONVICINI	97	CLEO	$E^{ee}_{cm} = 10.6$ GeV

$\Gamma(\mu^- \pi^0 \pi^0)/\Gamma_{total}$ — Γ_{233}/Γ

Test of lepton family number conservation.

VALUE	CL%	DOCUMENT ID		TECN	COMMENT
$<14 \times 10^{-6}$	90	BONVICINI	97	CLEO	$E^{ee}_{cm} = 10.6$ GeV

$\Gamma(e^- \eta\eta)/\Gamma_{total}$ — Γ_{234}/Γ

Test of lepton family number conservation.

VALUE	CL%	DOCUMENT ID		TECN	COMMENT
$<35 \times 10^{-6}$	90	BONVICINI	97	CLEO	$E^{ee}_{cm} = 10.6$ GeV

$\Gamma(\mu^- \eta\eta)/\Gamma_{total}$ — Γ_{235}/Γ

Test of lepton family number conservation.

VALUE	CL%	DOCUMENT ID		TECN	COMMENT
$<60 \times 10^{-6}$	90	BONVICINI	97	CLEO	$E^{ee}_{cm} = 10.6$ GeV

$\Gamma(e^- \pi^0 \eta)/\Gamma_{total}$ — Γ_{236}/Γ

Test of lepton family number conservation.

VALUE	CL%	DOCUMENT ID		TECN	COMMENT
$<24 \times 10^{-6}$	90	BONVICINI	97	CLEO	$E^{ee}_{cm} = 10.6$ GeV

$\Gamma(\mu^- \pi^0 \eta)/\Gamma_{total}$ — Γ_{237}/Γ

Test of lepton family number conservation.

VALUE	CL%	DOCUMENT ID		TECN	COMMENT
$<22 \times 10^{-6}$	90	BONVICINI	97	CLEO	$E^{ee}_{cm} = 10.6$ GeV

$\Gamma(p e^- e^-)/\Gamma_{total}$ — Γ_{238}/Γ

VALUE	CL%	DOCUMENT ID		TECN	COMMENT
$<3.0 \times 10^{-8}$	90	SAHOO	20	BELL	921 fb^{-1} $E^{ee}_{cm} = 10.6$ GeV

$\Gamma(\overline{p} e^+ e^-)/\Gamma_{total}$ — Γ_{239}/Γ

VALUE	CL%	DOCUMENT ID		TECN	COMMENT
$<3.0 \times 10^{-8}$	90	SAHOO	20	BELL	921 fb^{-1} $E^{ee}_{cm} = 10.6$ GeV

$\Gamma(\overline{p} e^+ \mu^-)/\Gamma_{total}$ — Γ_{240}/Γ

VALUE	CL%	DOCUMENT ID		TECN	COMMENT
$<2.0 \times 10^{-8}$	90	SAHOO	20	BELL	921 fb^{-1} $E^{ee}_{cm} = 10.6$ GeV

$\Gamma(\overline{p} e^- \mu^+)/\Gamma_{total}$ — Γ_{241}/Γ

VALUE	CL%	DOCUMENT ID		TECN	COMMENT
$<1.8 \times 10^{-8}$	90	SAHOO	20	BELL	921 fb^{-1} $E^{ee}_{cm} = 10.6$ GeV

$\Gamma(p \mu^- \mu^-)/\Gamma_{total}$ — Γ_{242}/Γ

VALUE	CL%	DOCUMENT ID		TECN	COMMENT
$<4.0 \times 10^{-8}$	90	SAHOO	20	BELL	921 fb^{-1} $E^{ee}_{cm} = 10.6$ GeV

• • • We do not use the following data for averages, fits, limits, etc. • • •

$<4.4 \times 10^{-7}$	90	AAIJ	13AH	LHCB	1.0 fb^{-1}, pp at 7 TeV

$\Gamma(\overline{p} \mu^+ \mu^-)/\Gamma_{total}$ — Γ_{243}/Γ

VALUE	CL%	DOCUMENT ID		TECN	COMMENT
$<1.8 \times 10^{-8}$	90	SAHOO	20	BELL	921 fb^{-1} $E^{ee}_{cm} = 10.6$ GeV

• • • We do not use the following data for averages, fits, limits, etc. • • •

$<3.3 \times 10^{-7}$	90	AAIJ	13AH	LHCB	1.0 fb^{-1}, pp at 7 TeV

$\Gamma(\overline{p}\gamma)/\Gamma_{total}$ — Γ_{244}/Γ

Test of lepton number and baryon number conservation.

VALUE	CL%	DOCUMENT ID		TECN	COMMENT
$< 3.5 \times 10^{-6}$	90	GODANG	99	CLEO	$E^{ee}_{cm} = 10.6$ GeV

• • • We do not use the following data for averages, fits, limits, etc. • • •

$<29 \times 10^{-5}$	90	ALBRECHT	92K	ARG	$E^{ee}_{cm} = 10$ GeV

$\Gamma(\overline{p}\pi^0)/\Gamma_{total}$ — Γ_{245}/Γ

Test of lepton number and baryon number conservation.

VALUE	CL%	DOCUMENT ID		TECN	COMMENT
$<15 \times 10^{-6}$	90	GODANG	99	CLEO	$E^{ee}_{cm} = 10.6$ GeV

• • • We do not use the following data for averages, fits, limits, etc. • • •

$<66 \times 10^{-5}$	90	ALBRECHT	92K	ARG	$E^{ee}_{cm} = 10$ GeV

$\Gamma(\overline{p}2\pi^0)/\Gamma_{total}$ — Γ_{246}/Γ

Test of lepton number and baryon number conservation.

VALUE	CL%	DOCUMENT ID		TECN	COMMENT
$<33 \times 10^{-6}$	90	GODANG	99	CLEO	$E^{ee}_{cm} = 10.6$ GeV

$\Gamma(\overline{p}\eta)/\Gamma_{total}$ — Γ_{247}/Γ

Test of lepton number and baryon number conservation.

VALUE	CL%	DOCUMENT ID		TECN	COMMENT
$< 8.9 \times 10^{-6}$	90	GODANG	99	CLEO	$E^{ee}_{cm} = 10.6$ GeV

• • • We do not use the following data for averages, fits, limits, etc. • • •

$<130 \times 10^{-5}$	90	ALBRECHT	92K	ARG	$E^{ee}_{cm} = 10$ GeV

$\Gamma(\overline{p}\pi^0\eta)/\Gamma_{total}$ — Γ_{248}/Γ

Test of lepton number and baryon number conservation.

VALUE	CL%	DOCUMENT ID		TECN	COMMENT
$<27 \times 10^{-6}$	90	GODANG	99	CLEO	$E^{ee}_{cm} = 10.6$ GeV

$\Gamma(\Lambda\pi^-)/\Gamma_{total}$ — Γ_{249}/Γ

Test of lepton number and baryon number conservation.

VALUE	CL%	DOCUMENT ID		TECN	COMMENT
$<4.7 \times 10^{-8}$	90	ADACHI	24Q	BELL	364 fb^{-1}, $E^{ee}_{cm} = 10.6$ GeV

• • • We do not use the following data for averages, fits, limits, etc. • • •

$<7.2 \times 10^{-8}$	90	MIYAZAKI	06	BELL	154 fb^{-1}, $E^{ee}_{cm} = 10.6$ GeV

$\Gamma(\overline{\Lambda}\pi^-)/\Gamma_{total}$ — Γ_{250}/Γ

Test of lepton number and baryon number conservation.

VALUE	CL%	DOCUMENT ID		TECN	COMMENT
$< 4.3 \times 10^{-8}$	90	ADACHI	24Q	BELL	364 fb^{-1}, $E^{ee}_{cm} = 10.6$ GeV

• • • We do not use the following data for averages, fits, limits, etc. • • •

$<14 \times 10^{-8}$	90	MIYAZAKI	06	BELL	154 fb^{-1}, $E^{ee}_{cm} = 10.6$ GeV

$\Gamma(e^- \text{light boson})/\Gamma_{total}$ — Γ_{251}/Γ

VALUE	CL%	DOCUMENT ID		TECN	COMMENT
$<4.5 \times 10^{-4}$	90	[1] UNO	25	BELL	800 fb^{-1}, $E^{ee}_{cm} = 10.6$ GeV

[1] UNO 25 limit holds for bosons with mass = 0.0 GeV. For masses between 0.0 and 1.6 GeV, the limit varies in the range $(0.3–6.0) \times 10^{-4}$.

$\Gamma(\mu^- \text{light boson})/\Gamma_{total}$ — Γ_{252}/Γ

VALUE	CL%	DOCUMENT ID		TECN	COMMENT
$<2.8 \times 10^{-4}$	90	[1] UNO	25	BELL	800 fb^{-1}, $E^{ee}_{cm} = 10.6$ GeV

[1] UNO 25 limit holds for bosons with mass = 0.0 GeV. For masses between 0.0 and 1.6 GeV, the limit varies in the range $(0.1–3.3) \times 10^{-4}$.

$\Gamma(e^- \text{light boson})/\Gamma(e^- \overline{\nu}_e \nu_\tau)$ — Γ_{251}/Γ_5

Test of lepton family number conservation.

• • • We do not use the following data for averages, fits, limits, etc. • • •

VALUE	CL%	DOCUMENT ID		TECN	COMMENT
<0.0053	95	[1] ADACHI	23A	BELL	$E^{ee}_{cm} = 10.58$ GeV
<0.008	95	[2] BRYMAN	21	RVUE	
<0.015	95	[3] ALBRECHT	95G	ARG	$E^{ee}_{cm} = 9.4–10.6$ GeV
<0.018	95	[4] ALBRECHT	90E	ARG	$E^{ee}_{cm} = 9.4–10.6$ GeV
<0.040	95	[5] BALTRUSAIT...85		MRK3	$E^{ee}_{cm} = 3.77$ GeV

[1] ADACHI 23A limit holds for bosons with mass = 0.0 GeV. The limit rises to 9.7×10^{-3} for a mass of 1.0 GeV, then falls to 1.1×10^{-3} at the upper mass limit of 1.6 GeV.

[2] BRYMAN 21 reports indirect limits obtained from the consistency of the world averages of $B(\tau^- \to e^- \overline{\nu}_e \nu_\tau)$ and $B(\tau^- \to \mu^- \overline{\nu}_\mu \nu_\tau)$ with their Standard Model predictions, without a simulation of the efficiency as a function of the X mass for the searched decay modes to be detected as the corresponding Standard Model decay modes.

[3] ALBRECHT 95G limit holds for bosons with mass < 0.4 GeV. The limit rises to 0.036 for a mass of 1.0 GeV, then falls to 0.006 at the upper mass limit of 1.6 GeV.

[4] ALBRECHT 90E limit applies for spinless boson with mass < 100 MeV, and rises to 0.050 for mass = 500 MeV.

[5] BALTRUSAITIS 85 limit applies for spinless boson with mass < 100 MeV.

$\Gamma(\mu^- \text{light boson})/\Gamma(e^- \overline{\nu}_e \nu_\tau)$ — Γ_{252}/Γ_5

Test of lepton family number conservation.

• • • We do not use the following data for averages, fits, limits, etc. • • •

VALUE	CL%	DOCUMENT ID		TECN	COMMENT
<0.0034	95	[1] ADACHI	23A	BELL	$E^{ee}_{cm} = 10.58$ GeV
<0.011	95	[2] BRYMAN	21	RVUE	
<0.026	95	[3] ALBRECHT	95G	ARG	$E^{ee}_{cm} = 9.4–10.6$ GeV
<0.033	95	[4] ALBRECHT	90E	ARG	$E^{ee}_{cm} = 9.4–10.6$ GeV
<0.125	95	[5] BALTRUSAIT...85		MRK3	$E^{ee}_{cm} = 3.77$ GeV

[1] ADACHI 23A limit holds for bosons with mass = 0.0 GeV. The limit rises to 12.2×10^{-3} for a mass of 1.0 GeV, then falls to 0.7×10^{-3} at the upper mass limit of 1.6 GeV.

[2] BRYMAN 21 reports indirect limits obtained from the consistency of the world averages of $B(\tau^- \to e^- \overline{\nu}_e \nu_\tau)$ and $B(\tau^- \to \mu^- \overline{\nu}_\mu \nu_\tau)$ with their Standard Model predictions, without a simulation of the efficiency as a function of the X mass for the searched decay modes to be detected as the corresponding Standard Model decay modes.

[3] ALBRECHT 95G limit holds for bosons with mass < 1.3 GeV. The limit rises to 0.034 for a mass of 1.4 GeV, then falls to 0.003 at the upper mass limit of 1.6 GeV.

[4] ALBRECHT 90E limit applies for spinless boson with mass < 100 MeV, and rises to 0.071 for mass $= 500$ MeV.

[5] BALTRUSAITIS 85 limit applies for spinless boson with mass < 100 MeV.

τ-DECAY PARAMETERS

See the related review(s):

τ-Lepton Decay Parameters

ρ(e or μ) PARAMETER

($V-A$) theory predicts $\rho = 0.75$.

VALUE	EVTS	DOCUMENT ID		TECN	COMMENT
0.745±0.008 OUR FIT					
0.749±0.008 OUR AVERAGE					
0.742±0.014±0.006	81k	HEISTER	01E	ALEP	1991–1995 LEP runs
0.775±0.023±0.020	36k	ABREU	00L	DLPH	1992–1995 runs
0.781±0.028±0.018	46k	ACKERSTAFF	99D	OPAL	1990–1995 LEP runs
0.762±0.035	54k	ACCIARRI	98R	L3	1991–1995 LEP runs
0.731±0.031		[1] ALBRECHT	98	ARG	E^{ee}_{cm} = 9.5–10.6 GeV
0.72 ±0.09 ±0.03		[2] ABE	97O	SLD	1993–1995 SLC runs
0.747±0.010±0.006	55k	ALEXANDER	97F	CLEO	E^{ee}_{cm} = 10.6 GeV
0.79 ±0.10 ±0.10	3732	FORD	87B	MAC	E^{ee}_{cm} = 29 GeV
0.71 ±0.09 ±0.03	1426	BEHRENDS	85	CLEO	e^+e^- near $\Upsilon(4S)$
• • • We do not use the following data for averages, fits, limits, etc. • • •					
0.735±0.013±0.008	31k	AMMAR	97B	CLEO	Repl. by ALEXANDER 97F
0.794±0.039±0.031	18k	ACCIARRI	96H	L3	Repl. by ACCIARRI 98R
0.732±0.034±0.020	8.2k	[3] ALBRECHT	95	ARG	E^{ee}_{cm} = 9.5–10.6 GeV
0.738±0.038		[4] ALBRECHT	95C	ARG	Repl. by ALBRECHT 98
0.751±0.039±0.022		BUSKULIC	95D	ALEP	Repl. by HEISTER 01E
0.742±0.035±0.020	8000	ALBRECHT	90E	ARG	E^{ee}_{cm} = 9.4–10.6 GeV

[1] Combined fit to ARGUS tau decay parameter measurements in ALBRECHT 98, ALBRECHT 95C, ALBRECHT 93G, and ALBRECHT 94E. ALBRECHT 98 use tau pair events of the type $\tau^-\tau^+ \to (\ell^- \overline{\nu}_\ell \nu_\tau)(\pi^+\pi^0\overline{\nu}_\tau)$, and their charged conjugates.

[2] ABE 97O assume $\eta = 0$ in their fit. Letting η vary in the fit gives a ρ value of 0.69 ± 0.13 ± 0.05.

[3] Value is from a simultaneous fit for the ρ and η decay parameters to the lepton energy spectrum. Not independent of ALBRECHT 90E ρ(e or μ) value which assumes $\eta = 0$. Result is strongly correlated with ALBRECHT 95C.

[4] Combined fit to ARGUS tau decay parameter measurements in ALBRECHT 95C, ALBRECHT 93G, and ALBRECHT 94E.

ρ(e) PARAMETER

($V-A$) theory predicts $\rho = 0.75$.

VALUE	EVTS	DOCUMENT ID		TECN	COMMENT
0.747±0.010 OUR FIT					
0.744±0.010 OUR AVERAGE					
0.747±0.019±0.014	44k	HEISTER	01E	ALEP	1991–1995 LEP runs
0.744±0.036±0.037	17k	ABREU	00L	DLPH	1992–1995 runs
0.779±0.047±0.029	25k	ACKERSTAFF	99D	OPAL	1990–1995 LEP runs
0.68 ±0.04 ±0.07		[1] ALBRECHT	98	ARG	E^{ee}_{cm} = 9.5–10.6 GeV
0.71 ±0.14 ±0.05		ABE	97O	SLD	1993–1995 SLC runs
0.747±0.012±0.004	34k	ALEXANDER	97F	CLEO	E^{ee}_{cm} = 10.6 GeV
0.735±0.036±0.020	4.7k	[2] ALBRECHT	95	ARG	E^{ee}_{cm} = 9.5–10.6 GeV
0.79 ±0.08 ±0.06	3230	[3] ALBRECHT	93G	ARG	E^{ee}_{cm} = 9.4–10.6 GeV
0.64 ±0.06 ±0.07	2753	JANSSEN	89	CBAL	E^{ee}_{cm} = 9.4–10.6 GeV
0.62 ±0.17 ±0.14	1823	FORD	87B	MAC	E^{ee}_{cm} = 29 GeV
0.60 ±0.13	699	BEHRENDS	85	CLEO	e^+e^- near $\Upsilon(4S)$
0.72 ±0.10 ±0.11	594	BACINO	79B	DLCO	E^{ee}_{cm} = 3.5–7.4 GeV
• • • We do not use the following data for averages, fits, limits, etc. • • •					
0.732±0.014±0.009	19k	AMMAR	97B	CLEO	Repl. by ALEXANDER 97F
0.793±0.050±0.025		BUSKULIC	95D	ALEP	Repl. by HEISTER 01E
0.747±0.045±0.028	5106	ALBRECHT	90E	ARG	Repl. by ALBRECHT 95

[1] ALBRECHT 98 use tau pair events of the type $\tau^-\tau^+ \to (\ell^- \overline{\nu}_\ell \nu_\tau)(\pi^+\pi^0\overline{\nu}_\tau)$, and their charged conjugates.

[2] ALBRECHT 95 use tau pair events of the type $\tau^-\tau^+ \to (\ell^- \overline{\nu}_\ell \nu_\tau)(h^+h^-h^+(\pi^0)\overline{\nu}_\tau)$ and their charged conjugates.

[3] ALBRECHT 93G use tau pair events of the type $\tau^-\tau^+ \to (\mu^- \overline{\nu}_\mu \nu_\tau)(e^+\nu_e\overline{\nu}_\tau)$ and their charged conjugates.

ρ(μ) PARAMETER

($V-A$) theory predicts $\rho = 0.75$.

VALUE	EVTS	DOCUMENT ID		TECN	COMMENT
0.763±0.020 OUR FIT					
0.770±0.022 OUR AVERAGE					
0.776±0.045±0.019	46k	HEISTER	01E	ALEP	1991–1995 LEP runs
0.999±0.098±0.045	22k	ABREU	00L	DLPH	1992–1995 runs
0.777±0.044±0.016	27k	ACKERSTAFF	99D	OPAL	1990–1995 LEP runs
0.69 ±0.06 ±0.06		[1] ALBRECHT	98	ARG	E^{ee}_{cm} = 9.5–10.6 GeV
0.54 ±0.28 ±0.14		ABE	97O	SLD	1993–1995 SLC runs
0.750±0.017±0.045	22k	ALEXANDER	97F	CLEO	E^{ee}_{cm} = 10.6 GeV
0.76 ±0.07 ±0.08	3230	ALBRECHT	93G	ARG	E^{ee}_{cm} = 9.4–10.6 GeV
0.734±0.055±0.027	3041	ALBRECHT	90E	ARG	E^{ee}_{cm} = 9.4–10.6 GeV
0.89 ±0.14 ±0.08	1909	FORD	87B	MAC	E^{ee}_{cm} = 29 GeV
0.81 ±0.13	727	BEHRENDS	85	CLEO	e^+e^- near $\Upsilon(4S)$
• • • We do not use the following data for averages, fits, limits, etc. • • •					
0.747±0.048±0.044	13k	AMMAR	97B	CLEO	Repl. by ALEXANDER 97F
0.693±0.057±0.028		BUSKULIC	95D	ALEP	Repl. by HEISTER 01E

[1] ALBRECHT 98 use tau pair events of the type $\tau^-\tau^+ \to (\ell^- \overline{\nu}_\ell \nu_\tau)(\pi^+\pi^0\overline{\nu}_\tau)$, and their charged conjugates.

ξ(e or μ) PARAMETER

($V-A$) theory predicts $\xi = 1$.

VALUE	EVTS	DOCUMENT ID		TECN	COMMENT
0.985±0.030 OUR FIT					
0.981±0.031 OUR AVERAGE					
0.986±0.068±0.031	81k	HEISTER	01E	ALEP	1991–1995 LEP runs
0.929±0.070±0.030	36k	ABREU	00L	DLPH	1992–1995 runs
0.98 ±0.22 ±0.10	46k	ACKERSTAFF	99D	OPAL	1990–1995 LEP runs
0.70 ±0.16	54k	ACCIARRI	98R	L3	1991–1995 LEP runs
1.03 ±0.11		[1] ALBRECHT	98	ARG	E^{ee}_{cm} = 9.5–10.6 GeV
1.05 ±0.35 ±0.04		[2] ABE	97O	SLD	1993–1995 SLC runs
1.007±0.040±0.015	55k	ALEXANDER	97F	CLEO	E^{ee}_{cm} = 10.6 GeV
• • • We do not use the following data for averages, fits, limits, etc. • • •					
0.94 ±0.21 ±0.07	18k	ACCIARRI	96H	L3	Repl. by ACCIARRI 98R
0.97 ±0.14		[3] ALBRECHT	95C	ARG	Repl. by ALBRECHT 98
1.18 ±0.15 ±0.16		BUSKULIC	95D	ALEP	Repl. by HEISTER 01E
0.90 ±0.15 ±0.10	3230	[4] ALBRECHT	93G	ARG	E^{ee}_{cm} = 9.4–10.6 GeV

[1] Combined fit to ARGUS tau decay parameter measurements in ALBRECHT 98, ALBRECHT 95C, ALBRECHT 93G, and ALBRECHT 94E. ALBRECHT 98 use tau pair events of the type $\tau^-\tau^+ \to (\ell^- \overline{\nu}_\ell \nu_\tau)(\pi^+\pi^0\overline{\nu}_\tau)$, and their charged conjugates.

[2] ABE 97O assume $\eta = 0$ in their fit. Letting η vary in the fit gives a ξ value of 1.02 ± 0.36 ± 0.05.

[3] Combined fit to ARGUS tau decay parameter measurements in ALBRECHT 95C, ALBRECHT 93G, and ALBRECHT 94E. ALBRECHT 95C uses events of the type $\tau^-\tau^+ \to (\ell^- \overline{\nu}_\ell \nu_\tau)(h^+h^-h^+\overline{\nu}_\tau)$ and their charged conjugates.

[4] ALBRECHT 93G measurement determines $|\xi|$ for the case $\xi(e) = \xi(\mu)$, but the authors point out that other LEP experiments determine the sign to be positive.

ξ(e) PARAMETER

($V-A$) theory predicts $\xi = 1$.

VALUE	EVTS	DOCUMENT ID		TECN	COMMENT
0.994±0.040 OUR FIT					
1.00 ±0.04 OUR AVERAGE					
1.011±0.094±0.038	44k	HEISTER	01E	ALEP	1991–1995 LEP runs
1.01 ±0.12 ±0.05	17k	ABREU	00L	DLPH	1992–1995 runs
1.13 ±0.39 ±0.14	25k	ACKERSTAFF	99D	OPAL	1990–1995 LEP runs
1.11 ±0.20 ±0.08		[1] ALBRECHT	98	ARG	E^{ee}_{cm} = 9.5–10.6 GeV
1.16 ±0.52 ±0.06		ABE	97O	SLD	1993–1995 SLC runs
0.979±0.048±0.016	34k	ALEXANDER	97F	CLEO	E^{ee}_{cm} = 10.6 GeV
• • • We do not use the following data for averages, fits, limits, etc. • • •					
1.03 ±0.23 ±0.09		BUSKULIC	95D	ALEP	Repl. by HEISTER 01E

[1] ALBRECHT 98 use tau pair events of the type $\tau^-\tau^+ \to (\ell^- \overline{\nu}_\ell \nu_\tau)(\pi^+\pi^0\overline{\nu}_\tau)$, and their charged conjugates.

ξ(μ) PARAMETER

($V-A$) theory predicts $\xi = 1$.

VALUE	EVTS	DOCUMENT ID		TECN	COMMENT
1.030±0.059 OUR FIT					
1.06 ±0.06 OUR AVERAGE					
1.030±0.120±0.050	46k	HEISTER	01E	ALEP	1991–1995 LEP runs
1.16 ±0.19 ±0.06	22k	ABREU	00L	DLPH	1992–1995 runs
0.79 ±0.41 ±0.09	27k	ACKERSTAFF	99D	OPAL	1990–1995 LEP runs
1.26 ±0.27 ±0.14		[1] ALBRECHT	98	ARG	E^{ee}_{cm} = 9.5–10.6 GeV
0.75 ±0.50 ±0.14		ABE	97O	SLD	1993–1995 SLC runs
1.054±0.069±0.047	22k	ALEXANDER	97F	CLEO	E^{ee}_{cm} = 10.6 GeV
• • • We do not use the following data for averages, fits, limits, etc. • • •					
1.23 ±0.22 ±0.10		BUSKULIC	95D	ALEP	Repl. by HEISTER 01E

[1] ALBRECHT 98 use tau pair events of the type $\tau^-\tau^+ \to (\ell^- \overline{\nu}_\ell \nu_\tau)(\pi^+\pi^0\overline{\nu}_\tau)$, and their charged conjugates.

η(e or μ) PARAMETER

($V-A$) theory predicts $\eta = 0$.

VALUE	EVTS	DOCUMENT ID		TECN	COMMENT
0.013±0.020 OUR FIT					
0.015±0.021 OUR AVERAGE					
0.012±0.026±0.004	81k	HEISTER	01E	ALEP	1991–1995 LEP runs
−0.005±0.036±0.037		ABREU	00L	DLPH	1992–1995 runs
0.027±0.055±0.005	46k	ACKERSTAFF	99D	OPAL	1990–1995 LEP runs
0.27 ±0.14	54k	ACCIARRI	98R	L3	1991–1995 LEP runs
−0.13 ±0.47 ±0.15		ABE	97O	SLD	1993–1995 SLC runs
−0.015±0.061±0.062	31k	AMMAR	97B	CLEO	E^{ee}_{cm} = 10.6 GeV
0.03 ±0.18 ±0.12	8.2k	ALBRECHT	95	ARG	E^{ee}_{cm} = 9.5–10.6 GeV
• • • We do not use the following data for averages, fits, limits, etc. • • •					
0.25 ±0.17 ±0.11	18k	ACCIARRI	96H	L3	Repl. by ACCIARRI 98R
−0.04 ±0.15 ±0.11		BUSKULIC	95D	ALEP	Repl. by HEISTER 01E

Int. J. Mod. Phys. A 2026.41. Downloaded from www.worldscientific.com
by UNIVERSITY OF CALIFORNIA @ BERKELEY on 09/16/26. Re-use and distribution is strictly not permitted, except for Open Access articles.

Int. J. Mod. Phys. A 2026.41. Downloaded from www.worldscientific.com
by UNIVERSITY OF CALIFORNIA @ BERKELEY on 09/16/26. Re-use and distribution is strictly not permitted, except for Open Access articles.

$\eta(\mu)$ PARAMETER

($V-A$) theory predicts $\eta = 0$.

VALUE	EVTS	DOCUMENT ID		TECN	COMMENT
0.094±0.073 OUR FIT					
0.17 ±0.15 OUR AVERAGE		Error includes scale factor of 1.2.			
0.160±0.150±0.060	46k	HEISTER	01E	ALEP	1991–1995 LEP runs
0.72 ±0.32 ±0.15		ABREU	00L	DLPH	1992–1995 runs
−0.59 ±0.82 ±0.45		[1] ABE	97O	SLD	1993–1995 SLC runs
0.010±0.149±0.171	13k	[2] AMMAR	97B	CLEO	E^{ee}_{cm}= 10.6 GeV
• • • We do not use the following data for averages, fits, limits, etc. • • •					
0.010±0.065±0.001	27k	[3] ACKERSTAFF	99D	OPAL	1990–1995 LEP runs
−0.24 ±0.23 ±0.18		BUSKULIC	95D	ALEP	Repl. by HEISTER 01E

[1] Highly correlated (corr. = 0.92) with ABE 97O $\rho(\mu)$ measurement.
[2] Highly correlated (corr. = 0.949) with AMMAR 97B $\rho(\mu)$ value.
[3] ACKERSTAFF 99D result is dominated by a constraint on η from the OPAL measurements of the τ lifetime and B($\tau^- \to \mu^- \overline{\nu}_\mu \nu_\tau$) assuming lepton universality for the total coupling strength.

$(\delta\xi)(e$ or $\mu)$ PARAMETER

($V-A$) theory predicts $(\delta\xi) = 0.75$.

VALUE	EVTS	DOCUMENT ID		TECN	COMMENT
0.746±0.021 OUR FIT					
0.744±0.022 OUR AVERAGE					
0.776±0.045±0.024	81k	HEISTER	01E	ALEP	1991–1995 LEP runs
0.779±0.070±0.028	36k	ABREU	00L	DLPH	1992–1995 runs
0.65 ±0.14 ±0.07	46k	ACKERSTAFF	99D	OPAL	1990–1995 LEP runs
0.70 ±0.11	54k	ACCIARRI	98R	L3	1991–1995 LEP runs
0.63 ±0.09		[1] ALBRECHT	98	ARG	E^{ee}_{cm}= 9.5–10.6 GeV
0.88 ±0.27 ±0.04		[2] ABE	97O	SLD	1993–1995 SLC runs
0.745±0.026±0.009	55k	ALEXANDER	97F	CLEO	E^{ee}_{cm}= 10.6 GeV
• • • We do not use the following data for averages, fits, limits, etc. • • •					
0.81 ±0.14 ±0.06	18k	ACCIARRI	96H	L3	Repl. by ACCIARRI 98R
0.65 ±0.12		[3] ALBRECHT	95C	ARG	Repl. by ALBRECHT 98
0.88 ±0.11 ±0.07		BUSKULIC	95D	ALEP	Repl. by HEISTER 01E

[1] Combined fit to ARGUS tau decay parameter measurements in ALBRECHT 98, ALBRECHT 95C, ALBRECHT 93G, and ALBRECHT 94E. ALBRECHT 98 use tau pair events of the type $\tau^-\tau^+ \to (\ell^-\overline{\nu}_\ell\nu_\tau)(\pi^+\pi^0\overline{\nu}_\tau)$, and their charged conjugates.
[2] ABE 97O assume $\eta = 0$ in their fit. Letting η vary in the fit gives a $(\delta\xi)$ value of 0.87 ± 0.27 ± 0.04.
[3] Combined fit to ARGUS tau decay parameter measurements in ALBRECHT 95C, ALBRECHT 93G, and ALBRECHT 94E. ALBRECHT 95C uses events of the type $\tau^-\tau^+ \to (\ell^-\overline{\nu}_\ell\nu_\tau)\,(h^+h^-h^+\overline{\nu}_\tau)$ and their charged conjugates.

$(\delta\xi)(e)$ PARAMETER

($V-A$) theory predicts $(\delta\xi) = 0.75$.

VALUE	EVTS	DOCUMENT ID		TECN	COMMENT
0.734±0.028 OUR FIT					
0.731±0.029 OUR AVERAGE					
0.778±0.066±0.024	44k	HEISTER	01E	ALEP	1991–1995 LEP runs
0.85 ±0.12 ±0.04	17k	ABREU	00L	DLPH	1992–1995 runs
0.72 ±0.31 ±0.14	25k	ACKERSTAFF	99D	OPAL	1990–1995 LEP runs
0.56 ±0.14 ±0.06		[1] ALBRECHT	98	ARG	E^{ee}_{cm}= 9.5–10.6 GeV
0.85 ±0.43 ±0.08		ABE	97O	SLD	1993–1995 SLC runs
0.720±0.032±0.010	34k	ALEXANDER	97F	CLEO	E^{ee}_{cm}= 10.6 GeV
• • • We do not use the following data for averages, fits, limits, etc. • • •					
1.11 ±0.17 ±0.07		BUSKULIC	95D	ALEP	Repl. by HEISTER 01E

[1] ALBRECHT 98 use tau pair events of the type $\tau^-\tau^+ \to (\ell^-\overline{\nu}_\ell\nu_\tau)(\pi^+\pi^0\overline{\nu}_\tau)$, and their charged conjugates.

$(\delta\xi)(\mu)$ PARAMETER

($V-A$) theory predicts $(\delta\xi) = 0.75$.

VALUE	EVTS	DOCUMENT ID		TECN	COMMENT
0.778±0.037 OUR FIT					
0.79 ±0.04 OUR AVERAGE					
0.786±0.066±0.028	46k	HEISTER	01E	ALEP	1991–1995 LEP runs
0.86 ±0.13 ±0.04	22k	ABREU	00L	DLPH	1992–1995 runs
0.63 ±0.23 ±0.05	27k	ACKERSTAFF	99D	OPAL	1990–1995 LEP runs
0.73 ±0.18 ±0.10		[1] ALBRECHT	98	ARG	E^{ee}_{cm}= 9.5–10.6 GeV
0.82 ±0.32 ±0.07		ABE	97O	SLD	1993–1995 SLC runs
0.786±0.041±0.032	22k	ALEXANDER	97F	CLEO	E^{ee}_{cm}= 10.6 GeV
• • • We do not use the following data for averages, fits, limits, etc. • • •					
0.71 ±0.14 ±0.06		BUSKULIC	95D	ALEP	Repl. by HEISTER 01E

[1] ALBRECHT 98 use tau pair events of the type $\tau^-\tau^+ \to (\ell^-\overline{\nu}_\ell\nu_\tau)(\pi^+\pi^0\overline{\nu}_\tau)$, and their charged conjugates.

$\xi(\pi)$ PARAMETER

($V-A$) theory predicts $\xi(\pi) = 1$.

VALUE	EVTS	DOCUMENT ID		TECN	COMMENT
0.993±0.022 OUR FIT					
0.994±0.023 OUR AVERAGE					
0.994±0.020±0.014	27k	HEISTER	01E	ALEP	1991–1995 LEP runs
0.81 ±0.17 ±0.02		ABE	97O	SLD	1993–1995 SLC runs
1.03 ±0.06 ±0.04	2.0k	COAN	97	CLEO	E^{ee}_{cm}= 10.6 GeV
• • • We do not use the following data for averages, fits, limits, etc. • • •					
0.987±0.057±0.027		BUSKULIC	95D	ALEP	Repl. by HEISTER 01E
0.95 ±0.11 ±0.05		[1] BUSKULIC	94D	ALEP	1990+1991 LEP run

[1] Superseded by BUSKULIC 95D.

$\xi(\rho)$ PARAMETER

($V-A$) theory predicts $\xi(\rho) = 1$.

VALUE	EVTS	DOCUMENT ID		TECN	COMMENT
0.994±0.008 OUR FIT					
0.994±0.009 OUR AVERAGE					
0.987±0.012±0.011	59k	HEISTER	01E	ALEP	1991–1995 LEP runs
0.99 ±0.12 ±0.04		ABE	97O	SLD	1993–1995 SLC runs
0.995±0.010±0.003	66k	ALEXANDER	97F	CLEO	E^{ee}_{cm}= 10.6 GeV
1.022±0.028±0.030	1.7k	[1] ALBRECHT	94E	ARG	E^{ee}_{cm}= 9.4–10.6 GeV
• • • We do not use the following data for averages, fits, limits, etc. • • •					
1.045±0.058±0.032		BUSKULIC	95D	ALEP	Repl. by HEISTER 01E
1.03 ±0.11 ±0.05		[2] BUSKULIC	94D	ALEP	1990+1991 LEP run

[1] ALBRECHT 94E measure the square of this quantity and use the sign determined by ALBRECHT 90I to obtain the quoted result.
[2] Superseded by BUSKULIC 95D.

$\xi(a_1)$ PARAMETER

($V-A$) theory predicts $\xi(a_1) = 1$.

VALUE	EVTS	DOCUMENT ID		TECN	COMMENT
1.001±0.027 OUR FIT					
1.002±0.028 OUR AVERAGE					
1.000±0.016±0.024	35k	[1] HEISTER	01E	ALEP	1991–1995 LEP runs
1.02 ±0.13 ±0.03	17.2k	ASNER	00	CLEO	E^{ee}_{cm}= 10.6 GeV
1.29 ±0.26 ±0.11	7.4k	[2] ACKERSTAFF	97R	OPAL	1992–1994 LEP runs
0.85 $^{+0.15}_{-0.17}$ ±0.05		ALBRECHT	95C	ARG	E^{ee}_{cm}= 9.5–10.6 GeV
1.25 ±0.23 $^{+0.15}_{-0.08}$	7.5k	ALBRECHT	93C	ARG	E^{ee}_{cm}= 9.4–10.6 GeV
• • • We do not use the following data for averages, fits, limits, etc. • • •					
1.08 $^{+0.46}_{-0.41}$ $^{+0.14}_{-0.25}$	2.6k	[3] AKERS	95P	OPAL	Repl. by ACKERSTAFF 97R
0.937±0.116±0.064		BUSKULIC	95D	ALEP	Repl. by HEISTER 01E

[1] HEISTER 01E quote 1.000 ± 0.016 ± 0.013 ± 0.020 where the errors are statistical, systematic, and an uncertainty due to the final state model. We combine the systematic error and model uncertainty.
[2] ACKERSTAFF 97R obtain this result with a model independent fit to the hadronic structure functions. Fitting with the model of Kuhn and Santamaria (ZPHY **C48**, 445 (1990)) gives 0.87 ± 0.16 ± 0.04, and with the model of of Isgur *et al.* (PR **D39**,1357 (1989)) they obtain 1.20 ± 0.21 ± 0.14.
[3] AKERS 95P obtain this result with a model independent fit to the hadronic structure functions. Fitting with the model of Kuhn and Santamaria (ZPHY **C48**, 445 (1990)) gives 0.87 ± 0.27$^{+0.05}_{-0.06}$, and with the model of of Isgur *et al.* (PR **D39**,1357 (1989)) they obtain 1.10 ± 0.31$^{+0.13}_{-0.14}$.

ξ(all hadronic modes) PARAMETER

($V-A$) theory predicts $\xi = 1$.

VALUE	EVTS	DOCUMENT ID		TECN	COMMENT
0.995±0.007 OUR FIT					
0.997±0.007 OUR AVERAGE					
0.992±0.007±0.008	102k	[1] HEISTER	01E	ALEP	1991–1995 LEP runs
0.997±0.027±0.011	39k	[2] ABREU	00L	DLPH	1992–1995 runs
1.02 ±0.13 ±0.03	17.2k	[3] ASNER	00	CLEO	E^{ee}_{cm}= 10.6 GeV
1.032±0.031	37k	[4] ACCIARRI	98R	L3	1991–1995 LEP runs
0.93 ±0.10 ±0.04		ABE	97O	SLD	1993–1995 SLC runs
1.29 ±0.26 ±0.11	7.4k	[5] ACKERSTAFF	97R	OPAL	1992–1994 LEP runs
0.995±0.010±0.003	66k	[6] ALEXANDER	97F	CLEO	E^{ee}_{cm}= 10.6 GeV
1.03 ±0.06 ±0.04	2.0k	[7] COAN	97	CLEO	E^{ee}_{cm}= 10.6 GeV
1.017±0.039		[8] ALBRECHT	95C	ARG	E^{ee}_{cm}= 9.5–10.6 GeV
1.25 ±0.23 $^{+0.15}_{-0.08}$	7.5k	[9] ALBRECHT	93C	ARG	E^{ee}_{cm}= 9.4–10.6 GeV
• • • We do not use the following data for averages, fits, limits, etc. • • •					
0.970±0.053±0.011	14k	[10] ACCIARRI	96H	L3	Repl. by ACCIARRI 98R
1.08 $^{+0.46}_{-0.41}$ $^{+0.14}_{-0.25}$	2.6k	[11] AKERS	95P	OPAL	Repl. by ACKERSTAFF 97R
1.006±0.032±0.019		[12] BUSKULIC	95D	ALEP	Repl. by HEISTER 01E
1.022±0.028±0.030	1.7k	[13] ALBRECHT	94E	ARG	E^{ee}_{cm}= 9.4–10.6 GeV
0.99 ±0.07 ±0.04		[14] BUSKULIC	94D	ALEP	1990+1991 LEP run
1.14 ±0.34 $^{+0.34}_{-0.17}$	3.9k	[9] ALBRECHT	90I	ARG	Repl. by ALBRECHT 93C

[1] HEISTER 01E quote 0.992 ± 0.007 ± 0.006 ± 0.005 where the errors are statistical, systematic, and an uncertainty due to the final state model. We combine the systematic error and model uncertainty. They use $\tau \to \pi\nu_\tau$, $\tau \to K\nu_\tau$, $\tau \to \rho\nu_\tau$, and $\tau \to a_1\nu_\tau$ decays.
[2] ABREU 00L use $\tau^- \to h^- \geq 0\pi^0\nu_\tau$ decays.
[3] ASNER 00 use $\tau^- \to \pi^- 2\pi^0\nu_\tau$ decays.
[4] ACCIARRI 98R use $\tau \to \pi\nu_\tau$, $\tau \to K\nu_\tau$, and $\tau \to \rho\nu_\tau$ decays.
[5] ACKERSTAFF 97R use $\tau \to a_1\nu_\tau$ decays.
[6] ALEXANDER 97F use $\tau \to \rho\nu_\tau$ decays.
[7] COAN 97 use h^+h^- energy correlations.
[8] Combined fit to ARGUS tau decay parameter measurements in ALBRECHT 95C, ALBRECHT 93G, and ALBRECHT 94E.
[9] Uses $\tau \to a_1\nu_\tau$ decays. Replaced by ALBRECHT 95C.
[10] ACCIARRI 96H use $\tau \to \pi\nu_\tau$, $\tau \to K\nu_\tau$, and $\tau \to \rho\nu_\tau$ decays.
[11] AKERS 95P use $\tau \to a_1\nu_\tau$ decays.
[12] BUSKULIC 95D use $\tau \to \pi\nu_\tau$, $\tau \to \rho\nu_\tau$, and $\tau \to a_1\nu_\tau$ decays.
[13] ALBRECHT 94E measure the square of this quantity and use the sign determined by ALBRECHT 90I to obtain the quoted result. Uses $\tau \to a_1\nu_\tau$ decays. Replaced by ALBRECHT 95C.
[14] BUSKULIC 94D use $\tau \to \pi\nu_\tau$ and $\tau \to \rho\nu_\tau$ decays. Superseded by BUSKULIC 95D.

Int. J. Mod
-use and distribution is strictly not permitted, except for Open Access articles.
by UNIVERSITY OF CALIFORNIA @ BERK
Downloaded from www.worldscientific.com

$\xi'(\mu)$ PARAMETER

($V-A$) theory predicts $\xi' = 1$.

VALUE	EVTS	DOCUMENT ID		TECN	COMMENT
0.22±0.94±0.42	165	BODROV	23	BELL	$E^{ee}_{\rm cm} = 10.6$ GeV

$\overline{\eta}(\mu)$ PARAMETER

($V-A$) theory predicts $\overline{\eta}(\mu) = 0$.

VALUE	EVTS	DOCUMENT ID		TECN	COMMENT
−1.3±1.5±0.8	71k	[1] SHIMIZU	18A	BELL	$\tau^- \to \nu_\tau \mu^- \overline{\nu}_\mu \gamma$

[1] SHIMIZU 18A measurement procedure fits a distribution affected by $\overline{\eta}(\mu)$, $\xi\kappa(\mu)$ and $\eta''(\mu)$, floating $\overline{\eta}(\mu)$ and $\xi\kappa(\mu)$ and fixing $\eta''(\mu) = 0$. The contribution of $\eta''(\mu)$ is suppressed by m_μ/m_τ.

$(\xi\kappa)(e$ or $\mu)$ PARAMETER

($V-A$) theory predicts $(\xi\kappa)(e$ or $\mu) = 0$.

VALUE	EVTS	DOCUMENT ID		TECN	COMMENT
0.5±0.4±0.2	149k	[1,2] SHIMIZU	18A	BELL	$\tau^- \to \nu_\tau e^- \overline{\nu}_e \gamma$ and $\tau^- \to \nu_\tau \mu^- \overline{\nu}_\mu \gamma$

[1] SHIMIZU 18A measurement procedure fits a distribution of radiative tau decays into both electrons and muons affected by $\overline{\eta}(e$ or $\mu)$, $\xi\kappa(e$ or $\mu)$ and $\eta''(e$ or $\mu)$, floating $\overline{\eta}(e$ or $\mu)$ and $\xi\kappa(e$ or $\mu)$ and fixing $\eta''(e$ or $\mu) = 0$. The contribution of $\eta''(e$ or $\mu)$ is suppressed by m_e/m_τ for tau decaying to electrons and by m_μ/m_τ for tau decaying to muons.

[2] Error correlated with SHIMIZU 18A $(\xi\kappa)(e)$ and $(\xi\kappa)(\mu)$ values.

$(\xi\kappa)(e)$ PARAMETER

($V-A$) theory predicts $(\xi\kappa)(e) = 0$.

VALUE	EVTS	DOCUMENT ID		TECN	COMMENT
−0.4±0.8±0.9	78k	[1,2] SHIMIZU	18A	BELL	$\tau^- \to \nu_\tau e^- \overline{\nu}_e \gamma$

[1] SHIMIZU 18A measurement procedure fits a distribution affected by $\overline{\eta}(e)$, $(\xi\kappa)(e)$ and $\eta''(e)$, floating $(\xi\kappa)(e)$ and fixing $\overline{\eta}(e) = 0$ and $\eta''(e) = 0$. The contribution of $\eta''(e)$ is suppressed by m_e/m_τ.

[2] Error correlated with SHIMIZU 18A $(\xi\kappa)(e$ or $\mu)$ value.

$(\xi\kappa)(\mu)$ PARAMETER

($V-A$) theory predicts $(\xi\kappa)(\mu) = 0$.

VALUE	EVTS	DOCUMENT ID		TECN	COMMENT
0.8±0.5±0.3	71k	[1,2] SHIMIZU	18A	BELL	$\tau^- \to \nu_\tau \mu^- \overline{\nu}_\mu \gamma$

[1] SHIMIZU 18A measurement procedure fits a distribution affected by $\overline{\eta}(\mu)$, $\xi\kappa(\mu)$ and $\eta''(\mu)$, floating $\overline{\eta}(\mu)$ and $\xi\kappa(\mu)$ and fixing $\eta''(\mu) = 0$. The contribution of $\eta''(\mu)$ is suppressed by m_μ/m_τ.

[2] Error correlated with SHIMIZU 18A $(\xi\kappa)(e$ or $\mu)$ value.

τ REFERENCES

AAD 25BB JHEP 2510 054 G. Aad et al. (ATLAS Collab.)
ADACHI 25AB JHEP 2512 169 I. Adachi et al. (BELLE II Collab.)
ADACHI 25P JHEP 2508 092 I. Adachi et al. (BELLE II Collab.)
UNO 25 JHEP 2508 155 K. Uno et al. (BELLE Collab.)
ADACHI 24K JHEP 2408 205 I. Adachi et al. (BELLE II Collab.)
ADACHI 24Q PR D110 112003 I. Adachi et al. (BELLE II Collab.)
ADACHI 24R JHEP 2409 062 I. Adachi et al. (BELLE II Collab.)
HAYRAPETY... 24J PL B853 138633 A. Hayrapetyan et al. (CMS Collab.)
AAD 23BM PRL 131 151802 G. Aad et al. (ATLAS Collab.)
ADACHI 23A PRL 130 181803 I. Adachi et al. (BELLE II Collab.)
ADACHI 23C PR D108 032006 I. Adachi et al. (BELLE II Collab.)
ANASHIN 23A PPN 54 185 V.V. Anashin et al. (VEPP-4M KEDR Collab.)
BODROV 23 PRL 131 021801 D. Bodrov et al. (BELLE Collab.)
Also PR D108 012003 D. Bodrov et al. (BELLE Collab.)
TSUZUKI 23 JHEP 2306 118 N. Tsuzuki et al. (BELLE Collab.)
TUMASYAN 23AS PRL 131 151803 A. Tumasyan et al. (CMS Collab.)
INAMI 22 JHEP 2204 110 K. Inami et al. (BELLE Collab.)
BRYMAN 21 PR D104 075032 D.A. Bryman, S. Ito, R. Shrock (BRCO, TRIU+)
SIRUNYAN 21D JHEP 2101 163 A.M. Sirunyan et al. (CMS Collab.)
UNO 21 JHEP 2110 019 K. Uno et al. (BELLE Collab.)
SAHOO 20 PR D102 111101 D. Sahoo et al. (BELLE Collab.)
JIN 19 PR D100 071101 Y. Jin et al. (BELLE Collab.)
LEES 18B PR D98 032010 J.P. Lees et al. (BABAR Collab.)
SHIMIZU 18A PTEP 2018 023C01 N. Shimizu et al. (BELLE Collab.)
AAD 16BA EPJ C76 232 G.Aad et al. (ATLAS Collab.)
AAIJ 15AI JHEP 1502 121 R. Aaij et al. (LHCb Collab.)
LEES 15G PR D91 051103 J.P. Lees et al. (BABAR Collab.)
ABLIKIM 14D PR D90 012001 M. Ablikim et al. (BESIII Collab.)
BELOUS 14 PRL 112 031801 K. Belous et al. (BELLE Collab.)
LEVICHEV 14 SPU 57 66 E.B. Levichev et al.
RYU 14 PR D89 072009 S. Ryu et al. (BELLE Collab.)
AAIJ 13AH PL B724 36 R. Aaij et al. (LHCb Collab.)
MIYAZAKI 13 PL B719 346 Y. Miyazaki et al. (BELLE Collab.)
LEES 12M PR D85 031102 J.P. Lees et al. (BABAR Collab.)
Also PR D85 099904 (errat.) J.P. Lees et al. (BABAR Collab.)
LEES 12X PR D86 092010 J.P. Lees et al. (BABAR Collab.)
LEES 12Y PR D86 092013 J.P. Lees et al. (BABAR Collab.)
PDG 12 PR D86 010001 J. Beringer et al. (PDG Collab.)
DEL-AMO-SA... 11E PR D83 032002 P. del Amo Sanchez et al. (BABAR Collab.)
MIYAZAKI 11 PL B699 251 Y. Miyazaki et al. (BELLE Collab.)
AUBERT 10B PRL 104 021802 B. Aubert et al. (BABAR Collab.)
AUBERT 10F PRL 105 051602 B. Aubert et al. (BABAR Collab.)
HAYASAKA 10 PL B687 139 K. Hayasaka et al. (BELLE Collab.)
LEE 10 PR D81 113007 M.J. Lee et al. (BELLE Collab.)
LEES 10A PR D81 111101 J.P. Lees et al. (BABAR Collab.)
MIYAZAKI 10 PL B682 355 Y. Miyazaki et al. (BELLE Collab.)
MIYAZAKI 10A PL B692 4 Y. Miyazaki et al. (BELLE Collab.)
AUBERT 09AK PR D80 092005 B. Aubert et al. (BABAR Collab.)
AUBERT 09D PR D79 012004 B. Aubert et al. (BABAR Collab.)
AUBERT 09W PRL 103 021801 B. Aubert et al. (BABAR Collab.)
GROZIN 09A PAN 72 1203 A.G. Grozin, I.B. Khriplovich, A.S. Rudenko (NOVO)
INAMI 09 PL B672 209 K. Inami et al. (BELLE Collab.)
MIYAZAKI 09 PL B672 317 Y. Miyazaki et al. (BELLE Collab.)
AUBERT 08 PRL 100 011801 B. Aubert et al. (BABAR Collab.)
AUBERT 08AE PR D77 112002 B. Aubert et al. (BABAR Collab.)
AUBERT 08K PRL 100 071802 B. Aubert et al. (BABAR Collab.)
FUJIKAWA 08 PR D78 072006 M. Fujikawa et al. (BELLE Collab.)
HAYASAKA 08 PL B666 16 K. Hayasaka et al. (BELLE Collab.)
MIYAZAKI 08 PL B660 154 Y. Miyazaki et al. (BELLE Collab.)
NISHIO 08 PL B664 35 Y. Nishio et al. (BELLE Collab.)
ANASHIN 07 JETPL 85 347 V.V. Anashin et al. (KEDR Collab.)
Translated from ZETFP 85 429.
AUBERT 07AP PR D76 051104 B. Aubert et al. (BABAR Collab.)
AUBERT 07BK PRL 99 251803 B. Aubert et al. (BABAR Collab.)
AUBERT 07I PRL 98 061803 B. Aubert et al. (BABAR Collab.)
BELOUS 07 PRL 99 011801 K. Belous et al. (BELLE Collab.)
EIDELMAN 07 MPL A22 159 S. Eidelman, M. Passera (NOVO, PADO)
EPIFANOV 07 PL B654 65 D. Epifanov et al. (BELLE Collab.)
MIYAZAKI 07 PL B648 341 Y. Miyazaki et al. (BELLE Collab.)
ABDALLAH 06A EPJ C46 1 J. Abdallah et al. (DELPHI Collab.)
AUBERT 06C PRL 96 041801 B. Aubert et al. (BABAR Collab.)
AUBERT,B 06 PR D73 112003 B. Aubert et al. (BABAR Collab.)
INAMI 06 PL B643 5 K. Inami et al. (BELLE Collab.)
MIYAZAKI 06 PL B632 51 Y. Miyazaki et al. (BELLE Collab.)
MIYAZAKI 06A PL B639 159 Y. Miyazaki et al. (BELLE Collab.)
PDG 06 JP G33 1 W.-M. Yao et al. (PDG Collab.)
YUSA 06 PL B640 138 Y. Yusa et al. (BELLE Collab.)
ARMS 05 PRL 94 241802 K. Arms et al. (CLEO Collab.)
AUBERT,B 05A PRL 95 041802 B. Aubert et al. (BABAR Collab.)
AUBERT,B 05F PR D72 012003 B. Aubert et al. (BABAR Collab.)
AUBERT,B 05W PR D72 072001 B. Aubert et al. (BABAR Collab.)
AUBERT,BE 05D PRL 95 191801 B. Aubert et al. (BABAR Collab.)
ENARI 05 PL B622 218 Y. Enari et al. (BELLE Collab.)
HAYASAKA 05 PL B613 20 K. Hayasaka et al. (BELLE Collab.)
SCHAEL 05C PRPL 421 191 S. Schael et al. (ALEPH Collab.)
ABBIENDI 04J EPJ C35 437 G. Abbiendi et al. (OPAL Collab.)
ABDALLAH 04K EPJ C35 159 J. Abdallah et al. (DELPHI Collab.)
ABDALLAH 04T EPJ C36 283 J. Abdallah et al. (DELPHI Collab.)
ABE 04B PRL 92 171802 K. Abe et al. (BELLE Collab.)
ACHARD 04G PL B585 53 P. Achard et al. (L3 Collab.)
AUBERT 04J PRL 92 121801 B. Aubert et al. (BABAR Collab.)
ENARI 04 PRL 93 081803 Y. Enari et al. (BELLE Collab.)
PDG 04 PL B592 1 S. Eidelman et al. (PDG Collab.)
YUSA 04 PL B589 103 Y. Yusa et al. (BELLE Collab.)
ABBIENDI 03 PL B551 35 G. Abbiendi et al. (OPAL Collab.)
BRIERE 03 PRL 90 181802 R. A. Briere et al. (CLEO Collab.)
HEISTER 03F EPJ C30 291 A. Heister et al. (ALEPH Collab.)
INAMI 03 PL B551 16 K. Inami et al. (BELLE Collab.)
CHEN 02C PR D66 071101 S. Chen et al. (CLEO Collab.)
REGAN 02 PRL 88 071805 B.C. Regan et al.
ABBIENDI 01J EPJ C19 653 G. Abbiendi et al. (OPAL Collab.)
ABREU 01M EPJ C20 617 P. Abreu et al. (DELPHI Collab.)
ACCIARRI 01F PL B507 47 M. Acciarri et al. (L3 Collab.)
ACHARD 01D PL B519 189 P. Achard et al. (L3 Collab.)
ANASTASSOV 01 PRL 86 4467 A. Anastassov et al. (CLEO Collab.)
HEISTER 01E EPJ C22 217 A. Heister et al. (ALEPH Collab.)
ABBIENDI 00A PL B492 23 G. Abbiendi et al. (OPAL Collab.)
ABBIENDI 00C EPJ C13 213 G. Abbiendi et al. (OPAL Collab.)
ABBIENDI 00D EPJ C13 197 G. Abbiendi et al. (OPAL Collab.)
ABREU 00L EPJ C16 229 P. Abreu et al. (DELPHI Collab.)
ACCIARRI 00B PL B479 67 M. Acciarri et al. (L3 Collab.)
AHMED 00 PR D61 071101 S. Ahmed et al. (CLEO Collab.)
ALBRECHT 00 PL B485 37 H. Albrecht et al. (ARGUS Collab.)
ASNER 00 PR D61 012002 D.M. Asner et al. (CLEO Collab.)
ASNER 00B PR D62 072006 D.M. Asner et al. (CLEO Collab.)
BERGFELD 00 PRL 84 830 T. Bergfeld et al. (CLEO Collab.)
BROWDER 00 PR D61 052004 T.E. Browder et al. (CLEO Collab.)
EDWARDS 00A PR D61 072003 K.W. Edwards et al. (CLEO Collab.)
GONZALEZ-S... 00 NP B582 3 G.A. Gonzalez-Sprinberg et al.
ABBIENDI 99H PL B447 134 G. Abbiendi et al. (OPAL Collab.)
ABREU 99X EPJ C10 201 P. Abreu et al. (DELPHI Collab.)
ACKERSTAFF 99D EPJ C8 3 K. Ackerstaff et al. (OPAL Collab.)
ACKERSTAFF 99E EPJ C8 183 K. Ackerstaff et al. (OPAL Collab.)
BARATE 99K EPJ C10 1 R. Barate et al. (ALEPH Collab.)
BARATE 99R EPJ C11 599 R. Barate et al. (ALEPH Collab.)
BISHAI 99 PRL 82 281 M. Bishai et al. (CLEO Collab.)
GODANG 99 PR D59 091303 R. Godang et al. (CLEO Collab.)
RICHICHI 99 PR D60 112002 S.J. Richichi et al. (CLEO Collab.)
ACCIARRI 98C PL B426 207 M. Acciarri et al. (L3 Collab.)
ACCIARRI 98E PL B434 169 M. Acciarri et al. (L3 Collab.)
ACCIARRI 98R PL B438 405 M. Acciarri et al. (L3 Collab.)
ACKERSTAFF 98M EPJ C4 193 K. Ackerstaff et al. (OPAL Collab.)
ACKERSTAFF 98N PL B431 188 K. Ackerstaff et al. (OPAL Collab.)
ALBRECHT 98 PL B431 179 H. Albrecht et al. (ARGUS Collab.)
BARATE 98 EPJ C1 65 R. Barate et al. (ALEPH Collab.)
BARATE 98E EPJ C4 29 R. Barate et al. (ALEPH Collab.)
BLISS 98 PR D57 5903 D.W. Bliss et al. (CLEO Collab.)
ABE 97O PRL 78 4691 K. Abe et al. (SLD Collab.)
ACKERSTAFF 97J PL B404 213 K. Ackerstaff et al. (OPAL Collab.)
ACKERSTAFF 97L ZPHY C74 403 K. Ackerstaff et al. (OPAL Collab.)
ACKERSTAFF 97R ZPHY C75 593 K. Ackerstaff et al. (OPAL Collab.)
ALEXANDER 97F PR D56 5320 J.P. Alexander et al. (CLEO Collab.)
AMMAR 97B PRL 78 4686 R. Ammar et al. (CLEO Collab.)
ANASTASSOV 97 PR D55 2559 A. Anastassov et al. (CLEO Collab.)
Also PR D58 119903 (errat.) A. Anastassov et al. (CLEO Collab.)
ANDERSON 97 PRL 79 3814 S. Anderson et al. (CLEO Collab.)
AVERY 97 PR D55 1119 P. Avery et al. (CLEO Collab.)
BARATE 97I ZPHY C74 387 R. Barate et al. (ALEPH Collab.)
BARATE 97R PL B414 362 R. Barate et al. (ALEPH Collab.)
BERGFELD 97 PRL 79 2406 T. Bergfeld et al. (CLEO Collab.)
BONVICINI 97 PRL 79 1221 G. Bonvicini et al. (CLEO Collab.)
BUSKULIC 97C ZPHY C74 263 D. Buskulic et al. (ALEPH Collab.)
COAN 97 PR D55 7291 T.E. Coan et al. (CLEO Collab.)
EDWARDS 97 PR D55 3919 K.W. Edwards et al. (CLEO Collab.)
EDWARDS 97B PR D56 5297 K.W. Edwards et al. (CLEO Collab.)
ESCRIBANO 97 PL B395 369 R. Escribano, E. Masso (BARC, PARIT)
ABREU 96B PL B365 448 P. Abreu et al. (DELPHI Collab.)
ACCIARRI 96H PL B377 313 M. Acciarri et al. (L3 Collab.)
ACCIARRI 96K PL B389 187 M. Acciarri et al. (L3 Collab.)
ALAM 96 PRL 76 2637 M.S. Alam et al. (CLEO Collab.)
ALBRECHT 96E PRPL 276 223 H. Albrecht et al. (ARGUS Collab.)
ALEXANDER 96D PL B369 163 G. Alexander et al. (OPAL Collab.)
ALEXANDER 96E PL B374 341 G. Alexander et al. (OPAL Collab.)
ALEXANDER 96S PL B388 437 G. Alexander et al. (OPAL Collab.)
BAI 96 PR D53 20 J.Z. Bai et al. (BES Collab.)
BALEST 96 PL B388 402 R. Balest et al. (CLEO Collab.)
BARTELT 96 PRL 76 4119 J.E. Bartelt et al. (CLEO Collab.)
BUSKULIC 96 ZPHY C70 579 D. Buskulic et al. (ALEPH Collab.)
BUSKULIC 96C ZPHY C70 561 D. Buskulic et al. (ALEPH Collab.)
COAN 96 PR D53 6037 T.E. Coan et al. (CLEO Collab.)
ABE 95Y PR D52 4828 K. Abe et al. (SLD Collab.)
ABREU 95T PL B357 715 P. Abreu et al. (DELPHI Collab.)
ABREU 95U PL B359 411 P. Abreu et al. (DELPHI Collab.)
ACCIARRI 95 PL B345 93 M. Acciarri et al. (L3 Collab.)
ACCIARRI 95F PL B352 487 M. Acciarri et al. (L3 Collab.)
AKERS 95F ZPHY C66 31 R. Akers et al. (OPAL Collab.)
AKERS 95I ZPHY C66 543 R. Akers et al. (OPAL Collab.)
AKERS 95P ZPHY C67 45 R. Akers et al. (OPAL Collab.)
AKERS 95Y ZPHY C68 555 R. Akers et al. (OPAL Collab.)
ALBRECHT 95 PL B341 441 H. Albrecht et al. (ARGUS Collab.)

Int. J. Mod. Phys. A 2026.41. Downloaded from www.worldscientific.com
by UNIVERSITY OF CALIFORNIA @ BERKELEY on 09/16/26. Re-use and distribution is strictly not permitted, except for Open Access articles.

ALBRECHT	95C	PL B349 576	H. Albrecht *et al.*	(ARGUS Collab.)
ALBRECHT	95G	ZPHY C68 25	H. Albrecht *et al.*	(ARGUS Collab.)
ALBRECHT	95H	ZPHY C68 215	H. Albrecht *et al.*	(ARGUS Collab.)
BALEST	95C	PRL 75 3809	R. Balest *et al.*	(CLEO Collab.)
BERNABEU	95	NP B436 474	J. Bernabeu *et al.*	
BUSKULIC	95C	PL B346 371	D. Buskulic *et al.*	(ALEPH Collab.)
BUSKULIC	95D	PL B346 379	D. Buskulic *et al.*	(ALEPH Collab.)
Also		PL B363 265 (errat.)	D. Buskulic *et al.*	(ALEPH Collab.)
ABREU	94K	PL B334 435	P. Abreu *et al.*	(DELPHI Collab.)
AKERS	94E	PL B328 207	R. Akers *et al.*	(OPAL Collab.)
AKERS	94G	PL B339 278	R. Akers *et al.*	(OPAL Collab.)
ALBRECHT	94E	PL B337 383	H. Albrecht *et al.*	(ARGUS Collab.)
ARTUSO	94	PRL 72 3762	M. Artuso *et al.*	(CLEO Collab.)
BARTELT	94	PRL 73 1890	J.E. Bartelt *et al.*	(CLEO Collab.)
BATTLE	94	PRL 73 1079	M. Battle *et al.*	(CLEO Collab.)
BAUER	94	PR D50 13	D.A. Bauer *et al.*	(TPC/2gamma Collab.)
BUSKULIC	94D	PL B321 168	D. Buskulic *et al.*	(ALEPH Collab.)
BUSKULIC	94E	PL B332 209	D. Buskulic *et al.*	(ALEPH Collab.)
BUSKULIC	94F	PL B332 219	D. Buskulic *et al.*	(ALEPH Collab.)
GIBAUT	94B	PRL 73 934	D. Gibaut *et al.*	(CLEO Collab.)
ADRIANI	93M	PRPL 236 1	O. Adriani *et al.*	(L3 Collab.)
ALBRECHT	93C	ZPHY C58 61	H. Albrecht *et al.*	(ARGUS Collab.)
ALBRECHT	93G	PL B316 608	H. Albrecht *et al.*	(ARGUS Collab.)
BALEST	93	PR D47 3671	R. Balest *et al.*	(CLEO Collab.)
BEAN	93	PRL 70 138	A. Bean *et al.*	(CLEO Collab.)
BORTOLETTO	93	PRL 71 1791	D. Bortoletto *et al.*	(CLEO Collab.)
ESCRIBANO	93	PL B301 419	R. Escribano, E. Masso	(BARC)
PROCARIO	93	PRL 70 1207	M. Procario *et al.*	(CLEO Collab.)
ABREU	92N	ZPHY C55 555	P. Abreu *et al.*	(DELPHI Collab.)
ACTON	92F	PL B281 405	D.P. Acton *et al.*	(OPAL Collab.)
ACTON	92H	PL B288 373	P.D. Acton *et al.*	(OPAL Collab.)
AKERIB	92	PRL 69 3610	D.S. Akerib *et al.*	(CLEO Collab.)
Also		PRL 71 3395 (errat.)	D.S. Akerib *et al.*	(CLEO Collab.)
ALBRECHT	92D	ZPHY C53 367	H. Albrecht *et al.*	(ARGUS Collab.)
ALBRECHT	92K	ZPHY C55 179	H. Albrecht *et al.*	(ARGUS Collab.)
ALBRECHT	92M	PL B292 221	H. Albrecht *et al.*	(ARGUS Collab.)
ALBRECHT	92Q	ZPHY C56 339	H. Albrecht *et al.*	(ARGUS Collab.)
AMMAR	92	PR D45 3976	R. Ammar *et al.*	(CLEO Collab.)
ARTUSO	92	PRL 69 3278	M. Artuso *et al.*	(CLEO Collab.)
BAI	92	PRL 69 3021	J.Z. Bai *et al.*	(BES Collab.)
BATTLE	92	PL B291 488	M. Battle *et al.*	(CLEO Collab.)
BUSKULIC	92J	PL B297 459	D. Buskulic *et al.*	(ALEPH Collab.)
DECAMP	92C	ZPHY C54 211	D. Decamp *et al.*	(ALEPH Collab.)
ADEVA	91F	PL B265 451	B. Adeva *et al.*	(L3 Collab.)
ALBRECHT	91D	PL B260 259	H. Albrecht *et al.*	(ARGUS Collab.)
ALEXANDER	91D	PL B266 201	G. Alexander *et al.*	(OPAL Collab.)
ANTREASYAN	91	PL B259 216	D. Antreasyan *et al.*	(Crystal Ball Collab.)
GRIFOLS	91	PL B255 611	J.A. Grifols, A. Mendez	(BARC)
ABACHI	90	PR D41 1414	S. Abachi *et al.*	(HRS Collab.)
ALBRECHT	90E	PL B246 278	H. Albrecht *et al.*	(ARGUS Collab.)
ALBRECHT	90I	PL B250 164	H. Albrecht *et al.*	(ARGUS Collab.)
BEHREND	90	ZPHY C46 537	H.J. Behrend *et al.*	(CELLO Collab.)
BOWCOCK	90	PR D41 805	T.J.V. Bowcock *et al.*	(CLEO Collab.)
DELAGUILA	90	PL B252 116	F. del Aguila, M. Sher	(BARC, WILL)
GOLDBERG	90	PL B251 223	M. Goldberg *et al.*	(CLEO Collab.)
WU	90	PR D41 2339	D.Y. Wu *et al.*	(Mark II Collab.)
ABACHI	89B	PR D40 902	S. Abachi *et al.*	(HRS Collab.)
BEHREND	89B	PL B222 163	H.J. Behrend *et al.*	(CELLO Collab.)
JANSSEN	89	PL B228 273	H. Janssen *et al.*	(Crystal Ball Collab.)
KLEINWORT	89	ZPHY C42 7	C. Kleinwort *et al.*	(JADE Collab.)
ADEVA	88	PR D38 2665	B. Adeva *et al.*	(Mark-J Collab.)
ALBRECHT	88B	PL B202 149	H. Albrecht *et al.*	(ARGUS Collab.)
ALBRECHT	88L	ZPHY C41 1	H. Albrecht *et al.*	(ARGUS Collab.)
ALBRECHT	88M	ZPHY C41 405	H. Albrecht *et al.*	(ARGUS Collab.)
AMIDEI	88	PR D37 1750	D. Amidei *et al.*	(Mark II Collab.)
BEHREND	88	PL B200 226	H.J. Behrend *et al.*	(CELLO Collab.)
BRAUNSCH...	88C	ZPHY C39 331	W. Braunschweig *et al.*	(TASSO Collab.)
KEH	88	PL B212 123	S. Keh *et al.*	(Crystal Ball Collab.)
TSCHIRHART	88	PL B205 407	R. Tschirhart *et al.*	(HRS Collab.)
ABACHI	87B	PL B197 291	S. Abachi *et al.*	(HRS Collab.)
ABACHI	87C	PRL 59 2519	S. Abachi *et al.*	(HRS Collab.)
ADLER	87B	PRL 59 1527	J. Adler *et al.*	(Mark III Collab.)
AIHARA	87B	PR D35 1553	H. Aihara *et al.*	(TPC Collab.)
AIHARA	87C	PRL 59 751	H. Aihara *et al.*	(TPC Collab.)
ALBRECHT	87L	PL B185 223	H. Albrecht *et al.*	(ARGUS Collab.)
ALBRECHT	87P	PL B199 580	H. Albrecht *et al.*	(ARGUS Collab.)
BAND	87	PL B198 297	H.R. Band *et al.*	(MAC Collab.)
BAND	87B	PRL 59 415	H.R. Band *et al.*	(MAC Collab.)
BARINGER	87	PRL 59 1993	P. Baringer *et al.*	(CLEO Collab.)
BEBEK	87C	PR D36 690	C. Bebek *et al.*	(CLEO Collab.)
BURCHAT	87	PR D35 27	P.R. Burchat *et al.*	(Mark II Collab.)
BYLSMA	87	PR D35 2269	B.G. Bylsma *et al.*	(HRS Collab.)
COFFMAN	87	PR D36 2185	D.M. Coffman *et al.*	(Mark III Collab.)
DERRICK	87	PL B189 260	M. Derrick *et al.*	(HRS Collab.)
FORD	87	PR D35 408	W.T. Ford *et al.*	(MAC Collab.)
FORD	87B	PR D36 1971	W.T. Ford *et al.*	(MAC Collab.)
GAN	87	PRL 59 411	K.K. Gan *et al.*	(Mark II Collab.)
GAN	87B	PL B197 561	K.K. Gan *et al.*	(Mark II Collab.)
AIHARA	86E	PRL 57 1836	H. Aihara *et al.*	(TPC Collab.)
BARTEL	86D	PL B182 216	W. Bartel *et al.*	(JADE Collab.)
PDG	86	PL 170B 1	M. Aguilar-Benitez *et al.*	(CERN, CIT+)
RUCKSTUHL	86	PRL 56 2132	W. Ruckstuhl *et al.*	(DELCO Collab.)
SCHMIDKE	86	PRL 57 527	W.B. Schmidke *et al.*	(Mark II Collab.)
YELTON	86	PRL 56 812	J.M. Yelton *et al.*	(Mark II Collab.)
ALTHOFF	85	ZPHY C26 521	M. Althoff *et al.*	(TASSO Collab.)
ASH	85B	PRL 55 2118	W.W. Ash *et al.*	(MAC Collab.)
BALTRUSAIT...	85	PRL 55 1842	R.M. Baltrusaitis *et al.*	(Mark III Collab.)
BARTEL	85F	PL 161B 188	W. Bartel *et al.*	(JADE Collab.)
BEHRENDS	85	PR D32 2468	S. Behrends *et al.*	(CLEO Collab.)
BELTRAMI	85	PRL 54 1775	I. Beltrami *et al.*	(HRS Collab.)
BERGER	85	ZPHY C28 1	C. Berger *et al.*	(PLUTO Collab.)
BURCHAT	85	PRL 54 2489	P.R. Burchat *et al.*	(Mark II Collab.)
FERNANDEZ	85	PRL 54 1624	E. Fernandez *et al.*	(MAC Collab.)
MILLS	85	PRL 54 624	G.B. Mills *et al.*	(DELCO Collab.)
AIHARA	84C	PR D30 2436	H. Aihara *et al.*	(TPC Collab.)
BEHREND	84	ZPHY C23 103	H.J. Behrend *et al.*	(CELLO Collab.)
MILLS	84	PRL 52 1944	G.B. Mills *et al.*	(DELCO Collab.)
BEHREND	83C	PL 127B 270	H.J. Behrend *et al.*	(CELLO Collab.)
SILVERMAN	83	PR D27 1196	D.J. Silverman, G.L. Shaw	(UCI)
BEHREND	82	PL 114B 282	H.J. Behrend *et al.*	(CELLO Collab.)
BLOCKER	82B	PRL 48 1586	C.A. Blocker *et al.*	(Mark II Collab.)
BLOCKER	82D	PL 109B 119	C.A. Blocker *et al.*	(Mark II Collab.) J
FELDMAN	82	PRL 48 66	G.J. Feldman *et al.*	(Mark II Collab.)
HAYES	82	PR D25 2869	K.G. Hayes *et al.*	(Mark II Collab.)
BERGER	81B	PL 99B 489	C. Berger *et al.*	(PLUTO Collab.)
DORFAN	81	PRL 46 215	J.M. Dorfan *et al.*	(Mark II Collab.)
BRANDELIK	80	PL 92B 199	R. Brandelik *et al.*	(TASSO Collab.)
ZHOLENTZ	80	PL 96B 214	A.A. Zholents *et al.*	(NOVO)
Also		SJNP 34 814	A.A. Zholents *et al.*	(NOVO)
		Translated from YAF 34 1471.		
BACINO	79B	PRL 42 749	W.J. Bacino *et al.*	(DELCO Collab.)
KIRKBY	79	SLAC-PUB-2419	J. Kirkby	(SLAC) J
Batavia Lepton Photon Conference.				
BACINO	78B	PRL 41 13	W.J. Bacino *et al.*	(DELCO Collab.) J
Also		Tokyo Conf. 249	J. Kirz	(STON)
Also		PL 96B 214	A.A. Zholents *et al.*	(NOVO)
BRANDELIK	78	PL 73B 109	R. Brandelik *et al.*	(DASP Collab.) J
FELDMAN	78	Tokyo Conf. 777	G.J. Feldman	(SLAC) J
JAROS	78	PRL 40 1120	J. Jaros *et al.*	(LGW Collab.)
PERL	75	PRL 35 1489	M.L. Perl *et al.*	(LBL, SLAC)

OTHER RELATED PAPERS

DAVIER	06	RMP 78 1043	M. Davier, A. Hocker, Z. Zhang	(LALO, PARIN+)
RAHAL-CAL...	98	IJMP A13 695	G. Rahal-Callot	(ETH)
GENTILE	96	PRPL 274 287	S. Gentile, M. Pohl	(ROMAI, ETH)
WEINSTEIN	93	ARNPS 43 457	A.J. Weinstein, R. Stroynowski	(CIT, SMU)
PERL	92	RPP 55 653	M.L. Perl	(SLAC)
PICH	90	MPL A5 1995	A. Pich	(VALE)
BARISH	88	PRPL 157 1	B.C. Barish, R. Stroynowski	(CIT)
GAN	88	IJMP A3 531	K.K. Gan, M.L. Perl	(SLAC)
HAYES	88	PR D38 3351	K.G. Hayes, M.L. Perl	(SLAC)
PERL	80	ARNPS 30 299	M.L. Perl	(SLAC)

Heavy Charged Lepton Searches

Charged Heavy Lepton MASS LIMITS

Sequential Charged Heavy Lepton ($L^{\pm}$) MASS LIMITS

These experiments assumed that a fourth generation $L^{\pm}$ decayed to a fourth generation ν_L (or L^0) where ν_L was stable, or that $L^{\pm}$ decays to a light ν_ℓ via mixing.

See the "Quark and Lepton Compositeness, Searches for" Listings for limits on radiatively decaying excited leptons, *i.e.* $\ell^* \to \ell\gamma$. See the "WIMPs and other Particle Searches" section for heavy charged particle search limits in which the charged particle could be a lepton.

VALUE (GeV)	*CL%*	*DOCUMENT ID*		*TECN*	*COMMENT*
>100.8	95	ACHARD	01B	L3	Decay to νW
>101.9	95	ACHARD	01B	L3	$m_L - m_{L^0} > 15$ GeV
• • • We do not use the following data for averages, fits, limits, etc. • • •					
> 81.5	95	ACKERSTAFF	98C	OPAL	Assumed $m_{L^\pm} - m_{L^0} > 8.4$ GeV
> 80.2	95	ACKERSTAFF	98C	OPAL	$m_{L^0} > m_{L^\pm}$ and $L^\pm \to \nu W$
< 48 or > 61	95	[1] ACCIARRI	96G	L3	
> 63.9	95	ALEXANDER	96P	OPAL	Decay to massless ν's
> 63.5	95	BUSKULIC	96S	ALEP	$m_L - m_{L^0} > 7$ GeV
> 65	95	BUSKULIC	96S	ALEP	Decay to massless ν's
none 10–225		[2] AHMED	94	CNTR	H1 Collab. at HERA
none 12.6–29.6	95	KIM	91B	AMY	Massless ν assumed
> 44.3	95	AKRAWY	90G	OPAL	
none 0.5–10	95	[3] RILES	90	MRK2	For (m_{L^0}-m_{L^0})> 0.25–0.4GeV
> 8		[4] STOKER	89	MRK2	For ($m_{L^+} - m_{L^0}$)= 0.4 GeV
> 12		[4] STOKER	89	MRK2	For m_{L^0}=0.9 GeV
none 18.4–27.6	95	[5] ABE	88	VNS	
> 25.5	95	[6] ADACHI	88B	TOPZ	
none 1.5–22.0	95	BEHREND	88C	CELL	
> 41	90	[7] ALBAJAR	87B	UA1	
> 22.5	95	[8] ADEVA	85	MRKJ	
> 18.0	95	[9] BARTEL	83	JADE	
none 4–14.5	95	[10] BERGER	81B	PLUT	
> 15.5	95	[11] BRANDELIK	81	TASS	
> 13.		[12] AZIMOV	80		
> 16.	95	[13] BARBER	80B	CNTR	
> 0.490		[14] ROTHE	69	RVUE	

[1] ACCIARRI 96G assumes LEP result that the associated neutral heavy lepton mass > 40 GeV.

[2] The AHMED 94 limits are from a search for neutral and charged sequential heavy leptons at HERA via the decay channels $L^- \to e\gamma$, $L^- \to \nu W^-$, $L^- \to eZ$; and $L^0 \to \nu\gamma$, $L^0 \to e^- W^+$, $L^- \to \nu Z$, where the W decays to $\ell\nu_\ell$, or to jets, and Z decays to $\ell^+\ell^-$ or jets.

[3] RILES 90 limits were the result of a special analysis of the data in the case where the mass difference $m_{L^-} - m_{L^0}$ was allowed to be quite small, where L^0 denotes the neutrino into which the sequential charged lepton decays. With a slightly reduced $m_{L^\pm}$ range, the mass difference extends to about 4 GeV.

[4] STOKER 89 (Mark II at PEP) gives bounds on charged heavy lepton (L^+) mass for the generalized case in which the corresponding neutral heavy lepton (L^0) in the SU(2) doublet is not of negligible mass.

[5] ABE 88 search for L^+ and $L^- \to$ hadrons looking for acoplanar jets. The bound is valid for $m_\nu < 10$ GeV.

[6] ADACHI 88B search for hadronic decays giving acoplanar events with large missing energy. $E_{cm}{}^{ee} = 52$ GeV.

[7] Assumes associated neutrino is approximately massless.

[8] ADEVA 85 analyze one-isolated-muon data and sensitive to τ <10 nanosec. Assume B(lepton) = 0.30. $E_{cm} = 40$–47 GeV.

[9] BARTEL 83 limit is from PETRA e^+e^- experiment with average $E_{cm} = 34.2$ GeV.

[10] BERGER 81B is DESY DORIS and PETRA experiment. Looking for $e^+e^- \to L^+L^-$.

[11] BRANDELIK 81 is DESY-PETRA experiment. Looking for $e^+e^- \to L^+L^-$.

[12] AZIMOV 80 estimated probabilities for $M + N$ type events in $e^+e^- \to L^+L^-$ deducing semi-hadronic decay multiplicities of L from e^+e^- annihilation data at $E_{cm} = (2/3)m_L$. Obtained above limit comparing these with e^+e^- data (BRANDELIK 80).

[13] BARBER 80B looked for $e^+e^- \to L^+L^-$, $L \to \nu_L^+ X$ with MARK-J at DESY-PETRA.

[14] ROTHE 69 examines previous data on μ pair production and π and K decays.

Int. J. Mod
by UNIVERSITY OF CALIFORNIA @ BERK
wnloaded from www.worldscientific.com
-use and distribution is strictly not permitted, except for Open Access articles.

Stable Charged Heavy Lepton ($L^{\pm}$) MASS LIMITS

VALUE (GeV)	CL%	DOCUMENT ID		TECN
>102.6	95	ACHARD	01B	L3
• • • We do not use the following data for averages, fits, limits, etc. • • •				
> 28.2	95	[15] ADACHI	90C	TOPZ
none 18.5–42.8	95	AKRAWY	90O	OPAL
> 26.5	95	DECAMP	90F	ALEP
none m_{μ}–36.3	95	SODERSTROM	90	MRK2

[15] ADACHI 90C put lower limits on the mass of stable charged particles with electric charge Q satisfying $2/3 < Q/e < 4/3$ and with spin 0 or 1/2. We list here the special case for a stable charged heavy lepton.

Charged Long-Lived Heavy Lepton MASS LIMITS

VALUE (GeV)	CL%	DOCUMENT ID		TECN	CHG	COMMENT
• • • We do not use the following data for averages, fits, limits, etc. • • •						
>574	95	CHATRCHYAN	13AB	CMS		Leptons singlet model
>102.0	95	ABBIENDI	03L	OPAL		pair produced in e^+e^-
> 0.1		[16] ANSORGE	73B	HBC	–	Long-lived
none 0.55–4.5		[17] BUSHNIN	73	CNTR	–	Long-lived
none 0.2–0.92		[18] BARNA	68	CNTR	–	Long-lived
none 0.97–1.03		[18] BARNA	68	CNTR	–	Long-lived

[16] ANSORGE 73B looks for electron pair production and electron-like Bremsstrahlung.
[17] BUSHNIN 73 is SERPUKHOV 70 GeV p experiment. Masses assume mean life above 7×10^{-10} and 3×10^{-8} respectively. Calculated from cross section (see "Charged Quasi-Stable Lepton Production Differential Cross Section" below) and 30 GeV muon pair production data.
[18] BARNA 68 is SLAC photoproduction experiment.

Doubly-Charged Heavy Lepton MASS LIMITS

VALUE (GeV)	CL%	DOCUMENT ID		TECN	CHG
• • • We do not use the following data for averages, fits, limits, etc. • • •					
none 1–9 GeV	90	[19] CLARK	81	SPEC	++

[19] CLARK 81 is FNAL experiment with 209 GeV muons. Bounds apply to μ_P which couples with full weak strength to muon. See also section on "Doubly-Charged Lepton Production Cross Section."

Doubly-Charged Lepton Production Cross Section (μN Scattering)

VALUE (cm^2)	EVTS	DOCUMENT ID		TECN	CHG
• • • We do not use the following data for averages, fits, limits, etc. • • •					
$<6. \times 10^{-38}$	0	[20] CLARK	81	SPEC	++

[20] CLARK 81 is FNAL experiment with 209 GeV muon. Looked for μ^+ nucleon $\rightarrow \overline{\mu}^0_P$ X, $\overline{\mu}^0_P \rightarrow \mu^+\mu^-\overline{\nu}_\mu$ and $\mu^+ n \rightarrow \mu^{++}_P$ X, $\mu^{++}_P \rightarrow 2\mu^+\nu_\mu$. Above limits are for $\sigma\times$BR taken from their mass-dependence plot figure 2.

REFERENCES FOR Heavy Charged Lepton Searches

CHATRCHYAN	13AB	JHEP 1307 122	S. Chatrchyan *et al.*	(CMS Collab.)
Also		JHEP 2211 149 (errat.)	S. Chatrchyan *et al.*	(CMS Collab.)
ABBIENDI	03L	PL B572 8	G. Abbiendi *et al.*	(OPAL Collab.)
ACHARD	01B	PL B517 75	P. Achard *et al.*	(L3 Collab.)
ACKERSTAFF	98C	EPJ C1 45	K. Ackerstaff *et al.*	(OPAL Collab.)
ACCIARRI	96G	PL B377 304	M. Acciarri *et al.*	(L3 Collab.)
ALEXANDER	96P	PL B385 433	G. Alexander *et al.*	(OPAL Collab.)
BUSKULIC	96S	PL B384 439	D. Buskulic *et al.*	(ALEPH Collab.)
AHMED	94	PL B340 205	T. Ahmed *et al.*	(H1 Collab.)
KIM	91B	IJMP A6 2583	G.N. Kim *et al.*	(AMY Collab.)
ADACHI	90C	PL B244 352	I. Adachi *et al.*	(TOPAZ Collab.)
AKRAWY	90G	PL B240 250	M.Z. Akrawy *et al.*	(OPAL Collab.)
AKRAWY	90O	PL B252 290	M.Z. Akrawy *et al.*	(OPAL Collab.)
DECAMP	90F	PL B236 511	D. Decamp *et al.*	(ALEPH Collab.)
RILES	90	PR D42 1	K. Riles *et al.*	(Mark II Collab.)
SODERSTROM	90	PRL 64 2980	E. Soderstrom *et al.*	(Mark II Collab.)
STOKER	89	PR D39 1811	D.P. Stoker *et al.*	(Mark II Collab.)
ABE	88	PRL 61 915	K. Abe *et al.*	(VENUS Collab.)
ADACHI	88B	PR D37 1339	I. Adachi *et al.*	(TOPAZ Collab.)
BEHREND	88C	ZPHY C41 7	H.J. Behrend *et al.*	(CELLO Collab.)
ALBAJAR	87B	PL B185 241	C. Albajar *et al.*	(UA1 Collab.)
ADEVA	85	PL 152B 439	B. Adeva *et al.*	(Mark-J Collab.)
Also		PRPL 109 131	B. Adeva *et al.*	(Mark-J Collab.)
BARTEL	83	PL 123B 353	W. Bartel *et al.*	(JADE Collab.)
BERGER	81B	PL 99B 489	C. Berger *et al.*	(PLUTO Collab.)
BRANDELIK	81	PL 99B 163	R. Brandelik *et al.*	(TASSO Collab.)
CLARK	81	PRL 46 299	A.R. Clark *et al.*	(UCB, LBL, FNAL+)
Also		PR D25 2762	W.H. Smith *et al.*	(LBL, FNAL, PRIN)
AZIMOV	80	JETPL 32 664	Y.I. Azimov, V.A. Khoze	(PNPI)
		Translated from ZETFP 32 677.		
BARBER	80B	PRL 45 1904	D.P. Barber *et al.*	(Mark-J Collab.)
BRANDELIK	80	PL 92B 199	R. Brandelik *et al.*	(TASSO Collab.)
ANSORGE	73B	PR D7 26	R.E. Ansorge *et al.*	(CAVE)
BUSHNIN	73	NP B58 476	Y.B. Bushnin *et al.*	(SERP)
Also		PL 42B 136	S.V. Golovkin *et al.*	(SERP)
ROTHE	69	NP B10 241	K.W. Rothe, A.M. Wolsky	(PENN)
BARNA	68	PR 173 1391	A. Barna *et al.*	(SLAC, STAN)

OTHER RELATED PAPERS

PERL	81	SLAC-PUB-2752	M.L. Perl	(SLAC)
Physics in Collision Conference.				

Neutrino Properties

NEUTRINO PROPERTIES

Revised July 2023 by P. Vogel (Caltech) and A. Piepke (University of Alabama).

The Neutrino Properties Listings concern measurements of various properties of neutrinos. Nearly all of the measurements, so far only limits, actually concern superpositions of the mass eigenstates ν_i, which are in turn related to the weak eigenstates ν_ℓ, via the neutrino mixing matrix

$$|\nu_\ell\rangle = \sum_i U_{\ell i}\,|\nu_i\rangle \ .$$

In the analogous case of quark mixing via the CKM matrix, the smallness of the off-diagonal terms (small mixing angles) permits a "dominant eigenstate" approximation. However, the results of neutrino oscillation searches show that the mixing matrix contains two large mixing angles and a third angle that is not exceedingly small. We cannot therefore associate any particular state $|\nu_i\rangle$ with any particular lepton label e, μ or τ. Nevertheless, note that in the standard labeling the $|\nu_1\rangle$ has the largest $|\nu_e\rangle$ component ($\sim 2/3$), $|\nu_2\rangle$ contains $\sim 1/3$ of the $|\nu_e\rangle$ component and $|\nu_3\rangle$ contains only a small $\sim 2.5\%$ $|\nu_e\rangle$ component.

Neutrinos are produced in weak decays with a definite lepton flavor, and are typically detected by the charged current weak interaction again associated with a specific lepton flavor. Hence, the listings for the neutrino mass that follow are separated into the three associated charged lepton categories. Other properties (mean lifetime, magnetic moment, charge and charge radius) are no longer separated this way. If needed, the associated lepton flavor is reported in the footnotes.

Measured quantities (mass-squared, magnetic moments, mean lifetimes, *etc.*) all depend upon the mixing parameters $|U_{\ell i}|^2$, but to some extent also on experimental conditions (e.g., on energy resolution). Many of these observables, in particular mass-squared, cannot distinguish between Dirac and Majorana neutrinos and are unaffected by CP phases.

Direct neutrino mass measurements are usually based on the analysis of the kinematics of charged particles (leptons, pions) emitted together with neutrinos (flavor states) in various weak decays. The most sensitive neutrino mass measurement to date, involving electron type antineutrinos, is based on fitting the shape of the beta spectrum. The quantity $m^{2(eff)}_{\nu_e} = \sum_i |U_{ei}|^2 m^2_{\nu_i}$ is determined or constrained, where the sum is over all mass eigenvalues m_{ν_i} that are too close together to be resolved experimentally. (The quantity $m^{eff}_{\nu_e} \equiv \sqrt{m^{2(eff)}_{\nu_e}}$ is often denoted $\langle m_\beta \rangle$ in the literature.) If the energy resolution is better than $\Delta m^2_{ij} \equiv m^2_{\nu_i} - m^2_{\nu_j}$, the corresponding heavier m_{ν_i} and mixing parameter could be determined by fitting the resulting spectral anomaly (step or kink).

Int. J. Mod. Phys. A 2026.41. Downloaded from www.worldscientific.com by UNIVERSITY OF CALIFORNIA @ BERKELEY on 09/16/26. Re-use and distribution is strictly not permitted, except for Open Access articles.

The dependence of m_{ν_e} on the mass of the lightest neutrino is shown in Fig. 14.11 of the *Neutrino Masses, Mixing, and Oscillations* review. In the case of inverted ordering there is a minimum possible value of $m_{\nu_e}^{eff}$, approximately $\sqrt{(\Delta m_{32}^2)} \sim$ 50 meV. If $m_{\nu_e}^{eff}$ is found to be larger than this value, it is impossible, based on this information only, to decide which ordering is realized in nature. On the other hand, if the $m_{\nu_e}^{eff}$ is less than ~50 meV, only the normal mass ordering is possible.

A limit on $m_{\nu_e}^{2(eff)}$ implies an upper limit on the minimum value m_{min}^2 of $m_{\nu_i}^2$, independent of the mixing parameters U_{ei}: $m_{min}^2 \leq m_{\nu_e}^{2(eff)}$. However, if and when the value of $m_{\nu_e}^{2(eff)}$ is determined then its combination with the results derived from neutrino oscillations that give us the values of the neutrino mass-squared differences $\Delta m_{ij}^2 \equiv m_i^2 - m_j^2$, including eventually also their signs, and the mixing parameters $|U_{ei}|^2$, the individual neutrino mass squares $m_{\nu_j}^2 = m_{\nu_e}^{2(eff)} - \sum_i |U_{ei}|^2 \Delta m_{ij}^2$ can be determined.

So far solar, reactor, atmospheric and accelerator neutrino oscillation experiments can be consistently described using three active neutrino flavors, i.e. two mass splittings and three mixing angles. However, several experiments with radioactive sources, reactors, and accelerators imply the possible existence of one or more non-interacting, i.e. sterile, neutrino species that might be observable since they couple, albeit weakly, to the flavor neutrinos $|\nu_l\rangle$. In that case, the neutrino mixing matrix would be $n \times n$ unitary matrix with $n > 3$.

Combined three neutrino analyses determine the squared mass differences and all three mixing angles to within reasonable accuracy. For given $|\Delta m_{ij}^2|$ a limit on $m_{\nu_e}^{2(eff)}$ from beta decay defines an upper limit on the maximum value m_{max} of m_{ν_i}: $m_{max}^2 \leq m_{\nu_e}^{2(eff)} + \sum_{i<j} |\Delta m_{ij}^2|$. The analysis of the low energy beta decay of tritium, combined with the oscillation results, thus limits *all* active neutrino masses. Traditionally, experimental neutrino mass limits obtained from pion decay $\pi^+ \to \mu^+ + \nu_\mu$ or the shape of the spectrum of decay products of the τ lepton did not distinguish between flavor and mass eigenstates. These results are reported as limits of the μ and τ based neutrino mass. After the determination of the $|\Delta m_{ij}^2|$'s and the mixing angles θ_{ij}, the corresponding neutrino mass limits are no longer competitive with those derived from low energy beta decays.

The spread of arrival times of the neutrinos from SN1987A, coupled with the measured neutrino energies, provided a time-of-flight limit on a quantity similar to $\langle m_\beta \rangle \equiv \sqrt{m_{\nu_e}^{2(eff)}}$. This statement, clothed in various degrees of sophistication, has been the basis for a very large number of papers. The resulting limits, however, are no longer comparable with the limits from tritium beta decay.

Constraint, or eventually a value, of the sum of the neutrino masses m_{tot} can be determined from the analysis of the cosmic microwave background anisotropy, combined with the galaxy redshift surveys and other data. These limits are reported in a separate table (Sum of Neutrino Masses, m_{tot}). Obviously, m_{tot} represents an upper limit for all m_i values. Note that many reported m_{tot} limits are considerably more stringent than the listed $m_{\nu_e}^{eff}$ limits. Discussion concerning the model dependence of the m_{tot} limit is continuing.

$\overline{\nu}$ MASS (electron based)

Those limits given below are for the square root of $m_{\nu_e}^{2(\mathrm{eff})} \equiv \sum_i |U_{ei}|^2 m_{\nu_i}^2$. Limits that come from the kinematics of ^{3}H $\beta^- \overline{\nu}$ decay are the square roots of the limits for $m_{\nu_e}^{2(\mathrm{eff})}$. Obtained from the measurements reported in the Listings for "$\overline{\nu}$ Mass Squared," below.

VALUE (eV)	CL%	DOCUMENT ID		TECN	COMMENT
< 0.45	90	[1] AKER	25A	SPEC	^{3}H β decay
• • • We do not use the following data for averages, fits, limits, etc. • • •					
<155	90	[2] ESFAHANI	23	CRES	^{3}H β decay
< 0.8	90	[3] AKER	22	SPEC	^{3}H β decay
< 1.1	90	[4] AKER	19	SPEC	^{3}H β decay
< 2.05	95	[5] ASEEV	11	SPEC	^{3}H β decay
< 5.8	95	[6] PAGLIAROLI	10	ASTR	SN1987A
< 2.3	95	[7] KRAUS	05	SPEC	^{3}H β decay
< 21.7	90	[8] ARNABOLDI	03A	BOLO	^{187}Re β decay
< 5.7	95	[9] LOREDO	02	ASTR	SN1987A
< 2.5	95	[10] LOBASHEV	99	SPEC	^{3}H β decay
< 2.8	95	[11] WEINHEIMER	99	SPEC	^{3}H β decay
< 4.35	95	[12] BELESEV	95	SPEC	^{3}H β decay
< 12.4	95	[13] CHING	95	SPEC	^{3}H β decay
< 92	95	[14] HIDDEMANN	95	SPEC	^{3}H β decay
15^{+32}_{-15}		HIDDEMANN	95	SPEC	^{3}H β decay
< 19.6	95	KERNAN	95	ASTR	SN 1987A
< 7.0	95	[15] STOEFFL	95	SPEC	^{3}H β decay
< 7.2	95	[16] WEINHEIMER	93	SPEC	^{3}H β decay
< 11.7	95	[17] HOLZSCHUH	92B	SPEC	^{3}H β decay
< 13.1	95	[18] KAWAKAMI	91	SPEC	^{3}H β decay
< 9.3	95	[19] ROBERTSON	91	SPEC	^{3}H β decay
< 14	95	AVIGNONE	90	ASTR	SN 1987A
< 16		SPERGEL	88	ASTR	SN 1987A
17 to 40		[20] BORIS	87	SPEC	^{3}H β decay

[1] AKER 25A use data collected by the KATRIN experiment, a precision analysis of the Tritium β spectrum, to formulate a bound on the neutrino mass. The combined analysis of 7 science runs is reported. Supersedes AKER 19 and AKER 22.

[2] ESFAHANI 23 report the first continuous-spectrum measurement of ^{3}H β decay, using cyclotron radiation emission spectroscopy (CRES) and a small demonstration detector. The energy resolution at the endpoint is demonstrated using ^{83m}Kr and a kinematical neutrino mass limit derived from the spectral shape. A frequentist analysis obtained a limit of <152 eV.

[3] AKER 22 derive an upper limit on the kinematical neutrino mass using Tritium β-decay and the KATRIN spectrometer. The constraint is based on combining the first two science runs. Supersedes AKER 19.

[4] AKER 19 report a neutrino mass limit, derived from the first month of data collected by the KATRIN tritium endpoint experiment. The analysis of the electron kinematics shows no evidence for neutrino mass. The quoted result is based on a frequentist analysis of the data following the method described in LOKHOV 15. Using the method of Feldman and Cousins, the derived upper limit is < 0.8 eV at 90% C.L. Superseded by AKER 22.

[5] ASEEV 11 report the analysis of the entire beta endpoint data, taken with the Troitsk integrating electrostatic spectrometer between 1997 and 2002 (some of the earlier runs were rejected), using a windowless gaseous tritium source. The fitted value of m_ν, based on the method of Feldman and Cousins, is obtained from the upper limit of the fit for m_ν^2. Previous analysis problems were resolved by careful monitoring of the tritium gas column density. Supersedes LOBASHEV 99 and BELESEV 95.

[6] PAGLIAROLI 10 is critical of the likelihood method used by LOREDO 02.

[7] KRAUS 05 is a continuation of the work reported in WEINHEIMER 99. This result represents the final analysis of data taken from 1997 to 2001. Various sources of systematic uncertainties have been identified and quantified. The background has been reduced compared to the initial running period. A spectral anomaly at the endpoint, reported in LOBASHEV 99, was not observed.

[8] ARNABOLDI 03A *et al.* report kinematical neutrino mass limit using β-decay of ^{187}Re. Bolometric $AgReO_4$ micro-calorimeters are used. Mass bound is substantially weaker than those derived from tritium β-decays but has different systematic uncertainties.

[9] LOREDO 02 updates LOREDO 89.

[10] LOBASHEV 99 report a new measurement which continues the work reported in BELESEV 95. This limit depends on phenomenological fit parameters used to derive their best fit to m_ν^2, making unambiguous interpretation difficult. See the footnote under "$\overline{\nu}$ Mass Squared."

[11] WEINHEIMER 99 presents two analyses which exclude the spectral anomaly and result in an acceptable m_ν^2. We report the most conservative limit, but the other is nearly the same. See the footnote under "$\overline{\nu}$ Mass Squared."

[12] BELESEV 95 (Moscow) use an integral electrostatic spectrometer with adiabatic magnetic collimation and a gaseous tritium sources. A fit to a normal Kurie plot above 18300–18350 eV (to avoid a low-energy anomaly) plus a monochromatic line 7–15 eV below the endpoint yields $m_\nu^2 = -4.1 \pm 10.9$ eV^2, leading to this Bayesian limit.

[13] CHING 95 quotes results previously given by SUN 93; no experimental details are given. A possible explanation for consistently negative values of m_ν^2 is given.

[14] HIDDEMANN 95 (Munich) experiment uses atomic tritium embedded in a metal-dioxide lattice. Bayesian limit calculated from the weighted mean $m_\nu^2 = 221 \pm 4244$ eV^2 from the two runs listed below.

[15] STOEFFL 95 (LLNL) result is the Bayesian limit obtained from the m_ν^2 errors given below but with m_ν^2 set equal to 0. The anomalous endpoint accumulation leads to a value of m_ν^2 which is negative by more than 5 standard deviations.

[16] WEINHEIMER 93 (Mainz) is a measurement of the endpoint of the tritium β spectrum using an electrostatic spectrometer with a magnetic guiding field. The source is molecular tritium frozen onto an aluminum substrate.

[17] HOLZSCHUH 92B (Zurich) result is obtained from the measurement $m_\nu^2 = -24 \pm 48 \pm 61$ (1σ errors), in eV^2, using the PDG prescription for conversion to a limit in m_ν.

[18] KAWAKAMI 91 (Tokyo) experiment uses tritium-labeled arachidic acid. This result is the Bayesian limit obtained from the m_ν^2 limit with the errors combined in quadrature. This was also done in ROBERTSON 91, although the authors report a different procedure.

[19] ROBERTSON 91 (LANL) experiment uses gaseous molecular tritium. The result is in strong disagreement with the earlier claims by the ITEP group [LUBIMOV 80, BORIS 87 (+ BORIS 88 erratum)] that m_ν lies between 17 and 40 eV. However, the probability of a positive m^2 is only 3% if statistical and systematic error are combined in quadrature.

[20] See also comment in BORIS 87B and erratum in BORIS 88.

$\overline{\nu}$ MASS SQUARED (electron based)

Given troubling systematics which result in improbably negative estimators of $m_{\nu_e}^{2(\mathrm{eff})} \equiv \sum_i |U_{ei}|^2\, m_{\nu_i}^2$, in many experiments, we use only KRAUS 05, LOBASHEV 99, and AKER 25A for our average.

VALUE (eV^2)	DOCUMENT ID		TECN	COMMENT
$-0.14^{+0.13}_{-0.15}$ OUR AVERAGE				
$-0.14^{+0.13}_{-0.15}$	[1] AKER	25A	SPEC	^{3}H β decay
-0.67 ± 2.53	[2] ASEEV	11	SPEC	^{3}H β decay
$-0.6 \pm 2.2 \pm 2.1$	[3] KRAUS	05	SPEC	^{3}H β decay
• • • We do not use the following data for averages, fits, limits, etc. • • •				
0.1 ± 0.3	[4] AKER	22	SPEC	^{3}H β decay
$-1.0^{+0.9}_{-1.1}$	[5] AKER	19	SPEC	^{3}H β decay
$-1.9 \pm 3.4 \pm 2.2$	[6] LOBASHEV	99	SPEC	^{3}H β decay
$-3.7 \pm 5.3 \pm 2.1$	[7] WEINHEIMER	99	SPEC	^{3}H β decay
-22 ± 4.8	[8] BELESEV	95	SPEC	^{3}H β decay
129 ± 6010	[9] HIDDEMANN	95	SPEC	^{3}H β decay
313 ± 5994	[9] HIDDEMANN	95	SPEC	^{3}H β decay
$-130 \pm 20 \pm 15$	[10] STOEFFL	95	SPEC	^{3}H β decay
$-31 \pm 75 \pm 48$	[11] SUN	93	SPEC	^{3}H β decay
$-39 \pm 34 \pm 15$	[12] WEINHEIMER	93	SPEC	^{3}H β decay
$-24 \pm 48 \pm 61$	[13] HOLZSCHUH	92B	SPEC	^{3}H β decay
$-65 \pm 85 \pm 65$	[14] KAWAKAMI	91	SPEC	^{3}H β decay
$-147 \pm 68 \pm 41$	[15] ROBERTSON	91	SPEC	^{3}H β decay

[1] AKER 25A use data collected by the KATRIN experiment, a precision analysis of the Tritium β spectrum, to formulate a bound on the squared neutrino mass. The combined analysis of 7 science runs is reported. Supersedes AKER 19 and AKER 22.

[2] ASEEV 11 report the analysis of the entire beta endpoint data, taken with the Troitsk integrating electrostatic spectrometer between 1997 and 2002, using a windowless gaseous tritium source. The analysis does not use the two additional fit parameters (see LOBASHEV 99) for a step-like structure near the endpoint. Using only the runs where the tritium gas column density was carefully monitored the need for such parameters was eliminated. Supersedes LOBASHEV 99 and BELESEV 95.

[3] KRAUS 05 is a continuation of the work reported in WEINHEIMER 99. This result represents the final analysis of data taken from 1997 to 2001. Problems with significantly negative squared neutrino masses, observed in some earlier experiments, have been resolved in this work.

[4] AKER 22 report results from the analysis of the Tritium β spectrum using the combined data set collected by the KATRIN experiment in the first two science runs. Supersedes AKER 19.

[5] AKER 19 use the first month of data collected by the KATRIN experiment to determine m_ν^2. The result is consistent with a neutrino mass of zero and is used to place a limit on m_ν. Superseded by AKER 22.

[6] LOBASHEV 99 report a new measurement which continues the work reported in BELESEV 95. The data were corrected for electron trapping effects in the source, eliminating the dependence of the fitted neutrino mass on the fit interval. The analysis assuming a pure beta spectrum yields significantly negative fitted $m_\nu^2 \approx -(20\text{–}10)$ eV^2. This problem is attributed to a discrete spectral anomaly of about 6×10^{-11} intensity with a time-dependent energy of 5–15 eV below the endpoint. The data analysis accounts for this anomaly by introducing two extra phenomenological fit parameters resulting in a best fit of $m_\nu^2 = -1.9 \pm 3.4 \pm 2.2$ eV^2 which is used to derive a neutrino mass limit. However, the introduction of phenomenological fit parameters which are correlated with the derived m_ν^2 limit makes unambiguous interpretation of this result difficult.

[7] WEINHEIMER 99 is a continuation of the work reported in WEINHEIMER 93 . Using a lower temperature of the frozen tritium source eliminated the dewetting of the T_2 film, which introduced a dependence of the fitted neutrino mass on the fit interval in the earlier work. An indication for a spectral anomaly reported in LOBASHEV 99 has been seen, but its time dependence does not agree with LOBASHEV 99. Two analyses, which exclude the spectral anomaly either by choice of the analysis interval or by using a particular data set which does not exhibit the anomaly, result in acceptable m_ν^2 fits and are used to derive the neutrino mass limit published by the authors. We list the most conservative of the two.

[8] BELESEV 95 (Moscow) use an integral electrostatic spectrometer with adiabatic magnetic collimation and a gaseous tritium sources. This value comes from a fit to a normal Kurie plot above 18300–18350 eV (to avoid a low-energy anomaly), including the effects of an apparent peak 7–15 eV below the endpoint.

[9] HIDDEMANN 95 (Munich) experiment uses atomic tritium embedded in a metal-dioxide lattice. They quote measurements from two data sets.

[10] STOEFFL 95 (LLNL) uses a gaseous source of molecular tritium. An anomalous pileup of events at the endpoint leads to the negative value for m_ν^2. The authors acknowledge that "the negative value for the best fit of m_ν^2 has no physical meaning" and discuss possible explanations for this effect.

[11] SUN 93 uses a tritiated hydrocarbon source. See also CHING 95.

[12] WEINHEIMER 93 (Mainz) is a measurement of the endpoint of the tritium β spectrum using an electrostatic spectrometer with a magnetic guiding field. The source is molecular tritium frozen onto an aluminum substrate.

[13] HOLZSCHUH 92B (Zurich) source is a monolayer of tritiated hydrocarbon.

[14] KAWAKAMI 91 (Tokyo) experiment uses tritium-labeled arachidic acid.

[15] ROBERTSON 91 (LANL) experiment uses gaseous molecular tritium. The result is in strong disagreement with the earlier claims by the ITEP group [LUBIMOV 80, BORIS 87 (+ BORIS 88 erratum)] that m_ν lies between 17 and 40 eV. However, the probability of a positive m_ν^2 is only 3% if statistical and systematic error are combined in quadrature.

ν MASS (electron based)

These are measurement of m_ν (in contrast to $m_{\overline{\nu}}$, given above). The masses can be different for a Dirac neutrino in the absence of CPT invariance. The possible distinction between ν and $\overline{\nu}$ properties is usually ignored elsewhere in these Listings.

VALUE (eV)	CL%	DOCUMENT ID		TECN	COMMENT
< 27	90	[1] ALPERT	25	CNTR	^{163}Ho decay
• • • We do not use the following data for averages, fits, limits, etc. • • •					
<460	68	YASUMI	94	CNTR	^{163}Ho decay
<225	95	SPRINGER	87	CNTR	^{163}Ho decay

[1] ALPERT 25 report a kinematical neutrino mass limit, derived from observing 6×10^7 ^{163}Ho EC-decays. The HOLMES bolometric micro-calorimeter array is used. The limit is obtained by means of a Bayesian analysis. The quoted 90% is for Credibility, not Confidence Level.

ν MASS (muon based)

Limits given below are for the square root of $m_{\nu_\mu}^{2(\mathrm{eff})} \equiv \sum_i |U_{\mu i}|^2\, m_{\nu_i}^2$.

In some of the COSM papers listed below, the authors did not distinguish between weak and mass eigenstates.

OUR EVALUATION is based on OUR AVERAGE for the $\pi^\pm$ mass and the ASSAMAGAN 96 value for the muon momentum for the π^+ decay at rest. The limit is calculated using the unified classical analysis of FELDMAN 98 for a Gaussian distribution near a physical boundary. WARNING: since $m_{\nu_\mu}^{2(\mathrm{eff})}$ is calculated from the differences of large numbers, it and the corresponding limits are extraordinarily sensitive to small changes in the pion mass, the decay muon momentum, and their errors. For example, the limits obtained using JECKELMANN 94, LENZ 98, and the weighted averages are 0.15, 0.29, and 0.19 MeV, respectively.

VALUE (MeV)	CL%	DOCUMENT ID		TECN	COMMENT
<0.19 (CL = 90%) OUR EVALUATION					
<0.17	90	[1] ASSAMAGAN	96	SPEC	$m_\nu^2 = -0.016 \pm 0.023$
• • • We do not use the following data for averages, fits, limits, etc. • • •					
<0.15		[2] DOLGOV	95	COSM	Nucleosynthesis
<0.48		[3] ENQVIST	93	COSM	Nucleosynthesis
<0.3		[4] FULLER	91	COSM	Nucleosynthesis
<0.42		[4] LAM	91	COSM	Nucleosynthesis
<0.50	90	[5] ANDERHUB	82	SPEC	$m_\nu^2 = -0.14 \pm 0.20$
<0.65	90	CLARK	74	ASPK	$K_{\mu 3}$ decay

[1] ASSAMAGAN 96 measurement of p_μ from $\pi^+ \to \mu^+\nu$ at rest combined with JECKELMANN 94 Solution B pion mass yields $m_\nu^2 = -0.016 \pm 0.023$ with corresponding Bayesian limit listed above. If Solution A is used, $m_\nu^2 = -0.143 \pm 0.024$ MeV^2. Replaces ASSAMAGAN 94.

[2] DOLGOV 95 removes earlier assumptions (DOLGOV 93) about thermal equilibrium below T_{QCD} for wrong-helicity Dirac neutrinos (ENQVIST 93, FULLER 91) to set more stringent limits.

[3] ENQVIST 93 bases limit on the fact that thermalized wrong-helicity Dirac neutrinos would speed up expansion of early universe, thus reducing the primordial abundance. FULLER 91 exploits the same mechanism but in the older calculation obtains a larger

Int. J. Mod
by UNIVERSITY OF CALIFORNIA @ BERK
wnloaded from www.worldscientific.com
-use and distribution is strictly not permitted, except for Open Access articles.

Int. J. Mod. Phys. A 2026.41. Downloaded from www.worldscientific.com by UNIVERSITY OF CALIFORNIA @ BERKELEY on 09/16/26. Re-use and distribution is strictly not permitted, except for Open Access articles.

production rate for these states, and hence a lower limit. Neutrino lifetime assumed to exceed nucleosynthesis time, ~ 1 s.

[4] Assumes neutrino lifetime >1 s. For Dirac neutrinos only. See also ENQVIST 93.

[5] ANDERHUB 82 kinematics is insensitive to the pion mass.

ν MASS (tau based)

The limits given below are the square roots of limits for $m^{2(\mathrm{eff})}_{\nu_\tau} \equiv \sum_i |U_{\tau i}|^2\, m^2_{\nu_i}$.

In some of the ASTR and COSM papers listed below, the authors did not distinguish between weak and mass eigenstates.

VALUE (MeV)	CL%	EVTS	DOCUMENT ID		TECN	COMMENT
< 18.2	95		[1] BARATE	98F	ALEP	1991–1995 LEP runs
• • • We do not use the following data for averages, fits, limits, etc. • • •						
< 28	95		[2] ATHANAS	00	CLEO	E^{ee}_{cm}= 10.6 GeV
< 27.6	95		[3] ACKERSTAFF	98T	OPAL	1990–1995 LEP runs
< 30	95	473	[4] AMMAR	98	CLEO	E^{ee}_{cm} = 10.6 GeV
< 60	95		[5] ANASTASSOV	97	CLEO	E^{ee}_{cm}= 10.6 GeV
< 0.37 or >22			[6] FIELDS	97	COSM	Nucleosynthesis
< 68	95		[7] SWAIN	97	THEO	m_τ, τ_τ, τ partial widths
< 29.9	95		[8] ALEXANDER	96M	OPAL	1990–1994 LEP runs
<149			[9] BOTTINO	96	THEO	π, μ, τ leptonic decays
<1 or >25			[10] HANNESTAD	96C	COSM	Nucleosynthesis
< 71	95		[11] SOBIE	96	THEO	m_τ, τ_τ, B($\tau^- \to e^- \overline{\nu}_e \nu_\tau$)
< 24	95	25	[12] BUSKULIC	95H	ALEP	1991–1993 LEP runs
< 0.19			[13] DOLGOV	95	COSM	Nucleosynthesis
< 3			[14] SIGL	95	ASTR	SN 1987A
< 0.4 or > 30			[15] DODELSON	94	COSM	Nucleosynthesis
< 0.1 or > 50			[16] KAWASAKI	94	COSM	Nucleosynthesis
155–225			[17] PERES	94	THEO	π,K,μ,τ weak decays
< 32.6	95	113	[18] CINABRO	93	CLEO	$E^{ee}_{\mathrm{cm}} \approx$ 10.6 GeV
< 0.3 or > 35			[19] DOLGOV	93	COSM	Nucleosynthesis
< 0.74			[20] ENQVIST	93	COSM	Nucleosynthesis
< 31	95	19	[21] ALBRECHT	92M	ARG	E^{ee}_{cm}= 9.4–10.6 GeV
< 0.3			[22] FULLER	91	COSM	Nucleosynthesis
< 0.5 or > 25			[23] KOLB	91	COSM	Nucleosynthesis
< 0.42			[22] LAM	91	COSM	Nucleosynthesis

[1] BARATE 98F result based on kinematics of 2939 $\tau^- \to 2\pi^-\pi^+\nu_\tau$ and 52 $\tau^- \to 3\pi^- 2\pi^+ (\pi^0)\nu_\tau$ decays. If possible 2.5% excited a_1 decay is included in 3-prong sample analysis, limit increases to 19.2 MeV.

[2] ATHANAS 00 bound comes from analysis of $\tau^- \to \pi^-\pi^+\pi^-\pi^0\nu_\tau$ decays.

[3] ACKERSTAFF 98T use $\tau \to 5\pi^\pm\nu_\tau$ decays to obtain a limit of 43.2 MeV (95%CL). They combine this with ALEXANDER 96M value using $\tau \to 3h^\pm\nu_\tau$ decays to obtain quoted limit.

[4] AMMAR 98 limit comes from analysis of $\tau^- \to 3\pi^- 2\pi^+\nu_\tau$ and $\tau^- \to 2\pi^-\pi^+ 2\pi^0\nu_\tau$ decay modes.

[5] ANASTASSOV 97 derive limit by comparing their m_τ measurement (which depends on m_{ν_τ}) to BAI 96 m_τ threshold measurement.

[6] FIELDS 97 limit for a Dirac neutrino. For a Majorana neutrino the mass region < 0.93 or >31 MeV is excluded. These bounds assume N_ν <4 from nucleosynthesis; a wider excluded region occurs with a smaller N_ν upper limit.

[7] SWAIN 97 derive their limit from the Standard Model relationships between the tau mass, lifetime, branching fractions for $\tau^- \to e^-\overline{\nu}_e\nu_\tau$, $\tau^- \to \mu^-\overline{\nu}_\mu\nu_\tau$, $\tau^- \to \pi^-\nu_\tau$, and $\tau^- \to K^-\nu_\tau$, and the muon mass and lifetime by assuming lepton universality and using world average values. Limit is reduced to 48 MeV when the CLEO τ mass measurement (BALEST 93) is included; see CLEO's more recent m_{ν_τ} limit (ANASTASSOV 97). Consideration of mixing with a fourth generation heavy neutrino yields $\sin^2\theta_L < 0.016$ (95%CL).

[8] ALEXANDER 96M bound comes from analyses of $\tau^- \to 3\pi^- 2\pi^+\nu_\tau$ and $\tau^- \to h^- h^- h^+\nu_\tau$ decays.

[9] BOTTINO 96 assumes three generations of neutrinos with mixing, finds consistency with massless neutrinos with no mixing based on 1995 data for masses, lifetimes, and leptonic partial widths.

[10] HANNESTAD 96C limit is on the mass of a Majorana neutrino. This bound assumes $N_\nu < 4$ from nucleosynthesis. A wider excluded region occurs with a smaller N_ν upper limit. This paper is the corrected version of HANNESTAD 96; see the erratum: HANNESTAD 96B.

[11] SOBIE 96 derive their limit from the Standard Model relationship between the tau mass, lifetime, and leptonic branching fraction, and the muon mass and lifetime, by assuming lepton universality and using world average values.

[12] BUSKULIC 95H bound comes from a two-dimensional fit of the visible energy and invariant mass distribution of $\tau \to 5\pi(\pi^0)\nu_\tau$ decays. Replaced by BARATE 98F.

[13] DOLGOV 95 removes earlier assumptions (DOLGOV 93) about thermal equilibrium below T_{QCD} for wrong-helicity Dirac neutrinos (ENQVIST 93, FULLER 91) to set more stringent limits. DOLGOV 96 argues that a possible window near 20 MeV is excluded.

[14] SIGL 95 exclude massive Dirac or Majorana neutrinos with lifetimes between 10^{-3} and 10^8 seconds if the decay products are predominantly γ or e^+e^-.

[15] DODELSON 94 calculate constraints on ν_τ mass and lifetime from nucleosynthesis for 4 generic decay modes. Limits depend strongly on decay mode. Quoted limit is valid for all decay modes of Majorana neutrinos with lifetime greater than about 300 s. For Dirac neutrinos limits change to < 0.3 or > 33.

[16] KAWASAKI 94 excluded region is for Majorana neutrino with lifetime >1000 s. Other limits are given as a function of ν_τ lifetime for decays of the type $\nu_\tau \to \nu_\mu\phi$ where ϕ is a Nambu-Goldstone boson.

[17] PERES 94 used PDG 92 values for parameters to obtain a value consistent with mixing. Reexamination by BOTTINO 96 which included radiative corrections and 1995 PDG parameters resulted in two allowed regions, m_3 < 70 MeV and 140 MeV m_3 < 149 MeV.

[18] CINABRO 93 bound comes from analysis of $\tau^- \to 3\pi^- 2\pi^+\nu_\tau$ and $\tau^- \to 2\pi^-\pi^+ 2\pi^0\nu_\tau$ decay modes.

[19] DOLGOV 93 assumes neutrino lifetime >100 s. For Majorana neutrinos, the low mass limit is 0.5 MeV. KAWANO 92 points out that these bounds can be overcome for a Dirac neutrino if it possesses a magnetic moment. See also DOLGOV 96.

[20] ENQVIST 93 bases limit on the fact that thermalized wrong-helicity Dirac neutrinos would speed up expansion of early universe, thus reducing the primordial abundance. FULLER 91 exploits the same mechanism but in the older calculation obtains a larger production rate for these states, and hence a lower limit. Neutrino lifetime assumed to exceed nucleosynthesis time, ~ 1 s.

[21] ALBRECHT 92M reports measurement of a slightly lower τ mass, which has the effect of reducing the ν_τ mass reported in ALBRECHT 88B. Bound is from analysis of $\tau^- \to 3\pi^- 2\pi^+\nu_\tau$ mode.

[22] Assumes neutrino lifetime >1 s. For Dirac neutrinos. See also ENQVIST 93.

[23] KOLB 91 exclusion region is for Dirac neutrino with lifetime >1 s; other limits are given.

Revised August 2025 by K.A. Olive (University of Minnesota).

Neutrinos decouple from thermal equilibrium in the early universe at temperatures $\mathcal{O}(1)$ MeV. The limits on low mass ($m_\nu \lesssim 1$ MeV) neutrinos apply to m_{tot} given by

$$m_{\mathrm{tot}} = \sum_\nu m_\nu \ .$$

Stable neutrinos in this mass range decouple from the thermal bath while still relativistic and make a contribution to the total energy density of the Universe which is given by

$$\rho_\nu = m_{\mathrm{tot}} n_\nu \simeq m_{\mathrm{tot}}(3/11)(3.045/3)^{3/4} n_\gamma \ ,$$

where the factor 3/11 is the ratio of (light) neutrinos to photons and the factor $(3.045/3)^{3/4}$ corrects for the fact that the effective number of neutrinos in the standard model is 3.045 when taking into account e^+e^- annihilation during neutrino decoupling. Writing $\Omega_\nu = \rho_\nu/\rho_c$, where ρ_c is the critical energy density of the Universe, and using $n_\gamma = 410.7\ \mathrm{cm}^{-3}$, we have

$$\Omega_\nu h^2 \simeq m_{\mathrm{tot}}/(93\ \mathrm{eV}) \ .$$

While an upper limit to the matter density of $\Omega_m h^2 < 0.12$ would constrain $m_{\mathrm{tot}} < 11$ eV, much stronger constraints are obtained from the observations of the CMB, combined with lensing and baryon acoustic oscillations data. These combine to give an upper limit of around 0.12 eV, and may, in the near future, be able to provide a lower bound on the sum of the neutrino masses. The current lower bound of $m_{\mathrm{tot}} > 0.06$ eV implies a lower limit of $\Omega_\nu h^2 > 6 \times 10^{-4}$. See our review on "Neutrinos in Cosmology" for more details.

Int. J. Mod
by UNIVERSITY OF CALIFORNIA @ BERK
wnloaded from www.worldscientific.com
-use and distribution is strictly not permitted, except for Open Access articles.

SUM OF THE NEUTRINO MASSES, m_{tot}

This is a sum of the neutrino masses, m_{tot}, as defined in the above note, of effectively stable neutrinos, i.e. those with mean lifetimes on cosmological scales. When necessary, we have generalized the results reported so they apply to m_{tot}. For other limits, see SZALAY 76, VYSOTSKY 77, BERNSTEIN 81, FREESE 84, SCHRAMM 84, and COWSIK 85. For more information see a note on "Neutrinos in Cosmology" in this *Review*.

VALUE (eV)	CL%	DOCUMENT ID		TECN	COMMENT
• • • We do not use the following data for averages, fits, limits, etc. • • •					
< 0.064	95	[1] ABDUL-KARIM	25	COSM	DESI
< 0.08	95	[2] IVANOV	25	COSM	EFT
< 0.19	95	[3] SHAO	25	COSM	
< 0.13	95	[4] MADHAVAC...	24	COSM	ACT
< 0.082	95	[5] BRIEDEN	22	COSM	BOSS, eBOSS, and CMB
< 0.116	95	[6] KUMAR	22	COMS	BOSS and CMB
< 0.14	95	[7] TANSERI	22	COSM	BOSS and CMB
< 0.13	95	[8] ABBOTT	21A	COSM	DES and Planck
< 0.12	95	[9] ALAM	21	COSM	
< 0.09	95	[10] DI-VALENT...	21	COSM	
< 0.16	95	[11] GARNY	21	COSM	
< 0.06–0.14	95	[12] STOCKER	21	COSM	Normal mass ordering
< 0.12	95	[13] AGHANIM	20	COSM	
< 0.15	95	[14] CHOUDHURY	20	COSM	Normal mass hierarchy
< 0.16	95	[15] IVANOV	20	COSM	Planck and BOSS
< 0.11	95	[16] PALANQUE-...	20	COSM	Lyman alpha and CMB
< 0.26	95	[17] LOUREIRO	19	COSM	
< 0.18	95	[18] UPADHYE	19	COSM	BOSS and CMB
< 0.152	95	[19] CHOUDHURY	18	COSM	
$0.064\ ^{+0.061}_{-0.005}$	95	[20] SIMPSON	17	COSM	
< 0.14	95	[21] YECHE	17	COSM	BOSS and XQ-100
< 0.0926	90	[22] DIVALENTINO	16	COSM	
< 0.18	95	[23] HUANG	16	COSM	Normal mass hierarchy
< 0.14	95	[24] ROSSI	15	COSM	
< 0.23	95	[25] ADE	14	COSM	Planck
0.320 ± 0.081		[26] BATTYE	14	COSM	
0.35 ± 0.10		[27] BEUTLER	14	COSM	BOSS
$0.22\ ^{+0.09}_{-0.10}$		[28] COSTANZI	14	COSM	
0.32 ± 0.11		[29] HOU	14	COSM	
< 0.26	95	[30] LEISTEDT	14	COSM	
< 0.18	95	[31] RIEMER-SOR...	14	COSM	
< 0.24	68	[32] MORESCO	12	COSM	
< 0.29	95	[33] XIA	12	COSM	
< 0.81	95	[34] SAITO	11	COSM	SDSS
< 0.44	95	[35] HANNESTAD	10	COSM	
< 0.6	95	[36] SEKIGUCHI	10	COSM	
< 0.28	95	[37] THOMAS	10	COSM	
< 1.1		[38] ICHIKI	09	COSM	
< 1.3	95	[39] KOMATSU	09	COSM	WMAP
< 1.2		[40] TERENO	09	COSM	
< 0.33		[41] VIKHLININ	09	COSM	
< 0.28		[42] BERNARDIS	08	COSM	
< 0.17–2.3		[43] FOGLI	07	COSM	
< 0.42	95	[44] KRISTIANSEN	07	COSM	
< 0.63–2.2		[45] ZUNCKEL	07	COSM	
< 0.24	95	[46] CIRELLI	06	COSM	
< 0.62	95	[47] HANNESTAD	06	COSM	
< 1.2		[48] SANCHEZ	06	COSM	
< 0.17	95	[46] SELJAK	06	COSM	
< 2.0	95	[49] ICHIKAWA	05	COSM	
< 0.75		[50] BARGER	04	COSM	
< 1.0		[51] CROTTY	04	COSM	
< 0.7		[52] SPERGEL	03	COSM	WMAP
< 0.9		[53] LEWIS	02	COSM	
< 4.2		[54] WANG	02	COSM	CMB
< 2.7		[55] FUKUGITA	00	COSM	
< 5.5		[56] CROFT	99	ASTR	Ly α power spec
<180		SZALAY	74	COSM	
<132		COWSIK	72	COSM	
<280		MARX	72	COSM	
<400		GERSHTEIN	66	COSM	

[1] ABDUL-KARIM 25 uses DESI DR2 data in combination with CMB measurements. The limit weakens to < 0.16 eV in the $w_0 w_a$ model. This updates ADAME 25A.

[2] IVANOV 25 combines an effective field theory likelihood with Planck and BAO data.

[3] SHAO 25 uses Planck CMB data with ACT lensing data, SN IA data from Pantheon+, and BAO data from SDSS and DESI. Relaxed limit assumes dynamical dark energy.

[4] MADHAVACHERIL 24 combines ACT lensing data with Planck CMB anisotropies as well as galaxy BAO and optical depth information from the SRoll2 reanalysis of the Planck data.

[5] BRIEDEN 22 combines redshift-space distortions and the shape of the matter power spectrum from BOSS and eBOSS data together with Planck CMB data. Absent the CMB data, the limit is 0.40 eV.

[6] KUMAR 22 combine the reconstructed galaxy power spectrum from BOSS data with Planck CMB data.

[7] TANSERI 22 combines BOSS galaxy clustering data with measurements of CMB data. Updates VAGNOZZI 17.

[8] ABBOTT 21A combines Dark Energy Survey (DES) year 3 results with Planck CMB lensing measurements.

[9] ALAM 21 limit on the sum of neutrino masses by the eBOSS collaboration is based on galaxy, quasar, and Lyman-α 3D clustering data combined with Planck temperature and polarization CMB and supernovae data.

[10] DI-VALENTINO 21 combines CMB temperature and polarization, SNIa luminosity distances and baryon acoustic oscillations data.

[11] GARNY 21 employs a model for the Lyman-α flux power spectrum to set a limit using BOSS data. When combined with Planck CMB temperature and polarization data, a 95% CL range 0.10–0.13 eV is found.

[12] STOCKER 21 use terrestrial and cosmological experiments to set a 95% CL range on the sum of neutrino masses of 0.058–0.139 eV for normal ordering and 0.098–0.174 eV for inverse ordering. They also set an upper limit of 0.037 eV (NO) and 0.042 eV (IO) for the lightest neutrino mass.

[13] AGHANIM 20 limit on the sum of neutrino masses from Planck data combined with lensing and baryon acoustic oscillations (BAO). Without BAO, the limit relaxes to <0.24 eV. Several other limits are quoted based on different combinations of data.

[14] CHOUDHURY 20 combines 2018 Planck CMB temperature and polarization data plus lensing, together with baryon acoustic oscillation data from BOSS, MGS, and 6dFGS. Assumes ΛCDM model. The upper limit is 0.17 eV for the inverted hierarchy, and 0.12 eV for degenerate neutrinos. Limits are also derived for extended cosmological models.

[15] IVANOV 20 combines 2018 Planck CMB data with baryon acoustic oscillation data from BOSS. This study is based on a full-shape likelihood for the redshift-space galaxy power spectrum of the BOSS data.

[16] PALANQUE-DELABROUILLE 20 combine Lyman alpha and Planck temperature and polarization data. Limit improves to 0.09 eV when CMB lensing and baryon acoustic oscillation data are included.

[17] LOUREIRO 19 combines data from large scale structure, cosmic microwave background, type Ia supernovae and big bang nucleosynthesis using physically motivated neutrino mass models.

[18] UPADHYE 19 uses the shape of the BOSS redshift-space galaxy power spectrum in combination with the CMB, and supernovae data. Limit weakens to < 0.54 eV if the dark energy equation of state is allowed to vary.

[19] CHOUDHURY 18 combines 2015 Planck CMB temperature data, information from the optical depth to reionization from Planck 2016 intermediate results together with baryon acoustic oscillation data from BOSS, MGS, and 6dFGS as well as supernovae Type Ia data from the Pantheon Sample. The limit is strengthened to 0.118 eV when high-l CMB polarization data is also included.

[20] SIMPSON 17 uses a combination of laboratory and cosmological measurements to determine the light neutrino masses and argue that there is strong evidence for the normal mass ordering.

[21] Constrains the total mass of neutrinos using the Lyman-alpha forest power spectrum with BOSS (mid-resolution), XQ-100 (high-resolution) and CMB. Without the CMB data, the limit relaxes to 0.8 eV. Supersedes PALANQUE-DELABROUILLE 15A.

[22] Constrains the total mass of neutrinos from Planck CMB data combined with baryon acoustic oscillation and Planck cluster data.

[23] Constrains the total mass of neutrinos from BAO data from SDSS-III/BOSS combined with CMB data from Planck. Limit quoted for normal mass hierarchy. The limit for the inverted mass hierarchy is 0.20 eV and for the degenerate mass hierarchy it is 0.15 eV.

[24] ROSSI 15 sets limits on the sum of neutrino masses using BOSS Lyman alpha forest data combined with Planck CMB data and baryon acoustic oscillations.

[25] Constrains the total mass of neutrinos from Planck CMB data along with WMAP polarization, high L, and BAO data.

[26] Finite neutrino mass fit to resolve discrepancy between CMB and lensing measurements.

[27] Fit to the total mass of neutrinos from BOSS data along with WMAP CMB data and data from other BAO constraints and weak lensing.

[28] Fit to the total mass of neutrinos from Planck CMB data along with BAO.

[29] Fit based on the SPT-SZ survey combined with CMB, BAO, and H_0 data.

[30] Constraints the total mass of neutrinos (marginalizing over the effective number of neutrino species) from CMB, CMB lensing, BAO, and galaxy clustering data.

[31] Constrains the total mass of neutrinos from Planck CMB data combined with baryon acoustic oscillation data from BOSS, 6dFGS, SDSS, WiggleZ data on the galaxy power spectrum, and HST data on the Hubble parameter. The limit is increased to 0.25 eV if a lower bound to the sum of neutrino masses of 0.04 eV is assumed.

[32] Constrains the total mass of neutrinos from observational Hubble parameter data with seven-year WMAP data and the most recent estimate of H_0.

[33] Constrains the total mass of neutrinos from the CFHTLS combined with seven-year WMAP data and a prior on the Hubble parameter. Limit is relaxed to 0.41 eV when small scales affected by non-linearities are removed.

[34] Constrains the total mass of neutrinos from the Sloan Digital Sky Survey and the five-year WMAP data.

[35] Constrains the total mass of neutrinos from the 7-year WMAP data including SDSS and HST data. Limit relaxes to 1.19 eV when CMB data is used alone. Supersedes HANNESTAD 06.

[36] Constrains the total mass of neutrinos from a combination of CMB data, a recent measurement of H_0 (SHOES), and baryon acoustic oscillation data from SDSS.

[37] Constrains the total mass of neutrinos from SDSS MegaZ LRG DR7 galaxy clustering data combined with CMB, HST, supernovae and baryon acoustic oscillation data. Limit relaxes to 0.47 eV when the equation of state parameter, $w \neq 1$.

[38] Constrains the total mass of neutrinos from weak lensing measurements when combined with CMB. Limit improves to 0.54 eV when supernovae and baryon acoustic oscillation observations are included. Assumes ΛCDM model.

Int. J. Mod. Phys. A 2026.41. Downloaded from www.worldscientific.com by UNIVERSITY OF CALIFORNIA @ BERKELEY on 09/16/26. Re-use and distribution is strictly not permitted, except for Open Access articles.

[39] Constrains the total mass of neutrinos from five-year WMAP data. Limit improves to 0.67 eV when supernovae and baryon acoustic oscillation observations are included. Limits quoted assume the ΛCDM model. Supersedes SPERGEL 07.

[40] Constrains the total mass of neutrinos from weak lensing measurements when combined with CMB. Limit improves to $0.03 < \Sigma m_\nu < 0.54$ eV when supernovae and baryon acoustic oscillation observations are included. The slight preference for massive neutrinos at the two-sigma level disappears when systematic errors are taken into account. Assumes ΛCDM model.

[41] Constrains the total mass of neutrinos from recent Chandra X-ray observations of galaxy clusters when combined with CMB, supernovae, and baryon acoustic oscillation measurements. Assumes flat universe and constant dark-energy equation of state, w.

[42] Constraints the total mass of neutrinos from recent CMB and SOSS LRG power spectrum data along with bias mass relations from SDSS, DEEP2, and Lyman-Break Galaxies. It assumes ΛCDM model. Limit degrades to 0.59 eV in a more general wCDM model.

[43] Constrains the total mass of neutrinos from neutrino oscillation experiments and cosmological data. The most conservative limit uses only WMAP three-year data, while the most stringent limit includes CMB, large-scale structure, supernova, and Lyman-alpha data.

[44] Constrains the total mass of neutrinos from recent CMB, large scale structure, SN1a, and baryon acoustic oscillation data. The limit relaxes to 1.75 when WMAP data alone is used with no prior. Paper shows results with several combinations of data sets. Supersedes KRISTIANSEN 06.

[45] Constrains the total mass of neutrinos from the CMB and the large scale structure data. The most conservative limit is obtained when generic initial conditions are allowed.

[46] Constrains the total mass of neutrinos from recent CMB, large scale structure, Lyman-alpha forest, and SN1a data.

[47] Constrains the total mass of neutrinos from recent CMB and large scale structure data. See also GOOBAR 06. Superseded by HANNESTAD 10.

[48] Constrains the total mass of neutrinos from the CMB and the final 2dF Galaxy Redshift Survey.

[49] Constrains the total mass of neutrinos from the CMB experiments alone, assuming ΛCDM Universe. FUKUGITA 06 show that this result is unchanged by the 3-year WMAP data.

[50] Constrains the total mass of neutrinos from the power spectrum of fluctuations derived from the Sloan Digital Sky Survey and the 2dF galaxy redshift survey, WMAP and 27 other CMB experiments and measurements by the HST Key project.

[51] Constrains the total mass of neutrinos from the power spectrum of fluctuations derived from the Sloan Digital Sky Survey, the 2dF galaxy redshift survey, WMAP and ACBAR. The limit is strengthened to 0.6 eV when measurements by the HST Key project and supernovae data are included.

[52] Constrains the fractional contribution of neutrinos to the total matter density in the Universe from WMAP data combined with other CMB measurements, the 2dfGRS data, and Lyman α data. The limit does not noticeably change if the Lyman α data are not used.

[53] LEWIS 02 constrains the total mass of neutrinos from the power spectrum of fluctuations derived from the CMB, HST Key project, 2dF galaxy redshift survey, supernovae type Ia, and BBN.

[54] WANG 02 constrains the total mass of neutrinos from the power spectrum of fluctuations derived from the CMB and other cosmological data sets such as galaxy clustering and the Lyman α forest.

[55] FUKUGITA 00 is a limit on neutrino masses from structure formation. The constraint is based on the clustering scale σ_8 and the COBE normalization and leads to a conservative limit of 0.9 eV assuming 3 nearly degenerate neutrinos. The quoted limit is on the sum of the light neutrino masses.

[56] CROFT 99 result based on the power spectrum of the Ly α forest. If $\Omega_{\rm matter} < 0.5$, the limit is improved to $m_\nu < 2.4\ (\Omega_{\rm matter}/0.17\text{–}1)$ eV.

Limits on MASSES of Light Stable Right-Handed ν (with necessarily suppressed interaction strengths)

VALUE (eV)	DOCUMENT ID		TECN	COMMENT
• • • We do not use the following data for averages, fits, limits, etc. • • •				
<100–200	[1] OLIVE	82	COSM	Dirac ν
<200–2000	[1] OLIVE	82	COSM	Majorana ν

[1] Depending on interaction strength G_R where $G_R < G_F$.

Limits on MASSES of Heavy Stable Right-Handed ν (with necessarily suppressed interaction strengths)

VALUE (GeV)	DOCUMENT ID		TECN	COMMENT
• • • We do not use the following data for averages, fits, limits, etc. • • •				
> 10	[1] OLIVE	82	COSM	G_R/G_F <0.1
>100	[1] OLIVE	82	COSM	G_R/G_F <0.01

[1] These results apply to heavy Majorana neutrinos and are summarized by the equation: m_ν >1.2 GeV (G_F/G_R). The bound saturates, and if G_R is too small no mass range is allowed.

ν CHARGE

e = electron charge is the unit of values listed below.

VALUE (e)	CL%	DOCUMENT ID		TECN	COMMENT
<4 $\times 10^{-35}$	95	[1] CAPRINI	05	COSM	charge neutral universe
• • • We do not use the following data for averages, fits, limits, etc. • • •					
$-3.6\text{–}4.7 \times 10^{-13}$	90	[2] DEMIRCI	25A		Solar $\nu - e$ scattering
$-1.6\text{–}3.7 \times 10^{-13}$	90	[3] DEMIRCI	25A		Solar $\nu - e$ scattering
$<2.24 \times 10^{-13}$	90	[4] AALBERS	23A	LZ	Solar ν spectrum
$<1.5 \times 10^{-13}$	90	[5] ATZORI-COR...	23	FIT	solar neutrinos
$<3.3 \times 10^{-12}$	90	[6] BONET	22A	CONU	nuclear reactor
$<5.4 \times 10^{-12}$	90	[7] ABE	20E	XMAS	solar neutrinos
$1.7\text{–}2.3 \times 10^{-12}$	68	[8] KHAN	20		spectral fit of XENON1T
$<3 \times 10^{-8}$	95	[9] DELLA-VALLE	16	LASR	magnetic dichroism
$<2.1 \times 10^{-12}$	90	[10] CHEN	14A	TEXO	nuclear reactor
$<1.5 \times 10^{-12}$	90	[11] STUDENIKIN	14		nuclear reactor
$<3.7 \times 10^{-12}$	90	[12] GNINENKO	07	RVUE	nuclear reactor
$<2 \times 10^{-14}$		[13] RAFFELT	99	ASTR	red giant luminosity
$<6 \times 10^{-14}$		[14] RAFFELT	99	ASTR	solar cooling
$<4 \times 10^{-4}$		[15] BABU	94	RVUE	BEBC beam dump
$<3 \times 10^{-4}$		[16] DAVIDSON	91	RVUE	SLAC e^- beam dump
$<2 \times 10^{-15}$		[17] BARBIELLINI	87	ASTR	SN 1987A
$<1 \times 10^{-13}$		[18] BERNSTEIN	63	ASTR	solar energy losses

[1] CAPRINI 05 limit derived from the lack of a charge asymmetry in the universe. Limit assumes that charge asymmetries between particles are not anti-correlated.

[2] DEMIRCI 25A analyzed 1540 kg·y of Xe exposure of the TPC-based PandaX-4T dark matter search. Elastic solar neutrino-electron scattering is used to derive a bound on the millicharge of neutrinos.

[3] DEMIRCI 25A analyzed 1600 kg·y of Xe exposure of the TPC-based XENONnT dark matter search. Elastic solar neutrino-electron scattering is used to derive a bound on the millicharge of neutrinos.

[4] AALBERS 23A utilize the first 60 days of data collected by the LZ dark matter search to place a limit on the electric charge of solar neutrinos. Low energy electron-recoil events are utilized. This LZ-collaboration analysis supersedes that of the external authors in ATZORI-CORONA 23 because of a more complete treatment of experiment uncertainties.

[5] ATZORI-CORONA 23 use LUX-ZEPLIN dark matter search data published by AALBERS 23 to place a limit on neutrino millicharge.

[6] BONET 22A use data collected by four low-threshold Ge detectors, placed 17.1 m from one of the cores of the nuclear reactors at Brokdorf to derive this limit. A spectral analysis is performed on reactor on and off data.

[7] ABE 20E obtains this result by assuming that the low-energy excess events in the XMASS detector are produced by neutrino millicharge which is common for all three neutrino flavors.

[8] KHAN 20 performed a constrained spectral fit analysis of the excess observed in the electron recoil energy spectrum by the XENON1T experiment. This range of neutrino millicharge values is one of the possible interpretations of these excess events. For the individual flavor constraints at 90% C.L. see the original reference.

[9] DELLA-VALLE 16 obtain a limit on the charge of neutrinos valid for masses of less than 10 meV. For heavier neutrinos the limit increases as a power of mass, reaching 10^{-6} e for $m = 100$ meV.

[10] CHEN 14A use the Multi-Configuration RRPA method to analyze reactor $\overline{\nu}_e$ scattering on Ge atoms with 300 eV recoil energy threshold to obtain this limit.

[11] STUDENIKIN 14 uses the limit on μ_ν from BEDA 13 and the 2.8 keV threshold of the electron recoil energy to obtain this limit.

[12] GNINENKO 07 use limit on $\overline{\nu}_e$ magnetic moment from LI 03B to derive this result. The limit is considerably weaker than the limits on the charge of ν_e and $\overline{\nu}_e$ from various astrophysics considerations.

[13] This RAFFELT 99 limit applies to all neutrino flavors which are light enough (<5 keV) to be emitted from globular-cluster red giants.

[14] This RAFFELT 99 limit is derived from the helioseismological limit on a new energy-loss channel of the Sun, and applies to all neutrino flavors which are light enough (<1 keV) to be emitted from the sun.

[15] BABU 94 use COOPER-SARKAR 92 limit on ν magnetic moment to derive quoted result. It applies to ν_τ.

[16] DAVIDSON 91 use data from early SLAC electron beam dump experiment to derive charge limit as a function of neutrino mass. It applies to ν_τ.

[17] Exact BARBIELLINI 87 limit depends on assumptions about the intergalactic or galactic magnetic fields and about the direct distance and time through the field. It applies to ν_e.

[18] The limit applies to all flavors.

ν (MEAN LIFE) / MASS

Measures $\left[\sum |U_{\ell j}|^2\ \Gamma_j\ m_j\right]^{-1}$, where the sum is over mass eigenstates which cannot be resolved experimentally. Some of the limits constrain the radiative decay and are based on the limit of the corresponding photon flux. Other apply to the decay of a heavier neutrino into the lighter one and a Majoron or other invisible particle. Many of these limits apply to any ν within the indicated mass range.

Limits on the radiative decay are either directly based on the limits of the corresponding photon flux, or are derived from the limits on the neutrino magnetic moments. In the later case the transition rate for $\nu_i \to \nu_j + \gamma$ is constrained by $\Gamma_{ij} = \frac{1}{\tau_{ij}} = \frac{(m_i^2 - m_j^2)^3}{m_i^3}\ \mu_{ij}^2$ where μ_{ij} is the neutrino transition moment in the mass eigenstates basis. Typically, the limits on lifetime based on the magnetic moments are many orders of magnitude more restrictive than limits based on the nonobservation of photons.

VALUE (s/eV)	CL%	DOCUMENT ID		TECN	COMMENT
> 15.4	90	[1] KRAKAUER	91	CNTR	$\nu_\mu, \overline{\nu}_\mu$ at LAMPF
> 7 $\times 10^9$		[2] RAFFELT	85	ASTR	
> 300	90	[3] REINES	74	CNTR	$\overline{\nu}_e$

• • • We do not use the following data for averages, fits, limits, etc. • • •

> 20–450	95	[4] VALERA	24	ASTR	ν_2 and ν_3 non-radiative decay
$> 1.2 \times 10^5$	90	[5] IVANEZ-BAL...	23	ASTR	SN1987A, nonradiative decay
$> 8.08 \times 10^{-5}$	90	[6] AHARMIM	19	SNO	ν_2 invisible nonradiative decay
$> 1.92 \times 10^{-3}$	90	[7] AHARMIM	19	FIT	ν_2 invisible nonradiative decay
6–26×10^9	95	[8] ESCUDERO	19	COSM	Invisible decay $m_\nu \geq 0.05$ eV
$> 10^5 - 10^{10}$	95	[9] CECCHINI	11	ASTR	$\nu_2 \rightarrow \nu_1$ radiative decay
		[10] MIRIZZI	07	CMB	radiative decay
		[11] MIRIZZI	07	CIB	radiative decay
		[12] WONG	07	CNTR	Reactor $\overline{\nu}_e$
> 0.11	90	[13] XIN	05	CNTR	Reactor ν_e
		[14] XIN	05	CNTR	Reactor ν_e
> 0.004	90	[15] AHARMIM	04	SNO	quasidegen. ν masses
$> 4.4 \times 10^{-5}$	90	[15] AHARMIM	04	SNO	hierarchical ν masses
$\gtrsim 100$	95	[16] CECCHINI	04	ASTR	Radiative decay for ν mass > 0.01 eV
> 0.067	90	[17] EGUCHI	04	KLND	quasidegen. ν masses
$> 1.1 \times 10^{-3}$	90	[17] EGUCHI	04	KLND	hierarchical ν masses
$> 8.7 \times 10^{-5}$	99	[18] BANDYOPA...	03	FIT	nonradiative decay
≥ 4200	90	[19] DERBIN	02B	CNTR	Solar pp and Be ν
$> 2.8 \times 10^{-5}$	99	[20] JOSHIPURA	02B	FIT	nonradiative decay
		[21] DOLGOV	99	COSM	
		[22] BILLER	98	ASTR	$m_\nu = 0.05$–1 eV
$> 2.8 \times 10^{15}$		[23,24] BLUDMAN	92	ASTR	$m_\nu < 50$ eV
none $10^{-12} - 5 \times 10^4$		[25] DODELSON	92	ASTR	$m_\nu = 1$–300 keV
$< 10^{-12}$ or $> 5 \times 10^4$		[25] DODELSON	92	ASTR	$m_\nu = 1$–300 keV
		[26] GRANEK	91	COSM	Decaying L^0
> 6.4	90	[27] KRAKAUER	91	CNTR	ν_e at LAMPF
$> 1.1 \times 10^{15}$		[28] WALKER	90	ASTR	$m_\nu = 0.03 - \sim 2$ MeV
$> 6.3 \times 10^{15}$		[24,29] CHUPP	89	ASTR	$m_\nu < 20$ eV
$> 1.7 \times 10^{15}$		[24] KOLB	89	ASTR	$m_\nu < 20$ eV
		[30] RAFFELT	89	RVUE	$\overline{\nu}$ (Dirac, Majorana)
		[31] RAFFELT	89B	ASTR	
$> 8.3 \times 10^{14}$		[32] VONFEILIT...	88	ASTR	
> 22	68	[33] OBERAUER	87		$\overline{\nu}_R$ (Dirac)
> 38	68	[33] OBERAUER	87		$\overline{\nu}$ (Majorana)
> 59	68	[33] OBERAUER	87		$\overline{\nu}_L$ (Dirac)
> 30	68	KETOV	86	CNTR	$\overline{\nu}$ (Dirac)
> 20	68	KETOV	86	CNTR	$\overline{\nu}$ (Majorana)
		[34] BINETRUY	84	COSM	$m_\nu \sim 1$ MeV
> 0.11	90	[35] FRANK	81	CNTR	$\nu\overline{\nu}$ LAMPF
$> 2 \times 10^{21}$		[36] STECKER	80	ASTR	$m_\nu = 10$–100 eV
$> 1.0 \times 10^{-2}$	90	[35] BLIETSCHAU	78	HLBC	ν_μ, CERN GGM
$> 1.7 \times 10^{-2}$	90	[35] BLIETSCHAU	78	HLBC	$\overline{\nu}_\mu$, CERN GGM
$< 3 \times 10^{-11}$		[37] FALK	78	ASTR	$m_\nu < 10$ MeV
$> 2.2 \times 10^{-3}$	90	[35] BARNES	77	DBC	ν, ANL 12-ft
		[38] COWSIK	77	ASTR	
$> 3. \times 10^{-3}$	90	[35] BELLOTTI	76	HLBC	ν, CERN GGM
$> 1.3 \times 10^{-2}$	90	[35] BELLOTTI	76	HLBC	$\overline{\nu}$, CERN GGM

[1] KRAKAUER 91 quotes the limit $\tau/m_{\nu_1} > (0.75a^2 + 21.65a + 26.3)$ s/eV, where a is a parameter describing the asymmetry in the neutrino decay defined as $dN_\gamma/d\cos\theta = (1/2)(1 + a\cos\theta)$ The parameter $a = 0$ for a Majorana neutrino, but can vary from -1 to 1 for a Dirac neutrino. The bound given by the authors is the most conservative (which applies for $a = -1$).

[2] RAFFELT 85 limit on the radiative decay is from solar x- and γ-ray fluxes. Limit depends on ν flux from pp, now established from GALLEX and SAGE to be > 0.5 of expectation.

[3] REINES 74 looked for ν of nonzero mass decaying radiatively to a neutral of lesser mass $+ \gamma$. Used liquid scintillator detector near fission reactor. Finds lab lifetime 6×10^7 s or more. Above value of (mean life)/mass assumes average effective neutrino energy of 0.2 MeV. To obtain the limit 6×10^7 s REINES 74 assumed that the full $\overline{\nu}_e$ reactor flux could be responsible for yielding decays with photon energies in the interval 0.1 MeV – 0.5 MeV. This represents some overestimate so their lower limit is an over-estimate of the lab lifetime (VOGEL 84). If so, OBERAUER 87 may be comparable or better.

[4] VALERA 24 reports limits using IceCube data. Authors caution that the limits on ν_2 and ν_3 are correlated.

[5] IVANEZ-BALLESTEROS 23 reports a limit on the lifetime-to-mass ratio of the mass eigenstates ν_1 and ν_2 for inverted mass ordering. No limit was obtained in the case of normal mass ordering.

[6] AHARMIM 19 quotes the limit τ/m_{ν_2} for invisible nonradiative decay of ν_2. They obtained this result by analyzing the entire SNO dataset, allowing for the decay of ν_2 which would cause an energy-dependent distortion of the survival probability of electron-type solar neutrinos.

[7] AHARMIM 19 quotes the limit τ/m_{ν_2} for invisible nonradiative decay of ν_2. They obtained this result by combining the τ/m_{ν_2} measurements from SNO and other solar neutrino experiments (Super-Kamiokande, KamLAND, and Borexino ^{8}B results; Borexino and KamLAND ^{7}Be results; the combined gallium interaction rate from GNO, GALLEX, and SAGE; and the chlorine interaction rate from Homestake). The quoted limit at 99% CL is $> 1.04 \times 10^{-3}$.

[8] ESCUDERO 19 sets limits on invisible neutrino decays using Planck 2018 data of $\tau > 1.3$–0.3×10^9 s at 95% C.L. Values in the range $\tau = 2$–16×10^9 s are preferred at 95% C.L. when Planck polarization data is included. Limits scale as $(m_\nu/0.05\text{ eV})^3$.

[9] CECCHINI 11 search for radiative decays of solar neutrinos into visible photons during the 2006 total solar eclipse. The range of (mean life)/mass values corresponds to a range of ν_1 masses between 10^{-4} and 0.1 eV.

[10] MIRIZZI 07 determine a limit on the neutrino radiative decay from analysis of the maximum allowed distortion of the CMB spectrum as measured by the COBE/FIRAS. For the decay $\nu_2 \rightarrow \nu_1$ the lifetime limit is $\lesssim 4 \times 10^{20}$ s for $m_{min} \lesssim 0.14$ eV. For transition with the $|\Delta m_{31}|$ mass difference the lifetime limit is $\sim 2 \times 10^{19}$ s for $m_{min} \lesssim 0.14$ eV and $\sim 5 \times 10^{20}$ s for $m_{min} \gtrsim 0.14$ eV.

[11] MIRIZZI 07 determine a limit on the neutrino radiative decay from analysis of the cosmic infrared background (CIB) using the Spitzer Observatory data. For transition with the $|\Delta m_{31}|$ mass difference they obtain the lifetime limit $\sim 10^{20}$ s for $m_{min} \lesssim 0.14$ eV.

[12] WONG 07 use their limit on the neutrino magnetic moment together with the assumed experimental value of $\Delta m^2_{13} \sim 2 \times 10^{-3}$ eV^2 to obtain $\tau_{13}/m_1^3 > 3.2 \times 10^{27}$ s/eV^3 for the radiative decay in the case of the inverted mass hierarchy. Similarly to RAFFELT 89 this limit can be violated if electric and magnetic moments are equal to each other. Analogous, but numerically somewhat different limits are obtained for τ_{23} and τ_{21}.

[13] XIN 05 search for the γ from radiative decay of ν_e produced by the electron capture on ^{51}Cr. No events were seen and the limit on τ/m_ν was derived. This is a weaker limit on the decay of ν_e than KRAKAUER 91.

[14] XIN 05 use their limit on the neutrino magnetic moment of ν_e together with the assumed experimental value of $\Delta m^2_{1,3} \sim 2 \times 10^{-3}$ eV^2 to obtain $\tau_{13}/m_1^3 > 1 \times 10^{23}$ s/eV^3 for the radiative decay in the case of the inverted mass hierarchy. Similarly to RAFFELT 89 this limit can be violated if electric and magnetic moments are equal to each other. Analogous, but numerically somewhat different limits are obtained for τ_{23} and τ_{21}. Again, this limit is specific for ν_e.

[15] AHARMIM 04 obtained these results from the solar $\overline{\nu}_e$ flux limit set by the SNO measurement assuming ν_2 decay through nonradiative process $\nu_2 \rightarrow \overline{\nu}_1 X$, where X is a Majoron or other invisible particle. Limits are given for the cases of quasidegenerate and hierarchical neutrino masses.

[16] CECCHINI 04 obtained this bound through the observations performed on the occasion of the 21 June 2001 total solar eclipse, looking for visible photons from radiative decays of solar neutrinos. Limit is a τ/m_{ν_2} in $\nu_2 \rightarrow \nu_1\gamma$. Limit ranges from ~ 100 to 10^7 s/eV for $0.01 < m_{\nu_1} < 0.1$ eV.

[17] EGUCHI 04 obtained these results from the solar $\overline{\nu}_e$ flux limit set by the KamLAND measurement assuming ν_2 decay through nonradiative process $\nu_2 \rightarrow \overline{\nu}_1 X$, where X is a Majoron or other invisible particle. Limits are given for the cases of quasidegenerate and hierarchical neutrino masses.

[18] The ratio of the lifetime over the mass derived by BANDYOPADHYAY 03 is for ν_2. They obtained this result using the following solar-neutrino data: total rates measured in Cl and Ga experiments, the Super-Kamiokande's zenith-angle spectra, and SNO's day and night spectra. They assumed that ν_1 is the lowest mass, stable or nearly stable neutrino state and ν_2 decays through nonradiative Majoron emission process, $\nu_2 \rightarrow \overline{\nu}_1 + J$, or through nonradiative process with all the final state particles being sterile. The best fit is obtained in the region of the LMA solution.

[19] DERBIN 02B (also BACK 03B) obtained this bound for the radiative decay from the results of background measurements with Counting Test Facility (the prototype of the Borexino detector). The laboratory gamma spectrum is given as $dN_\gamma/d\cos\theta = (1/2)(1 + \alpha\cos\theta)$ with $\alpha = 0$ for a Majorana neutrino, and α varying to -1 to 1 for a Dirac neutrino. The listed bound is for the case of $\alpha = 0$. The most conservative bound 1.5×10^3 s eV^{-1} is obtained for the case of $\alpha = -1$.

[20] The ratio of the lifetime over the mass derived by JOSHIPURA 02B is for ν_2. They obtained this result from the total rates measured in all solar neutrino experiments. They assumed that ν_1 is the lowest mass, stable or nearly stable neutrino state and ν_2 decays through nonradiative process like Majoron emission decay, $\nu_2 \rightarrow \nu_1' + J$ where ν_1' state is sterile. The exact limit depends on the specific solution of the solar neutrino problem. The quoted limit is for the LMA solution.

[21] DOLGOV 99 places limits in the (Majorana) τ-associated ν mass-lifetime plane based on nucleosynthesis. Results would be considerably modified if neutrino oscillations exist.

[22] BILLER 98 use the observed TeV γ-ray spectra to set limits on the mean life of any radiatively decaying neutrino between 0.05 and 1 eV. Curve shows $\tau_\nu/B_\gamma > 0.15 \times 10^{21}$ s at 0.05 eV, $> 1.2 \times 10^{21}$ s at 0.17 eV, $> 3 \times 10^{21}$ s at 1 eV, where B_γ is the branching ratio to photons.

[23] BLUDMAN 92 sets additional limits by this method for higher mass ranges. Cosmological limits are also obtained.

[24] Limit on the radiative decay based on nonobservation of γ's in coincidence with ν's from SN 1987A.

[25] DODELSON 92 range is for wrong-helicity keV mass Dirac ν's from the core of neutron star in SN 1987A decaying to ν's that would have interacted in KAM2 or IMB detectors.

[26] GRANEK 91 considers heavy neutrino decays to $\gamma\nu_L$ and $3\nu_L$, where $m_{\nu_L} < 100$ keV. Lifetime is calculated as a function of heavy neutrino mass, branching ratio into $\gamma\nu_L$, and m_{ν_L}.

[27] KRAKAUER 91 quotes the limit for ν_e, $\tau/m_\nu > (0.3a^2 + 9.8a + 15.9)$ s/eV, where a is a parameter describing the asymmetry in the radiative neutrino decay defined as $dN_\gamma/d\cos\theta = (1/2)(1 + a\cos\theta)$ $a = 0$ for a Majorana neutrino, but can vary from -1 to 1 for a Dirac neutrino. The bound given by the authors is the most conservative (which applies for $a = -1$).

[28] WALKER 90 uses SN 1987A γ flux limits after 289 days.

[29] CHUPP 89 should be multiplied by a branching ratio (about 1) and a detection efficiency (about 1/4), and pertains to radiative decay of any neutrino to a lighter or sterile neutrino.

Int. J. Mod
by UNIVERSITY OF CALIFORNIA @ BERK
wnloaded from www.worldscientific.com
-use and distribution is strictly not permitted, except for Open Access articles.

Int. J. Mod. Phys. A 2026.41. Downloaded from www.worldscientific.com
by UNIVERSITY OF CALIFORNIA @ BERKELEY on 09/16/26. Re-use and distribution is strictly not permitted, except for Open Access articles.

[30] RAFFELT 89 uses KYULDJIEV 84 to obtain $\tau m^3 > 3 \times 10^{18}$ s eV^3 (based on $\overline{\nu}_e e^-$ cross sections). The bound for the radiative decay is not valid if electric and magnetic transition moments are equal for Dirac neutrinos.

[31] RAFFELT 89B analyze stellar evolution and exclude the region $3 \times 10^{12} < \tau m^3 < 3 \times 10^{21}$ s eV^3.

[32] Model-dependent theoretical analysis of SN1987A neutrinos. Quoted limit is for $\left[\sum_j |U_{\ell j}|^2 \Gamma_j m_j\right]^{-1}$, where $\ell = \mu, \tau$. Limit is 3.3×10^{14} s/eV for $\ell = e$.

[33] OBERAUER 87 looks for photons and e^+e^- pairs from radiative decays of reactor neutrinos.

[34] BINETRUY 84 finds $\tau < 10^8$ s for neutrinos in a radiation-dominated universe.

[35] These experiments look for $\nu_k \rightarrow \nu_j \gamma$ or $\overline{\nu}_k \rightarrow \overline{\nu}_j \gamma$.

[36] STECKER 80 limit based on UV background; result given is $\tau > 4 \times 10^{22}$ s at m_ν=20 eV.

[37] FALK 78 finds lifetime constraints based on supernova energetics.

[38] COWSIK 77 considers variety of scenarios. For neutrinos produced in the big bang, present limits on optical photon flux require $\tau > 10^{23}$ s for $m_\nu \sim 1$ eV. See also COWSIK 79 and GOLDMAN 79.

ν MAGNETIC MOMENT

The coupling of neutrinos to an electromagnetic field is a characterized by a 3×3 matrix λ of the magnetic (μ) and electric (d) dipole moments ($\lambda = \mu - id$). For Majorana neutrinos the matrix λ is antisymmetric and only transition moments are allowed, while for Dirac neutrinos λ is a general 3×3 matrix. In the standard electroweak theory extended to include neutrino masses (see FUJIKAWA 80) $\mu_\nu = 3eG_F m_\nu/(8\pi^2\sqrt{2}) = 3.2 \times 10^{-19}(m_\nu/\text{eV})\mu_B$, i.e. it is unobservably small given the known small neutrino masses. In more general models there is no longer a proportionality between neutrino mass and its magnetic moment, even though only massive neutrinos have nonvanishing magnetic moments without fine tuning.

Laboratory bounds on λ are obtained via elastic ν-e scattering, where the scattered neutrino is not observed. The combinations of matrix elements of λ that are constrained by various experiments depend on the initial neutrino flavor and on its propagation between source and detector (e.g., solar ν_e and reactor $\overline{\nu}_e$ do not constrain the same combinations). The listings below therefore identify the initial neutrino flavor.

Other limits, e.g. from various stellar cooling processes, apply to all neutrino flavors. Analogous flavor independent, but weaker, limits are obtained from the analysis of $e^+e^- \rightarrow \nu\overline{\nu}\gamma$ collider experiments.

VALUE (10^{-10} μ_B)	CL%	DOCUMENT ID		TECN	COMMENT
< 0.064	90	[1] APRILE	22B	XENT	Solar ν spectrum
< 0.29	90	[2] BEDA	13	CNTR	Reactor $\overline{\nu}_e$
< 6.8	90	[3] AUERBACH	01	LSND	$\nu_e e$, $\nu_\mu e$ scattering
< 3900	90	[4] SCHWIENHO...	01	DONU	$\nu_\tau e^- \rightarrow \nu_\tau e^-$
• • • We do not use the following data for averages, fits, limits, etc. • • •					
< 5.6	90	[5] ALPIZAR-VE...	25	CNTR	Reactor $\overline{\nu}_e$
< 0.137	90	[6] DEMIRCI	25A		Solar $\nu - e$ scattering
< 0.072	90	[7] DEMIRCI	25A		Solar $\nu - e$ scattering
< 0.23	90	[8] ZENG	25	PAND	Solar ν spectrum
< 0.16		[9] CARENZA	24A	COSM	
< 0.136	90	[10] AALBERS	23A	LZ	Solar ν spectrum
< 0.11	90	[11] ATZORI-COR...	23	FIT	Solar ν spectrum
< 0.75	90	[12] BONET	22A	CONU	Reactor $\overline{\nu}_e$
< 2.8	90	[13] COLOMA	22	CNTR	Reactor $\overline{\nu}_e$
< 1.8	90	[14] ABE	20E	XMAS	Solar ν spectrum
0.14–0.29	90	[15] APRILE	20	XE1T	Solar ν spectrum
< 0.012	95	[16] CAPOZZI	20	ASTR	Tip of the Red-Giant Branch
0.2–0.4	68	[17] KHAN	20		Spectral fit of XENON1T
< 0.28	90	[18] AGOSTINI	17A	BORX	Solar ν spectrum
< 0.022	90	[19] ARCEO-DIAZ	15	ASTR	Red giants
< 0.1	95	[20] CORSICO	14	ASTR	
< 0.05	95	[21] MILLER-BER...	14B	ASTR	
< 0.045	95	[22] VIAUX	13A	ASTR	Globular cluster M5
< 0.32	90	[23] BEDA	10	CNTR	Reactor $\overline{\nu}_e$
< 2.2	90	[24] DENIZ	10	TEXO	Reactor $\overline{\nu}_e$
< 0.011–0.027		[25] KUZNETSOV	09	ASTR	$\nu_L \rightarrow \nu_R$ in SN1987A
< 0.54	90	[26] ARPESELLA	08A	BORX	Solar ν spectrum
< 0.58	90	[27] BEDA	07	CNTR	Reactor $\overline{\nu}_e$
< 0.74	90	[28] WONG	07	CNTR	Reactor $\overline{\nu}_e$
< 0.9	90	[29] DARAKTCH...	05		Reactor $\overline{\nu}_e$
< 130	90	[30] XIN	05	CNTR	Reactor ν_e
< 37	95	[31] GRIFOLS	04	FIT	Solar ^{8}B ν (SNO NC)
< 3.6	90	[32] LIU	04	SKAM	Solar ν spectrum
< 1.1	90	[33] LIU	04	SKAM	Solar ν spectrum (LMA region)
< 5.5	90	[34] BACK	03B	CNTR	Solar pp and Be ν
< 1.0	90	[35] DARAKTCH...	03		Reactor $\overline{\nu}_e$
< 1.3	90	[36] LI	03B	CNTR	Reactor $\overline{\nu}_e$
< 2	90	[37] GRIMUS	02	FIT	solar + reactor (Majorana ν)
<80000	90	[38] TANIMOTO	00	RVUE	$e^+e^- \rightarrow \nu\overline{\nu}\gamma$
< 0.01–0.04		[39] AYALA	99	ASTR	$\nu_L \rightarrow \nu_R$ in SN1987A
< 1.5	90	[40] BEACOM	99	SKAM	Solar ν spectrum
< 0.03		[41] RAFFELT	99	ASTR	Red giant luminosity
< 4		[42] RAFFELT	99	ASTR	Solar cooling
<44000	90	ABREU	97J	DLPH	$e^+e^- \rightarrow \nu\overline{\nu}\gamma$ at LEP
<33000	90	[43] ACCIARRI	97Q	L3	$e^+e^- \rightarrow \nu\overline{\nu}\gamma$ at LEP
< 0.62		[44] ELMFORS	97	COSM	Depolarization in early universe plasma
<27000	95	[45] ESCRIBANO	97	RVUE	$\Gamma(Z \rightarrow \nu\nu)$ at LEP
< 30	90	VILAIN	95B	CHM2	$\nu_\mu e \rightarrow \nu_\mu e$
<55000	90	GOULD	94	RVUE	$e^+e^- \rightarrow \nu\overline{\nu}\gamma$ at LEP
< 1.9	95	[46] DERBIN	93	CNTR	Reactor $\overline{\nu}e \rightarrow \overline{\nu}e$
< 5400	90	[47] COOPER-...	92	BEBC	$\nu_\tau e^- \rightarrow \nu_\tau e^-$
< 2.4	90	[48] VIDYAKIN	92	CNTR	Reactor $\overline{\nu}e \rightarrow \overline{\nu}e$
<56000	90	DESHPANDE	91	RVUE	$e^+e^- \rightarrow \nu\overline{\nu}\gamma$
< 100	95	[49] DORENBOS...	91	CHRM	$\nu_\mu e \rightarrow \nu_\mu e$
< 8.5	90	AHRENS	90	CNTR	$\nu_\mu e \rightarrow \nu_\mu e$
< 10.8	90	[50] KRAKAUER	90	CNTR	LAMPF $\nu e \rightarrow \nu e$
< 7.4	90	[50] KRAKAUER	90	CNTR	LAMPF $(\nu_\mu, \overline{\nu}_\mu)e$ elast.
< 0.02		[51] RAFFELT	90	ASTR	Red giant luminosity
< 0.1		[52] RAFFELT	89B	ASTR	Cooling helium stars
		[53] FUKUGITA	88	COSM	Primordial magn. fields
<40000	90	[54] GROTCH	88	RVUE	$e^+e^- \rightarrow \nu\overline{\nu}\gamma$
≤ .3		[52] RAFFELT	88B	ASTR	He burning stars
< 0.11		[52] FUKUGITA	87	ASTR	Cooling helium stars
< 0.0006		[55] NUSSINOV	87	ASTR	Cosmic EM backgrounds
< 0.1–0.2		MORGAN	81	COSM	^{4}He abundance
< 0.85		BEG	78	ASTR	Stellar plasmons
< 0.6		[56] SUTHERLAND	76	ASTR	Red giants + degenerate dwarfs
< 81		[57] KIM	74	RVUE	$\overline{\nu}_\mu e \rightarrow \overline{\nu}_\mu e$
< 1		BERNSTEIN	63	ASTR	Solar cooling
< 14		COWAN	57	CNTR	Reactor $\overline{\nu}$

[1] APRILE 22B use data collected with the XENONnT dark matter detector to place a limit on an enhanced magnetic moment of solar neutrinos. Supersedes APRILE 20.

[2] BEDA 13 report $\overline{\nu}_e e^-$ scattering results, using the Kalinin Nuclear Power Plant and a shielded Ge detector. The recoil electron spectrum is analyzed between 2.5 and 55 keV. Supersedes BEDA 07. Supersedes BEDA 10. This is the most stringent limit on the magnetic moment of reactor $\overline{\nu}_e$.

[3] AUERBACH 01 limit is based on the LSND ν_e and ν_μ electron scattering measurements. The limit is slightly more stringent than KRAKAUER 90.

[4] SCHWIENHORST 01 quote an experimental sensitivity of 4.9×10^{-7}.

[5] ALPIZAR-VENEGAS 25 use data collected by the CONUS+ coherent nucleus scattering experiment, conducted at 20.7 m distance to the Leibstadt nuclear power plant in Switzerland. The authors are not members of the CONUS+ collaboration and used public data to derive a limit on the magnetic moment of $\overline{\nu}_e$.

[6] DEMIRCI 25A analyzed 1540 kg·y of Xe exposure of the TPC-based PandaX-4T dark matter search. Elastic solar neutrino-electron scattering is used to derive a bound on the magnetic moment of neutrinos.

[7] DEMIRCI 25A analyzed 1600 kg·y of Xe exposure of the TPC-based XENONnT dark matter search. Elastic solar neutrino-electron scattering is used to derive a bound on the magnetic moment of neutrinos.

[8] ZENG 25 use data of the PandaX-4T dark matter detector to derive a limit on the anomalous magnetic moment of solar neutrinos.

[9] CARENZA 24A derive the limit from the production of right-handed neutrinos in the early universe.

[10] AALBERS 23A utilize the first 60 days of data collected by the LZ dark matter search to place a limit on the magnetic moment of solar neutrinos. Low energy electron-recoil events are utilized. This LZ-collaboration analysis supersedes that of the external authors in ATZORI-CORONA 23 because of a more complete treatment of experiment uncertainties.

[11] ATZORI-CORONA 23 use LUX-ZEPLIN dark matter search data published by AALBERS 23 to place a limit on an enhanced magnetic moment of solar neutrinos.

[12] BONET 22A use data collected by four low-threshold Ge detectors, placed 17.1 m from one of the cores of the nuclear reactors at Brokdorf to derive this limit. A spectral analysis is performed on reactor on and off data.

[13] COLOMA 22 present a re-analysis of data taken by the COHERENT and Dresden-II experiments. The combination of both experiments is used to place a limit on the magnetic moment of electron-type neutrinos. The presented value is one-sided limit as recommended by the authors; the two-sided limit is $< 3.2 \times 10^{-10} \mu_B$ at 90% C.L. Results based on Fef and YBe quenching models are reported in the paper. The authors are not part of either collaboration.

[14] ABE 20E observed an excess of low-energy events in the XMASS detector, which could be interpreted as a signal produced by a neutrino magnetic moment with this magnitude.

[15] APRILE 20 observed an excess of low-energy events in the XENON1T detector, which could be interpreted as a signal produced by a neutrino magnetic moment with this magnitude.

[16] CAPOZZI 20 obtains a limit on the neutrino dipole moment from the brightness of the tip of the red-giant branch in ω Centauri. A similar limit of $\mu_\nu < 1.5 \times 10^{-12}$ μ_B is obtained in NGC 4258.

[17] KHAN 20 performed a constrained spectral fit analysis of the excess observed in the electron recoil energy spectrum by the XENON1T experiment. This range of the μ_B values is one of the possible interpretations of these excess events. For the individual flavor constraints at 90% C.L. see the original reference.

[18] AGOSTINI 17A obtained this limit using the shape of the recoil electron energy spectrum from the Borexino Phase-II 1291.5 live days of solar neutrino data and the constraints on the sum of the solar neutrino fluxes from the radiochemical gallium experiments

SAGE, Gallex, and GNO. Without radiochemical constraints, the 90% C.L. limit of $< 4.0 \times 10^{-11} \mu_B$ is obtained.

[19] ARCEO-DIAZ 15 constrains the neutrino magnetic moment from observation of the tip of the red giant branch in the globular cluster ω-Centauri.

[20] CORSICO 14 constrains the neutrino magnetic moment from observations of white drarf pulsations.

[21] MILLER-BERTOLAMI 14B constrains the neutrino magnetic moment from observations of the white dwarf luminosity function of the Galactic disk.

[22] VIAUX 13A constrains the neutrino magnetic moment from observations of the globular cluster M5.

[23] BEDA 10 report $\overline{\nu}_e e^-$ scattering results, using the Kalinin Nuclear Power Plant and a shielded Ge detector. The recoil electron spectrum is analyzed between 2.9 and 45 keV. Supersedes BEDA 07. Superseded by BEDA 13.

[24] DENIZ 10 observe reactor $\overline{\nu}_e e$ scattering with recoil kinetic energies 3–8 MeV using CsI(Tl) detectors. The observed rate and spectral shape are consistent with the Standard Model prediction, leading to the reported constraint on $\overline{\nu}_e$ magnetic moment.

[25] KUZNETSOV 09 obtain a limit on the flavor averaged magnetic moment of Dirac neutrinos from the time averaged neutrino signal of SN1987A. Improves and supersedes the analysis of BARBIERI 88 and AYALA 99.

[26] ARPESELLA 08A obtained this limit using the shape of the recoil electron energy spectrum from the Borexino 192 live days of solar neutrino data.

[27] BEDA 07 performed search for electromagnetic $\overline{\nu}_e$-e scattering at Kalininskaya nuclear reactor. A Ge detector with active and passive shield was used and the electron recoil spectrum between 3.0 and 61.3 keV analyzed. Superseded by BEDA 10.

[28] WONG 07 performed search for non-standard $\overline{\nu}_e$-e scattering at the Kuo-Sheng nuclear reactor. Ge detector equipped with active anti-Compton shield is used. Most stringent laboratory limit on magnetic moment of reactor $\overline{\nu}_e$. Supersedes LI 03B.

[29] DARAKTCHIEVA 05 present the final analysis of the search for non-standard $\overline{\nu}_e$-e scattering component at Bugey nuclear reactor. Full kinematical event reconstruction of both the kinetic energy above 700 keV and scattering angle of the recoil electron, by use of TPC. Most stringent laboratory limit on magnetic moment. Supersedes DARAKTCHIEVA 03.

[30] XIN 05 evaluated the ν_e flux at the Kuo-Sheng nuclear reactor and searched for non-standard ν_e-e scattering. Ge detector equipped with active anti-Compton shield was used. This laboratory limit on magnetic moment is considerably less stringent than the limits for reactor $\overline{\nu}_e$, but is specific to ν_e.

[31] GRIFOLS 04 obtained this bound using the SNO data of the solar ^{8}B neutrino flux measured with deuteron breakup. This bound applies to $\mu_{\rm eff} = (\mu_{21}^2 + \mu_{22}^2 + \mu_{23}^2)^{1/2}$.

[32] LIU 04 obtained this limit using the shape of the recoil electron energy spectrum from the Super-Kamiokande-I 1496 days of solar neutrino data. Neutrinos are assumed to have only diagonal magnetic moments, $\mu_{\nu 1} = \mu_{\nu 2}$. This limit corresponds to the oscillation parameters in the vacuum oscillation region.

[33] LIU 04 obtained this limit using the shape of the recoil electron energy spectrum from the Super-Kamiokande-I 1496 live-day solar neutrino data, by limiting the oscillation parameter region in the LMA region allowed by solar neutrino experiments plus KamLAND. $\mu_{\nu 1} = \mu_{\nu 2}$ is assumed. In the LMA region, the same limit would be obtained even if neutrinos have off-diagonal magnetic moments.

[34] BACK 03B obtained this bound from the results of background measurements with Counting Test Facility (the prototype of the Borexino detector). Standard Solar Model flux was assumed. This μ_ν can be different from the reactor μ_ν in certain oscillation scenarios (see BEACOM 99).

[35] DARAKTCHIEVA 03 searched for non-standard $\overline{\nu}_e$-e scattering component at Bugey nuclear reactor. Full kinematical event reconstruction by use of TPC. Superseded by DARAKTCHIEVA 05.

[36] LI 03B used Ge detector in active shield near nuclear reactor to test for nonstandard $\overline{\nu}_e$-e scattering.

[37] GRIMUS 02 obtain stringent bounds on all Majorana neutrino transition moments from a simultaneous fit of LMA-MSW oscillation parameters and transition moments to global solar neutrino data + reactor data. Using only solar neutrino data, a 90% CL bound of $6.3 \times 10^{-10} \mu_B$ is obtained.

[38] TANIMOTO 00 combined $e^+ e^- \rightarrow \nu\overline{\nu}\gamma$ data from VENUS, TOPAZ, and AMY.

[39] AYALA 99 improves the limit of BARBIERI 88.

[40] BEACOM 99 obtain the limit using the shape, but not the absolute magnitude which is affected by oscillations, of the solar neutrino spectrum obtained by Superkamiokande (825 days). This μ_ν can be different from the reactor μ_ν in certain oscillation scenarios.

[41] RAFFELT 99 is an update of RAFFELT 90. This limit applies to all neutrino flavors which are light enough (< 5 keV) to be emitted from globular-cluster red giants. This limit pertains equally to electric dipole moments and magnetic transition moments, and it applies to both Dirac and Majorana neutrinos.

[42] RAFFELT 99 is essentially an update of BERNSTEIN 63, but is derived from the helioseismological limit on a new energy-loss channel of the Sun. This limit applies to all neutrino flavors which are light enough (<1 keV) to be emitted from the Sun. This limit pertains equally to electric dipole and magnetic transition moments, and it applies to both Dirac and Majorana neutrinos.

[43] ACCIARRI 97Q result applies to both direct and transition magnetic moments and for q^2=0.

[44] ELMFORS 97 calculate the rate of depolarization in a plasma for neutrinos with a magnetic moment and use the constraints from a big-bang nucleosynthesis on additional degrees of freedom.

[45] Applies to absolute value of magnetic moment.

[46] DERBIN 93 determine the cross section for 0.6–2.0 MeV electron energy as $(1.28 \pm 0.63) \times \sigma_{\rm weak}$. However, the (reactor on – reactor off)/(reactor off) is only $\sim 1/100$.

[47] COOPER-SARKAR 92 assume $f_{D_s}/f_\pi = 2$ and D_s, $\overline{D}_s$ production cross section = 2.6 μb to calculate ν flux.

[48] VIDYAKIN 92 limit is from a $e\overline{\nu}_e$ elastic scattering experiment. No experimental details are given except for the cross section from which this limit is derived. Signal/noise was 1/10. The limit uses $\sin^2\theta_W = 0.23$ as input.

[49] DORENBOSCH 91 corrects an incorrect statement in DORENBOSCH 89 that the ν magnetic moment is $< 1 \times 10^{-9}$ at the 95%CL. DORENBOSCH 89 measures both $\nu_\mu e$ and $\overline{\nu} e$ elastic scattering and assume $\mu(\nu) = \mu(\overline{\nu})$.

[50] KRAKAUER 90 experiment fully reported in ALLEN 93.

[51] RAFFELT 90 limit applies for a diagonal magnetic moment of a Dirac neutrino, or for a transition magnetic moment of a Majorana neutrino. In the latter case, the same analysis gives $< 1.4 \times 10^{-12}$. Limit at 95%CL obtained from δM_c.

[52] Significant dependence on details of stellar models.

[53] FUKUGITA 88 find magnetic dipole moments of any two neutrino species are bounded by $\mu < 10^{-16}$ $[10^{-9}\ G/B_0]$ where B_0 is the present-day intergalactic field strength.

[54] GROTCH 88 combined data from MAC, ASP, CELLO, and Mark J.

[55] For m_ν = 8–200 eV. NUSSINOV 87 examines transition magnetic moments for $\nu_\mu \rightarrow \nu_e$ and obtain $< 3 \times 10^{-15}$ for $m_\nu > 16$ eV and $< 6 \times 10^{-14}$ for $m_\nu > 4$ eV.

[56] We obtain above limit from SUTHERLAND 76 using their limit $f < 1/3$.

[57] KIM 74 is a theoretical analysis of $\overline{\nu}_\mu$ reaction data.

NEUTRINO CHARGE RADIUS SQUARED

We report limits on the so-called neutrino charge radius squared. While the straight-forward definition of a neutrino charge radius has been proven to be gauge-dependent and, hence, unphysical (LEE 77C), there have been recent attempts to define a physically observable neutrino charge radius (BERNABEU 00, BERNABEU 02). The issue is still controversial (FUJIKAWA 03, BERNABEU 03). A more general interpretation of the experimental results is that they are limits on certain nonstandard contributions to neutrino scattering.

VALUE (10^{-32} cm^2)	CL%	DOCUMENT ID		TECN	COMMENT
2.2 $^{+2.4}_{-2.3}$	68	[1] ATZORI-COR...25		FIT	Global fit to νES, CEνNS data
• • • We do not use the following data for averages, fits, limits, etc. • • •					
−70.01 to 28.52	90	[2] DEMIRCI	25A		Solar $\nu - e$ scattering
−54.36 to 12.90	90	[3] DEMIRCI	25A		Solar $\nu - e$ scattering
−27.5 to 3	90	[4] CADEDDU	18		ν_μ coherent scat. on CsI
− 2.1 to 3.3	90	[5] DENIZ	10	TEXO	Reactor $\overline{\nu}_e e$
− 0.53 to 0.68	90	[6] HIRSCH	03		$\nu_\mu e$ scat.
− 8.2 to 9.9	90	[7] HIRSCH	03		anomalous $e^+ e^- \rightarrow \nu\overline{\nu}\gamma$
− 2.97 to 4.14	90	[8] AUERBACH	01	LSND	$\nu_e e \rightarrow \nu_e e$
− 0.6 to 0.6	90	VILAIN	95B	CHM2	$\nu_\mu e$ elastic scat.
0.9 ±2.7		ALLEN	93	CNTR	LAMPF $\nu e \rightarrow \nu e$
< 2.3	95	MOURAO	92	ASTR	HOME/KAM2 ν rates
< 7.3	90	[9] VIDYAKIN	92	CNTR	Reactor $\overline{\nu} e \rightarrow \overline{\nu} e$
1.1 ±2.3		ALLEN	91	CNTR	Repl. by ALLEN 93
− 1.1 ±1.0		[10] AHRENS	90	CNTR	$\nu_\mu e$ elastic scat.
− 0.3 ±1.5		[10] DORENBOS...	89	CHRM	$\nu_\mu e$ elastic scat.
		[11] GRIFOLS	89B	ASTR	SN 1987A

[1] ATZORI-CORONA 25 reports the limit of ν_e charge radius squared by performing a global fit to νES and CEνNS data from BNL-E734, CCFR, CHARM-II, COHERENT, CONUS+, LAMPF, LSND, nuGEN, and TEXONO. Limits for the ν_μ and ν_τ charge radii squared are also reported.

[2] DEMIRCI 25A analyzed 1540 kg·y of Xe exposure of the TPC-based PandaX-4T dark matter search. Elastic solar neutrino-electron scattering is used to derive a bound on the square of the charge radius of neutrinos.

[3] DEMIRCI 25A analyzed 1600 kg·y of Xe exposure of the TPC-based XENONnT dark matter search. Elastic solar neutrino-electron scattering is used to derive a bound on the square of the charge radius of neutrinos.

[4] CADEDDU 18 use the data of the COHERENT experiment, AKIMOV 18. The limit is $\langle r_\nu^2 \rangle$ for ν_μ obtained from the time-dependent data. Weaker limits were obtained for charge radii of ν_e and for transition charge radii. The published value was divided by 2 to conform to the convention of this table.

[5] DENIZ 10 observe reactor $\overline{\nu}_e e$ scattering with recoil kinetic energies 3–8 MeV using CsI(Tl) detectors. The observed rate and spectral shape are consistent with the Standard Model prediction, leading to the reported constraint on $\overline{\nu}_e$ charge radius.

[6] Based on analysis of CCFR 98 results. Limit is on $\langle r_V^2 \rangle + \langle r_A^2 \rangle$. The CHARM II and E734 at BNL results are reanalyzed, and weaker bounds on the charge radius squared than previously published are obtained. The NuTeV result is discussed; when tentatively interpreted as ν_μ charge radius it implies $\langle r_V^2 \rangle + \langle r_A^2 \rangle = (4.20 \pm 1.64) \times 10^{-33}$ cm^2.

[7] Results of LEP-2 are interpreted as limits on the axial-vector charge radius squared of a Majorana ν_τ. Slightly weaker limits for both vector and axial-vector charge radius squared are obtained for the Dirac case, and somewhat weaker limits are obtained from the analysis of lower energy data (LEP-1.5 and TRISTAN).

[8] AUERBACH 01 measure $\nu_e e$ elastic scattering with LSND detector. The cross section agrees with the Standard Model expectation, including the charge and neutral current interference. The 90% CL applies to the range shown.

[9] VIDYAKIN 92 limit is from a $e\overline{\nu}$ elastic scattering experiment. No experimental details are given except for the cross section from which this limit is derived. Signal/noise was 1/10. The limit uses $\sin^2\theta_W = 0.23$ as input.

Int. J. Mod
by UNIVERSITY OF CALIFORNIA @ BERK
wnloaded from www.worldscientific.com
-use and distribution is strictly not permitted, except for Open Access articles.

[10] Result is obtained from reanalysis given in ALLEN 91, followed by our reduction to obtain 1 σ errors.

[11] GRIFOLS 89B sets a limit of $\langle r^2 \rangle < 0.2 \times 10^{-32}\,\mathrm{cm}^2$ for right-handed neutrinos.

REFERENCES FOR Neutrino Properties

ABDUL-KARIM 25 PR D112 083515 M. Abdul Karim *et al.* (DESI Collab.)
ADAME 25A JCAP 2507 028 A.G. Adame *et al.* (DESI Collab.)
AKER 25A SCI 388 180 M. Aker *et al.* (KATRIN Collab.)
ALPERT 25 PRL 135 141801 B.K. Alpert *et al.* (HOLMES Collab.)
ALPIZAR-VE... 25 PR D111 053001 M. Alpizar-Venegas *et al.* (UNAM)
ATZORI-COR... 25 PRL 135 231803 M. Atzori Corona *et al.* (ROMA3, CAGLI, INFN)
DEMIRCI 25A PR D112 095035 M. Demirci *et al.* (KARAD, WISC)
IVANOV 25 PRL 134 091001 M.M. Ivanov, M.W. Toomey, N.G. Karacayli (MIT+)
SHAO 25 PR D111 083535 H. Shao *et al.* (PRIN, PENN, CAMB)
ZENG 25 PRL 134 041001 X. Zeng *et al.* (PandaX-4T Collab.)
CARENZA 24A PR D110 023510 P. Carenza *et al.*
MADHAVAC... 24 APJ 962 113 M.S. Madhavacheril *et al.* (ACT Collab.)
VALERA 24 PR D110 043004 V.B. Valera *et al.*
AALBERS 23 PRL 131 041002 J. Aalbers *et al.* (LZ Collab.)
AALBERS 23A PR D108 072006 J. Aalbers *et al.* (LZ Collab.)
ATZORI-COR... 23 PR D107 053001 M. Atzori Corona *et al.* (CAGL, CAGLI)
ESFAHANI 23 PRL 131 102502 A.A. Esfahani *et al.* (Project 8 Collab.)
IVANEZ-BAL... 23 PL B847 138252 P. Ivanez-Ballesteros, M.C. Volpe (CNRS, UPCIT)
AKER 22 NATP 18 160 M. Aker *et al.* (KATRIN Collab.)
APRILE 22B PRL 129 161805 E. Aprile *et al.* (XENONnT Collab.)
BONET 22A EPJ C82 813 H. Bonet *et al.* (CONUS Collab.)
BRIEDEN 22 JCAP 2208 024 S. Brieden, Hector Gil-Marin, Licia Verde
COLOMA 22 JHEP 2205 037 P. Coloma *et al.* (IFT, OSU, STON, ICREA+)
KUMAR 22 JCAP 2209 060 S. Kumar, R. Nunes, P.Yadav
TANSERI 22 JHEAP 36 1 I. Tanseri *et al.*
ABBOTT 21A PR D105 023520 T.C.M. Abbott *et al.* (DES Collab.)
ALAM 21 PR D103 083533 S. Alam *et al.* (eBOSS Collab.)
DI-VALENT... 21 PR D104 083504 E. Di Valentino, S. Gariazzo, O. Mena (DURH+)
GARNY 21 JCAP 2103 049 M. Garny *et al.*
STOCKER 21 PR D103 123508 P. Stocker *et al.* (GAMBIT Collab.)
ABE 20E PL B809 135741 K. Abe *et al.* (XMASS Collab.)
AGHANIM 20 AA 641 A6 N. Aghanim *et al.* (Planck Collab.)
APRILE 20 PR D102 072004 E. Aprile *et al.* (XENON Collab.)
CAPOZZI 20 PR D102 083007 F. Capozzi, G. Raffelt (MPIM)
CHOUDHURY 20 JCAP 2007 037 S.R. Choudhury, S. Hannestad (IITB, AARH)
IVANOV 20 PR D101 083504 M.M. Ivanov, M. Simonovic, M. Zaldarriaga (NYU,+)
KHAN 20 PL B809 135782 A.N. Khan (MPIK)
PALANQUE-... 20 JCAP 2004 038 N. Palanque-Delabrouille *et al.* (SACL+)
AHARMIM 19 PR D99 032013 B. Aharmim *et al.* (SNO Collab.)
AKER 19 PRL 123 221802 M. Aker *et al.* (KATRIN Collab.)
Also PR D104 012005 M. Aker *et al.* (KATRIN Collab.)
ESCUDERO 19 PR D100 103531 M. Escudero, M. Fairbairn (LOKC)
LOUREIRO 19 PRL 123 081301 A. Loureiro *et al.*
UPADHYE 19 JCAP 1905 041 A. Upadhye (WISC)
AKIMOV 18 arXiv:1804.09459 D. Akimov *et al.* (COHERENT Collab.)
CADEDDU 18 PR D98 113010 M. Cadeddu *et al.*
Also PR D101 059902 (errat.) M. Cadeddu *et al.*
CHOUDHURY 18 JCAP 1809 017 S.R. Choudhury, S. Choubey
AGOSTINI 17A PR D96 091103 M. Agostini *et al.* (Borexino Collab.)
SIMPSON 17 JCAP 1706 029 F. Simpson *et al.* (BARC)
VAGNOZZI 17 PR D96 123503 S. Vagnozzi *et al.*
YECHE 17 JCAP 1706 047 C. Yeche *et al.*
DELLA-VALLE 16 EPJ C76 24 F. Della Valle *et al.* (PVLAS Collab.)
DIVALENTINO 16 PR D93 083527 E. Di Valentino *et al.*
HUANG 16 EPJ C76 489 Q.-G. Huang, K. Wang, S. Wang
ARCEO-DIAZ 15 ASP 70 1 S. Arceo-Diaz *et al.*
LOKHOV 15 PPN 46 347 A.V. Lokhov, F.V. Tkachov
Translated from FECAY 46 3.
PALANQUE-... 15A JCAP 1511 011 N. Palanque-Delabrouille *et al.*
ROSSI 15 PR D92 063505 G. Rossi *et al.*
ADE 14 AA 571 A16 P.A.R. Ade *et al.* (Planck Collab.)
BATTYE 14 PRL 112 051303 R.A. Battye, A. Moss (MCHS, NOTT)
BEUTLER 14 MNRAS 444 3501 F. Beutler *et al.* (BOSS Collab.)
CHEN 14A PR D90 011301 J.-W. Chen *et al.* (TEXONO Collab.)
CORSICO 14 JCAP 1408 054 A.H. Corsico
COSTANZI 14 JCAP 1410 081 M. Costanzi *et al.* (TRST, TRSTI)
HOU 14 APJ 782 74 Z. Hou *et al.*
LEISTEDT 14 PRL 113 041301 B. Leistedt, H.V. Peiris, L. Verde
MILLER-BER... 14B AA 562 A123 M.M. Miller Bertolami (MPIG, LAPL)
RIEMER-SOR... 14 PR D89 103505 S. Riemer-Sorensen, D. Parkinson, T.M. Davis
STUDENIKIN 14 EPL 107 21001 A.I. Studenikin
BEDA 13 PPNL 10 139 A.G. Beda *et al.* (GEMMA Collab.)
VIAUX 13A PRL 111 231301 N. Viaux *et al.*
MORESCO 12 JCAP 1207 053 M. Moresco *et al.*
XIA 12 JCAP 1206 010 J.-Q. Xia *et al.*
ASEEV 11 PR D84 112003 V.N. Aseev *et al.*
CECCHINI 11 ASP 34 486 S. Cecchini *et al.*
SAITO 11 PR D83 043529 S. Saito, M. Takada, A. Taruya
BEDA 10 PPNL 7 406 A.G. Beda *et al.* (GEMMA Collab.)
DENIZ 10 PR D81 072001 M. Deniz *et al.* (TEXONO Collab.)
HANNESTAD 10 JCAP 1008 001 S. Hannestad *et al.*
PAGLIAROLI 10 ASP 33 287 G. Pagliaroli, F. Rossi-Torres, E. Vissani (INFN+)
SEKIGUCHI 10 JCAP 1003 015 T. Sekiguchi *et al.*
THOMAS 10 PRL 105 031301 S.A. Thomas, F.B. Abdalla, O. Lahav (LOUC)
ICHIKI 09 PR D79 023520 K. Ichiki, M. Takada, T. Takahashi
KOMATSU 09 APJS 180 330 E. Komatsu *et al.*
KUZNETSOV 09 IJMP A24 5977 A.V. Kuznetsov, N.V. Mikheev, A.A. Okrugin (YARO)
TERENO 09 AA 500 657 I. Tereno *et al.*
VIKHLININ 09 APJ 692 1060 A. Vikhlinin *et al.*
ARPESELLA 08A PRL 101 091302 C. Arpesella *et al.* (Borexino Collab.)
BERNARDIS 08 PR D78 083535 F. De Bernardis *et al.*
BEDA 07 PAN 70 1873 A.G. Beda *et al.*
Translated from YAF 70 1925.
FOGLI 07 PR D75 053001 G.L. Fogli *et al.*
GNINENKO 07 PR D75 075014 S.N. Gninenko, N.V. Krasnikov, A. Rubbia
KRISTIANSEN 07 PR D75 083510 J. Kristiansen, O. Elgaroy, H. Dahle
MIRIZZI 07 PR D76 053007 A. Mirizzi, D. Montanino, P.D. Serpico
SPERGEL 07 APJS 170 377 D.N. Spergel *et al.*
WONG 07 PR D75 012001 H.T. Wong *et al.* (TEXONO Collab.)
ZUNCKEL 07 JCAP 0708 004 C. Zunckel, P. Ferreira
CIRELLI 06 JCAP 0612 013 M. Cirelli *et al.*
FUKUGITA 06 PR D74 027302 M. Fukugita *et al.*
GOOBAR 06 JCAP 0606 019 A. Goobar *et al.*
HANNESTAD 06 JCAP 0611 016 S. Hannestad, G. Raffelt
KRISTIANSEN 06 PR D74 123005 J. Kristiansen, O. Elgaroy, H. Eriksen
SANCHEZ 06 MNRAS 366 189 A.G. Sanchez *et al.*
SELJAK 06 JCAP 0610 014 U. Seljak, A. Slosar, P. McDonald
CAPRINI 05 JCAP 0502 006 C. Caprini, P.G. Ferreira (GEVA, OXFTP)
DARAKTCH... 05 PL B615 153 Z. Daraktchieva *et al.* (MUNU Collab.)
ICHIKAWA 05 PR D71 043001 K. Ichikawa, M. Fukugita, M. Kawasaki (ICRR)
KRAUS 05 EPJ C40 447 Ch. Kraus *et al.*
XIN 05 PR D72 012006 B. Xin *et al.* (TEXONO Collab.)
AHARMIM 04 PR D70 093014 B. Aharmim *et al.* (SNO Collab.)
BARGER 04 PL B595 55 V. Barger, D. Marfatia, A. Tregre
CECCHINI 04 ASP 21 183 S. Cecchini *et al.* (BGNA+)
CROTTY 04 PR D69 123007 P. Crotty, J. Lesgourgues, S. Pastor
EGUCHI 04 PRL 92 071301 K. Eguchi *et al.* (KamLAND Collab.)
GRIFOLS 04 PL B587 184 J.A. Grifols, E. Masso, S. Mohanty (BARC, AHMED)
LIU 04 PRL 93 021802 D.W. Liu *et al.* (Super-Kamiokande Collab.)
ARNABOLDI 03A PRL 91 161802 C. Arnaboldi *et al.*
BACK 03B PL B563 35 H.O. Back *et al.* (Borexino Collab.)
BANDYOPA... 03 PL B555 33 A. Bandyopadhyay, S. Choubey, S. Goswami (SAHA+)
BERNABEU 03 hep-ph/0303202 J. Bernabeu, J. Papavassiliou, J. Vidal
DARAKTCH... 03 PL B564 190 Z. Daraktchieva *et al.* (MUNU Collab.)
FUJIKAWA 03 hep-ph/0303188 K. Fujikawa, R. Shrock
HIRSCH 03 PR D67 033005 M. Hirsch, E. Nardi, D. Restrepo
LI 03B PRL 90 131802 H.B. Li *et al.* (TEXONO Collab.)
SPERGEL 03 APJS 148 175 D.N. Spergel *et al.*
BERNABEU 02 PRL 89 101802 J. Bernabeu, J. Papavassiliou, J. Vidal
Also PRL 89 229902 (errat.) J. Bernabeu, J. Papavassiliou, J. Vidal
DERBIN 02B JETPL 76 409 A.V. Derbin, O.Ju. Smirnov
Translated from ZETFP 76 483.
GRIMUS 02 NP B648 376 W. Grimus *et al.*
JOSHIPURA 02B PR D66 113008 A.S. Joshipura, E. Masso, S. Mohanty
LEWIS 02 PR D66 103511 A. Lewis, S. Bridle
LOREDO 02 PR D65 063002 T.J. Loredo, D.Q. Lamb
WANG 02 PR D65 123001 X. Wang, M. Tegmark, M. Zaldarriaga
AUERBACH 01 PR D63 112001 L.B. Auerbach *et al.* (LSND Collab.)
SCHWIENHO... 01 PL B513 23 R. Schwienhorst *et al.* (DONUT Collab.)
ATHANAS 00 PR D61 052002 M. Athanas *et al.* (CLEO Collab.)
BERNABEU 00 PR D62 113012 J. Bernabeu *et al.*
FUKUGITA 00 PRL 84 1082 M. Fukugita, G.C. Liu, N. Sugiyama
TANIMOTO 00 PL B478 1 N. Tanimoto *et al.*
AYALA 99 PR D59 111901 A. Ayala, J.C. D'Olivo, M. Torres
BEACOM 99 PRL 83 5222 J.F. Beacom, P. Vogel
CROFT 99 PRL 83 1092 R.A.C. Croft, W. Hu, R. Dave
DOLGOV 99 NP B548 385 A.D. Dolgov *et al.*
LOBASHEV 99 PL B460 227 V.M. Lobashev *et al.*
RAFFELT 99 PRPL 320 319 G.G. Raffelt
WEINHEIMER 99 PL B460 219 Ch. Weinheimer *et al.*
ACKERSTAFF 98T EPJ C5 229 K. Ackerstaff *et al.* (OPAL Collab.)
AMMAR 98 PL B431 209 R. Ammar *et al.* (CLEO Collab.)
BARATE 98F EPJ C2 395 R. Barate *et al.* (ALEPH Collab.)
BILLER 98 PRL 80 2992 S.D. Biller *et al.* (WHIPPLE Collab.)
FELDMAN 98 PR D57 3873 G.J. Feldman, R.D. Cousins
LENZ 98 PL B416 50 S. Lenz *et al.*
ABREU 97J ZPHY C74 577 P. Abreu *et al.* (DELPHI Collab.)
ACCIARRI 97Q PL B412 201 M. Acciarri *et al.* (L3 Collab.)
ANASTASSOV 97 PR D55 2559 A. Anastassov *et al.* (CLEO Collab.)
Also PR D58 119903 (errat.) A. Anastassov *et al.* (CLEO Collab.)
ELMFORS 97 NP B503 3 P. Elmfors *et al.*
ESCRIBANO 97 PL B395 369 R. Escribano, E. Masso (BARC, PARIT)
FIELDS 97 ASP 6 169 B.D. Fields, K. Kainulainen, K.A. Olive (NDAM+)
SWAIN 97 PR D55 1 J. Swain, L. Taylor (NEAS)
ALEXANDER 96M ZPHY C72 231 G. Alexander *et al.* (OPAL Collab.)
ASSAMAGAN 96 PR D53 6065 K.A. Assamagan *et al.* (PSI, ZURI, VILL+)
BAI 96 PR D53 20 J.Z. Bai *et al.* (BES Collab.)
BOTTINO 96 PR D53 6361 A. Bottino *et al.*
DOLGOV 96 PL B383 193 A.D. Dolgov, S. Pastor, J.W.F. Valle (IFIC, VALE)
HANNESTAD 96 PRL 76 2848 S. Hannestad, J. Madsen (AARH)
HANNESTAD 96B PRL 77 5148 (errat.) S. Hannestad, J. Madsen (AARH)
HANNESTAD 96C PR D54 7894 S. Hannestad, J. Madsen (AARH)
SOBIE 96 ZPHY C70 383 R.J. Sobie, R.K. Keeler, I. Lawson (VICT)
BELESEV 95 PL B350 263 A.I. Belesev *et al.* (INRM, KIAE)
BUSKULIC 95H PL B349 585 D. Buskulic *et al.* (ALEPH Collab.)
CHING 95 IJMP A10 2841 C.R. Ching *et al.* (CST, BEIJT, CIAE)
DOLGOV 95 PR D51 4129 A.D. Dolgov, K. Kainulainen, I.Z. Rothstein (MICH+)
HIDDEMANN 95 JP G21 639 K.H. Hiddemann, H. Daniel, O. Schwentker (TUM)
KERNAN 95 NP B437 243 P.J. Kernan, L.M. Krauss (CASE)
SIGL 95 PR D51 1499 G. Sigl, M.S. Turner (FNAL, EFI)
STOEFFL 95 PRL 75 3237 W. Stoeffl, D.J. Decman (LLNL)
VILAIN 95B PL B345 115 P. Vilain *et al.* (CHARM II Collab.)
ASSAMAGAN 94 PL B335 231 K.A. Assamagan *et al.* (PSI, ZURI, VILL+)
BABU 94 PL B321 140 K.S. Babu, T.M. Gould, I.Z. Rothstein (BART+)
DODELSON 94 PR D49 5068 S. Dodelson, G. Gyuk, M.S. Turner (FNAL, CHIC+)
GOULD 94 PL B333 545 T.M. Gould, I.Z. Rothstein (JHU, MICH)
JECKELMANN 94 PL B335 326 B. Jeckelmann, P.F.A. Goudsmit, H.J. Leisi (WABRN+)
KAWASAKI 94 NP B419 105 M. Kawasaki *et al.* (OSU)
PERES 94 PR D50 513 O.L.G. Peres, V. Pleitez, R. Zukanovich Funchal
YASUMI 94 PL B334 229 S. Yasumi *et al.* (KEK, TSUK, KYOT+)
ALLEN 93 PR D47 11 R.C. Allen *et al.* (UCI, LANL, ANL+)
BALEST 93 PR D47 3671 R. Balest *et al.* (CLEO Collab.)
CINABRO 93 PRL 70 3700 D. Cinabro *et al.* (CLEO Collab.)
DERBIN 93 JETPL 57 768 A.V. Derbin *et al.* (PNPI)
Translated from ZETFP 57 755.
DOLGOV 93 PRL 71 476 A.D. Dolgov, I.Z. Rothstein (MICH)
ENQVIST 93 PL B301 376 K. Enqvist, H. Uibo (NORD)
SUN 93 CJNP 15 261 H.C. Sun *et al.* (CIAE, CST, BEIJT)
WEINHEIMER 93 PL B300 210 C. Weinheimer *et al.* (MAINZ)
ALBRECHT 92M PL B292 221 H. Albrecht *et al.* (ARGUS Collab.)
BLUDMAN 92 PR D45 4720 S.A. Bludman (CFPA)
COOPER-... 92 PL B280 153 A.M. Cooper-Sarkar *et al.* (BEBC WA66 Collab.)
DODELSON 92 PRL 68 2572 S. Dodelson, J.A. Frieman, M.S. Turner (FNAL+)
HOLZSCHUH 92B PL B287 381 E. Holzschuh, M. Fritschi, W. Kundig (ZURI)
KAWANO 92 PL B275 487 L.H. Kawano *et al.* (CIT, UCSD, LLL+)
MOURAO 92 PL B285 364 A.M. Mourao, J. Pulido, J.P. Ralston (LISB, LISBT+)
PDG 92 PR D45 S1 K. Hikasa *et al.* (KEK, LBL, BOST+)
VIDYAKIN 92 JETPL 55 206 G.S. Vidyakin *et al.* (KIAE)
Translated from ZETFP 55 212.
ALLEN 91 PR D43 1 R.C. Allen *et al.* (UCI, LANL, UMD)
DAVIDSON 91 PR D43 2314 S. Davidson, B.A. Campbell, D. Bailey (ALBE+)
DESHPANDE 91 PR D43 943 N.G. Deshpande, K.V.L. Sarma (OREG, TATA)
DORENBOS... 91 ZPHY C51 142 (errat.) J. Dorenbosch *et al.* (CHARM Collab.)
FULLER 91 PR D43 3136 G.M. Fuller, R.A. Malaney (UCSD)
GRANEK 91 IJMP A6 2387 H. Granek, B.H.J. McKellar (MELB)
KAWAKAMI 91 PL B256 105 H. Kawakami *et al.* (INUS, TOHOK, TINT+)
KOLB 91 PRL 67 533 E.W. Kolb *et al.* (FNAL, CHIC)
KRAKAUER 91 PR D44 6 D.A. Krakauer *et al.* (LAMPF E225 Collab.)
LAM 91 PR D44 3345 W.P. Lam, K.W. Ng (AST)
ROBERTSON 91 PRL 67 957 R.G.H. Robertson *et al.* (LASL, LLL)
AHRENS 90 PR D41 3297 L.A. Ahrens *et al.* (BNL, BROW, HIRO+)
AVIGNONE 90 PR D41 682 F.T. Avignone, J.I. Collar (SCUC)
KRAKAUER 90 PL B252 177 D.A. Krakauer *et al.* (LAMPF E225 Collab.)
RAFFELT 90 PRL 64 2856 G.G. Raffelt (MPIM)
WALKER 90 PR D41 689 T.P. Walker (HARV)
CHUPP 89 PRL 62 505 E.L. Chupp, W.T. Vestrand, C. Reppin (UNH, MPIM)
DORENBOS... 89 ZPHY C41 567 J. Dorenbosch *et al.* (CHARM Collab.)
GRIFOLS 89B PR D40 3819 J.A. Grifols, E. Masso (BARC)
KOLB 89 PRL 62 509 E.W. Kolb, M.S. Turner (CHIC, FNAL)
LOREDO 89 ANYAS 571 601 T.J. Loredo, D.Q. Lamb (CHIC)
RAFFELT 89 PR D39 2066 G.G. Raffelt (PRIN, UCB)
RAFFELT 89B APJ 336 61 G. Raffelt, D. Dearborn, J. Silk (UCB, LLL)
ALBRECHT 88B PL B202 149 H. Albrecht *et al.* (ARGUS Collab.)

Int. J. Mod. Phys. A 2026.41. Downloaded from www.worldscientific.com
by UNIVERSITY OF CALIFORNIA @ BERKELEY on 09/16/26. Re-use and distribution is strictly not permitted, except for Open Access articles.

BARBIERI	88	PRL 61 27	R. Barbieri, R.N. Mohapatra	(PISA, UMD)
BORIS	88	PRL 61 245 (errat.)	S.D. Boris *et al.*	(ITEP, ASCI)
FUKUGITA	88	PRL 60 879	M. Fukugita *et al.*	(KYOTU, MPIM, UCB)
GROTCH	88	ZPHY C39 553	H. Grotch, R.W. Robinett	(PSU)
RAFFELT	88B	PR D37 549	G.G. Raffelt, D.S.P. Dearborn	(UCB, LLL)
SPERGEL	88	PL B200 366	D.N. Spergel, J.N. Bahcall	(IAS)
VONFEILIT...	88	PL B200 580	F. von Feilitzsch, L. Oberauer	(TUM)
BARBIELLINI	87	NAT 329 21	G. Barbiellini, G. Cocconi	(CERN)
BORIS	87	PRL 58 2019	S.D. Boris *et al.*	(ITEP, ASCI)
Also		PRL 61 245 (errat.)	S.D. Boris *et al.*	(ITEP, ASCI)
BORIS	87B	JETPL 45 333	S.D. Boris *et al.*	(ITEP)
		Translated from ZETFP 45 267.		
FUKUGITA	87	PR D36 3817	M. Fukugita, S. Yazaki	(KYOTU, TOKY)
NUSSINOV	87	PR D36 2278	S. Nussinov, Y. Rephaeli	(TELA)
OBERAUER	87	PL B198 113	L.F. Oberauer, F. von Feilitzsch, R.L. Mossbauer	
SPRINGER	87	PR A35 679	P.T. Springer *et al.*	(LLNL)
KETOV	86	JETPL 44 146	S.N. Ketov *et al.*	(KIAE)
		Translated from ZETFP 44 114.		
COWSIK	85	PL 151B 62	R. Cowsik	(TATA)
RAFFELT	85	PR D31 3002	G.G. Raffelt	(MPIM)
BINETRUY	84	PL 134B 174	P. Binetruy, G. Girardi, P. Salati	(LAPP)
FREESE	84	NP B233 167	K. Freese, D.N. Schramm	(CHIC, FNAL)
KYULDJIEV	84	NP B243 387	A.V. Kyuldjiev	(SOFI)
SCHRAMM	84	PL 141B 337	D.N. Schramm, G. Steigman	(FNAL, BART)
VOGEL	84	PR D30 1505	P. Vogel	
ANDERHUB	82	PL 114B 76	H.B. Anderhub *et al.*	(ETH, SIN)
OLIVE	82	PR D25 213	K.A. Olive, M.S. Turner	(CHIC, UCSB)
BERNSTEIN	81	PL 101B 39	J. Bernstein, G. Feinberg	(STEV, COLU)
FRANK	81	PR D24 2001	J.S. Frank *et al.*	(LASL, YALE, MIT+)
MORGAN	81	PL 102B 247	J.A. Morgan	(SUSS)
FUJIKAWA	80	PRL 45 963	K. Fujikawa, R. Shrock	(STON)
LUBIMOV	80	PL 94B 266	V.A. Lyubimov *et al.*	(ITEP)
STECKER	80	PRL 45 1460	F.W. Stecker	(NASA)
COWSIK	79	PR D19 2219	R. Cowsik	(TATA)
GOLDMAN	79	PR D19 2215	T. Goldman, G.J. Stephenson	(LASL)
BEG	78	PR D17 1395	M.A.B. Beg, W.J. Marciano, M. Ruderman	(ROCK+)
BLIETSCHAU	78	NP B133 205	J. Blietschau *et al.*	(Gargamelle Collab.)
FALK	78	PL 79B 511	S.W. Falk, D.N. Schramm	(CHIC)
BARNES	77	PRL 38 1049	V.E. Barnes *et al.*	(PURD, ANL)
COWSIK	77	PRL 39 784	R. Cowsik	(MPIM, TATA)
LEE	77C	PR D16 1444	B.W. Lee, R.E. Shrock	(STON)
VYSOTSKY	77	JETPL 26 188	M.I. Vysotsky, A.D. Dolgov, Y.B. Zeldovich	(ITEP)
		Translated from ZETFP 26 200.		
BELLOTTI	76	LNC 17 553	E. Bellotti *et al.*	(MILA)
SUTHERLAND	76	PR D13 2700	P. Sutherland *et al.*	(PENN, COLU, NYU)
SZALAY	76	AA 49 437	A.S. Szalay, G. Marx	(EOTV)
CLARK	74	PR D9 533	A.R. Clark *et al.*	(LBL)
KIM	74	PR D9 3050	J.E. Kim, V.S. Mathur, S. Okubo	(ROCH)
REINES	74	PRL 32 180	F. Reines, H.W. Sobel, H.S. Gurr	(UCI)
SZALAY	74	APAH 35 8	A.S. Szalay, G. Marx	(EOTV)
COWSIK	72	PRL 29 669	R. Cowsik, J. McClelland	(UCB)
MARX	72	Nu Conf. Budapest	G. Marx, A.S. Szalay	(EOTV)
GERSHTEIN	66	JETPL 4 120	S.S. Gershtein, Y.B. Zeldovich	(KIAM)
		Translated from ZETFP 4 189.		
BERNSTEIN	63	PR 132 1227	J. Bernstein, M. Ruderman, G. Feinberg	(NYU+)
COWAN	57	PR 107 528	C.L. Cowan, F. Reines	(LANL)

Number of Neutrino Types

The neutrinos referred to in this section are those of the Standard SU(2)×U(1) Electroweak Model possibly extended to allow nonzero neutrino masses. Light neutrinos are those with $m < m_Z/2$. The limits are on the number of neutrino mass eigenstates, including ν_1, ν_2, and ν_3.

THE NUMBER OF LIGHT NEUTRINO TYPES FROM COLLIDER EXPERIMENTS

Revised June 2020 by C.-J. Lin (LBNL). Written by D. Karlen (University of Victoria and TRIUMF).

The most precise measurements of the number of light neutrino types, N_ν, come from studies of Z production in e^+e^- collisions. The invisible partial width, $\Gamma_{\rm inv}$, is determined by subtracting the measured visible partial widths, corresponding to Z decays into quarks and charged leptons, from the total Z width. The invisible width is assumed to be due to N_ν light neutrino species each contributing the neutrino partial width Γ_ν as given by the Standard Model. In order to reduce the model dependence, the Standard Model value for the ratio of the neutrino to charged leptonic partial widths, $(\Gamma_\nu/\Gamma_\ell)_{\rm SM} = 1.991 \pm 0.001$, is used instead of $(\Gamma_\nu)_{\rm SM}$ to determine the number of light neutrino types:

$$N_\nu = \frac{\Gamma_{\rm inv}}{\Gamma_\ell}\left(\frac{\Gamma_\ell}{\Gamma_\nu}\right)_{\rm SM} \quad . \tag{1}$$

The combined result from the four LEP experiments is $N_\nu = 2.984 \pm 0.008$ [1]. Recent analyses applied corrections to the LEP result [1] by including the effect of correlated luminosity systematics and also using an improved Bhabha cross section calculation [2,3] to obtain $N_\nu = 2.9963 \pm 0.0074$.

In the past, when only small samples of Z decays had been recorded by the LEP experiments and by the Mark II at SLC, the uncertainty in N_ν was reduced by using Standard Model fits to the measured hadronic cross sections at several center-of-mass energies near the Z resonance. Since this method is much more dependent on the Standard Model, the approach described above is favored.

Before SLC and LEP, limits on the number of neutrino generations were placed by experiments at lower-energy e^+e^- colliders by measuring the cross section of the process $e^+e^- \to \nu\overline{\nu}\gamma$. The ASP, CELLO, MAC, MARK J, and VENUS experiments observed a total of 3.9 events above background [4], leading to a 95% CL limit of $N_\nu < 4.8$. This process has a much larger cross section at center-of-mass energies near the Z mass and has been measured at LEP by the ALEPH, DELPHI, L3, and OPAL experiments [5]. These experiments have observed several thousand such events, and the combined result is $N_\nu = 3.00 \pm 0.08$. The same process has also been measured by the LEP experiments at much higher center-of-mass energies, between 130 and 208 GeV, in searches for new physics [6]. Combined with the lower energy data, the result is $N_\nu = 2.92 \pm 0.05$.

Experiments at $p\overline{p}$ colliders also placed limits on N_ν by determining the total Z width from the observed ratio of $W^\pm \to \ell^\pm\nu$ to $Z \to \ell^+\ell^-$ events [7]. This involved a calculation that assumed Standard Model values for the total W width and the ratio of W and Z leptonic partial widths, and used an estimate of the ratio of Z to W production cross sections. Now that the Z width is very precisely known from the LEP experiments, the approach is now one of those used to determine the W width.

References

1. ALEPH, DELPHI, L3, OPAL, and SLD Collaborations, and LEP Electroweak Working Group, and SLD Electroweak Group, and SLD Heavy Flavour Group, Phys. Reports **427**, 257 (2006).
2. P. Janot and S. Jadach, Phys. Lett. **B803**, 135319 (2020).
3. G. Voutsinas *et al.*, Phys. Lett. **B800**, 135068 (2020).
4. VENUS: K. Abe *et al.*, Phys. Lett. **B232**, 431 (1989); ASP: C. Hearty *et al.*, Phys. Rev. **D39**, 3207 (1989); CELLO: H.J. Behrend *et al.*, Phys. Lett. **B215**, 186 (1988); MAC: W.T. Ford *et al.*, Phys. Rev. **D33**, 3472 (1986); MARK J: H. Wu, Ph.D. Thesis, Univ. Hamburg (1986).
5. L3: M. Acciarri *et al.*, Phys. Lett. **B431**, 199 (1998); DELPHI: P. Abreu *et al.*, Z. Phys. **C74**, 577 (1997); OPAL: R. Akers *et al.*, Z. Phys. **C65**, 47 (1995); ALEPH: D. Buskulic *et al.*, Phys. Lett. **B313**, 520 (1993).
6. DELPHI: J. Abdallah *et al.*, Eur. Phys. J. **C38**, 395 (2005); L3: P. Achard *et al.*, Phys. Lett. **B587**, 16 (2004); ALEPH: A. Heister *et al.*, Eur. Phys. J. **C28**, 1 (2003); OPAL: G. Abbiendi *et al.*, Eur. Phys. J. **C18**, 253 (2000).
7. UA1: C. Albajar *et al.*, Phys. Lett. **B198**, 271 (1987); UA2: R. Ansari *et al.*, Phys. Lett. **B186**, 440 (1987).

Int. J. Mod
by UNIVERSITY OF CALIFORNIA @ BERK
wnloaded from www.worldscientific.com
-use and distribution is strictly not permitted, except for Open Access articles.

Int. J. Mod. Phys. A 2026.41. Downloaded from www.worldscientific.com by UNIVERSITY OF CALIFORNIA @ BERKELEY on 09/16/26. Re-use and distribution is strictly not permitted, except for Open Access articles.

Number from e^+e^- Colliders

Number of Light ν Types

VALUE	DOCUMENT ID		TECN
2.9963±0.0074	[1] JANOT	20	
• • • We do not use the following data for averages, fits, limits, etc. • • •			
2.9918±0.0081	[2] VOUTSINAS	20	
2.9840±0.0082	[3] LEP-SLC	06	RVUE
3.00 ±0.05	[4] LEP	92	RVUE

[1] JANOT 20 applies a correction to LEP-SLC 06 using an updated Bhabha cross section calculation. This result also includes a correction to account for correlated luminosity bias as presented in VOUTSINAS 20.

[2] VOUTSINAS 20 applies a correction to LEP-SLC 06 to account for correlated luminosity bias.

[3] Combined fit from ALEPH, DELPHI, L3 and OPAL Experiments.

[4] Simultaneous fits to all measured cross section data from all four LEP experiments.

Number of Light ν Types from Direct Measurement of Invisible Z Width

In the following, the invisible Z width is obtained from studies of single-photon events from the reaction $e^+e^- \rightarrow \nu\overline{\nu}\gamma$. All are obtained from LEP runs in the E^{ee}_{cm} range 88–209 GeV.

VALUE	DOCUMENT ID		TECN	COMMENT
2.92±0.05 OUR AVERAGE Error includes scale factor of 1.2.				
2.84±0.10±0.14	ABDALLAH	05B	DLPH	$\sqrt{s}$ = 180–209 GeV
2.98±0.05±0.04	ACHARD	04E	L3	1990-2000 LEP runs
2.86±0.09	HEISTER	03C	ALEP	$\sqrt{s}$ = 189–209 GeV
2.69±0.13±0.11	ABBIENDI,G	00D	OPAL	1998 LEP run
2.89±0.32±0.19	ABREU	97J	DLPH	1993–1994 LEP runs
3.23±0.16±0.10	AKERS	95C	OPAL	1990–1992 LEP runs
2.68±0.20±0.20	BUSKULIC	93L	ALEP	1990–1991 LEP runs
• • • We do not use the following data for averages, fits, limits, etc. • • •				
2.84±0.15±0.14	ABREU	00Z	DLPH	1997–1998 LEP runs
3.01±0.08	ACCIARRI	99R	L3	1991–1998 LEP runs
3.1 ±0.6 ±0.1	ADAM	96C	DLPH	$\sqrt{s}$ = 130, 136 GeV

Limits from Astrophysics and Cosmology

Effective Number of Light ν Types

"Light" means here with a mass < about 1 MeV. The quoted values correspond to N_{eff}, where N_{eff} = 3.045 in the Standard Model with N_ν = 3. See also reviews on "Big-Bang Nucleosynthesis" and "Neutrinos in Cosmology."

VALUE	CL%	DOCUMENT ID		TECN	COMMENT
• • • We do not use the following data for averages, fits, limits, etc. • • •					
$3.23^{+0.35}_{-0.34}$	95	[1] ELBERS	25	COSM	DESI
3.12±0.38	95	[2] BRIEDEN	22	COSM	BOSS, eBOSS, CMB
2.90±0.15	68	[3] KUMAR	22	COSM	BOSS + CMB
2.89±0.14	68	[4] YEH	22	COSM	BBN + CMB
2.99±0.17	68	[5] AGHANIM	20	COSM	
2.84±0.15	68	[6] FIELDS	20	COSM	BBN
2.88±0.17	68	[7] IVANOV	20	COSM	Planck and BOSS
2.3–3.2	95	[8] VERDE	17	COSM	
2.88±0.16	68	[9] CYBURT	16	COSM	BBN
2.88±0.20	95	[10] ROSSI	15	COSM	
3.3 ±0.5	95	[11] ADE	14	COSM	Planck
$3.78^{+0.31}_{-0.30}$		[12] COSTANZI	14	COSM	
3.29±0.31		[13] HOU	14	COSM	
< 3.80	95	[14] LEISTEDT	14	COSM	
< 4.10	95	[15] MORESCO	12	COSM	
< 5.79	95	[16] XIA	12	COSM	
< 4.08	95	MANGANO	11	COSM	BBN
0.9–8.2		[17] ICHIKAWA	07	COSM	
3–7	95	[18] CIRELLI	06	COSM	
2.7–4.6	95	[19] HANNESTAD	06	COSM	
3.6–7.4	95	[18] SELJAK	06	COSM	
< 4.4		[20] CYBURT	05	COSM	
< 3.3		[21] BARGER	03C	COSM	
1.4–6.8		[22] CROTTY	03	COSM	
1.9–6.6		[22] PIERPAOLI	03	COSM	
2–4		LISI	99	COSM	BBN
< 4.3		OLIVE	99	COSM	BBN
< 4.9		COPI	97		Cosmology
< 3.6		HATA	97B		High D/H quasar abs.
< 4.0		OLIVE	97		BBN; high ^{4}He and ^{7}Li
< 4.7		CARDALL	96B	COSM	High D/H quasar abs.
< 3.9		FIELDS	96	COSM	BBN; high ^{4}He and ^{7}Li
< 4.5		KERNAN	96	COSM	High D/H quasar abs.
< 3.6		OLIVE	95		BBN; $\geq$ 3 massless ν
< 3.3		WALKER	91		Cosmology
< 3.4		OLIVE	90		Cosmology
< 4		YANG	84		Cosmology
< 4		YANG	79		Cosmology
< 7		STEIGMAN	77		Cosmology
		PEEBLES	71		Cosmology
<16		[23] SHVARTSMAN	69		Cosmology
		HOYLE	64		Cosmology

[1] ELBERS 25 uses DESI DR2 data in combination with CMB measurements.

[2] BRIEDEN 22 combines large scale structure data from BOSS and eBOSS including the shape of the matter power spectrum with Planck CMB data.

[3] KUMAR 22 combine the reconstructed galaxy power spectrum from BOSS data with Planck CMB data.

[4] YEH 22 combines Planck 2018 CMB data with BBN and observations of deuterium and Helium-4. Supersedes FIELDS 20.

[5] AGHANIM 20 best fit on number of neutrino types is based on Planck data combined with lensing and baryon acoustic oscillations (BAO). Without BAO, they find $2.89^{+0.18}_{-0.19}$. Several other values are quoted using different combinations of data.

[6] FIELDS 20 combines Planck 2018 CMB data with BBN and observations of deuterium and Helium-4.

[7] IVANOV 20 combines 2018 Planck CMB data with baryon acoustic oscillation data from BOSS. This study is based on a full-shape likelihood for the redshift-space galaxy power spectrum of the BOSS data.

[8] Uses Planck Data combined with an independent standard measure of distance to the sound horizon to set a limit on the total number of neutrinos. Only CMB and early-time information are used.

[9] CYBURT 16 combines Planck 2015 CMB data with BBN and observations of deuterium and Helium-4.

[10] ROSSI 15 sets limits on the number of neutrino types using BOSS Lyman alpha forest data combined with Planck CMB data and baryon acoustic oscillations.

[11] Fit to the number of neutrino degrees of freedom from Planck CMB data along with WMAP polarization, high L, and BAO data.

[12] Fit to the number of neutrinos degrees of freedom from Planck CMB data along with BAO, shear and cluster data.

[13] Fit based on the SPT-SZ survey combined with CMB, BAO, and H_0 data.

[14] Constrains the number of neutrino degrees of freedom (marginalizing over the total mass) from CMB, CMB lensing, BAO, and galaxy clustering data.

[15] Limit on the number of light neutrino types from observational Hubble parameter data with seven-year WMAP data, SPT, and the most recent estimate of H_0. Best fit is 3.45 ± 0.65.

[16] Limit on the number of light neutrino types from the CFHTLS combined with seven-year WMAP data and a prior on the Hubble parameter. Best fit is $4.17^{+1.62}_{-1.26}$. Limit is relaxed to $3.98^{+2.02}_{-1.20}$ when small scales affected by non-linearities are removed.

[17] Constrains the number of neutrino types from recent CMB and large scale structure data. No priors on other cosmological parameters are used.

[18] Constrains the number of neutrino types from recent CMB, large scale structure, Lyman-alpha forest, and SN1a data. The slight preference for $N_\nu > 3$ comes mostly from the Lyman-alpha forest data.

[19] Constrains the number of neutrino types from recent CMB and large scale structure data. See also HAMANN 07.

[20] Limit on the number of neutrino types based on ^{4}He and D/H abundance assuming a baryon density fixed to the WMAP data. Limit relaxes to 4.6 if D/H is not used or to 5.8 if only D/H and the CMB are used. See also CYBURT 01 and CYBURT 03.

[21] Limit on the number of neutrino types based on combination of WMAP data and big-bang nucleosynthesis. The limit from WMAP data alone is 8.3. See also KNELLER 01. $N_\nu \geq 3$ is assumed to compute the limit.

[22] 95% confidence level range on the number of neutrino flavors from WMAP data combined with other CMB measurements, the 2dfGRS data, and HST data.

[23] SHVARTSMAN 69 limit inferred from his equations.

Number Coupling with Less Than Full Weak Strength

VALUE	DOCUMENT ID		TECN
• • • We do not use the following data for averages, fits, limits, etc. • • •			
<20	[1] OLIVE	81C	COSM
<20	[1] STEIGMAN	79	COSM

[1] Limit varies with strength of coupling. See also WALKER 91.

REFERENCES FOR Limits on Number of Neutrino Types

ELBERS	25	PR D112 083513	W. Elbers *et al.*	(DESI Collab.)
BRIEDEN	22	JCAP 2208 024	S. Brieden, Hector Gil-Marin, Licia Verde	
KUMAR	22	JCAP 2209 060	S. Kumar, R. Nunes, P.Yadav	
YEH	22	JCAP 2210 046	T.-H. Yeh *et al.*	(ILL, MINN)
AGHANIM	20	AA 641 A6	N. Aghanim *et al.*	(Planck Collab.)
FIELDS	20	JCAP 2003 010	B. Fields *et al.*	(ILL, MINN)
Also		JCAP 2011 E02 (errat.)	B. Fields *et al.*	(ILL, MINN)
IVANOV	20	PR D101 083504	M.M. Ivanov, M. Simonovic, M. Zaldarriaga	(NYU,+)
JANOT	20	PL B803 135319	P. Janot, S. Jadach	(CERN, CRAC)
VOUTSINAS	20	PL B800 135068	G. Voutsinas *et al.*	(CERN, BOHR)
VERDE	17	JCAP 1704 023	L. Verde *et al.*	
CYBURT	16	RMP 88 015004	R.H. Cyburt *et al.*	(MSU, ILL, MINN)
ROSSI	15	PR D92 063505	G. Rossi *et al.*	
ADE	14	AA 571 A16	P.A.R. Ade *et al.*	(Planck Collab.)
COSTANZI	14	JCAP 1410 081	M. Costanzi *et al.*	(TRST, TRSTI)
HOU	14	APJ 782 74	Z. Hou *et al.*	
LEISTEDT	14	PRL 113 041301	B. Leistedt, H.V. Peiris, L. Verde	
MORESCO	12	JCAP 1207 053	M. Moresco *et al.*	
XIA	12	JCAP 1206 010	J.-Q. Xia *et al.*	
MANGANO	11	PL B701 296	G. Mangano, P. Serpico	
HAMANN	07	JCAP 0708 021	J. Hamann *et al.*	
ICHIKAWA	07	JCAP 0705 007	K. Ichikawa, M. Kawasaki, F. Takahashi	
CIRELLI	06	JCAP 0612 013	M. Cirelli *et al.*	
HANNESTAD	06	JCAP 0611 016	S. Hannestad, G. Raffelt	

LEP-SLC	06	PRPL 427 257	ALEPH, DELPHI, L3, OPAL, SLD and working groups	
SELJAK	06	JCAP 0610 014	U. Seljak, A. Slosar, P. McDonald	
ABDALLAH	05B	EPJ C38 395	J. Abdallah *et al.*	(DELPHI Collab.)
CYBURT	05	ASP 23 313	R.H. Cyburt *et al.*	
ACHARD	04E	PL B587 16	P. Achard *et al.*	(L3 Collab.)
BARGER	03C	PL B566 8	V. Barger *et al.*	
CROTTY	03	PR D67 123005	P. Crotty, J. Lesgourgues, S. Pastor	
CYBURT	03	PL B567 227	R.H. Cyburt, B.D. Fields, K.A. Olive	
HEISTER	03C	EPJ C28 1	A. Heister *et al.*	(ALEPH Collab.)
PIERPAOLI	03	MNRAS 342 L63	E. Pierpaoli	
CYBURT	01	ASP 17 87	R.H. Cyburt, B.D. Fields, K.A. Olive	
KNELLER	01	PR D64 123506	J.P. Kneller *et al.*	
ABBIENDI,G	00D	EPJ C18 253	G. Abbiendi *et al.*	(OPAL Collab.)
ABREU	00Z	EPJ C17 53	P. Abreu *et al.*	(DELPHI Collab.)
ACCIARRI	99R	PL B470 268	M. Acciarri *et al.*	(L3 Collab.)
LISI	99	PR D59 123520	E. Lisi, S. Sarkar, F.L. Villante	
OLIVE	99	ASP 11 403	K.A. Olive, D. Thomas	
ABREU	97J	ZPHY C74 577	P. Abreu *et al.*	(DELPHI Collab.)
COPI	97	PR D55 3389	C.J. Copi, D.N. Schramm, M.S. Turner	(CHIC)
HATA	97B	PR D55 540	N. Hata *et al.*	(OSU, PENN)
OLIVE	97	ASP 7 27	K.A. Olive, D. Thomas	(MINN, FLOR)
ADAM	96C	PL B380 471	W. Adam *et al.*	(DELPHI Collab.)
CARDALL	96B	APJ 472 435	C.Y. Cardall, G.M. Fuller	(UCSD)
FIELDS	96	New Ast 1 77	B.D. Fields *et al.*	(NDAM, CERN, MINN+)
KERNAN	96	PR D54 3681	P.S. Kernan, S. Sarkar	(CASE, OXFTP)
AKERS	95C	ZPHY C65 47	R. Akers *et al.*	(OPAL Collab.)
OLIVE	95	PL B354 357	K.A. Olive, G. Steigman	(MINN, OSU)
BUSKULIC	93L	PL B313 520	D. Buskulic *et al.*	(ALEPH Collab.)
LEP	92	PL B276 247	LEP Collabs.	(LEP, ALEPH, DELPHI, L3, OPAL)
WALKER	91	APJ 376 51	T.P. Walker *et al.*	(HSCA, OSU, CHIC+)
OLIVE	90	PL B236 454	K.A. Olive *et al.*	(MINN, CHIC, OSU+)
YANG	84	APJ 281 493	J. Yang *et al.*	(CHIC, BART)
OLIVE	81C	NP B180 497	K.A. Olive, D.N. Schramm, G. Steigman	(CHIC+)
STEIGMAN	79	PRL 43 239	G. Steigman, K.A. Olive, D.N. Schramm	(BART+)
YANG	79	APJ 227 697	J. Yang *et al.*	(CHIC, YALE, UVA)
STEIGMAN	77	PL 66B 202	G. Steigman, D.N. Schramm, J.E. Gunn	(YALE, CHIC+)
PEEBLES	71	Physical Cosmology Princeton Univ. Press (1971)	P.Z. Peebles	(PRIN)
SHVARTSMAN	69	JETPL 9 184 Translated from ZETFP 9 315.	V.F. Shvartsman	(MOSU)
HOYLE	64	NAT 203 1108	F. Hoyle, R.J. Tayler	(CAMB)

Double-β Decay

OMITTED FROM SUMMARY TABLE

For a discussion of the double-β decay, see sections 14.9.2 and 14.9.3 of the review "14. Neutrino Masses, Mixing, and Oscillations."

See the related review(s):

Neutrino Masses, Mixing, and Oscillations

Half-life 0ν double-β decay

In most cases the transitions (Z,A) $\rightarrow$ (Z+2,A) $+ 2e^-$ to the 0^+ ground state of the final nucleus are listed. We also list transitions that decrease the nuclear charge ($2e^+$, e^+ CC and double EC) and transitions to an excited state of the final nucleus (0^+_i, 2^+, and 2^+_i). In the following Listings only the best or comparable limits for the half-lives of each transition are reported and only those with about $T_{1/2} > 10^{23}$ years that are relevant for particle physics.

$t_{1/2}(10^{23}$ yr)	CL%	ISOTOPE	TRANSITION	METHOD	DOCUMENT ID	
• • • We do not use the following data for averages, fits, limits, etc. • • •						
>3800	90	^{136}Xe		KamLAND-Zen	[1] ABE	25C
> 350	90	^{130}Te		CUORE	[2] ADAMS	25B
> 29	90	^{100}Mo		AMoRE-I	[3] AGRAWAL	25
> 76	90	^{76}Ge	g.s. $\rightarrow 0^+_1$	MAJORANA	[4] ARNQUIST	25
> 35	90	^{76}Ge	g.s. $\rightarrow 2^+_1$	MAJORANA	[4] ARNQUIST	25
> 66	90	^{76}Ge	g.s. $\rightarrow 2^+_2$	MAJORANA	[4] ARNQUIST	25
> 21	90	^{136}Xe		PandaX-4T	[5] ZHANG	25
> 3	90	^{134}Xe		PandaX-4T	[6] YAN	24
> 830	90	^{76}Ge		MAJORANA	[7] ARNQUIST	23
> 2.1	90	^{100}Mo	g.s. $\rightarrow 2^+_1$	CUPID-Mo	[8] AUGIER	23
> 1.2	90	^{100}Mo	g.s. $\rightarrow 0^+_1$	CUPID-Mo	[8] AUGIER	23
> 13	90	^{136}Xe		NEXT	[9] NOVELLA	23
> 220	90	^{130}Te		CUORE	[10] ADAMS	22A
> 36	90	^{128}Te		CUORE	[11] ADAMS	22B
> 12	90	^{136}Xe		XENON1T	[12] APRILE	22A
> 18	90	^{100}Mo		CUPID-Mo	[13] AUGIER	22
> 46	90	^{82}Se		CUPID-0	[14] AZZOLINI	22
> 1.8	90	^{82}Se	g.s. $\rightarrow 0^+_1$	CUPID-0	[15] AZZOLINI	22
> 3.0	90	^{82}Se	g.s. $\rightarrow 2^+_1$	CUPID-0	[16] AZZOLINI	22
> 3.2	90	^{82}Se	g.s. $\rightarrow 2^+_2$	CUPID-0	[17] AZZOLINI	22
> 59	90	^{130}Te	g.s. $\rightarrow 0^+_1$	CUORE	[18] ADAMS	21A
> 15	90	^{100}Mo		CUPID-Mo	[19] ARMENGAUD	21
> 39.9	90	^{76}Ge	g.s. $\rightarrow 0^+_1$	MAJORANA-Dem	[20] ARNQUIST	21
> 21.2	90	^{76}Ge	g.s. $\rightarrow 2^+_1$	MAJORANA-Dem	[21] ARNQUIST	21
> 9.7	90	^{76}Ge	g.s. $\rightarrow 2^+_2$	MAJORANA-Dem	[22] ARNQUIST	21
>1800	90	^{76}Ge		GERDA	[23] AGOSTINI	20B
> 14	90	^{130}Te	g.s. $\rightarrow 0^+_1$	CUORE-0	[24] ALDUINO	19
> 350	90	^{136}Xe		EXO-200	[25] ANTON	19
> 2.4	90	^{136}Xe		PANDAX-II	[26] NI	19
> 150	90	^{130}Te		CUORE	[27] ALDUINO	18
> 2.5	90	^{82}Se		NEMO-3	[28] ARNOLD	18
> 2.2	90	^{116}Cd		AURORA	[29] BARABASH	18
> 1.1	90	^{134}Xe		EXO-200	[30] ALBERT	17C
> 1	90	^{116}Cd		NEMO-3	[31] ARNOLD	17
> 40	90	^{130}Te		CUORICINO	[32] ALDUINO	16
> 260	90	^{136}Xe	g.s.$\rightarrow 2^+_1$	KamLAND-Zen	[33] ASAKURA	16
> 260	90	^{136}Xe	g.s.$\rightarrow 2^+_2$	KamLAND-Zen	[34] ASAKURA	16
> 240	90	^{136}Xe	g.s.$\rightarrow 0^+_1$	KamLAND-Zen	[35] ASAKURA	16
> 11	90	^{100}Mo		NEMO-3	[36] ARNOLD	15
> 9.4	90	^{130}Te	g.s. $\rightarrow 0^+_1$	CUORICINO	[37] ANDREOTTI	12
> 0.58	90	^{48}Ca		CaF_2 scint.	[38] UMEHARA	08
> 0.89	90	^{100}Mo	g.s. $\rightarrow 0^+_1$	NEMO-3	[39] ARNOLD	07
> 1.6	90	^{100}Mo	g.s. $\rightarrow 2^+$	NEMO-3	[40] ARNOLD	07
> 1.1	90	^{128}Te		Cryog. det.	[41] ARNABOLDI	03
> 1.7	90	^{116}Cd		$^{116}CdWO_4$ scint.	[42] DANEVICH	03
> 157	90	^{76}Ge		Enriched HPGe	[43] AALSETH	02B

[1] ABE 25C use the complete data set of the KamLAND-Zen experiment, corresponding to a ^{136}Xe exposure of 2097 kg·yr. The experiment made use of 745 kg of isotopically enriched xenon. The presented result utilizes data acquired during both phases of the experiment.

[2] ADAMS 25B use 567.0 kg·yr of ^{130}Te exposure of the CUORE high-resolution bolometric calorimeter to place a limit on this decay. CUORE operates in the LNGS laboratory.

[3] AGRAWAL 25 report a new half-life limit for the $0\nu\beta\beta$ decay of ^{100}Mo, derived from 3.89 kg·yr of isotope exposure of the AMoRE-I experiment, conducted in the Yangyang Underground Laboratory in Korea.

[4] ARNQUIST 25 use the final data set collected by the MAJORANA DEMONSTRATOR experiment to place a limit on the $0\nu\beta\beta$ half-life of ^{76}Ge to one of the excited states of ^{76}Se. The data set corresponds to a ^{76}Ge isotope exposure of 98.2 kg·yr.

[5] ZHANG 25 make use of 44.6 kg·y of ^{136}Xe isotope exposure in the PandaX-4T TPC, using natural xenon, to place a limit on the $0\nu\beta\beta$ decay half-life of ^{136}Xe.

[6] YAN 24 make use of 17.9 kg·y of ^{134}Xe isotope exposure in the PandaX-4T TPC, using natural xenon, to place a limit on the $0\nu\beta\beta$ decay half-life of ^{134}Xe.

[7] ARNQUIST 23 use the final data set of the MAJORANA DEMONSTRATOR experiment, operating enriched in ^{76}Ge detectors, to set this limit on the $0\nu\beta\beta$ half-life of ^{76}Ge. The exposure is 64.5 kg·yr. A median sensitivity of 8.1×10^{25} yr is reported.

[8] AUGIER 23 utilize the complete data, set collected by the CUPID-Mo bolometric calorimeter with particle ID and located at the LSM, to study various double beta decays of ^{100}Mo to excited states of the daughter nucleus. An exposure of 1.47 kg·yr of ^{100}Mo is available.

[9] NOVELLA 23 use data collected by the NEXT-White experiment to limit the $0\nu\ \beta\beta$ half-life of ^{136}Xe. The experiment contains 3.5 kg of enriched Xe and is based on a high-pressure gas TPC. Two different limits are reported, based on different data analysis approaches, $> 5.5 \times 10^{23}$ yr and $> 13 \times 10^{23}$ yr.

[10] ADAMS 22A use the CUORE TeO_2 experiment with an exposure of 288.8 kg·yr of ^{130}Te to place a limit on its $0\nu\ \beta\beta$ decay. The median sensitivity is reported as 280×10^{23} yr. Superseeds ADAMS 20A.

[11] ADAMS 22B use the CUORE bolometric calorimeter to place a limit on the $0\nu\beta\beta$ decay half-life of ^{128}Te.

[12] APRILE 22A use 36.16 kg·yr of ^{136}Xe exposure of the XENON1T not enriched detector to establish the stated limit.

[13] AUGIER 22 use the final data set of the CUPID-Mo cryogenic calorimeter, utilizing enriched $Li_2{}^{100}MoO_4$ and an isotope exposure of 1.47 kg·y, to place a limit on the $0\nu\beta\beta$ decay half-life.

[14] AZZOLINI 22 use the CUPID-0 scintillating cryogenic bolometer to set a limit on the $0\nu\beta\beta$ half-life of ^{82}Se. The analyzed isotope exposure is 8.82 kg·yr. A median sensitivity of 7×10^{24} yr is reported. Supersedes AZZOLINI 19.

[15] AZZOLINI 22 use CUPID-0 data with an isotope exposure of 8.82 kg·yr to set a limit on the $0\nu\beta\beta$ decay to the first excited 0^+ state.

[16] AZZOLINI 22 use CUPID-0 data with an isotope exposure of 8.82 kg·yr to set a limit on the $0\nu\beta\beta$ decay to the first excited 2^+ state.

[17] AZZOLINI 22 use CUPID-0 data with an isotope exposure of 8.82 kg·yr to set a limit on the $0\nu\beta\beta$ decay to the second excited 2^+ state.

[18] ADAMS 21A et al. used 101.76 kg yr of ^{130}Te exposure of the CUORE (LNGS) bolometric detector to place a limit on the decay to the first excited state of ^{130}Xe, superseding ALDUINO 19 as the most restrictive bound on this particular decay.

[19] ARMENGAUD 21 use the CUPID-Mo 4.2 kg array of enriched $Li_2{}^{100}MoO_4$ scintillating bolometers, with 1.17 kg·yr exposure, to set this limit.

[20] ARNQUIST 21 use the MAJORANA demonstrator to set this limit for the $0\nu\ \beta\beta$ decay to the first excited 0^+ state, with a 41.9 kg yr isotopic exposure. The median sensitivity is 39.9×10^{23} yr.

[21] ARNQUIST 21 use the MAJORANA demonstrator to set this limit for the $0\nu\ \beta\beta$ decay to the first excited 2^+ state, with a 41.9 kg yr isotopic exposure. The median sensitivity is 21.2×10^{23} yr.

[22] ARNQUIST 21 use the MAJORANA demonstrator to set this limit for the $0\nu\ \beta\beta$ decay to the second excited 2^+ state, with a 41.9 kg yr isotopic exposure. The median sensitivity is 18.6×10^{23} yr.

Int. J. Mod. Phys. A 2026.41. Downloaded from www.worldscientific.com by UNIVERSITY OF CALIFORNIA @ BERKELEY on 09/16/26. Re-use and distribution is strictly not permitted, except for Open Access articles.

Int. J. Mod. Phys. A 2026.41. Downloaded from www.worldscientific.com by UNIVERSITY OF CALIFORNIA @ BERKELEY on 09/16/26. Re-use and distribution is strictly not permitted, except for Open Access articles.

[23] AGOSTINI 20B present the final data set of the GERDA experiment, searching for $0\nu\ \beta\beta$ decay of ^{76}Ge with isotopically enriched, high resolution Ge detectors. A final exposure of 127.2 kg·yr is reported. The experiment reports the lowest background and longest half life limit ever achieved by any double beta decay experiment. The reported experiment sensitivity equals the limit. Supersedes AGOSTINI 19.

[24] ALDUINO 19 use the combined data of the CUORICINO and CUORE-0 experiments to place a lower limit on the half life of the $0\nu\ \beta\beta$ decay of ^{130}Te to the first excited 0^+ state of ^{130}Xe. Supersedes ANDREOTTI 12.

[25] ANTON 19 uses he complete dataset of the EXO-200 detector to search for the $0\nu\ \beta\beta$ decay. The exposure is 234.1 kg yr. The median sensitivity is 5.0×10^{25} yr. Supersedes ALBERT 18 and ALBERT 14B.

[26] NI 19 use the PandaX-II dual phase TPC at CJPL to search for the $0\nu\ \beta\beta$ decay of ^{136}Xe. The half-life limit 2.4×10^{23} yr is obtained from 22.2 kg yr exposure with a sensitivity of 1.9×10^{23} yr.

[27] ALDUINO 18 uses the CUORE detector to search for the $0\nu\ \beta\beta$ decay of ^{130}Te. The exposure is 86.3 kg·year of natural TeO_2 corresponding to 24.0 kg·year for ^{130}Te. The median sensitivity is 0.7×10^{25} yr. The limit is obtained combining the new data from CUORE with those of CUORE0 (9.8 kg·year of ^{130}Te) and Cuoricino (19.8 kg·year of ^{130}Te).

[28] ARNOLD 18 use the NEMO-3 tracking detector to place a limit on the $0\nu\beta\beta$ decay of ^{82}Se. This is a slightly weaker limit than in BARABASH 11A, using the same detector. Supersedes ARNOLD 05A.

[29] BARABASH 18 use 1.162 kg of $^{116}CdWO_4$ scintillating crystals to obtain this limit. Supersedes DANEVICH 03 with analogous source and is more sensitive than ARNOLD 17.

[30] ALBERT 17C uses the EXO-200 detector that contains 19.098 ± 0.014% admixture of ^{134}Xe to search for the 0ν and $2\nu\ \beta\beta$ decay modes. The exposure is 29.6 kg·year. The median sensitivity is 1.9×10^{21} years.

[31] ARNOLD 17 use the NEMO-3 tracking calorimeter, containing 410 g of enriched ^{116}Cd exposed for 5.26 yr, to determine the half-life limit. Supersedes BARABASH 11A.

[32] ALDUINO 16 report result obtained with 9.8 kg·y of data collected with the CUORE-0 bolometer, combined with data from the CUORICINO. Supersedes ALFONSO 15.

[33] ASAKURA 16 use the KamLAND-Zen liquid scintillator calorimeter (^{136}Xe 89.5 kg yr) to place a limit on the $0\nu\beta\beta$-decay into the first excited state of the daughter nuclide.

[34] ASAKURA 16 use the KamLAND-Zen liquid scintillator calorimeter (^{136}Xe 89.5 kg yr) to place a limit on the $0\nu\beta\beta$-decay into the second excited state of the daughter nuclide.

[35] ASAKURA 16 use the KamLAND-Zen liquid scintillator calorimeter (^{136}Xe 89.5 kg yr) to place a limit on the $0\nu\beta\beta$-decay into the third excited state of the daughter nuclide.

[36] ARNOLD 15 use the NEMO-3 tracking calorimeter with 34.3 kg yr exposure to determine the limit of $0\nu\beta\beta$-half life of ^{100}Mo. Supersedes ARNOLD 2005A and BARABASH 11A.

[37] ANDREOTTI 12 use high resolution TeO_2 bolometric calorimeter to search for the $0\nu\beta\beta$ decay of ^{130}Te leading to the excited 0^1_+ state at 1793.5 keV.

[38] UMEHARA 08 use CaF_2 scintillation calorimeter to search for double beta decay of ^{48}Ca. Limit is significantly more stringent than quoted sensitivity: 18×10^{21} years.

[39] Limit on 0ν-decay to the first excited 0^+_1-state of daughter nucleus using NEMO-3 tracking calorimeter. Supersedes DASSIE 95.

[40] Limit on 0ν-decay to the first excited 2^+-state of daughter nucleus using NEMO-3 tracking calorimeter.

[41] Supersedes ALESSANDRELLO 00. Array of TeO_2 crystals in high resolution cryogenic calorimeter. Some enriched in ^{128}Te. Ground state to ground state decay.

[42] Limit on $0\nu\beta\beta$ decay of ^{116}Cd using enriched $CdWO_4$ scintillators. Supersedes DANEVICH 00.

[43] AALSETH 02B limit is based on 117 mol·yr of data using enriched Ge detectors. Background reduction by means of pulse shape analysis is applied to part of the data set. Reported limit is slightly less restrictive than that in KLAPDOR-KLEINGROTHAUS 01 However, it excludes part of the allowed half-life range reported in KLAPDOR-KLEINGROTHAUS 01B for the same nuclide. The analysis has been criticized in KLAPDOR-KLEINGROTHAUS 04B. The criticism was addressed and disputed in AALSETH 04.

Half-life measurements of the two-neutrino double-β decay

The measured half-life values for the transitions (Z,A) → (Z+2,A) + $2e^-$ + $2\overline{\nu}_e$ to the 0^+ ground state of the final nucleus are listed. We also list the transitions to an excited state of the final nucleus (0^+_i, etc.). We report only the measuremetnts with the smallest (or comparable) uncertainty for each transition.

$t_{1/2}$ (10^{20} yr)			ISOTOPE	TRANSITION	METHOD	DOCUMENT ID	
• • • We do not use the following data for averages, fits, limits, etc. • • •							
9.32	$^{+0.05}_{-0.04}$	± 0.07	^{130}Te		CUORE	[1] ADAMS	25A
1.03	$^{+0.38}_{-0.29}$		^{150}Nd	g.s. → 0^+_1	STELLA	[2] BARABASH	25
440	$^{+160}_{-90}$		^{82}Se	g.s. → 0^+_1	OBELIX	[3] BARABASH	25A
103	± 15	± 8	^{124}Xe	2νDEC	PandaX-4T	[4] BO	25A
109	± 14	± 5	^{124}Xe	2νDEC	LZ	[5] AALBERS	24C
20.22	± 0.18	± 0.38	^{76}Ge		GERDA	[6] AGOSTINI	23
1.11	$^{+0.19}_{-0.14}$	$^{+0.17}_{-0.15}$	^{150}Nd	$0^+ \to 0^+_1$	NEMO-3	[7] AGUERRE	23
7.5	± 0.8	$^{+0.4}_{-0.3}$	^{100}Mo	$0^+ \to 0^+_1$	CUPID-Mo	[8] AUGIER	23
0.0707	± 0.0002	± 0.0011	^{100}Mo		CUPID-Mo	[9] AUGIER	23A
0.869	± 0.005	$^{+0.009}_{-0.006}$	^{82}Se		CUPID-0	[10] AZZOLINI	23A
21.6	$^{+6.2}_{-4.0}$	$^{+4.0}_{-2.9}$	^{136}Xe		NEXT	[11] NOVELLA	23
21900	±700		^{128}Te		CUORE	[12] ADAMS	22B
110	± 20	±10	^{124}Xe		XENON1T	[13] APRILE	22A
118	± 13	±14	^{124}Xe		XENONnT	[14] APRILE	22B
23.4	$^{+0.8}_{-4.6}$	$^{+3.0}_{-1.7}$	^{136}Xe		NEXT	[15] NOVELLA	22
180	± 50	±10	^{124}Xe	2νDEC	XENON1T	[16] APRILE	19E
0.0680	± 0.0001	$^{+0.0038}_{-0.0040}$	^{100}Mo		NEMO-3	[17] ARNOLD	19
0.939	± 0.017	± 0.058	^{82}Se		NEMO-3	[18] ARNOLD	18
0.263	$^{+0.011}_{-0.012}$		^{116}Cd		AURORA	[19] BARABASH	18
> 0.87			^{134}Xe		EXO-200	[20] ALBERT	17C
8.2	± 0.2	± 0.6	^{130}Te		CUORE-0	[21] ALDUINO	17
0.274	± 0.004	± 0.018	^{116}Cd		NEMO-3	[22] ARNOLD	17
0.64	$^{+0.07}_{-0.06}$	$^{+0.12}_{-0.09}$	^{48}Ca		NEMO-3	[23] ARNOLD	16
0.0934	± 0.0022	$^{+0.0062}_{-0.0060}$	^{150}Nd		NEMO-3	[24] ARNOLD	16A
19.26	± 0.94		^{76}Ge		GERDA	[25] AGOSTINI	15A
0.0693	± 0.0004		^{100}Mo		NEMO-3	[26] ARNOLD	15
21.65	± 0.16	± 0.59	^{136}Xe		EXO-200	[27] ALBERT	14
92	$^{+55}_{-26}$	±13	^{78}Kr		BAKSAN	[28] GAVRILYAK	13
23.8	± 0.2	± 1.4	^{136}Xe		KamLAND-Z	[29] GANDO	12A
7.0	± 0.9	± 1.1	^{130}Te		NEMO-3	[30] ARNOLD	11
0.235	± 0.014	± 0.016	^{96}Zr		NEMO-3	[31] ARGYRIADES	10
6.9	$^{+1.0}_{-0.8}$	± 0.7	^{100}Mo	$0^+ \to 0^+_1$	Ge coinc.	[32] BELLI	10
5.7	$^{+1.3}_{-0.9}$	± 0.8	^{100}Mo	$0^+ \to 0^+_1$	NEMO-3	[33] ARNOLD	07
0.96	± 0.03	± 0.10	^{82}Se		NEMO-3	[34] ARNOLD	05A
0.29	$^{+0.04}_{-0.03}$		^{116}Cd		$CdWO_4$ sc.	[35] DANEVICH	03

[1] ADAMS 25A derive an improved $2\nu\beta\beta$ measurement of the half-life of ^{130}Te from 1038 kg·yr of TeO_2 exposure, with natural Te, of the CUORE experiment.

[2] BARABASH 25 use the STELLA low background Ge detectors at LNGS to search for $2\nu\beta\beta$ decay of ^{150}Nd to excited states of ^{150}Sm. The observation of $2\nu\beta\beta$ decay to 0^+_1 exited state is reported. The reported half-life value is obtained interpreting an excess observed at 334 keV as an indication of this decay.

[3] BARABASH 25A use the OBELIX Ge detector counting facility at the Laboratoire Souterrain de Modane to observe the $2\nu\beta\beta$ decay of ^{82}Se to the 0^+_1 excited state of ^{82}Kr.

[4] BO 25A use data collected by the PandaX-4T experiment to determine the half-life of ^{124}Xe against 2νDEC. 1.73 ton·yr of xenon exposure were analyzed. Data-derived capture fractions are used in the analysis.

[5] AALBERS 24C report the observation of ^{124}Xe 2νDEC. 1.39 kg·yr of isotopic exposure of the LZ dark matter experiment, collected during the first science run, were analyzed. The same capture fractions as used in APRILE 22A were assumed.

[6] AGOSTINI 23 report an updated value for the $2\nu\ \beta\beta$ half-life of ^{76}Ge; the final result of the GERDA Phase II experiment. A subset of the data, corresponding to an exposure of exposure is 11.8 kg·yr, is utilized. This is one of the most precise measurements of $2\nu\ \beta\beta$ decay reported in the literature. An effective nuclear matrix element of 0.101 ± 0.001 is derived from this result.

[7] AGUERRE 23 report the results of a 5.25 yr search for the $2\nu\ \beta\beta$ decay to the exited $0^+ \to 0^+_1$ state of the daughter nucleus, using the NEMO-3 tracking calorimeter. 36.6g of ^{150}Nd isotope were available for the measurement of this decay rate.

[8] AUGIER 23 utilize the complete data, set collected by the CUPID-Mo bolometric calorimeter with particle ID and located at the LSM, to measure the ^{100}Mo $2\nu\beta\beta$ half-life to excited 0^+_1 state of the daughter nucleus. An exposure of 1.47 kg·yr of ^{100}Mo is available.

[9] AUGIER 23A use full data set collected by the CUPID-Mo experiment to derive an improved $2\nu\ \beta\beta$ g.s. to g.s. half-life of ^{100}Mo. An exposure of 1.48 kg·yr of ^{100}Mo is utilized. Supersedes ARMENGAUD 20.

[10] AZZOLINI 23A report an improved measurement of the $2\nu\ \beta\beta$ decay with an exposure of 8.82 kg·yr of ^{82}Se, collected with the CUPID-0 detector. Superseded AZZOLINI 19B.

[11] NOVELLA 23 used the NEXT-White experiment, with a fiducial mass of 3.5 kg of enriched xenon, to measure the $2\nu\ \beta\beta$ g.s. to g.s. half-life of ^{136}Xe. The experiment is based on a high-pressure gas TPC. Supersedes NOVELLA 22.

[12] ADAMS 22B derive the $2\nu\beta\beta$ half-life of ^{128}Te from data of the CUORE bolometric calorimeter and the half-live ratio for ^{130}Te / ^{128}Te reported in BERNATOWICZ 92.

[13] APRILE 22A report an improved ^{124}Xe 2νDEC half-life measurement for ^{124}Xe, using data collected by the XENON1T detector with an isotopically not enriched Xe target. The analyzed ^{124}Xe exposure is 0.87 kg·yr. The statistical significance of the signal is 7.0 sigma. The stated half-life considers captures from the K shell up to the N5 shell. This result supersedes APRILE 19E, which exclusively considered captures from the K shell.

[14] APRILE 22B use data collected by the XENONnT dark matter experiment to derive an improved ^{124}Xe 2νDEC half-life measurement for ^{124}Xe. This result supersedes APRILE 22A.

[15] NOVELLA 22 report on a high-pressure gas TPC at Canfranc underground laboratory, filled with 3.5 kg (fiducial) xenon gas, used to measure the $2\nu\ \beta\beta$ decay of ^{136}Xe. Topological track reconstruction is utilized in the data analysis. The measurement is based on comparing runs with isotopically enriched and depleted xenon. Other measurements with smaller error exist.

[16] APRILE 19E report first measurement of two-neutrino double electron capture in ^{124}Xe using the XENON1T detector with a 0.73 t-yr exposure. An excess of 126 ± 29 events

is observed at 64.3 ± 0.6 keV decay energy, corresponding to $\sqrt{\Delta\chi^2} = 4.4$ with respect to the background-only hypothesis.

[17] ARNOLD 19 use the NEMO-3 tracking calorimeter with 34.3 kg y exposure to determine the $2\nu\ \beta\beta$ half-life of ^{100}Mo. Supersedes ARNOLD 15.

[18] ARNOLD 18 use the NEMO-3 tracking detector to determine the $2\nu\beta\beta$ half-life of ^{82}Se. 0.93 kg of ^{82}Se was observed for 5.25 y. The half-life value was obtained based on the single-state-dominance (SSD) hypothesis, preferred in this case by about 2 σ. Supersedes ARNOLD 05A.

[19] BARABASH 18 use 1.162 kg of $^{116}CdWO_4$ scintillating crystals to obtain this value. Supersedes DANEVICH 03 with analogous source and agrees with ARNOLD 17 with the NEMO-3 detector.

[20] ALBERT 17C uses the EXO-200 detector that contains 19.098 ± 0.014% admixture of ^{134}Xe to search for the $2\nu\ \beta\beta$ decay mode. The exposure is 29.6 kg·year. The median sensitivity is 1.2×10^{21} years.

[21] ALDUINO 17 use the CUORE-0 detector containing 10.8 kg of ^{130}Te in 52 crystals of TeO_2. The exposure was 9.3 kg yr of ^{130}Te. This is a more accurate rate determination than in ARNOLD 11 and BARABASH 11A.

[22] ARNOLD 17 use the NEMO-3 tracking calorimeter, containing 410 grams of enriched ^{116}Cd exposed for 5.26 years, to determine the half-life value.

[23] ARNOLD 16 use the NEMO-3 detector and a source of 6.99 g of ^{48}Ca. The half-life is based on 36.7 g year exposure. It is consistent, although somewhat longer, than the previous determinations of the half-life. Supersedes BARABASH 11A.

[24] ARNOLD 16A use the NEMO-3 tracking calorimeter, containing 36.6 g of ^{150}Nd exposed for 1918.5 days, to determine the half-life. Supersedes ARGYRIADES 09.

[25] AGOSTINI 15A use 17.9 kg yr exposure of the GERDA calorimeter to derive an improved measurement of the $2\nu\beta\beta$ decay half life of ^{76}Ge.

[26] ARNOLD 15 use the NEMO-3 tracking calorimeter with 34.3 kg yr exposure to determine the $2\nu\beta\beta$-half life of ^{100}Mo. Supersedes ARNOLD 05A and ARNOLD 04.

[27] ALBERT 14 use the EXO-200 tracking detector for a re-measurement of the $2\nu\beta\beta$-half life of ^{136}Xe. A nuclear matrix element of 0.0218 ± 0.0003 MeV^{-1} is derived from this data. Supersedes ACKERMAN 11.

[28] GAVRILYAK 13 use a proportional counter filled with Kr gas to search for the 2ν2K decay of ^{78}Kr. Data with the enriched and depleted Kr were used to determine signal and background. A 2.5σ excess of events obtained with the enriched sample is interpreted as an indication for the presence of this decay.

[29] GANDO 12A use a modification of the existing KamLAND detector. The $\beta\beta$ decay source/detector is 13 tons of enriched ^{136}Xe-loaded scintillator contained in an inner balloon. The $2\nu\beta\beta$ decay rate is derived from the fit to the spectrum between 0.5 and 4.8 MeV. This result is in agreement with ACKERMAN 11.

[30] ARNOLD 11 use enriched ^{130}Te in the NEMO-3 detector to measure the $2\nu\ \beta\beta$ decay rate. This result is in agreement with, but more accurate than ARNABOLDI 03.

[31] ARGYRIADES 10 use 9.4 ± 0.2 g of ^{96}Zr in NEMO-3 detector and identify its $2\nu\beta\beta$ decay. The result is in agreement and supersedes ARNOLD 99.

[32] BELLI 10 use enriched ^{100}Mo with 4 HP Ge detectors to record the 590.8 and 539.5 keV γ rays from the decay of the 0^+_1 state in ^{100}Ru both in singles and coincidences. This result confirms the measurement of KIDD 09 and ARNOLD 07 and supersedes them.

[33] First exclusive measurement of 2ν-decay to the first excited 0^+_1-state of daughter nucleus. ARNOLD 07 use the NEMO-3 tracking calorimeter to detect all particles emitted in decay. Result agrees with the inclusive ($0\nu + 2\nu$) measurement of DEBRAECKELEER 01.

[34] ARNOLD 05A use the NEMO-3 tracking detector to determine the $2\nu\beta\beta$ half-life of ^{82}Se with high statistics and low background (389 days of data taking). Supersedes ARNOLD 04.

[35] DANEVICH 03 is calorimetric measurement of $2\nu\beta\beta$ ground state decay of ^{116}Cd using enriched $CdWO_4$ scintillators. Agrees with EJIRI 95 and ARNOLD 96. Supersedes DANEVICH 00.

$\langle m_{ee} \rangle$, The Effective Weighted Sum of Majorana Neutrino Masses Contributing to Neutrinoless Double-β Decay

$\langle m_{ee} \rangle = |\Sigma U^2_{ei} m_{\nu_i}|$, $i = 1,2,3$. It is assumed that ν_i are Majorana particles and that the transition is dominated by the known (light) neutrinos. Note that U^2_{ei} and not $|U_{ei}|^2$ occur in the sum, and that consequently cancellations are possible. The experiments obtain the limits on $\langle m_\nu \rangle$ from the measured ones on $T_{1/2}$ using a range of nuclear matrix elements (NME), which is reflected in the spread of $\langle m_\nu \rangle$. Different experiments may choose different NME. All assume $g_A = 1.27$. In the following Listings, only the best or comparable limits for each isotope are reported. When not mentioned explicitly the transition is between ground states, but transitions between excited states are also reported.

VALUE (eV)	*ISOTOPE*	*METHOD*	*DOCUMENT ID*	
• • • We do not use the following data for averages, fits, limits, etc. • • •				
< 0.028–0.122	^{136}Xe	KamLAND-Zen	[1] ABE	25C
< 0.07–0.25	^{130}Te	CUORE	[2] ADAMS	25B
< 0.21–0.61	^{100}Mo	AMoRE-I	[3] AGRAWAL	25
< 0.4–1.6	^{136}Xe	PandaX-4T	[4] ZHANG	25
< 0.113–0.269	^{76}Ge	MAJORANA	[5] ARNQUIST	23
< 0.48–3.19	^{136}Xe	NEXT	[6] NOVELLA	23
< 0.09–0.305	^{130}Te	CUORE	[7] ADAMS	22A
< 0.8–2.5	^{136}Xe	XENON1T	[8] APRILE	22A
< 0.28–0.49	^{100}Mo	CUPID-Mo	[9] AUGIER	22
< 0.263–0.545	^{82}Se	CUPID-0	[10] AZZOLINI	22
< 0.31–0.54	^{100}Mo	CUPID-Mo	[11] ARMENGAUD	21
< 0.079–0.180	^{76}Ge	GERDA	[12] AGOSTINI	20B
< 1.2–2.1	^{100}Mo	AMoRE	[13] ALENKOV	19
< 0.093–0.286	^{136}Xe	EXO-200	[14] ANTON	19
< 1.3–3.5	^{136}Xe	PANDAX-II	[15] NI	19
< 0.11–0.52	^{130}Te	CUORE	[16] ALDUINO	18
< 1.2–3.0	^{82}Se	NEMO-3	[17] ARNOLD	18
< 1.0–1.7	^{116}Cd	AURORA	[18] BARABASH	18
< 1.4–2.5	^{116}Cd	NEMO-3	[19] ARNOLD	17
< 0.27–0.76	^{130}Te	CUORICINO	[20] ALDUINO	16
< 1.6–5.3	^{150}Nd	NEMO-3	[21] ARNOLD	16A
< 0.33–0.62	^{100}Mo	NEMO-3	[22] ARNOLD	15
< 7.2–19.5	^{96}Zr	NEMO-3	[23] ARGYRIADES	10
< 3.5–22	^{48}Ca	CaF_2 scint.	[24] UMEHARA	08
< 1.5–1.7	^{116}Cd	$^{116}CdWO_4$ scint.	[25] DANEVICH	03

[1] ABE 25C use the complete data set of the KamLAND-Zen experiment, corresponding to a ^{136}Xe exposure of 2097 kg·yr. The experiment made use of 745 kg of isotopically enriched xenon. The stated range of effective Majorana neutrino masses corresponds to the authors' assessment of nuclear matrix element variability.

[2] ADAMS 25B use 567.0 kg·yr of ^{130}Te exposure of the CUORE high-resolution bolometric calorimeter to place a limit on the effective Majorana neutrino mass. The range corresponds to the authors' assessment of nuclear matrix element variability.

[3] AGRAWAL 25 derive a range of upper limits on the effective Majorana neutrino mass, using 3.89 kg·yr of isotope exposure of the AMoRE-I experiment. The experiment is conducted in the Yangyang Underground Laboratory in Korea. The reported range is due to the authors' evaluation of the spread of relevant nuclear matrix elements.

[4] ZHANG 25 make use of 44.6 kg·y of ^{136}Xe isotope exposure in the PandaX-4T TPC, using natural xenon, to place a limit on the $0\nu\beta\beta$ decay half-life of ^{136}Xe. The derived range of effective Majorana neutrino masses reflects the author's evaluation of the spread of relevant nuclear matrix elements.

[5] ARNQUIST 23 use the final data set of the MAJORANA DEMONSTRATOR experiment, with 64.5 kg·yr of isotop exposure, to derive an upper limit for $\langle m_{\beta\beta} \rangle$. The range reflects the author's assessment of the variability of the theoretically calculated nuclear matrix elements.

[6] NOVELLA 23 use data collected with the NEXT-White experiment to derive a range of upper limits for $\langle m_{\beta\beta} \rangle$. The range reflects the author's assessment of the variability of the theoretically calculated nuclear matrix elements and both half-life limits stated in NOVELLA 23.

[7] ADAMS 22A use 1038.4 kg·yr of TeO_2 exposure collected by the CUORE experiment to determine this range of limits. The range reflects the uncertainty of nuclear matrix element calculations needed for the conversion of half-life to neutrino mass.

[8] APRILE 22A use data taken with the XENON1T detector to limit the Majorana neutrino mass. 36.16 kg·yr of ^{136}Xe exposure were utilized. The reported range of limits is due to uncertainties in the nuclear matrix elements.

[9] AUGIER 22 use the final data set of the CUPID-Mo cryogenic calorimeter with an isotop exposure of 1.47 kg·y to derive a range of neutrino mass limits. The range reflects the authors' estimate of the spread of nuclear matrix element calculations.

[10] AZZOLINI 22 use 8.82 kg·yr of isotopic exposure of the CPID-0 scintillating cryogenic bolometer to set this range of neutrino mass limits. The range reflects the authors' estimate of the spread of nuclear matrix element calculations.

[11] ARMENGAUD 21 use the CUPID-Mo demonstrator, with 1.17 kg·yr exposure of ^{100}Mo, to set this limit. The range reflects the estimated uncertainty of the calculated nuclear matrix elements.

[12] AGOSTINI 20B use the final data set of the GERDA experiment, representing an exposure of 127.2 kg·yr to derive an upper limit for $\langle m_{\beta\beta} \rangle$. Isotopically enriched Ge detectors were used. The range reflects the variability of the theoretically calculated nuclear matrix elements. Supersedes AGOSTINI 19.

[13] ALENKOV 19 report the range of the effective masses $\langle m_{\beta\beta} \rangle$ corresponding to the $0\nu\ \beta\beta$ decay half-life limit. It is based on the 52.1 kg·d exposure of ^{100}Mo, in the Yangyang underground laboratory. The median sensitivity is 1.1×10^{23} years. The range of $\langle m_{\beta\beta} \rangle$ reflects the uncertainty of nuclear matrix elements.

[14] ANTON 19 uses the complete dataset of the EXO-200 experiment to obtain these limits. The spread reflect the uncertainty in the nuclear matrix elements. Supersedes ALBERT 18 and ALBERT 14B.

[15] NI 19 use the PandaX-II dual phase TPC at CJPL to search for the $0\nu\ \beta\beta$ decay of ^{136}Xe with 22.2 kg yr exposure. The range in the $m_{\beta\beta}$ limit of 1.3–3.5 eV reflects the range of the calculated nuclear matrix elements. The sensitivity is 1.9×10^{23} yr.

[16] ALDUINO 18 use the combined data of CUORE, CUORE0, and Cuoricino to obtain this limit.

[17] ARNOLD 18 use the NEMO-3 tracking detector to constrain the $0\nu\beta\beta$ decay of ^{82}Se. The limit on $\langle m_{\beta\beta} \rangle$ is obtained assuming light neutrino exchange; the range reflects different calculations of the nuclear matrix elements. This is a somewhat weaker limit than in BARABASH 11A using the same detector.

[18] BARABASH 18 use 1.162 kg of $^{116}CdWO_4$ scintillating crystals to obtain these limits. The spread reflects the estimated uncertainty in the nuclear matrix element. Supersedes DANEVICH 03.

[19] ARNOLD 17 utilize NEMO-3 data, taken with enriched ^{116}Cd to limit the effective Majorana neutrino mass. The reported range results from the use of different nuclear matrix elements. Supersedes BARABASH 11A.

[20] ALDUINO 16 place a limit on the effective Majorana neutrino mass using the combined data of the CUORE-0 and CUORICINO experiments. The range reflects the authors' evaluation of the variability of the nuclear matrix elements. Supersededs ALFONSO 15.

[21] ARNOLD 16A limit is derived from data taken with the NEMO-3 detector and ^{150}Nd. A range of nuclear matrix elements that include the effect of nuclear deformation have been used. Supersedes ARGYRIADES 09.

Int. J. Mod
by UNIVERSITY OF CALIFORNIA @ BERK
wnloaded from www.worldscientific.com
-use and distribution is strictly not permitted, except for Open Access articles.

Int. J. Mod. Phys. A 2026.41. Downloaded from www.worldscientific.com
by UNIVERSITY OF CALIFORNIA @ BERKELEY on 09/16/26. Re-use and distribution is strictly not permitted, except for Open Access articles.

[22] ARNOLD 15 use the NEMO-3 tracking calorimeter with 34.3 kg yr exposure to determine the neutrino mass limit based on the $0\nu\beta\beta$-half life of ^{100}Mo. The spread range reflects different nuclear matrix elements. Supersedes ARNOLD 14 and BARABASH 11A.

[23] ARGYRIADES 10 use ^{96}Zr and the NEMO-3 tracking detector to obtain the reported mass limit. The range reflects the fluctuation of the nuclear matrix elements considered.

[24] Limit was obtained using CaF_2 scintillation calorimeter to search for double beta decay of ^{48}Ca. Reported range of limits reflects spread of QRPA and SM matrix element calculations used. Supersedes OGAWA 04.

[25] Limit for $\langle m_\nu \rangle$ is based on the nuclear matrix elements of STAUDT 90 and ARNOLD 96. Supersedes DANEVICH 00.

Limits on Lepton-Number Violating ($V+A$) Current Admixture

Considering that a number of experiments earlier than 1989 did not distinguish between λ and η, we list only results from that year on. $\langle\lambda\rangle = \lambda\sum U_{ej}V_{ej}$ and $\langle\eta\rangle = \eta\sum U_{ej}V_{ej}$, where the sum is over the number of neutrino generations. This sum vanishes for massless or unmixed neutrinos. In the following Listings, only best or comparable limits or lifetimes for each isotope are reported.

$\langle\lambda\rangle$ (10^{-6})	CL%	$\langle\eta\rangle$ (10^{-8})	CL%	ISOTOPE	METHOD	DOCUMENT ID	
• • • We do not use the following data for averages, fits, limits, etc. • • •							
$<$ 2.2–2.6	90	$<$ 1.7–2.1	90	^{82}Se	NEMO-3	[1] ARNOLD	18
$<$ 1.8–22	90	$<$ 1.6–21	90	^{116}Cd	AURORA	[2] BARABASH	18
$<$ 0.9–1.3	90	$<$ 0.5–0.8	90	^{100}Mo	NEMO-3	[3] ARNOLD	14
$<$120	90			^{100}Mo	$0^+ \to 2^+$	[4] ARNOLD	07
$0.692^{+0.058}_{-0.056}$	68	$0.305^{+0.026}_{-0.025}$	68	^{76}Ge	Enriched HP Ge	[5] KLAPDOR-K...	06A
$<$ 2.5	90			^{100}Mo	0ν, NEMO-3	[6] ARNOLD	05A
$<$ 3.8	90			^{82}Se	0ν, NEMO-3	[7] ARNOLD	05A
$<$ 1.5–2.0	90			^{100}Mo	0ν, NEMO-3	[8] ARNOLD	04
$<$ 3.2–3.8	90			^{82}Se	0ν, NEMO-3	[9] ARNOLD	04
$<$ 1.6–2.4	90	$<$ 0.9–5.3	90	^{130}Te	Cryog. det.	[10] ARNABOLDI	03
$<$ 2.2	90	$<$2.5	90	^{116}Cd	$^{116}CdWO_4$ scint.	[11] DANEVICH	03
$<$ 3.2–4.7	90	$<$ 2.4–2.7	90	^{100}Mo	ELEGANT V	[12] EJIRI	01
$<$ 1.1	90	$<$0.64	90	^{76}Ge	Enriched HP Ge	[13] GUENTHER	97
$<$ 4.4	90	$<$2.3	90	^{136}Xe	TPC	[14] VUILLEUMIER	93
		$<$5.3		^{128}Te	Geochem	[15] BERNATOW...	92

[1] ARNOLD 18 use the NEMO03 tracking detector, with 0.93 kg of ^{82}Se mass and 5.25 y exposure to obtain the limits for the hypothetical right-handed currents. Supersedes ARNOLD 05A.

[2] BARABASH 18 use 1.162 kg of $^{116}CdWO_4$ scintillating crystals to obtain this limits for the hypothetical right-handed currents in the $0\nu\beta\beta$ decay of ^{116}Cd.

[3] ARNOLD 14 is based on 34.7 kg yr of exposure of the NEMO-3 tracking calorimeter. The reported range limit on $\langle\lambda\rangle$ and $\langle\eta\rangle$ reflects the nuclear matrix element uncertainty in ^{100}Mo.

[4] ARNOLD 07 use NEMO-3 half life limit for 0ν-decay of ^{100}Mo to the first excited 2^+-state of daughter nucleus to limit the right-right handed admixture of weak currents $\langle\lambda\rangle$. This limit is not competitive when compared to the decay to the ground state.

[5] Re-analysis of data originally published in KLAPDOR-KLEINGROTHAUS 04A. Modified pulse shape analysis leads the authors to claim 6σ statistical evidence for observation of 0ν-decay. Authors use matrix element of MUTO 89 to determine $\langle\lambda\rangle$ and $\langle\eta\rangle$. Uncertainty of nuclear matrix element is not reflected in stated errors.

[6] ARNOLD 05A derive limit for $\langle\lambda\rangle$ based on ^{100}Mo data collected with NEMO-3 detector. No limit for $\langle\eta\rangle$ is given. Supersedes ARNOLD 04.

[7] ARNOLD 05A derive limit for $\langle\lambda\rangle$ based on ^{82}Se data collected with NEMO-3 detector. No limit for $\langle\eta\rangle$ is given. Supersedes ARNOLD 04.

[8] ARNOLD 04 use the matrix elements of SUHONEN 94 to obtain a limit for $\langle\lambda\rangle$, no limit for $\langle\eta\rangle$ is given. This limit is more stringent than the limit in EJIRI 01 for the same nucleus.

[9] ARNOLD 04 use the matrix elements of TOMODA 91 and SUHONEN 91 to obtain a limit for $\langle\lambda\rangle$, no limit for $\langle\eta\rangle$ is given.

[10] Supersedes ALESSANDRELLO 00. Cryogenic calorimeter search. Reported a range reflecting uncertainty in nuclear matrix element calculations.

[11] Limits for $\langle\lambda\rangle$ and $\langle\eta\rangle$ are based on nuclear matrix elements of STAUDT 90. Supersedes DANEVICH 00.

[12] The range of the reported $\langle\lambda\rangle$ and $\langle\eta\rangle$ values reflects the spread of the nuclear matrix elements. On axis value assuming $\langle m_\nu\rangle$=0 and $\langle\lambda\rangle$=$\langle\eta\rangle$=0, respectively.

[13] GUENTHER 97 limits use the matrix elements of STAUDT 90. Supersedes BALYSH 95 and BALYSH 92.

[14] VUILLEUMIER 93 uses the matrix elements of MUTO 89. Based on a half-life limit 2.6×10^{23} y at 90%CL.

[15] BERNATOWICZ 92 takes the measured geochemical decay width as a limit on the 0ν width, and uses the SUHONEN 91 coefficients to obtain the least restrictive limit on η. Further details of the experiment are given in BERNATOWICZ 93.

Double-β Decay REFERENCES

ABE	25C	PRL 135 262501	S. Abe *et al.*	(KamLAND-Zen Collab.)
ADAMS	25A	PRL 135 082501	D.Q. Adams *et al.*	(CUORE Collab.)
ADAMS	25B	SCI 390 1029	D.Q. Adams *et al.*	(CUORE Collab.)
AGRAWAL	25	PRL 134 082501	A. Agrawal *et al.*	(AMoRE Collab.)
ARNQUIST	25	PRL 134 242501	I.J. Arnquist *et al.*	(MAJORANA Collab.)
BARABASH	25	EPJ C85 174	A.S. Barabash *et al.*	(STELLA Collab.)
BARABASH	25A	PPN 56 831	A.S. Barabash *et al.*	(OBELIX Collab.)
BO	25A	JHEP 2505 119	Z. Bo *et al.*	(PandaX-4T Collab.)
ZHANG	25	SCIB 70 1779	S. Zhang *et al.*	(PandaX-4T Collab.)
AALBERS	24C	JP G52 015103	J. Aalbers *et al.*	(LZ Collab.)
YAN	24	PRL 132 152502	X. Yan *et al.*	(PandaX-4T Collab.)
AGOSTINI	23	PRL 131 142501	M. Agostini *et al.*	(GERDA Collab.)
AGUERRE	23	EPJ C83 1117	X. Aguerre *et al.*	(NEMO-3 Collab.)
ARNQUIST	23	PRL 130 062501	I.J. Arnquist *et al.*	(MAJORANA Collab.)
AUGIER	23	PR C107 025503	C. Augier *et al.*	(CUPID-Mo Collab.)
AUGIER	23A	PRL 131 162501	C. Augier *et al.*	(CUPID-Mo Collab.)
AZZOLINI	23A	PRL 131 222501	O. Azzolini *et al.*	(CUPID-0 Collab.)
NOVELLA	23	JHEP 2309 190	P. Novella *et al.*	(NEXT Collab.)
ADAMS	22A	NAT 604 53	D.Q. Adams *et al.*	(CUORE Collab.)
ADAMS	22B	PRL 129 222501	D.Q. Adams *et al.*	(CUORE Collab.)
APRILE	22A	PR C106 024328	E. Aprile *et al.*	(XENON1T Collab.)
APRILE	22B	PRL 129 161805	E. Aprile *et al.*	(XENONnT Collab.)
AUGIER	22	EPJ C82 1033	C. Augier *et al.*	(CUPID-Mo Collab.)
AZZOLINI	22	PRL 129 111801	O. Azzolini *et al.*	(CUPID-0 Collab.)
NOVELLA	22	PR C105 055501	P. Novella *et al.*	(NEXT Collab.)
ADAMS	21A	EPJ C81 567	D.Q. Adams *et al.*	(CUORE Collab.)
ARMENGAUD	21	PRL 126 181802	E. Armengaud *et al.*	(CUPID-Mo Collab.)
ARNQUIST	21	PR C103 015501	I.J. Arnquist *et al.*	(MAJORANA Collab.)
ADAMS	20A	PRL 124 122501	D.Q. Adams *et al.*	(CUORE Collab.)
AGOSTINI	20B	PRL 125 252502	M. Agostini *et al.*	(GERDA Collab.)
ARMENGAUD	20	EPJ C80 674	E. Armengaud *et al.*	(CUPID-Mo Collab.)
AGOSTINI	19	SCI 365 1445	M. Agostini *et al.*	(GERDA Collab.)
ALDUINO	19	EPJ C79 795	C. Alduino *et al.*	(CUORE Collab.)
ALENKOV	19	EPJ C79 791	V. Alenkov *et al.*	(AMoRE Collab.)
ANTON	19	PRL 123 161802	G. Anton *et al.*	(EXO-200 Collab.)
APRILE	19E	NAT 568 532	E. Aprile *et al.*	(XENON1T Collab.)
ARNOLD	19	EPJ C79 440	R. Arnold *et al.*	(NEMO-3 Collab.)
AZZOLINI	19	PRL 123 032501	O. Azzolini *et al.*	(CUPID-0 Collab.)
AZZOLINI	19B	PRL 123 262501	O. Azzolini *et al.*	(CUPID-0 Collab.)
NI	19	CP C43 113001	K. Ni *et al.*	(PandaX-II Collab.)
ALBERT	18	PRL 120 072701	J.B. Albert *et al.*	(EXO-200 Collab.)
ALDUINO	18	PRL 120 132501	C. Alduino *et al.*	(CUORE Collab.)
ARNOLD	18	EPJ C78 821	R. Arnold *et al.*	(NEMO-3 Collab.)
BARABASH	18	PR D98 092007	A.S. Barabash *et al.*	(AURORA Collab.)
ALBERT	17C	PR D96 092001	J.B. Albert *et al.*	(EXO-200 Collab.)
ALDUINO	17	EPJ C77 13	C. Alduino *et al.*	(CUORE Collab.)
ARNOLD	17	PR D95 012007	R. Arnold *et al.*	(NEMO-3 Collab.)
ALDUINO	16	PR C93 045503	C. Alduino *et al.*	(CUORE Collab.)
ARNOLD	16	PR D93 112008	R. Arnold *et al.*	(NEMO-3 Collab.)
ARNOLD	16A	PR D94 072003	R. Arnold *et al.*	(NEMO-3 Collab.)
ASAKURA	16	NP A946 171	K. Asakura *et al.*	(KamLAND-Zen Collab.)
AGOSTINI	15A	EPJ C75 416	M. Agostini *et al.*	(GERDA Collab.)
ALFONSO	15	PRL 115 102502	K. Alfonso *et al.*	(CUORE Collab.)
ARNOLD	15	PR D92 072011	R. Arnold *et al.*	(NEMO-3 Collab.)
ALBERT	14	PR C89 015502	J. Albert *et al.*	(EXO-200 Collab.)
ALBERT	14B	NAT 510 229	J.B. Albert *et al.*	(EXO-200 Collab.)
ARNOLD	14	PR D89 111101	R. Arnold *et al.*	(NEMO-3 Collab.)
GAVRILYAK	13	PR C87 035501	Yu.M. Gavrilyuk *et al.*	
ANDREOTTI	12	PR C85 045503	E. Andreotti *et al.*	(CUORICINO Collab.)
GANDO	12A	PR C85 045504	A. Gando *et al.*	(KamLAND-Zen Collab.)
ACKERMAN	11	PRL 107 212501	N. Ackerman *et al.*	(EXO Collab.)
ARNOLD	11	PRL 107 062504	R. Arnold *et al.*	(NEMO-3 Collab.)
BARABASH	11A	PAN 74 312	A.S. Barabash *et al.*	(NEMO-3 Collab.)
		Translated from YAF 74 330.		
ARGYRIADES	10	NP A847 168	J. Argyriades *et al.*	(NEMO-3 Collab.)
BELLI	10	NP A846 143	P. Belli *et al.*	(DAMA-INR Collab.)
ARGYRIADES	09	PR C80 032501	J. Argyriades *et al.*	(NEMO-3 Collab.)
KIDD	09	NP A821 251	M. Kidd *et al.*	
UMEHARA	08	PR C78 058501	S. Umehara *et al.*	
ARNOLD	07	NP A781 209	R. Arnold *et al.*	(NEMO-3 Collab.)
KLAPDOR-K...	06A	MPL A21 1547	H.V. Klapdor-Kleingrothaus, I.V. Krivosheina	
ARNOLD	05A	PRL 95 182302	R. Arnold *et al.*	(NEMO-3 Collab.)
AALSETH	04	PR D70 078302	C.E. Aalseth *et al.*	
ARNOLD	04	JETPL 80 377	R. Arnold *et al.*	(NEMO-3 Collab.)
		Translated from ZETFP 80 429.		
KLAPDOR-K...	04A	PL B586 198	H.V. Klapdor-Kleingrothaus *et al.*	
KLAPDOR-K...	04B	PR D70 078301	H.V. Klapdor-Kleingrothaus, A. Dietz, I.V. Krivosheina	
OGAWA	04	NP A730 215	I. Ogawa *et al.*	
ARNABOLDI	03	PL B557 167	C. Arnaboldi *et al.*	
DANEVICH	03	PR C68 035501	F.A. Danevich *et al.*	
AALSETH	02B	PR D65 092007	C.E. Aalseth *et al.*	(IGEX Collab.)
DEBRAECKEL...	01	PRL 86 3510	L. De Braeckeleer *et al.*	
EJIRI	01	PR C63 065501	H. Ejiri *et al.*	
KLAPDOR-K...	01	EPJ A12 147	H.V. Klapdor-Kleingrothaus *et al.*	
KLAPDOR-K...	01B	MPL A16 2409	H.V. Klapdor-Kleingrothaus *et al.*	
ALESSAND...	00	PL B486 13	A. Alessandrello *et al.*	
DANEVICH	00	PR C62 045501	F.A. Danevich *et al.*	
ARNOLD	99	NP A658 299	R. Arnold *et al.*	(NEMO Collab.)
GUENTHER	97	PR D55 54	M. Gunther *et al.*	(Heidelberg-Moscow Collab.)
ARNOLD	96	ZPHY C72 239	R. Arnold *et al.*	(BCEN, CAEN, JINR+)
BALYSH	95	PL B356 450	A. Balysh *et al.*	(Heidelberg-Moscow Collab.)
DASSIE	95	PR D51 2090	D. Dassie *et al.*	(NEMO Collab.)
EJIRI	95	JPSJ 64 339	H. Ejiri *et al.*	(OSAK, KIEV)
SUHONEN	94	PR C49 3055	J. Suhonen, O. Civitarese	
BERNATOW...	93	PR C47 806	T. Bernatowicz *et al.*	(WUSL, TATA)
VUILLEUMIER	93	PR D48 1009	J.C. Vuilleumier *et al.*	(NEUC, CIT, VILL)
BALYSH	92	PL B283 32	A. Balysh *et al.*	(MPIK, KIAE, SASSO)
BERNATOW...	92	PRL 69 2341	T. Bernatowicz *et al.*	(WUSL, TATA)
SUHONEN	91	NP A535 509	J. Suhonen, S.B. Khadkikar, A. Faessler	(JYV+)
TOMODA	91	RPP 54 53	T. Tomoda	
STAUDT	90	EPL 13 31	A. Staudt, K. Muto, H.V. Klapdor-Kleingrothaus	
MUTO	89	ZPHY A334 187	K. Muto, E. Bender, H.V. Klapdor	(TINT, MPIK)

Neutrino Mixing

With the possible exceptions of "short-baseline anomalies," such as LSND, all neutrino data can be described within the framework of a 3×3 mixing matrix between the mass eigenstates ν_1, ν_2, and ν_3, leading to the flavor eigenstates ν_e, ν_μ, and ν_τ, as described in the review *"Neutrino masses, mixing and oscillations."*

The Listings are divided in the following sections:

Int. J. Mod
by UNIVERSITY OF CALIFORNIA @ BERK
wnloaded from www.worldscientific.com
-use and distribution is strictly not permitted, except for Open Access articles.

(A) Neutrino fluxes and event ratios: shows measurements which correspond to various oscillation tests for Accelerator, Reactor, Atmospheric, and Solar neutrino experiments. Typically, ratios involve a measurement in a realm sensitive to oscillations compared to one for which no oscillation effect is expected.

(B) Neutrino mixing parameters: shows measurements of $\sin^2(\theta_{12})$, $\sin^2(\theta_{23})$, $\sin^2(\theta_{13})$, Δm^2_{21}, Δm^2_{32}, and δ_{CP} as extracted from the measured data in the quoted publications in the frame of the three-neutrino mixing scheme. The quoted averages are not the result of a global fit, as in the review *"Neutrino masses, mixing, and oscillations,"* and, as a consequence, might slightly differ from them. In some cases, measurements depend on the mass order (normal when $\Delta m^2_{32} > 0$ or inverted when $\Delta m^2_{32} < 0$) or octant of θ_{23} (lower when $\theta_{23} < 45°$ or upper when $\theta_{23} > 45°$).

(C) Other neutrino mixing results:

The LSND anomaly [AGUILAR 01], reported a signal which is consistent with $\overline{\nu}_\mu \to \overline{\nu}_e$ oscillations. In a three neutrino framework, this would be a measurement of θ_{12} and Δm^2_{21}. This does not appear to be consistent with the interpretation of other neutrino data. It has been interpreted as evidence for a 4th "sterile" neutrino. The following listings include results which might be relevant towards understanding this observation. They include searches for $\nu_\mu \to \nu_e$, $\overline{\nu}_\mu \to \overline{\nu}_e$, sterile neutrino oscillations, and others.

(A) Neutrino fluxes and event ratios

Events (observed/expected) from accelerator ν_μ experiments.

Some neutrino oscillation experiments compare the flux in two or more detectors. This is usually quoted as the ratio of the event rate in the far detector to the expected rate based on an extrapolation from the near detector in the absence of oscillations.

VALUE	DOCUMENT ID		TECN	COMMENT
• • • We do not use the following data for averages, fits, limits, etc. • • •				
1.01 ± 0.10	[1] ABE	14B	T2K	ν_e rate in T2K near detect.
0.71 ± 0.08	[2] AHN	06A	K2K	K2K to Super-K
0.64 ± 0.05	[3] MICHAEL	06	MINS	All charged current events
$0.71 {}^{+0.08}_{-0.09}$	[4] ALIU	05	K2K	KEK to Super-K
$0.70 {}^{+0.10}_{-0.11}$	[5] AHN	03	K2K	KEK to Super-K

[1] The rate of ν_e from μ decay was measured to be 0.68 ± 0.30 compared to the predicted flux. From K decay 1.10 ± 0.14 compared to the predicted flux.

[2] Based on the observation of 112 events when $158.1 {}^{+9.2}_{-8.6}$ were expected without oscillations. Including not only the number of events but also the shape of the energy distribution, the evidence for oscillation is at the level of about 4.3 σ. Supersedes ALIU 05.

[3] This ratio is based on the observation of 215 events compared to an expectation of 336 ± 14 without oscillations. See also ADAMSON 08.

[4] This ratio is based on the observation of 107 events at the far detector 250 km away from KEK, and an expectation of $151 {}^{+12}_{-10}$.

[5] This ratio is based on the observation of 56 events with an expectation of $80.1 {}^{+6.2}_{-5.4}$.

Events (observed/expected) from reactor $\overline{\nu}_e$ experiments.

The quoted values are the ratios of the measured reactor $\overline{\nu}_e$ event rate at the quoted distances, and the rate expected without oscillations. The expected rate is based on the experimental data for the most significant reactor fuels (^{235}U, ^{239}Pu, ^{241}Pu) and on calculations for ^{238}U.

A recent re-evaluation of the spectral conversion of electron to $\overline{\nu}_e$ in MUELLER 11 results in an upward shift of the reactor $\overline{\nu}_e$ spectrum by 3% and, thus, might require revisions to the ratios listed in this table.

VALUE	DOCUMENT ID		TECN	COMMENT
• • • We do not use the following data for averages, fits, limits, etc. • • •				
$0.948 \pm 0.008 \pm 0.033$	[1] ALMAZAN	20	RHF	RHF reactor at ILL
0.952 ± 0.027	[2] ADEY	19	DAYA	DayaBay, Ling Ao/Ao II reactors
	[3] AN	16	DAYA	DayaBay, Ling Ao/Ao II reactors
$1.08 \pm 0.21 \pm 0.16$	[4] DENIZ	10	TEXO	Kuo-Sheng reactor, 28 m
$0.658 \pm 0.044 \pm 0.047$	[5] ARAKI	05	KLND	Japanese react. $\sim$ 180 km
$0.611 \pm 0.085 \pm 0.041$	[6] EGUCHI	03	KLND	Japanese react. $\sim$ 180 km
$1.01 \pm 0.024 \pm 0.053$	[7] BOEHM	01		Palo Verde react. 0.75–0.89 km
$1.01 \pm 0.028 \pm 0.027$	[8] APOLLONIO	99	CHOZ	Chooz reactors 1 km
$0.987 \pm 0.006 \pm 0.037$	[9] GREENWOOD	96		Savannah River, 18.2 m
$0.988 \pm 0.004 \pm 0.05$	ACHKAR	95	CNTR	Bugey reactor, 15 m
$0.994 \pm 0.010 \pm 0.05$	ACHKAR	95	CNTR	Bugey reactor, 40 m
$0.915 \pm 0.132 \pm 0.05$	ACHKAR	95	CNTR	Bugey reactor, 95 m
$0.987 \pm 0.014 \pm 0.027$	[10] DECLAIS	94	CNTR	Bugey reactor, 15 m
$0.985 \pm 0.018 \pm 0.034$	KUVSHINN...	91	CNTR	Rovno reactor
$1.05 \pm 0.02 \pm 0.05$	VUILLEUMIER	82		Gösgen reactor
$0.955 \pm 0.035 \pm 0.110$	[11] KWON	81		$\overline{\nu}_e p \to e^+ n$
0.89 ± 0.15	[11] BOEHM	80		$\overline{\nu}_e p \to e^+ n$

[1] ALMAZAN 20 use the RHF research reactor at ILL to compare their measured antineutrino event rate to the calculation by HUBER 11. Reported $0.948 \pm 0.008 \pm 0.023 \pm 0.023$ measurement with uncertainties from statistics, systematic, and model. Note that this result is obtained for highly enriched ^{235}U reactor fuel while most other reactor experiments utilize a low-enrichment mix of fissile nuclides.

[2] ADEY 19 present a re-analysis of 1230 days of Daya Bay near detector data with reduced systematic uncertainties on the neutron detection efficiency. Note that ADEY 19 report the measured to predicted antineutrino ratio using the reactor model of MUELLER 11 (Huber-Mueller model). The ratio using the older ILL-Vogel model is $1.001 \pm 0.015 \pm 0.027$.

[3] AN 16 use 217 days of data (338k events) to determine the neutrino flux ratio relative to the prediction of Mueller-Huber and ILL-Vogel models (see AN 16 for details). The reported flux ratios were corrected for θ_{13} oscillation effect. The flux measurement is consistent with results from previous short-baseline reactor experiments. The measured inverse beta decay yield is $(1.55 \pm 0.04) \times 10^{-18}$ cm^2/(GW day) or $\sigma_f = (5.92 \pm 0.14) \times 10^{-43}$ cm^2/fission. About 4σ excess of events was observed in the 4–6 MeV prompt energy region.

[4] DENIZ 10 observe reactor $\overline{\nu}_e e$ scattering with recoil kinetic energies 3–8 MeV using CsI(Tl) detectors. The observed rate is consistent with the Standard Model prediction, leading to a constraint on $\sin^2\theta_W = 0.251 \pm 0.031(\text{stat}) \pm 0.024(\text{sys})$.

[5] Updated result of KamLAND, including the data used in EGUCHI 03. Note that the survival probabilities for different periods are not directly comparable because the effective baseline varies with power output of the reactor sources involved, and there were large variations in the reactor power production in Japan in 2003.

[6] EGUCHI 03 observe reactor neutrino disappearance at $\sim$ 180 km baseline to various Japanese nuclear power reactors.

[7] BOEHM 01 search for neutrino oscillations at 0.75 and 0.89 km distance from the Palo Verde reactors.

[8] APOLLONIO 99, APOLLONIO 98 search for neutrino oscillations at 1.1 km fixed distance from Chooz reactors. They use $\overline{\nu}_e p \to e^+ n$ in Gd-loaded scintillator target. APOLLONIO 99 supersedes APOLLONIO 98. See also APOLLONIO 03 for detailed description.

[9] GREENWOOD 96 search for neutrino oscillations at 18 m and 24 m from the reactor at Savannah River.

[10] DECLAIS 94 result based on integral measurement of neutrons only. Result is ratio of measured cross section to that expected in standard *V-A* theory. Replaced by ACHKAR 95.

[11] KWON 81 represents an analysis of a larger set of data from the same experiment as BOEHM 80.

Atmospheric neutrinos

Neutrinos and antineutrinos produced in the atmosphere induce μ-like and e-like events in underground detectors. The ratio of the numbers of the two kinds of events is defined as μ/e. It has the advantage that systematic effects, such as flux uncertainty, tend to cancel, for both experimental and theoretical values of the ratio. The "ratio of the ratios" of experimental to theoretical μ/e, $R(\mu/e)$, or that of experimental to theoretical μ/total, $R(\mu/\text{total})$ with total $= \mu + e$, is reported below. If the actual value is not unity, the value obtained in a given experiment may depend on the experimental conditions. In addition, the measured "up-down asymmetry" for μ ($N_{up}(\mu)/N_{down}(\mu)$) or e ($N_{up}(e)/N_{down}(e)$) is reported. The expected "up-down asymmetry" is nearly unity if there is no neutrino oscillation.

R(μ/e) = (Measured Ratio μ/e) / (Expected Ratio μ/e)

VALUE	DOCUMENT ID		TECN	COMMENT
• • • We do not use the following data for averages, fits, limits, etc. • • •				
$0.658 \pm 0.016 \pm 0.035$	[1] ASHIE	05	SKAM	sub-GeV
$0.702 {}^{+0.032}_{-0.030} \pm 0.101$	[2] ASHIE	05	SKAM	multi-GeV
$0.69 \pm 0.10 \pm 0.06$	[3] SANCHEZ	03	SOU2	Calorimeter raw data
	[4] FUKUDA	96B	KAMI	Water Cherenkov
$1.00 \pm 0.15 \pm 0.08$	[5] DAUM	95	FREJ	Calorimeter
$0.60 {}^{+0.06}_{-0.05} \pm 0.05$	[6] FUKUDA	94	KAMI	sub-GeV
$0.57 {}^{+0.08}_{-0.07} \pm 0.07$	[7] FUKUDA	94	KAMI	multi-Gev
	[8] BECKER-SZ...	92B	IMB	Water Cherenkov

[1] ASHIE 05 results are based on an exposure of 92 kton yr during the complete Super-Kamiokande I running period. The analyzed data sample consists of fully-contained

Int. J. Mod. Phys. A 2026.41. Downloaded from www.worldscientific.com by UNIVERSITY OF CALIFORNIA @ BERKELEY on 09/16/26. Re-use and distribution is strictly not permitted, except for Open Access articles.

single-ring e-like events with 0.1 GeV/c $< p_e$ and μ-like events 0.2 GeV/c $< p_\mu$, both having a visible energy $<$ 1.33 GeV. These criteria match the definition used by FUKUDA 94.

[2] ASHIE 05 results are based on an exposure of 92 kton yr during the complete Super-Kamiokande I running period. The analyzed data sample consists of fully-contained single-ring events with visible energy $>$ 1.33 GeV and partially-contained events. All partially-contained events are classified as μ-like.

[3] SANCHEZ 03 result is based on an exposure of 5.9 kton yr, and updates ALLISON 99 result. The analyzed data sample consists of fully-contained e-flavor and μ-flavor events having lepton momentum $>$ 0.3 GeV/c.

[4] FUKUDA 96B studied neutron background in the atmospheric neutrino sample observed in the Kamiokande detector. No evidence for the background contamination was found.

[5] DAUM 95 results are based on an exposure of 2.0 kton yr which includes the data used by BERGER 90B. This ratio is for the contained and semicontained events. DAUM 95 also report $R(\mu/e) = 0.99 \pm 0.13 \pm 0.08$ for the total neutrino induced data sample which includes upward going stopping muons and horizontal muons in addition to the contained and semicontained events.

[6] FUKUDA 94 result is based on an exposure of 7.7 kton yr and updates the HIRATA 92 result. The analyzed data sample consists of fully-contained e-like events with $0.1 < p_e < 1.33$ GeV/c and fully-contained μ-like events with $0.2 < p_\mu < 1.5$ GeV/c.

[7] FUKUDA 94 analyzed the data sample consisting of fully contained events with visible energy $>$ 1.33 GeV and partially contained μ-like events.

[8] BECKER-SZENDY 92B reports the fraction of nonshowering events (mostly muons from atmospheric neutrinos) as $0.36 \pm 0.02 \pm 0.02$, as compared with expected fraction $0.51 \pm 0.01 \pm 0.05$. After cutting the energy range to the Kamiokande limits, BEIER 92 finds $R(\mu/e)$ very close to the Kamiokande value.

R(ν_μ) = (Measured Flux of ν_μ) / (Expected Flux of ν_μ)

VALUE	DOCUMENT ID		TECN	COMMENT
• • • We do not use the following data for averages, fits, limits, etc. • • •				
0.84 ± 0.12	[1] ADAMSON	06	MINS	MINOS atmospheric
$0.72 \pm 0.026 \pm 0.13$	[2] AMBROSIO	01	MCRO	upward through-going
$0.57 \pm 0.05 \pm 0.15$	[3] AMBROSIO	00	MCRO	upgoing partially contained
$0.71 \pm 0.05 \pm 0.19$	[4] AMBROSIO	00	MCRO	downgoing partially contained + upgoing stopping
$0.74 \pm 0.036 \pm 0.046$	[5] AMBROSIO	98	MCRO	Streamer tubes
	[6] CASPER	91	IMB	Water Cherenkov
	[7] AGLIETTA	89	NUSX	
0.95 ± 0.22	[8] BOLIEV	81		Baksan
0.62 ± 0.17	CROUCH	78		Case Western/UCI

[1] ADAMSON 06 uses a measurement of 107 total neutrinos compared to an expected rate of 127 $\pm$ 13 without oscillations.

[2] AMBROSIO 01 result is based on the upward through-going muon tracks with $E_\mu > 1$ GeV. The data came from three different detector configurations, but the statistics is largely dominated by the full detector run, from May 1994 to December 2000. The total live time, normalized to the full detector configuration, is 6.17 years. The first error is the statistical error, the second is the systematic error, dominated by the theoretical error in the predicted flux.

[3] AMBROSIO 00 result is based on the upgoing partially contained event sample. It came from 4.1 live years of data taking with the full detector, from April 1994 to February 1999. The average energy of atmospheric muon neutrinos corresponding to this sample is 4 GeV. The first error is statistical, the second is the systematic error, dominated by the 25% theoretical error in the rate (20% in the flux and 15% in the cross section, added in quadrature). Within statistics, the observed deficit is uniform over the zenith angle.

[4] AMBROSIO 00 result is based on the combined samples of downgoing partially contained events and upgoing stopping events. These two subsamples could not be distinguished due to the lack of timing information. The result came from 4.1 live years of data taking with the full detector, from April 1994 to February 1999. The average energy of atmospheric muon neutrinos corresponding to this sample is 4 GeV. The first error is statistical, the second is the systematic error, dominated by the 25% theoretical error in the rate (20% in the flux and 15% in the cross section, added in quadrature). Within statistics, the observed deficit is uniform over the zenith angle.

[5] AMBROSIO 98 result is for all nadir angles and updates AHLEN 95 result. The lower cutoff on the muon energy is 1 GeV. In addition to the statistical and systematic errors, there is a Monte Carlo flux error (theoretical error) of ± 0.13. With a neutrino oscillation hypothesis, the fit either to the flux or zenith distribution independently yields $\sin^2 2\theta$=1.0 and $\Delta(m^2) \sim$ a few times 10^{-3} eV^2. However, the fit to the observed zenith distribution gives a maximum probability for χ^2 of only 5% for the best oscillation hypothesis.

[6] CASPER 91 correlates showering/nonshowering signature of single-ring events with parent atmospheric-neutrino flavor. They find nonshowering ($\approx \nu_\mu$ induced) fraction is $0.41 \pm 0.03 \pm 0.02$, as compared with expected 0.51 ± 0.05 (syst).

[7] AGLIETTA 89 finds no evidence for any anomaly in the neutrino flux. They define ρ = (measured number of ν_e's)/(measured number of ν_μ's). They report ρ(measured)=ρ(expected) $= 0.96^{+0.32}_{-0.28}$.

[8] From this data BOLIEV 81 obtain the limit $\Delta(m^2) \leq 6 \times 10^{-3}$ eV^2 for maximal mixing, $\nu_\mu \not\to \nu_\mu$ type oscillation.

R(μ/total) = (Measured Ratio μ/total) / (Expected Ratio μ/total)

VALUE	DOCUMENT ID		TECN	COMMENT
• • • We do not use the following data for averages, fits, limits, etc. • • •				
$1.1^{+0.07}_{-0.12} \pm 0.11$	[1] CLARK	97	IMB	multi-GeV

[1] CLARK 97 obtained this result by an analysis of fully contained and partially contained events in the IMB water-Cherenkov detector with visible energy $>$ 0.95 GeV.

$N_{up}(\mu)/N_{down}(\mu)$

VALUE	DOCUMENT ID		TECN	COMMENT
• • • We do not use the following data for averages, fits, limits, etc. • • •				
0.71 ± 0.06	[1] ADAMSON	12B	MINS	contained-vertex muons
$0.551^{+0.035}_{-0.033} \pm 0.004$	[2] ASHIE	05	SKAM	multi-GeV

[1] ADAMSON 12B reports the atmospheric neutrino results obtained with MINOS far detector in 2,553 live days (an exposure of 37.9 kton·yr). This result is obtained with a sample of high resolution contained-vertex muons. The quoted error is statistical only.

[2] ASHIE 05 results are based on an exposure of 92 kton yr during the complete Super-Kamiokande I running period. The analyzed data sample consists of fully-contained single-ring μ-like events with visible energy $>$ 1.33 GeV and partially-contained events. All partially-contained events are classified as μ-like. Upward-going events are those with $-1 <$ cos(zenith angle) < -0.2 and downward-going events are those with 0.2$<$ cos(zenith angle) $<$1. The μ-like up-down ratio for the multi-GeV data deviates from 1 (the expectation for no atmospheric ν_μ oscillations) by more than 12 standard deviations.

$N_{up}(e)/N_{down}(e)$

VALUE	DOCUMENT ID		TECN	COMMENT
• • • We do not use the following data for averages, fits, limits, etc. • • •				
$0.961^{+0.086}_{-0.079} \pm 0.016$	[1] ASHIE	05	SKAM	multi-GeV

[1] ASHIE 05 results are based on an exposure of 92 kton yr during the complete Super-Kamiokande I running period. The analyzed data sample consists of fully-contained single-ring e-like events with visible energy $>$ 1.33 GeV. Upward-going events are those with $-1 <$ cos(zenith angle) < -0.2 and downward-going events are those with 0.2 $<$ cos(zenith angle) $<$ 1. The e-like up-down ratio for the multi-GeV data is consistent with 1 (the expectation for no atmospheric ν_e oscillations).

R(up/down; μ) = (Measured up/down; μ) / (Expected up/down; μ)

VALUE	DOCUMENT ID		TECN	COMMENT
• • • We do not use the following data for averages, fits, limits, etc. • • •				
$0.62 \pm 0.05 \pm 0.02$	[1] ADAMSON	12B	MINS	contained-vertex muons
$0.62^{+0.19}_{-0.14} \pm 0.02$	[2] ADAMSON	06	MINS	atmospheric ν with far detector

[1] ADAMSON 12B reports the atmospheric neutrino results obtained with MINOS far detector in 2,553 live days (an exposure of 37.9 kton·yr). This result is obtained with a sample of high resolution contained-vertex muons. The expected ratio is calculated with no neutrino oscillation.

[2] ADAMSON 06 result is obtained with the MINOS far detector with an exposure of 4.54 kton yr. The expected ratio is calculated with no neutrino oscillation.

N(μ^+)/N(μ^-)

VALUE	DOCUMENT ID		TECN	COMMENT
• • • We do not use the following data for averages, fits, limits, etc. • • •				
$0.46^{+0.05}_{-0.04}$	[1,2] ADAMSON	12B	MINS	contained-vertex muons
$0.63^{+0.09}_{-0.08}$	[1,3] ADAMSON	12B	MINS	ν-induced rock-muons

[1] ADAMSON 12B reports the atmospheric neutrino results obtained with MINOS far detector in 2,553 live days (an exposure of 37.9 kton·yr). The muon charge ratio N(μ^+)/N(μ^-) represents the $\overline{\nu}_\mu/\nu_\mu$ ratio.

[2] This result is obtained with a charge-separated sample of high resolution contained-vertex muons. The quoted error is statistical only.

[3] This result is obtained with a charge-separated sample of high resolution neutrino-induced rock-muons. The quoted error is statistical only.

R(μ^+/μ^-) = (Measured N(μ^+)/N(μ^-)) / (Expected N(μ^+)/N(μ^-))

VALUE	DOCUMENT ID		TECN	COMMENT
• • • We do not use the following data for averages, fits, limits, etc. • • •				
$0.93 \pm 0.09 \pm 0.09$	[1,2] ADAMSON	12B	MINS	contained-vertex muons
$1.29^{+0.19}_{-0.17} \pm 0.16$	[1,3] ADAMSON	12B	MINS	ν-induced rock-muons
$1.03 \pm 0.08 \pm 0.08$	[1,4] ADAMSON	12B	MINS	contained
$1.39^{+0.35}_{-0.46}{}^{+0.08}_{-0.14}$	[5] ADAMSON	07	MINS	Upward and horizontal μ with far detector
$0.96^{+0.38}_{-0.27} \pm 0.15$	[6] ADAMSON	06	MINS	atmospheric ν with far detector

[1] ADAMSON 12B reports the atmospheric neutrino results obtained with MINOS far detector in 2,553 live days (an exposure of 37.9 kton·yr). The muon charge ratio N(μ^+)/N(μ^-) represents the $\overline{\nu}_\mu/\nu_\mu$ ratio. As far as the same oscillation parameters are used for ν and $\overline{\nu}$, the expected $\overline{\nu}_\mu/\nu_\mu$ ratio is almost entirely independent of any input oscillations.

[2] This result is obtained with a charge-separated sample of high resolution contained-vertex muons.

[3] This result is obtained with a charge-separated sample of high resolution neutrino-induced rock-muons.

[4] The charge-separated samples of high resolution contained-vertex muons and neutrino-induced rock-muons are combined to obtain this result which is consistent with unity.

[5] ADAMSON 07 result is obtained with the MINOS far detector in 854.24 live days, based on neutrino-induced upward-going and horizontal muons. This result is consistent with CPT conservation.

[6] ADAMSON 06 result is obtained with the MINOS far detector with an exposure of 4.54 kton yr, based on contained events. The expected ratio is calculated by assuming the same oscillation parameters for neutrinos and antineutrinos.

Solar neutrinos

Solar neutrinos are produced by thermonuclear fusion reactions in the Sun. Radiochemical experiments measure particular combinations of fluxes from various neutrino-producing reactions, whereas water-Cherenkov experiments mainly measure a flux of neutrinos from decay of ^{8}B. Solar neutrino fluxes are composed of all active neutrino species, ν_e, ν_μ, and ν_τ. In addition, some other mechanisms may cause antineutrino components in solar neutrino fluxes. Each measurement method is sensitive to a particular component or a combination of components of solar neutrino fluxes.

ν_e Capture Rates from Radiochemical Experiments

1 SNU (Solar Neutrino Unit) = 10^{-36} captures per atom per second.

VALUE (SNU)	DOCUMENT ID		TECN	COMMENT
• • • We do not use the following data for averages, fits, limits, etc. • • •				
$73.4\ ^{+6.1}_{-6.0}\ ^{+3.7}_{-4.1}$	[1] KAETHER	10		GALX reanalysis
$67.6 \pm 4.0 \pm 3.2$	[2] KAETHER	10		GNO+GALX reanalysis combined
$65.4\ ^{+3.1}_{-3.0}\ ^{+2.6}_{-2.8}$	[3] ABDURASHI...	09	SAGE	^{71}Ga $\rightarrow$ ^{71}Ge
$62.9\ ^{+5.5}_{-5.3} \pm 2.5$	[4] ALTMANN	05	GNO	^{71}Ga $\rightarrow$ ^{71}Ge
$69.3 \pm 4.1 \pm 3.6$	[5] ALTMANN	05	GNO	GNO + GALX combined
$77.5 \pm 6.2\ ^{+4.3}_{-4.7}$	[6] HAMPEL	99	GALX	^{71}Ga $\rightarrow$ ^{71}Ge
$2.56 \pm 0.16 \pm 0.16$	[7] CLEVELAND	98	HOME	^{37}Cl $\rightarrow$ ^{37}Ar

[1] KAETHER 10 reports the reanalysis results of a complete GALLEX data (GALLEX I+II+III+IV, reported in HAMPEL 99) based on the event selection with a new pulse shape analysis, which provides a better background reduction than the rise time analysis adopted in HAMPEL 99.

[2] Combined result of GALLEX I+II+III+IV reanalysis and GNO I+II+III (ALTMANN 05).

[3] ABDURASHITOV 09 reports a combined analysis of 168 extractions of the SAGE solar neutrino experiment during the period January 1990 through December 2007, and updates the ABDURASHITOV 02 result. The data are consistent with the assumption that the solar neutrino production rate is constant in time. Note that a $\sim$ 15% systematic uncertainty in the overall normalization may be added to the ABDURASHITOV 09 result, because calibration experiments for gallium solar neutrino measurements using intense ^{51}Cr (twice by GALLEX and once by SAGE) and ^{37}Ar (by SAGE) result in an average ratio of 0.87 $\pm$ 0.05 of the observed to calculated rates.

[4] ALTMANN 05 reports the complete result from the GNO solar neutrino experiment (GNO I+II+III), which is the successor project of GALLEX. Experimental technique of GNO is essentially the same as that of GALLEX. The run data cover the period 20 May 1998 through 9 April 2003.

[5] Combined result of GALLEX I+II+III+IV (HAMPEL 99) and GNO I+II+III.

[6] HAMPEL 99 report the combined result for GALLEX I+II+III+IV (65 runs in total), which update the HAMPEL 96 result. The GALLEX IV result (12 runs) is 118.4 $\pm$ 17.8 $\pm$ 6.6 SNU. (HAMPEL 99 discuss the consistency of partial results with the mean.) The GALLEX experimental program has been completed with these runs. The total run data cover the period 14 May 1991 through 23 January 1997. A total of 300 ^{71}Ge events were observed. Note that a $\sim$ 15% systematic uncertainty in the overall normalization may be added to the HAMPEL 99 result, because calibration experiments for gallium solar neutrino measurements using intense ^{51}Cr (twice by GALLEX and once by SAGE) and ^{37}Ar (by SAGE) result in an average ratio of 0.87$\pm$0.05 of the observed to calculated rates.

[7] CLEVELAND 98 is a detailed report of the ^{37}Cl experiment at the Homestake Mine. The average solar neutrino-induced ^{37}Ar production rate from 108 runs between 1970 and 1994 updates the DAVIS 89 result.

ϕ_{ES} (^{8}B)

^{8}B solar-neutrino flux measured via νe elastic scattering. This process is sensitive to all active neutrino flavors, but with reduced sensitivity to ν_μ, ν_τ due to the cross-section difference, $\sigma(\nu_{\mu,\tau} e) \sim 0.16\sigma(\nu_e e)$. If the ^{8}B solar-neutrino flux involves nonelectron flavor active neutrinos, their contribution to the flux is $\sim$ 0.16 times of ν_e.

VALUE (10^6 cm^{-2}s^{-1})	DOCUMENT ID		TECN	COMMENT
• • • We do not use the following data for averages, fits, limits, etc. • • •				
$2.314 \pm 0.014 \pm 0.040$	[1] ABE	24B	SKAM	SK-IV average flux
$2.336 \pm 0.011 \pm 0.043$	[2] ABE	24B	SKAM	SK-I+II+III+IV average flux
$2.32\ ^{+0.18}_{-0.17}\ ^{+0.07}_{-0.05}$	[3] ALLEGA	24	SNO+	Water phase; average flux
$2.57\ ^{+0.17}_{-0.18}\ ^{+0.07}_{-0.07}$	[4] AGOSTINI	20A	BORX	average flux
$2.53\ ^{+0.31}_{-0.28}\ ^{+0.13}_{-0.10}$	[5] ANDERSON	19	SNO+	Water phase; average flux
$2.57\ ^{+0.17}_{-0.18}\ ^{+0.07}_{-0.07}$	[6] AGOSTINI	18B	BORX	average flux
$2.345 \pm 0.014 \pm 0.036$	[7] ABE	16C	SKAM	SK-I+II+III+IV average flux
$2.308 \pm 0.020\ ^{+0.039}_{-0.040}$	[8] ABE	16C	SKAM	SK-IV average flux
$2.250\ ^{+0.030}_{-0.029} \pm 0.038$	[8] ABE	16C	SKAM	SK-IV day flux
$2.364 \pm 0.029 \pm 0.040$	[8] ABE	16C	SKAM	SK-IV night flux
$2.404 \pm 0.039 \pm 0.053$	[9] ABE	16C	SKAM	SK-III average flux
$2.41 \pm 0.05\ ^{+0.16}_{-0.15}$	[10] ABE	11	SKAM	SK-II average flux
$2.38 \pm 0.02 \pm 0.08$	[11] ABE	11	SKAM	SK-I average flux
$2.77 \pm 0.26 \pm 0.32$	[12] ABE	11B	KLND	average flux
$2.4 \pm 0.4 \pm 0.1$	[13] BELLINI	10A	BORX	average flux
$1.77\ ^{+0.24}_{-0.21}\ ^{+0.09}_{-0.10}$	[14] AHARMIM	08	SNO	Phase III
$2.38 \pm 0.05\ ^{+0.16}_{-0.15}$	[15] CRAVENS	08	SKAM	average flux
$2.35 \pm 0.02 \pm 0.08$	[16] HOSAKA	06	SKAM	average flux
$2.35 \pm 0.22 \pm 0.15$	[17] AHARMIM	05A	SNO	Salty D_2O; ^{8}B shape not constrained
$2.34 \pm 0.23\ ^{+0.15}_{-0.14}$	[17] AHARMIM	05A	SNO	Salty D_2O; ^{8}B shape constrained
$2.39\ ^{+0.24}_{-0.23} \pm 0.12$	[18] AHMAD	02	SNO	average flux
$2.39 \pm 0.34\ ^{+0.16}_{-0.14}$	[19] AHMAD	01	SNO	average flux
$2.80 \pm 0.19 \pm 0.33$	[20] FUKUDA	96	KAMI	average flux
2.70 ± 0.27	[20] FUKUDA	96	KAMI	day flux
$2.87\ ^{+0.27}_{-0.26}$	[20] FUKUDA	96	KAMI	night flux

[1] ABE 24B reports the Super-Kamiokande-IV results for 2970 live days from September 2008 to May 2018. The electron kinetic energy threshold for most of this period was 3.49 MeV. During 53 live days of water convection studies, the electron kinetic energy threshold was 5.49 MeV. Supersedes ABE 16C.

[2] ABE 24B reports the full Super-Kamiokande I to IV results for 5805 live days. Supersedes ABE 16C.

[3] ALLEGA 24 reports this result from the $\nu_e e$ elastic scattering rate using the full data from the SNO+ detector's initial water phase. The events over the reconstructed electron kinetic energy range of 3.5–15 MeV were analyzed. Supersedes ANDERSON 19.

[4] AGOSTINI 20A obtained this result from the $\nu_e e$ elastic scattering rate over the period between January 2008 and December 2016. Uses the same data as AGOSTINI 18B, but the analysis technique is significantly improved.

[5] ANDERSON 19 reports this result from the $\nu_e e$ elastic scattering rate using a 69.2 kton·day (or 114.7 days) of exposure from May through December, 2017 during the SNO+ detector's water commissioning phase. The events over the reconstructed electron kinetic energy range of 5–15 MeV were analyzed. Superseded by ALLEGA 24.

[6] AGOSTINI 18B obtained this result from the $\nu_e e$ elastic scattering rate over the period between January 2008 and December 2016.

[7] ABE 16C reports the combined results of the four phases of the Super-Kamiokande average flux measurements. Here the revised Super-Kamiokande-III result is used. Superseded by ABE 24B.

[8] ABE 16C reports the Super-Kamiokande-IV results for 1664 live days from September 2008 to February 2014. The analysis threshold is total electron energy of 4.0 MeV. Superseded by ABE 24B.

[9] ABE 16C revised the Super-Kamiokande-III average flux value reported in ABE 11. Super-Kamiokande-III results are for 548 live days from August 4, 2006 to August 18, 2008. The analysis threshold is 5.0 MeV, but the event sample in the 5.0–6.5 MeV total electron energy range has a total live time of 298 days. Superseded by ABE 24B.

[10] ABE 11 recalculated the Super-Kamiokande-II results using ^{8}B spectrum of WINTER 06A.

[11] ABE 11 recalculated the Super-Kamiokande-I results using ^{8}B spectrum of WINTER 06A.

[12] ABE 11B use a 123 kton·day exposure of the KamLAND liquid scintillation detector to measure the ^{8}B solar neutrino flux. They utilize $\nu - e$ elastic scattering above a reconstructed-energy threshold of 5.5 MeV, corresponding to 5 MeV electron recoil energy. 299 electron recoil candidate events are reported, of which 157 $\pm$ 23.6 are assigned to background.

[13] BELLINI 10A reports the Borexino result with 3 MeV energy threshold for scattered electrons. The data correspond to 345.3 live days with a target mass of 100 t, between July 15, 2007 and August 23, 2009.

[14] AHARMIM 08 reports the results from SNO Phase III measurement using an array of ^{3}He proportional counters to measure the rate of NC interactions in heavy water, over the period between November 27, 2004 and November 28, 2006, corresponding to 385.17 live days. A simultaneous fit was made for the number of NC events detected by the proportional counters and the numbers of NC, CC, and ES events detected by the PMTs, where the spectral distributions of the ES and CC events were not constrained to the ^{8}B shape.

[15] CRAVENS 08 reports the Super-Kamiokande-II results for 791 live days from December 2002 to October 2005. The photocathode coverage of the detector is 19% (reduced from 40% of that of Super-Kamiokande-I due to an accident in 2001). The analysis threshold for the average flux is 7 MeV.

[16] HOSAKA 06 reports the final results for 1496 live days with Super-Kamiokande-I between May 31, 1996 and July 15, 2001, and replace FUKUDA 02 results. The analysis threshold is 5 MeV except for the first 280 live days (6.5 MeV).

[17] AHARMIM 05A measurements were made with dissolved NaCl (0.195% by weight) in heavy water over the period between July 26, 2001 and August 28, 2003, corresponding to 391.4 live days, and update AHMED 04A. The *CC*, *ES*, and *NC* events were statistically separated. In one method, the ^{8}B energy spectrum was not constrained. In the other method, the constraint of an undistorted ^{8}B energy spectrum was added for comparison with AHMAD 02 results.

[18] AHMAD 02 reports the ^{8}B solar-neutrino flux measured via νe elastic scattering above the kinetic energy threshold of 5 MeV. The data correspond to 306.4 live days with SNO between November 2, 1999 and May 28, 2001, and updates AHMAD 01 results.

[19] AHMAD 01 reports the ^{8}B solar-neutrino flux measured via νe elastic scattering above the kinetic energy threshold of 6.75 MeV. The data correspond to 241 live days with SNO between November 2, 1999 and January 15, 2001.

Int. J. Mod
by UNIVERSITY OF CALIFORNIA @ BERK
wnloaded from www.worldscientific.com
-use and distribution is strictly not permitted, except for Open Access articles.

Int. J. Mod. Phys. A 2026.41. Downloaded from www.worldscientific.com by UNIVERSITY OF CALIFORNIA @ BERKELEY on 09/16/26. Re-use and distribution is strictly not permitted, except for Open Access articles.

[20] FUKUDA 96 results are for a total of 2079 live days with Kamiokande II and III from January 1987 through February 1995, covering the entire solar cycle 22, with threshold $E_e > 9.3$ MeV (first 449 days), > 7.5 MeV (middle 794 days), and > 7.0 MeV (last 836 days). These results update the HIRATA 90 result for the average ^{8}B solar-neutrino flux and HIRATA 91 result for the day-night variation in the ^{8}B solar-neutrino flux. The total data sample was also analyzed for short-term variations: within experimental errors, no strong correlation of the solar-neutrino flux with the sunspot numbers was found.

ϕ_{CC} (^{8}B)

^{8}B solar-neutrino flux measured with charged-current reaction which is sensitive exclusively to ν_e.

VALUE (10^6 cm^{-2}s^{-1})	DOCUMENT ID		TECN	COMMENT
• • • We do not use the following data for averages, fits, limits, etc. • • •				
$1.67^{+0.05}_{-0.04}{}^{+0.07}_{-0.08}$	[1] AHARMIM	08	SNO	Phase III
$1.68\pm0.06^{+0.08}_{-0.09}$	[2] AHARMIM	05A	SNO	Salty D_2O; ^{8}B shape not const.
$1.72\pm0.05\pm0.11$	[2] AHARMIM	05A	SNO	Salty D_2O; ^{8}B shape constrained
$1.76^{+0.06}_{-0.05}\pm0.09$	[3] AHMAD	02	SNO	average flux
$1.75\pm0.07^{+0.12}_{-0.11}\pm0.05$	[4] AHMAD	01	SNO	average flux

[1] AHARMIM 08 reports the results from SNO Phase III measurement using an array of ^{3}He proportional counters to measure the rate of NC interactions in heavy water, over the period between November 27, 2004 and November 28, 2006, corresponding to 385.17 live days. A simultaneous fit was made for the number of NC events detected by the proportional counters and the numbers of NC, CC, and ES events detected by the PMTs, where the spectral distributions of the ES and CC events were not constrained to the ^{8}B shape.

[2] AHARMIM 05A measurements were made with dissolved NaCl (0.195% by weight) in heavy water over the period between July 26, 2001 and August 28, 2003, corresponding to 391.4 live days, and update AHMED 04A. The *CC*, *ES*, and *NC* events were statistically separated. In one method, the ^{8}B energy spectrum was not constrained. In the other method, the constraint of an undistorted ^{8}B energy spectrum was added for comparison with AHMAD 02 results.

[3] AHMAD 02 reports the SNO result of the ^{8}B solar-neutrino flux measured with charged-current reaction on deuterium, $\nu_e d \rightarrow pp e^-$, above the kinetic energy threshold of 5 MeV. The data correspond to 306.4 live days with SNO between November 2, 1999 and May 28, 2001, and updates AHMAD 01 results. The complete description of the SNO Phase I data set is given in AHARMIM 07.

[4] AHMAD 01 reports the first SNO result of the ^{8}B solar-neutrino flux measured with the charged-current reaction on deuterium, $\nu_e d \rightarrow pp e^-$, above the kinetic energy threshold of 6.75 MeV. The data correspond to 241 live days with SNO between November 2, 1999 and January 15, 2001.

ϕ_{NC} (^{8}B)

^{8}B solar neutrino flux measured with neutral-current reaction, which is equally sensitive to ν_e, ν_μ, and ν_τ.

VALUE (10^6 cm^{-2}s^{-1})	CL%	DOCUMENT ID		TECN	COMMENT
• • • We do not use the following data for averages, fits, limits, etc. • • •					
$4.7\ ^{+3.6}_{-2.3}$		[1] APRILE	24A	XENT	CEνNS, liquid Xe detector
8.4 ± 3.1		[2] BO	24	PNDX	CEνNS, liquid Xe detector
<9.0	90	[3] MA	23A	PNDX	CEνNS, liquid Xe detector
$5.25\pm0.16\ ^{+0.11}_{-0.13}$		[4] AHARMIM	13	SNO	All three phases combined
$5.140^{+0.160}_{-0.158}{}^{+0.132}_{-0.117}$		[5] AHARMIM	10	SNO	Phase I+II, low threshold
$5.54\ ^{+0.33}_{-0.31}{}^{+0.36}_{-0.34}$		[6] AHARMIM	08	SNO	Phase III, prop. counter + PMT
$4.94\pm0.21\ ^{+0.38}_{-0.34}$		[7] AHARMIM	05A	SNO	Salty D_2O; ^{8}B shape not const.
$4.81\pm0.19\ ^{+0.28}_{-0.27}$		[7] AHARMIM	05A	SNO	Salty D_2O; ^{8}B shape constrained
$5.09\ ^{+0.44}_{-0.43}{}^{+0.46}_{-0.43}$		[8] AHMAD	02	SNO	average flux; ^{8}B shape const.
$6.42\pm1.57\ ^{+0.55}_{-0.58}$		[8] AHMAD	02	SNO	average flux; ^{8}B shape not const.

[1] APRILE 24A reports measurements of ^{8}B solar neutrinos through coherent scattering with xenon nuclei based on an exposure of 3.51 ton-yr with the XENONnT experiment.

[2] BO 24 reports measurements of ^{8}B solar neutrinos through coherent scattering with xenon nuclei in the commissioning run and the first science run of the PandaX-4T experiment. Supersedes MA 23A.

[3] MA 23A searched for ^{8}B solar neutrinos elastically scattered off xenon nuclei in the commissioning phase of the PANDAX-4T experiment with an effective exposure of 0.48 ton-yr. This experiment is dedicated to dark matter direct search using a dual-phase xenon TPC with a sensitive volume of 3.7 tons of liquid Xe. Superseded by BO 24.

[4] AHARMIM 13 obtained this result from a combined analysis of the data from all three phases, SNO-I, II, and III. The measurement of the ^{8}B flux mostly comes from the NC signal, however, CC contribution is included in the fit.

[5] AHARMIM 10 reports this result from a joint analysis of SNO Phase I+II data with the "effective electron kinetic energy" threshold of 3.5 MeV. This result is obtained with a "binned-histogram unconstrained fit" where binned probability distribution functions of the neutrino signal observables were used without any model constraints on the shape of the neutrino spectrum.

[6] AHARMIM 08 reports the results from SNO Phase III measurement using an array of ^{3}He proportional counters to measure the rate of NC interactions in heavy water, over the period between November 27, 2004 and November 28, 2006, corresponding to 385.17 live days. A simultaneous fit was made for the number of NC events detected by the proportional counters and the numbers of NC, CC, and ES events detected by the PMTs, where the spectral distributions of the ES and CC events were not constrained to the ^{8}B shape.

[7] AHARMIM 05A measurements were made with dissolved NaCl (0.195% by weight) in heavy water over the period between July 26, 2001 and August 28, 2003, corresponding to 391.4 live days, and update AHMED 04A. The *CC*, *ES*, and *NC* events were statistically separated. In one method, the ^{8}B energy spectrum was not constrained. In the other method, the constraint of an undistorted ^{8}B energy spectrum was added for comparison with AHMAD 02 results.

[8] AHMAD 02 reports the first SNO result of the ^{8}B solar-neutrino flux measured with the neutral-current reaction on deuterium, $\nu_\ell d \rightarrow np\nu_\ell$, above the neutral-current reaction threshold of 2.2 MeV. The data correspond to 306.4 live days with SNO between November 2, 1999 and May 28, 2001. The complete description of the SNO Phase I data set is given in AHARMIM 07.

$\phi_{\nu_\mu+\nu_\tau}$ (^{8}B)

Nonelectron-flavor active neutrino component (ν_μ and ν_τ) in the ^{8}B solar-neutrino flux.

VALUE (10^6 cm^{-2}s^{-1})	DOCUMENT ID		TECN	COMMENT
• • • We do not use the following data for averages, fits, limits, etc. • • •				
$3.26\pm0.25^{+0.40}_{-0.35}$	[1] AHARMIM	05A	SNO	From ϕ_{NC}, ϕ_{CC}, and ϕ_{ES}; ^{8}B shape not const.
$3.09\pm0.22^{+0.30}_{-0.27}$	[1] AHARMIM	05A	SNO	From ϕ_{NC}, ϕ_{CC}, and ϕ_{ES}; ^{8}B shape constrained
$3.41\pm0.45^{+0.48}_{-0.45}$	[2] AHMAD	02	SNO	From ϕ_{NC}, ϕ_{CC}, and ϕ_{ES}
3.69 ± 1.13	[3] AHMAD	01		Derived from SNO+SuperKam, water Cherenkov

[1] AHARMIM 05A measurements were made with dissolved NaCl (0.195% by weight) in heavy water over the period between July 26, 2001 and August 28, 2003, corresponding to 391.4 live days, and update AHMED 04A. The *CC*, *ES*, and *NC* events were statistically separated. In one method, the ^{8}B energy spectrum was not constrained. In the other method, the constraint of an undistorted ^{8}B energy spectrum was added for comparison with AHMAD 02 results.

[2] AHMAD 02 deduced the nonelectron-flavor active neutrino component (ν_μ and ν_τ) in the ^{8}B solar-neutrino flux, by combining the charged-current result, the νe elastic-scattering result and the neutral-current result. The complete description of the SNO Phase I data set is given in AHARMIM 07.

[3] AHMAD 01 deduced the nonelectron-flavor active neutrino component (ν_μ and ν_τ) in the ^{8}B solar-neutrino flux, by combining the SNO charged-current result (AHMAD 01) and the Super-Kamiokande νe elastic-scattering result (FUKUDA 01).

Total Flux of Active *pp* Solar Neutrinos

Total flux of active neutrinos (ν_e,ν_μ,ν_τ).

VALUE (10^{10} cm^{-2}s^{-1})	DOCUMENT ID		TECN	COMMENT
• • • We do not use the following data for averages, fits, limits, etc. • • •				
$6.1\pm0.5^{+0.3}_{-0.5}$	[1] AGOSTINI	18B	BORX	$\nu_e e$ scattering rate

[1] AGOSTINI 18B obtained this result from the measured $\nu_e e$ elastic scattering rate over the period between December 2011 and May 2016, assuming the MSW-LMA oscillation parameters derived by ESTEBAN 17. Assuming a high-metalicity standard solar model, the electron neutrino survival probability for the *pp* solar neutrino is calculated to be 0.57 ± 0.09.

Total Flux of Active ^{7}Be Solar Neutrinos

Total flux of active neutrinos (ν_e,ν_μ,ν_τ).

VALUE (10^9 cm^{-2}s^{-1})	DOCUMENT ID		TECN	COMMENT
• • • We do not use the following data for averages, fits, limits, etc. • • •				
$4.99\pm0.11^{+0.06}_{-0.08}$	[1] AGOSTINI	18B	BORX	$\nu_e e$ scattering rate

[1] AGOSTINI 18B obtained this result from the measured $\nu_e e$ elastic scattering rate over the period between December 2011 and May 2016, assuming the MSW-LMA oscillation parameters derived by ESTEBAN 17. Assuming a high-metalicity standard solar model, the electron neutrino survival probability for the ^{7}Be solar neutrino is calculated to be 0.53 ± 0.05.

Total Flux of Active *pep* Solar Neutrinos

Total flux of active neutrinos (ν_e,ν_μ,ν_τ).

VALUE (10^8 cm^{-2}s^{-1})	DOCUMENT ID		TECN	COMMENT
• • • We do not use the following data for averages, fits, limits, etc. • • •				
$1.27\pm0.19^{+0.08}_{-0.12}$	[1] AGOSTINI	18B	BORX	$\nu_e e$ scattering rate

[1] AGOSTINI 18B obtained this result from the measured $\nu_e e$ elastic scattering rate over the period between December 2011 and May 2016, assuming the MSW-LMA oscillation parameters derived by ESTEBAN 17 and a high-metalicity standard solar model. The

electron neutrino survival probability for the pep solar neutrino is calculated to be 0.43 ± 0.11.

Total Flux of Active ^{8}B Solar Neutrinos

Total flux of active neutrinos (ν_e, ν_μ, and ν_τ).

VALUE (10^6 cm^{-2}s^{-1})	DOCUMENT ID		TECN	COMMENT
• • • We do not use the following data for averages, fits, limits, etc. • • •				
$5.95\ ^{+0.75}_{-0.71}\ ^{+0.28}_{-0.30}$	[1] ANDERSON	19	SNO+	Water phase; $\nu_e e$ scattering rate
$5.68\ ^{+0.39}_{-0.41}\ ^{+0.03}_{-0.03}$	[2] AGOSTINI	18B	BORX	From $\nu_e e$ scattering rate
$5.25\ \pm0.16\ ^{+0.11}_{-0.13}$	[3] AHARMIM	13	SNO	All three phases combined
$5.046\ ^{+0.159}_{-0.152}\ ^{+0.107}_{-0.123}$	[4] AHARMIM	10	SNO	From ϕ_{NC} in Phase I+II, low threshold
$5.54\ ^{+0.33}_{-0.31}\ ^{+0.36}_{-0.34}$	[5] AHARMIM	08	SNO	ϕ_{NC} in Phase III
$4.94\ \pm0.21\ ^{+0.38}_{-0.34}$	[6] AHARMIM	05A	SNO	From ϕ_{NC}; ^{8}B shape not const.
$4.81\ \pm0.19\ ^{+0.28}_{-0.27}$	[6] AHARMIM	05A	SNO	From ϕ_{NC}; ^{8}B shape constrained
$5.09\ ^{+0.44}_{-0.43}\ ^{+0.46}_{-0.43}$	[7] AHMAD	02	SNO	Direct measurement from ϕ_{NC}
$5.44\ \pm0.99$	[8] AHMAD	01		Derived from SNO+SuperKam, water Cherenkov

[1] ANDERSON 19 reports this result from the measured $\nu_e e$ elastic scattering rate using a 69.2 kton·day (or 114.7 days) of exposure from May through December, 2017 during the SNO+ detector's water commissioning phase, assuming the neutrino mixing parameters given in PDG 16 and a standard solar model given in BAHCALL 05.

[2] AGOSTINI 18B obtained this result from the measured $\nu_e e$ elastic scattering rate over the period between January 2008 and December 2016, assuming the MSW-LMA oscillation parameters derived by ESTEBAN 17. Assuming a high-metalicity standard solar model, the electron neutrino survival probability for the ^{8}B solar neutrino is calculated to be 0.37 ± 0.08.

[3] AHARMIM 13 obtained this result from a combined analysis of the data from all three phases, SNO-I, II, and III. The measurement of the ^{8}B flux mostly comes from the NC signal, however, CC contribution is included in the fit.

[4] AHARMIM 10 reports this result from a joint analysis of SNO Phase I+II data with the "effective electron kinetic energy" threshold of 3.5 MeV. This result is obtained with the assumption of unitarity, which relates the NC, CC, and ES rates. The data were fit with the free parameters directly describing the total ^{8}B neutrino flux and the energy-dependent ν_e survival probability.

[5] AHARMIM 08 reports the results from SNO Phase III measurement using an array of ^{3}He proportional counters to measure the rate of NC interactions in heavy water, over the period between November 27, 2004 and November 28, 2006, corresponding to 385.17 live days. A simultaneous fit was made for the number of NC events detected by the proportional counters and the numbers of NC, CC, and ES events detected by the PMTs, where the spectral distributions of the ES and CC events were not constrained to the ^{8}B shape.

[6] AHARMIM 05A measurements were made with dissolved NaCl (0.195% by weight) in heavy water over the period between July 26, 2001 and August 28, 2003, corresponding to 391.4 live days, and update AHMED 04A. The CC, ES, and NC events were statistically separated. In one method, the ^{8}B energy spectrum was not constrained. In the other method, the constraint of an undistorted ^{8}B energy spectrum was added for comparison with AHMAD 02 results.

[7] AHMAD 02 determined the total flux of active ^{8}B solar neutrinos by directly measuring the neutral-current reaction, $\nu_\ell d \rightarrow np\nu_\ell$, which is equally sensitive to ν_e, ν_μ, and ν_τ. The complete description of the SNO Phase I data set is given in AHARMIM 07.

[8] AHMAD 01 deduced the total flux of active ^{8}B solar neutrinos by combining the SNO charged-current result (AHMAD 01) and the Super-Kamiokande νe elastic-scattering result (FUKUDA 01).

Total Flux of Active CNO Solar Neutrinos

Total flux of active neutrinos (ν_e,ν_μ,ν_τ).

VALUE (10^8 cm^{-2} s^{-1})	CL%	DOCUMENT ID		TECN	COMMENT
• • • We do not use the following data for averages, fits, limits, etc. • • •					
$6.7^{+1.2}_{-0.8}$		[1] BASILICO	23	BORX	$\nu_e e$ directional + spectral information
$6.6^{+2.0}_{-0.9}$		[2] APPEL	22	BORX	$\nu_e e$ scattering rate
$7.0^{+3.0}_{-2.0}$		[3] AGOSTINI	20D	BORX	$\nu_e e$ scattering rate
<7.9	95	[4] AGOSTINI	18B	BORX	$\nu_e e$ scattering rate

[1] BASILICO 23 obtained this result by combining the newly developed Correlated Integrated Directionality (CID)-based CNO result obtained by using the complete Borexino data-taking period from 2007 to 2021, with a spectral fit of the Phase-III dataset (from July 2016 to October 2021, characterized by a thermally stable detector). Note that the directional information is independent from the spectral information on which the previous CNO solar neutrino measurements by Borexino were based. Neutrino flavor conversion was taken into account.

[2] APPEL 22 obtained this result from the measured $\nu_e e$ elastic scattering rate over the period between January 2017 and October 2021, assuming the MSW-LMA oscillation parameters derived by ESTEBAN 20A. The exposure corresponding to this data is 1431.6 days × 71.3 tons.

[3] AGOSTINI 20D obtained this result from the measured $\nu_e e$ elastic scattering rate over the period between July 2016 to February 2020, assuming the MSW-LMA oscillation parameters derived by CAPOZZI 18.

[4] AGOSTINI 18B obtained this result from an upper limit of the $\nu_e e$ elastic scattering rate for the CNO neutrinos over the period between December 2011 and May 2016, assuming the MSW-LMA oscillation parameters derived by ESTEBAN 17.

Total Flux of Active hep Solar Neutrinos

Total flux of active neutrinos (ν_e,ν_μ,ν_τ).

VALUE (10^5 cm^{-2}s^{-1})	CL%	DOCUMENT ID		TECN	COMMENT
• • • We do not use the following data for averages, fits, limits, etc. • • •					
<1.8	90	[1] AGOSTINI	20A	BORX	$\nu_e e$ scattering and ^{12}C(ν,ν')^{12}C*
<0.3	90	[2] AHARMIM	20	SNO	CC, NC, $\nu_e e$ scattering
<2.2	90	[3] AGOSTINI	18B	BORX	$\nu_e e$ scattering rate

[1] AGOSTINI 20A obtained this result from an upper limit of the $\nu_e e$ elastic scattering rate and NC-mediated inelastic scattering on carbon nuclei with 15.1 MeV deexcitation γ-ray for the hep neutrino. The dataset corresponds to an effective exposure of 0.745 kt·yr from November 2009 to October 2017. A FADC DAQ system, optimized for the acquisition of high-energy events was used for data collection. The MSW-LMA oscillation parameters derived by ESTEBAN 17 were assumed.

[2] AHARMIM 20 uses the entire SNO dataset, corresponding to 2.47 kton·yrs of exposure after fiducialization. With the D_2O target, SNO was sensitive to charged current, neutral current, and elastic scattering channels.

[3] AGOSTINI 18B obtained this result from an upper limit of the $\nu_e e$ elastic scattering rate for the hep neutrino using the dataset corresponding to an exposure of 0.8 kt·yr and assuming the MSW-LMA oscillation parameters derived by ESTEBAN 17.

Day-Night Asymmetry (^{8}B)

$A = (\phi_{\rm night} - \phi_{\rm day}) / \phi_{\rm average}$

VALUE (units 10^{-2})	DOCUMENT ID		TECN	COMMENT
$2.86 \pm 0.85 \pm 0.32$	[1] ABE	24B	SKAM	SK combined; Based on ϕ_{ES}
• • • We do not use the following data for averages, fits, limits, etc. • • •				
$2.62 \pm 1.07 \pm 0.30$	[2] ABE	24B	SKAM	SK-IV; Based on ϕ_{ES}
$3.3\ \pm1.0\ \pm0.5$	[3] ABE	16C	SKAM	SK combined; Based on ϕ_{ES}
$3.6\ \pm1.6\ \pm0.6$	[4] ABE	16C	SKAM	SK-IV; Based on ϕ_{ES}
$3.2\ \pm1.1\ \pm0.5$	[5] RENSHAW	14	SKAM	Based on ϕ_{ES}
$6.3\ \pm4.2\ \pm3.7$	[6] CRAVENS	08	SKAM	Based on ϕ_{ES}
$2.1\ \pm2.0\ ^{+1.2}_{-1.3}$	[7] HOSAKA	06	SKAM	Based on ϕ_{ES}
$1.7\ \pm1.6\ ^{+1.2}_{-1.3}$	[8] HOSAKA	06	SKAM	Fitted in the LMA region
$-5.6\ \pm7.4\ \pm5.3$	[9] AHARMIM	05A	SNO	From salty SNO ϕ_{CC}
$-3.7\ \pm6.3\ \pm3.2$	[9] AHARMIM	05A	SNO	From salty SNO ϕ_{CC}; const. of no ϕ_{NC} asymmetry
$14.0\ \pm6.3\ ^{+1.5}_{-1.4}$	[10] AHMAD	02B	SNO	Derived from SNO ϕ_{CC}
$7.0\ \pm4.9\ ^{+1.3}_{-1.2}$	[11] AHMAD	02B	SNO	Const. of no ϕ_{NC} asymmetry

[1] ABE 24B reports the combined day-night flux asymmetry results of the four phases (5805 live days) of the Super-Kamiokande measurements. Amplitude fit method is used. Supersedes ABE 16C.

[2] ABE 24B reports the day-night flux asymmetry of the Super-Kamiokande IV data (2970 live days). Amplitude fit method is used. Supersedes ABE 16C.

[3] ABE 16C reports the combined day-night flux asymmetry results of the four phases of the Super-Kamiokande measurements. Amplitude fit method is used. See footnote to RENSHAW 14. Superseded by ABE 24B.

[4] ABE 16C reports the Super-Kamiokande-IV results for 1664 live days from September 2008 to February 2014. The analysis threshold for day-night flux asymmetry is recoil electron energy of 4.49 MeV (total electron energy of 5.0 MeV). Amplitude fit method is used. See footnote to RENSHAW 14. Superseded by ABE 24B.

[5] RENSHAW 14 obtains this result by using the "amplitude fit" introduced in SMY 04. The data from the Super-Kamiokande(SK)-I, -II, -III, and 1306 live days of the SK-IV measurements are used. The analysis threshold is recoil-electron kinetic energy of 4.5 MeV for SK-III, and SK-IV except for 250 live days in SK-III (6.0 MeV). The analysis threshold for SK-I and SK-II is the same as in the previous reports. (Note that in the previous SK solar-neutrino results, the analysis threshold is quoted as recoil-electron total energy.) This day-night asymmetry result is consistent with neutrino oscillations for 4×10^{-5} eV^2 $< \Delta m^2_{21} < 7 \times 10^{-5}$ eV^2 and large mixing values of θ_{12} at the 68% CL.

[6] CRAVENS 08 reports the Super-Kamiokande-II results for 791 live days from December 2002 to October 2005. The photocathode coverage of the detector is 19% (reduced from 40% of that of Super-Kamiokande-I due to an accident in 2001). The analysis threshold for the day and night fluxes is 7.5 MeV except for the first 159 live days (8.0 MeV).

[7] HOSAKA 06 reports the final results for 1496 live days with Super-Kamiokande-I between May 31, 1996 and July 15, 2001, and replace FUKUDA 02 results. The analysis threshold is 5 MeV except for the first 280 live days (6.5 MeV).

[8] This result with reduced statistical uncertainty is obtained by assuming two-neutrino oscillations within the LMA (large mixing angle) region and by fitting the time variation of the solar neutrino flux measured via ν_e elastic scattering to the variations expected from neutrino oscillations. For details, see SMY 04. There is an additional small systematic error of ±0.0004 coming from uncertainty of oscillation parameters.

[9] AHARMIM 05A measurements were made with dissolved NaCl (0.195% by weight) in heavy water over the period between July 26, 2001 and August 28, 2003, with 176.5 days of the live time recorded during the day and 214.9 days during the night. This result is obtained with the spectral distribution of the CC events not constrained to the ^{8}B shape.

[10] AHMAD 02B results are based on the charged-current interactions recorded between November 2, 1999 and May 28, 2001, with the day and night live times of 128.5 and

Int. J. Mod
by UNIVERSITY OF CALIFORNIA @ BERK
wnloaded from www.worldscientific.com
-use and distribution is strictly not permitted, except for Open Access articles.

Int. J. Mod. Phys. A 2026.41. Downloaded from www.worldscientific.com
by UNIVERSITY OF CALIFORNIA @ BERKELEY on 09/16/26. Re-use and distribution is strictly not permitted, except for Open Access articles.

177.9 days, respectively. The complete description of the SNO Phase I data set is given in AHARMIM 07.

[11] AHMAD 02B results are derived from the charged-current interactions, neutral-current interactions, and νe elastic scattering, with the total flux of active neutrinos constrained to have no asymmetry. The data were recorded between November 2, 1999 and May 28, 2001, with the day and night live times of 128.5 and 177.9 days, respectively. The complete description of the SNO Phase I data set is given in AHARMIM 07.

ϕ_{ES} (^{7}Be)

^{7}Be solar-neutrino flux measured via ν_e elastic scattering. This process is sensitive to all active neutrino flavors, but with reduced sensitivity to ν_μ, ν_τ due to the cross-section difference, $\sigma(\nu_{\mu,\tau}\, e) \sim 0.2\ \sigma(\nu_e\, e)$. If the ^{7}Be solar-neutrino flux involves nonelectron flavor active neutrinos, their contribution to the flux is $\sim$ 0.2 times that of ν_e.

VALUE (10^9 cm^{-2} s^{-1})	DOCUMENT ID		TECN	COMMENT
• • • We do not use the following data for averages, fits, limits, etc. • • •				
3.26±0.52	[1] GANDO	15	KLND	average flux
3.10±0.15	[2] BELLINI	11A	BORX	average flux

[1] GANDO 15 uses 165.4 kton·day exposure of the KamLAND liquid scintillator detector to measure the 862 keV ^{7}Be solar neutrino flux via $\nu - e$ elastic scattering

[2] BELLINI 11A reports the ^{7}Be solar neutrino flux measured via $\nu - e$ elastic scattering. The data correspond to 740.7 live days between May 16, 2007 and May 8, 2010, and also correspond to 153.6 ton·year fiducial exposure. BELLINI 11A measured the 862 keV ^{7}Be solar neutrino flux, which is an 89.6% branch of the ^{7}Be solar neutrino flux, to be $(2.78 \pm 0.13) \times 10^9$ cm^{-2} s^{-1}. Supercedes ARPESELLA 08A.

ϕ_{ES} (pep)

pep solar-neutrino flux measured via ν_e elastic scattering. This process is sensitive to all active neutrino flavors, but with reduced sensitivity to ν_μ, ν_τ due to the cross section difference, $\sigma(\nu_{\mu,\tau}\ e) \sim\ 0.2\ \sigma(\nu_e\, e)$. If the pep solar-neutrino flux involves non-electron flavor active neutrinos, their contribution to the flux is $\sim$ 0.2 times that of ν_e.

VALUE (10^8 cm^{-2}s^{-1})	DOCUMENT ID		TECN	COMMENT
• • • We do not use the following data for averages, fits, limits, etc. • • •				
1.0±0.2	[1] BELLINI	12A	BORX	average flux

[1] BELLINI 12A reports 1.44 MeV pep solar-neutrino flux measured via ν_e elastic scattering. The data were collected between January 13, 2008 and May 9, 2010, corresponding to 20,4009 ton·day fiducial exposure. The listed flux value is calculated from the observed rate of pep solar neutrino interactions in Borexino (3.1 ± 0.6 ± 0.3 counts/(day·100 ton)) and the corresponding rate expected for no neutrino flavor oscillations (4.47 ± 0.05 counts/(day·100 ton)), using the SSM prediction for the pep solar neutrino flux of $(1.441 \pm 0.012) \times 10^8$ cm^{-2}s^{-1}.

ϕ_{ES} (CNO)

CNO solar-neutrino flux measured via ν_e elastic scattering. This process is sensitive to all active neutrino flavors, but with reduced sensitivity to ν_μ, ν_τ due to the cross section difference, $\sigma(\nu_{\mu,\tau}\ e) \sim\ 0.2\ \sigma(\nu_e\, e)$. If the CNO solar-neutrino flux involves non-electron flavor active neutrinos, their contribution to the flux is $\sim$ 0.2 times that of ν_e.

VALUE (10^8 cm^{-2}s^{-1})	CL%	DOCUMENT ID		TECN	COMMENT
• • • We do not use the following data for averages, fits, limits, etc. • • •					
<7.7	90	[1] BELLINI	12A	BORX	MSW-LMA solution assumed

[1] BELLINI 12A reports an upper limit of the CNO solar neutrino flux measured via ν_e elastic scattering. The data were collected between January 13, 2008 and May 9, 2010, corresponding to 20,409 ton·day fiducial exposure.

$\phi_{ES}(pp)$

pp solar-neutrino flux measured via νe elastic scattering. This process is sensitive to all active neutrino flavors, but with reduced sensitivity to ν_μ, ν_τ due to the cross section difference, $\sigma(\nu_{\mu,\tau}\ e) \sim\ 0.3\ \sigma(\nu_e\, e)$. If the pp solar-neutrino flux involves nonelectron flavor active neutrinos, their contribution to the flux is $\sim$ 0.3 times of ν_e.

VALUE (10^{10} cm^{-2} s^{-1})	CL%	DOCUMENT ID		TECN	COMMENT
• • • We do not use the following data for averages, fits, limits, etc. • • •					
<23.3	90	[1] LU	24	PNDX	average flux
4.4±0.5		[2] BELLINI	14A	BORX	average flux

[1] LU 24 searched for pp solar neutrinos via νe elastic scattering using PandaX-4T commissioning data. By fitting the measured energy spectrum of events in the 24–144 keV recoil electron kinetic energy, the number of pp + ^{7}Be neutrinos is measured to be 231 ± 113 ± 287 events. The pp neutrino flux is estimated using the expected ratio of pp to ^{7}Be fluxes and their contributions to the measured energy range.

[2] BELLINI 14A reports pp solar-neutrino flux measured via νe elastic scattering. The data were collected between January 2012 and May 2013, corresponding to 408 days of data. The pp neutrino interaction rate in Borexino is measured to be 144 ± 13 ± 10 counts/(day·100 ton) by fitting the measured energy spectrum of events in the 165–590 keV recoil electron kinetic energy window with the expected signal + background spectrum. The listed flux value $\phi_{ES}(pp)$ is calculated from the observed rate and the number of $(3.307 \pm 0.003) \times 10^{31}$ electrons for 100 tons of the Borexino scintillator, and the $\nu_e\, e$ integrated cross section over the pp neutrino spectrum, $\sigma(\nu_e\, e) = 11.38 \times 10^{-46}$ cm^2.

$\phi_{CC}(pp)$

pp solar-neutrino flux measured with charged-current reaction which is sensitive exclusively to ν_e.

VALUE (10^{10} cm^{-2} s^{-1})	DOCUMENT ID		TECN	COMMENT
• • • We do not use the following data for averages, fits, limits, etc. • • •				
3.38±0.47	[1] ABDURASHI...	09	FIT	Fit existing solar-ν data

[1] ABDURASHITOV 09 reports the pp solar-neutrino flux derived from the Ga solar neutrino capture rate by subtracting contributions from ^{8}B, ^{7}Be, pep and CNO solar neutrino fluxes determined by other solar neutrino experiments as well as neutrino oscillation parameters determined from available world neutrino oscillation data.

ϕ_{ES} (hep)

hep solar-neutrino flux measured via νe elastic scattering. This process is sensitive to all active neutrino flavors, but with reduced sensitivity to ν_μ, ν_τ due to the cross-section difference, $\sigma(\nu_{\mu,\tau}\, e) \sim 0.16\sigma(\nu_e\, e)$. If the hep solar-neutrino flux involves nonelectron flavor active neutrinos, their contribution to the flux is $\sim$ 0.16 times of ν_e.

VALUE (10^3 cm^{-2}s^{-1})	CL%	DOCUMENT ID		TECN
• • • We do not use the following data for averages, fits, limits, etc. • • •				
<73	90	[1] HOSAKA	06	SKAM

[1] HOSAKA 06 result is obtained from the recoil electron energy window of 18–21 MeV, and updates FUKUDA 01 result.

$\phi_{\overline{\nu}_e}$ (^{8}B)

Searches are made for electron antineutrino flux from the Sun. Flux limits listed here are derived relative to the BS05(OP) Standard Solar Model ^{8}B solar neutrino flux (5.69×10^6 cm^{-2} s^{-1}), with an assumption that solar $\overline{\nu}_e$s follow an unoscillated ^{8}B neutrino spectrum.

VALUE (%)	CL%	DOCUMENT ID		TECN	COMMENT
• • • We do not use the following data for averages, fits, limits, etc. • • •					
<0.0072	90	[1] AGOSTINI	21	BORX	$E_{\overline{\nu}_e}$ > 1.8 MeV
<0.013	90	[2] BELLINI	11	BORX	$E_{\overline{\nu}_e}$ > 1.8 MeV
<1.9	90	[3] BALATA	06	CNTR	1.8< $E_{\overline{\nu}_e}$ < 20.0 MeV
<0.72	90	AHARMIM	04	SNO	4.0< $E_{\overline{\nu}_e}$ < 14.8 MeV
<0.022	90	EGUCHI	04	KLND	8.3< $E_{\overline{\nu}_e}$ < 14.8 MeV
<0.7	90	GANDO	03	SKAM	8.0< $E_{\overline{\nu}_e}$ < 20.0 MeV
<1.7	90	AGLIETTA	96	LSD	7< $E_{\overline{\nu}_e}$ < 17 MeV

[1] AGOSTINI 21 derived this result relative to the Standard Solar Model ^{8}B solar neutrino flux, under an assumption of high solar metallicity, of 5.46 $(1 \pm 0.12) \times 10^6$ cm^{-2}s^{-1} (see VINYOLES 17).

[2] Superseded by AGOSTINI 21.

[3] BALATA 06 obtained this result from the search for $\overline{\nu}_e$ interactions with Counting Test Facility (the prototype of the Borexino detector).

(B) Three-neutrino mixing parameters

$\sin^2(\theta_{12})$

If an experiment reports $\sin^2(2\,\theta_{12})$ we convert the value to $\sin^2(\,\theta_{12})$.

VALUE	DOCUMENT ID		TECN	COMMENT
0.307±0.012	[1] ABE	24B	FIT	KamLAND+global solar; 3ν
• • • We do not use the following data for averages, fits, limits, etc. • • •				
$0.62\ ^{+0.16}_{-0.40}$	[2] ABREU	25A	FIT	SNO+
0.308±0.013	[3] ABREU	25A	FIT	SNO+, KamLAND, global solar
0.306±0.013	[4] ABE	24B	FIT	global solar; 3ν
$0.324^{+0.027}_{-0.023}$	[5] ABE	24B	FIT	SK-I+II+III+IV; 3ν
0.318±0.016	[6] SALAS	21	FIT	global fit
0.304±0.012	[7] ESTEBAN	20A	FIT	Global fit
$0.320^{+0.020}_{-0.016}$	DE-SALAS	18	FIT	Global fit
$0.307^{+0.013}_{-0.012}$	[8] ABE	16C	FIT	KamLAND+global solar; 3ν
0.310±0.014	[9] ABE	16C	FIT	SKAM+SNO; 3ν
$0.334^{+0.027}_{-0.023}$	[10] ABE	16C	FIT	SK-I+II+III+IV; 3ν
$0.327^{+0.026}_{-0.031}$	[11] ABE	16C	FIT	SK-IV; 3ν
0.323±0.016	[12] FORERO	14	FIT	3ν
$0.304^{+0.013}_{-0.012}$	[13] GONZALEZ...	14	FIT	Either mass ordering; global fit
$0.299^{+0.014}_{-0.014}$	[14,15] AHARMIM	13	FIT	global solar: 2ν
$0.307^{+0.016}_{-0.013}$	[15,16] AHARMIM	13	FIT	global solar: 3ν
$0.304^{+0.022}_{-0.018}$	[15,17] AHARMIM	13	FIT	KamLAND + global solar: 3ν

$0.304^{+0.014}_{-0.013}$	[18] GANDO	13	FIT	KamLAND + global solar + SBL + accelerator: 3ν
$0.304^{+0.014}_{-0.013}$	[19] GANDO	13	FIT	KamLAND + global solar: 3ν
$0.325^{+0.039}_{-0.039}$	[20] GANDO	13	FIT	KamLAND: 3ν
$0.30^{+0.02}_{-0.01}$	[21] ABE	11	FIT	KamLAND + global solar: 2ν
$0.30^{+0.02}_{-0.01}$	[22] ABE	11	FIT	global solar: 2ν
$0.31^{+0.03}_{-0.02}$	[23] ABE	11	FIT	KamLAND + global solar: 3ν
$0.31^{+0.03}_{-0.03}$	[24] ABE	11	FIT	global solar: 3ν
$0.314^{+0.015}_{-0.012}$	[25] BELLINI	11A	FIT	KamLAND + global solar: 2ν
$0.319^{+0.017}_{-0.015}$	[26] BELLINI	11A	FIT	global solar: 2ν
$0.311^{+0.016}_{-0.016}$	[27] GANDO	11	FIT	KamLAND + solar: 3ν
$0.304^{+0.046}_{-0.042}$	[28] GANDO	11	FIT	KamLAND: 3ν
$0.314^{+0.018}_{-0.014}$	[29,30] AHARMIM	10	FIT	KamLAND + global solar: 2ν
$0.314^{+0.017}_{-0.020}$	[29,31] AHARMIM	10	FIT	global solar: 2ν
$0.319^{+0.019}_{-0.016}$	[29,32] AHARMIM	10	FIT	KamLAND + global solar: 3ν
$0.319^{+0.023}_{-0.024}$	[29,33] AHARMIM	10	FIT	global solar: 3ν
$0.36^{+0.05}_{-0.04}$	[34] ABE	08A	FIT	KamLAND
0.32 ± 0.03	[35] ABE	08A	FIT	KamLAND + global fit
0.32 ± 0.02	[36] AHARMIM	08	FIT	KamLAND + global solar
$0.31^{+0.04}_{-0.04}$	[37] HOSAKA	06	FIT	KamLAND + global solar
$0.31^{+0.04}_{-0.03}$	[38] HOSAKA	06	FIT	SKAM+SNO+KamLAND
$0.31^{+0.03}_{-0.04}$	[39] HOSAKA	06	FIT	SKAM+SNO
$0.31^{+0.02}_{-0.03}$	[40] AHARMIM	05A	FIT	KamLAND + global solar
0.25–0.39	[41] AHARMIM	05A	FIT	global solar
0.29 ± 0.03	[42] ARAKI	05	FIT	KamLAND + global solar
$0.29^{+0.03}_{-0.02}$	[43] AHMED	04A	FIT	KamLAND + global solar
0.23–0.37	[44] AHMED	04A	FIT	global solar
$0.31^{+0.04}_{-0.04}$	[45] SMY	04	FIT	KamLAND + global solar
$0.29^{+0.04}_{-0.04}$	[46] SMY	04	FIT	global solar
$0.32^{+0.06}_{-0.05}$	[47] SMY	04	FIT	SKAM + SNO
0.19–0.33	[48] AHMAD	02B	FIT	global solar
0.19–0.39	[49] FUKUDA	02	FIT	global solar

[1] ABE 24B obtained this result by a three-neutrino oscillation analysis, with a constraint of $\sin^2(\theta_{13}) = 0.0218 \pm 0.0007$ coming from reactor neutrino experiments, using all solar and KamLAND data. The result includes the full Super-Kamiokande I to IV data. *CPT* invariance is assumed. Supersedes ABE 16C.

[2] ABREU 25A report reactor anti-neutrino disappearance, observed using 286 ton-yr of data collected by the SNO+ experiment. The result is based on an extended log likelihood fit to unbinned data performed on the prompt energy distribution.

[3] ABREU 25A combine results from a spectral fit to 286 ton-yr of SNO+ with KamLAND and all solar data, as reported in ABE 16C, to obtain an improved measurement of the mixing angle. *CPT* invariance is assumed.

[4] ABE 24B obtained this result by a three-neutrino oscillation analysis, with a constraint of $\sin^2(\theta_{13}) = 0.0218 \pm 0.0007$ coming from reactor neutrino experiments, using all solar data. *CPT* invariance is assumed. Supersedes ABE 16C.

[5] ABE 24B obtained this result by a three-neutrino oscillation analysis, with a constraint of $\sin^2(\theta_{13}) = 0.0218 \pm 0.0007$ coming from reactor neutrino experiments and a constraint on ^{8}B(hep) flux based on the SNO neutral current event rate, using full Super-Kamiokande (I+II+III+IV) data. *CPT* invariance is assumed. Supersedes ABE 16C.

[6] SALAS 21 reports results of a global fit to neutrino oscillation data available at the time of the Neutrino 2020 conference.

[7] ESTEBAN 20A reports results of a global fit to neutrino oscillation data available at the time of the Neutrino2020 conference.

[8] ABE 16C obtained this result by a three-neutrino oscillation analysis, with a constraint of $\sin^2(\theta_{13}) = 0.0219 \pm 0.0014$ coming from reactor neutrino experiments, using all solar data and KamLAND data. *CPT* invariance is assumed. Superseded by ABE 24B.

[9] ABE 16C obtained this result by a three-neutrino oscillation analysis, with a constraint of $\sin^2(\theta_{13}) = 0.0219 \pm 0.0014$ coming from reactor neutrino experiments, using Super-Kamiokande (I+II+III+IV) and SNO data. Superseded by ABE 24B.

[10] ABE 16C obtained this result by a three-neutrino oscillation analysis, with a constraint of $\sin^2(\theta_{13}) = 0.0219 \pm 0.0014$ coming from reactor neutrino experiments, by combining the four phases of the Super-Kamiokande solar data. Superseded by ABE 24B.

[11] ABE 16C obtained this result by a three-neutrino oscillation analysis, with a constraint of $\sin^2(\theta_{13}) = 0.0219 \pm 0.0014$ coming from reactor neutrino experiments, using the Super-Kamiokande-IV data. Superseded by ABE 24B.

[12] FORERO 14 performs a global fit to neutrino oscillations using solar, reactor, long-baseline accelerator, and atmospheric neutrino data.

[13] GONZALEZ-GARCIA 14 result comes from a frequentist global fit. The corresponding Bayesian global fit to the same data results are reported in BERGSTROM 15 as $0.304^{+0.013}_{-0.012}$ for normal and $0.305^{+0.012}_{-0.013}$ for inverted mass ordering.

[14] AHARMIM 13 obtained this result by a two-neutrino oscillation analysis using global solar neutrino data.

[15] AHARMIM 13 global solar neutrino data include SNO's all-phases-combined analysis results on the total active ^{8}B neutrino flux and energy-dependent ν_e survival probability parameters, measurements of Cl (CLEVELAND 98), Ga (ABDURASHITOV 09 which contains combined analysis with GNO (ALTMANN 05 and Ph.D. thesis of F. Kaether)), and ^{7}Be (BELLINI 11A) rates, and ^{8}B solar-neutrino recoil electron measurements of SK-I (HOSAKA 06) zenith, SK-II (CRAVENS 08) and SK-III (ABE 11) day/night spectra, and Borexino (BELLINI 10A) spectra.

[16] AHARMIM 13 obtained this result by a three-neutrino oscillation analysis with the value of Δm^2_{32} fixed to 2.45×10^{-3} eV^2, using global solar neutrino data.

[17] AHARMIM 13 obtained this result by a three-neutrino oscillation analysis with the value of Δm^2_{32} fixed to 2.45×10^{-3} eV^2, using global solar neutrino and KamLAND (GANDO 11) data. CPT invariance is assumed.

[18] GANDO 13 obtained this result by a three-neutrino oscillation analysis using KamLAND, global solar neutrino, short-baseline (SBL) reactor, and accelerator data, assuming *CPT* invariance. Supersedes GANDO 11.

[19] GANDO 13 obtained this result by a three-neutrino oscillation analysis using KamLAND and global solar neutrino data, assuming CPT invariance. Supersedes GANDO 11.

[20] GANDO 13 obtained this result by a three-neutrino oscillation analysis using KamLAND data. Supersedes GANDO 11.

[21] ABE 11 obtained this result by a two-neutrino oscillation analysis using solar neutrino data including Super-Kamiokande, SNO, Borexino (ARPESELLA 08A), Homestake, GALLEX/GNO, SAGE, and KamLAND data. CPT invariance is assumed.

[22] ABE 11 obtained this result by a two-neutrino oscillation analysis using solar neutrino data including Super-Kamiokande, SNO, Borexino (ARPESELLA 08A), Homestake, GALLEX/GNO, and SAGE data.

[23] ABE 11 obtained this result by a three-neutrino oscillation analysis with the value of Δm^2_{32} fixed to 2.4×10^{-3} eV^2, using solar neutrino data including Super-Kamiokande, SNO, Borexino (ARPESELLA 08A), Homestake, GALLEX/GNO, SAGE, and KamLAND data. The normal neutrino mass ordering and CPT invariance are assumed.

[24] ABE 11 obtained this result by a three-neutrino oscillation analysis with the value of Δm^2_{32} fixed to 2.4×10^{-3} eV^2, using solar neutrino data including Super-Kamiokande, SNO, Borexino (ARPESELLA 08A), Homestake, and GALLEX/GNO data. The normal neutrino mass ordering is assumed.

[25] BELLINI 11A obtained this result by a two-neutrino oscillation analysis using KamLAND, Homestake, SAGE, Gallex, GNO, Kamiokande, Super-Kamiokande, SNO, and Borexino (BELLINI 11A) data and the SSM flux prediction in SERENELLI 11 (Astrophysical Journal **743** 24 (2011)) with the exception that the ^{8}B flux was left free. CPT invariance is assumed.

[26] BELLINI 11A obtained this result by a two-neutrino oscillation analysis using Homestake, SAGE, Gallex, GNO, Kamiokande, Super-Kamiokande, SNO, and Borexino (BELLINI 11A) data and the SSM flux prediction in SERENELLI 11 (Astrophysical Journal **743** 24 (2011)) with the exception that the ^{8}B flux was left free.

[27] GANDO 11 obtain this result with three-neutrino fit using the KamLAND + solar data. Superseded by GANDO 13.

[28] GANDO 11 obtain this result with three-neutrino fit using the KamLAND data only. Superseded by GANDO 13.

[29] AHARMIM 10 global solar neutrino data include SNO's low-energy-threshold analysis survival probability day/night curves, SNO Phase III integral rates (AHARMIM 08), Cl (CLEVELAND 98), SAGE (ABDURASHITOV 09), Gallex/GNO (HAMPEL 99, ALTMANN 05), Borexino (ARPESELLA 08A), SK-I zenith (HOSAKA 06), and SK-II day/night spectra (CRAVENS 08).

[30] AHARMIM 10 obtained this result by a two-neutrino oscillation analysis using global solar neutrino data and KamLAND data (ABE 08A). *CPT* invariance is assumed.

[31] AHARMIM 10 obtained this result by a two-neutrino oscillation analysis using global solar neutrino data.

[32] AHARMIM 10 obtained this result by a three-neutrino oscillation analysis with the value of Δm^2_{31} fixed to 2.3×10^{-3} eV^2, using global solar neutrino data and KamLAND data (ABE 08A). *CPT* invariance is assumed.

[33] AHARMIM 10 obtained this result by a three-neutrino oscillation analysis with the value of Δm^2_{31} fixed to 2.3×10^{-3} eV^2, using global solar neutrino data.

[34] ABE 08A obtained this result by a rate + shape + time combined geoneutrino and reactor two-neutrino fit for Δm^2_{21} and $\tan^2\theta_{12}$, using KamLAND data only. Superseded by GANDO 11.

[35] ABE 08A obtained this result by means of a two-neutrino fit using KamLAND, Homestake, SAGE, GALLEX, GNO, SK (zenith angle and E-spectrum), the SNO χ^2-map, and solar flux data. *CPT* invariance is assumed. Superseded by GANDO 11.

[36] The result given by AHARMIM 08 is $\theta = (34.4^{+1.3}_{-1.2})^\circ$. This result is obtained by a two-neutrino oscillation analysis using solar neutrino data including those of Borexino (ARPESELLA 08A) and Super-Kamiokande-I (HOSAKA 06), and KamLAND data (ABE 08A). *CPT* invariance is assumed.

[37] HOSAKA 06 obtained this result by a two-neutrino oscillation analysis using SK ν_e data, CC data from other solar neutrino experiments, and KamLAND data (ARAKI 05). *CPT* invariance is assumed.

[38] HOSAKA 06 obtained this result by a two-neutrino oscillation analysis using the data from Super-Kamiokande, SNO (AHMAD 02 and AHMAD 02B), and KamLAND (ARAKI 05) experiments. *CPT* invariance is assumed.

[39] HOSAKA 06 obtained this result by a two-neutrino oscillation analysis using the Super-Kamiokande and SNO (AHMAD 02 and AHMAD 02B) solar neutrino data.

[40] The result given by AHARMIM 05A is $\theta = (33.9 \pm 1.6)^\circ$. This result is obtained by a two-neutrino oscillation analysis using SNO pure deuteron and salt phase data, SK ν_e data, Cl and Ga CC data, and KamLAND data (ARAKI 05). *CPT* invariance is assumed. AHARMIM 05A also quotes $\theta = (33.9^{+2.4}_{-2.2})^\circ$ as the error enveloping the 68% CL two-dimensional region. This translates into $\sin^2 2\,\theta = 0.86^{+0.05}_{-0.06}$.

Int. J. Mod
by UNIVERSITY OF CALIFORNIA @ BERK
wnloaded from www.worldscientific.com
-use and distribution is strictly not permitted, except for Open Access articles.

Int. J. Mod. Phys. A 2026.41. Downloaded from www.worldscientific.com
by UNIVERSITY OF CALIFORNIA @ BERKELEY on 09/16/26. Re-use and distribution is strictly not permitted, except for Open Access articles.

[41] AHARMIM 05A obtained this result by a two-neutrino oscillation analysis using the data from all solar neutrino experiments. The listed range of the parameter envelops the 95% CL two-dimensional region shown in figure 35a of AHARMIM 05A. AHARMIM 05A also quotes $\tan^2\theta = 0.45^{+0.09}_{-0.08}$ as the error enveloping the 68% CL two-dimensional region. This translates into $\sin^2 2\,\theta = 0.86^{+0.05}_{-0.07}$.

[42] ARAKI 05 obtained this result by a two-neutrino oscillation analysis using KamLAND and solar neutrino data. *CPT* invariance is assumed. The 1σ error shown here is translated from the number provided by the KamLAND collaboration, $\tan^2\theta = 0.40^{+0.07}_{-0.05}$. The corresponding number quoted in ARAKI 05 is $\tan^2\theta = 0.40^{+0.10}_{-0.07}$ ($\sin^2 2\,\theta = 0.82 \pm 0.07$), which envelops the 68% CL two-dimensional region.

[43] The result given by AHMED 04A is $\theta = (32.5^{+1.7}_{-1.6})^\circ$. This result is obtained by a two-neutrino oscillation analysis using solar neutrino and KamLAND data (EGUCHI 03). *CPT* invariance is assumed. AHMED 04A also quotes $\theta = (32.5^{+2.4}_{-2.3})^\circ$ as the error enveloping the 68% CL two-dimensional region. This translates into $\sin^2 2\,\theta = 0.82 \pm 0.06$.

[44] AHMED 04A obtained this result by a two-neutrino oscillation analysis using the data from all solar neutrino experiments. The listed range of the parameter envelops the 95% CL two-dimensional region shown in Fig. 5(a) of AHMED 04A. The best-fit point is $\Delta(m^2) = 6.5 \times 10^{-5}$ eV^2, $\tan^2\theta = 0.40$ ($\sin^2 2\,\theta = 0.82$).

[45] The result given by SMY 04 is $\tan^2\theta = 0.44 \pm 0.08$. This result is obtained by a two-neutrino oscillation analysis using solar neutrino and KamLAND data (IANNI 03). *CPT* invariance is assumed.

[46] SMY 04 obtained this result by a two-neutrino oscillation analysis using the data from all solar neutrino experiments. The 1σ errors are read from Fig. 6(a) of SMY 04.

[47] SMY 04 obtained this result by a two-neutrino oscillation analysis using the Super-Kamiokande and SNO (AHMAD 02 and AHMAD 02B) solar neutrino data. The 1σ errors are read from Fig. 6(a) of SMY 04.

[48] AHMAD 02B obtained this result by a two-neutrino oscillation analysis using the data from all solar neutrino experiments. The listed range of the parameter envelops the 95% CL two-dimensional region shown in Fig. 4(b) of AHMAD 02B. The best fit point is $\Delta(m^2) = 5.0 \times 10^{-5}$ eV^2 and $\tan\theta = 0.34$ ($\sin^2 2\,\theta = 0.76$).

[49] FUKUDA 02 obtained this result by a two-neutrino oscillation analysis using the data from all solar neutrino experiments. The listed range of the parameter envelops the 95% CL two-dimensional region shown in Fig. 4 of FUKUDA 02. The best fit point is $\Delta(m^2) = 6.9 \times 10^{-5}$ eV^2 and $\tan^2\theta = 0.38$ ($\sin^2 2\,\theta = 0.80$).

Δm^2_{21}

VALUE (10^{-5} eV^2)	DOCUMENT ID		TECN	COMMENT
7.60±0.17 OUR AVERAGE				
$7.96^{+0.48}_{-0.42}$	[1] ABREU	25A	FIT	SNO+
$8.85^{+1.10}_{-1.33}$	[2] ALLEGA	25	FIT	SNO+
$7.50^{+0.19}_{-0.18}$	[3] ABE	24B	FIT	KamLAND + global solar; 3ν
• • • We do not use the following data for averages, fits, limits, etc. • • •				
$7.58^{+0.18}_{-0.17}$	[4] ABREU	25A	FIT	SNO+, KamLAND, global solar
$6.10^{+1.26}_{-0.86}$	[5] ABE	24B	FIT	SK-I+II+III+IV; 3ν
$6.10^{+1.04}_{-0.75}$	[6] ABE	24B	FIT	SKAM+SNO; 3ν
$6.9\ ^{+1.6}_{-1.2}$	[7] ABE	24B	FIT	SK-IV; 3ν
$7.50^{+0.22}_{-0.20}$	[8] SALAS	21	FIT	global fit
$7.42^{+0.21}_{-0.20}$	[9] ESTEBAN	20A	FIT	Global fit
$7.55^{+0.20}_{-0.16}$	DE-SALAS	18	FIT	Global fit
$7.49^{+0.19}_{-0.18}$	[10] ABE	16C	FIT	KamLAND+global solar; 3ν
$4.8\ ^{+1.3}_{-0.6}$	[11] ABE	16C	FIT	SKAM+SNO; 3ν
$4.8\ ^{+1.5}_{-0.8}$	[12] ABE	16C	FIT	SK-I+II+III+IV; 3ν
$3.2\ ^{+2.8}_{-0.2}$	[13] ABE	16C	FIT	SK-IV; 3ν
$7.6\ ^{+0.19}_{-0.18}$	[14] FORERO	14	FIT	3ν
$7.50^{+0.19}_{-0.17}$	[15] GONZALEZ...	14	FIT	Either mass ordering; global fit
$5.13^{+1.29}_{-0.96}$	[16,17] AHARMIM	13	FIT	global solar: 2ν
$5.13^{+1.49}_{-0.98}$	[17,18] AHARMIM	13	FIT	global solar: 3ν
$7.46^{+0.20}_{-0.19}$	[17,19] AHARMIM	13	FIT	KamLAND + global solar: 3ν
7.53 ± 0.18	[20] GANDO	13	FIT	KamLAND + global solar + SBL + accelerator: 3ν
$7.53^{+0.19}_{-0.18}$	[21] GANDO	13	FIT	KamLAND + global solar: 3ν
$7.54^{+0.19}_{-0.18}$	[22] GANDO	13	FIT	KamLAND: 3ν
$7.6\ \pm0.2$	[23] ABE	11	FIT	KamLAND + global solar: 2ν
$6.2\ ^{+1.1}_{-1.9}$	[24] ABE	11	FIT	global solar: 2ν
$7.7\ \pm0.3$	[25] ABE	11	FIT	KamLAND + global solar: 3ν
$6.0\ ^{+2.2}_{-2.5}$	[26] ABE	11	FIT	global solar: 3ν
$7.50^{+0.16}_{-0.24}$	[27] BELLINI	11A	FIT	KamLAND + global solar: 2ν
$5.2\ ^{+1.5}_{-0.9}$	[28] BELLINI	11A	FIT	global solar: 2ν
$7.50^{+0.19}_{-0.20}$	[29] GANDO	11	FIT	KamLAND + solar: 3ν
7.49 ± 0.20	[30] GANDO	11	FIT	KamLAND: 3ν
$7.59^{+0.20}_{-0.21}$	[31,32] AHARMIM	10	FIT	KamLAND + global solar: 2ν
$5.89^{+2.13}_{-2.16}$	[31,33] AHARMIM	10	FIT	global solar: 2ν
7.59 ± 0.21	[31,34] AHARMIM	10	FIT	KamLAND + global solar: 3ν
$6.31^{+2.49}_{-2.58}$	[31,35] AHARMIM	10	FIT	global solar: 3ν
$7.58^{+0.14}_{-0.13}\pm0.15$	[36] ABE	08A	FIT	KamLAND
7.59 ± 0.21	[37] ABE	08A	FIT	KamLAND + global solar
$7.59^{+0.19}_{-0.21}$	[38] AHARMIM	08	FIT	KamLAND + global solar
$8.0\ \pm0.3$	[39] HOSAKA	06	FIT	KamLAND + global solar
$8.0\ \pm0.3$	[40] HOSAKA	06	FIT	SKAM+SNO+KamLAND
$6.3\ ^{+3.7}_{-1.5}$	[41] HOSAKA	06	FIT	SKAM+SNO
5–12	[42] HOSAKA	06	FIT	SKAM day/night in the LMA region
$8.0\ ^{+0.4}_{-0.3}$	[43] AHARMIM	05A	FIT	KamLAND + global solar LMA
3.3–14.4	[44] AHARMIM	05A	FIT	global solar
$7.9\ ^{+0.4}_{-0.3}$	[45] ARAKI	05	FIT	KamLAND + global solar
$7.1\ ^{+1.0}_{-0.3}$	[46] AHMED	04A	FIT	KamLAND + global solar
3.2–13.7	[47] AHMED	04A	FIT	global solar
$7.1\ ^{+0.6}_{-0.5}$	[48] SMY	04	FIT	KamLAND + global solar
$6.0\ ^{+1.7}_{-1.6}$	[49] SMY	04	FIT	global solar
$6.0\ ^{+2.5}_{-1.6}$	[50] SMY	04	FIT	SKAM + SNO
2.8–12.0	[51] AHMAD	02B	FIT	global solar
3.2–19.1	[52] FUKUDA	02	FIT	global solar

[1] ABREU 25A report the observation of reactor anti-neutrino disappearance, using 286 ton·yr of data collected by the SNO+ experiment. The result is based on an extended log likelihood fit to unbinned data performed on the prompt energy distribution.

[2] ALLEGA 25 use the reactor anti-neutrino signal collected during 125.4 days of data taking with the partially liquid scintillator filled SNO+ detector to determine Δm^2_{21} by means of a spectral fit. Because of the low signal strength of 9.53 ± 0.30 inverse beta decay events, $\sin^2(\theta_{12})$ was fixed to the value given in PDG 20.

[3] ABE 24B obtained this result by a three-neutrino oscillation analysis, with a constraint of $\sin^2(\theta_{13}) = 0.0218 \pm 0.0007$ coming from reactor neutrino experiments, using all solar and KamLAND data. The result includes the full Super-Kamiokande I to IV data. *CPT* invariance is assumed. Supersedes ABE 16C.

[4] ABREU 25A combine results from a spectral fit to 286 ton·yr of SNO+ with KamLAND and all solar data, as reported in ABE 16C, to obtain an improved measurement of the mass difference. *CPT* invariance is assumed.

[5] ABE 24B obtained this result by a three-neutrino oscillation analysis, with a constraint of $\sin^2(\theta_{13}) = 0.0218 \pm 0.0007$ coming from reactor neutrino experiments and a constraint on ^{8}B(hep) flux based on the SNO neutral current event rate, using the full Super-Kamiokande I to IV data. Supersedes ABE 16C.

[6] ABE 24B obtained this result by a three-neutrino oscillation analysis, with a constraint of $\sin^2(\theta_{13}) = 0.0218 \pm 0.0007$ coming from reactor neutrino experiments, using SNO and full Super-Kamiokande I to IV data. Supersedes ABE 16C.

[7] ABE 24B obtained this result by a three-neutrino oscillation analysis, with a constraint of $\sin^2(\theta_{13}) = 0.0218 \pm 0.0007$ coming from reactor neutrino experiments and a constraint on ^{8}B(hep) flux based on the SNO neutral current event rate, using the full Super-Kamiokande IV data. Supersedes ABE 16C.

[8] SALAS 21 reports results of a global fit to neutrino oscillation data available at the time of the Neutrino 2020 conference.

[9] ESTEBAN 20A reports results of a global fit to neutrino oscillation data available at the time of the Neutrino2020 conference.

[10] ABE 16C obtained this result by a three-neutrino oscillation analysis, with a constraint of $\sin^2(\theta_{13}) = 0.0219 \pm 0.0014$ coming from reactor neutrino experiments, using all solar data and KamLAND data. *CPT* invariance is assumed.

[11] ABE 16C obtained this result by a three-neutrino oscillation analysis, with a constraint of $\sin^2(\theta_{13}) = 0.0219 \pm 0.0014$ coming from reactor neutrino experiments, using Super-Kamiokande (I+II+III+IV) and SNO data. Superseded by ABE 24B.

[12] ABE 16C obtained this result by a three-neutrino oscillation analysis, with a constraint of $\sin^2(\theta_{13}) = 0.0219 \pm 0.0014$ coming from reactor neutrino experiments, by combining the four phases of the Super-Kamiokande solar data. Superseded by ABE 24B.

[13] ABE 16C obtained this result by a three-neutrino oscillation analysis, with a constraint of $\sin^2(\theta_{13}) = 0.0219 \pm 0.0014$ coming from reactor neutrino experiments, using the Super-Kamiokande-IV data.

[14] FORERO 14 performs a global fit to Δm^2_{21} using solar, reactor, long-baseline accelerator, and atmospheric neutrino data.

[15] GONZALEZ-GARCIA 14 result comes from a frequentist global fit. The corresponding Bayesian global fit to the same data results are reported in BERGSTROM 15 as $(7.50^{+0.19}_{-0.17}) \times 10^{-5}$ eV^2 for normal and $(7.50^{+0.18}_{-0.17}) \times 10^{-5}$ eV^2 for inverted mass ordering.

[16] AHARMIM 13 obtained this result by a two-neutrino oscillation analysis using global solar neutrino data.

[17] AHARMIM 13 global solar neutrino data include SNO's all-phases-combined analysis results on the total active ^{8}B neutrino flux and energy-dependent ν_e survival probability

Int. J. Mod
by UNIVERSITY OF CALIFORNIA @ BERK
wnloaded from www.worldscientific.com
-use and distribution is strictly not permitted, except for Open Access articles.

parameters, measurements of Cl (CLEVELAND 98), Ga (ABDURASHITOV 09 which contains combined analysis with GNO (ALTMANN 05 and Ph.D. thesis of F. Kaether)), and ^{7}Be (BELLINI 11A) rates, and ^{8}B solar-neutrino recoil electron measurements of SK-I (HOSAKA 06) zenith, SK-II (CRAVENS 08), and SK-III (ABE 11) day/night spectra, and Borexino (BELLINI 10A) spectra.

[18] AHARMIM 13 obtained this result by a three-neutrino oscillation analysis with the value of Δm^2_{31} fixed to 2.45×10^{-3} eV^2, using global solar neutrino data.

[19] AHARMIM 13 obtained this result by a three-neutrino oscillation analysis with the value of Δm^2_{31} fixed to 2.45×10^{-3} eV^2, using global solar neutrino and KamLAND data (GANDO 11). CPT invariance is assumed.

[20] GANDO 13 obtained this result by a three-neutrino oscillation analysis using KamLAND, global solar neutrino, short-baseline (SBL) reactor, and accelerator data, assuming CPT invariance. Supersedes GANDO 11.

[21] GANDO 13 obtained this result by a three-neutrino oscillation analysis using KamLAND and global solar neutrino data, assuming CPT invariance. Supersedes GANDO 11.

[22] GANDO 13 obtained this result by a three-neutrino oscillation analysis using KamLAND data. Supersedes GANDO 11.

[23] ABE 11 obtained this result by a two-neutrino oscillation analysis using solar neutrino data including Super-Kamiokande, SNO, Borexino (ARPESELLA 08A), Homestake, GALLEX/GNO, SAGE, and KamLAND data. CPT invariance is assumed.

[24] ABE 11 obtained this result by a two-neutrino oscillation analysis using solar neutrino data including Super-Kamiokande, SNO, Borexino (ARPESELLA 08A), Homestake, GALLEX/GNO, and SAGE data.

[25] ABE 11 obtained this result by a three-neutrino oscillation analysis with the value of Δm^2_{32} fixed to 2.4×10^{-3} eV^2, using solar neutrino data including Super-Kamiokande, SNO, Borexino (ARPESELLA 08A), Homestake, GALLEX/GNO, SAGE, and KamLAND data. The normal neutrino mass ordering and CPT invariance are assumed.

[26] ABE 11 obtained this result by a three-neutrino oscillation analysis with the value of Δm^2_{32} fixed to 2.4×10^{-3} eV^2, using solar neutrino data including Super-Kamiokande, SNO, Borexino (ARPESELLA 08A), Homestake, and GALLEX/GNO data. The normal neutrino mass ordering is assumed.

[27] BELLINI 11A obtained this result by a two-neutrino oscillation analysis using KamLAND, Homestake, SAGE, Gallex, GNO, Kamiokande, Super-Kamiokande, SNO, and Borexino (BELLINI 11A) data and the SSM flux prediction in SERENELLI 11 (Astrophysical Journal **743** 24 (2011)) with the exception that the ^{8}B flux was left free. CPT invariance is assumed.

[28] BELLINI 11A obtained this result by a two-neutrino oscillation analysis using Homestake, SAGE, Gallex, GNO, Kamiokande, Super-Kamiokande, SNO, and Borexino (BELLINI 11A) data and the SSM flux prediction in SERENELLI 11 (Astrophysical Journal **743** 24 (2011)) with the exception that the ^{8}B flux was left free.

[29] GANDO 11 obtain this result with three-neutrino fit using the KamLAND + solar data. Superseded by GANDO 13.

[30] GANDO 11 obtain this result with three-neutrino fit using the KamLAND data only. Supersedes ABE 08A.

[31] AHARMIM 10 global solar neutrino data include SNO's low-energy-threshold analysis survival probability day/night curves, SNO Phase III integral rates (AHARMIM 08), Cl (CLEVELAND 98), SAGE (ABDURASHITOV 09), Gallex/GNO (HAMPEL 99, ALTMANN 05), Borexino (ARPESELLA 08A), SK-I zenith (HOSAKA 06), and SK-II day/night spectra (CRAVENS 08).

[32] AHARMIM 10 obtained this result by a two-neutrino oscillation analysis using global solar neutrino data and KamLAND data (ABE 08A). *CPT* invariance is assumed.

[33] AHARMIM 10 obtained this result by a two-neutrino oscillation analysis using global solar neutrino data.

[34] AHARMIM 10 obtained this result by a three-neutrino oscillation analysis with the value of Δm^2_{31} fixed to 2.3×10^{-3} eV^2, using global solar neutrino data and KamLAND data (ABE 08A). *CPT* invariance is assumed.

[35] AHARMIM 10 obtained this result by a three-neutrino oscillation analysis with the value of Δm^2_{31} fixed to 2.3×10^{-3} eV^2, using global solar neutrino data.

[36] ABE 08A obtained this result by a rate + shape + time combined geoneutrino and reactor two-neutrino fit for Δm^2_{21} and $\tan^2\theta_{12}$, using KamLAND data only. Superseded by GANDO 11.

[37] ABE 08A obtained this result by means of a two-neutrino fit using KamLAND, Homestake, SAGE, GALLEX, GNO, SK (zenith angle and E-spectrum), the SNO χ^2-map, and solar flux data. *CPT* invariance is assumed. Superseded by GANDO 11.

[38] AHARMIM 08 obtained this result by a two-neutrino oscillation analysis using all solar neutrino data including those of Borexino (ARPESELLA 08A) and Super-Kamiokande-I (HOSAKA 06), and KamLAND data (ABE 08A). *CPT* invariance is assumed.

[39] HOSAKA 06 obtained this result by a two-neutrino oscillation analysis using solar neutrino and KamLAND data (ARAKI 05). *CPT* invariance is assumed.

[40] HOSAKA 06 obtained this result by a two-neutrino oscillation analysis using the data from Super-Kamiokande, SNO (AHMAD 02 and AHMAD 02B), and KamLAND (ARAKI 05) experiments. *CPT* invariance is assumed.

[41] HOSAKA 06 obtained this result by a two-neutrino oscillation analysis using the Super-Kamiokande and SNO (AHMAD 02 and AHMAD 02B) solar neutrino data.

[42] HOSAKA 06 obtained this result from the consistency between the observed and expected day-night flux asymmetry amplitude. The listed 68% CL range is derived from the 1σ boundary of the amplitude fit to the data. Oscillation parameters are constrained to be in the LMA region. The mixing angle is fixed at $\tan^2\theta = 0.44$ because the fit depends only very weekly on it.

[43] AHARMIM 05A obtained this result by a two-neutrino oscillation analysis using solar neutrino and KamLAND data (ARAKI 05). *CPT* invariance is assumed. AHARMIM 05A also quotes $\Delta(m^2) = (8.0^{+0.6}_{-0.4}) \times 10^{-5}$ eV^2 as the error enveloping the 68% CL two-dimensional region.

[44] AHARMIM 05A obtained this result by a two-neutrino oscillation analysis using the data from all solar neutrino experiments. The listed range of the parameter envelops the 95% CL two-dimensional region shown in figure 35a of AHARMIM 05A. AHARMIM 05A also quotes $\Delta(m^2) = (6.5^{+4.4}_{-2.3}) \times 10^{-5}$ eV^2 as the error enveloping the 68% CL two-dimensional region.

[45] ARAKI 05 obtained this result by a two-neutrino oscillation analysis using KamLAND and solar neutrino data. *CPT* invariance is assumed. The 1σ error shown here is provided by the KamLAND collaboration. The error quoted in ARAKI 05, $\Delta(m^2) = (7.9^{+0.6}_{-0.5}) \times 10^{-5}$, envelops the 68% CL two-dimensional region.

[46] AHMED 04A obtained this result by a two-neutrino oscillation analysis using solar neutrino and KamLAND data (EGUCHI 03). *CPT* invariance is assumed. AHMED 04A also quotes $\Delta(m^2) = (7.1^{+1.2}_{-0.6}) \times 10^{-5}$ eV^2 as the error enveloping the 68% CL two-dimensional region.

[47] AHMED 04A obtained this result by a two-neutrino oscillation analysis using the data from all solar neutrino experiments. The listed range of the parameter envelops the 95% CL two-dimensional region shown in Fig. 5(a) of AHMED 04A. The best-fit point is $\Delta(m^2) = 6.5 \times 10^{-5}$ eV^2, $\tan^2\theta = 0.40$ ($\sin^2 2\,\theta = 0.82$).

[48] SMY 04 obtained this result by a two-neutrino oscillation analysis using solar neutrino and KamLAND data (IANNI 03). *CPT* invariance is assumed.

[49] SMY 04 obtained this result by a two-neutrino oscillation analysis using the data from all solar neutrino experiments. The 1σ errors are read from Fig. 6(a) of SMY 04.

[50] SMY 04 obtained this result by a two-neutrino oscillation analysis using the Super-Kamiokande and SNO (AHMAD 02 and AHMAD 02B) solar neutrino data. The 1σ errors are read from Fig. 6(a) of SMY 04.

[51] AHMAD 02B obtained this result by a two-neutrino oscillation analysis using the data from all solar neutrino experiments. The listed range of the parameter envelops the 95% CL two-dimensional region shown in Fig. 4(b) of AHMAD 02B. The best fit point is $\Delta(m^2) = 5.0 \times 10^{-5}$ eV^2 and $\tan\theta = 0.34$ ($\sin^2 2\,\theta = 0.76$).

[52] FUKUDA 02 obtained this result by a two-neutrino oscillation analysis using the data from all solar neutrino experiments. The listed range of the parameter envelops the 95% CL two-dimensional region shown in Fig. 4 of FUKUDA 02. The best fit point is $\Delta(m^2) = 6.9 \times 10^{-5}$ eV^2 and $\tan^2\theta = 0.38$ ($\sin^2 2\,\theta = 0.80$).

$\sin^2(\theta_{23})$

The reported limits below correspond to the projection onto the $\sin^2(\theta_{23})$ axis of the 90% CL contours in the $\sin^2(\theta_{23}) - \Delta m^2_{32}$ plane presented by the authors. Unless otherwise specified, the limits are 90% CL and the reported uncertainties are 68% CL.

If an experiment reports $\sin^2(2\,\theta_{23})$ we convert the value to $\sin^2(\,\theta_{23})$.

VALUE	DOCUMENT ID		TECN	COMMENT
$0.523^{+0.031}_{-0.027}$ OUR FIT Error includes scale factor of 1.3. Assuming inverted mass ordering				
0.533 ± 0.018 OUR FIT Assuming normal mass ordering				
$0.54\ ^{+0.04}_{-0.03}$	[1] ABBASI	25	ICCB	Normal mass ordering
$0.559^{+0.018}_{-0.078}$	[2] ABE	25B	T2K	Normal mass ordering; , θ_{13} constrained
$0.51\ ^{+0.04}_{-0.05}$	[3] AIELLO	24	KM3N	Both mass orderings
$0.45\ ^{+0.06}_{-0.03}$	[4] WESTER	24	SKAM	Normal mass ordering, θ_{13} constrained
$0.45\ ^{+0.08}_{-0.03}$	[4] WESTER	24	SKAM	Inverted mass ordering, θ_{13} constrained
$0.57\ ^{+0.03}_{-0.04}$	[5] ACERO	22	NOVA	Normal mass ordering; octant II for θ_{23}
$0.56\ ^{+0.04}_{-0.03}$	[5] ACERO	22	NOVA	Inverted mass ordering; octant II for θ_{23}
$0.43\ ^{+0.20}_{-0.04}$	[6] ADAMSON	20A	MINS	Normal mass ordering
$0.42\ ^{+0.07}_{-0.03}$	[6] ADAMSON	20A	MINS	Inverted mass ordering
• • • We do not use the following data for averages, fits, limits, etc. • • •				
$0.468^{+0.106}_{-0.025}$	[7] ABE	25	SKT2	Both mass orderings
$0.561^{+0.021}_{-0.039}$	[8] ABUBAKAR	25	FIT	Normal mass ordering, T2K+NOvA fit
$0.563^{+0.021}_{-0.039}$	[8] ABUBAKAR	25	FIT	Inverted mass ordering, T2K+NOvA fit
$0.56\ ^{+0.03}_{-0.12}$	[9] ACERO	24	NOVA	Normal mass ordering
0.56 ± 0.01	[9] ACERO	24	NOVA	Inverted mass ordering
0.51 ± 0.05	[10] ABBASI	23	ICCB	Normal mass ordering
$0.47\ ^{+0.11}_{-0.02}$	[11] ABE	23D	T2K	ν_μ disappearance
$0.45\ ^{+0.16}_{-0.04}$	[11] ABE	23D	T2K	$\overline{\nu}_\mu$ disappearance
$0.561^{+0.021}_{-0.032}$	[12] ABE	23F	T2K	Normal mass ordering
$0.563^{+0.017}_{-0.032}$	[12] ABE	23F	T2K	Inverted mass ordering
$0.51\ ^{+0.06}_{-0.07}$	[13] ABE	21A	T2K	ν_μ disappearance
$0.43\ ^{+0.21}_{-0.05}$	[13] ABE	21A	T2K	$\overline{\nu}_\mu$ disappearance
0.574 ± 0.014	[14] SALAS	21	FIT	Normal mass ordering, global fit

Int. J. Mod. Phys. A 2026.41. Downloaded from www.worldscientific.com
by UNIVERSITY OF CALIFORNIA @ BERKELEY on 09/16/26. Re-use and distribution is strictly not permitted, except for Open Access articles.

$0.578^{+0.010}_{-0.017}$	[14] SALAS	21	FIT	Inverted mass ordering, global fit
0.455	[15] AARTSEN	20	ICCB	For both mass orderings
$0.53^{+0.03}_{-0.04}$	[16] ABE	20F	T2K	Both mass orderings
$0.573^{+0.016}_{-0.020}$	[17] ESTEBAN	20A	FIT	Normal mass ordering, global fit
$0.575^{+0.016}_{-0.019}$	[17] ESTEBAN	20A	FIT	Inverted mass ordering, global fit
$0.58^{+0.04}_{-0.13}$	[18] AARTSEN	19C	ICCB	
$0.56^{+0.04}_{-0.03}$	[19] ACERO	19	NOVA	Normal mass order; octant II for θ_{23}
$0.48^{+0.04}_{-0.03}$	[19,20] ACERO	19	NOVA	Normal mass order; octant I for θ_{23}
$0.56^{+0.04}_{-0.03}$	[19,20] ACERO	19	NOVA	Inverted mass order; octant II for θ_{23}
$0.47^{+0.04}_{-0.03}$	[19,20] ACERO	19	NOVA	Inverted mass order; octant I for θ_{23}
$0.49^{+0.30}_{-0.28}$	AGAFONOVA	19	OPER	
$0.50^{+0.20}_{-0.19}$	[21] ALBERT	19	ANTR	Atmospheric ν, deep sea telescope
$0.51^{+0.07}_{-0.09}$	[22] AARTSEN	18A	ICCB	Normal mass ordering
$0.587^{+0.036}_{-0.069}$	[23] ABE	18B	SKAM	3ν osc: normal mass ordering, θ_{13} free
$0.551^{+0.044}_{-0.075}$	[23] ABE	18B	SKAM	3ν osc: inverted mass ordering, θ_{13} free
$0.588^{+0.031}_{-0.064}$	[24] ABE	18B	SKAM	Normal mass ordering, θ_{13} constrained
$0.575^{+0.036}_{-0.073}$	[24] ABE	18B	SKAM	Inverted mass ordering, θ_{13} constrained
$0.526^{+0.032}_{-0.036}$	[25] ABE	18G	T2K	Normal mass ordering, θ_{13} constrained
$0.530^{+0.030}_{-0.034}$	[25] ABE	18G	T2K	Inverted mass ordering, θ_{13} constrained
0.56 ± 0.04	[26] ACERO	18	NOVA	Normal mass order; octant II for θ_{23}
0.47 ± 0.04	[26] ACERO	18	NOVA	Normal mass order; octant I for θ_{23}
$0.547^{+0.020}_{-0.030}$	DE-SALAS	18	FIT	Normal mass ordering, global fit
$0.551^{+0.018}_{-0.030}$	DE-SALAS	18	FIT	Inverted mass order, global fit
$0.532^{+0.061}_{-0.087}$	[27] ABE	17A	T2K	Normal mass ordering
$0.534^{+0.061}_{-0.087}$	[27] ABE	17A	T2K	Inverted mass ordering
$0.51^{+0.08}_{-0.07}$	ABE	17C	T2K	Normal mass ordering with neutrinos
$0.42^{+0.25}_{-0.07}$	ABE	17C	T2K	Normal mass ordering with antineutrinos
$0.52^{+0.075}_{-0.09}$	ABE	17C	T2K	normal mass ordering with neutrinos and antineutrinos
$0.55^{+0.05}_{-0.09}$	[27] ABE	17F	T2K	Normal mass ordering
$0.55^{+0.05}_{-0.08}$	[27] ABE	17F	T2K	Inverted mass ordering
$0.404^{+0.022}_{-0.030}$	[28] ADAMSON	17A	NOVA	Normal mass ordering; octant I for θ_{23}
$0.624^{+0.022}_{-0.030}$	[28] ADAMSON	17A	NOVA	Normal mass ordering; octant II for θ_{23}
$0.398^{+0.030}_{-0.022}$	[28] ADAMSON	17A	NOVA	Inverted mass ordering; octant I for θ_{23}
$0.618^{+0.022}_{-0.030}$	[28] ADAMSON	17A	NOVA	Inverted mass ordering; octant II for θ_{23}
$0.45^{+0.19}_{-0.07}$	[29] ABE	16D	T2K	3ν osc; normal mass ordering; $\overline{\nu}$ beam
0.38 to 0.65	[30] ADAMSON	16A	NOVA	normal mass ordering
0.37 to 0.64	[30] ADAMSON	16A	NOVA	Inverted mass ordering
$0.53^{+0.09}_{-0.12}$	[31] AARTSEN	15A	ICCB	Normal mass ordering
$0.51^{+0.09}_{-0.11}$	[31] AARTSEN	15A	ICCB	Inverted mass ordering
$0.514^{+0.055}_{-0.056}$	[32] ABE	14	T2K	3ν osc.; normal mass ordering
0.511 ± 0.055	[32] ABE	14	T2K	3ν osc.; inverted mass ordering
$0.41^{+0.23}_{-0.06}$	[33] ADAMSON	14	MINS	Normal mass ordering
$0.41^{+0.26}_{-0.07}$	[33] ADAMSON	14	MINS	Inverted mass ordering
$0.567^{+0.032}_{-0.128}$	[34] FORERO	14	FIT	Normal mass ordering
$0.573^{+0.025}_{-0.043}$	[34] FORERO	14	FIT	Inverted mass ordering
$0.452^{+0.052}_{-0.028}$	[35] GONZALEZ...	14	FIT	Normal mass ordering; global fit
$0.579^{+0.025}_{-0.037}$	[35] GONZALEZ...	14	FIT	Inverted mass ordering; global fit
0.24 to 0.76	[36] AARTSEN	13B	ICCB	DeepCore, 2ν oscillation
0.514 ± 0.082	[37] ABE	13G	T2K	3ν osc.; normal mass ordering
$0.388^{+0.051}_{-0.053}$	[38] ADAMSON	13B	MINS	Beam + Atmospheric; identical ν & $\overline{\nu}$
0.3 to 0.7	[39] ABE	12A	T2K	Off-axis beam
0.28 to 0.72	[40] ADAMSON	12	MINS	$\overline{\nu}$ beam
0.25 to 0.75	[41,42] ADAMSON	12B	MINS	MINOS atmospheric
0.27 to 0.73	[41,43] ADAMSON	12B	MINS	MINOS pure atmospheric ν
0.21 to 0.79	[41,43] ADAMSON	12B	MINS	MINOS pure atmospheric $\overline{\nu}$
0.15 to 0.85	[44] ADRIAN-MAR..	12	ANTR	Atmospheric ν with deep see telescope
0.39 to 0.61	[45] ABE	11C	SKAM	Super-Kamiokande
0.34 to 0.66	ADAMSON	11	MINS	2ν osc.; maximal mixing
$0.31^{+0.10}_{-0.07}$	[46] ADAMSON	11B	MINS	$\overline{\nu}$ beam
0.41 to 0.59	[47] WENDELL	10	SKAM	3ν osc. with solar terms; θ_{13}=0
0.39 to 0.61	[48] WENDELL	10	SKAM	3ν osc.; normal mass ordering
0.37 to 0.63	[49] WENDELL	10	SKAM	3ν osc.; inverted mass ordering
0.31 to 0.69	ADAMSON	08A	MINS	MINOS
0.05 to 0.95	[50] ADAMSON	06	MINS	Atmospheric ν with far detector
0.18 to 0.82	[51] AHN	06A	K2K	KEK to Super-K
0.23 to 0.77	[52] MICHAEL	06	MINS	MINOS
0.18 to 0.82	[53] ALIU	05	K2K	KEK to Super-K
0.18 to 0.82	[54] ALLISON	05	SOU2	
0.36 to 0.64	[55] ASHIE	05	SKAM	Super-Kamiokande
0.28 to 0.72	[56] AMBROSIO	04	MCRO	MACRO
0.34 to 0.66	[57] ASHIE	04	SKAM	L/E distribution
0.08 to 0.92	[58] AHN	03	K2K	KEK to Super-K
0.13 to 0.87	[59] AMBROSIO	03	MCRO	MACRO
0.26 to 0.74	[60] AMBROSIO	03	MCRO	MACRO
0.15 to 0.85	[61] SANCHEZ	03	SOU2	Soudan-2 Atmospheric
0.28 to 0.72	[62] AMBROSIO	01	MCRO	Upward μ
0.29 to 0.71	[63] AMBROSIO	01	MCRO	Upward μ
0.13 to 0.87	[64] FUKUDA	99C	SKAM	Upward μ
0.23 to 0.77	[65] FUKUDA	99D	SKAM	Upward μ
0.08 to 0.92	[66] FUKUDA	99D	SKAM	Stop μ / through
0.29 to 0.71	[67] FUKUDA	98C	SKAM	Super-Kamiokande
0.08 to 0.92	[68] HATAKEYAMA	98	KAMI	Kamiokande
0.24 to 0.76	[69] HATAKEYAMA	98	KAMI	Kamiokande
0.20 to 0.80	[70] FUKUDA	94	KAMI	Kamiokande

[1] ABBASI 25 uses atmospheric neutrino data measured between 2012 and 2021 with the low-energy subdetector DeepCore of the IceCube neutrino telescope. Supersedes ABBASI 23.

[2] ABE 25B results are based on data collected between 2010 and 2020 in (anti)neutrino mode and include a neutrino beam exposure of 1.97×10^{21} (1.63×10^{21}) protons on target. Supersedes ABE 23F.

[3] AIELLO 24 uses atmospheric neutrino data measured between January 2020 and November 2021 with the first six detection units of ORCA, corresponding to 433 kton·yrs.

[4] WESTER 24 uses 484.2 kton·years of Super-Kamiokande I-IV atmospheric neutrino data to obtain this result. The fit is performed over the three parameters, Δm^2_{32}, $\sin^2(\theta_{23})$, and δ, while the solar parameters and $\sin^2(\theta_{13})$ are fixed to $\Delta m^2_{21} = (7.53 \pm 0.18) \times 10^{-5}$ eV^2, $\sin^2(\theta_{12}) = 0.307 \pm 0.013$, and $\sin^2(\theta_{13}) = 0.0220 \pm 0.0007$. Supersedes ABE 18B.

[5] ACERO 22 uses data from Jun 29, 2016 to Feb 26, 2019 (12.5×10^{20} POT) and Feb 6, 2014 to Mar 20, 2020 (13.6×10^{20} POT). Best fit for octant I (lower octant) is 0.46 for both normal and inverted mass orderings. The uncertainties are reported relative to the global minima in normal mass ordering. Supersedes ACERO 19.

[6] ADAMSON 20A uses the complete dataset from MINOS and MINOS+ experiments. The data were collected using a total exposure of 23.76×10^{20} protons on target and 60.75 kton·yr exposure to atmospheric neutrinos. Supersedes ADAMSON 14.

[7] ABE 25 reports the results of a joint analysis of Super-Kamiokande atmospheric neutrino data and T2K beam neutrino data, using 3244.4 days of atmospheric data and a (anti)neutrino beam exposure of 1.97×10^{21} (1.63×10^{21}) protons on target.

[8] ABUBAKAR 25 results are based on the joint analysis of data sets from NOvA and T2K experiments. The reactor constraint on θ_{13} is applied in the fits.

[9] ACERO 24 reanalyzed the dataset first examined in ACERO 22 using an alternative statistical approach based on Bayesian Markov chain Monte Carlo.

[10] ABBASI 23 uses atmospheric neutrino data measured between 2011 and 2019 with the low-energy subdetector DeepCore of the IceCube neutrino telescope. Supersedes AARTSEN 18A.

[11] ABE 23D uses the same dataset as ABE 23F. The measurement of $\sin^2(\theta_{23})$ is performed independently for ν_μ and $\overline{\nu}_\mu$.

[12] ABE 23F results are based on data collected between 2010 and 2020 in (anti)neutrino mode and include a neutrino beam exposure of 1.97×10^{21} (1.63×10^{21}) protons on target. Supersedes ABE 20F.

[13] ABE 21A results are based on 1.49×10^{21} POT in neutrino mode and 1.64×10^{21} POT in antineutrino mode.

[14] SALAS 21 reports results of a global fit to neutrino oscillation data available at the time of the Neutrino 2020 conference.

[15] AARTSEN 20 uses the data taken between May 2012 and April 2014 with the low-energy subdetector DeepCore of the IceCube neutrino telescope. The reconstructed energy range is between 4 (5) and 90 (80) GeV for the main (confirmatory) analysis. Though the observed best-fit is in the lower octant for both mass orderings, a substantial range of $\sin^2(\theta_{23}) > 0.5$ is still compatible with the observed data for both mass orderings.

[16] ABE 20F results are based on data collected between 2009 and 2018 in (anti)neutrino mode and include a neutrino beam exposure of 1.49×10^{21} (1.64×10^{21}) protons on target. Supersedes ABE 18G.

[17] ESTEBAN 20A reports results of a global fit to neutrino oscillation data available at the time of the Neutrino2020 conference.

[18] AARTSEN 19C uses three years (April 2012 – May 2015) of neutrino data from full sky with reconstructed energies between 5.6 and 56 GeV, measured with the low-energy subdetector DeepCore of the IceCube neutrino telescope. AARTSEN 19C adopts looser event selection criteria to prioritize the efficiency of selecting neutrino events, different from tighter event selection criteria which closely follow the criteria used by AARTSEN 18A to measure the ν_μ disappearance.

[19] ACERO 19 is based on a sample size of 12.33×10^{20} protons on target. The fit combines both antineutrino and neutrino data to extract the oscillation parameters. The results favor the normal mass ordering by 1.9 σ and θ_{23} values in octant II by 1.6 σ. Supersedes ACERO 18.

[20] Errors are from normal mass ordering and θ_{13} octant II fits.

[21] ALBERT 19 measured the oscillation parameters of atmospheric neutrinos with the ANTARES deep sea neutrino telescope using the data taken from 2007 to 2016 (2830 days of total live time). Supersedes ADRIAN-MARTINEZ 12.

[22] AARTSEN 18A uses three years (April 2012 – May 2015) of neutrino data from full sky with reconstructed energies between 5.6 and 56 GeV, measured with the low-energy subdetector DeepCore of the IceCube neutrino telescope. AARTSEN 18A also reports the best fit result for the inverted mass ordering as $\Delta m^2_{32} = -2.32 \times 10^{-3}$ eV^2 and $\sin^2(\theta_{23}) = 0.51$. Uncertainties for the inverted mass ordering fits were not provided. Supersedes AARTSEN 15A.

[23] ABE 18B uses 328 kton-years of Super-Kamiokande I-IV atmospheric neutrino data to obtain this result. The fit is performed over the four parameters, Δm^2_{32}, $\sin^2\theta_{23}$, $\sin^2\theta_{13}$, and δ, while the solar parameters are fixed to $\Delta m^2_{21} = (7.53 \pm 0.18) \times 10^{-5}$ eV^2 and $\sin^2\theta_{12} = 0.304 \pm 0.014$. Superseded by WESTER 24.

[24] ABE 18B uses 328 kton-years of Super-Kamiokande I-IV atmospheric neutrino data to obtain this result. The fit is performed over the three parameters, Δm^2_{32}, $\sin^2(\theta_{23})$, and δ, while the solar parameters and $\sin^2(\theta_{13})$ are fixed to $\Delta m^2_{21} = (7.53 \pm 0.18) \times 10^{-5}$ eV^2, $\sin^2(\theta_{12}) = 0.304 \pm 0.014$, and $\sin^2(\theta_{13}) = 0.0219 \pm 0.0012$. Superseded by WESTER 24.

[25] ABE 18G data prefers normal mass ordering is with a posterior probability of 87%. Supersedes ABE 17F.

[26] ACERO 18 performs a joint fit to the data for ν_μ disappearance and ν_e appearance. The overall best fit favors normal mass ordering and θ_{23} in octant II. No 1σ confidence intervals are presented for the inverted mass ordering scenarios. Superseded by ACERO 19.

[27] Errors are from the projections of the 68% contour on 2D plot of Δm^2 versus $\sin^2(\theta_{23})$. ABE 17F supersedes ABE 17A. Superseded by ABE 18G.

[28] Superseded by ACERO 18.

[29] ABE 16D reports oscillation results using $\overline{\nu}_\mu$ disappearance in an off-axis beam.

[30] ADAMSON 16A obtains $\sin^2(\theta_{23})$ in the 68% C.L. range [0.38, 0.65] ([0.37, 0.64]), with two statistically degenerate best-fit values of 0.44 and 0.59 (0.44 and 0.59) for normal (inverted) mass ordering. Superseded by ADAMSON 17A.

[31] AARTSEN 15A obtains this result by a three-neutrino oscillation analysis using 10–100 GeV muon neutrino sample from a total of 953 days of measurement with the low-energy subdetector DeepCore of the IceCube neutrino telescope. Superseded by AARTSEN 18A.

[32] ABE 14 results are based on ν_μ disappearance using three-neutrino oscillation fit. The confidence intervals are derived from one dimensional profiled likelihoods. Superseded by ABE 17A.

[33] ADAMSON 14 uses a complete set of accelerator and atmospheric data. The analysis combines the ν_μ disappearance and ν_e appearance data using three-neutrino oscillation fit. The fit results are obtained for normal and inverted mass ordering assumptions. The best fit is for first θ_{23} octant and inverted mass ordering.

[34] FORERO 14 performs a global fit to neutrino oscillations using solar, reactor, long-baseline accelerator, and atmospheric neutrino data.

[35] GONZALEZ-GARCIA 14 result comes from a frequentist global fit. The corresponding Bayesian global fit to the same data results are reported in BERGSTROM 15 as 68% CL intervals of 0.433–0.496 or 0.530–0.594 for normal and 0.514–0.612 for inverted mass ordering.

[36] AARTSEN 13B obtained this result by a two-neutrino oscillation analysis using 20–100 GeV muon neutrino sample from a total of 318.9 days of live-time measurement with the low-energy subdetector DeepCore of the IceCube neutrino telescope.

[37] The best fit value is $\sin^2(\theta_{23}) = 0.514 \pm 0.082$. Superseded by ABE 14.

[38] ADAMSON 13B obtained this result from ν_μ and $\overline{\nu}_\mu$ disappearance using ν_μ (10.71×10^{20} POT) and $\overline{\nu}_\mu$ (3.36×10^{20} POT) beams, and atmospheric (37.88kton-years) data from MINOS The fit assumed two-flavor neutrino hypothesis and identical ν_μ and $\overline{\nu}_\mu$ oscillation parameters. Superseded by ADAMSON 14.

[39] ABE 12A obtained this result by a two-neutrino oscillation analysis. The best-fit point is $\sin^2(2\theta_{23}) = 0.98$.

[40] ADAMSON 12 is a two-neutrino oscillation analysis using antineutrinos. The best fit value is $\sin^2(2\theta_{23}) = 0.95^{+0.10}_{-0.11} \pm 0.01$.

[41] ADAMSON 12B obtained this result by a two-neutrino oscillation analysis of the L/E distribution using 37.9 kton-yr atmospheric neutrino data with the MINOS far detector.

[42] The best fit point is $\Delta m^2 = 0.0019$ eV^2 and $\sin^2 2\theta = 0.99$. The 90% single-parameter confidence interval at the best fit point is $\sin^2 2\theta > 0.86$.

[43] The data are separated into pure samples of ν and $\overline{\nu}$, and separate oscillation parameters for ν and $\overline{\nu}$s are fit to the data. The best fit point is (Δm^2, $\sin^2 2\theta$) = (0.0022 eV^2, 0.99) and ($\Delta\overline{m}^2$, $\sin^2 2\overline{\theta}$) = (0.0016 eV^2, 1.00). The quoted result is taken from the 90% C.L. contour in the (Δm^2, $\sin^2 2\theta$) plane obtained by minimizing the four parameter log-likelihood function with respect to the other oscillation parameters.

[44] ADRIAN-MARTINEZ 12 measured the oscillation parameters of atmospheric neutrinos with the ANTARES deep sea neutrino telescope using the data taken from 2007 to 2010 (863 days of total live time). Superseded by ALBERT 19.

[45] ABE 11C obtained this result by a two-neutrino oscillation analysis using the Super-Kamiokande-I+II+III atmospheric neutrino data. ABE 11C also reported results under a two-neutrino disappearance model with separate mixing parameters between ν and $\overline{\nu}$, and obtained $\sin^2 2\theta > 0.93$ for ν and $\sin^2 2\theta > 0.83$ for $\overline{\nu}$ at 90% C.L.

[46] ADAMSON 11B obtained this result by a two-neutrino oscillation analysis of antineutrinos in an antineutrino enhanced beam with 1.71×10^{20} protons on target. This results is consistent with the neutrino measurements of ADAMSON 11 at 2% C.L.

[47] WENDELL 10 obtained this result ($\sin^2\theta_{23} = 0.407$–$0.583$) by a three-neutrino oscillation analysis using the Super-Kamiokande-I+II+III atmospheric neutrino data, assuming $\theta_{13} = 0$ but including the solar oscillation parameters Δm^2_{21} and $\sin^2\theta_{12}$ in the fit.

[48] WENDELL 10 obtained this result ($\sin^2\theta_{23} = 0.43$–0.61) by a three-neutrino oscillation analysis with one mass scale dominance ($\Delta m^2_{21} = 0$) using the Super-Kamiokande-I+II+III atmospheric neutrino data, and updates the HOSAKA 06A result.

[49] WENDELL 10 obtained this result ($\sin^2\theta_{23} = 0.44$–0.63) by a three-neutrino oscillation analysis with one mass scale dominance ($\Delta m^2_{21} = 0$) using the Super-Kamiokande-I+II+III atmospheric neutrino data, and updates the HOSAKA 06A result.

[50] ADAMSON 06 obtained this result by a two-neutrino oscillation analysis of the L/E distribution using 4.54 kton yr atmospheric neutrino data with the MINOS far detector.

[51] Supercedes ALIU 05.

[52] MICHAEL 06 best fit is for maximal mixing. See also ADAMSON 08.

[53] The best fit is for maximal mixing.

[54] ALLISON 05 result is based upon atmospheric neutrino interactions including upward-stopping muons, with an exposure of 5.9 kton yr. From a two-flavor oscillation analysis the best-fit point is $\Delta m^2 = 0.0017$ eV^2 and $\sin^2(2\theta) = 0.97$.

[55] ASHIE 05 obtained this result by a two-neutrino oscillation analysis using 92 kton yr atmospheric neutrino data from the complete Super-Kamiokande I running period.

[56] AMBROSIO 04 obtained this result, without using the absolute normalization of the neutrino flux, by combining the angular distribution of upward through-going muon tracks with $E_\mu > 1$ GeV, N_{low} and N_{high}, and the numbers of InDown + UpStop and InUp events. Here, N_{low} and N_{high} are the number of events with reconstructed neutrino energies < 30 GeV and > 130 GeV, respectively. InDown and InUp represent events with downward and upward-going tracks starting inside the detector due to neutrino interactions, while UpStop represents entering upward-going tracks which stop in the detector. The best fit is for maximal mixing.

[57] ASHIE 04 obtained this result from the L(flight length)/E(estimated neutrino energy) distribution of ν_μ disappearance probability, using the Super-Kamiokande-I 1489 live-day atmospheric neutrino data.

[58] There are several islands of allowed region from this K2K analysis, extending to high values of Δm^2. We only include the one that overlaps atmospheric neutrino analyses. The best fit is for maximal mixing.

[59] AMBROSIO 03 obtained this result on the basis of the ratio R = N_{low}/N_{high}, where N_{low} and N_{high} are the number of upward through-going muon events with reconstructed neutrino energy < 30 GeV and > 130 GeV, respectively. The data came from the full detector run started in 1994. The method of FELDMAN 98 is used to obtain the limits.

[60] AMBROSIO 03 obtained this result by using the ratio R and the angular distribution of the upward through-going muons. R is given in the previous note and the angular distribution is reported in AMBROSIO 01. The method of FELDMAN 98 is used to obtain the limits. The best fit is to maximal mixing.

[61] SANCHEZ 03 is based on an exposure of 5.9 kton yr. The result is obtained using a likelihood analysis of the neutrino L/E distribution for a selection μ flavor sample while the e-flavor sample provides flux normalization. The method of FELDMAN 98 is used to obtain the allowed region. The best fit is $\sin^2(2\theta) = 0.97$.

[62] AMBROSIO 01 result is based on the angular distribution of upward through-going muon tracks with $E_\mu > 1$ GeV. The data came from three different detector configurations, but the statistics is largely dominated by the full detector run, from May 1994 to December 2000. The total live time, normalized to the full detector configuration is 6.17 years. The best fit is obtained outside the physical region. The method of FELDMAN 98 is used to obtain the limits. The best fit is for maximal mixing.

[63] AMBROSIO 01 result is based on the angular distribution and normalization of upward through-going muon tracks with $E_\mu > 1$ GeV. See the previous footnote.

[64] FUKUDA 99C obtained this result from a total of 537 live days of upward through-going muon data in Super-Kamiokande between April 1996 to January 1998. With a threshold of $E_\mu > 1.6$ GeV, the observed flux is $(1.74 \pm 0.07 \pm 0.02) \times 10^{-13}$ cm^{-2}s^{-1}sr^{-1}. The best fit is $\sin^2(2\theta) = 0.95$.

[65] FUKUDA 99D obtained this result from a simultaneous fitting to zenith angle distributions of upward-stopping and through-going muons. The flux of upward-stopping muons of minimum energy of 1.6 GeV measured between April 1996 and January 1998 is $(0.39 \pm 0.04 \pm 0.02) \times 10^{-13}$ cm^{-2}s^{-1}sr^{-1}. This is compared to the expected flux of $(0.73 \pm 0.16$ (theoretical error)$) \times 10^{-13}$ cm^{-2}s^{-1}sr^{-1}. The best fit is to maximal mixing.

[66] FUKUDA 99D obtained this result from the zenith dependence of the upward-stopping/through-going flux ratio. The best fit is to maximal mixing.

[67] FUKUDA 98C obtained this result by an analysis of 33.0 kton yr atmospheric neutrino data. The best fit is for maximal mixing.

[68] HATAKEYAMA 98 obtained this result from a total of 2456 live days of upward-going muon data in Kamiokande between December 1985 and May 1995. With a threshold of $E_\mu > 1.6$ GeV, the observed flux of upward through-going muons is $(1.94 \pm 0.10^{+0.07}_{-0.06}) \times 10^{-13}$ cm^{-2}s^{-1}sr^{-1}. This is compared to the expected flux of $(2.46 \pm 0.54$ (theoretical error)$) \times 10^{-13}$ cm^{-2}s^{-1}sr^{-1}. The best fit is for maximal mixing.

[69] HATAKEYAMA 98 obtained this result from a combined analysis of Kamiokande contained events (FUKUDA 94) and upward going muon events. The best fit is $\sin^2(2\theta) = 0.95$.

[70] FUKUDA 94 obtained the result by a combined analysis of sub- and multi-GeV atmospheric neutrino events in Kamiokande. The best fit is for maximal mixing.

Δm^2_{32}

The sign of Δm^2_{32} is not known at this time. If given, values are shown separately for the normal and inverted mass ordering. Unless otherwise specified, the ranges below correspond to the projection onto the Δm^2_{32} axis of the 90% CL contours in the $\sin^2(2\theta_{23}) - \Delta m^2_{32}$ plane presented by the authors. If uncertainties are reported with the value, they correspond to one standard deviation uncertainty.

Int. J. Mod
by UNIVERSITY OF CALIFORNIA @ BERK
wnloaded from www.worldscientific.com
-use and distribution is strictly not permitted, except for Open Access articles.

Int. J. Mod. Phys. A 2026.41. Downloaded from www.worldscientific.com
by UNIVERSITY OF CALIFORNIA @ BERKELEY on 09/16/26. Re-use and distribution is strictly not permitted, except for Open Access articles.

VALUE (10^{-3} eV^2)	DOCUMENT ID		TECN	COMMENT
-2.52 ± 0.04 OUR FIT	Error includes scale factor of 1.3. Assuming inverted ordering			
2.445 ± 0.023 OUR FIT	Assuming normal ordering			
$2.40\ ^{+0.05}_{-0.04}$	[1] ABBASI	25	ICCB	Normal mass ordering
$2.506\ ^{+0.039}_{-0.052}$	[2] ABE	25B	T2K	Normal mass ordering, θ_{13} constrained
2.52 ± 0.12	[3] JEON	25	RENO	Normal mass ordering
-2.62 ± 0.12	[3] JEON	25	RENO	Inverted mass ordering
$2.10\ ^{+0.25}_{-0.35}$	[4,5] AIELLO	24	KM3N	Normal mass ordering
-2.33 to -1.84	[4,6] AIELLO	24	KM3N	Inverted mass ordering
$2.72\ ^{+0.14}_{-0.15}$	[7] AN	24A	DAYA	Normal mass ordering
$-2.83\ ^{+0.15}_{-0.14}$	[7] AN	24A	DAYA	Inverted mass ordering
$2.40\ ^{+0.07}_{-0.09}$	[8] WESTER	24	SKAM	Normal mass ordering, θ_{13} constrained
$-2.48\ ^{+0.06}_{-0.12}$	[8] WESTER	24	SKAM	Inverted mass ordering, θ_{13} constrained
2.47 ± 0.06	[9] AN	23	DAYA	Normal mass ordering
-2.57 ± 0.06	[9] AN	23	DAYA	Inverted mass ordering
2.41 ± 0.07	[10] ACERO	22	NOVA	Normal mass ordering, octant II for θ_{23}, θ_{13} constrained
-2.45 ± 0.06	[10] ACERO	22	NOVA	Inverted mass ordering, octant II for θ_{23}, θ_{13} constrained
$2.40\ ^{+0.08}_{-0.09}$	[11] ADAMSON	20A	MINS	Accel., atmospheric, normal mass ordering
$-2.45\ ^{+0.08}_{-0.07}$	[11] ADAMSON	20A	MINS	Accel., atmospheric, inverted mass ordering
• • • We do not use the following data for averages, fits, limits, etc. • • •				
$2.520\ ^{+0.048}_{-0.058}$	[12] ABE	25	SKT2	Normal mass ordering
$-2.555\ ^{+0.048}_{-0.052}$	[12,13] ABE	25	SKT2	Inverted mass ordering
$2.43\ ^{+0.04}_{-0.03}$	[14] ABUBAKAR	25	FIT	Normal mass ordering, joint T2K and NOvA fit
$-2.48\ ^{+0.03}_{-0.04}$	[14] ABUBAKAR	25	FIT	Inverted mass ordering, joint T2K and NOvA fit
$2.39\ ^{+0.07}_{-0.06}$	[15] ACERO	24	NOVA	Normal mass ordering
-2.44 ± 0.03	[15] ACERO	24	NOVA	Inverted mass ordering
2.41 ± 0.07	[16] ABBASI	23	ICCB	Normal mass ordering
$2.48\ ^{+0.05}_{-0.06}$	[17] ABE	23D	T2K	ν_μ disappearance
$2.53\ ^{+0.10}_{-0.11}$	[17] ABE	23D	T2K	$\overline{\nu}_\mu$ disappearance
$2.494\ ^{+0.041}_{-0.058}$	[18] ABE	23F	T2K	Normal mass ordering, θ_{13} constrained
$-2.54\ ^{+0.042}_{-0.056}$	[18,19] ABE	23F	T2K	Inverted mass ordering, θ_{13} constrained
$2.47\ ^{+0.08}_{-0.09}$	[20] ABE	21A	T2K	ν_μ disappearance
$2.50\ ^{+0.18}_{-0.13}$	[20] ABE	21A	T2K	$\overline{\nu}_\mu$ disappearance
2.45 ± 0.07	[21] ABE	20F	T2K	Normal mass ordering, θ_{13} constrained
-2.51 ± 0.07	[21,22] ABE	20F	T2K	Inverted mass ordering, θ_{13} constrained
$2.517\ ^{+0.026}_{-0.028}$	[23] ESTEBAN	20A	FIT	Normal mass ordering, global fit
$-2.498\ ^{+0.028}_{-0.028}$	[23] ESTEBAN	20A	FIT	Inverted mass ordering, global fit
$2.55\ ^{+0.12}_{-0.11}$	[24] AARTSEN	19C	ICCB	
$2.48\ ^{+0.11}_{-0.06}$	[25] ACERO	19	NOVA	Normal mass ordering, octant II for θ_{23}
$-2.54\ ^{+0.06}_{-0.11}$	[25] ACERO	19	NOVA	Inverted mass ordering, octant II for θ_{23}
< 4.1 at 90% CL	AGAFONOVA	19	OPER	
$2.0\ ^{+0.4}_{-0.3}$	[26] ALBERT	19	ANTR	Atmospheric ν, deep sea telescope
$2.31\ ^{+0.11}_{-0.13}$	[27] AARTSEN	18A	ICCB	Normal mass ordering
$2.50\ ^{+0.13}_{-0.31}$	[28] ABE	18B	SKAM	3ν osc: normal mass ordering, θ_{13} free
$-2.28\ ^{+0.33}_{-0.13}$	[28] ABE	18B	SKAM	3ν osc: inverted mass ordering, θ_{13} free
$2.50\ ^{+0.13}_{-0.20}$	[29] ABE	18B	SKAM	Normal mass ordering, θ_{13} constrained
$-2.58\ ^{+0.08}_{-0.37}$	[29] ABE	18B	SKAM	Inverted mass ordering, θ_{13} constrained
$2.463\ ^{+0.071}_{-0.070}$	[30] ABE	18G	T2K	Normal mass ordering, θ_{13} constrained
-2.507 ± 0.070	[30,31] ABE	18G	T2K	Inverted mass ordering, θ_{13} constrained
$2.44\ ^{+0.08}_{-0.07}$	[32] ACERO	18	NOVA	Normal mass order, octant II for θ_{23}
$2.45\ ^{+0.07}_{-0.08}$	[32,33] ACERO	18	NOVA	Normal mass order; octant I for θ_{23}
$2.471\ ^{+0.068}_{-0.070}$	[34] ADEY	18A	DAYA	Normal mass ordering
$-2.575\ ^{+0.068}_{-0.070}$	[34] ADEY	18A	DAYA	Inverted mass ordering
$2.7\ ^{+0.7}_{-0.6}$	[35] AGAFONOVA	18	OPER	OPERA ν_τ appearance
2.63 ± 0.14	[36] BAK	18	RENO	Normal mass ordering
-2.73 ± 0.14	[36] BAK	18	RENO	Inverted mass ordering
2.42 ± 0.03	DE-SALAS	18	FIT	Normal mass ordering, global fit
$-2.50\ ^{+0.03}_{-0.04}$	DE-SALAS	18	FIT	Inverted mass order, global fit
$2.57\ ^{+0.21}_{-0.23}\ ^{+0.12}_{-0.13}$	[37] SEO	18	RENO	Normal mass ordering
$-2.67\ ^{+0.23}_{-0.21}\ ^{+0.13}_{-0.12}$	[37] SEO	18	RENO	Inverted mass ordering
$2.53\ ^{+0.15}_{-0.13}$	ABE	17C	T2K	Normal mass ordering with neutrinos
$2.55\ ^{+0.33}_{-0.27}$	ABE	17C	T2K	Normal mass ordering with antineutrinos
$2.55\ ^{+0.08}_{-0.08}$	ABE	17C	T2K	Normal mass ordering with neutrinos and antineutrinos
$-2.63\ ^{+0.08}_{-0.08}$	ABE	17C	T2K	Inverted mass ordering with neutrinos and antineutrinos
2.54 ± 0.08	[38] ABE	17F	T2K	Normal mass ordering; $\nu+\overline{\nu}$
-2.51 ± 0.08	[38] ABE	17F	T2K	Inverted mass ordering; $\nu+\overline{\nu}$
2.67 ± 0.11	[39] ADAMSON	17A	NOVA	3ν osc; normal mass ordering
-2.72 ± 0.11	[39] ADAMSON	17A	NOVA	3ν osc; inverted mass ordering
$2.45 \pm 0.06 \pm 0.06$	[40] AN	17A	DAYA	Normal mass ordering
$-2.56 \pm 0.06 \pm 0.06$	[40] AN	17A	DAYA	Inverted mass ordering
$2.51\ ^{+0.29}_{-0.25}$	[41] ABE	16D	T2K	3ν osc.; normal mass ordering; $\overline{\nu}$ beam
$2.52\ ^{+0.20}_{-0.18}$	[42] ADAMSON	16A	NOVA	3ν osc; normal mass ordering
-2.56 ± 0.19	[42] ADAMSON	16A	NOVA	3ν osc; inverted mass ordering
$2.56\ ^{+0.21}_{-0.23}\ ^{+0.12}_{-0.13}$	[43] CHOI	16	RENO	3ν osc; normal mass ordering
$-2.69\ ^{+0.23}_{-0.21}\ ^{+0.13}_{-0.12}$	[43] CHOI	16	RENO	3ν osc; inverted mass ordering
$2.72\ ^{+0.19}_{-0.20}$	[44] AARTSEN	15A	ICCB	Normal mass ordering
$-2.73\ ^{+0.21}_{-0.18}$	[44] AARTSEN	15A	ICCB	Inverted mass ordering
2.0–5.0	[45] AGAFONOVA	15A	OPER	90% CL, 5 events
2.37 ± 0.11	[46] AN	15	DAYA	3ν osc.; normal mass ordering
-2.47 ± 0.11	[46] AN	15	DAYA	3ν osc.; inverted mass ordering
2.51 ± 0.10	[47] ABE	14	T2K	3ν osc.; normal mass ordering
-2.56 ± 0.10	[47] ABE	14	T2K	3ν osc.; inverted mass ordering
2.37 ± 0.09	[48] ADAMSON	14	MINS	Accel., atmospheric, normal mass ordering
$-2.41\ ^{+0.09}_{-0.12}$	[48] ADAMSON	14	MINS	Accel., atmsopheric, inverted mass ordering
$2.54\ ^{+0.19}_{-0.20}$	[49] AN	14	DAYA	3ν osc.; normal mass ordering
$-2.64\ ^{+0.20}_{-0.19}$	[49] AN	14	DAYA	3ν osc.; inverted mass ordering
$2.48\ ^{+0.05}_{-0.07}$	[50] FORERO	14	FIT	3ν; normal mass ordering
$-2.38\ ^{+0.06}_{-0.05}$	[50] FORERO	14	FIT	3ν; inverted mass ordering
2.457 ± 0.047	[51,52] GONZALEZ...	14	FIT	Normal mass ordering; global fit
$-2.449\ ^{+0.047}_{-0.048}$	[51] GONZALEZ...	14	FIT	Inverted mass ordering; global fit
$2.3\ ^{+0.6}_{-0.5}$	[53] AARTSEN	13B	ICCB	DeepCore, 2ν oscillation
$2.44\ ^{+0.17}_{-0.15}$	[54] ABE	13G	T2K	3ν osc.; normal mass ordering
$2.41\ ^{+0.09}_{-0.10}$	[55] ADAMSON	13B	MINS	2ν osc.; beam + atmospheric; identical ν & $\overline{\nu}$
2.2–3.1	[56] ABE	12A	T2K	off-axis beam
$2.62\ ^{+0.31}_{-0.28} \pm 0.09$	[57] ADAMSON	12	MINS	$\overline{\nu}$ beam
1.35–2.55	[58,59] ADAMSON	12B	MINS	MINOS atmospheric
1.4–5.6	[58,60] ADAMSON	12B	MINS	MINOS pure atmospheric ν
0.9–2.5	[58,60] ADAMSON	12B	MINS	MINOS pure atmospheric $\overline{\nu}$
1.8–5.0	[61] ADRIAN-MAR...	12	ANTR	Atmospheric ν with deep sea telescope
1.3–4.0	[62] ABE	11C	SKAM	atmospheric $\overline{\nu}$
$2.32\ ^{+0.12}_{-0.08}$	ADAMSON	11	MINS	2ν oscillation; maximal mixing
$3.36\ ^{+0.46}_{-0.40}$	[63] ADAMSON	11B	MINS	$\overline{\nu}$ beam
< 3.37	[64] ADAMSON	11C	MINS	MINOS
1.9–2.6	[65] WENDELL	10	SKAM	3ν osc.; normal mass ordering
-1.7– -2.7	[65] WENDELL	10	SKAM	3ν osc.; inverted mass ordering
2.43 ± 0.13	ADAMSON	08A	MINS	MINOS
0.07–50	[66] ADAMSON	06	MINS	atmospheric ν with far detector
1.9–4.0	[67,68] AHN	06A	K2K	KEK to Super-K
2.2–3.8	[69] MICHAEL	06	MINS	MINOS
1.9–3.6	[67] ALIU	05	K2K	KEK to Super-K

0.3–12	[70] ALLISON	05	SOU2	
1.5–3.4	[71] ASHIE	05	SKAM	atmospheric neutrino
0.6–8.0	[72] AMBROSIO	04	MCRO	MACRO
1.9 to 3.0	[73] ASHIE	04	SKAM	L/E distribution
1.5–3.9	[74] AHN	03	K2K	KEK to Super-K
0.25–9.0	[75] AMBROSIO	03	MCRO	MACRO
0.6–7.0	[76] AMBROSIO	03	MCRO	MACRO
0.15–15	[77] SANCHEZ	03	SOU2	Soudan-2 Atmospheric
0.6–15	[78] AMBROSIO	01	MCRO	upward μ
1.0–6.0	[79] AMBROSIO	01	MCRO	upward μ
1.0–50	[80] FUKUDA	99C	SKAM	upward μ
1.5–15.0	[81] FUKUDA	99D	SKAM	upward μ
0.7–18	[82] FUKUDA	99D	SKAM	stop μ / through
0.5–6.0	[83] FUKUDA	98C	SKAM	Super-Kamiokande
0.55–50	[84] HATAKEYAMA	98	KAMI	Kamiokande
4–23	[85] HATAKEYAMA	98	KAMI	Kamiokande
5–25	[86] FUKUDA	94	KAMI	Kamiokande

[1] ABBASI 25 uses atmospheric neutrino data measured between 2012 and 2021 with the low-energy subdetector DeepCore of the IceCube neutrino telescope. Supersedes ABBASI 23.

[2] ABE 25B results are based on data collected between 2010 and 2020 in (anti)neutrino mode and include a neutrino beam exposure of 1.97×10^{21} (1.63×10^{21}) protons on target. Supersedes ABE 23F.

[3] JEON 25 report results derived using the full data set of the RENO reactor anti-neutrino oscillation experiment, conducted at the Hanbit nuclear power plant in Korea. The result summarizes 3800 live days of detector operation. A rate and shape analysis is performed using data collected with near (294 m from reactors) and far detectors (1382 m from reactors). Values of $\sin^2\theta_{12}$ and Δm^2_{21} taken from the 2024 issue of the RPP (PDG 24) are used to determine these values for both possible mass orderings. This result superseded BAK 18.

[4] AIELLO 24 uses atmospheric neutrino data measured between January 2020 and November 2021 with the first six detection units of ORCA, corresponding to 433 kton-yrs.

[5] AIELLO 24 reports $\Delta m^2_{31} = (2.18^{+0.25}_{-0.35}) \times 10^{-3}$ eV^2 for normal mass ordering. We convert to Δm^2_{32} using PDG 24 value of $\Delta m^2_{21} = (7.53 \pm 0.18) \times 10^{-5}$ eV^2.

[6] AIELLO 24 reports $\Delta m^2_{31} = -2.25 \times 10^{-3}$ to -1.76×10^{-3} eV^2 at 68% CL for inverted mass ordering. We convert to Δm^2_{32} using PDG 24 value of $\Delta m^2_{21} = (7.53 \pm 0.18) \times 10^{-5}$ eV^2. The inverted mass ordering is disfavored with a p-value of 0.25.

[7] AN 24A report results from 1958 days of data taking with the Daya Bay experiment. This analysis makes use of neutron capture on protons and is independent of previous results in AN 23, utilizing neutron capture on Gd.

[8] WESTER 24 uses 484.2 kton-years of Super-Kamiokande I-IV atmospheric neutrino data to obtain this result. The fit is performed over the three parameters, Δm^2_{32}, $\sin^2(\theta_{23})$, and δ, while the solar parameters and $\sin^2(\theta_{13})$ are fixed to $\Delta m^2_{21} = (7.53 \pm 0.18) \times 10^{-5}$ eV^2, $\sin^2(\theta_{12}) = 0.307 \pm 0.013$, and $\sin^2(\theta_{13}) = 0.0220 \pm 0.0007$. Supersedes ABE 18B.

[9] AN 23 reports results derived from the complete data set collected by the Daya-Bay experiment, corresponding to 3158 days of operation, resulting in 5.55×10^6 $\overline{\nu}_e$ candidate events. Solar oscillation parameters are fixed in the analysis to $\sin^2(\theta_{12}) = 0.307 \pm 0.013$, $\Delta m^2_{21} = (7.53 \pm 0.18) \times 10^{-5}$ eV^2 from PDG 20. Supersedes ADEY 18A.

[10] ACERO 22 uses data from Jun 29, 2016 to Feb 26, 2019 (12.5×10^{20} POT) and Feb 6, 2014 to Mar 20, 2020 (13.6×10^{20} POT). For normal mass ordering and θ_{23} octant I (lower octant), best fit is 0.00239 eV^2; for inverted mass ordering and octant I, best fit is -0.00244 eV^2. Uncertainties are reported relative to the global minima in normal mass ordering. Supersedes ACERO 19.

[11] ADAMSON 20A uses the complete dataset from MINOS and MINOS+ experiments. The data were collected using a total exposure of 23.76×10^{20} protons on target and 60.75 kton·yr exposure to atmospheric neutrinos. Supersedes ADAMSON 14.

[12] ABE 25 reports the results of a joint analysis of Super-Kamiokande atmospheric neutrino data and T2K beam neutrino data, using 3244.4 days of atmospheric data and a (anti)neutrino beam exposure of 1.97×10^{21} (1.63×10^{21}) protons on target.

[13] ABE 25 reports $-\Delta m^2_{13}-=(2.480^{+0.052}_{-0.048}) \times 10^{-3}$ eV^2 for inverted mass ordering. We convert to Δm^2_{32} using PDG 24 value of $\Delta m^2_{21} = (7.53 \pm 0.18) \times 10^{-5}$ eV^2.

[14] ABUBAKAR 25 results are based on the joint analysis of data sets from NOvA and T2K experiments. The reactor constraint on θ_{13} is applied in the fits.

[15] ACERO 24 reanalyzed the dataset first examined in ACERO 22 using an alternative statistical approach based on Bayesian Markov chain Monte Carlo.

[16] ABBASI 23 uses atmospheric neutrino data measured between 2011 and 2019 with the low-energy subdetector DeepCore of the IceCube neutrino telescope. Supersedes AARTSEN 18A.

[17] ABE 23D uses the same dataset as ABE 23F. The measurement of Δm^2_{32} is performed independently for ν_μ and $\overline{\nu}_\mu$.

[18] ABE 23F results are based on data collected between 2010 and 2020 in (anti)neutrino mode and include a neutrino beam exposure of 1.97×10^{21} (1.63×10^{21}) protons on target. Supersedes ABE 20F.

[19] ABE 23F reports $\Delta m^2_{13}=(2.463^{+0.042}_{-0.056}) \times 10^{-3}$ eV^2 for inverted mass ordering. We convert to Δm^2_{32} using PDG 23 value of $\Delta m^2_{21} = (7.53 \pm 0.18) \times 10^{-5}$ eV^2.

[20] ABE 21A results are based on 1.49×10^{21} POT in neutrino mode and 1.64×10^{21} POT in antineutrino mode.

[21] ABE 20F results are based on data collected between 2009 and 2018 in (anti)neutrino mode and include a neutrino beam exposure of 1.49×10^{21} (1.64×10^{21}) protons on target. Supersedes ABE 18G.

[22] ABE 20F reports $\Delta m^2_{13}=(2.43 \pm 0.07) \times 10^{-3}$ eV^2 for inverted mass ordering. We convert to Δm^2_{32} using PDG 20 value of $\Delta m^2_{21} = (7.53 \pm 0.18) \times 10^{-5}$ eV^2.

[23] ESTEBAN 20A reports results of a global fit to neutrino oscillation data available at the time of the Neutrino2020 conference.

[24] AARTSEN 19C uses three years (April 2012 – May 2015) of neutrino data from full sky with reconstructed energies between 5.6 and 56 GeV, measured with the low-energy subdetector DeepCore of the IceCube neutrino telescope. AARTSEN 19C adopts looser event selection criteria to prioritize the efficiency of selecting neutrino events, different from tighter event selection criteria which closely follow the criteria used by AARTSEN 18A to measure the ν_μ disappearance.

[25] ACERO 19 is based on a sample size of 12.33×10^{20} protons on target. The fit combines both antineutrino and neutrino data to extract the oscillation parameters. The results favor the normal mass ordering by 1.9 σ and θ_{23} values in octant II by 1.6 σ. Superseded by ACERO 22.

[26] ALBERT 19 measured the oscillation parameters of atmospheric neutrinos with the ANTARES deep sea neutrino telescope using the data taken from 2007 to 2016 (2830 days of total live time). Supersedes ADRIAN-MARTINEZ 12.

[27] AARTSEN 18A uses three years (April 2012 – May 2015) of neutrino data from full sky with reconstructed energies between 5.6 and 56 GeV, measured with the low-energy subdetector DeepCore of the IceCube neutrino telescope. AARTSEN 18A also reports the best fit values for the inverted mass ordering as $\Delta m^2_{32} = -2.32 \times 10^{-3}$ eV^2 and $\sin^2(\theta_{23}) = 0.51$. Uncertainties for the inverted mass ordering fits were not provided. Supersedes AARTSEN 15A.

[28] ABE 18B uses 328 kton-years of Super-Kamiokande I-IV atmospheric neutrino data to obtain this result. The fit is performed over the four parameters, Δm^2_{32}, $\sin^2\theta_{23}$, $\sin^2\theta_{13}$, and δ, while the solar parameters are fixed to $\Delta m^2_{21}= (7.53 \pm 0.18) \times 10^{-5}$ eV^2 and $\sin^2\theta_{12} = 0.304 \pm 0.014$.

[29] ABE 18B uses 328 kton-years of Super-Kamiokande I-IV atmospheric neutrino data to obtain this result. The fit is performed over the three parameters, Δm^2_{32}, $\sin^2(\theta_{23})$, and δ, while the solar parameters and $\sin^2(\theta_{13})$ are fixed to $\Delta m^2_{21}= (7.53 \pm 0.18) \times 10^{-5}$ eV^2, $\sin^2(\theta_{12}) = 0.304 \pm 0.014$, and $\sin^2(\theta_{13}) = 0.0219 \pm 0.0012$. Superseded by WESTER 24.

[30] ABE 18G data prefers normal ordering with a posterior probability of 87%. Supersedes ABE 17F.

[31] ABE 18G reports $\Delta m^2_{13}=(2.432 \pm 0.070) \times 10^{-3}$ eV^2 for inverted mass ordering. We convert to Δm^2_{32} using PDG 18 value of $\Delta m^2_{21}=(7.53 \pm 0.18) \times 10^{-5}$ eV^2.

[32] ACERO 18 performs a joint fit to the data for ν_μ disappearance and ν_e appearance. The overall best fit favors normal mass ordering and θ_{23} in octant II. No 1σ confidence intervals are presented for the inverted mass ordering scenarios. Superseded by ACERO 19.

[33] The error for octant I is taken from the result for octant II.

[34] ADEY 18A reports results from analysis of 1958 days of data taking with the Daya-Bay experiment, with 3.9×10^6 $\overline{\nu}_e$ candidates. The fit to the data gives $\Delta m^2_{ee} = (2.522^{+0.068}_{-0.070}) \times 10^{-3}$ eV^2. Solar oscillation parameters are fixed in the analysis using the global averages, $\sin^2(\theta_{12}) = 0.307^{+0.013}_{-0.012}$, $\Delta m^2_{21} = (7.53 \pm 0.18) \times 10^{-5}$ eV^2, from PDG 18. Supersedes AN 17A.

[35] AGAFONOVA 18 assumes maximal θ_{23} mixing.

[36] BAK 18 reports results of the RENO experiment using about 2200 live-days of data taken with detectors placed at 410.6 and 1445.7 m from reactors of the Hanbit Nuclear Power Plant. We convert the results to Δm^2_{32} using the PDG 18 values of $\sin^2\theta_{12} = 0.307^{+0.013}_{-0.012}$ and $\Delta m^2_{21} = (7.53 \pm 0.18) \times 10^{-5}$ eV^2. Supersedes SEO 18.

[37] SEO 18 reports result of the RENO experiment from a rate and shape analysis of 500 days of data. A simultaneous fit to θ_{13} and Δm^2_{ee} yields $\Delta m^2_{ee} = (2.62^{+0.21+0.12}_{-0.23-0.13}) \times 10^{-3}$ eV^2. We convert the results to Δm^2_{32} using the PDG 18 values of $\sin^2\theta_{12}$ and Δm^2_{21}. SEO 18 is a detailed description of the results published in CHOI 16, which it supersedes. Superseded by BAK 18

[38] ABE 17F confidence intervals are obtained using a frequentist analysis including θ_{13} constraint from reactor experiments. Bayesian intervals based on Markov Chain Monte Carlo method are also provided by the authors. Superseded by ABE 18G.

[39] Superseded by ACERO 18.

[40] AN 17A report results from combined rate and spectral shape analysis of 1230 days of data taken with the Daya Bay reactor experiment. The data set contains more than 2.5×10^6 inverse beta-decay events with neutron capture on Gd. The fit to the data gives $\Delta^2_{ee}=(2.50 \pm 0.06 \pm 0.06) \times 10^{-3}$ eV. Superseded by ADEY 18A.

[41] ABE 16D reports oscillation results using $\overline{\nu}_\mu$ disappearance in an off-axis beam.

[42] Superseded by ADAMSON 17A.

[43] CHOI 16 reports result of the RENO experiment from a rate and shape analysis of 500 days of data. A simultaneous fit to θ_{13} and Δm^2_{ee} yields $\Delta m^2_{ee} = (2.62^{+0.21+0.12}_{-0.23-0.13}) \times 10^{-3}$ eV. We convert the results to Δm^2_{32} using PDG 18 values of $\sin^2(\theta_{12})$ and Δm^2_{21}.

[44] AARTSEN 15A obtains this result by a three-neutrino oscillation analysis using 10–100 GeV muon neutrino sample from a total of 953 days of measurements with the low-energy subdetector DeepCore of the IceCube neutrino telescope. Superseded by AARTSEN 18A.

[45] AGAFONOVA 15A result is based on 5 $\nu_\mu \to \nu_\tau$ appearance candidates with an expected background of 0.25 $\pm$ 0.05 events. The best fit is for $\Delta m^2_{32}=3.3 \times 10^{-3}$ eV^2.

[46] AN 15 uses all eight identical detectors, with four placed near the reactor cores and the remaining four at the far hall to determine prompt energy spectra. The results correspond to the exposure of 6.9×10^5 GW$_{th}$-ton-days. They derive $\Delta m^2_{ee} = (2.42 \pm 0.11) \times 10^{-3}$ eV^2. Assuming the normal (inverted) ordering, the fitted $\Delta m^2_{32} = (2.37 \pm 0.11) \times 10^{-3}$ ($(2.47 \pm 0.11) \times 10^{-3}$) eV^2. Superseded by AN 17A.

Int. J. Mod
by UNIVERSITY OF CALIFORNIA @ BERK
wnloaded from www.worldscientific.com
-use and distribution is strictly not permitted, except for Open Access articles.

Int. J. Mod. Phys. A 2026.41. Downloaded from www.worldscientific.com
by UNIVERSITY OF CALIFORNIA @ BERKELEY on 09/16/26. Re-use and distribution is strictly not permitted, except for Open Access articles.

[47] ABE 14 results are based on ν_μ disappearance using three-neutrino oscillation fit. The confidence intervals are derived from one dimensional profiled likelihoods. In ABE 14 the inverted mass ordering result is reported as $\Delta m^2_{13} = (2.48 \pm 0.10) \times 10^{-3}$ eV^2 which we converted to Δm^2_{32} by adding PDG 14 value of $\Delta m^2_{21} = (7.53 \pm 0.18) \times 10^{-5}$ eV^2. Superseded by ABE 17C.

[48] ADAMSON 14 uses a complete set of accelerator and atmospheric data. The analysis combines The analysis combines the ν_μ disappearance and ν_e appearance data using three-neutrino oscillation fit. The fit results are obtained for normal and inverted mass ordering assumptions.

[49] AN 14 uses six identical detectors, with three placed near the reactor cores (flux-weighted baselines of 512 and 561 m) and the remaining three at the far hall (at the flux averaged distance of 1579 m from all six reactor cores) to determine prompt energy spectra and derive $\Delta m^2_{ee} = (2.59^{+0.19}_{-0.20}) \times 10^{-3}$ eV^2. Assuming the normal (inverted) ordering, the fitted $\Delta m^2_{32} = (2.54^{+0.19}_{-0.20}) \times 10^{-3}$ ($(2.64^{+0.19}_{-0.20}) \times 10^{-3}$) eV^2. Superseded by AN 15.

[50] FORERO 14 performs a global fit to Δm^2_{31} using solar, reactor, long-baseline accelerator, and atmospheric neutrino data.

[51] GONZALEZ-GARCIA 14 result comes from a frequentist global fit. The corresponding Bayesian global fit to the same data results are reported in BERGSTROM 15 as $(2.460 \pm 0.046) \times 10^{-3}$ eV^2 for normal and $(2.445^{+0.047}_{-0.045}) \times 10^{-3}$ eV^2 for inverted mass ordering.

[52] The value for normal mass ordering is actually a measurement of Δm^2_{31} which differs from Δm^2_{32} by a much smaller value of Δm^2_{12}.

[53] AARTSEN 13B obtained this result by a two-neutrino oscillation analysis using 20–100 GeV muon neutrino sample from a total of 318.9 days of live-time measurement with the low-energy subdetector DeepCore of the IceCube neutrino telescope.

[54] Based on the observation of 58 ν_μ events with 205 ± 17(syst) expected in the absence of neutrino oscillations. Superseded by ABE 14.

[55] ADAMSON 13B obtained this result from ν_μ and $\overline{\nu}_\mu$ disappearance using ν_μ (10.71×10^{20} POT) and $\overline{\nu}_\mu$ (3.36×10^{20} POT) beams, and atmospheric (37.88 kton-years) data from MINOS. The fit assumed two-flavor neutrino hypothesis and identical ν_μ and $\overline{\nu}_\mu$ oscillation parameters.

[56] ABE 12A obtained this result by a two-neutrino oscillation analysis. The best-fit point is $\Delta m^2_{32} = 2.65 \times 10^{-3}$ eV^2.

[57] ADAMSON 12 is a two-neutrino oscillation analysis using antineutrinos.

[58] ADAMSON 12B obtained this result by a two-neutrino oscillation analysis of the L/E distribution using 37.9 kton·yr atmospheric neutrino data with the MINOS far detector.

[59] The 90% single-parameter confidence interval at the best fit point is $\Delta m^2 = 0.0019 \pm 0.0004$ eV^2.

[60] The data are separated into pure samples of ν and $\overline{\nu}$, and separate oscillation parameters for ν and $\overline{\nu}$s are fit to the data. The best fit point is (Δm^2, $\sin^2 2\theta$) = (0.0022 eV^2, 0.99) and ($\Delta\overline{m}^2$, $\sin^2 2\overline{\theta}$) = (0.0016 eV^2, 1.00). The quoted result is taken from the 90% C.L. contour in the (Δm^2, $\sin^2 2\theta$) plane obtained by minimizing the four parameter log-likelihood function with respect to the other oscillation parameters.

[61] ADRIAN-MARTINEZ 12 measured the oscillation parameters of atmospheric neutrinos with the ANTARES deep sea neutrino telescope using the data taken from 2007 to 2010 (863 days of total live time). Superseded by ALBERT 19

[62] ABE 11C obtained this result by a two-neutrino oscillation analysis with separate mixing parameters between neutrinos and antineutrinos, using the Super-Kamiokande-I+II+III atmospheric neutrino data. The corresponding 90% CL neutrino oscillation parameter range obtained from this analysis is $\Delta m^2 = 1.7$–3.0×10^{-3} eV^2.

[63] ADAMSON 11B obtained this result by a two-neutrino oscillation analysis of antineutrinos in an antineutrino enhanced beam with 1.71×10^{20} protons on target. This results is consistent with the neutrino measurements of ADAMSON 11 at 2% C.L.

[64] ADAMSON 11C obtains this result based on a study of antineutrinos in a neutrino beam and assumes maximal mixing in the two-flavor approximation.

[65] WENDELL 10 obtained this result by a three-neutrino oscillation analysis with one mass scale dominance ($\Delta m^2_{21} = 0$) using the Super-Kamiokande-I+II+III atmospheric neutrino data, and updates the HOSAKA 06A result.

[66] ADAMSON 06 obtained this result by a two-neutrino oscillation analysis of the L/E distribution using 4.54 kton yr atmospheric neutrino data with the MINOS far detector.

[67] The best fit in the physical region is for $\Delta m^2 = 2.8 \times 10^{-3}$ eV^2.

[68] Supercedes ALIU 05.

[69] MICHAEL 06 best fit is 2.74×10^{-3} eV^2. See also ADAMSON 08.

[70] ALLISON 05 result is based on an atmospheric neutrino observation with an exposure of 5.9 kton yr. From a two-flavor oscillation analysis the best-fit point is $\Delta m^2 = 0.0017$ eV^2 and $\sin^2 2\,\theta = 0.97$.

[71] ASHIE 05 obtained this result by a two-neutrino oscillation analysis using 92 kton yr atmospheric neutrino data from the complete Super-Kamiokande I running period. The best fit is for $\Delta m^2 = 2.1 \times 10^{-3}$ eV^2.

[72] AMBROSIO 04 obtained this result, without using the absolute normalization of the neutrino flux, by combining the angular distribution of upward through-going muon tracks with $E_\mu > 1$ GeV, N_{low} and N_{high}, and the numbers of InDown + UpStop and InUp events. Here, N_{low} and N_{high} are the number of events with reconstructed neutrino energies < 30 GeV and > 130 GeV, respectively. InDown and InUp represent events with downward and upward-going tracks starting inside the detector due to neutrino interactions, while UpStop represents entering upward-going tracks which stop in the detector. The best fit is for $\Delta m^2 = 2.3 \times 10^{-3}$ eV^2.

[73] ASHIE 04 obtained this result from the L(flight length)/E(estimated neutrino energy) distribution of ν_μ disappearance probability, using the Super-Kamiokande-I 1489 live-day atmospheric neutrino data. The best fit is for $\Delta m^2 = 2.4 \times 10^{-3}$ eV^2.

[74] There are several islands of allowed region from this K2K analysis, extending to high values of Δm^2. We only include the one that overlaps atmospheric neutrino analyses. The best fit is for $\Delta m^2 = 2.8 \times 10^{-3}$ eV^2.

[75] AMBROSIO 03 obtained this result on the basis of the ratio $R = N_{low}/N_{high}$, where N_{low} and N_{high} are the number of upward through-going muon events with reconstructed neutrino energy < 30 GeV and > 130 GeV, respectively. The data came from the full detector run started in 1994. The method of FELDMAN 98 is used to obtain the limits. The best fit is for $\Delta m^2 = 2.5 \times 10^{-3}$ eV^2.

[76] AMBROSIO 03 obtained this result by using the ratio R and the angular distribution of the upward through-going muons. R is given in the previous note and the angular distribution is reported in AMBROSIO 01. The method of FELDMAN 98 is used to obtain the limits. The best fit is for $\Delta m^2 = 2.5 \times 10^{-3}$ eV^2.

[77] SANCHEZ 03 is based on an exposure of 5.9 kton yr. The result is obtained using a likelihood analysis of the neutrino L/E distribution for a selection μ flavor sample while the e-flavor sample provides flux normalization. The method of FELDMAN 98 is used to obtain the allowed region. The best fit is for $\Delta m^2 = 5.2 \times 10^{-3}$ eV^2.

[78] AMBROSIO 01 result is based on the angular distribution of upward through-going muon tracks with $E_\mu > 1$ GeV. The data came from three different detector configurations, but the statistics is largely dominated by the full detector run, from May 1994 to December 2000. The total live time, normalized to the full detector configuration is 6.17 years. The best fit is obtained outside the physical region. The method of FELDMAN 98 is used to obtain the limits.

[79] AMBROSIO 01 result is based on the angular distribution and normalization of upward through-going muon tracks with $E_\mu > 1$ GeV. See the previous footnote.

[80] FUKUDA 99C obtained this result from a total of 537 live days of upward through-going muon data in Super-Kamiokande between April 1996 to January 1998. With a threshold of $E_\mu > 1.6$ GeV, the observed flux is $(1.74 \pm 0.07 \pm 0.02) \times 10^{-13}$ cm^{-2}s^{-1}sr^{-1}. The best fit is for $\Delta m^2 = 5.9 \times 10^{-3}$ eV^2.

[81] FUKUDA 99D obtained this result from a simultaneous fitting to zenith angle distributions of upward-stopping and through-going muons. The flux of upward-stopping muons of minimum energy of 1.6 GeV measured between April 1996 and January 1998 is $(0.39 \pm 0.04 \pm 0.02) \times 10^{-13}$ cm^{-2}s^{-1}sr^{-1}. This is compared to the expected flux of (0.73 ± 0.16 (theoretical error)) $\times 10^{-13}$ cm^{-2}s^{-1}sr^{-1}. The best fit is for $\Delta m^2 = 3.9 \times 10^{-3}$ eV^2.

[82] FUKUDA 99D obtained this result from the zenith dependence of the upward-stopping/through-going flux ratio. The best fit is for $\Delta m^2 = 3.1 \times 10^{-3}$ eV^2.

[83] FUKUDA 98C obtained this result by an analysis of 33.0 kton yr atmospheric neutrino data. The best fit is for $\Delta m^2 = 2.2 \times 10^{-3}$ eV^2.

[84] HATAKEYAMA 98 obtained this result from a total of 2456 live days of upward-going muon data in Kamiokande between December 1985 and May 1995. With a threshold of $E_\mu > 1.6$ GeV, the observed flux of upward through-going muons is $(1.94 \pm 0.10^{+0.07}_{-0.06}) \times 10^{-13}$ cm^{-2}s^{-1}sr^{-1}. This is compared to the expected flux of (2.46 ± 0.54 (theoretical error)) $\times 10^{-13}$ cm^{-2}s^{-1}sr^{-1}. The best fit is for $\Delta m^2 = 2.2 \times 10^{-3}$ eV^2.

[85] HATAKEYAMA 98 obtained this result from a combined analysis of Kamiokande contained events (FUKUDA 94) and upward going muon events. The best fit is for $\Delta m^2 = 13 \times 10^{-3}$ eV^2.

[86] FUKUDA 94 obtained the result by a combined analysis of sub- and multi-GeV atmospheric neutrino events in Kamiokande. The best fit is for $\Delta m^2 = 16 \times 10^{-3}$ eV^2.

$\sin^2(\theta_{13})$

At present time direct measurements of $\sin^2(\theta_{13})$ are derived from the reactor $\overline{\nu}_e$ disappearance at distances corresponding to the Δm^2_{32} value, i.e. L $\sim$ 1km. Alternatively, limits can also be obtained from the analysis of the solar neutrino data and accelerator-based $\nu_\mu \to \nu_e$ experiments.

If an experiment reports $\sin^2(2\,\theta_{13})$ we convert the value to $\sin^2(\theta_{13})$.

VALUE (units 10^{-2})	CL%	DOCUMENT ID		TECN	COMMENT
2.17 ± 0.07 OUR AVERAGE		Error includes scale factor of 1.4.			
$2.36^{+0.12}_{-0.11} \pm 0.11$		[1] JEON	25	RENO	Yonggwang reactors
2.2 ± 0.5		[2] ACERO	24	NOVA	Both mass orderings
2.128 ± 0.057		[3] AN	24A	DAYA	DayaBay, Ling Ao/Ao II reactors
$2.80^{+0.28}_{-0.65}$		[4] ABE	23F	T2K	Normal mass ordering
2.70 ± 0.37		[5] DE-KERRET	20	DCHZ	Chooz reactors
• • • We do not use the following data for averages, fits, limits, etc. • • •					
$2.28^{+0.42}_{-0.33}$		[6] ABUBAKAR	25	FIT	Normal mass ordering, T2K + NOvA fit
1.94 ± 0.13		[7] AN	24A	DAYA	DayaBay, Ling Ao reactors
$3.10^{+0.30}_{-0.69}$		[4] ABE	23F	T2K	Inverted mass ordering
2.170 ± 0.063		[8] AN	23	DAYA	DayaBay, Ling Ao/Ao II reactors
2.41 ± 0.45		[9] ABRAHAO	21	DCHZ	Chooz reactors
$2.200^{+0.069}_{-0.062}$		[10] SALAS	21	FIT	Normal mass ordering, global fit
$2.225^{+0.064}_{-0.070}$		[10] SALAS	21	FIT	Inverted mass ordering, global fit
$2.219^{+0.062}_{-0.063}$		[11] ESTEBAN	20A	FIT	Normal mass ordering, global fit
$2.238^{+0.063}_{-0.062}$		[11] ESTEBAN	20A	FIT	Inverted mass ordering, global fit

$2.22 \pm 0.21 \pm 0.37$		[12] SHIN	20	RENO	Yonggwang reactors
< 3.9	68	AGAFONOVA	19	OPER	
$1.8 \; {}^{+2.9}_{-1.3}$		[13] ABE	18B	SKAM	3ν osc: normal mass ordering, θ_{13} free
$0.8 \; {}^{+1.7}_{-0.7}$		[13] ABE	18B	SKAM	3ν osc: inverted mass ordering, θ_{13} free
2.188 ± 0.076		[14] ADEY	18A	DAYA	DayaBay, LingAo/Ao II reactors
<12	90	[15] AGAFONOVA	18A	OPER	OPERA: ν_e appearance
2.29 ± 0.18		[16] BAK	18	RENO	Yonggwang reactors
$2.160 \; {}^{+0.083}_{-0.069}$		DE-SALAS	18	FIT	Normal mass ordering, global fit
$2.220 \; {}^{+0.074}_{-0.076}$		DE-SALAS	18	FIT	Inverted mass ordering, global fit
$2.09 \pm 0.23 \pm 0.16$		[17] SEO	18	RENO	Yonggwang reactors
2.7 ± 0.7		[18] ABE	17F	T2K	Normal mass ordering, T2K only
$2.149 \pm 0.071 \pm 0.050$		[19] AN	17A	DAYA	DayaBay, LingAo/Ao II reactors
$2.25 \; {}^{+0.87}_{-0.86}$		[20] ABE	16B	DCHZ	Chooz reactors
1.81 ± 0.29		[21] AN	16A	DAYA	DayaBay, Ling Ao/Ao II reactors
$2.09 \pm 0.23 \pm 0.16$		[22] CHOI	16	RENO	Yonggwang reactors
2.15 ± 0.13		[23] AN	15	DAYA	DayaBay, Ling Ao/Ao II reactors
$2.6 \; {}^{+1.2}_{-1.1}$		[24] ABE	14A	DCHZ	Chooz reactors
$3.0 \; {}^{+1.3}_{-1.0}$		[25] ABE	14C	T2K	Inverted mass ordering
$3.6 \; {}^{+1.0}_{-0.9}$		[25] ABE	14C	T2K	Normal mass ordering
$2.3 \; {}^{+0.9}_{-0.8}$		[26] ABE	14H	DCHZ	Chooz reactors
2.3 ± 0.2		[27] AN	14	DAYA	DayaBay, Ling Ao/Ao II reactors
2.12 ± 0.47		[28] AN	14B	DAYA	DayaBay, Ling Ao/Ao II reactors
2.34 ± 0.20		[29] FORERO	14	FIT	Normal mass ordering
2.40 ± 0.19		[29] FORERO	14	FIT	Inverted mass ordering
2.18 ± 0.10		[30] GONZALEZ...	14	FIT	Normal mass ordering; global fit
$2.19 \; {}^{+0.11}_{-0.10}$		[30] GONZALEZ...	14	FIT	Inverted mass ordering; global fit
$2.5 \pm 0.9 \pm 0.9$		[31] ABE	13C	DCHZ	Chooz reactors
$2.3 \; {}^{+1.3}_{-1.0}$		[32] ABE	13E	T2K	Normal mass ordering
$2.8 \; {}^{+1.6}_{-1.2}$		[32] ABE	13E	T2K	Inverted mass ordering
$1.6 \; {}^{+1.3}_{-0.9}$		[33] ADAMSON	13A	MINS	Normal mass ordering
$3.0 \; {}^{+1.8}_{-1.6}$		[33] ADAMSON	13A	MINS	Inverted mass ordering
<13	90	AGAFONOVA	13	OPER	OPERA: 3ν
< 3.6	95	[34] AHARMIM	13	FIT	global solar: 3ν
$2.3 \pm 0.3 \pm 0.1$		[35] AN	13	DAYA	DayaBay, LIng Ao/Ao II reactors
$2.2 \pm 1.1 \pm 0.8$		[36] ABE	12	DCHZ	Chooz reactors
$2.8 \pm 0.8 \pm 0.7$		[37] ABE	12B	DCHZ	Chooz reactors
$2.9 \pm 0.3 \pm 0.5$		[38] AHN	12	RENO	Yonggwang reactors
$2.4 \pm 0.4 \pm 0.1$		[39] AN	12	DAYA	DayaBay, Ling Ao/Ao II reactors
$2.5 \; {}^{+1.8}_{-1.6}$		[40] ABE	11	FIT	KamLAND + global solar
< 6.1	95	[41] ABE	11	FIT	Global solar
1.3 to 5.6	68	[42] ABE	11A	T2K	Normal mass ordering
1.5 to 5.6	68	[43] ABE	11A	T2K	Inverted mass ordering
0.3 to 2.3	68	[44] ADAMSON	11D	MINS	Normal mass ordering
0.8 to 3.9	68	[45] ADAMSON	11D	MINS	Inverted mass ordering
8 ± 3		[46] FOGLI	11	FIT	Global neutrino data
7.8 ± 6.2		[47] GANDO	11	FIT	KamLAND + solar: 3ν
12.4 ± 13.3		[48] GANDO	11	FIT	KamLAND: 3ν
$3 \; {}^{+9}_{-7}$	90	[49] ADAMSON	10A	MINS	Normal mass ordering
$6 \; {}^{+14}_{-6}$	90	[50] ADAMSON	10A	MINS	Inverted mass ordering
$8 \; {}^{+8}_{-7}$		[51,52] AHARMIM	10	FIT	KamLAND + global solar: 3ν
< 30	95	[51,53] AHARMIM	10	FIT	global solar: 3ν
< 15	90	[54] WENDELL	10	SKAM	3ν osc.; normal m ordering
< 33	90	[54] WENDELL	10	SKAM	3ν osc.; inverted m ordering
$11 \; {}^{+11}_{-8}$		[55] ADAMSON	09	MINS	Normal mass ordering
$18 \; {}^{+15}_{-11}$		[56] ADAMSON	09	MINS	Inverted mass ordering
6 ± 4		[57] FOGLI	08	FIT	Global neutrino data
8 ± 7		[58] FOGLI	08	FIT	Solar + KamLAND data
5 ± 5		[59] FOGLI	08	FIT	Atmospheric + LBL + CHOOZ
< 36	90	[60] YAMAMOTO	06	K2K	Accelerator experiment
< 48	90	[61] AHN	04	K2K	Accelerator experiment
< 36	90	[62] BOEHM	01		Palo Verde react.
< 45	90	[63] BOEHM	00		Palo Verde react.
< 15	90	[64] APOLLONIO	99	CHOZ	Reactor Experiment

[1] JEON 25 report results derived using the full data set of the RENO reactor anti-neutrino oscillation experiment, conducted at the Hanbit nuclear power plant in Korea. The result summarizes 3800 live days of detector operation. A rate and shape analysis is performed using data collected with near (294 m from reactors) and far detectors (1382 m from reactors). This result superseded BAK 18 and SHIN 20.

[2] ACERO 24 reanalyzed the NOvA dataset of 13.6×10^{20} POT in neutrino beam node and 12.5×10^{20} POT in antineutrino mode using Bayesian statistical approach. The reported value $\sin^2(2\theta_{13}) = 0.087^{+0.020}_{-0.016}$ marginalized over both mass orderings.

[3] AN 24A performed a combined analysis of data taken by the Daya Bay experiment. 1958 days use neutron capture on protons, 3158 days neutron capture on Gd, as reported in AN 23. Combining these data sets results in 8% error reduction compared to AN 23.

[4] ABE 23F results are based on data collected between 2010 and 2020 in (anti)neutrino mode and include a neutrino beam exposure of 1.97×10^{21} (1.63×10^{21}) protons on target.

[5] DE-KERRET 20 uses 481 days of data from single detector operation and also 384 days of data with both near and far detectors operating. A rate and shape analysis is performed on combined neutron captures on H and Gd. Supersedes ABE 16B.

[6] ABUBAKAR 25 results are based on the joint analysis of data sets from NOvA and T2K experiments. No reactor constraint.

[7] AN 24A report results from 1958 days of data taking with the Daya Bay experiment. This analysis makes use of neutron capture on protons and is independent of previous results in AN 23, utilizing neutron capture on Gd.

[8] AN 23 reports results derived from the complete data set collected by the Daya-Bay experiment, corresponding to 3158 days of operation, resulting in 5.55×10^6 $\overline{\nu}_e$ candidate events. Solar oscillation parameters are fixed in the analysis to $\sin^2(\theta_{12}) = 0.307 \pm 0.013$, $\Delta m^2_{21} = (7.53 \pm 0.18) \times 10^{-5}$ eV^2 from PDG 20. Supersedes ADEY 18A.

[9] ABRAHAO 21 uses 865 days of data collected in both near and far detectors with at least one reactor in operation. The analysis is based on a background model independent approach, so called Reactor Rate Modulation, to determine the mixing angle θ_{13}. Adding the background model reduces the uncertainty to 0.0041. Supersedes ABE 16B.

[10] SALAS 21 reports results of a global fit to neutrino oscillation data available at the time of the Neutrino 2020 conference.

[11] ESTEBAN 20A reports results of a global fit to neutrino oscillation data available at the time of the Neutrino2020 conference.

[12] SHIN 20 uses the RENO detector and 1500 live days of data. The near (far) detector observed 567,690 (90,747) $\overline{\nu}_e$ candidate events with a delayed neutron capture on hydrogen. The extracted value of $\sin^2\theta_{13}$ is consistent with the previous analysis with neutron capture on Gd in BAK 18.

[13] ABE 18B uses 328 kton-years of Super-Kamiokande I-IV atmospheric neutrino data to obtain this result. The fit is performed over the four parameters, Δm^2_{32}, $\sin^2\theta_{23}$, $\sin^2\theta_{13}$, and δ, while the solar parameters are fixed to $\Delta m^2_{21} = (7.53 \pm 0.18) \times 10^{-5}$ eV^2 and $\sin^2\theta_{12} = 0.304 \pm 0.014$.

[14] ADEY 18A reports results from analysis of 1958 days of data taking with the Daya-Bay experiment, with 3.9×10^6 $\overline{\nu}_e$ candidates. The fit to the data gives $\Delta m^2_{ee} = (2.522^{+0.068}_{-0.070}) \times 10^{-3}$ eV^2. Solar oscillation parameters are fixed in the analysis using the global averages, $\sin^2(\theta_{12}) = 0.307^{+0.013}_{-0.012}$, $\Delta m^2_{21} = (7.53 \pm 0.18) \times 10^{-5}$ eV^2, from PDG 18. Supersedes AN 17A.

[15] AGAFONOVA 18A reports $\sin^2(2\theta_{13}) < 0.43$ at 90% C.L. The result on the sterile neutrino search in the context of 3+1 model is also reported. A 90% C.L. upper limit on $\sin^2(2\theta_{\mu e)} = 0.021$ for $\Delta m^2_{41} \geq 0.1$ eV^2 is set.

[16] BAK 18 reports results of the RENO experiment using about 2200 live-days of data taken with detectors placed at 410.6 and 1445.7 m from reactors of the Hanbit Nuclear Power Plant. Supersedes SEO 18.

[17] SEO 18 reports results of the RENO experiment using about 500 days of data, performing a rate and shape analysis. Compared to AHN 12, a significant reduction of the systematic uncertainties is reported. A 3% excess of events near 5 MeV of the prompt energy is observed. SEO 18 is a detailed description of the results published in CHOI 16, which it supersedes. Superseded by BAK 18.

[18] Using T2K data only. For inverted mass ordering, all values of θ_{13} are ruled out at 68% CL.

[19] AN 17A reports results from combined rate and spectral shape analysis of 1230 days of data taken with the Daya Bay reactor experiment. The data set contains more than 2.5×10^6 inverse beta-decay events with neutron capture on Gd. A simultaneous fit to θ_{13} and Δm^2_{ee} is performed. Superseded by ADEY 18A.

[20] ABE 16B uses 455.57 live days of data from a detector 1050 m away from two reactor cores of the Chooz nuclear power station, to determine the mixing parameter $\sin^2(2\theta_{13})$. This analysis uses 7.15 reactor-off days for constraining backgrounds. A rate and shape analysis is performed on combined neutron captures on H and Gd. Supersedes ABE 14H and ABE 13C.

[21] AN 16A uses data from the eight antineutrino detectors (404 days) and six antineutrino detectors (217 days) runs to determine the mixing parameter $\sin^2(2\theta_{13})$ using the neutron capture on H only. Supersedes AN 14B.

[22] CHOI 16 reports results of the RENO experiment using about 500 days of data, performing a rate and shape analysis. Compared to AHN 12, a significant reduction of the systematic uncertainties is reported. A 3% excess of events near 5 MeV of the prompt energy is observed. Supersedes AHN 12.

[23] AN 15 uses all eight identical detectors, with four placed near the reactor cores and the remaining four at the far hall to determine the mixing angle θ_{13} using the $\overline{\nu}_e$ observed interaction rates with neutron capture on Gd and energy spectra. The result corresponds to the exposure of 6.9×10^5 GW$_{th}$-ton-days. Superseded by AN 17A.

[24] ABE 14A uses 467.9 live days of one detector, 1050 m away from two reactor cores of the Chooz nuclear power station, to determine the mixing parameter $\sin^2(2\,\theta_{13})$. The

Int. J. Mod
by UNIVERSITY OF CALIFORNIA @ BERK
wnloaded from www.worldscientific.com
-use and distribution is strictly not permitted, except for Open Access articles.

Int. J. Mod. Phys. A 2026.41. Downloaded from www.worldscientific.com by UNIVERSITY OF CALIFORNIA @ BERKELEY on 09/16/26. Re-use and distribution is strictly not permitted, except for Open Access articles.

Bugey4 data (DECLAIS 94) is used to constrain the neutrino flux. The data set includes 7.24 reactor-off days. A "rate-modulation" analysis is performed. Supercedes ABE 12B.

[25] ABE 14C result is for ν_e appearance and assumes $\Delta m^2_{32} = 2.4 \times 10^{-3}$ eV^2, $\sin^2(\theta_{23}) = 0.5$, and $\delta = 0$.

[26] ABE 14H uses 467.9 live days of one detector, 1050 m away from two reactor cores of the Chooz nuclear power station, to determine the mixing parameter $\sin^2(2\,\theta_{13})$. The Bugey4 data (DECLAIS 94) is used to constrain the neutrino flux. The data set includes 7.24 reactor-off days. A rate and shape analysis is performed. Superceded by ABE 16B.

[27] AN 14 uses six identical detectors, with three placed near the reactor cores (flux-weighted baselines of 512 and 561 m) and the remaining three at the far hall (at the flux averaged distance of 1579 m from all six reactor cores) to determine the mixing angle θ_{13} using the $\overline{\nu}_e$ observed interaction rates with neutron capture on Gd and energy spectra. Supersedes AN 13 and superseded by AN 15.

[28] AN 14B uses six identical anti-neutrino detectors with flux-weighted baselines of $\sim$ 500 m and $\sim$ 1.6 km to six power reactors. This rate analysis uses a 217-day data set and neutron capture on protons (not Gd) only. $\Delta m^2_{31} = 2.32 \times 10^{-3}$ eV^2 is assumed. Superseded by AN 16A.

[29] FORERO 14 performs a global fit to neutrino oscillations using solar, reactor, long-baseline accelerator, and atmospheric neutrino data.

[30] GONZALEZ-GARCIA 14 result comes from a frequentist global fit. The corresponding Bayesian global fit to the same data results are reported in BERGSTROM 15 as $(2.18^{+0.10}_{-0.11}) \times 10^{-2}$ eV^2 for normal and $(2.19^{+0.12}_{-0.10}) \times 10^{-2}$ eV^2 for inverted mass ordering.

[31] ABE 13C uses delayed neutron capture on hydrogen instead of on Gd used previously. The physical volume is thus three times larger. The fit is based on the rate and shape analysis as in ABE 12B. The Bugey4 data (DECLAIS 94) is used to constrain the neutrino flux. Superseded by ABE 16B.

[32] ABE 13E assumes maximal θ_{23} mixing and *CP* phase $\delta = 0$.

[33] ADAMSON 13A results obtained from ν_e appearance, assuming $\delta = 0$, and $\sin^2(2\,\theta_{23}) = 0.957$.

[34] AHARMIM 13 obtained this result by a three-neutrino oscillation analysis with the value of Δm^2_{32} fixed to 2.45×10^{-3} eV^2, using global solar neutrino data. AHARMIM 13 global solar neutrino data include SNO's all-phases-combined analysis results on the total active ^{8}B neutrino flux and energy-dependent ν_e survival probability parameters, measurements of Cl (CLEVELAND 98), Ga (ABDURASHITOV 09 which contains combined analysis with GNO (ALTMANN 05 and Ph.D. thesis of F. Kaether)), and ^{7}Be (BELLINI 11A) rates, and ^{8}B solar-neutrino recoil electron measurements of SK-I (HOSAKA 06) zenith, SK-II (CRAVENS 08) and SK-III (ABE 11) day/night spectra, and Borexino (BELLINI 10A) spectra. AHARMIM 13 also reported a result combining global solar and KamLAND data, which is $\sin^2(2\,\theta_{13}) = (9.1^{+2.9}_{-3.1}) \times 10^{-2}$.

[35] AN 13 uses six identical detectors, with three placed near the reactor cores (flux-weighted baselines of 498 and 555 m) and the remaining three at the far hall (at the flux averaged distance of 1628 m from all six reactor cores) to determine the $\overline{\nu}_e$ interaction rate ratios. Superseded by AN 14.

[36] ABE 12 determines the $\overline{\nu}_e$ interaction rate in a single detector, located 1050 m from the cores of two reactors. A rate and shape analysis is performed. The rate normalization is fixed by the results of the Bugey4 reactor experiment, thus avoiding any dependence on possible very short baseline oscillations. The value of $\Delta m^2_{31} = 2.4 \times 10^{-3}$ eV^2 is used in the analysis. Superseded by ABE 12B.

[37] ABE 12B determines the neutrino mixing angle θ_{13} using a single detector, located 1050 m from the cores of two reactors. This result is based on a spectral shape and rate analysis. The Bugey4 data (DECLAIS 94) is used to constrain the neutrino flux. Superseded by ABE 14A.

[38] AHN 12 uses two identical detectors, placed at flux weighted distances of 408.56 m and 1433.99 m from six reactor cores, to determine the mixing angle θ_{13}. This rate-only analysis excludes the no-oscillation hypothesis at 4.9 standard deviations. The value of $\Delta m^2_{31} = (2.32^{+0.12}_{-0.08}) \times 10^{-3}$ eV^2 was assumed in the analysis. Superseded by CHOI 16.

[39] AN 12 uses six identical detectors with three placed near the reactor cores (flux-weighted baselines of 470 m and 576 m) and the remaining three at the far hall (at the flux averaged distance of 1648 m from all six reactor cores) to determine the mixing angle θ_{13} using the $\overline{\nu}_e$ observed interaction rate ratios. This rate-only analysis excludes the no-oscillation hypothesis at 5.2 standard deviations. The value of $\Delta m^2_{31} = (2.32^{+0.12}_{-0.08}) \times 10^{-3}$ eV^2 was assumed in the analysis. Superseded by AN 13.

[40] ABE 11 obtained this result by a three-neutrino oscillation analysis with the value of Δm^2_{32} fixed to 2.4×10^{-3} eV^2, using solar neutrino data including Super-Kamiokande, SNO, Borexino (ARPESELLA 08A), Homestake, GALLEX/GNO, SAGE, and KamLAND data. This result implies an upper bound of $\sin^2\theta_{13} < 0.059$ (95% CL) or $\sin^2 2\theta_{13} < 0.22$ (95% CL). The normal neutrino mass ordering and CPT invariance are assumed.

[41] ABE 11 obtained this result by a three-neutrino oscillation analysis with the value of Δm^2_{32} fixed to 2.4×10^{-3} eV^2, using solar neutrino data including Super-Kamiokande, SNO, Borexino (ARPESELLA 08A), Homestake, and GALLEX/GNO data. The normal neutrino mass ordering is assumed.

[42] The quoted limit is for $\Delta m^2_{32} = 2.4 \times 10^{-3}$ eV^2, $\theta_{23} = \pi/2$, $\delta = 0$, and the normal mass ordering. For other values of δ, the 68% region spans from 0.03 to 0.25, and the 90% region from 0.02 to 0.32.

[43] The quoted limit is for $\Delta m^2_{32} = 2.4 \times 10^{-3}$ eV^2, $\theta_{23} = \pi/2$, $\delta = 0$, and the inverted mass ordering. For other values of δ, the 68% region spans from 0.04 to 0.30, and the 90% region from 0.02 to 0.39.

[44] The quoted limit is for $\Delta m^2_{32} = 2.32 \times 10^{-3}$ eV^2, $\theta_{23} = \pi/2$, $\delta = 0$, and the normal mass ordering. For other values of δ, the 68% region spans from 0.02 to 0.12, and the 90% region from 0 to 0.16.

[45] The quoted limit is for $\Delta m^2_{32} = 2.32 \times 10^{-3}$ eV^2, $\theta_{23} = \pi/2$, $\delta = 0$, and the inverted mass ordering. For other values of δ, the 68% region spans from 0.02 to 0.16, and the 90% region from 0 to 0.21.

[46] FOGLI 11 obtained this result from an analysis using the atmospheric, accelerator long baseline, CHOOZ, solar, and KamLAND data. Recently, MUELLER 11 suggested an average increase of about 3.5% in normalization of the reactor $\overline{\nu}_e$ fluxess, and using these fluxes, the fitted result becomes 0.10 ± 0.03.

[47] GANDO 11 report $\sin^2\theta_{13} = 0.020 \pm 0.016$. This result was obtained with three-neutrino fit using the KamLAND + solar data.

[48] GANDO 11 report $\sin^2\theta_{13} = 0.032 \pm 0.037$. This result was obtained with three-neutrino fit using the KamLAND data only.

[49] This result corresponds to the limit of <0.12 at 90% CL for $\Delta m^2_{32} = 2.43 \times 10^{-3}$ eV^2, $\theta_{23} = \pi/2$, and $\delta = 0$. For other values of δ, the 90% CL region spans from 0 to 0.16.

[50] This result corresponds to the limit of <0.20 at 90% CL for $\Delta m^2_{32} = 2.43 \times 10^{-3}$ eV^2, $\theta_{23} = \pi/2$, and $\delta = 0$. For other values of δ, the 90% CL region spans from 0 to 0.21.

[51] AHARMIM 10 global solar neutrino data include SNO's low-energy-threshold analysis survival probability day/night curves, SNO Phase III integral rates (AHARMIM 08), Cl (CLEVELAND 98), SAGE (ABDURASHITOV 09), Gallex/GNO (HAMPEL 99, ALTMANN 05), Borexino (ARPESELLA 08A), SK-I zenith (HOSAKA 06), and SK-II day/night spectra (CRAVENS 08).

[52] AHARMIM 10 obtained this result by a three-neutrino oscillation analysis with the value of Δm^2_{31} fixed to 2.3×10^{-3} eV^2, using global solar neutrino data and KamLAND data (ABE 08A). *CPT* invariance is assumed. This result implies an upper bound of $\sin^2\theta_{13} < 0.057$ (95% CL) or $\sin^2 2\theta_{13} < 0.22$ (95% CL).

[53] AHARMIM 10 obtained this result by a three-neutrino oscillation analysis with the value of Δm^2_{31} fixed to 2.3×10^{-3} eV^2, using global solar neutrino data.

[54] WENDELL 10 obtained this result by a three-neutrino oscillation analysis with one mass scale dominance ($\Delta m^2_{21} = 0$) using the Super-Kamiokande-I+II+III atmospheric neutrino data, and updates the HOSAKA 06A result.

[55] The quoted limit is for $\Delta m^2_{32} = 2.43 \times 10^{-3}$ eV^2, $\theta_{23} = \pi/2$, and $\delta = 0$. For other values of δ, the 68% CL region spans from 0.02 to 0.26.

[56] The quoted limit is for $\Delta m^2_{32} = 2.43 \times 10^{-3}$ eV^2, $\theta_{23} = \pi/2$, and $\delta = 0$. For other values of δ, the 68% CL region spans from 0.04 to 0.34.

[57] FOGLI 08 obtained this result from a global analysis of all neutrino oscillation data, that is, solar + KamLAND + atmospheric + accelerator long baseline + CHOOZ.

[58] FOGLI 08 obtained this result from an analysis using the solar and KamLAND neutrino oscillation data.

[59] FOGLI 08 obtained this result from an analysis using the atmospheric, accelerator long baseline, and CHOOZ neutrino oscillation data.

[60] YAMAMOTO 06 searched for $\nu_\mu \to \nu_e$ appearance. Assumes $2\,\sin^2(2\theta_{\mu e}) = \sin^2(2\theta_{13})$. The quoted limit is for $\Delta m^2_{32} = 1.9 \times 10^{-3}$ eV^2. That value of Δm^2_{32} is the one-σ low value for AHN 06A. For the AHN 06A best fit value of 2.8×10^{-3} eV^2, the $\sin^2(2\theta_{13})$ limit is < 0.26. Supersedes AHN 04.

[61] AHN 04 searched for $\nu_\mu \to \nu_e$ appearance. Assuming $2\,\sin^2(2\,\theta_{\mu_e}) = \sin^2(2\,\theta_{13})$, a limit on $\sin^2(2\,\theta_{\mu_e})$ is converted to a limit on $\sin^2(2\,\theta_{13})$.The quoted limit is for $\Delta m^2_{32} = 1.9 \times 10^{-3}$ eV^2. That value of Δm^2_{32} is the one-σ low value for ALIU 05. For the ALIU 05 best fit value of 2.8×10^{-3} eV^2, the $\sin^2(2\,\theta_{13})$ limit is < 0.30.

[62] The quoted limit is for $\Delta m^2_{32} = 1.9 \times 10^{-3}$ eV^2. That value of Δm^2_{32} is the 1-σ low value for ALIU 05. For the ALIU 05 best fit value of 2.8×10^{-3} eV^2, the $\sin^2 2\,\theta_{13}$ limit is < 0.19. In this range, the θ_{13} limit is larger for lower values of Δm^2_{32}, and smaller for higher values of Δm^2_{32}.

[63] The quoted limit is for $\Delta m^2_{32} = 1.9 \times 10^{-3}$ eV^2. That value of Δm^2_{32} is the 1-σ low value for ALIU 05. For the ALIU 05 best fit value of 2.8×10^{-3} eV^2, the $\sin^2 2\,\theta_{13}$ limit is < 0.23.

[64] The quoted limit is for $\Delta m^2_{32} = 2.43 \times 10^{-3}$ eV^2. That value of Δm^2_{32} is the central value for ADAMSON 08. For the ADAMSON 08 1-σ low value of 2.30×10^{-3} eV^2, the $\sin^2 2\,\theta_{13}$ limit is < 0.16. See also APOLLONIO 03 for a detailed description of the experiment.

CP violating phase

δ, *CP* violating phase

Measurements of δ come from atmospheric and accelarator experiments looking at ν_e appearance. We encode values between 0 and 2π, though it is equivalent to use $-\pi$ to π.

VALUE (π rad)	CL%	DOCUMENT ID		TECN	COMMENT
$1.21^{+0.19}_{-0.17}$ OUR AVERAGE	Error includes scale factor of 1.2.				
$1.31^{+0.39}_{-0.15}$		[1] ABE	25B	T2K	Normal mass ordering, θ_{13} constrained
$1.44^{+0.24}_{-0.40}$		[2] WESTER	24	SKAM	Normal mass ordering, θ_{13} constrained
$0.82^{+0.27}_{-0.87}$		[3,4] ACERO	22	NOVA	Normal mass ordering, octant II for θ_{23}, θ_{13} constrained
• • • We do not use the following data for averages, fits, limits, etc. • • •					
$1.44^{+0.23}_{-0.30}$		[5] ABE	25	SKT2	Both mass orderings, θ_{13} constrained
$1.13^{+0.35}_{-0.21}$		[6] ABUBAKAR	25	FIT	Normal mass ordering, joint T2K and NOvA fit

$1.37^{+0.31}_{-0.20}$		[7] ABE	23F	T2K	Normal mass ordering, θ_{13} constrained
$1.52^{+0.27}_{-0.30}$		[3,8] ACERO	22	NOVA	Inverted mass ordering, octant II for θ_{23}, θ_{13} constrained
$1.08^{+0.13}_{-0.12}$		[9] SALAS	21	FIT	Normal mass ordering, global fit
$1.58^{+0.15}_{-0.16}$		[9] SALAS	21	FIT	Inverted mass ordering, global fit
$1.40^{+0.22}_{-0.18}$		[10] ABE	20F	T2K	Normal mass ordering
$1.09^{+0.15}_{-0.13}$		[11] ESTEBAN	20A	FIT	Normal mass ordering, global fit
$1.57^{+0.14}_{-0.17}$		[11] ESTEBAN	20A	FIT	Inverted mass ordering, global fit
$0.0\ ^{+1.3}_{-0.4}$		[12] ACERO	19	NOVA	Normall mass ordering, octant II for θ_{23}
$1.33^{+0.46}_{-0.53}$		[13] ABE	18B	SKAM	3ν osc: normal mass ordering, θ_{13} free
$1.22^{+0.76}_{-0.67}$		[13] ABE	18B	SKAM	3ν osc: inverted mass ordering, θ_{13} free
$1.33^{+0.45}_{-0.51}$		[14] ABE	18B	SKAM	Normal mass ordering, θ_{13} constrained
$1.33^{+0.48}_{-0.53}$		[14] ABE	18B	SKAM	3ν osc: inverted mass ordering, θ_{13} constrained
1.40 ± 0.20		[15] ABE	18G	T2K	Normal mass ordering, θ_{13} constrained
$1.54^{+0.14}_{-0.12}$	95	[15] ABE	18G	T2K	Inverted mass ordering, θ_{13} constrained
$1.21^{+0.91}_{-0.30}$		[16] ACERO	18	NOVA	Normal mass ordering, octant II for θ_{23}
$1.46^{+0.56}_{-0.42}$		[16] ACERO	18	NOVA	Normal mass order; octant I for θ_{23}
$1.32^{+0.21}_{-0.15}$		DE-SALAS	18	FIT	Normal mass ordering, global fit
$1.56^{+0.13}_{-0.15}$		DE-SALAS	18	FIT	Inverted mass ordering, global fit
$1.45^{+0.27}_{-0.26}$		[17] ABE	17F	T2K	Normal mass ordering
$1.54^{+0.22}_{-0.23}$		[17] ABE	17F	T2K	Inverted mass ordering
$1.50^{+0.53}_{-0.57}$		[18] ADAMSON	17B	NOVA	Inverted mass ordering; θ_{23} in octant II
$0.74^{+0.57}_{-0.93}$		[18] ADAMSON	17B	NOVA	Normal mass ordering; θ_{23} in octant II
$1.48^{+0.69}_{-0.58}$		[18] ADAMSON	17B	NOVA	Normal mass ordering; θ_{23} in octant I
0.0 to 0.1, 0.5 to 2.0	90	[18,19] ADAMSON	16	NOVA	Inverted mass ordering
0.0 to 2.0	90	[19] ADAMSON	16	NOVA	Normal mass ordering
0 to 0.15, 0.83 to 2	90	ABE	15D	T2K	Normal mass ordering
1.09 to 1.92	90	ABE	15D	T2K	Inverted mass ordering
0.05 to 1.2	90	[20] ADAMSON	14	MINS	Normal mass ordering
$1.34^{+0.64}_{-0.38}$		FORERO	14	FIT	Normal mass ordering
$1.48^{+0.34}_{-0.32}$		FORERO	14	FIT	Inverted mass ordering
$1.70^{+0.22}_{-0.39}$		[21] GONZALEZ...	14	FIT	Normal mass ordering; global fit
$1.41^{+0.35}_{-0.34}$		[21] GONZALEZ...	14	FIT	Inverted mass ordering; global fit
0 to 1.5 or 1.9 to 2	90	[22] ADAMSON	13A	MINS	Normal mass ordering

[1] ABE 25B results are based on data collected between 2010 and 2020 in (anti)neutrino mode and include a neutrino beam exposure of 1.97×10^{21} (1.63×10^{21}) protons on target. For inverted mass ordering, the quoted result is $1.54^{+0.18}_{-0.19}$ π rad. Supersedes ABE 23F.

[2] WESTER 24 uses 484.2 kton-years of Super-Kamiokande I-IV atmospheric neutrino data to obtain this result. The fit is performed over the three parameters, Δm^2_{32}, $\sin^2(\theta_{23})$, and δ, while the solar parameters and $\sin^2(\theta_{13})$ are fixed to $\Delta m^2_{21} = (7.53\pm0.18)\times10^{-5}$ eV^2, $\sin^2(\theta_{12}) = 0.307\pm0.013$, and $\sin^2(\theta_{13}) = 0.0220\pm0.0007$. Supersedes ABE 18B.

[3] ACERO 22 uses data from Jun 29, 2016 to Feb 26, 2019 (12.5×10^{20} POT) and Feb 6, 2014 to Mar 20, 2020 (13.6×10^{20} POT). Results for normal and inverted mass ordering, and θ_{23} octant I and II are presented. Supersedes ACERO 19.

[4] For the octant I (lower octant), the 68% CL allowed region is discontinuous, and all delta values are allowed at 90% CL.

[5] ABE 25 reports the results of a joint analysis of Super-Kamiokande atmospheric neutrino data and T2K beam neutrino data, using 3244.4 days of atmospheric data and a (anti)neutrino beam exposure of 1.97×10^{21} (1.63×10^{21}) protons on target.

[6] ABUBAKAR 25 results are based on the joint analysis of data sets from NOvA and T2K experiments. The reactor constraint on θ_{13} is applied in the fits.

[7] ABE 23F results are based on data collected between 2010 and 2020 in (anti)neutrino mode and include a neutrino beam exposure of 1.97×10^{21} (1.63×10^{21}) protons on target. For inverted mass ordering, the quoted result is $1.54^{+0.18}_{-0.19}$ π rad. Supersedes ABE 20F.

[8] The inverted mass ordering is rejected at 1.0 σ. The error bars are reported relative to the global minima in normal mass ordering.

[9] SALAS 21 reports results of a global fit to neutrino oscillation data available at the time of the Neutrino 2020 conference.

[10] ABE 20F results are based on data collected between 2009 and 2018 in (anti)neutrino mode and include a neutrino beam exposure of 1.49×10^{21} (1.64×10^{21}) protons on target. For inverted mass ordering, the quoted result is $1.56^{+0.15}_{-0.17}$ π rad. Supersedes ABE 18G.

[11] ESTEBAN 20A reports results of a global fit to neutrino oscillation data available at the time of the Neutrino 2020 conference.

[12] ACERO 19 is based on a sample size of 1.33×10^{20} protons on target with combined antineutrino and neutrino data. Superseded by ACERO 22.

[13] ABE 18B uses 328 kton-years of Super-Kamiokande I-IV atmospheric neutrino data to obtain this result. The fit is performed over the four parameters, Δm^2_{32}, $\sin^2\theta_{23}$, $\sin^2\theta_{13}$, and δ, while the solar parameters are fixed to $\Delta m^2_{21} = (7.53\pm0.18)\times10^{-5}$ eV^2 and $\sin^2\theta_{12} = 0.304\pm0.014$. Superseded by WESTER 24.

[14] ABE 18B uses 328 kton-years of Super-Kamiokande I-IV atmospheric neutrino data to obtain this result. The fit is performed over the three parameters, Δm^2_{32}, $\sin^2\theta_{23}$, and δ, while the solar parameters and $\sin^2\theta_{23}$ are fixed to $\Delta m^2_{21} = (7.53\pm0.18)\times10^{-5}$ eV^2, $\sin^2\theta_{12} = 0.304\pm0.014$, and $\sin^2\theta_{13} = 0.0219\pm0.0012$. Superseded by WESTER 24.

[15] ABE 18G confidence intervals are marginalized over both mass orderings. Normal order preferred with a posterior probability of 87%. The 1-sigma result for normal mass ordering used in the average was provided by the experiment via private communications. Supersedes ABE 17F.

[16] ACERO 18 performs a joint fit to the data for ν_μ disappearance and ν_e appearance. The overall best fit favors normal mass ordering and θ_{23} in octant II. No 1σ confidence intervals are presented for the inverted mass ordering scenarios. Superseded by ACERO 19.

[17] ABE 17F confidence intervals are obtained using a frequentist analysis including θ_{13} constraint from reactor experiments. Bayesian intervals based on Markov Chain Monte Carlo method are also provided by the authors. Superseded by ABE 18G.

[18] Errors are projections of 68% C.L. curve of δ_{CP} vs. $\sin^2\theta_{23}$.

[19] ADAMSON 16 result is based on a data sample with 2.74×10^{20} protons on target. The likelihood-based analysis observed 6 ν_e events with an expected background of 0.99 ± 0.11 events.

[20] ADAMSON 14 result is based on three-flavor formalism and $\theta_{23} > \pi/4$. Likelihood as a function of δ is also shown for the other three combinations of hierarchy and θ_{23} octants; all values of δ are allowed at 90% C.L.

[21] GONZALEZ-GARCIA 14 result comes from a frequentist global fit. The corresponding Bayesian global fit to the same data results are reported in BERGSTROM 15 as 68% CL intervals of 1.24–1.94 for normal and 1.15–1.77 for inverted mass ordering.

[22] ADAMSON 13A result is based on ν_e appearance in MINOS and the calculated $\sin^2(2\theta_{23}) = 0.957$, $\theta_{23} > \pi/4$, and normal mass hierarchy. Likelihood as a function of δ is also shown for the other three combinations of hierarchy and θ_{23} octants; all values of δ are allowed at 90% C.L.

(C) Other neutrino mixing results

The LSND collaboration reported in AGUILAR 01 a signal which is consistent with $\overline{\nu}_\mu \to \overline{\nu}_e$ oscillations. In a three neutrino framework, this would be a measurement of θ_{12} and Δm^2_{21}. This does not appear to be consistent with most of the other neutrino data. The following listings include results from $\nu_\mu \to \nu_e$, $\overline{\nu}_\mu \to \overline{\nu}_e$ appearance and ν_μ, $\overline{\nu}_\mu$, ν_e, and $\overline{\nu}_e$ disappearance experiments, and searches for CPT violation.

$\Delta(m^2)$ for $\sin^2(2\theta) = 1$ $(\nu_\mu \to \nu_e)$

VALUE (eV^2)	CL%	DOCUMENT ID		TECN	COMMENT
• • • We do not use the following data for averages, fits, limits, etc. • • •					
0.03 to 0.55	90	[1] AGUILAR-AR...	21	MBNE	MiniBooNE $\nu,\overline{\nu}$ combined
0.03 to 0.05	90	[2] AGUILAR-AR...	18C	MBNE	MiniBooNE $\nu,\overline{\nu}$ combined
0.015 to 0.050	90	[3] AGUILAR-AR...	13A	MBNE	MiniBooNE
<0.34	90	[4] MAHN	12	MBNE	MiniBooNE/SciBooNE
<0.034	90	AGUILAR-AR...	07	MBNE	MiniBooNE
<0.0008	90	AHN	04	K2K	Water Cherenkov
<0.4	90	ASTIER	03	NOMD	CERN SPS
<2.4	90	AVVAKUMOV	02	NTEV	NUTEV FNAL
		[5] AGUILAR	01	LSND	$\nu\mu \to \nu_e$ osc.prob.
0.03 to 0.3	95	[6] ATHANASSO...	98	LSND	$\nu_\mu \to \nu_e$
<2.3	90	[7] LOVERRE	96		CHARM/CDHS
<0.9	90	VILAIN	94C	CHM2	CERN SPS
<0.09	90	ANGELINI	86	HLBC	BEBC CERN PS

[1] AGUILAR-AREVALO 21 result is based on a total of 18.75×10^{20} POT in neutrino mode, and 11.27×10^{20} POT in anti-neutrino mode. Best fit at 0.043 eV^2. The allowed region does not extend to large Δm^2. The quoted value is the entire allowed region of Δm^2 at 90% C.L. for all values of $\sin^2(2\theta)$. Supersedes AGUILAR-AREVALO 18C.

[2] AGUILAR-AREVALO 18C result is based on $\nu_\mu \to \nu_e$ appearance of 460.5 ± 99.0 events; The best fit value is $\Delta m^2 = 0.041$ eV^2. Superseded by AGUILAR-AREVALO 21.

[3] AGUILAR-AREVALO 13A result is based on $\nu_\mu \to \nu_e$ appearance of 162.0 ± 47.8 events; marginally compatible with twoneutrino oscillations. The best fit value is $\Delta m^2 = 3.14$ eV^2.

[4] MAHN 12 is a combined spectral fit of MiniBooNE and SciBooNE neutrino data with the range of Δm^2 up to 25 eV^2. The best limit is 0.04 at 7 eV^2.

[5] AGUILAR 01 is the final analysis of the LSND full data set. Search is made for the $\nu_\mu \to \nu_e$ oscillations using ν_μ from π^+ decay in flight by observing beam-on electron events from $\nu_e C \to e^- X$. Present analysis results in $8.1\pm12.2\pm1.7$ excess events in the $60<E_e<200$ MeV energy range, corresponding to oscillation probability of

Int. J. Mod
by UNIVERSITY OF CALIFORNIA @ BERK
wnloaded from www.worldscientific.com
-use and distribution is strictly not permitted, except for Open Access articles.

Int. J. Mod. Phys. A 2026.41. Downloaded from www.worldscientific.com
by UNIVERSITY OF CALIFORNIA @ BERKELEY on 09/16/26. Re-use and distribution is strictly not permitted, except for Open Access articles.

$0.10 \pm 0.16 \pm 0.04\%$. This is consistent, though less significant, with the previous result of ATHANASSOPOULOS 98, which it supersedes. The present analysis uses selection criteria developed for the decay at rest region, and is less effective in removing the background above 60 MeV than ATHANASSOPOULOS 98.

[6] ATHANASSOPOULOS 98 is a search for the $\nu_\mu \rightarrow \nu_e$ oscillations using ν_μ from π^+ decay in flight. The 40 observed beam-on electron events are consistent with $\nu_e C \rightarrow e^- X$; the expected background is 21.9 ± 2.1. Authors interpret this excess as evidence for an oscillation signal corresponding to oscillations with probability $(0.26 \pm 0.10 \pm 0.05)\%$. Although the significance is only $2.3\,\sigma$, this measurement is an important and consistent cross check of ATHANASSOPOULOS 96 who reported evidence for $\overline{\nu}_\mu \rightarrow \overline{\nu}_e$ oscillations from μ^+ decay at rest. See also ATHANASSOPOULOS 98B.

[7] LOVERRE 96 uses the charged-current to neutral-current ratio from the combined CHARM (ALLABY 86) and CDHS (ABRAMOWICZ 86) data from 1986.

$\sin^2(2\theta)$ for "Large" $\Delta(m^2)$ $(\nu_\mu \rightarrow \nu_e)$

VALUE (units 10^{-3})	CL%	DOCUMENT ID		TECN	COMMENT
• • • We do not use the following data for averages, fits, limits, etc. • • •					
6 to 1000	90	[1] AGUILAR-AR...	21	MBNE	MiniBooNE; $\nu + \overline{\nu}$
< 5	90	[2] AGUILAR-AR...	18C	MBNE	MiniBooNE; $\nu + \overline{\nu}$
< 7.2	90	AGAFONOVA	13	OPER	$\Delta(m^2) > 0.1$ eV^2
0.8 to 3	90	[3] AGUILAR-AR...	13A	MBNE	MiniBooNE
< 11	90	[4] ANTONELLO	13	ICAR	$\nu_\mu \rightarrow \nu_e$
< 6.8	90	[5] ANTONELLO	13A	ICAR	$\nu_\mu \rightarrow \nu_e$
<100	90	[6] MAHN	12	MBNE	MiniBooNE/SciBooNE
< 1.8	90	[7] AGUILAR-AR...	07	MBNE	MiniBooNE
<110	90	[8] AHN	04	K2K	Water Cherenkov
< 1.4	90	ASTIER	03	NOMD	CERN SPS
< 1.6	90	AVVAKUMOV	02	NTEV	NUTEV FNAL
		[9] AGUILAR	01	LSND	$\nu_\mu \rightarrow \nu_e$ osc.prob.
0.5 to 30	95	[10] ATHANASSO...	98	LSND	$\nu_\mu \rightarrow \nu_e$
< 3.0	90	[11] LOVERRE	96		CHARM/CDHS
< 9.4	90	VILAIN	94C	CHM2	CERN SPS
< 5.6	90	[12] VILAIN	94C	CHM2	CERN SPS

[1] AGUILAR-AREVALO 21 result is based on a total of 18.75×10^{20} POT in neutrino mode, and 11.27×10^{20} POT in anti-neutrino mode. The best fit value is $\sin^2(2\theta)$=0.807. The allowed region does not extend to large Δm^2. The quoted value is the entire allowed region of $\sin^2(2\theta)$ at 90% C.L. for all values of Δm^2. Supersedes AGUILAR-AREVALO 18C.

[2] AGUILAR-AREVALO 18C result is based on $\nu_\mu \rightarrow \nu_e$ appearance of 460.5 ± 99.0 events; The best fit value is $\sin^2(2\theta) = 0.92$. The quoted limit for the two-neutrino mixing angle θ is valid above $\Delta m^2 = 0.59$ eV^2. Superseded by AGUILAR-AREVALO 21.

[3] AGUILAR-AREVALO 13A result is based on $\nu_\mu \rightarrow \nu_e$ appearance of 162.0 ± 47.8 events; marginally compatible with two neutrino oscillations. The best fit value is $\sin^2(2\theta) = 0.002$.

[4] ANTONELLO 13 use the ICARUS T600 detector at LNGS and ~ 20 GeV beam of ν_μ from CERN 730 km away to search for an excess of ν_e events. Two events are found with 3.7 ± 0.6 expected from conventional sources. This result excludes some parts of the parameter space expected by LSND. Superseded by ANTONELLO 13A.

[5] Based on four events with a background of 6.4 ± 0.9 from conventional sources with an average energy of 20 GeV and 730 km from the source of ν_μ.

[6] MAHN 12 is a combined fit of MiniBooNE and SciBooNE neutrino data.

[7] The limit is $\sin^2 2\theta < 0.9 \times 10^{-3}$ at $\Delta m^2 = 2$ eV^2. That value of Δm^2 corresponds to the smallest mixing angle consistent with the reported signal from LSND in AGUILAR 01.

[8] The limit becomes $\sin^2 2\theta < 0.15$ at $\Delta m^2 = 2.8 \times 10^{-3}$ eV^2, the bets-fit value of the ν_μ disappearance analysis in K2K.

[9] AGUILAR 01 is the final analysis of the LSND full data set of the search for the $\nu_\mu \rightarrow \nu_e$ oscillations. See footnote in preceding table for further details.

[10] ATHANASSOPOULOS 98 report $(0.26 \pm 0.10 \pm 0.05)\%$ for the oscillation probability; the value of $\sin^2 2\theta$ for large Δm^2 is deduced from this probability. See footnote in preceding table for further details, and see the paper for a plot showing allowed regions. If effect is due to oscillation, it is most likely to be intermediate $\sin^2 2\theta$ and Δm^2. See also ATHANASSOPOULOS 98B.

[11] LOVERRE 96 uses the charged-current to neutral-current ratio from the combined CHARM (ALLABY 86) and CDHS (ABRAMOWICZ 86) data from 1986.

[12] VILAIN 94C limit derived by combining the ν_μ and $\overline{\nu}_\mu$ data assuming *CP* conservation.

$\Delta(m^2)$ for $\sin^2(2\theta) = 1$ $(\overline{\nu}_\mu \rightarrow \overline{\nu}_e)$

VALUE (eV^2)	CL%	DOCUMENT ID		TECN	COMMENT
• • • We do not use the following data for averages, fits, limits, etc. • • •					
0.023 to 0.060	90	[1] AGUILAR-AR...	13A	MBNE	MiniBooNE
<0.16	90	[2] CHENG	12	MBNE	MiniBooNE/SciBooNE
0.03–0.09	90	[3] AGUILAR-AR...	10	MBNE	$E_\nu > 475$ MeV
0.03–0.07	90	[4] AGUILAR-AR...	10	MBNE	$E_\nu > 200$ MeV
<0.06	90	AGUILAR-AR...	09B	MBNE	MiniBooNE
<0.055	90	[5] ARMBRUSTER	02	KAR2	Liquid Sci. calor.
<2.6	90	AVVAKUMOV	02	NTEV	NUTEV FNAL
0.03–0.05		[6] AGUILAR	01	LSND	LAMPF
0.05–0.08	90	[7] ATHANASSO...	96	LSND	LAMPF
0.048–0.090	80	[8] ATHANASSO...	95		
<0.07	90	[9] HILL	95		
<0.9	90	VILAIN	94C	CHM2	CERN SPS
<0.14	90	[10] FREEDMAN	93	CNTR	LAMPF

[1] Based on $\overline{\nu}_\mu \rightarrow \overline{\nu}_e$ appearance of 78.4 ± 28.5 events. The best fit values are $\Delta m^2 = 0.043$ eV^2 and $\sin^2 2\theta = 0.88$.

[2] CHENG 12 is a combined fit of MiniBooNE and SciBooNE antineutrino data.

[3] This value is for a two neutrino oscillation analysis for excess antineutrino events with $E_\nu > 475$ MeV. The best fit is at 0.07. The allowed region is consistent with LSND reported by AGUILAR 01. Supercedes AGUILAR-AREVALO 09B.

[4] This value is for a two neutrino oscillation analysis for excess antineutrino events with $E_\nu > 200$ MeV with subtraction of the expected 12 events low energy excess seen in the neutrino component of the beam. The best fit value is 0.007 for $\Delta(m^2) = 4.4$ eV^2.

[5] ARMBRUSTER 02 is the final analysis of the KARMEN 2 data for 17.7 m distance from the ISIS stopped pion and muon neutrino source. It is a search for $\overline{\nu}_e$, detected by the inverse β-decay reaction on protons and ^{12}C. 15 candidate events are observed, and 15.8 ± 0.5 background events are expected, hence no oscillation signal is detected. The results exclude large regions of the parameter area favored by the LSND experiment.

[6] AGUILAR 01 is the final analysis of the LSND full data set. It is a search for $\overline{\nu}_e$ 30 m from LAMPF beam stop. Neutrinos originate mainly for π^+ decay at rest. $\overline{\nu}_e$ are detected through $\overline{\nu}_e p \rightarrow e^+ n$ ($20 < E_{e^+} < 60$ MeV) in delayed coincidence with $np \rightarrow d\gamma$. Authors observe $87.9 \pm 22.4 \pm 6.0$ total excess events. The observation is attributed to $\overline{\nu}_\mu \rightarrow \overline{\nu}_e$ oscillations with the oscillation probability of $0.264 \pm 0.067 \pm 0.045\%$, consistent with the previously published result. Taking into account all constraints, the most favored allowed region of oscillation parameters is a band of $\Delta(m^2)$ from 0.2–2.0 eV^2. Supersedes ATHANASSOPOULOS 95, ATHANASSOPOULOS 96, and ATHANASSOPOULOS 98.

[7] ATHANASSOPOULOS 96 is a search for $\overline{\nu}_e$ 30 m from LAMPF beam stop. Neutrinos originate mainly from π^+ decay at rest. $\overline{\nu}_e$ could come from either $\overline{\nu}_\mu \rightarrow \overline{\nu}_e$ or $\nu_e \rightarrow \overline{\nu}_e$; our entry assumes the first interpretation. They are detected through $\overline{\nu}_e p \rightarrow e^+ n$ (20 MeV $< E_{e^+} <$60 MeV) in delayed coincidence with $np \rightarrow d\gamma$. Authors observe $51 \pm 20 \pm 8$ total excess events over an estimated background 12.5 ± 2.9. ATHANASSOPOULOS 96B is a shorter version of this paper.

[8] ATHANASSOPOULOS 95 error corresponds to the 1.6σ band in the plot. The expected background is 2.7 ± 0.4 events. Corresponds to an oscillation probability of $(0.34^{+0.20}_{-0.18} \pm 0.07)\%$. For a different interpretation, see HILL 95. Replaced by ATHANASSOPOULOS 96.

[9] HILL 95 is a report by one member of the LSND Collaboration, reporting a different conclusion from the analysis of the data of this experiment (see ATHANASSOPOULOS 95). Contrary to the rest of the LSND Collaboration, Hill finds no evidence for the neutrino oscillation $\overline{\nu}_\mu \rightarrow \overline{\nu}_e$ and obtains only upper limits.

[10] FREEDMAN 93 is a search at LAMPF for $\overline{\nu}_e$ generated from any of the three neutrino types ν_μ, $\overline{\nu}_\mu$, and ν_e which come from the beam stop. The $\overline{\nu}_e$'s would be detected by the reaction $\overline{\nu}_e p \rightarrow e^+ n$. FREEDMAN 93 replaces DURKIN 88.

$\sin^2(2\theta)$ for "Large" $\Delta(m^2)$ $(\overline{\nu}_\mu \rightarrow \overline{\nu}_e)$

VALUE (units 10^{-3})	CL%	DOCUMENT ID		TECN	COMMENT
• • • We do not use the following data for averages, fits, limits, etc. • • •					
<640	90	[1] ANTONELLO	13A	ICAR	$\overline{\nu}_e$ appearance
<150	90	[2] CHENG	12	MBNE	MiniBooNE/SciBooNE
0.4–9.0	99	[3] AGUILAR-AR...	10	MBNE	$E_\nu > 475$ MeV
0.4–9.0	99	[4] AGUILAR-AR...	10	MBNE	$E_\nu > 200$ MeV
< 3.3	90	[5] AGUILAR-AR...	09B	MBNE	MiniBooNE
< 1.7	90	[6] ARMBRUSTER	02	KAR2	Liquid Sci. calor.
< 1.1	90	AVVAKUMOV	02	NTEV	NUTEV FNAL
5.3±1.3±9.0		[7] AGUILAR	01	LSND	LAMPF
6.2±2.4±1.0		[8] ATHANASSO...	96	LSND	LAMPF
3–12	80	[9] ATHANASSO...	95		
< 6	90	[10] HILL	95		

[1] ANTONELLO 13A obtained the limit by assuming $\overline{\nu}_\mu \rightarrow \overline{\nu}_e$ oscillation from the $\sim 2\%$ of $\overline{\nu}_\mu$ evnets contamination in the CNGS beam.

[2] CHENG 12 is a combined fit of MiniBooNE and SciBooNE antineutrino data.

[3] This value is for a two neutrino oscillation analysis for excess antineutrino events with $E_\nu > 475$ MeV. At 90% CL there is no solution at high $\Delta(m^2)$. The best fit is at maximal mixing. The allowed region is consistent with LSND reported by AGUILAR 01. Supercedes AGUILAR-AREVALO 09B.

[4] This value is for a two neutrino oscillation analysis for excess antineutrino events with $E_\nu > 200$ MeV with subtraction of the expected 12 events low energy excess seen in the neutrino component of the beam. At 90% CL there is no solution at high $\Delta(m^2)$. The best fit value is 0.007 for $\Delta(m^2) = 4.4$ eV^2.

[5] This result is inconclusive with respect to small amplitude mixing suggested by LSND.

[6] ARMBRUSTER 02 is the final analysis of the KARMEN 2 data. See footnote in the preceding table for further details, and the paper for the exclusion plot.

[7] AGUILAR 01 is the final analysis of the LSND full data set. The deduced oscillation probability is $0.264 \pm 0.067 \pm 0.045\%$; the value of $\sin^2 2\theta$ for large $\Delta(m^2)$ is twice this probability (although these values are excluded by other constraints). See footnote in preceding table for further details, and the paper for a plot showing allowed regions. Supersedes ATHANASSOPOULOS 95, ATHANASSOPOULOS 96, and ATHANASSOPOULOS 98.

[8] ATHANASSOPOULOS 96 reports $(0.31 \pm 0.12 \pm 0.05)\%$ for the oscillation probability; the value of $\sin^2 2\theta$ for large $\Delta(m^2)$ should be twice this probability. See footnote in preceding table for further details, and see the paper for a plot showing allowed regions.

[9] ATHANASSOPOULOS 95 error corresponds to the 1.6σ band in the plot. The expected background is 2.7 ± 0.4 events. Corresponds to an oscillation probability of

$(0.34^{+0.20}_{-0.18} \pm 0.07)$%. For a different interpretation, see HILL 95. Replaced by ATHANASSOPOULOS 96.

[10] HILL 95 is a report by one member of the LSND Collaboration, reporting a different conclusion from the analysis of the data of this experiment (see ATHANASSOPOULOS 95). Contrary to the rest of the LSND Collaboration, Hill finds no evidence for the neutrino oscillation $\overline{\nu}_\mu \rightarrow \overline{\nu}_e$ and obtains only upper limits.

Sterile neutrino limits

$\Delta(m^2)$ for $\sin^2(2\theta) = 1$ ($\nu_\mu \rightarrow \nu_s$)

ν_s means ν_τ or any sterile (noninteracting) ν.

VALUE (10^{-5} eV^2)	CL%	DOCUMENT ID		TECN	COMMENT
• • • We do not use the following data for averages, fits, limits, etc. • • •					
<3000 (or <550)	90	[1] OYAMA	89	KAMI	Water Cherenkov
< 4.2 or > 54.	90	BIONTA	88	IMB	Flux has ν_μ, $\overline{\nu}_\mu$, ν_e, and $\overline{\nu}_e$

[1] OYAMA 89 gives a range of limits, depending on assumptions in their analysis. They argue that the region $\Delta(m^2) = (100\text{–}1000) \times 10^{-5}$ eV^2 is not ruled out by any data for large mixing.

Search for ν_μ or $\nu_e \rightarrow \nu_s$

VALUE	CL%	DOCUMENT ID		TECN	COMMENT
• • • We do not use the following data for averages, fits, limits, etc. • • •					
<0.0018	95	[1] ACHARYA	25D	SPEC	T β decay
<0.042	95	[2] ANDRIAMIR...	25		PROSPECT-I
<0.01	95	[3] AN	24		DayaBay
< 0.033–0.108	90	[4] AUGIER	24		^{100}Mo $2\nu\beta\beta$ decay
<5 $\times 10^{-4}$	95	[5] AKER	23		T β decay
<0.05	95	[6] ALMAZAN	23		STEREO
<0.02	95	[7] AKER	22A	SPEC	T β decay
<0.0035	95	[8] ATIF	22		RENO, NEOS
$0.42^{+0.15}_{-0.17}$	68	[9] BARINOV	22A		BEST
<0.05	95	[10] ANDRIAMIR...	21		PROSPECT
<0.005	95	[11] SEREBROV	21		Neutrino-4
<0.008	95	[12] SKROBOVA	20		DANSS
<0.01	90	[13] ALEKSEEV	18		DANSS
<0.06	90	[14] ALMAZAN	18		STEREO
<0.1	95	[15] ASHENFELT...	18		PROSPECT
<0.4	90	[16] AARTSEN	17B	ICCB	IceCube-DeepCore
<8 $\times 10^{-3}$	95	[17] ABDURASHI...	17		T β decay
<1 $\times 10^{-2}$	90	[18] KO	17	NEOS	
<2 $\times 10^{-2}$	90	[19] AARTSEN	16	ICCB	IceCube
<4.5 $\times 10^{-4}$	95	[20] ADAMSON	16B		MINOS, DayaBay
<8.6 $\times 10^{-2}$	95	[21] ADAMSON	16C	MINS	
<1.1 $\times 10^{-2}$	95	[22] AN	16B	DAYA	
		[23] AMBROSIO	01	MCRO	matter effects
		[24] FUKUDA	00	SKAM	neutral currents + matter effects

[1] ACHARYA 25D analyze 3.6×10^7 tritium β decay events, collected by the KATRIN experiment, to place a limit on the admixture of sterile neutrinos. A 3+1 neutrino mixing model is assumed. The value reported here corresponds to approximately $\Delta m^2_{41} \sim 300$ eV^2, where their sensitivity is maximal in a two-dimensional Δm^2_{41} versus $\sin^2(2\theta_{ee})$ plot. We convert the limit to $\sin^2(\theta_{ee})$.

[2] ANDRIAMIRADO 25 report results derived from the complete dataset collected by the PROSPECT-I detector in 2018. Their disappearance search for $\overline{\nu}_e \rightarrow \overline{\nu}_s$ oscillations at 7–9 m distance to the HFIR reactor at ORNL shows no evidence for oscillations. The data is interpreted in a 3+1 mixing model and results are reported in a Δm^2_{41} versus $\sin^2(2\theta_{14})$ exclusion plot. The most sensitive $\sin^2(2\theta_{14})$ exclusion is reported here. It is taken from figure 4 and corresponds to Δm^2_{41} at $\simeq 3$ eV^2.

[3] AN 24 use the full data set of the Daya Bay reactor experiment, corresponding to 3158 days of detector operation, to place a limit on $\overline{\nu}_e \rightarrow \overline{\nu}_s$ oscillations. The result is in terms of $\sin^2(2\theta_{14})$ for 0.01 eV^2 $< \Delta m^2_{41} <$ 0.1 eV^2. A 3+1 mixing model is assumed.

[4] AUGIER 24 use of 1.47 kg·yr of ^{100}Mo exposure of the CUPID-Mo scintillating cryogenic calorimeter, operated at the Laboratoire Souterrain de Modane, to place a range of limits on the admixture of sterile neutrinos. Two different $2\nu\beta\beta$ spectral analysis approaches are used. $\sin^2(\theta_{14})$ is given for sterile neutrino masses ranging from 0.5 to 1.5 MeV. The limit above is for 0.5 MeV mass.

[5] AKER 23 assume a 3+1 neutrino mixing model, use low-rate commissioning data of the KATRIN tritium β decay experiment to place a limit on $\sin^2(\theta_{14})$ for a admixture sterile neutrino mass m_4 of $\sim$ 300 eV.

[6] ALMAZAN 23 use inverse beta decay data collected by the STEREO experiment, placed 9 to 11 m from the ILL research reactor, to search for $\overline{\nu}_e \rightarrow \overline{\nu}_s$ oscillations. The ILL research reactor uses highly enriched ^{235}U fuel. No indication of the oscillation to sterile neutrinos is found, the stated limit on $\sin^2(2\theta_{14})$ correspond to $\Delta m^2_{41} \sim 1$ eV^2 where the exclusion is maximal. Supersedes ALMAZAN 18.

[7] AKER 22A uses the first two science runs of the KATRIN tritium β decay neutrino mass experiment to search for an admixture of sterile neutrinos. No evidence is found for a spectral anomaly, indicating such admixture. The resulting limit is on $\sin^2(2\theta_{14})$ for sterile neutrino masses $m_4 < 40$ eV. It is most restrictive at $\Delta m^2_{41} \sim 400$ eV^2. A 3+1 model is assumed.

[8] ATIF 22 report results from the combined analysis of the RENO (419 m) and NEOS (24 m) experiments data, collected at the Hanbit Nuclear Power Plant. Results, in terms of $\sin^2(2\theta_{14})$, constrain for $\overline{\nu}_e \rightarrow \overline{\nu}_s$ oscillations. The authors report both excluded and allowed parameter combinations. The exclusion result reported here is based on the Feldman-Cousins method and for $\Delta m^2_{41} \simeq 0.55$ eV^2. Part of the allowed area is excluded by the STEREO and PROSPECT experiments.

[9] BARINOV 22A report an event deficit observed using the segmented Baksan Ga neutrino detector, exposed to a 3.4 MCi ^{51}Cr source. Equal suppression factors are observed for the inner and outer segments. The deficit is interpreted as evidence for oscillations to sterile neutrinos. The result is in terms of $\sin^2(2\theta_{14})$, for a best fit of $\Delta m^2_{41} = 3.3^{+\infty}_{-2.3}$ eV^2. Some, but not all, of the allowed neutrino parameter space conflicts with other experiments.

[10] ANDRIAMIRADO 21 reports a search for $\overline{\nu}_e \rightarrow \overline{\nu}_s$ oscillations at the HFIR research reactor, at baselines from 6.7 to 9.2 m. The reactor has a ^{235}U core. 4 tons of ^{6}Li-doped liquid scintillator are used in a segmented detector. Oscillations into sterile neutrinos are disfavored. The stated limit for $\sin^2(2\theta_{14})$ is for $\Delta m^2_{41} \sim 2$ eV^2 where the sensitivity is maximal.

[11] SEREBROV 21 searches for $\overline{\nu}_e \rightarrow \overline{\nu}_s$ oscillations with a moveable detector with baseline 6–12 m from the SM-3 research reactor with highly enriched ^{235}U fuel. Analyzing the L/E dependence a χ^2 minimum is found at $\Delta m^2_{41} = 7.3 \pm 0.13 \pm 1.16$ eV^2 and $\sin^2(2\theta_{14}) = 0.36 \pm 0.12$. The quoted limit of 0.005 for $\sin^2(2\theta_{14})$ corresponds to $\Delta m^2_{41} \sim 2$ eV^2. This is the result from 720 days of reactor ON and 860 days of reactor OFF measurements. The significance of the χ^2 minimum is 2.9 σ. Supersedes SEREBROV 20, SEREBROV 19 and SEREBROV 18A.

[12] SKROBOVA 20 searches for $\overline{\nu}_e - \overline{\nu}_s$ oscillations using the DANSS detector at 10.7, 11.2, and 12.7 m from the 3.1 GW$_{th}$ power reactor. The DANSS detector is highly segmented and moveable; the positions are changed usually 3 times a week. The analysis is based on the ratio of the events at top and bottom position; the middle position is used for checks of consistency. No evidence for sterile neutrinos is found. The quoted limit 0.008, the smallest excluded $\sin^2(2\theta_{14})$, corresponds to $\Delta m^2_{41} \sim 1.0$ eV^2. Supersedes ALEKSEEV 18.

[13] ALEKSEEV 18 searches for $\overline{\nu}_e \rightarrow \overline{\nu}_s$ oscillations using the DANSS detector at 10.7, 11.2, and 12.7 m from the 3.1 GW$_{th}$ power reactor. The DANSS detector is highly segmented and moveable; the positions are changed usually 3 times a week. The analysis is based on the ratio of the events at top and bottom position; the middle position is used for checks of consistency. The best fit point is at $\Delta m^2_{41} = 1.4$ eV^2 and $\sin^2(2\theta_{14}) = 0.05$ with $\Delta\chi^2 = 13.1$ (statistical errors only) compared to the fit with 3 active neutrinos only. The quoted limit of 0.01 for $\sin^2(2\theta_{14})$ corresponds to $\Delta m^2_{41} \sim 1.0$ eV^2. Superseded by SKROBOVA 20.

[14] ALMAZAN 18 searches for the $\overline{\nu}_e \rightarrow \overline{\nu}_s$ oscillations with baseline from 9.4 to 11.1 m from the ILL research reactor with highly enriched ^{235}U fuel. The STEREO detector consists of six separated cells with Gd loaded scintillator, with 15 m water equivalent overburden. The detected rate is 396.3 ± 4.7 $\overline{\nu}_e$/day with signal to background ratio of about 0.9. The reported results corresponds to 66 days of reactor-on. The analysis uses the relative rates normalized to the cell number 1. No indication of the oscillation to the sterile neutrinos is found, the stated limit on $\sin^2(2\theta_{14})$ correspond to $\Delta m^2_{41} \sim$ 3.5 eV^2 where the exclusion is maximal. Superseded by ALMAZAN 23.

[15] ASHENFELTER 18 searches for the $\overline{\nu}_e \rightarrow \overline{\nu}_s$ oscillations at baseline from 6.7 to 9.2 m from the 85 MW research reactor with pure ^{235}U core. The segmented 4 ton ^{6}Li-doped liquid scintillator is operated with about 1 m water equivalent overburden and recorded 25461 ± 283 IBD events. No indication of oscillations into sterile neutrinos was observed. The stated limit for $\sin^2(2\theta_{14})$ is for $\Delta m^2_{41} \sim 2$ eV^2 where the sensitivity is maximal.

[16] AARTSEN 17B uses three years of upward-going atmospheric neutrino data in the energy range of 10-60 GeV to constrain their disappearance into light sterile neutrinos. The reported limit $\sin^2\theta_{24} < 0.11$ at 90% C.L. is for $\Delta m^2_{41} = 1.0$ eV^2. We convert the result to $\sin^2 2\theta_{24}$ for the listing. AARTSEN 17B also reports $\cos^2\theta_{24} \cdot \sin^2\theta_{34} < 0.15$ at 90% C.L. for $\Delta m^2_{41} = 1.0$ eV^2.

[17] ABDURASHITOV 17 use the Troitsk nu-mass experiment to search for sterile neutrinos with mass 0.1 - 2 keV. We convert the reported limit from U^2_{e4} <0.002 to $\sin^2 2\theta_{14}$ <0.008 assume $U_{e4} \sim \sin\theta_{14}$. The stated limit corresponds to the smallest U^2_{e4}. The exclusion curve begins at U^2_{e4} of 0.02 for $m_4 = 0.1$ keV.

[18] KO 17 reports on short baseline reactor oscillation search ($\overline{\nu}_e \rightarrow \overline{\nu}_s$), motivated be the so-called "reactor antineutrino anomaly". The experiment is conducted at 23.7 m from the core of unit 5 of the Hanbit Nuclear Power Complex in Korea. the reported limited on $\sin^2(2\theta_{41})$ for sterile neutrinos was determined using the reactor antineutrino spectrum determined by the Daya Bay experiment for Δm^2_{14} around 0.55 eV^2 where the sensitivity is maximal. A fraction of the parameter space derived from the "reactor antineutrino anomaly" is excluded by this work. Compared to reactor models an event excess is observed at about 5 MeV, in agreement with other experiments.

[19] AARTSEN 16 use one year of upward-going atmospheric muon neutrino data in the energy range of 320 GeV to 20 TeV to constrain their disappearance into light sterile neutrinos. Sterile neutrinos are expected to produce distinctive zenith distribution for these energies for 0.01 $\leq \Delta m^2 \leq 10$ eV^2. The stated limit is for $\sin^2 2\theta_{24}$ at Δm^2 around 0.3 eV^2.

[20] ADAMSON 16B combine the results of AN 16B, ADAMSON 16C, and Bugey-3 reactor experiments to constrain ν_μ to ν_e mixing through oscillations into light sterile neutrinos. The stated limit for $\sin^2 2\theta_{\mu e}$ is at $|\Delta m^2_{41}| = 1.2$ eV^2.

[21] ADAMSON 16C use the NuMI beam and exposure of 10.56×10^{20} protons on target to search for the oscillation of ν_μ dominated beam into light sterile neutrinos with detectors at 1.04 and 735 km. The reported limit $\sin^2(\theta_{24}) < 0.022$ at 95% C.L. is for $|\Delta m^2_{41}| = 0.5$ eV^2. We convert the result to $\sin^2(2\theta_{24})$ for the listing.

Int. J. Mod
by UNIVERSITY OF CALIFORNIA @ BERK
wnloaded from www.worldscientific.com
-use and distribution is strictly not permitted, except for Open Access articles.

Int. J. Mod. Phys. A 2026.41. Downloaded from www.worldscientific.com
by UNIVERSITY OF CALIFORNIA @ BERKELEY on 09/16/26. Re-use and distribution is strictly not permitted, except for Open Access articles.

[22] AN 16B utilize 621 days of data to place limits on the $\overline{\nu}_e$ disappearance into a light sterile neutrino. The stated limit corresponds to the smallest $\sin^2(2\theta_{14})$ at $|\Delta m^2_{41}| \sim 3 \times 10^{-2}$ eV^2 (obtained from Figure 3 in AN 16B). The exclusion curve begins at $|\Delta m^2_{41}| \sim 1.5 \times 10^{-4}$ eV^2 and extends to ~ 0.25 eV^2. The analysis assumes $\sin^2(2\theta_{12}) = 0.846 \pm 0.021$, $\Delta m^2_{21} = (7.53 \pm 0.18) \times 10^{-5}$ eV^2, and $|\Delta m^2_{32}| = (2.44 \pm 0.06) \times 10^{-3}$ eV^2.

[23] AMBROSIO 01 tested the pure 2-flavor $\nu_\mu \rightarrow \nu_s$ hypothesis using matter effects which change the shape of the zenith-angle distribution of upward through-going muons. With maximum mixing and Δm^2around 0.0024 eV^2, the $\nu_\mu \rightarrow \nu_s$ oscillation isdisfavored with 99% confidence level with respect to the $\nu_\mu \rightarrow \nu_\tau$ hypothesis.

[24] FUKUDA 00 tested the pure 2-flavor $\nu_\mu \rightarrow \nu_s$ hypothesis using three complementary atmospheric-neutrino data samples. With this hypothesis, zenith-angle distributions are expected to show characteristic behavior due to neutral currents and matter effects. In the Δm^2 and $\sin^2 2\theta$region preferred by the Super-Kamiokande data, the $\nu_\mu \rightarrow \nu_s$ hypothesis isrejected at the 99% confidence level, while the $\nu_\mu \rightarrow \nu_\tau$hypothesis consistently fits all of the data sample.

CPT tests

$\langle \Delta m^2_{21} - \Delta \overline{m}^2_{21} \rangle$

VALUE (10^{-4} eV^2)	*CL%*	*DOCUMENT ID*		*TECN*	*COMMENT*
<1.1	99.7	[1] DEGOUVEA	05	FIT	solar vs. reactor

[1] DEGOUVEA 05 obtained this bound at the 3σ CL from the KamLAND (ARAKI 05) and solar neutrino data.

$\langle \Delta m^2_{32} - \Delta \overline{m}^2_{32} \rangle$

VALUE (10^{-3} eV^2)	*CL%*	*DOCUMENT ID*		*TECN*	*COMMENT*
$\mathbf{-0.12^{+0.26}_{-0.24}}$		[1] ADAMSON	13B	MINS	beam and atmosperic
• • • We do not use the following data for averages, fits, limits, etc. • • •					
$0.6\ ^{+2.4}_{-0.8}$	90	[2] ADAMSON	12B	MINS	MINOS atmospheric

[1] ADAMSON 13B quotes this difference as a negative of our convention.

[2] The quoted result is the single-parameter 90% C.L. interval determined from the 90% C.L. contour in the (Δm^2, $\Delta \overline{m}^2$) plane, which is obtained by minimizing the four parameter log-likelihood function with respect to the other oscillation parameters.

REFERENCES FOR Neutrino Mixing

ABBASI	25	PRL 134 091801	R. Abbasi *et al.*	(IceCube Collab.)
ABE	25	PRL 134 011801	K. Abe *et al.*	(Super-Kamiokande Collab.+)
ABE	25B	PRL 135 261801	K. Abe *et al.*	(T2K Collab.)
ABREU	25A	PRL 135 121801	M. Abreu *et al.*	(SNO+ Collab.)
ABUBAKAR	25	NAT 646 818	S. Abubakar *et al.*	(T2K and NOvA Collab.)
ACHARYA	25D	NAT 648 70	H. Acharya *et al.*	(KATRIN Collab.)
ALLEGA	25	EPJ C85 17	A. Allega *et al.*	(SNO+ Collab.)
Also		EPJ C85 296 (errat.)	A. Allega *et al.*	(SNO+ Collab.)
ANDRIAMIR...	25	PRL 134 151802	M. Andriamirado *et al.*	(PROSPECT Collab.)
JEON	25	PR D111 112006	S. Jeon *et al.*	(RENO Collab.)
ABE	24B	PR D109 092001	K. Abe *et al.*	(Super-Kamiokande Collab.)
ACERO	24	PR D110 012005	M.A. Acero *et al.*	(NOvA Collab.)
AIELLO	24	JHEP 2410 206	S. Aiello *et al.*	(KM3Net Collab.)
ALLEGA	24	PR D110 122003	A. Allega *et al.*	(SNO+ Collab.)
AN	24	PRL 133 051801	F.P. An *et al.*	(Daya Bay Collab.)
AN	24A	PRL 133 151801	F.P. An *et al.*	(Daya Bay Collab.)
APRILE	24A	PRL 133 191002	E. Aprile *et al.*	(XENON Collab.)
AUGIER	24	EPJ C84 925	C. Augier *et al.*	(CUPID-Mo Collab.)
BO	24	PRL 133 191001	Z. Bo *et al.*	(PandaX-4T Collab.)
LU	24	CP C48 091001	X. Lu *et al.*	(PandaX-4T Collab.)
PDG	24	PR D110 030001	S. Navas *et al.*	(PDG Collab.)
WESTER	24	PR D109 072014	T. Wester *et al.*	(Super-Kamiokande Collab.)
ABBASI	23	PR D108 012014	R. Abbasi *et al.*	(IceCube Collab.)
ABE	23D	PR D108 072011	K. Abe *et al.*	(T2K Collab.)
ABE	23F	EPJ C83 782	K. Abe *et al.*	(T2K Collab.)
AKER	23	EPJ C83 763	M. Aker *et al.*	(KATRIN Collab.)
ALMAZAN	23	NAT 613 257	H. Almazan *et al.*	(STEREO Collab.)
AN	23	PRL 130 161802	F.P. An *et al.*	(Daya Bay Collab.)
BASILICO	23	PR D108 102005	D. Basilico *et al.*	(Borexino Collab.)
MA	23A	PRL 130 021802	W. Ma *et al.*	(PandaX-4T Collab.)
PDG	23	RPP 2023 at pdg.lbl.gov	R.L. Workman *et al.*	(PDG Collab.)
ACERO	22	PR D106 032004	M.A. Acero *et al.*	(NOvA Collab.)
AKER	22A	PR D105 072004	M. Aker *et al.*	(KATRIN Collab.)
APPEL	22	PRL 129 252701	S. Appel *et al.*	(Borexino Collab.)
ATIF	22	PR D105 L111101	Z. Atif *et al.*	(RENO and NEOS Collab.)
BARINOV	22A	PR C105 065502	V.V. Barinov *et al.*	(BEST Collab.)
Also		PRL 128 232501	V.V. Barinov *et al.*	(BEST Collab.)
ABE	21A	PR D103 L011101	K. Abe *et al.*	(T2K Collab.)
ABRAHAO	21	JHEP 2101 190	T. Abrahao *et al.*	(Double Chooz Collab.)
AGOSTINI	21	ASP 125 102509	M. Agostini *et al.*	(Borexino Collab.)
AGUILAR-AR...	21	PR D103 052002	A.A. Aguilar-Arevalo *et al.*	(MiniBooNE Collab.)
ANDRIAMIR...	21	PR D103 032001	M. Andriamirado *et al.*	(PROSPECT Collab.)
SALAS	21	JHEP 2102 071	P.F. de Salas *et al.*	(STOH, VALE, INFN+)
SEREBROV	21	PR D104 032003	A.P. Serebrov *et al.*	(Neutrino-4 Collab.)
AARTSEN	20	EPJ C80 9	M.G. Aartsen *et al.*	(IceCube Collab.)
ABE	20F	NAT 580 339	K. Abe *et al.*	(T2K Collab.)
Also		PR D103 112008	K. Abe *et al.*	(T2K Collab.)
ADAMSON	20A	PRL 125 131802	P. Adamson *et al.*	(MINOS+ Collab.)
AGOSTINI	20A	PR D101 062001	M. Agostini *et al.*	(Borexino Collab.)
AGOSTINI	20D	NAT 587 577	M. Agostini *et al.*	(Borexino Collab.)
AHARMIM	20	PR D102 062006	B. Aharmim *et al.*	(SNO Collab.)
ALMAZAN	20	PRL 125 201801	H. Almazan *et al.*	(STEREO Collab.)
DE-KERRET	20	NATP 16 558	H. de Karret *et al.*	(Double Chooz Collab.)
ESTEBAN	20A	JHEP 2009 178	I. Esteban *et al.*	(NuFIT Collab.)
PDG	20	PTEP 2020 083C01	P.A. Zyla *et al.*	(PDG Collab.)
SEREBROV	20	JETPL 112 199	A.P. Serebrov, R.M. Samoilov	(PNPI)
		Translated from ZETFP 112 211.		
SHIN	20	JHEP 2004 029	C.D. Shin *et al.*	(RENO Collab.)
SKROBOVA	20	IJMP A35 2044015	N. Skrobova	(DANSS Collab.)
AARTSEN	19C	PR D99 032007	M.G. Aartsen *et al.*	(IceCube Collab.)
ACERO	19	PRL 123 151803	M.A. Acero *et al.*	(NOvA Collab.)
ADEY	19	PR D100 052004	D. Adey *et al.*	(Daya Bay Collab.)
AGAFONOVA	19	PR D100 051301	N. Agafonova *et al.*	(OPERA Collab.)
ALBERT	19	JHEP 1906 113	A. Albert *et al.*	(ANTARES Collab.)
ANDERSON	19	PR D99 012012	M. Anderson *et al.*	(SNO+ Collab.)
SEREBROV	19	JETPL 109 213	A.P. Serebrov *et al.*	(Neutrino-4 Collab.)
AARTSEN	18A	PRL 120 071801	M.G. Aartsen *et al.*	(IceCube Collab.)
ABE	18B	PR D97 072001	K. Abe *et al.*	(Super-Kamiokande Collab.)
ABE	18G	PRL 121 171802	K. Abe *et al.*	(T2K Collab.)
ACERO	18	PR D98 032012	M.A. Acero *et al.*	(NOvA Collab.)
ADEY	18A	PRL 121 241805	D. Adey *et al.*	(Daya Bay Collab.)
AGAFONOVA	18	PRL 120 211801	N. Agafonova *et al.*	(OPERA Collab.)
AGAFONOVA	18A	JHEP 1806 151	N. Agafonova *et al.*	(OPERA Collab.)
AGOSTINI	18B	NAT 562 505	M. Agostini *et al.*	(Borexino Collab.)
AGUILAR-AR...	18C	PRL 121 221801	A.A. Aguilar-Arevalo *et al.*	(MiniBooNE Collab.)
ALEKSEEV	18	PL B787 56	I. Alekseev *et al.*	(DANSS Collab.)
ALMAZAN	18	PRL 121 161801	H. Almazan *et al.*	(STEREO Collab.)
ASHENFELT...	18	PRL 121 251802	J. Ashenfelter *et al.*	(PROSPECT Collab.)
BAK	18	PRL 121 201801	G. Bak *et al.*	(RENO Collab.)
CAPOZZI	18	PPNP 102 48	F. Capozzi *et al.*	
DE-SALAS	18	PL B782 633	P.F. de Salas *et al.*	
PDG	18	PR D98 030001	M. Tanabashi *et al.*	(PDG Collab.)
SEO	18	PR D98 012002	S.H. Seo *et al.*	(RENO Collab.)
SEREBROV	18A	PPN 49 701	A.P. Serebrov *et al.*	(Neutrino-4 Collab.)
AARTSEN	17B	PR D95 112002	M.G. Aartsen *et al.*	(IceCube Collab.)
ABDURASHI...	17	JETPL 105 753	J.N. Abdurashitov *et al.*	(Troitsk nu-mass Collab.)
ABE	17A	PRL 118 151801	K. Abe *et al.*	(T2K Collab.)
ABE	17C	PR D96 011102	K. Abe *et al.*	(T2K Collab.)
ABE	17F	PR D96 092006	K. Abe *et al.*	(T2K Collab.)
Also		PR D98 019902 (errat.)	K. Abe *et al.*	(T2K Collab.)
ADAMSON	17A	PRL 118 151802	P. Adamson *et al.*	(NOvA Collab.)
ADAMSON	17B	PRL 118 231801	P. Adamson *et al.*	(NOvA Collab.)
AN	17A	PR D95 072006	F.P. An *et al.*	(Daya Bay Collab.)
ESTEBAN	17	JHEP 1701 087	I. Esteban *et al.*	
KO	17	PRL 118 121802	Y.J. Ko *et al.*	(NEOS Collab.)
VINYOLES	17	APJ 835 202	N. Vinyoles *et al.*	
AARTSEN	16	PRL 117 071801	M.G. Aartsen *et al.*	(IceCube Collab.)
ABE	16B	JHEP 1601 163	Y. Abe *et al.*	(Double Chooz Collab.)
ABE	16C	PR D94 052010	K. Abe *et al.*	(Super-Kamiokande Collab.)
ABE	16D	PRL 116 181801	K. Abe *et al.*	(T2K Collab.)
ADAMSON	16	PRL 116 151806	P. Adamson *et al.*	(NOvA Collab.)
ADAMSON	16A	PR D93 051104	P. Adamson *et al.*	(NOvA Collab.)
ADAMSON	16B	PRL 117 151801	P. Adamson *et al.*	(Daya Bay and MINOS Collab.)
ADAMSON	16C	PRL 117 151803	P. Adamson *et al.*	(MINOS Collab.)
AN	16	PRL 116 061801	F.P. An *et al.*	(Daya Bay Collab.)
AN	16A	PR D93 072011	F.P. An *et al.*	(Daya Bay Collab.)
AN	16B	PRL 117 151802	F.P. An *et al.*	(Daya Bay Collab.)
CHOI	16	PRL 116 211801	J.H. Choi *et al.*	(RENO Collab.)
PDG	16	CP C40 100001	C. Patrignani *et al.*	(PDG Collab.)
AARTSEN	15A	PR D91 072004	M.G. Aartsen	(IceCube Collab.)
ABE	15D	PR D91 072010	K. Abe *et al.*	(T2K Collab.)
AGAFONOVA	15A	PRL 115 121802	N. Agafonova *et al.*	(OPERA Collab.)
AN	15	PRL 115 111802	F.P. An *et al.*	(Daya Bay Collab.)
BERGSTROM	15	JHEP 1509 200	J. Bergstrom *et al.*	(BARC, STON, MADU+)
GANDO	15	PR C92 055808	A. Gando *et al.*	(KamLAND Collab.)
ABE	14	PRL 112 181801	K. Abe *et al.*	(T2K Collab.)
Also		PR D91 072010	K. Abe *et al.*	(T2K Collab.)
ABE	14A	PL B735 51	Y. Abe *et al.*	(Double Chooz Collab.)
ABE	14B	PR D89 092003	K. Abe *et al.*	(T2K Collab.)
ABE	14C	PRL 112 061802	K. Abe *et al.*	(T2K Collab.)
ABE	14H	JHEP 1410 086	Y. Abe *et al.*	(Double Chooz Collab.)
Also		JHEP 1502 074 (errat.)	Y. Abe *et al.*	(Double Chooz Collab.)
ADAMSON	14	PRL 112 191801	P. Adamson *et al.*	(MINOS Collab.)
AN	14	PRL 112 061801	F.P. An *et al.*	(Daya Bay Collab.)
AN	14B	PR D90 071101	F.P. An *et al.*	(Daya Bay Collab.)
BELLINI	14A	NAT 512 383	G. Bellini *et al.*	(Borexino Collab.)
FORERO	14	PR D90 093006	D.V. Forero, M. Tortola, J.W.F. Valle	
GONZALEZ...	14	JHEP 1411 052	M.C. Gonzalez-Garcia, M. Maltoni, T. Schwetz	
PDG	14	CP C38 070001	K. Olive *et al.*	(PDG Collab.)
RENSHAW	14	PRL 112 091805	A. Renshaw *et al.*	(Super-Kamiokande Collab.)
AARTSEN	13B	PRL 111 081801	M.G. Aartsen *et al.*	(IceCube Collab.)
ABE	13C	PL B723 66	Y. Abe *et al.*	(Double Chooz Collab.)
ABE	13E	PR D88 032002	K. Abe *et al.*	(T2K Collab.)
ABE	13G	PRL 111 211803	K. Abe *et al.*	(T2K Collab.)
ADAMSON	13A	PRL 110 171801	P. Adamson *et al.*	(MINOS Collab.)
ADAMSON	13B	PRL 110 251801	P. Adamson *et al.*	(MINOS Collab.)
AGAFONOVA	13	JHEP 1307 004	N. Agafonova *et al.*	(OPERA Collab.)
AGUILAR-AR...	13A	PRL 110 161801	A.A. Aguilar-Arevalo *et al.*	(MiniBooNE Collab.)
AHARMIM	13	PR C88 025501	B. Aharmim *et al.*	(SNO Collab.)
AN	13	CP C37 011001	F.P. An *et al.*	(Daya Bay Collab.)
ANTONELLO	13	EPJ C73 2345	M. Antonello *et al.*	(ICARUS Collab.)
ANTONELLO	13A	EPJ C73 2599	M. Antonello *et al.*	(ICARUS Collab.)
GANDO	13	PR D88 033001	A. Gando *et al.*	(KamLAND Collab.)
ABE	12	PRL 108 131801	Y. Abe *et al.*	(Double Chooz Collab.)
ABE	12A	PR D85 031103	K. Abe *et al.*	(T2K Collab.)
ABE	12B	PR D86 052008	Y. Abe *et al.*	(Double Chooz Collab.)
ADAMSON	12	PRL 108 191801	P. Adamson *et al.*	(MINOS Collab.)
ADAMSON	12B	PR D86 052007	P. Adamson *et al.*	(MINOS Collab.)
ADRIAN-MAR...	12	PL B714 224	S. Adrian-Martinez *et al.*	(ANTARES Collab.)
AHN	12	PRL 108 191802	J.K. Ahn *et al.*	(RENO Collab.)
AN	12	PRL 108 171803	F.P. An *et al.*	(Daya Bay Collab.)
BELLINI	12A	PRL 108 051302	G. Bellini *et al.*	(Borexino Collab.)
CHENG	12	PR D86 052009	G. Cheng *et al.*	(MiniBooNE/SciBooNE Collab.)
MAHN	12	PR D85 032007	K.B.M. Mahn *et al.*	(MiniBooNE/SciBooNE Collab.)
ABE	11	PR D83 052010	K. Abe *et al.*	(Super-Kamiokande Collab.)
ABE	11A	PRL 107 041801	K. Abe *et al.*	(T2K Collab.)
ABE	11B	PR C84 035804	S. Abe *et al.*	(KamLAND Collab.)
ABE	11C	PRL 107 241801	K. Abe *et al.*	(Super-Kamiokande Collab.)
ADAMSON	11	PRL 106 181801	P. Adamson *et al.*	(MINOS Collab.)
ADAMSON	11B	PRL 107 021801	P. Adamson *et al.*	(MINOS Collab.)
ADAMSON	11C	PR D84 071103	P. Adamson *et al.*	(MINOS Collab.)
ADAMSON	11D	PRL 107 181802	P. Adamson *et al.*	(MINOS Collab.)
BELLINI	11	PL B696 191	G. Bellini *et al.*	(Borexino Collab.)
BELLINI	11A	PRL 107 141302	G. Bellini *et al.*	(Borexino Collab.)
FOGLI	11	PR D84 053007	G.L. Fogli *et al.*	
GANDO	11	PR D83 052002	A. Gando *et al.*	(KamLAND Collab.)
HUBER	11	PR C84 024617	P. Huber	(VPI)
Also		PR C85 029901 (errat.)	P. Huber	(VPI)
MUELLER	11	PR C83 054615	Th.A Mueller *et al.*	
SERENELLI	11	APJ 743 24	A.M. Serenelli, W.C. Haxton, C. Pena-Garay	
ADAMSON	10A	PR D82 051102	P. Adamson *et al.*	(MINOS Collab.)
AGUILAR-AR...	10	PRL 105 181801	A.A. Aguillar-Arevalo *et al.*	(MiniBooNE Collab.)
AHARMIM	10	PR C81 055504	B. Aharmim *et al.*	(SNO Collab.)
BELLINI	10A	PR D82 033006	G. Bellini *et al.*	(Borexino Collab.)
DENIZ	10	PR D81 072001	M. Deniz *et al.*	(TEXONO Collab.)
KAETHER	10	PL B685 47	F. Kaether *et al.*	
WENDELL	10	PR D81 092004	R. Wendell *et al.*	(Super-Kamiokande Collab.)
ABDURASHI...	09	PR C80 015807	J.N. Abdurashitov *et al.*	(SAGE Collab.)
ADAMSON	09	PRL 103 261802	P. Adamson *et al.*	(MINOS Collab.)
AGUILAR-AR...	09B	PRL 103 111801	A.A. Aguilar-Arevalo *et al.*	(MiniBooNE Collab.)

ABE	08A	PRL 100 221803	S. Abe *et al.*	(KamLAND Collab.)
Also		PRL 101 119904E	S. Abe *et al.*	(KamLAND Collab.)
ADAMSON	08	PR D77 072002	P. Adamson *et al.*	(MINOS Collab.)
ADAMSON	08A	PRL 101 131802	P. Adamson *et al.*	(MINOS Collab.)
AHARMIM	08	PRL 101 111301	B. Aharmim *et al.*	(SNO Collab.)
Also		PR C87 015502	B. Aharmim *et al.*	(SNO Collab.)
ARPESELLA	08A	PRL 101 091302	C. Arpesella *et al.*	(Borexino Collab.)
CRAVENS	08	PR D78 032002	J.P. Cravens *et al.*	(Super-Kamiokande Collab.)
FOGLI	08	PRL 101 141801	G.L. Fogli	
ADAMSON	07	PR D75 092003	P. Adamson *et al.*	(MINOS Collab.)
AGUILAR-AR...	07	PRL 98 231801	A.A. Aguilar-Arevalo *et al.*	(MiniBooNE Collab.)
AHARMIM	07	PR C75 045502	B. Aharmim *et al.*	(SNO Collab.)
ADAMSON	06	PR D73 072002	P. Adamson *et al.*	(MINOS Collab.)
AHN	06A	PR D74 072003	M.H. Ahn *et al.*	(K2K Collab.)
BALATA	06	EPJ C47 21	M. Balata *et al.*	(Borexino Collab.)
HOSAKA	06	PR D73 112001	J. Hosaka *et al.*	(Super-Kamiokande Collab.)
HOSAKA	06A	PR D74 032002	J. Hosaka *et al.*	(Super-Kamiokande Collab.)
MICHAEL	06	PRL 97 191801	D. Michael *et al.*	(MINOS Collab.)
WINTER	06A	PR C73 025503	W.T. Winter *et al.*	
YAMAMOTO	06	PRL 96 181801	S. Yamamoto *et al.*	(K2K Collab.)
AHARMIM	05A	PR C72 055502	B. Aharmim *et al.*	(SNO Collab.)
ALIU	05	PRL 94 081802	E. Aliu *et al.*	(K2K Collab.)
ALLISON	05	PR D72 052005	W.W.M. Allison *et al.*	(SOUDAN-2 Collab.)
ALTMANN	05	PL B616 174	M. Altmann *et al.*	(GNO Collab.)
ARAKI	05	PRL 94 081801	T. Araki *et al.*	(KamLAND Collab.)
ASHIE	05	PR D71 112005	Y. Ashie *et al.*	(Super-Kamiokande Collab.)
BAHCALL	05	APJ 621 L85	J.N. Bahcall, A.M. Serenelli, S. Basu	(IAS+)
DEGOUVEA	05	PR D71 093002	A. de Gouvea, C. Pena-Garay	
AHARMIM	04	PR D70 093014	B. Aharmim *et al.*	(SNO Collab.)
AHMED	04A	PRL 92 181301	S.N. Ahmed *et al.*	(SNO Collab.)
AHN	04	PRL 93 051801	M.H. Ahn *et al.*	(K2K Collab.)
AMBROSIO	04	EPJ C36 323	M. Ambrosio *et al.*	(MACRO Collab.)
ASHIE	04	PRL 93 101801	Y. Ashie *et al.*	(Super-Kamiokande Collab.)
EGUCHI	04	PRL 92 071301	K. Eguchi *et al.*	(KamLAND Collab.)
SMY	04	PR D69 011104	M.B. Smy *et al.*	(Super-Kamiokande Collab.)
AHN	03	PRL 90 041801	M.H. Ahn *et al.*	(K2K Collab.)
AMBROSIO	03	PL B566 35	M. Ambrosio *et al.*	(MACRO Collab.)
APOLLONIO	03	EPJ C27 331	M. Apollonio *et al.*	(CHOOZ Collab.)
ASTIER	03	PL B570 19	P. Astier *et al.*	(NOMAD Collab.)
EGUCHI	03	PRL 90 021802	K. Eguchi *et al.*	(KamLAND Collab.)
GANDO	03	PRL 90 171302	Y. Gando *et al.*	(Super-Kamiokande Collab.)
IANNI	03	JP G29 2107	A. Ianni	(INFN Gran Sasso)
SANCHEZ	03	PR D68 113004	M. Sanchez *et al.*	(Soudan 2 Collab.)
ABDURASHI...	02	JETP 95 181	J.N. Abdurashitov *et al.*	(SAGE Collab.)
		Translated from ZETF 122 211.		
AHMAD	02	PRL 89 011301	Q.R. Ahmad *et al.*	(SNO Collab.)
AHMAD	02B	PRL 89 011302	Q.R. Ahmad *et al.*	(SNO Collab.)
ARMBRUSTER	02	PR D65 112001	B. Armbruster *et al.*	(KARMEN 2 Collab.)
AVVAKUMOV	02	PRL 89 011804	S. Avvakumov *et al.*	(NuTeV Collab.)
FUKUDA	02	PL B539 179	S. Fukuda *et al.*	(Super-Kamiokande Collab.)
AGUILAR	01	PR D64 112007	A. Aguilar *et al.*	(LSND Collab.)
AHMAD	01	PRL 87 071301	Q.R. Ahmad *et al.*	(SNO Collab.)
AMBROSIO	01	PL B517 59	M. Ambrosio *et al.*	(MACRO Collab.)
BOEHM	01	PR D64 112001	F. Boehm *et al.*	
FUKUDA	01	PRL 86 5651	S. Fukuda *et al.*	(Super-Kamiokande Collab.)
AMBROSIO	00	PL B478 5	M. Ambrosio *et al.*	(MACRO Collab.)
BOEHM	00	PRL 84 3764	F. Boehm *et al.*	
FUKUDA	00	PRL 85 3999	S. Fukuda *et al.*	(Super-Kamiokande Collab.)
ALLISON	99	PL B449 137	W.W.M. Allison *et al.*	(Soudan 2 Collab.)
APOLLONIO	99	PL B466 415	M. Apollonio *et al.*	(CHOOZ Collab.)
Also		PL B472 434 (errat.)	M. Apollonio *et al.*	(CHOOZ Collab.)
FUKUDA	99C	PRL 82 2644	Y. Fukuda *et al.*	(Super-Kamiokande Collab.)
FUKUDA	99D	PL B467 185	Y. Fukuda *et al.*	(Super-Kamiokande Collab.)
HAMPEL	99	PL B447 127	W. Hampel *et al.*	(GALLEX Collab.)
AMBROSIO	98	PL B434 451	M. Ambrosio *et al.*	(MACRO Collab.)
APOLLONIO	98	PL B420 397	M. Apollonio *et al.*	(CHOOZ Collab.)
ATHANASSO...	98	PRL 81 1774	C. Athanassopoulos *et al.*	(LSND Collab.)
ATHANASSO...	98B	PR C58 2489	C. Athanassopoulos *et al.*	(LSND Collab.)
CLEVELAND	98	APJ 496 505	B.T. Cleveland *et al.*	(Homestake Collab.)
FELDMAN	98	PR D57 3873	G.J. Feldman, R.D. Cousins	
FUKUDA	98C	PRL 81 1562	Y. Fukuda *et al.*	(Super-Kamiokande Collab.)
HATAKEYAMA	98	PRL 81 2016	S. Hatakeyama *et al.*	(Kamiokande Collab.)
CLARK	97	PRL 79 345	R. Clark *et al.*	(IMB Collab.)
AGLIETTA	96	JETPL 63 791	M. Aglietta *et al.*	(LSD Collab.)
		Translated from ZETFP 63 753.		
ATHANASSO...	96	PR C54 2685	C. Athanassopoulos *et al.*	(LSND Collab.)
ATHANASSO...	96B	PRL 77 3082	C. Athanassopoulos *et al.*	(LSND Collab.)
FUKUDA	96	PRL 77 1683	Y. Fukuda *et al.*	(Kamiokande Collab.)
FUKUDA	96B	PL B388 397	Y. Fukuda *et al.*	(Kamiokande Collab.)
GREENWOOD	96	PR D53 6054	Z.D. Greenwood *et al.*	(UCI, SVR, SCUC)
HAMPEL	96	PL B388 384	W. Hampel *et al.*	(GALLEX Collab.)
LOVERRE	96	PL B370 156	P.F. Loverre	
ACHKAR	95	NP B434 503	B. Achkar *et al.*	(SING, SACLD, CPPM, CDEF+)
AHLEN	95	PL B357 481	S.P. Ahlen *et al.*	(MACRO Collab.)
ATHANASSO...	95	PRL 75 2650	C. Athanassopoulos *et al.*	(LSND Collab.)
DAUM	95	ZPHY C66 417	K. Daum *et al.*	(FREJUS Collab.)
HILL	95	PRL 75 2654	J.E. Hill	(PENN)
DECLAIS	94	PL B338 383	Y. Declais *et al.*	
FUKUDA	94	PL B335 237	Y. Fukuda *et al.*	(Kamiokande Collab.)
VILAIN	94C	ZPHY C64 539	P. Vilain *et al.*	(CHARM II Collab.)
FREEDMAN	93	PR D47 811	S.J. Freedman *et al.*	(LAMPF E645 Collab.)
BECKER-SZ...	92B	PR D46 3720	R.A. Becker-Szendy *et al.*	(IMB Collab.)
BEIER	92	PL B283 446	E.W. Beier *et al.*	(KAM2 Collab.)
Also		PTRSL A346 63	E.W. Beier, E.D. Frank	(PENN)
HIRATA	92	PL B280 146	K.S. Hirata *et al.*	(Kamiokande II Collab.)
CASPER	91	PRL 66 2561	D. Casper *et al.*	(IMB Collab.)
HIRATA	91	PRL 66 9	K.S. Hirata *et al.*	(Kamiokande II Collab.)
KUVSHINN...	91	JETPL 54 253	A.A. Kuvshinnikov *et al.*	(KIAE)
BERGER	90B	PL B245 305	C. Berger *et al.*	(FREJUS Collab.)
HIRATA	90	PRL 65 1297	K.S. Hirata *et al.*	(Kamiokande II Collab.)
AGLIETTA	89	EPL 8 611	M. Aglietta *et al.*	(FREJUS Collab.)
DAVIS	89	ARNPS 39 467	R. Davis, A.K. Mann, L. Wolfenstein	(BNL, PENN+)
OYAMA	89	PR D39 1481	Y. Oyama *et al.*	(Kamiokande II Collab.)
BIONTA	88	PR D38 768	R.M. Bionta *et al.*	(IMB Collab.)
DURKIN	88	PRL 61 1811	L.S. Durkin *et al.*	(OSU, ANL, CIT+)
ABRAMOWICZ	86	PRL 57 298	H. Abramowicz *et al.*	(CDHS Collab.)
ALLABY	86	PL B177 446	J.V. Allaby *et al.*	(CHARM Collab.)
ANGELINI	86	PL B179 307	C. Angelini *et al.*	(PISA, ATHU, PADO+)
VUILLEUMIER	82	PL 114B 298	J.L. Vuilleumier *et al.*	(CIT, SIN, MUNI)
BOLIEV	81	SJNP 34 787	M.M. Boliev *et al.*	(INRM)
		Translated from YAF 34 1418.		
KWON	81	PR D24 1097	H. Kwon *et al.*	(CIT, ISNG, MUNI)
BOEHM	80	PL 97B 310	F. Boehm *et al.*	(ILLG, CIT, ISNG, MUNI)
CROUCH	78	PR D18 2239	M.F. Crouch *et al.*	(CASE, UCI, WITW)

Heavy Neutral Leptons, Searches for

OMITTED FROM SUMMARY TABLE

We define searches for Heavy Neutral Leptons (HNLs) as searches for Dirac or Majorana fermions with sterile neutrino quantum numbers, that are heavy enough to not disrupt the simplest Big Bang Nucleosynthesis bounds and/or unstable on cosmological timescales: Typically HNLs have mass $\sim$ MeV or higher.

Searches for these particles generically set bounds on the mixing between the HNL and the active neutrinos, as parametrized by the extended 3×4 PMNS matrix elements $U_{\ell x}$ (see the "Neutrino mass, mixing and oscillations" review) where $\ell = e$, μ or τ, and we denote the HNL as ν_x. While many measurements may be interpreted to place bounds on various combinations of these matrix elements, we quote below limits only for those cases in which one matrix element is assumed to be much larger than the other two, i.e. $\left|U_{\ell x}\right| \gg \left|U_{\ell' x}\right|$ for $\ell' \neq \ell$.

Experimental searches make use of various different strategies, including e.g. resonance searches in missing mass decay distributions or specific final states, searches for lepton number violating decays, and trilepton signatures. The resulting bounds on $U_{\ell x}$ are typically dependent on the HNL mass. The quoted limits below are either the best limit near an experimental kinematic threshold, or a characteristic value in the mass range of the experimental sensitivity.

Limits on heavy neutral lepton mixing parameters

Limits on $|U_{ex}|^2$

Quoted limits are either the best limit near the kinematic threshold of the experiment, or a characteristic value in the mass range of the experimental sensitivity

VALUE	CL%	DOCUMENT ID		TECN	COMMENT
$<3 \times 10^{-7}$	95	[1] AAD	25AF	ATLS	$m_{\nu_x} \sim$ 10 GeV
$<1 \times 10^{-6}$	90	[2] DREWES	25	RVUE	$m_{\nu_x} \sim$ 10 MeV
$<5 \times 10^{-7}$	95	[3] HAYRAPETY...	25O	CMS	$m_{\nu_x} \sim$ 10 GeV
<0.1	95	[4] AAD	24AW	ATLS	$m_{\nu_x} \sim$ 1 TeV
$<3 \times 10^{-4}$	95	[5] AAD	24BU	ATLS	$m_{\nu_x} \sim$ 20–50 GeV
$<4 \times 10^{-6}$	95	[6] HAYRAPETY...	24AB	CMS	$m_{\nu_x} \sim$ 20–60 GeV
$<1 \times 10^{-3}$	95	[6] HAYRAPETY...	24AB	CMS	$m_{\nu_x} \gtrsim m_W$
$<1 \times 10^{-5}$	95	[7] HAYRAPETY...	24S	CMS	$m_{\nu_x} \sim$ 2.5 GeV
$<3 \times 10^{-4}$	90	[8] AGNES	23A	DS50	$m_{\nu_x} \sim$ 7–35 keV
$<3 \times 10^{-8}$	90	[9] BAROUKI	22	RVUE	Near $m_{D_s} - m_e$ kin. thres.
$<1 \times 10^{-6}$	95	[10] TUMASYAN	22AD	CMS	$m_{\nu_x} \sim$ 8–14 GeV, pp at 13 TeV
$<2 \times 10^{-4}$	95	[11] FRIEDRICH	21		Near $m_{^7\mathrm{Be}} - m_{^7\mathrm{Li}}$ kin. thres.
$<1 \times 10^{-9}$	90	[12] CORTINA-GIL	20	NA62	$m_{\nu_x} \sim$ 150–400 MeV
$<2 \times 10^{-5}$	95	[13] AAD	19F	ATLS	$m_{\nu_x} \sim$ 15–40 GeV
$<1 \times 10^{-9}$	90	[14] ABE	19B	T2K	Near $m_K - m_e$ kin. thres.
$<1 \times 10^{-4}$	90	[15] ABLIKIM	19AL	BES3	$m_{\nu_x} \sim$ 0.3–0.7 GeV
$<2 \times 10^{-7}$	90	[16] BRYMAN	19	RVUE	$m_{\nu_x} \sim$ 55 MeV
$<1 \times 10^{-8}$	90	[17] AGUILAR-AR...	18A	PIEN	$m_{\nu_x} \sim$ 60–120 MeV
$<3 \times 10^{-7}$	90	[18] CORTINA-GIL	18	NA62	$m_{\nu_x} \sim$ 200–400 MeV
$<1 \times 10^{-6}$	90	[19] PARK	16	BELL	$m_{\nu_x} \sim$ 1.4 GeV
$<3 \times 10^{-5}$	90	[20] LIVENTSEV	13	BELL	Near $m_{\nu_x} \sim$ 2–2.5 GeV
$<3 \times 10^{-5}$	95	[21] ABREU	97I	DLPH	$m_{\nu_x} \sim$ 6–50 GeV
$<2 \times 10^{-5}$	95	[22] ABREU	97I	DLPH	Near $m_{\nu_x} \sim$ 3.5 GeV
$<1 \times 10^{-5}$	90	[23] BARANOV	93		Near $m_\pi - m_e$ kin. thres.
$<2 \times 10^{-7}$	90	[23] BARANOV	93		Near $m_K - m_e$ kin. thres.
$<1 \times 10^{-7}$		[24,25] BERNARDI	88	CNTR	Near $m_\pi - m_e$ kin. thres.
$<2 \times 10^{-9}$		[25,26] BERNARDI	88	CNTR	Near $m_K - m_e$ kin. thres.
$<1 \times 10^{-7}$	90	[27] DORENBOS...	86	CHRM	Near $m_D - m_e$ kin. thres.
$<1 \times 10^{-7}$	90	[28] COOPER-...	85	BEBC	Near $m_D - m_e$ kin. thres.
• • • We do not use the following data for averages, fits, limits, etc. • • •					
not seen		[29] ABLIKIM	25BC	BES3	$m_{\nu_x} \sim$ 0.2–0.8 GeV
$<1 \times 10^{-6}$	95	[30] HAYRAPETY...	24V	CMS	Superseded by HAYRAPETYAN 24O. $m_{\nu_x} \sim$ 10 GeV
$<5 \times 10^{-7}$	95	[31] AAD	23AO	ATLS	Superseded by AAD 25AF. $m_{\nu_x} \sim$ 3–15 GeV, pp at 13 TeV
$<2 \times 10^{-5}$	95	[32] SIRUNYAN	18K	CMS	$m_{\nu_x} \sim$ 20–60 GeV
$<1 \times 10^{-2}$	95	[32] SIRUNYAN	18K	CMS	$m_{\nu_x} \gtrsim m_W$

Int. J. Mod
by UNIVERSITY OF CALIFORNIA @ BERK
wnloaded from www.worldscientific.com
-use and distribution is strictly not permitted, except for Open Access articles.

Int. J. Mod. Phys. A 2026.41. Downloaded from www.worldscientific.com
by UNIVERSITY OF CALIFORNIA @ BERKELEY on 09/16/26. Re-use and distribution is strictly not permitted, except for Open Access articles.

[1] AAD 25AF searches for $W \to e\nu_X$ with displaced decay $\nu_X \to ee\nu$, $\nu_X \to e\mu\nu$ or $\nu_X \to e\pi$ over the range $m_{\nu_X} \sim$ 0.5–16 GeV. Limits are set for both Dirac and Majorana HNLs, as well as for for case in which the mixing coefficients to all three lepton generations are non-zero.

[2] DREWES 25 searches for displaced decays $\nu_X \to e^+e^-\nu_e$ from solar-produced HNLs, mainly via ^{8}B $\to$ ^{8}Be$e\nu_X$, over the range $m_{\nu_X} \sim$ 1–16 MeV. Limits are derived using data from the space-based detectors Ulysses and the Solar and Heliospheric Observatory. Limits are set for both Dirac and Majorana HNLs, being slightly stronger for the latter.

[3] HAYRAPETYAN 25O searches for $W \to e\nu_X$ with displaced decay $\nu_X \to ej$, i.e. with one jet, over the range $m_{\nu_X} \sim$ 1–16.5 GeV. Limits are set for both Dirac and Majorana HNLs, as well as for the $e\mu j$ final states in terms of the product of electron and muon-HNL couplings.

[4] AAD 24AW search for scattering of same-sign boson pairs into same-sign electron pairs, mediated by a virtual Majorana HNL, in the HNL mass range 50 GeV to 20 TeV. Limits are also set for $|V_{eX} V^*_{\mu X}|$.

[5] AAD 24BU search for same-sign electron pairs in semileptonic decays of top quarks via a Majorana HNL, in the HNL mass range 15–75 GeV.

[6] HAYRAPETYAN 24AB search for $W \to e\nu_X \to ee\ell\nu_\ell$ prompt decays assuming coupling to a single SM generation, between 10–1500 GeV. Above m_{ν_X} ¿ m_W, sensitivity is greatly reduced by the required virtuality of the HNL. Results are quoted for a mass range below m_W and just above m_W, for Majorana HNLs. Similar (weaker) limits also for Dirac HNLs are presented.

[7] HAYRAPETYAN 24S search for $W \to e\nu_X$ followed by ν_X displaced decay in flight to electromagnetic and hadronic showers in the CMS muon chamber, in the mass range $m_{\nu_X} \sim$ 1–3 GeV. Limits are set for both Majorana and Dirac HNLs. This long-lived particle style search results in an exclusion region in the coupling-mass plane whose upper contour is determined by an insufficiently long HNL lifetime to reach the muon chambers, and lower contour by insufficient HNL production. The intersection of these, and thus the extent of the experimental sensitivity, occurs at $m_{\nu_X} \sim$ 3 GeV.

[8] Search for ionization signals in an LArTPC. Assumes the candidate particle is 100% of dark matter.

[9] Reanalysis of BEBC results (cf. COOPER-SARKAR 85) to update searches for $D_s^\pm \to \nu_X e^\pm$ using a corrected formula for the HNL decay probabilities, additional production channels, and an improved fit for the charm meson distributions. Assumes a Majorana HNL.

[10] TUMASYAN 22AD search for $W \to e\nu_X$, $\nu_X \to e\mu\nu_\mu$ and set limits for Dirac and Majorana Heavy Neutral Leptons. The data correspond to an integrated luminosity of 138 fb^{-1}.

[11] Search in electron capture decay ^{7}Be $\to$ ^{7}Liν_X. Kinematic threshold is $\sim$ 850 keV.

[12] Search for $K^+ \to e^+\nu_X$. Assumes lifetime of ν_X > 50 ns.

[13] Limit from prompt lepton number violating trilepton search.

[14] $K^+ \to e^+\nu_X$, with ν_X decay through U_{eX}. ABE 19B also considers bounds on $|U_{\ell X} U_{\ell' X}|$ for combinations of lepton flavors in the ν_X decay final state.

[15] Searches for a Majorana Heavy Neutral Lepton producing a $\pi^- e^+$ resonance in the same sign dilepton decay $D \to K\pi^- e^+ e^+$.

[16] BRYMAN 19 sets best limits $|U_{eX}|^2 < 1\times10^{-4}$–$2\times10^{-7}$ in the mass range $m_{\nu_X} \sim$ 2–55 MeV, respectively, using the precision branching ratio measurement in AGUILAR-AREVALO 15. See also BRYMAN 19A.

[17] Search for $\pi^+ \to e^+\nu_X$.

[18] Search for $K^+ \to e^+\nu_X$.

[19] PARK 16 quotes an approximate limit B($B^+ \to e^+\nu_X$) < 3×10^{-6} in the mass range $m_{\nu_X} \sim$ 0.2–1.4 GeV.

[20] Search for $B^+ \to e^+\nu_X$.

[21] Search for prompt ν_X decay signatures.

[22] Search for displaced ν_X decay signatures.

[23] Searches for K or $\pi \to e^+\nu_X$, $\nu_X \to e^+e^-\nu_e$ using a beam dump experiment at the 70 GeV Serpukhov proton synchrotron. BARANOV 93 also considers limits for $|U_{eX} U_{\mu X}|$ from K or $\pi \to \mu^+\nu_X$, $\nu_X \to e^+e^-\nu_e$.

[24] $\pi^+ \to e^+\nu_X$, with ν_X decay through U_{eX}.

[25] BERNARDI 88 also considers bounds on $|U_{eX} U_{\mu X}|$.

[26] $K^+ \to e^+\nu_X$, with ν_X decay through U_{eX}.

[27] $D^+ \to e^+\nu_X$, with $\nu_X \to e^-\ell^+\nu_\ell$.

[28] $D^+ \to e^+\nu_X$, with $\nu_X \to e^-\ell^+\nu_\ell$ or $\nu_X \to e^-\pi^+$.

[29] ABLIKIM 25BC search for $D_s^+ \to \phi e^+\nu_X$, $\nu_X \to \pi^- e^+$ in the mass range 0.2–0.8 GeV, and set limits on its branching fraction in the range 10^{-5}–10^{-2} at 90% CL, respectively.

[30] HAYRAPETYAN 24V searches for $W \to e\nu_X$ with displaced decay $\nu_X \to ej$, i.e. with one jet, over the range $m_{\nu_X} \sim$ 2–20 GeV. Limits are set for both Dirac and Majorana HNLs.

[31] AAD 23AO search for $W \to \nu_X e$, for both Majorana and Dirac HNL scenarios. Also consider scenarios involving multiflavor mixing, with correspondingly weaker limits.

[32] Superseded by HAYRAPETYAN 24AB.

Limits on $|U_{\mu X}|^2$

Quoted limits are either the best limit near the kinematic threshold of the experiment, or a characteristic value in the mass range of the experimental sensitivity

VALUE	CL%	DOCUMENT ID		TECN	COMMENT
$<1 \times 10^{-7}$	95	[1] AAD	25AF	ATLS	$m_{\nu_X} \sim$ 12 GeV
$<2 \times 10^{-7}$	95	[2] HAYRAPETY...	25O	CMS	$m_{\nu_X} \sim$ 10 GeV
$<1 \times 10^{-4}$	95	[3] AAD	24BU	ATLS	$m_{\nu_X} \sim$ 20–50 GeV
$<3 \times 10^{-8}$	90	[4] ABRATENKO	24	MBNE	Near $m_K - m_\pi - m_\mu$ kin. thres.
$<1 \times 10^{-6}$	90	[4] ABRATENKO	24	MBNE	$m_{\nu_X} \sim$ 150 MeV
$<3 \times 10^{-6}$	95	[5] HAYRAPETY...	24AB	CMS	$m_{\nu_X} \sim$ 20–60 GeV
$<1 \times 10^{-3}$	95	[5] HAYRAPETY...	24AB	CMS	$m_{\nu_X} \gtrsim m_W$
$<3 \times 10^{-5}$	95	[6] HAYRAPETY...	24AC	CMS	$m_{\nu_X} \sim$ 1–3 GeV
$<5 \times 10^{-6}$	95	[7] HAYRAPETY...	24S	CMS	$m_{\nu_X} \sim$ 3 GeV
<0.1	95	[8] AAD	23CE	ATLS	Near $m_{\nu_X} \sim$ 0.1–2 TeV
<0.1	95	[9] TUMASYAN	23AC	CMS	Near $m_{\nu_X} \sim$ 0.1–3 TeV
$<5 \times 10^{-9}$	90	[10] ABRATENKO	22A	MBNE	Near $m_K - m_\mu$ kin. thres.
$<3 \times 10^{-7}$	95	[11] TUMASYAN	22AD	CMS	$m_{\nu_X} \sim$ 8–14 GeV, pp at 13 TeV
$<1 \times 10^{-3}$	95	[12] AAIJ	21AA	LHCB	$m_{\nu_X} \sim$ 5–50 GeV, pp at 7, 8 TeV
$<2 \times 10^{-4}$	95	[13] AAIJ	21AA	LHCB	$m_{\nu_X} \sim$ 5–50 GeV, pp at 7, 8 TeV
$<5 \times 10^{-9}$	90	[14,15] CORTINA-GIL	21	NA62	Near $m_K - m_\mu$ kin. thres.
$<2 \times 10^{-2}$	90	[16] PRIM	20	BELL	$m_{\nu_X} \sim$ 1 GeV
$<2 \times 10^{-5}$	95	[17] AAD	19F	ATLS	$m_{\nu_X} \sim$ 10–50 GeV
$<2 \times 10^{-6}$	95	[18] AAD	19F	ATLS	$m_{\nu_X} \sim$ 10 GeV
$<1 \times 10^{-9}$	90	[19] ABE	19B	T2K	Near $m_K - m_\mu$ kin. thres.
$<5 \times 10^{-6}$	90	[20,21] AGUILAR-AR...	19B	PIEN	$m_{\nu_X} \sim$ 16–30 MeV
$<1 \times 10^{-5}$	90	[21] AGUILAR-AR...	19B	PIEN	Near $m_\pi - m_\mu$ kin. thres.
$<3 \times 10^{-7}$	90	[14] CORTINA-GIL	18	NA62	$m_{\nu_X} \sim$ 250–350 MeV
$<3 \times 10^{-6}$	90	[14] LAZZERONI	17A	NA62	Near $m_K - m_\mu$ kin. thres.
$<5 \times 10^{-2}$	90	[22] PARK	16	BELL	$m_{\nu_X} \sim$ 1.4 GeV
$<1 \times 10^{-8}$	90	[14] ARTAMONOV	15A	B949	$m_{\nu_X} \sim$ 200–300 MeV
$<3 \times 10^{-5}$	90	[23] LIVENTSEV	13	BELL	Near $m_{\nu_X} \sim$ 2–2.5 GeV
$<2.0 \times 10^{-8}$	95	[24] DAUM	00	KARM	$m_{\nu_X} =$ 33.905 MeV
$<8 \times 10^{-8}$	90	[25] VAITAITIS	99	CCFR	Near $m_K - m_\mu$ kin. thres.
$<6 \times 10^{-8}$	90	[26] VAITAITIS	99	CCFR	Near $m_{D_s} - m_\mu$ kin. thres.
$<3 \times 10^{-5}$	95	[27] ABREU	97I	DLPH	$m_{\nu_X} \sim$ 6–50 GeV
$<2 \times 10^{-5}$	95	[28] ABREU	97I	DLPH	Near $m_{\nu_X} \sim$ 3.5 GeV
$<3 \times 10^{-5}$	90	[29] VILAIN	95C	CHM2	Near $m_K - m_\mu$ kin. thres.
$<3 \times 10^{-8}$		[30,31] BERNARDI	88	CNTR	Near $m_\mu + m_\pi$ kin. thres.
$<2 \times 10^{-9}$		[31,32] BERNARDI	88	CNTR	Near $m_K - m_\mu$ kin. thres.
$<1 \times 10^{-7}$	90	[33] DORENBOS...	86	CHRM	Near $m_D - m_\mu$ kin. thres.
$<1 \times 10^{-7}$	90	[34] COOPER-...	85	BEBC	Near $m_D - m_\mu$ kin. thres.
$<1 \times 10^{-6}$	90	[35] HAYANO	82	CNTR	$m_{\nu_X} \sim$ 200–300 MeV
• • • We do not use the following data for averages, fits, limits, etc. • • •					
$<5 \times 10^{-7}$	95	[36] HAYRAPETY...	24V	CMS	Superseded by HAYRAPETYAN 24O. $m_{\nu_X} \sim$ 10 GeV
$<5 \times 10^{-7}$	95	[37] AAD	23AO	ATLS	Superseded by AAD 25AF. $m_{\nu_X} \sim$ 3–15 GeV, pp at 13 TeV
$<1 \times 10^{-7}$	90	[38] ABRATENKO	20	MBNE	Superseded by ABRATENKO 22A
$<2 \times 10^{-5}$	95	[39] SIRUNYAN	18K	CMS	$m_{\nu_X} \sim$ 20–60 GeV
$<5 \times 10^{-3}$	95	[39] SIRUNYAN	18K	CMS	$m_{\nu_X} \gtrsim m_W$

[1] AAD 25AF searches for $W \to \mu\nu_X$ with displaced decay $\nu_X \to \mu\mu\nu$, $\nu_X \to e\mu\nu$ or $\nu_X \to \mu\pi$ over the range $m_{\nu_X} \sim$ 0.5–16 GeV. Limits are set for both Dirac and Majorana HNLs, as well as for for case in which the mixing coefficients to all three lepton generations are non-zero.

[2] HAYRAPETYAN 25O searches for $W \to \mu\nu_X$ with displaced decay $\nu_X \to \mu j$, i.e. with one jet, over the range $m_{\nu_X} \sim$ 1–16.5 GeV. Limits are set for both Dirac and Majorana HNLs, as well as for the $e\mu j$ final states in terms of the product of electron and muon-HNL couplings.

[3] AAD 24BU search for same-sign muon pairs in semileptonic decays of top quarks via a Majorana HNL, in the HNL mass range 15–75 GeV.

[4] ABRATENKO 24 search for $K^+ \to \mu^+\nu_X$, with $\nu_X \to \nu_\mu e^+e^-$ and $\nu_X \to \nu_\mu\pi^0 \to \nu_\mu\gamma\gamma$ in the mass ranges $m_{\nu_X} \sim$ 10–150 MeV and $m_{\nu_X} \sim$ 150–245 MeV, respectively, for the case of a Majorana HNL. The π^0 mode dominates above $m_{\nu_X} \sim$ 150 MeV.

[5] HAYRAPETYAN 24AB search for $W \to \mu\nu_X \to \mu\mu\ell\nu_\ell$ prompt decays assuming coupling to a single SM generation, between 10–1500 GeV. Above m_{ν_X} ¿ m_W, sensitivity is greatly reduced by the required virtuality of the HNL. Results are quoted for a mass range below m_W and just above m_W, for Majorana HNLs. Similar (weaker) limits also for Dirac HNLs are presented.

[6] HAYRAPETYAN 24AC search for $B \to X\mu\nu_X$ and $B \to \mu\nu_X$ followed by displaced $\nu_X \to \mu\pi^\pm$ decay, where X is an unreconstructed hadronic system, for Majorana HNLs. Also considers mixed flavor scenarios with $e\mu$ final state lepton pairs, and presents similar (weaker) limits for Dirac HNLs.

[7] HAYRAPETYAN 24S search for $W \to \mu\nu_X$ followed by ν_X displaced decay in flight to electromagnetic and hadronic showers in the CMS muon chamber, in the mass range $m_{\nu_X} \sim$ 1–3 GeV. Limits are set for both Majorana and Dirac HNLs. This long-lived particle style search results in an exclusion region in the coupling-mass plane whose upper contour is determined by an insufficiently long HNL lifetime to reach the muon chambers, and lower contour by insufficient HNL production. The intersection of these, and thus the extent of the experimental sensitivity, occurs at $m_{\nu_X} \sim$ 3.5 GeV.

[8] AAD 23CE search for Majorana HNLs via vector boson fusion $W^\pm W^\pm \to \mu^\pm\mu^\pm$. Limits set in a m_{ν_X} mass range from 50 GeV up to 20 TeV, using the Phenomenological Type-I Seesaw model as a benchmark scenario.

[9] TUMASYAN 23AC search for Majorana HNLs via vector boson fusion $W^\pm W^\pm \to \mu^\pm\mu^\pm$. Limits set in a m_{ν_X} mass range from 50 GeV up to 25 TeV.

[10] ABRATENKO 22A search for $K^+ \to \mu^+\nu_X$, with $\nu_X \to \mu^\mp\pi^\pm$, in the mass range $m_{\nu_X} \sim$ 246–385 MeV. Also considers limits from $\nu_X \to \mu^-\pi^+$ only, for the case of a Dirac HNL.

[11] TUMASYAN 22AD search for $W \to \mu\nu_X$, $\nu_X \to \mu e\nu_e$ and set limits for Dirac and Majorana Heavy Neutral Leptons. The data correspond to an integrated luminosity of 138 fb^{-1}.

[12] Limit from prompt lepton number conserving $W \to \mu\mu j$ search.

[13] Limit from prompt lepton number violating $W \to \mu\mu j$ search.

[14] Search for $K^+ \to \mu^+\nu_X$.

[15] Assumes a lifetime exceeding 50 ns, and searches over m_{ν_X} range 200–384 MeV.

[16] Search for $B^+ \to \mu^+\nu_X$ in the mass range $m_{\nu_X} \sim$ 0–1.5 GeV.

[17] Limit from prompt lepton number violating trilepton search.

[18] Limit from displaced lepton violating or conserving trilepton searches.

[19] $K^+ \to \mu^+\nu_X$, with ν_X decay through $U_{\mu X}$. ABE 19B also considers bounds on $|U_{\ell X}\ U_{\ell' X}|$ for combinations of lepton flavors in the ν_X decay final state.

[20] Limit requires muon kinetic energy > 1.2 MeV.

[21] Search for $\pi^+ \to \mu^+\nu_X$.

[22] PARK 16 quotes an approximate limit $B(B^+ \to \mu^+\nu_X) < 3\times10^{-6}$ in the mass range $m_{\nu_X} \sim$ 0.2–1.4 GeV.

[23] Search for $B^+ \to \mu^+\nu_X$.

[24] DAUM 00 quotes a branching ratio bound $B(\pi^+ \to \mu^+\nu_X) < 6.0\times10^{-10}$ at 95% CL.

[25] $K^+ \to \mu^+\nu_X$, with $\nu_X \to \mu X$.

[26] $D_s \to \mu^+\nu_X$, with $\nu_X \to \mu X$.

[27] Search for prompt ν_X decay signatures.

[28] Search for displaced ν_X decay signatures.

[29] Search for Heavy Neutral Leptons produced by neutral current muon neutrino interactions, with $\nu_X \to \mu^+\mu^-\nu_\mu$.

[30] $K^+ \to \mu^+\nu_X$, with ν_X decay through $U_{\mu X}$ and $m_{\nu_X} < m_\mu + m_\pi$.

[31] BERNARDI 88 also considers bounds on $|U_{eX}\ U_{\mu X}|$.

[32] $K^+ \to \mu^+\nu_X$, with $\nu_X \to \mu^-\pi^+$.

[33] $D^+ \to \mu^+\nu_X$, with $\nu_X \to \mu^-\ell^+\nu_\ell$.

[34] $D^+ \to \mu^+\nu_X$, with $\nu_X \to \mu^-\ell^+\nu_\ell$ or $\nu_X \to \mu^-\pi^+$.

[35] Search for $K^+ \to \mu^+\nu_X(\gamma)$.

[36] HAYRAPETYAN 24V searches for $W \to \mu\nu_X$ with displaced decay $\nu_X \to \mu j$, i.e. with one jet, over the range $m_{\nu_X} \sim$ 2–20 GeV. Limits are set for both Dirac and Majorana HNLs.

[37] AAD 23AO search for $W \to \nu_X\mu$, for both Majorana and Dirac HNL scenarios. Also consider scenarios involving multiflavor mixing, with correspondingly weaker limits.

[38] $K^+ \to \mu^+\nu_X$, with $\nu_X \to \mu^-\pi^+$, in the mass range $m_{\nu_X} \sim$ 260–385 MeV. ABRATENKO 20 also considers $\nu_X \to \mu^+\pi^-$ for the case of a Majorana HNL.

[39] Superseded by HAYRAPETYAN 24AB.

Limits on $|U_{\tau X}|^2$

Quoted limits are either the best limit near the kinematic threshold of the experiment, or a characteristic value in the mass range of the experimental sensitivity

VALUE	CL%	DOCUMENT ID		TECN	COMMENT
<0.1	95	[1] AAD	24BU	ATLS	$m_{\nu_X} \sim$ 20–50 GeV
$<6\times10^{-4}$	95	[2] HAYRAPETY...	24AB	CMS	$m_{\nu_X} \sim$ 20–60 GeV
$<1\times10^{-1}$	95	[2] HAYRAPETY...	24AB	CMS	$m_{\nu_X} \gtrsim m_W$
$<3\times10^{-4}$	95	[3] HAYRAPETY...	24S	CMS	$m_{\nu_X} \sim$ 2 GeV
$<1\times10^{-2}$	95	[4] HAYRAPETY...	24V	CMS	$m_{\nu_X} \sim$ 3–20 GeV
$<1\times10^{-3}$	90	[5] NAYAK	24	BELL	Near $m_\tau - m_\pi$ kin. thres.
$<1\times10^{-5}$	95	[6] LEES	23A	BABR	Near $m_\tau - 3m_\pi$ kin. thres.
$<2\times10^{-6}$	90	[7] BAROUKI	22	RVUE	Near $m_\tau - m_\nu$ kin. thres.
$<3\times10^{-4}$	90	[8] ACCIARRI	21	ARNT	Near $m_{\nu_X} \lesssim$ 970 MeV
$<3\times10^{-6}$	90	[9] BOIARSKA	21	RVUE	Near $m_{\nu_X} \sim$ 0.8–1.6 GeV
$<2\times10^{-4}$	90	[10] ORLOFF	02	CHRM	Near $m_D - m_\tau$ kin. thres.
$<1\times10^{-4}$	90	[11] ORLOFF	02	CHRM	$m_{\nu_X} \sim$ 200–250 MeV
$<3\times10^{-5}$	95	[12] ABREU	97I	DLPH	$m_{\nu_X} \sim$ 6–50 GeV
$<2\times10^{-5}$	95	[13] ABREU	97I	DLPH	Near $m_{\nu_X} \sim$ 3.5 GeV
• • • We do not use the following data for averages, fits, limits, etc. • • •					
		[14] LIVENTSEV	23	BELL	Near $m_{\nu_X} \sim$ 0.8–1.2 GeV
		[15] TUMASYAN	22H	CMS	pp at 13 TeV

[1] AAD 24BU search for same-sign tau pairs in semileptonic decays of top quarks via a Majorana HNL, in the HNL mass range 15–75 GeV.

[2] HAYRAPETYAN 24AB search for $W \to \tau\nu_X \to \tau\tau\ell\nu_\ell$ prompt decays assuming coupling to a single SM generation, between 10–1500 GeV. Above m_{ν_X} ¿ m_W, sensitivity is greatly reduced by the required virtuality of the HNL. Results are quoted for a mass range below m_W and just above m_W, for Majorana HNLs. Similar (weaker) limits also for Dirac HNLs are presented.

[3] HAYRAPETYAN 24S search for $W \to \tau\nu_X$ followed by ν_X displaced decay in flight to electromagnetic and hadronic showers in the CMS muon chamber, in the mass range $m_{\nu_X} \sim$ 1–2 GeV. Limits are set for both Majorana and Dirac HNLs. This long-lived particle style search results in an exclusion region in the coupling-mass plane whose upper contour is determined by an insufficiently long HNL lifetime to reach the muon chambers, and lower contour by insufficient HNL production. The intersection of these, and thus the extent of the experimental sensitivity, occurs at $m_{\nu_X} \sim$ 2 GeV.

[4] HAYRAPETYAN 24V searches for $W \to \tau\nu_X$ with displaced decay $\nu_X \to \tau j$, i.e. with one jet, over the range $m_{\nu_X} \sim$ 3–20 GeV. Limits are set for both Dirac and Majorana HNLs.

[5] NAYAK 24 searches for $\tau \to \pi\nu_X$ with displaced decay $\nu_X \to \nu_\tau\mu^+\mu^-$ in the Belle central drift chamber (CDC). This long-lived particle style search results in an exclusion region in the coupling-mass plane whose upper contour is determined by an insufficiently long HNL lifetime to reach the CDC, and lower contour by insufficient HNL production. Limits are set for both Dirac and Majorana HNLs.

[6] Search for $\tau^\pm \to \pi^\pm\pi^+\pi^-\nu_X$.

[7] Reanalysis of BEBC results (cf. COOPER-SARKAR 85) to include searches for $D_s^\pm \to \nu_\tau\tau^\pm$, $\tau^\pm \to \nu_X\pi^\pm$, $\nu_X\rho^\pm$, or $\nu_X\nu_\tau\ell^\pm$ via $U_{\tau X}$. Assumes a Majorana HNL.

[8] Search for $\nu_X \to \mu^+\mu^-\nu$.

[9] Reanalysis of CHARM results (cf. ORLOFF 02) to include searches for $\nu_X \to \nu\ell^+\ell^-$ decays, and including the production of HNLs from τ decays.

[10] $D_s \to \tau^+\nu_X$, with ν_X decay via $U_{\tau X}$.

[11] $D_s \to \nu_\tau\tau^+$, $\tau^+ \to \nu_X X$, with ν_X decay via $U_{\tau X}$.

[12] Search for prompt ν_X decay signatures.

[13] Search for displaced ν_X decay signatures. Kinematical suppression of $\nu_X \to \tau X$ at lower masses leads to rapid loosening of the $|U_{\tau X}|$ bound compared to that for $|U_{eX}|$ and $|U_{\mu X}|$.

[14] Search for $\tau \to \pi\nu_X$, $\nu_X \to \pi e$ or $\pi\mu$ in the range 0.2–1.6 GeV. LIVENTSEV 23 reports results for the sum $\Sigma_{\ell=e,\mu,\tau}|U_{\ell X}|^2$ in a model-dependent context, but which may be roughly reinterpreted as a limit $|U_{eX}\ U_{\tau X}|^2 + |U_{\mu X}\ U_{\tau X}|^2 \lesssim 5\times10^{-9}$ in either Majorana or Dirac HNL scenarios.

[15] TUMASYAN 22H sets limits on an approximately mass-degenerate vector-like lepton SU(2) doublet coupling to the τ. Some of the reported signal region distributions might be used to set limits for heavy neutral leptons coupled to the τ. The data correspond to an integrated luminosity of 138 fb^{-1}.

REFERENCES FOR Heavy Neutral Leptons, Searches for

AAD	25AF	JHEP 2507 196	G. Aad et al.	(ATLAS Collab.)
ABLIKIM	25BC	JHEP 2501 109	M. Ablikim et al.	(BESIII Collab.)
DREWES	25	PR D111 095001	M. Drewes, J. Heisig, V. Weber	(LOUV, AACH)
HAYRAPETY...	25O	JHEP 2502 036	A. Hayrapetyan et al.	(CMS Collab.)
AAD	24AW	PL B856 138865	G. Aad et al.	(ATLAS Collab.)
AAD	24BU	PR D110 112004	G. Aad et al.	(ATLAS Collab.)
ABRATENKO	24	PRL 132 041801	P. Abratenko et al.	(MicroBooNE Collab.)
HAYRAPETY...	24AB	JHEP 2406 123	A. Hayrapetyan et al.	(CMS Collab.)
HAYRAPETY...	24AC	JHEP 2406 183	A. Hayrapetyan et al.	(CMS Collab.)
HAYRAPETY...	24O	PR D109 112003	A. Hayrapetyan et al.	(CMS Collab.)
HAYRAPETY...	24S	PR D110 012004	A. Hayrapetyan et al.	(CMS Collab.)
HAYRAPETY...	24V	JHEP 2403 105	A. Hayrapetyan et al.	(CMS Collab.)
NAYAK	24	PR D109 L111102	M. Nayak et al.	(BELLE Collab.)
AAD	23AO	PRL 131 061803	G. Aad et al.	(ATLAS Collab.)
AAD	23CE	EPJ C83 824	G. Aad et al.	(ATLAS Collab.)
AGNES	23A	PRL 130 101002	P. Agnes et al.	(DarkSide-50 Collab.)
LEES	23A	PR D107 052009	J.P. Lees et al.	(BABAR Collab.)
LIVENTSEV	23	PRL 131 211802	D. Liventsev et al.	(BELLE Collab.)
TUMASYAN	23AC	PRL 131 011803	A. Tumasyan et al.	(CMS Collab.)
ABRATENKO	22A	PR D106 092006	P. Abratenko et al.	(MicroBooNE Collab.)
BAROUKI	22	SCP 13 118	R. Barouki, G. Marocco, S. Sarkar	(OXF)
TUMASYAN	22AD	JHEP 2207 081	A. Tumasyan et al.	(CMS Collab.)
TUMASYAN	22H	PR D105 112007	A. Tumasyan et al.	(CMS Collab.)
AAIJ	21AA	EPJ C81 248	R. Aaij et al.	(LHCb Collab.)
ACCIARRI	21	PRL 127 121801	R. Acciarri et al.	(ArgoNeuT Collab.)
BOIARSKA	21	PR D104 095019	I. Boiarska et al.	(BOHR, LEID)
CORTINA-GIL	21	PL B816 136259	E. Cortina Gil et al.	(NA62 Collab.)
FRIEDRICH	21	PRL 126 021803	S. Friedrich et al.	(BeEST Collab.)
ABRATENKO	20	PR D101 052001	P. Abratenko et al.	(MiniBooNE Collab.)
CORTINA-GIL	20	PL B807 135599	E. Cortina Gil et al.	(NA62 Collab.)
PRIM	20	PR D101 032007	M.T. Prim et al.	(BELLE Collab.)
AAD	19F	JHEP 1910 265	G. Aad et al.	(ATLAS Collab.)
ABE	19B	PR D100 052006	K. Abe et al.	(T2K Collab.)
ABLIKIM	19AL	PR D99 112002	M. Ablikim et al.	(BESIII Collab.)
AGUILAR-AR...	19B	PL B798 134980	A. Aguilar-Arevalo et al.	(PIENU Collab.)
BRYMAN	19	PR D100 053006	D.A. Bryman, R. Shrock	(BRCO, TRIU, STON)
BRYMAN	19A	PR D100 073011	D.A. Bryman, R. Shrock	(BRCO, TRIU, STON)
AGUILAR-AR...	18A	PR D97 072012	A. Aguilar-Arevalo et al.	(PIENU Collab.)
CORTINA-GIL	18	PL B778 137	E. Cortina Gil et al.	(NA62 Collab.)
SIRUNYAN	18K	PRL 120 221801	A.M. Sirunyan et al.	(CMS Collab.)
LAZZERONI	17A	PL B772 712	C. Lazzeroni et al.	(NA62 Collab.)
PARK	16	PR D94 012003	C.-S. Park et al.	(BELLE Collab.)
AGUILAR-AR...	15	PRL 115 071801	A. Aguilar-Arevalo et al.	(PIENU Collab.)
ARTAMONOV	15A	PR D91 052001	A.V. Artamanov et al.	(E949 Collab.)

Int. J. Mod
by UNIVERSITY OF CALIFORNIA @ BERK
wnloaded from www.worldscientific.com
-use and distribution is strictly not permitted, except for Open Access articles.

LIVENTSEV	13	PR D87 071102	D. Liventsev *et al.*	(BELLE Collab.)
Also		PR D95 099903 (errat.)	D. Liventsev *et al.*	(BELLE Collab.)
ORLOFF	02	PL B550 8	J. Orloff *et al.*	(CHARM Collab.)
DAUM	00	PRL 85 1815	M. Daum *et al.*	(KARMEN Collab.)
VAITAITIS	99	PRL 83 4943	A. Vaitaitis *et al.*	(CCFR Collab.)
ABREU	97I	ZPHY C74 57	P. Abreu *et al.*	(DELPHI Collab.)
Also		ZPHY C75 580 (errat.)	P. Abreu *et al.*	(DELPHI Collab.)
VILAIN	95C	PL B351 387	P. Vilain *et al.*	(CHARM II Collab.)
Also		PL B343 453	P. Vilain *et al.*	(CHARM II Collab.)
BARANOV	93	PL B302 336	S.A. Baranov *et al.*	(JINR, SERP, BUDA)
BERNARDI	88	PL B203 332	G. Bernardi *et al.*	(PARIN, CERN, INFN+)
DORENBOS...	86	PL 166B 473	J. Dorenbosch *et al.*	(CHARM Collab.)
COOPER-...	85	PL 160B 207	A.M. Cooper-Sarkar *et al.*	(CERN, LOIC+)
HAYANO	82	PRL 49 1305	R.S. Hayano *et al.*	(TOKY, KEK, TSUK)

Int. J. Mod. Phys. A 2026.41. Downloaded from www.worldscientific.com
by UNIVERSITY OF CALIFORNIA @ BERKELEY on 09/16/26. Re-use and distribution is strictly not permitted, except for Open Access articles.

Int. J. Mod
by UNIVERSITY OF CALIFORNIA @ BERK
wnloaded from www.worldscientific.com
-use and distribution is strictly not permitted, except for Open Access articles.

QUARKS

u 1447
d 1447
s 1447
c 1451
b 1453
t 1455
b' (Fourth Generation) Quark 1477
t' (Fourth Generation) Quark 1480
Free Quark Searches 1482

Related Reviews in Volume 1

60. Quark masses 861
61. Top quark (rev.) 871

Int. J. Mod. Phys. A 2026.41. Downloaded from www.worldscientific.com
by UNIVERSITY OF CALIFORNIA @ BERKELEY on 09/16/26. Re-use and distribution is strictly not permitted, except for Open Access articles.

Phys. A 2026.41. Downloaded from www.worldscientific.com
by UNIVERSITY OF CA[redacted]ELEY on 09/16/26. Re-use and distribution is strictly not permitted, except for Open Access articles.

Int. J. Mod. Phys. A 2026.41. Downloaded from www.worldscientific.com
by UNIVERSITY OF CALIFORNIA @ BERKELEY on 09/16/26. Re-use and distribution is strictly not permitted, except for Open Access articles.

QUARKS

See the related review(s):

Quark Masses

u

$I(J^P) = \frac{1}{2}(\frac{1}{2}^+)$

Mass $m = 2.16 \pm 0.07$ MeV Charge $= \frac{2}{3}\,e$ $I_z = +\frac{1}{2}$

$m_u/m_d = 0.462 \pm 0.020$

d

$I(J^P) = \frac{1}{2}(\frac{1}{2}^+)$

Mass $m = 4.70 \pm 0.07$ MeV Charge $= -\frac{1}{3}\,e$ $I_z = -\frac{1}{2}$

$m_s/m_d = 17$–22

$\overline{m} = (m_u + m_d)/2 = 3.49 \pm 0.07$ MeV

s

$I(J^P) = 0(\frac{1}{2}^+)$

Mass $m = 92.9 \pm 0.7$ MeV Charge $= -\frac{1}{3}\,e$ Strangeness $= -1$

$(m_s - (m_u + m_d)/2)/(m_d - m_u) = 27.33^{+0.18}_{-0.14}$

Light Quarks (u, d, s)

OMITTED FROM SUMMARY TABLE

See the related review(s):

Quark Masses

u-QUARK MASS

The u-, d-, and s-quark masses are estimates of so-called "current-quark masses," in a mass- independent subtraction scheme such as $\overline{\text{MS}}$. The ratios m_u/m_d and m_s/m_d are extracted from pion and kaon masses using chiral symmetry. The estimates of d and u masses are not without controversy and remain under active investigation. Within the literature there are even suggestions that the u quark could be essentially massless. The s-quark mass is estimated from SU(3) splittings in hadron masses.

We have normalized the $\overline{\text{MS}}$ masses at a renormalization scale of $\mu = 2$ GeV. Results quoted in the literature at $\mu = 1$ GeV have been rescaled by dividing by 1.35. The values of "Our Evaluation" were determined in part via Figures 2 and 3 in the "Quark masses" review.

$\overline{\text{MS}}$ MASS (MeV)	CL%	DOCUMENT ID		TECN
2.16 ±0.07 (CL = 90%) OUR EVALUATION		See the ideogram below.		
2.6 ±0.4		[1] DOMINGUEZ	19	THEO
2.130±0.041		[2] BAZAVOV	18	LATT
2.27 ±0.06 ±0.06		[3] FODOR	16	LATT
2.36 ±0.24		[4] CARRASCO	14	LATT
2.24 ±0.10 ±0.34		[5] BLUM	10	LATT
2.01 ±0.14		[6] MCNEILE	10	LATT
• • • We do not use the following data for averages, fits, limits, etc. • • •				
2.57 ±0.26 ±0.07		[7] AOKI	12	LATT
2.15 ±0.03 ±0.10		[8] DURR	11	LATT
1.9 ±0.2		[9] BAZAVOV	10	LATT
2.01 ±0.14		[6] DAVIES	10	LATT
2.9 ±0.2		[10] DOMINGUEZ	09	THEO
2.9 ±0.8		[11] DEANDREA	08	THEO
3.02 ±0.33		[12] BLUM	07	LATT
2.7 ±0.4		[13] JAMIN	06	THEO
1.9 ±0.2		[14] MASON	06	LATT
2.8 ±0.2		[15] NARISON	06	THEO
1.7 ±0.3		[16] AUBIN	04A	LATT

[1] DOMINGUEZ 19 determine the quark mass from a QCD finite energy sum rule for the divergence of the axial current.

[2] BAZAVOV 18 determine the quark masses using a lattice computation with staggered fermions and four active quark flavors.

[3] FODOR 16 is a lattice simulation with $n_f = 2 + 1$ dynamical flavors and includes partially quenched QED effects.

[4] CARRASCO 14 is a lattice QCD computation of light quark masses using $2 + 1 + 1$ dynamical quarks, with $m_u = m_d \neq m_s \neq m_c$. The u and d quark masses are obtained separately by using the K meson mass splittings and lattice results for the electromagnetic contributions.

[5] BLUM 10 determines light quark masses using a QCD plus QED lattice computation of the electromagnetic mass splittings of the low-lying hadrons. The lattice simulations use 2+1 dynamical quark flavors.

[6] DAVIES 10 and MCNEILE 10 determine $\overline{m}_c(\mu)/\overline{m}_s(\mu) = 11.85 \pm 0.16$ using a lattice computation with $n_f = 2 + 1$ dynamical fermions of the pseudoscalar meson masses. Mass m_u is obtained from this using the value of m_c from ALLISON 08 or MCNEILE 10 and the BAZAVOV 10 values for the light quark mass ratios, $m_s/\overline{m}$ and m_u/m_d.

[7] AOKI 12 is a lattice computation using $1 + 1 + 1$ dynamical quark flavors.

[8] DURR 11 determine quark mass from a lattice computation of the meson spectrum using $n_f = 2 + 1$ dynamical flavors. The lattice simulations were done at the physical quark mass, so that extrapolation in the quark mass was not needed. The individual m_u, m_d values are obtained using the lattice determination of the average mass m_{ud} and of the ratio m_s/m_{ud} and the value of $Q = (m_s^2 - m_{\text{ud}}^2)\,/\,(m_d^2 - m_u^2)$ as determined from $\eta \to 3\pi$ decays.

[9] BAZAVOV 10 is a lattice computation using 2+1 dynamical quark flavors.

[10] DOMINGUEZ 09 use QCD finite energy sum rules for the two-point function of the divergence of the axial vector current computed to order α_s^4.

[11] DEANDREA 08 determine $m_u - m_d$ from $\eta \to 3\pi^0$, and combine with the PDG 06 lattice average value of $m_u + m_d = 7.6 \pm 1.6$ to determine m_u and m_d.

[12] BLUM 07 determine quark masses from the pseudoscalar meson masses using a QED plus QCD lattice computation with two dynamical quark flavors.

[13] JAMIN 06 determine m_u(2 GeV) by combining the value of m_s obtained from the spectral function for the scalar $K\pi$ form factor with other determinations of the quark mass ratios.

[14] MASON 06 extract light quark masses from a lattice simulation using staggered fermions with an improved action, and three dynamical light quark flavors with degenerate u and d quarks. Perturbative corrections were included at NNLO order. The quark masses m_u and m_d were determined from their $(m_u + m_d)/2$ measurement and AUBIN 04A m_u/m_d value.

[15] NARISON 06 uses sum rules for $e^+e^- \to$ hadrons to order α_s^3 to determine m_s combined with other determinations of the quark mass ratios.

[16] AUBIN 04A employ a partially quenched lattice calculation of the pseudoscalar meson masses.

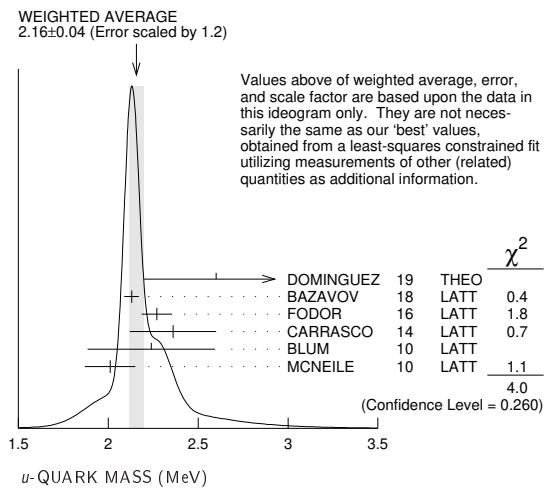

d-QUARK MASS

See the comment for the u quark above.

We have normalized the $\overline{\text{MS}}$ masses at a renormalization scale of $\mu = 2$ GeV. Results quoted in the literature at $\mu = 1$ GeV have been rescaled by dividing by 1.35. The values of "Our Evaluation" were determined in part via Figures 2 and 3 in the "Quark masses" review.

$\overline{\text{MS}}$ MASS (MeV)	CL%	DOCUMENT ID		TECN
4.70 ±0.07 (CL = 90%) OUR EVALUATION		See the ideogram below.		
5.3 ±0.4		[1] DOMINGUEZ	19	THEO
4.675±0.056		[2] BAZAVOV	18	LATT
4.67 ±0.06 ±0.06		[3] FODOR	16	LATT
5.03 ±0.26		[4] CARRASCO	14	LATT
4.65 ±0.15 ±0.32		[5] BLUM	10	LATT
4.77 ±0.15		[6] MCNEILE	10	LATT
• • • We do not use the following data for averages, fits, limits, etc. • • •				
3.68 ±0.29 ±0.10		[7] AOKI	12	LATT
4.79 ±0.07 ±0.12		[8] DURR	11	LATT
4.6 ±0.3		[9] BAZAVOV	10	LATT
4.79 ±0.16		[6] DAVIES	10	LATT
5.3 ±0.4		[10] DOMINGUEZ	09	THEO
4.7 ±0.8		[11] DEANDREA	08	THEO
5.49 ±0.39		[12] BLUM	07	LATT
4.8 ±0.5		[13] JAMIN	06	THEO
4.4 ±0.3		[14] MASON	06	LATT
5.1 ±0.4		[15] NARISON	06	THEO
3.9 ±0.5		[16] AUBIN	04A	LATT

[1] DOMINGUEZ 19 determine the quark mass from a QCD finite energy sum rule for the divergence of the axial current.

[2] BAZAVOV 18 determine the quark masses using a lattice computation with staggered fermions and four active quark flavors.

[3] FODOR 16 is a lattice simulation with $n_f = 2 + 1$ dynamical flavors and includes partially quenched QED effects.

by UNIVERSITY OF CA . Phys. A 2026.41. Downloaded from www.worldscientific.com
ELEY on 09/16/26. Re-use and distribution is strictly not permitted, except for Open Access articles.

[4] CARRASCO 14 is a lattice QCD computation of light quark masses using $2+1+1$ dynamical quarks, with $m_u = m_d \neq m_s \neq m_c$. The u and d quark masses are obtained separately by using the K meson mass splittings and lattice results for the electromagnetic contributions.

[5] BLUM 10 determines light quark masses using a QCD plus QED lattice computation of the electromagnetic mass splittings of the low-lying hadrons. The lattice simulations use 2+1 dynamical quark flavors.

[6] DAVIES 10 and MCNEILE 10 determine $\overline{m}_c(\mu)/\overline{m}_s(\mu) = 11.85 \pm 0.16$ using a lattice computation with $n_f = 2+1$ dynamical fermions of the pseudoscalar meson masses. Mass m_d is obtained from this using the value of m_c from ALLISON 08 or MCNEILE 10 and the BAZAVOV 10 values for the light quark mass ratios, $m_s/\overline{m}$ and m_u/m_d.

[7] AOKI 12 is a lattice computation using $1+1+1$ dynamical quark flavors.

[8] DURR 11 determine quark mass from a lattice computation of the meson spectrum using $n_f = 2+1$ dynamical flavors. The lattice simulations were done at the physical quark mass, so that extrapolation in the quark mass was not needed. The individual m_u, m_d values are obtained using the lattice determination of the average mass $m_{\rm ud}$ and of the ratio $m_s/m_{\rm ud}$ and the value of $Q = (m_s^2 - m_{\rm ud}^2)\ /\ (m_d^2 - m_u^2)$ as determined from $\eta \to 3\pi$ decays.

[9] BAZAVOV 10 is a lattice computation using 2+1 dynamical quark flavors.

[10] DOMINGUEZ 09 use QCD finite energy sum rules for the two-point function of the divergence of the axial vector current computed to order α_s^4.

[11] DEANDREA 08 determine $m_u - m_d$ from $\eta \to 3\pi^0$, and combine with the PDG 06 lattice average value of $m_u + m_d = 7.6 \pm 1.6$ to determine m_u and m_d.

[12] BLUM 07 determine quark masses from the pseudoscalar meson masses using a QED plus QCD lattice computation with two dynamical quark flavors.

[13] JAMIN 06 determine m_d(2 GeV) by combining the value of m_s obtained from the spectral function for the scalar $K\pi$ form factor with other determinations of the quark mass ratios.

[14] MASON 06 extract light quark masses from a lattice simulation using staggered fermions with an improved action, and three dynamical light quark flavors with degenerate u and d quarks. Perturbative corrections were included at NNLO order. The quark masses m_u and m_d were determined from their $(m_u + m_d)/2$ measurement and AUBIN 04A m_u/m_d value.

[15] NARISON 06 uses sum rules for $e^+e^- \to$ hadrons to order α_s^3 to determine m_s combined with other determinations of the quark mass ratios.

[16] AUBIN 04A perform three flavor dynamical lattice calculation of pseudoscalar meson masses, with continuum estimate of electromagnetic effects in the kaon masses, and one-loop perturbative renormalization constant.

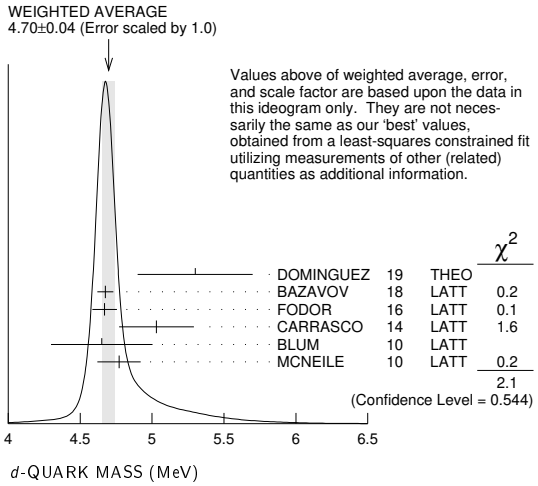

$\overline{m} = (m_u + m_d)/2$

See the comments for the u quark above.

We have normalized the $\overline{\rm MS}$ masses at a renormalization scale of $\mu = 2$ GeV. Results quoted in the literature at $\mu = 1$ GeV have been rescaled by dividing by 1.35. The values of "Our Evaluation" were determined in part via Figures 2 and 3 in the "Quark masses" review.

$\overline{\rm MS}$ MASS (MeV)	CL%	DOCUMENT ID		TECN
3.49 ±0.07 (CL = 90%) OUR EVALUATION See the ideogram below.				
$3.636 \pm 0.066^{+0.060}_{-0.057}$		[1] ALEXANDROU	21	LATT
3.54 ±0.12 ±0.09		[2] BRUNO	20	LATT
3.9 ±0.3		[3] DOMINGUEZ	19	THEO
$4.7\ ^{+0.8}_{-0.7}$		[4] YUAN	17	THEO
3.70 ±0.17		[5] CARRASCO	14	LATT
3.45 ±0.12		[6] ARTHUR	13	LATT
3.469±0.047±0.048		[7] DURR	11	LATT
3.6 ±0.2		[8] BLOSSIER	10	LATT
3.39 ±0.06		[9] MCNEILE	10	LATT
• • • We do not use the following data for averages, fits, limits, etc. • • •				
3.59 ±0.21		[10] AOKI	11A	LATT
3.40 ±0.07		[9] DAVIES	10	LATT
4.1 ±0.2		[11] DOMINGUEZ	09	THEO
3.72 ±0.41		[12] ALLTON	08	LATT
3.85 ±0.12 ±0.4		[13] BLOSSIER	08	LATT
≥ 4.85 ±0.20		[14] DOMINGUEZ...	08B	THEO
$3.55\ ^{+0.65}_{-0.28}$		[15] ISHIKAWA	08	LATT
4.026±0.048		[16] NAKAMURA	08	LATT
4.25 ±0.35		[17] BLUM	07	LATT
4.08 ±0.25 ±0.42		[18] GOCKELER	06	LATT
4.7 ±0.2 ±0.3		[19] GOCKELER	06A	LATT
3.2 ±0.3		[20] MASON	06	LATT
3.95 ±0.3		[21] NARISON	06	THEO
2.8 ±0.3		[22] AUBIN	04	LATT
4.29 ±0.14 ±0.65		[23] AOKI	03	LATT
3.223±0.3		[24] AOKI	03B	LATT
4.4 ±0.1 ±0.4		[25] BECIREVIC	03	LATT
4.1 ±0.3 ±1.0		[26] CHIU	03	LATT

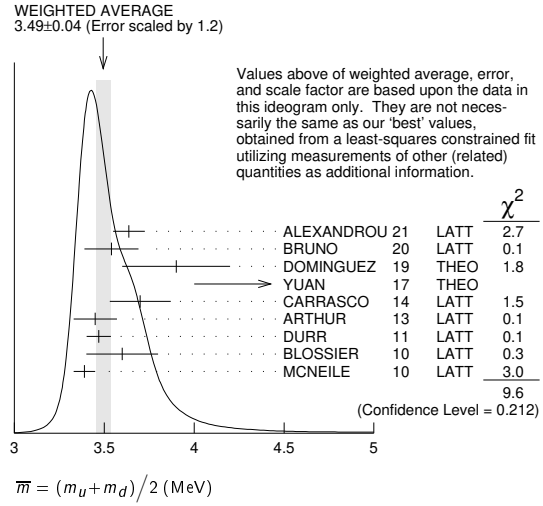

[1] ALEXANDROU 21 determines the quark mass using a lattice calculation of the meson and baryon masses with a twisted mass fermion action. The simulations are carried out using 2+1+1 dynamical quarks with $m_u = m_d \neq m_s \neq m_c$, including gauge ensembles close to the physical pion point.

[2] BRUNO 20 determines the light quark mass using a lattice calculation with $n_f = 2+1$ flavors of Wilson fermions. The scale has been set from f_π and f_K. The tuning was done using the masses of the lightest (π) and strange (K) pseudoscalar mesons.

[3] DOMINGUEZ 19 determine the quark mass from a QCD finite energy sum rule for the divergence of the axial current.

[4] YUAN 17 determine $\overline{m}$ using QCD sum rules in the isospin I=0 scalar channel. At the end of the "Numerical Results" section of YUAN 17 the authors discuss the significance of their larger value of the light quark mass compared to previous determinations.

[5] CARRASCO 14 is a lattice QCD computation of light quark masses using $2+1+1$ dynamical quarks, with $m_u = m_d \neq m_s \neq m_c$. The u and d quark masses are obtained separately by using the K meson mass splittings and lattice results for the electromagnetic contributions.

[6] ARTHUR 13 is a lattice computation using 2+1 dynamical domain wall fermions. Masses at $\mu = 3$ GeV have been converted to $\mu = 2$ GeV using conversion factors given in their paper.

[7] DURR 11 determine quark mass from a lattice computation of the meson spectrum using $n_f = 2+1$ dynamical flavors. The lattice simulations were done at the physical quark mass, so that extrapolation in the quark mass was not needed.

[8] BLOSSIER 10 determines quark masses from a computation of the hadron spectrum using n_f=2 dynamical twisted-mass Wilson fermions.

[9] DAVIES 10 and MCNEILE 10 determine $\overline{m}_c(\mu)/\overline{m}_s(\mu) = 11.85 \pm 0.16$ using a lattice computation with $n_f = 2+1$ dynamical fermions of the pseudoscalar meson masses. Mass $\overline{m}$ is obtained from this using the value of m_c from ALLISON 08 or MCNEILE 10 and the BAZAVOV 10 values for the light quark mass ratio, $m_s/\overline{m}$.

[10] AOKI 11A determine quark masses from a lattice computation of the hadron spectrum using $n_f = 2+1$ dynamical flavors of domain wall fermions.

[11] DOMINGUEZ 09 use QCD finite energy sum rules for the two-point function of the divergence of the axial vector current computed to order α_s^4.

[12] ALLTON 08 use a lattice computation of the π, K, and Ω masses with 2+1 dynamical flavors of domain wall quarks, and non-perturbative renormalization.

[13] BLOSSIER 08 use a lattice computation of pseudoscalar meson masses and decay constants with 2 dynamical flavors and non-perturbative renormalization.

[14] DOMINGUEZ-CLARIMON 08B obtain an inequality from sum rules for the scalar two-point correlator.

[15] ISHIKAWA 08 use a lattice computation of the light meson spectrum with 2+1 dynamical flavors of $\mathcal{O}(a)$ improved Wilson quarks, and one-loop perturbative renormalization.

[16] NAKAMURA 08 do a lattice computation using quenched domain wall fermions and non-perturbative renormalization.

[17] BLUM 07 determine quark masses from the pseudoscalar meson masses using a QED plus QCD lattice computation with two dynamical quark flavors.

[18] GOCKELER 06 use an unquenched lattice computation of the axial Ward Identity with $n_f = 2$ dynamical light quark flavors, and non-perturbative renormalization, to obtain $\overline{m}$(2 GeV) $= 4.08 \pm 0.25 \pm 0.19 \pm 0.23$ MeV, where the first error is statistical, the second and third are systematic due to the fit range and force scale uncertainties, respectively. We have combined the systematic errors linearly.

Int. J. Mod. Phys. A 2026.41. Downloaded from www.worldscientific.com by UNIVERSITY OF CALIFORNIA @ BERKELEY on 09/16/26. Re-use and distribution is strictly not permitted, except for Open Access articles.

[19] GOCKELER 06A use an unquenched lattice computation of the pseudoscalar meson masses with $n_f = 2$ dynamical light quark flavors, and non-perturbative renormalization.

[20] MASON 06 extract light quark masses from a lattice simulation using staggered fermions with an improved action, and three dynamical light quark flavors with degenerate u and d quarks. Perturbative corrections were included at NNLO order.

[21] NARISON 06 uses sum rules for $e^+e^- \to$ hadrons to order α_s^3 to determine m_s combined with other determinations of the quark mass ratios.

[22] AUBIN 04 perform three flavor dynamical lattice calculation of pseudoscalar meson masses, with one-loop perturbative renormalization constant.

[23] AOKI 03 uses quenched lattice simulation of the meson and baryon masses with degenerate light quarks. The extrapolations are done using quenched chiral perturbation theory.

[24] The errors given in AOKI 03B were $^{+0.046}_{-0.069}$. We changed them to ± 0.3 for calculating the overall best values. AOKI 03B uses lattice simulation of the meson and baryon masses with two dynamical light quarks. Simulations are performed using the $\mathcal{O}(a)$ improved Wilson action.

[25] BECIREVIC 03 perform quenched lattice computation using the vector and axial Ward identities. Uses $\mathcal{O}(a)$ improved Wilson action and nonperturbative renormalization.

[26] CHIU 03 determines quark masses from the pion and kaon masses using a lattice simulation with a chiral fermion action in quenched approximation.

m_u/m_d MASS RATIO

VALUE	CL%	DOCUMENT ID		TECN	COMMENT
0.462 ±0.020 (CL = 90%) OUR EVALUATION					See the ideogram below.
0.485 ±0.011 ±0.016		[1] FODOR	16	LATT	
0.4482 $^{+0.0173}_{-0.0206}$		[2] BASAK	15	LATT	
0.470 ±0.056		[3] CARRASCO	14	LATT	
0.42 ±0.01 ±0.04		[4] BAZAVOV	10	LATT	
0.4818 ±0.0096 ±0.0860		[5] BLUM	10	LATT	
• • • We do not use the following data for averages, fits, limits, etc. • • •					
0.698 ±0.051		[6] AOKI	12	LATT	
0.550 ±0.031		[7] BLUM	07	LATT	
0.43 ±0.08		[8] AUBIN	04A	LATT	
0.410 ±0.036		[9] NELSON	03	LATT	
0.553 ±0.043		[10] LEUTWYLER	96	THEO	Compilation

[1] FODOR 16 is a lattice simulation with $n_f = 2 + 1$ dynamical flavors and includes partially quenched QED effects.

[2] BASAK 15 is a lattice computation using 2+1 dynamical quark flavors.

[3] CARRASCO 14 is a lattice QCD computation of light quark masses using $2 + 1 + 1$ dynamical quarks, with $m_u = m_d \neq m_s \neq m_c$. The u and d quark masses are obtained separately by using the K meson mass splittings and lattice results for the electromagnetic contributions.

[4] BAZAVOV 10 is a lattice computation using 2+1 dynamical quark flavors.

[5] BLUM 10 is a lattice computation using 2+1 dynamical quark flavors.

[6] AOKI 12 is a lattice computation using $1 + 1 + 1$ dynamical quark flavors.

[7] BLUM 07 determine quark masses from the pseudoscalar meson masses using a QED plus QCD lattice computation with two dynamical quark flavors.

[8] AUBIN 04A perform three flavor dynamical lattice calculation of pseudoscalar meson masses, with continuum estimate of electromagnetic effects in the kaon masses.

[9] NELSON 03 computes coefficients in the order p^4 chiral Lagrangian using a lattice calculation with three dynamical flavors. The ratio m_u/m_d is obtained by combining this with the chiral perturbation theory computation of the meson masses to order p^4.

[10] LEUTWYLER 96 uses a combined fit to $\eta \to 3\pi$ and $\psi' \to J/\psi\ (\pi,\eta)$ decay rates, and the electromagnetic mass differences of the π and K.

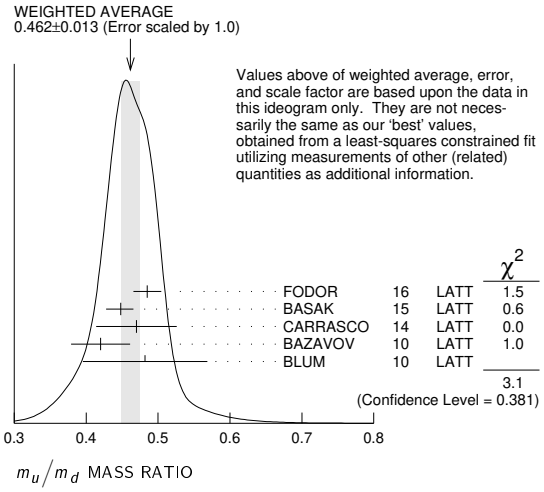

s-QUARK MASS

See the comment for the u quark above.

We have normalized the $\overline{\text{MS}}$ masses at a renormalization scale of $\mu = 2$ GeV. Results quoted in the literature at $\mu = 1$ GeV have been rescaled by dividing by 1.35.

$\overline{\text{MS}}$ MASS (MeV)	CL%	DOCUMENT ID		TECN
92.9 ± 0.7 (CL = 90%) OUR EVALUATION				See the ideogram below.
92.38 ± 0.43		[1] COLQUHOUN	26	LATT
98.7 ± 2.4 $^{+4.0}_{-3.2}$		[2] ALEXANDROU	21	LATT
95.7 ± 2.5 ± 2.4		[3] BRUNO	20	LATT
92.47 ± 0.69		[4] BAZAVOV	18	LATT
93.85 ± 0.75		[5] LYTLE	18	LATT
87.6 ± 6.0		[6] ANANTHANA..	16	THEO
99.6 ± 4.3		[7] CARRASCO	14	LATT
94.4 ± 2.3		[8] ARTHUR	13	LATT
94 ± 9		[9] BODENSTEIN	13	THEO
95.5 ± 1.1 ± 1.5		[10] DURR	11	LATT
• • • We do not use the following data for averages, fits, limits, etc. • • •				
93.6 ± 0.8		[11] CHAKRABOR..	15	LATT
102 ± 3 ± 1		[12] FRITZSCH	12	LATT
96.2 ± 2.7		[13] AOKI	11A	LATT
95 ± 6		[14] BLOSSIER	10	LATT
97.6 ± 2.9 ± 5.5		[15] BLUM	10	LATT
92.4 ± 1.5		[16] DAVIES	10	LATT
92.2 ± 1.3		[16] MCNEILE	10	LATT
107.3 ±11.7		[17] ALLTON	08	LATT
105 ± 3 ± 9		[18] BLOSSIER	08	LATT
102 ± 8		[19] DOMINGUEZ	08A	THEO
90.1 $^{+17.2}_{-6.1}$		[20] ISHIKAWA	08	LATT
105.6 ± 1.2		[21] NAKAMURA	08	LATT
119.5 ± 9.3		[22] BLUM	07	LATT
105 ± 6 ± 7		[23] CHETYRKIN	06	THEO
111 ± 6 ±10		[24] GOCKELER	06	LATT
119 ± 5 ± 8		[25] GOCKELER	06A	LATT
92 ± 9		[26] JAMIN	06	THEO
87 ± 6		[27] MASON	06	LATT
104 ±15		[28] NARISON	06	THEO
≥ 71 ± 4, ≤ 151 ± 14		[29] NARISON	06	THEO
96 $^{+5}_{-3}$ $^{+16}_{-18}$		[30] BAIKOV	05	THEO
81 ±22		[31] GAMIZ	05	THEO
125 ±28		[32] GORBUNOV	05	THEO
93 ±32		[33] NARISON	05	THEO
76 ± 8		[34] AUBIN	04	LATT
116 ± 6 ± 0.65		[35] AOKI	03	LATT
84.5 $^{+12}_{-1.7}$		[36] AOKI	03B	LATT
106 ± 2 ± 8		[37] BECIREVIC	03	LATT
92 ± 9 ±16		[38] CHIU	03	LATT
117 ±17		[39] GAMIZ	03	THEO
103 ±17		[40] GAMIZ	03	THEO

[1] COLQUHOUN 26 value comes from lattice computation of the pseudoscalar correlator. Quenched QED corrections are included.

[2] ALEXANDROU 21 determines the quark mass using a lattice calculation of the meson and baryon masses with a twisted mass fermion action. The simulations are carried out using 2+1+1 dynamical quarks with $m_u = m_d \neq m_s \neq m_c$, including gauge ensembles close to the physical pion point.

[3] BRUNO 20 determines the light quark mass using a lattice calculation with $n_f = 2+1$ flavors of Wilson fermions. The scale has been set from f_π and f_K. The tuning was done using the masses of the lightest (π) and strange (K) pseudoscalar mesons.

[4] BAZAVOV 18 determine the quark masses using a lattice computation with staggered fermions and four active quark flavors.

[5] LYTLE 18 combined with CHAKRABORTY 2015 determine $\overline{m}_s(3\text{ GeV}) = 84.78 \pm 0.65$ MeV from a lattice simulation with $n_f = 2+1+1$ flavors. They also determine the quoted value $\overline{m}_s(2\text{ GeV})$ for $n_f = 4$ dynamical flavors.

[6] ANANTHANARAYAN 16 determine $\overline{m}_s(2\text{ GeV}) = 106.70 \pm 9.36$ MeV and 74.47 ± 7.77 MeV from fits to ALEPH and OPAL τ decay data, respectively. We have used the weighted average of the two.

[7] CARRASCO 14 is a lattice QCD computation of light quark masses using $2 + 1 + 1$ dynamical quarks, with $m_u = m_d \neq m_s \neq m_c$. The u and d quark masses are obtained separately by using the K meson mass splittings and lattice results for the electromagnetic contributions.

[8] ARTHUR 13 is a lattice computation using 2+1 dynamical domain wall fermions. Masses at $\mu = 3$ GeV have been converted to $\mu = 2$ GeV using conversion factors given in their paper.

[9] BODENSTEIN 13 determines m_s from QCD finite energy sum rules, and the perturbative computation of the pseudoscalar correlator to five-loop order.

[10] DURR 11 determine quark mass from a lattice computation of the meson spectrum using $n_f = 2 + 1$ dynamical flavors. The lattice simulations were done at the physical quark mass, so that extrapolation in the quark mass was not needed.

[11] CHAKRABORTY 15 is a lattice QCD computation that determines m_c and m_c/m_s using pseudoscalar mesons masses tuned on gluon field configurations with 2+1+1 dynamical flavors of HISQ quarks with u/d masses down to the physical value.

[12] FRITZSCH 12 determine m_s using a lattice computation with $n_f = 2$ dynamical flavors.

[13] AOKI 11A determine quark masses from a lattice computation of the hadron spectrum using $n_f = 2 + 1$ dynamical flavors of domain wall fermions.

[14] BLOSSIER 10 determines quark masses from a computation of the hadron spectrum using n_f=2 dynamical twisted-mass Wilson fermions.

[15] BLUM 10 determines light quark masses using a QCD plus QED lattice computation of the electromagnetic mass splittings of the low-lying hadrons. The lattice simulations use 2+1 dynamical quark flavors.

[16] DAVIES 10 and MCNEILE 10 determine $\overline{m}_c(\mu)/\overline{m}_s(\mu) = 11.85 \pm 0.16$ using a lattice computation with $n_f = 2 + 1$ dynamical fermions of the pseudoscalar meson masses. Mass m_s is obtained from this using the value of m_c from ALLISON 08 or MCNEILE 10.

by UNIVERSITY OF CA . Phys. A 2026.41. Downloaded from www.worldscientific.com
ELEY on 09/16/26. Re-use and distribution is strictly not permitted, except for Open Access articles.

[17] ALLTON 08 use a lattice computation of the π, K, and Ω masses with 2+1 dynamical flavors of domain wall quarks, and non-perturbative renormalization.
[18] BLOSSIER 08 use a lattice computation of pseudoscalar meson masses and decay constants with 2 dynamical flavors and non-perturbative renormalization.
[19] DOMINGUEZ 08A make determination from QCD finite energy sum rules for the pseudoscalar two-point function computed to order α_s^4.
[20] ISHIKAWA 08 use a lattice computation of the light meson spectrum with 2+1 dynamical flavors of $\mathcal{O}(a)$ improved Wilson quarks, and one-loop perturbative renormalization.
[21] NAKAMURA 08 do a lattice computation using quenched domain wall fermions and non-perturbative renormalization.
[22] BLUM 07 determine quark masses from the pseudoscalar meson masses using a QED plus QCD lattice computation with two dynamical quark flavors.
[23] CHETYRKIN 06 use QCD sum rules in the pseudoscalar channel to order α_s^4.
[24] GOCKELER 06 use an unquenched lattice computation of the axial Ward Identity with $n_f = 2$ dynamical light quark flavors, and non-perturbative renormalization, to obtain $\overline{m}_s(2\text{ GeV}) = 111 \pm 6 \pm 4 \pm 6$ MeV, where the first error is statistical, the second and third are systematic due to the fit range and force scale uncertainties, respectively. We have combined the systematic errors linearly.
[25] GOCKELER 06A use an unquenched lattice computation of the pseudoscalar meson masses with $n_f = 2$ dynamical light quark flavors, and non-perturbative renormalization.
[26] JAMIN 06 determine $\overline{m}_s(2\text{ GeV})$ from the spectral function for the scalar $K\pi$ form factor.
[27] MASON 06 extract light quark masses from a lattice simulation using staggered fermions with an improved action, and three dynamical light quark flavors with degenerate u and d quarks. Perturbative corrections were included at NNLO order.
[28] NARISON 06 uses sum rules for $e^+e^- \to$ hadrons to order α_s^3.
[29] NARISON 06 obtains the quoted range from positivity of the spectral functions.
[30] BAIKOV 05 determines $\overline{m}_s(M_\tau) = 100^{+5}_{-3}{}^{+17}_{-19}$ from sum rules using the strange spectral function in τ decay. The computations were done to order α_s^3, with an estimate of the α_s^4 terms. We have converted the result to $\mu = 2$ GeV.
[31] GAMIZ 05 determines $\overline{m}_s(2\text{ GeV})$ from sum rules using the strange spectral function in τ decay. The computations were done to order α_s^2, with an estimate of the α_s^3 terms.
[32] GORBUNOV 05 use hadronic tau decays to N3LO, including power corrections.
[33] NARISON 05 determines $\overline{m}_s(2\text{ GeV})$ from sum rules using the strange spectral function in τ decay. The computations were done to order α_s^3.
[34] AUBIN 04 perform three flavor dynamical lattice calculation of pseudoscalar meson masses, with one-loop perturbative renormalization constant.
[35] AOKI 03 uses quenched lattice simulation of the meson and baryon masses with degenerate light quarks. The extrapolations are done using quenched chiral perturbation theory. Determines $m_s = 113.8 \pm 2.3^{+5.8}_{-2.9}$ using K mass as input and $m_s = 142.3 \pm 5.8^{+22}_{-0}$ using ϕ mass as input. We have performed a weighted average of these values.
[36] AOKI 03B uses lattice simulation of the meson and baryon masses with two dynamical light quarks. Simulations are performed using the $\mathcal{O}(a)$ improved Wilson action.
[37] BECIREVIC 03 perform quenched lattice computation using the vector and axial Ward identities. Uses $\mathcal{O}(a)$ improved Wilson action and nonperturbative renormalization. They also quote $\overline{m}/m_s = 24.3 \pm 0.2 \pm 0.6$.
[38] CHIU 03 determines quark masses from the pion and kaon masses using a lattice simulation with a chiral fermion action in quenched approximation.
[39] GAMIZ 03 determines m_s from SU(3) breaking in the τ hadronic width. The value of V_{us} is chosen to satisfy CKM unitarity.
[40] GAMIZ 03 determines m_s from SU(3) breaking in the τ hadronic width. The value of V_{us} is taken from the PDG.

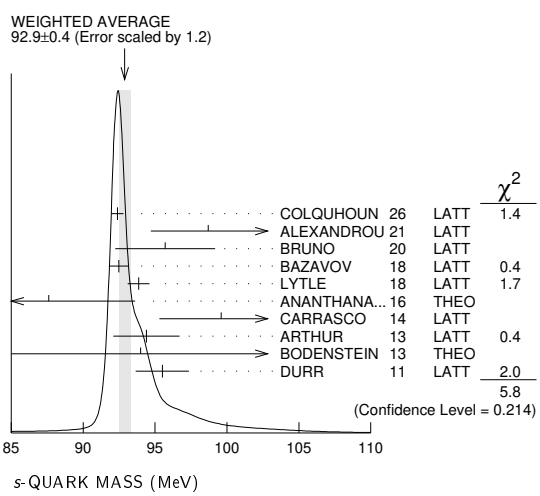

OTHER LIGHT QUARK MASS RATIOS

m_s/m_d MASS RATIO

VALUE	DOCUMENT ID		TECN	COMMENT
17–22 OUR EVALUATION				
20.0	[1] GAO	97	THEO	
18.9±0.8	[2] LEUTWYLER	96	THEO	Compilation
21	[3] DONOGHUE	92	THEO	
18	[4] GERARD	90	THEO	
18 to 23	[5] LEUTWYLER	90B	THEO	

[1] GAO 97 uses electromagnetic mass splittings of light mesons.
[2] LEUTWYLER 96 uses a combined fit to $\eta \to 3\pi$ and $\psi' \to J/\psi\,(\pi,\eta)$ decay rates, and the electromagnetic mass differences of the π and K.
[3] DONOGHUE 92 result is from a combined analysis of meson masses, $\eta \to 3\pi$ using second-order chiral perturbation theory including nonanalytic terms, and $(\psi(2S) \to J/\psi(1S)\,\pi)/(\psi(2S) \to J/\psi(1S)\,\eta)$.
[4] GERARD 90 uses large N and η-η' mixing.
[5] LEUTWYLER 90B determines quark mass ratios using second-order chiral perturbation theory for the meson and baryon masses, including nonanalytic corrections. Also uses Weinberg sum rules to determine L_7.

$m_s/\overline{m}$ MASS RATIO

$\overline{m} \equiv (m_u + m_d)/2$

VALUE	CL%	DOCUMENT ID		TECN
$27.33^{+0.18}_{-0.14}$ (CL = 90%) OUR EVALUATION		See the ideogram below.		
$27.17 \pm 0.32^{+0.56}_{-0.38}$		[1] ALEXANDROU	21	LATT
27.0 ±1.0 ±0.4		[2] BRUNO	20	LATT
$27.35 \pm 0.05^{+0.10}_{-0.07}$		[3] BAZAVOV	14A	LATT
26.66±0.32		[4] CARRASCO	14	LATT
27.36±0.54		[5] ARTHUR	13	LATT
27.53±0.20±0.08		[6] DURR	11	LATT
• • • We do not use the following data for averages, fits, limits, etc. • • •				
26.8 ±1.4		[7] AOKI	11A	LATT
27.3 ±0.9		[8] BLOSSIER	10	LATT
28.8 ±1.65		[9] ALLTON	08	LATT
27.3 ±0.3 ±1.2		[10] BLOSSIER	08	LATT
23.5 ±1.5		[11] OLLER	07A	THEO
27.4 ±0.4		[12] AUBIN	04	LATT

[1] ALEXANDROU 21 determines the quark mass using a lattice calculation of the meson and baryon masses with a twisted mass fermion action. The simulations are carried out using 2+1+1 dynamical quarks with $m_u = m_d \neq m_s \neq m_c$, including gauge ensembles close to the physical pion point.
[2] BRUNO 20 determines the light quark mass using a lattice calculation with $n_f = 2+1$ flavors of Wilson fermions. The scale has been set from f_π and f_K. The tuning was done using the masses of the lightest (π) and strange (K) pseudoscalar mesons.
[3] BAZAVOV 14A is a lattice computation using 4 dynamical flavors of HISQ fermions.
[4] CARRASCO 14 is a lattice QCD computation of light quark masses using $2+1+1$ dynamical quarks, with $m_u = m_d \neq m_s \neq m_c$. The u and d quark masses are obtained separately by using the K meson mass splittings and lattice results for the electromagnetic contributions.
[5] ARTHUR 13 is a lattice computation using 2+1 dynamical domain wall fermions.
[6] DURR 11 determine quark mass from a lattice computation of the meson spectrum using $n_f = 2+1$ dynamical flavors. The lattice simulations were done at the physical quark mass, so that extrapolation in the quark mass was not needed.
[7] AOKI 11A determine quark masses from a lattice computation of the hadron spectrum using $n_f = 2+1$ dynamical flavors of domain wall fermions.
[8] BLOSSIER 10 determines quark masses from a computation of the hadron spectrum using n_f=2 dynamical twisted-mass Wilson fermions.
[9] ALLTON 08 use a lattice computation of the π, K, and Ω masses with 2+1 dynamical flavors of domain wall quarks, and non-perturbative renormalization.
[10] BLOSSIER 08 use a lattice computation of pseudoscalar meson masses and decay constants with 2 dynamical flavors and non-perturbative renormalization.
[11] OLLER 07A use unitarized chiral perturbation theory to order p^4.
[12] Three flavor dynamical lattice calculation of pseudoscalar meson masses.

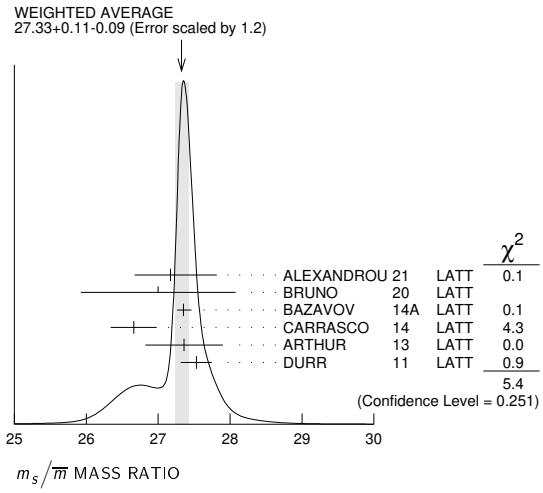

Q MASS RATIO

$Q \equiv \sqrt{(m^2{}_s - \overline{m}^2)/(m^2{}_d - m^2{}_u)}$; $\overline{m} \equiv (m_u + m_d)/2$

VALUE	DOCUMENT ID		TECN
• • • We do not use the following data for averages, fits, limits, etc. • • •			
22.1±0.7	[1] COLANGELO	18	THEO
22.0±0.7	[2] COLANGELO	17	THEO

Int. J. Mod. Phys. A 2026.41. Downloaded from www.worldscientific.com by UNIVERSITY OF CALIFORNIA @ BERKELEY on 09/16/26. Re-use and distribution is strictly not permitted, except for Open Access articles.

21.6±1.1	[3] GUO	17	THEO
23.4±0.4±0.5	[4] FODOR	16	LATT
21.4±0.4	[5] GUO	15F	THEO
22.8±0.4	[6] MARTEMYA...	05	THEO
22.7±0.8	[7] ANISOVICH	96	THEO

[1] COLANGELO 18 obtain Q from a dispersive analysis of $\eta \to 3\pi$ decay.

[2] COLANGELO 17 obtain Q from a dispersive analysis of KLOE collaboration data on $\eta \to \pi^+\pi^-\pi^0$ decays and chiral perturbation theory input.

[3] GUO 17 determine Q from a dispersive model fit to KLOE and WASA-at-COSY data on $\eta \to \pi^+\pi^-\pi^0$ decay and matching to chiral perturbation theory.

[4] FODOR 16 is a lattice simulation with $n_f = 2+1$ dynamical flavors and includes partially quenched QED effects.

[5] GUO 15F determine Q from a Khuri-Treiman analysis of $\eta \to 3\pi$ decays.

[6] MARTEMYANOV 05 determine Q from $\eta \to 3\pi$ decay.

[7] ANISOVICH 96 find Q from $\eta \to \pi^+\pi^-\pi^0$ decay using dispersion relations and chiral perturbation theory.

LIGHT QUARKS (u, d, s) REFERENCES

COLQUHOUN	26	PR D113 074522	B. Colquhoun *et al.*	(HPQCD Collab.)
ALEXANDROU	21	PR D104 074515	C. Alexandrou *et al.*	(ETM Collab.)
BRUNO	20	EPJ C80 169	M. Bruno *et al.*	(ALPHA Collab.)
DOMINGUEZ	19	JHEP 1902 057	C.A. Dominguez, A. Mes, K. Schilcher	(CAPE, MAINZ)
BAZAVOV	18	PR D98 054517	A. Bazavov *et al.*	(Fermilab Lattice, MILC, TUMQCD)
COLANGELO	18	EPJ C78 947	G. Colangelo *et al.*	
LYTLE	18	PR D98 014513	A.T. Lytle *et al.*	(HPQCD Collab.)
COLANGELO	17	PRL 118 022001	G. Colangelo *et al.*	(BERN, IND, JLAB)
GUO	17	PL B771 497	P. Guo *et al.*	
YUAN	17	PR D96 014034	J.-M. Yuan *et al.*	
ANANTHANA...	16	PR D94 116014	B. Ananthanarayan, D. Das	(BANG, AHMED)
FODOR	16	PRL 117 082001	Z. Fodor *et al.*	(BMW Collab.)
BASAK	15	JPCS 640 012052	S. Basak *et al.*	(MILC Collab.)
CHAKRABOR...	15	PR D91 054508	B. Chakraborty *et al.*	(HPQCD Collab.)
GUO	15F	PR D92 054016	P. Guo *et al.*	
BAZAVOV	14A	PR D90 074509	A. Bazavov *et al.*	(Fermi-LAT and MILC Collabs.)
CARRASCO	14	NP B887 19	N. Carrasco *et al.*	(European Twisted Mass Collab.)
ARTHUR	13	PR D87 094514	R. Arthur *et al.*	(RBC and UKQCD Collabs.)
BODENSTEIN	13	JHEP 1307 138	S. Bodenstein, C.A. Dominguez, K. Schilcher	
AOKI	12	PR D86 034507	S. Aoki *et al.*	(PACS-CS Collab.)
FRITZSCH	12	NP B865 397	P. Fritzsch *et al.*	(ALPHA Collab.)
AOKI	11A	PR D83 074508	Y. Aoki *et al.*	(RBC-UKQCD Collab.)
DURR	11	PL B701 265	S. Durr *et al.*	(BMW Collab.)
BAZAVOV	10	RMP 82 1349	A. Bazavov *et al.*	(MILC Collab.)
BLOSSIER	10	PR D82 114513	B. Blossier *et al.*	(ETM Collab.)
BLUM	10	PR D82 094508	T. Blum *et al.*	
DAVIES	10	PRL 104 132003	C.T.H. Davies *et al.*	(HPQCD Collab.)
MCNEILE	10	PR D82 034512	C. McNeile *et al.*	(HPQCD Collab.)
DOMINGUEZ	09	PR D79 014009	C.A. Dominguez *et al.*	
ALLISON	08	PR D78 054513	I. Allison *et al.*	(HPQCD Collab.)
ALLTON	08	PR D78 114509	C. Allton *et al.*	(RBC and UKQCD Collabs.)
BLOSSIER	08	JHEP 0804 020	B. Blossier *et al.*	(ETM Collab.)
DEANDREA	08	PR D78 034032	A. Deandrea, A. Nehme, P. Talavera	
DOMINGUEZ	08A	JHEP 0805 020	C.A. Dominguez *et al.*	
DOMINGUEZ...	08B	PL B660 49	A. Dominguez-Clarimon, E. de Rafael, J. Taron	
ISHIKAWA	08	PR D78 011502	T. Ishikawa *et al.*	(CP-PACS and JLQCD Collabs.)
NAKAMURA	08	PR D78 034502	Y. Nakamura *et al.*	(CP-PACS Collab.)
BLUM	07	PR D76 114508	T. Blum *et al.*	(RBC Collab.)
OLLER	07A	EPJ A34 371	J.A. Oller, L. Roca	
CHETYRKIN	06	EPJ C46 721	K.G. Chetyrkin, A. Khodjamirian	
GOCKELER	06	PR D73 054508	M. Gockeler *et al.*	(QCDSF and UKQCD Collabs)
GOCKELER	06A	PL B639 307	M. Gockeler *et al.*	(QCDSF and UKQCD Collabs)
JAMIN	06	PR D74 074009	M. Jamin, J.A. Oller, A. Pich	
MASON	06	PR D73 114501	Q. Mason *et al.*	(HPQCD Collab.)
NARISON	06	PR D74 034013	S. Narison	
PDG	06	JP G33 1	W.-M. Yao *et al.*	(PDG Collab.)
BAIKOV	05	PRL 95 012003	P.A. Baikov, K.G. Chetyrkin, J.H. Kuhn	
GAMIZ	05	PRL 94 011803	E. Gamiz *et al.*	
GORBUNOV	05	PR D71 013002	D.S. Gorbunov, A.A. Pivovarov	
MARTEMYA...	05	PR D71 017501	B.V. Martemyanov, V.S. Sopov	
NARISON	05	PL B626 101	S. Narison	
AUBIN	04	PR D70 031504	C. Aubin *et al.*	(HPQCD, MILC, UKQCD Collabs.)
AUBIN	04A	PR D70 114501	C. Aubin *et al.*	(MILC Collab.)
AOKI	03	PR D67 034503	S. Aoki *et al.*	(CP-PACS Collab.)
AOKI	03B	PR D68 054502	S. Aoki *et al.*	(CP-PACS Collab.)
BECIREVIC	03	PL B558 69	D. Becirevic, V. Lubicz, C. Tarantino	
CHIU	03	NP B673 217	T.-W. Chiu, T.-H. Hsieh	
GAMIZ	03	JHEP 0301 060	E. Gamiz *et al.*	
NELSON	03	PRL 90 021601	D. Nelson, G.T. Fleming, G.W. Kilcup	
GAO	97	PR D56 4115	D.-N. Gao, B.A. Li, M.-L. Yan	
ANISOVICH	96	PL B375 335	A.V. Anisovich, H. Leutwyler	
LEUTWYLER	96	PL B378 313	H. Leutwyler	
DONOGHUE	92	PRL 69 3444	J.F. Donoghue, B.R. Holstein, D. Wyler	(MASA+)
GERARD	90	MPL A5 391	J.M. Gerard	(MPIM)
LEUTWYLER	90B	NP B337 108	H. Leutwyler	(BERN)

c

$I(J^P) = 0(\frac{1}{2}^+)$

Charge $= \frac{2}{3}\,e$ Charm $= +1$

c-QUARK MASS

The c-quark mass corresponds to the "running" mass m_c ($\mu = m_c$) in the $\overline{\text{MS}}$ scheme. We have converted masses in other schemes to the $\overline{\text{MS}}$ scheme using two-loop QCD perturbation theory with $\alpha_s(\mu{=}m_c) = 0.38 \pm 0.03$. The value 1.2729 ± 0.0045 GeV for the $\overline{\text{MS}}$ mass corresponds to 1.65 ± 0.02 GeV for the pole mass (see the "Note on Quark Masses").

$\overline{\text{MS}}$ MASS (GeV)	CL%	DOCUMENT ID		TECN
1.2729±0.0045 (CL = 90%) OUR EVALUATION		See the ideogram below.		
1.2716±0.0082		[1] COLQUHOUN	26	LATT
1.316 ±0.022 $^{+0.019}_{-0.010}$		[2] ALEXANDROU	21	LATT
1.296 ±0.019		[3] HEITGER	21	LATT
1.2723±0.0078		[4] HATTON	20	LATT
1.266 ±0.006		[5] NARISON	20	THEO
1.290 $^{+0.077}_{-0.053}$		[6] ABRAMOWICZ	18	HERA
1.273 ±0.010		[7] BAZAVOV	18	LATT
1.2737±0.0077		[8] LYTLE	18	LATT
1.223 ±0.033		[9] PESET	18	THEO
1.279 ±0.008		[10] CHETYRKIN	17	THEO
1.272 ±0.008		[11] ERLER	17	THEO
1.246 ±0.023		[12] KIYO	16	THEO
1.288 ±0.020		[13] DEHNADI	15	THEO
1.348 ±0.046		[14] CARRASCO	14	LATT
1.24 ±0.03 $^{+0.03}_{-0.07}$		[15] ALEKHIN	13	THEO
1.159 ±0.075		[16] SAMOYLOV	13	NOMD
1.278 ±0.009		[17] BODENSTEIN	11	THEO
1.28 $^{+0.07}_{-0.06}$		[18] LASCHKA	11	THEO
1.196 ±0.059 ±0.050		[19] AUBERT	10A	BABR
1.25 ±0.04		[20] SIGNER	09	THEO
• • • We do not use the following data for averages, fits, limits, etc. • • •				
1.263 ±0.014		[21] NARISON	18A	THEO
1.264 ±0.006		[22] NARISON	18B	THEO
1.335 ±0.043 $^{+0.040}_{-0.011}$		[23] BERTONE	16	THEO
1.2715±0.0095		[24] CHAKRABOR..	15	LATT
1.26 ±0.05 ±0.04		[25] ABRAMOWICZ	13C	COMB
1.282 ±0.011 ±0.022		[26] DEHNADI	13	THEO
1.286 ±0.066		[27] NARISON	13	THEO
1.36 ±0.04 ±0.10		[28] ALEKHIN	12	THEO
1.261 ±0.016		[29] NARISON	12A	THEO
1.01 ±0.09 ±0.03		[30] ALEKHIN	11	THEO
1.28 ±0.04		[31] BLOSSIER	10	LATT
1.299 ±0.026		[32] BODENSTEIN	10	THEO
1.273 ±0.006		[33] MCNEILE	10	LATT
1.261 ±0.018		[34] NARISON	10	THEO
1.279 ±0.013		[35] CHETYRKIN	09	THEO
1.268 ±0.009		[36] ALLISON	08	LATT
1.286 ±0.013		[37] KUHN	07	THEO
1.295 ±0.015		[38] BOUGHEZAL	06	THEO
1.24 ±0.09		[39] BUCHMUEL...	06	THEO
1.224 ±0.017 ±0.054		[40] HOANG	06	THEO
1.33 ±0.10		[41] AUBERT	04X	THEO
1.29 ±0.07		[42] HOANG	04	THEO
1.319 ±0.028		[43] DEDIVITIIS	03	LATT
1.19 ±0.11		[44] EIDEMULLER	03	THEO
1.289 ±0.043		[45] ERLER	03	THEO
1.26 ±0.02		[46] ZYABLYUK	03	THEO

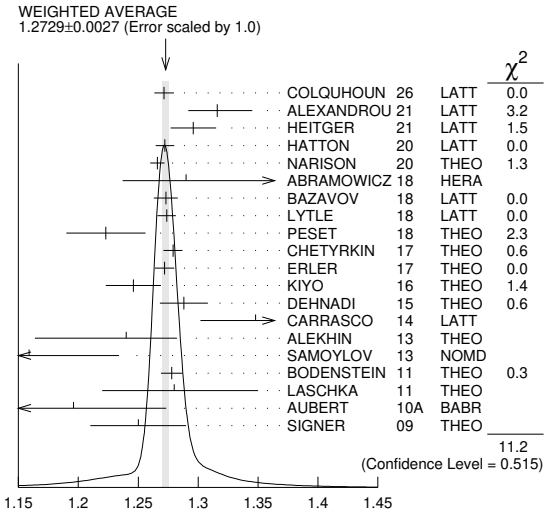

[1] COLQUHOUN 26 value comes from lattice computation of the pseudoscalar correlator. Quenched QED corrections are included.

[2] ALEXANDROU 21 determines the quark mass using a lattice calculation of the meson and baryon masses with a twisted mass fermion action. We have converted $\overline{m}_c(3\text{ GeV}) = 1.036 \pm 0.017^{+0.015}_{-0.008}$ to $\overline{m}_c(\overline{m}_c)$. The simulations are carried out using 2+1+1 dynamical quarks with $m_u = m_d \neq m_s \neq m_c$, including gauge ensembles close to the physical pion point.

[3] HEITGER 21 determines the charm quark mass using a $n_f = 2{+}1$ flavor lattice QCD simulation with non-perturbatively O(a) improved Wilson fermions. They also determine $\overline{m}_c(3\text{ GeV}) = 1.007 \pm 0.016$ GeV.

[4] HATTON 20 determines the charm quark mass with a lattice QCD + quenched QED simulation using the HISQ action and including $n_f = 2{+}1{+}1$ flavors of sea quarks. m_c is tuned from the J/ψ meson mass giving $\overline{m}_c(3\text{ GeV}) = 0.9841 \pm 0.0051$ GeV.

[5] NARISON 20 determines the quark mass using QCD Laplace sum rules from the B_c mass, combined with previous determinations of the QCD condensates and c and b masses.

Phys. A 2026.41. Downloaded from www.worldscientific.com
by UNIVERSITY OF CA ELEY on 09/16/26. Re-use and distribution is strictly not permitted, except for Open Access articles.

[6] ABRAMOWICZ 18 determine $\overline{m}_c(\overline{m}_c) = 1.290^{+0.046}_{-0.041}{}^{+0.062}_{-0.014}{}^{+0.003}_{-0.031}$ from the production of c quarks in ep collisions at HERA using combined H1 and ZEUS data. The experimental/fitting errors, and those from modeling and parameterization have been combined in quadrature.

[7] BAZAVOV 18 determine the quark masses using a lattice computation with staggered fermions and four active quark flavors.

[8] LYTLE 18 combined with CHAKRABORTY 15 determine $\overline{m}_c(3\text{ GeV}) = 0.9874(48)$ GeV from a lattice simulation with $n_f = 2+1+1$ flavors. They also determine the quoted value $\overline{m}_c(\overline{m}_c)$ for $n_f = 4$ dynamical flavors.

[9] PESET 18 determine $\overline{m}_c(\overline{m}_c)$ and $\overline{m}_b(\overline{m}_b)$ using an N3LO calculation of the η_c, η_b and B_c masses.

[10] CHETYRKIN 17 determine $\overline{m}_c(\mu = 3\text{ GeV}) = 0.993 \pm 0.008$ GeV and $\overline{m}_c(\overline{m}_c)$ from a four-loop sum-rule computation of the cross-section for $e^+e^- \to$ hadrons in the charm threshold region.

[11] ERLER 17 determine $\overline{m}_c(\overline{m}_c) = 1.272 \pm 0.008$ GeV from a three-loop QCD sum-rule computation of the vector current correlator. This result is for fixed $\alpha_s(M_Z) = 0.1182$. Including an α_s uncertainty of ± 0.0016, the charm mass error increases from 8 to 9 MeV.

[12] KIYO 16 determine $\overline{m}_c(\overline{m}_c)$ from the $J/\psi(1S)$ mass at order α_s^3 (N3LO).

[13] DEHNADI 15 determine $\overline{m}_c(\overline{m}_c)$ using sum rules for $e^+e^- \to$ hadrons at order α_s^3 (N3LO), and fitting to both experimental data and lattice results.

[14] CARRASCO 14 is a lattice QCD computation of light quark masses using $2+1+1$ dynamical quarks, with $m_u = m_d \neq m_s \neq m_c$. The u and d quark masses are obtained separately by using the K meson mass splittings and lattice results for the electromagnetic contributions.

[15] ALEKHIN 13 determines m_c from charm production in deep inelastic scattering at HERA using approximate NNLO QCD.

[16] SAMOYLOV 13 determines m_c from a study of charm dimuon production in neutrino-iron scattering using the NLO QCD result for the charm quark production cross section.

[17] BODENSTEIN 11 determine $\overline{m}_c(3\text{ GeV}) = 0.987 \pm 0.009$ GeV and $\overline{m}_c(\overline{m}_c) = 1.278 \pm 0.009$ GeV using QCD sum rules for the charm quark vector current correlator.

[18] LASCHKA 11 determine the c mass from the charmonium spectrum. The theoretical computation uses the heavy $Q\overline{Q}$ potential to order $1/m_Q$ obtained by matching the short-distance perturbative result onto lattice QCD result at larger scales.

[19] AUBERT 10A determine the b- and c-quark masses from a fit to the inclusive decay spectra in semileptonic B decays in the kinetic scheme (and convert it to the $\overline{\text{MS}}$ scheme).

[20] SIGNER 09 determines the c-quark mass using non-relativistic sum rules to analyze the $e^+e^- \to c\overline{c}$ cross-section near threshold. Also determine the PS mass $m_{PS}(\mu_F = 0.7$ GeV$) = 1.50 \pm 0.04$ GeV.

[21] NARISON 18A determines simultaneously $\overline{m}_c(\overline{m}_c)$ and the 4-dimension gluon condensate using QCD exponential sum rules and their ratios evaluated at the optimal scale $\mu = 2.85$ GeV at N2LO-N3LO of perturbative QCD and including condensates up to dimension 6–8 in the (axial-)vector and (pseudo-)scalar charmonium channels.

[22] NARISON 18B determines $\overline{m}_c(\overline{m}_c)$ using QCD vector moment sum rules and their ratios at N2LO-N3LO of perturbative QCD and including condensates up to dimension 8.

[23] BERTONE 16 determine $\overline{m}_c(\overline{m}_c)$ from HERA deep inelastic scattering data using the FONLL scheme. Also determine $\overline{m}_c(\overline{m}_c) = 1.318 \pm 0.054^{+0.490}_{-0.022}$ using the fixed flavor number scheme.

[24] CHAKRABORTY 15 is a lattice QCD computation using 2+1+1 dynamical flavors. Moments of pseudoscalar current-current correlators are matched to α_s^3-accurate QCD perturbation theory with the η_c meson mass tuned to experiment.

[25] ABRAMOWICZ 13C determines m_c from charm production in deep inelastic ep scattering, using the QCD prediction at NLO order. The uncertainties from model and parameterization assumptions, and the value of α_s, of ± 0.03, ± 0.02, and ± 0.02 respectively, have been combined in quadrature.

[26] DEHNADI 13 determines m_c using QCD sum rules for the charmonium spectrum and charm continuum to order α_s^3 (N3LO). The statistical and systematic experimental errors of ± 0.006 and ± 0.009 have been combined in quadrature. The theoretical uncertainties ± 0.019 from truncation of the perturbation series, ± 0.010 from α_s, and ± 0.002 from the gluon condensate have been combined in quadrature.

[27] NARISON 13 determines m_c using QCD spectral sum rules to order α_s^2 (NNLO) and including condensates up to dimension 6.

[28] ALEKHIN 12 determines m_c from heavy quark production in deep inelastic scattering at HERA using approximate NNLO QCD.

[29] NARISON 12A determines m_c using sum rules for the vector current correlator to order α_s^3, including the effect of gluon condensates up to dimension eight.

[30] ALEKHIN 11 determines m_c from heavy quark production in deep inelastic scattering using fixed target and HERA data, and approximate NNLO QCD.

[31] BLOSSIER 10 determines quark masses from a computation of the hadron spectrum using n_f=2 dynamical twisted-mass Wilson fermions.

[32] BODENSTEIN 10 determines $\overline{m}_c(3\text{ GeV}) = 1.008 \pm 0.026$ GeV using finite energy sum rules for the vector current correlator. The authors have converted this to $\overline{m}_c(\overline{m}_c)$ using $\alpha_s(M_Z) = 0.1189 \pm 0.0020$.

[33] MCNEILE 10 determines m_c by comparing the order α_s^3 perturbative results for the pseudo-scalar current to lattice simulations with $n_f = 2+1$ sea-quarks by the HPQCD collaboration.

[34] NARISON 10 determines m_c from ratios of moments of vector current correlators computed to order α_s^3 and including the dimension-six gluon condensate.

[35] CHETYRKIN 09 determine m_c and m_b from the $e^+e^- \to Q\overline{Q}$ cross-section and sum rules, using an order α_s^3 computation of the heavy quark vacuum polarization. They also determine $m_c(3\text{ GeV}) = 0.986 \pm 0.013$GeV.

[36] ALLISON 08 determine m_c by comparing four-loop perturbative results for the pseudo-scalar current correlator to lattice simulations by the HPQCD collaboration. The result has been updated in MCNEILE 10.

[37] KUHN 07 determine $\overline{m}_c(\mu = 3\text{ GeV}) = 0.986 \pm 0.013$ GeV and $\overline{m}_c(\overline{m}_c)$ from a four-loop sum-rule computation of the cross-section for $e^+e^- \to$ hadrons in the charm threshold region.

[38] BOUGHEZAL 06 result comes from the first moment of the hadronic production cross-section to order α_s^3.

[39] BUCHMUELLER 06 determine m_b and m_c by a global fit to inclusive B decay spectra.

[40] HOANG 06 determines $\overline{m}_c(\overline{m}_c)$ from a global fit to inclusive B decay data. The B decay distributions were computed to order $\alpha_s^2\beta_0$, and the conversion between different m_c mass schemes to order α_s^3.

[41] AUBERT 04X obtain m_c from a fit to the hadron mass and lepton energy distributions in semileptonic B decay. The paper quotes values in the kinetic scheme. The $\overline{\text{MS}}$ value has been provided by the BABAR collaboration.

[42] HOANG 04 determines $\overline{m}_c(\overline{m}_c)$ from moments at order α_s^2 of the charm production cross-section in e^+e^- annihilation.

[43] DEDIVITIIS 03 use a quenched lattice computation of heavy-heavy and heavy-light meson masses.

[44] EIDEMULLER 03 determines m_b and m_c using QCD sum rules.

[45] ERLER 03 determines m_b and m_c using QCD sum rules. Includes recent BES data.

[46] ZYABLYUK 03 determines m_c by using QCD sum rules in the pseudoscalar channel and comparing with the η_c mass.

m_c/m_s MASS RATIO

The ratio is that of the $\overline{\text{MS}}$ masses at a common scale, for four dynamical quark flavors.

VALUE	CL%	DOCUMENT ID		TECN
11.761±0.047 (CL = 90%) OUR EVALUATION		See the ideogram below.		
$11.48 \pm 0.12 \; ^{+0.25}_{-0.19}$		[1] ALEXANDROU	21	LATT
11.783±0.025		[2] BAZAVOV	18	LATT
11.652±0.065		[3] CHAKRABOR..	15	LATT
11.62 ±0.16		[4] CARRASCO	14	LATT
11.27 ±0.30 ±0.26		[5] DURR	12	LATT
11.85 ±0.16		[6] DAVIES	10	LATT
• • • We do not use the following data for averages, fits, limits, etc. • • •				
$11.747 \pm 0.019^{+0.059}_{-0.043}$		[7] BAZAVOV	14A	LATT
12.0 ±0.3		[8] BLOSSIER	10	LATT

[1] ALEXANDROU 21 determines the quark mass using a lattice calculation of the meson and baryon masses with a twisted mass fermion action. The simulations are carried out using 2+1+1 dynamical quarks with $m_u = m_d \neq m_s \neq m_c$, including gauge ensembles close to the physical pion point.

[2] BAZAVOV 18 determine the quark masses using a lattice computation with staggered fermions and four active quark flavors.

[3] CHAKRABORTY 15 is a lattice QCD computation on gluon field configurations with 2+1+1 dynamical flavors of HISQ quarks with u/d masses down to the physical value. m_c and m_s are tuned from pseudoscalar meson masses.

[4] CARRASCO 14 is a lattice QCD computation of light quark masses using $2+1+1$ dynamical quarks, with $m_u = m_d \neq m_s \neq m_c$. The u and d quark masses are obtained separately by using the K meson mass splittings and lattice results for the electromagnetic contributions.

[5] DURR 12 determine m_c/m_s using a lattice computation with $n_f = 2$ dynamical fermions. The result is combined with other determinations of m_c to obtain $m_s(2\text{ GeV}) = 97.0 \pm 2.6 \pm 2.5$ MeV.

[6] DAVIES 10 determine m_c/m_s from meson masses calculated on gluon fields including u, d, and s sea quarks with lattice spacing down to 0.045 fm. The Highly Improved Staggered quark formalism is used for the valence quarks.

[7] BAZAVOV 14A is a lattice computation using 4 dynamical flavors of HISQ fermions.

[8] BLOSSIER 10 determine m_c/m_s from a computation of the hadron spectrum using n_f = 2 dynamical twisted-mass Wilson fermions.

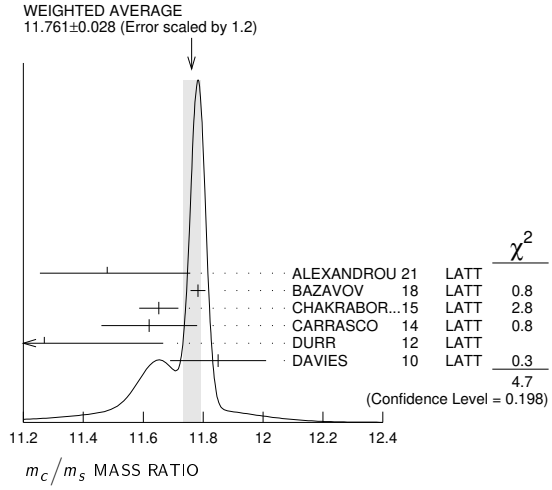

m_b/m_c MASS RATIO

The ratio is that of the $\overline{\text{MS}}$ masses at a common scale, for four dynamical quark flavors.

VALUE	DOCUMENT ID		TECN
4.58 ±0.01 OUR EVALUATION			
4.580±0.007 OUR AVERAGE			
4.586±0.012	[1] HATTON	21	LATT
4.578±0.008	[2] BAZAVOV	18	LATT
4.528±0.054	[3] CHAKRABOR..	15	LATT

[1] HATTON 21 determine $\overline{m}_b(\mu)/\overline{m}_c(\mu) = 4.586 \pm 0.012$ at $\mu = 3$ GeV with a lattice QCD + quenched QED simulation using the HISQ action and including n_f =2+1+1 flavors of sea quarks. The ratio depends weakly on μ because of QED effects.

Int. J. Mod. Phys. A 2026.41. Downloaded from www.worldscientific.com by UNIVERSITY OF CALIFORNIA @ BERKELEY on 09/16/26. Re-use and distribution is strictly not permitted, except for Open Access articles.

[2] BAZAVOV 18 determine the quark masses using a lattice computation with staggered fermions and four active quark flavors for the u, d, s, c quarks and five active flavors for the b quark.

[3] CHAKRABORTY 15 is a lattice computation using 4 dynamical quark flavors.

$m_b - m_c$ QUARK MASS DIFFERENCE

VALUE (GeV)		DOCUMENT ID		TECN
3.45 ±0.05 OUR EVALUATION				
• • • We do not use the following data for averages, fits, limits, etc. • • •				
3.472±0.032		[1] AUBERT	10A	BABR
3.42 ±0.06		[2] ABDALLAH	06B	DLPH
3.44 ±0.03		[3] AUBERT	04X	BABR
3.41 ±0.01		[3] BAUER	04	THEO

[1] AUBERT 10A determine the b- and c-quark masses from a fit to the inclusive decay spectra in semileptonic B decays in the kinetic scheme.

[2] ABDALLAH 06B determine $m_b - m_c$ from moments of the hadron invariant mass and lepton energy spectra in semileptonic inclusive B decays.

[3] Determine $m_b - m_c$ from a global fit to inclusive B decay spectra.

c-QUARK REFERENCES

COLQUHOUN	26	PR D113 074522	B. Colquhoun *et al.*	(HPQCD Collab.)
ALEXANDROU	21	PR D104 074515	C. Alexandrou *et al.*	(ETM Collab.)
HATTON	21	PR D103 114508	D. Hatton *et al.*	(HPQCD Collab.)
HEITGER	21	JHEP 2105 288	J. Heitger, F. Joswig, S. Kuberski	(ALPHA Collab.)
HATTON	20	PR D102 054511	D. Hatton *et al.*	(HPQCD Collab.)
NARISON	20	PL B802 135221	S. Narison	(MONP)
ABRAMOWICZ	18	EPJ C78 473	H. Abramowicz *et al.*	(H1 and ZEUS Collabs.)
BAZAVOV	18	PR D98 054517	A. Bazavov *et al.*	(Fermilab Lattice, MILC, TUMQCD)
LYTLE	18	PR D98 014513	A.T. Lytle *et al.*	(HPQCD Collab.)
NARISON	18A	IJMP A33 1850045	S. Narison	(MONP)
NARISON	18B	PL B784 261	S. Narison	(MONP)
PESET	18	JHEP 1809 167	C. Peset, A. Pineda, J. Segovia	(BARC, TUM)
CHETYRKIN	17	PR D96 116007	K.G. Chetyrkin *et al.*	
ERLER	17	EPJ C77 99	J. Erler, P. Masjuan, H. Spiesberger	
BERTONE	16	JHEP 1608 050	V. Bertone *et al.*	(xFitter Developers)
KIYO	16	PL B752 122	Y. Kiyo, G. Mishima, Y. Sumino	
CHAKRABOR...	15	PR D91 054508	B. Chakraborty *et al.*	(HPQCD Collab.)
DEHNADI	15	JHEP 1508 155	B. Dehnadi, A.H. Hoang, V. Mateu	
BAZAVOV	14A	PR D90 074509	A. Bazavov *et al.*	(Fermi-LAT and MILC Collabs.)
CARRASCO	14	NP B887 19	N. Carrasco *et al.*	(European Twisted Mass Collab.)
ABRAMOWICZ	13C	EPJ C73 2311	H. Abramovicz *et al.*	(H1 and Zeus Collabs.)
ALEKHIN	13	PL B720 172	S. Alekhin *et al.*	(SERP, DESYZ, WUPP+)
DEHNADI	13	JHEP 1309 103	B. Dehnadi *et al.*	(SHRZ, VIEN, MPIM+)
NARISON	13	PL B718 1321	S. Narison	(MONP)
SAMOYLOV	13	NP B876 339	O. Samoylov *et al.*	(NOMAD Collab.)
ALEKHIN	12	PL B718 550	S. Alekhin *et al.*	(SERP, WUPP, DESY+)
DURR	12	PRL 108 122003	S. Durr, G. Koutsou	(WUPP, JULI, CYPR)
NARISON	12A	PL B706 412	S. Narison	(MONP)
ALEKHIN	11	PL B699 345	S. Alekhin, S. Moch	(DESY, SERP)
BODENSTEIN	11	PR D83 074014	S. Bodenstein *et al.*	
LASCHKA	11	PR D83 094002	A. Laschka, N. Kaiser, W. Weise	
AUBERT	10A	PR D81 032003	B. Aubert *et al.*	(BABAR Collab.)
BLOSSIER	10	PR D82 114513	B. Blossier *et al.*	(ETM Collab.)
BODENSTEIN	10	PR D82 114013	S. Bodenstein *et al.*	
DAVIES	10	PRL 104 132003	C.T.H. Davies *et al.*	(HPQCD Collab.)
MCNEILE	10	PR D82 034512	C. McNeile *et al.*	(HPQCD Collab.)
NARISON	10	PL B693 559	S. Narison	(MONP)
Also		PL B705 544 (errat.)	S. Narison	(MONP)
CHETYRKIN	09	PR D80 074010	K.G. Chetyrkin *et al.*	(KARL, BNL)
SIGNER	09	PL B672 333	A. Signer	(DURH)
ALLISON	08	PR D78 054513	I. Allison *et al.*	(HPQCD Collab.)
KUHN	07	NP B778 192	J.H. Kuhn, M. Steinhauser, C. Sturm	
ABDALLAH	06B	EPJ C45 35	J. Abdallah *et al.*	(DELPHI Collab.)
BOUGHEZAL	06	PR D74 074006	R. Boughezal, M. Czakon, T. Schutzmeier	
BUCHMUEL...	06	PR D73 073008	O.L. Buchmueller, H.U. Flacher	(RHBL)
HOANG	06	PL B633 526	A.H. Hoang, A.V. Manohar	
AUBERT	04X	PRL 93 011803	B. Aubert *et al.*	(BABAR Collab.)
BAUER	04	PR D70 094017	C. Bauer *et al.*	
HOANG	04	PL B594 127	A.H. Hoang, M. Jamin	
DEDIVITIIS	03	NP B675 309	G.M. de Divitiis *et al.*	
EIDEMULLER	03	PR D67 113002	M. Eidemuller	
ERLER	03	PL B558 125	J. Erler, M. Luo	
ZYABLYUK	03	JHEP 0301 081	K.N. Zyablyuk	(ITEP)

b

$I(J^P) = 0(\frac{1}{2}^+)$

Charge $= -\frac{1}{3}\ e$ Bottom $= -1$

b-QUARK MASS

b-quark mass corresponds to the "running mass" $\overline{m}_b(\mu = \overline{m}_b)$ in the $\overline{\text{MS}}$ scheme. We have converted masses in other schemes to the $\overline{\text{MS}}$ mass using two-loop QCD perturbation theory with $\alpha_s(\mu = \overline{m}_b) = 0.223 \pm 0.008$. The value 4.186 ± 0.006 GeV for the $\overline{\text{MS}}$ mass corresponds to 4.788 ± 0.016 GeV for the pole mass, using the two-loop conversion formula. A discussion of masses in different schemes can be found in the "Note on Quark Masses."

$\overline{\text{MS}}$ MASS (GeV)	CL%	DOCUMENT ID		TECN
4.186 ±0.006 (CL = 90%) OUR EVALUATION See the ideogram below.				
4.1923±0.0063		[1] COLQUHOUN	26	LATT
$3.94\ ^{+0.46}_{-0.40}$		[2] APARISI	22	THEO
4.202 ±0.021		[3] HATTON	21	LATT
4.197 ±0.008		[4] NARISON	20	THEO
$4.049\ ^{+0.138}_{-0.118}$		[5] ABRAMOWICZ	18	HERA
4.195 ±0.014		[6] BAZAVOV	18	LATT
4.186 ±0.037		[7] PESET	18	THEO
4.197 ±0.022		[8] KIYO	16	THEO
4.183 ±0.037		[9] ALBERTI	15	THEO
$4.203\ ^{+0.016}_{-0.034}$		[10] BENEKE	15	THEO
4.196 ±0.023		[11] COLQUHOUN	15	LATT
4.176 ±0.023		[12] DEHNADI	15	THEO
4.21 ±0.11		[13] BERNARDONI	14	LATT
4.169 ±0.002 ±0.008		[14] PENIN	14	THEO
4.166 ±0.043		[15] LEE	13O	LATT
4.247 ±0.034		[16] LUCHA	13	THEO
4.171 ±0.009		[17] BODENSTEIN	12	THEO
4.29 ±0.14		[18] DIMOPOUL...	12	LATT
$4.18\ ^{+0.05}_{-0.04}$		[19] LASCHKA	11	THEO
4.186 ±0.044 ±0.015		[20] AUBERT	10A	BABR
4.163 ±0.016		[21] CHETYRKIN	09	THEO
4.243 ±0.049		[22] SCHWANDA	08	BELL
• • • We do not use the following data for averages, fits, limits, etc. • • •				
4.184 ±0.011		[23] NARISON	18A	THEO
4.188 ±0.008		[24] NARISON	18B	THEO
4.07 ±0.17		[25] ABRAMOWICZ	14A	ZEUS
4.201 ±0.043		[26] AYALA	14A	THEO
4.236 ±0.069		[27] NARISON	13	THEO
4.213 ±0.059		[28] NARISON	13A	THEO
4.235 ±0.003 ±0.055		[29] HOANG	12	THEO
4.212 ±0.032		[30] NARISON	12	THEO
4.177 ±0.011		[31] NARISON	12	THEO
4.171 ±0.014		[32] NARISON	12A	THEO
4.164 ±0.023		[33] MCNEILE	10	LATT
4.173 ±0.010		[34] NARISON	10	THEO
5.26 ±1.2		[35] ABDALLAH	08D	DLPH
4.42 ±0.06 ±0.08		[36] GUAZZINI	08	LATT
4.347 ±0.048 ±0.08		[37] DELLA-MOR...	07	LATT
4.164 ±0.025		[38] KUHN	07	THEO
4.19 ±0.40		[39] ABDALLAH	06D	DLPH
4.205 ±0.058		[40] BOUGHEZAL	06	THEO
4.20 ±0.04		[41] BUCHMUEL...	06	THEO
4.19 ±0.06		[42] PINEDA	06	THEO
4.4 ±0.3		[43] GRAY	05	LATT
4.22 ±0.06		[44] AUBERT	04X	THEO
4.17 ±0.03		[45] BAUER	04	THEO
4.22 ±0.11		[46] HOANG	04	THEO
4.25 ±0.11		[47] MCNEILE	04	LATT
4.22 ±0.09		[48] BAUER	03	THEO
4.19 ±0.05		[49] BORDES	03	THEO
4.20 ±0.09		[50] CORCELLA	03	THEO
4.33 ±0.10		[51] DEDIVITIIS	03	LATT
4.24 ±0.10		[52] EIDEMULLER	03	THEO
4.207 ±0.03		[53] ERLER	03	THEO
4.33 ±0.06 ±0.10		[54] MAHMOOD	03	CLEO
4.190 ±0.032		[55] BRAMBILLA	02	THEO
4.346 ±0.070		[56] PENIN	02	THEO

[1] COLQUHOUN 26 value comes from lattice computation of the pseudoscalar correlator. Quenched QED corrections are included.

[2] APARISI 22 determine m_b at the Higgs mass, $\overline{m}_b(m_H) = 2.60\ ^{+0.36}_{-0.31}$ GeV from Higgs boson decay rates at the LHC, which is used to obtain $\overline{m}_b(\overline{m}_b)$.

[3] HATTON 21 determine $\overline{m}_b(3\text{ GeV}) = 4.513 \pm 0.026$ GeV using a lattice QCD + quenched QED simulation using the HISQ action and including $n_f = 2+1+1$ flavors of sea quarks, by combining their $\overline{m}_b/\overline{m}_c$ and $\overline{m}_c$ determinations.

[4] NARISON 20 determines the quark mass using QCD Laplace sum rules from the B_c mass, combined with previous determinations of the QCD condensates and c and b masses.

[5] ABRAMOWICZ 18 determine $\overline{m}_b(\overline{m}_b) = 4.049\ ^{+0.104+0.090+0.001}_{-0.109-0.032-0.031}$ from the production of b quarks in ep collisions at HERA using combined H1 and ZEUS data. The experimental/fitting errors, and those from modeling and parameterization have been combined in quadrature.

[6] BAZAVOV 18 determine the b mass using a lattice computation with staggered fermions and five active quark flavors.

[7] PESET 18 determine $\overline{m}_c(\overline{m}_c)$ and $\overline{m}_b(\overline{m}_b)$ using an N3LO calculation of the η_c, η_b and B_c masses.

[8] KIYO 16 determine $\overline{m}_b(\overline{m}_b)$ from the $\Upsilon(1S)$ mass at order α_s^3 (N3LO).

[9] ALBERTI 15 determine $\overline{m}_b(\overline{m}_b)$ from fits to inclusive $B \to X_c e \overline{\nu}$ decay. They also find $m_b^{\text{kin}}(1\text{ GeV}) = 4.553 \pm 0.020$ GeV.

[10] BENEKE 15 determine $\overline{m}_b(\overline{m}_b)$ using sum rules for $e^+e^- \to$ hadrons at order N3LO including finite m_c effects. They find $m_b^{\text{PS}}(2\text{ GeV}) = 4.532\ ^{+0.013}_{-0.039}$ GeV, and $\overline{m}_b(\overline{m}_b) = 4.193\ ^{+0.022}_{-0.035}$ GeV. The value quoted is obtained using the four-loop conversion given in BENEKE 16.

[11] COLQUHOUN 15 determine $\overline{m}_b(\overline{m}_b)$ from moments of the vector current correlator computed with a lattice simulation using the NRQCD action.

[12] DEHNADI 15 determine $\overline{m}_b(\overline{m}_b)$ using sum rules for $e^+e^- \to$ hadrons at order α_s^3 (N3LO), and fitting to both experimental data and lattice results.

[13] BERNARDONI 14 determine m_b from $n_f = 2$ lattice calculations using heavy quark effective theory non-perturbatively renormalized and matched to QCD at $1/m$ order.

[14] PENIN 14 determine $\overline{m}_b(\overline{m}_b) = 4.169 \pm 0.008 \pm 0.002 \pm 0.002$ using an estimate of the order α_s^3 b-quark vacuum polarization function in the threshold region, including finite m_c effects. The errors of ±0.008 from theoretical uncertainties, and ±0.002 from α_s have been combined in quadrature.

[15] LEE 13O determines m_b using lattice calculations of the Υ and B_s binding energies in NRQCD, including three light dynamical quark flavors. The quark mass shift in NRQCD is determined to order α_s^2, with partial α_s^3 contributions.

by UNIVERSITY OF CA Phys. A 2026.41. Downloaded from www.worldscientific.com
ELEY on 09/16/26. Re-use and distribution is strictly not permitted, except for Open Access articles.

[16] LUCHA 13 determines m_b from QCD sum rules for heavy-light currents using the lattice value for f_B of 191.5 ± 7.3 GeV.

[17] BODENSTEIN 12 determine m_b using sum rules for the vector current correlator and the $e^+e^- \to Q\overline{Q}$ total cross-section.

[18] DIMOPOULOS 12 determine quark masses from a lattice computation using $n_f = 2$ dynamical flavors of twisted mass fermions.

[19] LASCHKA 11 determine the b mass from the charmonium spectrum. The theoretical computation uses the heavy $Q\overline{Q}$ potential to order $1/m_Q$ obtained by matching the short-distance perturbative result onto lattice QCD result at larger scales.

[20] AUBERT 10A determine the b- and c-quark masses from a fit to the inclusive decay spectra in semileptonic B decays in the kinetic scheme (and convert it to the $\overline{\text{MS}}$ scheme).

[21] CHETYRKIN 09 determine m_c and m_b from the $e^+e^- \to Q\overline{Q}$ cross-section and sum rules, using an order α_s^3 (N3LO) computation of the heavy quark vacuum polarization.

[22] SCHWANDA 08 measure moments of the inclusive photon spectrum in $B \to X_s\gamma$ decay to determine m_b^{1S}. We have converted this to $\overline{\text{MS}}$ scheme.

[23] NARISON 18A determines $\overline{m}_b(\overline{m}_b)$ as a function of α_s using QCD exponential sum rules and their ratios evaluated at the optimal scale $\mu = 9.5$ GeV at N2LO-N3LO of perturbative QCD and including condensates up to dimension 6–8 in the (axial-)vector and (pseudo-)scalar bottomonium channels.

[24] NARISON 18B determines $\overline{m}_b(\overline{m}_b)$ using QCD vector moment sum rules and their ratios at N2LO-N3LO of perturbative QCD and including condensates up to dimension 8.

[25] ABRAMOWICZ 14A determine $\overline{m}_b(\overline{m}_b) = 4.07 \pm 0.14^{+0.01}_{-0.07}{}^{+0.05}_{-0.00}{}^{+0.08}_{-0.05}$ from the production of b quarks in ep collisions at HERA. The errors due to fitting, modeling, PDF parameterization, and theoretical QCD uncertainties due to the values of α_s, m_c, and the renormalization scale μ have been combined in quadrature.

[26] AYALA 14A determine $\overline{m}_b(\overline{m}_b)$ from the $\Upsilon(1S)$ mass computed to N3LO order in perturbation theory using a renormalon subtracted scheme.

[27] NARISON 13 determines m_b using QCD spectral sum rules to order α_s^2 (NNLO) and including condensates up to dimension 6.

[28] NARISON 13A determines m_b using HQET sum rules to order α_s^2 (NNLO) and the B meson mass and decay constant.

[29] HOANG 12 determine m_b using non-relativistic sum rules for the Υ system at order α_s^2 (NNLO) with renormalization group improvement.

[30] NARISON 12 determines m_b using exponential sum rules for the vector current correlator to order α_s^3, including the effect of gluon condensates up to dimension eight.

[31] Determines m_b to order α_s^3 (N3LO), including the effect of gluon condensates up to dimension eight combining the methods of NARISON 12 and NARISON 12A.

[32] NARISON 12A determines m_b using sum rules for the vector current correlator to order α_s^3, including the effect of gluon condensates up to dimension eight.

[33] MCNEILE 10 determines m_b by comparing order α_s^3 (N3LO) perturbative results for the pseudo-scalar current to lattice simulations with $n_f = 2+1$ sea-quarks by the HPQCD collaboration.

[34] NARISON 10 determines m_b from ratios of moments of vector current correlators computed to order α_s^3 and including the dimension-six gluon condensate. These values are taken from the erratum to that reference.

[35] ABDALLAH 08D determine $\overline{m}_b(M_Z) = 3.76 \pm 1.0$ GeV from a leading order study of four-jet rates at LEP.

[36] GUAZZINI 08 determine $\overline{m}_b(\overline{m}_b)$ from a quenched lattice simulation of heavy meson masses. The ±0.08 is an estimate of the quenching error.

[37] DELLA-MORTE 07 determine $\overline{m}_b(\overline{m}_b)$ from a computation of the spin-averaged B meson mass using quenched lattice HQET at order $1/m$. The ±0.08 is an estimate of the quenching error.

[38] KUHN 07 determine $\overline{m}_b(\mu = 10\text{ GeV}) = 3.609 \pm 0.025$ GeV and $\overline{m}_b(\overline{m}_b)$ from a four-loop sum-rule computation of the cross-section for $e^+e^- \to$ hadrons in the bottom threshold region.

[39] ABDALLAH 06D determine $m_b(M_Z) = 2.85 \pm 0.32$ GeV from Z-decay three-jet events containing a b-quark.

[40] BOUGHEZAL 06 $\overline{\text{MS}}$ scheme result comes from the first moment of the hadronic production cross-section to order α_s^3.

[41] BUCHMUELLER 06 determine m_b and m_c by a global fit to inclusive B decay spectra.

[42] PINEDA 06 $\overline{\text{MS}}$ scheme result comes from a partial NNLL evaluation (complete at order α_s^2 (NNLO)) of sum rules of the bottom production cross-section in e^+e^- annihilation.

[43] GRAY 05 determines $\overline{m}_b(\overline{m}_b)$ from a lattice computation of the Υ spectrum. The simulations have 2+1 dynamical light flavors. The b quark is implemented using NRQCD.

[44] AUBERT 04X obtain m_b from a fit to the hadron mass and lepton energy distributions in semileptonic B decay. The paper quotes values in the kinetic scheme. The $\overline{\text{MS}}$ value has been provided by the BABAR collaboration.

[45] BAUER 04 determine m_b, m_c and $m_b - m_c$ by a global fit to inclusive B decay spectra.

[46] HOANG 04 determines $\overline{m}_b(\overline{m}_b)$ from moments at order α_s^2 of the bottom production cross-section in e^+e^- annihilation.

[47] MCNEILE 04 use lattice QCD with dynamical light quarks and a static heavy quark to compute the masses of heavy-light mesons.

[48] BAUER 03 determine the b quark mass by a global fit to B decay observables. The experimental data includes lepton energy and hadron invariant mass moments in semileptonic $B \to X_c\ell\nu_\ell$ decay, and the inclusive photon spectrum in $B \to X_s\gamma$ decay. The theoretical expressions used are of order $1/m^3$, and $\alpha_s^2\beta_0$.

[49] BORDES 03 determines m_b using QCD finite energy sum rules to order α_s^2.

[50] CORCELLA 03 determines $\overline{m}_b$ using sum rules computed to order α_s^2. Includes charm quark mass effects.

[51] DEDIVITIIS 03 use a quenched lattice computation of heavy-heavy and heavy-light meson masses.

[52] EIDEMULLER 03 determines $\overline{m}_b$ and $\overline{m}_c$ using QCD sum rules.

[53] ERLER 03 determines $\overline{m}_b$ and $\overline{m}_c$ using QCD sum rules. Includes recent BES data.

[54] MAHMOOD 03 determines m_b^{1S} by a fit to the lepton energy moments in $B \to X_c\ell\nu_\ell$ decay. The theoretical expressions used are of order $1/m^3$ and $\alpha_s^2\beta_0$. We have converted their result to the $\overline{\text{MS}}$ scheme.

[55] BRAMBILLA 02 determine $\overline{m}_b(\overline{m}_b)$ from a computation of the $\Upsilon(1S)$ mass to order α_s^4, including finite m_c corrections.

[56] PENIN 02 determines $\overline{m}_b$ from the spectrum of the Υ system.

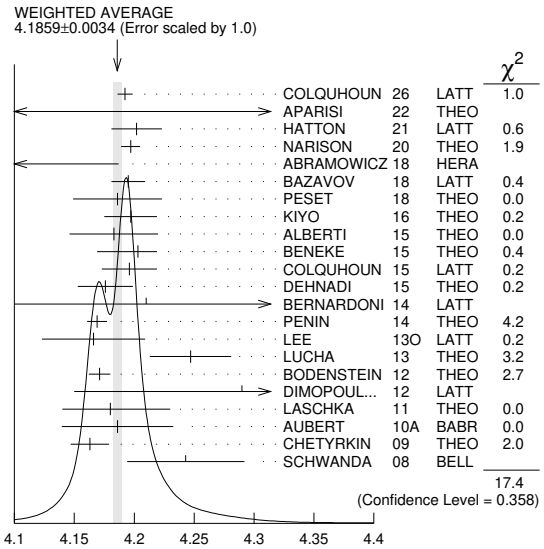

b-QUARK $\overline{\text{MS}}$ MASS (GeV)

m_b/m_s MASS RATIO

VALUE	DOCUMENT ID		TECN
53.88±0.12 OUR AVERAGE			
53.94±0.12	[1] BAZAVOV	18	LATT
52.55±0.55	[2] CHAKRABOR..	15	LATT

[1] BAZAVOV 18 determine the quark masses using a lattice computation with staggered fermions and four active quark flavors for the u, d, s, c quarks and five active flavors for the b quark.

[2] CHAKRABORTY 15 determine m_b/m_s from lattice QCD using the HISQ action and including $n_f = 2+1+1$ flavors of sea quarks.

b-QUARK REFERENCES

COLQUHOUN	26	PR D113 074522	B. Colquhoun *et al.*	(HPQCD Collab.)
APARISI	22	PRL 128 122001	J. Aparisi *et al.*	(VALE, WIEN, PSI+)
HATTON	21	PR D103 114508	D. Hatton *et al.*	(HPQCD Collab.)
NARISON	20	PL B802 135221	S. Narison	(MONP)
ABRAMOWICZ	18	EPJ C78 473	H. Abramowicz *et al.*	(H1 and ZEUS Collabs.)
BAZAVOV	18	PR D98 054517	A. Bazavov *et al.*	(Fermilab Lattice, MILC, TUMQCD)
NARISON	18A	IJMP A33 1850045	S. Narison	(MONP)
NARISON	18B	PL B784 261	S. Narison	(MONP)
PESET	18	JHEP 1809 167	C. Peset, A. Pineda, J. Segovia	(BARC, TUM)
BENEKE	16	PoS RADCOR2015 035	M. Beneke *et al.*	
KIYO	16	PL B752 122	Y. Kiyo, G. Mishima, Y. Sumino	
ALBERTI	15	PRL 114 061802	A. Alberti *et al.*	
BENEKE	15	NP B891 42	M. Beneke *et al.*	
CHAKRABOR...	15	PR D91 054508	B. Chakraborty *et al.*	(HPQCD Collab.)
COLQUHOUN	15	PR D91 074514	B. Colquhoun *et al.*	(HPQCD Collab.)
DEHNADI	15	JHEP 1508 155	B. Dehnadi, A.H. Hoang, V. Mateu	
ABRAMOWICZ	14A	JHEP 1409 127	H. Abramowicz *et al.*	(ZEUS Collab.)
AYALA	14A	JHEP 1409 045	C. Ayala, G. Cvetic, A. Pineda	
BERNARDONI	14	PL B730 171	F. Bernardoni *et al.*	(ALPHA Collab.)
PENIN	14	JHEP 1404 120	A.A. Penin, N. Zerf	
LEE	13O	PR D87 074018	A.J. Lee *et al.*	(HPQCD Collab.)
LUCHA	13	PR D88 056011	W. Lucha, D. Melikhov, S. Simula	(VIEN, MOSU+)
NARISON	13	PL B718 1321	S. Narison	(MONP)
NARISON	13A	PL B721 269	S. Narison	(MONP)
BODENSTEIN	12	PR D85 034003	S. Bodenstein *et al.*	(CAPE, VALE, MAINZ+)
DIMOPOUL...	12	JHEP 1201 046	P. Dimopoulos *et al.*	(ETM Collab.)
HOANG	12	JHEP 1210 188	A.H. Hoang, P. Ruiz-Femenia, M. Stahlhofen	(WIEN+)
NARISON	12	PL B707 259	S. Narison	(MONP)
NARISON	12A	PL B706 412	S. Narison	(MONP)
LASCHKA	11	PR D83 094002	A. Laschka, N. Kaiser, W. Weise	
AUBERT	10A	PR D81 032003	B. Aubert *et al.*	(BABAR Collab.)
MCNEILE	10	PR D82 034512	C. McNeile *et al.*	(HPQCD Collab.)
NARISON	10	PL B693 559	S. Narison	(MONP)
Also		PL B705 544 (errat.)	S. Narison	(MONP)
CHETYRKIN	09	PR D80 074010	K.G. Chetyrkin *et al.*	(KARL, BNL)
ABDALLAH	08D	EPJ C55 525	J. Abdallah *et al.*	(DELPHI Collab.)
GUAZZINI	08	JHEP 0801 076	D. Guazzini, R. Sommer, N. Tantalo	
SCHWANDA	08	PR D78 032016	C. Schwanda *et al.*	(BELLE Collab.)
DELLA-MOR...	07	JHEP 0701 007	M. Della Morte *et al.*	
KUHN	07	NP B778 192	J.H. Kuhn, M. Steinhauser, C. Sturm	
ABDALLAH	06D	EPJ C46 569	J. Abdallah *et al.*	(DELPHI Collab.)
BOUGHEZAL	06	PR D74 074006	R. Boughezal, M. Czakon, T. Schutzmeier	
BUCHMUEL...	06	PR D73 073008	O.L. Buchmueller, H.U. Flacher	(RHBL)
PINEDA	06	PR D73 111501	A. Pineda, A. Signer	
GRAY	05	PR D72 094507	A. Gray *et al.*	(HPQCD and UKQCD Collab.)
AUBERT	04X	PRL 93 011803	B. Aubert *et al.*	(BABAR Collab.)
BAUER	04	PR D70 094017	C. Bauer *et al.*	
HOANG	04	PL B594 127	A.H. Hoang, M. Jamin	
MCNEILE	04	PL B600 77	C. McNeile, C. Michael, G. Thompson	(UKQCD Collab.)
BAUER	03	PR D67 054012	C.W. Bauer *et al.*	
BORDES	03	PL B562 81	J. Bordes, J. Penarrocha, K. Schilcher	
CORCELLA	03	PL B554 133	G. Corcella, A.H. Hoang	
DEDIVITIIS	03	NP B675 309	G.M. de Divitiis *et al.*	
EIDEMULLER	03	PR D67 113002	M. Eidemuller	

Int. J. Mod. Phys. A 2026.41. Downloaded from www.worldscientific.com
by UNIVERSITY OF CALIFORNIA @ BERKELEY on 09/16/26. Re-use and distribution is strictly not permitted, except for Open Access articles.

ERLER	03	PL B558 125	J. Erler, M. Luo	
MAHMOOD	03	PR D67 072001	A.H. Mahmood *et al.*	(CLEO Collab.)
BRAMBILLA	02	PR D65 034001	N. Brambilla, Y. Sumino, A. Vairo	
PENIN	02	PL B538 335	A. Penin, M. Steinhauser	

t

$I(J^P) = 0(\frac{1}{2}^+)$

Charge $= \frac{2}{3}\ e$ Top $= +1$

See the related review(s):

Top Quark

t-QUARK MASS

We first list the direct measurements of the top quark mass which employ the event kinematics and then list the measurements which extract a top quark mass from the measured $t\bar{t}$ cross-section using theory calculations. A discussion of the definition of the top quark mass in these measurements can be found in the review "The Top Quark."

For earlier search limits see PDG 96, Physical Review **D54** 1 (1996). We no longer include a compilation of indirect top mass determinations from Standard Model Electroweak fits in the Listings (our last compilation can be found in the Listings of the 2007 partial update). For a discussion of current results see the reviews "The Top Quark" and "Electroweak Model and Constraints on New Physics."

t-Quark Mass (Direct Measurements)

The following measurements extract a t-quark mass from the kinematics of $t\bar{t}$ events. They are sensitive to the top quark mass used in the MC generator that is usually interpreted as the pole mass, but the theoretical uncertainty in this interpretation is hard to quantify. See the review "The Top Quark" and references therein for more information.

OUR AVERAGE of 172.60 ± 0.27 GeV is an average of top mass measurements from LHC and Tevatron Runs. The latest Tevatron average, 174.30 ± 0.35 ± 0.54 GeV, was provided by the Tevatron Electroweak Working Group (TEVEWWG).

VALUE (GeV)	DOCUMENT ID		TECN	COMMENT
172.60 ± 0.27 OUR AVERAGE	Error includes scale factor of 1.5. See the ideogram below.			
172.95 ± 0.53	[1] AAD	25H	ATLS	boosted top; ℓ+jets channel
172.52 ± 0.14 ± 0.30	[2] HAYRAPETY...	24F	LHC	ATLAS+CMS combined
174.41 ± 0.39 ± 0.71	[3] AAD	23N	ATLS	leptonic invariant mass in ℓ+jets channel
171.77 ± 0.37	[4] TUMASYAN	23BB	CMS	$\ell + \geq 4$j ($2b$)
173.06 ± 0.24 ± 0.80	[5] TUMASYAN	23Z	CMS	boosted top; ℓ+jets channel
$172.13^{+0.76}_{-0.77}$	[6] TUMASYAN	21G	CMS	t-channel single top production
172.6 ± 2.5	[7] SIRUNYAN	20AR	CMS	jet mass from boosted top
172.34 ± 0.20 ± 0.70	[8] SIRUNYAN	19AP	CMS	≥ 6 jets ($\geq 2b$)
$172.33 \pm 0.14^{+0.66}_{-0.72}$	[9] SIRUNYAN	19AR	CMS	dilepton channel ($e\mu$, $2e$, 2μ)
174.30 ± 0.35 ± 0.54	[10] TEVEWWG	16	TEVA	Tevatron combination
• • • We do not use the following data for averages, fits, limits, etc. • • •				
172.08 ± 0.39 ± 0.82	[11] AABOUD	19AC	ATLS	$\ell + \geq 4$j ($2b$)
172.69 ± 0.25 ± 0.41	[12] AABOUD	19AC	ATLS	7, 8 TeV ATLAS combination, superseded by HAYRAPETYAN 24F
172.26 ± 0.07 ± 0.61	[13] SIRUNYAN	19AP	CMS	lepton+jets, all-jets channels
172.25 ± 0.08 ± 0.62	[14] SIRUNYAN	18DE	CMS	$\ell + \geq 4$j ($2b$)
173.72 ± 0.55 ± 1.01	[15] AABOUD	17AH	ATLS	≥ 5 jets ($2b$)
174.95 ± 0.40 ± 0.64	[16] ABAZOV	17B	D0	ℓ + jets and dilepton channels
$172.95 \pm 0.77^{+0.97}_{-0.93}$	[17] SIRUNYAN	17L	CMS	t-channel single top production
170.8 ± 9.0	[18] SIRUNYAN	17N	CMS	jet mass in highly-boosted $t\bar{t}$ events
$172.22 \pm 0.18^{+0.89}_{-0.93}$	[19] SIRUNYAN	17O	CMS	Dilepton channel
172.99 ± 0.41 ± 0.74	[20] AABOUD	16T	ATLS	dilepton channel
172.84 ± 0.34 ± 0.61	[21] AABOUD	16T	ATLS	combination of ATLAS
173.32 ± 1.36 ± 0.85	[22] ABAZOV	16	D0	$\ell\ell + \not{E}_T + \geq 2$j ($\geq 2b$)
173.93 ± 1.61 ± 0.88	[23] ABAZOV	16D	D0	$\ell\ell + \not{E}_T + \geq 2$j ($\geq 2b$)
172.35 ± 0.16 ± 0.48	[24,25] KHACHATRY...	16AK	CMS	$\ell + \geq 4$j ($2b$)
172.32 ± 0.25 ± 0.59	[24,25] KHACHATRY...	16AK	CMS	≥ 6 jets ($2b$)
172.82 ± 0.19 ± 1.22	[24,26] KHACHATRY...	16AK	CMS	$(e e/\mu\mu)+\not{E}_T+ \geq 2b, e\mu+ \geq 2b$
172.44 ± 0.13 ± 0.47	[27] KHACHATRY...	16AK	CMS	7, 8 TeV CMS combination, superseded by HAYRAPETYAN 24F
$173.68 \pm 0.20^{+1.58}_{-0.97}$	[28] KHACHATRY...	16AL	CMS	semi- + di-leptonic channels
173.5 ± 3.0 ± 0.9	[29] KHACHATRY...	16CB	CMS	$t \to (W \to \ell\nu)(b \to J/\psi X \to \mu^+\mu^- X)$
175.1 ± 1.4 ± 1.2	[30] AAD	15AW	ATLS	small $\not{E}_T$, ≥ 6 jets ($2b$-tag)
172.99 ± 0.48 ± 0.78	[31] AAD	15BF	ATLS	ℓ + jets and dilepton
171.5 ± 1.9 ± 2.5	[32] AALTONEN	15D	CDF	$\ell\ell + \not{E}_T + \geq 2$j
$175.07 \pm 1.19^{+1.55}_{-1.58}$	[33] AALTONEN	14N	CDF	small $\not{E}_T$, 6–8 jets ($\geq 1b$-tag)
174.98 ± 0.58 ± 0.49	[34] ABAZOV	14C	D0	$\ell + \not{E}_T$ + 4 jets (≥ 1 b-tag)
173.49 ± 0.69 ± 1.21	[35] CHATRCHYAN	14C	CMS	≥ 6 jets (≥ 2 b-tag)
173.93 ± 1.64 ± 0.87	[36] AALTONEN	13H	CDF	$\not{E}_T + \geq 4$ jets (≥ 1 b)
$173.9 \pm 0.9\ ^{+1.7}_{-2.1}$	[37] CHATRCHYAN	13S	CMS	$\ell\ell+\not{E}_T+ \geq 2b$-tag ($MT2_{(T)}$)
174.5 ± 0.6 ± 2.3	[38] AAD	12I	ATLS	$\ell+\not{E}_T+ \geq 4$ jets (≥ 1 b), MT
172.85 ± 0.71 ± 0.85	[39] AALTONEN	12AI	CDF	$\ell+\not{E}_T+ \geq 4$j (0,1,2b) template
172.7 ± 9.3 ± 3.7	[40] AALTONEN	12AL	CDF	$\tau_h + \not{E}_T$ +4j ($\geq 1b$)
173.18 ± 0.56 ± 0.75	[41] AALTONEN	12AP	TEVA	CDF, D0 combination
172.5 ± 1.4 ± 1.5	[42] AALTONEN	12G	CDF	6–8 jets with ≥ 1 b
173.7 ± 2.8 ± 1.5	[43] ABAZOV	12AB	D0	$\ell\ell + \not{E}_T + \geq 2$ j (νWT)
173.9 ± 1.9 ± 1.6	[44] ABAZOV	12AB	D0	$\ell\ell+\not{E}_T+ \geq 2$j ($\nu$WT+MWT)
172.5 ± 0.4 ± 1.5	[45] CHATRCHYAN	12BA	CMS	$\ell\ell+\not{E}_T+ \geq 2$j ($\geq 1b$), AMWT
173.49 ± 0.43 ± 0.98	[46] CHATRCHYAN	12BP	CMS	$\ell+\not{E}_T+ \geq 4$j ($\geq 2b$)
172.4 ± 1.4 ± 1.3	[47] AALTONEN	11AC	CDF	$\ell + \not{E}_T$ + 4 jets (≥ 1 b-tag)
172.3 ± 2.4 ± 1.0	[48] AALTONEN	11AK	CDF	Repl. by AALTONEN 13H
172.1 ± 1.1 ± 0.9	[49] AALTONEN	11E	CDF	ℓ + jets and dilepton
176.9 ± 8.0 ± 2.7	[50] AALTONEN	11T	CDF	$\ell + \not{E}_T$ + 4 jets (≥ 1 b-tag), $p_T(\ell)$ shape
174.94 ± 0.83 ± 1.24	[51] ABAZOV	11P	D0	$\ell + \not{E}_T$ + 4 jets (≥ 1 b-tag)
174.0 ± 1.8 ± 2.4	[52] ABAZOV	11R	D0	dilepton + $\not{E}_T$ + ≥ 2 jets
175.5 ± 4.6 ± 4.6	[53] CHATRCHYAN	11F	CMS	dilepton + $\not{E}_T$ + jets
173.0 ± 0.9 ± 0.9	[54] AALTONEN	10AE	CDF	$\ell + \not{E}_T$ + 4 jets (≥ 1 b-tag), ME method
169.3 ± 2.7 ± 3.2	[55] AALTONEN	10C	CDF	dilepton + b-tag (MT2+NWA)
170.7 ± 6.3 ± 2.6	[56] AALTONEN	10D	CDF	$\ell + \not{E}_T$ + 4 jets (b-tag)
$174.8 \pm 2.4\ ^{+1.2}_{-1.0}$	[57] AALTONEN	10E	CDF	≥ 6 jets, vtx b-tag
180.5 ± 12.0 ± 3.6	[58] AALTONEN	09AK	CDF	$\ell + \not{E}_T$ + jets (soft μ b-tag)
172.7 ± 1.8 ± 1.2	[59] AALTONEN	09J	CDF	$\ell + \not{E}_T$ + 4 jets (b-tag)
171.1 ± 3.7 ± 2.1	[60] AALTONEN	09K	CDF	6 jets, vtx b-tag
171.9 ± 1.7 ± 1.1	[61] AALTONEN	09L	CDF	ℓ + jets, $\ell\ell$ + jets
171.2 ± 2.7 ± 2.9	[62] AALTONEN	09O	CDF	dilepton
$165.5\ ^{+3.4}_{-3.3} \pm 3.1$	[63] AALTONEN	09X	CDF	$\ell\ell + \not{E}_T$ ($\nu\phi$ weighting)
174.7 ± 4.4 ± 2.0	[64] ABAZOV	09AH	D0	dilepton + b-tag (νWT+MWT)
$170.7\ ^{+4.2}_{-3.9} \pm 3.5$	[65,66] AALTONEN	08C	CDF	dilepton, $\sigma_{t\bar{t}}$ constrained
171.5 ± 1.8 ± 1.1	[67] ABAZOV	08AH	D0	$\ell + \not{E}_T$ + 4 jets
177.1 ± 4.9 ± 4.7	[68,69] AALTONEN	07	CDF	6 jets with ≥ 1 b vtx
$172.3\ ^{+10.8}_{-9.6} \pm 10.8$	[70] AALTONEN	07B	CDF	≥ 4 jets (b-tag)
174.0 ± 2.2 ± 4.8	[71] AALTONEN	07D	CDF	≥ 6 jets, vtx b-tag
170.8 ± 2.2 ± 1.4	[72,73] AALTONEN	07I	CDF	lepton + jets (b-tag)
$173.7 \pm 4.4\ ^{+2.1}_{-2.0}$	[69,74] ABAZOV	07F	D0	lepton + jets
176.2 ± 9.2 ± 3.9	[75] ABAZOV	07W	D0	dilepton (MWT)
179.5 ± 7.4 ± 5.6	[75] ABAZOV	07W	D0	dilepton (νWT)
164.5 ± 3.9 ± 3.9	[73,76] ABULENCIA	07D	CDF	dilepton
$180.7\ ^{+15.5}_{-13.4} \pm 8.6$	[77] ABULENCIA	07J	CDF	lepton + jets
$170.3\ ^{+4.1}_{-4.5} \pm 1.2\ ^{+1.2}_{-1.8}$	[73,78] ABAZOV	06U	D0	lepton + jets (b-tag)
$173.2\ ^{+2.6}_{-2.4} \pm 3.2$	[79,80] ABULENCIA	06D	CDF	lepton + jets
$173.5\ ^{+3.7}_{-3.6} \pm 1.3$	[66,79] ABULENCIA	06D	CDF	lepton + jets
165.2 ± 6.1 ± 3.4	[73,81] ABULENCIA	06G	CDF	dilepton
170.1 ± 6.0 ± 4.1	[66,82] ABULENCIA	06V	CDF	dilepton
178.5 ± 13.7 ± 7.7	[83,84] ABAZOV	05	D0	6 or more jets
180.1 ± 3.6 ± 3.9	[85,86] ABAZOV	04G	D0	lepton + jets
176.1 ± 5.1 ± 5.3	[87] AFFOLDER	01	CDF	lepton + jets
176.1 ± 6.6	[88] AFFOLDER	01	CDF	dilepton, lepton+jets, all-jets
172.1 ± 5.2 ± 4.9	[89] ABBOTT	99G	D0	di-lepton, lepton+jets
176.0 ± 6.5	[90,91] ABE	99B	CDF	dilepton, lepton+jets, all-jets
167.4 ± 10.3 ± 4.8	[91,92] ABE	99B	CDF	dilepton
168.4 ± 12.3 ± 3.6	[86] ABBOTT	98D	D0	dilepton
173.3 ± 5.6 ± 5.5	[86,93] ABBOTT	98F	D0	lepton + jets
175.9 ± 4.8 ± 5.3	[92,94] ABE	98E	CDF	lepton + jets
161 ± 17 ± 10	[92] ABE	98F	CDF	dilepton
172.1 ± 5.2 ± 4.9	[95] BHAT	98B	RVUE	dilepton and lepton+jets
173.8 ± 5.0	[96] BHAT	98B	RVUE	dilepton, lepton+jets, all-jets
173.3 ± 5.6 ± 6.2	[86] ABACHI	97E	D0	lepton + jets
186 ± 10 ± 5.7	[92,97] ABE	97R	CDF	6 or more jets
$199\ ^{+19}_{-21} \pm 22$	ABACHI	95	D0	lepton + jets
176 ± 8 ± 10	ABE	95F	CDF	lepton + b-jet
$174 \pm 10\ ^{+13}_{-12}$	ABE	94E	CDF	lepton + b-jet

[1] AAD 25H based on 140 fb^{-1} of pp data at $\sqrt{s}$ = 13 TeV. The error is the sum of the systematic (±0.46) and statistical (±0.27) uncertainties. The mean of the invariant mass of the reconstructed large-radius jet is simultaneously fitted with m_{jj} and m_{tj} to reduce the uncertainties from jet-energy scale and modelling of the recoil in the top decay.

[2] HAYRAPETYAN 24F based on up to 5 and 20 fb^{-1} of pp data at $\sqrt{s}$ = 7 and 8 TeV, respectively. The combination includes 15 input measurements in $t\bar{t}$ events that exploit both semileptonic and hadronic decays of the top quark as well as t-channel single-top events.

[3] AAD 23N based on 36.1 fb^{-1} of pp data at $\sqrt{s}$ = 13 TeV. The second error is the sum of systematic (±0.66) and that from changing parton-shower gluon recoil scheme (±0.25) uncertainties. The distribution of the invariant mass $m_{\ell\mu}$ (ℓ from W and μ from b-hadron decay) is used, which is less sensitive to jet energy uncertainties and top production modelling.

[4] TUMASYAN 23BB based on 36.3 fb^{-1} of pp data at $\sqrt{s}$ = 13 TeV. For each event, the mass is reconstructed from a kinematic fit of the decay products to a $t\bar{t}$ hypothesis. A profile likelihood method is applied using up to four observables per event.

[5] TUMASYAN 23Z based on 138 fb^{-1} of pp data at $\sqrt{s}$ = 13 TeV. The second error is the sum of experimental (±0.61), model (±0.47), and theoretical (±0.23) uncertainties. The products of the hadronic decay of a top quark with p_T > 400 GeV, in the ℓ + jets

by UNIVERSITY OF CA Phys. A 2026.41. Downloaded from www.worldscientific.com
ELEY on 09/16/26. Re-use and distribution is strictly not permitted, except for Open Access articles.

channel of $t\bar{t}$, are reconstructed as a single jet. The top quark mass is determined from the normalized differential cross section measurement in the $m_{\rm jet}$ distribution.

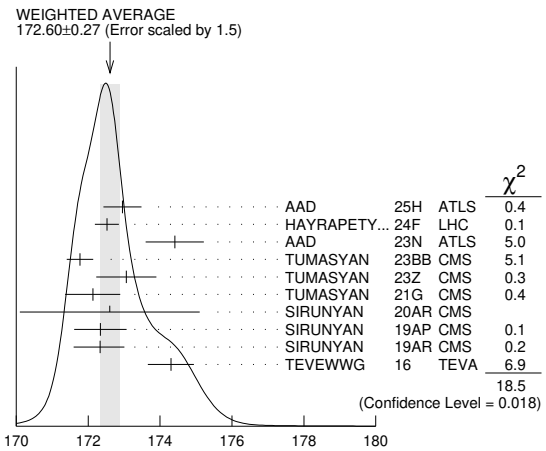

[6] TUMASYAN 21G based on 35.9 fb^{-1} of pp data at $\sqrt{s}$ = 13 TeV. Events are selected by requiring 1ℓ + 2jets($1b$ jet) final state.

[7] SIRUNYAN 20AR based on 35.9 fb^{-1} of pp data at $\sqrt{s}$ = 13 TeV. The products of the hadronic decay of a top quark with p_T > 400 GeV, in the ℓ + jets channel of $t\bar{t}$ are reconstructed as a single jet. The top quark mass is determined from the normalized differential cross section measurement in the $m_{\rm jet}$ distribution.

[8] SIRUNYAN 19AP based on 35.9 fb^{-1} of pp data at $\sqrt{s}$ = 13 TeV. A kinematical fit is applied to each event assuming the signal event topology. m_t is determined simultaneously with a jet energy scale factor (JSF). The second error represents stat.+JSF. Modeling uncertainties are larger than in the measurements at $\sqrt{s}$ = 7 and 8 TeV because of the use of new alternative color reconnection models.

[9] SIRUNYAN 19AR based on 35.9 fb^{-1} of pp data at $\sqrt{s}$ = 13 TeV. Obtained from a simultaneous fit of the cross section and the top quark mass in the POWHEG simulation. The cross section is used also to extract the $\overline{\rm MS}$ mass and the strong coupling constant for different PDF sets.

[10] TEVEWWG 16 is the latest Tevatron average (July 2016) provided by the Tevatron Electroweak Working Group. It takes correlated uncertainties into account and has a χ^2 of 10.8 for 11 degrees of freedom.

[11] AABOUD 19AC based on 20.2 fb^{-1} in pp collisions at $\sqrt{s}$ = 8 TeV. Uses optimized event selection to suppress less-well-reconstructed events and template fits to determine m_t together with a global jet energy scale factor and a relative b-to-light-jet energy scale factor.

[12] AABOUD 19AC is an ATLAS combination of 7 and 8 TeV top-quark mass determination in the dilepton, lepton + jets, and all jets channels.

[13] SIRUNYAN 19AP based on 35.9 fb^{-1} of pp data at $\sqrt{s}$ = 13 TeV. A combined measurement using the lepton+jets and all-jets channels through a single likelihood function. See SIRUNYAN 18DE.

[14] SIRUNYAN 18DE based on 35.9 fb^{-1} of pp data at $\sqrt{s}$ = 13 TeV. m_t is determined simultaneously with an overall jet energy scale factor constrained by the mass of the hadronically decayed W. Compared to the Run 1 analysis a more advanced treatment of modeling uncertainties are employed, in particular concerning color-reconnection models. Superseded by TUMASYAN 23BB.

[15] AABOUD 17AH based on 20.2 fb^{-1} of pp data at $\sqrt{s}$ = 8 TeV. Uses template fits to the ratio of the masses of three-jets (from t candidate) and dijets (from W candidate), to suppress jet energy scale uncertainty. Large QCD background is modelled using a data-driven method.

[16] ABAZOV 17B is a combination of measurements of the top quark mass by D0 in the lepton+jets and dilepton channels, using all data collected in Run I (1992–1996) at $\sqrt{s}$ = 1.8 TeV and Run II (2001–2011) at $\sqrt{s}$ = 1.96 TeV of the Tevatron, corresponding to integrated luminosities of 0.1 fb^{-1} and 9.7 fb^{-1}, respectively.

[17] SIRUNYAN 17L based on 19.7 fb^{-1} of pp data at $\sqrt{s}$ = 8 TeV. m_t is reconstructed from a fit to the invariant mass distribution of $\mu\nu b$, where p_T^{miss} and W mass constraint are used to reconstruct ν momentum. The number of events for various contributions, except for the t-channel single top one, are fixed to the values extracted from simulation. Superseded by TUMASYAN 21G.

[18] SIRUNYAN 17N based on 19.7 fb^{-1} of pp data at $\sqrt{s}$ = 8 TeV. The fully hadronic decay of a highly-boosted t is reconstructed in the ℓ+jets channel and unfolded at the particle level. The sensitivity of the peak position of the m_{jet} distribution is used to test quality of the modelling by the simulation.

[19] SIRUNYAN 17O based on 19.7 fb^{-1} of pp data at $\sqrt{s}$ = 8 TeV. Analysis is based on the kinematical observables $M(b\ell)$, M_{T2} and $M(b\ell\nu)$. A fit is performed to determine m_t and an overall jet energy scale factor simultaneously.

[20] AABOUD 16T based on 20.2 fb^{-1} of pp data at $\sqrt{s}$ = 8 TeV. The analysis is refined using the p_T and invariant mass distributions of ℓ+b-jet system. A combination with measurements from $\sqrt{s}$ = 7 TeV data in the dilepton and lepton+jets channels gives 172.84 ± 0.34 ± 0.61 GeV.

[21] AABOUD 16T is an ATLAS combination of 8 TeV top-quark mass in the dilepton channel with previous measurements from $\sqrt{s}$ = 7 TeV data in the dilepton and lepton + jets channels.

[22] ABAZOV 16 based on 9.7 fb^{-1} of data in $p\overline{p}$ collisions at $\sqrt{s}$ = 1.96 TeV. Employs improved fit to minimize statistical errors and improved jet energy calibration, using lepton + jets mode, which reduces error of jet energy scale. Based on previous determination in ABAZOV 12AB with increased integrated luminosity and improved fit and calibrations.

[23] ABAZOV 16D based on 9.7 fb^{-1} of data in $p\overline{p}$ collisions at $\sqrt{s}$ = 1.96 TeV, using the matrix element technique. Based on previous determination in ABAZOV 11R with increased integrated luminosity. There is a strong correlation with the determination in ABAZOV 16. (See ABAZOV 17B.)

[24] KHACHATRYAN 16AK based on 19.7 fb^{-1} of pp data at $\sqrt{s}$ = 8 TeV. Combination of the three top mass measurements in KHACHATRYAN 16AK and with the CMS results at $\sqrt{s}$ = 7 TeV gives 172.44 ± 0.13 ± 0.47 GeV.

[25] The top mass and jet energy scale factor are determined by a fit.

[26] Uses the analytical matrix weighting technique method.

[27] KHACHATRYAN 16AK based on 19.7 fb^{-1} of pp data at $\sqrt{s}$ = 8 TeV. Combination of the three top mass measurements in KHACHATRYAN 16AK and with the CMS results at $\sqrt{s}$ = 7 TeV.

[28] KHACHATRYAN 16AL based on 19.7 fb^{-1} in pp collisions at $\sqrt{s}$ = 8 TeV. Determined from the invariant mass distribution of leptons and reconstructed secondary vertices from b decays using only charged particles. The uncertainty is dominated by modeling of b fragmentation and top p_T distribution.

[29] KHACHATRYAN 16CB based on 666 candidate reconstructed events corresponding to 19.7 fb^{-1} of pp data at $\sqrt{s}$ = 8 TeV. The measurement exploits correlation of m_t with M($J/\psi\ell$) in the same top quark decay, using a high-purity event sample. A study on modeling of b-quark fragmentation is given in Sec.3.3.

[30] AAD 15AW based on 4.6 fb^{-1} of pp data at $\sqrt{s}$ = 7 TeV. Uses template fits to the ratio of the masses of three-jets (from t candidate) and dijets (from W candidate). Large background from multijet production is modeled with data-driven methods.

[31] AAD 15BF based on 4.6 fb^{-1} in pp collisions at $\sqrt{s}$ = 7 TeV. Using a three-dimensional template likelihood technique the lepton plus jets (≥ 1b-tagged) channel gives 172.33 ± 0.75 ± 1.02 GeV, while exploiting a one dimensional template method using $m_{\ell b}$ the dilepton channel (1 or 2b-tags) gives 173.79 ± 0.54 ± 1.30 GeV. The results are combined.

[32] AALTONEN 15D based on 9.1 fb^{-1} of $p\overline{p}$ data at $\sqrt{s}$ = 1.96 TeV. Uses a template technique to fit a distribution of a variable defined by a linear combination of variables sensitive and insensitive to jet energy scale to optimize reduction of systematic errors. b-tagged and non-b-tagged events are separately analyzed and combined.

[33] Based on 9.3 fb^{-1} of $p\overline{p}$ data at $\sqrt{s}$ = 1.96 TeV. Multivariate algorithm is used to discriminate signal from backgrounds, and templates are used to measure m_t.

[34] Based on 9.7 fb^{-1} of $p\overline{p}$ data at $\sqrt{s}$ = 1.96 TeV. A matrix element method is used to calculate the probability of an event to be signal or background, and the overall jet energy scale is constrained *in situ* by m_W. See ABAZOV 15G for further details.

[35] Based on 3.54 fb^{-1} of pp data at $\sqrt{s}$ = 7 TeV. The mass is reconstructed for each event employing a kinematic fit of the jets to a ttbar hypothesis. The combination with the pervious CMS measurements in the dilepton and the lepton+jets channels gives 173.54 ± 0.33 ± 0.96 GeV.

[36] Based on 8.7 fb^{-1} in $p\overline{p}$ collisions at $\sqrt{s}$ = 1.96 TeV. Events with an identified charged lepton or small $\not{E}_T$ are rejected from the event sample, so that the measurement is statistically independent from those in the ℓ + jets and all hadronic channels while being sensitive to those events with a τ lepton in the final state.

[37] Based on 5.0 fb^{-1} of pp data at $\sqrt{s}$ = 7 TeV. CHATRCHYAN 13S studied events with di-lepton + $\not{E}_T$ + ≥ 2 b-jets, and looked for kinematical endpoints of MT2, MT2$_T$, and subsystem variables.

[38] AAD 12I based on 1.04 fb^{-1} of pp data at $\sqrt{s}$ = 7 TeV. Uses 2d-template analysis (MT) with m_t and jet energy scale factor (JSF) from m_W mass fit.

[39] Based on 8.7 fb^{-1} of data in $p\overline{p}$ collisions at 1.96 TeV. The JES is calibrated by using the dijet mass from the W boson decay.

[40] Use the ME method based on 2.2 fb^{-1} of data in $p\overline{p}$ collisions at 1.96 TeV.

[41] Combination based on up to 5.8 fb^{-1} of data in $p\overline{p}$ collisions at 1.96 TeV.

[42] Based on 5.8 fb^{-1} of data in $p\overline{p}$ collisions at 1.96 TeV the quoted value is m_t = 172.5 ± 1.4(stat)±1.0(JES)±1.1(syst) GeV. The measurement is performed with a liklihood fit technique which simultaneously determines m_t and JES (Jet Energy Scale).

[43] Based on 4.3 fb^{-1} of data in p-pbar collisions at 1.96 TeV. The measurement reduces the JES uncertainty by using the single lepton channel study of ABAZOV 11P.

[44] Combination with the result in 1 fb^{-1} of preceding data reported in ABAZOV 09AH as well as the MWT result of ABAZOV 11R with a statistical correlation of 60%.

[45] Based on 5.0 fb^{-1} of pp data at $\sqrt{s}$ = 7 TeV. Uses an analytical matrix weighting technique (AMWT) and full kinematic analysis (KIN).

Int. J. Mod. Phys. A 2026.41. Downloaded from www.worldscientific.com by UNIVERSITY OF CALIFORNIA @ BERKELEY on 09/16/26. Re-use and distribution is strictly not permitted, except for Open Access articles.

[46] Based on 5.0 fb^{-1} of pp data at $\sqrt{s}$ = 7 TeV. The first error is statistical and JES combined, and the second is systematic. Ideogram method is used to obtain 2D liklihood for the kinematical fit with two parameters mtop and JES.

[47] Based on 3.2 fb^{-1} in $p\overline{p}$ collisions at $\sqrt{s}$ = 1.96 TeV. The first error is from statistics and JES combined, and the latter is from the other systematic uncertainties. The result is obtained using an unbinned maximum likelihood method where the top quark mass and the JES are measured simultaneously, with Δ_{JES} = 0.3 ± 0.3(stat).

[48] Based on 5.7 fb^{-1} in $p\overline{p}$ collisions at $\sqrt{s}$ = 1.96 TeV. Events with an identified charged lepton or small $\not{E}_T$ are rejected from the event sample, so that the measurement is statistically independent from those in the ℓ + jets and all hadronic channels while being sensitive to those events with a τ lepton in the final state. Supersedes AALTONEN 07B.

[49] AALTONEN 11E based on 5.6 fb^{-1} in $p\overline{p}$ collisions at $\sqrt{s}$ = 1.96 TeV. Employs a multi-dimensional template likelihood technique where the lepton plus jets (one or two b-tags) channel gives 172.2 ± 1.2 ± 0.9 GeV while the dilepton channel yields 170.3 ± 2.0 ± 3.1 GeV. The results are combined. OUR EVALUATION includes the measurement in the dilepton channel only.

[50] Uses a likelihood fit of the lepton p_T distribution based on 2.7 fb^{-1} in $p\overline{p}$ collisions at $\sqrt{s}$ = 1.96 TeV.

[51] Based on 3.6 fb^{-1} in $p\overline{p}$ collisions at $\sqrt{s}$ = 1.96 TeV. ABAZOV 11P reports 174.94 ± 0.83 ± 0.78 ± 0.96 GeV, where the first uncertainty is from statistics, the second from JES, and the last from other systematic uncertainties. We combine the JES and systematic uncertainties. A matrix-element method is used where the JES uncertainty is constrained by the W mass. ABAZOV 11P describes a measurement based on 2.6 fb^{-1} that is combined with ABAZOV 08AH, which employs an independent 1 fb^{-1} of data.

[52] Based on a matrix-element method which employs 5.4 fb^{-1} in $p\overline{p}$ collisions at $\sqrt{s}$ = 1.96 TeV. Superseded by ABAZOV 12AB.

[53] Based on 36 pb^{-1} of pp collisions at $\sqrt{s}$ = 7 TeV. A Kinematic Method using b-tagging and an analytical Matrix Weighting Technique give consistent results and are combined. Superseded by CHATRCHYAN 12BA.

[54] Based on 5.6 fb^{-1} in $p\overline{p}$ collisions at $\sqrt{s}$ = 1.96 TeV. The likelihood calculated using a matrix element method gives m_t = 173.0 ± 0.7(stat) ± 0.6(JES) ± 0.9(syst) GeV, for a total uncertainty of 1.2 GeV.

[55] Based on 3.4 fb^{-1} of $p\overline{p}$ collisions at $\sqrt{s}$ = 1.96 TeV. The result is obtained by combining the MT2 variable method and the NWA (Neutrino Weighting Algorithm). The MT2 method alone gives $m_t = 168.0^{+4.8}_{-4.0}$(stat) ± 2.9(syst) GeV with smaller systematic error due to small JES uncertainty.

[56] Based on 1.9 fb^{-1} in $p\overline{p}$ collisions at $\sqrt{s}$ = 1.96 TeV. The result is from the measurement using the transverse decay length of b-hadrons and that using the transverse momentum of the W decay muons, which are both insensitive to the JES (jet energy scale) uncertainty. OUR EVALUATION uses only the measurement exploiting the decay length significance which yields $166.9^{+9.5}_{-8.5}$(stat) ± 2.9 (syst) GeV. The measurement that uses the lepton transverse momentum is excluded from the average because of a statistical correlation with other samples.

[57] Based on 2.9 fb^{-1} of $p\overline{p}$ collisions at $\sqrt{s}$ = 1.96 TeV. The first error is from statistics and JES uncertainty, and the latter is from the other systematics. Neural-network-based kinematical selection of 6 highest E_T jets with a vtx b-tag is used to distinguish signal from background. Superseded by AALTONEN 12G.

[58] Based on 2 fb^{-1} of data at $\sqrt{s}$ = 1.96 TeV. The top mass is obtained from the measurement of the invariant mass of the lepton (e or μ) from W decays and the soft μ in b-jet. The result is insensitive to jet energy scaling.

[59] Based on 1.9 fb^{-1} of data at $\sqrt{s}$ = 1.96 TeV. The first error is from statistics and jet energy scale uncertainty, and the latter is from the other systematics. Matrix element method with effective propagators.

[60] Based on 943 pb^{-1} of data at $\sqrt{s}$ = 1.96 TeV. The first error is from statistical and jet-energy-scale uncertainties, and the latter is from other systematics. AALTONEN 09K selected 6 jet events with one or more vertex b-tags and used the tree-level matrix element to construct template models of signal and background.

[61] Based on 1.9 fb^{-1} of data at $\sqrt{s}$ = 1.96 TeV. The first error is from statistical and jet-energy-scale (JES) uncertainties, and the second is from other systematics. Events with lepton + jets and those with dilepton + jets were simultaneously fit to constrain m_t and JES. Lepton + jets data only give m_t = 171.8 ± 2.2 GeV, and dilepton data only give $m_t = 171.2^{+5.3}_{-5.1}$ GeV.

[62] Based on 2 fb^{-1} of data at $\sqrt{s}$ = 1.96 TeV. Matrix Element method. Optimal selection criteria for candidate events with two high p_T leptons, high $\not{E}_T$, and two or more jets with and without b-tag are obtained by neural network with neuroevolution technique to minimize the statistical error of m_t.

[63] Based on 2.9 fb^{-1} of data at $\sqrt{s}$ = 1.96 TeV. Mass m_t is estimated from the likelihood for the eight-fold kinematical solutions in the plane of the azimuthal angles of the two neutrino momenta.

[64] Based on 1 fb^{-1} of data at $\sqrt{s}$ = 1.96 TeV. Events with two identified leptons, and those with one lepton plus one isolated track and a b-tag were used to constrain m_t. The result is a combination of the νWT (ν Weighting Technique) result of 176.2 ± 4.8 ± 2.1 GeV and the MWT (Matrix-element Weighting Technique) result of 173.2 ± 4.9 ± 2.0 GeV.

[65] Reports measurement of $170.7^{+4.2}_{-3.9}$ ± 2.6 ± 2.4 GeV based on 1.2 fb^{-1} of data at $\sqrt{s}$ = 1.96 TeV. The last error is due to the theoretical uncertainty on $\sigma_{t\overline{t}}$. Without the cross-section constraint a top mass of $169.7^{+5.2}_{-4.9}$ ± 3.1 GeV is obtained.

[66] Template method.

[67] Result is based on 1 fb^{-1} of data at $\sqrt{s}$ = 1.96 TeV. The first error is from statistics and jet energy scale uncertainty, and the latter is from the other systematics.

[68] Based on 310 pb^{-1} of data at $\sqrt{s}$ = 1.96 TeV.

[69] Ideogram method.

[70] Based on 311 pb^{-1} of data at $\sqrt{s}$ = 1.96 TeV. Events with 4 or more jets with E_T > 15 GeV, significant missing E_T, and secondary vertex b-tag are used in the fit. About 44% of the signal acceptance is from $\tau\nu$ + 4 jets. Events with identified e or μ are vetoed to provide a statistically independent measurement.

[71] Based on 1.02 fb^{-1} of data at $\sqrt{s}$ = 1.96 TeV. Superseded by AALTONEN 12G.

[72] Based on 955 pb^{-1} of data $\sqrt{s}$ = 1.96 TeV. m_t and JES (Jet Energy Scale) are fitted simultaneously, and the first error contains the JES contribution of 1.5 GeV.

[73] Matrix element method.

[74] Based on 425 pb^{-1} of data at $\sqrt{s}$ = 1.96 TeV. The first error is a combination of statistics and JES (Jet Energy Scale) uncertainty, which has been measured simultaneously to give JES = 0.989 ± 0.029(stat).

[75] Based on 370 pb^{-1} of data at $\sqrt{s}$ = 1.96 TeV. Combined result of MWT (Matrix-element Weighting Technique) and νWT (ν Weighting Technique) analyses is 178.1 ± 6.7 ± 4.8 GeV.

[76] Based on 1.0 fb^{-1} of data at $\sqrt{s}$ = 1.96 TeV. ABULENCIA 07D improves the matrix element description by including the effects of initial-state radiation.

[77] Based on 695 pb^{-1} of data at $\sqrt{s}$ = 1.96 TeV. The transverse decay length of the b hadron is used to determine m_t, and the result is free from the JES (jet energy scale) uncertainty.

[78] Based on ~ 400 pb^{-1} of data at $\sqrt{s}$ = 1.96 TeV. The first error includes statistical and systematic jet energy scale uncertainties, the second error is from the other systematics. The result is obtained with the b-tagging information. The result without b-tagging is $169.2^{+5.0}_{-7.4}{}^{+1.5}_{-1.4}$ GeV. Superseded by ABAZOV 08AH.

[79] Based on 318 pb^{-1} of data at $\sqrt{s}$ = 1.96 TeV.

[80] Dynamical likelihood method.

[81] Based on 340 pb^{-1} of data at $\sqrt{s}$ = 1.96 TeV.

[82] Based on 360 pb^{-1} of data at $\sqrt{s}$ = 1.96 TeV.

[83] Based on 110.2 ± 5.8 pb^{-1} at $\sqrt{s}$ = 1.8 TeV.

[84] Based on the all hadronic decays of $t\overline{t}$ pairs. Single b-quark tagging via the decay chain $b \to c \to \mu$ was used to select signal enriched multijet events. The result was obtained by the maximum likelihood method after bias correction.

[85] Obtained by re-analysis of the lepton + jets candidate events that led to ABBOTT 98F. It is based upon the maximum likelihood method which makes use of the leading order matrix elements.

[86] Based on 125 ± 7 pb^{-1} of data at $\sqrt{s}$ = 1.8 TeV.

[87] Based on ~ 106 pb^{-1} of data at $\sqrt{s}$= 1.8 TeV.

[88] Obtained by combining the measurements in the lepton + jets [AFFOLDER 01], all-jets [ABE 97R, ABE 99B], and dilepton [ABE 99B] decay topologies.

[89] Obtained by combining the D0 result m_t (GeV) = 168.4 ± 12.3 ± 3.6 from 6 di-lepton events (see also ABBOTT 98D) and m_t (GeV) = 173.3 ± 5.6 ± 5.5 from lepton+jet events (ABBOTT 98F).

[90] Obtained by combining the CDF results of m_t (GeV)=167.4 ± 10.3 ± 4.8 from 8 dilepton events, m_t (GeV)=175.9 ± 4.8 ± 5.3 from lepton+jet events (ABE 98E), and m_t (GeV)=186.0 ± 10.0 ± 5.7 from all-jet events (ABE 97R). The systematic errors in the latter two measurements are changed in this paper.

[91] See AFFOLDER 01 for details of systematic error re-evaluation.

[92] Based on 109 ± 7 pb^{-1} of data at $\sqrt{s}$ = 1.8 TeV.

[93] See ABAZOV 04G.

[94] The updated systematic error is listed. See AFFOLDER 01, appendix C.

[95] Obtained by combining the DØ results of m_t(GeV)=168.4 ± 12.3 ± 3.6 from 6 dilepton events and m_t(GeV)=173.3 ± 5.6 ± 5.5 from 77 lepton+jet events.

[96] Obtained by combining the DØ results from dilepton and lepton+jet events, and the CDF results (ABE 99B) from dilepton, lepton+jet events, and all-jet events.

[97] Based on the first observation of all hadronic decays of $t\overline{t}$ pairs. Single b-quark tagging with jet-shape variable constraints was used to select signal enriched multi-jet events. The updated systematic error is listed. See AFFOLDER 01, appendix C.

t-Quark Mass from Cross-Section Measurements

The top quark $\overline{\text{MS}}$ or pole mass can be extracted from a measurement of $\sigma(t\overline{t})$ by using theory calculations. We quote below the $\overline{\text{MS}}$ mass. See the review "The Top Quark" and references therein for more information.

VALUE (GeV)	DOCUMENT ID		TECN	COMMENT
$162.5^{+2.1}_{-1.5}$ OUR AVERAGE				
$162.9 \pm 0.5 \pm 1.0^{+2.1}_{-1.2}$	[1] AAD	19G	ATLS	$\ell + \not{E}_T + \geq 5\ j\ (2b\text{-}j)$
$160.0^{+4.8}_{-4.3}$	[2] ABAZOV	11S	D0	$\sigma(t\overline{t})$ + theory
• • • We do not use the following data for averages, fits, limits, etc. • • •				
	[3] ABAZOV	09AG	D0	cross sects, theory + exp
	[4] ABAZOV	09R	D0	cross sects, theory + exp

[1] AAD 19G based on 20.2 fb^{-1} of data in pp collisions at $\sqrt{s}$ = 8 TeV. Normalized $t\overline{t}$ + 1-jet differential cross section as a function of $t\overline{t}j$ invariant mass is measured in the ℓ + jets mode. The unfolded parton-level distribution is compared with the NLO QCD prediction. The three errors are from statitics, systematics, and theory.

[2] Based on 5.3 fb^{-1} in $p\overline{p}$ collisions at $\sqrt{s}$ = 1.96 TeV. ABAZOV 11S uses the measured $t\overline{t}$ production cross section of $8.13^{+1.02}_{-0.90}$ pb [ABAZOV 11E] in the lepton plus jets channel to obtain the top quark $\overline{\text{MS}}$ mass by using an approximate NNLO computation (MOCH 08, LANGENFELD 09). The corresponding top quark pole mass is $167.5^{+5.4}_{-4.9}$ GeV. A different theory calculation (AHRENS 10, AHRENS 10A) is also used and yields $m_t^{\overline{\text{MS}}} = 154.5^{+5.0}_{-4.3}$ GeV.

[3] Based on 1 fb^{-1} of data at $\sqrt{s}$ = 1.96 TeV. Uses the ℓ + jets, $\ell\ell$, and $\ell\tau$ + jets channels. ABAZOV 09AG extract the pole mass of the top quark using two different calculations that yield $169.1^{+5.9}_{-5.2}$ GeV (MOCH 08, LANGENFELD 09) and $168.2^{+5.9}_{-5.4}$ GeV (KIDONAKIS 08).

[4] Based on 1 fb^{-1} of data at $\sqrt{s}$ = 1.96 TeV. Uses the $\ell\ell$ and $\ell\tau$ + jets channels. ABAZOV 09R extract the pole mass of the top quark using two different calculations that yield $173.3^{+9.8}_{-8.6}$ GeV (MOCH 08, LANGENFELD 09) and $171.5^{+9.9}_{-8.8}$ GeV (CACCIARI 08).

t-Quark Pole Mass from Cross-Section Measurements

VALUE (GeV)	DOCUMENT ID		TECN	COMMENT
172.1 ±0.6 OUR AVERAGE				
170.7 ±0.3 ±1.4±0.3±0.2	[1] AAD	25BI	ATLS	$t\overline{t}$+jet; $e^{\pm}\mu^{\mp}$ mode
173.4 $^{+1.8}_{-2.0}$	[2] AAD	23AY	LHC	$e^{\pm}\mu^{\mp}$ pair; ATLAS + CMS combined
172.93±1.36	[3] TUMASYAN	23R	CMS	$t\overline{t}$+jet; $\ell^{\pm}\ell^{\mp}$ mode
173.1 $^{+2.0}_{-2.1}$	[4] AAD	20Q	ATLS	$e + \mu$ + 1 or 2 b-jets
171.1 ±0.4 ±0.9$^{+0.7}_{-0.3}$	[5] AAD	19G	ATLS	ℓ+$\not{E}_T$+ $\geq$ 5 j (2b-j)
170.6 ±2.7	[6] SIRUNYAN	17W	CMS	ℓ + $\geq$ 1j
172.8 ±1.1 $^{+3.3}_{-3.1}$	[7] ABAZOV	16F	D0	$\ell\ell$, ℓ+jets channels
173.7 $^{+2.3}_{-2.1}$	[8] AAD	15BW	ATLS	ℓ+$\not{E}_T$+ $\geq$ 5j (2b-tag)
• • • We do not use the following data for averages, fits, limits, etc. • • •				
170.5 ±0.8	[9] SIRUNYAN	20BV	CMS	$t\overline{t}$ normalized multi-differential x-sections
173.2 ±0.9 ±0.8±1.2	[10] AABOUD	17BC	ATLS	$e + \mu$ + $\geq$ 1b jets
173.8 $^{+1.7}_{-1.8}$	[11] KHACHATRY...	16AW	CMS	$e + \mu$ + $\not{E}_T$ + $\geq$ 0j
172.9 $^{+2.5}_{-2.6}$	[12] AAD	14AY	ATLS	pp at $\sqrt{s}$ = 7, 8 TeV
176.7 $^{+3.0}_{-2.8}$	[13] CHATRCHYAN	14	CMS	pp at $\sqrt{s}$ = 7 TeV

[1] AAD 25BI based on 140 fb^{-1} of data in pp collisions at $\sqrt{s}$ = 13 TeV. Normalized $t\overline{t}$ + 1-jet differential cross section as a function of the inverse of the $t\overline{t}j$ invariant mass is measured in the dilepton mode. The unfolded parton-level distribution is compared with the NLO QCD predictions with and without the top-quark decays and the quoted value corresponds to the stable top quarks. The four errors are from statitics, systematics, scale, and PDF+α_s.

[2] AAD 23AY based on 5 fb^{-1} and 20 fb^{-1} of pp data at $\sqrt{s}$ = 7 TeV and 8 TeV, respectively. The result is obtained from the combined inclusive cross section measurements and the NNLO+NNLL predictions fixing $\alpha_s(m_Z) = 0.118$.

[3] TUMASYAN 23R based on 36.3 fb^{-1} of data in pp collisions at $\sqrt{s}$ = 13 TeV. Normalized $t\overline{t}$ + 1-jet differential cross section as a function of $t\overline{t}j$ invariant mass is measured in the dilepton mode. The unfolded parton-level distribution is compared with the NLO QCD prediction. The result depends on the PDF and ABMP16NLO is used.

[4] AAD 20Q based on 36.1 fb^{-1} of pp data at $\sqrt{s}$ = 13 TeV. The result is obtained from the inclusive cross section measurement and the NNLO+NNLL prediction.

[5] AAD 19G based on 20.2 fb^{-1} of data in pp collisions at $\sqrt{s}$ = 8 TeV. Normalized $t\overline{t}$ + 1-jet differential cross section as a function of $t\overline{t}j$ invariant mass is measured in the ℓ + jets mode. The unfolded parton-level distribution is compared with the NLO QCD prediction. The three errors are from statitics, systematics, and theory.

[6] SIRUNYAN 17W based on 2.2 fb^{-1} of pp data at $\sqrt{s}$ = 13 TeV. Events are categorized according to the jet multiplicity and the number of b-tagged jets. The pole mass is obtained from the inclusive cross section measurement and the NNLO prediction.

[7] ABAZOV 16F based on 9.7 fb^{-1} of data in $p\overline{p}$ collisions at $\sqrt{s}$ = 1.96 TeV. The result is obtained from the inclusive cross section measurement and the NNLO+NNLL prediction.

[8] AAD 15BW based on 4.6 fb^{-1} of pp data at $\sqrt{s}$ = 7 TeV. Uses normalized differential cross section for $t\overline{t}$ + 1 jet as a function of the inverse of the invariant mass of the $t\overline{t}$ + 1 jet system. The measured cross section is corrected to the parton level. Then a fit to the data using NLO + parton shower prediction is performed.

[9] SIRUNYAN 20BV based on 35.9 fb^{-1} of pp data at $\sqrt{s}$ = 13 TeV. The error accounts for both experimental and theoretical uncertainties. Events containing two oppositely charged leptons are used. The pole mass is particularly sensitive to the $t\overline{t}$ invariant mass distribution close to the threshold. However, the Coulomb and soft gluon resummation effects are not taken into account, hence, an additional theoretical uncertainty of order +1 GeV is assumed.

[10] AABOUD 17BC based on 20.2 fb^{-1} of pp data at $\sqrt{s}$ = 8 TeV. The pole mass is extracted from a fit of NLO predictions to eight single lepton and dilepton differential distributions, while simultaneously constraining uncertainties due to PDFs and QCD scales. The three reported uncertainties come from statistics, experimental systematics, and theoretical sources.

[11] KHACHATRYAN 16AW based on 5.0 fb^{-1} of pp collisions at 7 TeV and 19.7 fb^{-1} at 8 TeV. The 7 TeV data include those used in CHATRCHYAN 14. The result is obtained from the inclusive cross sections.

[12] AAD 14AY used $\sigma(t\overline{t})$ for $e\mu$ events. The result is a combination of the measurements m_t = 171.4 ± 2.6 GeV based on 4.6 fb^{-1} of data at 7 TeV and m_t = 174.1 ± 2.6 GeV based on 20.3 fb^{-1} of data at 8 TeV.

[13] CHATRCHYAN 14 used $\sigma(t\overline{t})$ from pp collisions at $\sqrt{s}$ = 7 TeV measured in CHATRCHYAN 12AX to obtain m_t(pole) for $\alpha_s(m_Z)$ = 0.1184 ± 0.0007. The errors have been corrected in KHACHATRYAN 14K.

$m_t - m_{\overline{t}}$

Test of CPT conservation. OUR AVERAGE assumes that the systematic uncertainties are uncorrelated.

VALUE (GeV)	DOCUMENT ID		TECN	COMMENT
−0.15±0.20 OUR AVERAGE	Error includes scale factor of 1.1.			
0.83 $^{+1.79}_{-1.35}$	[1] TUMASYAN	21G	CMS	t-channel single top production
−0.15±0.19±0.09	[2] CHATRCHYAN	17	CMS	ℓ + $\not{E}_T$ + $\geq$ 4j ($\geq$ 1b j)
0.67±0.61±0.41	[3] AAD	14	ATLS	ℓ + $\not{E}_T$ + $\geq$ 4j ($\geq$ 2 b-tags)
−1.95±1.11±0.59	[4] AALTONEN	13E	CDF	ℓ + $\not{E}_T$ + $\geq$ 4j (0,1,2 b-tags)
−0.44±0.46±0.27	[5] CHATRCHYAN	12Y	CMS	ℓ + $\not{E}_T$ + $\geq$ 4j
0.8 ±1.8 ±0.5	[6] ABAZOV	11T	D0	ℓ + $\not{E}_T$ + 4 jets ($\geq$ 1 b-tag)
• • • We do not use the following data for averages, fits, limits, etc. • • •				
−3.3 ±1.4 ±1.0	[7] AALTONEN	11K	CDF	Repl. by AALTONEN 13E
3.8 ±3.4 ±1.2	[8] ABAZOV	09AA	D0	ℓ + $\not{E}_T$ + 4 jets ($\geq$ 1 b-tag)

[1] TUMASYAN 21G based on 35.9 fb^{-1} of pp data at $\sqrt{s}$ = 13 TeV. Events are selected by requiring 1ℓ + 2jets(1b jet) final state. An average top mass of $172.13^{+0.76}_{-0.77}$ GeV/c^2 is obtained.

[2] CHATRCHYAN 17 based on 19.6 fb^{-1} of pp data at $\sqrt{s}$ = 8 TeV and an average top mass of 172.84 ± 0.10 (stat) GeV is obtained.

[3] Based on 4.7 fb^{-1} of pp data at $\sqrt{s}$ = 7 TeV and an average top mass of 172.5 GeV/c^2.

[4] Based on 8.7 fb^{-1} of $p\overline{p}$ collisions at $\sqrt{s}$ = 1.96 TeV and an average top mass of 172.5 GeV/c^2.

[5] Based on 4.96 fb^{-1} of pp data at $\sqrt{s}$ = 7 TeV. Based on the fitted m_t for ℓ^+ and ℓ^- events using the Ideogram method.

[6] Based on a matrix-element method which employs 3.6 fb^{-1} in $p\overline{p}$ collisions at $\sqrt{s}$ = 1.96 TeV.

[7] Based on a template likelihood technique which employs 5.6 fb^{-1} in $p\overline{p}$ collisions at $\sqrt{s}$ = 1.96 TeV.

[8] Based on 1 fb^{-1} of data in $p\overline{p}$ collisions at $\sqrt{s}$ = 1.96 TeV.

t-quark DECAY WIDTH

VALUE (GeV)	CL%	DOCUMENT ID		TECN	COMMENT
$1.42^{+0.19}_{-0.15}$ OUR AVERAGE	Error includes scale factor of 1.4.				
1.76±0.33 $^{+0.79}_{-0.68}$		[1] AABOUD	18AZ	ATLS	ℓ+$\not{E}_T$+ $\geq$ 4j ($\geq$ 1 b)
1.36±0.02 $^{+0.14}_{-0.11}$		[2] KHACHATRY...	14E	CMS	$\ell\ell$+$\not{E}_T$+2-4jets (0-2b-tag)
2.00 $^{+0.47}_{-0.43}$		[3] ABAZOV	12T	D0	$\Gamma(t \to bW)/B(t \to bW)$
• • • We do not use the following data for averages, fits, limits, etc. • • •					
< 6.38	95	[4] AALTONEN	13Z	CDF	ℓ+$\not{E}_T$+ $\geq$ 4j ($\geq$ 0 b), direct
1.99 $^{+0.69}_{-0.55}$		[5] ABAZOV	11B	D0	Repl. by ABAZOV 12T
> 1.21	95	[5] ABAZOV	11B	D0	$\Gamma(t \to Wb)$
< 7.6	95	[6] AALTONEN	10AC	CDF	ℓ + jets, direct
<13.1	95	[7] AALTONEN	09M	CDF	m_t(rec) distribution

[1] Based on 20.2 fb^{-1} of pp data at $\sqrt{s}$ = 8 TeV. Γ_t is measured using a template fit to the reconstructed invariant mass of the b-jet of the semileptonically decaying top quark and the corresponding lepton, and the angular distance between j_b and j_l in hadronic top decay. Signal templates are generated by reweighting events at parton-level to Breit-Wigner distribution with different Γ_t hypotheses for m_t = 172.5 GeV. The result is consistent with the NNLO SM prediction of 1.322 GeV.

[2] Based on 19.7 fb^{-1} of pp data at $\sqrt{s}$ = 8 TeV. The result is obtained by combining the measurement of $R = \Gamma(t \to Wb)/\Gamma(t \to Wq\ (q{=}b,s,d))$ and a previous CMS measurement of the t-channel single top production cross section of CHATRCHYAN 12BQ, by using the theoretical calculation of $\Gamma(t \to Wb)$ for m_t = 172.5 GeV.

[3] Based on 5.4 fb^{-1} of data in $p\overline{p}$ collisions at 1.96 TeV. $\Gamma(t \to bW) = 1.87^{+0.44}_{-0.40}$ GeV is obtained from the observed t-channel single top quark production cross section, whereas $B(t \to bW) = 0.90 \pm 0.04$ is used assuming $\sum_q B(t \to qW) = 1$. The result is valid for m_t = 172.5 GeV. See the paper for the values for m_t = 170 or 175 GeV.

[4] Based on 8.7 fb^{-1} of data. The two sided 68% CL interval is 1.10 GeV < Γ_t < 4.05 GeV for m_t = 172.5 GeV.

[5] Based on 2.3 fb^{-1} in $p\overline{p}$ collisions at $\sqrt{s}$ = 1.96 TeV. ABAZOV 11B extracted Γ_t from the partial width $\Gamma(t \to Wb) = 1.92^{+0.58}_{-0.51}$ GeV measured using the t-channel single top production cross section, and the branching fraction $br\, t \to Wb = 0.962^{+0.068}_{-0.066}(\text{stat})^{+0.064}_{-0.052}(\text{syst})$. The $\Gamma(t \to Wb)$ measurement gives the 95% CL lowerbound of $\Gamma(t \to Wb)$ and hence that of Γ_t.

[6] Results are based on 4.3 fb^{-1} of data in $p\overline{p}$ collisions at $\sqrt{s}$ = 1.96 TeV. The top quark mass and the hadronically decaying W boson mass are reconstructed for each candidate events and compared with templates of different top quark width. The two sided 68% CL interval is 0.3 GeV< Γ_t < 4.4 GeV for m_t = 172.5 GeV.

[7] Based on 955 pb^{-1} of $p\overline{p}$ collision data at $\sqrt{s}$ = 1.96 TeV. AALTONEN 09M selected $t\overline{t}$ candidate events for the ℓ + $\not{E}_T$ + jets channel with one or two b-tags, and examine the decay width dependence of the reconstructed m_t distribution. The result is for m_t =175 GeV, whereas the upper limit is lower for smaller m_t.

by UNIVERSITY OF CA Phys. A 2026.41. Downloaded from www.worldscientific.com
ELEY on 09/16/26. Re-use and distribution is strictly not permitted, except for Open Access articles.

Int. J. Mod. Phys. A 2026.41. Downloaded from www.worldscientific.com
by UNIVERSITY OF CALIFORNIA @ BERKELEY on 09/16/26. Re-use and distribution is strictly not permitted, except for Open Access articles.

t DECAY MODES

	Mode		Fraction (Γ_i/Γ)	Confidence level
Γ_1	$W q (q = b, s, d)$			
Γ_2	$W b$			
Γ_3	$e \nu_e b$		(11.10 ± 0.30) %	
Γ_4	$\mu \nu_\mu b$		(11.40 ± 0.20) %	
Γ_5	$\tau \nu_\tau b$		(10.7 ± 0.5) %	
Γ_6	$q \overline{q} b$		(66.5 ± 1.4) %	
Γ_7	$\gamma q (q=u,c)$		[a] $< 9.5 \times 10^{-6}$	95%
Γ_8	$H^+ b,\ H^+ \to \tau \nu_\tau$			
Γ_9	$a q (q=u, c)$		$< 1 \times 10^{-3}$	95%
	$\Delta T = 1$ weak neutral current ($T1$) modes			
Γ_{10}	$Z q (q=u,c)$	$T1$	[b] $< 1.2 \times 10^{-4}$	95%
Γ_{11}	$H u$	$T1$	$< 1.9 \times 10^{-4}$	95%
Γ_{12}	$H c$	$T1$	$< 3.4 \times 10^{-4}$	95%
Γ_{13}	$\ell^+ \overline{q} q' (q=d,s,b;\ q'=u,c)$	$T1$	$< 1.6 \times 10^{-3}$	95%
	Lepton Family number (LF) violating modes			
Γ_{14}	$e^\pm \mu^\mp c$	LF	$< 2.16 \times 10^{-7}$	95%
Γ_{15}	$e^\pm \mu^\mp u$	LF	$< 1.2 \times 10^{-8}$	95%
Γ_{16}	$\mu^\pm \tau^\mp q$	LF		
	Baryon number (B) violating modes			
Γ_{17}	$e^+ \overline{u} \overline{d}$	B		
Γ_{18}	$\mu^+ \overline{u} \overline{d}$	B		
Γ_{19}	$e^+ \overline{c} \overline{d}$	B		
Γ_{20}	$\mu^+ \overline{c} \overline{d}$	B		
Γ_{21}	$e^+ \overline{u} \overline{s}$	B		
Γ_{22}	$\mu^+ \overline{u} \overline{s}$	B		
Γ_{23}	$e^+ \overline{c} \overline{s}$	B		
Γ_{24}	$\mu^+ \overline{c} \overline{s}$	B		
Γ_{25}	$e^+ \overline{u} \overline{b}$	B		
Γ_{26}	$\mu^+ \overline{u} \overline{b}$	B		
Γ_{27}	$e^+ \overline{c} \overline{b}$	B		
Γ_{28}	$\mu^+ \overline{c} \overline{b}$	B		

[a] This limit is for $\Gamma(t \to \gamma q)/\Gamma(t \to W b)$.

[b] This limit is for $\Gamma(t \to Z q)/\Gamma(t \to W b)$.

t BRANCHING RATIOS

$\Gamma(W b)/\Gamma(W q(q=b,s,d))$ — Γ_2/Γ_1

OUR AVERAGE assumes that the systematic uncertainties are uncorrelated.

VALUE	DOCUMENT ID		TECN	COMMENT
0.957±0.034 OUR AVERAGE	Error includes scale factor of 1.5. See the ideogram below.			
0.87 ±0.07	[1] AALTONEN	14G	CDF	$\ell\ell + \not{E}_T + \geq 2$j (0,1,2 b-tag)
1.014±0.003±0.032	[2] KHACHATRY...	14E	CMS	$\ell\ell + \not{E}_T$ + 2,3,4j (0–2b-tag)
0.94 ±0.09	[3] AALTONEN	13G	CDF	$\ell + \not{E}_T + \geq 3$jets ($\geq 1 b$-tag)
0.90 ±0.04	[4] ABAZOV	11X	D0	
• • • We do not use the following data for averages, fits, limits, etc. • • •				
$0.97 \ ^{+0.09}_{-0.08}$	[5] ABAZOV	08M	D0	ℓ + n jets with 0,1,2 b-tag
$1.03 \ ^{+0.19}_{-0.17}$	[6] ABAZOV	06K	D0	
$1.12 \ ^{+0.21}_{-0.19} \ ^{+0.17}_{-0.13}$	[7] ACOSTA	05A	CDF	Repl. by AALTONEN 13G
$0.94 \ ^{+0.26}_{-0.21} \ ^{+0.17}_{-0.12}$	[8] AFFOLDER	01C	CDF	

[1] Based on 8.7 fb^{-1} of data. This measurement gives $|V_{tb}| = 0.93 \pm 0.04$ and $|V_{tb}| > 0.85$ (95% CL) in the SM.

[2] Based on 19.7 fb^{-1} of pp data at $\sqrt{s} = 8$ TeV. The result is obtained by counting the number of b jets per $t\overline{t}$ signal events in the dilepton channel. The $t\overline{t}$ production cross section is measured to be $\sigma(t\overline{t}) = 238 \pm 1 \pm 15$ pb, in good agreement with the SM prediction and the latest CMS measurement of CHATRCHYAN 14F. The measurement gives $R > 0.995$ (95% CL), or $|V_{tb}| > 0.975$ (95% CL) in the SM, requiring $R \leq 1$.

[3] Based on 8.7 fb^{-1} of $p\overline{p}$ collisions at $\sqrt{s} = 1.96$ TeV. Measure the fraction of $t \to W b$ decays simultaneously with the $t\overline{t}$ cross section. The correlation coefficient between those two measurements is -0.434. Assume unitarity of the 3×3 CKM matrix and set $|V_{tb}| > 0.89$ at 95% CL.

[4] Based on 5.4 fb^{-1} of data. The error is statistical and systematic combined. The result is a combination of 0.95 ± 0.07 from ℓ + jets channel and 0.86 ± 0.05 from $\ell\ell$ channel. $|V^{tb}| = 0.95 \pm 0.02$ follows from the result by assuming unitarity of the 3x3 CKM matrix.

[5] Result is based on 0.9 fb^{-1} of data. The 95% CL lower bound R > 0.79 gives $|V_{tb}| > 0.89$ (95% CL).

[6] ABAZOV 06K result is from the analysis of $t\overline{t} \to \ell\nu + \geq 3$ jets with 230 pb^{-1} of data at $\sqrt{s} = 1.96$ TeV. It gives R > 0.61 and $|V_{tb}| > 0.78$ at 95% CL. Superseded by ABAZOV 08M.

[7] ACOSTA 05A result is from the analysis of lepton + jets and di-lepton + jets final states of $t\overline{t}$ candidate events with ~ 162 pb^{-1} of data at $\sqrt{s} = 1.96$ TeV. The first error is statistical and the second systematic. It gives R > 0.61, or $|V_{tb}| > 0.78$ at 95% CL.

[8] AFFOLDER 01C measures the top-quark decay width ratio $R = \Gamma(W b)/\Gamma(W q)$, where q is a d, s, or b quark, by using the number of events with multiple b tags. The first error is statistical and the second systematic. A numerical integration of the likelihood function gives $R > 0.61$ (0.56) at 90% (95%) CL. By assuming three generation unitarity, $|V_{tb}| = 0.97 \ ^{+0.16}_{-0.12}$ or $|V_{tb}| > 0.78$ (0.75) at 90% (95%) CL is obtained. The result is based on 109 pb^{-1} of data at $\sqrt{s} = 1.8$ TeV.

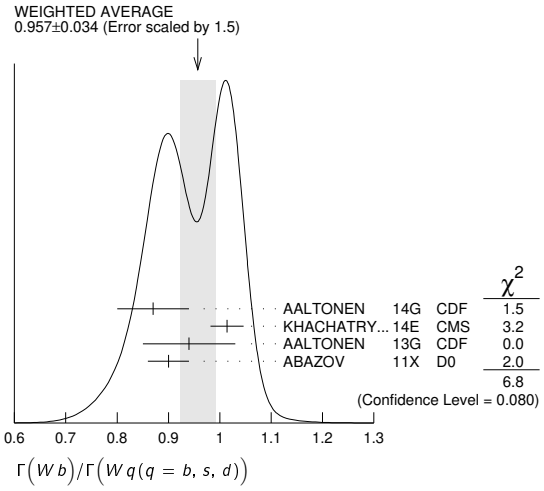

$\Gamma(e\nu_e b)/\Gamma_{total}$ — Γ_3/Γ

VALUE	DOCUMENT ID		TECN	COMMENT
0.111±0.003	[1] AAD	15CC	ATLS	ℓ+jets, $\ell\ell$+jets, $\ell\tau_h$+jets

[1] AAD 15CC based on 4.6 fb^{-1} of pp data at $\sqrt{s} = 7$ TeV. The original value is given by $13.3 \pm 0.4 \pm 0.5$%, which includes electrons from the decay of τ leptons. It is assumed that the top branching ratios to leptons and jets add up to one and that only SM processes contribute to the background. The event selection criteria are optimized for the $\ell\tau_h$ + jets channel. We have converted the original value to eliminate contributions of electrons from τ's, by using the AAD 15CC measurements of the branching ratios to μ and τ channels, as well as the PDG values of τ branching ratios into e and μ channels.

$\Gamma(\mu\nu_\mu b)/\Gamma_{total}$ — Γ_4/Γ

VALUE	DOCUMENT ID		TECN	COMMENT
0.114±0.002	[1] AAD	15CC	ATLS	ℓ+jets, $\ell\ell$+jets, $\ell\tau_h$+jets

[1] AAD 15CC based on 4.6 fb^{-1} of pp data at $\sqrt{s} = 7$ TeV. The original value is given by $13.4 \pm 0.3 \pm 0.5$%, which includes muons from the decay of τ leptons. It is assumed that the top branching ratios to leptons and jets add up to one and that only SM processes contribute to the background. The event selection criteria are optimized for the $\ell\tau_h$ + jets channel. We have converted the original value to eliminate contributions of muons from τ's, by using the AAD 15CC measurements of the branching ratios to μ and τ channels, as well as the PDG values of τ branching ratios into e and τ channels.

$\Gamma(\tau\nu_\tau b)/\Gamma_{total}$ — Γ_5/Γ

VALUE	DOCUMENT ID		TECN	COMMENT
0.107 ±0.005 OUR AVERAGE				
0.1050±0.0009±0.0071	[1] SIRUNYAN	20V	CMS	$\ell\tau_h$ + ≥ 3 jets ($\geq 1 b$-tag)
0.112 ±0.009	[2] AAD	15CC	ATLS	ℓ+jets, $\ell\ell$+jets, $\ell\tau_h$+jets
0.096 ±0.028	[3] AALTONEN	14A	CDF	$\ell + \tau_h + \geq 2$jets ($\geq 1 b$-tag)
• • • We do not use the following data for averages, fits, limits, etc. • • •				
	[4] ABULENCIA	06R	CDF	$\ell\tau$ + jets
	[5] ABE	97V	CDF	$\ell\tau$ + jets

[1] SIRUNYAN 20V based on 35.9 fb^{-1} of pp data at $\sqrt{s} = 13$ TeV. $t\overline{t}$ events are selected in the $t\overline{t} \to (\ell\nu_\ell)(\tau_h\nu_\tau)b\overline{b}$ mode, where τ_h refers to the hadronic decays of τ. The branching ratio is determined with respect to the $t\overline{t}$ inclusive cross section extrapolated from the light dilepton mode. The ratio of the $t\overline{t}$ production cross sections in the $\ell\tau_h$ and $\ell\ell$ channels yields $0.973 \pm 0.009 \pm 0.066$, consistent with lepton universality.

[2] AAD 15CC based on 4.6 fb^{-1} of pp data at $\sqrt{s} = 7$ TeV. The original value is given by $7.0 \pm 0.3 \pm 0.5$%, which includes only the hadronic decay of τ leptons. It is assumed that the top branching ratios to leptons and jets add up to one and that only SM processes contribute to the background. The event selection criteria are optimized for the $\ell\tau_h$ + jets channel. We have converted the original value to include leptonic decays of τ's, by using the AAD 15CC measurements of the branching ratios to e and μ channels, as well as the PDG values of τ branching ratios into e and μ channels.

[3] Based on 9 fb^{-1} of data. The measurement is in the channel $t\overline{t} \to (b\ell\nu)(b\tau\nu)$, where τ decays into hadrons (τ_h), and ℓ (e or μ) include ℓ from τ decays (τ_ℓ). The result is consistent with lepton universality.

[4] ABULENCIA 06R looked for $t\overline{t} \to (\ell\nu_\ell)(\tau\nu_\tau)b\overline{b}$ events in 194 pb^{-1} of $p\overline{p}$ collisions at $\sqrt{s} = 1.96$ TeV. 2 events are found where 1.00 ± 0.17 signal and 1.29 ± 0.25 background events are expected, giving a 95% CL upper bound for the partial width ratio $\Gamma(t \to \tau\nu q)\ /\ \Gamma_{SM}(t \to \tau\nu q) < 5.2$.

[5] ABE 97V searched for $t\overline{t} \to (\ell\nu_\ell)(\tau\nu_\tau)b\overline{b}$ events in 109 pb^{-1} of $p\overline{p}$ collisions at $\sqrt{s} = 1.8$ TeV. They observed 4 candidate events where one expects ~ 1 signal and ~ 2 background events. Three of the four observed events have jets identified as b candidates.

$\Gamma(q\overline{q}b)/\Gamma_{total}$ — Γ_6/Γ

VALUE	DOCUMENT ID		TECN	COMMENT
0.665±0.004±0.013	[1] AAD	15CC	ATLS	$\ell\ell$+jets, $\ell\ell$+jets, $\ell\tau_h$+jets

[1] AAD 15CC based on 4.6 fb^{-1} of pp data at $\sqrt{s} = 7$ TeV. Branching ratio of top quark into b and jets. It is assumed that the top branching ratios to leptons and jets add up to one and that only SM processes contribute to the background. The event selection criteria are optimized for the $\ell\tau_h$ + jets channel.

Phys. A 2026.41. Downloaded from www.worldscientific.com
by UNIVERSITY OF CA ELEY on 09/16/26. Re-use and distribution is strictly not permitted, except for Open Access articles.

$\Gamma(\gamma q(q=u,c))/\Gamma_{total}$ — Γ_7/Γ

VALUE	CL%	DOCUMENT ID		TECN	COMMENT
<0.95 $\times 10^{-5}$	95	[1] HAYRAPETY...	24L	CMS	B($t \to \gamma u$)
<1.51 $\times 10^{-5}$	95	[2] HAYRAPETY...	24L	CMS	B($t \to \gamma c$)
<0.85 $\times 10^{-5}$	95	[3] AAD	23	ATLS	B($t \to \gamma u$), left-handed $tu\gamma$ coupling
<4.2 $\times 10^{-5}$	95	[3] AAD	23	ATLS	B($t \to \gamma c$), left-handed $tc\gamma$ coupling
<1.2 $\times 10^{-5}$	95	[3] AAD	23	ATLS	B($t \to \gamma u$), right-handed $tu\gamma$ coupling
<4.5 $\times 10^{-5}$	95	[3] AAD	23	ATLS	B($t \to \gamma c$), right-handed $tc\gamma$ coupling
<5.9 $\times 10^{-3}$	95	[4] CHEKANOV	03	ZEUS	B($t \to \gamma u$)
• • • We do not use the following data for averages, fits, limits, etc. • • •					
<2.8 $\times 10^{-5}$	95	[5] AAD	20B	ATLS	Repl. by AAD 23
<6.1 $\times 10^{-5}$	95	[5] AAD	20B	ATLS	Repl. by AAD 23
<2.2 $\times 10^{-4}$	95	[5] AAD	20B	ATLS	Repl. by AAD 23
<1.8 $\times 10^{-4}$	95	[5] AAD	20B	ATLS	Repl. by AAD 23
<1.3 $\times 10^{-4}$	95	[6] KHACHATRY...	16AS	CMS	Repl. by HAYRAPETYAN 24L
<1.7 $\times 10^{-3}$	95	[6] KHACHATRY...	16AS	CMS	Repl. by HAYRAPETYAN 24L
<0.0064	95	[7] AARON	09A	H1	$t \to \gamma u$
<0.0465	95	[8] ABDALLAH	04C	DLPH	B(tc or γu)
<0.0132	95	[9] AKTAS	04	H1	B($t \to \gamma u$)
<0.041	95	[10] ACHARD	02J	L3	B($t \to \gamma c$ or γu)
<0.032	95	[11] ABE	98G	CDF	$t\bar{t} \to (Wb)(\gamma c$ or $\gamma u)$

[1] HAYRAPETYAN 24L based on 138 fb^{-1} of data in pp collisions at $\sqrt{s}$ = 13 TeV. FCNC through single top production in association with a photon, and $t\bar{t}$ production with a top quark decaying into a photon and up-quark, are searched for. Bounds on the anomalous FCNC coupling is given by $\kappa_{tu\gamma} < 6.2 \times 10^{-3}$.

[2] HAYRAPETYAN 24L based on 138 fb^{-1} of data in pp collisions at $\sqrt{s}$ = 13 TeV. FCNC through single top production in association with a photon, and $t\bar{t}$ production with a top quark decaying into a photon and charm-quark, are searched for. Bounds on the anomalous FCNC coupling is given by $\kappa_{tc\gamma} < 7.7 \times 10^{-3}$.

[3] AAD 23 based on 139 fb^{-1} of data in pp collisions at $\sqrt{s}$ = 13 TeV. Anomalous FCNC left-handed and right-handed couplings are searched for through the single top production in association with a photon and in the decay of a top quark in the $t\bar{t}$ production. The SM predictions of the corresponding branching ratios are of the order of 10^{-14}.

[4] CHEKANOV 03 looked for single top production via FCNC in the reaction $e^{\pm}p \to e^{\pm}$ (t or $\bar{t}$) X in 130.1 pb^{-1} of data at $\sqrt{s}$=300–318 GeV. No evidence for top production and its decay into bW was found. The result is obtained for m_t=175 GeV when B(γc)=B(Zq)=0, where q is a u or c quark. Bounds on the effective t-u-γ and t-u-Z couplings are found in their Fig. 4. The conversion to the constraint listed is from private communication, E. Gallo, January 2004.

[5] AAD 20B based on 81 fb^{-1} of data in pp collisions at $\sqrt{s}$ = 13 TeV. FCNC through single top production in association with a photon is searched for in the mode $\ell\gamma + \not{E}_T$ + 1j (b-tag). Anomalous FCNC left-handed and right-handed couplings are searched for, which result in different kinematical properties of top decay such as the lepton distribution. Limits are set on the $tq\gamma$ couplings in an effective field theory.

[6] KHACHATRYAN 16AS based on 19.8 fb^{-1} of data in pp collisions at $\sqrt{s}$ = 8 TeV. FCNC through single top production in association with a photon is searched for in the mode $\mu + \gamma + \not{E}_T + \geq$1$j$ (0,1b). Bounds on the anomalous FCNC couplings are given by $\kappa_{tu\gamma} < 0.025$ and $\kappa_{tc\gamma} < 0.091$.

[7] AARON 09A looked for single top production via FCNC in $e^{\pm}p$ collisions at HERA with 474 pb^{-1}. The upper bound of the cross section gives the bound on the FCNC coupling $\kappa_{tu\gamma}/\Lambda < 1.03$ TeV^{-1}, which corresponds to the result for m_t = 175 GeV.

[8] ABDALLAH 04C looked for single top production via FCNC in the reaction $e^+e^- \to \bar{t}c$ or $\bar{t}u$ in 541 pb^{-1} of data at $\sqrt{s}$=189–208 GeV. No deviation from the SM is found, which leads to the bound on B($t \to \gamma q$), where q is a u or a c quark, for m_t = 175 GeV when B($t \to Zq$)=0 is assumed. The conversion to the listed bound is from private communication, O. Yushchenko, April 2005. The bounds on the effective t-q-γ and t-q-Z couplings are given in their Fig. 7 and Table 4, for m_t = 170–180 GeV, where most conservative bounds are found by choosing the chiral couplings to maximize the negative interference between the virtual γ and Z exchange amplitudes.

[9] AKTAS 04 looked for single top production via FCNC in $e^{\pm}$ collisions at HERA with 118.3 pb^{-1}, and found 5 events in the e or μ channels. By assuming that they are due to statistical fluctuation, the upper bound on the $tu\gamma$ coupling $\kappa_{tu\gamma} < 0.27$ (95% CL) is obtained. The conversion to the partial width limit, when B(γc) = B(Zu) = B(Zc) = 0, is from private communication, E. Perez, May 2005.

[10] ACHARD 02J looked for single top production via FCNC in the reaction $e^+e^- \to \bar{t}c$ or $\bar{t}u$ in 634 pb^{-1} of data at $\sqrt{s}$= 189–209 GeV. No deviation from the SM is found, which leads to a bound on the top-quark decay branching fraction B(γq), where q is a u or c quark. The bound assumes B(Zq)=0 and is for m_t= 175 GeV; bounds for m_t=170 GeV and 180 GeV and B(Zq) $\neq$ 0 are given in Fig. 5 and Table 7.

[11] ABE 98G looked for $t\bar{t}$ events where one t decays into $q\gamma$ while the other decays into bW. The quoted bound is for $\Gamma(\gamma q)/\Gamma(Wb)$.

$\Gamma(H^+b,\ H^+ \to \tau\nu_\tau)/\Gamma_{total}$ — Γ_8/Γ

VALUE (%)	CL%	DOCUMENT ID		TECN
<0.25	95	[1] AABOUD	18BW	ATLS

[1] AABOUD 18BW based on 36.1 fb^{-1} of pp data at $\sqrt{s}$ = 13 TeV. In the mass range of m_{H^+} = 90–160 GeV, assuming the SM cross section for the $t\bar{t}$ production, the upper limit for the branching fraction B($t \to bH^+$) $\times$ B($H^+ \to \tau\nu_\tau$) ranges between 0.25% and 0.031%.

$\Gamma(aq(q=u,c))/\Gamma_{total}$ — Γ_9/Γ

VALUE (%)	CL%	DOCUMENT ID		TECN	COMMENT
<0.1	95	[1] AAD	24BN	ATLS	displaced jets

[1] AAD 24BN based on 140 fb^{-1} of pp data at $\sqrt{s}$ = 13 TeV. Long-lived axionlike particles which decay hadronically are searched for in the decay of the top quark. The upper limit on the branching ratio is obtained between 1.6 < $c\tau_a$ < 130 mm and for 40 < m_a < 55 GeV.

$\Gamma(Zq(q=u,c))/\Gamma_{total}$ — Γ_{10}/Γ

Test for ΔT=1 weak neutral current. Allowed by higher-order electroweak interaction.

VALUE (units 10^{-3})	CL%	DOCUMENT ID		TECN	COMMENT
< 0.062	95	[1] AAD	23AS	ATLS	B($t \to Zu$), left-handed tuZ coupling
< 0.13	95	[1] AAD	23AS	ATLS	B($t \to Zc$), left-handed tcZ coupling
< 0.066	95	[1] AAD	23AS	ATLS	B($t \to Zu$), right-handed tuZ coupling
< 0.12	95	[1] AAD	23AS	ATLS	B($t \to Zc$), right-handed tcZ coupling
< 0.22	95	[2] SIRUNYAN	17E	CMS	$t \to Zu$
< 0.49	95	[2] SIRUNYAN	17E	CMS	$t \to Zc$
< 0.7	95	[3] AAD	16D	ATLS	$t \to Zq$ (q = u, c)
• • • We do not use the following data for averages, fits, limits, etc. • • •					
< 0.17	95	[4] AABOUD	18AT	ATLS	$t \to Zu$
< 0.24	95	[4] AABOUD	18AT	ATLS	$t \to Zc$
< 0.6	95	[5] CHATRCHYAN	14S	CMS	$t \to Zq$ (q = u, c)
< 0.5	95	[6] CHATRCHYAN	14S	CMS	$t \to Zq$ (q = u, c)
< 2.1	95	[7] CHATRCHYAN	13F	CMS	$t \to Zq$ (q = u, c)
< 7.3	95	[8] AAD	12BT	ATLS	$t\bar{t} \to \ell^+\ell^-\ell'^{\pm} + \not{E}_T$ + jets
<32	95	[9] ABAZOV	11M	D0	$t \to Zq$ (q = u, c)
<83	95	[10] AALTONEN	09AL	CDF	$t \to Zq$ (q=c)
<37	95	[11] AALTONEN	08AD	CDF	$t \to Zq$ (q = u, c)
< 1.59 $\times 10^2$	95	[12] ABDALLAH	04C	DLPH	$e^+e^- \to \bar{t}c$ or $\bar{t}u$
< 1.37 $\times 10^2$	95	[13] ACHARD	02J	L3	$e^+e^- \to \bar{t}c$ or $\bar{t}u$
< 1.4 $\times 10^2$	95	[14] HEISTER	02Q	ALEP	$e^+e^- \to \bar{t}c$ or $\bar{t}u$
< 1.37 $\times 10^2$	95	[15] ABBIENDI	01T	OPAL	$e^+e^- \to \bar{t}c$ or $\bar{t}u$
< 1.7 $\times 10^2$	95	[16] BARATE	00S	ALEP	$e^+e^- \to \bar{t}c$ or $\bar{t}u$
< 3.3 $\times 10^2$	95	[17] ABE	98G	CDF	$t\bar{t} \to (Wb)(Zc$ or $Zu)$

[1] AAD 23AS based on 139 fb^{-1} of data in pp collisions at $\sqrt{s}$ = 13 TeV. Anomalous FCNC left-handed and right-handed couplings are searched for through the single top production in association with a Z boson and in the decay of a top quark in the $t\bar{t}$ production. Events with 3ℓ + $\geq$ 1 jet(s) (1b-tagged) + $\not{E}_T$ are used. The SM predictions of the corresponding branching ratios are of the order of 10^{-14}.

[2] SIRUNYAN 17E based on 19.7 fb^{-1} of pp data at $\sqrt{s}$ = 8 TeV. The final states $t\bar{t} \to \ell^+\ell^-\ell'^{\pm}\nu$ + jets (ℓ, ℓ' = e, μ) are investigated and the cross section $\sigma(pp \to tZq \to \ell\nu b\ell^+\ell^-q) = 10^{+8}_{-7}$ fb is measured, giving no sign of FCNC decays of the top quark.

[3] AAD 16D based on 20.3 fb^{-1} of pp data at $\sqrt{s}$ = 8 TeV. The FCNC decay is searched for in $t\bar{t}$ events in the final state $(bW)(qZ)$ when both W and Z decay leptonically, giving 3 charged leptons.

[4] Based on 36.1 fb^{-1} of pp data at $\sqrt{s}$ = 13 TeV. The final states $t\bar{t} \to \ell^+\ell^-\ell'^{\pm}\nu$ + jets (ℓ, ℓ' = e, μ) are investigated and no significant excess over the SM background contributions is observed.

[5] Based on 19.7 fb^{-1} of pp data at $\sqrt{s}$ = 8 TeV. The flavor changing decay is searched for in $t\bar{t}$ events in the final state $(bW)(qZ)$ when both W and Z decay leptoically, giving 3 charged leptons.

[6] CHATRCHYAN 14S combined search limit from this and CHATRCHYAN 13F data.

[7] Based on 5.0 fb^{-1} of pp data at $\sqrt{s}$ = 7 TeV. Search for FCNC decays of the top quark in $t\bar{t} \to \ell^+\ell^-\ell'^{\pm}\nu$ + jets (ℓ, ℓ' = e, μ) final states found no excess of signal events.

[8] Based on 2.1 fb^{-1} of pp data at $\sqrt{s}$ = 7 TeV.

[9] Based on 4.1 fb^{-1} of data. ABAZOV 11M searched for FCNC decays of the top quark in $t\bar{t} \to \ell^+\ell^-\ell'^{\pm}\nu$ + jets (ℓ, ℓ' = e, μ) final states, and absence of the signal gives the bound.

[10] Based on $p\bar{p}$ data of 1.52 fb^{-1}. AALTONEN 09AL compared $t\bar{t} \to WbWb \to \ell\nu bjjb$ and $t\bar{t} \to ZcWb \to \ell\ell cjjb$ decay chains, and absence of the latter signal gives the bound. The result is for 100% longitudinally polarized Z boson and the theoretical $t\bar{t}$ production cross section The results for different Z polarizations and those without the cross section assumption are given in their Table XII.

[11] Result is based on 1.9 fb^{-1} of data at $\sqrt{s}$ = 1.96 TeV. $t\bar{t} \to WbZq$ or $ZqZq$ processes have been looked for in Z + $\geq$ 4 jet events with and without b-tag. No signal leads to the bound B($t \to Zq$) < 0.037 (0.041) for m_t = 175 (170) GeV.

[12] ABDALLAH 04C looked for single top production via FCNC in the reaction $e^+e^- \to \bar{t}c$ or $\bar{t}u$ in 541 pb^{-1} of data at $\sqrt{s}$=189–208 GeV. No deviation from the SM is found, which leads to the bound on B($t \to Zq$), where q is a u or a c quark, for m_t = 175 GeV when B($t \to \gamma q$)=0 is assumed. The conversion to the listed bound is from private communication, O. Yushchenko, April 2005. The bounds on the effective t-q-γ and t-q-Z couplings are given in their Fig. 7 and Table 4, for m_t = 170–180 GeV, where most conservative bounds are found by choosing the chiral couplings to maximize the negative interference between the virtual γ and Z exchange amplitudes.

[13] ACHARD 02J looked for single top production via FCNC in the reaction $e^+e^- \to \bar{t}c$ or $\bar{t}u$ in 634 pb^{-1} of data at $\sqrt{s}$= 189–209 GeV. No deviation from the SM is found, which leads to a bound on the top-quark decay branching fraction B(Zq), where q is a u or c quark. The bound assumes B(γq)=0 and is for m_t= 175 GeV; bounds for m_t=170 GeV and 180 GeV and B(γq) $\neq$0 are given in Fig. 5 and Table 7. Table 6 gives constraints on t-c-e-e four-fermi contact interactions.

[14] HEISTER 02Q looked for single top production via FCNC in the reaction $e^+e^- \to \bar{t}c$ or $\bar{t}u$ in 214 pb^{-1} of data at $\sqrt{s}$= 204–209 GeV. No deviation from the SM is found, which leads to a bound on the branching fraction B(Zq), where q is a u or c quark. The bound assumes B(γq)=0 and is for m_t= 174 GeV. Bounds on the effective t- (c or u)-γ and t- (c or u)- Z couplings are given in their Fig. 2.

[15] ABBIENDI 01T looked for single top production via FCNC in the reaction $e^+e^- \to \bar{t}c$ or $\bar{t}u$ in 600 pb^{-1} of data at $\sqrt{s}$= 189–209 GeV. No deviation from the SM is found, which leads to bounds on the branching fractions B(Zq) and B(γq), where q is a u or c quark. The result is obtained for m_t= 174 GeV. The upper bound becomes 9.7%

Int. J. Mod. Phys. A 2026.41. Downloaded from www.worldscientific.com
by UNIVERSITY OF CALIFORNIA @ BERKELEY on 09/16/26. Re-use and distribution is strictly not permitted, except for Open Access articles.

(20.6%) for m_t= 169 (179) GeV. Bounds on the effective t- (c or u)-γ and t- (c or u)-Z couplings are given in their Fig. 4.

[16] BARATE 00S looked for single top production via FCNC in the reaction $e^+ e^- \rightarrow \bar{t} c$ or $\bar{t} u$ in 411 pb^{-1} of data at c.m. energies between 189 and 202 GeV. No deviation from the SM is found, which leads to a bound on the branching fraction. The bound assumes B(γq)=0. Bounds on the effective t- (c or u)-γ and t- (c or u)-Z couplings are given in their Fig. 4.

[17] ABE 98G looked for $t\bar{t}$ events where one t decays into three jets and the other decays into qZ with $Z \rightarrow \ell\ell$. The quoted bound is for $\Gamma(Zq)/\Gamma(Wb)$.

$\Gamma(Hu)/\Gamma_{\text{total}}$ — Γ_{11}/Γ

VALUE (units 10^{-4})	CL%	DOCUMENT ID		TECN	COMMENT
< 1.9	95	[1] TUMASYAN	22A	CMS	$t \rightarrow Hu$ ($H \rightarrow \gamma\gamma$)
• • • We do not use the following data for averages, fits, limits, etc. • • •					
< 7.2	95	[2] HAYRAPETY...	25AD	CMS	2ℓ (same sign) + $\geq$ 1j
< 2.8	95	[3] AAD	24AU	ATLS	$pp \rightarrow tH$ or $t \rightarrow Hu$ ($H \rightarrow WW, ZZ, \tau\tau$)
< 2.6	95	[4] AAD	24AU	ATLS	$pp \rightarrow tH$ or $t \rightarrow Hu$ (combined $H \rightarrow WW, ZZ, \tau\tau, \gamma\gamma, bb$)
< 3.8	95	[5] AAD	23CJ	ATLS	$pp \rightarrow tH$ or $t \rightarrow Hu$ ($H \rightarrow \gamma\gamma$)
< 4.0	95	[6] AAD	23CJ	ATLS	$pp \rightarrow tH$ or $t \rightarrow Hu$ (combined with $H \rightarrow \gamma\gamma$, $H \rightarrow bb$, $H \rightarrow \tau\tau$)
< 6.9	95	[7] AAD	23H	ATLS	$pp \rightarrow tH$ or $t \rightarrow Hu$ ($H \rightarrow \tau_h\tau_h$)
< 7.9	95	[8] TUMASYAN	22K	CMS	$t \rightarrow Hu$ ($H \rightarrow bb$)
<52	95	[9] AABOUD	19S	ATLS	$t \rightarrow Hu$ ($H \rightarrow bb$)
<17	95	[10] AABOUD	19S	ATLS	$t \rightarrow Hu$ ($H \rightarrow \tau\tau$)
<12	95	[11] AABOUD	19S	ATLS	combination of $t \rightarrow Hu$ ($H \rightarrow WW, ZZ, \tau\tau, \gamma\gamma, b\bar{b}$)
<19	95	[12] AABOUD	18X	ATLS	$t \rightarrow Hu$ ($H \rightarrow WW, ZZ, \tau\tau$)
<47	95	[13] SIRUNYAN	18BC	CMS	$t \rightarrow Hu$ ($H \rightarrow bb$)
<24	95	[14] AABOUD	17AV	ATLS	$t \rightarrow Hu$ ($H \rightarrow \gamma\gamma$)
<55	95	[15] KHACHATRY...	17I	CMS	$t \rightarrow Hu$ ($H \rightarrow WW, ZZ, \tau\tau, \gamma\gamma, b\bar{b}$)
<61	95	[16] AAD	15CO	ATLS	$t \rightarrow Hu$ ($H \rightarrow bb$)
<79	95	[17] AAD	14AA	ATLS	$t \rightarrow Hq$ (q=u,c; $H \rightarrow \gamma\gamma$)

[1] TUMASYAN 22A based on 137 fb^{-1} at $\sqrt{s}$ = 13 TeV of pp data. The processes considered include both the associated production of a single top quark with a Higgs boson and the decay $t \rightarrow Hu$ in $t\bar{t}$ production using $H \rightarrow \gamma\gamma$.

[2] HAYRAPETYAN 25AD based on 138 fb^{-1} at $\sqrt{s}$ = 13 TeV of pp data. Events with t and H are considered, which are produced via $t\bar{t}$ or single-t productions and anomalous Hut couplings.

[3] AAD 24AU based on 140 fb^{-1} at $\sqrt{s}$ = 13 TeV of pp data. The processes considered include both the associated production of a single top quark with a Higgs boson and the decay $t \rightarrow Hu$ in $t\bar{t}$ production using three Higgs decay modes.

[4] AAD 24AU based on 140 fb^{-1} at $\sqrt{s}$ = 13 TeV of pp data. The processes considered include both the associated production of a single top quark with a Higgs boson and the decay $t \rightarrow Hu$ in $t\bar{t}$ production using five Higgs decay modes.

[5] AAD 23CJ based on 139 fb^{-1} at $\sqrt{s}$ = 13 TeV of pp data. The processes considered include both the associated production of a single top quark with a Higgs boson and the decay $t \rightarrow Hu$ in $t\bar{t}$ production using $H \rightarrow \gamma\gamma$. Limits on the SMEFT Wilson coefficients are derived.

[6] AAD 23CJ based on 139 fb^{-1} at $\sqrt{s}$ = 13 TeV of pp data. The results are combined with searches in the $H \rightarrow \gamma\gamma$, $H \rightarrow bb$, and $H \rightarrow \tau\tau$ final states. Limits on the SMEFT Wilson coefficients are also derived.

[7] AAD 23H based on 139 fb^{-1} at $\sqrt{s}$ = 13 TeV of pp data. The limits are set using events with two hadronically decaying τ in the ℓ + multiple jets.

[8] TUMASYAN 22K based on 137 fb^{-1} at $\sqrt{s}$ = 13 TeV of pp data. Uses events with one isolated lepton and multiple jets (including $\geq$ 2b-jets). Deep neural networks are used for kinematical event reconstruction.

[9] AABOUD 19S based on 36.1 fb^{-1} at $\sqrt{s}$ = 13 TeV of pp data. Uses events with one isolated lepton and multiple jets (several of them b-tagged with high purity). A multivariate analysis is performed to distinguish the signal from backgrounds.

[10] AABOUD 19S based on 36.1 fb^{-1} at $\sqrt{s}$ = 13 TeV of pp data. Uses events with one or two hadronically decaying τ and multiple jets. A multivariate analysis is performed to distinguish the signal from backgrounds.

[11] AABOUD 19S based on 36.1 fb^{-1} at $\sqrt{s}$ = 13 TeV of pp data. The searches using $H \rightarrow bb$ and $H \rightarrow \tau_h\tau_h$ are combined with searches in diphoton and multilepton final states. The upper limit on the Yukawa coupling $|Y_{tuH}|$ < 0.066 (95% CL) is obtained.

[12] AABOUD 18X based on 36.1 fb^{-1} at $\sqrt{s}$ = 13 TeV of pp data. $\ell\ell$(same sign) + $\geq$ 4j mode and $\ell\ell\ell$ + $\geq$ 2j mode are targeted and specialized boosted decision trees are used to distinguish signals from backgrounds.

[13] SIRUNYAN 18BC based on 35.9 fb^{-1} at $\sqrt{s}$ = 13 TeV of pp data. Two channels $pp \rightarrow tH$ and $pp \rightarrow t\bar{t}$ in final states with one isolated lepton and >=3 jets with >=2 b jets are considered assuming a single tHu FCNC coupling. Reconstructed kinematical variables are fed into a multivariate analysis and no significant deviation is observed from the predicted background.

[14] AABOUD 17AV based on 36.1 fb^{-1} at $\sqrt{s}$ = 13 TeV of pp data. Search for $t\bar{t}$ events, where the other top quark decays hadronically or semi-leptonically.

[15] KHACHATRYAN 17I based on 19.7 fb^{-1} of pp data at $\sqrt{s}$ = 8 TeV, using the topologies $t\bar{t} \rightarrow Hq+Wb$, where q=u, c.

[16] AAD 15CO based on 20.3 fb^{-1} at $\sqrt{s}$ = 8 TeV of pp data. Searches for $t\bar{t}$ events, where the other top quark decays semi-leptonically. Exploits high multiplicity of b-jets and uses a likelihood discriminant. Combining with other ATLAS searches for different Higgs decay modes, B($t \rightarrow Hc$) < 0.46% and B($t \rightarrow Hu$) < 0.45% are obtained.

[17] AAD 14AA based on 4.7 fb^{-1} at $\sqrt{s}$ = 7 TeV and 20.3 fb^{-1} at $\sqrt{s}$ = 8 TeV of pp data. The upper-bound is for the sum of Br($t \rightarrow Hc$) and Br($t \rightarrow Hu$). Search for $t\bar{t}$ events, where the other top quark decays hadronically or semi-leptonically. The upper bound constrains the H-t-c Yukawa couplings $\sqrt{|Y^H_{tc_L}|^2 + |Y^H_{tc_R}|^2}$ < 0.17 (95% CL).

$\Gamma(Hc)/\Gamma_{\text{total}}$ — Γ_{12}/Γ

VALUE (units 10^{-4})	CL%	DOCUMENT ID		TECN	COMMENT
< 3.4	95	[1] AAD	24AU	ATLS	$pp \rightarrow tH$ or $t \rightarrow Hc$ (combined $H \rightarrow WW, ZZ, \tau\tau, \gamma\gamma, bb$)
• • • We do not use the following data for averages, fits, limits, etc. • • •					
< 4.3	95	[2] HAYRAPETY...	25AD	CMS	2ℓ (same sign) + $\geq$ 1j
< 3.3	95	[3] AAD	24AU	ATLS	$pp \rightarrow tH$ or $t \rightarrow Hc$ ($H \rightarrow WW, ZZ, \tau\tau$)
< 4.3	95	[4] AAD	23CJ	ATLS	$pp \rightarrow tH$ or $t \rightarrow Hc$ ($H \rightarrow \gamma\gamma$)
< 5.8	95	[5] AAD	23CJ	ATLS	$pp \rightarrow tH$ or $t \rightarrow Hc$ (combined with $H \rightarrow \gamma\gamma$, $H \rightarrow bb$, $H \rightarrow \tau_h\tau_h$)
< 9.4	95	[6] AAD	23H	ATLS	$pp \rightarrow tH$ or $t \rightarrow Hc$ ($H \rightarrow \tau_h\tau_h$)
< 7.3	95	[7] TUMASYAN	22A	CMS	$t \rightarrow Hc$ ($H \rightarrow \gamma\gamma$)
< 9.4	95	[8] TUMASYAN	22K	CMS	$t \rightarrow Hc$ ($H \rightarrow bb$)
<11	95	[9] AABOUD	19S	ATLS	combination of $t \rightarrow Hc$ ($H \rightarrow WW, ZZ, \tau\tau, \gamma\gamma, b\bar{b}$)
<42	95	[10] AABOUD	19S	ATLS	$t \rightarrow Hc$ ($H \rightarrow bb$)
<19	95	[11] AABOUD	19S	ATLS	$t \rightarrow Hc$ ($H \rightarrow \tau\tau$)
<16	95	[12] AABOUD	18X	ATLS	$t \rightarrow Hc$ ($H \rightarrow WW, ZZ, \tau\tau$)
<47	95	[13] SIRUNYAN	18BC	CMS	$t \rightarrow Hc$ ($H \rightarrow bb$)
<22	95	[14] AABOUD	17AV	ATLS	$t \rightarrow Hc$ ($H \rightarrow \gamma\gamma$)
<40	95	[15] KHACHATRY...	17I	CMS	$t \rightarrow Hc$ ($H \rightarrow WW, ZZ, \tau\tau, \gamma\gamma, b\bar{b}$)
<56	95	[16] AAD	15CO	ATLS	$t \rightarrow Hc$ ($H \rightarrow bb$)
<79	95	[17] AAD	14AA	ATLS	$t \rightarrow Hq$ (q=u,c; $H \rightarrow \gamma\gamma$)
< 1.3 × 10^2	95	[18] CHATRCHYAN	14R	CMS	$t \rightarrow Hc$ ($H \rightarrow \geq 2\ \ell$)
<56	95	[19] KHACHATRY...	14Q	CMS	$t \rightarrow Hc$ ($H \rightarrow \gamma\gamma$ or leptons)

[1] AAD 24AU based on 140 fb^{-1} at $\sqrt{s}$ = 13 TeV of pp data. The processes considered include both the associated production of a single top quark with a Higgs boson and the decay $t \rightarrow Hc$ in $t\bar{t}$ production using five Higgs decay modes.

[2] HAYRAPETYAN 25AD based on 138 fb^{-1} at $\sqrt{s}$ = 13 TeV of pp data. Events with t and H are considered, which are produced via $t\bar{t}$ or single-t productions and anomalous Hct couplings.

[3] AAD 24AU based on 140 fb^{-1} at $\sqrt{s}$ = 13 TeV of pp data. The processes considered include both the associated production of a single top quark with a Higgs boson and the decay $t \rightarrow Hc$ in $t\bar{t}$ production using three Higgs decay modes.

[4] AAD 23CJ based on 139 fb^{-1} at $\sqrt{s}$ = 13 TeV of pp data. The processes considered include both the associated production of a single top quark with a Higgs boson and the decay $t \rightarrow Hc$ in $t\bar{t}$ production using $H \rightarrow \gamma\gamma$. Limits on the SMEFT Wilson coefficients are derived.

[5] AAD 23CJ based on 139 fb^{-1} at $\sqrt{s}$ = 13 TeV of pp data. The results are combined with searches in the $H \rightarrow \gamma\gamma$, $H \rightarrow bb$, and $H \rightarrow \tau\tau$ final states. Limits on the SMEFT Wilson coefficients are also derived.

[6] AAD 23H based on 139 fb^{-1} at $\sqrt{s}$ = 13 TeV of pp data. Uses events with one or two hadronically decaying τ and multiple jets. The limit corresponds to $(4.8^{+2.2}_{-1.4}) \times 10^{-4}$ measurement.

[7] TUMASYAN 22A based on 137 fb^{-1} at $\sqrt{s}$ = 13 TeV of pp data. The processes considered include both the associated production of a single top quark with a Higgs boson and the decay $t \rightarrow Hc$ in $t\bar{t}$ production using $H \rightarrow \gamma\gamma$.

[8] TUMASYAN 22K based on 137 fb^{-1} at $\sqrt{s}$ = 13 TeV of pp data. Uses events with one isolated lepton and multiple jets (including $\geq$ 2b-jets). Deep neural networks are used for kinematical event reconstruction.

[9] AABOUD 19S based on 36.1 fb^{-1} at $\sqrt{s}$ = 13 TeV of pp data. The searches using $H \rightarrow bb$ and $H \rightarrow \tau_h\tau_h$ are combined with searches in diphoton and multilepton final states. The upper limit on the Yukawa coupling $|Y_{tcH}|$ < 0.064 (95% CL) is obtained.

[10] AABOUD 19S based on 36.1 fb^{-1} at $\sqrt{s}$ = 13 TeV of pp data. Uses events with one isolated lepton and multiple jets (several of them b-tagged with high purity). A multivariate analysis is performed to distinguish the signal from backgrounds.

[11] AABOUD 19S based on 36.1 fb^{-1} at $\sqrt{s}$ = 13 TeV of pp data. Uses events with one or two hadronically decaying τ and multiple jets. A multivariate analysis is performed to distinguish the signal from backgrounds.

[12] AABOUD 18X based on 36.1 fb^{-1} at $\sqrt{s}$ = 13 TeV of pp data. $\ell\ell$(same sign) + $\geq$ 4j mode and $\ell\ell\ell$ + $\geq$ 2j mode are targeted and specialized boosted decision trees are used to distinguish signals from backgrounds.

[13] SIRUNYAN 18BC based on 35.9 fb^{-1} at $\sqrt{s}$ = 13 TeV of pp data. Two channels $pp \rightarrow tH$ and $pp \rightarrow t\bar{t}$ in final states with one isolated lepton and >=3 jets with >=2 b jets are considered assuming a single tHc FCNC coupling. Reconstructed kinematical variables are fed into a multivariate analysis and no significant deviation is observed from the predicted background.

[14] AABOUD 17AV based on 36.1 fb^{-1} at $\sqrt{s}$ = 13 TeV of pp data. Search for $t\bar{t}$ events, where the other top quark decays hadronically or semi-leptonically. The upper bound on the H-t-c Yukawa couplings is 0.090 (95% CL).

[15] KHACHATRYAN 17I based on 19.7 fb^{-1} of pp data at $\sqrt{s}$ = 8 TeV, using the topologies $t\bar{t} \rightarrow Hq+Wb$, where q=u, c.

[16] AAD 15CO based on 20.3 fb^{-1} at $\sqrt{s}$ = 8 TeV of pp data. Searches for $t\bar{t}$ events, where the other top quark decays semi-leptonically. Exploits high multiplicity of b-jets and uses a likelihood discriminant. Combining with other ATLAS searches for different Higgs decay modes, B($t \rightarrow Hc$) < 0.46% and B($t \rightarrow Hu$) < 0.45% are obtained.

[17] AAD 14AA based on 4.7 fb^{-1} at $\sqrt{s}$ = 7 TeV and 20.3 fb^{-1} at $\sqrt{s}$ = 8 TeV of pp data. The upper-bound is for the sum of Br($t \rightarrow Hc$) and Br($t \rightarrow Hu$). Search for $t\bar{t}$ events, where the other top quark decays hadronically or semi-leptonically. The upper bound constrains the H-t-c Yukawa couplings $\sqrt{|Y^H_{tc_L}|^2 + |Y^H_{tc_R}|^2}$ < 0.17 (95% CL).

[18] Based on 19.5 fb^{-1} of pp data at $\sqrt{s}$ = 8 TeV. Search for final states with 3 or more isolated high E_T charged leptons (ℓ = e, μ) bounds the $t \rightarrow Hc$ decay in $t\bar{t}$ events

when H decays contain a pair of leptons. The upper bound constrains the H-t-c Yukawa couplings $\sqrt{|Y^H_{t\,c_L}|^2 + |Y^H_{t\,c_R}|^2} < 0.21$ (95% CL).

[19] KHACHATRYAN 14Q based on 19.5 fb^{-1} at $\sqrt{s} = 8$ TeV of pp data. Search for final states with ≥ 3 isolated charged leptons or with a photon pair accompanied by ≥ 1 lepton(s).

$\Gamma(\ell^+ \overline{q} q' (q{=}d,s,b; q'{=}u,c))/\Gamma_{total}$ — Γ_{13}/Γ

VALUE	CL%	DOCUMENT ID	TECN	COMMENT
$<1.6 \times 10^{-3}$	95	[1] CHATRCHYAN 14O	CMS	μ + dijets
• • • We do not use the following data for averages, fits, limits, etc. • • •				
$<1.7 \times 10^{-3}$	95	[1] CHATRCHYAN 14O	CMS	e + dijets

[1] Based on 19.5 fb^{-1} of pp data at $\sqrt{s} = 8$ TeV. Baryon number violating decays of the top quark are searched for in $t\overline{t}$ production events where one of the pair decays into hadronic three jets.

$\Gamma(e^\pm \mu^\mp c)/\Gamma_{total}$ — Γ_{14}/Γ

VALUE	CL%	DOCUMENT ID	TECN	COMMENT
$<2.16 \times 10^{-7}$	95	[1] HAYRAPETY...25J	CMS	$e^\pm \mu^\mp \ell + \geq 1$j($\leq 1b$-tag)
• • • We do not use the following data for averages, fits, limits, etc. • • •				
$<8.9 \times 10^{-7}$	95	[2] TUMASYAN 22Z	CMS	pp at 13 TeV

[1] HAYRAPETYAN 25J based on 138 fb^{-1} of pp data at $\sqrt{s} = 13$ TeV. Searches are performed for the charged-LFV interactions through $c \to e\mu t$ or $t \to e\mu c$ process. The data are consistent with the SM expectations, and the 95% CL upper limits of 4.98×10^{-7}, 3.69×10^{-7}, 2.16×10^{-7} are set on the branching ratios for tensorlike, vectorlike, and scalarlike interactions, respectively.

[2] TUMASYAN 22Z analysis includes both the production ($c \to e\mu t$) and decay ($t \to e\mu c$) modes of the top quark through CLFV interactions. With no significant excess over the standard model expectation, the limits are set at 95% CL on the B($t \to e\mu c$) of 1.31×10^{-6}, 0.89×10^{-6}, 2.59×10^{-6} for vector-, scalar-, and tensor-like CLFV four-fermion effective interactions, respectively.

$\Gamma(e^\pm \mu^\mp u)/\Gamma_{total}$ — Γ_{15}/Γ

VALUE	CL%	DOCUMENT ID	TECN	COMMENT
$<1.2 \times 10^{-8}$	95	[1] HAYRAPETY...25J	CMS	$e^\pm \mu^\mp \ell + \geq 1$j($\leq 1b$-tag)
• • • We do not use the following data for averages, fits, limits, etc. • • •				
$<7 \times 10^{-8}$	95	[2] TUMASYAN 22Z	CMS	pp at 13 TeV

[1] HAYRAPETYAN 25J based on 138 fb^{-1} of pp data at $\sqrt{s} = 13$ TeV. Searches are performed for the charged-LFV interactions through $u \to e\mu t$ or $t \to e\mu u$ process. The data are consistent with the SM expectations, and the 95% CL upper limits of 3.2×10^{-8}, 2.2×10^{-8}, 1.2×10^{-8} are set on the branching ratios for tensorlike, vectorlike, and scalarlike interactions, respectively.

[2] TUMASYAN 22Z analysis includes both the production ($u \to e\mu t$) and decay ($t \to e\mu u$) modes of the top quark through CLFV interactions. With no significant excess over the standard model expectation, the limits are set at 95% CL on the B($t \to e\mu u$) of 0.13×10^{-6}, 0.07×10^{-6}, 0.25×10^{-6} for vector-, scalar-, and tensor-like CLFV four-fermion effective interactions, respectively.

$\Gamma(\mu^\pm \tau^\mp q)/\Gamma_{total}$ — Γ_{16}/Γ

VALUE (units 10^{-7})	CL%	DOCUMENT ID	TECN	COMMENT
< (0.4, 0.8, 1.2)	95	[1] HAYRAPETY...25AO	CMS	$q = u$; pp at 13 TeV
• • • We do not use the following data for averages, fits, limits, etc. • • •				
< (8.1, 17.1, 20.5)	95	[1] HAYRAPETY...25AO	CMS	$q = c$; pp at 13 TeV
<8.7	95	[2] AAD 24W	ATLS	pp at 13 TeV

[1] HAYRAPETYAN 25AO analysis includes both the production ($q \to \mu\tau t$) and decay ($t \to \mu\tau q$) modes of the top quark through CLFV interactions, where $q = u$ or c. With no significant excess over the standard model expectation, upper limits are set on Wilson coefficients of dimension-6 EFT operators. The three values correspond to scalar, vector, and tensor-like operators.

[2] AAD 24W analysis includes both the production ($q \to \mu\tau t$) and decay ($t \to \mu\tau q$) modes of the top quark through CLFV interactions, where $q = u, c$. With no significant excess over the standard model expectation, upper limits are set on Wilson coefficients of SMEFT as well as leptoquark coupling strengths for various leptoquark masses.

$\Gamma(e^+ \overline{u}\overline{d})/\Gamma_{total}$ — Γ_{17}/Γ

VALUE (units 10^{-6})	CL%	DOCUMENT ID	TECN	COMMENT
<0.011	95	[1] HAYRAPETY...24E	CMS	C_s; pp at 13 TeV
<0.003	95	[1] HAYRAPETY...24E	CMS	C_t; pp at 13 TeV

[1] HAYRAPETYAN 24E based on 138 fb^{-1} of pp data at $\sqrt{s} = 13$ TeV. A search is performed for a baryon-number-violating interactions in top quark production and decay, using events with $\ell^\pm \ell^\mp + 1b$-jet. Upper limits are placed on the couplings of the 24 baryon-number-violating dimension-six operators involving the top quark, setting only one of them as non-zero each time. They are translated to limits on the branching fractions of the top quark.

$\Gamma(\mu^+ \overline{u}\overline{d})/\Gamma_{total}$ — Γ_{18}/Γ

VALUE (units 10^{-6})	CL%	DOCUMENT ID	TECN	COMMENT
<0.006	95	[1] HAYRAPETY...24E	CMS	C_s; pp at 13 TeV
<0.002	95	[1] HAYRAPETY...24E	CMS	C_t; pp at 13 TeV

[1] HAYRAPETYAN 24E based on 138 fb^{-1} of pp data at $\sqrt{s} = 13$ TeV. A search is performed for a baryon-number-violating interactions in top quark production and decay, using events with $\ell^\pm \ell^\mp + 1b$-jet. Upper limits are placed on the couplings of the 24 baryon-number-violating dimension-six operators involving the top quark, setting only one of them as non-zero each time. They are translated to limits on the branching fractions of the top quark.

$\Gamma(e^+ \overline{c}\overline{d})/\Gamma_{total}$ — Γ_{19}/Γ

VALUE (units 10^{-6})	CL%	DOCUMENT ID	TECN	COMMENT
<0.164	95	[1] HAYRAPETY...24E	CMS	C_s; pp at 13 TeV
<0.050	95	[1] HAYRAPETY...24E	CMS	C_t; pp at 13 TeV

[1] HAYRAPETYAN 24E based on 138 fb^{-1} of pp data at $\sqrt{s} = 13$ TeV. A search is performed for a baryon-number-violating interactions in top quark production and decay, using events with $\ell^\pm \ell^\mp + 1b$-jet. Upper limits are placed on the couplings of the 24 baryon-number-violating dimension-six operators involving the top quark, setting only one of them as non-zero each time. They are translated to limits on the branching fractions of the top quark.

$\Gamma(\mu^+ \overline{c}\overline{d})/\Gamma_{total}$ — Γ_{20}/Γ

VALUE (units 10^{-6})	CL%	DOCUMENT ID	TECN	COMMENT
<0.095	95	[1] HAYRAPETY...24E	CMS	C_s; pp at 13 TeV
<0.030	95	[1] HAYRAPETY...24E	CMS	C_t; pp at 13 TeV

[1] HAYRAPETYAN 24E based on 138 fb^{-1} of pp data at $\sqrt{s} = 13$ TeV. A search is performed for a baryon-number-violating interactions in top quark production and decay, using events with $\ell^\pm \ell^\mp + 1b$-jet. Upper limits are placed on the couplings of the 24 baryon-number-violating dimension-six operators involving the top quark, setting only one of them as non-zero each time. They are translated to limits on the branching fractions of the top quark.

$\Gamma(e^+ \overline{u}\overline{s})/\Gamma_{total}$ — Γ_{21}/Γ

VALUE (units 10^{-6})	CL%	DOCUMENT ID	TECN	COMMENT
<0.050	95	[1] HAYRAPETY...24E	CMS	C_s; pp at 13 TeV
<0.015	95	[1] HAYRAPETY...24E	CMS	C_t; pp at 13 TeV

[1] HAYRAPETYAN 24E based on 138 fb^{-1} of pp data at $\sqrt{s} = 13$ TeV. A search is performed for a baryon-number-violating interactions in top quark production and decay, using events with $\ell^\pm \ell^\mp + 1b$-jet. Upper limits are placed on the couplings of the 24 baryon-number-violating dimension-six operators involving the top quark, setting only one of them as non-zero each time. They are translated to limits on the branching fractions of the top quark.

$\Gamma(\mu^+ \overline{u}\overline{s})/\Gamma_{total}$ — Γ_{22}/Γ

VALUE (units 10^{-6})	CL%	DOCUMENT ID	TECN	COMMENT
<0.030	95	[1] HAYRAPETY...24E	CMS	C_s; pp at 13 TeV
<0.009	95	[1] HAYRAPETY...24E	CMS	C_t; pp at 13 TeV

[1] HAYRAPETYAN 24E based on 138 fb^{-1} of pp data at $\sqrt{s} = 13$ TeV. A search is performed for a baryon-number-violating interactions in top quark production and decay, using events with $\ell^\pm \ell^\mp + 1b$-jet. Upper limits are placed on the couplings of the 24 baryon-number-violating dimension-six operators involving the top quark, setting only one of them as non-zero each time. They are translated to limits on the branching fractions of the top quark.

$\Gamma(e^+ \overline{c}\overline{s})/\Gamma_{total}$ — Γ_{23}/Γ

VALUE (units 10^{-6})	CL%	DOCUMENT ID	TECN	COMMENT
<0.786	95	[1] HAYRAPETY...24E	CMS	C_s; pp at 13 TeV
<0.229	95	[1] HAYRAPETY...24E	CMS	C_t; pp at 13 TeV

[1] HAYRAPETYAN 24E based on 138 fb^{-1} of pp data at $\sqrt{s} = 13$ TeV. A search is performed for a baryon-number-violating interactions in top quark production and decay, using events with $\ell^\pm \ell^\mp + 1b$-jet. Upper limits are placed on the couplings of the 24 baryon-number-violating dimension-six operators involving the top quark, setting only one of them as non-zero each time. They are translated to limits on the branching fractions of the top quark.

$\Gamma(\mu^+ \overline{c}\overline{s})/\Gamma_{total}$ — Γ_{24}/Γ

VALUE (units 10^{-6})	CL%	DOCUMENT ID	TECN	COMMENT
<0.468	95	[1] HAYRAPETY...24E	CMS	C_s; pp at 13 TeV
<0.138	95	[1] HAYRAPETY...24E	CMS	C_t; pp at 13 TeV

[1] HAYRAPETYAN 24E based on 138 fb^{-1} of pp data at $\sqrt{s} = 13$ TeV. A search is performed for a baryon-number-violating interactions in top quark production and decay, using events with $\ell^\pm \ell^\mp + 1b$-jet. Upper limits are placed on the couplings of the 24 baryon-number-violating dimension-six operators involving the top quark, setting only one of them as non-zero each time. They are translated to limits on the branching fractions of the top quark.

$\Gamma(e^+ \overline{u}\overline{b})/\Gamma_{total}$ — Γ_{25}/Γ

VALUE (units 10^{-6})	CL%	DOCUMENT ID	TECN	COMMENT
<0.154	95	[1] HAYRAPETY...24E	CMS	C_s; pp at 13 TeV
<0.045	95	[1] HAYRAPETY...24E	CMS	C_t; pp at 13 TeV

[1] HAYRAPETYAN 24E based on 138 fb^{-1} of pp data at $\sqrt{s} = 13$ TeV. A search is performed for a baryon-number-violating interactions in top quark production and decay, using events with $\ell^\pm \ell^\mp + 1b$-jet. Upper limits are placed on the couplings of the 24 baryon-number-violating dimension-six operators involving the top quark, setting only one of them as non-zero each time. They are translated to limits on the branching fractions of the top quark.

$\Gamma(\mu^+ \overline{u}\overline{b})/\Gamma_{total}$ — Γ_{26}/Γ

VALUE (units 10^{-6})	CL%	DOCUMENT ID	TECN	COMMENT
<0.087	95	[1] HAYRAPETY...24E	CMS	C_s; pp at 13 TeV
<0.028	95	[1] HAYRAPETY...24E	CMS	C_t; pp at 13 TeV

[1] HAYRAPETYAN 24E based on 138 fb^{-1} of pp data at $\sqrt{s} = 13$ TeV. A search is performed for a baryon-number-violating interactions in top quark production and decay, using events with $\ell^\pm \ell^\mp + 1b$-jet. Upper limits are placed on the couplings of the 24 baryon-number-violating dimension-six operators involving the top quark, setting only one of them as non-zero each time. They are translated to limits on the branching fractions of the top quark.

by UNIVERSITY OF CALIFORNIA BERKELEY on 09/16/26. Re-use and distribution is strictly not permitted, except for Open Access articles.
Phys. A 2026.41. Downloaded from www.worldscientific.com

Int. J. Mod. Phys. A 2026.41. Downloaded from www.worldscientific.com
by UNIVERSITY OF CALIFORNIA @ BERKELEY on 09/16/26. Re-use and distribution is strictly not permitted, except for Open Access articles.

$\Gamma(e^+\overline{c}\overline{b})/\Gamma_{total}$ — Γ_{27}/Γ

VALUE (units 10^{-6})	CL%	DOCUMENT ID		TECN	COMMENT
<2.090	95	[1] HAYRAPETY...24E		CMS	C_s; pp at 13 TeV
<0.652	95	[1] HAYRAPETY...24E		CMS	C_t; pp at 13 TeV

[1] HAYRAPETYAN 24E based on 138 fb^{-1} of pp data at $\sqrt{s}$ = 13 TeV. A search is performed for a baryon-number-violating interactions in top quark production and decay, using events with $\ell^\pm\ell^\mp$ + 1b-jet. Upper limits are placed on the couplings of the 24 baryon-number-violating dimension-six operators involving the top quark, setting only one of them as non-zero each time. They are translated to limits on the branching fractions of the top quark.

$\Gamma(\mu^+\overline{c}\overline{b})/\Gamma_{total}$ — Γ_{28}/Γ

VALUE (units 10^{-6})	CL%	DOCUMENT ID		TECN	COMMENT
<1.521	95	[1] HAYRAPETY...24E		CMS	C_s; pp at 13 TeV
<0.455	95	[1] HAYRAPETY...24E		CMS	C_t; pp at 13 TeV

[1] HAYRAPETYAN 24E based on 138 fb^{-1} of pp data at $\sqrt{s}$ = 13 TeV. A search is performed for a baryon-number-violating interactions in top quark production and decay, using events with $\ell^\pm\ell^\mp$ + 1b-jet. Upper limits are placed on the couplings of the 24 baryon-number-violating dimension-six operators involving the top quark, setting only one of them as non-zero each time. They are translated to limits on the branching fractions of the top quark.

t-quark EW Couplings

W helicity fractions in top decays. F_0 is the fraction of longitudinal and F_+ the fraction of right-handed W bosons. F_{V+A} is the fraction of $V+A$ current in top decays. The effective Lagrangian (cited by ABAZOV 08AI) has terms f_1^L and f_1^R for $V-A$ and $V+A$ couplings, f_2^L and f_2^R for tensor couplings with b_R and b_L respectively.

F_0

VALUE	DOCUMENT ID		TECN	COMMENT
0.693±0.013 OUR AVERAGE				
0.693±0.009±0.011	[1] AAD	20Y	LHC	ATLAS+CMS combined
0.726±0.066±0.067	[2] AALTONEN	13D	CDF	$F_0 = B(t \to W_0 b)$
0.682±0.030±0.033	[3] CHATRCHYAN	13BH	CMS	$F_0 = B(t \to W_0 b)$
0.67 ±0.07	[4] AAD	12BG	ATLS	$F_0 = B(t \to W_0 b)$
0.722±0.062±0.052	[5] AALTONEN	12Z	TEVA	$F_0 = B(t \to W_0 b)$
0.669±0.078±0.065	[6] ABAZOV	11C	D0	$F_0 = B(t \to W_0 b)$
0.91 ±0.37 ±0.13	[7] AFFOLDER	00B	CDF	$F_0 = B(t \to W_0 b)$
• • • We do not use the following data for averages, fits, limits, etc. • • •				
0.70 ±0.05	[8] AABOUD	17BB	ATLS	$F_0 = 1 - f_1$, Repl by AAD 20Y
0.681±0.012±0.023	[9] KHACHATRY...16BU		CMS	$F_0 = B(t \to W_0 b)$, Repl by AAD 20Y
0.70 ±0.07 ±0.04	[10] AALTONEN	10Q	CDF	Repl. by AALTONEN 12Z
0.62 ±0.10 ±0.05	[11] AALTONEN	09Q	CDF	Repl. by AALTONEN 10Q
0.425±0.166±0.102	[12] ABAZOV	08B	D0	Repl. by ABAZOV 11C
0.85 $^{+0.15}_{-0.22}$ ±0.06	[13] ABULENCIA	07I	CDF	$F_0 = B(t \to W_0 b)$
0.74 $^{+0.22}_{-0.34}$	[14] ABULENCIA	06U	CDF	$F_0 = B(t \to W_0 b)$
0.56 ±0.31	[15] ABAZOV	05G	D0	$F_0 = B(t \to W_0 b)$

[1] AAD 20Y based on about 20 fb^{-1} of pp data at $\sqrt{s}$ = 8 TeV for each experiment. The first error stands for the sum of the statistical and background uncertainties, and the second error for the remaining systematic uncertainties. The measurements used events with one lepton and different jet multiplicities in the final state. The result is consistent with the NNLO SM prediction of 0.687 ± 0.005 for m_t = 172.8 ± 1.3 GeV.

[2] Based on 8.7 fb^{-1} of data in $p\overline{p}$ collisions at $\sqrt{s}$ = 1.96 TeV using $t\overline{t}$ events with $\ell + \not{E}_T + \geq 4$ jets(≥ 1 b), and under the constraint $F_0 + F_+ + F_- = 1$. The statstical errors of F_0 and F_+ are correlated with correlation coefficient $\rho(F_0,F_+) = -0.69$.

[3] Based on 5.0 fb^{-1} of pp data at $\sqrt{s}$ = 7 TeV. CHATRCHYAN 13BH studied tt events with large $\not{E}_T$ and $\ell + \geq 4$ jets using a constrained kinematic fit.

[4] Based on 1.04 fb^{-1} of pp data at $\sqrt{s}$ = 7 TeV. AAD 12BG studied tt events with large $\not{E}_T$ and either $\ell + \geq 4$j or $\ell\ell + \geq 2$j. The uncertainties are not independent, $\rho(F_0,F_-) = -0.96$.

[5] Based on 2.7 and 5.1 fb^{-1} of CDF data in ℓ + jets and dilepton channels, and 5.4 fb^{-1} of D0 data in ℓ + jets and dilepton channels. $F_0 = 0.682 \pm 0.035 \pm 0.046$ if $F_+ = 0.0017(1)$, while $F_+ = -0.015 \pm 0.018 \pm 0.030$ if $F_0 = 0.688(4)$, where the assumed fixed values are the SM prediction for $m_t = 173.3 \pm 1.1$ GeV and $m_W = 80.399 \pm 0.023$ GeV.

[6] Results are based on 5.4 fb^{-1} of data in $p\overline{p}$ collisions at 1.96 TeV, including those of ABAZOV 08B. Under the SM constraint of $f_0 = 0.698$ (for m_t = 173.3 GeV, m_W = 80.399 GeV), $f_+ = 0.010 \pm 0.022 \pm 0.030$ is obtained.

[7] AFFOLDER 00B studied the angular distribution of leptonic decays of W bosons in $t \to Wb$ events. The ratio F_0 is the fraction of the helicity zero (longitudinal) W bosons in the decaying top quark rest frame. $B(t \to W_+ b)$ is the fraction of positive helicity (right-handed) positive charge W bosons in the top quark decays. It is obtained by assuming the Standard Model value of F_0.

[8] AABOUD 17BB based on 20.2 fb^{-1} of pp data at $\sqrt{s}$ = 8 TeV. Triple-differential decay rate of top quark in the t-channel single-top production is used to simultaneously determine five generalized Wtb couplings as well as the top polarization. No assumption is made for the other couplings. See this paper for constraints on other couplings not included here. The paper reported f_1, and we converted it to F_0.

[9] KHACHATRYAN 16BU based on 19.8 fb^{-1} of pp data at $\sqrt{s}$ = 8 TeV using $t\overline{t}$ events with $\ell + \not{E}_T + \geq 4$ jets(≥ 2 b). The errors of F_0 and F_- are correlated with a correlation coefficient $\rho(F_0, F_-) = -0.87$. The result is consistent with the NNLO SM prediction of 0.687 ± 0.005 for m_t = 172.8 ± 1.3 GeV.

[10] Results are based on 2.7 fb^{-1} of data in $p\overline{p}$ collisions at $\sqrt{s}$ = 1.96 TeV. F_0 result is obtained by assuming $F_+ = 0$, while F_+ result is obtained for $F_0 = 0.70$, the SM value. Model independent fits for the two fractions give $F_0 = 0.88 \pm 0.11 \pm 0.06$ and $F_+ = -0.15 \pm 0.07 \pm 0.06$ with correlation coefficient of −0.59. The results are for m_t = 175 GeV.

[11] Results are based on 1.9 fb^{-1} of data in $p\overline{p}$ collisions at $\sqrt{s}$ = 1.96 TeV. F_0 result is obtained assuming $F_+ = 0$, while F_+ result is obtained for $F_0 = 0.70$, the SM values. Model independent fits for the two fractions give $F_0 = 0.66 \pm 0.16 \pm 0.05$ and $F_+ = -0.03 \pm 0.06 \pm 0.03$.

[12] Based on 1 fb^{-1} at $\sqrt{s}$ = 1.96 TeV.

[13] Based on 318 pb^{-1} of data at $\sqrt{s}$ = 1.96 TeV.

[14] Based on 200 pb^{-1} of data at $\sqrt{s}$ = 1.96 TeV. $t \to Wb \to \ell\nu b$ ($\ell = e$ or μ). The errors are stat + syst.

[15] ABAZOV 05G studied the angular distribution of leptonic decays of W bosons in $t\overline{t}$ candidate events with lepton + jets final states, and obtained the fraction of longitudinally polarized W under the constraint of no right-handed current, $F_+ = 0$. Based on 125 pb^{-1} of data at $\sqrt{s}$ = 1.8 TeV.

F_-

VALUE	CL%	DOCUMENT ID		TECN	COMMENT
0.315±0.010 OUR AVERAGE					
0.315±0.006±0.009		[1] AAD	20Y	LHC	ATLAS+CMS combined
0.310±0.022±0.022		[2] CHATRCHYAN	13BH	CMS	$F_- = B(t \to W_- b)$
0.32 ±0.04		[3] AAD	12BG	ATLS	$F_- = B(t \to W_- b)$
• • • We do not use the following data for averages, fits, limits, etc. • • •					
> 0.264 ± 0.044	95	[4] AABOUD	17BB	ATLS	$F_- = f_1(1 - f_1^+)$, Repl. by AAD 20Y
0.323±0.008±0.014		[5] KHACHATRY...16BU		CMS	$F_- = B(t \to W_- b)$, Repl. by AAD 20Y

[1] AAD 20Y based on about 20 fb^{-1} of pp data at $\sqrt{s}$ = 8 TeV for each experiment. The first error stands for the sum of the statistical and background uncertainties, and the second error for the remaining systematic uncertainties. The measurements used events with one lepton and different jet multiplicities in the final state. The result is consistent with the NNLO SM prediction of 0.311 ± 0.005 for m_t = 172.8 ± 1.3 GeV.

[2] Based on 5.0 fb^{-1} of pp data at $\sqrt{s}$ = 7 TeV. CHATRCHYAN 13BH studied tt events with large $\not{E}_T$ and $\ell + \geq 4$ jets using a constrained kinematic fit.

[3] Based on 1.04 fb^{-1} of pp data at $\sqrt{s}$ = 7 TeV. AAD 12BG studied tt events with large $\not{E}_T$ and either $\ell + \geq 4$j or $\ell\ell + \geq 2$j. The uncertainties are not independent, $\rho(F_0,F_-) = -0.96$.

[4] AABOUD 17BB based on 20.2 fb^{-1} of pp data at $\sqrt{s}$ = 8 TeV. Triple-differential decay rate of top quark in the t-channel single-top production is used to simultaneously determine five generalized Wtb couplings as well as the top polarization. No assumption is made for the other couplings. The authors reported $f_1 = 0.30 \pm 0.05$ and $f_1^+ < 0.120$ which we converted to $F_- = f_1(1 - f_1^+)$. See this paper for constraints on other couplings not included here.

[5] KHACHATRYAN 16BU based on 19.8 fb^{-1} of pp data at $\sqrt{s}$ = 8 TeV using $t\overline{t}$ events with $\ell + \not{E}_T + \geq 4$ jets(≥ 2 b). The errors of F_0 and F_- are correlated with a correlation coefficient $\rho(F_0, F_-) = -0.87$. The result is consistent with the NNLO SM prediction of 0.311 ± 0.005 for m_t = 172.8 ± 1.3 GeV.

F_+

VALUE	CL%	DOCUMENT ID		TECN	COMMENT
−0.005±0.007 OUR AVERAGE					
−0.008±0.005±0.006		[1] AAD	20Y	LHC	ATLAS+CMS combined
−0.045±0.044±0.058		[2] AALTONEN	13D	CDF	$F_+ = B(t \to W_+ b)$
0.008±0.012±0.014		[3] CHATRCHYAN	13BH	CMS	$F_+ = B(t \to W_+ b)$
0.01 ±0.05		[4] AAD	12BG	ATLS	$F_+ = B(t \to W_+ b)$
0.023±0.041±0.034		[5] ABAZOV	11C	D0	$F_+ = B(t \to W_+ b)$
0.11 ±0.15		[6] AFFOLDER	00B	CDF	$F_+ = B(t \to W_+ b)$
• • • We do not use the following data for averages, fits, limits, etc. • • •					
< 0.036 ± 0.006	95	[7] AABOUD	17BB	ATLS	$F_+ = f_1 f_1^+$, Repl. by AAD 20Y
−0.004±0.005±0.014		[8] KHACHATRY...16BU		CMS	$F_+ = B(t \to W_+ b)$, Repl. by AAD 20Y
−0.033±0.034±0.031		[9] AALTONEN	12Z	TEVA	$F_+ = B(t \to W_+ b)$
−0.01 ±0.02 ±0.05		[10] AALTONEN	10Q	CDF	Repl. by AALTONEN 13D
−0.04 ±0.04 ±0.03		[11] AALTONEN	09Q	CDF	Repl. by AALTONEN 10Q
0.119±0.090±0.053		[12] ABAZOV	08B	D0	Repl. by ABAZOV 11C
0.056±0.080±0.057		[13] ABAZOV	07D	D0	$F_+ = B(t \to W_+ b)$
0.05 $^{+0.11}_{-0.05}$ ±0.03		[14] ABULENCIA	07I	CDF	$F_+ = B(t \to W_+ b)$
< 0.26	95	[14] ABULENCIA	07I	CDF	$F_+ = B(t \to W_+ b)$
< 0.27	95	[15] ABULENCIA	06U	CDF	$F_+ = B(t \to W_+ b)$
0.00 ±0.13 ±0.07		[16] ABAZOV	05L	D0	$F_+ = B(t \to W_+ b)$
< 0.25	95	[16] ABAZOV	05L	D0	$F_+ = B(t \to W_+ b)$
< 0.24	95	[17] ACOSTA	05D	CDF	$F_+ = B(t \to W_+ b)$

[1] AAD 20Y based on about 20 fb^{-1} of pp data at $\sqrt{s}$ = 8 TeV for each experiment. The first error stands for the sum of the statistical and background uncertainties, and the second error for the remaining systematic uncertainties. The measurements used events with one lepton and different jet multiplicities in the final state. The result is estimated from the measurements of F_0 and F_- assuming unitarity. The value is consistent with the NNLO SM prediction of 0.0017 ± 0.0001 for m_t = 172.8 ± 1.3 GeV.

[2] Based on 8.7 fb^{-1} of data in $p\overline{p}$ collisions at $\sqrt{s}$ = 1.96 TeV using $t\overline{t}$ events with $\ell + \not{E}_T + \geq 4$ jets(≥ 1 b), and under the constraint $F_0 + F_+ + F_- = 1$. The statstical errors of F_0 and F_+ are correlated with correlation coefficient $\rho(F_0,F_+) = -0.69$.

[3] Based on 5.0 fb^{-1} of pp data at $\sqrt{s}$ = 7 TeV. CHATRCHYAN 13BH studied tt events with large $\not{E}_T$ and $\ell + \geq 4$ jets using a constrained kinematic fit.

[4] Based on 1.04 fb^{-1} of pp data at $\sqrt{s}$ = 7 TeV. AAD 12BG studied tt events with large $\not{E}_T$ and either $\ell + \geq 4$j or $\ell\ell + \geq 2$j.

[5] Results are based on 5.4 fb^{-1} of data in $p\overline{p}$ collisions at 1.96 TeV, including those of ABAZOV 08B. Under the SM constraint of f_0 = 0.698 (for m_t = 173.3 GeV, m_W = 80.399 GeV), f_+ = 0.010 ± 0.022 ± 0.030 is obtained.

[6] AFFOLDER 00B studied the angular distribution of leptonic decays of W bosons in $t \to Wb$ events. The ratio F_0 is the fraction of the helicity zero (longitudinal) W bosons in the decaying top quark rest frame. B($t \to W_+ b$) is the fraction of positive helicity (right-handed) positive charge W bosons in the top quark decays. It is obtained by assuming the Standard Model value of F_0.

[7] AABOUD 17BB based on 20.2 fb^{-1} of pp data at $\sqrt{s}$ = 8 TeV. Triple-differential decay rate of top quark in the t-channel single-top production is used to simultaneously determine five generalized Wtb couplings as well as the top polarization. No assumption is made for the other couplings. The authors reported f_1 = 0.30 ± 0.05 and f_1^+ < 0.120 which we converted to $F_+ = f_1\ f_1^+$. See this paper for constraints on other couplings not included here.

[8] KHACHATRYAN 16BU based on 19.8 fb^{-1} of pp data at $\sqrt{s}$ = 8 TeV using $t\overline{t}$ events with $\ell + \not{E}_T + \geq 4$ jets($\geq 2\ b$). The result is consistent with the NNLO SM prediction of 0.0017 ± 0.0001 for m_t = 172.8 ± 1.3 GeV.

[9] Based on 2.7 and 5.1 fb^{-1} of CDF data in $\ell +$ jets and dilepton channels, and 5.4 fb^{-1} of D0 data in $\ell +$ jets and dilepton channels. F_0 = 0.682 ± 0.035 ± 0.046 if F_+ = 0.0017(1), while F_+ = −0.015 ± 0.018 ± 0.030 if F_0 = 0.688(4), where the assumed fixed values are the SM prediction for m_t = 173.3 ± 1.1 GeV and m_W = 80.399 ± 0.023 GeV.

[10] Results are based on 2.7 fb^{-1} of data in $p\overline{p}$ collisions at $\sqrt{s}$ = 1.96 TeV. F_0 result is obtained by assuming F_+ = 0, while F_+ result is obtained for F_0 = 0.70, the SM value. Model independent fits for the two fractions give F_0 = 0.88 ± 0.11 ± 0.06 and F_+ = −0.15 ± 0.07 ± 0.06 with correlation coefficient of −0.59. The results are for m_t = 175 GeV.

[11] Results are based on 1.9 fb^{-1} of data in $p\overline{p}$ collisions at $\sqrt{s}$ = 1.96 TeV. F_0 result is obtained assuming F_+ = 0, while F_+ result is obtained for F_0 = 0.70, the SM values. Model independent fits for the two fractions give F_0 = 0.66 ± 0.16 ± 0.05 and F_+ = −0.03 ± 0.06 ± 0.03.

[12] Based on 1 fb^{-1} at $\sqrt{s}$ = 1.96 TeV.

[13] Based on 370 pb^{-1} of data at $\sqrt{s}$ = 1.96 TeV, using the $\ell +$ jets and dilepton decay channels. The result assumes F_0 = 0.70, and it gives F_+ < 0.23 at 95% CL.

[14] Based on 318 pb^{-1} of data at $\sqrt{s}$ = 1.96 TeV.

[15] Based on 200 pb^{-1} of data at $\sqrt{s}$ = 1.96 TeV. $t \to Wb \to \ell\nu b$ ($\ell = e$ or μ). The errors are stat + syst.

[16] ABAZOV 05L studied the angular distribution of leptonic decays of W bosons in $t\overline{t}$ events, where one of the W's from t or $\overline{t}$ decays into e or μ and the other decays hadronically. The fraction of the "+" helicity W boson is obtained by assuming F_0 = 0.7, which is the generic prediction for any linear combination of V and A currents. Based on 230 ± 15 pb^{-1} of data at $\sqrt{s}$ = 1.96 TeV.

[17] ACOSTA 05D measures the $m^2_{\ell+b}$ distribution in $t\overline{t}$ production events where one or both W's decay leptonically to $\ell = e$ or μ, and finds a bound on the V+A coupling of the tbW vertex. By assuming the SM value of the longitudinal W fraction F_0 = B($t \to W_0 b$) = 0.70, the bound on F_+ is obtained. If the results are combined with those of AFFOLDER 00B, the bounds become F_{V+A} < 0.61 (95% CL) and F_+ < 0.18 (95 %CL), respectively. Based on 109 ± 7 pb^{-1} of data at $\sqrt{s}$ = 1.8 TeV (run I).

F_{V+A}

VALUE	CL%	DOCUMENT ID		TECN	COMMENT
< 0.29	95	[1] ABULENCIA	07G	CDF	F_{V+A} = B($t \to Wb_R$)
• • • We do not use the following data for averages, fits, limits, etc. • • •					
−0.06±0.22±0.12		[1] ABULENCIA	07G	CDF	F_{V+A} = B($t \to Wb_R$)
< 0.80	95	[2] ACOSTA	05D	CDF	F_{V+A} = B($t \to Wb_R$)

[1] Based on 700 pb^{-1} of data at $\sqrt{s}$ = 1.96 TeV.

[2] ACOSTA 05D measures the $m^2_{\ell+b}$ distribution in $t\overline{t}$ production events where one or both W's decay leptonically to $\ell = e$ or μ, and finds a bound on the V+A coupling of the tbW vertex. By assuming the SM value of the longitudinal W fraction F_0 = B($t \to W_0 b$) = 0.70, the bound on F_+ is obtained. If the results are combined with those of AFFOLDER 00B, the bounds become F_{V+A} < 0.61 (95% CL) and F_+ < 0.18 (95 %CL), respectively. Based on 109 ± 7 pb^{-1} of data at $\sqrt{s}$ = 1.8 TeV (run I).

f_1^R

VALUE	CL%	DOCUMENT ID		TECN	COMMENT
• • • We do not use the following data for averages, fits, limits, etc. • • •					
−0.11 < f_1^R < 0.16	95	[1] AAD	20Y	LHC	ATLAS+CMS combined
$\lvert f_1^R/f_2^L\rvert$ < 0.37	95	[2] AABOUD	17BB	ATLS	t-channel single top
$\lvert f_1^R\rvert$ < 0.16	95	[3] KHACHATRY...	17G	CMS	t-channel single-t prod.
−0.20 < Re($V_{tb}\ f_1^R$) < 0.23	95	[4] AAD	12BG	ATLS	Constr. on Wtb vtx
$(V_{tb}\ f_1^R)^2$ < 0.93	95	[5] ABAZOV	12E	D0	Single-top
$\lvert f_1^R\rvert^2$ < 0.30	95	[6] ABAZOV	12I	D0	single-t + W helicity
$\lvert f_1^R\rvert^2$ < 1.01	95	[7] ABAZOV	09J	D0	$\lvert f_1^L\rvert$ = 1, $\lvert f_2^L\rvert$=$\lvert f_2^R\rvert$=0
$\lvert f_1^R\rvert^2$ < 2.5	95	[8] ABAZOV	08AI	D0	$\lvert f_1^L\rvert^2 = 1.8^{+1.0}_{-1.3}$

[1] AAD 20Y based on about 20 fb^{-1} of pp data at $\sqrt{s}$ = 8 TeV for each experiment. The measurements used events with one lepton and different jet multiplicities in the final state. The measurements of F_0 and F_- are used to set the limit. The limit is obtained by assuming the other couplings to have their SM values.

[2] AABOUD 17BB based on 20.2 fb^{-1} of pp data at $\sqrt{s}$ = 8 TeV. Triple-differential decay rate of top quark is used to simultaneously determine five generalized Wtb couplings as well as the top polarization. No assumption is made for the other couplings. See this paper for constraints on other couplings not included here.

[3] KHACHATRYAN 17G based on 5.0 and 19.7 fb^{-1} of pp data at $\sqrt{s}$ = 7 and 8 TeV, respectively. A Bayesian neural network technique is used to discriminate between signal and backgrounds. This is a 95% CL exclusion limit obtained by a three-dimensional fit with simultaneous variation of (f_1^L, f_1^R, f_2^R).

[4] Based on 1.04 fb^{-1} of pp data at $\sqrt{s}$ = 7 TeV. AAD 12BG studied tt events with large $\not{E}_T$ and either $\ell + \geq 4$j or $\ell\ell + \geq 2$j.

[5] Based on 5.4 fb^{-1} of data. For each value of the form factor quoted the other two are assumed to have their SM value. Their Fig. 4 shows two-dimensional posterior probability density distributions for the anomalous couplings.

[6] Based on 5.4 fb^{-1} of data in $p\overline{p}$ collisions at 1.96 TeV. Results are obtained by combining the limits from the W helicity measurements and those from the single top quark production.

[7] Based on 1 fb^{-1} of data at $p\overline{p}$ collisions $\sqrt{s}$ = 1.96 TeV. Combined result of the W helicity measurement in $t\overline{t}$ events (ABAZOV 08B) and the search for anomalous tbW couplings in the single top production (ABAZOV 08AI). Constraints when f_1^L and one of the anomalous couplings are simultaneously allowed to vary are given in their Fig. 1 and Table 1.

[8] Result is based on 0.9 fb^{-1} of data at $\sqrt{s}$ = 1.96 TeV. Single top quark production events are used to measure the Lorentz structure of the tbW coupling. The upper bounds on the non-standard couplings are obtained when only one non-standard coupling is allowed to be present together with the SM one, $f_1^L = V^*_{tb}$.

f_2^L

VALUE	CL%	DOCUMENT ID		TECN	COMMENT
• • • We do not use the following data for averages, fits, limits, etc. • • •					
−0.08 < f_2^L < 0.05	95	[1] AAD	20Y	LHC	ATLAS+CMS combined
$\lvert f_2^L/f_1^L\rvert$ < 0.29	95	[2] AABOUD	17BB	ATLS	t-channel single top
$\lvert f_2^L\rvert$ < 0.057	95	[3] KHACHATRY...	17G	CMS	t-channel single-t prod.
−0.14 < Re(f_2^L) < 0.11	95	[4] AAD	12BG	ATLS	Constr. on Wtb vtx
$(V_{tb}\ f_2^L)^2$ < 0.13	95	[5] ABAZOV	12E	D0	Single-top
$\lvert f_2^L\rvert^2$ < 0.05	95	[6] ABAZOV	12I	D0	single-t + W helicity
$\lvert f_2^L\rvert^2$ < 0.28	95	[7] ABAZOV	09J	D0	$\lvert f_1^L\rvert$ = 1, $\lvert f_1^R\rvert$=$\lvert f_2^R\rvert$=0
$\lvert f_2^L\rvert^2$ < 0.5	95	[8] ABAZOV	08AI	D0	$\lvert f_1^L\rvert^2 = 1.4^{+0.6}_{-0.5}$

[1] AAD 20Y based on about 20 fb^{-1} of pp data at $\sqrt{s}$ = 8 TeV for each experiment. The measurements used events with one lepton and different jet multiplicities in the final state. The measurements of F_0 and F_- are used to set the limit. The limit is obtained by assuming the other couplings to have their SM values.

[2] AABOUD 17BB based on 20.2 fb^{-1} of pp data at $\sqrt{s}$ = 8 TeV. Triple-differential decay rate of top quark is used to simultaneously determine five generalized Wtb couplings as well as the top polarization. No assumption is made for the other couplings. See this paper for constraints on other couplings not included here.

[3] KHACHATRYAN 17G based on 5.0 and 19.7 fb^{-1} of pp data at $\sqrt{s}$ = 7 and 8 TeV, respectively. A Bayesian neural network technique is used to discriminate between signal and backgrounds. This is a 95% CL exclusion limit obtained by a three-dimensional fit with simultaneous variation of (f_1^L, f_2^L, f_2^R).

[4] Based on 1.04 fb^{-1} of pp data at $\sqrt{s}$ = 7 TeV. AAD 12BG studied tt events with large $\not{E}_T$ and either $\ell + \geq 4$j or $\ell\ell + \geq 2$j.

[5] Based on 5.4 fb^{-1} of data. For each value of the form factor quoted the other two are assumed to have their SM value. Their Fig. 4 shows two-dimensional posterior probability density distributions for the anomalous couplings.

[6] Based on 5.4 fb^{-1} of data in $p\overline{p}$ collisions at 1.96 TeV. Results are obtained by combining the limits from the W helicity measurements and those from the single top quark production.

[7] Based on 1 fb^{-1} of data at $p\overline{p}$ collisions $\sqrt{s}$ = 1.96 TeV. Combined result of the W helicity measurement in $t\overline{t}$ events (ABAZOV 08B) and the search for anomalous tbW couplings in the single top production (ABAZOV 08AI). Constraints when f_1^L and one of the anomalous couplings are simultaneously allowed to vary are given in their Fig. 1 and Table 1.

[8] Result is based on 0.9 fb^{-1} of data at $\sqrt{s}$ = 1.96 TeV. Single top quark production events are used to measure the Lorentz structure of the tbW coupling. The upper bounds on the non-standard couplings are obtained when only one non-standard coupling is allowed to be present together with the SM one, $f_1^L = V^*_{tb}$.

f_2^R

VALUE	CL%	DOCUMENT ID		TECN	COMMENT
• • • We do not use the following data for averages, fits, limits, etc. • • •					
−0.04 < f_2^R < 0.02	95	[1] AAD	20Y	LHC	ATLAS+CMS combined
−0.12 < Re(f_2^R/f_1^L) < 0.17	95	[2] AABOUD	17BB	ATLS	t-channel single top
−0.07 < Im(f_2^R/f_1^L) < 0.06	95	[2] AABOUD	17BB	ATLS	t-channel single top
−0.18 < Im(f_2^R) < 0.06	95	[3] AABOUD	17I	ATLS	t-channel single top
−0.049 < f_2^R < 0.048	95	[4] KHACHATRY...	17G	CMS	t-channel single top
−0.36 < Re(f_2^R/f_1^L) < 0.10	95	[5] AAD	16AK	ATLS	Single-top
−0.17 < Im(f_2^R/f_1^L) < 0.23	95	[5] AAD	16AK	ATLS	Single-top
−0.08 < Re(f_2^R) < 0.04	95	[6] AAD	12BG	ATLS	Constr. on Wtb vtx
$(V_{tb}\ f_2^R)^2$ < 0.06	95	[7] ABAZOV	12E	D0	Single-top
$\lvert f_2^R\rvert^2$ < 0.12	95	[8] ABAZOV	12I	D0	single-t + W helicity
$\lvert f_2^R\rvert^2$ < 0.23	95	[9] ABAZOV	09J	D0	$\lvert f_1^L\rvert$=1, $\lvert f_1^R\rvert$=$\lvert f_2^L\rvert$=0
$\lvert f_2^R\rvert^2$ < 0.3	95	[10] ABAZOV	08AI	D0	$\lvert f_1^L\rvert^2 = 1.4^{+0.9}_{-0.8}$

[1] AAD 20Y based on about 20 fb^{-1} of pp data at $\sqrt{s}$ = 8 TeV for each experiment. The measurements used events with one lepton and different jet multiplicities in the final state. The measurements of F_0 and F_- are used to set the limit. The limit is obtained by assuming the other couplings to have their SM values.

[2] AABOUD 17BB based on 20.2 fb^{-1} of pp data at $\sqrt{s}$ = 8 TeV. Triple-differential decay rate of top quark is used to simultaneously determine five generalized Wtb couplings as well as the top polarization. No assumption is made for the other couplings. See this paper for constraints on other couplings not included here.

Phys. A 2026.41. Downloaded from www.worldscientific.com
by UNIVERSITY OF CA ELEY on 09/16/26. Re-use and distribution is strictly not permitted, except for Open Access articles.

Int. J. Mod. Phys. A 2026.41. Downloaded from www.worldscientific.com
by UNIVERSITY OF CALIFORNIA @ BERKELEY on 09/16/26. Re-use and distribution is strictly not permitted, except for Open Access articles.

[3] AABOUD 17I based on 20.2 fb^{-1} of pp data at $\sqrt{s}$ = 8 TeV. A cut-based analysis is used to discriminate between signal and backgrounds. All anomalous couplings other than $\mathrm{Im}(f)_2^R$ are assumed to be zero. See this paper for a number of other asymmetries and measurements that are not included here.

[4] KHACHATRYAN 17G based on 5.0 and 19.7 fb^{-1} of pp data at $\sqrt{s}$ = 7 and 8 TeV, respectively. A Bayesian neural network technique is used to discriminate between signal and backgrounds. This is a 95% CL exclusion limit obtained by a three-dimensional fit with simultaneous variation of (f_1^L, f_2^L, f_2^R).

[5] AAD 16AK based on 4.6 fb^{-1} of pp data at $\sqrt{s}$ = 7 TeV. The results are obtained from an analysis of angular distributions of the decay products of single top quarks, assuming f_1^R=f_2^L=0. The fraction of decays containing transversely polarized W is measured to be $F_+ + F_- = 0.37 \pm 0.07$.

[6] Based on 1.04 fb^{-1} of pp data at $\sqrt{s}$ = 7 TeV. AAD 12BG studied tt events with large $\not{E}_T$ and either $\ell + \geq$ 4j or $\ell\ell + \geq$ 2j.

[7] Based on 5.4 fb^{-1} of data. For each value of the form factor quoted the other two are assumed to have their SM value. Their Fig. 4 shows two-dimensional posterior probability density distributions for the anomalous couplings.

[8] Based on 5.4 fb^{-1} of data in $p\overline{p}$ collisions at 1.96 TeV. Results are obtained by combining the limits from the W helicity measurements and those from the single top quark production.

[9] Based on 1 fb^{-1} of data at $p\overline{p}$ collisions $\sqrt{s}$ = 1.96 TeV. Combined result of the W helicity measurement in $t\overline{t}$ events (ABAZOV 08B) and the search for anomalous tbW couplings in the single top production (ABAZOV 08AI). Constraints when f_1^L and one of the anomalous couplings are simultaneously allowed to vary are given in their Fig. 1 and Table 1.

[10] Result is based on 0.9 fb^{-1} of data at $\sqrt{s}$ = 1.96 TeV. Single top quark production events are used to measure the Lorentz structure of the tbW coupling. The upper bounds on the non-standard couplings are obtained when only one non-standard coupling is allowed to be present together with the SM one, $f_1^L = V^*_{tb}$.

$|f_{LV} V_{tb}|$

Assumed that the top-quark-related CKM matrix elements obey the relation $|V_{td}|$, $|V_{ts}| \ll |V_{tb}|$ and a form factor f_{LV} is determined for each production mode and centre-of-mass energy.

VALUE	DOCUMENT ID		TECN	COMMENT
0.999±0.017 OUR AVERAGE				
1.015±0.031	[1] AAD	24AL	ATLS	13 TeV, t-channel single top
0.97 ±0.10	[2] AAD	24BS	ATLS	13 TeV, Wt production
$0.94\ ^{+0.11}_{-0.10}$	[3] AAD	24M	ATLS	5.02 TeV, t-channel single top
0.988±0.024	[4] SIRUNYAN	20AZ	CMS	13 TeV, t-channel single top
1.02 ±0.04 ±0.02	[5] AABOUD	19R	LHC	ATLAS + CMS at 7, 8 TeV

[1] AAD 24AL based on 140 fb^{-1} of data at $\sqrt{s}$ = 13 TeV. The value is extracted by dividing the measured value $\sigma(tq + \overline{t}q)$ = 221 ± 13 pb by the SM expectation of 214.2 ± 3.4(scale+PDF)±1.8(Δm_{top}) pb in the t-channel single-top production mode. Restricting $0 < |V_{tb}| < 1$ and setting f_{LV} = 1, a lower limit $|V_{tb}| > 0.95$ (95% CL) is obtained within the SM.

[2] AAD 24BS based on 140 fb^{-1} of data at $\sqrt{s}$ = 13 TeV. The value is extracted by comparing the measured cross section for a single top quark in association with a W boson with the SM prediction.

[3] AAD 24M based on 255 pb^{-1} of data at $\sqrt{s}$ = 5.02 TeV. The value is extracted from the cross section of the t-channel single-top production $\sigma(tq + \overline{t}q) = 27.1\ ^{+4.4}_{-4.1}\ ^{+4.4}_{-3.7}$ pb.

[4] SIRUNYAN 20AZ based on 35.9 fb^{-1} of pp data at $\sqrt{s}$ = 13 TeV. Final states enriched in single top quark t-channel events are used. Several theories beyond the standard model are considered, and by releasing all constraints among the involved parameters. Under the standard model assumption of CKM unitarity, the values are found to be $|V_{tb}| >$ 0.970 and $|V_{td}|^2 + |V_{ts}|^2 < 0.057$, both at 95% CL.

[5] The combination of single-top production cross-section measurements in the t-channel, tW, and s-channel production modes from ATLAS and CMS at $\sqrt{s}$ = 7 and 8 TeV.

$|f_{LV}\sqrt{|V_{td}|^2 + |V_{ts}|^2}|$

Assumed that the top-quark-related CKM matrix elements obey the relation $|V_{td}|$,$|V_{ts}| \ll |V_{tb}|$ and a form factor f_{LV} is determined for each production mode andcentre-of-mass energy.

VALUE	DOCUMENT ID		TECN	COMMENT
• • • We do not use the following data for averages, fits, limits, etc. • • •				
0.24±0.12	[1] SIRUNYAN	20AZ	CMS	t-channel single top

[1] We report the square root of SIRUNYAN 20AZ result based on 35.9 fb^{-1} of pp data at $\sqrt{s}$ = 13 TeV measured $|V_{td}|^2 + |V_{ts}|^2 = 0.06 \pm 0.06$ using final states enriched in single top quark t-channel events by releasing all constraints from unitarity of the CKM matrix within the SM. Under the standard model assumption of CKM unitarity,the values are found to be $|V_{tb}| > 0.970$ and $|V_{td}|^2 + |V_{ts}|^2 < 0.057$, both at 95% CL.

CP-odd EW dipole couplings

VALUE	DOCUMENT ID		TECN	COMMENT
• • • We do not use the following data for averages, fits, limits, etc. • • •				
$-2.7 < c^I_{tW} < 2.5$	[1] HAYRAPETY...	25AJ	CMS	$t\overline{t}Z$, tZq
$-0.2 < c^I_{tZ} < 2.0$	[1] HAYRAPETY...	25AJ	CMS	$t\overline{t}Z$, tZq

[1] HAYRAPETYAN 25AJ based on 173 fb^{-1} of pp data at $\sqrt{s}$ = 13 TeV and 13.6 TeV. CP-odd observables constructed using machine-learning techniques are exploited. The obtained results are consistent with the SM prediction within 2σ. The obtained limits are for the Wilson coefficients of CP-odd dimension-6 SMEFT operators.

Chromo-magnetic dipole moment μ_t=$g_s\hat{\mu}_t/m_t$

VALUE	CL%	DOCUMENT ID		TECN	COMMENT
• • • We do not use the following data for averages, fits, limits, etc. • • •					
$-0.024\ ^{+0.013}_{-0.009}\ ^{+0.016}_{-0.011}$		[1] SIRUNYAN	20AM	CMS	ℓ+jets
$-0.014 < \hat{\mu}_t < 0.004$	95	[2] SIRUNYAN	19BX	CMS	$\ell\ell + \geq$ 2j ($\geq$ 1b)
$-0.053 < \mathrm{Re}(\hat{\mu}_t) < 0.026$	95	[3] KHACHATRY...	16AI	CMS	$\ell\ell + \geq$ 2j ($\geq$ 1b)

[1] SIRUNYAN 20AM based on 35.9 fb^{-1} of pp data at $\sqrt{s}$ = 13 TeV. $t\overline{t}$ with low and high boosts are reconstructed through a fit of the kinematic distributions. The $q\overline{q}$ initial subprocess is separated using different dependencies of the distributions on the initial states, and the linearized forward-backward asymmetry is measured to be $A^{(1)}_{FB} = 0.048\ ^{+0.095}_{-0.087}\ ^{+0.020}_{-0.029}$.

[2] SIRUNYAN 19BX based on 35.9 fb^{-1} of pp data at $\sqrt{s}$ = 13 TeV. A set of parton-level normalized differential cross sections is measured to extract coefficients of the spin-dependent $t\overline{t}$ production density matrix. The coefficients are compared with the NLO MC simulations and with the NLO QCD calculation including EW corrections.

[3] KHACHATRYAN 16AI based on 19.5 fb^{-1} of pp data at $\sqrt{s}$ = 8 TeV, using lepton angular distributions as a function of the $t\overline{t}$-system kinematical variables.

Chromo-electric dipole moment $d_t = g_s\hat{d}_t/m_t$

VALUE	CL%	DOCUMENT ID		TECN	COMMENT
• • • We do not use the following data for averages, fits, limits, etc. • • •					
$\lvert\hat{d}_t\rvert < 0.015$	95	[1] TUMASYAN	23J	CMS	ℓ+jets
$-0.014 < \hat{d}_t < 0.027$	95	[2] TUMASYAN	23U	CMS	dilepton channel; $\epsilon(p_t p_{\overline{t}} p_{\ell^+} p_{\ell^-})$
$-0.019 < \hat{d}_t < 0.019$	95	[2] TUMASYAN	23U	CMS	dilepton channel; $\epsilon(p_b p_{\overline{b}} p_{\ell^+} p_{\ell^-})$
$\lvert\hat{d}_t\rvert < 0.03$	95	[3] SIRUNYAN	20AM	CMS	ℓ+jets
$-0.020 < \hat{d}_t < 0.012$	95	[4] SIRUNYAN	19BX	CMS	$\ell\ell + \geq$ 2j ($\geq$ 1b)
$-0.068 < \mathrm{Im}(\hat{d}_t) < 0.067$	95	[5] KHACHATRY...	16AI	CMS	$\ell\ell + \geq$ 2j ($\geq$ 1b)

[1] TUMASYAN 23J based on 138 fb^{-1} of pp data at $\sqrt{s}$ = 13 TeV. Four T-odd triple products of momenta of the final-state particles are measured to constrain the dimensionless chromoelectric top quark dipole moment. No evidence of CP-violating effects is found, which is consistent with the SM expectation.

[2] TUMASYAN 23U based on 35.9 fb^{-1} of pp data at $\sqrt{s}$ = 13 TeV. CP-odd Lorentz pseudo-scalar products $O_1 = \epsilon(p_t p_{\overline{t}} p_{\ell^+} p_{\ell^-})$ and $O_3 = \epsilon(p_b p_{\overline{b}} p_{\ell^+} p_{\ell^-})$ constructed from the momenta of t, $\overline{t}$, ℓ^+, ℓ^- and of b, $\overline{b}$, ℓ^+, ℓ^-, respectively, are measured and used to constrain the dimensionless chromoelectric top quark dipole moment. No evidence for CP-violating effects is found, which is consistent with the SM expectation.

[3] SIRUNYAN 20AM based on 35.9 fb^{-1} of pp data at $\sqrt{s}$ = 13 TeV. $t\overline{t}$ with low and high boosts are reconstructed through a fit of the kinematic distributions. The $q\overline{q}$ initial subprocess is separated using different dependencies of the distributions on the initial states, and the linearized forward-backward asymmetry is measured to be $A^{(1)}_{FB} = 0.048\ ^{+0.095}_{-0.087}\ ^{+0.020}_{-0.029}$.

[4] SIRUNYAN 19BX based on 35.9 fb^{-1} of pp data at $\sqrt{s}$ = 13 TeV. A set of parton-level normalized differential cross sections is measured to extract coefficients of the spin-dependent $t\overline{t}$ production density matrix and constrain the anomalous chromomagnetic and chromoelectric dipole moments of the top quark. The coefficients are compared with the NLO MC simulations and with the NLO QCD calculation including EW corrections.

[5] KHACHATRYAN 16AI based on 19.5 fb^{-1} of pp data at $\sqrt{s}$ = 8 TeV, using lepton angular distributions as a function of the $t\overline{t}$-system kinematical variables.

Spin Correlation in $t\overline{t}$ Production in $p\overline{p}$ Collisions

C is the correlation strength parameter, f is the ratio of events with correlated t and $\overline{t}$ spins (SM prediction: f = 1), and κ is the spin correlation coefficient. See "The Top Quark" review for more information.

VALUE	DOCUMENT ID		TECN	COMMENT
• • • We do not use the following data for averages, fits, limits, etc. • • •				
0.89±0.22	[1] ABAZOV	16A	D0	f ($\ell\ell + \geq$ 2 jets, $\ell + \geq$ 4 jets)
0.85±0.29	[2] ABAZOV	12B	D0	f ($\ell\ell + \geq$ 2 jets, $\ell + \geq$ 4 jets)
$1.15\ ^{+0.42}_{-0.43}$	[3] ABAZOV	12B	D0	f ($\ell + \not{E}_T + \geq$ 4 jets)
$0.60\ ^{+0.50}_{-0.16}$	[4] AALTONEN	11AR	CDF	κ ($\ell + \not{E}_T + \geq$ 4 jets)
$0.74\ ^{+0.40}_{-0.41}$	[5] ABAZOV	11AE	D0	f ($\ell\ell + \not{E}_T + \geq$ 2 jets)
0.10±0.45	[6] ABAZOV	11AF	D0	C ($\ell\ell + \not{E}_T + \geq$ 2 jets)

[1] ABAZOV 16A based on 9.7 fb^{-1} of data. A matrix element method is used. It corresponds to evidence of spin correlation at 4.2σ and is in agreement with the NLO SM prediction $0.80\ ^{+0.01}_{-0.02}$.

[2] This is a combination of the lepton + jets analysis presented in ABAZOV 12B and the dilepton measurement of ABAZOV 11AE. It provides a 3.1 σ evidence for the $t\overline{t}$ spin correlation.

[3] Based on 5.3 fb^{-1} of data. The error is statistical and systematic combined. A matrix element method is used.

[4] Based on 4.3 fb^{-1} of data. The measurement is based on the angular study of the top quark decay products in the helicity basis.The theory prediction is $\kappa \approx$ 0.40.

[5] Based on 5.4 fb^{-1} of data using a matrix element method. The error is statistical and systematic combined. The no-correlation hypothesis is excluded at the 97.7% CL.

[6] Based on 5.4 fb^{-1} of data. The error is statistical and systematic combined. The NLO QCD prediction is C = 0.78 ± 0.03. The neutrino weighting method is used for reconstruction of kinematics.

Spin Correlation in $t\overline{t}$ Production in pp Collisions

Spin correlation, f_{SM}, measures the strength of the correlation between the spins of the pair produced $t\overline{t}$. f_{SM} =1 for the SM, while f_{SM} =0 for no spin correlation.

VALUE	DOCUMENT ID		TECN	COMMENT
• • • We do not use the following data for averages, fits, limits, etc. • • •				
	[1] AAD	24CO	ATLS	tr(C) in $e^\pm\mu^\mp + \geq$ 2j ($\geq$ 1b)
	[2] HAYRAPETY...	24AS	CMS	C_{ij} in ℓ + jets mode
0.90±0.07±0.09±0.01	[3] SIRUNYAN	19BX	CMS	C_{kk} in $\ell\ell + \geq$ 2j ($\geq$ 1b)
$1.13 \pm 0.32 \pm 0.32\ ^{+0.10}_{-0.13}$	[3] SIRUNYAN	19BX	CMS	C_{rr} in $\ell\ell + \geq$ 2j ($\geq$ 1b)
1.01±0.04±0.05±0.01	[3] SIRUNYAN	19BX	CMS	C_{nn} in $\ell\ell + \geq$ 2j ($\geq$ 1b)

$0.94 \pm 0.17 \pm 0.26 \pm 0.01$	[3] SIRUNYAN	19BX	CMS	$C_{rk}+C_{kr}$ in $\ell\ell + \geq 2j$ ($\geq 1b$)
$0.98 \pm 0.03 \pm 0.04 \pm 0.01$	[3] SIRUNYAN	19BX	CMS	$(C_{kk}+C_{rr}+C_{nn})/3$ in $\ell\ell + \geq 2j$ ($\geq 1b$)
$0.74 \pm 0.07 \pm 0.19^{+0.06}_{-0.08}$	[3] SIRUNYAN	19BX	CMS	$A^{lab}_{cos\phi}$ in $\ell\ell + \geq 2j$ ($\geq 1b$)
$1.05 \pm 0.03 \pm 0.08^{+0.09}_{-0.12}$	[3] SIRUNYAN	19BX	CMS	$A_{\lvert\Delta\phi(\ell\ell)\rvert}$ in $\ell\ell + \geq 2j$ ($\geq 1b$)
$1.12^{+0.12}_{-0.15}$	[4] KHACHATRY...	16AI	CMS	$\ell\ell + \geq 2j$ ($\geq 1b$)
$0.72 \pm 0.08^{+0.15}_{-0.13}$	[5] KHACHATRY...	16X	CMS	$\mu + 4,5j$
$1.20 \pm 0.05 \pm 0.13$	[6] AAD	15J	ATLS	$\Delta\phi(\ell\ell)$ in $\ell\ell + \geq 2j$($\geq 1b$)
$1.19 \pm 0.09 \pm 0.18$	[7] AAD	14BB	ATLS	$\Delta\phi(\ell\ell)$ in $\ell\ell + \geq 2j$ events
$1.12 \pm 0.11 \pm 0.22$	[7] AAD	14BB	ATLS	$\Delta\phi(\ell j)$ in $\ell + \geq 4j$ events
$0.87 \pm 0.11 \pm 0.14$	[7,8] AAD	14BB	ATLS	S-ratio in $\ell\ell + \geq 2j$ events
$0.75 \pm 0.19 \pm 0.23$	[7,9] AAD	14BB	ATLS	$\cos\theta(\ell^+)\cos\theta(\ell^-)$ in $\ell\ell + \geq 2j$ events
$0.83 \pm 0.14 \pm 0.18$	[7,10] AAD	14BB	ATLS	$\cos\theta(\ell^+)\cos\theta(\ell^-)$ in $\ell\ell + \geq 2j$ events

[1] AAD 24CO based on 140 fb^{-1} of pp data at $\sqrt{s}$ = 13 TeV. The measured lepton distributions are consistent with SM predictions. Entanglement is observed from the measurement close to the $t\overline{t}$ threshold region, 340 GeV $< m(t\overline{t}) <$ 380 GeV, with more than 5σ significance.

[2] HAYRAPETYAN 24AS based on 138 fb^{-1} of pp data at $\sqrt{s}$ = 13 TeV. The measured polarization vector (P_i) and spin correlation matrix (C_{ij}) are consistent with SM predictions. Entanglement is observed from the measurement of $\widetilde{D} = (C_{nn} - C_{rr} - C_{kk})/3$ in the high $t\overline{t}$ mass region, $m(t\overline{t}) >$ 800 GeV and $|\cos\theta| < 0.4$, with a significance of 6.1σ.

[3] SIRUNYAN 19BX based on 35.9 fb^{-1} of pp data at $\sqrt{s}$ = 13 TeV. A set of parton-level normalized differential cross sections sensitive to coefficients of the spin-dependent $t\overline{t}$ production density matrix is measured. The distributions and coefficients are compared with the NLO MC simulations and with the NLO QCD calculation including EW corrections. Three errors are from statistics, experimental systematics, and theory.

[4] KHACHATRYAN 16AI based on 19.5 fb^{-1} of pp data at $\sqrt{s}$ = 8 TeV, using lepton angular distributions as a function of the $t\overline{t}$-system kinematical variables.

[5] KHACHATRYAN 16X based on 19.7 fb^{-1} of pp data at $\sqrt{s}$ = 8 TeV. Uses a template fit method. Spin correlation strength in the helicity basis is given by $A_{\rm hel} = 0.23 \pm 0.03^{+0.05}_{-0.04}$.

[6] AAD 15J based on 20.3 fb^{-1} of pp data at $\sqrt{s}$ = 8 TeV. Uses a fit including a linear superposition of $\Delta\phi$ distribution from the SM NLO simulation with coefficient f_{SM} and from $t\overline{t}$ simulation without spin correlation with coefficient $(1 - f_{SM})$.

[7] Based on 4.6 fb^{-1} of pp data at $\sqrt{s}$ =7 TeV. The results are for m_t = 172.5 GeV.

[8] The S-ratio is defined as the SM spin correlation in the like-helicity gluon-gluon collisions normalized to the no spin correlation case; see eq.(6) for the LO expression.

[9] The polar angle correlation along the helicity axis.

[10] The polar angle correlation along the direction which maximizes the correlation.

t-quark FCNC Couplings κ^{utg}/Λ and κ^{ctg}/Λ

VALUE (TeV^{-1})	CL%	DOCUMENT ID		TECN	COMMENT
• • • We do not use the following data for averages, fits, limits, etc. • • •					
		[1] AAD	22T	ATLS	$ug \to t$, $cg \to t$
<0.0041	95	[2] KHACHATRY...	17G	CMS	$\lvert\kappa^{tug}\rvert/\Lambda$
<0.018	95	[2] KHACHATRY...	17G	CMS	$\lvert\kappa^{tcg}\rvert/\Lambda$
<0.010	95	[3] AAD	16AS	ATLS	κ^{tug}/Λ
<0.023	95	[3] AAD	16AS	ATLS	κ^{tcg}/Λ
<0.0069	95	[4] AAD	12BP	ATLS	t^{tug}/Λ ($t^{tcg} = 0$)
<0.016	95	[4] AAD	12BP	ATLS	t^{tcg}/Λ ($t^{tug} = 0$)
<0.013	95	[5] ABAZOV	10K	D0	κ^{tug}/Λ
<0.057	95	[5] ABAZOV	10K	D0	κ^{tcg}/Λ
<0.018	95	[6] AALTONEN	09N	CDF	κ^{tug}/Λ ($\kappa^{tcg} = 0$)
<0.069	95	[6] AALTONEN	09N	CDF	κ^{tcg}/Λ ($\kappa^{tug} = 0$)
<0.037	95	[7] ABAZOV	07V	D0	κ^{utg}/Λ
<0.15	95	[7] ABAZOV	07V	D0	κ^{ctg}/Λ

[1] AAD 22T based on 139 fb^{-1} of pp data at $\sqrt{s}$ = 13 TeV. The results are obtained from the 95% CL upper limits on the single top-quark productions $\sigma(ug \to t)\cdot B(t \to bW)\cdot B(W \to \ell\nu) <$ 3.0 pb and $\sigma(cg \to t)\cdot B(t \to bW)\cdot B(W \to \ell\nu) <$ 4.7 pb. These are interpreted as limits on couplings in an EFT $|C^{ut}_{uG}|/\Lambda^2 <$ 0.057 TeV^{-2} and $|C^{ct}_{uG}|/\Lambda^2 <$ 0.14 TeV^{-2}. The results also correspond to $B(t \to ug) < 6.1 \times 10^{-5}$ and $B(t \to cg) < 3.7 \times 10^{-4}$.

[2] KHACHATRYAN 17G based on 5.0 and 19.7 fb^{-1} of pp data at $\sqrt{s}$ = 7 and 8 TeV, respectively. t-channel single top production is used. The result corresponds to $B(t \to ug) < 2.0 \times 10^{-5}$ or $B(t \to cg) < 4.1 \times 10^{-4}$.

[3] AAD 16AS based on 20.3 fb^{-1} of pp data at $\sqrt{s}$ = 8 TeV. The results are obtained from the 95% CL upper limit on the single top-quark production $\sigma(qg \to t)\cdot B(t \to bW)B(W \to l\nu) <$ 2.9 pb, $B(t \to ug) < 4.0 \times 10^{-5}$ and $B(t \to cg) < 20 \times 10^{-5}$.

[4] Based on 2.05 fb^{-1} of pp data at $\sqrt{s}$ = 7 TeV. The results are obtained from the 95% CL upper limit on the single top-quark production $\sigma(qg \to t)\cdot B(t \to bW) <$ 3.9 pb, for q=u or q=c, $B(t \to ug) < 5.7 \times 10^{-5}$ and $B(t \to ug) < 2.7 \times 10^{-4}$.

[5] Based on 2.3 fb^{-1} of data in $p\overline{p}$ collisions at $\sqrt{s}$ = 1.96 TeV. Upper limit of single top quark production cross section 0.20 pb and 0.27 pb via FCNC t-u-g and t-c-g couplings, respectively, lead to the bounds without assuming the absence of the other coupling. $B(t \to u + g) < 2.0 \times 10^{-4}$ and $B(t \to c + g) < 3.9 \times 10^{-3}$ follow.

[6] Based on 2.2 fb^{-1} of data in $p\overline{p}$ collisions at $\sqrt{s}$ = 1.96 TeV. Upper limit of single top quark production cross section $\sigma(u(c) + g \to t) <$ 1.8 pb (95% CL) via FCNC t-u-g and t-c-g couplings lead to the bounds. $B(t \to u + g) < 3.9 \times 10^{-4}$ and $B(t \to c + g) < 5.7 \times 10^{-3}$ follow.

[7] Result is based on 230 pb^{-1} of data at $\sqrt{s}$ = 1.96 TeV. Absence of single top quark production events via FCNC t-u-g and t-c-g couplings lead to the upper bounds on the dimensionised couplings, κ^{utg}/Λ and κ^{ctg}/Λ, respectively.

Mixing Angle of CP-even and CP-odd t-Quark Yukawa Couplings

VALUE (°)	DOCUMENT ID		TECN	COMMENT
11^{+52}_{-73}	[1] AAD	24J	ATLS	$t\overline{t}H$, tH ($H \to bb$)

[1] AAD 24J based on 139 fb^{-1} of data at $\sqrt{s}$ = 13 TeV. Events containing one or two leptons (e, μ) are used. The SM branching ratio for the Higgs boson decay into bb is assumed. The result is consistent with the SM prediction of no CP-odd coupling, α = 0.

t-Quark Yukawa Coupling from $t\overline{t}$ Kinematic Distributions in pp Collisions

The ratio of t-quark Yukawa coupling to its standard model predicted value.

VALUE	DOCUMENT ID		TECN	COMMENT
• • • We do not use the following data for averages, fits, limits, etc. • • •				
$1.16^{+0.24}_{-0.35}$	[1] SIRUNYAN	20BH	CMS	$\ell\ell$ (ℓ=e,μ) + jets ($\geq 2b$j) + $\not{E}_T$
$1.07^{+0.34}_{-0.43}$	[2] SIRUNYAN	19BY	CMS	ℓ+jets, $t\overline{t}$ threshold

[1] SIRUNYAN 20BH based on 137 fb^{-1} of data at $\sqrt{s}$ = 13 TeV. Kinematic distributions of $t\overline{t}$ are compared with predictions by different values of the top Yukawa coupling in loop corrections, where the scaling of the SM coupling is used within the κ-framework. The $\not{E}_T$ cut applies only to the same-flavor dilepton, not $e\mu$ events.

[2] SIRUNYAN 19BY based on 35.8 fb^{-1} of data at $\sqrt{s}$ = 13 TeV. Experimental sensitivity is enhanced in the low $M_{t\overline{t}}$ region. The distributions of $M_{t\overline{t}}$, $|y_t - y_{\overline{t}}|$, and the number of reconstructed jets are compared with predictions by different Yukawa couplings which include NNLO QCD and NLO EW corrections.

$\sigma(Ht\overline{t})$ /$\sigma(Ht\overline{t})_{SM}$

VALUE	CL%	DOCUMENT ID		TECN	COMMENT
• • • We do not use the following data for averages, fits, limits, etc. • • •					
$0.33 \pm 0.17 \pm 0.21$		[1] HAYRAPETY...	25R	CMS	$Ht\overline{t}$ ($H \to b\overline{b}$)
$1.43^{+0.33}_{-0.31}{}^{+0.21}_{-0.15}$		[2] AAD	20Z	ATLS	$Ht\overline{t}$ ($H \to \gamma\gamma$)
$1.38^{+0.29}_{-0.27}{}^{+0.21}_{-0.11}$		[3] SIRUNYAN	20AS	CMS	$Ht\overline{t}$ ($H \to \gamma\gamma$)
$0.72 \pm 0.24 \pm 0.38$		[4] SIRUNYAN	19R	CMS	$Ht\overline{t}$ ($H \to b\overline{b}$, $t\overline{t} \to \ell$+jets or dilepton)
$0.9 \pm 0.7 \pm 1.3$		[5] SIRUNYAN	18BD	CMS	$Ht\overline{t}$ ($H \to b\overline{b}$, $t\overline{t} \to$ all jets)
$1.26^{+0.31}_{-0.26}$		[6] SIRUNYAN	18L	CMS	combination of CMS
<6.7	95	[7] AAD	15	ATLS	$Ht\overline{t}$; $H \to \gamma\gamma$
2.8 ± 1.0		[8] KHACHATRY...	14H	CMS	$H \to b\overline{b}$, $\tau_h\tau_h$, $\gamma\gamma$, WW/ZZ(leptons)

[1] HAYRAPETYAN 25R based on 138 fb^{-1} of data at 13 TeV. An upper limit (95% CL) is set on the tH production rate of 14.6 times the SM prediction. Constraints on the strength and structure of the tH coupling are obtained.

[2] AAD 20Z based on 139 fb^{-1} of pp data at 13 TeV. Assuming a CP-even coupling the $t\overline{t}H$ process is observed with a significance of 5.2 σ, and the measured $\sigma_{t\overline{t}H} \cdot B_{\gamma\gamma} = 1.64^{+0.38}_{-0.36}{}^{+0.17}_{-0.14}$ fb. A CP-mixing angle $|\alpha| > 43°$ is excluded at 95% CL.

[3] SIRUNYAN 20AS based on 137 fb^{-1} of pp data at 13 TeV. The $t\overline{t}H$ process is observed with a significance of 6.6 σ, and the measured $\sigma_{t\overline{t}H} \cdot B_{\gamma\gamma} = 1.56^{+0.33}_{-0.30}{}^{+0.09}_{-0.08}$ fb. The fractional contribution of the CP-odd component is measured to be $f^{t\overline{t}H}_{CP} = 0.00 \pm 0.33$.

[4] SIRUNYAN 19R based on 35.9 fb^{-1} of pp data at 13 TeV. Multivariate techniques are employed to separate the signal from the dominant $t\overline{t}$+jets background. The result is for m_H = 125 GeV. The measured ratio corresponds to a signal significance of 1.6σ above the background-only hypothesis.

[5] SIRUNYAN 18BD based on 35.9 fb^{-1} of pp data at 13 TeV. A combined fit of signal and background templates to data is performed in six event categories separated by jet and b-jet multiplicities. An upper limit of 3.8 is obtained for the cross section ratio.

[6] SIRUNYAN 18L based on up to 5.1, 19.7, and 35.9 fb^{-1} of pp data at 7, 8, and 13 TeV, respectively. An excess of events is observed, with a significance of 5.2 standard deviations, over the expectation from the background-only hypothesis. The result is for the Higgs boson mass of 125.09 GeV.

[7] Based on 4.5 fb^{-1} of data at 7 TeV and 20.3 fb^{-1} at 8 TeV. The result is for m_H = 125.4 GeV. The measurement constrains the top quark Yukawa coupling strength parameter $\kappa_t = Y_t/Y_t^{SM}$ to be $-1.3 < \kappa_t < 8.0$ (95% CL).

[8] Based on 5.1 fb^{-1} of pp data at 7 TeV and 19.7 fb^{-1} at 8 TeV. The results are obtained by assuming the SM decay branching fractions for the Higgs boson of mass 125.6 GeV. The signal strength for individual Higgs decay channels are given in Fig. 13, and the preferred region in the (κ_V, κ_f) space is given in Fig. 14.

Single t-Quark Production Cross Section in $p\overline{p}$ Collisions at $\sqrt{s}$ = 1.8 TeV

Direct probe of the tbW coupling and possible new physics at $\sqrt{s}$ = 1.8 TeV.

VALUE (pb)	CL%	DOCUMENT ID		TECN	COMMENT
• • • We do not use the following data for averages, fits, limits, etc. • • •					
<24	95	[1] ACOSTA	04H	CDF	$p\overline{p} \to tb + X$, $tqb + X$
<18	95	[2] ACOSTA	02	CDF	$p\overline{p} \to tb + X$
<13	95	[3] ACOSTA	02	CDF	$p\overline{p} \to tqb + X$

[1] ACOSTA 04H bounds single top-quark production from the s-channel W-exchange process, $q'\overline{q} \to t\overline{b}$, and the t-channel W-exchange process, $q'g \to qt\overline{b}$. Based on $\sim$106 pb^{-1} of data.

[2] ACOSTA 02 bounds the cross section for single top-quark production via the s-channel W-exchange process, $q'\overline{q} \to t\overline{b}$. Based on $\sim$106 pb^{-1} of data.

[3] ACOSTA 02 bounds the cross section for single top-quark production via the t-channel W-exchange process, $q'g \to qt\overline{b}$. Based on $\sim$106 pb^{-1} of data.

Phys. A 2026.41. Downloaded from www.worldscientific.com
by UNIVERSITY OF CA ELEY on 09/16/26. Re-use and distribution is strictly not permitted, except for Open Access articles.

Int. J. Mod. Phys. A 2026.41. Downloaded from www.worldscientific.com
by UNIVERSITY OF CALIFORNIA @ BERKELEY on 09/16/26. Re-use and distribution is strictly not permitted, except for Open Access articles.

Single t-Quark Production Cross Section in $p\overline{p}$ Collisions at $\sqrt{s}$ = 1.96 TeV

Direct probes of the tbW coupling and possible new physics at $\sqrt{s}$ = 1.96 TeV.
OUR AVERAGE assumes that the systematic uncertainties are uncorrelated.

VALUE (pb)	CL%	DOCUMENT ID		TECN	COMMENT
• • • We do not use the following data for averages, fits, limits, etc. • • •					
$3.53^{+1.25}_{-1.16}$		[1] AALTONEN	16	CDF	s- + t-channels ($0\ell+\not{E}_T$ + 2,3j ($\geq 1b$-tag))
$2.25^{+0.29}_{-0.31}$		[2] AALTONEN	15H	TEVA	t-channel
$3.30^{+0.52}_{-0.40}$		[2,3] AALTONEN	15H	TEVA	s- + t-channels
$1.12^{+0.61}_{-0.57}$		[4] AALTONEN	14K	CDF	s-channel ($0\ell+\not{E}_T$+2,3j ($\geq 1b$-tag))
$1.41^{+0.44}_{-0.42}$		[5] AALTONEN	14L	CDF	s-channel ($\ell+\not{E}_T$+2j ($\geq 1b$-tag))
$1.29^{+0.26}_{-0.24}$		[6] AALTONEN	14M	TEVA	s-channel (CDF + D0)
$3.04^{+0.57}_{-0.53}$		[7] AALTONEN	14O	CDF	$s + t + Wt$ ($\ell + \not{E}_T$ + 2 or 3 jets ($\geq 1b$-tag))
$1.10^{+0.33}_{-0.31}$		[8] ABAZOV	13O	D0	s-channel
$3.07^{+0.54}_{-0.49}$		[8] ABAZOV	13O	D0	t-channel
$4.11^{+0.60}_{-0.55}$		[8] ABAZOV	13O	D0	s- + t-channels
0.98 ± 0.63		[9] ABAZOV	11AA	D0	s-channel
2.90 ± 0.59		[9] ABAZOV	11AA	D0	t-channel
$3.43^{+0.73}_{-0.74}$		[10] ABAZOV	11AD	D0	s- + t-channels
$1.8\ ^{+0.7}_{-0.5}$		[11] AALTONEN	10AB	CDF	s-channel
$0.8\ \pm0.4$		[11] AALTONEN	10AB	CDF	t-channel
$4.9\ ^{+2.5}_{-2.2}$		[12] AALTONEN	10U	CDF	$\not{E}_T$ + jets decay
$3.14^{+0.94}_{-0.80}$		[13] ABAZOV	10	D0	t-channel
1.05 ± 0.81		[13] ABAZOV	10	D0	s-channel
< 7.3	95	[14] ABAZOV	10J	D0	τ + jets decay
$2.3\ ^{+0.6}_{-0.5}$		[15] AALTONEN	09AT	CDF	s- + t-channel
3.94 ± 0.88		[16] ABAZOV	09Z	D0	s- + t-channel
$2.2\ ^{+0.7}_{-0.6}$		[17] AALTONEN	08AH	CDF	s- + t-channel
$4.7\ \pm1.3$		[18] ABAZOV	08I	D0	s- + t-channel
$4.9\ \pm1.4$		[19] ABAZOV	07H	D0	s- + t-channel
< 6.4	95	[20] ABAZOV	05P	D0	$p\overline{p} \to tb + X$
< 5.0	95	[20] ABAZOV	05P	D0	$p\overline{p} \to tqb + X$
<10.1	95	[21] ACOSTA	05N	CDF	$p\overline{p} \to tqb + X$
<13.6	95	[21] ACOSTA	05N	CDF	$p\overline{p} \to tb + X$
<17.8	95	[21] ACOSTA	05N	CDF	$p\overline{p} \to tb + X$, $tqb + X$

[1] AALTONEN 16 based on 9.5 fb^{-1} of data. This includes, as a part, the result of AALTONEN 14K. Combination of this result with that of AALTONEN 14O gives a $s + t$ cross section of $3.02^{+0.49}_{-0.48}$ pb and $|V_{tb}| > 0.84$ (95% CL).

[2] AALTONEN 15H based on 9.7 fb^{-1} of data per experiment. The result is for m_t = 172.5 GeV, and is a combination of the CDF measurements (AALTONEN 16) and the D0 measurements (ABAZOV 13O) on the t-channel single t-quark production cross section. The result is consistent with the NLO+NNLL SM prediction and gives $|V_{tb}| = 1.02^{+0.06}_{-0.05}$ and $|V_{tb}| > 0.92$ (95% CL).

[3] AALTONEN 15H is a combined measurement of s-channel single top cross section by CDF + D0. AALTONEN 14M is not included.

[4] Based on 9.45 fb^{-1} of data, using neural networks to separate signal from backgrounds. The result is for m_t = 172.5 GeV. Combination of this result with the CDF measurement in the 1 lepton channel AALTONEN 14L gives $1.36^{+0.37}_{-0.32}$ pb, consistent with the SM prediction, and is 4.2 sigma away from the background only hypothesis.

[5] Based on 9.4 fb^{-1} of data, using neural networks to separate signal from backgrounds. The result is for m_t = 172.5 GeV. The result is 3.8 sigma away from the background only hypothesis.

[6] Based on 9.7 fb^{-1} of data per experiment. The result is for m_t = 172.5 GeV, and is a combination of the CDF measurements AALTONEN 14L, AALTONEN 14K and the D0 measurement ABAZOV 13O on the s-channel single t-quark production cross section. The result is consistent with the SM prediction of 1.05 ± 0.06 pb and the significance of the observation is of 6.3 standard deviations.

[7] Based on 7.5 fb^{-1} of data. Neural network is used to discriminate signals (s-, t- and Wt-channel single top production) from backgrounds. The result is consistent with the SM prediction, and gives $|V_{tb}| = 0.95 \pm 0.09(\text{stat + syst}) \pm 0.05(\text{theory})$ and $|V_{tb}| > 0.78$ (95% CL). The result is for m_t = 172.5 GeV.

[8] Based on 9.7 fb^{-1} of data. Events with $\ell + \not{E}_T$ + 2 or 3 jets (1 or 2 b-tag) are analysed, assuming m_t = 172.5 GeV. The combined s- + t-channel cross section gives $|V_{tb}\ f_1^L| = 1.12^{+0.09}_{-0.08}$, or $|V_{tb}| > 0.92$ at 95% CL for $f_1^L = 1$ and a flat prior within $0 \leq |V_{tb}|^2 \leq 1$.

[9] Based on 5.4 fb^{-1} of data. The error is statistical + systematic combined. The results are for m_t = 172.5 GeV. Results for other m_t values are given in Table 2 of ABAZOV 11AA.

[10] Based on 5.4 fb^{-1} of data and for m_t = 172.5 GeV. The error is statistical + systematic combined. Results for other m_t values are given in Table III of ABAZOV 11AD. The result is obtained by assuming the SM ratio between tb (s-channel) and tqb (t-channel) productions, and gives $|V_{tb}\ f_1^L| = 1.02^{+0.10}_{-0.11}$, or $|V_{tb}| > 0.79$ at 95% CL for a flat prior within $0 < |V_{tb}|^2 < 1$.

[11] Based on 3.2 fb^{-1} of data. For combined s- + t-channel result see AALTONEN 09AT.

[12] Result is based on 2.1 fb^{-1} of data. Events with large missing E_T and jets with at least one b-jet without identified electron or muon are selected. Result is obtained when observed 2.1 σ excess over the background originates from the signal for m_t = 175 GeV, giving $|V_{tb}| = 1.24^{+0.34}_{-0.29} \pm 0.07$(theory).

[13] Result is based on 2.3 fb^{-1} of data. Events with isolated $\ell + \not{E}_T$ + 2 ,3, 4 jets with one or two b-tags are selected. The analysis assumes m_t = 170 GeV.

[14] Result is based on 4.8 fb^{-1} of data. Events with an isolated reconstructed tau lepton, missing E_T + 2, 3 jets with one or two b-tags are selected. When combined with ABAZOV 09Z result for $e + \mu$ channels, the s- and t-channels combined cross section is $3.84^{+0.89}_{-0.83}$ pb.

[15] Based on 3.2 fb^{-1} of data. Events with isolated $\ell + \not{E}_T$ + jets with at least one b-tag are analyzed and s- and t-channel single top events are selected by using the likelihood function, matrix element, neural-network, boosted decision tree, likelihood function optimized for s-channel process, and neural-networked based analysis of events with $\not{E}_T$ that has sensitivity for $W \to \tau\nu$ decays. The result is for m_t = 175 GeV, and the mean value decreases by 0.02 pb/GeV for smaller m_t. The signal has 5.0 sigma significance. The result gives $|V_{tb}| = 0.91 \pm 0.11$ (stat+syst) ± 0.07 (theory), or $|V_{tb}| > 0.71$ at 95% CL.

[16] Based on 2.3 fb^{-1} of data. Events with isolated $\ell + \not{E}_T + \geq 2$ jets with 1 or 2 b-tags are analyzed and s- and t-channel single top events are selected by using boosted decision tree, Bayesian neural networks and the matrix element method. The signal has 5.0 sigma significance. The result gives $|V_{tb}| = 1.07 \pm 0.12$, or $|V_{tb}| > 0.78$ at 95% CL. The analysis assumes m_t = 170 GeV.

[17] Result is based on 2.2 fb^{-1} of data. Events with isolated $\ell + \not{E}_T$ + 2, 3 jets with at least one b-tag are selected, and s- and t-channel single top events are selected by using likelihood, matrix element, and neural network discriminants. The result can be interpreted as $|V_{tb}| = 0.88^{+0.13}_{-0.12}$(stat + syst) ± 0.07(theory), and $|V_{tb}| > 0.66$ (95% CL) under the $|V_{tb}| < 1$ constraint.

[18] Result is based on 0.9 fb^{-1} of data. Events with isolated $\ell + \not{E}_T$ + 2, 3, 4 jets with one or two b-vertex-tag are selected, and contributions from W + jets, $t\overline{t}$, s- and t-channel single top events are identified by using boosted decision trees, Bayesian neural networks, and matrix element analysis. The result can be interpreted as the measurement of the CKM matrix element $|V_{tb}| = 1.31^{+0.25}_{-0.21}$, or $|V_{tb}| > 0.68$ (95% CL) under the $|V_{tb}| < 1$ constraint.

[19] Result is based on 0.9 fb^{-1} of data. This result constrains V_{tb} to $0.68 < |V_{tb}| \leq 1$ at 95% CL.

[20] ABAZOV 05P bounds single top-quark production from either the s-channel W-exchange process, $q'\overline{q} \to t\overline{b}$, or the t-channel W-exchange process, $q'g \to qt\overline{b}$, based on $\sim$ 230 pb^{-1} of data.

[21] ACOSTA 05N bounds single top-quark production from the t-channel W-exchange process ($q'g \to qt\overline{b}$), the s-channel W-exchange process ($q'\overline{q} \to t\overline{b}$), and from the combined cross section of t- and s-channel. Based on $\sim$ 162 pb^{-1} of data.

Production Cross Section in pp Collisions at $\sqrt{s}$ = 5.02 TeV

VALUE (pb)	DOCUMENT ID		TECN	COMMENT
• • • We do not use the following data for averages, fits, limits, etc. • • •				
$19.8^{+3.9}_{-3.1}{}^{+2.9}_{-2.2}$	[1] AAD	24M	ATLS	$\sigma(tq)$, $\ell+\not{E}_T$+2 j (1b, 1 forward j)
$7.3^{+3.2}_{-2.1}{}^{+2.8}_{-1.5}$	[1] AAD	24M	ATLS	$\sigma(\overline{t}q)$, $\ell+\not{E}_T$+2 j (1b, 1 forward j)

[1] AAD 24M based on 255 pb^{-1} of data. The sum and ratio of the cross sections are measured to be $\sigma(tq + \overline{t}q)$=$27.1^{+4.4}_{-4.1}{}^{+4.4}_{-3.7}$ pb and $\sigma(tq)/\sigma(\overline{t}q) = 2.73^{+1.43}_{-0.82}{}^{+1.01}_{-0.29}$, respectively. All results are in agreement with the SM.

t-channel Single t Production Cross Section in pp Collisions at $\sqrt{s}$ = 7 TeV

Direct probe of the tbW coupling and possible new physics at $\sqrt{s}$ = 7 TeV.

VALUE (pb)	DOCUMENT ID		TECN	COMMENT
• • • We do not use the following data for averages, fits, limits, etc. • • •				
$67.5\pm\ 5.7$	[1] AABOUD	19R	LHC	combination of ATLAS+CMS
$68\ \pm\ 2\ \pm\ 8$	[2] AAD	14BI	ATLS	$\ell + \not{E}_T$ + 2j or 3j
$83\ \pm\ 4\ ^{+20}_{-19}$	[3] AAD	12CH	ATLS	t-channel $\ell+\not{E}_T$+ (2,3)j (1b)
$67.2\pm\ 6.1$	[4] CHATRCHYAN	12BQ	CMS	t-channel $\ell + \not{E}_T$+ $\geq$ 2j (1b)
$83.6\pm29.8\pm\ 3.3$	[5] CHATRCHYAN	11R	CMS	t-channel

[1] AABOUD 19R based on 1.17 to 5.1 fb^{-1} of data from ATLAS and CMS at 7 TeV.

[2] Based on 4.59 fb^{-1} of data, using neural networks for signal and background separation. $\sigma(tq) = 46 \pm 1 \pm 6$ pb and $\sigma(\overline{t}q) = 23 \pm 1 \pm 3$ pb are separately measured, as well as their ratio $R = \sigma(tq)/\sigma(\overline{t}q) = 2.04 \pm 0.13 \pm 0.12$. The results are for m_t = 172.5 GeV, and those for other m_t values are given by eq.(4) and Table IV. The measurements give $|V_{tb}| = 1.02 \pm 0.07$ or $|V_{tb}| > 0.88$ (95% CL).

[3] Based on 1.04 fb^{-1} of data. The result gives $|V_{tb}| = 1.13^{+0.14}_{-0.13}$ from the ratio σ(exp)/σ(th), where σ(th) is the SM prediction for $|V_{tb}| = 1$. The 95% CL lower bound of $|V_{tb}| > 0.75$ is found if $|V_{tb}| < 1$ is assumed. $\sigma(t) = 59^{+18}_{-16}$ pb and $\sigma(\overline{t}) = 33^{+13}_{-12}$ pb are found for the separate single t and $\overline{t}$ production cross sections, respectively. The results assume m_t = 172.5 GeV for the acceptance.

[4] Based on 1.17 fb^{-1} of data for $\ell = \mu$, 1.56 fb^{-1} of data for $\ell = e$ at 7 TeV collected during 2011. The result gives $|V_{tb}| = 1.020 \pm 0.046$(meas) ± 0.017(th). The 95% CL lower bound of $|V_{tb}| > 0.92$ is found if $|V_{tb}| < 1$ is assumed. The results assume m_t = 172.5 GeV for the acceptance.

[5] Based on 36 pb^{-1} of data. The first error is statistical + systematic combined, the second is luminosity. The result gives $|V_{tb}| = 1.114 \pm 0.22$(exp) ± 0.02(th) from the ratio σ(exp)/σ(th), where σ(th) is the SM prediction for $|V_{tb}| = 1$. The 95% CL lower bound of $|V_{tb}| > 0.62$ (0.68) is found from the 2D (BDT) analysis under the constraint $0 < |V_{tb}|^2 < 1$.

by UNIVERSITY OF CALIFORNIA SANTA BARBARA on 09/16/26. Re-use and distribution is strictly not permitted, except for Open Access articles.
Phys. A 2026.41. Downloaded from www.worldscientific.com

t-channel Single t Production Cross Section in pp Collisions at $\sqrt{s}$ = 8 TeV

VALUE (pb)	DOCUMENT ID		TECN	COMMENT
• • • We do not use the following data for averages, fits, limits, etc. • • •				
87.7±5.8	[1] AABOUD	19R	LHC	combination of ATLAS+CMS
$89.6^{+7.1}_{-6.3}$	[2] AABOUD	17T	ATLS	$\ell+\not{E}_T+2$ j (1b j)
83.6±2.3±7.4	[3] KHACHATRY...	14F	CMS	$\ell+\not{E}_T+\geq 2$ j (1,2 b, 1 forward j)

[1] AABOUD 19R based on 12.2 to 20.3 fb^{-1} of data from ATLAS and CMS at 8 TeV.
[2] AABOUD 17T based on 20.2 fb^{-1} of data. A maximum-likelihood fit to neural-network discriminant distributions is used to separate signal and background events. Individual cross sections are measured as $\sigma(tq) = 56.7^{+4.3}_{-3.8}$ pb and $\sigma(\overline{t}q) = 32.9^{+3.0}_{-2.7}$ pb, while their ratio is given by $\sigma(tq)/\sigma(\overline{t}q) = 1.72 \pm 0.09$. A lower limit $|V_{tb}| > 0.92$ (95% CL) is obtained. Measured total and differential cross sections are described well by the SM.
[3] Based on 19.7 fb^{-1} of data. The t and $\overline{t}$ production cross sections are measured separately as $\sigma_{t-ch.}(t) = 53.8 \pm 1.5 \pm 4.4$ pb and $\sigma_{t-ch.}(\overline{t}) = 27.6 \pm 1.3 \pm 3.7$ pb, respectively, as well as their ratio $R_{t-ch} = \sigma_{t-ch.}(t)/\sigma_{t-ch.}(\overline{t}) = 1.95 \pm 0.10 \pm 0.19$, in agreement with the SM predictions. Combination with a previous CMS result at $\sqrt{s}$ = 7 TeV [CHATRCHYAN 12BQ] gives $|V_{tb}| = 0.998 \pm 0.038 \pm 0.016$. Also obtained is the ratio $R_{8/7} = \sigma_{t-ch.}(8\text{TeV})/\sigma_{t-ch.}(7\text{TeV}) = 1.24 \pm 0.08 \pm 0.12$.

s-channel Single t Production Cross Section in pp Collisions at $\sqrt{s}$ = 8 TeV

VALUE (pb)	DOCUMENT ID		TECN	COMMENT
• • • We do not use the following data for averages, fits, limits, etc. • • •				
4.9±1.4	[1] AABOUD	19R	LHC	ATLAS + CMS
$4.8\pm0.8^{+1.6}_{-1.3}$	[2] AAD	16U	ATLS	$\ell + \not{E}_T + 2b$
13.4±7.3	[3] KHACHATRY...	16AZ	CMS	$\ell + \not{E}_T + 2b$
5.0±4.3	[4] AAD	15A	ATLS	$\ell + \not{E}_T + 2b$

[1] AABOUD 19R based on 12.2 to 20.3 fb^{-1} of data from ATLAS and CMS at 8 TeV.
[2] AAD 16U based on 20.3 fb^{-1} of data, using a maximum-likelihood fit of a matrix element method discriminant. The same data set as in AAD 15A is used. The result corresponds to an observed significance of 3.2σ.
[3] KHACHATRYAN 16AZ based on 19.7 fb^{-1} of data, using a multivariate analysis to separate signal and backgrounds. The same method is applied to 5.1 fb^{-1} of data at $\sqrt{s}$ = 7 TeV, giving 7.1 ± 8.1 pb. Combining both measurements, the observed significance is 2.5σ. A best fit value of 2.0 ± 0.9 is obtained for the combined ratio of the measured values and SM expectations.
[4] AAD 15A based on 20.3 fb^{-1} of data, using a multivariate analysis to separate signal and backgrounds. The 95% CL upper bound of the cross section is 14.6 pb. The results are consistent with the SM prediction of 5.61 ± 0.22 pb at approximate NNLO.

t-channel Single t Production Cross Section in pp Collisions at $\sqrt{s}$ = 13 TeV

VALUE (pb)	DOCUMENT ID		TECN	COMMENT
• • • We do not use the following data for averages, fits, limits, etc. • • •				
137± 8	[1] AAD	24AL	ATLS	$\sigma(tq)$, $\ell+\not{E}_T+2$ j (1b, 1 forward j)
84^{+6}_{-5}	[1] AAD	24AL	ATLS	$\sigma(\overline{t}q)$, $\ell+\not{E}_T+2$ j (1b, 1 forward j)
130± 1±19	[2] SIRUNYAN	20D	CMS	$\sigma(tq)$, $\ell+\not{E}_T+\geq 2$ j
77± 1±12	[2] SIRUNYAN	20D	CMS	$\sigma(\overline{t}q)$, $\ell+\not{E}_T+\geq 2$ j
156± 5±27± 3	[3,4] AABOUD	17H	ATLS	$\sigma(tq)$, $\ell+\not{E}_T+2$ j (1b, 1 forward j)
91± 4±18± 2	[3,4] AABOUD	17H	ATLS	$\sigma(\overline{t}q)$, $\ell+\not{E}_T+2$ j (1b, 1 forward j)
154± 8± 9±19±4	[5] SIRUNYAN	17AA	CMS	$\sigma(tq)$, $\mu+\geq 2$ j (1b)
85±10± 4±11±2	[5] SIRUNYAN	17AA	CMS	$\sigma(\overline{t}q)$, $\mu+\geq 2$ j (1b)

[1] AAD 24AL based on 140 fb^{-1} of data. The cross section ratio is measured to be $\sigma(tq)/\sigma(\overline{t}q) = 1.636 \pm 0.036 \pm 0.034$. A lower limit $|V_{tb}| > 0.95$ (95% CL) is obtained. All results are in agreement with the SM. The measurements are used to constrain a four-quark operator and a Higgs-quark operator in SMEFT.
[2] SIRUNYAN 20D based on 35.9 fb^{-1} of data. Different categories of jet and b jet multiplicity and multivariate discriminators are used to separate signal and background events. The cross section ratio is measured to be $\sigma(tq)/\sigma(\overline{t}q) = 1.68 \pm 0.02 \pm 0.05$. CKM matrix element is obtained as $|f_{LV} V_{tb}| = 0.98 \pm 0.07(\text{exp}) \pm 0.02(\text{theo})$ where f_{LV} is an anomalous form factor. All results are in agreement with the SM.
[3] AABOUD 17H based on 3.2 fb^{-1} of data. A maximum-likelihood fit to neural-network discriminant distributions is used to separate signal and background events. The third error is for luminosity. The cross section ratio is measured to be $\sigma(tq)/\sigma(\overline{t}q) = 1.72 \pm 0.09 \pm 0.18$. A lower limit $|V_{tb}| > 0.84$ (95% CL) is obtained. All results are in agreement with the SM.
[4] Superseded by AAD 24AL.
[5] SIRUNYAN 17AA based on 2.2 fb^{-1} of data. A multivariate discriminator is used to separate signal and background events. The four errors are from statitics, experimental systematics, theory, and luminosity. The cross section ratio is measured to be $\sigma(tq)/\sigma(\overline{t}q) = 1.81 \pm 0.18 \pm 0.15$. CKM matrix element is obtained as $|V_{tb}| = 1.05 \pm 0.07(\text{exp}) \pm 0.02(\text{theo})$. All results are in agreement with the SM.

s-channel Single t Production Cross Section in pp Collisions at $\sqrt{s}$ = 13 TeV

VALUE (pb)	DOCUMENT ID		TECN	COMMENT
• • • We do not use the following data for averages, fits, limits, etc. • • •				
$8.2^{+3.5}_{-2.9}$	[1] AAD	23E	ATLS	$\ell + \not{E}_T + 2b$

[1] AAD 23E based on 139 fb^{-1} of data. The signal significance is 3.3σ over the background-only hypothesis. The result is consistent with the NLO SM prediction of $10.32^{+0.40}_{-0.36}$ pb.

Wt Production Cross Section in pp Collisions at $\sqrt{s}$ = 7 TeV

VALUE (pb)	DOCUMENT ID		TECN	COMMENT
• • • We do not use the following data for averages, fits, limits, etc. • • •				
16.3±4.1	[1] AABOUD	19R	LHC	ATLAS + CMS combined
16^{+5}_{-4}	[2] CHATRCHYAN	13C	CMS	$t+W$ channel, $2\ell+\not{E}_T+1b$
[1] AABOUD 19R based on 1.17 to 5.1 fb^{-1} of data from ATLAS and CMS at 7 TeV.				

[2] Based on 4.9 fb^{-1} of data. The result gives $V_{tb} = 1.01^{+0.16}_{-0.13}(\text{exp})^{+0.03}_{-0.04}(\text{th})$. $V_{tb} > 0.79$ (95% CL) if $V_{tb} < 1$ is assumed. The results assume m_t = 172.5 GeV for the acceptance.

Wt Production Cross Section in pp Collisions at $\sqrt{s}$ = 8 TeV

VALUE (pb)	DOCUMENT ID		TECN	COMMENT
• • • We do not use the following data for averages, fits, limits, etc. • • •				
26 ±7	[1] AAD	21AT	ATLS	$\ell+\geq 3$j
23.1±3.6	[2] AABOUD	19R	LHC	ATLAS + CMS combined
$23.0\pm1.3^{+3.2}_{-3.5}\pm1.1$	[3] AAD	16B	ATLS	$2\ell+\not{E}_T+1b$
23.4±5.4	[4] CHATRCHYAN	14AC	CMS	$t+W$ channel, $2\ell+\not{E}_T+1b$

[1] AAD 21AT based on 20.2 fb^{-1} of data. In this single lepton channel, only single neutrino is emitted, so that both W and t can be reconstructed. A neural network is trained to separate signal from background. The measured cross section agrees with the NLO+NNLL SM prediction of 22.4 ± 0.6(scale) ±1.4(PDF) pb.
[2] AABOUD 19R based on 12.2 to 20.3 fb^{-1} of data from ATLAS and CMS at 8 TeV.
[3] AAD 16B based on 20.3 fb^{-1} of data. The result gives $|V_{tb}| = 1.01 \pm 0.10$ and $|V_{tb}| > 0.80$ (95% CL) without assuming unitarity of the CKM matrix. The results assume m_t = 172.5 GeV for the acceptance.
[4] Based on 12.2 fb^{-1} of data. Events with two oppositely charged leptons, large $\not{E}_T$ and a b-tagged jet are selected, and a multivariate analysis is used to separate the signal from the backgrounds. The result is consistent with the SM prediction of 22.2 ± 0.6(scale) ±1.4(PDF) pb at approximate NNLO.

Wt Production Cross Section in pp Collisions at $\sqrt{s}$ = 13 TeV

VALUE (pb)	DOCUMENT ID		TECN	COMMENT
• • • We do not use the following data for averages, fits, limits, etc. • • •				
$75 \pm 1 \;^{+15}_{-14} \pm 1$	[1] AAD	24BS	ATLS	$e^{\pm}\mu^{\mp}+\not{E}_T+1$j($b$-tag)
$79.2\pm 0.9^{+7.7}_{-8.0}\pm1.2$	[2] TUMASYAN	23T	CMS	$e^{\pm}\mu^{\mp}+\geq 1$j(b-tag)
89 ± 4 ±12	[3] TUMASYAN	21E	CMS	1ℓ + jets
$94 \pm 10 \;^{+28}_{-22} \pm 2$	[4] AABOUD	18H	ATLS	$\ell^+\ell^- + \geq 1$j
63.1± 1.8± 6.4±2.1	[5] SIRUNYAN	18DL	CMS	$e^{\pm}\mu^{\mp}+\geq 1$j(b-tag)

[1] AAD 24BS based on 140 fb^{-1} of data. The errors quoted are statistical, systematic, and the uncertainty from luminosity. The result is consistent with the NLO+NNLL SM prediction of $79.3^{+1.9}_{-1.8}$(scale) ± 2.2(PDF) pb.
[2] TUMASYAN 23T based on 138 fb^{-1} of data. The result is consistent with the NNLO SM prediction. The differential cross sections are measured as a function of six kinematical variables and are consistent with the NLO SM prediction.
[3] TUMASYAN 21E based on 36 fb^{-1} of data. A boosted decision tree is used to separate the signal from the dominant $t\overline{t}$ backgrounds. The result corresponds to an observation with a significance exceeding 5 σ and is consistent with the NNLO QCD prediction of 71.7 ± 1.8(scale) ± 3.4(PDF) pb or with the approximate NNNLO SM prediction of $79.5^{+1.9}_{-1.8}(\text{scale})^{+2.0}_{-1.4}(\text{PDF})$ pb.
[4] AABOUD 18H based on 3.2 fb^{-1} of data. The last error is from luminosity. A multivariate analysis is used to separate the signal from the backgrounds. The result is consistent with the NLO+NNLL SM prediction of 71.7 ± 1.8(scale) ± 3.4(PDF) pb.
[5] SIRUNYAN 18DL based on 35.9 fb^{-1} of data. The last error is from luminosity. A multivariate analysis is used to separate the signal from the backgrounds. The result is consistent with the NLO+NNLL SM prediction of 71.7 ± 1.8(scale) ± 3.4(PDF) pb.

Wt Production Cross Section in pp Collisions at $\sqrt{s}$ = 13.6 TeV

VALUE (pb)	DOCUMENT ID		TECN	COMMENT
• • • We do not use the following data for averages, fits, limits, etc. • • •				
$82.3\pm2.1^{+9.9}_{-9.7}\pm3.3$	[1] HAYRAPETY...	25N	CMS	$e^{\pm}\mu^{\mp}$ + 1,2j($\geq 1b$-tag)

[1] HAYRAPETYAN 25N based on 34.7 fb^{-1} of data. The result is consistent with the approximate-N^{3}LO + N^{3}LL SM prediction of $87.9^{+2.0}_{-1.9}$(scale) ± 2.4(PDF+α_s) pb and with other measurements. The last uncertainty of the quoted result is due to the beam luminosity.

Zt Production Cross Section in pp Collisions at $\sqrt{s}$ = 13 TeV

VALUE (fb)	DOCUMENT ID		TECN	COMMENT
• • • We do not use the following data for averages, fits, limits, etc. • • •				
810 ± 70 ± 60	[1] HAYRAPETY...	25S	CMS	$70 < m_{\ell^+\ell^-} < 110$ GeV
$87.9^{+7.5}_{-7.3}{}^{+7.3}_{-6.0}$	[2] TUMASYAN	22L	CMS	$3\ell + \geq 2$j ($\geq 1bj$)
97 ± 13 ± 7	[3] AAD	20AB	ATLS	3ℓ + 1,2j + 1bj
$111 \pm 13 \;^{+11}_{-9}$	[4] SIRUNYAN	19BF	CMS	$3\ell + \geq 2$j ($\geq 1bj$)
600 ±170 ±140	[5] AABOUD	18AE	ATLS	3ℓ + 1j + 1bj
$123 \;^{+33}_{-31} \;^{+29}_{-23}$	[6] SIRUNYAN	18Z	CMS	3ℓ + 1j + 1bj

[1] HAYRAPETYAN 25S based on 138 fb^{-1} of data. Events with 3 or more leptons are used. It is in agreement with the NLO SM prediction of 820 ± 50 fb.
[2] TUMASYAN 22L based on 138 fb^{-1} of data at 13 TeV. The result is for a dilepton invariant masses above 30 GeV. It agrees with the NLO SM prediction of $94.2^{+1.9}_{-1.8}(\text{scale})\pm2.5(\text{PDF})$ fb. The ratio of t and $\overline{t}$ production cross sections is measured as $2.37^{+0.56}_{-0.42}{}^{+0.27}_{-0.13}$. The spin asymmetry is measured to be 0.54 ± 0.16 ± 0.06. Both measurements are in agreement with the SM predictions.
[3] AAD 20AB based on 139 fb^{-1} of data at 13 TeV. Neural networks are used to discriminate tZq signal from backgrounds. The result is for the cross section $\sigma(pp \rightarrow t\ell^+\ell^- q)$, including non-resonant dilepton pairs, for dilepton invariant masses above 30 GeV and is consistent with the NLO SM prediction of 102^{+5}_{-2} fb.

Int. J. Mod. Phys. A 2026.41. Downloaded from www.worldscientific.com
by UNIVERSITY OF CALIFORNIA @ BERKELEY on 09/16/26. Re-use and distribution is strictly not permitted, except for Open Access articles.

[4] SIRUNYAN 19BF based on 77.4 fb^{-1} of data. Two BDT's are used in the analysis: one to discriminate prompt leptons from non-prompt ones; and one to discriminate tZq signal from backgrounds. The result is for the cross section $\sigma(pp \to tZq \to t\ell^+\ell^-q)$ for dilepton invariant masses above 30 GeV and is consistent with the NLO SM prediction of 94.2 ± 3.1 fb.

[5] AABOUD 18AE based on 36.1 fb^{-1} of data. A multivariate analysis is used to separate the signal from the backgrounds. The result is consistent with the NLO SM prediction of 800 fb with a scale uncertainty of $^{+6.1}_{-7.4}$%.

[6] SIRUNYAN 18Z based on 35.9 fb^{-1} of data. A multivariate analysis is used to separate the signal from the backgrounds. The result is for the cross section $\sigma(pp \to tZq \to Wb\ell^+\ell^-q)$ and is consistent with the NLO SM prediction of $94.2^{+1.9}_{-1.8}$(scale) ± 2.5(PDF) fb. Superseded by SIRUNYAN 19BF.

Ht Production Cross Section in pp Collisions at $\sqrt{s}$ = 13 TeV

VALUE (fb)	DOCUMENT ID		TECN	COMMENT
• • • We do not use the following data for averages, fits, limits, etc. • • •				
720±270	[1] AAD	25BD	ATLS	$\ell + H(H \to b\overline{b}, WW^*, \tau\tau, ZZ^*)$

[1] AAD 25BD based on 140 fb^{-1} of data. The observed significance is 2.8σ. The ratio between the measured cross section and the SM prediction is 8.1 ± 2.6 ± 2.0.

γt Production Cross Section in pp Collisions at $\sqrt{s}$ = 13 TeV

VALUE (fb)	DOCUMENT ID		TECN	COMMENT
• • • We do not use the following data for averages, fits, limits, etc. • • •				
	[1] AAD	23BN	ATLS	$\gamma + \ell +$ jets $+ \not{E}_T$

[1] AAD 23BN measured fiducial cross section for $pp \to t\gamma$ at 13 TeV with 139 fb^{-1} of data. The measured cross section is 688 ± 23^{+75}_{-71} fb, to be compared with the NLO SM prediction of 515^{+36}_{-42} fb.

tWZ Production Cross Section in pp Collisions at $\sqrt{s}$ = 13 TeV

VALUE (fb)	DOCUMENT ID		TECN	COMMENT
354±54±95	[1] HAYRAPETY...24K		CMS	$\geq 3\ell + 1bj + 2$, 3j or boosted t
• • • We do not use the following data for averages, fits, limits, etc. • • •				
1140±50±40	[2] HAYRAPETY...25S		CMS	$\sigma(t\overline{t}Z + tWZ)$

[1] Reported a statistical significance of 3.4 standard deviations based on 138 fb^{-1} of data at 13 TeV.

[2] HAYRAPETYAN 25S based on 138 fb^{-1} of data. Events with 3 or more leptons are used. It is about 2σ larger than the NLO SM prediction.

Single t-Quark Production Cross Section in ep Collisions

VALUE (pb)	CL%	DOCUMENT ID		TECN	COMMENT
• • • We do not use the following data for averages, fits, limits, etc. • • •					
<0.25	95	[1] AARON	09A	H1	$e^\pm p \to e^\pm tX$
<0.55	95	[2] AKTAS	04	H1	$e^\pm p \to e^\pm tX$
<0.225	95	[3] CHEKANOV	03	ZEUS	$e^\pm p \to e^\pm tX$

[1] AARON 09A looked for single top production via FCNC in $e^\pm p$ collisions at HERA with 474 pb^{-1} of data at $\sqrt{s}$ = 301–319 GeV. The result supersedes that of AKTAS 04.

[2] AKTAS 04 looked for single top production via FCNC in $e^\pm$ collisions at HERA with 118.3 pb^{-1}, and found 5 events in the e or μ channels while 1.31 ± 0.22 events are expected from the Standard Model background. No excess was found for the hadronic channel. The observed cross section of $\sigma(ep \to etX) = 0.29^{+0.15}_{-0.14}$ pb at $\sqrt{s}$ = 319 GeV gives the quoted upper bound if the observed events are due to statistical fluctuation.

[3] CHEKANOV 03 looked in 130.1 pb^{-1} of data at $\sqrt{s}$ = 301 and 318 GeV. The limit is for $\sqrt{s}$ = 318 GeV and assumes m_t = 175 GeV.

$t\overline{t}$ Production Cross Section in $p\overline{p}$ Collisions at $\sqrt{s}$ = 1.8 TeV

Only the final combined $t\overline{t}$ production cross sections obtained from Tevatron Run I by the CDF and D0 experiments are quoted below.

VALUE (pb)	DOCUMENT ID		TECN	COMMENT
• • • We do not use the following data for averages, fits, limits, etc. • • •				
5.69±1.21±1.04	[1] ABAZOV	03A	D0	Combined Run I data
$6.5\ ^{+1.7}_{-1.4}$	[2] AFFOLDER	01A	CDF	Combined Run I data

[1] Combined result from 110 pb^{-1} of Tevatron Run I data. Assume m_t = 172.1 GeV.

[2] Combined result from 105 pb^{-1} of Tevatron Run I data. Assume m_t = 175 GeV.

$t\overline{t}$ Production Cross Section in $p\overline{p}$ Collisions at $\sqrt{s}$ = 1.96 TeV

Unless otherwise noted the first quoted error is from statistics, the second from systematic uncertainties, and the third from luminosity. If only two errors are quoted the luminosity is included in the systematic uncertainties.

VALUE (pb)	DOCUMENT ID		TECN	COMMENT
• • • We do not use the following data for averages, fits, limits, etc. • • •				
$7.26 \pm 0.13^{+0.57}_{-0.50}$	[1] ABAZOV	16F	D0	$\ell\ell$, ℓ+jets channels
8.1 ±2.1	[2] AALTONEN	14A	CDF	$\ell + \tau_h + \geq$ 2jets ($\geq 1b$-tag)
7.60±0.20±0.29±0.21	[3] AALTONEN	14H	TEVA	$\ell\ell$, ℓ+jets, all-jets channels
8.0 ±0.7 ±0.6 ±0.5	[4] ABAZOV	14K	D0	$\ell + \not{E}_T + \geq 4$ jets ($\geq 1b$-tag)
7.09±0.84	[5] AALTONEN	13AB	CDF	$\ell\ell + \not{E}_T + \geq 2$ jets
7.5 ±1.0	[6] AALTONEN	13G	CDF	$\ell + \not{E}_T + \geq$ 3jets ($\geq 1b$-tag)
8.8 ±3.3 ±2.2	[7] AALTONEN	12AL	CDF	$\tau_h + \not{E}_T$ +4j ($\geq 1b$)
8.5 ±0.6 ±0.7	[8] AALTONEN	11D	CDF	$\ell + \not{E}_T$ + jets ($\geq 1b$-tag)
7.64±0.57±0.45	[9] AALTONEN	11W	CDF	$\ell + \not{E}_T$ + jets ($\geq 1b$-tag)
7.99±0.55±0.76±0.46	[10] AALTONEN	11Y	CDF	$\not{E}_T + \geq$ 4jets (0,1,2 b-tag)
$7.78^{+0.77}_{-0.64}$	[11] ABAZOV	11E	D0	$\ell + \not{E}_T + \geq 2$ jets
$7.56^{+0.63}_{-0.56}$	[12] ABAZOV	11Z	D0	Combination
6.27±0.73±0.63±0.39	[13] AALTONEN	10AA	CDF	Repl. by AALTONEN 13AB
7.2 ±0.5 ±1.0 ±0.4	[14] AALTONEN	10E	CDF	$\geq$ 6 jets, vtx b-tag
7.8 ±2.4 ±1.6 ±0.5	[15] AALTONEN	10V	CDF	$\ell + \geq$ 3 jets, soft-e b-tag
7.70±0.52	[16] AALTONEN	10W	CDF	$\ell + \not{E}_T + \geq$ 3 jets + b-tag, norm. to $\sigma(Z \to \ell\ell)_{TH}$
6.9 ±2.0	[17] ABAZOV	10I	D0	$\geq$ 6 jets with 2 b-tags
$6.9 \pm 1.2\ ^{+0.8}_{-0.7} \pm 0.4$	[18] ABAZOV	10Q	D0	τ_h + jets
$9.6 \pm 1.2\ ^{+0.6}_{-0.5} \pm 0.6$	[19] AALTONEN	09AD	CDF	$\ell\ell + \not{E}_T$ / vtx b-tag
$9.1 \pm 1.1\ ^{+1.0}_{-0.9} \pm 0.6$	[20] AALTONEN	09H	CDF	$\ell + \geq$ 3 jets+$\not{E}_T$/soft μ b-tag
$8.18^{+0.98}_{-0.87}$	[21] ABAZOV	09AG	D0	ℓ + jets, $\ell\ell$ and $\ell\tau$ + jets
$7.5 \pm 1.0\ ^{+0.7}_{-0.6}\ ^{+0.6}_{-0.5}$	[22] ABAZOV	09R	D0	$\ell\ell$ and $\ell\tau$ + jets
$8.18^{+0.90}_{-0.84} \pm 0.50$	[23] ABAZOV	08M	D0	ℓ + n jets with 0,1,2 b-tag
7.62±0.85	[24] ABAZOV	08N	D0	ℓ + n jets + b-tag or kinematics
$8.5\ ^{+2.7}_{-2.2}$	[25] ABULENCIA	08	CDF	$\ell^+\ell^-$ ($\ell = e, \mu$)
$8.3 \pm 1.0\ ^{+2.0}_{-1.5} \pm 0.5$	[26] AALTONEN	07D	CDF	$\geq$ 6 jets, vtx b-tag
7.4 ±1.4 ±1.0	[27] ABAZOV	07O	D0	$\ell\ell$ + jets, vtx b-tag
$4.5\ ^{+2.0}_{-1.9}\ ^{+1.4}_{-1.1} \pm 0.3$	[28] ABAZOV	07P	D0	$\geq$ 6 jets, vtx b-tag
$6.4\ ^{+1.3}_{-1.2} \pm 0.7 \pm 0.4$	[29] ABAZOV	07R	D0	$\ell + \geq$ 4 jets
6.6 ±0.9 ±0.4	[30] ABAZOV	06X	D0	ℓ + jets, vtx b-tag
$8.7 \pm 0.9\ ^{+1.1}_{-0.9}$	[31] ABULENCIA	06Z	CDF	ℓ + jets, vtx b-tag
$5.8 \pm 1.2\ ^{+0.9}_{-0.7}$	[32] ABULENCIA,A	06C	CDF	missing E_T + jets, vtx b-tag
$7.5 \pm 2.1\ ^{+3.3}_{-2.2}\ ^{+0.5}_{-0.4}$	[33] ABULENCIA,A	06E	CDF	6–8 jets, b-tag
$8.9 \pm 1.0\ ^{+1.1}_{-1.0}$	[34] ABULENCIA,A	06F	CDF	$\ell + \geq$ 3 jets, b-tag
$8.6\ ^{+1.6}_{-1.5} \pm 0.6$	[35] ABAZOV	05Q	D0	ℓ + n jets
$8.6\ ^{+3.2}_{-2.7} \pm 1.1 \pm 0.6$	[36] ABAZOV	05R	D0	di-lepton + n jets
$6.7\ ^{+1.4}_{-1.3}\ ^{+1.6}_{-1.1} \pm 0.4$	[37] ABAZOV	05X	D0	ℓ + jets / kinematics
$5.3 \pm 3.3\ ^{+1.3}_{-1.0}$	[38] ACOSTA	05S	CDF	ℓ + jets / soft μ b-tag
6.6 ±1.1 ±1.5	[39] ACOSTA	05T	CDF	ℓ + jets / kinematics
$6.0\ ^{+1.5}_{-1.6}\ ^{+1.2}_{-1.3}$	[40] ACOSTA	05U	CDF	ℓ + jets/kinematics + vtx b-tag
$5.6\ ^{+1.2}_{-1.1}\ ^{+0.9}_{-0.6}$	[41] ACOSTA	05V	CDF	ℓ + n jets
$7.0\ ^{+2.4}_{-2.1}\ ^{+1.6}_{-1.1} \pm 0.4$	[42] ACOSTA	04I	CDF	di-lepton + jets + missing ET

[1] ABAZOV 16F based on 9.7 fb^{-1} of data. The result is for m_t = 172.5 GeV, and the m_t dependence is shown in Table V and Fig. 9. The result agrees with the NNLO+NNLL SM prediction of $7.35^{+0.23}_{-0.27}$ pb.

[2] Based on 9 fb^{-1} of data. The measurement is in the channel $t\overline{t} \to (b\ell\nu)(b\tau\nu)$, where τ decays into hadrons (τ_h), and ℓ (e or μ) include ℓ from τ decays (τ_ℓ). The result is for m_t = 173 GeV.

[3] Based on 8.8 fb^{-1} of data. Combination of CDF and D0 measurements given, respectively, by $\sigma(t\overline{t}$; CDF) = 7.63 ± 0.31 ± 0.36 ± 0.16 pb, $\sigma(t\overline{t}$; D0) = 7.56 ± 0.20 ± 0.32 ± 0.46 pb. All the results are for m_t = 172.5 GeV. The m_t dependence of the mean value is parametrized in eq. (1) and shown in Fig. 2.

[4] Based on 9.7 fb^{-1} of data. Differential cross sections with respect to m_{tt}, $|y(\text{top})|$, E_T(top) are shown in Figs. 9, 10, 11, respectively, and are compared to the predictions of MC models.

[5] Based on 8.8 fb^{-1} of $p\overline{p}$ collisions at $\sqrt{s}$ = 1.96 TeV.

[6] Based on 8.7 fb^{-1} of $p\overline{p}$ collisions at $\sqrt{s}$ = 1.96 TeV. Measure the $t\overline{t}$ cross section simultaneously with the fraction of $t \to Wb$ decays. The correlation coefficient between those two measurements is −0.434. Assume unitarity of the 3×3 CKM matrix and set $|V_{tb}| > 0.89$ at 95% CL.

[7] Based on 2.2 fb^{-1} of data in $p\overline{p}$ collisions at 1.96 TeV. The result assumes the acceptance for m_t = 172.5 GeV.

[8] Based on 1.12 fb^{-1} and assumes m_t = 175 GeV, where the cross section changes by ±0.1 pb for every ∓1 GeV shift in m_t. AALTONEN 11D fits simultaneously the $t\overline{t}$ production cross section and the b-tagging efficiency and find improvements in both measurements.

[9] Based on 2.7 fb^{-1}. The first error is from statistics and systematics, the second is from luminosity. The result is for m_t = 175 GeV. AALTONEN 11W fits simultaneously a jet flavor discriminator between b-, c-, and light-quarks, and find significant reduction in the systematic error.

[10] Based on 2.2 fb^{-1}. The result is for m_t = 172.5 GeV. AALTONEN 11Y selects multi-jet events with large $\not{E}_T$, and vetoes identified electrons and muons.

[11] Based on 5.3 fb^{-1}. The error is statistical + systematic + luminosity combined. The result is for m_t = 172.5 GeV. The results for other m_t values are given in Table XII and eq.(10) of ABAZOV 11E.

[12] Combination of a dilepton measurement presented in ABAZOV 11Z (based on 5.4 fb^{-1}), which yields $7.36^{+0.90}_{-0.79}$ (stat+syst) pb, and the lepton + jets measurement of ABAZOV 11E. The result is for m_t = 172.5 GeV. The results for other m_t values is given by eq.(5) of ABAZOV 11A.

[13] Based on 2.8 fb^{-1}. The result is for m_t = 175 GeV.

[14] Based on 2.9 fb^{-1}. Result is obtained from the fraction of signal events in the top quark mass measurement in the all hadronic decay channel.

[15] Based on 1.7 fb^{-1}. The result is for m_t = 175 GeV. AALTONEN 10V uses soft electrons from b-hadron decays to suppress W+jets background events.

by UNIVERSITY OF CALIFORNIA SANTA CRUZ on 09/16/26. Re-use and distribution is strictly not permitted, except for Open Access articles.
Int. J. Phys. A 2026.41. Downloaded from www.worldscientific.com

[16] Based on 4.6 fb^{-1}. The result is for m_t = 172.5 GeV. The ratio $\sigma(t\bar{t} \to \ell$+jets) / $\sigma(Z/\gamma^* \to \ell\ell)$ is measured and then multiplied by the theoretical $Z/\gamma^* \to \ell\ell$ cross section of $\sigma(Z/\gamma^* \to \ell\ell)$ = 251.3 ± 5.0 pb, which is free from the luminosity error.

[17] Based on 1 fb^{-1}. The result is for m_t = 175 GeV. 7.9 ± 2.3 pb is found for m_t = 170 GeV. ABAZOV 10I uses a likelihood discriminant to separate signal from background, where the background model was created from lower jet-multiplicity data.

[18] Based on 1 fb^{-1}. The result is for m_t = 170 GeV. For m_t = 175 GeV, the result is $6.3^{+1.2}_{-1.1}$(stat)±0.7(syst)±0.4(lumi) pb. Cross section of $t\bar{t}$ production has been measured in the $t\bar{t} \to \tau_h +$ jets topology, where τ_h denotes hadronically decaying τ leptons. The result for the cross section times the branching ratio is $\sigma(t\bar{t}) \cdot$ B($t\bar{t} \to \tau_h +$ jets) = $0.60^{+0.23}_{-0.22}{}^{+0.15}_{-0.14}$ ± 0.04 pb for m_t = 170 GeV.

[19] Based on 1.1 fb^{-1}. The result is for B($W \to \ell\nu$) = 10.8% and m_t = 175 GeV; the mean value is 9.8 for m_t = 172.5 GeV and 10.1 for m_t = 170 GeV. AALTONEN 09AD used high p_T e or μ with an isolated track to select $t\bar{t}$ decays into dileptons including $\ell = \tau$. The result is based on the candidate event samples with and without vertex b-tag.

[20] Based on 2 fb^{-1}. The result is for m_t = 175 GeV; the mean value is 3% higher for m_t = 170 GeV and 4% lower for m_t = 180 GeV.

[21] Result is based on 1 fb^{-1} of data. The result is for m_t = 170 GeV, and the mean value decreases with increasing m_t; see their Fig. 2. The result is obtained after combining ℓ + jets, $\ell\ell$, and $\ell\tau$ final states, and the ratios of the extracted cross sections are $R^{\ell\ell/\ell j} = 0.86^{+0.19}_{-0.17}$ and $R^{\ell\tau/\ell\ell-\ell j} = 0.97^{+0.32}_{-0.29}$, consistent with the SM expectation of R = 1. This leads to the upper bound of B($t \to bH^+$) as a function of m_{H^+}. Results are shown in their Fig. 1 for B($H^+ \to \tau\nu$) = 1 and B($H^+ \to c\bar{s}$) = 1 cases. Comparison of the m_t dependence of the extracted cross section and a partial NNLO prediction gives $m_t = 169.1^{+5.9}_{-5.2}$ GeV.

[22] Result is based on 1 fb^{-1} of data. The result is for m_t = 170 GeV, and the mean value changes by −0.07 [m_t(GeV)−170] pb near the reference m_t value. Comparison of the m_t dependence of the extracted cross section and a partial NNLO QCD prediction gives $m_t = 171.5^{+9.9}_{-8.8}$ GeV. The $\ell\tau$ channel alone gives $7.6^{+4.9}_{-4.3}{}^{+3.5}_{-3.4}{}^{+1.4}_{-0.9}$ pb and the $\ell\ell$ channel gives $7.5^{+1.2}_{-1.1}{}^{+0.7}_{-0.6}{}^{+0.7}_{-0.5}$ pb.

[23] Result is based on 0.9 fb^{-1} of data. The first error is from stat + syst, while the latter error is from luminosity. The result is for m_t=175 GeV, and the mean value changes by −0.09 pb·[m_t(GeV)−175].

[24] Result is based on 0.9 fb^{-1} of data. The cross section is obtained from the $\ell + \geq 3$jet event rates with 1 or 2 b-tag, and also from the kinematical likelihood analysis of the ℓ+ 3, 4 jet events. The result is for m_t= 172.6 GeV, and its m_t dependence shown in Fig. 3 leads to the constraint m_t = 170 ± 7 GeV when compared to the SM prediction.

[25] Result is based on 360 pb^{-1} of data. Events with high p_T oppositely charged dileptons $\ell^+\ell^-$ ($\ell = e, \mu$) are used to obtain cross sections for $t\bar{t}$, W^+W^-, and $Z \to \tau^+\tau^-$ production processes simultaneously. The other cross sections are given in Table IV.

[26] Based on 1.02 fb^{-1} of data. Result is for m_t = 175 GeV. Secondary vertex b-tag and neural network selections are used to achieve a signal-to-background ratio of about 1/2.

[27] Based on 425 pb^{-1} of data. Result is for m_t = 175 GeV. For m_t = 170.9 GeV, 7.8 ± 1.8(stat + syst) pb is obtained.

[28] Based on 405 ± 25 pb^{-1} of data. Result is for m_t = 175 GeV. The last error is for luminosity. Secondary vertex b-tag and neural network are used to separate the signal events from the background.

[29] Based on 425 pb^{-1} of data. Assumes m_t = 175 GeV.

[30] Based on ∼ 425 pb^{-1}. Assuming m_t = 175 GeV. The first error is combined statistical and systematic, the second one is luminosity.

[31] Based on ∼ 318 pb^{-1}. Assuming m_t = 178 GeV. The cross section changes by ±0.08 pb for each ∓ GeV change in the assumed m_t. Result is for at least one b-tag. For at least two b-tagged jets, $t\bar{t}$ signal of significance greater than 5σ is found, and the cross section is $10.1^{+1.6}_{-1.4}{}^{+2.0}_{-1.3}$ pb for m_t = 178 GeV.

[32] Based on ∼ 311 pb^{-1}. Assuming m_t = 178 GeV. For m_t = 175 GeV, the result is $6.0 \pm 1.2^{+0.9}_{-0.7}$. This is the first CDF measurement without lepton identification, and hence it has sensitivity to the $W \to \tau\nu$ mode.

[33] ABULENCIA,A 06E measures the $t\bar{t}$ production cross section in the all hadronic decay mode by selecting events with 6 to 8 jets and at least one b-jet. S/B = 1/5 has been achieved. Based on 311 pb^{-1}. Assuming m_t = 178 GeV.

[34] Based on ∼ 318 pb^{-1}. Assuming m_t = 178 GeV. Result is for at least one b-tag. For at least two b-tagged jets, the cross section is $11.1^{+2.3}_{-1.9}{}^{+2.5}_{-1.9}$ pb.

[35] ABAZOV 05Q measures the top-quark pair production cross section with ∼ 230 pb^{-1} of data, based on the analysis of W plus n-jet events where W decays into e or μ plus neutrino, and at least one of the jets is b-jet like. The first error is statistical and systematic, and the second accounts for the luminosity uncertainty. The result assumes m_t = 175 GeV; the mean value changes by (175−m_t(GeV)) × 0.06 pb in the mass range 160 to 190 GeV.

[36] ABAZOV 05R measures the top-quark pair production cross section with 224–243 pb^{-1} of data, based on the analysis of events with two charged leptons in the final state. The result assumes m_t = 175 GeV; the mean value changes by (175−m_t(GeV)) × 0.08 pb in the mass range 160 to 190 GeV.

[37] Based on 230 pb^{-1}. Assuming m_t = 175 GeV.

[38] Based on 194 pb^{-1}. Assuming m_t = 175 GeV.

[39] Based on 194 ± 11 pb^{-1}. Assuming m_t = 175 GeV.

[40] Based on 162 ± 10 pb^{-1}. Assuming m_t = 175 GeV.

[41] ACOSTA 05V measures the top-quark pair production cross section with ∼ 162 pb^{-1} data, based on the analysis of W plus n-jet events where W decays into e or μ plus neutrino, and at least one of the jets is b-jet like. Assumes m_t = 175 GeV.

[42] ACOSTA 04I measures the top-quark pair production cross section with 197 ± 12 pb^{-1} data, based on the analysis of events with two charged leptons in the final state. Assumes m_t = 175 GeV.

Ratio of the Production Cross Sections of $t\bar{t}\gamma$ to $t\bar{t}$ at $\sqrt{s}$ = 1.96 TeV

VALUE	DOCUMENT ID		TECN	COMMENT
• • • We do not use the following data for averages, fits, limits, etc. • • •				
0.024±0.009	[1] AALTONEN	11Z	CDF	$E_T(\gamma) > 10$ GeV, $\lvert\eta(\gamma)\rvert < 1.0$

[1] Based on 6.0 fb^{-1} of data. The error is statistical and systematic combined. Events with lepton + $\not{E}_T$ + $\geq$ 3 jets($\geq 1b$) with and without central, high E_T photon are measured. The result is consistent with the SM prediction of 0.024±0.005. The absolute production cross section is measured to be 0.18 ± 0.08 fb. The statistical significance is 3.0 standard deviations.

tt Production Cross Section in pp Collisions at $\sqrt{s}$ = 7 TeV

VALUE (pb)	CL%	DOCUMENT ID		TECN	COMMENT
• • • We do not use the following data for averages, fits, limits, etc. • • •					
<1.7	95	[1] AAD	12BE	ATLS	$\ell^+\ell^+ + \not{E}_T + \geq 2$j +HT

[1] Based on 1.04 fb^{-1} of pp data at $\sqrt{s}$ = 7 TeV. The upper bounds are the same for LL, LR and RR chiral components of the two top quarks.

tt or $\overline{tt}$ Production Cross Section in pp Collisions at $\sqrt{s}$ = 13 TeV

VALUE (fb)	CL%	DOCUMENT ID		TECN	COMMENT
• • • We do not use the following data for averages, fits, limits, etc. • • •					
<1.6	95	[1] AAD	25T	ATLS	2ℓ(same sign) + $\geq 2b$-jets

[1] AAD 25T based on 140 fb^{-1} of data. Searches are performed for the production of same-sign top quark pairs, where the SM cross section is predicted to be about 4×10^{-12} fb. Signal process is simulated using the SMEFT framework as originating from 4 up-type-quark pointlike interactions.

$t\bar{t}$ Production Cross Section in pp Collisions at $\sqrt{s}$ = 5.02 TeV

Unless otherwise noted the first quoted error is from statistics, the second from systematic uncertainties, and the third from luminosity. If only two errors are quoted the luminosity is included in the systematic uncertainties.

VALUE (pb)	DOCUMENT ID		TECN	COMMENT
• • • We do not use the following data for averages, fits, limits, etc. • • •				
$62.5 \pm 1.6^{+2.6}_{-2.5} \pm 1.2$	[1] HAYRAPETY...	25U	CMS	ℓ + jets(≥ 1 b-jet)
62.3±1.5±2.4±1.2	[2] HAYRAPETY...	25U	CMS	ℓ+jets, $\ell\ell$+jets
67.5±0.9±2.6	[3] AAD	23J	ATLS	dilepton + single ℓ channels
60.7±5.0±2.8±1.1	[4] TUMASYAN	22T	CMS	$e + \mu + \geq 2$ jets
63.0±4.1±3.0	[5] TUMASYAN	22T	CMS	combination of $e + \mu + \geq 2$ jets, ℓ+jets
69.5±6.1±5.6±1.6	[6] SIRUNYAN	18AQ	CMS	ℓ+jets, $\ell\ell$+jets

[1] HAYRAPETYAN 25U based on 302 pb^{-1} of data. Multivariate analysis techniques are used to enhance S/N ratio. The result is consistent with the NNLO SM prediction $69.5^{+3.5}_{-3.7}$ pb within 2σ.

[2] Combination of the measurement by HAYRAPETYAN 25U and the measurement in the $\ell\ell$+jets channel by TUMASYAN 22T. The result is consistent with the NNLO SM prediction $69.5^{+3.5}_{-3.7}$ pb within 2σ.

[3] AAD 23J based on 257 pb^{-1} of data from pp collisions. The second error is the sum of systematics (±2.3), luminosity(±1.1) and beam energy (±0.2) uncertainties. The result agrees with the NNLO+NNLL SM prediction $68.2^{+5.2}_{-5.3}$ pb.

[4] TUMASYAN 22T based on 302 pb^{-1} of data from pp collisions at $\sqrt{s}$ = 5.02 TeV. The errors are from statistics, systematics and luminosity.

[5] Combination of the measurement by TUMASYAN 22T and the measurement in the ℓ+jets channel by SIRUNYAN 18AQ. The errors are from statistics and systematics + luminosity. The result is in agreement with the NNLO+NNLL SM prediction $66.8^{+2.9}_{-3.1}$ pb.

[6] SIRUNYAN 18AQ based on 27.4 pb^{-1} of data from pp collisions at $\sqrt{s}$ = 5.02 TeV. The result is in agreement with the NNLO SM prediction $68.9^{+1.9}_{-2.3}$(scale)±2.3(PDF)$^{+1.4}_{-1.0}$(α_s) pb.

$t\bar{t}$ Production Cross Section in pp Collisions at $\sqrt{s}$ = 7 TeV

Unless otherwise noted the first quoted error is from statistics, the second from systematic uncertainties, and the third from luminosity. If only two errors are quoted the luminosity is included in the systematic uncertainties.

VALUE (pb)	DOCUMENT ID		TECN	COMMENT
• • • We do not use the following data for averages, fits, limits, etc. • • •				
$168.5 \pm 0.7^{+6.2}_{-5.9}{}^{+3.4}_{-3.2}$	[1] AABOUD	23	ATLS	$1\ell + \not{E}_T + \geq 3$j (0,1,2 b-tagged j)
178.5± 4.7	[2] AAD	23AY	LHC	$e^\pm\mu^\mp$ pair; ATLAS+CMS combined
161.7± 6.0±12.0± 3.6	[3] KHACHATRY...	17B	CMS	$\ell + \not{E}_T + \geq 4$j ($\geq 1b$)
$173.6 \pm 2.1^{+4.5}_{-4.0} \pm 3.8$	[4] KHACHATRY...	16AW	CMS	$e + \mu + \not{E}_T + \geq 0$j
$181.2 \pm 2.8^{+10.8}_{-10.6}$	[5] AAD	15BO	ATLS	$e + \mu + \not{E}_T + \geq 0$j
178 ± 3 ±16 ± 3	[6] AAD	15CC	ATLS	ℓ+jets, $\ell\ell$+jets, $\ell\tau_h$+jets
	[7] AAIJ	15R	LHCB	$\mu + \geq 1$j(b-tag) forward region
182.9± 3.1± 6.4	[8] AAD	14AY	ATLS	$e + \mu + 1$ or 2b jets
194 ±18 ±46	[9] AAD	13X	ATLS	$\tau_h + \not{E}_T + \geq 5$j ($\geq 2b$)
139 ±10 ±26	[10] CHATRCHYAN	13AY	CMS	≥ 6 jets with 2 b-tags
158.1± 2.1±10.8	[11] CHATRCHYAN	13BB	CMS	$\ell + \not{E}_T$ + jets(≥ 1 b-tag)
152 ±12 ±32	[12] CHATRCHYAN	13BE	CMS	$\tau_h + \not{E}_T + \geq 4$ jets (≥ 1 b)
177 ±20 ±14 ± 7	[13] AAD	12B	ATLS	Repl. by AAD 12BF
$176 \pm 5^{+14}_{-11} \pm 8$	[14] AAD	12BF	ATLS	$\ell\ell + \not{E}_T + \geq 2$j
$187 \pm 11^{+18}_{-17} \pm 6$	[15] AAD	12BO	ATLS	$\ell + \not{E}_T + \geq 3$j with b-tag
186 ±13 ±20 ± 7	[16] AAD	12CG	ATLS	$\ell + \tau_h + \not{E}_T + \geq 2$j ($\geq 1b$)
143 ±14 ±22 ± 3	[17] CHATRCHYAN	12AC	CMS	$\ell + \tau_h + \not{E}_T + \geq 2$j ($\geq 1b$)
$161.9 \pm 2.5^{+5.1}_{-5.0} \pm 3.6$	[18] CHATRCHYAN	12AX	CMS	$\ell\ell + \not{E}_T + \geq 2b$

Int. J. Mod. Phys. A 2026.41. Downloaded from www.worldscientific.com
by UNIVERSITY OF CALIFORNIA @ BERKELEY on 09/16/26. Re-use and distribution is strictly not permitted, except for Open Access articles.

145 ±31 $^{+42}_{-27}$	[19] AAD	11A	ATLS	$\ell+\not{E}_T+\geq 4$j, $\ell\ell+\not{E}_T+\geq 2$j
173 $^{+39}_{-32}$ ± 7	[20] CHATRCHYAN	11AA	CMS	$\ell+\not{E}_T+\geq 3$ jets
168 ±18 ±14 ± 7	[21] CHATRCHYAN	11F	CMS	$\ell\ell+\not{E}_T+$ jets
154 ±17 ± 6	[22] CHATRCHYAN	11Z	CMS	Combination
194 ±72 ±24 ±21	[23] KHACHATRY...	11A	CMS	$\ell\ell+\not{E}_T+\geq 2$ jets

[1] AABOUD 23 based on 4.6 fb^{-1} of data. The measurement is performed using a multivariate event classifier based on a binary learning algorithm which differentiates $t\overline{t}$ events from backgrounds in a three-dimensional space. The result is in agreement with the NNLO+NNLL SM prediction of 177^{+5}_{-6}(scale)±9(PDF+α_s) pb for m_t = 172.5 GeV. Compared to the measured cross section using the dilepton mode of AAD 14AY, significance of discrepancy is between 1.9σ to 2.1σ.

[2] AAD 23AY based on 5 fb^{-1} of data using m_t = 172.5 GeV. The ratio of the combined cross section at $\sqrt{s}$ = 8 TeV to this one at $\sqrt{s}$ = 7 TeV is determined as 1.363 ± 0.032. The values of the cross sections as well as the ratio are consistent with the NNLO+NNLL SM predictions.

[3] KHACHATRYAN 17B based on 5.0 fb^{-1} of data, using a binned likelihood fit of templates to the data. Also the ratio $\sigma(t\overline{t}$; 8 TeV)/$\sigma(t\overline{t}$; 7 TeV) = 1.43 ± 0.04 ± 0.07 ± 0.05 is reported. The results are in agreement with NNLO SM predictions.

[4] KHACHATRYAN 16AW based on 5.0 fb^{-1} of data, using a binned likelihood fit to differential distributions of b-tagged and non-b-tagged jets. The result is in good agreement with NNLO SM predictions.

[5] Based on 4.6 fb^{-1} of data. Uses a template fit to distributions of $\not{E}_T$ and jet multiplicities to measure simultaneously $t\overline{t}$, WW, and $Z/\gamma^* \rightarrow \tau\tau$ cross sections, assuming m_t = 172.5 GeV.

[6] AAD 15CC based on 4.6 fb^{-1} of data. The event selection criteria are optimized for the $\ell\tau_h$ + jets channel. Using only this channel 183 ± 9 ± 23 ± 3 pb is derived for the cross section.

[7] AAIJ 15R, based on 1.0 fb^{-1} of data, reports 0.239 ± 0.053 ± 0.033 ± 0.024 pb cross section for the forward fiducial region $p_T(\mu)$ > 25 GeV, 2.0 < $\eta(\mu)$ < 4.5, 50 GeV < $p_T(b)$ < 100 GeV, 2.2 < $\eta(b)$ < 4.2, $\Delta R(\mu,b)$ > 0.5, and $p_T(\mu+b)$ > 20 GeV. The three errors are from statistics, systematics, and theory. The result agrees with the SM NLO prediction.

[8] AAD 14AY reports 182.9 ± 3.1 ± 4.2 ± 3.6 ± 3.3 pb value based on 4.6 fb^{-1} of data. The four errors are from statistics, systematic, luminosity, and the 0.66% beam energy uncertainty. We have combined the systematic uncertainties in quadrature. The result is for m_t = 172.5GeV; for other m_t, $\sigma(m_t) = \sigma$(172.5GeV)×[1−0.0028×(m_t − 172.5GeV)]. The result is consistent with the SM prediction at NNLO.

[9] Based on 1.67 fb^{-1} of data. The result uses the acceptance for m_t = 172.5 GeV.

[10] Based on 3.54 fb^{-1} of data.

[11] Based on 2.3 fb^{-1} of data.

[12] Based on 3.9 fb^{-1} of data.

[13] Based on 35 pb^{-1} of data for an assumed top quark mass of m_t = 172.5 GeV.

[14] Based on 0.70 fb^{-1} of data. The 3 errors are from statistics, systematics, and luminosity. The result uses the acceptance for m_t = 172.5 GeV.

[15] Based on 35 pb^{-1} of data. The 3 errors are from statistics, systematics, and luminosity. The result uses the acceptance for m_t = 172.5 GeV and 173 ± 17^{+18}_{-16} ± 6 pb is found without the b-tag.

[16] Based on 2.05 fb^{-1} of data. The hadronic τ candidates are selected using a BDT technique. The 3 errors are from statistics, systematics, and luminosity. The result uses the acceptance for m_t = 172.5 GeV.

[17] Based on 2.0 fb^{-1} and 2.2 fb^{-1} of data for $\ell = e$ and $\ell = \mu$, respectively. The 3 errors are from statistics, systematics, and luminosity. The result uses the acceptance for m_t = 172.5 GeV.

[18] Based on 2.3 fb^{-1} of data. The 3 errors are from statistics, systematics, and luminosity. The result uses the profile likelihood-ratio (PLB) method and an assumed m_t of 172.5 GeV.

[19] Based on 2.9 pb^{-1} of data. The result for single lepton channels is 142 ± 34^{+50}_{-31} pb, while for the dilepton channels is 151^{+78+37}_{-62-24} pb.

[20] Result is based on 36 pb^{-1} of data. The first uncertainty corresponds to the statistical and systematic uncertainties, and the second corresponds to the luminosity.

[21] Based on 36 pb^{-1} of data. The ratio of $t\overline{t}$ and Z/γ^* cross sections is measured as $\sigma(pp \rightarrow t\overline{t})/\sigma(pp \rightarrow Z/\gamma^* \rightarrow e^+e^-/\mu^+\mu^-)$ = 0.175 ± 0.018(stat) ± 0.015(syst) for 60 < $m_{\ell\ell}$ < 120 GeV, for which they use an NNLO prediction for the denominator cross section of 972 ± 42 pb.

[22] Result is based on 36 pb^{-1} of data. The first error is from statistical and systematic uncertainties, and the second from luminosity. This is a combination of a measurement in the dilepton channel (CHATRCHYAN 11F) and the measurement in the ℓ + jets channel (CHATRCHYAN 11Z) which yields 150 ± 9 ± 17 ± 6 pb.

[23] Result is based on 3.1 ± 0.3 pb^{-1} of data.

$t\overline{t}$ Production Cross Section in pp Collisions at $\sqrt{s}$ = 8 TeV

Unless otherwise noted the first quoted error is from statistics, the second from systematic uncertainties, and the third from luminosity. If only two errors are quoted the luminosity is included in the systematic uncertainties.

VALUE (pb)	DOCUMENT ID		TECN	COMMENT
• • • We do not use the following data for averages, fits, limits, etc. • • •				
$243.3^{+6.0}_{-5.9}$	[1] AAD	23AY	LHC	$e^{\pm}\mu^{\mp}$ pair; ATLAS+CMS combined
248.3±0.7±13.4±4.7	[2] AABOUD	18BH	ATLS	$\ell+\not{E}_T+\geq 4$j ($\geq 1b$)
239 ±4 ±28 ±5	[3] AABOUD	17Z	ATLS	$\tau_h+\not{E}_T+\geq 2$j ($\geq 2b$)
228.5±3.8±13.7±6.0	[4] KHACHATRY...	17B	CMS	$\ell+\not{E}_T+\geq 4$j ($\geq 1b$)
242.9±1.7± 8.6	[5] AAD	16BK	ATLS	$e+\mu+1$ or $2b$ jets
$244.9\pm1.4^{+6.3}_{-5.5}\pm6.4$	[6] KHACHATRY...	16AW	CMS	$e+\mu+\not{E}_T+\geq 0$j
275.6±6.1±37.8±7.2	[7] KHACHATRY...	16BC	CMS	≥ 6j ($\geq 2b$)
260 ±1 $^{+24}_{-25}$	[8] AAD	15BP	ATLS	$\ell+\not{E}_T+\geq 3$j ($\geq 1b$)
	[9] AAIJ	15R	LHCB	$\mu+\geq 1$j(b-tag) forward region
242.4±1.7±10.2	[10] AAD	14AY	ATLS	$e+\mu+1$ or $2b$ jets
239 ±2 ±11 ±6	[11] CHATRCHYAN	14F	CMS	$\ell\ell+\not{E}_T+\geq 2$j (≥ 1 b-tag)
257 ±3 ±24 ±7	[12] KHACHATRY...	14S	CMS	$\ell+\tau_h+\not{E}_T+\geq 2$j ($\geq 1b$)

[1] AAD 23AY based on 20 fb^{-1} of data using m_t = 172.5 GeV. The ratio of this cross section at $\sqrt{s}$ = 8 TeV to the combined cross section at $\sqrt{s}$ = 7 TeV is determined as 1.363 ± 0.032. The values of cross sections as well as their ratio are consistent with the NNLO+NNLL SM predictions.

[2] AABOUD 18BH based on 20.2 fb^{-1} of data. The result is for m_t = 172.5 GeV. To reduce effects of uncertainties in the jet energy scale and b-tagging efficiency, they are included as nuisance parameters in the fit of discriminant distributions, after separating selected events into three regions. Furthermore the W+jets background distribution is modelled using Z+jets event data.

[3] AABOUD 17Z based on 20.2 fb^{-1} of data, using the mode $t\overline{t} \rightarrow \tau\nu q'\overline{q}b\overline{b}$ with τ decaying hadronically. Single prong and 3 prong decays of τ are separately analyzed. The result is consistent with the SM. The third quoted uncertainty is due to luminosity.

[4] KHACHATRYAN 17B based on 19.6 fb^{-1} of data, using a binned likelihood fit of templates to the data. Also the ratio $\sigma(t\overline{t}$; 8 TeV)/$\sigma(t\overline{t}$; 7 TeV) = 1.43 ± 0.04 ± 0.07 ± 0.05 is reported. The results are in agreement with NNLO SM predictions.

[5] AAD 16BK is an update of the value from AAD 14AY using the improved luminosity calibration. The value 242.9 ± 1.7 ± 5.5 ± 5.1 ± 4.2 pb is reported, where we have combined the systematic uncertainties in quadrature. Also the ratio $\sigma(t\overline{t}$; 8TeV)/$\sigma(t\overline{t}$; 7TeV) = 1.328 ± 0.024 ± 0.015 ± 0.038 ± 0.001 has been updated. The former result is consistent with the SM predictions at NNLO, while the latter result is 2.1 σ below the expectation.

[6] KHACHATRYAN 16AW based on 19.7 fb^{-1} of data, using a binned likelihood fit to differential distributions of b-tagged and non-b-tagged jets. The result is in good agreement with NNLO SM predictions.

[7] KHACHATRYAN 16BC based on 18.4 fb^{-1} of data. The last uncertainty is due to luminosity. Cuts on kinematical fit probability and $\Delta R(b,b)$ are imposed. The major QCD background is determined from the data. The result is for m_t = 172.5 GeV and in agreement with the SM prediction. The top quark p_T spectra, also measured, are significantly softer than theoretical predictions.

[8] AAD 15BP based on 20.3 fb^{-1} of data. The result is for m_t = 172.5 GeV and in agreement with the SM prediction 253^{+13}_{-15} pb at NNLO+NNLL. Superseded by AABOUD 18BH.

[9] AAIJ 15R, based on 2.0 fb^{-1} of data, reports 0.289 ± 0.043 ± 0.040 ± 0.029 pb cross section for the forward fiducial region $p_T(\mu)$ > 25 GeV, 2.0 < $\eta(\mu)$ < 4.5, 50 GeV < $p_T(b)$ < 100 GeV, 2.2 < $\eta(b)$ < 4.2, $\Delta R(\mu,b)$ > 0.5, and $p_T(\mu+b)$ > 20 GeV. The three errors are from statistics, systematics, and theory. The result agrees with the SM NLO prediction.

[10] AAD 14AY reports 242.4 ± 1.7 ± 5.5 ± 7.5 ± 4.2 pb value based on 20.3 fb^{-1} of data. The four errors are from statistics, systematic, luminosity, and the 0.66% beam energy uncertainty. We have combined the systematic uncertainties in quadrature. The result is for m_t = 172.5GeV; for other m_t, $\sigma(m_t) = \sigma$(172.5GeV)×[1−0.0028×(m_t − 172.5GeV)]. Also measured is the ratio $\sigma(t\overline{t}$; 8TeV)/$\sigma(t\overline{t}$; 7TeV) = 1.326 ± 0.024 ± 0.015 ± 0.049 ± 0.001. The results are consistent with the SM predictions at NNLO.

[11] Based on 5.3 fb^{-1} of data. The result is for m_t = 172.5 GeV, and a parametrization is given in eq.(6.1) for the mean value at other m_t values. The result is in agreement with the SM prediction $252.9^{+6.4}_{-8.6}$ pb at NNLO.

[12] Based on 19.6 fb^{-1} of data. The measurement is in the channel $t\overline{t} \rightarrow (b\ell\nu)(b\tau\nu)$, where τ decays into hadrons (τ_h). The result is for m_t = 172.5 GeV. For m_t = 173.3 GeV, the cross section is lower by 3.1 pb.

$t\overline{t}$ Production Cross Section in pp Collisions at $\sqrt{s}$ = 13 TeV

VALUE (pb)	DOCUMENT ID		TECN	COMMENT
• • • We do not use the following data for averages, fits, limits, etc. • • •				
829 ± 1 ±15.4	[1] AAD	23S	ATLS	$e^{\pm}\mu^{\mp}+1$ or 2 b-jets
791 ± 1 ±21 ±14	[2] TUMASYAN	21J	CMS	1ℓ + jets
830 ± 0.4±36 ±14	[3] AAD	20AH	ATLS	$\ell+\geq 4$ jets ($\geq 1b$-tag)
826.4± 3.6±11.5±15.8	[4] AAD	20Q	ATLS	$e\mu+1$ or 2 b-jets
781 ± 7 ±62 ±20	[5] SIRUNYAN	20V	CMS	$\ell\tau_h+\geq 3$ jets ($\geq 1b$-tag)
803 ± 2 ±25 ±20	[6] SIRUNYAN	19AR	CMS	dilepton channel ($e\mu$,2e,2μ)
	[7] SIRUNYAN	19P	CMS	dilepton channel
815 ± 9 ±38 ±19	[8] KHACHATRY...	17N	CMS	$e\mu+\geq 2$j ($\geq 1b$ j)
888 ± 2 $^{+26}_{-28}$ ±20	[9] SIRUNYAN	17W	CMS	$\ell+\geq 1$j
818 ± 8 ±35	[10] AABOUD	16R	ATLS	$e+\mu+1$ or $2b$ jets
746 ±58 ±53 ±36	[11] KHACHATRY...	16J	CMS	$e+\mu+\geq 2$j

[1] AAD 23S based on 140 fb^{-1} of data at 13 TeV. The second error is the sum of systematic effects (±13), luminosity (±8), and beam energy (±2) uncertainties. This measurement supersedes that of AAD 20Q. The result is in good agreement with the NNLO+NNLL SM prediction.

[2] TUMASYAN 21J result is based on 137 fb^{-1} of data. The last uncertainty is due to the beam luminosity. The result is in agreement with the SM prediction of 832^{+40}_{-46} pb at NNLO+NNLL. Measurements of differential and double-differential cross sections are also presented.

[3] AAD 20AH based on 139 fb^{-1} of data. The last quoted uncertainty is due to the beam luminosity. The result is for m_t = 172.5 GeV and in agreement with the SM prediction of 832^{+20}_{-29}(scale)±35(PDF+α(s)) pb at NNLO+NNLL.

[4] AAD 20Q reports 826.4 ± 3.6 ± 11.5 ± 15.7 ± 1.9 pb based on 36.1 fb^{-1} of data at 13 TeV. The four errors stem from statistics, systematic effects, luminosity, and beam energy, respectively. We have combined luminosity and beam energy uncertainties in quadrature. The result is in agreement with the SM prediction 832^{+20}_{-29}(scale)±35(PDF+α(s)) pb at NNLO+NNLL for m_t = 172.5 GeV .

[5] SIRUNYAN 20V based on 35.9 fb^{-1} of pp data at $\sqrt{s}$ = 13 TeV. The last uncertainty is due to beam luminosity. The $t\overline{t}$ production cross section is measured in the $t\overline{t} \rightarrow (\ell\nu_\ell)(\tau_h\nu_\tau)b\overline{b}$ final state, where τ_h refers to the hadronic decays of τ. The result is for m_t = 172.5 GeV and in agreement with the SM prediction at NNLO+NNLL.

[6] SIRUNYAN 19AR based on 35.9 fb^{-1} of data. Obtained from the visible cross section measured using a template fit to multidifferential distributions categorized according to the b-tagged jet multiplicity. The result is for m_t = 172.5 GeV and in agreement with the SM prediction at NNLO+NNLL.

[7] SIRUNYAN 19P reports differential $t\overline{t}$ cross sections measured using dilepton events at 13 TeV with 35.9 fb^{-1} and compared to NLO predictions.

[8] KHACHATRYAN 17N based on 2.2 fb^{-1} of data. The last quoted uncertainty is due to the beam luminosity. This measurement supersedes that of KHACHATRYAN 16J.

[9] SIRUNYAN 17W based on 2.2 fb^{-1} of pp data at $\sqrt{s}$ = 13 TeV. Events are categorized according to the jet multiplicity and the number of b-tagged jets. A likelihood fit is performed to the event distributions to compare to the NNLO+NNLL prediction.

[10] AABOUD 16R reported value 818 ± 8 ± 27 ± 19 ± 12 pb based on 3.2 fb^{-1} of data. The four errors are from statistics, systematic, luminosity, and beam energy. We have combined the systematic uncertainties in quadrature. The result is in agreement with the SM prediction 832^{+20}_{-29}(scale)±35(PDF+α(s)) pb at NNLO+NNLL for m_t = 172.5 GeV .

[11] KHACHATRYAN 16J based on 43 pb^{-1} of data. The last uncertainty is due to luminosity. The result is for m_t = 172.5 GeV and in agreement with the SM prediction 832^{+20}_{-29}(scale)±35(PDF+α(s)) pb at NNLO+NNLL.

$t\overline{t}$ Production Cross Section in pp Collisions at $\sqrt{s}$ = 13.6 TeV

VALUE (pb)	DOCUMENT ID		TECN	COMMENT
• • • We do not use the following data for averages, fits, limits, etc. • • •				
850±3±27	[1,2] AAD	24	ATLS	$e^{\pm}\mu^{\mp}$ + 1 or 2 b-jets

[1] AAD 24 based on 29 fb^{-1} of data. The last error includes the luminosity uncertainty of ±20 pb. The result is for m_t = 172.5 GeV and in agreement with the SM prediction of 924^{+32}_{-40} (scale+PDF+α_s) pb. The ratio of the $t\overline{t}$ to the Z production cross section is also measured as 1.145 ± 0.003 ± 0.021 ± 0.002, which is consistent with the SM prediction of $1.238^{+0.063}_{-0.071}$ (scale+PDF+α_s). The uncertainties of luminosity and lepton efficiency largely cancel in the ratio.

[2] AAD 24BC based on 29 fb^{-1} of data. The same data sample as AAD 24 is used to measure the ratios of the $t\overline{t}$ to the $W^{\pm}$, W^{+} and W^{-} production cross sections.

$t\overline{t}$ Production Cross Section in p-Nucleus Collisions

VALUE (nb)	DOCUMENT ID		TECN	COMMENT
• • • We do not use the following data for averages, fits, limits, etc. • • •				
$58.1\pm2.0^{+4.8}_{-4.4}$	[1] AAD	24CC	ATLS	$p-$Pb collisions, $\ell+\geq$ 4j, $\ell^+\ell^-+\geq$ 2j
45 ±8	[2] SIRUNYAN	17CQ	CMS	$p-$Pb collisions, $\ell+\geq$ 4j

[1] AAD 24CC based on 165 nb^{-1} of proton-lead collision data at a nucleon-nucleon c.m. energy of 8.16 TeV. Top quark pair production is observed with more than 5σ significance in each mode. The nuclear modification factor is measured to be R_{pA} = 1.090 ± 0.039(stat)$^{+0.094}_{-0.087}$(syst). The results agree with theory predictions.

[2] SIRUNYAN 17CQ based on 174 nb^{-1} of proton-lead collision data at a nucleon-nucleon c.m. energy of 8.16 TeV. Top quark pair production is observed with more than 5σ significance. The measured cross section is consistent with the expectation from the scaled pp data as well as perturbative QCD calculations.

$t\overline{t}$ Production Cross Section in Nucleus-Nucleus Collisions

VALUE (μbarn)	DOCUMENT ID		TECN	COMMENT
• • • We do not use the following data for averages, fits, limits, etc. • • •				
$3.6\ ^{+1.0}_{-0.9}\ ^{+0.8}_{-0.5}$	[1] AAD	25D	ATLS	Pb-Pb collisions, $e\mu$ + $\geq$ 2-jets
$2.03^{+0.71}_{-0.64}$	[2] SIRUNYAN	20BC	CMS	Pb-Pb collisions, dilepton + b-jets
$2.54^{+0.84}_{-0.74}$	[3] SIRUNYAN	20BC	CMS	Pb-Pb collisions, dilepton only

[1] AAD 25D based on 1.9 nb^{-1} of lead-lead collision data at a nucleon-nucleon c.m. energy of 5.02 TeV. The significance of the signal observation is 5.0σ.

[2] SIRUNYAN 20BC based on (1.7 ± 0.1) nb^{-1} of lead-lead collision data at a nucleon-nucleon c.m. energy of 5.02 TeV. It makes use of the final-state dilepton kinematic properties together with requirements on the number of b-jets. The measured value is compatible with QCD predictions.

[3] SIRUNYAN 20BC based on (1.7 ± 0.1) nb^{-1} of lead-lead collision data at a nucleon-nucleon c.m. energy of 5.02 TeV. It makes use of the final-state dilepton kinematic properties alone. The measured value is compatible with QCD predictions.

$t\overline{t}\ t\overline{t}$ Production Cross Section in pp Collisions at $\sqrt{s}$ = 8 TeV

VALUE (fb)	CL%	DOCUMENT ID		TECN	COMMENT
• • • We do not use the following data for averages, fits, limits, etc. • • •					
<23	95	[1] AAD	15AR	ATLS	$\ell+\not{E}_T+\geq$ 5j ($\geq$ 2 b)
<70	95	[2] AAD	15BY	ATLS	$\geq$ 2$\ell+\not{E}_T+\geq$ 2j ($\geq$ 1 b)
<32	95	[3] KHACHATRY...	14R	CMS	$\ell+\not{E}_T+\geq$ 6j ($\geq$ 2 b)

[1] AAD 15AR based on 20.3 fb^{-1} of data. A fit to H_T distributions in multi-channels classified by the number of jets and of b-tagged jets is performed.

[2] AAD 15BY based on 20.3 fb^{-1} of data. A same-sign lepton pair is required. An excess over the SM prediction reaches 2.5σ for hypotheses involving heavy resonances decaying into $t\overline{t}t\overline{t}$.

[3] Based on 19.6 fb^{-1} of data, using a multivariate analysis to separate signal from backgrounds. About $\sigma(t\overline{t}t\overline{t})$ = 1 fb is expected in the SM.

$t\overline{t}\ t\overline{t}$ Production Cross Section in pp Collisions at $\sqrt{s}$ = 13 TeV

VALUE (fb)	CL%	DOCUMENT ID		TECN	COMMENT
• • • We do not use the following data for averages, fits, limits, etc. • • •					
$22.5^{+6.6}_{-5.5}$		[1] AAD	23BC	ATLS	(same-sign 2ℓ) or $\geq$ 3ℓ
$17.7^{+3.7+2.3}_{-3.5-1.9}$		[2] HAYRAPETY...	23B	CMS	(same-sign 2ℓ), 3ℓ, 4ℓ
$36\ ^{+12}_{-11}$		[3] TUMASYAN	23AQ	CMS	(0,1 ℓ) + ($\ell^{\pm}\ell^{\mp}$) channels
17 ± 4 ±3		[4] TUMASYAN	23AQ	CMS	CMS combined
$26\ ^{+17}_{-15}$		[5] AAD	21BC	ATLS	ℓ or $\ell^+\ell^-$ + jets
$24\ ^{+7}_{-6}$		[6] AAD	21BC	ATLS	combination of 1ℓ/2ℓ(OS) and 2ℓ(SS)/3ℓ
$24\ ^{+7}_{-6}$		[7] AAD	20AR	ATLS	(same-sign 2ℓ) or $\geq$ 3ℓ + jets
$12.6^{+5.8}_{-5.2}$		[8] SIRUNYAN	20C	CMS	(same-sign 2ℓ) or 3ℓ + jets
<47	95	[9] AABOUD	19AP	ATLS	ℓ + $\ell^+\ell^-$ channels
<49	95	[10] AABOUD	19AP	ATLS	combination of ATLAS
$13\ ^{+11}_{-9}$		[11] SIRUNYAN	19CN	CMS	combination of CMS
<48	95	[12] SIRUNYAN	19CN	CMS	ℓ+jets, $\ell^+\ell^-$+jets channels
<69	95	[13] AABOUD	18CE	ATLS	$\geq$ 2ℓ(same sign) + $\not{E}_T$ + $\geq$ 1bj
$16.9^{+13.8}_{-11.4}$		[14] SIRUNYAN	18BU	CMS	$t\overline{t}t\overline{t}\rightarrow$ (same sign 2ℓ or $\geq$ 3ℓ) + $\geq$ 4 j ($\geq$ 2b)
<94	95	[15] SIRUNYAN	17AB	CMS	ℓ+jets, $\ell^+\ell^-$+jets channels
<42	95	[16] SIRUNYAN	17S	CMS	(same sign 2ℓ)+$\not{E}_T$+ $\geq$ 2j

[1] AAD 23BC result is based on 140 fb^{-1} of data. The result corresponds to observed significance of 6.1 σ.

[2] HAYRAPETYAN 23B based on 138 fb^{-1} of data. Improvements include the identification of leptons and jets from b hadrons, and from the revised analysis strategy for the signal-background separation by application of machine learning techniques. The result corresponds to the observed significance of 5.6 σ and is in agreement with the NLO (QCD+EW) SM prediction of $13.4^{+1.0}_{-1.8}$ fb including soft-gluon emission corrections at the next-to-leading logarithmic accuracy.

[3] TUMASYAN 23AQ based on up to 138 fb^{-1} of data. The all-hadronic final state is included for the first time.

[4] TUMASYAN 23AQ based on up to 138 fb^{-1} of data. It combines earlier CMS results, giving the observed significance of 4.0σ.

[5] AAD 21BC result is based on 139 fb^{-1} of data. The events are categorized according to the number of jets and how likely to contain b-hadrons and a multivariate analysis is used to discriminate the signal from backgrounds. The result corresponds to observed significance of 1.9 σ.

[6] AAD 21BC combines the results of the four-top-quark production cross section measured from the 1ℓ/opposite-sign 2ℓ channel with that from the same-sign 2ℓ/3ℓ channel (AAD 20AR). The result corresponds to observed significance of 4.7 σ and is consistent within 2.0 σ with the NLO (QCD+EW) SM prediction of 12.0 ± 2.4 fb.

[7] AAD 20AR based on 139 fb^{-1} of data. Jet multiplicity, jet flavor and event kinematics are used in a multivariate analysis to discriminate the signal from backgrounds. The result corresponds to observed significance of 4.3σ and is consistent within 1.7σ with the NLO (QCD+EW) SM prediction of 12.0 ± 2.4 fb.

[8] SIRUNYAN 20C based on 137 fb^{-1} of data. Both cut-based and multivariate approaches are taken to discriminate the signal from backgrounds. The result is in agreement with the NLO (QCD+EW) SM prediction of $12.0^{+2.2}_{-2.5}$ fb. The measurement constrains the top quark Yukawa coupling strength parameter to be $|Y_t/Y_t^{SM}|$ < 1.7 (95% CL). It is also used to constrain an oblique parameter of the Higgs boson. Superseded by HAYRAPETYAN 23B.

[9] AABOUD 19AP based on 36.1 fb^{-1} of data. The upper limit corresponds to 5.1 times the NLO SM cross section.

[10] AABOUD 19AP limit from data combined with AABOUD 18CE. The upper limit corresponds to 5.3 times the NLO SM cross section. Also a limit on the four-top-quark contact interaction of $|C_{4t}|/\Lambda^2$ < 1.9 TeV^{-2} (95% CL) is obtained in an EFT model.

[11] SIRUNYAN 19CN based on 35.8 fb^{-1} of data, combined with SIRUNYAN 18BU. The results are also interpreted in the effective field theory framework.

[12] SIRUNYAN 19CN based on 35.8 fb^{-1} of data. A multivariate analysis using global event and jet propoerties is performed to discriminate from $t\overline{t}$ background.

[13] AABOUD 18CE based on 36.1 fb^{-1} of proton-proton data taken at $\sqrt{s}$ = 13 TeV. Events including a same-sign lepton pair are used. The result is consistent with the NLO SM cross section of 9.2 fb.

[14] SIRUNYAN 18BU based on 35.9 fb^{-1} of proton-proton data taken at $\sqrt{s}$ = 13 TeV. Yields from signal regions and control regions defined based on N_{jets}, N_b and N_l are combined in a maximum-likelihood fit. The result is in agreement with the NLO SM prediction $9.2^{+2.9}_{-2.4}$ fb. The measurement constrains the top quark Yukawa coupling strength parameter to be $|Y_t/Y_t^{SM}|$ < 2.1 (95% CL).

[15] SIRUNYAN 17AB based on 2.6 fb^{-1} of data. A multivariate analysis is used to discriminate between $t\overline{t}t\overline{t}$ signal and $t\overline{t}$ background. A combination with a previous search (CMS, KHACHATRYAN 16BJ) in the same-sign dilepton channel gives an upper limit of 69 fb (95% CL), corresponding to 7.4·(SM prediction).

[16] SIRUNYAN 17S based on 35.9 fb^{-1}. The limit is in agreement with the NLO SM prediction $9.2^{+2.9}_{-2.4}$ fb. Superseded by SIRUNYAN 18BU. The signal events are also used to constrain various new physics models.

$t\overline{t}W$ Production Cross Section in pp Collisions at $\sqrt{s}$ = 8 TeV

VALUE (fb)	DOCUMENT ID		TECN	COMMENT
• • • We do not use the following data for averages, fits, limits, etc. • • •				
170^{+90}_{-80}±70	[1] KHACHATRY...	14N	CMS	$t\overline{t}W\rightarrow$ same sign dilepton + $\not{E}_T$ + jets

[1] Based on 19.5 fb^{-1} of data. The result is consistent with the SM prediction of $\sigma(t\overline{t}W)$ = 206^{+21}_{-23} fb.

$t\overline{t}W$ Production Cross Section in pp Collisions at $\sqrt{s}$ = 13 TeV

VALUE (pb)	DOCUMENT ID		TECN	COMMENT
• • • We do not use the following data for averages, fits, limits, etc. • • •				
0.880±0.080	[1] AAD	24AI	ATLS	2ℓ (same sign) or 3ℓ
0.868±0.040±0.051	[2] TUMASYAN	23AN	CMS	2 or 3 ℓ + $\not{E}_T$ + jets
0.87 ±0.13 ±0.14	[3] AABOUD	19AR	ATLS	2,3,4ℓ + $\not{E}_T$ + jets
$0.77\ ^{+0.12}_{-0.11}\ ^{+0.13}_{-0.12}$	[4] SIRUNYAN	18BS	CMS	$t\overline{t}W\rightarrow$ same sign dilepton + $\not{E}_T$ + jets

[1] AAD 24AI result is based on 140 fb^{-1} of data. The result is consistent with the SM prediction 0.745 ± 0.050(scale)±0.013(two loop approx.)±0.019(PDF α(S)) pb. The inclusive relative charge asymmetry of $t\overline{t}W^+$ and $t\overline{t}W^-$ is measured to be 0.33 ± 0.05 in agreement with the SM prediction of 0.322 ± 0.003(scale)±0.007(PDF).

J. Phys. A 2026.41. Downloaded from www.worldscientific.com
by UNIVERSITY OF CA ELEY on 09/16/26. Re-use and distribution is strictly not permitted, except for Open Access articles.

Int. J. Mod. Phys. A 2026.41. Downloaded from www.worldscientific.com
by UNIVERSITY OF CALIFORNIA @ BERKELEY on 09/16/26. Re-use and distribution is strictly not permitted, except for Open Access articles.

[2] TUMASYAN 23AN result is based on 138 fb^{-1} of proton-proton data. The $t\bar{t}W^+$ and $t\bar{t}W^-$ production cross sections, respectively, are measured as $0.553 \pm 0.030 \pm 0.030$ pb and $0.343 \pm 0.026 \pm 0.025$ pb. The results are within 2σ deviations from the NLO FxFx SM predictions, $0.592^{+0.155}_{-0.097}$ pb ($t\bar{t}W$), $0.384^{+0.053}_{-0.033}$ pb ($t\bar{t}W^+$) and $0.198^{+0.026}_{-0.017}$ pb ($t\bar{t}W^-$).

[3] AABOUD 19AR result is based on 35.9 fb^{-1} of data. $t\bar{t}W$ and $t\bar{t}Z$ cross sections are simultaneously measured using a combined fit to the events divided into multiple regions. The result is consistent with the SM prediction at NLO $0.60^{+0.08}_{-0.07}$ pb. It is also used to constrain the Wilson coefficients for dimension-six operators which modify the $t\bar{t}Z$ vertex.

[4] SIRUNYAN 18BS result is based on 35.9 fb^{-1} of proton-proton data taken at $\sqrt{s}$ = 13 TeV. The result is consistent with the SM prediction and is used to constrain the Wilson coefficients for dimension-six operators describing new interactions. The result is consistent with the SM prediction at NLO 0.628 ± 0.082 pb.

$t\bar{t}Z$ Production Cross Section in pp Collisions at $\sqrt{s}$ = 8 TeV

VALUE (fb)	DOCUMENT ID	TECN	COMMENT
• • • We do not use the following data for averages, fits, limits, etc. • • •			
$200^{+80}_{-70}{}^{+40}_{-30}$	[1] KHACHATRY...14N	CMS	$t\bar{t}Z \to 3,4\ \ell + \not{E}_T$ + jets

[1] Based on 19.5 fb^{-1} of data. The result is consistent with the SM prediction of $\sigma(t\bar{t}Z) = 197^{+22}_{-25}$ fb.

$t\bar{t}Z$ Production Cross Section in pp Collisions at $\sqrt{s}$ = 13 TeV

VALUE (pb)	DOCUMENT ID	TECN	COMMENT
• • • We do not use the following data for averages, fits, limits, etc. • • •			
$1.14 \pm 0.05 \pm 0.04$	[1] HAYRAPETY...25S	CMS	$\sigma(t\bar{t}Z + tWZ)$
$0.86 \pm 0.04 \pm 0.04$	[2] AAD 24AN	ATLS	2,3,4ℓ + jets
$0.99 \pm 0.05 \pm 0.08$	[3,4] AAD 21AS	ATLS	3,4ℓ + jets
$0.95 \pm 0.05 \pm 0.06$	[5] SIRUNYAN 20AB	CMS	3,4ℓ + jets
$0.95 \pm 0.08 \pm 0.10$	[6] AABOUD 19AR	ATLS	2,3,4$\ell + \not{E}_T$ + jets
$0.99^{+0.09}_{-0.08}{}^{+0.12}_{-0.10}$	[7] SIRUNYAN 18BS	CMS	$t\bar{t}Z \to 3,4\ \ell + \not{E}_T$ + jets

[1] HAYRAPETYAN 25S based on 138 fb^{-1} of data. Events with 3 or more leptons are used. It is about 2σ larger than the NLO SM prediction.

[2] AAD 24AN based on 140 fb^{-1} of data. The result is consistent with the NLO+NNLL SM prediction including EW corrections of $0.863^{+0.073}_{-0.085}$(scale) ± 0.028(PDF + α_s) pb. Also overall the differential cross sections are in good agreement with the SM predictions. All hadronic decays of $t\bar{t}$ are also included.

[3] AAD 21AS based on 139 fb^{-1} of data. The result is consistent with the SM prediction of $0.88^{+0.09}_{-0.10}$ pb which includes NLO QCD+EW corrections. Also overall the differential cross sections are in good agreement with the SM predictions.

[4] Superseded by AAD 24AN

[5] SIRUNYAN 20AB based on 77.5 fb^{-1} of data at 13 TeV. The result is consistent with the NLO SM prediction of 0.84 ± 0.10 pb. Differential cross sections are measured and used to constrain the anomalous couplings and Wilson coefficients for the $t\bar{t}Z$ interaction.

[6] AABOUD 19AR based on 35.9 fb^{-1} of data. $t\bar{t}W$ and $t\bar{t}Z$ cross sections are simultaneously measured using a combined fit to the events divided into multiple regions. The result is consistent with the SM prediction at NLO $0.88^{+0.09}_{-0.11}$ pb. It is also used to constrain the Wilson coefficients for dimension-six operators which modify the $t\bar{t}Z$ vertex.

[7] Based on 35.9 fb^{-1} of proton-proton data taken at $\sqrt{s}$ = 13 TeV. The result is consistent with the SM prediction and is used to constrain the Wilson coefficients for dimension-six operators describing new interactions. The result is consistent with the SM prediction at NLO 0.839 ± 0.101 pb.

$t\bar{t}H$ Production Cross Section in pp Collisions at $\sqrt{s}$ = 13 TeV

VALUE (fb)	DOCUMENT ID	TECN	COMMENT
• • • We do not use the following data for averages, fits, limits, etc. • • •			
$411 \pm 54^{+85}_{-75}$	[1] AAD 25AJ	ATLS	$H \to b\bar{b}$
$33 \pm 31^{+22}_{-17}$	[2] AAD 22Q	ATLS	$H \to \tau\tau$
$670 \pm 90^{+110}_{-100}$	[3] AABOUD 18BK	ATLS	$H \to b\bar{b}$, WW^* $\tau\tau$, $\gamma\gamma$, ZZ^*

[1] AAD 25AJ based on 140 fb^{-1} of data. The observed significance is 4.6σ. The measurement is consistent with the NLO SM prediction of 507^{+35}_{-50} fb.

[2] AAD 22Q based on 139 fb^{-1} of data. The measured value includes B($H \to \tau\tau$) and corresponds to the rapidity range $|y_H| < 2.5$. The value is consistent with the SM prediction, where B($H \to \tau\tau$) = 6.3% for m_H = 125.09 GeV.

[3] AABOUD 18BK based on 79.8 fb^{-1} of data. The observed significance is 5.8σ relative to the background-only hypothesis. The measurement is consistent with the NLO SM prediction of 507^{+35}_{-50} fb. See Table 3 and Fig. 5 for measurements of individual modes. Combined with the measurements at 7 and 8 TeV, the observed significance is 6.3σ.

$t\bar{t}\gamma$ Production Cross Section in pp Collisions at $\sqrt{s}$ = 13 TeV

VALUE (pb)	DOCUMENT ID	TECN	COMMENT
• • • We do not use the following data for averages, fits, limits, etc. • • •			
	[1] AAD 24BY	ATLS	single lepton + dilepton channels
	[2] TUMASYAN 22W	CMS	$1\gamma + \ell^+\ell^-$ + $\geq$ 1bj
	[3] TUMASYAN 21H	CMS	$pp \to t\bar{t}\gamma$
	[4] AABOUD 19AD	ATLS	$pp \to t\bar{t}\gamma$

[1] AAD 24BY measured fiducial inclusive and differential cross-sections for $pp \to t\bar{t}\gamma$ at 13 TeV with 140 fb^{-1} of data. The results are in agreement with the SM predictions. The results are used to constrain anomalous couplings of the top quark in the SMEFT framework.

[2] TUMASYAN 22W measured fiducial inclusive and differential cross-sections for $pp \to t\bar{t}\gamma$ at 13 TeV with 138 fb^{-1} of data. The results are in agreement with the SM predictions. The results are used to constrain anomalous couplings of the top quark in the SMEFT framework.

[3] TUMASYAN 21H measured fiducial inclusive and differential cross-sections for $pp \to t\bar{t}\gamma$ at 13 TeV with 137 fb^{-1} of data. The results are in agreement with the SM predictions. The results are used to constrain anomalous couplings of the top quark in the SMEFT framework.

[4] AABOUD 19AD measured fiducial inclusive and differential cross-sections for $pp \to t\bar{t}\gamma$ at 13 TeV with 36.1 fb^{-1} of data. The results are in agreement with the theoretical predictions.

f(Q_0): $t\bar{t}$ Fraction of Events with a Veto on Additional Central Jet Activity in pp Collisions at $\sqrt{s}$ = 7 TeV

Q_0 denotes the threshold of the additional jet p_T.

VALUE (%)	DOCUMENT ID	TECN	COMMENT
• • • We do not use the following data for averages, fits, limits, etc. • • •			
$80.0 \pm 1.1 \pm 1.6$	[1] CHATRCHYAN 14AE	CMS	Q_0 = 75 GeV ($|y|$ <2.4)
$92.0 \pm 0.7 \pm 0.8$	[1] CHATRCHYAN 14AE	CMS	Q_0= 150 GeV ($|y|$ <2.4)
$98.0 \pm 0.3 \pm 0.3$	[1] CHATRCHYAN 14AE	CMS	Q_0= 300 GeV ($|y|$ <2.4)
$56.4 \pm 1.3^{+2.6}_{-2.8}$	[2] AAD 12BL	ATLS	Q_0 = 25 GeV ($|y|$ <2.1)
$84.7 \pm 0.9 \pm 1.0$	[2] AAD 12BL	ATLS	Q_0 = 75 GeV ($|y|$ <2.1)
$95.2^{+0.5}_{-0.6} \pm 0.4$	[2] AAD 12BL	ATLS	Q_0= 150 GeV ($|y|$ <2.1)

[1] CHATRCHYAN 15 based on 5.0 fb^{-1} of data. The $t\bar{t}$ events are selected in the dilepton and lepton + jets decay channels. For other values of Q_0 see Table 5.

[2] Based on 2.05 fb^{-1} of data. The $t\bar{t}$ events are selected in the dilepton decay channel with two identified b-jets.

Fraction of $t\bar{t}$ + multi-jet Events in pp Collisions at $\sqrt{s}$ = 7 TeV

VALUE	DOCUMENT ID	TECN	COMMENT
• • • We do not use the following data for averages, fits, limits, etc. • • •			
	[1] AAD 15D	ATLS	$\ell + \not{E}_T$ + nj (n=3 to 8)
0.332 ± 0.090	[2] CHATRCHYAN 14AE	CMS	$t\bar{t}(\ell\ell)$ + 0 jet (E_T > 30GeV)
0.436 ± 0.098	[2] CHATRCHYAN 14AE	CMS	$t\bar{t}(\ell\ell)$ + 1 jet (E_T > 30GeV)
0.232 ± 0.125	[2] CHATRCHYAN 14AE	CMS	$t\bar{t}(\ell\ell)$ + $\geq$ 2 jet (E_T > 30GeV)

[1] Based on 4.6 fb^{-1} of data. Fiducial $t\bar{t}$ production cross section is presented as a function of the jet multiplicity for up to eight jets with the jet p_T threshold of 25, 40, 60, and 80 GeV, and as a function of jet p_T up to the 5th jet. MC models can be discriminated by using data for high jet multiplicity and by p_T distributions of the leading and 5th jet.

[2] Based on 5.0 fb^{-1} of data. Events with two oppositely charged leptons, large $\not{E}_T$ and jets with at least 1 b-tag are used to measure the fraction of $t\bar{t}$ plus additional jets. The gap fraction (n=0 jet rate) as a function of the jet p_T and that of H_T, the scalar sum of the p_T's of additional jets, is shown in Fig. 8.

$t\bar{t}$ Charge Asymmetry (A_C) in pp Collisions at $\sqrt{s}$ = 7 TeV

A_C = (N($\Delta|y|$ >0) − N($\Delta|y|$ <0)) / (N($\Delta|y|$ >0) + N($\Delta|y|$ <0)) where $\Delta|y| = |y_t| - |y_{\bar{t}}|$ is the difference between the absolute values of the top and antitop rapidities and N is the number of events with $\Delta|y|$ positive or negative.

VALUE (%)	DOCUMENT ID	TECN	COMMENT
• • • We do not use the following data for averages, fits, limits, etc. • • •			
$0.5 \pm 0.7 \pm 0.6$	[1] AABOUD 18AM	LHC	ATLAS+CMS combination (lepton + jets)
$2.1 \pm 2.5 \pm 1.7$	[2] AAD 15AJ	ATLS	$\ell\ell + \not{E}_T$ + $\geq$ 2j
0.6 ± 1.0	[3] AAD 14I	ATLS	$\ell + \not{E}_T$ + $\geq$ 4j ($\geq$ 1b)
$-1.0 \pm 1.7 \pm 0.8$	[4] CHATRCHYAN 14D	CMS	$\ell\ell + \not{E}_T$ + $\geq$ 2j ($\geq$ 1b)
$-1.9 \pm 2.8 \pm 2.4$	[5] AAD 12BK	ATLS	$\ell + \not{E}_T$ + $\geq$ 4j ($\geq$ 1b)
$0.4 \pm 1.0 \pm 1.1$	[6] CHATRCHYAN 12BB	CMS	$\ell + \not{E}_T$ + $\geq$ 4j ($\geq$ 1b)
$-1.3 \pm 2.8^{+2.9}_{-3.1}$	[7] CHATRCHYAN 12BS	CMS	$\ell + \not{E}_T$ + $\geq$ 4j ($\geq$ 1b)

[1] ATLAS and CMS combination based on the data of AAD 14I and CHATRCHYAN 12BB. It takes into account the correlations of the measurements and systematic errors. The result is in agreement with the SM prediction (NLO QCD + NLO EW).

[2] AAD 15AJ based on 4.6 fb^{-1} of data. After kinematic reconstruction the top quark momenta are corrected for detector resolution and acceptance effects by unfolding, using parton level information of the MC generators. The lepton charge asymmetry is measured as $A_C^\ell = 0.024 \pm 0.015 \pm 0.009$. All the measurements are consistent with the SM predictions.

[3] Based on 4.7 fb^{-1} of data. The result is consistent with the SM prediction of A_C = 0.0123 ± 0.0005. The asymmetry is 0.011 ± 0.018 if restricted to those events where $\beta_Z(t\bar{t}) > 0.6$, which is also consistent with the SM prediction of $0.020^{+0.006}_{-0.007}$.

[4] Based on 5.0 fb^{-1} of data. The lepton charge asymmetry is measured as $A_C^\ell = 0.009 \pm 0.0010 \pm 0.006$. A_C^ℓ dependences on $m_{t\bar{t}}$, $|y(t\bar{t})|$, and $p_T(t\bar{t})$ are given in Fig. 5. All measurements are consistent with the SM predictions.

[5] Based on 1.04 fb^{-1} of data. The result is consistent with A_C = 0.006 ± 0.002 (MC at NLO). No significant dependence of A_C on $m_{t\bar{t}}$ is observed.

[6] Based on 5.0 fb^{-1} of data at 7 TeV.

[7] Based on 1.09 fb^{-1} of data. The result is consistent with the SM predictions.

$t\bar{t}$ Charge Asymmetry (A_C) in pp Collisions at $\sqrt{s}$ = 8 TeV

VALUE (%)	DOCUMENT ID	TECN	COMMENT
• • • We do not use the following data for averages, fits, limits, etc. • • •			
$0.55 \pm 0.23 \pm 0.25$	[1] AABOUD 18AM	LHC	ATLAS+CMS combination (lepton + jets)
2.1 ± 1.6	[2] AAD 16AE	ATLS	$\ell\ell + \not{E}_T$ + $\geq$ 2j

Phys. A 2026.41. Downloaded from www.worldscientific.com
by UNIVERSITY OF CA LEY on 09/16/26. Re-use and distribution is strictly not permitted, except for Open Access articles.

0.9 ±0.5	[3] AAD	16AZ	ATLS	$\ell + \not{E}_T + \geq 4$j
4.2 ±3.2	[4] AAD	16T	ATLS	$m_{t\overline{t}} > 0.75$ TeV, $\|\|y_t\| - \|y_{\overline{t}}\|\| < 2$, $\ell + \not{E}_T$ + jets
1.1 ±1.1 ±0.7	[5] KHACHATRY...16AD		CMS	$\ell\ell + \not{E}_T + \geq 2$j ($\geq 1$b)
0.33±0.26±0.33	[6] KHACHATRY...16AH		CMS	$\ell + \not{E}_T + \geq 4$j ($\geq 1$b)
0.10±0.68±0.37	[7] KHACHATRY...16T		CMS	$\ell + \not{E}_T + \geq 4$j ($\geq 1$b)

[1] ATLAS and CMS combination based on the data of AAD 16AZ and KHACHATRYAN 16AH. It takes into account the correlations of the measurements and systematic errors. A combination of the differential measurements of the charge asymmetry is also presented. The results are in agreement with the SM prediction (NNLO QCD + NLO EW).

[2] AAD 16AE is based on 20.3 fb^{-1} of data. After kinematic reconstruction, the top quark momenta are corrected for detector resolution and acceptance effects by unfolding, using parton level information of the MC generators. The lepton charge asymmetry is measured as $A_C^{\ell\ell} = 0.008 \pm 0.006$. All the measurements are consistent with the SM predictions.

[3] AAD 16AZ based on 20.3 fb^{-1} of data. All the differential and inclusive measurements are statistically limited and consistent with the SM predictions.

[4] AAD 16T based on 20.3 fb^{-1} of data. Uses reconstruction techniques for the decay topology of highly boosted top quarks. The observed asymmetry is transformed by unfolding to a parton-level result in the shown fiducial region. The result is consistent with the NLO SM prediction.

[5] KHACHATRYAN 16AD based on 19.5 fb^{-1} of data. The lepton charge asymmetry is measured as $A_C^{\ell\ell} = 0.003 \pm 0.006 \pm 0.003$. All the measurements are consistent with the SM predictions.

[6] KHACHATRYAN 16AH based on 19.6 fb^{-1} of data. The same data set as in KHACHATRYAN 16T is used. A template technique is used, which is sensitive to the charge anti-symmetric component of the $t\overline{t}$ rapidity distributions and statistically advantageous. The result is consistent with the SM predictions.

[7] KHACHATRYAN 16T based on 19.7 fb^{-1} of data. The same data set as in KHACHATRYAN 16AH is used. After kinematic reconstruction the top quark momenta are corrected for detector resolution and acceptance effects by unfolding, using parton level information of the MC generators. All the measurements are consistent with the SM predictions.

$t\overline{t}$ Charge Asymmetry (A_C) in pp Collisions at $\sqrt{s} = 13$ TeV

VALUE (%)	DOCUMENT ID		TECN	COMMENT
• • • We do not use the following data for averages, fits, limits, etc. • • •				
0.68±0.15	[1] AAD	23BA	ATLS	single lepton + dilepton channels
$0.42^{+0.64}_{-0.69}$	[2] TUMASYAN	23BD	CMS	$M_{t\overline{t}} > 750$GeV, single-ℓ channel

[1] AAD 23BA is based on 139 fb^{-1} of data. Inclusive $t\overline{t}$ charge asymmetry is measured to be nonzero with 4.7σ significance. Also differential $t\overline{t}$ as well as lepton charge asymmetries are measured. All the results are consistent with the SM predictions which include NNLO QCD + NLO EW corrections.

[2] TUMASYAN 23BD is based on 138 fb^{-1} of data. $t\overline{t}$ charge asymmetry for highly Lorentz-boosted top quarks is measured and is in agreement with the NNLO QCD + NLO EW corrected SM prediction of $0.94^{+0.05}_{-0.07}$%. The event selection is optimized for highly-boosted top quarks.

$t\overline{t}W$ leptonic Charge Asymmetry (A_C^{ℓ}) in pp Collisions at $\sqrt{s} = 13$ TeV

VALUE	DOCUMENT ID		TECN	COMMENT
• • • We do not use the following data for averages, fits, limits, etc. • • •				
−0.12±0.14±0.05	[1] AAD	23AA	ATLS	$\ell\ell\ell + \geq 1b$

[1] AAD 23AA is based on 139 fb^{-1} of data. The charge-asymmetry in a fiducial volume at particle level is also reported at $-0.11 \pm 0.17 \pm 0.05$. All the results are consistent with the SM predictions which include NLO QCD + NLO EW corrections.

$t\overline{t}\gamma$ Charge Asymmetry (A_C) in pp Collisions at $\sqrt{s} = 13$ TeV

VALUE	DOCUMENT ID		TECN	COMMENT
• • • We do not use the following data for averages, fits, limits, etc. • • •				
−0.003±0.029	[1] AAD	23AW	ATLS	$\gamma\ell + \geq 4$j ($\geq 1b$)

[1] AAD 23AW is based on 139 fb^{-1} of data. The measurement is in agreement with the Standard Model expectation.

t-quark Polarization in $t\overline{t}$ Events in $p\overline{p}$ Collisions at $\sqrt{s} = 1.96$ TeV

VALUE	DOCUMENT ID		TECN	COMMENT
• • • We do not use the following data for averages, fits, limits, etc. • • •				
0.070±0.055	[1] ABAZOV	17	D0	$\ell + \not{E}_T + \geq 3$j($\geq 1b$)
−0.102±0.061	[2] ABAZOV	17	D0	$\ell + \not{E}_T + \geq 3$j($\geq 1b$)
0.040±0.035	[3] ABAZOV	17	D0	$\ell + \not{E}_T + \geq 3$j($\geq 1b$)
0.113±0.091±0.019	[4] ABAZOV	15K	D0	A_{FB}^{ℓ} in $\ell\ell + \not{E}_T + \geq 2$j($\geq 1b$)

[1] ABAZOV 17 based on 9.7 fb^{-1} of data. The value is top quark polarization times spin analyzing power in the beam basis. Combination with the result of ABAZOV 15K yields 0.081 ± 0.048. This result together with the helicity polarization is shown in a 2-dimensional plot in Fig.4. These results are consistent with the SM prediction.

[2] ABAZOV 17 based on 9.7 fb^{-1} of data. The value is top quark polarization times spin analyzing power in the helicity basis. The result is consistent with the SM prediction. This result together with the beam polarization is shown in a 2-dimensional plot in Fig.4.

[3] ABAZOV 17 based on 9.7 fb^{-1} of data. The value is top quark polarization times spin analyzing power in the transverse basis. The result is consistent with the SM prediction.

[4] ABAZOV 15K based on 9.7 fb^{-1} of data. The value is top quark polarization times spin analyzing power in the beam basis. The result is consistent with the SM prediction of -0.0019 ± 0.0005.

t-quark Polarization in $t\overline{t}$ Events in pp Collisions at $\sqrt{s} = 7$ TeV

The double differential distribution in polar angles, θ_1 (θ_2) of the decay particle of the top (anti-top) decay products, is parametrized as $(1/\sigma)d\sigma/(d\cos\theta_1\ d\cos\theta_2) = (1/4)\ (1 + A_t \cos\theta_1 + A_{\overline{t}} \cos\theta_2 - C \cos\theta_1 \cos\theta_2)$. The charged lepton is used to tag t or $\overline{t}$. The coefficient A_t and $A_{\overline{t}}$ measure the average helicity of t and $\overline{t}$, respectively. $A_{CPC} = A_t = A_{\overline{t}}$ assumes CP conservation, whereas $A_{CPV} = A_t = -A_{\overline{t}}$ corresponds to maximal CP violation.

VALUE	DOCUMENT ID		TECN	COMMENT
• • • We do not use the following data for averages, fits, limits, etc. • • •				
−0.035±0.014±0.037	[1] AAD	13BE	ATLS	A_{CPC}
$0.020 \pm 0.016^{+0.013}_{-0.017}$	[1] AAD	13BE	ATLS	A_{CPV}

[1] Based on 4.7 fb^{-1} of data using the final states containing one or two isolated electrons or muons and jets with at least one b-tag.

t-quark Polarization in $t\overline{t}$ Events in pp Collisions at $\sqrt{s} = 8$ TeV

A_t, $A_{\overline{t}}$, A_{CPC}, A_{CPV}, and A_C are defined in header texts in the subsections, just above.

VALUE	DOCUMENT ID		TECN	COMMENT
• • • We do not use the following data for averages, fits, limits, etc. • • •				
−0.044±0.038±0.027	[1] AABOUD	17G	ATLS	A_t
−0.064±0.040±0.027	[1] AABOUD	17G	ATLS	$A_{\overline{t}}$
0.296±0.093±0.037	[1] AABOUD	17G	ATLS	A_C
−0.022±0.058	[2] KHACHATRY...16AI		CMS	A_{CPC}
0.000±0.016	[2] KHACHATRY...16AI		CMS	A_{CPV}

[1] AABOUD 17G based on 20.2 fb^{-1} of pp data, using events with two leptons and two or more jets with at least one b-tag. Determined from measurements of 15 top quark spin observables. The second error corresponds to a variation of m_t about 172.5 GeV by 0.7 GeV. The values are consistent with the NLO SM predictions.

[2] KHACHATRYAN 16AI based on 19.5 fb^{-1} of pp data at $\sqrt{s} = 8$ TeV, using events with two leptons and two or more jets with at least one b-tag. Determined from the lepton angular distributions as a function of the $t\overline{t}$-system kinematical variables.

t-quark Polarization in Single Top Events in pp Collisions at $\sqrt{s} = 8$ TeV

VALUE	CL%	DOCUMENT ID		TECN	COMMENT
• • • We do not use the following data for averages, fits, limits, etc. • • •					
>0.72	95	[1] AABOUD	17BB	ATLS	$\alpha_\ell P$; t-channel
0.97±0.05±0.11		[2] AABOUD	17I	ATLS	$\alpha_\ell P$; t-channel
0.25±0.08±0.14		[3] AABOUD	17I	ATLS	$(F_+ + F_-)P$; t-channel
0.26±0.03±0.10		[4] KHACHATRY...16BO		CMS	$(\alpha_\mu P)/2$; t-channel

[1] AABOUD 17BB based on 20.2 fb^{-1} of pp data. Triple-differential decay rate of top quark is used to simultaneously determine five generalized Wtb couplings as well as the top polarization. α_ℓ denotes the spin analyzing power of charged lepton, and the spin axis of the top polarization P is taken along the spectator-quark momentum in the top rest frame. The value is compatible with the SM prediction of about 0.9.

[2] AABOUD 17I based on 20.2 fb^{-1} of pp data. A cut-based analysis is used to discriminate between signal and backgrounds. α_ℓ denotes the spin analyzing power of charged lepton, and the spin axis of the top polarization P is taken along the spectator-quark momentum in the top rest frame. See this paper for a number of other asymmetries and measurements that are not included here.

[3] AABOUD 17I based on 20.2 fb^{-1} of pp data. A cut-based analysis is used to discriminate between signal and backgrounds. $F_\pm$ denotes W helicity fraction, and the spin axis of the top polarization P is taken along the spectator-quark momentum in the top rest frame. See this paper for a number of other asymmetries and measurements that are not included here.

[4] KHACHATRYAN 16BO based on 19.7 fb^{-1} of data. A high-purity sample with a muon is selected by a multivariate analysis. The value is the top spin asymmetry, given by one half of the spin analyzing power α_μ (=1 at LO of SM) times the top polarization, P, where the spin axis is defined as the direction of the untagged jet in the top rest frame. The value is compatible with the SM prediction of 0.44 with a 2.0σ deviation.

t-quark Polarization in Single Top Events in pp Collisions at $\sqrt{s} = 13$ TeV

VALUE	DOCUMENT ID		TECN	COMMENT
• • • We do not use the following data for averages, fits, limits, etc. • • •				
0.01 ±0.18	[1] AAD	22Z	ATLS	$P_{x'}$ (t, transverse component)
−0.029±0.027	[1] AAD	22Z	ATLS	$P_{y'}$ (t, normal component)
0.91 ±0.10	[1] AAD	22Z	ATLS	$P_{z'}$ (t, parallel component)
−0.02 ±0.20	[1] AAD	22Z	ATLS	$P_{x'}$ ($\overline{t}$, transverse component)
−0.007±0.051	[1] AAD	22Z	ATLS	$P_{y'}$ ($\overline{t}$, normal component)
−0.79 ±0.16	[1] AAD	22Z	ATLS	$P_{z'}$ ($\overline{t}$, parallel component)
0.440±0.070	[2] SIRUNYAN	20R	CMS	$(\alpha_\ell P)/2$; t-channel

[1] AAD 22Z based on 139 fb^{-1} of data. Three components of t or $\overline{t}$ polarization vector (defined in the t or $\overline{t}$ rest frame) are measured in t-channel single top production using ℓ momentum distribution in the $\ell + \not{E}_T$ + 2j (with 1 of them b-jet) channel. The measured values are in agreement with NNLO SM prediction. Constraints on the Wilson coefficients of SMEFT are obtained as -0.9 < C_{tW} < 1.4 and -0.8 < C_{ltW} < 0.2.

[2] SIRUNYAN 20R based on 36.1 fb^{-1} of data. Differential cross sections for t-channel single top production are measured using 1ℓ + 2,3-jet mode and found to be in good agreement with SM predictions. The value is the top spin asymmetry, given by 1/2 of the spin analyzing power α_ℓ (=1 at LO of SM) times the top polarization P, where the spin axis is defined as the direction of the spectator quark in the top rest frame at the parton level. It is in good agreement with the NLO SM prediction of 0.436.

$gg \rightarrow t\overline{t}$ Fraction in $p\overline{p}$ Collisions at $\sqrt{s} = 1.96$ TeV

VALUE	CL%	DOCUMENT ID		TECN	COMMENT
• • • We do not use the following data for averages, fits, limits, etc. • • •					
<0.33	68	[1] AALTONEN	09F	CDF	$t\overline{t}$ correlations
0.07±0.14±0.07		[2] AALTONEN	08AG	CDF	low p_T number of tracks

[1] Based on 955 pb^{-1}. AALTONEN 09F used differences in the $t\overline{t}$ production angular distribution and polarization correlation to descriminate between $gg \rightarrow t\overline{t}$ and $q\overline{q} \rightarrow t\overline{t}$ subprocesses. The combination with the result of AALTONEN 08AG gives $0.07^{+0.15}_{-0.07}$.

[2] Result is based on 0.96 fb^{-1} of data. The contribution of the subprocesses $gg \rightarrow t\overline{t}$ and $q\overline{q} \rightarrow t\overline{t}$ is distinguished by using the difference between quark and gluon initiated jets in the number of small p_T (0.3 GeV < p_T < 3 GeV) charged particles in the central region ($|\eta| < 1.1$).

Int. J. Mod. Phys. A 2026.41. Downloaded from www.worldscientific.com
by UNIVERSITY OF CALIFORNIA @ BERKELEY on 09/16/26. Re-use and distribution is strictly not permitted, except for Open Access articles.

A_{FB} of $t\overline{t}$ in $p\overline{p}$ Collisions at $\sqrt{s}$ = 1.96 TeV

A_{FB} = Forward-backward asymmetry.

VALUE (%)	DOCUMENT ID		TECN	COMMENT
• • • We do not use the following data for averages, fits, limits, etc. • • •				
$12.8 \pm 2.1 \pm 1.4$	[1] AALTONEN	18	TEVA	CDF, D0 combination
$17.5 \pm 5.6 \pm 3.1$	[2] ABAZOV	15K	D0	A^{ℓ}_{FB} in $\ell\ell + \not{E}_T + \geq 2j(\geq 1b)$
7.2 ± 6.0	[3] AALTONEN	14F	CDF	A^{ℓ}_{FB} in dilepton channel ($\ell\ell + \not{E}_T + \geq 2j$)
7.6 ± 8.2	[3] AALTONEN	14F	CDF	$A^{\ell\ell}_{FB}$ in dilepton channel ($\ell\ell + \not{E}_T + \geq 2j$)
$4.2 \pm 2.3^{+1.7}_{-2.0}$	[4] ABAZOV	14G	D0	A^{ℓ}_{FB} ($\ell + \not{E}_T + \geq 3j$ ($0,1 \geq 2b$))
10.6 ± 3.0	[5] ABAZOV	14H	D0	A_{FB} ($\ell + \not{E}_T + \geq 3j$ ($\geq 1b$))
20.1 ± 6.7	[6] AALTONEN	13AD	CDF	a_1/a_0 in $\ell + \not{E}_T + \geq 4j$ ($\geq 1b$)
-0.2 ± 3.1	[6] AALTONEN	13AD	CDF	a_3, a_5, a_7 in $\ell + \not{E}_T + \geq 4j$ ($\geq 1b$)
16.4 ± 4.7	[7] AALTONEN	13S	CDF	$\ell + \not{E}_T + \geq 4$ jets($\geq 1b$-tag)
$9.4^{+3.2}_{-2.9}$	[8] AALTONEN	13X	CDF	$\ell + \not{E}_T + \geq 4$ jets (≥ 1 b-tag)
11.8 ± 3.2	[9] ABAZOV	13A	D0	$\ell\ell$ & $\ell+$ jets comb.
-11.6 ± 15.3	[10] AALTONEN	11F	CDF	$m_{t\overline{t}} < 450$ GeV
47.5 ± 11.4	[10] AALTONEN	11F	CDF	$m_{t\overline{t}} > 450$ GeV
19.6 ± 6.5	[11] ABAZOV	11AH	D0	$\ell + \not{E}_T + \geq 4$ jets($\geq 1b$-tag)
17 ± 8	[12] AALTONEN	08AB	CDF	$p\overline{p}$ frame
24 ± 14	[12] AALTONEN	08AB	CDF	$t\overline{t}$ frame
$12 \pm 8 \pm 1$	[13] ABAZOV	08L	D0	$\ell + \not{E}_T + \geq 4$ jets

[1] AALTONEN 18 based on 9–10 fb^{-1} of $p\overline{p}$ data at $\sqrt{s}$ = 1.96 TeV. The value is the asymmetry in the number of reconstructed $t\overline{t}$ events with rapidity $y_t > y_{\overline{t}}$ and those with $y_t < y_{\overline{t}}$. The combined fits to CDF and D0 single lepton and $\ell\ell$ asymmetries give $A^{\ell}_{FB} = 0.073 \pm 0.016 \pm 0.012$ and $A^{\ell\ell}_{FB} = 0.108 \pm 0.043 \pm 0.016$, respectively. The results are consistent with the SM predictions.

[2] ABAZOV 15K based on 9.7 fb^{-1} of data. The result is consistent with the SM predictions. By combining with the previous D0 measurement in the ℓ + jet channel ABAZOV 14H, $A^{\ell}_{FB} = 0.118 \pm 0.025 \pm 0.013$ is obtained.

[3] AALTONEN 14F based on 9.1 fb^{-1} of data. A^{ℓ}_{FB} and $A^{\ell\ell}_{FB}$ denote, respectively, the asymmetries $(N(x>0) - N(x<0))/N_{tot}$ for $x = q_{\ell}\eta_{\ell}$ (q_{ℓ} is the charge of ℓ) and $x = \eta_{\ell^+} - \eta_{\ell^-}$. Both results are consistent with the SM predictions. By combining with the previous CDF measurement in the ℓ+jet channel AALTONEN 13X, $A^{\ell}_{FB} = 0.098^{+0.028}_{-0.026}$ is obtained. The combined result is about two sigma larger than the SM prediction of $A^{\ell}_{FB} = 0.038 \pm 0.003$.

[4] Based on 9.7 fb^{-1} of $p\overline{p}$ data at $\sqrt{s}$ = 1.96 TeV. The asymmetry is corrected for the production level for events with $|y_l| < 1.5$. Asymmetry as functions of $E_T(\ell)$ and $|y_l|$ are given in Figs. 7 and 8, respectively. Combination with the asymmetry measured in the dilepton channel [ABAZOV 13P] gives $A^{\ell}_{FB} = 4.2 \pm 2.0 \pm 1.4$ %, in agreement with the SM prediction of 2.0%.

[5] Based on 9.7 fb^{-1} of data of $p\overline{p}$ data at $\sqrt{s}$=1.96 TeV. The measured asymmetry is in agreement with the SM predictions of 8.8 ± 0.9 % [BERNREUTHER 12], which includes the EW effects. The dependences of the asymmetry on $|y(t) - y(\overline{t})|$ and $m_{t\overline{t}}$ are shown in Figs. 9 and 10, respectively.

[6] Based on 9.4 fb^{-1} of data. Reported A_{FB} values come from the determination of a_i coefficients of $d\sigma/d(\cos\theta_t) = \Sigma_i\, a_i P_i(\cos(\theta_t))$ measurement. The result of $a_1/a_0 = (40 \pm 12)$% seems higher than the NLO SM prediction of (15^{+7}_{-3})%.

[7] Based on 9.4 fb^{-1} of data. The quoted result is the asymmetry at the parton level.

[8] Based on 9.4 fb^{-1} of data. The observed asymmetry is to be compared with the SM prediction of $A^{\ell}_{FB} = 0.038 \pm 0.003$.

[9] Based on 5.4 fb^{-1} of data. ABAZOV 13A studied the dilepton channel of the $t\overline{t}$ events and measured the leptonic forward-backward asymmetry to be $A^{\ell}_{FB} = 5.8 \pm 5.1 \pm 1.3$%, which is consistent with the SM (QCD+EW) prediction of 4.7 ± 0.1%. The result is obtained after combining the measurement (15.2 ± 4.0%) in the ℓ + jets channel ABAZOV 11AH. The top quark helicity is measured by using the neutrino weighting method to be consistent with zero in both dilepton and ℓ + jets channels.

[10] Based on 5.3 fb^{-1} of data. The error is statistical and systematic combined. Events with lepton + $\not{E}_T$ + $\geq$ 4jets($\geq 1b$) are used. AALTONEN 11F also measures the asymmetry as a function of the rapidity difference $|y_t - y_{\overline{t}}|$. The NLO QCD predictions [MCFM] are (4.0 ± 0.6)% and (8.8 ± 1.3)% for $m_{t\overline{t}} < 450$ and > 450 GeV, respectively.

[11] Based on 5.4 fb^{-1} of data. The error is statistical and systematic combined. The quoted asymmetry is obtained after unfolding to be compared with the MC@NLO prediction of (5.0 ± 0.1)%. No significant difference between the $m_{t\overline{t}} < 450$ and > 450 GeV data samples is found. A corrected asymmetry based on the lepton from a top quark decay of (15.2 ± 4.0)% is measured to be compared to the MC@NLO prediction of (2.1 ± 0.1)%.

[12] Result is based on 1.9 fb^{-1} of data. The FB asymmetry in the $t\overline{t}$ events has been measured in the ℓ + jets mode, where the lepton charge is used as the flavor tag. The asymmetry in the $p\overline{p}$ frame is defined in terms of $\cos(\theta)$ of hadronically decaying t-quark momentum, whereas that in the $t\overline{t}$ frame is defined in terms of the t and $\overline{t}$ rapidity difference. The results are consistent ($\leq 2\,\sigma$) with the SM predictions.

[13] Result is based on 0.9 fb^{-1} of data. The asymmetry in the number of $t\overline{t}$ events with $y_t > y_{\overline{t}}$ and those with $y_t < y_{\overline{t}}$ has been measured in the lepton + jets final state. The observed value is consistent with the SM prediction of 0.8% by MC@NLO, and an upper bound on the $Z' \to t\overline{t}$ contribution for the SM Z-like couplings is given in in Fig. 2 for 350 GeV $< m_{Z'} <$ 1 TeV.

t-Quark Electric Charge

VALUE	DOCUMENT ID		TECN	COMMENT
$0.64 \pm 0.02 \pm 0.08$	[1] AAD	13AY	ATLS	$\ell + \not{E}_T + \geq 4$ jets (≥ 1 b)
• • • We do not use the following data for averages, fits, limits, etc. • • •				
	[2] ABAZOV	14D	D0	$\ell + \not{E}_T + \geq 4$ jets (≥ 2 b)
	[3] AALTONEN	13J	CDF	$p\overline{p}$ at 1.96 TeV
	[4] AALTONEN	10S	CDF	Repl. by AALTONEN 13J
	[5] ABAZOV	07C	D0	fraction of $|q|$=4e/3 pair

[1] AAD 13AY result is based on 2.05 fb^{-1} of pp data at $\sqrt{s}$ = 7 TeV, the result is obtained by reconstructing $t\overline{t}$ events in the lepton + jets final state, where b-jet charges are tagged by the jet-charge algorithm. This measurement excludes the charge $-4/3$ assignment to the top quark at more than 8 standard deviations.

[2] ABAZOV 14D result is based on 5.3 fb^{-1} of $p\overline{p}$ data at $\sqrt{s}$=1.96 TeV. The electric charge of $b + W$ system in $t\overline{t}$ candidate events is measured from the charges of the leptons from W decay and in b jets. Under the assumption that the $b + W$ system consists of the sum of the top quark and the charge $-4/3$ quark b'(-4/3) of the same mass, the top quark fraction is found to be $f = 0.88 \pm 0.13$ (stat)± 0.11 (syst), or the upper bound for the b'(-4/3) contamination of $1 - f < 0.46$ (95% CL).

[3] AALTONEN 13J excludes the charge $-4/3$ assignment to the top quark at 99% CL, using 5.6 fb^{-1} of data in $p\overline{p}$ collisions at $\sqrt{s}$ = 1.96 TeV. Result is obtained by reconstructing $t\overline{t}$ events in the lepton + jets final state, where b-jet charges are tagged by the jet-charge algorithm.

[4] AALTONEN 10S excludes the charge $-4/3$ assignment for the top quark [CHANG 99] at 95%CL, using 2.7 fb^{-1} of data in $p\overline{p}$ collisions at $\sqrt{s}$ = 1.96 TeV. Result is obtained by reconstructing $t\overline{t}$ events in the lepton + jets final state, where b-jet charges are tagged by the SLT (soft lepton tag) algorithm.

[5] ABAZOV 07C reports an upper limit $\rho < 0.80$ (90% CL) on the fraction ρ of exotic quark pairs $Q\overline{Q}$ with electric charge $|q| = 4e/3$ in $t\overline{t}$ candidate events with high p_T lepton, missing E_T and ≥ 4 jets. The result is obtained by measuring the fraction of events in which the quark pair decays into $W^- + b$ and $W^+ + \overline{b}$, where b and $\overline{b}$ jets are discriminated by using the charge and momenta of tracks within the jet cones. The maximum CL at which the model of CHANG 99 can be excluded is 92%. Based on 370 pb^{-1} of data at $\sqrt{s}$ = 1.96 TeV.

t-Quark REFERENCES

AAD	25AJ	EPJ C85 210	G. Aad et al.	(ATLAS Collab.)
AAD	25BD	JHEP 2510 093	G. Aad et al.	(ATLAS Collab.)
AAD	25BI	JHEP 2512 023	G. Aad et al.	(ATLAS Collab.)
AAD	25D	PRL 134 142301	G. Aad et al.	(ATLAS Collab.)
AAD	25H	PL B867 139608	G. Aad et al.	(ATLAS Collab.)
AAD	25T	JHEP 2502 084	G. Aad et al.	(ATLAS Collab.)
HAYRAPETY...	25AD	PR D112 032008	A. Hayrapetyan et al.	(CMS Collab.)
HAYRAPETY...	25AJ	PL B869 139857	A. Hayrapetyan et al.	(CMS Collab.)
HAYRAPETY...	25AO	JHEP 2512 065	A. Hayrapetyan et al.	(CMS Collab.)
HAYRAPETY...	25J	PR D111 012009	A. Hayrapetyan et al.	(CMS Collab.)
HAYRAPETY...	25N	JHEP 2501 107	A. Hayrapetyan et al.	(CMS Collab.)
HAYRAPETY...	25R	JHEP 2502 097	A. Hayrapetyan et al.	(CMS Collab.)
HAYRAPETY...	25S	JHEP 2502 177	A. Hayrapetyan et al.	(CMS Collab.)
HAYRAPETY...	25U	JHEP 2504 099	A. Hayrapetyan et al.	(CMS Collab.)
AAD	24	PL B848 138376	G. Aad et al.	(ATLAS Collab.)
AAD	24AI	JHEP 2405 131	G. Aad et al.	(ATLAS Collab.)
Also		JHEP 2511 127 (errat.)	G. Aad et al.	(ATLAS Collab.)
AAD	24AL	JHEP 2405 305	G. Aad et al.	(ATLAS Collab.)
Also		JHEP 2506 024 (errat.)	G. Aad et al.	(ATLAS Collab.)
AAD	24AN	JHEP 2407 163	G. Aad et al.	(ATLAS Collab.)
AAD	24AU	EPJ C84 757	G. Aad et al.	(ATLAS Collab.)
AAD	24BC	PL B854 138725	G. Aad et al.	(ATLAS Collab.)
AAD	24BN	PRL 133 161803	G. Aad et al.	(ATLAS Collab.)
AAD	24BS	PR D110 072010	G. Aad et al.	(ATLAS Collab.)
AAD	24BY	JHEP 2410 191	G. Aad et al.	(ATLAS Collab.)
AAD	24CC	JHEP 2411 101	G. Aad et al.	(ATLAS Collab.)
AAD	24CO	NAT 633 542	G. Aad et al.	(ATLAS Collab.)
AAD	24J	PL B849 138469	G. Aad et al.	(ATLAS Collab.)
AAD	24M	PL B854 138726	G. Aad et al.	(ATLAS Collab.)
AAD	24W	PR D110 012014	G. Aad et al.	(ATLAS Collab.)
HAYRAPETY...	24AS	PR D110 112016	A. Hayrapetyan et al.	(CMS Collab.)
HAYRAPETY...	24E	PRL 132 241802	A. Hayrapetyan et al.	(CMS Collab.)
HAYRAPETY...	24F	PRL 132 261902	A. Hayrapetyan et al.	(ATLAS and CMS Collab.)
HAYRAPETY...	24K	PL B855 138815	A. Hayrapetyan et al.	(CMS Collab.)
HAYRAPETY...	24L	PR D109 072004	A. Hayrapetyan et al.	(CMS Collab.)
AABOUD	23	PR D108 032014	M. Aaboud et al.	(ATLAS Collab.)
AAD	23	PL B842 137379	G. Aad et al.	(ATLAS Collab.)
Also		PL B847 138286 (errat.)	G. Aad et al.	(ATLAS Collab.)
AAD	23AA	JHEP 2307 033	G. Aad et al.	(ATLAS Collab.)
AAD	23AS	PR D108 032019	G. Aad et al.	(ATLAS Collab.)
AAD	23AW	PL B843 137848	G. Aad et al.	(ATLAS Collab.)
AAD	23AY	JHEP 2307 213	G. Aad et al.	(ATLAS and CMS Collabs.)
AAD	23BA	JHEP 2308 077	G. Aad et al.	(ATLAS Collab.)
AAD	23BC	EPJ C83 496	G. Aad et al.	(ATLAS Collab.)
Also		EPJ C84 156 (errat.)	G. Aad et al.	(ATLAS Collab.)
AAD	23BN	PRL 131 181901	G. Aad	(ATLAS Collab.)
AAD	23CJ	JHEP 2312 195	G. Aad et al.	(ATLAS Collab.)
AAD	23E	JHEP 2306 191	G. Aad et al.	(ATLAS Collab.)
AAD	23H	JHEP 2306 155	G. Aad et al.	(ATLAS Collab.)
AAD	23J	JHEP 2306 138	G. Aad et al.	(ATLAS Collab.)
AAD	23N	JHEP 2306 019	G. Aad et al.	(ATLAS Collab.)
AAD	23S	JHEP 2307 141	G. Aad et al.	(ATLAS Collab.)
HAYRAPETY...	23B	PL B847 138290	A. Hayrapetyan et al.	(CMS Collab.)
TUMASYAN	23AN	JHEP 2307 219	A. Tumasyan et al.	(CMS Collab.)
TUMASYAN	23AQ	PL B844 138076	A. Tumasyan et al.	(CMS Collab.)
TUMASYAN	23BB	EPJ C83 963	A. Tumasyan et al.	(CMS Collab.)
TUMASYAN	23BD	PL B846 137703	A. Tumasyan et al.	(CMS Collab.)
TUMASYAN	23J	JHEP 2306 081	A. Tumasyan et al.	(CMS Collab.)
TUMASYAN	23R	JHEP 2307 077	A. Tumasyan et al.	(CMS Collab.)
TUMASYAN	23T	JHEP 2307 046	A. Tumasyan et al.	(CMS Collab.)
TUMASYAN	23U	JHEP 2307 023	A. Tumasyan et al.	(CMS Collab.)
TUMASYAN	23Z	EPJ C83 560	A. Tumasyan et al.	(CMS Collab.)
AAD	22Q	JHEP 2208 175	G. Aad et al.	(ATLAS Collab.)
AAD	22T	EPJ C82 334	G. Aad et al.	(ATLAS Collab.)
AAD	22Z	JHEP 2211 040	G. Aad et al.	(ATLAS Collab.)
TUMASYAN	22A	PRL 129 032001	A. Tumasyan et al.	(CMS Collab.)
TUMASYAN	22K	JHEP 2202 169	A. Tumasyan et al.	(CMS Collab.)
TUMASYAN	22L	JHEP 2202 107	A. Tumasyan et al.	(CMS Collab.)
TUMASYAN	22T	JHEP 2204 144	A. Tumasyan et al.	(CMS Collab.)
TUMASYAN	22W	JHEP 2205 091	A. Tumasyan et al.	(CMS Collab.)
TUMASYAN	22Z	JHEP 2206 082	A. Tumasyan et al.	(CMS Collab.)
AAD	21AS	EPJ C81 737	G. Aad et al.	(ATLAS Collab.)
AAD	21AT	EPJ C81 720	G. Aad et al.	(ATLAS Collab.)
AAD	21BC	JHEP 2111 118	G. Aad et al.	(ATLAS Collab.)
TUMASYAN	21E	JHEP 2111 111	A. Tumasyan et al.	(CMS Collab.)
TUMASYAN	21G	JHEP 2112 161	A. Tumasyan et al.	(CMS Collab.)
TUMASYAN	21H	JHEP 2112 180	A. Tumasyan et al.	(CMS Collab.)
TUMASYAN	21J	PR D104 092013	A. Tumasyan et al.	(CMS Collab.)
AAD	20AB	JHEP 2007 124	G. Aad et al.	(ATLAS Collab.)
AAD	20AH	PL B810 135797	G. Aad et al.	(ATLAS Collab.)

Phys. A 2026.41. Downloaded from www.worldscientific.com
by UNIVERSITY OF CA LEY on 09/16/26. Re-use and distribution is strictly not permitted, except for Open Access articles.

AAD	20AR	EPJ C80 1085	G. Aad *et al.*	(ATLAS Collab.)
AAD	20B	PL B800 135082	G. Aad *et al.*	(ATLAS Collab.)
AAD	20Q	EPJ C80 528	G. Aad *et al.*	(ATLAS Collab.)
AAD	20Y	JHEP 2008 051	G. Aad *et al.*	(ATLAS and CMS Collabs.)
AAD	20Z	PRL 125 061802	G. Aad *et al.*	(ATLAS Collab.)
SIRUNYAN	20AB	JHEP 2003 056	A.M. Sirunyan *et al.*	(CMS Collab.)
SIRUNYAN	20AM	JHEP 2006 146	A.M. Sirunyan *et al.*	(CMS Collab.)
SIRUNYAN	20AR	PRL 124 202001	A.M. Sirunyan *et al.*	(CMS Collab.)
SIRUNYAN	20AS	PRL 125 061801	A.M. Sirunyan *et al.*	(CMS Collab.)
SIRUNYAN	20AZ	PL B808 135609	A.M. Sirunyan *et al.*	(CMS Collab.)
SIRUNYAN	20BC	PRL 125 222001	A.M. Sirunyan *et al.*	(CMS Collab.)
SIRUNYAN	20BH	PR D102 092013	A.M. Sirunyan *et al.*	(CMS Collab.)
SIRUNYAN	20BV	EPJ C80 658	A.M. Sirunyan *et al.*	(CMS Collab.)
SIRUNYAN	20C	EPJ C80 75	A.M. Sirunyan *et al.*	(CMS Collab.)
SIRUNYAN	20D	PL B800 135042	A.M. Sirunyan *et al.*	(CMS Collab.)
SIRUNYAN	20R	EPJ C80 370	A.M. Sirunyan *et al.*	(CMS Collab.)
SIRUNYAN	20V	JHEP 2002 191	A.M. Sirunyan *et al.*	(CMS Collab.)
AABOUD	19AC	EPJ C79 290	M. Aaboud *et al.*	(ATLAS Collab.)
AABOUD	19AD	EPJ C79 382	M. Aaboud *et al.*	(ATLAS Collab.)
AABOUD	19AP	PR D99 052009	M. Aaboud *et al.*	(ATLAS Collab.)
AABOUD	19AR	PR D99 072009	M. Aaboud *et al.*	(ATLAS Collab.)
AABOUD	19R	JHEP 1905 088	M. Aaboud *et al.*	(ATLAS and CMS Collabs.)
AABOUD	19S	JHEP 1905 123	M. Aaboud *et al.*	(ATLAS Collab.)
AAD	19G	JHEP 1911 150	G. Aad *et al.*	(ATLAS Collab.)
SIRUNYAN	19AP	EPJ C79 313	A.M. Sirunyan *et al.*	(CMS Collab.)
SIRUNYAN	19AR	EPJ C79 368	A.M. Sirunyan *et al.*	(CMS Collab.)
SIRUNYAN	19BF	PRL 122 132003	A.M. Sirunyan *et al.*	(CMS Collab.)
SIRUNYAN	19BX	PR D100 072002	A.M. Sirunyan *et al.*	(CMS Collab.)
SIRUNYAN	19BY	PR D100 072007	A.M. Sirunyan *et al.*	(CMS Collab.)
SIRUNYAN	19CN	JHEP 1911 082	A.M. Sirunyan *et al.*	(CMS Collab.)
SIRUNYAN	19P	JHEP 1902 149	A.M. Sirunyan *et al.*	(CMS Collab.)
SIRUNYAN	19R	JHEP 1903 026	A.M. Sirunyan *et al.*	(CMS Collab.)
AABOUD	18AE	PL B780 557	M. Aaboud *et al.*	(ATLAS Collab.)
AABOUD	18AM	JHEP 1804 033	M. Aaboud *et al.*	(ATLAS and CMS Collabs.)
AABOUD	18AT	JHEP 1807 176	M. Aaboud *et al.*	(ATLAS Collab.)
AABOUD	18AZ	EPJ C78 129	M. Aaboud *et al.*	(ATLAS Collab.)
AABOUD	18BH	EPJ C78 487	M. Aaboud *et al.*	(ATLAS Collab.)
AABOUD	18BK	PL B784 173	M. Aaboud *et al.*	(ATLAS Collab.)
AABOUD	18BW	JHEP 1809 139	M. Aaboud *et al.*	(ATLAS Collab.)
AABOUD	18CE	JHEP 1812 039	M. Aaboud *et al.*	(ATLAS Collab.)
AABOUD	18H	JHEP 1801 063	M. Aaboud *et al.*	(ATLAS Collab.)
AABOUD	18X	PR D98 032002	M. Aaboud *et al.*	(ATLAS Collab.)
AALTONEN	18	PRL 120 042001	T. Aaltonen *et al.*	(CDF and D0 Collabs.)
SIRUNYAN	18AQ	JHEP 1803 115	A.M. Sirunyan *et al.*	(CMS Collab.)
SIRUNYAN	18BC	JHEP 1806 102	A.M. Sirunyan *et al.*	(CMS Collab.)
SIRUNYAN	18BD	JHEP 1806 101	A.M. Sirunyan *et al.*	(CMS Collab.)
SIRUNYAN	18BS	JHEP 1808 011	A.M. Sirunyan *et al.*	(CMS Collab.)
SIRUNYAN	18BU	EPJ C78 140	A.M. Sirunyan *et al.*	(CMS Collab.)
SIRUNYAN	18DE	EPJ C78 891	A.M. Sirunyan *et al.*	(CMS Collab.)
Also		EPJ C82 323 (errat.)	A.M. Sirunyan *et al.*	(CMS Collab.)
SIRUNYAN	18DL	JHEP 1810 117	A.M. Sirunyan *et al.*	(CMS Collab.)
SIRUNYAN	18L	PRL 120 231801	A.M. Sirunyan *et al.*	(CMS Collab.)
SIRUNYAN	18Z	PL B779 358	A.M. Sirunyan *et al.*	(CMS Collab.)
AABOUD	17AH	JHEP 1709 118	M. Aaboud *et al.*	(ATLAS Collab.)
AABOUD	17AV	JHEP 1710 129	M. Aaboud *et al.*	(ATLAS Collab.)
AABOUD	17BB	JHEP 1712 017	M. Aaboud *et al.*	(ATLAS Collab.)
AABOUD	17BC	EPJ C77 804	M. Aaboud *et al.*	(ATLAS Collab.)
AABOUD	17G	JHEP 1703 113	M. Aaboud *et al.*	(ATLAS Collab.)
AABOUD	17H	JHEP 1704 086	M. Aaboud *et al.*	(ATLAS Collab.)
AABOUD	17I	JHEP 1704 124	M. Aaboud *et al.*	(ATLAS Collab.)
AABOUD	17T	EPJ C77 531	M. Aaboud *et al.*	(ATLAS Collab.)
AABOUD	17Z	PR D95 072003	M. Aaboud *et al.*	(ATLAS Collab.)
ABAZOV	17	PR D95 011101	V.M. Abazov *et al.*	(D0 Collab.)
ABAZOV	17B	PR D95 112004	V.M. Abazov *et al.*	(D0 Collab.)
CHATRCHYAN	17	PL B770 50	S. Chatrchyan *et al.*	(CMS Collab.)
KHACHATRY...	17B	EPJ C77 15	V. Khachatryan *et al.*	(CMS Collab.)
KHACHATRY...	17G	JHEP 1702 028	V. Khachatryan *et al.*	(CMS Collab.)
KHACHATRY...	17I	JHEP 1702 079	V. Khachatryan *et al.*	(CMS Collab.)
KHACHATRY...	17N	EPJ C77 172	V. Khachatryan *et al.*	(CMS Collab.)
SIRUNYAN	17AA	PL B772 752	A.M. Sirunyan *et al.*	(CMS Collab.)
SIRUNYAN	17AB	PL B772 336	A.M. Sirunyan *et al.*	(CMS Collab.)
SIRUNYAN	17CQ	PRL 119 242001	A.M. Sirunyan *et al.*	(CMS Collab.)
SIRUNYAN	17E	JHEP 1707 003	A.M. Sirunyan *et al.*	(CMS Collab.)
SIRUNYAN	17L	EPJ C77 354	A.M. Sirunyan *et al.*	(CMS Collab.)
SIRUNYAN	17N	EPJ C77 467	A.M. Sirunyan *et al.*	(CMS Collab.)
SIRUNYAN	17O	PR D96 032002	A.M. Sirunyan *et al.*	(CMS Collab.)
SIRUNYAN	17S	EPJ C77 578	A.M. Sirunyan *et al.*	(CMS Collab.)
SIRUNYAN	17W	JHEP 1709 051	A.M. Sirunyan *et al.*	(CMS Collab.)
AABOUD	16R	PL B761 136	M. Aaboud *et al.*	(ATLAS Collab.)
AABOUD	16T	PL B761 350	M. Aaboud *et al.*	(ATLAS Collab.)
AAD	16AE	PR D94 032006	G. Aad *et al.*	(ATLAS Collab.)
AAD	16AK	JHEP 1604 023	G. Aad *et al.*	(ATLAS Collab.)
AAD	16AS	EPJ C76 55	G. Aad *et al.*	(ATLAS Collab.)
Also		EPJ C82 70 (errat.)	G. Aad *et al.*	(ATLAS Collab.)
AAD	16AZ	EPJ C76 87	G. Aad *et al.*	(ATLAS Collab.)
AAD	16B	JHEP 1601 064	G. Aad *et al.*	(ATLAS Collab.)
AAD	16BK	EPJ C76 642	G. Aad *et al.*	(ATLAS Collab.)
AAD	16D	EPJ C76 12	G. Aad *et al.*	(ATLAS Collab.)
AAD	16T	PL B756 52	G. Aad *et al.*	(ATLAS Collab.)
AAD	16U	PL B756 228	G. Aad *et al.*	(ATLAS Collab.)
AALTONEN	16	PR D93 032011	T. Aaltonen *et al.*	(CDF Collab.)
ABAZOV	16	PL B752 18	V.M. Abazov *et al.*	(D0 Collab.)
ABAZOV	16A	PL B757 199	V.M. Abazov *et al.*	(D0 Collab.)
ABAZOV	16D	PR D94 032004	V.M. Abazov *et al.*	(D0 Collab.)
ABAZOV	16F	PR D94 092004	V.M. Abazov *et al.*	(D0 Collab.)
KHACHATRY...	16AD	PL B760 365	V. Khachatryan *et al.*	(CMS Collab.)
KHACHATRY...	16AH	PR D93 034014	V. Khachatryan *et al.*	(CMS Collab.)
KHACHATRY...	16AI	PR D93 052007	V. Khachatryan *et al.*	(CMS Collab.)
KHACHATRY...	16AK	PR D93 072004	V. Khachatryan *et al.*	(CMS Collab.)
KHACHATRY...	16AL	PR D93 092006	V. Khachatryan *et al.*	(CMS Collab.)
KHACHATRY...	16AS	JHEP 1604 035	V. Khachatryan *et al.*	(CMS Collab.)
KHACHATRY...	16AW	JHEP 1608 029	V. Khachatryan *et al.*	(CMS Collab.)
KHACHATRY...	16AZ	JHEP 1609 027	V. Khachatryan *et al.*	(CMS Collab.)
KHACHATRY...	16BC	EPJ C76 128	V. Khachatryan *et al.*	(CMS Collab.)
KHACHATRY...	16BJ	EPJ C76 439	V. Khachatryan *et al.*	(CMS Collab.)
KHACHATRY...	16BO	JHEP 1604 073	V. Khachatryan *et al.*	(CMS Collab.)
KHACHATRY...	16BU	PL B762 512	V. Khachatryan *et al.*	(CMS Collab.)
KHACHATRY...	16CB	JHEP 1612 123	V. Khachatryan *et al.*	(CMS Collab.)
KHACHATRY...	16J	PRL 116 052002	V. Khachatryan *et al.*	(CMS Collab.)
KHACHATRY...	16T	PL B757 154	V. Khachatryan *et al.*	(CMS Collab.)
KHACHATRY...	16X	PL B758 321	V. Khachatryan *et al.*	(CMS Collab.)
TEVEWWG	16	arXiv:1608.01881	Tevatron Electroweak Working Group	
AAD	15	PL B740 222	G. Aad *et al.*	(ATLAS Collab.)
AAD	15A	PL B740 118	G. Aad *et al.*	(ATLAS Collab.)
AAD	15AJ	JHEP 1505 061	G. Aad *et al.*	(ATLAS Collab.)
AAD	15AR	JHEP 1508 105	G. Aad *et al.*	(ATLAS Collab.)
AAD	15AW	EPJ C75 158	G. Aad *et al.*	(ATLAS Collab.)
AAD	15BF	EPJ C75 330	G. Aad *et al.*	(ATLAS Collab.)
AAD	15BO	PR D91 052005	G. Aad *et al.*	(ATLAS Collab.)
AAD	15BP	PR D91 112013	G. Aad *et al.*	(ATLAS Collab.)
AAD	15BW	JHEP 1510 121	G. Aad *et al.*	(ATLAS Collab.)
AAD	15BY	JHEP 1510 150	G. Aad *et al.*	(ATLAS Collab.)
AAD	15CC	PR D92 072005	G. Aad *et al.*	(ATLAS Collab.)
AAD	15CO	JHEP 1512 061	G. Aad *et al.*	(ATLAS Collab.)
AAD	15D	JHEP 1501 020	G. Aad *et al.*	(ATLAS Collab.)
AAD	15J	PRL 114 142001	G. Aad *et al.*	(ATLAS Collab.)
AAIJ	15R	PRL 115 112001	R. Aaij *et al.*	(LHCb Collab.)
AALTONEN	15D	PR D92 032003	T. Aaltonen *et al.*	(CDF Collab.)
AALTONEN	15H	PRL 115 152003	T. Aaltonen *et al.*	(CDF, D0 Collab.)
ABAZOV	15G	PR D91 112003	V.M. Abazov *et al.*	(D0 Collab.)
ABAZOV	15K	PR D92 052007	V.M. Abazov *et al.*	(D0 Collab.)
CHATRCHYAN	15	EPJ C75 216 (errat.)	S. Chatrchyan *et al.*	(CMS Collab.)
AAD	14	PL B728 363	G. Aad *et al.*	(ATLAS Collab.)
AAD	14AA	JHEP 1406 008	G. Aad *et al.*	(ATLAS Collab.)
AAD	14AY	EPJ C74 3109	G. Aad *et al.*	(ATLAS Collab.)
AAD	14BB	PR D90 112016	G. Aad *et al.*	(ATLAS Collab.)
AAD	14BI	PR D90 112006	G. Aad *et al.*	(ATLAS Collab.)
AAD	14I	JHEP 1402 107	G. Aad *et al.*	(ATLAS Collab.)
AALTONEN	14A	PR D89 091101	T. Aaltonen *et al.*	(CDF Collab.)
AALTONEN	14F	PRL 113 042001	T. Aaltonen *et al.*	(CDF Collab.)
Also		PRL 117 199901 (errat.)	T. Aaltonen *et al.*	(CDF Collab.)
AALTONEN	14G	PRL 112 221801	T. Aaltonen *et al.*	(CDF Collab.)
AALTONEN	14H	PR D89 072001	T. Aaltonen *et al.*	(CDF and D0 Collab.)
AALTONEN	14K	PRL 112 231805	T. Aaltonen *et al.*	(CDF Collab.)
AALTONEN	14L	PRL 112 231804	T. Aaltonen *et al.*	(CDF Collab.)
AALTONEN	14M	PRL 112 231803	T. Aaltonen *et al.*	(CDF and D0 Collab.)
AALTONEN	14N	PR D90 091101	T. Aaltonen *et al.*	(CDF Collab.)
AALTONEN	14O	PRL 113 261804	T. Aaltonen *et al.*	(CDF Collab.)
ABAZOV	14C	PRL 113 032002	V.M. Abazov *et al.*	(D0 Collab.)
Also		PR D91 112003	V.M. Abazov *et al.*	(D0 Collab.)
ABAZOV	14D	PR D90 051101	V.M. Abazov *et al.*	(D0 Collab.)
ABAZOV	14G	PR D90 072001	V.M. Abazov *et al.*	(D0 Collab.)
ABAZOV	14H	PR D90 072011	V.M. Abazov *et al.*	(D0 Collab.)
ABAZOV	14K	PR D90 092006	V.M. Abazov *et al.*	(D0 Collab.)
CHATRCHYAN	14	PL B728 496	S. Chatrchyan *et al.*	(CMS Collab.)
CHATRCHYAN	14AC	PRL 112 231802	S. Chatrchyan *et al.*	(CMS Collab.)
CHATRCHYAN	14AE	EPJ C74 3014	S. Chatrchyan *et al.*	(CMS Collab.)
Also		EPJ C75 216 (errat.)	S. Chatrchyan *et al.*	(CMS Collab.)
CHATRCHYAN	14C	EPJ C74 2758	S. Chatrchyan *et al.*	(CMS Collab.)
CHATRCHYAN	14D	JHEP 1404 191	S. Chatrchyan *et al.*	(CMS Collab.)
CHATRCHYAN	14F	JHEP 1402 024	S. Chatrchyan *et al.*	(CMS Collab.)
CHATRCHYAN	14O	PL B731 173	S. Chatrchyan *et al.*	(CMS Collab.)
CHATRCHYAN	14R	PR D90 032006	S. Chatrchyan *et al.*	(CMS Collab.)
CHATRCHYAN	14S	PRL 112 171802	S. Chatrchyan *et al.*	(CMS Collab.)
KHACHATRY...	14E	PL B736 33	V. Khachartryan *et al.*	(CMS Collab.)
KHACHATRY...	14F	JHEP 1406 090	V. Khachartryan *et al.*	(CMS Collab.)
KHACHATRY...	14H	JHEP 1409 087	V. Khachartryan *et al.*	(CMS Collab.)
KHACHATRY...	14K	PL B738 526 (errat.)	S. Chatrchyan *et al.*	(CMS Collab.)
KHACHATRY...	14N	EPJ C74 3060	V. Khachartryan *et al.*	(CMS Collab.)
KHACHATRY...	14Q	PR D90 112013	V. Khachatryan *et al.*	(CMS Collab.)
KHACHATRY...	14R	JHEP 1411 154	V. Khachartryan *et al.*	(CMS Collab.)
KHACHATRY...	14S	PL B739 23	V. Khachartryan *et al.*	(CMS Collab.)
AAD	13AY	JHEP 1311 031	G. Aad *et al.*	(ATLAS Collab.)
AAD	13BE	PRL 111 232002	G. Aad *et al.*	(ATLAS Collab.)
AAD	13X	EPJ C73 2328	G. Aad *et al.*	(ATLAS Collab.)
AALTONEN	13AB	PR D88 091103	T. Aaltonen *et al.*	(CDF Collab.)
AALTONEN	13AD	PRL 111 182002	T. Aaltonen *et al.*	(CDF Collab.)
AALTONEN	13D	PR D87 031104	T. Aaltonen *et al.*	(CDF Collab.)
AALTONEN	13E	PR D87 052013	T. Aaltonen *et al.*	(CDF Collab.)
AALTONEN	13G	PR D87 111101	T. Aaltonen *et al.*	(CDF Collab.)
AALTONEN	13H	PR D88 011101	T. Aaltonen *et al.*	(CDF Collab.)
AALTONEN	13J	PR D88 032003	T. Aaltonen *et al.*	(CDF Collab.)
AALTONEN	13S	PR D87 092002	T. Aaltonen *et al.*	(CDF Collab.)
AALTONEN	13X	PR D88 072003	T. Aaltonen *et al.*	(CDF Collab.)
AALTONEN	13Z	PRL 111 202001	T. Aaltonen *et al.*	(CDF Collab.)
ABAZOV	13A	PR D87 011103	V.M. Abazov *et al.*	(D0 Collab.)
ABAZOV	13O	PL B726 656	V.M. Abazov *et al.*	(D0 Collab.)
ABAZOV	13P	PR D88 112002	V.M. Abazov *et al.*	(D0 Collab.)
CHATRCHYAN	13AY	JHEP 1305 065	S. Chatrchyan *et al.*	(CMS Collab.)
CHATRCHYAN	13BB	PL B720 83	S. Chatrchyan *et al.*	(CMS Collab.)
CHATRCHYAN	13BE	EPJ C73 2386	S. Chatrchyan *et al.*	(CMS Collab.)
CHATRCHYAN	13BH	JHEP 1310 167	S. Chatrchyan *et al.*	(CMS Collab.)
CHATRCHYAN	13C	PRL 110 022003	S. Chatrchyan *et al.*	(CMS Collab.)
CHATRCHYAN	13F	PL B718 1252	S. Chatrchyan *et al.*	(CMS Collab.)
CHATRCHYAN	13S	EPJ C73 2494	S. Chatrchyan *et al.*	(CMS Collab.)
AAD	12B	PL B707 459	G. Aad *et al.*	(ATLAS Collab.)
AAD	12BE	JHEP 1204 069	G. Aad *et al.*	(ATLAS Collab.)
AAD	12BF	JHEP 1205 059	G. Aad *et al.*	(ATLAS Collab.)
AAD	12BG	JHEP 1206 088	G. Aad *et al.*	(ATLAS Collab.)
AAD	12BK	EPJ C72 2039	G. Aad *et al.*	(ATLAS Collab.)
AAD	12BL	EPJ C72 2043	G. Aad *et al.*	(ATLAS Collab.)
AAD	12BO	PL B711 244	G. Aad *et al.*	(ATLAS Collab.)
AAD	12BP	PL B712 351	G. Aad *et al.*	(ATLAS Collab.)
AAD	12BT	JHEP 1209 139	G. Aad *et al.*	(ATLAS Collab.)
AAD	12CG	PL B717 89	G. Aad *et al.*	(ATLAS Collab.)
AAD	12CH	PL B717 330	G. Aad *et al.*	(ATLAS Collab.)
AAD	12I	EPJ C72 2046	G. Aad *et al.*	(ATLAS Collab.)
AALTONEN	12AI	PRL 109 152003	T. Aaltonen *et al.*	(CDF Collab.)
AALTONEN	12AL	PRL 109 192001	T. Aaltonen *et al.*	(CDF Collab.)
AALTONEN	12AP	PR D86 092003	T. Aaltonen *et al.*	(CDF, D0 Collab.)
AALTONEN	12G	PL B714 24	T. Aaltonen *et al.*	(CDF Collab.)
AALTONEN	12Z	PR D85 071106	T. Aaltonen *et al.*	(CDF, D0 Collab.)
ABAZOV	12AB	PR D86 051103	V.M. Abazov *et al.*	(D0 Collab.)
ABAZOV	12B	PRL 108 032004	V.M. Abazov *et al.*	(D0 Collab.)
ABAZOV	12E	PL B708 21	V.M. Abazov *et al.*	(D0 Collab.)
ABAZOV	12I	PL B713 165	V.M. Abazov *et al.*	(D0 Collab.)
ABAZOV	12T	PR D85 091104	V.M. Abazov *et al.*	(D0 Collab.)
BERNREUTH...	12	PR D86 034026	W. Bernreuther, Z.-G. Si	(AACH, SHDN)
CHATRCHYAN	12AC	PR D85 112007	S. Chatrchyan *et al.*	(CMS Collab.)
CHATRCHYAN	12AX	JHEP 1211 067	S. Chatrchyan *et al.*	(CMS Collab.)
CHATRCHYAN	12BA	EPJ C72 2202	S. Chatrchyan *et al.*	(CMS Collab.)
CHATRCHYAN	12BB	PL B717 129	S. Chatrchyan *et al.*	(CMS Collab.)
CHATRCHYAN	12BP	JHEP 1212 105	S. Chatrchyan *et al.*	(CMS Collab.)
CHATRCHYAN	12BQ	JHEP 1212 035	S. Chatrchyan *et al.*	(CMS Collab.)
CHATRCHYAN	12BS	PL B709 28	S. Chatrchyan *et al.*	(CMS Collab.)
CHATRCHYAN	12Y	JHEP 1206 109	S. Chatrchyan *et al.*	(CMS Collab.)
AAD	11A	EPJ C71 1577	G. Aad *et al.*	(ATLAS Collab.)
AALTONEN	11AC	PR D84 071105	T. Aaltonen *et al.*	(CDF Collab.)
AALTONEN	11AK	PRL 107 232002	T. Aaltonen *et al.*	(CDF Collab.)
AALTONEN	11AR	PR D83 031104	T. Aaltonen *et al.*	(CDF Collab.)
AALTONEN	11D	PR D83 071102	T. Aaltonen *et al.*	(CDF Collab.)
AALTONEN	11E	PR D83 111101	T. Aaltonen *et al.*	(CDF Collab.)
AALTONEN	11F	PR D83 112003	T. Aaltonen *et al.*	(CDF Collab.)
AALTONEN	11K	PRL 106 152001	T. Aaltonen *et al.*	(CDF Collab.)
AALTONEN	11T	PL B698 371	T. Aaltonen *et al.*	(CDF Collab.)
AALTONEN	11W	PR D84 031101	T. Aaltonen *et al.*	(CDF Collab.)
AALTONEN	11Y	PR D84 032003	T. Aaltonen *et al.*	(CDF Collab.)
AALTONEN	11Z	PR D84 031104	T. Aaltonen *et al.*	(CDF Collab.)
ABAZOV	11A	PL B695 88	V.M. Abazov *et al.*	(D0 Collab.)
ABAZOV	11AA	PL B705 313	V.M. Abazov *et al.*	(D0 Collab.)
ABAZOV	11AD	PR D84 112001	V.M. Abazov *et al.*	(D0 Collab.)
ABAZOV	11AE	PRL 107 032001	V.M. Abazov *et al.*	(D0 Collab.)
ABAZOV	11AF	PL B702 16	V.M. Abazov *et al.*	(D0 Collab.)
ABAZOV	11AH	PR D84 112005	V.M. Abazov *et al.*	(D0 Collab.)

Int. J. Mod. Phys. A 2026.41. Downloaded from www.worldscientific.com
by UNIVERSITY OF CALIFORNIA @ BERKELEY on 09/16/26. Re-use and distribution is strictly not permitted, except for Open Access articles.

ABAZOV	11B	PRL 106 022001	V.M. Abazov *et al.*	(D0 Collab.)
ABAZOV	11C	PR D83 032009	V.M. Abazov *et al.*	(D0 Collab.)
ABAZOV	11E	PR D84 012008	V.M. Abazov *et al.*	(D0 Collab.)
ABAZOV	11M	PL B701 313	V.M. Abazov *et al.*	(D0 Collab.)
ABAZOV	11P	PR D84 032004	V.M. Abazov *et al.*	(D0 Collab.)
ABAZOV	11R	PRL 107 082004	V.M. Abazov *et al.*	(D0 Collab.)
ABAZOV	11S	PL B703 422	V.M. Abazov *et al.*	(D0 Collab.)
ABAZOV	11T	PR D84 052005	V.M. Abazov *et al.*	(D0 Collab.)
ABAZOV	11X	PRL 107 121802	V.M. Abazov *et al.*	(D0 Collab.)
ABAZOV	11Z	PL B704 403	V.M. Abazov *et al.*	(D0 Collab.)
CHATRCHYAN	11AA	EPJ C71 1721	S. Chatrchyan *et al.*	(CMS Collab.)
CHATRCHYAN	11F	JHEP 1107 049	S. Chatrchyan *et al.*	(CMS Collab.)
CHATRCHYAN	11R	PRL 107 091802	S. Chatrchyan *et al.*	(CMS Collab.)
CHATRCHYAN	11Z	PR D84 092004	S. Chatrchyan *et al.*	(CMS Collab.)
KHACHATRY...	11A	PL B695 424	V. Khachatryan *et al.*	(CMS Collab.)
AALTONEN	10AA	PR D82 052002	T. Aaltonen *et al.*	(CDF Collab.)
AALTONEN	10AB	PR D82 112005	T. Aaltonen *et al.*	(CDF Collab.)
AALTONEN	10AC	PRL 105 232003	T. Aaltonen *et al.*	(CDF Collab.)
AALTONEN	10AE	PRL 105 252001	T. Aaltonen *et al.*	(CDF Collab.)
AALTONEN	10C	PR D81 031102	T. Aaltonen *et al.*	(CDF Collab.)
AALTONEN	10D	PR D81 032002	T. Aaltonen *et al.*	(CDF Collab.)
AALTONEN	10E	PR D81 052011	T. Aaltonen *et al.*	(CDF Collab.)
AALTONEN	10Q	PRL 105 042002	T. Aaltonen *et al.*	(CDF Collab.)
AALTONEN	10S	PRL 105 101801	T. Aaltonen *et al.*	(CDF Collab.)
AALTONEN	10U	PR D81 072003	T. Aaltonen *et al.*	(CDF Collab.)
AALTONEN	10V	PR D81 092002	T. Aaltonen *et al.*	(CDF Collab.)
AALTONEN	10W	PRL 105 012001	T. Aaltonen *et al.*	(CDF Collab.)
ABAZOV	10	PL B682 363	V.M. Abazov *et al.*	(D0 Collab.)
ABAZOV	10I	PR D82 032002	V.M. Abazov *et al.*	(D0 Collab.)
ABAZOV	10J	PL B690 5	V.M. Abazov *et al.*	(D0 Collab.)
ABAZOV	10K	PL B693 81	V.M. Abazov *et al.*	(D0 Collab.)
ABAZOV	10Q	PR D82 071102	V.M. Abazov *et al.*	(D0 Collab.)
AHRENS	10	JHEP 1009 097	V. Ahrens *et al.*	(MAINZ, HEIDH)
AHRENS	10A	NPBPS 205-206 48	V. Ahrens *et al.*	(MAINZ, HEIDH)
AALTONEN	09AD	PR D79 112007	T. Aaltonen *et al.*	(CDF Collab.)
AALTONEN	09AK	PR D80 051104	T. Aaltonen *et al.*	(CDF Collab.)
AALTONEN	09AL	PR D80 052001	T. Aaltonen *et al.*	(CDF Collab.)
AALTONEN	09AT	PRL 103 092002	T. Aaltonen *et al.*	(CDF Collab.)
AALTONEN	09F	PR D79 031101	T. Aaltonen *et al.*	(CDF Collab.)
AALTONEN	09H	PR D79 052007	T. Aaltonen *et al.*	(CDF Collab.)
AALTONEN	09J	PR D79 072001	T. Aaltonen *et al.*	(CDF Collab.)
AALTONEN	09K	PR D79 072010	T. Aaltonen *et al.*	(CDF Collab.)
AALTONEN	09L	PR D79 092005	T. Aaltonen *et al.*	(CDF Collab.)
AALTONEN	09M	PRL 102 042001	T. Aaltonen *et al.*	(CDF Collab.)
AALTONEN	09N	PRL 102 151801	T. Aaltonen *et al.*	(CDF Collab.)
AALTONEN	09O	PRL 102 152001	T. Aaltonen *et al.*	(CDF Collab.)
AALTONEN	09Q	PL B674 160	T. Aaltonen *et al.*	(CDF Collab.)
AALTONEN	09X	PR D79 072005	T. Aaltonen *et al.*	(CDF Collab.)
AARON	09A	PL B678 450	F.D. Aaron *et al.*	(H1 Collab.)
ABAZOV	09AA	PRL 103 132001	V.M. Abazov *et al.*	(D0 Collab.)
ABAZOV	09AG	PR D80 071102	V.M. Abazov *et al.*	(D0 Collab.)
ABAZOV	09AH	PR D80 092006	V.M. Abazov *et al.*	(D0 Collab.)
ABAZOV	09J	PRL 102 092002	V.M. Abazov *et al.*	(D0 Collab.)
ABAZOV	09R	PL B679 177	V.M. Abazov *et al.*	(D0 Collab.)
ABAZOV	09Z	PRL 103 092001	V.M. Abazov *et al.*	(D0 Collab.)
LANGENFELD	09	PR D80 054009	U. Langenfeld, S. Moch, P. Uwer	
AALTONEN	08AB	PRL 101 202001	T. Aaltonen *et al.*	(CDF Collab.)
AALTONEN	08AD	PRL 101 192002	T. Aaltonen *et al.*	(CDF Collab.)
AALTONEN	08AG	PR D78 111101	T. Aaltonen *et al.*	(CDF Collab.)
AALTONEN	08AH	PRL 101 252001	T. Aaltonen *et al.*	(CDF Collab.)
AALTONEN	08C	PRL 100 062005	T. Aaltonen *et al.*	(CDF Collab.)
ABAZOV	08AH	PRL 101 182001	V.M. Abazov *et al.*	(D0 Collab.)
ABAZOV	08AI	PRL 101 221801	V.M. Abazov *et al.*	(D0 Collab.)
ABAZOV	08B	PRL 100 062004	V.M. Abazov *et al.*	(D0 Collab.)
ABAZOV	08I	PR D78 012005	V.M. Abazov *et al.*	(D0 Collab.)
ABAZOV	08L	PRL 100 142002	V.M. Abazov *et al.*	(D0 Collab.)
ABAZOV	08M	PRL 100 192003	V.M. Abazov *et al.*	(D0 Collab.)
ABAZOV	08N	PRL 100 192004	V.M. Abazov *et al.*	(D0 Collab.)
ABULENCIA	08	PR D78 012003	A. Abulencia *et al.*	(CDF Collab.)
CACCIARI	08	JHEP 0809 127	M. Cacciari *et al.*	
KIDONAKIS	08	PR D78 074005	N. Kidonakis, R. Vogt	
MOCH	08	PR D78 034003	S. Moch, P. Uwer	(BERL, KARLE)
AALTONEN	07	PRL 98 142001	T. Aaltonen *et al.*	(CDF Collab.)
AALTONEN	07B	PR D75 111103	T. Aaltonen *et al.*	(CDF Collab.)
AALTONEN	07D	PR D76 072009	T. Aaltonen *et al.*	(CDF Collab.)
AALTONEN	07I	PRL 99 182002	T. Aaltonen *et al.*	(CDF Collab.)
ABAZOV	07C	PRL 98 041801	V.M. Abazov *et al.*	(D0 Collab.)
ABAZOV	07D	PR D75 031102	V.M. Abazov *et al.*	(D0 Collab.)
ABAZOV	07F	PR D75 092001	V.M. Abazov *et al.*	(D0 Collab.)
ABAZOV	07H	PRL 98 181802	V.M. Abazov *et al.*	(D0 Collab.)
ABAZOV	07O	PR D76 052006	V.M. Abazov *et al.*	(D0 Collab.)
ABAZOV	07P	PR D76 072007	V.M. Abazov *et al.*	(D0 Collab.)
ABAZOV	07R	PR D76 092007	V.M. Abazov *et al.*	(D0 Collab.)
ABAZOV	07V	PRL 99 191802	V.M. Abazov *et al.*	(D0 Collab.)
ABAZOV	07W	PL B655 7	V.M. Abazov *et al.*	(D0 Collab.)
ABULENCIA	07D	PR D75 031105	A. Abulencia *et al.*	(CDF Collab.)
ABULENCIA	07G	PRL 98 072001	A. Abulencia *et al.*	(CDF Collab.)
ABULENCIA	07I	PR D75 052001	A. Abulencia *et al.*	(CDF Collab.)
ABULENCIA	07J	PR D75 071102	A. Abulencia *et al.*	(CDF Collab.)
ABAZOV	06K	PL B639 616	V.M. Abazov *et al.*	(D0 Collab.)
ABAZOV	06U	PR D74 092005	V.M. Abazov *et al.*	(D0 Collab.)
ABAZOV	06X	PR D74 112004	V.M. Abazov *et al.*	(D0 Collab.)
ABULENCIA	06D	PRL 96 022004	A. Abulencia *et al.*	(CDF Collab.)
Also		PR D73 032003	A. Abulencia *et al.*	(CDF Collab.)
Also		PR D73 092002	A. Abulencia *et al.*	(CDF Collab.)
ABULENCIA	06G	PRL 96 152002	A. Abulencia *et al.*	(CDF Collab.)
Also		PR D74 032009	A. Abulencia *et al.*	(CDF Collab.)
ABULENCIA	06R	PL B639 172	A. Abulencia *et al.*	(CDF Collab.)
ABULENCIA	06U	PR D73 111103	A. Abulencia *et al.*	(CDF Collab.)
ABULENCIA	06V	PR D73 112006	A. Abulencia *et al.*	(CDF Collab.)
ABULENCIA	06Z	PRL 97 082004	A. Abulencia *et al.*	(CDF Collab.)
ABULENCIA,A	06C	PRL 96 202002	A. Abulencia *et al.*	(CDF Collab.)
ABULENCIA,A	06E	PR D74 072005	A. Abulencia *et al.*	(CDF Collab.)
ABULENCIA,A	06F	PR D74 072006	A. Abulencia *et al.*	(CDF Collab.)
ABAZOV	05	PL B606 25	V.M. Abazov *et al.*	(D0 Collab.)
ABAZOV	05G	PL B617 1	V.M. Abazov *et al.*	(D0 Collab.)
ABAZOV	05L	PR D72 011104	V.M. Abazov *et al.*	(D0 Collab.)
ABAZOV	05P	PL B622 265	V.M. Abazov *et al.*	(D0 Collab.)
Also		PL B517 282	V.M. Abazov *et al.*	(D0 Collab.)
Also		PR D63 031101	B. Abbott *et al.*	(D0 Collab.)
Also		PR D75 092007	V.M. Abazov *et al.*	(D0 Collab.)
ABAZOV	05Q	PL B626 35	V.M. Abazov *et al.*	(D0 Collab.)
ABAZOV	05R	PL B626 55	V.M. Abazov *et al.*	(D0 Collab.)
ABAZOV	05X	PL B626 45	V.M. Abazov *et al.*	(D0 Collab.)
ACOSTA	05A	PRL 95 102002	D. Acosta *et al.*	(CDF Collab.)
ACOSTA	05D	PR D71 031101	D. Acosta *et al.*	(CDF Collab.)
ACOSTA	05N	PR D71 012005	D. Acosta *et al.*	(CDF Collab.)
ACOSTA	05S	PR D72 032002	D. Acosta *et al.*	(CDF Collab.)
ACOSTA	05T	PR D72 052003	D. Acosta *et al.*	(CDF Collab.)
ACOSTA	05U	PR D71 072005	D. Acosta *et al.*	(CDF Collab.)
ACOSTA	05V	PR D71 052003	D. Acosta *et al.*	(CDF Collab.)
ABAZOV	04G	NAT 429 638	V.M. Abazov *et al.*	(D0 Collab.)
ABDALLAH	04C	PL B590 21	J. Abdallah *et al.*	(DELPHI Collab.)
ACOSTA	04H	PR D69 052003	D. Acosta *et al.*	(CDF Collab.)
ACOSTA	04I	PRL 93 142001	D. Acosta *et al.*	(CDF Collab.)
AKTAS	04	EPJ C33 9	A. Aktas *et al.*	(H1 Collab.)
ABAZOV	03A	PR D67 012004	V.M. Abazov *et al.*	(D0 Collab.)
CHEKANOV	03	PL B559 153	S. Chekanov *et al.*	(ZEUS Collab.)
ACHARD	02J	PL B549 290	P. Achard *et al.*	(L3 Collab.)
ACOSTA	02	PR D65 091102	D. Acosta *et al.*	(CDF Collab.)
HEISTER	02Q	PL B543 173	A. Heister *et al.*	(ALEPH Collab.)
ABBIENDI	01T	PL B521 181	G. Abbiendi *et al.*	(OPAL Collab.)
AFFOLDER	01	PR D63 032003	T. Affolder *et al.*	(CDF Collab.)
AFFOLDER	01A	PR D64 032002	T. Affolder *et al.*	(CDF Collab.)
AFFOLDER	01C	PRL 86 3233	T. Affolder *et al.*	(CDF Collab.)
AFFOLDER	00B	PRL 84 216	T. Affolder *et al.*	(CDF Collab.)
BARATE	00S	PL B494 33	S. Barate *et al.*	(ALEPH Collab.)
ABBOTT	99G	PR D60 052001	B. Abbott *et al.*	(D0 Collab.)
ABE	99B	PRL 82 271	F. Abe *et al.*	(CDF Collab.)
Also		PRL 82 2808 (errat.)	F. Abe *et al.*	(CDF Collab.)
CHANG	99	PR D59 091503	D. Chang, W. Chang, E. Ma	
ABBOTT	98D	PRL 80 2063	B. Abbott *et al.*	(D0 Collab.)
ABBOTT	98F	PR D58 052001	B. Abbott *et al.*	(D0 Collab.)
ABE	98E	PRL 80 2767	F. Abe *et al.*	(CDF Collab.)
ABE	98F	PRL 80 2779	F. Abe *et al.*	(CDF Collab.)
ABE	98G	PRL 80 2525	F. Abe *et al.*	(CDF Collab.)
BHAT	98B	IJMP A13 5113	P.C. Bhat, H.B. Prosper, S.S. Snyder	
ABACHI	97E	PRL 79 1197	S. Abachi *et al.*	(D0 Collab.)
ABE	97R	PRL 79 1992	F. Abe *et al.*	(CDF Collab.)
ABE	97V	PRL 79 3585	F. Abe *et al.*	(CDF Collab.)
PDG	96	PR D54 1	R. M. Barnett *et al.*	(PDG Collab.)
ABACHI	95	PRL 74 2632	S. Abachi *et al.*	(D0 Collab.)
ABE	95F	PRL 74 2626	F. Abe *et al.*	(CDF Collab.)
ABE	94E	PR D50 2966	F. Abe *et al.*	(CDF Collab.)
Also		PRL 73 225	F. Abe *et al.*	(CDF Collab.)

b' (4th Generation) Quark, Searches for

$b'(-1/3)$-quark/hadron mass limits in $p\overline{p}$ and pp collisions

VALUE (GeV)	CL%	DOCUMENT ID		TECN	COMMENT
>1530	95	[1] AAD	24BP	ATLS	$B(b' \to Wu) = 1$
>1540	95	[2] HAYRAPETY...	24AQ	CMS	$B(b' \to Zb) = 1$
>1570	95	[2] HAYRAPETY...	24AQ	CMS	$B(b' \to Hb) = 1$
>1560	95	[3] TUMASYAN	23V	CMS	$B(b' \to Wt) = 1$
>1570	95	[4] SIRUNYAN	20BI	CMS	$B(b' \to Hb) = 1$
>1000	95	[5] AABOUD	18CE	ATLS	$\geq 2\ell + \not{E}_T + \geq 1bj$
> 950	95	[6] AABOUD	18CL	ATLS	Wt, Zb, hb modes
>1010	95	[7,8] AABOUD	18CP	ATLS	$2,3\ell$, singlet model
>1140	95	[6,9] AABOUD	18CP	ATLS	$2,3\ell$, doublet model
>1220	95	[10,11] AABOUD	18CR	ATLS	singlet b'. ATLAS Combination
>1370	95	[10,12] AABOUD	18CR	ATLS	b' in a weak isospin doublet (t',b'). ATLAS combination.
> 730	95	[13] SIRUNYAN	17AU	CMS	
> 810	95	[14] AAD	15Z	ATLS	
> 190	95	[15] ABAZOV	08X	D0	$c\tau$= 200mm
> 190	95	[16] ACOSTA	03	CDF	quasi-stable b'
• • • We do not use the following data for averages, fits, limits, etc. • • •					
>1460	95	[17] AAD	23AG	ATLS	$B(b' \to Wt) = 1$
>1420	95	[18] AAD	23AV	ATLS	$B(b' \to Zb) = 1$
>1390	95	[4] SIRUNYAN	20BI	CMS	$B(b' \to Zb) = 1$
>1130	95	[19] SIRUNYAN	19AQ	CMS	$B(b' \to Zb) = 1$
>1230	95	[20] SIRUNYAN	19BW	CMS	$B(b' \to Wt) = 1$
>1350	95	[21] AABOUD	18AW	ATLS	$B(b' \to Wt) = 1$
> 910	95	[22] SIRUNYAN	18BM	CMS	Wt, Zb, hb modes
> 845	95	[23] SIRUNYAN	18Q	CMS	$B(b' \to Wu) = 1$
> 880	95	[24] KHACHATRY...	16AN	CMS	$B(b' \to Wt) = 1$
<350, 580–635, >700	95	[25] AAD	15AR	ATLS	$B(b' \to Hb) = 1$
> 620	95	[26] AAD	15BY	ATLS	Wt, Zb, hb modes
> 730	95	[27] AAD	15BY	ATLS	$B(b' \to Wt) = 1$
> 690	95	[28] AAD	15CN	ATLS	$B(b' \to Wq) = 1$ (q=u)
> 755	95	[29] AAD	14AZ	ATLS	$B(b' \to Wt) = 1$
> 675	95	[30] CHATRCHYAN	13I	CMS	$B(b' \to Wt) = 1$
> 480	95	[31] AAD	12AT	ATLS	$B(b' \to Wt) = 1$
> 400	95	[32] AAD	12AU	ATLS	$B(b' \to Zb) = 1$
> 350	95	[33] AAD	12BC	ATLS	$B(b' \to Wq) = 1$ (q=u,c)
> 450	95	[34] AAD	12BE	ATLS	$B(b' \to Wt) = 1$
> 685	95	[35] CHATRCHYAN	12BH	CMS	$m_{t'} = m_{b'}$
> 611	95	[36] CHATRCHYAN	12X	CMS	$B(b' \to Wt) = 1$
> 372	95	[37] AALTONEN	11J	CDF	$b' \to Wt$
> 361	95	[38] CHATRCHYAN	11L	CMS	Repl. by CHATRCHYAN 12X
> 338	95	[39] AALTONEN	10H	CDF	$b' \to Wt$
> 380–430	95	[40] FLACCO	10	RVUE	$m_{b'} > m_{t'}$
> 268	95	[41,42] AALTONEN	07C	CDF	$B(b' \to Zb) = 1$
> 199	95	[43] AFFOLDER	00	CDF	NC: $b' \to Zb$
> 148	95	[44] ABE	98N	CDF	NC: $b' \to Zb$ + vertex
> 96	95	[45] ABACHI	97D	D0	NC: $b' \to b\gamma$
> 128	95	[46] ABACHI	95F	D0	$\ell\ell$ + jets, ℓ + jets
> 75	95	[47] MUKHOPAD...	93	RVUE	NC: $b' \to b\ell\ell$
> 85	95	[48] ABE	92	CDF	CC: $\ell\ell$
> 72	95	[49] ABE	90B	CDF	CC: $e + \mu$

> 54	95	[50] AKESSON	90	UA2	CC: e + jets + $\not{E}_T$
> 43	95	[51] ALBAJAR	90B	UA1	CC: μ + jets
> 34	95	[52] ALBAJAR	88	UA1	CC: e or μ + jets

[1] AAD 24BP based on 140 fb^{-1} of pp data at $\sqrt{s}$ = 13 TeV. Limit on pair-production of heavy vectorlike quarks where each decays into a W boson and a light quark. Used events with $\ell + \not{E}_T$ + multiple jets + 1 boosted-W-jet.

[2] HAYRAPETYAN 24AQ based on 138 fb^{-1} of pp data at $\sqrt{s}$ = 13 TeV. Pair production of vector-like b' is searched for in the fully hadronic final states and those containing $\ell^+\ell^-$ from a Z boson. The data are consistent with the SM background predictions and limits are obtained for different branching ratios B($b' \rightarrow Hb$), B($b' \rightarrow Zb$), B($b' \rightarrow Wt$).

[3] TUMASYAN 23V based on 138 fb^{-1} of pp data at $\sqrt{s}$ = 13 TeV. Pair production of vector-like b' is seached for in the single-lepton, same-sign charge dilepton and multi-lepton channels. The data are consistent with the SM background predictions and limits are obtained for different branching ratios.

[4] SIRUNYAN 20BI based on 137 fb^{-1} of pp data at $\sqrt{s}$ = 13 TeV. Pair production of vector-like b' is seached for with each b' decaying into Zb or hb. Analysis focuses on final states consisting of jets from six quarks. Mass limits are obtained for a variety of branching ratios of b' decays.

[5] AABOUD 18CE based on 36.1 fb^{-1} of proton-proton data taken at $\sqrt{s}$ = 13 TeV. Events including a same-sign lepton pair are used. The limit is for a singlet model, assuming the branching ratios of b' into Zb, Wt and Hb as predicted by the model.

[6] AABOUD 18CL, AABOUD 18CP based on 36.1 fb^{-1} of pp data at $\sqrt{s}$ = 13 TeV. The limit is for the pair-produced vector-like b' using all-hadronic final state. The analysis is particularly powerful for the $b' \rightarrow hb$ mode. Assuming the pure decay only in this mode sets a limit $m_{b'}$ > 1010 GeV.

[7] AABOUD 18CP based on 36.1 fb^{-1} of pp data at $\sqrt{s}$ = 13 TeV. Pair and single production of vector-like b' are seached for with at least one b' decaying into Zb. In the case of B($b' \rightarrow Zb$) = 1, the limit is $m_{b'}$ > 1220 GeV.

[8] The limit is for the singlet model, assuming that the branching ratios into Wt, Zb, hb add up to one.

[9] The limit is for the doublet model, assuming that the branching ratios into Wt, Zb, hb add up to one.

[10] AABOUD 18CR based on 36.1 fb^{-1} of pp data at $\sqrt{s}$ = 13 TeV. A combination of searches for the pair-produced vector-like b' in various decay channels ($b' \rightarrow Wt$, Zb, hb). Also a model-independent limit is obtained as $m_{b'}$ > 1.03 TeV, assuming that the branching ratios into Zb, Wt, and hb add up to one.

[11] The limit is for the singlet b'.

[12] The limit is for b' in a weak isospin doublet (t',b') and $|V_{t'b}| \ll |V_{tb'}|$. For a b' in a doublet with a charge −4/3 vector-like quark, the limit $m_{b'}$ > 1.14 TeV is obtained.

[13] SIRUNYAN 17AU based on 2.3–2.6 fb^{-1} of pp data at $\sqrt{s}$ = 13 TeV. Limit on pair-produced singlet vector-like b' using one lepton and several jets. The mass bound is given for a b' transforming as a singlet under the electroweak symmetry group, assumed to decay through W, Z or Higgs boson (which decays to jets) and to a third generation quark.

[14] AAD 15Z based on 20.3 fb^{-1} of pp data at $\sqrt{s}$ = 8 TeV. Used events with $\ell + \not{E}_T$ + ≥ 6j (≥ 1 b) and at least one pair of jets from weak boson decay, primarily designed to select the signature $b'\overline{b}' \rightarrow WWt\overline{t} \rightarrow WWWWb\overline{b}$. This is a limit on pair-produced vector-like b'. The lower mass limit is 640 GeV for a vector-like singlet b'.

[15] Result is based on 1.1 fb^{-1} of data. No signal is found for the search of long-lived particles which decay into final states with two electrons or photons, and upper bound on the cross section times branching fraction is obtained for 2 < cτ< 7000 mm; see Fig. 3. 95% CL excluded region of b' lifetime and mass is shown in Fig. 4.

[16] ACOSTA 03 looked for long-lived fourth generation quarks in the data sample of 90 pb^{-1} of $\sqrt{s}$=1.8 TeV $p\overline{p}$ collisions by using the muon-like penetration and anomalously high ionization energy loss signature. The corresponding lower mass bound for the charge (2/3)e quark (t') is 220 GeV. The t' bound is higher than the b' bound because t' is more likely to produce charged hadrons than b'. The 95% CL upper bounds for the production cross sections are given in their Fig. 3.

[17] AAD 23AG based on 139 fb^{-1} of pp data at $\sqrt{s}$ = 13 TeV. Pair production of vector-like top or bs is searched for in the mode 1ℓ + ≥ 4j(≥ 1b-tagged) + $\not{E}_T$. The data are consistent with the SM background predictions and limits are obtained for different branching ratios. Masses below 1.59 TeV are excluded assuming a mass-degenerate vector-like doublet (t',b') model.

[18] AAD 23AV based on 139 fb^{-1} of pp data at $\sqrt{s}$ = 13 TeV. Pair production of vector-like b' is searched for in the mode $\ell^\pm\ell^\mp$ + ≥ 2j (≥ 1b-tagged) + $\not{E}_T$ or with 3ℓ. The data are consistent with the SM background predictions and limits are obtained for different branching ratios.

[19] SIRUNYAN 19AQ based on 35.9 fb^{-1} of pp data at $\sqrt{s}$ = 13 TeV. Pair production of vector-like b' is seached for with one b' decaying into Zb and the other b' decaying into Wt, Zb, hb. Events with an opposite-sign lepton pair consistent with coming from Z and jets are used. Mass limits are obtained for a variety of branching ratios of b'.

[20] SIRUNYAN 19BW based on 35.9 fb^{-1} of pp data at $\sqrt{s}$ = 13 TeV. The limit is for the pair-produced vector-like b' using all-hadronic final state. The analysis is made for the Zb, Wt, hb modes and mass limits are obtained for a variety of branching ratios.

[21] AABOUD 18AW based on 36.1 fb^{-1} of pp data at $\sqrt{s}$ = 13 TeV. The limit is for the pair-produced vector-like b' using lepton-plus-jets final state. The search is also sensitive to the decays into Zb and Hb final states.

[22] SIRUNYAN 18BM based on 35.9 fb^{-1} of pp data at $\sqrt{s}$ = 13 TeV. The limit is for the pair-produced vector-like b'. Three channels (single lepton, same-charge 2 leptons, or at least 3 leptons) are considered for various branching fraction combinations. Assuming B(tW) = 1, the limit is 1240 GeV and for B(bZ) = 1 it is 960 GeV.

[23] SIRUNYAN 18Q based on 19.7 fb^{-1} of pp data at $\sqrt{s}$ = 8 TeV. The limit is for the pair-produced vector-like b' that couple only to light quarks. Upper cross section limits on the single production of a b' and constraints for other decay channels (Zq and Hq) are also given in the paper.

[24] KHACHATRYAN 16AN based on 19.7 fb^{-1} of pp data at $\sqrt{s}$ = 8 TeV. Limit on pair-produced vector-like b' using 1, 2, and >2 leptons as well as fully hadronic final states. Other limits depending on the branching fractions to tW, bZ, and bH are given in Table IX.

[25] AAD 15AR based on 20.3 fb^{-1} of pp data at $\sqrt{s}$ = 8 TeV. Used lepton-plus-jets final state. See Fig. 24 for mass limits in the plane of B($b' \rightarrow Wt$) vs. B($b' \rightarrow Hb$) from $b'\overline{b}' \rightarrow Hb + X$ searches.

[26] AAD 15BY based on 20.3 fb^{-1} of pp data at $\sqrt{s}$ = 8 TeV. Limit on pair-produced vector-like b' assuming the branching fractions to W, Z, and h modes of the singlet model. Used events containing ≥ 2ℓ + $\not{E}_T$ + ≥ 2j (≥ 1 b) and including a same-sign lepton pair.

[27] AAD 15BY based on 20.3 fb^{-1} of pp data at $\sqrt{s}$ = 8 TeV. Limit on pair-produced chiral b'-quark. Used events containing ≥ 2ℓ + $\not{E}_T$ + ≥ 2j (≥ 1 b) and including a same-sign lepton pair.

[28] AAD 15CN based on 20.3 fb^{-1} of pp data at $\sqrt{s}$ = 8 TeV. Limit on pair-production of chiral b'-quark. Used events with $\ell + \not{E}_T$ + ≥ 4j (non-b-tagged). Limits on a heavy vector-like quark, which decays into Wq, Zq, hq, are presented in the plane B($Q \rightarrow Wq$) vs. B($Q \rightarrow hq$) in Fig. 12.

[29] Based on 20.3 fb^{-1} of pp data at $\sqrt{s}$ = 8 TeV. No significant excess over SM expectation is found in the search for pair production or single production of b' in the events with dilepton from a high p_T Z and additional jets (≥ 1 b-tag). If instead of B($b' \rightarrow Wt$) = 1 an electroweak singlet with B($b' \rightarrow Wt$) ∼ 0.45 is assumed, the limit reduces to 685 GeV.

[30] Based on 5.0 fb^{-1} of pp data at $\sqrt{s}$ = 7 TeV. CHATRCHYAN 13I looked for events with one isolated electron or muon, large $\not{E}_T$, and at least four jets with large transverse momenta, where one jet is likely to originate from the decay of a bottom quark.

[31] Based on 1.04 fb^{-1} of pp data at $\sqrt{s}$ = 7 TeV. No signal is found for the search of heavy quark pair production that decay into W and a t quark in the events with a high p_T isolated lepton, large $\not{E}_T$, and at least 6 jets in which one, two or more dijets are from W.

[32] Based on 2.0 fb^{-1} of pp data at $\sqrt{s}$ = 7 TeV. No $b' \rightarrow Zb$ invariant mass peak is found in the search of heavy quark pair production that decay into Z and a b quark in events with $Z \rightarrow e^+e^-$ and at least one b-jet. The lower mass limit is 358 GeV for a vector-like singlet b' mixing solely with the third SM generation.

[33] Based on 1.04 fb^{-1} of pp data at $\sqrt{s}$ = 7 TeV. No signal is found for the search of heavy quark pair production that decay into W and a quark in the events with dileptons, large $\not{E}_T$, and ≥ 2 jets.

[34] Based on 1.04 fb^{-1} of pp data at $\sqrt{s}$ = 7 TeV. AAD 12BE looked for events with two isolated like-sign leptons and at least 2 jets, large $\not{E}_T$ and H$_T$ > 350 GeV.

[35] Based on 5 fb^{-1} of pp data at $\sqrt{s}$ = 7 TeV. CHATRCHYAN 12BH searched for QCD and EW production of single and pair of degenerate 4'th generation quarks that decay to bW or tW. Absence of signal in events with one lepton, same-sign dileptons or tri-leptons gives the bound. With a mass difference of 25 GeV/c^2 between $m_{t'}$ and $m_{b'}$, the corresponding limit shifts by about ±20 GeV/c^2.

[36] Based on 4.9 fb^{-1} of pp data at $\sqrt{s}$ = 7 TeV. CHATRCHYAN 12X looked for events with trileptons or same-sign dileptons and at least one b jet.

[37] Based on 4.8 fb^{-1} of data in $p\overline{p}$ collisions at 1.96 TeV. AALTONEN 11J looked for events with $\ell + \not{E}_T$ + ≥ 5j (≥ 1 b or c). No signal is observed and the bound $\sigma(b'\overline{b}')$ < 30 fb for $m_{b'}$ > 375 GeV is found for B($b' \rightarrow Wt$) = 1.

[38] Based on 34 pb^{-1} of data in pp collisions at 7 TeV. CHATRCHYAN 11L looked for multi-jet events with trileptons or same-sign dileptons. No excess above the SM background excludes $m_{b'}$ between 255 and 361 GeV at 95% CL for B($b' \rightarrow Wt$) = 1.

[39] Based on 2.7 fb^{-1} of data in $p\overline{p}$ collisions at $\sqrt{s}$ = 1.96 TeV. AALTONEN 10H looked for pair production of heavy quarks which decay into tW^- or tW^+, in events with same sign dileptons (e or μ), several jets and large missing E_T. The result is obtained for b' which decays into tW^-. For the charge 5/3 quark ($T_{5/3}$) which decays into tW^+, $m_{T_{5/3}}$ > 365 GeV (95% CL) is found when it has the charge −1/3 partner B of the same mass.

[40] FLACCO 10 result is obtained from AALTONEN 10H result of $m_{b'}$ > 338 GeV, by relaxing the condition B($b' \rightarrow Wt$) = 100% when $m_{b'} > m_{t'}$.

[41] Result is based on 1.06 fb^{-1} of data. No excess from the SM Z+jet events is found when Z decays into ee or $\mu\mu$. The $m_{b'}$ bound is found by comparing the resulting upper bound on $\sigma(b'\overline{b}')$ [1-(1-B($b' \rightarrow Zb$))^2] and the LO estimate of the b' pair production cross section shown in Fig. 38 of the article.

[42] HUANG 08 reexamined the b' mass lower bound of 268 GeV obtained in AALTONEN 07C that assumes B($b' \rightarrow Zb$) = 1, which does not hold for $m_{b'}$ > 255 GeV. The lower mass bound is given in the plane of sin^2($\theta_{tb'}$) and $m_{b'}$.

[43] AFFOLDER 00 looked for b' that decays in to b+Z. The signal searched for is $bbZZ$ events where one Z decays into e^+e^- or $\mu^+\mu^-$ and the other Z decays hadronically. The bound assumes B($b' \rightarrow Zb$)= 100%. Between 100 GeV and 199 GeV, the 95%CL upper bound on $\sigma(b' \rightarrow \overline{b'})$×B^2($b' \rightarrow Zb$) is also given (see their Fig. 2).

[44] ABE 98N looked for $Z \rightarrow e^+e^-$ decays with displaced vertices. Quoted limit assumes B($b' \rightarrow Zb$)=1 and $c\tau_{b'}$=1 cm. The limit is lower than m_Z+m_b (∼ 96 GeV) if $c\tau$> 22 cm or $c\tau$< 0.009 cm. See their Fig. 4.

[45] ABACHI 97D searched for b' that decays mainly via FCNC. They obtained 95%CL upper bounds on B($b'\overline{b}' \rightarrow \gamma$+ 3 jets) and B($b'\overline{b}' \rightarrow 2\gamma$+ 2 jets), which can be interpreted as the lower mass bound $m_{b'}$ >m_Z+m_b.

[46] ABACHI 95F bound on the top-quark also applies to b' and t' quarks that decay predominantly into W. See FROGGATT 97.

[47] MUKHOPADHYAYA 93 analyze CDF dilepton data of ABE 92G in terms of a new quark decaying via flavor-changing neutral current. The above limit assumes B($b' \rightarrow b\ell^+\ell^-$)=1%. For an exotic quark decaying only via virtual Z [B($b\ell^+\ell^-$) = 3%], the limit is 85 GeV.

[48] ABE 92 dilepton analysis limit of >85 GeV at CL=95% also applies to b' quarks, as discussed in ABE 90B.

[49] ABE 90B exclude the region 28–72 GeV.

[50] AKESSON 90 searched for events having an electron with p_T > 12 GeV, missing momentum > 15 GeV, and a jet with E_T > 10 GeV, $|\eta|$ < 2.2, and excluded $m_{b'}$ between 30 and 69 GeV.

Int. J. Mod. Phys. A 2026.41. Downloaded from www.worldscientific.com
by UNIVERSITY OF CALIFORNIA BERKELEY on 09/16/26. Re-use and distribution is strictly not permitted, except for Open Access articles.

Int. J. Mod. Phys. A 2026.41. Downloaded from www.worldscientific.com
by UNIVERSITY OF CALIFORNIA @ BERKELEY on 09/16/26. Re-use and distribution is strictly not permitted, except for Open Access articles.

[51] For the reduction of the limit due to non-charged-current decay modes, see Fig. 19 of ALBAJAR 90B.

[52] ALBAJAR 88 study events at E_{cm} = 546 and 630 GeV with a muon or isolated electron, accompanied by one or more jets and find agreement with Monte Carlo predictions for the production of charm and bottom, without the need for a new quark. The lower mass limit is obtained by using a conservative estimate for the $b'\overline{b}'$ production cross section and by assuming that it cannot be produced in W decays. The value quoted here is revised using the full $O(\alpha_s^3)$ cross section of ALTARELLI 88.

$b'(-1/3)$ mass limits from single production in $p\overline{p}$ and pp collisions

VALUE (GeV)	CL%	DOCUMENT ID		TECN	COMMENT
>3000	95	[1] TUMASYAN	22O	CMS	$g\,b \to b' \to t\,W$, B($b' \to t\,W$)=1
> 693	95	[2] ABAZOV	11F	D0	$q\,u \to q'\,b' \to q'(W\,u)$ $\widetilde{\kappa}_{u\,b'}$=1, B($b' \to W\,u$)=1
> 430	95	[2] ABAZOV	11F	D0	$q\,d \to q\,b' \to q(Z\,d)$ $\widetilde{\kappa}_{d\,b'}=\sqrt{2}$, B($b' \to Z\,d$)=1
• • • We do not use the following data for averages, fits, limits, etc. • • •					
		[3] AAD	23CQ	ATLS	$b' \to b\,h$ ($h \to b\overline{b}$)
>2600	95	[4] SIRUNYAN	21AG	CMS	$g\,b \to b' \to t\,W$, B($b' \to t\,W$)=1
		[5] SIRUNYAN	19AI	CMS	$b\,Z/t\,W \to b' \to t\,W$
>1500	95	[6] AAD	16AH	ATLS	$g\,b \to b' \to t\,W$, B($b' \to t\,W$)=1
>1390	95	[7] KHACHATRY...	16I	CMS	$g\,b \to b'_L \to t\,W$, B($b'_L \to t\,W$)=1
>1430	95	[8] KHACHATRY...	16I	CMS	$g\,b \to b'_R \to t\,W$, B($b'_R \to t\,W$)=1
>1530	95	[9] KHACHATRY...	16I	CMS	$g\,b \to b' \to t\,W$, B($b' \to t\,W$)=1

[1] TUMASYAN 22O based on 138 fb^{-1} of data in pp collisions at 13 TeV. No significant excess over SM expectation is found in the search for a left-handed b' assuming 100% decay to $t\,W$ using a t-tagged jet and a lepton from W. The model assumes that the b' has the excited quark couplings. The bound is from a statistical combination with an earlier analysis by SIRUNYAN 21AG. The 95% CL bounds are also set as 3.0, 3.0, and 3.2 TeV, respectively, for left-handed, right-handed, and vector-like couplings.

[2] ABAZOV 11F based on 5.4 fb^{-1} of data in ppbar collisions at 1.96 TeV. ABAZOV 11F looked for single production of b' via the W or Z coupling to the first generation up or down quarks, respectively. Model independent cross section limits for the single production processes $p\overline{p} \to b'q \to W\,u\,q$, and $p\overline{p} \to b'q \to Z\,d\,q$ are given in Figs. 3 and 4, respectively, and the mass limits are obtained for the model of ATRE 09 with degenerate bi-doublets of vector-like quarks.

[3] AAD 23CQ based on 139 fb^{-1} of data in pp collisions at 13 TeV. No significant excess over SM expectation is found. Limits on mass and production cross section of a vector-like b' are obtained in several theoretical scenarios determined by the couplings between b' and W, Z, h.

[4] SIRUNYAN 21AG based on 137 fb^{-1} of data in pp collisions at 13 TeV. No significant excess over SM expectation is found in the search for a left-handed b' assuming 100% decay to $t\,W$ using all hadronic final states, where t and W are tagged as single jets, respectively. The model assumes that the b' has the excited quark couplings. The 95% CL bounds are also set as 2.8 and 3.1 TeV, respectively, for the right-handed and vector-like couplings.

[5] SIRUNYAN 19AI based on 35.9 fb^{-1} of pp data at $\sqrt{s}$ = 13 TeV. Exclusion limits are set on the product of the production cross section and branching fraction for the $b'(-1/3)+\ b$ and $b'(-1/3)+\ t$ modes as a function of the vector-like quark mass in Figs. 7 and 8 and in Tab. 2 for relative vector-like quark widths between 1 and 30% for left- and right-handed vector-like quark couplings. No significant deviation from the SM prediction is observed.

[6] AAD 16AH based on 20.3 fb^{-1} of data in pp collisions at 8 TeV. No significant excess over SM expectation is found in the search for a vector-like b' in the single-lepton and dilepton channels (ℓ or $\ell\ell$) + 1,2,3 j ($\geq 1b$). The model assumes that the b' has the excited quark couplings.

[7] Based on 19.7 fb^{-1} of data in pp collisions at 8 TeV. Limit on left-handed b' assuming 100% decay to $t\,W$ and using all-hadronic, lepton + jets, and dilepton final states.

[8] Based on 19.7 fb^{-1} of data in pp collisions at 8 TeV. Limit on right-handed b' assuming 100% decay to $t\,W$ and using all-hadronic, lepton + jets, and dilepton final states.

[9] Based on 19.7 fb^{-1} of data in pp collisions at 8 TeV. Limit on vector-like b' assuming 100% decay to $t\,W$ and using all-hadronic, lepton+jets, and dilepton final states.

MASS LIMITS for b' (4th Generation) Quark or Hadron in e^+e^- Collisions

Search for hadrons containing a fourth-generation $-1/3$ quark denoted b'.

The last column specifies the assumption for the decay mode ($C\,C$ denotes the conventional charged-current decay) and the event signature which is looked for.

VALUE (GeV)	CL%	DOCUMENT ID		TECN	COMMENT
>46.0	95	[1] DECAMP	90F	ALEP	any decay
• • • We do not use the following data for averages, fits, limits, etc. • • •					
none 96–103	95	[2] ABDALLAH	07	DLPH	$b' \to b\,Z$, $c\,W$
		[3] ADRIANI	93G	L3	Quarkonium
>44.7	95	ADRIANI	93M	L3	$\Gamma(Z)$
>45	95	ABREU	91F	DLPH	$\Gamma(Z)$
none 19.4–28.2	95	ABE	90D	VNS	Any decay; event shape
>45.0	95	ABREU	90D	DLPH	B($C\,C$) = 1; event shape
>44.5	95	[4] ABREU	90D	DLPH	$b' \to c\,H^-$, $H^- \to \overline{c}\,s$, $\tau^-\,\nu$
>40.5	95	[5] ABREU	90D	DLPH	$\Gamma(Z \to$ hadrons)
>28.3	95	ADACHI	90	TOPZ	B(FCNC)=100%; isol. γ or 4 jets
>41.4	95	[6] AKRAWY	90B	OPAL	Any decay; acoplanarity
>45.2	95	[6] AKRAWY	90B	OPAL	B($C\,C$) = 1; acoplanarity
>46	95	[7] AKRAWY	90J	OPAL	$b' \to \gamma$ + any
>27.5	95	[8] ABE	89E	VNS	B($C\,C$) =1; μ, e
none 11.4–27.3	95	[9] ABE	89G	VNS	B($b' \to b\gamma$) > 10%; isolated γ
>44.7	95	[10] ABRAMS	89C	MRK2	B($C\,C$)= 100%; isol. track
>42.7	95	[10] ABRAMS	89C	MRK2	B($b\,g$)= 100%; event shape
>42.0	95	[10] ABRAMS	89C	MRK2	Any decay; event shape
>28.4	95	[11,12] ADACHI	89C	TOPZ	B($C\,C$) =1; μ
>28.8	95	[13] ENO	89	AMY	B($C\,C$) $\gtrsim$90%; μ, e
>27.2	95	[13,14] ENO	89	AMY	any decay; event shape
>29.0	95	[13] ENO	89	AMY	B($b' \to b\,g$) $\gtrsim$ 85%; event shape
>24.4	95	[15] IGARASHI	88	AMY	μ,e
>23.8	95	[16] SAGAWA	88	AMY	event shape
>22.7	95	[17] ADEVA	86	MRKJ	μ
>21		[18] ALTHOFF	84C	TASS	R, event shape
>19		[19] ALTHOFF	84I	TASS	Aplanarity

[1] DECAMP 90F looked for isolated charged particles, for isolated photons, and for four-jet final states. The modes $b' \to b\,g$ for B($b' \to b\,g$) > 65% $b' \to b\gamma$ for B($b' \to b\gamma$) > 5% are excluded. Charged Higgs decay were not discussed.

[2] ABDALLAH 07 searched for b' pair production at E_{cm}=196–209 GeV, with 420 pb^{-1}. No signal leads to the 95% CL upper limits on B($b' \to b\,Z$) and B($b' \to c\,W$) for $m_{b'}$ = 96 to 103 GeV.

[3] ADRIANI 93G search for vector quarkonium states near Z and give limit on quarkonium–Z mixing parameter δm^2 <(10–30) GeV^2 (95%CL) for the mass 88–94.5 GeV. Using Richardson potential, a 1S ($b'\overline{b}'$) state is excluded for the mass range 87.7–94.7 GeV. This range depends on the potential choice.

[4] ABREU 90D assumed $m_{H^-} < m_{b'} - 3$ GeV.

[5] Superseded by ABREU 91F.

[6] AKRAWY 90B search was restricted to data near the Z peak at E_{cm} = 91.26 GeV at LEP. The excluded region is between 23.6 and 41.4 GeV if no H^+ decays exist. For charged Higgs decays the excluded regions are between (m_{H^+} + 1.5 GeV) and 45.5 GeV.

[7] AKRAWY 90J search for isolated photons in hadronic Z decay and derive B($Z \to b'\overline{b}'$)·B($b' \to \gamma$X)/B($Z \to$ hadrons) < 2.2×10^{-3}. Mass limit assumes B($b' \to \gamma$X) > 10%.

[8] ABE 89E search at E_{cm} = 56–57 GeV at TRISTAN for multihadron events with a spherical shape (using thrust and acoplanarity) or containing isolated leptons.

[9] ABE 89G search was at E_{cm} = 55–60.8 GeV at TRISTAN.

[10] If the photonic decay mode is large (B($b' \to b\gamma$) > 25%), the ABRAMS 89C limit is 45.4 GeV. The limit for for Higgs decay ($b' \to c\,H^-$, $H^- \to \overline{c}s$) is 45.2 GeV.

[11] ADACHI 89C search was at E_{cm} = 56.5–60.8 GeV at TRISTAN using multi-hadron events accompanying muons.

[12] ADACHI 89C also gives limits for any mixture of $C\,C$ and $b\,g$ decays.

[13] ENO 89 search at E_{cm} = 50–60.8 at TRISTAN.

[14] ENO 89 considers arbitrary mixture of the charged current, $b\,g$, and $b\gamma$ decays.

[15] IGARASHI 88 searches for leptons in low-thrust events and gives $\Delta R(b')$ < 0.26 (95% CL) assuming charged current decay, which translates to $m_{b'}$ > 24.4 GeV.

[16] SAGAWA 88 set limit σ(top) < 6.1 pb at CL=95% for top-flavored hadron production from event shape analyses at E_{cm} = 52 GeV. By using the quark parton model cross-section formula near threshold, the above limit leads to lower mass bounds of 23.8 GeV for charge $-1/3$ quarks.

[17] ADEVA 86 give 95%CL upper bound on an excess of the normalized cross section, ΔR, as a function of the minimum c.m. energy (see their figure 3). Production of a pair of 1/3 charge quarks is excluded up to E_{cm} = 45.4 GeV.

[18] ALTHOFF 84C narrow state search sets limit $\Gamma(e^+e^-)$B(hadrons) <2.4 keV CL = 95% and heavy charge 1/3 quark pair production m >21 GeV, CL = 95%.

[19] ALTHOFF 84I exclude heavy quark pair production for 7 <m <19 GeV (1/3 charge) using aplanarity distributions (CL = 95%).

REFERENCES FOR Searches for (Fourth Generation) b' Quark

AAD	24BP	PR D110 052009	G. Aad et al.	(ATLAS Collab.)
HAYRAPETY...	24AQ	PR D110 052004	A. Hayrapetyan et al.	(CMS Collab.)
AAD	23AG	EPJ C83 719	G. Aad et al.	(ATLAS Collab.)
AAD	23AV	PL B843 138019	G. Aad et al.	(ATLAS Collab.)
AAD	23CQ	JHEP 2311 168	G. Aad et al.	(ATLAS Collab.)
TUMASYAN	23V	JHEP 2307 020	A. Tumasyan et al.	(CMS Collab.)
TUMASYAN	22O	JHEP 2204 048	A. Tumasyan et al.	(CMS Collab.)
SIRUNYAN	21AG	JHEP 2112 106	A.M. Sirunyan et al.	(CMS Collab.)
SIRUNYAN	20BI	PR D102 112004	A.M. Sirunyan et al.	(CMS Collab.)
SIRUNYAN	19AI	EPJ C79 90	A.M. Sirunyan et al.	(CMS Collab.)
SIRUNYAN	19AQ	EPJ C79 364	A.M. Sirunyan et al.	(CMS Collab.)
SIRUNYAN	19BW	PR D100 072001	A.M. Sirunyan et al.	(CMS Collab.)
AABOUD	18AW	JHEP 1808 048	M. Aaboud et al.	(ATLAS Collab.)
AABOUD	18CE	JHEP 1812 039	M. Aaboud et al.	(ATLAS Collab.)
AABOUD	18CL	PR D98 092005	M. Aaboud et al.	(ATLAS Collab.)
AABOUD	18CP	PR D98 112010	M. Aaboud et al.	(ATLAS Collab.)
AABOUD	18CR	PRL 121 211801	M. Aaboud et al.	(ATLAS Collab.)
SIRUNYAN	18BM	JHEP 1808 177	A.M. Sirunyan et al.	(CMS Collab.)
SIRUNYAN	18Q	PR D97 072008	A.M. Sirunyan et al.	(CMS Collab.)
SIRUNYAN	17AU	JHEP 1711 085	A.M. Sirunyan et al.	(CMS Collab.)
AAD	16AH	JHEP 1602 110	G. Aad et al.	(ATLAS Collab.)
KHACHATRY...	16AN	PR D93 112009	V. Khachatryan et al.	(CMS Collab.)
KHACHATRY...	16I	JHEP 1601 166	V. Khachatryan et al.	(CMS Collab.)
AAD	15AR	JHEP 1508 105	G. Aad et al.	(ATLAS Collab.)
AAD	15BY	JHEP 1510 150	G. Aad et al.	(ATLAS Collab.)
AAD	15CN	PR D92 112007	G. Aad et al.	(ATLAS Collab.)
AAD	15Z	PR D91 112011	G. Aad et al.	(ATLAS Collab.)
AAD	14AZ	JHEP 1411 104	G. Aad et al.	(ATLAS Collab.)
CHATRCHYAN	13I	JHEP 1301 154	S. Chatrchyan et al.	(CMS Collab.)
AAD	12AT	PRL 109 032001	G. Aad et al.	(ATLAS Collab.)

AAD	12AU	PRL 109 071801	G. Aad *et al.*	(ATLAS Collab.)
AAD	12BC	PR D86 012007	G. Aad *et al.*	(ATLAS Collab.)
AAD	12BE	JHEP 1204 069	G. Aad *et al.*	(ATLAS Collab.)
CHATRCHYAN	12BH	PR D86 112003	S. Chatrchyan *et al.*	(CMS Collab.)
CHATRCHYAN	12X	JHEP 1205 123	S. Chatrchyan *et al.*	(CMS Collab.)
AALTONEN	11J	PRL 106 141803	T. Aaltonen *et al.*	(CDF Collab.)
ABAZOV	11F	PRL 106 081801	V.M. Abazov *et al.*	(D0 Collab.)
CHATRCHYAN	11L	PL B701 204	S. Chatrchyan *et al.*	(CMS Collab.)
AALTONEN	10H	PRL 104 091801	T. Aaltonen *et al.*	(CDF Collab.)
FLACCO	10	PRL 105 111801	C.J. Flacco *et al.*	(UCI, HAIF)
ATRE	09	PR D79 054018	A. Atre *et al.*	
ABAZOV	08X	PRL 101 111802	V.M. Abazov *et al.*	(D0 Collab.)
HUANG	08	PR D77 037302	P.Q. Hung, M. Sher	(UVA, WILL)
AALTONEN	07C	PR D76 072006	T. Aaltonen *et al.*	(CDF Collab.)
ABDALLAH	07	EPJ C50 507	J. Abdallah *et al.*	(DELPHI Collab.)
ACOSTA	03	PRL 90 131801	D. Acosta *et al.*	(CDF Collab.)
AFFOLDER	00	PRL 84 835	A. Affolder *et al.*	(CDF Collab.)
ABE	98N	PR D58 051102	F. Abe *et al.*	(CDF Collab.)
ABACHI	97D	PRL 78 3818	S. Abachi *et al.*	(D0 Collab.)
FROGGATT	97	ZPHY C73 333	C.D. Froggatt, D.J. Smith, H.B. Nielsen	(GLAS+)
ABACHI	95F	PR D52 4877	S. Abachi *et al.*	(D0 Collab.)
ADRIANI	93G	PL B313 326	O. Adriani *et al.*	(L3 Collab.)
ADRIANI	93M	PRPL 236 1	O. Adriani *et al.*	(L3 Collab.)
MUKHOPAD...	93	PR D48 2105	B. Mukhopadhyaya, D.P. Roy	(TATA)
ABE	92	PRL 68 447	F. Abe *et al.*	(CDF Collab.)
Also		PR D45 3921	F. Abe *et al.*	(CDF Collab.)
ABE	92G	PR D45 3921	F. Abe *et al.*	(CDF Collab.)
ABREU	91F	NP B367 511	P. Abreu *et al.*	(DELPHI Collab.)
ABE	90B	PRL 64 147	F. Abe *et al.*	(CDF Collab.)
ABE	90D	PL B234 382	K. Abe *et al.*	(VENUS Collab.)
ABREU	90D	PL B242 536	P. Abreu *et al.*	(DELPHI Collab.)
ADACHI	90	PL B234 197	I. Adachi *et al.*	(TOPAZ Collab.)
AKESSON	90	ZPHY C46 179	T. Akesson *et al.*	(UA2 Collab.)
AKRAWY	90B	PL B236 364	M.Z. Akrawy *et al.*	(OPAL Collab.)
AKRAWY	90J	PL B246 285	M.Z. Akrawy *et al.*	(OPAL Collab.)
ALBAJAR	90B	ZPHY C48 1	C. Albajar *et al.*	(UA1 Collab.)
DECAMP	90F	PL B236 511	D. Decamp *et al.*	(ALEPH Collab.)
ABE	89E	PR D39 3524	K. Abe *et al.*	(VENUS Collab.)
ABE	89G	PRL 63 1776	K. Abe *et al.*	(VENUS Collab.)
ABRAMS	89C	PRL 63 2447	G.S. Abrams *et al.*	(Mark II Collab.)
ADACHI	89C	PL B229 427	I. Adachi *et al.*	(TOPAZ Collab.)
ENO	89	PRL 63 1910	S. Eno *et al.*	(AMY Collab.)
ALBAJAR	88	ZPHY C37 505	C. Albajar *et al.*	(UA1 Collab.)
ALTARELLI	88	NP B308 724	G. Altarelli *et al.*	(CERN, ROMA, ETH)
IGARASHI	88	PRL 60 2359	S. Igarashi *et al.*	(AMY Collab.)
SAGAWA	88	PRL 60 93	H. Sagawa *et al.*	(AMY Collab.)
ADEVA	86	PR D34 681	B. Adeva *et al.*	(Mark-J Collab.)
ALTHOFF	84C	PL 138B 441	M. Althoff *et al.*	(TASSO Collab.)
ALTHOFF	84I	ZPHY C22 307	M. Althoff *et al.*	(TASSO Collab.)

t' (4th Generation) Quark, Searches for

t'(2/3)-quark/hadron mass limits in $p\overline{p}$ and pp collisions

VALUE (GeV)	CL%	DOCUMENT ID		TECN	COMMENT
>1530	95	[1] AAD	24BP	ATLS	$B(t' \to Wq) = 1$ (q=d,s)
>1700	95	[2] AAD	24N	ATLS	$B(t' \to Wb) = 1$
>1360	95	[3] AAD	24N	ATLS	$B(t' \to Wb : Ht : Zt) = 1/2 : 1/4 : 1/4$
>1600	95	[4] AAD	23AV	ATLS	$B(t' \to Zt) = 1$
> 960	95	[5] TUMASYAN	23AX	CMS	EW production, $t' \to Ht$ ($H \to \gamma\gamma$)
>1500	95	[6] TUMASYAN	23V	CMS	$B(t' \to ht) = 1$
> 980	95	[7] AABOUD	18CE	ATLS	$\geq 2\ell + \not{E}_T + \geq 1b$j
>1030	95	[8,9] AABOUD	18CP	ATLS	2,3ℓ, singlet model
>1210	95	[8,10] AABOUD	18CP	ATLS	2,3ℓ, doublet model
>1310	95	[11,12] AABOUD	18CR	ATLS	singlet t'. ATLAS combination
>1370	95	[11,13] AABOUD	18CR	ATLS	t' in a weak isospin doublet (t',b'). ATLAS combination.
>1140	95	[14] SIRUNYAN	18BM	CMS	Wb, Zt, ht modes
> 845	95	[15] SIRUNYAN	18Q	CMS	$B(t' \to Wq) = 1$ (q=d,s)
> 860	95	[16] SIRUNYAN	17AU	CMS	
> 735	95	[17] AAD	14AZ	ATLS	$B(b' \to Wt) = 1$
> 350	95	[18] AAD	12BC	ATLS	$B(t' \to Wq)$=1 (q=d,s,b)
> 420	95	[19] AAD	12C	ATLS	$t' \to Xt$ (m_X < 140 GeV)
> 685	95	[20] CHATRCHYAN	12BH	CMS	$m_{b'} = m_{t'}$
> 557	95	[21] CHATRCHYAN	12P	CMS	$t'\overline{t}' \to W^+ b W^- \overline{b} \to b\ell^+\nu\overline{b}\ell^-\overline{\nu}$
• • • We do not use the following data for averages, fits, limits, etc. • • •					
>1470	95	[22] AAD	23AG	ATLS	$B(t' \to Zt) = 1$
>1280	95	[23] SIRUNYAN	19AQ	CMS	$B(t' \to Zt) = 1$
>1370	95	[24] SIRUNYAN	19BW	CMS	$B(t' \to ht) = 1$
>1010	95	[25] AABOUD	18CL	ATLS	$B(t' \to ht) = 1$
>1295	95	[26] SIRUNYAN	18W	CMS	$B(t' \to Wb) = 1$
>1160	95	[27] AABOUD	17L	ATLS	$B(t' \to Zt) = 1$
> 770	95	[28] AAD	15AR	ATLS	$B(t' \to Wb) = 1$
> 590	95	[29] AAD	15BY	ATLS	Wb, Zt, ht modes
> 745	95	[30] KHACHATRY...	15AI	CMS	$B(t' \to ht) = 1$
> 700	95	[31] CHATRCHYAN	14A	CMS	$B(t' \to Wb) = 1$
> 706	95	[31] CHATRCHYAN	14A	CMS	$B(t' \to Zt) = 1$
> 782	95	[31] CHATRCHYAN	14A	CMS	$B(t' \to ht) = 1$
> 656	95	[32] AAD	13F	ATLS	$B(t' \to Wb) = 1$
> 625	95	[33] CHATRCHYAN	13I	CMS	$B(t' \to Zt) = 1$
> 404	95	[34] AAD	12AR	ATLS	$B(t' \to Wb) = 1$
> 570	95	[35] CHATRCHYAN	12BC	CMS	$t'\overline{t}' \to W^+ b W^- \overline{b}$
> 400	95	[36] AALTONEN	11AH	CDF	$t' \to Xt$ (m_X < 70 GeV)
> 358	95	[37] AALTONEN	11AL	CDF	$t' \to Wb$
> 340	95	[37] AALTONEN	11AL	CDF	$t' \to Wq$ (q=d,s,b)
> 360	95	[38] AALTONEN	11O	CDF	$t' \to Xt$ (m_X < 100 GeV)
> 285	95	[39] ABAZOV	11Q	D0	$t' \to Wq$ (q=d,s,b)
> 256	95	[40,41] AALTONEN	08H	CDF	$t' \to Wq$

[1] AAD 24BP based on 140 fb^{-1} of pp data at $\sqrt{s}$ = 13 TeV. Limit on pair-production of heavy vectorlike quarks where each decays into a W boson and a light quark. Used events with $\ell + \not{E}_T$ + multiple jets + 1 boosted-W-jet.

[2] AAD 24N based on 140 fb^{-1} of pp data at $\sqrt{s}$ = 13 TeV. Pair production of vector-like t' is searched for in the lepton+jets mode. The limit is for t' in a weak isospin doublet. The data are consistent with the SM background predictions and limits are obtained for different branching ratios. The same limits also apply to t' of charge $-4/3$.

[3] AAD 24N based on 140 fb^{-1} of pp data at $\sqrt{s}$ = 13 TeV. Pair production of vector-like t' is searched for in the lepton+jets mode. The limit is for a singlet model. The data are consistent with the SM background predictions and limits are obtained for different branching ratios.

[4] AAD 23AV based on 139 fb^{-1} of pp data at $\sqrt{s}$ = 13 TeV. Pair production of vector-like t' is searched for in the mode $\ell^\pm\ell^\mp + \geq 2$j ($\geq$ 1b-tagged) + $\not{E}_T$ or with 3ℓ. The data are consistent with the SM background predictions and limits are obtained for different branching ratios.

[5] TUMASYAN 23AX based on 138 fb^{-1} of pp data at $\sqrt{s}$ = 13 TeV. A vector-like t' is seached for in the $t + H$ ($H \to \gamma\gamma$) decay channel. EW production via a coupling to third-generation quarks of κ_T = 0.25 is assumed. The branching fractions are assumed to be 50, 25, and 25%, respectively, for bW, tZ, and tH decays.

[6] TUMASYAN 23V based on 138 fb^{-1} of pp data at $\sqrt{s}$ = 13 TeV. Pair production of vector-like t' is seached for in the single-lepton, same-sign charge dilepton and multi-lepton channels. The data are consistent with the SM background predictions and limits are obtained for different branching ratios. Masses below 1.48 TeV are excluded for all decays to third generation quarks.

[7] AABOUD 18CE based on 36.1 fb^{-1} of proton-proton data taken at $\sqrt{s}$ = 13 TeV. Events including a same-sign lepton pair are used. The limit is for a singlet model, assuming the branching ratios of t' into Zt, Wb and Ht as predicted by the model.

[8] AABOUD 18CP based on 36.1 fb^{-1} of pp data at $\sqrt{s}$ = 13 TeV. Pair and single production of vector-like t' are seached for with at least one t' decaying into Zt. In the case of $B(t' \to Zt) = 1$, the limit is $m_{t'} > 1340$ GeV.

[9] The limit is for the singlet model, assuming that the branching ratios into Zt, Wb, and Ht add up to one.

[10] The limit is for the doublet model, assuming that the branching ratios into Zt, Wb, and Ht add up to one.

[11] AABOUD 18CR based on 36.1 fb^{-1} of pp data at $\sqrt{s}$ = 13 TeV. A combination of searches for the pair-produced vector-like t' in various decay channels ($t' \to Wb$, Zt, ht). Also a model-independent limit is obtained as $m_{t'} > 1.31$ TeV, assuming that the branching ratios into Zt, Wb and ht add up to one.

[12] The limit is for the singlet t'.

[13] The limit is for t' in a weak isospin doublet (t',b') and $|V_{t'b}| \ll |V_{tb'}|$.

[14] SIRUNYAN 18BM based on 35.9 fb^{-1} of pp data at $\sqrt{s}$ = 13 TeV. The limit is for the pair-produced vector-like t'. Three channels (single lepton, same-charge 2 leptons, or at least 3 leptons) are considered for various branching fraction combinations. Assuming $B(tH) = 1$, the limit is 1270 GeV and for $B(tZ) = 1$ it is 1300 GeV.

[15] SIRUNYAN 18Q based on 19.7 fb^{-1} of pp data at $\sqrt{s}$ = 8 TeV. The limit is for the pair-produced vector-like t' that couple only to light quarks. Constraints for other decay channels (Zq and Hq) are also given in the paper.

[16] SIRUNYAN 17AU based on 2.3-2.6 fb^{-1} of pp data at $\sqrt{s}$ = 13 TeV. Limit on pair-produced singlet vector-like t' using one lepton and several jets. The mass bound is given for a t' transforming as a singlet under the electroweak symmetry group, assumed to decay through W, Z or Higgs boson (which decays to jets) and to a third generation quark. For a doublet, the limit is >830 GeV. Other limits are also given in the paper.

[17] Based on 20.3 fb^{-1} of pp data at $\sqrt{s}$ = 8 TeV. No significant excess over SM expectation is found in the search for pair production or single production of t' in the events with dilepton from a high p_T Z and additional jets ($\geq$ 1 b-tag). If instead of $B(b' \to Wt) = 1$ an electroweak singlet with $B(b' \to Wt) \sim 0.45$ is assumed, the limit reduces to 685 GeV.

[18] Based on 1.04 fb^{-1} of pp data at $\sqrt{s}$ = 7 TeV. No signal is found for the search of heavy quark pair production that decay into W and a quark in the events with dileptons, large $\not{E}_T$, and $\geq$ 2 jets.

[19] Based on 1.04 fb^{-1} of data in pp collisions at 7 TeV. AAD 12C looked for $t'\overline{t}'$ production followed by t' decaying into a top quark and X, an invisible particle, in a final state with an isolated high-P_T lepton, four or more jets, and a large missing transverse energy. No excess over the SM $t\overline{t}$ production gives the upper limit on $t'\overline{t}'$ production cross section as a function of $m_{t'}$ and m_X. The result is obtained for $B(t' \to Wt) = 1$.

[20] Based on 5 fb^{-1} of pp data at $\sqrt{s}$ = 7 TeV. CHATRCHYAN 12BH searched for QCD and EW production of single and pair of degenerate 4'th generation quarks that decay to Wb or Wt. Absence of signal in events with one lepton, same-sign dileptons or tri-leptons gives the bound. With a mass difference of 25 GeV/c^2 between $m_{t'}$ and $m_{b'}$, the corresponding limit shifts by about $\pm$20 GeV/c^2.

[21] Based on 5.0 fb^{-1} of pp data at $\sqrt{s}$ = 7 TeV. CHATRCHYAN 12P looked for $t'\overline{t}'$ production events with two isolated high p_T leptons, large $\not{E}_T$, and 2 high p_T jets with b-tag. The absence of signal above the SM background gives the limit for $B(t' \to Wb) = 1$.

[22] AAD 23AG based on 139 fb^{-1} of pp data at $\sqrt{s}$ = 13 TeV. Pair production of vector-like top or bs is searched for in the mode 1$\ell + \geq$ 4j($\geq$ 1b-tagged) + $\not{E}_T$. The data are consistent with the SM background predictions and limits are obtained for different branching ratios. Masses below 1.59 TeV are excluded assuming a mass-degenerate vector-like doublet (t',b') model.

[23] SIRUNYAN 19AQ based on 35.9 fb^{-1} of pp data at $\sqrt{s}$ = 13 TeV. Pair production of vector-like t' is seached for with one t' decaying into Zt and the other t' decaying into Wb, Zt, ht. Events with an opposite-sign lepton pair consistent with coming from Z and jets are used. Mass limits are obtained for a variety of branching ratios of t'.

Int. J. Mod. Phys. A 2026.41. Downloaded from www.worldscientific.com
by UNIVERSITY OF CALIFORNIA BERKELEY on 09/16/26. Re-use and distribution is strictly not permitted, except for Open Access articles.

Int. J. Mod. Phys. A 2026.41. Downloaded from www.worldscientific.com
by UNIVERSITY OF CALIFORNIA @ BERKELEY on 09/16/26. Re-use and distribution is strictly not permitted, except for Open Access articles.

[24] SIRUNYAN 19BW based on 35.9 fb^{-1} of pp data at $\sqrt{s}$ = 13 TeV. The limit is for the pair-produced vector-like t' using all-hadronic final state. The analysis is made for the Wb, Zt, ht modes and mass limits are obtained for a variety of branching ratios.

[25] AABOUD 18CL based on 36.1 fb^{-1} of pp data at $\sqrt{s}$ = 13 TeV. The limit is for the pair-produced vector-like t' using all-hadronic final state. The analysis is also made for the Wb, Zt, ht modes and mass limits are obtained for a variety of branching ratios.

[26] SIRUNYAN 18W based on 35.8 fb^{-1} of pp data at $\sqrt{s}$ = 13 TeV. The limit is for the vector-like t' pair-produced by strong interaction using lepton-plus-jets mode and assuming that B($t' \rightarrow Wb$) is 100%. Generally the measurement sets upper limits on the product of the production cross section and branching faction to Wb for any new pair-produced heavy quark decaying to this channel as a narrow resonance.

[27] AABOUD 17L based on 36.1 fb^{-1} of pp data at $\sqrt{s}$ = 13 TeV. No signal is found in the search for heavy quark pair production that decay into Zt followed by $Z \rightarrow \nu\nu$ in the events with one lepton, large $\not{E}_T$, and ≥ 4 jets. The lower mass limit 0.87 (1.05) TeV is obtained for the singlet (doublet) model with other possible decay modes.

[28] AAD 15AR based on 20.3 fb^{-1} of pp data at $\sqrt{s}$ = 8 TeV. Used lepton-plus-jets final state. See Fig. 20 for mass limits in the plane of B($t' \rightarrow Ht$) vs. B($t' \rightarrow Wb$) from a combination of $t'\overline{t}' \rightarrow Wb + X$ and $t'\overline{t}' \rightarrow Ht + X$ searches. Any branching ratio scenario is excluded for mass below 715 GeV.

[29] AAD 15BY based on 20.3 fb^{-1} of pp data at $\sqrt{s}$ = 8 TeV. Limit on pair-produced vector-like t' assuming the branching fractions to W, Z, and h modes of the singlet model. Used events containing $\geq 2\ell + \not{E}_T + \geq 2$j ($\geq 1$ b) and including a same-sign lepton pair.

[30] KHACHATRYAN 15AI based on 19.7 fb^{-1} of pp data at $\sqrt{s}$ = 8 TeV. The search exploits all-hadronic final states by tagging boosted Higgs boson using jet substructure and b-tagging.

[31] Based on 19.5 fb^{-1} of pp data at $\sqrt{s}$ = 8TeV. The t' quark is pair produced and is assumed to decay into three different final states of bW, tZ, and th. The search is carried out using events with at least one isolated lepton.

[32] Based on 4.7 fb^{-1} of pp data at $\sqrt{s}$ = 7 TeV. No signal is found for the search of heavy quark pair production that decay into W and a b quark in the events with a high p_T isolated lepton, large $\not{E}_T$ and at least 3 jets ($\geq$ 1 b-tag). Vector-like quark of charge 2/3 with 400 < $m_{t'}$ < 550 GeV and B($t' \rightarrow Wb$) > 0.63 is excluded at 95% CL.

[33] Based on 5.0 fb^{-1} of pp data at $\sqrt{s}$ = 7 TeV. CHATRCHYAN 13I looked for events with one isolated electron or muon, large $\not{E}_T$, and at least four jets with large transverse momenta, where one jet is likely to originate from the decay of a bottom quark.

[34] Based on 1.04 fb^{-1} of pp data at $\sqrt{s}$ = 7 TeV. No signal is found in the search for pair produced heavy quarks that decay into W boson and a b quark in the events with a high p_T isolated lepton, large $\not{E}_T$ and at least 3 jets (≥ 1 b-tag).

[35] Based on 5.0 fb^{-1} of pp data at $\sqrt{s}$ = 7 TeV. CHATRCHYAN 12BC looked for $t'\overline{t}'$ production events with a single isolated high p_T lepton, large $\not{E}_T$ and at least 4 high p_T jets with a b-tag. The absence of signal above the SM background gives the limit for B($t' \rightarrow Wb$) = 1.

[36] Based on 5.7 fb^{-1} of data in $p\overline{p}$ collisions at 1.96 TeV. AALTONEN 11AH looked for $t'\overline{t}'$ production followed by t' decaying into a top quark and X, an invisible particle, in the all hadronic decay mode of $t\overline{t}$. No excess over the SM $t\overline{t}$ production gives the upper limit on $t'\overline{t}'$ production cross section as a function of $m_{t'}$ and m_X. The result is obtained for B($t' \rightarrow Xt$) = 1.

[37] Based on 5.6 fb^{-1} of data in ppbar collisions at 1.96 TeV. AALTONEN 11AL looked for $\ell + \geq 4$j events and set upper limits on $\sigma(t'\overline{t}')$ as functions of $m_{t'}$.

[38] Based on 4.8 fb^{-1} of data in $p\overline{p}$ collisions at 1.96 TeV. AALTONEN 11O looked for $t'\overline{t}'$ production signal when t' decays into a top quark and X, an invisible particle, in $\ell + \not{E}_T +$ jets channel. No excess over the SM $t\overline{t}$ production gives the upper limit on $t'\overline{t}'$ production cross section as a function of $m_{t'}$ and m_X. The result is obtained for B($t' \rightarrow Xt$) = 1.

[39] Based on 5.3 fb^{-1} of data in $p\overline{p}$ collisions at 1.96 TeV. ABAZOV 11Q looked for $\ell + \not{E}_T + \geq 4$j events and set upper limits on $\sigma(t'\overline{t}')$ as functions of $m_{t'}$.

[40] Searches for pair production of a new heavy top-like quark t' decaying to a W boson and another quark by fitting the observed spectrum of total transverse energy and reconstructed t' mass in the lepton + jets events.

[41] HUANG 08 reexamined the t' mass lower bound of 256 GeV obtained in AALTONEN 08H that assumes B($b' \rightarrow qZ$) = 1 for $q = u, c$ which does not hold when $m_{b'} < m_{t'} - m_W$ or the mixing $\sin^2(\theta_{bt'})$ is so tiny that the decay occurs outside of the vertex detector. Fig. 1 gives that lower bound on $m_{t'}$ in the plane of $\sin^2(\theta_{bt'})$ and $m_{b'}$.

t'(5/3)-quark/hadron mass limits in $p\overline{p}$ and pp collisions

VALUE (GeV)	CL%	DOCUMENT ID		TECN	COMMENT
>1460	95	[1] AAD	23AG	ATLS	$t'(5/3) \rightarrow tW^+$
>1330	95	[2] SIRUNYAN	19T	CMS	$t'_R(5/3) \rightarrow tW^+$
>1300	95	[2] SIRUNYAN	19T	CMS	$t'_L(5/3) \rightarrow tW^+$
>1190	95	[3] AABOUD	18CE	ATLS	$\geq 2\ell + \not{E}_T + \geq 1bj$
>1020	95	[4] SIRUNYAN	17J	CMS	$t'_R(5/3) \rightarrow tW^+$
> 990	95	[4] SIRUNYAN	17J	CMS	$t'_L(5/3) \rightarrow tW^+$
> 750	95	[5] AAD	15BY	ATLS	$t'(5/3) \rightarrow tW^+$
> 840	95	[6] AAD	15Z	ATLS	$t'(5/3) \rightarrow tW^+$
> 800	95	[7] CHATRCHYAN	14T	CMS	$t'(5/3) \rightarrow tW^+$
• • • We do not use the following data for averages, fits, limits, etc. • • •					
>1350	95	[8] AABOUD	18AW	ATLS	$t'(5/3) \rightarrow tW^+$

[1] AAD 23AG based on 139 fb^{-1} of pp data at $\sqrt{s}$ = 13 TeV. Pair production of vector-like top or b' is seached for in the mode $1\ell + \geq 4$j($\geq$ 1b-tagged) + $\not{E}_T$. The data are consistent with the SM background predictions and limits are obtained for different branching ratios.

[2] SIRUNYAN 19T based on 35.9 fb^{-1} of pp data at $\sqrt{s}$ = 13 TeV. Signals are searched in the final states of t' pair production, with same-sign leptons (which come from a t' decay) or a single lepton (which comes from a W out of 4Ws), along with jets, and no excess over the SM expectation is found.

[3] AABOUD 18CE based on 36.1 fb^{-1} of proton-proton data taken at $\sqrt{s}$ = 13 TeV. Events including a same-sign lepton pair are used. The limit is for the pair-produced vector-like t'. With single t' production included, assuming $t'tW$ coupling of one, the limit is $m_{t'}$ > 1.6 TeV.

[4] SIRUNYAN 17J based on 2.3 fb^{-1} of pp data at $\sqrt{s}$ = 13 TeV. Signals are searched in the final states of t' pair production, with same-sign leptons (which come from a t' decay) or a single lepton (which comes from a W out of 4Ws), along with jets, and no excess over the SM expectation is found.

[5] AAD 15BY based on 20.3 fb^{-1} of pp data at $\sqrt{s}$ = 8 TeV. Limit on $t'(5/3)$ in pair and single production assuming its coupling to Wt is equal to one. Used events containing $\geq 2\ell + \not{E}_T + \geq 2$j ($\geq 1$ b) and including a same-sign lepton pair.

[6] AAD 15Z based on 20.3 fb^{-1} of pp data at $\sqrt{s}$ = 8 TeV. Used events with $\ell + \not{E}_T + \geq 6$j ($\geq 1$ b) and at least one pair of jets from weak boson decay, sensitive to the final state $b\overline{b}W^+W^-W^+W^-$.

[7] CHATRCHYAN 14T based on 19.5 fb^{-1} of pp data at $\sqrt{s}$ = 8 TeV. Non-observation of anomaly in H_T distribution in the same-sign dilepton events leads to the limit when pair produced $t'(5/3)$ quark decays exclusively into t and W^+, resulting in the final state with $b\overline{b}W^+W^-W^+W^-$.

[8] AABOUD 18AW based on 36.1 fb^{-1} of pp data at $\sqrt{s}$ = 13 TeV. Limit on $t'(5/3)$ in pair production assuming its coupling to Wt is equal to one. Lepton-plus-jets final state is used, characterized by $\ell + \not{E}_T +$ jets (≥ 1 b-tagged).

$t'(2/3)$ mass limits from single production in $p\overline{p}$ and pp collisions

VALUE (GeV)	CL%	EVTS	DOCUMENT ID		TECN	COMMENT
>2100	95		[1] AAD	25I	ATLS	$qg \rightarrow q't'b$, $t' \rightarrow Ht$ or $t' \rightarrow Zt$
>1800	95		[2] AAD	24AK	ATLS	$qg \rightarrow q't'b$, B($t' \rightarrow Wb$) = 0.5
> 950	95		[3] AAD	16AV	ATLS	$qg \rightarrow q't'b$, B($t' \rightarrow Wb$)=0.5
> 403	95		[4] ABAZOV	11F	D0	$qd \rightarrow q't' \rightarrow q'(Wd)$ $\widetilde{\kappa}_{dt'}$=1, B($t' \rightarrow Wd$)=1
> 551	95		[4] ABAZOV	11F	D0	$qu \rightarrow qt' \rightarrow q(Zu)$ $\widetilde{\kappa}_{ut'}=\sqrt{2}$, B($t' \rightarrow Zu$)=1
• • • We do not use the following data for averages, fits, limits, etc. • • •						
			[5] AAD	25BH	ATLS	$t' \rightarrow Wb$
>1850	95	ATLS	[6] AAD	25S	ATLS	$qg \rightarrow q't'b$, $t' \rightarrow Wb$
			[7] AAD	24V	ATLS	$t' \rightarrow Zt$
			[8] HAYRAPETY...	24AR	CMS	$t' \rightarrow Zt$, Ht
			[9] AAD	22G	ATLS	$t' \rightarrow Ht$, singlet t'
			[10] TUMASYAN	22X	CMS	$t' \rightarrow Zt$

[1] AAD 25I based on 139 fb^{-1} of pp data at $\sqrt{s}$ = 13 TeV. No significant excess over SM expectation is found in the search for a vector-like t' decaying into tZ or tH in hadronic and semileptonic final states. The highest mass bound is obtained for the SU(2) singlet t' with electroweak coupling, κ, of 0.5, and $\Gamma_{t'}/m_{t'}$ = 0.5.

[2] AAD 24AK based on 139 fb^{-1} of pp data at $\sqrt{s}$ = 13 TeV. No significant excess over SM expectation is found in the search for a vector-like t' in events with a reconstructed boosted top quark and a large missing transverse momentum. B($t' \rightarrow Wb$) + B($t' \rightarrow tZ$) + B($t' \rightarrow tH$) = 1 and B($t' \rightarrow tZ$) = B($t' \rightarrow tH$) = 1/4 are assumed.

[3] AAD 16AV based on 20.3 fb^{-1} of pp data at $\sqrt{s}$ = 8 TeV. No significant excess over SM expectation is found in the search for a fully reconstructed vector-like t' in the mode $\ell + \not{E}_T + \geq 2j$ ($\geq 1b$). A veto on massive large-radius jets is used to reject the $t\overline{t}$ background.

[4] ABAZOV 11F based on 5.4 fb^{-1} of data in ppbar collisions at 1.96 TeV. It looked for single production of t' via the Z or E coupling to the first generation up or down quarks, respectively. Model independent cross section limits for the single production processes $p\overline{p} \rightarrow t'q \rightarrow (Wd)q$, and $p\overline{p} \rightarrow t'q \rightarrow (Zd)q$ are given in Figs. 3 and 4, respectively, and the mass limits are obtained for the model of ATRE 09 with degenerate bi-doublets of vector-like quarks.

[5] AAD 25BH based on 140 fb^{-1} of pp data at $\sqrt{s}$ = 13 TeV. No significant excess over SM expectation is found in the search for a vector-like t' decaying into bW in semileptonic final states. Upper limits are set on the cross section times branching ratio and on the coupling of t' to the SM sector. Also similar limits are set for t' with charge -4/3.

[6] AAD 25S based on 139 fb^{-1} of pp data at $\sqrt{s}$ = 13 TeV. No significant excess over SM expectation is found in the search for a vector-like t' decaying into bW in the fully hadronic final states using a highly boosted W jet. The mass bound is obtained for the global coupling parameter κ = 0.7. The corresponding mass bound for a vector-like quark Y with electric charge -4/3 is 2.35 TeV.

[7] AAD 24V based on 139 fb^{-1} of pp data at $\sqrt{s}$ = 13 TeV. No significant excess over SM expectation is found in the search for a vector-like t' in the Zt decay channel, which consists of a pair of opposite-sign leptons from a Z-boson, b-tagged jets and forward jets. The mass range above 1 TeV is targeted and 95% CL limits on the mass and coupling strength of t' are set, in the singlet and doublet scenarios.

[8] HAYRAPETYAN 24AR based on 138 fb^{-1} of pp data at $\sqrt{s}$ = 13 TeV. No deviation from the SM expectation is found in the search for a vector-like t' in the all-hadronic final state where the t' is reconstructed as five jets, with three of them being b-jets. 95% CL upper limits are set on the product of the t'-production cross section and the branching ratio B($t' \rightarrow tZ$) or B($t' \rightarrow tH$).

[9] AAD 22G based on 139 fb^{-1} of pp data at $\sqrt{s}$ = 13 TeV. No significant excess over SM expectation is found in the search for a vector-like t' in the Ht decay channel, where H and t are reconstructed as single jets. The mass range between 1.0 and 2.3 TeV is targeted and 95% CL limits on the production section times the decay branching fraction are set depending on the coupling and mass of t'.

[10] TUMASYAN 22X based on 137 fb^{-1} of pp data at $\sqrt{s}$ = 13 TeV. No significant excess over SM expectation is found in the search for a vector-like t' in the Zt decay channel, where Z decays to neutrinos and t decays hadronically. The 95% CL limits on the production section times the decay branching fraction are set depending on the coupling and mass of t'.

by UNIVERSITY OF CA . Phys. A 2026.41. Downloaded from www.worldscientific.com
ELEY on 09/16/26. Re-use and distribution is strictly not permitted, except for Open Access articles.

$t'(5/3)$ mass limits from single production in $p\overline{p}$ and pp collisions

VALUE (GeV)	DOCUMENT ID	TECN	COMMENT
• • • We do not use the following data for averages, fits, limits, etc. • • •			
	[1] SIRUNYAN 19AI	CMS	$tW \to t'(5/3) \to tW$

[1] SIRUNYAN 19AI based on 35.9 fb^{-1} of pp data at $\sqrt{s} = 13$ TeV. Exclusion limits are set on the product of the production cross section and branching fraction for the $b'(-1/3) + t$ and $t'(5/3) + t$ modes as a function of the vector-like quark mass in Fig. 8 and Tab. 2 for relative vector-like quark widths between 1 and 30% for left- and right-handed vector-like quark couplings. No significant deviation from the SM prediction is observed.

REFERENCES FOR Searches for (Fourth Generation) t' Quark

AAD	25BH	JHEP 2512 012	G. Aad et al.	(ATLAS Collab.)
AAD	25I	PR D111 012012	G. Aad et al.	(ATLAS Collab.)
AAD	25S	JHEP 2502 075	G. Aad et al.	(ATLAS Collab.)
AAD	24AK	JHEP 2405 263	G. Aad et al.	(ATLAS Collab.)
AAD	24BP	PR D110 052009	G. Aad et al.	(ATLAS Collab.)
AAD	24N	PL B854 138743	G. Aad et al.	(ATLAS Collab.)
AAD	24V	PR D109 112012	G. Aad et al.	(ATLAS Collab.)
HAYRAPETY...	24AR	PR D110 072012	A. Hayrapetyan et al.	(CMS Collab.)
AAD	23AG	EPJ C83 719	G. Aad et al.	(ATLAS Collab.)
AAD	23AV	PL B843 138019	G. Aad et al.	(ATLAS Collab.)
TUMASYAN	23AX	JHEP 2309 057	A. Tumasyan et al.	(CMS Collab.)
TUMASYAN	23V	JHEP 2307 020	A. Tumasyan et al.	(CMS Collab.)
AAD	22G	PR D105 092012	G. Aad et al.	(ATLAS Collab.)
TUMASYAN	22X	JHEP 2205 093	A. Tumasyan et al.	(CMS Collab.)
SIRUNYAN	19AI	EPJ C79 90	A.M. Sirunyan et al.	(CMS Collab.)
SIRUNYAN	19AQ	EPJ C79 364	A.M. Sirunyan et al.	(CMS Collab.)
SIRUNYAN	19BW	PR D100 072001	A.M. Sirunyan et al.	(CMS Collab.)
SIRUNYAN	19T	JHEP 1903 082	A.M. Sirunyan et al.	(CMS Collab.)
AABOUD	18AW	JHEP 1808 048	M. Aaboud et al.	(ATLAS Collab.)
AABOUD	18CE	JHEP 1812 039	M. Aaboud et al.	(ATLAS Collab.)
AABOUD	18CL	PR D98 092005	M. Aaboud et al.	(ATLAS Collab.)
AABOUD	18CP	PR D98 112010	M. Aaboud et al.	(ATLAS Collab.)
AABOUD	18CR	PRL 121 211801	M. Aaboud et al.	(ATLAS Collab.)
SIRUNYAN	18BM	JHEP 1808 177	A.M. Sirunyan et al.	(CMS Collab.)
SIRUNYAN	18Q	PR D97 072008	A.M. Sirunyan et al.	(CMS Collab.)
SIRUNYAN	18W	PL B779 82	A.M. Sirunyan et al.	(CMS Collab.)
AABOUD	17L	JHEP 1708 052	M. Aaboud et al.	(ATLAS Collab.)
SIRUNYAN	17AU	JHEP 1711 085	A.M. Sirunyan et al.	(CMS Collab.)
SIRUNYAN	17J	JHEP 1708 073	A.M. Sirunyan et al.	(CMS Collab.)
AAD	16AV	EPJ C76 442	G. Aad et al.	(ATLAS Collab.)
AAD	15AR	JHEP 1508 105	G. Aad et al.	(ATLAS Collab.)
AAD	15BY	JHEP 1510 150	G. Aad et al.	(ATLAS Collab.)
AAD	15Z	PR D91 112011	G. Aad et al.	(ATLAS Collab.)
KHACHATRY...	15AI	JHEP 1506 080	V. Khachatryan et al.	(CMS Collab.)
AAD	14AZ	JHEP 1411 104	G. Aad et al.	(ATLAS Collab.)
CHATRCHYAN	14A	PL B729 149	S. Chatrchyan et al.	(CMS Collab.)
CHATRCHYAN	14T	PRL 112 171801	S. Chatrchyan et al.	(CMS Collab.)
AAD	13F	PL B718 1284	G. Aad et al.	(ATLAS Collab.)
CHATRCHYAN	13I	JHEP 1301 154	S. Chatrchyan et al.	(CMS Collab.)
AAD	12AR	PRL 108 261802	G. Aad et al.	(ATLAS Collab.)
AAD	12BC	PR D86 012007	G. Aad et al.	(ATLAS Collab.)
AAD	12C	PRL 108 041805	G. Aad et al.	(ATLAS Collab.)
CHATRCHYAN	12BC	PL B718 307	S. Chatrchyan et al.	(CMS Collab.)
CHATRCHYAN	12BH	PR D86 112003	S. Chatrchyan et al.	(CMS Collab.)
CHATRCHYAN	12P	PL B716 103	S. Chatrchyan et al.	(CMS Collab.)
AALTONEN	11AH	PRL 107 191803	T. Aaltonen et al.	(CDF Collab.)
AALTONEN	11AL	PRL 107 261801	T. Aaltonen et al.	(CDF Collab.)
AALTONEN	11O	PRL 106 191801	T. Aaltonen et al.	(CDF Collab.)
ABAZOV	11F	PRL 106 081801	V.M. Abazov et al.	(D0 Collab.)
ABAZOV	11Q	PRL 107 082001	V.M. Abazov et al.	(D0 Collab.)
ATRE	09	PR D79 054018	A. Atre et al.	
AALTONEN	08H	PRL 100 161803	T. Aaltonen et al.	(CDF Collab.)
HUANG	08	PR D77 037302	P.Q. Hung, M. Sher	(UVA, WILL)

Free Quark Searches

FREE QUARK SEARCHES

Quarks are fractionally charged particles, the constituents of hadrons, with charges 1/3 e or 2/3 e. The charge of every known charged system is an integer multiple of 1/3 e. Quantum Chromodynamics predicts that quarks cannot be observed as freely propagating particles, being confined inside hadrons or deconfined in quark-gluon plasma (QGP). We observe the top quark decaying as still free, because its lifetime is too short to allow its hadronization. Experiments have produced no evidence for free propagating quarks.

Reviews can be found in Refs. 1–5.

References

1. M.L. Perl, E.R. Lee, and D. Lomba, Mod. Phys. Lett. **A19**, 2595 (2004).
2. P.F. Smith, Ann. Rev. Nucl. and Part. Sci. **39**, 73 (1989).
3. L. Lyons, Phys. Reports **129**, 225 (1985).
4. M. Marinelli and G. Morpurgo, Phys. Reports **85**, 161 (1982).
5. L.W. Jones, Rev. Mod. Phys. **49**, 717 (1977).

Quark Production Cross Section — Accelerator Searches

X-SECT (cm^2)	CHG (e/3)	MASS (GeV)	ENERGY (GeV)	BEAM	EVTS	DOCUMENT ID		TECN
<1.7-2.3E−39	±2	100–600	7000	pp	0	[1] CHATRCHYAN	13AR	CMS
<14-5.4E−39	±1	100–600	7000	pp	0	[1] CHATRCHYAN	13AR	CMS
<1.3E−36	±2	45–84	130–172	e^+e^-	0	ABREU	97D	DLPH
<2.E−35	+2	250	1800	$p\overline{p}$	0	[2] ABE	92J	CDF
<1.E−35	+4	250	1800	$p\overline{p}$	0	[2] ABE	92J	CDF
<3.8E−28			14.5A	^{28}Si–Pb	0	[3] HE	91	PLAS
<3.2E−28			14.5A	^{28}Si–Cu	0	[3] HE	91	PLAS
<1.E−40	±1,2	<10		$p,\nu,\overline{\nu}$	0	BERGSMA	84B	CHRM
<1.E−36	±1,2	<9	200	μ	0	AUBERT	83C	SPEC
<2.E−10	±2,4	1–3	200	p	0	[4] BUSSIERE	80	CNTR
<5.E−38	+1,2	>5	300	p	0	[5,6] STEVENSON	79	CNTR
<1.E−33	±1	<20	52	pp	0	BASILE	78	SPEC
<9.E−39	±1,2	<6	400	p	0	[5] ANTREASYAN	77	SPEC
<8.E−35	+1,2	<20	52	pp	0	[7] FABJAN	75	CNTR
<5.E−38	−1,2	4–9	200	p	0	NASH	74	CNTR
<1.E−32	+2,4	4–24	52	pp	0	ALPER	73	SPEC
<5.E−31	+1,2,4	<12	300	p	0	LEIPUNER	73	CNTR
<6.E−34	±1,2	<13	52	pp	0	BOTT	72	CNTR
<1.E−36	−4	4	70	p	0	ANTIPOV	71	CNTR
<1.E−35	±1,2	2	28	p	0	[8] ALLABY	69B	CNTR
<4.E−37	−2	<5	70	p	0	[4] ANTIPOV	69	CNTR
<3.E−37	−1,2	2–5	70	p	0	[8] ANTIPOV	69B	CNTR
<1.E−35	+1,2	<7	30	p	0	DORFAN	65	CNTR
<2.E−35	−2	< 2.5–5	30	p	0	[9] FRANZINI	65B	CNTR
<5.E−35	+1,2	<2.2	21	p	0	BINGHAM	64	HLBC
<1.E−32	+1,2	<4.0	28	p	0	BLUM	64	HBC
<1.E−35	+1,2	<2.5	31	p	0	[9] HAGOPIAN	64	HBC
<1.E−34	+1	<2	28	p	0	LEIPUNER	64	CNTR
<1.E−33	+1,2	<2.4	24	p	0	MORRISON	64	HBC

[1] CHATRCHYAN 13AR limits assume pair-produced long-lived spin-1/2 particles neutral under $SU(3)_C$ and $SU(2)_L$.
[2] ABE 92J flux limits decrease as the mass increases from 50 to 500 GeV.
[3] HE 91 limits are for charges of the form $N\pm1/3$ from 23/3 to 38/3.
[4] Hadronic or leptonic quarks.
[5] Cross section cm^2/GeV^2.
[6] 3×10^{-5} <lifetime < 1×10^{-3} s.
[7] Includes BOTT 72 results.
[8] Assumes isotropic cm production.
[9] Cross section inferred from flux.

Quark Differential Production Cross Section — Accelerator Searches

X-SECT (cm^{2}sr^{-1}GeV^{-1})	CHG e/3	MASS (GeV)	ENERGY (GeV)	BEAM	EVTS	DOCUMENT ID		TECN
<4.E−36	−2,4	1.5–6	70	p	0	BALDIN	76	CNTR
<2.E−33	±4	5–20	52	pp	0	ALBROW	75	SPEC
<5.E−34	<7	7–15	44	pp	0	JOVANOV...	75	CNTR
<5.E−35			20	γ	0	[1] GALIK	74	CNTR
<9.E−35	−1,2		200	p	0	NASH	74	CNTR
<4.E−36	−4	2.3–2.7	70	p	0	ANTIPOV	71	CNTR
<3.E−35	±1,2	<2.7	27	p	0	ALLABY	69B	CNTR
<7.E−38	−1,2	<2.5	70	p	0	ANTIPOV	69B	CNTR

[1] Cross section in cm^2/sr/equivalent quanta.

Quark Flux — Accelerator Searches

The definition of FLUX depends on the experiment

(a) is the ratio of measured free quarks to predicted free quarks if there is no "confinement."
(b) is the probability of fractional charge on nuclear fragments. Energy is in GeV/nucleon.
(c) is the 90%CL upper limit on fractionally-charged particles produced per interaction.
(d) is quarks per collision.
(e) is inclusive quark-production cross-section ratio to $\sigma(e^+e^- \to \mu^+\mu^-)$.
(f) is quark flux per charged particle.
(g) is the flux per ν-event.
(h) is quark yield per π^- yield.
(i) is 2-body exclusive quark-production cross-section ratio to $\sigma(e^+e^- \to \mu^+\mu^-)$.

FLUX		CHG (e/3)	MASS (GeV)	ENRGY (GeV)	BEAM	EVTS	DOCUMENT ID		TECN
<1.6E−3	b	see note		200	^{32}S–Pb	0	[1] HUENTRUP	96	PLAS
<6.2E−4	b	see note		10.6	^{32}S–Pb	0	[1] HUENTRUP	96	PLAS
<0.94E−4	e	±2	2–30	88–94	e^+e^-	0	AKERS	95R	OPAL
<1.7E−4	e	±2	30–40	88–94	e^+e^-	0	AKERS	95R	OPAL
<3.6E−4	e	±4	5–30	88–94	e^+e^-	0	AKERS	95R	OPAL
<1.9E−4	e	±4	30–45	88–94	e^+e^-	0	AKERS	95R	OPAL
<2.E−3	e	+1	5–40	88–94	e^+e^-	0	[2] BUSKULIC	93C	ALEP
<6.E−4	e	+2	5–30	88–94	e^+e^-	0	[2] BUSKULIC	93C	ALEP
<1.2E−3	e	+4	15–40	88–94	e^+e^-	0	[2] BUSKULIC	93C	ALEP
<3.6E−4	i	+4	5.0–10.2	88–94	e^+e^-	0	BUSKULIC	93C	ALEP
<3.6E−4	i	+4	16.5–26.0	88–94	e^+e^-	0	BUSKULIC	93C	ALEP
<6.9E−4	i	+4	26.0–33.3	88–94	e^+e^-	0	BUSKULIC	93C	ALEP

Int. J. Mod. Phys. A 2026.41. Downloaded from www.worldscientific.com
by UNIVERSITY OF CALIFORNIA @ BERKELEY on 09/16/26. Re-use and distribution is strictly not permitted, except for Open Access articles.

<9.1E−4	i	+4	33.3–38.6	88–94	e^+e^-	0	BUSKULIC	93C	ALEP
<1.1E−3	i	+4	38.6–44.9	88–94	e^+e^-	0	BUSKULIC	93C	ALEP
<1.6E−4	b	see note		see note		0	[3] CECCHINI	93	PLAS
	b	4,5,7,8		2.1A	^{16}O	0,2,0,6	[4] GHOSH	92	EMUL
<6.4E−5	g	1			$\nu,\overline{\nu}$	1	[5] BASILE	91	CNTR
<3.7E−5	g	2			$\nu,\overline{\nu}$	0	[5] BASILE	91	CNTR
<3.9E−5	g	1			$\nu,\overline{\nu}$	1	[6] BASILE	91	CNTR
<2.8E−5	g	2			$\nu,\overline{\nu}$	0	[6] BASILE	91	CNTR
<1.9E−4	c			14.5A	^{28}Si–Pb	0	[7] HE	91	PLAS
<3.9E−4	c			14.5A	^{28}Si–Cu	0	[7] HE	91	PLAS
<1.E−9	c	±1,2,4		14.5A	^{16}O–Ar	0	MATIS	91	MDRP
<5.1E−10	c	±1,2,4		14.5A	^{16}O–Hg	0	MATIS	91	MDRP
<8.1E−9	c	±1,2,4		14.5A	Si–Hg	0	MATIS	91	MDRP
<1.7E−6	c	±1,2,4		60A	^{16}O–Hg	0	MATIS	91	MDRP
<3.5E−7	c	±1,2,4		200A	^{16}O–Hg	0	MATIS	91	MDRP
<1.3E−6	c	±1,2,4		200A	S–Hg	0	MATIS	91	MDRP
<5E−2	e	2	19–27	52–60	e^+e^-	0	ADACHI	90C	TOPZ
<5E−2	e	4	<24	52–60	e^+e^-	0	ADACHI	90C	TOPZ
<1.E−4	e	+2	<3.5	10	e^+e^-	0	BOWCOCK	89B	CLEO
<1.E−6	d	±1,2		60	^{16}O–Hg	0	CALLOWAY	89	MDRP
<3.5E−7	d	±1,2		200	^{16}O–Hg	0	CALLOWAY	89	MDRP
<1.3E−6	d	±1,2		200	S–Hg	0	CALLOWAY	89	MDRP
<1.2E−10	d	±1	1	800	p–Hg	0	MATIS	89	MDRP
<1.1E−10	d	±2	1	800	p–Hg	0	MATIS	89	MDRP
<1.2E−10	d	±1	1	800	p–N_2	0	MATIS	89	MDRP
<7.7E−11	d	±2	1	800	p–N_2	0	MATIS	89	MDRP
<6.E−9	h	−5	0.9–2.3	12	p	0	NAKAMURA	89	SPEC
<5.E−5	g	1,2	<0.5		$\nu,\overline{\nu}d$	0	ALLASIA	88	BEBC
<3.E−4	b	See note		14.5	^{16}O–Pb	0	[8] HOFFMANN	88	PLAS
<2.E−4	b	See note		200	^{16}O–Pb	0	[9] HOFFMANN	88	PLAS
<8E−5	b	19,20,22,23		200A			GERBIER	87	PLAS
<2.E−4	a	±1,2	<300	320	$\overline{p}p$	0	LYONS	87	MLEV
<1.E−9	c	±1,2,4,5		14.5	^{16}O–Hg	0	SHAW	87	MDRP
<3.E−3	d	−1,2,3,4,6	<5	2	Si–Si	0	[10] ABACHI	86C	CNTR
<1.E−4	e	±1,2,4	<4	10	e^+e^-	0	ALBRECHT	85G	ARG
<6.E−5	b	±1,2	1	540	$p\overline{p}$	0	BANNER	85	UA2
<5.E−3	e	−4	1–8	29	e^+e^-	0	AIHARA	84	TPC
<1.E−2	e	±1,2	1–13	29	e^+e^-	0	AIHARA	84B	TPC
<2.E−4	b	±1		72	^{40}Ar	0	[11] BARWICK	84	CNTR
<1.E−4	e	±2	<0.4	1.4	e^+e^-	0	BONDAR	84	OLYA
<5.E−1	e	±1,2	<13	29	e^+e^-	0	GURYN	84	CNTR
<3.E−3	b	±1,2	<2	540	$p\overline{p}$	0	BANNER	83	CNTR
<1.E−4	b	±1,2		106	^{56}Fe	0	LINDGREN	83	CNTR
<3.E−3	b	>|±0.1|		74	^{40}Ar	0	[11] PRICE	83	PLAS
<1.E−2	e	±1,2	<14	29	e^+e^-	0	MARINI	82B	CNTR
<8.E−2	e	±1,2	<12	29	e^+e^-	0	ROSS	82	CNTR
<3.E−4	e	±2	1.8–2	7	e^+e^-	0	WEISS	81	MRK2
<5.E−2	e	+1,2,4,5	2–12	27	e^+e^-	0	BARTEL	80	JADE
<2.E−5	g	1,2			ν	0	[5,6] BASILE	80	CNTR
<3.E−10	f	±2,4	1–3	200	p	0	[12] BOZZOLI	79	CNTR
<6.E−11	f	±1	<21	52	pp	0	BASILE	78	SPEC
<5.E−3	g				ν_μ	0	BASILE	78B	CNTR
<2.E−9	f	±1	<26	62	pp	0	BASILE	77	SPEC
<7.E−10	f	+1,2	<20	52	p	0	[13] FABJAN	75	CNTR
		+1,2	>4.5		γ	0	[5,6] GALIK	74	CNTR
		+1,2	>1.5	12	e^-	0	[5,6] BELLAMY	68	CNTR
		+1,2	>0.9		γ	0	[6] BATHOW	67	CNTR
		+1,2	>0.9	6	γ	0	[6] FOSS	67	CNTR

[1] HUENTRUP 96 quote 95% CL limits for production of fragments with charge differing by as much as ±1/3 (in units of e) for charge $6 \le Z \le 10$.
[2] BUSKULIC 93C limits for inclusive quark production are more conservative if the ALEPH hadronic fragmentation function is assumed.
[3] CECCHINI 93 limit at 90%CL for $23/3 \le Z \le 40/3$, for 16*A* GeV O, 14.5*A* Si, and 200*A* S incident on Cu target. Other limits are 2.3×10^{-4} for $17/3 \le Z \le 20/3$ and 1.2×10^{-4} for $20/3 \le Z \le 23/3$.
[4] GHOSH 92 reports measurement of spallation fragment charge based on ionization in emulsion. Out of 650 measured tracks, 2 were consistent with charge $5e/3$, and 4 with $7e/3$.
[5] Hadronic quark.
[6] Leptonic quark.
[7] HE 91 limits are for charges of the form $N\pm1/3$ from 23/3 to 38/3, and correspond to cross-section limits of 380μb (Pb) and 320μb (Cu).
[8] The limits apply to projectile fragment charges of 17, 19, 20, 22, 23 in units of $e/3$.
[9] The limits apply to projectile fragment charges of 16, 17, 19, 20, 22, 23 in units of $e/3$.
[10] Flux limits and mass range depend on charge.
[11] Bound to nuclei.
[12] Quark lifetimes $> 1 \times 10^{-8}$ s.
[13] One candidate m <0.17 GeV.

Quark Flux — Cosmic Ray Searches

Shielding values followed with an asterisk indicate altitude in km. Shielding values not followed with an asterisk indicate sea level in kg/cm^2.

FLUX (cm^{-2}sr^{-1}s^{-1})	CHG ($e/3$)	MASS (GeV)	SHIELDING	DOCUMENT ID		TECN
< 6.2E−10	±2			[1] ALEMANNO	22	DAMP
< 1.E−8	±1/6–1/10			[2] AGNESE	15	CDMS
< 9.2E−15	±1		3800	[3] AMBROSIO	00C	MCRO
<2.1E−15	±1			MORI	91	KAM2
<2.3E−15	±2			MORI	91	KAM2
<2.E−10	±1,2		0.3	WADA	88	CNTR
	±4		0.3	[4] WADA	88	CNTR
	±4		0.3	[5] WADA	86	CNTR
<1.E−12	±2,3/2		−70.	[6] KAWAGOE	84B	PLAS
<9.E−10	±1,2		0.3	WADA	84B	CNTR
<4.E−9	±4		0.3	WADA	84B	CNTR
<2.E−12	±1,2,3		−0.3 *	MASHIMO	83	CNTR
<3.E−10	±1,2		0.3	MARINI	82	CNTR
<2.E−11	±1,2			MASHIMO	82	CNTR
<8.E−10	±1,2		0.3	[6] NAPOLITANO	82	CNTR
				[7] YOCK	78	CNTR
<1.E−9				[8] BRIATORE	76	ELEC
<2.E−11	+1			[9] HAZEN	75	CC
<2.E−10	+1,2			KRISOR	75	CNTR
<1.E−7	+1,2			[9,10] CLARK	74B	CC
<3.E−10	+1	>20		KIFUNE	74	CNTR
<8.E−11	+1			[9] ASHTON	73	CNTR
<2.E−8	+1,2			HICKS	73B	CNTR
<5.E−10	+4		2.8 *	BEAUCHAMP	72	CNTR
<1.E−10	+1,2			[9] BOHM	72B	CNTR
<1.E−10	+1,2		2.8 *	COX	72	ELEC
<3.E−10	+2			CROUCH	72	CNTR
<3.E−8			7	[8] DARDO	72	CNTR
<4.E−9	+1			[9] EVANS	72	CC
<2.E−9		>10		[8] TONWAR	72	CNTR
<2.E−10	+1		2.8 *	CHIN	71	CNTR
<3.E−10	+1,2			[9] CLARK	71B	CC
<1.E−10	+1,2			[9] HAZEN	71	CC
<5.E−10	+1,2		3.5 *	BOSIA	70	CNTR
	+1,2	<6.5		[9] CHU	70	HLBC
<2.E−9	+1			FAISSNER	70B	CNTR
<2.E−10	+1,2		0.8 *	KRIDER	70	CNTR
<5.E−11	+2			CAIRNS	69	CC
<8.E−10	+1,2	<10		FUKUSHIMA	69	CNTR
	+2			[9,11] MCCUSKER	69	CC
<1.E−10		>5	1.7,3.6	[8] BJORNBOE	68	CNTR
<1.E−8	±1,2,4		6.3,.2 *	[6] BRIATORE	68	CNTR
<3.E−8		>2		FRANZINI	68	CNTR
<9.E−11	±1,2			GARMIRE	68	CNTR
<4.E−10	±1			HANAYAMA	68	CNTR
<3.E−8		>15		KASHA	68	OSPK
<2.E−10	+2			KASHA	68B	CNTR
<2.E−10	+4			KASHA	68C	CNTR
<2.E−10	+2		6	BARTON	67	CNTR
<2.E−7	+4		0.008,0.5 *	BUHLER	67	CNTR
<5.E−10	1,2		0.008,0.5 *	BUHLER	67B	CNTR
<4.E−10	+1,2			GOMEZ	67	CNTR
<2.E−9	+2			KASHA	67	CNTR
<2.E−10	+2		220	BARTON	66	CNTR
<2.E−9	+1,2		0.5 *	BUHLER	66	CNTR
<3.E−9	+1,2			KASHA	66	CNTR
<2.E−9	+1,2			LAMB	66	CNTR
<2.E−8	+1,2	>7	2.8 *	DELISE	65	CNTR
<5.E−8	+2	>2.5	0.5 *	MASSAM	65	CNTR
<2.E−8	+1		2.5 *	BOWEN	64	CNTR
<2.E−7	+1		0.8	SUNYAR	64	CNTR

[1] ALEMANNO 22 uses data from the DAMPE satellite, with calorimetry and tracking to search for fractionally charged particles with $q = \pm 2/3e$ with a exposure time of 2.3×10^7 s.
[2] See AGNESE 15 Fig.6 for limits on vertical density as function of charge extending to $|q|/e < 1/10$.
[3] AMBROSIO 00C limit is below 11×10^{-15} for $0.25 < q/e < 0.5$, and is changing rapidly near $q/e = 2/3$, where it is 2×10^{-14}.
[4] Distribution in celestial sphere was described as anisotropic.
[5] With telescope axis at zenith angle 40° to the south.
[6] Leptonic quarks.
[7] Lifetime $> 10^{-8}$ s; charge ±0.70, 0.68, 0.42; and mass >4.4, 4.8, and 20 GeV, respectively.
[8] Time delayed air shower search.
[9] Prompt air shower search.
[10] Also $e/4$ and $e/6$ charges.
[11] No events in subsequent experiments.

Quark Density — Matter Searches

QUARKS/ NUCLEON	CHG ($e/3$)	MASS (GeV)	MATERIAL/METHOD	EVTS	DOCUMENT ID	
<1.17E−22			silicone oil drops	0	[1] LEE	02
<4.71E−22			silicone oil drops	1	[2] HALYO	00
<4.7E−21	±1,2		silicone oil drops	0	MAR	96
<8.E−22	+2		Si/infrared photoionization	0	PERERA	93
<5.E−27	±1,2		sea water/levitation	0	HOMER	92
<4.E−20	±1,2		meteorites/mag. levitation	0	JONES	89
<1.E−19	±1,2		various/spectrometer	0	MILNER	87
<5.E−22	±1,2		W/levitation	0	SMITH	87
<3.E−20	+1,2		org liq/droplet tower	0	VANPOLEN	87
<6.E−20	−1,2		org liq/droplet tower	0	VANPOLEN	87

<3.E−21	±1		Hg drops-untreated	0	SAVAGE	86
<3.E−22	±1,2		levitated niobium	0	SMITH	86
<2.E−26	±1,2		^{4}He/levitation	0	SMITH	86B
<2.E−20	>±1	0.2–250	niobium+tungs/ion	0	MILNER	85
<1.E−21	±1		levitated niobium	0	SMITH	85
	+1,2	<100	niobium/mass spec	0	KUTSCHERA	84
<5.E−22			levitated steel	0	MARINELLI	84
<9.E−20	± <13		water/oil drop	0	JOYCE	83
<2.E−21	> | ± 1/2|		levitated steel	0	LIEBOWITZ	83
<1.E−19	±1,2		photo ion spec	0	VANDESTEEG	83
<2.E−20			mercury/oil drop	0	[3] HODGES	81
1.E−20	+1		levitated niobium	4	[4] LARUE	81
1.E−20	−1		levitated niobium	4	[4] LARUE	81
<1.E−21			levitated steel	0	MARINELLI	80B
<6.E−16			helium/mass spec	0	BOYD	79
1.E−20	+1		levitated niobium	2	[4] LARUE	79
<4.E−28			earth+/ion beam	0	OGOROD...	79
<5.E−15	+1		tungs./mass spec	0	BOYD	78
<5.E−16	+3	<1.7	hydrogen/mass spec	0	BOYD	78B
<1.E−21	±2,4		water/ion beam	0	LUND	78
<6.E−15	>1/2		levitated tungsten	0	PUTT	78
<1.E−22			metals/mass spec	0	SCHIFFER	78
<5.E−15			levitated tungsten ox	0	BLAND	77
<3.E−21			levitated iron	0	GALLINARO	77
2.E−21	−1		levitated niobium	1	[4] LARUE	77
4.E−21	+1		levitated niobium	2	[4] LARUE	77
<1.E−13	+3	<7.7	hydrogen/mass spec	0	MULLER	77
<5.E−27			water+/ion beam	0	OGOROD...	77
<1.E−21			lunar+/ion spec	0	STEVENS	76
<1.E−15	+1	<60	oxygen+/ion spec	0	ELBERT	70
<5.E−19			levitated graphite	0	MORPURGO	70
<5.E−23			water+/atom beam	0	COOK	69
<1.E−17	±1,2		levitated graphite	0	BRAGINSK	68
<1.E−17			water+/uv spec	0	RANK	68
<3.E−19	±1		levitated iron	0	STOVER	67
<1.E−10			sun/uv spec	0	[5] BENNETT	66
<1.E−17	+1,2		meteorites+/ion beam	0	CHUPKA	66
<1.E−16	±1		levitated graphite	0	GALLINARO	66
<1.E−22			argon/electrometer	0	HILLAS	59
	−2		levitated oil	0	MILLIKAN	10

[1] 95% CL limit for fractional charge particles with $0.18e \leq |Q_{residual}| \leq 0.82e$ in total of 70.1 mg of silicone oil.
[2] 95% CL limit for particles with fractional charge $|Q_{residual}| > 0.16e$ in total of 17.4 mg of silicone oil.
[3] Also set limits for $Q = \pm e/6$.
[4] Note that in PHILLIPS 88 these authors report a subtle magnetic effect which could account for the apparent fractional charges.
[5] Limit inferred by JONES 77B.

REFERENCES FOR Free Quark Searches

ALEMANNO 22 PR D106 063026 F. Alemanno et al. (DAMPE Collab.)
AGNESE 15 PRL 114 111302 R. Agnese et al. (CDMS Collab.)
CHATRCHYAN 13AR PR D87 092008 S. Chatrchyan et al. (CMS Collab.)
Also PR D106 099903 (errat.) S. Chatrchyan et al. (CMS Collab.)
LEE 02 PR D66 012002 I.T. Lee et al.
AMBROSIO 00C PR D62 052003 M. Ambrosio et al. (MACRO Collab.)
HALYO 00 PRL 84 2576 V. Halyo et al.
ABREU 97D PL B396 315 P. Abreu et al. (DELPHI Collab.)
HUENTRUP 96 PR C53 358 G. Huentrup et al. (SIEG)
MAR 96 PR D53 6017 N.M. Mar et al. (SLAC, SCHAF, LANL, UCI)
AKERS 95R ZPHY C67 203 R. Akers et al. (OPAL Collab.)
BUSKULIC 93C PL B303 198 D. Buskulic et al. (ALEPH Collab.)
CECCHINI 93 ASP 1 369 S. Cecchini et al.
PERERA 93 PRL 70 1053 A.G.U. Perera et al. (PITT)
ABE 92J PR D46 1889 F. Abe et al. (CDF Collab.)
GHOSH 92 NC 105A 99 D. Ghosh et al. (JADA, BANGB)
HOMER 92 ZPHY C55 549 G.J. Homer et al. (RAL, SHMP, LOQM)
BASILE 91 NC 104A 405 M. Basile et al. (BGNA, INFN, CERN, PLRM+)
HE 91 PR C44 1672 Y.B. He, P.B. Price (UCB)
MATIS 91 NP A525 513 H.S. Matis et al. (LBL, SFSU, UCI+)
MORI 91 PR D43 2843 M. Mori et al. (Kamiokande II Collab.)
ADACHI 90C PL B244 352 I. Adachi et al. (TOPAZ Collab.)
BOWCOCK 89B PR D40 263 T.J.V. Bowcock et al. (CLEO Collab.)
CALLOWAY 89 PL B232 549 D. Calloway et al. (SFSU, UCI, LBL+)
JONES 89 ZPHY C43 349 W.G. Jones et al. (LOIC, RAL)
MATIS 89 PR D39 1851 H.S. Matis et al. (LBL, SFSU, UCI+)
NAKAMURA 89 PR D39 1261 T.T. Nakamura et al. (KYOT, TMTC)
ALLASIA 88 PR D37 219 D. Allasia et al. (WA25 Collab.)
HOFFMANN 88 PL B200 583 A. Hofmann et al. (SIEG, USF)
PHILLIPS 88 NIM A264 125 J.D. Phillips, W.M. Fairbank, J. Navarro (STAN)
WADA 88 NC 11C 229 T. Wada, Y. Yamashita, I. Yamamoto (OKAY)
GERBIER 87 PRL 59 2535 G. Gerbier et al. (UCB, CERN)
LYONS 87 ZPHY C36 363 L. Lyons et al. (OXF, RAL, LOIC)
MILNER 87 PR D36 37 R.E. Milner et al. (CIT)
SHAW 87 PR D36 3533 G.L. Shaw et al. (UCI, LBL, LANL, SFSU)
SMITH 87 PL B197 447 P.F. Smith et al. (RAL, LOIC)
VANPOLEN 87 PR D36 1983 J. van Polen, R.T. Hagstrom, G. Hirsch (ANL+)
ABACHI 86C PR D33 2733 S. Abachi et al. (UCLA, LBL, UCD)
SAVAGE 86 PL 167B 481 M.L. Savage et al. (SFSU)
SMITH 86 PL B171 129 P.F. Smith et al. (RAL, LOIC)
SMITH 86B PL B181 407 P.F. Smith et al. (RAL, LOIC)
WADA 86 NC 9C 358 T. Wada (OKAY)
ALBRECHT 85G PL 156B 134 H. Albrecht et al. (ARGUS Collab.)
BANNER 85 PL 156B 129 M. Banner et al. (UA2 Collab.)
MILNER 85 PRL 54 1472 R.E. Milner et al. (CIT)
SMITH 85 PL 153B 188 P.F. Smith et al. (RAL, LOIC)
AIHARA 84 PRL 52 168 H. Aihara et al. (TPC Collab.)
AIHARA 84B PRL 52 2332 H. Aihara et al. (TPC Collab.)
BARWICK 84 PR D30 691 S.W. Barwick, J.A. Musser, J.D. Stevenson (UCB)
BERGSMA 84B ZPHY C24 217 F. Bergsma et al. (CHARM Collab.)
BONDAR 84 JETPL 40 1265 A.E. Bondar et al. (NOVO)
Translated from ZETFP 40 440.
GURYN 84 PL 139B 313 W. Guryn et al. (FRAS, LBL, NWES, STAN+)
KAWAGOE 84B LNC 41 604 K. Kawagoe et al. (TOKY)
KUTSCHERA 84 PR D29 791 W. Kutschera et al. (ANL, FNAL)
MARINELLI 84 PL 137B 439 M. Marinelli, G. Morpurgo (GENO)
WADA 84B LNC 40 329 T. Wada, Y. Yamashita, I. Yamamoto (OKAY)
AUBERT 83C PL 133B 461 J.J. Aubert et al. (EMC Collab.)
BANNER 83 PL 121B 187 M. Banner et al. (UA2 Collab.)
JOYCE 83 PRL 51 731 D.C. Joyce et al. (SFSU)
LIEBOWITZ 83 PRL 50 1640 D. Liebowitz, M. Binder, K.O.H. Ziock (UVA)
LINDGREN 83 PRL 51 1621 M.A. Lindgren et al. (SFSU, UCR, UCI+)
MASHIMO 83 PL 128B 327 T. Mashimo et al. (ICEPP)
PRICE 83 PRL 50 566 P.B. Price et al. (UCB)
VANDESTEEG 83 PRL 50 1234 M.J.H. van de Steeg, H.W.H.M. Jongbloets, P. Wyder
MARINI 82 PR D26 1777 A. Marini et al. (FRAS, LBL, NWES, STAN+)
MARINI 82B PRL 48 1649 A. Marini et al. (FRAS, LBL, NWES, STAN+)
MASHIMO 82 JPSJ 51 3067 T. Mashimo, K. Kawagoe, M. Koshiba (INUS)
NAPOLITANO 82 PR D25 2837 J. Napolitano et al. (STAN, FRAS, LBL+)
ROSS 82 PL 118B 199 M.C. Ross et al. (FRAS, LBL, NWES, STAN+)
HODGES 81 PRL 47 1651 C.L. Hodges et al. (UCR, SFSU)
LARUE 81 PRL 46 967 G.S. Larue, J.D. Phillips, W.M. Fairbank (STAN)
WEISS 81 PL 101B 439 J.M. Weiss et al. (SLAC, LBL, UCB)
BARTEL 80 ZPHY C6 295 W. Bartel et al. (JADE Collab.)
BASILE 80 LNC 29 251 M. Basile et al. (BGNA, CERN, FRAS, ROMA+)
BUSSIERE 80 NP B174 1 A. Bussiere et al. (BGNA, SACL, LAPP)
MARINELLI 80B PL 94B 433 M. Marinelli, G. Morpurgo (GENO)
Also PL 94B 427 M. Marinelli, G. Morpurgo (GENO)
BOYD 79 PRL 43 1288 R.N. Boyd et al. (OSU)
BOZZOLI 79 NP B159 363 W. Bozzoli et al. (BGNA, LAPP, SACL+)
LARUE 79 PRL 42 142 G.S. Larue, W.M. Fairbank, J.D. Phillips (STAN)
Also PRL 42 1019 G.S. Larue, W.M. Fairbank, J.D. Phillips
OGOROD... 79 JETP 49 953 D.D. Ogorodnikov, I.M. Samoilov, A.M. Solntsev
Translated from ZETF 76 1881.
STEVENSON 79 PR D20 82 M.L. Stevenson (LBL)
BASILE 78 NC 45A 171 M. Basile et al. (CERN, BGNA)
BASILE 78B NC 45A 281 M. Basile et al. (CERN, BGNA)
BOYD 78 PRL 40 216 R.N. Boyd et al. (ROCH)
BOYD 78B PL 72B 484 R.N. Boyd et al. (ROCH)
LUND 78 RA 25 75 T. Lund, R. Brandt, Y. Fares (MARB)
PUTT 78 PR D17 1466 G.D. Putt, P.C.M. Yock (AUCK)
SCHIFFER 78 PR D17 2241 J.P. Schiffer et al. (CHIC, ANL)
YOCK 78 PR D18 641 P.C.M. Yock (AUCK)
ANTREASYAN 77 PRL 39 513 D. Antreasyan et al. (EFI, PRIN)
BASILE 77 NC 40A 41 M. Basile et al. (CERN, BGNA)
BLAND 77 PRL 39 369 R.W. Bland et al. (SFSU)
GALLINARO 77 PRL 38 1255 G. Gallinaro, M. Marinelli, G. Morpurgo (GENO)
JONES 77B RMP 49 717 L.W. Jones
LARUE 77 PRL 38 1011 G.S. Larue, W.M. Fairbank, A.F. Hebard (STAN)
MULLER 77 SCI 196 521 R.A. Muller et al. (LBL)
OGOROD... 77 JETP 45 857 D.D. Ogorodnikov, I.M. Samoilov, A.M. Solntsev
Translated from ZETF 72 1633.
BALDIN 76 SJNP 22 264 B.Y. Baldin et al. (JINR)
Translated from YAF 22 512.
BRIATORE 76 NC 31A 553 L. Briatore et al. (LCGT, FRAS, FREIB)
STEVENS 76 PR D14 716 C.M. Stevens, J.P. Schiffer, W. Chupka (ANL)
ALBROW 75 NP B97 189 M.G. Albrow et al. (CERN, DARE, FOM+)
FABJAN 75 NP B101 349 C.W. Fabjan et al. (CERN, MPIM)
HAZEN 75 NP B95 189 W.E. Hazen et al. (MICH, LEED)
JOVANOV... 75 PL 56B 105 J.V. Jovanovich et al. (MANI, AACH, CERN+)
KRISOR 75 NC 27A 132 K. Krisor (AACH3)
CLARK 74B PR D10 2721 A.F. Clark et al. (LLL)
GALIK 74 PR D9 1856 R.S. Galik et al. (SLAC, FNAL)
KIFUNE 74 JPSJ 36 629 T. Kifune et al. (TOKY, KEK)
NASH 74 PRL 32 858 T. Nash et al. (FNAL, CORN, NYU)
ALPER 73 PL 46B 265 B. Alper et al. (CERN, LIVP, LUND, BOHR+)
ASHTON 73 JP A6 577 F. Ashton et al. (DURH)
HICKS 73B NC 14A 65 R.B. Hicks, R.W. Flint, S. Standil (MANI)
LEIPUNER 73 PRL 31 1226 L.B. Leipuner et al. (BNL, YALE)
BEAUCHAMP 72 PR D6 1211 W.T. Beauchamp et al. (ARIZ)
BOHM 72B PRL 28 326 A. Bohm et al. (AACH)
BOTT 72 PL 40B 693 M. Bott-Bodenhausen et al. (CERN, MPIM)
COX 72 PR D6 1203 A.J. Cox et al. (ARIZ)
CROUCH 72 PR D5 2667 M.F. Crouch, K. Mori, G.R. Smith (CASE)
DARDO 72 NC 9A 319 M. Dardo et al. (TORI)
EVANS 72 PRSE A70 143 G.R. Evans et al. (EDIN, LEED)
TONWAR 72 JP A5 569 S.C. Tonwar, S. Naranan, B.V. Sreekantan (TATA)
ANTIPOV 71 NP B29 374 Y.M. Antipov et al. (SERP)
CHIN 71 NC 2A 419 S. Chin et al. (OSAK)
CLARK 71B PRL 27 51 A.F. Clark et al. (LLL, LBL)
HAZEN 71 PRL 26 582 W.E. Hazen (MICH)
BOSIA 70 NC 66A 167 G.F. Bosia, L. Briatore (TORI)
CHU 70 PRL 24 917 W.T. Chu et al. (OSU, ROSE, KANS)
Also PRL 25 550 W.W.M. Allison et al. (ANL)
ELBERT 70 NP B20 217 J.W. Elbert et al. (WISC)
FAISSNER 70B PRL 24 1357 H. Faissner et al. (AACH3)
KRIDER 70 PR D1 835 E.P. Krider, T. Bowen, R.M. Kalbach (ARIZ)
MORPURGO 70 NIM 79 95 G. Morpurgo, G. Gallinaro, G. Palmieri (GENO)
ALLABY 69B NC 64A 75 J.V. Allaby et al. (CERN)
ANTIPOV 69 PL 29B 245 Y.M. Antipov et al. (SERP)
ANTIPOV 69B PL 30B 576 Y.M. Antipov et al. (SERP)
CAIRNS 69 PR 186 1394 I. Cairns et al. (SYDN)
COOK 69 PR 188 2092 D.D. Cook et al. (ILL)
FUKUSHIMA 69 PR 178 2058 Y. Fukushima et al. (TOKY)
MCCUSKER 69 PRL 23 658 C.B.A. McCusker, I. Cairns (SYDN)
BELLAMY 68 PR 166 1391 E.H. Bellamy et al. (STAN, SLAC)
BJORNBOE 68 NC B53 241 J. Bjornboe et al. (BOHR, TATA, BERN+)
BRAGINSK 68 JETP 27 51 V.B. Braginsky et al. (MOSU)
Translated from ZETF 54 91.
BRIATORE 68 NC 57A 850 L. Briatore et al. (TORI, CERN, BGNA)
FRANZINI 68 PRL 21 1013 P. Franzini, S. Shulman (COLU)
GARMIRE 68 PR 166 1280 G. Garmire, C. Leong, V. Sreekantan (MIT)
HANAYAMA 68 CJP 46 S734 Y. Hanayama et al. (OSAK)
KASHA 68 PR 172 1297 H. Kasha, R.J. Stefanski (BNL, YALE)
KASHA 68B PRL 20 217 H. Kasha et al. (BNL, YALE)
KASHA 68C CJP 46 S730 H. Kasha et al. (BNL, YALE)
RANK 68 PR 176 1635 D. Rank (MICH)
BARTON 67 PRSL 90 87 J.C. Barton (NPOL)
BATHOW 67 PL 25B 163 G. Bathow et al. (DESY)
BUHLER 67 NC 49A 209 A. Buhler-Broglin et al. (CERN, BGNA)
BUHLER 67B NC 51A 837 A. Buhler-Broglin et al. (CERN, BGNA+)
FOSS 67 PL 25B 166 J. Foss et al. (MIT)
GOMEZ 67 PRL 18 1022 R. Gomez et al. (CIT)
KASHA 67 PR 154 1263 H. Kasha et al. (BNL, YALE)
STOVER 67 PR 164 1599 R.W. Stover, T.I. Moran, J.W. Trischka (SYRA)
BARTON 66 PL 21 360 J.C. Barton, C.T. Stockel (NPOL)
BENNETT 66 PRL 17 1196 W.R. Bennett (YALE)
BUHLER 66 NC 45A 520 A. Buhler-Broglin et al. (CERN, BGNA+)
CHUPKA 66 PRL 17 60 W.A. Chupka, J.P. Schiffer, C.M. Stevens (ANL)
GALLINARO 66 PL 23 609 G. Gallinaro, G. Morpurgo (GENO)
KASHA 66 PR 150 1140 H. Kasha, L.B. Leipuner, R.K. Adair (BNL, YALE)
LAMB 66 PRL 17 1068 R.C. Lamb et al. (ANL)
DELISE 65 PR 140 B458 D.A. de Lise, T. Bowen (ARIZ)
DORFAN 65 PRL 14 999 D.E. Dorfan et al. (COLU)

Phys. A 2026.41. Downloaded from www.worldscientific.com
by UNIVERSITY OF CA LEY on 09/16/26. Re-use and distribution is strictly not permitted, except for Open Access articles.

FRANZINI	65B	PRL 14 196	P. Franzini *et al.*	(BNL, COLU)
MASSAM	65	NC 40A 589	T. Massam, T. Muller, A. Zichichi	(CERN)
BINGHAM	64	PL 9 201	H.H. Bingham *et al.*	(CERN, EPOL)
BLUM	64	PRL 13 353A	W. Blum *et al.*	(CERN)
BOWEN	64	PRL 13 728	T. Bowen *et al.*	(ARIZ)
HAGOPIAN	64	PRL 13 280	V. Hagopian *et al.*	(PENN, BNL)
LEIPUNER	64	PRL 12 423	L.B. Leipuner *et al.*	(BNL, YALE)
MORRISON	64	PL 9 199	D.R.O. Morrison	(CERN)
SUNYAR	64	PR 136 B1157	A.W. Sunyar, A.Z. Schwarzschild, P.I. Connors	(BNL)
HILLAS	59	NAT 184 B92	A.M. Hillas, T.E. Cranshaw	(AERE)
MILLIKAN	10	Phil Mag 19 209	R.A. Millikan	(CHIC)

OTHER RELATED PAPERS

LYONS Review	85	PRPL C129 225	L. Lyons	(OXF)
MARINELLI Review	82	PRPL 85 161	M. Marinelli, G. Morpurgo	(GENO)

Int. J. Mod. Phys. A 2026.41. Downloaded from www.worldscientific.com
by UNIVERSITY OF CALIFORNIA @ BERKELEY on 09/16/26. Re-use and distribution is strictly not permitted, except for Open Access articles.

Phys. A 2026.41. Downloaded from www.worldscientific.com
by UNIVERSITY OF CA[redacted]ELEY on 09/16/26. Re-use and distribution is strictly not permitted, except for Open Access articles.

Int. J. Mod. Phys. A 2026.41. Downloaded from www.worldscientific.com
by UNIVERSITY OF CALIFORNIA @ BERKELEY on 09/16/26. Re-use and distribution is strictly not permitted, except for Open Access articles.

LIGHT UNFLAVORED MESONS ($S = C = B = 0$)

- $\pi^{\pm}$ . . . 1491
- π^0 . . . 1494
- η . . . 1496
- $f_0(500)$ aka σ; was $f_0(600)$, $f_0(400-1200)$ . . . 1502
- $\rho(770)$ . . . 1504
- $\omega(782)$ . . . 1510
- $\eta'(958)$ . . . 1516
- $f_0(980)$ . . . 1523
- $a_0(980)$ . . . 1526
- $\phi(1020)$ . . . 1527
- $h_1(1170)$ . . . 1535
- $b_1(1235)$ . . . 1536
- $a_1(1260)$ . . . 1537
- $f_2(1270)$ . . . 1539
- $f_1(1285)$ . . . 1543
- $\eta(1295)$ . . . 1546
- $\pi(1300)$ . . . 1546
- $a_2(1320)$ . . . 1547
- $f_0(1370)$ . . . 1551
  - $\pi_1(1400)$ . . . 1553
- $\eta(1405)$ . . . 1554
- $h_1(1415)$ . . . 1557
- $f_1(1420)$ . . . 1557
- $\omega(1420)$ . . . 1559
  - $f_2(1430)$ . . . 1560
- $a_0(1450)$ . . . 1561
- $\rho(1450)$ . . . 1562
- $\eta(1475)$ . . . 1565
- $f_0(1500)$ . . . 1566
  - $f_1(1510)$ . . . 1569
- $f_2'(1525)$ . . . 1570
- $f_2(1565)$ . . . 1574
  - $\rho(1570)$ . . . 1575
  - $h_1(1595)$ . . . 1575
- $\pi_1(1600)$ . . . 1575
- $a_1(1640)$ . . . 1577
  - $f_2(1640)$ . . . 1578
- $\eta_2(1645)$ . . . 1578
- $\omega(1650)$ . . . 1578
- $\omega_3(1670)$ . . . 1580
- $\pi_2(1670)$ . . . 1580
- $\phi(1680)$ . . . 1582
- $\rho_3(1690)$ . . . 1584
- $\rho(1700)$ . . . 1587
- $a_2(1700)$ . . . 1591
  - $a_0(1710)$ . . . 1592
- $f_0(1710)$ . . . 1593
  - $X(1750)$ . . . 1595
  - $\eta(1760)$ . . . 1596
- $\pi(1800)$ . . . 1596
  - $f_0(1810)$ . . . 1597
  - $f_2(1810)$ . . . 1599
  - $X(1835)$ . . . 1600
- $\phi_3(1850)$ . . . 1601
  - $\eta_1(1855)$ . . . 1602
- $\eta_2(1870)$ . . . 1602
- $\pi_2(1880)$ . . . 1602
  - $\rho(1900)$ . . . 1603
  - $f_2(1910)$ . . . 1603
  - $a_0(1950)$ . . . 1604
- $f_2(1950)$ . . . 1605
- $a_4(1970)$ . . . 1606
  - $\rho_3(1990)$ . . . 1607
  - $\pi_2(2005)$ . . . 1607
- $f_2(2010)$ . . . 1607
- $f_0(2020)$ . . . 1608
- $f_4(2050)$ . . . 1608
  - $\pi_2(2100)$ . . . 1610
  - $f_0(2100)$ . . . 1610
- $f_2(2150)$ . . . 1611
  - $\rho(2150)$ . . . 1612
- $\phi(2170)$ . . . 1614
  - $f_0(2200)$ . . . 1616
  - $f_J(2220)$ . . . 1616
  - $\omega(2220)$ . . . 1617
  - $\eta(2225)$ . . . 1618
  - $\rho_3(2250)$ . . . 1618
- $f_2(2300)$ . . . 1619
  - $f_4(2300)$ . . . 1619
  - $f_0(2330)$ . . . 1620
- $f_2(2340)$ . . . 1620
  - $\rho_5(2350)$ . . . 1621
  - $\eta(2370)$ . . . 1621
  - $f_0(2470)$ . . . 1622
  - $f_6(2510)$ . . . 1622

STRANGE MESONS ($S = \pm 1, C = B = 0$)

- $K^{\pm}$ . . . 1623
- K^0 . . . 1638
- K^0_S . . . 1639
- K^0_L . . . 1643
- $K^*_0(700)$ aka κ; was $K^*_0(800)$ . . . 1658
- $K^*(892)$ . . . 1659
- $K_1(1270)$ . . . 1662
- $K_1(1400)$ . . . 1664
- $K^*(1410)$ . . . 1665
- $K^*_0(1430)$ . . . 1665
- $K^*_2(1430)$ . . . 1666
- $K(1460)$ . . . 1669
  - $K_2(1580)$ . . . 1669
  - $K(1630)$ . . . 1669
- $K_1(1650)$ . . . 1670
- $K^*(1680)$ . . . 1670
- $K_2(1770)$ . . . 1671
- $K^*_3(1780)$ . . . 1671
- $K_2(1820)$ . . . 1672
  - $K(1830)$ . . . 1673
- $K^*_0(1950)$ . . . 1673
- $K^*_2(1980)$ . . . 1674
- $K^*_4(2045)$ . . . 1674
  - $K_2(2250)$ . . . 1675
  - $K_3(2320)$ . . . 1675
  - $K^*_5(2380)$ . . . 1676
  - $K_4(2500)$ . . . 1676
  - $K(3100)$ aka $K^*_J(3100)$ . . . 1676

CHARMED MESONS ($C = \pm 1$)

- $D^{\pm}$ . . . 1677
- D^0 . . . 1698
- $D^*(2007)^0$ . . . 1738
- $D^*(2010)^{\pm}$ . . . 1739
- $D^*_0(2300)$ was $D^*_0(2400)$ . . . 1741
- $D_1(2420)$ . . . 1741

• Indicates the particle is in the Meson Summary Table

(Continued on the next page)

- $D_1(2430)^0$ . . . 1743
- $D_2^*(2460)$ . . . 1743
  $D_0(2550)^0$ . . . 1745
  $D_1^*(2600)^0$ was $D(2600)$ . . . 1745
  $D^*(2640)^\pm$ . . . 1746
  $D_2(2740)^0$ was $D(2740)^0$ . . . 1746
- $D_3^*(2750)$ . . . 1747
  $D_1^*(2760)^0$ . . . 1747
  $D_2^*(3000)^0$ . . . 1748

CHARMED, STRANGE MESONS ($C = S = \pm 1$)

- $D_s^\pm$ . . . 1749
- $D_s^{*\pm}$ . . . 1768
- $D_{s0}^*(2317)^\pm$ . . . 1769
- $D_{s1}(2460)^\pm$ . . . 1769
- $D_{s1}(2536)^\pm$ . . . 1771
- $D_{s2}^*(2573)$ . . . 1772
  $D_{s0}(2590)^+$ . . . 1773
- $D_{s1}^*(2700)^\pm$ . . . 1773
  $D_{s1}^*(2860)^\pm$ was $D_{sJ}^*(2860)$ . . . 1774
- $D_{s3}^*(2860)^\pm$ . . . 1774
  $D_{sJ}(3040)^\pm$ . . . 1774

BOTTOM MESONS ($B = \pm 1$)

- $B^\pm$ . . . 1776
- B^0 . . . 1849
- $B^\pm/B^0$ ADMIXTURE . . . 1929
- $B^\pm/B^0/B_s^0/b$-baryon ADMIXTURE . . . 1951
  V_{cb} and V_{ub} CKM Matrix Elements . . . 1959
- B^* . . . 1961
- $B_1(5721)$ . . . 1961
  $B_J^*(5732)$ . . . 1962
- $B_2^*(5747)$ . . . 1962
  $B_J(5840)$ . . . 1963
- $B_J(5970)$ . . . 1963

BOTTOM, STRANGE MESONS ($B = \pm 1, S = \mp 1$)

- B_s^0 . . . 1965
- B_s^* . . . 1994
- $B_{s1}(5830)^0$ . . . 1994
- $B_{s2}^*(5840)^0$ . . . 1994
  $B_{sJ}^*(5850)$ . . . 1995
  $B_{sJ}(6063)^0$ . . . 1995
  $B_{sJ}(6114)^0$ . . . 1995

BOTTOM, CHARMED MESONS ($B = C = \pm 1$)

- B_c^+ . . . 1996
  $B_c(1P)^\pm$ . . . 2000
- $B_c(2S)^\pm$ . . . 2001

$c\bar{c}$ MESONS

- $\eta_c(1S)$ . . . 2002
- $J/\psi(1S)$ . . . 2012
- $\chi_{c0}(1P)$ . . . 2042
- $\chi_{c1}(1P)$ . . . 2054
- $h_c(1P)$ . . . 2064
- $\chi_{c2}(1P)$ . . . 2067
- $\eta_c(2S)$ . . . 2080
- $\psi(2S)$ . . . 2083
- $\psi(3770)$ . . . 2102
- $\psi_2(3823)$ was $\psi(3823)$, $X(3823)$ . . . 2110
- $\psi_3(3842)$ . . . 2111
  $\chi_{c0}(3860)$ . . . 2111
- $\chi_{c1}(3872)$ aka $X(3872)$ . . . 2111
- $\chi_{c0}(3915)$ was $X(3915)$ . . . 2116
- $\chi_{c2}(3930)$ . . . 2117
  $X(3940)$ . . . 2117
- $\psi(4040)$ . . . 2118
- $\chi_{c1}(4140)$ was $X(4140)$ . . . 2121
- $\psi(4160)$ . . . 2122
  $X(4160)$ . . . 2125
  $T_{c\bar{c}}(4250)^+$ . . . 2189
- $\psi(4230)$ aka $Y(4260)$; was $X(4260)$ . . . 2125
- $\chi_{c1}(4274)$ was $X(4274)$ . . . 2131
  $X(4350)$ . . . 2132
- $\psi(4360)$ aka $Y(4360)$; was $X(4360)$ . . . 2132
- $\psi(4415)$ . . . 2135
  $\chi_{c0}(4500)$ was $X(4500)$ . . . 2137
  $X(4630)$ . . . 2138
- $\psi(4660)$ aka $Y(4660)$; was $X(4660)$ . . . 2138
  $\chi_{c1}(4685)$ . . . 2140
  $\chi_{c0}(4700)$ was $X(4700)$ . . . 2141

$b\bar{b}$ MESONS

- $\eta_b(1S)$ . . . 2143
- $\Upsilon(1S)$ . . . 2144
- $\chi_{b0}(1P)$ . . . 2151
- $\chi_{b1}(1P)$ . . . 2153
- $h_b(1P)$ . . . 2155
- $\chi_{b2}(1P)$ . . . 2155
  $\eta_b(2S)$ . . . 2157
- $\Upsilon(2S)$ . . . 2157
- $\Upsilon_2(1D)$ was $\Upsilon(1D)$ . . . 2163
- $\chi_{b0}(2P)$ . . . 2163
- $\chi_{b1}(2P)$ . . . 2165
- $h_b(2P)$ . . . 2168
- $\chi_{b2}(2P)$ . . . 2168
- $\Upsilon(3S)$ . . . 2170
- $\chi_{b1}(3P)$ . . . 2174
- $\chi_{b2}(3P)$ . . . 2174
- $\Upsilon(4S)$ aka $\Upsilon(10580)$ . . . 2175
  $\Upsilon(10753)$ . . . 2177
- $\Upsilon(10860)$ . . . 2177
- $\Upsilon(11020)$ . . . 2181

OTHER MESONS

  $T^*_{\overline{cs}0}(2870)^0$ was $X_0(2900)$ . . . 2183
  $T^*_{\overline{cs}1}(2900)^0$ was $X_1(2900)$ . . . 2183
  $T^*_{c\bar{s}0}(2900)$ . . . 2184
  $T_{cc}(3875)^+$ . . . 2184
- $T_{c\bar{c}1}(3900)$ was $Z_c(3900)$, $X(3900)$ . . . 2184
  $T_{c\overline{cs}1}(4000)$ was $Z_{cs}(4000)$ . . . 2186
- $T_{c\bar{c}}(4020)$ was $X(4020)$ . . . 2186
  $T_{c\bar{c}}(4050)^+$ was $X(4050)$ . . . 2187
  $T_{c\bar{c}}(4055)^+$ was $X(4055)^\pm$ . . . 2188
  $T_{c\bar{c}}(4100)^+$ was $X(4100)^\pm$ . . . 2188
  $T_{c\bar{c}1}(4200)^+$ was $Z_c(4200)$, $X(4200)^\pm$ . . . 2188
  $T_{c\overline{cs}1}(4220)^+$ was $Z_{cs}(4220)^+$ . . . 2189
  $T_{c\bar{c}0}(4240)^+$ was $R_{c0}(4240)$, $X(4240)^\pm$ . . . 2189
  $T_{c\bar{c}}(4250)^+$ was $X(4250)^\pm$ . . . 2189
- $T_{c\bar{c}1}(4430)^+$ was $Z_c(4430)$, $X(4430)^\pm$ . . . 2189
  $T_{b\bar{s}}(5568)^+$ was $X(5568)^\pm$ . . . 2190
  $T_{cc\overline{cc}}(6600)$ . . . 2191
- $T_{cc\overline{cc}}(6900)^0$ was $X(6900)$ . . . 2191
  $T_{cc\overline{cc}}(7100)$ . . . 2191
- $T_{b\bar{b}1}(10610)$ was $Z_b(10610)$, $X(10610)$ . . . 2192

(Continued on next page.)

• Indicates the particle is in the Meson Summary Table

Int. J. Mod. Phys. A 2026.41. Downloaded from www.worldscientific.com
by [redacted] LIFORNIA @ BERKELEY on 09/16/26. Re-use and distribution is strictly not permitted, except for Open Access articles.

• $T_{b\overline{b}1}(10650)$ was $Z_b(10650)$, $X(10650)^{\pm}$ 2193
Further States 2194

• Indicates the particle is in the Meson Summary Table

Notes in the Listings

Charged kaon mass 1623
Dalitz plot parameters for $K \to 3\pi$ decays 1632
CP-violation in $K_S \to 3\pi$ 1642
Heavy Flavor Averaging Group (rev.) 1775
Charmonium system 2002
Branching ratios of $\psi(2S)$ and $\chi_{c0,1,2}$ (rev.) 2041
Bottomonium system 2142
Width determination of the Υ states 2142

Related Reviews in Volume 1

62. Form factors for semileptonic kaon ($K_{\ell 3}$), radiative pion ($\pi_{\ell 2\gamma}$) & kaon ($K_{\ell 2\gamma}$) decays (rev.) 911
63. Spectroscopy of light meson resonances (rev.) 914
64. Scalar mesons below 1 GeV (rev.) 928
65. Rare kaon decays (rev.) 937
66. CPT invariance tests in neutral kaon decay 943
67. V_{ud}, V_{us}, Cabibbo angle, and CKM unitarity (rev.) . . . 945
68. CP-violation in K_L decays 949
69. Review of multibody charm analyses (rev.) 952
70. D^0–$\overline{D}^0$ mixing (rev.) 958
71. Leptonic decays of charged pseudoscalar mesons (rev.) . . 969
72. Production and decay of b-flavored hadrons (rev.) 980
73. Polarization in B decays (rev.) 992
74. B^0–$\overline{B}^0$ mixing (rev.) 996
75. Semileptonic B decays, V_{cb} and V_{ub} (rev.) 1003
76. CKM angles from B hadrons, determination of (rev.) . . 1021
77. Spectroscopy of mesons containing two heavy quarks (rev.) 1026
78. Heavy non-$q\overline{q}$ mesons (rev.) 1035

Int. J. Mod. Phys. A 2026.41. Downloaded from www.worldscientific.com
by UNIVERSITY OF CALIFORNIA @ BERKELEY on 09/16/26. Re-use and distribution is strictly not permitted, except for Open Access articles.

Int. J. Mod. Phys. A 2026.41. Downloaded from www.worldscientific.com
by [redacted]LIFORNIA @ BERKELEY on 09/16/26. Re-use and distribution is strictly not permitted, except for Open Access articles.

Int. J. Mod. Phys. A 2026.41. Downloaded from www.worldscientific.com
by UNIVERSITY OF CALIFORNIA @ BERKELEY on 09/16/26. Re-use and distribution is strictly not permitted, except for Open Access articles.

LIGHT UNFLAVORED MESONS ($S = C = B = 0$)

For $I = 1$ (π, b, ρ, a): $u\overline{d}$, $(u\overline{u} - d\overline{d})/\sqrt{2}$, $d\overline{u}$;
for $I = 0$ (η, η', h, h', ω, ϕ, f, f'): $c_1(u\overline{u} + d\overline{d}) + c_2(s\overline{s})$

$\pi^{\pm}$

$I^G(J^P) = 1^-(0^-)$

We have omitted some results that have been superseded by later experiments. The omitted results may be found in our 1988 edition Physics Letters **B204** 1 (1988).

$\pi^{\pm}$ MASS

The most accurate charged pion mass measurements are based upon x-ray wavelength measurements for transitions in π^--mesonic atoms. The observed line is the blend of three components, corresponding to different K-shell occupancies. JECKELMANN 94 revisits the occupancy question, with the conclusion that two sets of occupancy ratios, resulting in two different pion masses (Solutions A and B), are equally probable. We choose the higher Solution B since only this solution is consistent with a positive mass-squared for the muon neutrino, given the precise muon momentum measurements now available (DAUM 91, ASSAMAGAN 94, and ASSAMAGAN 96) for the decay of pions at rest. Earlier mass determinations with pi-mesonic atoms may have used incorrect K-shell screening corrections.

Measurements with an error of > 0.005 MeV have been omitted from this Listing.

VALUE (MeV)	DOCUMENT ID		TECN	CHG	COMMENT
139.57039±0.00018 OUR FIT	Error includes scale factor of 1.8.				
139.57039±0.00017 OUR AVERAGE	Error includes scale factor of 1.6. See the ideogram below.				
139.57021±0.00014	[1] DAUM	19	SPEC		$\pi^+ \to \mu^+ \nu_\mu$
139.57077±0.00018	[2] TRASSINELLI	16	CNTR		X-ray transitions in pionic N2
139.57071±0.00053	[3] LENZ	98	CNTR	−	pionic N2-atoms gas target
139.56995±0.00035	[4] JECKELMANN	94	CNTR	−	π^- atom, Soln. B
• • • We do not use the following data for averages, fits, limits, etc. • • •					
139.57022±0.00014	[5] ASSAMAGAN	96	SPEC	+	$\pi^+ \to \mu^+ \nu_\mu$
139.56782±0.00037	[6] JECKELMANN	94	CNTR	−	π^- atom, Soln. A
139.56996±0.00067	[7] DAUM	91	SPEC	+	$\pi^+ \to \mu^+ \nu$
139.56752±0.00037	[8] JECKELMANN	86B	CNTR	−	Mesonic atoms
139.5704 ±0.0011	[7] ABELA	84	SPEC	+	See DAUM 91
139.5664 ±0.0009	[9] LU	80	CNTR	−	Mesonic atoms
139.5686 ±0.0020	CARTER	76	CNTR	−	Mesonic atoms
139.5660 ±0.0024	[9,10] MARUSHEN...	76	CNTR	−	Mesonic atoms

[1] DAUM 19 value is based on their previous (1991+1996) measurements of the μ^+ momentum of 29.79200 ± 0.00011 MeV for π^+ decay at rest. It also uses m_μ = 105.658 3745 ± 0.0000024 MeV, and assumes conservatively m_{ν_μ} = 2.0 ± 2.0 MeV. It is the most precise charged pion mass determination.

[2] TRASSINELLI 16 use the muonic oxygen line for online energy calibration of the pionic line.

[3] LENZ 98 result does not suffer K-electron configuration uncertainties as does JECKELMANN 94.

[4] JECKELMANN 94 Solution B (dominant 2-electron K-shell occupancy), chosen for consistency with positive $m^2_{\nu_\mu}$.

[5] ASSAMAGAN 96 measures the μ^+ momentum p_μ in $\pi^+ \to \mu^+ \nu_\mu$ decay at rest to be 29.79200 ± 0.00011 MeV/c. Combined with the μ^+ mass and the assumption m_{ν_μ} = 0, this gives the π^+ mass above; if $m_{\nu_\mu} > 0$, m_{π^+} given above is a lower limit. Combined instead with m_μ and (assuming CPT) the π^- mass of JECKELMANN 94, p_μ gives an upper limit on m_{ν_μ} (see the ν_μ).

[6] JECKELMANN 94 Solution A (small 2-electron K-shell occupancy) in combination with either the DAUM 91 or ASSAMAGAN 94 pion decay muon momentum measurement yields a significantly negative $m^2_{\nu_\mu}$. It is accordingly not used in our fits.

[7] The DAUM 91 value includes the ABELA 84 result. The value is based on a measurement of the μ^+ momentum for π^+ decay at rest, p_μ = 29.79179 ± 0.00053 MeV, uses m_μ = 105.658 389 ± 0.000034 MeV, and assumes that m_{ν_μ} = 0. The last assumption means that in fact the value is a lower limit.

[8] JECKELMANN 86B gives m_π/m_e = 273.12677(71). We use m_e = 0.51099906(15) MeV from COHEN 87. The authors note that two solutions for the probability distribution of K-shell occupancy fit equally well, and use other data to choose the lower of the two possible $\pi^\pm$ masses.

[9] These values are scaled with a new wavelength-energy conversion factor $V\lambda$ = 1.23984244(37) × 10^{-6} eV m from COHEN 87. The LU 80 screening correction relies upon a theoretical calculation of inner-shell refilling rates.

[10] This MARUSHENKO 76 value used at the authors' request to use the accepted set of calibration γ energies. Error increased from 0.0017 MeV to include QED calculation error of 0.0017 MeV (12 ppm).

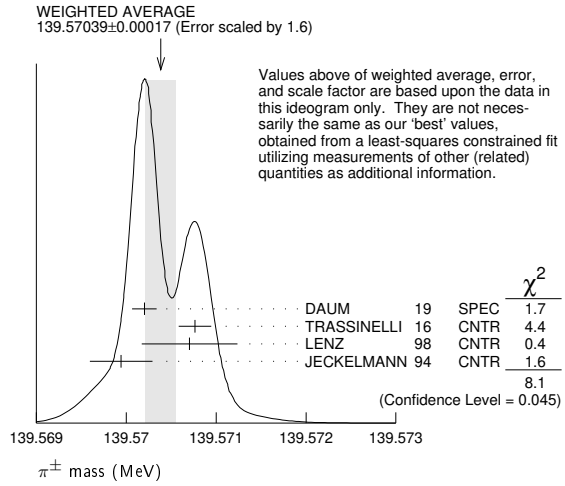

$m_{\pi^+} - m_{\mu^+}$

Measurements with an error > 0.05 MeV have been omitted from this Listing.

VALUE (MeV)	EVTS	DOCUMENT ID		TECN	CHG	COMMENT
• • • We do not use the following data for averages, fits, limits, etc. • • •						
33.91157±0.00067		[1] DAUM	91	SPEC	+	$\pi^+ \to \mu^+ \nu$
33.9111 ±0.0011		ABELA	84	SPEC		See DAUM 91
33.925 ±0.025		BOOTH	70	CNTR	+	Magnetic spect.
33.881 ±0.035	145	HYMAN	67	HEBC	+	K^- He

[1] The DAUM 91 value assumes that m_{ν_μ} = 0 and uses our m_μ = 105.658389 ± 0.000034 MeV.

$(m_{\pi^+} - m_{\pi^-}) / m_{\text{average}}$

A test of CPT invariance.

VALUE (units 10^{-4})	DOCUMENT ID		TECN
2±5	AYRES	71	CNTR

$\pi^{\pm}$ MEAN LIFE

Measurements with an error > 0.02 × 10^{-8} s have been omitted.

VALUE (10^{-8} s)	DOCUMENT ID		TECN	CHG	COMMENT
2.6033 ±0.0005 OUR AVERAGE	Error includes scale factor of 1.2.				
2.60361±0.00052	[1] KOPTEV	95	SPEC	+	Surface μ^+'s
2.60231±0.00050±0.00084	NUMAO	95	SPEC	+	Surface μ^+'s
2.609 ±0.008	DUNAITSEV	73	CNTR	+	
2.602 ±0.004	AYRES	71	CNTR	±	
2.604 ±0.005	NORDBERG	67	CNTR	+	
2.602 ±0.004	ECKHAUSE	65	CNTR	+	
• • • We do not use the following data for averages, fits, limits, etc. • • •					
2.640 ±0.008	[2] KINSEY	66	CNTR	+	

[1] KOPTEV 95 combines the statistical and systematic errors; the statistical error dominates.

[2] Systematic errors in the calibration of this experiment are discussed by NORDBERG 67.

$(\tau_{\pi^+} - \tau_{\pi^-}) / \tau_{\text{average}}$

A test of CPT invariance.

VALUE (units 10^{-4})	DOCUMENT ID		TECN
5.5± 7.1	AYRES	71	CNTR
• • • We do not use the following data for averages, fits, limits, etc. • • •			
−14 ±29	PETRUKHIN	68	CNTR
40 ±70	BARDON	66	CNTR
23 ±40	[1] LOBKOWICZ	66	CNTR

[1] This is the most conservative value given by LOBKOWICZ 66.

π ELECTRIC POLARIZABILITY α_π

See HOLSTEIN 14 for a general review on hadron polarizability.

VALUE (10^{-4} fm^3)	EVTS	DOCUMENT ID		TECN	COMMENT
2.0±0.6±0.7	63k	[1] ADOLPH	15A	SPEC	$\pi^-\gamma \to \pi^-\gamma$ Compton scatt.

[1] Value is derived assuming $\alpha_\pi = -\beta_\pi$.

Int. J. Mod. Phys. A 2026.41. Downloaded from www.worldscientific.com
by UNIVERSITY OF CALIFORNIA @ BERKELEY on 09/16/26. Re-use and distribution is strictly not permitted, except for Open Access articles.

π^+ DECAY MODES

π^- modes are charge conjugates of the modes below.

For decay limits to particles which are not established, see the section on Searches for Axions and Other Very Light Bosons.

	Mode		Fraction (Γ_i/Γ)	Confidence level
Γ_1	$\mu^+\nu_\mu$	[a]	(99.98770 ± 0.00004) %	
Γ_2	$\mu^+\nu_\mu\gamma$	[b]	$(2.00\pm0.25)\times10^{-4}$	
Γ_3	$e^+\nu_e$	[a]	$(1.230\pm0.004)\times10^{-4}$	
Γ_4	$e^+\nu_e\gamma$	[b]	$(7.39\pm0.05)\times10^{-7}$	
Γ_5	$e^+\nu_e\pi^0$		$(1.036\pm0.006)\times10^{-8}$	
Γ_6	$e^+\nu_e e^+e^-$		$(3.2\pm0.5)\times10^{-9}$	
Γ_7	$\mu^+\nu_\mu\nu\overline{\nu}$		$<9\times10^{-6}$	90%
Γ_8	$e^+\nu_e\nu\overline{\nu}$		$<1.6\times10^{-7}$	90%
	Lepton Family number (LF) or Lepton number (L) violating modes			
Γ_9	$\mu^+\overline{\nu}_e$	L [c]	$<1.5\times10^{-3}$	90%
Γ_{10}	$\mu^+\nu_e$	LF [c]	$<8.0\times10^{-3}$	90%
Γ_{11}	$\mu^-e^+e^+\nu$	LF	$<1.6\times10^{-6}$	90%

[a] Measurements of $\Gamma(e^+\nu_e)/\Gamma(\mu^+\nu_\mu)$ always include decays with γ's, and measurements of $\Gamma(e^+\nu_e\gamma)$ and $\Gamma(\mu^+\nu_\mu\gamma)$ never include low-energy γ's. Therefore, since no clean separation is possible, we consider the modes with γ's to be subreactions of the modes without them, and let $[\Gamma(e^+\nu_e)+\Gamma(\mu^+\nu_\mu)]/\Gamma_{\rm total}=100\%$.

[b] See the Particle Listings below for the energy limits used in this measurement; low-energy γ's are not included.

[c] Derived from an analysis of neutrino-oscillation experiments.

π^+ BRANCHING RATIOS

$\Gamma(e^+\nu_e)/\Gamma_{\rm total}$ — Γ_3/Γ

See note [a] in the list of π^+ decay modes just above, and see also the next block of data. See also the note on "Decay Constants of Charged Pseudoscalar Mesons" in the D_s^+ Listings.

VALUE (units 10^{-4})	DOCUMENT ID
1.230±0.004 OUR EVALUATION	

$[\Gamma(e^+\nu_e)+\Gamma(e^+\nu_e\gamma)]/[\Gamma(\mu^+\nu_\mu)+\Gamma(\mu^+\nu_\mu\gamma)]$ — $(\Gamma_3+\Gamma_4)/(\Gamma_1+\Gamma_2)$

See note [a] in the list of π^+ decay modes above. See NUMAO 92 for a discussion of e-μ universality. See also the note on "Decay Constants of Charged Pseudoscalar Mesons" in the D_s^+ Listings.

VALUE (units 10^{-4})	EVTS	DOCUMENT ID		TECN	CHG	COMMENT
1.2327±0.0023 OUR AVERAGE						
$1.2344\pm0.0023\pm0.0019$	400k	AGUILAR-AR...	15	CNTR	+	Stopping π^+
$1.2346\pm0.0035\pm0.0036$	120k	CZAPEK	93	CALO		Stopping π^+
$1.2265\pm0.0034\pm0.0044$	190k	BRITTON	92	CNTR		Stopping π^+
1.218 ± 0.014	32k	BRYMAN	86	CNTR		Stopping π^+
• • • We do not use the following data for averages, fits, limits, etc. • • •						
1.273 ± 0.028	11k	[1] DICAPUA	64	CNTR		
1.21 ± 0.07		ANDERSON	60	SPEC		

[1] DICAPUA 64 has been updated using the current mean life.

$\Gamma(\mu^+\nu_\mu\gamma)/\Gamma_{\rm total}$ — Γ_2/Γ

Note that measurements here do not cover the full kinematic range.

VALUE (units 10^{-4})	EVTS	DOCUMENT ID		TECN	CHG	COMMENT
2.0 ±0.24±0.08		[1] BRESSI	98	CALO	+	Stopping π^+
• • • We do not use the following data for averages, fits, limits, etc. • • •						
1.24 ± 0.25	26	CASTAGNOLI	58	EMUL		$KE_\mu<3.38$ MeV

[1] BRESSI 98 result is given for $E_\gamma>1$ MeV only. Result agrees with QED expectation, 2.283×10^{-4} and does not confirm discrepancy of earlier experiment CASTAGNOLI 58.

$\Gamma(e^+\nu_e\gamma)/\Gamma_{\rm total}$ — Γ_4/Γ

The very different values reflect the very different kinematic ranges covered (bigger range, bigger value). And none of them covers the whole kinematic range.

VALUE (units 10^{-8})	EVTS	DOCUMENT ID		TECN	COMMENT
73.86±0.54	65k	[1] BYCHKOV	09	PIBE	$e^+\nu\gamma$ at rest
• • • We do not use the following data for averages, fits, limits, etc. • • •					
16.1 ± 2.3		[2] BOLOTOV	90B	SPEC	17 GeV $\pi^-\to e^-\overline{\nu}_e\gamma$
5.6 ± 0.7	226	[3] STETZ	78	SPEC	$P_e>56$ MeV/c
3.0	143	DEPOMMIER	63B	CNTR	$(KE)_{e^+\gamma}>48$ MeV

[1] This BYCHKOV 09 value is for $E_\gamma>10$ MeV and $\Theta_{e^+\gamma}>40^\circ$.

[2] BOLOTOV 90B is for $E_\gamma>21$ MeV, $E_e>70-0.8E_\gamma$.

[3] STETZ 78 is for an $e^-\gamma$ opening angle $>132^\circ$. Obtains 3.7 when using same cutoffs as DEPOMMIER 63B.

$\Gamma(e^+\nu_e\pi^0)/\Gamma_{\rm total}$ — Γ_5/Γ

VALUE (units 10^{-8})	EVTS	DOCUMENT ID		TECN	CHG	COMMENT
1.036±0.006 OUR AVERAGE						
1.036 ± 0.006	64k	[1,2] POCANIC	04	PIBE	+	π decay at rest
1.026 ± 0.039	1224	[3] MCFARLANE	85	CNTR	+	Decay in flight
$1.00\ ^{+0.08}_{-0.10}$	332	DEPOMMIER	68	CNTR	+	
1.07 ± 0.21	38	[4] BACASTOW	65	OSPK	+	
1.10 ± 0.26		[4] BERTRAM	65	OSPK	+	
1.1 ± 0.2	43	[4] DUNAITSEV	65	CNTR	+	
0.97 ± 0.20	36	[4] BARTLETT	64	OSPK	+	
• • • We do not use the following data for averages, fits, limits, etc. • • •						
1.15 ± 0.22	52	[4] DEPOMMIER	63	CNTR	+	See DEPOMMIER 68

[1] POCANIC 04 normalizes to $e^+\nu_e$ decays, using the PDG 2004 value $B(\pi^+\to e^+\nu_e)=(1.230\pm0.004)\times10^{-4}$. We add their statistical (0.004×10^{-8}), systematic (0.004×10^{-8}) and systematic error due to the uncertainty of $B(\pi^+\to e^+\nu_e)$ (0.003×10^{-8}) in quadrature.

[2] This result can be used to calculate V_{ud} from pion beta decay: $V_{ud}^{PIBETA}=0.9728\pm0.0030$.

[3] MCFARLANE 85 combines a measured rate (0.394 ± 0.015)/s with 1982 PDG mean life.

[4] DEPOMMIER 68 says the result of DEPOMMIER 63 is at least 10% too large because of a systematic error in the π^0 detection efficiency, and that this may be true of all the previous measurements (also V. Soergel, private communication, 1972).

$\Gamma(e^+\nu_e e^+e^-)/\Gamma(\mu^+\nu_\mu)$ — Γ_6/Γ_1

VALUE (units 10^{-9})	CL%	EVTS	DOCUMENT ID		TECN	COMMENT
3.2 ±0.5 ±0.2		98	EGLI	89	SPEC	Uses $R_{\rm PCAC}=0.068\pm0.004$
• • • We do not use the following data for averages, fits, limits, etc. • • •						
$0.46\pm0.16\pm0.07$		7	[1] BARANOV	92	SPEC	Stopped π^+
<4.8	90		KORENCHE...	76B	SPEC	
<34	90		KORENCHE...	71	OSPK	

[1] This measurement by BARANOV 92 is of the structure-dependent part of the decay. The value depends on values assumed for ratios of form factors.

$\Gamma(\mu^+\nu_\mu\nu\overline{\nu})/\Gamma(\mu^+\nu_\mu)$ — Γ_7/Γ_1

VALUE	CL%	EVTS	DOCUMENT ID		TECN	COMMENT
$<8.6\times10^{-6}$	90	9.1M	AGUILAR-AR...	20A	SPEC	fit E_μ spectrum

$\Gamma(e^+\nu_e\nu\overline{\nu})/\Gamma_{\rm total}$ — Γ_8/Γ

VALUE	CL%	EVTS	DOCUMENT ID		TECN	COMMENT
$<1.6\times10^{-7}$	90	1.3M	AGUILAR-AR...	20A	SPEC	fit E_e spectrum
• • • We do not use the following data for averages, fits, limits, etc. • • •						
$<5\times10^{-6}$	90		PICCIOTTO	88	SPEC	

$\Gamma(\mu^+\overline{\nu}_e)/\Gamma_{\rm total}$ — Γ_9/Γ

Forbidden by total lepton number conservation. See the note on "Decay Constants of Charged Pseudoscalar Mesons" in the D_s^+ Listings.

VALUE (units 10^{-3})	CL%	DOCUMENT ID		TECN	COMMENT
<1.5	90	[1] COOPER	82	HLBC	Wideband ν beam

[1] COOPER 82 limit on $\overline{\nu}_e$ observation is here interpreted as a limit on lepton number violation.

$\Gamma(\mu^+\nu_e)/\Gamma_{\rm total}$ — Γ_{10}/Γ

Forbidden by lepton family number conservation.

VALUE (units 10^{-3})	CL%	DOCUMENT ID		TECN	COMMENT
<8.0	90	[1] COOPER	82	HLBC	Wideband ν beam

[1] COOPER 82 limit on ν_e observation is here interpreted as a limit on lepton family number violation.

$\Gamma(\mu^-e^+e^+\nu)/\Gamma_{\rm total}$ — Γ_{11}/Γ

Forbidden by lepton family number conservation.

VALUE (units 10^{-6})	CL%	DOCUMENT ID		TECN	CHG
<1.6	90	BARANOV	91B	SPEC	+
• • • We do not use the following data for averages, fits, limits, etc. • • •					
<7.7	90	KORENCHE...	87	SPEC	+

π^+ — POLARIZATION OF EMITTED μ^+

$\pi^+\to\mu^+\nu$

Tests the Lorentz structure of leptonic charged weak interactions.

VALUE	CL%	DOCUMENT ID		TECN	CHG	COMMENT
• • • We do not use the following data for averages, fits, limits, etc. • • •						
$<(-0.9959)$	90	[1] FETSCHER	84	RVUE	+	
-0.99 ± 0.16		[2] ABELA	83	SPEC	−	μ X-rays

[1] FETSCHER 84 uses only the measurement of CARR 83.

[2] Sign of measurement reversed in ABELA 83 to compare with μ^+ measurements.

See the related review(s):

Form Factors for Semileptonic Kaon ($K_{\ell3}$), Radiative Pion ($\pi_{\ell2\gamma}$) and Kaon ($K_{\ell2\gamma}$) Decays

Int. J. Mod. Phys. A 2026.41. Downloaded from www.worldscientific.com
by UNIVERSITY OF CALIFORNIA @ BERKELEY on 09/16/26. Re-use and distribution is strictly not permitted, except for Open Access articles.

$\pi^{\pm}$ FORM FACTORS

F_V, VECTOR FORM FACTOR

VALUE	EVTS	DOCUMENT ID		TECN	COMMENT
0.0254±0.0017 OUR AVERAGE					
0.0258±0.0017	65k	[1] BYCHKOV	09	PIBE	$e^+\nu\gamma$ at rest
0.014 ±0.009		[2] BOLOTOV	90B	SPEC	17 GeV $\pi^- \to e^-\overline{\nu}_e\gamma$
$0.023\ ^{+0.015}_{-0.013}$	98	EGLI	89	SPEC	$\pi^+ \to e^+\nu_e e^+e^-$

[1] The BYCHKOV 09 F_A and F_V results are highly (anti-)correlated: $F_A + 1.0286\ F_V = 0.03853 \pm 0.00014$.
[2] BOLOTOV 90B only determines the absolute value.

F_A, AXIAL-VECTOR FORM FACTOR

VALUE	EVTS	DOCUMENT ID		TECN	COMMENT
0.0119±0.0001	65k	[1,2] BYCHKOV	09	PIBE	$e^+\nu\gamma$ at rest
• • • We do not use the following data for averages, fits, limits, etc. • • •					
0.0115±0.0004	41k	[1,3] FRLEZ	04	PIBE	$\pi^+ \to e^+\nu\gamma$ at rest
0.0106±0.0060		[1,4] BOLOTOV	90B	SPEC	17 GeV $\pi^- \to e^-\overline{\nu}_e\gamma$
$0.021\ ^{+0.011}_{-0.013}$	98	EGLI	89	SPEC	$\pi^+ \to e^+\nu_e e^+e^-$
0.0135±0.0016		[1,4] BAY	86	SPEC	$\pi^+ \to e^+\nu\gamma$
0.006 ±0.003		[1,4] PIILONEN	86	SPEC	$\pi^+ \to e^+\nu\gamma$
0.011 ±0.003		[1,4,5] STETZ	78	SPEC	$\pi^+ \to e^+\nu\gamma$

[1] These values come from fixing the vector form factor at the CVC prediction, $F_V = 0.0259 \pm 0.0005$.
[2] When F_V is released, the BYCHKOV 09 F_A is 0.0117 ± 0.0017, and F_A and F_V results are highly (anti-)correlated: $F_A + 1.0286\ F_V = 0.03853 \pm 0.00014$.
[3] The sign of $\gamma = F_A / F_V$ is determined to be positive.
[4] Only the absolute value of F_A is determined.
[5] The result of STETZ 78 has a two-fold ambiguity. We take the solution compatible with later determinations.

VECTOR FORM FACTOR SLOPE PARAMETER *a*

This is a in $F_V(q^2) = F_V(0)\ (1 + a\ q^2)$

VALUE	EVTS	DOCUMENT ID		TECN	COMMENT
0.10±0.06	65k	BYCHKOV	09	PIBE	$e^+\nu\gamma$ at rest

R, SECOND AXIAL-VECTOR FORM FACTOR

VALUE	EVTS	DOCUMENT ID		TECN	COMMENT
$\mathbf{0.059^{+0.009}_{-0.008}}$	98	EGLI	89	SPEC	$\pi^+ \to e^+\nu_e e^+e^-$

$\pi^{\pm}$ CHARGE RADIUS

The charge radius of the pion $\sqrt{\langle r^2_\pi \rangle}$ is defined in relation to the form factor of the pion electromagnetic vertex, called vector form factor VFF, F^V_π. The VFF is a function of the squared four-momentum transfer t, or of the squared c.m. energy s, depending on the channel in which the photon exchange takes place. In both cases, it is related to the slope of the VFF at zero, namely

$$\langle r^2_\pi \rangle = 6\ \frac{dF^V_\pi(q)}{dq}(q{=}0) \text{ where } q = t,\ s.$$

The quantity cannot be measured directly. It can be extracted from the cross sections of three processes: pion electroproduction, $eN \to eN\pi$, and pion electron scattering $e\pi \to e\pi$, for the t channel, and positron electron annihilation into two charged pions, $e^+e^- \to \pi^+\pi^-$, for the s channel. We encode all measurements, but we do not use electroproduction data in averaging because the extraction of the pion radius involves, in this case, theoretical uncertainties that cannot be controlled at the needed level of accuracy. In case of analyses based on the same data set, as ANANTHANARAYAN 17 and COLANGELO 19, which cannot be averaged, we combine the results into a common value, with the uncertainty range chosen to cover both analyses. Note that for consistency the form factor needs to be defined in both channels with the vacuum polarisation removed. For details see COLANGELO 19 or Appendix B of ANANTHANARAYAN 16A.

VALUE (fm)		DOCUMENT ID		TECN	COMMENT
0.659 ±0.004 OUR AVERAGE					
0.656 ±0.005		[1] PDG	19	FIT	
0.65 ±0.05	±0.06	ESCHRICH	01	CNTR	$\pi e \to \pi e$
0.663 ±0.006		AMENDOLIA	86	CNTR	$\pi e \to \pi e$
0.663 ±0.023		DALLY	82	CNTR	$\pi e \to \pi e$
• • • We do not use the following data for averages, fits, limits, etc. • • •					
0.640 ±0.007		[2] CUI	21A	FIT	Fit existing data
0.655 ±0.004		[3] COLANGELO	19	FIT	Fit existing data
0.657 ±0.003		[4] ANANTHANA..	17	FIT	Fit existing data
0.6603±0.0005	±0.0004	[5] HANHART	17	FIT	Fit existing data
0.740 ±0.031		[6] LIESENFELD	99	CNTR	$ep \to e\pi^+n$
0.661 ±0.012		[7] BIJNENS	98	CNTR	χPT extraction
0.660 ±0.024		AMENDOLIA	84	CNTR	$\pi e \to \pi e$
0.711 ±0.009	±0.016	[6] BEBEK	78	CNTR	$eN \to e\pi N$
0.678 ±0.004	±0.008	[8] QUENZER	78	CNTR	$e^+e^- \to \pi^+\pi^-$
$0.78\ ^{+0.09}_{-0.10}$		ADYLOV	77	CNTR	$\pi e \to \pi e$
$0.74\ ^{+0.11}_{-0.13}$		BARDIN	77	CNTR	$ep \to e\pi^+n$
0.56 ±0.04		DALLY	77	CNTR	$\pi e \to \pi e$

[1] This value combines the measurements of ANANTHANARAYAN 17 and COLANGELO 19 which are based on the same data set. The uncertainty range is chosen to cover both results.
[2] CUI 21A perform a fit including spacelike data only. Employ a new mathematical procedure based on interpolation via continued fractions augmented by statistical sampling. Also do not impose the charge conserving normalization condition F(0) = 1.
[3] COLANGELO 19 fit existing F_V data, using an extended Omnes dispersive representation. This analysis is based on the same data set of ANANTHANARAYAN 17 . Accordingly, they cannot be averaged. We combine the results into a common value, with the uncertainty range chosen to cover the uncertainty ranges of both analyses.
[4] ANANTHANARAYAN 17 fit existing F_V data, using a mixed phase-modulus dispersive representation. This analysis is based on the same data set of COLANGELO 19. Accordingly, they cannot be averaged. We combine the results into a common value, with the uncertainty range chosen to cover the uncertainty ranges of both analyses.
[5] According to the authors the uncertainty could be underestimated. The value quoted omits the BaBar data AUBERT 09.
[6] The extractions could contain an additional theoretical uncertainty which cannot be sufficiently quantified.
[7] BIJNENS 98 fits existing data.
[8] The extraction is based on a parametrization that does not have correct analytic properties.

$\pi^{\pm}$ REFERENCES

We have omitted some papers that have been superseded by later experiments. The omitted papers may be found in our 1988 edition Physics Letters **B204** 1 (1988).

CUI	21A	PL B822 136631	Z.-F. Cui *et al.*	(NJU, ECT, HZDR)
AGUILAR-AR...	20A	PR D102 012001	A. Aguilar-Arevalo *et al.*	(PIENU Collab.)
COLANGELO	19	JHEP 1902 006	G. Colangelo, M. Hoferichter, P. Stoffer	(BERN+)
DAUM	19	PL B796 11	M. Daum, R. Frosch, P.-R. Kettle	(PSI)
PDG	19	RPP 2019 at pdg.lbl.gov	M. Tanabashi *et al.*	(PDG Collab.)
ANANTHANA...	17	PRL 119 132002	B. Ananthanarayan, I. Caprini, D. Das	
HANHART	17	EPJ C77 98	C. Hanhart *et al.*	
ANANTHANA...	16A	PR D93 116007	B. Ananthanarayan *et al.*	
TRASSINELLI	16	PL B759 583	M. Trassinelli *et al.*	
ADOLPH	15A	PRL 114 062002	C. Adolph *et al.*	(COMPASS Collab.)
AGUILAR-AR...	15	PRL 115 071801	A. Aguilar-Arevalo *et al.*	(PIENU Collab.)
HOLSTEIN	14	ARNPS 64 51	B. Holstein, S. Scherer	(MASA, MAINZ)
AUBERT	09	PR D79 011102	B. Aubert *et al.*	(BABAR Collab.)
BYCHKOV	09	PRL 103 051802	M. Bychkov *et al.*	(PSI PIBETA Collab.)
FRLEZ	04	PRL 93 181804	E. Frlez *et al.*	(PSI PIBETA Collab.)
POCANIC	04	PRL 93 181803	D. Pocanic *et al.*	(PSI PIBETA Collab.)
ESCHRICH	01	PL B522 233	I. Eschrich *et al.*	(FNAL SELEX Collab.)
LIESENFELD	99	PL B468 20	A. Liesenfeld *et al.*	
BIJNENS	98	JHEP 9805 014	J. Bijnens *et al.*	
BRESSI	98	NP B513 555	G. Bressi *et al.*	
LENZ	98	PL B416 50	S. Lenz *et al.*	
ASSAMAGAN	96	PR D53 6065	K.A. Assamagan *et al.*	(PSI, ZURI, VILL+)
KOPTEV	95	JETPL 61 877	V.P. Koptev *et al.*	(PNPI)
		Translated from ZETFP 61 865.		
NUMAO	95	PR D52 4855	T. Numao *et al.*	(TRIU, BRCO)
ASSAMAGAN	94	PL B335 231	K.A. Assamagan *et al.*	(PSI, ZURI, VILL+)
JECKELMANN	94	PL B335 326	B. Jeckelmann, P.F.A. Goudsmit, H.J. Leisi	(WABRN+)
CZAPEK	93	PRL 70 17	G. Czapek *et al.*	(BERN, VILL)
BARANOV	92	SJNP 55 1644	V.A. Baranov *et al.*	(JINR)
		Translated from YAF 55 2940.		
BRITTON	92	PRL 68 3000	D.I. Britton *et al.*	(TRIU, CARL)
Also		PR D49 28	D.I. Britton *et al.*	(TRIU, CARL)
NUMAO	92	MPL A7 3357	T. Numao	(TRIU)
BARANOV	91B	SJNP 54 790	V.A. Baranov *et al.*	(JINR)
		Translated from YAF 54 1298.		
DAUM	91	PL B265 425	M. Daum *et al.*	(VILL)
BOLOTOV	90B	PL B243 308	V.N. Bolotov *et al.*	(INRM)
EGLI	89	PL B222 533	S. Egli *et al.*	(SINDRUM Collab.)
Also		PL B175 97	S. Egli *et al.*	(AACH3, ETH, SIN, ZURI)
PDG	88	PL B204 1	G.P. Yost *et al.*	(LBL+)
PICCIOTTO	88	PR D37 1131	C.E. Picciotto *et al.*	(TRIU, CNRC)
COHEN	87	RMP 59 1121	E.R. Cohen, B.N. Taylor	(RISC, NBS)
KORENCHE...	87	SJNP 46 192	S.M. Korenchenko *et al.*	(JINR)
		Translated from YAF 46 313.		
AMENDOLIA	86	NP B277 168	S.R. Amendolia *et al.*	(CERN NA7 Collab.)
BAY	86	PL B174 445	A. Bay *et al.*	(LAUS, ZURI)
BRYMAN	86	PR D33 1211	D.A. Bryman *et al.*	(TRIU, CNRC)
Also		PRL 50 7	D.A. Bryman *et al.*	(TRIU, CNRC)
JECKELMANN	86B	NP A457 709	B. Jeckelmann *et al.*	(ETH, FRIB)
Also		PRL 56 1444	B. Jeckelmann *et al.*	(ETH, FRIB)
PIILONEN	86	PRL 57 1402	L.E. Piilonen *et al.*	(LANL, TEMP, CHIC)
MCFARLANE	85	PR D32 547	W.K. McFarlane *et al.*	(TEMP, LANL)
ABELA	84	PL 146B 431	R. Abela *et al.*	(SIN)
Also		PL 74B 126	M. Daum *et al.*	(SIN)
Also		PR D20 2692	M. Daum *et al.*	(SIN)
AMENDOLIA	84	PL 146B 116	S.R. Amendolia *et al.*	(CERN NA7 Collab.)
FETSCHER	84	PL 140B 117	W. Fetscher	(ETH)
ABELA	83	NP A395 413	R. Abela *et al.*	(BASL, KARLK, KARLE)
CARR	83	PRL 51 627	J. Carr *et al.*	(LBL, NWES, TRIU)
COOPER	82	PL 112B 97	A.M. Cooper *et al.*	(RL)
DALLY	82	PRL 48 375	E.B. Dally *et al.*	
LU	80	PRL 45 1066	D.C. Lu *et al.*	(YALE, COLU, JHU)
BEBEK	78	PR D17 1693	C.J. Bebek *et al.*	
QUENZER	78	PL 76B 512	A. Quenzer *et al.*	(LALO)
STETZ	78	NP B138 285	A.W. Stetz *et al.*	(LBL, UCLA)
ADYLOV	77	NP B128 461	G.T. Adylov *et al.*	
BARDIN	77	NP B120 45	G. Bardin *et al.*	
DALLY	77	PRL 39 1176	E.B. Dally *et al.*	
CARTER	76	PRL 37 1380	A.L. Carter *et al.*	(CARL, CNRC, CHIC+)
KORENCHE...	76B	JETP 44 35	S.M. Korenchenko *et al.*	(JINR)
		Translated from ZETF 71 69.		
MARUSHEN...	76	JETPL 23 72	V.I. Marushenko *et al.*	(PNPI)
		Translated from ZETFP 23 80.		
Also		Private Comm.	R.E. Shafer	(FNAL)
Also		Private Comm.	A. Smirnov	(PNPI)
DUNAITSEV	73	SJNP 16 292	A.F. Dunaitsev *et al.*	(SERP)
		Translated from YAF 16 524.		
AYRES	71	PR D3 1051	D.S. Ayres *et al.*	(LRL, UCSB)
Also		PR 157 1288	D.S. Ayres *et al.*	(LRL)
Also		PRL 21 261	D.S. Ayres *et al.*	(LRL, UCSB)
Also		Thesis UCRL 18369	D.S. Ayres	(LRL)
Also		PRL 23 1267	A.J. Greenberg *et al.*	(LRL, UCSB)
KORENCHE...	71	SJNP 13 189	S.M. Korenchenko *et al.*	(JINR)
		Translated from YAF 13 339.		
BOOTH	70	PL 32B 723	P.S.L. Booth *et al.*	(LIVP)
DEPOMMIER	68	NP B4 189	P. Depommier *et al.*	(CERN)
PETRUKHIN	68	JINR P1 3862	V.I. Petrukhin *et al.*	(JINR)

HYMAN	67	PL 25B 376	L.G. Hyman *et al.*	(ANL, CMU, NWES)
NORDBERG	67	PL 24B 594	M.E. Nordberg, F. Lobkowicz, R.L. Burman	(ROCH)
BARDON	66	PRL 16 775	M. Bardon *et al.*	(COLU)
KINSEY	66	PR 144 1132	K.F. Kinsey, F. Lobkowicz, M.E. Nordberg	(ROCH)
LOBKOWICZ	66	PRL 17 548	F. Lobkowicz *et al.*	(ROCH, BNL)
BACASTOW	65	PR 139 B407	R.B. Bacastow *et al.*	(LRL, SLAC)
BERTRAM	65	PR 139 B617	W.K. Bertram *et al.*	(MICH, CMU)
DUNAITSEV	65	JETP 20 58	A.F. Dunaitsev *et al.*	(JINR)
		Translated from ZETF 47 84.		
ECKHAUSE	65	PL 19 348	M. Eckhause *et al.*	(WILL)
BARTLETT	64	PR 136 B1452	D. Bartlett *et al.*	(COLU)
DICAPUA	64	PR 133 B1333	M. di Capua *et al.*	(COLU)
Also		Private Comm.	L. Pondrom	(WISC)
DEPOMMIER	63	PL 5 61	P. Depommier *et al.*	(CERN)
DEPOMMIER	63B	PL 7 285	P. Depommier *et al.*	(CERN)
ANDERSON	60	PR 119 2050	H.L. Anderson *et al.*	(EFI)
CASTAGNOLI	58	PR 112 1779	C. Castagnoli, M. Muchnik	(ROMA)

π^0

$I^G(J^{PC}) = 1^-(0^{-+})$

We have omitted some results that have been superseded by later experiments. The omitted results may be found in our 1988 edition Physics Letters **B204** 1 (1988).

π^0 MASS

The value is calculated from $m_{\pi^\pm}$ and $(m_{\pi^\pm} - m_{\pi^0})$. See also the notes under the $\pi^\pm$ Mass Listings.

VALUE (MeV)	DOCUMENT ID
134.9768±0.0005 OUR FIT	Error includes scale factor of 1.1.

$m_{\pi^\pm} - m_{\pi^0}$

Measurements with an error > 0.01 MeV have been omitted.

VALUE (MeV)	DOCUMENT ID		TECN	COMMENT
4.5936 ±0.0005 OUR FIT				
4.5936 ±0.0005 OUR AVERAGE				
4.59364±0.00048	CRAWFORD	91	CNTR	$\pi^- p \to \pi^0 n$, n TOF
4.5930 ±0.0013	CRAWFORD	86	CNTR	$\pi^- p \to \pi^0 n$, n TOF
• • • We do not use the following data for averages, fits, limits, etc. • • •				
4.59366±0.00048	CRAWFORD	88B	CNTR	See CRAWFORD 91
4.6034 ±0.0052	VASILEVSKY	66	CNTR	
4.6056 ±0.0055	CZIRR	63	CNTR	

π^0 MEAN LIFE

Most experiments measure the π^0 width which we convert to a lifetime. ATHERTON 85 is the only direct measurement of the π^0 lifetime. The two Primakoff measurements from 1970 have been excluded from our average because they suffered model-related systematics unknown at the time. More information on the π^0 lifetime can be found in BERNSTEIN 13.

VALUE (10^{-17} s)	EVTS	DOCUMENT ID		TECN	COMMENT
8.43 ±0.13 OUR AVERAGE		Error includes scale factor of 1.2.			
8.337±0.056±0.112		[1] LARIN	20	PRMX	Primakoff effect
8.5 ±1.1		[2] BYCHKOV	09	PIBE	$\pi^+ \to e^+ \nu\gamma$ at rest
8.4 ±0.5 ±0.5	1182	[3] WILLIAMS	88	CBAL	$e^+ e^- \to e^+ e^- \pi^0$
8.97 ±0.22 ±0.17		ATHERTON	85	CNTR	Direct measurement
8.2 ±0.4		[4] BROWMAN	74	CNTR	Primakoff effect
• • • We do not use the following data for averages, fits, limits, etc. • • •					
8.32 ±0.15 ±0.18		[5] LARIN	11	PRMX	Primakoff effect
5.6 ±0.6		BELLETTINI	70	CNTR	Primakoff effect
9 ±0.68		KRYSHKIN	70	CNTR	Primakoff effect
7.3 ±1.1		BELLETTINI	65B	CNTR	Primakoff effect

[1] LARIN 20 reported this lifetime value from a measurement of $\Gamma(\pi^0 \to \gamma\gamma) = 7.802 \pm 0.052 \pm 0.105$ eV, combining data from PrimEX-II on 12C and 28Si targets with previous PrimEx-I LARIN 11 measurements. This result supersedes LARIN 11.

[2] BYCHKOV 09 obtains this using the conserved-vector-current relation between the vector form factor F_V and the π^0 lifetime.

[3] WILLIAMS 88 gives $\Gamma(\gamma\gamma) = 7.7 \pm 0.5 \pm 0.5$ eV. We give here $\tau = \hbar/\Gamma(\text{total})$.

[4] BROWMAN 74 gives a π^0 width $\Gamma = 8.02 \pm 0.42$ eV. The mean life is $\hbar/\Gamma$.

[5] LARIN 11 reported $\Gamma(\pi^0 \to \gamma\gamma) = 7.82 \pm 0.14 \pm 0.17$ eV which we converted to mean life $\tau = \hbar/\Gamma(\text{total})$.

π^0 DECAY MODES

For decay limits to particles which are not established, see the appropriate Search sections (A^0 (axion) and Other Light Boson (X^0) Searches, etc.).

	Mode	Fraction (Γ_i/Γ)	Scale factor/ Confidence level
Γ_1	2γ	(98.823±0.034) %	S=1.5
Γ_2	$e^+ e^- \gamma$	(1.174±0.035) %	S=1.5
Γ_3	γpositronium	(1.82 ±0.29) $\times 10^{-9}$	
Γ_4	$e^+ e^+ e^- e^-$	(3.34 ±0.16) $\times 10^{-5}$	
Γ_5	$e^+ e^-$	(6.46 ±0.33) $\times 10^{-8}$	
Γ_6	4γ	< 2 $\times 10^{-8}$	CL=90%
Γ_7	invisible	< 4.4 $\times 10^{-9}$	CL=90%
Γ_8	$\nu_e \overline{\nu}_e$	< 1.7 $\times 10^{-6}$	CL=90%
Γ_9	$\nu_\mu \overline{\nu}_\mu$	< 1.6 $\times 10^{-6}$	CL=90%
Γ_{10}	$\nu_\tau \overline{\nu}_\tau$	< 2.1 $\times 10^{-6}$	CL=90%
Γ_{11}	$\gamma\nu\overline{\nu}$	< 1.9 $\times 10^{-7}$	CL=90%

Charge conjugation (C) or Lepton Family number (LF) violating modes

Γ_{12}	3γ	C	< 3.1 $\times 10^{-8}$	CL=90%
Γ_{13}	$\mu^+ e^-$	LF	< 3.8 $\times 10^{-10}$	CL=90%
Γ_{14}	$\mu^- e^+$	LF	< 3.2 $\times 10^{-10}$	CL=90%
Γ_{15}	$\mu^+ e^- + \mu^- e^+$	LF	< 3.6 $\times 10^{-10}$	CL=90%

CONSTRAINED FIT INFORMATION

An overall fit to 2 branching ratios uses 6 measurements and one constraint to determine 3 parameters. The overall fit has a χ^2 = 4.6 for 4 degrees of freedom.

The following *off-diagonal* array elements are the correlation coefficients $\langle \delta x_i \delta x_j \rangle / (\delta x_i \cdot \delta x_j)$, in percent, from the fit to the branching fractions, $x_i \equiv \Gamma_i/\Gamma_{\text{total}}$. The fit constrains the x_i whose labels appear in this array to sum to one.

	x_1	x_2
x_2	−100	
x_4	0	−1

π^0 BRANCHING RATIOS

$\Gamma(e^+ e^- \gamma)/\Gamma(2\gamma)$ — Γ_2/Γ_1

VALUE (%)	EVTS	DOCUMENT ID		TECN	COMMENT
1.188 ±0.035 OUR FIT	Error includes scale factor of 1.5.				
1.188 ±0.034 OUR AVERAGE	Error includes scale factor of 1.4. See the ideogram below.				
1.140 ±0.024 ±0.033	12.5k	[1] BEDDALL	08	ALEP	$e^+ e^- \to Z \to$ hadrons
1.25 ±0.04		SCHARDT	81	SPEC	$\pi^- p \to n\pi^0$
1.166 ±0.047	3k	[2] SAMIOS	61	HBC	$\pi^- p \to n\pi^0$
1.17 ±0.15	27	BUDAGOV	60	HBC	
• • • We do not use the following data for averages, fits, limits, etc. • • •					
1.1559±0.0047±0.0106	60k	[3] ABOUZAID	19	KTEV	$K_L \to 3\pi^0$ in flight
1.196		JOSEPH	60	THEO	QED calculation

[1] BEDDALL 08 value is obtained from ALEPH archived data.

[2] SAMIOS 61 value uses a Panofsky ratio = 1.62.

[3] ABOUZAID 19 measured a value of (0.3920 ± 0.0016 ± 0.0036)% from 1999 KTEV data in $K_L \to 3\pi^0 \to 5\gamma e^+ e^-$ decays, normalised to $K_L \to 3\pi^0$, for m(ee) > 15 MeV and then extrapolated it to the full m(ee) range using the Mikaelian and Smith predictions for the mass spectrum.

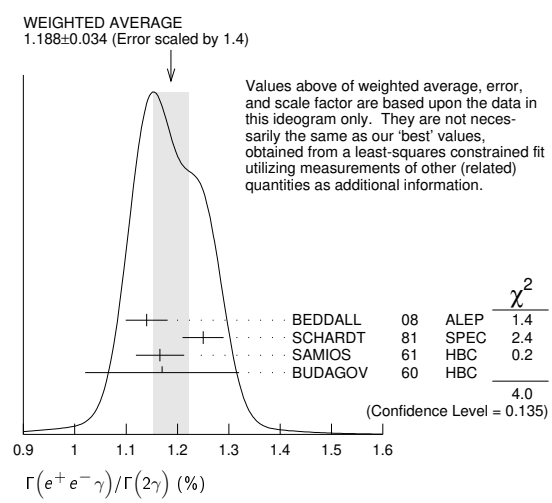

$\Gamma(\gamma\text{positronium})/\Gamma(2\gamma)$ — Γ_3/Γ_1

VALUE (units 10^{-9})	EVTS	DOCUMENT ID		TECN	COMMENT
1.84±0.29	277	AFANASYEV	90	CNTR	pC 70 GeV

$\Gamma(e^+ e^+ e^- e^-)/\Gamma(2\gamma)$ — Γ_4/Γ_1

VALUE (units 10^{-5})	EVTS	DOCUMENT ID		TECN	COMMENT
3.38±0.16 OUR FIT					
3.38±0.16 OUR AVERAGE					
3.46±0.19	30.5k	[1] ABOUZAID	08D	KTEV	$K_L^0 \to \pi^0 \pi^0 \pi^0_{DD}$
3.18±0.30	146	[2] SAMIOS	62B	HBC	

Int. J. Mod. Phys. A 2026.41. Downloaded from www.worldscientific.com
by [redacted]LIFORNIA @ BERKELEY on 09/16/26. Re-use and distribution is strictly not permitted, except for Open Access articles.

[1] This ABOUZAID 08D value includes all radiative final states. The error includes both statistical and systematic errors. The correlation between the Dalitz-pair planes gives a direct measurement of the π^0 parity. The $\pi^0 2\gamma^*$ form factor is measured and limits are placed on a scalar contribution to the decay.

[2] SAMIOS 62B value uses a Panofsky ratio = 1.62.

$\Gamma(e^+e^-)/\Gamma_{total}$ — Γ_5/Γ

Experimental results are listed; branching ratios corrected for radiative effects are given in the footnotes. BERMAN 60 found $B(\pi^0 \to e^+e^-) \geq 4.69 \times 10^{-8}$ via an exact QED calculation.

VALUE (units 10^{-8})	EVTS	DOCUMENT ID		TECN	CHG	COMMENT
6.46±0.33 OUR AVERAGE						
6.44±0.25±0.22	794	[1] ABOUZAID	07	KTEV		$K^0_L \to 3\pi^0$ in flight
6.9 ±2.3 ±0.6	21	[2] DESHPANDE	93	SPEC		$K^+ \to \pi^+\pi^0$
7.6 $^{+2.9}_{-2.8}$ ±0.5	8	[3] MCFARLAND	93	SPEC		$K^0_L \to 3\pi^0$ in flight
• • • We do not use the following data for averages, fits, limits, etc. • • •						
6.09±0.40±0.24	275	[4] ALAVI-HARATI	99C	SPEC	0	Repl. by ABOUZAID 07

[1] ABOUZAID 07 result is for $m_{e^+e^-}/m_{\pi^0} > 0.95$. With radiative corrections the result becomes $(7.48 \pm 0.29 \pm 0.25) \times 10^{-8}$.

[2] The DESHPANDE 93 result with bremsstrahlung radiative corrections is $(8.0 \pm 2.6 \pm 0.6) \times 10^{-8}$.

[3] The MCFARLAND 93 result is for $B[\pi^0 \to e^+e^-, (m_{e^+e^-}/m_{\pi^0})^2 > 0.95]$. With radiative corrections it becomes $(8.8 \pm^{4.5}_{-3.2} \pm 0.6) \times 10^{-8}$.

[4] ALAVI-HARATI 99C quote result for $B[\pi^0 \to e^+e^-, (m_{e^+e^-}/m_{\pi^0})^2 > 0.95]$ to minimize radiative contributions from $\pi^0 \to e^+e^-\gamma$. After radiative corrections they obtain $(7.04 \pm 0.46 \pm 0.28) \times 10^{-8}$.

$\Gamma(e^+e^-)/\Gamma(2\gamma)$ — Γ_5/Γ_1

VALUE (units 10^{-7})	CL%	EVTS	DOCUMENT ID		TECN	COMMENT
• • • We do not use the following data for averages, fits, limits, etc. • • •						
<1.3	90		NIEBUHR	89	SPEC	$\pi^- p \to \pi^0 n$ at rest
<5.3	90		ZEPHAT	87	SPEC	$\pi^- p \to \pi^0 n$ 0.3 GeV/c
1.7 ±0.6 ±0.3		59	FRANK	83	SPEC	$\pi^- p \to n\pi^0$
1.8 ±0.6		58	MISCHKE	82	SPEC	See FRANK 83
2.23 $^{+2.40}_{-1.10}$	90	8	FISCHER	78B	SPRK	$K^+ \to \pi^+\pi^0$

$\Gamma(4\gamma)/\Gamma_{total}$ — Γ_6/Γ

VALUE (units 10^{-8})	CL%	EVTS	DOCUMENT ID		TECN	COMMENT
< 2	90		MCDONOUGH	88	CBOX	$\pi^- p$ at rest
• • • We do not use the following data for averages, fits, limits, etc. • • •						
<160	90		BOLOTOV	86C	CALO	
<440	90	0	AUERBACH	80	CNTR	

$\Gamma(\text{invisible})/\Gamma_{total}$ — Γ_7/Γ

The limits apply to all "invisible" channels, including in particular neutrino-antineutrino final states, obtained with laboratory experiments. Astrophysical and cosmological limits exist and are many orders of magnitude lower, but they are model dependent.

VALUE	CL%	DOCUMENT ID		TECN	COMMENT
< 4.4 × 10^{-9}	90	CORTINA-GIL	21C	SPEC	$K^+ \to \pi^+\pi^0(\gamma)$
• • • We do not use the following data for averages, fits, limits, etc. • • •					
< 0.27 × 10^{-6}	90	ARTAMONOV	05A	B949	$K^+ \to \pi^+\pi^0$
< 0.83 × 10^{-6}	90	ATIYA	91	B787	$K^+ \to \pi^+\nu\nu'$
<24 × 10^{-6}	90	HERCZEG	81	RVUE	$K^+ \to \pi^+\nu\nu'$

$\Gamma(\nu_e\overline{\nu}_e)/\Gamma_{total}$ — Γ_8/Γ

VALUE (units 10^{-6})	CL%	DOCUMENT ID		TECN	COMMENT
<1.7	90	DORENBOS...	88	CHRM	Beam dump, prompt ν
• • • We do not use the following data for averages, fits, limits, etc. • • •					
<3.1	90	[1] HOFFMAN	88	RVUE	Beam dump, prompt ν

[1] HOFFMAN 88 analyzes data from a 400-GeV BEBC beam-dump experiment.

$\Gamma(\nu_\mu\overline{\nu}_\mu)/\Gamma_{total}$ — Γ_9/Γ

VALUE (units 10^{-6})	CL%	EVTS	DOCUMENT ID		TECN	COMMENT
<1.6	90	8.7	AUERBACH	04	LSND	800 MeV p on Cu
<3.1	90		[1] HOFFMAN	88	RVUE	Beam dump, prompt ν
• • • We do not use the following data for averages, fits, limits, etc. • • •						
<7.8	90		DORENBOS...	88	CHRM	Beam dump, prompt ν

[1] HOFFMAN 88 analyzes data from a 400-GeV BEBC beam-dump experiment.

$\Gamma(\nu_\tau\overline{\nu}_\tau)/\Gamma_{total}$ — Γ_{10}/Γ

VALUE (units 10^{-6})	CL%	DOCUMENT ID		TECN	COMMENT
<2.1	90	[1] HOFFMAN	88	RVUE	Beam dump, prompt ν
• • • We do not use the following data for averages, fits, limits, etc. • • •					
<4.1	90	DORENBOS...	88	CHRM	Beam dump, prompt ν

[1] HOFFMAN 88 analyzes data from a 400-GeV BEBC beam-dump experiment.

$\Gamma(\gamma\nu\overline{\nu})/\Gamma_{total}$ — Γ_{11}/Γ

Standard Model prediction is 6×10^{-18}.

VALUE	CL%	DOCUMENT ID		TECN	COMMENT
<1.9 × 10^{-7}	90	CORTINA-GIL	19	SPEC	$K^+ \to \pi^+\gamma\nu\overline{\nu}$
• • • We do not use the following data for averages, fits, limits, etc. • • •					
<6 × 10^{-4}	90	ATIYA	92	CNTR	$K^+ \to \gamma\nu\overline{\nu}\pi^+$

$\Gamma(3\gamma)/\Gamma_{total}$ — Γ_{12}/Γ

Forbidden by C invariance.

VALUE (units 10^{-8})	CL%	EVTS	DOCUMENT ID		TECN	COMMENT
< 3.1	90		MCDONOUGH	88	CBOX	$\pi^- p$ at rest
• • • We do not use the following data for averages, fits, limits, etc. • • •						
< 38	90	0	HIGHLAND	80	CNTR	
<150	90	0	AUERBACH	78	CNTR	
<490	90	0	[1] DUCLOS	65	CNTR	
<490	90		[1] KUTIN	65	CNTR	

[1] These experiments give $B(3\gamma/2\gamma) < 5.0 \times 10^{-6}$.

$\Gamma(\mu^+e^-)/\Gamma_{total}$ — Γ_{13}/Γ

Forbidden by lepton family number conservation.

VALUE (units 10^{-9})	CL%	EVTS	DOCUMENT ID		TECN	COMMENT
< 0.38	90	0	APPEL	00	SPEC	$K^+ \to \pi^+\mu^+e^-$
• • • We do not use the following data for averages, fits, limits, etc. • • •						
<16	90		LEE	90	SPEC	$K^+ \to \pi^+\mu^+e^-$
<78	90		CAMPAGNARI	88	SPEC	See LEE 90

$\Gamma(\mu^-e^+)/\Gamma_{total}$ — Γ_{14}/Γ

Forbidden by lepton family number conservation.

VALUE	CL%	DOCUMENT ID		TECN	COMMENT
<3.2 × 10^{-10}	90	ALIBERTI	21	NA62	$K^+ \to \pi^+e^+\mu^-$
• • • We do not use the following data for averages, fits, limits, etc. • • •					
<3.4 × 10^{-9}	90	APPEL	00B	B865	$K^+ \to \pi^+e^+\mu^-$

$[\Gamma(\mu^+e^-) + \Gamma(\mu^-e^+)]/\Gamma_{total}$ — Γ_{15}/Γ

Forbidden by lepton family number conservation.

VALUE (units 10^{-9})	CL%	DOCUMENT ID		TECN	COMMENT
< 0.36	90	ABOUZAID	08C	KTEV	$K^0_L \to 2\pi^0\mu^\pm e^\mp$
• • • We do not use the following data for averages, fits, limits, etc. • • •					
< 17.2	90	KROLAK	94	E799	In $K^0_L \to 3\pi^0$
<140		HERCZEG	84	RVUE	$K^+ \to \pi^+\mu e$
< 2 × 10^{-6}		HERCZEG	84	THEO	$\mu^- \to e^-$ conversion
< 70	90	BRYMAN	82	RVUE	$K^+ \to \pi^+\mu e$

π^0 ELECTROMAGNETIC FORM FACTOR

The amplitude for the process $\pi^0 \to e^+e^-\gamma$ contains a form factor $F(x)$ at the $\pi^0\gamma\gamma$ vertex, where $x = [m_{e^+e^-}/m_{\pi^0}]^2$. The parameter a in the linear expansion $F(x) = 1 + ax$ is listed below.

All the measurements except that of BEHREND 91 are in the time-like region of momentum transfer.

LINEAR COEFFICIENT OF π^0 ELECTROMAGNETIC FORM FACTOR

VALUE (units 10^{-2})	EVTS	DOCUMENT ID		TECN	COMMENT
3.32± 0.29 OUR AVERAGE					
3.0 ± 1.0	0.4M	[1] ADLARSON	17A	SPEC	$\gamma p \to \pi^0 p$, $\pi^0 \to e^+e^-\gamma$
3.68± 0.51±0.25	1.1M	LAZZERONI	17	SPEC	$K^\pm \to \pi^0\pi^\pm$; $\pi^0 \to e^+e^-\gamma$
2.6 ± 2.4 ±4.8	7.5k	FARZANPAY	92	SPEC	$\pi^- p \to \pi^0 n$ at rest
2.5 ± 1.4 ±2.6	54k	MEIJERDREES	92B	SPEC	$\pi^- p \to \pi^0 n$ at rest
3.26± 0.26±0.26	127	[2] BEHREND	91	CELL	$e^+e^- \to e^+e^-\pi^0$
−11 ± 3 ±8	32k	FONVIEILLE	89	SPEC	Radiation corr.
• • • We do not use the following data for averages, fits, limits, etc. • • •					
12 $^{+5}_{-4}$		[3] TUPPER	83	THEO	FISCHER 78 data
10 ± 3	31k	[4] FISCHER	78	SPEC	Radiation corr.
1 ±11	2.2k	DEVONS	69	OSPK	No radiation corr.
−15 ±10	7.6k	KOBRAK	61	HBC	No radiation corr.
−24 ±16	3.0k	SAMIOS	61	HBC	No radiation corr.

[1] ADLARSON 17A use the A2 tagged photon facility at the Mainz Microtron, MAMI to measure π^0 Dalitz decay. The error is the total estimated experimental uncertainty .

[2] BEHREND 91 estimates that their systematic error is of the same order of magnitude as their statistical error, and so we have included a systematic error of this magnitude. The value of a is obtained by extrapolation from the region of large space-like momentum transfer assuming vector dominance.

[3] TUPPER 83 is a theoretical analysis of FISCHER 78 including 2-photon exchange in the corrections.

[4] The FISCHER 78 error is statistical only. The result without radiation corrections is +0.05 ± 0.03.

π^0 REFERENCES

We have omitted some papers that have been superseded by later experiments. The omitted papers may be found in our 1988 edition Physics Letters **B204** 1 (1988).

ALIBERTI	21	PRL 127 131802	R. Aliberti *et al.*	(NA62 Collab.)
CORTINA-GIL	21C	JHEP 2102 201	E. Cortina Gil *et al.*	(NA62 Collab.)
LARIN	20	SCI 368 506	I. Larin *et al.*	(PrimEx II Collab.)
ABOUZAID	19	PR D100 032003	E. Abouzaid *et al.*	(KTeV Collab.)
CORTINA-GIL	19	JHEP 1905 182	E. Cortina Gil *et al.*	(NA62 Collab.)
ADLARSON	17A	PR C95 025202	P. Adlarson *et al.*	(A2 Collab. at MAMI)
LAZZERONI	17	PL B768 38	C. Lazzeroni *et al.*	(NA62 Collab.)
BERNSTEIN	13	RMP 85 49	A.M. Bernstein, B. R. Holstein	(AMHT, MIT)

Int. J. Mod. Phys. A 2026.41. Downloaded from www.worldscientific.com
by UNIVERSITY OF CALIFORNIA @ BERKELEY on 09/16/26. Re-use and distribution is strictly not permitted, except for Open Access articles.

LARIN	11	PRL 106 162303	I. Larin *et al.*	(PrimEx Collab.)
BYCHKOV	09	PRL 103 051802	M. Bychkov *et al.*	(PSI PIBETA Collab.)
ABOUZAID	08C	PRL 100 131803	E. Abouzaid *et al.*	(FNAL KTeV Collab.)
ABOUZAID	08D	PRL 100 182001	E. Abouzaid *et al.*	(FNAL KTeV Collab.)
BEDDALL	08	EPJ C54 365	A. Beddall, A. Beddall	(UGAZ)
ABOUZAID	07	PR D75 012004	E. Abouzaid *et al.*	(KTeV Collab.)
ARTAMONOV	05A	PR D72 091102	A.V. Artamonov *et al.*	(BNL E949 Collab.)
AUERBACH	04	PRL 92 091801	L.B. Auerbach *et al.*	(LSND Collab.)
APPEL	00	PRL 85 2450	R. Appel *et al.*	(BNL 865 Collab.)
Also		Thesis, Yale Univ.	D.R. Bergman	
Also		Thesis, Univ. Zurich	S. Pislak	
APPEL	00B	PRL 85 2877	R. Appel *et al.*	(BNL 865 Collab.)
ALAVI-HARATI	99C	PRL 83 922	A. Alavi-Harati *et al.*	(FNAL KTeV Collab.)
KROLAK	94	PL B320 407	P. Krolak *et al.*	(EFI, UCLA, COLO, ELMT+)
DESHPANDE	93	PRL 71 27	A. Deshpande *et al.*	(BNL E851 Collab.)
MCFARLAND	93	PRL 71 31	K.S. McFarland *et al.*	(EFI, UCLA, COLO+)
ATIYA	92	PRL 69 733	M.S. Atiya *et al.*	(BNL, LANL, PRIN+)
FARZANPAY	92	PL B278 413	F. Farzanpay *et al.*	(ORST, TRIU, BRCO+)
MEIJERDREES	92B	PR D45 1439	R. Meijer Drees *et al.*	(PSI SINDRUM-I Collab.)
ATIYA	91	PRL 66 2189	M.S. Atiya *et al.*	(BNL, LANL, PRIN+)
BEHREND	91	ZPHY C49 401	H.J. Behrend *et al.*	(CELLO Collab.)
CRAWFORD	91	PR D43 46	J.F. Crawford *et al.*	(VILL, UVA)
AFANASYEV	90	PL B236 116	L.G. Afanasyev *et al.*	(JINR, MOSU, SERP)
Also		SJNP 51 664	L.G. Afanasyev *et al.*	(JINR)
		Translated from YAF 51 1040.		
LEE	90	PRL 64 165	A.M. Lee *et al.*	(BNL, FNAL, VILL, WASH+)
FONVIEILLE	89	PL B233 65	H. Fonvieille *et al.*	(CLER, LYON, SACL)
NIEBUHR	89	PR D40 2796	C. Niebuhr *et al.*	(SINDRUM Collab.)
CAMPAGNARI	88	PRL 61 2062	C. Campagnari *et al.*	(BNL, FNAL, PSI+)
CRAWFORD	88B	PL B213 391	J.F. Crawford *et al.*	(PSI, UVA)
DORENBOS...	88	ZPHY C40 497	J. Dorenbosch *et al.*	(CHARM Collab.)
HOFFMAN	88	PL B208 149	C.M. Hoffman	(LANL)
MCDONOUGH	88	PR D38 2121	J.M. McDonough *et al.*	(TEMP, LANL, CHIC)
PDG	88	PL B204 1	G.P. Yost *et al.*	(LBL+)
WILLIAMS	88	PR D38 1365	D.A. Williams *et al.*	(Crystal Ball Collab.)
ZEPHAT	87	JP G13 1375	A.G. Zephat *et al.*	(OMICRON Collab.)
BOLOTOV	86C	JETPL 43 520	V.N. Bolotov *et al.*	(INRM)
		Translated from ZETFP 43 405.		
CRAWFORD	86	PRL 56 1043	J.F. Crawford *et al.*	(SIN, UVA)
ATHERTON	85	PL 158B 81	H.W. Atherton *et al.*	(CERN, ISU, LUND+)
HERCZEG	84	PR D29 1954	P. Herczeg, C.M. Hoffman	(LANL)
FRANK	83	PR D28 423	J.S. Frank *et al.*	(LANL, ARZS)
TUPPER	83	PR D28 2905	G.B. Tupper, T.R. Grose, M.A. Samuel	(OKSU)
BRYMAN	82	PR D26 2538	D.A. Bryman	(TRIU)
MISCHKE	82	PRL 48 1153	R.E. Mischke *et al.*	(LANL, ARZS)
HERCZEG	81	PL 100B 347	P. Herczeg, C.M. Hoffman	(LANL)
SCHARDT	81	PR D23 639	M.A. Schardt *et al.*	(ARZS, LANL)
AUERBACH	80	PL 90B 317	L.B. Auerbach *et al.*	(TEMP, LASL)
HIGHLAND	80	PRL 44 628	V.L. Highland *et al.*	(TEMP, LASL)
AUERBACH	78	PRL 41 275	L.B. Auerbach *et al.*	(TEMP, LASL)
FISCHER	78	PL 73B 359	J. Fischer *et al.*	(GEVA, SACL)
FISCHER	78B	PL 73B 364	J. Fischer *et al.*	(GEVA, SACL)
BROWMAN	74	PRL 33 1400	A. Browman *et al.*	(CORN, BING)
BELLETTINI	70	NC 66A 243	G. Bellettini *et al.*	(PISA, BONN)
KRYSHKIN	70	JETP 30 1037	V.I. Kryshkin, A.G. Sterligov, Y.P. Usov	(TMSK)
		Translated from ZETF 57 1917.		
DEVONS	69	PR 184 1356	S. Devons *et al.*	(COLU, ROMA)
VASILEVSKY	66	PL 23 281	I.M. Vasilevsky *et al.*	(JINR)
BELLETTINI	65B	NC 40A 1139	G. Bellettini *et al.*	(PISA, FIRZ)
DUCLOS	65	PL 19 253	J. Duclos *et al.*	(CERN, HEID)
KUTIN	65	JETPL 2 243	V.M. Kutjin, V.I. Petrukhin, Y.D. Prokoshkin	(JINR)
		Translated from ZETFP 2 387.		
CZIRR	63	PR 130 341	J.B. Czirr	(LRL)
SAMIOS	62B	PR 126 1844	N.P. Samios *et al.*	(COLU, BNL)
KOBRAK	61	NC 20 1115	H. Kobrak	(EFI)
SAMIOS	61	PR 121 275	N.P. Samios	(COLU, BNL)
BERMAN	60	NC 18 1192	S. Berman, D. Geffen	
BUDAGOV	60	JETP 11 755	Y.A. Budagov *et al.*	(JINR)
		Translated from ZETF 38 1047.		
JOSEPH	60	NC 16 997	D.W. Joseph	(EFI)

η

$I^G(J^{PC}) = 0^+(0^{-+})$

We have omitted some results that have been superseded by later experiments. The omitted results may be found in our 1988 edition Physics Letters **B204** (1988).

η MASS

Recent measurements resolve the obvious inconsistency in previous η mass measurements in favor of the higher value first reported by NA48 (LAI 02). We use only precise measurements consistent with this higher mass value for our η mass average.

VALUE (MeV)	*EVTS*	*DOCUMENT ID*		*TECN*	*COMMENT*
547.862±0.017 OUR AVERAGE					
547.865±0.031±0.062		NIKOLAEV	14	CRYB	$\gamma p \to p \eta$
547.873±0.005±0.027	1M	GOSLAWSKI	12	SPEC	$dp \to {}^3\mathrm{He}\,\eta$
547.874±0.007±0.029		AMBROSINO	07B	KLOE	$e^+e^- \to \phi \to \eta\gamma$
547.785±0.017±0.057	16k	MILLER	07	CLEO	$\psi(2S) \to J/\psi\eta$
547.843±0.030±0.041	1134	LAI	02	NA48	$\eta \to 3\pi^0$
• • • We do not use the following data for averages, fits, limits, etc. • • •					
547.311±0.028±0.032		[1] ABDEL-BARY	05	SPEC	$dp \to {}^3\mathrm{He}\,\eta$
547.12 ±0.06 ±0.25		KRUSCHE	95D	SPEC	$\gamma p \to \eta p$, threshold
547.30 ±0.15		PLOUIN	92	SPEC	$dp \to {}^3\mathrm{He}\,\eta$
547.45 ±0.25		DUANE	74	SPEC	$\pi^- p \to n$ neutrals
548.2 ±0.65		FOSTER	65C	HBC	
549.0 ±0.7	148	FOELSCHE	64	HBC	
548.0 ±1.0	91	ALFF-...	62	HBC	
549.0 ±1.2	53	BASTIEN	62	HBC	

[1] ABDEL-BARY 05 disagrees significantly with recent measurements of similar or better precision. See comment in the header.

η WIDTH

This is the partial decay rate $\Gamma(\eta \to \gamma\gamma)$ divided by the fitted branching fraction for that mode. See the note at the start of the $\Gamma(2\gamma)$ data block, next below.

VALUE (keV)	*DOCUMENT ID*
1.31±0.05 OUR FIT	

η DECAY MODES

	Mode	Fraction (Γ_i/Γ)	Scale factor/ Confidence level
	Neutral modes		
Γ_1	neutral modes	(71.95±0.29) %	S=1.3
Γ_2	2γ	(39.36±0.18) %	S=1.1
Γ_3	$3\pi^0$	(32.56±0.21) %	S=1.2
Γ_4	$\pi^0 2\gamma$	(2.55±0.22) $\times 10^{-4}$	
Γ_5	$2\pi^0 2\gamma$	< 1.2 $\times 10^{-3}$	CL=90%
Γ_6	4γ	< 2.8 $\times 10^{-4}$	CL=90%
Γ_7	invisible	< 2.4 $\times 10^{-5}$	CL=90%
	Charged modes		
Γ_8	charged modes	(28.05±0.29) %	S=1.3
Γ_9	$\pi^+\pi^-\pi^0$	(23.02±0.25) %	S=1.2
Γ_{10}	$\pi^+\pi^-\gamma$	(4.28±0.07) %	S=1.1
Γ_{11}	$e^+e^-\gamma$	(6.96±0.18) $\times 10^{-3}$	
Γ_{12}	$\mu^+\mu^-\gamma$	(2.98±0.13) $\times 10^{-4}$	
Γ_{13}	e^+e^-	< 7 $\times 10^{-7}$	CL=90%
Γ_{14}	$\mu^+\mu^-$	(5.8 ±0.8) $\times 10^{-6}$	
Γ_{15}	$2e^+2e^-$	(2.40±0.22) $\times 10^{-5}$	
Γ_{16}	$\pi^+\pi^-e^+e^-(\gamma)$	(2.76±0.16) $\times 10^{-4}$	S=1.5
Γ_{17}	$e^+e^-\mu^+\mu^-$	< 6.88 $\times 10^{-6}$	CL=90%
Γ_{18}	$2\mu^+2\mu^-$	(5.0 ±1.3) $\times 10^{-9}$	
Γ_{19}	$\mu^+\mu^-\pi^+\pi^-$	< 4.0 $\times 10^{-7}$	CL=90%
Γ_{20}	$\pi^+e^-\overline{\nu}_e$ + c.c.	< 1.7 $\times 10^{-4}$	CL=90%
Γ_{21}	$\pi^+\pi^-2\gamma$	< 2.1 $\times 10^{-3}$	
Γ_{22}	$\pi^+\pi^-\pi^0\gamma$	< 6 $\times 10^{-4}$	CL=90%
Γ_{23}	$\pi^0\mu^+\mu^-\gamma$	< 3 $\times 10^{-6}$	CL=90%
	Charge conjugation (*C*), Parity (*P*), Charge conjugation × Parity (*CP*), or Lepton Family number (*LF*) violating modes		
Γ_{24}	$\pi^0\gamma$ *C*	[a] < 9 $\times 10^{-5}$	CL=90%
Γ_{25}	$\pi^+\pi^-$ *P,CP*	< 4.4 $\times 10^{-6}$	CL=90%
Γ_{26}	$2\pi^0$ *P,CP*	< 3.5 $\times 10^{-4}$	CL=90%
Γ_{27}	$2\pi^0\gamma$ *C*	< 5 $\times 10^{-4}$	CL=90%
Γ_{28}	$3\pi^0\gamma$ *C*	< 6 $\times 10^{-5}$	CL=90%
Γ_{29}	3γ *C*	< 1.6 $\times 10^{-5}$	CL=90%
Γ_{30}	$4\pi^0$ *P,CP*	< 6.9 $\times 10^{-7}$	CL=90%
Γ_{31}	$\pi^0e^+e^-$ *C*	[b] < 8 $\times 10^{-6}$	CL=90%
Γ_{32}	$\pi^0\mu^+\mu^-$ *C*	[b] < 5 $\times 10^{-6}$	CL=90%
Γ_{33}	$\mu^+e^- + \mu^-e^+$ *LF*	< 6 $\times 10^{-6}$	CL=90%
Γ_{34}	$\pi^+\pi^+e^-e^-$ + c.c. *LF*	< 4.6 $\times 10^{-6}$	CL=90%

[a] Forbidden by angular momentum conservation.

[b] *C* parity forbids this to occur as a single-photon process.

CONSTRAINED FIT INFORMATION

An overall fit to 2 decay rate and 22 branching ratios uses 58 measurements and one constraint to determine 9 parameters. The overall fit has a $\chi^2 = 49.2$ for 50 degrees of freedom.

The following *off-diagonal* array elements are the correlation coefficients $\langle \delta x_i \delta x_j \rangle / (\delta x_i \cdot \delta x_j)$, in percent, from the fit to the branching fractions, $x_i \equiv \Gamma_i/\Gamma_{\mathrm{total}}$. The fit constrains the x_i whose labels appear in this array to sum to one.

	x_2	x_3	x_4	x_9	x_{10}	x_{11}	x_{12}	x_{16}
x_3	12							
x_4	4	0						
x_9	−69	−77	−3					
x_{10}	−48	−53	−2	53				
x_{11}	−3	−3	0	−2	−1			
x_{12}	0	0	0	0	0	0		
x_{16}	0	0	0	0	0	0	0	
Γ	−13	−1	−32	9	6	0	0	0

Int. J. Mod. Phys. A 2026.41. Downloaded from www.worldscientific.com
by LIFORNIA @ BERKELEY on 09/16/26. Re-use and distribution is strictly not permitted, except for Open Access articles.

Int. J. Mod. Phys. A 2026.41. Downloaded from www.worldscientific.com
by UNIVERSITY OF CALIFORNIA @ BERKELEY on 09/16/26. Re-use and distribution is strictly not permitted, except for Open Access articles.

	Mode	Rate (keV)	Scale factor
Γ_2	2γ	0.515 ±0.018	
Γ_3	$3\pi^0$	0.426 ±0.015	
Γ_4	$\pi^0 2\gamma$	(3.34 ±0.28) × 10^{-4}	
Γ_9	$\pi^+\pi^-\pi^0$	0.301 ±0.011	
Γ_{10}	$\pi^+\pi^-\gamma$	0.0559±0.0022	
Γ_{11}	$e^+e^-\gamma$	0.0091±0.0004	
Γ_{12}	$\mu^+\mu^-\gamma$	(3.90 ±0.22) × 10^{-4}	
Γ_{16}	$\pi^+\pi^-e^+e^-(\gamma)$	(3.61 ±0.24) × 10^{-4}	1.3

η DECAY RATES

$\Gamma(2\gamma)$ — Γ_2

See the table immediately above giving the fitted decay rates. Following the advice of NEFKENS 02, we have removed the Primakoff-effect measurement from the average. See also the "Note on the Decay Width $\Gamma(\eta \to \gamma\gamma)$," in our 1994 edition, Phys. Rev. **D50**, 1 August 1994, Part I, p. 1451, for a discussion of the various measurements.

VALUE (keV)	EVTS	DOCUMENT ID		TECN	COMMENT
0.515±0.018 OUR FIT					
0.516±0.018 OUR AVERAGE					
0.520±0.020±0.013		BABUSCI	13A	KLOE	$e^+e^- \to e^+e^-\eta$
0.51 ±0.12 ±0.05	36	BARU	90	MD1	$e^+e^- \to e^+e^-\eta$
0.490±0.010±0.048	2287	ROE	90	ASP	$e^+e^- \to e^+e^-\eta$
0.514±0.017±0.035	1295	WILLIAMS	88	CBAL	$e^+e^- \to e^+e^-\eta$
0.53 ±0.04 ±0.04		BARTEL	85E	JADE	$e^+e^- \to e^+e^-\eta$
• • • We do not use the following data for averages, fits, limits, etc. • • •					
0.476±0.062		[1] RODRIGUES	08	CNTR	Reanalysis
0.64 ±0.14 ±0.13		AIHARA	86	TPC	$e^+e^- \to e^+e^-\eta$
0.56 ±0.16	56	WEINSTEIN	83	CBAL	$e^+e^- \to e^+e^-\eta$
0.324±0.046		BROWMAN	74B	CNTR	Primakoff effect
1.00 ±0.22		[2] BEMPORAD	67	CNTR	Primakoff effect

[1] RODRIGUES 08 uses a more sophisticated calculation for the inelastic background due to incoherent photoproduction to reanalyze the η photoproduction data on Be and Cu at 9 GeV from BROWMAN 74B. This brings the value of $\Gamma(\eta \to 2\gamma)$ in line with direct measurements of the width. The error here is only statistical.

[2] BEMPORAD 67 gives $\Gamma(2\gamma) = 1.21 \pm 0.26$ keV assuming $\Gamma(2\gamma)/\Gamma(\text{total}) = 0.314$. Bemporad private communication gives $\Gamma(2\gamma)^2/\Gamma(\text{total}) = 0.380 \pm 0.083$. We evaluate this using $\Gamma(2\gamma)/\Gamma(\text{total}) = 0.38 \pm 0.01$. Not included in average because the uncertainty resulting from the separation of the coulomb and nuclear amplitudes has apparently been underestimated.

$\Gamma(\pi^0 2\gamma)$ — Γ_4

VALUE (eV)	EVTS	DOCUMENT ID		TECN	COMMENT
0.334±0.028 OUR FIT					
0.33 ±0.03	1200	NEFKENS	14	CRYB	$\gamma p \to \eta p$

η BRANCHING RATIOS

Neutral modes

$\Gamma(\text{neutral modes})/\Gamma_{\text{total}}$ — $\Gamma_1/\Gamma = (\Gamma_2+\Gamma_3+\Gamma_4)/\Gamma$

VALUE	EVTS	DOCUMENT ID		TECN	COMMENT
0.7195±0.0029 OUR FIT Error includes scale factor of 1.3.					
0.705 ±0.008	16k	BASILE	71D	CNTR	MM spectrometer
• • • We do not use the following data for averages, fits, limits, etc. • • •					
0.79 ±0.08		BUNIATOV	67	OSPK	

$\Gamma(2\gamma)/\Gamma_{\text{total}}$ — Γ_2/Γ

VALUE (units 10^{-2})	EVTS	DOCUMENT ID		TECN	COMMENT
39.36±0.18 OUR FIT Error includes scale factor of 1.1.					
39.53±0.33 OUR AVERAGE					
39.86±0.04±0.99	2m	[1] ABLIKIM	21AM	BES3	$J/\psi \to \gamma\eta$
39.49±0.17±0.30	65k	ABEGG	96	SPEC	$pd \to {}^3\text{He}\eta$
• • • We do not use the following data for averages, fits, limits, etc. • • •					
38.45±0.40±0.36	14k	[2] LOPEZ	07	CLEO	$\psi(2S) \to J/\psi\eta$

[1] ABLIKIM 21AM normalize the branching ratio $(\eta \to \gamma\gamma)$ to $B(J/\psi \to \gamma\eta)$, which they measured absolutely.

[2] Not independent of other results listed for LOPEZ 07. Assuming decays of $\eta \to \gamma\gamma$, $3\pi^0$, $\pi^+\pi^-\pi^0$, $\pi^+\pi^-\gamma$, and $e^+e^-\gamma$ account for all η decays within a contribution of 0.3% to the systematic error.

$\Gamma(2\gamma)/\Gamma(\text{neutral modes})$ — $\Gamma_2/\Gamma_1 = \Gamma_2/(\Gamma_2+\Gamma_3+\Gamma_4)$

VALUE	EVTS	DOCUMENT ID		TECN	COMMENT
0.5471±0.0018 OUR FIT					
0.548 ±0.023 OUR AVERAGE Error includes scale factor of 1.5.					
0.535 ±0.018		BUTTRAM	70	OSPK	
0.59 ±0.033		BUNIATOV	67	OSPK	
• • • We do not use the following data for averages, fits, limits, etc. • • •					
0.52 ±0.09	88	ABROSIMOV	80	HLBC	
0.60 ±0.14	113	KENDALL	74	OSPK	
0.57 ±0.09		STRUGALSKI	71	HLBC	
0.579 ±0.052		FELDMAN	67	OSPK	
0.416 ±0.044		DIGIUGNO	66	CNTR	Error doubled
0.44 ±0.07		GRUNHAUS	66	OSPK	
0.39 ±0.06		[1] JONES	66	CNTR	

[1] This result from combining cross sections from two different experiments.

$\Gamma(3\pi^0)/\Gamma_{\text{total}}$ — Γ_3/Γ

VALUE (units 10^{-2})	EVTS	DOCUMENT ID		TECN	COMMENT
32.56±0.21 OUR FIT Error includes scale factor of 1.2.					
31.96±0.07±0.84	280k	[1] ABLIKIM	21AM	BES3	$J/\psi \to \gamma\eta$
• • • We do not use the following data for averages, fits, limits, etc. • • •					
34.03±0.56±0.49	1821	[2] LOPEZ	07	CLEO	$\psi(2S) \to J/\psi\eta$

[1] ABLIKIM 21AM normalize the branching ratio $(\eta \to 3\pi^0)$ to $B(J/\psi \to \gamma\eta)$, which they measured absolutely.

[2] Not independent of other results listed for LOPEZ 07. Assuming decays of $\eta \to \gamma\gamma$, $3\pi^0$, $\pi^+\pi^-\pi^0$, $\pi^+\pi^-\gamma$, and $e^+e^-\gamma$ account for all η decays within a contribution of 0.3% to the systematic error.

$\Gamma(3\pi^0)/\Gamma(\text{neutral modes})$ — $\Gamma_3/\Gamma_1 = \Gamma_3/(\Gamma_2+\Gamma_3+\Gamma_4)$

VALUE	EVTS	DOCUMENT ID		TECN	COMMENT
0.4526±0.0019 OUR FIT					
0.439 ±0.024		BUTTRAM	70	OSPK	
• • • We do not use the following data for averages, fits, limits, etc. • • •					
0.44 ±0.08	75	ABROSIMOV	80	HLBC	
0.32 ±0.09		STRUGALSKI	71	HLBC	
0.41 ±0.033		BUNIATOV	67	OSPK	Not indep. of $\Gamma(2\gamma)/\Gamma(\text{neutral modes})$
0.177 ±0.035		FELDMAN	67	OSPK	
0.209 ±0.054		DIGIUGNO	66	CNTR	Error doubled
0.29 ±0.10		GRUNHAUS	66	OSPK	

$\Gamma(3\pi^0)/\Gamma(2\gamma)$ — Γ_3/Γ_2

VALUE	EVTS	DOCUMENT ID		TECN	COMMENT
0.827±0.006 OUR FIT					
0.829±0.007 OUR AVERAGE					
0.884±0.022±0.019	1821	LOPEZ	07	CLEO	$\psi(2S) \to J/\psi\eta$
0.817±0.012±0.032	17.4k	[1] AKHMETSHIN	05	CMD2	$e^+e^- \to \phi \to \eta\gamma$
0.826±0.024		ACHASOV	00D	SND	$e^+e^- \to \phi \to \eta\gamma$
0.832±0.005±0.012		KRUSCHE	95D	SPEC	$\gamma p \to \eta p$, threshold
0.841±0.034		AMSLER	93	CBAR	$\bar{p}p \to \pi^+\pi^-\eta$ at rest
0.822±0.009		ALDE	84	GAM2	
• • • We do not use the following data for averages, fits, limits, etc. • • •					
0.796±0.016±0.016		ACHASOV	00	SND	See ACHASOV 00D
0.91 ±0.14		COX	70B	HBC	
0.75 ±0.09		DEVONS	70	OSPK	
0.88 ±0.16		BALTAY	67D	DBC	
1.1 ±0.2		CENCE	67	OSPK	
1.25 ±0.39		BACCI	63	CNTR	Inverse BR reported

[1] Uses result from AKHMETSHIN 01B.

$\Gamma(\pi^0 2\gamma)/\Gamma_{\text{total}}$ — Γ_4/Γ

Early results are summarized in the review by LANDSBERG 85.

VALUE (units 10^{-4})	CL%	EVTS	DOCUMENT ID		TECN	COMMENT
2.55±0.22 OUR FIT						
2.21±0.24±0.47		≈ 500	[1] PRAKHOV	08	CRYB	$\pi^-p \to \eta n \approx$ threshold
• • • We do not use the following data for averages, fits, limits, etc. • • •						
3.5 ±0.7 ±0.6		1.6k	[2,3] PRAKHOV	05	CRYB	See PRAKHOV 08
<8.4	90	7	ACHASOV	01D	SND	$e^+e^- \to \phi \to \eta\gamma$
<30	90	0	DAVYDOV	81	GAM2	$\pi^-p \to \eta n$

[1] PRAKHOV 08 is a reanalysis of the data of PRAKHOV 05, using for the first time the invariant-mass spectrum of the two photons.

[2] Normalized using $\Gamma(\eta \to 2\gamma)/\Gamma = 0.3943 \pm 0.0026$.

[3] This measurement and the independent analysis of the same data by KNECHT 04 both imply a lower value of $\Gamma(\pi^0 2\gamma)$ than the one obtained by ALDE 84 from $\Gamma(\pi^0 2\gamma)/\Gamma(2\gamma)$.

$\Gamma(\pi^0 2\gamma)/\Gamma(2\gamma)$ — Γ_4/Γ_2

VALUE (units 10^{-3})	EVTS	DOCUMENT ID		TECN	CHG	COMMENT
0.65±0.06 OUR FIT						
1.8 ±0.4		ALDE	84	GAM2	0	
• • • We do not use the following data for averages, fits, limits, etc. • • •						
2.5 ±0.6	70	BINON	82	GAM2		See ALDE 84

$\Gamma(\pi^0 2\gamma)/\Gamma(3\pi^0)$ — Γ_4/Γ_3

VALUE (units 10^{-4})	DOCUMENT ID		TECN	COMMENT
7.8±0.7 OUR FIT				
• • • We do not use the following data for averages, fits, limits, etc. • • •				
8.3±2.8±1.4	[1] KNECHT	04	CRYB	$\pi^-p \to n\eta$

[1] Independent analysis of same data as PRAKHOV 05.

$\Gamma(2\pi^0 2\gamma)/\Gamma_{\text{total}}$ — Γ_5/Γ

VALUE	CL%	DOCUMENT ID		TECN	COMMENT
<1.2 × 10^{-3}	90	[1] NEFKENS	05A	CRYB	p(720 MeV/c) $\pi^- \to n\eta$
• • • We do not use the following data for averages, fits, limits, etc. • • •					
<4.0 × 10^{-3}	90	BLIK	07	GAM4	$\pi^-p \to \eta n$

[1] Measurement is done in limited $\gamma\gamma$ energy range.

$\Gamma(4\gamma)/\Gamma_{\text{total}}$ — Γ_6/Γ

VALUE	CL%	DOCUMENT ID		TECN	COMMENT
<2.8 × 10^{-4}	90	BLIK	07	GAM4	$\pi^-p \to \eta n$

Int. J. Mod. Phys. A 2026.41. Downloaded from www.worldscientific.com by LIFORNIA @ BERKELEY on 09/16/26. Re-use and distribution is strictly not permitted, except for Open Access articles.

$\Gamma(\text{invisible})/\Gamma_{\text{total}}$ — Γ_7/Γ

VALUE	CL%	DOCUMENT ID		TECN	COMMENT
$<2.4\times10^{-5}$	90	[1] ABLIKIM	25BS	BES3	$e^+e^-\to J/\psi\to\phi\eta$
• • • We do not use the following data for averages, fits, limits, etc. • • •					
$<1.1\times10^{-4}$	90	[2] ANDREEV	24D	SPEC	$\pi^-+\text{Fe}\to\eta X$

[1] ABLIKIM 25BS result is based on a total of $(8774.0\pm39.4)\times10^6$ J/ψ decays.
[2] ANDREEV 24D result is based on 2.9×10^9 pions on an active dump target.

$\Gamma(\text{invisible})/\Gamma(2\gamma)$ — Γ_7/Γ_2

VALUE	CL%	DOCUMENT ID		TECN	COMMENT
$<2.6\times10^{-4}$	90	[1] ABLIKIM	13	BES3	$J/\psi\to\phi\eta$
• • • We do not use the following data for averages, fits, limits, etc. • • •					
$<1.65\times10^{-3}$	90	[2] ABLIKIM	06Q	BES2	$J/\psi\to\phi\eta$

[1] Based on 225M J/ψ decays.
[2] Based on 58M J/ψ decays.

Charged modes

$\Gamma(\text{charged modes})/\Gamma_{\text{total}}$ — $\Gamma_8/\Gamma=(\Gamma_9+\Gamma_{10}+\Gamma_{11}+\Gamma_{12}+\Gamma_{16})/\Gamma$

VALUE	DOCUMENT ID
0.2805±0.0029 OUR FIT Error includes scale factor of 1.3.	

$\Gamma(\pi^+\pi^-\pi^0)/\Gamma_{\text{total}}$ — Γ_9/Γ

VALUE (units 10^{-2})	EVTS	DOCUMENT ID		TECN	COMMENT
23.02±0.25 OUR FIT Error includes scale factor of 1.2.					
23.04±0.03±0.54	60k	[1] ABLIKIM	21AM	BES3	$J/\psi\to\gamma\eta$
• • • We do not use the following data for averages, fits, limits, etc. • • •					
22.60±0.35±0.29	3915	[2] LOPEZ	07	CLEO	$\psi(2S)\to J/\psi\eta$

[1] ABLIKIM 21AM normalize the branching ratio $(\eta\to\pi^+\pi^-\pi^0)$ to $B(J/\psi\to\gamma\eta)$, which they measured absolutely.
[2] Not independent of other results listed for LOPEZ 07. Assuming decays of $\eta\to\gamma\gamma$, $3\pi^0$, $\pi^+\pi^-\pi^0$, $\pi^+\pi^-\gamma$, and $e^+e^-\gamma$ account for all η decays within a contribution of 0.3% to the systematic error.

$\Gamma(\text{neutral modes})/\Gamma(\pi^+\pi^-\pi^0)$ — $\Gamma_1/\Gamma_9=(\Gamma_2+\Gamma_3+\Gamma_4)/\Gamma_9$

VALUE	EVTS	DOCUMENT ID		TECN
3.13±0.05 OUR FIT Error includes scale factor of 1.3.				
3.26±0.30 OUR AVERAGE				
2.54±1.89	74	KENDALL	74	OSPK
3.4 ±1.1	29	AGUILAR-...	72B	HBC
2.83±0.80	70	[1] BLOODWO...	72B	HBC
3.6 ±0.6	244	FLATTE	67B	HBC
2.89±0.56		ALFF-...	66	HBC
3.6 ±0.8	50	KRAEMER	64	DBC
3.8 ±1.1		PAULI	64	DBC

[1] Error increased from published value 0.5 by Bloodworth (private communication).

$\Gamma(2\gamma)/\Gamma(\pi^+\pi^-\pi^0)$ — Γ_2/Γ_9

VALUE	EVTS	DOCUMENT ID		TECN	COMMENT
1.710±0.025 OUR FIT Error includes scale factor of 1.2.					
1.70 ±0.04 OUR AVERAGE					
1.704±0.032±0.026	3915	[1] LOPEZ	07	CLEO	$\psi(2S)\to J/\psi\eta$
1.61 ±0.14		ABLIKIM	06E	BES2	$e^+e^-\to J/\psi\to\eta\gamma$
1.78 ±0.10 ±0.13	1077	AMSLER	95	CBAR	$\bar{p}p\to\pi^+\pi^-\eta$ at rest
1.72 ±0.25	401	BAGLIN	69	HLBC	
1.61 ±0.39		FOSTER	65	HBC	

[1] LOPEZ 07 reports $\Gamma(\eta\to\pi^+\pi^-\pi^0)/\Gamma(\eta\to2\gamma)=\Gamma_9/\Gamma_2=0.587\pm0.011\pm0.009$.

$\Gamma(3\pi^0)/\Gamma(\pi^+\pi^-\pi^0)$ — Γ_3/Γ_9

VALUE	EVTS	DOCUMENT ID		TECN	COMMENT
1.415±0.023 OUR FIT Error includes scale factor of 1.2.					
1.48 ±0.05 OUR AVERAGE					
1.46 ±0.03 ±0.09		ACHASOV	06A	SND	$e^+e^-\to\eta\gamma$
1.52 ±0.04 ±0.08	23k	[1] AKHMETSHIN	01B	CMD2	$e^+e^-\to\phi\to\eta\gamma$
1.44 ±0.09 ±0.10	1627	AMSLER	95	CBAR	$\bar{p}p\to\pi^+\pi^-\eta$ at rest
$1.50\ ^{+0.15}_{-0.29}$	199	BAGLIN	69	HLBC	
$1.47\ ^{+0.20}_{-0.17}$		BULLOCK	68	HLBC	
• • • We do not use the following data for averages, fits, limits, etc. • • •					
1.3 ±0.4		BAGLIN	67B	HLBC	
0.90 ±0.24		FOSTER	65	HBC	
2.0 ±1.0		FOELSCHE	64	HBC	
0.83 ±0.32		CRAWFORD	63	HBC	

[1] AKHMETSHIN 01B uses results from AKHMETSHIN 99F.

$\Gamma(\pi^+\pi^-\pi^0)/[\Gamma(2\gamma)+\Gamma(3\pi^0)]$ — $\Gamma_9/(\Gamma_2+\Gamma_3)$

VALUE	DOCUMENT ID		TECN	COMMENT
0.320 ±0.005 OUR FIT Error includes scale factor of 1.2.				
0.304 ±0.012	ACHASOV	00D	SND	$e^+e^-\to\phi\to\eta\gamma$
• • • We do not use the following data for averages, fits, limits, etc. • • •				
0.3141±0.0081±0.0058	ACHASOV	00B	SND	See ACHASOV 00D

$\Gamma(\pi^+\pi^-\gamma)/\Gamma_{\text{total}}$ — Γ_{10}/Γ

VALUE (units 10^{-2})	EVTS	DOCUMENT ID		TECN	COMMENT
4.28±0.07 OUR FIT Error includes scale factor of 1.1.					
4.38±0.02±0.10	200k	[1] ABLIKIM	21AM	BES3	$J/\psi\to\gamma\eta$
• • • We do not use the following data for averages, fits, limits, etc. • • •					
3.96±0.14±0.14	859	[2] LOPEZ	07	CLEO	$\psi(2S)\to J/\psi\eta$

[1] ABLIKIM 21AM normalize the branching ratio $(\eta\to\pi^+\pi^-\gamma)$ to $B(J/\psi\to\gamma\eta)$, which they measured absolutely.
[2] Not independent of other results listed for LOPEZ 07. Assuming decays of $\eta\to\gamma\gamma$, $3\pi^0$, $\pi^+\pi^-\pi^0$, $\pi^+\pi^-\gamma$, and $e^+e^-\gamma$ account for all η decays within a contribution of 0.3% to the systematic error.

$\Gamma(\pi^+\pi^-\gamma)/\Gamma(\pi^+\pi^-\pi^0)$ — Γ_{10}/Γ_9

VALUE	EVTS	DOCUMENT ID		TECN	COMMENT
0.1858±0.0025 OUR FIT					
0.1847±0.0030 OUR AVERAGE Error includes scale factor of 1.1.					
0.1856±0.0005±0.0028	200k	BABUSCI	13	KLOE	$e^+e^-\to\phi\to\eta\gamma$
0.175 ±0.007 ±0.006	859	LOPEZ	07	CLEO	$\psi(2S)\to J/\psi\eta$
• • • We do not use the following data for averages, fits, limits, etc. • • •					
0.209 ±0.004	18k	THALER	73	ASPK	
0.201 ±0.006	7250	GORMLEY	70	ASPK	
0.28 ±0.04		BALTAY	67B	DBC	
0.25 ±0.035		LITCHFIELD	67	DBC	
0.30 ±0.06		CRAWFORD	66	HBC	
0.196 ±0.041		FOSTER	65C	HBC	

$\Gamma(e^+e^-\gamma)/\Gamma_{\text{total}}$ — Γ_{11}/Γ

VALUE (units 10^{-3})	EVTS	DOCUMENT ID		TECN	COMMENT
6.96±0.18 OUR FIT					
6.92±0.18 OUR AVERAGE					
6.79±0.05±0.36	21774	ABLIKIM	25CL	BES3	$e^+e^-\to J/\psi\to\gamma\eta'\to\gamma\eta\pi^+\pi^-$
7.07±0.05±0.23	23k	ABLIKIM	24M	BES3	$e^+e^-\to J/\psi\to\gamma\eta/\eta'$
6.6 ±0.4 ±0.4	1345	BERGHAUSER	11	SPEC	$\gamma p\to p\eta$
7.8 ±0.5 ±0.8	435 ± 31	BERLOWSKI	08	WASA	$pd\to{}^3\text{He}\,\eta$
5.15±0.62±0.74	283	ACHASOV	01B	SND	$e^+e^-\to\phi\to\eta\gamma$
7.10±0.64±0.46	323	AKHMETSHIN	01	CMD2	$e^+e^-\to\phi\to\eta\gamma$
• • • We do not use the following data for averages, fits, limits, etc. • • •					
9.4 ±0.7 ±0.5	172	[1] LOPEZ	07	CLEO	$\psi(2S)\to J/\psi\eta$

[1] Not independent of other results listed for LOPEZ 07. Assuming decays of $\eta\to\gamma\gamma$, $3\pi^0$, $\pi^+\pi^-\pi^0$, $\pi^+\pi^-\gamma$, and $e^+e^-\gamma$ account for all η decays within a contribution of 0.3% to the systematic error.

$\Gamma(e^+e^-\gamma)/\Gamma(\pi^+\pi^-\gamma)$ — Γ_{11}/Γ_{10}

VALUE	EVTS	DOCUMENT ID		TECN	COMMENT
0.163±0.005 OUR FIT Error includes scale factor of 1.1.					
0.237±0.021±0.015	172	LOPEZ	07	CLEO	$\psi(2S)\to J/\psi\eta$

$\Gamma(e^+e^-\gamma)/\Gamma(\pi^+\pi^-\pi^0)$ — Γ_{11}/Γ_9

VALUE (units 10^{-2})	EVTS	DOCUMENT ID		TECN	COMMENT
3.02±0.08 OUR FIT Error includes scale factor of 1.1.					
2.1 ±0.5	80	JANE	75B	OSPK	See the erratum

$\Gamma(\text{neutral modes})/[\Gamma(\pi^+\pi^-\pi^0)+\Gamma(\pi^+\pi^-\gamma)+\Gamma(e^+e^-\gamma)]$ — $\Gamma_1/(\Gamma_9+\Gamma_{10}+\Gamma_{11})=(\Gamma_2+\Gamma_3+\Gamma_4)/(\Gamma_9+\Gamma_{10}+\Gamma_{11})$

VALUE	EVTS	DOCUMENT ID		TECN
2.57±0.04 OUR FIT Error includes scale factor of 1.3.				
2.64±0.23		BALTAY	67B	DBC
• • • We do not use the following data for averages, fits, limits, etc. • • •				
4.5 ±1.0	280	[1] JAMES	66	HBC
3.20±1.26	53	[1] BASTIEN	62	HBC
2.5 ±1.0	10	[1] PICKUP	62	HBC

[1] These experiments are not used in the averages as they do not separate clearly $\eta\to\pi^+\pi^-\pi^0$ and $\eta\to\pi^+\pi^-\gamma$ from each other. The reported values thus probably contain some unknown fraction of $\eta\to\pi^+\pi^-\gamma$.

$\Gamma(2\gamma)/[\Gamma(\pi^+\pi^-\pi^0)+\Gamma(\pi^+\pi^-\gamma)+\Gamma(e^+e^-\gamma)]$ — $\Gamma_2/(\Gamma_9+\Gamma_{10}+\Gamma_{11})$

VALUE	EVTS	DOCUMENT ID		TECN
1.406±0.020 OUR FIT Error includes scale factor of 1.2.				
1.1 ±0.4 OUR AVERAGE				
1.51 ±0.93	75	KENDALL	74	OSPK
0.99 ±0.48		CRAWFORD	63	HBC

$\Gamma(\mu^+\mu^-\gamma)/\Gamma_{\text{total}}$ — Γ_{12}/Γ

VALUE (units 10^{-4})	EVTS	DOCUMENT ID		TECN	COMMENT
2.98±0.13 OUR FIT					
2.98±0.13 OUR AVERAGE					
2.97±0.12±0.07	648	ABLIKIM	25CL	BES3	$e^+e^-\to J/\psi\to\gamma\eta'\to\gamma\eta\pi^+\pi^-$
3.1 ±0.4	600	DZHELYADIN	80	SPEC	$\pi^-p\to\eta n$
• • • We do not use the following data for averages, fits, limits, etc. • • •					
1.5 ±0.75	100	BUSHNIN	78	SPEC	See DZHELYADIN 80

Int. J. Mod. Phys. A 2026.41. Downloaded from www.worldscientific.com
by UNIVERSITY OF CALIFORNIA @ BERKELEY on 09/16/26. Re-use and distribution is strictly not permitted, except for Open Access articles.

$\Gamma(e^+e^-)/\Gamma_{total}$ — Γ_{13}/Γ

VALUE	CL%	DOCUMENT ID		TECN	COMMENT
<7 × 10⁻⁷	90	ACHASOV	18B	CNTR	Inverse reaction $e^+e^- \to \eta$
• • • We do not use the following data for averages, fits, limits, etc. • • •					
<2.3 × 10⁻⁶	90	AGAKISHIEV	14		$pp \to \eta + X$
<5.6 × 10⁻⁶	90	[1] AGAKISHIEV	12A	SPEC	$pp \to \eta + X$
<2.7 × 10⁻⁵	90	BERLOWSKI	08	WASA	$pd \to {}^3$He η
<0.77 × 10⁻⁴	90	BROWDER	97B	CLE2	$e^+e^- \simeq 10.5$ GeV
<2 × 10⁻⁴	90	WHITE	96	SPEC	$pd \to \eta\, {}^3$He
<3 × 10⁻⁴	90	DAVIES	74	RVUE	Uses ESTEN 67

[1] AGAKISHIEV 12A uses a data sample of 3.5 GeV proton beam collisions on liquid hydrogen target collected by the HADES detector.

$\Gamma(\mu^+\mu^-)/\Gamma_{total}$ — Γ_{14}/Γ

VALUE (units 10⁻⁶)	CL%	EVTS	DOCUMENT ID		TECN	COMMENT
5.8±0.8 OUR AVERAGE						
5.7±0.7±0.5		114	ABEGG	94	SPEC	$pd \to \eta\, {}^3$He
6.5±2.1		27	DZHELYADIN	80B	SPEC	$\pi^- p \to \eta n$
• • • We do not use the following data for averages, fits, limits, etc. • • •						
$5.6^{+0.6}_{-0.7}$±0.5		100	KESSLER	93	SPEC	See ABEGG 94
< 20	95	0	WEHMANN	68	OSPK	

$\Gamma(\mu^+\mu^-)/\Gamma(2\gamma)$ — Γ_{14}/Γ_2

VALUE (units 10⁻⁵)	DOCUMENT ID		TECN
• • • We do not use the following data for averages, fits, limits, etc. • • •			
5.9±2.2	HYAMS	69	OSPK

$\Gamma(2e^+2e^-)/\Gamma_{total}$ — Γ_{15}/Γ

VALUE (units 10⁻⁵)	CL%	EVTS	DOCUMENT ID		TECN	COMMENT
2.4±0.2±0.1		362	[1] AMBROSINO	11B	KLOE	$e^+e^- \to \phi \to \eta\gamma$
• • • We do not use the following data for averages, fits, limits, etc. • • •						
<9.7	90		BERLOWSKI	08	WASA	$pd \to {}^3$He η
<6.9	90		AKHMETSHIN	01	CMD2	$e^+e^- \to \phi \to \eta\gamma$

[1] This measurement is fully inclusive (includes "$2e^+2e^-\gamma$" channel).

$\Gamma(\pi^+\pi^-e^+e^-(\gamma))/\Gamma_{total}$ — Γ_{16}/Γ

VALUE (units 10⁻⁴)	EVTS	DOCUMENT ID		TECN	COMMENT
2.76±0.16 OUR FIT Error includes scale factor of 1.5.					
2.76±0.16 OUR AVERAGE Error includes scale factor of 1.5.					
3.07±0.12±0.19	680	ABLIKIM	25AV	BES3	10B $e^+e^- \to J/\psi \to \gamma\eta$
2.68±0.09±0.07	1.5k	[1] AMBROSINO	09B	KLOE	$e^+e^- \to \phi \to \eta\gamma$
• • • We do not use the following data for averages, fits, limits, etc. • • •					
$4.3\ ^{+2.0}_{-1.6}$ ±0.4	16	BERLOWSKI	08	WASA	$pd \to {}^3$He η
4.3 ±1.3 ±0.4	16	BARGHOLTZ	07	CNTR	See BERLOWSKI 08
$3.7\ ^{+2.5}_{-1.8}$ ±0.3	4	AKHMETSHIN	01	CMD2	$e^+e^- \to \phi \to \eta\gamma$

[1] This AMBROSINO 09B value includes radiative events.

$\Gamma(e^+e^-\mu^+\mu^-)/\Gamma_{total}$ — Γ_{17}/Γ

VALUE	CL%	DOCUMENT ID		TECN	COMMENT
<6.88 × 10⁻⁶	90	ABLIKIM	25N	BES3	10B $J/\psi \to \gamma\eta$
• • • We do not use the following data for averages, fits, limits, etc. • • •					
<1.6 × 10⁻⁴	90	BERLOWSKI	08	WASA	$pd \to {}^3$Heη

$\Gamma(2\mu^+2\mu^-)/\Gamma(\mu^+\mu^-)$ — Γ_{18}/Γ_{14}

VALUE (units 10⁻⁴)	EVTS	DOCUMENT ID		TECN	COMMENT
8.6±1.4±1.2	49.6	HAYRAPETY...	23A	CMS	pp at 13 TeV

$\Gamma(\mu^+\mu^-\pi^+\pi^-)/\Gamma_{total}$ — Γ_{19}/Γ

VALUE	CL%	DOCUMENT ID		TECN	COMMENT
<4.0 × 10⁻⁷	90	ABLIKIM	25AV	BES3	10B $e^+e^- \to J/\psi \to \gamma\eta$
• • • We do not use the following data for averages, fits, limits, etc. • • •					
<3.6 × 10⁻⁴	90	BERLOWSKI	08	WASA	$pd \to {}^3$He η

$\Gamma(\pi^+e^-\overline{\nu}_e + \text{c.c.})/\Gamma(\pi^+\pi^-\pi^0)$ — Γ_{20}/Γ_9

VALUE	CL%	DOCUMENT ID		TECN	COMMENT
<7.3 × 10⁻⁴	90	ABLIKIM	13G	BES3	$J/\psi \to \phi\eta$

$\Gamma(\pi^+\pi^-2\gamma)/\Gamma(\pi^+\pi^-\pi^0)$ — Γ_{21}/Γ_9

VALUE	CL%	DOCUMENT ID		TECN
< 9 × 10⁻³		PRICE	67	HBC
• • • We do not use the following data for averages, fits, limits, etc. • • •				
<16 × 10⁻³	95	BALTAY	67B	DBC

$\Gamma(\pi^+\pi^-\pi^0\gamma)/\Gamma(\pi^+\pi^-\pi^0)$ — Γ_{22}/Γ_9

VALUE	CL%	EVTS	DOCUMENT ID		TECN
<0.24 × 10⁻²	90	0	THALER	73	ASPK
• • • We do not use the following data for averages, fits, limits, etc. • • •					
<1.7 × 10⁻²	90		ARNOLD	68	HLBC
<1.6 × 10⁻²	95		BALTAY	67B	DBC
<7.0 × 10⁻²			FLATTE	67	HBC
<0.9 × 10⁻²			PRICE	67	HBC

$\Gamma(\pi^0\mu^+\mu^-\gamma)/\Gamma_{total}$ — Γ_{23}/Γ

VALUE	CL%	DOCUMENT ID		TECN	COMMENT
<3 × 10⁻⁶	90	DZHELYADIN	81	SPEC	$\pi^- p \to \eta n$

Forbidden modes

$\Gamma(\pi^0\gamma)/\Gamma_{total}$ — Γ_{24}/Γ

Forbidden by angular momentum conservation.

VALUE	CL%	DOCUMENT ID		TECN	COMMENT
<9 × 10⁻⁵	90	NEFKENS	05A	CRYB	p(720 MeV/c) $\pi^- \to n\eta$

$\Gamma(\pi^+\pi^-)/\Gamma_{total}$ — Γ_{25}/Γ

Forbidden by P and CP invariance.

VALUE	CL%	EVTS	DOCUMENT ID		TECN	COMMENT
< 4.4 × 10⁻⁶	90	83M	[1] BABUSCI	20A	KLOE	$e^+e^- \to \phi \to \eta\gamma$
• • • We do not use the following data for averages, fits, limits, etc. • • •						
< 5.3 × 10⁻¹⁷			[2] ZHEVLAKOV	19	THEO	from nEDM limits
< 1.6 × 10⁻⁵	90	25M	AAIJ	17D	LHCB	in $D \to \pi\pi\pi$ decays
< 3.9 × 10⁻⁴	90	225M	ABLIKIM	11G	BES3	$e^+e^- \to J/\psi \to \eta\gamma$
< 1.3 × 10⁻⁵	90	16M	AMBROSINO	05A	KLOE	$e^+e^- \to \phi \to \eta\gamma$
< 3.3 × 10⁻⁴	90		AKHMETSHIN	99B	CMD2	$e^+e^- \to \phi \to \eta\gamma$
< 9 × 10⁻⁴	90		AKHMETSHIN	97C	CMD2	See AKHMETSHIN 99B
<15 × 10⁻⁴		0	THALER	73	ASPK	

[1] BABUSCI 20A combines new data with the previous AMBROSINO 05A data, and thus supersedes AMBROSINO 05A.
[2] ZHEVLAKOV 19 derives the value from the experimental limits of nEDM by a calculation using an effective Lagrangian.

$\Gamma(2\pi^0)/\Gamma_{total}$ — Γ_{26}/Γ

Forbidden by P and CP invariance.

VALUE	CL%	EVTS	DOCUMENT ID		TECN	COMMENT
<3.5 × 10⁻⁴	90		BLIK	07	GAM4	$\pi^- p \to \eta n$
• • • We do not use the following data for averages, fits, limits, etc. • • •						
<2.7 × 10⁻¹⁷			[1] ZHEVLAKOV	19	THEO	from nEDM limits
<6.9 × 10⁻⁴	90	225M	ABLIKIM	11G	BES3	$e^+e^- \to J/\psi \to \eta\gamma$
<4.3 × 10⁻⁴	90		AKHMETSHIN	99C	CMD2	$e^+e^- \to \phi \to \eta\gamma$
<6 × 10⁻⁴	90		[2] ACHASOV	98	SND	$e^+e^- \to \phi \to \eta\gamma$

[1] ZHEVLAKOV 19 derives the value from the experimental limits of nEDM by a calculation using an effective Lagrangian.
[2] ACHASOV 98 observes one event in a $\pm 3\sigma$ region around the η mass, while a Monte Carlo calculation gives 10 ± 5 events. The limit here is the Poisson upper limit for one observed event and no background.

$\Gamma(2\pi^0\gamma)/\Gamma_{total}$ — Γ_{27}/Γ

Forbidden by C invariance.

VALUE	CL%	DOCUMENT ID		TECN	CHG	COMMENT
< 5 × 10⁻⁴	90	NEFKENS	05	CRYB	0	p(720 MeV/c) $\pi^- \to n\eta$
• • • We do not use the following data for averages, fits, limits, etc. • • •						
<17 × 10⁻⁴	90	BLIK	07	GAM4		$\pi^- p \to \eta n$

$\Gamma(3\pi^0\gamma)/\Gamma_{total}$ — Γ_{28}/Γ

Forbidden by C invariance.

VALUE	CL%	DOCUMENT ID		TECN	CHG	COMMENT
< 6 × 10⁻⁵	90	NEFKENS	05	CRYB	0	p(720 MeV/c) $\pi^- \to n\eta$
• • • We do not use the following data for averages, fits, limits, etc. • • •						
<24 × 10⁻⁵	90	BLIK	07	GAM4		$\pi^- p \to \eta n$

$\Gamma(3\gamma)/\Gamma_{total}$ — Γ_{29}/Γ

Forbidden by C invariance.

VALUE	CL%	DOCUMENT ID		TECN	COMMENT
• • • We do not use the following data for averages, fits, limits, etc. • • •					
<16 × 10⁻⁵	90	BLIK	07	GAM4	$\pi^- p \to \eta n$
< 4 × 10⁻⁵	90	NEFKENS	05A	CRYB	p(720 MeV/c) $\pi^- \to n\eta$

$\Gamma(3\gamma)/\Gamma(2\gamma)$ — Γ_{29}/Γ_2

VALUE	CL%	DOCUMENT ID		TECN	CHG
<1.2 × 10⁻³	95	ALDE	84	GAM2	0

$\Gamma(3\gamma)/\Gamma(3\pi^0)$ — Γ_{29}/Γ_3

VALUE	CL%	DOCUMENT ID		TECN	COMMENT
<4.9 × 10⁻⁵	90	ALOISIO	04	KLOE	$\phi \to \eta\gamma$

$\Gamma(4\pi^0)/\Gamma_{total}$ — Γ_{30}/Γ

Forbidden by P and CP invariance.

VALUE	CL%	DOCUMENT ID		TECN	COMMENT
< 6.9 × 10⁻⁷	90	PRAKHOV	00	CRYB	$\pi^- p \to n\eta$, 720 MeV/c
• • • We do not use the following data for averages, fits, limits, etc. • • •					
<200 × 10⁻⁷	90	BLIK	07	GAM4	$\pi^- p \to \eta n$

$\Gamma(\pi^0e^+e^-)/\Gamma_{total}$ — Γ_{31}/Γ

C parity forbids this to occur as a single-photon process.

VALUE	CL%	DOCUMENT ID		TECN	COMMENT
• • • We do not use the following data for averages, fits, limits, etc. • • •					
< 7.5 × 10⁻⁶	90	ADLARSON	18C	WASA	$pd \to \eta\, {}^3$He
< 1.6 × 10⁻⁴	90	MARTYNOV	76	HLBC	
< 8.4 × 10⁻⁴	90	BAZIN	68	DBC	
<70 × 10⁻⁴		RITTENBERG	65	HBC	

Int. J. Mod. Phys. A 2026.41. Downloaded from www.worldscientific.com by LIFORNIA @ BERKELEY on 09/16/26. Re-use and distribution is strictly not permitted, except for Open Access articles.

$\Gamma(\pi^0 e^+ e^-)/\Gamma(\pi^+\pi^-\pi^0)$ — Γ_{31}/Γ_9

C parity forbids this to occur as a single-photon process.

VALUE	CL%	DOCUMENT ID		TECN	COMMENT
< 3.28×10^{-5}	90	ADLARSON	18C	WASA	$pd \to \eta\, {}^3$He
• • • We do not use the following data for averages, fits, limits, etc. • • •					
< 1.9×10^{-4}	90	JANE	75	OSPK	
< 42×10^{-4}	90	BAGLIN	67	HLBC	
< 16×10^{-4}	90	BILLING	67	HLBC	
< 77×10^{-4}		FOSTER	65B	HBC	
< 110×10^{-4}		PRICE	65	HBC	

$\Gamma(\pi^0\mu^+\mu^-)/\Gamma_{total}$ — Γ_{32}/Γ

C parity forbids this to occur as a single-photon process.

VALUE	CL%	DOCUMENT ID		TECN	COMMENT
< 5×10^{-6}	90	DZHELYADIN	81	SPEC	$\pi^- p \to \eta n$
• • • We do not use the following data for averages, fits, limits, etc. • • •					
$<500 \times 10^{-6}$		WEHMANN	68	OSPK	

$[\Gamma(\mu^+ e^-) + \Gamma(\mu^- e^+)]/\Gamma_{total}$ — Γ_{33}/Γ

Forbidden by lepton family number conservation.

VALUE	CL%	DOCUMENT ID		TECN	COMMENT
$<6 \times 10^{-6}$	90	WHITE	96	SPEC	$pd \to \eta\, {}^3$He

$\Gamma(\pi^+\pi^+ e^- e^- + c.c.)/\Gamma_{total}$ — Γ_{34}/Γ

VALUE	CL%	DOCUMENT ID		TECN	COMMENT
$<4.6 \times 10^{-6}$	90	[1] ABLIKIM	25CA	BES3	$J/\psi \to \phi\eta$

[1] ABLIKIM 25CA determine the upper limit from 0 observed events relative to the $B(\eta \to \gamma\gamma) = (39.36 \pm 0.18)\%$ branching fraction, as this ratio has the smallest uncertainty.

η C-NONCONSERVING DECAY PARAMETERS

$\pi^+\pi^-\pi^0$ LEFT-RIGHT ASYMMETRY PARAMETER

Measurements with an error $> 1.0 \times 10^{-2}$ have been omitted.

VALUE (units 10^{-2})	EVTS	DOCUMENT ID		TECN
$0.09^{+0.11}_{-0.12}$ OUR AVERAGE				
$+0.09 \pm 0.10^{+0.09}_{-0.14}$	1.34M	AMBROSINO	08D	KLOE
0.28 ± 0.26	165k	JANE	74	OSPK
-0.05 ± 0.22	220k	LAYTER	72	ASPK
• • • We do not use the following data for averages, fits, limits, etc. • • •				
1.5 ± 0.5	37k	[1] GORMLEY	68C	ASPK

[1] The GORMLEY 68C asymmetry is probably due to unmeasured ($\mathbf{E} \times \mathbf{B}$) spark chamber effects. New experiments with ($\mathbf{E} \times \mathbf{B}$) controls don't observe an asymmetry.

$\pi^+\pi^-\pi^0$ SEXTANT ASYMMETRY PARAMETER

Measurements with an error $> 2.0 \times 10^{-2}$ have been omitted.

VALUE (units 10^{-2})	EVTS	DOCUMENT ID		TECN
$0.12^{+0.10}_{-0.11}$ OUR AVERAGE				
$+0.08 \pm 0.10^{+0.08}_{-0.13}$	1.34M	AMBROSINO	08D	KLOE
0.20 ± 0.25	165k	JANE	74	OSPK
0.10 ± 0.22	220k	LAYTER	72	ASPK
0.5 ± 0.5	37k	GORMLEY	68C	WIRE

$\pi^+\pi^-\pi^0$ QUADRANT ASYMMETRY PARAMETER

VALUE (units 10^{-2})	EVTS	DOCUMENT ID		TECN
-0.09 ± 0.09 OUR AVERAGE				
$-0.05 \pm 0.10^{+0.03}_{-0.05}$	1.34M	AMBROSINO	08D	KLOE
-0.30 ± 0.25	165k	JANE	74	OSPK
-0.07 ± 0.22	220k	LAYTER	72	ASPK

$\pi^+\pi^-\gamma$ LEFT-RIGHT ASYMMETRY PARAMETER

Measurements with an error $> 2.0 \times 10^{-2}$ have been omitted.

VALUE (units 10^{-2})	EVTS	DOCUMENT ID		TECN
0.9 ± 0.4 OUR AVERAGE				
1.2 ± 0.6	35k	JANE	74B	OSPK
0.5 ± 0.6	36k	THALER	72	ASPK
1.22 ± 1.56	7257	GORMLEY	70	ASPK

$\pi^+\pi^-\gamma$ PARAMETER β (D-wave)

Sensitive to a D-wave contribution: $dN/d\cos\theta = \sin^2\theta\ (1 + \beta\ \cos^2\theta)$.

VALUE	EVTS	DOCUMENT ID		TECN
-0.02 ± 0.07 OUR AVERAGE Error includes scale factor of 1.3.				
0.11 ± 0.11	35k	JANE	74B	OSPK
-0.060 ± 0.065	7250	GORMLEY	70	WIRE
• • • We do not use the following data for averages, fits, limits, etc. • • •				
0.12 ± 0.06		[1] THALER	72	ASPK

[1] The authors don't believe this indicates D-wave because the dependence of β on the γ energy is inconsistent with the theoretical prediction. A $\cos^2\theta$ dependence can also come from P- and F-wave interference.

η CP-NONCONSERVING DECAY PARAMETER

$\pi^+\pi^- e^+ e^-$ DECAY-PLANE ASYMMETRY PARAMETER A_ϕ

In the η rest frame, the total momentum of the e^+e^- pair is equal and opposite to that of the $\pi^+\pi^-$ pair. Let $\hat{z}$ be the unit vector along the momentum of the e^+e^- pair; let $\hat{n}_{ee}$ and $\hat{n}_{\pi\pi}$ be the unit vectors normal to the e^+e^- and $\pi^+\pi^-$ planes; and let ϕ be the angle between the two normals. Then

$$\sin\phi\cos\phi = [(\hat{n}_{ee} \times \hat{n}_{\pi\pi}) \cdot \hat{z}]\ (\hat{n}_{ee} \cdot \hat{n}_{\pi\pi})\ ,$$

and

$$A_\phi \equiv \frac{N_{\sin\phi\cos\phi>0} - N_{\sin\phi\cos\phi<0}}{N_{\sin\phi\cos\phi>0} + N_{\sin\phi\cos\phi<0}}\ .$$

VALUE (units 10^{-2})	EVTS	DOCUMENT ID		TECN	COMMENT
-1.6 ± 2.6 OUR AVERAGE					
$-4.04 \pm 4.69 \pm 0.14$	680	ABLIKIM	25AV	BES3	10B $e^+e^- \to J/\psi \to \eta\gamma$
$-0.6 \pm 2.5 \pm 1.8$	1.5k	AMBROSINO	09B	KLOE	$e^+e^- \to \phi \to \eta\gamma$

ENERGY DEPENDENCE OF $\eta \to 3\pi$ DALITZ PLOTS

PARAMETERS FOR $\eta \to \pi^+\pi^-\pi^0$

See the "Note on η Decay Parameters," page 1454, in our 1994 edition (Physical Review **D50** 1173 (1994)). The following experiments fit to one or more of the coefficients a, b, c, d, e, f or g for $|\text{matrix element}|^2 = 1 + ay + by^2 + cx + dx^2 + exy + fy^3 + gx^2y$.

VALUE	EVTS	DOCUMENT ID		TECN	COMMENT
• • • We do not use the following data for averages, fits, limits, etc. • • •					
	631k	[1] ABLIKIM	23AN	BES3	$J/\psi \to \gamma\eta$
	4.7M	[2] ANASTASI	16A	KLOE	$e^+e^- \to \phi \to \eta\gamma$
	79k	ABLIKIM	15G	BES3	$e^+e^- \to J/\psi \to \gamma\eta$
	174k	ADLARSON	14A	WASA	$pd \to \eta\, {}^3$He
	1.34M	AMBROSINO	08D	KLOE	
	3230	[3] ABELE	98D	CBAR	$\bar{p}p \to \pi^0\pi^0\eta$ at rest
	1077	[4] AMSLER	95	CBAR	$\bar{p}p \to \pi^+\pi^-\eta$ at rest
	81k	LAYTER	73	ASPK	
	220k	LAYTER	72	ASPK	
	1138	CARPENTER	70	HBC	
	349	DANBURG	70	DBC	
	7250	GORMLEY	70	WIRE	
	526	BAGLIN	69	HLBC	
	7170	CNOPS	68	OSPK	
	37k	GORMLEY	68C	WIRE	
	1300	CLPWY	66	HBC	
	705	LARRIBE	66	HBC	

[1] ABLIKIM 23AN fit the Dalitz plot density distribution with two parameter sets (a, b, d, f), and (a, b, d, f, g).
[2] ANASTASI 16A measure the Dalitz parameters a, b, d, f, and g. This is the first measurement of g.
[3] ABELE 98D obtains $a = -1.22 \pm 0.07$ and $b = 0.22 \pm 0.11$ when c (or d) is fixed at 0.06.
[4] AMSLER 95 fits to $(1+ay+by^2)$ and obtains $a = -0.94 \pm 0.15$ and $b = 0.11 \pm 0.27$.

α PARAMETER FOR $\eta \to 3\pi^0$

See the "Note on η Decay Parameters" in our 1994 edition, Phys. Rev. **D50**, 1 August 1994, Part I, p. 1454. The value here is of α in $|\text{matrix element}|^2 = 1 + 2\alpha z$.

VALUE	EVTS	DOCUMENT ID		TECN	COMMENT
-0.0296 ± 0.0016 OUR AVERAGE Error includes scale factor of 1.7. See the ideogram below.					
$-0.0406 \pm 0.0035 \pm 0.0008$	272k	ABLIKIM	23AN	BES3	$J/\psi \to \gamma\eta$
$-0.0265 \pm 0.0010 \pm 0.0009$	7M	PRAKHOV	18	CRYB	$\gamma p \to p\eta$
$-0.055 \pm 0.014 \pm 0.004$	33k	ABLIKIM	15G	BES3	$e^+e^- \to J/\psi \to \gamma\eta$
$-0.0301 \pm 0.0035^{+0.0022}_{-0.0035}$	512k	AMBROSINO	10A	KLOE	$e^+e^- \to \phi \to \eta\gamma$
$-0.027 \pm 0.008 \pm 0.005$	120k	[1] ADOLPH	09	WASA	$pp \to pp\eta$
$-0.0322 \pm 0.0012 \pm 0.0022$	3M	[2] PRAKHOV	09	CRYB	$\gamma p \to p\eta$
$-0.032 \pm 0.002 \pm 0.002$	1.8M	[2] UNVERZAGT	09	CRYB	$\gamma p \to p\eta$
$-0.026 \pm 0.010 \pm 0.010$	75k	BASHKANOV	07	WASA	$pp \to pp\eta$
$-0.010 \pm 0.021 \pm 0.010$	12k	ACHASOV	01C	SND	$e^+e^- \to \phi \to \eta\gamma$
-0.031 ± 0.004	1M	TIPPENS	01	CRYB	$\pi^- p \to n\eta$, 720 MeV
$-0.052 \pm 0.017 \pm 0.010$	98k	ABELE	98C	CBAR	$\bar{p}p \to 5\pi^0$
-0.022 ± 0.023	50k	ALDE	84	GAM2	
• • • We do not use the following data for averages, fits, limits, etc. • • •					
$-0.038 \pm 0.003\ ^{+0.012}_{-0.008}$	1.34M	[3] AMBROSINO	08D	KLOE	
-0.32 ± 0.37	192	BAGLIN	70	HLBC	

[1] This ADOLPH 09 result is independent of the BASHKANOV 07 result.
[2] The PRAKHOV 09 and UNVERZAGT 09 results are independent.
[3] This AMBROSINO 08D value is an indirect result using $\eta \to \pi^+\pi^0\pi^-$ events and a rescattering matrix that mixes isospin decay amplitudes.

Int. J. Mod. Phys. A 2026.41. Downloaded from www.worldscientific.com
by UNIVERSITY OF CALIFORNIA @ BERKELEY on 09/16/26. Re-use and distribution is strictly not permitted, except for Open Access articles.

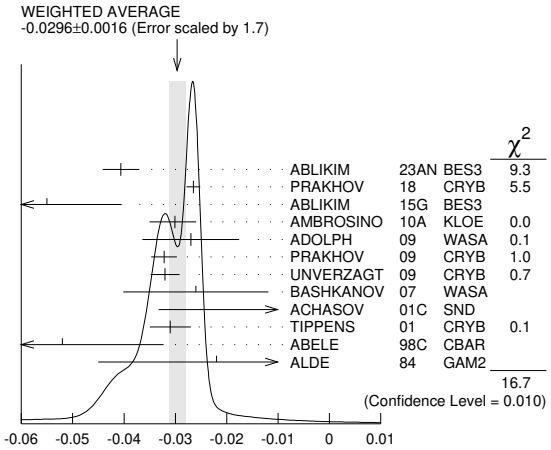

PARAMETER Λ IN $\eta \to \ell^+\ell^-\gamma$ DECAY

In the pole approximation the electromagnetic transition form factor for a resonance of mass M is given by the expression:

$$|F|^2 = (1 - M^2_{\ell\ell}/\Lambda^2)^{-2},$$

where for the parameter Λ vector dominance predicts Λ ≈ 0.770 GeV.

VALUE (GeV/c^2)	EVTS	DOCUMENT ID		TECN	COMMENT
0.731 ±0.013 OUR AVERAGE		Error includes scale factor of 1.3. See the ideogram below.			
0.765 ±0.018	45k	[1] ABLIKIM	25CL	BES3	$e^+e^- \to J/\psi \to \gamma\eta/\eta'$ and $e^+e^- \to J/\psi \to \gamma\eta' \to \gamma\eta\pi^+\pi^-$
0.780 ±0.081	22k	[2] ABLIKIM	25CL	BES3	$e^+e^- \to J/\psi \to \gamma\eta' \to \gamma\eta\pi^+\pi^-$
0.712 ±0.020		[3] ADLARSON	17B	A2MM	$\gamma p \to \eta p$
0.7191±0.0125±0.0093		[4] ARNALDI	16	NA60	400 GeV p-A collisions
0.716 ±0.031 ±0.009		[5] ARNALDI	09	NA60	158A In−In collisions
0.72 ±0.09	600	DZHELYADIN	80	SPEC	$\pi^-p \to \eta n, \eta \to \gamma\mu^+\mu^-$
• • • We do not use the following data for averages, fits, limits, etc. • • •					
0.774 ±0.022	22k	[6] ABLIKIM	25CL	BES3	$e^+e^- \to J/\psi \to \gamma\eta' \to \gamma\eta\pi^+\pi^-$
0.749 ±0.027 ±0.008	23k	ABLIKIM	24M	BES3	$e^+e^- \to J/\psi \to \gamma\eta/\eta'$

[1] ABLIKIM 25CL reports $\Lambda^{-2}(\eta \to \gamma e^+e^-) = 1.707 \pm 0.081$ (GeV/c^2)$^{-2}$ for the combined sample of ABLIKIM 25CL and ABLIKIM 24M, which we converted to the quoted Λ value and uncertainty (total=statistical plus systematic).

[2] ABLIKIM 25CL reports $\Lambda^{-2}(\eta \to \gamma\mu^+\mu^-) = 1.645 \pm 0.343 \pm 0.017$ (GeV/c^2)$^{-2}$ which we converted to the quoted Λ value and uncertainty (total=statistical plus systematic).

[3] ADLARSON 17B reports $\Lambda^{-2}(\eta \to \gamma e^+e^-) = 1.97 \pm 0.11$ (GeV/c^2)$^{-2}$ which we converted to the quoted Λ value and uncertainty (total=statistical plus systematic).

[4] ARNALDI 16 reports $\Lambda^{-2}(\eta \to \gamma\mu^+\mu^-) = 1.934 \pm 0.067 \pm 0.050$ (GeV/c^2)$^{-2}$ which we converted to the quoted Λ value.

[5] ARNALDI 09 reports $\Lambda^{-2}(\eta \to \gamma\mu^+\mu^-) = 1.95 \pm 0.17 \pm 0.05$ (GeV/c^2)$^{-2}$ which we converted to the quoted Λ value.

[6] ABLIKIM 25CL reports $\Lambda^{-2}(\eta \to \gamma e^+e^-) = 1.668 \pm 0.096$ (GeV/c^2)$^{-2}$ which we converted to the quoted Λ value and uncertainty (total=statistical plus systematic).

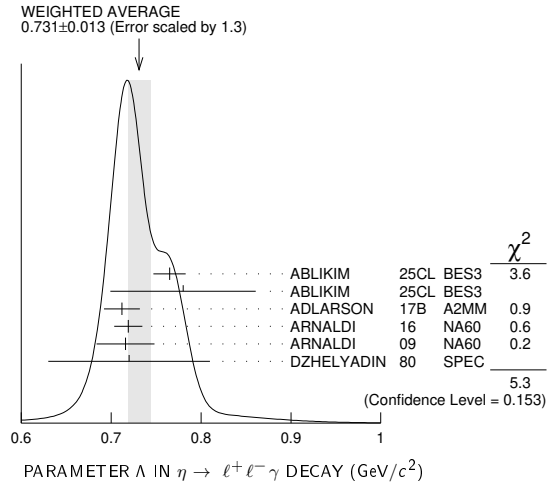

η REFERENCES

ABLIKIM	25AV	PR D111 072008	M. Ablikim *et al.*	(BESIII Collab.)
ABLIKIM	25BS	PRL 135 151804	M. Ablikim *et al.*	(BESIII Collab.)
ABLIKIM	25CA	PR D112 112021	M. Ablikim *et al.*	(BESIII Collab.)
ABLIKIM	25CL	PR D112 052007	M. Ablikim *et al.*	(BESIII Collab.)
ABLIKIM	25N	PR D111 052002	M. Ablikim *et al.*	(BESIII Collab.)
ABLIKIM	24M	PR D109 072001	M. Ablikim *et al.*	(BESIII Collab.)
ANDREEV	24D	PRL 133 121803	Yu.M. Andreev *et al.*	(NA64 Collab.)
ABLIKIM	23AN	PR D107 092007	M. Ablikim *et al.*	(BESIII Collab.)
HAYRAPETY...	23A	PRL 131 091903	A. Hayrapetyan *et al.*	(CMS Collab.)
ABLIKIM	21AM	PR D104 092004	M. Ablikim *et al.*	(BESIII Collab.)
BABUSCI	20A	JHEP 2010 047	D. Babusci *et al.*	(KLOE-2 Collab.)
ZHEVLAKOV	19	PR D99 031703	A.S. Zhevlakov *et al.*	(TMSK, MAINZ, TUBIN+)
ACHASOV	18B	PR D98 052007	M.N. Achasov *et al.*	(SND Collab.)
ADLARSON	18C	PL B784 378	P. Adlarson *et al.*	(WASA-at-COSY Collab.)
PRAKHOV	18	PR C97 065203	S. Prakhov *et al.*	(A2 Collab. at MAMI)
AAIJ	17D	PL B764 233	R. Aaij *et al.*	(LHCb Collab.)
ADLARSON	17B	PR C95 035208	P. Adlarson *et al.*	(A2 Collab. at MAMI)
ANASTASI	16A	JHEP 1605 019	A. Anastasi *et al.*	(KLOE-2 Collab.)
ARNALDI	16	PL B757 437	R. Arnaldi *et al.*	(NA60 Collab.)
ABLIKIM	15G	PR D92 012014	M. Ablikim *et al.*	(BESIII Collab.)
ADLARSON	14A	PR C90 045207	P. Adlarson *et al.*	(WASA-at-COSY Collab.)
AGAKISHIEV	14	PL B731 265	G. Agakishiev *et al.*	(HADES Collab.)
NEFKENS	14	PR C90 025206	B.M.K. Nefkens *et al.*	(A2 Collab. at MAMI)
NIKOLAEV	14	EPJ A50 58	A. Nikolaev *et al.*	(MAMI-B, MAINZ, BONN)
ABLIKIM	13	PR D87 012009	M. Ablikim *et al.*	(BESIII Collab.)
ABLIKIM	13G	PR D87 032006	M. Ablikim *et al.*	(BESIII Collab.)
BABUSCI	13	PL B718 910	D. Babusci *et al.*	(KLOE/KLOE-2 Collab.)
BABUSCI	13A	JHEP 1301 119	D. Babusci *et al.*	(KLOE-2 Collab.)
AGAKISHIEV	12A	EPJ A48 64	G. Agakishiev *et al.*	(HADES Collab.)
GOSLAWSKI	12	PR D85 112011	P. Goslawski *et al.*	(COSY-ANKE Collab.)
ABLIKIM	11G	PR D84 032006	M. Ablikim *et al.*	(BESIII Collab.)
AMBROSINO	11B	PL B702 324	F. Ambrosino *et al.*	(KLOE Collab.)
BERGHAUSER	11	PL B701 562	H. Berghauser *et al.*	(GIES, UCLA, GUTE)
AMBROSINO	10A	PL B694 16	F. Ambrosino *et al.*	(KLOE Collab.)
ADOLPH	09	PL B677 24	C. Adolph *et al.*	(WASA-at-COSY Collab.)
AMBROSINO	09B	PL B675 283	F. Ambrosino *et al.*	(KLOE Collab.)
ARNALDI	09	PL B677 260	R. Arnaldi *et al.*	(NA60 Collab.)
PRAKHOV	09	PR C79 035204	S. Prakhov *et al.*	(MAMI-C Crystal Ball Collab.)
UNVERZAGT	09	EPJ A39 169	M. Unverzagt *et al.*	(MAMI-B Crystal Ball Collab.)
AMBROSINO	08D	JHEP 0805 006	F. Ambrosino *et al.*	(DAPHNE KLOE Collab.)
BERLOWSKI	08	PR D77 032004	M. Berlowski *et al.*	(CELSIUS/WASA Collab.)
PRAKHOV	08	PR C78 015206	S. Prakhov *et al.*	(BNL Crystal Ball Collab.)
RODRIGUES	08	PRL 101 012301	T.E. Rodrigues *et al.*	(USP, FESP, UNESP+)
AMBROSINO	07B	JHEP 0712 073	F. Ambrosino *et al.*	(KLOE Collab.)
BARGHOLTZ	07	PL B644 299	Chr. Bargholtz *et al.*	(CELSIUS/WASA Collab.)
BASHKANOV	07	PR C76 048201	M. Bashkanov *et al.*	(CELSIUS/WASA Collab.)
BLIK	07	PAN 70 693	A.M. Blik *et al.*	(GAMS Collab.)
		Translated from YAF 70 724.		
LOPEZ	07	PRL 99 122001	A. Lopez *et al.*	(CLEO Collab.)
MILLER	07	PRL 99 122002	D.H. Miller *et al.*	(CLEO Collab.)
ABLIKIM	06E	PR D73 052008	M. Ablikim *et al.*	(BES Collab.)
ABLIKIM	06Q	PRL 97 202002	M. Ablikim *et al.*	(BES Collab.)
ACHASOV	06A	PR D74 014016	M.N. Achasov *et al.*	(SND Collab.)
ABDEL-BARY	05	PL B619 281	M. Abdel-Bary *et al.*	(GEM Collab.)
AKHMETSHIN	05	PL B605 26	R.R. Akhmetshin *et al.*	(Novosibirsk CMD-2 Collab.)
AMBROSINO	05A	PL B606 276	F. Ambrosino *et al.*	(KLOE Collab.)
NEFKENS	05	PRL 94 041601	B.M.K. Nefkens *et al.*	(BNL Crystal Ball Collab.)
NEFKENS	05A	PR C72 035212	B.M.K. Nefkens *et al.*	(BNL Crystal Ball Collab.)
PRAKHOV	05	PR C72 025201	S. Prakhov *et al.*	(BNL Crystal Ball Collab.)
ALOISIO	04	PL B591 49	A. Aloisio *et al.*	(KLOE Collab.)
KNECHT	04	PL B589 14	N. Knecht *et al.*	
LAI	02	PL B533 196	A. Lai *et al.*	(CERN NA48 Collab.)
NEFKENS	02	PS T99 114	B.M.K. Nefkens, J.W. Price	(UCLA)
ACHASOV	01B	PL B504 275	M.N. Achasov *et al.*	(Novosibirsk SND Collab.)
ACHASOV	01C	JETPL 73 451	M.N. Achasov *et al.*	(Novosibirsk SND Collab.)
		Translated from ZETFP 73 511.		
ACHASOV	01D	NP B600 3	M.N. Achasov *et al.*	(Novosibirsk SND Collab.)
AKHMETSHIN	01	PL B501 191	R.R. Akhmetshin *et al.*	(Novosibirsk CMD-2 Collab.)
AKHMETSHIN	01B	PL B509 217	R.R. Akhmetshin *et al.*	(Novosibirsk CMD-2 Collab.)
TIPPENS	01	PRL 87 192001	W.B. Tippens *et al.*	(BNL Crystal Ball Collab.)
ACHASOV	00	EPJ C12 25	M.N. Achasov *et al.*	(Novosibirsk SND Collab.)
ACHASOV	00B	JETP 90 17	M.N. Achasov *et al.*	(Novosibirsk SND Collab.)
		Translated from ZETF 117 22.		
ACHASOV	00D	JETPL 72 282	M.N. Achasov *et al.*	(Novosibirsk SND Collab.)
		Translated from ZETFP 72 411.		
PRAKHOV	00	PRL 84 4802	S. Prakhov *et al.*	(BNL Crystal Ball Collab.)
AKHMETSHIN	99B	PL B462 371	R.R. Akhmetshin *et al.*	(Novosibirsk CMD-2 Collab.)
AKHMETSHIN	99C	PL B462 380	R.R. Akhmetshin *et al.*	(Novosibirsk CMD-2 Collab.)
AKHMETSHIN	99F	PL B460 242	R.R. Akhmetshin *et al.*	(Novosibirsk CMD-2 Collab.)
ABELE	98C	PL B417 193	A. Abele *et al.*	(Crystal Barrel Collab.)
ABELE	98D	PL B417 197	A. Abele *et al.*	(Crystal Barrel Collab.)
ACHASOV	98	PL B425 388	M.N. Achasov *et al.*	(Novosibirsk SND Collab.)
AKHMETSHIN	97C	PL B415 452	R.R. Akhmetshin *et al.*	(Novosibirsk CMD-2 Collab.)
BROWDER	97B	PR D56 5359	T.E. Browder *et al.*	(CLEO Collab.)
ABEGG	96	PR D53 11	R. Abegg *et al.*	(Saturne SPES2 Collab.)
WHITE	96	PR D53 6658	D.B. White *et al.*	(Saturne SPES2 Collab.)
AMSLER	95	PL B346 203	C. Amsler *et al.*	(Crystal Barrel Collab.)
KRUSCHE	95D	ZPHY A351 237	B. Krusche *et al.*	(TAPS + A2 Collab.)
ABEGG	94	PR D50 92	R. Abegg *et al.*	(Saturne SPES2 Collab.)
PDG	94	PR D50 1173	L. Montanet *et al.*	(CERN, LBL, BOST+)
AMSLER	93	ZPHY C58 175	C. Amsler *et al.*	(Crystal Barrel Collab.)
KESSLER	93	PRL 70 892	R.S. Kessler *et al.*	(Saturne SPES2 Collab.)
PLOUIN	92	PL B276 526	F. Plouin *et al.*	(Saturne SPES4 Collab.)
BARU	90	ZPHY C48 581	S.E. Baru *et al.*	(MD-1 Collab.)
ROE	90	PR D41 17	N.A. Roe *et al.*	(ASP Collab.)
WILLIAMS	88	PR D38 1365	D.A. Williams *et al.*	(Crystal Ball Collab.)
AIHARA	86	PR D33 844	H. Aihara *et al.*	(TPC-2γ Collab.)
BARTEL	85E	PL 160B 421	W. Bartel *et al.*	(JADE Collab.)
LANDSBERG	85	PRPL 128 301	L.G. Landsberg	(SERP)
ALDE	84	ZPHY C25 225	D.M. Alde *et al.*	(SERP, BELG, LAPP)
Also		SJNP 40 918	D.M. Alde *et al.*	(SERP, BELG, LAPP)
		Translated from YAF 40 1447.		
WEINSTEIN	83	PR D28 2896	A.J. Weinstein *et al.*	(Crystal Ball Collab.)
BINON	82	SJNP 36 391	F.G. Binon *et al.*	(SERP, BELG, LAPP+)
		Translated from YAF 36 670.		
Also		NC 71A 497	F.G. Binon *et al.*	(SERP, BELG, LAPP+)
DAVYDOV	81	LNC 32 45	V.A. Davydov *et al.*	(SERP, BELG, LAPP+)
Also		SJNP 33 825	V.A. Davydov *et al.*	(SERP, BELG, LAPP+)
		Translated from YAF 33 1534.		
DZHELYADIN	81	PL 105B 239	R.I. Dzhelyadin *et al.*	(SERP)
Also		SJNP 33 822	R.I. Dzhelyadin *et al.*	(SERP)
		Translated from YAF 33 1529.		
ABROSIMOV	80	SJNP 31 195	A.T. Abrosimov *et al.*	(JINR)
		Translated from YAF 31 371.		
DZHELYADIN	80	PL 94B 548	R.I. Dzhelyadin *et al.*	(SERP)
Also		SJNP 32 516	R.I. Dzhelyadin *et al.*	(SERP)
		Translated from YAF 32 998.		
DZHELYADIN	80B	PL 97B 471	R.I. Dzhelyadin *et al.*	(SERP)
Also		SJNP 32 518	R.I. Dzhelyadin *et al.*	(SERP)
		Translated from YAF 32 1002.		

Int. J. Mod. Phys. A 2026.41. Downloaded from www.worldscientific.com
by UNIVERSITY OF CALIFORNIA @ BERKELEY on 09/16/26. Re-use and distribution is strictly not permitted, except for Open Access articles.

BUSHNIN	78	PL 79B 147	Y.B. Bushnin *et al.*	(SERP)
Also		SJNP 28 775	Y.B. Bushnin *et al.*	(SERP)
		Translated from YAF 28 1507.		
MARTYNOV	76	SJNP 23 48	A.S. Martynov *et al.*	(JINR)
		Translated from YAF 23 93.		
JANE	75	PL 59B 99	M.R. Jane *et al.*	(RHEL, LOWC)
JANE	75B	PL 59B 103	M.R. Jane *et al.*	(RHEL, LOWC)
Also		PL 73B 503	M.R. Jane	
Erratum in private communication.				
BROWMAN	74B	PRL 32 1067	A. Browman *et al.*	(CORN, BING)
DAVIES	74	NC 24A 324	J.D. Davies, J.G. Guy, R.K.P. Zia	(BIRM, RHEL+)
DUANE	74	PRL 32 425	A. Duane *et al.*	(LOIC, SHMP)
JANE	74	PL 48B 260	M.R. Jane *et al.*	(RHEL, LOWC, SUSS)
JANE	74B	PL 48B 265	M.R. Jane *et al.*	(RHEL, LOWC, SUSS)
KENDALL	74	NC 21A 387	B.N. Kendall *et al.*	(BROW, BARI, MIT)
LAYTER	73	PR D7 2565	J.G. Layter *et al.*	(COLU)
THALER	73	PR D7 2569	J.J. Thaler *et al.*	(COLU)
AGUILAR-...	72B	PR D6 29	M. Aguilar-Benitez *et al.*	(BNL)
BLOODWO...	72B	NP B39 525	I.J. Bloodworth *et al.*	(TNTO)
LAYTER	72	PRL 29 316	J.G. Layter *et al.*	(COLU)
THALER	72	PRL 29 313	J.J. Thaler *et al.*	(COLU)
BASILE	71D	NC 3A 796	M. Basile *et al.*	(CERN, BGNA, STRB)
STRUGALSKI	71	NP B27 429	Z.S. Strugalski *et al.*	(JINR)
BAGLIN	70	NP B22 66	C. Baglin *et al.*	(EPOL, MADR, STRB)
BUTTRAM	70	PRL 25 1358	M.T. Buttram, M.N. Kreisler, R.E. Mischke	(PRIN)
CARPENTER	70	PR D1 1303	D.W. Carpenter *et al.*	(DUKE)
COX	70B	PRL 24 534	B. Cox, L. Fortney, J.P. Golson	(DUKE)
DANBURG	70	PR D2 2564	J.S. Danburg *et al.*	(LRL)
DEVONS	70	PR D1 1936	S. Devons *et al.*	(COLU, SYRA)
GORMLEY	70	PR D2 501	M. Gormley *et al.*	(COLU, BNL)
Also		Thesis Nevis 181	M. Gormley	(COLU)
BAGLIN	69	PL 29B 445	C. Baglin *et al.*	(EPOL, UCB, MADR, STRB)
Also		NP B22 66	C. Baglin *et al.*	(EPOL, MADR, STRB)
HYAMS	69	PL 29B 128	B.D. Hyams *et al.*	(CERN, MPIM)
ARNOLD	68	PL 27B 466	R.G. Arnold *et al.*	(STRB, MADR, EPOL+)
BAZIN	68	PRL 20 895	M.J. Bazin *et al.*	(PRIN, QUKI)
BULLOCK	68	PL 27B 402	F.W. Bullock *et al.*	(LOUC)
CNOPS	68	PRL 21 1609	A.M. Cnops *et al.*	(BNL, ORNL, UCND+)
GORMLEY	68C	PRL 21 402	M. Gormley *et al.*	(COLU, BNL)
WEHMANN	68	PRL 20 748	A.W. Wehmann *et al.*	(HARV, CASE, SLAC+)
BAGLIN	67	PL 24B 637	C. Baglin *et al.*	(EPOL, UCB)
BAGLIN	67B	BAPS 12 567	C. Baglin *et al.*	(EPOL, UCB)
BALTAY	67B	PRL 19 1498	C. Baltay *et al.*	(COLU, STON)
BALTAY	67D	PRL 19 1495	C. Baltay *et al.*	(COLU, BRAN)
BEMPORAD	67	PL 25B 380	C. Bemporad *et al.*	(PISA, BONN)
Also		Private Comm.	I. Ion	
BILLING	67	PL 25B 435	K.D. Billing *et al.*	(LOUC, OXF)
BUNIATOV	67	PL 25B 560	S.A. Bunyatov *et al.*	(CERN, KARL)
CENCE	67	PRL 19 1393	R.J. Cence *et al.*	(HAWA, LRL)
ESTEN	67	PL 24B 115	M.J. Esten *et al.*	(LOUC, OXF)
FELDMAN	67	PRL 18 868	M. Feldman *et al.*	(PENN)
FLATTE	67	PRL 18 976	S.M. Flatte	(LRL)
FLATTE	67B	PR 163 1441	S.M. Flatte, C.G. Wohl	(LRL)
LITCHFIELD	67	PL 24B 486	P.J. Litchfield *et al.*	(RHEL, SACL)
PRICE	67	PRL 18 1207	L.R. Price, F.S. Crawford	(LRL)
ALFF-...	66	PR 145 1072	C. Alff-Steinberger *et al.*	(COLU, RUTG)
CLPWY	66	PR 149 1044	C. Baltay	(SCUC, LRL, PURD, WISC, YALE)
CRAWFORD	66	PRL 16 333	F.S. Crawford, L.R. Price	(LRL)
DIGIUGNO	66	PRL 16 767	G. di Giugno *et al.*	(NAPL, TRST, FRAS)
GRUNHAUS	66	Thesis	J. Grunhaus	(COLU)
JAMES	66	PR 142 896	F.E. James, H.L. Kraybill	(YALE, BNL)
JONES	66	PL 23 597	W.G. Jones *et al.*	(LOIC, RHEL)
LARRIBE	66	PL 23 600	A. Larribe *et al.*	(SACL, RHEL)
FOSTER	65	PR 138 B652	M. Foster *et al.*	(WISC, PURD)
FOSTER	65B	Athens Conf.	M. Foster, M. Good, M. Meer	(WISC)
FOSTER	65C	Thesis	M. Foster	(WISC)
PRICE	65	PRL 15 123	L.R. Price, F.S. Crawford	(LRL)
RITTENBERG	65	PRL 15 556	A. Rittenberg, G.R. Kalbfleisch	(LRL, BNL)
FOELSCHE	64	PR 134 B1138	H.W.J. Foelsche, H.L. Kraybill	(YALE)
KRAEMER	64	PR 136 B496	R.W. Kraemer *et al.*	(JHU, NWES, WOOD)
PAULI	64	PL 13 351	E. Pauli, A. Muller	(SACL)
BACCI	63	PRL 11 37	C. Bacci *et al.*	(ROMA, FRAS)
CRAWFORD	63	PRL 10 546	F.S.Jr. Crawford, L.J. Lloyd, E.C. Fowler	(LRL+)
Also		PRL 16 907	F.S. Crawford, L.J. Lloyd, E.C. Fowler	(LRL+)
ALFF-...	62	PRL 9 322	C. Alff-Steinberger *et al.*	(COLU, RUTG)
BASTIEN	62	PRL 8 114	P.L. Bastien *et al.*	(LRL)
PICKUP	62	PRL 8 329	E. Pickup, D.K. Robinson, E.O. Salant	(CNRC+)

$f_0(500)$

$I^G(J^{PC}) = 0^+(0^{++})$

also known as σ; was $f_0(600)$, $f_0(400–1200)$

See the related review(s):

Scalar Mesons below 1 GeV

$f_0(500)$ T-MATRIX POLE $\sqrt{s}$

Note that $\Gamma = -2\,\mathrm{Im}(\sqrt{s})$.

VALUE (MeV)	*DOCUMENT ID*		*TECN*	*COMMENT*
(400–550)−*i*(200–350) OUR ESTIMATE (see Fig. 64.3 in the review)				
$(458 \pm 7^{+4}_{-10}) - i(245 \pm 6^{+7}_{-10})$	[1] DANILKIN	21	RVUE	Compilation
$(410 \pm 20) - i(240 \pm 15)$	SARANTSEV	21	RVUE	$J/\psi(1S) \to \gamma(\pi\pi, K\overline{K}, \eta\eta, \omega\phi)$
$(512 \pm 15) - i(188 \pm 12)$	[2] ABLIKIM	17	BES3	$J/\psi \to \gamma 3\pi$
$(440 \pm 10) - i(238 \pm 10)$	[3] ALBALADEJO	12	RVUE	Compilation
$(445 \pm 25) - i(278^{+22}_{-18})$	[4,5] GARCIA-MAR..	11	RVUE	Compilation
$(457^{+14}_{-13}) - i(279^{+11}_{-7})$	[4,6] GARCIA-MAR..	11	RVUE	Compilation
$(442^{+5}_{-8}) - i(274^{+6}_{-5})$	[7] MOUSSALLAM	11	RVUE	Compilation
$(452 \pm 13) - i(259 \pm 16)$	[8] MENNESSIER	10	RVUE	Compilation
$(448 \pm 43) - i(266 \pm 43)$	[9] MENNESSIER	10	RVUE	Compilation
$(455 \pm 6^{+31}_{-13}) - i(278 \pm 6^{+34}_{-43})$	[10] CAPRINI	08	RVUE	Compilation
$(463 \pm 6^{+31}_{-17}) - i(259 \pm 6^{+33}_{-34})$	[11] CAPRINI	08	RVUE	Compilation
$(552^{+84}_{-106}) - i(232^{+81}_{-72})$	[12] ABLIKIM	07A	BES2	$\psi(2S) \to \pi^+\pi^- J/\psi$
$(466 \pm 18) - i(223 \pm 28)$	[13] BONVICINI	07	CLEO	$D^+ \to \pi^-\pi^+\pi^+$
$(472 \pm 30) - i(271 \pm 30)$	[14] BUGG	07A	RVUE	Compilation
$(484 \pm 17) - i(255 \pm 10)$	GARCIA-MAR..	07	RVUE	Compilation
$(430) - i(325)$	[15] ANISOVICH	06	RVUE	Compilation
$(441^{+16}_{-8}) - i(272^{+9}_{-12.5})$	[16] CAPRINI	06	RVUE	$\pi\pi \to \pi\pi$
$(470 \pm 50) - i(285 \pm 25)$	[17] ZHOU	05	RVUE	
$(541 \pm 39) - i(252 \pm 42)$	[18] ABLIKIM	04A	BES2	$J/\psi \to \omega\pi^+\pi^-$
$(528 \pm 32) - i(207 \pm 23)$	[19] GALLEGOS	04	RVUE	Compilation
$(533 \pm 25) - i(249 \pm 25)$	[20] BUGG	03	RVUE	
$517 - i240$	BLACK	01	RVUE	$\pi\pi \to \pi\pi$
$(470 \pm 30) - i(295 \pm 20)$	[16] COLANGELO	01	RVUE	$\pi\pi \to \pi\pi$
$(535^{+48}_{-36}) - i(155^{+76}_{-53})$	[21] ISHIDA	01		$\Upsilon(3S) \to \Upsilon\pi\pi$
$610 \pm 14 - i(310 \pm 13)$	[22] SUROVTSEV	01	RVUE	$\pi\pi \to \pi\pi, K\overline{K}$
$(540^{+36}_{-29}) - i(193^{+32}_{-40})$	ISHIDA	00B		$p\overline{p} \to \pi^0\pi^0\pi^0$
$445 - i235$	HANNAH	99	RVUE	π scalar form factor
$(523 \pm 12) - i(259 \pm 7)$	KAMINSKI	99	RVUE	$\pi\pi \to \pi\pi, K\overline{K}, \sigma\sigma$
$442 - i\ 227$	OLLER	99	RVUE	$\pi\pi \to \pi\pi, K\overline{K}$
$469 - i203$	OLLER	99B	RVUE	$\pi\pi \to \pi\pi, K\overline{K}$
$445 - i221$	OLLER	99C	RVUE	$\pi\pi \to \pi\pi, K\overline{K}, \eta\eta$
$420 - i\ 212$	LOCHER	98	RVUE	$\pi\pi \to \pi\pi$, $K\overline{K}$
$440 - i245$	[23] DOBADO	97	RVUE	Compilation
$(602 \pm 26) - i(196 \pm 27)$	[24] ISHIDA	97		$\pi\pi \to \pi\pi$
$(537 \pm 20) - i(250 \pm 17)$	[25] KAMINSKI	97B	RVUE	$\pi\pi \to \pi\pi, K\overline{K}, 4\pi$
$470 - i250$	[26,27] TORNQVIST	96	RVUE	$\pi\pi \to \pi\pi, K\overline{K}, K\pi, \eta\pi$
$387 - i305$	[27,28] JANSSEN	95	RVUE	$\pi\pi \to \pi\pi, K\overline{K}$
$420 - i370$	[29] ACHASOV	94	RVUE	$\pi\pi \to \pi\pi$
$(506 \pm 10) - i(247 \pm 3)$	KAMINSKI	94	RVUE	$\pi\pi \to \pi\pi, K\overline{K}$
$370 - i356$	[30] ZOU	94B	RVUE	$\pi\pi \to \pi\pi, K\overline{K}$
$408 - i342$	[27,30] ZOU	93	RVUE	$\pi\pi \to \pi\pi, K\overline{K}$
$470 - i208$	[31] VANBEVEREN	86	RVUE	$\pi\pi \to \pi\pi, K\overline{K}, \eta\eta, \ldots$
$(750 \pm 50) - i(450 \pm 50)$	[32] ESTABROOKS	79	RVUE	$\pi\pi \to \pi\pi, K\overline{K}$
$(660 \pm 100) - i(320 \pm 70)$	PROTOPOP...	73	HBC	$\pi\pi \to \pi\pi, K\overline{K}$
$650 - i370$	[33] BASDEVANT	72	RVUE	$\pi\pi \to \pi\pi$

[1] Data driven analysis using partial-wave dispersion relations.
[2] S-matrix pole; 8595 events.
[3] Applying the chiral unitary approach at NLO to the K_{e4} data of BATLEY 10 and $\pi N \to \pi\pi N$ data of HYAMS 73, GRAYER 74, and PROTOPOPESCU 73.
[4] Uses the K_{e4} data of BATLEY 10C and the $\pi N \to \pi\pi N$ data of HYAMS 73, GRAYER 74, and PROTOPOPESCU 73.
[5] Analytic continuation using Roy equations.
[6] Analytic continuation using GKPY equations.
[7] Using Roy equations.
[8] Average of three variants of the analytic K-matrix model. Uses the K_{e4} data of BATLEY 08A and the $\pi N \to \pi\pi N$ data of HYAMS 73 and GRAYER 74.
[9] Average of the analyses of three data sets in the K-matrix model. Uses the data of BATLEY 08A, HYAMS 73, and GRAYER 74, partially of COHEN 80 or ETKIN 82B.
[10] From the K_{e4} data of BATLEY 08A and $\pi N \to \pi\pi N$ data of HYAMS 73.
[11] From the K_{e4} data of BATLEY 08A and $\pi N \to \pi\pi N$ data of PROTOPOPESCU 73, GRAYER 74, and ESTABROOKS 74.
[12] From a mean of three different $f_0(500)$ parametrizations. Uses 40k events.
[13] From an isobar model using 2.6k events.
[14] Reanalysis of ABLIKIM 04A, PISLAK 01, and HYAMS 73 data.
[15] Using the N/D method.
[16] From the solution of the Roy equation (ROY 71) for the isoscalar S-wave and using a phase-shift analysis of HYAMS 73 and PROTOPOPESCU 73 data.
[17] Reanalysis of the data from PROTOPOPESCU 73, ESTABROOKS 74, GRAYER 74, ROSSELET 77, PISLAK 03, and AKHMETSHIN 04.
[18] From a mean of six different analyses and $f_0(500)$ parameterizations.
[19] Using data on $\psi(2S) \to J/\psi\pi\pi$ from BAI 00E and on $\Upsilon(nS) \to \Upsilon(mS)\pi\pi$ from BUTLER 94B and ALEXANDER 98.
[20] From a combined analysis of HYAMS 73, AUGUSTIN 89, AITALA 01B, and PISLAK 01.
[21] A similar analysis (KOMADA 01) finds $(580^{+79}_{-30}) - i(190^{+107}_{-49})$ MeV.
[22] Coupled channel reanalysis of BATON 70, BENSINGER 71, BAILLON 72, HYAMS 73, HYAMS 75, ROSSELET 77, COHEN 80, and ETKIN 82B using the uniformizing variable.
[23] Using the inverse amplitude method and data of ESTABROOKS 73, GRAYER 74, and PROTOPOPESCU 73.
[24] Reanalysis of data from HYAMS 73, GRAYER 74, SRINIVASAN 75, and ROSSELET 77 using the interfering amplitude method.
[25] Average and spread of 4 variants ("up" and "down") of KAMINSKI 97B 3-channel model.
[26] Uses data from BEIER 72B, OCHS 73, HYAMS 73, GRAYER 74, ROSSELET 77, CASON 83, ASTON 88, and ARMSTRONG 91B. Coupled channel analysis with flavor symmetry and all light two-pseudoscalars systems.
[27] Demonstrates explicitly that $f_0(500)$ and $f_0(1370)$ are two different poles.
[28] Analysis of data from FALVARD 88.
[29] Analysis of data from OCHS 73, ESTABROOKS 75, ROSSELET 77, and MUKHIN 80.
[30] Analysis of data from OCHS 73, GRAYER 74, and ROSSELET 77.
[31] Coupled-channel analysis using data from PROTOPOPESCU 73, HYAMS 73, HYAMS 75, GRAYER 74, ESTABROOKS 74, ESTABROOKS 75, FROGGATT 77, CORDEN 79, BISWAS 81.
[32] Analysis of data from APEL 72C, GRAYER 74, CASON 76, PAWLICKI 77. Includes spread and errors of 4 solutions.
[33] Analysis of data from BATON 70, BENSINGER 71, COLTON 71, BAILLON 72,PROTOPOPESCU 73, and WALKER 67.

$f_0(500)$ BREIT-WIGNER MASS

VALUE (MeV)	*DOCUMENT ID*		*TECN*	*COMMENT*
400 to 800 OUR ESTIMATE				
• • • We do not use the following data for averages, fits, limits, etc. • • •				
513 ± 32	[34] MURAMATSU	02	CLEO	$e^+e^- \approx 10$ GeV

Int. J. Mod. Phys. A 2026.41. Downloaded from www.worldscientific.com
by UNIVERSITY OF CALIFORNIA @ BERKELEY on 09/16/26. Re-use and distribution is strictly not permitted, except for Open Access articles.

$478^{+24}_{-23}\pm17$		AITALA	01B	E791	$D^+ \to \pi^-\pi^+\pi^+$
563^{+58}_{-29}	[35]	ISHIDA	01		$\Upsilon(3S) \to \Upsilon\pi\pi$
555	[36]	ASNER	00	CLE2	$\tau^- \to \pi^-\pi^0\pi^0\nu_\tau$
540 ± 36		ISHIDA	00B		$p\overline{p} \to \pi^0\pi^0\pi^0$
750 ± 4		ALEKSEEV	99	SPEC	$1.78\ \pi^- p_{\rm polar} \to \pi^-\pi^+ n$
744 ± 5		ALEKSEEV	98	SPEC	$1.78\ \pi^- p_{\rm polar} \to \pi^-\pi^+ n$
759 ± 5	[37]	TROYAN	98		$5.2\ np \to np\pi^+\pi^-$
780 ± 30		ALDE	97	GAM2	$450\ pp \to pp\pi^0\pi^0$
585 ± 20	[38]	ISHIDA	97		$\pi\pi \to \pi\pi$
761 ± 12	[39]	SVEC	96	RVUE	6–$17\ \pi N_{\rm polar} \to \pi^+\pi^- N$
~ 860	[40,41]	TORNQVIST	96	RVUE	$\pi\pi \to \pi\pi$, $K\overline{K}$, $K\pi$, $\eta\pi$
1165 ± 50	[42,43]	ANISOVICH	95	RVUE	$\pi^- p \to \pi^0\pi^0 n$, $\overline{p}p \to \pi^0\pi^0\pi^0$, $\pi^0\pi^0\eta$, $\pi^0\eta\eta$
414 ± 20	[39]	AUGUSTIN	89	DM2	

[34] Statistical uncertainty only.
[35] A similar analysis (KOMADA 01) finds 526^{+48}_{-37} MeV.
[36] From the best fit of the Dalitz plot.
[37] 6σ effect, no PWA.
[38] Reanalysis of data from HYAMS 73, GRAYER 74, SRINIVASAN 75, and ROSSELET 77 using the interfering amplitude method.
[39] Breit-Wigner fit to S-wave intensity measured in $\pi N \to \pi^-\pi^+ N$ on polarized targets. The fit does not include $f_0(980)$.
[40] Uses data from ASTON 88, OCHS 73, HYAMS 73, ARMSTRONG 91B, GRAYER 74, CASON 83, ROSSELET 77, and BEIER 72B. Coupled channel analysis with flavor symmetry and all light two-pseudoscalars systems.
[41] Also observed by ASNER 00 in $\tau^- \to \pi^-\pi^0\pi^0\nu_\tau$ decays.
[42] Uses $\pi^0\pi^0$ data from ANISOVICH 94, AMSLER 94D, and ALDE 95B, $\pi^+\pi^-$ data from OCHS 73, GRAYER 74 and ROSSELET 77, and $\eta\eta$ data from ANISOVICH 94.
[43] The pole is on Sheet III. Demonstrates explicitly that $f_0(500)$ and $f_0(1370)$ are two different poles.

$f_0(500)$ BREIT-WIGNER WIDTH

VALUE (MeV)		DOCUMENT ID		TECN	COMMENT
100 to 800 OUR ESTIMATE					
• • • We do not use the following data for averages, fits, limits, etc. • • •					
335 ± 67	[44]	MURAMATSU	02	CLEO	$e^+e^- \approx 10$ GeV
$324^{+42}_{-40}\pm21$		AITALA	01B	E791	$D^+ \to \pi^-\pi^+\pi^+$
372^{+229}_{-95}	[45]	ISHIDA	01		$\Upsilon(3S) \to \Upsilon\pi\pi$
540	[46]	ASNER	00	CLE2	$\tau^- \to \pi^-\pi^0\pi^0\nu_\tau$
372 ± 80		ISHIDA	00B		$p\overline{p} \to \pi^0\pi^0\pi^0$
119 ± 13		ALEKSEEV	99	SPEC	$1.78\ \pi^- p_{\rm polar} \to \pi^-\pi^+ n$
77 ± 22		ALEKSEEV	98	SPEC	$1.78\ \pi^- p_{\rm polar} \to \pi^-\pi^+ n$
35 ± 12	[47]	TROYAN	98		$5.2\ np \to np\pi^+\pi^-$
780 ± 60		ALDE	97	GAM2	$450\ pp \to pp\pi^0\pi^0$
385 ± 70	[48]	ISHIDA	97		$\pi\pi \to \pi\pi$
290 ± 54	[49]	SVEC	96	RVUE	6–$17\ \pi N_{\rm polar} \to \pi^+\pi^- N$
~ 880	[50,51]	TORNQVIST	96	RVUE	$\pi\pi \to \pi\pi$, $K\overline{K}$, $K\pi$, $\eta\pi$
460 ± 40	[52,53]	ANISOVICH	95	RVUE	$\pi^- p \to \pi^0\pi^0 n$, $\overline{p}p \to \pi^0\pi^0\pi^0$, $\pi^0\pi^0\eta$, $\pi^0\eta\eta$
494 ± 58	[49]	AUGUSTIN	89	DM2	

[44] Statistical uncertainty only.
[45] A similar analysis (KOMADA 01) finds 301^{+145}_{-100} MeV.
[46] From the best fit of the Dalitz plot.
[47] 6σ effect, no PWA.
[48] Reanalysis of data from HYAMS 73, GRAYER 74, SRINIVASAN 75, and ROSSELET 77 using the interfering amplitude method.
[49] Breit-Wigner fit to S-wave intensity measured in $\pi N \to \pi^-\pi^+ N$ on polarized targets. The fit does not include $f_0(980)$.
[50] Uses data from ASTON 88, OCHS 73, HYAMS 73, ARMSTRONG 91B, GRAYER 74, CASON 83, ROSSELET 77, and BEIER 72B. Coupled channel analysis with flavor symmetry and all light two-pseudoscalars systems.
[51] Also observed by ASNER 00 in $\tau^- \to \pi^-\pi^0\pi^0\nu_\tau$ decays.
[52] Uses $\pi^0\pi^0$ data from ANISOVICH 94, AMSLER 94D, and ALDE 95B, $\pi^+\pi^-$ data from OCHS 73, GRAYER 74 and ROSSELET 77, and $\eta\eta$ data from ANISOVICH 94.
[53] The pole is on Sheet III. Demonstrates explicitly that $f_0(500)$ and $f_0(1370)$ are two different poles.

$f_0(500)$ DECAY MODES

	Mode	Fraction (Γ_i/Γ)
Γ_1	$\pi\pi$	seen
Γ_2	$\gamma\gamma$	seen

$f_0(500)$ PARTIAL WIDTHS

$\Gamma(\gamma\gamma)$ Γ_2

VALUE (keV)		DOCUMENT ID		TECN	COMMENT
• • • We do not use the following data for averages, fits, limits, etc. • • •					
$1.37\pm13\ ^{+0.09}_{-0.06}$	[54]	DANILKIN	21	RVUE	Compilation
2.05 ± 0.21	[55]	DAI	14A	RVUE	Compilation
1.7 ± 0.4	[56]	HOFERICHT...	11	RVUE	Compilation
3.08 ± 0.82	[57]	MENNESSIER	11	RVUE	Compilation
$2.08\pm0.2\ ^{+0.07}_{-0.04}$	[58]	MOUSSALLAM	11	RVUE	Compilation
2.08	[59]	MAO	09	RVUE	Compilation
1.2 ± 0.4	[60]	BERNABEU	08	RVUE	
3.9 ± 0.6	[57]	MENNESSIER	08	RVUE	$\gamma\gamma \to \pi^+\pi^-$, $\pi^0\pi^0$
1.8 ± 0.4	[61]	OLLER	08	RVUE	Compilation
1.68 ± 0.15	[61,62]	OLLER	08A	RVUE	Compilation
3.1 ± 0.5	[63,64]	PENNINGTON	08	RVUE	Compilation
2.4 ± 0.4	[64,65]	PENNINGTON	08	RVUE	Compilation
4.1 ± 0.3	[66]	PENNINGTON	06	RVUE	$\gamma\gamma \to \pi^0\pi^0$
3.8 ± 1.5	[67,68]	BOGLIONE	99	RVUE	$\gamma\gamma \to \pi^+\pi^-$, $\pi^0\pi^0$
5.4 ± 2.3	[67]	MORGAN	90	RVUE	$\gamma\gamma \to \pi^+\pi^-$, $\pi^0\pi^0$
10 ± 6		COURAU	86	DM1	$e^+e^- \to \pi^+\pi^-e^+e^-$

[54] Using the value of the coupled channel analysis.
[55] Using dispersive analysis with phases from GARCIA-MARTIN 11A and BUETTIKER 04 as input.
[56] Using Roy-Steiner equations with $\pi\pi$ phase shifts from an update of COLANGELO 01 and from GARCIA-MARTIN 11A.
[57] Using an analytic K-matrix model.
[58] Using dispersion integral with phase input from Roy equations and data from MARSISKE 90, BOYER 90, BEHREND 92, UEHARA 08A, and MORI 07.
[59] Used dispersion theory. The value quoted used the $f_0(500)$ pole position of $457 - i276$ MeV.
[60] Using p, n polarizabilities from PDG 06 and fitting to $\pi\pi$ phase motion from GARCIA-MARTIN 07 and σ-poles from GARCIA-MARTIN 07 and CAPRINI 06.
[61] Using twice-subtracted dispersion integrals.
[62] Supersedes OLLER 08.
[63] Solution A (preferred solution based on χ^2-analysis).
[64] Dispersion theory based amplitude analysis of BOYER 90, MARSISKE 90, BEHREND 92, and MORI 07.
[65] Solution B (worse than solution A; still acceptable when systematic uncertainties are included).
[66] Using unitarity and the σ pole position from CAPRINI 06.
[67] This width could equally well be assigned to the $f_0(1370)$. The authors analyse data from BOYER 90 and MARSISKE 90 and report strong correlation with $\gamma\gamma$ width of $f_2(1270)$.
[68] Supersedes MORGAN 90.

$f_0(500)$ REFERENCES

DANILKIN	21	PR D103 114023	I. Danilkin, O. Deineka, M. Vanderhaeghen	(MAINZ)
SARANTSEV	21	PL B816 136227	A.V. Sarantsev *et al.*	(BONN, PNPI)
ABLIKIM	17	PRL 118 012001	M. Ablikim *et al.*	(BESIII Collab.)
DAI	14A	PR D90 036004	L.-Y. Dai, M.R. Pennington	(CEBAF)
ALBALADEJO	12	PR D86 034003	M. Albaladejo, J.A. Oller	(MURC)
GARCIA-MAR...	11	PRL 107 072001	R. Garcia-Martin *et al.*	(MADR, CRAC)
GARCIA-MAR...	11A	PR D83 074004	R. Garcia-Martin *et al.*	(MADR, CRAC)
HOFERICHT...	11	EPJ C71 1743	M. Hoferichter, D.R. Phillips, C. Schat	(BONN+)
MENNESSIER	11	PL B696 40	G. Mennessier, S. Narison, X.-G. Wang	
MOUSSALLAM	11	EPJ C71 1814	B. Moussallam	
BATLEY	10	PL B686 101	J.R. Batley *et al.*	(CERN NA48/2 Collab.)
BATLEY	10C	EPJ C70 635	J.R. Batley *et al.*	(CERN NA48/2 Collab.)
MENNESSIER	10	PL B688 59	G. Mennessier, S. Narison, X.-G. Wang	
MAO	09	PR D79 116008	Y. Mao *et al.*	
BATLEY	08A	EPJ C54 411	J.R. Batley *et al.*	(CERN NA48/2 Collab.)
BERNABEU	08	PRL 100 241804	J. Bernabeu, J. Prades	(IFIC, GRAN)
CAPRINI	08	PR D77 114019	I. Caprini	
MENNESSIER	08	PL B665 205	G. Mennessier, S. Narison, W. Ochs	
OLLER	08	PL B659 201	J.A. Oller, L. Roca, C. Schat	(MURC, UBA)
OLLER	08A	EPJ A37 15	J.A. Oller, L. Roca	(MURC)
PENNINGTON	08	EPJ C56 1	M.R. Pennington *et al.*	
UEHARA	08A	PR D78 052004	S. Uehara *et al.*	(BELLE Collab.)
ABLIKIM	07A	PL B645 19	M. Ablikim *et al.*	(BES Collab.)
BONVICINI	07	PR D76 012001	G. Bonvicini *et al.*	(CLEO Collab.)
BUGG	07A	JP G34 151	D.V. Bugg *et al.*	
GARCIA-MAR...	07	PR D76 074034	R. Garcia-Martin, J.R. Pelaez, F.J. Yndurain	
MORI	07	PR D75 051101	T. Mori *et al.*	(BELLE Collab.)
ANISOVICH	06	IJMP A21 3615	V.V. Anisovich	
CAPRINI	06	PRL 96 132001	I. Caprini, G. Colangelo, H. Leutwyler	(BCIP+)
PDG	06	JP G33 1	W.-M. Yao *et al.*	(PDG Collab.)
PENNINGTON	06	PRL 97 011601	M.R. Pennington	
ZHOU	05	JHEP 0502 043	Z.Y. Zhou *et al.*	
ABLIKIM	04A	PL B598 149	M. Ablikim *et al.*	(BES Collab.)
AKHMETSHIN	04	PL B578 285	R.R. Akhmetshin *et al.*	(Novosibirsk CMD-2 Collab.)
BUETTIKER	04	EPJ C33 409	P. Buettiker, S. Descotes-Genon, B. Moussallam	
GALLEGOS	04	PR D69 074033	A. Gallegos *et al.*	
BUGG	03	PL B572 1	D.V. Bugg	
PISLAK	03	PR D67 072004	S. Pislak *et al.*	(BNL E865 Collab.)
Also		PR D81 119903E	S. Pislak *et al.*	(BNL E865 Collab.)
MURAMATSU	02	PRL 89 251802	H. Muramatsu *et al.*	(CLEO Collab.)
Also		PRL 90 059901 (errat.)	H. Muramatsu *et al.*	(CLEO Collab.)
AITALA	01B	PRL 86 770	E.M. Aitala *et al.*	(FNAL E791 Collab.)
BLACK	01	PR D64 014031	D. Black *et al.*	
COLANGELO	01	NP B603 125	G. Colangelo, J. Gasser, H. Leytwyler	
ISHIDA	01	PL B518 47	M. Ishida *et al.*	
KOMADA	01	PL B508 31	T. Komada *et al.*	
PISLAK	01	PRL 87 221801	S. Pislak *et al.*	(BNL E865 Collab.)
Also		PR D67 072004	S. Pislak *et al.*	(BNL E865 Collab.)
Also		PRL 105 019901E	S. Pislak *et al.*	(BNL E865 Collab.)
SUROVTSEV	01	PR D63 054024	Y.S. Surovtsev, D. Krupa, M. Nagy	
ASNER	00	PR D61 012002	D.M. Asner *et al.*	(CLEO Collab.)
BAI	00E	PR D62 032002	J. Bai *et al.*	(BES Collab.)
ISHIDA	00B	PTP 104 203	M. Ishida *et al.*	
ALEKSEEV	99	NP B541 3	I.G. Alekseev *et al.*	
BOGLIONE	99	EPJ C9 11	M. Boglione, M.R. Pennington	
HANNAH	99	PR D60 017502	T. Hannah	
KAMINSKI	99	EPJ C9 141	R. Kaminski, L. Lesniak, B. Loiseau	(CRAC, PARIN)
OLLER	99	PR D60 099906 (errat.)	J.A. Oller *et al.*	
OLLER	99B	NP A652 407 (errat.)	J.A. Oller, E. Oset	
OLLER	99C	PR D60 074023	J.A. Oller, E. Oset	
ALEKSEEV	98	PAN 61 174	I.G. Alekseev *et al.*	
ALEXANDER	98	PR D58 052004	J.P. Alexander *et al.*	(CLEO Collab.)
LOCHER	98	EPJ C4 317	M.P. Locher *et al.*	(PSI)
TROYAN	98	JINRRC 5-91 33	Yu. Troyan *et al.*	

ALDE	97	PL B397 350	D.M. Alde *et al.*	(GAMS Collab.)
DOBADO	97	PR D56 3057	A. Dobado, J.R. Pelaez	
ISHIDA	97	PTP 98 1005	S. Ishida *et al.*	(TOKY, MIYA, KEK)
KAMINSKI	97B	PL B413 130	R. Kaminski, L. Lesniak, B. Loiseau	(CRAC, IPN)
Also		PTP 95 745	S. Ishida *et al.*	(TOKY, MIYA, KEK)
SVEC	96	PR D53 2343	M. Svec	(MCGI)
TORNQVIST	96	PRL 76 1575	N.A. Tornqvist, M. Roos	(HELS)
ALDE	95B	ZPHY C66 375	D.M. Alde *et al.*	(GAMS Collab.)
ANISOVICH	95	PL B355 363	V.V. Anisovich *et al.*	(PNPI, SERP)
JANSSEN	95	PR D52 2690	G. Janssen *et al.*	(STON, ADLD, JULI)
ACHASOV	94	PR D49 5779	N.N. Achasov, G.N. Shestakov	(NOVM)
AMSLER	94D	PL B333 277	C. Amsler *et al.*	(Crystal Barrel Collab.)
ANISOVICH	94	PL B323 233	V.V. Anisovich *et al.*	(Crystal Barrel Collab.)
BUTLER	94B	PR D49 40	F. Butler *et al.*	(CLEO Collab.)
KAMINSKI	94	PR D50 3145	R. Kaminski, L. Lesniak, J.P. Maillet	(CRAC+)
ZOU	94B	PR D50 591	B.S. Zou, D.V. Bugg	(LOQM)
ZOU	93	PR D48 3948	B.S. Zou, D.V. Bugg	(LOQM)
BEHREND	92	ZPHY C56 381	H.J. Behrend	(CELLO Collab.)
ARMSTRONG	91B	ZPHY C52 389	T.A. Armstrong *et al.*	(ATHU, BARI, BIRM+)
BOYER	90	PR D42 1350	J. Boyer *et al.*	(Mark II Collab.)
MARSISKE	90	PR D41 3324	H. Marsiske *et al.*	(Crystal Ball Collab.)
MORGAN	90	ZPHY C48 623	D. Morgan, M.R. Pennington	(RAL, DURH)
AUGUSTIN	89	NP B320 1	J.E. Augustin, G. Cosme	(DM2 Collab.)
ASTON	88	NP B296 493	D. Aston *et al.*	(SLAC, NAGO, CINC, INUS)
FALVARD	88	PR D38 2706	A. Falvard *et al.*	(CLER, FRAS, LALO+)
COURAU	86	NP B271 1	A. Courau *et al.*	(CLER, LALO)
VANBEVEREN	86	ZPHY C30 615	E. van Beveren *et al.*	(NIJM, BIEL)
CASON	83	PR D28 1586	N.M. Cason *et al.*	(NDAM, ANL)
ETKIN	82B	PR D25 1786	A. Etkin *et al.*	(BNL, CUNY, TUFTS, VAND)
BISWAS	81	PRL 47 1378	N.N. Biswas *et al.*	(NDAM, ANL)
COHEN	80	PR D22 2595	D. Cohen *et al.*	(ANL) IJP
MUKHIN	80	JETPL 32 601	K.N. Mukhin *et al.*	(KIAE)
		Translated from ZETFP 32 616.		
CORDEN	79	NP B157 250	M.J. Corden *et al.*	(BIRM, RHEL, TELA+) JP
ESTABROOKS	79	PR D19 2678	P. Estabrooks	(CARL)
FROGGATT	77	NP B129 89	C.D. Froggatt, J.L. Petersen	(GLAS, NORD)
PAWLICKI	77	PR D15 3196	A.J. Pawlicki *et al.*	(ANL) IJ
ROSSELET	77	PR D15 574	L. Rosselet *et al.*	(GEVA, SACL)
CASON	76	PRL 36 1485	N.M. Cason *et al.*	(NDAM, ANL) IJ
ESTABROOKS	75	NP B95 322	P.G. Estabrooks, A.D. Martin	(DURH)
HYAMS	75	NP B100 205	B.D. Hyams *et al.*	(CERN, MPIM)
SRINIVASAN	75	PR D12 681	V. Srinivasan *et al.*	(NDAM, ANL)
ESTABROOKS	74	NP B79 301	P.G. Estabrooks, A.D. Martin	(DURH)
GRAYER	74	NP B75 189	G. Grayer *et al.*	(CERN, MPIM)
ESTABROOKS	73	Tallahassee	P.G. Estabrooks *et al.*	(CERN, MPIM)
HYAMS	73	NP B64 134	B.D. Hyams *et al.*	(CERN, MPIM)
OCHS	73	Thesis	W. Ochs	(MPIM, MUNI)
PROTOPOP...	73	PR D7 1279	S.D. Protopopescu *et al.*	(LBL)
APEL	72C	PL 41B 542	W.D. Apel *et al.*	(KARLK, KARLE, PISA)
BAILLON	72	PL 38B 555	P.H. Baillon *et al.*	(SLAC)
BASDEVANT	72	PL 41B 178	J.L. Basdevant, C.D. Froggatt, J.L. Petersen	(CERN)
BEIER	72B	PRL 29 511	E.W. Beier *et al.*	(PENN)
BENSINGER	71	PL 36B 134	J.R. Bensinger *et al.*	(WISC)
COLTON	71	PR D3 2028	E.P. Colton *et al.*	(LBL, FNAL, UCLA+)
ROY	71	PL 36B 353	S.M. Roy	
BATON	70	PL 33B 528	J.P. Baton, G. Laurens, J. Reignier	(SACL)
WALKER	67	RMP 39 695	W.D. Walker	(WISC)

$\rho(770)$

$I^G(J^{PC}) = 1^+(1^{--})$

$\rho(770)$ T-MATRIX POLE $\sqrt{s}$

Note that $\Gamma = -2\,\mathrm{Im}(\sqrt{s})$.

VALUE (MeV)	DOCUMENT ID		TECN	COMMENT
(761–765) − *i* (71–74) OUR ESTIMATE				
$(762.5 \pm 1.7) - i\,(73.2 \pm 1.1)$	[1] HOFERICHT...	24	RVUE	Compilation
$(763.7^{+1.7}_{-1.5}) - i\,(73.2^{+1.0}_{-1.1})$	[2] GARCIA-MAR...	11	RVUE	Compilation
$(754 \pm 18) - i\,(74 \pm 10)$	[3] PELAEZ	04A	RVUE	$\pi\pi \to \pi\pi$
$(762.4 \pm 1.8) - i\,(72.6 \pm 1.4)$	COLANGELO	01	RVUE	$\pi\pi \to \pi\pi$

[1] Update of GARCIA-MARTIN 11 with input for $\pi\pi$ T-matrix from HOFERICHTER 16.
[2] Reanalysis of the K_{e4} data of BATLEY 10C and the $\pi N \to \pi\pi N$ data of HYAMS 73, GRAYER 74, and PROTOPOPESCU 73 using GKPY equations.
[3] Reanalysis of data from PROTOPOPESCU 73, ESTABROOKS 74, GRAYER 74, and COHEN 80 in the unitarized ChPT model.

$\rho(770)$ MASS

We no longer list S-wave Breit-Wigner fits, or data with high combinatorial background.

NEUTRAL ONLY, e^+e^-

VALUE (MeV)	EVTS	DOCUMENT ID		TECN	COMMENT
775.26±0.23 OUR AVERAGE					
775.3 ±0.5 ±0.6		[1] ACHASOV	21	SND	$e^+e^- \to \pi^+\pi^-$
775.02±0.35		[2] LEES	12G	BABR	$e^+e^- \to \pi^+\pi^-\gamma$
775.97±0.46±0.70	900k	[3] AKHMETSHIN	07		$e^+e^- \to \pi^+\pi^-$
774.6 ±0.4 ±0.5	800k	[4,5] ACHASOV	06	SND	$e^+e^- \to \pi^+\pi^-$
775.65±0.64±0.50	114k	[6,7] AKHMETSHIN	04	CMD2	$e^+e^- \to \pi^+\pi^-$
775.9 ±0.5 ±0.5	1.98M	[8] ALOISIO	03	KLOE	$1.02\ e^+e^- \to \pi^+\pi^-\pi^0$
775.8 ±0.9 ±2.0	500k	[8] ACHASOV	02	SND	$1.02\ e^+e^- \to \pi^+\pi^-\pi^0$
775.9 ±1.1		[9] BARKOV	85	OLYA	$e^+e^- \to \pi^+\pi^-$
• • • We do not use the following data for averages, fits, limits, etc. • • •					
775.4 ±0.1	34M	[10] IGNATOV	24	CMD3	$e^+e^- \to \pi^+\pi^-$
763.49±0.53		[11] BARTOS	17	RVUE	$e^+e^- \to \pi^+\pi^-$
758.23±0.46		[12] BARTOS	17A	RVUE	$e^+e^- \to \pi^+\pi^-$
775.8 ±0.5 ±0.3	1.98M	[13] ALOISIO	03	KLOE	$1.02\ e^+e^- \to \pi^+\pi^-\pi^0$
775.9 ±0.6 ±0.5	1.98M	[14] ALOISIO	03	KLOE	$1.02\ e^+e^- \to \pi^+\pi^-\pi^0$
775.0 ±0.6 ±1.1	500k	[15] ACHASOV	02	SND	$1.02\ e^+e^- \to \pi^+\pi^-\pi^0$
775.1 ±0.7 ±5.3		[16] BENAYOUN	98	RVUE	$e^+e^- \to \pi^+\pi^-$, $\mu^+\mu^-$
770.5 ±1.9 ±5.1		[17] GARDNER	98	RVUE	0.28–$0.92\ e^+e^- \to \pi^+\pi^-$
764.1 ±0.7		[18] O'CONNELL	97	RVUE	$e^+e^- \to \pi^+\pi^-$
757.5 ±1.5		[19] BERNICHA	94	RVUE	$e^+e^- \to \pi^+\pi^-$
768 ±1		[20] GESHKEN...	89	RVUE	$e^+e^- \to \pi^+\pi^-$

[1] From a fit of the cross section in the energy range $0.525 < \sqrt{s} < 0.883$ GeV parameterized by the sum of the Breit-Wigner amplitudes for the $\rho(770)$, ω and $\rho(1450)$ resonances.
[2] Using the GOUNARIS 68 parametrization with the complex phase of the $\rho-\omega$ interference and leaving the masses and widths of the $\rho(1450)$, $\rho(1700)$, and $\rho(2150)$ resonances as free parameters of the fit.
[3] A combined fit of AKHMETSHIN 07, AULCHENKO 06, and AULCHENKO 05.
[4] Supersedes ACHASOV 05A.
[5] A fit of the SND data from 400 to 1000 MeV using parameters of the $\rho(1450)$ and $\rho(1700)$ from a fit of the data of BARKOV 85, BISELLO 89 and ANDERSON 00A.
[6] Using the GOUNARIS 68 parametrization with the complex phase of the ρ-ω interference.
[7] Update of AKHMETSHIN 02.
[8] Assuming $m_{\rho^+} = m_{\rho^-}$, $\Gamma_{\rho^+} = \Gamma_{\rho^-}$.
[9] From the GOUNARIS 68 parametrization of the pion form factor.
[10] From a fit of the pion form factor in the energy range $0.32 < \sqrt{s} < 1.2$ GeV using the GOUNARIS 68 parametrization with the complex phase of the $\rho-\omega$ interference with ω and ϕ masses and widths constrained by the values and their errors from PDG 22, and leaving $\rho(1450)$, $\rho(1700)$ resonances as free parameters of the fit. Systematic errors not estimated.
[11] Applies the Unitary & Analytic Model of the pion electromagnetic form factor of DUBNICKA 10 to analyze the data of LEES 12G and ABLIKIM 16C.
[12] Applies the Unitary & Analytic Model of the pion electromagnetic form factor of DUBNICKA 10 to analyze the data of ACHASOV 06, AKHMETSHIN 07, AUBERT 09AS, and AMBROSINO 11A.
[13] Assuming $m_{\rho^+} = m_{\rho^-} = m_{\rho^0}$, $\Gamma_{\rho^+} = \Gamma_{\rho^-} = \Gamma_{\rho^0}$.
[14] Without limitations on masses and widths.
[15] Assuming $m_{\rho^0} = m_{\rho^\pm}$, $g_{\rho^0\pi\pi} = g_{\rho^\pm\pi\pi}$.
[16] Using the data of BARKOV 85 in the hidden local symmetry model.
[17] From the fit to $e^+e^- \to \pi^+\pi^-$ data from the compilations of HEYN 81 and BARKOV 85, including the GOUNARIS 68 parametrization of the pion form factor.
[18] A fit of BARKOV 85 data assuming the direct $\omega\pi\pi$ coupling.
[19] Applying the S-matrix formalism to the BARKOV 85 data.
[20] Includes BARKOV 85 data. Model-dependent width definition.

CHARGED ONLY, τ DECAYS and e^+e^-

VALUE (MeV)	EVTS	DOCUMENT ID		TECN	CHG	COMMENT
775.11±0.34 OUR AVERAGE						
774.6 ±0.2 ±0.5	5.4M	[1,2] FUJIKAWA	08	BELL	±	$\tau^- \to \pi^-\pi^0\nu_\tau$
775.5 ±0.7		[2,3] SCHAEL	05C	ALEP		$\tau^- \to \pi^-\pi^0\nu_\tau$
775.5 ±0.5 ±0.4	1.98M	[4] ALOISIO	03	KLOE		$1.02\ e^+e^- \to \pi^+\pi^-\pi^0$
775.1 ±1.1 ±0.5	87k	[5,6] ANDERSON	00A	CLE2		$\tau^- \to \pi^-\pi^0\nu_\tau$
• • • We do not use the following data for averages, fits, limits, etc. • • •						
761.60±0.95		[7] BARTOS	17A	RVUE		$\tau^- \to \pi^-\pi^0\nu_\tau$
774.8 ±0.6 ±0.4	1.98M	[8] ALOISIO	03	KLOE	−	$1.02\ e^+e^- \to \pi^+\pi^-\pi^0$
776.3 ±0.6 ±0.7	1.98M	[8] ALOISIO	03	KLOE	+	$1.02\ e^+e^- \to \pi^+\pi^-\pi^0$
773.9 ±2.0 $^{+0.3}_{-1.0}$		[9] SANZ-CILLERO	03	RVUE		$\tau^- \to \pi^-\pi^0\nu_\tau$
774.5 ±0.7 ±1.5	500k	[4] ACHASOV	02	SND	±	$1.02\ e^+e^- \to \pi^+\pi^-\pi^0$
775.1 ±0.5		[10] PICH	01	RVUE		$\tau^- \to \pi^-\pi^0\nu_\tau$

[1] $|F_\pi(0)|^2$ fixed to 1.
[2] From the GOUNARIS 68 parametrization of the pion form factor.
[3] The error combines statistical and systematic uncertainties. Supersedes BARATE 97M.
[4] Assuming $m_{\rho^+} = m_{\rho^-}$, $\Gamma_{\rho^+} = \Gamma_{\rho^-}$.
[5] $\rho(1700)$ mass and width fixed at 1700 MeV and 235 MeV respectively.
[6] From the GOUNARIS 68 parametrization of the pion form factor. The second error is a model error taking into account different parametrizations of the pion form factor.
[7] Applies the Unitary & Analytic Model of the pion electromagnetic form factor of DUBNICKA 10 to analyze the data of FUJIKAWA 08.
[8] Without limitations on masses and widths.
[9] Using the data of BARATE 97M and the effective chiral Lagrangian.
[10] From a fit of the model-independent parameterization of the pion form factor to the data of BARATE 97M.

MIXED CHARGES, OTHER REACTIONS

VALUE (MeV)	EVTS	DOCUMENT ID		TECN	CHG	COMMENT
763.0±0.3±1.2	600k	[1] ABELE	99E	CBAR	0±	$0.0\ \bar{p}p \to \pi^+\pi^-\pi^0$

[1] Assuming the equality of ρ^+ and ρ^- masses and widths.

CHARGED ONLY, HADROPRODUCED

VALUE (MeV)	EVTS	DOCUMENT ID		TECN	CHG	COMMENT
766.5±1.1 OUR AVERAGE						
763.7±3.2		ABELE	97	CBAR		$\bar{p}n \to \pi^-\pi^0\pi^0$
768 ±9		AGUILAR-...	91	EHS		$400\ pp$
767 ±3	2935	[1] CAPRARO	87	SPEC	−	$200\ \pi^-\mathrm{Cu} \to \pi^-\pi^0\mathrm{Cu}$
761 ±5	967	[1] CAPRARO	87	SPEC	−	$200\ \pi^-\mathrm{Pb} \to \pi^-\pi^0\mathrm{Pb}$
771 ±4		HUSTON	86	SPEC	+	$202\ \pi^+\mathrm{A} \to \pi^+\pi^0\mathrm{A}$
766 ±7	6500	[2] BYERLY	73	OSPK	−	$5\ \pi^-p$
766.8±1.5	9650	[3] PISUT	68	RVUE	−	1.7–$3.2\ \pi^-p$, $t < 10$
767 ±6	900	[1] EISNER	67	HBC	−	$4.2\ \pi^-p$, $t < 10$

Int. J. Mod. Phys. A 2026.41. Downloaded from www.worldscientific.com
by CALIFORNIA @ BERKELEY on 09/16/26. Re-use and distribution is strictly not permitted, except for Open Access articles.

[1] Mass errors enlarged by us to $\Gamma/\sqrt{N}$; see the note with the $K^*(892)$ mass.
[2] Phase shift analysis. Systematic errors added corresponding to spread of different fits.
[3] From fit of 3-parameter relativistic P-wave Breit-Wigner to total mass distribution. Includes BATON 68, MILLER 67B, ALFF-STEINBERGER 66, HAGOPIAN 66, HAGOPIAN 66B, JACOBS 66B, JAMES 66, WEST 66, BLIEDEN 65 and CARMONY 64.

NEUTRAL ONLY, PHOTOPRODUCED

VALUE (MeV)	EVTS	DOCUMENT ID		TECN	COMMENT
769.6± 0.8 OUR AVERAGE					
774 ± 3		[1] AAIJ	25AG	LHCB	5 TeV PbPb → PbPb$\pi^+\pi^-$
769.5± 1.2±2.0		[2] ACHARYA	20F	ALCE	5 TeV PbPb → PbPb$\pi^+\pi^-$
770.8± 1.3$^{+2.3}_{-2.4}$	900k	ANDREEV	20	H1	$ep \to e\pi^+\pi^- p$
771 ± 2 $^{+2}_{-1}$	63.5k	[3] ABRAMOWICZ	12	ZEUS	$ep \to e\pi^+\pi^- p$
770 ± 2 ±1	79k	[4] BREITWEG	98B	ZEUS	50–100 γp
767.6± 2.7		BARTALUCCI	78	CNTR	$\gamma p \to e^+e^- p$
775 ± 5		GLADDING	73	CNTR	2.9–4.7 γp
767 ± 4	1930	BALLAM	72	HBC	2.8 γp
770 ± 4	2430	BALLAM	72	HBC	4.7 γp
765 ±10		ALVENSLEB...	70	CNTR	γA, $t<0.01$
767.7± 1.9	140k	BIGGS	70	CNTR	<4.1 γC → $\pi^+\pi^-$C
765 ± 5	4000	ASBURY	67B	CNTR	γ + Pb
• • • We do not use the following data for averages, fits, limits, etc. • • •					
773 ± 1		[5] SIRUNYAN	19CS	CMS	5 TeV PbPb → PbPb$\pi^+\pi^-$
776.2± 0.6	384k	[6] ADAMCZYK	17A	STAR	AuAu → AuAu$\pi^+\pi^-$
771 ± 2	79k	[7] BREITWEG	98B	ZEUS	50–100 γp

[1] Using the parametrisation as in ANDREEV 20 with ρ-ω interference with the additional presence of two Breit-Wigner resonances for excited ρ states.
[2] From the parametrization according to SOEDING 66 plus an additional constant term.
[3] Using the KUHN 90 parametrization of the pion form factor, neglecting $\rho-\omega$ interference.
[4] From the parametrization according to SOEDING 66.
[5] Including interference with direct $\pi\pi$ production and ρ-ω interference, statistical error only.
[6] From the parametrization according to SOEDING 66 with an additional relativistic Breit-Wigner component to account for ω photoproduction. Systematic errors not evaluated.
[7] From the parametrization according to ROSS 66.

NEUTRAL ONLY, OTHER REACTIONS

VALUE (MeV)	EVTS	DOCUMENT ID		TECN	COMMENT
769.0 ±0.9 OUR AVERAGE		Error includes scale factor of 1.4.			See the ideogram below.
765 ±6		BERTIN	97C	OBLX	0.0 $\overline{p}p \to \pi^+\pi^-\pi^0$
773 ±1.6		WEIDENAUER	93	ASTE	$\overline{p}p \to \pi^+\pi^-\omega$
762.6 ±2.6		AGUILAR-...	91	EHS	400 pp
770 ±2		[1] HEYN	81	RVUE	Pion form factor
768 ±4		[2,3] BOHACIK	80	RVUE	
769 ±3		[4] WICKLUND	78	ASPK	3,4,6 $\pi^\pm N$
768 ±1	76k	DEUTSCH...	76	HBC	16 $\pi^+ p$
767 ±4	4100	ENGLER	74	DBC	6 $\pi^+ n \to \pi^+\pi^- p$
775 ±4	32k	[2] PROTOPOP...	73	HBC	7.1 $\pi^+ p$, $t<0.4$
764 ±3	6.8k	[5] RATCLIFF	72	ASPK	15 $\pi^- p$, $t<0.3$
774 ±3	1.7k	REYNOLDS	69	HBC	2.26 $\pi^- p$
769.2 ±1.5	13.3k	[6] PISUT	68	RVUE	1.7–3.2 $\pi^- p$, $t<10$
• • • We do not use the following data for averages, fits, limits, etc. • • •					
774.34±0.18±0.35	970k	[7] ABLIKIM	18C	BES3	$\eta'(958) \to \gamma\pi^+\pi^-$
772.93±0.18±0.34	970k	[8] ABLIKIM	18C	BES3	$\eta'(958) \to \gamma\pi^+\pi^-$
773.5 ±2.5		[9] COLANGELO	01	RVUE	$\pi\pi \to \pi\pi$
762.3 ±0.5 ±1.2	600k	[10] ABELE	99E	CBAR	0.0 $\overline{p}p \to \pi^+\pi^-\pi^0$
777 ±2	4.9k	[11] ADAMS	97	E665	470 $\mu p \to \mu XB$
770 ±2		[12] BOGOLYUB...	97	MIRA	32 $\overline{p}p \to \pi^+\pi^-$X
768 ±8		[12] BOGOLYUB...	97	MIRA	32 $pp \to \pi^+\pi^-$X
761.1 ±2.9		DUBNICKA	89	RVUE	π form factor
777.4 ±2.0		[13] CHABAUD	83	ASPK	17 $\pi^- p$ polarized
769.5 ±0.7		[2,3] LANG	79	RVUE	
770 ±9		[3] ESTABROOKS	74	RVUE	17 $\pi^- p \to \pi^+\pi^- n$
773.5 ±1.7	11.2k	[14] JACOBS	72	HBC	2.8 $\pi^- p$
775 ±3	2.2k	[15] HYAMS	68	OSPK	11.2 $\pi^- p$

[1] HEYN 81 includes all spacelike and timelike F_π values until 1978.
[2] From pole extrapolation.
[3] From phase shift analysis of GRAYER 74 data.
[4] Phase shift analysis. Systematic errors added corresponding to spread of different fits.
[5] Published values contain misprints. Corrected by private communication RATCLIFF 74.
[6] Includes MALAMUD 69, ARMENISE 68, BACON 67, HUWE 67, MILLER 67B, ALFF-STEINBERGER 66, HAGOPIAN 66, HAGOPIAN 66B, JACOBS 66B, JAMES 66, WEST 66, GOLDHABER 64, ABOLINS 63.
[7] From a fit to $\pi^+\pi^-$ mass using $\rho(770)$ (parametrized with the Gounaris-Sakurai approach), $\omega(782)$, and box anomaly components.
[8] From a fit to $\pi^+\pi^-$ mass using $\rho(770)$ (parametrized with the Gounaris-Sakurai approach), $\omega(782)$, and $\rho(1450)$ components.
[9] Breit-Wigner mass from a phase-shift analysis of HYAMS 73 and PROTOPOPESCU 73 data.
[10] Using relativistic Breit-Wigner and taking into account ρ-ω interference.
[11] Systematic errors not evaluated.
[12] Systematic effects not studied.
[13] From fit of 3-parameter relativistic Breit-Wigner to helicity-zero part of P-wave intensity. CHABAUD 83 includes data of GRAYER 74.
[14] Mass errors enlarged by us to $\Gamma/\sqrt{N}$; see the note with the $K^*(892)$ mass.
[15] Of HYAMS 68 six parametrizations, this is theoretically soundest. MR

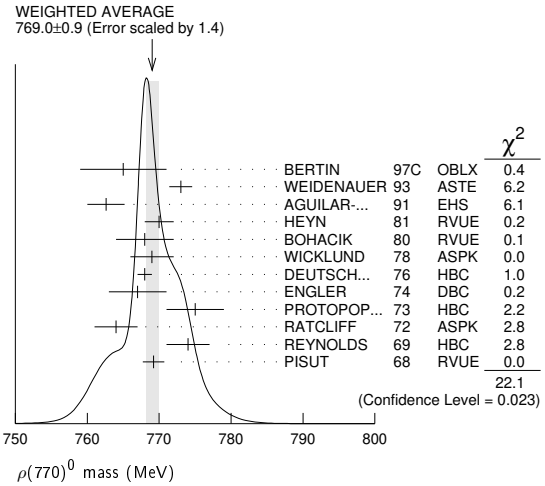

$m_{\rho(770)^0} - m_{\rho(770)^\pm}$

VALUE (MeV)	EVTS	DOCUMENT ID		TECN	CHG	COMMENT
−0.7 ±0.8 OUR AVERAGE		Error includes scale factor of 1.5. See the ideogram below.				
−2.4 ±0.8		[1] SCHAEL	05C	ALEP		$\tau^- \to \pi^-\pi^0\nu_\tau$
0.4 ±0.7 ±0.6	1.98M	[2] ALOISIO	03	KLOE		1.02 $e^+e^- \to \pi^+\pi^-\pi^0$
1.3 ±1.1 ±2.0	500k	[2] ACHASOV	02	SND		1.02 $e^+e^- \to \pi^+\pi^-\pi^0$
1.6 ±0.6 ±1.7	600k	ABELE	99E	CBAR	±0	0.0 $\overline{p}p \to \pi^+\pi^-\pi^0$
−4 ±4	3000	[3] REYNOLDS	69	HBC	−0	2.26 $\pi^- p$
−5 ±5	3600	[3] FOSTER	68	HBC	±0	0.0 $\overline{p}p$
2.4 ±2.1	22950	[4] PISUT	68	RVUE		$\pi N \to \rho N$
• • • We do not use the following data for averages, fits, limits, etc. • • •						
−3.37±1.06		[5] BARTOS	17A	RVUE		$e^+e^- \to \pi^+\pi^-$, $\tau^- \to \pi^-\pi^0\nu_\tau$

[1] From the combined fit of the τ^- data from ANDERSON 00A and SCHAEL 05C and e^+e^- data from the compilation of BARKOV 85, AKHMETSHIN 04, and ALOISIO 05. Supersedes BARATE 97M.
[2] Assuming $m_{\rho^+} = m_{\rho^-}$, $\Gamma_{\rho^+} = \Gamma_{\rho^-}$.
[3] From quoted masses of charged and neutral modes.
[4] Includes MALAMUD 69, ARMENISE 68, BATON 68, BACON 67, HUWE 67, MILLER 67B, ALFF-STEINBERGER 66, HAGOPIAN 66, HAGOPIAN 66B, JACOBS 66B, JAMES 66, WEST 66, BLIEDEN 65, CARMONY 64, GOLDHABER 64, ABOLINS 63.
[5] Applies the Unitary & Analytic Model of the pion electromagnetic form factor of DUBNICKA 10 to analyze the data of ACHASOV 06, AKHMETSHIN 07, AUBERT 09AS, AMBROSINO 11A, and FUJIKAWA 08.

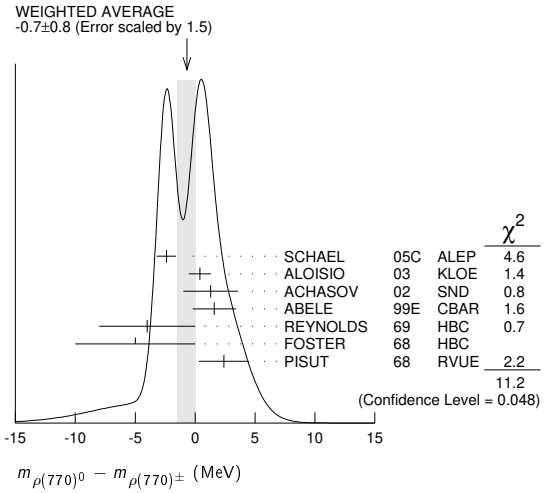

$m_{\rho(770)^+} - m_{\rho(770)^-}$

VALUE (MeV)	EVTS	DOCUMENT ID		TECN	COMMENT
• • • We do not use the following data for averages, fits, limits, etc. • • •					
1.5±0.8±0.7	1.98M	[1] ALOISIO	03	KLOE	1.02 $e^+e^- \to \pi^+\pi^-\pi^0$

[1] Without limitations on masses and widths.

Int. J. Mod. Phys. A 2026.41. Downloaded from www.worldscientific.com
by UNIVERSITY OF CALIFORNIA @ BERKELEY on 09/16/26. Re-use and distribution is strictly not permitted, except for Open Access articles.

Int. J. Mod. Phys. A 2026.41. Downloaded from www.worldscientific.com
by CALIFORNIA @ BERKELEY on 09/16/26. Re-use and distribution is strictly not permitted, except for Open Access articles.

$\rho(770)$ RANGE PARAMETER

The range parameter R enters an energy-dependent correction to the width, of the form $(1 + q_r^2 R^2) / (1 + q^2 R^2)$, where q is the momentum of one of the pions in the $\pi\pi$ rest system. At resonance, $q = q_r$.

VALUE (GeV^{-1})	DOCUMENT ID		TECN	CHG	COMMENT
$5.3^{+0.9}_{-0.7}$	[1] CHABAUD	83	ASPK	0	17 $\pi^- p$ polarized

[1] The old PISUT 68 value, properly corrected, was 3.2 ± 0.6.

$\rho(770)$ WIDTH

We no longer list S-wave Breit-Wigner fits, or data with high combinatorial background.

NEUTRAL ONLY, e^+e^-

VALUE (MeV)	EVTS	DOCUMENT ID		TECN	COMMENT
147.4 ±0.8 OUR AVERAGE		Error includes scale factor of 2.0.			See the ideogram below.
145.6 ±0.6 ±0.8		[1] ACHASOV	21	SND	$e^+e^- \to \pi^+\pi^-$
149.59±0.67		[2] LEES	12G	BABR	$e^+e^- \to \pi^+\pi^-\gamma$
145.98±0.75±0.50	900k	[3] AKHMETSHIN	07		$e^+e^- \to \pi^+\pi^-$
146.1 ±0.8 ±1.5	800k	[4,5] ACHASOV	06	SND	$e^+e^- \to \pi^+\pi^-$
143.85±1.33±0.80	114k	[6,7] AKHMETSHIN	04	CMD2	$e^+e^- \to \pi^+\pi^-$
147.3 ±1.5 ±0.7	1.98M	[8] ALOISIO	03	KLOE	1.02 $e^+e^- \to \pi^+\pi^-\pi^0$
151.1 ±2.6 ±3.0	500k	[8] ACHASOV	02	SND	1.02 $e^+e^- \to \pi^+\pi^-\pi^0$
150.5 ±3.0		[9] BARKOV	85	OLYA	$e^+e^- \to \pi^+\pi^-$
• • • We do not use the following data for averages, fits, limits, etc. • • •					
148.76±0.17	34M	[10] IGNATOV	24	CMD3	$e^+e^- \to \pi^+\pi^-$
144.06±0.85		[11] BARTOS	17	RVUE	$e^+e^- \to \pi^+\pi^-$
144.56±0.80		[12] BARTOS	17A	RVUE	$e^+e^- \to \pi^+\pi^-$
143.9 ±1.3 ±1.1	1.98M	[13] ALOISIO	03	KLOE	1.02 $e^+e^- \to \pi^+\pi^-\pi^0$
147.4 ±1.5 ±0.7	1.98M	[14] ALOISIO	03	KLOE	1.02 $e^+e^- \to \pi^+\pi^-\pi^0$
149.8 ±2.2 ±2.0	500k	[15] ACHASOV	02	SND	1.02 $e^+e^- \to \pi^+\pi^-\pi^0$
147.9 ±1.5 ±7.5		[16] BENAYOUN	98	RVUE	$e^+e^- \to \pi^+\pi^-$, $\mu^+\mu^-$
153.5 ±1.3 ±4.6		[17] GARDNER	98	RVUE	0.28–0.92 $e^+e^- \to \pi^+\pi^-$
145.0 ±1.7		[18] O'CONNELL	97	RVUE	$e^+e^- \to \pi^+\pi^-$
142.5 ±3.5		[19] BERNICHA	94	RVUE	$e^+e^- \to \pi^+\pi^-$
138 ±1		[20] GESHKEN...	89	RVUE	$e^+e^- \to \pi^+\pi^-$

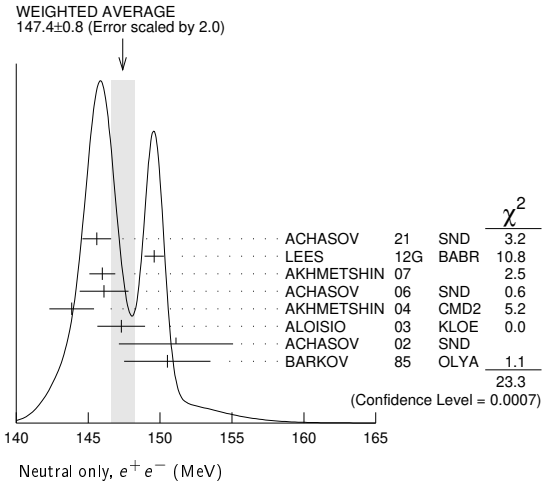

[1] From a fit of the cross section in the energy range $0.525 < \sqrt{s} < 0.883$ GeV parameterized by the sum of the Breit-Wigner amplitudes for the $\rho(770)$, ω and $\rho(1450)$ resonances.
[2] Using the GOUNARIS 68 parametrization with the complex phase of the ρ–ω interference and leaving the masses and widths of the $\rho(1450)$, $\rho(1700)$, and $\rho(2150)$ resonances as free parameters of the fit.
[3] A combined fit of AKHMETSHIN 07, AULCHENKO 06, and AULCHENKO 05.
[4] Supersedes ACHASOV 05A.
[5] A fit of the SND data from 400 to 1000 MeV using parameters of the $\rho(1450)$ and $\rho(1700)$ from a fit of the data of BARKOV 85, BISELLO 89 and ANDERSON 00A.
[6] Using the GOUNARIS 68 parametrization with the complex phase of the ρ–ω interference.
[7] From a fit in the energy range 0.61 to 0.96 GeV. Update of AKHMETSHIN 02.
[8] Assuming $m_{\rho^+} = m_{\rho^-}$, $\Gamma_{\rho^+} = \Gamma_{\rho^-}$.
[9] From the GOUNARIS 68 parametrization of the pion form factor.
[10] From a fit of the pion form factor in the energy range $0.32 < \sqrt{s} < 1.2$ GeV using the GOUNARIS 68 parametrization with the complex phase of the $\rho-\omega$ interference with ω and ϕ masses and widths constrained by the values and their errors from PDG 22, and leaving $\rho(1450)$, $\rho(1700)$ resonances as free parameters of the fit. Systematic errors not estimated.
[11] Applies the Unitary & Analytic Model of the pion electromagnetic form factor of DUBNICKA 10 to analyze the data of LEES 12G and ABLIKIM 16C.
[12] Applies the Unitary & Analytic Model of the pion electromagnetic form factor of DUBNICKA 10 to analyze the data of ACHASOV 06, AKHMETSHIN 07, AUBERT 09AS, and AMBROSINO 11A.
[13] Assuming $m_{\rho^+} = m_{\rho^-} = m_{\rho^0}$, $\Gamma_{\rho^+} = \Gamma_{\rho^-} = \Gamma_{\rho^0}$.
[14] Without limitations on masses and widths.
[15] Assuming $m_{\rho^0} = m_{\rho^\pm}$, $g_{\rho^0\pi\pi} = g_{\rho^\pm\pi\pi}$.
[16] Using the data of BARKOV 85 in the hidden local symmetry model.
[17] From the fit to $e^+e^- \to \pi^+\pi^-$ data from the compilations of HEYN 81 and BARKOV 85, including the GOUNARIS 68 parametrization of the pion form factor.
[18] A fit of BARKOV 85 data assuming the direct $\omega\pi\pi$ coupling.
[19] Applying the S-matrix formalism to the BARKOV 85 data.
[20] Includes BARKOV 85 data. Model-dependent width definition.

CHARGED ONLY, τ DECAYS and e^+e^-

VALUE (MeV)	EVTS	DOCUMENT ID		TECN	CHG	COMMENT
149.1 ±0.8 OUR FIT						
149.1 ±0.8 OUR AVERAGE						
148.1 ±0.4 ±1.7	5.4M	[1,2] FUJIKAWA	08	BELL	±	$\tau^- \to \pi^-\pi^0\nu_\tau$
149.0 ±1.2		[2,3] SCHAEL	05C	ALEP		$\tau^- \to \pi^-\pi^0\nu_\tau$
149.9 ±2.3 ±2.0	500k	[4] ACHASOV	02	SND	±	1.02 $e^+e^- \to \pi^+\pi^-\pi^0$
150.4 ±1.4 ±1.4	87k	[5,6] ANDERSON	00A	CLE2		$\tau^- \to \pi^-\pi^0\nu_\tau$
• • • We do not use the following data for averages, fits, limits, etc. • • •						
139.90±0.46		[7] BARTOS	17A	RVUE		$\tau^- \to \pi^-\pi^0\nu_\tau$
143.7 ±1.3 ±1.2	1.98M	[4] ALOISIO	03	KLOE	±	1.02 $e^+e^- \to \pi^+\pi^-\pi^0$
142.9 ±1.3 ±1.4	1.98M	[8] ALOISIO	03	KLOE	−	1.02 $e^+e^- \to \pi^+\pi^-\pi^0$
144.7 ±1.4 ±1.2	1.98M	[8] ALOISIO	03	KLOE	+	1.02 $e^+e^- \to \pi^+\pi^-\pi^0$
150.2 ±2.0 $^{+0.7}_{-1.6}$		[9] SANZ-CILLERO	03	RVUE		$\tau^- \to \pi^-\pi^0\nu_\tau$
150.9 ±2.2 ±2.0	500k	[10] ACHASOV	02	SND		1.02 $e^+e^- \to \pi^+\pi^-\pi^0$

[1] $|F_\pi(0)|^2$ fixed to 1.
[2] From the GOUNARIS 68 parametrization of the pion form factor.
[3] The error combines statistical and systematic uncertainties. Supersedes BARATE 97M.
[4] Assuming $m_{\rho^+} = m_{\rho^-}$, $\Gamma_{\rho^+} = \Gamma_{\rho^-}$.
[5] $\rho(1700)$ mass and width fixed at 1700 MeV and 235 MeV respectively.
[6] From the GOUNARIS 68 parametrization of the pion form factor. The second error is a model error taking into account different parametrizations of the pion form factor.
[7] Applies the Unitary & Analytic Model of the pion electromagnetic form factor of DUBNICKA 10 to analyze the data of FUJIKAWA 08.
[8] Without limitations on masses and widths.
[9] Using the data of BARATE 97M and the effective chiral Lagrangian.
[10] Assuming $m_{\rho^0} = m_{\rho^\pm}$, $g_{\rho^0\pi\pi} = g_{\rho^\pm\pi\pi}$.

MIXED CHARGES, OTHER REACTIONS

VALUE (MeV)	EVTS	DOCUMENT ID		TECN	CHG	COMMENT
149.5±1.3	600k	[1] ABELE	99E	CBAR	0±	0.0 $\overline{p}p \to \pi^+\pi^-\pi^0$

[1] Assuming the equality of ρ^+ and ρ^- masses and widths.

CHARGED ONLY, HADROPRODUCED

VALUE (MeV)	EVTS	DOCUMENT ID		TECN	CHG	COMMENT
150.2± 2.4 OUR FIT						
150.2± 2.4 OUR AVERAGE						
152.8± 4.3		ABELE	97	CBAR		$\overline{p}n \to \pi^-\pi^0\pi^0$
155 ±11	2.9k	[1] CAPRARO	87	SPEC	−	200 π^-Cu $\to \pi^-\pi^0$Cu
154 ±20	967	[1] CAPRARO	87	SPEC	−	200 π^-Pb $\to \pi^-\pi^0$Pb
150 ± 5		HUSTON	86	SPEC	+	202 π^+A $\to \pi^+\pi^0$A
146 ±12	6.5k	[2] BYERLY	73	OSPK	−	5 π^-p
148.2± 4.1	9.6k	[3] PISUT	68	RVUE	−	1.7–3.2 π^-p, t <10
146 ±13	900	EISNER	67	HBC	−	4.2 π^-p, t <10
• • • We do not use the following data for averages, fits, limits, etc. • • •						
137.0± 0.4		[4] ABLIKIM	17	BES3		$J/\psi \to \gamma 3\pi$

[1] Width errors enlarged by us to $4\Gamma/\sqrt{N}$; see the note with the $K^*(892)$ mass.
[2] Phase shift analysis. Systematic errors added corresponding to spread of different fits.
[3] From fit of 3-parameter relativistic P-wave Breit-Wigner to total mass distribution. Includes BATON 68, MILLER 67B, ALFF-STEINBERGER 66, HAGOPIAN 66, HAGOPIAN 66B, JACOBS 66B, JAMES 66, WEST 66, BLIEDEN 65 and CARMONY 64.
[4] S-matrix pole at a fixed ρ meson mass of 775.49 MeV.

NEUTRAL ONLY, PHOTOPRODUCED

VALUE (MeV)	EVTS	DOCUMENT ID		TECN	COMMENT
152.3± 1.7 OUR AVERAGE					
148 ± 7		[1] AAIJ	25AG	LHCB	5 TeV PbPb $\to$ PbPb$\pi^+\pi^-$
156 ± 2 ± 3		[2] ACHARYA	20F	ALCE	5 TeV PbPb $\to$ PbPb$\pi^+\pi^-$
151.3± 2.2$^{+1.6}_{-2.8}$	900k	ANDREEV	20	H1	$ep \to e\pi^+\pi^-p$
155 ± 5 ± 2	63.5k	[3] ABRAMOWICZ	12	ZEUS	$ep \to e\pi^+\pi^-p$
146 ± 3 ±13	79k	[4] BREITWEG	98B	ZEUS	50–100 γp
150.9± 3.0		BARTALUCCI	78	CNTR	$\gamma p \to e^+e^-p$
• • • We do not use the following data for averages, fits, limits, etc. • • •					
148 ± 3		[5] SIRUNYAN	19CS	CMS	5 TeV PbPb $\to$ PbPb$\pi^+\pi^-$
156 ± 1	384k	[6] ADAMCZYK	17A	STAR	AuAu $\to$ AuAu$\pi^+\pi^-$

Int. J. Mod. Phys. A 2026.41. Downloaded from www.worldscientific.com by UNIVERSITY OF CALIFORNIA @ BERKELEY on 09/16/26. Re-use and distribution is strictly not permitted, except for Open Access articles.

138 ± 3	79k	[7] BREITWEG	98B	ZEUS	50–100 γp
147 ±11		GLADDING	73	CNTR	2.9–4.7 γp
155 ±12	2430	BALLAM	72	HBC	4.7 γp
145 ±13	1930	BALLAM	72	HBC	2.8 γp
140 ± 5		ALVENSLEB...	70	CNTR	γA, t <0.01
146.1± 2.9	140k	BIGGS	70	CNTR	<4.1 γC → $\pi^+\pi^-$C
160 ±10		LANZEROTTI	68	CNTR	γp
130 ± 5	4000	ASBURY	67B	CNTR	γ + Pb

[1] Using the parametrisation as in ANDREEV 20 with ρ-ω interference with the additional presence of two Breit-Wigner resonances for excited ρ states.
[2] From the parametrization according to SOEDING 66 plus an additional constant term.
[3] Using the KUHN 90 parametrization of the pion form factor, neglecting $\rho-\omega$ interference.
[4] From the parametrization according to SOEDING 66.
[5] Including interference with direct $\pi\pi$ production and ρ-ω interference, statistical error only.
[6] From the parametrization according to SOEDING 66 with an additional relativistic Breit-Wigner component to account for ω photoproduction. Systematic errors not evaluated.
[7] From the parametrization according to ROSS 66.

NEUTRAL ONLY, OTHER REACTIONS

VALUE (MeV)	EVTS	DOCUMENT ID		TECN	COMMENT
150.9 ± 1.7 OUR AVERAGE		Error includes scale factor of 1.1.			
122 ±20		BERTIN	97C	OBLX	0.0 $\overline{p}p \to \pi^+\pi^-\pi^0$
145.7 ± 5.3		WEIDENAUER	93	ASTE	$\overline{p}p \to \pi^+\pi^-\omega$
144.9 ± 3.7		DUBNICKA	89	RVUE	π form factor
148 ± 6		[1,2] BOHACIK	80	RVUE	
152 ± 9		[3] WICKLUND	78	ASPK	3,4,6 $\pi^\pm p N$
154 ± 2	76k	DEUTSCH...	76	HBC	16 $\pi^+ p$
157 ± 8	6.8k	[4] RATCLIFF	72	ASPK	15 $\pi^- p$, t <0.3
143 ± 8	1.7k	REYNOLDS	69	HBC	2.26 $\pi^- p$
• • • We do not use the following data for averages, fits, limits, etc. • • •					
150.85± 0.55±0.67	970k	[5] ABLIKIM	18C	BES3	$\eta'(958) \to \gamma\pi^+\pi^-$
150.18± 0.55±0.65	970k	[6] ABLIKIM	18C	BES3	$\eta'(958) \to \gamma\pi^+\pi^-$
147.0 ± 2.5	600k	[7] ABELE	99E	CBAR	0.0 $\overline{p}p \to \pi^+\pi^-\pi^0$
146 ± 3	4.9k	[8] ADAMS	97	E665	470 $\mu p \to \mu XB$
$160.0^{+4.1}_{-4.0}$		[9] CHABAUD	83	ASPK	17 $\pi^- p$ polarized
155 ± 1		[10] HEYN	81	RVUE	π form factor
148.0 ± 1.3		[1,2] LANG	79	RVUE	
146 ±14	4.1k	ENGLER	74	DBC	6 $\pi^+ n \to \pi^+\pi^- p$
143 ±13		[2] ESTABROOKS	74	RVUE	17 $\pi^- p \to \pi^+\pi^- n$
160 ±10	32k	[1] PROTOPOP...	73	HBC	7.1 $\pi^+ p$, t <0.4
145 ±12	2.2k	[3,11] HYAMS	68	OSPK	11.2 $\pi^- p$
163 ±15	13.3k	[12] PISUT	68	RVUE	1.7–3.2 $\pi^- p$, t <10

[1] From pole extrapolation.
[2] From phase shift analysis of GRAYER 74 data.
[3] Width errors enlarged by us to $4\Gamma/\sqrt{N}$; see the note with the $K^*(892)$ mass.
[4] Published values contain misprints. Corrected by private communication RATCLIFF 74.
[5] From a fit to $\pi^+\pi^-$ mass using $\rho(770)$ (parametrized with the Gounaris-Sakurai approach), $\omega(782)$, and box anomaly components.
[6] From a fit to $\pi^+\pi^-$ mass using $\rho(770)$ (parametrized with the Gounaris-Sakurai approach), $\omega(782)$, and $\rho(1450)$ components.
[7] Using relativistic Breit-Wigner and taking into account ρ-ω interference.
[8] Systematic errors not evaluated.
[9] From fit of 3-parameter relativistic Breit-Wigner to helicity-zero part of P-wave intensity. CHABAUD 83 includes data of GRAYER 74.
[10] HEYN 81 includes all spacelike and timelike F_π values until 1978.
[11] Of HYAMS 68 six parametrizations this is theoretically soundest. MR
[12] Includes MALAMUD 69, ARMENISE 68, BACON 67, HUWE 67, MILLER 67B, ALFF-STEINBERGER 66, HAGOPIAN 66, HAGOPIAN 66B, JACOBS 66B, JAMES 66, WEST 66, GOLDHABER 64, ABOLINS 63.

$\Gamma_{\rho(770)^0} - \Gamma_{\rho(770)^\pm}$

VALUE (MeV)	EVTS	DOCUMENT ID		TECN	COMMENT
0.3 ±1.3 OUR AVERAGE		Error includes scale factor of 1.4.			
−0.2 ±1.0		[1] SCHAEL	05C	ALEP	$\tau^- \to \pi^-\pi^0\nu_\tau$
3.6 ±1.8 ±1.7	1.98M	[2] ALOISIO	03	KLOE	1.02 $e^+e^- \to \pi^+\pi^-\pi^0$
• • • We do not use the following data for averages, fits, limits, etc. • • •					
4.66±0.85		[3] BARTOS	17A	RVUE	$e^+e^- \to \pi^+\pi^-$, $\tau^- \to \pi^-\pi^0\nu_\tau$

[1] From the combined fit of the τ^- data from ANDERSON 00A and SCHAEL 05C and e^+e^- data from the compilation of BARKOV 85, AKHMETSHIN 04, and ALOISIO 05. Supersedes BARATE 97M.
[2] Assuming $m_{\rho^+} = m_{\rho^-}$, $\Gamma_{\rho^+} = \Gamma_{\rho^-}$.
[3] Applies the Unitary & Analytic Model of the pion electromagnetic form factor of DUBNICKA 10 to analyze the data of ACHASOV 06, AKHMETSHIN 07, AUBERT 09AS, AMBROSINO 11A, and FUJIKAWA 08.

$\Gamma_{\rho(770)^+} - \Gamma_{\rho(770)^-}$

VALUE	EVTS	DOCUMENT ID		TECN	COMMENT
1.8±2.0±0.5	1.98M	[1] ALOISIO	03	KLOE	1.02 $e^+e^- \to \pi^+\pi^-\pi^0$

[1] Without limitations on masses and widths.

$\rho(770)$ DECAY MODES

	Mode	Fraction (Γ_i/Γ)	Scale factor/ Confidence level
Γ_1	$\pi\pi$	~ 100 %	
	$\rho(770)^\pm$ decays		
Γ_2	$\pi^\pm\pi^0$	~ 100 %	
Γ_3	$\pi^\pm\gamma$	(4.5 ±0.5) × 10^{-4}	S=2.2
Γ_4	$\pi^\pm\eta$	< 6 × 10^{-3}	CL=84%
Γ_5	$\pi^\pm\pi^+\pi^-\pi^0$	< 2.0 × 10^{-3}	CL=84%
	$\rho(770)^0$ decays		
Γ_6	$\pi^+\pi^-$	~ 100 %	
Γ_7	$\pi^+\pi^-\gamma$	(9.9 ±1.6) × 10^{-3}	
Γ_8	$\pi^0\gamma$	(4.7 ±0.8) × 10^{-4}	S=1.7
Γ_9	$\eta\gamma$	(3.00±0.21) × 10^{-4}	
Γ_{10}	$\pi^0\pi^0\gamma$	(4.5 ±0.8) × 10^{-5}	
Γ_{11}	$\mu^+\mu^-$	[a] (4.55±0.28) × 10^{-5}	
Γ_{12}	e^+e^-	[a] (4.72±0.05) × 10^{-5}	
Γ_{13}	$\pi^+\pi^-\pi^0$	(9 ±4) × 10^{-5}	
Γ_{14}	$\pi^+\pi^-\pi^+\pi^-$	(1.8 ±0.9) × 10^{-5}	
Γ_{15}	$\pi^+\pi^-\pi^0\pi^0$	(1.6 ±0.8) × 10^{-5}	
Γ_{16}	$\pi^0 e^+e^-$	< 1.2 × 10^{-5}	CL=90%
Γ_{17}	ηe^+e^-		

[a] The $\omega\rho$ interference is then due to $\omega\rho$ mixing only, and is expected to be small. If $e\mu$ universality holds, $\Gamma(\rho^0 \to \mu^+\mu^-) = \Gamma(\rho^0 \to e^+e^-) \times 0.99785$.

CONSTRAINED FIT INFORMATION

An overall fit to the total width and a partial width uses 10 measurements and one constraint to determine 3 parameters. The overall fit has a $\chi^2 = 10.7$ for 8 degrees of freedom.

The following *off-diagonal* array elements are the correlation coefficients $\langle \delta p_i \delta p_j \rangle / (\delta p_i \cdot \delta p_j)$, in percent, from the fit to parameters p_i, including the branching fractions, $x_i \equiv \Gamma_i/\Gamma_{\rm total}$. The fit constrains the x_i whose labels appear in this array to sum to one.

	x_2	x_3
x_3	−100	
Γ	15	−15

	Mode	Rate (MeV)	Scale factor
Γ_2	$\pi^\pm\pi^0$	150.2 ±2.4	
Γ_3	$\pi^\pm\gamma$	0.068±0.007	2.3

CONSTRAINED FIT INFORMATION

An overall fit to the total width, a partial width, and 7 branching ratios uses 21 measurements and one constraint to determine 9 parameters. The overall fit has a $\chi^2 = 9.5$ for 13 degrees of freedom.

The following *off-diagonal* array elements are the correlation coefficients $\langle \delta p_i \delta p_j \rangle / (\delta p_i \cdot \delta p_j)$, in percent, from the fit to parameters p_i, including the branching fractions, $x_i \equiv \Gamma_i/\Gamma_{\rm total}$. The fit constrains the x_i whose labels appear in this array to sum to one.

	x_6	x_7	x_8	x_9	x_{10}	x_{11}	x_{12}	x_{14}
x_7	−100							
x_8	−5	0						
x_9	−1	0	1					
x_{10}	−1	0	0	0				
x_{11}	2	−3	0	0	0			
x_{12}	0	0	−6	−9	0	0		
x_{14}	−1	0	0	0	0	0	0	
Γ	0	0	3	5	0	0	−54	0

	Mode	Rate (MeV)	Scale factor
Γ_6	$\pi^+\pi^-$	147.5 ±0.9	
Γ_7	$\pi^+\pi^-\gamma$	1.48 ±0.24	
Γ_8	$\pi^0\gamma$	0.070 ±0.012	1.7
Γ_9	$\eta\gamma$	0.0447 ±0.0032	
Γ_{10}	$\pi^0\pi^0\gamma$	0.0066 ±0.0012	
Γ_{11}	$\mu^+\mu^-$	[a] 0.0068 ±0.0004	
Γ_{12}	e^+e^-	[a] 0.00704±0.00006	
Γ_{14}	$\pi^+\pi^-\pi^+\pi^-$	0.0027 ±0.0014	

Int. J. Mod. Phys. A 2026.41. Downloaded from www.worldscientific.com by LIFORNIA @ BERKELEY on 09/16/26. Re-use and distribution is strictly not permitted, except for Open Access articles.

$\rho(770)$ PARTIAL WIDTHS

$\Gamma(\pi^\pm\gamma)$ — Γ_3

VALUE (keV)	DOCUMENT ID		TECN	CHG	COMMENT
68 ±7 OUR FIT Error includes scale factor of 2.3.					
68 ±7 OUR AVERAGE Error includes scale factor of 2.2. See the ideogram below.					
81 ±4 ±4	CAPRARO	87	SPEC	−	200 $\pi^- A \to \pi^- \pi^0 A$
59.8±4.0	HUSTON	86	SPEC	+	202 $\pi^+ A \to \pi^+ \pi^0 A$
71 ±7	JENSEN	83	SPEC	−	156–260 $\pi^- A \to \pi^- \pi^0 A$

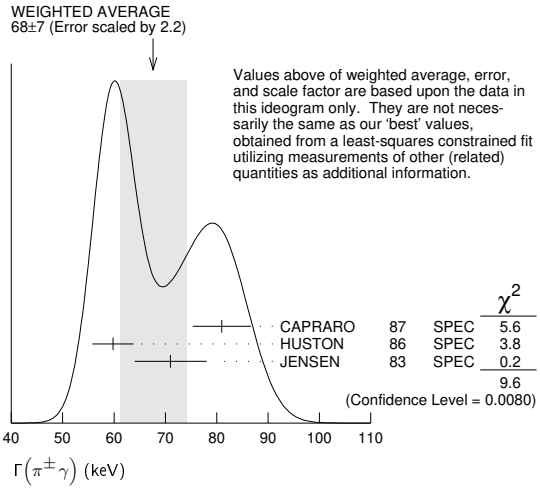

$\Gamma(\pi^0\gamma)$ — Γ_8

VALUE (keV)	EVTS	DOCUMENT ID		TECN	COMMENT
• • • We do not use the following data for averages, fits, limits, etc. • • •					
77±17±11	36500	[1] ACHASOV	03	SND	0.60–0.97 $e^+e^- \to \pi^0\gamma$
121±31		DOLINSKY	89	ND	$e^+e^- \to \pi^0\gamma$

[1] Using Γ_{total}= 147.9 ± 1.3 MeV and B($\rho \to \pi^0\gamma$) from ACHASOV 03.

$\Gamma(\eta\gamma)$ — Γ_9

VALUE (keV)	DOCUMENT ID		TECN	COMMENT
• • • We do not use the following data for averages, fits, limits, etc. • • •				
62±17	[1] DOLINSKY	89	ND	$e^+e^- \to \eta\gamma$

[1] Solution corresponding to constructive ω-ρ interference.

$\Gamma(e^+e^-)$ — Γ_{12}

VALUE (keV)	EVTS	DOCUMENT ID		TECN	COMMENT
7.04 ±0.06 OUR FIT					
7.04 ±0.06 OUR AVERAGE					
7.048±0.057±0.050	900k	[1] AKHMETSHIN	07		$e^+e^- \to \pi^+\pi^-$
7.06 ±0.11 ±0.05	114k	[2,3] AKHMETSHIN	04	CMD2	$e^+e^- \to \pi^+\pi^-$
6.77 ±0.10 ±0.30		BARKOV	85	OLYA	$e^+e^- \to \pi^+\pi^-$
• • • We do not use the following data for averages, fits, limits, etc. • • •					
7.12 ±0.02 ±0.11	800k	[4] ACHASOV	06	SND	$e^+e^- \to \pi^+\pi^-$
6.3 ±0.1		[5] BENAYOUN	98	RVUE	$e^+e^- \to \pi^+\pi^-$, $\mu^+\mu^-$

[1] A combined fit of AKHMETSHIN 07, AULCHENKO 06, and AULCHENKO 05.
[2] Using the GOUNARIS 68 parametrization with the complex phase of the ρ-ω interference.
[3] From a fit in the energy range 0.61 to 0.96 GeV. Update of AKHMETSHIN 02.
[4] Supersedes ACHASOV 05A.
[5] Using the data of BARKOV 85 in the hidden local symmetry model.

$\Gamma(\pi^+\pi^-\pi^+\pi^-)$ — Γ_{14}

VALUE (keV)	EVTS	DOCUMENT ID		TECN	COMMENT
• • • We do not use the following data for averages, fits, limits, etc. • • •					
2.8±1.4±0.5	153	AKHMETSHIN	00	CMD2	0.6–0.97 $e^+e^- \to \pi^+\pi^-\pi^+\pi^-$

$\rho(770)\ \Gamma(e^+e^-)\Gamma(i)/\Gamma^2(total)$

$\Gamma(e^+e^-)/\Gamma_{total} \times \Gamma(\pi^+\pi^-)/\Gamma_{total}$ — $\Gamma_{12}/\Gamma \times \Gamma_6/\Gamma$

VALUE (units 10^{-5})	EVTS	DOCUMENT ID		TECN	COMMENT
4.89 ±0.04 OUR AVERAGE					
4.889±0.015±0.039		[1] ACHASOV	21	SND	$e^+e^- \to \pi^+\pi^-$
4.876±0.023±0.064	800k	[2,3] ACHASOV	06	SND	$e^+e^- \to \pi^+\pi^-$
• • • We do not use the following data for averages, fits, limits, etc. • • •					
4.72 ±0.02		[4] BENAYOUN	10	RVUE	0.4–1.05 e^+e^-

[1] From a fit of the cross section in the energy range $0.525 < \sqrt{s} < 0.883$ GeV parameterized by the sum of the Breit-Wigner amplitudes for the $\rho(770)$, ω and $\rho(1450)$ resonances.
[2] Supersedes ACHASOV 05A.
[3] A fit of the SND data from 400 to 1000 MeV using parameters of the $\rho(1450)$ and $\rho(1700)$ from a fit of the data of BARKOV 85, BISELLO 89 and ANDERSON 00A.
[4] A simultaneous fit of $e^+e^- \to \pi^+\pi^-$, $\pi^+\pi^-\pi^0$, $\pi^0\gamma$, $\eta\gamma$ data.

$\Gamma(e^+e^-)/\Gamma_{total} \times \Gamma(\eta\gamma)/\Gamma_{total}$ — $\Gamma_{12}/\Gamma \times \Gamma_9/\Gamma$

VALUE (units 10^{-8})	EVTS	DOCUMENT ID		TECN	COMMENT
1.42±0.10 OUR FIT					
1.45±0.12 OUR AVERAGE					
1.32±0.14±0.08	33k	[1] ACHASOV	07B	SND	0.6–1.38 $e^+e^- \to \eta\gamma$
1.50±0.65±0.09	17.4k	[2] AKHMETSHIN	05	CMD2	0.60-1.38 $e^+e^- \to \eta\gamma$
1.61±0.20±0.11	23k	[3,4] AKHMETSHIN	01B	CMD2	$e^+e^- \to \eta\gamma$
1.85±0.49		[5] DOLINSKY	89	ND	$e^+e^- \to \eta\gamma$
• • • We do not use the following data for averages, fits, limits, etc. • • •					
1.05±0.02		[6] BENAYOUN	10	RVUE	0.4–1.05 e^+e^-

[1] From a combined fit of $\sigma(e^+e^- \to \eta\gamma)$ with $\eta \to 3\pi^0$ and $\eta \to \pi^+\pi^-\pi^0$, and fixing B($\eta \to 3\pi^0$) / B($\eta \to \pi^+\pi^-\pi^0$) = 1.44 ± 0.04. Recalculated by us from the cross section at the peak. Supersedes ACHASOV 00D and ACHASOV 06A.
[2] From the $\eta \to 2\gamma$ decay and using B($\eta \to \gamma\gamma$)= 39.43 ± 0.26%.
[3] From the $\eta \to 3\pi^0$ decay and using B($\eta \to 3\pi^0$)= (32.24 ± 0.29) × 10^{-2}.
[4] The combined fit from 600 to 1380 MeV taking into account $\rho(770)$, $\omega(782)$, $\phi(1020)$, and $\rho(1450)$ (mass and width fixed at 1450 MeV and 310 MeV respectively).
[5] Recalculated by us from the cross section in the peak.
[6] A simultaneous fit of $e^+e^- \to \pi^+\pi^-$, $\pi^+\pi^-\pi^0$, $\pi^0\gamma$, $\eta\gamma$ data.

$\Gamma(e^+e^-)/\Gamma_{total} \times \Gamma(\pi^0\gamma)/\Gamma_{total}$ — $\Gamma_{12}/\Gamma \times \Gamma_8/\Gamma$

VALUE (units 10^{-8})	EVTS	DOCUMENT ID		TECN	COMMENT
2.2 ±0.4 OUR FIT Error includes scale factor of 1.7.					
2.21 ±0.34 OUR AVERAGE Error includes scale factor of 1.6. See the ideogram below.					
1.98 ±0.22 ±0.10		[1] ACHASOV	16A	SND	0.60-1.38 $e^+e^- \to \pi^0\gamma$
$2.90\ ^{+0.60}_{-0.55}$ ±0.18	18k	AKHMETSHIN	05	CMD2	0.60-1.38 $e^+e^- \to \pi^0\gamma$
3.61 ±0.74 ±0.49	10k	[2] DOLINSKY	89	ND	$e^+e^- \to \pi^0\gamma$
• • • We do not use the following data for averages, fits, limits, etc. • • •					
1.875±0.026		[3] BENAYOUN	10	RVUE	0.4–1.05 e^+e^-
2.37 ±0.53 ±0.33	36k	[4] ACHASOV	03	SND	0.60–0.97 $e^+e^- \to \pi^0\gamma$

[1] From the VMD model with the prho(770), $\omega(782)$, $\phi(1020)$ resonances, and an additional resonance describing the total contribution of the $\rho(1450)$ and $\omega(1420)$ states. Supersedes ACHASOV 03.
[2] Recalculated by us from the cross section in the peak.
[3] A simultaneous fit of $e^+e^- \to \pi^+\pi^-$, $\pi^+\pi^-\pi^0$, $\pi^0\gamma$, $\eta\gamma$ data.
[4] Using $\sigma_{\phi \to \pi^0\gamma}$ from ACHASOV 00 and m_ρ = 775.97 MeV in the model with the energy-independent phase of ρ-ω interferenceequal to $(-10.2 \pm 7.0)^\circ$.

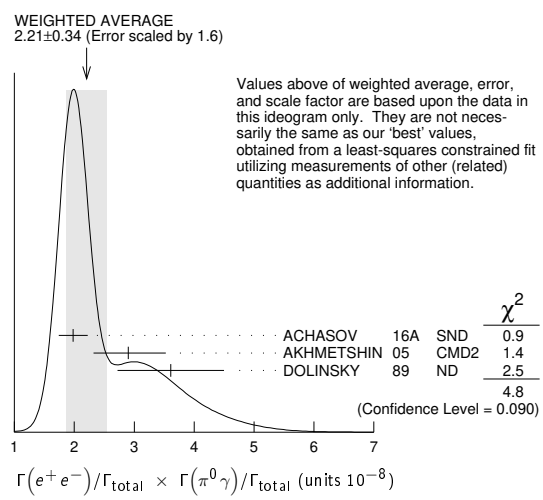

$\Gamma(e^+e^-)/\Gamma_{total} \times \Gamma(\pi^+\pi^-\pi^0)/\Gamma_{total}$ — $\Gamma_{12}/\Gamma \times \Gamma_{13}/\Gamma$

VALUE (units 10^{-9})	EVTS	DOCUMENT ID		TECN	COMMENT
• • • We do not use the following data for averages, fits, limits, etc. • • •					
0.903±0.076		[1] BENAYOUN	10	RVUE	0.4–1.05 e^+e^-
$4.58\ ^{+2.46}_{-1.64}$ ±1.56	1.2M	[2] ACHASOV	03D	RVUE	0.44–2.00 $e^+e^- \to \pi^+\pi^-\pi^0$

[1] A simultaneous fit of $e^+e^- \to \pi^+\pi^-$, $\pi^+\pi^-\pi^0$, $\pi^0\gamma$, $\eta\gamma$ data.
[2] Statistical significance is less than 3 σ.

$\rho(770)$ BRANCHING RATIOS

$\Gamma(\pi^\pm\eta)/\Gamma(\pi\pi)$ — Γ_4/Γ_1

VALUE (units 10^{-4})	CL%	DOCUMENT ID		TECN	CHG	COMMENT
<60	84	FERBEL	66	HBC	±	$\pi^\pm p$ above 2.5

$\Gamma(\pi^\pm\pi^+\pi^-\pi^0)/\Gamma(\pi\pi)$ — Γ_5/Γ_1

VALUE (units 10^{-4})	CL%	DOCUMENT ID		TECN	CHG	COMMENT
<20	84	FERBEL	66	HBC	±	$\pi^\pm p$ above 2.5
• • • We do not use the following data for averages, fits, limits, etc. • • •						
35±40		JAMES	66	HBC	+	2.1 $\pi^+ p$

Int. J. Mod. Phys. A 2026.41. Downloaded from www.worldscientific.com
by UNIVERSITY OF CALIFORNIA @ BERKELEY on 09/16/26. Re-use and distribution is strictly not permitted, except for Open Access articles.

$\Gamma(\pi^+\pi^-\gamma)/\Gamma_{total}$ — Γ_7/Γ

VALUE	CL%	DOCUMENT ID		TECN	COMMENT
0.0099±0.0016 OUR FIT					
0.0099±0.0016		[1] DOLINSKY	91	ND	$e^+e^- \to \pi^+\pi^-\gamma$
• • • We do not use the following data for averages, fits, limits, etc. • • •					
0.0111±0.0014		[2] VASSERMAN	88	ND	$e^+e^- \to \pi^+\pi^-\gamma$
<0.005	90	[3] VASSERMAN	88	ND	$e^+e^- \to \pi^+\pi^-\gamma$

[1] Bremsstrahlung from a decay pion and for photon energy above 50 MeV.
[2] Superseded by DOLINSKY 91.
[3] Structure radiation due to quark rearrangement in the decay.

$\Gamma(\pi^0\gamma)/\Gamma_{total}$ — Γ_8/Γ

VALUE (units 10^{-4})	EVTS	DOCUMENT ID		TECN	COMMENT
• • • We do not use the following data for averages, fits, limits, etc. • • •					
4.20±0.52		[1] ACHASOV	16A	SND	0.60–1.38 $e^+e^- \to \pi^0\gamma$
$6.21^{+1.28}_{-1.18}\pm0.39$	18k	[2,3] AKHMETSHIN	05	CMD2	0.60-1.38 $e^+e^- \to \pi^0\gamma$
5.22±1.17±0.75	36k	[3,4] ACHASOV	03	SND	0.60–0.97 $e^+e^- \to \pi^0\gamma$
6.8 ±1.7		[5] BENAYOUN	96	RVUE	0.54-1.04 $e^+e^- \to \pi^0\gamma$
7.9 ±2.0		[3] DOLINSKY	89	ND	$e^+e^- \to \pi^0\gamma$

[1] Using $B(\rho \to e^+e^-)$ from PDG 15. Supersedes ACHASOV 03.
[2] Using $B(\rho \to e^+e^-) = (4.67 \pm 0.09) \times 10^{-5}$.
[3] Not independent of the corresponding $\Gamma(e^+e^-) \times \Gamma(\pi^0\gamma)/\Gamma^2_{total}$.
[4] Using $B(\rho \to e^+e^-) = (4.54 \pm 0.10) \times 10^{-5}$.
[5] Reanalysis of DRUZHININ 84, DOLINSKY 89, and DOLINSKY 91 taking into account a triangle anomaly contribution.

$\Gamma(\eta\gamma)/\Gamma_{total}$ — Γ_9/Γ

VALUE (units 10^{-4})	EVTS	DOCUMENT ID		TECN	CHG	COMMENT
3.00±0.21 OUR FIT						
2.90±0.32 OUR AVERAGE						
2.79±0.34±0.03	33k	[1] ACHASOV	07B	SND		0.6–1.38 $e^+e^- \to \eta\gamma$
3.6 ±0.9		[2] ANDREWS	77	CNTR	0	6.7–10 γCu
• • • We do not use the following data for averages, fits, limits, etc. • • •						
3.21±1.39±0.20	17.4k	[3,4] AKHMETSHIN	05	CMD2		0.60-1.38 $e^+e^- \to \eta\gamma$
3.39±0.42±0.23		[2,5,6] AKHMETSHIN	01B	CMD2		$e^+e^- \to \eta\gamma$
$1.9\ ^{+0.6}_{-0.8}$		[7] BENAYOUN	96	RVUE		0.54-1.04 $e^+e^- \to \eta\gamma$
4.0 ±1.1		[2,4] DOLINSKY	89	ND		$e^+e^- \to \eta\gamma$

[1] ACHASOV 07B reports $[\Gamma(\rho(770) \to \eta\gamma)/\Gamma_{total}] \times [B(\rho(770) \to e^+e^-)] = (1.32 \pm 0.14 \pm 0.08) \times 10^{-8}$ which we divide by our best (shown rounded) value $B(\rho(770) \to e^+e^-) = (4.72 \pm 0.05) \times 10^{-5}$. Our first error is their experiment's error and our second error is the systematic error from using our best (shown rounded) value. Supersedes ACHASOV 00D and ACHASOV 06A.
[2] Solution corresponding to constructive ω-ρ interference.
[3] Using $B(\rho \to e^+e^-) = (4.67 \pm 0.09) \times 10^{-5}$ and $B(\eta \to \gamma\gamma) = 39.43 \pm 0.26\%$.
[4] Not independent of the corresponding $\Gamma(e^+e^-) \times \Gamma(\eta\gamma)/\Gamma^2_{total}$.
[5] The combined fit from 600 to 1380 MeV taking into account $\rho(770)$, $\omega(782)$, $\phi(1020)$, and $\rho(1450)$ (mass and width fixed at 1450 MeV and 310 MeV respectively).
[6] Using $B(\rho \to e^+e^-) = (4.75 \pm 0.10) \times 10^{-5}$ from AKHMETSHIN 02 and $B(\eta \to 3\pi^0) = (32.24 \pm 0.29) \times 10^{-2}$.
[7] Reanalysis of DRUZHININ 84, DOLINSKY 89, and DOLINSKY 91 taking into account a triangle anomaly contribution. Constructive ρ-ω interference solution.

$\Gamma(\pi^0\pi^0\gamma)/\Gamma_{total}$ — Γ_{10}/Γ

VALUE (units 10^{-5})	EVTS	DOCUMENT ID		TECN	COMMENT
4.5±0.8 OUR FIT					
$4.5^{+0.9}_{-0.8}$ OUR AVERAGE					
$5.2^{+1.5}_{-1.3}\pm0.6$	190	[1] AKHMETSHIN	04B	CMD2	0.6–0.97 $e^+e^- \to \pi^0\pi^0\gamma$
$4.1^{+1.0}_{-0.9}\pm0.3$	295	[2] ACHASOV	02F	SND	0.36–0.97 $e^+e^- \to \pi^0\pi^0\gamma$
• • • We do not use the following data for averages, fits, limits, etc. • • •					
$4.8^{+3.4}_{-1.8}\pm0.5$	63	[3] ACHASOV	00G	SND	$e^+e^- \to \pi^0\pi^0\gamma$

[1] This branching ratio includes the conventional VMD mechanism $\rho \to \omega\pi^0$, $\omega \to \pi^0\gamma$, and the new decay mode $\rho \to f_0(500)\gamma$, $f_0(500) \to \pi^0\pi^0$ with a branching ratio $(2.0^{+1.1}_{-0.9} \pm 0.3) \times 10^{-5}$ differing from zero by 2.0 standard deviations.
[2] This branching ratio includes the conventional VMD mechanism $\rho \to \omega\pi^0$, $\omega \to \pi^0\gamma$ and the new decay mode $\rho \to f_0(500)\gamma$, $f_0(500) \to \pi^0\pi^0$ with a branching ratio $(1.9^{+0.9}_{-0.8} \pm 0.4) \times 10^{-5}$ differing from zero by 2.4 standard deviations. Supersedes ACHASOV 00G.
[3] Superseded by ACHASOV 02F.

$\Gamma(\mu^+\mu^-)/\Gamma(\pi^+\pi^-)$ — Γ_{11}/Γ_6

VALUE (units 10^{-5})	DOCUMENT ID		TECN	COMMENT
4.60±0.28 OUR FIT				
4.6 ±0.2 ±0.2	ANTIPOV	89	SIGM	π^-Cu $\to \mu^+\mu^-\pi^-$Cu
• • • We do not use the following data for averages, fits, limits, etc. • • •				
$8.2\ ^{+1.6}_{-3.6}$	[1] ROTHWELL	69	CNTR	Photoproduction
5.6 ±1.5	[2] WEHMANN	69	OSPK	12 π^-C, Fe
$9.7\ ^{+3.1}_{-3.3}$	[3,4] HYAMS	67	OSPK	11 π^-Li, H

[1] Possibly large ρ-ω interference leads us to increase the minus error.
[2] Result contains 11 ± 11% correction using SU(3) for central value. The error on the correction takes account of possible ρ-ω interference and the upper limit agrees with the upper limit of $\omega \to \mu^+\mu^-$ from this experiment.
[3] But he even enlarges his error to take residual ω contamination into account. Since his value is high, seems the other experiments also can't have too many ω's. But maybe Hyams has additional μ's from $\rho \to \pi\pi$, decaying π's.
[4] HYAMS 67's mass resolution is 20 MeV. The ω region was excluded.

$\Gamma(e^+e^-)/\Gamma(\pi\pi)$ — Γ_{12}/Γ_1

VALUE (units 10^{-4})	DOCUMENT ID		TECN	COMMENT
• • • We do not use the following data for averages, fits, limits, etc. • • •				
0.40±0.05	[1,2] BENAKSAS	72	OSPK	$e^+e^- \to \pi^+\pi^-$

[1] The ρ' contribution is not taken into account.
[2] Barkov excludes Auslender and Benaksas for large statistical and systematic errors.

$\Gamma(\pi^+\pi^-\pi^0)/\Gamma_{total}$ — Γ_{13}/Γ

VALUE (units 10^{-4})	CL%	EVTS	DOCUMENT ID		TECN	COMMENT
0.88±0.23±0.30			[1] LEES	21B	BABR	10.5 $e^+e^- \to \pi^+\pi^-\pi^0\gamma$
• • • We do not use the following data for averages, fits, limits, etc. • • •						
$1.01^{+0.54}_{-0.36}\pm0.34$		1.2M	[2] ACHASOV	03D	RVUE	0.44–2.00 $e^+e^- \to \pi^+\pi^-\pi^0$
<1.2	90		VASSERMAN	88B	ND	$e^+e^- \to \pi^+\pi^-\pi^0$

[1] From the cross section for $e^+e^- \to \pi^+\pi^-\pi^0$ with contributions from $\rho(770)$, $\omega(782)$, $\phi(1020)$, $\omega(1420)$, and $\omega(1650)$. Statistical evidence is more than 6 σ.
[2] Statistical significance is less than 3σ.

$\Gamma(\pi^+\pi^-\pi^0)/\Gamma(\pi\pi)$ — Γ_{13}/Γ_1

VALUE	CL%	DOCUMENT ID		TECN	CHG	COMMENT
• • • We do not use the following data for averages, fits, limits, etc. • • •						
~ 0.01		BRAMON	86	RVUE	0	$J/\psi \to \omega\pi^0$
<0.01	84	[1] ABRAMS	71	HBC	0	3.7 π^+p

[1] Model dependent, assumes I = 1, 2, or 3 for the 3π system.

$\Gamma(\pi^+\pi^-\pi^+\pi^-)/\Gamma_{total}$ — Γ_{14}/Γ

VALUE (units 10^{-5})	CL%	EVTS	DOCUMENT ID		TECN	COMMENT
1.8±0.9 OUR FIT						
1.8±0.9±0.3		153	AKHMETSHIN	00	CMD2	0.6–0.97 $e^+e^- \to \pi^+\pi^-\pi^+\pi^-$
• • • We do not use the following data for averages, fits, limits, etc. • • •						
<20	90		KURDADZE	88	OLYA	$e^+e^- \to \pi^+\pi^-\pi^+\pi^-$

$\Gamma(\pi^+\pi^-\pi^+\pi^-)/\Gamma(\pi\pi)$ — Γ_{14}/Γ_1

VALUE (units 10^{-4})	CL%	DOCUMENT ID		TECN	CHG	COMMENT
• • • We do not use the following data for averages, fits, limits, etc. • • •						
<15	90	ERBE	69	HBC	0	2.5–5.8 γp
<20		CHUNG	68	HBC	0	3.2,4.2 π^-p
<20	90	HUSON	68	HLBC	0	16.0 π^-p
<80		JAMES	66	HBC	0	2.1 π^+p

$\Gamma(\pi^+\pi^-\pi^0\pi^0)/\Gamma_{total}$ — Γ_{15}/Γ

VALUE (units 10^{-5})	CL%	DOCUMENT ID		TECN	COMMENT
1.60±0.74±0.18		[1] ACHASOV	09A	SND	$e^+e^- \to \pi^+\pi^-\pi^0\pi^0$
• • • We do not use the following data for averages, fits, limits, etc. • • •					
< 4	90	AULCHENKO	87C	ND	$e^+e^- \to \pi^+\pi^-\pi^0\pi^0$
<20	90	KURDADZE	86	OLYA	$e^+e^- \to \pi^+\pi^-\pi^0\pi^0$

[1] Assuming no interference between the ρ and ω contributions.

$\Gamma(\pi^0e^+e^-)/\Gamma_{total}$ — Γ_{16}/Γ

VALUE (units 10^{-5})	CL%	DOCUMENT ID		TECN	COMMENT
<1.2	90	ACHASOV	08	SND	0.36–0.97 $e^+e^- \to \pi^0e^+e^-$
• • • We do not use the following data for averages, fits, limits, etc. • • •					
<1.6		AKHMETSHIN	05A	CMD2	0.72-0.84 e^+e^-

$\Gamma(\eta e^+e^-)/\Gamma_{total}$ — Γ_{17}/Γ

VALUE (units 10^{-5})	DOCUMENT ID		TECN	COMMENT
• • • We do not use the following data for averages, fits, limits, etc. • • •				
<0.7	AKHMETSHIN	05A	CMD2	0.72-0.84 e^+e^-

$\rho(770)$ REFERENCES

AAIJ	25AG	JHEP 2511 103	R. Aaij et al.	(LHCb Collab.)
HOFERICHT...	24	PL B853 138698	M. Hoferichter et al.	(BERN, MADU, BONN+)
IGNATOV	24	PR D109 112002	F.V. Ignatov et al.	(CMD-3 Collab.)
PDG	22	PTEP 2022 083C01	R.L. Workman et al.	(PDG Collab.)
ACHASOV	21	JHEP 2101 113	M.N. Achasov et al.	(SND Collab.)
LEES	21B	PR D104 112003	J.P. Lees et al.	(BABAR Collab.)
ACHARYA	20F	JHEP 2006 035	S. Acharya et al.	(ALICE Collab.)
ANDREEV	20	EPJ C80 1189	V. Andreev et al.	(H1 Collab.)
SIRUNYAN	19CS	EPJ C79 702	A.M. Sirunyan	(CMS Collab.)
ABLIKIM	18C	PRL 120 242003	M. Ablikim et al.	(BESIII Collab.)
ABLIKIM	17	PRL 118 012001	M. Ablikim et al.	(BESIII Collab.)
ADAMCZYK	17A	PR C96 054904	L. Adamczyk et al.	(STAR Collab.)
BARTOS	17	PR D96 113004	E. Bartos et al.	

Int. J. Mod. Phys. A 2026.41. Downloaded from www.worldscientific.com by CALIFORNIA @ BERKELEY on 09/16/26. Re-use and distribution is strictly not permitted, except for Open Access articles.

BARTOS 17A IJMP A32 1750154 E. Bartos et al.
ABLIKIM 16C PL B753 629 M. Ablikim et al. (BESIII Collab.)
ACHASOV 16A PR D93 092001 M.N. Achasov et al. (SND Collab.)
HOFERICHT... 16 PRPL 625 1 M. Hoferichter et al. (WASH, BONN)
PDG 15 RPP 2015 at pdg.lbl.gov (PDG Collab.)
ABRAMOWICZ 12 EPJ C72 1869 H. Abramowicz et al. (ZEUS Collab.)
LEES 12G PR D86 032013 J.P. Lees et al. (BABAR Collab.)
AMBROSINO 11A PL B700 102 F. Ambrosino et al. (KLOE Collab.)
GARCIA-MAR... 11 PRL 107 072001 R. Garcia-Martin et al. (MADR, CRAC)
BATLEY 10C EPJ C70 635 J.R. Batley et al. (CERN NA48/2 Collab.)
BENAYOUN 10 EPJ C65 211 M. Benayoun et al.
DUBNICKA 10 APS 60 1 S. Dubnicka, A.Z. Dubnickova
ACHASOV 09A JETP 109 379 M.N. Achasov et al. (SND Collab.)
Translated from ZETF 136 442.
AUBERT 09AS PRL 103 231801 B. Aubert et al. (BABAR Collab.)
ACHASOV 08 JETP 107 61 M.N. Achasov et al. (SND Collab.)
Translated from ZETF 134 80.
FUJIKAWA 08 PR D78 072006 M. Fujikawa et al. (BELLE Collab.)
ACHASOV 07B PR D76 077101 M.N. Achasov et al. (SND Collab.)
AKHMETSHIN 07 PL B648 28 R.R. Akhmetshin et al. (Novosibirsk CMD-2 Collab.)
ACHASOV 06 JETP 103 380 M.N. Achasov et al. (Novosibirsk SND Collab.)
Translated from ZETF 130 437.
ACHASOV 06A PR D74 014016 M.N. Achasov et al. (SND Collab.)
AULCHENKO 06 JETPL 84 413 V.M. Aulchenko et al. (Novosibirsk CMD-2 Collab.)
Translated from ZETFP 84 491.
ACHASOV 05A JETP 101 1053 M.N. Achasov et al. (Novosibirsk SND Collab.)
Translated from ZETF 128 1201.
AKHMETSHIN 05 PL B605 26 R.R. Akhmetshin et al. (Novosibirsk CMD-2 Collab.)
AKHMETSHIN 05A PL B613 29 R.R. Akhmetshin et al. (Novosibirsk CMD-2 Collab.)
ALOISIO 05 PL B606 12 A. Aloisio et al. (KLOE Collab.)
AULCHENKO 05 JETPL 82 743 V.M. Aulchenko et al. (Novosibirsk CMD-2 Collab.)
Translated from ZETFP 82 841.
SCHAEL 05C PRPL 421 191 S. Schael et al. (ALEPH Collab.)
AKHMETSHIN 04 PL B578 285 R.R. Akhmetshin et al. (Novosibirsk CMD-2 Collab.)
AKHMETSHIN 04B PL B580 119 R.R. Akhmetshin et al. (Novosibirsk CMD-2 Collab.)
PELAEZ 04A MPL A19 2879 J.R. Pelaez (MADU)
ACHASOV 03 PL B559 171 M.N. Achasov et al. (Novosibirsk SND Collab.)
ACHASOV 03D PR D68 052006 M.N. Achasov et al. (Novosibirsk SND Collab.)
ALOISIO 03 PL B561 55 A. Aloisio et al. (KLOE Collab.)
SANZ-CILLERO 03 EPJ C27 587 J.J. Sanz-Cillero, A. Pich
ACHASOV 02 PR D65 032002 M.N. Achasov et al. (Novosibirsk SND Collab.)
ACHASOV 02F PL B537 201 M.N. Achasov et al. (Novosibirsk SND Collab.)
AKHMETSHIN 02 PL B527 161 R.R. Akhmetshin et al. (Novosibirsk CMD-2 Collab.)
AKHMETSHIN 01B PL B509 217 R.R. Akhmetshin et al. (Novosibirsk CMD-2 Collab.)
COLANGELO 01 NP B603 125 G. Colangelo, J. Gasser, H. Leytwyler
PICH 01 PR D63 093005 A. Pich, J. Portoles
ACHASOV 00 EPJ C12 25 M.N. Achasov et al. (Novosibirsk SND Collab.)
ACHASOV 00D JETPL 72 282 M.N. Achasov et al. (Novosibirsk SND Collab.)
Translated from ZETFP 72 411.
ACHASOV 00G JETPL 71 355 M.N. Achasov et al. (Novosibirsk SND Collab.)
Translated from ZETFP 71 519.
AKHMETSHIN 00 PL B475 190 R.R. Akhmetshin et al. (Novosibirsk CMD-2 Collab.)
ANDERSON 00A PR D61 112002 S. Anderson et al. (CLEO Collab.)
ABELE 99E PL B469 270 A. Abele et al. (Crystal Barrel Collab.)
BENAYOUN 98 EPJ C2 269 M. Benayoun et al. (IPNP, NOVO, ADLD+)
BREITWEG 98B EPJ C2 247 J. Breitweg et al. (ZEUS Collab.)
GARDNER 98 PR D57 2716 S. Gardner, H.B. O'Connell
Also PR D62 019903 (errat.) S. Gardner, H.B. O'Connell
ABELE 97 PL B391 191 A. Abele et al. (Crystal Barrel Collab.)
ADAMS 97 ZPHY C74 237 M.R. Adams et al. (E665 Collab.)
BARATE 97M ZPHY C76 15 R. Barate et al. (ALEPH Collab.)
BERTIN 97C PL B408 476 A. Bertin et al. (OBELIX Collab.)
BOGOLYUB... 97 PAN 60 46 M.Y. Bogolyubsky et al. (MOSU, SERP)
Translated from YAF 60 53.
O'CONNELL 97 NP A623 559 H.B. O'Connell et al. (ADLD)
BENAYOUN 96 ZPHY C72 221 M. Benayoun et al. (IPNP, NOVO)
BERNICHA 94 PR D50 4454 A. Bernicha, G. Lopez Castro, J. Pestieau (LOUV+)
WEIDENAUER 93 ZPHY C59 387 P. Weidenauer et al. (ASTERIX Collab.)
AGUILAR-... 91 ZPHY C50 405 M. Aguilar-Benitez et al. (LEBC-EHS Collab.)
DOLINSKY 91 PRPL 202 99 S.I. Dolinsky et al. (NOVO)
KUHN 90 ZPHY C48 445 J.H. Kuhn et al. (MPIM)
ANTIPOV 89 ZPHY C42 185 Y.M. Antipov et al. (SERP, JINR, BGNA+)
BISELLO 89 PL B220 321 D. Bisello et al. (DM2 Collab.)
DOLINSKY 89 ZPHY C42 511 S.I. Dolinsky et al. (NOVO)
DUBNICKA 89 JP G15 1349 S. Dubnicka et al. (JINR, SLOV)
GESHKEN... 89 ZPHY C45 351 B.V. Geshkenbein (ITEP)
KURDADZE 88 JETPL 47 512 L.M. Kurdadze et al. (NOVO)
Translated from ZETFP 47 432.
VASSERMAN 88 SJNP 47 1035 I.B. Vasserman et al. (NOVO)
Translated from YAF 47 1635.
VASSERMAN 88B SJNP 48 480 I.B. Vasserman et al. (NOVO)
Translated from YAF 48 753.
AULCHENKO 87C IYF 87-90 Preprint V.M. Aulchenko et al. (NOVO)
CAPRARO 87 NP B288 659 L. Capraro et al. (CLER, FRAS, MILA+)
BRAMON 86 PL B173 97 A. Bramon, J. Casulleras (BARC)
HUSTON 86 PR D33 3199 J. Huston et al. (ROCH, FNAL, MINN)
KURDADZE 86 JETPL 43 643 L.M. Kurdadze et al. (NOVO)
Translated from ZETFP 43 497.
BARKOV 85 NP B256 365 L.M. Barkov et al. (NOVO)
DRUZHININ 84 PL 144B 136 V.P. Druzhinin et al. (NOVO)
CHABAUD 83 NP B223 1 V. Chabaud et al. (CERN, CRAC, MPIM)
JENSEN 83 PR D27 26 T. Jensen et al. (ROCH, FNAL, MINN)
HEYN 81 ZPHY C7 169 M.F. Heyn, C.B. Lang (GRAZ)
BOHACIK 80 PR D21 1342 J. Bohacik, H. Kuhnelt (SLOV, WIEN)
COHEN 80 PR D22 2595 D. Cohen et al. (ANL)
LANG 79 PR D19 956 C.B. Lang, A. Mas-Parareda (GRAZ)
BARTALUCCI 78 NC 44A 587 S. Bartalucci et al. (DESY, FRAS)
WICKLUND 78 PR D17 1197 A.B. Wicklund et al. (ANL)
ANDREWS 77 PRL 38 198 D.E. Andrews et al. (ROCH)
DEUTSCH... 76 NP B103 426 M. Deutschmann et al. (AACH3, BERL, BONN+)
ENGLER 74 PR D10 2070 A. Engler et al. (CMU, CASE)
ESTABROOKS 74 NP B79 301 P.G. Estabrooks, A.D. Martin (DURH)
GRAYER 74 NP B75 189 G. Grayer et al. (CERN, MPIM)
RATCLIFF 74 Private Comm.
BYERLY 73 PR D7 637 W.L. Byerly et al. (MICH)
GLADDING 73 PR D8 3721 G.E. Gladding et al. (HARV)
HYAMS 73 NP B64 134 B.D. Hyams et al. (CERN, MPIM)
PROTOPOP... 73 PR D7 1279 S.D. Protopopescu et al. (LBL)
BALLAM 72 PR D5 545 J. Ballam et al. (SLAC, LBL, TUFTS)
BENAKSAS 72 PL 39B 289 D. Benaksas et al. (ORSAY)
JACOBS 72 PR D6 1291 L.D. Jacobs (SACL)
RATCLIFF 72 PL 38B 345 B.N. Ratcliff et al. (SLAC)
ABRAMS 71 PR D4 653 G.S. Abrams et al. (LBL)
ALVENSLEB... 70 PRL 24 786 H. Alvensleben et al. (DESY)
BIGGS 70 PRL 24 1197 P.J. Biggs et al. (DARE)
ERBE 69 PR 188 2060 R. Erbe et al. (German Bubble Chamber Collab.)
MALAMUD 69 Argonne Conf. 93 E.I. Malamud, P.E. Schlein (UCLA)
REYNOLDS 69 PR 184 1424 B.G. Reynolds et al. (FSU)
ROTHWELL 69 PRL 23 1521 P.L. Rothwell et al. (NEAS)
WEHMANN 69 PR 178 2095 A.A. Wehmann et al. (HARV, CASE, SLAC+)
ARMENISE 68 NC 54A 999 N. Armenise et al. (BARI, BGNA, FIRZ+)
BATON 68 PR 176 1574 J.P. Baton, G. Laurens (SACL)
CHUNG 68 PR 165 1491 S.U. Chung et al. (LRL)
FOSTER 68 NP B6 107 M. Foster et al. (CERN, CDEF)
GOUNARIS 68 PRL 21 244 G.J. Gounaris, J.J. Sakurai
HUSON 68 PL 28B 208 R. Huson et al. (ORSAY, MILA, UCLA)
HYAMS 68 NP B7 1 B.D. Hyams et al. (CERN, MPIM)
LANZEROTTI 68 PR 166 1365 L.J. Lanzerotti et al. (HARV)
PISUT 68 NP B6 325 J. Pisut, M. Roos (CERN)
ASBURY 67B PRL 19 865 J.G. Asbury et al. (DESY, COLU)
BACON 67 PR 157 1263 T.C. Bacon et al. (BNL)
EISNER 67 PR 164 1699 R.L. Eisner et al. (PURD)
HUWE 67 PL 24B 252 D.O. Huwe et al. (COLU)
HYAMS 67 PL 24B 634 B.D. Hyams et al. (CERN, MPIM)
MILLER 67B PR 153 1423 D.H. Miller et al. (PURD)
ALFF-... 66 PR 145 1072 C. Alff-Steinberger et al. (COLU, RUTG)
FERBEL 66 PL 21 111 T. Ferbel (ROCH)
HAGOPIAN 66 PR 145 1128 V. Hagopian et al. (PENN, SACL)
HAGOPIAN 66B PR 152 1183 V. Hagopian, Y.L. Pan (PENN, LRL)
JACOBS 66B UCRL 16877 L.D. Jacobs (LRL)
JAMES 66 PR 142 896 F.E. James, H.L. Kraybill (YALE, BNL)
ROSS 66 PR 149 1172 M. Ross, L. Stodolsky
SOEDING 66 PL B19 702 P. Soeding (HAMB)
WEST 66 PR 149 1089 E. West et al. (WISC)
BLIEDEN 65 PL 19 444 H.R. Blieden et al. (CERN MMS Collab.)
CARMONY 64 PRL 12 254 D.D. Carmony et al. (UCB)
GOLDHABER 64 PRL 12 336 G. Goldhaber et al. (LRL, UCB)
ABOLINS 63 PRL 11 381 M.A. Abolins et al. (UCSD)

$\omega(782)$

$I^G(J^{PC}) = 0^-(1^{--})$

$\omega(782)$ MASS

VALUE (MeV)	EVTS	DOCUMENT ID		TECN	COMMENT
782.66±0.13 OUR AVERAGE		Error includes scale factor of 2.0.			See the ideogram below.
777.9 $\pm 2.2\ ^{+4.3}_{-2.2}$	900k	ANDREEV	20	H1	$ep \to e\pi^+\pi^-p$
783.20±0.13±0.16	18680	AKHMETSHIN	05	CMD2	0.60–1.38 $e^+e^- \to \pi^0\gamma$
782.68±0.09±0.04	11200	[1] AKHMETSHIN	04	CMD2	$e^+e^- \to \pi^+\pi^-\pi^0$
782.79±0.08±0.09	1.2M	[2] ACHASOV	03D	RVUE	0.44–2.00 $e^+e^- \to \pi^+\pi^-\pi^0$
781.96±0.17±0.80	11k	[3] AMSLER	94C	CBAR	0.0 $\overline{p}p \to \omega\eta\pi^0$
782.08±0.36±0.82	3463	[4] AMSLER	94C	CBAR	0.0 $\overline{p}p \to \omega\eta\pi^0$
781.96±0.13±0.17	15k	AMSLER	93B	CBAR	0.0 $\overline{p}p \to \omega\pi^0\pi^0$
782.4 ±0.2	270k	WEIDENAUER	93	ASTE	$\overline{p}p \to 2\pi^+2\pi^-\pi^0$
782.4 ±0.5	7000	[5] KEYNE	76	CNTR	$\pi^-p \to \omega n$
• • • We do not use the following data for averages, fits, limits, etc. • • •					
782.83±0.02±0.05		[6] FEDOTOVICH	25A	CMD3	0.66–0.98 $e^+e^- \to \pi^+\pi^-\pi^0$
782.43±0.03	34M	[7] IGNATOV	24	CMD3	$e^+e^- \to \pi^+\pi^-$
782.58±0.03±0.01		[8] HOID	20	RVUE	$e^+e^- \to \pi^0\gamma$
781.68±0.09±0.03		[9] COLANGELO	19	RVUE	$e^+e^- \to \pi^+\pi^-$
782.63±0.03±0.01		[10] HOFERICHT...	19	RVUE	$e^+e^- \to \pi^+\pi^-\pi^0$
782.4 ±0.8	384k	[11] ADAMCZYK	17A	STAR	$AuAu \to AuAu\pi^+\pi^-$
781.91±0.24		[12] LEES	12G	BABR	$e^+e^- \to \pi^+\pi^-\gamma$
782.7 ±0.1 ±1.5	19500	[13] WURZINGER	95	SPEC	1.33 $pd \to {}^3\mathrm{He}\omega$
781.78±0.10		[13] BARKOV	87	CMD	$e^+e^- \to \pi^+\pi^-\pi^0$
782.2 ±0.4	1488	[14] KURDADZE	83B	OLYA	$e^+e^- \to \pi^+\pi^-\pi^0$
783.3 ±0.4	433	CORDIER	80	DM1	$e^+e^- \to \pi^+\pi^-\pi^0$
782.5 ±0.8	33260	ROOS	80	RVUE	0.0–3.6 $\overline{p}p$
782.6 ±0.8	3000	BENKHEIRI	79	OMEG	9–12 $\pi^\pm p$
781.8 ±0.6	1430	COOPER	78B	HBC	0.7–0.8 $\overline{p}p \to 5\pi$
782.7 ±0.9	535	VANAPEL...	78	HBC	7.2 $\overline{p}p \to \overline{p}p\omega$
783.5 ±0.8	2100	GESSAROLI	77	HBC	11 $\pi^-p \to \omega n$
782.5 ±0.8	418	AGUILAR-...	72B	HBC	3.9,4.6 K^-p
783.4 ±1.0	248	BIZZARRI	71	HBC	0.0 $p\overline{p} \to K^+K^-\omega$
781.0 ±0.6	510	BIZZARRI	71	HBC	0.0 $p\overline{p} \to K_1K_1\omega$
783.7 ±1.0	3583	[15] COYNE	71	HBC	3.7 $\pi^+p \to p\pi^+\pi^+\pi^-\pi^0$
784.1 ±1.2	750	ABRAMOVI...	70	HBC	3.9 π^-p
783.2 ±1.6		[16] BIGGS	70B	CNTR	<4.1 $\gamma C \to \pi^+\pi^-C$
782.4 ±0.5	2400	BIZZARRI	69	HBC	0.0 $\overline{p}p$

[1] Update of AKHMETSHIN 00C.

[2] From the combined fit of ANTONELLI 92, ACHASOV 01E, ACHASOV 02E, and ACHASOV 03D data on the $\pi^+\pi^-\pi^0$ and ANTONELLI 92 on the $\omega\pi^+\pi^-$ final states. Supersedes ACHASOV 99E and ACHASOV 02E.

[3] From the $\eta \to \gamma\gamma$ decay.

[4] From the $\eta \to 3\pi^0$ decay.

[5] Observed by threshold-crossing technique. Mass resolution = 4.8 MeV FWHM.

[6] From a VMD fit of the Born cross section allowing for interference of ρ, ω, ϕ, $\omega(1420)$, and $\omega(1650)$. The parameters of ρ, ϕ, $\omega(1420)$, and $\omega(1650)$ are fixed to their PDG 20 values.

[7] From a fit of the pion form factor in the energy range $0.32 < \sqrt{s} < 1.2$ GeV using the GOUNARIS 68 parametrization with the complex phase of the $\rho-\omega$ interference leaving $\rho(1450)$, $\rho(1700)$ resonances as free parameters of the fit. Systematic errors not estimated.

[8] The values were extracted from a dispersively improved Breit-Wigner parameterization and do not include vacuum polarization. Inclusion of vacuum polarization gives 782.736± 0.024 MeV.

[9] The ω mass was extracted from a dispersively improved Breit-Wigner parameterization, the ω width fixed at 8.49 ± 0.08 MeV. The value does not include vacuum polarization which would shift the mass to 781.81 ± 0.09 ± 0.03 MeV. The mixing parameter is assumed real valued.

[10] The values were extracted from a dispersively improved Breit-Wigner parameterization and do not include vacuum polarization.

[11] From the parametrization according to SOEDING 66 with an additional relativistic Breit-Wigner component to account for ω photoproduction. Systematic errors not evaluated.
[12] From the $\rho-\omega$ interference in the $\pi^+\pi^-$ mass spectrum using the Breit-Wigner for the ω and leaving its mass and width as free parameters of the fit.
[13] Systematic uncertainties underestimated.
[14] Systematic uncertainties not estimated.
[15] From best-resolution sample of COYNE 71.
[16] From ω-ρ interference in the $\pi^+\pi^-$ mass spectrum assuming ω width 12.6 MeV.

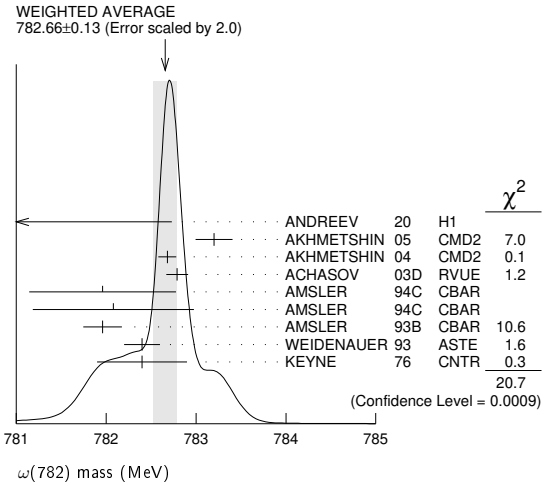

$\omega(782)$ WIDTH

VALUE (MeV)	EVTS	DOCUMENT ID		TECN	COMMENT
8.68±0.13 OUR AVERAGE					
8.68±0.23±0.10	11200	[1] AKHMETSHIN	04	CMD2	$e^+e^- \to \pi^+\pi^-\pi^0$
8.68±0.04±0.15	1.2M	[2] ACHASOV	03D	RVUE	0.44–2.00 $e^+e^- \to \pi^+\pi^-\pi^0$
• • • We do not use the following data for averages, fits, limits, etc. • • •					
8.62±0.06±0.09		[3] FEDOTOVICH	25A	CMD3	0.66–0.98 $e^+e^- \to \pi^+\pi^-\pi^0$
8.57±0.06	34M	[4] IGNATOV	24	CMD3	$e^+e^- \to \pi^+\pi^-$
8.65±0.06±0.01		[5] HOID	20	RVUE	$e^+e^- \to \pi^0\gamma$
8.71±0.04±0.04		[6] HOFERICHT...	19	RVUE	$e^+e^- \to \pi^+\pi^-\pi^0$
8.13±0.45		[7] LEES	12G	BABR	$e^+e^- \to \pi^+\pi^-\gamma$
8.2 ±0.3	19500	[8] WURZINGER	95	SPEC	1.33 $pd \to {}^3\mathrm{He}\omega$
8.4 ±0.1		[9] AULCHENKO	87	ND	$e^+e^- \to \pi^+\pi^-\pi^0$
8.30±0.40		[8] BARKOV	87	CMD	$e^+e^- \to \pi^+\pi^-\pi^0$
9.8 ±0.9	1488	[10] KURDADZE	83B	OLYA	$e^+e^- \to \pi^+\pi^-\pi^0$
9.0 ±0.8	433	[8] CORDIER	80	DM1	$e^+e^- \to \pi^+\pi^-\pi^0$
12 ±2	1430	COOPER	78B	HBC	0.7–0.8 $\bar{p}p \to 5\pi$
9.4 ±2.5	2100	GESSAROLI	77	HBC	11 $\pi^-p \to \omega n$
10.22±0.43	20000	[11] KEYNE	76	CNTR	$\pi^-p \to \omega n$
13.3 ±2	418	AGUILAR-...	72B	HBC	3.9,4.6 K^-p
9.1 ±0.8	451	[8] BENAKSAS	72B	OSPK	$e^+e^- \to \pi^+\pi^-\pi^0$
10.5 ±1.5		BORENSTEIN	72	HBC	2.18 K^-p
7.70±0.9 ±1.15	940	BROWN	72	MMS	2.5 $\pi^-p \to nMM$
10.3 ±1.4	510	BIZZARRI	71	HBC	0.0 $p\bar{p} \to K_1K_1\omega$
12.8 ±3.0	248	BIZZARRI	71	HBC	0.0 $p\bar{p} \to K^+K^-\omega$
9.5 ±1.0	3583	COYNE	71	HBC	3.7 $\pi^+p \to p\pi^+\pi^+\pi^-\pi^0$

[1] Update of AKHMETSHIN 00C.
[2] From the combined fit of ANTONELLI 92, ACHASOV 01E, ACHASOV 02E, and ACHASOV 03D data on the $\pi^+\pi^-\pi^0$ and ANTONELLI 92 on the $\omega\pi^+\pi^-$ final states. Supersedes ACHASOV 99E and ACHASOV 02E.
[3] From a VMD fit of the born cross section allowing for interference of ρ, ω, ϕ, $\omega(1420)$, and $\omega(1650)$. The parameters of ρ, ϕ, $\omega(1420)$, and $\omega(1650)$ are fixed to their PDG 20 values.
[4] From a fit of the pion form factor in the energy range $0.32 < \sqrt{s} < 1.2$ GeV using the GOUNARIS 68 parametrization with the complex phase of the $\rho-\omega$ interference leaving $\rho(1450)$, $\rho(1700)$ resonances as free parameters of the fit. Systematic errors not estimated.
[5] The values were extracted from a dispersively improved Breit-Wigner parameterization and do not include vacuum polarization. Inclusion of vacuum polarization gives 8.63 ± 0.05 MeV.
[6] The values were extracted from a dispersively improved Breit-Wigner parameterization and do not include vacuum polarization.
[7] From the $\rho-\omega$ interference in the $\pi^+\pi^-$ mass spectrum using the Breit-Wigner for the ω and leaving its mass and width as free parameters of the fit.
[8] Systematic uncertainties underestimated.
[9] Relativistic Breit-Wigner includes radiative corrections. Systematic uncertainties not estimated.
[10] Systematic uncertainties not estimated.
[11] Observed by threshold-crossing technique. Mass resolution = 4.8 MeV FWHM.

$\omega(782)$ DECAY MODES

	Mode	Fraction (Γ_i/Γ)	Scale factor/ Confidence level
Γ_1	$\pi^+\pi^-\pi^0$	(89.2 ±0.7) %	
Γ_2	$\pi^0\gamma$	(8.33±0.25) %	S=2.1
Γ_3	$\pi^+\pi^-$	(1.53±0.12) %	S=1.2
Γ_4	neutrals (excluding $\pi^0\gamma$)	$(7\ {}^{+7}_{-5}) \times 10^{-3}$	S=1.1
Γ_5	$\eta\gamma$	$(4.5 \pm 0.4) \times 10^{-4}$	S=1.1
Γ_6	$\pi^0e^+e^-$	$(7.7 \pm 0.6) \times 10^{-4}$	
Γ_7	$\pi^0\mu^+\mu^-$	$(1.34\pm0.18) \times 10^{-4}$	S=1.5
Γ_8	ηe^+e^-		
Γ_9	e^+e^-	$(7.41\pm0.19) \times 10^{-5}$	S=1.8
Γ_{10}	$\pi^+\pi^-\pi^0\pi^0$	$< 2 \times 10^{-4}$	CL=90%
Γ_{11}	$\pi^+\pi^-e^+e^-$	$< 2.8 \times 10^{-6}$	CL=90%
Γ_{12}	$\pi^+\pi^-\gamma$	$< 3.6 \times 10^{-3}$	CL=95%
Γ_{13}	$\pi^+\pi^-\pi^+\pi^-$	$< 1 \times 10^{-3}$	CL=90%
Γ_{14}	$\pi^0\pi^0\gamma$	$(6.7 \pm 1.1) \times 10^{-5}$	
Γ_{15}	$\eta\pi^0\gamma$	$< 3.3 \times 10^{-5}$	CL=90%
Γ_{16}	$\mu^+\mu^-$	$(7.4 \pm 1.8) \times 10^{-5}$	
Γ_{17}	3γ	$< 1.9 \times 10^{-4}$	CL=95%
	Charge conjugation (C) violating modes		
Γ_{18}	$\eta\pi^0$ C	$< 2.1 \times 10^{-4}$	CL=90%
Γ_{19}	$2\pi^0$ C	$< 2.2 \times 10^{-4}$	CL=90%
Γ_{20}	$3\pi^0$ C	$< 2.3 \times 10^{-4}$	CL=90%
Γ_{21}	invisible	$< 7 \times 10^{-5}$	CL=90%

CONSTRAINED FIT INFORMATION

An overall fit to 15 branching ratios uses 49 measurements and one constraint to determine 10 parameters. The overall fit has a $\chi^2 = 48.9$ for 40 degrees of freedom.

The following *off-diagonal* array elements are the correlation coefficients $\langle \delta x_i \delta x_j \rangle / (\delta x_i \cdot \delta x_j)$, in percent, from the fit to the branching fractions, $x_i \equiv \Gamma_i/\Gamma_{total}$. The fit constrains the x_i whose labels appear in this array to sum to one.

	x_1	x_2	x_3	x_4	x_5	x_6	x_7	x_9	x_{14}
x_2	24								
x_3	−18	−4							
x_4	−93	−55	1						
x_5	7	16	−1	−12					
x_6	−1	0	0	0	0				
x_7	0	0	0	0	0	0			
x_9	−28	−59	5	44	−28	0	0		
x_{14}	1	4	0	−2	1	0	0	−2	
x_{16}	0	0	0	0	0	0	0	0	0

$\omega(782)$ PARTIAL WIDTHS

$\Gamma(\pi^0\gamma)$ — Γ_2

VALUE (keV)	EVTS	DOCUMENT ID		TECN	COMMENT
• • • We do not use the following data for averages, fits, limits, etc. • • •					
880±50	7815	[1] ACHASOV	13	SND	1.05–2.00 $e^+e^- \to \pi^0\pi^0\gamma$
788±12±27	36500	[2] ACHASOV	03	SND	0.60–0.97 $e^+e^- \to \pi^0\gamma$
764±51	10625	DOLINSKY	89	ND	$e^+e^- \to \pi^0\gamma$

[1] Systematic uncertainty not estimated.
[2] Using $\Gamma_\omega = 8.44 \pm 0.09$ MeV and $B(\omega \to \pi^0\gamma)$ from ACHASOV 03.

$\Gamma(\eta\gamma)$ — Γ_5

VALUE (keV)	DOCUMENT ID		TECN	COMMENT
• • • We do not use the following data for averages, fits, limits, etc. • • •				
6.1±2.5	[1] DOLINSKY	89	ND	$e^+e^- \to \eta\gamma$

[1] Using $\Gamma_\omega = 8.4 \pm 0.1$ MeV and $B(\omega \to \eta\gamma)$ from DOLINSKY 89.

$\Gamma(e^+e^-)$ — Γ_9

VALUE (keV)	EVTS	DOCUMENT ID		TECN	COMMENT
0.60 ±0.02 OUR EVALUATION					
• • • We do not use the following data for averages, fits, limits, etc. • • •					
0.591±0.015	11200	[1,2] AKHMETSHIN	04	CMD2	$e^+e^- \to \pi^+\pi^-\pi^0$
0.653±0.003±0.021	1.2M	[3] ACHASOV	03D	RVUE	0.44–2.00 $e^+e^- \to \pi^+\pi^-\pi^0$
0.600±0.031	10625	DOLINSKY	89	ND	$e^+e^- \to \pi^0\gamma$

[1] Using $B(\omega \to \pi^+\pi^-\pi^0) = 0.891 \pm 0.007$ and $\Gamma_{total} = 8.44 \pm 0.09$ MeV.
[2] Update of AKHMETSHIN 00C.
[3] Using ACHASOV 03, ACHASOV 03D and $B(\omega \to \pi^+\pi^-) = (1.70 \pm 0.28)\%$.

Int. J. Mod. Phys. A 2026.41. Downloaded from www.worldscientific.com
by UNIVERSITY OF CALIFORNIA @ BERKELEY on 09/16/26. Re-use and distribution is strictly not permitted, except for Open Access articles.

Int. J. Mod. Phys. A 2026.41. Downloaded from www.worldscientific.com
by LIFORNIA @ BERKELEY on 09/16/26. Re-use and distribution is strictly not permitted, except for Open Access articles.

$\omega(782)$ $\Gamma(i)\Gamma(e^+e^-)/\Gamma(\text{total})$

$\Gamma(\pi^+\pi^-\pi^0) \times \Gamma(e^+e^-)/\Gamma_{\text{total}}$ — $\Gamma_1\Gamma_9/\Gamma$

VALUE (eV)	DOCUMENT ID		TECN	COMMENT
569.8±3.1±8.2	[1] LEES	21B	BABR	10.5 $e^+e^- \to \pi^+\pi^-\pi^0\gamma$

[1] From the cross section for $e^+e^- \to \pi^+\pi^-\pi^0$ with contributions from $\rho(770)$, $\omega(782)$, $\phi(1020)$, $\omega(1420)$, and $\omega(1650)$.

$\omega(782)$ $\Gamma(e^+e^-)\Gamma(i)/\Gamma^2(\text{total})$

$\Gamma(e^+e^-)/\Gamma_{\text{total}} \times \Gamma(\pi^+\pi^-\pi^0)/\Gamma_{\text{total}}$ — $\Gamma_9/\Gamma \times \Gamma_1/\Gamma$

VALUE (units 10^{-5})	EVTS	DOCUMENT ID		TECN	COMMENT
6.61±0.16 OUR FIT Error includes scale factor of 2.0.					
6.45±0.15 OUR AVERAGE Error includes scale factor of 1.5. See the ideogram below.					
6.82±0.04±0.23	123k	[1] IGNATOV	24	CMD3	$e^+e^- \to \pi^+\pi^-\pi^0$
6.24±0.11±0.08	11.2k	[2] AKHMETSHIN	04	CMD2	$e^+e^- \to \pi^+\pi^-\pi^0$
6.74±0.04±0.24	1.2M	[3,4] ACHASOV	03D	RVUE	0.44–2.00 $e^+e^- \to \pi^+\pi^-\pi^0$
6.37±0.35		[3] DOLINSKY	89	ND	$e^+e^- \to \pi^+\pi^-\pi^0$
• • • We do not use the following data for averages, fits, limits, etc. • • •					
6.20±0.13		[5] BENAYOUN	10	RVUE	0.4–1.05 e^+e^-
6.70±0.06±0.27		[6] AUBERT,B	04N	BABR	10.6 $e^+e^- \to \pi^+\pi^-\pi^0\gamma$
6.45±0.24		[7] BARKOV	87	CMD	$e^+e^- \to \pi^+\pi^-\pi^0$
5.79±0.42	1488	[8] KURDADZE	83B	OLYA	$e^+e^- \to \pi^+\pi^-\pi^0$
5.89±0.54	433	[7] CORDIER	80	DM1	$e^+e^- \to \pi^+\pi^-\pi^0$
7.54±0.84	451	[7] BENAKSAS	72B	OSPK	$e^+e^- \to \pi^+\pi^-\pi^0$

[1] From a fit of the cross section using a VMD model which includes the interference of the ω and ϕ and non-resonant background, with some parameters, including ϕ mass and width, fixed at their PDG 22 values.
[2] Update of AKHMETSHIN 00C.
[3] Recalculated by us from the cross section in the peak.
[4] From the combined fit of ANTONELLI 92, ACHASOV 01E, ACHASOV 02E, and ACHASOV 03D data on the $\pi^+\pi^-\pi^0$ and ANTONELLI 92 on the $\omega\pi^+\pi^-$ final states. Supersedes ACHASOV 99E and ACHASOV 02E.
[5] A simultaneous fit of $e^+e^- \to \pi^+\pi^-$, $\pi^+\pi^-\pi^0$, $\pi^0\gamma$, $\eta\gamma$ data.
[6] Superseeded by LEES 21B.
[7] Recalculated by us from the cross section in the peak. Systematic uncertainties underestimated.
[8] Recalculated by us from the cross section in the peak. Systematic uncertainties not estimated.

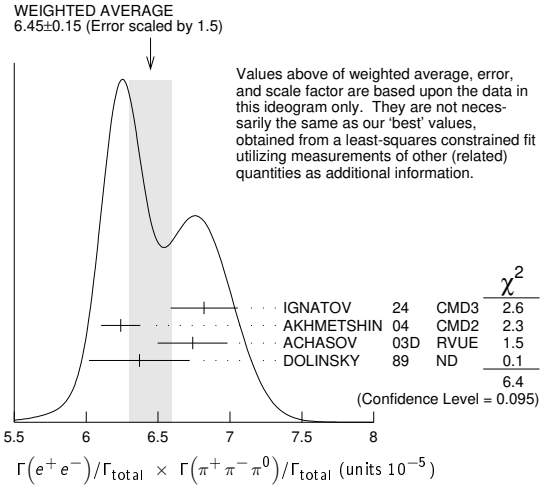

$\Gamma(e^+e^-)/\Gamma_{\text{total}} \times \Gamma(\pi^0\gamma)/\Gamma_{\text{total}}$ — $\Gamma_9/\Gamma \times \Gamma_2/\Gamma$

VALUE (units 10^{-6})	EVTS	DOCUMENT ID		TECN	COMMENT
6.17 ±0.16 OUR FIT Error includes scale factor of 2.0.					
6.34 ±0.10 OUR AVERAGE					
6.336±0.056±0.089		[1] ACHASOV	16A	SND	0.60–1.38 $e^+e^- \to \pi^0\gamma$
6.47 ±0.14 ±0.39	18k	AKHMETSHIN	05	CMD2	0.60–1.38 $e^+e^- \to \pi^0\gamma$
6.34 ±0.21 ±0.21	10k	[2] DOLINSKY	89	ND	$e^+e^- \to \pi^0\gamma$
• • • We do not use the following data for averages, fits, limits, etc. • • •					
6.80 ±0.13		[3] BENAYOUN	10	RVUE	0.4–1.05 e^+e^-
6.50 ±0.11 ±0.20	36k	[4] ACHASOV	03	SND	0.60–0.97 $e^+e^- \to \pi^0\gamma$

[1] From the VMD model with the interfering $\rho(770)$, $\omega(782)$, $\phi(1020)$, and an additional resonance describing the total contribution of the $\rho(1450)$ and $\omega(1420)$ states. Supersedes ACHASOV 03.
[2] Recalculated by us from the cross section in the peak.
[3] A simultaneous fit of $e^+e^- \to \pi^+\pi^-$, $\pi^+\pi^-\pi^0$, $\pi^0\gamma$, $\eta\gamma$ data.
[4] Using $\sigma(\phi \to \pi^0\gamma)$ from ACHASOV 00 and m_ω = 782.57 MeV in the model with the energy-independent phase of ρ-ω interferenceequal to $(-10.2 \pm 7.0)^\circ$.

$\Gamma(e^+e^-)/\Gamma_{\text{total}} \times \Gamma(\pi^+\pi^-)/\Gamma_{\text{total}}$ — $\Gamma_9/\Gamma \times \Gamma_3/\Gamma$

VALUE (units 10^{-6})	EVTS	DOCUMENT ID		TECN	COMMENT
1.225±0.030 OUR AVERAGE Error includes scale factor of 1.3. See the ideogram below.					
1.204±0.013±0.023	34M	[1] IGNATOV	24	CMD3	$e^+e^- \to \pi^+\pi^-$
1.318±0.051±0.021		[2] ACHASOV	21	SND	$e^+e^- \to \pi^+\pi^-$
1.225±0.058±0.041	800k	[3] ACHASOV	06	SND	$e^+e^- \to \pi^+\pi^-$
• • • We do not use the following data for averages, fits, limits, etc. • • •					
1.166±0.036		[4] BENAYOUN	13	RVUE	0.4–1.05 e^+e^-
1.05 ±0.08		[5] DAVIER	13	RVUE	$e^+e^- \to \pi^+\pi^-(\gamma)$

[1] From a fit of the pion form factor in the energy range $0.32 < \sqrt{s} < 1.2$ GeV using the GOUNARIS 68 parametrization with the complex phase of the $\rho-\omega$ interference with ω and ϕ masses and widths constrained by the values and their errors from PDG 22, and leaving $\rho(1450)$, $\rho(1700)$ resonances as free parameters of the fit.
[2] From a fit of the cross section in the energy range $0.525 < \sqrt{s} < 0.883$ GeV parameterized by the sum of the Breit-Wigner amplitudes for the $\rho(770)$, ω and $\rho(1450)$ resonances. The measured phase of the $\rho(770)$—ω interference is $(110.7 \pm 1.5 \pm 1.0)^\circ$.
[3] Supersedes ACHASOV 05A.
[4] A simultaneous fit to $e^+e^- \to \pi^+\pi^-$, $\pi^+\pi^-\pi^0$, $\pi^0\gamma$, $\eta\gamma$, $K\overline{K}$, and $\tau^- \to \pi^-\pi^0\nu_\tau$ data. Supersedes BENAYOUN 10.
[5] From $e^+e^- \to \pi^+\pi^-(\gamma)$ data of LEES 12G.

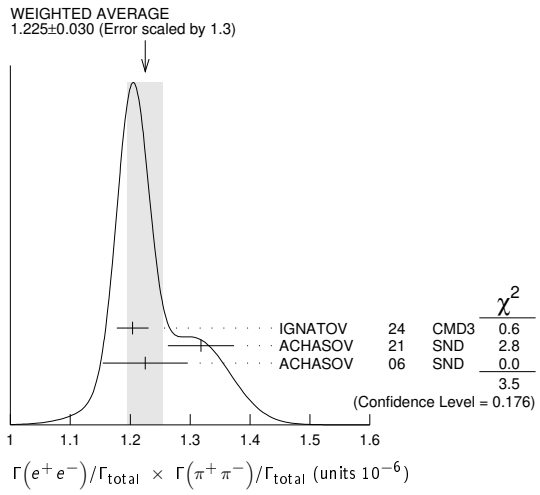

$\Gamma(e^+e^-)/\Gamma_{\text{total}} \times \Gamma(\eta\gamma)/\Gamma_{\text{total}}$ — $\Gamma_9/\Gamma \times \Gamma_5/\Gamma$

VALUE (units 10^{-8})	EVTS	DOCUMENT ID		TECN	COMMENT
3.32±0.28 OUR FIT Error includes scale factor of 1.1.					
3.18±0.28 OUR AVERAGE					
3.10±0.31±0.11	33k	[1] ACHASOV	07B	SND	0.6–1.38 $e^+e^- \to \eta\gamma$
$3.17^{+1.85}_{-1.31}\pm0.21$	17.4k	[2] AKHMETSHIN	05	CMD2	0.60–1.38 $e^+e^- \to \eta\gamma$
3.41±0.52±0.21	23k	[3,4] AKHMETSHIN	01B	CMD2	$e^+e^- \to \eta\gamma$
• • • We do not use the following data for averages, fits, limits, etc. • • •					
4.50±0.10		[5] BENAYOUN	10	RVUE	0.4–1.05 e^+e^-

[1] From a combined fit of $\sigma(e^+e^- \to \eta\gamma)$ with $\eta \to 3\pi^0$ and $\eta \to \pi^+\pi^-\pi^0$, and fixing $B(\eta \to 3\pi^0)$ / $B(\eta \to \pi^+\pi^-\pi^0)$ = 1.44 ± 0.04. Recalculated by us from the cross section at the peak. Supersedes ACHASOV 00D and ACHASOV 06A.
[2] From the $\eta \to 2\gamma$ decay and using $B(\eta \to \gamma\gamma)$= 39.43 ± 0.26%.
[3] From the $\eta \to 3\pi^0$ decay and using $B(\eta \to 3\pi^0)$= $(32.24 \pm 0.29) \times 10^{-2}$.
[4] The combined fit from 600 to 1380 MeV taking into account $\rho(770)$, $\omega(782)$, $\phi(1020)$, and $\rho(1450)$ (mass and width fixed at 1450 MeV and 310 MeV respectively).
[5] A simultaneous fit of $e^+e^- \to \pi^+\pi^-$, $\pi^+\pi^-\pi^0$, $\pi^0\gamma$, $\eta\gamma$ data.

$\Gamma(e^+e^-)/\Gamma_{\text{total}} \times \Gamma(\mu^+\mu^-)/\Gamma_{\text{total}}$ — $\Gamma_9/\Gamma \times \Gamma_{16}/\Gamma$

VALUE (units 10^{-9})	EVTS	DOCUMENT ID		TECN	COMMENT
4.3±1.8±2.2	4.5 M	[1] ANASTASI	17	KLOE	$e^+e^- \to \mu^+\mu^-\gamma$

[1] From a fit of the real part of the vacuum polarization by a sum of the leptonic and hadronic contributions, where the hadronic contribution is parametrized as a sum of Breit-Wigner resonances $\omega(782)$, $\phi(1020)$ and using a GOUNARIS 68 parametrization for the $\rho(770)$, and a non-resonant term.

$\omega(782)$ BRANCHING RATIOS

$\Gamma(\pi^+\pi^-\pi^0)/\Gamma_{\text{total}}$ — Γ_1/Γ

NIECKNIG 12 describes final-state interactions between the three pions in a dispersive framework using data on the $\pi\pi$ P-wave scattering phase shift.

VALUE	EVTS	DOCUMENT ID		TECN	COMMENT
• • • We do not use the following data for averages, fits, limits, etc. • • •					
0.9024±0.0019		[1] AMBROSINO	08G	KLOE	1.0–1.03 $e^+e^- \to \pi^+\pi^-2\pi^0$, $2\pi^0\gamma$
0.8965±0.0016±0.0048	1.2M	[2,3] ACHASOV	03D	RVUE	0.44–2.00 $e^+e^- \to \pi^+\pi^-\pi^0$
0.880 ±0.020 ±0.032	11200	[3,4] AKHMETSHIN	00C	CMD2	$e^+e^- \to \pi^+\pi^-\pi^0$
0.8942±0.0062		[3] DOLINSKY	89	ND	$e^+e^- \to \pi^+\pi^-\pi^0$

[1] Not independent of $\Gamma(\pi^0\gamma)$ / $\Gamma(\pi^+\pi^-\pi^0)$ from AMBROSINO 08G.
[2] Using ACHASOV 03, ACHASOV 03D and $B(\omega \to \pi^+\pi^-)$ = (1.70 ± 0.28)%.
[3] Not independent of the corresponding $\Gamma(e^+e^-) \times \Gamma(\pi^+\pi^-\pi^0)/\Gamma^2_{\text{total}}$.
[4] Using $\Gamma(e^+e^-)$=0.60 ± 0.02 keV.

Int. J. Mod. Phys. A 2026.41. Downloaded from www.worldscientific.com by UNIVERSITY OF CALIFORNIA @ BERKELEY on 09/16/26. Re-use and distribution is strictly not permitted, except for Open Access articles.

$\Gamma(\pi^0\gamma)/\Gamma_{total}$ — Γ_2/Γ

VALUE (units 10^{-2})	EVTS	DOCUMENT ID		TECN	COMMENT
• • • We do not use the following data for averages, fits, limits, etc. • • •					
8.88±0.18		[1] ACHASOV	16A	SND	0.60–1.38 $e^+e^- \to \pi^0\gamma$
8.09±0.14		[2] AMBROSINO	08G	KLOE	$e^+e^- \to \pi^+\pi^-2\pi^0$, $2\pi^0\gamma$
9.06±0.20±0.57	18k	[3,4] AKHMETSHIN	05	CMD2	0.60-1.38 $e^+e^- \to \pi^0\gamma$
9.34±0.15±0.31	36k	[4] ACHASOV	03	SND	0.60–0.97 $e^+e^- \to \pi^0\gamma$
8.65±0.16±0.42	1.2M	[5,6] ACHASOV	03D	RVUE	0.44–2.00 $e^+e^- \to \pi^+\pi^-\pi^0$
8.39±0.24	9k	[7] BENAYOUN	96	RVUE	$e^+e^- \to \pi^0\gamma$
8.88±0.62	10k	[4] DOLINSKY	89	ND	$e^+e^- \to \pi^0\gamma$

[1] Using $B(\omega \to e^+e^-)$ from PDG 15. Supersedes ACHASOV 03.
[2] Not independent of $\Gamma(\pi^0\gamma)$ / $\Gamma(\pi^+\pi^-\pi^0)$ from AMBROSINO 08G.
[3] Using $B(\omega \to e^+e^-) = (7.14 \pm 0.13) \times 10^{-5}$.
[4] Not independent of the corresponding $\Gamma(e^+e^-) \times \Gamma(\pi^0\gamma)/\Gamma^2_{total}$.
[5] Using ACHASOV 03, ACHASOV 03D and $B(\omega \to \pi^+\pi^-) = (1.70 \pm 0.28)\%$.
[6] Not independent of the corresponding $\Gamma(e^+e^-) \times \Gamma(\pi^+\pi^-\pi^0)/\Gamma^2_{total}$.
[7] Reanalysis of DRUZHININ 84, DOLINSKY 89, DOLINSKY 91 taking into account the triangle anomaly contributions.

$\Gamma(\pi^0\gamma)/\Gamma(\pi^+\pi^-\pi^0)$ — Γ_2/Γ_1

VALUE (units 10^{-2})	DOCUMENT ID		TECN	COMMENT
9.33±0.28 OUR FIT Error includes scale factor of 2.3.				
9.05±0.27 OUR AVERAGE Error includes scale factor of 1.8.				
8.97±0.16	AMBROSINO	08G	KLOE	$e^+e^- \to \pi^+\pi^-2\pi^0$, $2\pi^0\gamma$
9.94±0.36±0.38	[1] AULCHENKO	00A	SND	$e^+e^- \to \pi^+\pi^-2\pi^0$, $2\pi^0\gamma$
8.4 ±1.3	KEYNE	76	CNTR	$\pi^-p \to \omega n$
10.9 ±2.5	BENAKSAS	72C	OSPK	$e^+e^- \to \pi^0\gamma$
8.1 ±2.0	BALDIN	71	HLBC	2.9 π^+p
13 ±4	JACQUET	69B	HLBC	2.05 $\pi^+p \to \pi^+p\omega$
• • • We do not use the following data for averages, fits, limits, etc. • • •				
9.7 ±0.2 ±0.5	[2,3] ACHASOV	03D	RVUE	0.44–2.00 $e^+e^- \to \pi^+\pi^-\pi^0$
9.9 ±0.7	[2] DOLINSKY	89	ND	$e^+e^- \to \pi^0\gamma$

[1] From $\sigma_0^{\omega\pi^0 \to \pi^0\pi^0\gamma}(m_\phi)/\sigma_0^{\omega\pi^0 \to \pi^+\pi^-\pi^0\pi^0}(m_\phi)$ with a phase-space correction factor of 1/1.023.
[2] Not independent of the corresponding $\Gamma(e^+e^-) \times \Gamma(\pi^0\gamma)/\Gamma^2_{total}$.
[3] Using ACHASOV 03. Based on 1.2M events.

$\Gamma(\pi^+\pi^-)/\Gamma_{total}$ — Γ_3/Γ

See also $\Gamma(\pi^+\pi^-)/\Gamma(\pi^+\pi^-\pi^0)$.

VALUE (units 10^{-2})	EVTS	DOCUMENT ID		TECN	COMMENT
1.53±0.12 OUR FIT Error includes scale factor of 1.2.					
1.49±0.13 OUR AVERAGE Error includes scale factor of 1.3. See the ideogram below.					
1.46±0.12±0.02	900k	[1] AKHMETSHIN	07		$e^+e^- \to \pi^+\pi^-$
1.30±0.24±0.05	11.2k	[2] AKHMETSHIN	04	CMD2	$e^+e^- \to \pi^+\pi^-$
$2.38^{+1.77}_{-0.90}$±0.18	5.4k	[3] ACHASOV	02E	SND	1.1–1.38 $e^+e^- \to \pi^+\pi^-\pi^0$
2.3 ±0.5		BARKOV	85	OLYA	$e^+e^- \to \pi^+\pi^-$
1.6 $^{+0.9}_{-0.7}$		QUENZER	78	DM1	$e^+e^- \to \pi^+\pi^-$
3.6 ±1.9		BENAKSAS	72	OSPK	$e^+e^- \to \pi^+\pi^-$
• • • We do not use the following data for averages, fits, limits, etc. • • •					
1.29±0.22±0.03	970k	[4,5] ABLIKIM	18C	BES3	$\eta'(958) \to \gamma\pi^+\pi^-$
1.28±0.22±0.03	970k	[6,7] ABLIKIM	18C	BES3	$\eta'(958) \to \gamma\pi^+\pi^-$
1.52±0.08		[8] HANHART	18	RVUE	$e^+e^- \to \pi^+\pi^-$
1.75±0.11	4.5M	[9] ACHASOV	05A	SND	$e^+e^- \to \pi^+\pi^-$
2.01±0.29		[10] BENAYOUN	03	RVUE	$e^+e^- \to \pi^+\pi^-$
1.9 ±0.3		[11] GARDNER	99	RVUE	$e^+e^- \to \pi^+\pi^-$
2.3 ±0.4		[12] BENAYOUN	98	RVUE	$e^+e^- \to \pi^+\pi^-$, $\mu^+\mu^-$
1.0 ±0.11		[13] WICKLUND	78	ASPK	3,4,6 $\pi^\pm N$
1.22±0.30		ALVENSLEB...	71C	CNTR	Photoproduction
1.3 $^{+1.2}_{-0.9}$		MOFFEIT	71	HBC	2.8,4.7 γp
0.80$^{+0.28}_{-0.20}$		[14] BIGGS	70B	CNTR	4.2γC $\to \pi^+\pi^-$C

[1] A combined fit of AKHMETSHIN 07, AULCHENKO 06, and AULCHENKO 05.
[2] Update of AKHMETSHIN 02.
[3] From the $m_{\pi^+\pi^-}$ spectrum taking into account the interference of the $\rho\pi$ and $\omega\pi$ amplitudes.
[4] From a fit to $\pi^+\pi^-$ mass using $\rho(770)$ (parametrized with the Gounaris-Sakurai approach), $\omega(782)$, and box anomaly components.
[5] ABLIKIM 18C reports $[\Gamma(\omega(782) \to \pi^+\pi^-)/\Gamma_{total}] \times [B(\eta'(958) \to \omega\gamma)] = (3.25 \pm 0.21 \pm 0.52) \times 10^{-4}$ which we divide by our best (shown rounded) value $B(\eta'(958) \to \omega\gamma) = (2.52 \pm 0.07) \times 10^{-2}$. Our first error is their experiment's error and our second error is the systematic error from using our best (shown rounded) value.
[6] From a fit to $\pi^+\pi^-$ mass using $\rho(770)$ (parametrized with the Gounaris-Sakurai approach), $\omega(782)$, and $\rho(1450)$ components.
[7] ABLIKIM 18C reports $[\Gamma(\omega(782) \to \pi^+\pi^-)/\Gamma_{total}] \times [B(\eta'(958) \to \omega\gamma)] = (3.22 \pm 0.21 \pm 0.52) \times 10^{-4}$ which we divide by our best (shown rounded) value $B(\eta'(958) \to \omega\gamma) = (2.52 \pm 0.07) \times 10^{-2}$. Our first error is their experiment's error and our second error is the systematic error from using our best (shown rounded) value.
[8] Dispersive analysis. Value extracted from average of data from AUBERT 09AS, AKHMETSHIN 07, ACHASOV 06, AMBROSINO 11A, BABUSCI 13D, ABLIKIM 16B normalised by PDG 16 evaluation for $\Gamma(\omega \to e^+e^-)$.
[9] Using $\Gamma(\omega \to e^+e^-)$ from the 2004 Edition of this Review (PDG 04).
[10] Using the data of AKHMETSHIN 02 in the hidden local symmetry model.
[11] Using the data of BARKOV 85.
[12] Using the data of BARKOV 85 in the hidden local symmetry model.
[13] From a model-dependent analysis assuming complete coherence.
[14] Re-evaluated under $\Gamma(\pi^+\pi^-)/\Gamma(\pi^+\pi^-\pi^0)$ by BEHREND 71 using more accurate $\omega \to \rho$ photoproduction cross-section ratio.

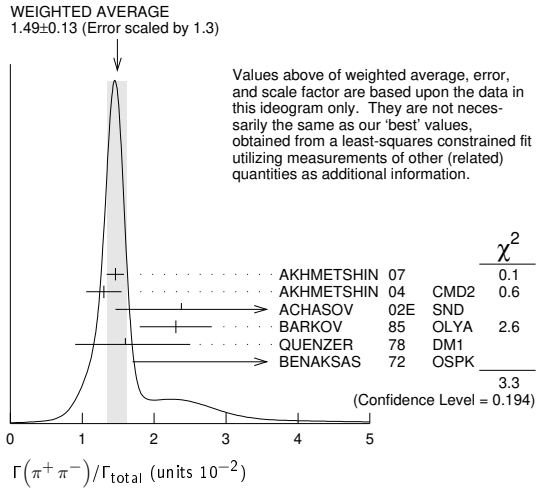

$\Gamma(\pi^+\pi^-)/\Gamma(\pi^+\pi^-\pi^0)$ — Γ_3/Γ_1

See also $\Gamma(\pi^+\pi^-)/\Gamma_{total}$.

VALUE	DOCUMENT ID		TECN	COMMENT
0.0172±0.0014 OUR FIT Error includes scale factor of 1.2.				
0.026 ±0.005 OUR AVERAGE				
0.021 $^{+0.028}_{-0.009}$	[1,2] RATCLIFF	72	ASPK	15 $\pi^-p \to n2\pi$
0.028 ±0.006	[1] BEHREND	71	ASPK	Photoproduction
0.022 $^{+0.009}_{-0.01}$	[3] ROOS	70	RVUE	

[1] The fitted width of these data is 160 MeV in agreement with present average, thus the ω contribution is overestimated. Assuming ρ width 145 MeV.
[2] Significant interference effect observed. NB of $\omega \to 3\pi$ comes from an extrapolation.
[3] ROOS 70 combines ABRAMOVICH 70 and BIZZARRI 70.

$\Gamma(\pi^+\pi^-)/\Gamma(\pi^0\gamma)$ — Γ_3/Γ_2

VALUE	EVTS	DOCUMENT ID		TECN	COMMENT
0.20±0.04	1.98M	[1] ALOISIO	03	KLOE	1.02 $e^+e^- \to \pi^+\pi^-\pi^0$

[1] Using the data of ALOISIO 02D.

$\Gamma(\text{neutrals})/\Gamma_{total}$ — $(\Gamma_2+\Gamma_4)/\Gamma$

VALUE	EVTS	DOCUMENT ID		TECN	COMMENT
0.091±0.006 OUR FIT					
0.081±0.011 OUR AVERAGE					
0.075±0.025		BIZZARRI	71	HBC	0.0 $p\overline{p}$
0.079±0.019		DEINET	69B	OSPK	1.5 π^-p
0.084±0.015		BOLLINI	68C	CNTR	2.1 π^-p
• • • We do not use the following data for averages, fits, limits, etc. • • •					
0.073±0.018	42	BASILE	72B	CNTR	1.67 π^-p

$\Gamma(\text{neutrals})/\Gamma(\pi^+\pi^-\pi^0)$ — $(\Gamma_2+\Gamma_4)/\Gamma_1$

VALUE	EVTS	DOCUMENT ID		TECN	COMMENT
0.102±0.008 OUR FIT					
0.103$^{+0.011}_{-0.010}$ OUR AVERAGE					
0.15 ±0.04	46	AGUILAR-...	72B	HBC	3.9,4.6 K^-p
0.10 ±0.03	19	BARASH	67B	HBC	0.0 $\overline{p}p$
0.134±0.026	850	DIGIUGNO	66B	CNTR	1.4 π^-p
0.097±0.016	348	FLATTE	66	HBC	1.4 – 1.7 $K^-p \to \Lambda$MM
0.06 $^{+0.05}_{-0.02}$		JAMES	66	HBC	2.1 π^+p
0.08 ±0.03	35	KRAEMER	64	DBC	1.2 π^+d
• • • We do not use the following data for averages, fits, limits, etc. • • •					
0.11 ±0.02	20	BUSCHBECK	63	HBC	1.5 K^-p

$\Gamma(\pi^0\gamma)/\Gamma(\text{neutrals})$ — $\Gamma_2/(\Gamma_2+\Gamma_4)$

VALUE	CL%	DOCUMENT ID		TECN	COMMENT
• • • We do not use the following data for averages, fits, limits, etc. • • •					
0.78±0.07		[1] DAKIN	72	OSPK	1.4 $\pi^-p \to n$MM
>0.81	90	DEINET	69B	OSPK	

[1] Error statistical only. Authors obtain good fit also assuming $\pi^0\gamma$ as the only neutral decay.

Int. J. Mod. Phys. A 2026.41. Downloaded from www.worldscientific.com by CALIFORNIA @ BERKELEY on 09/16/26. Re-use and distribution is strictly not permitted, except for Open Access articles.

$\Gamma(\text{neutrals})/\Gamma(\text{charged particles})$ — $(\Gamma_2+\Gamma_4)/(\Gamma_1+\Gamma_3)$

VALUE	DOCUMENT ID		TECN	COMMENT
0.100±0.008 OUR FIT				
0.124±0.021	FELDMAN	67C	OSPK	1.2 $\pi^- p$

$\Gamma(\eta\gamma)/\Gamma_{\text{total}}$ — Γ_5/Γ

VALUE (units 10^{-4})	EVTS	DOCUMENT ID		TECN	COMMENT
4.5 ±0.4 OUR FIT Error includes scale factor of 1.1.					
6.3 ±1.3 OUR AVERAGE Error includes scale factor of 1.2.					
6.6 ±1.7		[1] ABELE	97E	CBAR	0.0 $\overline{p}p \to 5\gamma$
8.3 ±2.1		ALDE	93	GAM2	38$\pi^- p \to \omega n$
3.0 $^{+2.5}_{-1.8}$		[2] ANDREWS	77	CNTR	6.7–10 γ Cu
• • • We do not use the following data for averages, fits, limits, etc. • • •					
4.2 ±0.4 ±0.1	33k	[3] ACHASOV	07B	SND	0.6–1.38 $e^+e^- \to \eta\gamma$
4.44$^{+2.59}_{-1.83}$±0.28	17.4k	[4,5] AKHMETSHIN	05	CMD2	0.60-1.38 $e^+e^- \to \eta\gamma$
5.10±0.72±0.34	23k	[6] AKHMETSHIN	01B	CMD2	$e^+e^- \to \eta\gamma$
0.7 to 5.5		[7] CASE	00	CBAR	0.0 $p\overline{p} \to \eta\eta\gamma$
6.56$^{+2.41}_{-2.55}$	3525	[2,8] BENAYOUN	96	RVUE	$e^+e^- \to \eta\gamma$
7.3 ±2.9		[2,4] DOLINSKY	89	ND	$e^+e^- \to \eta\gamma$

[1] No flat $\eta\eta\gamma$ background assumed.
[2] Solution corresponding to constructive ω-ρ interference.
[3] ACHASOV 07B reports $[\Gamma(\omega(782) \to \eta\gamma)/\Gamma_{\text{total}}] \times [B(\omega(782) \to e^+e^-)] = (3.10 \pm 0.31 \pm 0.11) \times 10^{-8}$ which we divide by our best (shown rounded) value $B(\omega(782) \to e^+e^-) = (7.41 \pm 0.19) \times 10^{-5}$. Our first error is their experiment's error and our second error is the systematic error from using our best (shown rounded) value. Supersedes ACHASOV 00D and ACHASOV 06A.
[4] Not independent of the corresponding $\Gamma(e^+e^-) \times \Gamma(\eta\gamma)/\Gamma^2_{\text{total}}$.
[5] Using $B(\omega \to e^+e^-) = (7.14 \pm 0.13) \times 10^{-5}$ and $B(\eta \to \gamma\gamma) = 39.43 \pm 0.26\%$.
[6] Using $B(\omega \to e^+e^-) = (7.07 \pm 0.19) \times 10^{-5}$ and using $B(\eta \to 3\pi^0) = (32.24 \pm 0.29) \times 10^{-2}$. Solution corresponding to constructive ω-ρ interference. The combined fit from 600 to 1380 MeV taking into account $\rho(770)$, $\omega(782)$, $\phi(1020)$, and $\rho(1450)$ (mass and width fixed at 1450 MeV and 310 MeV respectively). Not independent of the corresponding $\Gamma(e^+e^-) \times \Gamma(\eta\gamma)/\Gamma^2_{\text{total}}$.
[7] Depending on the degree of coherence with the flat $\eta\eta\gamma$ background and using $B(\omega \to \pi^0\gamma) = (8.5 \pm 0.5) \times 10^{-2}$.
[8] Reanalysis of DRUZHININ 84, DOLINSKY 89, DOLINSKY 91 taking into account the triangle anomaly contributions.

$\Gamma(\eta\gamma)/\Gamma(\pi^0\gamma)$ — Γ_5/Γ_2

VALUE	DOCUMENT ID		TECN	COMMENT
• • • We do not use the following data for averages, fits, limits, etc. • • •				
0.0098±0.0024	[1] ALDE	93	GAM2	38$\pi^- p \to \omega n$
0.0082±0.0033	[2] DOLINSKY	89	ND	$e^+e^- \to \eta\gamma$
0.010 ±0.045	APEL	72B	OSPK	4–8 $\pi^- p \to n3\gamma$

[1] Model independent determination.
[2] Solution corresponding to constructive ω-ρ interference.

$\Gamma(\pi^0 e^+e^-)/\Gamma_{\text{total}}$ — Γ_6/Γ

VALUE (units 10^{-4})	EVTS	DOCUMENT ID		TECN	COMMENT
7.7 ±0.6 OUR FIT					
7.7 ±0.6 OUR AVERAGE					
7.61±0.53±0.64		ACHASOV	08	SND	0.36–0.97 $e^+e^- \to \pi^0 e^+e^-$
8.19±0.71±0.62		AKHMETSHIN	05A	CMD2	0.72-0.84 e^+e^-
5.9 ±1.9	43	DOLINSKY	88	ND	$e^+e^- \to \pi^0 e^+e^-$

$\Gamma(\pi^0\mu^+\mu^-)/\Gamma_{\text{total}}$ — Γ_7/Γ

VALUE (units 10^{-4})	EVTS	DOCUMENT ID		TECN	COMMENT
1.34±0.18 OUR FIT Error includes scale factor of 1.5.					
1.34±0.19 OUR AVERAGE Error includes scale factor of 1.5. See the ideogram below.					
1.41±0.09±0.15		ARNALDI	16	NA60	400 GeV (p-A) collisions
1.72±0.25±0.14	3k	ARNALDI	09	NA60	158A In–In collisions
0.96±0.23		DZHELYADIN	81B	CNTR	25–33 $\pi^- p \to \omega n$

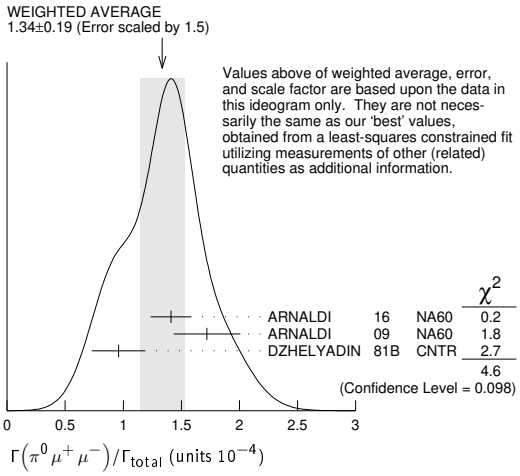

$\Gamma(\eta e^+e^-)/\Gamma_{\text{total}}$ — Γ_8/Γ

VALUE (units 10^{-5})	DOCUMENT ID		TECN	COMMENT
• • • We do not use the following data for averages, fits, limits, etc. • • •				
<1.1	AKHMETSHIN	05A	CMD2	0.72-0.84 e^+e^-

$\Gamma(e^+e^-)/\Gamma_{\text{total}}$ — Γ_9/Γ

VALUE (units 10^{-4})	EVTS	DOCUMENT ID		TECN	COMMENT
0.741±0.019 OUR FIT Error includes scale factor of 1.8.					
• • • We do not use the following data for averages, fits, limits, etc. • • •					
0.700±0.016	11200	[1,2] AKHMETSHIN	04	CMD2	$e^+e^- \to \pi^+\pi^-\pi^0$
0.752±0.004±0.024	1.2M	[2,3] ACHASOV	03D	RVUE	0.44–2.00 $e^+e^- \to \pi^+\pi^-\pi^0$
0.714±0.036		[2] DOLINSKY	89	ND	$e^+e^- \to \pi^+\pi^-\pi^0$
0.72 ±0.03		[2] BARKOV	87	CMD	$e^+e^- \to \pi^+\pi^-\pi^0$
0.64 ±0.04	1488	[2] KURDADZE	83B	OLYA	$e^+e^- \to \pi^+\pi^-\pi^0$
0.675±0.069	433	[2] CORDIER	80	DM1	$e^+e^- \to \pi^+\pi^-\pi^0$
0.83 ±0.10	451	[2] BENAKSAS	72B	OSPK	$e^+e^- \to \pi^+\pi^-\pi^0$
0.77 ±0.06		[4] AUGUSTIN	69D	OSPK	$e^+e^- \to \pi^+\pi^-\pi^0$
0.65 ±0.13	33	[5] ASTVACAT...	68	OSPK	Assume SU(3)+mixing

[1] Using $B(\omega \to \pi^+\pi^-\pi^0) = 0.891 \pm 0.007$. Update of AKHMETSHIN 00C.
[2] Not independent of the corresponding $\Gamma(e^+e^-) \times \Gamma(\pi^+\pi^-\pi^0)/\Gamma^2_{\text{total}}$.
[3] Using ACHASOV 03, ACHASOV 03D and $B(\omega \to \pi^+\pi^-) = (1.70 \pm 0.28)\%$.
[4] Rescaled by us to correspond to ω width 8.4 MeV. Systematic errors underestimated.
[5] Not resolved from ρ decay. Error statistical only.

$\Gamma(\pi^+\pi^-\pi^0\pi^0)/\Gamma_{\text{total}}$ — Γ_{10}/Γ

VALUE (units 10^{-4})	CL%	DOCUMENT ID		TECN	COMMENT
< 2	90	ACHASOV	09A	SND	$e^+e^- \to \pi^+\pi^-\pi^0\pi^0$
• • • We do not use the following data for averages, fits, limits, etc. • • •					
<200	90	KURDADZE	86	OLYA	$e^+e^- \to \pi^+\pi^-\pi^0\pi^0$

$\Gamma(\pi^+\pi^-e^+e^-)/\Gamma_{\text{total}}$ — Γ_{11}/Γ

VALUE	CL%	DOCUMENT ID		TECN	COMMENT
<2.8 × 10^{-6}	90	ABLIKIM	25CI	BES3	$J/\psi \to \omega\eta$

$\Gamma(\pi^+\pi^-\gamma)/\Gamma_{\text{total}}$ — Γ_{12}/Γ

VALUE	CL%	DOCUMENT ID		TECN	COMMENT
<0.0036	95	WEIDENAUER	90	ASTE	$p\overline{p} \to \pi^+\pi^-\pi^+\pi^-\gamma$
• • • We do not use the following data for averages, fits, limits, etc. • • •					
<0.004	95	BITYUKOV	88B	SPEC	32 $\pi^- p \to \pi^+\pi^-\gamma X$

$\Gamma(\pi^+\pi^-\gamma)/\Gamma(\pi^+\pi^-\pi^0)$ — Γ_{12}/Γ_1

VALUE	CL%	DOCUMENT ID		TECN	COMMENT
• • • We do not use the following data for averages, fits, limits, etc. • • •					
<0.066	90	KALBFLEISCH	75	HBC	2.18 $K^- p \to \Lambda\pi^+\pi^-\gamma$
<0.05	90	FLATTE	66	HBC	1.2 – 1.7 $K^- p \to \Lambda\pi^+\pi^-\gamma$

$\Gamma(\pi^+\pi^-\pi^+\pi^-)/\Gamma_{\text{total}}$ — Γ_{13}/Γ

VALUE	CL%	DOCUMENT ID		TECN	COMMENT
<1 × 10^{-3}	90	KURDADZE	88	OLYA	$e^+e^- \to \pi^+\pi^-\pi^+\pi^-$

$\Gamma(\pi^0\pi^0\gamma)/\Gamma_{\text{total}}$ — Γ_{14}/Γ

VALUE (units 10^{-5})	EVTS	DOCUMENT ID		TECN	COMMENT
6.7±1.1 OUR FIT					
6.5±1.2 OUR AVERAGE					
6.4$^{+2.4}_{-2.0}$±0.8	190	[1] AKHMETSHIN	04B	CMD2	0.6–0.97 $e^+e^- \to \pi^0\pi^0\gamma$
6.6$^{+1.4}_{-1.3}$±0.6	295	ACHASOV	02F	SND	0.36–0.97 $e^+e^- \to \pi^0\pi^0\gamma$
• • • We do not use the following data for averages, fits, limits, etc. • • •					
11.8$^{+2.1}_{-1.9}$±1.4	190	[2] AKHMETSHIN	04B	CMD2	0.6–0.97 $e^+e^- \to \pi^0\pi^0\gamma$
7.8±2.7±2.0	63	[1,3] ACHASOV	00G	SND	$e^+e^- \to \pi^0\pi^0\gamma$
12.7±2.3±2.5	63	[2,3] ACHASOV	00G	SND	$e^+e^- \to \pi^0\pi^0\gamma$

[1] In the model assuming the $\rho \to \pi^0\pi^0\gamma$ decay via the $\omega\pi$ and $f_0(500)\gamma$ mechanisms.
[2] In the model assuming the $\rho \to \pi^0\pi^0\gamma$ decay via the $\omega\pi$ mechanism only.
[3] Superseded by ACHASOV 02F.

$\Gamma(\pi^0\pi^0\gamma)/\Gamma(\pi^+\pi^-\pi^0)$ — Γ_{14}/Γ_1

VALUE	CL%	DOCUMENT ID		TECN	COMMENT
<0.00045	90	DOLINSKY	89	ND	$e^+e^- \to \pi^0\pi^0\gamma$
• • • We do not use the following data for averages, fits, limits, etc. • • •					
<0.08	95	JACQUET	69B	HLBC	2.05 $\pi^+ p \to \pi^+ p\omega$

$\Gamma(\pi^0\pi^0\gamma)/\Gamma(\pi^0\gamma)$ — Γ_{14}/Γ_2

VALUE (units 10^{-4})	CL%	EVTS	DOCUMENT ID		TECN	COMMENT
8.0±1.3 OUR FIT						
8.5±2.9		40 ± 14	ALDE	94B	GAM2	38$\pi^- p \to \pi^0\pi^0\gamma n$
• • • We do not use the following data for averages, fits, limits, etc. • • •						
< 50	90		DOLINSKY	89	ND	$e^+e^- \to \pi^0\pi^0\gamma$
<1800	95		KEYNE	76	CNTR	$\pi^- p \to \omega n$
<1500	90		BENAKSAS	72C	OSPK	e^+e^-
<1400			BALDIN	71	HLBC	2.9 $\pi^+ p$
<1000	90		BARMIN	64	HLBC	1.3–2.8 $\pi^- p$

Int. J. Mod. Phys. A 2026.41. Downloaded from www.worldscientific.com
by UNIVERSITY OF CALIFORNIA @ BERKELEY on 09/16/26. Re-use and distribution is strictly not permitted, except for Open Access articles.

$\Gamma(\pi^0\pi^0\gamma)/\Gamma(\text{neutrals})$ — $\Gamma_{14}/(\Gamma_2+\Gamma_4)$

VALUE	CL%	DOCUMENT ID		TECN	COMMENT
• • • We do not use the following data for averages, fits, limits, etc. • • •					
0.22 ± 0.07		[1] DAKIN	72	OSPK	$1.4\ \pi^- p \to n$MM
<0.19	90	DEINET	69B	OSPK	

[1] See $\Gamma(\pi^0\gamma)/\Gamma(\text{neutrals})$.

$\Gamma(\eta\pi^0\gamma)/\Gamma_{total}$ — Γ_{15}/Γ

VALUE (units 10^{-5})	CL%	DOCUMENT ID		TECN	COMMENT
<3.3	90	AKHMETSHIN	04B	CMD2	0.6–0.97 $e^+e^- \to \eta\pi^0\gamma$

$\Gamma(\mu^+\mu^-)/\Gamma_{total}$ — Γ_{16}/Γ

VALUE (units 10^{-5})	EVTS	DOCUMENT ID		TECN	COMMENT
7.4±1.8 OUR FIT					
7.4±1.8 OUR AVERAGE					
$6.6\pm1.4\pm1.7$	4.5 M	[1] ANASTASI	17	KLOE	$e^+e^- \to \mu^+\mu^-\gamma$
$9.0\pm2.9\pm1.1$	18	HEISTER	02C	ALEP	$Z \to \mu^+\mu^- + X$

[1] Assuming lepton universality in the decay $\omega \to \ell^+\ell^-$ and correcting for different phase space between electron and muon final states.

$\Gamma(\mu^+\mu^-)/\Gamma(\pi^+\pi^-\pi^0)$ — Γ_{16}/Γ_1

VALUE (units 10^{-3})	CL%	DOCUMENT ID		TECN	COMMENT
<0.2	90	WILSON	69	OSPK	$12\ \pi^- C \to$ Fe
• • • We do not use the following data for averages, fits, limits, etc. • • •					
<1.7	74	FLATTE	66	HBC	$1.2-1.7\ K^- p \to \Lambda\mu^+\mu^-$
<1.2		BARBARO-...	65	HBC	$2.7\ K^- p$

$\Gamma(\pi^0\mu^+\mu^-)/\Gamma(\mu^+\mu^-)$ — Γ_7/Γ_{16}

VALUE	EVTS	DOCUMENT ID		TECN	COMMENT
• • • We do not use the following data for averages, fits, limits, etc. • • •					
1.2 ± 0.6	30	[1] DZHELYADIN	79	CNTR	$25-33\ \pi^- p$

[1] Superseded by DZHELYADIN 81B result above.

$\Gamma(3\gamma)/\Gamma_{total}$ — Γ_{17}/Γ

VALUE (units 10^{-4})	CL%	DOCUMENT ID		TECN	COMMENT
<1.9	95	[1] ABELE	97E	CBAR	$0.0\ \bar{p}p \to 5\gamma$
• • • We do not use the following data for averages, fits, limits, etc. • • •					
<2	90	[1] PROKOSHKIN	95	GAM2	$38\ \pi^- p \to 3\gamma n$

[1] From direct 3γ decay search.

$\Gamma(\eta\pi^0)/\Gamma_{total}$ — Γ_{18}/Γ

Violates C conservation.

VALUE	CL%	DOCUMENT ID		TECN	COMMENT
• • • We do not use the following data for averages, fits, limits, etc. • • •					
<0.001	90	ALDE	94B	GAM2	$38\pi^- p \to \eta\pi^0 n$

$[\Gamma(\eta\gamma)+\Gamma(\eta\pi^0)]/\Gamma(\pi^+\pi^-\pi^0)$ — $(\Gamma_5+\Gamma_{18})/\Gamma_1$

VALUE	CL%	DOCUMENT ID		TECN	COMMENT
<0.016	90	[1] FLATTE	66	HBC	$1.2-1.7\ K^- p \to \Lambda\pi^+\pi^-$ MM
• • • We do not use the following data for averages, fits, limits, etc. • • •					
<0.045	95	JACQUET	69B	HLBC	$2.05\ \pi^+ p \to \pi^+ p\omega$

[1] Restated by us using $B(\eta \to \text{charged modes}) = 29.2\%$.

$\Gamma(\eta\pi^0)/\Gamma(\pi^0\gamma)$ — Γ_{18}/Γ_2

Violates C conservation.

VALUE (units 10^{-3})	CL%	DOCUMENT ID		TECN	COMMENT
<2.6	90	[1] STAROSTIN	09	CRYM	$\gamma p \to \eta\pi^0 p$

[1] STAROSTIN 09 reports $[\Gamma(\omega(782) \to \eta\pi^0)/\Gamma(\omega(782) \to \pi^0\gamma)] \times [B(\eta \to 2\gamma)] < 1.01\times10^{-3}$ which we divide by our best (shown rounded) value $B(\eta \to 2\gamma) = 39.36\times10^{-2}$.

$\Gamma(2\pi^0)/\Gamma(\pi^0\gamma)$ — Γ_{19}/Γ_2

Violates C conservation and Bose-Einstein statistics.

VALUE (units 10^{-3})	CL%	DOCUMENT ID		TECN	COMMENT
<2.59	90	STAROSTIN	09	CRYM	$\gamma p \to 2\pi^0 p$

$\Gamma(3\pi^0)/\Gamma_{total}$ — Γ_{20}/Γ

Violates C conservation.

VALUE	CL%	DOCUMENT ID		TECN	COMMENT
• • • We do not use the following data for averages, fits, limits, etc. • • •					
$<3\times10^{-4}$	90	PROKOSHKIN	95	GAM2	$38\ \pi^- p \to 3\pi^0 n$

$\Gamma(3\pi^0)/\Gamma(\pi^0\gamma)$ — Γ_{20}/Γ_2

Violates C conservation.

VALUE (units 10^{-3})	CL%	DOCUMENT ID		TECN	COMMENT
<2.72	90	STAROSTIN	09	CRYM	$\gamma p \to 3\pi^0 p$

$\Gamma(3\pi^0)/\Gamma(\pi^+\pi^-\pi^0)$ — Γ_{20}/Γ_1

Violates C conservation.

VALUE	CL%	DOCUMENT ID		COMMENT
• • • We do not use the following data for averages, fits, limits, etc. • • •				
<0.009	90	BARBERIS	01	$450\ pp \to p_f 3\pi^0 p_s$

$\Gamma(\text{invisible})/\Gamma(\pi^+\pi^-\pi^0)$ — Γ_{21}/Γ_1

VALUE	CL%	DOCUMENT ID		TECN	COMMENT
$<8.1\times10^{-5}$	90	ABLIKIM	18S	BES3	$J/\psi \to \omega\eta \to \omega\pi^+\pi^-\pi^0$

PARAMETER Λ IN $\omega \to \pi^0\ell^+\ell^-$ DECAY

In the pole approximation the electromagnetic transition form factor for a resonance of mass M is given by the expression:

$$|F|^2 = (1 - M^2/\Lambda^2)^{-2},$$

where for the parameter Λ vector dominance predicts $\Lambda = M_\rho \approx 0.770$ GeV. The ARNALDI 09 measurement is in obvious conflict with this expectation. Note that for $\eta \to \gamma\mu^+\mu^-$ decay ARNALDI 09 and DZHELYADIN 80 obtain the value of Λ consistent with vector dominance.

PARAMETER Λ IN $\omega \to \pi^0\mu^+\mu^-$ DECAY

VALUE (GeV)	EVTS	DOCUMENT ID		TECN	COMMENT
0.670 ±0.006 OUR AVERAGE					
$0.6707\pm0.0039\pm0.0056$		[1] ARNALDI	16	NA60	400 GeV (p-A) collisions
$0.668\ \pm0.009\ \pm0.003$	3k	[2] ARNALDI	09	NA60	158A In−In collisions
• • • We do not use the following data for averages, fits, limits, etc. • • •					
$0.65\ \pm0.03$		DZHELYADIN	81B	CNTR	$25-33\ \pi^- p \to \omega n$

[1] ARNALDI 16 reports $\Lambda^{-2}(\omega) = 2.223 \pm 0.026 \pm 0.037$ GeV^{-2} which we converted to the quoted Λ value.

[2] ARNALDI 09 reports $\Lambda^{-2}(\omega) = 2.24 \pm 0.06 \pm 0.02$ GeV^{-2} which we converted to the quoted Λ value.

PARAMETER Λ IN $\omega \to \pi^0 e^+e^-$ DECAY

VALUE (GeV)	EVTS	DOCUMENT ID		TECN	COMMENT
0.709±0.037	1.1k	[1] ADLARSON	17B	A2MM	$\gamma p \to \omega p$

[1] ADLARSON 17B reports $\Lambda^{-2}(\omega\pi^0) = 1.99 \pm 0.21$ GeV^{-2} that we converted to the quoted Λ value.

ENERGY DEPENDENCE OF $\omega \to \pi^+\pi^-\pi^0$ DALITZ PLOT

The following experiments fit to one or more of the coefficients α, β, γ for $|\text{matrix element}|^2 \propto P\,(1 + 2\alpha Z + 2\beta Z^{3/2}\sin(3\phi) + 2\gamma Z^2 + O(Z^{5/2}))$ where P is the P-wave phase-space factor and Z, ϕ are kinematical variables as defined in ADLARSON 17.

VALUE	EVTS	DOCUMENT ID		TECN	COMMENT
0.133 ±0.008 OUR AVERAGE					
$0.1321\pm0.0067\pm0.0046$	260k	[1] ABLIKIM	18AD	BES3	$J/\psi \to \omega\eta$
$0.147\ \pm0.036$	44k	ADLARSON	17	WASA	α in $pd \to {}^3$He ω, $pp \to pp\omega$

[1] Keeping a term linear in Z only. A fit with the terms proportional to Z and $Z^{3/2}$ gives $\alpha = 0.133 \pm 0.041$ and $\beta = 0.037 \pm 0.054$.

$\omega(782)$ REFERENCES

ABLIKIM	25CI	CP C49 103002	M. Ablikim et al.	(BESIII Collab.)
FEDOTOVICH	25A	PPN 56 814	G.V. Fedotovich et al.	(CMD-3 Collab.)
IGNATOV	24	PR D109 112002	F.V. Ignatov et al.	(CMD-3 Collab.)
PDG	22	PTEP 2022 083C01	R.L. Workman et al.	(PDG Collab.)
ACHASOV	21	JHEP 2101 113	M.N. Achasov et al.	(SND Collab.)
LEES	21B	PR D104 112003	J.P. Lees et al.	(BABAR Collab.)
ANDREEV	20	EPJ C80 1189	V. Andreev et al.	(H1 Collab.)
HOID	20	EPJ C80 988	B.-L. Hoid, M. Hoferichter, B. Kubis	(BONN, BERN)
PDG	20	PTEP 2020 083C01	P.A. Zyla et al.	(PDG Collab.)
COLANGELO	19	JHEP 1902 006	G. Colangelo, M. Hoferichter, P. Stoffer	(BERN+)
HOFERICHT...	19	JHEP 1908 137	M. Hoferichter, B.-L. Hoid, B. Kubis	(WASH, BONN)
ABLIKIM	18AD	PR D98 112007	M. Ablikim et al.	(BESIII Collab.)
ABLIKIM	18C	PRL 120 242003	M. Ablikim et al.	(BESIII Collab.)
ABLIKIM	18S	PR D98 032001	M. Ablikim et al.	(BESIII Collab.)
HANHART	18	EPJ C78 450	C. Hanhart et al.	
ADAMCZYK	17A	PR C96 054904	L. Adamczyk et al.	(STAR Collab.)
ADLARSON	17	PL B770 418	P. Adlarson et al.	(WASA-at-COSY Collab.)
ADLARSON	17B	PR C95 035208	P. Adlarson et al.	(A2 Collab. at MAMI)
ANASTASI	17	PL B767 485	A. Anastasi et al.	(KLOE-2 Collab.)
ABLIKIM	16B	PL B753 103	M. Ablikim et al.	(BESIII Collab.)
ACHASOV	16A	PR D93 092001	M.N. Achasov et al.	(SND Collab.)
ARNALDI	16	PL B757 437	R. Arnaldi et al.	(NA60 Collab.)
PDG	16	CP C40 100001	C. Patrignani et al.	(PDG Collab.)
PDG	15	RPP 2015 at pdg.lbl.gov		(PDG Collab.)
ACHASOV	13	PR D88 054013	M.N. Achasov et al.	(SND Collab.)
BABUSCI	13D	PL B720 336	D. Babusci et al.	(CATA, CALB, BARI)
BENAYOUN	13	EPJ C73 2453	M. Benayoun, P. David, L. DelBuono	(PARIN, BERLIN+)
DAVIER	13	EPJ C73 2597	M. Davier et al.	
LEES	12G	PR D86 032013	J.P. Lees et al.	(BABAR Collab.)
NIECKNIG	12	EPJ C72 2014	F. Niecknig, B. Kubis, S.P. Schneider	(BONN)
AMBROSINO	11A	PL B700 102	F. Ambrosino et al.	(KLOE Collab.)
BENAYOUN	10	EPJ C65 211	M. Benayoun et al.	
ACHASOV	09A	JETP 109 379	M.N. Achasov et al.	(SND Collab.)
		Translated from ZETF 136 442.		
ARNALDI	09	PL B677 260	R. Arnaldi et al.	(NA60 Collab.)
AUBERT	09AS	PRL 103 231801	B. Aubert et al.	(BABAR Collab.)
STAROSTIN	09	PR C79 065201	A. Starostin et al.	(Crystal Ball Collab. at MAMI)
ACHASOV	08	JETP 107 61	M.N. Achasov et al.	(SND Collab.)
		Translated from ZETF 134 80.		
AMBROSINO	08G	PL B669 223	F. Ambrosino et al.	(KLOE Collab.)
ACHASOV	07B	PR D76 077101	M.N. Achasov et al.	(SND Collab.)
AKHMETSHIN	07	PL B648 28	R.R. Akhmetshin et al.	(Novosibirsk CMD-2 Collab.)
ACHASOV	06	JETP 103 380	M.N. Achasov et al.	(Novosibirsk SND Collab.)
		Translated from ZETF 130 437.		

ACHASOV	06A	PR D74 014016	M.N. Achasov *et al.*	(SND Collab.)
AULCHENKO	06	JETPL 84 413	V.M. Aulchenko *et al.*	(Novosibirsk CMD-2 Collab.)
		Translated from ZETFP 84 491.		
ACHASOV	05A	JETP 101 1053	M.N. Achasov *et al.*	(Novosibirsk SND Collab.)
		Translated from ZETF 128 1201.		
AKHMETSHIN	05	PL B605 26	R.R. Akhmetshin *et al.*	(Novosibirsk CMD-2 Collab.)
AKHMETSHIN	05A	PL B613 29	R.R. Akhmetshin *et al.*	(Novosibirsk CMD-2 Collab.)
AULCHENKO	05	JETPL 82 743	V.M. Aulchenko *et al.*	(Novosibirsk CMD-2 Collab.)
		Translated from ZETFP 82 841.		
AKHMETSHIN	04	PL B578 285	R.R. Akhmetshin *et al.*	(Novosibirsk CMD-2 Collab.)
AKHMETSHIN	04B	PL B580 119	R.R. Akhmetshin *et al.*	(Novosibirsk CMD-2 Collab.)
AUBERT,B	04N	PR D70 072004	B. Aubert *et al.*	(BABAR Collab.)
PDG	04	PL B592 1	S. Eidelman *et al.*	(PDG Collab.)
ACHASOV	03	PL B559 171	M.N. Achasov *et al.*	(Novosibirsk SND Collab.)
ACHASOV	03D	PR D68 052006	M.N. Achasov *et al.*	(Novosibirsk SND Collab.)
ALOISIO	03	PL B561 55	A. Aloisio *et al.*	(KLOE Collab.)
BENAYOUN	03	EPJ C29 397	M. Benayoun *et al.*	
ACHASOV	02E	PR D66 032001	M.N. Achasov *et al.*	(Novosibirsk SND Collab.)
ACHASOV	02F	PL B537 201	M.N. Achasov *et al.*	(Novosibirsk SND Collab.)
AKHMETSHIN	02	PL B527 161	R.R. Akhmetshin *et al.*	(Novosibirsk CMD-2 Collab.)
ALOISIO	02D	PL B537 21	A. Aloisio *et al.*	(KLOE Collab.)
HEISTER	02C	PL B528 19	A. Heister *et al.*	(ALEPH Collab.)
ACHASOV	01E	PR D63 072002	M.N. Achasov *et al.*	(Novosibirsk SND Collab.)
AKHMETSHIN	01B	PL B509 217	R.R. Akhmetshin *et al.*	(Novosibirsk CMD-2 Collab.)
BARBERIS	01	PL B507 14	D. Barberis *et al.*	
ACHASOV	00	EPJ C12 25	M.N. Achasov *et al.*	(Novosibirsk SND Collab.)
ACHASOV	00D	JETPL 72 282	M.N. Achasov *et al.*	(Novosibirsk SND Collab.)
		Translated from ZETFP 72 411.		
ACHASOV	00G	JETPL 71 355	M.N. Achasov *et al.*	(Novosibirsk SND Collab.)
		Translated from ZETFP 71 519.		
AKHMETSHIN	00C	PL B476 33	R.R. Akhmetshin *et al.*	(Novosibirsk CMD-2 Collab.)
AULCHENKO	00A	JETP 90 927	V.M. Aulchenko *et al.*	(Novosibirsk SND Collab.)
		Translated from ZETF 117 1067.		
CASE	00	PR D61 032002	T. Case *et al.*	(Crystal Barrel Collab.)
ACHASOV	99E	PL B462 365	M.N. Achasov *et al.*	(Novosibirsk SND Collab.)
GARDNER	99	PR D59 076002	S. Gardner, H.B. O'Connell	
BENAYOUN	98	EPJ C2 269	M. Benayoun *et al.*	(IPNP, NOVO, ADLD+)
ABELE	97E	PL B411 361	A. Abele *et al.*	(Crystal Barrel Collab.)
BENAYOUN	96	ZPHY C72 221	M. Benayoun *et al.*	(IPNP, NOVO)
PROKOSHKIN	95	PD 40 273	Y.D. Prokoshkin, V.D. Samoilenko	(SERP)
		Translated from DANS 342 610.		
WURZINGER	95	PR C51 443	R. Wurzinger *et al.*	(BONN, ORSAY, SACL+)
ALDE	94B	PL B340 122	D.M. Alde *et al.*	(SERP, BELG, LANL, LAPP+)
AMSLER	94C	PL B327 425	C. Amsler *et al.*	(Crystal Barrel Collab.)
ALDE	93	PAN 56 1229	D.M. Alde *et al.*	(SERP, LAPP, LANL, BELG+)
		Translated from YAF 56 137.		
Also		ZPHY C61 35	D.M. Alde *et al.*	(SERP, LAPP, LANL, BELG+)
AMSLER	93B	PL B311 362	C. Amsler *et al.*	(Crystal Barrel Collab.)
WEIDENAUER	93	ZPHY C59 387	P. Weidenauer *et al.*	(ASTERIX Collab.)
ANTONELLI	92	ZPHY C56 15	A. Antonelli *et al.*	(DM2 Collab.)
DOLINSKY	91	PRPL 202 99	S.I. Dolinsky *et al.*	(NOVO)
WEIDENAUER	90	ZPHY C47 353	P. Weidenauer *et al.*	(ASTERIX Collab.)
DOLINSKY	89	ZPHY C42 511	S.I. Dolinsky *et al.*	(NOVO)
BITYUKOV	88B	SJNP 47 800	S.I. Bityukov *et al.*	(SERP)
		Translated from YAF 47 1258.		
DOLINSKY	88	SJNP 48 277	S.I. Dolinsky *et al.*	(NOVO)
		Translated from YAF 48 442.		
KURDADZE	88	JETPL 47 512	L.M. Kurdadze *et al.*	(NOVO)
		Translated from ZETFP 47 432.		
AULCHENKO	87	PL B186 432	V.M. Aulchenko *et al.*	(NOVO)
BARKOV	87	JETPL 46 164	L.M. Barkov *et al.*	(NOVO)
		Translated from ZETFP 46 132.		
KURDADZE	86	JETPL 43 643	L.M. Kurdadze *et al.*	(NOVO)
		Translated from ZETFP 43 497.		
BARKOV	85	NP B256 365	L.M. Barkov *et al.*	(NOVO)
DRUZHININ	84	PL 144B 136	V.P. Druzhinin *et al.*	(NOVO)
KURDADZE	83B	JETPL 36 274	A.M. Kurdadze *et al.*	(NOVO)
		Translated from ZETFP 36 221.		
DZHELYADIN	81B	PL 102B 296	R.I. Dzhelyadin *et al.*	(SERP)
CORDIER	80	NP B172 13	A. Cordier *et al.*	(LALO)
DZHELYADIN	80	PL 94B 548	R.I. Dzhelyadin *et al.*	(SERP)
ROOS	80	LNC 27 321	M. Roos, A. Pellinen	(HELS)
BENKHEIRI	79	NP B150 268	P. Benkheiri *et al.*	(EPOL, CERN, CDEF+)
DZHELYADIN	79	PL 84B 143	R.I. Dzhelyadin *et al.*	(SERP)
COOPER	78B	NP B146 1	A.M. Cooper *et al.*	(TATA, CERN, CDEF+)
QUENZER	78	PL 76B 512	A. Quenzer *et al.*	(LALO)
VANAPEL...	78	NP B133 245	G.W. van Apeldoorn *et al.*	(ZEEM)
WICKLUND	78	PR D17 1197	A.B. Wicklund *et al.*	(ANL)
ANDREWS	77	PRL 38 198	D.E. Andrews *et al.*	(ROCH)
GESSAROLI	77	NP B126 382	R. Gessaroli *et al.*	(BGNA, FIRZ, GENO+)
KEYNE	76	PR D14 28	J. Keyne *et al.*	(LOIC, SHMP)
Also		PR D8 2789	D.M. Binnie *et al.*	(LOIC, SHMP)
KALBFLEISCH	75	PR D11 987	G.R. Kalbfleisch, R.C. Strand, J.W. Chapman	(BNL+)
AGUILAR-...	72B	PR D6 29	M. Aguilar-Benitez *et al.*	(BNL)
APEL	72B	PL 41B 234	W.D. Apel *et al.*	(KARLK, KARLE, PISA)
BASILE	72B	Phil. Conf. 153	M. Basile *et al.*	(CERN)
BENAKSAS	72	PL 39B 289	D. Benaksas *et al.*	(ORSAY)
BENAKSAS	72B	PL 42B 507	D. Benaksas *et al.*	(ORSAY)
BENAKSAS	72C	PL 42B 511	D. Benaksas *et al.*	(ORSAY)
BORENSTEIN	72	PR D5 1559	S.R. Borenstein *et al.*	(BNL, MICH)
BROWN	72	PL 42B 117	R.M. Brown *et al.*	(ILL, ILLC)
DAKIN	72	PR D6 2321	J.T. Dakin *et al.*	(PRIN)
RATCLIFF	72	PL 38B 345	B.N. Ratcliff *et al.*	(SLAC)
ALVENSLEB...	71C	PRL 27 888	H. Alvensleben *et al.*	(DESY)
BALDIN	71	SJNP 13 758	A.B. Baldin *et al.*	(ITEP)
		Translated from YAF 13 1318.		
BEHREND	71	PRL 27 61	H.J. Behrend *et al.*	(ROCH, CORN, FNAL)
BIZZARRI	71	NP B27 140	R. Bizzarri *et al.*	(CERN, CDEF)
COYNE	71	NP B32 333	D.G. Coyne *et al.*	(LRL)
MOFFEIT	71	NP B29 349	K.C. Moffeit *et al.*	(LRL, UCB, SLAC+)
ABRAMOVI...	70	NP B20 209	M. Abramovich *et al.*	(CERN)
BIGGS	70B	PRL 24 1201	P.J. Biggs *et al.*	(DARE)
BIZZARRI	70	PRL 25 1385	R. Bizzarri *et al.*	(ROMA, SYRA)
ROOS	70	DNPL/R7 173	M. Roos	(CERN)
Proc. Daresbury Study Weekend No. 1.				
AUGUSTIN	69D	PL 28B 513	J.E. Augustin *et al.*	(ORSAY)
BIZZARRI	69	NP B14 169	R. Bizzarri *et al.*	(CERN, CDEF)
DEINET	69B	PL 30B 426	W. Deinet *et al.*	(KARL, CERN)
JACQUET	69B	NC 63A 743	F. Jacquet *et al.*	(EPOL, BERG)
WILSON	69	Private Comm.	R. Wilson	(HARV)
Also		PR 178 2095	A.A. Wehmann *et al.*	(HARV, CASE, SLAC+)
ASTVACAT...	68	PL 27B 45	R.G. Astvatsaturov *et al.*	(JINR, MOSU)
BOLLINI	68C	NC 56A 531	D. Bollini *et al.*	(CERN, BGNA, STRB)
GOUNARIS	68	PRL 21 244	G.J. Gounaris, J.J. Sakurai	
BARASH	67B	PR 156 1399	N. Barash *et al.*	(COLU)
FELDMAN	67C	PR 159 1219	M. Feldman *et al.*	(PENN)
DIGIUGNO	66B	NC 44A 1272	G. Di Giugno *et al.*	(NAPL, FRAS, TRST)
FLATTE	66	PR 145 1050	S.M. Flatte *et al.*	(LRL)
JAMES	66	PR 142 896	F.E. James, H.L. Kraybill	(YALE, BNL)
SOEDING	66	PL B19 702	P. Soeding	(HAMB)
BARBARO-...	65	PRL 14 279	A. Barbaro-Galtieri, R.D. Tripp	(LRL)
BARMIN	64	JETP 18 1289	V.V. Barmin *et al.*	(ITEP)
		Translated from ZETF 45 1879.		
KRAEMER	64	PR 136 B496	R.W. Kraemer *et al.*	(JHU, NWES, WOOD)
BUSCHBECK	63	Siena Conf. 1 166	B. Buschbeck *et al.*	(VIEN, CERN, ANIK)

$\eta'(958)$

$I^G(J^{PC}) = 0^+(0^{-+})$

$\eta'(958)$ MASS

VALUE (MeV)	EVTS	DOCUMENT ID		TECN	COMMENT
957.78 ±0.06 OUR AVERAGE					
957.793±0.054±0.036	3.9k	LIBBY	08	CLEO	$J/\psi \to \gamma\eta'$
957.9 ±0.2 ±0.6	4800	WURZINGER	96	SPEC	1.68 $pd \to {}^3\mathrm{He}\eta'$
957.46 ±0.33		DUANE	74	MMS	$\pi^- p \to n$MM
958.2 ±0.5	1414	DANBURG	73	HBC	2.2 $K^- p \to \Lambda\eta'$
958 ±1	400	JACOBS	73	HBC	2.9 $K^- p \to \Lambda\eta'$
956.1 ±1.1	3415	[1] BASILE	71	CNTR	1.6 $\pi^- p \to n\eta'$
• • • We do not use the following data for averages, fits, limits, etc. • • •					
957.5 ±0.2		BAI	04J	BES2	$J/\psi \to \gamma\gamma\pi^+\pi^-$
959 ±1	630	[2] BELADIDZE	92C	VES	36 π^-Be $\to \pi^-\eta'\eta$Be
958 ±1	340	[2] ARMSTRONG	91B	OMEG	300 $pp \to pp\eta\pi^+\pi^-$
958.2 ±0.4	622	[2] AUGUSTIN	90	DM2	$J/\psi \to \gamma\eta\pi^+\pi^-$
957.8 ±0.2	2420	[2] AUGUSTIN	90	DM2	$J/\psi \to \gamma\gamma\pi^+\pi^-$
956.3 ±1.0	143	[2] GIDAL	87	MRK2	$e^+e^- \to e^+e^-\eta\pi^+\pi^-$
957.4 ±1.4	535	[3] BASILE	71	CNTR	1.6 $\pi^- p \to n\eta'$
957 ±1		RITTENBERG	69	HBC	1.7–2.7 $K^- p$

[1] Using all η' decays.
[2] Systematic uncertainty not estimated.
[3] Using η' decays into neutrals. Not independent of the other listed BASILE 71 η' mass measurement.

$\eta'(958)$ WIDTH

VALUE (MeV)	EVTS	DOCUMENT ID		TECN	CHG	COMMENT
0.188±0.006 OUR FIT						
0.230±0.021 OUR AVERAGE						
0.226±0.017±0.014	2300	CZERWINSKI	10	MMS		$pp \to pp\eta'$
0.40 ±0.22	4800	WURZINGER	96	SPEC		1.68 $pd \to {}^3\mathrm{He}\eta'$
0.28 ±0.10	1000	BINNIE	79	MMS	0	$\pi^- p \to n$MM
• • • We do not use the following data for averages, fits, limits, etc. • • •						
0.20 ±0.04		BAI	04J	BES2		$J/\psi \to \gamma\gamma\pi^+\pi^-$

$\eta'(958)$ DECAY MODES

	Mode	Fraction (Γ_i/Γ)	Confidence level
Γ_1	$\pi^+\pi^-\eta$	(42.5 ±0.5) %	
Γ_2	$\rho^0\gamma$ (including non-resonant $\pi^+\pi^-\gamma$)	(29.48 ±0.35) %	
Γ_3	$\rho^0\gamma$		
Γ_4	$\pi^0\pi^0\eta$	(22.4 ±0.5) %	
Γ_5	$\omega\gamma$	(2.52 ±0.07) %	
Γ_6	ωe^+e^-	(2.0 ±0.4) $\times 10^{-4}$	
Γ_7	$\gamma\gamma$	(2.307±0.033) %	
Γ_8	$3\pi^0$	(2.50 ±0.17) $\times 10^{-3}$	
Γ_9	$\mu^+\mu^-\gamma$	(1.13 ±0.28) $\times 10^{-4}$	
Γ_{10}	$\pi^+\pi^-\mu^+\mu^-$	(2.13 ±0.13) $\times 10^{-5}$	
Γ_{11}	$\pi^+\pi^-\pi^0$	(3.61 ±0.17) $\times 10^{-3}$	
Γ_{12}	$(\pi^+\pi^-\pi^0)$ S-wave	(3.8 ±0.5) $\times 10^{-3}$	
Γ_{13}	$\pi^\mp\rho^\pm$	(7.4 ±2.3) $\times 10^{-4}$	
Γ_{14}	$2(\pi^+\pi^-)$	(8.51 ±0.33) $\times 10^{-5}$	
Γ_{15}	$\pi^+\pi^-2\pi^0$	(2.11 ±0.15) $\times 10^{-4}$	
Γ_{16}	$2(\pi^+\pi^-)$ neutrals	< 1 %	95%
Γ_{17}	$2(\pi^+\pi^-)\pi^0$	< 1.8 $\times 10^{-3}$	90%
Γ_{18}	$2(\pi^+\pi^-)2\pi^0$	< 1 %	95%
Γ_{19}	$3(\pi^+\pi^-)$	< 3.1 $\times 10^{-5}$	90%
Γ_{20}	$K^\pm\pi^\mp$	< 4 $\times 10^{-5}$	90%
Γ_{21}	$\pi^+\pi^-e^+e^-$	(2.43 ±0.06) $\times 10^{-3}$	
Γ_{22}	$\pi^+e^-\nu_e +$ c.c.	< 2.1 $\times 10^{-4}$	90%
Γ_{23}	γe^+e^-	(4.80 ±0.15) $\times 10^{-4}$	
Γ_{24}	$\pi^0\gamma\gamma$	(3.20 ±0.24) $\times 10^{-3}$	
Γ_{25}	$\pi^0\gamma\gamma$ (non resonant)	(6.2 ±0.9) $\times 10^{-4}$	
Γ_{26}	$\eta\gamma\gamma$	< 1.33 $\times 10^{-4}$	90%
Γ_{27}	$4\pi^0$	< 1.2 $\times 10^{-5}$	90%
Γ_{28}	e^+e^-	< 5.6 $\times 10^{-9}$	90%
Γ_{29}	$e^+e^-e^+e^-$	(4.5 ±1.1) $\times 10^{-6}$	
Γ_{30}	$e^+e^-\mu^+\mu^-$	< 1.8 $\times 10^{-6}$	90%
Γ_{31}	$\mu^+\mu^-\mu^+\mu^-$	< 5 $\times 10^{-7}$	90%
Γ_{32}	invisible	< 2.1 $\times 10^{-4}$	90%
Γ_{33}	γ Dark Photon	5×10^{-7} to 3.5×10^{-6}	90%

Int. J. Mod. Phys. A 2026.41. Downloaded from www.worldscientific.com
by LIFORNIA @ BERKELEY on 09/16/26. Re-use and distribution is strictly not permitted, except for Open Access articles.

Int. J. Mod. Phys. A 2026.41. Downloaded from www.worldscientific.com
by UNIVERSITY OF CALIFORNIA @ BERKELEY on 09/16/26. Re-use and distribution is strictly not permitted, except for Open Access articles.

Charge conjugation (C), Parity (P), Lepton family number (LF) violating modes

Γ_{34}	$\pi^+\pi^-$	P,CP		< 1.8	$\times 10^{-5}$	90%
Γ_{35}	$\pi^0\pi^0$	P,CP		< 4	$\times 10^{-4}$	90%
Γ_{36}	$\pi^0 e^+ e^-$	C	[a]	< 1.4	$\times 10^{-3}$	90%
Γ_{37}	$\pi^0\rho^0$	C		< 4	%	90%
Γ_{38}	$\eta e^+ e^-$	C	[a]	< 2.4	$\times 10^{-3}$	90%
Γ_{39}	3γ	C		< 1.0	$\times 10^{-4}$	90%
Γ_{40}	$\mu^+\mu^-\pi^0$	C	[a]	< 6.0	$\times 10^{-5}$	90%
Γ_{41}	$\mu^+\mu^-\eta$	C	[a]	< 1.5	$\times 10^{-5}$	90%
Γ_{42}	$e\mu$	LF		< 4.7	$\times 10^{-4}$	90%
Γ_{43}	$\pi^+\pi^-$ALP $\rightarrow$ $\pi^+\pi^- e^+ e^-$			< 1.9	$\times 10^{-5}$	90%

[a] C parity forbids this to occur as a single-photon process.

CONSTRAINED FIT INFORMATION

An overall fit to the total width, a partial width, 2 combinations of partial widths obtained from integrated cross section, and 21 branching ratios uses 53 measurements and one constraint to determine 9 parameters. The overall fit has a $\chi^2 = 69.5$ for 45 degrees of freedom.

The following *off-diagonal* array elements are the correlation coefficients $\langle \delta p_i \delta p_j \rangle / (\delta p_i \cdot \delta p_j)$, in percent, from the fit to parameters p_i, including the branching fractions, $x_i \equiv \Gamma_i/\Gamma_{total}$. The fit constrains the x_i whose labels appear in this array to sum to one.

	x_1	x_2	x_4	x_5	x_7	x_8	x_{11}	x_{21}
x_2	−24							
x_4	−77	−42						
x_5	−7	−6	−2					
x_7	−11	−7	9	−1				
x_8	−17	−9	19	−1	2			
x_{11}	−1	−1	−1	0	0	0		
x_{21}	−5	19	−9	−1	−2	−2	0	
Γ	11	−9	−2	1	−40	0	0	−2

	Mode	Rate (MeV)
Γ_1	$\pi^+\pi^-\eta$	0.0799 ± 0.0029
Γ_2	$\rho^0\gamma$(including non-resonant $\pi^+\pi^-\gamma$)	0.0554 ± 0.0019
Γ_4	$\pi^0\pi^0\eta$	0.0421 ± 0.0017
Γ_5	$\omega\gamma$	0.00474 ± 0.00020
Γ_7	$\gamma\gamma$	0.00434 ± 0.00013
Γ_8	$3\pi^0$	$(4.7 \pm 0.4) \times 10^{-4}$
Γ_{11}	$\pi^+\pi^-\pi^0$	$(6.8 \pm 0.4) \times 10^{-4}$
Γ_{21}	$\pi^+\pi^- e^+ e^-$	$(4.57 \pm 0.19) \times 10^{-4}$

$\eta'(958)$ PARTIAL WIDTHS

$\Gamma(\gamma\gamma)$ — Γ_7

VALUE (keV)	EVTS	DOCUMENT ID		TECN	COMMENT
4.34±0.14 OUR FIT					
4.28±0.19 OUR AVERAGE					
$4.17 \pm 0.10 \pm 0.27$	2000	[1] ACCIARRI	98Q	L3	$e^+e^- \rightarrow e^+e^-\pi^+\pi^-\gamma$
$4.53 \pm 0.29 \pm 0.51$	266	KARCH	92	CBAL	$e^+e^- \rightarrow e^+e^-\eta\pi^0\pi^0$
$3.61 \pm 0.13 \pm 0.48$		[2] BEHREND	91	CELL	$e^+e^- \rightarrow e^+e^-\eta'(958)$
$4.6 \pm 1.1 \pm 0.6$	23	BARU	90	MD1	$e^+e^- \rightarrow e^+e^-\pi^+\pi^-\gamma$
$4.57 \pm 0.25 \pm 0.44$		BUTLER	90	MRK2	$e^+e^- \rightarrow e^+e^-\eta'(958)$
$5.08 \pm 0.24 \pm 0.71$	547	[3] ROE	90	ASP	$e^+e^- \rightarrow e^+e^-2\gamma$
$3.8 \pm 0.7 \pm 0.6$	34	AIHARA	88C	TPC	$e^+e^- \rightarrow e^+e^-\eta\pi^+\pi^-$
$4.9 \pm 0.5 \pm 0.5$	136	[4] WILLIAMS	88	CBAL	$e^+e^- \rightarrow e^+e^-2\gamma$
• • • We do not use the following data for averages, fits, limits, etc. • • •					
$4.7 \pm 0.6 \pm 0.9$	143	[5] GIDAL	87	MRK2	$e^+e^- \rightarrow e^+e^-\eta\pi^+\pi^-$
4.0 ± 0.9		[6] BARTEL	85E	JADE	$e^+e^- \rightarrow e^+e^-2\gamma$

[1] No non-resonant $\pi^+\pi^-$ contribution found.
[2] Reevaluated by us using $B(\eta' \rightarrow \rho(770)\gamma) = (30.2 \pm 1.3)\%$.
[3] Reevaluated by us using $B(\eta' \rightarrow \gamma\gamma) = (2.11 \pm 0.13)\%$.
[4] Reevaluated by us using $B(\eta' \rightarrow \gamma\gamma) = (2.11 \pm 0.13)\%$.
[5] Superseded by BUTLER 90.
[6] Systematic error not evaluated.

$\Gamma(e^+e^-)$ — Γ_{28}

VALUE (eV)	CL%	DOCUMENT ID		TECN	COMMENT
$<1.1 \times 10^{-3}$	90	[1,2] ACHASOV	15	SND	$0.958\ e^+e^- \rightarrow \pi\pi\eta$
• • • We do not use the following data for averages, fits, limits, etc. • • •					
$<2.0 \times 10^{-3}$	90	[2] ACHASOV	15	SND	$0.958\ e^+e^- \rightarrow \pi\pi\eta$
$<2.4 \times 10^{-3}$	90	[2] AKHMETSHIN	15	CMD3	$0.958\ e^+e^- \rightarrow \pi^+\pi^-\eta$

[1] Combining data of ACHASOV 15 and AKHMETSHIN 15.
[2] Using η and η' branching fractions from PDG 14.

$\eta'(958)$ $\Gamma(i)\Gamma(\gamma\gamma)/\Gamma(total)$

This combination of a partial width with the partial width into $\gamma\gamma$ and with the total width is obtained from the integrated cross section into channel(i) in the $\gamma\gamma$ annihilation.

$\Gamma(\gamma\gamma) \times \Gamma(\rho^0\gamma$(including non-resonant $\pi^+\pi^-\gamma)) / \Gamma_{total}$ — $\Gamma_7\Gamma_2/\Gamma$

VALUE (keV)	EVTS	DOCUMENT ID		TECN	COMMENT
1.28±0.04 OUR FIT					
1.26±0.07 OUR AVERAGE Error includes scale factor of 1.2.					
$1.09 \pm 0.04 \pm 0.13$		BEHREND	91	CELL	$e^+e^- \rightarrow e^+e^-\rho(770)^0\gamma$
$1.35 \pm 0.09 \pm 0.21$		AIHARA	87	TPC	$e^+e^- \rightarrow e^+e^-\rho\gamma$
$1.13 \pm 0.04 \pm 0.13$	867	ALBRECHT	87B	ARG	$e^+e^- \rightarrow e^+e^-\rho\gamma$
$1.53 \pm 0.09 \pm 0.21$		ALTHOFF	84E	TASS	$e^+e^- \rightarrow e^+e^-\rho\gamma$
$1.14 \pm 0.08 \pm 0.11$	243	BERGER	84B	PLUT	$e^+e^- \rightarrow e^+e^-\rho\gamma$
$1.73 \pm 0.34 \pm 0.35$	95	JENNI	83	MRK2	$e^+e^- \rightarrow e^+e^-\rho\gamma$
$1.49 \pm 0.13 \pm 0.027$	213	BARTEL	82B	JADE	$e^+e^- \rightarrow e^+e^-\rho\gamma$
• • • We do not use the following data for averages, fits, limits, etc. • • •					
$1.85 \pm 0.31 \pm 0.24$	43	BEHREND	82C	CELL	$e^+e^- \rightarrow e^+e^-\rho\gamma$

$\Gamma(\gamma\gamma) \times \Gamma(\pi^0\pi^0\eta)/\Gamma_{total}$ — $\Gamma_7\Gamma_4/\Gamma$

VALUE (keV)	DOCUMENT ID		TECN	COMMENT
0.97±0.04 OUR FIT Error includes scale factor of 1.1.				
0.92±0.06±0.11	[1] KARCH	92	CBAL	$e^+e^- \rightarrow e^+e^-\eta\pi^0\pi^0$
• • • We do not use the following data for averages, fits, limits, etc. • • •				
$0.95 \pm 0.05 \pm 0.08$	[2] KARCH	90	CBAL	$e^+e^- \rightarrow e^+e^-\eta\pi^0\pi^0$
$1.00 \pm 0.08 \pm 0.10$	[2,3] ANTREASYAN	87	CBAL	$e^+e^- \rightarrow e^+e^-\eta\pi^0\pi^0$

[1] Reevaluated by us using $B(\eta \rightarrow \gamma\gamma) = (39.21 \pm 0.34)\%$. Supersedes ANTREASYAN 87 and KARCH 90.
[2] Superseded by KARCH 92.
[3] Using $BR(\eta \rightarrow 2\gamma) = (38.9 \pm 0.5)\%$.

$\eta'(958)$ $\Gamma(i)\Gamma(e^+e^-)/\Gamma(total)$

$\Gamma(\pi^+\pi^-\eta) \times \Gamma(e^+e^-)/\Gamma_{total}$ — $\Gamma_1\Gamma_{28}/\Gamma$

VALUE (10^{-3} eV)	CL%	DOCUMENT ID		TECN	COMMENT
<1.0	90	[1] AKHMETSHIN	15	CMD3	$0.958\ e^+e^- \rightarrow \pi^+\pi^-\eta$

[1] AKHMETSHIN 15 reports $[\Gamma(\eta'(958) \rightarrow \pi^+\pi^-\eta) \times \Gamma(\eta'(958) \rightarrow e^+e^-)/\Gamma_{total}] \times [B(\eta \rightarrow 2\gamma)] < 4.1 \times 10^{-4}$ eV which we divide by our best (shown rounded) value $B(\eta \rightarrow 2\gamma) = 39.36 \times 10^{-2}$.

$\eta'(958)$ BRANCHING RATIOS

$\Gamma(\pi^+\pi^-\eta)/\Gamma_{total}$ — Γ_1/Γ

VALUE (units 10^{-2})	EVTS	DOCUMENT ID		TECN	COMMENT
42.5 ±0.5 OUR FIT Error includes scale factor of 1.1.					
41.24±0.08±1.24	312k	ABLIKIM	19T	BES	$J/\psi \rightarrow \gamma\eta'$
• • • We do not use the following data for averages, fits, limits, etc. • • •					
$42.4 \pm 1.1 \pm 0.4$	1.2k	[1] PEDLAR	09	CLEO	$J/\psi \rightarrow \gamma\eta'$

[1] Not independent of other η' branching fractions and ratios in PEDLAR 09.

$\Gamma(\pi^+\pi^-\eta$(charged decay))$/\Gamma_{total}$ — $0.2805\Gamma_1/\Gamma$

VALUE	EVTS	DOCUMENT ID		TECN	COMMENT
0.1191±0.0015 OUR FIT Error includes scale factor of 1.1.					
• • • We do not use the following data for averages, fits, limits, etc. • • •					
0.123 ± 0.014	107	RITTENBERG	69	HBC	1.7–2.7 K^-p
0.10 ± 0.04	10	LONDON	66	HBC	2.24 $K^-p \rightarrow \Lambda 2\pi^+ 2\pi^-\pi^0$
0.07 ± 0.04	7	BADIER	65B	HBC	3 K^-p

$\Gamma(\pi^+\pi^-\eta$(neutral decay))$/\Gamma_{total}$ — $0.7195\Gamma_1/\Gamma$

VALUE	EVTS	DOCUMENT ID		TECN	COMMENT
0.306±0.004 OUR FIT Error includes scale factor of 1.1.					
• • • We do not use the following data for averages, fits, limits, etc. • • •					
0.314 ± 0.026	281	RITTENBERG	69	HBC	1.7–2.7 K^-p

$\Gamma(\rho^0\gamma$(including non-resonant $\pi^+\pi^-\gamma))/\Gamma_{total}$ — Γ_2/Γ

VALUE (units 10^{-2})	EVTS	DOCUMENT ID		TECN	COMMENT
29.5 ± 0.4 OUR FIT Error includes scale factor of 1.1.					
29.90± 0.03±0.55	913k	ABLIKIM	19T	BES	$J/\psi \rightarrow \gamma\eta'$
• • • We do not use the following data for averages, fits, limits, etc. • • •					
$28.7 \pm 0.7 \pm 0.4$	0.2k	[1] PEDLAR	09	CLEO	$J/\psi \rightarrow \gamma\eta'$
32.9 ± 3.3	298	RITTENBERG	69	HBC	1.7–2.7 K^-p
20 ± 10	20	LONDON	66	HBC	2.24 $K^-p \rightarrow \Lambda\pi^+\pi^-\gamma$
34 ± 9	35	BADIER	65B	HBC	3 K^-p

[1] Not independent of other η' branching fractions and ratios in PEDLAR 09.

$\Gamma(\rho^0\gamma)/\Gamma_{total}$ — Γ_3/Γ

VALUE (%)	EVTS	DOCUMENT ID		TECN	COMMENT
• • • We do not use the following data for averages, fits, limits, etc. • • •					
$33.34 \pm 0.06 \pm 1.60$	970k	[1] ABLIKIM	18C	BES3	$\eta'(958) \rightarrow \gamma\pi^+\pi^-$

34.43±0.52±1.97	970k	[2] ABLIKIM	18C	BES3	$\eta'(958) \to \gamma\pi^+\pi^-$

[1] From a fit to $\pi^+\pi^-$ mass using $\rho(770)$, $\omega(782)$, and box anomaly components.
[2] From a fit to $\pi^+\pi^-$ mass using $\rho(770)$, $\omega(782)$, and $\rho(1450)$ components.

$\Gamma(\rho^0\gamma(\text{including non-resonant}\,\pi^+\pi^-\gamma))/\Gamma(\pi^+\pi^-\eta)$ — Γ_2/Γ_1

VALUE	DOCUMENT ID		TECN	COMMENT
0.694±0.014 OUR FIT Error includes scale factor of 1.1.				
0.683±0.020 OUR AVERAGE				
0.677±0.024±0.011	PEDLAR	09	CLE3	$J/\psi \to \eta'\gamma$
0.69 ±0.03	ABLIKIM	06E	BES2	$J/\psi \to \eta'\gamma$

$\Gamma(\rho^0\gamma(\text{including non-resonant}\,\pi^+\pi^-\gamma))/\Gamma(\pi^+\pi^-\eta(\text{neutral decay}))$ — $\Gamma_2/0.714\Gamma_1$

VALUE	EVTS	DOCUMENT ID		TECN	COMMENT
0.972±0.019 OUR FIT Error includes scale factor of 1.1.					
0.97 ±0.09 OUR AVERAGE					
0.70 ±0.22		AMSLER	04B	CBAR	0 $\bar{p}p \to \pi^+\pi^-\eta$
1.07 ±0.17		BELADIDZE	92C	VES	36 π^-Be $\to \pi^-\eta'\eta$Be
0.92 ±0.14	473	DANBURG	73	HBC	2.2 $K^-p \to \Lambda X^0$
1.11 ±0.18	192	JACOBS	73	HBC	2.9 $K^-p \to \Lambda X^0$

$\Gamma(\pi^0\pi^0\eta)/\Gamma_{\text{total}}$ — Γ_4/Γ

VALUE (units 10^{-2})	EVTS	DOCUMENT ID		TECN	COMMENT
22.4 ±0.6 OUR FIT Error includes scale factor of 1.1.					
21.36±0.10±0.92	52k	ABLIKIM	19T	BES	$J/\psi \to \gamma\eta'$
• • • We do not use the following data for averages, fits, limits, etc. • • •					
23.5 ±1.3 ±0.4	3.2k	[1] PEDLAR	09	CLEO	$J/\psi \to \gamma\eta'$

[1] Not independent of other η' branching fractions and ratios in PEDLAR 09.

$\Gamma(\pi^0\pi^0\eta(3\pi^0\,\text{decay}))/\Gamma_{\text{total}}$ — $0.321\Gamma_4/\Gamma$

VALUE	EVTS	DOCUMENT ID		TECN	COMMENT
0.0718±0.0018 OUR FIT Error includes scale factor of 1.1.					
• • • We do not use the following data for averages, fits, limits, etc. • • •					
0.11 ±0.06	4	BENSINGER	70	DBC	2.2 π^+d

$\Gamma(\pi^0\pi^0\eta)/\Gamma(\pi^+\pi^-\eta)$ — Γ_4/Γ_1

VALUE	DOCUMENT ID		TECN	COMMENT
0.527±0.019 OUR FIT Error includes scale factor of 1.1.				
0.555±0.043±0.013	PEDLAR	09	CLE3	$J/\psi \to \eta'\gamma$

$\Gamma(\rho^0\gamma(\text{including non-resonant}\,\pi^+\pi^-\gamma))/\Gamma(\pi\pi\eta)$ — $\Gamma_2/(\Gamma_1+\Gamma_4)$

VALUE	DOCUMENT ID		TECN	COMMENT
0.455±0.008 OUR FIT Error includes scale factor of 1.1.				
0.43 ±0.02 ±0.02	BARBERIS	98C	OMEG	450 $pp \to p_f\eta' p_s$
• • • We do not use the following data for averages, fits, limits, etc. • • •				
0.31 ±0.15	DAVIS	68	HBC	5.5 K^-p

$\Gamma(\omega\gamma)/\Gamma_{\text{total}}$ — Γ_5/Γ

VALUE (units 10^{-2})	EVTS	DOCUMENT ID		TECN	COMMENT
2.52 ±0.07 OUR FIT					
2.50 ±0.07 OUR AVERAGE					
2.489±0.018±0.074	23k	ABLIKIM	19T	BES	$J/\psi \to \gamma\eta'$
2.55 ±0.03 ±0.16	33.2k	[1] ABLIKIM	15AD	BES3	$J/\psi \to \eta'\gamma$
• • • We do not use the following data for averages, fits, limits, etc. • • •					
2.34 ±0.30 ±0.04	70	[2] PEDLAR	09	CLEO	$J/\psi \to \gamma\eta'$

[1] Using $B(J/\psi \to \eta'\gamma) = (5.15 \pm 0.16)\times 10^{-3}$ and $B(\omega \to \pi^+\pi^-\pi^0) = (89.2 \pm 0.7)\%$.
[2] Not independent of other η' branching fractions and ratios in PEDLAR 09.

$\Gamma(\omega\gamma)/\Gamma(\pi^+\pi^-\eta)$ — Γ_5/Γ_1

VALUE	EVTS	DOCUMENT ID		TECN	COMMENT
0.0593±0.0018 OUR FIT Error includes scale factor of 1.1.					
0.055 ±0.007 ±0.001		PEDLAR	09	CLE3	$J/\psi \to \eta'\gamma$
• • • We do not use the following data for averages, fits, limits, etc. • • •					
0.068 ±0.013	68	ZANFINO	77	ASPK	8.4 π^-p

$\Gamma(\omega\gamma)/\Gamma(\pi^0\pi^0\eta)$ — Γ_5/Γ_4

VALUE	DOCUMENT ID		TECN	COMMENT
0.113±0.004 OUR FIT				
0.147±0.016	ALDE	87B	GAM2	38 $\pi^-p \to n4\gamma$

$\Gamma(\omega e^+e^-)/\Gamma(\omega\gamma)$ — Γ_6/Γ_5

VALUE (units 10^{-3})	DOCUMENT ID		TECN	COMMENT
• • • We do not use the following data for averages, fits, limits, etc. • • •				
7.71±1.34±0.54	[1] ABLIKIM	15AD	BES3	$J/\psi \to \eta'\gamma$

[1] Obtained from other ABLIKIM 15AD meausurements with common systematics taken into account.

$\Gamma(\omega e^+e^-)/\Gamma_{\text{total}}$ — Γ_6/Γ

VALUE (units 10^{-4})	EVTS	DOCUMENT ID		TECN	COMMENT
1.97±0.34±0.17	66	[1] ABLIKIM	15AD	BES3	$J/\psi \to \eta'\gamma$

[1] Using $B(J/\psi \to \eta'\gamma) = (5.15 \pm 0.16)\times 10^{-3}$ and $B(\omega \to \pi^+\pi^-\pi^0) = (89.2 \pm 0.7)\%$.

$\Gamma(\rho^0\gamma(\text{including non-resonant}\,\pi^+\pi^-\gamma))/[\Gamma(\pi^+\pi^-\eta)+\Gamma(\pi^0\pi^0\eta)+\Gamma(\omega\gamma)]$ — $\Gamma_2/(\Gamma_1+\Gamma_4+\Gamma_5)$

VALUE	DOCUMENT ID		TECN	COMMENT
0.438±0.008 OUR FIT Error includes scale factor of 1.1.				
• • • We do not use the following data for averages, fits, limits, etc. • • •				
0.25 ±0.14	DAUBER	64	HBC	1.95 K^-p

$[\Gamma(\pi^0\pi^0\eta(\text{charged decay}))+\Gamma(\omega(\text{charged decay})\gamma)]/\Gamma_{\text{total}}$ — $(0.286\Gamma_4+0.89\Gamma_5)/\Gamma$

VALUE	EVTS	DOCUMENT ID		TECN	COMMENT
0.0864±0.0017 OUR FIT Error includes scale factor of 1.1.					
• • • We do not use the following data for averages, fits, limits, etc. • • •					
0.045 ±0.029	42	RITTENBERG	69	HBC	1.7–2.7 K^-p

$\Gamma(\pi^+\pi^-\text{neutrals})/\Gamma_{\text{total}}$ — $(0.714\Gamma_1+0.286\Gamma_4+0.89\Gamma_5)/\Gamma$

VALUE	EVTS	DOCUMENT ID		TECN	COMMENT
0.3896±0.0027 OUR FIT Error includes scale factor of 1.1.					
• • • We do not use the following data for averages, fits, limits, etc. • • •					
0.4 ±0.1	39	LONDON	66	HBC	2.24 $K^-p \to \Lambda\pi^+\pi^-$neutrals
0.35 ±0.06	33	BADIER	65B	HBC	3 K^-p

$\Gamma(\gamma\gamma)/\Gamma_{\text{total}}$ — Γ_7/Γ

VALUE (units 10^{-2})	EVTS	DOCUMENT ID		TECN	COMMENT
2.307±0.035 OUR FIT Error includes scale factor of 1.1.					
2.31 ±0.06 OUR AVERAGE Error includes scale factor of 1.8.					
2.331±0.012±0.035	71k	ABLIKIM	19T	BES	$J/\psi \to \gamma\eta'$
1.99 $^{+0.31}_{-0.27}$ ±0.07	114	[1] WICHT	08	BELL	$B^\pm \to K^\pm\gamma\gamma$
2.00 ±0.18		[2] STANTON	80	SPEC	8.45 $\pi^-p \to n\pi^+\pi^-2\gamma$
• • • We do not use the following data for averages, fits, limits, etc. • • •					
2.25 ±0.16 ±0.03	0.3k	[3] PEDLAR	09	CLEO	$J/\psi \to \gamma\eta'$
1.8 ±0.2	6000	[4] APEL	79	NICE	15–40 $\pi^-p \to n2\gamma$
2.5 ±0.7		DUANE	74	MMS	$\pi^-p \to n$MM
1.71 ±0.33	68	DALPIAZ	72	CNTR	1.6 $\pi^-p \to nX^0$
2.0 $^{+0.8}_{-0.6}$	31	HARVEY	71	OSPK	3.65 $\pi^-p \to nX^0$

[1] WICHT 08 reports $[\Gamma(\eta'(958) \to \gamma\gamma)/\Gamma_{\text{total}}] \times [B(B^+ \to \eta' K^+)] = (1.40^{+0.16+0.15}_{-0.15-0.12})\times 10^{-6}$ which we divide by our best (shown rounded) value $B(B^+ \to \eta' K^+) = (7.04 \pm 0.25)\times 10^{-5}$. Our first error is their experiment's error and our second error is the systematic error from using our best (shown rounded) value.
[2] Includes APEL 79 result.
[3] Not independent of other η' branching fractions and ratios in PEDLAR 09.
[4] Data is included in STANTON 80 evaluation.

$\Gamma(\gamma\gamma)/\Gamma(\pi^+\pi^-\eta)$ — Γ_7/Γ_1

VALUE	DOCUMENT ID		TECN	COMMENT
0.0543±0.0012 OUR FIT Error includes scale factor of 1.1.				
0.053 ±0.004 ±0.001	PEDLAR	09	CLE3	$J/\psi \to \eta'\gamma$

$\Gamma(\gamma\gamma)/\Gamma(\rho^0\gamma(\text{including non-resonant}\,\pi^+\pi^-\gamma))$ — Γ_7/Γ_2

VALUE	DOCUMENT ID		TECN	COMMENT
0.0782±0.0016 OUR FIT Error includes scale factor of 1.1.				
0.080 ±0.008	ABLIKIM	06E	BES2	$J/\psi \to \eta'\gamma$

$\Gamma(\gamma\gamma)/\Gamma(\pi^0\pi^0\eta)$ — Γ_7/Γ_4

VALUE	DOCUMENT ID		TECN	COMMENT
0.1031±0.0028 OUR FIT				
0.105 ±0.010 OUR AVERAGE Error includes scale factor of 1.9.				
0.091 ±0.009	AMSLER	93	CBAR	0.0 $\bar{p}p$
0.112 ±0.002 ±0.006	ALDE	87B	GAM2	38 $\pi^-p \to n2\gamma$

$\Gamma(\gamma\gamma)/\Gamma(\pi^0\pi^0\eta(\text{neutral decay}))$ — $\Gamma_7/0.714\Gamma_4$

VALUE	EVTS	DOCUMENT ID		TECN	COMMENT
0.144±0.004 OUR FIT					
• • • We do not use the following data for averages, fits, limits, etc. • • •					
0.188±0.058	16	APEL	72	OSPK	3.8 $\pi^-p \to nX^0$

$\Gamma(\text{neutrals})/\Gamma_{\text{total}}$ — $(0.714\Gamma_4+0.09\Gamma_5+\Gamma_7)/\Gamma$

VALUE	EVTS	DOCUMENT ID		TECN	COMMENT
0.185±0.004 OUR FIT Error includes scale factor of 1.1.					
• • • We do not use the following data for averages, fits, limits, etc. • • •					
0.185±0.022	535	BASILE	71	CNTR	1.6 $\pi^-p \to nX^0$
0.189±0.026	123	RITTENBERG	69	HBC	1.7–2.7 K^-p

$\Gamma(3\pi^0)/\Gamma_{\text{total}}$ — Γ_8/Γ

VALUE (units 10^{-3})	EVTS	DOCUMENT ID		TECN	COMMENT
2.50 ±0.17 OUR FIT					
3.57 ±0.26 OUR AVERAGE					
3.522±0.082±0.254	2015	ABLIKIM	17	BES3	$J/\psi \to \gamma(3\pi^0)$
4.79 ±0.59 ±1.14	183	[1] ABLIKIM	15P	BES3	$J/\psi \to K^+K^-3\pi$
• • • We do not use the following data for averages, fits, limits, etc. • • •					
3.56 ±0.22 ±0.34	309	[2] ABLIKIM	12E	BES3	$J/\psi \to \gamma(3\pi^0)$

[1] We have added all systematic uncertainties in quadrature to a single value.
[2] Superseded by ABLIKIM 17.

Int. J. Mod. Phys. A 2026.41. Downloaded from www.worldscientific.com
by CALIFORNIA @ BERKELEY on 09/16/26. Re-use and distribution is strictly not permitted, except for Open Access articles.

Int. J. Mod. Phys. A 2026.41. Downloaded from www.worldscientific.com by UNIVERSITY OF CALIFORNIA @ BERKELEY on 09/16/26. Re-use and distribution is strictly not permitted, except for Open Access articles.

$\Gamma(3\pi^0)/\Gamma(\pi^0\pi^0\eta)$ — Γ_8/Γ_4

VALUE (units 10^{-4})	EVTS	DOCUMENT ID		TECN	COMMENT
112± 8 OUR FIT					
78±10 OUR AVERAGE					
86±19	235	BLIK	08	GAMS	32 $\pi^- p \to \eta' n$
74±15		ALDE	87B	GAM2	38 $\pi^- p \to n6\gamma$
75±18		BINON	84	GAM2	30–40 $\pi^- p \to n6\gamma$

$\Gamma(\mu^+\mu^-\gamma)/\Gamma(\gamma\gamma)$ — Γ_9/Γ_7

VALUE (units 10^{-3})	EVTS	DOCUMENT ID		TECN	COMMENT
4.9±1.2	33	VIKTOROV	80	CNTR	25,33 $\pi^- p \to 2\mu\gamma$

$\Gamma(\pi^+\pi^-\mu^+\mu^-)/\Gamma_{total}$ — Γ_{10}/Γ

VALUE (units 10^{-5})	CL%	EVTS	DOCUMENT ID		TECN	COMMENT
2.13±0.13 OUR AVERAGE						
2.15±0.13±0.02		434	[1] ABLIKIM	24AK	BES3	$J/\psi \to \gamma\eta'$
1.94±0.37±0.02		53	[2] ABLIKIM	21I	BES3	$J/\psi \to \gamma\eta'(958)$
• • • We do not use the following data for averages, fits, limits, etc. • • •						
< 2.9	90		[3] ABLIKIM	13O	BES3	$J/\psi \to \gamma\eta'$
<24	90		[4] NAIK	09	CLEO	$J/\psi \to \gamma\eta'$

[1] ABLIKIM 24AK reports $(2.16 \pm 0.12 \pm 0.06) \times 10^{-5}$ from a measurement of $[\Gamma(\eta'(958) \to \pi^+\pi^-\mu^+\mu^-)/\Gamma_{total}] \times [B(J/\psi(1S) \to \gamma\eta'(958))]$ assuming $B(J/\psi(1S) \to \gamma\eta'(958)) = (5.25 \pm 0.07) \times 10^{-3}$, which we rescale to our best (shown rounded) value $B(J/\psi(1S) \to \gamma\eta'(958)) = (5.28 \pm 0.06) \times 10^{-3}$. Our first error is their experiment's error and our second error is the systematic error from using our best (shown rounded) value.

[2] ABLIKIM 21I reports $(1.97 \pm 0.33 \pm 0.19) \times 10^{-5}$ from a measurement of $[\Gamma(\eta'(958) \to \pi^+\pi^-\mu^+\mu^-)/\Gamma_{total}] \times [B(J/\psi(1S) \to \gamma\eta'(958))]$ assuming $B(J/\psi(1S) \to \gamma\eta'(958)) = (5.21 \pm 0.17) \times 10^{-3}$, which we rescale to our best (shown rounded) value $B(J/\psi(1S) \to \gamma\eta'(958)) = (5.28 \pm 0.06) \times 10^{-3}$. Our first error is their experiment's error and our second error is the systematic error from using our best (shown rounded) value.

[3] Using $\Gamma_2/\Gamma = (29.3 \pm 0.6)\%$ from PDG 12.

[4] Not independent of measured value of Γ_{10}/Γ_1 from NAIK 09.

$\Gamma(\pi^+\pi^-\mu^+\mu^-)/\Gamma(\pi^+\pi^-\eta)$ — Γ_{10}/Γ_1

VALUE (units 10^{-3})	CL%	DOCUMENT ID		TECN	COMMENT
<0.5	90	[1] NAIK	09	CLEO	$J/\psi \to \gamma\eta'$

[1] NAIK 09 reports $[\Gamma(\eta'(958) \to \pi^+\pi^-\mu^+\mu^-)/\Gamma(\eta'(958) \to \pi^+\pi^-\eta)]$ / $[B(\eta \to 2\gamma)] < 1.3 \times 10^{-3}$ which we multiply by our best (shown rounded) value $B(\eta \to 2\gamma) = 39.36 \times 10^{-2}$.

$\Gamma(\pi^+\pi^-\mu^+\mu^-)/\Gamma(\rho^0\gamma(\text{including non-resonant } \pi^+\pi^-\gamma))$ — Γ_{10}/Γ_2

VALUE (units 10^{-4})	CL%	DOCUMENT ID		TECN	COMMENT
<1.0	90	ABLIKIM	13O	BES3	$J/\psi \to \gamma\eta'$

$\Gamma(\pi^+\pi^-\pi^0)/\Gamma_{total}$ — Γ_{11}/Γ

VALUE (units 10^{-3})	EVTS	DOCUMENT ID		TECN	COMMENT
3.61 ±0.18 OUR FIT					
3.61 ±0.18 OUR AVERAGE					
3.591±0.054±0.174	6067	ABLIKIM	17	BES3	$J/\psi \to \gamma(\pi^+\pi^-\pi^0)$
4.28 ±0.49 ±1.11	78	[1] ABLIKIM	15P	BES3	$J/\psi \to K^+K^-3\pi$
3.7 $^{+1.1}_{-0.9}$ ±0.4		[2] NAIK	09	CLEO	$J/\psi \to \gamma\eta'$
• • • We do not use the following data for averages, fits, limits, etc. • • •					
3.83 ±0.15 ±0.39	1014	[3] ABLIKIM	12E	BES3	$J/\psi \to \gamma(\pi^+\pi^-\pi^0)$

[1] We have added all systematic uncertainties in quadrature to a single value.

[2] Not independent of measured value of Γ_{11}/Γ_1 from NAIK 09.

[3] Superseded by ABLIKIM 17.

$\Gamma(\pi^+\pi^-\pi^0)/\Gamma(\pi^+\pi^-\eta)$ — Γ_{11}/Γ_1

VALUE (units 10^{-3})	EVTS	DOCUMENT ID		TECN	COMMENT
8.5 ±0.4 OUR FIT Error includes scale factor of 1.1.					
$8.27^{+2.49}_{-2.12}$±0.04	20	[1] NAIK	09	CLEO	$J/\psi \to \gamma\eta'$

[1] NAIK 09 reports $[\Gamma(\eta'(958) \to \pi^+\pi^-\pi^0)/\Gamma(\eta'(958) \to \pi^+\pi^-\eta)]$ / $[B(\eta \to 2\gamma)] = (21^{+6}_{-5} \pm 2) \times 10^{-3}$ which we multiply by our best (shown rounded) value $B(\eta \to 2\gamma) = (39.36 \pm 0.18) \times 10^{-2}$. Our first error is their experiment's error and our second error is the systematic error from using our best (shown rounded) value.

$\Gamma((\pi^+\pi^-\pi^0)\text{ S-wave})/\Gamma_{total}$ — Γ_{12}/Γ

VALUE (units 10^{-4})	EVTS	DOCUMENT ID		TECN	COMMENT
37.63±0.77±5.00	6580	[1] ABLIKIM	17	BES3	$J/\psi \to \gamma(\pi^+\pi^-\pi^0)$

[1] We have added all systematic uncertainties in quadrature.

$\Gamma(\pi^\mp\rho^\pm)/\Gamma_{total}$ — Γ_{13}/Γ

VALUE (units 10^{-4})	EVTS	DOCUMENT ID		TECN	COMMENT
7.44±0.60±2.23	1231	[1] ABLIKIM	17	BES3	$J/\psi \to \gamma(\pi^\mp\rho^\pm)$

[1] We have added all systematic uncertainties in quadrature.

$\Gamma(2(\pi^+\pi^-))/\Gamma_{total}$ — Γ_{14}/Γ

VALUE (units 10^{-5})	CL%	EVTS	DOCUMENT ID		TECN	COMMENT
8.51±0.32±0.10		1650	[1] ABLIKIM	24F	BES3	$J/\psi \to \gamma\eta'(958)$
• • • We do not use the following data for averages, fits, limits, etc. • • •						
8.3 ±0.9 ±0.1		199	[2,3] ABLIKIM	14M	BES3	$J/\psi \to \gamma\eta'$
< 24	90		[4] NAIK	09	CLEO	$J/\psi \to \gamma\eta'$
<1000	90		RITTENBERG	69	HBC	1.7–2.7 $K^- p$

[1] ABLIKIM 24F reports $(8.56 \pm 0.25 \pm 0.23) \times 10^{-5}$ from a measurement of $[\Gamma(\eta'(958) \to 2(\pi^+\pi^-))/\Gamma_{total}] \times [B(J/\psi(1S) \to \gamma\eta'(958))]$ assuming $B(J/\psi(1S) \to \gamma\eta'(958)) = (5.25 \pm 0.07) \times 10^{-3}$, which we rescale to our best (shown rounded) value $B(J/\psi(1S) \to \gamma\eta'(958)) = (5.28 \pm 0.06) \times 10^{-3}$. Our first error is their experiment's error and our second error is the systematic error from using our best (shown rounded) value.

[2] ABLIKIM 14M reports $[\Gamma(\eta'(958) \to 2(\pi^+\pi^-))/\Gamma_{total}] \times [B(J/\psi(1S) \to \gamma\eta'(958))] = (4.40 \pm 0.35 \pm 0.30) \times 10^{-7}$ which we divide by our best (shown rounded) value $B(J/\psi(1S) \to \gamma\eta'(958)) = (5.28 \pm 0.06) \times 10^{-3}$. Our first error is their experiment's error and our second error is the systematic error from using our best (shown rounded) value.

[3] Superseded by ABLIKIM 24F.

[4] Not independent of measured value of Γ_{14}/Γ_1 from NAIK 09.

$\Gamma(2(\pi^+\pi^-))/\Gamma(\pi^+\pi^-\eta)$ — Γ_{14}/Γ_1

VALUE (units 10^{-3})	CL%	DOCUMENT ID		TECN	COMMENT
<0.6	90	[1] NAIK	09	CLEO	$J/\psi \to \gamma\eta'$

[1] NAIK 09 reports $[\Gamma(\eta'(958) \to 2(\pi^+\pi^-))/\Gamma(\eta'(958) \to \pi^+\pi^-\eta)]$ / $[B(\eta \to 2\gamma)] < 1.4 \times 10^{-3}$ which we multiply by our best (shown rounded) value $B(\eta \to 2\gamma) = 39.36 \times 10^{-2}$.

$\Gamma(\pi^+\pi^-2\pi^0)/\Gamma_{total}$ — Γ_{15}/Γ

VALUE (units 10^{-4})	CL%	EVTS	DOCUMENT ID		TECN	COMMENT
2.11±0.15±0.02		865	[1] ABLIKIM	24F	BES3	$J/\psi \to \gamma\eta'(958)$
• • • We do not use the following data for averages, fits, limits, etc. • • •						
1.78±0.38±0.02		84	[2,3] ABLIKIM	14M	BES3	$J/\psi \to \gamma\eta'$
<27	90		[4] NAIK	09	CLEO	$J/\psi \to \gamma\eta'$

[1] ABLIKIM 24F reports $(2.12 \pm 0.12 \pm 0.10) \times 10^{-4}$ from a measurement of $[\Gamma(\eta'(958) \to \pi^+\pi^-2\pi^0)/\Gamma_{total}] \times [B(J/\psi(1S) \to \gamma\eta'(958))]$ assuming $B(J/\psi(1S) \to \gamma\eta'(958)) = (5.25 \pm 0.07) \times 10^{-3}$, which we rescale to our best (shown rounded) value $B(J/\psi(1S) \to \gamma\eta'(958)) = (5.28 \pm 0.06) \times 10^{-3}$. Our first error is their experiment's error and our second error is the systematic error from using our best (shown rounded) value.

[2] ABLIKIM 14M reports $[\Gamma(\eta'(958) \to \pi^+\pi^-2\pi^0)/\Gamma_{total}] \times [B(J/\psi(1S) \to \gamma\eta'(958))] = (9.38 \pm 1.79 \pm 0.89) \times 10^{-7}$ which we divide by our best (shown rounded) value $B(J/\psi(1S) \to \gamma\eta'(958)) = (5.28 \pm 0.06) \times 10^{-3}$. Our first error is their experiment's error and our second error is the systematic error from using our best (shown rounded) value.

[3] Superseded by ABLIKIM 24F.

[4] Not independent of measured value of Γ_{15}/Γ_1 from NAIK 09.

$\Gamma(\pi^+\pi^-2\pi^0)/\Gamma(\pi^+\pi^-\eta)$ — Γ_{15}/Γ_1

VALUE (units 10^{-3})	CL%	DOCUMENT ID		TECN	COMMENT
<6	90	[1] NAIK	09	CLEO	$J/\psi \to \gamma\eta'$

[1] NAIK 09 reports $[\Gamma(\eta'(958) \to \pi^+\pi^-2\pi^0)/\Gamma(\eta'(958) \to \pi^+\pi^-\eta)]$ / $[B(\eta \to 2\gamma)] < 15 \times 10^{-3}$ which we multiply by our best (shown rounded) value $B(\eta \to 2\gamma) = 39.36 \times 10^{-2}$.

$\Gamma(2(\pi^+\pi^-)\text{ neutrals})/\Gamma_{total}$ — Γ_{16}/Γ

VALUE	CL%	DOCUMENT ID		TECN	COMMENT
<0.01	95	DANBURG	73	HBC	2.2 $K^- p \to \Lambda X^0$
• • • We do not use the following data for averages, fits, limits, etc. • • •					
<0.01	90	RITTENBERG	69	HBC	1.7–2.7 $K^- p$

$\Gamma(2(\pi^+\pi^-)\pi^0)/\Gamma_{total}$ — Γ_{17}/Γ

VALUE	CL%	DOCUMENT ID		TECN	COMMENT
• • • We do not use the following data for averages, fits, limits, etc. • • •					
<0.002	90	[1] NAIK	09	CLEO	$J/\psi \to \gamma\eta'$
<0.01	90	RITTENBERG	69	HBC	1.7–2.7 $K^- p$

[1] Not independent of measured value of Γ_{17}/Γ_1 from NAIK 09.

$\Gamma(2(\pi^+\pi^-)\pi^0)/\Gamma(\pi^+\pi^-\eta)$ — Γ_{17}/Γ_1

VALUE (units 10^{-3})	CL%	DOCUMENT ID		TECN	COMMENT
<4	90	[1] NAIK	09	CLEO	$J/\psi \to \gamma\eta'$

[1] NAIK 09 reports $[\Gamma(\eta'(958) \to 2(\pi^+\pi^-)\pi^0)/\Gamma(\eta'(958) \to \pi^+\pi^-\eta)]$ / $[B(\eta \to 2\gamma)] < 11 \times 10^{-3}$ which we multiply by our best (shown rounded) value $B(\eta \to 2\gamma) = 39.36 \times 10^{-2}$.

$\Gamma(2(\pi^+\pi^-)2\pi^0)/\Gamma_{total}$ — Γ_{18}/Γ

VALUE	CL%	DOCUMENT ID		TECN	COMMENT
<0.01	95	KALBFLEISCH	64B	HBC	$K^- p \to \Lambda 2(\pi^+\pi^-)$+MM
• • • We do not use the following data for averages, fits, limits, etc. • • •					
<0.01	90	LONDON	66	HBC	Compilation

Int. J. Mod. Phys. A 2026.41. Downloaded from www.worldscientific.com by CALIFORNIA @ BERKELEY on 09/16/26. Re-use and distribution is strictly not permitted, except for Open Access articles.

$\Gamma(3(\pi^+\pi^-))/\Gamma_{total}$ — Γ_{19}/Γ

VALUE (units 10^{-5})	CL%	DOCUMENT ID		TECN	COMMENT
< 3.1	90	[1] ABLIKIM	13U	BES3	$J/\psi \to \gamma 3(\pi^+\pi^-)$
• • • We do not use the following data for averages, fits, limits, etc. • • •					
< 53	90	[2] NAIK	09	CLEO	$J/\psi \to \gamma\eta'$
<500	95	KALBFLEISCH	64B	HBC	$K^-p \to \Lambda 2(\pi^+\pi^-)$

[1] Using $B(J/\psi \to \gamma\eta'(958)) = (5.16 \pm 0.15) \times 10^{-3}$.
[2] Not independent of measured value of Γ_{19}/Γ_1 from NAIK 09.

$\Gamma(3(\pi^+\pi^-))/\Gamma(\pi^+\pi^-\eta)$ — Γ_{19}/Γ_1

VALUE (units 10^{-3})	CL%	DOCUMENT ID		TECN	COMMENT
<1.2	90	[1] NAIK	09	CLEO	$J/\psi \to \gamma\eta'$

[1] NAIK 09 reports $[\Gamma(\eta'(958) \to 3(\pi^+\pi^-))/\Gamma(\eta'(958) \to \pi^+\pi^-\eta)] / [B(\eta \to 2\gamma)] < 3.0 \times 10^{-3}$ which we multiply by our best (shown rounded) value $B(\eta \to 2\gamma) = 39.36 \times 10^{-2}$.

$\Gamma(K^\pm\pi^\mp)/\Gamma(\rho^0\gamma(\text{including non-resonant } \pi^+\pi^-\gamma))$ — Γ_{20}/Γ_2

VALUE	CL%	DOCUMENT ID		TECN	COMMENT
<1.3 × 10^{-4}	90	ABLIKIM	16M	BES3	$e^+e^- \to J/\psi \to$ hadrons

$\Gamma(\pi^+\pi^-e^+e^-)/\Gamma_{total}$ — Γ_{21}/Γ

VALUE (units 10^{-3})	CL%	EVTS	DOCUMENT ID		TECN	COMMENT
2.43±0.06 OUR FIT						
2.44±0.08±0.03		22725	[1] ABLIKIM	24AK	BES3	$J/\psi \to \gamma\eta'$
• • • We do not use the following data for averages, fits, limits, etc. • • •						
2.11±0.12±0.14		429	[2] ABLIKIM	13O	BES3	$J/\psi \to \gamma\eta'$
$2.5\ ^{+1.2}_{-0.9} \pm 0.5$			[3] NAIK	09	CLEO	$J/\psi \to \gamma\eta'$
<6	90		RITTENBERG	65	HBC	2.7 K^-p

[1] ABLIKIM 24AK reports $(2.45 \pm 0.02 \pm 0.08) \times 10^{-3}$ from a measurement of $[\Gamma(\eta'(958) \to \pi^+\pi^-e^+e^-)/\Gamma_{total}] \times [B(J/\psi(1S) \to \gamma\eta'(958))]$ assuming $B(J/\psi(1S) \to \gamma\eta'(958)) = (5.25 \pm 0.07) \times 10^{-3}$, which we rescale to our best (shown rounded) value $B(J/\psi(1S) \to \gamma\eta'(958)) = (5.28 \pm 0.06) \times 10^{-3}$. Our first error is their experiment's error and our second error is the systematic error from using our best (shown rounded) value.
[2] Using $\Gamma_2/\Gamma = (29.3 \pm 0.6)\%$ from PDG 12.
[3] Not independent of measured value of Γ_{21}/Γ_1 from NAIK 09.

$\Gamma(\pi^+\pi^-e^+e^-)/\Gamma(\pi^+\pi^-\eta)$ — Γ_{21}/Γ_1

VALUE (units 10^{-3})	EVTS	DOCUMENT ID		TECN	COMMENT
5.72±0.17 OUR FIT					
$5.51\ ^{+3.00}_{-2.30} \pm 0.03$	8	[1] NAIK	09	CLEO	$J/\psi \to \gamma\eta'$

[1] NAIK 09 reports $[\Gamma(\eta'(958) \to \pi^+\pi^-e^+e^-)/\Gamma(\eta'(958) \to \pi^+\pi^-\eta)] / [B(\eta \to 2\gamma)] = (14\ ^{+7}_{-5} \pm 3) \times 10^{-3}$ which we multiply by our best (shown rounded) value $B(\eta \to 2\gamma) = (39.36 \pm 0.18) \times 10^{-2}$. Our first error is their experiment's error and our second error is the systematic error from using our best (shown rounded) value.

$\Gamma(\pi^+\pi^-e^+e^-)/\Gamma(\rho^0\gamma(\text{including non-resonant } \pi^+\pi^-\gamma))$ — Γ_{21}/Γ_2

VALUE (units 10^{-3})	EVTS	DOCUMENT ID		TECN	COMMENT
8.24±0.21 OUR FIT					
8.20±0.16±0.27	2584	ABLIKIM	21J	BES3	$J/\psi \to \gamma\eta'$
• • • We do not use the following data for averages, fits, limits, etc. • • •					
7.2 ±0.4 ±0.5	429	[1] ABLIKIM	13O	BES3	$J/\psi \to \gamma\eta'$

[1] Superseded by ABLIKIM 21J.

$\Gamma(\pi^+e^-\nu_e + \text{c.c.})/\Gamma(\pi^+\pi^-\eta)$ — Γ_{22}/Γ_1

VALUE (units 10^{-4})	CL%	DOCUMENT ID		TECN	COMMENT
<5.0	90	ABLIKIM	13G	BES3	$J/\psi \to \phi\eta'$

$\Gamma(\gamma e^+e^-)/\Gamma_{total}$ — Γ_{23}/Γ

VALUE (units 10^{-4})	CL%	EVTS	DOCUMENT ID		TECN	COMMENT
4.80±0.14±0.05		7611	[1] ABLIKIM	24M	BES3	$e^+e^- \to J/\psi \to \gamma\eta'$
• • • We do not use the following data for averages, fits, limits, etc. • • •						
<9	90		BRIERE	00	CLEO	10.6 e^+e^-

[1] ABLIKIM 24M reports $(4.83 \pm 0.07 \pm 0.14) \times 10^{-4}$ from a measurement of $[\Gamma(\eta'(958) \to \gamma e^+e^-)/\Gamma_{total}] \times [B(J/\psi(1S) \to \gamma\eta'(958))]$ assuming $B(J/\psi(1S) \to \gamma\eta'(958)) = (5.25 \pm 0.07) \times 10^{-3}$, which we rescale to our best (shown rounded) value $B(J/\psi(1S) \to \gamma\eta'(958)) = (5.28 \pm 0.06) \times 10^{-3}$. Our first error is their experiment's error and our second error is the systematic error from using our best (shown rounded) value.

$\Gamma(\gamma e^+e^-)/\Gamma(\gamma\gamma)$ — Γ_{23}/Γ_7

VALUE (units 10^{-2})	EVTS	DOCUMENT ID		TECN	COMMENT
2.13±0.09±0.07	864	ABLIKIM	15O	BES3	$J/\psi \to \gamma e^+e^-$

$\Gamma(\pi^0\gamma\gamma)/\Gamma_{total}$ — Γ_{24}/Γ

VALUE (units 10^{-3})	EVTS	DOCUMENT ID		TECN	COMMENT
3.20±0.07±0.23	3.4k	ABLIKIM	17T	BES3	$J/\psi \to \gamma\eta'$

$\Gamma(\pi^0\gamma\gamma)/\Gamma(\pi^0\pi^0\eta)$ — Γ_{24}/Γ_4

VALUE (units 10^{-4})	CL%	DOCUMENT ID		TECN	COMMENT
<37	90	ALDE	87B	GAM2	38 $\pi^-p \to n4\gamma$

$\Gamma(\pi^0\gamma\gamma(\text{non resonant}))/\Gamma_{total}$ — Γ_{25}/Γ

VALUE (units 10^{-4})	EVTS	DOCUMENT ID		TECN	COMMENT
6.16±0.64±0.67	655	ABLIKIM	17T	BES3	$J/\psi \to \gamma\eta'$

$\Gamma(\eta\gamma\gamma)/\Gamma_{total}$ — Γ_{26}/Γ

VALUE	CL%	DOCUMENT ID		TECN	COMMENT
<1.33 × 10^{-4}	90	ABLIKIM	19AW	BES3	$J/\psi \to \gamma\eta' \to \gamma\gamma\gamma 2\gamma$

$\Gamma(4\pi^0)/\Gamma_{total}$ — Γ_{27}/Γ

VALUE	CL%	DOCUMENT ID		TECN	COMMENT
<1.2 × 10^{-5}	90	[1] ABLIKIM	24F	BES3	$J/\psi \to \gamma\eta'(958)$
• • • We do not use the following data for averages, fits, limits, etc. • • •					
<4.94 × 10^{-5}	90	[2] ABLIKIM	20E	BES3	$J/\psi \to \eta'\gamma$
<3.2 × 10^{-4}	90	DONSKOV	14	GAM4	32.5 $\pi^-p \to \eta' n$

[1] ABLIKIM 24F reports $< 1.24 \times 10^{-5}$ from a measurement of $[\Gamma(\eta'(958) \to 4\pi^0)/\Gamma_{total}] \times [B(J/\psi(1S) \to \gamma\eta'(958))]$ assuming $B(J/\psi(1S) \to \gamma\eta'(958)) = (5.25 \pm 0.07) \times 10^{-3}$, which we rescale to our best (shown rounded) value $B(J/\psi(1S) \to \gamma\eta'(958)) = 5.28 \times 10^{-3}$.
[2] Superseded by ABLIKIM 24F.

$\Gamma(4\pi^0)/\Gamma(\pi^0\pi^0\eta)$ — Γ_{27}/Γ_4

VALUE (units 10^{-4})	CL%	DOCUMENT ID		TECN	COMMENT
• • • We do not use the following data for averages, fits, limits, etc. • • •					
<23	90	ALDE	87B	GAM2	38 $\pi^-p \to n8\gamma$

$\Gamma(e^+e^-)/\Gamma_{total}$ — Γ_{28}/Γ

VALUE	CL%	DOCUMENT ID		TECN	COMMENT
< 5.6 × 10^{-9}	90	[1] ACHASOV	15	SND	0.958 $e^+e^- \to \pi\pi\eta$
• • • We do not use the following data for averages, fits, limits, etc. • • •					
<12 × 10^{-9}	90	[2] AKHMETSHIN	15	CMD3	0.958 $e^+e^- \to \pi^+\pi^-\eta$
< 2.1 × 10^{-7}	90	VOROBYEV	88	ND	$e^+e^- \to \pi^+\pi^-\eta$

[1] Combining data of ACHASOV 15 and AKHMETSHIN 15 and using $\Gamma(\eta') = 0.198 \pm 0.009$ MeV.
[2] Using $\Gamma_{\eta'(958)} = 198 \pm 9$ keV, $B(\eta'(958) \to \pi^+\pi^-\eta) = (42.9 \pm 0.7)\%$, and $B(\eta \to \gamma\gamma) = (39.41 \pm 0.20)\%$.

$\Gamma(e^+e^-e^+e^-)/\Gamma_{total}$ — Γ_{29}/Γ

VALUE (units 10^{-6})	EVTS	DOCUMENT ID		TECN	COMMENT
4.5±1.1±0.1	30	[1] ABLIKIM	22E	BES3	$J/\psi \to \gamma\eta'$

[1] ABLIKIM 22E reports $(4.5 \pm 1.0 \pm 0.5) \times 10^{-6}$ from a measurement of $[\Gamma(\eta'(958) \to e^+e^-e^+e^-)/\Gamma_{total}] \times [B(J/\psi(1S) \to \gamma\eta'(958))]$ assuming $B(J/\psi(1S) \to \gamma\eta'(958)) = (5.25 \pm 0.07) \times 10^{-3}$, which we rescale to our best (shown rounded) value $B(J/\psi(1S) \to \gamma\eta'(958)) = (5.28 \pm 0.06) \times 10^{-3}$. Our first error is their experiment's error and our second error is the systematic error from using our best (shown rounded) value.

$\Gamma(e^+e^-\mu^+\mu^-)/\Gamma_{total}$ — Γ_{30}/Γ

VALUE	CL%	DOCUMENT ID		TECN	COMMENT
<1.8 × 10^{-6}	90	[1] ABLIKIM	25N	BES3	$J/\psi \to \gamma\eta'$

[1] ABLIKIM 25N reports $< 1.75 \times 10^{-6}$ from a measurement of $[\Gamma(\eta'(958) \to e^+e^-\mu^+\mu^-)/\Gamma_{total}] \times [B(J/\psi(1S) \to \gamma\eta'(958))]$ assuming $B(J/\psi(1S) \to \gamma\eta'(958)) = (5.28 \pm 0.06) \times 10^{-3}$.

$\Gamma(\mu^+\mu^-\mu^+\mu^-)/\Gamma_{total}$ — Γ_{31}/Γ

VALUE	CL%	DOCUMENT ID		TECN	COMMENT
<5 × 10^{-7}	90	[1] ABLIKIM	25N	BES3	$J/\psi \to \gamma\eta'$

[1] ABLIKIM 25N reports $< 5.28 \times 10^{-7}$ from a measurement of $[\Gamma(\eta'(958) \to \mu^+\mu^-\mu^+\mu^-)/\Gamma_{total}] \times [B(J/\psi(1S) \to \gamma\eta'(958))]$ assuming $B(J/\psi(1S) \to \gamma\eta'(958)) = (5.28 \pm 0.06) \times 10^{-3}$.

$\Gamma(\pi^+\pi^-e^+e^-)/\Gamma(\pi^+\pi^-\mu^+\mu^-)$ — Γ_{21}/Γ_{10}

VALUE	EVTS	DOCUMENT ID		TECN	COMMENT
• • • We do not use the following data for averages, fits, limits, etc. • • •					
113.4±0.9±3.7	434	[1] ABLIKIM	24AK	BES3	$J/\psi \to \gamma\eta'$

[1] ABLIKIM 24AK value is not independent from the individual branching fraction measurements.

$\Gamma(\text{invisible})/\Gamma_{total}$ — Γ_{32}/Γ

VALUE	CL%	DOCUMENT ID		TECN	COMMENT
<2.1 × 10^{-4}	90	[1] ANDREEV	24D	NA64	CEX π^-Fe $\to \eta' X$
• • • We do not use the following data for averages, fits, limits, etc. • • •					
<9.5 × 10^{-4}	90	[2] NAIK	09	CLEO	$J/\psi \to \gamma\eta'$

[1] ANDREEV 24D result is based on 2.9×10^9 pions on active ^{26}Fe target.
[2] Not independent of measured value of Γ_{32}/Γ_1 from NAIK 09.

Int. J. Mod. Phys. A 2026.41. Downloaded from www.worldscientific.com
by UNIVERSITY OF CALIFORNIA @ BERKELEY on 09/16/26. Re-use and distribution is strictly not permitted, except for Open Access articles.

$\Gamma(\text{invisible})/\Gamma(\pi^+\pi^-\eta)$ — Γ_{32}/Γ_1

VALUE (units 10^{-3})	CL%	DOCUMENT ID		TECN	COMMENT
• • • We do not use the following data for averages, fits, limits, etc. • • •					
<2.1	90	[1] NAIK	09	CLEO	$J/\psi \to \gamma\eta'$

[1] NAIK 09 reports $[\Gamma(\eta'(958) \to \text{invisible})/\Gamma(\eta'(958) \to \pi^+\pi^-\eta)] / [B(\eta \to 2\gamma)] < 5.4 \times 10^{-3}$ which we multiply by our best (shown rounded) value $B(\eta \to 2\gamma) = 39.36 \times 10^{-2}$.

$\Gamma(\text{invisible})/\Gamma(\gamma\gamma)$ — Γ_{32}/Γ_7

VALUE	CL%	DOCUMENT ID		TECN	COMMENT
• • • We do not use the following data for averages, fits, limits, etc. • • •					
$<2.4 \times 10^{-2}$	90	ABLIKIM	13	BES3	$J/\psi \to \phi\eta'$
$<6.69 \times 10^{-2}$	90	ABLIKIM	06Q	BES	$J/\psi \to \phi\eta'$

$\Gamma(\gamma\,\text{Dark Photon})/\Gamma_{\text{total}}$ — Γ_{33}/Γ

VALUE (units 10^{-6})	CL%	EVTS	DOCUMENT ID		TECN	COMMENT
0.5 to 3.5	90	7611	[1] ABLIKIM	24M	BES3	$e^+e^- \to J/\psi \to \gamma\eta'$

[1] For a dark photon decaying to e^+e^- in the mass range 0 to 0.7 GeV.

$\Gamma(\pi^+\pi^-)/\Gamma_{\text{total}}$ — Γ_{34}/Γ

VALUE (units 10^{-4})	CL%	DOCUMENT ID		TECN	COMMENT
< 0.18	90	[1] AAIJ	17D	LHCB	$D^+_{(s)} \to \pi^+\pi^-\pi^+$
• • • We do not use the following data for averages, fits, limits, etc. • • •					
< 0.5	90	[2] ABLIKIM	11G	BES3	$J/\psi \to \gamma\pi^+\pi^-$
< 29	90	[3] MORI	07A	BELL	$\gamma\gamma \to \pi^+\pi^-$
< 3.3	90	[4] MORI	07A	BELL	$\gamma\gamma \to \pi^+\pi^-$
<800	95	DANBURG	73	HBC	2.2 $K^-p \to \Lambda X^0$
<200	90	RITTENBERG	69	HBC	1.7–2.7 K^-p

[1] Using branching fractions of $D^+_{(s)}$ decays from PDG 15.
[2] ABLIKIM 11G reports $[\Gamma(\eta'(958) \to \pi^+\pi^-)/\Gamma_{\text{total}}] \times [B(J/\psi(1S) \to \gamma\eta'(958))] < 2.84 \times 10^{-7}$ which we divide by our best (shown rounded) value $B(J/\psi(1S) \to \gamma\eta'(958)) = 5.28 \times 10^{-3}$.
[3] Taking into account interference with the $\gamma\gamma \to \pi^+\pi^-$ continuum.
[4] Without interference with the $\gamma\gamma \to \pi^+\pi^-$ continuum.

$\Gamma(\pi^0\pi^0)/\Gamma_{\text{total}}$ — Γ_{35}/Γ

VALUE	CL%	DOCUMENT ID		TECN	COMMENT
$<4 \times 10^{-4}$	90	[1] ABLIKIM	11G	BES3	$J/\psi \to \gamma\pi^0\pi^0$

[1] ABLIKIM 11G reports $[\Gamma(\eta'(958) \to \pi^+\pi^-)/\Gamma_{\text{total}}] \times [B(J/\psi(1S) \to \gamma\eta'(958))] < 2.84 \times 10^{-7}$ which we divide by our best (shown rounded) value $B(J/\psi(1S) \to \gamma\eta'(958)) = 5.28 \times 10^{-3}$.

$\Gamma(\pi^0\pi^0)/\Gamma(\pi^0\pi^0\eta)$ — Γ_{35}/Γ_4

VALUE (units 10^{-4})	CL%	DOCUMENT ID		TECN	COMMENT
<45	90	ALDE	87B	GAM2	38 $\pi^-p \to n4\gamma$

$\Gamma(\pi^0e^+e^-)/\Gamma_{\text{total}}$ — Γ_{36}/Γ

VALUE (units 10^{-3})	CL%	DOCUMENT ID		TECN	COMMENT
< 1.4	90	BRIERE	00	CLEO	10.6 e^+e^-
• • • We do not use the following data for averages, fits, limits, etc. • • •					
<13	90	RITTENBERG	65	HBC	2.7 K^-p

$\Gamma(\pi^0\rho^0)/\Gamma_{\text{total}}$ — Γ_{37}/Γ

VALUE	CL%	DOCUMENT ID		TECN	COMMENT
<0.04	90	RITTENBERG	65	HBC	2.7 K^-p

$\Gamma(\eta e^+e^-)/\Gamma_{\text{total}}$ — Γ_{38}/Γ

VALUE (units 10^{-3})	CL%	DOCUMENT ID		TECN	COMMENT
< 2.4	90	BRIERE	00	CLEO	10.6 e^+e^-
• • • We do not use the following data for averages, fits, limits, etc. • • •					
<11	90	RITTENBERG	65	HBC	2.7 K^-p

$\Gamma(3\gamma)/\Gamma(\pi^0\pi^0\eta)$ — Γ_{39}/Γ_4

VALUE (units 10^{-4})	CL%	DOCUMENT ID		TECN	COMMENT
<4.6	90	ALDE	87B	GAM2	38 $\pi^-p \to n3\gamma$

$\Gamma(\mu^+\mu^-\pi^0)/\Gamma_{\text{total}}$ — Γ_{40}/Γ

VALUE (units 10^{-5})	CL%	DOCUMENT ID		TECN	COMMENT
<6.0	90	DZHELYADIN	81	CNTR	30 $\pi^-p \to \eta'n$

$\Gamma(\mu^+\mu^-\eta)/\Gamma_{\text{total}}$ — Γ_{41}/Γ

VALUE (units 10^{-5})	CL%	DOCUMENT ID		TECN	COMMENT
<1.5	90	DZHELYADIN	81	CNTR	30 $\pi^-p \to \eta'n$

$\Gamma(e\mu)/\Gamma_{\text{total}}$ — Γ_{42}/Γ

VALUE (units 10^{-4})	CL%	DOCUMENT ID		TECN	COMMENT
<4.7	90	BRIERE	00	CLEO	10.6 e^+e^-

$\Gamma(\pi^+\pi^-\text{ALP} \to \pi^+\pi^-e^+e^-)/\Gamma(\pi^+\pi^-e^+e^-)$ — Γ_{43}/Γ_{21}

VALUE	CL%	DOCUMENT ID		TECN	COMMENT
$<7.8 \times 10^{-3}$	90	[1] ABLIKIM	24AK	BES3	$J/\psi \to \gamma\eta'$

[1] For a pseudoscalar ALP, with a mass in the range 0–500 MeV. The measured limit at the 90% credibility level as a function of the mass of ALP ranges from 0.1×10^{-3} to 7.8×10^{-3}.

$\eta'(958) \to \eta\pi\pi$ DECAY PARAMETERS

$$|\text{MATRIX ELEMENT}|^2 = |1 + \alpha Y|^2 + CX + DX^2$$

X and Y are Dalitz variables; α is complex and C, and D are real-valued. Parameters C and D are not necessarily equal to c and d, respectively, in the generalized parameterization following this one. May be different for $\eta'(958) \to \eta\pi^+\pi^-$ and $\eta'(958) \to \eta\pi^0\pi^0$ decays. Because of different initial assumptions and strong correlations of the parameters we do not average the parameters in the section below.

$Re(\alpha)$ decay parameter

VALUE	EVTS	DOCUMENT ID		TECN	COMMENT
• • • We do not use the following data for averages, fits, limits, etc. • • •					
$-0.034 \pm 0.002 \pm 0.002$	351k	ABLIKIM	18	BES3	$\eta' \to \eta\pi^+\pi^-$
$-0.054 \pm 0.004 \pm 0.001$	56k	ABLIKIM	18	BES3	$\eta' \to \eta\pi^0\pi^0$
$-0.033 \pm 0.005 \pm 0.003$	44k	[1] ABLIKIM	11	BES3	$J/\psi \to \gamma\eta\pi^+\pi^-$
$-0.072 \pm 0.012 \pm 0.006$	7k	[2] AMELIN	05A	VES	28 $\pi^-A \to \eta\pi^+\pi^-\pi^-A^*$
$-0.021 \pm 0.018 \pm 0.017$	6.7k	[3] BRIERE	00	CLEO	10.6 $e^+e^- \to \eta\pi^+\pi^-X$
$-0.058 \pm 0.013 \pm 0.003$	5.4k	[4] ALDE	86	GAM2	38 $\pi^-p \to n\eta\pi^0\pi^0$
-0.08 ± 0.03		[4,5] KALBFLEISCH	74	RVUE	$\eta' \to \eta\pi^+\pi^-$

[1] See ABLIKIM 11 for the full correlation matrix.
[2] Superseded by DOROFEEV 07, which found this parameterization unacceptable. See below.
[3] Assuming $\text{Im}(\alpha) = 0$, $C = 0$, and $D = 0$.
[4] Assuming $C = 0$.
[5] From the data of DAUBER 64, RITTENBERG 69, AGUILAR-BENITEZ 72B, JACOBS 73, and DANBURG 73.

$Im(\alpha)$ decay parameter

VALUE	EVTS	DOCUMENT ID		TECN	COMMENT
• • • We do not use the following data for averages, fits, limits, etc. • • •					
$0.000 \pm 0.019 \pm 0.001$	351k	ABLIKIM	18	BES3	$\eta' \to \eta\pi^+\pi^-$
$0.000 \pm 0.038 \pm 0.002$	56k	ABLIKIM	18	BES3	$\eta' \to \eta\pi^0\pi^0$
$0.000 \pm 0.049 \pm 0.001$	44k	[1] ABLIKIM	11	BES3	$J/\psi \to \gamma\eta\pi^+\pi^-$
$0.0 \pm 0.1 \pm 0.0$	7k	[2] AMELIN	05A	VES	28 $\pi^-A \to \eta\pi^+\pi^-\pi^-A^*$
$-0.00 \pm 0.13 \pm 0.00$	5.4k	[3] ALDE	86	GAM2	38 $\pi^-p \to n\eta\pi^0\pi^0$
0.0 ± 0.3		[3,4] KALBFLEISCH	74	RVUE	$\eta' \to \eta\pi^+\pi^-$

[1] See ABLIKIM 11 for the full correlation matrix.
[2] Superseded by DOROFEEV 07, which found this parameterization unacceptable. See below.
[3] Assuming $C = 0$.
[4] From the data of DAUBER 64, RITTENBERG 69, AGUILAR-BENITEZ 72B, JACOBS 73, and DANBURG 73.

C decay parameter

VALUE	EVTS	DOCUMENT ID		TECN	COMMENT
• • • We do not use the following data for averages, fits, limits, etc. • • •					
$0.0027 \pm 0.0024 \pm 0.0015$	351k	ABLIKIM	18	BES3	$\eta' \to \eta\pi^+\pi^-$
$0.018 \pm 0.009 \pm 0.003$	44k	[1] ABLIKIM	11	BES3	$J/\psi \to \gamma\eta\pi^+\pi^-$
$0.020 \pm 0.018 \pm 0.004$	7k	[2] AMELIN	05A	VES	28 $\pi^-A \to \eta\pi^+\pi^-\pi^-A^*$

[1] See ABLIKIM 11 for the full correlation matrix.
[2] Superseded by DOROFEEV 07, which found this parameterization unacceptable. See below.

D decay parameter

VALUE	EVTS	DOCUMENT ID		TECN	COMMENT
• • • We do not use the following data for averages, fits, limits, etc. • • •					
$-0.053 \pm 0.004 \pm 0.004$	351k	ABLIKIM	18	BES3	$\eta' \to \eta\pi^+\pi^-$
$-0.061 \pm 0.009 \pm 0.005$	56k	ABLIKIM	18	BES3	$\eta' \to \eta\pi^0\pi^0$
$-0.059 \pm 0.012 \pm 0.004$	44k	[1] ABLIKIM	11	BES3	$J/\psi \to \gamma\eta\pi^+\pi^-$
$-0.066 \pm 0.030 \pm 0.015$	7k	[2] AMELIN	05A	VES	28 $\pi^-A \to \eta\pi^+\pi^-\pi^-A^*$
$0.00 \pm 0.03 \pm 0.00$	5.4k	[3] ALDE	86	GAM2	38 $\pi^-p \to n\eta\pi^0\pi^0$
0		[3,4] KALBFLEISCH	74	RVUE	$\eta' \to \eta\pi^+\pi^-$

[1] See ABLIKIM 11 for the full correlation matrix.
[2] Superseded by DOROFEEV 07, which found this parameterization unacceptable. See below.
[3] Assuming $C = 0$.
[4] From the data of DAUBER 64, RITTENBERG 69, AGUILAR-BENITEZ 72B, JACOBS 73, and DANBURG 73.

Int. J. Mod. Phys. A 2026.41. Downloaded from www.worldscientific.com
by CALIFORNIA @ BERKELEY on 09/16/26. Re-use and distribution is strictly not permitted, except for Open Access articles.

$\eta'(958) \to \eta\pi\pi$ DECAY PARAMETERS

$|\text{MATRIX ELEMENT}|^2 \propto 1 + a\,Y + b\,Y^2 + c\,X + d\,X^2$

X and Y are Dalitz variables and a, b, c, and d are real-valued parameters. May be different for $\eta'(958) \to \eta\pi^+\pi^-$ and $\eta'(958) \to \eta\pi^0\pi^0$ decays. We do not average measurements in the section below because parameter values from each experiment are strongly correlated.

a decay parameter

VALUE	EVTS	DOCUMENT ID		TECN	COMMENT
• • • We do not use the following data for averages, fits, limits, etc. • • •					
$-0.077 \pm 0.003 \pm 0.001$		[1] ABLIKIM	23AH	BES3	$\eta' \to \eta\pi^0\pi^0$
$-0.056 \pm 0.004 \pm 0.002$	351k	ABLIKIM	18	BES3	$\eta' \to \eta\pi^+\pi^-$
$-0.087 \pm 0.009 \pm 0.006$	56k	ABLIKIM	18	BES3	$\eta' \to \eta\pi^0\pi^0$
$-0.074 \pm 0.008 \pm 0.006$	124k	ADLARSON	18A	A2MM	$\eta' \to \eta\pi^0\pi^0$
$-0.072 \pm 0.007 \pm 0.008$		[2] GONZALEZ-S...	18A	RVUE	$\eta' \to \eta\pi^0\pi^0$
$-0.047 \pm 0.011 \pm 0.003$	44k	[3] ABLIKIM	11	BES3	$J/\psi \to \gamma\eta\pi^+\pi^-$
$-0.066 \pm 0.016 \pm 0.003$	15k	[4] BLIK	09	GAM4	32.5 $\pi^- p \to \eta' n$
$-0.127 \pm 0.016 \pm 0.008$	20k	[5] DOROFEEV	07	VES	27 $\pi^- p \to \eta' n$, $\pi^- A \to \eta'\pi^- A^*$

[1] Fit IV, ignoring noncusp terms. Supersedes ABLIKIM 18.
[2] Theoretical analysis of ADLARSON 18A using resonance chiral perturbation theory to one loop.
[3] See ABLIKIM 11 for the full correlation matrix.
[4] From $\eta' \to \eta\pi^0\pi^0$ decay.
[5] From $\eta' \to \eta\pi^+\pi^-$ decay.

b decay parameter

VALUE	EVTS	DOCUMENT ID		TECN	COMMENT
• • • We do not use the following data for averages, fits, limits, etc. • • •					
$-0.066 \pm 0.006 \pm 0.001$		[1] ABLIKIM	23AH	BES3	$\eta' \to \eta\pi^0\pi^0$
$-0.049 \pm 0.006 \pm 0.006$	351k	ABLIKIM	18	BES3	$\eta' \to \eta\pi^+\pi^-$
$-0.073 \pm 0.014 \pm 0.005$	56k	ABLIKIM	18	BES3	$\eta' \to \eta\pi^0\pi^0$
$-0.063 \pm 0.014 \pm 0.005$	124k	ADLARSON	18A	A2MM	$\eta' \to \eta\pi^0\pi^0$
$-0.052 \pm 0.001 \pm 0.002$		[2] GONZALEZ-S...	18A	RVUE	$\eta' \to \eta\pi^0\pi^0$
$-0.069 \pm 0.019 \pm 0.009$	44k	[3] ABLIKIM	11	BES3	$J/\psi \to \gamma\eta\pi^+\pi^-$
$-0.063 \pm 0.028 \pm 0.004$	15k	[4] BLIK	09	GAM4	32.5 $\pi^- p \to \eta' n$
$-0.106 \pm 0.028 \pm 0.014$	20k	[5] DOROFEEV	07	VES	27 $\pi^- p \to \eta' n$, $\pi^- A \to \eta'\pi^- A^*$

[1] Fit IV, ignoring noncusp terms. Supersedes ABLIKIM 18.
[2] Theoretical analysis of ADLARSON 18A using resonance chiral perturbation theory to one loop.
[3] See ABLIKIM 11 for the full correlation matrix.
[4] From $\eta' \to \eta\pi^0\pi^0$ decay.
[5] From $\eta' \to \eta\pi^+\pi^-$ decay.

c decay parameter

VALUE	EVTS	DOCUMENT ID		TECN	COMMENT
• • • We do not use the following data for averages, fits, limits, etc. • • •					
$0.0027 \pm 0.0024 \pm 0.0018$	351k	ABLIKIM	18	BES3	$\eta' \to \eta\pi^+\pi^-$
$0.019 \pm 0.011 \pm 0.003$	44k	[1] ABLIKIM	11	BES3	$J/\psi \to \gamma\eta\pi^+\pi^-$
$-0.107 \pm 0.096 \pm 0.003$	15k	[2] BLIK	09	GAM4	32.5 $\pi^- p \to \eta' n$
$0.015 \pm 0.011 \pm 0.014$	20k	[3] DOROFEEV	07	VES	27 $\pi^- p \to \eta' n$, $\pi^- A \to \eta'\pi^- A^*$

[1] See ABLIKIM 11 for the full correlation matrix.
[2] From $\eta' \to \eta\pi^0\pi^0$ decay.
[3] From $\eta' \to \eta\pi^+\pi^-$ decay.

d decay parameter

VALUE	EVTS	DOCUMENT ID		TECN	COMMENT
• • • We do not use the following data for averages, fits, limits, etc. • • •					
$-0.068 \pm 0.004 \pm 0.001$		[1] ABLIKIM	23AH	BES3	$\eta' \to \eta\pi^0\pi^0$
$-0.063 \pm 0.004 \pm 0.003$	351k	ABLIKIM	18	BES3	$\eta' \to \eta\pi^+\pi^-$
$-0.074 \pm 0.009 \pm 0.004$	56k	ABLIKIM	18	BES3	$\eta' \to \eta\pi^0\pi^0$
$-0.050 \pm 0.009 \pm 0.005$	124k	ADLARSON	18A	A2MM	$\eta' \to \eta\pi^0\pi^0$
$-0.051 \pm 0.008 \pm 0.006$		[2] GONZALEZ-S...	18A	RVUE	$\eta' \to \eta\pi^0\pi^0$
$-0.073 \pm 0.012 \pm 0.003$	44k	[3] ABLIKIM	11	BES3	$J/\psi \to \gamma\eta\pi^+\pi^-$
$0.018 \pm 0.078 \pm 0.006$	15k	[4] BLIK	09	GAM4	32.5 $\pi^- p \to \eta' n$
$-0.082 \pm 0.017 \pm 0.008$	20k	[5] DOROFEEV	07	VES	27 $\pi^- p \to \eta' n$, $\pi^- A \to \eta'\pi^- A^*$

[1] Fit IV, ignoring noncusp terms. Supersedes ABLIKIM 18.
[2] Theoretical analysis of ADLARSON 18A using resonance chiral perturbation theory to one loop.
[3] See ABLIKIM 11 for the full correlation matrix.
[4] From $\eta' \to \eta\pi^0\pi^0$ decay. If $c \equiv 0$ from Bose-Einstein symmetry, $d = -0.067 \pm 0.020 \pm 0.003$.
[5] From $\eta' \to \eta\pi^+\pi^-$ decay.

$\eta'(958)$ β PARAMETER

$|\text{MATRIX ELEMENT}|^2 = (1 + 2\beta Z)$

See the "Note on η Decay Parameters" in our 1994 edition Physical Review **D50** 1173 (1994), p. 1454.

β decay parameter

VALUE	EVTS	DOCUMENT ID		TECN	COMMENT
-0.61 ± 0.08 OUR AVERAGE	Error includes scale factor of 1.2.				
$-0.640 \pm 0.046 \pm 0.047$	1.8k	ABLIKIM	15G	BES3	$J/\psi \to \gamma(\pi^0\pi^0\pi^0)$
-0.59 ± 0.18	235	BLIK	08	GAMS	32 $\pi^- p \to \eta' n$
-0.1 ± 0.3		ALDE	87B	GAM2	38 $\pi^- p \to n3\pi^0$

$\eta'(958)$ C-NONCONSERVING DECAY PARAMETER

See the note on η decay parameters in the Stable Particle Particle Listings for definition of this parameter.

DECAY ASYMMETRY PARAMETER FOR $\pi^+\pi^-\gamma$

VALUE	EVTS	DOCUMENT ID		TECN	COMMENT
-0.03 ± 0.04 OUR AVERAGE					
-0.019 ± 0.056		AIHARA	87	TPC	$2\gamma \to \pi^+\pi^-\gamma$
-0.069 ± 0.078	295	GRIGORIAN	75	STRC	2.1 $\pi^- p$
0.00 ± 0.10	103	KALBFLEISCH	75	HBC	2.18 $K^- p \to \Lambda\pi^+\pi^-\gamma$
• • • We do not use the following data for averages, fits, limits, etc. • • •					
0.07 ± 0.08	152	RITTENBERG	65	HBC	2.1–2.7 $K^- p$

$\eta'(958) \to \gamma\ell^+\ell^-$ TRANSITION FORM FACTOR SLOPE

Related to the effective virtual meson mass Λ, via slope $\approx \Lambda^{-2}$. See e.g. LANDSBERG 85, eq. (3.8), for a detailed definition.

VALUE (GeV^{-2})	EVTS	DOCUMENT ID		TECN	COMMENT
1.53 ± 0.04 OUR AVERAGE					
1.524 ± 0.041	7611	[1] ABLIKIM	24M	BES3	$e^+e^- \to J/\psi \to \gamma\eta'$
1.7 ± 0.4	33	[1] VIKTOROV	80		25,33 $\pi^- p \to 2\mu\gamma$
• • • We do not use the following data for averages, fits, limits, etc. • • •					
1.30 ± 0.19		[2] ABLIKIM	24AK	BES3	$\eta' \to \pi^+\pi^-\mu^+\mu^-$, $\pi^+\pi^-e^+e^-$
$1.60 \pm 0.17 \pm 0.08$	864	[1] ABLIKIM	15O	BES3	$\eta' \to \gamma e^+e^-$

[1] In the single-pole Ansatz where slope $= 1/(\Lambda^2 + \gamma^2)$ with Λ, γ being a Breit-Wigner mass, width for the effective contributing vector meson.
[2] From a weighted average of the $\eta' \to \pi^+\pi^-e^+e^-$ and $\eta' \to \pi^+\pi^-\mu^+\mu^-$ values. The uncertainty is obtained by combining statistical and systematic uncertainties. TFF slope values go between 1.10 ± 0.21 GeV^{-2} and 1.61 ± 0.71 GeV^{-2} for $\eta' \to \pi^+\pi^-e^+e^-$, and between 2.37 ± 0.49 GeV^{-2} and 2.88 ± 0.25 GeV^{-2} for $\eta' \to \pi^+\pi^-\mu^+\mu^-$, according to the solution of the fitting function model.

$\eta'(958)$ REFERENCES

ABLIKIM	25N	PR D111 052002	M. Ablikim *et al.*	(BESIII Collab.)
ABLIKIM	24AK	JHEP 2407 135	M. Ablikim *et al.*	(BESIII Collab.)
ABLIKIM	24F	PR D109 032006	M. Ablikim *et al.*	(BESIII Collab.)
ABLIKIM	24M	PR D109 072001	M. Ablikim *et al.*	(BESIII Collab.)
ANDREEV	24D	PRL 133 121803	Yu.M. Andreev *et al.*	(NA64 Collab.)
ABLIKIM	23AH	PRL 130 081901	M. Ablikim *et al.*	(BESIII Collab.)
ABLIKIM	22E	PR D105 112010	M. Ablikim *et al.*	(BESIII Collab.)
ABLIKIM	21I	PR D103 072006	M. Ablikim *et al.*	(BESIII Collab.)
ABLIKIM	21J	PR D103 092005	M. Ablikim *et al.*	(BESIII Collab.)
ABLIKIM	20E	PR D101 032001	M. Ablikim *et al.*	(BESIII Collab.)
ABLIKIM	19AW	PR D100 052015	M. Ablikim *et al.*	(BESIII Collab.)
ABLIKIM	19T	PRL 122 142002	M. Ablikim *et al.*	(BESIII Collab.)
ABLIKIM	18	PR D97 012003	M. Ablikim *et al.*	(BESIII Collab.)
ABLIKIM	18C	PRL 120 242003	M. Ablikim *et al.*	(BESIII Collab.)
ADLARSON	18A	PR D98 012001	P. Adlarson *et al.*	(A2 Collab. at MAMI)
GONZALEZ-S...	18A	EPJ C78 758	S. Gonzalez-Solis, E. Passemar	(BEIJ, IND+)
AAIJ	17D	PL B764 233	R. Aaij *et al.*	(LHCb Collab.)
ABLIKIM	17	PRL 118 012001	M. Ablikim *et al.*	(BESIII Collab.)
ABLIKIM	17T	PR D96 012005	M. Ablikim *et al.*	(BESIII Collab.)
ABLIKIM	16M	PR D93 072008	M. Ablikim *et al.*	(BESIII Collab.)
ABLIKIM	15AD	PR D92 051101	M. Ablikim *et al.*	(BESIII Collab.)
ABLIKIM	15G	PR D92 012014	M. Ablikim *et al.*	(BESIII Collab.)
ABLIKIM	15O	PR D92 012001	M. Ablikim *et al.*	(BESIII Collab.)
ABLIKIM	15P	PR D92 012007	M. Ablikim *et al.*	(BESIII Collab.)
ACHASOV	15	PR D91 092010	M.N. Achasov *et al.*	(SND Collab.)
AKHMETSHIN	15	PL B740 273	R.R. Akhmetshin *et al.*	(CMD-3 Collab.)
PDG	15	RPP 2015 at pdg.lbl.gov		(PDG Collab.)
ABLIKIM	14M	PRL 112 251801	M. Ablikim *et al.*	(BESIII Collab.)
DONSKOV	14	MPL A29 1450213	S. Donskov *et al.*	(GAMS-4π Collab.)
PDG	14	CP C38 070001	K. Olive *et al.*	(PDG Collab.)
ABLIKIM	13	PR D87 012009	M. Ablikim *et al.*	(BESIII Collab.)
ABLIKIM	13G	PR D87 032006	M. Ablikim *et al.*	(BESIII Collab.)
ABLIKIM	13O	PR D87 092011	M. Ablikim *et al.*	(BESIII Collab.)
ABLIKIM	13U	PR D88 091502	M. Ablikim *et al.*	(BESIII Collab.)
ABLIKIM	12E	PRL 108 182001	M. Ablikim *et al.*	(BESIII Collab.)
PDG	12	PR D86 010001	J. Beringer *et al.*	(PDG Collab.)
ABLIKIM	11	PR D83 012003	M. Ablikim *et al.*	(BESIII Collab.)
ABLIKIM	11G	PR D84 032006	M. Ablikim *et al.*	(BESIII Collab.)
CZERWINSKI	10	PRL 105 122001	E. Czerwinski *et al.*	(COSY-11 Collab.)
BLIK	09	PAN 72 231	A.M. Blik *et al.*	(IHEP (Protvino))
		Translated from YAF 72 258.		
NAIK	09	PRL 102 061801	P. Naik *et al.*	(CLEO Collab.)
PEDLAR	09	PR D79 111101	T.K. Pedlar *et al.*	(CLEO Collab.)
BLIK	08	PAN 71 2124	A. Blik *et al.*	(GAMS-4π Collab.)
		Translated from YAF 71 2161.		
LIBBY	08	PRL 101 182002	J. Libby *et al.*	(CLEO Collab.)
WICHT	08	PL B662 323	J. Wicht *et al.*	(BELLE Collab.)
DOROFEEV	07	PL B651 22	V. Dorofeev *et al.*	(VES Collab.)
MORI	07A	JPSJ 76 074102	T. Mori *et al.*	(BELLE Collab.)
ABLIKIM	06E	PR D73 052008	M. Ablikim *et al.*	(BES Collab.)
ABLIKIM	06Q	PRL 97 202002	M. Ablikim *et al.*	(BES Collab.)
AMELIN	05A	PAN 68 372	D.V. Amelin *et al.*	(VES Collab.)
		Translated from YAF 68 401.		

Int. J. Mod. Phys. A 2026.41. Downloaded from www.worldscientific.com
by UNIVERSITY OF CALIFORNIA @ BERKELEY on 09/16/26. Re-use and distribution is strictly not permitted, except for Open Access articles.

AMSLER	04B	EPJ C33 23	C. Amsler *et al.*	(Crystal Barrel Collab.)
BAI	04J	PL B594 47	J.Z. Bai *et al.*	(BES Collab.)
BRIERE	00	PRL 84 26	R. Briere *et al.*	(CLEO Collab.)
ACCIARRI	98Q	PL B418 399	M. Acciarri *et al.*	(L3 Collab.)
BARBERIS	98C	PL B440 225	D. Barberis *et al.*	(WA 102 Collab.)
WURZINGER	96	PL B374 283	R. Wurzinger *et al.*	(BONN, ORSAY, SACL+)
PDG	94	PR D50 1173	L. Montanet *et al.*	(CERN, LBL, BOST+)
AMSLER	93	ZPHY C58 175	C. Amsler *et al.*	(Crystal Barrel Collab.)
BELADIDZE	92C	SJNP 55 1535	G.M. Beladidze, S.I. Bityukov, G.V. Borisov	(SERP+)
		Translated from YAF 55 2748.		
KARCH	92	ZPHY C54 33	K. Karch *et al.*	(Crystal Ball Collab.)
ARMSTRONG	91B	ZPHY C52 389	T.A. Armstrong *et al.*	(ATHU, BARI, BIRM+)
BEHREND	91	ZPHY C49 401	H.J. Behrend *et al.*	(CELLO Collab.)
AUGUSTIN	90	PR D42 10	J.E. Augustin *et al.*	(DM2 Collab.)
BARU	90	ZPHY C48 581	S.E. Baru *et al.*	(MD-1 Collab.)
BUTLER	90	PR D42 1368	F. Butler *et al.*	(Mark II Collab.)
KARCH	90	PL B249 353	K. Karch *et al.*	(Crystal Ball Collab.)
ROE	90	PR D41 17	N.A. Roe *et al.*	(ASP Collab.)
AIHARA	88C	PR D38 1	H. Aihara *et al.*	(TPC-2γ Collab.)
VOROBYEV	88	SJNP 48 273	P.V. Vorobiev *et al.*	(NOVO)
		Translated from YAF 48 436.		
WILLIAMS	88	PR D38 1365	D.A. Williams *et al.*	(Crystal Ball Collab.)
AIHARA	87	PR D35 2650	H. Aihara *et al.*	(TPC-2γ Collab.) JP
ALBRECHT	87B	PL B199 457	H. Albrecht *et al.*	(ARGUS Collab.)
ALDE	87B	ZPHY C36 603	D.M. Alde *et al.*	(LANL, BELG, SERP, LAPP)
ANTREASYAN	87	PR D36 2633	D. Antreasyan *et al.*	(Crystal Ball Collab.)
GIDAL	87	PRL 59 2012	G. Gidal *et al.*	(LBL, SLAC, HARV)
ALDE	86	PL B177 115	D.M. Alde *et al.*	(SERP, BELG, LANL, LAPP)
BARTEL	85E	PL 160B 421	W. Bartel *et al.*	(JADE Collab.)
LANDSBERG	85	PRPL 128 301	L.G. Landsberg	(SERP)
ALTHOFF	84E	PL 147B 487	M. Althoff *et al.*	(TASSO Collab.)
BERGER	84B	PL 142B 125	C. Berger	(PLUTO Collab.)
BINON	84	PL 140B 264	F.G. Binon *et al.*	(SERP, BELG, LAPP+)
JENNI	83	PR D27 1031	P. Jenni *et al.*	(SLAC, LBL)
BARTEL	82B	PL 113B 190	W. Bartel *et al.*	(JADE Collab.)
BEHREND	82C	PL 114B 378	H.J. Behrend *et al.*	(CELLO Collab.)
Also		PL 125B 518 (errat.)	H.J. Behrend *et al.*	(CELLO Collab.)
DZHELYADIN	81	PL 105B 239	R.I. Dzhelyadin *et al.*	(SERP)
STANTON	80	PL B92 353	N.R. Stanton *et al.*	(OSU, CARL, MCGI+)
VIKTOROV	80	SJNP 32 520	V.A. Viktorov *et al.*	(SERP)
		Translated from YAF 32 1005.		
APEL	79	PL 83B 131	W.D. Apel, K.H. Augenstein, E. Bertolucci	(KARLK+)
BINNIE	79	PL 83B 141	D.M. Binnie *et al.*	(LOIC)
ZANFINO	77	PRL 38 930	C. Zanfino *et al.*	(CARL, MCGI, OHIO+)
GRIGORIAN	75	NP B91 232	A. Grigorian *et al.*	(+)
KALBFLEISCH	75	PR D11 987	G.R. Kalbfleisch, R.C. Strand, J.W. Chapman	(BNL+)
DUANE	74	PRL 32 425	A. Duane *et al.*	(LOIC, SHMP)
KALBFLEISCH	74	PR D10 916	G.R. Kalbfleisch	(BNL)
DANBURG	73	PR D8 3744	J.S. Danburg *et al.*	(BNL, MICH) JP
JACOBS	73	PR D8 18	S.M. Jacobs *et al.*	(BRAN, UMD, SYRA+) JP
AGUILAR-...	72B	PR D6 29	M. Aguilar-Benitez *et al.*	(BNL)
APEL	72	PL 40B 680	W.D. Apel *et al.*	(KARLK, KARLE, PISA)
DALPIAZ	72	PL 42B 377	P.F. Dalpiaz *et al.*	(CERN)
BASILE	71	NC 3A 371	M. Basile *et al.*	(CERN, BGNA, STRB)
HARVEY	71	PRL 27 885	E.H. Harvey *et al.*	(MINN, MICH)
BENSINGER	70	PL 33B 505	J.R. Bensinger *et al.*	(WISC)
RITTENBERG	69	Thesis UCRL 18863	A. Rittenberg	(LRL) I
DAVIS	68	PL 27B 532	R. Davis *et al.*	(NWES, ANL)
LONDON	66	PR 143 1034	G.W. London *et al.*	(BNL, SYRA) IJP
BADIER	65B	PL 17 337	J. Badier *et al.*	(EPOL, SACL, AMST)
RITTENBERG	65	PRL 15 556	A. Rittenberg, G.R. Kalbfleisch	(LRL, BNL)
DAUBER	64	PRL 13 449	P.M. Dauber *et al.*	(UCLA) JP
KALBFLEISCH	64B	PRL 13 349	G.R. Kalbfleisch, O.I. Dahl, A. Rittenberg	(LRL) JP

$f_0(980)$

$I^G(J^{PC}) = 0^+(0^{++})$

See the related review(s):

Scalar Mesons below 1 GeV

$f_0(980)$ T-MATRIX POLE $\sqrt{s}$

Note that $\Gamma = -2\,\mathrm{Im}(\sqrt{s})$.

VALUE (MeV)	*DOCUMENT ID*		*TECN*	*COMMENT*
(980–1010) − *i* (20–35) OUR ESTIMATE (see Fig. 64.4 in the review)				
$(1002 \pm 9) - i(23 \pm 8)$	[1] HOFERICHT...	24	RVUE	Compilation
$(993 \pm 2^{+2}_{-1}) - i(21 \pm 3^{+2}_{-4})$	[2] DANILKIN	21	RVUE	Compilation
$(1014 \pm 8) - i(35 \pm 5)$	SARANTSEV	21	RVUE	$J/\psi(1S) \to \gamma(\pi\pi, K\overline{K}, \eta\eta, \omega\phi)$
$(992.8 \pm 1.3) - i(30.7 \pm 2.3)$	[3] ALBRECHT	20	RVUE	$0.9\,\overline{p}p \to \pi^0\pi^0\eta$, $\pi^0\eta\eta$, $\pi^0 K^+K^-$
$(1003^{+5}_{-27}) - i(21^{+10}_{-8})$	[4] GARCIA-MAR...	11	RVUE	Compilation
$(996 \pm 7) - i(25^{+10}_{-6})$	[5] GARCIA-MAR...	11	RVUE	Compilation
$(996^{+4}_{-14}) - i(24^{+11}_{-3})$	[6] MOUSSALLAM	11	RVUE	Compilation
$(981 \pm 43) - i(18 \pm 11)$	[7] MENNESSIER	10	RVUE	Compilation
$(1030^{+30}_{-10}) - i(35^{+10}_{-16})$	[8] ANISOVICH	09	RVUE	$0.0\,\overline{p}p$, πN
$(973^{+39}_{-127}) - i(11^{+189}_{-11})$	[9] PELAEZ	04A	RVUE	$\pi\pi \to \pi\pi$

[1] Using the GKPY equations as GARCIA-MARTIN 11, but with different treatment of kaon thresholds and input for $\pi\pi/K\overline{K}$ T-matrix from HOFERICHTER 16.

[2] Data driven analysis using partial-wave dispersion relations.

[3] 5 poles, 5 channels, including scattering data from HYAMS 75 ($\pi\pi$), LONGACRE 86 ($K\overline{K}$), BINON 83 ($\eta\eta$), and BINON 84C ($\eta\eta'$). Based on 18.5k events. Second solution 977.8 ± 1.7 MeV.

[4] Reanalysis of the K_{e4} data of BATLEY 10C and the $\pi N \to \pi\pi N$ data of HYAMS 73, GRAYER 74, and PROTOPOPESCU 73 using Roy equations.

[5] Reanalysis of the K_{e4} data of BATLEY 10C and the $\pi N \to \pi\pi N$ data of HYAMS 73, GRAYER 74, and PROTOPOPESCU 73 using GKPY equations.

[6] Uses Roy equations.

[7] Average of the analyses of three data sets in the K-matrix model. Uses the data of BATLEY 08A, HYAMS 73 , and GRAYER 74 , partially of COHEN 80 or ETKIN 82B.

[8] On sheet II in a 2-pole solution. The other pole is found on sheet III at $(850 - i\,100)$ MeV.

[9] Reanalysis of data from PROTOPOPESCU 73, ESTABROOKS 74, GRAYER 74, and COHEN 80 in the unitarized ChPT model.

$f_0(980)$ MASS

VALUE (MeV)	*EVTS*	*DOCUMENT ID*		*TECN*	*COMMENT*
990 ± 20 OUR ESTIMATE					
• • • We do not use the following data for averages, fits, limits, etc. • • •					
$992.0^{+8.5}_{-7.5} \pm 8.6$		[1] AAIJ	19H	LHCB	$pp \to D^\pm X$
989.4 ± 1.3	424	ABLIKIM	15P	BES3	$J/\psi \to K^+K^-3\pi$
989.9 ± 0.4	706	ABLIKIM	12E	BES3	$J/\psi \to \gamma 3\pi$
$977^{+11}_{-9} \pm 1$	44	[2] ECKLUND	09	CLEO	4.17 $e^+e^- \to D_s^- D_s^{*+}$ + c.c.
$982.2 \pm 1.0^{+8.1}_{-8.0}$		[3] UEHARA	08A	BELL	10.6 $e^+e^- \to e^+e^-\pi^0\pi^0$
$976.8 \pm 0.3^{+10.1}_{-0.6}$	64k	[4] AMBROSINO	07	KLOE	1.02 $e^+e^- \to \pi^0\pi^0\gamma$
$984.7 \pm 0.4^{+2.4}_{-3.7}$	64k	[5] AMBROSINO	07	KLOE	1.02 $e^+e^- \to \pi^0\pi^0\gamma$
973 ± 3	262 ± 30	[6] AUBERT	07AK	BABR	10.6 $e^+e^- \to \phi\pi^+\pi^-\gamma$
970 ± 7	54 ± 9	[6] AUBERT	07AK	BABR	10.6 $e^+e^- \to \phi\pi^0\pi^0\gamma$
953 ± 20	2.6k	[7] BONVICINI	07	CLEO	$D^+ \to \pi^-\pi^+\pi^+$
$985.6^{+1.2}_{-1.5} \pm 1.1 \pm 1.6$		[8] MORI	07	BELL	10.6 $e^+e^- \to e^+e^-\pi^+\pi^-$
$983.0 \pm 0.6^{+4.0}_{-3.0}$		[9] AMBROSINO	06B	KLOE	1.02 $e^+e^- \to \pi^+\pi^-\gamma$
$977.3 \pm 0.9^{+3.7}_{-4.3}$		[10] AMBROSINO	06B	KLOE	1.02 $e^+e^- \to \pi^+\pi^-\gamma$
950 ± 9	4286	[11] GARMASH	06	BELL	$B^+ \to K^+\pi^+\pi^-$
965 ± 10		[12] ABLIKIM	05	BES2	$J/\psi \to \phi\pi^+\pi^-$, ϕK^+K^-
1031 ± 8		[13] ANISOVICH	03	RVUE	
1037 ± 31		TIKHOMIROV	03	SPEC	40.0 $\pi^- C \to K_S^0 K_S^0 K_L^0 X$
973 ± 1	2438	[14] ALOISIO	02D	KLOE	$e^+e^- \to \pi^0\pi^0\gamma$
$977 \pm 3 \pm 2$	848	[15] AITALA	01A	E791	$D_s^+ \to \pi^-\pi^+\pi^+$
969.8 ± 4.5	419	[16] ACHASOV	00H	SND	$e^+e^- \to \pi^0\pi^0\gamma$
985^{+16}_{-12}	419	[17,18] ACHASOV	00H	SND	$e^+e^- \to \pi^0\pi^0\gamma$
$976 \pm 5 \pm 6$		[19] AKHMETSHIN	99B	CMD2	$e^+e^- \to \pi^+\pi^-\gamma$
$977 \pm 3 \pm 6$	268	[19] AKHMETSHIN	99C	CMD2	$e^+e^- \to \pi^0\pi^0\gamma$
$975 \pm 4 \pm 6$		[20] AKHMETSHIN	99C	CMD2	$e^+e^- \to \pi^0\pi^0\gamma$
$975 \pm 4 \pm 6$		[21] AKHMETSHIN	99C	CMD2	$e^+e^- \to \pi^+\pi^-\gamma$, $\pi^0\pi^0\gamma$
985 ± 10		BARBERIS	99	OMEG	450 $pp \to p_s p_f K^+K^-$
982 ± 3		BARBERIS	99B	OMEG	450 $pp \to p_s p_f \pi^+\pi^-$
982 ± 3		BARBERIS	99C	OMEG	450 $pp \to p_s p_f \pi^0\pi^0$
$987 \pm 6 \pm 6$		[22] BARBERIS	99D	OMEG	450 $pp \to K^+K^-$, $\pi^+\pi^-$
989 ± 15		BELLAZZINI	99	GAM4	450 $pp \to pp\pi^0\pi^0$
991 ± 3		[23] KAMINSKI	99	RVUE	$\pi\pi \to \pi\pi$, $K\overline{K}$, $\sigma\sigma$
~ 980		[23] OLLER	99	RVUE	$\pi\pi \to \pi\pi$, $K\overline{K}$
~ 993.5		OLLER	99B	RVUE	$\pi\pi \to \pi\pi$, $K\overline{K}$
~ 987		[23] OLLER	99C	RVUE	$\pi\pi \to \pi\pi$, $K\overline{K}$, $\eta\eta$
957 ± 6		[24] ACKERSTAFF	98Q	OPAL	$Z \to f_0 X$
960 ± 10		ALDE	98	GAM4	
1015 ± 15		[23] ANISOVICH	98B	RVUE	Compilation
1008		[25] LOCHER	98	RVUE	$\pi\pi \to \pi\pi$, $K\overline{K}$
955 ± 10		[24] ALDE	97	GAM2	450 $pp \to pp\pi^0\pi^0$
994 ± 9		[26] BERTIN	97C	OBLX	0.0 $\overline{p}p \to \pi^+\pi^-\pi^0$
$993.2 \pm 6.5 \pm 6.9$		[27] ISHIDA	96	RVUE	$\pi\pi \to \pi\pi$, $K\overline{K}$
1006		TORNQVIST	96	RVUE	$\pi\pi \to \pi\pi$, $K\overline{K}$, $K\pi$, $\eta\pi$
997 ± 5	3k	[28] ALDE	95B	GAM2	38 $\pi^-p \to \pi^0\pi^0 n$
960 ± 10	10k	[29] ALDE	95B	GAM2	38 $\pi^-p \to \pi^0\pi^0 n$
994 ± 5		AMSLER	95B	CBAR	0.0 $\overline{p}p \to 3\pi^0$
~ 996		[30] AMSLER	95D	CBAR	0.0 $\overline{p}p \to \pi^0\pi^0\pi^0$, $\pi^0\eta\eta$, $\pi^0\pi^0\eta$
987 ± 6		[31] ANISOVICH	95	RVUE	
1015		JANSSEN	95	RVUE	$\pi\pi \to \pi\pi$, $K\overline{K}$
983		[32] BUGG	94	RVUE	$\overline{p}p \to \eta 2\pi^0$
973 ± 2		[33] KAMINSKI	94	RVUE	$\pi\pi \to \pi\pi$, $K\overline{K}$
988		[34] ZOU	94B	RVUE	
988 ± 10		[35] MORGAN	93	RVUE	$\pi\pi(K\overline{K}) \to \pi\pi(K\overline{K})$, $J/\psi \to \phi\pi\pi(K\overline{K})$, $D_s \to \pi(\pi\pi)$
971.1 ± 4.0		[24] AGUILAR-...	91	EHS	400 pp
979 ± 4		[36] ARMSTRONG	91	OMEG	300 $pp \to pp\pi\pi$, $pp K\overline{K}$
956 ± 12		BREAKSTONE	90	SFM	$pp \to pp\pi^+\pi^-$
959.4 ± 6.5		[24] AUGUSTIN	89	DM2	$J/\psi \to \omega\pi^+\pi^-$
978 ± 9		[24] ABACHI	86B	HRS	$e^+e^- \to \pi^+\pi^- X$
$985.0^{+9.0}_{-39.0}$		ETKIN	82B	MPS	23 $\pi^-p \to n 2K_S^0$

974 ± 4	[36] GIDAL	81	MRK2	$J/\psi \to \pi^+\pi^- X$
975	[37] ACHASOV	80	RVUE	
986 ±10	[36] AGUILAR-...	78	HBC	$0.7\,\overline{p}p \to K^0_S K^0_S$
969 ± 5	[36] LEEPER	77	ASPK	2–2.4 $\pi^- p \to \pi^+\pi^- n$, $K^+K^- n$
987 ± 7	[36] BINNIE	73	CNTR	$\pi^- p \to n$MM
1012 ± 6	[38] GRAYER	73	ASPK	$17\,\pi^- p \to \pi^+\pi^- n$
1007 ±20	[38] HYAMS	73	ASPK	$17\,\pi^- p \to \pi^+\pi^- n$
997 ± 6	[38] PROTOPOP...	73	HBC	$7\,\pi^+ p \to \pi^+ p\pi^+\pi^-$

[1] From the $D^\pm \to K^\pm K^+ K^-$ Dalitz plot fit with the Triple-M amplitude in the multi-meson model of AOUDE 18.
[2] Using a relativistic Breit-Wigner function and taking into account the finite D_s mass.
[3] Breit-Wigner mass. Using finite width corrections according to FLATTE 76 and ACHASOV 05, and the ratio $g_{f_0 KK}/g_{f_0\pi\pi} = 0$.
[4] In the kaon-loop fit.
[5] In the no-structure fit.
[6] Systematic errors not estimated.
[7] FLATTE 76 parameterization. $g_{f_0\pi\pi} = 329 \pm 96$ MeV/c^2 assuming $g_{f_0 K\overline{K}}/g_{f_0\pi\pi}$=2.
[8] Breit-Wigner mass. Using finite width corrections according to FLATTE 76 and ACHASOV 05, and the ratio $g_{f_0 KK}/g_{f_0\pi\pi} = 4.21 \pm 0.25 \pm 0.21$ from ABLIKIM 05.
[9] In the kaon-loop fit following formalism of ACHASOV 89.
[10] In the no-structure fit assuming a direct coupling of ϕ to $f_0\gamma$.
[11] FLATTE 76 parameterization. Supersedes GARMASH 05.
[12] FLATTE 76 parameterization, $g_{f_0 K\overline{K}}/g_{f_0\pi\pi} = 4.21 \pm 0.25 \pm 0.21$.
[13] K-matrix pole from combined analysis of $\pi^- p \to \pi^0\pi^0 n$, $\pi^- p \to K\overline{K}n$, $\pi^+\pi^- \to \pi^+\pi^-$, $\overline{p}p \to \pi^0\pi^0\pi^0$, $\pi^0\eta\eta$, $\pi^0\pi^0\eta$, $\pi^+\pi^-\pi^0$, $K^+K^-\pi^0$, $K^0_S K^0_S \pi^0$, $K^+K^0_S\pi^-$ at rest, $\overline{p}n \to \pi^-\pi^-\pi^+$, $K^0_S K^-\pi^0$, $K^0_S K^0_S \pi^-$ at rest.
[14] From the negative interference with the $f_0(500)$ meson of AITALA 01B using the ACHASOV 89 parameterization for the $f_0(980)$, a Breit-Wigner for the $f_0(500)$, and ACHASOV 01F for the $\rho\pi$ contribution.
[15] Coupled-channel Breit-Wigner, couplings g_π=0.09±0.01±0.01, g_K=0.02±0.04±0.03.
[16] Supersedes ACHASOV 98I. Using the model of ACHASOV 89.
[17] Supersedes ACHASOV 98I.
[18] In the "narrow resonance" approximation.
[19] Assuming $\Gamma(f_0)$= 40 MeV.
[20] From a narrow pole fit taking into account $f_0(980)$ and $f_0(1200)$ intermediate mechanisms.
[21] From the combined fit of the photon spectra in the reactions $e^+e^- \to \pi^+\pi^-\gamma$, $\pi^0\pi^0\gamma$.
[22] Supersedes BARBERIS 99 and BARBERIS 99B
[23] T-matrix pole.
[24] From invariant mass fit.
[25] On sheet II in a 2 pole solution. The other pole is found on sheet III at (1039−93i) MeV.
[26] On sheet II in a 2 pole solution. The other pole is found on sheet III at (963-29i) MeV.
[27] Reanalysis of data from HYAMS 73, GRAYER 74, SRINIVASAN 75, and ROSSELET 77 using the interfering amplitude method.
[28] At high $|t|$.
[29] At low $|t|$.
[30] On sheet II in a 4-pole solution, the other poles are found on sheet III at (953−55i) MeV and on sheet IV at (938−35i) MeV.
[31] Combined fit of ALDE 95B, ANISOVICH 94, AMSLER 94D.
[32] On sheet II in a 2 pole solution. The other pole is found on sheet III at (996−103i) MeV.
[33] From sheet II pole position.
[34] On sheet II in a 2 pole solution. The other pole is found on sheet III at (797−185i) MeV and can be interpreted as a shadow pole.
[35] On sheet II in a 2 pole solution. The other pole is found on sheet III at (978−28i) MeV.
[36] From coupled channel analysis.
[37] Coupled channel analysis with finite width corrections.
[38] Included in AGUILAR-BENITEZ 78 fit.

$f_0(980)$ WIDTH

Width determination very model dependent. Peak width in $\pi\pi$ is about 50 MeV, but decay width can be much larger.

VALUE (MeV)	EVTS	DOCUMENT ID		TECN	COMMENT
10 to 100 OUR ESTIMATE					
• • • We do not use the following data for averages, fits, limits, etc. • • •					
15.3± 4.7	424	ABLIKIM	15P	BES3	$J/\psi \to K^+K^- 3\pi$
9.5± 1.1	706	ABLIKIM	12E	BES3	$J/\psi \to \gamma 3\pi$
$91\ ^{+30}_{-22} \pm 3$	44	[1] ECKLUND	09	CLEO	4.17 $e^+e^- \to D^-_s D^{*+}_s$ + c.c.
$66.9 \pm 2.2\ ^{+17.6}_{-12.5}$		[2] UEHARA	08A	BELL	10.6 $e^+e^- \to e^+e^-\pi^0\pi^0$
65 ± 13	262 ± 30	[3] AUBERT	07AK	BABR	10.6 $e^+e^- \to \phi\pi^+\pi^-\gamma$
81 ± 21	54 ± 9	[3] AUBERT	07AK	BABR	10.6 $e^+e^- \to \phi\pi^0\pi^0\gamma$
$51.3\ ^{+20.8}_{-17.7} \pm ^{+13.2}_{-3.8}$		[4] MORI	07	BELL	10.6 $e^+e^- \to e^+e^-\pi^+\pi^-$
$61 \pm 9\ ^{+14}_{-8}$	2584	[5] GARMASH	05	BELL	$B^+ \to K^+\pi^+\pi^-$
64 ± 16		[6] ANISOVICH	03	RVUE	
121 ± 23		TIKHOMIROV	03	SPEC	40.0 $\pi^- C \to K^0_S K^0_S K^0_L X$
∼ 70		[7] BRAMON	02	RVUE	1.02 $e^+e^- \to \pi^0\pi^0\gamma$
44 ± 2 ± 2	848	[8] AITALA	01A	E791	$D^+_s \to \pi^-\pi^+\pi^+$
201 ± 28	419	[9] ACHASOV	00H	SND	$e^+e^- \to \pi^0\pi^0\gamma$
122 ± 13	419	[10,11] ACHASOV	00H	SND	$e^+e^- \to \pi^0\pi^0\gamma$
56 ± 20		[12] AKHMETSHIN	99C	CMD2	$e^+e^- \to \pi^0\pi^0\gamma$
65 ± 20		BARBERIS	99	OMEG	450 $pp \to p_s p_f K^+K^-$
80 ± 10		BARBERIS	99B	OMEG	450 $pp \to p_s p_f \pi^+\pi^-$
80 ± 10		BARBERIS	99C	OMEG	450 $pp \to p_s p_f \pi^0\pi^0$
48 ± 12 ± 8		[13] BARBERIS	99D	OMEG	450 $pp \to K^+K^-$, $\pi^+\pi^-$
65 ± 25		BELLAZZINI	99	GAM4	450 $pp \to pp\pi^0\pi^0$
71 ± 14		[14] KAMINSKI	99	RVUE	$\pi\pi \to \pi\pi$, $K\overline{K}$, $\sigma\sigma$
∼ 28		[14] OLLER	99	RVUE	$\pi\pi \to \pi\pi$, $K\overline{K}$
∼ 25		OLLER	99B	RVUE	$\pi\pi \to \pi\pi$, $K\overline{K}$
∼ 14		[14] OLLER	99C	RVUE	$\pi\pi \to \pi\pi$, $K\overline{K}$, $\eta\eta$
70 ± 20		ALDE	98	GAM4	
86 ± 16		[14] ANISOVICH	98B	RVUE	Compilation
54		[15] LOCHER	98	RVUE	$\pi\pi \to \pi\pi$, $K\overline{K}$
69 ± 15		[16] ALDE	97	GAM2	450 $pp \to pp\pi^0\pi^0$
38 ± 20		[17] BERTIN	97C	OBLX	0.0 $\overline{p}p \to \pi^+\pi^-\pi^0$
∼ 100		[18] ISHIDA	96	RVUE	$\pi\pi \to \pi\pi$, $K\overline{K}$
34		TORNQVIST	96	RVUE	$\pi\pi \to \pi\pi$, $K\overline{K}$, $K\pi$, $\eta\pi$
48 ± 10	3k	[19] ALDE	95B	GAM2	38 $\pi^- p \to \pi^0\pi^0 n$
95 ± 20	10k	[20] ALDE	95B	GAM2	38 $\pi^- p \to \pi^0\pi^0 n$
26 ± 10		AMSLER	95B	CBAR	0.0 $\overline{p}p \to 3\pi^0$
∼ 112		[21] AMSLER	95D	CBAR	0.0 $\overline{p}p \to \pi^0\pi^0\pi^0$, $\pi^0\eta\eta$, $\pi^0\pi^0\eta$
80 ± 12		[22] ANISOVICH	95	RVUE	
30		JANSSEN	95	RVUE	$\pi\pi \to \pi\pi$, $K\overline{K}$
74		[23] BUGG	94	RVUE	$\overline{p}p \to \eta 2\pi^0$
29 ± 2		[24] KAMINSKI	94	RVUE	$\pi\pi \to \pi\pi$, $K\overline{K}$
46		[25] ZOU	94B	RVUE	
48 ± 12		[26] MORGAN	93	RVUE	$\pi\pi(K\overline{K}) \to \pi\pi(K\overline{K})$, $J/\psi \to \phi\pi\pi(K\overline{K})$, $D_s \to \pi(\pi\pi)$
37.4± 10.6		[16] AGUILAR-...	91	EHS	400 pp
72 ± 8		[27] ARMSTRONG	91	OMEG	300 $pp \to pp\pi\pi$, $pp K\overline{K}$
110 ± 30		BREAKSTONE	90	SFM	$pp \to pp\pi^+\pi^-$
29 ± 13		[16] ABACHI	86B	HRS	$e^+e^- \to \pi^+\pi^- X$
120 ±281 ±20		ETKIN	82B	MPS	23 $\pi^- p \to n 2K^0_S$
28 ± 10		[27] GIDAL	81	MRK2	$J/\psi \to \pi^+\pi^- X$
70 to 300		[28] ACHASOV	80	RVUE	
100 ± 80		[29] AGUILAR-...	78	HBC	$0.7\,\overline{p}p \to K^0_S K^0_S$
30 ± 8		[27] LEEPER	77	ASPK	2–2.4 $\pi^- p \to \pi^+\pi^- n$, $K^+K^- n$
48 ± 14		[27] BINNIE	73	CNTR	$\pi^- p \to n$MM
32 ± 10		[30] GRAYER	73	ASPK	$17\,\pi^- p \to \pi^+\pi^- n$
30 ± 10		[30] HYAMS	73	ASPK	$17\,\pi^- p \to \pi^+\pi^- n$
54 ± 16		[30] PROTOPOP...	73	HBC	$7\,\pi^+ p \to \pi^+ p\pi^+\pi^-$

[1] Using a relativistic Breit-Wigner function and taking into account the finite D_s mass.
[2] Breit-Wigner $\pi\pi$ width. Using finite width corrections according to FLATTE 76 and ACHASOV 05, and the ratio $g_{f_0 KK}/g_{f_0\pi\pi} = 0$.
[3] Systematic errors not estimated.
[4] Breit-Wigner $\pi\pi$ width. Using finite width corrections according to FLATTE 76 and ACHASOV 05, and the ratio $g_{f_0 KK}/g_{f_0\pi\pi} = 4.21 \pm 0.25 \pm 0.21$ from ABLIKIM 05.
[5] Breit-Wigner, solution 1, PWA ambiguous.
[6] K-matrix pole from combined analysis of $\pi^- p \to \pi^0\pi^0 n$, $\pi^- p \to K\overline{K}n$, $\pi^+\pi^- \to \pi^+\pi^-$, $\overline{p}p \to \pi^0\pi^0\pi^0$, $\pi^0\eta\eta$, $\pi^0\pi^0\eta$, $\pi^+\pi^-\pi^0$, $K^+K^-\pi^0$, $K^0_S K^0_S \pi^0$, $K^+K^0_S\pi^-$ at rest, $\overline{p}n \to \pi^-\pi^-\pi^+$, $K^0_S K^-\pi^0$, $K^0_S K^0_S \pi^-$ at rest.
[7] Using the data of AKHMETSHIN 99C, ACHASOV 00H, and ALOISIO 02D.
[8] Breit-Wigner width.
[9] Supersedes ACHASOV 98I. Using the model of ACHASOV 89.
[10] Supersedes ACHASOV 98I.
[11] In the "narrow resonance" approximation.
[12] From the combined fit of the photon spectra in the reactions $e^+e^- \to \pi^+\pi^-\gamma$, $\pi^0\pi^0\gamma$.
[13] Supersedes BARBERIS 99 and BARBERIS 99B
[14] T-matrix pole.
[15] On sheet II in a 2 pole solution. The other pole is found on sheet III at (1039−93i) MeV.
[16] From invariant mass fit.
[17] On sheet II in a 2 pole solution. The other pole is found on sheet III at (963-29i) MeV.
[18] Reanalysis of data from HYAMS 73, GRAYER 74, SRINIVASAN 75, and ROSSELET 77 using the interfering amplitude method.
[19] At high $|t|$.
[20] At low $|t|$.
[21] On sheet II in a 4-pole solution, the other poles are found on sheet III at (953−55i) MeV and on sheet IV at (938−35i) MeV.
[22] Combined fit of ALDE 95B, ANISOVICH 94,
[23] On sheet II in a 2 pole solution. The other pole is found on sheet III at (996−103i) MeV.
[24] From sheet II pole position.

Int. J. Mod. Phys. A 2026.41. Downloaded from www.worldscientific.com
by LIFORNIA @ BERKELEY on 09/16/26. Re-use and distribution is strictly not permitted, except for Open Access articles.

[25] On sheet II in a 2 pole solution. The other pole is found on sheet III at $(797-185i)$ MeV and can be interpreted as a shadow pole.
[26] On sheet II in a 2 pole solution. The other pole is found on sheet III at $(978-28i)$ MeV.
[27] From coupled channel analysis.
[28] Coupled channel analysis with finite width corrections.
[29] From coupled channel fit to the HYAMS 73 and PROTOPOPESCU 73 data. With a simultaneous fit to the $\pi\pi$ phase-shifts, inelasticity and to the $K^0_S K^0_S$ invariant mass.
[30] Included in AGUILAR-BENITEZ 78 fit.

$f_0(980)$ DECAY MODES

	Mode	Fraction (Γ_i/Γ)
Γ_1	$\pi\pi$	seen
Γ_2	$K\overline{K}$	seen
Γ_3	$\gamma\gamma$	seen
Γ_4	e^+e^-	

$f_0(980)$ PARTIAL WIDTHS

$\Gamma(\gamma\gamma)$ — Γ_3

VALUE (keV)	DOCUMENT ID		TECN	COMMENT
$0.29\ ^{+0.11}_{-0.06}$ OUR AVERAGE				
$0.286\pm0.017\ ^{+0.211}_{-0.070}$	[1] UEHARA	08A	BELL	$10.6\ e^+e^-\to e^+e^-\pi^0\pi^0$
$0.205\ ^{+0.095}_{-0.083}\ ^{+0.147}_{-0.117}$	[2] MORI	07	BELL	$10.6\ e^+e^-\to e^+e^-\pi^+\pi^-$
$0.42\ \pm0.06\ \pm0.18$	[3] OEST	90	JADE	$e^+e^-\to e^+e^-\pi^0\pi^0$
• • • We do not use the following data for averages, fits, limits, etc. • • •				
$0.32\ \pm0.05$	[4] DAI	14A	RVUE	Compilation
$0.16\ \pm0.01$	[5] MENNESSIER	11	RVUE	
$0.29\ \pm0.21\ ^{+0.02}_{-0.07}$	[6] MOUSSALLAM	11	RVUE	Compilation
0.42	[7,8] PENNINGTON	08	RVUE	Compilation
0.10	[8,9] PENNINGTON	08	RVUE	Compilation
$0.28\ ^{+0.09}_{-0.13}$	[10] BOGLIONE	99	RVUE	$\gamma\gamma\to\pi^+\pi^-,\ \pi^0\pi^0$
$0.29\ \pm0.07\ \pm0.12$	[11,12] BOYER	90	MRK2	$e^+e^-\to e^+e^-\pi^+\pi^-$
$0.31\ \pm0.14\ \pm0.09$	[11,12] MARSISKE	90	CBAL	$e^+e^-\to e^+e^-\pi^0\pi^0$
$0.63\ \pm0.14$	[13] MORGAN	90	RVUE	$\gamma\gamma\to\pi^+\pi^-,\ \pi^0\pi^0$

[1] Using finite width corrections according to FLATTE 76 and ACHASOV 05, and the ratio $g_{f_0 KK}/g_{f_0\pi\pi}=0$.
[2] Using finite width corrections according to FLATTE 76 and ACHASOV 05, and the ratio $g_{f_0 KK}/g_{f_0\pi\pi}=4.21\pm0.25\pm0.21$ from ABLIKIM 05.
[3] OEST 90 quote systematic errors $^{+0.08}_{-0.18}$. We use ±0.18. Observed 60 events.
[4] Using dispersive analysis with phases from GARCIA-MARTIN 11A and BUETTIKER 04 as input.
[5] Uses an analytic K-matrix model. Compilation.
[6] Using dispersion integral with phase input from Roy equations and data from MARSISKE 90, BOYER 90, BEHREND 92, UEHARA 08A, and MORI 07.
[7] Solution A (preferred solution based on χ^2-analysis).
[8] Dispersion theory based amplitude analysis of BOYER 90, MARSISKE 90, BEHREND 92, and MORI 07.
[9] Solution B (worse than solution A; still acceptable when systematic uncertainties are included).
[10] Supersedes MORGAN 90.
[11] From analysis allowing arbitrary background unconstrained by unitarity.
[12] Data included in MORGAN 90, BOGLIONE 99 analyses.
[13] From amplitude analysis of BOYER 90 and MARSISKE 90, data corresponds to resonance parameters $m=989$ MeV, $\Gamma=61$ MeV.

$\Gamma(e^+e^-)$ — Γ_4

VALUE (eV)	CL%	DOCUMENT ID		TECN	COMMENT
<8.4	90	VOROBYEV	88	ND	$e^+e^-\to\pi^0\pi^0$

$f_0(980)$ BRANCHING RATIOS

$\Gamma(\pi\pi)/[\Gamma(\pi\pi)+\Gamma(K\overline{K})]$ — $\Gamma_1/(\Gamma_1+\Gamma_2)$

VALUE	EVTS	DOCUMENT ID		TECN	COMMENT
• • • We do not use the following data for averages, fits, limits, etc. • • •					
0.52 ± 0.12	9.9k	[1] AUBERT	06O	BABR	$B^\pm\to K^\pm\pi^\pm\pi^\mp$
$0.75\ ^{+0.11}_{-0.13}$		[2] ABLIKIM	05Q	BES2	$\chi_{c0}\to 2\pi^+2\pi^-$, $\pi^+\pi^-K^+K^-$
0.84 ± 0.02		[3] ANISOVICH	02D	SPEC	Combined fit
~ 0.68		OLLER	99B	RVUE	$\pi\pi\to\pi\pi,\ K\overline{K}$
0.67 ± 0.09		[4] LOVERRE	80	HBC	$4\ \pi^-p\to n2K^0_S$
$0.81\ ^{+0.09}_{-0.04}$		[4] CASON	78	STRC	$7\ \pi^-p\to n2K^0_S$
0.78 ± 0.03		[4] WETZEL	76	OSPK	$8.9\ \pi^-p\to n2K^0_S$

[1] Recalculated by us using $\Gamma(K^+K^-)\ /\ \Gamma(\pi^+\pi^-)=0.69\pm0.32$ from AUBERT 06O and isospin relations.
[2] Using data from ABLIKIM 04G.
[3] From a combined K-matrix analysis of Crystal Barrel ($p\overline{p}\to\pi^0\pi^0\pi^0$, $\pi^0\eta\eta$, $\pi^0\pi^0\eta$), GAMS ($\pi p\to\pi^0\pi^0 n$, $\eta\eta n$, $\eta\eta' n$), and BNL ($\pi p\to K\overline{K}n$) data.
[4] Measure $\pi\pi$ elasticity assuming two resonances coupled to the $\pi\pi$ and $K\overline{K}$ channels only.

$f_0(980)$ REFERENCES

HOFERICHT...	24	PL B853 138698	M. Hoferichter *et al.*	(BERN, MADU, BONN+)
DANILKIN	21	PR D103 114023	I. Danilkin, O. Deineka, M. Vanderhaeghen	(MAINZ)
SARANTSEV	21	PL B816 136227	A.V. Sarantsev *et al.*	(BONN, PNPI)
ALBRECHT	20	EPJ C80 453	M. Albrecht *et al.*	(Crystal Barrel Collab.)
AAIJ	19H	JHEP 1904 063	R. Aaij *et al.*	(LHCb Collab.)
AOUDE	18	PR D98 056021	R.T. Aoude *et al.*	
HOFERICHT...	16	PRPL 625 1	M. Hoferichter *et al.*	(WASH, BONN)
ABLIKIM	15P	PR D92 012007	M. Ablikim *et al.*	(BESIII Collab.)
DAI	14A	PR D90 036004	L.-Y. Dai, M.R. Pennington	(CEBAF)
ABLIKIM	12E	PRL 108 182001	M. Ablikim *et al.*	(BESIII Collab.)
GARCIA-MAR...	11	PRL 107 072001	R. Garcia-Martin *et al.*	(MADR, CRAC)
GARCIA-MAR...	11A	PR D83 074004	R. Garcia-Martin *et al.*	(MADR, CRAC)
MENNESSIER	11	PL B696 40	G. Mennessier, S. Narison, X.-G. Wang	
MOUSSALLAM	11	EPJ C71 1814	B. Moussallam	
BATLEY	10C	EPJ C70 635	J.R. Batley *et al.*	(CERN NA48/2 Collab.)
MENNESSIER	10	PL B688 59	G. Mennessier, S. Narison, X.-G. Wang	
ANISOVICH	09	IJMP A24 2481	V.V. Anisovich, A.V. Sarantsev	(PNPI)
ECKLUND	09	PR D80 052009	K.M. Ecklund *et al.*	(CLEO Collab.)
BATLEY	08A	EPJ C54 411	J.R. Batley *et al.*	(CERN NA48/2 Collab.)
PENNINGTON	08	EPJ C56 1	M.R. Pennington *et al.*	
UEHARA	08A	PR D78 052004	S. Uehara *et al.*	(BELLE Collab.)
AMBROSINO	07	EPJ C49 473	F. Ambrosino *et al.*	(KLOE Collab.)
AUBERT	07AK	PR D76 012008	B. Aubert *et al.*	(BABAR Collab.)
BONVICINI	07	PR D76 012001	G. Bonvicini *et al.*	(CLEO Collab.)
MORI	07	PR D75 051101	T. Mori *et al.*	(BELLE Collab.)
AMBROSINO	06B	PL B634 148	F. Ambrosino *et al.*	(KLOE Collab.)
AUBERT	06O	PR D74 032003	B. Aubert *et al.*	(BABAR Collab.)
GARMASH	06	PRL 96 251803	A. Garmash *et al.*	(BELLE Collab.)
ABLIKIM	05	PL B607 243	M. Ablikim *et al.*	(BES Collab.)
ABLIKIM	05Q	PR D72 092002	M. Ablikim *et al.*	(BES Collab.)
ACHASOV	05	PR D72 013006	N.N. Achasov, G.N. Shestakov	
GARMASH	05	PR D71 092003	A. Garmash *et al.*	(BELLE Collab.)
ABLIKIM	04G	PR D70 092002	M. Ablikim *et al.*	(BES Collab.)
BUETTIKER	04	EPJ C33 409	P. Buettiker, S. Descotes-Genon, B. Moussallam	
PELAEZ	04A	MPL A19 2879	J.R. Pelaez	(MADU)
ANISOVICH	03	EPJ A16 229	V.V. Anisovich *et al.*	
TIKHOMIROV	03	PAN 66 828	G.D. Tikhomirov *et al.*	
		Translated from YAF 66 860.		
ALOISIO	02D	PL B537 21	A. Aloisio *et al.*	(KLOE Collab.)
ANISOVICH	02D	PAN 65 1545	V.V. Anisovich *et al.*	
		Translated from YAF 65 1583.		
BRAMON	02	EPJ C26 253	A. Bramon *et al.*	
ACHASOV	01F	PR D63 094007	N.N. Achasov, V.V. Gubin	(Novosibirsk SND Collab.)
AITALA	01A	PRL 86 765	E.M. Aitala *et al.*	(FNAL E791 Collab.)
AITALA	01B	PRL 86 770	E.M. Aitala *et al.*	(FNAL E791 Collab.)
ACHASOV	00H	PL B485 349	M.N. Achasov *et al.*	(Novosibirsk SND Collab.)
AKHMETSHIN	99B	PL B462 371	R.R. Akhmetshin *et al.*	(Novosibirsk CMD-2 Collab.)
AKHMETSHIN	99C	PL B462 380	R.R. Akhmetshin *et al.*	(Novosibirsk CMD-2 Collab.)
BARBERIS	99	PL B453 305	D. Barberis *et al.*	(Omega Expt.)
BARBERIS	99B	PL B453 316	D. Barberis *et al.*	(Omega Expt.)
BARBERIS	99C	PL B453 325	D. Barberis *et al.*	(Omega Expt.)
BARBERIS	99D	PL B462 462	D. Barberis *et al.*	(Omega Expt.)
BELLAZZINI	99	PL B467 296	R. Bellazzini *et al.*	
BOGLIONE	99	EPJ C9 11	M. Boglione, M.R. Pennington	
KAMINSKI	99	EPJ C9 141	R. Kaminski, L. Lesniak, B. Loiseau	(CRAC, PARIN)
OLLER	99	PR D60 099906 (errat.)	J.A. Oller *et al.*	
OLLER	99B	NP A652 407 (errat.)	J.A. Oller, E. Oset	
OLLER	99C	PR D60 074023	J.A. Oller, E. Oset	
ACHASOV	98I	PL B440 442	M.N. Achasov *et al.*	
ACKERSTAFF	98Q	EPJ C4 19	K. Ackerstaff *et al.*	(OPAL Collab.)
ALDE	98	EPJ A3 361	D. Alde *et al.*	(GAM4 Collab.)
Also		PAN 62 405	D. Alde *et al.*	(GAMS Collab.)
		Translated from YAF 62 446.		
ANISOVICH	98B	SPU 41 419	V.V. Anisovich *et al.*	
		Translated from UFN 168 481.		
LOCHER	98	EPJ C4 317	M.P. Locher *et al.*	(PSI)
ALDE	97	PL B397 350	D.M. Alde *et al.*	(GAMS Collab.)
BERTIN	97C	PL B408 476	A. Bertin *et al.*	(OBELIX Collab.)
ISHIDA	96	PTP 95 745	S. Ishida *et al.*	(TOKY, MIYA, KEK)
TORNQVIST	96	PRL 76 1575	N.A. Tornqvist, M. Roos	(HELS)
ALDE	95B	ZPHY C66 375	D.M. Alde *et al.*	(GAMS Collab.)
AMSLER	95B	PL B342 433	C. Amsler *et al.*	(Crystal Barrel Collab.)
AMSLER	95D	PL B355 425	C. Amsler *et al.*	(Crystal Barrel Collab.)
ANISOVICH	95	PL B355 363	V.V. Anisovich *et al.*	(PNPI, SERP)
JANSSEN	95	PR D52 2690	G. Janssen *et al.*	(STON, ADLD, JULI)
AMSLER	94D	PL B333 277	C. Amsler *et al.*	(Crystal Barrel Collab.)
ANISOVICH	94	PL B323 233	V.V. Anisovich *et al.*	(Crystal Barrel Collab.)
BUGG	94	PR D50 4412	D.V. Bugg *et al.*	(LOQM)
KAMINSKI	94	PR D50 3145	R. Kaminski, L. Lesniak, J.P. Maillet	(CRAC+)
ZOU	94B	PR D50 591	B.S. Zou, D.V. Bugg	(LOQM)
MORGAN	93	PR D48 1185	D. Morgan, M.R. Pennington	(RAL, DURH)
BEHREND	92	ZPHY C56 381	H.J. Behrend	(CELLO Collab.)
AGUILAR-...	91	ZPHY C50 405	M. Aguilar-Benitez *et al.*	(LEBC-EHS Collab.)
ARMSTRONG	91	ZPHY C51 351	T.A. Armstrong *et al.*	(ATHU, BARI, BIRM+)
BOYER	90	PR D42 1350	J. Boyer *et al.*	(Mark II Collab.)
BREAKSTONE	90	ZPHY C48 569	A.M. Breakstone *et al.*	(ISU, BGNA, CERN+)
MARSISKE	90	PR D41 3324	H. Marsiske *et al.*	(Crystal Ball Collab.)
MORGAN	90	ZPHY C48 623	D. Morgan, M.R. Pennington	(RAL, DURH)
OEST	90	ZPHY C47 343	T. Oest *et al.*	(JADE Collab.)
ACHASOV	89	NP B315 465	N.N. Achasov, V.N. Ivanchenko	
AUGUSTIN	89	NP B320 1	J.E. Augustin, G. Cosme	(DM2 Collab.)
VOROBYEV	88	SJNP 48 273	P.V. Vorobiev *et al.*	(NOVO)
		Translated from YAF 48 436.		
ABACHI	86B	PRL 57 1990	S. Abachi *et al.*	(PURD, ANL, IND, MICH+)
LONGACRE	86	PL B177 223	R.S. Longacre *et al.*	(BNL, BRAN, CUNY+)
BINON	84C	NC 80A 363	F.G. Binon *et al.*	(BELG, LAPP, SERP+)
BINON	83	NC 78A 313	F.G. Binon *et al.*	(BELG, LAPP, SERP+)
ETKIN	82B	PR D25 1786	A. Etkin *et al.*	(BNL, CUNY, TUFTS, VAND)
GIDAL	81	PL 107B 153	G. Gidal *et al.*	(SLAC, LBL)
ACHASOV	80	SJNP 32 566	N.N. Achasov, S.A. Devyanin, G.N. Shestakov	(NOVM)
		Translated from YAF 32 1098.		
COHEN	80	PR D22 2595	D. Cohen *et al.*	(ANL) IJP
LOVERRE	80	ZPHY C6 187	P.F. Loverre *et al.*	(CERN, CDEF, MADR+) IJP
AGUILAR-...	78	NP B140 73	M. Aguilar-Benitez *et al.*	(MADR, BOMB+)
CASON	78	PRL 41 271	N.M. Cason *et al.*	(NDAM, ANL)
LEEPER	77	PR D16 2054	R.J. Leeper *et al.*	(ISU)
ROSSELET	77	PR D15 574	L. Rosselet *et al.*	(GEVA, SACL)
FLATTE	76	PL 63B 224	S.M. Flatte	(CERN)
WETZEL	76	NP B115 208	W. Wetzel *et al.*	(ETH, CERN, LOIC)
HYAMS	75	NP B100 205	B.D. Hyams *et al.*	(CERN, MPIM)
SRINIVASAN	75	PR D12 681	V. Srinivasan *et al.*	(NDAM, ANL)
ESTABROOKS	74	NP B79 301	P.G. Estabrooks, A.D. Martin	(DURH)
GRAYER	74	NP B75 189	G. Grayer *et al.*	(CERN, MPIM)
BINNIE	73	PRL 31 1534	D.M. Binnie *et al.*	(LOIC, SHMP)
GRAYER	73	Tallahassee	G. Grayer *et al.*	(CERN, MPIM)
HYAMS	73	NP B64 134	B.D. Hyams *et al.*	(CERN, MPIM)
PROTOPOP...	73	PR D7 1279	S.D. Protopopescu *et al.*	(LBL)

Int. J. Mod. Phys. A 2026.41. Downloaded from www.worldscientific.com
by UNIVERSITY OF CALIFORNIA @ BERKELEY on 09/16/26. Re-use and distribution is strictly not permitted, except for Open Access articles.

Int. J. Mod. Phys. A 2026.41. Downloaded from www.worldscientific.com
by UNIVERSITY OF CALIFORNIA @ BERKELEY on 09/16/26. Re-use and distribution is strictly not permitted, except for Open Access articles.

$a_0(980)$

$I^G(J^{PC}) = 1^-(0^{++})$

See the related review(s):
Scalar Mesons below 1 GeV

$a_0(980)$ T-MATRIX POLE $\sqrt{s}$

Note that $\Gamma = -2\,\mathrm{Im}(\sqrt{s})$.

VALUE (MeV)	DOCUMENT ID		TECN	COMMENT
(970–1020) − i (30–70) OUR ESTIMATE (see Fig. 64.2 in the review)				
$(1002.4 \pm 1.4 \pm 6.6) - i(63.5 \pm 2.9)$	[1] ALBRECHT	20	CBAR	$0.9\,\overline{p}p \to \pi^0\pi^0\eta$, $\pi^0\eta\eta$, $\pi^0 K^+K^-$
$(1000.7^{+12.9}_{-0.7}) - i(36.6^{+12.7}_{-2.6})$	[2] LU	20	RVUE	$\gamma\gamma \to \pi^0\eta$, $K^0_S K^0_S$
$(989 \pm 5) - i(40 \pm 5)$	[3] BUGG	08A	RVUE	$\overline{p}p$ annihilation data
$(1117^{+24}_{-320}) - i(12^{+43}_{-12})$	[4] PELAEZ	04A	RVUE	$\pi\pi \to \pi\pi, \pi K \to \pi K$
$(982 \pm 3) - i(46 \pm 4)$	[5] ABELE	98	CBAR	$0.0\,\overline{p}p \to K^0_L K^\pm\pi^\mp$

[1] Pole mass on sheet closest to the physical axis - the more remote pole is extracted at $(1004.1 \pm 1.5 \pm 6.5) - i(48.6 \pm 1.2 \pm 3.4)$ MeV.
[2] T-matrix pole on sheet II.
[3] T-matrix pole on sheet II. Parameterizes couplings to $\overline{K}K$, $\pi\eta$, and $\pi\eta'$. Uses AMSLER 94D and ABELE 98.
[4] Reanalysis of data from LINGLIN 73, ESTABROOKS 78, and ASTON 88 in the unitarized ChPT model.
[5] T-matrix pole on sheet II; the pole on sheet III is at $(1006 - i\,49)$ MeV.

$a_0(980)$ MASS

VALUE (MeV)	DOCUMENT ID
980±20 OUR ESTIMATE Mass determination very model dependent	

$\eta\pi$ FINAL STATE ONLY

VALUE (MeV)	EVTS	DOCUMENT ID		TECN	CHG	COMMENT
• • • We do not use the following data for averages, fits, limits, etc. • • •						
$982.5 \pm 1.6 \pm 1.1$	16.9k	[1] AMBROSINO	09F	KLOE		$1.02\,e^+e^- \to \eta\pi^0\gamma$
986 ± 4		ANISOVICH	09	RVUE		$0.0\,\overline{p}p$, πN
$982.3^{+0.6}_{-0.7} {}^{+3.1}_{-4.7}$		[2] UEHARA	09A	BELL		$\gamma\gamma \to \pi^0\eta$
$985 \pm 4 \pm 6$	318	ACHARD	02B	L3		$183–209\ e^+e^- \to e^+e^-\eta\pi^+\pi^-$
995^{+52}_{-10}	36	[3] ACHASOV	00F	SND		$e^+e^- \to \eta\pi^0\gamma$
994^{+33}_{-8}	36	[4] ACHASOV	00F	SND		$e^+e^- \to \eta\pi^0\gamma$
975 ± 7		BARBERIS	00H			$450\ pp \to p_f\eta\pi^0 p_s$
988 ± 8		BARBERIS	00H			$450\ pp \to \Delta_f^{++}\eta\pi^- p_s$
~ 1055		[5] OLLER	99	RVUE		$\eta\pi$, $K\overline{K}$
~ 1009.2		[5] OLLER	99B	RVUE		$\pi\pi \to \pi\pi$, $K\overline{K}$
993.1 ± 2.1		[6] TEIGE	99	B852		$18.3\ \pi^-p \to \eta\pi^+\pi^-n$
988 ± 6		[5] ANISOVICH	98B	RVUE		Compilation
987		TORNQVIST	96	RVUE		$\pi\pi \to \pi\pi$, $K\overline{K}$, $K\pi$, $\eta\pi$
991		JANSSEN	95	RVUE		$\eta\pi \to \eta\pi$, $K\overline{K}$, $K\pi$, $\eta\pi$
$984.45 \pm 1.23 \pm 0.34$		AMSLER	94C	CBAR		$0.0\,\overline{p}p \to \omega\eta\pi^0$
982 ± 2		[7] AMSLER	92	CBAR		$0.0\,\overline{p}p \to \eta\eta\pi^0$
984 ± 4	1040	[7] ARMSTRONG	91B	OMEG	±	$300\ pp \to pp\eta\pi^+\pi^-$
976 ± 6		ATKINSON	84E	OMEG	±	$25–55\ \gamma p \to \eta\pi n$
986 ± 3	500	[8] EVANGELIS...	81	OMEG	±	$12\ \pi^-p \to \eta\pi^+\pi^-\pi^-p$
990 ± 7	145	[8] GURTU	79	HBC	±	$4.2\ K^-p \to \Lambda\eta 2\pi$
980 ± 11	47	CONFORTO	78	OSPK	−	$4.5\ \pi^-p \to pX^-$
978 ± 16	50	CORDEN	78	OMEG	±	$12–15\ \pi^-p \to n\eta 2\pi$
977 ± 7		GRASSLER	77	HBC	−	$16\ \pi^\mp p \to p\eta 3\pi$
989 ± 4	70	WELLS	75	HBC	−	$3.1–6\ K^-p \to \Lambda\eta 2\pi$
972 ± 10	150	DEFOIX	72	HBC	±	$0.7\ \overline{p}p \to 7\pi$
970 ± 15	20	BARNES	69C	HBC	−	$4–5\ K^-p \to \Lambda\eta 2\pi$
980 ± 10		CAMPBELL	69	DBC	±	$2.7\ \pi^+d$
980 ± 10	15	MILLER	69B	HBC	−	$4.5\ K^-N \to \eta\pi\Lambda$
980 ± 10	30	AMMAR	68	HBC	±	$5.5\ K^-p \to \Lambda\eta 2\pi$

[1] Using the model of ACHASOV 89 and ACHASOV 03B.
[2] From a fit with the S-wave amplitude including two interfering Breit-Wigners plus a background term.
[3] Using the model of ACHASOV 89. Supersedes ACHASOV 98B.
[4] Using the model of JAFFE 77. Supersedes ACHASOV 98B.
[5] T-matrix pole.
[6] Breit-Wigner fit, average between $a_0^\pm$ and a_0^0. The fit favors a slightly heavier $a_0^\pm$.
[7] From a single Breit-Wigner fit.
[8] From $f_1(1285)$ decay.

$K\overline{K}$ ONLY

VALUE (MeV)	EVTS	DOCUMENT ID		TECN	COMMENT
• • • We do not use the following data for averages, fits, limits, etc. • • •					
$947.7^{+5.5}_{-5.0} \pm 6.6$		[1] AAIJ	19H	LHCB	$pp \to D^\pm X$
$925 \pm 5 \pm 8$	190k	[2] AAIJ	16N	LHCB	$D^0 \to K^0_S K^\pm\pi^\mp$
~ 1053		[3] OLLER	99C	RVUE	$\pi\pi \to \pi\pi$, $K\overline{K}$
975 ± 15		BERTIN	98B	OBLX	$0.0\,\overline{p}p \to K^\pm K_s\pi^\mp$
970 ± 10	316	DEBILLY	80	HBC	$1.2–2\ \overline{p}p \to f_1(1285)\omega$
1016 ± 10	100	[4] ASTIER	67	HBC	$0.0\,\overline{p}p$
1003.3 ± 7.0	143	[5,6] ROSENFELD	65	RVUE	

[1] From the $D^\pm \to K^\pm K^+K^-$ Dalitz plot fit with the Triple-M amplitude in the multi-meson model of AOUDE 18.
[2] Using a two-channel resonance parametrization with couplings fixed to ABELE 98.
[3] T-matrix pole.
[4] ASTIER 67 includes data of BARLOW 67, CONFORTO 67, ARMENTEROS 65.
[5] Note on J^P. Main argument for 0^+ is small Q value. Isotropy of decay distribution in $\overline{p}p$ at rest proves nothing. See discussion by Rosenfeld (Oxford) and Butterworth (Heidelberg).
[6] Plus systematic errors.

$a_0(980)$ WIDTH

VALUE (MeV)	EVTS	DOCUMENT ID		TECN	CHG	COMMENT
50 to 100 OUR ESTIMATE Width determination very model dependent. Peak width in $\eta\pi$ is about 60 MeV, but decay width can be much larger.						
• • • We do not use the following data for averages, fits, limits, etc. • • •						
$75.6 \pm 1.6\ {}^{+17.4}_{-10.0}$		[1] UEHARA	09A	BELL		$\gamma\gamma \to \pi^0\eta$
$50 \pm 13 \pm 4$	318	ACHARD	02B	L3		$183–209\ e^+e^- \to e^+e^-\eta\pi^+\pi^-$
72 ± 16		BARBERIS	00H			$450\ pp \to p_f\eta\pi^0 p_s$
61 ± 19		BARBERIS	00H			$450\ pp \to \Delta_f^{++}\eta\pi^- p_s$
~ 42		[2] OLLER	99	RVUE		$\eta\pi$, $K\overline{K}$
~ 112		[2] OLLER	99B	RVUE		$\pi\pi \to \eta\pi$, $K\overline{K}$
71 ± 7		TEIGE	99	B852		$18.3\ \pi^-p \to \eta\pi^+\pi^-n$
92 ± 20		[2] ANISOVICH	98B	RVUE		Compilation
65 ± 10		[3] BERTIN	98B	OBLX	±	$0.0\,\overline{p}p \to K^\pm K_s\pi^\mp$
~ 100		TORNQVIST	96	RVUE		$\pi\pi \to \pi\pi$, $K\overline{K}$, $K\pi$, $\eta\pi$
202		JANSSEN	95	RVUE		$\eta\pi \to \eta\pi$, $K\overline{K}$, $K\pi$, $\eta\pi$
$54.12 \pm 0.34 \pm 0.12$		AMSLER	94C	CBAR		$0.0\,\overline{p}p \to \omega\eta\pi^0$
54 ± 10		[4] AMSLER	92	CBAR		$0.0\,\overline{p}p \to \eta\eta\pi^0$
95 ± 14	1040	[4] ARMSTRONG	91B	OMEG	±	$300\ pp \to pp\eta\pi^+\pi^-$
62 ± 15	500	[5] EVANGELIS...	81	OMEG	±	$12\ \pi^-p \to \eta\pi^+\pi^-\pi^-p$
60 ± 20	145	[5] GURTU	79	HBC	±	$4.2\ K^-p \to \Lambda\eta 2\pi$
60^{+50}_{-30}	47	CONFORTO	78	OSPK	−	$4.5\ \pi^-p \to pX^-$
$86.0^{+60.0}_{-50.0}$	50	CORDEN	78	OMEG	±	$12–15\ \pi^-p \to n\eta 2\pi$
44 ± 22		GRASSLER	77	HBC	−	$16\ \pi^\mp p \to p\eta 3\pi$
80 to 300		[6] FLATTE	76	RVUE	−	$4.2\ K^-p \to \Lambda\eta 2\pi$
$16.0^{+25.0}_{-16.0}$	70	[7] WELLS	75	HBC	−	$3.1–6\ K^-p \to \Lambda\eta 2\pi$
30 ± 5	150	[8] DEFOIX	72	HBC	±	$0.7\ \overline{p}p \to 7\pi$
40 ± 15		CAMPBELL	69	DBC	±	$2.7\ \pi^+d$
60 ± 30	15	MILLER	69B	HBC	−	$4.5\ K^-N \to \eta\pi\Lambda$
80 ± 30	30	AMMAR	68	HBC	±	$5.5\ K^-p \to \Lambda\eta 2\pi$

[1] From a fit with the S-wave amplitude including two interfering Breit-Wigners plus a background term.
[2] T-matrix pole.
[3] The $\eta\pi$ width.
[4] From a single Breit-Wigner fit.
[5] From $f_1(1285)$ decay.
[6] Using a two-channel resonance parametrization of GAY 76B data.
[7] Weak evidence only for $a_0(980)^+$ production.
[8] This number has very little meaning. Error is much too small. Vlada

$K\overline{K}$ ONLY

VALUE (MeV)	EVTS	DOCUMENT ID		TECN	CHG	COMMENT
• • • We do not use the following data for averages, fits, limits, etc. • • •						
~ 48		[1] OLLER	99C	RVUE		$\pi\pi \to \pi\pi$, $K\overline{K}$
~ 25	100	[2] ASTIER	67	HBC	±	
57 ± 13	143	[3] ROSENFELD	65	RVUE	±	

[1] T-matrix pole.
[2] ASTIER 67 includes data of BARLOW 67, CONFORTO 67, ARMENTEROS 65.
[3] Plus systematic errors.

Int. J. Mod. Phys. A 2026.41. Downloaded from www.worldscientific.com by UNIVERSITY OF CALIFORNIA @ BERKELEY on 09/16/26. Re-use and distribution is strictly not permitted, except for Open Access articles.

$a_0(980)$ DECAY MODES

	Mode	Fraction (Γ_i/Γ)
Γ_1	$\eta\pi$	seen
Γ_2	$K\overline{K}$	seen
Γ_3	$\eta'\pi$	seen
Γ_4	$\rho\pi$	not seen
Γ_5	$\gamma\gamma$	seen
Γ_6	e^+e^-	

$a_0(980)$ PARTIAL WIDTHS

$\Gamma(\gamma\gamma)$ — Γ_5

VALUE (keV)	DOCUMENT ID		TECN
• • • We do not use the following data for averages, fits, limits, etc. • • •			
0.30 ± 0.10	[1] AMSLER	98	RVUE

[1] Using $\Gamma_{\gamma\gamma}B(a0(980) \to \eta\pi) = 0.24 \pm 0.08$ keV.

$a_0(980)$ $\Gamma(i)\Gamma(\gamma\gamma)/\Gamma(\text{total})$

$\Gamma(\eta\pi) \times \Gamma(\gamma\gamma)/\Gamma_{\text{total}}$ — $\Gamma_1\Gamma_5/\Gamma$

VALUE (keV)	EVTS	DOCUMENT ID		TECN	COMMENT
$0.21^{+0.08}_{-0.04}$ OUR AVERAGE					
$0.128^{+0.003}_{-0.002}{}^{+0.502}_{-0.043}$		[1] UEHARA	09A	BELL	$\gamma\gamma \to \pi^0\eta$
$0.28 \pm0.04 \pm0.10$	44	OEST	90	JADE	$e^+e^- \to e^+e^-\pi^0\eta$
$0.19 \pm0.07\ ^{+0.10}_{-0.07}$		ANTREASYAN	86	CBAL	$e^+e^- \to e^+e^-\pi^0\eta$

[1] From a fit with the S-wave amplitude including two interfering Breit-Wigners plus a background term.

$\Gamma(\eta\pi) \times \Gamma(e^+e^-)/\Gamma_{\text{total}}$ — $\Gamma_1\Gamma_6/\Gamma$

VALUE (eV)	CL%	DOCUMENT ID		TECN	COMMENT
<1.5	90	VOROBYEV	88	ND	$e^+e^- \to \pi^0\eta$

$a_0(980)$ BRANCHING RATIOS

$\Gamma(K\overline{K})/\Gamma(\eta\pi)$ — Γ_2/Γ_1

VALUE	DOCUMENT ID		TECN	CHG	COMMENT
0.172±0.019 OUR AVERAGE					
$0.137\pm0.036\pm0.042$	[1] ABLIKIM	22AH	BES3		$D_s^+ \to K_S^0 K^+\pi^0$
0.23 ± 0.05	[2] ABELE	98	CBAR		$0.0\,\overline{p}p \to K_L^0 K^\pm\pi^\mp$
$0.166\pm0.01 \pm0.02$	[3] BARBERIS	98C	OMEG		$450\,pp \to p_f\, f_1(1285)\, p_s$
• • • We do not use the following data for averages, fits, limits, etc. • • •					
$0.138\pm0.001\pm0.035$	[4] ALBRECHT	20	CBAR		$0.9\,\overline{p}p \to \pi^0\pi^0\eta$, $\pi^0\eta\eta$, $\pi^0 K^+K^-$
1.20 ± 0.15	[5] ANISOVICH	09	RVUE		$0.0\,\overline{p}p$, πN
$1.05 \pm0.07 \pm0.05$	[6] BUGG	08A	RVUE	0	$\overline{p}p \to \pi^0\pi^0\eta$
0.57 ± 0.16	[7] BARGIOTTI	03	OBLX		$\overline{p}p$
~ 0.60	OLLER	99B	RVUE		$\pi\pi \to \eta\pi$, $K\overline{K}$
0.7 ± 0.3	[3] CORDEN	78	OMEG		12–15 $\pi^-p \to n\eta 2\pi$
0.25 ± 0.08	[3] DEFOIX	72	HBC	±	$0.7\,\overline{p} \to 7\pi$

[1] Using $D_s^+ \to a_0(980)^+\pi^0$ from ABLIKIM 19BE.
[2] Using $\pi^0\pi^0\eta$ from AMSLER 94D.
[3] From the decay of $f_1(1285)$.
[4] Residues from T-matrix pole with 2 poles, 2 channels. Solution on adjacent sheet $0.149\pm0.001\pm0.039$.
[5] This is a ratio of couplings.
[6] A ratio of couplings, using AMSLER 94D and ABELE 98. Supersedes BUGG 94.
[7] Coupled channel analysis of $\pi^+\pi^-\pi^0$, $K^+K^-\pi^0$, and $K^\pm K_S^0\pi^\mp$.

$\Gamma(\eta'\pi)/\Gamma_{\text{total}}$ — Γ_3/Γ

VALUE	EVTS	DOCUMENT ID		TECN	COMMENT
seen	116k	[1] CHEN	20A	BELL	$D^0 \to K^-\pi^+\eta$

[1] From an amplitude analysis of the $D^0 \to K^-\pi^+\eta$ decay in a three-channel Flatte model with a 10.1 σ significance. Earlier observed by ABLIKIM 17K in the $\chi_{c1} \to \eta\pi^+\pi^-$ decay with a 8.9 σ significance.

$\Gamma(\rho\pi)/\Gamma(\eta\pi)$ — Γ_4/Γ_1

$\rho\pi$ forbidden.

VALUE	CL%	DOCUMENT ID		TECN	CHG	COMMENT
• • • We do not use the following data for averages, fits, limits, etc. • • •						
<0.25	70	[1] AMMAR	70	HBC	±	4.1,5.5 $K^-p \to \Lambda\eta 2\pi$

[1] Not clear if they really observed the $a_0(980)$ 3 standard deviations.

$a_0(980)$ REFERENCES

ABLIKIM	22AH	PRL 129 182001	M. Ablikim *et al.*	(BESIII Collab.)
ALBRECHT	20	EPJ C80 453	M. Albrecht *et al.*	(Crystal Barrel Collab.)
CHEN	20A	PR D102 012002	Y.Q. Chen *et al.*	(BELLE Collab.)
LU	20	EPJ C80 436	J. Lu, B. Moussallam	
AAIJ	19H	JHEP 1904 063	R. Aaij *et al.*	(LHCb Collab.)
ABLIKIM	19BE	PRL 123 112001	M. Ablikim *et al.*	(BESIII Collab.)
AOUDE	18	PR D98 056021	R.T. Aoude *et al.*	
ABLIKIM	17K	PR D95 032002	M. Ablikim *et al.*	(BESIII Collab.)
AAIJ	16N	PR D93 052018	R. Aaij *et al.*	(LHCb Collab.)
AMBROSINO	09F	PL B681 5	F. Ambrosino *et al.*	(KLOE Collab.)
ANISOVICH	09	IJMP A24 2481	V.V. Anisovich, A.V. Sarantsev	(PNPI)
UEHARA	09A	PR D80 032001	S. Uehara *et al.*	(BELLE Collab.)
BUGG	08A	PR D78 074023	D.V. Bugg	(LOQM)
PELAEZ	04A	MPL A19 2879	J.R. Pelaez	(MADU)
ACHASOV	03B	PR D68 014006	N.N. Achsaov, A.V. Kiselev	
BARGIOTTI	03	EPJ C26 371	M. Bargiotti *et al.*	(OBELIX Collab.)
ACHARD	02B	PL B526 269	P. Achard *et al.*	(L3 Collab.)
ACHASOV	00F	PL B479 53	M.N. Achasov *et al.*	(Novosibirsk SND Collab.)
BARBERIS	00H	PL B488 225	D. Barberis *et al.*	(WA 102 Collab.)
OLLER	99	PR D60 099906 (errat.)	J.A. Oller *et al.*	
OLLER	99B	NP A652 407 (errat.)	J.A. Oller, E. Oset	
OLLER	99C	PR D60 074023	J.A. Oller, E. Oset	
TEIGE	99	PR D59 012001	S. Teige *et al.*	(BNL E852 Collab.)
ABELE	98	PR D57 3860	A. Abele *et al.*	(Crystal Barrel Collab.)
ACHASOV	98B	PL B438 441	M.N. Achasov *et al.*	(Novosibirsk SND Collab.)
AMSLER	98	RMP 70 1293	C. Amsler	
ANISOVICH	98B	SPU 41 419	V.V. Anisovich *et al.*	
		Translated from UFN 168 481.		
BARBERIS	98C	PL B440 225	D. Barberis *et al.*	(WA 102 Collab.)
BERTIN	98B	PL B434 180	A. Bertin *et al.*	(OBELIX Collab.)
TORNQVIST	96	PRL 76 1575	N.A. Tornqvist, M. Roos	(HELS)
JANSSEN	95	PR D52 2690	G. Janssen *et al.*	(STON, ADLD, JULI)
AMSLER	94C	PL B327 425	C. Amsler *et al.*	(Crystal Barrel Collab.)
AMSLER	94D	PL B333 277	C. Amsler *et al.*	(Crystal Barrel Collab.)
BUGG	94	PR D50 4412	D.V. Bugg *et al.*	(LOQM)
AMSLER	92	PL B291 347	C. Amsler *et al.*	(Crystal Barrel Collab.)
ARMSTRONG	91B	ZPHY C52 389	T.A. Armstrong *et al.*	(ATHU, BARI, BIRM+)
OEST	90	ZPHY C47 343	T. Oest *et al.*	(JADE Collab.)
ACHASOV	89	NP B315 465	N.N. Achasov, V.N. Ivanchenko	
ASTON	88	NP B296 493	D. Aston *et al.*	(SLAC, NAGO, CINC, INUS)
VOROBYEV	88	SJNP 48 273	P.V. Vorobiev *et al.*	(NOVO)
		Translated from YAF 48 436.		
ANTREASYAN	86	PR D33 1847	D. Antreasyan *et al.*	(Crystal Ball Collab.)
ATKINSON	84E	PL 138B 459	M. Atkinson *et al.*	(BONN, CERN, GLAS+)
EVANGELIS...	81	NP B178 197	C. Evangelista *et al.*	(BARI, BONN, CERN+)
DEBILLY	80	NP B176 1	L. de Billy *et al.*	(CURIN, LAUS, NEUC+)
GURTU	79	NP B151 181	A. Gurtu *et al.*	(CERN, ZEEM, NIJM, OXF)
CONFORTO	78	LNC 23 419	B. Conforto *et al.*	(RHEL, TNTO, CHIC+)
CORDEN	78	NP B144 253	M.J. Corden *et al.*	(BIRM, RHEL, TELA+)
ESTABROOKS	78	NP B133 490	P.G. Estabrooks *et al.*	(MCGI, CARL, DURH+)
GRASSLER	77	NP B121 189	H. Grassler *et al.*	(AACH3, BERL, BONN+)
JAFFE	77	PR D15 267,281	R. Jaffe	(MIT)
FLATTE	76	PL 63B 224	S.M. Flatte	(CERN)
GAY	76B	PL 63B 220	J.B. Gay *et al.*	(CERN, AMST, NIJM) JP
WELLS	75	NP B101 333	J. Wells *et al.*	(OXF)
LINGLIN	73	NP B55 408	D. Linglin	(CERN)
DEFOIX	72	NP B44 125	C. Defoix *et al.*	(CDEF, CERN)
AMMAR	70	PR D2 430	R. Ammar *et al.*	(KANS, NWES, ANL, WISC)
BARNES	69C	PRL 23 610	V.E. Barnes *et al.*	(BNL, SYRA)
CAMPBELL	69	PRL 22 1204	J.H. Campbell *et al.*	(PURD)
MILLER	69B	PL 29B 255	D.H. Miller *et al.*	(PURD)
Also		PR 188 2011	W.L. Yen *et al.*	(PURD)
AMMAR	68	PRL 21 1832	R. Ammar *et al.*	(NWES, ANL)
ASTIER	67	PL 25B 294	A. Astier *et al.*	(CDEF, CERN, IRAD)
Includes data of BARLOW 67, CONFORTO 67, and ARMENTEROS 65.				
BARLOW	67	NC 50A 701	J. Barlow *et al.*	(CERN, CDEF, IRAD, LIVP)
CONFORTO	67	NP B3 469	G. Conforto *et al.*	(CERN, CDEF, IPNP+)
ARMENTEROS	65	PL 17 344	R. Armenteros *et al.*	(CERN, CDEF)
ROSENFELD	65	Oxford Conf. 58	A.H. Rosenfeld	(LRL)

$\phi(1020)$

$I^G(J^{PC}) = 0^-(1^{--})$

$\phi(1020)$ MASS

VALUE (MeV)	EVTS	DOCUMENT ID		TECN	COMMENT
1019.460 ±0.016 OUR AVERAGE					
$1019.444 \pm0.013 \pm0.060$		DRUZHININ	25	SND	$e^+e^- \to K_L^0K_S^0$
1019.463 ± 0.061	2.3M	[1] KOZYREV	18	CMD3	$e^+e^- \to K^+K^-$, $K_S^0K_L^0$
$1019.462 \pm0.042 \pm0.056$	28k	[2] LEES	14H	BABR	$e^+e^- \to K_S^0K_L^0\gamma$
$1019.51 \pm0.02 \pm0.05$		[3] LEES	13Q	BABR	$e^+e^- \to K^+K^-\gamma$
$1019.30 \pm0.02 \pm0.10$	105k	AKHMETSHIN	06	CMD2	0.98–1.06 $e^+e^- \to \pi^+\pi^-\pi^0$
$1019.52 \pm0.05 \pm0.05$	17.4k	AKHMETSHIN	05	CMD2	0.60-1.38 $e^+e^- \to \gamma\gamma$
$1019.483 \pm0.011 \pm0.025$	272k	[4] AKHMETSHIN	04	CMD2	$e^+e^- \to K_L^0K_S^0$
1019.42 ± 0.05	1900k	[5] ACHASOV	01E	SND	$e^+e^- \to K^+K^-$, K_SK_L, $\pi^+\pi^-\pi^0$
$1019.40 \pm0.04 \pm0.05$	23k	AKHMETSHIN	01B	CMD2	$e^+e^- \to \eta\gamma$
1019.36 ± 0.12		[6] ACHASOV	00B	SND	$e^+e^- \to \eta\gamma$
$1019.38 \pm0.07 \pm0.08$	2200	[7] AKHMETSHIN	99F	CMD2	$e^+e^- \to \pi^+\pi^- \geq 2\gamma$
$1019.51 \pm0.07 \pm0.10$	11169	AKHMETSHIN	98	CMD2	$e^+e^- \to \pi^+\pi^-\pi^0$
1019.5 ± 0.4		BARBERIS	98	OMEG	$450\,pp \to pp2K^+2K^-$
1019.42 ± 0.06	55600	AKHMETSHIN	95	CMD2	$e^+e^- \to$ hadrons
1019.7 ± 0.3	2012	DAVENPORT	86	MPSF	$400\,pA \to 4KX$
$1019.7 \pm0.1 \pm0.1$	5079	ALBRECHT	85D	ARG	$10\,e^+e^- \to K^+K^-X$

1019.3 ±0.1		1500	ARENTON	82	AEMS	11.8 polar. $pp \to K K$
1019.67 ±0.17		25080	[8] PELLINEN	82	RVUE	
1019.52 ±0.13		3681	BUKIN	78C	OLYA	$e^+e^- \to$ hadrons
• • • We do not use the following data for averages, fits, limits, etc. • • •						
1019.443 ±0.010	±0.060	1.28M	[9,10] ACHASOV	24	SND	$e^+e^- \to K^0_L K^0_S$
1019.0330±0.0084			[11] DUBNICKA	24	RVUE	$e^+e^- \to K^+K^-$, $K^0_S K^0_L$
1019.761 ±0.130		34M	[12] IGNATOV	24	CMD3	$e^+e^- \to \pi^+\pi^-$
1018.4 ±0.5	±0.1		[13] ALBRECHT	20	CBAR	0.9 $\overline{p}p \to K^+K^-\pi^0$
1019.21 ±0.04	±0.03		[14] HOID	20	RVUE	$e^+e^- \to \pi^0\gamma$
1019.54 ±0.10	±0.51		[15] AAIJ	19H	LHCB	$pp \to D^\pm X$
1019.20 ±0.02	±0.01		[16] HOFERICHT...	19	RVUE	$e^+e^- \to \pi^+\pi^-\pi^0$
1019.469 ±0.061		1.7M	KOZYREV	18	CMD3	$e^+e^- \to K^+K^-$
1019.457 ±0.061		610k	KOZYREV	16	CMD3	$e^+e^- \to K^0_S K^0_L$
1019.48 ±0.01			LEES	13F	BABR	$D^+ \to K^+K^-\pi^+$
1019.441 ±0.008	±0.080	542k	[17] AKHMETSHIN	08	CMD2	1.02 $e^+e^- \to K^+K^-$
1019.63 ±0.07		12540	[18] AUBERT,B	05J	BABR	$D^0 \to \overline{K}^0 K^+K^-$
1019.8 ±0.7			ARMSTRONG	86	OMEG	85 $\pi^+/pp \to \pi^+/p4Kp$
1020.1 ±0.11		5526	[18] ATKINSON	86	OMEG	20–70 γp
1019.7 ±1.0			BEBEK	86	CLEO	$e^+e^- \to \Upsilon(4S)$
1019.411 ±0.008		642k	[19] DIJKSTRA	86	SPEC	100–200 $\pi^\pm$, $\overline{p}$, p, $K^\pm$, on Be
1020.9 ±0.2			[18] FRAME	86	OMEG	13 $K^+p \to \phi K^+p$
1021.0 ±0.2			[18] ARMSTRONG	83B	OMEG	18.5 $K^-p \to K^-K^+\Lambda$
1020.0 ±0.5			[18] ARMSTRONG	83B	OMEG	18.5 $K^-p \to K^-K^+\Lambda$
1019.7 ±0.3			[18] BARATE	83	GOLI	190 π^-Be $\to 2\mu$X
1019.8 ±0.2	±0.5	766	IVANOV	81	OLYA	1–1.4 $e^+e^- \to K^+K^-$
1019.4 ±0.5		337	COOPER	78B	HBC	0.7–0.8 $\overline{p}p \to K^0_S K^0_L \pi^+\pi^-$
1020 ±1		383	[18] BALDI	77	CNTR	10 $\pi^-p \to \pi^-\phi p$
1018.9 ±0.6		800	COHEN	77	ASPK	6 $\pi^\pm N \to K^+K^-N$
1019.7 ±0.5		454	KALBFLEISCH	76	HBC	2.18 $K^-p \to \Lambda K\overline{K}$
1019.4 ±0.8		984	BESCH	74	CNTR	2 $\gamma p \to pK^+K^-$
1020.3 ±0.4		100	BALLAM	73	HBC	2.8–9.3 γp
1019.4 ±0.7			BINNIE	73B	CNTR	$\pi^-p \to \phi n$
1019.6 ±0.5		120	[20] AGUILAR-...	72B	HBC	3.9,4.6 $K^-p \to \Lambda K^+K^-$
1019.9 ±0.5		100	[20] AGUILAR-...	72B	HBC	3.9,4.6 $K^-p \to K^-pK^+K^-$
1020.4 ±0.5		131	COLLEY	72	HBC	10 $K^+p \to K^+p\phi$
1019.9 ±0.3		410	STOTTLE...	71	HBC	2.9 $K^-p \to \Sigma/\Lambda K\overline{K}$

[1] Average of KOZYREV 16 and KOZYREV 18 values taking into account the correlated uncertainties. Supersedes individual KOZYREV 16 and KOZYREV 18 results.
[2] Using a vector meson dominance model with contribution from $\phi(1020)$ and higher mass excitations of $\rho(770)$, $\omega(782)$, and $\phi(1020)$.
[3] Using a phenomenological model based on KUHN 90 with a sum of Breit-Wigner resonances for $\rho(770)$, $\omega(782)$, $\phi(1020)$ and their higher mass excitations.
[4] Update of AKHMETSHIN 99D
[5] From the combined fit assuming that the total $\phi(1020)$ production cross section is saturated by those of K^+K^-, $K_S K_L$, $\pi^+\pi^-\pi^0$, and $\eta\gamma$ decays modes and using ACHASOV 00B for the $\eta\gamma$ decay mode.
[6] Using a total width of 4.43 ± 0.05 MeV. Systematic uncertainty included.
[7] Using a total width of 4.43 ± 0.05 MeV.
[8] PELLINEN 82 review includes AKERLOF 77, DAUM 81, BALDI 77, AYRES 74, DEGROOT 74.
[9] From a fit of the cross section in the energy region $1.000 < \sqrt{s} < 1.100$ GeV using a vector meson dominance model with contribution from $\phi(1020)$, $\rho(770)$, $\omega(782)$ and higher vector resonances.
[10] Superseded by DRUZHININ 25.
[11] From the fit to data of CMD3, BABAR and BES3.
[12] From a fit of the pion form factor in the energy range $0.32 < \sqrt{s} < 1.2$ GeV using the GOUNARIS 68 parametrization with the complex phase of the $\rho-\omega$ interference leaving $\rho(1450)$, $\rho(1700)$ resonances as free parameters of the fit. Systematic errors not estimated.
[13] Width fixed at 4.2 MeV.
[14] The values were extracted from a dispersively improved Breit-Wigner parameterization and do not include vacuum polarization. Inclusion of vacuum polarization gives 1019.457 ± 0.020 MeV.
[15] From the $D^\pm \to K^\pm K^+K^-$ Dalitz plot fit with the Triple-M amplitude in the multi-meson model of AOUDE 18.
[16] The values were extracted from a dispersively improved Breit-Wigner parameterization and do not include vacuum polarization.
[17] Strongly correlated with AKHMETSHIN 04.
[18] Systematic errors not evaluated.
[19] Weighted and scaled average of 12 measurements of DIJKSTRA 86.
[20] Mass errors enlarged by us to $\Gamma/\sqrt{N}$; see the note with the $K^*(892)$ mass.

$\phi(1020)$ WIDTH

VALUE (MeV)	EVTS	DOCUMENT ID		TECN	COMMENT
4.249±0.013 OUR AVERAGE		Error includes scale factor of 1.1.			
4.234±0.22 ±0.12		DRUZHININ	25	SND	$e^+e^- \to K^0_L K^0_S$
4.245±0.013	2.3M	[1] KOZYREV	18	CMD3	$e^+e^- \to K^+K^-$, $K^0_S K^0_L$
4.205±0.103±0.067	28k	[2] LEES	14H	BABR	$e^+e^- \to K^0_S K^0_L \gamma$
4.29 ±0.04 ±0.07		[3] LEES	13Q	BABR	$e^+e^- \to K^+K^-\gamma$
4.30 ±0.06 ±0.17	105k	AKHMETSHIN	06	CMD2	0.98–1.06 $e^+e^- \to \pi^+\pi^-\pi^0$
4.280±0.033±0.025	272k	[4] AKHMETSHIN	04	CMD2	$e^+e^- \to K^0_L K^0_S$
4.21 ±0.04	1900k	[5] ACHASOV	01E	SND	$e^+e^- \to K^+K^-$, $K_S K_L$, $\pi^+\pi^-\pi^0$
4.44 ±0.09	55600	AKHMETSHIN	95	CMD2	$e^+e^- \to$ hadrons
4.5 ±0.7	1500	ARENTON	82	AEMS	11.8 polar. $pp \to KK$
4.2 ±0.6	766	[6] IVANOV	81	OLYA	1–1.4 $e^+e^- \to K^+K^-$
4.3 ±0.6		[6] CORDIER	80	DM1	$e^+e^- \to \pi^+\pi^-\pi^0$
4.36 ±0.29	3681	[6] BUKIN	78C	OLYA	$e^+e^- \to$ hadrons
4.4 ±0.6	984	[6] BESCH	74	CNTR	2 $\gamma p \to pK^+K^-$
4.67 ±0.72	681	[6] BALAKIN	71	OSPK	$e^+e^- \to$ hadrons
4.09 ±0.29		BIZOT	70	OSPK	$e^+e^- \to$ hadrons
• • • We do not use the following data for averages, fits, limits, etc. • • •					
4.212±0.20 ±0.13	1.28M	[7,8] ACHASOV	24	SND	$e^+e^- \to K^0_L K^0_S$
4.151±0.018		[9] DUBNICKA	24	RVUE	$e^+e^- \to K^+K^-$, $K^0_S K^0_L$
4.681±0.277	34M	[10] IGNATOV	24	CMD3	$e^+e^- \to \pi^+\pi^-$
4.07 ±0.13 ±0.01		[11] HOID	20	RVUE	$e^+e^- \to \pi^0\gamma$
4.23 ±0.04 ±0.02		[12] HOFERICHT...	19	RVUE	$e^+e^- \to \pi^+\pi^-\pi^0$
4.249±0.015	1.7M	KOZYREV	18	CMD3	$e^+e^- \to K^+K^-$
4.240±0.017	610k	KOZYREV	16	CMD3	$e^+e^- \to K^0_S K^0_L$
4.37 ±0.02		LEES	13F	BABR	$D^+ \to K^+K^-\pi^+$
4.24 ±0.02 ±0.03	542k	[13] AKHMETSHIN	08	CMD2	1.02 $e^+e^- \to K^+K^-$
4.28 ±0.13	12540	[14] AUBERT,B	05J	BABR	$D^0 \to \overline{K}^0 K^+K^-$
4.45 ±0.06	271k	DIJKSTRA	86	SPEC	100 π^-Be
3.6 ±0.8	337	[6] COOPER	78B	HBC	0.7–0.8 $\overline{p}p \to K^0_S K^0_L \pi^+\pi^-$
4.5 ±0.50	1300	[6,14] AKERLOF	77	SPEC	400 $pA \to K^+K^-X$
4.5 ±0.8	500	[6,14] AYRES	74	ASPK	3–6 $\pi^-p \to K^+K^-n$, $K^-p \to K^+K^-\Lambda/\Sigma^0$
3.81 ±0.37		COSME	74B	OSPK	$e^+e^- \to K^0_L K^0_S$
3.8 ±0.7	454	[6] BORENSTEIN	72	HBC	2.18 $K^-p \to K\overline{K}n$

[1] Average of KOZYREV 16 and KOZYREV 18 values taking into account the correlated uncertainties. Supersedes individual KOZYREV 16 and KOZYREV 18 results.
[2] Using a vector meson dominance model with contribution from $\phi(1020)$ and higher mass excitations of $\rho(770)$, $\omega(782)$, and $\phi(1020)$.
[3] Using a phenomenological model based on KUHN 90 with a sum of Breit-Wigner resonances for $\rho(770)$, $\omega(782)$, $\phi(1020)$ and their higher mass excitations.
[4] Update of AKHMETSHIN 99D
[5] From the combined fit assuming that the total $\phi(1020)$ production cross section is saturated by those of K^+K^-, $K_S K_L$, $\pi^+\pi^-\pi^0$, and $\eta\gamma$ decays modes and using ACHASOV 00B for the $\eta\gamma$ decay mode.
[6] Width errors enlarged by us to $4\Gamma/\sqrt{N}$; see the note with the $K^*(892)$ mass.
[7] From a fit of the cross section in the energy region $1.000 < \sqrt{s} < 1.100$ GeV using a vector meson dominance model with contribution from $\phi(1020)$, $\rho(770)$, $\omega(782)$ and higher vector resonances.
[8] Superseded by DRUZHININ 25.
[9] From the fit to data of CMD3, BABAR and BES3.
[10] From a fit of the pion form factor in the energy range $0.32 < \sqrt{s} < 1.2$ GeV using the GOUNARIS 68 parametrization with the complex phase of the $\rho-\omega$ interference leaving $\rho(1450)$, $\rho(1700)$ resonances as free parameters of the fit. Systematic errors not estimated.
[11] The values were extracted from a dispersively improved Breit-Wigner parameterization.
[12] The values were extracted from a dispersively improved Breit-Wigner parameterization and do not include vacuum polarization.
[13] Strongly correlated with AKHMETSHIN 04.
[14] Systematic errors not evaluated.

$\phi(1020)$ DECAY MODES

	Mode	Fraction (Γ_i/Γ)	Scale factor/ Confidence level
Γ_1	K^+K^-	(50.1 ±0.6) %	S=1.6
Γ_2	$K^0_L K^0_S$	(33.6 ±0.4) %	S=1.3
Γ_3	$\rho\pi + \pi^+\pi^-\pi^0$	(14.7 ±0.4) %	S=1.5
Γ_4	$\pi^+\pi^-\pi^0$		
Γ_5	$\eta\gamma$	(1.306±0.024) %	S=1.2
Γ_6	$\pi^0\gamma$	(1.33 ±0.05) $\times 10^{-3}$	
Γ_7	$\ell^+\ell^-$	—	
Γ_8	e^+e^-	(2.963±0.034) $\times 10^{-4}$	S=1.4
Γ_9	$\mu^+\mu^-$	(2.86 ±0.22) $\times 10^{-4}$	S=1.2
Γ_{10}	ηe^+e^-	(1.08 ±0.04) $\times 10^{-4}$	
Γ_{11}	$\pi^+\pi^-$	(9.5 ±1.9) $\times 10^{-5}$	S=2.0

Int. J. Mod. Phys. A 2026.41. Downloaded from www.worldscientific.com
by LIFORNIA @ BERKELEY on 09/16/26. Re-use and distribution is strictly not permitted, except for Open Access articles.

Γ_{12}	$\omega\pi^0$	$(4.7 \pm 0.5) \times 10^{-5}$	
Γ_{13}	$\omega\gamma$	< 5 %	CL=84%
Γ_{14}	$\rho\gamma$	$< 1.2 \times 10^{-5}$	CL=90%
Γ_{15}	$\pi^+\pi^-\gamma$	$(4.1 \pm 1.3) \times 10^{-5}$	
Γ_{16}	$f_0(980)\gamma$	$(3.22 \pm 0.19) \times 10^{-4}$	S=1.1
Γ_{17}	$\pi^0\pi^0\gamma$	$(1.13 \pm 0.06) \times 10^{-4}$	
Γ_{18}	$\pi^+\pi^-\pi^+\pi^-$	$(3.9 {}^{+2.8}_{-2.2}) \times 10^{-6}$	
Γ_{19}	$\pi^+\pi^+\pi^-\pi^-\pi^0$	$< 4.6 \times 10^{-6}$	CL=90%
Γ_{20}	$\pi^0 e^+ e^-$	$(1.33 {}^{+0.07}_{-0.10}) \times 10^{-5}$	
Γ_{21}	$\pi^0\eta\gamma$	$(7.27 \pm 0.30) \times 10^{-5}$	S=1.5
Γ_{22}	$a_0(980)\gamma$	$(7.6 \pm 0.6) \times 10^{-5}$	
Γ_{23}	$K^0\overline{K}^0\gamma$	$< 1.9 \times 10^{-8}$	CL=90%
Γ_{24}	$\eta'(958)\gamma$	$(6.23 \pm 0.21) \times 10^{-5}$	
Γ_{25}	$\eta\pi^0\pi^0\gamma$	$< 2 \times 10^{-5}$	CL=90%
Γ_{26}	$\mu^+\mu^-\gamma$	$(1.4 \pm 0.5) \times 10^{-5}$	
Γ_{27}	$\rho\gamma\gamma$	$< 1.2 \times 10^{-4}$	CL=90%
Γ_{28}	$\eta\pi^+\pi^-$	$< 1.8 \times 10^{-5}$	CL=90%
Γ_{29}	$\eta\mu^+\mu^-$	$< 9.4 \times 10^{-6}$	CL=90%
Γ_{30}	$\eta U \to \eta e^+ e^-$	$< 1 \times 10^{-6}$	CL=90%
Γ_{31}	invisible	$< 1.7 \times 10^{-4}$	CL=90%

Lepton Family number (*LF*) violating modes

Γ_{32}	$e^\pm\mu^\mp$	*LF*	$< 2 \times 10^{-6}$	CL=90%
Γ_{33}	$\pi^+\pi^+e^-e^-$	*L*	$< 1.3 \times 10^{-5}$	CL=90%

CONSTRAINED FIT INFORMATION

An overall fit to 30 branching ratios uses 84 measurements and one constraint to determine 14 parameters. The overall fit has a $\chi^2 = 98.5$ for 71 degrees of freedom.

The following *off-diagonal* array elements are the correlation coefficients $\langle \delta x_i \delta x_j \rangle / (\delta x_i \cdot \delta x_j)$, in percent, from the fit to the branching fractions, $x_i \equiv \Gamma_i/\Gamma_{total}$. The fit constrains the x_i whose labels appear in this array to sum to one.

	x_1	x_2	x_3	x_5	x_6	x_8	x_9	x_{11}	x_{12}	x_{16}
x_2	−70									
x_3	−67	−6								
x_5	−25	28	0							
x_6	−14	17	1	8						
x_8	60	−77	−3	−37	−23					
x_9	−6	7	0	3	2	−9				
x_{11}	−4	4	0	2	1	−6	1			
x_{12}	−5	6	0	3	2	−8	1	0		
x_{16}	0	0	0	0	0	0	0	0	0	
x_{17}	−12	15	0	18	4	−19	2	1	2	0
x_{18}	−1	1	0	1	0	−2	0	0	0	0
x_{22}	0	0	0	0	0	0	0	0	0	0
x_{24}	−8	9	0	32	3	−12	1	1	1	0

	x_{17}	x_{18}	x_{22}
x_{18}	0		
x_{22}	0	0	
x_{24}	6	0	0

$\phi(1020)$ PARTIAL WIDTHS

$\Gamma(\eta\gamma)$ — Γ_5

VALUE (keV)	DOCUMENT ID		TECN	COMMENT
• • • We do not use the following data for averages, fits, limits, etc. • • •				
$58.9 \pm 0.5 \pm 2.4$	ACHASOV	00	SND	$e^+e^- \to \eta\gamma$

$\Gamma(\pi^0\gamma)$ — Γ_6

VALUE (keV)	DOCUMENT ID		TECN	COMMENT
• • • We do not use the following data for averages, fits, limits, etc. • • •				
$5.40 \pm 0.16 {}^{+0.43}_{-0.40}$	ACHASOV	00	SND	$e^+e^- \to \pi^0\gamma$

$\Gamma(\ell^+\ell^-)$ — Γ_7

VALUE (keV)	DOCUMENT ID		TECN	COMMENT
• • • We do not use the following data for averages, fits, limits, etc. • • •				
$1.320 \pm 0.017 \pm 0.015$	[1] AMBROSINO	05	KLOE	$1.02\ e^+e^- \to \mu^+\mu^-$

[1] Weighted average of Γ_{ee} and $\sqrt{\Gamma_{ee}\Gamma_{\mu\mu}}$ from AMBROSINO 05 assuming lepton universality.

$\Gamma(e^+e^-)$ — Γ_8

VALUE (keV)	DOCUMENT ID		TECN	COMMENT
1.27 ±0.04 OUR EVALUATION				
1.251±0.021 OUR AVERAGE Error includes scale factor of 1.1.				
$1.235 \pm 0.006 \pm 0.022$	[1] AKHMETSHIN	11	CMD2	$1.02\ e^+e^- \to \phi$
$1.32 \pm 0.05 \pm 0.03$	[2] AMBROSINO	05	KLOE	$1.02\ e^+e^- \to e^+e^-$
1.28 ± 0.05	AKHMETSHIN	95	CMD2	$1.02\ e^+e^- \to \phi$

[1] Combined analysis of the CMD-2 data on $\phi \to K^+K^-$, $K^0_S K^0_L$, $\pi^+\pi^-\pi^0$, $\eta\gamma$ assuming that the sum of their branching fractions is 0.99741 ± 0.00007.

[2] From forward-backward asymmetry and using $\Gamma_{total} = 4.26 \pm 0.05$ MeV from the 2004 edition of this Review.

$(\Gamma(e^+e^-) \times \Gamma(\mu^+\mu^-))^{1/2}$ — $(\Gamma_8\Gamma_9)^{1/2}$

VALUE (keV)	DOCUMENT ID		TECN	COMMENT
1.320±0.018±0.017	AMBROSINO	05	KLOE	$1.02\ e^+e^- \to \mu^+\mu^-$

$\phi(1020)$ $\Gamma(i)\Gamma(e^+e^-)/\Gamma(total)$

$\Gamma(K^+K^-) \times \Gamma(e^+e^-)/\Gamma_{total}$ — $\Gamma_1\Gamma_8/\Gamma$

VALUE (keV)	EVTS	DOCUMENT ID		TECN	COMMENT
0.6340±0.0070±0.0039		[1] LEES	13Q	BABR	$e^+e^- \to K^+K^-\gamma$
• • • We do not use the following data for averages, fits, limits, etc. • • •					
$0.669 \pm 0.001 \pm 0.023$	1.7M	KOZYREV	18	CMD3	$e^+e^- \to K^+K^-$

[1] Using a phenomenological model based on KUHN 90 with a sum of Breit-Wigner resonances for $\rho(770)$, $\omega(782)$, $\phi(1020)$ and their higher mass excitations. The first error combines statistical and systematic uncertainties. The second one is due to the parametrization of the charged kaon form factor and mass calibration.

$\Gamma(K^0_L K^0_S) \times \Gamma(e^+e^-)/\Gamma_{total}$ — $\Gamma_2\Gamma_8/\Gamma$

VALUE (keV)	EVTS	DOCUMENT ID		TECN	COMMENT
0.4200±0.0033±0.0123	28k	[1] LEES	14H	BABR	$e^+e^- \to K^0_S K^0_L\gamma$

[1] Using a vector meson dominance model with contribution from $\phi(1020)$ and higher mass excitations of $\rho(770)$, $\omega(782)$, and $\phi(1020)$.

$[\Gamma(\rho\pi) + \Gamma(\pi^+\pi^-\pi^0)] \times \Gamma(e^+e^-)/\Gamma_{total}$ — $\Gamma_3\Gamma_8/\Gamma$

VALUE (eV)	DOCUMENT ID		TECN	COMMENT
184.1±2.1±8.0	[1] LEES	21B	BABR	$10.5\ e^+e^- \to \pi^+\pi^-\pi^0\gamma$

[1] From the cross section for $e^+e^- \to \pi^+\pi^-\pi^0$ with contributions from $\rho(770)$, $\omega(782)$, $\phi(1020)$, $\omega(1420)$, and $\omega(1650)$.

$\phi(1020)$ $\Gamma(i)\Gamma(e^+e^-)/\Gamma^2(total)$

$\Gamma(K^+K^-)/\Gamma_{total} \times \Gamma(e^+e^-)/\Gamma_{total}$ — $\Gamma_1/\Gamma \times \Gamma_8/\Gamma$

VALUE (units 10^{-5})	EVTS	DOCUMENT ID		TECN	COMMENT
14.85 ±0.30 OUR FIT Error includes scale factor of 1.6.					
14.6 ±0.5 OUR AVERAGE Error includes scale factor of 1.8. See the ideogram below.					
15.789 ± 0.541	1.7M	KOZYREV	18	CMD3	$e^+e^- \to K^+K^-$
$14.27 \pm 0.05 \pm 0.31$	542k	AKHMETSHIN	08	CMD2	$1.02\ e^+e^- \to K^+K^-$
$13.93 \pm 0.14 \pm 0.99$	1000k	[1] ACHASOV	01E	SND	$e^+e^- \to K^+K^-$, $K_S K_L$, $\pi^+\pi^-\pi^0$

[1] From the combined fit assuming that the total $\phi(1020)$ production cross section is saturated by those of K^+K^-, $K_S K_L$, $\pi^+\pi^-\pi^0$, and $\eta\gamma$ decays modes and using ACHASOV 00B for the $\eta\gamma$ decay mode.

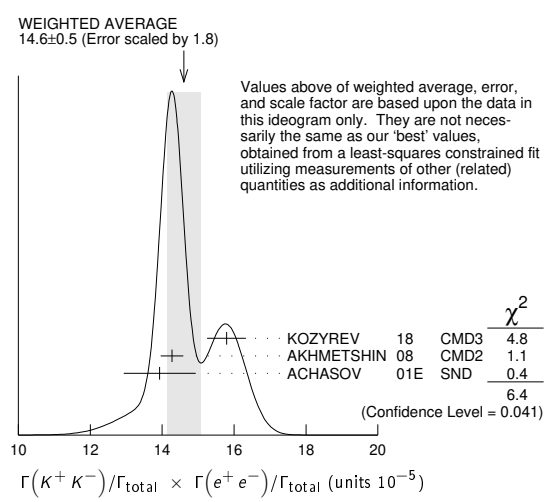

$\Gamma(K^0_L K^0_S)/\Gamma_{total} \times \Gamma(e^+e^-)/\Gamma_{total}$ — $\Gamma_2/\Gamma \times \Gamma_8/\Gamma$

VALUE (units 10^{-5})	EVTS	DOCUMENT ID		TECN	COMMENT
9.96 ±0.08 OUR FIT					
9.93 ±0.08 OUR AVERAGE					
$9.83 \pm 0.04 \pm 0.10$		DRUZHININ	25	SND	$e^+e^- \to K^0_L K^0_S$
10.078 ± 0.223	610k	[1] KOZYREV	16	CMD3	$e^+e^- \to K^0_S K^0_L$

Int. J. Mod. Phys. A 2026.41. Downloaded from www.worldscientific.com
by UNIVERSITY OF CALIFORNIA @ BERKELEY on 09/16/26. Re-use and distribution is strictly not permitted, except for Open Access articles.

10.01 ±0.04 ±0.17	272k	[2] AKHMETSHIN 04	CMD2	$e^+e^- \to K^0_L K^0_S$
10.27 ±0.07 ±0.34	500k	[3] ACHASOV 01E	SND	$e^+e^- \to K^+K^-$, $K_S K_L$, $\pi^+\pi^-\pi^0$
• • • We do not use the following data for averages, fits, limits, etc. • • •				
9.85 ±0.03 ±0.10	1.28M	[4,5] ACHASOV 24	SND	$e^+e^- \to K^0_L K^0_S$

[1] KOZYREV 16 also reports $\Gamma(e^+e^-)$ B($\phi \to K^0_S K^0_L$) = (0.428 ± 0.001 ± 0.009) keV.
[2] Update of AKHMETSHIN 99D
[3] From the combined fit assuming that the total $\phi(1020)$ production cross section is saturated by those of K^+K^-, $K_S K_L$, $\pi^+\pi^-\pi^0$, and $\eta\gamma$ decays modes and using ACHASOV 00B for the $\eta\gamma$ decay mode.
[4] From a fit of the cross section in the energy region $1.000 < \sqrt{s} < 1.100$ GeV using a vector meson dominance model with contribution from $\phi(1020)$, $\rho(770)$, $\omega(782)$ and higher vector resonances.
[5] Superseded by DRUZHININ 25.

$[\Gamma(\rho\pi) + \Gamma(\pi^+\pi^-\pi^0)]/\Gamma_{total} \times \Gamma(e^+e^-)/\Gamma_{total}$ — $\Gamma_3/\Gamma \times \Gamma_8/\Gamma$

VALUE (units 10^{-5})	EVTS	DOCUMENT ID		TECN	COMMENT
4.35 ±0.13 OUR FIT Error includes scale factor of 1.4.					
4.51 ±0.14 OUR AVERAGE					
4.51 ±0.16 ±0.11	105k	AKHMETSHIN 06		CMD2	0.98–1.06 $e^+e^- \to \pi^+\pi^-\pi^0$
4.665±0.042±0.261	400k	[1] ACHASOV 01E		SND	$e^+e^- \to K^+K^-$, $K_S K_L$, $\pi^+\pi^-\pi^0$
4.35 ±0.27 ±0.08	11169	[2] AKHMETSHIN 98		CMD2	$e^+e^- \to \pi^+\pi^-\pi^0$
• • • We do not use the following data for averages, fits, limits, etc. • • •					
4.38 ±0.12		BENAYOUN 10		RVUE	0.4–1.05 e^+e^-
4.30 ±0.08 ±0.21		[3] AUBERT,B 04N		BABR	10.6 $e^+e^- \to \pi^+\pi^-\pi^0\gamma$

[1] From the combined fit assuming that the total $\phi(1020)$ production cross section is saturated by those of K^+K^-, $K_S K_L$, $\pi^+\pi^-\pi^0$, and $\eta\gamma$ decays modes and using ACHASOV 00B for the $\eta\gamma$ decay mode.
[2] Recalculated by us from the cross section in the peak.
[3] Superseeded by LEES 21B.

$\Gamma(\eta\gamma)/\Gamma_{total} \times \Gamma(e^+e^-)/\Gamma_{total}$ — $\Gamma_5/\Gamma \times \Gamma_8/\Gamma$

VALUE (units 10^{-6})	EVTS	DOCUMENT ID		TECN	COMMENT
3.87 ±0.07 OUR FIT Error includes scale factor of 1.2.					
3.93 ±0.09 OUR AVERAGE Error includes scale factor of 1.3. See the ideogram below.					
4.050±0.067±0.118	33k	[1] ACHASOV 07B		SND	0.6–1.38 $e^+e^- \to \eta\gamma$
$4.093^{+0.040}_{-0.043}$±0.247	17.4k	[2] AKHMETSHIN 05		CMD2	0.60–1.38 $e^+e^- \to \eta\gamma$
3.850±0.041±0.159	23k	[3,4] AKHMETSHIN 01B		CMD2	$e^+e^- \to \eta\gamma$
4.00 ±0.04 ±0.11		[5] ACHASOV 00		SND	$e^+e^- \to \eta\gamma$
3.53 ±0.08 ±0.17	2200	[6,7] AKHMETSHIN 99F		CMD2	$e^+e^- \to \eta\gamma$
• • • We do not use the following data for averages, fits, limits, etc. • • •					
4.19 ±0.06		[8] BENAYOUN 10		RVUE	0.4–1.05 e^+e^-

[1] From a combined fit of $\sigma(e^+e^- \to \eta\gamma)$ with $\eta \to 3\pi^0$ and $\eta \to \pi^+\pi^-\pi^0$, and fixing B($\eta \to 3\pi^0$) / B($\eta \to \pi^+\pi^-\pi^0$) = 1.44 ± 0.04. Recalculated by us from the cross section at the peak. Supersedes ACHASOV 00D and ACHASOV 06A.
[2] From the $\eta \to 2\gamma$ decay and using B($\eta \to \gamma\gamma$) = 39.43 ± 0.26%.
[3] From the $\eta \to 3\pi^0$ decay and using B($\eta \to 3\pi^0$)= (32.24 ± 0.29) × 10^{-2}.
[4] The combined fit from 600 to 1380 MeV taking into account $\rho(770)$, $\omega(782)$, $\phi(1020)$, and $\rho(1450)$ (mass and width fixed at 1450 MeV and 310 MeV respectively).
[5] From the $\eta \to 2\gamma$ decay and using B($\eta \to 2\gamma$) =(39.21 ± 0.34) × 10^{-2}.
[6] Recalculated by the authors from the cross section in the peak.
[7] From the $\eta \to \pi^+\pi^-\pi^0$ decay and using B($\eta \to \pi^+\pi^-\pi^0$) =(23.1 ± 0.5) × 10^{-2}.
[8] A simultaneous fit of $e^+e^- \to \pi^+\pi^-$, $\pi^+\pi^-\pi^0$, $\pi^0\gamma$, $\eta\gamma$ data.

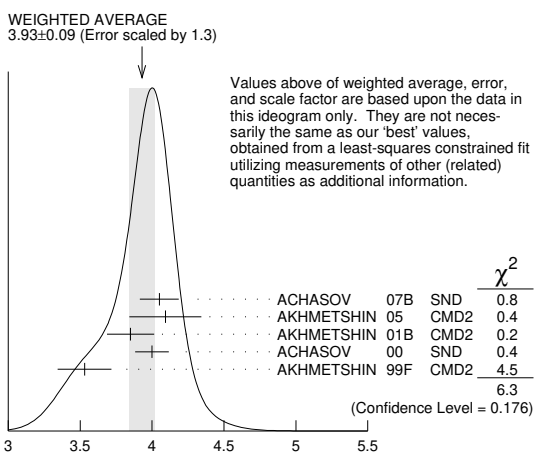

$\Gamma(\pi^0\gamma)/\Gamma_{total} \times \Gamma(e^+e^-)/\Gamma_{total}$ — $\Gamma_6/\Gamma \times \Gamma_8/\Gamma$

VALUE (units 10^{-7})	EVTS	DOCUMENT ID		TECN	COMMENT
3.94±0.16 OUR FIT					
3.95±0.17 OUR AVERAGE					
4.04±0.09±0.19		[1] ACHASOV 16A		SND	0.60–1.38 $e^+e^- \to \pi^0\gamma$
3.75±0.11±0.29	18k	AKHMETSHIN 05		CMD2	0.60–1.38 $e^+e^- \to \pi^0\gamma$
• • • We do not use the following data for averages, fits, limits, etc. • • •					
4.29±0.11		[2] BENAYOUN 10		RVUE	0.4–1.05 e^+e^-
$3.67\pm0.10^{+0.27}_{-0.25}$		[3] ACHASOV 00		SND	$e^+e^- \to \pi^0\gamma$

[1] From the VMD model with the interfering $\rho(770)$, $\omega(782)$, $\phi(1020)$ resonances, and an additional resonance describing the total contribution of the $\rho(1450)$ and $\omega(1420)$ states. Supersedes ACHASOV 00.
[2] A simultaneous fit of $e^+e^- \to \pi^+\pi^-$, $\pi^+\pi^-\pi^0$, $\pi^0\gamma$, $\eta\gamma$ data.
[3] From the $\pi^0 \to 2\gamma$ decay and using B($\pi^0 \to 2\gamma$) = (98.798 ± 0.032) × 10^{-2}.

$\Gamma(\mu^+\mu^-)/\Gamma_{total} \times \Gamma(e^+e^-)/\Gamma_{total}$ — $\Gamma_9/\Gamma \times \Gamma_8/\Gamma$

VALUE (units 10^{-8})	DOCUMENT ID		TECN	COMMENT
8.5 ±0.6 OUR FIT Error includes scale factor of 1.2.				
8.8 ±0.9 OUR AVERAGE Error includes scale factor of 1.5. See the ideogram below.				
8.36±0.59±0.37	ACHASOV 01G		SND	$e^+e^- \to \mu^+\mu^-$
9.9 ±1.4 ±0.9	[1] ACHASOV 99C		SND	$e^+e^- \to \mu^+\mu^-$
14.4 ±3.0	[2] VASSERMAN 81		OLYA	$e^+e^- \to \mu^+\mu^-$
8.6 ±5.9	[2] AUGUSTIN 73		OSPK	$e^+e^- \to \mu^+\mu^-$

[1] Recalculated by the authors from the cross section in the peak.
[2] Recalculated by us from the cross section in the peak.

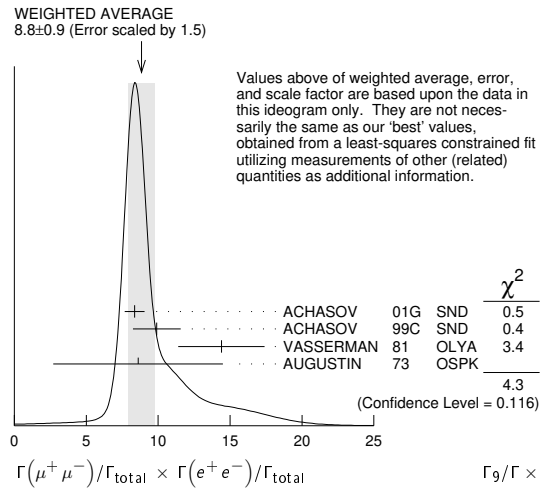

$\Gamma(\pi^+\pi^-)/\Gamma_{total} \times \Gamma(e^+e^-)/\Gamma_{total}$ — $\Gamma_{11}/\Gamma \times \Gamma_8/\Gamma$

VALUE (units 10^{-8})	EVTS	DOCUMENT ID		TECN	COMMENT
2.8 ±0.6 OUR FIT Error includes scale factor of 2.0.					
2.8 ±0.5 OUR AVERAGE Error includes scale factor of 1.8. See the ideogram below.					
3.51±0.33±0.24	34M	[1] IGNATOV 24		CMD3	$e^+e^- \to \pi^+\pi^-$
2.1 ±0.3 ±0.3		[2] ACHASOV 00C		SND	$e^+e^- \to \pi^+\pi^-$
$1.95^{+1.15}_{-0.87}$		[3] GOLUBEV 86		ND	$e^+e^- \to \pi^+\pi^-$
$6.01^{+3.19}_{-2.51}$		[3] VASSERMAN 81		OLYA	$e^+e^- \to \pi^+\pi^-$
• • • We do not use the following data for averages, fits, limits, etc. • • •					
3.31±0.99		[4] BENAYOUN 13		RVUE	0.4–1.05 e^+e^-

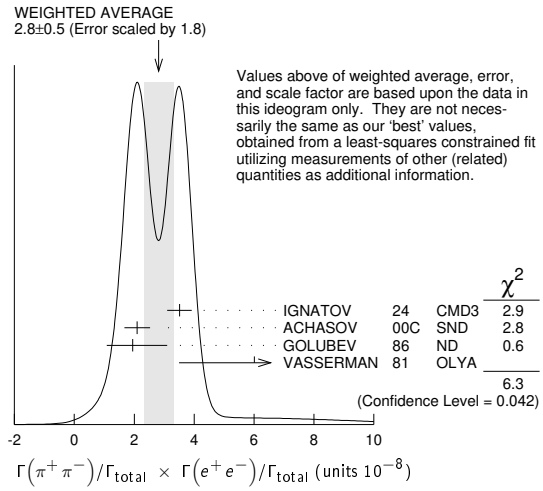

Int. J. Mod. Phys. A 2026.41. Downloaded from www.worldscientific.com
by [redacted]LIFORNIA @ BERKELEY on 09/16/26. Re-use and distribution is strictly not permitted, except for Open Access articles.

Int. J. Mod. Phys. A 2026.41. Downloaded from www.worldscientific.com by UNIVERSITY OF CALIFORNIA @ BERKELEY on 09/16/26. Re-use and distribution is strictly not permitted, except for Open Access articles.

[1] From a fit of the pion form factor in the energy range $0.32 < \sqrt{s} < 1.2$ GeV using the GOUNARIS 68 parametrization with the complex phase of the $\rho-\omega$ interference with ω and ϕ masses and widths constrained by the values and their errors from PDG 22, and leaving $\rho(1450)$, $\rho(1700)$ resonances as free parameters of the fit. A fit without the constraints from PDG 22 gives a value $\Gamma(e^+e^-)\times\Gamma(\pi^+\pi^-)/\Gamma^2_{\rm total} = (3.65\pm0.24)\times10^{-8}$.

[2] Recalculated by the authors from the cross section in the peak.

[3] Recalculated by us from the cross section in the peak.

[4] A simultaneous fit to $e^+e^-\to\pi^+\pi^-$, $\pi^+\pi^-\pi^0$, $\pi^0\gamma$, $\eta\gamma$, $K\overline{K}$, and $\tau^-\to\pi^-\pi^0\nu_\tau$ data.

$\Gamma(\omega\pi^0)/\Gamma_{\rm total}\times\Gamma(e^+e^-)/\Gamma_{\rm total}$ — $\Gamma_{12}/\Gamma\times\Gamma_8/\Gamma$

VALUE (units 10^{-8})	DOCUMENT ID	TECN	COMMENT
1.40±0.15 OUR FIT			
1.37±0.17±0.01	[1,2] AMBROSINO 08G	KLOE	$e^+e^-\to\pi^+\pi^-2\pi^0$, $2\pi^0\gamma$

[1] Recalculated by the authors from the cross section at the peak.

[2] AMBROSINO 08G reports $[\Gamma(\phi(1020)\to\omega\pi^0)/\Gamma_{\rm total}\times\Gamma(\phi(1020)\to e^+e^-)/\Gamma_{\rm total}]\times[B(\omega(782)\to\pi^+\pi^-\pi^0)] = (1.22\pm0.13\pm0.08)\times10^{-8}$ which we divide by our best (shown rounded) value $B(\omega(782)\to\pi^+\pi^-\pi^0) = (89.2\pm0.7)\times10^{-2}$. Our first error is their experiment's error and our second error is the systematic error from using our best (shown rounded) value.

$\Gamma(\pi^0\pi^0\gamma)/\Gamma_{\rm total}\times\Gamma(e^+e^-)/\Gamma_{\rm total}$ — $\Gamma_{17}/\Gamma\times\Gamma_8/\Gamma$

VALUE (units 10^{-8})	DOCUMENT ID	TECN	COMMENT
3.34±0.17 OUR FIT			
$\mathbf{3.33^{+0.04+0.19}_{-0.09-0.20}}$	[1] AMBROSINO 07	KLOE	$e^+e^-\to\pi^0\pi^0\gamma$

[1] Calculated by the authors from the cross section at the peak.

$\Gamma(\pi^+\pi^-\pi^+\pi^-)/\Gamma_{\rm total}\times\Gamma(e^+e^-)/\Gamma_{\rm total}$ — $\Gamma_{18}/\Gamma\times\Gamma_8/\Gamma$

VALUE (units 10^{-9})	EVTS	DOCUMENT ID	TECN	COMMENT
$\mathbf{1.2\ ^{+0.8}_{-0.7}}$ **OUR FIT**				
1.17±0.52±0.64	3285	[1] AKHMETSHIN 00E	CMD2	$e^+e^-\to\pi^+\pi^-\pi^+\pi^-$

[1] Recalculated by the authors from the cross section in the peak.

$\phi(1020)$ BRANCHING RATIOS

$\Gamma(K^+K^-)/\Gamma_{\rm total}$ — Γ_1/Γ

VALUE	EVTS	DOCUMENT ID	TECN	COMMENT
0.501±0.006 OUR FIT Error includes scale factor of 1.6.				
0.493±0.010 OUR AVERAGE				
0.492±0.012	2913	AKHMETSHIN 95	CMD2	$e^+e^-\to K^+K^-$
0.44 ±0.05	321	KALBFLEISCH 76	HBC	2.18 $K^-p\to\Lambda K^+K^-$
0.49 ±0.06	270	DEGROOT 74	HBC	4.2 $K^-p\to\Lambda\phi$
0.540±0.034	565	BALAKIN 71	OSPK	$e^+e^-\to K^+K^-$
0.48 ±0.04	252	LINDSEY 66	HBC	2.1–2.7 $K^-p\to\Lambda K^+K^-$
• • • We do not use the following data for averages, fits, limits, etc. • • •				
0.493±0.003±0.007		[1] AKHMETSHIN 11	CMD2	1.02 $e^+e^-\to K^+K^-$
0.476±0.017	1000k	[2] ACHASOV 01E	SND	$e^+e^-\to K^+K^-$, K_SK_L, $\pi^+\pi^-\pi^0$

[1] Combined analysis of the CMD-2 data on $\phi\to K^+K^-$, $K^0_SK^0_L$, $\pi^+\pi^-\pi^0$, $\eta\gamma$ assuming that the sum of their branching fractions is 0.99741 ± 0.00007.

[2] Using $B(\phi\to e^+e^-) = (2.93\pm0.14)\times10^{-4}$.

$\Gamma(K^0_LK^0_S)/\Gamma_{\rm total}$ — Γ_2/Γ

VALUE	EVTS	DOCUMENT ID	TECN	COMMENT
0.336±0.004 OUR FIT Error includes scale factor of 1.3.				
0.331±0.009 OUR AVERAGE				
0.335±0.010	40644	AKHMETSHIN 95	CMD2	$e^+e^-\to K^0_LK^0_S$
0.326±0.035		DOLINSKY 91	ND	$e^+e^-\to K^0_LK^0_S$
0.310±0.024		DRUZHININ 84	ND	$e^+e^-\to K^0_LK^0_S$
• • • We do not use the following data for averages, fits, limits, etc. • • •				
0.336±0.002±0.006		[1] AKHMETSHIN 11	CMD2	1.02 $e^+e^-\to K^0_SK^0_L$
0.351±0.013	500k	[2] ACHASOV 01E	SND	$e^+e^-\to K^+K^-$, K_SK_L, $\pi^+\pi^-\pi^0$
0.27 ±0.03	133	KALBFLEISCH 76	HBC	2.18 $K^-p\to\Lambda K^0_LK^0_S$
0.257±0.030	95	[3] BALAKIN 71	OSPK	$e^+e^-\to K^0_LK^0_S$
0.40 ±0.04	167	LINDSEY 66	HBC	2.1–2.7 $K^-p\to\Lambda K^0_LK^0_S$

[1] Combined analysis of the CMD-2 data on $\phi\to K^+K^-$, $K^0_SK^0_L$, $\pi^+\pi^-\pi^0$, $\eta\gamma$ assuming that the sum of their branching fractions is 0.99741 ± 0.00007.

[2] Using $B(\phi\to e^+e^-) = (2.93\pm0.14)\times10^{-4}$.

[3] Balakin error increased by Paul.

$\Gamma(K^0_LK^0_S)/\Gamma(K^+K^-)$ — Γ_2/Γ_1

VALUE (units 10^{-2})	EVTS	DOCUMENT ID	TECN	COMMENT
67.1± 1.4 OUR FIT Error includes scale factor of 1.5.				
74.0± 3.1 OUR AVERAGE				
70 ± 6	2732	BUKIN 78C	OLYA	$e^+e^-\to K^0_LK^0_S$
82 ± 8		LOSTY 78	HBC	4.2 $K^-p\to\phi$hyperon
71 ± 5		LAVEN 77	HBC	10 $K^-p\to K^+K^-\Lambda$
71 ± 8		LYONS 77	HBC	3–4 $K^-p\to\Lambda\phi$
89 ±10	144	AGUILAR-... 72B	HBC	3.9,4.6 K^-p
• • • We do not use the following data for averages, fits, limits, etc. • • •				
59.3± 2.3±2.1	665k	[1] ABLIKIM 25BR	BES3	$D^+_s\to\phi(\to K^0_SK^0_L)\pi^+$
64.4± 1.7		[2] DUBNICKA 24	RVUE	$e^+e^-\to K^+K^-$, $K^0_SK^0_L$
63.8± 2.2	2.3M	[3] KOZYREV 18	CMD3	$e^+e^-\to K^0_LK^0_S$, K^+K^-
68 ± 3		[4] AKHMETSHIN 95	CMD2	$e^+e^-\to K^0_LK^0_S$, K^+K^-

[1] From a measurement of $D^+_s\to\phi(\to K^0_SK^0_L)\pi^+$ using the PDG 24 value for $B(D^+_s\to\phi(\to K^+K^-)\pi^+)$.

[2] From a fit to CMD3, BABAR and BES3 data.

[3] The prediction taking into account phase-space difference, radiative corrections, isospin breaking, and the Sommerfeld-Gamow-Sakharov factor gives 0.630.

[4] Theoretical analysis of BRAMON 00 taking into account phase-space difference, electromagnetic radiative corrections, as well as isospin breaking, predicts 0.62. FLOREZ-BAEZ 08 predicts 0.63 considering also structure-dependent radiative corrections. FISCHBACH 02 calculates additional corrections caused by the close threshold and predicts 0.68. See also BENAYOUN 01 and DUBYNSKIY 07. BENAYOUN 12 obtains 0.71±0.01 in the HLS model.

$\Gamma(K^0_LK^0_S)/\Gamma(K\overline{K})$ — $\Gamma_2/(\Gamma_1+\Gamma_2)$

VALUE	EVTS	DOCUMENT ID	TECN	COMMENT
0.402±0.005 OUR FIT Error includes scale factor of 1.5.				
0.45 ±0.04 OUR AVERAGE				
0.44 ±0.07		[1] LONDON 66	HBC	2.24 $K^-p\to\Lambda K\overline{K}$
0.48 ±0.07	52	BADIER 65B	HBC	3 K^-p
0.40 ±0.10	34	SCHLEIN 63	HBC	1.95 $K^-p\to\Lambda K\overline{K}$

[1] This is probably not affected by their controversial background subtraction; the value is from their numbers of K_1K_2 vs K^+K^- events.

$[\Gamma(\rho\pi)+\Gamma(\pi^+\pi^-\pi^0)]/\Gamma_{\rm total}$ — Γ_3/Γ

VALUE	EVTS	DOCUMENT ID	TECN	COMMENT
0.147±0.004 OUR FIT Error includes scale factor of 1.5.				
0.151±0.009 OUR AVERAGE Error includes scale factor of 1.7.				
0.161±0.008	11761	AKHMETSHIN 95	CMD2	$e^+e^-\to\pi^+\pi^-\pi^0$
0.143±0.007		DOLINSKY 91	ND	$e^+e^-\to\pi^+\pi^-\pi^0$
• • • We do not use the following data for averages, fits, limits, etc. • • •				
0.155±0.002±0.005		[1] AKHMETSHIN 11	CMD2	1.02 $e^+e^-\to\pi^+\pi^-\pi^0$
0.159±0.008	400k	[2] ACHASOV 01E	SND	$e^+e^-\to K^+K^-$, K_SK_L, $\pi^+\pi^-\pi^0$
0.145±0.009±0.003	11169	[3] AKHMETSHIN 98	CMD2	$e^+e^-\to\pi^+\pi^-\pi^0$
0.139±0.007		[4] PARROUR 76B	OSPK	e^+e^-

[1] Combined analysis of the CMD-2 data on $\phi\to K^+K^-$, $K^0_SK^0_L$, $\pi^+\pi^-\pi^0$, $\eta\gamma$ assuming that the sum of their branching fractions is 0.99741 ± 0.00007.

[2] Using $B(\phi\to e^+e^-) = (2.93\pm0.14)\times10^{-4}$.

[3] Using $B(\phi\to e^+e^-) = (2.99\pm0.08)\times10^{-4}$.

[4] Using $\Gamma(\phi) = 4.1$ MeV. If interference between the $\rho\pi$ and 3π modes is neglected, the fraction of the $\rho\pi$ is more than 80% at the 90% confidence level.

$[\Gamma(\rho\pi)+\Gamma(\pi^+\pi^-\pi^0)]/\Gamma(K^+K^-)$ — Γ_3/Γ_1

VALUE	EVTS	DOCUMENT ID	TECN	COMMENT
0.293±0.011 OUR FIT Error includes scale factor of 1.6.				
0.229±0.014 OUR AVERAGE				
0.230±0.014±0.010		[1] ABLIKIM 25A	BES3	$D^+_s\to\phi\pi^+$
0.222±0.019±0.016		[2] ABLIKIM 25F	BES3	$D^+_s\to\phi\rho^+$
0.28 ±0.09	34	AGUILAR-... 72B	HBC	3.9,4.6 K^-p

[1] Using ABLIKIM 21AE.

[2] Using ABLIKIM 21U.

$[\Gamma(\rho\pi)+\Gamma(\pi^+\pi^-\pi^0)]/\Gamma(K\overline{K})$ — $\Gamma_3/(\Gamma_1+\Gamma_2)$

VALUE	DOCUMENT ID	TECN	COMMENT
0.175±0.006 OUR FIT Error includes scale factor of 1.5.			
0.24 ±0.04 OUR AVERAGE			
0.237±0.039	CERRADA 77B	HBC	4.2 $K^-p\to\Lambda3\pi$
0.30 ±0.15	LONDON 66	HBC	2.24 $K^-p\to\Lambda\pi^+\pi^-\pi^0$

$[\Gamma(\rho\pi)+\Gamma(\pi^+\pi^-\pi^0)]/\Gamma(K^0_LK^0_S)$ — Γ_3/Γ_2

VALUE	EVTS	DOCUMENT ID	TECN	COMMENT
0.437±0.013 OUR FIT Error includes scale factor of 1.4.				
0.51 ±0.05 OUR AVERAGE				
0.56 ±0.07	3681	BUKIN 78C	OLYA	$e^+e^-\to K^0_LK^0_S$, $\pi^+\pi^-\pi^0$
0.47 ±0.06	516	COSME 74	OSPK	$e^+e^-\to\pi^+\pi^-\pi^0$

$\Gamma(\pi^+\pi^-\pi^0)/\Gamma_{\rm total}$ — Γ_4/Γ

VALUE	CL%	EVTS	DOCUMENT ID	TECN	COMMENT
• • • We do not use the following data for averages, fits, limits, etc. • • •					
≃ 0.0087		1.98M	[1,2] ALOISIO 03	KLOE	1.02 $e^+e^-\to\pi^+\pi^-\pi^0$
<0.0006	90		[3] ACHASOV 02	SND	1.02 $e^+e^-\to\pi^+\pi^-\pi^0$
<0.23	90		[3] CORDIER 80	DM1	$e^+e^-\to\pi^+\pi^-\pi^0$
<0.20	90		[3] PARROUR 76B	OSPK	$e^+e^-\to\pi^+\pi^-\pi^0$

[1] From a fit without limitations on charged and neutral ρ masses and widths.

[2] Adding the direct and $\omega\pi$ contributions and considering the interference between the $\rho\pi$ and $\pi^+\pi^-\pi^0$.

[3] Neglecting the interference between the $\rho\pi$ and $\pi^+\pi^-\pi^0$.

Int. J. Mod. Phys. A 2026.41. Downloaded from www.worldscientific.com by CALIFORNIA @ BERKELEY on 09/16/26. Re-use and distribution is strictly not permitted, except for Open Access articles.

$\Gamma(\eta\gamma)/\Gamma_{total}$ — Γ_5/Γ

VALUE (units 10^{-2})	EVTS	DOCUMENT ID		TECN	COMMENT
1.306±0.024 OUR FIT	Error includes scale factor of 1.2.				
1.26 ±0.04 OUR AVERAGE					
1.246±0.025±0.057	10k	[1] ACHASOV	98F	SND	$e^+e^- \to 7\gamma$
1.18 ±0.11	279	[2] AKHMETSHIN	95	CMD2	$e^+e^- \to \pi^+\pi^- 3\gamma$
1.30 ±0.06		[3] DRUZHININ	84	ND	$e^+e^- \to 3\gamma$
1.4 ±0.2		[4] DRUZHININ	84	ND	$e^+e^- \to 6\gamma$
0.88 ±0.20	290	KURDADZE	83C	OLYA	$e^+e^- \to 3\gamma$
1.35 ±0.29		ANDREWS	77	CNTR	6.7–10 γCu
1.5 ±0.4	54	[3] COSME	76	OSPK	e^+e^-
• • • We do not use the following data for averages, fits, limits, etc. • • •					
1.38 ±0.02 ±0.02		[5] AKHMETSHIN	11	CMD2	$1.02\ e^+e^- \to \eta\gamma$
1.37 ±0.05 ±0.02	33k	[6] ACHASOV	07B	SND	0.6–$1.38\ e^+e^- \to \eta\gamma$
1.373±0.014±0.085	17.4k	[7,8] AKHMETSHIN	05	CMD2	0.60–$1.38\ e^+e^- \to \eta\gamma$
1.287±0.013±0.063		[9,10] AKHMETSHIN	01B	CMD2	$e^+e^- \to \eta\gamma$
1.338±0.012±0.052		[11] ACHASOV	00	SND	$e^+e^- \to \eta\gamma$
1.18 ±0.03 ±0.06	2200	[12] AKHMETSHIN	99F	CMD2	$e^+e^- \to \eta\gamma$
1.21 ±0.07		[13] BENAYOUN	96	RVUE	0.54–$1.04\ e^+e^- \to \eta\gamma$

[1] Using $B(\phi \to e^+e^-) = (2.99 \pm 0.08) \times 10^{-4}$ and $B(\eta \to 3\pi^0) = (32.2 \pm 0.4) \times 10^{-2}$.
[2] From $\pi^+\pi^-\pi^0$ decay mode of η.
[3] From 2γ decay mode of η.
[4] From $3\pi^0$ decay mode of η.
[5] Combined analysis of the CMD-2 data on $\phi \to K^+K^-$, $K^0_S K^0_L$, $\pi^+\pi^-\pi^0$, $\eta\gamma$ assuming that the sum of their branching fractions is 0.99741 ± 0.00007.
[6] ACHASOV 07B reports $[\Gamma(\phi(1020) \to \eta\gamma)/\Gamma_{total}] \times [B(\phi(1020) \to e^+e^-)] = (4.050 \pm 0.067 \pm 0.118) \times 10^{-6}$ which we divide by our best (shown rounded) value $B(\phi(1020) \to e^+e^-) = (2.963 \pm 0.034) \times 10^{-4}$. Our first error is their experiment's error and our second error is the systematic error from using our best (shown rounded) value. Supersedes ACHASOV 00D and ACHASOV 06A.
[7] Using $B(\phi \to e^+e^-) = (2.98 \pm 0.04) \times 10^{-4}$ and $B(\eta \to \gamma\gamma) = 39.43 \pm 0.26\%$.
[8] Not independent of the corresponding $\Gamma(e^+e^-) \times \Gamma(\eta\gamma)/\Gamma^2_{total}$.
[9] Using $B(\phi \to e^+e^-) = (2.99 \pm 0.08) \times 10^{-4}$ and $B(\eta \to 3\pi^0) = (32.24 \pm 0.29) \times 10^{-2}$.
[10] The combined fit from 600 to 1380 MeV taking into account $\rho(770)$, $\omega(782)$, $\phi(1020)$, and $\rho(1450)$ (mass and width fixed at 1450 MeV and 310 MeV respectively).
[11] From the $\eta \to 2\gamma$ decay and using $B(\phi \to e^+e^-) = (2.99 \pm 0.08) \times 10^{-4}$.
[12] From $\pi^+\pi^-\pi^0$ decay mode of η and using $B(\phi \to e^+e^-) = (2.99 \pm 0.08) \times 10^{-4}$.
[13] Reanalysis of DRUZHININ 84, DOLINSKY 89, and DOLINSKY 91 taking into account a triangle anomaly contribution.

$\Gamma(\pi^0\gamma)/\Gamma_{total}$ — Γ_6/Γ

VALUE (units 10^{-3})	EVTS	DOCUMENT ID		TECN	COMMENT
1.33 ±0.05 OUR FIT					
1.31 ±0.13 OUR AVERAGE					
1.30 ±0.13		DRUZHININ	84	ND	$e^+e^- \to 3\gamma$
1.4 ±0.5	32	COSME	76	OSPK	e^+e^-
• • • We do not use the following data for averages, fits, limits, etc. • • •					
1.367±0.072		[1] ACHASOV	16A	SND	0.60–$1.38\ e^+e^- \to \pi^0\gamma$
1.258±0.037±0.077	18k	[2,3] AKHMETSHIN	05	CMD2	0.60-$1.38\ e^+e^- \to \pi^0\gamma$
$1.226 \pm 0.036^{+0.096}_{-0.089}$		[4] ACHASOV	00	SND	$e^+e^- \to \pi^0\gamma$
1.26 ±0.17		[5] BENAYOUN	96	RVUE	0.54-$1.04\ e^+e^- \to \pi^0\gamma$

[1] Using $B(\phi \to e^+e^-)$ from PDG 15. Supersedes ACHASOV 00.
[2] Using $B(\phi \to e^+e^-) = (2.98 \pm 0.04) \times 10^{-4}$.
[3] Not independent of the corresponding $\Gamma(e^+e^-) \times \Gamma(\pi^0\gamma)/\Gamma^2_{total}$.
[4] From the $\pi^0 \to 2\gamma$ decay and using $B(\phi \to e^+e^-) = (2.99 \pm 0.08) \times 10^{-4}$.
[5] Reanalysis of DRUZHININ 84, DOLINSKY 89, and DOLINSKY 91 taking into account a triangle anomaly contribution.

$\Gamma(\eta\gamma)/\Gamma(\pi^0\gamma)$ — Γ_5/Γ_6

VALUE	DOCUMENT ID		TECN	COMMENT
• • • We do not use the following data for averages, fits, limits, etc. • • •				
$10.9 \pm 0.3^{+0.7}_{-0.8}$	ACHASOV	00	SND	$e^+e^- \to \eta\gamma, \pi^0\gamma$

$\Gamma(e^+e^-)/\Gamma_{total}$ — Γ_8/Γ

VALUE (units 10^{-4})	EVTS	DOCUMENT ID		TECN	COMMENT
2.963±0.034 OUR FIT	Error includes scale factor of 1.4.				
2.98 ±0.07 OUR AVERAGE	Error includes scale factor of 1.1.				
2.93 ±0.14	1900k	[1] ACHASOV	01E	SND	$e^+e^- \to K^+K^-$, $K_S K_L$, $\pi^+\pi^-\pi^0$
2.88 ±0.09	55600	AKHMETSHIN	95	CMD2	$e^+e^- \to$ hadrons
3.00 ±0.21	3681	BUKIN	78C	OLYA	$e^+e^- \to$ hadrons
3.10 ±0.14		[2] PARROUR	76	OSPK	e^+e^-
3.3 ±0.3		COSME	74	OSPK	$e^+e^- \to$ hadrons
2.81 ±0.25	681	BALAKIN	71	OSPK	$e^+e^- \to$ hadrons
3.50 ±0.27		CHATELUS	71	OSPK	e^+e^-

[1] From the combined fit assuming that the total $\phi(1020)$ production cross section is saturated by those of K^+K^-, $K_S K_L$, $\pi^+\pi^-\pi^0$, and $\eta\gamma$ decays modes and using ACHASOV 00B for the $\eta\gamma$ decay mode.
[2] Using total width 4.2 MeV. They detect 3π mode and observe significant interference with ω tail. This is accounted for in the result quoted above.

$\Gamma(\mu^+\mu^-)/\Gamma_{total}$ — Γ_9/Γ

VALUE (units 10^{-4})	DOCUMENT ID		TECN	COMMENT
2.86 ±0.22 OUR FIT	Error includes scale factor of 1.2.			
2.96 ±0.16 OUR AVERAGE	Error includes scale factor of 1.1.			
2.69 ±0.46	[1] HAYES	71	CNTR	8.3,9.8 γC $\to \mu^+\mu^-$X
2.17 ±0.60	[1] EARLES	70	CNTR	6.0 γC $\to \mu^+\mu^-$X
• • • We use the following data for averages but not for fits. • • •				
3.045±0.049±0.148	[2] AAIJ	24B	LHCB	D^+, $D^+_s \to \pi^+\phi$
• • • We do not use the following data for averages, fits, limits, etc. • • •				
2.87 ±0.20 ±0.14	[3] ACHASOV	01G	SND	$e^+e^- \to \mu^+\mu^-$
3.30 ±0.45 ±0.32	[4] ACHASOV	99C	SND	$e^+e^- \to \mu^+\mu^-$
4.83 ±1.02	[5] VASSERMAN	81	OLYA	$e^+e^- \to \mu^+\mu^-$
2.87 ±1.98	[5] AUGUSTIN	73	OSPK	$e^+e^- \to \mu^+\mu^-$

[1] Neglecting interference between resonance and continuum.
[2] Value not independent from the measurement of $B(\phi \to \mu^+\mu^-)/B(\phi \to e^+e^-)$.
[3] Using $B(\phi \to e^+e^-) = (2.91 \pm 0.07) \times 10^{-4}$.
[4] Using $B(\phi \to e^+e^-) = (2.99 \pm 0.08) \times 10^{-4}$.
[5] Recalculated by us using $B(\phi \to e^+e^-) = (2.99 \pm 0.08) \times 10^{-4}$.

$\Gamma(\mu^+\mu^-)/\Gamma(e^+e^-)$ — Γ_9/Γ_8

VALUE	EVTS	DOCUMENT ID		TECN	COMMENT
1.022±0.012±0.048	24k	AAIJ	24B	LHCB	D^+, $D^+_s \to \pi^+\phi$
• • • We do not use the following data for averages, fits, limits, etc. • • •					
1.026±0.020±0.056	7.5k	AAIJ	24B	LHCB	$D^+ \to \pi^+\phi$
1.017±0.013±0.051	16.7k	AAIJ	24B	LHCB	$D^+_s \to \pi^+\phi$

$\Gamma(\eta e^+e^-)/\Gamma_{total}$ — Γ_{10}/Γ

VALUE (units 10^{-4})	EVTS	DOCUMENT ID		TECN	COMMENT
1.08 ±0.04 OUR AVERAGE					
1.075±0.007±0.038	30k	[1] BABUSCI	15	KLOE	$1.02\ e^+e^- \to \eta e^+e^-$
1.19 ±0.19 ±0.12	213	[2] ACHASOV	01B	SND	$e^+e^- \to \eta e^+e^-$
1.14 ±0.10 ±0.06	355	[3] AKHMETSHIN	01	CMD2	$e^+e^- \to \eta e^+e^-$
• • • We do not use the following data for averages, fits, limits, etc. • • •					
1.13 ±0.14 ±0.07	183	[4] AKHMETSHIN	01	CMD2	$e^+e^- \to \eta e^+e^-$
1.21 ±0.14 ±0.09	130	[5] AKHMETSHIN	01	CMD2	$e^+e^- \to \eta e^+e^-$
1.04 ±0.20 ±0.08	42	[6] AKHMETSHIN	01	CMD2	$e^+e^- \to \eta e^+e^-$
$1.3\ ^{+0.8}_{-0.6}$	7	GOLUBEV	85	ND	$e^+e^- \to \eta e^+e^-$

[1] Using $B(\eta \to 3\pi^0) = (32.57 \pm 0.23)\%$ from PDG 12.
[2] Using $B(\eta \to \gamma\gamma) = (39.25 \pm 0.32)\%$, $B(\phi \to \eta\gamma) = (1.26 \pm 0.06)\%$, and $B(\phi \to e^+e^-) = (3.00 \pm 0.06) \times 10^{-4}$.
[3] The average of the branching ratios separately obtained from the $\eta \to \gamma\gamma$, $3\pi^0$, $\pi^+\pi^-\pi^0$ decays.
[4] From $\eta \to \gamma\gamma$ decays and using $B(\eta \to \gamma\gamma) = (39.33 \pm 0.25) \times 10^{-2}$, $B(\eta \to \pi^+\pi^-\gamma) = (4.75 \pm 11) \times 10^{-2}$, and $B(\phi \to \eta\gamma) = (1.297 \pm 0.033) \times 10^{-2}$.
[5] From $\eta \to 3\pi^0$ decays and using $B(\pi^0 \to \gamma\gamma) = (98.798 \pm 0.033) \times 10^{-2}$, $B(\eta \to 3\pi^0) = (32.24 \pm 0.29) \times 10^{-2}$, $B(\eta \to \pi^+\pi^-\gamma) = (4.75 \pm 0.11) \times 10^{-2}$, and $B(\phi \to \eta\gamma) = (1.297 \pm 0.033) \times 10^{-2}$.
[6] From $\eta \to \pi^+\pi^-\pi^0$ decays and using $B(\pi^0 \to \gamma\gamma) = (98.798 \pm 0.033) \times 10^{-2}$, $B(\pi^0 \to e^+e^-\gamma) = (1.198 \pm 0.032) \times 10^{-2}$, $B(\eta \to \pi^+\pi^-\pi^0) = (23.0 \pm 0.4) \times 10^{-2}$, $B(\phi \to \pi^+\pi^-\pi^0) = (15.5 \pm 0.6) \times 10^{-2}$, and $B(\phi \to \eta\gamma) = (1.297 \pm 0.033) \times 10^{-2}$.

$\Gamma(\pi^+\pi^-)/\Gamma_{total}$ — Γ_{11}/Γ

VALUE (units 10^{-4})	CL%	DOCUMENT ID		TECN	COMMENT
• • • We do not use the following data for averages, fits, limits, etc. • • •					
0.71±0.11±0.09		[1] ACHASOV	00C	SND	$e^+e^- \to \pi^+\pi^-$
$0.65\ ^{+0.38}_{-0.29}$		[1] GOLUBEV	86	ND	$e^+e^- \to \pi^+\pi^-$
$2.01\ ^{+1.07}_{-0.84}$		[1] VASSERMAN	81	OLYA	$e^+e^- \to \pi^+\pi^-$
<6.6	95	BUKIN	78B	OLYA	$e^+e^- \to \pi^+\pi^-$
<2.7	95	ALVENSLEB...	72	CNTR	6.7 γC $\to$ C$\pi^+\pi^-$

[1] Using $B(\phi \to e^+e^-) = (2.99 \pm 0.08) \times 10^{-4}$.

$\Gamma(\omega\pi^0)/\Gamma_{total}$ — Γ_{12}/Γ

VALUE (units 10^{-5})	DOCUMENT ID		TECN	COMMENT
4.7±0.5 OUR FIT				
$\mathbf{5.2^{+1.3}_{-1.1}}$	[1,2] AULCHENKO	00A	SND	$e^+e^- \to \pi^+\pi^-\pi^0\pi^0$
• • • We do not use the following data for averages, fits, limits, etc. • • •				
4.4±0.6	[3] AMBROSINO	08G	KLOE	$e^+e^- \to \pi^+\pi^- 2\pi^0$, $2\pi^0\gamma$
~ 5.4	[4] ACHASOV	00E	SND	$e^+e^- \to \pi^0\pi^0\gamma$
$5.5\ ^{+1.6}_{-1.4} \pm 0.3$	[2,5] AULCHENKO	00A	SND	$e^+e^- \to \pi^+\pi^-\pi^0\pi^0$
$4.8\ ^{+1.9}_{-1.7} \pm 0.8$	[4] ACHASOV	99	SND	$e^+e^- \to \pi^+\pi^-\pi^0\pi^0$

[1] Using the 1996 and 1998 data.
[2] (2.3 ± 0.3)% correction for other decay modes of the $\omega(782)$ applied.
[3] Not independent of the corresponding $\Gamma(\omega\pi^0) \times \Gamma(e^+e^-) / \Gamma^2(total)$.
[4] Using the 1996 data.
[5] Using the 1998 data.

Int. J. Mod. Phys. A 2026.41. Downloaded from www.worldscientific.com
by UNIVERSITY OF CALIFORNIA @ BERKELEY on 09/16/26. Re-use and distribution is strictly not permitted, except for Open Access articles.

$\Gamma(\omega\gamma)/\Gamma_{total}$ — Γ_{13}/Γ

VALUE	CL%	DOCUMENT ID		TECN	COMMENT
<0.05	84	LINDSEY	66	HBC	2.1–2.7 $K^- p \to \Lambda\pi^+\pi^-$ neutrals

$\Gamma(\rho\gamma)/\Gamma_{total}$ — Γ_{14}/Γ

VALUE (units 10^{-4})	CL%	DOCUMENT ID		TECN	COMMENT
< 0.12	90	[1] AKHMETSHIN 99B		CMD2	$e^+e^- \to \pi^+\pi^-\gamma$
• • • We do not use the following data for averages, fits, limits, etc. • • •					
< 7	90	AKHMETSHIN 97C		CMD2	$e^+e^- \to \pi^+\pi^-\gamma$
<200	84	LINDSEY	66	HBC	2.1–2.7 $K^- p \to \Lambda\pi^+\pi^-$ neutrals

[1] Supersedes AKHMETSHIN 97C.

$\Gamma(\pi^+\pi^-\gamma)/\Gamma_{total}$ — Γ_{15}/Γ

VALUE (units 10^{-4})	CL%	EVTS	DOCUMENT ID		TECN	COMMENT
0.41±0.12±0.04		30175	[1] AKHMETSHIN 99B		CMD2	$e^+e^- \to \pi^+\pi^-\gamma$
• • • We do not use the following data for averages, fits, limits, etc. • • •						
< 0.3	90		[2] AKHMETSHIN 97C		CMD2	$e^+e^- \to \pi^+\pi^-\gamma$
<600	90		KALBFLEISCH 75		HBC	2.18 $K^- p \to \Lambda\pi^+\pi^-\gamma$
< 70	90		COSME 74		OSPK	$e^+e^- \to \pi^+\pi^-\gamma$
<400	90		LINDSEY 65		HBC	2.1–2.7 $K^- p \to \Lambda\pi^+\pi^-$ neutrals

[1] For $E_\gamma > 20$ MeV and assuming that $B(\phi(1020) \to f_0(980)\gamma)$ is negligible. Supersedes AKHMETSHIN 97C.
[2] For $E_\gamma > 20$ MeV and assuming that $B(\phi(1020) \to f_0(980)\gamma)$ is negligible.

$\Gamma(f_0(980)\gamma)/\Gamma_{total}$ — Γ_{16}/Γ

VALUE (units 10^{-4})	CL%	EVTS	DOCUMENT ID		TECN	COMMENT
3.22±0.19 OUR FIT Error includes scale factor of 1.1.						
3.21±0.19 OUR AVERAGE						
$3.21^{+0.03}_{-0.09}\pm0.18$			[1] AMBROSINO 07		KLOE	$e^+e^- \to \pi^0\pi^0\gamma$
2.90±0.21±1.54			[2] AKHMETSHIN 99C		CMD2	$e^+e^- \to \pi^+\pi^-\gamma$, $\pi^0\pi^0\gamma$
• • • We do not use the following data for averages, fits, limits, etc. • • •						
4.47±0.21		2438	[3] ALOISIO 02D		KLOE	$e^+e^- \to \pi^0\pi^0\gamma$
3.5 ±0.3 $^{+1.3}_{-0.5}$		419	[4,5] ACHASOV 00H		SND	$e^+e^- \to \pi^0\pi^0\gamma$
1.93±0.46±0.50		27188	[6] AKHMETSHIN 99B		CMD2	$e^+e^- \to \pi^+\pi^-\gamma$
3.05±0.25±0.72		268	[7] AKHMETSHIN 99C		CMD2	$e^+e^- \to \pi^0\pi^0\gamma$
1.5 ±0.5		268	[8] AKHMETSHIN 99C		CMD2	$e^+e^- \to \pi^0\pi^0\gamma$
3.42±0.30±0.36		164	[4] ACHASOV 98I		SND	$e^+e^- \to 5\gamma$
< 1	90		[9] AKHMETSHIN 97C		CMD2	$e^+e^- \to \pi^+\pi^-\gamma$
< 7	90		[10] AKHMETSHIN 97C		CMD2	$e^+e^- \to \pi^+\pi^-\gamma$
< 20	90		DRUZHININ 87		ND	$e^+e^- \to \pi^0\pi^0\gamma$

[1] Obtained by the authors taking into account the $\pi^+\pi^-$ decay mode. Includes a component due to $\pi\pi$ production via the $f_0(500)$ meson. Supersedes ALOISIO 02D.
[2] From the combined fit of the photon spectra in the reactions $e^+e^- \to \pi^+\pi^-\gamma$, $\pi^0\pi^0\gamma$.
[3] From the negative interference with the $f_0(500)$ meson of AITALA 01B using the ACHASOV 89 parameterization for the $f_0(980)$, a Breit-Wigner for the $f_0(500)$, and ACHASOV 01F for the $\rho\pi$ contribution. Superseded by AMBROSINO 07.
[4] Assuming that the $\pi^0\pi^0\gamma$ final state is completely determined by the $f_0\gamma$ mechanism, neglecting the decay $B(\phi \to K\overline{K}\gamma)$ and using $B(f_0 \to \pi^+\pi^-) = 2B(f_0 \to \pi^0\pi^0)$.
[5] Using the value $B(\phi \to \eta\gamma) = (1.338 \pm 0.053) \times 10^{-2}$.
[6] For $E_\gamma > 20$ MeV. Supersedes AKHMETSHIN 97C.
[7] Neglecting other intermediate mechanisms ($\rho\pi$, $\sigma\gamma$).
[8] A narrow pole fit taking into account $f_0(980)$ and $f_0(1200)$ intermediate mechanisms.
[9] For destructive interference with the Bremsstrahlung process
[10] For constructive interference with the Bremsstrahlung process

$\Gamma(f_0(980)\gamma)/\Gamma(\eta\gamma)$ — Γ_{16}/Γ_5

VALUE (units 10^{-2})	EVTS	DOCUMENT ID		TECN	COMMENT
2.47±0.15 OUR FIT Error includes scale factor of 1.1.					
2.6 ±0.2 $^{+0.8}_{-0.3}$	419	[1] ACHASOV 00H		SND	$e^+e^- \to \pi^0\pi^0\gamma$

[1] Assuming that the $\pi^0\pi^0\gamma$ final state is completely determined by the $f_0\gamma$ mechanism, neglecting the decay $B(\phi \to K\overline{K}\gamma)$ and using $B(f_0 \to \pi^+\pi^-) = 2B(f_0 \to \pi^0\pi^0)$.

$\Gamma(\pi^0\pi^0\gamma)/\Gamma_{total}$ — Γ_{17}/Γ

VALUE (units 10^{-4})	CL%	EVTS	DOCUMENT ID		TECN	COMMENT
1.07 ±0.06 OUR AVERAGE						
$1.07\ ^{+0.01}_{-0.03}\ ^{+0.06}_{-0.06}$			[1] AMBROSINO 07		KLOE	$e^+e^- \to \pi^0\pi^0\gamma$
1.08 ±0.17 ±0.09		268	AKHMETSHIN 99C		CMD2	$e^+e^- \to \pi^0\pi^0\gamma$
• • • We do not use the following data for averages, fits, limits, etc. • • •						
1.09 ±0.03 ±0.05		2438	ALOISIO 02D		KLOE	$e^+e^- \to \pi^0\pi^0\gamma$
1.158±0.093±0.052		419	[2,3] ACHASOV 00H		SND	$e^+e^- \to \pi^0\pi^0\gamma$
<10	90		DRUZHININ 87		ND	$e^+e^- \to 5\gamma$

[1] Supersedes ALOISIO 02D.
[2] Using the value $B(\phi \to \eta\gamma) = (1.338 \pm 0.053) \times 10^{-2}$.
[3] Supersedes ACHASOV 98I. Excluding $\omega\pi^0$.

$\Gamma(\pi^0\pi^0\gamma)/\Gamma(\eta\gamma)$ — Γ_{17}/Γ_5

VALUE (units 10^{-2})	EVTS	DOCUMENT ID		TECN	COMMENT
0.86 ±0.04 OUR FIT					
0.865±0.070±0.017	419	[1] ACHASOV 00H		SND	$e^+e^- \to \pi^0\pi^0\gamma$
• • • We do not use the following data for averages, fits, limits, etc. • • •					
0.90 ±0.08 ±0.07	164	ACHASOV 98I		SND	$e^+e^- \to 5\gamma$

[1] Supersedes ACHASOV 98I. Excluding $\omega\pi^0$.

$\Gamma(\pi^+\pi^-\pi^+\pi^-)/\Gamma_{total}$ — Γ_{18}/Γ

VALUE (units 10^{-6})	CL%	EVTS	DOCUMENT ID		TECN	COMMENT
6.5 ±2.7 ±1.6		6.8k	[1] AKHMETSHIN 17		CMD3	$e^+e^- \to \pi^+\pi^-\pi^+\pi^-$
• • • We do not use the following data for averages, fits, limits, etc. • • •						
3.93±1.74±2.14		3.3k	AKHMETSHIN 00E		CMD2	$e^+e^- \to \pi^+\pi^-\pi^+\pi^-$
< 870	90		CORDIER 79		WIRE	$e^+e^- \to \pi^+\pi^-\pi^+\pi^-$

[1] Using the cross section at the ϕ meson peak $\sigma(\phi) = 4172 \pm 42$ nb, the nonresonant cross section $\sigma(0) = 1.263 \pm 0.027$ nb and $\mathrm{Re}(Z) = 0.146 \pm 0.030$, $\mathrm{Im}(Z) = -0.002 \pm 0.024$ for the complex amplitude of the $\phi \to \pi^+\pi^-\pi^+\pi^-$ transition.

$\Gamma(\pi^+\pi^+\pi^-\pi^-\pi^0)/\Gamma_{total}$ — Γ_{19}/Γ

VALUE (units 10^{-6})	CL%	DOCUMENT ID		TECN	COMMENT
< 4.6	90	AKHMETSHIN 00E		CMD2	$e^+e^- \to \pi^+\pi^-\pi^+\pi^-\pi^0$
• • • We do not use the following data for averages, fits, limits, etc. • • •					
<150	95	BARKOV 88		CMD	$e^+e^- \to \pi^+\pi^-\pi^+\pi^-\pi^0$

$\Gamma(\pi^0 e^+e^-)/\Gamma_{total}$ — Γ_{20}/Γ

VALUE (units 10^{-5})	CL%	EVTS	DOCUMENT ID		TECN	COMMENT
$1.33^{+0.07}_{-0.10}$ OUR AVERAGE						
$1.35\pm0.05\ ^{+0.05}_{-0.10}$		9.5k	[1] ANASTASI 16B		KLOE	$e^+e^- \to \pi^0 e^+e^-$
1.01±0.28±0.29		52	[2] ACHASOV 02D		SND	$e^+e^- \to \pi^0 e^+e^-$
1.22±0.34±0.21		46	[3] AKHMETSHIN 01C		CMD2	$e^+e^- \to \pi^0 e^+e^-$
• • • We do not use the following data for averages, fits, limits, etc. • • •						
<12	90		DOLINSKY 88		ND	$e^+e^- \to \pi^0 e^+e^-$

[1] Using $B(\pi^0 \to \gamma\gamma)$ from the 2014 Edition of this Review (PDG 14).
[2] Using various branching ratios from the 2000 Edition of this Review (PDG 00).
[3] Using $B(\pi^0 \to \gamma\gamma) = 0.98798 \pm 0.00032$, $B(\phi \to \eta\gamma) = (1.297 \pm 0.033) \times 10^{-2}$, and $B(\eta \to \pi^+\pi^-\gamma) = (4.75 \pm 0.11) \times 10^{-2}$.

$\Gamma(\pi^0\eta\gamma)/\Gamma_{total}$ — Γ_{21}/Γ

VALUE (units 10^{-5})	CL%	EVTS	DOCUMENT ID		TECN	COMMENT
7.27±0.30 OUR AVERAGE Error includes scale factor of 1.5. See the ideogram below.						
7.06±0.22		16.9k	[1] AMBROSINO 09F		KLOE	$1.02\ e^+e^- \to \eta\pi^0\gamma$
8.51±0.51±0.57		607	[2] ALOISIO 02C		KLOE	$e^+e^- \to \eta\pi^0\gamma$
7.96±0.60±0.40		197	[3] ALOISIO 02C		KLOE	$e^+e^- \to \eta\pi^0\gamma$
8.8 ±1.4 ±0.9		36	[4] ACHASOV 00F		SND	$e^+e^- \to \eta\pi^0\gamma$
9.0 ±2.4 ±1.0		80	AKHMETSHIN 99C		CMD2	$e^+e^- \to \eta\pi^0\gamma$
• • • We do not use the following data for averages, fits, limits, etc. • • •						
7.01±0.10±0.20		13.3k	[2,5] AMBROSINO 09F		KLOE	$1.02\ e^+e^- \to \eta\pi^0\gamma$
7.12±0.13±0.22		3.6k	[3,6] AMBROSINO 09F		KLOE	$1.02\ e^+e^- \to \eta\pi^0\gamma$
8.3 ±2.3 ±1.2		20	ACHASOV 98B		SND	$e^+e^- \to 5\gamma$
<250	90		DOLINSKY 91		ND	$e^+e^- \to \pi^0\eta\gamma$

[1] Combined results of $\eta \to \gamma\gamma$ and $\eta \to \pi^+\pi^-\pi^0$ decay modes measurements.
[2] From the decay mode $\eta \to \gamma\gamma$.
[3] From the decay mode $\eta \to \pi^+\pi^-\pi^0$.
[4] Supersedes ACHASOV 98B.
[5] Using $B(\phi \to \eta\gamma) = (1.304 \pm 0.025)\%$, $B(\eta \to 3\pi^0) = (32.56 \pm 0.23)\%$, and $B(\eta \to \gamma\gamma) = (39.31 \pm 0.20)\%$.
[6] Using $B(\phi \to \eta\gamma) = (1.304 \pm 0.025)\%$, $B(\eta \to 3\pi^0) = (32.56 \pm 0.23)\%$, and $B(\eta \to \pi^+\pi^-\pi^0) = (22.73 \pm 0.28)\%$.

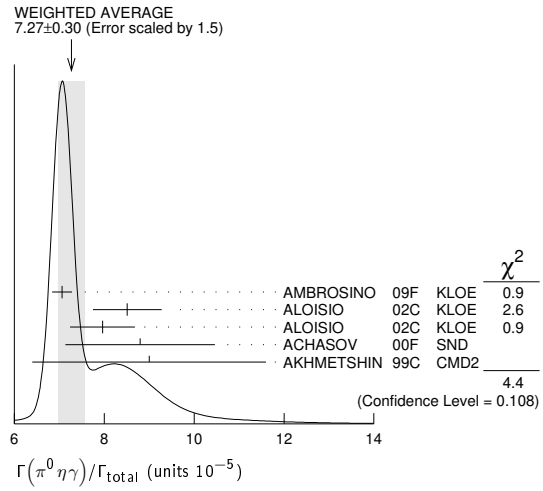

Int. J. Mod. Phys. A 2026.41. Downloaded from www.worldscientific.com by CALIFORNIA @ BERKELEY on 09/16/26. Re-use and distribution is strictly not permitted, except for Open Access articles.

$\Gamma(a_0(980)\gamma)/\Gamma_{total}$ — Γ_{22}/Γ

VALUE (units 10^{-5})	CL%	EVTS	DOCUMENT ID		TECN	COMMENT
7.6±0.6 OUR FIT						
7.6±0.6 OUR AVERAGE						
7.4±0.7			[1] ALOISIO	02C	KLOE	$e^+e^- \to \eta\pi^0\gamma$
8.8±1.7		36	[2] ACHASOV	00F	SND	$e^+e^- \to \eta\pi^0\gamma$
• • • We do not use the following data for averages, fits, limits, etc. • • •						
11 ±2			[3] GOKALP	02	RVUE	$e^+e^- \to \eta\pi^0\gamma$
<500	90		DOLINSKY	91	ND	$e^+e^- \to \pi^0\eta\gamma$

[1] Using $M_{a_0(980)}$=984.8 MeV and assuming $a_0(980)\gamma$ dominance.
[2] Assuming $a_0(980)\gamma$ dominance in the $\eta\pi^0\gamma$ final state.
[3] Using data of ACHASOV 00F.

$\Gamma(f_0(980)\gamma)/\Gamma(a_0(980)\gamma)$ — Γ_{16}/Γ_{22}

VALUE	DOCUMENT ID		TECN	COMMENT
6.1±0.6	[1] ALOISIO	02C	KLOE	$e^+e^- \to \eta\pi^0\gamma$

[1] Using results of ALOISIO 02D and assuming that $f_0(980)$ decays into $\pi\pi$ only and $a_0(980)$ into $\eta\pi$ only.

$\Gamma(K^0\overline{K}^0\gamma)/\Gamma_{total}$ — Γ_{23}/Γ

VALUE	CL%	DOCUMENT ID		TECN	COMMENT
<1.9 × 10^{-8}	90	AMBROSINO	09C	KLOE	$e^+e^- \to K^0_S K^0_S \gamma$

$\Gamma(\eta'(958)\gamma)/\Gamma_{total}$ — Γ_{24}/Γ

VALUE (units 10^{-5})	CL%	EVTS	DOCUMENT ID		TECN	COMMENT
6.23±0.21 OUR FIT						
6.24±0.30 OUR AVERAGE						
6.23±0.27±0.12		3407	[1] AMBROSINO	07A	KLOE	1.02 $e^+e^- \to \pi^+\pi^- 7\gamma$
6.7 $^{+2.8}_{-2.4}$ ±0.8		12	[2] AULCHENKO	03B	SND	$e^+e^- \to \eta'\gamma$
• • • We do not use the following data for averages, fits, limits, etc. • • •						
6.7 $^{+5.0}_{-4.2}$ ±1.5		7	AULCHENKO	03B	SND	$e^+e^- \to 7\gamma$
6.10±0.61±0.43		120	[3] ALOISIO	02E	KLOE	1.02 $e^+e^- \to \pi^+\pi^- 3\gamma$
8.2 $^{+2.1}_{-1.9}$ ±1.1		21	[4] AKHMETSHIN	00B	CMD2	$e^+e^- \to \pi^+\pi^- 3\gamma$
4.9 $^{+2.2}_{-1.8}$ ±0.6		9	[5] AKHMETSHIN	00F	CMD2	$e^+e^- \to \pi^+\pi^-\pi^+\pi^- \geq 2\gamma$
6.4 ±1.6		30	[6] AKHMETSHIN	00F	CMD2	$e^+e^- \to \eta'(958)\gamma$
6.7 $^{+3.4}_{-2.9}$ ±1.0		5	[7] AULCHENKO	99	SND	$e^+e^- \to \pi^+\pi^- 3\gamma$
<11	90		AULCHENKO	98	SND	$e^+e^- \to 7\gamma$
12 $^{+7}_{-5}$ ±2		6	[4] AKHMETSHIN	97B	CMD2	$e^+e^- \to \pi^+\pi^- 3\gamma$
<41	90		DRUZHININ	87	ND	$e^+e^- \to \gamma\eta\pi^+\pi^-$

[1] AMBROSINO 07A reports $[\Gamma(\phi(1020) \to \eta'(958)\gamma)/\Gamma_{total}]$ / $[B(\phi(1020) \to \eta\gamma)] = (4.77 \pm 0.09 \pm 0.19) \times 10^{-3}$ which we multiply by our best (shown rounded) value $B(\phi(1020) \to \eta\gamma) = (1.306 \pm 0.024) \times 10^{-2}$. Our first error is their experiment's error and our second error is the systematic error from using our best (shown rounded) value.
[2] Averaging AULCHENKO 03B with AULCHENKO 99.
[3] Using $B(\phi \to \eta\gamma)$= (1.297 ± 0.033)%.
[4] Using the value $B(\phi \to \eta\gamma) = (1.26 \pm 0.06) \times 10^{-2}$.
[5] Using $B(\phi \to K^0_L K^0_S) = (33.8 \pm 0.6)$%.
[6] Averaging AKHMETSHIN 00B with AKHMETSHIN 00F.
[7] Using the value $B(\eta' \to \eta\pi^+\pi^-)$= $(43.7 \pm 1.5) \times 10^{-2}$ and $B(\eta \to \gamma\gamma)$= $(39.25 \pm 0.31) \times 10^{-2}$.

$\Gamma(\eta'(958)\gamma)/\Gamma(K^0_L K^0_S)$ — Γ_{24}/Γ_2

VALUE (units 10^{-4})	EVTS	DOCUMENT ID		TECN	COMMENT
1.85±0.06 OUR FIT					
1.46 $^{+0.64}_{-0.54}$ ±0.18	9	[1] AKHMETSHIN	00F	CMD2	$e^+e^- \to \pi^+\pi^-\pi^+\pi^- \geq 2\gamma$

[1] Using various branching ratios of K^0_S, K^0_L, η, η' from the 2000 edition (The European Physical Journal **C15** 1 (2000)) of this Review.

$\Gamma(\eta'(958)\gamma)/\Gamma(\eta\gamma)$ — Γ_{24}/Γ_5

VALUE (units 10^{-3})	EVTS	DOCUMENT ID		TECN	COMMENT
4.77±0.15 OUR FIT					
4.78±0.20 OUR AVERAGE					
4.77±0.09±0.19	3407	AMBROSINO	07A	KLOE	1.02 $e^+e^- \to \pi^+\pi^- 7\gamma$
4.70±0.47±0.31	120	[1] ALOISIO	02E	KLOE	1.02 $e^+e^- \to \pi^+\pi^- 3\gamma$
6.5 $^{+1.7}_{-1.5}$ ±0.8	21	AKHMETSHIN	00B	CMD2	$e^+e^- \to \pi^+\pi^- 3\gamma$
• • • We do not use the following data for averages, fits, limits, etc. • • •					
9.5 $^{+5.2}_{-4.0}$ ±1.4	6	[2] AKHMETSHIN	97B	CMD2	$e^+e^- \to \pi^+\pi^- 3\gamma$

[1] From the decay mode $\eta' \to \eta\pi^+\pi^-$, $\eta \to \gamma\gamma$.
[2] Superseded by AKHMETSHIN 00B.

$\Gamma(\eta\pi^0\pi^0\gamma)/\Gamma_{total}$ — Γ_{25}/Γ

VALUE (units 10^{-5})	CL%	DOCUMENT ID		TECN	COMMENT
<2	90	AULCHENKO	98	SND	$e^+e^- \to 7\gamma$

$\Gamma(\mu^+\mu^-\gamma)/\Gamma_{total}$ — Γ_{26}/Γ

VALUE (units 10^{-5})	EVTS	DOCUMENT ID		TECN	COMMENT
1.43±0.45±0.14	27188	[1] AKHMETSHIN	99B	CMD2	$e^+e^- \to \mu^+\mu^-\gamma$
• • • We do not use the following data for averages, fits, limits, etc. • • •					
2.3 ±1.0	824 ± 33	[2] AKHMETSHIN	97C	CMD2	$e^+e^- \to \mu^+\mu^-\gamma$

[1] For $E_\gamma > 20$ MeV. Supersedes AKHMETSHIN 97C.
[2] For $E_\gamma > 20$ MeV.

$\Gamma(\rho\gamma\gamma)/\Gamma_{total}$ — Γ_{27}/Γ

VALUE (units 10^{-4})	CL%	DOCUMENT ID		TECN	COMMENT
<1.2	90	AULCHENKO	08	CMD2	$\phi \to \pi^+\pi^-\gamma\gamma$
• • • We do not use the following data for averages, fits, limits, etc. • • •					
<5	90	AKHMETSHIN	98	CMD2	$e^+e^- \to \pi^+\pi^-\gamma\gamma$

$\Gamma(\eta\pi^+\pi^-)/\Gamma_{total}$ — Γ_{28}/Γ

VALUE (units 10^{-5})	CL%	DOCUMENT ID		TECN	COMMENT
< 1.8	90	AKHMETSHIN	00E	CMD2	$e^+e^- \to \pi^+\pi^-\pi^+\pi^-\pi^0$
• • • We do not use the following data for averages, fits, limits, etc. • • •					
< 6.1	90	AULCHENKO	08	CMD2	$\phi \to \eta\pi^+\pi^-$
<30	90	AKHMETSHIN	98	CMD2	$e^+e^- \to \pi^+\pi^-\gamma\gamma$

$\Gamma(\eta\mu^+\mu^-)/\Gamma_{total}$ — Γ_{29}/Γ

VALUE (units 10^{-6})	CL%	DOCUMENT ID		TECN	COMMENT
<9.4	90	AKHMETSHIN	01	CMD2	$e^+e^- \to \eta e^+e^-$

$\Gamma(\eta U \to \eta e^+e^-)/\Gamma_{total}$ — Γ_{30}/Γ

VALUE	CL%	DOCUMENT ID		TECN	COMMENT
<1 × 10^{-6}	90	[1] BABUSCI	13B	KLOE	1.02 $e^+e^- \to \eta e^+e^-$

[1] For a narrow vector U with mass between 5 and 470 MeV, from the combined analysis of $\eta \to \pi^+\pi^-\pi^0$ and $\eta \to \pi^0\pi^0\pi^0$ from ARCHILLI 12. Measured 90% CL limits as a function of m_U range from 2.2×10^{-8} to 10^{-6}.

$\Gamma(\text{invisible})/\Gamma(K^+K^-)$ — Γ_{31}/Γ_1

VALUE	CL%	DOCUMENT ID		TECN	COMMENT
<3.4 × 10^{-4}	90	ABLIKIM	18S	BES3	$J/\psi \to \phi\eta \to \phi\pi^+\pi^-\pi^0$

Lepton Family number (LF) violating modes

$\Gamma(e^\pm\mu^\mp)/\Gamma_{total}$ — Γ_{32}/Γ

VALUE	CL%	DOCUMENT ID		TECN	COMMENT
<2 × 10^{-6}	90	ACHASOV	10A	SND	$e^+e^- \to e^\pm\mu^\mp$

$\Gamma(\pi^+\pi^+e^-e^-)/\Gamma_{total}$ — Γ_{33}/Γ

VALUE	CL%	DOCUMENT ID		TECN	COMMENT
<1.3 × 10^{-5}	90	[1] ABLIKIM	25AK	BES3	$J/\psi \to \phi\eta$

[1] $B(\phi \to K^+K^-)$ = (49.2 ± 0.5)% was used.

$\pi^+\pi^-\pi^0$ / $\rho\pi$ AMPLITUDE RATIO a_1 IN DECAY OF $\phi \to \pi^+\pi^-\pi^0$

NIECKNIG 12 describes final-state interactions between the three pions in a dispersive framework using data on the $\pi\pi$ P-wave scattering phase shift.

VALUE (units 10^{-2})	CL%	EVTS	DOCUMENT ID		TECN	COMMENT
9.1±1.2 OUR AVERAGE						
10.1±4.4±1.7		80k	[1] AKHMETSHIN	06	CMD2	1.017–1.021 $e^+e^- \to \pi^+\pi^-\pi^0$
9.0±1.1±0.6		1.98M	[2,3] ALOISIO	03	KLOE	1.02 $e^+e^- \to \pi^+\pi^-\pi^0$
• • • We do not use the following data for averages, fits, limits, etc. • • •						
$-6 < a_1 < 6$		500k	[3] ACHASOV	02	SND	$e^+e^- \to \pi^+\pi^-\pi^0$
$-16 < a_1 < 11$	90	9.8k	[1,4] AKHMETSHIN	98	CMD2	$e^+e^- \to \pi^+\pi^-\gamma\gamma$

[1] Dalitz plot analysis taking into account interference between the contact and $\rho\pi$ amplitudes.
[2] From a fit without limitations on charged and neutral ρ masses and widths.
[3] Recalculated by us to match the notations of AKHMETSHIN 98.
[4] Assuming zero phase for the contact term.

PARAMETER β IN $\phi \to Pe^+e^-$ DECAYS

In the one-pole approximation the electromagnetic transition form factor for $\phi \to Pe^+e^-$ ($P = \pi,\eta$) is given as a function of the e^+e^- invariant mass squared, q^2, by the expression:

$$|F(q^2)|^2 = (1 - q^2/\Lambda^2)^{-2},$$

where vector meson dominance predicts parameter $\Lambda \approx 0.770$ GeV ($\Lambda^{-2} \approx 1.687$ GeV^{-2}). The slope of this form factor, $\beta = dF/dq^2(q^2{=}0)$, equals Λ^{-2} in this approximation.

The measurements below obtain β in the one-pole approximation.

PARAMETER β IN $\phi \to \pi^0e^+e^-$ DECAY

VALUE (GeV^{-2})	EVTS	DOCUMENT ID		TECN	COMMENT
2.02±0.11	9.5k	[1] ANASTASI	16B	KLOE	1.02 $e^+e^- \to \pi^0e^+e^-$

[1] The error combines statistical and systematic uncertainties.

Int. J. Mod. Phys. A 2026.41. Downloaded from www.worldscientific.com
by UNIVERSITY OF CALIFORNIA @ BERKELEY on 09/16/26. Re-use and distribution is strictly not permitted, except for Open Access articles.

PARAMETER β IN $\phi \to \eta e^+ e^-$ DECAY

VALUE (GeV^{-2})	EVTS	DOCUMENT ID		TECN	COMMENT
1.29±0.13 OUR AVERAGE					
$1.28 \pm 0.10^{+0.09}_{-0.08}$	30k	BABUSCI	15	KLOE	$1.02\ e^+e^- \to \eta e^+e^-$
3.8 ±1.8	213	[1] ACHASOV	01B	SND	$1.02\ e^+e^- \to \eta e^+e^-$

[1] The uncertainty is statistical only. The systematic one is negligible, in comparison.

$\phi(1020)$ REFERENCES

ABLIKIM	25A	PRL 134 011904	M. Ablikim et al.	(BESIII Collab.)
ABLIKIM	25AK	CP C49 043001	M. Ablikim et al.	(BESIII Collab.)
ABLIKIM	25BR	PRL 135 161902	M. Ablikim et al.	(BESIII Collab.)
ABLIKIM	25F	PRL 134 201902	M. Ablikim et al.	(BESIII Collab.)
DRUZHININ	25	PPN 56 405	V.P. Druzhinin et al.	(SND Collab.)
AAIJ	24B	JHEP 2405 293	R. Aaij et al.	(LHCb Collab.)
ACHASOV	24	PR D110 072001	M.N. Achasov et al.	(SND Collab.)
DUBNICKA	24	PR D110 054019	S. Dubnicka et al.	(SLOV, CMNS)
IGNATOV	24	PR D109 112002	F.V. Ignatov et al.	(CMD-3 Collab.)
PDG	24	PR D110 030001	S. Navas et al.	(PDG Collab.)
PDG	22	PTEP 2022 083C01	R.L. Workman et al.	(PDG Collab.)
ABLIKIM	21AE	PR D104 012016	M. Ablikim et al.	(BESIII Collab.)
ABLIKIM	21U	PR D104 032011	M. Ablikim et al.	(BESIII Collab.)
LEES	21B	PR D104 112003	J.P. Lees et al.	(BABAR Collab.)
ALBRECHT	20	EPJ C80 453	M. Albrecht et al.	(Crystal Barrel Collab.)
HOID	20	EPJ C80 988	B.-L. Hoid, M. Hoferichter, B. Kubis	(BONN, BERN)
AAIJ	19H	JHEP 1904 063	R. Aaij et al.	(LHCb Collab.)
HOFERICHT...	19	JHEP 1908 137	M. Hoferichter, B.-L. Hoid, B. Kubis	(WASH, BONN)
ABLIKIM	18S	PR D98 032001	M. Ablikim et al.	(BESIII Collab.)
AOUDE	18	PR D98 056021	R.T. Aoude et al.	
KOZYREV	18	PL B779 64	E.A. Kozyrev et al.	(CMD-3 Collab.)
AKHMETSHIN	17	PL B768 345	R.R. Akhmetshin et al.	(CMD-3 Collab.)
ACHASOV	16A	PR D93 092001	M.N. Achasov et al.	(SND Collab.)
ANASTASI	16B	PL B757 362	A. Anastasi et al.	(KLOE-2 Collab.)
KOZYREV	16	PL B760 314	E.A. Kozyrev et al.	(CMD-3 Collab.)
BABUSCI	15	PL B742 1	D. Babusci et al.	(KLOE-2 Collab.)
PDG	15	RPP 2015 at pdg.lbl.gov		(PDG Collab.)
LEES	14H	PR D89 092002	J.P. Lees et al.	(BABAR Collab.)
PDG	14	CP C38 070001	K. Olive et al.	(PDG Collab.)
BABUSCI	13B	PL B720 111	D. Babusci et al.	(KLOE-2 Collab.)
BENAYOUN	13	EPJ C73 2453	M. Benayoun, P. David, L. DelBuono	(PARIN, BERLIN+)
LEES	13F	PR D87 052010	J.P. Lees et al.	(BABAR Collab.)
LEES	13Q	PR D88 032013	J.P. Lees et al.	(BABAR Collab.)
ARCHILLI	12	PL B706 251	F. Archilli et al.	(KLOE-2 Collab.)
BENAYOUN	12	EPJ C72 1848	M. Benayoun et al.	
NIECKNIG	12	EPJ C72 2014	F. Niecknig, B. Kubis, S.P. Schneider	(BONN)
PDG	12	PR D86 010001	J. Beringer et al.	(PDG Collab.)
AKHMETSHIN	11	PL B695 412	R.R. Akhmetshin et al.	(CMD-2 Collab.)
ACHASOV	10A	PR D81 057102	M.N. Achasov et al.	(Novosibirsk SND Collab.)
BENAYOUN	10	EPJ C65 211	M. Benayoun et al.	
AMBROSINO	09C	PL B679 10	F. Ambrosino et al.	(KLOE Collab.)
AMBROSINO	09F	PL B681 5	F. Ambrosino et al.	(KLOE Collab.)
AKHMETSHIN	08	PL B669 217	R.R. Akhmetshin et al.	(CMD-2 Collab.)
AMBROSINO	08G	PL B669 223	F. Ambrosino et al.	(KLOE Collab.)
AULCHENKO	08	JETPL 88 85	V. Aulchenko et al.	(CMD-2 Collab.)
		Translated from ZETFP 88 93.		
FLOREZ-BAEZ	08	PR D78 077301	F.V. Florez-Baez, G. Lopez Castro	
ACHASOV	07B	PR D76 077101	M.N. Achasov et al.	(SND Collab.)
AMBROSINO	07	EPJ C49 473	F. Ambrosino et al.	(KLOE Collab.)
AMBROSINO	07A	PL B648 267	F. Ambrosino et al.	(KLOE Collab.)
DUBYNSKIY	07	PR D75 113001	S. Dubynskiy et al.	
ACHASOV	06A	PR D74 014016	M.N. Achasov et al.	(SND Collab.)
AKHMETSHIN	06	PL B642 203	R.R. Akhmetshin et al.	(CMD-2 Collab.)
AKHMETSHIN	05	PL B605 26	R.R. Akhmetshin et al.	(Novosibirsk CMD-2 Collab.)
AMBROSINO	05	PL B608 199	F. Ambrosino et al.	(KLOE Collab.)
AUBERT,B	05J	PR D72 052008	B. Aubert et al.	(BABAR Collab.)
AKHMETSHIN	04	PL B578 285	R.R. Akhmetshin et al.	(Novosibirsk CMD-2 Collab.)
AUBERT,B	04N	PR D70 072004	B. Aubert et al.	(BABAR Collab.)
ALOISIO	03	PL B561 55	A. Aloisio et al.	(KLOE Collab.)
AULCHENKO	03B	JETP 97 24	V.M. Aulchenko et al.	(Novosibirsk SND Collab.)
		Translated from ZETF 124 28.		
ACHASOV	02	PR D65 032002	M.N. Achasov et al.	(Novosibirsk SND Collab.)
ACHASOV	02D	JETPL 75 449	M.N. Achasov et al.	(Novosibirsk SND Collab.)
		Translated from ZETFP 75 539.		
ALOISIO	02C	PL B536 209	A. Aloisio et al.	(KLOE Collab.)
ALOISIO	02D	PL B537 21	A. Aloisio et al.	(KLOE Collab.)
ALOISIO	02E	PL B541 45	A. Aloisio et al.	(KLOE Collab.)
FISCHBACH	02	PL B526 355	E. Fischbach, A.W. Overhauser, B. Woodahl	
GOKALP	02	JP G28 2783	A. Gokalp et al.	
ACHASOV	01B	PL B504 275	M.N. Achasov et al.	(Novosibirsk SND Collab.)
ACHASOV	01E	PR D63 072002	M.N. Achasov et al.	(Novosibirsk SND Collab.)
ACHASOV	01F	PR D63 094007	N.N. Achasov, V.V. Gubin	(Novosibirsk SND Collab.)
ACHASOV	01G	PRL 86 1698	M.N. Achasov et al.	(Novosibirsk SND Collab.)
AITALA	01B	PRL 86 770	E.M. Aitala et al.	(FNAL E791 Collab.)
AKHMETSHIN	01	PL B501 191	R.R. Akhmetshin et al.	(Novosibirsk CMD-2 Collab.)
AKHMETSHIN	01B	PL B509 217	R.R. Akhmetshin et al.	(Novosibirsk CMD-2 Collab.)
AKHMETSHIN	01C	PL B503 237	R.R. Akhmetshin et al.	(Novosibirsk CMD-2 Collab.)
BENAYOUN	01	EPJ C22 503	M. Benayoun, H.B. O'Connell	
ACHASOV	00	EPJ C12 25	M.N. Achasov et al.	(Novosibirsk SND Collab.)
ACHASOV	00B	JETP 90 17	M.N. Achasov et al.	(Novosibirsk SND Collab.)
		Translated from ZETF 117 22.		
ACHASOV	00C	PL B474 188	M.N. Achasov et al.	(Novosibirsk SND Collab.)
ACHASOV	00D	JETPL 72 282	M.N. Achasov et al.	(Novosibirsk SND Collab.)
		Translated from ZETFP 72 411.		
ACHASOV	00E	NP B569 158	M.N. Achasov et al.	(Novosibirsk SND Collab.)
ACHASOV	00F	PL B479 53	M.N. Achasov et al.	(Novosibirsk SND Collab.)
ACHASOV	00H	PL B485 349	M.N. Achasov et al.	(Novosibirsk SND Collab.)
AKHMETSHIN	00B	PL B473 337	R.R. Akhmetshin et al.	(Novosibirsk CMD-2 Collab.)
AKHMETSHIN	00E	PL B491 81	R.R. Akhmetshin et al.	(Novosibirsk CMD-2 Collab.)
AKHMETSHIN	00F	PL B494 26	R.R. Akhmetshin et al.	(Novosibirsk CMD-2 Collab.)
AULCHENKO	00A	JETP 90 927	V.M. Aulchenko et al.	(Novosibirsk SND Collab.)
		Translated from ZETF 117 1067.		
BRAMON	00	PL B486 406	A. Bramon et al.	
PDG	00	EPJ C15 1	D.E. Groom et al.	(PDG Collab.)
ACHASOV	99	PL B449 122	M.N. Achasov et al.	
ACHASOV	99C	PL B456 304	M.N. Achasov et al.	
AKHMETSHIN	99B	PL B462 371	R.R. Akhmetshin et al.	(Novosibirsk CMD-2 Collab.)
AKHMETSHIN	99C	PL B462 380	R.R. Akhmetshin et al.	(Novosibirsk CMD-2 Collab.)
AKHMETSHIN	99D	PL B466 385	R.R. Akhmetshin et al.	
Also		PL B508 217 (errat.)	R.R. Akhmetshin et al.	(Novosibirsk CMD-2 Collab.)
AKHMETSHIN	99F	PL B460 242	R.R. Akhmetshin et al.	(Novosibirsk CMD-2 Collab.)
AULCHENKO	99	JETPL 69 97	V.M. Aulchenko et al.	
		Translated from ZETFP 69 87.		
ACHASOV	98B	PL B438 441	M.N. Achasov et al.	(Novosibirsk SND Collab.)
ACHASOV	98F	JETPL 68 573	M.N. Achasov et al.	(Novosibirsk SND Collab.)
ACHASOV	98I	PL B440 442	M.N. Achasov et al.	
AKHMETSHIN	98	PL B434 426	R.R. Akhmetshin et al.	(CMD-2 Collab.)
AULCHENKO	98	PL B436 199	V.M. Aulchenko et al.	(Novosibirsk SND Collab.)
BARBERIS	98	PL B432 436	D. Barberis et al.	(Omega Expt.)
AKHMETSHIN	97B	PL B415 445	R.R. Akhmetshin et al.	(NOVO, BOST, PITT+)
AKHMETSHIN	97C	PL B415 452	R.R. Akhmetshin et al.	(Novosibirsk CMD-2 Collab.)
BENAYOUN	96	ZPHY C72 221	M. Benayoun et al.	(IPNP, NOVO)
AKHMETSHIN	95	PL B364 199	R.R. Akhmetshin et al.	(Novosibirsk CMD-2 Collab.)
DOLINSKY	91	PRPL 202 99	S.I. Dolinsky et al.	(NOVO)
KUHN	90	ZPHY C48 445	J.H. Kuhn et al.	(MPIM)
ACHASOV	89	NP B315 465	N.N. Achasov, V.N. Ivanchenko	
DOLINSKY	89	ZPHY C42 511	S.I. Dolinsky et al.	(NOVO)
BARKOV	88	SJNP 47 248	L.M. Barkov et al.	(NOVO)
		Translated from YAF 47 393.		
DOLINSKY	88	SJNP 48 277	S.I. Dolinsky et al.	(NOVO)
		Translated from YAF 48 442.		
DRUZHININ	87	ZPHY C37 1	V.P. Druzhinin et al.	(NOVO)
ARMSTRONG	86	PL 166B 245	T.A. Armstrong et al.	(ATHU, BARI, BIRM+)
ATKINSON	86	ZPHY C30 521	M. Atkinson et al.	(BONN, CERN, GLAS+)
BEBEK	86	PRL 56 1893	C. Bebek et al.	(CLEO Collab.)
DAVENPORT	86	PR D33 2519	T.F. Davenport	(TUFTS, ARIZ, FNAL, FSU, NDAM+)
DIJKSTRA	86	ZPHY C31 375	H. Dijkstra et al.	(ANIK, BRIS, CERN+)
FRAME	86	NP B276 667	D. Frame et al.	(GLAS)
GOLUBEV	86	SJNP 44 409	V.B. Golubev et al.	(NOVO)
		Translated from YAF 44 633.		
ALBRECHT	85D	PL 153B 343	H. Albrecht et al.	(ARGUS Collab.)
GOLUBEV	85	SJNP 41 756	V.B. Golubev et al.	(NOVO)
		Translated from YAF 41 1183.		
DRUZHININ	84	PL 144B 136	V.P. Druzhinin et al.	(NOVO)
ARMSTRONG	83B	NP B224 193	T.A. Armstrong et al.	(BARI, BIRM, CERN+)
BARATE	83	PL 121B 449	R. Barate et al.	(SACL, LOIC, SHMP, IND)
KURDADZE	83C	JETPL 38 366	L.M. Kurdadze et al.	(NOVO)
		Translated from ZETFP 38 306.		
ARENTON	82	PR D25 2241	M.W. Arenton et al.	(ANL, ILL)
PELLINEN	82	PS 25 599	A. Pellinen, M. Roos	(HELS)
DAUM	81	PL 100B 439	C. Daum et al.	(AMST, BRIS, CERN, CRAC+)
IVANOV	81	PL 107B 297	P.M. Ivanov et al.	(NOVO)
Also		Private Comm.	S.I. Eidelman	(NOVO)
VASSERMAN	81	PL 99B 62	I.B. Vasserman et al.	(NOVO)
Also		SJNP 35 240	L.M. Kurdadze et al.	
		Translated from YAF 35 352.		
CORDIER	80	NP B172 13	A. Cordier et al.	(LALO)
CORDIER	79	PL 81B 389	A. Cordier et al.	(LALO)
BUKIN	78B	SJNP 27 521	A.D. Bukin et al.	(NOVO)
		Translated from YAF 27 985.		
BUKIN	78C	SJNP 27 516	A.D. Bukin et al.	(NOVO)
		Translated from YAF 27 976.		
COOPER	78B	NP B146 1	A.M. Cooper et al.	(TATA, CERN, CDEF+)
LOSTY	78	NP B133 38	M.J. Losty et al.	(CERN, AMST, NIJM+)
AKERLOF	77	PRL 39 861	C.W. Akerlof et al.	(FNAL, MICH, PURD)
ANDREWS	77	PRL 38 198	D.E. Andrews et al.	(ROCH)
BALDI	77	PL 68B 381	R. Baldi et al.	(GEVA)
CERRADA	77B	NP B126 241	M. Cerrada et al.	(AMST, CERN, NIJM+)
COHEN	77	PRL 38 269	D. Cohen et al.	(ANL)
LAVEN	77	NP B127 43	H. Laven et al.	(AACH3, BERL, CERN, LOIC+)
LYONS	77	NP B125 207	L. Lyons, A.M. Cooper, A.G. Clark	(OXF)
COSME	76	PL 63B 352	G. Cosme et al.	(ORSAY)
KALBFLEISCH	76	PR D13 22	G.R. Kalbfleisch, R.C. Strand, J.W. Chapman	(BNL+)
PARROUR	76	PL 63B 357	G. Parrour et al.	(ORSAY)
PARROUR	76B	PL 63B 362	G. Parrour et al.	(ORSAY)
KALBFLEISCH	75	PR D11 987	G.R. Kalbfleisch, R.C. Strand, J.W. Chapman	(BNL+)
AYRES	74	PRL 32 1463	D.S. Ayres et al.	(ANL)
BESCH	74	NP B70 257	H.J. Besch et al.	(BONN)
COSME	74	PL 48B 155	G. Cosme et al.	(ORSAY)
COSME	74B	PL 48B 159	G. Cosme et al.	(ORSAY)
DEGROOT	74	NP B74 77	A.J. de Groot et al.	(AMST, NIJM)
AUGUSTIN	73	PRL 30 462	J.E. Augustin et al.	(ORSAY)
BALLAM	73	PR D7 3150	J. Ballam et al.	(SLAC, LBL)
BINNIE	73B	PR D8 2789	D.M. Binnie et al.	(LOIC, SHMP)
AGUILAR-...	72B	PR D6 29	M. Aguilar-Benitez et al.	(BNL)
ALVENSLEB...	72	PRL 28 66	H. Alvensleben et al.	(MIT, DESY)
BORENSTEIN	72	PR D5 1559	S.R. Borenstein et al.	(BNL, MICH)
COLLEY	72	NP B50 1	D.C. Colley et al.	(BIRM, GLAS)
BALAKIN	71	PL 34B 328	V.E. Balakin et al.	(NOVO)
CHATELUS	71	Thesis LAL 1247	Y. Chatelus	(STRB)
Also		PL 32B 416	J.C. Bizot et al.	(ORSAY)
HAYES	71	PR D4 899	S. Hayes et al.	(CORN)
STOTTLE...	71	Thesis ORO 2504 170	A.R. Stottlemyer	(UMD)
BIZOT	70	PL 32B 416	J.C. Bizot et al.	(ORSAY)
Also		Liverpool Sym. 69	J.P. Perez-y-Jorba	
EARLES	70	PRL 25 1312	D.R. Earles et al.	(NEAS)
GOUNARIS	68	PRL 21 244	G.J. Gounaris, J.J. Sakurai	
LINDSEY	66	PR 147 913	J.S. Lindsey, G. Smith	(LRL)
LONDON	66	PR 143 1034	G.W. London et al.	(BNL, SYRA) IGJPC
BADIER	65B	PL 17 337	J. Badier et al.	(EPOL, SACL, AMST)
LINDSEY	65	PRL 15 221	J.S. Lindsey, G.A. Smith	(LRL)
LINDSEY 65 data included in LINDSEY 66.				
SCHLEIN	63	PRL 10 368	P.E. Schlein et al.	(UCLA) IGJP

$h_1(1170)$

$I^G(J^{PC}) = 0^-(1^{+-})$

$h_1(1170)$ MASS

VALUE (MeV)	DOCUMENT ID		TECN	CHG	COMMENT
1166± 5±3	[1] ANDO	92	SPEC		$8\ \pi^- p \to \pi^+\pi^-\pi^0 n$
• • • We do not use the following data for averages, fits, limits, etc. • • •					
1168± 4	ANDO	92	SPEC		$8\ \pi^- p \to \pi^+\pi^-\pi^0 n$
1190±60	[2] DANKOWY...	81	SPEC	0	$8\ \pi p \to 3\pi n$

[1] Average and spread of values using 2 variants of the model of BOWLER 75.
[2] Uses the model of BOWLER 75.

$h_1(1170)$ WIDTH

VALUE (MeV)	DOCUMENT ID		TECN	CHG	COMMENT
375± 6±34	[3] ANDO	92	SPEC		$8\ \pi^- p \to \pi^+\pi^-\pi^0 n$
• • • We do not use the following data for averages, fits, limits, etc. • • •					
345± 6	ANDO	92	SPEC		$8\ \pi^- p \to \pi^+\pi^-\pi^0 n$
320±50	[4] DANKOWY...	81	SPEC	0	$8\ \pi p \to 3\pi n$

[3] Average and spread of values using 2 variants of the model of BOWLER 75.
[4] Uses the model of BOWLER 75.

$h_1(1170)$ DECAY MODES

	Mode	Fraction (Γ_i/Γ)
Γ_1	$\rho\pi$	seen

$h_1(1170)$ BRANCHING RATIOS

$\Gamma(\rho\pi)/\Gamma_{total}$ — **Γ_1/Γ**

VALUE	DOCUMENT ID		TECN	COMMENT
• • • We do not use the following data for averages, fits, limits, etc. • • •				
seen	ANDO	92	SPEC	$8\ \pi^- p \to \pi^+\pi^-\pi^0 n$
seen	ATKINSON	84	OMEG	20–70 $\gamma p \to \pi^+\pi^-\pi^0 p$
seen	DANKOWY...	81	SPEC	$8\ \pi p \to 3\pi n$

$h_1(1170)$ REFERENCES

ANDO	92	PL B291 496	A. Ando *et al.*	(KEK, KYOT, NIRS, SAGA+)
ATKINSON	84	NP B231 15	M. Atkinson *et al.*	(BONN, CERN, GLAS+)
DANKOWY...	81	PRL 46 580	J.A. Dankowych *et al.*	(TNTO, BNL, CARL+)
BOWLER	75	NP B97 227	M.G. Bowler *et al.*	(OXFTP, DARE)

$b_1(1235)$

$I^G(J^{PC}) = 1^+(1^{+-})$

$b_1(1235)$ MASS

VALUE (MeV)	EVTS	DOCUMENT ID		TECN	CHG	COMMENT
1229.5 ± 3.2 OUR AVERAGE		Error includes scale factor of 1.6.				See the ideogram below.
1225 ± 5		WEIDENAUER	93	ASTE		$\overline{p}p \to 2\pi^+2\pi^-\pi^0$
1235 ±15		ALDE	92C	GAM2		38,100 $\pi^- p \to \omega\pi^0 n$
1236 ±16		FUKUI	91	SPEC		8.95 $\pi^- p \to \omega\pi^0 n$
1222 ± 6		ATKINSON	84E	OMEG	±	25–55 $\gamma p \to \omega\pi X$
1237 ± 7		ATKINSON	84E	OMEG	0	25–55 $\gamma p \to \omega\pi X$
1239 ± 5		EVANGELIS...	81	OMEG	−	12 $\pi^- p \to \omega\pi p$
1251 ± 8	450	GESSAROLI	77	HBC	−	11 $\pi^- p \to \pi^-\omega p$
1245 ±11	890	FLATTE	76C	HBC	−	4.2 $K^- p \to \pi^-\omega\Sigma^+$
1222 ± 4	1400	CHALOUPKA	74	HBC	−	3.9 $\pi^- p$
1220 ± 7	600	KARSHON	74B	HBC	+	4.9 $\pi^+ p$
• • • We do not use the following data for averages, fits, limits, etc. • • •						
1190 ±10		AUGUSTIN	89	DM2	±	$e^+e^- \to 5\pi$
1213 ± 5		ATKINSON	84C	OMEG	0	20–70 γp
1271 ±11		COLLICK	84	SPEC	+	200 $\pi^+ Z \to Z\pi\omega$

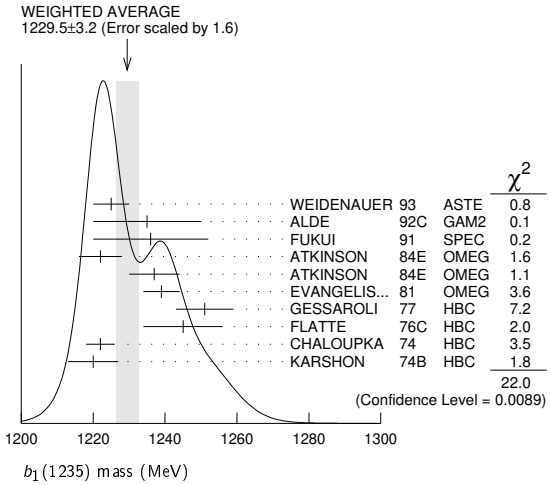

$b_1(1235)$ WIDTH

VALUE (MeV)	EVTS	DOCUMENT ID		TECN	CHG	COMMENT
142± 9 OUR AVERAGE		Error includes scale factor of 1.2.				
113±12		WEIDENAUER	93	ASTE		$\overline{p}p \to 2\pi^+2\pi^-\pi^0$
160±30		ALDE	92C	GAM2		38,100 $\pi^- p \to \omega\pi^0 n$
151±31		FUKUI	91	SPEC		8.95 $\pi^- p \to \omega\pi^0 n$
170±15		EVANGELIS...	81	OMEG	−	12 $\pi^- p \to \omega\pi p$
170±50	225	BALTAY	78B	HBC	+	15 $\pi^+ p \to p4\pi$
155±32	450	GESSAROLI	77	HBC	−	11 $\pi^- p \to \pi^-\omega p$
182±45	890	FLATTE	76C	HBC	−	4.2 $K^- p \to \pi^-\omega\Sigma^+$
135±20	1400	CHALOUPKA	74	HBC	−	3.9 $\pi^- p$
156±22	600	KARSHON	74B	HBC	+	4.9 $\pi^+ p$
• • • We do not use the following data for averages, fits, limits, etc. • • •						
210±19		AUGUSTIN	89	DM2	±	$e^+e^- \to 5\pi$
231±14		ATKINSON	84C	OMEG	0	20–70 γp
232±29		COLLICK	84	SPEC	+	200 $\pi^+ Z \to Z\pi\omega$

$b_1(1235)$ DECAY MODES

	Mode	Fraction (Γ_i/Γ)	Confidence level
Γ_1	$\omega\pi$ [D/S amplitude ratio = 0.277 ± 0.027]	seen	
Γ_2	$\pi^\pm\gamma$	$(1.6\pm0.4)\times10^{-3}$	
Γ_3	$\eta\rho$	seen	
Γ_4	$\pi^+\pi^+\pi^-\pi^0$	< 50 %	84%
Γ_5	$K^*(892)^\pm K^\mp$	seen	
Γ_6	$(K\overline{K})^\pm\pi^0$	< 8 %	90%
Γ_7	$K^0_S K^0_L \pi^\pm$	< 6 %	90%
Γ_8	$K^0_S K^0_S \pi^\pm$	< 2 %	90%
Γ_9	$\phi\pi$	< 1.5 %	84%

$b_1(1235)$ PARTIAL WIDTHS

$\Gamma(\pi^\pm\gamma)$ — **Γ_2**

VALUE (keV)	DOCUMENT ID		TECN	CHG	COMMENT
230±60	COLLICK	84	SPEC	+	200 $\pi^+ Z \to Z\pi\omega$

$b_1(1235)$ D-wave/S-wave AMPLITUDE RATIO IN DECAY OF $b_1(1235) \to \omega\pi$

VALUE	EVTS	DOCUMENT ID		TECN	CHG	COMMENT
0.277±0.027 OUR AVERAGE		Error includes scale factor of 2.4.				See the ideogram below.
0.269±0.009±0.010		NOZAR	02	MPS	−	18 $\pi^- p \to \omega\pi^- p$
0.23 ±0.03		AMSLER	94C	CBAR		0.0 $\overline{p}p \to \omega\eta\pi^0$
0.45 ±0.04		AMSLER	93B	CBAR		0.0 $\overline{p}p \to \omega\pi^0\pi^0$
0.235±0.047		ATKINSON	84C	OMEG		20–70 γp
$0.4\ ^{+0.1}_{-0.1}$		GESSAROLI	77	HBC	−	11 $\pi^- p \to \pi^-\omega p$
0.21 ±0.08		CHUNG	75B	HBC	+	7.1 $\pi^+ p$
0.3 ±0.1		CHALOUPKA	74	HBC	−	3.9–7.5 $\pi^- p$
0.35 ±0.25	600	KARSHON	74B	HBC	+	4.9 $\pi^+ p$

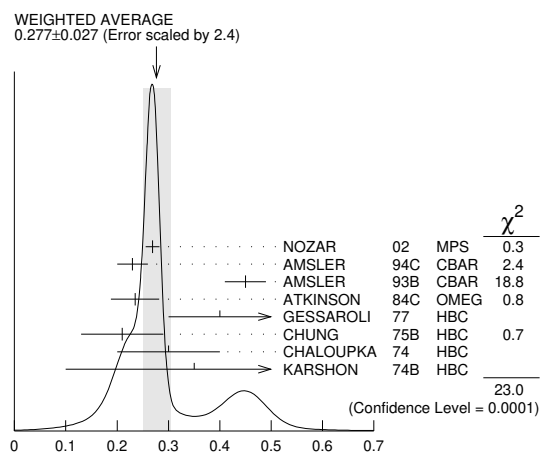

$b_1(1235)$ D-wave/S-wave AMPLITUDE PHASE DIFFERENCE IN DECAY OF $b_1(1235) \to \omega\pi$

VALUE (°)	DOCUMENT ID		TECN	CHG	COMMENT
10.5±2.4±3.9	NOZAR	02	MPS	−	18 $\pi^- p \to \omega\pi^- p$

$b_1(1235)$ BRANCHING RATIOS

$\Gamma(\eta\rho)/\Gamma(\omega\pi)$ — **Γ_3/Γ_1**

VALUE	DOCUMENT ID		TECN	COMMENT
<0.10	ATKINSON	84D	OMEG	20–70 γp

$\Gamma(\pi^+\pi^+\pi^-\pi^0)/\Gamma(\omega\pi)$ — **Γ_4/Γ_1**

VALUE	DOCUMENT ID		TECN	CHG	COMMENT
<0.5	ABOLINS	63	HBC	+	3.5 $\pi^+ p$

Int. J. Mod. Phys. A 2026.41. Downloaded from www.worldscientific.com
by [redacted]LIFORNIA @ BERKELEY on 09/16/26. Re-use and distribution is strictly not permitted, except for Open Access articles.

Int. J. Mod. Phys. A 2026.41. Downloaded from www.worldscientific.com by UNIVERSITY OF CALIFORNIA @ BERKELEY on 09/16/26. Re-use and distribution is strictly not permitted, except for Open Access articles.

$\Gamma(K^*(892)^\pm K^\mp)/\Gamma_{total}$ — Γ_5/Γ

VALUE	DOCUMENT ID		TECN	COMMENT
seen	[1] ABLIKIM	10E	BES2	$J/\psi \to K^\pm K^0_S \pi^\mp \pi^0$

[1] From a fit including ten additional resonances and energy-independent Breit-Wigner width.

$\Gamma((K\overline{K})^\pm \pi^0)/\Gamma(\omega\pi)$ — Γ_6/Γ_1

VALUE	CL%	DOCUMENT ID		TECN	CHG	COMMENT
<0.08	90	BALTAY	67	HBC	$\pm$	0.0 $\overline{p}p$

$\Gamma(K^0_S K^0_L \pi^\pm)/\Gamma(\omega\pi)$ — Γ_7/Γ_1

VALUE	CL%	DOCUMENT ID		TECN	CHG	COMMENT
<0.06	90	BALTAY	67	HBC	$\pm$	0.0 $\overline{p}p$

$\Gamma(K^0_S K^0_S \pi^\pm)/\Gamma(\omega\pi)$ — Γ_8/Γ_1

VALUE	CL%	DOCUMENT ID		TECN	CHG	COMMENT
<0.02	90	BALTAY	67	HBC	$\pm$	0.0 $\overline{p}p$

$\Gamma(\phi\pi)/\Gamma(\omega\pi)$ — Γ_9/Γ_1

VALUE	CL%	DOCUMENT ID		TECN	CHG	COMMENT
<0.004	95	VIKTOROV	96	SPEC	0	32.5 $\pi^- p \to K^+ K^- \pi^0 n$
• • • We do not use the following data for averages, fits, limits, etc. • • •						
<0.04	95	BIZZARRI	69	HBC	$\pm$	0.0 $\overline{p}p$
<0.015		DAHL	67	HBC		1.6–4.2 $\pi^- p$

$b_1(1235)$ REFERENCES

ABLIKIM	10E	PL B693 88	M. Ablikim *et al.*	(BES II Collab.)
NOZAR	02	PL B541 35	M. Nozar *et al.*	
VIKTOROV	96	PAN 59 1184 Translated from YAF 59 1239.	V.A. Viktorov *et al.*	(SERP)
AMSLER	94C	PL B327 425	C. Amsler *et al.*	(Crystal Barrel Collab.)
AMSLER	93B	PL B311 362	C. Amsler *et al.*	(Crystal Barrel Collab.)
WEIDENAUER	93	ZPHY C59 387	P. Weidenauer *et al.*	(ASTERIX Collab.)
ALDE	92C	ZPHY C54 553	D.M. Alde *et al.*	(BELG, SERP, KEK, LANL+)
FUKUI	91	PL B257 241	S. Fukui *et al.*	(SUGI, NAGO, KEK, KYOT+)
AUGUSTIN	89	NP B320 1	J.E. Augustin, G. Cosme	(DM2 Collab.)
ATKINSON	84C	NP B243 1	M. Atkinson *et al.*	(BONN, CERN, GLAS+) JP
ATKINSON	84D	NP B242 269	M. Atkinson *et al.*	(BONN, CERN, GLAS+)
ATKINSON	84E	PL 138B 459	M. Atkinson *et al.*	(BONN, CERN, GLAS+)
COLLICK	84	PRL 53 2374	B. Collick *et al.*	(MINN, ROCH, FNAL)
EVANGELIS...	81	NP B178 197	C. Evangelista *et al.*	(BARI, BONN, CERN+)
BALTAY	78B	PR D17 62	C. Baltay *et al.*	(COLU, BING)
GESSAROLI	77	NP B126 382	R. Gessaroli *et al.*	(BGNA, FIRZ, GENO+) JP
FLATTE	76C	PL 64B 225	S.M. Flatte *et al.*	(CERN, AMST, NIJM+) JP
CHUNG	75B	PR D11 2426	S.U. Chung *et al.*	(BNL, LBL, UCSC) JP
CHALOUPKA	74	PL 51B 407	V. Chaloupka *et al.*	(CERN) JP
KARSHON	74B	PR D10 3608	U. Karshon *et al.*	(REHO) JP
BIZZARRI	69	NP B14 169	R. Bizzarri *et al.*	(CERN, CDEF)
BALTAY	67	PRL 18 93	C. Baltay *et al.*	(COLU)
DAHL	67	PR 163 1377	O.I. Dahl *et al.*	(LRL)
ABOLINS	63	PRL 11 381	M.A. Abolins *et al.*	(UCSD)

$a_1(1260)$

$I^G(J^{PC}) = 1^-(1^{++})$

See also our review under the $a_1(1260)$ in PDG 06, Journal of Physics **G33** 1 (2006).

$a_1(1260)$ T-MATRIX POLE $\sqrt{s}$

Note that $\Gamma = -2\,\mathrm{Im}(\sqrt{s})$.

VALUE (MeV)	DOCUMENT ID	TECN	COMMENT
$(1209^{+13}_{-10}) - i(288^{+45}_{-12})$ OUR ESTIMATE			
$(1209 \pm 4^{+12}_{-9}) - i\,(288 \pm 6^{+45}_{-10})$	MIKHASENKO 18	RVUE	$\tau^- \to \pi^-\pi^+\pi^-\nu_\tau$

$a_1(1260)$ MASS

VALUE (MeV)	EVTS	DOCUMENT ID		TECN	COMMENT
1230 ±40 OUR ESTIMATE					
1202 ±15 OUR AVERAGE Error includes scale factor of 2.7. See the ideogram below.					
1195.05 ± 1.05 ± 6.33	894k	[1] AAIJ	18AI	LHCB	$D^0 \to K^\mp\pi^\pm\pi^\pm\pi^\mp$
1299 $^{+12}_{-28}$	46M	[2,3] AGHASYAN	18B	COMP	190 $\pi^- p \to \pi^-\pi^+\pi^- p$
1225 ± 9 ±20	7k	[1,4] DARGENT	17	RVUE	$D^0 \to \pi^-\pi^+\pi^-\pi^+$
• • • We do not use the following data for averages, fits, limits, etc. • • •					
1255 ± 6 $^{+7}_{-17}$	420k	[5] ALEKSEEV	10	COMP	190 $\pi^- Pb \to \pi^-\pi^-\pi^+ Pb'$
1243 ±12 ±20		[6] AUBERT	07AU	BABR	10.6 $e^+e^- \to \rho^0\rho^\pm\pi^\mp\gamma$
1230–1270	6360	[7] LINK	07A	FOCS	$D^0 \to \pi^-\pi^+\pi^-\pi^+$
1203 ± 3		[8] GOMEZ-DUM...	04	RVUE	$\tau^+ \to \pi^+\pi^+\pi^-\nu_\tau$
1330 ±24	90k	SALVINI	04	OBLX	$\overline{p}p \to 2\pi^+2\pi^-$
1331 ±10 ± 3	37k	[9] ASNER	00	CLE2	10.6 $e^+e^- \to \tau^+\tau^-$, $\tau^- \to \pi^-\pi^0\pi^0\nu_\tau$
1255 ± 7 ± 6	5904	[10] ABREU	98G	DLPH	e^+e^-
1207 ± 5 ± 8	5904	[11] ABREU	98G	DLPH	e^+e^-
1196 ± 4 ± 5	5904	[12,13] ABREU	98G	DLPH	e^+e^-
1240 ±10		BARBERIS	98B		450 $pp \to p_f\pi^+\pi^-\pi^0 p_s$
1262 ± 9 ± 7		[10,14] ACKERSTAFF	97R	OPAL	E^{ee}_{cm}= 88–94, $\tau \to 3\pi\nu$
1210 ± 7 ± 2		[11,14] ACKERSTAFF	97R	OPAL	E^{ee}_{cm}= 88–94, $\tau \to 3\pi\nu$
1211 ± 7 $^{+50}_{-0}$		[11] ALBRECHT	93C	ARG	$\tau^+ \to \pi^+\pi^+\pi^-\nu$
1121 ± 8		[15] ANDO	92	SPEC	8 $\pi^- p \to \pi^+\pi^-\pi^0 n$
1242 ±37		[16] IVANOV	91	RVUE	$\tau \to \pi^+\pi^+\pi^-\nu$
1260 ±14		[17] IVANOV	91	RVUE	$\tau \to \pi^+\pi^+\pi^-\nu$
1250 ± 9		[18] IVANOV	91	RVUE	$\tau \to \pi^+\pi^+\pi^-\nu$
1208 ±15		ARMSTRONG	90	OMEG	300.0 $pp \to pp\pi^+\pi^-\pi^0$
1220 ±15		[19] ISGUR	89	RVUE	$\tau^+ \to \pi^+\pi^+\pi^-\nu$
1260 ±25		[20] BOWLER	88	RVUE	
1166 ±18 ±11		BAND	87	MAC	$\tau^+ \to \pi^+\pi^+\pi^-\nu$
1164 ±41 ±23		BAND	87	MAC	$\tau^+ \to \pi^+\pi^0\pi^0\nu$
1250 ±40		[19] TORNQVIST	87	RVUE	
1046 ±11		ALBRECHT	86B	ARG	$\tau^+ \to \pi^+\pi^+\pi^-\nu$
1056 ±20 ±15		RUCKSTUHL	86	DLCO	$\tau^+ \to \pi^+\pi^+\pi^-\nu$
1194 ±14 ±10		SCHMIDKE	86	MRK2	$\tau^+ \to \pi^+\pi^+\pi^-\nu$
1255 ±23		BELLINI	85	SPEC	40 $\pi^- A \to \pi^-\pi^+\pi^- A$
1240 ±80		[21] DANKOWY...	81	SPEC	8.45 $\pi^- p \to n3\pi$
1280 ±30		[21] DAUM	81B	CNTR	63,94 $\pi^- p \to p3\pi$
1041 ±13		[22] GAVILLET	77	HBC	4.2 $K^- p \to \Sigma 3\pi$

[1] Using Breit–Wigner functions and the covariant tensor formalism with exponential form factors, including the symmetrized $f_0\pi$ and $\rho\pi$ channels, as well as their interference.
[2] Statistical error negligible.
[3] Using Breit–Wigner functions and the helicity formalism with Blatt–Weisskopf form factors, including the symmetrized $\rho\pi$ channel.
[4] Reanalysis of CLEO data using Breit-Wigner parameterization.
[5] Superseded by AGHASYAN 18B.
[6] The $\rho^\pm\pi^\mp$ state can be also due to the $\pi(1300)$.
[7] Using the Breit-Wigner parameterization; strong correlation between mass and width.
[8] Using the data of BARATE 98R.
[9] From a fit to the 3π mass spectrum including the $K\overline{K}^*(892)$ threshold.
[10] Uses the model of KUHN 90.
[11] Uses the model of ISGUR 89.
[12] Includes the effect of a possible a_1' state.
[13] Uses the model of FEINDT 90.
[14] Supersedes AKERS 95P.
[15] Average and spread of values using 2 variants of the model of BOWLER 75.
[16] Reanalysis of RUCKSTUHL 86.
[17] Reanalysis of SCHMIDKE 86.
[18] Reanalysis of ALBRECHT 86B.
[19] From a combined reanalysis of ALBRECHT 86B, SCHMIDKE 86, and RUCKSTUHL 86.
[20] From a combined reanalysis of ALBRECHT 86B and DAUM 81B.
[21] Uses the model of BOWLER 75.
[22] Produced in K^- backward scattering.

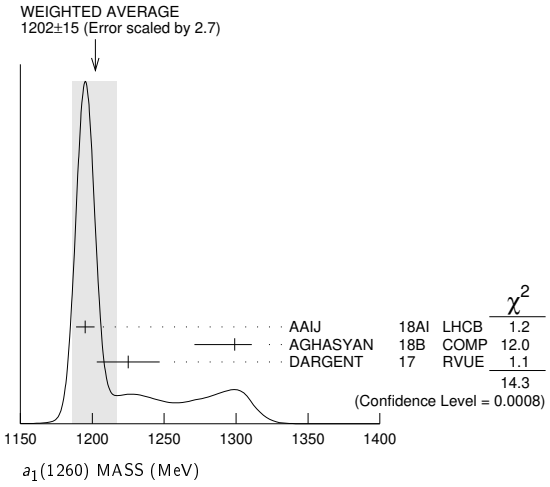

$a_1(1260)$ WIDTH

VALUE (MeV)	EVTS	DOCUMENT ID		TECN	COMMENT
250 to 600 OUR ESTIMATE					
422 ± 12 OUR AVERAGE					
422.01 ± 2.10 ± 12.72	894k	[1] AAIJ	18AI	LHCB	$D^0 \to K^\mp\pi^\pm\pi^\pm\pi^\mp$
380 ± 80	46M	[2,3] AGHASYAN	18B	COMP	190 $\pi^- p \to \pi^-\pi^+\pi^- p$
430 ± 24 ± 31		[1,4] DARGENT	17	RVUE	$D^0 \to \pi^-\pi^+\pi^-\pi^+$
• • • We do not use the following data for averages, fits, limits, etc. • • •					
367 ± 9 $^{+28}_{-25}$	420k	[5] ALEKSEEV	10	COMP	190 $\pi^- Pb \to \pi^-\pi^-\pi^+ Pb'$
410 ± 31 ± 30		[6] AUBERT	07AU	BABR	10.6 $e^+e^- \to \rho^0\rho^\pm\pi^\mp\gamma$

520–680		6360	[7] LINK	07A	FOCS	$D^0 \to \pi^-\pi^+\pi^-\pi^+$
480 ± 20			[8] GOMEZ-DUM..	04	RVUE	$\tau^+ \to \pi^+\pi^+\pi^-\nu_\tau$
580 ± 41		90k	SALVINI	04	OBLX	$\bar{p}p \to 2\pi^+2\pi^-$
460 ± 85		205	[9] DRUTSKOY	02	BELL	$B \to D^{(*)}K^-K^{*0}$
814 ± 36	± 13	37k	[10] ASNER	00	CLE2	10.6 $e^+e^- \to \tau^+\tau^-$, $\tau^- \to \pi^-\pi^0\pi^0\nu_\tau$
450 ± 50		22k	[11] AKHMETSHIN	99E	CMD2	1.05–1.38 $e^+e^- \to \pi^+\pi^-\pi^0\pi^0$
570 ± 10			[12] BONDAR	99	RVUE	$e^+e^- \to 4\pi$, $\tau \to 3\pi\nu_\tau$
587 ± 27	± 21	5904	[13] ABREU	98G	DLPH	e^+e^-
478 ± 3	± 15	5904	[14] ABREU	98G	DLPH	e^+e^-
425 ± 14	± 8	5904	[15,16] ABREU	98G	DLPH	e^+e^-
400 ± 35			BARBERIS	98B		450 $pp \to p_f\pi^+\pi^-\pi^0 p_s$
621 ± 32	± 58		[13,17] ACKERSTAFF	97R	OPAL	E^{ee}_{cm}= 88–94, $\tau \to 3\pi\nu$
457 ± 15	± 17		[14,17] ACKERSTAFF	97R	OPAL	E^{ee}_{cm}= 88–94, $\tau \to 3\pi\nu$
446 ± 21	$^{+140}_{-0}$		[14] ALBRECHT	93C	ARG	$\tau^+ \to \pi^+\pi^+\pi^-\nu$
239 ± 11			ANDO	92	SPEC	8 $\pi^-p \to \pi^+\pi^-\pi^0 n$
266 ± 13	± 4		[18] ANDO	92	SPEC	8 $\pi^-p \to \pi^+\pi^-\pi^0 n$
465	$^{+228}_{-143}$		[19] IVANOV	91	RVUE	$\tau \to \pi^+\pi^+\pi^-\nu$
298	$^{+40}_{-34}$		[20] IVANOV	91	RVUE	$\tau \to \pi^+\pi^+\pi^-\nu$
488 ± 32			[21] IVANOV	91	RVUE	$\tau \to \pi^+\pi^+\pi^-\nu$
430 ± 50			ARMSTRONG	90	OMEG	300.0$pp \to pp\pi^+\pi^-\pi^0$
420 ± 40			[22] ISGUR	89	RVUE	$\tau^+ \to \pi^+\pi^+\pi^-\nu$
396 ± 43			[23] BOWLER	88	RVUE	
405 ± 75	± 25		BAND	87	MAC	$\tau^+ \to \pi^+\pi^+\pi^-\nu$
419 ±108	± 57		BAND	87	MAC	$\tau^+ \to \pi^+\pi^0\pi^0\nu$
521 ± 27			ALBRECHT	86B	ARG	$\tau^+ \to \pi^+\pi^+\pi^-\nu$
476	$^{+132}_{-120}$	± 54	RUCKSTUHL	86	DLCO	$\tau^+ \to \pi^+\pi^+\pi^-\nu$
462 ± 56	± 30		SCHMIDKE	86	MRK2	$\tau^+ \to \pi^+\pi^+\pi^-\nu$
292 ± 40			BELLINI	85	SPEC	40 $\pi^-A \to \pi^-\pi^+\pi^-A$
380 ±100			[24] DANKOWY...	81	SPEC	8.45 $\pi^-p \to n3\pi$
300 ± 50			[24] DAUM	81B	CNTR	63,94 $\pi^-p \to p3\pi$
230 ± 50			[25] GAVILLET	77	HBC	4.2 $K^-p \to \Sigma 3\pi$

[1] Using Breit–Wigner functions and the covariant tensor formalism with equational form factors, including the symmetrized $f_0\pi$ and $\rho\pi$ channels, as well as their interference.
[2] Statistical error negligible.
[3] Using Breit–Wigner functions and the helicity formalism with Blatt–Weisskopf form factors, including the symmetrized $\rho\pi$ channel.
[4] Reanalysis of CLEO data using Breit-Wigner parameterization.
[5] Superseded by AGHASYAN 18B.
[6] The $\rho^\pm\pi^\mp$ state can be also due to the $\pi(1300)$.
[7] Using the Breit-Wigner parameterization; strong correlation between mass and width.
[8] Using the data of BARATE 98R.
[9] From a fit of the K^-K^{*0} distribution assuming m_{a_1}= 1230 MeV and purely resonant production of the K^-K^{*0} system.
[10] From a fit to the 3π mass spectrum including the $K\overline{K}^*(892)$ threshold.
[11] Using the $a_1(1260)$ mass of 1230 MeV.
[12] From AKHMETSHIN 99E and ASNER 00 data using the $a_1(1260)$ mass of 1230 MeV.
[13] Uses the model of KUHN 90.
[14] Uses the model of ISGUR 89.
[15] Includes the effect of a possible a_1' state.
[16] Uses the model of FEINDT 90.
[17] Supersedes AKERS 95P.
[18] Average and spread of values using 2 variants of the model of BOWLER 75.
[19] Reanalysis of RUCKSTUHL 86.
[20] Reanalysis of SCHMIDKE 86.
[21] Reanalysis of ALBRECHT 86B.
[22] From a combined reanalysis of ALBRECHT 86B, SCHMIDKE 86, and RUCKSTUHL 86.
[23] From a combined reanalysis of ALBRECHT 86B and DAUM 81B.
[24] Uses the model of BOWLER 75.
[25] Produced in K^- backward scattering.

$a_1(1260)$ DECAY MODES

	Mode	Fraction (Γ_i/Γ)
Γ_1	3π	seen
Γ_2	$(\rho\pi)_{S-\text{wave}}$, $\rho \to \pi\pi$	seen
Γ_3	$(\rho\pi)_{D-\text{wave}}$, $\rho \to \pi\pi$	seen
Γ_4	$(\rho(1450)\pi)_{S-\text{wave}}$, $\rho \to \pi\pi$	seen
Γ_5	$(\rho(1450)\pi)_{D-\text{wave}}$, $\rho \to \pi\pi$	seen
Γ_6	$f_0(500)\pi$, $f_0 \to \pi\pi$	seen
Γ_7	$f_0(980)\pi$, $f_0 \to \pi\pi$	seen
Γ_8	$f_0(1370)\pi$, $f_0 \to \pi\pi$	seen
Γ_9	$f_2(1270)\pi$, $f_2 \to \pi\pi$	seen
Γ_{10}	$\pi^+\pi^-\pi^0$	seen
Γ_{11}	$\pi^0\pi^0\pi^0$	not seen
Γ_{12}	$KK\pi$	seen
Γ_{13}	$K^*(892)K$	seen
Γ_{14}	$\pi\gamma$	seen

$a_1(1260)$ PARTIAL WIDTHS

$\Gamma(\pi\gamma)$ — Γ_{14}

VALUE (keV)	DOCUMENT ID		TECN	COMMENT
640±246	ZIELINSKI	84C	SPEC	200 $\pi^+Z \to Z3\pi$

D-wave/S-wave AMPLITUDE RATIO IN DECAY OF $a_1(1260) \to \rho\pi$

VALUE	DOCUMENT ID		TECN	COMMENT
−0.062±0.020 OUR AVERAGE	Error includes scale factor of 2.3. See the ideogram below.			
−0.043±0.009±0.005	LINK	07A	FOCS	$D^0 \to \pi^-\pi^+\pi^-\pi^+$
−0.14 ±0.04 ±0.07	[1] CHUNG	02	B852	18.3 $\pi^-p \to \pi^+\pi^-\pi^-p$
−0.10 ±0.02 ±0.02	[2,3] ACKERSTAFF	97R	OPAL	E^{ee}_{cm}= 88–94, $\tau \to 3\pi\nu$
−0.11 ±0.02	[2] ALBRECHT	93C	ARG	$\tau^+ \to \pi^+\pi^+\pi^-\nu$

[1] Deck-type background not subtracted.
[2] Uses the model of ISGUR 89.
[3] Supersedes AKERS 95P.

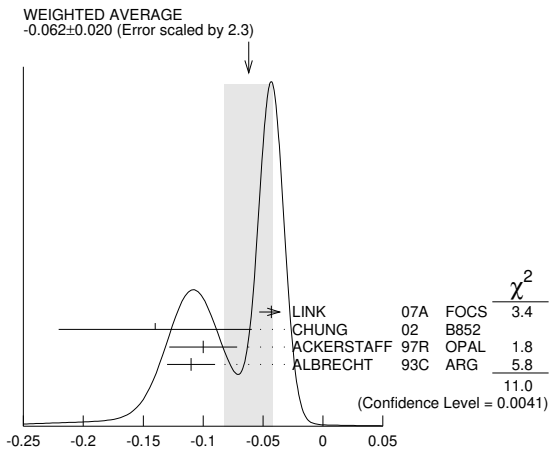

D-wave/S-wave AMPLITUDE RATIO IN DECAY OF $a_1(1260) \to \rho\pi$

$a_1(1260)$ BRANCHING RATIOS

$\Gamma((\rho\pi)_{S-\text{wave}}, \rho \to \pi\pi)/\Gamma_{\text{total}}$ — Γ_2/Γ

VALUE (units 10^{-2})	EVTS	DOCUMENT ID		TECN	COMMENT
• • • We do not use the following data for averages, fits, limits, etc. • • •					
60.19	37k	[1] ASNER	00	CLE2	10.6 $e^+e^- \to \tau^+\tau^-$, $\tau^- \to \pi^-\pi^0\pi^0\nu_\tau$

[1] From a fit to the Dalitz plot.

$\Gamma((\rho\pi)_{D-\text{wave}}, \rho \to \pi\pi)/\Gamma_{\text{total}}$ — Γ_3/Γ

VALUE (units 10^{-2})	EVTS	DOCUMENT ID		TECN	COMMENT
• • • We do not use the following data for averages, fits, limits, etc. • • •					
1.30±0.60±0.22	37k	[1] ASNER	00	CLE2	10.6 $e^+e^- \to \tau^+\tau^-$, $\tau^- \to \pi^-\pi^0\pi^0\nu_\tau$

[1] From a fit to the Dalitz plot.

$\Gamma((\rho(1450)\pi)_{S-\text{wave}}, \rho \to \pi\pi)/\Gamma_{\text{total}}$ — Γ_4/Γ

VALUE (units 10^{-2})	EVTS	DOCUMENT ID		TECN	COMMENT
• • • We do not use the following data for averages, fits, limits, etc. • • •					
0.56±0.84±0.32	37k	[1,2] ASNER	00	CLE2	10.6 $e^+e^- \to \tau^+\tau^-$, $\tau^- \to \pi^-\pi^0\pi^0\nu_\tau$

[1] From a fit to the Dalitz plot.
[2] Assuming for $\rho(1450)$ mass and width of 1370 and 386 MeV respectively.

$\Gamma((\rho(1450)\pi)_{D-\text{wave}}, \rho \to \pi\pi)/\Gamma_{\text{total}}$ — Γ_5/Γ

VALUE (units 10^{-2})	EVTS	DOCUMENT ID		TECN	COMMENT
• • • We do not use the following data for averages, fits, limits, etc. • • •					
2.04±1.20±0.28	37k	[1,2] ASNER	00	CLE2	10.6 $e^+e^- \to \tau^+\tau^-$, $\tau^- \to \pi^-\pi^0\pi^0\nu_\tau$

[1] From a fit to the Dalitz plot.
[2] Assuming for $\rho(1450)$ mass and width of 1370 and 386 MeV respectively.

Int. J. Mod. Phys. A 2026.41. Downloaded from www.worldscientific.com
by [redacted]LIFORNIA @ BERKELEY on 09/16/26. Re-use and distribution is strictly not permitted, except for Open Access articles.

Int. J. Mod. Phys. A 2026.41. Downloaded from www.worldscientific.com
by UNIVERSITY OF CALIFORNIA @ BERKELEY on 09/16/26. Re-use and distribution is strictly not permitted, except for Open Access articles.

$\Gamma(f_0(500)\pi,\ f_0 \to \pi\pi)/\Gamma_{total}$ — Γ_6/Γ

VALUE (units 10^{-2})	EVTS	DOCUMENT ID		TECN	COMMENT
• • • We do not use the following data for averages, fits, limits, etc. • • •					
seen		CHUNG	02	B852	18.3 $\pi^- p \to \pi^+\pi^-\pi^- p$
18.76±4.29±1.48	37k	[1,2] ASNER	00	CLE2	10.6 $e^+e^- \to \tau^+\tau^-$, $\tau^- \to \pi^-\pi^0\pi^0\nu_\tau$

[1] From a fit to the Dalitz plot.
[2] Assuming for $f_0(500)$ (σ) mass and width of 860 and 880 MeV respectively.

$\Gamma(f_0(500)\pi,\ f_0 \to \pi\pi)/[\Gamma((\rho\pi)_{S\text{-wave}},\ \rho \to \pi\pi) + \Gamma((\rho\pi)_{S\text{-wave}},\ \rho \to \pi\pi)]$ — $\Gamma_6/(\Gamma_2+\Gamma_2)$

VALUE	EVTS	DOCUMENT ID		TECN	COMMENT
• • • We do not use the following data for averages, fits, limits, etc. • • •					
0.06 ±0.05	90k	SALVINI	04	OBLX	$\overline{p}p \to 2\pi^+2\pi^-$
∼ 0.3	28k	AKHMETSHIN	99E	CMD2	1.05–1.38 $e^+e^- \to \pi^+\pi^-\pi^+\pi^-$
0.003±0.003		[1] LONGACRE	82	RVUE	

[1] Uses multichannel Aitchison-Bowler model (BOWLER 75). Uses data from GAVILLET 77, DAUM 80, and DANKOWYCH 81.

$\Gamma(f_0(980)\pi,\ f_0 \to \pi\pi)/\Gamma_{total}$ — Γ_7/Γ

VALUE	EVTS	DOCUMENT ID		TECN	COMMENT
seen		[1] ALEXEEV	21	COMP	$\pi^- p \to \pi^-\pi^+\pi^- p$
• • • We do not use the following data for averages, fits, limits, etc. • • •					
not seen	37k	ASNER	00	CLE2	10.6 $e^+e^- \to \tau^+\tau^-$, $\tau^- \to \pi^-\pi^0\pi^0\nu_\tau$

[1] The $a_1(1260)^- \to f_0(980)\pi^-$ decay mode via the Triangle Singularity mechanism from MIKHASENKO 15 and ACETI 16 explains the $a_1(1420)^-$ signal observed by ADOLPH 15C.

$\Gamma(f_0(1370)\pi,\ f_0 \to \pi\pi)/\Gamma_{total}$ — Γ_8/Γ

VALUE (units 10^{-2})	EVTS	DOCUMENT ID		TECN	COMMENT
• • • We do not use the following data for averages, fits, limits, etc. • • •					
7.40±2.71±1.26	37k	[1,2] ASNER	00	CLE2	10.6 $e^+e^- \to \tau^+\tau^-$, $\tau^- \to \pi^-\pi^0\pi^0\nu_\tau$

[1] From a fit to the Dalitz plot.
[2] Assuming for $f_0(1370)$ mass and width of 1186 and 350 MeV respectively.

$\Gamma(f_2(1270)\pi,\ f_2 \to \pi\pi)/\Gamma_{total}$ — Γ_9/Γ

VALUE (units 10^{-2})	EVTS	DOCUMENT ID		TECN	COMMENT
• • • We do not use the following data for averages, fits, limits, etc. • • •					
1.19±0.49±0.17	37k	[1,2] ASNER	00	CLE2	10.6 $e^+e^- \to \tau^+\tau^-$, $\tau^- \to \pi^-\pi^0\pi^0\nu_\tau$

[1] From a fit to the Dalitz plot.
[2] Assuming for $f_2(1270)$ mass and width of 1275 and 185 MeV respectively.

$\Gamma(\pi^+\pi^-\pi^0)/\Gamma_{total}$ — Γ_{10}/Γ

VALUE	DOCUMENT ID		COMMENT
seen	BARBERIS	98B	450 $pp \to p_f\pi^+\pi^-\pi^0 p_s$

$\Gamma(\pi^0\pi^0\pi^0)/\Gamma(\pi^+\pi^-\pi^0)$ — Γ_{11}/Γ_{10}

VALUE	CL%	DOCUMENT ID		COMMENT
• • • We do not use the following data for averages, fits, limits, etc. • • •				
<0.008	90	[1] BARBERIS	01	450 $pp \to p_f 3\pi^0 p_s$

[1] Inconsistent with observations of $\sigma\pi$, $f_0(1370)\pi$, and $f_2(1270)\pi$ decay modes.

$\Gamma(K^*(892)K)/\Gamma_{total}$ — Γ_{13}/Γ

VALUE (units 10^{-2})	EVTS	DOCUMENT ID		TECN	COMMENT
• • • We do not use the following data for averages, fits, limits, etc. • • •					
2.2±0.5	2255	[1] COAN	04	CLEO	$\tau^- \to K^-\pi^-K^+\nu_\tau$
8 to 15	205	[2] DRUTSKOY	02	BELL	$B \to D^{(*)}K^-K^{*0}$
3.3±0.5±0.1	37k	[3] ASNER	00	CLE2	10.6 $e^+e^- \to \tau^+\tau^-$, $\tau^- \to \pi^-\pi^0\pi^0\nu_\tau$
2.6±0.3		[4] BARATE	99R	ALEP	$\tau \to K\overline{K}\pi\nu_\tau$

[1] Using structure functions from KUHN 92 and DECKER 93A and $B(\tau^- \to K^-\pi^-K^+\nu_\tau) = (0.155 \pm 0.006 \pm 0.009)\%$ from BRIERE 03.
[2] From a comparison to ALAM 94 assuming purely resonant production of the K^-K^{*0} system.
[3] From a fit to the 3π mass spectrum including the $K\overline{K}^*(892)$ threshold.
[4] Assuming $a_1(1260)$ dominance and taking $B(\tau \to a_1(1260)\nu_\tau)$ from BUSKULIC 96.

$a_1(1260)$ REFERENCES

ALEXEEV	21	PRL 127 082501	G.D. Alexeev et al.	(COMPASS Collab.)
AAIJ	18AI	EPJ C78 443	R. Aaij et al.	(LHCb Collab.)
AGHASYAN	18B	PR D98 092003	M. Aghasyan et al.	(COMPASS Collab.)
MIKHASENKO	18	PR D98 096021	M. Mikhasenko et al.	(JPAC Collab.)
DARGENT	17	JHEP 1705 143	P. dArgent et al.	(HEID, BRIS)
ACETI	16	PR D94 096015	F. Aceti, L.R. Dai, E. Oset	(IFIC, LNUDA)
ADOLPH	15C	PRL 115 082001	C. Adolph et al.	(COMPASS Collab.)
MIKHASENKO	15	PR D91 094015	M. Mikhasenko, B. Ketzer, A. Sarantsev	(BONN+)
ALEKSEEV	10	PRL 104 241803	M.G. Alekseev et al.	(COMPASS Collab.)
AUBERT	07AU	PR D76 092005	B. Aubert et al.	(BABAR Collab.)
LINK	07A	PR D75 052003	J.M. Link et al.	(FNAL FOCUS Collab.)
PDG	06	JP G33 1	W.-M. Yao et al.	(PDG Collab.)
COAN	04	PRL 92 232001	T.E. Coan et al.	(CLEO Collab.)
GOMEZ-DUM...	04	PR D69 073002	D. Gomez Dumm, A. Pich, J. Portoles	
SALVINI	04	EPJ C35 21	P. Salvini et al.	(OBELIX Collab.)
BRIERE	03	PRL 90 181802	R. A. Briere et al.	(CLEO Collab.)
CHUNG	02	PR D65 072001	S.U. Chung et al.	(BNL E852 Collab.)
DRUTSKOY	02	PL B542 171	A. Drutskoy et al.	(BELLE Collab.)
BARBERIS	01	PL B507 14	D. Barberis et al.	
ASNER	00	PR D61 012002	D.M. Asner et al.	(CLEO Collab.)
AKHMETSHIN	99E	PL B466 392	R.R. Akhmetshin et al.	(Novosibirsk CMD-2 Collab.)
BARATE	99R	EPJ C11 599	R. Barate et al.	(ALEPH Collab.)
BONDAR	99	PL B466 403	A.E. Bondar et al.	(Novosibirsk CMD-2 Collab.)
ABREU	98G	PL B426 411	P. Abreu et al.	(DELPHI Collab.)
BARATE	98R	EPJ C4 409	R. Barate et al.	(ALEPH Collab.)
BARBERIS	98B	PL B422 399	D. Barberis et al.	(WA 102 Collab.)
ACKERSTAFF	97R	ZPHY C75 593	K. Ackerstaff et al.	(OPAL Collab.)
BUSKULIC	96	ZPHY C70 579	D. Buskulic et al.	(ALEPH Collab.)
AKERS	95P	ZPHY C67 45	R. Akers et al.	(OPAL Collab.)
ALAM	94	PR D50 43	M.S. Alam et al.	(CLEO Collab.)
ALBRECHT	93C	ZPHY C58 61	H. Albrecht et al.	(ARGUS Collab.)
DECKER	93A	ZPHY C58 445	R. Decker et al.	
ANDO	92	PL B291 496	A. Ando et al.	(KEK, KYOT, NIRS, SAGA+)
KUHN	92	ZPHY C56 661	J.H. Kuhn, E. Mirkes	
IVANOV	91	ZPHY C49 563	Y.P. Ivanov, A.A. Osipov, M.K. Volkov	(JINR)
ARMSTRONG	90	ZPHY C48 213	T.A. Armstrong, M. Benayoun, W. Beusch	(WA76 Coll.)
FEINDT	90	ZPHY C48 681	M. Feindt	(HAMB)
KUHN	90	ZPHY C48 445	J.H. Kuhn et al.	(MPIM)
ISGUR	89	PR D39 1357	N. Isgur, C. Morningstar, C. Reader	(TNTO)
BOWLER	88	PL B209 99	M.G. Bowler	(OXF)
BAND	87	PL B198 297	H.R. Band et al.	(MAC Collab.)
TORNQVIST	87	ZPHY C36 695	N.A. Tornqvist	(HELS)
ALBRECHT	86B	ZPHY C33 7	H. Albrecht et al.	(ARGUS Collab.)
RUCKSTUHL	86	PRL 56 2132	W. Ruckstuhl et al.	(DELCO Collab.)
SCHMIDKE	86	PRL 57 527	W.B. Schmidke et al.	(Mark II Collab.)
BELLINI	85	SJNP 41 781	D. Bellini et al.	
		Translated from YAF 41 1223.		
ZIELINSKI	84C	PRL 52 1195	M. Zielinski et al.	(ROCH, MINN, FNAL)
LONGACRE	82	PR D26 82	R.S. Longacre	(BNL)
DANKOWY...	81	PRL 46 580	J.A. Dankowych et al.	(TNTO, BNL, CARL+)
DAUM	81B	NP B182 269	C. Daum et al.	(AMST, CERN, CRAC, MPIM+)
DAUM	80	PL 89B 281	C. Daum et al.	(AMST, CERN, CRAC, MPIM+) JP
GAVILLET	77	PL 69B 119	P. Gavillet et al.	(AMST, CERN, NIJM+) JP
BOWLER	75	NP B97 227	M.G. Bowler et al.	(OXFTP, DARE)

$f_2(1270)$

$I^G(J^{PC}) = 0^+(2^{++})$

$f_2(1270)$ T-MATRIX POLE $\sqrt{s}$

Note that $\Gamma = -2\,\mathrm{Im}(\sqrt{s})$.

VALUE (MeV)	DOCUMENT ID		TECN	COMMENT
(1260–1283) − i (90–110) OUR ESTIMATE				
(1226.2 ± 8.6 ± 8.8) − i (78.9 ± 7.5 ± 11.7)	ABLIKIM	25CD	BES3	$e^+e^- \to \psi(2S)$
(1268 ± 8) − i (101 ± 6)	RODAS	22	RVUE	$J/\psi(1S) \to \gamma(\pi\pi,\ K\overline{K})$
(1263.3 ± 0.2 ± 1.5) − i (96.9 ± 0.2 ± 0.8)	ALBRECHT	20	RVUE	$\overline{p}p \to \pi^0\pi^0\eta,\ \pi^0\eta\eta,\ \pi^0K^+K^-$
(1270 ± 8) − i (97 ± 8)	[1] ANISOVICH	09	RVUE	0.0 $\overline{p}p$, πN
(1278 ± 5) − i (102 ± 10)	[1] BERTIN	97C	OBLX	0.0 $\overline{p}p \to \pi^+\pi^-\pi^0$

[1] Amplitude did not include dispersive corrections.

$f_2(1270)$ MASS

VALUE (MeV)	EVTS	DOCUMENT ID		TECN	COMMENT
1275.4± 0.8 OUR AVERAGE		Error includes scale factor of 1.1.			
1275.8± 1.0±0.4		[1] BOGOLYUB...	13	SPEC	$7\pi^+(K^+,p)A \to n\gamma + X$
1262 $^{+1}_{-2}$ ±8		[2] ABLIKIM	06V	BES2	$e^+e^- \to J/\psi \to \gamma\pi^+\pi^-$
1275 ±15		ABLIKIM	05	BES2	$J/\psi \to \phi\pi^+\pi^-$
1283 ± 5		ALDE	98	GAM4	100 $\pi^- p \to \pi^0\pi^0 n$
1272 ± 8	200k	PROKOSHKIN	94	GAM2	38 $\pi^- p \to \pi^0\pi^0 n$
1269.7± 5.2	5730	AUGUSTIN	89	DM2	$e^+e^- \to 5\pi$
1283 ± 8	400	[3] ALDE	87	GAM4	100 $\pi^- p \to 4\pi^0 n$
1274 ± 5		[3] AUGUSTIN	87	DM2	$J/\psi \to \gamma\pi^+\pi^-$
1283 ± 6		[4] LONGACRE	86	MPS	22 $\pi^- p \to n2K^0_S$
1276 ± 7		COURAU	84	DLCO	$e^+e^- \to e^+e^-\pi^+\pi^-$
1273.3± 2.3		[5] CHABAUD	83	ASPK	17 $\pi^- p$ polarized
1280 ± 4		[6] CASON	82	STRC	8 $\pi^+ p \to \Delta^{++}\pi^0\pi^0$
1281 ± 7	11600	GIDAL	81	MRK2	J/ψ decay
1282 ± 5		[7] CORDEN	79	OMEG	12–15 $\pi^- p \to n2\pi$
1269 ± 4	10k	APEL	75	NICE	40 $\pi^- p \to n2\pi^0$
1272 ± 4	4600	ENGLER	74	DBC	6 $\pi^+ n \to \pi^+\pi^- p$
1277 ± 4	5300	FLATTE	71	HBC	7.0 $\pi^+ p$
1273 ± 8		[3] STUNTEBECK	70	HBC	8 $\pi^- p$, 5.4 $\pi^+ d$
1265 ± 8		BOESEBECK	68	HBC	8 $\pi^+ p$
• • • We do not use the following data for averages, fits, limits, etc. • • •					
1257 ± 6		[8] KLEMPT	22	RVUE	$J/\psi(1S) \to \gamma\pi^0\pi^0$, $\gamma K^0_S K^0_S$
1263 ±12		CARVER	21	CLAS	$\gamma p \to \pi^0\pi^0 p$
1259 ± 4 ±4	1.7k	[9,10] DOBBS	15		$J/\psi \to \gamma\pi^+\pi^-$
1267 ± 4 ±3	1.5k	[9,10] DOBBS	15		$\psi(2S) \to \gamma\pi^+\pi^-$
1277 ± 6	870	[11] SCHEGELSKY	06A	RVUE	$\gamma\gamma \to K^0_S K^0_S$
1251 ±10		TIKHOMIROV	03	SPEC	40.0 $\pi^- C \to K^0_S K^0_S K^0_L X$
1260 ±10		[12] ALDE	97	GAM2	450 $pp \to pp\pi^0\pi^0$

1278 ± 6		[12] GRYGOREV	96	SPEC	40 $\pi^- N \to K^0_S K^0_S X$
1262 ±11		AGUILAR-...	91	EHS	400 pp
1275 ±10		AKER	91	CBAR	0.0 $\overline{p}p \to 3\pi^0$
1220 ±10		BREAKSTONE	90	SFM	$pp \to pp\pi^+\pi^-$
1288 ±12		ABACHI	86B	HRS	$e^+e^- \to \pi^+\pi^- X$
1284 ±30	3k	BINON	83	GAM2	38 $\pi^- p \to n2\eta$
1280 ±20	3k	APEL	82	CNTR	25 $\pi^- p \to n2\pi^0$
1284 ±10	16000	DEUTSCH...	76	HBC	16 $\pi^+ p$
1258 ±10	600	TAKAHASHI	72	HBC	8 $\pi^- p \to n2\pi$
1275 ±13		ARMENISE	70	HBC	9 $\pi^+ n \to p\pi^+\pi^-$
1261 ± 5	1960	[3] ARMENISE	68	DBC	5.1 $\pi^+ n \to p\pi^+ MM^-$
1270 ±10	360	[3] ARMENISE	68	DBC	5.1 $\pi^+ n \to p\pi^0 MM$
1268 ± 6		[13] JOHNSON	68	HBC	3.7–4.2 $\pi^- p$

[1] Averaged over six nuclear targets, no statistically significant dependence on target nucleus observed.
[2] Breit-Wigner mass.
[3] Mass errors enlarged by us to $\Gamma/\sqrt{N}$; see the note with the $K^*(892)$ mass.
[4] From a partial-wave analysis of data using a K-matrix formalism with 5 poles.
[5] From an energy-independent partial-wave analysis.
[6] From an amplitude analysis of the reaction $\pi^+\pi^- \to 2\pi^0$.
[7] From an amplitude analysis of $\pi^+\pi^- \to \pi^+\pi^-$ scattering data.
[8] Fit of the tensor partial waves from BES3 in the multipole basis.
[9] Using CLEO-c data but not authored by the CLEO Collaboration.
[10] From a fit to a Breit-Wigner line shape with fixed $\Gamma = 185$ MeV.
[11] From analysis of L3 data at 91 and 183–209 GeV.
[12] Systematic uncertainties not estimated.
[13] JOHNSON 68 includes BONDAR 63, LEE 64, DERADO 65, EISNER 67.

$f_2(1270)$ WIDTH

VALUE (MeV)	EVTS	DOCUMENT ID		TECN	COMMENT
$\mathbf{186.6^{+2.8}_{-2.2}}$ **OUR FIT** Error includes scale factor of 1.5.					
$\mathbf{185.8^{+2.8}_{-2.1}}$ **OUR AVERAGE** Error includes scale factor of 1.6. See the ideogram below.					
190.3± 1.9± 1.8		[1] BOGOLYUB...	13	SPEC	$7\pi^+(K^+,p)A \to n\gamma + X$
175^{+6}_{-4} ±10		[2] ABLIKIM	06V	BES2	$e^+e^- \to J/\psi \to \gamma\pi^+\pi^-$
190 ±20		ABLIKIM	05	BES2	$J/\psi \to \phi\pi^+\pi^-$
171 ±10		ALDE	98	GAM4	100 $\pi^- p \to \pi^0\pi^0 n$
192 ± 5	200k	PROKOSHKIN	94	GAM2	38 $\pi^- p \to \pi^0\pi^0 n$
180 ±24		AGUILAR-...	91	EHS	400 pp
169 ± 9	5730	[3] AUGUSTIN	89	DM2	$e^+e^- \to 5\pi$
150 ±30	400	[3] ALDE	87	GAM4	100 $\pi^- p \to 4\pi^0 n$
186^{+9}_{-2}		[4] LONGACRE	86	MPS	22 $\pi^- p \to n2K^0_S$
$179.2^{+6.9}_{-6.6}$		[5] CHABAUD	83	ASPK	17 $\pi^- p$ polarized
160 ±11		DENNEY	83	LASS	10 $\pi^+ N$
196 ±10	3k	APEL	82	CNTR	25 $\pi^- p \to n2\pi^0$
152 ± 9		[6] CASON	82	STRC	8 $\pi^+ p \to \Delta^{++}\pi^0\pi^0$
186 ±27	11600	GIDAL	81	MRK2	J/ψ decay
216 ±13		[7] CORDEN	79	OMEG	12–15 $\pi^- p \to n2\pi$
190 ±10	10k	APEL	75	NICE	40 $\pi^- p \to n2\pi^0$
192 ±16	4600	ENGLER	74	DBC	6 $\pi^+ n \to \pi^+\pi^- p$
183 ±15	5300	FLATTE	71	HBC	7 $\pi^+ p \to \Delta^{++} f_2$
196 ±30		[3] STUNTEBECK	70	HBC	8 $\pi^- p$, 5.4 $\pi^+ d$
216 ±20	1960	[3] ARMENISE	68	DBC	5.1 $\pi^+ n \to p\pi^+ MM^-$
128 ±27		[3] BOESEBECK	68	HBC	8 $\pi^+ p$
176 ±21		[3,8] JOHNSON	68	HBC	3.7–4.2 $\pi^- p$
• • • We do not use the following data for averages, fits, limits, etc. • • •					
168 ± 7		[9] KLEMPT	22	RVUE	$J/\psi(1S) \to \gamma\pi^0\pi^0$, $\gamma K^0_S K^0_S$
183 ± 2		CARVER	21	CLAS	$\gamma p \to \pi^0\pi^0 p$
195 ±15	870	[10] SCHEGELSKY	06A	RVUE	$\gamma\gamma \to K^0_S K^0_S$
121 ±26		TIKHOMIROV	03	SPEC	40.0 $\pi^- C \to K^0_S K^0_S K^0_L X$
187 ±20		[11] ALDE	97	GAM2	450 $pp \to pp\pi^0\pi^0$
184 ±10		[11] GRYGOREV	96	SPEC	40 $\pi^- N \to K^0_S K^0_S X$
200 ±10		AKER	91	CBAR	0.0 $\overline{p}p \to 3\pi^0$
240 ±40	3k	BINON	83	GAM2	38 $\pi^- p \to n2\eta$
187 ±30	650	[3] ANTIPOV	77	CIBS	25 $\pi^- p \to p3\pi$
225 ±38	16000	DEUTSCH...	76	HBC	16 $\pi^+ p$
166 ±28	600	[3] TAKAHASHI	72	HBC	8 $\pi^- p \to n2\pi$
173 ±53		[3] ARMENISE	70	HBC	9 $\pi^+ n \to p\pi^+\pi^-$

[1] Averaged over six nuclear targets, no statistically significant dependence on target nucleus observed.
[2] Breit-Wigner width
[3] Width errors enlarged by us to $4\Gamma/\sqrt{N}$; see the note with the $K^*(892)$ mass.
[4] From a partial-wave analysis of data using a K-matrix formalism with 5 poles.
[5] From an energy-independent partial-wave analysis.
[6] From an amplitude analysis of the reaction $\pi^+\pi^- \to 2\pi^0$.
[7] From an amplitude analysis of $\pi^+\pi^- \to \pi^+\pi^-$ scattering data.
[8] JOHNSON 68 includes BONDAR 63, LEE 64, DERADO 65, EISNER 67.
[9] Fit of the tensor partial waves from BES3 in the multipole basis.
[10] From analysis of L3 data at 91 and 183–209 GeV.
[11] Systematic uncertainties not estimated.

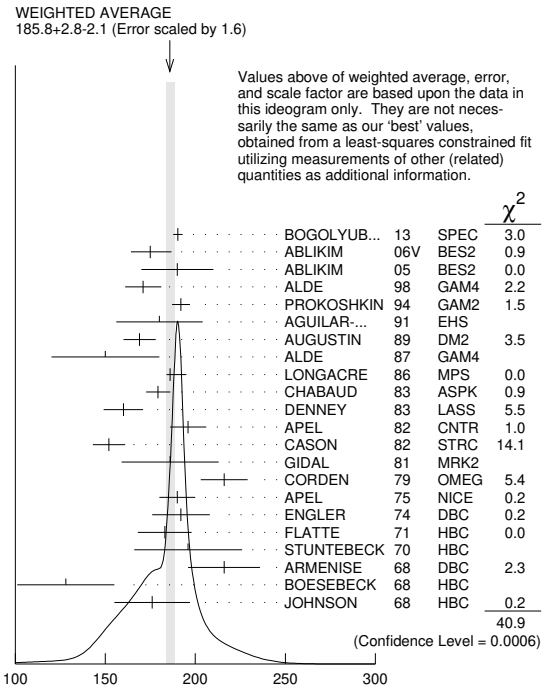

$f_2(1270)$ DECAY MODES

	Mode	Fraction (Γ_i/Γ)	Scale factor/ Confidence level
Γ_1	$\pi\pi$	$(84.3^{+2.8}_{-1.0})$ %	S=1.2
Γ_2	$\pi^+\pi^- 2\pi^0$	$(7.7^{+1.2}_{-3.1})$ %	S=1.2
Γ_3	$K\overline{K}$	(4.6 ±0.4) %	S=2.7
Γ_4	$2\pi^+ 2\pi^-$	(2.8 ±0.4) %	S=1.2
Γ_5	$\eta\eta$	(4.0 ±0.8) $\times 10^{-3}$	S=2.1
Γ_6	$4\pi^0$	(3.0 ±1.0) $\times 10^{-3}$	
Γ_7	$\gamma\gamma$	(1.42±0.24) $\times 10^{-5}$	S=1.4
Γ_8	$\eta\pi\pi$	< 8 $\times 10^{-3}$	CL=95%
Γ_9	$K^0 K^- \pi^+$ + c.c.	< 3.4 $\times 10^{-3}$	CL=95%
Γ_{10}	e^+e^-	< 6 $\times 10^{-10}$	CL=90%

CONSTRAINED FIT INFORMATION

An overall fit to the total width, 4 partial widths, a combination of partial widths obtained from integrated cross sections, and 6 branching ratios uses 44 measurements and one constraint to determine 8 parameters. The overall fit has a $\chi^2 = 82.3$ for 37 degrees of freedom.

The following *off-diagonal* array elements are the correlation coefficients $\langle \delta p_i \delta p_j \rangle / (\delta p_i \cdot \delta p_j)$, in percent, from the fit to parameters p_i, including the branching fractions, $x_i \equiv \Gamma_i/\Gamma_{total}$. The fit constrains the x_i whose labels appear in this array to sum to one.

	x_1	x_2	x_3	x_4	x_5	x_6	x_7
x_2	−91						
x_3	10	−39					
x_4	10	−38	1				
x_5	1	−6	0	0			
x_6	0	−7	0	0	0		
x_7	4	1	−15	0	0	0	
Γ	−72	66	−10	−7	−1	0	−6

	Mode	Rate (MeV)	Scale factor
Γ_1	$\pi\pi$	$157.2^{+5.0}_{-1.0}$	
Γ_2	$\pi^+\pi^- 2\pi^0$	$14.3^{+2.3}_{-6.0}$	1.3

Int. J. Mod. Phys. A 2026.41. Downloaded from www.worldscientific.com
by LIFORNIA @ BERKELEY on 09/16/26. Re-use and distribution is strictly not permitted, except for Open Access articles.

Γ_3	$K\overline{K}$	8.5	± 0.8	2.8
Γ_4	$2\pi^+ 2\pi^-$	5.2	± 0.7	1.2
Γ_5	$\eta\eta$	0.75	± 0.14	2.1
Γ_6	$4\pi^0$	0.56	± 0.19	
Γ_7	$\gamma\gamma$	0.0026	± 0.0005	1.4

$f_2(1270)$ PARTIAL WIDTHS

$\Gamma(\pi\pi)$ — Γ_1

VALUE (MeV)	EVTS	DOCUMENT ID		TECN	COMMENT
$157.2^{+5.0}_{-1.0}$ OUR FIT					
$157.0^{+6.0}_{-1.0}$		[1] LONGACRE	86	MPS	$22\ \pi^- p \to n 2K^0_S$
• • • We do not use the following data for averages, fits, limits, etc. • • •					
152 ± 8	870	[2] SCHEGELSKY	06A	RVUE	$\gamma\gamma \to K^0_S K^0_S$

[1] From a partial-wave analysis of data using a K-matrix formalism with 5 poles.
[2] From analysis of L3 data at 91 and 183–209 GeV and using SU(3) relations.

$\Gamma(K\overline{K})$ — Γ_3

VALUE (MeV)	EVTS	DOCUMENT ID		TECN	COMMENT
8.5 ± 0.8 OUR FIT Error includes scale factor of 2.8.					
$9.0^{+0.7}_{-0.3}$		[1] LONGACRE	86	MPS	$22\ \pi^- p \to n 2K^0_S$
• • • We do not use the following data for averages, fits, limits, etc. • • •					
7.5 ± 2.0	870	[2] SCHEGELSKY	06A	RVUE	$\gamma\gamma \to K^0_S K^0_S$

[1] From a partial-wave analysis of data using a K-matrix formalism with 5 poles.
[2] From analysis of L3 data at 91 and 183–209 GeV and using SU(3) relations.

$\Gamma(\eta\eta)$ — Γ_5

VALUE (MeV)	EVTS	DOCUMENT ID		TECN	COMMENT
0.75 ± 0.14 OUR FIT Error includes scale factor of 2.1.					
1.0 ± 0.1		[1] LONGACRE	86	MPS	$22\ \pi^- p \to n 2K^0_S$
• • • We do not use the following data for averages, fits, limits, etc. • • •					
1.8 ± 0.4	870	[2] SCHEGELSKY	06A	RVUE	$\gamma\gamma \to K^0_S K^0_S$

[1] From a partial-wave analysis of data using a K-matrix formalism with 5 poles.
[2] From analysis of L3 data at 91 and 183–209 GeV and using SU(3) relations.

$\Gamma(\gamma\gamma)$ — Γ_7

The value of this width depends on the theoretical model used. Unitary approaches with scalars typically (with exception of PENNINGTON 08) give values clustering around 2.6 keV; without an S-wave contribution, values are systematically higher (typically around 3 keV).

VALUE (keV)	EVTS	DOCUMENT ID		TECN	COMMENT
2.6 ± 0.5 OUR FIT Error includes scale factor of 1.4.					
2.93 ± 0.40		[1] DAI	14A	RVUE	Compilation
• • • We do not use the following data for averages, fits, limits, etc. • • •					
3.14 ± 0.20		[2,3] PENNINGTON	08	RVUE	Compilation
3.82 ± 0.30		[3,4] PENNINGTON	08	RVUE	Compilation
2.55 ± 0.15	870	[5] SCHEGELSKY	06A	RVUE	$\gamma\gamma \to K^0_S K^0_S$
2.84 ± 0.35		BOGLIONE	99	RVUE	$\gamma\gamma \to \pi^+\pi^-, \pi^0\pi^0$
$2.93 \pm 0.23 \pm 0.32$		[6] YABUKI	95	VNS	
$2.58 \pm 0.13^{+0.36}_{-0.27}$		[7] BEHREND	92	CELL	$e^+e^- \to e^+e^-\pi^+\pi^-$
$3.10 \pm 0.35 \pm 0.35$		[8] BLINOV	92	MD1	$e^+e^- \to e^+e^-\pi^+\pi^-$
$2.27 \pm 0.47 \pm 0.11$		ADACHI	90D	TOPZ	$e^+e^- \to e^+e^-\pi^+\pi^-$
$3.15 \pm 0.04 \pm 0.39$		BOYER	90	MRK2	$e^+e^- \to e^+e^-\pi^+\pi^-$
$3.19 \pm 0.16^{+0.29}_{-0.28}$		MARSISKE	90	CBAL	$e^+e^- \to e^+e^-\pi^0\pi^0$
2.35 ± 0.65		[9] MORGAN	90	RVUE	$\gamma\gamma \to \pi^+\pi^-, \pi^0\pi^0$
$3.19 \pm 0.09^{+0.22}_{-0.38}$	2177	OEST	90	JADE	$e^+e^- \to e^+e^-\pi^0\pi^0$
$3.2 \pm 0.1 \pm 0.4$		[10] AIHARA	86B	TPC	$e^+e^- \to e^+e^-\pi^+\pi^-$
$2.5 \pm 0.1 \pm 0.5$		BEHREND	84B	CELL	$e^+e^- \to e^+e^-\pi^+\pi^-$
$2.85 \pm 0.25 \pm 0.5$		[11] BERGER	84	PLUT	$e^+e^- \to e^+e^- 2\pi$
$2.70 \pm 0.05 \pm 0.20$		COURAU	84	DLCO	$e^+e^- \to e^+e^-\pi^+\pi^-$
$2.52 \pm 0.13 \pm 0.38$		[12] SMITH	84C	MRK2	$e^+e^- \to e^+e^-\pi^+\pi^-$
$2.7 \pm 0.2 \pm 0.6$		EDWARDS	82F	CBAL	$e^+e^- \to e^+e^- 2\pi^0$
$2.9\ ^{+0.6}_{-0.4} \pm 0.6$		[13] EDWARDS	82F	CBAL	$e^+e^- \to e^+e^- 2\pi^0$
$3.2 \pm 0.2 \pm 0.6$		BRANDELIK	81B	TASS	$e^+e^- \to e^+e^-\pi^+\pi^-$
$3.6 \pm 0.3 \pm 0.5$		ROUSSARIE	81	MRK2	$e^+e^- \to e^+e^-\pi^+\pi^-$
2.3 ± 0.8		[14] BERGER	80B	PLUT	e^+e^-

[1] Based on a K-matrix analysis of BELLE data from MORI 07, UEHARA 08A, UEHARA 09 and UEHARA 13. The width is derived for the pole on the third sheet which is closest to the physical axis. Supersedes PENNINGTON 08.
[2] Solution A (preferred solution based on χ^2-analysis).
[3] Dispersion theory based amplitude analysis of BOYER 90, MARSISKE 90, BEHREND 92, and MORI 07.
[4] Solution B (worse than solution A; still acceptable when systematic uncertainties are included).
[5] From analysis of L3 data at 91 and 183–209 GeV and using SU(3) relations.
[6] With a narrow scalar state around 1220 MeV.
[7] Using a unitarized model with a 300 - 500 keV wide scalar at 1100 MeV.
[8] Using the unitarized model of LYTH 85.
[9] Error includes spread of different solutions. Data of MARK2 and CRYSTAL BALL used in the analysis. Authors report strong correlations with $\gamma\gamma$ width of $f_0(1370)$: $\Gamma(f_2) + 1/4\ \Gamma(f^0) = 3.6 \pm 0.3$ KeV.
[10] Radiative corrections modify the partial widths; for instance the COURAU 84 value becomes 2.66 ± 0.21 in the calculation of LANDRO 86.
[11] Using the MENNESSIER 83 model.
[12] Superseded by BOYER 90.
[13] If helicity = 2 assumption is not made.
[14] Using mass, width and $B(f_2(1270) \to 2\pi)$ from PDG 78.

$\Gamma(e^+e^-)$ — Γ_{10}

VALUE (eV)	CL%	DOCUMENT ID		TECN	COMMENT
<0.11	90	ACHASOV	00K	SND	$e^+e^- \to \pi^0\pi^0$
• • • We do not use the following data for averages, fits, limits, etc. • • •					
<1.7	90	VOROBYEV	88	ND	$e^+e^- \to \pi^0\pi^0$

$f_2(1270)\ \Gamma(i)\Gamma(\gamma\gamma)/\Gamma(\text{total})$

$\Gamma(K\overline{K}) \times \Gamma(\gamma\gamma)/\Gamma_{\text{total}}$ — $\Gamma_3\Gamma_7/\Gamma$

VALUE (keV)	DOCUMENT ID		TECN	COMMENT
0.121 ± 0.020 OUR FIT Error includes scale factor of 1.3.				
$0.091 \pm 0.007 \pm 0.027$	[1] ALBRECHT	90G	ARG	$e^+e^- \to e^+e^- K^+K^-$
• • • We do not use the following data for averages, fits, limits, etc. • • •				
$0.104 \pm 0.007 \pm 0.072$	[2] ALBRECHT	90G	ARG	$e^+e^- \to e^+e^- K^+K^-$

[1] Using an incoherent background.
[2] Using a coherent background.

$\Gamma(\eta\eta) \times \Gamma(\gamma\gamma)/\Gamma_{\text{total}}$ — $\Gamma_5\Gamma_7/\Gamma$

VALUE (eV)	DOCUMENT ID		TECN	COMMENT
$11.5^{+1.8}_{-2.0}{}^{+4.5}_{-3.7}$	[1] UEHARA	10A	BELL	$10.6\ e^+e^- \to e^+e^-\eta\eta$

[1] Including interference with the $f'_2(1525)$ (parameters fixed to the values from the 2008 edition of this review, PDG 08) and $f_0(Y)$.

Helicity-0/Helicity-2 RATIO IN $\gamma\gamma \to f_2(1270) \to \pi\pi$

VALUE (units 10^{-2})	DOCUMENT ID		TECN	COMMENT
$3.7 \pm 0.3^{+15.9}_{-2.9}$	UEHARA	08A	BELL	$10.6\ e^+e^- \to e^+e^-\pi^0\pi^0$
• • • We do not use the following data for averages, fits, limits, etc. • • •				
9.5 ± 1.8	[1] DAI	14A	RVUE	Compilation
13	[2,3] PENNINGTON	08	RVUE	Compilation
26	[3,4] PENNINGTON	08	RVUE	Compilation

[1] Based on a K-matrix analysis of BELLE data from MORI 07, UEHARA 08A, UEHARA 09 and UEHARA 13. The width is derived for the pole on the third sheet which is closest to the physical axis.
[2] Solution A (preferred solution based on χ^2-analysis).
[3] Dispersion theory based amplitude analysis of BOYER 90, MARSISKE 90, BEHREND 92, and MORI 07.
[4] Solution B (worse than solution A; still acceptable when systematic uncertainties are included).

$f_2(1270)$ BRANCHING RATIOS

$\Gamma(\pi\pi)/\Gamma_{\text{total}}$ — Γ_1/Γ

VALUE	EVTS	DOCUMENT ID		TECN	COMMENT
$0.843^{+0.028}_{-0.010}$ OUR FIT Error includes scale factor of 1.2.					
0.837 ± 0.020 OUR AVERAGE					
0.849 ± 0.025		CHABAUD	83	ASPK	$17\ \pi^- p$ polarized
0.85 ± 0.05	250	BEAUPRE	71	HBC	$8\ \pi^+ p \to \Delta^{++} f_2$
0.8 ± 0.04	600	OH	70	HBC	$1.26\ \pi^- p \to \pi^+\pi^- n$
• • • We do not use the following data for averages, fits, limits, etc. • • •					
$0.856 \pm 0.001 \pm 0.05$	[1] ALBRECHT	20	RVUE		$0.9\ \overline{p}p \to \pi^0\pi^0\eta$, $\pi^0\eta\eta$, $\pi^0 K^+K^-$

[1] Residue from T-matrix pole, 4 poles, 4 channels, including scattering data from HYAMS 75 ($\pi\pi$), LONGACRE 86 ($K\overline{K}$), BINON 83 ($\eta\eta$).

$\Gamma(\pi^+\pi^-2\pi^0)/\Gamma(\pi\pi)$ — Γ_2/Γ_1

Should be twice $\Gamma(2\pi^+2\pi^-)/\Gamma(\pi\pi)$ if decay is $\rho\rho$. (See ASCOLI 68D.)

VALUE	EVTS	DOCUMENT ID		TECN	COMMENT
$0.091^{+0.015}_{-0.040}$ OUR FIT Error includes scale factor of 1.2.					
0.15 ± 0.06	600	EISENBERG	74	HBC	$4.9\ \pi^+ p \to \Delta^{++} f_2$
• • • We do not use the following data for averages, fits, limits, etc. • • •					
0.07		EMMS	75D	DBC	$4\ \pi^+ n \to p f_2$

$\Gamma(K\overline{K})/\Gamma_{\text{total}}$ — Γ_3/Γ

VALUE	DOCUMENT ID		TECN	COMMENT
• • • We do not use the following data for averages, fits, limits, etc. • • •				
$0.033 \pm 0.001 \pm 0.005$	[1] ALBRECHT	20	RVUE	$0.9\ \overline{p}p \to \pi^0\pi^0\eta$, $\pi^0\eta\eta$, $\pi^0 K^+K^-$

[1] Residue from T-matrix pole, 4 poles, 4 channels, including scattering data from HYAMS 75 ($\pi\pi$), LONGACRE 86 ($K\overline{K}$), BINON 83 ($\eta\eta$).

Int. J. Mod. Phys. A 2026.41. Downloaded from www.worldscientific.com
by UNIVERSITY OF CALIFORNIA @ BERKELEY on 09/16/26. Re-use and distribution is strictly not permitted, except for Open Access articles.

Int. J. Mod. Phys. A 2026.41. Downloaded from www.worldscientific.com by CALIFORNIA @ BERKELEY on 09/16/26. Re-use and distribution is strictly not permitted, except for Open Access articles.

$\Gamma(K\overline{K})/\Gamma(\pi\pi)$ — Γ_3/Γ_1

We average only experiments which either take into account $f_2(1270)$-$a_2(1320)$ interference explicitly or demonstrate that $a_2(1320)$ production is negligible.

VALUE	EVTS	DOCUMENT ID		TECN	COMMENT
$0.054^{+0.005}_{-0.006}$ OUR FIT Error includes scale factor of 2.7.					
$0.041^{+0.004}_{-0.005}$ OUR AVERAGE					
0.045 ± 0.01		[1] BARGIOTTI	03	OBLX	$\overline{p}p$
$0.037^{+0.008}_{-0.021}$		ETKIN	82B	MPS	$23\ \pi^-p\to n2K^0_S$
0.045 ± 0.009		CHABAUD	81	ASPK	$17\ \pi^-p$ polarized
0.039 ± 0.008		LOVERRE	80	HBC	$4\ \pi^-p\to K\overline{K}N$
• • • We do not use the following data for averages, fits, limits, etc. • • •					
0.052 ± 0.025		ABLIKIM	04E	BES2	$J/\psi\to\omega K^+K^-$
0.036 ± 0.005		[2] COSTA	80	OMEG	1–$2.2\ \pi^-p\to K^+K^-n$
0.030 ± 0.005		[3] MARTIN	79	RVUE	
0.027 ± 0.009		[4] POLYCHRO...	79	STRC	$7\ \pi^-p\to n2K^0_S$
0.025 ± 0.015		EMMS	75D	DBC	$4\ \pi^+n\to pf_2$
0.031 ± 0.012	20	ADERHOLZ	69	HBC	$8\ \pi^+p\to K^+K^-\pi^+p$

[1] Coupled channel analysis of $\pi^+\pi^-\pi^0$, $K^+K^-\pi^0$, and $K^\pm K^0_S\pi^\mp$.
[2] Re-evaluated by CHABAUD 83.
[3] Includes PAWLICKI 77 data.
[4] Takes into account the $f_2(1270)$-$f'_2(1525)$ interference.

$\Gamma(2\pi^+2\pi^-)/\Gamma(\pi\pi)$ — Γ_4/Γ_1

VALUE	EVTS	DOCUMENT ID		TECN	COMMENT
0.033 ± 0.005 OUR FIT Error includes scale factor of 1.2.					
0.033 ± 0.004 OUR AVERAGE Error includes scale factor of 1.1.					
0.024 ± 0.006	160	EMMS	75D	DBC	$4\ \pi^+n\to pf_2$
0.051 ± 0.025	70	EISENBERG	74	HBC	$4.9\ \pi^+p\to\Delta^{++}f_2$
$0.043^{+0.007}_{-0.011}$	285	[1] LOUIE	74	HBC	$3.9\ \pi^-p\to nf_2$
0.037 ± 0.007	154	ANDERSON	73	DBC	$6\ \pi^+n\to pf_2$
0.047 ± 0.013		OH	70	HBC	$1.26\ \pi^-p\to\pi^+\pi^-n$

[1] LOUIE 74 was quoted as 0.065 in PDG 74. Factor 2/3 to go from $\pi^+\pi^-\to\pi\pi$ forgotten. Mike L.

$\Gamma(\eta\eta)/\Gamma_{total}$ — Γ_5/Γ

VALUE (units 10^{-3})	DOCUMENT ID		TECN	COMMENT
4.0 ± 0.8 OUR FIT Error includes scale factor of 2.1.				
2.9 ± 0.5 OUR AVERAGE				
2.7 ± 0.7	BINON	05	GAMS	$33\ \pi^-p\to\eta\eta n$
2.8 ± 0.7	ALDE	86D	GAM4	$100\ \pi^-p\to2\eta n$
5.2 ± 1.7	BINON	83	GAM2	$38\ \pi^-p\to2\eta n$
• • • We do not use the following data for averages, fits, limits, etc. • • •				
$4.0\pm1.0\pm2.0$	[1] ALBRECHT	20	RVUE	$0.9\ \overline{p}p\to\pi^0\pi^0\eta$, $\pi^0\eta\eta$, $\pi^0K^+K^-$

[1] Residue from T-matrix pole, 4 poles, 4 channels, including scattering data from HYAMS 75 ($\pi\pi$), LONGACRE 86 ($K\overline{K}$), BINON 83 ($\eta\eta$).

$\Gamma(\eta\eta)/\Gamma(\pi\pi)$ — Γ_5/Γ_1

VALUE	CL%	DOCUMENT ID		TECN	COMMENT
0.003±0.001		BARBERIS	00E		$450\ pp\to p_f\eta\eta p_s$
• • • We do not use the following data for averages, fits, limits, etc. • • •					
<0.05	95	EDWARDS	82F	CBAL	$e^+e^-\to e^+e^-2\eta$
<0.016	95	EMMS	75D	DBC	$4\ \pi^+n\to pf_2$
<0.09	95	EISENBERG	74	HBC	$4.9\ \pi^+p\to\Delta^{++}f_2$

$\Gamma(4\pi^0)/\Gamma_{total}$ — Γ_6/Γ

VALUE	EVTS	DOCUMENT ID		TECN	COMMENT
0.0030 ± 0.0010 OUR FIT					
$0.003\ \pm0.001$	400 ± 50	ALDE	87	GAM4	$100\ \pi^-p\to4\pi^0n$

$\Gamma(\gamma\gamma)/\Gamma_{total}$ — Γ_7/Γ

VALUE (units 10^{-5})	DOCUMENT ID		TECN	COMMENT
• • • We do not use the following data for averages, fits, limits, etc. • • •				
$1.57\pm0.01^{+1.39}_{-0.14}$	UEHARA	08A	BELL	$10.6\ e^+e^-\to e^+e^-\pi^0\pi^0$

$\Gamma(\eta\pi\pi)/\Gamma(\pi\pi)$ — Γ_8/Γ_1

VALUE	CL%	DOCUMENT ID		TECN	COMMENT
<0.010	95	EMMS	75D	DBC	$4\ \pi^+n\to pf_2$

$\Gamma(K^0K^-\pi^++\text{c.c.})/\Gamma(\pi\pi)$ — Γ_9/Γ_1

VALUE	CL%	DOCUMENT ID		TECN	COMMENT
<0.004	95	EMMS	75D	DBC	$4\ \pi^+n\to pf_2$

$\Gamma(e^+e^-)/\Gamma_{total}$ — Γ_{10}/Γ

VALUE (units 10^{-10})	CL%	DOCUMENT ID		TECN	COMMENT
<6	90	ACHASOV	00K	SND	$e^+e^-\to\pi^0\pi^0$

$f_2(1270)$ REFERENCES

ABLIKIM	25CD	JHEP 2510 081	M. Ablikim *et al.*	(BESIII Collab.)
KLEMPT	22	PL B830 137171	E. Klempt *et al.*	(BONN)
RODAS	22	EPJ C82 80	A. Rodas *et al.*	(JPAC Collab.)
CARVER	21	PRL 126 082002	M. Carver *et al.*	(CLAS Collab.)
ALBRECHT	20	EPJ C80 453	M. Albrecht *et al.*	(Crystal Barrel Collab.)
DOBBS	15	PR D91 052006	S. Dobbs *et al.*	(NWES)
DAI	14A	PR D90 036004	L.-Y. Dai, M.R. Pennington	(CEBAF)
BOGOLYUB...	13	PAN 76 1324	M.Yu. Bogolyubsky *et al.*	(HYPERON-M Collab.)
		Translated from YAF 76 1389.		
UEHARA	13	PTEP 2013 123C01	S. Uehara *et al.*	(BELLE Collab.)
UEHARA	10A	PR D82 114031	S. Uehara *et al.*	(BELLE Collab.)
ANISOVICH	09	IJMP A24 2481	V.V. Anisovich, A.V. Sarantsev	(PNPI)
UEHARA	09	PR D79 052009	S. Uehara *et al.*	(BELLE Collab.)
PDG	08	PL B667 1	C. Amsler *et al.*	(PDG Collab.)
PENNINGTON	08	EPJ C56 1	M.R. Pennington *et al.*	
UEHARA	08A	PR D78 052004	S. Uehara *et al.*	(BELLE Collab.)
MORI	07	PR D75 051101	T. Mori *et al.*	(BELLE Collab.)
ABLIKIM	06V	PL B642 441	M. Ablikim *et al.*	(BES Collab.)
SCHEGELSKY	06A	EPJ A27 207	V.A. Schegelsky *et al.*	
ABLIKIM	05	PL B607 243	M. Ablikim *et al.*	(BES Collab.)
BINON	05	PAN 68 960	F. Binon *et al.*	
		Translated from YAF 68 998.		
ABLIKIM	04E	PL B603 138	M. Ablikim *et al.*	(BES Collab.)
BARGIOTTI	03	EPJ C26 371	M. Bargiotti *et al.*	(OBELIX Collab.)
TIKHOMIROV	03	PAN 66 828	G.D. Tikhomirov *et al.*	
		Translated from YAF 66 860.		
ACHASOV	00K	PL B492 8	M.N. Achasov *et al.*	(Novosibirsk SND Collab.)
BARBERIS	00E	PL B479 59	D. Barberis *et al.*	(WA 102 Collab.)
BOGLIONE	99	EPJ C9 11	M. Boglione, M.R. Pennington	
ALDE	98	EPJ A3 361	D. Alde *et al.*	(GAM4 Collab.)
Also		PAN 62 405	D. Alde *et al.*	(GAMS Collab.)
		Translated from YAF 62 446.		
ALDE	97	PL B397 350	D.M. Alde *et al.*	(GAMS Collab.)
BERTIN	97C	PL B408 476	A. Bertin *et al.*	(OBELIX Collab.)
GRYGOREV	96	PAN 59 2105	V.K. Grigoriev, O.N. Baloshin, B.P. Barkov	(ITEP)
		Translated from YAF 59 2187.		
YABUKI	95	JPSJ 64 435	F. Yabuki *et al.*	(VENUS Collab.)
PROKOSHKIN	94	PD 39 420	Y.D. Prokoshkin, A.A. Kondashov	(SERP)
		Translated from DANS 336 613.		
BEHREND	92	ZPHY C56 381	H.J. Behrend	(CELLO Collab.)
BLINOV	92	ZPHY C53 33	A.E. Blinov *et al.*	(NOVO)
AGUILAR-...	91	ZPHY C50 405	M. Aguilar-Benitez *et al.*	(LEBC-EHS Collab.)
AKER	91	PL B260 249	E. Aker *et al.*	(Crystal Barrel Collab.)
ADACHI	90D	PL B234 185	I. Adachi *et al.*	(TOPAZ Collab.)
ALBRECHT	90G	ZPHY C48 183	H. Albrecht *et al.*	(ARGUS Collab.)
BOYER	90	PR D42 1350	J. Boyer *et al.*	(Mark II Collab.)
BREAKSTONE	90	ZPHY C48 569	A.M. Breakstone *et al.*	(ISU, BGNA, CERN+)
MARSISKE	90	PR D41 3324	H. Marsiske *et al.*	(Crystal Ball Collab.)
MORGAN	90	ZPHY C48 623	D. Morgan, M.R. Pennington	(RAL, DURH)
OEST	90	ZPHY C47 343	T. Oest *et al.*	(JADE Collab.)
AUGUSTIN	89	NP B320 1	J.E. Augustin, G. Cosme	(DM2 Collab.)
VOROBYEV	88	SJNP 48 273	P.V. Vorobiev *et al.*	(NOVO)
		Translated from YAF 48 436.		
ALDE	87	PL B198 286	D.M. Alde *et al.*	(LANL, BRUX, SERP, LAPP)
AUGUSTIN	87	ZPHY C36 369	J.E. Augustin *et al.*	(LALO, CLER, FRAS+)
ABACHI	86B	PRL 57 1990	S. Abachi *et al.*	(PURD, ANL, IND, MICH+)
AIHARA	86B	PRL 57 404	H. Aihara *et al.*	(TPC-2γ Collab.)
ALDE	86D	NP B269 485	D.M. Alde *et al.*	(BELG, LAPP, SERP, CERN+)
LANDRO	86	PL B172 445	M. Landro, K.J. Mork, H.A. Olsen	(UTRO)
LONGACRE	86	PL B177 223	R.S. Longacre *et al.*	(BNL, BRAN, CUNY+)
LYTH	85	JP G11 459	D.H. Lyth	
BEHREND	84B	ZPHY C23 223	H.J. Behrend *et al.*	(CELLO Collab.)
BERGER	84	ZPHY C26 199	C. Berger *et al.*	(PLUTO Collab.)
COURAU	84	PL 147B 227	A. Courau *et al.*	(CIT, SLAC)
SMITH	84C	PR D30 851	J.R. Smith *et al.*	(SLAC, LBL, HARV)
BINON	83	NC 78A 313	F.G. Binon *et al.*	(BELG, LAPP, SERP+)
Also		SJNP 38 561	F.G. Binon *et al.*	(BELG, LAPP, SERP+)
		Translated from YAF 38 934.		
CHABAUD	83	NP B223 1	V. Chabaud *et al.*	(CERN, CRAC, MPIM)
DENNEY	83	PR D28 2726	D.L. Denney *et al.*	(IOWA, MICH)
MENNESSIER	83	ZPHY C16 241	G. Mennessier	(MONP)
APEL	82	NP B201 197	W.D. Apel *et al.*	(KARLK, KARLE, PISA, SERP+)
CASON	82	PRL 48 1316	N.M. Cason *et al.*	(NDAM, ANL)
EDWARDS	82F	PL 110B 82	C. Edwards *et al.*	(CIT, HARV, PRIN+)
ETKIN	82B	PR D25 1786	A. Etkin *et al.*	(BNL, CUNY, TUFTS, VAND)
BRANDELIK	81B	ZPHY C10 117	R. Brandelik *et al.*	(TASSO Collab.)
CHABAUD	81	APP B12 575	V. Chabaud *et al.*	(CERN, CRAC, MPIM)
GIDAL	81	PL 107B 153	G. Gidal *et al.*	(SLAC, LBL)
ROUSSARIE	81	PL 105B 304	A. Roussarie *et al.*	(SLAC, LBL)
BERGER	80B	PL 94B 254	C. Berger *et al.*	(PLUTO Collab.)
COSTA	80	NP B175 402	G. Costa *et al.*	(BARI, BONN, CERN, GLAS+)
LOVERRE	80	ZPHY C6 187	P.F. Loverre *et al.*	(CERN, CDEF, MADR+)
CORDEN	79	NP B157 250	M.J. Corden *et al.*	(BIRM, RHEL, TELA+)
MARTIN	79	NP B158 520	A.D. Martin, E.N. Ozmutlu	(DURH)
POLYCHRO...	79	PR D19 1317	V.A. Polychronakos *et al.*	(NDAM, ANL)
PDG	78	PL 75B 1	C. Bricman *et al.*	
ANTIPOV	77	NP B119 45	Y.M. Antipov *et al.*	(SERP, GEVA)
PAWLICKI	77	PR D15 3196	A.J. Pawlicki *et al.*	(ANL)
DEUTSCH...	76	NP B103 426	M. Deutschmann *et al.*	(AACH3, BERL, BONN+)
APEL	75	PL 57B 398	W.D. Apel *et al.*	(KARLK, KARLE, PISA, SERP+)
EMMS	75D	NP B96 155	M.J. Emms *et al.*	(BIRM, DURH, RHEL)
HYAMS	75	NP B100 205	B.D. Hyams *et al.*	(CERN, MPIM)
EISENBERG	74	PL 52B 239	Y. Eisenberg *et al.*	(REHO)
ENGLER	74	PR D10 2070	A. Engler *et al.*	(CMU, CASE)
LOUIE	74	PL 48B 385	J. Louie *et al.*	(SACL, CERN)
PDG	74	PL 50B 1	V. Chaloupka *et al.*	
ANDERSON	73	PRL 31 562	J.C. Anderson *et al.*	(CMU, CASE)
TAKAHASHI	72	PR D6 1266	K. Takahashi *et al.*	(TOHOK, PENN, NDAM+)
BEAUPRE	71	NP B28 77	J.V. Beaupre *et al.*	(AACH, BERL, CERN)
FLATTE	71	PL 34B 551	S.M. Flatte *et al.*	(LBL)
ARMENISE	70	LNC 4 199	N. Armenise *et al.*	(BARI, BGNA, FIRZ)
OH	70	PR D1 2494	B.Y. Oh *et al.*	(WISC, TNTO) JP
STUNTEBECK	70	PL 32B 391	P.H. Stuntebeck *et al.*	(NDAM)
ADERHOLZ	69	NP B11 259	M. Aderholz *et al.*	(AACH3, BERL, CERN+)
ARMENISE	68	NC 54A 999	N. Armenise *et al.*	(BARI, BGNA, FIRZ+)
ASCOLI	68D	PRL 21 1712	G. Ascoli *et al.*	(ILL)
BOESEBECK	68	NP B4 501	K. Boesebeck *et al.*	(AACH, BERL, CERN)
JOHNSON	68	PR 176 1651	P.B. Johnson *et al.*	(NDAM, PURD, SLAC)
EISNER	67	PR 164 1699	R.L. Eisner *et al.*	(PURD)
DERADO	65	PRL 14 872	I. Derado *et al.*	(NDAM)
LEE	64	PRL 12 342	Y.Y. Lee *et al.*	(MICH)
BONDAR	63	PL 5 153	L. Bondar *et al.*	(AACH, BIRM, BONN, DESY+)

Int. J. Mod. Phys. A 2026.41. Downloaded from www.worldscientific.com
by UNIVERSITY OF CALIFORNIA @ BERKELEY on 09/16/26. Re-use and distribution is strictly not permitted, except for Open Access articles.

$f_1(1285)$

$I^G(J^{PC}) = 0^+(1^{++})$

$f_1(1285)$ MASS

VALUE (MeV)	EVTS	DOCUMENT ID		TECN	COMMENT
1281.8 ± 0.5 OUR AVERAGE		Error includes scale factor of 1.7. See the ideogram below.			
1283.5 ± 1.5	360	AAIJ	25F	LHCB	$B \to (K^0_S K\pi) K$
1280.2 ± 0.6 $^{+1.2}_{-1.5}$	126k	ABLIKIM	23M	BES3	$J/\psi \to \gamma K^0_S K^0_S \pi^0$
1281.0 ± 0.8		DICKSON	16	CLAS	2.55 $\gamma p \to \eta\pi^+\pi^- p$
1287.4 ± 3.0	87	ABLIKIM	15P	BES3	$J/\psi \to K^+K^-3\pi$
1281.16 ± 0.39 ± 0.45		[1] LEES	12X	BABR	$\tau^- \to \pi^- f_1(1285)\nu_\tau$
1285.1 ± 1.0 $^{+1.6}_{-0.3}$		[2] ABLIKIM	11J	BES3	$J/\psi \to \omega(\eta\pi^+\pi^-)$
1281 ± 2 ± 1		AUBERT	07AU	BABR	10.6 $e^+e^- \to f_1(1285)\pi^+\pi^-\gamma$
1276.1 ± 8.1 ± 8.0	203	BAI	04J	BES2	$J/\psi \to \gamma\gamma\pi^+\pi^-$
1274 ± 6	237	ABDALLAH	03H	DLPH	91.2 $e^+e^- \to K^0_S K^\pm\pi^\mp + X$
1280 ± 4		ACCIARRI	01G	L3	
1288 ± 4 ± 5	20k	ADAMS	01B	B852	18 GeV $\pi^- p \to K^+K^-\pi^0 n$
1284 ± 6	1400	ALDE	97B	GAM4	100 $\pi^- p \to \eta\pi^0\pi^0 n$
1281 ± 1		BARBERIS	97B	OMEG	450 $pp \to pp2(\pi^+\pi^-)$
1281 ± 1		BARBERIS	97C	OMEG	450 $pp \to pp K^0_S K^\pm\pi^\mp$
1280 ± 2		[3] ANTINORI	95	OMEG	300,450 $pp \to pp2(\pi^+\pi^-)$
1282.2 ± 1.5		LEE	94	MPS2	18 $\pi^- p \to K^+\overline{K}^0 2\pi^- p$
1279 ± 5		FUKUI	91C	SPEC	8.95 $\pi^- p \to \eta\pi^+\pi^- n$
1278 ± 2	140	ARMSTRONG	89	OMEG	300 $pp \to K\overline{K}\pi pp$
1278 ± 2		ARMSTRONG	89G	OMEG	85 $\pi^+ p \to 4\pi\pi p$, $pp \to 4\pi pp$
1280.1 ± 2.1	60	RATH	89	MPS	21.4 $\pi^- p \to K^0_S K^0_S \pi^0 n$
1285 ± 1	4750	[4] BIRMAN	88	MPS	8 $\pi^- p \to K^+\overline{K}^0\pi^- n$
1280 ± 1	504	BITYUKOV	88	SPEC	32.5 $\pi^- p \to K^+K^-\pi^0 n$
1280 ± 4		ANDO	86	SPEC	8 $\pi^- p \to \eta\pi^+\pi^- n$
1277 ± 2	420	REEVES	86	SPEC	6.6 $p\overline{p} \to KK\pi X$
1285 ± 2		CHUNG	85	SPEC	8 $\pi^- p \to NK\overline{K}\pi$
1279 ± 2	604	ARMSTRONG	84	OMEG	85 $\pi^+ p \to K\overline{K}\pi\pi p$, $pp \to K\overline{K}\pi pp$
1286 ± 1		CHAUVAT	84	SPEC	ISR 31.5 pp
1278 ± 4		EVANGELIS...	81	OMEG	12 $\pi^- p \to \eta\pi^+\pi^-\pi^- p$
1283 ± 3	103	DIONISI	80	HBC	4 $\pi^- p \to K\overline{K}\pi n$
1282 ± 2	320	NACASCH	78	HBC	0.7,0.76 $\overline{p}p \to K\overline{K}3\pi$
1279 ± 5	210	GRASSLER	77	HBC	16 $\pi^\mp p$
1286 ± 3	180	DUBOC	72	HBC	1.2 $\overline{p}p \to 2K4\pi$
1283 ± 5		DAHL	67	HBC	1.6–4.2 $\pi^- p$
• • • We do not use the following data for averages, fits, limits, etc. • • •					
1289.3 ± 2.8	234	ABLIKIM	19BA	BES3	$e^+e^- \to \psi(2S)$
1284.2 ± 2.2		[5] AAIJ	14Y	LHCB	$\overline{B}^0_{(s)} \to J/\psi(2\pi^+\pi^-)$
1281.9 ± 0.5		[5] SOSA	99	SPEC	$pp \to p_{slow}(K^0_S K^+\pi^-)\, p_{fast}$
1282.8 ± 0.6		[5] SOSA	99	SPEC	$pp \to p_{slow}(K^0_S K^-\pi^+)\, p_{fast}$
1270 ±10		AMELIN	95	VES	37 $\pi^- N \to \pi^-\pi^+\pi^-\gamma N$
1280 ± 2		ABATZIS	94	OMEG	450 $pp \to pp2(\pi^+\pi^-)$
1282 ± 4		ARMSTRONG	93C	E760	$\overline{p}p \to \pi^0\eta\eta \to 6\gamma$
1270 ± 6 ±10		ARMSTRONG	92C	OMEG	300 $pp \to pp\pi^+\pi^-\gamma$
1281 ± 1		ARMSTRONG	89E	OMEG	300 $pp \to pp2(\pi^+\pi^-)$
1279 ± 6 ±10	16	BECKER	87	MRK3	$e^+e^- \to \phi K\overline{K}\pi$
1286 ± 9		GIDAL	87	MRK2	$e^+e^- \to e^+e^-\eta\pi^+\pi^-$
1287 ± 5	353	BITYUKOV	84B	SPEC	32 $\pi^- p \to K^+K^-\pi^0 n$
~ 1279		[6] TORNQVIST	82B	RVUE	
1275 ± 6	31	BROMBERG	80	SPEC	100 $\pi^- p \to K\overline{K}\pi X$
1288 ± 9	200	GURTU	79	HBC	4.2 $K^- p \to n\eta 2\pi$
~ 1275.0	46	[7] STANTON	79	CNTR	8.5 $\pi^- p \to n2\gamma 2\pi$
1271 ±10	34	CORDEN	78	OMEG	12–15 $\pi^- p \to K^+K^-\pi n$
1295 ±12	85	CORDEN	78	OMEG	12–15 $\pi^- p \to n5\pi$
1292 ±10	150	DEFOIX	72	HBC	0.7 $\overline{p}p \to 7\pi$
1280 ± 3	500	[8] THUN	72	MMS	13.4 $\pi^- p$
1303 ± 8		BARDADIN-...	71	HBC	8 $\pi^+ p \to p6\pi$
1283 ± 6		BOESEBECK	71	HBC	16.0 $\pi p \to p5\pi$
1270 ±10		CAMPBELL	69	DBC	2.7 $\pi^+ d$
1285 ± 7		LORSTAD	69	HBC	0.7 $\overline{p}p$, 4,5-body
1290 ± 7		D'ANDLAU	68	HBC	1.2 $\overline{p}p$, 5–6 body

[1] Using the $2\pi^+2\pi^-$ and $\pi^+\pi^-\eta$ modes of $f_1(1285)$ decay.
[2] The selected process is $J/\psi \to \omega a_0(980)\pi$.
[3] Supersedes ABATZIS 94, ARMSTRONG 89E.
[4] From partial wave analysis of $K^+\overline{K}^0\pi^-$ system.
[5] No systematic error given.
[6] From a unitarized quark-model calculation.
[7] From phase shift analysis of $\eta\pi^+\pi^-$ system.
[8] Seen in the missing mass spectrum.

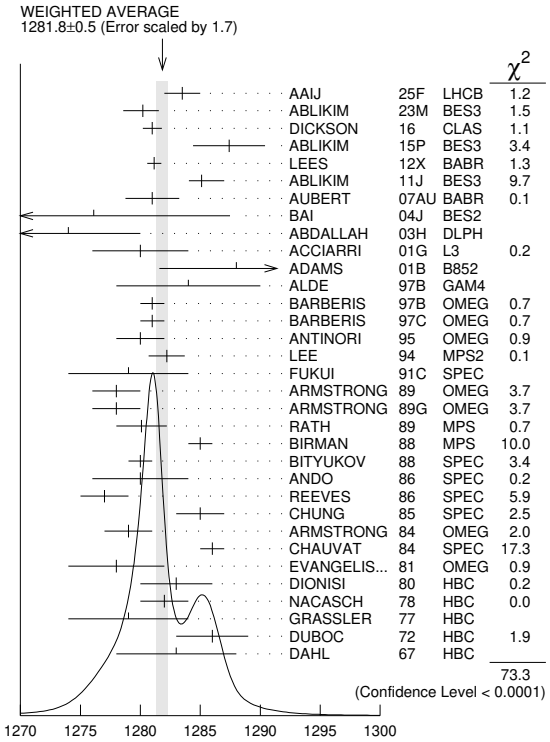

$f_1(1285)$ WIDTH

Only experiments giving width error less than 20 MeV are kept for averaging.

VALUE (MeV)	EVTS	DOCUMENT ID		TECN	COMMENT
23.0 ± 1.0 OUR AVERAGE		Error includes scale factor of 1.5. See the ideogram below.			
27.4 ± 5.6	360	AAIJ	25F	LHCB	$B \to (K^0_S K\pi) K$
28.2 ± 1.1 $^{+5.5}_{-2.9}$	126k	ABLIKIM	23M	BES3	$J/\psi \to \gamma K^0_S K^0_S \pi^0$
18.4 ± 1.4		DICKSON	16	CLAS	2.55 $\gamma p \to \eta\pi^+\pi^- p$
18.3 ± 6.3	87	ABLIKIM	15P	BES3	$J/\psi \to K^+K^-3\pi$
22.0 ± 3.1 $^{+2.0}_{-1.5}$		[1] ABLIKIM	11J	BES3	$J/\psi \to \omega(\eta\pi^+\pi^-)$
35 ± 6 ± 4		AUBERT	07AU	BABR	10.6 $e^+e^- \to f_1(1285)\pi^+\pi^-\gamma$
40.0 ± 8.6 ± 9.3	203	BAI	04J	BES2	$J/\psi \to \gamma\gamma\pi^+\pi^-$
29 ±12	237	ABDALLAH	03H	DLPH	91.2 $e^+e^- \to K^0_S K^\pm\pi^\mp + X$
45 ± 9 ± 7	20k	ADAMS	01B	B852	18 GeV $\pi^- p \to K^+K^-\pi^0 n$
55 ±18	1400	ALDE	97B	GAM4	100 $\pi^- p \to \eta\pi^0\pi^0 n$
24 ± 3		BARBERIS	97B	OMEG	450 $pp \to pp2(\pi^+\pi^-)$
20 ± 2		BARBERIS	97C	OMEG	450 $pp \to pp K^0_S K^\pm\pi^\mp$
36 ± 5		[2] ANTINORI	95	OMEG	300,450 $pp \to pp2(\pi^+\pi^-)$
29.0 ± 4.1		LEE	94	MPS2	18 $\pi^- p \to K^+\overline{K}^0 2\pi^- p$
25 ± 4	140	ARMSTRONG	89	OMEG	300 $pp \to K\overline{K}\pi pp$
22 ± 2	4750	[3] BIRMAN	88	MPS	8 $\pi^- p \to K^+\overline{K}^0\pi^- n$
25 ± 4	504	BITYUKOV	88	SPEC	32.5 $\pi^- p \to K^+K^-\pi^0 n$
19 ± 5		ANDO	86	SPEC	8 $\pi^- p \to \eta\pi^+\pi^- n$
32 ± 8	420	REEVES	86	SPEC	6.6 $p\overline{p} \to KK\pi X$
22 ± 2		CHUNG	85	SPEC	8 $\pi^- p \to NK\overline{K}\pi$
32 ± 3	604	ARMSTRONG	84	OMEG	85 $\pi^+ p \to K\overline{K}\pi\pi p$, $pp \to K\overline{K}\pi pp$
24 ± 3		CHAUVAT	84	SPEC	ISR 31.5 pp
29 ±10	103	DIONISI	80	HBC	4 $\pi^- p \to K\overline{K}\pi n$
28.3 ± 6.7	320	NACASCH	78	HBC	0.7,0.76 $\overline{p}p \to K\overline{K}3\pi$

Int. J. Mod. Phys. A 2026.41. Downloaded from www.worldscientific.com
by CALIFORNIA @ BERKELEY on 09/16/26. Re-use and distribution is strictly not permitted, except for Open Access articles.

• • • We do not use the following data for averages, fits, limits, etc. • • •

17.1 ± 3.4	234	ABLIKIM	19BA	BES3	$e^+e^- \to \psi(2S)$
32.4 ± 5.8		[4] AAIJ	14Y	LHCB	$\overline{B}^0_{(s)} \to J/\psi 2(\pi^+\pi^-)$
18.2 ± 1.2		[4] SOSA	99	SPEC	$pp \to p_{slow}\ (K^0_S K^+\pi^-)\ p_{fast}$
19.4 ± 1.5		[4] SOSA	99	SPEC	$pp \to p_{slow}\ (K^0_S K^-\pi^+)\ p_{fast}$
40 ± 5		ABATZIS	94	OMEG	450 $pp \to pp2(\pi^+\pi^-)$
31 ± 5		ARMSTRONG	89E	OMEG	300 $pp \to pp2(\pi^+\pi^-)$
41 ± 12		ARMSTRONG	89G	OMEG	85 $\pi^+p \to 4\pi\pi p$, $pp \to 4\pi pp$
17.9 ± 10.9	60	RATH	89	MPS	21.4 $\pi^-p \to K^0_S K^0_S \pi^0 n$
14 $^{+20}_{-14}$ ± 10	16	BECKER	87	MRK3	$e^+e^- \to \phi K\overline{K}\pi$
26 ± 12		EVANGELIS...	81	OMEG	12 $\pi^-p \to \eta\pi^+\pi^-\pi^-p$
25 ± 15	200	GURTU	79	HBC	4.2 $K^-p \to n\eta 2\pi$
~ 10		[5] STANTON	79	CNTR	8.5 $\pi^-p \to n2\gamma 2\pi$
24 ± 18	210	GRASSLER	77	HBC	16 $\pi^\mp p$
28 ± 5	150	[6] DEFOIX	72	HBC	0.7 $\overline{p}p \to 7\pi$
46 ± 9	180	[6] DUBOC	72	HBC	1.2 $\overline{p}p \to 2K4\pi$
37 ± 5	500	[7] THUN	72	MMS	13.4 π^-p
10 ± 10		BOESEBECK	71	HBC	16.0 $\pi p \to p5\pi$
30 ± 15		CAMPBELL	69	DBC	2.7 π^+d
60 ± 15		[6] LORSTAD	69	HBC	0.7 $\overline{p}p$, 4,5-body
35 ± 10		[6] DAHL	67	HBC	1.6–4.2 π^-p

[1] The selected process is $J/\psi \to \omega a_0(980)\pi$.
[2] Supersedes ABATZIS 94, ARMSTRONG 89E.
[3] From partial wave analysis of $K^+\overline{K}^0\pi^-$ system.
[4] No systematic error given.
[5] From phase shift analysis of $\eta\pi^+\pi^-$ system.
[6] Resolution is not unfolded.
[7] Seen in the missing mass spectrum.

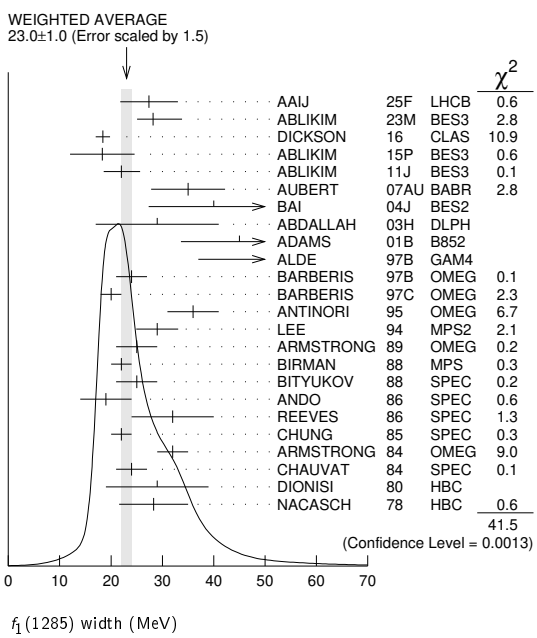

$f_1(1285)$ DECAY MODES

	Mode	Fraction (Γ_i/Γ)	Scale factor/ Confidence level
Γ_1	4π	(32.7 ± 1.8) %	S=1.2
Γ_2	$\pi^0\pi^0\pi^+\pi^-$	(21.8 ± 1.2) %	S=1.2
Γ_3	$2\pi^+2\pi^-$	(10.9 ± 0.6) %	S=1.2
Γ_4	$\rho^0\pi^+\pi^-$	(10.9 ± 0.6) %	S=1.2
Γ_5	$\rho^0\rho^0$	seen	
Γ_6	$4\pi^0$	< 7 $\times 10^{-4}$	CL=90%
Γ_7	$\eta\pi^+\pi^-$	(35 ± 15) %	
Γ_8	$\eta\pi\pi$	(52.2 ± 1.9) %	S=1.2
Γ_9	$a_0(980)\pi$ [ignoring $a_0(980) \to K\overline{K}$]	(38 ± 4) %	
Γ_{10}	$\eta\pi\pi$ [excluding $a_0(980)\pi$]	(14 ± 4) %	
Γ_{11}	$K\overline{K}\pi$	(9.0 ± 0.4) %	S=1.1
Γ_{12}	$K\overline{K}^*(892)$	not seen	
Γ_{13}	$\pi^+\pi^-\pi^0$	(3.0 ± 0.9) $\times 10^{-3}$	
Γ_{14}	$\rho^\pm\pi^\mp$	< 3.1 $\times 10^{-3}$	CL=95%
Γ_{15}	$\gamma\rho^0$	(6.1 ± 1.0) %	S=1.7
Γ_{16}	$\phi\gamma$	seen	
Γ_{17}	e^+e^-	< 9.4 $\times 10^{-9}$	CL=90%
Γ_{18}	$\gamma\gamma^*$		
Γ_{19}	$\gamma\gamma$		

CONSTRAINED FIT INFORMATION

An overall fit to 6 branching ratios uses 18 measurements and one constraint to determine 5 parameters. The overall fit has a χ^2 = 24.0 for 14 degrees of freedom.

The following *off-diagonal* array elements are the correlation coefficients $\langle \delta x_i \delta x_j \rangle / (\delta x_i \cdot \delta x_j)$, in percent, from the fit to the branching fractions, $x_i \equiv \Gamma_i/\Gamma_{total}$. The fit constrains the x_i whose labels appear in this array to sum to one.

	x_1	x_9	x_{10}	x_{11}
x_9	−29			
x_{10}	−12	−89		
x_{11}	22	−9	−4	
x_{15}	−24	−8	−3	−27

$f_1(1285)$ $\Gamma(i)\Gamma(\gamma\gamma)/\Gamma(total)$

$\Gamma(\eta\pi\pi) \times \Gamma(\gamma\gamma)/\Gamma_{total}$ — $\Gamma_8\Gamma_{19}/\Gamma = (\Gamma_9+\Gamma_{10})\Gamma_{19}/\Gamma$

VALUE (keV)	CL%	DOCUMENT ID		TECN	COMMENT
<0.62	95	GIDAL	87	MRK2	$e^+e^- \to e^+e^-\eta\pi^+\pi^-$

$\Gamma(\eta\pi\pi) \times \Gamma(\gamma\gamma^*)/\Gamma_{total}$ — $\Gamma_8\Gamma_{18}/\Gamma = (\Gamma_9+\Gamma_{10})\Gamma_{18}/\Gamma$

VALUE (keV)	EVTS	DOCUMENT ID		TECN	COMMENT
1.4 ±0.4 OUR AVERAGE		Error includes scale factor of 1.4.			
1.18 ± 0.25 ± 0.20	26	[1,2] AIHARA	88B	TPC	$e^+e^- \to e^+e^-\eta\pi^+\pi^-$
2.30 ± 0.61 ± 0.42		[1,3] GIDAL	87	MRK2	$e^+e^- \to e^+e^-\eta\pi^+\pi^-$
• • • We do not use the following data for averages, fits, limits, etc. • • •					
1.8 ± 0.3 ± 0.3	420	[4] ACHARD	02B	L3	183–209 $e^+e^- \to e^+e^-\eta\pi^+\pi^-$

[1] Assuming a ρ-pole form factor.
[2] Published value multiplied by $\eta\pi\pi$ branching ratio 0.49.
[3] Published value divided by 2 and multiplied by the $\eta\pi\pi$ branching ratio 0.49.
[4] Published value multiplied by the $\eta\pi\pi$ branching ratio 0.52.

$f_1(1285)$ BRANCHING RATIOS

$\Gamma(K\overline{K}\pi)/\Gamma(4\pi)$ — Γ_{11}/Γ_1

VALUE	DOCUMENT ID		TECN	COMMENT
0.274 ± 0.017 OUR FIT	Error includes scale factor of 1.4.			
0.271 ± 0.016 OUR AVERAGE	Error includes scale factor of 1.2.			
0.265 ± 0.014	[1] BARBERIS	97C	OMEG	450 $pp \to pp K^0_S K^\pm\pi^\mp$
0.28 ± 0.05	[2] ARMSTRONG	89E	OMEG	300 $pp \to pp f_1(1285)$
0.37 ± 0.03 ± 0.05	[3] ARMSTRONG	89G	OMEG	85 $\pi p \to 4\pi X$

[1] Using $2(\pi^+\pi^-)$ data from BARBERIS 97B.
[2] Assuming $\rho\pi\pi$ and $a_0(980)\pi$ intermediate states.
[3] 4π consistent with being entirely $\rho\pi\pi$.

$\Gamma(\pi^0\pi^0\pi^+\pi^-)/\Gamma_{total}$ — $\Gamma_2/\Gamma = \frac{2}{3}\Gamma_1/\Gamma$

VALUE	DOCUMENT ID
0.218 ± 0.012 OUR FIT	Error includes scale factor of 1.2.

$\Gamma(2\pi^+2\pi^-)/\Gamma_{total}$ — $\Gamma_3/\Gamma = \frac{1}{3}\Gamma_1/\Gamma$

VALUE	DOCUMENT ID
0.109 ± 0.006 OUR FIT	Error includes scale factor of 1.2.

$\Gamma(\rho^0\pi^+\pi^-)/\Gamma_{total}$ — $\Gamma_4/\Gamma = \frac{1}{3}\Gamma_1/\Gamma$

VALUE	DOCUMENT ID
0.109 ± 0.006 OUR FIT	Error includes scale factor of 1.2.

$\Gamma(\rho^0\pi^+\pi^-)/\Gamma(2\pi^+2\pi^-)$ — Γ_4/Γ_3

VALUE	DOCUMENT ID		TECN	COMMENT
• • • We do not use the following data for averages, fits, limits, etc. • • •				
1.0 ± 0.4	GRASSLER	77	HBC	16 GeV $\pi^\pm p$

$\Gamma(\rho^0\rho^0)/\Gamma_{total}$ — Γ_5/Γ

VALUE	DOCUMENT ID		COMMENT
seen	BARBERIS	00C	450 $pp \to p_f 4\pi p_s$

$\Gamma(4\pi^0)/\Gamma_{total}$ — Γ_6/Γ

VALUE (units 10^{-4})	CL%	DOCUMENT ID		TECN	COMMENT
<7	90	ALDE	87	GAM4	100 $\pi^-p \to 4\pi^0 n$

$\Gamma(\pi^+\pi^-\pi^0)/\Gamma(\eta\pi^+\pi^-)$ — Γ_{13}/Γ_7

VALUE (%)	EVTS	DOCUMENT ID		TECN	COMMENT
0.86 ± 0.16 ± 0.20	2.3k	[1] DOROFEEV	11	VES	$\pi^-N \to \pi^- f_1(1285) N$

[1] Value obtained selecting the region corresponding to $f_0(980)$ in the $\pi^+\pi^-$ mass spectrum.

Int. J. Mod. Phys. A 2026.41. Downloaded from www.worldscientific.com by UNIVERSITY OF CALIFORNIA @ BERKELEY on 09/16/26. Re-use and distribution is strictly not permitted, except for Open Access articles.

$\Gamma(\eta\pi\pi)/\Gamma_{total}$ — $\Gamma_8/\Gamma = (\Gamma_9+\Gamma_{10})/\Gamma$

VALUE	DOCUMENT ID
0.522±0.019 OUR FIT Error includes scale factor of 1.2.	

$\Gamma(4\pi)/\Gamma(\eta\pi\pi)$ — $\Gamma_1/\Gamma_8 = \Gamma_1/(\Gamma_9+\Gamma_{10})$

VALUE	DOCUMENT ID		TECN	COMMENT
0.63±0.06 OUR FIT Error includes scale factor of 1.2.				
0.41±0.14 OUR AVERAGE				
0.37±0.11±0.11	BOLTON	92	MRK3	$J/\psi \to \gamma f_1(1285)$
0.64±0.40	GURTU	79	HBC	4.2 $K^- p$
• • • We do not use the following data for averages, fits, limits, etc. • • •				
0.93±0.30	[1] GRASSLER	77	HBC	16 $\pi^\mp p$

[1] Assuming $\rho\pi\pi$ and $a_0(980)\pi$ intermediate states.

$\Gamma(2\pi^+2\pi^-)/\Gamma(\eta\pi\pi)$ — Γ_3/Γ_8

VALUE	DOCUMENT ID		TECN	COMMENT
0.28±0.02±0.02	[1] LEES	12X	BABR	$\tau^- \to \pi^- f_1(1285)\nu_\tau$

[1] Assuming $B(f_1(1285) \to \pi\pi\eta) = 3/2\ B(f_1(1285) \to \pi^+\pi^-\eta)$.

$\Gamma(a_0(980)\pi$ [ignoring $a_0(980) \to K\overline{K}$])$/\Gamma(\eta\pi\pi)$ — $\Gamma_9/\Gamma_8 = \Gamma_9/(\Gamma_9+\Gamma_{10})$

VALUE	CL%	DOCUMENT ID		TECN	COMMENT
0.72±0.08 OUR FIT					
0.72±0.07 OUR AVERAGE					
0.74±0.02±0.09		DICKSON	16	CLAS	$\gamma p \to f_1(1285) p$
0.72±0.15		GURTU	79	HBC	4.2 $K^- p$
$0.6^{+0.3}_{-0.2}$		CORDEN	78	OMEG	12–15 $\pi^- p$
• • • We do not use the following data for averages, fits, limits, etc. • • •					
>0.69	95	ACHARD	02B	L3	183–209 $e^+e^- \to e^+e^-\eta\pi^+\pi^-$
0.28±0.07		ALDE	97B	GAM4	100 $\pi^- p \to \eta\pi^0\pi^0 n$
1.0 ±0.3		GRASSLER	77	HBC	16 $\pi^\mp p$

$\Gamma(K\overline{K}\pi)/\Gamma(\eta\pi\pi)$ — $\Gamma_{11}/\Gamma_8 = \Gamma_{11}/(\Gamma_9+\Gamma_{10})$

VALUE	DOCUMENT ID		TECN	COMMENT
0.172±0.011 OUR FIT				
0.176±0.012 OUR AVERAGE				
0.216±0.010±0.031	DICKSON	16	CLAS	$\gamma p \to f_1(1285) p$
0.166±0.01 ±0.008	BARBERIS	98C	OMEG	450 $pp \to p_f f_1(1285) p_s$
0.42 ±0.15	GURTU	79	HBC	4.2 $K^- p$
0.5 ±0.2	[1] CORDEN	78	OMEG	12–15 $\pi^- p$
0.20 ±0.08	[2] DEFOIX	72	HBC	0.7 $\overline{p}p \to 7\pi$
0.16 ±0.08	CAMPBELL	69	DBC	2.7 $\pi^+ d$

[1] CORDEN 78 assumes low-mass $\eta\pi\pi$ region is dominantly 1^{++}. See BARBERIS 98C and MANAK 00A for discussion.
[2] $K\overline{K}$ system characterized by the $I = 1$ threshold enhancement. (See under $a_0(980)$).

$\Gamma(K\overline{K}^*(892))/\Gamma_{total}$ — Γ_{12}/Γ

VALUE	DOCUMENT ID		TECN	COMMENT
not seen	NACASCH	78	HBC	0.7,0.76 $\overline{p}p \to K\overline{K}3\pi$
• • • We do not use the following data for averages, fits, limits, etc. • • •				
seen	[1] ACHARD	07	L3	183–209 $e^+e^- \to e^+e^- K^0_S K^\pm\pi^\mp$

[1] A clear signal of 19.8 ± 4.4 events observed at high Q^2.

$\Gamma(\pi^+\pi^-\pi^0)/\Gamma_{total}$ — Γ_{13}/Γ

VALUE (%)	EVTS	DOCUMENT ID		TECN	COMMENT
0.30±0.055±0.074	2.3k	[1] DOROFEEV	11	VES	$\pi^- N \to \pi^- f_1(1285) N$

[1] Value obtained selecting the region corresponding to $f_0(980)$ in the $\pi^+\pi^-$ mass spectrum. The sytematic error includes the uncertainty on the partial width $f_1 \to \eta\pi\pi$ obtained from PDG 10 data.

$\Gamma(\rho^\pm\pi^\mp)/\Gamma_{total}$ — Γ_{14}/Γ

VALUE (%)	CL%	DOCUMENT ID		TECN	COMMENT
<0.31	95	DOROFEEV	11	VES	$\pi^- N \to \pi^- f_1(1285) N$

$\Gamma(\gamma\rho^0)/\Gamma_{total}$ — Γ_{15}/Γ

VALUE (units 10^{-2})	CL%	DOCUMENT ID		TECN	COMMENT
6.1±1.0 OUR FIT Error includes scale factor of 1.7.					
• • • We do not use the following data for averages, fits, limits, etc. • • •					
2.8±0.7±0.6		[1] AMELIN	95	VES	37 $\pi^- N \to \pi^-\pi^+\pi^-\gamma N$
<5	95	BITYUKOV	91B	SPEC	32 $\pi^- p \to \pi^+\pi^-\gamma n$

[1] Not an independent measurement.

$\Gamma(\gamma\rho^0)/\Gamma(2\pi^+2\pi^-)$ — $\Gamma_{15}/\Gamma_3 = \Gamma_{15}/\frac{1}{3}\Gamma_1$

VALUE	DOCUMENT ID		TECN	COMMENT
0.55±0.10 OUR FIT Error includes scale factor of 1.5.				
0.45±0.18	[1] COFFMAN	90	MRK3	$J/\psi \to \gamma\gamma\pi^+\pi^-$

[1] Using $B(J/\psi \to \gamma f_1(1285) \to \gamma\gamma\rho^0) = 0.25 \times 10^{-4}$ and $B(J/\psi \to \gamma f_1(1285) \to \gamma 2\pi^+ 2\pi^-) = 0.55 \times 10^{-4}$ given by MIR 88.

$\Gamma(\eta\pi\pi)/\Gamma(\gamma\rho^0)$ — $\Gamma_8/\Gamma_{15} = (\Gamma_9+\Gamma_{10})/\Gamma_{15}$

VALUE	DOCUMENT ID		TECN	COMMENT
8.6±1.6 OUR FIT Error includes scale factor of 1.9.				
8.5±2.0 OUR AVERAGE Error includes scale factor of 2.2. See the ideogram below.				
21.3±4.4	DICKSON	16	CLAS	$\gamma p \to f_1(1285) p$
10.0±1.0±2.0	BARBERIS	98C	OMEG	450 $pp \to p_f f_1(1285) p_s$
7.5±1.0	[1] ARMSTRONG	92C	OMEG	300 $pp \to pp\pi^+\pi^-\gamma$, $pp\eta\pi^+\pi^-$

[1] Published value multiplied by 1.5.

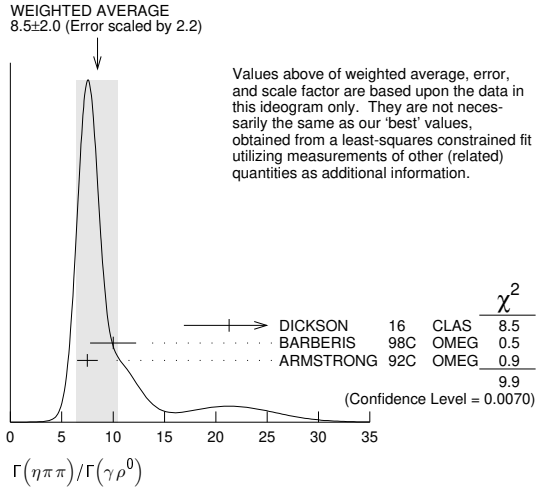

$\Gamma(\gamma\rho^0)/\Gamma(K\overline{K}\pi)$ — Γ_{15}/Γ_{11}

VALUE	CL%	DOCUMENT ID		TECN	COMMENT
• • • We do not use the following data for averages, fits, limits, etc. • • •					
>0.035	90	[1] COFFMAN	90	MRK3	$J/\psi \to \gamma\gamma\pi^+\pi^-$

[1] Using $B(J/\psi \to \gamma f_1(1285) \to \gamma\gamma\rho^0) = 0.25 \times 10^{-4}$ and $B(J/\psi \to \gamma f_1(1285) \to \gamma K\overline{K}\pi) = < 0.72 \times 10^{-3}$.

$\Gamma(\phi\gamma)/\Gamma_{total}$ — Γ_{16}/Γ

VALUE	DOCUMENT ID		TECN	COMMENT
seen	[1] ABLIKIM	25P	BES3	$J/\psi \to \gamma\gamma\phi$

[1] From a partial wave analysis of $J/\psi \to \gamma\gamma\phi$ with significance 17.3σ.

$\Gamma(\phi\gamma)/\Gamma(K\overline{K}\pi)$ — Γ_{16}/Γ_{11}

VALUE (units 10^{-2})	CL%	EVTS	DOCUMENT ID		TECN	COMMENT
0.82±0.21±0.20		19	BITYUKOV	88	SPEC	32.5 $\pi^- p \to K^+K^-\pi^0 n$
• • • We do not use the following data for averages, fits, limits, etc. • • •						
<0.50	95		BARBERIS	98C	OMEG	450 $pp \to p_f f_1(1285) p_s$
<0.93	95		AMELIN	95	VES	37 $\pi^- N \to \pi^-\pi^+\pi^-\gamma N$

$\Gamma(e^+e^-)/\Gamma_{total}$ — Γ_{17}/Γ

VALUE	CL%	DOCUMENT ID		TECN	COMMENT
$<9.4 \times 10^{-9}$	90	[1] ACHASOV	20	SND	$e^+e^- \to \eta\pi^0\pi^0$

[1] ACHASOV 20 reports two candidate events corresponding to a significance of 2.5 σ and the branching fraction of $(5.1^{+3.7}_{-2.7}) \times 10^{-9}$.

$f_1(1285)$ REFERENCES

AAIJ	25F	PR D111 092009	R. Aaij *et al.*	(LHCb Collab.)
ABLIKIM	25P	PR D111 052011	M. Ablikim *et al.*	(BESIII Collab.)
ABLIKIM	23M	JHEP 2303 121	M. Ablikim *et al.*	(BESIII Collab.)
ACHASOV	20	PL B800 135074	M.N. Achasov *et al.*	(SND Collab.)
ABLIKIM	19BA	PR D100 092003	M. Ablikim *et al.*	(BESIII Collab.)
DICKSON	16	PR C93 065202	R. Dickson *et al.*	(JLab CLAS Collab.)
ABLIKIM	15P	PR D92 012007	M. Ablikim *et al.*	(BESIII Collab.)
AAIJ	14Y	PRL 112 091802	R. Aaij *et al.*	(LHCb Collab.)
LEES	12X	PR D86 092010	J.P. Lees *et al.*	(BABAR Collab.)
ABLIKIM	11J	PRL 107 182001	M. Ablikim *et al.*	(BESIII Collab.)
DOROFEEV	11	EPJ A47 68	V. Dorofeev *et al.*	(SERP, MIPT)
PDG	10	JP G37 075021	K. Nakamura *et al.*	(PDG Collab.)
ACHARD	07	JHEP 0703 018	P. Achard *et al.*	(L3 Collab.)
AUBERT	07AU	PR D76 092005	B. Aubert *et al.*	(BABAR Collab.)
BAI	04J	PL B594 47	J.Z. Bai *et al.*	(BES Collab.)
ABDALLAH	03H	PL B569 129	J. Abdallah *et al.*	(DELPHI Collab.)
ACHARD	02B	PL B526 269	P. Achard *et al.*	(L3 Collab.)
ACCIARRI	01G	PL B501 1	M. Acciarri *et al.*	(L3 Collab.)
ADAMS	01B	PL B516 264	G.S. Adams *et al.*	(BNL E852 Collab.)
BARBERIS	00C	PL B471 440	D. Barberis *et al.*	(WA 102 Collab.)
MANAK	00A	PR D62 012003	J.J. Manak *et al.*	(BNL E852 Collab.)
SOSA	99	PRL 83 913	M. Sosa *et al.*	
BARBERIS	98C	PL B440 225	D. Barberis *et al.*	(WA 102 Collab.)
ALDE	97B	PAN 60 386	D. Alde *et al.*	(GAMS Collab.)
		Translated from YAF 60 458.		
BARBERIS	97B	PL B413 217	D. Barberis *et al.*	(WA 102 Collab.)
BARBERIS	97C	PL B413 225	D. Barberis *et al.*	(WA 102 Collab.)
AMELIN	95	ZPHY C66 71	D.V. Amelin *et al.*	(VES Collab.)
ANTINORI	95	PL B353 589	F. Antinori *et al.*	(ATHU, BARI, BIRM+)
ABATZIS	94	PL B324 509	S. Abatzis *et al.*	(ATHU, BARI, BIRM+)
LEE	94	PL B323 227	J.H. Lee *et al.*	(BNL, IND, KYUN, MASD+)
ARMSTRONG	93C	PL B307 394	T.A. Armstrong *et al.*	(FNAL, FERR, GENO+)
ARMSTRONG	92C	ZPHY C54 371	T.A. Armstrong *et al.*	(ATHU, BARI, BIRM+)
BOLTON	92	PL B278 495	T. Bolton *et al.*	(Mark III Collab.)
BITYUKOV	91B	SJNP 54 318	S.I. Bityukov *et al.*	(SERP)
		Translated from YAF 54 529.		

FUKUI	91C	PL B267 293	S. Fukui *et al.*	(SUGI, NAGO, KEK, KYOT+)
COFFMAN	90	PR D41 1410	D.M. Coffman *et al.*	(Mark III Collab.)
ARMSTRONG	89	PL B221 216	T.A. Armstrong *et al.*	(CERN, CDEF, BIRM+) JPC
ARMSTRONG	89E	PL B228 536	T.A. Armstrong, M. Benayoun	(ATHU, BARI, BIRM+)
ARMSTRONG	89G	ZPHY C43 55	T.A. Armstrong *et al.*	(CERN, BIRM, BARI+)
RATH	89	PR D40 693	M.G. Rath *et al.*	(NDAM, BRAN, BNL, CUNY+)
AIHARA	88B	PL B209 107	H. Aihara *et al.*	(TPC-2γ Collab.)
BIRMAN	88	PRL 61 1557	A. Birman *et al.*	(BNL, FSU, IND, MASD) JP
BITYUKOV	88	PL B203 327	S.I. Bityukov *et al.*	(SERP)
MIR	88	Photon-Photon 88, 126 Conference	R. Mir	(Mark III Collab.)
ALDE	87	PL B198 286	D.M. Alde *et al.*	(LANL, BRUX, SERP, LAPP)
BECKER	87	PRL 59 186	J.J. Becker *et al.*	(Mark III Collab.)
GIDAL	87	PRL 59 2012	G. Gidal *et al.*	(LBL, SLAC, HARV)
ANDO	86	PRL 57 1296	A. Ando *et al.*	(KEK, KYOT, NIRS, SAGA+) IJP
REEVES	86	PR D34 1960	D.F. Reeves *et al.*	(FLOR, BNL, IND+) JP
CHUNG	85	PRL 55 779	S.U. Chung *et al.*	(BNL, FLOR, IND+) JP
ARMSTRONG	84	PL 146B 273	T.A. Armstrong *et al.*	(ATHU, BARI, BIRM+) JP
BITYUKOV	84B	PL 144B 133	S.I. Bityukov *et al.*	(SERP)
CHAUVAT	84	PL 148B 382	P. Chauvat *et al.*	(CERN, CLER, UCLA+)
TORNQVIST	82B	NP B203 268	N.A. Tornqvist	(HELS)
EVANGELIS...	81	NP B178 197	C. Evangelista *et al.*	(BARI, BONN, CERN+)
BROMBERG	80	PR D22 1513	C.M. Bromberg *et al.*	(CIT, FNAL, ILLC+)
DIONISI	80	NP B169 1	C. Dionisi *et al.*	(CERN, MADR, CDEF+)
GURTU	79	NP B151 181	A. Gurtu *et al.*	(CERN, ZEEM, NIJM, OXF)
STANTON	79	PRL 42 346	N.R. Stanton *et al.*	(OSU, CARL, MCGI+) JP
CORDEN	78	NP B144 253	M.J. Corden *et al.*	(BIRM, RHEL, TELA+) JP
NACASCH	78	NP B135 203	R. Nacasch *et al.*	(PARIS, MADR, CERN)
GRASSLER	77	NP B121 189	H. Grassler *et al.*	(AACH3, BERL, BONN+)
DEFOIX	72	NP B44 125	C. Defoix *et al.*	(CDEF, CERN)
DUBOC	72	NP B46 429	J. Duboc *et al.*	(PARIS, LIVP)
THUN	72	PRL 28 1733	R. Thun *et al.*	(STON, NEAS)
BARDADIN-...	71	PR D4 2711	M. Bardadin-Otwinowska *et al.*	(WARS)
BOESEBECK	71	PL 34B 659	K. Boesebeck	(AACH, BERL, BONN, CERN, CRAC+)
CAMPBELL	69	PRL 22 1204	J.H. Campbell *et al.*	(PURD)
LORSTAD	69	NP B14 63	B. Lorstad *et al.*	(CDEF, CERN) JP
D'ANDLAU	68	NP B5 693	C. d'Andlau *et al.*	(CDEF, CERN, IRAD+) IJP
DAHL	67	PR 163 1377	O.I. Dahl *et al.*	(LRL) IJP

$\eta(1295)$

$I^G(J^{PC}) = 0^+(0^{-+})$

See the review on "Spectroscopy of Light Meson Resonances."

$\eta(1295)$ MASS

VALUE (MeV)	EVTS	DOCUMENT ID		TECN	COMMENT
1294±4 OUR AVERAGE	Error includes scale factor of 1.6. See the ideogram below.				
1302±9±8	20k	ADAMS	01B	B852	18 GeV $\pi^- p \to K^+ K^- \pi^0 n$
1282±5	9082	MANAK	00A	MPS	18 $\pi^- p \to \eta\pi^+\pi^- n$
1299±4	2100	ALDE	97B	GAM4	100 $\pi^- p \to \eta\pi^0\pi^0 n$
1295±4		FUKUI	91C	SPEC	8.95 $\pi^- p \to \eta\pi^+\pi^- n$
• • • We do not use the following data for averages, fits, limits, etc. • • •					
1264±8		[1] AUGUSTIN	90	DM2	$J/\psi \to \gamma\eta\pi^+\pi^-$
∼ 1275		STANTON	79	CNTR	8.4 $\pi^- p \to n\eta 2\pi$

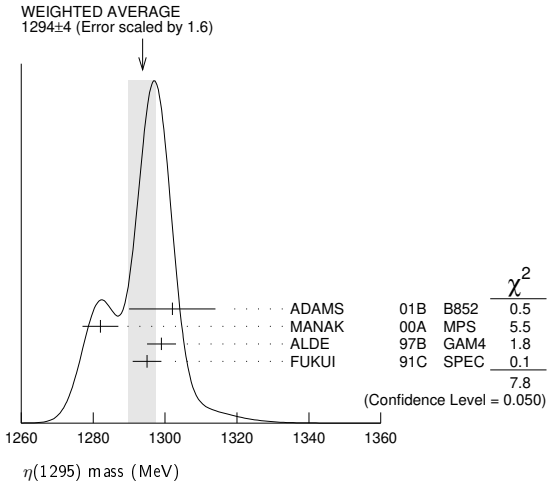

[1] PWA analysis of AUGUSTIN 92 assigns 0^{-+} quantum numbers to this state rather than 1^{++} as before.

$\eta(1295)$ WIDTH

VALUE (MeV)	EVTS	DOCUMENT ID		TECN	COMMENT
55± 5 OUR AVERAGE					
57±23±21	20k	ADAMS	01B	B852	18 GeV $\pi^- p \to K^+ K^- \pi^0 n$
66±13	9082	MANAK	00A	MPS	18 $\pi^- p \to \eta\pi^+\pi^- n$
53± 6		FUKUI	91C	SPEC	8.95 $\pi^- p \to \eta\pi^+\pi^- n$
• • • We do not use the following data for averages, fits, limits, etc. • • •					
<40	2100	ALDE	97B	GAM4	100 $\pi^- p \to \eta\pi^0\pi^0 n$
44±20		[1] AUGUSTIN	90	DM2	$J/\psi \to \gamma\eta\pi^+\pi^-$
∼ 70		STANTON	79	CNTR	8.4 $\pi^- p \to n\eta 2\pi$

[1] PWA analysis of AUGUSTIN 92 assigns 0^{-+} quantum numbers to this state rather than 1^{++} as before.

$\eta(1295)$ DECAY MODES

	Mode	Fraction (Γ_i/Γ)
Γ_1	$\eta\pi^+\pi^-$	seen
Γ_2	$a_0(980)\pi$	seen
Γ_3	$\gamma\gamma$	
Γ_4	$\eta\pi^0\pi^0$	seen
Γ_5	$\eta(\pi\pi)_{S\text{-wave}}$	seen
Γ_6	$\sigma\eta$	seen
Γ_7	$K\overline{K}\pi$	seen

$\eta(1295)$ $\Gamma(i)\Gamma(\gamma\gamma)/\Gamma(\text{total})$

$\Gamma(\eta\pi^+\pi^-) \times \Gamma(\gamma\gamma)/\Gamma_{\text{total}}$ — $\Gamma_1\Gamma_3/\Gamma$

VALUE (keV)	CL%	DOCUMENT ID		TECN	COMMENT
<0.066	95	ACCIARRI	01G	L3	183–202 $e^+e^- \to e^+e^-\eta\pi^+\pi^-$
• • • We do not use the following data for averages, fits, limits, etc. • • •					
<0.6	90	AIHARA	88C	TPC	$e^+e^- \to e^+e^-\eta\pi^+\pi^-$
<0.3		ANTREASYAN	87	CBAL	$e^+e^- \to e^+e^-\eta\pi\pi$

$\Gamma(K\overline{K}\pi) \times \Gamma(\gamma\gamma)/\Gamma_{\text{total}}$ — $\Gamma_7\Gamma_3/\Gamma$

VALUE (keV)	CL%	DOCUMENT ID		TECN	COMMENT
• • • We do not use the following data for averages, fits, limits, etc. • • •					
<0.014	90	[1,2] AHOHE	05	CLE2	10.6 $e^+e^- \to e^+e^- K^0_S K^\pm\pi^\mp$

[1] Using $\eta(1295)$ mass and width 1294 MeV and 55 MeV, respectively.
[2] Assuming three-body phase-space decay to $K^0_S K^\pm\pi^\mp$.

$\eta(1295)$ BRANCHING RATIOS

$\Gamma(a_0(980)\pi)/\Gamma_{\text{total}}$ — Γ_2/Γ

VALUE	DOCUMENT ID		TECN	COMMENT
• • • We do not use the following data for averages, fits, limits, etc. • • •				
not seen	BERTIN	97	OBLX	0.0 $\overline{p}p \to K^\pm(K^0)\pi^\mp\pi^+\pi^-$
seen	BIRMAN	88	MPS	8 $\pi^- p \to K^+\overline{K}^0\pi^- n$
large	ANDO	86	SPEC	8 $\pi^- p \to \eta\pi^+\pi^- n$
large	STANTON	79	CNTR	8.4 $\pi^- p \to n\eta 2\pi$

$\Gamma(a_0(980)\pi)/\Gamma(\eta\pi^0\pi^0)$ — Γ_2/Γ_4

VALUE	DOCUMENT ID		TECN	COMMENT
0.65±0.10	[1] ALDE	97B	GAM4	100 $\pi^- p \to \eta\pi^0\pi^0 n$

[1] Assuming that $a_0(980)$ decays only to $\eta\pi$.

$\Gamma(\eta(\pi\pi)_{S\text{-wave}})/\Gamma(\eta\pi^0\pi^0)$ — Γ_5/Γ_4

VALUE	DOCUMENT ID		TECN	COMMENT
0.35±0.10	ALDE	97B	GAM4	100 $\pi^- p \to \eta\pi^0\pi^0 n$

$\Gamma(a_0(980)\pi)/\Gamma(\sigma\eta)$ — Γ_2/Γ_6

VALUE	EVTS	DOCUMENT ID		TECN	COMMENT
0.48±0.22	9082	MANAK	00A	MPS	18 $\pi^- p \to \eta\pi^+\pi^- n$

$\eta(1295)$ REFERENCES

AHOHE	05	PR D71 072001	R. Ahohe *et al.*	(CLEO Collab.)
ACCIARRI	01G	PL B501 1	M. Acciarri *et al.*	(L3 Collab.)
ADAMS	01B	PL B516 264	G.S. Adams *et al.*	(BNL E852 Collab.)
MANAK	00A	PR D62 012003	J.J. Manak *et al.*	(BNL E852 Collab.)
ALDE	97B	PAN 60 386 Translated from YAF 60 458.	D. Alde *et al.*	(GAMS Collab.)
BERTIN	97	PL B400 226	A. Bertin *et al.*	(OBELIX Collab.)
AUGUSTIN	92	PR D46 1951	J.E. Augustin, G. Cosme	(DM2 Collab.)
FUKUI	91C	PL B267 293	S. Fukui *et al.*	(SUGI, NAGO, KEK, KYOT+)
AUGUSTIN	90	PR D42 10	J.E. Augustin *et al.*	(DM2 Collab.)
AIHARA	88C	PR D38 1	H. Aihara *et al.*	(TPC-2γ Collab.)
BIRMAN	88	PRL 61 1557	A. Birman *et al.*	(BNL, FSU, IND, MASD) JP
ANTREASYAN	87	PR D36 2633	D. Antreasyan *et al.*	(Crystal Ball Collab.)
ANDO	86	PRL 57 1296	A. Ando *et al.*	(KEK, KYOT, NIRS, SAGA+) IJP
STANTON	79	PRL 42 346	N.R. Stanton *et al.*	(OSU, CARL, MCGI+) JP

$\pi(1300)$

$I^G(J^{PC}) = 1^-(0^{-+})$

$\pi(1300)$ MASS

VALUE (MeV)	EVTS	DOCUMENT ID		TECN	COMMENT
1300±100 OUR ESTIMATE					
• • • We do not use the following data for averages, fits, limits, etc. • • •					
1128± 26±70		DARGENT	17	RVUE	$D^0 \to \pi^-\pi^+\pi^-\pi^+$
1345± 8±10	18k	[1] SCHEGELSKY	06	RVUE	$\gamma\gamma \to \pi^+\pi^-\pi^0$
1200± 40	90k	SALVINI	04	OBLX	$\overline{p}p \to 2\pi^+ 2\pi^-$

Int. J. Mod. Phys. A 2026.41. Downloaded from www.worldscientific.com
by [redacted]LIFORNIA @ BERKELEY on 09/16/26. Re-use and distribution is strictly not permitted, except for Open Access articles.

Int. J. Mod. Phys. A 2026.41. Downloaded from www.worldscientific.com by UNIVERSITY OF CALIFORNIA @ BERKELEY on 09/16/26. Re-use and distribution is strictly not permitted, except for Open Access articles.

1343± 15±24	CHUNG	02	B852	18.3 $\pi^- p \to \pi^+\pi^-\pi^- p$
1375± 40	ABELE	01	CBAR	0.0 $\overline{p}d \to \pi^- 4\pi^0 p$
1275± 15	BERTIN	97D	OBLX	0.05 $\overline{p}p \to 2\pi^+ 2\pi^-$
∼ 1114	ABELE	96	CBAR	0.0 $\overline{p}p \to 5\pi^0$
1190± 30	ZIELINSKI	84	SPEC	200 $\pi^+ Z \to Z 3\pi$
1240± 30	BELLINI	82	SPEC	40 $\pi^- A \to A 3\pi$
1273± 50	[2] AARON	81	RVUE	
1342± 20	BONESINI	81	OMEG	12 $\pi^- p \to p 3\pi$
∼ 1400	DAUM	81B	SPEC	63,94 $\pi^- p$

[1] From analysis of L3 data at 183–209 GeV.
[2] Uses multichannel Aitchison-Bowler model (BOWLER 75). Uses data from DAUM 80 and DANKOWYCH 81.

$\pi(1300)$ WIDTH

VALUE (MeV)	EVTS	DOCUMENT ID		TECN	COMMENT
200 to 600 OUR ESTIMATE					
• • • We do not use the following data for averages, fits, limits, etc. • • •					
314± 39±66		DARGENT	17	RVUE	$D^0 \to \pi^-\pi^+\pi^-\pi^+$
260± 20±30	18k	[3] SCHEGELSKY	06	RVUE	$\gamma\gamma \to \pi^+\pi^-\pi^0$
470±120	90k	SALVINI	04	OBLX	$\overline{p}p \to 2\pi^+ 2\pi^-$
449± 39±47		CHUNG	02	B852	18.3 $\pi^- p \to \pi^+\pi^-\pi^- p$
268± 50		ABELE	01	CBAR	0.0 $\overline{p}d \to \pi^- 4\pi^0 p$
218±100		BERTIN	97D	OBLX	0.05 $\overline{p}p \to 2\pi^+ 2\pi^-$
∼ 340		ABELE	96	CBAR	0.0 $\overline{p}p \to 5\pi^0$
440± 80		ZIELINSKI	84	SPEC	200 $\pi^+ Z \to Z 3\pi$
360±120		BELLINI	82	SPEC	40 $\pi^- A \to A 3\pi$
580±100		[4] AARON	81	RVUE	
220± 70		BONESINI	81	OMEG	12 $\pi^- p \to p 3\pi$
∼ 600		DAUM	81B	SPEC	63,94 $\pi^- p$

[3] From analysis of L3 data at 183–209 GeV.
[4] Uses multichannel Aitchison-Bowler model (BOWLER 75). Uses data from DAUM 80 and DANKOWYCH 81.

$\pi(1300)$ DECAY MODES

	Mode	Fraction (Γ_i/Γ)
Γ_1	$\rho\pi$	seen
Γ_2	$\pi(\pi\pi)_{S\text{-wave}}$	seen
Γ_3	$\gamma\gamma$	

$\pi(1300)$ $\Gamma(i)\Gamma(\gamma\gamma)/\Gamma(\text{total})$

$\Gamma(\rho\pi) \times \Gamma(\gamma\gamma)/\Gamma_{\text{total}}$ — $\Gamma_1\Gamma_3/\Gamma$

VALUE (keV)	CL%	DOCUMENT ID		TECN	COMMENT
<0.085	90	ACCIARRI	97T	L3	$e^+e^- \to e^+e^-\pi^+\pi^-\pi^0$
• • • We do not use the following data for averages, fits, limits, etc. • • •					
<0.8	95	[5] SCHEGELSKY	06	RVUE	$\gamma\gamma \to \pi^+\pi^-\pi^0$
<0.54	90	ALBRECHT	97B	ARG	$e^+e^- \to e^+e^-\pi^+\pi^-\pi^0$

[5] From analysis of L3 data at 183–209 GeV.

$\pi(1300)$ BRANCHING RATIOS

$\Gamma(\pi(\pi\pi)_{S\text{-wave}})/\Gamma(\rho\pi)$ — Γ_2/Γ_1

VALUE	CL%	EVTS	DOCUMENT ID		TECN	COMMENT
• • • We do not use the following data for averages, fits, limits, etc. • • •						
2.2 ±0.4		90k	SALVINI	04	OBLX	$\overline{p}p \to 2\pi^+ 2\pi^-$
seen			CHUNG	02	B852	18.3 $\pi^- p \to \pi^+ 2\pi^- p$
<0.15	90		ABELE	01	CBAR	0.0 $\overline{p}d \to \pi^- 4\pi^0 p$
2.12			[6] AARON	81	RVUE	

[6] Uses multichannel Aitchison-Bowler model (BOWLER 75). Uses data from DAUM 80 and DANKOWYCH 81.

$\pi(1300)$ REFERENCES

DARGENT	17	JHEP 1705 143	P. dArgent *et al.*	(HEID, BRIS)
SCHEGELSKY	06	EPJ A27 199	V.A. Schegelsky *et al.*	
SALVINI	04	EPJ C35 21	P. Salvini *et al.*	(OBELIX Collab.)
CHUNG	02	PR D65 072001	S.U. Chung *et al.*	(BNL E852 Collab.)
ABELE	01	EPJ C19 667	A. Abele *et al.*	(Crystal Barrel Collab.)
ACCIARRI	97T	PL B413 147	M. Acciarri *et al.*	(L3 Collab.)
ALBRECHT	97B	ZPHY C74 469	H. Albrecht *et al.*	(ARGUS Collab.)
BERTIN	97D	PL B414 220	A. Bertin *et al.*	(OBELIX Collab.)
ABELE	96	PL B380 453	A. Abele *et al.*	(Crystal Barrel Collab.)
ZIELINSKI	84	PR D30 1855	M. Zielinski *et al.*	(ROCH, MINN, FNAL)
BELLINI	82	PRL 48 1697	G. Bellini *et al.*	(MILA, BGNA, JINR)
AARON	81	PR D24 1207	R.A. Aaron, R.S. Longacre	(NEAS, BNL)
BONESINI	81	PL 103B 75	M. Bonesini *et al.*	(MILA, LIVP, DARE+)
DANKOWY...	81	PRL 46 580	J.A. Dankowych *et al.*	(TNTO, BNL, CARL+)
DAUM	81B	NP B182 269	C. Daum *et al.*	(AMST, CERN, CRAC, MPIM+)
DAUM	80	PL 89B 281	C. Daum *et al.*	(AMST, CERN, CRAC, MPIM+)
BOWLER	75	NP B97 227	M.G. Bowler *et al.*	(OXFTP, DARE)

$a_2(1320)$

$I^G(J^{PC}) = 1^-(2^{++})$

$a_2(1320)$ T-MATRIX POLE $\sqrt{s}$

Note that $\Gamma = -2\,\mathrm{Im}(\sqrt{s})$.

VALUE (MeV)	DOCUMENT ID		TECN	COMMENT
(1305–1321)−i(52–58) OUR ESTIMATE				
$(1318.7 \pm 1.9 \pm 1.3) - i(53.8 \pm 2.3^{+1.7}_{-0.9})$	[1] KOPF	21	RVUE	0.9 $p\overline{p} \to \pi^0\pi^0\eta$, $\pi^0\eta\eta$, $\pi^0 K^+K^-$ and 191 $\pi^- p \to \pi^-\pi^-\pi^+ p$
$(1312.5 \pm 0.7 \pm 2.6) - i(53.5 \pm 0.6 \pm 1.9)$	[2] ALBRECHT	20	RVUE	0.9 $\overline{p}p \to \pi^0\pi^0\eta$, $\pi^0\eta\eta$, $\pi^0 K^+K^-$
$(1306.0 \pm 0.8 \pm 1.3) - i(57.2 \pm 0.8 \pm 0.0)$	[3] RODAS	19	RVUE	91 $\pi^- p \to \eta^{(\prime)}\pi^- p$
$(1309 \pm 4) - i\,(55 \pm 2)$	[4] ANISOVICH	09	RVUE	$\overline{p}p$, πN

[1] Extraction based on a combined fit of Crystal Barrel and $\pi\pi$ scattering data (ALBRECHT 20), and COMPASS data (ADOLPH 15), using a coupled-channel model of $\eta\pi$, $\eta'\pi$ and $K\overline{K}$ systems.
[2] T-matrix pole with 2 poles, 2 channels ($\pi^0\eta$ and $K\overline{K}$).
[3] Coupled-channel analysis of both the $\eta\pi$ and $\eta'\pi$ systems using ADOLPH 15 data. Supersedes JACKURA 18. Performed by JPAC.
[4] Amplitude did not include dispersive corrections. From analysis of $\eta\pi$ mode.

$a_2(1320)$ MASS

VALUE (MeV)	DOCUMENT ID
1318.2±0.6 OUR AVERAGE Includes data from the 4 datablocks that follow this one. Error includes scale factor of 1.2.	

3π MODE

VALUE (MeV)	EVTS	DOCUMENT ID		TECN	CHG	COMMENT
The data in this block is included in the average printed for a previous datablock.						
1318.6± 1.3 OUR AVERAGE Error includes scale factor of 1.4. See the ideogram below.						
$1314.5^{+4.0}_{-3.3}$	46M	[1] AGHASYAN	18B	COMP		190 $\pi^- p \to \pi^-\pi^+\pi^- p$
1326 ± 2 ±2		CHUNG	02	B852		18.3 $\pi^- p \to \pi^+\pi^-\pi^- p$
1317 ± 3		BARBERIS	98B			450 $pp \to p_f\pi^+\pi^-\pi^0 p_s$
1323 ± 4 ±3		ACCIARRI	97T	L3		$e^+e^- \to e^+e^-\pi^+\pi^-\pi^0$
1320 ± 7		ALBRECHT	97B	ARG		$e^+e^- \to e^+e^-\pi^+\pi^-\pi^0$
1311.3± 1.6±3.0	72.4k	AMELIN	96	VES		36 $\pi^- p \to \pi^+\pi^-\pi^0 n$
1310 ± 5		ARMSTRONG	90	OMEG	0	300.0 $pp \to pp\pi^+\pi^-\pi^0$
1323.8± 2.3	4022	AUGUSTIN	89	DM2	±	$J/\psi \to \rho^\pm a_2^\mp$
1320.6± 3.1	3562	AUGUSTIN	89	DM2	0	$J/\psi \to \rho^0 a_2^0$
1317 ± 2	25k	[2] DAUM	80C	SPEC	−	63,94 $\pi^- p \to 3\pi p$
1320 ±10	1097	[2] BALTAY	78B	HBC	+0	15 $\pi^+ p \to p 4\pi$
1306 ± 8		FERRERSORIA	78	OMEG	−	9 $\pi^- p \to p 3\pi$
1318 ± 7	1.6k	[2] EMMS	75	DBC	0	4 $\pi^+ n \to p(3\pi)^0$
1315 ± 5		[2] ANTIPOV	73C	CNTR	−	25,40 $\pi^- p \to p\eta\pi^-$
1306 ± 9	1580	CHALOUPKA	73	HBC	−	3.9 $\pi^- p$
• • • We do not use the following data for averages, fits, limits, etc. • • •						
1321 ± 1 $^{+0}_{-7}$	420k	[3] ALEKSEEV	10	COMP		190 $\pi^- Pb \to \pi^-\pi^-\pi^+ Pb'$
1300 ± 2 ±4	18k	[4] SCHEGELSKY	06	RVUE	0	$\gamma\gamma \to \pi^+\pi^-\pi^0$
1305 ±14		CONDO	93	SHF		$\gamma p \to n\pi^+\pi^+\pi^-$
1310 ± 2		[2] EVANGELIS...	81	OMEG	−	12 $\pi^- p \to 3\pi p$
1343 ±11	490	BALTAY	78B	HBC	0	15 $\pi^+ p \to \Delta 3\pi$
1309 ± 5	5k	BINNIE	71	MMS	−	$\pi^- p$ near a_2 threshold
1299 ± 6	28k	BOWEN	71	MMS	−	5 $\pi^- p$
1300 ± 6	24k	BOWEN	71	MMS	+	5 $\pi^+ p$
1309 ± 4	17k	BOWEN	71	MMS	−	7 $\pi^- p$
1306 ± 4	941	ALSTON-...	70	HBC	+	7.0 $\pi^+ p \to 3\pi p$

[1] Statistical error negligible.
[2] From a fit to $J^P = 2^+$ $\rho\pi$ partial wave.
[3] Superseded by AGHASYAN 2018B.
[4] From analysis of L3 data at 183–209 GeV.

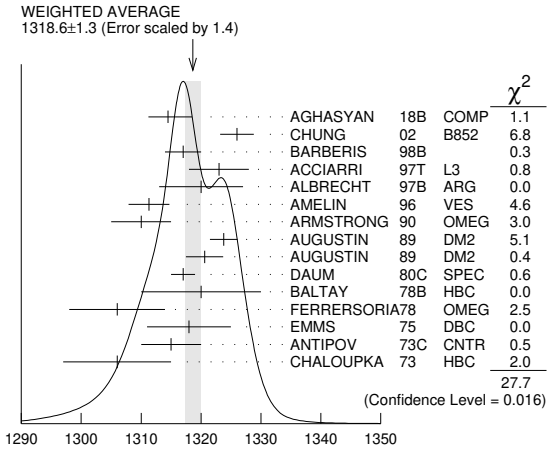

$K\overline{K}$ MODE

VALUE (MeV)	EVTS	DOCUMENT ID		TECN	CHG	COMMENT
The data in this block is included in the average printed for a previous datablock.						
1318.1± 0.7 OUR AVERAGE						
1319 ± 5	4700	[1,2] CLELAND	82B	SPEC	+	50 $\pi^+ p \to K^0_S K^+ p$
1324 ± 6	5200	[1,2] CLELAND	82B	SPEC	−	50 $\pi^- p \to K^0_S K^- p$
1320 ± 2	4000	CHABAUD	80	SPEC	−	17 $\pi^- A \to K^0_S K^- A$
1312 ± 4	11000	CHABAUD	78	SPEC	−	9.8 $\pi^- p \to K^- K^0_S p$
1316 ± 2	4730	CHABAUD	78	SPEC	−	18.8 $\pi^- p \to K^- K^0_S p$
1318 ± 1		[1,3] MARTIN	78D	SPEC	−	10 $\pi^- p \to K^0_S K^- p$
1320 ± 2	2724	MARGULIE	76	SPEC	−	23 $\pi^- p \to K^- K^0_S p$
1313 ± 4	730	FOLEY	72	CNTR	−	20.3 $\pi^- p \to K^- K^0_S p$
1319 ± 3	1500	[3] GRAYER	71	ASPK	−	17.2 $\pi^- p \to K^- K^0_S p$
• • • We do not use the following data for averages, fits, limits, etc. • • •						
1304 ±10	870	[4] SCHEGELSKY	06A	RVUE	0	$\gamma\gamma \to K^0_S K^0_S$
1330 ±11	1000	[1,2] CLELAND	82B	SPEC	+	30 $\pi^+ p \to K^0_S K^+ p$
1324 ± 5	350	HYAMS	78	ASPK	+	12.7 $\pi^+ p \to K^+ K^0_S p$

[1] From a fit to $J^P = 2^+$ partial wave.
[2] Number of events evaluated by us.
[3] Systematic error in mass scale subtracted.
[4] From analysis of L3 data at 91 and 183–209 GeV.

$\eta\pi$ MODE

VALUE (MeV)	EVTS	DOCUMENT ID		TECN	CHG	COMMENT
The data in this block is included in the average printed for a previous datablock.						
1317.7± 1.4 OUR AVERAGE						
1308 ± 9		BARBERIS	00H			450 $pp \to p_f \eta\pi^0 p_s$
1316 ± 9		BARBERIS	00H			450 $pp \to \Delta_f^{++} \eta\pi^- p_s$
1317 ± 1 ±2		THOMPSON	97	MPS		18 $\pi^- p \to \eta\pi^- p$
1315 ± 5 ±2		[1] AMSLER	94D	CBAR		0.0 $\overline{p}p \to \pi^0\pi^0\eta$
1325.1± 5.1		AOYAGI	93	BKEI		$\pi^- p \to \eta\pi^- p$
1317.7± 1.4±2.0		BELADIDZE	93	VES		37$\pi^- N \to \eta\pi^- N$
1323 ± 8	1000	[2] KEY	73	OSPK	−	6 $\pi^- p \to p\pi^- \eta$
• • • We do not use the following data for averages, fits, limits, etc. • • •						
1307 ± 1 ±6		[3] JACKURA	18	RVUE		$\pi^- p \to \eta\pi^- p$
1315 ±12		[4] ADOLPH	15	COMP		191 $\pi^- p \to \eta^{(\prime)}\pi^- p$
1324 ± 5		ARMSTRONG	93C	E760	0	$\overline{p}p \to \pi^0\eta\eta \to 6\gamma$
1336.2± 1.7	2561	DELFOSSE	81	SPEC	+	$\pi^\pm p \to p\pi^\pm\eta$
1330.7± 2.4	1653	DELFOSSE	81	SPEC	−	$\pi^\pm p \to p\pi^\pm\eta$
1324 ± 8	6200	[2,5] CONFORTO	73	OSPK	−	6 $\pi^- p \to p\,\mathrm{MM}^-$

[1] The systematic error of 2 MeV corresponds to the spread of solutions.
[2] Error includes 5 MeV systematic mass-scale error.
[3] Superseded by RODAS 19.
[4] ADOLPH 15 value is derived from a Breit-Wigner fit with mass-dependent width taking the $\eta\pi$ and $\rho\pi$ channels into account.
[5] Missing mass with enriched MMS = $\eta\pi^-$, $\eta = 2\gamma$.

$\eta'\pi$ MODE

VALUE (MeV)	DOCUMENT ID		TECN	COMMENT
The data in this block is included in the average printed for a previous datablock.				
1322 ± 7 OUR AVERAGE				
1318 ± 8 $^{+3}_{-5}$	IVANOV	01	B852	18 $\pi^- p \to \eta'\pi^- p$
1327.0±10.7	BELADIDZE	93	VES	37$\pi^- N \to \eta'\pi^- N$

$a_2(1320)$ WIDTH

VALUE (MeV)	DOCUMENT ID
107 ±5 OUR ESTIMATE	
107.8±1.2 OUR AVERAGE Includes data from the 4 datablocks that follow this one.	

3π MODE

VALUE (MeV)	EVTS	DOCUMENT ID		TECN	CHG	COMMENT
The data in this block is included in the average printed for a previous datablock.						
105.0$^{+1.7}_{-1.9}$ OUR AVERAGE						
106.6$^{+3.4}_{-7.0}$	46M	[1] AGHASYAN	18B	COMP		190 $\pi^- p \to \pi^-\pi^+\pi^- p$
108 ± 3 ±15		CHUNG	02	B852		18.3 $\pi^- p \to \pi^+\pi^-\pi^- p$
120 ±10		BARBERIS	98B			450 $pp \to p_f \pi^+\pi^-\pi^0 p_s$
105 ±10 ±11		ACCIARRI	97T	L3		$e^+e^- \to e^+e^-\pi^+\pi^-\pi^0$
120 ±10		ALBRECHT	97B	ARG		$e^+e^- \to e^+e^-\pi^+\pi^-\pi^0$
103.0± 6.0± 3.3	72.4k	AMELIN	96	VES		36 $\pi^- p \to \pi^+\pi^-\pi^0 n$
120 ±10		ARMSTRONG	90	OMEG	0	300.0$pp \to pp\pi^+\pi^-\pi^0$
107.0± 9.7	4022	AUGUSTIN	89	DM2	±	$J/\psi \to \rho^\pm a_2^\mp$
118.5±12.5	3562	AUGUSTIN	89	DM2	0	$J/\psi \to \rho^0 a_2^0$
97 ± 5		[2] EVANGELIS...	81	OMEG	−	12 $\pi^- p \to 3\pi p$
96 ± 9	25k	[2] DAUM	80C	SPEC	−	63,94 $\pi^- p \to 3\pi p$
110 ±15	1097	[2] BALTAY	78B	HBC	+0	15 $\pi^+ p \to p4\pi$
112 ±18	1.6k	[2] EMMS	75	DBC	0	4 $\pi^+ n \to p(3\pi)^0$
122 ±14	1.2k	[2,3] WAGNER	75	HBC	0	7 $\pi^+ p \to \Delta^{++}(3\pi)^0$
115 ±15		[2] ANTIPOV	73C	CNTR	−	25,40 $\pi^- p \to p\eta\pi^-$
99 ±15	1580	CHALOUPKA	73	HBC	−	3.9 $\pi^- p$
105 ± 5	28k	BOWEN	71	MMS	−	5 $\pi^- p$
99 ± 5	24k	BOWEN	71	MMS	+	5 $\pi^+ p$
103 ± 5	17k	BOWEN	71	MMS	−	7 $\pi^- p$
• • • We do not use the following data for averages, fits, limits, etc. • • •						
110 ± 2 $^{+2}_{-15}$	420k	[4] ALEKSEEV	10	COMP		190 $\pi^- Pb \to \pi^-\pi^-\pi^+ Pb'$
117 ± 6 ±20	18k	[5] SCHEGELSKY	06	RVUE	0	$\gamma\gamma \to \pi^+\pi^-\pi^0$
120 ±40		CONDO	93	SHF		$\gamma p \to n\pi^+\pi^+\pi^-$
115 ±14	490	BALTAY	78B	HBC	0	15 $\pi^+ p \to \Delta 3\pi$
72 ±16	5k	BINNIE	71	MMS	−	$\pi^- p$ near a_2 threshold
79 ±12	941	ALSTON-...	70	HBC	+	7.0 $\pi^+ p \to 3\pi p$

[1] Statistical error negligible.
[2] From a fit to $J^P = 2^+$ $\rho\pi$ partial wave.
[3] Width errors enlarged by us to $4\Gamma/\sqrt{N}$; see the note with the $K^*(892)$ mass.
[4] Superseded by AGHASYAN 2018B.
[5] From analysis of L3 data at 183–209 GeV.

$K\overline{K}$ MODE

VALUE (MeV)	EVTS	DOCUMENT ID		TECN	CHG	COMMENT
The data in this block is included in the average printed for a previous datablock.						
109.8± 2.4 OUR AVERAGE						
112 ±20	4700	[1,2] CLELAND	82B	SPEC	+	50 $\pi^+ p \to K^0_S K^+ p$
120 ±25	5200	[1,2] CLELAND	82B	SPEC	−	50 $\pi^- p \to K^0_S K^- p$
106 ± 4	4000	CHABAUD	80	SPEC	−	17 $\pi^- A \to K^0_S K^- A$
126 ±11	11000	CHABAUD	78	SPEC	−	9.8 $\pi^- p \to K^- K^0_S p$
101 ± 8	4730	CHABAUD	78	SPEC	−	18.8 $\pi^- p \to K^- K^0_S p$
113 ± 4		[1,3] MARTIN	78D	SPEC	−	10 $\pi^- p \to K^0_S K^- p$
105 ± 8	2724	[3] MARGULIE	76	SPEC	−	23 $\pi^- p \to K^- K^0_S p$
113 ±19	730	FOLEY	72	CNTR	−	20.3 $\pi^- p \to K^- K^0_S p$
123 ±13	1500	[3] GRAYER	71	ASPK	−	17.2 $\pi^- p \to K^- K^0_S p$
• • • We do not use the following data for averages, fits, limits, etc. • • •						
120 ±15	870	[4] SCHEGELSKY	06A	RVUE	0	$\gamma\gamma \to K^0_S K^0_S$
121 ±51	1000	[1,2] CLELAND	82B	SPEC	+	30 $\pi^+ p \to K^0_S K^+ p$
110 ±18	350	HYAMS	78	ASPK	+	12.7 $\pi^+ p \to K^+ K^0_S p$

[1] From a fit to $J^P = 2^+$ partial wave.
[2] Number of events evaluated by us.
[3] Width errors enlarged by us to $4\Gamma/\sqrt{N}$; see the note with the $K^*(892)$ mass.
[4] From analysis of L3 data at 91 and 183–209 GeV.

$\eta\pi$ MODE

VALUE (MeV)	EVTS	DOCUMENT ID		TECN	CHG	COMMENT
The data in this block is included in the average printed for a previous datablock.						
111.1± 2.4 OUR AVERAGE						
115 ±20		BARBERIS	00H			450 $pp \to p_f \eta\pi^0 p_s$
112 ±14		BARBERIS	00H			450 $pp \to \Delta_f^{++} \eta\pi^- p_s$
112 ± 3 ±2		[1] AMSLER	94D	CBAR		0.0 $\overline{p}p \to \pi^0\pi^0\eta$
103 ± 6 ±3		BELADIDZE	93	VES		37$\pi^- N \to \eta\pi^- N$
112.2± 5.7	2561	DELFOSSE	81	SPEC	+	$\pi^\pm p \to p\pi^\pm\eta$
116.6± 7.7	1653	DELFOSSE	81	SPEC	−	$\pi^\pm p \to p\pi^\pm\eta$
108 ± 9	1000	KEY	73	OSPK	−	6 $\pi^- p \to p\pi^- \eta$

Int. J. Mod. Phys. A 2026.41. Downloaded from www.worldscientific.com
by CALIFORNIA @ BERKELEY on 09/16/26. Re-use and distribution is strictly not permitted, except for Open Access articles.

Int. J. Mod. Phys. A 2026.41. Downloaded from www.worldscientific.com
by UNIVERSITY OF CALIFORNIA @ BERKELEY on 09/16/26. Re-use and distribution is strictly not permitted, except for Open Access articles.

• • • We do not use the following data for averages, fits, limits, etc. • • •

112 ± 1 ± 8		[2] JACKURA	18	RVUE	$\pi^- p \to \eta\pi^- p$
119 ± 14		[3] ADOLPH	15	COMP	191 $\pi^- p \to \eta^{(\prime)}\pi^- p$
127 ± 2 ± 2		[4] THOMPSON	97	MPS	18 $\pi^- p \to \eta\pi^- p$
118 ± 10		ARMSTRONG	93C	E760	0 $\overline{p}p \to \pi^0\eta\eta \to 6\gamma$
104 ± 9	6200	[5] CONFORTO	73	OSPK	− 6 $\pi^- p \to p$ MM$^-$

[1] The systematic error of 2 MeV corresponds to the spread of solutions.
[2] Superseded by RODAS 19.
[3] ADOLPH 15 value is derived from a Breit-Wigner fit with mass-dependent width taking the $\eta\pi$ and $\rho\pi$ channels into account.
[4] Resolution is not unfolded.
[5] Missing mass with enriched MMS = $\eta\pi^-$, $\eta = 2\gamma$.

$\eta'\pi$ MODE

VALUE (MeV)	DOCUMENT ID	TECN	COMMENT
The data in this block is included in the average printed for a previous datablock.			
119±25 OUR AVERAGE			
140±35±20	IVANOV 01	B852	18 $\pi^- p \to \eta'\pi^- p$
106±32	BELADIDZE 93	VES	37$\pi^- N \to \eta'\pi^- N$

$a_2(1320)$ DECAY MODES

	Mode	Fraction (Γ_i/Γ)	Scale factor/ Confidence level
Γ_1	3π	(70.1 ±2.7) %	S=1.2
Γ_2	$\rho(770)\pi$		
Γ_3	$f_2(1270)\pi$		
Γ_4	$\rho(1450)\pi$		
Γ_5	$\eta\pi$	(14.5 ±1.2) %	
Γ_6	$\omega\pi\pi$	(10.6 ±3.2) %	S=1.3
Γ_7	$K\overline{K}$	(4.9 ±0.8) %	
Γ_8	$\eta'(958)\pi$	(5.5 ±0.9) $\times 10^{-3}$	
Γ_9	$\pi^\pm\gamma$	(2.91±0.27) $\times 10^{-3}$	
Γ_{10}	$\gamma\gamma$	(9.4 ±0.7) $\times 10^{-6}$	
Γ_{11}	e^+e^-	< 5 $\times 10^{-9}$	CL=90%

CONSTRAINED FIT INFORMATION

An overall fit to 5 branching ratios uses 18 measurements and one constraint to determine 4 parameters. The overall fit has a χ^2 = 9.3 for 15 degrees of freedom.

The following *off-diagonal* array elements are the correlation coefficients $\langle \delta x_i \delta x_j \rangle / (\delta x_i \cdot \delta x_j)$, in percent, from the fit to the branching fractions, $x_i \equiv \Gamma_i/\Gamma_{total}$. The fit constrains the x_i whose labels appear in this array to sum to one.

	x_1	x_5	x_6
x_5	10		
x_6	−89	−46	
x_7	−1	−2	−24

$a_2(1320)$ PARTIAL WIDTHS

$\Gamma(\eta\pi)$ — Γ_5

VALUE (MeV)	EVTS	DOCUMENT ID	TECN	CHG	COMMENT
• • • We do not use the following data for averages, fits, limits, etc. • • •					
18.5±3.0	870	[1] SCHEGELSKY 06A	RVUE	0	$\gamma\gamma \to K^0_S K^0_S$

[1] From analysis of L3 data at 91 and 183–209 GeV, using $\Gamma(a_2(1320) \to \gamma\gamma)$ = 0.91 keV and SU(3) relations.

$\Gamma(K\overline{K})$ — Γ_7

VALUE (MeV)	EVTS	DOCUMENT ID	TECN	CHG	COMMENT
• • • We do not use the following data for averages, fits, limits, etc. • • •					
$7.0^{+2.0}_{-1.5}$	870	[1] SCHEGELSKY 06A	RVUE	0	$\gamma\gamma \to K^0_S K^0_S$

[1] From analysis of L3 data at 91 and 183–209 GeV, using $\Gamma(a_2(1320) \to \gamma\gamma)$ = 0.91 keV and SU(3) relations.

$\Gamma(\pi^\pm\gamma)$ — Γ_9

VALUE (keV)	EVTS	DOCUMENT ID	TECN	CHG	COMMENT
311± 25 OUR AVERAGE					
358± 6±42		[1] ADOLPH 14	COMP	−	190 π^-Pb → $\pi^+\pi^-\pi^-$Pb′
284± 25±25	7.1k	MOLCHANOV 01	SELX		600 $\pi^- A \to \pi^+\pi^-\pi^- A$
295± 60		CIHANGIR 82	SPEC	+	200 π^+A
• • • We do not use the following data for averages, fits, limits, etc. • • •					
461±110		[2] MAY 77	SPEC	±	9.7 γA

[1] Primakoff reaction using $a_2(1320) \to 3\pi$ branching ratio of 70.1%.
[2] Assuming one-pion exchange.

$\Gamma(\gamma\gamma)$ — Γ_{10}

VALUE (keV)	EVTS	DOCUMENT ID	TECN	CHG	COMMENT
1.00±0.06 OUR AVERAGE					
0.98±0.05±0.09		ACCIARRI 97T	L3		$e^+e^- \to e^+e^-\pi^+\pi^-\pi^0$
0.96±0.03±0.13		ALBRECHT 97B	ARG		$e^+e^- \to e^+e^-\pi^+\pi^-\pi^0$
1.26±0.26±0.18	36	BARU 90	MD1		$e^+e^- \to e^+e^-\pi^+\pi^-\pi^0$
1.00±0.07±0.15	415	BEHREND 90C	CELL	0	$e^+e^- \to e^+e^-\pi^+\pi^-\pi^0$
1.03±0.13±0.21		BUTLER 90	MRK2		$e^+e^- \to e^+e^-\pi^+\pi^-\pi^0$
1.01±0.14±0.22	85	OEST 90	JADE		$e^+e^- \to e^+e^-\pi^0\eta$
0.90±0.27±0.15	56	[1] ALTHOFF 86	TASS	0	$e^+e^- \to e^+e^-3\pi$
1.14±0.20±0.26		[2] ANTREASYAN 86	CBAL	0	$e^+e^- \to e^+e^-\pi^0\eta$
1.06±0.18±0.19		BERGER 84C	PLUT	0	$e^+e^- \to e^+e^-3\pi$
• • • We do not use the following data for averages, fits, limits, etc. • • •					
$0.81\pm0.19^{+0.42}_{-0.11}$	35	[1] BEHREND 82C	CELL	0	$e^+e^- \to e^+e^-3\pi$
0.77±0.18±0.27	22	[2] EDWARDS 82F	CBAL	0	$e^+e^- \to e^+e^-\pi^0\eta$

[1] From $\rho\pi$ decay mode.
[2] From $\eta\pi^0$ decay mode.

$\Gamma(e^+e^-)$ — Γ_{11}

VALUE (eV)	CL%	DOCUMENT ID	TECN	COMMENT
< 0.56	90	ACHASOV 00K	SND	$e^+e^- \to \pi^0\pi^0$
• • • We do not use the following data for averages, fits, limits, etc. • • •				
<25	90	VOROBYEV 88	ND	$e^+e^- \to \pi^0\eta$

$a_2(1320)$ $\Gamma(i)\Gamma(\gamma\gamma)/\Gamma(\text{total})$

$\Gamma(3\pi) \times \Gamma(\gamma\gamma)/\Gamma_{total}$ — $\Gamma_1\Gamma_{10}/\Gamma$

VALUE (keV)	EVTS	DOCUMENT ID	TECN	COMMENT
• • • We do not use the following data for averages, fits, limits, etc. • • •				
0.65±0.02±0.02	18k	[1] SCHEGELSKY 06	RVUE	$\gamma\gamma \to \pi^+\pi^-\pi^0$

[1] From analysis of L3 data at 183–209 GeV.

$\Gamma(\eta\pi) \times \Gamma(\gamma\gamma)/\Gamma_{total}$ — $\Gamma_5\Gamma_{10}/\Gamma$

VALUE (keV)	DOCUMENT ID	TECN	COMMENT
• • • We do not use the following data for averages, fits, limits, etc. • • •			
$0.145^{+0.097}_{-0.034}$	[1] UEHARA 09A	BELL	$e^+e^- \to e^+e^-\eta\pi^0$

[1] From the D_2-wave. The fraction of the D_0-wave is $3.4^{+2.3}_{-1.1}$%.

$\Gamma(K\overline{K}) \times \Gamma(\gamma\gamma)/\Gamma_{total}$ — $\Gamma_7\Gamma_{10}/\Gamma$

VALUE (keV)	DOCUMENT ID	TECN	COMMENT
0.126±0.007±0.028	[1] ALBRECHT 90G	ARG	$e^+e^- \to e^+e^-K^+K^-$
• • • We do not use the following data for averages, fits, limits, etc. • • •			
0.081±0.006±0.027	[2] ALBRECHT 90G	ARG	$e^+e^- \to e^+e^-K^+K^-$

[1] Using an incoherent background.
[2] Using a coherent background.

$a_2(1320)$ BRANCHING RATIOS

$[\Gamma(f_2(1270)\pi) + \Gamma(\rho(1450)\pi)]/\Gamma(\rho(770)\pi)$ — $(\Gamma_3+\Gamma_4)/\Gamma_2$

VALUE	CL%	DOCUMENT ID	TECN	CHG	COMMENT
<0.12	90	ABRAMOVI... 70B	HBC	−	3.93 $\pi^- p$

$\Gamma(\rho(770)\pi)/\Gamma(f_2(1270)\pi)$ — Γ_2/Γ_3

VALUE	EVTS	DOCUMENT ID	TECN	COMMENT
$\mathbf{16.5^{+1.2}_{-2.4}}$	46M	[1] AGHASYAN 18B	COMP	190 $\pi^- p \to \pi^-\pi^+\pi^- p$

[1] Statistical error negligible.

$\Gamma(\eta\pi)/\Gamma(3\pi)$ — Γ_5/Γ_1

VALUE	EVTS	DOCUMENT ID	TECN	CHG	COMMENT
0.207±0.018 OUR FIT					
0.213±0.020 OUR AVERAGE					
0.18 ±0.05		FORINO 76	HBC		11 $\pi^- p$
0.22 ±0.05	52	ANTIPOV 73	CNTR	−	40 $\pi^- p$
0.211±0.044	149	CHALOUPKA 73	HBC	−	3.9 $\pi^- p$
0.246±0.042	167	ALSTON-... 71	HBC	+	7.0 $\pi^+ p$
0.25 ±0.09	15	BOECKMANN 70	HBC	+	5.0 $\pi^+ p$
0.23 ±0.08	22	ASCOLI 68	HBC	−	5 $\pi^- p$
0.12 ±0.08		CHUNG 68	HBC	−	3.2 $\pi^- p$
0.22 ±0.09		CONTE 67	HBC	−	11.0 $\pi^- p$

$\Gamma(\omega\pi\pi)/\Gamma(3\pi)$ — Γ_6/Γ_1

VALUE	EVTS	DOCUMENT ID	TECN	CHG	COMMENT
0.15±0.05 OUR FIT Error includes scale factor of 1.3.					
0.15±0.05 OUR AVERAGE Error includes scale factor of 1.3. See the ideogram below.					
0.28±0.09	60	DIAZ 74	DBC	0	6 $\pi^+ n$
0.18±0.08		[1] KARSHON 74	HBC		Avg. of above two
0.10±0.05	279	[2] CHALOUPKA 73	HBC	−	3.9 $\pi^- p$

Int. J. Mod. Phys. A 2026.41. Downloaded from www.worldscientific.com
by CALIFORNIA @ BERKELEY on 09/16/26. Re-use and distribution is strictly not permitted, except for Open Access articles.

• • • We do not use the following data for averages, fits, limits, etc. • • •

0.29±0.08	140	[1] KARSHON	74	HBC	0	4.9 $\pi^+ p$
0.10±0.04	60	[1] KARSHON	74	HBC	+	4.9 $\pi^+ p$
0.19±0.08		DEFOIX	73	HBC	0	0.7 $\overline{p}p$

[1] KARSHON 74 suggest an additional $I = 0$ state strongly coupled to $\omega\pi\pi$ which could explain discrepancies in branching ratios and masses. We use a central value and a systematic spread.

[2] Decays to $b_1(1040)\pi$, $b_1 \to \omega\pi$. Error increased to account for possible systematic errors of complicated analysis.

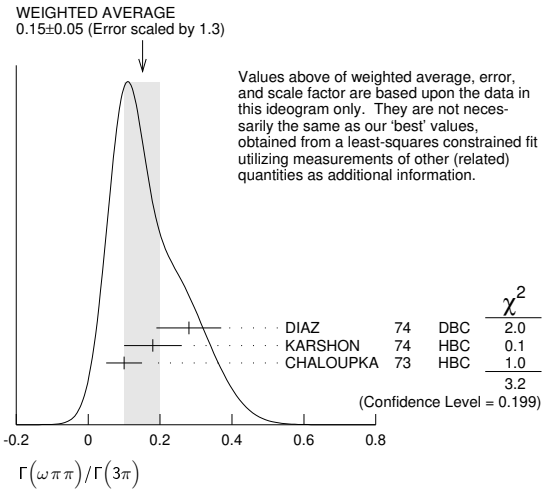

$\Gamma(K\overline{K})/\Gamma(3\pi)$ — Γ_7/Γ_1

VALUE	EVTS	DOCUMENT ID		TECN	CHG	COMMENT
0.070±0.012 OUR FIT						
0.078±0.017		CHABAUD	78	RVUE		
• • • We do not use the following data for averages, fits, limits, etc. • • •						
0.011±0.003		[1] BERTIN	98B	OBLX		0.0 $\overline{p}p \to K^\pm K_S \pi^\mp$
0.056±0.014	50	[2] CHALOUPKA	73	HBC	−	3.9 $\pi^- p$
0.097±0.018	113	[2] ALSTON-...	71	HBC	+	7.0 $\pi^+ p$
0.06 ±0.03		[2] ABRAMOVI...	70B	HBC	−	3.93 $\pi^- p$
0.054±0.022		[2] CHUNG	68	HBC	−	3.2 $\pi^- p$

[1] Using 4π data from BERTIN 97D.

[2] Included in CHABAUD 78 review.

$\Gamma(K\overline{K})/\Gamma(\eta\pi)$ — Γ_7/Γ_5

VALUE	DOCUMENT ID		TECN	COMMENT
• • • We do not use the following data for averages, fits, limits, etc. • • •				
0.31 $\pm0.22\ ^{+0.09}_{-0.11}$	[1] KOPF	21	RVUE	0.9 $p\overline{p} \to \pi^0\pi^0\eta$, $\pi^0\eta\eta$, $\pi^0 K^+ K^-$ and 191 $\pi^- p \to \pi^-\pi^-\pi^+ p$
0.352±0.011±0.175	[2] ALBRECHT	20	RVUE	0.9 $\overline{p}p \to \pi^0\pi^0\eta$, $\pi^0\eta\eta$, $\pi^0 K^+ K^-$
0.08 ±0.02	[3] BERTIN	98B	OBLX	0.0 $\overline{p}p \to K^\pm K_S \pi^\mp$

[1] From T-matrix pole based on combined fit of Crystal Barrel and $\pi\pi$ scattering data (ALBRECHT 20), and COMPASS data (ADOLPH 15), using a coupled-channel model of $\eta\pi$, $\eta'\pi$ and $K\overline{K}$ systems.

[2] Residues from T-matrix pole with 2 poles, 2 channels ($\pi^0\eta$ and $K\overline{K}$).

[3] Using $\eta\pi\pi$ data from AMSLER 94D.

$\Gamma(\eta\pi)/[\Gamma(3\pi)+\Gamma(\eta\pi)+\Gamma(K\overline{K})]$ — $\Gamma_5/(\Gamma_1+\Gamma_5+\Gamma_7)$

VALUE	EVTS	DOCUMENT ID		TECN	CHG	COMMENT
0.162±0.012 OUR FIT						
0.140±0.028 OUR AVERAGE						
0.13 ±0.04		ESPIGAT	72	HBC	±	0.0 $\overline{p}p$
0.15 ±0.04	34	BARNHAM	71	HBC	+	3.7 $\pi^+ p$

$\Gamma(K\overline{K})/[\Gamma(3\pi)+\Gamma(\eta\pi)+\Gamma(K\overline{K})]$ — $\Gamma_7/(\Gamma_1+\Gamma_5+\Gamma_7)$

VALUE	EVTS	DOCUMENT ID		TECN	CHG	COMMENT
0.054±0.009 OUR FIT						
0.048±0.012 OUR AVERAGE						
0.05 ±0.02		TOET	73	HBC	+	5 $\pi^+ p$
0.09 ±0.04		TOET	73	HBC	0	5 $\pi^+ p$
0.03 ±0.02	8	[1] DAMERI	72	HBC	−	11 $\pi^- p$
0.06 ±0.03	17	BARNHAM	71	HBC	+	3.7 $\pi^+ p$
• • • We do not use the following data for averages, fits, limits, etc. • • •						
0.020±0.004		[2] ESPIGAT	72	HBC	±	0.0 $\overline{p}p$

[1] Montanet agrees. Vlada.

[2] Not averaged because of discrepancy between masses from $K\overline{K}$ and $\rho\pi$ modes.

$\Gamma(\eta'(958)\pi)/\Gamma_{total}$ — Γ_8/Γ

VALUE	CL%	DOCUMENT ID		TECN	CHG	COMMENT
• • • We do not use the following data for averages, fits, limits, etc. • • •						
<0.006	95	ALDE	92B	GAM2		38,100 $\pi^- p \to \eta'\pi^0 n$
<0.02	97	BARNHAM	71	HBC	+	3.7 $\pi^+ p$
0.004±0.004		[1] BOESEBECK	68	HBC	+	8 $\pi^+ p$

[1] No longer valid since $\Gamma(K\overline{K})/\Gamma(3\pi)$ value has changed (MORRISON 71).

$\Gamma(\eta'(958)\pi)/\Gamma(3\pi)$ — Γ_8/Γ_1

VALUE	CL%	DOCUMENT ID		TECN	CHG	COMMENT
• • • We do not use the following data for averages, fits, limits, etc. • • •						
<0.011	90	EISENSTEIN	73	HBC	−	5 $\pi^- p$
<0.04		ALSTON-...	71	HBC	+	7.0 $\pi^+ p$
$0.04\ ^{+0.03}_{-0.04}$		BOECKMANN	70	HBC	0	5.0 $\pi^+ p$

$\Gamma(\eta'(958)\pi)/\Gamma(\eta\pi)$ — Γ_8/Γ_5

VALUE	DOCUMENT ID		TECN	COMMENT
0.038±0.005 OUR AVERAGE				
0.05 ±0.02	ADOLPH	15	COMP	191 $\pi^- p \to \eta^{(\prime)}\pi^- p$
0.032±0.009	ABELE	97C	CBAR	0.0 $\overline{p}p \to \pi^0\pi^0\eta'$
0.047±0.010±0.004	[1] BELADIDZE	93	VES	37$\pi^- N \to a_2^- N$
0.034±0.008±0.005	BELADIDZE	92	VES	36π^- C $\to a_2^-$ C
• • • We do not use the following data for averages, fits, limits, etc. • • •				
$0.046\pm0.015\ ^{+0.07}_{-0.006}$	[2] KOPF	21	RVUE	0.9 $p\overline{p} \to \pi^0\pi^0\eta$, $\pi^0\eta\eta$, $\pi^0 K^+ K^-$ and 191 $\pi^- p \to \pi^-\pi^-\pi^+ p$

[1] Using $B(\eta' \to \pi^+\pi^-\eta) = 0.441$, $B(\eta \to \gamma\gamma) = 0.389$ and $B(\eta \to \pi^+\pi^-\pi^0) = 0.236$.

[2] From T-matrix pole based on combined fit of Crystal Barrel and $\pi\pi$ scattering data (ALBRECHT 20), and COMPASS data (ADOLPH 15), using a coupled-channel model of $\eta\pi$, $\eta'\pi$ and $K\overline{K}$ systems.

$\Gamma(\pi^\pm\gamma)/\Gamma_{total}$ — Γ_9/Γ

VALUE	DOCUMENT ID		TECN	COMMENT
• • • We do not use the following data for averages, fits, limits, etc. • • •				
$0.005\ ^{+0.005}_{-0.003}$	[1] EISENBERG	72	HBC	4.3,5.25,7.5 γp

[1] Pion-exchange model used in this estimation.

$\Gamma(e^+e^-)/\Gamma_{total}$ — Γ_{11}/Γ

VALUE (units 10^{-9})	CL%	DOCUMENT ID		TECN	COMMENT
• • • We do not use the following data for averages, fits, limits, etc. • • •					
<6	90	ACHASOV	00K	SND	$e^+e^- \to \pi^0\pi^0$

$a_2(1320)$ REFERENCES

KOPF	21	EPJ C81 1056	B. Kopf *et al.*	(BOCH)
ALBRECHT	20	EPJ C80 453	M. Albrecht *et al.*	(Crystal Barrel Collab.)
RODAS	19	PRL 122 042002	A. Rodas *et al.*	(JPAC Collab.)
AGHASYAN	18B	PR D98 092003	M. Aghasyan *et al.*	(COMPASS Collab.)
JACKURA	18	PL B779 464	A. Jackura *et al.*	(JPAC and COMPASS Collab.)
ADOLPH	15	PL B740 303	M. Adolph *et al.*	(COMPASS Collab.)
ADOLPH	14	EPJ A50 79	C. Adolph *et al.*	(COMPASS Collab.)
ALEKSEEV	10	PRL 104 241803	M.G. Alekseev *et al.*	(COMPASS Collab.)
ANISOVICH	09	IJMP A24 2481	V.V. Anisovich, A.V. Sarantsev	(PNPI)
UEHARA	09A	PR D80 032001	S. Uehara *et al.*	(BELLE Collab.)
SCHEGELSKY	06	EPJ A27 199	V.A. Schegelsky *et al.*	
SCHEGELSKY	06A	EPJ A27 207	V.A. Schegelsky *et al.*	
CHUNG	02	PR D65 072001	S.U. Chung *et al.*	(BNL E852 Collab.)
IVANOV	01	PRL 86 3977	E.I. Ivanov *et al.*	(BNL E852 Collab.)
MOLCHANOV	01	PL B521 171	V.V. Molchanov *et al.*	(FNAL SELEX Collab.)
ACHASOV	00K	PL B492 8	M.N. Achasov *et al.*	(Novosibirsk SND Collab.)
BARBERIS	00H	PL B488 225	D. Barberis *et al.*	(WA 102 Collab.)
BARBERIS	98B	PL B422 399	D. Barberis *et al.*	(WA 102 Collab.)
BERTIN	98B	PL B434 180	A. Bertin *et al.*	(OBELIX Collab.)
ABELE	97C	PL B404 179	A. Abele *et al.*	(Crystal Barrel Collab.)
ACCIARRI	97T	PL B413 147	M. Acciarri *et al.*	(L3 Collab.)
ALBRECHT	97B	ZPHY C74 469	H. Albrecht *et al.*	(ARGUS Collab.)
THOMPSON	97	PRL 79 1630	D.R. Thompson *et al.*	(BNL E852 Collab.)
AMELIN	96	ZPHY C70 71	D.V. Amelin *et al.*	(SERP, TBIL)
AMSLER	94D	PL B333 277	C. Amsler *et al.*	(Crystal Barrel Collab.)
AOYAGI	93	PL B314 246	H. Aoyagi *et al.*	(BKEI Collab.)
ARMSTRONG	93C	PL B307 394	T.A. Armstrong *et al.*	(FNAL, FERR, GENO+)
BELADIDZE	93	PL B313 276	G.M. Beladidze *et al.*	(VES Collab.)
CONDO	93	PR D48 3045	G.T. Condo *et al.*	(SLAC Hybrid Collab.)
ALDE	92B	ZPHY C54 549	D.M. Alde *et al.*	(SERP, BELG, LANL, LAPP+)
BELADIDZE	92	ZPHY C54 235	G.M. Beladidze *et al.*	(VES Collab.)
ALBRECHT	90G	ZPHY C48 183	H. Albrecht *et al.*	(ARGUS Collab.)
ARMSTRONG	90	ZPHY C48 213	T.A. Armstrong, M. Benayoun, W. Beusch	(WA76 Coll.)
BARU	90	ZPHY C48 581	S.E. Baru *et al.*	(MD-1 Collab.)
BEHREND	90C	ZPHY C46 583	H.J. Behrend *et al.*	(CELLO Collab.)
BUTLER	90	PR D42 1368	F. Butler *et al.*	(Mark II Collab.)
OEST	90	ZPHY C47 343	T. Oest *et al.*	(JADE Collab.)
AUGUSTIN	89	NP B320 1	J.E. Augustin, G. Cosme	(DM2 Collab.)
VOROBYEV	88	SJNP 48 273	P.V. Vorobiev *et al.*	(NOVO)
		Translated from YAF 48 436.		
ALTHOFF	86	ZPHY C31 537	M. Althoff *et al.*	(TASSO Collab.)
ANTREASYAN	86	PR D33 1847	D. Antreasyan *et al.*	(Crystal Ball Collab.)
BERGER	84C	PL 149B 427	C. Berger *et al.*	(PLUTO Collab.)
BEHREND	82C	PL 114B 378	H.J. Behrend *et al.*	(CELLO Collab.)
Also		PL 125B 518 (errat.)	H.J. Behrend *et al.*	(CELLO Collab.)
CIHANGIR	82	PL 117B 123	S. Cihangir *et al.*	(FNAL, MINN, ROCH)
CLELAND	82B	NP B208 228	W.E. Cleland *et al.*	(DURH, GEVA, LAUS+)
EDWARDS	82F	PL 110B 82	C. Edwards *et al.*	(CIT, HARV, PRIN+)

Int. J. Mod. Phys. A 2026.41. Downloaded from www.worldscientific.com
by UNIVERSITY OF CALIFORNIA @ BERKELEY on 09/16/26. Re-use and distribution is strictly not permitted, except for Open Access articles.

DELFOSSE	81	NP B183 349	A. Delfosse *et al.*	(GEVA, LAUS)
EVANGELIS...	81	NP B178 197	C. Evangelista *et al.*	(BARI, BONN, CERN+)
CHABAUD	80	NP B175 189	V. Chabaud *et al.*	(CERN, MPIM, AMST)
DAUM	80C	PL 89B 276	C. Daum *et al.*	(AMST, CERN, CRAC, MPIM+) JP
BALTAY	78B	PR D17 62	C. Baltay *et al.*	(COLU, BING)
CHABAUD	78	NP B145 349	V. Chabaud *et al.*	(CERN, MPIM)
FERRERSORIA	78	PL 74B 287	A. Ferrer Soria *et al.*	(ORSAY, CERN, CDEF+)
HYAMS	78	NP B146 303	B.D. Hyams *et al.*	(CERN, MPIM, ATEN)
MARTIN	78D	PL 74B 417	A.D. Martin *et al.*	(DURH, GEVA) JP
MAY	77	PR D16 1983	E.N. May *et al.*	(ROCH, CORN)
FORINO	76	NC 35A 465	A. Forino *et al.*	(BGNA, FIRZ, GENO, MILA+)
MARGULIE	76	PR D14 667	M. Margulies *et al.*	(BNL, CUNY)
EMMS	75	PL 58B 117	M.J. Emms *et al.*	(BIRM, DURH, RHEL) JP
WAGNER	75	PL 58B 201	F. Wagner, M. Tabak, D.M. Chew	(LBL) JP
DIAZ	74	PRL 32 260	J. Diaz *et al.*	(CASE, CMU)
KARSHON	74	PRL 32 852	U. Karshon *et al.*	(REHO)
ANTIPOV	73	NP B63 175	Y.M. Antipov *et al.*	(CERN, SERP) JP
ANTIPOV	73C	NP B63 153	Y.M. Antipov *et al.*	(CERN, SERP) JP
CHALOUPKA	73	PL 44B 211	V. Chaloupka *et al.*	(CERN)
CONFORTO	73	PL 45B 154	G. Conforto *et al.*	(EFI, FNAL, TNTO+)
DEFOIX	73	PL 43B 141	C. Defoix *et al.*	(CDEF)
EISENSTEIN	73	PR D7 278	L. Eisenstein *et al.*	(ILL)
KEY	73	PRL 30 503	A.W. Key *et al.*	(TNTO, EFI, FNAL, WISC)
TOET	73	NP B63 248	D.Z. Toet *et al.*	(NIJM, BONN, DURH, TORI)
DAMERI	72	NC 9A 1	M. Dameri *et al.*	(GENO, MILA, SACL)
EISENBERG	72	PR D5 15	Y. Eisenberg *et al.*	(REHO, SLAC, TELA)
ESPIGAT	72	NP B36 93	P. Espigat *et al.*	(CERN, CDEF)
FOLEY	72	PR D6 747	K.J. Foley *et al.*	(BNL, CUNY)
ALSTON-...	71	PL 34B 156	M. Alston-Garnjost *et al.*	(LRL)
BARNHAM	71	PRL 26 1494	K.W.J. Barnham *et al.*	(LBL)
BINNIE	71	PL 36B 257	D.M. Binnie *et al.*	(LOIC, SHMP)
BOWEN	71	PRL 26 1663	D.R. Bowen *et al.*	(NEAS, STON)
GRAYER	71	PL 34B 333	G. Grayer *et al.*	(CERN, MPIM)
ABRAMOVI...	70B	NP B23 466	M. Abramovich *et al.*	(CERN) JP
ALSTON-...	70	PL 33B 607	M. Alston-Garnjost *et al.*	(LRL)
BOECKMANN	70	NP B16 221	K. Boeckmann *et al.*	(BONN, DURH, NIJM+)
ASCOLI	68	PRL 20 1321	G. Ascoli *et al.*	(ILL) JP
BOESEBECK	68	NP B4 501	K. Boesebeck *et al.*	(AACH, BERL, CERN)
CHUNG	68	PR 165 1491	S.U. Chung *et al.*	(LRL)
CONTE	67	NC 51A 175	F. Conte *et al.*	(GENO, HAMB, MILA, SACL)

$f_0(1370)$

$I^G(J^{PC}) = 0^+(0^{++})$

See the review on "Spectroscopy of Light Meson Resonances" and a note on "Non-$q\overline{q}$ Candidates" in PDG 06, Journal of Physics **G33** 1 (2006).

$f_0(1370)$ T-MATRIX POLE $\sqrt{s}$

Note that $\Gamma = -2\,\mathrm{Im}(\sqrt{s})$.

VALUE (MeV)	DOCUMENT ID		TECN	COMMENT
(1250–1440) $-i$ (60–300) OUR ESTIMATE				
$(1297.4 \pm 56.9 \pm 29.4) - i(125.8 \pm 71.5 \pm 44.0)$	ABLIKIM	25CD	BES3	$e^+e^- \to \psi(2S)$
$(1245 \pm 40) - i(300^{+30}_{-70})$	[1] PELAEZ	23	RVUE	Compilation
$(1380^{+70}_{-60}) - i(220^{+80}_{-70})$	[2] PELAEZ	23	RVUE	Compilation
$(1370 \pm 40) - i(195 \pm 20)$	SARANTSEV	21	RVUE	$J/\psi(1S) \to \gamma(\pi\pi, K\overline{K}, \eta\eta, \omega\phi)$
$(1280.6 \pm 1.6 \pm 47.4) - i(205.2 \pm 1.7 \pm 20.7)$	[3] ALBRECHT	20	RVUE	$0.9\,\overline{p}p \to \pi^0\pi^0\eta, \pi^0\eta\eta, \pi^0 K^+K^-$
$(1290 \pm 50) - i(170^{+20}_{-40})$	[4] ANISOVICH	09	RVUE	$0.0\,\overline{p}p, \pi N$
$(1373 \pm 15) - i(137 \pm 10)$	[5] BARGIOTTI	03	OBLX	$\overline{p}p$
$(1302 \pm 17) - i(166 \pm 18)$	[6] BARBERIS	00C		$450\,pp \to p_f 4\pi p_s$
$(1312 \pm 25 \pm 10) - i(109 \pm 22 \pm 15)$	BARBERIS	99D	OMEG	$450\,pp \to K^+K^-, \pi^+\pi^-$
$(1406 \pm 19) - i(80 \pm 6)$	[7] KAMINSKI	99	RVUE	$\pi\pi \to \pi\pi, K\overline{K}, \sigma\sigma$
$(1300 \pm 20) - i(120 \pm 20)$	ANISOVICH	98B	RVUE	Compilation
$(1290 \pm 15) - i(145 \pm 15)$	BARBERIS	97B	OMEG	$450\,pp \to pp2(\pi^+\pi^-)$
$(1548 \pm 40) - i(560 \pm 40)$	BERTIN	97C	OBLX	$0.0\,\overline{p}p \to \pi^+\pi^-\pi^0$
$(1380 \pm 40) - i(180 \pm 25)$	ABELE	96B	CBAR	$0.0\,\overline{p}p \to \pi^0 K^0_L K^0_L$
$(1300 \pm 15) - i(115 \pm 8)$	BUGG	96	RVUE	
$(1330 \pm 50) - i(150 \pm 40)$	[8] AMSLER	95B	CBAR	$\overline{p}p \to 3\pi^0$
$(1360 \pm 35) - i(150–300)$	[8] AMSLER	95C	CBAR	$\overline{p}p \to \pi^0\eta\eta$
$(1390 \pm 30) - i(190 \pm 40)$	[9] AMSLER	95D	CBAR	$\overline{p}p \to 3\pi^0, \pi^0\eta\eta, \pi^0\pi^0\eta$
$1346 - i249$	[10,11] JANSSEN	95	RVUE	$\pi\pi \to \pi\pi, K\overline{K}$
$1214 - i168$	[11,12] TORNQVIST	95	RVUE	$\pi\pi \to \pi\pi, K\overline{K}, K\pi, \eta\pi$
$1364 - i139$	AMSLER	94D	CBAR	$\overline{p}p \to \pi^0\pi^0\eta$
$(1365^{+20}_{-55}) - i(134 \pm 35)$	ANISOVICH	94	CBAR	$\overline{p}p \to 3\pi^0, \pi^0\eta\eta$
$(1340 \pm 40) - i(127^{+30}_{-20})$	[13] BUGG	94	RVUE	$\overline{p}p \to 3\pi^0, \eta\eta\pi^0, \eta\pi^0\pi^0$
$(1430 \pm 5) - i(73 \pm 13)$	[14] KAMINSKI	94	RVUE	$\pi\pi \to \pi\pi, K\overline{K}$
$1420 - i220$	[15] AU	87	RVUE	$\pi\pi \to \pi\pi, K\overline{K}$

[1] From forward dispersion relation applied to $\pi\pi$ scattering data.
[2] From partial-wave dispersion relation applied to $\pi\pi \to \overline{K}K$ data.
[3] T-matrix pole, 5 poles, 5 channels, including scattering data from HYAMS 75 ($\pi\pi$), LONGACRE 86 ($K\overline{K}$), BINON 83 ($\eta\eta$), and BINON 84C ($\eta\eta'$).
[4] Another pole is found at $(1510 \pm 130) - i\,(800^{+100}_{-150})$ MeV.
[5] Coupled channel analysis of $\pi^+\pi^-\pi^0$, $K^+K^-\pi^0$, and $K^\pm K^0_S\pi^\mp$.
[6] Average between $\pi^+\pi^-2\pi^0$ and $2(\pi^+\pi^-)$.
[7] T-matrix pole on sheet $---$.
[8] Supersedes ANISOVICH 94.
[9] Coupled-channel analysis of $\overline{p}p \to 3\pi^0$, $\pi^0\eta\eta$, and $\pi^0\pi^0\eta$ on sheet IV. Demonstrates explicitly that $f_0(500)$ and $f_0(1370)$ are two different poles.
[10] Analysis of data from FALVARD 88.
[11] The pole is on Sheet III. Demonstrates explicitly that $f_0(500)$ and $f_0(1370)$ are two different poles.
[12] Uses data from BEIER 72B, OCHS 73, HYAMS 73, GRAYER 74, ROSSELET 77, CASON 83, ASTON 88, and ARMSTRONG 91B. Coupled channel analysis with flavor symmetry and all light two-pseudoscalars systems.
[13] Reanalysis of ANISOVICH 94 data.
[14] T-matrix pole on sheet III.
[15] Analysis of data from OCHS 73,GRAYER 74, BECKER 79, and CASON 83.

$f_0(1370)$ BREIT-WIGNER MASS

VALUE (MeV)	DOCUMENT ID
1200 to 1500 OUR ESTIMATE	

$\pi\pi$ MODE

VALUE (MeV)	EVTS	DOCUMENT ID		TECN	COMMENT
• • • We do not use the following data for averages, fits, limits, etc. • • •					
1400 ± 40		[1] AUBERT	09L	BABR	$B^\pm \to \pi^\pm\pi^\pm\pi^\mp$
1470^{+72}_{-255}		[2] UEHARA	08A	BELL	$10.6\,e^+e^- \to e^+e^-\pi^0\pi^0$
1259 ± 55	2.6k	BONVICINI	07	CLEO	$D^+ \to \pi^-\pi^+\pi^+$
$1309 \pm 15 \pm 15$		[3] BUGG	07A	RVUE	$0.0\,p\overline{p} \to 3\pi^0$
1449 ± 13	4.3k	[4] GARMASH	06	BELL	$B^+ \to K^+\pi^+\pi^-$
1350 ± 50		ABLIKIM	05	BES2	$J/\psi \to \phi\pi^+\pi^-$
$1265 \pm 30^{+20}_{-35}$		ABLIKIM	05Q	BES2	$\psi(2S) \to \gamma\pi^+\pi^-K^+K^-$
$1434 \pm 18 \pm 9$	848	AITALA	01A	E791	$D^+_s \to \pi^-\pi^+\pi^+$
1308 ± 10		BARBERIS	99B	OMEG	$450\,pp \to p_s p_f \pi^+\pi^-$
1315 ± 50		BELLAZZINI	99	GAM4	$450\,pp \to pp\pi^0\pi^0$
1315 ± 30		ALDE	98	GAM4	$100\,\pi^-p \to \pi^0\pi^0 n$
1280 ± 55		BERTIN	98	OBLX	0.05–$0.405\,\overline{n}p \to \pi^+\pi^+\pi^-$
1186		[5,6] TORNQVIST	95	RVUE	$\pi\pi \to \pi\pi, K\overline{K}, K\pi, \eta\pi$
1472 ± 12		ARMSTRONG	91	OMEG	$300\,pp \to pp\pi\pi, pp K\overline{K}$
1275 ± 20		BREAKSTONE	90	SFM	$62\,pp \to pp\pi^+\pi^-$
1420 ± 20		AKESSON	86	SPEC	$63\,pp \to pp\pi^+\pi^-$
1256		FROGGATT	77	RVUE	$\pi^+\pi^-$ channel

[1] Breit-Wigner mass.
[2] Breit-Wigner mass. May also be the $f_0(1500)$.
[3] Reanalysis of ABELE 96C data.
[4] Also observed by GARMASH 07 in $B^0 \to K^0_S\pi^+\pi^-$ decays. Supersedes GARMASH 05.
[5] Uses data from BEIER 72B, OCHS 73, HYAMS 73, GRAYER 74, ROSSELET 77, CASON 83, ASTON 88, and ARMSTRONG 91B. Coupled channel analysis with flavor symmetry and all light two-pseudoscalars systems.
[6] Also observed by ASNER 00 in $\tau^- \to \pi^-\pi^0\pi^0\nu_\tau$ decays

$K\overline{K}$ MODE

VALUE (MeV)	EVTS	DOCUMENT ID		TECN	COMMENT
• • • We do not use the following data for averages, fits, limits, etc. • • •					
$1422 \pm 15 \pm 28$		[1] AAIJ	19H	LHCB	$pp \to D^\pm X$
$1360 \pm 31 \pm 28$	430	[2,3] DOBBS	15		$J/\psi \to \gamma K^+K^-$
$1350 \pm 48 \pm 15$	168	[2,3] DOBBS	15		$\psi(2S) \to \gamma K^+K^-$
1440 ± 6		VLADIMIRSK...	06	SPEC	$40\,\pi^-p \to K^0_S K^0_S n$
1391 ± 10		TIKHOMIROV	03	SPEC	$40.0\,\pi^-C \to K^0_S K^0_S K^0_L X$
1440 ± 50		BOLONKIN	88	SPEC	$40\,\pi^-p \to K^0_S K^0_S n$
1463 ± 9		ETKIN	82B	MPS	$23\,\pi^-p \to n2K^0_S$
1425 ± 15		WICKLUND	80	SPEC	$6\,\pi N \to K^+K^-N$
~ 1300		POLYCHRO...	79	STRC	$7\,\pi^-p \to n2K^0_S$

[1] From the $D^\pm \to K^\pm K^+K^-$ Dalitz plot fit with the isobar model A.
[2] Using CLEO-c data but not authored by the CLEO Collaboration.
[3] From a fit to a Breit-Wigner line shape with fixed $\Gamma = 346$ MeV.

4π MODE $2(\pi\pi)_S + \rho\rho$

VALUE (MeV)	EVTS	DOCUMENT ID		TECN	COMMENT
• • • We do not use the following data for averages, fits, limits, etc. • • •					
1395 ± 40		ABELE	01	CBAR	$0.0\,\overline{p}d \to \pi^-4\pi^0 p$
1374 ± 38		AMSLER	94	CBAR	$0.0\,\overline{p}p \to \pi^+\pi^-3\pi^0$
1345 ± 12		ADAMO	93	OBLX	$\overline{n}p \to 3\pi^+2\pi^-$
1386 ± 30		GASPERO	93	DBC	$0.0\,\overline{p}n \to 2\pi^+3\pi^-$
~ 1410	5751	[1] BETTINI	66	DBC	$0.0\,\overline{p}n \to 2\pi^+3\pi^-$

[1] $\rho\rho$ dominant.

$\eta\eta$ MODE

VALUE (MeV)	DOCUMENT ID		TECN	COMMENT
• • • We do not use the following data for averages, fits, limits, etc. • • •				
$1262^{+51}_{-78} + {}^{82}_{-103}$	[1] UEHARA	10A	BELL	$10.6\,e^+e^- \to e^+e^-\eta\eta$
1430	AMSLER	92	CBAR	$0.0\,\overline{p}p \to \pi^0\eta\eta$
1220 ± 40	ALDE	86D	GAM4	$100\,\pi^-p \to n2\eta$

[1] Breit-Wigner mass. May also be the $f_0(1500)$.

Int. J. Mod. Phys. A 2026.41. Downloaded from www.worldscientific.com by CALIFORNIA @ BERKELEY on 09/16/26. Re-use and distribution is strictly not permitted, except for Open Access articles.

COUPLED CHANNEL MODE

VALUE (MeV)	DOCUMENT ID		TECN	COMMENT
• • • We do not use the following data for averages, fits, limits, etc. • • •				
$1330.2^{+5.9}_{-6.5}\pm5.1$	[1] AAIJ	19H	LHCB	$pp \to D^\pm X$
1306 ±20	[2] ANISOVICH	03	RVUE	

[1] From the $D^\pm \to K^\pm K^+ K^-$ Dalitz plot fit with the Triple-M amplitude in the multi-meson model of AOUDE 18.
[2] K-matrix pole from combined analysis of $\pi^- p \to \pi^0\pi^0 n$, $\pi^- p \to K\overline{K} n$, $\pi^+\pi^- \to \pi^+\pi^-$, $\overline{p}p \to \pi^0\pi^0\pi^0$, $\pi^0\eta\eta$, $\pi^0\pi^0\eta$, $\pi^+\pi^-\pi^0$, $K^+K^-\pi^0$, $K^0_S K^0_S \pi^0$, $K^+ K^0_S \pi^-$ at rest, $\overline{p}n \to \pi^-\pi^-\pi^+$, $K^0_S K^-\pi^0$, $K^0_S K^0_S \pi^-$ at rest.

$f_0(1370)$ BREIT-WIGNER WIDTH

VALUE (MeV)	DOCUMENT ID
200 to 500 OUR ESTIMATE	

$\pi\pi$ MODE

VALUE (MeV)	EVTS	DOCUMENT ID		TECN	COMMENT
• • • We do not use the following data for averages, fits, limits, etc. • • •					
300± 80		[1] AUBERT	09L	BABR	$B^\pm \to \pi^\pm\pi^\pm\pi^\mp$
90^{+2+50}_{-1-22}		[2] UEHARA	08A	BELL	10.6 $e^+e^- \to e^+e^-\pi^0\pi^0$
298± 21	2.6k	BONVICINI	07	CLEO	$D^+ \to \pi^-\pi^+\pi^+$
126± 25	4286	[3] GARMASH	06	BELL	$B^+ \to K^+\pi^+\pi^-$
265± 40		ABLIKIM	05	BES2	$J/\psi \to \phi\pi^+\pi^-$
$350\pm100^{+105}_{-60}$		ABLIKIM	05Q	BES2	$\psi(2S) \to \gamma\pi^+\pi^- K^+K^-$
173± 32± 6	848	AITALA	01A	E791	$D^+_s \to \pi^-\pi^+\pi^+$
222± 20		BARBERIS	99B	OMEG	450 $pp \to p_s p_f \pi^+\pi^-$
255± 60		BELLAZZINI	99	GAM4	450 $pp \to pp\pi^0\pi^0$
190± 50		ALDE	98	GAM4	100 $\pi^- p \to \pi^0\pi^0 n$
323± 13		BERTIN	98	OBLX	0.05–0.405 $\overline{n}p \to \pi^+\pi^+\pi^-$
350		[4,5] TORNQVIST	95	RVUE	$\pi\pi \to \pi\pi$, $K\overline{K}$, $K\pi$, $\eta\pi$
195± 33		ARMSTRONG	91	OMEG	300 $pp \to pp\pi\pi$, $pp K\overline{K}$
285± 60		BREAKSTONE	90	SFM	62 $pp \to pp\pi^+\pi^-$
460± 50		AKESSON	86	SPEC	63 $pp \to pp\pi^+\pi^-$
~ 400		[6] FROGGATT	77	RVUE	$\pi^+\pi^-$ channel

[1] The systematic errors are not reported.
[2] Breit-Wigner width. May also be the $f_0(1500)$.
[3] Also observed by GARMASH 07 in $B^0 \to K^0_S\pi^+\pi^-$ decays. Supersedes GARMASH 05.
[4] Uses data from BEIER 72B, OCHS 73, HYAMS 73, GRAYER 74, ROSSELET 77, CASON 83, ASTON 88, and ARMSTRONG 91B. Coupled channel analysis with flavor symmetry and all light two-pseudoscalars systems.
[5] Also observed by ASNER 00 in $\tau^- \to \pi^-\pi^0\pi^0\nu_\tau$ decays
[6] Width defined as distance between 45 and 135° phase shift.

$K\overline{K}$ MODE

VALUE (MeV)	DOCUMENT ID		TECN	COMMENT
• • • We do not use the following data for averages, fits, limits, etc. • • •				
324± 38±42	[1] AAIJ	19H	LHCB	$pp \to D^\pm X$
121± 15	VLADIMIRSK...	06	SPEC	40 $\pi^- p \to K^0_S K^0_S n$
55± 26	TIKHOMIROV	03	SPEC	40.0 $\pi^- C \to K^0_S K^0_S K^0_L X$
250± 80	BOLONKIN	88	SPEC	40 $\pi^- p \to K^0_S K^0_S n$
118^{+138}_{-16}	ETKIN	82B	MPS	23 $\pi^- p \to n2K^0_S$
160± 30	WICKLUND	80	SPEC	6 $\pi N \to K^+K^- N$
~ 150	POLYCHRO...	79	STRC	7 $\pi^- p \to n2K^0_S$

[1] From the $D^\pm \to K^\pm K^+ K^-$ Dalitz plot fit with the isobar model A.

4π MODE $2(\pi\pi)_S+\rho\rho$

VALUE (MeV)	EVTS	DOCUMENT ID		TECN	COMMENT
• • • We do not use the following data for averages, fits, limits, etc. • • •					
275±55		ABELE	01	CBAR	0.0 $\overline{p}d \to \pi^-4\pi^0 p$
375±61		AMSLER	94	CBAR	0.0 $\overline{p}p \to \pi^+\pi^-3\pi^0$
398±26		ADAMO	93	OBLX	$\overline{n}p \to 3\pi^+2\pi^-$
310±50		GASPERO	93	DBC	0.0 $\overline{p}n \to 2\pi^+3\pi^-$
~ 90	5751	[1] BETTINI	66	DBC	0.0 $\overline{p}n \to 2\pi^+3\pi^-$

[1] $\rho\rho$ dominant.

$\eta\eta$ MODE

VALUE (MeV)	DOCUMENT ID		TECN	COMMENT
• • • We do not use the following data for averages, fits, limits, etc. • • •				
$484^{+246+246}_{-170-263}$	[1] UEHARA	10A	BELL	10.6 $e^+e^- \to e^+e^-\eta\eta$
250	AMSLER	92	CBAR	0.0 $\overline{p}p \to \pi^0\eta\eta$
320± 40	ALDE	86D	GAM4	100 $\pi^- p \to n2\eta$

[1] Breit-Wigner width. May also be the $f_0(1500)$.

COUPLED CHANNEL MODE

VALUE (MeV)	DOCUMENT ID		TECN
• • • We do not use the following data for averages, fits, limits, etc. • • •			
147^{+30}_{-50}	[1] ANISOVICH	03	RVUE

[1] K-matrix pole from combined analysis of $\pi^- p \to \pi^0\pi^0 n$, $\pi^- p \to K\overline{K} n$, $\pi^+\pi^- \to \pi^+\pi^-$, $\overline{p}p \to \pi^0\pi^0\pi^0$, $\pi^0\eta\eta$, $\pi^0\pi^0\eta$, $\pi^+\pi^-\pi^0$, $K^+K^-\pi^0$, $K^0_S K^0_S \pi^0$, $K^+ K^0_S \pi^-$ at rest, $\overline{p}n \to \pi^-\pi^-\pi^+$, $K^0_S K^-\pi^0$, $K^0_S K^0_S \pi^-$ at rest.

$f_0(1370)$ DECAY MODES

	Mode	Fraction (Γ_i/Γ)
Γ_1	$\pi\pi$	seen
Γ_2	4π	seen
Γ_3	$4\pi^0$	seen
Γ_4	$2\pi^+2\pi^-$	seen
Γ_5	$\pi^+\pi^-2\pi^0$	seen
Γ_6	$\rho\rho$	seen
Γ_7	$2(\pi\pi)_S$-wave	seen
Γ_8	$\pi(1300)\pi$	seen
Γ_9	$a_1(1260)\pi$	seen
Γ_{10}	$\eta\eta$	seen
Γ_{11}	$K\overline{K}$	seen
Γ_{12}	$K\overline{K}n\pi$	not seen
Γ_{13}	6π	not seen
Γ_{14}	$\omega\omega$	not seen
Γ_{15}	$\gamma\gamma$	seen
Γ_{16}	e^+e^-	not seen

$f_0(1370)$ PARTIAL WIDTHS

$\Gamma(\gamma\gamma)$ — Γ_{15}

See $\gamma\gamma$ widths under $f_0(500)$ and MORGAN 90.

$\Gamma(e^+e^-)$ — Γ_{16}

VALUE (eV)	CL%	DOCUMENT ID		TECN	COMMENT
<20	90	VOROBYEV	88	ND	$e^+e^- \to \pi^0\pi^0$

$f_0(1370)$ $\Gamma(i)\Gamma(\gamma\gamma)/\Gamma(\text{total})$

$\Gamma(\eta\eta) \times \Gamma(\gamma\gamma)/\Gamma_{\text{total}}$ — $\Gamma_{10}\Gamma_{15}/\Gamma$

VALUE (eV)	DOCUMENT ID		TECN	COMMENT
• • • We do not use the following data for averages, fits, limits, etc. • • •				
$121^{+133+169}_{-53-106}$	[1] UEHARA	10A	BELL	10.6 $e^+e^- \to e^+e^-\eta\eta$

[1] Including interference with the $f'_2(1525)$ (parameters fixed to the values from the 2008 edition of this review, PDG 08) and $f_2(1270)$. May also be the $f_0(1500)$.

$f_0(1370)$ BRANCHING RATIOS

$\Gamma(\pi\pi)/\Gamma_{\text{total}}$ — Γ_1/Γ

VALUE	CL%	DOCUMENT ID		TECN	COMMENT
• • • We do not use the following data for averages, fits, limits, etc. • • •					
<0.10	95	OCHS	13	RVUE	
0.26±0.09		BUGG	96	RVUE	
<0.15		[1] AMSLER	94	CBAR	$\overline{p}p \to \pi^+\pi^-3\pi^0$
<0.06		GASPERO	93	DBC	0.0 $\overline{p}n \to$ hadrons

[1] Using AMSLER 95B ($3\pi^0$).

$\Gamma(4\pi)/\Gamma_{\text{total}}$ — $\Gamma_2/\Gamma = (\Gamma_3+\Gamma_4+\Gamma_5)/\Gamma$

VALUE	DOCUMENT ID		TECN	COMMENT
• • • We do not use the following data for averages, fits, limits, etc. • • •				
>0.72	GASPERO	93	DBC	0.0 $\overline{p}n \to$ hadrons

$\Gamma(4\pi^0)/\Gamma(4\pi)$ — Γ_3/Γ_2

VALUE	DOCUMENT ID		TECN	COMMENT
• • • We do not use the following data for averages, fits, limits, etc. • • •				
seen	ABELE	96	CBAR	0.0 $\overline{p}p \to 5\pi^0$
0.068±0.005	[1] GASPERO	93	DBC	0.0 $\overline{p}n \to$ hadrons

[1] Model-dependent evaluation.

$\Gamma(2\pi^+2\pi^-)/\Gamma(4\pi)$ — $\Gamma_4/\Gamma_2 = \Gamma_4/(\Gamma_3+\Gamma_4+\Gamma_5)$

VALUE	DOCUMENT ID		TECN	COMMENT
• • • We do not use the following data for averages, fits, limits, etc. • • •				
0.420±0.014	[1] GASPERO	93	DBC	0.0 $\overline{p}n \to 2\pi^+3\pi^-$

[1] Model-dependent evaluation.

$\Gamma(\pi^+\pi^-2\pi^0)/\Gamma(4\pi)$ — $\Gamma_5/\Gamma_2 = \Gamma_5/(\Gamma_3+\Gamma_4+\Gamma_5)$

VALUE	DOCUMENT ID		TECN	COMMENT
• • • We do not use the following data for averages, fits, limits, etc. • • •				
0.512±0.019	[1] GASPERO	93	DBC	0.0 $\overline{p}n \to$ hadrons

[1] Model-dependent evaluation.

Int. J. Mod. Phys. A 2026.41. Downloaded from www.worldscientific.com
by UNIVERSITY OF CALIFORNIA @ BERKELEY on 09/16/26. Re-use and distribution is strictly not permitted, except for Open Access articles.

$\Gamma(\rho\rho)/\Gamma(4\pi)$ — Γ_6/Γ_2

VALUE	DOCUMENT ID		TECN	COMMENT
• • • We do not use the following data for averages, fits, limits, etc. • • •				
0.26 ± 0.07	ABELE	01B	CBAR	$0.0\ \overline{p}d \to 5\pi p$

$\Gamma(2(\pi\pi)_{S\text{-wave}})/\Gamma(\pi\pi)$ — Γ_7/Γ_1

VALUE	DOCUMENT ID		TECN	COMMENT
• • • We do not use the following data for averages, fits, limits, etc. • • •				
5.6 ± 2.6	[1] ABELE	01	CBAR	$0.0\ \overline{p}d \to \pi^- 4\pi^0 p$

[1] From the combined data of ABELE 96 and ABELE 96C.

$\Gamma(2(\pi\pi)_{S\text{-wave}})/\Gamma(4\pi)$ — Γ_7/Γ_2

VALUE	DOCUMENT ID		TECN	COMMENT
• • • We do not use the following data for averages, fits, limits, etc. • • •				
0.51 ± 0.09	ABELE	01B	CBAR	$0.0\ \overline{p}d \to 5\pi p$

$\Gamma(\rho\rho)/\Gamma(2(\pi\pi)_{S\text{-wave}})$ — Γ_6/Γ_7

VALUE	DOCUMENT ID		TECN	COMMENT
• • • We do not use the following data for averages, fits, limits, etc. • • •				
large	BARBERIS	00C		$450\ pp \to p_f 4\pi p_s$
1.6 ± 0.2	AMSLER	94	CBAR	$\overline{p}p \to \pi^+\pi^- 3\pi^0$
~ 0.65	GASPERO	93	DBC	$0.0\ \overline{p}n \to$ hadrons

$\Gamma(\pi(1300)\pi)/\Gamma(4\pi)$ — Γ_8/Γ_2

VALUE	DOCUMENT ID		TECN	COMMENT
• • • We do not use the following data for averages, fits, limits, etc. • • •				
0.17 ± 0.06	ABELE	01B	CBAR	$0.0\ \overline{p}d \to 5\pi p$

$\Gamma(a_1(1260)\pi)/\Gamma(4\pi)$ — Γ_9/Γ_2

VALUE	DOCUMENT ID		TECN	COMMENT
• • • We do not use the following data for averages, fits, limits, etc. • • •				
0.06 ± 0.02	ABELE	01B	CBAR	$0.0\ \overline{p}d \to 5\pi p$

$\Gamma(\eta\eta)/\Gamma(4\pi)$ — $\Gamma_{10}/\Gamma_2 = \Gamma_{10}/(\Gamma_3+\Gamma_4+\Gamma_5)$

VALUE	DOCUMENT ID		TECN	COMMENT
• • • We do not use the following data for averages, fits, limits, etc. • • •				
$(28 \pm 11) \times 10^{-3}$	[1] ANISOVICH	02D	SPEC	Combined fit
$(4.7 \pm 2.0) \times 10^{-3}$	BARBERIS	00E		$450\ pp \to p_f \eta\eta p_s$

[1] From a combined K-matrix analysis of Crystal Barrel (0. $p\overline{p} \to \pi^0\pi^0\pi^0$, $\pi^0\eta\eta$, $\pi^0\pi^0\eta$), GAMS ($\pi p \to \pi^0\pi^0 n$, $\eta\eta n$, $\eta\eta' n$), and BNL ($\pi p \to K\overline{K}n$) data.

$\Gamma(K\overline{K})/\Gamma_{total}$ — Γ_{11}/Γ

VALUE	DOCUMENT ID		TECN
• • • We do not use the following data for averages, fits, limits, etc. • • •			
0.35 ± 0.13	BUGG	96	RVUE

$\Gamma(K\overline{K})/\Gamma(\pi\pi)$ — Γ_{11}/Γ_1

VALUE	DOCUMENT ID		TECN	COMMENT
• • • We do not use the following data for averages, fits, limits, etc. • • •				
0.08 ± 0.08	ABLIKIM	05	BES2	$J/\psi \to \phi\pi^+\pi^-$, ϕK^+K^-
0.91 ± 0.20	[1] BARGIOTTI	03	OBLX	$\overline{p}p$
0.12 ± 0.06	[2] ANISOVICH	02D	SPEC	Combined fit
$0.46 \pm 0.15 \pm 0.11$	BARBERIS	99D	OMEG	$450\ pp \to K^+K^-, \pi^+\pi^-$

[1] Coupled channel analysis of $\pi^+\pi^-\pi^0$, $K^+K^-\pi^0$, and $K^\pm K^0_S \pi^\mp$.

[2] From a combined K-matrix analysis of Crystal Barrel (0. $p\overline{p} \to \pi^0\pi^0\pi^0$, $\pi^0\eta\eta$, $\pi^0\pi^0\eta$), GAMS ($\pi p \to \pi^0\pi^0 n$, $\eta\eta n$, $\eta\eta' n$), and BNL ($\pi p \to K\overline{K}n$) data.

$\Gamma(K\overline{K}n\pi)/\Gamma_{total}$ — Γ_{12}/Γ

VALUE	DOCUMENT ID		TECN	COMMENT
• • • We do not use the following data for averages, fits, limits, etc. • • •				
<0.03	GASPERO	93	DBC	$0.0\ \overline{p}n \to$ hadrons

$\Gamma(6\pi)/\Gamma_{total}$ — Γ_{13}/Γ

VALUE	DOCUMENT ID		TECN	COMMENT
• • • We do not use the following data for averages, fits, limits, etc. • • •				
<0.22	GASPERO	93	DBC	$0.0\ \overline{p}n \to$ hadrons

$\Gamma(\omega\omega)/\Gamma_{total}$ — Γ_{14}/Γ

VALUE	DOCUMENT ID		TECN	COMMENT
• • • We do not use the following data for averages, fits, limits, etc. • • •				
<0.13	GASPERO	93	DBC	$0.0\ \overline{p}n \to$ hadrons

$f_0(1370)$ REFERENCES

ABLIKIM 25CD JHEP 2510 081 M. Ablikim et al. (BESIII Collab.)
PELAEZ 23 PRL 130 051902 J.R. Pelaez, A. Rodas, J. Ruiz de Elvira (MADU+)
SARANTSEV 21 PL B816 136227 A.V. Sarantsev et al. (BONN, PNPI)
ALBRECHT 20 EPJ C80 453 M. Albrecht et al. (Crystal Barrel Collab.)
AAIJ 19H JHEP 1904 063 R. Aaij et al. (LHCb Collab.)
AOUDE 18 PR D98 056021 R.T. Aoude et al.
DOBBS 15 PR D91 052006 S. Dobbs et al. (NWES)
OCHS 13 JP G40 043001 W. Ochs
UEHARA 10A PR D82 114031 S. Uehara et al. (BELLE Collab.)
ANISOVICH 09 IJMP A24 2481 V.V. Anisovich, A.V. Sarantsev (PNPI)
AUBERT 09L PR D79 072006 B. Aubert et al. (BABAR Collab.)
PDG 08 PL B667 1 C. Amsler et al. (PDG Collab.)
UEHARA 08A PR D78 052004 S. Uehara et al. (BELLE Collab.)
BONVICINI 07 PR D75 012001 G. Bonvicini et al. (CLEO Collab.)
BUGG 07A JP G34 151 D.V. Bugg et al.
GARMASH 07 PR D75 012006 A. Garmash et al. (BELLE Collab.)
GARMASH 06 PRL 96 251803 A. Garmash et al. (BELLE Collab.)
PDG 06 JP G33 1 W.-M. Yao et al. (PDG Collab.)
VLADIMIRSK... 06 PAN 69 493 V.V. Vladimirsky et al. (ITEP, Moscow)
Translated from YAF 69 515.
ABLIKIM 05 PL B607 243 M. Ablikim et al. (BES Collab.)
ABLIKIM 05Q PR D72 092002 M. Ablikim et al. (BES Collab.)
GARMASH 05 PR D71 092003 A. Garmash et al. (BELLE Collab.)
ANISOVICH 03 EPJ A16 229 V.V. Anisovich et al.
BARGIOTTI 03 EPJ C26 371 M. Bargiotti et al. (OBELIX Collab.)
TIKHOMIROV 03 PAN 66 828 G.D. Tikhomirov et al.
Translated from YAF 66 860.
ANISOVICH 02D PAN 65 1545 V.V. Anisovich et al.
Translated from YAF 65 1583.
ABELE 01 EPJ C19 667 A. Abele et al. (Crystal Barrel Collab.)
ABELE 01B EPJ C21 261 A. Abele et al. (Crystal Barrel Collab.)
AITALA 01A PRL 86 765 E.M. Aitala et al. (FNAL E791 Collab.)
ASNER 00 PR D61 012002 D.M. Asner et al. (CLEO Collab.)
BARBERIS 00C PL B471 440 D. Barberis et al. (WA 102 Collab.)
BARBERIS 00E PL B479 59 D. Barberis et al. (WA 102 Collab.)
BARBERIS 99B PL B453 316 D. Barberis et al. (Omega Expt.)
BARBERIS 99D PL B462 462 D. Barberis et al. (Omega Expt.)
BELLAZZINI 99 PL B467 296 R. Bellazzini et al.
KAMINSKI 99 EPJ C9 141 R. Kaminski, L. Lesniak, B. Loiseau (CRAC, PARIN)
ALDE 98 EPJ A3 361 D. Alde et al. (GAM4 Collab.)
Also PAN 62 405 D. Alde et al. (GAMS Collab.)
Translated from YAF 62 446.
ANISOVICH 98B SPU 41 419 V.V. Anisovich et al.
Translated from UFN 168 481.
BERTIN 98 PR D57 55 A. Bertin et al. (OBELIX Collab.)
BARBERIS 97B PL B413 217 D. Barberis et al. (WA 102 Collab.)
BERTIN 97C PL B408 476 A. Bertin et al. (OBELIX Collab.)
ABELE 96 PL B380 453 A. Abele et al. (Crystal Barrel Collab.)
ABELE 96B PL B385 425 A. Abele et al. (Crystal Barrel Collab.)
ABELE 96C NP A609 562 A. Abele et al. (Crystal Barrel Collab.)
BUGG 96 NP B471 59 D.V. Bugg, A.V. Sarantsev, B.S. Zou (LOQM, PNPI)
AMSLER 95B PL B342 433 C. Amsler et al. (Crystal Barrel Collab.)
AMSLER 95C PL B353 571 C. Amsler et al. (Crystal Barrel Collab.)
AMSLER 95D PL B355 425 C. Amsler et al. (Crystal Barrel Collab.)
JANSSEN 95 PR D52 2690 G. Janssen et al. (STON, ADLD, JULI)
TORNQVIST 95 ZPHY C68 647 N.A. Tornqvist (HELS)
AMSLER 94 PL B322 431 C. Amsler et al. (Crystal Barrel Collab.) JPC
AMSLER 94D PL B333 277 C. Amsler et al. (Crystal Barrel Collab.)
ANISOVICH 94 PL B323 233 V.V. Anisovich et al. (Crystal Barrel Collab.) JPC
BUGG 94 PR D50 4412 D.V. Bugg et al. (LOQM)
KAMINSKI 94 PR D50 3145 R. Kaminski, L. Lesniak, J.P. Maillet (CRAC+)
ADAMO 93 NP A558 13C A. Adamo et al. (OBELIX Collab.) JPC
GASPERO 93 NP A562 407 M. Gaspero (ROMA1) JPC
AMSLER 92 PL B291 347 C. Amsler et al. (Crystal Barrel Collab.)
ARMSTRONG 91 ZPHY C51 351 T.A. Armstrong et al. (ATHU, BARI, BIRM+)
ARMSTRONG 91B ZPHY C52 389 T.A. Armstrong et al. (ATHU, BARI, BIRM+)
BREAKSTONE 90 ZPHY C48 569 A.M. Breakstone et al. (ISU, BGNA, CERN+)
MORGAN 90 ZPHY C48 623 D. Morgan, M.R. Pennington (RAL, DURH)
ASTON 88 NP B296 493 D. Aston et al. (SLAC, NAGO, CINC, INUS)
BOLONKIN 88 NP B309 426 B.V. Bolonkin et al. (ITEP, SERP)
FALVARD 88 PR D38 2706 A. Falvard et al. (CLER, FRAS, LALO+)
VOROBYEV 88 SJNP 48 273 P.V. Vorobiev et al. (NOVO)
Translated from YAF 48 436.
AU 87 PR D35 1633 K.L. Au, D. Morgan, M.R. Pennington (DURH, RAL)
AKESSON 86 NP B264 154 T. Akesson et al. (Axial Field Spec. Collab.)
ALDE 86D NP B269 485 D.M. Alde et al. (BELG, LAPP, SERP, CERN+)
LONGACRE 86 PL B177 223 R.S. Longacre et al. (BNL, BRAN, CUNY+)
BINON 84C NC 80A 363 F.G. Binon et al. (BELG, LAPP, SERP+)
BINON 83 NC 78A 313 F.G. Binon et al. (BELG, LAPP, SERP+)
CASON 83 PR D28 1586 N.M. Cason et al. (NDAM, ANL)
ETKIN 82B PR D25 1786 A. Etkin et al. (BNL, CUNY, TUFTS, VAND)
WICKLUND 80 PRL 45 1469 A.B. Wicklund et al. (ANL)
BECKER 79 NP B151 46 H. Becker et al. (MPIM, CERN, ZEEM, CRAC)
POLYCHRO... 79 PR D19 1317 V.A. Polychronakos et al. (NDAM, ANL)
FROGGATT 77 NP B129 89 C.D. Froggatt, J.L. Petersen (GLAS, NORD)
ROSSELET 77 PR D15 574 L. Rosselet et al. (GEVA, SACL)
HYAMS 75 NP B100 205 B.D. Hyams et al. (CERN, MPIM)
GRAYER 74 NP B75 189 G. Grayer et al. (CERN, MPIM)
HYAMS 73 NP B64 134 B.D. Hyams et al. (CERN, MPIM)
OCHS 73 Thesis W. Ochs (MPIM, MUNI)
BEIER 72B PRL 29 511 E.W. Beier et al. (PENN)
BETTINI 66 NC 42A 695 A. Bettini et al. (PADO, PISA)

$\pi_1(1400)$

$I^G(J^{PC}) = 1^-(1^{-+})$

OMITTED FROM SUMMARY TABLE

Coupled channel analyses favor the existence of only one broad 1^{-+} isovector state consistent with $\pi_1(1600)$ in the 1400–1600 MeV region. See the review on "Spectroscopy of Light Meson Resonances". See also $\pi_1(1600)$.

Int. J. Mod. Phys. A 2026.41. Downloaded from www.worldscientific.com
by [redacted]LIFORNIA @ BERKELEY on 09/16/26. Re-use and distribution is strictly not permitted, except for Open Access articles.

$\eta(1405)$

$I^G(J^{PC}) = 0^+(0^{-+})$

See also the $\eta(1475)$.

$\eta(1405)$ MASS

VALUE (MeV)	DOCUMENT ID
$1408.0^{+1.8}_{-1.2}$ OUR AVERAGE Includes data from the 2 datablocks that follow this one. Error includes scale factor of 2.1. See the ideogram below.	

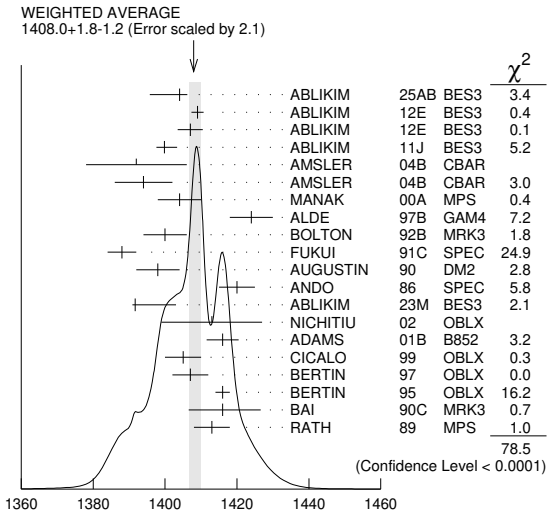

$\eta\pi\pi$ MODE

VALUE (MeV)	EVTS	DOCUMENT ID		TECN	COMMENT
The data in this block is included in the average printed for a previous datablock.					
1405.5 ± 2.3 OUR AVERAGE Error includes scale factor of 2.2. See the ideogram below.					
$1404^{+0.8+2.0}_{-1.5-8.1}$		[1] ABLIKIM	25AB	BES3	$J/\psi \to \gamma\pi^0 f_0(980) \to \gamma\pi^0\pi^0\pi^0$
1409.0 ± 1.7	743	ABLIKIM	12E	BES3	$J/\psi \to \gamma(\pi^+\pi^-\pi^0)$
1407.0 ± 3.5	198	ABLIKIM	12E	BES3	$J/\psi \to \gamma(\pi^0\pi^0\pi^0)$
$1399.8 \pm 2.2^{+2.8}_{-0.1}$		[2] ABLIKIM	11J	BES3	$J/\psi \to \omega(\eta\pi^+\pi^-)$
1392 ± 14	900 ± 375	AMSLER	04B	CBAR	$0\,\overline{p}p \to \pi^+\pi^-\pi^+\pi^-\eta$
1394 ± 8	6.6 ± 2.0k	AMSLER	04B	CBAR	$0\,\overline{p}p \to \pi^+\pi^-\pi^0\pi^0\eta$
1404 ± 6	9082	MANAK	00A	MPS	$18\,\pi^-p \to \eta\pi^+\pi^-n$
1424 ± 6	2200	ALDE	97B	GAM4	$100\,\pi^-p \to \eta\pi^0\pi^0n$
1400 ± 6		[3] BOLTON	92B	MRK3	$J/\psi \to \gamma\eta\pi^+\pi^-$
1388 ± 4		FUKUI	91C	SPEC	$8.95\,\pi^-p \to \eta\pi^+\pi^-n$
1398 ± 6	261	[4] AUGUSTIN	90	DM2	$J/\psi \to \gamma\eta\pi^+\pi^-$
1420 ± 5		ANDO	86	SPEC	$8\,\pi^-p \to \eta\pi^+\pi^-n$
• • • We do not use the following data for averages, fits, limits, etc. • • •					
1404.0 ± 11.0	195	ABLIKIM	19BA	BES3	$e^+e^- \to \psi(2S)$
1385 ± 7		BAI	99	BES	$J/\psi \to \gamma\eta\pi^+\pi^-$
1409 ± 3		[5] AMSLER	95F	CBAR	$0\,\overline{p}p \to \pi^+\pi^-\pi^0\pi^0\eta$

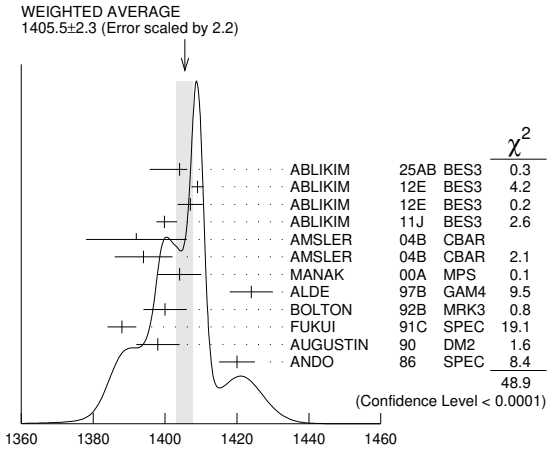

[1] ABLIKIM 25AB measured $J/\psi \to \gamma\eta(1405) \to \gamma\pi^0 f_0(980)$ / 0^{++} *PHSP* $\to \gamma\pi^0\pi^0\pi^0$. Here $\gamma\pi^0 f_0(980)$ / 0^{++} *PHSP* indicates an intermediate state which could be either $\gamma\pi^0 f_0(980)$ or $\gamma\pi^0\, 0^{++}$ phase space.
[2] The selected process is $J/\psi \to \omega a_0(980)\pi$.
[3] From fit to the $a_0(980)\pi\, 0^{-+}$ partial wave.
[4] Best fit with a single Breit Wigner.
[5] Superseded by AMSLER 04B.

$K\overline{K}\pi$ MODE ($a_0(980)\pi$ or direct $K\overline{K}\pi$)

VALUE (MeV)	EVTS	DOCUMENT ID		TECN	COMMENT
The data in this block is included in the average printed for a previous datablock.					
$1413.5^{+2.0}_{-0.9}$ OUR AVERAGE Error includes scale factor of 1.3. See the ideogram below.					
$1391.7 \pm 0.7^{+11.3}_{-0.3}$	126k	[1] ABLIKIM	23M	BES3	$J/\psi \to \gamma K^0_S K^0_S \pi^0$
1413 ± 14	3651	[2] NICHITIU	02	OBLX	$0\,\overline{p}p \to K^+K^-\pi^+\pi^-\pi^0$
$1416 \pm 4 \pm 2$	20k	ADAMS	01B	B852	18 GeV $\pi^-p \to K^+K^-\pi^0 n$
1405 ± 5		[3] CICALO	99	OBLX	$0\,\overline{p}p \to K^\pm K^0_S \pi^\mp\pi^+\pi^-$
1407 ± 5		[3] BERTIN	97	OBLX	$0\,\overline{p}p \to K^\pm(K^0)\pi^\mp\pi^+\pi^-$
1416 ± 2		[3] BERTIN	95	OBLX	$0\,\overline{p}p \to K\overline{K}\pi\pi\pi$
$1416 \pm 8\ ^{+7}_{-5}$	700	[4] BAI	90C	MRK3	$J/\psi \to \gamma K^0_S K^\pm\pi^\mp$
1413 ± 5		[4] RATH	89	MPS	$21.4\,\pi^-p \to nK^0_S K^0_S \pi^0$
• • • We do not use the following data for averages, fits, limits, etc. • • •					
1459 ± 5		[5] AUGUSTIN	92	DM2	$J/\psi \to \gamma K\overline{K}\pi$

[1] ABLIKIM 23M reports for this state a significance from the fit much higher than 35 σ.
[2] Decaying dominantly directly to $K^+K^-\pi^0$.
[3] Decaying into $(K\overline{K})_S\pi$, $(K\pi)_S\overline{K}$, and $a_0(980)\pi$.
[4] From fit to the $a_0(980)\pi\, 0^{-+}$ partial wave. Cannot rule out a $a_0(980)\pi\, 1^{++}$ partial wave.
[5] Excluded from averaging because averaging would be meaningless.

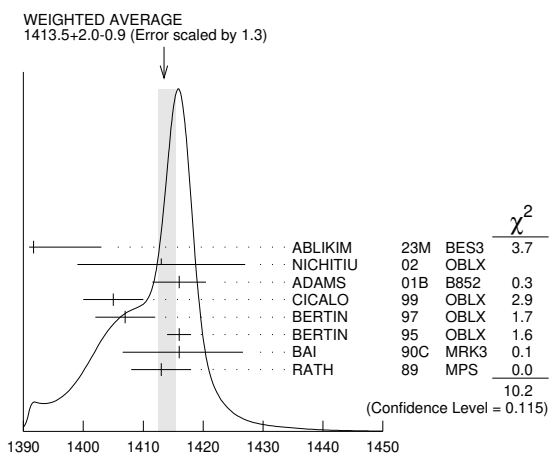

$\pi\pi\gamma$ MODE

VALUE (MeV)	EVTS	DOCUMENT ID		TECN	COMMENT
1403 ± 17 OUR AVERAGE Error includes scale factor of 1.8.					
1390 ± 12	235 ± 91	AMSLER	04B	CBAR	$0\,\overline{p}p \to \pi^+\pi^-\pi^+\pi^-\eta$
$1424 \pm 10 \pm 11$	547	BAI	04J	BES2	$J/\psi \to \gamma\gamma\pi^+\pi^-$
• • • We do not use the following data for averages, fits, limits, etc. • • •					
1401 ± 18		[1,2] AUGUSTIN	90	DM2	$J/\psi \to \pi^+\pi^-\gamma\gamma$
1432 ± 8		[2] COFFMAN	90	MRK3	$J/\psi \to \pi^+\pi^-2\gamma$

[1] Best fit with a single Breit Wigner.
[2] This peak in the $\gamma\rho$ channel may not be related to the $\eta(1405)$.

4π MODE

VALUE (MeV)	EVTS	DOCUMENT ID		TECN	COMMENT
• • • We do not use the following data for averages, fits, limits, etc. • • •					
1420 ± 20		BUGG	95	MRK3	$J/\psi \to \gamma\pi^+\pi^-\pi^+\pi^-$
1489 ± 12	3270	[1] BISELLO	89B	DM2	$J/\psi \to 4\pi\gamma$

[1] Estimated by us from various fits.

$\phi\gamma$ MODE

VALUE (MeV)	DOCUMENT ID		TECN	COMMENT
$1422.0 \pm 2.1^{+5.9}_{-7.8}$	[1] ABLIKIM	25P	BES3	$J/\psi \to \gamma\gamma\phi$

[1] From a partial wave analysis of $J/\psi \to \gamma\gamma\phi$ with significance 18.9σ.

$K\overline{K}\pi$ MODE (unresolved)

VALUE (MeV)	EVTS	DOCUMENT ID		TECN	COMMENT
• • • We do not use the following data for averages, fits, limits, etc. • • •					
1452.7 ± 3.3	191	[1,2] ABLIKIM	13M	BES3	$\psi(2S) \to \omega K K\pi$

Int. J. Mod. Phys. A 2026.41. Downloaded from www.worldscientific.com
by UNIVERSITY OF CALIFORNIA @ BERKELEY on 09/16/26. Re-use and distribution is strictly not permitted, except for Open Access articles.

1437.6 ± 3.2	249 ± 35	[1,2] ABLIKIM	08E	BES2	$J/\psi \to \omega K^0_S K^+ \pi^-$ + c.c.
1445.9 ± 5.7	62 ± 18	[1,2] ABLIKIM	08E	BES2	$J/\psi \to \omega K^+ K^- \pi^0$
1442 ± 10	410	[1] BAI	98C	BES	$J/\psi \to \gamma K^+ K^- \pi^0$
1445 ± 8	693	[1] AUGUSTIN	90	DM2	$J/\psi \to \gamma K^0_S K^\pm \pi^\mp$
1433 ± 8	296	[1] AUGUSTIN	90	DM2	$J/\psi \to \gamma K^+ K^- \pi^0$
1413 ± 8	500	[1] DUCH	89	ASTE	$\overline{p}p \to \pi^+\pi^- K^\pm \pi^\mp K^0$
1453 ± 7	170	[1] RATH	89	MPS	21.4 $\pi^- p \to K^0_S K^0_S \pi^0 n$
1419 ± 1	8800	[1] BIRMAN	88	MPS	8 $\pi^- p \to K^+ \overline{K}^0 \pi^- n$
1424 ± 3	620	[1] REEVES	86	SPEC	6.6 $p\overline{p} \to K\overline{K}\pi X$
1421 ± 2		[1] CHUNG	85	SPEC	8 $\pi^- p \to K\overline{K}\pi n$
1440 $^{+20}_{-15}$	174	[1] EDWARDS	82E	CBAL	$J/\psi \to \gamma K^+ K^- \pi^0$
1440 $^{+10}_{-15}$		[1] SCHARRE	80	MRK2	$J/\psi \to \gamma K^0_S K^\pm \pi^\mp$
1425 ± 7	800	[1,3] BAILLON	67	HBC	0 $\overline{p}p \to K\overline{K}\pi\pi\pi$

[1] These experiments identify only one pseudoscalar in the 1400–1500 range. Data could also refer to $\eta(1475)$.
[2] Systematic uncertainty not evaluated.
[3] From best fit of 0^{-+} partial wave , 50% $K^*(892)\,K$, 50% $a_0(980)\,\pi$.

$\eta(1405)$ WIDTH

VALUE (MeV)	DOCUMENT ID
$49.8^{+2.3}_{-2.0}$ OUR AVERAGE Includes data from the 2 datablocks that follow this one. Error includes scale factor of 1.6. See the ideogram below.	

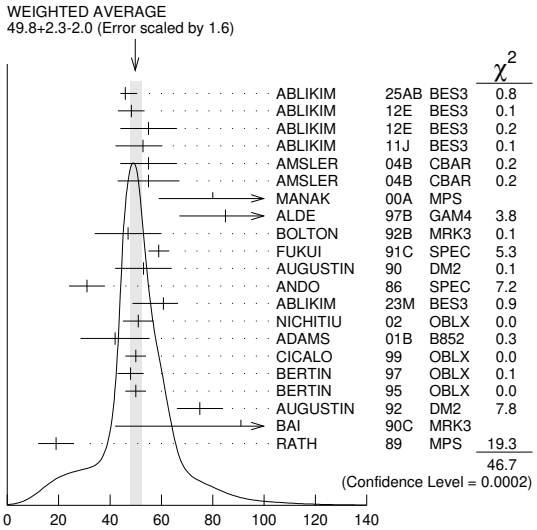

$\eta\pi\pi$ MODE

VALUE (MeV)	EVTS	DOCUMENT ID	TECN	COMMENT
The data in this block is included in the average printed for a previous datablock.				
$51.1^{+2.8}_{-2.1}$ OUR AVERAGE Error includes scale factor of 1.3. See the ideogram below.				
46 $^{+1.8+4.2}_{-2.0-0.0}$		[1] ABLIKIM	25AB BES3	$J/\psi \to \gamma\pi^0 f_0(980) \to \gamma\pi^0\pi^0\pi^0$
48.3 ± 5.2	743	ABLIKIM	12E BES3	$J/\psi \to \gamma(\pi^+\pi^-\pi^0)$
55.0 ± 11.0	198	ABLIKIM	12E BES3	$J/\psi \to \gamma(\pi^0\pi^0\pi^0)$
52.8 ± 7.6 $^{+0.1}_{-7.6}$		[2] ABLIKIM	11J BES3	$J/\psi \to \omega(\eta\pi^+\pi^-)$
55 ± 11	900	AMSLER	04B CBAR	0 $\overline{p}p \to \pi^+\pi^-\pi^+\pi^-\eta$
55 ± 12	6.6k	AMSLER	04B CBAR	0 $\overline{p}p \to \pi^+\pi^-\pi^0\pi^0\gamma$
80 ± 21	9.0k	MANAK	00A MPS	18 $\pi^- p \to \eta\pi^+\pi^- n$
85 ± 18	2.2k	ALDE	97B GAM4	100 $\pi^- p \to \eta\pi^0\pi^0 n$
47 ± 13		[3] BOLTON	92B MRK3	$J/\psi \to \gamma\eta\pi^+\pi^-$
59 ± 4		FUKUI	91C SPEC	8.95 $\pi^- p \to \eta\pi^+\pi^- n$
53 ± 11		[4] AUGUSTIN	90 DM2	$J/\psi \to \gamma\eta\pi^+\pi^-$
31 ± 7		ANDO	86 SPEC	8 $\pi^- p \to \eta\pi^+\pi^- n$
• • • We do not use the following data for averages, fits, limits, etc. • • •				
79.0 ± 16.0	195	ABLIKIM	19BA BES3	$e^+e^- \to \psi(2S)$
86 ± 10		[5] AMSLER	95F CBAR	0 $\overline{p}p \to \pi^+\pi^-\pi^0\pi^0\eta$

[1] ABLIKIM 25AB measured $J/\psi \to \gamma\eta(1405) \to \gamma\pi^0 f_0(980)$ / 0^{++} *PHSP* $\to \gamma\pi^0\pi^0\pi^0$. Here $\gamma\pi^0 f_0(980)$ / 0^{++} *PHSP* indicates an intermediate state which could be either $\gamma\pi^0 f_0(980)$ or $\gamma\pi^0\,0^{++}$ phase space.
[2] The selected process is $J/\psi \to \omega a_0(980)\pi$.
[3] From fit to the $a_0(980)\,\pi\;0^{-+}$ partial wave.
[4] From $\eta\pi^+\pi^-$ mass distribution – mainly $a_0(980)\,\pi$ – no spin–parity determination available.
[5] Superseded by AMSLER 04B.

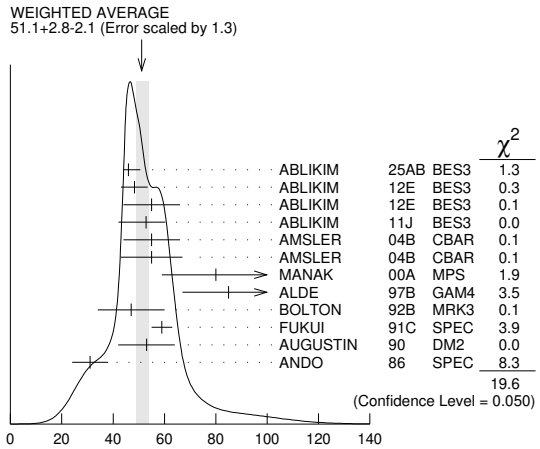

$K\overline{K}\pi$ MODE ($a_0(980)\pi$ or direct $K\overline{K}\pi$)

VALUE (MeV)	EVTS	DOCUMENT ID	TECN	COMMENT
The data in this block is included in the average printed for a previous datablock.				
49 ± 4 OUR AVERAGE Error includes scale factor of 2.0. See the ideogram below.				
60.8 ± 1.2 $^{+5.5}_{-12.0}$	126k	ABLIKIM	23M BES3	$J/\psi \to \gamma K^0_S K^0_S \pi^0$
51 ± 6	3651	[1] NICHITIU	02 OBLX	0 $\overline{p}p \to K^+K^-\pi^+\pi^-\pi^0$
42 ± 10 ± 9	20k	ADAMS	01B B852	18 GeV $\pi^- p \to K^+K^-\pi^0 n$
50 ± 4		CICALO	99 OBLX	0 $\overline{p}p \to K^\pm K^0_S \pi^\mp\pi^+\pi^-$
48 ± 5		[2] BERTIN	97 OBLX	0.0 $\overline{p}p \to K^\pm(K^0)\pi^\mp\pi^+\pi^-$
50 ± 4		[2] BERTIN	95 OBLX	0 $\overline{p}p \to K\overline{K}\pi\pi\pi$
75 ± 9		AUGUSTIN	92 DM2	$J/\psi \to \gamma K\overline{K}\pi$
91 $^{+67}_{-31}$ $^{+15}_{-38}$		[3] BAI	90C MRK3	$J/\psi \to \gamma K^0_S K^\pm\pi^\mp$
19 ± 7		[3] RATH	89 MPS	21.4 $\pi^- p \to n K^0_S K^0_S \pi^0$

[1] Decaying dominantly directly to $K^+K^-\pi^0$.
[2] Decaying into $(K\overline{K})_S\pi$, $(K\pi)_S\overline{K}$, and $a_0(980)\,\pi$.
[3] From fit to the $a_0(980)\,\pi\;0^{-+}$ partial wave , but $a_0(980)\,\pi\;1^{++}$ cannot be excluded.

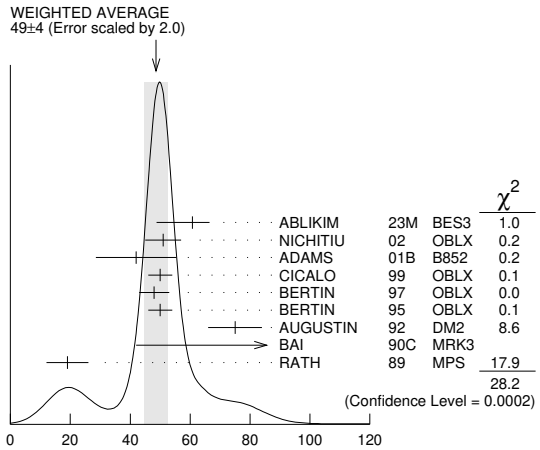

$\pi\pi\gamma$ MODE

VALUE (MeV)	EVTS	DOCUMENT ID	TECN	COMMENT
89 ± 17 OUR AVERAGE Error includes scale factor of 1.7.				
64 ± 18	235 ± 91	AMSLER	04B CBAR	0 $\overline{p}p \to \pi^+\pi^-\pi^+\pi^-\gamma$
101.0 ± 8.8 ± 8.8	547	BAI	04J BES2	$J/\psi \to \gamma\gamma\pi^+\pi^-$
• • • We do not use the following data for averages, fits, limits, etc. • • •				
174 ± 44		AUGUSTIN	90 DM2	$J/\psi \to \pi^+\pi^-\gamma\gamma$
90 ± 26		[1] COFFMAN	90 MRK3	$J/\psi \to \pi^+\pi^-2\gamma$

[1] This peak in the $\gamma\rho$ channel may not be related to the $\eta(1405)$.

4π MODE

VALUE (MeV)	EVTS	DOCUMENT ID	TECN	COMMENT
• • • We do not use the following data for averages, fits, limits, etc. • • •				
160 ± 30		BUGG	95 MRK3	$J/\psi \to \gamma\pi^+\pi^-\pi^+\pi^-$
144 ± 13	3270	[1] BISELLO	89B DM2	$J/\psi \to 4\pi\gamma$

[1] Estimated by us from various fits.

Int. J. Mod. Phys. A 2026.41. Downloaded from www.worldscientific.com by CALIFORNIA @ BERKELEY on 09/16/26. Re-use and distribution is strictly not permitted, except for Open Access articles.

$\phi\gamma$ MODE

VALUE (MeV)	DOCUMENT ID		TECN	COMMENT
$86.3\pm2.7^{+6.6}_{-17.4}$	[1] ABLIKIM	25P	BES3	$J/\psi \to \gamma\gamma\phi$

[1] From a partial wave analysis of $J/\psi \to \gamma\gamma\phi$ with significance 18.9σ.

$K\overline{K}\pi$ MODE (unresolved)

VALUE (MeV)	EVTS	DOCUMENT ID		TECN	COMMENT
• • • We do not use the following data for averages, fits, limits, etc. • • •					
45.9 ± 8.2	191	[1,2] ABLIKIM	13M	BES3	$\psi(2S) \to \omega K K \pi$
48.9 ± 9.0	249 ± 35	[1,2] ABLIKIM	08E	BES2	$J/\psi \to \omega K^0_S K^+\pi^-$ + c.c.
34.2 ± 18.5	62 ± 18	[1,2] ABLIKIM	08E	BES2	$J/\psi \to \omega K^+ K^-\pi^0$
93 ± 14	296	[1] AUGUSTIN	90	DM2	$J/\psi \to \gamma K^+ K^-\pi^0$
105 ± 10	693	[1] AUGUSTIN	90	DM2	$J/\psi \to \gamma K^0_S K^\pm\pi^\mp$
62 ± 16	500	[1] DUCH	89	ASTE	$\overline{p}p \to K\overline{K}\pi\pi\pi$
100 ± 11	170	[1] RATH	89	MPS	$21.4\ \pi^- p \to K^0_S K^0_S \pi^0 n$
66 ± 2	8800	[1] BIRMAN	88	MPS	$8\ \pi^- p \to K^+\overline{K}^0\pi^- n$
60 ± 10	620	[1] REEVES	86	SPEC	$6.6\ p\overline{p} \to K K\pi$X
60 ± 10		[1] CHUNG	85	SPEC	$8\ \pi^- p \to K\overline{K}\pi n$
$55\ ^{+20}_{-30}$	174	[1] EDWARDS	82E	CBAL	$J/\psi \to \gamma K^+ K^-\pi^0$
$50\ ^{+30}_{-20}$		[1] SCHARRE	80	MRK2	$J/\psi \to \gamma K^0_S K^\pm\pi^\mp$
80 ± 10	800	[1,3] BAILLON	67	HBC	$0.0\ \overline{p}p \to K\overline{K}\pi\pi\pi$

[1] These experiments identify only one pseudoscalar in the 1400–1500 range. Data could also refer to $\eta(1475)$.
[2] Systematic uncertainty not evaluated.
[3] From best fit to 0^{-+} partial wave , 50% $K^*(892)\,K$, 50% $a_0(980)\,\pi$.

$\eta(1405)$ DECAY MODES

	Mode	Fraction (Γ_i/Γ)	Confidence level
Γ_1	$K\overline{K}\pi$	seen	
Γ_2	$\eta\pi\pi$	seen	
Γ_3	$a_0(980)\,\pi$	seen	
Γ_4	$\eta(\pi\pi)_{S\text{-wave}}$	seen	
Γ_5	$f_0(980)\,\pi^0 \to \pi^+\pi^-\pi^0$		
Γ_6	$f_0(980)\,\eta$	seen	
Γ_7	4π	seen	
Γ_8	$\rho\rho$	<58 %	99.85%
Γ_9	$\gamma\gamma$		
Γ_{10}	$\rho^0\gamma$	seen	
Γ_{11}	$\phi\gamma$	seen	
Γ_{12}	$K^*(892)\,K$	seen	

$\eta(1405)$ $\Gamma(i)\Gamma(\gamma\gamma)/\Gamma(\text{total})$

$\Gamma(K\overline{K}\pi)\times\Gamma(\gamma\gamma)/\Gamma_{\text{total}}$ — $\Gamma_1\Gamma_9/\Gamma$

VALUE (keV)	CL%	DOCUMENT ID		TECN	COMMENT
• • • We do not use the following data for averages, fits, limits, etc. • • •					
<0.035	90	[1,2] AHOHE	05	CLE2	$10.6\ e^+e^- \to e^+e^- K^0_S K^\pm\pi^\mp$

[1] Using $\eta(1405)$ mass and width 1410 MeV and 51 MeV, respectively.
[2] Assuming three-body phase-space decay to $K^0_S K^\pm\pi^\mp$.

$\Gamma(\eta\pi\pi)\times\Gamma(\gamma\gamma)/\Gamma_{\text{total}}$ — $\Gamma_2\Gamma_9/\Gamma$

VALUE (keV)	CL%	DOCUMENT ID		TECN	COMMENT
<0.095	95	ACCIARRI	01G	L3	$183\text{–}202\ e^+e^- \to e^+e^-\eta\pi^+\pi^-$

$\Gamma(\rho^0\gamma)\times\Gamma(\gamma\gamma)/\Gamma_{\text{total}}$ — $\Gamma_{10}\Gamma_9/\Gamma$

VALUE (keV)	CL%	DOCUMENT ID		TECN	COMMENT
• • • We do not use the following data for averages, fits, limits, etc. • • •					
<1.5	95	ALTHOFF	84E	TASS	$e^+e^- \to e^+e^-\pi^+\pi^-\gamma$

$\eta(1405)$ BRANCHING RATIOS

$\Gamma(\eta\pi\pi)/\Gamma(K\overline{K}\pi)$ — Γ_2/Γ_1

VALUE	CL%	DOCUMENT ID		TECN	COMMENT
1.09±0.48		[1] AMSLER	04B	CBAR	$0\ \overline{p}p \to \pi^+\pi^-\pi^+\pi^-\eta$
• • • We do not use the following data for averages, fits, limits, etc. • • •					
<0.5	90	EDWARDS	83B	CBAL	$J/\psi \to \eta\pi\pi\gamma$
<1.1	90	SCHARRE	80	MRK2	$J/\psi \to \eta\pi\pi\gamma$
<1.5	95	FOSTER	68B	HBC	$0.0\ \overline{p}p$

[1] Using the data of BAILLON 67 on $\overline{p}p \to K\overline{K}\pi$.

$\Gamma(\rho^0\gamma)/\Gamma(\eta\pi\pi)$ — Γ_{10}/Γ_2

VALUE	DOCUMENT ID		TECN	COMMENT
0.111±0.064	AMSLER	04B	CBAR	$0\ \overline{p}p$

$\Gamma(a_0(980)\pi)/\Gamma(K\overline{K}\pi)$ — Γ_3/Γ_1

VALUE	EVTS	DOCUMENT ID		TECN	COMMENT
• • • We do not use the following data for averages, fits, limits, etc. • • •					
~ 0.15		[1] BERTIN	95	OBLX	$0\ \overline{p}p \to K\overline{K}\pi\pi\pi$
~ 0.8	500	[1] DUCH	89	ASTE	$\overline{p}p \to \pi^+\pi^- K^\pm\pi^\mp K^0$
~ 0.75		[1] REEVES	86	SPEC	$6.6\ p\overline{p} \to K K\pi$X

[1] Assuming that the $a_0(980)$ decays only into $K\overline{K}$.

$\Gamma(a_0(980)\pi)/\Gamma(\eta\pi\pi)$ — Γ_3/Γ_2

VALUE	EVTS	DOCUMENT ID		TECN	COMMENT
• • • We do not use the following data for averages, fits, limits, etc. • • •					
0.29 ± 0.10		ABELE	98E	CBAR	$0\ p\overline{p} \to \eta\pi^0\pi^0\pi^0$
0.19 ± 0.04	2200	[1] ALDE	97B	GAM4	$100\ \pi^- p \to \eta\pi^0\pi^0 n$
$0.56\pm0.04\pm0.03$		[1] AMSLER	95F	CBAR	$0\ \overline{p}p \to \pi^+\pi^-\pi^0\pi^0\eta$

[1] Assuming that the $a_0(980)$ decays only into $\eta\pi$.

$\Gamma(a_0(980)\pi)/\Gamma(\eta(\pi\pi)_{S\text{-wave}})$ — Γ_3/Γ_4

VALUE	EVTS	DOCUMENT ID		TECN	COMMENT
• • • We do not use the following data for averages, fits, limits, etc. • • •					
0.91 ± 0.12		ANISOVICH	01	SPEC	$0.0\ \overline{p}p \to \eta\pi^+\pi^-\pi^+\pi^-$
0.15 ± 0.04	9082	[1] MANAK	00A	MPS	$18\ \pi^- p \to \eta\pi^+\pi^- n$
$0.70\pm0.12\pm0.20$		[2] BAI	99	BES	$J/\psi \to \gamma\eta\pi^+\pi^-$

[1] Statistical error only.
[2] Assuming that the $a_0(980)$ decays only into $\eta\pi$.

$\Gamma(\rho^0\gamma)/\Gamma(K\overline{K}\pi)$ — Γ_{10}/Γ_1

VALUE	DOCUMENT ID		TECN	COMMENT
0.0152±0.0038	[1] COFFMAN	90	MRK3	$J/\psi \to \gamma\gamma\pi^+\pi^-$

[1] Using $B(J/\psi \to \gamma\eta(1405) \to \gamma K\overline{K}\pi)=4.2\times10^{-3}$ and $B(J/\psi \to \gamma\eta(1405) \to \gamma\gamma\rho^0)=6.4\times10^{-5}$.

$\Gamma(\gamma\gamma)/\Gamma(K\overline{K}\pi)$ — Γ_9/Γ_1

VALUE	CL%	DOCUMENT ID		TECN	COMMENT
$<1.78\times10^{-3}$	90	[1] ABLIKIM	18O	BES3	$\psi(2S) \to \pi^+\pi^-\gamma\gamma$

[1] Using results from BAI 00D.

$\Gamma(\eta(\pi\pi)_{S\text{-wave}})/\Gamma(\eta\pi\pi)$ — Γ_4/Γ_2

VALUE	EVTS	DOCUMENT ID		TECN	COMMENT
• • • We do not use the following data for averages, fits, limits, etc. • • •					
0.81 ± 0.04	2200	ALDE	97B	GAM4	$100\ \pi^- p \to \eta\pi^0\pi^0 n$

$\Gamma(f_0(980)\eta)/\Gamma(\eta\pi\pi)$ — Γ_6/Γ_2

VALUE	DOCUMENT ID		TECN	COMMENT
• • • We do not use the following data for averages, fits, limits, etc. • • •				
0.32 ± 0.07	[1] ANISOVICH	00	SPEC	$0.9\text{–}1.2\ \overline{p}p \to \eta 3\pi^0$

[1] Using preliminary Crystal Barrel data.

$\Gamma(f_0(980)\pi^0 \to \pi^+\pi^-\pi^0)/\Gamma_{\text{total}}$ — Γ_5/Γ

VALUE	EVTS	DOCUMENT ID		TECN	COMMENT
seen	203	[1] ABLIKIM	24I	BES3	$J/\psi \to e^+e^-\eta(1405)$
seen	743	[2] ABLIKIM	12E	BES3	$J/\psi \to \gamma\eta(1405)$
• • • We do not use the following data for averages, fits, limits, etc. • • •					
not seen		[3] ABLIKIM	17AJ	BES3	$\psi(2S) \to \gamma\pi^+\pi^-\pi^0$

[1] ABLIKIM 24I reports $B(J/\psi \to e^+e^-\eta(1405) \to f_0(980)\pi^0 \to \pi^+\pi^-\pi^0) = (2.04\pm0.20\pm0.08)\times10^{-7}$.
[2] ABLIKIM 12E reports $B(J/\psi \to \gamma\eta(1405) \to f_0(980)\pi^0 \to \pi^+\pi^-\pi^0) = (1.5\pm0.11\pm0.11)\times10^{-5}$ and $B(J/\psi \to \gamma\eta(1405) \to f_0(980)\pi^0 \to \pi^0\pi^0\pi^0) = (7.10\pm0.82\pm0.72)\times10^{-6}$.
[3] ABLIKIM 17AJ reports $B(\psi(2S) \to \gamma\eta(1405) \to \gamma f_0(980)\pi^0 \to \gamma\pi^+\pi^-\pi^0) < 5.0\times10^{-7}$.

$\Gamma(\rho\rho)/\Gamma_{\text{total}}$ — Γ_8/Γ

VALUE	CL%	DOCUMENT ID		TECN	COMMENT
<0.58	99.85	[1,2] AMSLER	04B	CBAR	$0\ \overline{p}p$

[1] Assuming that the $\eta(1405)$ decays are saturated by the $\pi\pi\eta$, $K\overline{K}\pi$ and $\rho\rho$ modes.
[2] Using the data of BAILLON 67 on $\overline{p}p \to K\overline{K}\pi$.

$\Gamma(K^*(892)\,K)/\Gamma(a_0(980)\pi)$ — Γ_{12}/Γ_3

VALUE	DOCUMENT ID		TECN	COMMENT
• • • We do not use the following data for averages, fits, limits, etc. • • •				
0.084 ± 0.024	[1] ADAMS	01B	B852	18 GeV $\pi^- p \to K^+K^-\pi^0 n$

[1] Statistical error only.

$\Gamma(\phi\gamma)/\Gamma_{\text{total}}$ — Γ_{11}/Γ

VALUE	DOCUMENT ID		TECN	COMMENT
seen	[1] ABLIKIM	25P	BES3	$J/\psi \to \gamma\gamma\phi$

[1] From a partial wave analysis of $J/\psi \to \gamma\gamma\phi$ with significance 18.9σ.

$\Gamma(\phi\gamma)/\Gamma(\rho^0\gamma)$ — Γ_{11}/Γ_{10}

VALUE	CL%	DOCUMENT ID		TECN	COMMENT
• • • We do not use the following data for averages, fits, limits, etc. • • •					
0.09 ± 0.03		[1] ABLIKIM	18I	BES3	$J/\psi \to \gamma\gamma\phi(1020)$
0.13 ± 0.04		[2] ABLIKIM	18I	BES3	$J/\psi \to \gamma\gamma\phi(1020)$
<0.77	95	[3] BAI	04J	BES2	$J/\psi \to \gamma\gamma K^+K^-$

Int. J. Mod. Phys. A 2026.41. Downloaded from www.worldscientific.com by UNIVERSITY OF CALIFORNIA @ BERKELEY on 09/16/26. Re-use and distribution is strictly not permitted, except for Open Access articles.

[1] Constructive interference between $X(1835)$ and $\eta(1405)/\eta(1475)$ decays to $\gamma\phi$ is assumed. Also see $\eta(1475)$. ABLIKIM 18I reports the inverse as 11.10 ± 3.5.
[2] Destructive interference between $X(1835)$ and $\eta(1405)/\eta(1475)$ decays to $\gamma\phi$ is assumed. Also see $\eta(1475)$. ABLIKIM 18I reports the inverse as 7.53 ± 2.49.
[3] Calculated by us from $B(J/\psi \to \eta(1405)\gamma \to \phi\gamma\gamma) < 0.82 \times 10^{-4}$ and $B(J/\psi \to \eta(1405)\gamma \to \rho^0\gamma\gamma) = (1.07 \pm 0.17 \pm 0.11) \times 10^{-4}$.

$\eta(1405)$ REFERENCES

ABLIKIM	25AB	PR D112 032007	M. Ablikim et al.	(BESIII Collab.)
ABLIKIM	25P	PR D111 052011	M. Ablikim et al.	(BESIII Collab.)
ABLIKIM	24I	PR D109 012007	M. Ablikim et al.	(BESIII Collab.)
ABLIKIM	23M	JHEP 2303 121	M. Ablikim et al.	(BESIII Collab.)
ABLIKIM	19BA	PR D100 092003	M. Ablikim et al.	(BESIII Collab.)
ABLIKIM	18I	PR D97 051101	M. Ablikim et al.	(BESIII Collab.)
ABLIKIM	18O	PR D97 072014	M. Ablikim et al.	(BESIII Collab.)
ABLIKIM	17AJ	PR D96 112008	M. Ablikim et al.	(BESIII Collab.)
ABLIKIM	13M	PR D87 092006	M. Ablikim et al.	(BESIII Collab.)
ABLIKIM	12E	PRL 108 182001	M. Ablikim et al.	(BESIII Collab.)
ABLIKIM	11J	PRL 107 182001	M. Ablikim et al.	(BESIII Collab.)
ABLIKIM	08E	PR D77 032005	M. Ablikim et al.	(BES Collab.)
AHOHE	05	PR D71 072001	R. Ahohe et al.	(CLEO Collab.)
AMSLER	04B	EPJ C33 23	C. Amsler et al.	(Crystal Barrel Collab.)
BAI	04J	PL B594 47	J.Z. Bai et al.	(BES Collab.)
NICHITIU	02	PL B545 261	F. Nichitiu et al.	(OBELIX Collab.)
ACCIARRI	01G	PL B501 1	M. Acciarri et al.	(L3 Collab.)
ADAMS	01B	PL B516 264	G.S. Adams et al.	(BNL E852 Collab.)
ANISOVICH	01	NP A690 567	A.V. Anisovich et al.	
ANISOVICH	00	PL B472 168	A.V. Anisovich et al.	
BAI	00D	PL B476 25	J.Z. Bai et al.	(BES Collab.)
MANAK	00A	PR D62 012003	J.J. Manak et al.	(BNL E852 Collab.)
BAI	99	PL B446 356	J.Z. Bai et al.	(BES Collab.)
CICALO	99	PL B462 453	C. Cicalo et al.	(OBELIX Collab.)
ABELE	98E	NP B514 45	A. Abele et al.	(Crystal Barrel Collab.)
BAI	98C	PL B440 217	J.Z. Bai et al.	(BES Collab.)
ALDE	97B	PAN 60 386	D. Alde et al.	(GAMS Collab.)
		Translated from YAF 60 458.		
BERTIN	97	PL B400 226	A. Bertin et al.	(OBELIX Collab.)
AMSLER	95F	PL B358 389	C. Amsler et al.	(Crystal Barrel Collab.)
BERTIN	95	PL B361 187	A. Bertin et al.	(OBELIX Collab.)
BUGG	95	PL B353 378	D.V. Bugg et al.	(LOQM, PNPI, WASH)
AUGUSTIN	92	PR D46 1951	J.E. Augustin, G. Cosme	(DM2 Collab.)
BOLTON	92B	PRL 69 1328	T. Bolton et al.	(Mark III Collab.)
FUKUI	91C	PL B267 293	S. Fukui et al.	(SUGI, NAGO, KEK, KYOT+)
AUGUSTIN	90	PR D42 10	J.E. Augustin et al.	(DM2 Collab.)
BAI	90C	PRL 65 2507	Z. Bai et al.	(Mark III Collab.)
COFFMAN	90	PR D41 1410	D.M. Coffman et al.	(Mark III Collab.)
BISELLO	89B	PR D39 701	G. Busetto et al.	(DM2 Collab.)
DUCH	89	ZPHY C45 223	K.D. Duch et al.	(ASTERIX Collab.) JP
RATH	89	PR D40 693	M.G. Rath et al.	(NDAM, BRAN, BNL, CUNY+)
BIRMAN	88	PRL 61 1557	A. Birman et al.	(BNL, FSU, IND, MASD) JP
ANDO	86	PRL 57 1296	A. Ando et al.	(KEK, KYOT, NIRS, SAGA+) IJP
REEVES	86	PR D34 1960	D.F. Reeves et al.	(FLOR, BNL, IND+) JP
CHUNG	85	PRL 55 779	S.U. Chung et al.	(BNL, FLOR, IND+) JP
ALTHOFF	84E	PL 147B 487	M. Althoff et al.	(TASSO Collab.)
EDWARDS	83B	PRL 51 859	C. Edwards et al.	(CIT, HARV, PRIN+)
EDWARDS	82E	PRL 49 259	C. Edwards et al.	(CIT, HARV, PRIN+)
Also		PRL 50 219	C. Edwards et al.	(CIT, HARV, PRIN+)
SCHARRE	80	PL 97B 329	D.L. Scharre et al.	(SLAC, LBL)
FOSTER	68B	NP B8 174	M. Foster et al.	(CERN, CDEF)
BAILLON	67	NC 50A 393	P.H. Baillon et al.	(CERN, CDEF, IRAD)

$h_1(1415)$

$I^G(J^{PC}) = 0^-(1^{+-})$

$h_1(1415)$ MASS

VALUE (MeV)	EVTS	DOCUMENT ID		TECN	COMMENT
1409^{+9}_{-8} OUR AVERAGE		Error includes scale factor of 1.9. See the ideogram below.			
$1384 \pm 6\ ^{+9}_{-0}$		[1] ABLIKIM	22C	BES3	$J/\psi \to \gamma\eta'\eta' \to 4/5\,\gamma 2(\pi^+\pi^-)$
$1423 \pm 2.1 \pm 7.3$	2.2k	[2] ABLIKIM	18AB	BES3	$J/\psi \to \eta' h_1 \to \eta' K^* \overline{K}$
$1412 \pm 4 \pm 8$		[2] ABLIKIM	15M	BES3	$\psi(2S) \to \gamma\chi_{c1,2} \to \gamma\phi(h_1 \to K^*\overline{K})$
1440 ± 60		ABELE	97H	CBAR	$\overline{p}p \to K^0_L K^0_S \pi^0\pi^0$
1380 ± 20		ASTON	88C	LASS	$11\ K^- p \to K^0_S K^\pm \pi^\mp \Lambda$

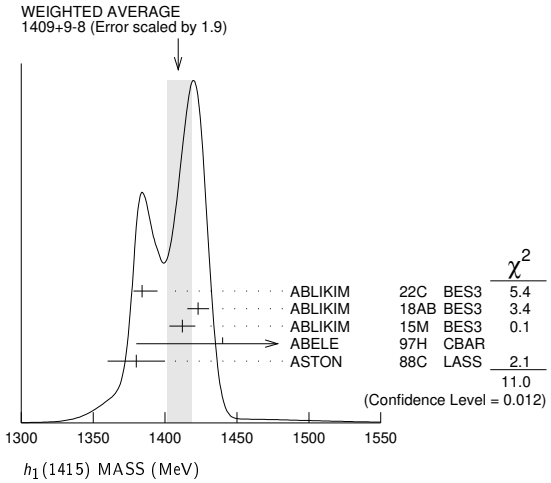

[1] From a partial wave analysis of the systems (γX), with $X \to \eta'\eta'$, and $(\eta' X)$, with $X \to \gamma\eta'$ in the decay $J/\psi \to \gamma\eta'\eta'$. The intermediate resonance X is parametrized by a constant-width, relativistic Breit-Wigner.
[2] Final states $K^+K^-\pi^0$ and $K^0_S K^\pm\pi^\mp$.

$h_1(1415)$ WIDTH

VALUE (MeV)	EVTS	DOCUMENT ID		TECN	COMMENT
78 ± 11 OUR AVERAGE					
$66 \pm 10\ ^{+12}_{-10}$		[1] ABLIKIM	22C	BES3	$J/\psi \to \gamma\eta'\eta' \to 4/5\,\gamma 2(\pi^+\pi^-)$
$90.3 \pm 9.8 \pm 17.5$	2.2k	[2] ABLIKIM	18AB	BES3	$J/\psi \to \eta' h_1 \to \eta' K^* \overline{K}$
$84 \pm 12 \pm 40$		[2] ABLIKIM	15M	BES3	$\psi(2S) \to \gamma\chi_{c1,2} \to \gamma\phi(h_1 \to K^*\overline{K})$
170 ± 80		ABELE	97H	CBAR	$\overline{p}p \to K^0_L K^0_S \pi^0\pi^0$
80 ± 30		ASTON	88C	LASS	$11\ K^- p \to K^0_S K^\pm \pi^\mp \Lambda$

[1] From a partial wave analysis of the systems (γX), with $X \to \eta'\eta'$, and $(\eta' X)$, with $X \to \gamma\eta'$ in the decay $J/\psi \to \gamma\eta'\eta'$. The intermediate resonance X is parametrized by a constant-width, relativistic Breit-Wigner.
[2] Final states $K^+K^-\pi^0$ and $K^0_S K^\pm\pi^\mp$.

$h_1(1415)$ DECAY MODES

	Mode
Γ_1	$K\overline{K}^*(892) +$ c.c.

$h_1(1415)$ REFERENCES

ABLIKIM	22C	PR D105 072002	M. Ablikim et al.	(BESIII Collab.)
ABLIKIM	18AB	PR D98 072005	M. Ablikim et al.	(BESIII Collab.)
ABLIKIM	15M	PR D91 112008	M. Ablikim et al.	(BESIII Collab.)
ABELE	97H	PL B415 280	A. Abele et al.	(Crystal Barrel Collab.)
ASTON	88C	PL B201 573	D. Aston et al.	(SLAC, NAGO, CINC, INUS)

$f_1(1420)$

$I^G(J^{PC}) = 0^+(1^{++})$

See the review on "Spectroscopy of Light Meson Resonances."

$f_1(1420)$ MASS

VALUE (MeV)	EVTS	DOCUMENT ID		TECN	COMMENT
$1427.7^{+1.7}_{-1.4}$ OUR AVERAGE		Error includes scale factor of 2.1. See the ideogram below.			
$1418\ ^{+1.7}_{-2.1} \pm 2.0 \pm 2.2$		[1] ABLIKIM	25AB	BES3	$J/\psi \to \gamma\pi^0 f_0(980) \to \gamma\pi^0\pi^0\pi^0$
$1433.5 \pm 1.1\ ^{+27.9}_{-0.7}$	126k	ABLIKIM	23M	BES3	$J/\psi \to \gamma K^0_S K^0_S \pi^0$
$1434 \pm 5 \pm 5$	133	[2] ACHARD	07	L3	183–209 $e^+e^- \to e^+e^- K^0_S K^\pm\pi^\mp$
1426 ± 6	711	ABDALLAH	03H	DLPH	91.2 $e^+e^- \to K^0_S K^\pm\pi^\mp + X$
1420 ± 14	3651	NICHITIU	02	OBLX	0 $\overline{p}p \to K^+K^-\pi^+\pi^-\pi^0$
$1428 \pm 4 \pm 2$	20k	ADAMS	01B	B852	18 GeV $\pi^- p \to K^+K^-\pi^0 n$
1426 ± 1		BARBERIS	97C	OMEG	450 $pp \to pp K^0_S K^\pm\pi^\mp$
1425 ± 8		BERTIN	97	OBLX	0.0 $\overline{p}p \to K^\pm(K^0)\pi^\mp\pi^+\pi^-$
1430 ± 4		[3] ARMSTRONG	92E	OMEG	85,300 π^+p, $pp \to \pi^+p$, $pp(K\overline{K}\pi)$
1462 ± 20		[4] AUGUSTIN	92	DM2	$J/\psi \to \gamma K\overline{K}\pi$
$1443\ ^{+7}_{-6} \pm 3 \pm 2$	1100	BAI	90C	MRK3	$J/\psi \to \gamma K^0_S K^\pm\pi^\mp$
1425 ± 10	17	BEHREND	89	CELL	$\gamma\gamma \to K^0_S K^\pm\pi^\mp$
$1442 \pm 5\ ^{+10}_{-17}$	111	BECKER	87	MRK3	e^+e^-, $\omega K\overline{K}\pi$
1423 ± 4		GIDAL	87B	MRK2	$e^+e^- \to e^+e^- K\overline{K}\pi$
1417 ± 13	13	AIHARA	86C	TPC	$e^+e^- \to e^+e^- K\overline{K}\pi$
1422 ± 3		CHAUVAT	84	SPEC	ISR 31.5 pp
1440 ± 10		[5] BROMBERG	80	SPEC	100 $\pi^- p \to K\overline{K}\pi X$
1426 ± 6	221	DIONISI	80	HBC	4 $\pi^- p \to K\overline{K}\pi n$
1420 ± 20		DAHL	67	HBC	1.6–4.2 $\pi^- p$
• • • We do not use the following data for averages, fits, limits, etc. • • •					
1430.8 ± 0.9		[6] SOSA	99	SPEC	$pp \to p_{slow}(K^0_S K^+\pi^-)\,p_{fast}$
1433.4 ± 0.8		[6] SOSA	99	SPEC	$pp \to p_{slow}(K^0_S K^-\pi^+)\,p_{fast}$
1435 ± 9		PROKOSHKIN	97B	GAM4	100 $\pi^- p \to \eta\pi^0\pi^0 n$
1429 ± 3	389	ARMSTRONG	89	OMEG	300 $pp \to K\overline{K}\pi pp$

1425 ± 2	1520	ARMSTRONG	84	OMEG	85 $\pi^+ p$, $pp \to (\pi^+, p)(K\overline{K}\pi)p$
~ 1420		BITYUKOV	84	SPEC	32 $K^- p \to K^+ K^- \pi^0 Y$

[1] ABLIKIM 25AB measured $J/\psi \to \gamma f_1(1420) \to \gamma\pi^0 f_0(980)$ / 0^{++} *PHSP* $\to \gamma\pi^0\pi^0\pi^0$. Here $\gamma\pi^0 f_0(980)$ / 0^{++} *PHSP* indicates an intermediate state which could be either $\gamma\pi^0 f_0(980)$ or $\gamma\pi^0$ 0^{++} phase space.
[2] From a fit with a width fixed at 55 MeV.
[3] This result supersedes ARMSTRONG 84, ARMSTRONG 89.
[4] From fit to the $K^*(892)K$ 1^{++} partial wave.
[5] Mass error increased to account for $a_0(980)$ mass cut uncertainties.
[6] No systematic error given.

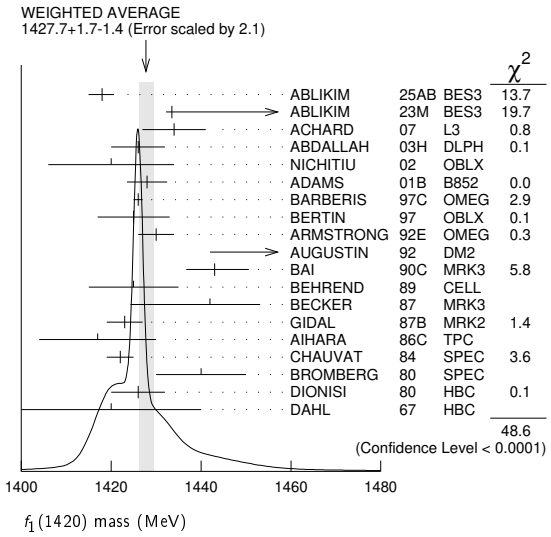

$f_1(1420)$ WIDTH

VALUE (MeV)	EVTS	DOCUMENT ID		TECN	COMMENT
55.4± 3.2 OUR AVERAGE		Error includes scale factor of 1.3. See the ideogram below.			
$46^{+3.4}_{-2.3}{}^{+6.1}_{-11.0}$		[7] ABLIKIM	25AB	BES3	$J/\psi \to \gamma\pi^0 f_0(980) \to \gamma\pi^0\pi^0\pi^0$
$95.9 \pm 2.3^{+13.6}_{-10.9}$	126k	ABLIKIM	23M	BES3	$J/\psi \to \gamma K^0_S K^0_S \pi^0$
51 ±14	711	ABDALLAH	03H	DLPH	91.2 $e^+e^- \to K^0_S K^\pm\pi^\mp + X$
61 ± 8	3651	NICHITIU	02	OBLX	0 $\overline{p}p \to K^+K^-\pi^+\pi^-\pi^0$
38 ± 9 ± 6	20k	ADAMS	01B	B852	18 GeV $\pi^- p \to K^+K^-\pi^0 n$
58 ± 4		BARBERIS	97C	OMEG	450 $pp \to pp K^0_S K^\pm\pi^\mp$
45 ±10		BERTIN	97	OBLX	0.0 $\overline{p}p \to K^\pm(K^0)\pi^\mp\pi^+\pi^-$
58 ±10		[8] ARMSTRONG	92E	OMEG	85,300 $\pi^+ p$, $pp \to \pi^+ p$, $pp(K\overline{K}\pi)$
129 ±41		[9] AUGUSTIN	92	DM2	$J/\psi \to \gamma K\overline{K}\pi$
$68^{+29}_{-18} \pm 8 \pm 9$	1100	BAI	90C	MRK3	$J/\psi \to \gamma K^0_S K^\pm\pi^\mp$
42 ±22	17	BEHREND	89	CELL	$\gamma\gamma \to K^0_S K^\pm\pi^\mp$
$40^{+17}_{-13} \pm 5$	111	BECKER	87	MRK3	$e^+e^- \to \omega K\overline{K}\pi$
35^{+47}_{-20}	13	AIHARA	86C	TPC	$e^+e^- \to e^+e^- K\overline{K}\pi$
47 ±10		CHAUVAT	84	SPEC	ISR 31.5 pp
62 ±14		BROMBERG	80	SPEC	100 $\pi^- p \to K\overline{K}\pi X$
40 ±15	221	DIONISI	80	HBC	4 $\pi^- p \to K\overline{K}\pi n$
60 ±20		DAHL	67	HBC	1.6–4.2 $\pi^- p$
• • • We do not use the following data for averages, fits, limits, etc. • • •					
68.7± 2.9		[10] SOSA	99	SPEC	$pp \to p_{slow}(K^0_S K^+\pi^-)\, p_{fast}$
58.8± 3.3		[10] SOSA	99	SPEC	$pp \to p_{slow}(K^0_S K^-\pi^+)\, p_{fast}$
90 ±25		PROKOSHKIN	97B	GAM4	100 $\pi^- p \to \eta\pi^0\pi^0 n$
58 ± 8	389	ARMSTRONG	89	OMEG	300 $pp \to K\overline{K}\pi pp$
62 ± 5	1520	ARMSTRONG	84	OMEG	85 $\pi^+ p$, $pp \to (\pi^+, p)(K\overline{K}\pi)p$
~ 50		BITYUKOV	84	SPEC	32 $K^- p \to K^+K^-\pi^0 Y$

[7] ABLIKIM 25AB measured $J/\psi \to \gamma f_1(1420) \to \gamma\pi^0 f_0(980)$ / 0^{++} *PHSP* $\to \gamma\pi^0\pi^0\pi^0$. Here $\gamma\pi^0 f_0(980)$ / 0^{++} *PHSP* indicates an intermediate state which could be either $\gamma\pi^0 f_0(980)$ or $\gamma\pi^0$ 0^{++} phase space.
[8] This result supersedes ARMSTRONG 84, ARMSTRONG 89.
[9] From fit to the $K^*(892)K$ 1^{++} partial wave.
[10] No systematic error given.

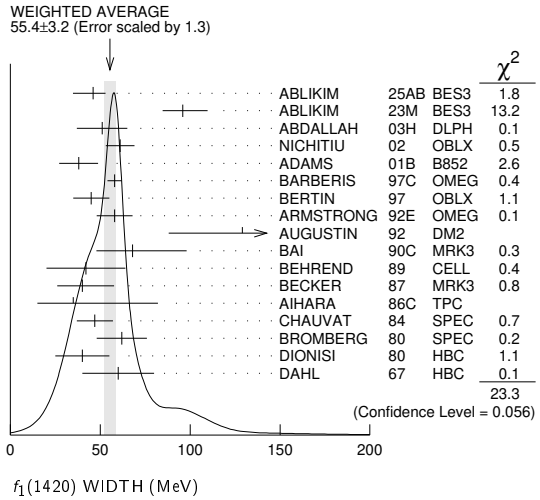

$f_1(1420)$ DECAY MODES

	Mode	Fraction (Γ_i/Γ)
Γ_1	$K\overline{K}\pi$	seen
Γ_2	$K\overline{K}^*(892)+$ c.c.	seen
Γ_3	$\eta\pi\pi$	possibly seen
Γ_4	$a_0(980)\pi$	
Γ_5	$\pi\pi\rho$	
Γ_6	4π	
Γ_7	$\rho^0\gamma$	
Γ_8	$\phi\gamma$	seen

$f_1(1420)$ $\Gamma(i)\Gamma(\gamma\gamma)/\Gamma(\text{total})$

$\Gamma(K\overline{K}\pi) \times \Gamma(\gamma\gamma^*)/\Gamma_{total}$

VALUE (keV)	CL%	EVTS	DOCUMENT ID		TECN	COMMENT
1.9±0.4 OUR AVERAGE						
3.2±0.6±0.7		133	[11,12] ACHARD	07	L3	183–209 $e^+e^- \to e^+e^- K^0_S K^\pm\pi^\mp$
3.0±0.9±0.7			[13,14] BEHREND	89	CELL	$e^+e^- \to e^+e^- K^0_S K\pi$
$2.3^{+1.0}_{-0.9} \pm 0.8$			HILL	89	JADE	$e^+e^- \to e^+e^- K^\pm K^0_S \pi^\mp$
1.3±0.5±0.3			AIHARA	88B	TPC	$e^+e^- \to e^+e^- K^\pm K^0_S \pi^\mp$
1.6±0.7±0.3			[13,15] GIDAL	87B	MRK2	$e^+e^- \to e^+e^- K\overline{K}\pi$
• • • We do not use the following data for averages, fits, limits, etc. • • •						
<8.0	95		JENNI	83	MRK2	$e^+e^- \to e^+e^- K\overline{K}\pi$

[11] From a fit with a width fixed at 55 MeV.
[12] The form factor parameter from the fit is 926 ± 78 MeV.
[13] Assume a ρ-pole form factor.
[14] A ϕ - pole form factor gives considerably smaller widths.
[15] Published value divided by 2.

$f_1(1420)$ BRANCHING RATIOS

$\Gamma(K\overline{K}^*(892)+\text{c.c.})/\Gamma(K\overline{K}\pi)$ — Γ_2/Γ_1

VALUE	DOCUMENT ID		TECN	COMMENT
• • • We do not use the following data for averages, fits, limits, etc. • • •				
0.76±0.06	BROMBERG	80	SPEC	100 $\pi^- p \to K\overline{K}\pi X$
0.86±0.12	DIONISI	80	HBC	4 $\pi^- p \to K\overline{K}\pi n$

$\Gamma(\pi\pi\rho)/\Gamma(K\overline{K}\pi)$ — Γ_5/Γ_1

VALUE	CL%	DOCUMENT ID		TECN	COMMENT
• • • We do not use the following data for averages, fits, limits, etc. • • •					
<0.3	95	CORDEN	78	OMEG	12–15 $\pi^- p$
<2.0		DAHL	67	HBC	1.6–4.2 $\pi^- p$

$\Gamma(\eta\pi\pi)/\Gamma(K\overline{K}\pi)$ — Γ_3/Γ_1

VALUE	CL%	DOCUMENT ID		TECN	COMMENT
<0.1	95	ARMSTRONG	91B	OMEG	300 $pp \to pp\eta\pi^+\pi^-$
• • • We do not use the following data for averages, fits, limits, etc. • • •					
1.35±0.75		KOPKE	89	MRK3	$J/\psi \to \omega\eta\pi\pi(K\overline{K}\pi)$

Int. J. Mod. Phys. A 2026.41. Downloaded from www.worldscientific.com
by LIFORNIA @ BERKELEY on 09/16/26. Re-use and distribution is strictly not permitted, except for Open Access articles.

Int. J. Mod. Phys. A 2026.41. Downloaded from www.worldscientific.com
by UNIVERSITY OF CALIFORNIA @ BERKELEY on 09/16/26. Re-use and distribution is strictly not permitted, except for Open Access articles.

<0.6	90	GIDAL	87	MRK2	$e^+e^- \to e^+e^-\eta\pi^+\pi^-$
<0.5	95	CORDEN	78	OMEG	12–15 π^-p
1.5 ±0.8		DEFOIX	72	HBC	0.7 $\bar{p}p$

$\Gamma(a_0(980)\pi)/\Gamma(\eta\pi\pi)$ — Γ_4/Γ_3

VALUE	CL%	DOCUMENT ID		TECN	COMMENT
• • • We do not use the following data for averages, fits, limits, etc. • • •					
>0.1	90	PROKOSHKIN	97B	GAM4	100 $\pi^-p \to \eta\pi^0\pi^0 n$
not seen in either mode		ANDO	86	SPEC	8 π^-p
not seen in either mode		CORDEN	78	OMEG	12–15 π^-p
0.4±0.2		DEFOIX	72	HBC	0.7 $\bar{p}p \to 7\pi$

$\Gamma(4\pi)/\Gamma(K\overline{K}^*(892)+\text{c.c.})$ — Γ_6/Γ_2

VALUE	CL%	DOCUMENT ID		TECN	COMMENT
• • • We do not use the following data for averages, fits, limits, etc. • • •					
<0.90	95	DIONISI	80	HBC	4 π^-p

$\Gamma(K\overline{K}\pi)/[\Gamma(K\overline{K}^*(892)+\text{c.c.})+\Gamma(a_0(980)\pi)]$ — $\Gamma_1/(\Gamma_2+\Gamma_4)$

VALUE	DOCUMENT ID		TECN	COMMENT
• • • We do not use the following data for averages, fits, limits, etc. • • •				
0.65±0.27	[16] DIONISI	80	HBC	4 π^-p

[16] Calculated using $\Gamma(K\overline{K})/\Gamma(\eta\pi) = 0.24 \pm 0.07$ for $a_0(980)$ fractions.

$\Gamma(a_0(980)\pi)/\Gamma(K\overline{K}^*(892)+\text{c.c.})$ — Γ_4/Γ_2

VALUE	CL%	DOCUMENT ID		TECN	COMMENT
0.042±0.014 OUR AVERAGE					
0.44 ±0.19		ABLIKIM	21U	BES3	$D_s^+ \to f_1(1420)\pi^+$
0.04 ±0.01 ±0.01		BARBERIS	98C	OMEG	450 $pp \to p_f f_1(1420) p_s$
• • • We do not use the following data for averages, fits, limits, etc. • • •					
<0.04	68	ARMSTRONG	84	OMEG	85 π^+p

$\Gamma(4\pi)/\Gamma(K\overline{K}\pi)$ — Γ_6/Γ_1

VALUE	CL%	DOCUMENT ID		TECN	COMMENT
<0.62	95	ARMSTRONG	89G	OMEG	85 $\pi p \to 4\pi X$

$\Gamma(\rho^0\gamma)/\Gamma_{\text{total}}$ — Γ_7/Γ

VALUE	CL%	DOCUMENT ID		TECN	COMMENT
<0.08	95	[17] ARMSTRONG	92C	SPEC	300 $pp \to pp\pi^+\pi^-\gamma$

[17] Using the data on the $\overline{K}K\pi$ mode from ARMSTRONG 89.

$\Gamma(\rho^0\gamma)/\Gamma(K\overline{K}\pi)$ — Γ_7/Γ_1

VALUE	CL%	DOCUMENT ID		TECN	COMMENT
<0.02	95	BARBERIS	98C	OMEG	450 $pp \to p_f f_1(1420) p_s$

$\Gamma(\phi\gamma)/\Gamma_{\text{total}}$ — Γ_8/Γ

VALUE	DOCUMENT ID		TECN	COMMENT
seen	[18] ABLIKIM	25P	BES3	$J/\psi \to \gamma\gamma\phi$

[18] From a partial wave analysis of $J/\psi \to \gamma\gamma\phi$ with significance 9.0σ.

$\Gamma(\phi\gamma)/\Gamma(K\overline{K}\pi)$ — Γ_8/Γ_1

VALUE	DOCUMENT ID		TECN	COMMENT
0.003±0.001±0.001	BARBERIS	98C	OMEG	450 $pp \to p_f f_1(1420) p_s$

$f_1(1420)$ REFERENCES

ABLIKIM	25AB	PR D112 032007	M. Ablikim *et al.*	(BESIII Collab.)
ABLIKIM	25P	PR D111 052011	M. Ablikim *et al.*	(BESIII Collab.)
ABLIKIM	23M	JHEP 2303 121	M. Ablikim *et al.*	(BESIII Collab.)
ABLIKIM	21U	PR D104 032011	M. Ablikim *et al.*	(BESIII Collab.)
ACHARD	07	JHEP 0703 018	P. Achard *et al.*	(L3 Collab.)
ABDALLAH	03H	PL B569 129	J. Abdallah *et al.*	(DELPHI Collab.)
NICHITIU	02	PL B545 261	F. Nichitiu *et al.*	(OBELIX Collab.)
ADAMS	01B	PL B516 264	G.S. Adams *et al.*	(BNL E852 Collab.)
SOSA	99	PRL 83 913	M. Sosa *et al.*	
BARBERIS	98C	PL B440 225	D. Barberis *et al.*	(WA 102 Collab.)
BARBERIS	97C	PL B413 225	D. Barberis *et al.*	(WA 102 Collab.)
BERTIN	97	PL B400 226	A. Bertin *et al.*	(OBELIX Collab.)
PROKOSHKIN	97B	PD 42 298	Yu.D. Prokoshkin, S.A. Sadovsky	
		Translated from DANS 354 751.		
ARMSTRONG	92C	ZPHY C54 371	T.A. Armstrong *et al.*	(ATHU, BARI, BIRM+)
ARMSTRONG	92E	ZPHY C56 29	T.A. Armstrong *et al.*	(ATHU, BARI, BIRM+) JPC
AUGUSTIN	92	PR D46 1951	J.E. Augustin, G. Cosme	(DM2 Collab.)
ARMSTRONG	91B	ZPHY C52 389	T.A. Armstrong *et al.*	(ATHU, BARI, BIRM+)
BAI	90C	PRL 65 2507	Z. Bai *et al.*	(Mark III Collab.)
ARMSTRONG	89	PL B221 216	T.A. Armstrong *et al.*	(CERN, CDEF, BIRM+) JPC
ARMSTRONG	89G	ZPHY C43 55	T.A. Armstrong *et al.*	(CERN, BIRM, BARI+)
BEHREND	89	ZPHY C42 367	H.J. Behrend *et al.*	(CELLO Collab.)
HILL	89	ZPHY C42 355	P. Hill *et al.*	(JADE Collab.) JP
KOPKE	89	PRPL 174 67	L. Kopke *et al.*	(CERN)
AIHARA	88B	PL B209 107	H. Aihara *et al.*	(TPC-2γ Collab.)
BECKER	87	PRL 59 186	J.J. Becker *et al.*	(Mark III Collab.) JP
GIDAL	87	PRL 59 2012	G. Gidal *et al.*	(LBL, SLAC, HARV)
GIDAL	87B	PRL 59 2016	G. Gidal *et al.*	(LBL, SLAC, HARV)
AIHARA	86C	PRL 57 2500	H. Aihara *et al.*	(TPC-2γ Collab.) JP
ANDO	86	PRL 57 1296	A. Ando *et al.*	(KEK, KYOT, NIRS, SAGA+)
ARMSTRONG	84	PL 146B 273	T.A. Armstrong *et al.*	(ATHU, BARI, BIRM+) JP
BITYUKOV	84	SJNP 39 735	S. Bityukov *et al.*	(SERP)
		Translated from YAF 39 1165.		
CHAUVAT	84	PL 148B 382	P. Chauvat *et al.*	(CERN, CLER, UCLA+)
JENNI	83	PR D27 1031	P. Jenni *et al.*	(SLAC, LBL)
BROMBERG	80	PR D22 1513	C.M. Bromberg *et al.*	(CIT, FNAL, ILLC+)
DIONISI	80	NP B169 1	C. Dionisi *et al.*	(CERN, MADR, CDEF+) IJP
CORDEN	78	NP B144 253	M.J. Corden *et al.*	(BIRM, RHEL, TELA+)
DEFOIX	72	NP B44 125	C. Defoix *et al.*	(CDEF, CERN)
DAHL	67	PR 163 1377	O.I. Dahl *et al.*	(LRL) IJP
Also		PRL 14 1074	D.H. Miller *et al.*	(LRL, UCB)

$\omega(1420)$

$I^G(J^{PC}) = 0^-(1^{--})$

See also the $\omega(1650)$ particle listing.

$\omega(1420)$ MASS

VALUE (MeV)	EVTS	DOCUMENT ID		TECN	COMMENT
1410± 60 OUR ESTIMATE					
• • • We do not use the following data for averages, fits, limits, etc. • • •					
1350± 43		[1] DIMOVA	25	SND	$e^+e^- \to \pi^+\pi^-\pi^0$
1350± 43		[2] ACHASOV	24A	SND	$e^+e^- \to \pi^+\pi^-\pi^0$
1418± 30± 10	824	[3] AKHMETSHIN	17A	CMD3	1.4–2.0 $e^+e^- \to \omega\eta$
1470± 50	13.1k	[4] AULCHENKO	15A	SND	1.05–1.80 $e^+e^- \to \pi^+\pi^-\pi^0$
1382± 23± 70		AUBERT	07AU	BABR	10.6 $e^+e^- \to \omega\pi^+\pi^-\gamma$
1350± 20± 20		AUBERT,B	04N	BABR	10.6 $e^+e^- \to \pi^+\pi^-\pi^0\gamma$
1400± 50±130	1.2M	[5] ACHASOV	03D	RVUE	0.44–2.00 $e^+e^- \to \pi^+\pi^-\pi^0$
1450± 10		[6] HENNER	02	RVUE	1.2–2.0 $e^+e^- \to \rho\pi, \omega\pi\pi$
1373± 70	177	[7] AKHMETSHIN	00D	CMD2	1.2–1.38 $e^+e^- \to \omega\pi^+\pi^-$
1370± 25	5095	ANISOVICH	00H	SPEC	0.0 $p\bar{p} \to \omega\pi^0\pi^0\pi^0$
1400^{+100}_{-200}		[8] ACHASOV	98H	RVUE	$e^+e^- \to \pi^+\pi^-\pi^0$
~ 1400		[9] ACHASOV	98H	RVUE	$e^+e^- \to \omega\pi^+\pi^-$
~ 1460		[10] ACHASOV	98H	RVUE	$e^+e^- \to K^+K^-$
1440± 70		[11] CLEGG	94	RVUE	
1419± 31	315	[12] ANTONELLI	92	DM2	1.34–2.4$e^+e^- \to \rho\pi$

[1] From a fit to the cross section with contributions from $\omega(782)$, $\phi(1020)$, $\omega(1420)$, and $\omega(1650)$. An alternative fit which also includes $\phi(1680)$ gives 1374 ± 27 MeV with a worse χ^2. Supersedes ACHASOV 24A.

[2] From a fit to the cross section including contribution from $\omega(782)$, $\phi(1020)$, $\omega(1420)$, and $\omega(1650)$. Supersedes ACHASOV 20A.

[3] From a fit of the interfering $\omega(1420)$ and $\omega(1650)$ with a relative phase of π and other parameters floating.

[4] From a fit with contributions from $\omega(782)$, $\phi(1020)$, $\omega(1420)$, and $\omega(1650)$. See ACHASOV 20A for a further analysis of the $\pi^+\pi^-\pi^0$ data.

[5] From the combined fit of ANTONELLI 92, ACHASOV 01E, ACHASOV 02E, and ACHASOV 03D data on the $\pi^+\pi^-\pi^0$ and ANTONELLI 92 on the $\omega\pi^+\pi^-$ final states. Supersedes ACHASOV 99E and ACHASOV 02E.

[6] Using results of CORDIER 81 and preliminary data of DOLINSKY 91 and ANTONELLI 92.

[7] Using the data of AKHMETSHIN 00D and ANTONELLI 92. The $\rho\pi$ dominance for the energy dependence of the $\omega(1420)$ and $\omega(1650)$ width assumed.

[8] Using data from BARKOV 87, DOLINSKY 91, and ANTONELLI 92.

[9] Using the data from ANTONELLI 92.

[10] Using the data from IVANOV 81 and BISELLO 88B.

[11] From a fit to two Breit-Wigner functions and using the data of DOLINSKY 91 and ANTONELLI 92.

[12] From a fit to two Breit-Wigner functions interfering between them and with the ω,ϕ tails with fixed (+,−,+) phases.

$\omega(1420)$ WIDTH

VALUE (MeV)	EVTS	DOCUMENT ID		TECN	COMMENT
290±190 OUR ESTIMATE					
• • • We do not use the following data for averages, fits, limits, etc. • • •					
590± 90		[1] DIMOVA	25	SND	$e^+e^- \to \pi^+\pi^-\pi^0$
590± 90		[2] ACHASOV	24A	SND	$e^+e^- \to \pi^+\pi^-\pi^0$
440±125	267	[3] ACHASOV	20B	SND	$e^+e^- \to \omega\eta \to \eta\pi^0\gamma$
104± 35± 10	824	[4] AKHMETSHIN	17A	CMD3	1.4–2.0 $e^+e^- \to \omega\eta$
880±170	13.1k	[5] AULCHENKO	15A	SND	1.05–1.80 $e^+e^- \to \pi^+\pi^-\pi^0$
480±180		[6] ACHASOV	10D	SND	1.075–2.0 $e^+e^- \to \pi^0\gamma$
130± 50±100		AUBERT	07AU	BABR	10.6 $e^+e^- \to \omega\pi^+\pi^-\gamma$
450± 70± 70		AUBERT,B	04N	BABR	10.6 $e^+e^- \to \pi^+\pi^-\pi^0\gamma$
870^{+500}_{-300}±450	1.2M	[7] ACHASOV	03D	RVUE	0.44–2.00 $e^+e^- \to \pi^+\pi^-\pi^0$
199± 15		[8] HENNER	02	RVUE	1.2–2.0 $e^+e^- \to \rho\pi, \omega\pi\pi$
188± 45	177	[9] AKHMETSHIN	00D	CMD2	1.2–1.38 $e^+e^- \to \omega\pi^+\pi^-$
360^{+100}_{-60}	5095	ANISOVICH	00H	SPEC	0.0 $p\bar{p} \to \omega\pi^0\pi^0\pi^0$
240± 70		[10] CLEGG	94	RVUE	
174± 59	315	[11] ANTONELLI	92	DM2	1.34–2.4$e^+e^- \to \rho\pi$

[1] From a fit to the cross section with contributions from $\omega(782)$, $\phi(1020)$, $\omega(1420)$, and $\omega(1650)$. An alternative fit which also includes $\phi(1680)$ gives 720 ± 98 MeV with a worse χ^2. Supersedes ACHASOV 24A.

[2] From a fit to the cross section including contribution from $\omega(782)$, $\phi(1020)$, $\omega(1420)$, and $\omega(1650)$. Supersedes ACHASOV 20A.

[3] From a fit with contributions from $\omega(1420)$, $\omega(1650)$, and $\phi(1680)$. The mass of $\omega(1420)$ is fixed to the PDG 18 value of 1420 MeV.

[4] From a fit of the interfering $\omega(1420)$ and $\omega(1650)$ with a relative phase of π and other parameters floating.

[5] From a fit with contributions from $\omega(782)$, $\phi(1020)$, $\omega(1420)$, and $\omega(1650)$. See ACHASOV 20A for a further analysis of the $\pi^+\pi^-\pi^0$ data.
[6] From a fit of a VMD model with two effective resonances with masses of 1450 MeV and 1700 MeV to describe the excited vector states $\omega(1420)$, $\rho(1450)$, $\omega(1650)$, and $\rho(1700)$. Systematic errors not evaluated.
[7] From the combined fit of ANTONELLI 92, ACHASOV 01E, ACHASOV 02E, and ACHASOV 03D data on the $\pi^+\pi^-\pi^0$ and ANTONELLI 92 on the $\omega\pi^+\pi^-$ final states. Supersedes ACHASOV 99E and ACHASOV 02E.
[8] Using results of CORDIER 81 and preliminary data of DOLINSKY 91 and ANTONELLI 92.
[9] Using the data of AKHMETSHIN 00D and ANTONELLI 92. The $\rho\pi$ dominance for the energy dependence of the $\omega(1420)$ and $\omega(1650)$ width assumed.
[10] From a fit to two Breit-Wigner functions and using the data of DOLINSKY 91 and ANTONELLI 92.
[11] From a fit to two Breit-Wigner functions interfering between them and with the ω,ϕ tails with fixed $(+,-,+)$ phases.

$\omega(1420)$ DECAY MODES

	Mode	Fraction (Γ_i/Γ)
Γ_1	$\rho\pi$	seen
Γ_2	$\rho(1450)\pi$	possibly seen
Γ_3	$\omega\pi\pi$	seen
Γ_4	$\omega\eta$	possibly seen
Γ_5	$b_1(1235)\pi$	seen
Γ_6	e^+e^-	seen
Γ_7	$\pi^0\gamma$	

$\omega(1420)$ $\Gamma(i)\Gamma(e^+e^-)/\Gamma^2(\text{total})$

$\Gamma(\rho\pi)/\Gamma_{\text{total}} \times \Gamma(e^+e^-)/\Gamma_{\text{total}}$ — $\Gamma_1/\Gamma \times \Gamma_6/\Gamma$

VALUE (units 10^{-6})	EVTS	DOCUMENT ID		TECN	COMMENT
• • • We do not use the following data for averages, fits, limits, etc. • • •					
0.73 ±0.08	13.1k	[1] AULCHENKO	15A	SND	1.05–1.80 $e^+e^- \to \pi^+\pi^-\pi^0$
0.82 ±0.05 ±0.06		AUBERT,B	04N	BABR	10.6 $e^+e^- \to \pi^+\pi^-\pi^0\gamma$
0.65 ±0.13 ±0.21	1.2M	[2,3] ACHASOV	03D	RVUE	0.44–2.00 $e^+e^- \to \pi^+\pi^-\pi^0$
0.625±0.160		[4,5] CLEGG	94	RVUE	
0.466±0.178		[6,7] ANTONELLI	92	DM2	1.34–2.4 $e^+e^- \to \rho\pi$

[1] From a fit with contributions from $\omega(782)$, $\phi(1020)$, $\omega(1420)$, and $\omega(1650)$. See ACHASOV 20A for a further analysis of the $\pi^+\pi^-\pi^0$ data.
[2] Calculated by us from the cross section at the peak.
[3] From the combined fit of ANTONELLI 92, ACHASOV 01E, ACHASOV 02E, and ACHASOV 03D data on the $\pi^+\pi^-\pi^0$ and ANTONELLI 92 on the $\omega\pi^+\pi^-$ final states. Supersedes ACHASOV 99E and ACHASOV 02E.
[4] From a fit to two Breit-Wigner functions and using the data of DOLINSKY 91 and ANTONELLI 92.
[5] From the partial and leptonic width given by the authors.
[6] From a fit to two Breit-Wigner functions interfering between them and with the ω,ϕ tails with fixed $(+,-,+)$ phases.
[7] From the product of the leptonic width and partial branching ratio given by the authors.

$\Gamma(\omega\pi\pi)/\Gamma_{\text{total}} \times \Gamma(e^+e^-)/\Gamma_{\text{total}}$ — $\Gamma_3/\Gamma \times \Gamma_6/\Gamma$

VALUE (units 10^{-8})	DOCUMENT ID		TECN	COMMENT
• • • We do not use the following data for averages, fits, limits, etc. • • •				
19.7±5.7	AUBERT	07AU	BABR	10.6 $e^+e^- \to \omega\pi^+\pi^-\gamma$
1.9±1.9	[1] AKHMETSHIN	00D	CMD2	1.2–2.4 $e^+e^- \to \omega\pi^+\pi^-$

[1] Using the data of AKHMETSHIN 00D and ANTONELLI 92. The $\rho\pi$ dominance for the energy dependence of the $\omega(1420)$ and $\omega(1650)$ width assumed.

$\Gamma(\omega\eta)/\Gamma_{\text{total}} \times \Gamma(e^+e^-)/\Gamma_{\text{total}}$ — $\Gamma_4/\Gamma \times \Gamma_6/\Gamma$

VALUE (units 10^{-8})	EVTS	DOCUMENT ID		TECN	COMMENT
• • • We do not use the following data for averages, fits, limits, etc. • • •					
2.5±0.6	267	[1] ACHASOV	20B	SND	$e^+e^- \to \omega\eta \to \eta\pi^0\gamma$
$2.1^{+1.0}_{-0.8}$		ACHASOV	19	SND	$e^+e^- \to \pi^+\pi^-\pi^0\eta$
5.0±2.6±0.3	824	[2] AKHMETSHIN	17A	CMD3	1.4–2.0 $e^+e^- \to \omega\eta$
$1.6^{+0.9}_{-0.7}$	898	[3] ACHASOV	16B	SND	1.34–2.00 $e^+e^- \to \omega\eta$

[1] From a fit with contributions from $\omega(1420)$, $\omega(1650)$, and $\phi(1680)$. The mass of $\omega(1420)$ is fixed to the PDG 18 value of 1420 MeV. Fixing also the width of $\omega(1420)$ to the PDG 18 value of 220 MeV results in $(3.0 \pm 1.6) \times 10^{-8}$ measurement.
[2] From a fit of the interfering $\omega(1420)$ and $\omega(1650)$ with a relative phase of π and other parameters floating. From an alternative fit $\Gamma(\omega(1420) \to \omega\eta)/\Gamma_{\text{total}} \times \Gamma(\omega(1420) \to e^+e^-) = 5.3 \pm 1.6$ eV.
[3] From a fit with contributions from $\omega(1420)$, $\omega(1650)$, and $\phi(1680)$. The mass and the width of $\omega(1420)$ are fixed to the 2014 edition (PDG 14) of this review.

$\Gamma(\pi^0\gamma)/\Gamma_{\text{total}} \times \Gamma(e^+e^-)/\Gamma_{\text{total}}$ — $\Gamma_7/\Gamma \times \Gamma_6/\Gamma$

VALUE (units 10^{-8})	DOCUMENT ID		TECN	COMMENT
• • • We do not use the following data for averages, fits, limits, etc. • • •				
0.23±0.14	[1] ACHASOV	10D	SND	1.075–2.0 $e^+e^- \to \pi^0\gamma$
$2.03^{+0.70}_{-0.75}$	[2] AKHMETSHIN	05	CMD2	0.60–1.38 $e^+e^- \to \pi^0\gamma$

[1] From a fit of a VMD model with two effective resonances with masses of 1450 MeV and 1700 MeV to describe the excited vector states $\omega(1420)$, $\rho(1450)$, $\omega(1650)$, and $\rho(1700)$. Systematic errors not evaluated.
[2] Using 1420 MeV and 220 MeV for the $\omega(1420)$ mass and width.

$\omega(1420)$ BRANCHING RATIOS

$\Gamma(\rho\pi)/\Gamma_{\text{total}}$ — Γ_1/Γ

VALUE	DOCUMENT ID		TECN	COMMENT
seen	[1] DIMOVA	25	SND	$e^+e^- \to \pi^+\pi^-\pi^0$
• • • We do not use the following data for averages, fits, limits, etc. • • •				
seen	ACHASOV	20A	SND	1.15–2.00 $e^+e^- \to \pi^+\pi^-\pi^0$
0.699±0.029	[2] HENNER	02	RVUE	1.2–2.0 $e^+e^- \to \rho\pi, \omega\pi\pi$

[1] From a fit to the cross section with contributions from $\omega(782)$, $\phi(1020)$, $\omega(1420)$, and $\omega(1650)$.
[2] Assuming that the $\omega(1420)$ decays into $\rho\pi$ and $\omega\pi\pi$ only.

$\Gamma(\rho(1450)\pi)/\Gamma_{\text{total}}$ — Γ_2/Γ

VALUE	DOCUMENT ID		TECN	COMMENT
possibly seen	[1] DIMOVA	25	SND	$e^+e^- \to \pi^+\pi^-\pi^0$

[1] From a fit to the cross section with contributions from $\omega(782)$, $\phi(1020)$, $\omega(1420)$, and $\omega(1650)$.

$\Gamma(\omega\pi\pi)/\Gamma_{\text{total}}$ — Γ_3/Γ

VALUE	DOCUMENT ID		TECN	COMMENT
• • • We do not use the following data for averages, fits, limits, etc. • • •				
0.301±0.029	[1] HENNER	02	RVUE	1.2–2.0 $e^+e^- \to \rho\pi, \omega\pi\pi$
possibly seen	AKHMETSHIN	00D	CMD2	$e^+e^- \to \omega\pi^+\pi^-$

[1] Assuming that the $\omega(1420)$ decays into $\rho\pi$ and $\omega\pi\pi$ only.

$\Gamma(\omega\pi\pi)/\Gamma(b_1(1235)\pi)$ — Γ_3/Γ_5

VALUE	EVTS	DOCUMENT ID		TECN	COMMENT
• • • We do not use the following data for averages, fits, limits, etc. • • •					
0.60±0.16	5095	ANISOVICH	00H	SPEC	0.0 $p\overline{p} \to \omega\pi^0\pi^0\pi^0$

$\Gamma(e^+e^-)/\Gamma_{\text{total}}$ — Γ_6/Γ

VALUE (units 10^{-7})	EVTS	DOCUMENT ID		TECN	COMMENT
• • • We do not use the following data for averages, fits, limits, etc. • • •					
~ 6.6	1.2M	[1,2] ACHASOV	03D	RVUE	0.44–2.00 $e^+e^- \to \pi^+\pi^-\pi^0$
23 ±1		[3] HENNER	02	RVUE	1.2–2.0 $e^+e^- \to \rho\pi, \omega\pi\pi$

[1] Assuming that the $\omega(1420)$ decays into $\rho\pi$ only.
[2] Calculated by us from the cross section at the peak.
[3] Assuming that the $\omega(1420)$ decays into $\rho\pi$ and $\omega\pi\pi$ only.

$\omega(1420)$ REFERENCES

DIMOVA	25	PPN 56 820	T.V. Dimova et al.	(SND Collab.)
ACHASOV	24A	PAN 87 747	M.N. Achasov et al.	(SND Collab.)
ACHASOV	20A	EPJ C80 993	M.N. Achasov et al.	(SND Collab.)
ACHASOV	20B	EPJ C80 1008	M.N. Achasov et al.	(SND Collab.)
ACHASOV	19	PR D99 112004	M.N. Achasov et al.	(SND Collab.)
PDG	18	PR D98 030001	M. Tanabashi et al.	(PDG Collab.)
AKHMETSHIN	17A	PL B773 150	R.R. Akhmetshin et al.	(CMD-3 Collab.)
ACHASOV	16B	PR D94 092002	M.N. Achasov et al.	(SND Collab.)
AULCHENKO	15A	JETP 121 27	V.M. Aulchenko et al.	(SND Collab.)
		Translated from ZETF 148 34.		
PDG	14	CP C38 070001	K. Olive et al.	(PDG Collab.)
ACHASOV	10D	PR D98 112001	M.N. Achasov et al.	(SND Collab.)
AUBERT	07AU	PR D76 092005	B. Aubert et al.	(BABAR Collab.)
AKHMETSHIN	05	PL B605 26	R.R. Akhmetshin et al.	(Novosibirsk CMD-2 Collab.)
AUBERT,B	04N	PR D70 072004	B. Aubert et al.	(BABAR Collab.)
ACHASOV	03D	PR D68 052006	M.N. Achasov et al.	(Novosibirsk SND Collab.)
ACHASOV	02E	PR D66 032001	M.N. Achasov et al.	(Novosibirsk SND Collab.)
HENNER	02	EPJ C26 3	V.K. Henner et al.	
ACHASOV	01E	PR D63 072002	M.N. Achasov et al.	(Novosibirsk SND Collab.)
AKHMETSHIN	00D	PL B489 125	R.R. Akhmetshin et al.	(Novosibirsk CMD-2 Collab.)
ANISOVICH	00H	PL B485 341	A.V. Anisovich et al.	
ACHASOV	99E	PL B462 365	M.N. Achasov et al.	(Novosibirsk SND Collab.)
ACHASOV	98H	PR D57 4334	N.N. Achasov, A.A. Kozhevnikov	
CLEGG	94	ZPHY C62 455	A.B. Clegg, A. Donnachie	(LANC, MCHS)
ANTONELLI	92	ZPHY C56 15	A. Antonelli et al.	(DM2 Collab.)
DOLINSKY	91	PRPL 202 99	S.I. Dolinsky et al.	(NOVO)
BISELLO	88B	ZPHY C39 13	D. Bisello et al.	(PADO, CLER, FRAS+)
BARKOV	87	JETPL 46 164	L.M. Barkov et al.	(NOVO)
		Translated from ZETFP 46 132.		
CORDIER	81	PL 106B 155	A. Cordier et al.	(ORSAY)
IVANOV	81	PL 107B 297	P.M. Ivanov et al.	(NOVO)

$f_2(1430)$

$I^G(J^{PC}) = 0^+(2^{++})$

OMITTED FROM SUMMARY TABLE

This entry lists nearby peaks observed in the D wave of the $K\overline{K}$ and $\pi^+\pi^-$ systems. Seen by LEES 21A with 4.4 σ significance. Needs confirmation.

$f_2(1430)$ MASS

VALUE (MeV)	DOCUMENT ID		TECN	COMMENT
≈ 1430 OUR ESTIMATE				
• • • We do not use the following data for averages, fits, limits, etc. • • •				
1440±11±3	LEES	21A	BABR	$\gamma\gamma \to \eta_c(1S) \to \eta'\pi^+\pi^-$

Int. J. Mod. Phys. A 2026.41. Downloaded from www.worldscientific.com
by CALIFORNIA @ BERKELEY on 09/16/26. Re-use and distribution is strictly not permitted, except for Open Access articles.

1453± 4	[1] VLADIMIRSK...01		SPEC	40 $\pi^- p \to K^0_S K^0_S n$
1421± 5	AUGUSTIN	87	DM2	$J/\psi \to \gamma\pi^+\pi^-$
1480±50	AKESSON	86	SPEC	$pp \to pp\pi^+\pi^-$
1436^{+26}_{-16}	DAUM	84	CNTR	17–18 $\pi^- p \to K^+ K^- n$
1412± 3	DAUM	84	CNTR	63 $\pi^- p \to K^0_S K^0_S n$, $K^+ K^- n$
1439^{+5}_{-6}	[2] BEUSCH	67	OSPK	5,7,12 $\pi^- p \to K^0_S K^0_S n$

[1] $J^{PC} = 0^{++}$ or 2^{++}.
[2] Not seen by WETZEL 76.

$f_2(1430)$ WIDTH

VALUE (MeV)	DOCUMENT ID		TECN	COMMENT
• • • We do not use the following data for averages, fits, limits, etc. • • •				
46±15±5	LEES	21A	BABR	$\gamma\gamma \to \eta_c(1S) \to \eta'\pi^+\pi^-$
13± 5	[3] VLADIMIRSK...01		SPEC	40 $\pi^- p \to K^0_S K^0_S n$
30± 9	AUGUSTIN	87	DM2	$J/\psi \to \gamma\pi^+\pi^-$
150±50	AKESSON	86	SPEC	$pp \to pp\pi^+\pi^-$
81^{+56}_{-29}	DAUM	84	CNTR	17–18 $\pi^- p \to K^+ K^- n$
14± 6	DAUM	84	CNTR	63 $\pi^- p \to K^0_S K^0_S n$, $K^+ K^- n$
43^{+17}_{-18}	[4] BEUSCH	67	OSPK	5,7,12 $\pi^- p \to K^0_S K^0_S n$

[3] $J^{PC} = 0^{++}$ or 2^{++}.
[4] Not seen by WETZEL 76.

$f_2(1430)$ DECAY MODES

	Mode
Γ_1	$K\overline{K}$
Γ_2	$\pi\pi$

$f_2(1430)$ REFERENCES

LEES	21A	PR D104 072002	J.P. Lees *et al.*	(BABAR Collab.)
VLADIMIRSK...	01	PAN 64 1895 Translated from YAF 64 1979.	V.V. Vladimirsky *et al.*	
AUGUSTIN	87	ZPHY C36 369	J.E. Augustin *et al.*	(LALO, CLER, FRAS+)
AKESSON	86	NP B264 154	T. Akesson *et al.*	(Axial Field Spec. Collab.)
DAUM	84	ZPHY C23 339	C. Daum *et al.*	(AMST, CERN, CRAC, MPIM+) JP
WETZEL	76	NP B115 208	W. Wetzel *et al.*	(ETH, CERN, LOIC)
BEUSCH	67	PL 25B 357	W. Beusch *et al.*	(ETH, CERN)

$a_0(1450)$

$I^G(J^{PC}) = 1^-(0^{++})$

See the review on "Spectroscopy of Light Meson Resonances."

$a_0(1450)$ T-MATRIX POLE $\sqrt{s}$

Note that $\Gamma = -2\,\mathrm{Im}(\sqrt{s})$.

VALUE (MeV)	DOCUMENT ID		TECN	COMMENT
(1290–1500) − *i* (30–140) OUR ESTIMATE				
(1302.1 ± 1.1 ± 3.9) − *i* (56.2 ± 0.7 ± 1.7)	[1] ALBRECHT	20	RVUE	0.9 $\overline{p}p \to \pi^0\pi^0\eta$, $\pi^0\eta\eta$, $\pi^0 K^+ K^-$
(1515 ± 30) − *i* (115 ± 18)	ANISOVICH	09	RVUE	0.0 $\overline{p}p$, πN
(1432±13±25)−*i*(98±5±5)	[2] BUGG	08A	RVUE	$\overline{p}p$
(1441^{+40}_{-15}) − *i* (55 ± 7)	[3] BAKER	03	SPEC	$\overline{p}p \to \omega\pi^+\pi^-\pi^0$
(1303 ± 16) − *i* (46 ± 8)	[4] BARGIOTTI	03	OBLX	$\overline{p}p$
(1296 ± 10) − *i* (41 ± 11)	AMSLER	02	CBAR	0.9 $\overline{p}p \to \pi^0\pi^0\eta$
(1565 ± 30) − *i* (146 ± 20)	ANISOVICH	98B	RVUE	Compilation
(1470 ± 25)−*i*(132 ± 15)	[5] AMSLER	95D	CBAR	0.0 $\overline{p}p \to \pi^0\pi^0\pi^0$, $\pi^0\eta\eta$, $\pi^0\pi^0\eta$

[1] T-matrix pole, 2 poles, 2 channels ($\pi\eta$, $K\overline{K}$).
[2] Using data from AMSLER 94D, ABELE 98, and BAKER 03. Supersedes BUGG 94.
[3] From the pole position of a fitted Breit-Wigner amplitude.
[4] Coupled channel analysis of $\pi^+\pi^-\pi^0$, $K^+K^-\pi^0$, and $K^\pm K^0_S\pi^\mp$.
[5] Coupled-channel analysis of AMSLER 95B, AMSLER 95C, and AMSLER 94D.

$a_0(1450)$ MASS

VALUE (MeV)	EVTS	DOCUMENT ID		TECN	COMMENT
1439 ±34 OUR AVERAGE		Error includes scale factor of 1.8.			
1480 ±30		ABELE	98	CBAR	0.0 $\overline{p}p \to K^0_L K^\pm\pi^\mp$
1410 ±25		ETKIN	82C	MPS	23 $\pi^- p \to n2K^0_S$
• • • We do not use the following data for averages, fits, limits, etc. • • •					
1458 ±14 ±15	190k	[1] AAIJ	16N	LHCB	$D^0 \to K^0_S K^\pm\pi^\mp$
$1316.8^{+0.7+24.7}_{-1.0-4.6}$		[2] UEHARA	09A	BELL	$\gamma\gamma \to \pi^0\eta$
1477 ±10	80k	[3] UMAN	06	E835	5.2 $\overline{p}p \to \eta\eta\pi^0$
1290 ±10		[4] BERTIN	98B	OBLX	0.0 $\overline{p}p \to K^\pm K_s\pi^\mp$
1450 ±40		AMSLER	94D	CBAR	0.0 $\overline{p}p \to \pi^0\pi^0\eta$
∼ 1300		MARTIN	78	SPEC	10 $K^\pm p \to K^0_S\pi p$
1255 ± 5		[5] CASON	76		

[1] Using a model with Gaussian constraints to the PDG averaged values.
[2] May be a different state.
[3] Statistical error only.
[4] Not confirmed by BUGG 08A.
[5] Isospin 0 not excluded.

$a_0(1450)$ WIDTH

VALUE (MeV)	EVTS	DOCUMENT ID		TECN	COMMENT
258 ±14 OUR AVERAGE					
265 ±15		ABELE	98	CBAR	0.0 $\overline{p}p \to K^0_L K^\pm\pi^\mp$
230 ±30		ETKIN	82C	MPS	23 $\pi^- p \to n2K^0_S$
• • • We do not use the following data for averages, fits, limits, etc. • • •					
282 ±12 ±13	190k	[1] AAIJ	16N	LHCB	$D^0 \to K^0_S K^\pm\pi^\mp$
$65.0^{+2.1+99.1}_{-5.4-32.6}$		[2] UEHARA	09A	BELL	$\gamma\gamma \to \pi^0\eta$
267 ±11	80k	[3] UMAN	06	E835	5.2 $\overline{p}p \to \eta\eta\pi^0$
80 ± 5		[4] BERTIN	98B	OBLX	0.0 $\overline{p}p \to K^\pm K_s\pi^\mp$
270 ±40		AMSLER	94D	CBAR	0.0 $\overline{p}p \to \pi^0\pi^0\eta$
∼ 250		MARTIN	78	SPEC	10 $K^\pm p \to K^0_S\pi p$
79 ±10		[5] CASON	76		

[1] Using a model with Gaussian constraints to the PDG averaged values.
[2] May be a different state.
[3] Statistical error only.
[4] Not confirmed by BUGG 08A.
[5] Isospin 0 not excluded.

$a_0(1450)$ DECAY MODES

Branching fractions are given relative to the one **DEFINED AS 1**.

	Mode	Fraction (Γ_i/Γ)
Γ_1	$\pi\eta$	0.093±0.020
Γ_2	$\pi\eta'(958)$	0.033±0.017
Γ_3	$K\overline{K}$	0.082±0.028
Γ_4	$\omega\pi\pi$	**DEFINED AS 1**
Γ_5	$a_0(980)\pi\pi$	seen
Γ_6	$\gamma\gamma$	seen

$a_0(1450)$ $\Gamma(i)\Gamma(\gamma\gamma)/\Gamma(\text{total})$

$\Gamma(\pi\eta) \times \Gamma(\gamma\gamma)/\Gamma_{\text{total}}$ — $\Gamma_1\Gamma_6/\Gamma$

VALUE (eV)	DOCUMENT ID		TECN	COMMENT
• • • We do not use the following data for averages, fits, limits, etc. • • •				
$432\pm6^{+1073}_{-256}$	[1] UEHARA	09A	BELL	$\gamma\gamma \to \pi^0\eta$

[1] May be a different state.

$a_0(1450)$ BRANCHING RATIOS

$\Gamma(\pi\eta'(958))/\Gamma(\pi\eta)$ — Γ_2/Γ_1

VALUE	DOCUMENT ID		TECN	COMMENT
0.35±0.16	[1] ABELE	98	CBAR	0.0 $\overline{p}p \to K^0_L K^\pm\pi^\mp$
• • • We do not use the following data for averages, fits, limits, etc. • • •				
0.43±0.19	ABELE	97C	CBAR	0.0 $\overline{p}p \to \pi^0\pi^0\eta'$

[1] Using $\pi^0\eta$ from AMSLER 94D.

$\Gamma(K\overline{K})/\Gamma(\pi\eta)$ — Γ_3/Γ_1

VALUE	DOCUMENT ID		TECN	COMMENT
0.88 ±0.23	[1] ABELE	98	CBAR	0.0 $\overline{p}p \to K^0_L K^\pm\pi^\mp$
• • • We do not use the following data for averages, fits, limits, etc. • • •				
1.887±0.041±0.97	[2] ALBRECHT	20	RVUE	0.9 $\overline{p}p \to \pi^0\pi^0\eta$, $\pi^0\eta\eta$, $\pi^0 K^+ K^-$

[1] Using $\pi^0\eta$ from AMSLER 94D.
[2] Residues from T-matrix pole, 2 poles, 2 channels ($\pi\eta$, $K\overline{K}$).

$\Gamma(\omega\pi\pi)/\Gamma(\pi\eta)$ — Γ_4/Γ_1

VALUE	EVTS	DOCUMENT ID		TECN	COMMENT
10.7±2.3	35280	[1] BAKER	03	SPEC	$\overline{p}p \to \omega\pi^+\pi^-\pi^0$

[1] Using results on $\overline{p}p \to a_0(1450)^0\pi^0$, $a_0(1450) \to \eta\pi^0$ from ABELE 96C and assuming the $\omega\rho$ mechanism for the $\omega\pi\pi$ state.

$\Gamma(a_0(980)\pi\pi)/\Gamma_{\text{total}}$ — Γ_5/Γ

VALUE	DOCUMENT ID		TECN	COMMENT
seen	BUGG	08A	RVUE	$\overline{p}p$

$\Gamma(a_0(980)\pi\pi)/\Gamma(\pi\eta)$ — Γ_5/Γ_1

VALUE	DOCUMENT ID		TECN	CHG	COMMENT
• • • We do not use the following data for averages, fits, limits, etc. • • •					
≤ 4.3	ANISOVICH	01	RVUE	0	$\overline{p}p \to \eta 2\pi^+ 2\pi^-$

Int. J. Mod. Phys. A 2026.41. Downloaded from www.worldscientific.com
by UNIVERSITY OF CALIFORNIA @ BERKELEY on 09/16/26. Re-use and distribution is strictly not permitted, except for Open Access articles.

Int. J. Mod. Phys. A 2026.41. Downloaded from www.worldscientific.com by CALIFORNIA @ BERKELEY on 09/16/26. Re-use and distribution is strictly not permitted, except for Open Access articles.

$\Gamma(\gamma\gamma)/\Gamma_{total}$ — Γ_6/Γ

VALUE	DOCUMENT ID		TECN	COMMENT
seen	[1] UEHARA	09A	BELL	$\gamma\gamma \to \pi^0\eta$

[1] May be a different state.

$a_0(1450)$ REFERENCES

ALBRECHT	20	EPJ C80 453	M. Albrecht *et al.*	(Crystal Barrel Collab.)
AAIJ	16N	PR D93 052018	R. Aaij *et al.*	(LHCb Collab.)
ANISOVICH	09	IJMP A24 2481	V.V. Anisovich, A.V. Sarantsev	(PNPI)
UEHARA	09A	PR D80 032001	S. Uehara *et al.*	(BELLE Collab.)
BUGG	08A	PR D78 074023	D.V. Bugg	(LOQM)
UMAN	06	PR D73 052009	I. Uman *et al.*	(FNAL E835)
BAKER	03	PL B563 140	C.A. Baker *et al.*	
BARGIOTTI	03	EPJ C26 371	M. Bargiotti *et al.*	(OBELIX Collab.)
AMSLER	02	EPJ C23 29	C. Amsler *et al.*	(Crystal Barrel Collab.)
ANISOVICH	01	NP A690 567	A.V. Anisovich *et al.*	
ABELE	98	PR D57 3860	A. Abele *et al.*	(Crystal Barrel Collab.)
ANISOVICH	98B	SPU 41 419	V.V. Anisovich *et al.*	
		Translated from UFN 168 481.		
BERTIN	98B	PL B434 180	A. Bertin *et al.*	(OBELIX Collab.)
ABELE	97C	PL B404 179	A. Abele *et al.*	(Crystal Barrel Collab.)
ABELE	96C	NP A609 562	A. Abele *et al.*	(Crystal Barrel Collab.)
AMSLER	95B	PL B342 433	C. Amsler *et al.*	(Crystal Barrel Collab.)
AMSLER	95C	PL B353 571	C. Amsler *et al.*	(Crystal Barrel Collab.)
AMSLER	95D	PL B355 425	C. Amsler *et al.*	(Crystal Barrel Collab.)
AMSLER	94D	PL B333 277	C. Amsler *et al.*	(Crystal Barrel Collab.) IGJPC
BUGG	94	PR D50 4412	D.V. Bugg *et al.*	(LOQM)
ETKIN	82C	PR D25 2446	A. Etkin *et al.*	(BNL, CUNY, TUFTS, VAND)
MARTIN	78	NP B134 392	A.D. Martin *et al.*	(DURH, GEVA)
CASON	76	PRL 36 1485	N.M. Cason *et al.*	(NDAM, ANL)

$\rho(1450)$

$I^G(J^{PC}) = 1^+(1^{--})$

$\rho(1450)$ MASS

$\rho(1450)$ MASS

VALUE (MeV)	DOCUMENT ID
1465 ± 25 OUR ESTIMATE This is only an educated guess; the error given is larger than the error on the average of the published values.	

$\eta\rho^0$ MODE

VALUE (MeV)	EVTS	DOCUMENT ID		TECN	COMMENT
• • • We do not use the following data for averages, fits, limits, etc. • • •					
1506 ± 11	13.4k	[1] GRIBANOV	20	CMD3	1.1–2.0 $e^+e^- \to \eta\pi^+\pi^-$
1500 ± 10	7.4k	[2] ACHASOV	18	SND	1.22–2.00 $e^+e^- \to \eta\pi^+\pi^-$
1497 ± 14		[3] AKHMETSHIN	01B	CMD2	$e^+e^- \to \eta\gamma$
1421 ± 15		[4] AKHMETSHIN	00D	CMD2	$e^+e^- \to \eta\pi^+\pi^-$
1470 ± 20		ANTONELLI	88	DM2	$e^+e^- \to \eta\pi^+\pi^-$
1446 ± 10		FUKUI	88	SPEC	8.95 $\pi^-p \to \eta\pi^+\pi^-n$

[1] Mass and width of the $\rho(770)$ fixed at 775 and 149 MeV, respectively; solution 2 of model 2, $\eta \to \gamma\gamma$ decays used.
[2] From the combined fit of AULCHENKO 15 and ACHASOV 18 in the model with the interfering $\rho(1450)$, $\rho(1700)$ and $\rho(2150)$ with the parameters of the $\rho(1450)$ and $\rho(1700)$ floating and the mass and width of the $\rho(2150)$ fixed at 2155 MeV and 320 MeV, respectively. The phases of the resonances are π, 0 and π, respectively.
[3] Using the data of AKHMETSHIN 01B on $e^+e^- \to \eta\gamma$, AKHMETSHIN 00D and ANTONELLI 88 on $e^+e^- \to \eta\pi^+\pi^-$.
[4] Using the data of ANTONELLI 88, DOLINSKY 91, and AKHMETSHIN 00D. The energy-independent width of the $\rho(1450)$ and $\rho(1700)$ mesons assumed.

$\omega\pi$ MODE

VALUE (MeV)	EVTS	DOCUMENT ID		TECN	COMMENT
• • • We do not use the following data for averages, fits, limits, etc. • • •					
1510 ± 7	10.2k	[1] ACHASOV	16D	SND	1.05–2.00 $e^+e^- \to \pi^0\pi^0\gamma$
$1544 \pm 22^{+11}_{-46}$	821	[2] MATVIENKO	15	BELL	$\overline{B}^0 \to D^{*+}\omega\pi^-$
1491 ± 19	7815	[3] ACHASOV	13	SND	1.05–2.00 $e^+e^- \to \pi^0\pi^0\gamma$
1582 ± 17 ± 25	2382	[4] AKHMETSHIN	03B	CMD2	$e^+e \to \pi^0\pi^0\gamma$
$1349 \pm 25^{+10}_{-5}$	341	[5] ALEXANDER	01B	CLE2	$B \to D^{(*)}\omega\pi^-$
1523 ± 10		[6] EDWARDS	00A	CLE2	$\tau^- \to \omega\pi^-\nu_\tau$
1463 ± 25		[7] CLEGG	94	RVUE	
1250		[8] ASTON	80C	OMEG	20–70 $\gamma p \to \omega\pi^0 p$
1290 ± 40		[8] BARBER	80C	SPEC	3–5 $\gamma p \to \omega\pi^0 p$

[1] From a phenomenological model based on vector meson dominance with interfering $\rho(770)$, $\rho(1450)$, and $\rho(1700)$. The $\rho(1700)$ mass and width are fixed at 1720 MeV and 250 MeV, respectively. Systematic uncertainties not estimated. Supersedes ACHASOV 13.
[2] Using Breit-Wigner parameterization of the $\rho(1450)$ and assuming equal probabilities of the $\rho(1450) \to \pi\pi$ and $\rho(1450) \to \omega\pi$ decays.
[3] From a phenomenological model based on vector meson dominance with the interfering $\rho(1450)$ and $\rho(1700)$ and their widths fixed at 400 and 250 MeV, respectively. Systematic uncertainty not estimated.
[4] Using the data of AKHMETSHIN 03B and BISELLO 91B assuming the $\omega\pi^0$ and $\pi^+\pi^-$ mass dependence of the total width. $\rho(1700)$ mass and width fixed at 1700 MeV and 240 MeV, respectively.
[5] Using Breit-Wigner parameterization of the $\rho(1450)$ and assuming the $\omega\pi^-$ mass dependence for the total width.
[6] Mass-independent width parameterization. $\rho(1700)$ mass and width fixed at 1700 MeV and 235 MeV respectively.
[7] Using data from BISELLO 91B, DOLINSKY 86 and ALBRECHT 87L.
[8] Not separated from $b_1(1235)$, not pure $J^P = 1^-$ effect.

4π MODE

VALUE (MeV)	DOCUMENT ID		TECN	COMMENT
• • • We do not use the following data for averages, fits, limits, etc. • • •				
1385 ± 14 ± 36	[1] ACHARYA	26	ALCE	5 TeV PbPb $\to$ PbPb4π
1435 ± 40	ABELE	01B	CBAR	0.0 $\overline{p}n \to 2\pi^-2\pi^0\pi^+$
1350 ± 50	ACHASOV	97	RVUE	$e^+e^- \to 2(\pi^+\pi^-)$
1449 ± 4	[2] ARMSTRONG	89E	OMEG	300 $pp \to pp2(\pi^+\pi^-)$

[1] From a two Breit-Wigner resonance fit to the 4π mass distribution produced in ultraperipheral Pb−Pb collisions.
[2] Not clear whether this observation has I=1 or 0.

$\pi\pi$ MODE

VALUE (MeV)		EVTS	DOCUMENT ID		TECN	COMMENT
• • • We do not use the following data for averages, fits, limits, etc. • • •						
1350	± 20		[1] AAIJ	25AG	LHCB	5 TeV PbPb $\to$ PbPb$\pi^+\pi^-$
1226.22 ± 24.76		34M	[2] IGNATOV	24	CMD3	$e^+e^- \to \pi^+\pi^-$
1326.35 ± 3.46			[3] BARTOS	17	RVUE	$e^+e^- \to \pi^+\pi^-$
1342.31 ± 46.62			[4] BARTOS	17A	RVUE	$e^+e^- \to \pi^+\pi^-$
1373.83 ± 11.37			[5] BARTOS	17A	RVUE	$\tau^- \to \pi^-\pi^0\nu_\tau$
1429	± 41	20k	[6] LEES	17C	BABR	$J/\psi \to \pi^+\pi^-\pi^0$
1350	± 20	$^{+20}_{-30}$ 63.5k	[7] ABRAMOWICZ	12	ZEUS	$ep \to e\pi^+\pi^-p$
1493	± 15		[8] LEES	12G	BABR	$e^+e^- \to \pi^+\pi^-\gamma$
1446	± 7	± 28 5.4M	[9,10] FUJIKAWA	08	BELL	$\tau^- \to \pi^-\pi^0\nu_\tau$
1328	± 15		[11] SCHAEL	05C	ALEP	$\tau^- \to \pi^-\pi^0\nu_\tau$
1406	± 15	87k	[9,12] ANDERSON	00A	CLE2	$\tau^- \to \pi^-\pi^0\nu_\tau$
∼ 1368			[13] ABELE	99C	CBAR	0.0 $\overline{p}d \to \pi^+\pi^-\pi^-p$
1348	± 33		BERTIN	98	OBLX	0.05–0.405 $\overline{n}p \to 2\pi^+\pi^-$
1411	± 14		[14] ABELE	97	CBAR	$\overline{p}n \to \pi^-\pi^0\pi^0$
1370	$^{+90}_{-70}$		ACHASOV	97	RVUE	$e^+e^- \to \pi^+\pi^-$
1359	± 40		[12] BERTIN	97C	OBLX	0.0 $\overline{p}p \to \pi^+\pi^-\pi^0$
1282	± 37		BERTIN	97D	OBLX	0.05 $\overline{p}p \to 2\pi^+2\pi^-$
1424	± 25		BISELLO	89	DM2	$e^+e^- \to \pi^+\pi^-$
1265.5	± 75.3		DUBNICKA	89	RVUE	$e^+e^- \to \pi^+\pi^-$
1292	± 17		[15] KURDADZE	83	OLYA	0.64–1.4 $e^+e^- \to \pi^+\pi^-$

[1] Using the parametrisation as in ANDREEV 20 with ρ-ω interference with the additional presence of two Breit-Wigner resonances for excited ρ states.
[2] From a fit of the pion form factor using the GOUNARIS 68 parametrization with the complex phase of the $\rho - \omega$ interference leaving $\rho(1450)$, $\rho(1700)$ resonances as free parameters of the fit. The fit uses also data from CMD-2 and DM2 experiments. Systematic errors not estimated.
[3] Applies the Unitary & Analytic Model of the pion electromagnetic form factor of DUBNICKA 10 to analyze the data of LEES 12G and ABLIKIM 16C.
[4] Applies the Unitary & Analytic Model of the pion electromagnetic form factor of DUBNICKA 10 to analyze the data of ACHASOV 06, AKHMETSHIN 07, AUBERT 09AS, and AMBROSINO 11A.
[5] Applies the Unitary & Analytic Model of the pion electromagnetic form factor of DUBNICKA 10 to analyze the data of FUJIKAWA 08.
[6] From a Dalitz plot analysis in an isobar model with $\rho(1450)$ and $\rho(1700)$ masses and widths floating.
[7] Using the KUHN 90 parametrization of the pion form factor, neglecting ρ−ω interference.
[8] Using the GOUNARIS 68 parametrization of the pion form factor leaving the masses and widths of the $\rho(1450)$, $\rho(1700)$, and $\rho(2150)$ resonances as free parameters of the fit.
[9] From the GOUNARIS 68 parametrization of the pion form factor.
[10] $|F_\pi(0)|^2$ fixed to 1.
[11] From the combined fit of the τ^- data from ANDERSON 00A and SCHAEL 05C and e^+e^- data from the compilation of BARKOV 85, AKHMETSHIN 04, and ALOISIO 05. $\rho(1700)$ mass and width fixed at 1713 MeV and 235 MeV, respectively. Supersedes BARATE 97M.
[12] $\rho(1700)$ mass and width fixed at 1700 MeV and 235 MeV, respectively.
[13] $\rho(1700)$ mass and width fixed at 1780 MeV and 275 MeV respectively.
[14] T-matrix pole.
[15] Using for $\rho(1700)$ mass and width 1600 ± 20 and 300 ± 10 MeV respectively.

$K\overline{K}$ MODE

VALUE (MeV)	EVTS	DOCUMENT ID		TECN	CHG	COMMENT
• • • We do not use the following data for averages, fits, limits, etc. • • •						
1208 ± 8 ± 9	190k	[1] AAIJ	16N	LHCB		$D^0 \to K^0_S K^\pm\pi^\mp$
1422.8 ± 6.5	27k	[2] ABELE	99D	CBAR	±	0.0 $\overline{p}p \to K^+K^-\pi^0$

[1] Using the GOUNARIS 68 parameterization with fixed width.
[2] K-matrix pole. Isospin not determined, could be $\omega(1420)$.

$K\overline{K}^*(892)$ + c.c. MODE

VALUE (MeV)	EVTS	DOCUMENT ID		TECN	COMMENT
• • • We do not use the following data for averages, fits, limits, etc. • • •					
1502 ± 11	9.1k	[1] FEDOTOVICH	25	CMD3	$e^+e^- \to K^0_S K^\pm\pi^\mp$
1505 ± 19 ± 7		AUBERT	08S	BABR	10.6 $e^+e^- \to K\overline{K}^*(892)\gamma$

[1] Using a vector dominance fit with contributions from $\phi(1680)$ and $\rho(1450)$.

$m_{\rho(1450)^0} - m_{\rho(1450)^\pm}$

VALUE (MeV)	DOCUMENT ID		TECN	COMMENT
• • • We do not use the following data for averages, fits, limits, etc. • • •				
−31.53 ± 47.99	[1] BARTOS	17A	RVUE	$e^+e^- \to \pi^+\pi^-$, $\tau^- \to \pi^-\pi^0\nu_\tau$

[1] Applies the Unitary & Analytic Model of the pion electromagnetic form factor of DUBNICKA 10 to analyze the data of ACHASOV 06, AKHMETSHIN 07, AUBERT 09AS, AMBROSINO 11A, and FUJIKAWA 08.

$\rho(1450)$ WIDTH

$\rho(1450)$ WIDTH

VALUE (MeV)	DOCUMENT ID	TECN	COMMENT
400± 60 OUR ESTIMATE This is only an educated guess; the error given is larger than the error on the average of the published values.			
• • • We do not use the following data for averages, fits, limits, etc. • • •			
480±180	[1] ACHASOV 10D	SND	1.075–2.0 $e^+e^- \to \pi^0\gamma$

[1] From a fit of a VMD model with two effective resonances with masses of 1450 MeV and 1700 MeV to describe the excited vector states $\omega(1420)$, $\rho(1450)$, $\omega(1650)$, and $\rho(1700)$. Systematic errors not evaluated.

$\eta\rho^0$ MODE

VALUE (MeV)	EVTS	DOCUMENT ID	TECN	COMMENT
• • • We do not use the following data for averages, fits, limits, etc. • • •				
321±27	13.4k	[1] GRIBANOV 20	CMD3	1.1–2.0 $e^+e^- \to \eta\pi^+\pi^-$
280±20	7.4k	[2] ACHASOV 18	SND	1.22–2.00 $e^+e^- \to \eta\pi^+\pi^-$
226±44		[3] AKHMETSHIN 01B	CMD2	$e^+e^- \to \eta\gamma$
211±31		[4] AKHMETSHIN 00D	CMD2	$e^+e^- \to \eta\pi^+\pi^-$
230±30		ANTONELLI 88	DM2	$e^+e^- \to \eta\pi^+\pi^-$
60±15		FUKUI 88	SPEC	8.95 $\pi^-p \to \eta\pi^+\pi^-n$

[1] Mass and width of the $\rho(770)$ fixed at 775 and 149 MeV, respectively; solution 2 of model 2, $\eta \to \gamma\gamma$ decays used.
[2] From the combined fit of AULCHENKO 15 and ACHASOV 18 in the model with the interfering $\rho(1450)$, $\rho(1700)$ and $\rho(2150)$ with the parameters of the $\rho(1450)$ and $\rho(1700)$ floating and the mass and width of the $\rho(2150)$ fixed at 2155 MeV and 320 MeV, respectively. The phases of the resonances are π, 0 and π, respectively.
[3] Using the data of AKHMETSHIN 01B on $e^+e^- \to \eta\gamma$, AKHMETSHIN 00D and ANTONELLI 88 on $e^+e^- \to \eta\pi^+\pi^-$.
[4] Using the data of ANTONELLI 88, DOLINSKY 91, and AKHMETSHIN 00D. The energy-independent width of the $\rho(1450)$ and $\rho(1700)$ mesons assumed.

$\omega\pi$ MODE

VALUE (MeV)	EVTS	DOCUMENT ID	TECN	COMMENT
• • • We do not use the following data for averages, fits, limits, etc. • • •				
440± 40	10.2k	[1] ACHASOV 16D	SND	1.05–2.00 $e^+e^- \to \pi^0\pi^0\gamma$
303^{+31+69}_{-52-7}	821	[2] MATVIENKO 15	BELL	$\overline{B}^0 \to D^{*+}\omega\pi^-$
429± 42±10	2382	[3] AKHMETSHIN 03B	CMD2	$e^+e \to \pi^0\pi^0\gamma$
$547\pm 86^{+46}_{-45}$	341	[4] ALEXANDER 01B	CLE2	$B \to D^{(*)}\omega\pi^-$
400± 35		[5] EDWARDS 00A	CLE2	$\tau^- \to \omega\pi^-\nu_\tau$
311± 62		[6] CLEGG 94	RVUE	
300		[7] ASTON 80C	OMEG	20–70 $\gamma p \to \omega\pi^0 p$
320±100		[7] BARBER 80C	SPEC	3–5 $\gamma p \to \omega\pi^0 p$

[1] From a phenomenological model based on vector meson dominance with interfering $\rho(770)$, $\rho(1450)$, and $\rho(1700)$. The $\rho(1700)$ mass and width are fixed at 1720 MeV and 250 MeV, respectively. Systematic uncertainties not estimated. Supersedes ACHASOV 13.
[2] Using Breit-Wigner parameterization of the $\rho(1450)$ and assuming equal probabilities of the $\rho(1450) \to \pi\pi$ and $\rho(1450) \to \omega\pi$ decays.
[3] Using the data of AKHMETSHIN 03B and BISELLO 91B assuming the $\omega\pi^0$ and $\pi^+\pi^-$ mass dependence of the total width. $\rho(1700)$ mass and width fixed at 1700 MeV and 240 MeV, respectively.
[4] Using Breit-Wigner parameterization of the $\rho(1450)$ and assuming the $\omega\pi^-$ mass dependence for the total width.
[5] Mass-independent width parameterization. $\rho(1700)$ mass and width fixed at 1700 MeV and 235 MeV respectively.
[6] Using data from BISELLO 91B, DOLINSKY 86 and ALBRECHT 87L.
[7] Not separated from $b_1(1235)$, not pure $J^P = 1^-$ effect.

4π MODE

VALUE (MeV)	DOCUMENT ID	TECN	COMMENT
• • • We do not use the following data for averages, fits, limits, etc. • • •			
431± 36±82	[1] ACHARYA 26	ALCE	5 TeV PbPb $\to$ PbPb4π
325±100	ABELE 01B	CBAR	0.0 $\overline{p}n \to 2\pi^-2\pi^0\pi^+$

[1] From a two Breit-Wigner resonance fit to the 4π mass distribution produced in ultraperipheral Pb–Pb collisions.

$\pi\pi$ MODE

VALUE (MeV)	EVTS	DOCUMENT ID	TECN	COMMENT
• • • We do not use the following data for averages, fits, limits, etc. • • •				
320 ± 40		[1] AAIJ 25AG	LHCB	5 TeV PbPb $\to$ PbPb$\pi^+\pi^-$
272.97± 45.53	34M	[2] IGNATOV 24	CMD3	$e^+e^- \to \pi^+\pi^-$
324.13± 12.01		[3] BARTOS 17	RVUE	$e^+e^- \to \pi^+\pi^-$
492.17±138.38		[4] BARTOS 17A	RVUE	$e^+e^- \to \pi^+\pi^-$
340.87± 23.84		[5] BARTOS 17A	RVUE	$\tau^- \to \pi^-\pi^0\nu_\tau$
576 ± 29	20k	[6] LEES 17C	BABR	$J/\psi \to \pi^+\pi^-\pi^0$
460 ± 30 $^{+40}_{-45}$	63.5k	[7] ABRAMOWICZ 12	ZEUS	$ep \to e\pi^+\pi^-p$
427 ± 31		[8] LEES 12G	BABR	$e^+e^- \to \pi^+\pi^-\gamma$
434 ± 16 ±60	5.4M	[9,10] FUJIKAWA 08	BELL	$\tau^- \to \pi^-\pi^0\nu_\tau$
468 ± 41		[11] SCHAEL 05C	ALEP	$\tau^- \to \pi^-\pi^0\nu_\tau$
455 ± 41	87k	[9,12] ANDERSON 00A	CLE2	$\tau^- \to \pi^-\pi^0\nu_\tau$
∼ 374		[13] ABELE 99C	CBAR	0.0 $\overline{p}d \to \pi^+\pi^-\pi^-p$
275 ± 10		BERTIN 98	OBLX	0.05–0.405 $\overline{n}p \to \pi^+\pi^+\pi^-$
343 ± 20		[14] ABELE 97	CBAR	$\overline{p}n \to \pi^-\pi^0\pi^0$
310 ± 40		[12] BERTIN 97C	OBLX	0.0 $\overline{p}p \to \pi^+\pi^-\pi^0$
236 ± 36		BERTIN 97D	OBLX	0.05 $\overline{p}p \to 2\pi^+2\pi^-$
269 ± 31		BISELLO 89	DM2	$e^+e^- \to \pi^+\pi^-$
391 ± 70		DUBNICKA 89	RVUE	$e^+e^- \to \pi^+\pi^-$
218 ± 46		[15] KURDADZE 83	OLYA	0.64–1.4 $e^+e^- \to \pi^+\pi^-$

[1] Using the parametrisation as in ANDREEV 20 with ρ-ω interference with the additional presence of two Breit-Wigner resonances for excited ρ states.
[2] From a fit of the pion form factor using the GOUNARIS 68 parametrization with the complex phase of the $\rho-\omega$ interference leaving $\rho(1450)$, $\rho(1700)$ resonances as free parameters of the fit. The fit uses also data from CMD-2 and DM2 experiments. Systematic errors not estimated.
[3] Applies the Unitary & Analytic Model of the pion electromagnetic form factor of DUBNICKA 10 to analyze the data of LEES 12G and ABLIKIM 16C.
[4] Applies the Unitary & Analytic Model of the pion electromagnetic form factor of DUBNICKA 10 to analyze the data of ACHASOV 06, AKHMETSHIN 07, AUBERT 09AS, and AMBROSINO 11A.
[5] Applies the Unitary & Analytic Model of the pion electromagnetic form factor of DUBNICKA 10 to analyze the data of FUJIKAWA 08.
[6] From a Dalitz plot analysis in an isobar model with $\rho(1450)$ and $\rho(1700)$ masses and widths floating.
[7] Using the KUHN 90 parametrization of the pion form factor, neglecting $\rho-\omega$ interference.
[8] Using the GOUNARIS 68 parametrization of the pion form factor leaving the masses and widths of the $\rho(1450)$, $\rho(1700)$, and $\rho(2150)$ resonances as free parameters of the fit.
[9] From the GOUNARIS 68 parametrization of the pion form factor.
[10] $|F_\pi(0)|^2$ fixed to 1.
[11] From the combined fit of the τ^- data from ANDERSON 00A and SCHAEL 05C and e^+e^- data from the compilation of BARKOV 85, AKHMETSHIN 04, and ALOISIO 05. $\rho(1700)$ mass and width fixed at 1713 MeV and 235 MeV, respectively. Supersedes BARATE 97M.
[12] $\rho(1700)$ mass and width fixed at 1700 MeV and 235 MeV, respectively.
[13] $\rho(1700)$ mass and width fixed at 1780 MeV and 275 MeV respectively.
[14] T-matrix pole.
[15] Using for $\rho(1700)$ mass and width 1600 ± 20 and 300 ± 10 MeV respectively.

$K\overline{K}$ MODE

VALUE (MeV)	EVTS	DOCUMENT ID	TECN	CHG	COMMENT
• • • We do not use the following data for averages, fits, limits, etc. • • •					
410 ±19 ±35	190k	[1] AAIJ 16N	LHCB		$D^0 \to K^0_S K^\pm\pi^\mp$
146.5±10.5	27k	[2] ABELE 99D	CBAR	±	0.0 $\overline{p}p \to K^+K^-\pi^0$

[1] Using the GOUNARIS 68 parameterization with fixed mass.
[2] K-matrix pole. Isospin not determined, could be $\omega(1420)$.

$K\overline{K}^*(892)$ + c.c. MODE

VALUE (MeV)	EVTS	DOCUMENT ID	TECN	COMMENT
• • • We do not use the following data for averages, fits, limits, etc. • • •				
315±27	9.1k	[1] FEDOTOVICH 25	CMD3	$e^+e^- \to K^0_S K^\pm\pi^\mp$
418±25±4		AUBERT 08S	BABR	10.6 $e^+e^- \to K\overline{K}^*(892)\gamma$

[1] Using a vector dominance fit with contributions from $\phi(1680)$ and $\rho(1450)$.

$\Gamma_{\rho(1450)^0} - \Gamma_{\rho(1450)^\pm}$

VALUE (MeV)	DOCUMENT ID	TECN	COMMENT
• • • We do not use the following data for averages, fits, limits, etc. • • •			
151.30±140.42	[1] BARTOS 17A	RVUE	$e^+e^- \to \pi^+\pi^-$, $\tau^- \to \pi^-\pi^0\nu_\tau$

[1] Applies the Unitary & Analytic Model of the pion electromagnetic form factor of DUBNICKA 10 to analyze the data of ACHASOV 06, AKHMETSHIN 07, AUBERT 09AS, AMBROSINO 11A, and FUJIKAWA 08.

$\rho(1450)$ DECAY MODES

	Mode	Fraction (Γ_i/Γ)
Γ_1	$\pi\pi$	seen
Γ_2	$\pi^+\pi^-$	seen
Γ_3	4π	seen
Γ_4	$\omega\pi$	
Γ_5	$a_1(1260)\pi$	
Γ_6	$h_1(1170)\pi$	
Γ_7	$\pi(1300)\pi$	
Γ_8	$\rho\rho$	
Γ_9	$\rho(\pi\pi)S$-wave	
Γ_{10}	e^+e^-	seen
Γ_{11}	$\eta\rho$	seen
Γ_{12}	$a_2(1320)\pi$	not seen
Γ_{13}	$K\overline{K}$	seen
Γ_{14}	K^+K^-	seen
Γ_{15}	$K\overline{K}^*(892)$ + c.c.	possibly seen

Int. J. Mod. Phys. A 2026.41. Downloaded from www.worldscientific.com
by UNIVERSITY OF CALIFORNIA @ BERKELEY on 09/16/26. Re-use and distribution is strictly not permitted, except for Open Access articles.

Γ_{16}	$\pi^0\gamma$	seen
Γ_{17}	$\eta\gamma$	seen
Γ_{18}	$f_0(500)\gamma$	not seen
Γ_{19}	$f_0(980)\gamma$	not seen
Γ_{20}	$f_0(1370)\gamma$	not seen
Γ_{21}	$f_2(1270)\gamma$	not seen

$\rho(1450)$ $\Gamma(i)\Gamma(e^+e^-)/\Gamma(\text{total})$

$\Gamma(\pi\pi) \times \Gamma(e^+e^-)/\Gamma_{\text{total}}$ — $\Gamma_1\Gamma_{10}/\Gamma$

VALUE (keV)	DOCUMENT ID		TECN	COMMENT
• • • We do not use the following data for averages, fits, limits, etc. • • •				
0.12	[1] DIEKMAN	88	RVUE	$e^+e^- \to \pi^+\pi^-$
$0.027^{+0.015}_{-0.010}$	[2] KURDADZE	83	OLYA	0.64–1.4 $e^+e^- \to \pi^+\pi^-$

[1] Using total width = 235 MeV.
[2] Using for $\rho(1700)$ mass and width 1600 ± 20 and 300 ± 10 MeV respectively.

$\Gamma(\eta\rho) \times \Gamma(e^+e^-)/\Gamma_{\text{total}}$ — $\Gamma_{11}\Gamma_{10}/\Gamma$

VALUE (eV)	EVTS	DOCUMENT ID		TECN	COMMENT
• • • We do not use the following data for averages, fits, limits, etc. • • •					
335±27±20	13.4k	[1] GRIBANOV	20	CMD3	1.1–2.0 $e^+e^- \to \eta\pi^+\pi^-$
210±24±10		[2] LEES	18	BABR	$e^+e^- \to \eta\pi^+\pi^-$
74±20		[3] AKHMETSHIN	00D	CMD2	$e^+e^- \to \eta\pi^+\pi^-$
91±19		ANTONELLI	88	DM2	$e^+e^- \to \eta\pi^+\pi^-$

[1] Mass and width of the $\rho(770)$ fixed at 775 and 149 MeV, respectively; solution 2 of model 2, $\eta \to \gamma\gamma$ decays used.
[2] Includes non-resonant contribution. The selected fit model includes three ρ excited states. Model uncertainty is 20%.
[3] Using the data of ANTONELLI 88, DOLINSKY 91, and AKHMETSHIN 00D. The energy-independent width of the $\rho(1450)$ and $\rho(1700)$ mesons assumed.

$\Gamma(K\overline{K}^*(892)+\text{c.c.}) \times \Gamma(e^+e^-)/\Gamma_{\text{total}}$ — $\Gamma_{15}\Gamma_{10}/\Gamma$

VALUE (eV)	EVTS	DOCUMENT ID		TECN	COMMENT
• • • We do not use the following data for averages, fits, limits, etc. • • •					
119±14±15	9.1k	[1] FEDOTOVICH	25	CMD3	$e^+e^- \to K^0_S K^\pm\pi^\mp$
127±15± 6		AUBERT	08S	BABR	10.6 $e^+e^- \to K\overline{K}^*(892)\gamma$

[1] Using a vector dominance fit with contributions from $\phi(1680)$ and $\rho(1450)$.

$\Gamma(\eta\gamma) \times \Gamma(e^+e^-)/\Gamma_{\text{total}}$ — $\Gamma_{17}\Gamma_{10}/\Gamma$

VALUE (eV)	DOCUMENT ID		TECN	COMMENT
• • • We do not use the following data for averages, fits, limits, etc. • • •				
<16.4	[1] AKHMETSHIN	05	CMD2	0.60-1.38 $e^+e^- \to \eta\gamma$
2.2±0.5±0.3	[2] AKHMETSHIN	01B	CMD2	$e^+e^- \to \eta\gamma$

[1] From 2γ decay mode of η using 1465 MeV and 310 MeV for the $\rho(1450)$ mass and width. Recalculated by us.
[2] Using the data of AKHMETSHIN 01B on $e^+e^- \to \eta\gamma$, AKHMETSHIN 00D and ANTONELLI 88 on $e^+e^- \to \eta\pi^+\pi^-$. Recalculated by us using width of 226 MeV.

$\rho(1450)$ $\Gamma(i)/\Gamma(\text{total}) \times \Gamma(e^+e^-)/\Gamma(\text{total})$

$\Gamma(\omega\pi)/\Gamma_{\text{total}} \times \Gamma(e^+e^-)/\Gamma_{\text{total}}$ — $\Gamma_4/\Gamma \times \Gamma_{10}/\Gamma$

VALUE (units 10^{-6})	EVTS	DOCUMENT ID		TECN	COMMENT
• • • We do not use the following data for averages, fits, limits, etc. • • •					
2.1±0.4	10.2k	[1] ACHASOV	16D	SND	1.05–2.00 $e^+e^- \to \pi^0\pi^0\gamma$
5.3±0.4	7815	[2] ACHASOV	13	SND	1.05–2.00 $e^+e^- \to \pi^0\pi^0\gamma$

[1] From a phenomenological model based on vector meson dominance with interfering $\rho(770)$, $\rho(1450)$, and $\rho(1700)$. The $\rho(1700)$ mass and width are fixed at 1720 MeV and 250 MeV, respectively. Systematic uncertainties not estimated. Supersedes ACHASOV 13.
[2] From a phenomenological model based on vector meson dominance with the interfering $\rho(1450)$ and $\rho(1700)$ and their widths fixed at 400 and 250 MeV, respectively. Systematic uncertainty not estimated.

$\Gamma(\eta\rho)/\Gamma_{\text{total}} \times \Gamma(e^+e^-)/\Gamma_{\text{total}}$ — $\Gamma_{11}/\Gamma \times \Gamma_{10}/\Gamma$

VALUE (units 10^{-7})	EVTS	DOCUMENT ID		TECN	COMMENT
• • • We do not use the following data for averages, fits, limits, etc. • • •					
7.3±0.3	7.4k	[1] ACHASOV	18	SND	1.22–2.00 $e^+e^- \to \eta\pi^+\pi^-$
$4.3^{+1.1}_{-0.9}\pm0.2$	4.9k	[2] AULCHENKO	15	SND	1.22–2.00 $e^+e^- \to \eta\pi^+\pi^-$

[1] From the combined fit of AULCHENKO 15 and ACHASOV 18 in the model with the interfering $\rho(1450)$, $\rho(1700)$ and $\rho(2150)$ with the parameters of the $\rho(1450)$ and $\rho(1700)$ floating and the mass and width of the $\rho(2150)$ fixed at 2155 MeV and 320 MeV, respectively. The phases of the resonances are π, 0 and π, respectively.
[2] From a fit to the $e^+e^- \to \eta\pi^+\pi^-$ cross section with vector meson dominance model including $\rho(770)$, $\rho(1450)$, and $\rho(1700)$ decaying exclusively via $\eta\rho(770)$. Masses and widths of vector states are fixed to PDG 14. Coupling constants are assumed to be real.

$\Gamma(\pi^0\gamma)/\Gamma_{\text{total}} \times \Gamma(e^+e^-)/\Gamma_{\text{total}}$ — $\Gamma_{16}/\Gamma \times \Gamma_{10}/\Gamma$

VALUE (units 10^{-9})	DOCUMENT ID		TECN	COMMENT
• • • We do not use the following data for averages, fits, limits, etc. • • •				
2.3±1.4	[1] ACHASOV	10D	SND	1.075–2.0 $e^+e^- \to \pi^0\gamma$

[1] From a fit of a VMD model with two effective resonances with masses of 1450 MeV and 1700 MeV to describe the excited vector states $\omega(1420)$, $\rho(1450)$, $\omega(1650)$, and $\rho(1700)$. Systematic errors not evaluated.

$\Gamma(f_0(500)\gamma)/\Gamma_{\text{total}} \times \Gamma(e^+e^-)/\Gamma_{\text{total}}$ — $\Gamma_{18}/\Gamma \times \Gamma_{10}/\Gamma$

VALUE (units 10^{-9})	CL%	DOCUMENT ID		TECN	COMMENT
<4.0	90	ACHASOV	11	SND	$e^+e^- \to \pi^0\pi^0\gamma$

$\Gamma(f_0(980)\gamma)/\Gamma_{\text{total}} \times \Gamma(e^+e^-)/\Gamma_{\text{total}}$ — $\Gamma_{19}/\Gamma \times \Gamma_{10}/\Gamma$

VALUE (units 10^{-9})	CL%	DOCUMENT ID		TECN	COMMENT
<2.6	90	ACHASOV	11	SND	$e^+e^- \to \pi^0\pi^0\gamma$

$\Gamma(f_0(1370)\gamma)/\Gamma_{\text{total}} \times \Gamma(e^+e^-)/\Gamma_{\text{total}}$ — $\Gamma_{20}/\Gamma \times \Gamma_{10}/\Gamma$

VALUE (units 10^{-9})	CL%	DOCUMENT ID		TECN	COMMENT
<3.5	90	ACHASOV	11	SND	$e^+e^- \to \pi^0\pi^0\gamma$

$\Gamma(f_2(1270)\gamma)/\Gamma_{\text{total}} \times \Gamma(e^+e^-)/\Gamma_{\text{total}}$ — $\Gamma_{21}/\Gamma \times \Gamma_{10}/\Gamma$

VALUE (units 10^{-9})	CL%	DOCUMENT ID		TECN	COMMENT
<0.8	90	[1] ACHASOV	11	SND	$e^+e^- \to \pi^0\pi^0\gamma$

[1] Using Breit-Wigner parametrization of the $\rho(1450)$ with mass and width of 1465 MeV and 400 MeV, respectively.

$\rho(1450)$ BRANCHING RATIOS

$\Gamma(\pi\pi)/\Gamma(4\pi)$ — Γ_1/Γ_3

VALUE	DOCUMENT ID		TECN	COMMENT
• • • We do not use the following data for averages, fits, limits, etc. • • •				
0.37±0.10	[1,2] ABELE	01B	CBAR	0.0 $\overline{p}n \to 5\pi$

[1] $\omega\pi$ not included.
[2] Using ABELE 97.

$\Gamma(K^+K^-)/\Gamma(\pi^+\pi^-)$ — Γ_{14}/Γ_2

VALUE (%)	EVTS	DOCUMENT ID		TECN	COMMENT
30.7±8.4±8.2	20k	[1] LEES	17C	BABR	$J/\psi \to h^+h^-\pi^0$

[1] From Dalitz plot analyses in isobar models.

$\Gamma(\omega\pi)/\Gamma_{\text{total}}$ — Γ_4/Γ

VALUE	EVTS	DOCUMENT ID		TECN	COMMENT
• • • We do not use the following data for averages, fits, limits, etc. • • •					
seen	821	[1] MATVIENKO	15	BELL	$\overline{B}^0 \to D^{*+}\omega\pi^-$
seen	1.6k	ACHASOV	12	SND	$e^+e^- \to \pi^0\pi^0\gamma$
~ 0.21		CLEGG	94	RVUE	

[1] Using Breit-Wigner parameterization of the $\rho(1450)$ and assuming equal probabilities of the $\rho(1450) \to \pi\pi$ and $\rho(1450) \to \omega\pi$ decays.

$\Gamma(\pi\pi)/\Gamma(\omega\pi)$ — Γ_1/Γ_4

VALUE	DOCUMENT ID		TECN
• • • We do not use the following data for averages, fits, limits, etc. • • •			
~ 0.32	CLEGG	94	RVUE

$\Gamma(\omega\pi)/\Gamma(4\pi)$ — Γ_4/Γ_3

VALUE	DOCUMENT ID		TECN
• • • We do not use the following data for averages, fits, limits, etc. • • •			
<0.14	CLEGG	88	RVUE

$\Gamma(a_1(1260)\pi)/\Gamma(4\pi)$ — Γ_5/Γ_3

VALUE	DOCUMENT ID		TECN	COMMENT
• • • We do not use the following data for averages, fits, limits, etc. • • •				
0.27±0.08	[1] ABELE	01B	CBAR	0.0 $\overline{p}n \to 5\pi$

[1] $\omega\pi$ not included.

$\Gamma(h_1(1170)\pi)/\Gamma(4\pi)$ — Γ_6/Γ_3

VALUE	DOCUMENT ID		TECN	COMMENT
• • • We do not use the following data for averages, fits, limits, etc. • • •				
0.08±0.04	[1] ABELE	01B	CBAR	0.0 $\overline{p}n \to 5\pi$

[1] $\omega\pi$ not included.

$\Gamma(\pi(1300)\pi)/\Gamma(4\pi)$ — Γ_7/Γ_3

VALUE	DOCUMENT ID		TECN	COMMENT
• • • We do not use the following data for averages, fits, limits, etc. • • •				
0.37±0.13	[1] ABELE	01B	CBAR	0.0 $\overline{p}n \to 5\pi$

[1] $\omega\pi$ not included.

$\Gamma(\rho\rho)/\Gamma(4\pi)$ — Γ_8/Γ_3

VALUE	DOCUMENT ID		TECN	COMMENT
• • • We do not use the following data for averages, fits, limits, etc. • • •				
0.11±0.05	[1] ABELE	01B	CBAR	0.0 $\overline{p}n \to 5\pi$

[1] $\omega\pi$ not included.

Int. J. Mod. Phys. A 2026.41. Downloaded from www.worldscientific.com
by [redacted]LIFORNIA @ BERKELEY on 09/16/26. Re-use and distribution is strictly not permitted, except for Open Access articles.

Int. J. Mod. Phys. A 2026.41. Downloaded from www.worldscientific.com
by UNIVERSITY OF CALIFORNIA @ BERKELEY on 09/16/26. Re-use and distribution is strictly not permitted, except for Open Access articles.

$\Gamma(\rho(\pi\pi)_{S\text{-wave}})/\Gamma(4\pi)$ — Γ_9/Γ_3

VALUE	DOCUMENT ID		TECN	COMMENT
• • • We do not use the following data for averages, fits, limits, etc. • • •				
0.17 ± 0.09	[1] ABELE	01B	CBAR	$0.0\ \overline{p}n \to 5\pi$

[1] $\omega\pi$ not included.

$\Gamma(\eta\rho)/\Gamma_{\text{total}}$ — Γ_{11}/Γ

VALUE	EVTS	DOCUMENT ID		TECN	COMMENT
seen	35	[1] ACHASOV	14	SND	1.15–$2.00\ e^+e^- \to \eta\gamma$
• • • We do not use the following data for averages, fits, limits, etc. • • •					
<0.04		DONNACHIE	87B	RVUE	

[1] From a phenomenological model based on vector meson dominance with $\rho(1450)$ and $\phi(1680)$ masses and widths from the PDG 12.

$\Gamma(\eta\rho)/\Gamma(\omega\pi)$ — Γ_{11}/Γ_4

VALUE	DOCUMENT ID		TECN	COMMENT
• • • We do not use the following data for averages, fits, limits, etc. • • •				
0.081 ± 0.020	[1,2] AULCHENKO	15	SND	1.22–$2.00\ e^+e^- \to \eta\pi^+\pi^-$
~ 0.24	[3] DONNACHIE	91	RVUE	
>2	FUKUI	91	SPEC	$8.95\ \pi^-p \to \omega\pi^0 n$

[1] From a fit to the $e^+e^- \to \eta\pi^+\pi^-$ cross section with vector meson dominance model including $\rho(770)$, $\rho(1450)$, and $\rho(1700)$ decaying exclusively via $\eta\rho(770)$. Masses and widths of vector states are fixed to PDG 14. Coupling constants are assumed to be real.
[2] Reports the inverse of the quoted value as 12.3 ± 3.1.
[3] Using data from BISELLO 91B, DOLINSKY 86 and ALBRECHT 87L.

$\Gamma(\pi\pi)/\Gamma(\eta\rho)$ — Γ_1/Γ_{11}

VALUE	DOCUMENT ID		TECN	COMMENT
• • • We do not use the following data for averages, fits, limits, etc. • • •				
1.3 ± 0.4	[1] AULCHENKO	15	SND	1.22–$2.00\ e^+e^- \to \eta\pi^+\pi^-$

[1] From a fit to the $e^+e^- \to \eta\pi^+\pi^-$ cross section with vector meson dominance model including $\rho(770)$, $\rho(1450)$, and $\rho(1700)$ decaying exclusively via $\eta\rho(770)$. Masses and widths of vector states are fixed to PDG 14. Coupling constants are assumed to be real.

$\Gamma(a_2(1320)\pi)/\Gamma_{\text{total}}$ — Γ_{12}/Γ

VALUE	DOCUMENT ID		TECN	COMMENT
• • • We do not use the following data for averages, fits, limits, etc. • • •				
not seen	AMELIN	00	VES	$37\ \pi^-p \to \eta\pi^+\pi^-n$

$\Gamma(K\overline{K})/\Gamma(\omega\pi)$ — Γ_{13}/Γ_4

VALUE	DOCUMENT ID		TECN
• • • We do not use the following data for averages, fits, limits, etc. • • •			
<0.08	[1] DONNACHIE	91	RVUE

[1] Using data from BISELLO 91B, DOLINSKY 86 and ALBRECHT 87L.

$\Gamma(K\overline{K}^*(892)+\text{c.c.})/\Gamma_{\text{total}}$ — Γ_{15}/Γ

VALUE	DOCUMENT ID		TECN	COMMENT
• • • We do not use the following data for averages, fits, limits, etc. • • •				
possibly seen	COAN	04	CLEO	$\tau^- \to K^-\pi^-K^+\nu_\tau$

$\Gamma(\eta\gamma)/\Gamma_{\text{total}}$ — Γ_{17}/Γ

VALUE	EVTS	DOCUMENT ID		TECN	COMMENT
seen	35	[1] ACHASOV	14	SND	1.15–$2.00\ e^+e^- \to \eta\gamma$

[1] From a phenomenological model based on vector meson dominance with $\rho(1450)$ and $\phi(1680)$ masses and widths from the PDG 12.

$\rho(1450)$ REFERENCES

ACHARYA	26	PL B872 140006	S. Acharya *et al.*	(ALICE Collab.)
AAIJ	25AG	JHEP 2511 103	R. Aaij *et al.*	(LHCb Collab.)
FEDOTOVICH	25	PPN 56 434	G.V. Fedotovich *et al.*	(CMD-3 Collab.)
IGNATOV	24	PR D109 112002	F.V. Ignatov *et al.*	(CMD-3 Collab.)
ANDREEV	20	EPJ C80 1189	V. Andreev *et al.*	(H1 Collab.)
GRIBANOV	20	JHEP 2001 112	S.S. Gribanov *et al.*	(CMD-3 Collab.)
ACHASOV	18	PR D97 012008	M.N. Achasov *et al.*	(SND Collab.)
LEES	18	PR D97 052007	J.P. Lees *et al.*	(BABAR Collab.)
BARTOS	17	PR D96 113004	E. Bartos *et al.*	
BARTOS	17A	IJMP A32 1750154	E. Bartos *et al.*	
LEES	17C	PR D95 072007	J.P. Lees *et al.*	(BABAR Collab.)
AAIJ	16N	PR D93 052018	R. Aaij *et al.*	(LHCb Collab.)
ABLIKIM	16C	PL B753 629	M. Ablikim *et al.*	(BESIII Collab.)
ACHASOV	16D	PR D94 112001	M.N. Achasov *et al.*	(SND Collab.)
AULCHENKO	15	PR D91 052013	V.M. Aulchenko *et al.*	(SND Collab.)
MATVIENKO	15	PR D92 012013	D. Matvienko *et al.*	(BELLE Collab.)
ACHASOV	14	PR D90 032002	M.N. Achasov *et al.*	(SND Collab.)
PDG	14	CP C38 070001	K. Olive *et al.*	(PDG Collab.)
ACHASOV	13	PR D88 054013	M.N. Achasov *et al.*	(SND Collab.)
ABRAMOWICZ	12	EPJ C72 1869	H. Abramowicz *et al.*	(ZEUS Collab.)
ACHASOV	12	JETPL 94 734	M.N. Achasov *et al.*	
		Translated from ZETFP 94 796.		
LEES	12G	PR D86 032013	J.P. Lees *et al.*	(BABAR Collab.)
PDG	12	PR D86 010001	J. Beringer *et al.*	(PDG Collab.)
ACHASOV	11	JETP 113 75	M.N. Achasov *et al.*	(SND Collab.)
		Translated from ZETF 140 87.		
AMBROSINO	11A	PL B700 102	F. Ambrosino *et al.*	(KLOE Collab.)
ACHASOV	10D	PR D98 112001	M.N. Achasov *et al.*	(SND Collab.)
DUBNICKA	10	APS 60 1	S. Dubnicka, A.Z. Dubnickova	
AUBERT	09AS	PRL 103 231801	B. Aubert *et al.*	(BABAR Collab.)
AUBERT	08S	PR D77 092002	B. Aubert *et al.*	(BABAR Collab.)
FUJIKAWA	08	PR D78 072006	M. Fujikawa *et al.*	(BELLE Collab.)
AKHMETSHIN	07	PL B648 28	R.R. Akhmetshin *et al.*	(Novosibirsk CMD-2 Collab.)
ACHASOV	06	JETP 103 380	M.N. Achasov *et al.*	(Novosibirsk SND Collab.)
		Translated from ZETF 130 437.		
AKHMETSHIN	05	PL B605 26	R.R. Akhmetshin *et al.*	(Novosibirsk CMD-2 Collab.)
ALOISIO	05	PL B606 12	A. Aloisio *et al.*	(KLOE Collab.)
SCHAEL	05C	PRPL 421 191	S. Schael *et al.*	(ALEPH Collab.)
AKHMETSHIN	04	PL B578 285	R.R. Akhmetshin *et al.*	(Novosibirsk CMD-2 Collab.)
COAN	04	PRL 92 232001	T.E. Coan *et al.*	(CLEO Collab.)
AKHMETSHIN	03B	PL B562 173	R.R. Akhmetshin *et al.*	(Novosibirsk CMD-2 Collab.)
ABELE	01B	EPJ C21 261	A. Abele *et al.*	(Crystal Barrel Collab.)
AKHMETSHIN	01B	PL B509 217	R.R. Akhmetshin *et al.*	(Novosibirsk CMD-2 Collab.)
ALEXANDER	01B	PR D64 092001	J.P. Alexander *et al.*	(CLEO Collab.)
AKHMETSHIN	00D	PL B489 125	R.R. Akhmetshin *et al.*	(Novosibirsk CMD-2 Collab.)
AMELIN	00	NP A668 83	D. Amelin *et al.*	(VES Collab.)
ANDERSON	00A	PR D61 112002	S. Anderson *et al.*	(CLEO Collab.)
EDWARDS	00A	PR D61 072003	K.W. Edwards *et al.*	(CLEO Collab.)
ABELE	99C	PL B450 275	A. Abele *et al.*	(Crystal Barrel Collab.)
ABELE	99D	PL B468 178	A. Abele *et al.*	(Crystal Barrel Collab.)
BERTIN	98	PR D57 55	A. Bertin *et al.*	(OBELIX Collab.)
ABELE	97	PL B391 191	A. Abele *et al.*	(Crystal Barrel Collab.)
ACHASOV	97	PR D55 2663	N.N. Achasov *et al.*	(NOVM)
BARATE	97M	ZPHY C76 15	R. Barate *et al.*	(ALEPH Collab.)
BERTIN	97C	PL B408 476	A. Bertin *et al.*	(OBELIX Collab.)
BERTIN	97D	PL B414 220	A. Bertin *et al.*	(OBELIX Collab.)
CLEGG	94	ZPHY C62 455	A.B. Clegg, A. Donnachie	(LANC, MCHS)
BISELLO	91B	NPBPS B21 111	D. Bisello	(DM2 Collab.)
DOLINSKY	91	PRPL 202 99	S.I. Dolinsky *et al.*	(NOVO)
DONNACHIE	91	ZPHY C51 689	A. Donnachie, A.B. Clegg	(MCHS, LANC)
FUKUI	91	PL B257 241	S. Fukui *et al.*	(SUGI, NAGO, KEK, KYOT+)
KUHN	90	ZPHY C48 445	J.H. Kuhn *et al.*	(MPIM)
ARMSTRONG	89E	PL B228 536	T.A. Armstrong, M. Benayoun	(ATHU, BARI, BIRM+)
BISELLO	89	PL B220 321	D. Bisello *et al.*	(DM2 Collab.)
DUBNICKA	89	JP G15 1349	S. Dubnicka *et al.*	(JINR, SLOV)
ANTONELLI	88	PL B212 133	A. Antonelli *et al.*	(DM2 Collab.)
CLEGG	88	ZPHY C40 313	A.B. Clegg, A. Donnachie	(MCHS, LANC)
DIEKMAN	88	PRPL 159 99	B. Diekmann	(BONN)
FUKUI	88	PL B202 441	S. Fukui *et al.*	(SUGI, NAGO, KEK, KYOT+)
ALBRECHT	87L	PL B185 223	H. Albrecht *et al.*	(ARGUS Collab.)
DONNACHIE	87B	ZPHY C34 257	A. Donnachie, A.B. Clegg	(MCHS, LANC)
DOLINSKY	86	PL B174 453	S.I. Dolinsky *et al.*	(NOVO)
BARKOV	85	NP B256 365	L.M. Barkov *et al.*	(NOVO)
KURDADZE	83	JETPL 37 733	L.M. Kurdadze *et al.*	(NOVO)
		Translated from ZETFP 37 613.		
ASTON	80C	PL 92B 211	D. Aston	(BONN, CERN, EPOL, GLAS, LANC+)
BARBER	80C	ZPHY C4 169	D.P. Barber *et al.*	(DARE, LANC, SHEF)
GOUNARIS	68	PRL 21 244	G.J. Gounaris, J.J. Sakurai	

$\eta(1475)$

$I^G(J^{PC}) = 0^+(0^{-+})$

See the $\eta(1405)$ and the related review on "Spectroscopy of Light Meson Resonances."

$\eta(1475)$ MASS

VALUE (MeV)	EVTS	DOCUMENT ID		TECN	COMMENT
1476 ± 4 OUR AVERAGE		Error includes scale factor of 1.4. See the ideogram below.			
$1507.6 \pm 1.6\,^{+15.5}_{-32.2}$	126k	[1] ABLIKIM	23M	BES3	$J/\psi \to \gamma K^0_S K^0_S \pi^0$
$1469 \pm 14 \pm 13$	74	ACHARD	07	L3	183–$209\ e^+e^- \to e^+e^- K^0_S K^\pm \pi^\mp$
1460 ± 12	3651	NICHITIU	02	OBLX	$0\ \overline{p}p \to K^+K^-\pi^+\pi^-\pi^0$
$1485 \pm 8 \pm 5$	20k	ADAMS	01B	B852	$18\ \text{GeV}\ \pi^-p \to K^+K^-\pi^0 n$
1500 ± 10		CICALO	99	OBLX	$0\ \overline{p}p \to K^\pm K^0_S \pi^\mp \pi^+\pi^-$
1464 ± 10		BERTIN	97	OBLX	$0\ \overline{p}p \to K^\pm (K^0)\pi^\mp\pi^+\pi^-$
1460 ± 10		BERTIN	95	OBLX	$0\ \overline{p}p \to K\overline{K}\pi\pi\pi$
$1490\,^{+14}_{-8}\,^{+3}_{-16}$	1100	BAI	90C	MRK3	$J/\psi \to \gamma K^0_S K^\pm \pi^\mp$
1475 ± 4		RATH	89	MPS	$21.4\ \pi^-p \to n K^0_S K^0_S \pi^0$
• • • We do not use the following data for averages, fits, limits, etc. • • •					
$1477 \pm 7 \pm 13$		[2] ABLIKIM	18I	BES3	$J/\psi \to \gamma\gamma\phi(1020)$
$1565 \pm 8\,^{+0}_{-63}$		[3] ABLIKIM	15T	BES3	$J/\psi \to \gamma K^0_S K^0_S \eta$
1421 ± 14		AUGUSTIN	92	DM2	$J/\psi \to \gamma K\overline{K}\pi$

[1] ABLIKIM 23M reports for this state a significance from the fit much higher than 35 σ.
[2] From a fit to $\gamma\phi$ invariant mass. Angular analysis consistent with $J^{PC} = 0^{-+}$. Other J^{PC} not excluded.
[3] Could also be the $\eta(1405)$.

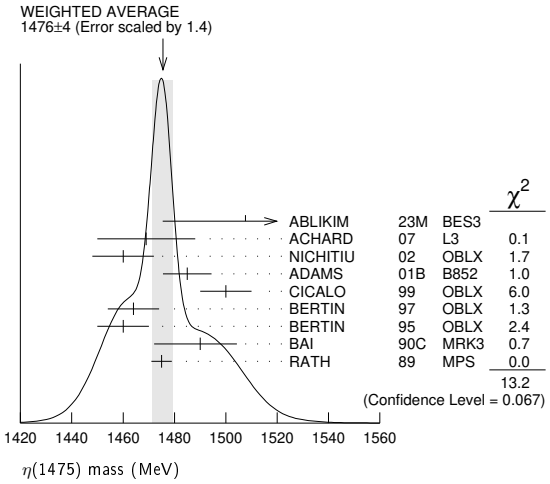

Int. J. Mod. Phys. A 2026.41. Downloaded from www.worldscientific.com
by CALIFORNIA @ BERKELEY on 09/16/26. Re-use and distribution is strictly not permitted, except for Open Access articles.

$\eta(1475)$ WIDTH

VALUE (MeV)	EVTS	DOCUMENT ID		TECN	COMMENT
96 ± 9 OUR AVERAGE		Error includes scale factor of 1.7. See the ideogram below.			
$115.8 \pm 2.4^{+14.8}_{-10.9}$	126k	ABLIKIM	23M	BES3	$J/\psi \to \gamma K^0_S K^0_S \pi^0$
67 ± 18 ± 7	74	ACHARD	07	L3	183–209 $e^+e^- \to e^+e^- K^0_S K^\pm \pi^\mp$
120 ± 15	3651	NICHITIU	02	OBLX	0 $\overline{p}p \to K^+K^-\pi^+\pi^-\pi^0$
98 ± 18 ± 3	20k	ADAMS	01B	B852	18 GeV $\pi^- p \to K^+K^-\pi^0 n$
100 ± 20		CICALO	99	OBLX	0 $\overline{p}p \to K^\pm K^0_S \pi^\mp \pi^+\pi^-$
105 ± 15		BERTIN	97	OBLX	0.0 $\overline{p}p \to K^\pm(K^0)\pi^\mp\pi^+\pi^-$
105 ± 15		BERTIN	95	OBLX	0 $\overline{p}p \to K\overline{K}\pi\pi\pi$
54^{+37}_{-21} $^{+13}_{-24}$		BAI	90C	MRK3	$J/\psi \to \gamma K^0_S K^\pm \pi^\mp$
51 ± 13		RATH	89	MPS	21.4 $\pi^- p \to n K^0_S K^0_S \pi^0$
• • • We do not use the following data for averages, fits, limits, etc. • • •					
118 ± 22 ± 17		[1] ABLIKIM	18I	BES3	$J/\psi \to \gamma\gamma\phi(1020)$
45^{+14}_{-13} $^{+21}_{-28}$		[2] ABLIKIM	15T	BES3	$J/\psi \to \gamma K^0_S K^0_S \eta$
63 ± 18		AUGUSTIN	92	DM2	$J/\psi \to \gamma K\overline{K}\pi$

[1] From a fit to $\gamma\phi$ invariant mass. Angular analysis consistent with $J^{PC} = 0^{-+}$. Other J^{PC} not excluded.
[2] Could also be the $\eta(1405)$.

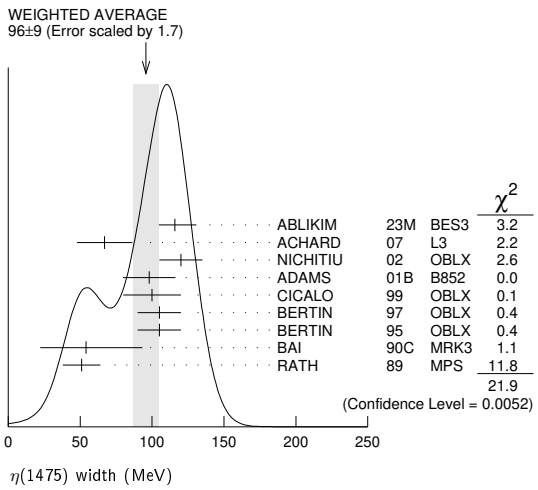

$\eta(1475)$ DECAY MODES

	Mode	Fraction (Γ_i/Γ)
Γ_1	$K\overline{K}\pi$	seen
Γ_2	$K\overline{K}^*(892)+$ c.c.	seen
Γ_3	$a_0(980)\pi$	seen
Γ_4	$\gamma\gamma$	seen
Γ_5	$K^0_S K^0_S \eta$	possibly seen
Γ_6	$\gamma\phi(1020)$	possibly seen

$\eta(1475)$ $\Gamma(i)\Gamma(\gamma\gamma)/\Gamma(\text{total})$

$\Gamma(K\overline{K}\pi) \times \Gamma(\gamma\gamma)/\Gamma_{\text{total}}$ — $\Gamma_1\Gamma_4/\Gamma$

VALUE (keV)	CL%	EVTS	DOCUMENT ID		TECN	COMMENT
0.23±0.05±0.05		74	[1] ACHARD	07	L3	183–209 $e^+e^- \to e^+e^- K^0_S K^\pm \pi^\mp$
• • • We do not use the following data for averages, fits, limits, etc. • • •						
< 0.089	90		[2,3] AHOHE	05	CLE2	10.6 $e^+e^- \to e^+e^- K^0_S K^\pm \pi^\mp$

[1] Supersedes ACCIARRI 01G. Using $B(K^0_S \to \pi^+\pi^-) = 0.6895$.
[2] Using $\eta(1475)$ mass of 1481 MeV and width of 48 MeV. The upper limit increases to 0.140 keV if the world average value, 87 MeV, of the width is used.
[3] Assuming three-body phase-space decay to $K^0_S K^\pm \pi^\mp$.

$\eta(1475)$ BRANCHING RATIOS

$\Gamma(K\overline{K}^*(892)+\text{c.c.})/\Gamma(K\overline{K}\pi)$ — Γ_2/Γ_1

VALUE	DOCUMENT ID		TECN	COMMENT
• • • We do not use the following data for averages, fits, limits, etc. • • •				
0.50±0.10	[1] BAILLON	67	HBC	0.0 $\overline{p}p \to K\overline{K}\pi\pi\pi$

[1] Data could also refer to $\eta(1405)$.

$\Gamma(K\overline{K}^*(892)+\text{c.c.})/[\Gamma(K\overline{K}^*(892)+\text{c.c.}) + \Gamma(a_0(980)\pi)]$ — $\Gamma_2/(\Gamma_2+\Gamma_3)$

VALUE	CL%	DOCUMENT ID		TECN	COMMENT
• • • We do not use the following data for averages, fits, limits, etc. • • •					
<0.25	90	EDWARDS	82E	CBAL	$J/\psi \to K^+K^-\pi^0\gamma$

$\Gamma(\gamma\gamma)/\Gamma(K\overline{K}\pi)$ — Γ_4/Γ_1

VALUE	CL%	DOCUMENT ID		TECN	COMMENT
<1.27 × 10⁻³	90	[1] ABLIKIM	18O	BES3	$\psi(2S) \to \pi^+\pi^-\gamma\gamma\gamma$

[1] Using results from BAI 00D.

$\Gamma(\gamma\phi(1020))/\Gamma_{\text{total}}$ — Γ_6/Γ

VALUE	DOCUMENT ID		TECN	COMMENT
possibly seen	[1] ABLIKIM	18I	BES3	$J/\psi \to \gamma\gamma\phi(1020)$

[1] Seen as a peak in $\gamma\phi$ invariant mass. Angular analysis consistent with $J^{PC} = 0^{-+}$. Other J^{PC} not excluded. Also see $\eta(1405)$.

$\eta(1475)$ REFERENCES

ABLIKIM	23M	JHEP 2303 121	M. Ablikim *et al.*	(BESIII Collab.)
ABLIKIM	18I	PR D97 051101	M. Ablikim *et al.*	(BESIII Collab.)
ABLIKIM	18O	PR D97 072014	M. Ablikim *et al.*	(BESIII Collab.)
ABLIKIM	15T	PRL 115 091803	M. Ablikim *et al.*	(BESIII Collab.)
ACHARD	07	JHEP 0703 018	P. Achard *et al.*	(L3 Collab.)
AHOHE	05	PR D71 072001	R. Ahohe *et al.*	(CLEO Collab.)
NICHITIU	02	PL B545 261	F. Nichitiu *et al.*	(OBELIX Collab.)
ACCIARRI	01G	PL B501 1	M. Acciarri *et al.*	(L3 Collab.)
ADAMS	01B	PL B516 264	G.S. Adams *et al.*	(BNL E852 Collab.)
BAI	00D	PL B476 25	J.Z. Bai *et al.*	(BES Collab.)
CICALO	99	PL B462 453	C. Cicalo *et al.*	(OBELIX Collab.)
BERTIN	97	PL B400 226	A. Bertin *et al.*	(OBELIX Collab.)
BERTIN	95	PL B361 187	A. Bertin *et al.*	(OBELIX Collab.)
AUGUSTIN	92	PR D46 1951	J.E. Augustin, G. Cosme	(DM2 Collab.)
BAI	90C	PRL 65 2507	Z. Bai *et al.*	(Mark III Collab.)
RATH	89	PR D40 693	M.G. Rath *et al.*	(NDAM, BRAN, BNL, CUNY+)
EDWARDS	82E	PRL 49 259	C. Edwards *et al.*	(CIT, HARV, PRIN+)
BAILLON	67	NC 50A 393	P.H. Baillon *et al.*	(CERN, CDEF, IRAD)

$f_0(1500)$

$I^G(J^{PC}) = 0^+(0^{++})$

See the review on "Spectroscopy of Light Meson Resonances."

$f_0(1500)$ T-MATRIX POLE $\sqrt{s}$

Note that $\Gamma = -2\,\text{Im}(\sqrt{s})$.

VALUE (MeV)	DOCUMENT ID		TECN	COMMENT
(1430–1530) − i (40–90) OUR ESTIMATE				
(1487.8 ± 7.7 ± 3.7) − i (46.1 ± 8.6 ± 6.6)	ABLIKIM	25CD	BES3	$e^+e^- \to \psi(2S)$
(1450 ± 10) − i (53 ± 8)	[1] RODAS	22	RVUE	$J/\psi(1S) \to \gamma(\pi\pi, K\overline{K})$
(1483 ± 15) − i (58 ± 6)	SARANTSEV	21	RVUE	$J/\psi(1S) \to \gamma(\pi\pi, K\overline{K}, \eta\eta, \omega\phi)$
$(1496 \pm 1.2^{+4.4}_{-26.4}) - i(40.4 \pm 0.3^{+10.0}_{-2.5})$	[2] ALBRECHT	20	RVUE	0.9 $\overline{p}p \to \pi^0\pi^0\eta$, $\pi^0\eta\eta$, $\pi^0 K^+K^-$
(1465 ± 18) − i (50 ± 9)	[3] ROPERTZ	18	RVUE	$\overline{B}^0_s \to J/\psi(\pi^+\pi^-/K^+K^-)$
(1486 ± 10) − i (57 ± 5)	ANISOVICH	09	RVUE	0.0 $\overline{p}p$, πN
$(1489^{+8}_{-4}) - i(51 \pm 5)$	[4] ANISOVICH	03	RVUE	
(1515 ± 12) − i (55 ± 12)	BARBERIS	00A		450 $pp \to p_f(\eta\eta', \eta'\eta')p_s$
(1511 ± 9) − i (51 ± 9)	[5] BARBERIS	00C		450 $pp \to p_f 4\pi p_s$
(1510 ± 8) − i (55 ± 8)	BARBERIS	00E		450 $pp \to p_f \eta\eta p_s$
(1502 ± 12 ± 10) − i (49 ± 9 ± 8)	[6] BARBERIS	99D	OMEG	450 $pp \to K^+K^-, \pi^+\pi^-$
(1447 ± 27) − i (54 ± 23)	[7] KAMINSKI	99	RVUE	$\pi\pi \to \pi\pi, K\overline{K}, \sigma\sigma$
(1499 ± 8) − i (65 ± 10)	ANISOVICH	98B	RVUE	Compilation.
(1510 ± 20) − i (60 ± 18)	BARBERIS	97B	OMEG	450 $pp \to pp2(\pi^+\pi^-)$
(1449 ± 20) − i (57 ± 15)	BERTIN	97C	OBLX	0.0 $\overline{p}p \to \pi^+\pi^-\pi^0$
(1515 ± 20) − i (53 ± 8)	ABELE	96B	CBAR	0.0 $\overline{p}p \to \pi^0 K^0_L K^0_L$
(1500 ± 8) − i (66 ± 8)	ABELE	96C	RVUE	Compilation.
(1500 ± 10) − i (77 ± 15)	[8] AMSLER	95D	CBAR	0.0 $\overline{p}p \to \pi^0\pi^0\pi^0$, $\pi^0\eta\eta$, $\pi^0\pi^0\eta$
$(1520 \pm 25) - i(74^{+10}_{-13})$	[9] ANISOVICH	94	CBAR	0.0 $\overline{p}p \to 3\pi^0, \pi^0\eta\eta$
(1505 ± 20) − i (75 ± 10)	[10] BUGG	94	RVUE	$\overline{p}p \to 3\pi^0, \eta\eta\pi^0, \eta\pi^0\pi^0$

[1] T-matrix pole from coupled channel K-matrix fit to data on $J/\psi \to \gamma\pi^0\pi^0$ (ABLIKIM 15AE) and $J/\psi \to \gamma K^0_S K^0_S$ (ABLIKIM 18AA).
[2] T-matrix pole, 5 poles, 5 channels, including scattering data from HYAMS 75 ($\pi\pi$), LONGACRE 86 ($K\overline{K}$), BINON 83 ($\eta\eta$), and BINON 84C ($\eta\eta'$).
[3] T-matrix pole of 3 channel unitary model fit to data from AAIJ 14BR and AAIJ 17V extracted using Pade approximants.
[4] Pole position from combined analysis of $\pi^-p \to \pi^0\pi^0 n$, $\pi^-p \to K\overline{K}n$, $\pi^+\pi^- \to \pi^+\pi^-$, $\overline{p}p \to \pi^0\pi^0\pi^0$, $\pi^0\eta\eta$, $\pi^0\pi^0\eta$, $\pi^+\pi^-\pi^0$, $K^+K^-\pi^0$, $K^0_S K^0_S \pi^0$, $K^+K^0_S\pi^-$ at rest, $\overline{p}n \to \pi^-\pi^-\pi^+$, $K^0_S K^-\pi^0$, $K^0_S K^0_S \pi^-$ at rest.
[5] Average between $\pi^+\pi^-2\pi^0$ and $2(\pi^+\pi^-)$.
[6] Supersedes BARBERIS 99 and BARBERIS 99B.

Int. J. Mod. Phys. A 2026.41. Downloaded from www.worldscientific.com
by UNIVERSITY OF CALIFORNIA @ BERKELEY on 09/16/26. Re-use and distribution is strictly not permitted, except for Open Access articles.

[7] T-matrix pole on sheet $- - +$.
[8] Coupled-channel analysis of AMSLER 95B, AMSLER 95C, and AMSLER 94D.
[9] From a simultaneous analysis of the annihilations $\overline{p}p \to 3\pi^0, \pi^0\eta\eta$.
[10] Reanalysis of ANISOVICH 94 data.

$f_0(1500)$ MASS

VALUE (MeV)	EVTS	DOCUMENT ID		TECN	COMMENT
1522 ±25		[1] BERTIN	98	OBLX	0.05–0.405 $\overline{n}p \to \pi^+\pi^+\pi^-$
• • • We do not use the following data for averages, fits, limits, etc. • • •					
1492.5 ± 3.6 $^{+2.4}_{-20.5}$		[2] ABLIKIM	22G	BES3	$J/\psi \to \gamma\pi^+\pi^-\eta'$
1447 ±16 ± 13	163	[3,4] DOBBS	15		$J/\psi \to \gamma\pi^+\pi^-$
1442 ± 9 ± 4	261	[3,4] DOBBS	15		$\psi(2S) \to \gamma\pi^+\pi^-$
1460.9 ± 2.9		[5] AAIJ	14BR	LHCB	$\overline{B}^0_s \to J/\psi\pi^+\pi^-$
1468 $^{+14}_{-15}$ $^{+23}_{-74}$	5.5k	[6] ABLIKIM	13N	BES3	$e^+e^- \to J/\psi \to \gamma\eta\eta$
1470 ±60	568	[7] KLEMPT	08	E791	$D^+_s \to \pi^-\pi^+\pi^+$
1470 $^{+6}_{-7}$ $^{+72}_{-255}$		[8] UEHARA	08A	BELL	10.6 $e^+e^- \to e^+e^-\pi^0\pi^0$
1466 ± 6 ± 20		[9] ABLIKIM	06V	BES2	$e^+e^- \to J/\psi \to \gamma\pi^+\pi^-$
1495 ± 4		AMSLER	06	CBAR	0.9 $\overline{p}p \to K^+K^-\pi^0$
1539 ±20	9.9k	AUBERT	06O	BABR	$B^+ \to K^+K^+K^-$
1473 ± 5	80k	[9,10] UMAN	06	E835	5.2 $\overline{p}p \to \eta\eta\pi^0$
1478 ± 6		VLADIMIRSK...	06	SPEC	40 $\pi^-p \to K^0_S K^0_S n$
1493 ± 7		[9] BINON	05	GAMS	33 $\pi^-p \to \eta\eta n$
1524 ±14	1400	[11] GARMASH	05	BELL	$B^+ \to K^+K^+K^-$
1490 ±30		[9] ABELE	01	CBAR	0.0 $\overline{p}d \to \pi^-4\pi^0 p$
1497 ±10		[9] BARBERIS	99	OMEG	450 $pp \to p_s p_f K^+K^-$
1502 ±10		[9] BARBERIS	99B	OMEG	450 $pp \to p_s p_f \pi^+\pi^-$
1530 ±45		[9] BELLAZZINI	99	GAM4	450 $pp \to pp\pi^0\pi^0$
1505 ±18		[9] FRENCH	99		300 $pp \to p_f(K^+K^-)p_s$
1580 ±80		[9] ALDE	98	GAM4	100 $\pi^-p \to \pi^0\pi^0 n$
~ 1520		REYES	98	SPEC	800 $pp \to p_s p_f K^0_S K^0_S$
~ 1475		FRABETTI	97D	E687	$D^\pm_s \to \pi^\mp\pi^\pm\pi^\pm$
~ 1505		ABELE	96	CBAR	0.0 $\overline{p}p \to 5\pi^0$
1460 ±20	120	[9] AMELIN	96B	VES	37 $\pi^-A \to \eta\eta\pi^-A$
1500 ± 8		BUGG	96	RVUE	
1500 ±15		[12] AMSLER	95B	CBAR	0.0 $\overline{p}p \to 3\pi^0$
1505 ±15		[13] AMSLER	95C	CBAR	0.0 $\overline{p}p \to \eta\eta\pi^0$
1445 ± 5		[14] ANTINORI	95	OMEG	300,450 $pp \to pp2(\pi^+\pi^-)$
1497 ±30		[9] ANTINORI	95	OMEG	300,450 $pp \to pp\pi^+\pi^-$
~ 1505		BUGG	95	MRK3	$J/\psi \to \gamma\pi^+\pi^-\pi^+\pi^-$
1446 ± 5		[9] ABATZIS	94	OMEG	450 $pp \to pp2(\pi^+\pi^-)$
1545 ±25		[9] AMSLER	94E	CBAR	0.0 $\overline{p}p \to \pi^0\eta\eta'$
1560 ±25		[9] AMSLER	92	CBAR	0.0 $\overline{p}p \to \pi^0\eta\eta$
1550 ±45 ± 30		[9] BELADIDZE	92C	VES	36 π^-Be $\to \pi^-\eta'\eta$Be
1449 ± 4		[9] ARMSTRONG	89E	OMEG	300 $pp \to pp2(\pi^+\pi^-)$
1610 ±20		[9] ALDE	88	GAM4	300 $\pi^-N \to \pi^-N2\eta$
~ 1525		ASTON	88D	LASS	11 $K^-p \to K^0_S K^0_S \Lambda$
1570 ±20	600	[9] ALDE	87	GAM4	100 $\pi^-p \to 4\pi^0 n$
1575 ±45		[15] ALDE	86D	GAM4	100 $\pi^-p \to 2\eta n$
1568 ±33		[9] BINON	84C	GAM2	38 $\pi^-p \to \eta\eta' n$
1592 ±25		[9] BINON	83	GAM2	38 $\pi^-p \to 2\eta n$
1525 ± 5		[9] GRAY	83	DBC	0.0 $\overline{p}N \to 3\pi$

[1] Breit-Wigner mass.
[2] The $\pi^+\pi^-$ mass spectrum is described by a coherent sum of two Breit-Wigner resonances, $f_0(1500)$ and a new $X(1540)$ with mass $1540.2 \pm 7.0^{+36.3}_{-6.1}$ MeV and width $157 \pm 19^{+11}_{-77}$ MeV.
[3] Using CLEO-c data but not authored by the CLEO Collaboration.
[4] From a fit to a Breit-Wigner line shape with fixed $\Gamma = 109$ MeV.
[5] Solution I, statistical error only.
[6] From partial wave analysis including all possible combinations of 0^{++}, 2^{++}, and 4^{++} resonances.
[7] Reanalysis of AITALA 01A data. This state could also be $f_0(1370)$.
[8] Breit-Wigner mass. May also be the $f_0(1370)$.
[9] Breit-Wigner mass.
[10] Statistical error only.
[11] Breit-Wigner, solution 1, PWA ambiguous.
[12] T-matrix pole, supersedes ANISOVICH 94.
[13] T-matrix pole, supersedes ANISOVICH 94 and AMSLER 92.
[14] Supersedes ABATZIS 94, ARMSTRONG 89E. Breit-Wigner mass.
[15] From central value and spread of two solutions. Breit-Wigner mass.

$f_0(1500)$ WIDTH

VALUE (MeV)	EVTS	DOCUMENT ID		TECN	COMMENT
108 ± 33		[1] BERTIN	98	OBLX	0.05–0.405 $\overline{n}p \to \pi^+\pi^+\pi^-$
• • • We do not use the following data for averages, fits, limits, etc. • • •					
107 ± $^{+21}_{-9}$		[2] ABLIKIM	22G	BES3	$J/\psi \to \gamma\pi^+\pi^-\eta'$
124 ± 7		[3] AAIJ	14BR	LHCB	$\overline{B}^0_s \to J/\psi\pi^+\pi^-$
136 $^{+41}_{-26}$ $^{+28}_{-100}$	5.5k	[4] ABLIKIM	13N	BES3	$e^+e^- \to J/\psi \to \gamma\eta\eta$
90 $^{+2}_{-1}$ $^{+50}_{-22}$		[5] UEHARA	08A	BELL	10.6 $e^+e^- \to e^+e^-\pi^0\pi^0$
108 $^{+14}_{-11}$ ± 25		[6] ABLIKIM	06V	BES2	$e^+e^- \to J/\psi \to \gamma\pi^+\pi^-$
121 ± 8		AMSLER	06	CBAR	0.9 $\overline{p}p \to K^+K^-\pi^0$
257 ± 33	9.9k	AUBERT	06O	BABR	$B^+ \to K^+K^+K^-$
108 ± 9	80k	[6,7] UMAN	06	E835	5.2 $\overline{p}p \to \eta\eta\pi^0$
119 ± 10		VLADIMIRSK...	06	SPEC	40 $\pi^-p \to K^0_S K^0_S n$
90 ± 15		[6] BINON	05	GAMS	33 $\pi^-p \to \eta\eta n$
136 ± 23	1400	[8] GARMASH	05	BELL	$B^+ \to K^+K^+K^-$
140 ± 40		[6] ABELE	01	CBAR	0.0 $\overline{p}d \to \pi^-4\pi^0 p$
104 ± 25		[6] BARBERIS	99	OMEG	450 $pp \to p_s p_f K^+K^-$
131 ± 15		[6] BARBERIS	99B	OMEG	450 $pp \to p_s p_f \pi^+\pi^-$
160 ± 50		[6] BELLAZZINI	99	GAM4	450 $pp \to pp\pi^0\pi^0$
100 ± 33		[6] FRENCH	99		300 $pp \to p_f(K^+K^-)p_s$
280 ±100		[6] ALDE	98	GAM4	100 $\pi^-p \to \pi^0\pi^0 n$
~ 100		FRABETTI	97D	E687	$D^\pm_s \to \pi^\mp\pi^\pm\pi^\pm$
~ 169		ABELE	96	CBAR	0.0 $\overline{p}p \to 5\pi^0$
100 ± 30	120	[6] AMELIN	96B	VES	37 $\pi^-A \to \eta\eta\pi^-A$
132 ± 15		BUGG	96	RVUE	
120 ± 25		[9] AMSLER	95B	CBAR	0.0 $\overline{p}p \to 3\pi^0$
120 ± 30		[10] AMSLER	95C	CBAR	0.0 $\overline{p}p \to \eta\eta\pi^0$
65 ± 10		[11] ANTINORI	95	OMEG	300,450 $pp \to pp2(\pi^+\pi^-)$
199 ± 30		[6] ANTINORI	95	OMEG	300,450 $pp \to pp\pi^+\pi^-$
56 ± 12		[6] ABATZIS	94	OMEG	450 $pp \to pp2(\pi^+\pi^-)$
100 ± 40		[6] AMSLER	94E	CBAR	0.0 $\overline{p}p \to \pi^0\eta\eta'$
245 ± 50		[6] AMSLER	92	CBAR	0.0 $\overline{p}p \to \pi^0\eta\eta$
153 ± 67 ± 50		[6] BELADIDZE	92C	VES	36 π^-Be $\to \pi^-\eta'\eta$Be
78 ± 18		[6] ARMSTRONG	89E	OMEG	300 $pp \to pp2(\pi^+\pi^-)$
170 ± 40		[6] ALDE	88	GAM4	300 $\pi^-N \to \pi^-N2\eta$
150 ± 20	600	[6] ALDE	87	GAM4	100 $\pi^-p \to 4\pi^0 n$
265 ± 65		[12] ALDE	86D	GAM4	100 $\pi^-p \to 2\eta n$
260 ± 60		[6] BINON	84C	GAM2	38 $\pi^-p \to \eta\eta' n$
210 ± 40		[6] BINON	83	GAM2	38 $\pi^-p \to 2\eta n$
101 ± 13		[6] GRAY	83	DBC	0.0 $\overline{p}N \to 3\pi$

[1] Breit-Wigner width.
[2] The $\pi^+\pi^-$ mass spectrum is described by a coherent sum of two Breit-Wigner resonances, $f_0(1500)$ and a new $X(1540)$ with mass $1540.2 \pm 7.0^{+36.3}_{-6.1}$ MeV and width $157 \pm 19^{+11}_{-77}$ MeV.
[3] Solution I, statistical error only.
[4] From partial wave analysis including all possible combinations of 0^{++}, 2^{++}, and 4^{++} resonances.
[5] Breit-Wigner width. May also be the $f_0(1370)$.
[6] Breit-Wigner width.
[7] Statistical error only.
[8] Breit-Wigner, solution 1, PWA ambiguous.
[9] T-matrix pole, supersedes ANISOVICH 94.
[10] T-matrix pole, supersedes ANISOVICH 94 and AMSLER 92.
[11] Supersedes ABATZIS 94, ARMSTRONG 89E. Breit-Wigner mass.
[12] From central value and spread of two solutions. Breit-Wigner mass.

$f_0(1500)$ DECAY MODES

	Mode	Fraction (Γ_i/Γ)	Scale factor
Γ_1	$\pi\pi$	(34.5±2.2) %	1.2
Γ_2	$\pi^+\pi^-$	seen	
Γ_3	$2\pi^0$	seen	
Γ_4	4π	(48.9±3.3) %	1.2
Γ_5	$4\pi^0$	seen	
Γ_6	$2\pi^+2\pi^-$	seen	
Γ_7	$2(\pi\pi)_S$-wave	seen	
Γ_8	$\rho\rho$	seen	
Γ_9	$\pi(1300)\pi$	seen	
Γ_{10}	$a_1(1260)\pi$	seen	
Γ_{11}	$\eta\eta$	(6.0±0.9) %	1.1
Γ_{12}	$\eta\eta'(958)$	(2.2±0.8) %	1.4
Γ_{13}	$K\overline{K}$	(8.5±1.0) %	1.1
Γ_{14}	$\gamma\gamma$	not seen	

Int. J. Mod. Phys. A 2026.41. Downloaded from www.worldscientific.com
by [redacted]LIFORNIA @ BERKELEY on 09/16/26. Re-use and distribution is strictly not permitted, except for Open Access articles.

CONSTRAINED FIT INFORMATION

An overall fit to 6 branching ratios uses 10 measurements and one constraint to determine 5 parameters. The overall fit has a $\chi^2 = 5.6$ for 6 degrees of freedom.

The following *off-diagonal* array elements are the correlation coefficients $\langle \delta x_i \delta x_j \rangle / (\delta x_i \cdot \delta x_j)$, in percent, from the fit to the branching fractions, $x_i \equiv \Gamma_i/\Gamma_{\rm total}$. The fit constrains the x_i whose labels appear in this array to sum to one.

x_4	−88			
x_{11}	27	−56		
x_{12}	3	−32	26	
x_{13}	43	−64	20	2
	x_1	x_4	x_{11}	x_{12}

$f_0(1500)$ $\Gamma(i)\Gamma(\gamma\gamma)/\Gamma(\text{total})$

$\Gamma(\pi\pi) \times \Gamma(\gamma\gamma)/\Gamma_{\rm total}$ — $\Gamma_1\Gamma_{14}/\Gamma$

VALUE (eV)	CL%	DOCUMENT ID		TECN	COMMENT
• • • We do not use the following data for averages, fits, limits, etc. • • •					
$33^{+12}_{-6}{}^{+1809}_{-21}$		[1] UEHARA	08A	BELL	$10.6\ e^+e^- \to e^+e^-\pi^0\pi^0$
not seen		ACCIARRI	01H	L3	$\gamma\gamma \to K^0_S K^0_S$, $E^{ee}_{\rm cm}$= 91, 183–209 GeV
<460	95	BARATE	00E	ALEP	$\gamma\gamma \to \pi^+\pi^-$

[1] May also be the $f_0(1370)$. Multiplied by us by 3 to obtain the $\pi\pi$ value.

$f_0(1500)$ BRANCHING RATIOS

$\Gamma(\pi\pi)/\Gamma_{\rm total}$ — Γ_1/Γ

VALUE	DOCUMENT ID		TECN	COMMENT
• • • We do not use the following data for averages, fits, limits, etc. • • •				
0.454±0.104	BUGG	96	RVUE	

$\Gamma(\pi^+\pi^-)/\Gamma_{\rm total}$ — Γ_2/Γ

VALUE	DOCUMENT ID		TECN	COMMENT
seen	BERTIN	98	OBLX	0.05–$0.405\ \overline{n}p \to \pi^+\pi^+\pi^-$
• • • We do not use the following data for averages, fits, limits, etc. • • •				
possibly seen	FRABETTI	97D	E687	$D^\pm_s \to \pi^\mp\pi^\pm\pi^\pm$

$\Gamma(4\pi)/\Gamma(\pi\pi)$ — Γ_4/Γ_1

VALUE	DOCUMENT ID		TECN	COMMENT
1.42±0.18 OUR FIT Error includes scale factor of 1.2.				
1.42±0.18 OUR AVERAGE Error includes scale factor of 1.2.				
1.37±0.16	BARBERIS	00D		$450\ pp \to p_f 4\pi p_s$
2.1 ±0.6	[1] AMSLER	98	RVUE	
• • • We do not use the following data for averages, fits, limits, etc. • • •				
2.1 ±0.2	[2] ANISOVICH	02D	SPEC	Combined fit
3.4 ±0.8	[1] ABELE	96	CBAR	$0.0\ \overline{p}p \to 5\pi^0$

[1] Excluding $\rho\rho$ contribution to 4π.
[2] From a combined K-matrix analysis of Crystal Barrel (0. $p\overline{p} \to \pi^0\pi^0\pi^0$, $\pi^0\eta\eta$, $\pi^0\pi^0\eta$), GAMS ($\pi p \to \pi^0\pi^0 n$, $\eta\eta n$, $\eta\eta' n$), and BNL ($\pi p \to K\overline{K}n$) data.

$\Gamma(2(\pi\pi)_{S\text{-wave}})/\Gamma(\pi\pi)$ — Γ_7/Γ_1

VALUE	DOCUMENT ID		TECN	COMMENT
• • • We do not use the following data for averages, fits, limits, etc. • • •				
0.42±0.26	[1] ABELE	01	CBAR	$0.0\ \overline{p}d \to \pi^-4\pi^0 p$

[1] From the combined data of ABELE 96 and ABELE 96C.

$\Gamma(2(\pi\pi)_{S\text{-wave}})/\Gamma(4\pi)$ — Γ_7/Γ_4

VALUE	DOCUMENT ID		TECN	COMMENT
• • • We do not use the following data for averages, fits, limits, etc. • • •				
0.26±0.07	ABELE	01B	CBAR	$0.0\ \overline{p}d \to 5\pi p$

$\Gamma(\rho\rho)/\Gamma(4\pi)$ — Γ_8/Γ_4

VALUE	DOCUMENT ID		TECN	COMMENT
• • • We do not use the following data for averages, fits, limits, etc. • • •				
0.13±0.08	ABELE	01B	CBAR	$0.0\ \overline{p}d \to 5\pi p$

$\Gamma(\rho\rho)/\Gamma(2(\pi\pi)_{S\text{-wave}})$ — Γ_8/Γ_7

VALUE	DOCUMENT ID		COMMENT
2.87±0.34 OUR AVERAGE Error includes scale factor of 1.1.			
3.3 ±0.5	BARBERIS	00C	$450\ pp \to p_f\pi^+\pi^-2\pi^0 p_s$
2.6 ±0.4	BARBERIS	00C	$450\ pp \to p_f 2(\pi^+\pi^-) p_s$

$\Gamma(\pi(1300)\pi)/\Gamma(4\pi)$ — Γ_9/Γ_4

VALUE	DOCUMENT ID		TECN	COMMENT
• • • We do not use the following data for averages, fits, limits, etc. • • •				
0.50±0.25	ABELE	01B	CBAR	$0.0\ \overline{p}d \to 5\pi p$

$\Gamma(a_1(1260)\pi)/\Gamma(4\pi)$ — Γ_{10}/Γ_4

VALUE	DOCUMENT ID		TECN	COMMENT
• • • We do not use the following data for averages, fits, limits, etc. • • •				
0.12±0.05	ABELE	01B	CBAR	$0.0\ \overline{p}d \to 5\pi p$

$\Gamma(\eta\eta)/\Gamma_{\rm total}$ — Γ_{11}/Γ

VALUE	DOCUMENT ID		TECN	COMMENT
• • • We do not use the following data for averages, fits, limits, etc. • • •				
large	ALDE	88	GAM4	$300\ \pi^- N \to \eta\eta\pi^- N$
large	BINON	83	GAM2	$38\ \pi^- p \to 2\eta n$

$\Gamma(\eta\eta)/\Gamma(\pi\pi)$ — Γ_{11}/Γ_1

VALUE	DOCUMENT ID		TECN	COMMENT
0.173±0.024 OUR FIT Error includes scale factor of 1.1.				
0.175±0.027 OUR AVERAGE				
0.18 ±0.03	BARBERIS	00E		$450\ pp \to p_f\eta\eta p_s$
0.157±0.060	[1] AMSLER	95D	CBAR	$0.0\ \overline{p}p \to \pi^0\pi^0\pi^0$, $\pi^0\eta\eta$, $\pi^0\pi^0\eta$
• • • We do not use the following data for averages, fits, limits, etc. • • •				
0.080±0.033	AMSLER	02	CBAR	$0.9\ \overline{p}p \to \pi^0\eta\eta$, $\pi^0\pi^0\pi^0$
0.11 ±0.03	[2] ANISOVICH	02D	SPEC	Combined fit
0.078±0.013	[3] ABELE	96C	RVUE	Compilation
0.230±0.097	[4] AMSLER	95C	CBAR	$0.0\ \overline{p}p \to \eta\eta\pi^0$

[1] Coupled-channel analysis of AMSLER 95B, AMSLER 95C, and AMSLER 94D.
[2] From a combined K-matrix analysis of Crystal Barrel (0. $p\overline{p} \to \pi^0\pi^0\pi^0$, $\pi^0\eta\eta$, $\pi^0\pi^0\eta$), GAMS ($\pi p \to \pi^0\pi^0 n$, $\eta\eta n$, $\eta\eta' n$), and BNL ($\pi p \to K\overline{K}n$) data.
[3] 2π width determined to be 60 ± 12 MeV.
[4] Using AMSLER 95B ($3\pi^0$).

$\Gamma(4\pi^0)/\Gamma(\eta\eta)$ — Γ_5/Γ_{11}

VALUE	DOCUMENT ID		TECN	COMMENT
• • • We do not use the following data for averages, fits, limits, etc. • • •				
0.8±0.3	ALDE	87	GAM4	$100\ \pi^- p \to 4\pi^0 n$

$\Gamma(\eta\eta'(958))/\Gamma(\pi\pi)$ — Γ_{12}/Γ_1

VALUE (units 10^{-2})	DOCUMENT ID		TECN	COMMENT
6.4±2.2 OUR FIT Error includes scale factor of 1.4.				
9.5±2.6	BARBERIS	00A		$450\ pp \to p_f\eta\eta p_s$
• • • We do not use the following data for averages, fits, limits, etc. • • •				
$16.6^{+4.2}_{-4.0}$	[1] ABLIKIM	22AS	BES3	$J/\psi(1S) \to \gamma\eta\eta'$
0.5±0.3	[2] ANISOVICH	02D	SPEC	Combined fit

[1] From a Breit-Wigner fit involving 9 resonances and a resonating exotic $\eta_1(1855) \to \eta\eta'$ P-wave.
[2] From a combined K-matrix analysis of Crystal Barrel (0. $p\overline{p} \to \pi^0\pi^0\pi^0$, $\pi^0\eta\eta$, $\pi^0\pi^0\eta$), GAMS ($\pi p \to \pi^0\pi^0 n$, $\eta\eta n$, $\eta\eta' n$), and BNL ($\pi p \to K\overline{K}n$) data.

$\Gamma(\eta\eta'(958))/\Gamma(\eta\eta)$ — Γ_{12}/Γ_{11}

VALUE	DOCUMENT ID		TECN	COMMENT
0.37±0.13 OUR FIT Error includes scale factor of 1.5.				
0.29±0.10	[1] AMSLER	95C	CBAR	$0.0\ \overline{p}p \to \eta\eta\pi^0$
• • • We do not use the following data for averages, fits, limits, etc. • • •				
0.05±0.03	[2] ANISOVICH	02D	SPEC	Combined fit
0.84±0.23	ABELE	96C	RVUE	Compilation
2.7 ±0.8	BINON	84C	GAM2	$38\ \pi^- p \to \eta\eta' n$

[1] Using AMSLER 94E ($\eta\eta'\pi^0$).
[2] From a combined K-matrix analysis of Crystal Barrel (0. $p\overline{p} \to \pi^0\pi^0\pi^0$, $\pi^0\eta\eta$, $\pi^0\pi^0\eta$), GAMS ($\pi p \to \pi^0\pi^0 n$, $\eta\eta n$, $\eta\eta' n$), and BNL ($\pi p \to K\overline{K}n$) data.

$\Gamma(K\overline{K})/\Gamma_{\rm total}$ — Γ_{13}/Γ

VALUE	DOCUMENT ID		TECN
• • • We do not use the following data for averages, fits, limits, etc. • • •			
0.044±0.021	BUGG	96	RVUE

$\Gamma(K\overline{K})/\Gamma(\pi\pi)$ — Γ_{13}/Γ_1

VALUE	DOCUMENT ID		TECN	COMMENT
0.246±0.025 OUR FIT				
0.236±0.026 OUR AVERAGE				
0.25 ±0.03	[1] BARGIOTTI	03	OBLX	$\overline{p}p$
0.19 ±0.07	[2] ABELE	98	CBAR	$0.0\ \overline{p}p \to K^0_L K^\pm\pi^\mp$
0.20 ±0.08	[3] ABELE	96B	CBAR	$0.0\ \overline{p}p \to \pi^0 K^0_L K^0_L$
• • • We do not use the following data for averages, fits, limits, etc. • • •				
0.16 ±0.05	[4] ANISOVICH	02D	SPEC	Combined fit
0.33 ±0.03 ±0.07	BARBERIS	99D	OMEG	$450\ pp \to K^+K^-$, $\pi^+\pi^-$

[1] Coupled channel analysis of $\pi^+\pi^-\pi^0$, $K^+K^-\pi^0$, and $K^\pm K^0_S\pi^\mp$.
[2] Using $\pi^0\pi^0$ from AMSLER 95B.
[3] Using AMSLER 95B ($3\pi^0$), AMSLER 94C ($2\pi^0\eta$) and SU(3).
[4] From a combined K-matrix analysis of Crystal Barrel (0. $p\overline{p} \to \pi^0\pi^0\pi^0$, $\pi^0\eta\eta$, $\pi^0\pi^0\eta$), GAMS ($\pi p \to \pi^0\pi^0 n$, $\eta\eta n$, $\eta\eta' n$), and BNL ($\pi p \to K\overline{K}n$) data.

Int. J. Mod. Phys. A 2026.41. Downloaded from www.worldscientific.com
by UNIVERSITY OF CALIFORNIA @ BERKELEY on 09/16/26. Re-use and distribution is strictly not permitted, except for Open Access articles.

$\Gamma(K\overline{K})/\Gamma(\eta\eta)$ — Γ_{13}/Γ_{11}

VALUE	CL%	DOCUMENT ID		TECN	COMMENT
1.43±0.24 OUR FIT		Error includes scale factor of 1.1.			
1.85±0.41		BARBERIS	00E		450 $pp \to p_f \eta\eta p_s$
• • • We do not use the following data for averages, fits, limits, etc. • • •					
1.5 ±0.6		[1] ANISOVICH	02D	SPEC	Combined fit
<0.4	90	[2] PROKOSHKIN	91	GAM4	300 $\pi^- p \to \pi^- p \eta\eta$
<0.6		[3] BINON	83	GAM2	38 $\pi^- p \to 2\eta n$

[1] From a combined K-matrix analysis of Crystal Barrel (0. $p\overline{p} \to \pi^0\pi^0\pi^0$, $\pi^0\eta\eta$, $\pi^0\pi^0\eta$), GAMS ($\pi p \to \pi^0\pi^0 n$, $\eta\eta n$, $\eta\eta' n$), and BNL ($\pi p \to K\overline{K} n$) data.
[2] Combining results of GAM4 with those of WA76 on $K\overline{K}$ central production.
[3] Using ETKIN 82B and COHEN 80.

$f_0(1500)$ REFERENCES

ABLIKIM	25CD	JHEP 2510 081	M. Ablikim *et al.*	(BESIII Collab.)
ABLIKIM	22AS	PR D106 072012	M. Ablikim *et al.*	(BESIII Collab.)
Also		PR D107 079901 (errat.)	M. Ablikim *et al.*	(BESIII Collab.)
ABLIKIM	22G	PRL 129 042001	M. Ablikim *et al.*	(BESIII Collab.)
RODAS	22	EPJ C82 80	A. Rodas *et al.*	(JPAC Collab.)
SARANTSEV	21	PL B816 136227	A.V. Sarantsev *et al.*	(BONN, PNPI)
ALBRECHT	20	EPJ C80 453	M. Albrecht *et al.*	(Crystal Barrel Collab.)
ABLIKIM	18AA	PR D98 072003	M. Ablikim *et al.*	(BESIII Collab.)
ROPERTZ	18	EPJ C78 1000	S. Ropertz, C. Hanhart, B. Kubis	(BONN, JULI)
AAIJ	17V	JHEP 1708 037	R. Aaij *et al.*	(LHCb Collab.)
ABLIKIM	15AE	PR D92 052003	M. Ablikim *et al.*	(BESIII Collab.)
DOBBS	15	PR D91 052006	S. Dobbs *et al.*	(NWES)
AAIJ	14BR	PR D89 092006	R. Aaij *et al.*	(LHCb Collab.)
ABLIKIM	13N	PR D87 092009	M. Ablikim *et al.*	(BESIII Collab.)
ANISOVICH	09	IJMP A24 2481	V.V. Anisovich, A.V. Sarantsev	(PNPI)
KLEMPT	08	EPJ C55 39	E. Klempt, M. Matveev, A.V. Sarantsev	(BONN+)
UEHARA	08A	PR D78 052004	S. Uehara *et al.*	(BELLE Collab.)
ABLIKIM	06V	PL B642 441	M. Ablikim *et al.*	(BES Collab.)
AMSLER	06	PL B639 165	C. Amsler *et al.*	(Crystal Barrel Collab.)
AUBERT	06O	PR D74 032003	B. Aubert *et al.*	(BABAR Collab.)
UMAN	06	PR D73 052009	I. Uman *et al.*	(FNAL E835)
VLADIMIRSK...	06	PAN 69 493	V.V. Vladimirsky *et al.*	(ITEP, Moscow)
		Translated from YAF 69 515.		
BINON	05	PAN 68 960	F. Binon *et al.*	
		Translated from YAF 68 998.		
GARMASH	05	PR D71 092003	A. Garmash *et al.*	(BELLE Collab.)
ANISOVICH	03	EPJ A16 229	V.V. Anisovich *et al.*	
BARGIOTTI	03	EPJ C26 371	M. Bargiotti *et al.*	(OBELIX Collab.)
AMSLER	02	EPJ C23 29	C. Amsler *et al.*	(Crystal Barrel Collab.)
ANISOVICH	02D	PAN 65 1545	V.V. Anisovich *et al.*	
		Translated from YAF 65 1583.		
ABELE	01	EPJ C19 667	A. Abele *et al.*	(Crystal Barrel Collab.)
ABELE	01B	EPJ C21 261	A. Abele *et al.*	(Crystal Barrel Collab.)
ACCIARRI	01H	PL B501 173	M. Acciarri *et al.*	(L3 Collab.)
AITALA	01A	PRL 86 765	E.M. Aitala *et al.*	(FNAL E791 Collab.)
BARATE	00E	PL B472 189	R. Barate *et al.*	(ALEPH Collab.)
BARBERIS	00A	PL B471 429	D. Barberis *et al.*	(WA 102 Collab.)
BARBERIS	00C	PL B471 440	D. Barberis *et al.*	(WA 102 Collab.)
BARBERIS	00D	PL B474 423	D. Barberis *et al.*	(WA 102 Collab.)
BARBERIS	00E	PL B479 59	D. Barberis *et al.*	(WA 102 Collab.)
BARBERIS	99	PL B453 305	D. Barberis *et al.*	(Omega Expt.)
BARBERIS	99B	PL B453 316	D. Barberis *et al.*	(Omega Expt.)
BARBERIS	99D	PL B462 462	D. Barberis *et al.*	(Omega Expt.)
BELLAZZINI	99	PL B467 296	R. Bellazzini *et al.*	
FRENCH	99	PL B460 213	B. French *et al.*	(WA76 Collab.)
KAMINSKI	99	EPJ C9 141	R. Kaminski, L. Lesniak, B. Loiseau	(CRAC, PARIN)
ABELE	98	PR D57 3860	A. Abele *et al.*	(Crystal Barrel Collab.)
ALDE	98	EPJ A3 361	D. Alde *et al.*	(GAM4 Collab.)
Also		PAN 62 405	D. Alde *et al.*	(GAMS Collab.)
		Translated from YAF 62 446.		
AMSLER	98	RMP 70 1293	C. Amsler	
ANISOVICH	98B	SPU 41 419	V.V. Anisovich *et al.*	
		Translated from UFN 168 481.		
BERTIN	98	PR D57 55	A. Bertin *et al.*	(OBELIX Collab.)
REYES	98	PRL 81 4079	M.A. Reyes *et al.*	
BARBERIS	97B	PL B413 217	D. Barberis *et al.*	(WA 102 Collab.)
BERTIN	97C	PL B408 476	A. Bertin *et al.*	(OBELIX Collab.)
FRABETTI	97D	PL B407 79	P.L. Frabetti *et al.*	(FNAL E687 Collab.)
ABELE	96	PL B380 453	A. Abele *et al.*	(Crystal Barrel Collab.)
ABELE	96B	PL B385 425	A. Abele *et al.*	(Crystal Barrel Collab.)
ABELE	96C	NP A609 562	A. Abele *et al.*	(Crystal Barrel Collab.)
AMELIN	96B	PAN 59 976	D.V. Amelin *et al.*	(SERP, TBIL)
		Translated from YAF 59 1021.		
BUGG	96	NP B471 59	D.V. Bugg, A.V. Sarantsev, B.S. Zou	(LOQM, PNPI)
AMSLER	95B	PL B342 433	C. Amsler *et al.*	(Crystal Barrel Collab.)
AMSLER	95C	PL B353 571	C. Amsler *et al.*	(Crystal Barrel Collab.)
AMSLER	95D	PL B355 425	C. Amsler *et al.*	(Crystal Barrel Collab.)
ANTINORI	95	PL B353 589	F. Antinori *et al.*	(ATHU, BARI, BIRM+)
BUGG	95	PL B353 378	D.V. Bugg *et al.*	(LOQM, PNPI, WASH)
ABATZIS	94	PL B324 509	S. Abatzis *et al.*	(ATHU, BARI, BIRM+)
AMSLER	94C	PL B327 425	C. Amsler *et al.*	(Crystal Barrel Collab.)
AMSLER	94D	PL B333 277	C. Amsler *et al.*	(Crystal Barrel Collab.)
AMSLER	94E	PL B340 259	C. Amsler *et al.*	(Crystal Barrel Collab.)
ANISOVICH	94	PL B323 233	V.V. Anisovich *et al.*	(Crystal Barrel Collab.)
BUGG	94	PR D50 4412	D.V. Bugg *et al.*	(LOQM)
AMSLER	92	PL B291 347	C. Amsler *et al.*	(Crystal Barrel Collab.)
BELADIDZE	92C	SJNP 55 1535	G.M. Beladidze, S.I. Bityukov, G.V. Borisov	(SERP+)
		Translated from YAF 55 2748.		
PROKOSHKIN	91	SPD 36 155	Y.D. Prokoshkin	(GAM2 and GAM4 Collab.)
		Translated from DANS 316 900.		
ARMSTRONG	89E	PL B228 536	T.A. Armstrong, M. Benayoun	(ATHU, BARI, BIRM+)
ALDE	88	PL B201 160	D.M. Alde *et al.*	(SERP, BELG, LANL, LAPP+)
ASTON	88D	NP B301 525	D. Aston *et al.*	(SLAC, NAGO, CINC, INUS)
ALDE	87	PL B198 286	D.M. Alde *et al.*	(LANL, BRUX, SERP, LAPP)
ALDE	86D	NP B269 485	D.M. Alde *et al.*	(BELG, LAPP, SERP, CERN+)
LONGACRE	86	PL B177 223	R.S. Longacre *et al.*	(BNL, BRAN, CUNY+)
BINON	84C	NC 80A 363	F.G. Binon *et al.*	(BELG, LAPP, SERP+)
BINON	83	NC 78A 313	F.G. Binon *et al.*	(BELG, LAPP, SERP+)
Also		SJNP 38 561	F.G. Binon *et al.*	(BELG, LAPP, SERP+)
		Translated from YAF 38 934.		
GRAY	83	PR D27 307	L. Gray *et al.*	(SYRA)
ETKIN	82B	PR D25 1786	A. Etkin *et al.*	(BNL, CUNY, TUFTS, VAND)
COHEN	80	PR D22 2595	D. Cohen *et al.*	(ANL)
HYAMS	75	NP B100 205	B.D. Hyams *et al.*	(CERN, MPIM)

$f_1(1510)$

$I^G(J^{PC}) = 0^+(1^{++})$

OMITTED FROM SUMMARY TABLE

See the review on "Spectroscopy of Light Meson Resonances."

$f_1(1510)$ MASS

VALUE (MeV)	EVTS	DOCUMENT ID		TECN	COMMENT
1518± 5 OUR AVERAGE		Error includes scale factor of 1.7. See the ideogram below.			
1530±10		ASTON	88C	LASS	11 $K^- p \to K^0_S K^\pm \pi^\mp \Lambda$
1512± 4	600	[1] BIRMAN	88	MPS	8 $\pi^- p \to K^+ \overline{K}^0 \pi^- n$
1526± 6	271	GAVILLET	82	HBC	4.2 $K^- p \to \Lambda K K \pi$
• • • We do not use the following data for averages, fits, limits, etc. • • •					
~ 1525		[2] BAUER	93B		$\gamma\gamma^* \to \pi^+\pi^-\pi^0\pi^0$

[1] From partial wave analysis of $K^+\overline{K}^0\pi^-$ state.
[2] Not seen by AIHARA 88C in the $K^0_S K^\pm \pi^\mp$ final state.

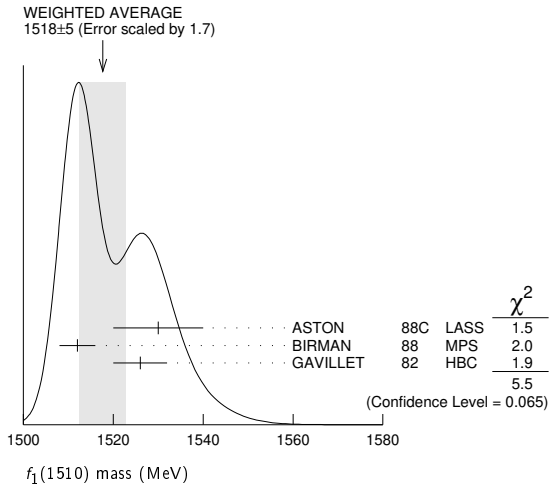

$f_1(1510)$ WIDTH

VALUE (MeV)	EVTS	DOCUMENT ID		TECN	COMMENT
73±25 OUR AVERAGE		Error includes scale factor of 2.5. See the ideogram below.			
100±40		ASTON	88C	LASS	11 $K^- p \to K^0_S K^\pm \pi^\mp \Lambda$
35±15	600	[3] BIRMAN	88	MPS	8 $\pi^- p \to K^+ \overline{K}^0 \pi^- n$
107±15	271	GAVILLET	82	HBC	4.2 $K^- p \to \Lambda K K \pi$

[3] From partial wave analysis of $K^+\overline{K}^0\pi^-$ state.

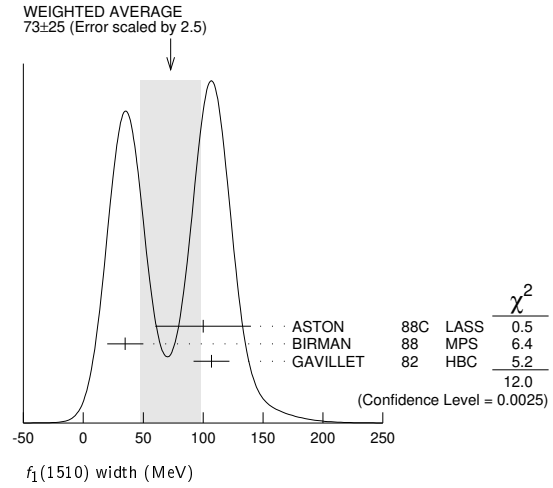

$f_1(1510)$ DECAY MODES

	Mode	Fraction (Γ_i/Γ)
Γ_1	$K\overline{K}^*(892)$ + c.c.	seen
Γ_2	$\pi^+\pi^-\eta'$	seen
Γ_3	$\gamma\phi$	seen

Int. J. Mod. Phys. A 2026.41. Downloaded from www.worldscientific.com
by CALIFORNIA @ BERKELEY on 09/16/26. Re-use and distribution is strictly not permitted, except for Open Access articles.

$f_1(1510)$ BRANCHING RATIOS

$\Gamma(\pi^+\pi^-\eta')/\Gamma_{total}$ — Γ_2/Γ

VALUE	EVTS	DOCUMENT ID		TECN	COMMENT
seen	230	ABLIKIM	11C	BES3	$J/\psi \to \gamma\pi^+\pi^-\eta'$

$\Gamma(\gamma\phi)/\Gamma_{total}$ — Γ_3/Γ

VALUE	DOCUMENT ID		TECN	COMMENT
seen	[4] ABLIKIM	25P	BES3	$J/\psi \to \gamma\gamma\phi$

[4] From a partial wave analysis of $J/\psi \to \gamma\gamma\phi$ with significance 5.3σ.

$f_1(1510)$ REFERENCES

ABLIKIM	25P	PR D111 052011	M. Ablikim *et al.*	(BESIII Collab.)
ABLIKIM	11C	PRL 106 072002	M. Ablikim *et al.*	(BESIII Collab.)
BAUER	93B	PR D48 3976	D.A. Bauer *et al.*	(SLAC)
AIHARA	88C	PR D38 1	H. Aihara *et al.*	(TPC-2γ Collab.)
ASTON	88C	PL B201 573	D. Aston *et al.*	(SLAC, NAGO, CINC, INUS) JP
BIRMAN	88	PRL 61 1557	A. Birman *et al.*	(BNL, FSU, IND, MASD) JP
GAVILLET	82	ZPHY C16 119	P. Gavillet *et al.*	(CERN, CDEF, PADO+)

$f'_2(1525)$

$I^G(J^{PC}) = 0^+(2^{++})$

$f'_2(1525)$ T-MATRIX POLE $\sqrt{s}$

Note that $\Gamma = -2\,\mathrm{Im}(\sqrt{s})$.

VALUE (MeV)	DOCUMENT ID		TECN	COMMENT
$(1515.7 \pm 4.3 \pm 3.3) - i(33.7 \pm 3.8 \pm 4.1)$	ABLIKIM	25CD	BES3	$e^+e^- \to \psi(2S)$

$f'_2(1525)$ MASS

VALUE (MeV)	DOCUMENT ID
1517.3±2.4 OUR AVERAGE Includes data from the 6 datablocks that follow this one. Error includes scale factor of 2.8. See the ideogram below.	

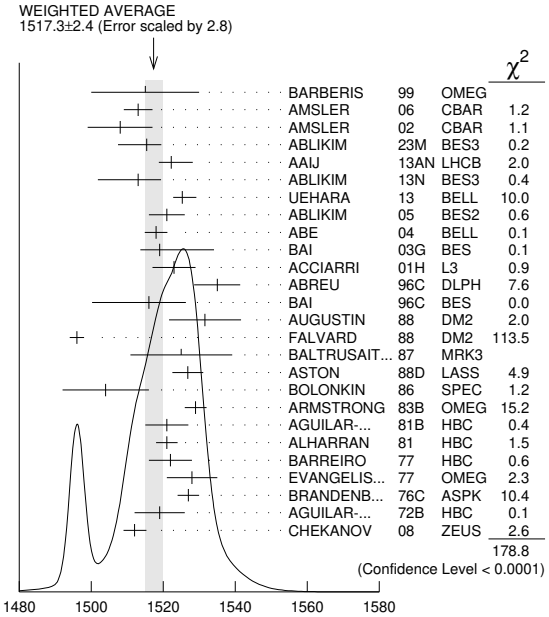

PRODUCED BY PION BEAM

VALUE (MeV)	EVTS	DOCUMENT ID		TECN	COMMENT
The data in this block is included in the average printed for a previous datablock.					
• • • We do not use the following data for averages, fits, limits, etc. • • •					
1521 ± 13		TIKHOMIROV	03	SPEC	$40.0\ \pi^- C \to K^0_S K^0_S K^0_L X$
1547^{+10}_{-2}		[1] LONGACRE	86	MPS	$22\ \pi^- p \to K^0_S K^0_S n$
1496^{+9}_{-8}		[2] CHABAUD	81	ASPK	$6\ \pi^- p \to K^+ K^- n$
1497^{+8}_{-9}		CHABAUD	81	ASPK	$18.4\ \pi^- p \to K^+ K^- n$
1492 ± 29		GORLICH	80	ASPK	$17\ \pi^- p$polarized $\to K^+ K^- n$
1502 ± 25		[3] CORDEN	79	OMEG	12–$15\ \pi^- p \to \pi^+\pi^- n$
1480	14	CRENNELL	66	HBC	$6.0\ \pi^- p \to K^0_S K^0_S n$

[1] From a partial-wave analysis of data using a K-matrix formalism with 5 poles.
[2] CHABAUD 81 is a reanalysis of PAWLICKI 77 data.
[3] From an amplitude analysis where the $f'_2(1525)$ width and elasticity are in complete disagreement with the values obtained from $K\overline{K}$ channel, making the solution dubious.

PRODUCED BY $K^\pm$ BEAM

VALUE (MeV)	EVTS	DOCUMENT ID		TECN	COMMENT
The data in this block is included in the average printed for a previous datablock.					
1518.0± 2.7 OUR AVERAGE Includes data from the datablock that follows this one. Error includes scale factor of 2.9. See the ideogram below.					
1526.8 ± 4.3		ASTON	88D	LASS	$11\ K^- p \to K^0_S K^0_S \Lambda$
1504 ± 12		BOLONKIN	86	SPEC	$40\ K^- p \to K^0_S K^0_S Y$
1529 ± 3		ARMSTRONG	83B	OMEG	$18.5\ K^- p \to K^- K^+ \Lambda$
1521 ± 6	650	AGUILAR-...	81B	HBC	$4.2\ K^- p \to \Lambda K^+ K^-$
1521 ± 3	572	ALHARRAN	81	HBC	$8.25\ K^- p \to \Lambda K\overline{K}$
1522 ± 6	123	BARREIRO	77	HBC	$4.15\ K^- p \to \Lambda K^0_S K^0_S$
1528 ± 7	166	EVANGELIS...	77	OMEG	$10\ K^- p \to K^+ K^-(\Lambda, \Sigma)$
1527 ± 3	120	BRANDENB...	76C	ASPK	$13\ K^- p \to K^+ K^-(\Lambda, \Sigma)$
1519 ± 7	100	AGUILAR-...	72B	HBC	$3.9, 4.6\ K^- p \to K\overline{K}(\Lambda, \Sigma)$
• • • We do not use the following data for averages, fits, limits, etc. • • •					
1514 ± 8	61	BINON	07	GAMS	$32.5\ K^- p \to \eta\eta(\Lambda/\Sigma^0)$
1513 ± 10		[1] BARKOV	99	SPEC	$40\ K^- p \to K^0_S K^0_S y$

[1] Systematic errors not estimated.

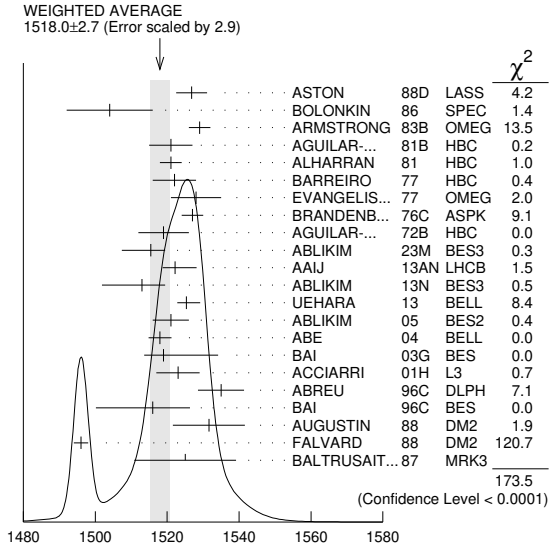

PRODUCED IN e^+e^- ANNIHILATION AND PARTICLE DECAYS

VALUE (MeV)	EVTS	DOCUMENT ID		TECN	COMMENT
The data in this block is included in the average printed for a previous datablock.					
1514 ± 4 OUR AVERAGE Error includes scale factor of 3.6. See the ideogram below.					
$1515.4 \pm 2.5^{+3.2}_{-7.6}$	126k	ABLIKIM	23M	BES3	$J/\psi \to \gamma K^0_S K^0_S \pi^0$
$1522.2 \pm 2.8^{+5.3}_{-2.0}$		AAIJ	13AN	LHCB	$\overline{B}^0_s \to J/\psi K^+ K^-$
$1513 \pm 5\ ^{+4}_{-10}$	5.5k	[1] ABLIKIM	13N	BES3	$e^+e^- \to J/\psi \to \gamma\eta\eta$
$1525.3^{+1.2}_{-1.4} \pm 3.7 \pm 2.1$		UEHARA	13	BELL	$\gamma\gamma \to K^0_S K^0_S$
1521 ± 5		ABLIKIM	05	BES2	$J/\psi \to \phi K^+ K^-$
$1518 \pm 1 \pm 3$		ABE	04	BELL	$10.6\ e^+e^- \to e^+e^- K^+ K^-$
$1519 \pm 2\ ^{+15}_{-5}$		BAI	03G	BES	$J/\psi \to \gamma K\overline{K}$
1523 ± 6	331	[2] ACCIARRI	01H	L3	$91, 183$–$209\ e^+e^- \to e^+e^- K^0_S K^0_S$
$1535 \pm 5 \pm 4$		ABREU	96C	DLPH	$Z^0 \to K^+ K^- + X$
$1516 \pm 5\ ^{+9}_{-15}$		BAI	96C	BES	$J/\psi \to \gamma K^+ K^-$
1531.6 ± 10.0		AUGUSTIN	88	DM2	$J/\psi \to \gamma K^+ K^-$
1496 ± 2		[3] FALVARD	88	DM2	$J/\psi \to \phi K^+ K^-$
$1525 \pm 10 \pm 10$		BALTRUSAIT...	87	MRK3	$J/\psi \to \gamma K^+ K^-$
• • • We do not use the following data for averages, fits, limits, etc. • • •					
1518 ± 3		[4] KLEMPT	22	RVUE	$J/\psi(1S) \to \gamma\pi^0\pi^0$, $\gamma K^0_S K^0_S$
1503 ± 11		[5] RODAS	22	RVUE	$J/\psi(1S) \to \gamma(\pi\pi, K\overline{K})$
$1532 \pm 3 \pm 6$	644	[6,7] DOBBS	15		$J/\psi \to \gamma K^+ K^-$
$1557 \pm 9 \pm 3$	113	[6,7] DOBBS	15		$\psi(2S) \to \gamma K^+ K^-$

Int. J. Mod. Phys. A 2026.41. Downloaded from www.worldscientific.com
by UNIVERSITY OF CALIFORNIA @ BERKELEY on 09/16/26. Re-use and distribution is strictly not permitted, except for Open Access articles.

1526 ± 7	29	[8] LEES	14H	BABR	$e^+e^- \to K^0_S K^0_S K^+ K^- \gamma$
1523 ± 5	870	[9] SCHEGELSKY	06A	RVUE	$\gamma\gamma \to K^0_S K^0_S$
1515 ± 5		[10] FALVARD	88	DM2	$J/\psi \to \phi K^+ K^-$

[1] From partial wave analysis including all possible combinations of 0^{++}, 2^{++}, and 4^{++} resonances.
[2] Supersedes ACCIARRI 95J.
[3] From an analysis including interference with $f_0(1710)$.
[4] Fit of the tensor partial waves from BES3 in the multipole basis.
[5] T-matrix pole from coupled channel K-matrix fit to data on $J/\psi \to \gamma\pi^0\pi^0$ (ABLIKIM 15AE) and $J/\psi \to \gamma K^0_S K^0_S$ (ABLIKIM 18AA).
[6] Using CLEO-c data but not authored by the CLEO Collaboration.
[7] From a fit to a Breit-Wigner line shape with fixed $\Gamma = 73$ MeV.
[8] From a fit to a Breit-Wigner line shape plus a second-order polynomial function. Systematic errors not evaluated.
[9] From analysis of L3 data at 91 and 183–209 GeV.
[10] From an analysis ignoring interference with $f_0(1710)$.

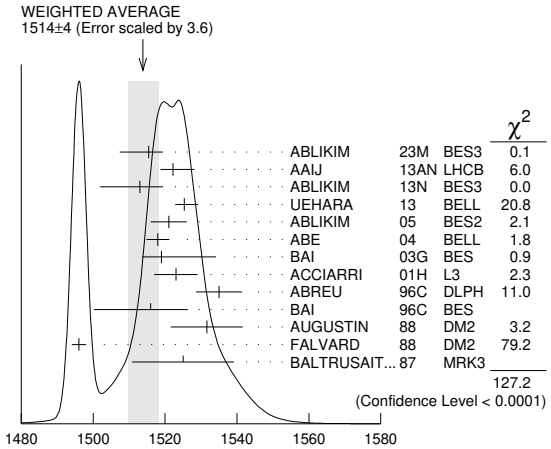

$f_2'(1525)$ mass, e^+e^- annihilation and particle decays (MeV)

PRODUCED IN $\overline{p}p$ ANNIHILATION

VALUE (MeV)	DOCUMENT ID		TECN	COMMENT
The data in this block is included in the average printed for a previous datablock.				
1512 ± 4 OUR AVERAGE				
1513 ± 4	AMSLER	06	CBAR	$0.9\ \overline{p}p \to K^+K^-\pi^0$
1508 ± 9	[1] AMSLER	02	CBAR	$0.9\ \overline{p}p \to \pi^0\eta, \pi^0\pi^0\pi^0$
• • • We do not use the following data for averages, fits, limits, etc. • • •				
1495.0± 1.1±8.1	[2] ALBRECHT	20	RVUE	$0.9\ \overline{p}p \to \pi^0\pi^0\eta,\ \pi^0\eta\eta,\ \pi^0K^+K^-$
1530 ±12	[3] ANISOVICH	09	RVUE	$0.0\ \overline{p}p,\ \pi N$

[1] T-matrix pole.
[2] T-matrix pole, 4 poles, 4 channels, including scattering data from HYAMS 75 ($\pi\pi$), LONGACRE 86 ($K\overline{K}$), BINON 83 ($\eta\eta$).
[3] 4-poles, 5-channel K matrix fit.

CENTRAL PRODUCTION

VALUE (MeV)	DOCUMENT ID		TECN	COMMENT
The data in this block is included in the average printed for a previous datablock.				
1515±15	BARBERIS	99	OMEG	450 $pp \to p_s p_f K^+K^-$

PRODUCED IN ep COLLISIONS

VALUE (MeV)	EVTS	DOCUMENT ID		TECN	COMMENT
The data in this block is included in the average printed for a previous datablock.					
$1512\pm3^{+1.4}_{-0.5}$		[1] CHEKANOV	08	ZEUS	$ep \to K^0_S K^0_S X$
• • • We do not use the following data for averages, fits, limits, etc. • • •					
1537^{+9}_{-8}	84	[2] CHEKANOV	04	ZEUS	$ep \to K^0_S K^0_S X$

[1] In the SU(3) based model with a specific interference pattern of the $f_2(1270)$, $a_2^0(1320)$, and $f_2'(1525)$ mesons incoherently added to the $f_0(1710)$ and non-resonant background.
[2] Systematic errors not estimated.

$f_2'(1525)$ WIDTH

VALUE (MeV)	DOCUMENT ID
72^{+7}_{-6} OUR FIT	
84.4±2.7 OUR AVERAGE Includes data from the 6 datablocks that follow this one. Error includes scale factor of 1.7. See the ideogram below.	

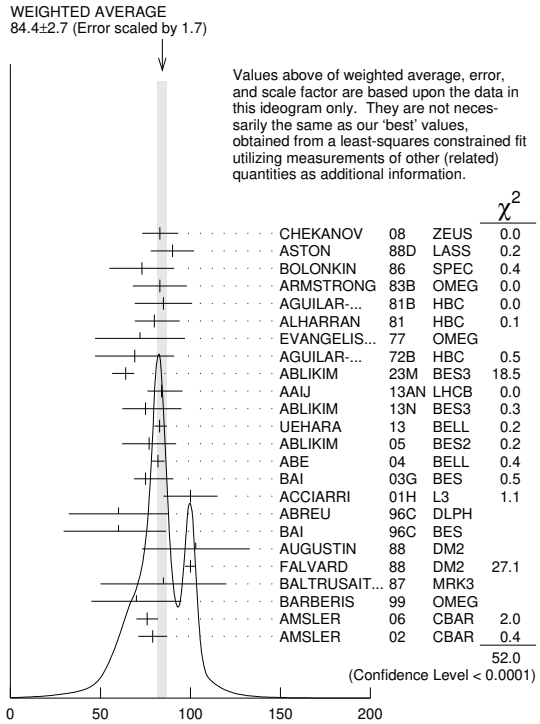

$f_2'(1525)$ WIDTH (MeV)

PRODUCED BY PION BEAM

VALUE (MeV)	DOCUMENT ID		TECN	COMMENT
The data in this block is included in the average printed for a previous datablock.				
• • • We do not use the following data for averages, fits, limits, etc. • • •				
102±42	TIKHOMIROV	03	SPEC	$40.0\ \pi^- C \to K^0_S K^0_S K^0_L X$
108^{+5}_{-2}	[1] LONGACRE	86	MPS	$22\ \pi^- p \to K^0_S K^0_S n$
69^{+22}_{-16}	[2] CHABAUD	81	ASPK	$6\ \pi^- p \to K^+K^- n$
137^{+23}_{-21}	CHABAUD	81	ASPK	$18.4\ \pi^- p \to K^+K^- n$
150^{+83}_{-50}	GORLICH	80	ASPK	$17\ \pi^- p$ polarized $\to K^+K^- n$
165±42	[3] CORDEN	79	OMEG	12–$15\ \pi^- p \to \pi^+\pi^- n$
92^{+39}_{-22}	[4] POLYCHRO...	79	STRC	$7\ \pi^- p \to n K^0_S K^0_S$

[1] From a partial-wave analysis of data using a K-matrix formalism with 5 poles.
[2] CHABAUD 81 is a reanalysis of PAWLICKI 77 data.
[3] From an amplitude analysis where the $f_2'(1525)$ width and elasticity are in complete disagreement with the values obtained from $K\overline{K}$ channel, making the solution dubious.
[4] From a fit to the D with $f_2(1270)$-$f_2'(1525)$ interference. Mass fixed at 1516 MeV.

PRODUCED BY $K^\pm$ BEAM

VALUE (MeV)	EVTS	DOCUMENT ID		TECN	COMMENT
The data in this block is included in the average printed for a previous datablock.					
82± 6 OUR AVERAGE					
90±12		ASTON	88D	LASS	$11\ K^-p \to K^0_S K^0_S \Lambda$
73±18		BOLONKIN	86	SPEC	$40\ K^-p \to K^0_S K^0_S Y$
83±15		ARMSTRONG	83B	OMEG	$18.5\ K^-p \to K^-K^+\Lambda$
85±16	650	AGUILAR-...	81B	HBC	$4.2\ K^-p \to \Lambda K^+K^-$
80^{+14}_{-11}	572	ALHARRAN	81	HBC	$8.25\ K^-p \to \Lambda K\overline{K}$
72±25	166	EVANGELIS...	77	OMEG	$10\ K^-p \to K^+K^-(\Lambda,\Sigma)$
69±22	100	AGUILAR-...	72B	HBC	$3.9,4.6\ K^-p \to K\overline{K}(\Lambda,\Sigma)$
• • • We do not use the following data for averages, fits, limits, etc. • • •					
92^{+25}_{-16}	61	BINON	07	GAMS	$32.5\ K^-p \to \eta\eta(\Lambda/\Sigma^0)$
75±20		[1] BARKOV	99	SPEC	$40\ K^-p \to K^0_S K^0_S y$
62^{+19}_{-14}	123	BARREIRO	77	HBC	$4.15\ K^-p \to \Lambda K^0_S K^0_S$
61± 8	120	BRANDENB...	76C	ASPK	$13\ K^-p \to K^+K^-(\Lambda,\Sigma)$

[1] Systematic errors not estimated.

PRODUCED IN e^+e^- ANNIHILATION AND PARTICLE DECAYS

VALUE (MeV)	EVTS	DOCUMENT ID		TECN	COMMENT
The data in this block is included in the average printed for a previous datablock.					
86 ± 4 OUR AVERAGE Error includes scale factor of 2.4. See the ideogram below.					
$64.0\pm 4.3^{+2.0}_{-6.1}$	126k	ABLIKIM	23M	BES3	$J/\psi \to \gamma K^0_S K^0_S \pi^0$

$84 \pm 6 \; {}^{+10}_{-5}$			AAIJ	13AN	LHCB	$\overline{B}^0_s \to J/\psi K^+ K^-$
$75 \; {}^{+12}_{-10} \; {}^{+16}_{-8}$	5.5k	[1]	ABLIKIM	13N	BES3	$e^+e^- \to J/\psi \to \gamma\eta\eta$
$82.9 \pm 2.1 \pm 3.3$			UEHARA	13	BELL	$\gamma\gamma \to K^0_S K^0_S$
77 ± 15			ABLIKIM	05	BES2	$J/\psi \to \phi K^+ K^-$
$82 \pm 2 \pm 3$			ABE	04	BELL	$10.6\ e^+e^- \to e^+e^- K^+ K^-$
$75 \pm 4 \; {}^{+15}_{-5}$			BAI	03G	BES	$J/\psi \to \gamma K\overline{K}$
100 ± 15	331	[2]	ACCIARRI	01H	L3	$91, 183–209\ e^+e^- \to e^+e^- K^0_S K^0_S$
$60 \pm 20 \pm 19$			ABREU	96C	DLPH	$Z^0 \to K^+ K^- + X$
$60 \pm 23 \; {}^{+13}_{-20}$			BAI	96C	BES	$J/\psi \to \gamma K^+ K^-$
103 ± 30			AUGUSTIN	88	DM2	$J/\psi \to \gamma K^+ K^-$
100 ± 3		[3]	FALVARD	88	DM2	$J/\psi \to \phi K^+ K^-$
85 ± 35			BALTRUSAIT...	87	MRK3	$J/\psi \to \gamma K^+ K^-$
• • • We do not use the following data for averages, fits, limits, etc. • • •						
78 ± 6		[4]	KLEMPT	22	RVUE	$J/\psi(1S) \to \gamma\pi^0\pi^0, \gamma K^0_S K^0_S$
84 ± 15		[5]	RODAS	22	RVUE	$J/\psi(1S) \to \gamma\ (\pi\pi, K\overline{K})$
37 ± 12	29	[6]	LEES	14H	BABR	$e^+e^- \to K^0_S K^0_S K^+ K^- \gamma$
104 ± 10	870	[7]	SCHEGELSKY	06A	RVUE	$\gamma\gamma \to K^0_S K^0_S$
62 ± 10		[8]	FALVARD	88	DM2	$J/\psi \to \phi K^+ K^-$

[1] From partial wave analysis including all possible combinations of 0^{++}, 2^{++}, and 4^{++} resonances.
[2] Supersedes ACCIARRI 95J.
[3] From an analysis including interference with $f_0(1710)$.
[4] Fit of the tensor partial waves from BES3 in the multipole basis.
[5] T-matrix pole from coupled channel K-matrix fit to data on $J/\psi \to \gamma\pi^0\pi^0$ (ABLIKIM 15AE) and $J/\psi \to \gamma K^0_S K^0_S$ (ABLIKIM 18AA).
[6] From a fit to a Breit-Wigner line shape plus a second-order polynomial function. Systematic errors not evaluated.
[7] From analysis of L3 data at 91 and 183–209 GeV.
[8] From an analysis ignoring interference with $f_0(1710)$.

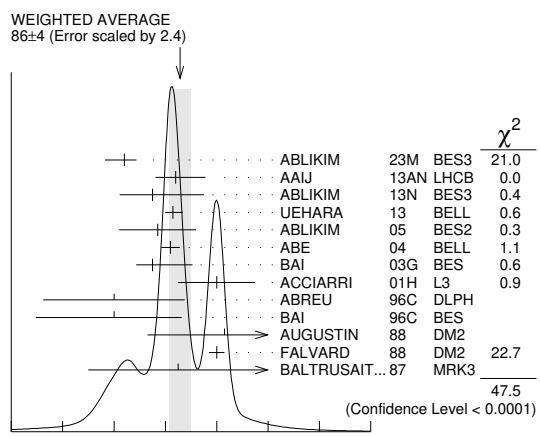

$f'_2(1525)$ width, e^+e^- annihilation and particle decays (MeV)

PRODUCED IN $\overline{p}p$ ANNIHILATION

VALUE (MeV)	DOCUMENT ID		TECN	COMMENT
The data in this block is included in the average printed for a previous datablock.				
77 ± 5 OUR AVERAGE				
76 ± 6	AMSLER	06	CBAR	$0.9\ \overline{p}p \to K^+ K^- \pi^0$
79 ± 8	[1] AMSLER	02	CBAR	$0.9\ \overline{p}p \to \pi^0\eta\eta, \pi^0\pi^0\pi^0$
• • • We do not use the following data for averages, fits, limits, etc. • • •				
$104.8 \pm 0.9 \pm 9.8$	[2] ALBRECHT	20	RVUE	$0.9\ \overline{p}p \to \pi^0\pi^0\eta, \pi^0\eta\eta, \pi^0 K^+ K^-$
128 ± 20	[3] ANISOVICH	09	RVUE	$0.0\ \overline{p}p, \pi N$

[1] T-matrix pole.
[2] T-matrix pole, 4 poles, 4 channels, including scattering data from HYAMS 75 ($\pi\pi$), LONGACRE 86 ($K\overline{K}$), BINON 83 ($\eta\eta$).
[3] K-matrix, 4-poles, 5-channel fit.

CENTRAL PRODUCTION

VALUE (MeV)	DOCUMENT ID		TECN	COMMENT
The data in this block is included in the average printed for a previous datablock.				
70 ± 25	BARBERIS	99	OMEG	$450\ pp \to p_s p_f K^+ K^-$

PRODUCED IN ep COLLISIONS

VALUE (MeV)	EVTS	DOCUMENT ID		TECN	COMMENT
The data in this block is included in the average printed for a previous datablock.					
$83 \pm 9 \; {}^{+5}_{-4}$		[1] CHEKANOV	08	ZEUS	$ep \to K^0_S K^0_S X$
• • • We do not use the following data for averages, fits, limits, etc. • • •					
$50 \; {}^{+34}_{-22}$	84	[2] CHEKANOV	04	ZEUS	$ep \to K^0_S K^0_S X$

[1] In the SU(3) based model with a specific interference pattern of the $f_2(1270)$, $a^0_2(1320)$, and $f'_2(1525)$ mesons incoherently added to the $f_0(1710)$ and non-resonant background.
[2] Systematic errors not estimated.

$f'_2(1525)$ DECAY MODES

	Mode	Fraction (Γ_i/Γ)
Γ_1	$K\overline{K}$	(88.8 ± 2.2) %
Γ_2	$\eta\eta$	(10.3 ± 2.2) %
Γ_3	$\pi\pi$	$(8.2 \pm 1.5) \times 10^{-3}$
Γ_4	$K\overline{K}^*(892) +$ c.c.	
Γ_5	$\pi K\overline{K}$	
Γ_6	$\pi\pi\eta$	
Γ_7	$\pi^+\pi^+\pi^-\pi^-$	
Γ_8	$\gamma\phi$	seen
Γ_9	$\gamma\gamma$	$(1.12 \pm 0.15) \times 10^{-6}$

CONSTRAINED FIT INFORMATION

An overall fit to 2 partial widths, a combination of partial widths obtained from integrated cross sections, and 3 branching ratios uses 16 measurements and one constraint to determine 5 parameters. The overall fit has a $\chi^2 = 14.2$ for 12 degrees of freedom.

The following *off-diagonal* array elements are the correlation coefficients $\langle \delta x_i \delta x_j \rangle / (\delta x_i \cdot \delta x_j)$, in percent, from the fit to the branching fractions, $x_i \equiv \Gamma_i/\Gamma_{total}$. The fit constrains the x_i whose labels appear in this array to sum to one.

	x_1	x_2	x_3	x_9
x_2	−100			
x_3	−5	−1		
x_9	0	0	1	
Γ	−28	28	−1	−62

	Mode	Rate (MeV)
Γ_1	$K\overline{K}$	$64 \; {}^{+6}_{-5}$
Γ_2	$\eta\eta$	7.4 ± 1.9
Γ_3	$\pi\pi$	0.59 ± 0.12
Γ_9	$\gamma\gamma$	$(8.1 \pm 0.9) \times 10^{-5}$

$f'_2(1525)$ PARTIAL WIDTHS

$\Gamma(K\overline{K})$ — Γ_1

VALUE (MeV)	DOCUMENT ID		TECN	COMMENT
$64 \; {}^{+6}_{-5}$ OUR FIT				
$63 \; {}^{+6}_{-5}$	[1] LONGACRE	86	MPS	$22\ \pi^- p \to K^0_S K^0_S n$

[1] From a partial-wave analysis of data using a K-matrix formalism with 5 poles.

$\Gamma(\eta\eta)$ — Γ_2

VALUE (MeV)	EVTS	DOCUMENT ID		TECN	COMMENT
7.4 ± 1.9 OUR FIT					
• • • We do not use the following data for averages, fits, limits, etc. • • •					
5.0 ± 0.8	870	[1] SCHEGELSKY	06A	RVUE	$\gamma\gamma \to K^0_S K^0_S$
$24 \; {}^{+3}_{-1}$		[2] LONGACRE	86	MPS	$22\ \pi^- p \to K^0_S K^0_S n$

[1] From analysis of L3 data at 91 and 183–209 GeV, using $\Gamma(f'_2(1525) \to K\overline{K}) = 68$ MeV and SU(3) relations.
[2] From a partial-wave analysis of data using a K-matrix formalism with 5 poles.

$\Gamma(\pi\pi)$ — Γ_3

VALUE (MeV)	EVTS	DOCUMENT ID		TECN	COMMENT
0.59 ± 0.12 OUR FIT					
$1.4 \; {}^{+1.0}_{-0.5}$		[1] LONGACRE	86	MPS	$22\ \pi^- p \to K^0_S K^0_S n$
• • • We do not use the following data for averages, fits, limits, etc. • • •					
$0.2 \; {}^{+1.0}_{-0.2}$	870	[2] SCHEGELSKY	06A	RVUE	$\gamma\gamma \to K^0_S K^0_S$

[1] From a partial-wave analysis of data using a K-matrix formalism with 5 poles.
[2] From analysis of L3 data at 91 and 183–209 GeV, using $\Gamma(f'_2(1525) \to K\overline{K}) = 68$ MeV and SU(3) relations.

Int. J. Mod. Phys. A 2026.41. Downloaded from www.worldscientific.com
by [redacted] LIFORNIA @ BERKELEY on 09/16/26. Re-use and distribution is strictly not permitted, except for Open Access articles.

Int. J. Mod. Phys. A 2026.41. Downloaded from www.worldscientific.com
by UNIVERSITY OF CALIFORNIA @ BERKELEY on 09/16/26. Re-use and distribution is strictly not permitted, except for Open Access articles.

$\Gamma(\gamma\gamma)$ — Γ_9

VALUE (keV)	EVTS	DOCUMENT ID		TECN	COMMENT
0.081±0.009 OUR FIT					
• • • We do not use the following data for averages, fits, limits, etc. • • •					
0.13 ±0.03	870	[1] SCHEGELSKY	06A	RVUE	$\gamma\gamma \to K^0_S K^0_S$

[1] From analysis of L3 data at 91 and 183–209 GeV, using $\Gamma(f'_2(1525) \to K\overline{K}) = 68$ MeV and SU(3) relations.

$\Gamma(K\overline{K})/\Gamma_{total}$ — Γ_1/Γ

VALUE	DOCUMENT ID		TECN	COMMENT
• • • We do not use the following data for averages, fits, limits, etc. • • •				
$0.746 \pm 0.002^{+0.166}_{-0.162}$	[1] ALBRECHT	20	RVUE	0.9 $\overline{p}p \to \pi^0\pi^0\eta$, $\pi^0\eta\eta$, $\pi^0 K^+K^-$

[1] Residue from T-matrix pole, 4 poles, 4 channels, including scattering data from HYAMS 75 ($\pi\pi$), LONGACRE 86 ($K\overline{K}$), BINON 83 ($\eta\eta$).

$f'_2(1525)$ $\Gamma(i)\Gamma(\gamma\gamma)/\Gamma(total)$

$\Gamma(K\overline{K}) \times \Gamma(\gamma\gamma)/\Gamma_{total}$ — $\Gamma_1\Gamma_9/\Gamma$

VALUE (keV)	EVTS	DOCUMENT ID		TECN	COMMENT
0.072 ±0.007 OUR FIT					
0.072 ±0.007 OUR AVERAGE					
0.048 $^{+0.067}_{-0.008}$ $^{+0.108}_{-0.012}$		UEHARA	13	BELL	$\gamma\gamma \to K^0_S K^0_S$
0.0564±0.0048±0.0116		ABE	04	BELL	10.6 $e^+e^- \to e^+e^-K^+K^-$
0.076 ±0.006 ±0.011	331	[1] ACCIARRI	01H	L3	$e^+e^- \to e^+e^-K^0_S K^0_S$
0.067 ±0.008 ±0.015		[2] ALBRECHT	90G	ARG	$e^+e^- \to e^+e^-K^+K^-$
0.11 $^{+0.03}_{-0.02}$ ±0.02		BEHREND	89C	CELL	$e^+e^- \to e^+e^-K^0_S K^0_S$
0.10 $^{+0.04}_{-0.03}$ $^{+0.03}_{-0.02}$		BERGER	88	PLUT	$e^+e^- \to e^+e^-K^0_S K^0_S$
0.12 ±0.07 ±0.04		[2] AIHARA	86B	TPC	$e^+e^- \to e^+e^-K^+K^-$
0.11 ±0.02 ±0.04		[2] ALTHOFF	83	TASS	$e^+e^- \to e^+e^-K\overline{K}$
• • • We do not use the following data for averages, fits, limits, etc. • • •					
0.0314±0.0050±0.0077		[3] ALBRECHT	90G	ARG	$e^+e^- \to e^+e^-K^+K^-$

[1] Supersedes ACCIARRI 95J. From analysis of L3 data at 91 and 183–209 GeV,
[2] Using an incoherent background.
[3] Using a coherent background.

$f'_2(1525)$ BRANCHING RATIOS

$\Gamma(\eta\eta)/\Gamma_{total}$ — Γ_2/Γ

VALUE	DOCUMENT ID		TECN	COMMENT
• • • We do not use the following data for averages, fits, limits, etc. • • •				
0.059±0.003±0.026	[1] ALBRECHT	20	RVUE	0.9 $\overline{p}p \to \pi^0\pi^0\eta$, $\pi^0\eta\eta$, $\pi^0K^+K^-$
seen	UEHARA	10A	BELL	10.6 $e^+e^- \to e^+e^-\eta\eta$
0.10 ±0.03	[2] PROKOSHKIN	91	GAM4	300 $\pi^-p \to \pi^-p\eta\eta$

[1] Residue from T-matrix pole, 4 poles, 4 channels, including scattering data from HYAMS 75 ($\pi\pi$), LONGACRE 86 ($K\overline{K}$), BINON 83 ($\eta\eta$).
[2] Combining results of GAM4 with those of WA76 on $K\overline{K}$ central production and results of CBAL, MRK3 and DM2 on $J/\psi \to \gamma\eta\eta$.

$\Gamma(\eta\eta)/\Gamma(K\overline{K})$ — Γ_2/Γ_1

VALUE	CL%	EVTS	DOCUMENT ID		TECN	COMMENT
0.116±0.028 OUR FIT						
0.115±0.028 OUR AVERAGE						
0.119±0.015±0.036		61	[1] BINON	07	GAMS	32.5 $K^-p \to \eta\eta(\Lambda/\Sigma^0)$
0.11 ±0.04			[2] PROKOSHKIN	91	GAM4	300 $\pi^-p \to \pi^-p\eta\eta$
• • • We do not use the following data for averages, fits, limits, etc. • • •						
< 0.14	90		BARBERIS	00E		450 $pp \to p_f\eta\eta p_s$
< 0.50			BARNES	67	HBC	4.6,5.0 K^-p

[1] Using the compilation of the cross sections for $f'_2(1525)$ production in K^-p collisions from ASTON 88D.
[2] Combining results of GAM4 with those of WA76 on $K\overline{K}$ central production and results of CBAL, MRK3 and DM2 on $J/\psi \to \gamma\eta\eta$.

$\Gamma(\pi\pi)/\Gamma_{total}$ — Γ_3/Γ

VALUE (units 10^{-2})	CL%	DOCUMENT ID		TECN	COMMENT
0.82±0.16 OUR FIT					
0.75±0.16 OUR AVERAGE					
0.7 ±0.2		COSTA	80	OMEG	10 $\pi^-p \to K^+K^-n$
2.7 $^{+7.1}_{-1.3}$		[1] GORLICH	80	ASPK	17,18 π^-p
0.75±0.25		[1,2] MARTIN	79	RVUE	
• • • We do not use the following data for averages, fits, limits, etc. • • •					
3.4 ±1.5 ±1.0		[3] ALBRECHT	20	RVUE	0.9 $\overline{p}p \to \pi^0\pi^0\eta$, $\pi^0\eta\eta$, $\pi^0K^+K^-$
< 6	95	AGUILAR-...	81B	HBC	4.2 $K^-p \to \Lambda K^+K^-$
19 ±3		CORDEN	79	OMEG	12–15 $\pi^-p \to \pi^+\pi^-n$
< 4.5	95	BARREIRO	77	HBC	4.15 $K^-p \to \Lambda K^0_S K^0_S$
1.2 ±0.4		[1] PAWLICKI	77	SPEC	6 $\pi N \to K^+K^-N$
< 6.3	90	BRANDENB...	76C	ASPK	13 $K^-p \to K^+K^-(\Lambda,\Sigma)$
< 0.86		[1] BEUSCH	75B	OSPK	8.9 $\pi^-p \to K^0\overline{K}^0n$

[1] Assuming that the $f'_2(1525)$ is produced by an one-pion exchange production mechanism.
[2] MARTIN 79 uses the PAWLICKI 77 data with different input value of the $f'_2(1525) \to K\overline{K}$ branching ratio.
[3] Residue from T-matrix pole, 4 poles, 4 channels, including scattering data from HYAMS 75 ($\pi\pi$), LONGACRE 86 ($K\overline{K}$), BINON 83 ($\eta\eta$).

$\Gamma(\pi\pi)/\Gamma(K\overline{K})$ — Γ_3/Γ_1

VALUE	DOCUMENT ID		TECN	COMMENT
0.0092±0.0018 OUR FIT				
0.075 ±0.035	AUGUSTIN	87	DM2	$J/\psi \to \gamma\pi^+\pi^-$

$[\Gamma(K\overline{K}^*(892)+c.c.)+\Gamma(\pi K\overline{K})]/\Gamma(K\overline{K})$ — $(\Gamma_4+\Gamma_5)/\Gamma_1$

VALUE	CL%	DOCUMENT ID		TECN	COMMENT
• • • We do not use the following data for averages, fits, limits, etc. • • •					
<0.35	95	AGUILAR-...	72B	HBC	3.9,4.6 K^-p
<0.4	67	AMMAR	67	HBC	

$\Gamma(\pi\pi\eta)/\Gamma(K\overline{K})$ — Γ_6/Γ_1

VALUE	CL%	DOCUMENT ID		TECN	COMMENT
• • • We do not use the following data for averages, fits, limits, etc. • • •					
<0.41	95	AGUILAR-...	72B	HBC	3.9,4.6 K^-p
<0.3	67	AMMAR	67	HBC	

$\Gamma(\pi^+\pi^+\pi^-\pi^-)/\Gamma(K\overline{K})$ — Γ_7/Γ_1

VALUE	CL%	DOCUMENT ID		TECN	COMMENT
• • • We do not use the following data for averages, fits, limits, etc. • • •					
<0.32	95	AGUILAR-...	72B	HBC	3.9,4.6 K^-p

$\Gamma(\gamma\phi)/\Gamma_{total}$ — Γ_8/Γ

VALUE	DOCUMENT ID		TECN	COMMENT
seen	[1] ABLIKIM	25P	BES3	$J/\psi \to \gamma\gamma\phi$

[1] From a partial wave analysis of $J/\psi \to \gamma\gamma\phi$ with significance 16.4σ.

$f'_2(1525)$ REFERENCES

ABLIKIM	25CD	JHEP 2510 081	M. Ablikim et al.	(BESIII Collab.)
ABLIKIM	25P	PR D111 052011	M. Ablikim et al.	(BESIII Collab.)
ABLIKIM	23M	JHEP 2303 121	M. Ablikim et al.	(BESIII Collab.)
KLEMPT	22	PL B830 137171	E. Klempt et al.	(BONN)
RODAS	22	EPJ C82 80	A. Rodas et al.	(JPAC Collab.)
ALBRECHT	20	EPJ C80 453	M. Albrecht et al.	(Crystal Barrel Collab.)
ABLIKIM	18AA	PR D98 072003	M. Ablikim et al.	(BESIII Collab.)
ABLIKIM	15AE	PR D92 052003	M. Ablikim et al.	(BESIII Collab.)
DOBBS	15	PR D91 052006	S. Dobbs et al.	(NWES)
LEES	14H	PR D89 092002	J.P. Lees et al.	(BABAR Collab.)
AAIJ	13AN	PR D87 072004	R. Aaij et al.	(LHCb Collab.)
ABLIKIM	13N	PR D87 092009	M. Ablikim et al.	(BESIII Collab.)
UEHARA	13	PTEP 2013 123C01	S. Uehara et al.	(BELLE Collab.)
UEHARA	10A	PR D82 114031	S. Uehara et al.	(BELLE Collab.)
ANISOVICH	09	IJMP A24 2481	V.V. Anisovich, A.V. Sarantsev	(PNPI)
CHEKANOV	08	PRL 101 112003	S. Chekanov et al.	(ZEUS Collab.)
BINON	07	PAN 70 1713	F. Binon et al.	(GAMS Collab.)
		Translated from YAF 70 1758.		
AMSLER	06	PL B639 165	C. Amsler et al.	(Crystal Barrel Collab.)
SCHEGELSKY	06A	EPJ A27 207	V.A. Schegelsky et al.	
ABLIKIM	05	PL B607 243	M. Ablikim et al.	(BES Collab.)
ABE	04	EPJ C32 323	K. Abe et al.	(BELLE Collab.)
CHEKANOV	04	PL B578 33	S. Chekanov et al.	(ZEUS Collab.)
BAI	03G	PR D68 052003	J.Z. Bai et al.	(BES Collab.)
TIKHOMIROV	03	PAN 66 828	G.D. Tikhomirov et al.	
		Translated from YAF 66 860.		
AMSLER	02	EPJ C23 29	C. Amsler et al.	(Crystal Barrel Collab.)
ACCIARRI	01H	PL B501 173	M. Acciarri et al.	(L3 Collab.)
BARBERIS	00E	PL B479 59	D. Barberis et al.	(WA 102 Collab.)
BARBERIS	99	PL B453 305	D. Barberis et al.	(Omega Expt.)
BARKOV	99	JETPL 70 248	B.P. Barkov et al.	
		Translated from ZETFP 70 242.		
ABREU	96C	PL B379 309	P. Abreu et al.	(DELPHI Collab.)
BAI	96C	PRL 77 3959	J.Z. Bai et al.	(BES Collab.)
ACCIARRI	95J	PL B363 118	M. Acciarri et al.	(L3 Collab.)
PROKOSHKIN	91	SPD 36 155	Y.D. Prokoshkin	(GAM2 and GAM4 Collab.)
		Translated from DANS 316 900.		
ALBRECHT	90G	ZPHY C48 183	H. Albrecht et al.	(ARGUS Collab.)
BEHREND	89C	ZPHY C43 91	H.J. Behrend et al.	(CELLO Collab.)
ASTON	88D	NP B301 525	D. Aston et al.	(SLAC, NAGO, CINC, INUS)
AUGUSTIN	88	PRL 60 2238	J.E. Augustin et al.	(DM2 Collab.)
BERGER	88	ZPHY C37 329	C. Berger et al.	(PLUTO Collab.)
FALVARD	88	PR D38 2706	A. Falvard et al.	(CLER, FRAS, LALO+)
AUGUSTIN	87	ZPHY C36 369	J.E. Augustin et al.	(LALO, CLER, FRAS+)
BALTRUSAIT...	87	PR D35 2077	R.M. Baltrusaitis et al.	(Mark III Collab.)
AIHARA	86B	PRL 57 404	H. Aihara et al.	(TPC-2γ Collab.)
BOLONKIN	86	SJNP 43 776	B.V. Bolonkin et al.	(ITEP) JP
		Translated from YAF 43 1211.		
LONGACRE	86	PL B177 223	R.S. Longacre et al.	(BNL, BRAN, CUNY+)
ALTHOFF	83	PL 121B 216	M. Althoff et al.	(TASSO Collab.)
ARMSTRONG	83B	NP B224 193	T.A. Armstrong et al.	(BARI, BIRM, CERN+)
BINON	83	NC 78A 313	F.G. Binon et al.	(BELG, LAPP, SERP+)
AGUILAR-...	81B	ZPHY C8 313	M. Aguilar-Benitez et al.	(CERN, CDEF+)
ALHARRAN	81	NP B191 26	S. Al-Harran et al.	(BIRM, CERN, GLAS+)
CHABAUD	81	APP B12 575	V. Chabaud et al.	(CERN, CRAC, MPIM)
COSTA	80	NP B175 402	G. Costa et al.	(BARI, BONN, CERN, GLAS+)
GORLICH	80	NP B174 16	L. Gorlich et al.	(CRAC, MPIM, CERN+)
CORDEN	79	NP B157 250	M.J. Corden et al.	(BIRM, RHEL, TELA+) JP
MARTIN	79	NP B158 520	A.D. Martin, E.N. Ozmutlu	(DURH)
POLYCHRO...	79	PR D19 1317	V.A. Polychronakos et al.	(NDAM, ANL)
BARREIRO	77	NP B121 237	F. Barreiro et al.	(CERN, AMST, NIJM+)
EVANGELIS...	77	NP B127 384	C. Evangelista et al.	(BARI, BONN, CERN+)
PAWLICKI	77	PR D15 3196	A.J. Pawlicki et al.	(ANL) IJP
BRANDENB...	76C	NP B104 413	G.W. Brandenburg et al.	(SLAC)
BEUSCH	75B	PL 60B 101	W. Beusch et al.	(CERN, ETH)
HYAMS	75	NP B100 205	B.D. Hyams et al.	(CERN, MPIM)
AGUILAR-...	72B	PR D6 29	M. Aguilar-Benitez et al.	(BNL)
AMMAR	67	PRL 19 1071	R. Ammar et al.	(NWES, ANL) JP
BARNES	67	PRL 19 964	V.E. Barnes et al.	(BNL, SYRA) IJPC
CRENNELL	66	PRL 16 1025	D.J. Crennell et al.	(BNL) I

Int. J. Mod. Phys. A 2026.41. Downloaded from www.worldscientific.com by CALIFORNIA @ BERKELEY on 09/16/26. Re-use and distribution is strictly not permitted, except for Open Access articles.

$f_2(1565)$

$I^G(J^{PC}) = 0^+(2^{++})$

Seen mostly in antinucleon-nucleon annihilation. See the review on "Spectroscopy of Light Meson Resonances."

$f_2(1565)$ T-MATRIX POLE $\sqrt{s}$

Note that $\Gamma = -2\,\mathrm{Im}(\sqrt{s})$.

VALUE (MeV)	DOCUMENT ID		TECN	COMMENT
(1495–1560) − i (40–110) OUR ESTIMATE				
$(1560 \pm 15) - i\,(140 \pm 20)$	[1] ANISOVICH	09	RVUE	0.0 $\overline{p}p$, πN
$(1552 \pm 13) - i\,(57 \pm 12)$	AMSLER	02	CBAR	0.9 $\overline{p}p \to \pi^0\eta\eta$, $\pi^0\pi^0\pi^0$
$(1507 \pm 15) - i\,(65 \pm 10)$	BERTIN	97C	OBLX	0.0 $\overline{p}p \to \pi^+\pi^-\pi^0$
$(1534 \pm 20) - i\,(90 \pm 30)$	[2] ABELE	96C	RVUE	Compilation
$(\sim 1552) - i\,(\sim 71)$	[3] AMSLER	95D	CBAR	0.0 $\overline{p}p \to \pi^0\pi^0\pi^0$, $\pi^0\eta\eta$, $\pi^0\pi^0\eta$

[1] On sheet II in a two-pole solution.
[2] T-matrix pole, large coupling to $\rho\rho$ and $\omega\omega$, could be $f_2(1640)$.
[3] Coupled-channel analysis of AMSLER 95B, AMSLER 95C, and AMSLER 94D.

$f_2(1565)$ MASS

VALUE (MeV)	DOCUMENT ID		TECN	COMMENT
1571±13 OUR AVERAGE				
1575±18	[1] BERTIN	98	OBLX	0.05–0.405 $\overline{n}p \to \pi^+\pi^+\pi^-$
1565±20	[1] MAY	90	ASTE	0.0 $\overline{p}p \to \pi^+\pi^-\pi^0$
• • • We do not use the following data for averages, fits, limits, etc. • • •				
1590±10	AMELIN	06	VES	36 $\pi^-p \to \omega\omega n$
1550±10±20	AMELIN	00	VES	37 $\pi^-p \to \eta\pi^+\pi^-n$
1598±11± 9	BAKER	99B	SPEC	0 $\overline{p}p \to \omega\omega\pi^0$
1598±72	BALOSHIN	95	SPEC	40 π^-C $\to K^0_S K^0_S$X
1566^{+80}_{-50}	[2] ANISOVICH	94	CBAR	0.0 $\overline{p}p \to 3\pi^0, \eta\eta\pi^0$
1502± 9	ADAMO	93	OBLX	$\overline{n}p \to \pi^+\pi^+\pi^-$
1488±10	[3] ARMSTRONG	93C	E760	$\overline{p}p \to \pi^0\eta\eta \to 6\gamma$
1508±10	[3] ARMSTRONG	93D	E760	$\overline{p}p \to 3\pi^0 \to 6\gamma$
1525±10	[3] ARMSTRONG	93D	E760	$\overline{p}p \to \eta\pi^0\pi^0 \to 6\gamma$
∼ 1504	[4] WEIDENAUER	93	ASTE	0.0 $\overline{p}N \to 3\pi^-2\pi^+$
1540±15	[3] ADAMO	92	OBLX	$\overline{n}p \to \pi^+\pi^+\pi^-$
1515±10	[5] AKER	91	CBAR	0.0 $\overline{p}p \to 3\pi^0$
1477± 5	BRIDGES	86C	DBC	0.0 $\overline{p}N \to 3\pi^-2\pi^+$

[1] Breit-Wigner mass.
[2] From a simultaneous analysis of the annihilations $\overline{p}p \to 3\pi^0, \pi^0\eta\eta$ including AKER 91 data.
[3] J^P not determined, could be partly $f_0(1500)$.
[4] J^P not determined.
[5] Superseded by AMSLER 95B.

$f_2(1565)$ WIDTH

VALUE (MeV)	DOCUMENT ID		TECN	COMMENT
132± 23 OUR AVERAGE	Error includes scale factor of 1.1.			
119± 24	[1] BERTIN	98	OBLX	0.05–0.405 $\overline{n}p \to \pi^+\pi^+\pi^-$
170± 40	[1] MAY	90	ASTE	0.0 $\overline{p}p \to \pi^+\pi^-\pi^0$
• • • We do not use the following data for averages, fits, limits, etc. • • •				
140± 11	[1,2] AMELIN	06	VES	36 $\pi^-p \to \omega\omega n$
130± 20±40	[1] AMELIN	00	VES	37 $\pi^-p \to \eta\pi^+\pi^-n$
263±101	BALOSHIN	95	SPEC	40 π^-C $\to K^0_S K^0_S$X
166^{+80}_{-20}	[3] ANISOVICH	94	CBAR	0.0 $\overline{p}p \to 3\pi^0, \eta\eta\pi^0$
130± 10	[4] ADAMO	93	OBLX	$\overline{n}p \to \pi^+\pi^+\pi^-$
148± 27	[5] ARMSTRONG	93C	E760	$\overline{p}p \to \pi^0\eta\eta \to 6\gamma$
103± 15	[5] ARMSTRONG	93D	E760	$\overline{p}p \to 3\pi^0 \to 6\gamma$
111± 10	[5] ARMSTRONG	93D	E760	$\overline{p}p \to \eta\pi^0\pi^0 \to 6\gamma$
∼ 206	[6] WEIDENAUER	93	ASTE	0.0 $\overline{p}N \to 3\pi^-2\pi^+$
132± 37	[5] ADAMO	92	OBLX	$\overline{n}p \to \pi^+\pi^+\pi^-$
120± 10	[7] AKER	91	CBAR	0.0 $\overline{p}p \to 3\pi^0$
116± 9	BRIDGES	86C	DBC	0.0 $\overline{p}N \to 3\pi^-2\pi^+$

[1] Breit-Wigner width.
[2] Supersedes the $\omega\omega$ state of BELADIDZE 92B earlier assigned to the $f_2(1640)$.
[3] From a simultaneous analysis of the annihilations $\overline{p}p \to 3\pi^0, \pi^0\eta\eta$ including AKER 91 data.
[4] Supersedes ADAMO 92.
[5] J^P not determined, could be partly $f_0(1500)$.
[6] J^P not determined.
[7] Superseded by AMSLER 95B.

$f_2(1565)$ DECAY MODES

	Mode	Fraction (Γ_i/Γ)
Γ_1	$\pi\pi$	seen
Γ_2	$\pi^+\pi^-$	seen
Γ_3	$\pi^0\pi^0$	seen
Γ_4	$\rho^0\rho^0$	seen
Γ_5	$2\pi^+2\pi^-$	seen
Γ_6	$\eta\eta$	seen
Γ_7	$\omega\omega$	seen
Γ_8	$K\overline{K}$	seen
Γ_9	$\gamma\gamma$	seen

$f_2(1565)$ PARTIAL WIDTHS

$\Gamma(\eta\eta)$ — Γ_6

VALUE (MeV)	EVTS	DOCUMENT ID		TECN	COMMENT
• • • We do not use the following data for averages, fits, limits, etc. • • •					
1.2±0.3	870	[1] SCHEGELSKY	06A	RVUE	$\gamma\gamma \to K^0_S K^0_S$

[1] From analysis of L3 data at 91 and 183–209 GeV, using $f_2(1565)$ mass of 1570 MeV, width of 160 MeV, $\Gamma(\pi\pi) = 25$ MeV, and SU(3) relations.

$\Gamma(K\overline{K})$ — Γ_8

VALUE (MeV)	EVTS	DOCUMENT ID		TECN	COMMENT
• • • We do not use the following data for averages, fits, limits, etc. • • •					
2.0±1.0	870	[1] SCHEGELSKY	06A	RVUE	$\gamma\gamma \to K^0_S K^0_S$

[1] From analysis of L3 data at 91 and 183–209 GeV, using $f_2(1565)$ mass of 1570 MeV, width of 160 MeV, $\Gamma(\pi\pi) = 25$ MeV, and SU(3) relations.

$\Gamma(\gamma\gamma)$ — Γ_9

VALUE (keV)	EVTS	DOCUMENT ID		TECN	COMMENT
• • • We do not use the following data for averages, fits, limits, etc. • • •					
0.70±0.14	870	[1] SCHEGELSKY	06A	RVUE	$\gamma\gamma \to K^0_S K^0_S$

[1] From analysis of L3 data at 91 and 183–209 GeV, using $f_2(1565)$ mass of 1570 MeV, width of 160 MeV, $\Gamma(\pi\pi) = 25$ MeV, and SU(3) relations.

$f_2(1565)$ BRANCHING RATIOS

$\Gamma(\pi\pi)/\Gamma_{total}$ — Γ_1/Γ

VALUE	DOCUMENT ID		TECN	COMMENT
• • • We do not use the following data for averages, fits, limits, etc. • • •				
seen	BAKER	99B	SPEC	0 $\overline{p}p \to \omega\omega\pi^0$

$\Gamma(\pi^+\pi^-)/\Gamma_{total}$ — Γ_2/Γ

VALUE	DOCUMENT ID		TECN	COMMENT
• • • We do not use the following data for averages, fits, limits, etc. • • •				
seen	BERTIN	98	OBLX	0.05–0.405 $\overline{n}p \to \pi^+\pi^+\pi^-$
not seen	[1] ANISOVICH	94B	RVUE	$\overline{p}p \to \pi^+\pi^-\pi^0$
seen	MAY	89	ASTE	$\overline{p}p \to \pi^+\pi^-\pi^0$

[1] ANISOVICH 94B is from a reanalysis of MAY 90.

$\Gamma(\pi^0\pi^0)/\Gamma_{total}$ — Γ_3/Γ

VALUE	DOCUMENT ID		TECN	COMMENT
seen	AMSLER	95B	CBAR	0.0 $\overline{p}p \to 3\pi^0$

$\Gamma(\pi^+\pi^-)/\Gamma(\rho^0\rho^0)$ — Γ_2/Γ_4

VALUE	DOCUMENT ID		TECN	COMMENT
• • • We do not use the following data for averages, fits, limits, etc. • • •				
0.042±0.013	BRIDGES	86B	DBC	$\overline{p}N \to 3\pi^-2\pi^+$

$\Gamma(\eta\eta)/\Gamma(\pi^0\pi^0)$ — Γ_6/Γ_3

VALUE	DOCUMENT ID		TECN	COMMENT
• • • We do not use the following data for averages, fits, limits, etc. • • •				
0.024±0.005±0.012	[1] ARMSTRONG	93C	E760	$\overline{p}p \to \pi^0\eta\eta \to 6\gamma$

[1] J^P not determined, could be partly $f_0(1500)$.

$\Gamma(\omega\omega)/\Gamma_{total}$ — Γ_7/Γ

VALUE	DOCUMENT ID		TECN	COMMENT
• • • We do not use the following data for averages, fits, limits, etc. • • •				
seen	BAKER	99B	SPEC	0 $\overline{p}p \to \omega\omega\pi^0$

$f_2(1565)$ REFERENCES

ANISOVICH 09 IJMP A24 2481 V.V. Anisovich, A.V. Sarantsev (PNPI)
AMELIN 06 PAN 69 690 D.V. Amelin *et al.* (VES Collab.)
Translated from YAF 69 715.
SCHEGELSKY 06A EPJ A27 207 V.A. Schegelsky *et al.*
AMSLER 02 EPJ C23 29 C. Amsler *et al.* (Crystal Barrel Collab.)
AMELIN 00 NP A668 83 D. Amelin *et al.* (VES Collab.)
BAKER 99B PL B467 147 C.A. Baker *et al.*

Int. J. Mod. Phys. A 2026.41. Downloaded from www.worldscientific.com
by UNIVERSITY OF CALIFORNIA @ BERKELEY on 09/16/26. Re-use and distribution is strictly not permitted, except for Open Access articles.

BERTIN	98	PR D57 55	A. Bertin *et al.*	(OBELIX Collab.)
BERTIN	97C	PL B408 476	A. Bertin *et al.*	(OBELIX Collab.)
ABELE	96C	NP A609 562	A. Abele *et al.*	(Crystal Barrel Collab.)
AMSLER	95B	PL B342 433	C. Amsler *et al.*	(Crystal Barrel Collab.)
AMSLER	95C	PL B353 571	C. Amsler *et al.*	(Crystal Barrel Collab.)
AMSLER	95D	PL B355 425	C. Amsler *et al.*	(Crystal Barrel Collab.)
BALOSHIN	95	PAN 58 46	O.N. Baloshin *et al.*	(ITEP)
		Translated from YAF 58 50.		
AMSLER	94D	PL B333 277	C. Amsler *et al.*	(Crystal Barrel Collab.)
ANISOVICH	94	PL B323 233	V.V. Anisovich *et al.*	(Crystal Barrel Collab.)
ANISOVICH	94B	PR D50 1972	V.V. Anisovich *et al.*	(LOQM)
ADAMO	93	NP A558 13C	A. Adamo *et al.*	(OBELIX Collab.)
ARMSTRONG	93C	PL B307 394	T.A. Armstrong *et al.*	(FNAL, FERR, GENO+)
ARMSTRONG	93D	PL B307 399	T.A. Armstrong *et al.*	(FNAL, FERR, GENO+)
WEIDENAUER	93	ZPHY C59 387	P. Weidenauer *et al.*	(ASTERIX Collab.)
ADAMO	92	PL B287 368	A. Adamo *et al.*	(OBELIX Collab.)
BELADIDZE	92B	ZPHY C54 367	G.M. Beladidze *et al.*	(VES Collab.)
AKER	91	PL B260 249	E. Aker *et al.*	(Crystal Barrel Collab.)
MAY	90	ZPHY C46 203	B. May *et al.*	(ASTERIX Collab.)
MAY	89	PL B225 450	B. May *et al.*	(ASTERIX Collab.) IJP
BRIDGES	86B	PRL 56 215	D.L. Bridges *et al.*	(SYRA, CASE)
BRIDGES	86C	PRL 57 1534	D.L. Bridges *et al.*	(SYRA)

$\rho(1570)$

$I^G(J^{PC}) = 1^+(1^{--})$

OMITTED FROM SUMMARY TABLE

May be an OZI-violating decay mode of $\rho(1700)$. See the review on "Spectroscopy of Light Meson Resonances."

$\rho(1570)$ MASS

VALUE (MeV)	EVTS	DOCUMENT ID		TECN	COMMENT
1570±36±62	54	[1] AUBERT	08S	BABR	10.6 $e^+e^- \to \phi\pi^0\gamma$
• • • We do not use the following data for averages, fits, limits, etc. • • •					
1614± 2		[2] ACHASOV	23A	SND	$e^+e^- \to \omega\pi^0$
1585±15		[3] ACHASOV	20C	SND	1.3–2.0 $e^+e^- \to K^+K^-\pi^0$
1480±40		[4] BITYUKOV	87	SPEC	32.5 $\pi^-p \to \phi\pi^0 n$

[1] From the fit with two resonances.
[2] From a vector dominance fit to the Born cross section between 1.05 and 2.0 GeV with $\rho(770)$, $\rho(1570)$, $\rho(1700)$, $\rho(2150)$. The fit also uses SND data from the VEPP-2M collider below 1.02 GeV and from LEES 17H and ABLIKIM 21A above 1.5 GeV.
[3] From a fit using a two resonance model in which the mass and width of the other resonance are fixed at the $\rho(1700)$ values from PDG 20.
[4] Systematic errors not estimated.

$\rho(1570)$ WIDTH

VALUE (MeV)	EVTS	DOCUMENT ID		TECN	COMMENT
144±75±43	54	[1] AUBERT	08S	BABR	10.6 $e^+e^- \to \phi\pi^0\gamma$
• • • We do not use the following data for averages, fits, limits, etc. • • •					
492± 4		[2] ACHASOV	23A	SND	$e^+e^- \to \omega\pi^0$
75±30		[3] ACHASOV	20C	SND	1.3–2.0 $e^+e^- \to K^+K^-\pi^0$
130±60		[4] BITYUKOV	87	SPEC	32.5 $\pi^-p \to \phi\pi^0 n$

[1] From the fit with two resonances.
[2] From a vector dominance fit to the Born cross section between 1.05 and 2.0 GeV with $\rho(770)$, $\rho(1570)$, $\rho(1700)$, $\rho(2150)$. The fit also uses SND data from the VEPP-2M collider below 1.02 GeV and from LEES 17H and ABLIKIM 21A above 1.5 GeV.
[3] From a fit using a two resonance model in which the mass and width of the other resonance are fixed at the $\rho(1700)$ values from PDG 20.
[4] Systematic errors not estimated.

$\rho(1570)$ DECAY MODES

	Mode	Fraction (Γ_i/Γ)
Γ_1	e^+e^-	seen
Γ_2	$\phi\pi$	not seen
Γ_3	$\omega\pi$	

$\rho(1570)$ $\Gamma(i)\Gamma(e^+e^-)/\Gamma(\text{total})$

$\Gamma(\phi\pi) \times \Gamma(e^+e^-)/\Gamma_{\text{total}}$ — $\Gamma_2\Gamma_1/\Gamma$

VALUE (eV)	CL%	EVTS	DOCUMENT ID		TECN	COMMENT
3.5±0.9±0.3		54	[1] AUBERT	08S	BABR	10.6 $e^+e^- \to \phi\pi^0\gamma$
• • • We do not use the following data for averages, fits, limits, etc. • • •						
<70	90		[2] AULCHENKO	87B	ND	$e^+e^- \to K^0_S K^0_L \pi^0$

[1] From the fit with two resonances.
[2] Using mass and width of BITYUKOV 87.

$\rho(1570)$ BRANCHING RATIOS

$\Gamma(\phi\pi)/\Gamma_{\text{total}}$ — Γ_2/Γ

VALUE	DOCUMENT ID		TECN	COMMENT
not seen	ABELE	97H	CBAR	$\overline{p}p \to K^0_L K^0_S \pi^0\pi^0$
• • • We do not use the following data for averages, fits, limits, etc. • • •				
<0.01	[1] DONNACHIE	91	RVUE	

[1] Using data from BISELLO 91B, DOLINSKY 86, and ALBRECHT 87L.

$\Gamma(\phi\pi)/\Gamma(\omega\pi)$ — Γ_2/Γ_3

VALUE	CL%	DOCUMENT ID		TECN	COMMENT
• • • We do not use the following data for averages, fits, limits, etc. • • •					
>0.5	95	BITYUKOV	87	SPEC	32.5 $\pi^-p \to \phi\pi^0 n$

$\rho(1570)$ REFERENCES

ACHASOV	23A	PR D108 092012	M.N. Achasov *et al.*	(SND Collab.)
ABLIKIM	21A	PL B813 136059	M. Ablikim *et al.*	(BESIII Collab.)
ACHASOV	20C	EPJ C80 1139	M.N. Achasov *et al.*	(SND Collab.)
PDG	20	PTEP 2020 083C01	P.A. Zyla *et al.*	(PDG Collab.)
LEES	17H	PR D96 092009	J.P. Lees *et al.*	(BABAR Collab.)
AUBERT	08S	PR D77 092002	B. Aubert *et al.*	(BABAR Collab.)
ABELE	97H	PL B415 280	A. Abele *et al.*	(Crystal Barrel Collab.)
BISELLO	91B	NPBPS B21 111	D. Bisello	(DM2 Collab.)
DONNACHIE	91	ZPHY C51 689	A. Donnachie, A.B. Clegg	(MCHS, LANC)
ALBRECHT	87L	PL B185 223	H. Albrecht *et al.*	(ARGUS Collab.)
AULCHENKO	87B	JETPL 45 145	V.M. Aulchenko *et al.*	(NOVO)
		Translated from ZETFP 45 118.		
BITYUKOV	87	PL B188 383	S.I. Bityukov *et al.*	(SERP)
DOLINSKY	86	PL B174 453	S.I. Dolinsky *et al.*	(NOVO)

$h_1(1595)$

$I^G(J^{PC}) = 0^-(1^{+-})$

OMITTED FROM SUMMARY TABLE

Seen in a partial-wave analysis of the $\omega\eta$ system produced in the reaction $\pi^-p \to \omega\eta n$ at 18 GeV/c.

$h_1(1595)$ MASS

VALUE (MeV)	DOCUMENT ID		TECN	COMMENT
$1594\pm15^{+10}_{-60}$	EUGENIO	01	SPEC	18 $\pi^-p \to \omega\eta n$

$h_1(1595)$ WIDTH

VALUE (MeV)	DOCUMENT ID		TECN	COMMENT
$384\pm60^{+70}_{-100}$	EUGENIO	01	SPEC	18 $\pi^-p \to \omega\eta n$

$h_1(1595)$ DECAY MODES

	Mode	Fraction (Γ_i/Γ)
Γ_1	$\omega\eta$	seen

$h_1(1595)$ REFERENCES

EUGENIO	01	PL B497 190	P. Eugenio *et al.*

$\pi_1(1600)$

$I^G(J^{PC}) = 1^-(1^{-+})$

Coupled channel analyses favor the existence of only one broad 1^{-+} isovector state consistent with $\pi_1(1600)$ in the 1400–1600 MeV region. Accordingly, the $\pi_1(1400)$ entries of the previous Reviews have been moved into this section. See the review on "Spectroscopy of Light Meson Resonances."

$\pi_1(1600)$ T-Matrix Pole $\sqrt{s}$

Note that $\Gamma = -2\,\mathrm{Im}(\sqrt{s})$.

VALUE (MeV)	DOCUMENT ID		TECN	COMMENT
(1480–1680) − i (150–300) OUR ESTIMATE				
$(1623 \pm 47^{+24}_{-75}) - i\,(228 \pm 44^{+72}_{-88})$	[1] KOPF	21	RVUE	0.9 $p\overline{p} \to \pi^0\pi^0\eta$, $\pi^0\eta\eta$, $\pi^0K^+K^-$ and 191 $\pi^-p \to \pi^-\pi^-\pi^+p$
$(1564 \pm 24 \pm 86) - i\,(246 \pm 27 \pm 51)$	[2] RODAS	19	RVUE	191 $\pi^-p \to \eta^{(\prime)}\pi^-p$
• • • We do not use the following data for averages, fits, limits, etc. • • •				
$(1405 \pm 4^{+15}_{-18}) - i\,(314 \pm 14^{+18}_{-69})$	[3] ALBRECHT	20	RVUE	$\overline{p}p \to \pi^0\pi^0\eta$

[1] From T-matrix pole based on combined fit of Crystal Barrel and $\pi\pi$ scattering data (ALBRECHT 20), and COMPASS data (ADOLPH 15), using a coupled-channel model of $\eta\pi$, $\eta'\pi$ and $K\overline{K}$ systems.
[2] The coupled-channel analysis of both the $\eta\pi$ and $\eta'\pi$ systems using ADOLPH 15 data.
[3] Superseded by KOPF 21.

Int. J. Mod. Phys. A 2026.41. Downloaded from www.worldscientific.com
by [redacted]LIFORNIA @ BERKELEY on 09/16/26. Re-use and distribution is strictly not permitted, except for Open Access articles.

$\pi_1(1600)$ MASS ($\eta\pi$ mode)

Not seen by PROKOSHKIN 95B, BUGG 94, APEL 81, BOUTEMEUR 90, and AGHASYAN 18B.

VALUE (MeV)	EVTS	DOCUMENT ID		TECN	CHG	COMMENT
1354 ±25 OUR AVERAGE		Error includes scale factor of 1.8. See the ideogram below.				
1257 ±20 ±25	23.5k	ADAMS	07B	B852		$18\ \pi^- p \to \eta\pi^0 n$
1384 ±20 ±35	90k	SALVINI	04	OBLX		$\overline{p}p \to 2\pi^+ 2\pi^-$
1360 ±25		ABELE	99	CBAR		$0.0\ \overline{p}p \to \pi^0\pi^0\eta$
1400 ±20 ±20		ABELE	98B	CBAR		$0.0\ \overline{p}n \to \pi^-\pi^0\eta$
1370 ±16 $^{+50}_{-30}$		[1] THOMPSON	97	MPS		$18\ \pi^- p \to \eta\pi^- p$
• • • We do not use the following data for averages, fits, limits, etc. • • •						
1323.1± 4.6		[2] AOYAGI	93	BKEI		$\pi^- p \to \eta\pi^- p$
1406 ±20		[3] ALDE	88B	GAM4	0	$100\ \pi^- p \to \eta\pi^0 n$

[1] Natural parity exchange, questioned by DZIERBA 03.
[2] Unnatural parity exchange.
[3] Seen in the P_0-wave intensity of the $\eta\pi^0$ system, unnatural parity exchange.

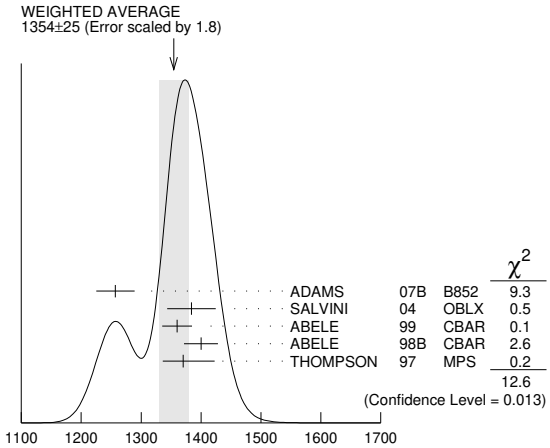

$\pi_1(1600)$ MASS (non-$\eta\pi$ mode)

VALUE (MeV)	EVTS	DOCUMENT ID		TECN	COMMENT
1645 $^{+40}_{-17}$ OUR AVERAGE		Error includes scale factor of 1.3. See the ideogram below.			
1600 $^{+110}_{-60}$	46M	[1] AGHASYAN	18B	COMP	$190\ \pi^- p \to \pi^-\pi^+\pi^- p$
1709± 24±41	69k	[2] KUHN	04	B852	$18\ \pi^- p \to \eta\pi^+\pi^-\pi^- p$
1597± 10 $^{+45}_{-10}$		[2] IVANOV	01	B852	$18\ \pi^- p \to \eta'\pi^- p$
• • • We do not use the following data for averages, fits, limits, etc. • • •					
1660± 10 $^{+0}_{-64}$	420k	[3] ALEKSEEV	10	COMP	$190\ \pi^- Pb \to \pi^-\pi^-\pi^+ Pb'$
1664± 8±10	145k	[4] LU	05	B852	$18\ \pi^- p \to \omega\pi^-\pi^0 p$
1593± 8 $^{+29}_{-47}$		[2,5] ADAMS	98B	B852	$18.3\ \pi^- p \to \pi^+\pi^-\pi^- p$

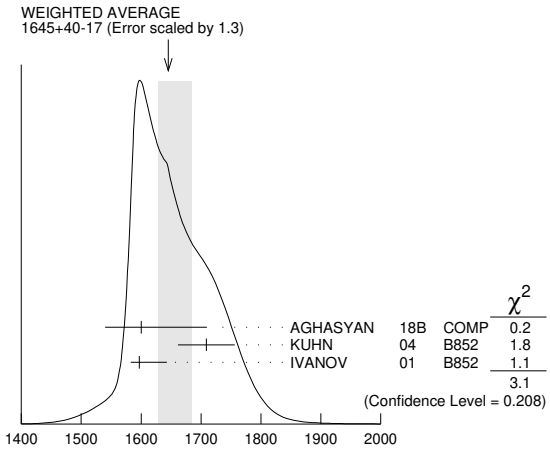

[1] Statistical error negligible. See also the review ALEXEEV 22.
[2] Natural parity exchange.
[3] Superseded by AGHASYAN 2018B.
[4] May be a different state: natural and unnatural parity exchanges.
[5] Superseded by DZIERBA 06 excluding this state in a more refined PWA analysis, with 2.6 M events of $\pi^- p \to \pi^-\pi^-\pi^+ p$ and 3 M events of $\pi^- p \to \pi^-\pi^0\pi^0 p$ of E852 data.

$\pi_1(1600)$ WIDTH ($\eta\pi$ mode)

Not seen by PROKOSHKIN 95B, BUGG 94, APEL 81, BOUTEMEUR 90, and AGHASYAN 18B.

VALUE (MeV)	EVTS	DOCUMENT ID		TECN	CHG	COMMENT
330 ±35 OUR AVERAGE						
354 ±64 ± 58	23.5k	ADAMS	07B	B852		$18\ \pi^- p \to \eta\pi^0 n$
378 ±50 ± 50	90k	SALVINI	04	OBLX		$\overline{p}p \to 2\pi^+ 2\pi^-$
220 ±90		ABELE	99	CBAR		$0.0\ \overline{p}p \to \pi^0\pi^0\eta$
310 ±50 $^{+50}_{-30}$		ABELE	98B	CBAR		$0.0\ \overline{p}n \to \pi^-\pi^0\eta$
385 ±40 $^{+65}_{-105}$		[1] THOMPSON	97	MPS		$18\ \pi^- p \to \eta\pi^- p$
• • • We do not use the following data for averages, fits, limits, etc. • • •						
143.2±12.5		[2] AOYAGI	93	BKEI		$\pi^- p \to \eta\pi^- p$
180 ±20		[3] ALDE	88B	GAM4	0	$100\ \pi^- p \to \eta\pi^0 n$

[1] Resolution is not unfolded, natural parity exchange, questioned by DZIERBA 03.
[2] Unnatural parity exchange.
[3] Seen in the P_0-wave intensity of the $\eta\pi^0$ system, unnatural parity exchange.

$\pi_1(1600)$ WIDTH (non-$\eta\pi$ mode)

VALUE (MeV)	EVTS	DOCUMENT ID		TECN	COMMENT
370 $^{+50}_{-60}$ OUR AVERAGE					
580 $^{+100}_{-230}$	46M	[1] AGHASYAN	18B	COMP	$190\ \pi^- p \to \pi^-\pi^+\pi^- p$
403± 80±115	69k	[2] KUHN	04	B852	$18\ \pi^- p \to \eta\pi^+\pi^-\pi^- p$
340± 40± 50		[2] IVANOV	01	B852	$18\ \pi^- p \to \eta'\pi^- p$
• • • We do not use the following data for averages, fits, limits, etc. • • •					
269± 21 $^{+42}_{-64}$	420k	[3] ALEKSEEV	10	COMP	$190\ \pi^- Pb \to \pi^-\pi^-\pi^+ Pb'$
185± 25± 28	145k	[4] LU	05	B852	$18\ \pi^- p \to \omega\pi^-\pi^0 p$
168± 20 $^{+150}_{-12}$		[2,5] ADAMS	98B	B852	$18.3\ \pi^- p \to \pi^+\pi^-\pi^- p$

[1] Statistical error negligible. See also the review ALEXEEV 22.
[2] Natural parity exchange.
[3] Superseded by AGHASYAN 2018B.
[4] May be a different state: natural and unnatural parity exchanges.
[5] Superseded by DZIERBA 06 excluding this state in a more refined PWA analysis, with 2.6 M events of $\pi^- p \to \pi^-\pi^-\pi^+ p$ and 3 M events of $\pi^- p \to \pi^-\pi^0\pi^0 p$ of E852 data.

$\pi_1(1600)$ DECAY MODES

	Mode	Fraction (Γ_i/Γ)
Γ_1	$\pi\pi\pi$	seen
Γ_2	$\rho^0\pi^-$	seen
Γ_3	$f_2(1270)\pi^-$	not seen
Γ_4	$b_1(1235)\pi$	seen
Γ_5	$\eta'(958)\pi^-$	seen
Γ_6	$\eta\pi$	seen
Γ_7	$f_1(1285)\pi$	seen

$\pi_1(1600)$ BRANCHING RATIOS

$\Gamma(\rho^0\pi^-)/\Gamma_{total}$ — Γ_2/Γ

VALUE	DOCUMENT ID		TECN	COMMENT
seen	ALEKSEEV	10	COMP	$190\ \pi^- Pb \to \pi^-\pi^-\pi^+ Pb'$
• • • We do not use the following data for averages, fits, limits, etc. • • •				
not seen	NOZAR	09	CLAS	$\gamma p \to 2\pi^+\pi^- n$
not seen	[1] DZIERBA	06	B852	$18\ \pi^- p$

[1] From the PWA analysis of 2.6 M $\pi^- p \to \pi^-\pi^-\pi^+ p$ and 3 M events of $\pi^- p \to \pi^-\pi^0\pi^0 p$ of E852 data. Supersedes ADAMS 98B.

$\Gamma(f_2(1270)\pi^-)/\Gamma_{total}$ — Γ_3/Γ

VALUE	DOCUMENT ID		TECN	COMMENT
not seen	[1] DZIERBA	06	B852	$18\ \pi^- p$

[1] From the PWA analysis of 2.6 M $\pi^- p \to \pi^-\pi^-\pi^+ p$ and 3 M events of $\pi^- p \to \pi^-\pi^0\pi^0 p$ of E852 data. Supersedes CHUNG 02.

$\Gamma(b_1(1235)\pi)/\Gamma_{total}$ — Γ_4/Γ

VALUE	EVTS	DOCUMENT ID		TECN	COMMENT
seen	35280	[1] BAKER	03	SPEC	$\overline{p}p \to \omega\pi^+\pi^-\pi^0$
• • • We do not use the following data for averages, fits, limits, etc. • • •					
seen	145k	LU	05	B852	$18\ \pi^- p \to \omega\pi^-\pi^0 p$

[1] $B((b_1\pi)_{D-wave})/B((b_1\pi)_{S\text{-wave}})=0.3 \pm 0.1$.

Int. J. Mod. Phys. A 2026.41. Downloaded from www.worldscientific.com
by UNIVERSITY OF CALIFORNIA @ BERKELEY on 09/16/26. Re-use and distribution is strictly not permitted, except for Open Access articles.

$\Gamma(\eta'(958)\pi^-)/\Gamma_{total}$ — Γ_5/Γ

VALUE	DOCUMENT ID		TECN	COMMENT
seen	IVANOV	01	B852	$18\ \pi^- p \to \eta' \pi^- p$

$\Gamma(\eta'(958)\pi^-)/\Gamma(\eta\pi)$ — Γ_5/Γ_6

VALUE	DOCUMENT ID		TECN	COMMENT
• • • We do not use the following data for averages, fits, limits, etc. • • •				
$5.54 \pm 1.1^{+1.8}_{-0.27}$	[1] KOPF	21	RVUE	$0.9\ p\overline{p} \to \pi^0\pi^0\eta$, $\pi^0\eta\eta$, $\pi^0 K^+ K^-$ and $191\ \pi^- p \to \pi^-\pi^-\pi^+ p$

[1] From T-matrix pole based on combined fit of Crystal Barrel and $\pi\pi$ scattering data (ALBRECHT 20), and COMPASS data (ADOLPH 15), using a coupled-channel model of $\eta\pi$, $\eta'\pi$ and $K\overline{K}$ systems.

$\Gamma(f_1(1285)\pi)/\Gamma(\eta'(958)\pi^-)$ — Γ_7/Γ_5

VALUE	EVTS	DOCUMENT ID		TECN	COMMENT
3.80±0.78	69k	[1] KUHN	04	B852	$18\ \pi^- p \to \eta\pi^+\pi^-\pi^- p$

[1] Using $\eta'(958)\pi$ data from IVANOV 01.

$\pi_1(1600)$ REFERENCES

ALEXEEV	22	PR D105 012005	G.D. Alexeev *et al.*	(COMPASS Collab.)
KOPF	21	EPJ C81 1056	B. Kopf *et al.*	(BOCH)
ALBRECHT	20	EPJ C80 453	M. Albrecht *et al.*	(Crystal Barrel Collab.)
RODAS	19	PRL 122 042002	A. Rodas *et al.*	(JPAC Collab.)
AGHASYAN	18B	PR D98 092003	M. Aghasyan *et al.*	(COMPASS Collab.)
ADOLPH	15	PL B740 303	M. Adolph *et al.*	(COMPASS Collab.)
ALEKSEEV	10	PRL 104 241803	M.G. Alekseev *et al.*	(COMPASS Collab.)
NOZAR	09	PRL 102 102002	M. Nozar *et al.*	(JLab CLAS Collab.)
ADAMS	07B	PL B657 27	G.S. Adams *et al.*	(BNL E852 Collab.)
DZIERBA	06	PR D73 072001	A.R. Dzierba *et al.*	(BNL E852 Collab.)
LU	05	PRL 94 032002	M. Lu *et al.*	(BNL E852 Collab.)
KUHN	04	PL B595 109	J. Kuhn *et al.*	(BNL E852 Collab.)
SALVINI	04	EPJ C35 21	P. Salvini *et al.*	(OBELIX Collab.)
BAKER	03	PL B563 140	C.A. Baker *et al.*	
DZIERBA	03	PR D67 094015	A.R. Dzierba *et al.*	
CHUNG	02	PR D65 072001	S.U. Chung *et al.*	(BNL E852 Collab.)
IVANOV	01	PRL 86 3977	E.I. Ivanov *et al.*	(BNL E852 Collab.)
ABELE	99	PL B446 349	A. Abele *et al.*	(Crystal Barrel Collab.)
ABELE	98B	PL B423 175	A. Abele *et al.*	(Crystal Barrel Collab.)
ADAMS	98B	PRL 81 5760	G.S. Adams *et al.*	(BNL E852 Collab.)
THOMPSON	97	PRL 79 1630	D.R. Thompson *et al.*	(BNL E852 Collab.)
PROKOSHKIN	95B	PAN 58 606	Y.D. Prokoshkin, S.A. Sadovsky	(SERP)
		Translated from YAF 58 662.		
BUGG	94	PR D50 4412	D.V. Bugg *et al.*	(LOQM)
AOYAGI	93	PL B314 246	H. Aoyagi *et al.*	(BKEI Collab.)
BOUTEMEUR	90	Hadron 89 Conf. p 119	M. Boutemeur, M. Poulet	(SERP, BELG, LANL+)
ALDE	88B	PL B205 397	D.M. Alde *et al.*	(SERP, BELG, LANL, LAPP)
APEL	81	NP B193 269	W.D. Apel *et al.*	(SERP, CERN)

$a_1(1640)$

$I^G(J^{PC}) = 1^-(1^{++})$

Possibly seen in the study of the hadronic structure in decay $\tau \to 3\pi\nu_\tau$ (ABREU 98G and ASNER 00).

$a_1(1640)$ MASS

VALUE (MeV)	EVTS	DOCUMENT ID		TECN	COMMENT
1655 ± 16 OUR AVERAGE		Error includes scale factor of 1.2.			
1700^{+35}_{-130}	46M	[1] AGHASYAN	18B	COMP	$190\ \pi^- p \to \pi^-\pi^+\pi^- p$
1691 ± 18 ± 30		DARGENT	17	RVUE	$D^0 \to \pi^-\pi^+\pi^-\pi^+$
1630 ± 20	35k	[2] BAKER	03	SPEC	$\overline{p}p \to \omega\pi^+\pi^-\pi^0$
1714 ± 9 ± 36		CHUNG	02	B852	$18.3\ \pi^- p \to \pi^+\pi^-\pi^- p$
1640 ± 12 ± 30		BAKER	99	SPEC	$1.94\ \overline{p}p \to 4\pi^0$
• • • We do not use the following data for averages, fits, limits, etc. • • •					
1670 ± 90		BELLINI	85	SPEC	$40\ \pi^- A \to \pi^-\pi^+\pi^- A$

[1] Statistical error negligible.
[2] Using the $a_1(1260)$ mass and width results of BOWLER 88.

$a_1(1640)$ WIDTH

VALUE (MeV)	EVTS	DOCUMENT ID		TECN	COMMENT
250 ± 40 OUR AVERAGE		Error includes scale factor of 1.8. See the ideogram below.			
510^{+170}_{-90}	46M	[1] AGHASYAN	18B	COMP	$190\ \pi^- p \to \pi^-\pi^+\pi^- p$
171 ± 33 ± 40		DARGENT	17	RVUE	$D^0 \to \pi^-\pi^+\pi^-\pi^+$
225 ± 30	35k	[2] BAKER	03	SPEC	$\overline{p}p \to \omega\pi^+\pi^-\pi^0$
308 ± 37 ± 62		CHUNG	02	B852	$18.3\ \pi^- p \to \pi^+\pi^-\pi^- p$
300 ± 22 ± 40		BAKER	99	SPEC	$1.94\ \overline{p}p \to 4\pi^0$
• • • We do not use the following data for averages, fits, limits, etc. • • •					
300 ± 100		BELLINI	85	SPEC	$40\ \pi^- A \to \pi^-\pi^+\pi^- A$

[1] Statistical error negligible.
[2] Using the $a_1(1260)$ mass and width results of BOWLER 88.

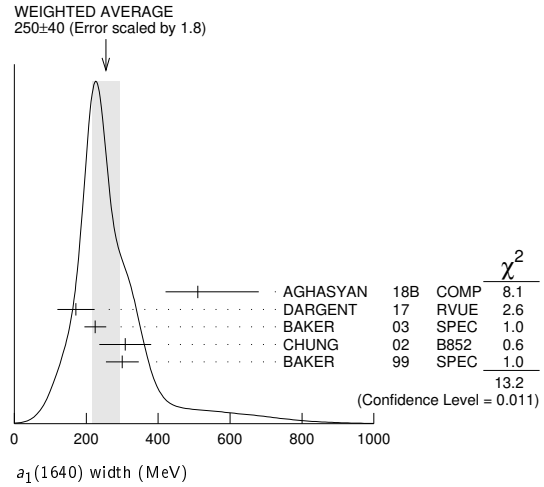

$a_1(1640)$ DECAY MODES

	Mode	Fraction (Γ_i/Γ)
Γ_1	$\pi\pi\pi$	seen
Γ_2	$f_2(1270)\pi$	seen
Γ_3	$\sigma\pi$	seen
Γ_4	$\rho\pi_{S-wave}$	seen
Γ_5	$\rho\pi_{D-wave}$	seen
Γ_6	$\omega\pi\pi$	seen
Γ_7	$f_1(1285)\pi$	seen
Γ_8	$a_1(1260)\eta$	not seen

$a_1(1640)$ BRANCHING RATIOS

$\Gamma(f_2(1270)\pi)/\Gamma(\sigma\pi)$ — Γ_2/Γ_3

VALUE	DOCUMENT ID		TECN	COMMENT
0.24±0.07	BAKER	99	SPEC	$1.94\ \overline{p}p \to 4\pi^0$

$\Gamma(\rho\pi_{D-wave})/\Gamma_{total}$ — Γ_5/Γ

VALUE	DOCUMENT ID		TECN	COMMENT
• • • We do not use the following data for averages, fits, limits, etc. • • •				
seen	CHUNG	02	B852	$18.3\ \pi^- p \to \pi^+\pi^-\pi^- p$
seen	AMELIN	95B	VES	$36\ \pi^- A \to \pi^+\pi^-\pi^- A$

$\Gamma(\omega\pi\pi)/\Gamma_{total}$ — Γ_6/Γ

VALUE	EVTS	DOCUMENT ID		TECN	COMMENT
• • • We do not use the following data for averages, fits, limits, etc. • • •					
seen	35280	[1] BAKER	03	SPEC	$\overline{p}p \to \omega\pi^+\pi^-\pi^0$

[1] Assuming the $\omega\rho$ mechanism for the $\omega\pi\pi$ state.

$\Gamma(f_1(1285)\pi)/\Gamma_{total}$ — Γ_7/Γ

VALUE	DOCUMENT ID		TECN	COMMENT
• • • We do not use the following data for averages, fits, limits, etc. • • •				
not seen	KUHN	04	B852	$18\ \pi^- p \to \eta\pi^+\pi^-\pi^- p$
seen	LEE	94	MPS2	$18\ \pi^- p \to K^+\overline{K}^0\pi^-\pi^- p$

$\Gamma(a_1(1260)\eta)/\Gamma_{total}$ — Γ_8/Γ

VALUE	DOCUMENT ID		TECN	COMMENT
not seen	KUHN	04	B852	$18\ \pi^- p \to \eta\pi^+\pi^-\pi^- p$

$a_1(1640)$ REFERENCES

AGHASYAN	18B	PR D98 092003	M. Aghasyan *et al.*	(COMPASS Collab.)
DARGENT	17	JHEP 1705 143	P. dArgent *et al.*	(HEID, BRIS)
KUHN	04	PL B595 109	J. Kuhn *et al.*	(BNL E852 Collab.)
BAKER	03	PL B563 140	C.A. Baker *et al.*	
CHUNG	02	PR D65 072001	S.U. Chung *et al.*	(BNL E852 Collab.)
ASNER	00	PR D61 012002	D.M. Asner *et al.*	(CLEO Collab.)
BAKER	99	PL B449 114	C.A. Baker *et al.*	
ABREU	98G	PL B426 411	P. Abreu *et al.*	(DELPHI Collab.)
AMELIN	95B	PL B356 595	D.V. Amelin *et al.*	(SERP, TBIL)
LEE	94	PL B323 227	J.H. Lee *et al.*	(BNL, IND, KYUN, MASD+)
BOWLER	88	PL B209 99	M.G. Bowler	(OXF)
BELLINI	85	SJNP 41 781	D. Bellini *et al.*	
		Translated from YAF 41 1223.		

Int. J. Mod. Phys. A 2026.41. Downloaded from www.worldscientific.com
by [redacted]LIFORNIA @ BERKELEY on 09/16/26. Re-use and distribution is strictly not permitted, except for Open Access articles.

$f_2(1640)$

$I^G(J^{PC}) = 0^+(2^{++})$

OMITTED FROM SUMMARY TABLE

$f_2(1640)$ MASS

VALUE (MeV)	DOCUMENT ID		TECN	COMMENT
1639± 6 OUR AVERAGE Error includes scale factor of 1.2.				
1620±16	BUGG	95	MRK3	$J/\psi \to \gamma\pi^+\pi^-\pi^+\pi^-$
1647± 7	ADAMO	92	OBLX	$\overline{n}p \to 3\pi^+2\pi^-$
1635± 7	ALDE	90	GAM2	$38\ \pi^-p \to \omega\omega n$
• • • We do not use the following data for averages, fits, limits, etc. • • •				
1640± 5	AMSLER	06	CBAR	$0.9\ \overline{p}p \to K^+K^-\pi^0$
1659± 6	VLADIMIRSK...	06	SPEC	$40\ \pi^-p \to K^0_SK^0_Sn$
1643± 7	[1] ALDE	89B	GAM2	$38\ \pi^-p \to \omega\omega n$

[1] Superseded by ALDE 90.

$f_2(1640)$ WIDTH

VALUE (MeV)	CL%	DOCUMENT ID		TECN	COMMENT
100^{+60}_{-40} OUR AVERAGE Error includes scale factor of 2.9.					
140^{+60}_{-20}		BUGG	95	MRK3	$J/\psi \to \gamma\pi^+\pi^-\pi^+\pi^-$
58±20		ADAMO	92	OBLX	$\overline{n}p \to 3\pi^+2\pi^-$
• • • We do not use the following data for averages, fits, limits, etc. • • •					
44± 9		AMSLER	06	CBAR	$0.9\ \overline{p}p \to K^+K^-\pi^0$
152±18		VLADIMIRSK...	06	SPEC	$40\ \pi^-p \to K^0_SK^0_Sn$
< 70	90	ALDE	90	GAM2	$38\ \pi^-p \to \omega\omega n$

$f_2(1640)$ DECAY MODES

	Mode	Fraction (Γ_i/Γ)
Γ_1	$\omega\omega$	seen
Γ_2	4π	seen
Γ_3	$K\overline{K}$	seen

$f_2(1640)$ BRANCHING RATIOS

$\Gamma(K\overline{K})/\Gamma_{total}$ — **Γ_3/Γ**

VALUE	DOCUMENT ID		TECN	COMMENT
seen	AMSLER	06	CBAR	$0.9\ \overline{p}p \to K^+K^-\pi^0$

$f_2(1640)$ REFERENCES

AMSLER	06	PL B639 165	C. Amsler *et al.*	(Crystal Barrel Collab.)
VLADIMIRSK...	06	PAN 69 493	V.V. Vladimirsky *et al.*	(ITEP, Moscow)
		Translated from YAF 69 515.		
BUGG	95	PL B353 378	D.V. Bugg *et al.*	(LOQM, PNPI, WASH) JP
ADAMO	92	PL B287 368	A. Adamo *et al.*	(OBELIX Collab.)
ALDE	90	PL B241 600	D.M. Alde *et al.*	(SERP, BELG, LANL, LAPP+)
ALDE	89B	PL B216 451	D.M. Alde *et al.*	(SERP, BELG, LANL, LAPP+) IGJPC

$\eta_2(1645)$

$I^G(J^{PC}) = 0^+(2^{-+})$

$\eta_2(1645)$ MASS

VALUE (MeV)	DOCUMENT ID		TECN	CHG	COMMENT
1617± 5 OUR AVERAGE					
1613± 8	BARBERIS	00B			$450\ pp \to p_f\eta\pi^+\pi^-p_s$
1617± 8	BARBERIS	00C			$450\ pp \to p_f4\pi p_s$
1620±20	BARBERIS	97B	OMEG		$450\ pp \to pp2(\pi^+\pi^-)$
1645±14±15	ADOMEIT	96	CBAR	0	$1.94\ \overline{p}p \to \eta3\pi^0$
• • • We do not use the following data for averages, fits, limits, etc. • • •					
1645± 6±20	ANISOVICH	00E	SPEC		0.9–$1.94\ \overline{p}p \to \eta3\pi^0$

$\eta_2(1645)$ WIDTH

VALUE (MeV)	DOCUMENT ID		TECN	CHG	COMMENT
181±11 OUR AVERAGE					
185±17	BARBERIS	00B			$450\ pp \to p_f\eta\pi^+\pi^-p_s$
177±18	BARBERIS	00C			$450\ pp \to p_f4\pi p_s$
180±25	BARBERIS	97B	OMEG		$450\ pp \to pp2(\pi^+\pi^-)$
180^{+40}_{-21}±25	ADOMEIT	96	CBAR	0	$1.94\ \overline{p}p \to \eta3\pi^0$
• • • We do not use the following data for averages, fits, limits, etc. • • •					
200±25	ANISOVICH	00E	SPEC		0.9–$1.94\ \overline{p}p \to \eta3\pi^0$

$\eta_2(1645)$ DECAY MODES

	Mode	Fraction (Γ_i/Γ)
Γ_1	$a_2(1320)\pi$	seen
Γ_2	$K\overline{K}\pi$	seen
Γ_3	$K^*\overline{K}$	seen
Γ_4	$\eta\pi^+\pi^-$	seen
Γ_5	$a_0(980)\pi$	seen
Γ_6	$f_2(1270)\eta$	not seen

$\eta_2(1645)$ BRANCHING RATIOS

$\Gamma(K\overline{K}\pi)/\Gamma(a_2(1320)\pi)$ — **Γ_2/Γ_1**

VALUE	DOCUMENT ID		TECN	COMMENT
0.07±0.03	[1] BARBERIS	97C	OMEG	$450\ pp \to ppK\overline{K}\pi$

[1] Using $2(\pi^+\pi^-)$ data from BARBERIS 97B.

$\Gamma(a_2(1320)\pi)/\Gamma(a_0(980)\pi)$ — **Γ_1/Γ_5**

VALUE	DOCUMENT ID		TECN	COMMENT
13.1±2.3 OUR AVERAGE				
13.5±4.6	[2] ANISOVICH	11	SPEC	0.9–$1.94\ p\overline{p}$
13.0±2.7	BARBERIS	00B		$450\ pp \to p_f\eta\pi^+\pi^-p_s$

[2] Reanalysis of ADOMEIT 96 and ANISOVICH 00E.

$\Gamma(f_2(1270)\eta)/\Gamma_{total}$ — **Γ_6/Γ**

VALUE	DOCUMENT ID		COMMENT
• • • We do not use the following data for averages, fits, limits, etc. • • •			
not seen	BARBERIS	00B	$450\ pp \to p_f\eta\pi^+\pi^-p_s$

$\eta_2(1645)$ REFERENCES

ANISOVICH	11	EPJ C71 1511	A.V. Anisovich *et al.*	(LOQM, RAL, PNPI)
ANISOVICH	00E	PL B477 19	A.V. Anisovich *et al.*	
BARBERIS	00B	PL B471 435	D. Barberis *et al.*	(WA 102 Collab.)
BARBERIS	00C	PL B471 440	D. Barberis *et al.*	(WA 102 Collab.)
BARBERIS	97B	PL B413 217	D. Barberis *et al.*	(WA 102 Collab.)
BARBERIS	97C	PL B413 225	D. Barberis *et al.*	(WA 102 Collab.)
ADOMEIT	96	ZPHY C71 227	J. Adomeit *et al.*	(Crystal Barrel Collab.)

$\omega(1650)$

$I^G(J^{PC}) = 0^-(1^{--})$

See also the $\omega(1420)$ particle listing.

$\omega(1650)$ MASS

VALUE (MeV)	EVTS	DOCUMENT ID		TECN	COMMENT
1670 ± 30 OUR ESTIMATE					
• • • We do not use the following data for averages, fits, limits, etc. • • •					
1643 ± 6		[1] DIMOVA	25	SND	$e^+e^- \to \pi^+\pi^-\pi^0$
1643 ± 6		[2] ACHASOV	24A	SND	$e^+e^- \to \pi^+\pi^-\pi^0$
1660.0± 8.4		[3] LICHARD	23	RVUE	$e^+e^- \to \omega\eta$
1698 ± 10	267	[4] ACHASOV	20B	SND	$e^+e^- \to \omega\eta \to \eta\pi^0\gamma$
1651 ± 3 $^{+16}_{-6}$	183k	[5] ABLIKIM	19AQ	BES	$J/\psi \to K^+K^-\pi^0$
1673 $^{+6}_{-7}$		ACHASOV	19	SND	$e^+e^- \to \pi^+\pi^-\pi^0\eta$
1671 ± 6 ±10	824	[6] AKHMETSHIN	17A	CMD3	1.4–$2.0\ e^+e^- \to \omega\eta$
1660 ± 10	898	[7] ACHASOV	16B	SND	1.34–$2.00\ e^+e^- \to \omega\eta$
1680 ± 10	13.1k	[8] AULCHENKO	15A	SND	1.05–$1.80\ e^+e^- \to \pi^+\pi^-\pi^0$
1667 ± 13 ± 6		AUBERT	07AU	BABR	$10.6\ e^+e^- \to \omega\pi^+\pi^-\gamma$
1645 ± 8	13	AUBERT	06D	BABR	$10.6\ e^+e^- \to \omega\eta\gamma$
1660 ± 10 ± 2		AUBERT,B	04N	BABR	$10.6\ e^+e^- \to \pi^+\pi^-\pi^0\gamma$
1770 ± 50 ±60	1.2M	[9] ACHASOV	03D	RVUE	0.44–$2.00\ e^+e^- \to \pi^+\pi^-\pi^0$
1619 ± 5		[10] HENNER	02	RVUE	1.2–$2.0\ e^+e^- \to \rho\pi, \omega\pi\pi$
1700 ± 20		EUGENIO	01	SPEC	$18\ \pi^-p \to \omega\eta n$
1705 ± 26	612	[11] AKHMETSHIN	00D	CMD2	$e^+e^- \to \omega\pi^+\pi^-$
1820 $^{+190}_{-150}$		[12] ACHASOV	98H	RVUE	$e^+e^- \to \pi^+\pi^-\pi^0$
1840 $^{+100}_{-70}$		[13] ACHASOV	98H	RVUE	$e^+e^- \to \omega\pi^+\pi^-$
1780 $^{+170}_{-300}$		[14] ACHASOV	98H	RVUE	$e^+e^- \to K^+K^-$
~ 2100		[15] ACHASOV	98H	RVUE	$e^+e^- \to K^0_SK^\pm\pi^\mp$
1606 ± 9		[16] CLEGG	94	RVUE	
1662 ± 13	750	[17] ANTONELLI	92	DM2	1.34–$2.4 e^+e^- \to \rho\pi, \omega\pi\pi$
1670 ± 20		ATKINSON	83B	OMEG	20–$70\ \gamma p \to 3\pi X$
1657 ± 13		CORDIER	81	DM1	$e^+e^- \to \omega2\pi$
1679 ± 34	21	ESPOSITO	80	FRAM	$e^+e^- \to 3\pi$
1652 ± 17		COSME	79	OSPK	$e^+e^- \to 3\pi$

Int. J. Mod. Phys. A 2026.41. Downloaded from www.worldscientific.com
by UNIVERSITY OF CALIFORNIA @ BERKELEY on 09/16/26. Re-use and distribution is strictly not permitted, except for Open Access articles.

[1] From a fit to the cross section with contributions from $\omega(782)$, $\phi(1020)$, $\omega(1420)$, and $\omega(1650)$. An alternative fit which also includes $\phi(1680)$ gives 1649 ± 9 MeV with a worse χ^2. Supersedes ACHASOV 24A.
[2] From a fit to the cross section including contribution from $\omega(782)$, $\phi(1020)$, $\omega(1420)$, and $\omega(1650)$. Supersedes ACHASOV 20A.
[3] From a VDM fit to AKHMETSHIN 17A $\omega\eta$ data with two additional resonances of low statistical evidences.
[4] From a fit with contributions from $\omega(1420)$, $\omega(1650)$, and $\phi(1680)$. The mass of $\omega(1420)$ is fixed to the PDG 18 value of 1420 MeV. Fixing also the width of $\omega(1420)$ to the PDG 18 value of 220 MeV results in 1694 ± 9 MeV measurement.
[5] Could also be $\rho(1700)$. Branching ratio $J/\psi \to X\pi^0 \to K^+K^-\pi^0 = (5.3\pm0.3^{+0.6}_{-0.5})\times 10^{-5}$.
[6] From a fit of the interfering $\omega(1420)$ and $\omega(1650)$ with a relative phase of π and other parameters floating.
[7] From a fit with contributions from $\omega(1420)$, $\omega(1650)$, and $\phi(1680)$.
[8] From a fit with contributions from $\omega(782)$, $\phi(1020)$, $\omega(1420)$, and $\omega(1650)$. See ACHASOV 20A for a further analysis of the $\pi^+\pi^-\pi^0$ data.
[9] From the combined fit of ANTONELLI 92, ACHASOV 01E, ACHASOV 02E, and ACHASOV 03D data on the $\pi^+\pi^-\pi^0$ and ANTONELLI 92 on the $\omega\pi^+\pi^-$ final states. Supersedes ACHASOV 99E and ACHASOV 02E.
[10] Using results of CORDIER 81 and preliminary data of DOLINSKY 91 and ANTONELLI 92.
[11] Using the data of AKHMETSHIN 00D and ANTONELLI 92. The $\rho\pi$ dominance for the energy dependence of the $\omega(1420)$ and $\omega(1650)$ width assumed.
[12] Using data from BARKOV 87, DOLINSKY 91, and ANTONELLI 92.
[13] Using the data from ANTONELLI 92.
[14] Using the data from IVANOV 81 and BISELLO 88B.
[15] Using the data from BISELLO 91C.
[16] From a fit to two Breit-Wigner functions and using the data of DOLINSKY 91 and ANTONELLI 92.
[17] From the combined fit of the $\rho\pi$ and $\omega\pi\pi$ final states.

$\omega(1650)$ WIDTH

VALUE (MeV)	EVTS	DOCUMENT ID		TECN	COMMENT
150± 50 OUR ESTIMATE					
• • • We do not use the following data for averages, fits, limits, etc. • • •					
148± 13		[1] DIMOVA	25	SND	$e^+e^- \to \pi^+\pi^-\pi^0$
148± 13		[2] ACHASOV	24A	SND	$e^+e^- \to \pi^+\pi^-\pi^0$
106± 15		[3] LICHARD	23	RVUE	$e^+e^- \to \omega\eta$
110± 16	267	[4] ACHASOV	20B	SND	$e^+e^- \to \omega\eta \to \eta\pi^0\gamma$
194± 8^{+15}_{-7}	183k	[5] ABLIKIM	19AQ	BES	$J/\psi \to K^+K^-\pi^0$
95± 11		ACHASOV	19	SND	$e^+e^- \to \pi^+\pi^-\pi^0\eta$
113± 9± 10	824	[6] AKHMETSHIN	17A	CMD3	1.4–2.0 $e^+e^- \to \omega\eta$
110± 20	898	[7] ACHASOV	16B	SND	1.34–2.00 $e^+e^- \to \omega\eta$
310± 30	13.1k	[8] AULCHENKO	15A	SND	1.05–1.80 $e^+e^- \to \pi^+\pi^-\pi^0$
222± 25± 20		AUBERT	07AU	BABR	10.6 $e^+e^- \to \omega\pi^+\pi^-\gamma$
114± 14	13	AUBERT	06D	BABR	10.6 $e^+e^- \to \omega\eta\gamma$
230± 30± 20		AUBERT,B	04N	BABR	10.6 $e^+e^- \to \pi^+\pi^-\pi^0\gamma$
$490^{+200}_{-150}\pm130$	1.2M	[9] ACHASOV	03D	RVUE	0.44–2.00 $e^+e^- \to \pi^+\pi^-\pi^0$
250± 14		[10] HENNER	02	RVUE	1.2–2.0 $e^+e^- \to \rho\pi, \omega\pi\pi$
250± 50		EUGENIO	01	SPEC	18 $\pi^-p \to \omega\eta n$
370± 25	612	[11] AKHMETSHIN	00D	CMD2	$e^+e^- \to \omega\pi^+\pi^-$
113± 20		[12] CLEGG	94	RVUE	
280± 24	750	[13] ANTONELLI	92	DM2	1.34–2.4 $e^+e^- \to \rho\pi, \omega\pi\pi$
160± 20		ATKINSON	83B	OMEG	20–70 $\gamma p \to 3\pi X$
136± 46		CORDIER	81	DM1	$e^+e^- \to \omega 2\pi$
99± 49	21	ESPOSITO	80	FRAM	$e^+e^- \to 3\pi$
42± 17		COSME	79	OSPK	$e^+e^- \to 3\pi$

[1] From a fit to the cross section with contributions from $\omega(782)$, $\phi(1020)$, $\omega(1420)$, and $\omega(1650)$. An alternative fit which also includes $\phi(1680)$ gives 165 ± 14 MeV with a worse χ^2. Supersedes ACHASOV 24A.
[2] From a fit to the cross section including contribution from $\omega(782)$, $\phi(1020)$, $\omega(1420)$, and $\omega(1650)$. Supersedes ACHASOV 20A.
[3] From a VDM fit to AKHMETSHIN 17A $\omega\eta$ data with two additional resonances of low statistical evidences.
[4] From a fit with contributions from $\omega(1420)$, $\omega(1650)$, and $\phi(1680)$. The mass of $\omega(1420)$ is fixed to the PDG 18 value of 1420 MeV. Fixing also the width of $\omega(1420)$ to the PDG 18 value of 220 MeV results in 94 ± 13 MeV measurement.
[5] Could also be $\rho(1700)$. Branching ratio $J/\psi \to X\pi^0 \to K^+K^-\pi^0 = (5.3\pm0.3^{+0.6}_{-0.5})\times 10^{-5}$.
[6] From a fit of the interfering $\omega(1420)$ and $\omega(1650)$ with a relative phase of π and other parameters floating.
[7] From a fit with contributions from $\omega(1420)$, $\omega(1650)$, and $\phi(1680)$.
[8] From a fit with contributions from $\omega(782)$, $\phi(1020)$, $\omega(1420)$, and $\omega(1650)$. See ACHASOV 20A for a further analysis of the $\pi^+\pi^-\pi^0$ data.
[9] From the combined fit of ANTONELLI 92, ACHASOV 01E, ACHASOV 02E, and ACHASOV 03D data on the $\pi^+\pi^-\pi^0$ and ANTONELLI 92 on the $\omega\pi^+\pi^-$ final states. Supersedes ACHASOV 99E and ACHASOV 02E.
[10] Using results of CORDIER 81 and preliminary data of DOLINSKY 91 and ANTONELLI 92.
[11] Using the data of AKHMETSHIN 00D and ANTONELLI 92. The $\rho\pi$ dominance for the energy dependence of the $\omega(1420)$ and $\omega(1650)$ width assumed.
[12] From a fit to two Breit-Wigner functions and using the data of DOLINSKY 91 and ANTONELLI 92.
[13] From the combined fit of the $\rho\pi$ and $\omega\pi\pi$ final states.

$\omega(1650)$ DECAY MODES

	Mode	Fraction (Γ_i/Γ)
Γ_1	$\rho\pi$	seen
Γ_2	$\rho(1450)\pi$	seen
Γ_3	$\omega\pi\pi$	seen
Γ_4	$\omega\eta$	seen
Γ_5	e^+e^-	seen
Γ_6	$\pi^0\gamma$	not seen

$\omega(1650)$ $\Gamma(i)\Gamma(e^+e^-)/\Gamma^2(\text{total})$

$\Gamma(\rho\pi)/\Gamma_{\text{total}} \times \Gamma(e^+e^-)/\Gamma_{\text{total}}$ — $\Gamma_1/\Gamma \times \Gamma_5/\Gamma$

VALUE (units 10^{-6})	EVTS	DOCUMENT ID		TECN	COMMENT
• • • We do not use the following data for averages, fits, limits, etc. • • •					
1.56 ±0.23	13.1k	[1] AULCHENKO	15A	SND	1.05–1.80 $e^+e^- \to \pi^+\pi^-\pi^0$
1.3 ±0.1 ±0.1		AUBERT,B	04N	BABR	10.6 $e^+e^- \to \pi^+\pi^-\pi^0\gamma$
1.2 $^{+0.4}_{-0.1}$ ±0.8	1.2M	[2,3] ACHASOV	03D	RVUE	0.44–2.00 $e^+e^- \to \pi^+\pi^-\pi^0$
0.921±0.230		[4,5] CLEGG	94	RVUE	
0.479±0.050	750	[6,7] ANTONELLI	92	DM2	1.34–2.4 $e^+e^- \to \rho\pi, \omega\pi\pi$

[1] From a fit with contributions from $\omega(782)$, $\phi(1020)$, $\omega(1420)$, and $\omega(1650)$. See ACHASOV 20A for a further analysis of the $\pi^+\pi^-\pi^0$ data.
[2] Calculated by us from the cross section at the peak.
[3] From the combined fit of ANTONELLI 92, ACHASOV 01E, ACHASOV 02E, and ACHASOV 03D data on the $\pi^+\pi^-\pi^0$ and ANTONELLI 92 on the $\omega\pi^+\pi^-$ final states. Supersedes ACHASOV 99E and ACHASOV 02E.
[4] From a fit to two Breit-Wigner functions and using the data of DOLINSKY 91 and ANTONELLI 92.
[5] From the partial and leptonic width given by the authors.
[6] From the combined fit of the $\rho\pi$ and $\omega\pi\pi$ final states.
[7] From the product of the leptonic width and partial branching ratio given by the authors.

$\Gamma(\omega\pi\pi)/\Gamma_{\text{total}} \times \Gamma(e^+e^-)/\Gamma_{\text{total}}$ — $\Gamma_3/\Gamma \times \Gamma_5/\Gamma$

VALUE (units 10^{-7})	EVTS	DOCUMENT ID		TECN	COMMENT
• • • We do not use the following data for averages, fits, limits, etc. • • •					
7.0 ±0.5		AUBERT	07AU	BABR	10.6 $e^+e^- \to \omega\pi^+\pi^-\gamma$
4.1 ±0.9 ±1.3	1.2M	[1,2] ACHASOV	03D	RVUE	0.44–2.00 $e^+e^- \to \pi^+\pi^-\pi^0$
5.40±0.95		[3] AKHMETSHIN	00D	CMD2	1.2–1.38 $e^+e^- \to \omega\pi^+\pi^-$
3.18±0.80		[4,5] CLEGG	94	RVUE	
6.07±0.61	750	[6,7] ANTONELLI	92	DM2	1.34–2.4 $e^+e^- \to \rho\pi, \omega\pi\pi$

[1] Calculated by us from the cross section at the peak.
[2] From the combined fit of ANTONELLI 92, ACHASOV 01E, ACHASOV 02E, and ACHASOV 03D data on the $\pi^+\pi^-\pi^0$ and ANTONELLI 92 on the $\omega\pi^+\pi^-$ final states. Supersedes ACHASOV 99E and ACHASOV 02E.
[3] Using the data of AKHMETSHIN 00D and ANTONELLI 92. The $\rho\pi$ dominance for the energy dependence of the $\omega(1420)$ and $\omega(1650)$ width assumed.
[4] From a fit to two Breit-Wigner functions and using the data of DOLINSKY 91 and ANTONELLI 92.
[5] From the partial and leptonic width given by the authors.
[6] From the combined fit of the $\rho\pi$ and $\omega\pi\pi$ final states.
[7] From the product of the leptonic width and partial branching ratio given by the authors.

$\Gamma(\omega\eta)/\Gamma_{\text{total}} \times \Gamma(e^+e^-)/\Gamma_{\text{total}}$ — $\Gamma_4/\Gamma \times \Gamma_5/\Gamma$

VALUE (units 10^{-7})	EVTS	DOCUMENT ID		TECN	COMMENT
• • • We do not use the following data for averages, fits, limits, etc. • • •					
6.4 ±0.9	267	[1] ACHASOV	20B	SND	$e^+e^- \to \omega\eta \to \eta\pi^0\gamma$
$5.62^{+0.45}_{-0.42}$		ACHASOV	19	SND	$e^+e^- \to \pi^+\pi^-\pi^0\eta$
4.5 ±0.3 ±0.3	824	[2] AKHMETSHIN	17A	CMD3	1.4–2.0 $e^+e^- \to \omega\eta$
4.4 ±0.5	898	[3] ACHASOV	16B	SND	1.34–2.00 $e^+e^- \to \omega\eta$
5.7 ±0.6	13	AUBERT	06D	BABR	10.6 $e^+e^- \to \omega\eta\gamma$
< 60 at 90% CL		[4] AKHMETSHIN	03B	CMD2	$e^+e \to \eta\pi^0\gamma$

[1] From a fit with contributions from $\omega(1420)$, $\omega(1650)$, and $\phi(1680)$. The mass of $\omega(1420)$ is fixed to the PDG 18 value of 1420 MeV. Fixing also the width of $\omega(1420)$ to the PDG 18 value of 220 MeV results in (5.4 ± 0.6) × 10^{-7} measurement.
[2] From a fit of the interfering $\omega(1420)$ and $\omega(1650)$ with a relative phase of π and other parameters floating. From an alternative fit $\Gamma(\omega(1650) \to \omega\eta)/\Gamma_{\text{total}} \times \Gamma(\omega(1650) \to e^+e^-) = 51 \pm 3$ eV.
[3] From a fit with contributions from $\omega(1420)$, $\omega(1650)$, and $\phi(1680)$.
[4] $\omega(1650)$ mass and width fixed at 1700 MeV and 250 MeV, respectively.

$\omega(1650)$ BRANCHING RATIOS

$\Gamma(\rho\pi)/\Gamma_{\text{total}}$ — Γ_1/Γ

VALUE	EVTS	DOCUMENT ID		TECN	COMMENT
• • • We do not use the following data for averages, fits, limits, etc. • • •					
not seen		[1] DIMOVA	25	SND	$e^+e^- \to \pi^+\pi^-\pi^0$
~ 0.65	1.2M	[2] ACHASOV	03D	RVUE	0.44–2.00 $e^+e^- \to \pi^+\pi^-\pi^0$
0.380±0.014		[3] HENNER	02	RVUE	1.2–2.0 $e^+e^- \to \rho\pi, \omega\pi\pi$

[1] From a fit to the cross section with contributions from $\omega(782)$, $\phi(1020)$, $\omega(1420)$, and $\omega(1650)$.
[2] From the combined fit of ANTONELLI 92, ACHASOV 01E, ACHASOV 02E, and ACHASOV 03D data on the $\pi^+\pi^-\pi^0$ and ANTONELLI 92 on the $\omega\pi^+\pi^-$ final states. Supersedes ACHASOV 99E and ACHASOV 02E.
[3] Assuming that the $\omega(1650)$ decays into $\rho\pi$ and $\omega\pi\pi$ only.

$\Gamma(\rho(1450)\pi)/\Gamma_{total}$ — Γ_2/Γ

VALUE	DOCUMENT ID		TECN	COMMENT
seen	ACHASOV	20A	SND	1.15–2.00 $e^+e^- \to \pi^+\pi^-\pi^0$
• • • We do not use the following data for averages, fits, limits, etc. • • •				
possibly seen	[1] DIMOVA	25	SND	$e^+e^- \to \pi^+\pi^-\pi^0$

[1] From a fit to the cross section with contributions from $\omega(782)$, $\phi(1020)$, $\omega(1420)$, and $\omega(1650)$.

$\Gamma(\omega\pi\pi)/\Gamma_{total}$ — Γ_3/Γ

VALUE	EVTS	DOCUMENT ID		TECN	COMMENT
• • • We do not use the following data for averages, fits, limits, etc. • • •					
~ 0.35	1.2M	[1] ACHASOV	03D	RVUE	0.44–2.00 $e^+e^- \to \pi^+\pi^-\pi^0$
0.620 ± 0.014		[2] HENNER	02	RVUE	1.2–2.0 $e^+e^- \to \rho\pi, \omega\pi\pi$

[1] From the combined fit of ANTONELLI 92, ACHASOV 01E, ACHASOV 02E, and ACHASOV 03D data on the $\pi^+\pi^-\pi^0$ and ANTONELLI 92 on the $\omega\pi^+\pi^-$ final states. Supersedes ACHASOV 99E and ACHASOV 02E.
[2] Assuming that the $\omega(1650)$ decays into $\rho\pi$ and $\omega\pi\pi$ only.

$\Gamma(e^+e^-)/\Gamma_{total}$ — Γ_5/Γ

VALUE (units 10^{-7})	EVTS	DOCUMENT ID		TECN	COMMENT
• • • We do not use the following data for averages, fits, limits, etc. • • •					
~ 18	1.2M	[1,2] ACHASOV	03D	RVUE	0.44–2.00 $e^+e^- \to \pi^+\pi^-\pi^0$
32 ± 1		[2] HENNER	02	RVUE	1.2–2.0 $e^+e^- \to \rho\pi, \omega\pi\pi$

[1] Calculated by us from the cross section at the peak.
[2] Assuming that the $\omega(1650)$ decays into $\rho\pi$ and $\omega\pi\pi$ only.

$\Gamma(\pi^0\gamma)/\Gamma_{total}$ — Γ_6/Γ

VALUE	DOCUMENT ID		TECN	COMMENT
not seen	[1] ACHASOV	10D	SND	1.075–2.0 $e^+e^- \to \pi^0\gamma$

[1] From a fit of a VMD model with two effective resonances with masses of 1450 MeV and 1700 MeV to describe the excited vector states $\omega(1420)$, $\rho(1450)$, $\omega(1650)$, and $\rho(1700)$. The width of the highest mass effective resonance is fixed at 315 MeV.

$\omega(1650)$ REFERENCES

DIMOVA	25	PPN 56 820	T.V. Dimova et al.	(SND Collab.)
ACHASOV	24A	PAN 87 747	M.N. Achasov et al.	(SND Collab.)
LICHARD	23	PR D108 092005	P. Lichard	(OPAV, CTUP)
ACHASOV	20A	EPJ C80 993	M.N. Achasov et al.	(SND Collab.)
ACHASOV	20B	EPJ C80 1008	M.N. Achasov et al.	(SND Collab.)
ABLIKIM	19AQ	PR D100 032004	M. Ablikim et al.	(BESIII Collab.)
ACHASOV	19	PR D99 112004	M.N. Achasov et al.	(SND Collab.)
PDG	18	PR D98 030001	M. Tanabashi et al.	(PDG Collab.)
AKHMETSHIN	17A	PL B773 150	R.R. Akhmetshin et al.	(CMD-3 Collab.)
ACHASOV	16B	PR D94 092002	M.N. Achasov et al.	(SND Collab.)
AULCHENKO	15A	JETP 121 27	V.M. Aulchenko et al.	(SND Collab.)
		Translated from ZETF 148 34.		
ACHASOV	10D	PR D98 112001	M.N. Achasov et al.	(SND Collab.)
AUBERT	07AU	PR D76 092005	B. Aubert et al.	(BABAR Collab.)
AUBERT	06D	PR D73 052003	B. Aubert et al.	(BABAR Collab.)
AUBERT,B	04N	PR D70 072004	B. Aubert et al.	(BABAR Collab.)
ACHASOV	03D	PR D68 052006	M.N. Achasov et al.	(Novosibirsk SND Collab.)
AKHMETSHIN	03B	PL B562 173	R.R. Akhmetshin et al.	(Novosibirsk CMD-2 Collab.)
ACHASOV	02E	PR D66 032001	M.N. Achasov et al.	(Novosibirsk SND Collab.)
HENNER	02	EPJ C26 3	V.K. Henner et al.	
ACHASOV	01E	PR D63 072002	M.N. Achasov et al.	(Novosibirsk SND Collab.)
EUGENIO	01	PL B497 190	P. Eugenio et al.	
AKHMETSHIN	00D	PL B489 125	R.R. Akhmetshin et al.	(Novosibirsk CMD-2 Collab.)
ACHASOV	99E	PL B462 365	M.N. Achasov et al.	(Novosibirsk SND Collab.)
ACHASOV	98H	PR D57 4334	N.N. Achasov, A.A. Kozhevnikov	
CLEGG	94	ZPHY C62 455	A.B. Clegg, A. Donnachie	(LANC, MCHS)
ANTONELLI	92	ZPHY C56 15	A. Antonelli et al.	(DM2 Collab.)
BISELLO	91C	ZPHY C52 227	D. Bisello et al.	(DM2 Collab.)
DOLINSKY	91	PRPL 202 99	S.I. Dolinsky et al.	(NOVO)
BISELLO	88B	ZPHY C39 13	D. Bisello et al.	(PADO, CLER, FRAS+)
BARKOV	87	JETPL 46 164	L.M. Barkov et al.	(NOVO)
		Translated from ZETFP 46 132.		
ATKINSON	83B	PL 127B 132	M. Atkinson et al.	(BONN, CERN, GLAS+)
CORDIER	81	PL 106B 155	A. Cordier et al.	(ORSAY)
IVANOV	81	PL 107B 297	P.M. Ivanov et al.	(NOVO)
ESPOSITO	80	LNC 28 195	B. Esposito et al.	(FRAS, NAPL, PADO+)
COSME	79	NP B152 215	G. Cosme et al.	(IPN)

$\omega_3(1670)$ — $I^G(J^{PC}) = 0^-(3^{--})$

$\omega_3(1670)$ MASS

VALUE (MeV)	EVTS	DOCUMENT ID		TECN	COMMENT
1667 ± 4 OUR AVERAGE					
$1665.3 \pm 5.2 \pm 4.5$	23400	AMELIN	96	VES	36 $\pi^-p \to \pi^+\pi^-\pi^0 n$
1685 ± 20	60	BAUBILLIER	79	HBC	8.2 K^-p backward
1673 ± 12	430	[1,2] BALTAY	78E	HBC	15 $\pi^+p \to \Delta 3\pi$
1650 ± 12		CORDEN	78B	OMEG	8–12 $\pi^-p \to N3\pi$
1669 ± 11	600	[2] WAGNER	75	HBC	7 $\pi^+p \to \Delta^{++}3\pi$
1678 ± 14	500	DIAZ	74	DBC	6 $\pi^+n \to p3\pi^0$
1660 ± 13	200	DIAZ	74	DBC	6 $\pi^+n \to p\omega\pi^0\pi^0$
1679 ± 17	200	MATTHEWS	71D	DBC	7.0 $\pi^+n \to p3\pi^0$
1670 ± 20		KENYON	69	DBC	8 $\pi^+n \to p3\pi^0$
• • • We do not use the following data for averages, fits, limits, etc. • • •					
~ 1700	110	[1] CERRADA	77B	HBC	4.2 $K^-p \to \Lambda 3\pi$
1636 ± 20		ARMENISE	68B	DBC	5.1 $\pi^+n \to p3\pi^0$

[1] Phase rotation seen for $J^P = 3^-$ $\rho\pi$ wave.
[2] From a fit to $I(J^P) = 0(3^-)$ $\rho\pi$ partial wave.

$\omega_3(1670)$ WIDTH

VALUE (MeV)	EVTS	DOCUMENT ID		TECN	COMMENT
168±10 OUR AVERAGE					
$149 \pm 19 \pm 7$	23400	AMELIN	96	VES	36 $\pi^-p \to \pi^+\pi^-\pi^0 n$
160 ± 80	60	[3] BAUBILLIER	79	HBC	8.2 K^-p backward
173 ± 16	430	[4,5] BALTAY	78E	HBC	15 $\pi^+p \to \Delta 3\pi$
253 ± 39		CORDEN	78B	OMEG	8–12 $\pi^-p \to N3\pi$
173 ± 28	600	[3,5] WAGNER	75	HBC	7 $\pi^+p \to \Delta^{++}3\pi$
167 ± 40	500	DIAZ	74	DBC	6 $\pi^+n \to p3\pi^0$
122 ± 39	200	DIAZ	74	DBC	6 $\pi^+n \to p\omega\pi^0\pi^0$
155 ± 40	200	[3] MATTHEWS	71D	DBC	7.0 $\pi^+n \to p3\pi^0$
• • • We do not use the following data for averages, fits, limits, etc. • • •					
100 ± 40		KENYON	69	DBC	8 $\pi^+n \to p3\pi^0$
112 ± 60		ARMENISE	68B	DBC	5.1 $\pi^+n \to p3\pi^0$

[3] Width errors enlarged by us to $4\Gamma/\sqrt{N}$; see the note with the $K^*(892)$ mass.
[4] Phase rotation seen for $J^P = 3^-$ $\rho\pi$ wave.
[5] From a fit to $I(J^P) = 0(3^-)$ $\rho\pi$ partial wave.

$\omega_3(1670)$ DECAY MODES

	Mode	Fraction (Γ_i/Γ)
Γ_1	$\rho\pi$	seen
Γ_2	$\omega\pi\pi$	seen
Γ_3	$b_1(1235)\pi$	possibly seen

$\omega_3(1670)$ BRANCHING RATIOS

$\Gamma(\omega\pi\pi)/\Gamma(\rho\pi)$ — Γ_2/Γ_1

VALUE	EVTS	DOCUMENT ID		TECN	COMMENT
• • • We do not use the following data for averages, fits, limits, etc. • • •					
0.71 ± 0.27	100	DIAZ	74	DBC	6 $\pi^+n \to p5\pi^0$

$\Gamma(b_1(1235)\pi)/\Gamma(\rho\pi)$ — Γ_3/Γ_1

VALUE	DOCUMENT ID		TECN	COMMENT
possibly seen	DIAZ	74	DBC	6 $\pi^+n \to p5\pi^0$

$\Gamma(b_1(1235)\pi)/\Gamma(\omega\pi\pi)$ — Γ_3/Γ_2

VALUE	CL%	DOCUMENT ID		TECN	COMMENT
• • • We do not use the following data for averages, fits, limits, etc. • • •					
>0.75	68	BAUBILLIER	79	HBC	8.2 K^-p backward

$\omega_3(1670)$ REFERENCES

AMELIN	96	ZPHY C70 71	D.V. Amelin et al.	(SERP, TBIL)
BAUBILLIER	79	PL 89B 131	M. Baubillier et al.	(BIRM, CERN, GLAS+)
BALTAY	78E	PRL 40 87	C. Baltay, C.V. Cautis, M. Kalelkar	(COLU) JP
CORDEN	78B	NP B138 235	M.J. Corden et al.	(BIRM, RHEL, TELA+)
CERRADA	77B	NP B126 241	M. Cerrada et al.	(AMST, CERN, NIJM+) JP
WAGNER	75	PL 58B 201	F. Wagner, M. Tabak, D.M. Chew	(LBL) JP
DIAZ	74	PRL 32 260	J. Diaz et al.	(CASE, CMU)
MATTHEWS	71D	PR D3 2561	J.A.J. Matthews et al.	(TNTO, WISC)
KENYON	69	PRL 23 146	I.R. Kenyon et al.	(BNL, UCND, ORNL)
ARMENISE	68B	PL 26B 336	N. Armenise et al.	(BARI, BGNA, FIRZ+)

$\pi_2(1670)$ — $I^G(J^{PC}) = 1^-(2^{-+})$

$\pi_2(1670)$ MASS

VALUE (MeV)	EVTS	DOCUMENT ID		TECN	CHG	COMMENT
$1670.6^{+2.9}_{-1.2}$ OUR AVERAGE Error includes scale factor of 1.3. See the ideogram below.						
$1642 \; {}^{+12}_{-1}$	46M	[1] AGHASYAN	18B	COMP		190 $\pi^-p \to \pi^-\pi^+\pi^-p$
$1749 \pm 10 \pm 100$	145k	LU	05	B852		18 $\pi^-p \to \omega\pi^-\pi^0 p$
$1676 \pm 3 \pm 8$		[2] CHUNG	02	B852		18.3 $\pi^-p \to \pi^+\pi^-\pi^-p$
$1685 \pm 10 \pm 30$		BARBERIS	01			450 $pp \to p_f 3\pi^0 p_s$
$1687 \pm 9 \pm 15$		AMELIN	99	VES		37 $\pi^-A \to \omega\pi^-\pi^0 A^*$

Int. J. Mod. Phys. A 2026.41. Downloaded from www.worldscientific.com
by CALIFORNIA @ BERKELEY on 09/16/26. Re-use and distribution is strictly not permitted, except for Open Access articles.

1669 ± 4			BARBERIS	98B			450 $pp \to p_f \rho\pi p_s$
1670 ± 4			BARBERIS	98B			450 $pp \to p_f f_2(1270)\pi p_s$
1690 ±14			[3] BERDNIKOV	94	VES		37 $\pi^- A \to K^+K^-\pi^- A$
1710 ±20		700	ANTIPOV	87	SIGM	−	50 π^- Cu $\to \mu^+\mu^-\pi^-$ Cu
1676 ± 6			[3] EVANGELIS...	81	OMEG	−	12 $\pi^- p \to 3\pi p$
1657 ±14			[3,4] DAUM	80D	SPEC	−	63–94 $\pi p \to 3\pi X$
1662 ±10		2000	[3] BALTAY	77	HBC	+	15 $\pi^+ p \to p 3\pi$
• • • We do not use the following data for averages, fits, limits, etc. • • •							
1658 ± 3	$^{+24}_{-8}$	420k	[5] ALEKSEEV	10	COMP		190 $\pi^- Pb \to \pi^-\pi^-\pi^+ Pb'$
1730 ±20			[6] AMELIN	95B	VES		36 $\pi^- A \to \pi^+\pi^-\pi^- A$
1742 ±31	± 49		ANTREASYAN	90	CBAL		$e^+e^- \to e^+e^-\pi^0\pi^0\pi^0$
1624 ±21			[2] BELLINI	85	SPEC		40 $\pi^- A \to \pi^-\pi^+\pi^- A$
1622 ±35			[7] BELLINI	85	SPEC		40 $\pi^- A \to \pi^-\pi^+\pi^- A$
1693 ±28			[8] BELLINI	85	SPEC		40 $\pi^- A \to \pi^-\pi^+\pi^- A$
1710 ±20			[9] DAUM	81B	SPEC	−	63,94 $\pi^- p$
1660 ±10			[3] ASCOLI	73	HBC	−	5–25 $\pi^- p \to p\pi_2$

[1] Statistical error negligible.
[2] From $f_2(1270)\pi$ decay.
[3] From a fit to $J^P = 2^-$ S-wave $f_2(1270)\pi$ partial wave.
[4] Clear phase rotation seen in 2^-S, 2^-P, 2^-D waves. We quote central value and spread of single-resonance fits to three channels.
[5] Superseded by AGHASYAN 2018B.
[6] J^{PC} ambiguous.
[7] From $\rho\pi$ decay.
[8] From $\sigma\pi$ decay.
[9] From a two-resonance fit to four 2^-0^+ waves. This should not be averaged with all the single resonance fits.

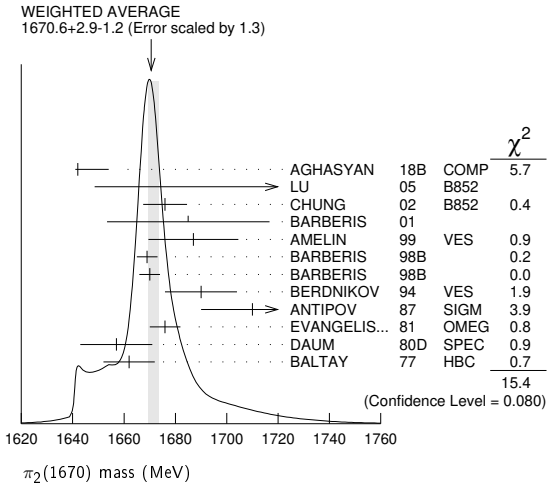

$\pi_2(1670)$ WIDTH

VALUE (MeV)	EVTS	DOCUMENT ID		TECN	CHG	COMMENT
258^{+8}_{-9} OUR AVERAGE	Error includes scale factor of 1.2.					
311^{+12}_{-23}	46M	[10] AGHASYAN	18B	COMP		190 $\pi^- p \to \pi^-\pi^+\pi^- p$
408 ± 60 ± 250	145k	LU	05	B852		18 $\pi^- p \to \omega\pi^-\pi^0 p$
254 ± 3 ± 31		[11] CHUNG	02	B852		18.3 $\pi^- p \to \pi^+\pi^-\pi^- p$
265 ± 30 ± 40		BARBERIS	01			450 $pp \to p_f 3\pi^0 p_s$
168 ± 43 ± 53		AMELIN	99	VES		37 $\pi^- A \to \omega\pi^-\pi^0 A^*$
268 ± 15		BARBERIS	98B			450 $pp \to p_f \rho\pi p_s$
256 ± 15		BARBERIS	98B			450 $pp \to p_f f_2(1270)\pi p_s$
190 ± 50		[12] BERDNIKOV	94	VES		37 $\pi^- A \to K^+K^-\pi^- A$
170 ± 80	700	ANTIPOV	87	SIGM	−	50 π^- Cu $\to \mu^+\mu^-\pi^-$ Cu
260 ± 20		[12] EVANGELIS...	81	OMEG	−	12 $\pi^- p \to 3\pi p$
219 ± 20		[12,13] DAUM	80D	SPEC	−	63–94 $\pi p \to 3\pi X$
285 ± 60	2000	[12] BALTAY	77	HBC	+	15 $\pi^+ p \to p 3\pi$
• • • We do not use the following data for averages, fits, limits, etc. • • •						
$271 \pm 9^{+22}_{-24}$	420k	[14] ALEKSEEV	10	COMP		190 $\pi^- Pb \to \pi^-\pi^-\pi^+ Pb'$
310 ± 20		[15] AMELIN	95B	VES		36 $\pi^- A \to \pi^+\pi^-\pi^- A$
236 ± 49 ± 36		ANTREASYAN	90	CBAL		$e^+e^- \to e^+e^-\pi^0\pi^0\pi^0$
304 ± 22		[11] BELLINI	85	SPEC		40 $\pi^- A \to \pi^-\pi^+\pi^- A$
404 ±108		[16] BELLINI	85	SPEC		40 $\pi^- A \to \pi^-\pi^+\pi^- A$
330 ± 90		[17] BELLINI	85	SPEC		40 $\pi^- A \to \pi^-\pi^+\pi^- A$
312 ± 50		[18] DAUM	81B	SPEC	−	63,94 $\pi^- p$
270 ± 60		[12] ASCOLI	73	HBC	−	5–25 $\pi^- p \to p\pi_2$

[10] Statistical error negligible.
[11] From $f_2(1270)\pi$ decay.
[12] From a fit to $J^P = 2^-$ $f_2(1270)\pi$ partial wave.
[13] Clear phase rotation seen in 2^-S, 2^-P, 2^-D waves. We quote central value and spread of single-resonance fits to three channels.
[14] Superseded by AGHASYAN 2018B.
[15] J^{PC} ambiguous.
[16] From $\rho\pi$ decay.
[17] From $\sigma\pi$ decay.
[18] From a two-resonance fit to four 2^-0^+ waves. This should not be averaged with all the single resonance fits.

$\pi_2(1670)$ DECAY MODES

	Mode	Fraction (Γ_i/Γ)	Confidence level
Γ_1	3π	(95.8±1.4) %	
Γ_2	$\pi^+\pi^-\pi^0$		
Γ_3	$\pi^0\pi^0\pi^0$		
Γ_4	$f_2(1270)\pi$	(56.3±3.2) %	
Γ_5	$\rho\pi$	(31 ±4) %	
Γ_6	$\sigma\pi$	(10 ±4) %	
Γ_7	$\pi(\pi\pi)_S$-wave	(8.7±3.4) %	
Γ_8	$\pi^\pm\pi^+\pi^-$	(53 ±4) %	
Γ_9	$K\overline{K}^*(892)+$ c.c.	(4.2±1.4) %	
Γ_{10}	$\omega\rho$	(2.7±1.1) %	
Γ_{11}	$\pi^\pm\gamma$	(7.0±1.2) $\times 10^{-4}$	
Γ_{12}	$\gamma\gamma$	< 2.8 $\times 10^{-7}$	90%
Γ_{13}	$\eta\pi$	< 5 %	
Γ_{14}	$\pi^\pm 2\pi^+ 2\pi^-$	< 5 %	
Γ_{15}	$\rho(1450)\pi$	< 3.6 $\times 10^{-3}$	97.7%
Γ_{16}	$b_1(1235)\pi$	< 1.9 $\times 10^{-3}$	97.7%
Γ_{17}	$f_1(1285)\pi$	possibly seen	
Γ_{18}	$a_2(1320)\pi$	not seen	

CONSTRAINED FIT INFORMATION

An overall fit to 4 branching ratios uses 6 measurements and one constraint to determine 4 parameters. The overall fit has a χ^2 = 1.9 for 3 degrees of freedom.

The following *off-diagonal* array elements are the correlation coefficients $\langle \delta x_i \delta x_j \rangle / (\delta x_i \cdot \delta x_j)$, in percent, from the fit to the branching fractions, $x_i \equiv \Gamma_i/\Gamma_{total}$. The fit constrains the x_i whose labels appear in this array to sum to one.

x_5	−53		
x_7	−29	−59	
x_9	−8	−21	−9
	x_4	x_5	x_7

$\pi_2(1670)$ PARTIAL WIDTHS

$\Gamma(\pi^\pm\gamma)$ — Γ_{11}

VALUE (keV)	DOCUMENT ID		TECN	CHG	COMMENT
181±11±27	[19] ADOLPH	14	COMP	−	190 π^-Pb $\to \pi^+\pi^-\pi^-$Pb$'$

[19] Primakoff reaction. Assumes incoherent $f_2(1270)\pi$ contribution to 3π final state and uses B($\pi_2(1670) \to f_2\pi$) = 56%.

$\Gamma(\gamma\gamma)$ — Γ_{12}

VALUE (keV)	CL%	DOCUMENT ID		TECN	CHG	COMMENT
<0.072	90	[20] ACCIARRI	97T	L3		$e^+e^- \to e^+e^-\pi^+\pi^-\pi^0$
• • • We do not use the following data for averages, fits, limits, etc. • • •						
<0.19	90	[20] ALBRECHT	97B	ARG		$e^+e^- \to e^+e^-\pi^+\pi^-\pi^0$
1.41 ±0.23±0.28		ANTREASYAN	90	CBAL	0	$e^+e^- \to e^+e^-\pi^0\pi^0\pi^0$
0.8 ±0.3 ±0.12		[21] BEHREND	90C	CELL	0	$e^+e^- \to e^+e^-\pi^+\pi^-\pi^0$
1.3 ±0.3 ±0.2		[22] BEHREND	90C	CELL	0	$e^+e^- \to e^+e^-\pi^+\pi^-\pi^0$

[20] Decaying into $f_2(1270)\pi$ and $\rho\pi$.
[21] Constructive interference between $f_2(1270)\pi$,$\rho\pi$ and background.
[22] Incoherent Ansatz.

Int. J. Mod. Phys. A 2026.41. Downloaded from www.worldscientific.com
by UNIVERSITY OF CALIFORNIA @ BERKELEY on 09/16/26. Re-use and distribution is strictly not permitted, except for Open Access articles.

Int. J. Mod. Phys. A 2026.41. Downloaded from www.worldscientific.com by CALIFORNIA @ BERKELEY on 09/16/26. Re-use and distribution is strictly not permitted, except for Open Access articles.

$\pi_2(1670)$ $\Gamma(i)\Gamma(\gamma\gamma)/\Gamma(\text{total})$

$\Gamma(\pi^+\pi^-\pi^0) \times \Gamma(\gamma\gamma)/\Gamma_{\text{total}}$ — $\Gamma_2\Gamma_{12}/\Gamma$

VALUE (keV)	CL%	DOCUMENT ID		TECN	COMMENT
<0.1	95	[23] SCHEGELSKY	06	RVUE	$\gamma\gamma \to \pi^+\pi^-\pi^0$

[23] From analysis of L3 data at 183–209 GeV.

$\pi_2(1670)$ BRANCHING RATIOS

$\Gamma(3\pi)/\Gamma_{\text{total}}$ — $\Gamma_1/\Gamma = (\Gamma_4+\Gamma_5+\Gamma_7)/\Gamma$

VALUE	DOCUMENT ID
0.958±0.014 OUR FIT	

$\Gamma(\pi^0\pi^0\pi^0)/\Gamma(\pi^+\pi^-\pi^0)$ — Γ_3/Γ_2

VALUE	DOCUMENT ID		COMMENT
0.29±0.03±0.05	BARBERIS	01	$450\ pp \to p_f 3\pi^0 p_s$

$\Gamma(\rho\pi)/0.565\Gamma(f_2(1270)\pi)$ — $\Gamma_5/0.565\Gamma_4$

(With $f_2(1270) \to \pi^+\pi^-$.)

VALUE	DOCUMENT ID		TECN	COMMENT
0.97±0.09 OUR AVERAGE	Error includes scale factor of 1.9.			
0.76±0.07±0.10	CHUNG	02	B852	$18.3\ \pi^- p \to \pi^+\pi^-\pi^- p$
1.01±0.05	BARBERIS	98B		$450\ pp \to p_f \pi^+\pi^-\pi^0 p_s$

$\Gamma(\sigma\pi)/\Gamma(f_2(1270)\pi)$ — Γ_6/Γ_4

VALUE	DOCUMENT ID		TECN	COMMENT
0.17±0.02±0.07	CHUNG	02	B852	$18.3\ \pi^- p \to \pi^+\pi^-\pi^- p$
• • • We do not use the following data for averages, fits, limits, etc. • • •				
0.24±0.10	[24,25] BAKER	99	SPEC	$1.94\ \bar{p}p \to 4\pi^0$

$\frac{1}{2}\Gamma(\rho\pi)/\Gamma(\pi^\pm\pi^+\pi^-)$ — $\frac{1}{2}\Gamma_5/\Gamma_8 = \frac{1}{2}\Gamma_5/(0.565\Gamma_4+\frac{1}{2}\Gamma_5+0.624\Gamma_7)$

VALUE	DOCUMENT ID		TECN	CHG	COMMENT
0.29±0.04 OUR FIT					
0.29±0.05	[26] DAUM	81B	SPEC		$63,94\ \pi^- p$
• • • We do not use the following data for averages, fits, limits, etc. • • •					
<0.3	BARTSCH	68	HBC	+	$8\ \pi^+ p \to 3\pi p$

$0.565\Gamma(f_2(1270)\pi)/\Gamma(\pi^\pm\pi^+\pi^-)$
$0.565\Gamma_4/\Gamma_8 = 0.565\Gamma_4/(0.565\Gamma_4+\frac{1}{2}\Gamma_5+0.624\Gamma_7)$

(With $f_2(1270) \to \pi^+\pi^-$.)

VALUE	DOCUMENT ID		TECN	CHG	COMMENT
0.604±0.035 OUR FIT					
0.60 ±0.05 OUR AVERAGE	Error includes scale factor of 1.3.				
0.61 ±0.04	[26] DAUM	81B	SPEC		$63,94\ \pi^- p$
$0.76\ ^{+0.24}_{-0.34}$	ARMENISE	69	DBC	+	$5.1\ \pi^+ d \to d 3\pi$
0.35 ±0.20	BALTAY	68	HBC	+	$7–8.5\ \pi^+ p$
• • • We do not use the following data for averages, fits, limits, etc. • • •					
0.59	BARTSCH	68	HBC	+	$8\ \pi^+ p \to 3\pi p$

$0.624\Gamma(\pi(\pi\pi)_{S\text{-wave}})/\Gamma(\pi^\pm\pi^+\pi^-)$
$0.624\Gamma_7/\Gamma_8 = 0.624\Gamma_7/(0.565\Gamma_4+\frac{1}{2}\Gamma_5+0.624\Gamma_7)$

(With $(\pi\pi)_{S\text{-wave}} \to \pi^+\pi^-$.)

VALUE	DOCUMENT ID		TECN	COMMENT
0.10±0.04 OUR FIT				
0.10±0.05	[26] DAUM	81B	SPEC	$63,94\ \pi^- p$

$\Gamma(K\overline{K}^*(892)+\text{c.c.})/\Gamma(f_2(1270)\pi)$ — Γ_9/Γ_4

VALUE	DOCUMENT ID		TECN	CHG	COMMENT
0.075±0.025 OUR FIT					
0.075±0.025	[27] ARMSTRONG	82B	OMEG	−	$16\ \pi^- p \to K^+K^-\pi^- p$

$\Gamma(\omega\rho)/\Gamma_{\text{total}}$ — Γ_{10}/Γ

VALUE	DOCUMENT ID		TECN	COMMENT
0.027±0.004±0.010	[28] AMELIN	99	VES	$37\ \pi^- A \to \omega\pi^-\pi^0 A^*$

$\Gamma(\eta\pi)/\Gamma(\pi^\pm\pi^+\pi^-)$ — $\Gamma_{13}/\Gamma_8 = \Gamma_{13}/(0.565\Gamma_4+\frac{1}{2}\Gamma_5+0.624\Gamma_7)$

(All η decays.)

VALUE	DOCUMENT ID		TECN	CHG	COMMENT
<0.09	BALTAY	68	HBC	+	$7–8.5\ \pi^+ p$
• • • We do not use the following data for averages, fits, limits, etc. • • •					
<0.10	CRENNELL	70	HBC	−	$6\ \pi^- p \to f_2\pi^- N$

$\Gamma(\pi^\pm 2\pi^+ 2\pi^-)/\Gamma(\pi^\pm\pi^+\pi^-)$ — $\Gamma_{14}/\Gamma_8 = \Gamma_{14}/(0.565\Gamma_4+\frac{1}{2}\Gamma_5+0.624\Gamma_7)$

VALUE	DOCUMENT ID		TECN	CHG	COMMENT
<0.10	CRENNELL	70	HBC	−	$6\ \pi^- p \to f_2\pi^- N$
• • • We do not use the following data for averages, fits, limits, etc. • • •					
<0.1	BALTAY	68	HBC	+	$7,8.5\ \pi^+ p$

$\Gamma(\rho(1450)\pi)/\Gamma_{\text{total}}$ — Γ_{15}/Γ

VALUE	CL%	DOCUMENT ID		TECN	COMMENT
<0.0036	97.7	AMELIN	99	VES	$37\ \pi^- A \to \omega\pi^-\pi^0 A^*$

$\Gamma(b_1(1235)\pi)/\Gamma_{\text{total}}$ — Γ_{16}/Γ

VALUE	CL%	DOCUMENT ID		TECN	COMMENT
<0.0019	97.7	AMELIN	99	VES	$37\ \pi^- A \to \omega\pi^-\pi^0 A^*$

$\Gamma(f_1(1285)\pi)/\Gamma_{\text{total}}$ — Γ_{17}/Γ

VALUE	EVTS	DOCUMENT ID		TECN	COMMENT
possibly seen	69k	KUHN	04	B852	$18\ \pi^- p \to \eta\pi^+\pi^-\pi^- p$

$\Gamma(a_2(1320)\pi)/\Gamma_{\text{total}}$ — Γ_{18}/Γ

VALUE	EVTS	DOCUMENT ID		TECN	COMMENT
not seen	69k	KUHN	04	B852	$18\ \pi^- p \to \eta\pi^+\pi^-\pi^- p$

D-wave/S-wave RATIO FOR $\pi_2(1670) \to f_2(1270)\pi$

VALUE	DOCUMENT ID		TECN	COMMENT
−0.18±0.06	[24] BAKER	99	SPEC	$1.94\ \bar{p}p \to 4\pi^0$
• • • We do not use the following data for averages, fits, limits, etc. • • •				
0.22±0.10	[26] DAUM	81B	SPEC	$63,94\ \pi^- p$

F-wave/P-wave RATIO FOR $\pi_2(1670) \to \rho\pi$

VALUE	DOCUMENT ID		TECN	COMMENT
−0.72±0.07±0.14	CHUNG	02	B852	$18.3\ \pi^- p \to \pi^+\pi^-\pi^- p$

[24] Using preliminary CBAR data.
[25] With the $\sigma\pi$ in L=2 and the $f_2(1270)\pi$ in L=0.
[26] From a two-resonance fit to four 2^-0^+ waves.
[27] From a partial-wave analysis of $K^+K^-\pi^-$ system.
[28] Normalized to the $B(\pi_2(1670) \to f_2\pi)$.

$\pi_2(1670)$ REFERENCES

AGHASYAN	18B	PR D98 092003	M. Aghasyan et al.	(COMPASS Collab.)
ADOLPH	14	EPJ A50 79	C. Adolph et al.	(COMPASS Collab.)
ALEKSEEV	10	PRL 104 241803	M.G. Alekseev et al.	(COMPASS Collab.)
SCHEGELSKY	06	EPJ A27 199	V.A. Schegelsky et al.	
LU	05	PRL 94 032002	M. Lu et al.	(BNL E852 Collab.)
KUHN	04	PL B595 109	J. Kuhn et al.	(BNL E852 Collab.)
CHUNG	02	PR D65 072001	S.U. Chung et al.	(BNL E852 Collab.)
BARBERIS	01	PL B507 14	D. Barberis et al.	
AMELIN	99	PAN 62 445	D.V. Amelin et al.	(VES Collab.)
		Translated from YAF 62 487.		
BAKER	99	PL B449 114	C.A. Baker et al.	
BARBERIS	98B	PL B422 399	D. Barberis et al.	(WA 102 Collab.)
ACCIARRI	97T	PL B413 147	M. Acciarri et al.	(L3 Collab.)
ALBRECHT	97B	ZPHY C74 469	H. Albrecht et al.	(ARGUS Collab.)
AMELIN	95B	PL B356 595	D.V. Amelin et al.	(SERP, TBIL)
BERDNIKOV	94	PL B337 219	E.B. Berdnikov et al.	(SERP, TBIL)
ANTREASYAN	90	ZPHY C48 561	D. Antreasyan et al.	(Crystal Ball Collab.)
BEHREND	90C	ZPHY C46 583	H.J. Behrend et al.	(CELLO Collab.)
ANTIPOV	87	EPL 4 403	Y.M. Antipov et al.	(SERP, JINR, INRM+)
BELLINI	85	SJNP 41 781	D. Bellini et al.	
		Translated from YAF 41 1223.		
ARMSTRONG	82B	NP B202 1	T.A. Armstrong, B. Baccari	(AACH3, BARI, BONN+)
DAUM	81B	NP B182 269	C. Daum et al.	(AMST, CERN, CRAC, MPIM+)
EVANGELIS...	81	NP B178 197	C. Evangelista et al.	(BARI, BONN, CERN+)
Also		NP B186 594	C. Evangelista	
DAUM	80D	PL 89B 285	C. Daum et al.	(AMST, CERN, CRAC, MPIM+) JP
BALTAY	77	PRL 39 591	C. Baltay, C.V. Cautis, M. Kalelkar	(COLU) JP
ASCOLI	73	PR D7 669	G. Ascoli	(ILL, TNTO, GENO, HAMB, MILA+) JP
CRENNELL	70	PRL 24 781	D.J. Crennell et al.	(BNL)
ARMENISE	69	LNC 2 501	N. Armenise et al.	(BARI, BGNA, FIRZ)
BALTAY	68	PRL 20 887	C. Baltay et al.	(COLU, ROCH, RUTG, YALE) I
BARTSCH	68	NP B7 345	J. Bartsch et al.	(AACH, BERL, CERN) JP

$\phi(1680)$

$I^G(J^{PC}) = 0^-(1^{--})$

$\phi(1680)$ MASS

e^+e^- PRODUCTION

VALUE (MeV)		EVTS	DOCUMENT ID		TECN	COMMENT
1680 ±20 OUR ESTIMATE						
• • • We do not use the following data for averages, fits, limits, etc. • • •						
1694 ± 5	±15	9.1k	[1] FEDOTOVICH	25	CMD3	$e^+e^- \to K^0_S K^\pm\pi^\mp$
1663 ± 5	$^{+16}_{-4}$		ABLIKIM	24CB	BES3	$J/\psi \to \phi\eta\pi^0$
1656.8± 4.9			[2] LICHARD	23	RVUE	$e^+e^- \to \Upsilon(nS) \to \phi\eta\gamma$
1683 ± 7	± 9		[3] ZHU	23	BELL	$e^+e^- \to \Upsilon(nS) \to \phi\eta\gamma$
1678 $^{+5}_{-3}$	± 7		[4] ZHU	23A	RVUE	$e^+e^- \to \eta\phi$
1673 ± 5			[5] ABLIKIM	22L	BES3	2.0–3.08 $e^+e^- \to K^+K^-\pi^0$
1680 $^{+12}_{-13}$	±21	1.8k	[6] ABLIKIM	20F	BES3	$\psi(2S) \to K^+K^-\eta$
1662 ±20			[7] ACHASOV	20C	SND	1.3–2.0 $e^+e^- \to K^+K^-\pi^0$
1641 $^{+24}_{-18}$			ACHASOV	19	SND	$e^+e^- \to \pi^+\pi^-\pi^0\eta$
1667 ± 5	±11	3k	[8] IVANOV	19A	CMD3	1.59–2.007 $e^+e^- \to K^+K^-\eta$
1700 ±23		2k	[9] ACHASOV	18A	SND	1.3–2.0 $e^+e^- \to K^0_S K^0_L\pi^0$
1674 ±12	± 6	6.2k	[10] LEES	14H	BABR	$e^+e^- \to K^0_S K^0_L\gamma$
1733 ±10	±10		[11] LEES	12F	BABR	10.6 $e^+e^- \to \phi\pi^+\pi^-\gamma$

1689 ± 7 ±10	4.8k	[12] SHEN	09	BELL	10.6 $e^+e^- \to K^+K^-\pi^+\pi^-\gamma$
1709 ±20 ±43		[13] AUBERT	08S	BABR	10.6 $e^+e^- \to$ hadrons
1623 ±20	948	[14] AKHMETSHIN	03	CMD2	1.05–1.38 $e^+e^- \to K^0_L K^0_S$
~ 1500		[15] ACHASOV	98H	RVUE	$e^+e^- \to \pi^+\pi^-\pi^0$, $\omega\pi^+\pi^-$, K^+K^-
~ 1900		[16] ACHASOV	98H	RVUE	$e^+e^- \to K^0_S K^\pm\pi^\mp$
1700 ±20		[17] CLEGG	94	RVUE	$e^+e^- \to K^+K^-$, $K^0_S K\pi$
1657 ±27	367	BISELLO	91C	DM2	$e^+e^- \to K^0_S K^\pm\pi^\mp$
1655 ±17		[18] BISELLO	88B	DM2	$e^+e^- \to K^+K^-$
1680 ±10		[19] BUON	82	DM1	$e^+e^- \to$ hadrons
1677 ±12		[20] MANE	82	DM1	$e^+e^- \to K^0_S K\pi$

[1] Using a vector dominance fit with contributions from $\phi(1680)$ and $\rho(1450)$.
[2] From a VDM fit to ZHU 23 $\eta\phi\gamma$ data with two resonances, $\phi(1680)$, $\phi(2170)$, and a third resonance with mass 1850.7 ± 5.3 MeV and width 25 ± 35 MeV of 1.7 σ statistical evidence.
[3] From a fit using a vector meson dominance model with contributions from $\phi(1680)$, $\phi(2170)$ and non resonant contribution.
[4] From the analysis of the combined measurements of $\sigma(e^+e^- \to \eta\phi)$ from BaBar, Belle, BESIII, CMD3.
[5] From a partial wave amplitude analysis at $\sqrt{s} = 2.125$ GeV which includes all the possible intermediate states that match J^{PC} conservation in the subsequent two-body decay. The intermediate states are parameterized with the relativistic Breit-Wigner functions. Statistical error only.
[6] Seen in $\psi(2S)$ decay with branching ratio $\psi(2S) \to X\eta \to K^+K^-\eta = (12.0 \pm 1.3^{+6.5}_{-6.9}) \times 10^{-6}$.
[7] From a fit using a vector meson dominance model with contribution from $\rho(770)$, $\omega(782)$, $\phi(1020)$, $\omega(1420)$, $\rho(1450)$.
[8] From a fit with coherent interference of the $\phi(1680)$ with a non-resonant contribution.
[9] Assuming the $K\overline{K}^*(892)+$ c.c. dynamics. Systematic uncertainties not estimated.
[10] Using a vector meson dominance model with contribution from $\phi(1020)$, $\phi(1680)$, and higher mass excitations of $\rho(770)$ and $\omega(782)$.
[11] Using events with $\pi\pi$ invariant mass less than 0.85 GeV.
[12] From a fit with two incoherent Breit-Wigners.
[13] From the simultaneous fit to the $K\overline{K}^*(892)+$ c.c. and $\phi\eta$ data from AUBERT 08S using the results of AUBERT 07AK.
[14] From the combined fit of AKHMETSHIN 03 and MANE 81 also including ρ, ω, and ϕ. Neither isospin nor flavor structure known.
[15] Using data from IVANOV 81, BARKOV 87, BISELLO 88B, DOLINSKY 91, and ANTONELLI 92.
[16] Using the data from BISELLO 91C.
[17] Using BISELLO 88B and MANE 82 data.
[18] From global fit including ρ, ω, ϕ and $\rho(1700)$ assume mass 1570 MeV and width 510 MeV for ρ radial excitation.
[19] From global fit of ρ, ω, ϕ and their radial excitations to channels $\omega\pi^+\pi^-$, K^+K^-, $K^0_S K^0_L$, $K^0_S K^\pm\pi^\mp$. Assume mass 1570 MeV and width 510 MeV for ρ radial excitations, mass 1570 and width 500 MeV for ω radial excitation.
[20] Fit to one channel only, neglecting interference with ω, $\rho(1700)$.

$p\overline{p}$ ANNIHILATION

VALUE (MeV)	DOCUMENT ID		TECN	COMMENT
• • • We do not use the following data for averages, fits, limits, etc. • • •				
1700 ± 8	[1] AMSLER	06	CBAR	0.9 $\overline{p}p \to K^+K^-\pi^0$

[1] Could also be $\rho(1700)$.

$\phi(1680)$ WIDTH

e^+e^- PRODUCTION

VALUE (MeV)	EVTS	DOCUMENT ID		TECN	COMMENT
150 ±50 OUR ESTIMATE This is only an educated guess; the error given is larger than the error on the average of the published values.					
• • • We do not use the following data for averages, fits, limits, etc. • • •					
204 ±18 ± 22	9.1k	[1] FEDOTOVICH	25	CMD3	$e^+e^- \to K^0_S K^\pm\pi^\mp$
159 ±15 ± 11		ABLIKIM	24CB	BES3	$J/\psi \to \phi\eta\pi^0$
150.8 ± 7.0		[2] LICHARD	23	RVUE	$e^+e^- \to \Upsilon(nS) \to \phi\eta\gamma$
149 ±12 ± 13		[3] ZHU	23	BELL	$e^+e^- \to \Upsilon(nS) \to \phi\eta\gamma$
156 ± 5 ± 9		[4] ZHU	23A	RVUE	$e^+e^- \to \eta\phi$
172 ± 8		[5] ABLIKIM	22L	BES3	2.0–3.08 $e^+e^- \to K^+K^-\pi^0$
185 $^{+30}_{-26}$ $^{+25}_{-47}$	1.8k	[6] ABLIKIM	20F	BES3	$\psi(2S) \to K^+K^-\eta$
159 ±32		[7] ACHASOV	20C	SND	1.3–2.0 $e^+e^- \to K^+K^-\pi^0$
103 $^{+26}_{-24}$		ACHASOV	19	SND	$e^+e^- \to \pi^+\pi^-\pi^0\eta$
176 ±23 ± 38	3k	[8] IVANOV	19A	CMD3	1.59–2.007 $e^+e^- \to K^+K^-\eta$
300 ±50	2k	[9] ACHASOV	18A	SND	1.3–2.0 $e^+e^- \to K^0_S K^0_L\pi^0$
165 ±38 ± 70	6.2k	[10] LEES	14H	BABR	$e^+e^- \to K^0_S K^0_L\gamma$
300 ±15 ± 37		[11] LEES	12F	BABR	10.6 $e^+e^- \to \phi\pi^+\pi^-\gamma$
211 ±14 ± 19	4.8k	[12] SHEN	09	BELL	10.6 $e^+e^- \to K^+K^-\pi^+\pi^-\gamma$
322 ±77 ±160		[13] AUBERT	08S	BABR	10.6 $e^+e^- \to$ hadrons
139 ±60	948	[14] AKHMETSHIN	03	CMD2	1.05–1.38 $e^+e^- \to K^0_L K^0_S$
300 ±60		[15] CLEGG	94	RVUE	$e^+e^- \to K^+K^-$, $K^0_S K\pi$
146 ±55	367	BISELLO	91C	DM2	$e^+e^- \to K^0_S K^\pm\pi^\mp$
207 ±45		[16] BISELLO	88B	DM2	$e^+e^- \to K^+K^-$
185 ±22		[17] BUON	82	DM1	$e^+e^- \to$ hadrons
102 ±36		[18] MANE	82	DM1	$e^+e^- \to K^0_S K\pi$

[1] Using a vector dominance fit with contributions from $\phi(1680)$ and $\rho(1450)$.
[2] From a VDM fit to ZHU 23 $\eta\phi\gamma$ data with two resonances, $\phi(1680)$, $\phi(2170)$, and a third resonance with mass 1850.7 ± 5.3 MeV and width 25 ± 35 MeV of 1.7 σ statistical evidence.
[3] From a fit using a vector meson dominance model with contributions from $\phi(1680)$, $\phi(2170)$ and non resonant contribution.
[4] From the analysis of the combined measurements of $\sigma(e^+e^- \to \eta\phi)$ from BaBar, Belle, BESIII, CMD3.
[5] From a partial wave amplitude analysis at $\sqrt{s} = 2.125$ GeV which includes all the possible intermediate states that match J^{PC} conservation in the subsequent two-body decay. The intermediate states are parameterized with the relativistic Breit-Wigner functions. Statistical error only.
[6] Seen in $\psi(2S)$ decay with branching ratio $\psi(2S) \to X\eta \to K^+K^-\eta = (12.0 \pm 1.3^{+6.5}_{-6.9}) \times 10^{-6}$.
[7] From a fit using a vector meson dominance model with contribution from $\rho(770)$, $\omega(782)$, $\phi(1020)$, $\omega(1420)$, $\rho(1450)$.
[8] From a fit with coherent interference of the $\phi(1680)$ with a non-resonant contribution.
[9] Assuming the $K\overline{K}^*(892)+$ c.c. dynamics. Systematic uncertainties not estimated.
[10] Using a vector meson dominance model with contribution from $\phi(1020)$, $\phi(1680)$, and higher mass excitations of $\rho(770)$ and $\omega(782)$.
[11] Using events with $\pi\pi$ invariant mass less than 0.85 GeV.
[12] From a fit with two incoherent Breit-Wigners.
[13] From the simultaneous fit to the $K\overline{K}^*(892)+$ c.c. and $\phi\eta$ data from AUBERT 08S using the results of AUBERT 07AK.
[14] From the combined fit of AKHMETSHIN 03 and MANE 81 also including ρ, ω, and ϕ. Neither isospin nor flavor structure known.
[15] Using BISELLO 88B and MANE 82 data.
[16] From global fit including ρ, ω, ϕ and $\rho(1700)$
[17] From global fit of ρ, ω, ϕ and their radial excitations to channels $\omega\pi^+\pi^-$, K^+K^-, $K^0_S K^0_L$, $K^0_S K^\pm\pi^\mp$. Assume mass 1570 MeV and width 510 MeV for ρ radial excitations, mass 1570 and width 500 MeV for ω radial excitation.
[18] Fit to one channel only, neglecting interference with ω, $\rho(1700)$.

$p\overline{p}$ ANNIHILATION

VALUE (MeV)	DOCUMENT ID		TECN	COMMENT
• • • We do not use the following data for averages, fits, limits, etc. • • •				
143 ± 24	[1] AMSLER	06	CBAR	0.9 $\overline{p}p \to K^+K^-\pi^0$

[1] Could also be $\rho(1700)$.

$\phi(1680)$ DECAY MODES

	Mode	Fraction (Γ_i/Γ)
Γ_1	$K\overline{K}^*(892)+$ c.c.	seen
Γ_2	$K^0_S K\pi$	seen
Γ_3	$K\overline{K}$	seen
Γ_4	$K^0_L K^0_S$	
Γ_5	e^+e^-	seen
Γ_6	$\omega\pi\pi$	not seen
Γ_7	$\phi\pi\pi$	
Γ_8	$K^+K^-\pi^+\pi^-$	seen
Γ_9	$\eta\phi$	seen
Γ_{10}	$\eta\gamma$	seen
Γ_{11}	$K^+K^-\pi^0$	
Γ_{12}	$\rho(770)\pi$	not seen
Γ_{13}	$f'_2(1525)\gamma$	not seen

$\phi(1680)$ $\Gamma(i)\Gamma(e^+e^-)/\Gamma(\text{total})$

This combination of a partial width with the partial width into e^+e^- and with the total width is obtained from the integrated cross section into channel (i) in e^+e^- annihilation. We list only data that have not been used to determine the partial width $\Gamma(i)$ or the branching ratio $\Gamma(i)/\text{total}$.

$\Gamma(K^0_L K^0_S) \times \Gamma(e^+e^-)/\Gamma_{\text{total}}$ — $\Gamma_4\Gamma_5/\Gamma$

VALUE (eV)	EVTS	DOCUMENT ID		TECN	COMMENT
• • • We do not use the following data for averages, fits, limits, etc. • • •					
14.3 ± 2.4 ± 6.2	6.2k	[1] LEES	14H	BABR	$e^+e^- \to K^0_S K^0_L\gamma$

[1] Using a vector meson dominance model with contribution from $\phi(1020)$, $\phi(1680)$, and higher mass excitations of $\rho(770)$ and $\omega(782)$.

$\Gamma(\phi\pi\pi) \times \Gamma(e^+e^-)/\Gamma_{\text{total}}$ — $\Gamma_7\Gamma_5/\Gamma$

VALUE (10^{-2} keV)	DOCUMENT ID		TECN	COMMENT
• • • We do not use the following data for averages, fits, limits, etc. • • •				
4.2 ± 0.2 ± 0.3	LEES	12F	BABR	10.6 $e^+e^- \to \phi\pi^+\pi^-\gamma$

$\Gamma(\eta\phi) \times \Gamma(e^+e^-)/\Gamma_{\text{total}}$ — $\Gamma_9\Gamma_5/\Gamma$

VALUE (eV)	EVTS	DOCUMENT ID		TECN	COMMENT
• • • We do not use the following data for averages, fits, limits, etc. • • •					
122 ± 6 ± 13		[1] ZHU	23	BELL	$e^+e^- \to \Upsilon(nS) \to \phi\eta\gamma$
$65^{+5}_{-4} \pm 13$ to $215^{+8}_{-5} \pm 11$		[2] ZHU	23A	RVUE	$e^+e^- \to \eta\phi$
94 ± 13 ± 15	3k	[3] IVANOV	19A	CMD3	1.59–2.007 $e^+e^- \to K^+K^-\eta$

Int. J. Mod. Phys. A 2026.41. Downloaded from www.worldscientific.com
by UNIVERSITY OF CALIFORNIA @ BERKELEY on 09/16/26. Re-use and distribution is strictly not permitted, except for Open Access articles.

[1] From a solution of the fit using a vector meson dominance model with contributions from $\phi(1680)$, $\phi(2170)$ and non resonant contribution. Other solutions with equal fit quality give (219 ± 15 ± 18) eV, (163 ± 11 ± 13) eV and (203 ± 12 ± 18) eV.
[2] From the analysis of the combined measurements of $\sigma(e^+e^- \to \eta\phi)$ from BaBar, Belle, BESIII, CMD3. Four solutions are found, with equal fit quality: (79 ± 4 ± 16) eV, (127 ± 5 ± 12) eV, $(65^{+5}_{-4} \pm 13)$ eV, $(215^{+8}_{-5} \pm 11)$ eV.
[3] From a fit with coherent interference of the $\phi(1680)$ with a non-resonant contribution.

$\Gamma(K\overline{K}^*(892)+\text{c.c.}) \times \Gamma(e^+e^-)/\Gamma_{total}$ — $\Gamma_1\Gamma_5/\Gamma$

VALUE (eV)	EVTS	DOCUMENT ID		TECN	COMMENT
• • • We do not use the following data for averages, fits, limits, etc. • • •					
427±40±21	9.1k	[1] FEDOTOVICH	25	CMD3	$e^+e^- \to K^0_S K^\pm\pi^\mp$

[1] Using a vector dominance fit with contributions from $\phi(1680)$ and $\rho(1450)$.

$\phi(1680)$ $\Gamma(i)\Gamma(e^+e^-)/\Gamma^2(\text{total})$

This combination of a branching ratio into channel (i) and branching ratio into e^+e^- is directly measured and obtained from the cross section at the peak. We list only data that have not been used to determine the branching ratio into (i) or e^+e^-.

$\Gamma(K^0_L K^0_S)/\Gamma_{total} \times \Gamma(e^+e^-)/\Gamma_{total}$ — $\Gamma_4/\Gamma \times \Gamma_5/\Gamma$

VALUE (units 10^{-6})	EVTS	DOCUMENT ID		TECN	COMMENT
• • • We do not use the following data for averages, fits, limits, etc. • • •					
0.131±0.059	948	[1] AKHMETSHIN	03	CMD2	1.05–1.38 $e^+e^- \to K^0_L K^0_S$

[1] From the combined fit of AKHMETSHIN 03 and MANE 81 also including ρ, ω, and ϕ. Neither isospin nor flavor structure known. Recalculated by us.

$\Gamma(K\overline{K}^*(892)+\text{c.c.})/\Gamma_{total} \times \Gamma(e^+e^-)/\Gamma_{total}$ — $\Gamma_1/\Gamma \times \Gamma_5/\Gamma$

VALUE (units 10^{-6})	EVTS	DOCUMENT ID		TECN	COMMENT
• • • We do not use the following data for averages, fits, limits, etc. • • •					
1.15±0.16±0.01		[1] AUBERT	08S	BABR	10.6 $e^+e^- \to K\overline{K}^*(892)\gamma$ + c.c.
3.29±1.57	367	[2] BISELLO	91C	DM2	1.35–2.40 $e^+e^- \to K^0_S K^\pm\pi^\mp$

[1] From the simultaneous fit to the $K\overline{K}^*(892)+$ c.c. and $\phi\eta$ data from AUBERT 08S using the results of AUBERT 07AK.
[2] Recalculated by us with the published value of $B(K\overline{K}^*(892) +$ c.c.$) \times \Gamma(e^+e^-)$.

$\Gamma(\phi\pi\pi)/\Gamma_{total} \times \Gamma(e^+e^-)/\Gamma_{total}$ — $\Gamma_7/\Gamma \times \Gamma_5/\Gamma$

VALUE (units 10^{-7})	EVTS	DOCUMENT ID		TECN	COMMENT
• • • We do not use the following data for averages, fits, limits, etc. • • •					
1.86±0.14±0.21	4.8k	[1] SHEN	09	BELL	10.6 $e^+e^- \to K^+K^-\pi^+\pi^-\gamma$

[1] Multiplied by 3/2 to take into account the $\phi\pi^0\pi^0$ mode. Using $B(\phi \to K^+K^-) = (49.2 \pm 0.6)\%$.

$\Gamma(\eta\phi)/\Gamma_{total} \times \Gamma(e^+e^-)/\Gamma_{total}$ — $\Gamma_9/\Gamma \times \Gamma_5/\Gamma$

VALUE (units 10^{-7})	EVTS	DOCUMENT ID		TECN	COMMENT
• • • We do not use the following data for averages, fits, limits, etc. • • •					
$5.64^{+1.74}_{-1.80}$		ACHASOV	19	SND	$e^+e^- \to \pi^+\pi^-\pi^0\eta$
5.3 ±0.6 ±0.9	3k	[1] IVANOV	19A	CMD3	1.59–2.007 $e^+e^- \to K^+K^-\eta$
4.3 ±1.0 ±0.9		[2] AUBERT	08S	BABR	10.6 $e^+e^- \to \phi\eta\gamma$

[1] From a fit with coherent interference of the $\phi(1680)$ with a non-resonant contribution.
[2] From the simultaneous fit to the $K\overline{K}^*(892)+$ c.c. and $\phi\eta$ data from AUBERT 08S using the results of AUBERT 07AK.

$\phi(1680)$ BRANCHING RATIOS

$\Gamma(K\overline{K}^*(892)+\text{c.c.})/\Gamma(K^0_S K\pi)$ — Γ_1/Γ_2

VALUE	DOCUMENT ID		TECN	COMMENT
dominant	MANE	82	DM1	$e^+e^- \to K^0_S K^\pm\pi^\mp$

$\Gamma(K\overline{K})/\Gamma(K\overline{K}^*(892)+\text{c.c.})$ — Γ_3/Γ_1

VALUE	DOCUMENT ID		TECN	COMMENT
• • • We do not use the following data for averages, fits, limits, etc. • • •				
0.07±0.01	BUON	82	DM1	e^+e^-

$\Gamma(\omega\pi\pi)/\Gamma(K\overline{K}^*(892)+\text{c.c.})$ — Γ_6/Γ_1

VALUE	DOCUMENT ID		TECN	COMMENT
<0.10	BUON	82	DM1	e^+e^-

$\Gamma(\eta\phi)/\Gamma_{total}$ — Γ_9/Γ

VALUE	EVTS	DOCUMENT ID		TECN	COMMENT
seen	35	[1] ACHASOV	14	SND	1.15–2.00 $e^+e^- \to \eta\gamma$

[1] From a phenomenological model based on vector meson dominance with $\rho(1450)$ and $\phi(1680)$ masses and widths from the PDG 12.

$\Gamma(\eta\phi)/\Gamma(K\overline{K}^*(892)+\text{c.c.})$ — Γ_9/Γ_1

VALUE	DOCUMENT ID		TECN	COMMENT
• • • We do not use the following data for averages, fits, limits, etc. • • •				
≈ 0.37	[1] AUBERT	08S	BABR	10.6 $e^+e^- \to$ hadrons

[1] From the fit including data from AUBERT 07AK.

$\Gamma(\eta\gamma)/\Gamma_{total}$ — Γ_{10}/Γ

VALUE	EVTS	DOCUMENT ID		TECN	COMMENT
seen	35	[1] ACHASOV	14	SND	1.15–2.00 $e^+e^- \to \eta\gamma$

[1] From a phenomenological model based on vector meson dominance with $\rho(1450)$ and $\phi(1680)$ masses and widths from the PDG 12.

$\Gamma(\rho(770)\pi)/\Gamma_{total}$ — Γ_{12}/Γ

VALUE	DOCUMENT ID		TECN	COMMENT
not seen	[1] DIMOVA	25	SND	$e^+e^- \to \pi^+\pi^-\pi^0$

[1] From a fit to the cross section with contributions from $\omega(782)$, $\phi(1020)$, $\omega(1420)$, $\omega(1650)$, and $\phi(1680)$.

$\Gamma(f'_2(1525)\gamma)/\Gamma_{total}$ — Γ_{13}/Γ

VALUE	DOCUMENT ID		TECN	COMMENT
not seen	[1] ACHASOV	22	SND	1.17–2.00 $e^+e^- \to \eta\eta\gamma$

[1] The 90% CL upper limit on the Born cross sections $\sigma(e^+e^- \to \phi(1680) \to f'_2(1525)\gamma \to \eta\eta\gamma)$ and $\sigma(e^+e^- \to \rho(1700) \to f_0(1500)\gamma \to \eta\eta\gamma)$ is 10.6 pb.

$\phi(1680)$ REFERENCES

DIMOVA	25	PPN 56 820	T.V. Dimova *et al.*	(SND Collab.)
FEDOTOVICH	25	PPN 56 434	G.V. Fedotovich *et al.*	(CMD-3 Collab.)
ABLIKIM	24CB	PR D110 112014	M. Ablikim *et al.*	(BESIII Collab.)
LICHARD	23	PR D108 092005	P. Lichard	(OPAV, CTUP)
ZHU	23	PR D107 012006	W. Zhu *et al.*	(BELLE Collab.)
ZHU	23A	CP C47 113003	W. Zhu, X. Wang	(RVUE)
ABLIKIM	22L	JHEP 2207 045	M. Ablikim *et al.*	(BESIII Collab.)
ACHASOV	22	EPJ C82 168	M.N. Achasov *et al.*	(SND Collab.)
ABLIKIM	20F	PR D101 032008	M. Ablikim *et al.*	(BESIII Collab.)
ACHASOV	20C	EPJ C80 1139	M.N. Achasov *et al.*	(SND Collab.)
ACHASOV	19	PR D99 112004	M.N. Achasov *et al.*	(SND Collab.)
IVANOV	19A	PL B798 134946	V.L. Ivanov *et al.*	(CMD-3 Collab.)
ACHASOV	18A	PR D97 032011	M.N. Achasov *et al.*	(SND Collab.)
ACHASOV	14	PR D90 032002	M.N. Achasov *et al.*	(SND Collab.)
LEES	14H	PR D89 092002	J.P. Lees *et al.*	(BABAR Collab.)
LEES	12F	PR D86 012008	J.P. Lees *et al.*	(BABAR Collab.)
PDG	12	PR D86 010001	J. Beringer *et al.*	(PDG Collab.)
SHEN	09	PR D80 031101	C.P. Shen *et al.*	(BELLE Collab.)
AUBERT	08S	PR D77 092002	B. Aubert *et al.*	(BABAR Collab.)
AUBERT	07AK	PR D76 012008	B. Aubert *et al.*	(BABAR Collab.)
AMSLER	06	PL B639 165	C. Amsler *et al.*	(Crystal Barrel Collab.)
AKHMETSHIN	03	PL B551 27	R.R. Akhmetshin *et al.*	(Novosibirsk CMD-2 Collab.)
Also		PAN 65 1222	E.V. Anashkin, V.M. Aulchenko, R.R. Akhmetshin	
		Translated from YAF 65 1255.		
ACHASOV	98H	PR D57 4334	N.N. Achasov, A.A. Kozhevnikov	
CLEGG	94	ZPHY C62 455	A.B. Clegg, A. Donnachie	(LANC, MCHS)
ANTONELLI	92	ZPHY C56 15	A. Antonelli *et al.*	(DM2 Collab.)
BISELLO	91C	ZPHY C52 227	D. Bisello *et al.*	(DM2 Collab.)
DOLINSKY	91	PRPL 202 99	S.I. Dolinsky *et al.*	(NOVO)
BISELLO	88B	ZPHY C39 13	D. Bisello *et al.*	(PADO, CLER, FRAS+)
BARKOV	87	JETPL 46 164	L.M. Barkov *et al.*	(NOVO)
		Translated from ZETFP 46 132.		
BUON	82	PL 118B 221	J. Buon *et al.*	(LALO, MONP)
MANE	82	PL 112B 178	F. Mane *et al.*	(LALO)
IVANOV	81	PL 107B 297	P.M. Ivanov *et al.*	(NOVO)
MANE	81	PL 99B 261	F. Mane *et al.*	(ORSAY)

$\rho_3(1690)$

$I^G(J^{PC}) = 1^+(3^{--})$

$\rho_3(1690)$ MASS

VALUE (MeV)	DOCUMENT ID
1688.8±2.1 OUR AVERAGE	Includes data from the 5 datablocks that follow this one.

2π MODE

VALUE (MeV)	EVTS	DOCUMENT ID		TECN	CHG	COMMENT
The data in this block is included in the average printed for a previous datablock.						
1686± 4 OUR AVERAGE						
1677±14		EVANGELIS...	81	OMEG	−	12 $\pi^-p \to 2\pi p$
1679±11	476	BALTAY	78B	HBC	0	15 $\pi^+p \to \pi^+\pi^-n$
1678±12	175	[1] ANTIPOV	77	CIBS	0	25 $\pi^-p \to p3\pi$
1690± 7	600	[1] ENGLER	74	DBC	0	6 $\pi^+n \to \pi^+\pi^-p$
1693± 8		[2] GRAYER	74	ASPK	0	17 $\pi^-p \to \pi^+\pi^-n$
1678±12		MATTHEWS	71C	DBC	0	7 π^+N
• • • We do not use the following data for averages, fits, limits, etc. • • •						
1734±10		[3] CORDEN	79	OMEG		12–15 $\pi^-p \to n2\pi$
1692±12		[2,4] ESTABROOKS	75	RVUE		17 $\pi^-p \to \pi^+\pi^-n$
1737±23		ARMENISE	70	DBC	0	9 π^+N
1650±35	122	BARTSCH	70B	HBC	+	8 $\pi^+p \to N2\pi$
1687±21		STUNTEBECK	70	HDBC	0	8 π^-p, 5.4 π^+d
1683±13		ARMENISE	68	DBC	0	5.1 π^+d
1670±30		GOLDBERG	65	HBC	0	6 π^+d, 8 π^-p

[1] Mass errors enlarged by us to $\Gamma/\sqrt{N}$; see the note with the $K^*(892)$ mass.
[2] Uses same data as HYAMS 75.
[3] From a phase shift solution containing a $f'_2(1525)$ width two times larger than the $K\overline{K}$ result.
[4] From phase-shift analysis. Error takes account of spread of different phase-shift solutions.

Int. J. Mod. Phys. A 2026.41. Downloaded from www.worldscientific.com
by CALIFORNIA @ BERKELEY on 09/16/26. Re-use and distribution is strictly not permitted, except for Open Access articles.

Int. J. Mod. Phys. A 2026.41. Downloaded from www.worldscientific.com
by UNIVERSITY OF CALIFORNIA @ BERKELEY on 09/16/26. Re-use and distribution is strictly not permitted, except for Open Access articles.

$K\overline{K}$ AND $K\overline{K}\pi$ MODES

VALUE (MeV)	EVTS	DOCUMENT ID		TECN	CHG	COMMENT
The data in this block is included in the average printed for a previous datablock.						
1696± 4 OUR AVERAGE						
1699± 5		ALPER	80	CNTR	0	62 $\pi^- p \to K^+ K^- n$
1698±12	6k	[5,6] MARTIN	78D	SPEC		10 $\pi p \to K^0_S K^- p$
1692± 6		BLUM	75	ASPK	0	18.4 $\pi^- p \to n K^+ K^-$
1690±16		ADERHOLZ	69	HBC	+	8 $\pi^+ p \to K\overline{K}\pi$
• • • We do not use the following data for averages, fits, limits, etc. • • •						
1694± 8		[7] COSTA	80	OMEG		10 $\pi^- p \to K^+ K^- n$

[5] From a fit to $J^P = 3^-$ partial wave.
[6] Systematic error on mass scale subtracted.
[7] They cannot distinguish between $\rho_3(1690)$ and $\omega_3(1670)$.

$(4\pi)^\pm$ MODE

VALUE (MeV)	EVTS	DOCUMENT ID		TECN	CHG	COMMENT
The data in this block is included in the average printed for a previous datablock.						
1686± 5 OUR AVERAGE Error includes scale factor of 1.1.						
1694± 6		[8] EVANGELIS...	81	OMEG	−	12 $\pi^- p \to p 4\pi$
1665±15	177	BALTAY	78B	HBC	+	15 $\pi^+ p \to p 4\pi$
1670±10		THOMPSON	74	HBC	+	13 $\pi^+ p$
1687±20		CASON	73	HBC	−	8,18.5 $\pi^- p$
1685±14		[9] CASON	73	HBC	−	8,18.5 $\pi^- p$
1680±40	144	BARTSCH	70B	HBC	+	8 $\pi^+ p \to N 4\pi$
1689±20	102	[9] BARTSCH	70B	HBC	+	8 $\pi^+ p \to N 2\rho$
1705±21		CASO	70	HBC	−	11.2 $\pi^- p \to n\rho 2\pi$
• • • We do not use the following data for averages, fits, limits, etc. • • •						
1718±10		[10] EVANGELIS...	81	OMEG	−	12 $\pi^- p \to p 4\pi$
1673± 9		[11] EVANGELIS...	81	OMEG	−	12 $\pi^- p \to p 4\pi$
1733± 9	66	[9] KLIGER	74	HBC	−	4.5 $\pi^- p \to p 4\pi$
1630±15		HOLMES	72	HBC	+	10–12 $K^+ p$
1720±15		BALTAY	68	HBC	+	7, 8.5 $\pi^+ p$

[8] From $\rho^- \rho^0$ mode, not independent of the other two EVANGELISTA 81 entries.
[9] From $\rho^\pm \rho^0$ mode.
[10] From $a_2(1320)^- \pi^0$ mode, not independent of the other two EVANGELISTA 81 entries.
[11] From $a_2(1320)^0 \pi^-$ mode, not independent of the other two EVANGELISTA 81 entries.

$\omega\pi$ MODE

VALUE (MeV)	DOCUMENT ID		TECN	CHG	COMMENT
The data in this block is included in the average printed for a previous datablock.					
1681± 7 OUR AVERAGE					
1670±25	[12] ALDE	95	GAM2		38 $\pi^- p \to \omega\pi^0 n$
1690±15	EVANGELIS...	81	OMEG	−	12 $\pi^- p \to \omega\pi p$
1666±14	GESSAROLI	77	HBC		11 $\pi^- p \to \omega\pi p$
1686± 9	THOMPSON	74	HBC	+	13 $\pi^+ p$
• • • We do not use the following data for averages, fits, limits, etc. • • •					
1654±24	BARNHAM	70	HBC	+	10 $K^+ p \to \omega\pi X$

[12] Supersedes ALDE 92C.

$\eta\pi^+\pi^-$ MODE

(For difficulties with MMS experiments, see the $a_2(1320)$ mini-review in the 1973 edition.)

VALUE (MeV)	DOCUMENT ID		TECN	CHG	COMMENT
The data in this block is included in the average printed for a previous datablock.					
1682±12 OUR AVERAGE					
1685±10±20	AMELIN	00	VES		37 $\pi^- p \to \eta\pi^+\pi^- n$
1680±15	FUKUI	88	SPEC	0	8.95 $\pi^- p \to \eta\pi^+\pi^- n$
• • • We do not use the following data for averages, fits, limits, etc. • • •					
1700±47	[13] ANDERSON	69	MMS	−	16 $\pi^- p$ backward
1632±15	[13,14] FOCACCI	66	MMS	−	7–12 $\pi^- p \to p$MM
1700±15	[13,14] FOCACCI	66	MMS	−	7–12 $\pi^- p \to p$MM
1748±15	[13,14] FOCACCI	66	MMS	−	7–12 $\pi^- p \to p$MM

[13] Seen in 2.5–3 GeV/c $\overline{p}p$. $2\pi^+ 2\pi^-$, with 0, 1, 2 $\pi^+\pi^-$ pairs in ρ band not seen by OREN 74 (2.3 GeV/c $\overline{p}p$) with more statistics. (Jan. 1976)
[14] Not seen by BOWEN 72.

$\rho_3(1690)$ WIDTH

2π, $K\overline{K}$, AND $K\overline{K}\pi$ MODES

VALUE (MeV)	DOCUMENT ID
161±10 OUR AVERAGE Includes data from the 5 datablocks that follow this one. Error includes scale factor of 1.5. See the ideogram below.	

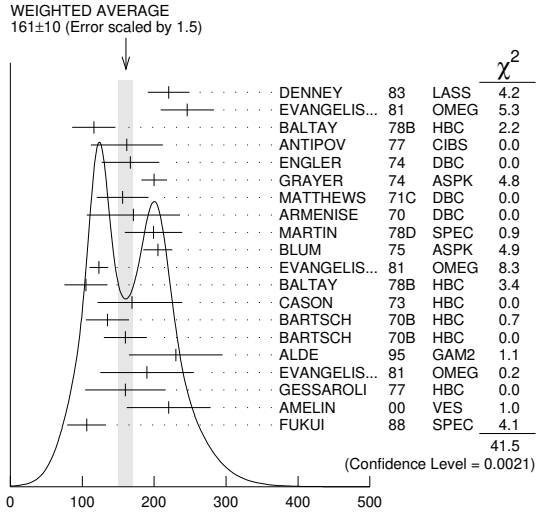

$\rho_3(1690)$ width, 2π, $K\overline{K}$, and $K\overline{K}\pi$ modes (MeV)

2π MODE

VALUE (MeV)	EVTS	DOCUMENT ID		TECN	CHG	COMMENT
The data in this block is included in the average printed for a previous datablock.						
186±14 OUR AVERAGE Error includes scale factor of 1.3. See the ideogram below.						
220±29		DENNEY	83	LASS		10 $\pi^+ N$
246±37		EVANGELIS...	81	OMEG	−	12 $\pi^- p \to 2\pi p$
116±30	476	BALTAY	78B	HBC	0	15 $\pi^+ p \to \pi^+\pi^- n$
162±50	175	[15] ANTIPOV	77	CIBS	0	25 $\pi^- p \to p 3\pi$
167±40	600	ENGLER	74	DBC	0	6 $\pi^+ n \to \pi^+\pi^- p$
200±18		[16] GRAYER	74	ASPK	0	17 $\pi^- p \to \pi^+\pi^- n$
156±36		MATTHEWS	71C	DBC	0	7 $\pi^+ N$
171±65		ARMENISE	70	DBC	0	9 $\pi^+ d$
• • • We do not use the following data for averages, fits, limits, etc. • • •						
322±35		[17] CORDEN	79	OMEG		12–15 $\pi^- p \to n 2\pi$
240±30		[16,18] ESTABROOKS	75	RVUE		17 $\pi^- p \to \pi^+\pi^- n$
180±30	122	BARTSCH	70B	HBC	+	8 $\pi^+ p \to N 2\pi$
267^{+72}_{-46}		STUNTEBECK	70	HDBC	0	8 $\pi^- p$, 5.4 $\pi^+ d$
188±49		ARMENISE	68	DBC	0	5.1 $\pi^+ d$
180±40		GOLDBERG	65	HBC	0	6 $\pi^+ d$, 8 $\pi^- p$

[15] Width errors enlarged by us to $4\Gamma/\sqrt{N}$; see the note with the $K^*(892)$ mass.
[16] Uses same data as HYAMS 75 and BECKER 79.
[17] From a phase shift solution containing a $f'_2(1525)$ width two times larger than the $K\overline{K}$ result.
[18] From phase-shift analysis. Error takes account of spread of different phase-shift solutions.

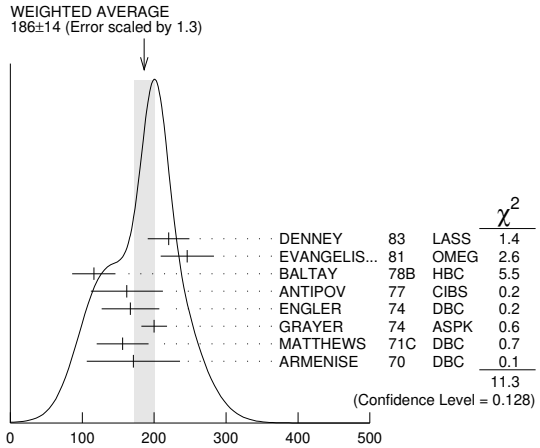

$\rho_3(1690)$ width, 2π mode (MeV)

$K\overline{K}$ AND $K\overline{K}\pi$ MODES

VALUE (MeV)	EVTS	DOCUMENT ID		TECN	CHG	COMMENT
The data in this block is included in the average printed for a previous datablock.						
204±18 OUR AVERAGE						
199±40	6000	[19] MARTIN	78D	SPEC		10 $\pi p \to K^0_S K^- p$
205±20		BLUM	75	ASPK	0	18.4 $\pi^- p \to n K^+ K^-$

Int. J. Mod. Phys. A 2026.41. Downloaded from www.worldscientific.com
by CALIFORNIA @ BERKELEY on 09/16/26. Re-use and distribution is strictly not permitted, except for Open Access articles.

• • • We do not use the following data for averages, fits, limits, etc. • • •

219± 4	ALPER	80	CNTR	0	62 $\pi^- p \to K^+ K^- n$
186±11	[20] COSTA	80	OMEG		10 $\pi^- p \to K^+ K^- n$
112±60	ADERHOLZ	69	HBC	+	8 $\pi^+ p \to K\overline{K}\pi$

[19] From a fit to $J^P = 3^-$ partial wave.
[20] They cannot distinguish between $\rho_3(1690)$ and $\omega_3(1670)$.

$(4\pi)^\pm$ MODE

VALUE (MeV)	EVTS	DOCUMENT ID		TECN	CHG	COMMENT
The data in this block is included in the average printed for a previous datablock.						
129±10 OUR AVERAGE						
123±13		[21] EVANGELIS...	81	OMEG	−	12 $\pi^- p \to p4\pi$
105±30	177	BALTAY	78B	HBC	+	15 $\pi^+ p \to p4\pi$
169^{+70}_{-48}		CASON	73	HBC	−	8,18.5 $\pi^- p$
135±30	144	BARTSCH	70B	HBC	+	8 $\pi^+ p \to N4\pi$
160±30	102	BARTSCH	70B	HBC	+	8 $\pi^+ p \to N2\rho$
• • • We do not use the following data for averages, fits, limits, etc. • • •						
230±28		[22] EVANGELIS...	81	OMEG	−	12 $\pi^- p \to p4\pi$
184±33		[23] EVANGELIS...	81	OMEG	−	12 $\pi^- p \to p4\pi$
150	66	[24] KLIGER	74	HBC	−	4.5 $\pi^- p \to p4\pi$
106±25		THOMPSON	74	HBC	+	13 $\pi^+ p$
125^{+83}_{-35}		[24] CASON	73	HBC	−	8,18.5 $\pi^- p$
130±30		HOLMES	72	HBC	+	10–12 $K^+ p$
180±30	90	[24] BARTSCH	70B	HBC	+	8 $\pi^+ p \to N a_2 \pi$
100±35		BALTAY	68	HBC	+	7, 8.5 $\pi^+ p$

[21] From $\rho^- \rho^0$ mode, not independent of the other two EVANGELISTA 81 entries.
[22] From $a_2(1320)^- \pi^0$ mode, not independent of the other two EVANGELISTA 81 entries.
[23] From $a_2(1320)^0 \pi^-$ mode, not independent of the other two EVANGELISTA 81 entries.
[24] From $\rho^\pm \rho^0$ mode.

$\omega\pi$ MODE

VALUE (MeV)	DOCUMENT ID		TECN	CHG	COMMENT
The data in this block is included in the average printed for a previous datablock.					
190±40 OUR AVERAGE					
230±65	[25] ALDE	95	GAM2		38 $\pi^- p \to \omega\pi^0 n$
190±65	EVANGELIS...	81	OMEG	−	12 $\pi^- p \to \omega\pi p$
160±56	GESSAROLI	77	HBC		11 $\pi^- p \to \omega\pi p$
• • • We do not use the following data for averages, fits, limits, etc. • • •					
89±25	THOMPSON	74	HBC	+	13 $\pi^+ p$
130^{+73}_{-43}	BARNHAM	70	HBC	+	10 $K^+ p \to \omega\pi X$

[25] Supersedes ALDE 92C.

$\eta\pi^+\pi^-$ MODE

(For difficulties with MMS experiments, see the $a_2(1320)$ mini-review in the 1973 edition.)

VALUE (MeV)	DOCUMENT ID		TECN	CHG	COMMENT
The data in this block is included in the average printed for a previous datablock.					
130±40 OUR AVERAGE Error includes scale factor of 1.8.					
220±30±50	AMELIN	00	VES		37 $\pi^- p \to \eta\pi^+\pi^- n$
106±27	FUKUI	88	SPEC	0	8.95 $\pi^- p \to \eta\pi^+\pi^- n$
• • • We do not use the following data for averages, fits, limits, etc. • • •					
195	[26] ANDERSON	69	MMS	−	16 $\pi^- p$ backward
< 21	[26,27] FOCACCI	66	MMS	−	7–12 $\pi^- p \to p$MM
< 30	[26,27] FOCACCI	66	MMS	−	7–12 $\pi^- p \to p$MM
< 38	[26,27] FOCACCI	66	MMS	−	7–12 $\pi^- p \to p$MM

[26] Seen in 2.5–3 GeV/c $\overline{p}p$. $2\pi^+2\pi^-$, with 0, 1, 2 $\pi^+\pi^-$ pairs in ρ^0 band not seen by OREN 74 (2.3 GeV/c $\overline{p}p$) with more statistics. (Jan. 1979)
[27] Not seen by BOWEN 72.

$\rho_3(1690)$ DECAY MODES

	Mode	Fraction (Γ_i/Γ)	Scale factor
Γ_1	4π	(71.1 ± 1.9) %	
Γ_2	$\pi^\pm\pi^+\pi^-\pi^0$	(67 ±22) %	
Γ_3	$\omega\pi$	(16 ± 6) %	
Γ_4	$\pi\pi$	(23.6 ± 1.3) %	
Γ_5	$K\overline{K}\pi$	(3.8 ± 1.2) %	
Γ_6	$K\overline{K}$	(1.58± 0.26) %	1.2
Γ_7	$\eta\pi^+\pi^-$	seen	
Γ_8	$\rho(770)\eta$	seen	
Γ_9	$\pi\pi\rho$	seen	
Γ_{10}	$a_2(1320)\pi$	seen	
Γ_{11}	$\rho\rho$	seen	
Γ_{12}	$\phi\pi$		
Γ_{13}	$\eta\pi$		
Γ_{14}	$\pi^\pm 2\pi^+ 2\pi^- \pi^0$		

CONSTRAINED FIT INFORMATION

An overall fit to 5 branching ratios uses 10 measurements and one constraint to determine 4 parameters. The overall fit has a χ^2 = 14.7 for 7 degrees of freedom.

The following *off-diagonal* array elements are the correlation coefficients $\langle \delta x_i \delta x_j \rangle / (\delta x_i \cdot \delta x_j)$, in percent, from the fit to the branching fractions, $x_i \equiv \Gamma_i/\Gamma_{total}$. The fit constrains the x_i whose labels appear in this array to sum to one.

	x_1	x_4	x_5
x_4	−77		
x_5	−74	17	
x_6	−15	2	0

$\rho_3(1690)$ BRANCHING RATIOS

$\Gamma(\pi\pi)/\Gamma_{total}$ — Γ_4/Γ

VALUE	DOCUMENT ID		TECN	CHG	COMMENT
0.236±0.013 OUR FIT					
0.243±0.013 OUR AVERAGE					
$0.259^{+0.018}_{-0.019}$	BECKER	79	ASPK	0	17 $\pi^- p$ polarized
0.23 ±0.02	CORDEN	79	OMEG		12–15 $\pi^- p \to n2\pi$
0.22 ±0.04	[28] MATTHEWS	71C	HDBC	0	7 $\pi^+ n \to \pi^- p$
• • • We do not use the following data for averages, fits, limits, etc. • • •					
0.245±0.006	[29] ESTABROOKS	75	RVUE		17 $\pi^- p \to \pi^+\pi^- n$

[28] One-pion-exchange model used in this estimation.
[29] From phase-shift analysis of HYAMS 75 data.

$\Gamma(\pi\pi)/\Gamma(\pi^\pm\pi^+\pi^-\pi^0)$ — Γ_4/Γ_2

VALUE	DOCUMENT ID		TECN	CHG	COMMENT
0.35±0.11	CASON	73	HBC	−	8,18.5 $\pi^- p$
• • • We do not use the following data for averages, fits, limits, etc. • • •					
<0.2	HOLMES	72	HBC	+	10–12 $K^+ p$
<0.12	BALLAM	71B	HBC	−	16 $\pi^- p$

$\Gamma(\pi\pi)/\Gamma(4\pi)$ — Γ_4/Γ_1

VALUE	DOCUMENT ID		TECN	CHG	COMMENT
0.332±0.026 OUR FIT Error includes scale factor of 1.1.					
0.30 ±0.10	BALTAY	78B	HBC	0	15 $\pi^+ p \to p4\pi$

$\Gamma(K\overline{K})/\Gamma(\pi\pi)$ — Γ_6/Γ_4

VALUE	DOCUMENT ID		TECN	CHG	COMMENT
0.067±0.011 OUR FIT Error includes scale factor of 1.2.					
$\mathbf{0.118^{+0.040}_{-0.032}}$ **OUR AVERAGE** Error includes scale factor of 1.7. See the ideogram below.					
$0.191^{+0.040}_{-0.037}$	GORLICH	80	ASPK	0	17,18 $\pi^- p$ polarized
0.08 ±0.03	BARTSCH	70B	HBC	+	8 $\pi^+ p$
$0.08^{+0.08}_{-0.03}$	CRENNELL	68B	HBC		6.0 $\pi^- p$

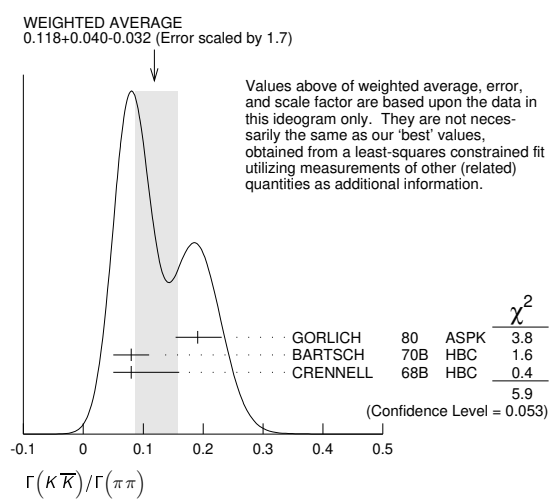

$\Gamma(K\overline{K}\pi)/\Gamma(\pi\pi)$ — Γ_5/Γ_4

VALUE	DOCUMENT ID		TECN	CHG	COMMENT
0.16±0.05 OUR FIT					
0.16±0.05	[30] BARTSCH	70B	HBC	+	8 $\pi^+ p$

[30] Increased by us to correspond to B($\rho_3(1690) \to \pi\pi$)=0.24.

Int. J. Mod. Phys. A 2026.41. Downloaded from www.worldscientific.com by UNIVERSITY OF CALIFORNIA @ BERKELEY on 09/16/26. Re-use and distribution is strictly not permitted, except for Open Access articles.

$[\Gamma(\pi\pi\rho) + \Gamma(a_2(1320)\pi) + \Gamma(\rho\rho)]/\Gamma(\pi^\pm\pi^+\pi^-\pi^0)$ — $(\Gamma_9+\Gamma_{10}+\Gamma_{11})/\Gamma_2$

VALUE	DOCUMENT ID		TECN	CHG	COMMENT
0.94±0.09 OUR AVERAGE					
0.96±0.21	BALTAY	78B	HBC	+	15 $\pi^+ p \to p4\pi$
0.88±0.15	BALLAM	71B	HBC	−	16 $\pi^- p$
1 ±0.15	BARTSCH	70B	HBC	+	8 $\pi^+ p$
consistent with 1	CASO	68	HBC	−	11 $\pi^- p$

$\Gamma(\rho\rho)/\Gamma(\pi^\pm\pi^+\pi^-\pi^0)$ — Γ_{11}/Γ_2

VALUE	EVTS	DOCUMENT ID		TECN	CHG	COMMENT
• • • We do not use the following data for averages, fits, limits, etc. • • •						
0.12±0.11		BALTAY	78B	HBC	+	15 $\pi^+ p \to p4\pi$
0.56	66	KLIGER	74	HBC	−	4.5 $\pi^- p \to p4\pi$
0.13±0.09		[31] THOMPSON	74	HBC	+	13 $\pi^+ p$
0.7 ±0.15		BARTSCH	70B	HBC	+	8 $\pi^+ p$

[31] $\rho\rho$ and $a_2(1320)\pi$ modes are indistinguishable.

$\Gamma(\rho\rho)/[\Gamma(\pi\pi\rho) + \Gamma(a_2(1320)\pi) + \Gamma(\rho\rho)]$ — $\Gamma_{11}/(\Gamma_9+\Gamma_{10}+\Gamma_{11})$

VALUE	DOCUMENT ID		TECN	CHG	COMMENT
• • • We do not use the following data for averages, fits, limits, etc. • • •					
0.48±0.16	CASO	68	HBC	−	11 $\pi^- p$

$\Gamma(a_2(1320)\pi)/\Gamma(\pi^\pm\pi^+\pi^-\pi^0)$ — Γ_{10}/Γ_2

VALUE	DOCUMENT ID		TECN	CHG	COMMENT
• • • We do not use the following data for averages, fits, limits, etc. • • •					
0.66±0.08	BALTAY	78B	HBC	+	15 $\pi^+ p \to p4\pi$
0.36±0.14	[32] THOMPSON	74	HBC	+	13 $\pi^+ p$
not seen	CASON	73	HBC	−	8,18.5 $\pi^- p$
0.6 ±0.15	BARTSCH	70B	HBC	+	8 $\pi^+ p$
0.6	BALTAY	68	HBC	+	7,8.5 $\pi^+ p$

[32] $\rho\rho$ and $a_2(1320)\pi$ modes are indistinguishable.

$\Gamma(\omega\pi)/\Gamma(\pi^\pm\pi^+\pi^-\pi^0)$ — Γ_3/Γ_2

VALUE	CL%	DOCUMENT ID		TECN	CHG	COMMENT
0.23±0.05 OUR AVERAGE		Error includes scale factor of 1.2.				
0.33±0.07		THOMPSON	74	HBC	+	13 $\pi^+ p$
0.12±0.07		BALLAM	71B	HBC	−	16 $\pi^- p$
0.25±0.10		BALTAY	68	HBC	+	7,8.5 $\pi^+ p$
0.25±0.10		JOHNSTON	68	HBC	−	7.0 $\pi^- p$
• • • We do not use the following data for averages, fits, limits, etc. • • •						
<0.11	95	BALTAY	78B	HBC	+	15 $\pi^+ p \to p4\pi$
<0.09		KLIGER	74	HBC	−	4.5 $\pi^- p \to p4\pi$

$\Gamma(\phi\pi)/\Gamma(\pi^\pm\pi^+\pi^-\pi^0)$ — Γ_{12}/Γ_2

VALUE	DOCUMENT ID		TECN	CHG	COMMENT
• • • We do not use the following data for averages, fits, limits, etc. • • •					
<0.11	BALTAY	68	HBC	+	7,8.5 $\pi^+ p$

$\Gamma(\pi^\pm 2\pi^+ 2\pi^- \pi^0)/\Gamma(\pi^\pm\pi^+\pi^-\pi^0)$ — Γ_{14}/Γ_2

VALUE	DOCUMENT ID		TECN	CHG	COMMENT
• • • We do not use the following data for averages, fits, limits, etc. • • •					
<0.15	BALTAY	68	HBC	+	7,8.5 $\pi^+ p$

$\Gamma(\eta\pi)/\Gamma(\pi^\pm\pi^+\pi^-\pi^0)$ — Γ_{13}/Γ_2

VALUE	DOCUMENT ID		TECN	CHG	COMMENT
• • • We do not use the following data for averages, fits, limits, etc. • • •					
<0.02	THOMPSON	74	HBC	+	13 $\pi^+ p$

$\Gamma(K\overline{K})/\Gamma_{total}$ — Γ_6/Γ

VALUE	DOCUMENT ID		TECN	CHG	COMMENT
0.0158±0.0026 OUR FIT	Error includes scale factor of 1.2.				
0.0130±0.0024 OUR AVERAGE					
0.013 ±0.003	COSTA	80	OMEG	0	10 $\pi^- p \to K^+ K^- n$
0.013 ±0.004	[33] MARTIN	78B	SPEC	−	10 $\pi p \to K^0_S K^- p$

[33] From $(\Gamma_4\Gamma_6)^{1/2} = 0.056 \pm 0.034$ assuming $B(\rho_3(1690) \to \pi\pi) = 0.24$.

$\Gamma(\omega\pi)/[\Gamma(\omega\pi) + \Gamma(\rho\rho)]$ — $\Gamma_3/(\Gamma_3+\Gamma_{11})$

VALUE	DOCUMENT ID		TECN	CHG	COMMENT
• • • We do not use the following data for averages, fits, limits, etc. • • •					
0.22±0.08	CASON	73	HBC	−	8,18.5 $\pi^- p$

$\Gamma(\eta\pi^+\pi^-)/\Gamma_{total}$ — Γ_7/Γ

VALUE	DOCUMENT ID		TECN	COMMENT
seen	FUKUI	88	SPEC	8.95 $\pi^- p \to \eta\pi^+\pi^- n$

$\Gamma(a_2(1320)\pi)/\Gamma(\rho(770)\eta)$ — Γ_{10}/Γ_8

VALUE	DOCUMENT ID		TECN	COMMENT
5.5±2.0	AMELIN	00	VES	37 $\pi^- p \to \eta\pi^+\pi^- n$

$\rho_3(1690)$ REFERENCES

AMELIN	00	NP A668 83	D. Amelin et al.	(VES Collab.)
ALDE	95	ZPHY C66 379	D.M. Alde et al.	(GAMS Collab.) JP
ALDE	92C	ZPHY C54 553	D.M. Alde et al.	(BELG, SERP, KEK, LANL+)
FUKUI	88	PL B202 441	S. Fukui et al.	(SUGI, NAGO, KEK, KYOT+)
DENNEY	83	PR D28 2726	D.L. Denney et al.	(IOWA, MICH)
EVANGELIS...	81	NP B178 197	C. Evangelista et al.	(BARI, BONN, CERN+)
ALPER	80	PL 94B 422	B. Alper et al.	(AMST, CERN, CRAC, MPIM+)
COSTA	80	NP B175 402	G. Costa et al.	(BARI, BONN, CERN, GLAS+)
GORLICH	80	NP B174 16	L. Gorlich et al.	(CRAC, MPIM, CERN+)
BECKER	79	NP B151 46	H. Becker et al.	(MPIM, CERN, ZEEM, CRAC)
CORDEN	79	NP B157 250	M.J. Corden et al.	(BIRM, RHEL, TELA+) JP
BALTAY	78B	PR D17 62	C. Baltay et al.	(COLU, BING)
MARTIN	78B	NP B140 158	A.D. Martin et al.	(DURH, GEVA)
MARTIN	78D	PL 74B 417	A.D. Martin et al.	(DURH, GEVA)
ANTIPOV	77	NP B119 45	Y.M. Antipov et al.	(SERP, GEVA)
GESSAROLI	77	NP B126 382	R. Gessaroli et al.	(BGNA, FIRZ, GENO+)
BLUM	75	PL 57B 403	W. Blum et al.	(CERN, MPIM) JP
ESTABROOKS	75	NP B95 322	P.G. Estabrooks, A.D. Martin	(DURH)
HYAMS	75	NP B100 205	B.D. Hyams et al.	(CERN, MPIM)
ENGLER	74	PR D10 2070	A. Engler et al.	(CMU, CASE)
GRAYER	74	NP B75 189	G. Grayer et al.	(CERN, MPIM)
KLIGER	74	SJNP 19 428	G.K. Kliger et al.	(ITEP)
		Translated from YAF 19 839.		
OREN	74	NP B71 189	Y. Oren et al.	(ANL, OXF)
THOMPSON	74	NP B69 220	G. Thompson et al.	(PURD)
CASON	73	PR D7 1971	N.M. Cason et al.	(NDAM)
BOWEN	72	PRL 29 890	D.R. Bowen et al.	(NEAS, STON)
HOLMES	72	PR D6 3336	R. Holmes et al.	(ROCH)
BALLAM	71B	PR D3 2606	J. Ballam et al.	(SLAC)
MATTHEWS	71C	NP B33 1	J.A.J. Matthews et al.	(TNTO, WISC) JP
ARMENISE	70	LNC 4 199	N. Armenise et al.	(BARI, BGNA, FIRZ)
BARNHAM	70	PRL 24 1083	K.W.J. Barnham et al.	(BIRM)
BARTSCH	70B	NP B22 109	J. Bartsch et al.	(AACH, BERL, CERN)
CASO	70	LNC 3 707	C. Caso et al.	(GENO, HAMB, MILA, SACL)
STUNTEBECK	70	PL 32B 391	P.H. Stuntebeck et al.	(NDAM)
ADERHOLZ	69	NP B11 259	M. Aderholz et al.	(AACH3, BERL, CERN+)
ANDERSON	69	PRL 22 1390	E.W. Anderson et al.	(BNL, CMU)
ARMENISE	68	NC 54A 999	N. Armenise et al.	(BARI, BGNA, FIRZ+) I
BALTAY	68	PRL 20 887	C. Baltay et al.	(COLU, ROCH, RUTG, YALE) I
CASO	68	NC 54A 983	C. Caso et al.	(GENO, HAMB, MILA, SACL)
CRENNELL	68B	PL 28B 136	D.J. Crennell et al.	(BNL)
JOHNSTON	68	PRL 20 1414	T.F. Johnston et al.	(TNTO, WISC) IJP
FOCACCI	66	PRL 17 890	M.N. Focacci et al.	(CERN)
GOLDBERG	65	PL 17 354	M. Goldberg et al.	(CERN, EPOL, ORSAY+)

$\rho(1700)$

$I^G(J^{PC}) = 1^+(1^{--})$

See the review on "Spectroscopy of Light Meson Resonances."

$\rho(1700)$ MASS

$\eta\rho^0$ AND $\pi^+\pi^-$ MODES

VALUE (MeV)	DOCUMENT ID
1720±20 OUR ESTIMATE	

$\eta\rho^0$ MODE

VALUE (MeV)	EVTS	DOCUMENT ID		TECN	COMMENT
The data in this block is included in the average printed for a previous datablock.					
• • • We do not use the following data for averages, fits, limits, etc. • • •					
1834±12	13.4k	[1] GRIBANOV	20	CMD3	1.1–2.0 $e^+e^- \to \eta\pi^+\pi^-$
1840±10	7.4k	[2] ACHASOV	18	SND	1.22–2.00 $e^+e^- \to \eta\pi^+\pi^-$
1740±20		ANTONELLI	88	DM2	$e^+e^- \to \eta\pi^+\pi^-$
1701±15		[3] FUKUI	88	SPEC	8.95 $\pi^- p \to \eta\pi^+\pi^- n$

[1] Mass and width of the $\rho(770)$ fixed at 775 and 149 MeV, respectively; solution 2 of model 2, $\eta \to \gamma\gamma$ decays used.

[2] From the combined fit of AULCHENKO 15 and ACHASOV 18 in the model with the interfering $\rho(1450)$, $\rho(1700)$ and $\rho(2150)$ with the parameters of the $\rho(1450)$ and $\rho(1700)$ floating and the mass and width of the $\rho(2150)$ fixed at 2155 MeV and 320 MeV, respectively. The phases of the resonances are π, 0 and π, respectively.

[3] Assuming $\rho^+ f_0(1370)$ decay mode interferes with $a_1(1260)^+\pi$ background. From a two Breit-Wigner fit.

$\pi\pi$ MODE

VALUE (MeV)	EVTS	DOCUMENT ID		TECN	COMMENT
The data in this block is included in the average printed for a previous datablock.					
• • • We do not use the following data for averages, fits, limits, etc. • • •					
1790 ±20		[1] AAIJ	25AG	LHCB	5 TeV PbPb → PbPb $\pi^+\pi^-$
1604.66±30.8	34M	[2] IGNATOV	24	CMD3	$e^+e^- \to \pi^+\pi^-$
1725 ±17		[3] ACHARYA	20F	ALCE	5 TeV PbPb → PbPb $\pi^+\pi^-$
1770.54± 5.49		[4] BARTOS	17	RVUE	$e^+e^- \to \pi^+\pi^-$
1718.50±65.44		[5] BARTOS	17A	RVUE	$e^+e^- \to \pi^+\pi^-$
1766.80±52.36		[6] BARTOS	17A	RVUE	$\tau^- \to \pi^-\pi^0\nu_\tau$
1644 ±36	20k	[7] LEES	17C	BABR	$J/\psi \to \pi^+\pi^-\pi^0$
1780 $^{+15}_{-20}$	63.5k	[8] ABRAMOWICZ	12	ZEUS	$ep \to e\pi^+\pi^- p$
1861 ±17		[9] LEES	12G	BABR	$e^+e^- \to \pi^+\pi^-\gamma$
1728 ±17 ±89	5.4M	[10,11] FUJIKAWA	08	BELL	$\tau^- \to \pi^-\pi^0\nu_\tau$
1780 $^{+37}_{-29}$		[12] ABELE	97	CBAR	$\overline{p}n \to \pi^-\pi^0\pi^0$
1719 ±15		[12] BERTIN	97C	OBLX	0.0 $\overline{p}p \to \pi^+\pi^-\pi^0$
1730 ±30		CLEGG	94	RVUE	$e^+e^- \to \pi^+\pi^-$

Int. J. Mod. Phys. A 2026.41. Downloaded from www.worldscientific.com by CALIFORNIA @ BERKELEY on 09/16/26. Re-use and distribution is strictly not permitted, except for Open Access articles.

1768	±21	BISELLO	89	DM2	$e^+e^- \to \pi^+\pi^-$
1745.7	±91.9	DUBNICKA	89	RVUE	$e^+e^- \to \pi^+\pi^-$
1546	±26	GESHKEN...	89	RVUE	
1650		[13] ERKAL	85	RVUE	20–70 $\gamma p \to \gamma\pi$
1550	±70	ABE	84B	HYBR	20 $\gamma p \to \pi^+\pi^- p$
1590	±20	[14] ASTON	80	OMEG	20–70 $\gamma p \to p2\pi$
1600	±10	[15] ATIYA	79B	SPEC	50 γC $\to$ C2π
1598	$^{+24}_{-22}$	BECKER	79	ASPK	17 $\pi^- p$ polarized
1659	±25	[13] LANG	79	RVUE	
1575		[13] MARTIN	78C	RVUE	17 $\pi^- p \to \pi^+\pi^- n$
1610	±30	[13] FROGGATT	77	RVUE	17 $\pi^- p \to \pi^+\pi^- n$
1590	±20	[16] HYAMS	73	ASPK	17 $\pi^- p \to \pi^+\pi^- n$

[1] Using the parametrisation as in ANDREEV 20 with ρ-ω interference with the additional presence of two Breit-Wigner resonances for excited ρ states.
[2] From a fit of the pion form factor using the GOUNARIS 68 parametrization with the complex phase of the $\rho-\omega$ interference leaving $\rho(1450)$, $\rho(1700)$ resonances as free parameters of the fit. The fit uses also data from CMD-2 and DM2 experiments. Systematic errors not estimated.
[3] J^{PC} not determined, could be $\rho_3(1690)$.
[4] Applies the Unitary & Analytic Model of the pion electromagnetic form factor of DUBNICKA 10 to analyze the data of LEES 12G and ABLIKIM 16C.
[5] Applies the Unitary & Analytic Model of the pion electromagnetic form factor of DUBNICKA 10 to analyze the data of ACHASOV 06, AKHMETSHIN 07, AUBERT 09AS, and AMBROSINO 11A.
[6] Applies the Unitary & Analytic Model of the pion electromagnetic form factor of DUBNICKA 10 to analyze the data of FUJIKAWA 08.
[7] From a Dalitz plot analysis in an isobar model with $\rho(1450)$ and $\rho(1700)$ masses and widths floating.
[8] Using the KUHN 90 parametrization of the pion form factor, neglecting $\rho-\omega$ interference.
[9] Using the GOUNARIS 68 parametrization of the pion form factor leaving the masses and widths of the $\rho(1450)$, $\rho(1700)$, and $\rho(2150)$ resonances as free parameters of the fit.
[10] $|F_\pi(0)|^2$ fixed to 1.
[11] From the GOUNARIS 68 parametrization of the pion form factor.
[12] T-matrix pole.
[13] From phase shift analysis of HYAMS 73 data.
[14] Simple relativistic Breit-Wigner fit with constant width.
[15] An additional 40 MeV uncertainty in both the mass and width is present due to the choice of the background shape.
[16] Included in BECKER 79 analysis.

$\pi\omega$ MODE

VALUE (MeV)	EVTS	DOCUMENT ID		TECN	COMMENT
• • • We do not use the following data for averages, fits, limits, etc. • • •					
1723± 2		[1] ACHASOV	23A	SND	$e^+e^- \to \omega\pi^0$
1708±41	7815	[2] ACHASOV	13	SND	1.05–2.00 $e^+e^- \to \pi^0\pi^0\gamma$
1550 to 1620		[3] ACHASOV	00I	SND	$e^+e^- \to \pi^0\pi^0\gamma$
1580 to 1710		[4] ACHASOV	00I	SND	$e^+e^- \to \pi^0\pi^0\gamma$
1710±90		ACHASOV	97	RVUE	$e^+e^- \to \omega\pi^0$

[1] From a vector dominance fit to the Born cross section between 1.05 and 2.0 GeV with $\rho(770)$, $\rho(1570)$, $\rho(1700)$, $\rho(2150)$. The fit also uses SND data from the VEPP-2M collider below 1.02 GeV and from LEES 17H and ABLIKIM 21A above 1.5GeV.
[2] From a phenomenological model based on vector meson dominance with the interfering $\rho(1450)$ and $\rho(1700)$ and their widths fixed at 400 and 250 MeV, respectively. Systematic uncertainty not estimated.
[3] Taking into account both $\rho(1450)$ and $\rho(1700)$ contributions. Using the data of ACHASOV 00I on $e^+e^- \to \omega\pi^0$ and of EDWARDS 00A on $\tau^- \to \omega\pi^-\nu_\tau$. $\rho(1450)$ mass and width fixed at 1400 MeV and 500 MeV respectively.
[4] Taking into account the $\rho(1700)$ contribution only. Using the data of ACHASOV 00I on $e^+e^- \to \omega\pi^0$ and of EDWARDS 00A on $\tau^- \to \omega\pi^-\nu_\tau$.

$K\overline{K}$ MODE

VALUE (MeV)	EVTS	DOCUMENT ID		TECN	CHG	COMMENT
• • • We do not use the following data for averages, fits, limits, etc. • • •						
1688.7± 3.1 $^{+141.1}_{-1.3}$		[1] ALBRECHT	20	RVUE		0.9 $\overline{p}p \to K^+K^-\pi^0$
1541 ±12 ± 33	190k	[2] AAIJ	16N	LHCB		$D^0 \to K^0_S K^\pm\pi^\mp$
1740.8±22.2	27k	[3] ABELE	99D	CBAR	±	0.0 $\overline{p}p \to K^+K^-\pi^0$
1582 ±36	1600	CLELAND	82B	SPEC	±	50 $\pi p \to K^0_S K^\pm p$

[1] T-matrix pole, 2 poles, 3 channels, including $\pi\pi$ scattering data from HYAMS 75.
[2] Using the GOUNARIS 68 parameterization with a fixed width. Value is average using different $K\pi$ S-wave parametrizations in fit.
[3] K-matrix pole. Isospin not determined, could be $\omega(1650)$ or $\phi(1680)$.

2 $(\pi^+\pi^-)$ MODE

VALUE (MeV)	EVTS	DOCUMENT ID		TECN	COMMENT
• • • We do not use the following data for averages, fits, limits, etc. • • •					
1663± 13±22		[1] ACHARYA	26	ALCE	5 TeV PbPb $\to$ PbPb4π
1851 $^{+27}_{-24}$		ACHASOV	97	RVUE	$e^+e^- \to 2(\pi^+\pi^-)$
1570± 20		[2] CORDIER	82	DM1	$e^+e^- \to 2(\pi^+\pi^-)$
1520± 30		[3] ASTON	81E	OMEG	20–70 $\gamma p \to p4\pi$
1654± 25		[4] DIBIANCA	81	DBC	$\pi^+ d \to pp2(\pi^+\pi^-)$
1666± 39		[2] BACCI	80	FRAG	$e^+e^- \to 2(\pi^+\pi^-)$
1780	34	KILLIAN	80	SPEC	11 $e^- p \to 2(\pi^+\pi^-)$
1500		[5] ATIYA	79B	SPEC	50 γC $\to$ C$4\pi^\pm$
1570± 60	65	[6] ALEXANDER	75	HBC	7.5 $\gamma p \to p4\pi$
1550± 60		[3] CONVERSI	74	OSPK	$e^+e^- \to 2(\pi^+\pi^-)$
1550± 50	160	SCHACHT	74	STRC	5.5–9 $\gamma p \to p4\pi$
1450±100	340	SCHACHT	74	STRC	9–18 $\gamma p \to p4\pi$
1430± 50	400	BINGHAM	72B	HBC	9.3 $\gamma p \to p4\pi$

[1] From a two Breit-Wigner resonance fit to the 4π mass distribution produced in ultraperipheral Pb–Pb collisions.
[2] Simple relativistic Breit-Wigner fit with model dependent width.
[3] Simple relativistic Breit-Wigner fit with constant width.
[4] One peak fit result.
[5] Parameters roughly estimated, not from a fit.
[6] Skew mass distribution compensated by Ross-Stodolsky factor.

$\pi^+\pi^-\pi^0\pi^0$ MODE

VALUE (MeV)	DOCUMENT ID		TECN	COMMENT
• • • We do not use the following data for averages, fits, limits, etc. • • •				
1660±30	ATKINSON	85B	OMEG	20–70 γp

$3(\pi^+\pi^-)$ AND $2(\pi^+\pi^-\pi^0)$ MODES

VALUE (MeV)	DOCUMENT ID		TECN	COMMENT
• • • We do not use the following data for averages, fits, limits, etc. • • •				
1730±34	[1] FRABETTI	04	E687	$\gamma p \to 3\pi^+ 3\pi^- p$
1783±15	CLEGG	90	RVUE	$e^+e^- \to 3(\pi^+\pi^-)2(\pi^+\pi^-\pi^0)$

[1] From a fit with two resonances with the JACOB 72 continuum.

$m_{\rho(1700)^0} - m_{\rho(1700)^\pm}$

VALUE (MeV)	DOCUMENT ID		TECN	COMMENT
• • • We do not use the following data for averages, fits, limits, etc. • • •				
−48.30±83.81	[1] BARTOS	17A	RVUE	$e^+e^- \to \pi^+\pi^-$, $\tau^- \to \pi^-\pi^0\nu_\tau$

[1] Applies the Unitary & Analytic Model of the pion electromagnetic form factor of DUBNICKA 10 to analyze the data of ACHASOV 06, AKHMETSHIN 07, AUBERT 09AS, AMBROSINO 11A, and FUJIKAWA 08.

$\rho(1700)$ WIDTH

$\eta\rho^0$ AND $\pi^+\pi^-$ MODES

VALUE (MeV)	DOCUMENT ID
250±100 OUR ESTIMATE	

$\eta\rho^0$ MODE

VALUE (MeV)	EVTS	DOCUMENT ID		TECN	COMMENT
The data in this block is included in the average printed for a previous datablock.					
• • • We do not use the following data for averages, fits, limits, etc. • • •					
47±19	13.4k	[1] GRIBANOV	20	CMD3	1.1–2.0 $e^+e^- \to \eta\pi^+\pi^-$
132±40	7.4k	[2] ACHASOV	18	SND	1.22–2.00 $e^+e^- \to \eta\pi^+\pi^-$
150±30		ANTONELLI	88	DM2	$e^+e^- \to \eta\pi^+\pi^-$
282±44		[3] FUKUI	88	SPEC	8.95 $\pi^- p \to \eta\pi^+\pi^- n$

[1] Mass and width of the $\rho(770)$ fixed at 775 and 149 MeV, respectively; solution 2 of model 2, $\eta \to \gamma\gamma$ decays used.
[2] From the combined fit of AULCHENKO 15 and ACHASOV 18 in the model with the interfering $\rho(1450)$, $\rho(1700)$ and $\rho(2150)$ with the parameters of the $\rho(1450)$ and $\rho(1700)$ floating and the mass and width of the $\rho(2150)$ fixed at 2155 MeV and 320 MeV, respectively. The phases of the resonances are π, 0 and π, respectively.
[3] Assuming $\rho^+ f_0(1370)$ decay mode interferes with $a_1(1260)^+\pi$ background. From a two Breit-Wigner fit.

$\pi\pi$ MODE

VALUE (MeV)	EVTS	DOCUMENT ID		TECN	COMMENT
The data in this block is included in the average printed for a previous datablock.					
• • • We do not use the following data for averages, fits, limits, etc. • • •					
290 ± 40		[1] AAIJ	25AG	LHCB	5 TeV PbPb $\to$ PbPb$\pi^+\pi^-$
249.39± 52.24	34M	[2] IGNATOV	24	CMD3	$e^+e^- \to \pi^+\pi^-$
143 ± 21		[3] ACHARYA	20F	ALCE	5 TeV PbPb $\to$ PbPb$\pi^+\pi^-$
268.98± 11.40		[4] BARTOS	17	RVUE	$e^+e^- \to \pi^+\pi^-$
489.58± 16.95		[5] BARTOS	17A	RVUE	$e^+e^- \to \pi^+\pi^-$
414.71±119.48		[6] BARTOS	17A	RVUE	$\tau^- \to \pi^-\pi^0\nu_\tau$
109 ± 19	20k	[7] LEES	17C	BABR	$J/\psi \to \pi^+\pi^-\pi^0$
310 ± 30	$^{+25}_{-35}$ 63.5k	[8] ABRAMOWICZ	12	ZEUS	$ep \to e\pi^+\pi^- p$
316 ± 26		[9] LEES	12G	BABR	$e^+e^- \to \pi^+\pi^-\gamma$
164 ± 21	$^{+89}_{-26}$ 5.4M	[10,11] FUJIKAWA	08	BELL	$\tau^- \to \pi^-\pi^0\nu_\tau$
275 ± 45		[12] ABELE	97	CBAR	$\overline{p}n \to \pi^-\pi^0\pi^0$
310 ± 40		[12] BERTIN	97C	OBLX	0.0 $\overline{p}p \to \pi^+\pi^-\pi^0$
400 ±100		CLEGG	94	RVUE	$e^+e^- \to \pi^+\pi^-$
224 ± 22		BISELLO	89	DM2	$e^+e^- \to \pi^+\pi^-$
242.5 ±163.0		DUBNICKA	89	RVUE	$e^+e^- \to \pi^+\pi^-$
620 ± 60		GESHKEN...	89	RVUE	
<315		[13] ERKAL	85	RVUE	20–70 $\gamma p \to \gamma\pi$
280 $^{+30}_{-80}$		ABE	84B	HYBR	20 $\gamma p \to \pi^+\pi^- p$
230 ± 80		[14] ASTON	80	OMEG	20–70 $\gamma p \to p2\pi$
283 ± 14		[15] ATIYA	79B	SPEC	50 γC $\to$ C2π
175 $^{+98}_{-53}$		BECKER	79	ASPK	17 $\pi^- p$ polarized
232 ± 34		[13] LANG	79	RVUE	
340		[13] MARTIN	78C	RVUE	17 $\pi^- p \to \pi^+\pi^- n$
300 ±100		[13] FROGGATT	77	RVUE	17 $\pi^- p \to \pi^+\pi^- n$
180 ± 50		[16] HYAMS	73	ASPK	17 $\pi^- p \to \pi^+\pi^- n$

Int. J. Mod. Phys. A 2026.41. Downloaded from www.worldscientific.com
by UNIVERSITY OF CALIFORNIA @ BERKELEY on 09/16/26. Re-use and distribution is strictly not permitted, except for Open Access articles.

[1] Using the parametrisation as in ANDREEV 20 with ρ-ω interference with the additional presence of two Breit-Wigner resonances for excited ρ states.
[2] From a fit of the pion form factor using the GOUNARIS 68 parametrization with the complex phase of the $\rho - \omega$ interference leaving $\rho(1450)$, $\rho(1700)$ resonances as free parameters of the fit. The fit uses also data from CMD-2 and DM2 experiments. Systematic errors not estimated.
[3] J^{PC} not determined, could be $\rho_3(1690)$.
[4] Applies the Unitary & Analytic Model of the pion electromagnetic form factor of DUBNICKA 10 to analyze the data of LEES 12G and ABLIKIM 16C.
[5] Applies the Unitary & Analytic Model of the pion electromagnetic form factor of DUBNICKA 10 to analyze the data of ACHASOV 06, AKHMETSHIN 07, AUBERT 09AS, and AMBROSINO 11A.
[6] Applies the Unitary & Analytic Model of the pion electromagnetic form factor of DUBNICKA 10 to analyze the data of FUJIKAWA 08.
[7] From a Dalitz plot analysis in an isobar model with $\rho(1450)$ and $\rho(1700)$ masses and widths floating.
[8] Using the KUHN 90 parametrization of the pion form factor, neglecting ρ–ω interference.
[9] Using the GOUNARIS 68 parametrization of the pion form factor leaving the masses and widths of the $\rho(1450)$, $\rho(1700)$, and $\rho(2150)$ resonances as free parameters of the fit.
[10] $|F_\pi(0)|^2$ fixed to 1.
[11] From the GOUNARIS 68 parametrization of the pion form factor.
[12] T-matrix pole.
[13] From phase shift analysis of HYAMS 73 data.
[14] Simple relativistic Breit-Wigner fit with constant width.
[15] An additional 40 MeV uncertainty in both the mass and width is present due to the choice of the background shape.
[16] Included in BECKER 79 analysis.

$K\overline{K}$ MODE

VALUE (MeV)	EVTS	DOCUMENT ID		TECN	CHG	COMMENT
• • • We do not use the following data for averages, fits, limits, etc. • • •						
$150.9 \pm 2.5^{+60}_{-10.6}$		[1] ALBRECHT	20	RVUE		0.9 $\overline{p}p \to K^+K^-\pi^0$
187.2 ± 26.7	27k	[2] ABELE	99D	CBAR	$\pm$	0.0 $\overline{p}p \to K^+K^-\pi^0$
265 ± 120	1600	CLELAND	82B	SPEC	$\pm$	50 $\pi p \to K^0_S K^\pm p$

[1] T-matrix pole, 2 poles, 3 channels, including $\pi\pi$ scattering data from HYAMS 75.
[2] K-matrix pole. Isospin not determined, could be $\omega(1650)$ or $\phi(1680)$.

$2(\pi^+\pi^-)$ MODE

VALUE (MeV)	EVTS	DOCUMENT ID		TECN	COMMENT
• • • We do not use the following data for averages, fits, limits, etc. • • •					
$357 \pm 31 \pm 49$		[1] ACHARYA	26	ALCE	5 TeV PbPb $\to$ PbPb4π
510 ± 40		[2] CORDIER	82	DM1	$e^+e^- \to 2(\pi^+\pi^-)$
400 ± 50		[3] ASTON	81E	OMEG	20–70 $\gamma p \to p4\pi$
400 ± 146		[4] DIBIANCA	81	DBC	$\pi^+ d \to pp2(\pi^+\pi^-)$
700 ± 160		[2] BACCI	80	FRAG	$e^+e^- \to 2(\pi^+\pi^-)$
100	34	KILLIAN	80	SPEC	11 $e^-p \to 2(\pi^+\pi^-)$
600		[5] ATIYA	79B	SPEC	50 γC $\to$ C$4\pi^\pm$
340 ± 160	65	[6] ALEXANDER	75	HBC	7.5 $\gamma p \to p4\pi$
360 ± 100		[3] CONVERSI	74	OSPK	$e^+e^- \to 2(\pi^+\pi^-)$
400 ± 120	160	[7] SCHACHT	74	STRC	5.5–9 $\gamma p \to p4\pi$
850 ± 200	340	[7] SCHACHT	74	STRC	9–18 $\gamma p \to p4\pi$
650 ± 100	400	BINGHAM	72B	HBC	9.3 $\gamma p \to p4\pi$

[1] From a two Breit-Wigner resonance fit to the 4π mass distribution produced in ultraperipheral Pb–Pb collisions.
[2] Simple relativistic Breit-Wigner fit with model-dependent width.
[3] Simple relativistic Breit-Wigner fit with constant width.
[4] One peak fit result.
[5] Parameters roughly estimated, not from a fit.
[6] Skew mass distribution compensated by Ross-Stodolsky factor.
[7] Width errors enlarged by us to $4\Gamma/\sqrt{N}$; see the note with the $K^*(892)$ mass.

$\pi^+\pi^-\pi^0\pi^0$ MODE

VALUE (MeV)	DOCUMENT ID		TECN	COMMENT
• • • We do not use the following data for averages, fits, limits, etc. • • •				
300 ± 50	ATKINSON	85B	OMEG	20–70 γp

$\omega\pi^0$ MODE

VALUE (MeV)	DOCUMENT ID		TECN	COMMENT
• • • We do not use the following data for averages, fits, limits, etc. • • •				
371 ± 3	[1] ACHASOV	23A	SND	$e^+e^- \to \omega\pi^0$
350 to 580	[2] ACHASOV	00I	SND	$e^+e^- \to \pi^0\pi^0\gamma$
490 to 1040	[3] ACHASOV	00I	SND	$e^+e^- \to \pi^0\pi^0\gamma$

[1] From a vector dominance fit to the Born cross section between 1.05 and 2.0 GeV with $\rho(770)$, $\rho(1570)$, $\rho(1700)$, $\rho(2150)$. The fit also uses SND data from the VEPP-2M collider below 1.02 GeV and from LEES 17H and ABLIKIM 21A above 1.5 GeV.
[2] Taking into account both $\rho(1450)$ and $\rho(1700)$ contributions. Using the data of ACHASOV 00I on $e^+e^- \to \omega\pi^0$ and of EDWARDS 00A on $\tau^- \to \omega\pi^-\nu_\tau$. $\rho(1450)$ mass and width fixed at 1400 MeV and 500 MeV respectively.
[3] Taking into account the $\rho(1700)$ contribution only. Using the data of ACHASOV 00I on $e^+e^- \to \omega\pi^0$ and of EDWARDS 00A on $\tau^- \to \omega\pi^-\nu_\tau$.

$3(\pi^+\pi^-)$ AND $2(\pi^+\pi^-\pi^0)$ MODES

VALUE (MeV)	DOCUMENT ID		TECN	COMMENT
• • • We do not use the following data for averages, fits, limits, etc. • • •				
315 ± 100	[1] FRABETTI	04	E687	$\gamma p \to 3\pi^+3\pi^- p$
285 ± 20	CLEGG	90	RVUE	$e^+e^- \to 3(\pi^+\pi^-)2(\pi^+\pi^-\pi^0)$

[1] From a fit with two resonances with the JACOB 72 continuum.

$\Gamma_{\rho(1700)^0} - \Gamma_{\rho(1700)^\pm}$

VALUE (MeV)	DOCUMENT ID		TECN	COMMENT
• • • We do not use the following data for averages, fits, limits, etc. • • •				
74.87 ± 120.67	[1] BARTOS	17A	RVUE	$e^+e^- \to \pi^+\pi^-, \tau^- \to \pi^-\pi^0\nu_\tau$

[1] Applies the Unitary & Analytic Model of the pion electromagnetic form factor of DUBNICKA 10 to analyze the data of ACHASOV 06, AKHMETSHIN 07, AUBERT 09AS, AMBROSINO 11A, and FUJIKAWA 08.

$\rho(1700)$ DECAY MODES

	Mode	Fraction (Γ_i/Γ)
Γ_1	4π	
Γ_2	$2(\pi^+\pi^-)$	seen
Γ_3	$\rho\pi\pi$	seen
Γ_4	$\rho^0\pi^+\pi^-$	seen
Γ_5	$\rho^0\pi^0\pi^0$	
Γ_6	$\rho^\pm\pi^\mp\pi^0$	seen
Γ_7	$a_1(1260)\pi$	seen
Γ_8	$h_1(1170)\pi$	seen
Γ_9	$\pi(1300)\pi$	seen
Γ_{10}	$\rho\rho$	seen
Γ_{11}	$\pi^+\pi^-$	seen
Γ_{12}	$\pi\pi$	seen
Γ_{13}	$K\overline{K}^*(892) +$ c.c.	seen
Γ_{14}	$\eta\rho$	seen
Γ_{15}	$a_2(1320)\pi$	not seen
Γ_{16}	$K\overline{K}$	seen
Γ_{17}	e^+e^-	seen
Γ_{18}	$\pi^0\omega$	seen
Γ_{19}	$\pi^0\gamma$	not seen
Γ_{20}	$f_0(1500)\gamma$	not seen

$\rho(1700)$ $\Gamma(i)\Gamma(e^+e^-)/\Gamma(\text{total})$

This combination of a partial width with the partial width into e^+e^- and with the total width is obtained from the cross-section into channel$_i$ in e^+e^- annihilation.

$\Gamma(2(\pi^+\pi^-)) \times \Gamma(e^+e^-)/\Gamma_{\text{total}}$ — $\Gamma_2\Gamma_{17}/\Gamma$

VALUE (keV)	DOCUMENT ID		TECN	COMMENT
• • • We do not use the following data for averages, fits, limits, etc. • • •				
2.6 ± 0.2	DELCOURT	81B	DM1	$e^+e^- \to 2(\pi^+\pi^-)$
2.83 ± 0.42	BACCI	80	FRAG	$e^+e^- \to 2(\pi^+\pi^-)$

$\Gamma(\pi^+\pi^-) \times \Gamma(e^+e^-)/\Gamma_{\text{total}}$ — $\Gamma_{11}\Gamma_{17}/\Gamma$

VALUE (keV)	DOCUMENT ID		TECN	COMMENT
• • • We do not use the following data for averages, fits, limits, etc. • • •				
0.13	[1] DIEKMAN	88	RVUE	$e^+e^- \to \pi^+\pi^-$
$0.029^{+0.016}_{-0.012}$	KURDADZE	83	OLYA	0.64–1.4 $e^+e^- \to \pi^+\pi^-$

[1] Using total width = 220 MeV.

$\Gamma(K\overline{K}^*(892) + \text{c.c.}) \times \Gamma(e^+e^-)/\Gamma_{\text{total}}$ — $\Gamma_{13}\Gamma_{17}/\Gamma$

VALUE (keV)	DOCUMENT ID		TECN	COMMENT
• • • We do not use the following data for averages, fits, limits, etc. • • •				
0.305 ± 0.071	[1] BIZOT	80	DM1	e^+e^-

[1] Model dependent.

$\Gamma(\eta\rho) \times \Gamma(e^+e^-)/\Gamma_{\text{total}}$ — $\Gamma_{14}\Gamma_{17}/\Gamma$

VALUE (eV)	EVTS	DOCUMENT ID		TECN	COMMENT
• • • We do not use the following data for averages, fits, limits, etc. • • •					
$1.35 \pm 0.53 \pm 0.08$	13.4k	[1] GRIBANOV	20	CMD3	1.1–2.0 $e^+e^- \to \eta\pi^+\pi^-$
$84 \pm 26 \pm 4$		[2] LEES	18	BABR	$e^+e^- \to \eta\pi^+\pi^-$
7 ± 3		ANTONELLI	88	DM2	$e^+e^- \to \eta\pi^+\pi^-$

[1] Mass and width of the $\rho(770)$ fixed at 775 and 149 MeV, respectively; solution 2 of model 2, $\eta \to \gamma\gamma$ decays used.
[2] Includes non-resonant contribution. The selected fit model includes three ρ excited states. Model uncertainty is 80%.

$\Gamma(K\overline{K}) \times \Gamma(e^+e^-)/\Gamma_{\text{total}}$ — $\Gamma_{16}\Gamma_{17}/\Gamma$

VALUE (keV)	DOCUMENT ID		TECN	COMMENT
• • • We do not use the following data for averages, fits, limits, etc. • • •				
0.035 ± 0.029	[1] BIZOT	80	DM1	e^+e^-

[1] Model dependent.

Int. J. Mod. Phys. A 2026.41. Downloaded from www.worldscientific.com by CALIFORNIA @ BERKELEY on 09/16/26. Re-use and distribution is strictly not permitted, except for Open Access articles.

$\Gamma(\rho\pi\pi) \times \Gamma(e^+e^-)/\Gamma_{total}$ — $\Gamma_3\Gamma_{17}/\Gamma$

VALUE (keV)	DOCUMENT ID		TECN	COMMENT
• • • We do not use the following data for averages, fits, limits, etc. • • •				
3.510 ± 0.090	[1] BIZOT	80	DM1	e^+e^-

[1] Model dependent.

$\rho(1700)$ $\Gamma(i)/\Gamma(total) \times \Gamma(e^+e^-)/\Gamma(total)$

$\Gamma(\pi^0\omega)/\Gamma_{total} \times \Gamma(e^+e^-)/\Gamma_{total}$ — $\Gamma_{18}/\Gamma \times \Gamma_{17}/\Gamma$

VALUE (units 10^{-6})	EVTS	DOCUMENT ID		TECN	COMMENT
• • • We do not use the following data for averages, fits, limits, etc. • • •					
0.09 ± 0.05	10.2k	[1] ACHASOV	16D	SND	1.05–2.00 $e^+e^- \to \pi^0\pi^0\gamma$
1.7 ± 0.4	7815	[2] ACHASOV	13	SND	1.05–2.00 $e^+e^- \to \pi^0\pi^0\gamma$

[1] From a phenomenological model based on vector meson dominance with interfering $\rho(700)$, $\rho(1450)$, and $\rho(1700)$. The $\rho(1700)$ mass and width are fixed at 1720 MeV and 250 MeV, respectively. Systematic uncertainty not estimated. Supersedes ACHASOV 13.

[2] From a phenomenological model based on vector meson dominance with the interfering $\rho(1450)$ and $\rho(1700)$ and their widths fixed at 400 and 250 MeV, respectively. Systematic uncertainty not estimated.

$\Gamma(\eta\rho)/\Gamma_{total} \times \Gamma(e^+e^-)/\Gamma_{total}$ — $\Gamma_{14}/\Gamma \times \Gamma_{17}/\Gamma$

VALUE (units 10^{-8})	EVTS	DOCUMENT ID		TECN	COMMENT
• • • We do not use the following data for averages, fits, limits, etc. • • •					
$8.3^{+3.8}_{-3.1}$	7.4k	[1] ACHASOV	18	SND	1.22–2.00 $e^+e^- \to \eta\pi^+\pi^-$

[1] From the combined fit of AULCHENKO 15 and ACHASOV 18 in the model with the interfering $\rho(1450)$, $\rho(1700)$ and $\rho(2150)$ with the parameters of the $\rho(1450)$ and $\rho(1700)$ floating and the mass and width of the $\rho(2150)$ fixed at 2155 MeV and 320 MeV, respectively. The phases of the resonances are π, 0 and π, respectively.

$\rho(1700)$ BRANCHING RATIOS

$\Gamma(\rho\pi\pi)/\Gamma(4\pi)$ — Γ_3/Γ_1

VALUE	DOCUMENT ID		TECN	COMMENT
• • • We do not use the following data for averages, fits, limits, etc. • • •				
0.28 ± 0.06	[1] ABELE	01B	CBAR	$0.0\ \overline{p}n \to 5\pi$

[1] $\omega\pi$ not included.

$\Gamma(\rho^0\pi^+\pi^-)/\Gamma(2(\pi^+\pi^-))$ — Γ_4/Γ_2

VALUE	EVTS	DOCUMENT ID		TECN	COMMENT
• • • We do not use the following data for averages, fits, limits, etc. • • •					
~ 1.0		DELCOURT	81B	DM1	$e^+e^- \to 2(\pi^+\pi^-)$
0.7 ± 0.1	500	SCHACHT	74	STRC	5.5–18 $\gamma p \to p4\pi$
0.80		[1] BINGHAM	72B	HBC	9.3 $\gamma p \to p4\pi$

[1] The $\pi\pi$ system is in S-wave.

$\Gamma(\rho^0\pi^0\pi^0)/\Gamma(\rho^\pm\pi^\mp\pi^0)$ — Γ_5/Γ_6

VALUE	DOCUMENT ID		TECN	CHG	COMMENT
• • • We do not use the following data for averages, fits, limits, etc. • • •					
<0.10	ATKINSON	85B	OMEG		20–70 γp
<0.15	ATKINSON	82	OMEG	0	20–70 $\gamma p \to p4\pi$

$\Gamma(a_1(1260)\pi)/\Gamma(4\pi)$ — Γ_7/Γ_1

VALUE	DOCUMENT ID		TECN	COMMENT
• • • We do not use the following data for averages, fits, limits, etc. • • •				
0.16 ± 0.05	[1] ABELE	01B	CBAR	$0.0\ \overline{p}n \to 5\pi$

[1] $\omega\pi$ not included.

$\Gamma(h_1(1170)\pi)/\Gamma(4\pi)$ — Γ_8/Γ_1

VALUE	DOCUMENT ID		TECN	COMMENT
• • • We do not use the following data for averages, fits, limits, etc. • • •				
0.17 ± 0.06	[1] ABELE	01B	CBAR	$0.0\ \overline{p}n \to 5\pi$

[1] $\omega\pi$ not included.

$\Gamma(\pi(1300)\pi)/\Gamma(4\pi)$ — Γ_9/Γ_1

VALUE	DOCUMENT ID		TECN	COMMENT
• • • We do not use the following data for averages, fits, limits, etc. • • •				
0.30 ± 0.10	[1] ABELE	01B	CBAR	$0.0\ \overline{p}n \to 5\pi$

[1] $\omega\pi$ not included.

$\Gamma(\rho\rho)/\Gamma(4\pi)$ — Γ_{10}/Γ_1

VALUE	DOCUMENT ID		TECN	COMMENT
• • • We do not use the following data for averages, fits, limits, etc. • • •				
0.09 ± 0.03	[1] ABELE	01B	CBAR	$0.0\ \overline{p}n \to 5\pi$

[1] $\omega\pi$ not included.

$\Gamma(\pi^+\pi^-)/\Gamma_{total}$ — Γ_{11}/Γ

VALUE	DOCUMENT ID		TECN	COMMENT
• • • We do not use the following data for averages, fits, limits, etc. • • •				
$0.108 \pm 0.017^{+0.162}_{-0.004}$	[1] ALBRECHT	20	RVUE	$0.9\ \overline{p}p \to K^+K^-\pi^0$
$0.287^{+0.043}_{-0.042}$	BECKER	79	ASPK	17 π^-p polarized
0.15 to 0.30	[2] MARTIN	78C	RVUE	17 $\pi^-p \to \pi^+\pi^-n$
<0.20	[3] COSTA...	77B	RVUE	$e^+e^- \to 2\pi, 4\pi$
0.30 ± 0.05	[2] FROGGATT	77	RVUE	17 $\pi^-p \to \pi^+\pi^-n$
<0.15	[4] EISENBERG	73	HBC	5 $\pi^+p \to \Delta^{++}2\pi$
0.25 ± 0.05	[5] HYAMS	73	ASPK	17 $\pi^-p \to \pi^+\pi^-n$

[1] Residue from T-matrix pole, 2 poles, 3 channels, Chew-Mandelstam functions and simplified analytic continuation for the 4π channel. Includes scattering data from HYAMS 75 and model-independent calculation of GARCIA-MARTIN 11A.

[2] From phase shift analysis of HYAMS 73 data.

[3] Estimate using unitarity, time reversal invariance, Breit-Wigner.

[4] Estimated using one-pion-exchange model.

[5] Included in BECKER 79 analysis.

$\Gamma(K\overline{K})/\Gamma_{total}$ — Γ_{16}/Γ

VALUE	DOCUMENT ID		TECN	COMMENT
• • • We do not use the following data for averages, fits, limits, etc. • • •				
$0.007 \pm 0.006^{+0.041}_{-0.002}$	[1] ALBRECHT	20	RVUE	$0.9\ \overline{p}p \to K^+K^-\pi^0$

[1] Residue from T-matrix pole, 2 poles, 3 channels, Chew-Mandelstam functions and simplified analytic continuation for the 4π channel. Includes scattering data from HYAMS 75 and model-independent calculation of GARCIA-MARTIN 11A.

$\Gamma(\pi^+\pi^-)/\Gamma(2(\pi^+\pi^-))$ — Γ_{11}/Γ_2

VALUE	DOCUMENT ID		TECN	COMMENT
• • • We do not use the following data for averages, fits, limits, etc. • • •				
0.13 ± 0.05	ASTON	80	OMEG	20–70 $\gamma p \to p2\pi$
<0.14	[1] DAVIER	73	STRC	6–18 $\gamma p \to p4\pi$
<0.2	[2] BINGHAM	72B	HBC	9.3 $\gamma p \to p2\pi$

[1] Upper limit is estimate.

[2] 2σ upper limit.

$\Gamma(\pi\pi)/\Gamma(4\pi)$ — Γ_{12}/Γ_1

VALUE	DOCUMENT ID		TECN	COMMENT
• • • We do not use the following data for averages, fits, limits, etc. • • •				
0.16 ± 0.04	[1,2] ABELE	01B	CBAR	$0.0\ \overline{p}n \to 5\pi$

[1] Using ABELE 97.

[2] $\omega\pi$ not included.

$\Gamma(K\overline{K}^*(892)+c.c.)/\Gamma_{total}$ — Γ_{13}/Γ

VALUE	DOCUMENT ID		TECN	COMMENT
• • • We do not use the following data for averages, fits, limits, etc. • • •				
possibly seen	COAN	04	CLEO	$\tau^- \to K^-\pi^-K^+\nu_\tau$

$\Gamma(K\overline{K}^*(892)+c.c.)/\Gamma(2(\pi^+\pi^-))$ — Γ_{13}/Γ_2

VALUE	DOCUMENT ID		TECN	COMMENT
• • • We do not use the following data for averages, fits, limits, etc. • • •				
0.15 ± 0.03	[1] DELCOURT	81B	DM1	$e^+e^- \to \overline{K}K\pi$

[1] Assuming $\rho(1700)$ and ω radial excitations to be degenerate in mass.

$\Gamma(\eta\rho)/\Gamma_{total}$ — Γ_{14}/Γ

VALUE	CL%	DOCUMENT ID		TECN	COMMENT
• • • We do not use the following data for averages, fits, limits, etc. • • •					
possibly seen		AKHMETSHIN	00D	CMD2	$e^+e^- \to \eta\pi^+\pi^-$
<0.04		DONNACHIE	87B	RVUE	
<0.02	58	ATKINSON	86B	OMEG	20–70 γp

$\Gamma(\eta\rho)/\Gamma(2(\pi^+\pi^-))$ — Γ_{14}/Γ_2

VALUE	DOCUMENT ID		TECN	COMMENT
• • • We do not use the following data for averages, fits, limits, etc. • • •				
0.123 ± 0.027	DELCOURT	82	DM1	$e^+e^- \to \pi^+\pi^-$ MM
~ 0.1	ASTON	80	OMEG	20–70 γp

$\Gamma(\pi^+\pi^-\text{neutrals})/\Gamma(2(\pi^+\pi^-))$ — $(\Gamma_5+\Gamma_6+0.714\Gamma_{14})/\Gamma_2$

VALUE	DOCUMENT ID		TECN	COMMENT
• • • We do not use the following data for averages, fits, limits, etc. • • •				
2.6 ± 0.4	[1] BALLAM	74	HBC	9.3 γp

[1] Upper limit. Background not subtracted.

$\Gamma(a_2(1320)\pi)/\Gamma_{total}$ — Γ_{15}/Γ

VALUE	DOCUMENT ID		TECN	COMMENT
• • • We do not use the following data for averages, fits, limits, etc. • • •				
not seen	AMELIN	00	VES	37 $\pi^-p \to \eta\pi^+\pi^-n$

$\Gamma(K\overline{K})/\Gamma(2(\pi^+\pi^-))$ — Γ_{16}/Γ_2

VALUE	CL%	DOCUMENT ID		TECN	CHG	COMMENT
• • • We do not use the following data for averages, fits, limits, etc. • • •						
0.015 ± 0.010		[1] DELCOURT	81B	DM1		$e^+e^- \to \overline{K}K$
<0.04	95	BINGHAM	72B	HBC	0	9.3 γp

[1] Assuming $\rho(1700)$ and ω radial excitations to be degenerate in mass.

Int. J. Mod. Phys. A 2026.41. Downloaded from www.worldscientific.com
by UNIVERSITY OF CALIFORNIA @ BERKELEY on 09/16/26. Re-use and distribution is strictly not permitted, except for Open Access articles.

$\Gamma(K\overline{K})/\Gamma(K\overline{K}^*(892)+\text{c.c.})$ — Γ_{16}/Γ_{13}

VALUE	DOCUMENT ID		TECN	COMMENT
• • • We do not use the following data for averages, fits, limits, etc. • • •				
0.052 ± 0.026	BUON	82	DM1	$e^+e^- \to$ hadrons

$\Gamma(\pi^0\omega)/\Gamma_{\text{total}}$ — Γ_{18}/Γ

VALUE	EVTS	DOCUMENT ID		TECN	COMMENT
• • • We do not use the following data for averages, fits, limits, etc. • • •					
not seen		MATVIENKO	15	BELL	$\overline{B}^0 \to D^{*+}\omega\pi^-$
seen	1.6k	ACHASOV	12	SND	$e^+e^- \to \pi^0\pi^0\gamma$
not seen	2382	AKHMETSHIN	03B	CMD2	$e^+e \to \pi^0\pi^0\gamma$
seen		ACHASOV	97	RVUE	$e^+e^- \to \omega\pi^0$

$\Gamma(\pi^0\gamma)/\Gamma_{\text{total}}$ — Γ_{19}/Γ

VALUE	DOCUMENT ID		TECN	COMMENT
not seen	[1] ACHASOV	10D	SND	1.075–2.0 $e^+e^- \to \pi^0\gamma$

[1] From a fit of a VMD model with two effective resonances with masses of 1450 MeV and 1700 MeV to describe the excited vector states $\omega(1420)$, $\rho(1450)$, $\omega(1650)$, and $\rho(1700)$. The width of the highest mass effective resonance is fixed at 315 MeV.

$\Gamma(f_0(1500)\gamma)/\Gamma_{\text{total}}$ — Γ_{20}/Γ

VALUE	DOCUMENT ID		TECN	COMMENT
not seen	[1] ACHASOV	22	SND	1.17–2.00 $e^+e^- \to \eta\eta\gamma$

[1] The 90% CL upper limit on the Born cross sections $\sigma(e^+e^- \to \phi(1680) \to f_2'(1525)\gamma \to \eta\eta\gamma)$ and $\sigma(e^+e^- \to \rho(1700) \to f_0(1500)\gamma \to \eta\eta\gamma)$ is 10.6 pb.

$\rho(1700)$ REFERENCES

ACHARYA	26	PL B872 140006	S. Acharya *et al.*	(ALICE Collab.)
AAIJ	25AG	JHEP 2511 103	R. Aaij *et al.*	(LHCb Collab.)
IGNATOV	24	PR D109 112002	F.V. Ignatov *et al.*	(CMD-3 Collab.)
ACHASOV	23A	PR D108 092012	M.N. Achasov *et al.*	(SND Collab.)
ACHASOV	22	EPJ C82 168	M.N. Achasov *et al.*	(SND Collab.)
ABLIKIM	21A	PL B813 136059	M. Ablikim *et al.*	(BESIII Collab.)
ACHARYA	20F	JHEP 2006 035	S. Acharya *et al.*	(ALICE Collab.)
ALBRECHT	20	EPJ C80 453	M. Albrecht *et al.*	(Crystal Barrel Collab.)
ANDREEV	20	EPJ C80 1189	V. Andreev *et al.*	(H1 Collab.)
GRIBANOV	20	JHEP 2001 112	S.S. Gribanov *et al.*	(CMD-3 Collab.)
ACHASOV	18	PR D97 012008	M.N. Achasov *et al.*	(SND Collab.)
LEES	18	PR D97 052007	J.P. Lees *et al.*	(BABAR Collab.)
BARTOS	17	PR D96 113004	E. Bartos *et al.*	
BARTOS	17A	IJMP A32 1750154	E. Bartos *et al.*	
LEES	17C	PR D95 072007	J.P. Lees *et al.*	(BABAR Collab.)
LEES	17H	PR D96 092009	J.P. Lees *et al.*	(BABAR Collab.)
AAIJ	16N	PR D93 052018	R. Aaij *et al.*	(LHCb Collab.)
ABLIKIM	16C	PL B753 629	M. Ablikim *et al.*	(BESIII Collab.)
ACHASOV	16D	PR D94 112001	M.N. Achasov *et al.*	(SND Collab.)
AULCHENKO	15	PR D91 052013	V.M. Aulchenko *et al.*	(SND Collab.)
MATVIENKO	15	PR D92 012013	D. Matvienko *et al.*	(BELLE Collab.)
ACHASOV	13	PR D88 054013	M.N. Achasov *et al.*	(SND Collab.)
ABRAMOWICZ	12	EPJ C72 1869	H. Abramowicz *et al.*	(ZEUS Collab.)
ACHASOV	12	JETPL 94 734	M.N. Achasov *et al.*	
		Translated from ZETFP 94 796.		
LEES	12G	PR D86 032013	J.P. Lees *et al.*	(BABAR Collab.)
AMBROSINO	11A	PL B700 102	F. Ambrosino *et al.*	(KLOE Collab.)
GARCIA-MAR...	11A	PR D83 074004	R. Garcia-Martin *et al.*	(MADR, CRAC)
ACHASOV	10D	PR D98 112001	M.N. Achasov *et al.*	(SND Collab.)
DUBNICKA	10	APS 60 1	S. Dubnicka, A.Z. Dubnickova	
AUBERT	09AS	PRL 103 231801	B. Aubert *et al.*	(BABAR Collab.)
FUJIKAWA	08	PR D78 072006	M. Fujikawa *et al.*	(BELLE Collab.)
AKHMETSHIN	07	PL B648 28	R.R. Akhmetshin *et al.*	(Novosibirsk CMD-2 Collab.)
ACHASOV	06	JETP 103 380	M.N. Achasov *et al.*	(Novosibirsk SND Collab.)
		Translated from ZETF 130 437.		
COAN	04	PRL 92 232001	T.E. Coan *et al.*	(CLEO Collab.)
FRABETTI	04	PL B578 290	P.L. Frabetti *et al.*	(FNAL E687 Collab.)
AKHMETSHIN	03B	PL B562 173	R.R. Akhmetshin *et al.*	(Novosibirsk CMD-2 Collab.)
ABELE	01B	EPJ C21 261	A. Abele *et al.*	(Crystal Barrel Collab.)
ACHASOV	00I	PL B486 29	M.N. Achasov *et al.*	(Novosibirsk SND Collab.)
AKHMETSHIN	00D	PL B489 125	R.R. Akhmetshin *et al.*	(Novosibirsk CMD-2 Collab.)
AMELIN	00	NP A668 83	D. Amelin *et al.*	(VES Collab.)
EDWARDS	00A	PR D61 072003	K.W. Edwards *et al.*	(CLEO Collab.)
ABELE	99D	PL B468 178	A. Abele *et al.*	(Crystal Barrel Collab.)
ABELE	97	PL B391 191	A. Abele *et al.*	(Crystal Barrel Collab.)
ACHASOV	97	PR D55 2663	N.N. Achasov *et al.*	(NOVM)
BERTIN	97C	PL B408 476	A. Bertin *et al.*	(OBELIX Collab.)
CLEGG	94	ZPHY C62 455	A.B. Clegg, A. Donnachie	(LANC, MCHS)
CLEGG	90	ZPHY C45 677	A.B. Clegg, A. Donnachie	(LANC, MCHS)
KUHN	90	ZPHY C48 445	J.H. Kuhn *et al.*	(MPIM)
BISELLO	89	PL B220 321	D. Bisello *et al.*	(DM2 Collab.)
DUBNICKA	89	JP G15 1349	S. Dubnicka *et al.*	(JINR, SLOV)
GESHKEN...	89	ZPHY C45 351	B.V. Geshkenbein	(ITEP)
ANTONELLI	88	PL B212 133	A. Antonelli *et al.*	(DM2 Collab.)
DIEKMAN	88	PRPL 159 99	B. Diekmann	(BONN)
FUKUI	88	PL B202 441	S. Fukui *et al.*	(SUGI, NAGO, KEK, KYOT+)
DONNACHIE	87B	ZPHY C34 257	A. Donnachie, A.B. Clegg	(MCHS, LANC)
ATKINSON	86B	ZPHY C30 531	M. Atkinson *et al.*	(BONN, CERN, GLAS+)
ATKINSON	85B	ZPHY C26 499	M. Atkinson *et al.*	(BONN, CERN, GLAS+)
ERKAL	85	ZPHY C29 485	C. Erkal, M.G. Olsson	(WISC)
ABE	84B	PRL 53 751	K. Abe *et al.*	(SLAC HFP Collab.)
KURDADZE	83	JETPL 37 733	L.M. Kurdadze *et al.*	(NOVO)
		Translated from ZETFP 37 613.		
ATKINSON	82	PL 108B 55	M. Atkinson *et al.*	(BONN, CERN, GLAS+)
BUON	82	PL 118B 221	J. Buon *et al.*	(LALO, MONP)
CLELAND	82B	NP B208 228	W.E. Cleland *et al.*	(DURH, GEVA, LAUS+)
CORDIER	82	PL 109B 129	A. Cordier *et al.*	(LALO)
DELCOURT	82	PL 113B 93	B. Delcourt *et al.*	(LALO)
ASTON	81E	NP B189 15	D. Aston	(BONN, CERN, EPOL, GLAS, LANC+)
DELCOURT	81B	Bonn Conf. 205	B. Delcourt	(ORSAY)
Also		PL 109B 129	A. Cordier *et al.*	(LALO)
DIBIANCA	81	PR D23 595	F.A. di Bianca *et al.*	(CASE, CMU)
ASTON	80	PL 92B 215	D. Aston	(BONN, CERN, EPOL, GLAS, LANC+)
BACCI	80	PL 95B 139	C. Bacci *et al.*	(ROMA, FRAS)
BIZOT	80	Madison Conf. 546	J.C. Bizot *et al.*	(LALO, MONP)
KILLIAN	80	PR D21 3005	T.J. Killian *et al.*	(CORN)
ATIYA	79B	PRL 43 1691	M.S. Atiya *et al.*	(COLU, ILL, FNAL)
BECKER	79	NP B151 46	H. Becker *et al.*	(MPIM, CERN, ZEEM, CRAC)
LANG	79	PR D19 956	C.B. Lang, A. Mas-Parareda	(GRAZ)
MARTIN	78C	ANP 114 1	A.D. Martin, M.R. Pennington	(CERN)
COSTA...	77B	PL 71B 345	B. Costa de Beauregard, B. Pire, T.N. Truong	(EPOL)
FROGGATT	77	NP B129 89	C.D. Froggatt, J.L. Petersen	(GLAS, NORD)
ALEXANDER	75	PL 57B 487	G. Alexander *et al.*	(TELA)
HYAMS	75	NP B100 205	B.D. Hyams *et al.*	(CERN, MPIM)
BALLAM	74	NP B76 375	J. Ballam *et al.*	(SLAC, LBL, MPIM)
CONVERSI	74	PL 52B 493	M. Conversi *et al.*	(ROMA, FRAS)
SCHACHT	74	NP B81 205	P. Schacht *et al.*	(MPIM)
DAVIER	73	NP B58 31	M. Davier *et al.*	(SLAC)
EISENBERG	73	PL 43B 149	Y. Eisenberg *et al.*	(REHO)
HYAMS	73	NP B64 134	B.D. Hyams *et al.*	(CERN, MPIM)
BINGHAM	72B	PL 41B 635	H.H. Bingham *et al.*	(LBL, UCB, SLAC) IGJP
JACOB	72	PR D5 1847	M. Jacob, R. Slansky	
GOUNARIS	68	PRL 21 244	G.J. Gounaris, J.J. Sakurai	

$a_2(1700)$

$I^G(J^{PC}) = 1^-(2^{++})$

$a_2(1700)$ T-MATRIX POLE $\sqrt{s}$

Note that $\Gamma = -2\,\text{Im}(\sqrt{s})$.

VALUE (MeV)	DOCUMENT ID		TECN	COMMENT
(1630–1780) − i (60–250) OUR ESTIMATE				
$(1686 \pm 22^{+19}_{-7}) - i\,(211 \pm 38^{+32}_{-29})$	[1] KOPF	21	RVUE	0.9 $p\overline{p} \to \pi^0\pi^0\eta$, $\pi^0\eta\eta$, $\pi^0K^+K^-$ and 191 $\pi^-p \to \pi^-\pi^-\pi^+p$
$(1638.9 \pm 2.3^{+57.4}_{-0.1}) - i(112.0 \pm 1.3^{+0.9}_{-24.2})$	[2] ALBRECHT	20	RVUE	0.9 $\overline{p}p \to \pi^0\pi^0\eta$, $\pi^0\eta\eta$, $\pi^0K^+K^-$
$(1722 \pm 15 \pm 67) - i(124 \pm 9 \pm 32)$	[3] RODAS	19	RVUE	191 $\pi^-p \to \eta'\pi^-p$
$(1698 \pm 44) - i\,(133 \pm 28)$	AMSLER	02	CBAR	0.9 $\overline{p}p \to \pi^0\eta\eta$

[1] Based on combined fit of Crystal Barrel and $\pi\pi$ scattering data (ALBRECHT 20), and COMPASS data (ADOLPH 15), using a coupled-channel model of $\eta\pi$, $\eta'\pi$ and $K\overline{K}$ systems.

[2] Based on 2 poles, 2 channels ($\pi\eta$, $K\overline{K}$).

[3] The coupled-channel analysis of both the $\eta\pi$ and $\eta'\pi$ systems using ADOLPH 15 data.

$a_2(1700)$ MASS

VALUE (MeV)	EVTS	DOCUMENT ID		TECN	COMMENT
1706±14 OUR AVERAGE	Error includes scale factor of 1.2.				
1681^{+22}_{-35}	46M	[1,2] AGHASYAN	18B	COMP	190 $\pi^-p \to \pi^-\pi^+\pi^-p$
$1726\pm12\pm25$		[2] ABLIKIM	17K	BES3	$\psi(2S) \to \gamma\eta\pi^+\pi^-$
$1722\pm\ 9\pm15$	18k	[3] SCHEGELSKY	06	RVUE	$\gamma\gamma \to \pi^+\pi^-\pi^0$
1660 ± 40		[2] ABELE	99B	CBAR	1.94 $\overline{p}p \to \pi^0\eta\eta$
• • • We do not use the following data for averages, fits, limits, etc. • • •					
$1720\pm10\pm60$		[4] JACKURA	18	RVUE	$\pi^-p \to \eta\pi^-p$
1675 ± 25		ANISOVICH	09	RVUE	0.0 $\overline{p}p$, πN
$1702\pm\ 7$	80k	[5] UMAN	06	E835	5.2 $\overline{p}p \to \eta\eta\pi^0$
$1721\pm13\pm44$	145k	LU	05	B852	18 $\pi^-p \to \omega\pi^-\pi^0p$
$1737\pm\ 5\pm\ 7$		ABE	04	BELL	10.6 $e^+e^- \to e^+e^-K^+K^-$
1767 ± 14	221	[6] ACCIARRI	01H	L3	$\gamma\gamma \to K^0_SK^0_S$, $E^{ee}_{\text{cm}}=$ 91, 183–209 GeV
~1775		[7] GRYGOREV	99	SPEC	40 $\pi^-p \to K^0_SK^0_Sn$
$1752\pm21\pm\ 4$		ACCIARRI	97T	L3	$\gamma\gamma \to \pi^+\pi^-\pi^0$

[1] Statistical error negligible.

[2] Breit-Wigner mass.

[3] From analysis of L3 data at 183–209 GeV.

[4] Superseded by RODAS 19.

[5] Statistical error only.

[6] Spin 2 dominant, isospin not determined, could also be I=1.

[7] Possibly two $J^P = 2^+$ resonances with isospins 0 and 1.

$a_2(1700)$ WIDTH

VALUE (MeV)	EVTS	DOCUMENT ID		TECN	COMMENT
380^{+60}_{-50} OUR AVERAGE	Error includes scale factor of 3.9. See the ideogram below.				
436^{+20}_{-16}	46M	[1,2] AGHASYAN	18B	COMP	190 $\pi^-p \to \pi^-\pi^+\pi^-p$
$190\pm\ 18\pm30$		[2] ABLIKIM	17K	BES3	$\psi(2S) \to \gamma\eta\pi^+\pi^-$
$336\pm\ 20\pm20$	18k	[3] SCHEGELSKY	06	RVUE	$\gamma\gamma \to \pi^+\pi^-\pi^0$
$280\pm\ 70$		[2] ABELE	99B	CBAR	1.94 $\overline{p}p \to \pi^0\eta\eta$
• • • We do not use the following data for averages, fits, limits, etc. • • •					
$280\pm\ 10\pm70$		[4] JACKURA	18	RVUE	$\pi^-p \to \eta\pi^-p$
270^{+50}_{-20}		ANISOVICH	09	RVUE	0.0 $\overline{p}p$, πN
$417\pm\ 19$	80k	[5] UMAN	06	E835	5.2 $\overline{p}p \to \eta\eta\pi^0$
$279\pm\ 49\pm66$	145k	LU	05	B852	18 $\pi^-p \to \omega\pi^-\pi^0p$
$151\pm\ 22\pm24$		ABE	04	BELL	10.6 $e^+e^- \to e^+e^-K^+K^-$
$187\pm\ 60$	221	[6] ACCIARRI	01H	L3	$\gamma\gamma \to K^0_SK^0_S$, $E^{ee}_{\text{cm}}=$ 91, 183–209 GeV
$150\pm110\pm34$		ACCIARRI	97T	L3	$\gamma\gamma \to \pi^+\pi^-\pi^0$

[1] Statistical error negligible.
[2] Breit-Wigner width.
[3] From analysis of L3 data at 183–209 GeV.
[4] Superseded by RODAS 19.
[5] Statistical error only.
[6] Spin 2 dominant, isospin not determined, could also be I=1.

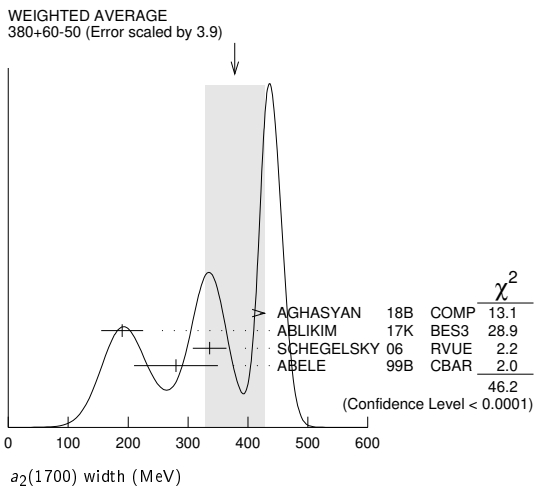

$a_2(1700)$ DECAY MODES

	Mode	Fraction (Γ_i/Γ)
Γ_1	$\eta\pi$	(2.5 ± 0.6) %
Γ_2	$\eta'\pi$	seen
Γ_3	$\gamma\gamma$	$(7.9\pm1.7)\times10^{-7}$
Γ_4	$\rho\pi$	seen
Γ_5	$f_2(1270)\pi$	seen
Γ_6	$K\overline{K}$	(1.3 ± 0.8) %
Γ_7	$\omega\pi^-\pi^0$	seen
Γ_8	$\omega\rho$	seen

$a_2(1700)$ PARTIAL WIDTHS

$\Gamma(\eta\pi)$ — Γ_1

VALUE (MeV)	EVTS	DOCUMENT ID	TECN	COMMENT
9.5±2.0	870	[1] SCHEGELSKY 06A	RVUE	$\gamma\gamma\to K^0_S K^0_S$

[1] From analysis of L3 data at 91 and 183–209 GeV, using $a_2(1700)$ mass of 1730 MeV and width of 340 MeV, and SU(3) relations.

$\Gamma(\gamma\gamma)$ — Γ_3

VALUE (keV)	EVTS	DOCUMENT ID	TECN	COMMENT
0.30±0.05	870	[1] SCHEGELSKY 06A	RVUE	$\gamma\gamma\to K^0_S K^0_S$

[1] From analysis of L3 data at 91 and 183–209 GeV, using $a_2(1700)$ mass of 1730 MeV and width of 340 MeV, and SU(3) relations.

$\Gamma(K\overline{K})$ — Γ_6

VALUE (MeV)	EVTS	DOCUMENT ID	TECN	COMMENT
5.0±3.0	870	[1] SCHEGELSKY 06A	RVUE	$\gamma\gamma\to K^0_S K^0_S$

[1] From analysis of L3 data at 91 and 183–209 GeV, using $a_2(1700)$ mass of 1730 MeV and width of 340 MeV, and SU(3) relations.

$a_2(1700)$ $\Gamma(i)\Gamma(\gamma\gamma)/\Gamma(\text{total})$

$[\Gamma(\rho\pi)+\Gamma(f_2(1270)\pi)]\times\Gamma(\gamma\gamma)/\Gamma_{\text{total}}$ — $(\Gamma_4+\Gamma_5)\Gamma_3/\Gamma$

VALUE (keV)	EVTS	DOCUMENT ID	TECN	COMMENT
0.29±0.04±0.02		ACCIARRI 97T	L3	$\gamma\gamma\to\pi^+\pi^-\pi^0$
• • • We do not use the following data for averages, fits, limits, etc. • • •				
$0.37^{+0.12}_{-0.08}\pm0.10$	18k	[1] SCHEGELSKY 06	RVUE	$\gamma\gamma\to\pi^+\pi^-\pi^0$

[1] From analysis of L3 data at 183–209 GeV.

$\Gamma(K\overline{K})\times\Gamma(\gamma\gamma)/\Gamma_{\text{total}}$ — $\Gamma_6\Gamma_3/\Gamma$

VALUE (eV)	DOCUMENT ID	TECN	COMMENT
• • • We do not use the following data for averages, fits, limits, etc. • • •			
20.6± 4.2± 4.6	[1] ABE 04	BELL	$10.6\ e^+e^-\to e^+e^-K^+K^-$
49 ±11 ±13	[2] ACCIARRI 01H	L3	$\gamma\gamma\to K^0_S K^0_S$, $E^{ee}_{\text{cm}}=91$, 183–209 GeV

[1] Assuming spin 2.
[2] Spin 2 dominant, isospin not determined, could also be I=1.

$a_2(1700)$ BRANCHING RATIOS

$\Gamma(\rho\pi)/\Gamma(f_2(1270)\pi)$ — Γ_4/Γ_5

VALUE	EVTS	DOCUMENT ID	TECN	COMMENT
• • • We do not use the following data for averages, fits, limits, etc. • • •				
$3.4\pm0.4\pm0.1$	18k	[1] SCHEGELSKY 06	RVUE	$\gamma\gamma\to\pi^+\pi^-\pi^0$

[1] From analysis of L3 data at 183–209 GeV.

$\Gamma(K\overline{K})/\Gamma(\eta\pi)$ — Γ_6/Γ_1

VALUE	DOCUMENT ID	TECN	COMMENT
• • • We do not use the following data for averages, fits, limits, etc. • • •			
$0.029\pm0.04\ ^{+0.011}_{-0.012}$	[1] KOPF 21	RVUE	$0.9\ p\overline{p}\to\pi^0\pi^0\eta$, $\pi^0\pi^0\eta\eta$, $\pi^0K^+K^-$ and $191\ \pi^-p\to\pi^-\pi^-\pi^+p$
$4.134\pm0.106^{+4.909}_{-2.988}$	[2] ALBRECHT 20	RVUE	$0.9\ \overline{p}p\to\pi^0\pi^0\eta$, $\pi^0\pi^0\eta\eta$, $\pi^0K^+K^-$

[1] From T-matrix pole based on combined fit of Crystal Barrel and $\pi\pi$ scattering data (ALBRECHT 20), and COMPASS data (ADOLPH 15), using a coupled-channel model of $\eta\pi$, $\eta'\pi$ and $K\overline{K}$ systems.
[2] Residues from T-matrix pole, 2 poles, 2 channels ($\pi\eta$, $K\overline{K}$).

$\Gamma(\eta'\pi)/\Gamma(\eta\pi)$ — Γ_2/Γ_1

VALUE	DOCUMENT ID	TECN	COMMENT
• • • We do not use the following data for averages, fits, limits, etc. • • •			
$0.035\pm0.044^{+0.069}_{-0.012}$	[1] KOPF 21	RVUE	$0.9\ p\overline{p}\to\pi^0\pi^0\eta$, $\pi^0\pi^0\eta\eta$, $\pi^0K^+K^-$ and $191\ \pi^-p\to\pi^-\pi^-\pi^+p$

[1] From T-matrix pole based on combined fit of Crystal Barrel and $\pi\pi$ scattering data (ALBRECHT 20), and COMPASS data (ADOLPH 15), using a coupled-channel model of $\eta\pi$, $\eta'\pi$ and $K\overline{K}$ systems.

$a_2(1700)$ REFERENCES

KOPF	21	EPJ C81 1056	B. Kopf *et al.*	(BOCH)
ALBRECHT	20	EPJ C80 453	M. Albrecht *et al.*	(Crystal Barrel Collab.)
RODAS	19	PRL 122 042002	A. Rodas *et al.*	(JPAC Collab.)
AGHASYAN	18B	PR D98 092003	M. Aghasyan *et al.*	(COMPASS Collab.)
JACKURA	18	PL B779 464	A. Jackura *et al.*	(JPAC and COMPASS Collab.)
ABLIKIM	17K	PR D95 032002	M. Ablikim *et al.*	(BESIII Collab.)
ADOLPH	15	PL B740 303	M. Adolph *et al.*	(COMPASS Collab.)
ANISOVICH	09	IJMP A24 2481	V.V. Anisovich, A.V. Sarantsev	(PNPI)
SCHEGELSKY	06	EPJ A27 199	V.A. Schegelsky *et al.*	
SCHEGELSKY	06A	EPJ A27 207	V.A. Schegelsky *et al.*	
UMAN	06	PR D73 052009	I. Uman *et al.*	(FNAL E835)
LU	05	PRL 94 032002	M. Lu *et al.*	(BNL E852 Collab.)
ABE	04	EPJ C32 323	K. Abe *et al.*	(BELLE Collab.)
AMSLER	02	EPJ C23 29	C. Amsler *et al.*	(Crystal Barrel Collab.)
ACCIARRI	01H	PL B501 173	M. Acciarri *et al.*	(L3 Collab.)
ABELE	99B	EPJ C8 67	A. Abele *et al.*	(Crystal Barrel Collab.)
GRYGOREV	99	PAN 62 470 Translated from YAF 62 513.	V.K. Grygorev *et al.*	
ACCIARRI	97T	PL B413 147	M. Acciarri *et al.*	(L3 Collab.)

$a_0(1710)$

$I^G(J^{PC}) = 1^-(0^{++})$

OMITTED FROM SUMMARY TABLE

Evidence for this state is also inferred from the interference of the K^+K^- and $K^0_S K^0_S$ decays of the $f_0(1710)$ in $D^+_s\to f_0(1710)\pi^+$, leading to a relative branching ratio an order of magnitude larger than expected from isospin symmetry (ABLIKIM 22F). See also the review on "Spectroscopy of Light Meson Resonances."

$a_0(1710)$ MASS

VALUE (MeV)	DOCUMENT ID	TECN	COMMENT
1713±19 OUR AVERAGE Error includes scale factor of 3.8. See the ideogram below.			
1736±10±12	[1] AAIJ 23AH	LHCB	$B^+\to K^+(K^0_S K\pi)$
1817± 8±20	[2] ABLIKIM 22AH	BES3	$D^+_s\to K^0_S K^+\pi^0$
1704± 5± 2	LEES 21A	BABR	$\eta_c(1S)\to\pi^+\pi^-\eta$

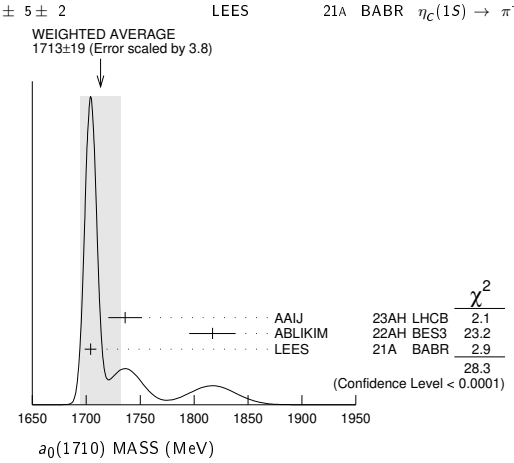

Int. J. Mod. Phys. A 2026.41. Downloaded from www.worldscientific.com
by [redacted]LIFORNIA @ BERKELEY on 09/16/26. Re-use and distribution is strictly not permitted, except for Open Access articles.

Int. J. Mod. Phys. A 2026.41. Downloaded from www.worldscientific.com
by UNIVERSITY OF CALIFORNIA @ BERKELEY on 09/16/26. Re-use and distribution is strictly not permitted, except for Open Access articles.

[1] From Dalitz plot analyses of $\eta_c(1S,2S) \to K^0_S K^+ \pi^- +$ c.c..

[2] Observed to decay into $K^0_S K^+$ in a Breit-Wigner amplitude analysis involving D^+_s decays into $\overline{K}^*(892)^0 K^+$, $\overline{K}^*(892)^+ K^0_S$, $\overline{K}^*(1410)^0 K^+$, $a_0(980)^+ \pi^0$, and $a_0(1817)^+ \pi^0$.

$a_0(1710)$ WIDTH

VALUE (MeV)	DOCUMENT ID		TECN	COMMENT
107±15 OUR AVERAGE				
134±17±61	[1] AAIJ	23AH	LHCB	$B^+ \to K^+(K^0_S K\pi)$
97±22±15	[2] ABLIKIM	22AH	BES3	$D^+_s \to K^0_S K^+ \pi^0$
110±15±11	LEES	21A	BABR	$\eta_c(1S) \to \pi^+\pi^-\eta$

[1] From Dalitz plot analyses of $\eta_c(1S,2S) \to K^0_S K^+ \pi^- +$ c.c..

[2] Observed to decay into $K^0_S K^+$ in a Breit-Wigner amplitude analysis involving D^+_s decays into $\overline{K}^*(892)^0 K^+$, $\overline{K}^*(892)^+ K^0_S$, $\overline{K}^*(1410)^0 K^+$, $a_0(980)^+ \pi^0$, and $a_0(1817)^+ \pi^0$.

$a_0(1710)$ DECAY MODES

	Mode	Fraction (Γ_i/Γ)
Γ_1	$\pi\eta$	seen
Γ_2	K^+K^-	seen
Γ_3	$K^0_S K^0_S$	seen
Γ_4	$K^0_S K^+$	seen

$a_0(1710)$ BRANCHING RATIOS

$\Gamma(\pi\eta)/\Gamma_{total}$ — Γ_1/Γ

VALUE	DOCUMENT ID		TECN	COMMENT
seen	LEES	21A	BABR	$\eta_c(1S) \to \pi^+\pi^-\eta$

$\Gamma(K^+K^-)/\Gamma(K^0_S K^0_S)$ — Γ_2/Γ_3

VALUE	DOCUMENT ID		TECN	COMMENT
0.32±0.12	[1] ABLIKIM	22F	BES3	$D^+_s \to K^0_S K^0_S \pi^+$

[1] Using $D^+_s \to K^+K^-\pi^+$ from ABLIKIM 21AE. The apparent violation of isospin symmetry may be due to a destructive interference with the $f_0(1710)$ in the K^+K^- channel, and a constructive interference in the $K^0_S K^0_S$ channel.

$\Gamma(K^0_S K^+)/\Gamma_{total}$ — Γ_4/Γ

VALUE	DOCUMENT ID		TECN	COMMENT
seen	ABLIKIM	22AH	BES3	$D^+_s \to K^0_S K^+ \pi^0$

$a_0(1710)$ REFERENCES

AAIJ	23AH	PR D108 032010	R. Aaij *et al.*	(LHCb Collab.)
ABLIKIM	22AH	PRL 129 182001	M. Ablikim *et al.*	(BESIII Collab.)
ABLIKIM	22F	PR D105 L051103	M. Ablikim *et al.*	(BESIII Collab.)
ABLIKIM	21AE	PR D104 012016	M. Ablikim *et al.*	(BESIII Collab.)
LEES	21A	PR D104 072002	J.P. Lees *et al.*	(BABAR Collab.)

$f_0(1710)$

$I^G(J^{PC}) = 0^+(0^{++})$

Evidence for two isoscalar scales, $f_0(1710)$ and $f_0(1810)$, was first reported by SARANTSEV 21 and ABLIKIM 22F. The data assignments to either $f_0(1710)$ or $f_0(1810)$ are tentative. See the review on "Spectroscopy of Light Meson Resonances."

$f_0(1710)$ T-MATRIX POLE $\sqrt{s}$

Note that $\Gamma = -2\,\mathrm{Im}(\sqrt{s})$.

VALUE (MeV)	DOCUMENT ID		TECN	COMMENT
(1680–1820) − i (50–180) OUR ESTIMATE				
(1770.7 ± 5.1 ± 4.2) − i (84.7 ± 3.8 ± 4.7)	ABLIKIM	25CD	BES3	$e^+e^- \to \psi(2S)$
(1769 ± 8) − i (78 ± 6)	[1] RODAS	22	RVUE	$J/\psi(1S) \to \gamma(\pi\pi, K\overline{K})$
(1700 ± 18) − i (127 ± 12)	SARANTSEV	21	RVUE	$J/\psi(1S) \to \gamma(\pi\pi, K\overline{K}, \eta\eta, \omega\phi)$
(1732 ± 15) − i (160^{+25}_{-10})	[2] ANISOVICH	03	RVUE	$\pi\pi$, $K\overline{K}$, $\eta\eta$, $\eta\eta'$, $\pi\pi\pi\pi$
(1698 ± 18) − i (60 ± 13)	BARBERIS	00E	OMEG	450 $pp \to p_f \eta\eta p_s$
(1770 ± 12) − i (110 ± 20)	[3] ANISOVICH	99B	SPEC	0.6–1.2 $p\overline{p} \to \eta\eta\pi^0$
(1727 ± 12 ± 11) − i (63 ± 8 ± 9)	BARBERIS	99D	OMEG	450 $pp \to K^+K^-$, $\pi^+\pi^-$
(1750 ± 30) − i (125 ± 70)	ANISOVICH	98B	RVUE	Compilation

[1] T-matrix pole from coupled channel K-matrix fit to data on $J/\psi \to \gamma\pi^0\pi^0$ (ABLIKIM 15AE) and $J/\psi \to \gamma K^0_S K^0_S$ (ABLIKIM 18AA).

[2] Solution I.

[3] Not seen by AMSLER 02.

$f_0(1710)$ Breit-Wigner MASS

VALUE (MeV)	EVTS	DOCUMENT ID		TECN	COMMENT
1723^{+7}_{-6} OUR AVERAGE		Error includes scale factor of 1.3. See the ideogram below.			
1723±11 ± 2		ABLIKIM	22F	BES3	$D^+_s \to K^0_S K^0_S \pi^+$
1757±24 ± 9		LEES	21A	BABR	$\eta_c(1S) \to \eta' K^+K^-$
1759± 6 $^{+14}_{-25}$	5.5k	[1] ABLIKIM	13N	BES3	$e^+e^- \to J/\psi \to \gamma\eta\eta$
1750$^{+6}_{-7}$ $^{+29}_{-18}$		[2] UEHARA	13	BELL	$\gamma\gamma \to K^0_S K^0_S$
1701± 5 $^{+9}_{-2}$	4k	[3] CHEKANOV	08	ZEUS	$ep \to K^0_S K^0_S X$
1738±30		ABLIKIM	04E	BES2	$J/\psi \to \omega K^+K^-$
1740± 4 $^{+10}_{-25}$		BAI	03G	BES	$J/\psi \to \gamma K\overline{K}$
1710±25		[4] FRENCH	99		300 $pp \to p_f(K^+K^-)p_s$
• • • We do not use the following data for averages, fits, limits, etc. • • •					
1744± 7 ± 5	381	[5,6] DOBBS	15		$J/\psi \to \gamma\pi^+\pi^-$
1705±11 ± 5	237	[5,6] DOBBS	15		$\psi(2S) \to \gamma\pi^+\pi^-$
1706± 4 ± 5	1.0k	[5,6] DOBBS	15		$J/\psi \to \gamma K^+K^-$
1690± 8 ± 3	349	[5,6] DOBBS	15		$\psi(2S) \to \gamma K^+K^-$
1750±13		AMSLER	06	CBAR	1.64 $\overline{p}p \to K^+K^-\pi^0$
1747± 5	80k	[7] UMAN	06	E835	5.2 $\overline{p}p \to \eta\eta\pi^0$
1776±15		VLADIMIRSK...	06	SPEC	40 $\pi^- p \to K^0_S K^0_S n$
1670±20		BINON	05	GAMS	33 $\pi^- p \to \eta\eta n$
1682±16		TIKHOMIROV	03	SPEC	40.0 $\pi^- C \to K^0_S K^0_S K^0_L X$
1670±26	3.6k	[8] NICHITIU	02	OBLX	0 $\overline{p}p \to K^+K^-\pi^+\pi^-\pi^0$
1730±15		BARBERIS	99	OMEG	450 $pp \to p_s p_f K^+K^-$
1750±20		BARBERIS	99B	OMEG	450 $pp \to p_s p_f \pi^+\pi^-$
1720±39		BAI	98H	BES	$J/\psi \to \gamma\pi^0\pi^0$
1775± 1.5	57	[9] BARKOV	98		$\pi^- p \to K^0_S K^0_S n$
1690±11		[10] ABREU	96C	DLPH	$Z^0 \to K^+K^- + X$
1696± 5 $^{+9}_{-34}$		[11] BAI	96C	BES	$J/\psi \to \gamma K^+K^-$
1781± 8 $^{+10}_{-31}$		BAI	96C	BES	$J/\psi \to \gamma K^+K^-$
1768±14		BALOSHIN	95	SPEC	40 $\pi^- C \to K^0_S K^0_S X$
1750±15		[12] BUGG	95	MRK3	$J/\psi \to \gamma\pi^+\pi^-\pi^+\pi^-$
1620±16		[11] BUGG	95	MRK3	$J/\psi \to \gamma\pi^+\pi^-\pi^+\pi^-$
1748±10		[13] ARMSTRONG	93C	E760	$\overline{p}p \to \pi^0\eta\eta \to 6\gamma$
∼ 1750		BREAKSTONE	93	SFM	$pp \to pp\pi^+\pi^-\pi^+\pi^-$
1744±15		[14] ALDE	92D	GAM2	38 $\pi^- p \to \eta\eta n$
1713±10		[15] ARMSTRONG	89D	OMEG	300 $pp \to pp K^+K^-$
1706±10		[15] ARMSTRONG	89D	OMEG	300 $pp \to pp K^0_S K^0_S$
1707±10		[13] AUGUSTIN	88	DM2	$J/\psi \to \gamma K^+K^-$, $K^0_S K^0_S$
1700±15		[11] BOLONKIN	88	SPEC	40 $\pi^- p \to K^0_S K^0_S n$
1720±60		BOLONKIN	88	SPEC	40 $\pi^- p \to K^0_S K^0_S n$
1638±10		[16] FALVARD	88	DM2	$J/\psi \to \phi K^+K^-$, $K^0_S K^0_S$
1690± 4		[17] FALVARD	88	DM2	$J/\psi \to \phi K^+K^-$, $K^0_S K^0_S$
1698±15		[13] AUGUSTIN	87	DM2	$J/\psi \to \gamma\pi^+\pi^-$
1720±10 ±10		[11] BALTRUSAIT...	87	MRK3	$J/\psi \to \gamma K^+K^-$
1755± 8		[18] ALDE	86C	GAM2	38 $\pi^- p \to n2\eta$
1730$^{+2}_{-10}$		[19] LONGACRE	86	RVUE	22 $\pi^- p \to n2K^0_S$
1742±15		[13] WILLIAMS	84	MPSF	200 $\pi^- N \to 2K^0_S X$
1670±50		BLOOM	83	CBAL	$J/\psi \to \gamma 2\eta$
1650±50		BURKE	82	MRK2	$J/\psi \to \gamma 2\rho$
1640±50		[20,21] EDWARDS	82D	CBAL	$J/\psi \to \gamma 2\eta$
1730±10 ±20		[22] ETKIN	82C	MPS	23 $\pi^- p \to n2K^0_S$

[1] From partial wave analysis including all possible combinations of 0^{++}, 2^{++}, and 4^{++} resonances.

[2] Spin 0 favored over spin 2.

[3] In the SU(3) based model with a specific interference pattern of the $f_2(1270)$, $a^0_2(1320)$, and $f'_2(1525)$ mesons incoherently added to the $f_0(1710)$ and non-resonant background.

[4] $J^P = 0^+$, supersedes ARMSTRONG 89D.

[5] Using CLEO-c data but not authored by the CLEO Collaboration.

[6] From a fit to a Breit-Wigner line shape with fixed $\Gamma = 135$ MeV.

[7] Systematic errors not estimated.

[8] Decaying to $f_0(1370)\pi\pi$.

[9] No J^{PC} determination.

[10] No J^{PC} determination, width not determined.

[11] $J^P = 2^+$.

[12] From a fit to the 0^+ partial wave.

[13] No J^{PC} determination.

[14] ALDE 92D combines all the GAMS-2000 data.

[15] $J^P = 2^+$, superseded by FRENCH 99.

[16] From an analysis ignoring interference with $f'_2(1525)$.

[17] From an analysis including interference with $f'_2(1525)$.

[18] Superseded by ALDE 92D.

[19] Uses MRK3 data. From a partial-wave analysis of data using a K-matrix formalism with 5 poles, but assuming spin 2. Fit with constrained inelasticity.

[20] $J^P = 2^+$ preferred.

[21] From fit neglecting nearby $f'_2(1525)$. Replaced by BLOOM 83.

[22] Superseded by LONGACRE 86.

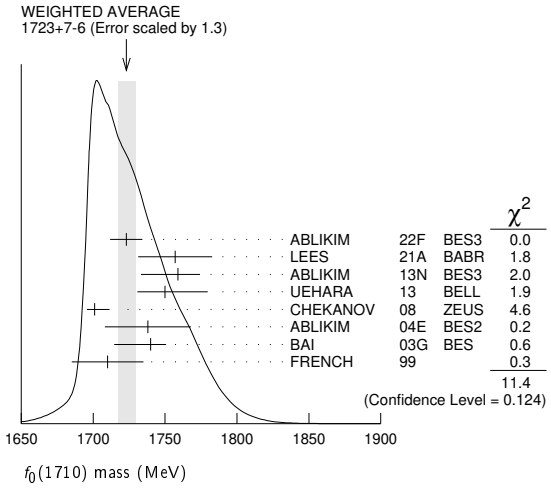

$f_0(1710)$ Breit-Wigner WIDTH

VALUE (MeV)	EVTS	DOCUMENT ID		TECN	COMMENT
149 ± 10 OUR AVERAGE		Error includes scale factor of 1.4. See the ideogram below.			
140 ± 14 ± 4		ABLIKIM	22F	BES3	$D_s^+ \to K_S^0 K_S^0 \pi^+$
175 ± 23 ± 4		LEES	21A	BABR	$\eta_c(1S) \to \eta' K^+ K^-$
172 ± 10 $^{+32}_{-16}$	5.5k	[1] ABLIKIM	13N	BES3	$e^+ e^- \to J/\psi \to \gamma\eta\eta$
139 $^{+11}_{-12}$ $^{+96}_{-50}$		[2] UEHARA	13	BELL	$\gamma\gamma \to K_S^0 K_S^0$
100 ± 24 $^{+7}_{-22}$	4k	[3] CHEKANOV	08	ZEUS	$ep \to K_S^0 K_S^0 X$
125 ± 20		ABLIKIM	04E	BES2	$J/\psi \to \omega K^+ K^-$
166 $^{+5}_{-8}$ $^{+15}_{-10}$		BAI	03G	BES	$J/\psi \to \gamma K \overline{K}$
105 ± 34		[4] FRENCH	99		300 $pp \to p_f(K^+K^-)p_s$
• • • We do not use the following data for averages, fits, limits, etc. • • •					
148 $^{+40}_{-30}$		AMSLER	06	CBAR	1.64 $\overline{p}p \to K^+ K^- \pi^0$
188 ± 13	80k	[5] UMAN	06	E835	5.2 $\overline{p}p \to \eta\eta\pi^0$
250 ± 30		VLADIMIRSK...	06	SPEC	40 $\pi^- p \to K_S^0 K_S^0 n$
260 ± 50		BINON	05	GAMS	33 $\pi^- p \to \eta\eta n$
102 ± 26		TIKHOMIROV	03	SPEC	40.0 $\overline{n}C \to K_S^0 K_S^0 K_L^0 X$
267 ± 44	3651	[6] NICHITIU	02	OBLX	0 $\overline{p}p \to K^+K^-\pi^+\pi^-\pi^0$
100 ± 25		BARBERIS	99	OMEG	450 $pp \to p_s p_f K^+ K^-$
160 ± 30		BARBERIS	99B	OMEG	450 $pp \to p_s p_f \pi^+\pi^-$
30 ± 7	57	[7] BARKOV	98		$\pi^- p \to K_S^0 K_S^0 n$
103 ± 18 $^{+30}_{-11}$		[8] BAI	96C	BES	$J/\psi \to \gamma K^+ K^-$
85 ± 24 $^{+22}_{-19}$		BAI	96C	BES	$J/\psi \to \gamma K^+ K^-$
56 ± 19		BALOSHIN	95	SPEC	40 $\pi^- C \to K_S^0 K_S^0 X$
160 ± 40		[9] BUGG	95	MRK3	$J/\psi \to \gamma\pi^+\pi^-\pi^+\pi^-$
160 $^{+60}_{-20}$		[8] BUGG	95	MRK3	$J/\psi \to \gamma\pi^+\pi^-\pi^+\pi^-$
264 ± 25		[10] ARMSTRONG	93C	E760	$\overline{p}p \to \pi^0\eta\eta \to 6\gamma$
200 to 300		BREAKSTONE	93	SFM	$pp \to pp\pi^+\pi^-\pi^+\pi^-$
< 80 90% CL		[11] ALDE	92D	GAM2	38 $\pi^- p \to \eta\eta N^*$
181 ± 30		[12] ARMSTRONG	89D	OMEG	300 $pp \to pp K^+ K^-$
104 ± 30		[12] ARMSTRONG	89D	OMEG	300 $pp \to pp K_S^0 K_S^0$
166.4 ± 33.2		[10] AUGUSTIN	88	DM2	$J/\psi \to \gamma K^+ K^-$, $K_S^0 K_S^0$
30 ± 20		[8] BOLONKIN	88	SPEC	40 $\pi^- p \to K_S^0 K_S^0 n$
350 ±150		BOLONKIN	88	SPEC	40 $\pi^- p \to K_S^0 K_S^0 n$
148 ± 17		[13] FALVARD	88	DM2	$J/\psi \to \phi K^+ K^-$, $K_S^0 K_S^0$
184 ± 6		[14] FALVARD	88	DM2	$J/\psi \to \phi K^+ K^-$, $K_S^0 K_S^0$
136 ± 28		[10] AUGUSTIN	87	DM2	$J/\psi \to \gamma\pi^+\pi^-$
130 ± 20		[8] BALTRUSAIT...	87	MRK3	$J/\psi \to \gamma K^+ K^-$
122 $^{+74}_{-15}$		[15] LONGACRE	86	RVUE	22 $\pi^- p \to n 2K_S^0$
57 ± 38		[16] WILLIAMS	84	MPSF	200 $\pi^- N \to 2K_S^0 X$
160 ± 80		BLOOM	83	CBAL	$J/\psi \to \gamma 2\eta$
200 ±100		BURKE	82	MRK2	$J/\psi \to \gamma 2\rho$
220 $^{+100}_{-70}$		[17,18] EDWARDS	82D	CBAL	$J/\psi \to \gamma 2\eta$
200 $^{+156}_{-9}$		[19] ETKIN	82B	MPS	23 $\pi^- p \to n 2K_S^0$

[1] From partial wave analysis including all possible combinations of 0^{++}, 2^{++}, and 4^{++} resonances.
[2] Spin 0 favored over spin 2.
[3] In the SU(3) based model with a specific interference pattern of the $f_2(1270)$, $a_2^0(1320)$, and $f_2'(1525)$ mesons incoherently added to the $f_0(1710)$ and non-resonant background.
[4] $J^P = 0^+$, supersedes ARMSTRONG 89D.
[5] Systematic errors not estimated.
[6] Decaying to $f_0(1370)\pi\pi$.
[7] No J^{PC} determination.
[8] $J^P = 2^+$.
[9] From a fit to the 0^+ partial wave.
[10] No J^{PC} determination.
[11] ALDE 92D combines all the GAMS-2000 data.
[12] $J^P = 2^+$, (0^+ excluded).
[13] From an analysis ignoring interference with $f_2'(1525)$.
[14] From an analysis including interference with $f_2'(1525)$.
[15] Uses MRK3 data. From a partial-wave analysis of data using a K-matrix formalism with 5 poles, but assuming spin 2. Fit with constrained inelasticity.
[16] No J^{PC} determination.
[17] $J^P = 2^+$ preferred.
[18] From fit neglecting nearby $f_2'(1525)$. Replaced by BLOOM 83.
[19] From an amplitude analysis of the $K_S^0 K_S^0$ system, superseded by LONGACRE 86.

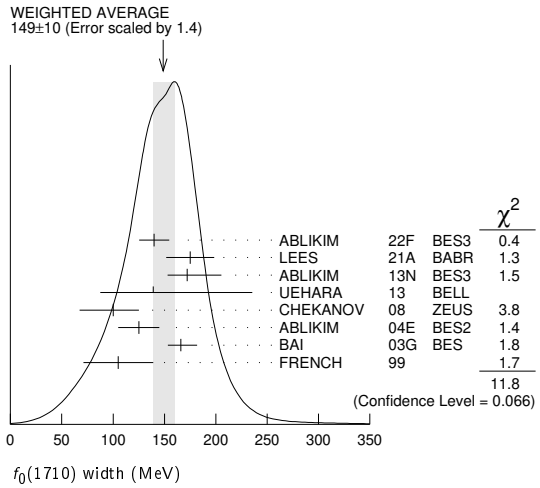

$f_0(1710)$ DECAY MODES

	Mode	Fraction (Γ_i/Γ)
Γ_1	$K\overline{K}$	seen
Γ_2	$\eta\eta$	seen
Γ_3	$\eta\eta'$	not seen
Γ_4	$\pi\pi$	seen
Γ_5	$\gamma\gamma$	seen
Γ_6	$\omega\omega$	seen

$f_0(1710)$ $\Gamma(i)\Gamma(\gamma\gamma)/\Gamma(\text{total})$

$\Gamma(K\overline{K}) \times \Gamma(\gamma\gamma)/\Gamma_{\text{total}}$ — $\Gamma_1\Gamma_5/\Gamma$

VALUE (eV)	CL%	DOCUMENT ID		TECN	COMMENT
12^{+3+227}_{-2-8}		UEHARA	13	BELL	$\gamma\gamma \to K_S^0 K_S^0$
• • • We do not use the following data for averages, fits, limits, etc. • • •					
<480	95	ALBRECHT	90G	ARG	$\gamma\gamma \to K^+ K^-$
<110	95	[1] BEHREND	89C	CELL	$\gamma\gamma \to K_S^0 K_S^0$
<280	95	[1] ALTHOFF	85B	TASS	$\gamma\gamma \to K\overline{K}\pi$

[1] Assuming helicity 2.

$\Gamma(\pi\pi) \times \Gamma(\gamma\gamma)/\Gamma_{\text{total}}$ — $\Gamma_4\Gamma_5/\Gamma$

VALUE (keV)	CL%	DOCUMENT ID		TECN	COMMENT
<0.82	95	[1] BARATE	00E	ALEP	$\gamma\gamma \to \pi^+\pi^-$

[1] Assuming spin 0.

$f_0(1710)$ BRANCHING RATIOS

$\Gamma(K\overline{K})/\Gamma_{\text{total}}$ — Γ_1/Γ

VALUE	EVTS	DOCUMENT ID		TECN	COMMENT
• • • We do not use the following data for averages, fits, limits, etc. • • •					
seen	1004	[1] DOBBS	15		$J/\psi \to \gamma K^+ K^-$
seen	349	[1] DOBBS	15		$\psi(2S) \to \gamma K^+ K^-$
0.36±0.12		ALBALADEJO	08	RVUE	
$0.38^{+0.09}_{-0.19}$		[2] LONGACRE	86	MPS	22 $\pi^- p \to n 2K_S^0$

[1] Using CLEO-c data but not authored by the CLEO Collaboration.
[2] From a partial-wave analysis of data using a K-matrix formalism with 5 poles, but assuming spin 2. Fit with constrained inelasticity.

Int. J. Mod. Phys. A 2026.41. Downloaded from www.worldscientific.com
by CALIFORNIA @ BERKELEY on 09/16/26. Re-use and distribution is strictly not permitted, except for Open Access articles.

Int. J. Mod. Phys. A 2026.41. Downloaded from www.worldscientific.com
by UNIVERSITY OF CALIFORNIA @ BERKELEY on 09/16/26. Re-use and distribution is strictly not permitted, except for Open Access articles.

$\Gamma(\eta\eta)/\Gamma_{total}$ — Γ_2/Γ

VALUE	DOCUMENT ID		TECN
• • • We do not use the following data for averages, fits, limits, etc. • • •			
0.22 ± 0.12	ALBALADEJO	08	RVUE
$0.18^{+0.03}_{-0.13}$	[1] LONGACRE	86	RVUE

[1] From a partial-wave analysis of data using a K-matrix formalism with 5 poles, but assuming spin 2. Fit with constrained inelasticity.

$\Gamma(\eta\eta)/\Gamma(K\overline{K})$ — Γ_2/Γ_1

VALUE	CL%	DOCUMENT ID		TECN	COMMENT
0.48 ± 0.15		BARBERIS	00E		450 $pp \to p_f \eta\eta p_s$
• • • We do not use the following data for averages, fits, limits, etc. • • •					
$0.46^{+0.70}_{-0.38}$		[1] ANISOVICH	02D	SPEC	Combined fit
<0.02	90	[2] PROKOSHKIN	91	GA24	300 $\pi^- p \to \pi^- p \eta\eta$

[1] From a combined K-matrix analysis of Crystal Barrel (0. $p\overline{p} \to \pi^0\pi^0\pi^0$, $\pi^0\eta\eta$, $\pi^0\pi^0\eta$), GAMS ($\pi p \to \pi^0\pi^0 n$, $\eta\eta n$, $\eta\eta' n$), and BNL ($\pi p \to K\overline{K} n$) data.

[2] Combining results of GAM4 with those of ARMSTRONG 89D.

$\Gamma(\pi\pi)/\Gamma_{total}$ — Γ_4/Γ

VALUE	EVTS	DOCUMENT ID		TECN	COMMENT
• • • We do not use the following data for averages, fits, limits, etc. • • •					
seen	381	[1] DOBBS	15		$J/\psi \to \gamma\pi^+\pi^-$
seen	237	[1] DOBBS	15		$\psi(2S) \to \gamma\pi^+\pi^-$
not seen		AMSLER	02	CBAR	0.9 $\overline{p}p \to \pi^0\eta\eta$, $\pi^0\pi^0\pi^0$
$0.039^{+0.002}_{-0.024}$		[2] LONGACRE	86	RVUE	

[1] Using CLEO-c data but not authored by the CLEO Collaboration.

[2] From a partial-wave analysis of data using a K-matrix formalism with 5 poles, but assuming spin 2. Fit with constrained inelasticity.

$\Gamma(\pi\pi)/\Gamma(K\overline{K})$ — Γ_4/Γ_1

VALUE	CL%	DOCUMENT ID		TECN	COMMENT
0.23 ± 0.05 OUR AVERAGE		Error includes scale factor of 1.2.			
$0.64 \pm 0.27 \pm 0.18$		LEES	18A	BABR	$\Upsilon(1S) \to \gamma\pi^+\pi^-$, γK^+K^-
$0.41^{+0.11}_{-0.17}$		ABLIKIM	06V	BES2	$e^+e^- \to J/\psi \to \gamma\pi^+\pi^-$
$0.2 \pm 0.024 \pm 0.036$		BARBERIS	99D	OMEG	450 $pp \to K^+K^-$, $\pi^+\pi^-$
0.39 ± 0.14		ARMSTRONG	91	OMEG	300 $pp \to pp\pi\pi$, $pp K\overline{K}$
• • • We do not use the following data for averages, fits, limits, etc. • • •					
0.32 ± 0.14		ALBALADEJO	08	RVUE	
< 0.11	95	[1] ABLIKIM	04E	BES2	$J/\psi \to \omega K^+K^-$
$5.8^{+9.1}_{-5.5}$		[2] ANISOVICH	02D	SPEC	Combined fit

[1] Using data from ABLIKIM 04A.

[2] From a combined K-matrix analysis of Crystal Barrel (0. $p\overline{p} \to \pi^0\pi^0\pi^0$, $\pi^0\eta\eta$, $\pi^0\pi^0\eta$), GAMS ($\pi p \to \pi^0\pi^0 n$, $\eta\eta n$, $\eta\eta' n$), and BNL ($\pi p \to K\overline{K} n$) data.

$\Gamma(\eta\eta')/\Gamma(\pi\pi)$ — Γ_3/Γ_4

VALUE	CL%	DOCUMENT ID		TECN	COMMENT
$<2.87 \times 10^{-3}$	90	[1] ABLIKIM	22AS	BES3	$J/\psi(1S) \to \gamma\eta\eta'$

[1] From a Breit-Wigner fit involving 9 resonances and a resonating exotic $\eta_1(1855) \to \eta\eta'$ P-wave.

$\Gamma(\omega\omega)/\Gamma_{total}$ — Γ_6/Γ

VALUE	EVTS	DOCUMENT ID		TECN	COMMENT
seen	180	ABLIKIM	06H	BES	$J/\psi \to \gamma\omega\omega$

$f_0(1710)$ REFERENCES

ABLIKIM	25CD	JHEP 2510 081	M. Ablikim et al.	(BESIII Collab.)
ABLIKIM	22AS	PR D106 072012	M. Ablikim et al.	(BESIII Collab.)
Also		PR D107 079901 (errat.)	M. Ablikim et al.	(BESIII Collab.)
ABLIKIM	22F	PR D105 L051103	M. Ablikim et al.	(BESIII Collab.)
RODAS	22	EPJ C82 80	A. Rodas et al.	(JPAC Collab.)
LEES	21A	PR D104 072002	J.P. Lees et al.	(BABAR Collab.)
SARANTSEV	21	PL B816 136227	A.V. Sarantsev et al.	(BONN, PNPI)
ABLIKIM	18AA	PR D98 072003	M. Ablikim et al.	(BESIII Collab.)
LEES	18A	PR D97 112006	J.P. Lees et al.	(BABAR Collab.)
ABLIKIM	15AE	PR D92 052003	M. Ablikim et al.	(BESIII Collab.)
DOBBS	15	PR D91 052006	S. Dobbs et al.	(NWES)
ABLIKIM	13N	PR D87 092009	M. Ablikim et al.	(BESIII Collab.)
UEHARA	13	PTEP 2013 123C01	S. Uehara et al.	(BELLE Collab.)
ALBALADEJO	08	PRL 101 252002	M. Albaladejo, J.A. Oller	
CHEKANOV	08	PRL 101 112003	S. Chekanov et al.	(ZEUS Collab.)
ABLIKIM	06H	PR D73 112007	M. Ablikim et al.	(BES Collab.)
ABLIKIM	06V	PL B642 441	M. Ablikim et al.	(BES Collab.)
AMSLER	06	PL B639 165	C. Amsler et al.	(Crystal Barrel Collab.)
UMAN	06	PR D73 052009	I. Uman et al.	(FNAL E835)
VLADIMIRSK...	06	PAN 69 493	V.V. Vladimirsky et al.	(ITEP, Moscow)
		Translated from YAF 69 515.		
BINON	05	PAN 68 960	F. Binon et al.	
		Translated from YAF 68 998.		
ABLIKIM	04A	PL B598 149	M. Ablikim et al.	(BES Collab.)
ABLIKIM	04E	PL B603 138	M. Ablikim et al.	(BES Collab.)
ANISOVICH	03	EPJ A16 229	V.V. Anisovich et al.	
BAI	03G	PR D68 052003	J.Z. Bai et al.	(BES Collab.)
TIKHOMIROV	03	PAN 66 828	G.D. Tikhomirov et al.	
		Translated from YAF 66 860.		
AMSLER	02	EPJ C23 29	C. Amsler et al.	(Crystal Barrel Collab.)
ANISOVICH	02D	PAN 65 1545	V.V. Anisovich et al.	
		Translated from YAF 65 1583.		
NICHITIU	02	PL B545 261	F. Nichitiu et al.	(OBELIX Collab.)
BARATE	00E	PL B472 189	R. Barate et al.	(ALEPH Collab.)
BARBERIS	00E	PL B479 59	D. Barberis et al.	(WA 102 Collab.)
ANISOVICH	99B	PL B449 154	A.V. Anisovich et al.	
BARBERIS	99	PL B453 305	D. Barberis et al.	(Omega Expt.)
BARBERIS	99B	PL B453 316	D. Barberis et al.	(Omega Expt.)
BARBERIS	99D	PL B462 462	D. Barberis et al.	(Omega Expt.)
FRENCH	99	PL B460 213	B. French et al.	(WA76 Collab.)
ANISOVICH	98B	SPU 41 419	V.V. Anisovich et al.	
		Translated from UFN 168 481.		
BAI	98H	PRL 81 1179	J.Z. Bai et al.	(BES Collab.)
BARKOV	98	JETPL 68 764	B.P. Barkov et al.	
ABREU	96C	PL B379 309	P. Abreu et al.	(DELPHI Collab.)
BAI	96C	PRL 77 3959	J.Z. Bai et al.	(BES Collab.)
BALOSHIN	95	PAN 58 46	O.N. Baloshin et al.	(ITEP)
		Translated from YAF 58 50.		
BUGG	95	PL B353 378	D.V. Bugg et al.	(LOQM, PNPI, WASH)
ARMSTRONG	93C	PL B307 394	T.A. Armstrong et al.	(FNAL, FERR, GENO+)
BREAKSTONE	93	ZPHY C58 251	A.M. Breakstone et al.	(IOWA, CERN, DORT+)
ALDE	92D	PL B284 457	D.M. Alde et al.	(GAM2 Collab.)
Also		SJNP 54 451	D.M. Alde et al.	(GAM2 Collab.)
		Translated from YAF 54 745.		
ARMSTRONG	91	ZPHY C51 351	T.A. Armstrong et al.	(ATHU, BARI, BIRM+)
PROKOSHKIN	91	SPD 36 155	Y.D. Prokoshkin	(GAM2 and GAM4 Collab.)
		Translated from DANS 316 900.		
ALBRECHT	90G	ZPHY C48 183	H. Albrecht et al.	(ARGUS Collab.)
ARMSTRONG	89D	PL B227 186	T.A. Armstrong, M. Benayoun	(ATHU, BARI, BIRM+)
BEHREND	89C	ZPHY C43 91	H.J. Behrend et al.	(CELLO Collab.)
AUGUSTIN	88	PRL 60 2238	J.E. Augustin et al.	(DM2 Collab.)
BOLONKIN	88	NP B309 426	B.V. Bolonkin et al.	(ITEP, SERP)
FALVARD	88	PR D38 2706	A. Falvard et al.	(CLER, FRAS, LALO+)
AUGUSTIN	87	ZPHY C36 369	J.E. Augustin et al.	(LALO, CLER, FRAS+)
BALTRUSAIT...	87	PR D35 2077	R.M. Baltrusaitis et al.	(Mark III Collab.)
ALDE	86C	PL B182 105	D.M. Alde et al.	(SERP, BELG, LANL, LAPP)
LONGACRE	86	PL B177 223	R.S. Longacre et al.	(BNL, BRAN, CUNY+)
ALTHOFF	85B	ZPHY C29 189	M. Althoff et al.	(TASSO Collab.)
WILLIAMS	84	PR D30 877	E.G.H. Williams et al.	(VAND, NDAM, TUFTS+)
BLOOM	83	ARNS 33 143	E.D. Bloom, C. Peck	(SLAC, CIT)
BURKE	82	PRL 49 632	D.L. Burke et al.	(LBL, SLAC)
EDWARDS	82D	PRL 48 458	C. Edwards et al.	(CIT, HARV, PRIN+)
ETKIN	82B	PR D25 1786	A. Etkin et al.	(BNL, CUNY, TUFTS, VAND)
ETKIN	82C	PR D25 2446	A. Etkin et al.	(BNL, CUNY, TUFTS, VAND)

$X(1750)$

$I^G(J^{PC}) = ?^-(1^{--})$

OMITTED FROM SUMMARY TABLE

The $X(1750)$ was separated from the $\phi(1680)$ in the 2022 listings due to its incompatible mass and incompatible pattern of $\overline{K}K$ and $\overline{K}^*(892)K$ branching fractions.

$X(1750)$ MASS

VALUE (MeV)	DOCUMENT ID		TECN	COMMENT
1753.8 ± 2.7 OUR AVERAGE				
$1784 \pm 12 \; ^{+0}_{-27}$	ABLIKIM	20F	BES3	$\psi(2S) \to K^+K^-\eta$
$1753.5 \pm 1.5 \pm 2.3$	LINK	02K	FOCS	20–160 $\gamma p \to K^+K^-p$
• • • We do not use the following data for averages, fits, limits, etc. • • •				
1726 ± 22	BUSENITZ	89	TPS	$\gamma p \to K^+K^-X$
1760 ± 20	ATKINSON	85C	OMEG	20–70 $\gamma p \to K\overline{K}X$
1690 ± 10	ASTON	81F	OMEG	25–70 $\gamma p \to K^+K^-X$

$X(1750)$ WIDTH

VALUE (MeV)	DOCUMENT ID		TECN	COMMENT
120 ± 10 OUR AVERAGE				
$106 \; ^{+22}_{-19} \; ^{+8}_{-36}$	ABLIKIM	20F	BES3	$\psi(2S) \to K^+K^-\eta$
$122.2 \pm 6.2 \pm 8.0$	LINK	02K	FOCS	20–160 $\gamma p \to K^+K^-p$
• • • We do not use the following data for averages, fits, limits, etc. • • •				
121 ± 47	BUSENITZ	89	TPS	$\gamma p \to K^+K^-X$
80 ± 40	ATKINSON	85C	OMEG	20–70 $\gamma p \to K\overline{K}X$
100 ± 40	ASTON	81F	OMEG	25–70 $\gamma p \to K^+K^-X$

$X(1750)$ DECAY MODES

	Mode	Fraction (Γ_i/Γ)
Γ_1	K^+K^-	seen
Γ_2	$\overline{K}^*(892)^0 K^0_S$	not seen
Γ_3	$K^*(892)^\pm K^\mp$	not seen
Γ_4	$\eta\phi$	not seen

$X(1750)$ BRANCHING RATIOS

$\Gamma(\overline{K}^*(892)^0 K^0_S)/\Gamma(K^+K^-)$ — Γ_2/Γ_1

VALUE	CL%	DOCUMENT ID		TECN	COMMENT
<0.065	90	LINK	02K	FOCS	$\gamma p \to K^+K^-p$

$\Gamma(K^*(892)^\pm K^\mp)/\Gamma(K^+K^-)$ — Γ_3/Γ_1

VALUE	CL%	DOCUMENT ID		TECN	COMMENT
<0.183	90	LINK	02K	FOCS	$\gamma p \to K^+K^-p$

$\Gamma(\eta\phi)/\Gamma_{total}$ — Γ_4/Γ

VALUE	DOCUMENT ID		TECN	COMMENT
not seen	[1] ZHU	23A	RVUE	$e^+e^- \to \eta\phi$

[1] Reported with a 2 σ significance in the fit and an upper limit of $\Gamma(e^+e^-)$ B($X(1750) \to \eta\phi$) in the range 136–322 eV.

Int. J. Mod. Phys. A 2026.41. Downloaded from www.worldscientific.com by [redacted]LIFORNIA @ BERKELEY on 09/16/26. Re-use and distribution is strictly not permitted, except for Open Access articles.

$X(1750)$ REFERENCES

ZHU	23A	CP C47 113003	W. Zhu, X. Wang	(RVUE)
ABLIKIM	20F	PR D101 032008	M. Ablikim *et al.*	(BESIII Collab.)
LINK	02K	PL B545 50	J.M. Link *et al.*	(FNAL FOCUS Collab.)
BUSENITZ	89	PR D40 1	J.K. Busenitz *et al.*	(ILL, FNAL)
ATKINSON	85C	ZPHY C27 233	M. Atkinson *et al.*	(BONN, CERN, GLAS+)
ASTON	81F	PL 104B 231	D. Aston	(BONN, CERN, EPOL, GLAS, LANC+)

$\eta(1760)$

$I^G(J^{PC}) = 0^+(0^{-+})$

OMITTED FROM SUMMARY TABLE

Seen by DM2 in the $\rho\rho$ system (BISELLO 89B). Structure in this region has been reported before in the same system (BALTRUSAITIS 86B) and in the $\omega\omega$ system (BALTRUSAITIS 85C, BISELLO 87).

$\eta(1760)$ MASS

VALUE (MeV)	EVTS	DOCUMENT ID		TECN	COMMENT
1751±15 OUR AVERAGE					
$1768^{+24}_{-25}\pm10$	465	[1] ZHANG	12A	BELL	$e^+e^- \to e^+e^-\eta'\pi^+\pi^-$
$1744\pm10\pm15$	1045	[2] ABLIKIM	06H	BES	$J/\psi \to \gamma\omega\omega$
• • • We do not use the following data for averages, fits, limits, etc. • • •					
$1703^{+12}_{-11}\pm2$		[3] ZHANG	12A	BELL	$e^+e^- \to e^+e^-\eta'\pi^+\pi^-$
1760 ± 11	320	[4] BISELLO	89B	DM2	$J/\psi \to 4\pi\gamma$

[1] From a single-resonance fit.
[2] From a partial wave analysis including $\eta(1760)$, $f_0(1710)$, $f_2(1640)$, and $f_2(1910)$.
[3] From a two-resonance fit.
[4] Estimated by us from various fits. Systematic uncertainties not estimated.

$\eta(1760)$ WIDTH

VALUE (MeV)	EVTS	DOCUMENT ID		TECN	COMMENT
240±30 OUR AVERAGE					
$224^{+62}_{-56}\pm25$	465	[5] ZHANG	12A	BELL	$e^+e^- \to e^+e^-\eta'\pi^+\pi^-$
$244^{+24}_{-21}\pm25$	1045	[6] ABLIKIM	06H	BES	$J/\psi \to \gamma\omega\omega$
• • • We do not use the following data for averages, fits, limits, etc. • • •					
$42^{+36}_{-22}\pm15$		[7] ZHANG	12A	BELL	$e^+e^- \to e^+e^-\eta'\pi^+\pi^-$
60 ± 16	320	[8] BISELLO	89B	DM2	$J/\psi \to 4\pi\gamma$

[5] From a single-resonance fit.
[6] From a partial wave analysis including $\eta(1760)$, $f_0(1710)$, $f_2(1640)$, and $f_2(1910)$.
[7] From a two-resonance fit.
[8] Estimated by us from various fits. Systematic uncertainties not estimated.

$\eta(1760)$ DECAY MODES

	Mode	Fraction (Γ_i/Γ)
Γ_1	4π	
Γ_2	$2\pi^+2\pi^-$	seen
Γ_3	$\pi^+\pi^-2\pi^0$	seen
Γ_4	$\rho^0\rho^0$	seen
Γ_5	$\rho^+\rho^-$	seen
Γ_6	$\omega\omega$	seen
Γ_7	$\eta'\pi^+\pi^-$	seen
Γ_8	$\gamma\gamma$	seen

$\eta(1760)$ $\Gamma(i)\Gamma(\gamma\gamma)/\Gamma(\text{total})$

$\Gamma(\eta'\pi^+\pi^-) \times \Gamma(\gamma\gamma)/\Gamma_{\text{total}}$ — $\Gamma_7\Gamma_8/\Gamma$

VALUE (eV)	EVTS	DOCUMENT ID		TECN	COMMENT
$\mathbf{28.2^{+7.9}_{-7.5}\pm3.7}$	465	[9] ZHANG	12A	BELL	$e^+e^- \to e^+e^-\eta'\pi^+\pi^-$
• • • We do not use the following data for averages, fits, limits, etc. • • •					
$3.0^{+2.0}_{-1.2}\pm0.8$	52	[10] ZHANG	12A	BELL	$e^+e^- \to e^+e^-\eta'\pi^+\pi^-$
$18^{+13}_{-10}\pm5$	315	[11] ZHANG	12A	BELL	$e^+e^- \to e^+e^-\eta'\pi^+\pi^-$

[9] From a single-resonance fit.
[10] From a two-resonance fit. For constructive interference with the $X(1835)$.
[11] From a two-resonance fit. For destructive interference with the $X(1835)$.

$\eta(1760)$ BRANCHING RATIOS

$\Gamma(2\pi^+2\pi^-)/\Gamma_{\text{total}}$ — Γ_2/Γ

VALUE	DOCUMENT ID		TECN	COMMENT
seen	BISELLO	89B	DM2	$J/\psi \to \gamma 2\pi^+2\pi^-$

$\Gamma(\pi^+\pi^-2\pi^0)/\Gamma_{\text{total}}$ — Γ_3/Γ

VALUE	DOCUMENT ID		TECN	COMMENT
seen	BISELLO	89B	DM2	$J/\psi \to \gamma\pi^+\pi^-2\pi^0$

$\Gamma(\rho^0\rho^0)/\Gamma_{\text{total}}$ — Γ_4/Γ

VALUE	DOCUMENT ID		TECN	COMMENT
seen	BISELLO	89B	DM2	$J/\psi \to \gamma\rho^0\rho^0$
seen	BALTRUSAIT...	86	MRK3	$J/\psi \to \gamma\rho^0\rho^0$

$\Gamma(\rho^+\rho^-)/\Gamma_{\text{total}}$ — Γ_5/Γ

VALUE	DOCUMENT ID		TECN	COMMENT
seen	BISELLO	89B	DM2	$J/\psi \to \gamma\rho^+\rho^-$
seen	BALTRUSAIT...	86	MRK3	$J/\psi \to \gamma\rho^+\rho^-$

$\Gamma(\omega\omega)/\Gamma_{\text{total}}$ — Γ_6/Γ

VALUE	DOCUMENT ID		TECN	COMMENT
seen	BISELLO	87	DM2	$J/\psi \to \omega\omega$
seen	BALTRUSAIT...	85C	MRK3	$J/\psi \to \gamma\omega\omega$

$\Gamma(\gamma\gamma)/\Gamma(\omega\omega)$ — Γ_8/Γ_6

VALUE	CL%	DOCUMENT ID		TECN	COMMENT
$\mathbf{<2.48\times10^{-3}}$	90	[12] ABLIKIM	18O	BES3	$\psi(2S) \to \pi^+\pi^-\gamma\gamma\gamma$

[12] Using results from ABLIKIM 06H.

$\eta(1760)$ REFERENCES

ABLIKIM	18O	PR D97 072014	M. Ablikim *et al.*	(BESIII Collab.)
ZHANG	12A	PR D86 052002	C.C. Zhang *et al.*	(BELLE Collab.)
ABLIKIM	06H	PR D73 112007	M. Ablikim *et al.*	(BES Collab.)
BISELLO	89B	PR D39 701	G. Busetto *et al.*	(DM2 Collab.)
BISELLO	87	PL B192 239	D. Bisello *et al.*	(PADO, CLER, FRAS+)
BALTRUSAIT...	86	PR D33 629	R.M. Baltrusaitis *et al.*	(Mark III Collab.)
BALTRUSAIT...	86B	PR D33 1222	R.M. Baltrusaitis *et al.*	(Mark III Collab.)
BALTRUSAIT...	85C	PRL 55 1723	R.M. Baltrusaitis *et al.*	(CIT, UCSC+)

$\pi(1800)$

$I^G(J^{PC}) = 1^-(0^{-+})$

See the review on "Spectroscopy of Light Meson Resonances."

$\pi(1800)$ MASS

VALUE (MeV)	EVTS	DOCUMENT ID		TECN	CHG	COMMENT
$\mathbf{1810^{+9}_{-11}}$ **OUR AVERAGE** Error includes scale factor of 2.2. See the ideogram below.						
1804^{+6}_{-9}	46M	[1] AGHASYAN	18B	COMP		190 $\pi^-p \to \pi^-\pi^+\pi^-p$
$1876\pm18\pm16$	4k	[2] EUGENIO	08	B852	–	18 $\pi^-p \to \eta\eta\pi^-p$
$1774\pm18\pm20$		[3] CHUNG	02	B852		18.3 $\pi^-p \to \pi^+\pi^-\pi^-p$
$1863\pm9\pm10$		[4] CHUNG	02	B852		18.3 $\pi^-p \to \pi^+\pi^-\pi^-p$
$1840\pm10\pm10$	1.2k	AMELIN	96B	VES	–	37 $\pi^-A \to \eta\eta\pi^-A$
$1775\pm7\pm10$		[5] AMELIN	95B	VES	–	36 $\pi^-A \to \pi^+\pi^-\pi^-A$
1790 ± 14		[6] BERDNIKOV	94	VES	–	37 $\pi^-A \to K^+K^-\pi^-A$
$1873\pm33\pm20$		BELADIDZE	92C	VES	–	36 $\pi^-\text{Be} \to \pi^-\eta'\eta\text{Be}$
$1814\pm10\pm23$	426	BITYUKOV	91	VES	–	36 $\pi^-\text{C} \to \pi^-\eta\eta\text{C}$
1770 ± 30	1.1k	BELLINI	82	SPEC	–	40 $\pi^-\text{A} \to 3\pi\text{A}$
• • • We do not use the following data for averages, fits, limits, etc. • • •						
$1785\pm9^{+12}_{-6}$	420k	[7] ALEKSEEV	10	COMP		190 $\pi^-Pb \to \pi^-\pi^-\pi^+Pb'$
$1737\pm5\pm15$		AMELIN	99	VES		37 $\pi^-A \to \omega\pi^-\pi^0A^*$

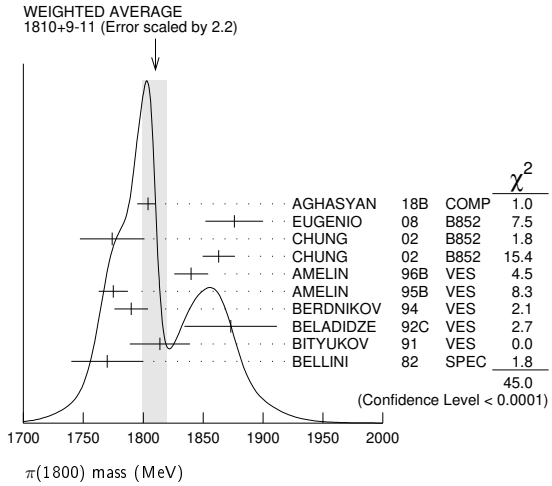

Int. J. Mod. Phys. A 2026.41. Downloaded from www.worldscientific.com by UNIVERSITY OF CALIFORNIA @ BERKELEY on 09/16/26. Re-use and distribution is strictly not permitted, except for Open Access articles.

[1] Statistical error negligible.
[2] From a single-pole fit.
[3] In the $f_0(980)\pi$ wave.
[4] In the $f_0(500)\pi$ wave.
[5] From a fit to $J^{PC} = 0^{-+}$ $f_0(980)\pi$, $f_0(1370)\pi$ waves.
[6] From a fit to $J^{PC} = 0^{-+}$ $K_0^*(1430)K^-$ and $f_0(980)\pi^-$ waves.
[7] Superseded by AGHASYAN 2018B.

$\pi(1800)$ WIDTH

VALUE (MeV)	EVTS	DOCUMENT ID		TECN	CHG	COMMENT
215^{+7}_{-8} OUR AVERAGE						
220^{+8}_{-11}	46M	[8] AGHASYAN	18B	COMP		190 $\pi^- p \to \pi^-\pi^+\pi^- p$
$221\pm26\pm38$	4k	[9] EUGENIO	08	B852	−	18 $\pi^- p \to \eta\eta\pi^- p$
$223\pm48\pm50$		[10] CHUNG	02	B852		18.3 $\pi^- p \to \pi^+\pi^-\pi^- p$
$191\pm21\pm20$		[11] CHUNG	02	B852		18.3 $\pi^- p \to \pi^+\pi^-\pi^- p$
$210\pm30\pm30$	1.2k	AMELIN	96B	VES	−	37 $\pi^- A \to \eta\eta\pi^- A$
$190\pm15\pm15$		[12] AMELIN	95B	VES	−	36 $\pi^- A \to \pi^+\pi^-\pi^- A$
210 ± 70		[13] BERDNIKOV	94	VES	−	37 $\pi^- A \to K^+K^-\pi^- A$
$225\pm35\pm20$		BELADIDZE	92C	VES	−	36 π^-Be $\to \pi^-\eta'\eta$Be
$205\pm18\pm32$	426	BITYUKOV	91	VES	−	36 π^-C $\to \pi^-\eta\eta$C
310 ± 50	1.1k	BELLINI	82	SPEC	−	40 π^-A $\to$ 3πA
• • • We do not use the following data for averages, fits, limits, etc. • • •						
$208\pm22^{+21}_{-37}$	420k	[14] ALEKSEEV	10	COMP		190 $\pi^- Pb \to \pi^-\pi^-\pi^+ Pb'$
$259\pm19\pm6$		AMELIN	99	VES		37 $\pi^- A \to \omega\pi^-\pi^0 A^*$

[8] Statistical error negligible.
[9] From a single-pole fit.
[10] In the $f_0(980)\pi$ wave.
[11] In the $f_0(500)\pi$ wave.
[12] From a fit to $J^{PC} = 0^{-+}$ $f_0(980)\pi$, $f_0(1370)\pi$ waves.
[13] From a fit to $J^{PC} = 0^{-+}$ $K_0^*(1430)K^-$ and $f_0(980)\pi^-$ waves.
[14] Superseded by AGHASYAN 2018B.

$\pi(1800)$ DECAY MODES

	Mode	Fraction (Γ_i/Γ)
Γ_1	$\pi^+\pi^-\pi^-$	seen
Γ_2	$f_0(500)\pi^-$	seen
Γ_3	$f_0(980)\pi^-$	seen
Γ_4	$f_0(1370)\pi^-$	seen
Γ_5	$f_0(1500)\pi^-$	not seen
Γ_6	$\rho\pi^-$	not seen
Γ_7	$\eta\eta\pi^-$	seen
Γ_8	$a_0(980)\eta$	seen
Γ_9	$a_2(1320)\eta$	not seen
Γ_{10}	$f_2(1270)\pi$	not seen
Γ_{11}	$f_0(1370)\pi^-$	not seen
Γ_{12}	$f_0(1500)\pi^-$	seen
Γ_{13}	$\eta\eta'(958)\pi^-$	seen
Γ_{14}	$K_0^*(1430)K^-$	seen
Γ_{15}	$K^*(892)K^-$	not seen

$\pi(1800)$ BRANCHING RATIOS

$\Gamma(f_0(980)\pi^-)/\Gamma(f_0(500)\pi^-)$ — Γ_3/Γ_2

VALUE	DOCUMENT ID		TECN	COMMENT
0.44±0.08±0.38	[15] CHUNG	02	B852	18.3 $\pi^- p \to \pi^+\pi^-\pi^- p$

$\Gamma(f_0(980)\pi^-)/\Gamma(f_0(1370)\pi^-)$ — Γ_3/Γ_4

VALUE	DOCUMENT ID		TECN	CHG	COMMENT
• • • We do not use the following data for averages, fits, limits, etc. • • •					
1.7±1.3	[16] AMELIN	95B	VES	−	36 $\pi^- A \to \pi^+\pi^-\pi^- A$

$\Gamma(f_0(1370)\pi^-)/\Gamma_{total}$ — Γ_4/Γ

VALUE	DOCUMENT ID		TECN	CHG	COMMENT
seen	BELLINI	82	SPEC	−	40 π^-A $\to$ 3πA

$\Gamma(f_0(1500)\pi^-)/\Gamma_{total}$ — Γ_5/Γ

VALUE	DOCUMENT ID		TECN	COMMENT
not seen	CHUNG	02	B852	18.3 $\pi^- p \to \pi^+\pi^-\pi^- p$

$\Gamma(\rho\pi^-)/\Gamma_{total}$ — Γ_6/Γ

VALUE	DOCUMENT ID		TECN	CHG	COMMENT
not seen	BELLINI	82	SPEC	−	40 π^-A $\to$ 3πA

$\Gamma(\rho\pi^-)/\Gamma(f_0(980)\pi^-)$ — Γ_6/Γ_3

VALUE	CL%	DOCUMENT ID		TECN	CHG	COMMENT
• • • We do not use the following data for averages, fits, limits, etc. • • •						
<0.25		CHUNG	02	B852		18.3 $\pi^- p \to \pi^+\pi^-\pi^- p$
<0.14	90	AMELIN	95B	VES	−	36 $\pi^- A \to \pi^+\pi^-\pi^- A$

$\Gamma(\eta\eta\pi^-)/\Gamma(\pi^+\pi^-\pi^-)$ — Γ_7/Γ_1

VALUE	EVTS	DOCUMENT ID		TECN	CHG	COMMENT
• • • We do not use the following data for averages, fits, limits, etc. • • •						
0.5±0.1	1200	[16] AMELIN	96B	VES	−	37 $\pi^- A \to \eta\eta\pi^- A$

$\Gamma(a_2(1320)\eta)/\Gamma_{total}$ — Γ_9/Γ

VALUE	DOCUMENT ID		TECN	COMMENT
not seen	EUGENIO	08	B852	18 $\pi^- p \to \eta\eta\pi^- p$

$\Gamma(f_2(1270)\pi)/\Gamma_{total}$ — Γ_{10}/Γ

VALUE	DOCUMENT ID		TECN	COMMENT
not seen	EUGENIO	08	B852	18 $\pi^- p \to \eta\eta\pi^- p$

$\Gamma(f_0(1370)\pi^-)/\Gamma_{total}$ — Γ_{11}/Γ

VALUE	DOCUMENT ID		TECN	COMMENT
not seen	EUGENIO	08	B852	18 $\pi^- p \to \eta\eta\pi^- p$

$\Gamma(f_0(1500)\pi^-)/\Gamma(a_0(980)\eta)$ — Γ_{12}/Γ_8

VALUE	EVTS	DOCUMENT ID		TECN	CHG	COMMENT
• • • We do not use the following data for averages, fits, limits, etc. • • •						
0.48 ±0.17	4k	[16,17] EUGENIO	08	B852	−	18 $\pi^- p \to \eta\eta\pi^- p$
$0.030^{+0.014}_{-0.011}$		[16] ANISOVICH	01B	SPEC	0	0.6–1.94 $p\overline{p} \to \eta\eta\pi^0\pi^0$
0.08 ±0.03	1200	[16,18] AMELIN	96B	VES	−	37 $\pi^- A \to \eta\eta\pi^- A$

$\Gamma(\eta\eta'(958)\pi^-)/\Gamma(\eta\eta\pi^-)$ — Γ_{13}/Γ_7

VALUE	EVTS	DOCUMENT ID		TECN	CHG	COMMENT
• • • We do not use the following data for averages, fits, limits, etc. • • •						
0.29±0.07		[16] BELADIDZE	92C	VES	−	36 π^-Be $\to \pi^-\eta'\eta$Be
0.3 ±0.1	426 ± 57	[16] BITYUKOV	91	VES	−	36 π^-C $\to \pi^-\eta\eta$C

$\Gamma(K_0^*(1430)K^-)/\Gamma_{total}$ — Γ_{14}/Γ

VALUE	DOCUMENT ID		TECN	CHG	COMMENT
seen	BERDNIKOV	94	VES	−	37 $\pi^- A \to K^+K^-\pi^- A$

$\Gamma(K^*(892)K^-)/\Gamma_{total}$ — Γ_{15}/Γ

VALUE	DOCUMENT ID		TECN	CHG	COMMENT
not seen	BERDNIKOV	94	VES	−	37 $\pi^- A \to K^+K^-\pi^- A$

[15] Assuming that $f_0(980)$ decays only to $\pi\pi$.
[16] Systematic errors not estimated.
[17] From a single-pole fit.
[18] Assuming that $f_0(1500)$ decays only to $\eta\eta$ and $a_0(980)$ decays only to $\eta\pi$.

$\pi(1800)$ REFERENCES

AGHASYAN	18B	PR D98 092003	M. Aghasyan *et al.*	(COMPASS Collab.)
ALEKSEEV	10	PRL 104 241803	M.G. Alekseev *et al.*	(COMPASS Collab.)
EUGENIO	08	PL B660 466	P. Eugenio *et al.*	(BNL E852 Collab.)
CHUNG	02	PR D65 072001	S.U. Chung *et al.*	(BNL E852 Collab.)
ANISOVICH	01B	PL B500 222	A.V. Anisovich *et al.*	
AMELIN	99	PAN 62 445 Translated from YAF 62 487.	D.V. Amelin *et al.*	(VES Collab.)
AMELIN	96B	PAN 59 976 Translated from YAF 59 1021.	D.V. Amelin *et al.*	(SERP, TBIL) IGJPC
AMELIN	95B	PL B356 595	D.V. Amelin *et al.*	(SERP, TBIL)
BERDNIKOV	94	PL B337 219	E.B. Berdnikov *et al.*	(SERP, TBIL)
BELADIDZE	92C	SJNP 55 1535 Translated from YAF 55 2748.	G.M. Beladidze, S.I. Bityukov, G.V. Borisov	(SERP+)
BITYUKOV	91	PL B268 137	S.I. Bityukov *et al.*	(SERP, TBIL)
BELLINI	82	PRL 48 1697	G. Bellini *et al.*	(MILA, BGNA, JINR)

$f_0(1810)$

$I^G(J^{PC}) = 0^+(0^{++})$

OMITTED FROM SUMMARY TABLE

was $f_0(1770)$

Evidence for two isoscalar scales, $f_0(1710)$ and $f_0(1810)$, was first reported by SARANTSEV 21 and ABLIKIM 22F. The data assignments to either $f_0(1710)$ or $f_0(1810)$ are tentative. See the review on "Spectroscopy of Light Meson Resonances."

$f_0(1810)$ T-MATRIX POLE $\sqrt{s}$

Note that $\Gamma = -2\,\mathrm{Im}(\sqrt{s})$.

VALUE (MeV)	DOCUMENT ID		TECN	COMMENT
$(1765 \pm 15) - i\,(90 \pm 10)$	SARANTSEV	21	RVUE	$J/\psi \to \gamma\,(\pi\pi,\ K\overline{K},\ \eta\eta,\ \omega\phi)$
$(1803\pm3.5^{+45.5}_{-10.4}) - i\,(145\pm2.5^{+16.3}_{-9.6})$	[1] ALBRECHT	20	RVUE	0.9 $\overline{p}p \to \pi^0\pi^0\eta$, $\pi^0\eta\eta$, $\pi^0 K^+K^-$

[1] T-matrix pole, 5 poles, 5 channels, including scattering data from HYAMS 75 ($\pi\pi$), LONGACRE 86 ($K\overline{K}$), BINON 83 ($\eta\eta$), and BINON 84C ($\eta\eta'$).

$f_0(1810)$ Breit-Wigner MASS

VALUE (MeV)	EVTS	DOCUMENT ID		TECN	COMMENT
1785 ± 13 OUR AVERAGE		Error includes scale factor of 1.7. See the ideogram below.			
$1834\pm14^{+2}_{-10}$		[1] GOTMAN	25	VES	29 π^-Be $\to$ A$\omega\phi$
1814 ± 31	7.2k	[2] KHOLODENK..	21	VES	29 $\pi^- p \to n\omega\phi$
$1795\pm7^{+23}_{-20}$		ABLIKIM	13J	BES3	$J/\psi \to \gamma\omega\phi$
$1765^{+4}_{-3}\pm13$		ABLIKIM	06V	BES2	$e^+e^- \to J/\psi \to \gamma\pi^+\pi^-$
$1760\pm15^{+15}_{-10}$		ABLIKIM	05Q	BES2	$\psi(2S) \to \gamma\pi^+\pi^- K^+K^-$
1740^{+30}_{-25}		BAI	00A	BES	$J/\psi \to \gamma(\pi^+\pi^-\pi^+\pi^-)$
• • • We do not use the following data for averages, fits, limits, etc. • • •					
$1834\pm14^{+2}_{-10}$		[3] DOROFEEV	24	VES	29 π^-Be $\to$ A$\omega\phi$
1814 ± 18		[4,5] AAIJ	14BR	LHCB	$\overline{B}^0_s \to J/\psi\pi^+\pi^-$
$1812^{+19}_{-26}\pm18$		[6] ABLIKIM	06J	BES2	$J/\psi \to \gamma\omega\phi$
1790^{+40}_{-30}		ABLIKIM	05	BES2	$J/\psi \to \phi\pi^+\pi^-$

[1] GOTMAN 25 attributes these data to the $f_0(1710)$.
[2] From partial wave analysis of $\omega\phi$ invariant mass including 0^{++}, 2^{++}, and 0^{-+} resonances.
[3] Superseded by GOTMAN 25.
[4] Second solution: 1800 ± 22 MeV. The fit favors $f_0(1810)$ to $f_0(1710)$.
[5] Statistical error only.
[6] Not seen by LIU 09 in $B^\pm \to K^\pm\omega\phi$.

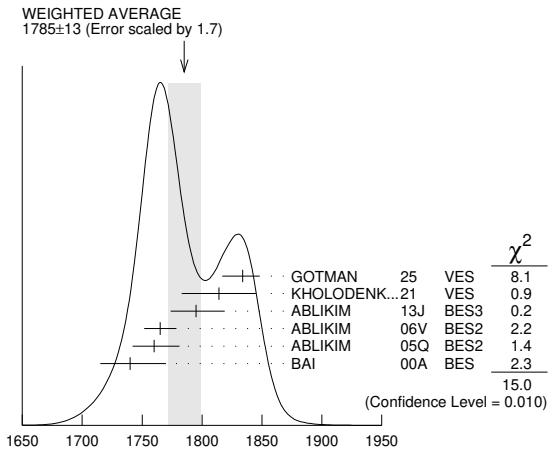

$f_0(1810)$ Breit-Wigner WIDTH

VALUE (MeV)	EVTS	DOCUMENT ID		TECN	COMMENT
137^{+15}_{-17} OUR AVERAGE		Error includes scale factor of 1.4. See the ideogram below.			
$114\pm15^{+5}_{-15}$		[1] GOTMAN	25	VES	29 π^-Be $\to$ A$\omega\phi$
182 ± 19	7.2k	[2] KHOLODENK..	21	VES	29 $\pi^- p \to n\omega\phi$
$95\pm10^{+78}_{-82}$		ABLIKIM	13J	BES3	$J/\psi \to \gamma\omega\phi$
$145\pm8\pm69$		ABLIKIM	06V	BES2	$e^+e^- \to J/\psi \to \gamma\pi^+\pi^-$
$125\pm25^{+10}_{-15}$		ABLIKIM	05Q	BES2	$\psi(2S) \to \gamma\pi^+\pi^- K^+K^-$
120^{+50}_{-40}		BAI	00A	BES	$J/\psi \to \gamma(\pi^+\pi^-\pi^+\pi^-)$
• • • We do not use the following data for averages, fits, limits, etc. • • •					
$114\pm15^{+5}_{-15}$		[3] DOROFEEV	24	VES	29 π^-Be $\to$ A$\omega\phi$
328 ± 34		[4,5] AAIJ	14BR	LHCB	$\overline{B}^0_s \to J/\psi\pi^+\pi^-$
$105\pm20\pm28$		[6] ABLIKIM	06J	BES2	$J/\psi \to \gamma\omega\phi$
270^{+60}_{-30}		[7] ABLIKIM	05	BES2	$J/\psi \to \phi\pi^+\pi^-$

[1] GOTMAN 25 attributes these data to the $f_0(1710)$.
[2] From partial wave analysis of $\omega\phi$ invariant mass including 0^{++}, 2^{++}, and 0^{-+} resonances.
[3] Superseded by GOTMAN 25.
[4] Second solution: 263 ± 30 MeV. The fit favors $f_0(1810)$ to $f_0(1710)$.
[5] Statistical error only.
[6] Not seen by LIU 09 in $B^\pm \to K^\pm\omega\phi$.
[7] $f_0(1710)$ width fixed to PDG value.

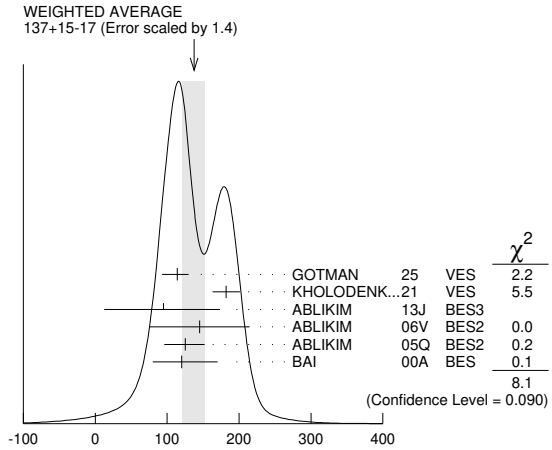

$f_0(1810)$ DECAY MODES

	Mode	Fraction (Γ_i/Γ)
Γ_1	$\pi\pi$	seen
Γ_2	$K\overline{K}$	seen
Γ_3	$\eta\eta$	seen
Γ_4	$\omega\phi$	seen

$f_0(1810)$ BRANCHING RATIOS

$\Gamma(\pi\pi)/\Gamma_{total}$ — Γ_1/Γ

VALUE	DOCUMENT ID		TECN	COMMENT
seen	SARANTSEV	21	RVUE	$J/\psi \to \gamma(\pi\pi,\ K\overline{K},\ \eta\eta,\ \omega\phi)$
seen	AAIJ	14BR	LHCB	$\overline{B}^0_s \to J/\psi\pi^+\pi^-$
seen	ABLIKIM	05	BES2	$J/\psi \to \phi\pi^+\pi^-$

$\Gamma(K\overline{K})/\Gamma_{total}$ — Γ_2/Γ

VALUE	DOCUMENT ID		TECN	COMMENT
seen	SARANTSEV	21	RVUE	$J/\psi \to \gamma(\pi\pi,\ K\overline{K},\ \eta\eta,\ \omega\phi)$

$\Gamma(\eta\eta)/\Gamma_{total}$ — Γ_3/Γ

VALUE	DOCUMENT ID		TECN	COMMENT
seen	SARANTSEV	21	RVUE	$J/\psi \to \gamma(\pi\pi,\ K\overline{K},\ \eta\eta,\ \omega\phi)$

$\Gamma(\omega\phi)/\Gamma_{total}$ — Γ_4/Γ

VALUE	EVTS	DOCUMENT ID		TECN	COMMENT
seen	7.2k	KHOLODENK..	21	VES	29 $\pi^- p \to n\omega\phi$
seen		SARANTSEV	21	RVUE	$J/\psi \to \gamma(\pi\pi,\ K\overline{K},\ \eta\eta,\ \omega\phi)$

$\Gamma(\pi\pi)/\Gamma_{total} \times \Gamma(\omega\phi)/\Gamma_{total}$ — $\Gamma_1/\Gamma \times \Gamma_4/\Gamma$

VALUE (units 10^{-3})	DOCUMENT ID		TECN	COMMENT
• • • We do not use the following data for averages, fits, limits, etc. • • •				
4.8 ± 1.2	[1] DOROFEEV	24	VES	29 π^-Be $\to$ A$\omega\phi$

[1] Using one-pion exchange. Assigning this resonance to be $f_0(1710)$ instead gives $B(f_0 \to \pi\pi) \times B(f_0 \to \omega\phi) = (3.9 \pm 1.0) \times 10^{-3}$.

$f_0(1810)$ REFERENCES

GOTMAN	25	PPN 56 743	V.G. Gotman *et al.*	(VES Collab.)
DOROFEEV	24	EPJ A60 105	V.A. Dorofeev *et al.*	(VES Collab.)
ABLIKIM	22F	PR D105 L051103	M. Ablikim *et al.*	(BESIII Collab.)
KHOLODENK...	21	PAN 83 1602	M.S. Kholodenko	(VES Collab.)
SARANTSEV	21	PL B816 136227	A.V. Sarantsev *et al.*	(BONN, PNPI)
ALBRECHT	20	EPJ C80 453	M. Albrecht *et al.*	(Crystal Barrel Collab.)
AAIJ	14BR	PR D89 092006	R. Aaij *et al.*	(LHCb Collab.)
ABLIKIM	13J	PR D87 032008	M. Ablikim *et al.*	(BESIII Collab.)
LIU	09	PR D79 071102	C. Liu *et al.*	(BELLE Collab.)
ABLIKIM	06J	PRL 96 162002	M. Ablikim *et al.*	(BES Collab.)
ABLIKIM	06V	PL B642 441	M. Ablikim *et al.*	(BES Collab.)
ABLIKIM	05	PL B607 243	M. Ablikim *et al.*	(BES Collab.)
ABLIKIM	05Q	PR D72 092002	M. Ablikim *et al.*	(BES Collab.)
BAI	00A	PL B472 207	J.Z. Bai *et al.*	(BES Collab.)
LONGACRE	86	PL B177 223	R.S. Longacre *et al.*	(BNL, BRAN, CUNY+)
BINON	84C	NC 80A 363	F.G. Binon *et al.*	(BELG, LAPP, SERP+)
BINON	83	NC 78A 313	F.G. Binon *et al.*	(BELG, LAPP, SERP+)
HYAMS	75	NP B100 205	B.D. Hyams *et al.*	(CERN, MPIM)

Int. J. Mod. Phys. A 2026.41. Downloaded from www.worldscientific.com
by CALIFORNIA @ BERKELEY on 09/16/26. Re-use and distribution is strictly not permitted, except for Open Access articles.

Int. J. Mod. Phys. A 2026.41. Downloaded from www.worldscientific.com by UNIVERSITY OF CALIFORNIA @ BERKELEY on 09/16/26. Re-use and distribution is strictly not permitted, except for Open Access articles.

$f_2(1810)$

$I^G(J^{PC}) = 0^+(2^{++})$

OMITTED FROM SUMMARY TABLE

Needs confirmation.

$f_2(1810)$ MASS

VALUE (MeV)		EVTS	DOCUMENT ID		TECN	COMMENT
1815 ±12			**OUR AVERAGE**			Error includes scale factor of 1.4. See the ideogram below.
$1822\ ^{+29}_{-24}\ ^{+66}_{-57}$	5.5k		[1] ABLIKIM	13N	BES3	$e^+e^- \to J/\psi \to \gamma\eta\eta$
$1737 \pm 9\ ^{+198}_{-65}$			[2] UEHARA	10A	BELL	10.6 $e^+e^- \to e^+e^-\eta\eta$
1800 ±30		40	ALDE	88D	GAM4	300 $\pi^-p \to \pi^-p4\pi^0$
1806 ±10		1600	ALDE	87	GAM4	100 $\pi^-p \to 4\pi^0 n$
1870 ±40			[3] ALDE	86D	GAM4	100 $\pi^-p \to \eta\eta n$
$1857\ ^{+35}_{-24}$			[4] COSTA	80	OMEG	10 $\pi^-p \to K^+K^-n$
• • • We do not use the following data for averages, fits, limits, etc. • • •						
$1845.0 \pm 2.2\ ^{+1.6}_{-7.2}$			[5] ALBRECHT	20	RVUE	0.9 $\overline{p}p \to \pi^0\pi^0\eta$, $\pi^0\eta\eta$, $\pi^0K^+K^-$
$1858\ ^{+18}_{-71}$			[6] LONGACRE	86	RVUE	Compilation
1799 ±15			[7] CASON	82	STRC	8 $\pi^+p \to \Delta^{++}\pi^0\pi^0$

[1] From partial wave analysis including all possible combinations of 0^{++}, 2^{++}, and 4^{++} resonances.
[2] Breit-Wigner mass. Could also be the $f_2(1910)$.
[3] Seen in only one solution.
[4] Error increased by spread of two solutions. Included in LONGACRE 86 global analysis.
[5] T-matrix pole, 4 poles, 4 channels, including scattering data from HYAMS 75 ($\pi\pi$), LONGACRE 86 ($K\overline{K}$), BINON 83 ($\eta\eta$).
[6] From a partial-wave analysis of data using a K-matrix formalism with 5 poles. Includes compilation of several other experiments.
[7] From an amplitude analysis of the reaction $\pi^+\pi^- \to 2\pi^0$. The resonance in the $2\pi^0$ final state is not confirmed by PROKOSHKIN 97.

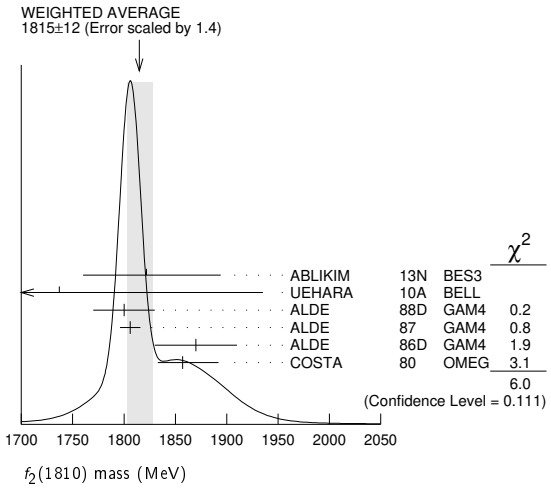

$f_2(1810)$ WIDTH

VALUE (MeV)		EVTS	DOCUMENT ID		TECN	COMMENT
197 ± 22			**OUR AVERAGE**			Error includes scale factor of 1.5. See the ideogram below.
$229\ ^{+52}_{-42}\ ^{+88}_{-155}$	5.5k		[1] ABLIKIM	13N	BES3	$e^+e^- \to J/\psi \to \gamma\eta\eta$
$228\ ^{+21}_{-20}\ ^{+234}_{-153}$			[2] UEHARA	10A	BELL	10.6 $e^+e^- \to e^+e^-\eta\eta$
160 ± 30		40	ALDE	88D	GAM4	300 $\pi^-p \to \pi^-p4\pi^0$
190 ± 20		1600	ALDE	87	GAM4	100 $\pi^-p \to 4\pi^0 n$
250 ± 30			[3] ALDE	86D	GAM4	100 $\pi^-p \to \eta\eta n$
$185\ ^{+102}_{-139}$			[4] COSTA	80	OMEG	10 $\pi^-p \to K^+K^-n$
• • • We do not use the following data for averages, fits, limits, etc. • • •						
$260.9 \pm 3.9\ ^{+199.9}_{-38.2}$			[5] ALBRECHT	20	RVUE	0.9 $\overline{p}p \to \pi^0\pi^0\eta$, $\pi^0\eta\eta$, $\pi^0K^+K^-$
$388\ ^{+15}_{-21}$			[6] LONGACRE	86	RVUE	Compilation
$280\ ^{+42}_{-35}$			[7] CASON	82	STRC	8 $\pi^+p \to \Delta^{++}\pi^0\pi^0$

[1] From partial wave analysis including all possible combinations of 0^{++}, 2^{++}, and 4^{++} resonances.
[2] Breit-Wigner width. Could also be the $f_2(1910)$.
[3] Seen in only one solution.
[4] Error increased by spread of two solutions. Included in LONGACRE 86 global analysis.
[5] T-matrix pole, 4 poles, 4 channels, including scattering data from HYAMS 75 ($\pi\pi$), LONGACRE 86 ($K\overline{K}$), BINON 83 ($\eta\eta$).
[6] From a partial-wave analysis of data using a K-matrix formalism with 5 poles. Includes compilation of several other experiments.
[7] From an amplitude analysis of the reaction $\pi^+\pi^- \to 2\pi^0$. The resonance in the $2\pi^0$ final state is not confirmed by PROKOSHKIN 97.

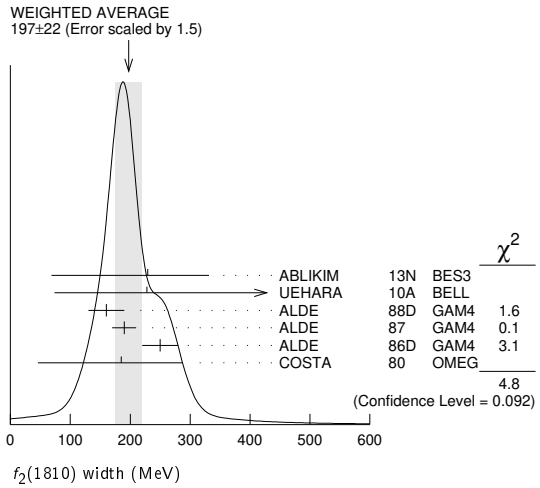

$f_2(1810)$ DECAY MODES

	Mode	Fraction (Γ_i/Γ)
Γ_1	$\pi\pi$	seen
Γ_2	$\eta\eta$	seen
Γ_3	$4\pi^0$	seen
Γ_4	K^+K^-	seen
Γ_5	$\gamma\gamma$	seen

$f_2(1810)$ $\Gamma(i)\Gamma(\gamma\gamma)/\Gamma(\text{total})$

$\Gamma(\eta\eta) \times \Gamma(\gamma\gamma)/\Gamma_{\text{total}}$ — **$\Gamma_2\Gamma_5/\Gamma$**

VALUE (eV)	DOCUMENT ID		TECN	COMMENT
$\mathbf{5.2\ ^{+0.9}_{-0.8}\ ^{+37.3}_{-4.5}}$	[1] UEHARA	10A	BELL	10.6 $e^+e^- \to e^+e^-\eta\eta$

[1] Including interference with the $f'_2(1525)$ (parameters fixed to the values from the 2008 edition of this review, PDG 08) and $f_2(1270)$. May also be the $f_0(1500)$.

$f_2(1810)$ BRANCHING RATIOS

$\Gamma(\pi\pi)/\Gamma_{\text{total}}$ — **Γ_1/Γ**

VALUE	DOCUMENT ID		TECN	COMMENT
• • • We do not use the following data for averages, fits, limits, etc. • • •				
not seen	AMSLER	02	CBAR	0.9 $\overline{p}p \to \pi^0\eta\eta$, $\pi^0\pi^0\pi^0$
not seen	PROKOSHKIN	97	GAM2	38 $\pi^-p \to \pi^0\pi^0 n$
$0.21\ ^{+0.02}_{-0.03}$	[1] LONGACRE	86	RVUE	Compilation
0.44 ± 0.03	[2] CASON	82	STRC	8 $\pi^+p \to \Delta^{++}\pi^0\pi^0$

[1] From a partial-wave analysis of data using a K-matrix formalism with 5 poles. Includes compilation of several other experiments.
[2] Included in LONGACRE 86 global analysis.

$\Gamma(\eta\eta)/\Gamma_{\text{total}}$ — **Γ_2/Γ**

VALUE	DOCUMENT ID		TECN	COMMENT
seen	ABLIKIM	13N	BES3	PWA of $J/\psi \to \gamma\eta\eta$
• • • We do not use the following data for averages, fits, limits, etc. • • •				
$0.008\ ^{+0.028}_{-0.003}$	[1] LONGACRE	86	RVUE	Compilation

[1] From a partial-wave analysis of data using a K-matrix formalism with 5 poles. Includes compilation of several other experiments.

$\Gamma(\pi\pi)/\Gamma(4\pi^0)$ — **Γ_1/Γ_3**

VALUE	DOCUMENT ID		TECN	COMMENT
• • • We do not use the following data for averages, fits, limits, etc. • • •				
<0.75	ALDE	87	GAM4	100 $\pi^-p \to 4\pi^0 n$

$\Gamma(4\pi^0)/\Gamma(\eta\eta)$ — **Γ_3/Γ_2**

VALUE	DOCUMENT ID		TECN	COMMENT
• • • We do not use the following data for averages, fits, limits, etc. • • •				
0.8 ± 0.3	ALDE	87	GAM4	100 $\pi^-p \to 4\pi^0 n$

Int. J. Mod. Phys. A 2026.41. Downloaded from www.worldscientific.com by CALIFORNIA @ BERKELEY on 09/16/26. Re-use and distribution is strictly not permitted, except for Open Access articles.

$\Gamma(K^+K^-)/\Gamma_{total}$ — Γ_4/Γ

VALUE	DOCUMENT ID		TECN	COMMENT
• • • We do not use the following data for averages, fits, limits, etc. • • •				
$0.003^{+0.019}_{-0.002}$	[1] LONGACRE	86	RVUE	Compilation
seen	COSTA	80	OMEG	$10\ \pi^- p \to K^+K^- n$

[1] From a partial-wave analysis of data using a K-matrix formalism with 5 poles. Includes compilation of several other experiments.

$f_2(1810)$ REFERENCES

ALBRECHT	20	EPJ C80 453	M. Albrecht *et al.*	(Crystal Barrel Collab.)
ABLIKIM	13N	PR D87 092009	M. Ablikim *et al.*	(BESIII Collab.)
UEHARA	10A	PR D82 114031	S. Uehara *et al.*	(BELLE Collab.)
PDG	08	PL B667 1	C. Amsler *et al.*	(PDG Collab.)
AMSLER	02	EPJ C23 29	C. Amsler *et al.*	(Crystal Barrel Collab.)
PROKOSHKIN	97	PD 42 117	Y.D. Prokoshkin *et al.*	(SERP)
		Translated from DANS 353 323.		
ALDE	88D	SJNP 47 810	D.M. Alde *et al.*	(SERP, BELG, LANL, LAPP+)
		Translated from YAF 47 1273.		
ALDE	87	PL B198 286	D.M. Alde *et al.*	(LANL, BRUX, SERP, LAPP)
ALDE	86D	NP B269 485	D.M. Alde *et al.*	(BELG, LAPP, SERP, CERN+)
LONGACRE	86	PL B177 223	R.S. Longacre *et al.*	(BNL, BRAN, CUNY+)
BINON	83	NC 78A 313	F.G. Binon *et al.*	(BELG, LAPP, SERP+)
CASON	82	PRL 48 1316	N.M. Cason *et al.*	(NDAM, ANL)
COSTA	80	NP B175 402	G. Costa *et al.*	(BARI, BONN, CERN, GLAS+)
HYAMS	75	NP B100 205	B.D. Hyams *et al.*	(CERN, MPIM)

$X(1835)$

$I^G(J^{PC}) = 0^+(0^{-+})$

OMITTED FROM SUMMARY TABLE

Could be a superposition of two states, one appearing as threshold enhancement in $p\overline{p}$ the other one with a lower mass at 1835 MeV. Coupled-channel analyses with more sophisticated model are needed.

$X(1835)$ MASS

VALUE (MeV)	EVTS	DOCUMENT ID		TECN	COMMENT
$1834.0^{+4.0}_{-3.0}$ OUR AVERAGE Error includes scale factor of 1.2.					
$1849.3\pm 3.0^{+7.6}_{-10.0}$		[1] ABLIKIM	25P	BES3	$J/\psi \to \gamma\gamma\phi$
$1832.5\pm 3.1\pm 2.5$	21k	[2] ABLIKIM	24B	BES3	$J/\psi \to \gamma 3(\pi^+\pi^-)$
$1825.3\pm 2.4^{+17.3}_{-2.4}$		[3] ABLIKIM	16J	BES3	$J/\psi \to \gamma\pi^+\pi^-\eta'$
$1844\pm 9^{+16}_{-25}$		[4] ABLIKIM	15T	BES3	$J/\psi \to \gamma K^0_S K^0_S \eta$
• • • We do not use the following data for averages, fits, limits, etc. • • •					
$1818\pm 9\pm 2.5$	37k	[5] ABLIKIM	24B	BES3	$J/\psi \to \gamma 3(\pi^+\pi^-)$
$1839\pm 26\pm 26$		[6] ABLIKIM	18I	BES3	$J/\psi \to \gamma\gamma\phi(1020)$
$1909.5\pm 15.9^{+9.4}_{-27.5}$		[7] ABLIKIM	16J	BES3	$J/\psi \to \gamma\pi^+\pi^-\eta'$
$1842.2\pm 4.2^{+7.1}_{-2.6}$	0.6k	[8] ABLIKIM	13U	BES3	$J/\psi \to \gamma 3(\pi^+\pi^-)$
$1832^{+19}_{-5}\pm 26$		[9] ABLIKIM	12D	BES3	$J/\psi \to \gamma p\overline{p}$
$1836.5\pm 3.0^{+5.6}_{-2.1}$	4265	[10] ABLIKIM	11C	BES3	$J/\psi \to \gamma\pi^+\pi^-\eta'$
$1877.3\pm 6.3^{+3.4}_{-7.4}$		[11] ABLIKIM	11J	BES3	$J/\psi \to \omega(\eta\pi^+\pi^-)$
$1837^{+10}_{-12}{}^{+9}_{-7}$	231	[12,13] ALEXANDER	10	CLEO	$J/\psi \to \gamma p\overline{p}$
$1833.7\pm 6.1\pm 2.7$	264	ABLIKIM	05R	BES2	$J/\psi \to \gamma\pi^+\pi^-\eta'$
1831 ± 7		[13,14] ABLIKIM	05R	BES2	$J/\psi \to \gamma p\overline{p}$
$1859^{+3}_{-10}{}^{+5}_{-25}$		[13] BAI	03F	BES2	$J/\psi \to \gamma p\overline{p}$

[1] From a partial wave analysis of $J/\psi \to \gamma\gamma\phi$ with significance 15.3σ. $J^{PC} = 0^{-+}$ established at 13.2σ.

[2] From a fit of the measured $3(\pi^+\pi^-)$ lineshape that accounts for the abrupt distortion observed at the $p\overline{p}$ threshold through interference with a second previously unseen narrow resonance near 1880 MeV. The fit uses Breit-Wigner functions for the signal shapes and includes known background contributions. A second solution of the fit gives 37k events.

[3] From a fit of the measured $\pi^+\pi^-\eta'$ lineshape that accounts for the abrupt distortion observed at the $p\overline{p}$ threshold through interference with a second previously unseen narrow resonance near 1870 MeV. The fit uses Breit-Wigner functions for the signal shapes and includes known backgrounds and contributors.

[4] Decay dominated by $f_0(980)\eta$ hence $I^G(J^{PC}) = 0^+(0^{-+})$.

[5] From a fit of the measured $3(\pi^+\pi^-)$ lineshape to a Flatte formula that accounts for the abrupt distortion observed at the $p\overline{p}$ threshold. The fit also includes known background contributions.

[6] From a fit to $\gamma\phi$ invariant mass. Angular analysis consistent with $J^{PC} = 0^{-+}$. Other J^{PC} not excluded. Superseded by ABLIKIM 25P.

[7] Pole mass from a fit of the measured $\pi^+\pi^-\eta'$ lineshape to a Flatte formula that accounts for the abrupt distortion observed at the $p\overline{p}$ threshold; the fit also includes known backgrounds and contributors, as well as an *ad hoc* Breit-Wigner function ($M \approx$ 1919 MeV; $\Gamma \approx$ 51 MeV) that is required for a good fit.

[8] Superseded by ABLIKIM 24B.

[9] From the fit including final state interaction effects in isospin 0 S-wave according to SIBIRTSEV 05A. Supersedes ABLIKIM 10G.

[10] From a fit of the $\pi^+\pi^-\eta'$ mass distribution to a combination of $\gamma f_1(1510)$, $\gamma X(1835)$, and two states $\gamma X(2120)$ and $\gamma\eta(2370)$, for $M(\pi^+\pi^-\eta') < 2.8$ GeV,and accounting for backgrounds from non-η' events and $J/\psi \to \pi^0\pi^+\pi^-\eta'$.

[11] The selected process is $J/\psi \to \omega a_0(980)\pi$ with $B(J/\psi \to \omega X \to \omega a_0(980)^\pm(\to \eta\pi^\pm)\pi^\mp) = (1.50 \pm 0.26^{+0.72}_{-0.36}) \times 10^{-4}$. Not seen in $J/\psi(1S) \to \omega K^+K^-\eta$ by ABLIKIM 24BQ with 90% CL upper limit of 9.55×10^{-7}. This state may be also due to $\eta_2(1870)$ or to a combination of $X(1835)$ and $\eta_2(1870)$.

[12] From a fit of the $p\overline{p}$ mass distribution to a combination of $\gamma X(1835)$, γR with $M(R) = 2100$ MeV and $\Gamma(R) = 160$ MeV, and $\gamma p\overline{p}$ phase space, for $M(p\overline{p}) < 2.85$ GeV.

[13] Evidence for a threshold enhancement in the $p\overline{p}$ mass spectrum was also reported by ABE 02K, AUBERT,B 05L, and WANG 05A in $B^+ \to p\overline{p}K^+$, WANG 05A in $B^0 \to p\overline{p}K^0_S$, ABE 02W in $\overline{B}^0 \to p\overline{p}D^0$, DEL-AMO-SANCHEZ 12 in $B \to D(D^*)p\overline{p}(\pi)$, and WEI 08 in $B^+ \to p\overline{p}\pi^+$ decays. Not seen by ATHAR 06 in $\Upsilon(1S) \to p\overline{p}\gamma$.

[14] From the fit including final state interaction effects in isospin 0 S-wave according to SIBIRTSEV 05A. Systematic errors not estimated.

$X(1835)$ WIDTH

VALUE (MeV)	CL%	EVTS	DOCUMENT ID		TECN	COMMENT
130 ± 50 OUR AVERAGE Error includes scale factor of 6.4. See the ideogram below.						
$179.6\pm 8.7^{+22.5}_{-27.9}$			[1] ABLIKIM	25P	BES3	$J/\psi \to \gamma\gamma\phi$
$80.7\pm 5.2\pm 7.7$		21k	[2] ABLIKIM	24B	BES3	$J/\psi \to \gamma 3(\pi^+\pi^-)$
$245.2\pm 13.1^{+4.6}_{-9.6}$			[3] ABLIKIM	16J	BES3	$J/\psi \to \gamma\pi^+\pi^-\eta'$
$192^{+20}_{-17}{}^{+62}_{-43}$			[4] ABLIKIM	15T	BES3	$J/\psi \to \gamma K^0_S K^0_S \eta$
• • • We do not use the following data for averages, fits, limits, etc. • • •						
$175\pm 57\pm 25$			[5] ABLIKIM	18I	BES3	$J/\psi \to \gamma\gamma\phi(1020)$
$273.5\pm 21.4^{+6.1}_{-64.0}$			[6] ABLIKIM	16J	BES3	$J/\psi \to \gamma\pi^+\pi^-\eta'$
$83\pm 14\pm 11$		0.6k	[7] ABLIKIM	13U	BES3	$J/\psi \to \gamma 3(\pi^+\pi^-)$
< 76	90		[8] ABLIKIM	12D	BES3	$J/\psi \to \gamma p\overline{p}$
$190\pm 9^{+38}_{-36}$		4265	[9] ABLIKIM	11C	BES3	$J/\psi \to \gamma\pi^+\pi^-\eta'$
$57\pm 12^{+19}_{-4}$			[10] ABLIKIM	11J	BES3	$J/\psi \to \omega(\eta\pi^+\pi^-)$
0^{+44}_{-0}		231	[11,12] ALEXANDER	10	CLEO	$J/\psi \to \gamma p\overline{p}$
$67.7\pm 20.3\pm 7.7$		264	ABLIKIM	05R	BES2	$J/\psi \to \gamma\pi^+\pi^-\eta'$
< 153	90		[12,13] ABLIKIM	05R	BES2	$J/\psi \to \gamma p\overline{p}$
< 30			[12] BAI	03F	BES2	$J/\psi \to \gamma p\overline{p}$

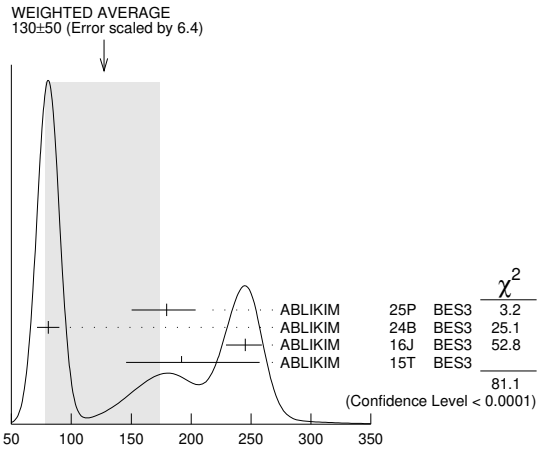

[1] From a partial wave analysis of $J/\psi \to \gamma\gamma\phi$ with significance 15.3σ. $J^{PC} = 0^{-+}$ established at 13.2σ.

[2] From a fit of the measured $3(\pi^+\pi^-)$ lineshape that accounts for the abrupt distortion observed at the $p\overline{p}$ threshold through interference with a second previously unseen narrow resonance near 1880 MeV. The fit uses Breit-Wigner functions for the signal shapes and includes known background contributions. A second solution of the fit gives 37k events.

[3] From a fit of the measured $\pi^+\pi^-\eta'$ lineshape that accounts for the abrupt distortion observed at the $p\overline{p}$ threshold through interference with a second previously unseen narrow resonance near 1870 MeV. The fit uses Breit-Wigner functions for the signal shapes and includes known backgrounds and contributors.

[4] Decay dominated by $f_0(980)\eta$ hence $I^G(J^{PC}) = 0^+(0^{-+})$.

[5] From a fit to $\gamma\phi$ invariant mass. Angular analysis consistent with $J^{PC} = 0^{-+}$. Other J^{PC} not excluded. Superseded by ABLIKIM 25P.

[6] Pole width from a fit of the measured $\pi^+\pi^-\eta'$ lineshape to a Flatte formula that accounts for the abrupt distortion observed at the $p\overline{p}$ threshold; the fit also includes known backgrounds and contributors, as well as an *ad hoc* Breit-Wigner function ($M \approx$ 1919 MeV; $\Gamma \approx$ 51 MeV) that is required for a good fit.

[7] Superseded by ABLIKIM 24B.

[8] From the fit including final state interaction effects in isospin 0 S-wave according to SIBIRTSEV 05A. Supersedes ABLIKIM 10G.

[9] From a fit of the $\pi^+\pi^-\eta'$ mass distribution to a combination of $\gamma f_1(1510)$, $\gamma X(1835)$, and two states $\gamma X(2120)$ and $\gamma\eta(2370)$, for $M(\pi^+\pi^-\eta') < 2.8$ GeV,and accounting for backgrounds from non-η' events and $J/\psi \to \pi^0\pi^+\pi^-\eta'$.

[10] The selected process is $J/\psi \to \omega a_0(980)\pi$ with $B(J/\psi \to \omega X \to \omega a_0(980)^{\pm}(\to \eta\pi^{\pm})\pi^{\mp}) = (1.50 \pm 0.26^{+0.72}_{-0.36}) \times 10^{-4}$. Not seen in $J/\psi(1S) \to \omega K^+ K^- \eta$ by ABLIKIM 24BQ with 90% CL upper limit of 9.55×10^{-7}. This state may be also due to $\eta_2(1870)$ or to a combination of $X(1835)$ and $\eta_2(1870)$.

[11] From a fit of the $p\overline{p}$ mass distribution to a combination of $\gamma X(1835)$, γR with $M(R) = 2100$ MeV and $\Gamma(R) = 160$ MeV, and $\gamma p\overline{p}$ phase space, for $M(p\overline{p}) < 2.85$ GeV.

[12] Evidence for a threshold enhancement in the $p\overline{p}$ mass spectrum was also reported by ABE 02K, AUBERT,B 05L, and WANG 05A in $B^+ \to p\overline{p}K^+$, WANG 05A in $B^0 \to p\overline{p}K^0_S$, ABE 02W in $\overline{B}^0 \to p\overline{p}D^0$, DEL-AMO-SANCHEZ 12 in $B \to D(D^*)p\overline{p}(\pi)$, and WEI 08 in $B^+ \to p\overline{p}\pi^+$ decays. Not seen by ATHAR 06 in $\Upsilon(1S) \to p\overline{p}\gamma$.

[13] From the fit including final state interaction effects in isospin 0 S-wave according to SIBIRTSEV 05A. Systematic errors not estimated.

$X(1835)$ DECAY MODES

	Mode	Fraction (Γ_i/Γ)
Γ_1	$p\overline{p}$	seen
Γ_2	$\eta'\pi^+\pi^-$	seen
Γ_3	$\gamma\gamma$	not seen
Γ_4	$K^0_S K^0_S \eta$	seen
Γ_5	$\gamma\phi(1020)$	seen
Γ_6	$3(\pi^+\pi^-)$	seen

$X(1835)$ $\Gamma(i)\Gamma(\gamma\gamma)/\Gamma(\text{total})$

$\Gamma(\eta'\pi^+\pi^-) \times \Gamma(\gamma\gamma)/\Gamma_{\text{total}}$ — $\Gamma_2\Gamma_3/\Gamma$

VALUE (eV)	CL%	DOCUMENT ID		TECN	COMMENT
• • • We do not use the following data for averages, fits, limits, etc. • • •					
<35.6	90	[1] ZHANG	12A	BELL	$e^+e^- \to e^+e^-\eta'\pi^+\pi^-$
<83	90	[2] ZHANG	12A	BELL	$e^+e^- \to e^+e^-\eta'\pi^+\pi^-$

[1] From a two-resonance fit and constructive interference of the $\eta(1760)$ and $X(1835)$, a significance of 2.8 σ.

[2] From a two-resonance fit and destructive interference of the $\eta(1760)$ and $X(1835)$, a significance of 2.8 σ.

$X(1835)$ BRANCHING RATIOS

$\Gamma(p\overline{p})/\Gamma(\eta'\pi^+\pi^-)$ — Γ_1/Γ_2

VALUE	DOCUMENT ID		TECN	COMMENT
• • • We do not use the following data for averages, fits, limits, etc. • • •				
0.333	ABLIKIM	05R	BES2	$J/\psi \to \gamma\pi^+\pi^-\eta'$

$\Gamma(\eta'\pi^+\pi^-)/\Gamma(K^0_S K^0_S \eta)$ — Γ_2/Γ_4

VALUE	DOCUMENT ID		TECN	COMMENT
• • • We do not use the following data for averages, fits, limits, etc. • • •				
6.7 ± 1.8	[1] ABLIKIM	15T	BES3	$J/\psi \to \gamma K^0_S K^0_S \eta$

[1] Using resutls from ABLIKIM 05R.

$\Gamma(\eta'\pi^+\pi^-)/\Gamma_{\text{total}}$ — Γ_2/Γ

VALUE	DOCUMENT ID		TECN	COMMENT
seen	[1] ABLIKIM	16J	BES3	$J/\psi \to \gamma\pi^+\pi^-\eta'$

[1] ABLIKIM 16J quotes $B(J/\psi \to \gamma X(1835)) \times B(X(1835) \to \pi^+\pi^-\eta') = (3.93 \pm 0.38^{+0.31}_{-0.84}) \times 10^{-4}$ from a fit of the measured $\pi^+\pi^-\eta'$ lineshape that accounts for the abrupt distortion observed at the $p\overline{p}$ threshold with a Flatte formula in addition to known backgrounds and contributors, as well as an *ad hoc* Breit-Wigner ($M \approx 1919$ MeV; $\Gamma \approx 51$ MeV) that is required for a good fit. Another explanation for the distortion provided by ABLIKIM 16J is that a second resonance near 1870 MeV interferes with the $X(1835)$; fits to this possibility yield product branching fraction values compatible with that shown within the respective systematic uncertainties.

$\Gamma(\gamma\phi(1020))/\Gamma_{\text{total}}$ — Γ_5/Γ

VALUE	DOCUMENT ID		TECN	COMMENT
seen	[1] ABLIKIM	25P	BES3	$J/\psi \to \gamma\gamma\phi$
• • • We do not use the following data for averages, fits, limits, etc. • • •				
possibly seen	[2] ABLIKIM	18I	BES3	$J/\psi \to \gamma\gamma\phi(1020)$

[1] From a partial wave analysis of $J/\psi \to \gamma\gamma\phi$ with significance 15.3σ. $J^{PC} = 0^{-+}$ established at 13.2σ.

[2] Seen as a peak in $\gamma\phi$ invariant mass. Angular analysis consistent with $J^{PC} = 0^{-+}$. Other J^{PC} not excluded. Superseded by ABLIKIM 25P.

$\Gamma(\gamma\gamma)/\Gamma(\eta'\pi^+\pi^-)$ — Γ_3/Γ_2

VALUE	CL%	DOCUMENT ID		TECN	COMMENT
$<9.80 \times 10^{-3}$	90	[1] ABLIKIM	18O	BES3	$\psi(2S) \to \pi^+\pi^-\gamma\gamma\gamma$

[1] Using results from ABLIKIM 16J.

$\Gamma(3(\pi^+\pi^-))/\Gamma_{\text{total}}$ — Γ_6/Γ

VALUE	EVTS	DOCUMENT ID		TECN	COMMENT
seen	21k	[1] ABLIKIM	24B	BES3	$J/\psi \to \gamma 3(\pi^+\pi^-)$
• • • We do not use the following data for averages, fits, limits, etc. • • •					
seen	0.6k	[2] ABLIKIM	13U	BES3	$J/\psi \to \gamma 3(\pi^+\pi^-)$

[1] ABLIKIM 24B quotes $B(J/\psi \to \gamma X(1835)) \times B(X(1835) \to 3(\pi^+\pi^-)) = (1.19 \pm 0.30 \pm 0.15) \times 10^{-5}$ for constructive interference and $(2.07 \pm 0.50 \pm 0.36) \times 10^{-5}$ for destructive interference from a fit of the measured $3(\pi^+\pi^-)$ lineshape that accounts for the abrupt distortion observed at the $p\overline{p}$ threshold through interference with a second narrow resonance near 1880 MeV. The solution for destructive interference gives 37k events.

[2] Superseded by ABLIKIM 24B.

$X(1835)$ REFERENCES

ABLIKIM	25P	PR D111 052011	M. Ablikim et al.	(BESIII Collab.)
ABLIKIM	24B	PRL 132 151901	M. Ablikim et al.	(BESIII Collab.)
ABLIKIM	24BQ	PR D110 052005	M. Ablikim et al.	(BESIII Collab.)
ABLIKIM	18I	PR D97 051101	M. Ablikim et al.	(BESIII Collab.)
ABLIKIM	18O	PR D97 072014	M. Ablikim et al.	(BESIII Collab.)
ABLIKIM	16J	PRL 117 042002	M. Ablikim et al.	(BESIII Collab.)
ABLIKIM	15T	PRL 115 091803	M. Ablikim et al.	(BESIII Collab.)
ABLIKIM	13U	PR D88 091502	M. Ablikim et al.	(BESIII Collab.)
ABLIKIM	12D	PRL 108 112003	M. Ablikim et al.	(BESIII Collab.) JPC
DEL-AMO-SA...	12	PR D85 092017	P. del Amo Sanchez et al.	(BABAR Collab.)
ZHANG	12A	PR D86 052002	C.C. Zhang et al.	(BELLE Collab.)
ABLIKIM	11C	PRL 106 072002	M. Ablikim et al.	(BESIII Collab.)
ABLIKIM	11J	PRL 107 182001	M. Ablikim et al.	(BESIII Collab.)
ABLIKIM	10G	CP C34 421	M. Ablikim et al.	(BESIII Collab.)
ALEXANDER	10	PR D82 092002	J.P. Alexander et al.	(CLEO Collab.)
WEI	08	PL B659 80	J.-T. Wei et al.	(BELLE Collab.)
ATHAR	06	PR D73 032001	S.B. Athar et al.	(CLEO Collab.)
ABLIKIM	05R	PRL 95 262001	M. Ablikim et al.	(BES Collab.)
AUBERT,B	05L	PR D72 051101	B. Aubert et al.	(BABAR Collab.)
SIBIRTSEV	05A	PR D71 054010	A. Sibirtsev, J. Haidenbauer	
WANG	05A	PL B617 141	M.-Z. Wang et al.	(BELLE Collab.)
BAI	03F	PRL 91 022001	J.Z. Bai et al.	(BES II Collab.)
ABE	02K	PRL 88 181803	K. Abe et al.	(BELLE Collab.)
ABE	02W	PRL 89 151802	K. Abe et al.	(BELLE Collab.)

$\phi_3(1850)$

$I^G(J^{PC}) = 0^-(3^{--})$

$\phi_3(1850)$ MASS

VALUE (MeV)	EVTS	DOCUMENT ID		TECN	COMMENT
1854 ± 7 OUR AVERAGE					
1855 ± 10		ASTON	88E	LASS	11 $K^-p \to K^-K^+\Lambda$, $K^0_S K^{\pm}\pi^{\mp}\Lambda$
1870^{+30}_{-20}	430	ARMSTRONG	82	OMEG	18.5 $K^-p \to K^-K^+\Lambda$
1850 ± 10	123	ALHARRAN	81B	HBC	8.25 $K^-p \to K\overline{K}\Lambda$

$\phi_3(1850)$ WIDTH

VALUE (MeV)	EVTS	DOCUMENT ID		TECN	COMMENT
87^{+28}_{-23} OUR AVERAGE Error includes scale factor of 1.2.					
64 ± 31		ASTON	88E	LASS	11 $K^-p \to K^-K^+\Lambda$, $K^0_S K^{\pm}\pi^{\mp}\Lambda$
160^{+90}_{-50}	430	ARMSTRONG	82	OMEG	18.5 $K^-p \to K^-K^+\Lambda$
80^{+40}_{-30}	123	ALHARRAN	81B	HBC	8.25 $K^-p \to K\overline{K}\Lambda$

$\phi_3(1850)$ DECAY MODES

	Mode	Fraction (Γ_i/Γ)
Γ_1	$K\overline{K}$	seen
Γ_2	$K\overline{K}^*(892) +$ c.c.	seen

$\phi_3(1850)$ BRANCHING RATIOS

$\Gamma(K\overline{K}^*(892) + \text{c.c.})/\Gamma(K\overline{K})$ — Γ_2/Γ_1

VALUE	DOCUMENT ID		TECN	COMMENT
$0.55^{+0.85}_{-0.45}$	ASTON	88E	LASS	11 $K^-p \to K^-K^+\Lambda$, $K^0_S K^{\pm}\pi^{\mp}\Lambda$
• • • We do not use the following data for averages, fits, limits, etc. • • •				
0.8 ± 0.4	ALHARRAN	81B	HBC	8.25 $K^-p \to K\overline{K}\pi\Lambda$

$\phi_3(1850)$ REFERENCES

ASTON	88E	PL B208 324	D. Aston et al.	(SLAC, NAGO, CINC, INUS) IGJPC
ARMSTRONG	82	PL 110B 77	T.A. Armstrong et al.	(BARI, BIRM, CERN+) JP
ALHARRAN	81B	PL 101B 357	S. Al-Harran et al.	(BIRM, CERN, GLAS+)

Int. J. Mod. Phys. A 2026.41. Downloaded from www.worldscientific.com
by UNIVERSITY OF CALIFORNIA @ BERKELEY on 09/16/26. Re-use and distribution is strictly not permitted, except for Open Access articles.

Meson Particle Listings

$\eta_1(1855)$, $\eta_2(1870)$, $\pi_2(1880)$

Int. J. Mod. Phys. A 2026.41. Downloaded from www.worldscientific.com by CALIFORNIA @ BERKELEY on 09/16/26. Re-use and distribution is strictly not permitted, except for Open Access articles.

$\eta_1(1855)$

$I^G(J^{PC}) = 0^+(1^{-+})$

OMITTED FROM SUMMARY TABLE

Meson with exotic (non-$q\overline{q}$) quantum numbers. A state decaying into $\eta\eta'$ with possible quantum numbers 1^{-+} was reported earlier in this mass region BARBERIS 00A in high energy central pp production and by ALDE 91B in $\pi^- p$ interactions, see the $f_2(1910)$, and the review on "Spectroscopy of Light Meson Resonances."

$\eta_1(1855)$ MASS

VALUE (MeV)	DOCUMENT ID		TECN	COMMENT
$1855 \pm 9^{+6}_{-1}$	[1] ABLIKIM	22AI	BES3	$J/\psi(1S) \to \gamma\eta\eta'$

[1] From a Breit-Wigner fit involving 9 resonances and the resonating exotic $\eta_1(1855) \to \eta\eta'$ P-wave. For analysis details see ABLIKIM 22AS.

$\eta_1(1855)$ WIDTH

VALUE (MeV)	DOCUMENT ID		TECN	COMMENT
$188 \pm 18^{+3}_{-8}$	[1] ABLIKIM	22AI	BES3	$J/\psi(1S) \to \gamma\eta\eta'$

[1] From a Breit-Wigner fit involving 9 resonances and the resonating exotic $\eta_1(1855) \to \eta\eta'$ P-wave. For analysis details see ABLIKIM 22AS.

$\eta_1(1855)$ DECAY MODES

	Mode	Fraction (Γ_i/Γ)
Γ_1	$\eta\eta'$	seen
Γ_2	$\eta\eta'$	

$\eta_1(1855)$ BRANCHING RATIOS

$\Gamma(\eta\eta')/\Gamma_{total}$ — Γ_1/Γ

VALUE	DOCUMENT ID		TECN	COMMENT
seen	ABLIKIM	22AI	BES3	$J/\psi \to \gamma\eta\eta'$
seen	BARBERIS	00A		$450\ pp \to p_f\eta\eta' p_s$
seen	ALDE	91B	GAM2	$38\ \pi^- p \to \eta\eta' n$
• • • We do not use the following data for averages, fits, limits, etc. • • •				
not seen	[1] ABLIKIM	25CJ	BES3	$\psi(2S) \to \gamma\chi_{c1} \to \eta\eta\eta'$

[1] ABLIKIM 25CJ reports $B(\chi_{c1} \to \eta_1(1855)\eta) \times B(\eta_1(1855) \to \eta\eta') < 9.79 \times 10^{-5}$ at 90% CL.

$\eta_1(1855)$ REFERENCES

ABLIKIM	25CJ	CP C49 123001	M. Ablikim *et al.*	(BESIII Collab.)
ABLIKIM	22AI	PRL 129 192002	M. Ablikim *et al.*	(BESIII Collab.)
Also		PR D106 072012	M. Ablikim *et al.*	(BESIII Collab.)
ABLIKIM	22AS	PR D106 072012	M. Ablikim *et al.*	(BESIII Collab.)
Also		PR D107 079901 (errat.)	M. Ablikim *et al.*	(BESIII Collab.)
BARBERIS	00A	PL B471 429	D. Barberis *et al.*	(WA 102 Collab.)
ALDE	91B	SJNP 54 455	D.M. Alde *et al.*	(SERP, BELG, LANL, LAPP+)
		Translated from YAF 54 751.		

$\eta_2(1870)$

$I^G(J^{PC}) = 0^+(2^{-+})$

$\eta_2(1870)$ MASS

VALUE (MeV)	EVTS	DOCUMENT ID		TECN	COMMENT
1842 ± 8 OUR AVERAGE					
1835 ± 12		BARBERIS	00B		$450\ pp \to p_f\eta\pi^+\pi^- p_s$
1844 ± 13		BARBERIS	00C		$450\ pp \to p_f 4\pi p_s$
1840 ± 25		BARBERIS	97B	OMEG	$450\ pp \to pp2(\pi^+\pi^-)$
1875 ± 20 ± 35		ADOMEIT	96	CBAR	$1.94\ \overline{p}p \to \eta 3\pi^0$
1881 ± 32 ± 40	26	KARCH	92	CBAL	$e^+e^- \to e^+e^-\eta\pi^0\pi^0$
• • • We do not use the following data for averages, fits, limits, etc. • • •					
1860 ± 5 ± 15		ANISOVICH	00E	SPEC	0.9–$1.94\ \overline{p}p \to \eta 3\pi^0$
1840 ± 15		BAI	99	BES	$J/\psi \to \gamma\eta\pi^+\pi^-$

$\eta_2(1870)$ WIDTH

VALUE (MeV)	EVTS	DOCUMENT ID		TECN	COMMENT
225 ± 14 OUR AVERAGE					
235 ± 22		BARBERIS	00B		$450\ pp \to p_f\eta\pi^+\pi^- p_s$
228 ± 23		BARBERIS	00C		$450\ pp \to p_f 4\pi p_s$
200 ± 40		BARBERIS	97B	OMEG	$450\ pp \to pp2(\pi^+\pi^-)$
200 ± 25 ± 45		ADOMEIT	96	CBAR	$1.94\ \overline{p}p \to \eta 3\pi^0$
221 ± 92 ± 44	26	KARCH	92	CBAL	$e^+e^- \to e^+e^-\eta\pi^0\pi^0$
• • • We do not use the following data for averages, fits, limits, etc. • • •					
$250 \pm 25^{+50}_{-35}$		ANISOVICH	00E	SPEC	0.9–$1.94\ \overline{p}p \to \eta 3\pi^0$
170 ± 40		BAI	99	BES	$J/\psi \to \gamma\eta\pi^+\pi^-$

$\eta_2(1870)$ DECAY MODES

	Mode	Fraction (Γ_i/Γ)
Γ_1	$\eta\pi\pi$	seen
Γ_2	$a_2(1320)\pi$	seen
Γ_3	$f_2(1270)\eta$	seen
Γ_4	$a_0(980)\pi$	seen
Γ_5	$\gamma\gamma$	seen

$\eta_2(1870)$ BRANCHING RATIOS

$\Gamma(a_2(1320)\pi)/\Gamma(f_2(1270)\eta)$ — Γ_2/Γ_3

VALUE	DOCUMENT ID		TECN	COMMENT
1.7 ± 0.4 OUR AVERAGE				
1.60 ± 0.40	[1] ANISOVICH	11	SPEC	0.9–$1.94\ p\overline{p}$
20.4 ± 6.6	BARBERIS	00B		$450\ pp \to p_f\eta\pi^+\pi^- p_s$
4.1 ± 2.3	ADOMEIT	96	CBAR	$1.94\ \overline{p}p \to \eta 3\pi^0$

[1] Reanalysis of ADOMEIT 96 and ANISOVICH 00E.

$\Gamma(a_2(1320)\pi)/\Gamma(a_0(980)\pi)$ — Γ_2/Γ_4

VALUE	DOCUMENT ID		COMMENT
32.6 ± 12.6	BARBERIS	00B	$450\ pp \to p_f\eta\pi^+\pi^- p_s$

$\Gamma(a_0(980)\pi)/\Gamma(f_2(1270)\eta)$ — Γ_4/Γ_3

VALUE	DOCUMENT ID		TECN	COMMENT
0.48 ± 0.45	[1] ANISOVICH	11	SPEC	0.9–$1.94\ p\overline{p}$

[1] Reanalysis of ADOMEIT 96 and ANISOVICH 00E.

$\Gamma(\gamma\gamma)/\Gamma_{total}$ — Γ_5/Γ

VALUE	DOCUMENT ID		TECN	COMMENT
seen	KARCH	92	CBAL	$e^+e^- \to e^+e^-\eta\pi^0\pi^0$

$\eta_2(1870)$ REFERENCES

ANISOVICH	11	EPJ C71 1511	A.V. Anisovich *et al.*	(LOQM, RAL, PNPI)
ANISOVICH	00E	PL B477 19	A.V. Anisovich *et al.*	
BARBERIS	00B	PL B471 435	D. Barberis *et al.*	(WA 102 Collab.)
BARBERIS	00C	PL B471 440	D. Barberis *et al.*	(WA 102 Collab.)
BAI	99	PL B446 356	J.Z. Bai *et al.*	(BES Collab.)
BARBERIS	97B	PL B413 217	D. Barberis *et al.*	(WA 102 Collab.)
ADOMEIT	96	ZPHY C71 227	J. Adomeit *et al.*	(Crystal Barrel Collab.)
KARCH	92	ZPHY C54 33	K. Karch *et al.*	(Crystal Ball Collab.)

$\pi_2(1880)$

$I^G(J^{PC}) = 1^-(2^{-+})$

$\pi_2(1880)$ MASS

VALUE (MeV)	EVTS	DOCUMENT ID		TECN	CHG	COMMENT
$\mathbf{1874^{+26}_{-5}}$ **OUR AVERAGE**	Error includes scale factor of 1.6. See the ideogram below.					
1847^{+20}_{-3}	46M	[1] AGHASYAN	18B	COMP		$190\ \pi^- p \to \pi^-\pi^+\pi^- p$
1929 ± 24 ± 18	4k	EUGENIO	08	B852	−	$18\ \pi^- p \to \eta\eta\pi^- p$
1876 ± 11 ± 67	145k	LU	05	B852	−	$18\ \pi^- p \to \omega\pi^-\pi^0 p$
2003 ± 88 ± 148	69k	KUHN	04	B852	−	$18\ \pi^- p \to \eta\pi^+\pi^-\pi^- p$
• • • We do not use the following data for averages, fits, limits, etc. • • •						
1880 ± 20		ANISOVICH	01B	SPEC	0	0.6–$1.94\ \overline{p}p \to \eta\eta\pi^0\pi^0$

[1] Statistical error negligible.

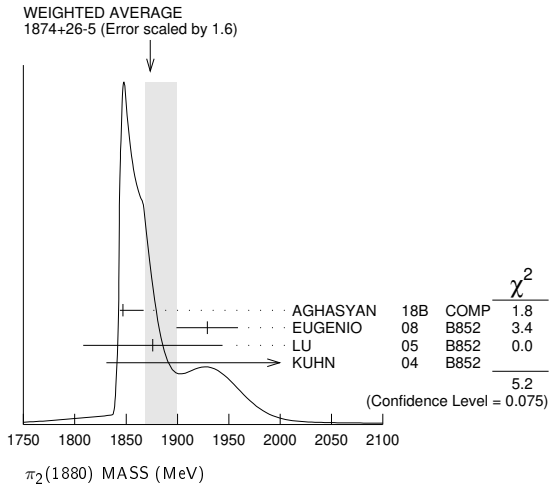

Int. J. Mod. Phys. A 2026.41. Downloaded from www.worldscientific.com
by UNIVERSITY OF CALIFORNIA @ BERKELEY on 09/16/26. Re-use and distribution is strictly not permitted, except for Open Access articles.

$\pi_2(1880)$ WIDTH

VALUE (MeV)	EVTS	DOCUMENT ID		TECN	CHG	COMMENT
237^{+33}_{-30} OUR AVERAGE		Error includes scale factor of 1.2.				
246^{+33}_{-28}	46M	[2] AGHASYAN	18B	COMP		190 $\pi^- p \to \pi^- \pi^+ \pi^- p$
$323 \pm 87 \pm 43$	4k	EUGENIO	08	B852	−	18 $\pi^- p \to \eta\eta\pi^- p$
$146 \pm 17 \pm 62$	145k	LU	05	B852	−	18 $\pi^- p \to \omega\pi^- \pi^0 p$
$306 \pm 132 \pm 121$	69k	KUHN	04	B852	−	18 $\pi^- p \to \eta\pi^+ \pi^- \pi^- p$
• • • We do not use the following data for averages, fits, limits, etc. • • •						
255 ± 45		ANISOVICH	01B	SPEC	0	0.6–1.94 $\overline{p}p \to \eta\eta\pi^0\pi^0$

[2] Statistical error negligible.

$\pi_2(1880)$ DECAY MODES

	Mode	Fraction (Γ_i/Γ)
Γ_1	$\eta\eta\pi^-$	seen
Γ_2	$a_0(980)\eta$	seen
Γ_3	$a_2(1320)\eta$	seen
Γ_4	$f_0(1500)\pi$	seen
Γ_5	$f_1(1285)\pi$	seen
Γ_6	$\omega\pi^-\pi^0$	seen

$\Gamma(a_2(1320)\eta)/\Gamma(f_1(1285)\pi)$ — Γ_3/Γ_5

VALUE	EVTS	DOCUMENT ID		TECN	CHG	COMMENT
• • • We do not use the following data for averages, fits, limits, etc. • • •						
22.7 ± 7.3	69k	KUHN	04	B852	−	18 $\pi^- p \to \eta\pi^+ \pi^- \pi^- p$

$\Gamma(f_0(1500)\pi)/\Gamma(a_0(980)\eta)$ — Γ_4/Γ_2

VALUE	DOCUMENT ID		TECN	CHG	COMMENT
• • • We do not use the following data for averages, fits, limits, etc. • • •					
$0.28^{+0.20}_{-0.15}$	[3] ANISOVICH	01B	SPEC	0	0.6–1.94 $\overline{p}p \to \eta\eta\pi^0\pi^0$

[3] Systematic errors not estimated.

$\pi_2(1880)$ REFERENCES

AGHASYAN	18B	PR D98 092003	M. Aghasyan *et al.*	(COMPASS Collab.)
EUGENIO	08	PL B660 466	P. Eugenio *et al.*	(BNL E852 Collab.)
LU	05	PRL 94 032002	M. Lu *et al.*	(BNL E852 Collab.)
KUHN	04	PL B595 109	J. Kuhn *et al.*	(BNL E852 Collab.)
ANISOVICH	01B	PL B500 222	A.V. Anisovich *et al.*	

$\rho(1900)$

$I^G(J^{PC}) = 1^+(1^{--})$

OMITTED FROM SUMMARY TABLE

See the review on "Spectroscopy of Light Meson Resonances."

$\rho(1900)$ MASS

VALUE (MeV)	EVTS	DOCUMENT ID		TECN	COMMENT
• • • We do not use the following data for averages, fits, limits, etc. • • •					
1880 ± 10		[1] ABLIKIM	22L	BES3	2.0–3.08 $e^+e^- \to K^+K^-\pi^0$
$1909 \pm 17 \pm 25$	54	[2] AUBERT	08S	BABR	10.6 $e^+e^- \to \phi\pi^0\gamma$
1880 ± 30		AUBERT	06D	BABR	10.6 $e^+e^- \to 3\pi^+3\pi^-\gamma$
1860 ± 20		AUBERT	06D	BABR	10.6 $e^+e^- \to 2(\pi^+\pi^-\pi^0)\gamma$
1910 ± 10		[3,4] FRABETTI	04	E687	$\gamma p \to 3\pi^+3\pi^- p$
1870 ± 10		ANTONELLI	96	SPEC	$e^+e^- \to$ hadrons

[1] From a partial wave amplitude analysis at $\sqrt{s} = 2.125$ GeV which includes all the possible intermediate states that match J^{PC} conservation in the subsequent two-body decay. The intermediate states are parameterized with the relativistic Breit-Wigner functions. Statistical error only.
[2] From the fit with two resonances.
[3] From a fit with two resonances with the JACOB 72 continuum.
[4] Supersedes FRABETTI 01.

$\rho(1900)$ WIDTH

VALUE (MeV)	EVTS	DOCUMENT ID		TECN	COMMENT
• • • We do not use the following data for averages, fits, limits, etc. • • •					
69 ± 15		[1] ABLIKIM	22L	BES3	2.0–3.08 $e^+e^- \to K^+K^-\pi^0$
$48 \pm 17 \pm 2$	54	[2] AUBERT	08S	BABR	10.6 $e^+e^- \to \phi\pi^0\gamma$
130 ± 30		AUBERT	06D	BABR	10.6 $e^+e^- \to 3\pi^+3\pi^-\gamma$
160 ± 20		AUBERT	06D	BABR	10.6 $e^+e^- \to 2(\pi^+\pi^-\pi^0)\gamma$
37 ± 13		[3,4] FRABETTI	04	E687	$\gamma p \to 3\pi^+3\pi^- p$
10 ± 5		ANTONELLI	96	SPEC	$e^+e^- \to$ hadrons

[1] From a partial wave amplitude analysis at $\sqrt{s} = 2.125$ GeV which includes all the possible intermediate states that match J^{PC} conservation in the subsequent two-body decay. The intermediate states are parameterized with the relativistic Breit-Wigner functions. Statistical error only.
[2] From the fit with two resonances.
[3] From a fit with two resonances with the JACOB 72 continuum.
[4] Supersedes FRABETTI 01.

$\rho(1900)$ $\Gamma(i)\Gamma(e^+e^-)/\Gamma^2(\text{total})$

$\Gamma(\phi\pi)/\Gamma_{total} \times \Gamma(e^+e^-)/\Gamma_{total}$ — $\Gamma_4/\Gamma \times \Gamma_6/\Gamma$

VALUE (units 10^{-8})	EVTS	DOCUMENT ID		TECN	COMMENT
• • • We do not use the following data for averages, fits, limits, etc. • • •					
$4.2 \pm 1.2 \pm 0.8$	54	[1] AUBERT	08S	BABR	10.6 $e^+e^- \to \phi\pi^0\gamma$

[1] From the fit with two resonances.

$\rho(1900)$ DECAY MODES

	Mode	Fraction (Γ_i/Γ)
Γ_1	6π	seen
Γ_2	$3\pi^+3\pi^-$	seen
Γ_3	$2\pi^+2\pi^-2\pi^0$	
Γ_4	$\phi\pi$	seen
Γ_5	hadrons	seen
Γ_6	e^+e^-	seen
Γ_7	$\overline{N}N$	not seen

$\rho(1900)$ BRANCHING RATIOS

$\Gamma(6\pi)/\Gamma_{total}$ — Γ_1/Γ

VALUE	EVTS	DOCUMENT ID		TECN	COMMENT
seen	8k	AKHMETSHIN	13	CMD3	$e^+e^- \to 3\pi^+3\pi^-$
not seen		AGNELLO	02	OBLX	$\overline{n}p \to 3\pi^+2\pi^-\pi^0$
seen		FRABETTI	01	E687	$\gamma p \to 3\pi^+3\pi^- p$
seen		ANTONELLI	96	SPEC	$e^+e^- \to$ hadrons

$\rho(1900)$ REFERENCES

ABLIKIM	22L	JHEP 2207 045	M. Ablikim *et al.*	(BESIII Collab.)
AKHMETSHIN	13	PL B723 82	R.R. Akhmetshin *et al.*	(CMD-3 Collab.)
AUBERT	08S	PR D77 092002	B. Aubert *et al.*	(BABAR Collab.)
AUBERT	06D	PR D73 052003	B. Aubert *et al.*	(BABAR Collab.)
FRABETTI	04	PL B578 290	P.L. Frabetti *et al.*	(FNAL E687 Collab.)
AGNELLO	02	PL B527 39	M. Agnello *et al.*	(OBELIX Collab.)
FRABETTI	01	PL B514 240	P.L. Frabetti *et al.*	(FNAL E687 Collab.)
ANTONELLI	96	PL B365 427	A. Antonelli *et al.*	(FENICE Collab.)
JACOB	72	PR D5 1847	M. Jacob, R. Slansky	

$f_2(1910)$

$I^G(J^{PC}) = 0^+(2^{++})$

OMITTED FROM SUMMARY TABLE

We list here three different peaks with close masses and widths seen in the mass distributions of $\omega\omega$, $\eta\eta'$, and K^+K^- final states. ALDE 91B argues that they are of different nature.

$f_2(1910)$ MASS

$f_2(1910)$ $\omega\omega$ MODE

VALUE (MeV)	DOCUMENT ID		TECN	COMMENT
1900± 9 OUR AVERAGE	Error includes scale factor of 1.4. See the ideogram below.			
1890 ± 10	[1] AMELIN	06	VES	36 $\pi^- p \to \omega\omega n$
1897 ± 11	BARBERIS	00F		450 $pp \to p_f \omega\omega p_s$
1924 ± 14	ALDE	90	GAM2	38 $\pi^- p \to \omega\omega n$

[1] Supersedes BELADIDZE 92B.

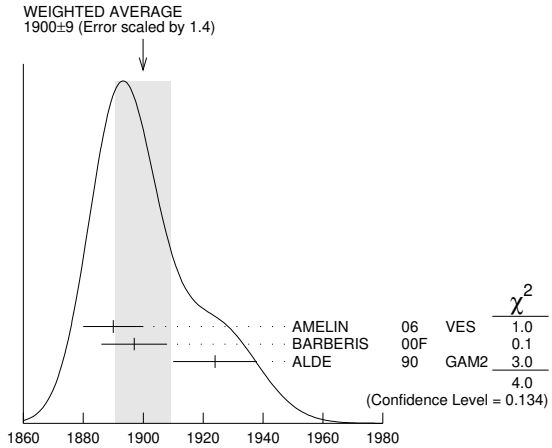

$f_2(1910)$ $\omega\omega$ MODE MASS (MeV)

Int. J. Mod. Phys. A 2026.41. Downloaded from www.worldscientific.com
by [redacted]LIFORNIA @ BERKELEY on 09/16/26. Re-use and distribution is strictly not permitted, except for Open Access articles.

$f_2(1910)$ $\eta\eta'$ MODE

VALUE (MeV)	DOCUMENT ID		TECN	COMMENT
1934±16	[1] BARBERIS	00A		450 $pp \to p_f \eta\eta' p_s$
• • • We do not use the following data for averages, fits, limits, etc. • • •				
1934±20	[2] ANISOVICH	00J	SPEC	
1911±10	ALDE	91B	GAM2	38 $\pi^- p \to \eta\eta' n$

[1] Also compatible with $J^{PC} = 1^{-+}$.
[2] Combined fit with $\eta\eta$, $\pi\pi$, and $\eta\pi\pi$.

$f_2(1910)$ K^+K^- MODE

VALUE (MeV)	DOCUMENT ID		TECN	COMMENT
• • • We do not use the following data for averages, fits, limits, etc. • • •				
1941±18	[1] AMSLER	06	CBAR	1.64 $\overline{p}p \to K^+K^-\pi^0$

[1] Tentative, could be $f_2(1950)$.

$f_2(1910)$ WIDTH

$f_2(1910)$ $\omega\omega$ MODE

VALUE (MeV)	DOCUMENT ID		TECN	COMMENT
167±21 OUR AVERAGE Error includes scale factor of 1.3. See the ideogram below.				
165±19	[1] AMELIN	06	VES	36 $\pi^- p \to \omega\omega n$
202±32	BARBERIS	00F		450 $pp \to p_f \omega\omega p_s$
91±50	ALDE	90	GAM2	38 $\pi^- p \to \omega\omega n$

[1] Supersedes BELADIDZE 92B.

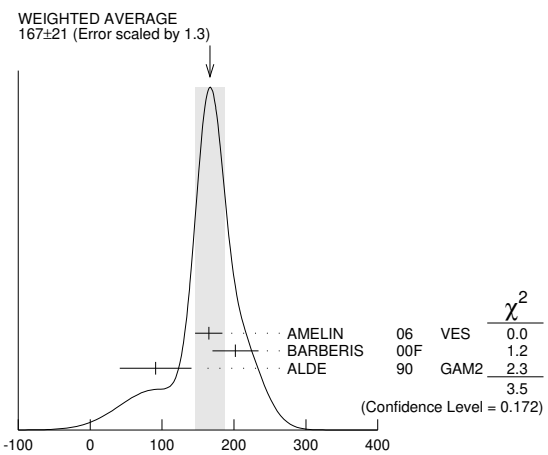

$f_2(1910)$ $\omega\omega$ mode width (MeV)

$f_2(1910)$ $\eta\eta'$ MODE

VALUE (MeV)	DOCUMENT ID		TECN	COMMENT
141±41	[1] BARBERIS	00A		450 $pp \to p_f \eta\eta' p_s$
• • • We do not use the following data for averages, fits, limits, etc. • • •				
271±25	[2] ANISOVICH	00J	SPEC	
90±35	ALDE	91B	GAM2	38 $\pi^- p \to \eta\eta' n$

[1] Also compatible with $J^{PC}=1^{-+}$.
[2] Combined fit with $\eta\eta$, $\pi\pi$, and $\eta\pi\pi$.

$f_2(1910)$ K^+K^- MODE

VALUE (MeV)	DOCUMENT ID		TECN	COMMENT
• • • We do not use the following data for averages, fits, limits, etc. • • •				
120±40	AMSLER	06	CBAR	1.64 $\overline{p}p \to K^+K^-\pi^0$

$f_2(1910)$ DECAY MODES

	Mode	Fraction (Γ_i/Γ)
Γ_1	$\pi^0\pi^0$	
Γ_2	K^+K^-	seen
Γ_3	$K^0_S K^0_S$	
Γ_4	$\eta\eta$	seen
Γ_5	$\omega\omega$	seen
Γ_6	$\eta\eta'$	seen
Γ_7	$\eta'\eta'$	
Γ_8	$\rho\rho$	seen
Γ_9	$a_2(1320)\pi$	seen
Γ_{10}	$f_2(1270)\eta$	seen

$f_2(1910)$ BRANCHING RATIOS

$\Gamma(K^+K^-)/\Gamma_{total}$ — Γ_2/Γ

VALUE	DOCUMENT ID		TECN	COMMENT
seen	[1] AMSLER	06	CBAR	1.64 $\overline{p}p \to K^+K^-\pi^0$

[1] Tentative, could be $f_2(1950)$.

$\Gamma(\pi^0\pi^0)/\Gamma(\eta\eta')$ — Γ_1/Γ_6

VALUE	DOCUMENT ID		TECN	COMMENT
• • • We do not use the following data for averages, fits, limits, etc. • • •				
<0.1	ALDE	89	GAM2	38$\pi^- p \to \eta\eta' n$

$\Gamma(K^0_S K^0_S)/\Gamma(\eta\eta')$ — Γ_3/Γ_6

VALUE	CL%	DOCUMENT ID		TECN	COMMENT
• • • We do not use the following data for averages, fits, limits, etc. • • •					
<0.066	90	BALOSHIN	86	SPEC	40$\pi p \to K^0_S K^0_S n$

$\Gamma(\eta\eta)/\Gamma(\eta\eta')$ — Γ_4/Γ_6

VALUE	CL%	DOCUMENT ID		TECN	COMMENT
• • • We do not use the following data for averages, fits, limits, etc. • • •					
<0.05	90	ALDE	91B	GAM2	38 $\pi^- p \to \eta\eta' n$

$\Gamma(\omega\omega)/\Gamma(\eta\eta')$ — Γ_5/Γ_6

VALUE	DOCUMENT ID		COMMENT
• • • We do not use the following data for averages, fits, limits, etc. • • •			
2.6±0.6	BARBERIS	00F	450 $pp \to p_f \omega\omega p_s$

$\Gamma(\eta'\eta')/\Gamma_{total}$ — Γ_7/Γ

VALUE	DOCUMENT ID		TECN	COMMENT
• • • We do not use the following data for averages, fits, limits, etc. • • •				
probably not seen	BARBERIS	00A		450 $pp \to p_f \eta'\eta' p_s$
possibly seen	BELADIDZE	92D	VES	37 $\pi^- p \to \eta'\eta' n$

$\Gamma(\rho\rho)/\Gamma(\omega\omega)$ — Γ_8/Γ_5

VALUE	DOCUMENT ID		COMMENT
• • • We do not use the following data for averages, fits, limits, etc. • • •			
2.6±0.4	BARBERIS	00F	450 $pp \to p_f \omega\omega p_s$

$\Gamma(f_2(1270)\eta)/\Gamma(a_2(1320)\pi)$ — Γ_{10}/Γ_9

VALUE	DOCUMENT ID		TECN	COMMENT
0.09±0.05	[1] ANISOVICH	11	SPEC	0.9–1.94 $p\overline{p}$

[1] Reanalysis of ADOMEIT 96 and ANISOVICH 00E.

$f_2(1910)$ REFERENCES

ANISOVICH	11	EPJ C71 1511	A.V. Anisovich *et al.*	(LOQM, RAL, PNPI)
AMELIN	06	PAN 69 690	D.V. Amelin *et al.*	(VES Collab.)
		Translated from YAF 69 715.		
AMSLER	06	PL B639 165	C. Amsler *et al.*	(Crystal Barrel Collab.)
ANISOVICH	00E	PL B477 19	A.V. Anisovich *et al.*	
ANISOVICH	00J	PL B491 47	A.V. Anisovich *et al.*	(RAL, LOQM, PNPI+)
BARBERIS	00A	PL B471 429	D. Barberis *et al.*	(WA 102 Collab.)
BARBERIS	00F	PL B484 198	D. Barberis *et al.*	(WA 102 Collab.)
ADOMEIT	96	ZPHY C71 227	J. Adomeit *et al.*	(Crystal Barrel Collab.)
BELADIDZE	92B	ZPHY C54 367	G.M. Beladidze *et al.*	(VES Collab.)
BELADIDZE	92D	ZPHY C57 13	G.M. Beladidze *et al.*	(VES Collab.)
ALDE	91B	SJNP 54 455	D.M. Alde *et al.*	(SERP, BELG, LANL, LAPP+)
		Translated from YAF 54 751.		
Also		PL B276 375	D.M. Alde *et al.*	(BELG, SERP, KEK, LANL+)
ALDE	90	PL B241 600	D.M. Alde *et al.*	(SERP, BELG, LANL, LAPP+)
ALDE	89	PL B216 447	D.M. Alde *et al.*	(SERP, BELG, LANL, LAPP)
Also		SJNP 48 1035	D.M. Alde *et al.*	(BELG, SERP, LANL, LAPP)
		Translated from YAF 48 1724.		
BALOSHIN	86	SJNP 43 959	O.N. Baloshin *et al.*	(ITEP)
		Translated from YAF 43 1487.		

$a_0(1950)$

$I^G(J^{PC}) = 1^-(0^{++})$

OMITTED FROM SUMMARY TABLE

Needs confirmation. Seen in $\gamma\gamma \to \eta_c(1S) \to K\overline{K}\pi$ by LEES 16A with significance 2.5 σ in $K^0_S K^\pm\pi^\mp$ and 4.2 σ in $K^+K^-\pi^0$.

$a_0(1950)$ MASS

VALUE (MeV)	EVTS	DOCUMENT ID		TECN	COMMENT
1931±14±22	12k	[1,2] LEES	16A	BABR	$\gamma\gamma \to \eta_c(1S) \to K\overline{K}\pi$
• • • We do not use the following data for averages, fits, limits, etc. • • •					
1949±32±76	8k	[1] LEES	16A	BABR	$\gamma\gamma \to \eta_c(1S) \to K^0_S K^\pm\pi^\mp$
1927±15±23	4k	[1] LEES	16A	BABR	$\gamma\gamma \to \eta_c(1S) \to K^+K^-\pi^0$

[1] From a model-independent partial wave analysis fit to a relativistic Breit-Wigner function with a floating width.
[2] Weighted average of the $K^0_S K^\pm$ and K^+K^- decay modes.

Int. J. Mod. Phys. A 2026.41. Downloaded from www.worldscientific.com
by UNIVERSITY OF CALIFORNIA @ BERKELEY on 09/16/26. Re-use and distribution is strictly not permitted, except for Open Access articles.

$a_0(1950)$ WIDTH

VALUE (MeV)	EVTS	DOCUMENT ID		TECN	COMMENT
271±22± 29	12k	[1,2] LEES	16A	BABR	$\gamma\gamma \to \eta_c(1S) \to K\overline{K}\pi$
• • • We do not use the following data for averages, fits, limits, etc. • • •					
265±36±110	8k	[1] LEES	16A	BABR	$\gamma\gamma \to \eta_c(1S) \to K^0_S K^\pm \pi^\mp$
274±28± 30	4k	[1] LEES	16A	BABR	$\gamma\gamma \to \eta_c(1S) \to K^+ K^- \pi^0$

[1] From a model-independent partial wave analysis fit to a relativistic Breit-Wigner function with a floating mass.
[2] Weighted average of the $K^0_S K^\pm$ and $K^+ K^-$ decay modes.

$a_0(1950)$ DECAY MODES

	Mode	Fraction (Γ_i/Γ)
Γ_1	$K\overline{K}$	seen

$a_0(1950)$ BRANCHING RATIOS

$\Gamma(K\overline{K})/\Gamma_{total}$ — Γ_1/Γ

VALUE	EVTS	DOCUMENT ID		TECN	COMMENT
seen	12k	[1] LEES	16A	BABR	$\gamma\gamma \to \eta_c(1S) \to K\overline{K}\pi$

[1] From a model-independent partial wave analysis.

$a_0(1950)$ REFERENCES

LEES 16A PR D93 012005 J.P. Lees et al. (BABAR Collab.)

$f_2(1950)$

$I^G(J^{PC}) = 0^+(2^{++})$

$f_2(1950)$ T-MATRIX POLE $\sqrt{s}$

Note that $\Gamma = -2\,\mathrm{Im}(\sqrt{s})$.

VALUE (MeV)	DOCUMENT ID		TECN	COMMENT
(1830–2020) − i (110–220) OUR ESTIMATE				
(2069.9 ± 22.2 ± 17.6) − i (130.0±26.0±19.3)	ABLIKIM	25CD	BES3	$e^+e^- \to \psi(2S)$
(1955 ± 75) − i (175 ± 57)	[1] RODAS	22	RVUE	$J/\psi(1S) \to \gamma(\pi\pi,\ K\overline{K})$
(1978.2 ± 1.8$^{+28.4}_{-16.9}$) − i (118.8 ± 0.8$^{+20.8}_{-7.8}$)	[2] ALBRECHT	20	RVUE	$0.9\ \overline{p}p \to \pi^0\pi^0\eta,\ \pi^0\eta\eta,\ \pi^0K^+K^-$
(1867 ± 46) − i (193 ± 29)	AMSLER	02	CBAR	$0.9\ \overline{p}p \to \pi^0\eta\eta,\ \pi^0\pi^0\pi^0$

[1] T-matrix pole from coupled channel K-matrix fit to data on $J/\psi \to \gamma\pi^0\pi^0$ (ABLIKIM 15AE) and $J/\psi \to \gamma K^0_S K^0_S$ (ABLIKIM 18AA).
[2] T-matrix pole, 4 poles, 4 channels, including scattering data from HYAMS 75 ($\pi\pi$), LONGACRE 86 ($K\overline{K}$), BINON 83 ($\eta\eta$).

$f_2(1950)$ MASS

VALUE (MeV)	DOCUMENT ID		TECN	COMMENT
1936±12 OUR AVERAGE	Error includes scale factor of 1.3. See the ideogram below.			
1940±50	BAI	00A	BES	$J/\psi \to \gamma(\pi^+\pi^-\pi^+\pi^-)$
1980±22	[1] BARBERIS	00C		$450\ pp \to pp4\pi$
1940±22	[2] BARBERIS	00C		$450\ pp \to pp2\pi2\pi^0$
1960±30	BARBERIS	97B	OMEG	$450\ pp \to pp2(\pi^+\pi^-)$
1918±12	ANTINORI	95	OMEG	$300,450\ pp \to pp2(\pi^+\pi^-)$
• • • We do not use the following data for averages, fits, limits, etc. • • •				
2038$^{+13+12}_{-11-73}$	[3] UEHARA	09	BELL	$10.6\ e^+e^- \to e^+e^-\pi^0\pi^0$
1930±25	[4] BINON	05	GAMS	$33\ \pi^-p \to \eta\eta n$
1980± 2±14	ABE	04	BELL	$10.6\ e^+e^- \to e^+e^-K^+K^-$
2010±25	ANISOVICH	00J	SPEC	
1980±50	ANISOVICH	99B	SPEC	$1.35–1.94\ p\overline{p} \to \eta\eta\pi^0$
∼ 1990	[5] OAKDEN	94	RVUE	$0.36–1.55\ \overline{p}p \to \pi\pi$
1950±15	[6] ASTON	91	LASS	$11\ K^-p \to \Lambda K\overline{K}\pi\pi$

[1] Decaying into $\pi^+\pi^-2\pi^0$.
[2] Decaying into $2(\pi^+\pi^-)$.
[3] Taking into account $f_4(2050)$.
[4] First solution, PWA is ambiguous.
[5] From solution B of amplitude analysis of data on $\overline{p}p \to \pi\pi$. See however KLOET 96 who fit $\pi^+\pi^-$ only and find waves only up to $J = 3$ to be important but not significantly resonant.
[6] Cannot determine spin to be 2.

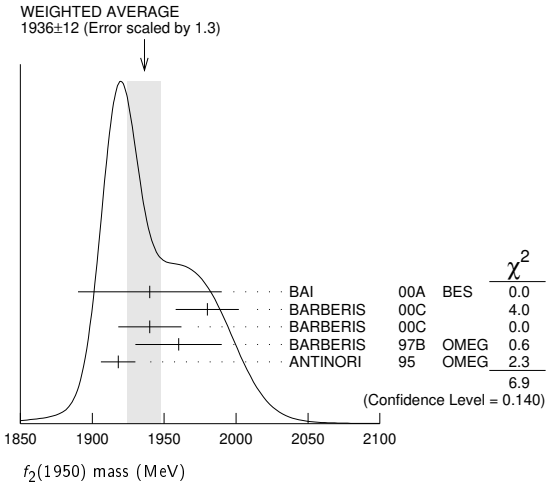

$f_2(1950)$ WIDTH

VALUE (MeV)	DOCUMENT ID		TECN	COMMENT
464± 24 OUR AVERAGE				
380$^{+120}_{-90}$	BAI	00A	BES	$J/\psi \to \gamma(\pi^+\pi^-\pi^+\pi^-)$
520± 50	[1] BARBERIS	00C		$450\ pp \to pp4\pi$
485± 55	[2] BARBERIS	00C		$450\ pp \to pp4\pi$
460± 40	BARBERIS	97B	OMEG	$450\ pp \to pp2(\pi^+\pi^-)$
390± 60	ANTINORI	95	OMEG	$300,450\ pp \to pp2(\pi^+\pi^-)$
• • • We do not use the following data for averages, fits, limits, etc. • • •				
441$^{+27+28}_{-25-192}$	[3] UEHARA	09	BELL	$10.6\ e^+e^- \to e^+e^-\pi^0\pi^0$
450± 50	[4] BINON	05	GAMS	$33\ \pi^-p \to \eta\eta n$
297± 12± 6	ABE	04	BELL	$10.6\ e^+e^- \to e^+e^-K^+K^-$
495± 35	ANISOVICH	00J	SPEC	
500±100	ANISOVICH	99B	SPEC	$1.35–1.94\ p\overline{p} \to \eta\eta\pi^0$
∼ 100	[5] OAKDEN	94	RVUE	$0.36–1.55\ \overline{p}p \to \pi\pi$
250± 50	[6] ASTON	91	LASS	$11\ K^-p \to \Lambda K\overline{K}\pi\pi$

[1] Decaying into $\pi^+\pi^-2\pi^0$.
[2] Decaying into $2(\pi^+\pi^-)$.
[3] Taking into account $f_4(2050)$.
[4] First solution, PWA is ambiguous.
[5] From solution B of amplitude analysis of data on $\overline{p}p \to \pi\pi$. See however KLOET 96 who fit $\pi^+\pi^-$ only and find waves only up to $J = 3$ to be important but not significantly resonant.
[6] Cannot determine spin to be 2.

$f_2(1950)$ DECAY MODES

	Mode	Fraction (Γ_i/Γ)
Γ_1	$K^*(892)\overline{K}^*(892)$	seen
Γ_2	$\pi\pi$	
Γ_3	$\pi^+\pi^-$	seen
Γ_4	$\pi^0\pi^0$	seen
Γ_5	4π	seen
Γ_6	$\pi^+\pi^-\pi^+\pi^-$	
Γ_7	$a_2(1320)\pi$	
Γ_8	$\eta\eta$	seen
Γ_9	$K\overline{K}$	seen
Γ_{10}	$\gamma\gamma$	seen
Γ_{11}	$\gamma\phi$	seen
Γ_{12}	$p\overline{p}$	seen

$f_2(1950)$ $\Gamma(i)\Gamma(\gamma\gamma)/\Gamma(total)$

$\Gamma(K\overline{K}) \times \Gamma(\gamma\gamma)/\Gamma_{total}$ — $\Gamma_9\Gamma_{10}/\Gamma$

VALUE (eV)	DOCUMENT ID		TECN	COMMENT
• • • We do not use the following data for averages, fits, limits, etc. • • •				
122±4±26	[1] ABE	04	BELL	$10.6\ e^+e^- \to e^+e^-K^+K^-$

[1] Assuming spin 2.

$\Gamma(\pi\pi) \times \Gamma(\gamma\gamma)/\Gamma_{total}$ — $\Gamma_2\Gamma_{10}/\Gamma$

VALUE	DOCUMENT ID		TECN	COMMENT
• • • We do not use the following data for averages, fits, limits, etc. • • •				
162$^{+69+1137}_{-42-204}$	[1] UEHARA	09	BELL	$10.6\ e^+e^- \to e^+e^-\pi^0\pi^0$

[1] Taking into account $f_4(2050)$.

Int. J. Mod. Phys. A 2026.41. Downloaded from www.worldscientific.com
by CALIFORNIA @ BERKELEY on 09/16/26. Re-use and distribution is strictly not permitted, except for Open Access articles.

$f_2(1950)$ BRANCHING RATIOS

$\Gamma(K^*(892)\overline{K}^*(892))/\Gamma_{total}$ — Γ_1/Γ

VALUE	DOCUMENT ID		TECN	CHG	COMMENT
seen	ASTON	91	LASS	0	11 $K^- p \to \Lambda K \overline{K} \pi \pi$

$\Gamma(a_2(1320)\pi)/\Gamma_{total}$ — Γ_7/Γ

VALUE	DOCUMENT ID		TECN	COMMENT
• • • We do not use the following data for averages, fits, limits, etc. • • •				
not seen	BARBERIS	00B		450 $pp \to p_f \eta \pi^+ \pi^- p_s$
not seen	BARBERIS	00C		450 $pp \to p_f 4\pi p_s$
possibly seen	BARBERIS	97B	OMEG	450 $pp \to pp2(\pi^+\pi^-)$

$\Gamma(\eta\eta)/\Gamma(4\pi)$ — Γ_8/Γ_5

VALUE	CL%	DOCUMENT ID		COMMENT
• • • We do not use the following data for averages, fits, limits, etc. • • •				
$<5.0\times10^{-3}$	90	BARBERIS	00E	450 $pp \to p_f \eta\eta p_s$

$\Gamma(\eta\eta)/\Gamma(\pi^+\pi^-)$ — Γ_8/Γ_3

VALUE	DOCUMENT ID		TECN	COMMENT
0.14±0.05	AMSLER	02	CBAR	0.9 $\overline{p}p \to \pi^0\eta\eta$, $\pi^0\pi^0\pi^0$

$\Gamma(\gamma\phi)/\Gamma_{total}$ — Γ_{11}/Γ

VALUE	DOCUMENT ID		TECN	COMMENT
seen	[1] ABLIKIM	25P	BES3	$J/\psi \to \gamma\gamma\phi$

[1] From a partial wave analysis of $J/\psi \to \gamma\gamma\phi$ with significance 13.1σ.

$\Gamma(p\overline{p})/\Gamma_{total}$ — Γ_{12}/Γ

VALUE	EVTS	DOCUMENT ID		TECN	COMMENT
seen	111	ALEXANDER	10	CLEO	$\psi(2S) \to \gamma p\overline{p}$

$f_2(1950)$ REFERENCES

ABLIKIM	25CD	JHEP 2510 081	M. Ablikim *et al.*	(BESIII Collab.)
ABLIKIM	25P	PR D111 052011	M. Ablikim *et al.*	(BESIII Collab.)
RODAS	22	EPJ C82 80	A. Rodas *et al.*	(JPAC Collab.)
ALBRECHT	20	EPJ C80 453	M. Albrecht *et al.*	(Crystal Barrel Collab.)
ABLIKIM	18AA	PR D98 072003	M. Ablikim *et al.*	(BESIII Collab.)
ABLIKIM	15AE	PR D92 052003	M. Ablikim *et al.*	(BESIII Collab.)
ALEXANDER	10	PR D82 092002	J.P. Alexander *et al.*	(CLEO Collab.)
UEHARA	09	PR D79 052009	S. Uehara *et al.*	(BELLE Collab.)
BINON	05	PAN 68 960	F. Binon *et al.*	
		Translated from YAF 68 998.		
ABE	04	EPJ C32 323	K. Abe *et al.*	(BELLE Collab.)
AMSLER	02	EPJ C23 29	C. Amsler *et al.*	(Crystal Barrel Collab.)
ANISOVICH	00J	PL B491 47	A.V. Anisovich *et al.*	(RAL, LOQM, PNPI+)
BAI	00A	PL B472 207	J.Z. Bai *et al.*	(BES Collab.)
BARBERIS	00B	PL B471 435	D. Barberis *et al.*	(WA 102 Collab.)
BARBERIS	00C	PL B471 440	D. Barberis *et al.*	(WA 102 Collab.)
BARBERIS	00E	PL B479 59	D. Barberis *et al.*	(WA 102 Collab.)
ANISOVICH	99B	PL B449 154	A.V. Anisovich *et al.*	
BARBERIS	97B	PL B413 217	D. Barberis *et al.*	(WA 102 Collab.)
KLOET	96	PR D53 6120	W.M. Kloet, F. Myhrer	(RUTG, NORD)
ANTINORI	95	PL B353 589	F. Antinori *et al.*	(ATHU, BARI, BIRM+) JP
OAKDEN	94	NP A574 731	M.N. Oakden, M.R. Pennington	(DURH)
ASTON	91	NPBPS B21 5	D. Aston *et al.*	(LASS Collab.)
LONGACRE	86	PL B177 223	R.S. Longacre *et al.*	(BNL, BRAN, CUNY+)
BINON	83	NC 78A 313	F.G. Binon *et al.*	(BELG, LAPP, SERP+)
HYAMS	75	NP B100 205	B.D. Hyams *et al.*	(CERN, MPIM)

$a_4(1970)$

$I^G(J^{PC}) = 1^-(4^{++})$

$a_4(1970)$ MASS

VALUE (MeV)	EVTS	DOCUMENT ID		TECN	CHG	COMMENT
1967±16 OUR AVERAGE		Error includes scale factor of 2.1. See the ideogram below.				
1935^{+11}_{-13}	46M	[1] AGHASYAN	18B	COMP		190 $\pi^- p \to \pi^-\pi^+\pi^- p$
1900^{+80}_{-20}		ADOLPH	15	COMP		191 $\pi^- p \to \eta^{(\prime)}\pi^- p$
1985±10±13	145k	LU	05	B852		18 $\pi^- p \to \omega\pi^-\pi^0 p$
1996±25±43		CHUNG	02	B852		18.3 $\pi^- p \to 3\pi p$
$2000\pm40^{+60}_{-20}$		IVANOV	01	B852		18 $\pi^- p \to \eta'\pi^- p$
2010±20		[2] ALDE	96	GAM2	0	38 $\pi^- p \to \eta\pi^0 n$
2040±30		[3] CLELAND	82B	SPEC	±	50 $\pi p \to K^0_S K^\pm p$
• • • We do not use the following data for averages, fits, limits, etc. • • •						
$1885\pm13^{+50}_{-2}$	420k	[4] ALEKSEEV	10	COMP		190 $\pi^- Pb \to \pi^-\pi^-\pi^+ Pb'$
2004± 6	80k	[5] UMAN	06	E835		5.2 $\overline{p}p \to \eta\eta\pi^0$
2005^{+25}_{-45}		[6] ANISOVICH	01F	SPEC		2.0 $\overline{p}p \to 3\pi^0$, $\pi^0\eta$, $\pi^0\eta'$
1944± 8±50		[7] AMELIN	99	VES		37 $\pi^- A \to \omega\pi^-\pi^0 A^*$
1903±10		[8] BALDI	78	SPEC	−	10 $\pi^- p \to pK^0_S K^-$
2030±50		[9] CORDEN	78C	OMEG	0	15 $\pi^- p \to 3\pi n$

[1] Statistical error negligible.
[2] From a simultaneous fit to the G_+ and G_0 wave intensities.
[3] From an amplitude analysis.
[4] Superseded by AGHASYAN 2018B.
[5] Statistical error only.
[6] From the combined analysis of ANISOVICH 99C, ANISOVICH 99E, and ANISOVICH 01F.
[7] May be a different state.
[8] From a fit to the Y^0_8 moment. Limited by phase space.
[9] $J^P = 4^+$ is favored, though $J^P = 2^+$ cannot be excluded.

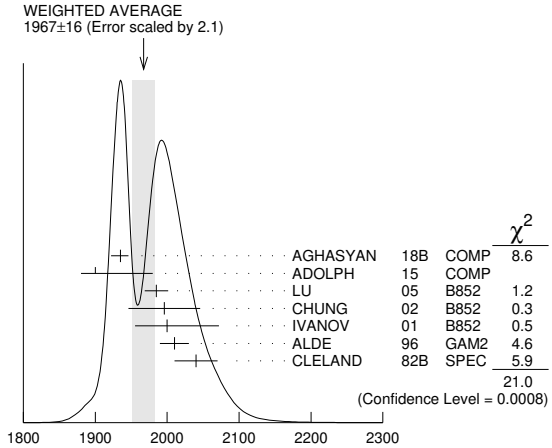

$a_4(1970)$ WIDTH

VALUE (MeV)	EVTS	DOCUMENT ID		TECN	CHG	COMMENT
$\mathbf{324^{+15}_{-18}}$ **OUR AVERAGE**						
333^{+16}_{-21}	46M	[1] AGHASYAN	18B	COMP		190 $\pi^- p \to \pi^-\pi^+\pi^- p$
300^{+80}_{-100}		ADOLPH	15	COMP		191 $\pi^- p \to \eta^{(\prime)}\pi^- p$
231± 30±46	145k	LU	05	B852		18 $\pi^- p \to \omega\pi^-\pi^0 p$
298± 81±85		CHUNG	02	B852		18.3 $\pi^- p \to 3\pi p$
$350\pm100^{+70}_{-50}$		IVANOV	01	B852		18 $\pi^- p \to \eta'\pi^- p$
370± 80		[2] ALDE	96	GAM2	0	38 $\pi^- p \to \eta\pi^0 n$
380±150		[3] CLELAND	82B	SPEC	±	50 $\pi p \to K^0_S K^\pm p$
• • • We do not use the following data for averages, fits, limits, etc. • • •						
$294\pm 25^{+46}_{-19}$	420k	[4] ALEKSEEV	10	COMP		190 $\pi^- Pb \to \pi^-\pi^-\pi^+ Pb'$
401± 16	80k	[5] UMAN	06	E835		5.2 $\overline{p}p \to \eta\eta\pi^0$
180± 30		[6] ANISOVICH	01F	SPEC		2.0 $\overline{p}p \to 3\pi^0$, $\pi^0\eta$, $\pi^0\eta'$
324± 26±75		[7] AMELIN	99	VES		37 $\pi^- A \to \omega\pi^-\pi^0 A^*$
166± 43		[8] BALDI	78	SPEC	−	10 $\pi^- p \to pK^0_S K^-$
510±200		[9] CORDEN	78C	OMEG	0	15 $\pi^- p \to 3\pi n$

[1] Statistical error negligible.
[2] From a simultaneous fit to the G_+ and G_0 wave intensities.
[3] From an amplitude analysis.
[4] Superseded by AGHASYAN 2018B.
[5] Statistical error only.
[6] From the combined analysis of ANISOVICH 99C, ANISOVICH 99E, and ANISOVICH 01F.
[7] May be a different state.
[8] From a fit to the Y^0_8 moment. Limited by phase space.
[9] $J^P = 4^+$ is favored, though $J^P = 2^+$ cannot be excluded.

$a_4(1970)$ DECAY MODES

	Mode	Fraction (Γ_i/Γ)
Γ_1	$K\overline{K}$	seen
Γ_2	$\pi^+\pi^-\pi^0$	seen
Γ_3	$\rho\pi$	seen
Γ_4	$f_2(1270)\pi$	seen
Γ_5	$\omega\pi^-\pi^0$	seen
Γ_6	$\omega\rho$	seen
Γ_7	$\eta\pi$	seen
Γ_8	$\eta'(958)\pi$	seen

$a_4(1970)$ BRANCHING RATIOS

$\Gamma(K\overline{K})/\Gamma_{total}$ — Γ_1/Γ

VALUE	DOCUMENT ID		TECN	CHG	COMMENT
seen	BALDI	78	SPEC	±	10 $\pi^- p \to K^0_S K^- p$

Int. J. Mod. Phys. A 2026.41. Downloaded from www.worldscientific.com by UNIVERSITY OF CALIFORNIA @ BERKELEY on 09/16/26. Re-use and distribution is strictly not permitted, except for Open Access articles.

$\Gamma(\pi^+\pi^-\pi^0)/\Gamma_{total}$ — Γ_2/Γ

VALUE	DOCUMENT ID		TECN	CHG	COMMENT
seen	CORDEN	78C	OMEG	0	15 $\pi^- p \to 3\pi n$

$\Gamma(\rho\pi)/\Gamma(f_2(1270)\pi)$ — Γ_3/Γ_4

VALUE	EVTS	DOCUMENT ID		TECN	COMMENT
$1.7^{+0.9}_{-0.8}$ OUR AVERAGE Error includes scale factor of 3.7.					
$2.9^{+0.6}_{-0.4}$	46M	[1] AGHASYAN	18B	COMP	190 $\pi^- p \to \pi^-\pi^+\pi^- p$
$1.1\pm0.2\pm0.2$		CHUNG	02	B852	18.3 $\pi^- p \to 3\pi p$

[1] Statistical error negligible.

$\Gamma(\eta\pi)/\Gamma_{total}$ — Γ_7/Γ

VALUE	DOCUMENT ID		TECN	CHG	COMMENT
seen	ALDE	96	GAM2	0	38 $\pi^- p \to \eta\pi^0 n$

$\Gamma(\eta'(958)\pi)/\Gamma(\eta\pi)$ — Γ_8/Γ_7

VALUE	DOCUMENT ID		TECN	COMMENT
0.23±0.07	ADOLPH	15	COMP	191 $\pi^- p \to \eta^{(\prime)}\pi^- p$

$\Gamma(\omega\rho)/\Gamma_{total}$ — Γ_6/Γ

VALUE	EVTS	DOCUMENT ID		TECN	COMMENT
seen	145k	LU	05	B852	18 $\pi^- p \to \omega\pi^-\pi^0 p$

$a_4(1970)$ REFERENCES

AGHASYAN	18B	PR D98 092003	M. Aghasyan *et al.*	(COMPASS Collab.)
ADOLPH	15	PL B740 303	M. Adolph *et al.*	(COMPASS Collab.)
ALEKSEEV	10	PRL 104 241803	M.G. Alekseev *et al.*	(COMPASS Collab.)
UMAN	06	PR D73 052009	I. Uman *et al.*	(FNAL E835)
LU	05	PRL 94 032002	M. Lu *et al.*	(BNL E852 Collab.)
CHUNG	02	PR D65 072001	S.U. Chung *et al.*	(BNL E852 Collab.)
ANISOVICH	01F	PL B517 261	A.V. Anisovich *et al.*	
IVANOV	01	PRL 86 3977	E.I. Ivanov *et al.*	(BNL E852 Collab.)
AMELIN	99	PAN 62 445 Translated from YAF 62 487.	D.V. Amelin *et al.*	(VES Collab.)
ANISOVICH	99C	PL B452 173	A.V. Anisovich *et al.*	
ANISOVICH	99E	PL B452 187	A.V. Anisovich *et al.*	
ALDE	96	PAN 59 982 Translated from YAF 59 1027.	S.V. Donskov *et al.*	(GAMS Collab.) IGJPC
CLELAND	82B	NP B208 228	W.E. Cleland *et al.*	(DURH, GEVA, LAUS+)
BALDI	78	PL 74B 413	R. Baldi *et al.*	(GEVA) JP
CORDEN	78C	NP B136 77	M.J. Corden *et al.*	(BIRM, RHEL, TELA+) JP

$\rho_3(1990)$

$I^G(J^{PC}) = 1^+(3^{--})$

OMITTED FROM SUMMARY TABLE

$\rho_3(1990)$ MASS

VALUE (MeV)	DOCUMENT ID		TECN	COMMENT
• • • We do not use the following data for averages, fits, limits, etc. • • •				
1982±14	[1] ANISOVICH	02	SPEC	0.6–1.9 $p\overline{p} \to \omega\pi^0$, $\omega\eta\pi^0$, $\pi^+\pi^-$
~ 2007	HASAN	94	RVUE	$\overline{p}p \to \pi\pi$

[1] From the combined analysis of ANISOVICH 00J, ANISOVICH 01D, ANISOVICH 01E, and ANISOVICH 02.

$\rho_3(1990)$ WIDTH

VALUE (MeV)	DOCUMENT ID		TECN	COMMENT
• • • We do not use the following data for averages, fits, limits, etc. • • •				
188±24	[2] ANISOVICH	02	SPEC	0.6–1.9 $p\overline{p} \to \omega\pi^0$, $\omega\eta\pi^0$, $\pi^+\pi^-$
~ 287	HASAN	94	RVUE	$\overline{p}p \to \pi\pi$

[2] From the combined analysis of ANISOVICH 00J, ANISOVICH 01D, ANISOVICH 01E, and ANISOVICH 02.

$\rho_3(1990)$ REFERENCES

ANISOVICH	02	PL B542 8	A.V. Anisovich *et al.*	
ANISOVICH	01D	PL B508 6	A.V. Anisovich *et al.*	
ANISOVICH	01E	PL B513 281	A.V. Anisovich *et al.*	
ANISOVICH	00J	PL B491 47	A.V. Anisovich *et al.*	(RAL, LOQM, PNPI+)
HASAN	94	PL B334 215	A. Hasan, D.V. Bugg	(LOQM)

$\pi_2(2005)$

$I^G(J^{PC}) = 1^-(2^{-+})$

OMITTED FROM SUMMARY TABLE

$\pi_2(2005)$ MASS

VALUE (MeV)	EVTS	DOCUMENT ID		TECN	COMMENT
1963^{+17}_{-27} OUR AVERAGE					
1962^{+17}_{-29}	46M	[1] AGHASYAN	18B	COMP	190 $\pi^- p \to \pi^-\pi^+\pi^- p$
1974±14±83	145k	LU	05	B852	18 $\pi^- p \to \omega\pi^-\pi^0 p$
• • • We do not use the following data for averages, fits, limits, etc. • • •					
2005±15		ANISOVICH	01F	SPEC	2.0 $\overline{p}p \to 3\pi^0$, $\pi^0\eta$, $\pi^0\eta'$

[1] Statistical uncertainty negligible.

$\pi_2(2005)$ WIDTH

VALUE (MeV)	EVTS	DOCUMENT ID		TECN	COMMENT
370^{+16}_{-90} OUR AVERAGE					
371^{+16}_{-120}	46M	[1] AGHASYAN	18B	COMP	190 $\pi^- p \to \pi^-\pi^+\pi^- p$
341± 61±139	145k	LU	05	B852	18 $\pi^- p \to \omega\pi^-\pi^0 p$
• • • We do not use the following data for averages, fits, limits, etc. • • •					
200± 40		ANISOVICH	01F	SPEC	2.0 $\overline{p}p \to 3\pi^0$, $\pi^0\eta$, $\pi^0\eta'$

[1] Statistical uncertainty negligible.

$\pi_2(2005)$ DECAY MODES

	Mode	Fraction (Γ_i/Γ)
Γ_1	$\pi^-\pi^+\pi^-$	seen
Γ_2	$\omega\pi^0\pi^-$	seen

$\pi_2(2005)$ BRANCHING RATIOS

$\Gamma(\pi^-\pi^+\pi^-)/\Gamma_{total}$ — Γ_1/Γ

VALUE	DOCUMENT ID		TECN	COMMENT
seen	AGHASYAN	18B	COMP	190 $\pi^- p \to \pi^-\pi^+\pi^- p$

$\Gamma(\omega\pi^0\pi^-)/\Gamma_{total}$ — Γ_2/Γ

VALUE	DOCUMENT ID		TECN	COMMENT
seen	LU	05	B852	18 $\pi^- p \to \omega\pi^-\pi^0 p$

$\pi_2(2005)$ REFERENCES

AGHASYAN	18B	PR D98 092003	M. Aghasyan *et al.*	(COMPASS Collab.)
LU	05	PRL 94 032002	M. Lu *et al.*	(BNL E852 Collab.)
ANISOVICH	01F	PL B517 261	A.V. Anisovich *et al.*	

$f_2(2010)$

$I^G(J^{PC}) = 0^+(2^{++})$

$f_2(2010)$ MASS

VALUE (MeV)	DOCUMENT ID		TECN	COMMENT
2011^{+62}_{-76}	[1] ETKIN	88	MPS	22 $\pi^- p \to \phi\phi n$
• • • We do not use the following data for averages, fits, limits, etc. • • •				
2062± 6^{+10}_{-7}	[2] ABLIKIM	22AS	BES3	$J/\psi(1S) \to \gamma\eta\eta'$
2005± 12	VLADIMIRSK...	06	SPEC	40 $\pi^- p \to K^0_S K^0_S n$
2049^{+35}_{-24}	[3] LONGACRE	04	RVUE	22 $\pi^- p \to \phi\phi n$, 450 $pp \to p_f 4\pi p_s$
1980± 20	[4] BOLONKIN	88	SPEC	40 $\pi^- p \to K^0_S K^0_S n$
2050^{+90}_{-50}	ETKIN	85	MPS	22 $\pi^- p \to 2\phi n$
2120^{+20}_{-120}	LINDENBAUM	84	RVUE	
2160± 50	ETKIN	82	MPS	22 $\pi^- p \to 2\phi n$

[1] Includes data of ETKIN 85. The percentage of the resonance going into $\phi\phi$ 2^{++} s_2, D_2, and D_0 is 98^{+1}_{-3}, 0^{+1}_{-0}, and 2^{+2}_{-1}, respectively.
[2] From a Breit-Wigner fit involving 9 resonances and a resonating exotic $\eta_1(1855) \to \eta\eta'$ P-wave.
[3] From a four pole K-matrix reanalysis of ETKIN 88 and BARBERIS 00C data.
[4] Statistically very weak, only 1.4 s.d.

$f_2(2010)$ WIDTH

VALUE (MeV)	DOCUMENT ID		TECN	COMMENT
202^{+67}_{-62}	[5] ETKIN	88	MPS	22 $\pi^- p \to \phi\phi n$
• • • We do not use the following data for averages, fits, limits, etc. • • •				
165± 17^{+10}_{-5}	[6] ABLIKIM	22AS	BES3	$J/\psi(1S) \to \gamma\eta\eta'$
209± 32	VLADIMIRSK...	06	SPEC	40 $\pi^- p \to K^0_S K^0_S n$
567^{+64}_{-71}	[7] LONGACRE	04	RVUE	22 $\pi^- p \to \phi\phi n$, 450 $pp \to p_f 4\pi p_s$
145± 50	[8] BOLONKIN	88	SPEC	40 $\pi^- p \to K^0_S K^0_S n$
200^{+160}_{-50}	ETKIN	85	MPS	22 $\pi^- p \to 2\phi n$
300^{+150}_{-50}	LINDENBAUM	84	RVUE	
310± 70	ETKIN	82	MPS	22 $\pi^- p \to 2\phi n$

[5] Includes data of ETKIN 85.
[6] From a Breit-Wigner fit involving 9 resonances and a resonating exotic $\eta_1(1855) \to \eta\eta'$ P-wave.
[7] From a four pole K-matrix reanalysis of ETKIN 88 and BARBERIS 00C data
[8] Statistically very weak, only 1.4 s.d.

Int. J. Mod. Phys. A 2026.41. Downloaded from www.worldscientific.com by CALIFORNIA @ BERKELEY on 09/16/26. Re-use and distribution is strictly not permitted, except for Open Access articles.

$f_2(2010)$ DECAY MODES

	Mode	Fraction (Γ_i/Γ)
Γ_1	$\phi\phi$	seen
Γ_2	$K\overline{K}$	seen
Γ_3	$\gamma\phi$	seen

$f_2(2010)$ BRANCHING RATIOS

$\Gamma(K\overline{K})/\Gamma_{total}$ — Γ_2/Γ

VALUE	DOCUMENT ID	TECN	COMMENT
seen	VLADIMIRSK...06	SPEC	$40\ \pi^- p \rightarrow K^0_S K^0_S n$

$\Gamma(\gamma\phi)/\Gamma_{total}$ — Γ_3/Γ

VALUE	DOCUMENT ID	TECN	COMMENT
seen	[9] ABLIKIM 25P	BES3	$J/\psi \rightarrow \gamma\gamma\phi$

[9] From a partial wave analysis of $J/\psi \rightarrow \gamma\gamma\phi$ with significance 11.3σ.

$f_2(2010)$ REFERENCES

ABLIKIM	25P	PR D111 052011	M. Ablikim *et al.*	(BESIII Collab.)
ABLIKIM	22AS	PR D106 072012	M. Ablikim *et al.*	(BESIII Collab.)
Also		PR D107 079901 (errat.)	M. Ablikim *et al.*	(BESIII Collab.)
VLADIMIRSK...	06	PAN 69 493	V.V. Vladimirsky *et al.*	(ITEP, Moscow)
		Translated from YAF 69 515.		
LONGACRE	04	PR D70 094041	R.S. Longacre, S.J. Lindenbaum	(BNL, CUNY)
BARBERIS	00C	PL B471 440	D. Barberis *et al.*	(WA 102 Collab.)
BOLONKIN	88	NP B309 426	B.V. Bolonkin *et al.*	(ITEP, SERP)
ETKIN	88	PL B201 568	A. Etkin *et al.*	(BNL, CUNY)
ETKIN	85	PL 165B 217	A. Etkin *et al.*	(BNL, CUNY)
LINDENBAUM	84	CNPP 13 285	S.J. Lindenbaum	(CUNY)
ETKIN	82	PRL 49 1620	A. Etkin *et al.*	(BNL, CUNY)
Also		Brighton Conf. 351	S.J. Lindenbaum	(BNL, CUNY)

$f_0(2020)$

$I^G(J^{PC}) = 0^+(0^{++})$

Needs confirmation.

$f_0(2020)$ T-MATRIX POLE $\sqrt{s}$

Note that $\Gamma = -2\,\mathrm{Im}(\sqrt{s})$.

VALUE (MeV)	DOCUMENT ID	TECN	COMMENT
(1870–2080) − i (120–240) OUR ESTIMATE			
$(2141.9 \pm 17.2 \pm 17.9) - i\,(138.8 \pm 10.0 \pm 14.4)$	ABLIKIM 25CD	BES3	$e^+e^- \rightarrow \psi(2S)$
$(2038 \pm 48) - i\,(156 \pm 41)$	[1] RODAS 22	RVUE	$J/\psi(1S) \rightarrow \gamma\,(\pi\pi,\ K\overline{K})$
$(1925 \pm 25) - i\,(160 \pm 18)$	SARANTSEV 21	RVUE	$J/\psi(1S) \rightarrow \gamma\,(\pi\pi,\ K\overline{K},\ \eta\eta,\ \omega\phi)$
$(1910 \pm 50) - i\,(199 \pm 40)$	[2] ROPERTZ 18	RVUE	$\overline{B}^0_s \rightarrow J/\psi(\pi^+\pi^- / K^+K^-)$
$(1992 \pm 16) - i\,(221 \pm 30)$	[3] BARBERIS 00C		$450\ pp \rightarrow p_f 4\pi p_s$
$(2020 \pm 35) - i\,(205 \pm 25)$	BARBERIS 97B	OMEG	$450\ pp \rightarrow pp2(\pi^+\pi^-)$

[1] T-matrix pole from coupled channel K-matrix fit to data on $J/\psi \rightarrow \gamma\pi^0\pi^0$ (ABLIKIM 15AE) and $J/\psi \rightarrow \gamma K^0_S K^0_S$ (ABLIKIM 18AA).
[2] T-matrix pole of 3 channel unitary model fit to data from AAIJ 14BR and AAIJ 17V extracted using Pade approximants.
[3] Average between $\pi^+\pi^- 2\pi^0$ and $2(\pi^+\pi^-)$.

$f_0(2020)$ MASS

VALUE (MeV)	EVTS	DOCUMENT ID	TECN	COMMENT
$1982 \pm 3^{+54}_{-0}$		[1] ABLIKIM 22C	BES3	$J/\psi \rightarrow \gamma\eta'\eta' \rightarrow 4/5\gamma 2(\pi^+\pi^-)$
• • • We do not use the following data for averages, fits, limits, etc. • • •				
$2010 \pm 6^{+6}_{-4}$		[2] ABLIKIM 22AS	BES3	$J/\psi(1S) \rightarrow \gamma\eta\eta'$
2037 ± 8	80k	[3] UMAN 06	E835	$5.2\ \overline{p}p \rightarrow \eta\eta\pi^0$
2040 ± 38		ANISOVICH 00J	SPEC	
2010 ± 60		ALDE 98	GAM4	$100\ \pi^- p \rightarrow \pi^0\pi^0 n$

[1] From a partial wave analysis of the systems (γX), with $X \rightarrow \eta'\eta'$, and $(\eta' X)$, with $X \rightarrow \gamma\eta'$ in the decay $J/\psi \rightarrow \gamma\eta'\eta'$. The intermediate resonance X is parametrized by a constant-width, relativistic Breit-Wigner.
[2] From a Breit-Wigner fit involving 9 resonances and a resonating exotic $\eta_1(1855) \rightarrow \eta\eta'$ P-wave.
[3] Statistical error only.

$f_0(2020)$ WIDTH

VALUE (MeV)	EVTS	DOCUMENT ID	TECN	COMMENT
$436 \pm 4^{+46}_{-49}$		[1] ABLIKIM 22C	BES3	$J/\psi \rightarrow \gamma\eta'\eta' \rightarrow 4/5\gamma 2(\pi^+\pi^-)$
• • • We do not use the following data for averages, fits, limits, etc. • • •				
$203 \pm 9^{+13}_{-11}$		[2] ABLIKIM 22AS	BES3	$J/\psi(1S) \rightarrow \gamma\eta\eta'$
296 ± 17	80k	[3] UMAN 06	E835	$5.2\ \overline{p}p \rightarrow \eta\eta\pi^0$
405 ± 40		ANISOVICH 00J	SPEC	
240 ± 100		ALDE 98	GAM4	$100\ \pi^- p \rightarrow \pi^0\pi^0 n$

[1] From a partial wave analysis of the systems (γX), with $X \rightarrow \eta'\eta'$, and $(\eta' X)$, with $X \rightarrow \gamma\eta'$ in the decay $J/\psi \rightarrow \gamma\eta'\eta'$. The intermediate resonance X is parametrized by a constant-width, relativistic Breit-Wigner.
[2] From a Breit-Wigner fit involving 9 resonances and a resonating exotic $\eta_1(1855) \rightarrow \eta\eta'$ P-wave.
[3] Statistical error only.

$f_0(2020)$ DECAY MODES

	Mode	Fraction (Γ_i/Γ)
Γ_1	$\rho\pi\pi$	seen
Γ_2	$\pi^0\pi^0$	seen
Γ_3	$\rho\rho$	seen
Γ_4	$\omega\omega$	seen
Γ_5	$\eta\eta$	seen
Γ_6	$\eta'\eta'$	seen

$f_0(2020)$ BRANCHING RATIOS

$\Gamma(\rho\rho)/\Gamma(\omega\omega)$ — Γ_3/Γ_4

VALUE	DOCUMENT ID	COMMENT
• • • We do not use the following data for averages, fits, limits, etc. • • •		
~ 3	BARBERIS 00F	$450\ pp \rightarrow p_f\omega\omega p_s$

$\Gamma(\eta\eta)/\Gamma_{total}$ — Γ_5/Γ

VALUE	DOCUMENT ID	TECN	COMMENT
seen	UMAN 06	E835	$5.2\ \overline{p}p \rightarrow \eta\eta\pi^0$

$\Gamma(\eta'\eta')/\Gamma_{total}$ — Γ_6/Γ

VALUE	DOCUMENT ID	TECN	COMMENT
seen	[1] ABLIKIM 22C	BES3	$J/\psi \rightarrow \gamma\eta'\eta' \rightarrow 4/5\gamma 2(\pi^+\pi^-)$

[1] From a partial wave analysis of the systems (γX), with $X \rightarrow \eta'\eta'$, and $(\eta' X)$, with $X \rightarrow \gamma\eta'$ in the decay $J/\psi \rightarrow \gamma\eta'\eta'$. The intermediate resonance X is parametrized by a constant-width, relativistic Breit-Wigner.

$f_0(2020)$ REFERENCES

ABLIKIM	25CD	JHEP 2510 081	M. Ablikim *et al.*	(BESIII Collab.)
ABLIKIM	22AS	PR D106 072012	M. Ablikim *et al.*	(BESIII Collab.)
Also		PR D107 079901 (errat.)	M. Ablikim *et al.*	(BESIII Collab.)
ABLIKIM	22C	PR D105 072002	M. Ablikim *et al.*	(BESIII Collab.)
RODAS	22	EPJ C82 80	A. Rodas *et al.*	(JPAC Collab.)
SARANTSEV	21	PL B816 136227	A.V. Sarantsev *et al.*	(BONN, PNPI)
ABLIKIM	18AA	PR D98 072003	M. Ablikim *et al.*	(BESIII Collab.)
ROPERTZ	18	EPJ C78 1000	S. Ropertz, C. Hanhart, B. Kubis	(BONN, JULI)
AAIJ	17V	JHEP 1708 037	R. Aaij *et al.*	(LHCb Collab.)
ABLIKIM	15AE	PR D92 052003	M. Ablikim *et al.*	(BESIII Collab.)
AAIJ	14BR	PR D89 092006	R. Aaij *et al.*	(LHCb Collab.)
UMAN	06	PR D73 052009	I. Uman *et al.*	(FNAL E835)
ANISOVICH	00J	PL B491 47	A.V. Anisovich *et al.*	(RAL, LOQM, PNPI+)
BARBERIS	00C	PL B471 440	D. Barberis *et al.*	(WA 102 Collab.)
BARBERIS	00F	PL B484 198	D. Barberis *et al.*	(WA 102 Collab.)
ALDE	98	EPJ A3 361	D. Alde *et al.*	(GAM4 Collab.)
Also		PAN 62 405	D. Alde *et al.*	(GAMS Collab.)
		Translated from YAF 62 446.		
BARBERIS	97B	PL B413 217	D. Barberis *et al.*	(WA 102 Collab.)

$f_4(2050)$

$I^G(J^{PC}) = 0^+(4^{++})$

$f_4(2050)$ MASS

VALUE (MeV)	EVTS	DOCUMENT ID	TECN	COMMENT
2018±11 OUR AVERAGE		Error includes scale factor of 2.1. See the ideogram below.		
1960 ± 15		AMELIN 06	VES	$36\ \pi^- p \rightarrow \omega\omega n$
2005 ± 10		[1] BINON 05	GAMS	$33\ \pi^- p \rightarrow \eta\eta n$
1998 ± 15		ALDE 98	GAM4	$100\ \pi^- p \rightarrow \pi^0\pi^0 n$
2060 ± 20		ALDE 90	GAM2	$38\ \pi^- p \rightarrow \omega\omega n$
2038 ± 30		AUGUSTIN 87	DM2	$J/\psi \rightarrow \gamma\pi^+\pi^-$
2086 ± 15		BALTRUSAIT...87	MRK3	$J/\psi \rightarrow \gamma\pi^+\pi^-$
2000 ± 60		ALDE 86D	GAM4	$100\ \pi^- p \rightarrow n2\eta$
2020 ± 20	40k	[2] BINON 84B	GAM2	$38\ \pi^- p \rightarrow n2\pi^0$
2015 ± 28		[3] CASON 82	STRC	$8\ \pi^+ p \rightarrow \Delta^{++}\pi^0\pi^0$
2031^{+25}_{-36}		ETKIN 82B	MPS	$23\ \pi^- p \rightarrow n2K^0_S$
2020 ± 30	700	APEL 75	NICE	$40\ \pi^- p \rightarrow n2\pi^0$
2050 ± 25		BLUM 75	ASPK	$18.4\ \pi^- p \rightarrow nK^+K^-$
• • • We do not use the following data for averages, fits, limits, etc. • • •				
1966 ± 25		[4] ANISOVICH 09	RVUE	$0.0\ \overline{p}p,\ \pi N$
$1885^{+14}_{-13}{}^{+218}_{-25}$		[5] UEHARA 09	BELL	$10.6\ e^+e^- \rightarrow e^+e^-\pi^0\pi^0$
2018 ± 6		ANISOVICH 00J	SPEC	$2.0\ \overline{p}p \rightarrow \eta\pi^0\pi^0,\ \pi^0\pi^0,\ \eta\eta,\ \eta\eta',\ \pi\pi$
~ 2000		[6] MARTIN 98	RVUE	$N\overline{N} \rightarrow \pi\pi$
~ 2010		[7] MARTIN 97	RVUE	$\overline{N}N \rightarrow \pi\pi$
~ 2040		[8] OAKDEN 94	RVUE	0.36–$1.55\ \overline{p}p \rightarrow \pi\pi$

Int. J. Mod. Phys. A 2026.41. Downloaded from www.worldscientific.com
by UNIVERSITY OF CALIFORNIA @ BERKELEY on 09/16/26. Re-use and distribution is strictly not permitted, except for Open Access articles.

~ 1990	[9] OAKDEN	94	RVUE	0.36–1.55 $\overline{p}p \to \pi\pi$
1978 ± 5	[10] ALPER	80	CNTR	62 $\pi^- p \to K^+ K^- n$
2040 ± 10	[10] ROZANSKA	80	SPRK	18 $\pi^- p \to p\overline{p}n$
1935 ± 13	[10] CORDEN	79	OMEG	12–15 $\pi^- p \to n2\pi$
1988 ± 7	EVANGELIS...	79B	OMEG	10 $\pi^- p \to K^+ K^- n$
1922 ± 14	[11] ANTIPOV	77	CIBS	25 $\pi^- p \to p3\pi$

[1] From the first PWA solution.
[2] From a partial-wave analysis of the data.
[3] From an amplitude analysis of the reaction $\pi^+\pi^- \to 2\pi^0$.
[4] K matrix pole.
[5] Taking into account the $f_2(1950)$. Helicity-2 production favored.
[6] Energy-dependent analysis.
[7] Single energy analysis.
[8] From solution A of amplitude analysis of data on $\overline{p}p \to \pi\pi$. See however KLOET 96 who fit $\pi^+\pi^-$ only and find waves only up to $J = 3$ to be important but not significantly resonant.
[9] From solution B of amplitude analysis of data on $\overline{p}p \to \pi\pi$. See however KLOET 96 who fit $\pi^+\pi^-$ only and find waves only up to $J = 3$ to be important but not significantly resonant.
[10] $I(J^P) = 0(4^+)$ from amplitude analysis assuming one-pion exchange.
[11] Width errors enlarged by us to $4\Gamma/\sqrt{N}$; see the note with the $K^*(892)$ mass.

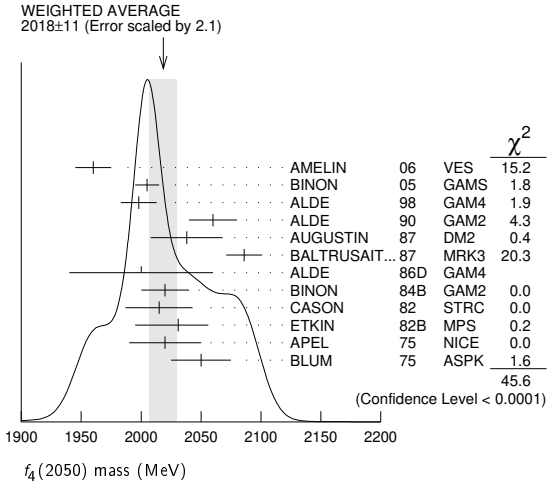

$f_4(2050)$ WIDTH

VALUE (MeV)	EVTS	DOCUMENT ID		TECN	COMMENT
237± 18 OUR AVERAGE		Error includes scale factor of 1.9. See the ideogram below.			
290± 20		AMELIN	06	VES	36 $\pi^- p \to \omega\omega n$
340± 80		[12] BINON	05	GAMS	33 $\pi^- p \to \eta\eta n$
395± 40		ALDE	98	GAM4	100 $\pi^- p \to \pi^0\pi^0 n$
170± 60		ALDE	90	GAM2	38 $\pi^- p \to \omega\omega n$
304± 60		AUGUSTIN	87	DM2	$J/\psi \to \gamma\pi^+\pi^-$
210± 63		BALTRUSAIT...	87	MRK3	$J/\psi \to \gamma\pi^+\pi^-$
400±100		ALDE	86D	GAM4	100 $\pi^- p \to n2\eta$
240± 40	40k	[13] BINON	84B	GAM2	38 $\pi^- p \to n2\pi^0$
190± 14		DENNEY	83	LASS	10 $\pi^+ n/\pi^+ p$
186^{+103}_{-58}		[14] CASON	82	STRC	8 $\pi^+ p \to \Delta^{++}\pi^0\pi^0$
305^{+36}_{-119}		ETKIN	82B	MPS	23 $\pi^- p \to n2K^0_S$
180± 60	700	APEL	75	NICE	40 $\pi^- p \to n2\pi^0$
225^{+120}_{-70}		BLUM	75	ASPK	18.4 $\pi^- p \to nK^+K^-$
• • • We do not use the following data for averages, fits, limits, etc. • • •					
260± 40		[15] ANISOVICH	09	RVUE	0.0 $\overline{p}p$, πN
$453 \pm 20^{+31}_{-129}$		[16] UEHARA	09	BELL	10.6 $e^+e^- \to e^+e^-\pi^0\pi^0$
182± 7		ANISOVICH	00J	SPEC	2.0 $\overline{p}p \to \eta\pi^0\pi^0$, $\pi^0\pi^0$, $\eta\eta$, $\eta\eta'$, $\pi\pi$
~ 170		[17] MARTIN	98	RVUE	$N\overline{N} \to \pi\pi$
~ 200		[18] MARTIN	97	RVUE	$\overline{N}N \to \pi\pi$
~ 60		[19] OAKDEN	94	RVUE	0.36–1.55 $\overline{p}p \to \pi\pi$
~ 80		[20] OAKDEN	94	RVUE	0.36–1.55 $\overline{p}p \to \pi\pi$
243± 16		[21] ALPER	80	CNTR	62 $\pi^- p \to K^+K^- n$
140± 15		[21] ROZANSKA	80	SPRK	18 $\pi^- p \to p\overline{p}n$
263± 57		[21] CORDEN	79	OMEG	12–15 $\pi^- p \to n2\pi$
100± 28		EVANGELIS...	79B	OMEG	10 $\pi^- p \to K^+K^- n$
107± 56		[22] ANTIPOV	77	CIBS	25 $\pi^- p \to p3\pi$

[12] From the first PWA solution.
[13] From a partial-wave analysis of the data.
[14] From an amplitude analysis of the reaction $\pi^+\pi^- \to 2\pi^0$.
[15] K matrix pole.
[16] Taking into account the $f_2(1950)$. Helicity-2 production favored.
[17] Energy-dependent analysis.
[18] Single energy analysis.
[19] From solution A of amplitude analysis of data on $\overline{p}p \to \pi\pi$. See however KLOET 96 who fit $\pi^+\pi^-$ only and find waves only up to $J = 3$ to be important but not significantly resonant.
[20] From solution B of amplitude analysis of data on $\overline{p}p \to \pi\pi$. See however KLOET 96 who fit $\pi^+\pi^-$ only and find waves only up to $J = 3$ to be important but not significantly resonant.
[21] $I(J^P) = 0(4^+)$ from amplitude analysis assuming one-pion exchange.
[22] Width errors enlarged by us to $4\Gamma/\sqrt{N}$; see the note with the $K^*(892)$ mass.

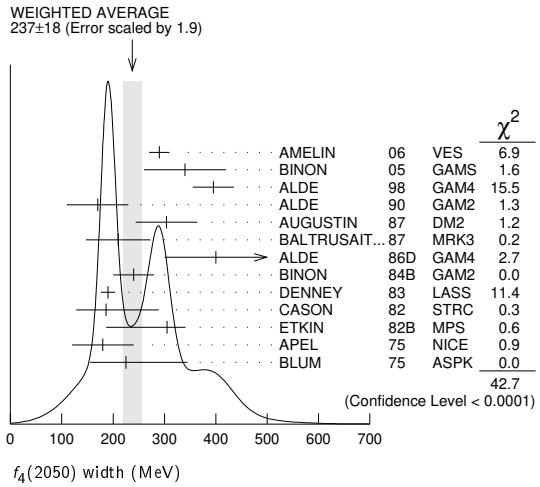

$f_4(2050)$ DECAY MODES

	Mode	Fraction (Γ_i/Γ)
Γ_1	$\omega\omega$	seen
Γ_2	$\pi\pi$	(17.0±1.5) %
Γ_3	$K\overline{K}$	$(6.8^{+3.4}_{-1.8}) \times 10^{-3}$
Γ_4	$\eta\eta$	$(2.1 \pm 0.8) \times 10^{-3}$
Γ_5	$4\pi^0$	< 1.2 %
Γ_6	$\gamma\gamma$	seen
Γ_7	$a_2(1320)\pi$	seen

$f_4(2050)$ $\Gamma(i)\Gamma(\gamma\gamma)/\Gamma(\text{total})$

$\Gamma(K\overline{K}) \times \Gamma(\gamma\gamma)/\Gamma_{\text{total}}$ — $\Gamma_3\Gamma_6/\Gamma$

VALUE (keV)	CL%	DOCUMENT ID		TECN	COMMENT
• • • We do not use the following data for averages, fits, limits, etc. • • •					
<0.29	95	ALTHOFF	85B	TASS	$\gamma\gamma \to K\overline{K}\pi$

$\Gamma(\pi\pi) \times \Gamma(\gamma\gamma)/\Gamma_{\text{total}}$ — $\Gamma_2\Gamma_6/\Gamma$

VALUE (eV)	CL%	EVTS	DOCUMENT ID		TECN	COMMENT
• • • We do not use the following data for averages, fits, limits, etc. • • •						
$23.1^{+3.6}_{-3.3}{}^{+70.5}_{-15.6}$			[23] UEHARA	09	BELL	10.6 $e^+e^- \to e^+e^-\pi^0\pi^0$
<1100	95	13 ± 4	OEST	90	JADE	$e^+e^- \to e^+e^-\pi^0\pi^0$

[23] Taking into account the $f_2(1950)$. Helicity-2 production favored.

$f_4(2050)$ BRANCHING RATIOS

$\Gamma(\omega\omega)/\Gamma_{\text{total}}$ — Γ_1/Γ

VALUE	DOCUMENT ID		TECN	COMMENT
seen	AMELIN	06	VES	36 $\pi^- p \to \omega\omega n$
• • • We do not use the following data for averages, fits, limits, etc. • • •				
not seen	BARBERIS	00F		450 $pp \to p_f\omega\omega p_s$

$\Gamma(\omega\omega)/\Gamma(\pi\pi)$ — Γ_1/Γ_2

VALUE	DOCUMENT ID		TECN	COMMENT
1.5±0.3	ALDE	90	GAM2	38 $\pi^- p \to \omega\omega n$

$\Gamma(\pi\pi)/\Gamma_{\text{total}}$ — Γ_2/Γ

VALUE	DOCUMENT ID		TECN	COMMENT
0.170±0.015 OUR AVERAGE				
0.18 ±0.03	[24] BINON	83C	GAM2	38 $\pi^- p \to n4\gamma$
0.16 ±0.03	[24] CASON	82	STRC	8 $\pi^+ p \to \Delta^{++}\pi^0\pi^0$
0.17 ±0.02	[24] CORDEN	79	OMEG	12–15 $\pi^- p \to n2\pi$

[24] Assuming one pion exchange.

Int. J. Mod. Phys. A 2026.41. Downloaded from www.worldscientific.com
by CALIFORNIA @ BERKELEY on 09/16/26. Re-use and distribution is strictly not permitted, except for Open Access articles.

$\Gamma(K\overline{K})/\Gamma(\pi\pi)$ — Γ_3/Γ_2

VALUE	DOCUMENT ID		TECN	COMMENT
$0.04^{+0.02}_{-0.01}$	ETKIN	82B	MPS	$23\ \pi^- p \to n 2K^0_S$

$\Gamma(\eta\eta)/\Gamma_{total}$ — Γ_4/Γ

VALUE (units 10^{-3})	DOCUMENT ID		TECN	COMMENT
2.1 ± 0.8	ALDE	86D	GAM4	$100\ \pi^- p \to n 4\gamma$

$\Gamma(4\pi^0)/\Gamma_{total}$ — Γ_5/Γ

VALUE	DOCUMENT ID		TECN	COMMENT
<0.012	ALDE	87	GAM4	$100\ \pi^- p \to 4\pi^0 n$

$\Gamma(a_2(1320)\pi)/\Gamma_{total}$ — Γ_7/Γ

VALUE	DOCUMENT ID		TECN	COMMENT
seen	AMELIN	00	VES	$37\ \pi^- p \to \eta\pi^+\pi^- n$

$f_4(2050)$ REFERENCES

ANISOVICH	09	IJMP A24 2481	V.V. Anisovich, A.V. Sarantsev	(PNPI)
UEHARA	09	PR D79 052009	S. Uehara *et al.*	(BELLE Collab.)
AMELIN	06	PAN 69 690	D.V. Amelin *et al.*	(VES Collab.)
		Translated from YAF 69 715.		
BINON	05	PAN 68 960	F. Binon *et al.*	
		Translated from YAF 68 998.		
AMELIN	00	NP A668 83	D. Amelin *et al.*	(VES Collab.)
ANISOVICH	00J	PL B491 47	A.V. Anisovich *et al.*	(RAL, LOQM, PNPI+)
BARBERIS	00F	PL B484 198	D. Barberis *et al.*	(WA 102 Collab.)
ALDE	98	EPJ A3 361	D. Alde *et al.*	(GAM4 Collab.)
Also		PAN 62 405	D. Alde *et al.*	(GAMS Collab.)
		Translated from YAF 62 446.		
MARTIN	98	PR C57 3492	B.R. Martin *et al.*	
MARTIN	97	PR C56 1114	B.R. Martin, G.C. Oades	(LOUC, AARH)
KLOET	96	PR D53 6120	W.M. Kloet, F. Myhrer	(RUTG, NORD)
OAKDEN	94	NP A574 731	M.N. Oakden, M.R. Pennington	(DURH)
ALDE	90	PL B241 600	D.M. Alde *et al.*	(SERP, BELG, LANL, LAPP+)
OEST	90	ZPHY C47 343	T. Oest *et al.*	(JADE Collab.)
ALDE	87	PL B198 286	D.M. Alde *et al.*	(LANL, BRUX, SERP, LAPP)
AUGUSTIN	87	ZPHY C36 369	J.E. Augustin *et al.*	(LALO, CLER, FRAS+)
BALTRUSAIT...	87	PR D35 2077	R.M. Baltrusaitis *et al.*	(Mark III Collab.)
ALDE	86D	NP B269 485	D.M. Alde *et al.*	(BELG, LAPP, SERP, CERN+)
ALTHOFF	85B	ZPHY C29 189	M. Althoff *et al.*	(TASSO Collab.)
BINON	84B	LNC 39 41	F.G. Binon *et al.*	(SERP, BELG, LAPP)
BINON	83C	SJNP 38 723	F.G. Binon *et al.*	(SERP, BRUX+)
		Translated from YAF 38 1199.		
DENNEY	83	PR D28 2726	D.L. Denney *et al.*	(IOWA, MICH)
CASON	82	PRL 48 1316	N.M. Cason *et al.*	(NDAM, ANL)
ETKIN	82B	PR D25 1786	A. Etkin *et al.*	(BNL, CUNY, TUFTS, VAND)
ALPER	80	PL 94B 422	B. Alper *et al.*	(AMST, CERN, CRAC, MPIM+)
ROZANSKA	80	NP B162 505	M. Rozanska *et al.*	(MPIM, CERN)
CORDEN	79	NP B157 250	M.J. Corden *et al.*	(BIRM, RHEL, TELA+) JP
EVANGELIS...	79B	NP B154 381	C. Evangelista *et al.*	(BARI, BONN, CERN+)
ANTIPOV	77	NP B119 45	Y.M. Antipov *et al.*	(SERP, GEVA)
APEL	75	PL 57B 398	W.D. Apel *et al.*	(KARLK, KARLE, PISA, SERP+) JP
BLUM	75	PL 57B 403	W. Blum *et al.*	(CERN, MPIM) JP

$\pi_2(2100)$

$I^G(J^{PC}) = 1^-(2^{-+})$

OMITTED FROM SUMMARY TABLE
Needs confirmation.

$\pi_2(2100)$ MASS

VALUE (MeV)	DOCUMENT ID		TECN	COMMENT
2090± 29 OUR AVERAGE				
2090± 30	[1] AMELIN	95B	VES	$36\ \pi^- A \to \pi^+\pi^-\pi^- A$
2100±150	[2] DAUM	81B	CNTR	$63{,}94\ \pi^- p \to 3\pi X$

[1] From a fit to $J^{PC} = 2^{-+}$ $f_2(1270)\pi$, $(\pi\pi)_S\pi$ waves.
[2] From a two-resonance fit to four 2^-0^+ waves.

$\pi_2(2100)$ WIDTH

VALUE (MeV)	DOCUMENT ID		TECN	COMMENT
620± 50 OUR AVERAGE Error includes scale factor of 1.2.				
520±100	[3] AMELIN	95B	VES	$36\ \pi^- A \to \pi^+\pi^-\pi^- A$
651± 50	[4] DAUM	81B	CNTR	$63{,}94\ \pi^- p \to 3\pi X$

[3] From a fit to $J^{PC} = 2^{-+}$ $f_2(1270)\pi$, $(\pi\pi)_S\pi$ waves.
[4] From a two-resonance fit to four 2^-0^+ waves.

$\pi_2(2100)$ DECAY MODES

	Mode	Fraction (Γ_i/Γ)
Γ_1	3π	seen
Γ_2	$\rho\pi$	seen
Γ_3	$f_2(1270)\pi$	seen
Γ_4	$(\pi\pi)_S\pi$	seen

$\pi_2(2100)$ BRANCHING RATIOS

$\Gamma(\rho\pi)/\Gamma(3\pi)$ — Γ_2/Γ_1

VALUE	DOCUMENT ID		TECN	COMMENT
0.19 ± 0.05	[5] DAUM	81B	CNTR	$63{,}94\ \pi^- p$

$\Gamma(f_2(1270)\pi)/\Gamma(3\pi)$ — Γ_3/Γ_1

VALUE	DOCUMENT ID		TECN	COMMENT
0.36 ± 0.09	[5] DAUM	81B	CNTR	$63{,}94\ \pi^- p$

$\Gamma((\pi\pi)_S\pi)/\Gamma(3\pi)$ — Γ_4/Γ_1

VALUE	DOCUMENT ID		TECN	COMMENT
0.45 ± 0.07	[5] DAUM	81B	CNTR	$63{,}94\ \pi^- p$

D-wave/S-wave RATIO FOR $\pi_2(2100) \to f_2(1270)\pi$

VALUE	DOCUMENT ID		TECN	COMMENT
0.39 ± 0.23	[5] DAUM	81B	CNTR	$63{,}94\ \pi^- p$

[5] From a two-resonance fit to four 2^-0^+ waves.

$\pi_2(2100)$ REFERENCES

AMELIN	95B	PL B356 595	D.V. Amelin *et al.*	(SERP, TBIL)
DAUM	81B	NP B182 269	C. Daum *et al.*	(AMST, CERN, CRAC, MPIM+)

$f_0(2100)$

$I^G(J^{PC}) = 0^+(0^{++})$

OMITTED FROM SUMMARY TABLE
Needs confirmation.

$f_0(2100)$ MASS

VALUE (MeV)	EVTS	DOCUMENT ID		TECN	COMMENT
2095^{+17}_{-19} OUR AVERAGE					
2116±27±17		LEES	21A	BABR	$\gamma\gamma \to \eta_c(1S) \to \eta'\pi^+\pi^-$
$2081 \pm 13^{+24}_{-36}$	5.5k	[1] ABLIKIM	13N	BES3	$e^+e^- \to J/\psi \to \gamma\eta\eta$
2090±30		BAI	00A	BES	$J/\psi \to \gamma(\pi^+\pi^-\pi^+\pi^-)$
• • • We do not use the following data for averages, fits, limits, etc. • • •					
2075±20		SARANTSEV	21	RVUE	$J/\psi(1S) \to \gamma\ (\pi\pi,\ K\overline{K},\ \eta\eta,\ \omega\phi)$
2090±10± 6	529	[2,3] DOBBS	15		$J/\psi \to \gamma\pi^+\pi^-$
2099±17± 8	283	[2,3] DOBBS	15		$\psi(2S) \to \gamma\pi^+\pi^-$
2105± 8	80k	[4] UMAN	06	E835	$5.2\ \overline{p}p \to \eta\eta\pi^0$
2102±13		[5] ANISOVICH	00J	SPEC	$2.0\ \overline{p}p \to \eta\pi^0\pi^0,\ \pi^0\pi^0,\ \eta\eta,\ \eta\eta',\ \pi^+\pi^-$
2105±10		ANISOVICH	99K	SPEC	$0.6\text{–}1.94\ \overline{p}p \to \eta\eta,\ \eta\eta'$
∼ 2104		BUGG	95		$J/\psi \to \gamma\pi^+\pi^-\pi^+\pi^-$
∼ 2122		HASAN	94	RVUE	$\overline{p}p \to \pi\pi$

[1] From partial wave analysis including all possible combinations of 0^{++}, 2^{++}, and 4^{++} resonances.
[2] Using CLEO-c data but not authored by the CLEO Collaboration.
[3] From a fit to a Breit-Wigner line shape with fixed $\Gamma = 209$ MeV.
[4] Statistical error only.
[5] Includes the data of ANISOVICH 00B indicating to exotic decay pattern.

$f_0(2100)$ WIDTH

VALUE (MeV)	EVTS	DOCUMENT ID		TECN	COMMENT
287^{+32}_{-24} OUR AVERAGE					
289± 34±15		LEES	21A	BABR	$\gamma\gamma \to \eta_c(1S) \to \eta'\pi^+\pi^-$
273^{+27+70}_{-24-23}	5.5k	[1] ABLIKIM	13N	BES3	$e^+e^- \to J/\psi \to \gamma\eta\eta$
330±100		BAI	00A	BES	$J/\psi \to \gamma(\pi^+\pi^-\pi^+\pi^-)$
• • • We do not use the following data for averages, fits, limits, etc. • • •					
260± 25		SARANTSEV	21	RVUE	$J/\psi(1S) \to \gamma\ (\pi\pi,\ K\overline{K},\ \eta\eta,\ \omega\phi)$
236± 14	80k	[2] UMAN	06	E835	$5.2\ \overline{p}p \to \eta\eta\pi^0$
211± 29		[3] ANISOVICH	00J	SPEC	$2.0\ \overline{p}p \to \eta\pi^0\pi^0,\ \pi^0\pi^0,\ \eta\eta,\ \eta\eta',\ \pi^+\pi^-$
200± 25		ANISOVICH	99K	SPEC	$0.6\text{–}1.94\ \overline{p}p \to \eta\eta,\ \eta\eta'$
∼ 203		BUGG	95		$J/\psi \to \gamma\pi^+\pi^-\pi^+\pi^-$
∼ 273		HASAN	94	RVUE	$\overline{p}p \to \pi\pi$

[1] From partial wave analysis including all possible combinations of 0^{++}, 2^{++}, and 4^{++} resonances.
[2] Statistical error only.
[3] Includes the data of ANISOVICH 00B indicating to exotic decay pattern.

$f_0(2100)$ REFERENCES

LEES	21A	PR D104 072002	J.P. Lees *et al.*	(BABAR Collab.)
SARANTSEV	21	PL B816 136227	A.V. Sarantsev *et al.*	(BONN, PNPI)
DOBBS	15	PR D91 052006	S. Dobbs *et al.*	(NWES)
ABLIKIM	13N	PR D87 092009	M. Ablikim *et al.*	(BESIII Collab.)
UMAN	06	PR D73 052009	I. Uman *et al.*	(FNAL E835)
ANISOVICH	00B	NP A662 319	A.V. Anisovich *et al.*	
ANISOVICH	00J	PL B491 47	A.V. Anisovich *et al.*	(RAL, LOQM, PNPI+)
BAI	00A	PL B472 207	J.Z. Bai *et al.*	(BES Collab.)
ANISOVICH	99K	PL B468 309	A.V. Anisovich *et al.*	
BUGG	95	PL B353 378	D.V. Bugg *et al.*	(LOQM, PNPI, WASH)
HASAN	94	PL B334 215	A. Hasan, D.V. Bugg	(LOQM)

Int. J. Mod. Phys. A 2026.41. Downloaded from www.worldscientific.com
by UNIVERSITY OF CALIFORNIA @ BERKELEY on 09/16/26. Re-use and distribution is strictly not permitted, except for Open Access articles.

$f_2(2150)$

$I^G(J^{PC}) = 0^+(2^{++})$

This entry was previously called T_0.

$f_2(2150)$ MASS

$f_2(2150)$ MASS, COMBINED MODES (MeV)

VALUE (MeV)	EVTS	DOCUMENT ID		TECN	COMMENT
2157±12 OUR AVERAGE Includes data from the datablock that follows this one.					
• • • We do not use the following data for averages, fits, limits, etc. • • •					
2170± 6	80k	[1] UMAN	06	E835	5.2 $\overline{p}p \to \eta\eta\pi^0$
2123^{+15}_{-33}		[2] LONGACRE	04	RVUE	22 $\pi^- p \to \phi\phi n$, 450 $pp \to p_f 4\pi p_s$

[1] Statistical error only.
[2] From a four pole K-matrix reanalysis of ETKIN 88 and BARBERIS 00C data.

$\eta\eta$ MODE

VALUE (MeV)	DOCUMENT ID		TECN	COMMENT
The data in this block is included in the average printed for a previous datablock.				
2157±12 OUR AVERAGE				
2151±16	BARBERIS	00E		450 $pp \to p_f \eta\eta p_s$
2175±20	PROKOSHKIN	95D	GAM4	300 $\pi^- N \to \pi^- N 2\eta$, 450 $pp \to pp2\eta$
2130±35	SINGOVSKI	94	GAM4	450 $pp \to pp2\eta$
• • • We do not use the following data for averages, fits, limits, etc. • • •				
2140±30	[3] ABELE	99B	CBAR	1.94 $\overline{p}p \to \pi^0\eta\eta$
2104±20	[4] ARMSTRONG	93C	E760	$\overline{p}p \to \pi^0\eta\eta \to 6\gamma$

[3] Spin not determined.
[4] No J^{PC} determination.

$\eta\pi\pi$ MODE

VALUE (MeV)	DOCUMENT ID		TECN	CHG	COMMENT
• • • We do not use the following data for averages, fits, limits, etc. • • •					
2135±20±45	[5] ADOMEIT	96	CBAR	0	1.94 $\overline{p}p \to \eta 3\pi^0$

[5] ANISOVICH 00E recommends to withdraw ADOMEIT 96 that assumed a single $J^P = 2^+$ resonance.

$\overline{p}p \to \pi\pi$

VALUE (MeV)	DOCUMENT ID		TECN	COMMENT
• • • We do not use the following data for averages, fits, limits, etc. • • •				
∼ 2090	[6] OAKDEN	94	RVUE	0.36–1.55 $\overline{p}p \to \pi\pi$
∼ 2120	[7] OAKDEN	94	RVUE	0.36–1.55 $\overline{p}p \to \pi\pi$
∼ 2170	[8] MARTIN	80B	RVUE	
∼ 2150	[8] MARTIN	80C	RVUE	
∼ 2150	[9] DULUDE	78B	OSPK	1–2 $\overline{p}p \to \pi^0\pi^0$

[6] OAKDEN 94 makes an amplitude analysis of LEAR data on $\overline{p}p \to \pi\pi$ using a method based on Barrelet zeros. This is solution A. The amplitude analysis of HASAN 94 includes earlier data as well, and assume that the data can be parametrized in terms of towers of nearly degenerate resonances on the leading Regge trajectory. See also KLOET 96 and MARTIN 97 who make related analyses.
[7] From solution B of amplitude analysis of data on $\overline{p}p \to \pi\pi$.
[8] $I(J^P) = 0(2^+)$ from simultaneous analysis of $p\overline{p} \to \pi^-\pi^+$ and $\pi^0\pi^0$.
[9] $I^G(J^P) = 0^+(2^+)$ from partial-wave amplitude analysis.

S-CHANNEL $\overline{p}p$, $\overline{N}N$ or $\overline{K}K$

VALUE (MeV)	DOCUMENT ID		TECN	CHG	COMMENT
• • • We do not use the following data for averages, fits, limits, etc. • • •					
2139^{+8}_{-9}	[10] EVANGELIS...	97	SPEC		0.6-2.4 $\overline{p}p \to K^0_S K^0_S$
∼ 2190	[10] CUTTS	78B	CNTR		0.97–3 $\overline{p}p \to \overline{N}N$
2155±15	[10,11] COUPLAND	77	CNTR	0	0.7–2.4 $\overline{p}p \to \overline{p}p$
2193± 2	[10,12] ALSPECTOR	73	CNTR		$\overline{p}p$ S channel

[10] Isospins 0 and 1 not separated.
[11] From a fit to the total elastic cross section.
[12] Referred to as T or T region by ALSPECTOR 73.

$K\overline{K}$ MODE

VALUE (MeV)	DOCUMENT ID		TECN	COMMENT
• • • We do not use the following data for averages, fits, limits, etc. • • •				
2200±13	VLADIMIRSK...	06	SPEC	40 $\pi^- p \to K^0_S K^0_S n$
2150±20	ABLIKIM	04E	BES2	$J/\psi \to \omega K^+ K^-$
2130±35	BARBERIS	99	OMEG	450 $pp \to p_s p_f K^+ K^-$

$f_2(2150)$ WIDTH

$f_2(2150)$ WIDTH, COMBINED MODES (MeV)

VALUE (MeV)	EVTS	DOCUMENT ID		TECN	COMMENT
152±30 OUR AVERAGE Includes data from the datablock that follows this one. Error includes scale factor of 1.4. See the ideogram below.					
• • • We do not use the following data for averages, fits, limits, etc. • • •					
182±11	80k	[13] UMAN	06	E835	5.2 $\overline{p}p \to \eta\eta\pi^0$
294^{+56}_{-55}		[14] LONGACRE	04	RVUE	22 $\pi^- p \to \phi\phi n$, 450 $pp \to p_f 4\pi p_s$

[13] Statistical error only.
[14] From a four pole K-matrix reanalysis of ETKIN 88 and BARBERIS 00C data.

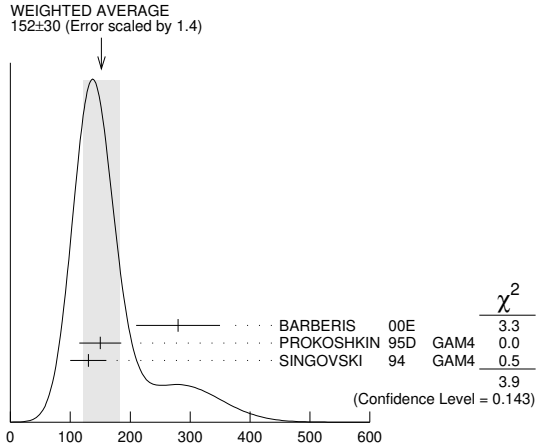

$f_2(2150)$ width, comibined modes (MeV)

$\eta\eta$ MODE

VALUE (MeV)	DOCUMENT ID		TECN	COMMENT
The data in this block is included in the average printed for a previous datablock.				
152±30 OUR AVERAGE Error includes scale factor of 1.4. See the ideogram below.				
280±70	BARBERIS	00E		450 $pp \to p_f \eta\eta p_s$
150±35	PROKOSHKIN	95D	GAM4	300 $\pi^- N \to \pi^- N 2\eta$, 450 $pp \to pp2\eta$
130±30	SINGOVSKI	94	GAM4	450 $pp \to pp2\eta$
• • • We do not use the following data for averages, fits, limits, etc. • • •				
310±50	[15] ABELE	99B	CBAR	1.94 $\overline{p}p \to \pi^0\eta\eta$
203±10	[16] ARMSTRONG	93C	E760	$\overline{p}p \to \pi^0\eta\eta \to 6\gamma$

[15] Spin not determined.
[16] No J^{PC} determination.

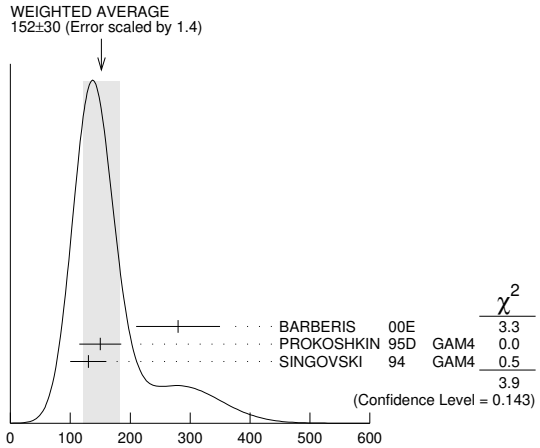

$f_2(2150)$ width, $\eta\eta$ mode (MeV)

$\eta\pi\pi$ MODE

VALUE (MeV)	DOCUMENT ID		TECN	CHG	COMMENT
• • • We do not use the following data for averages, fits, limits, etc. • • •					
250±25±45	[17] ADOMEIT	96	CBAR	0	1.94 $\overline{p}p \to \eta 3\pi^0$

[17] ANISOVICH 00E recommends to withdraw ADOMEIT 96 that assumed a single $J^P = 2^+$ resonance.

$\overline{p}p \to \pi\pi$

VALUE (MeV)	DOCUMENT ID		TECN	COMMENT
250 OUR ESTIMATE				
• • • We do not use the following data for averages, fits, limits, etc. • • •				
∼ 70	[18] OAKDEN	94	RVUE	0.36–1.55 $\overline{p}p \to \pi\pi$
∼ 250	[19] MARTIN	80B	RVUE	
∼ 250	[19] MARTIN	80C	RVUE	
∼ 250	[20] DULUDE	78B	OSPK	1–2 $\overline{p}p \to \pi^0\pi^0$

[18] See however KLOET 96 who fit $\pi^+\pi^-$ only and find waves only up to $J = 3$ to be important but not significantly resonant.
[19] $I(J^P) = 0(2^+)$ from simultaneous analysis of $p\overline{p} \to \pi^-\pi^+$ and $\pi^0\pi^0$.
[20] $I^G(J^P) = 0^+(2^+)$ from partial-wave amplitude analysis.

Int. J. Mod. Phys. A 2026.41. Downloaded from www.worldscientific.com
by CALIFORNIA @ BERKELEY on 09/16/26. Re-use and distribution is strictly not permitted, except for Open Access articles.

S-CHANNEL $\overline{p}p$, $\overline{N}N$ or $\overline{K}K$

VALUE (MeV)	DOCUMENT ID		TECN	CHG	COMMENT
• • • We do not use the following data for averages, fits, limits, etc. • • •					
56^{+31}_{-16}	[21] EVANGELIS...	97	SPEC		0.6-2.4 $\overline{p}p \to K^0_S K^0_S$
135 ± 75	[22,23] COUPLAND	77	CNTR	0	0.7–2.4 $\overline{p}p \to \overline{p}p$
98 ± 8	[23] ALSPECTOR	73	CNTR		$\overline{p}p$ S channel

[21] Isospin 0 and 2 not separated.
[22] From a fit to the total elastic cross section.
[23] Isospins 0 and 1 not separated.

$K\overline{K}$ MODE

VALUE (MeV)	DOCUMENT ID		TECN	COMMENT
• • • We do not use the following data for averages, fits, limits, etc. • • •				
91 ± 62	VLADIMIRSK...06		SPEC	40 $\pi^- p \to K^0_S K^0_S n$
150 ± 30	ABLIKIM	04E	BES2	$J/\psi \to \omega K^+ K^-$
270 ± 50	BARBERIS	99	OMEG	450 $pp \to p_s p_f K^+ K^-$

$f_2(2150)$ DECAY MODES

	Mode	Fraction (Γ_i/Γ)
Γ_1	$\pi\pi$	
Γ_2	$\phi\phi$	
Γ_3	$\eta\eta$	seen
Γ_4	$K\overline{K}$	seen
Γ_5	$f_2(1270)\eta$	seen
Γ_6	$a_2(1320)\pi$	seen
Γ_7	$p\overline{p}$	seen

$f_2(2150)$ BRANCHING RATIOS

$\Gamma(K\overline{K})/\Gamma(\eta\eta)$ — Γ_4/Γ_3

VALUE	CL%	DOCUMENT ID		TECN	COMMENT
1.28 ± 0.23		BARBERIS	00E		450 $pp \to p_f \eta\eta p_s$
• • • We do not use the following data for averages, fits, limits, etc. • • •					
<0.1	95	[24] PROKOSHKIN	95D	GAM4	300 $\pi^- N \to \pi^- N 2\eta$, 450 $pp \to pp2\eta$

[24] Using data from ARMSTRONG 89D.

$\Gamma(\pi\pi)/\Gamma(\eta\eta)$ — Γ_1/Γ_3

VALUE	CL%	DOCUMENT ID		TECN	COMMENT
• • • We do not use the following data for averages, fits, limits, etc. • • •					
<0.33	95	[25] PROKOSHKIN	95D	GAM4	300 $\pi^- N \to \pi^- N 2\eta$, 450 $pp \to pp2\eta$

[25] Derived from a $\pi^0\pi^0/\eta\eta$ limit.

$\Gamma(f_2(1270)\eta)/\Gamma(a_2(1320)\pi)$ — Γ_5/Γ_6

VALUE	DOCUMENT ID		TECN	COMMENT
0.79 ± 0.11	[26] ADOMEIT	96	CBAR	1.94 $\overline{p}p \to \eta 3\pi^0$

[26] Using $B(a_2(1320) \to \eta\pi) = 0.145$

$\Gamma(p\overline{p})/\Gamma_{total}$ — Γ_7/Γ

VALUE	EVTS	DOCUMENT ID		TECN	COMMENT
seen	73	ALEXANDER	10	CLEO	$\psi(2S) \to \gamma p\overline{p}$

$f_2(2150)$ REFERENCES

ALEXANDER	10	PR D82 092002	J.P. Alexander *et al.*	(CLEO Collab.)
UMAN	06	PR D73 052009	I. Uman *et al.*	(FNAL E835)
VLADIMIRSK...	06	PAN 69 493	V.V. Vladimirsky *et al.*	(ITEP, Moscow)
		Translated from YAF 69 515.		
ABLIKIM	04E	PL B603 138	M. Ablikim *et al.*	(BES Collab.)
LONGACRE	04	PR D70 094041	R.S. Longacre, S.J. Lindenbaum	(BNL, CUNY)
ANISOVICH	00E	PL B477 19	A.V. Anisovich *et al.*	
BARBERIS	00C	PL B471 440	D. Barberis *et al.*	(WA 102 Collab.)
BARBERIS	00E	PL B479 59	D. Barberis *et al.*	(WA 102 Collab.)
ABELE	99B	EPJ C8 67	A. Abele *et al.*	(Crystal Barrel Collab.)
BARBERIS	99	PL B453 305	D. Barberis *et al.*	(Omega Expt.)
EVANGELIS...	97	PR D56 3803	C. Evangelista *et al.*	(LEAR Collab.)
MARTIN	97	PR C56 1114	B.R. Martin, G.C. Oades	(LOUC, AARH)
ADOMEIT	96	ZPHY C71 227	J. Adomeit *et al.*	(Crystal Barrel Collab.)
KLOET	96	PR D53 6120	W.M. Kloet, F. Myhrer	(RUTG, NORD)
PROKOSHKIN	95D	PD 40 495	Y.D. Prokoshkin	(SERP) IGJPC
		Translated from DANS 344 469.		
HASAN	94	PL B334 215	A. Hasan, D.V. Bugg	(LOQM)
OAKDEN	94	NP A574 731	M.N. Oakden, M.R. Pennington	(DURH)
SINGOVSKI	94	NC A107 1911	A.V. Singovsky	(SERP)
ARMSTRONG	93C	PL B307 394	T.A. Armstrong *et al.*	(FNAL, FERR, GENO+)
ARMSTRONG	89D	PL B227 186	T.A. Armstrong, M. Benayoun	(ATHU, BARI, BIRM+)
ETKIN	88	PL B201 568	A. Etkin *et al.*	(BNL, CUNY)
MARTIN	80B	NP B176 355	B.R. Martin, D. Morgan	(LOUC, RHEL) JP
MARTIN	80C	NP B169 216	A.D. Martin, M.R. Pennington	(DURH) JP
CUTTS	78B	PR D17 16	D. Cutts *et al.*	(STON, WISC)
DULUDE	78B	PL 79B 335	R.S. Dulude *et al.*	(BROW, MIT, BARI) JP
COUPLAND	77	PL 71B 460	M. Coupland *et al.*	(LOQM, RHEL)
ALSPECTOR	73	PRL 30 511	J. Alspector *et al.*	(RUTG, UPNJ)

$\rho(2150)$

$I^G(J^{PC}) = 1^+(1^{--})$

OMITTED FROM SUMMARY TABLE

This entry was previously called $T_1(2190)$. See the review on "Spectroscopy of Light Meson Resonances."

$\rho(2150)$ MASS

e^+e^- PRODUCED

VALUE (MeV)		EVTS	DOCUMENT ID		TECN	COMMENT
• • • We do not use the following data for averages, fits, limits, etc. • • •						
2044 ± 31	± 4		[1] ABLIKIM	23BQ	BES3	$e^+e^- \to a_2(1320)^+\pi^- +$ c.c. $\to \eta\pi^+\pi^-$
2095 ± 4			[2] ACHASOV	23A	SND	$e^+e^- \to \omega\pi^0$
2034 ± 13	± 9		[3] ABLIKIM	21A	BES3	$e^+e^- \to \omega\pi^0$
2111 ± 43	± 25		[4] ABLIKIM	21X	BES3	$e^+e^- \to \eta'\pi^+\pi^-$
2255^{+17}_{-18}	$^{+50}_{-41}$	1.8k	[5] ABLIKIM	20F	BES3	$\psi(2S) \to K^+K^-\eta$
2201 ± 19			[6] LEES	20	BABR	$e^+e^- \to K^+K^-\gamma$
2227 ± 9	± 9		[7] LEES	20	RVUE	$e^+e^- \to K^+K^-$
2039 ± 8	$^{+36}_{-18}$		[8] ABLIKIM	19AQ	BES	$J/\psi \to K^+K^-\pi^0$
2239.2 ± 7.1	± 11.3		[9] ABLIKIM	19L	BES3	$e^+e^- \to K^+K^-$
2254 ± 22			[10] LEES	12G	BABR	$e^+e^- \to \pi^+\pi^-\gamma$
2150 ± 40	± 50		AUBERT	07AU	BABR	10.6 $e^+e^- \to f_1(1285)\pi^+\pi^-\gamma$
1990 ± 80			AUBERT	07AU	BABR	10.6 $e^+e^- \to \eta'\pi^+\pi^-\gamma$
2153 ± 37			BIAGINI	91	RVUE	$e^+e^- \to \pi^+\pi^-$, K^+K^-
2110 ± 50			[11] CLEGG	90	RVUE	$e^+e^- \to 3(\pi^+\pi^-)$, $2(\pi^+\pi^-\pi^0)$

[1] From a fit to the cross section between 2.00 and 3.08 GeV with a coherent sum of a Breit-Wigner resonance and a non-resonant contribution. Could be another state.
[2] From a vector dominance fit to the Born cross section between 1.05 and 2.0 GeV with $\rho(770)$, $\rho(1570)$, $\rho(1700)$, $\rho(2150)$. The fit also uses SND data from the VEPP-2M collider below 1.02 GeV and from LEES 17H and ABLIKIM 21A above 1.5 GeV.
[3] From a fit to the cross section between 2.00 and 3.08 GeV with a coherent sum of Breit-Wigner amplitudes, including contributions from $\rho(770)$, $\rho(1450)$ and $\rho(1700)$. Could be another state.
[4] From a Breit-Wigner fit to the Born cross section, including an s-dependent continuum amplitude.
[5] Seen in $\psi(2S)$ decay with branching ratio $\psi(2S) \to X\eta \to K^+K^-\eta = (21.7 \pm 1.9^{+7.7}_{-8.3}) \times 10^{-6}$.
[6] From the fit to the BABAR data of LEES 13Q assuming a coherent sum of a single Breit-Wigner resonance and a nonresonant contribution. The resonance significance is 3.5 σ.
[7] From the fit to the BABAR data of LEES 13Q and BESIII data of ABLIKIM 19L assuming a coherent sum of a single Breit-Wigner resonance and a nonresonant contribution.
[8] Could also be another state. Seen in J/ψ decay with branching ratio $J/\psi \to X\pi^0 \to K^+K^-\pi^0 = (6.7 \pm 1.1^{+2.2}_{-1.8}) \times 10^{-6}$.
[9] The observed structure can be due to both the $\phi(2170)$ and $\rho(2150)$.
[10] Using the GOUNARIS 68 parametrization of the pion form factor leaving the masses and widths of the $\rho(1450)$, $\rho(1700)$, and $\rho(2150)$ resonances as free parameters of the fit.
[11] Includes ATKINSON 85.

$\overline{p}p \to \pi\pi$

VALUE (MeV)	DOCUMENT ID		TECN	COMMENT
• • • We do not use the following data for averages, fits, limits, etc. • • •				
~ 2191	HASAN	94	RVUE	$\overline{p}p \to \pi\pi$
~ 2070	[1] OAKDEN	94	RVUE	0.36–1.55 $\overline{p}p \to \pi\pi$
~ 2170	[2] MARTIN	80B	RVUE	
~ 2100	[2] MARTIN	80C	RVUE	

[1] See however KLOET 96 who fit $\pi^+\pi^-$ only and find waves only up to $J = 3$ to be important but not significantly resonant.
[2] $I(J^P) = 1(1^-)$ from simultaneous analysis of $p\overline{p} \to \pi^-\pi^+$ and $\pi^0\pi^0$.

S-CHANNEL $\overline{N}N$

VALUE (MeV)	DOCUMENT ID		TECN	COMMENT
• • • We do not use the following data for averages, fits, limits, etc. • • •				
2110 ± 35	[1] ANISOVICH	02	SPEC	0.6–1.9 $p\overline{p} \to \omega\pi^0, \omega\eta\pi^0, \pi^+\pi^-$
~ 2190	[2] CUTTS	78B	CNTR	0.97–3 $\overline{p}p \to \overline{N}N$
2155 ± 15	[2,3] COUPLAND	77	CNTR	0.7–2.4 $\overline{p}p \to \overline{p}p$
2193 ± 2	[2,4] ALSPECTOR	73	CNTR	$\overline{p}p$ S channel
2190 ± 10	[5] ABRAMS	70	CNTR	S channel $\overline{p}N$

[1] From the combined analysis of ANISOVICH 00J, ANISOVICH 01D, ANISOVICH 01E, and ANISOVICH 02.
[2] Isospins 0 and 1 not separated.
[3] From a fit to the total elastic cross section.
[4] Referred to as T or T region by ALSPECTOR 73.
[5] Seen as bump in $I = 1$ state. See also COOPER 68. PEASLEE 75 confirm $\overline{p}p$ results of ABRAMS 70, no narrow structure.

$\pi^- p \to \omega\pi^0 n$

VALUE (MeV)	DOCUMENT ID		TECN	COMMENT
• • • We do not use the following data for averages, fits, limits, etc. • • •				
2140 ± 30	ALDE	95	GAM2	38 $\pi^- p \to \omega\pi^0 n$
2170 ± 30	ALDE	92C	GAM4	100 $\pi^- p \to \omega\pi^0 n$

Int. J. Mod. Phys. A 2026.41. Downloaded from www.worldscientific.com by UNIVERSITY OF CALIFORNIA @ BERKELEY on 09/16/26. Re-use and distribution is strictly not permitted, except for Open Access articles.

$\rho(2150)$ WIDTH

e^+e^- PRODUCED

VALUE (MeV)	EVTS	DOCUMENT ID		TECN	COMMENT
• • • We do not use the following data for averages, fits, limits, etc. • • •					
$163 \pm 69 \pm 24$		[1] ABLIKIM	23BQ	BES3	$e^+e^- \to a_2(1320)^+\pi^- +$ c.c. $\to \eta\pi^+\pi^-$
270 ± 3		[2] ACHASOV	23A	SND	$e^+e^- \to \omega\pi^0$
$234 \pm 30 \pm 25$		[3] ABLIKIM	21A	BES3	$e^+e^- \to \omega\pi^0$
$135 \pm 34 \pm 30$		[4] ABLIKIM	21X	BES3	$e^+e^- \to \eta'\pi^+\pi^-$
$460 {}^{+54}_{-48} {}^{+160}_{-90}$	1.8k	[5] ABLIKIM	20F	BES3	$\psi(2S) \to K^+K^-\eta$
70 ± 38		[6] LEES	20	BABR	$e^+e^- \to K^+K^-\gamma$
$127 \pm 14 \pm 4$		[7] LEES	20	RVUE	$e^+e^- \to K^+K^-$
$196 \pm 23 {}^{+25}_{-27}$		[8] ABLIKIM	19AQ	BES	$J/\psi \to K^+K^-\pi^0$
$139.8 \pm 12.3 \pm 20.6$		[9] ABLIKIM	19L	BES3	$e^+e^- \to K^+K^-$
109 ± 76		[10] LEES	12G	BABR	$e^+e^- \to \pi^+\pi^-\gamma$
$350 \pm 40 \pm 50$		AUBERT	07AU	BABR	10.6 $e^+e^- \to f_1(1285)\pi^+\pi^-\gamma$
310 ± 140		AUBERT	07AU	BABR	10.6 $e^+e^- \to \eta'\pi^+\pi^-\gamma$
389 ± 79		BIAGINI	91	RVUE	$e^+e^- \to \pi^+\pi^-$, K^+K^-
410 ± 100		[11] CLEGG	90	RVUE	$e^+e^- \to 3(\pi^+\pi^-)$, $2(\pi^+\pi^-\pi^0)$

[1] From a fit to the cross section between 2.00 and 3.08 GeV with a coherent sum of a Breit-Wigner resonance and a non-resonant contribution. Could be another state.

[2] From a vector dominance fit to the Born cross section between 1.05 and 2.0 GeV with $\rho(770)$, $\rho(1570)$, $\rho(1700)$, $\rho(2150)$. The fit also uses SND data from the VEPP-2M collider below 1.02 GeV and from LEES 17H and ABLIKIM 21A above 1.5 GeV.

[3] From a fit to the cross section between 2.00 and 3.08 GeV with a coherent sum of Breit-Wigner amplitudes, including contributions from $\rho(770)$, $\rho(1450)$ and $\rho(1700)$. Could be another state.

[4] From a Breit-Wigner fit to the Born cross section, including an s-dependent continuum amplitude.

[5] Seen in $\psi(2S)$ decay with branching ratio $\psi(2S) \to X\eta \to K^+K^-\eta = (21.7 \pm 1.9 {}^{+7.7}_{-8.3}) \times 10^{-6}$.

[6] From the fit to the BABAR data of LEES 13Q assuming a coherent sum of a single Breit-Wigner resonance and a nonresonant contribution. The resonance significance is 3.5 σ.

[7] From the fit to the BABAR data of LEES 13Q and BESIII data of ABLIKIM 19L assuming a coherent sum of a single Breit-Wigner resonance and a nonresonant contribution.

[8] Could also be another state. Seen in J/ψ decay with branching ratio $J/\psi \to X\pi^0 \to K^+K^-\pi^0 = (6.7 \pm 1.1 {}^{+2.2}_{-1.8}) \times 10^{-6}$.

[9] The observed structure can be due to both the $\phi(2170)$ and $\rho(2150)$.

[10] Using the GOUNARIS 68 parametrization of the pion form factor leaving the masses and widths of the $\rho(1450)$, $\rho(1700)$, and $\rho(2150)$ resonances as free parameters of the fit.

[11] Includes ATKINSON 85.

$\overline{p}p \to \pi\pi$

VALUE (MeV)	DOCUMENT ID		TECN	COMMENT
• • • We do not use the following data for averages, fits, limits, etc. • • •				
~ 296	HASAN	94	RVUE	$\overline{p}p \to \pi\pi$
~ 40	[1] OAKDEN	94	RVUE	0.36–1.55 $\overline{p}p \to \pi\pi$
~ 250	[2] MARTIN	80B	RVUE	
~ 200	[2] MARTIN	80C	RVUE	

[1] See however KLOET 96 who fit $\pi^+\pi^-$ only and find waves only up to $J = 3$ to be important but not significantly resonant.

[2] $I(J^P) = 1(1^-)$ from simultaneous analysis of $p\overline{p} \to \pi^-\pi^+$ and $\pi^0\pi^0$.

S-CHANNEL $\overline{N}N$

VALUE (MeV)	DOCUMENT ID		TECN	COMMENT
• • • We do not use the following data for averages, fits, limits, etc. • • •				
230 ± 50	[1] ANISOVICH	02	SPEC	0.6–1.9 $p\overline{p} \to \omega\pi^0$, $\omega\eta\pi^0$, $\pi^+\pi^-$
135 ± 75	[2,3] COUPLAND	77	CNTR	0.7–2.4 $\overline{p}p \to \overline{p}p$
98 ± 8	[3] ALSPECTOR	73	CNTR	$\overline{p}p$ S channel
~ 85	[4] ABRAMS	70	CNTR	S channel $\overline{p}N$

[1] From the combined analysis of ANISOVICH 00J, ANISOVICH 01D, ANISOVICH 01E, and ANISOVICH 02.

[2] From a fit to the total elastic cross section.

[3] Isospins 0 and 1 not separated.

[4] Seen as bump in $I = 1$ state. See also COOPER 68. PEASLEE 75 confirm $\overline{p}p$ results of ABRAMS 70, no narrow structure.

$\pi^-p \to \omega\pi^0 n$

VALUE (MeV)	DOCUMENT ID		TECN	COMMENT
• • • We do not use the following data for averages, fits, limits, etc. • • •				
320 ± 70	ALDE	95	GAM2	38 $\pi^-p \to \omega\pi^0 n$
~ 300	ALDE	92C	GAM4	100 $\pi^-p \to \omega\pi^0 n$

$\rho(2150)$ DECAY MODES

	Mode	Fraction (Γ_i/Γ)
Γ_1	e^+e^-	
Γ_2	$\pi^+\pi^-$	seen
Γ_3	K^+K^-	seen
Γ_4	$3(\pi^+\pi^-)$	seen
Γ_5	$2(\pi^+\pi^-\pi^0)$	seen
Γ_6	$\eta'\pi^+\pi^-$	seen
Γ_7	$f_1(1285)\pi^+\pi^-$	seen
Γ_8	$\omega\pi^0$	seen
Γ_9	$\omega\pi^0\eta$	seen
Γ_{10}	$a_2(1320)\pi$	
Γ_{11}	$p\overline{p}$	

$\rho(2150)$ $\Gamma(i)\Gamma(e^+e^-)/\Gamma(\text{total})$

$\Gamma(\eta'\pi^+\pi^-) \times \Gamma(e^+e^-)/\Gamma_{\text{total}}$ — $\Gamma_6\Gamma_1/\Gamma$

VALUE (eV)	DOCUMENT ID		TECN	COMMENT
• • • We do not use the following data for averages, fits, limits, etc. • • •				
$23.3 \pm 5.3 \pm 3.3$	[1] ABLIKIM	21X	BES3	$e^+e^- \to \eta'\pi^+\pi^-$

[1] From a Breit-Wigner fit to the Born cross section interfering constructively with the continuum. For destructive interference the value is $0.64 \pm 0.49 \pm 0.42$ eV.

$\Gamma(\omega\pi^0) \times \Gamma(e^+e^-)/\Gamma_{\text{total}}$ — $\Gamma_8\Gamma_1/\Gamma$

VALUE (eV)	DOCUMENT ID		TECN	COMMENT
• • • We do not use the following data for averages, fits, limits, etc. • • •				
$34 \pm 11 \pm 16$	ABLIKIM	21A	BES3	$e^+e^- \to \omega\pi^0$

$\Gamma(a_2(1320)\pi) \times \Gamma(e^+e^-)/\Gamma_{\text{total}}$ — $\Gamma_{10}\Gamma_1/\Gamma$

VALUE (eV)	DOCUMENT ID		TECN	COMMENT
• • • We do not use the following data for averages, fits, limits, etc. • • •				
$34.6 \pm 17.1 \pm 6.0$	[1] ABLIKIM	23BQ	BES3	$e^+e^- \to a_2(1320)^+\pi^-$+c.c. $\to \eta\pi^+\pi^-$

[1] From a solution of the fit to the cross section between 2.00 and 3.08 GeV using a coherent sum of a single Breit-Wigner resonance and a non-resonant contribution. $B(a_2(1320) \to \eta\pi) \times B(\eta \to \gamma\gamma)$ fixed to 0.057. Another solution with equal fit quality gives $137.1 \pm 73.3 \pm 2.1$ eV.

$\rho(2150)$ $\Gamma(i)\Gamma(e^+e^-)/\Gamma^2(\text{total})$

$\Gamma(f_1(1285)\pi^+\pi^-)/\Gamma_{\text{total}} \times \Gamma(e^+e^-)/\Gamma_{\text{total}}$ — $\Gamma_7/\Gamma \times \Gamma_1/\Gamma$

VALUE (units 10^{-7})	DOCUMENT ID		TECN	COMMENT
$3.1 \pm 0.6 \pm 0.5$	[1] AUBERT	07AU	BABR	10.6 $e^+e^- \to f_1(1285)\pi^+\pi^-\gamma$

[1] Calculated by us from the reported value of cross section at the peak.

$\Gamma(\eta'\pi^+\pi^-)/\Gamma_{\text{total}} \times \Gamma(e^+e^-)/\Gamma_{\text{total}}$ — $\Gamma_6/\Gamma \times \Gamma_1/\Gamma$

VALUE (units 10^{-8})	DOCUMENT ID		TECN	COMMENT
• • • We do not use the following data for averages, fits, limits, etc. • • •				
4.9 ± 1.9	[1] AUBERT	07AU	BABR	10.6 $e^+e^- \to \eta'\pi^+\pi^-\gamma$

[1] Calculated by us from the reported value of cross section at the peak.

$\rho(2150)$ REFERENCES

ABLIKIM	23BQ	PR D108 L111101	M. Ablikim *et al.*	(BESIII Collab.)
ACHASOV	23A	PR D108 092012	M.N. Achasov *et al.*	(SND Collab.)
ABLIKIM	21A	PL B813 136059	M. Ablikim *et al.*	(BESIII Collab.)
ABLIKIM	21X	PR D103 072007	M. Ablikim *et al.*	(BESIII Collab.)
ABLIKIM	20F	PR D101 032008	M. Ablikim *et al.*	(BESIII Collab.)
LEES	20	PR D101 012011	J.P. Lees *et al.*	(BESIII Collab.)
ABLIKIM	19AQ	PR D100 032004	M. Ablikim *et al.*	(BESIII Collab.)
ABLIKIM	19L	PR D99 032001	M. Ablikim *et al.*	(BESIII Collab.)
LEES	17H	PR D96 092009	J.P. Lees *et al.*	(BABAR Collab.)
LEES	13Q	PR D88 032013	J.P. Lees *et al.*	(BABAR Collab.)
LEES	12G	PR D86 032013	J.P. Lees *et al.*	(BABAR Collab.)
AUBERT	07AU	PR D76 092005	B. Aubert *et al.*	(BABAR Collab.)
ANISOVICH	02	PL B542 8	A.V. Anisovich *et al.*	
ANISOVICH	01D	PL B508 6	A.V. Anisovich *et al.*	
ANISOVICH	01E	PL B513 281	A.V. Anisovich *et al.*	
ANISOVICH	00J	PL B491 47	A.V. Anisovich *et al.*	(RAL, LOQM, PNPI+)
KLOET	96	PR D53 6120	W.M. Kloet, F. Myhrer	(RUTG, NORD)
ALDE	95	ZPHY C66 379	D.M. Alde *et al.*	(GAMS Collab.) JP
HASAN	94	PL B334 215	A. Hasan, D.V. Bugg	(LOQM)
OAKDEN	94	NP A574 731	M.N. Oakden, M.R. Pennington	(DURH)
ALDE	92C	ZPHY C54 553	D.M. Alde *et al.*	(BELG, SERP, KEK, LANL+)
BIAGINI	91	NC 104A 363	M.E. Biagini *et al.*	(FRAS, PRAG)
CLEGG	90	ZPHY C45 677	A.B. Clegg, A. Donnachie	(LANC, MCHS)
ATKINSON	85	ZPHY C29 333	M. Atkinson *et al.*	(BONN, CERN, GLAS+)
MARTIN	80B	NP B176 355	B.R. Martin, D. Morgan	(LOUC, RHEL) JP
MARTIN	80C	NP B169 216	A.D. Martin, M.R. Pennington	(DURH) JP
CUTTS	78B	PR D17 16	D. Cutts *et al.*	(STON, WISC)
COUPLAND	77	PL 71B 460	M. Coupland *et al.*	(LOQM, RHEL)
PEASLEE	75	PL 57B 189	D.C. Peaslee *et al.*	(CANB, BARI, BROW+)
ALSPECTOR	73	PRL 30 511	J. Alspector *et al.*	(RUTG, UPNJ)
ABRAMS	70	PR D1 1917	R.J. Abrams *et al.*	(BNL)
COOPER	68	PRL 20 1059	W.A. Cooper *et al.*	(ANL)
GOUNARIS	68	PRL 21 244	G.J. Gounaris, J.J. Sakurai	

$\phi(2170)$

$I^G(J^{PC}) = 0^-(1^{--})$

See the review on "Spectroscopy of Light Meson Resonances."

$\phi(2170)$ MASS

VALUE (MeV)	EVTS	DOCUMENT ID		TECN	COMMENT
2164 ± 5 OUR AVERAGE					
2164.7 ± 9.1 ± 3.1		[1] ABLIKIM	24AN	BES3	$e^+e^- \to K^0_S K^0_L \pi^0$
2178 ± 20 ± 5		[2] ABLIKIM	23AX	BES3	$e^+e^- \to \phi\pi^+\pi^-$
2190 ± 19 ± 37		[3] ABLIKIM	22L	BES3	2.0–3.08 $e^+e^- \to K^+K^-\pi^0$
2163.5 ± 6.2 ± 3.0		[4] ABLIKIM	21T	BES3	$e^+e^- \to \phi\eta$
2177.5 ± 4.8 ± 19.5		[5] ABLIKIM	20M	BES3	$e^+e^- \to \eta'\phi$
2126.5 ± 16.8 ± 12.4		[6] ABLIKIM	20S	BES3	$e^+e^- \to K^+K^-\pi^0\pi^0$
• • • We do not use the following data for averages, fits, limits, etc. • • •					
2191.6 ± 5.0		[7] CHEN	25D	RVUE	$e^+e^- \to K^+K^-$, $K^0_S K^0_L$
2215.7 ± 8.3		[8] LICHARD	23	RVUE	$e^+e^- \to \Upsilon(nS) \to \phi\eta\gamma$
2169 ± 5 ± 6		[9] ZHU	23A	RVUE	$e^+e^- \to \eta\phi$
2273.7 ± 5.7 ± 19.3		[10] ABLIKIM	21AP	BES3	$e^+e^- \to K^0_S K^0_L$
2135 ± 8 ± 9	95	ABLIKIM	19I	BES3	$e^+e^- \to \eta\phi f_0(980)$
2239.2 ± 7.1 ± 11.3		[11] ABLIKIM	19L	BES3	$e^+e^- \to K^+K^-$
2200 ± 6 ± 5	471	ABLIKIM	15H	BES3	$J/\psi \to \eta\phi\pi^+\pi^-$
2180 ± 8 ± 8		[12,13] LEES	12F	BABR	10.6 $e^+e^- \to \phi\pi^+\pi^-\gamma$
2079 ± 13 $^{+79}_{-28}$	4.8k	[14] SHEN	09	BELL	10.6 $e^+e^- \to K^+K^-\pi^+\pi^-\gamma$
2186 ± 10 ± 6	52	ABLIKIM	08F	BES	$J/\psi \to \eta\phi f_0(980)$
2125 ± 22 ± 10	483	AUBERT	08S	BABR	10.6 $e^+e^- \to \phi\eta\gamma$
2192 ± 14	116	[15] AUBERT	07AK	BABR	10.6 $e^+e^- \to K^+K^-\pi^+\pi^-\gamma$
2169 ± 20	149	[15] AUBERT	07AK	BABR	10.6 $e^+e^- \to K^+K^-\pi^0\pi^0\gamma$
2175 ± 10 ± 15	201	[13,16] AUBERT,BE	06D	BABR	10.6 $e^+e^- \to K^+K^-\pi\pi\gamma$

[1] Seen in $e^+e^- \to K^*(892)^0\overline{K}^0 \to K^0_S K^0_L \pi^0$ with a significance of 3.2σ.
[2] From a fit to the e^+e^- cross section between 2.00 and 3.08 GeV with a sum of Breit-Wigner amplitude and a non-resonant contribution.
[3] By a simultaneous fit of the $K^*_2(1430)^+K^-$ and $K^*(892)^+K^-$ intermediate channels in a partial-wave analysis, assuming the same structure, modelled with a coherent sum of a nonresonant component and a resonant component by a Breit-Wigner function.
[4] From a fit to the cross section below 3.5 GeV measured by BaBar and BESIII with a coherent sum of two modified Breit-Wigner amplitudes ($\phi(1680)$ and $\phi(2170)$) and a nonresonant term.
[5] From a fit using a coherent sum of a phase-space modified Breit-Wigner function and a phase-space term.
[6] By a simultaneous fit of the intermediate channels in a partial-wave analysis, assuming the same structure, modelled with a coherent sum of a nonresonant component and a resonant component by a Breit-Wigner function.
[7] From the combined analysis of the cross sections for $e^+e^- \to K^+K$ and $e^+e^- \to K^0_S K^0_L$ using data from ABLIKIM 19L and ABLIKIM 21AP. The parametrisation includes the interference between direct coupling process and resonance intermediate process with the isospin factor fixed to one. Other solutions which include additional vector resonances give 2190.0 ± 20.1 MeV and 2186.1 ± 6.2 MeV.
[8] From a VDM fit to ZHU 23 $\eta\phi\gamma$ data with two resonances, $\phi(1680)$, $\phi(2170)$, and a third resonance with mass 1850.7 ± 5.3 MeV and width 25 ± 35 MeV of 1.7 σ statistical evidence.
[9] From the analysis of the combined measurements of $\sigma(e^+e^- \to \eta\phi)$ from BaBar, Belle, BESIII, CMD3. The statistical significance for $\phi(2170)$ is 7.2 σ.
[10] From a fit to the cross section between 2.00 and 3.08 GeV with a sum of Breit-Wigner amplitude and a nonresonant contribution. The observed structure can be also due to $\rho(2150)$.
[11] The observed structure can be due to both the $\phi(2170)$ and $\rho(2150)$.
[12] Fit includes interference with the $\phi(1680)$.
[13] From the $\phi f_0(980)$ component.
[14] From a fit with two incoherent Breit-Wigners.
[15] From the $K^+K^- f_0(980)$ component.
[16] Superseded by LEES 12F.

$\phi(2170)$ WIDTH

VALUE (MeV)	EVTS	DOCUMENT ID		TECN	COMMENT
88 $^{+26}_{-21}$ OUR AVERAGE		Error includes scale factor of 2.5. See the ideogram below.			
32.4 ± 21.0 ± 1.8		[1] ABLIKIM	24AN	BES3	$e^+e^- \to K^0_S K^0_L \pi^0$
140 ± 36 ± 16		[2] ABLIKIM	23AX	BES3	$e^+e^- \to \phi\pi^+\pi^-$
191 ± 28 ± 60		[3] ABLIKIM	22L	BES3	2.0–3.08 $e^+e^- \to K^+K^-\pi^0$
31.1 $^{+21.1}_{-11.6}$ ± 1.1		[4] ABLIKIM	21T	BES3	$e^+e^- \to \phi\eta$
149.0 ± 15.6 ± 8.9		[5] ABLIKIM	20M	BES3	$e^+e^- \to \eta'\phi$
106.9 ± 32.1 ± 28.1		[6] ABLIKIM	20S	BES3	$e^+e^- \to K^+K^-\pi^0\pi^0$
• • • We do not use the following data for averages, fits, limits, etc. • • •					
86.1 ± 9.2		[7] CHEN	25D	RVUE	$e^+e^- \to K^+K^-$, $K^0_S K^0_L$
35 ± 23		[8] LICHARD	23	RVUE	$e^+e^- \to \Upsilon(nS) \to \phi\eta\gamma$
96 $^{+17}_{-14}$ ± 9		[9] ZHU	23A	RVUE	$e^+e^- \to \eta\phi$
86 ± 44 ± 51		[10] ABLIKIM	21AP	BES3	$e^+e^- \to K^0_S K^0_L$
104 ± 24 ± 12	95	ABLIKIM	19I	BES3	$e^+e^- \to \eta\phi f_0(980)$
139.8 ± 12.3 ± 20.6		[11] ABLIKIM	19L	BES3	$e^+e^- \to K^+K^-$
104 ± 15 ± 15	471	ABLIKIM	15H	BES3	$J/\psi \to \eta\phi\pi^+\pi^-$
77 ± 15 ± 10		[12,13] LEES	12F	BABR	10.6 $e^+e^- \to \phi\pi^+\pi^-\gamma$
192 ± 23 $^{+25}_{-61}$	4.8k	[14] SHEN	09	BELL	10.6 $e^+e^- \to K^+K^-\pi^+\pi^-\gamma$
65 ± 23 ± 17	52	ABLIKIM	08F	BES	$J/\psi \to \eta\phi f_0(980)$
61 ± 50 ± 13	483	AUBERT	08S	BABR	10.6 $e^+e^- \to \phi\eta\gamma$
71 ± 21	116	[15] AUBERT	07AK	BABR	10.6 $e^+e^- \to K^+K^-\pi^+\pi^-\gamma$
102 ± 27	149	[15] AUBERT	07AK	BABR	10.6 $e^+e^- \to K^+K^-\pi^0\pi^0\gamma$
58 ± 16 ± 20	201	[13,16] AUBERT,BE	06D	BABR	10.6 $e^+e^- \to K^+K^-\pi\pi\gamma$

[1] Seen in $e^+e^- \to K^*(892)^0\overline{K}^0 \to K^0_S K^0_L \pi^0$ with a significance of 3.2σ.
[2] From a fit to the e^+e^- cross section between 2.00 and 3.08 GeV with a sum of Breit-Wigner amplitude and a non-resonant contribution.
[3] By a simultaneous fit of the $K^*_2(1430)^+K^-$ and $K^*(892)^+K^-$ intermediate channels in a partial-wave analysis, assuming the same structure, modelled with a coherent sum of a nonresonant component and a resonant component by a Breit-Wigner function.
[4] From a fit to the cross section below 3.5 GeV measured by BaBar and BESIII with a coherent sum of two modified Breit-Wigner amplitudes ($\phi(1680)$ and $\phi(2170)$) and a nonresonant term.
[5] From a fit using a coherent sum of a phase-space modified Breit-Wigner function and a phase-space term.
[6] By a simultaneous fit of the intermediate channels in a partial-wave analysis, assuming the same structure, modelled with a coherent sum of a nonresonant component and a resonant component by a Breit-Wigner function.
[7] From the combined analysis of the cross sections for $e^+e^- \to K^+K$ and $e^+e^- \to K^0_S K^0_L$ using data from ABLIKIM 19L and ABLIKIM 21AP. The parametrisation includes the interference between direct coupling process and resonance intermediate process with the isospin factor fixed to one. Other solutions which include additional vector resonances give 85.9 ± 8.6 MeV and 86.4 ± 8.9 MeV.
[8] From a VDM fit to ZHU 23 $\eta\phi\gamma$ data with two resonances, $\phi(1680)$, $\phi(2170)$, and a third resonance with mass 1850.7 ± 5.3 MeV and width 25 ± 35 MeV of 1.7 σ statistical evidence.
[9] From the analysis of the combined measurements of $\sigma(e^+e^- \to \eta\phi)$ from BaBar, Belle, BESIII, CMD3. The statistical significance for $\phi(2170)$ is 7.2 σ.
[10] From a fit to the cross section between 2.00 and 3.08 GeV with a sum of Breit-Wigner amplitude and a nonresonant contribution. The observed structure can be also due to $\rho(2150)$.
[11] The observed structure can be due to both the $\phi(2170)$ and $\rho(2150)$.
[12] Fit includes interference with the $\phi(1680)$.
[13] From the $\phi f_0(980)$ component.
[14] From a fit with two incoherent Breit-Wigners.
[15] From the $K^+K^- f_0(980)$ component.
[16] Superseded by LEES 12F.

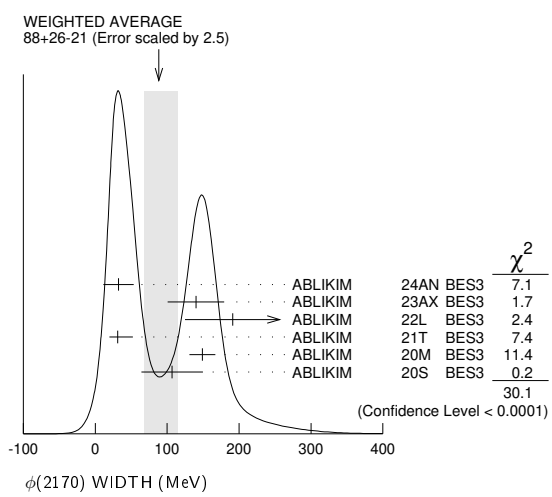

$\phi(2170)$ DECAY MODES

	Mode	Fraction (Γ_i/Γ)
Γ_1	e^+e^-	seen
Γ_2	$\phi\eta$	seen
Γ_3	$\phi\eta'$	seen
Γ_4	$\phi\pi\pi$	seen
Γ_5	$\phi f_0(980)$	seen
Γ_6	$K^0_S K^0_L$	
Γ_7	$K^+K^-\pi^+\pi^-$	
Γ_8	$K^+K^- f_0(980) \to K^+K^-\pi^+\pi^-$	seen
Γ_9	$K^+K^-\pi^0\pi^0$	
Γ_{10}	$K^+K^- f_0(980) \to K^+K^-\pi^0\pi^0$	seen
Γ_{11}	$K^{*0}K^\pm\pi^\mp$	not seen
Γ_{12}	$K^*(892)^0\overline{K}^*(892)^0$	not seen

Int. J. Mod. Phys. A 2026.41. Downloaded from www.worldscientific.com
by LIFORNIA @ BERKELEY on 09/16/26. Re-use and distribution is strictly not permitted, except for Open Access articles.

Int. J. Mod. Phys. A 2026.41. Downloaded from www.worldscientific.com by UNIVERSITY OF CALIFORNIA @ BERKELEY on 09/16/26. Re-use and distribution is strictly not permitted, except for Open Access articles.

Γ_{13} $K^*(892)^+ K^*(892)^-$
Γ_{14} $K^*(892)^+ K^- +$ c.c.
Γ_{15} $K^*(892)^0 \overline{K}^0$
Γ_{16} $K(1460)^+ K^-+$ c.c.
Γ_{17} $K_1(1270)^+ K^-+$ c.c.
Γ_{18} $K_1(1400)^+ K^-+$ c.c.
Γ_{19} $K_2^*(1430)^+ K^-+$ c.c.

$\phi(2170)$ $\Gamma(i)\Gamma(e^+e^-)/\Gamma(\text{total})$

$\Gamma(\phi\eta) \times \Gamma(e^+e^-)/\Gamma_{\text{total}}$ — $\Gamma_2\Gamma_1/\Gamma$

VALUE (eV)	CL%	EVTS	DOCUMENT ID		TECN	COMMENT
• • • We do not use the following data for averages, fits, limits, etc. • • •						
0.17	90		[1] ZHU	23	BELL	$e^+e^- \to \Upsilon(\text{nS}) \to \phi\eta\gamma$
$0.36^{+0.05}_{-0.03} \pm 0.07$ to $41 \pm 2 \pm 6$			[2] ZHU	23A	RVUE	$e^+e^- \to \eta\phi$
$0.24^{+0.12}_{-0.07}$			[3] ABLIKIM	21T	BES3	$e^+e^- \to \phi\eta$
$1.7 \pm 0.7 \pm 1.3$		483	AUBERT	08S	BABR	10.6 $e^+e^- \to \phi\eta\gamma$

[1] From a solution of the fit using a vector meson dominance model with contributions from $\phi(1680)$, $\phi(2170)$ and non resonant contribution with mass and width of $\phi(2170)$ fixed at 2163.5 MeV and 31.1 MeV respectively. Four solutions are found with equal fit quality giving 0.17 eV (solution I and II) and 18.6 eV (III and IV) at 90% CL.

[2] From the analysis of the combined measurements of $\sigma(e^+e^- \to \eta\phi)$ from BaBar, Belle, BESIII, CMD3. The statistical significance for $\phi(2170)$ is 7.2 σ. Four solutions are found, with equal fit quality: $(0.56^{+0.03}_{-0.02} \pm 0.07)$ eV, $(0.36^{+0.05}_{-0.03} \pm 0.07)$ eV, $(38 \pm 1 \pm 5)$ eV, $(41 \pm 2 \pm 6)$ eV.

[3] From a solution of the fit to the cross section below 3.5 GeV measured by BaBar and BESIII with a coherent sum of two modified Breit-Wigner amplitudes ($\phi(1680)$ and $\phi(2170)$) and a nonresonant term. The other solution gives $10.11^{+3.87}_{-3.13}$ eV.

$\Gamma(\phi\eta') \times \Gamma(e^+e^-)/\Gamma_{\text{total}}$ — $\Gamma_3\Gamma_1/\Gamma$

VALUE (eV)	DOCUMENT ID		TECN	COMMENT
7.1±0.7±0.7	[1] ABLIKIM	20M	BES3	$e^+e^- \to \eta'\phi$

[1] From a fit using a coherent sum of a phase-space modified Breit-Wigner function and a phase-space term.

$\Gamma(\phi f_0(980)) \times \Gamma(e^+e^-)/\Gamma_{\text{total}}$ — $\Gamma_5\Gamma_1/\Gamma$

VALUE (eV)	EVTS	DOCUMENT ID		TECN	COMMENT
• • • We do not use the following data for averages, fits, limits, etc. • • •					
$2.3 \pm 0.3 \pm 0.3$		[1,2] LEES	12F	BABR	10.6 $e^+e^- \to \phi\pi^+\pi^-\gamma$
$2.5 \pm 0.8 \pm 0.4$	201	[2,3] AUBERT,BE	06D	BABR	10.6 $e^+e^- \to K^+K^-\pi\pi\gamma$

[1] From a fit with constructive interference with the $\phi(1680)$. In a fit with destructive interference, the value is larger by a factor of 12.

[2] For $f_0(980) \to \pi\pi$.

[3] Superseded by LEES 12F.

$\Gamma(K_S^0 K_L^0) \times \Gamma(e^+e^-)/\Gamma_{\text{total}}$ — $\Gamma_6\Gamma_1/\Gamma$

VALUE (eV)	DOCUMENT ID		TECN	COMMENT
• • • We do not use the following data for averages, fits, limits, etc. • • •				
$0.9 \pm 0.6 \pm 0.7$	[1] ABLIKIM	21AP	BES3	$e^+e^- \to K_S^0 K_L^0$

[1] From a fit to the cross section between 2.00 and 3.08 GeV with a sum of Breit-Wigner amplitude and a nonresonant contribution. The observed structure can be also due to $\rho(2150)$.

$\Gamma(K^*(892)^+ K^*(892)^-) \times \Gamma(e^+e^-)/\Gamma_{\text{total}}$ — $\Gamma_{13}\Gamma_1/\Gamma$

VALUE (eV)	CL%	DOCUMENT ID		TECN	COMMENT
<1.9	90	[1] ABLIKIM	20S	BES3	$e^+e^- \to K^+K^-\pi^0\pi^0$

[1] By a simultaneous fit of the intermediate channels in a partial-wave analysis, assuming the same structure, modelled with a coherent sum of a nonresonant component and a resonant component by a Breit-Wigner function.

$\Gamma(K^*(892)^+ K^- + \text{c.c.}) \times \Gamma(e^+e^-)/\Gamma_{\text{total}}$ — $\Gamma_{14}\Gamma_1/\Gamma$

VALUE (eV)	DOCUMENT ID		TECN	COMMENT
• • • We do not use the following data for averages, fits, limits, etc. • • •				
1.0 ± 0.3	[1] ABLIKIM	22L	BES3	2.0–3.08 $e^+e^- \to K^+K^-\pi^0$

[1] From a solution of a simultaneous fit of the $K_2^*(1430)^+ K^-$ and $K^*(892)^+ K^-$ intermediate channels in a partial-wave analysis, assuming the same structure, modelled with a coherent sum of a nonresonant component and a resonant component by a Breit-Wigner function. The other solution gives 7.1 ± 0.9 eV. Significance 3.7 σ.

$\Gamma(K^*(892)^0 \overline{K}^0) \times \Gamma(e^+e^-)/\Gamma_{\text{total}}$ — $\Gamma_{15}\Gamma_1/\Gamma$

VALUE (eV)	DOCUMENT ID		TECN	COMMENT
• • • We do not use the following data for averages, fits, limits, etc. • • •				
$1.0 \pm 0.2 \pm 0.1$	[1] ABLIKIM	24AN	BES3	$e^+e^- \to K_S^0 K_L^0 \pi^0$
$73.6 \pm 4.4 \pm 2.0$	[2] ABLIKIM	24AN	BES3	$e^+e^- \to K_S^0 K_L^0 \pi^0$

[1] Solution 1 of 2. Seen in $e^+e^- \to K^*(892)^0 \overline{K}^0 \to K_S^0 K_L^0 \pi^0$ with a significance of 3.2σ.

[2] Solution 2 of 2. Seen in $e^+e^- \to K^*(892)^0 \overline{K}^0 \to K_S^0 K_L^0 \pi^0$ with a significance of 3.2σ.

$\Gamma(K(1460)^+ K^- + \text{c.c.}) \times \Gamma(e^+e^-)/\Gamma_{\text{total}}$ — $\Gamma_{16}\Gamma_1/\Gamma$

VALUE (eV)	DOCUMENT ID		TECN	COMMENT
• • • We do not use the following data for averages, fits, limits, etc. • • •				
3.0 ± 3.8	[1] ABLIKIM	20S	BES3	$e^+e^- \to K^+K^-\pi^0\pi^0$

[1] By a simultaneous fit of the intermediate channels in a partial-wave analysis, assuming the same structure, modelled with a coherent sum of a nonresonant component and a resonant component by a Breit-Wigner function.

$\Gamma(K_1(1270)^+ K^- + \text{c.c.}) \times \Gamma(e^+e^-)/\Gamma_{\text{total}}$ — $\Gamma_{17}\Gamma_1/\Gamma$

VALUE (eV)	CL%	DOCUMENT ID		TECN	COMMENT
<12.5	90	[1] ABLIKIM	20S	BES3	$e^+e^- \to K^+K^-\pi^0\pi^0$

[1] By a simultaneous fit of the intermediate channels in a partial-wave analysis, assuming the same structure, modelled with a coherent sum of a nonresonant component and a resonant component by a Breit-Wigner function. A second solution of the fit with equal fit quality gives an upper limit value of 297.6 eV.

$\Gamma(K_1(1400)^+ K^- + \text{c.c.}) \times \Gamma(e^+e^-)/\Gamma_{\text{total}}$ — $\Gamma_{18}\Gamma_1/\Gamma$

VALUE (eV)	DOCUMENT ID		TECN	COMMENT
• • • We do not use the following data for averages, fits, limits, etc. • • •				
4.7 ± 3.3	[1] ABLIKIM	20S	BES3	$e^+e^- \to K^+K^-\pi^0\pi^0$

[1] By a simultaneous fit of the intermediate channels in a partial-wave analysis, assuming the same structure, modelled with a coherent sum of a nonresonant component and a resonant component by a Breit-Wigner function. A second solution of the fit with equal fit quality gives a value of 98.8 ± 7.8 eV.

$\Gamma(K_2^*(1430)^+ K^- + \text{c.c.}) \times \Gamma(e^+e^-)/\Gamma_{\text{total}}$ — $\Gamma_{19}\Gamma_1/\Gamma$

VALUE (eV)	DOCUMENT ID		TECN	COMMENT
• • • We do not use the following data for averages, fits, limits, etc. • • •				
12.6 ± 2.4	[1] ABLIKIM	22L	BES3	2.0–3.08 $e^+e^- \to K^+K^-\pi^0$

[1] From a solution of a simultaneous fit of the $K_2^*(1430)^+ K^-$ and $K^*(892)^+ K^-$ intermediate channels in a partial-wave analysis, assuming the same structure, modelled with a coherent sum of a nonresonant component and a resonant component by a Breit-Wigner function. The other solution gives 161.1 ± 20.6 eV.

$\phi(2170)$ $\Gamma(i)\Gamma(e^+e^-)/\Gamma^2(\text{total})$

$\Gamma(\phi\pi\pi)/\Gamma_{\text{total}} \times \Gamma(e^+e^-)/\Gamma_{\text{total}}$ — $\Gamma_4/\Gamma \times \Gamma_1/\Gamma$

VALUE (units 10^{-7})	EVTS	DOCUMENT ID		TECN	COMMENT
• • • We do not use the following data for averages, fits, limits, etc. • • •					
$1.65 \pm 0.15 \pm 0.18$	4.8k	[1] SHEN	09	BELL	10.6 $e^+e^- \to K^+K^-\pi^+\pi^-\gamma$

[1] Multiplied by 3/2 to take into account the $\phi\pi^0\pi^0$ mode. Using $B(\phi \to K^+K^-) = (49.2 \pm 0.6)\%$.

$\phi(2170)$ BRANCHING RATIOS

$\Gamma(\phi\pi\pi)/\Gamma_{\text{total}}$ — Γ_4/Γ

VALUE	DOCUMENT ID		TECN	COMMENT
seen	[1] ABLIKIM	23AX	BES3	$e^+e^- \to \phi\pi^+\pi^-$

[1] From a fit to the e^+e^- cross section between 2.00 and 3.08 GeV with a sum of Breit-Wigner amplitude and a non-resonant contribution.

$\Gamma(K^+K^- f_0(980) \to K^+K^-\pi^+\pi^-)/\Gamma_{\text{total}}$ — Γ_8/Γ

VALUE	DOCUMENT ID		TECN	COMMENT
seen	AUBERT	07AK	BABR	10.6 $e^+e^- \to K^+K^-\pi^+\pi^-\gamma$

$\Gamma(K^+K^- f_0(980) \to K^+K^-\pi^0\pi^0)/\Gamma_{\text{total}}$ — Γ_{10}/Γ

VALUE	DOCUMENT ID		TECN	COMMENT
seen	AUBERT	07AK	BABR	10.6 $e^+e^- \to K^+K^-\pi^0\pi^0\gamma$

$\Gamma(K^{*0} K^\pm \pi^\mp)/\Gamma_{\text{total}}$ — Γ_{11}/Γ

VALUE	DOCUMENT ID		TECN	COMMENT
not seen	AUBERT	07AK	BABR	10.6 GeV e^+e^-

$\Gamma(K^*(892)^0 \overline{K}^*(892)^0)/\Gamma_{\text{total}}$ — Γ_{12}/Γ

VALUE	DOCUMENT ID		TECN	COMMENT
not seen	ABLIKIM	10C	BES2	$J/\psi \to \eta K^+\pi^- K^-\pi^+$

$\phi(2170)$ REFERENCES

CHEN	25D	EPJ C85 1388	D.-Y. Chen *et al.*	
ABLIKIM	24AN	JHEP 2401 180	M. Ablikim *et al.*	(BESIII Collab.)
ABLIKIM	23AX	PR D108 032011	M. Ablikim *et al.*	(BESIII Collab.)
LICHARD	23	PR D108 092005	P. Lichard	(OPAV, CTUP)
ZHU	23	PR D107 012006	W. Zhu *et al.*	(BELLE Collab.)
ZHU	23A	CP C47 113003	W. Zhu, X. Wang	(RVUE)
ABLIKIM	22L	JHEP 2207 045	M. Ablikim *et al.*	(BESIII Collab.)
ABLIKIM	21AP	PR D104 092014	M. Ablikim *et al.*	(BESIII Collab.)
ABLIKIM	21T	PR D104 032007	M. Ablikim *et al.*	(BESIII Collab.)
ABLIKIM	20M	PR D102 012008	M. Ablikim *et al.*	(BESIII Collab.)
ABLIKIM	20S	PRL 124 112001	M. Ablikim *et al.*	(BESIII Collab.)
ABLIKIM	19I	PR D99 012014	M. Ablikim *et al.*	(BESIII Collab.)
ABLIKIM	19L	PR D99 032001	M. Ablikim *et al.*	(BESIII Collab.)
ABLIKIM	15H	PR D91 052017	M. Ablikim *et al.*	(BESIII Collab.)
LEES	12F	PR D86 012008	J.P. Lees *et al.*	(BABAR Collab.)
ABLIKIM	10C	PL B685 27	M. Ablikim *et al.*	(BES II Collab.)
SHEN	09	PR D80 031101	C.P. Shen *et al.*	(BELLE Collab.)
ABLIKIM	08F	PRL 100 102003	M. Ablikim *et al.*	(BES Collab.)
AUBERT	08S	PR D77 092002	B. Aubert *et al.*	(BABAR Collab.)
AUBERT	07AK	PR D76 012008	B. Aubert *et al.*	(BABAR Collab.)
AUBERT,BE	06D	PR D74 091103	B. Aubert *et al.*	(BABAR Collab.)

Int. J. Mod. Phys. A 2026.41. Downloaded from www.worldscientific.com by CALIFORNIA @ BERKELEY on 09/16/26. Re-use and distribution is strictly not permitted, except for Open Access articles.

$f_0(2200)$

$I^G(J^{PC}) = 0^+(0^{++})$

OMITTED FROM SUMMARY TABLE

Seen in $K^0_S K^0_S$ (AUGUSTIN 88), K^+K^- (ABLIKIM 05Q) and $\eta\eta$ (BINON 05) system. Not seen in $\Upsilon(1S)$ radiative decays (BARU 89).

$f_0(2200)$ MASS

VALUE (MeV)	EVTS	DOCUMENT ID		TECN	COMMENT
2187±14 OUR AVERAGE					
$2170\pm20^{+10}_{-15}$		ABLIKIM	05Q	BES2	$\psi(2S) \to \gamma\pi^+\pi^-K^+K^-$
2197±17		[1] AUGUSTIN	88	DM2	$J/\psi \to \gamma K^0_S K^0_S$
• • • We do not use the following data for averages, fits, limits, etc. • • •					
2200±25		SARANTSEV	21	RVUE	$J/\psi(1S) \to \gamma(\pi\pi, K\overline{K}, \eta\eta, \omega\phi)$
2206±12± 8	381	[2,3] DOBBS	15		$J/\psi \to \gamma K^+K^-$
2188±17±16	203	[2,3] DOBBS	15		$\psi(2S) \to \gamma K^+K^-$
2210±50		[4] BINON	05	GAMS	$33\ \pi^-p \to \eta\eta n$
∼ 2122		HASAN	94	RVUE	$\overline{p}p \to \pi\pi$
∼ 2321		HASAN	94	RVUE	$\overline{p}p \to \pi\pi$

[1] Cannot determine spin to be 0.
[2] Using CLEO-c data but not authored by the CLEO Collaboration.
[3] From a fit to a Breit-Wigner line shape with fixed Γ = 238 MeV.
[4] First solution, PWA is ambiguous.

$f_0(2200)$ WIDTH

VALUE (MeV)	DOCUMENT ID		TECN	COMMENT
210±40 OUR AVERAGE				
$220\pm60^{+40}_{-45}$	ABLIKIM	05Q	BES2	$\psi(2S) \to \gamma\pi^+\pi^-K^+K^-$
201±51	[5] AUGUSTIN	88	DM2	$J/\psi \to \gamma K^0_S K^0_S$
• • • We do not use the following data for averages, fits, limits, etc. • • •				
150±30	SARANTSEV	21	RVUE	$J/\psi(1S) \to \gamma(\pi\pi, K\overline{K}, \eta\eta, \omega\phi)$
380±90	[6] BINON	05	GAMS	$33\ \pi^-p \to \eta\eta n$
∼ 273	HASAN	94	RVUE	$\overline{p}p \to \pi\pi$
∼ 223	HASAN	94	RVUE	$\overline{p}p \to \pi\pi$

[5] Cannot determine spin to be 0.
[6] First solution, PWA is ambiguous.

$f_0(2200)$ DECAY MODES

	Mode	Fraction (Γ_i/Γ)
Γ_1	$\gamma\phi$	seen

$f_0(2200)$ BRANCHING RATIOS

$\Gamma(\gamma\phi)/\Gamma_{total}$ — **Γ_1/Γ**

VALUE	DOCUMENT ID		TECN	COMMENT
seen	[7] ABLIKIM	25P	BES3	$J/\psi \to \gamma\gamma\phi$

[7] From a partial wave analysis of $J/\psi \to \gamma\gamma\phi$ with significance 6.3σ.

$f_0(2200)$ REFERENCES

ABLIKIM	25P	PR D111 052011	M. Ablikim *et al.*	(BESIII Collab.)
SARANTSEV	21	PL B816 136227	A.V. Sarantsev *et al.*	(BONN, PNPI)
DOBBS	15	PR D91 052006	S. Dobbs *et al.*	(NWES)
ABLIKIM	05Q	PR D72 092002	M. Ablikim *et al.*	(BES Collab.)
BINON	05	PAN 68 960 Translated from YAF 68 998.	F. Binon *et al.*	
HASAN	94	PL B334 215	A. Hasan, D.V. Bugg	(LOQM)
BARU	89	ZPHY C42 505	S.E. Baru *et al.*	(NOVO)
AUGUSTIN	88	PRL 60 2238	J.E. Augustin *et al.*	(DM2 Collab.)

$f_J(2220)$

$I^G(J^{PC}) = 0^+(2^{++}$ or $4^{++})$

OMITTED FROM SUMMARY TABLE

See our mini-review in the 2004 edition of this *Review*, PDG 04.

$f_J(2220)$ MASS

VALUE (MeV)	EVTS	DOCUMENT ID		TECN	COMMENT
2231.1± 3.5 OUR AVERAGE					
2235 ± 4 ± 6	74	BAI	96B	BES	$e^+e^- \to J/\psi \to \gamma\pi^+\pi^-$
$2230\ ^{+6}_{-7}\pm16$	46	BAI	96B	BES	$e^+e^- \to J/\psi \to \gamma K^+K^-$
$2232\ ^{+8}_{-7}\pm15$	23	BAI	96B	BES	$e^+e^- \to J/\psi \to \gamma K^0_S K^0_S$
2235 ± 4 ± 5	32	BAI	96B	BES	$e^+e^- \to J/\psi \to \gamma p\overline{p}$
$2209\ ^{+17}_{-15}\pm10$		ASTON	88F	LASS	$11\ K^-p \to K^+K^-\Lambda$
2230 ±20		BOLONKIN	88	SPEC	$40\ \pi^-p \to K^0_S K^0_S n$
2220 ±10	41	[1] ALDE	86B	GA24	$38\text{–}100\ \pi p \to n\eta\eta'$
2230 ± 6 ±14	93	BALTRUSAIT...	86D	MRK3	$e^+e^- \to \gamma K^+K^-$
2232 ± 7 ± 7	23	BALTRUSAIT...	86D	MRK3	$e^+e^- \to \gamma K^0_S K^0_S$
• • • We do not use the following data for averages, fits, limits, etc. • • •					
2223.9± 2.5		[2] VLADIMIRSK...	08	SPEC	$40\ \pi^-p \to K^0_S K^0_S n + m\pi^0$
2246 ±36		BAI	98H	BES	$J/\psi \to \gamma\pi^0\pi^0$

[1] ALDE 86B uses data from both the GAMS-2000 and GAMS-4000 detectors.
[2] $J^{PC} = 2^{++}$. Systematic uncertainties not evaluated

$f_J(2220)$ WIDTH

VALUE (MeV)	CL%	EVTS	DOCUMENT ID		TECN	COMMENT
23^{+8}_{-7} OUR AVERAGE						
$19\ ^{+13}_{-11}\pm12$		74	BAI	96B	BES	$e^+e^- \to J/\psi \to \gamma\pi^+\pi^-$
$20\ ^{+20}_{-15}\pm17$		46	BAI	96B	BES	$e^+e^- \to J/\psi \to \gamma K^+K^-$
$20\ ^{+25}_{-16}\pm14$		23	BAI	96B	BES	$e^+e^- \to J/\psi \to \gamma K^0_S K^0_S$
$15\ ^{+12}_{-9}\pm9$		32	BAI	96B	BES	$e^+e^- \to J/\psi \to \gamma p\overline{p}$
$60\ ^{+107}_{-57}$			ASTON	88F	LASS	$11\ K^-p \to K^+K^-\Lambda$
80± 30			BOLONKIN	88	SPEC	$40\ \pi^-p \to K^0_S K^0_S n$
$26\ ^{+20}_{-16}\pm17$		93	BALTRUSAIT...	86D	MRK3	$e^+e^- \to \gamma K^+K^-$
$18\ ^{+23}_{-15}\pm10$		23	BALTRUSAIT...	86D	MRK3	$e^+e^- \to \gamma K^0_S K^0_S$
• • • We do not use the following data for averages, fits, limits, etc. • • •						
8.6 ± 2.5			[1] VLADIMIRSK...	08	SPEC	$40\ \pi^-p \to K^0_S K^0_S n + m\pi^0$
<80	90		ALDE	87C	GAM2	$38\ \pi^-p \to \eta'\eta n$

[1] $J^{PC} = 2^{++}$. Systematic uncertainties not evaluated

$f_J(2220)$ DECAY MODES

	Mode	Fraction (Γ_i/Γ)
Γ_1	$\pi\pi$	not seen
Γ_2	$\pi^+\pi^-$	not seen
Γ_3	$K\overline{K}$	not seen
Γ_4	$p\overline{p}$	not seen
Γ_5	$\gamma\gamma$	not seen
Γ_6	$\eta\eta'(958)$	seen
Γ_7	$\phi\phi$	not seen
Γ_8	$\eta\eta$	not seen

$f_J(2220)$ $\Gamma(i)\Gamma(\gamma\gamma)/\Gamma(total)$

$\Gamma(K\overline{K}) \times \Gamma(\gamma\gamma)/\Gamma_{total}$ — **$\Gamma_3\Gamma_5/\Gamma$**

VALUE (eV)	CL%	DOCUMENT ID		TECN	COMMENT
< 1.4	95	[1] ACCIARRI	01H	L3	$\gamma\gamma \to K^0_S K^0_S$, E^{ee}_{cm} = 91, 183–209 GeV
• • • We do not use the following data for averages, fits, limits, etc. • • •					
< 5.6	95	[1] GODANG	97	CLE2	$\gamma\gamma \to K^0_S K^0_S$
< 86	95	[1] ALBRECHT	90G	ARG	$\gamma\gamma \to K^+K^-$
<1000	95	[2] ALTHOFF	85B	TASS	$\gamma\gamma$, $K\overline{K}\pi$

$\Gamma(\pi\pi) \times \Gamma(\gamma\gamma)/\Gamma_{total}$ — **$\Gamma_1\Gamma_5/\Gamma$**

VALUE (eV)	CL%	DOCUMENT ID		TECN	COMMENT
<2.5	95	ALAM	98C	CLE2	$\gamma\gamma \to \pi^+\pi^-$

[1] Assuming $J^P = 2^+$.
[2] True for $J^P = 0^+$ and $J^P = 2^+$.

$f_J(2220)$ $\Gamma(i)\Gamma(p\overline{p})/\Gamma^2(total)$

$\Gamma(p\overline{p})/\Gamma_{total} \times \Gamma(\pi\pi)/\Gamma_{total}$ — **$\Gamma_4/\Gamma \times \Gamma_1/\Gamma$**

VALUE (units 10^{-5})	CL%	DOCUMENT ID		TECN	COMMENT
<18	95	[1] AMSLER	01	CBAR	1.4–1.5 $p\overline{p} \to \pi^0\pi^0$
• • • We do not use the following data for averages, fits, limits, etc. • • •					
<(11–42)	99	[2] HASAN	96	SPEC	1.35–1.55 $p\overline{p} \to \pi^+\pi^-$

$\Gamma(p\overline{p})/\Gamma_{total} \times \Gamma(\phi\phi)/\Gamma_{total}$ — **$\Gamma_4/\Gamma \times \Gamma_7/\Gamma$**

VALUE (units 10^{-5})	CL%	DOCUMENT ID		TECN	COMMENT
<6	95	[3] EVANGELIS...	98	SPEC	1.1–2.0 $p\overline{p} \to \phi\phi$

Int. J. Mod. Phys. A 2026.41. Downloaded from www.worldscientific.com
by UNIVERSITY OF CALIFORNIA @ BERKELEY on 09/16/26. Re-use and distribution is strictly not permitted, except for Open Access articles.

$\Gamma(p\overline{p})/\Gamma_{total} \times \Gamma(\eta\eta)/\Gamma_{total}$ — $\Gamma_4/\Gamma \times \Gamma_8/\Gamma$

VALUE (units 10^{-5})	CL%	DOCUMENT ID		TECN	COMMENT
<4	95	[1] AMSLER	01	CBAR	1.4–1.5 $p\overline{p} \to \eta\eta$

[1] For $J^P = 2^+$ in the mass range 2222–2240 MeV and the total width between 10 and 20 MeV.
[2] For $J^P = 2^+$ and $J^P = 4^+$ in the mass range 2220–2245 MeV and the total width of 15 MeV.
[3] For $J^P = 2^+$, the mass of 2235 MeV and the total width of 15 MeV.

$f_J(2220)$ BRANCHING RATIOS

$\Gamma(\pi\pi)/\Gamma_{total}$ — Γ_1/Γ

VALUE	DOCUMENT ID		COMMENT
not seen	[1] DOBBS	15	$J/\psi \to \gamma\pi\pi$
not seen	[1] DOBBS	15	$\psi(2S) \to \gamma\pi\pi$

[1] Using CLEO-c data but not authored by the CLEO Collaboration.

$\Gamma(K\overline{K})/\Gamma_{total}$ — Γ_3/Γ

VALUE	DOCUMENT ID		COMMENT
not seen	[1] DOBBS	15	$J/\psi \to \gamma K\overline{K}$
not seen	[1] DOBBS	15	$\psi(2S) \to \gamma K\overline{K}$

[1] Using CLEO-c data but not authored by the CLEO Collaboration.

$\Gamma(\pi\pi)/\Gamma(K\overline{K})$ — Γ_1/Γ_3

VALUE	DOCUMENT ID		TECN	COMMENT
1.0±0.5	BAI	96B	BES	$e^+e^- \to J/\psi \to \gamma 2\pi, K\overline{K}$

$\Gamma(p\overline{p})/\Gamma_{total}$ — Γ_4/Γ

VALUE (units 10^{-4})	CL%	DOCUMENT ID		TECN	COMMENT
• • • We do not use the following data for averages, fits, limits, etc. • • •					
not seen		[1] AUBERT	07AV	BABR	$B \to p\overline{p}K^{(*)}$
not seen		WANG	05A	BELL	$B^+ \to \overline{p}pK^+$
<3.0	95	[2] EVANGELIS...	97	SPEC	1.96–2.40 $\overline{p}p \to K^0_S K^0_S$
<1.1	99.7	[3] BARNES	93	SPEC	1.3–1.57 $\overline{p}p \to K^0_S K^0_S$
<2.6	99.7	[3] BARDIN	87	CNTR	1.3–1.5 $\overline{p}p \to K^+K^-$
<3.6	99.7	[3] SCULLI	87	CNTR	1.29–1.55 $\overline{p}p \to K^+K^-$

[1] Assuming $\Gamma < 30$ MeV.
[2] Assuming $\Gamma \sim 20$ MeV, $J^P = 2^+$ and $B(f_J(2220) \to K\overline{K}) = 100\%$.
[3] Assuming $\Gamma = 30$–35 MeV, $J^P = 2^+$ and $B(f_J(2220) \to K\overline{K}) = 100\%$.

$\Gamma(p\overline{p})/\Gamma(K\overline{K})$ — Γ_4/Γ_3

VALUE	DOCUMENT ID		TECN	COMMENT
0.17±0.09	BAI	96B	BES	$e^+e^- \to J/\psi \to \gamma p\overline{p}, K\overline{K}$

$f_J(2220)$ REFERENCES

DOBBS	15	PR D91 052006	S. Dobbs *et al.*	(NWES)
VLADIMIRSK...	08	PAN 71 2129	V.V. Vladimirsky *et al.*	(ITEP)
		Translated from YAF 71 2166.		
AUBERT	07AV	PR D76 092004	B. Aubert *et al.*	(BABAR Collab.)
WANG	05A	PL B617 141	M.-Z. Wang *et al.*	(BELLE Collab.)
PDG	04	PL B592 1	S. Eidelman *et al.*	(PDG Collab.)
ACCIARRI	01H	PL B501 173	M. Acciarri *et al.*	(L3 Collab.)
AMSLER	01	PL B520 175	C. Amsler *et al.*	(Crystal Barrel Collab.)
ALAM	98C	PRL 81 3328	M.S. Alam *et al.*	(CLEO Collab.)
BAI	98H	PRL 81 1179	J.Z. Bai *et al.*	(BES Collab.)
EVANGELIS...	98	PR D57 5370	C. Evangelista *et al.*	(JETSET Collab.)
EVANGELIS...	97	PR D56 3803	C. Evangelista *et al.*	(LEAR Collab.)
GODANG	97	PRL 79 3829	R. Godang *et al.*	(CLEO Collab.)
BAI	96B	PRL 76 3502	J.Z. Bai *et al.*	(BES Collab.)
HASAN	96	PL B388 376	A. Hasan, D.V. Bugg	(BRUN, LOQM)
BARNES	93	PL B309 469	P.D. Barnes *et al.*	(PS185 Collab.)
ALBRECHT	90G	ZPHY C48 183	H. Albrecht *et al.*	(ARGUS Collab.)
ASTON	88F	PL B215 199	D. Aston *et al.*	(SLAC, NAGO, CINC, INUS) JP
BOLONKIN	88	NP B309 426	B.V. Bolonkin *et al.*	(ITEP, SERP)
ALDE	87C	SJNP 45 255	D. Alde *et al.*	
		Translated from YAF 45 405.		
BARDIN	87	PL B195 292	G. Bardin *et al.*	(SACL, FERR, CERN, PADO+)
SCULLI	87	PRL 58 1715	J. Sculli *et al.*	(NYU, BNL)
ALDE	86B	PL B177 120	D.M. Alde *et al.*	(SERP, BELG, LANL, LAPP)
BALTRUSAIT...	86D	PRL 56 107	R.M. Baltrusaitis	(CIT, UCSC, ILL, SLAC+)
ALTHOFF	85B	ZPHY C29 189	M. Althoff *et al.*	(TASSO Collab.)

OTHER RELATED PAPERS

DEL-AMO-SA...	10O	PRL 105 172001	P. del Amo Sanchez *et al.*	(BABAR Collab.)

$\omega(2220)$

$I^G(J^{PC}) = 0^-(1^{--})$

OMITTED FROM SUMMARY TABLE

$\omega(2220)$ MASS

VALUE (MeV)	DOCUMENT ID		TECN	COMMENT
2188±21 OUR AVERAGE	Error includes scale factor of 1.2.			
2153±30±31	[1] ABLIKIM	24AJ	BES3	$e^+e^- \to \omega\eta'$
2232±19±27	[2] ABLIKIM	23G	BES3	2.0–3.1 $e^+e^- \to \omega\pi\pi$
2176±24± 3	[3] ABLIKIM	21A	BES3	$e^+e^- \to \omega\eta$
• • • We do not use the following data for averages, fits, limits, etc. • • •				
2250±25±27	[4] ABLIKIM	23G	BES3	2.0–3.1 $e^+e^- \to \omega\pi^+\pi^-$
2222± 7± 2	[5] ABLIKIM	22I	BES3	2.0–3.8 $e^+e^- \to \omega\pi^0\pi^0$
2205±30	[6] ANISOVICH	02B	SPEC	0.6–1.9 $p\overline{p} \to \omega\eta, \omega\pi^0\pi^0$

[1] From a fit to the e^+e^- cross section between 2.00 and 3.08 GeV with a sum of Breit-Wigner amplitude and a non-resonant contribution.
[2] From a fit to $\omega\pi^+\pi^-$ and $\omega\pi^0\pi^0$ with a Breit-Wigner resonance interfering with the continuum. Supersedes ABLIKIM 22I.
[3] From a fit to the cross section between 2.00 and 3.08 GeV with a coherent sum of Breit-Wigner amplitudes, including contributions from $\omega(1420)$ and $\omega(1650)/\phi(1680)$.
[4] From a fit to $\omega\pi^+\pi^-$ with a Breit-Wigner resonance interfering with the continuum.
[5] From the fit to the cross section by the coherent sum of resonant component parametrized by a modified Breit-Wigner amplitude and a phase-space contribution for the continuum.
[6] From the combined analysis of ANISOVICH 00D, ANISOVICH 01C, and ANISOVICH 02B.

$\omega(2220)$ WIDTH

VALUE (MeV)	DOCUMENT ID		TECN	COMMENT
105±34 OUR AVERAGE				
167±77± 7	[1] ABLIKIM	24AJ	BES3	$e^+e^- \to \omega\eta'$
93±53±20	[2] ABLIKIM	23G	BES3	2.0–3.1 $e^+e^- \to \omega\pi\pi$
89±50± 5	[3] ABLIKIM	21A	BES3	$e^+e^- \to \omega\eta$
• • • We do not use the following data for averages, fits, limits, etc. • • •				
125±43±15	[4] ABLIKIM	23G	BES3	2.0–3.1 $e^+e^- \to \omega\pi^+\pi^-$
59±30± 6	[5] ABLIKIM	22I	BES3	2.0–3.8 $e^+e^- \to \omega\pi^0\pi^0$
350±90	[6] ANISOVICH	02B	SPEC	0.6–1.9 $p\overline{p} \to \omega\eta, \omega\pi^0\pi^0$

[1] From a fit to the e^+e^- cross section between 2.00 and 3.08 GeV with a sum of Breit-Wigner amplitude and a non-resonant contribution.
[2] From a fit to $\omega\pi^+\pi^-$ and $\omega\pi^0\pi^0$ with a Breit-Wigner resonance interfering with the continuum. Supersedes ABLIKIM 22I.
[3] From a fit to the cross section between 2.00 and 3.08 GeV with a coherent sum of Breit-Wigner amplitudes, including contributions from $\omega(1420)$ and $\omega(1650)/\phi(1680)$.
[4] From a fit to $\omega\pi^+\pi^-$ with a Breit-Wigner resonance interfering with the continuum.
[5] From the fit to the cross section by the coherent sum of resonant component parametrized by a modified Breit-Wigner amplitude and a phase-space contribution for the continuum.
[6] From the combined analysis of ANISOVICH 00D, ANISOVICH 01C, and ANISOVICH 02B.

$\omega(2220)$ DECAY MODES

	Mode	Fraction (Γ_i/Γ)
Γ_1	$\omega\pi\pi$	seen
Γ_2	$\omega\pi^+\pi^-$	seen
Γ_3	$\omega\pi^0\pi^0$	seen
Γ_4	$\omega\eta$	seen
Γ_5	$\omega\eta'$	seen
Γ_6	e^+e^-	seen

$\omega(2220)$ $\Gamma(i)\Gamma(e^+e^-)/\Gamma(total)$

$\Gamma(\omega\pi^0\pi^0) \times \Gamma(e^+e^-)/\Gamma_{total}$ — $\Gamma_3\Gamma_6/\Gamma$

VALUE (eV)	DOCUMENT ID		TECN	COMMENT
• • • We do not use the following data for averages, fits, limits, etc. • • •				
0.3±0.1±0.1	[1] ABLIKIM	22I	BES3	2.0–3.8 $e^+e^- \to \omega\pi^0\pi^0$

[1] Superseded by ABLIKIM 23G.

$\Gamma(\omega\pi^+\pi^-) \times \Gamma(e^+e^-)/\Gamma_{total}$ — $\Gamma_2\Gamma_6/\Gamma$

VALUE (eV)	DOCUMENT ID		TECN	COMMENT
• • • We do not use the following data for averages, fits, limits, etc. • • •				
0.9±0.4±0.4	[1] ABLIKIM	23G	BES3	2.0–3.1 $e^+e^- \to \omega\pi^+\pi^-$

[1] From a fit to $\omega\pi^+\pi^-$ with a Breit-Wigner resonance interfering with the continuum. Solution with constructive interference: 52.9 ± 17.0 ± 13.1 eV.

$\Gamma(\omega\pi\pi) \times \Gamma(e^+e^-)/\Gamma_{total}$ — $\Gamma_1\Gamma_6/\Gamma$

VALUE (eV)	DOCUMENT ID		TECN	COMMENT
0.9±0.5±0.2	[1] ABLIKIM	23G	BES3	2.0–3.1 $e^+e^- \to \omega\pi\pi$

[1] From a fit to $\omega\pi^+\pi^-$ and $\omega\pi^0\pi^0$ with a Breit-Wigner resonance interfering with the continuum. Solution with constructive interference: 61.1 ± 32.1 ± 15.4 eV. Supersedes ABLIKIM 22I.

$\Gamma(\omega\eta) \times \Gamma(e^+e^-)/\Gamma_{total}$ — $\Gamma_4\Gamma_6/\Gamma$

VALUE (eV)	DOCUMENT ID		TECN	COMMENT
0.43±0.15±0.04	[1] ABLIKIM	21A	BES3	$e^+e^- \to \omega\eta$

[1] For constructive interference with $\omega(1420)$ and $\omega(1650)/\phi(1680)$. For destructive interference: 1.25 ± 0.48 ± 0.18 eV.

$\Gamma(\omega\eta') \times \Gamma(e^+e^-)/\Gamma_{total}$ — $\Gamma_5\Gamma_6/\Gamma$

VALUE (eV)	DOCUMENT ID		TECN	COMMENT
4.2 ±1.5 OUR AVERAGE				
5.72±1.68±1.5	[1] ABLIKIM	24AJ	BES3	$e^+e^- \to \omega\eta'$
2.99±1.68±1.2	[2] ABLIKIM	24AJ	BES3	$e^+e^- \to \omega\eta'$

[1] Solution 1 of the two solutions.
[2] Solution 2 of the two solutions.

Int. J. Mod. Phys. A 2026.41. Downloaded from www.worldscientific.com by CALIFORNIA @ BERKELEY on 09/16/26. Re-use and distribution is strictly not permitted, except for Open Access articles.

$\omega(2220)$ REFERENCES

ABLIKIM	24AJ	JHEP 2407 093	M. Ablikim *et al.*	(BESIII Collab.)
ABLIKIM	23G	JHEP 2301 111	M. Ablikim *et al.*	(BESIII Collab.)
Also		JHEP 2303 093 (errat.)	M. Ablikim, et. al.	(BESIII Collab.)
ABLIKIM	22I	PR D105 032005	M. Ablikim *et al.*	(BESIII Collab.)
ABLIKIM	21A	PL B813 136059	M. Ablikim *et al.*	(BESIII Collab.)
ANISOVICH	02B	PL B542 19	A.V. Anisovich *et al.*	
ANISOVICH	01C	PL B507 23	A.V. Anisovich *et al.*	
ANISOVICH	00D	PL B476 15	A.V. Anisovich *et al.*	

$\eta(2225)$

$I^G(J^{PC}) = 0^+(0^{-+})$

OMITTED FROM SUMMARY TABLE

Seen in $J/\psi \to \gamma\phi\phi$. Possibly seen in $B \to \phi\phi K$ by LEES 11A.

$\eta(2225)$ MASS

VALUE (MeV)	EVTS	DOCUMENT ID		TECN	COMMENT
2221^{+13}_{-10} OUR AVERAGE					
$2216^{+4}_{-5}{}^{+21}_{-11}$		[1] ABLIKIM	16N	BES3	$J/\psi \to \gamma K^+K^-K^+K^-$
$2240^{+30}_{-20}{}^{+30}_{-20}$	196 ± 19	ABLIKIM	08I	BES	$J/\psi \to \gamma K^+K^-K^0_SK^0_L$
$2230 \pm 25 \pm 15$		BAI	90B	MRK3	$J/\psi \to \gamma K^+K^-K^+K^-$
$2214 \pm 20 \pm 13$		BAI	90B	MRK3	$J/\psi \to \gamma K^+K^-K^0_SK^0_L$
• • • We do not use the following data for averages, fits, limits, etc. • • •					
~ 2220		BISELLO	86B	DM2	$J/\psi \to \gamma K^+K^-K^+K^-$

[1] From a partial wave analysis of $J/\psi \to \gamma\phi\phi$ that also finds significant signals for for $\eta(2100)$, 0^{-+} phase space, $f_0(2100)$, $f_2(2010)$, $f_2(2300)$, $f_2(2340)$, and a previously unseen 0^{-+} state $X(2500)$ ($M = 2470^{+15}_{-19}{}^{+101}_{-23}$ MeV, $\Gamma = 230^{+64}_{-35}{}^{+56}_{-33}$ MeV).

$\eta(2225)$ WIDTH

VALUE (MeV)	EVTS	DOCUMENT ID		TECN	COMMENT
185^{+40}_{-20} OUR AVERAGE					
$185^{+12}_{-14}{}^{+43}_{-17}$		[1] ABLIKIM	16N	BES3	$J/\psi \to \gamma K^+K^-K^+K^-$
$190 \pm 30^{+60}_{-40}$	196 ± 19	ABLIKIM	08I	BES	$J/\psi \to \gamma K^+K^-K^0_SK^0_L$
$150^{+300}_{-60} \pm 60$		BAI	90B	MRK3	$J/\psi \to \gamma K^+K^-K^+K^-$
• • • We do not use the following data for averages, fits, limits, etc. • • •					
~ 80		BISELLO	86B	DM2	$J/\psi \to \gamma K^+K^-K^+K^-$

[1] From a partial wave analysis of $J/\psi \to \gamma\phi\phi$ that also finds significant signals for for $\eta(2100)$, 0^{-+} phase space, $f_0(2100)$, $f_2(2010)$, $f_2(2300)$, $f_2(2340)$, and a previously unseen 0^{-+} state $X(2500)$ ($M = 2470^{+15}_{-19}{}^{+101}_{-23}$ MeV, $\Gamma = 230^{+64}_{-35}{}^{+56}_{-33}$ MeV).

$\eta(2225)$ REFERENCES

ABLIKIM	16N	PR D93 112011	M. Ablikim	(BESIII Collab.)
LEES	11A	PR D84 012001	J.P. Lees *et al.*	(BABAR Collab.)
ABLIKIM	08I	PL B662 330	M. Ablikim *et al.*	(BES Collab.)
BAI	90B	PRL 65 1309	Z. Bai *et al.*	(Mark III Collab.)
BISELLO	86B	PL B179 294	D. Bisello *et al.*	(DM2 Collab.)

$\rho_3(2250)$

$I^G(J^{PC}) = 1^+(3^{--})$

OMITTED FROM SUMMARY TABLE

Contains results mostly from formation experiments. For further production experiments see the Further States entry. See also $\rho(2150)$, $f_2(2150)$, $f_4(2300)$, $\rho_5(2350)$.

$\rho_3(2250)$ MASS

$\overline{p}p \to \pi\pi$ or $K\overline{K}$

VALUE (MeV)	EVTS	DOCUMENT ID		TECN	CHG	COMMENT
• • • We do not use the following data for averages, fits, limits, etc. • • •						
$2248 \pm 17^{+59}_{-5}$	1.8k	[1] ABLIKIM	20F	BES3		$\psi(2S) \to K^+K^-\eta$
~ 2232		HASAN	94	RVUE		$\overline{p}p \to \pi\pi$
~ 2090		[2] OAKDEN	94	RVUE		0.36–1.55 $\overline{p}p \to \pi\pi$
~ 2250		[3] MARTIN	80B	RVUE		
~ 2300		[3] MARTIN	80C	RVUE		
~ 2140		[4] CARTER	78B	CNTR	0	0.7–2.4 $\overline{p}p \to K^-K^+$
~ 2150		[5] CARTER	77	CNTR	0	0.7–2.4 $\overline{p}p \to \pi\pi$

[1] Seen in $\psi(2S)$ decay with branching ratio $\psi(2S) \to X\eta \to K^+K^-\eta = (1.9 \pm 0.4^{+0.5}_{-1.3}) \times 10^{-6}$.
[2] See however KLOET 96 who fit $\pi^+\pi^-$ only and find waves only up to $J = 3$ to be important but not significantly resonant.
[3] $I(J^P) = 1(3^-)$ from simultaneous analysis of $p\overline{p} \to \pi^-\pi^+$ and $\pi^0\pi^0$.
[4] $I = 0, 1$. $J^P = 3^-$ from Barrelet-zero analysis.
[5] $I(J^P) = 1(3^-)$ from amplitude analysis.

S-CHANNEL $\overline{N}N$

VALUE (MeV)	DOCUMENT ID		TECN	CHG	COMMENT
• • • We do not use the following data for averages, fits, limits, etc. • • •					
2260 ± 20	[6] ANISOVICH	02	SPEC		0.6–1.9 $p\overline{p} \to \omega\pi^0$, $\omega\eta\pi^0$, $\pi^+\pi^-$
~ 2190	[7] CUTTS	78B	CNTR		0.97–3 $\overline{p}p \to \overline{N}N$
2155 ± 15	[7,8] COUPLAND	77	CNTR	0	0.7–2.4 $\overline{p}p \to \overline{p}p$
2193 ± 2	[7,9] ALSPECTOR	73	CNTR		$\overline{p}p$ S channel
2190 ± 10	[10] ABRAMS	70	CNTR		S channel $\overline{p}N$

[6] From the combined analysis of ANISOVICH 00J, ANISOVICH 01D, ANISOVICH 01E, and ANISOVICH 02.
[7] Isospins 0 and 1 not separated.
[8] From a fit to the total elastic cross section.
[9] Referred to as T or T region by ALSPECTOR 73.
[10] Seen as bump in $I = 1$ state. See also COOPER 68. PEASLEE 75 confirm $\overline{p}p$ results of ABRAMS 70, no narrow structure.

Other processes

VALUE (MeV)	DOCUMENT ID		TECN	COMMENT
• • • We do not use the following data for averages, fits, limits, etc. • • •				
$2290 \pm 20 \pm 30$	AMELIN	00	VES	37 $\pi^-p \to \eta\pi^+\pi^-n$

$\rho_3(2250)$ WIDTH

$\overline{p}p \to \pi\pi$ or $K\overline{K}$

VALUE (MeV)	EVTS	DOCUMENT ID		TECN	CHG	COMMENT
• • • We do not use the following data for averages, fits, limits, etc. • • •						
$185^{+31}_{-26}{}^{+17}_{-103}$	1.8k	[11] ABLIKIM	20F	BES3		$\psi(2S) \to K^+K^-\eta$
~ 220		HASAN	94	RVUE		$\overline{p}p \to \pi\pi$
~ 60		[12] OAKDEN	94	RVUE		0.36–1.55 $\overline{p}p \to \pi\pi$
~ 250		[13] MARTIN	80B	RVUE		
~ 200		[13] MARTIN	80C	RVUE		
~ 150		[14] CARTER	78B	CNTR	0	0.7–2.4 $\overline{p}p \to K^-K^+$
~ 200		[15] CARTER	77	CNTR	0	0.7–2.4 $\overline{p}p \to \pi\pi$

[11] Seen in $\psi(2S)$ decay with branching ratio $\psi(2S) \to X\eta \to K^+K^-\eta = (1.9 \pm 0.4^{+0.5}_{-1.3}) \times 10^{-6}$.
[12] See however KLOET 96 who fit $\pi^+\pi^-$ only and find waves only up to $J = 3$ to be important but not significantly resonant.
[13] $I(J^P) = 1(3^-)$ from simultaneous analysis of $p\overline{p} \to \pi^-\pi^+$ and $\pi^0\pi^0$.
[14] $I = 0, 1$. $J^P = 3^-$ from Barrelet-zero analysis.
[15] $I(J^P) = 1(3^-)$ from amplitude analysis.

S-CHANNEL $\overline{N}N$

VALUE (MeV)	DOCUMENT ID		TECN	CHG	COMMENT
• • • We do not use the following data for averages, fits, limits, etc. • • •					
160 ± 25	[16] ANISOVICH	02	SPEC		0.6–1.9 $p\overline{p} \to \omega\pi^0$, $\omega\eta\pi^0$, $\pi^+\pi^-$
135 ± 75	[17,18] COUPLAND	77	CNTR	0	0.7–2.4 $\overline{p}p \to \overline{p}p$
98 ± 8	[18] ALSPECTOR	73	CNTR		$\overline{p}p$ S channel
~ 85	[19] ABRAMS	70	CNTR		S channel $\overline{p}N$

[16] From the combined analysis of ANISOVICH 00J, ANISOVICH 01D, ANISOVICH 01E, and ANISOVICH 02.
[17] From a fit to the total elastic cross section.
[18] Isospins 0 and 1 not separated.
[19] Seen as bump in $I = 1$ state. See also COOPER 68. PEASLEE 75 confirm $\overline{p}p$ results of ABRAMS 70, no narrow structure.

Other processes

VALUE (MeV)	DOCUMENT ID		TECN	COMMENT
• • • We do not use the following data for averages, fits, limits, etc. • • •				
$230 \pm 50 \pm 80$	AMELIN	00	VES	37 $\pi^-p \to \eta\pi^+\pi^-n$

$\rho_3(2250)$ REFERENCES

ABLIKIM	20F	PR D101 032008	M. Ablikim *et al.*	(BESIII Collab.)
ANISOVICH	02	PL B542 8	A.V. Anisovich *et al.*	
ANISOVICH	01D	PL B508 6	A.V. Anisovich *et al.*	
ANISOVICH	01E	PL B513 281	A.V. Anisovich *et al.*	
AMELIN	00	NP A668 83	D. Amelin *et al.*	(VES Collab.)
ANISOVICH	00J	PL B491 47	A.V. Anisovich *et al.*	(RAL, LOQM, PNPI+)
KLOET	96	PR D53 6120	W.M. Kloet, F. Myhrer	(RUTG, NORD)
HASAN	94	PL B334 215	A. Hasan, D.V. Bugg	(LOQM)
OAKDEN	94	NP A574 731	M.N. Oakden, M.R. Pennington	(DURH)
MARTIN	80B	NP B176 355	B.R. Martin, D. Morgan	(LOUC, RHEL)JP
MARTIN	80C	NP B169 216	A.D. Martin, M.R. Pennington	(DURH)JP
CARTER	78B	NP B141 467	A.A. Carter	(LOQM)
CUTTS	78B	PR D17 16	D. Cutts *et al.*	(STON, WISC)
CARTER	77	PL 67B 117	A.A. Carter *et al.*	(LOQM, RHEL)JP
COUPLAND	77	PL 71B 460	M. Coupland *et al.*	(LOQM, RHEL)
PEASLEE	75	PL 57B 189	D.C. Peaslee *et al.*	(CANB, BARI, BROW+)
ALSPECTOR	73	PRL 30 511	J. Alspector *et al.*	(RUTG, UPNJ)
ABRAMS	70	PR D1 1917	R.J. Abrams *et al.*	(BNL)
COOPER	68	PRL 20 1059	W.A. Cooper *et al.*	(ANL)

Int. J. Mod. Phys. A 2026.41. Downloaded from www.worldscientific.com by UNIVERSITY OF CALIFORNIA @ BERKELEY on 09/16/26. Re-use and distribution is strictly not permitted, except for Open Access articles.

$f_2(2300)$

$I^G(J^{PC}) = 0^+(2^{++})$

$f_2(2300)$ MASS

VALUE (MeV)	DOCUMENT ID		TECN	COMMENT
2297±28	[1] ETKIN	88	MPS	$22\ \pi^- p \to \phi\phi n$
• • • We do not use the following data for averages, fits, limits, etc. • • •				
2262± 4±28	[2] ABLIKIM	21AI	BES3	3.51–4.60 $e^+e^- \to \phi\Lambda\overline{\Lambda}$
$2243^{+7}_{-6}{}^{+3}_{-29}$	[3] UEHARA	13	BELL	$\gamma\gamma \to K^0_S K^0_S$
2270±12	VLADIMIRSK...	06	SPEC	$40\ \pi^- p \to K^0_S K^0_S n$
2327± 9± 6	ABE	04	BELL	$10.6\ e^+e^- \to e^+e^- K^+K^-$
2340±13	[4] LONGACRE	04	RVUE	$22\ \pi^- p \to \phi\phi n$, $450\ pp \to p_f 4\pi p_s$
2231±10	BOOTH	86	OMEG	$85\ \pi^-$Be $\to 2\phi$Be
2220^{+90}_{-20}	LINDENBAUM	84	RVUE	
2320±40	ETKIN	82	MPS	$22\ \pi^- p \to 2\phi n$

[1] Includes data of ETKIN 85. The percentage of the resonance going into $\phi\phi$ 2^{++} S_2, D_2, and D_0 is 6^{+15}_{-5}, 25^{+18}_{-14}, and 69^{+16}_{-27}, respectively.
[2] Threshold enhancement in $\Lambda\overline{\Lambda}$, preferred J^{PC} are 2^{++}, 2^{-+}, or 1^{++}. Could be another state.
[3] Spin 2 preferred, tentatively assigned to $f_2(2300)$.
[4] From a four pole K-matrix reanalysis of ETKIN 88 and BARBERIS 00C data.

$f_2(2300)$ WIDTH

VALUE (MeV)	DOCUMENT ID		TECN	COMMENT
149±41	[1] ETKIN	88	MPS	$22\ \pi^- p \to \phi\phi n$
• • • We do not use the following data for averages, fits, limits, etc. • • •				
72± 5±43	[2] ABLIKIM	21AI	BES3	3.51–4.60 $e^+e^- \to \phi\Lambda\overline{\Lambda}$
$145\pm12^{+27}_{-34}$	[3] UEHARA	13	BELL	$\gamma\gamma \to K^0_S K^0_S$
90±29	VLADIMIRSK...	06	SPEC	$40\ \pi^- p \to K^0_S K^0_S n$
275±36±20	ABE	04	BELL	$10.6\ e^+e^- \to e^+e^- K^+K^-$
148^{+66}_{-32}	[4] LONGACRE	04	RVUE	$22\ \pi^- p \to \phi\phi n$, $450\ pp \to p_f 4\pi p_s$
133±50	BOOTH	86	OMEG	$85\ \pi^-$Be $\to 2\phi$Be
200±50	LINDENBAUM	84	RVUE	
220±70	ETKIN	82	MPS	$22\ \pi^- p \to 2\phi n$

[1] Includes data of ETKIN 85.
[2] Threshold enhancement in $\Lambda\overline{\Lambda}$, preferred J^{PC} are 2^{++}, 2^{-+}, or 1^{++}. Could be another state.
[3] Spin 2 preferred, tentatively assigned to $f_2(2300)$.
[4] From a four pole K-matrix reanalysis of ETKIN 88 and BARBERIS 00C data.

$f_2(2300)$ DECAY MODES

	Mode	Fraction (Γ_i/Γ)
Γ_1	$\phi\phi$	seen
Γ_2	$K\overline{K}$	seen
Γ_3	$\gamma\gamma$	seen
Γ_4	$\Lambda\overline{\Lambda}$	seen

$f_2(2300)$ $\Gamma(i)\Gamma(\gamma\gamma)/\Gamma(\text{total})$

$\Gamma(K\overline{K}) \times \Gamma(\gamma\gamma)/\Gamma_{\text{total}}$ — $\Gamma_2\Gamma_3/\Gamma$

VALUE (eV)	DOCUMENT ID		TECN	COMMENT
• • • We do not use the following data for averages, fits, limits, etc. • • •				
$3.2^{+0.5}_{-0.4}{}^{+1.3}_{-2.2}$	UEHARA	13	BELL	$\gamma\gamma \to K^0_S K^0_S$
44 ±6 ±12	[1] ABE	04	BELL	$10.6\ e^+e^- \to e^+e^- K^+K^-$

[1] Assuming spin 2.

$f_2(2300)$ BRANCHING RATIOS

$\Gamma(\phi\phi)/\Gamma_{\text{total}}$ — Γ_1/Γ

VALUE	DOCUMENT ID		TECN	COMMENT
seen	BOOTH	86	OMEG	$85\ \pi^-$Be $\to 2\phi$Be
seen	ETKIN	82	MPS	$22\ \pi^- p \to 2\phi n$

$\Gamma(K\overline{K})/\Gamma_{\text{total}}$ — Γ_2/Γ

VALUE	DOCUMENT ID		TECN	COMMENT
seen	VLADIMIRSK...	06	SPEC	$40\ \pi^- p \to K^0_S K^0_S n$
seen	ABE	04	BELL	$10.6\ e^+e^- \to e^+e^- K^+K^-$

$\Gamma(\gamma\gamma)/\Gamma_{\text{total}}$ — Γ_3/Γ

VALUE	DOCUMENT ID		TECN	COMMENT
seen	UEHARA	13	BELL	$\gamma\gamma \to K^0_S K^0_S$

$\Gamma(\Lambda\overline{\Lambda})/\Gamma_{\text{total}}$ — Γ_4/Γ

VALUE	DOCUMENT ID		TECN	COMMENT
seen	[1] ABLIKIM	21AI	BES3	3.51–4.60 $e^+e^- \to \phi\Lambda\overline{\Lambda}$

[1] Threshold enhancement in $\Lambda\overline{\Lambda}$, preferred J^{PC} are 2^{++}, 2^{-+}, or 1^{++}. Could be another state.

$f_2(2300)$ REFERENCES

ABLIKIM	21AI	PR D104 052006	M. Ablikim *et al.*	(BESIII Collab.)
UEHARA	13	PTEP 2013 123C01	S. Uehara *et al.*	(BELLE Collab.)
VLADIMIRSK...	06	PAN 69 493	V.V. Vladimirsky *et al.*	(ITEP, Moscow)
		Translated from YAF 69 515.		
ABE	04	EPJ C32 323	K. Abe *et al.*	(BELLE Collab.)
LONGACRE	04	PR D70 094041	R.S. Longacre, S.J. Lindenbaum	(BNL, CUNY)
BARBERIS	00C	PL B471 440	D. Barberis *et al.*	(WA 102 Collab.)
ETKIN	88	PL B201 568	A. Etkin *et al.*	(BNL, CUNY)
BOOTH	86	NP B273 677	P.S.L. Booth *et al.*	(LIVP, GLAS, CERN)
ETKIN	85	PL 165B 217	A. Etkin *et al.*	(BNL, CUNY)
LINDENBAUM	84	CNPP 13 285	S.J. Lindenbaum	(CUNY)
ETKIN	82	PRL 49 1620	A. Etkin *et al.*	(BNL, CUNY)

$f_4(2300)$

$I^G(J^{PC}) = 0^+(4^{++})$

OMITTED FROM SUMMARY TABLE

This entry was previously called $U_0(2350)$. Contains results mostly from formation experiments. For further production experiments see the Further States entry. See also $\rho(2150)$, $f_2(2150)$, $\rho_3(2250)$, $\rho_5(2350)$.

$f_4(2300)$ MASS

$\overline{p}p \to \pi\pi$ or $\overline{K}K$

VALUE (MeV)	DOCUMENT ID		TECN	COMMENT
• • • We do not use the following data for averages, fits, limits, etc. • • •				
~ 2314	HASAN	94	RVUE	$\overline{p}p \to \pi\pi$
~ 2300	[1] MARTIN	80B	RVUE	
~ 2300	[1] MARTIN	80C	RVUE	
~ 2340	[2] CARTER	78B	CNTR	0.7–2.4 $\overline{p}p \to K^-K^+$
~ 2330	DULUDE	78B	OSPK	1–2 $\overline{p}p \to \pi^0\pi^0$
~ 2310	[3] CARTER	77	CNTR	0.7–2.4 $\overline{p}p \to \pi\pi$

[1] $I(J^P) = 0(4^+)$ from simultaneous analysis of $p\overline{p} \to \pi^-\pi^+$ and $\pi^0\pi^0$.
[2] $I(J^P) = 0(4^+)$ from Barrelet-zero analysis.
[3] $I(J^P) = 0(4^+)$ from amplitude analysis.

S-CHANNEL $\overline{p}p$ or $\overline{N}N$

VALUE (MeV)	DOCUMENT ID		TECN	COMMENT
• • • We do not use the following data for averages, fits, limits, etc. • • •				
2283±17	[4] ANISOVICH	00J	SPEC	
~ 2380	[5] CUTTS	78B	CNTR	0.97–3 $\overline{p}p \to \overline{N}N$
2345±15	[5,6] COUPLAND	77	CNTR	0.7–2.4 $\overline{p}p \to \overline{p}p$
2359± 2	[5,7] ALSPECTOR	73	CNTR	$\overline{p}p$ S channel
2375±10	ABRAMS	70	CNTR	S channel $\overline{N}N$

[4] From the combined analysis of ANISOVICH 99C and ANISOVICH 99F on $\overline{p}p \to \eta\pi^0\pi^0$, $\pi^0\pi^0$, $\eta\eta$, $\eta\eta'$, $\pi^+\pi^-$.
[5] Isospins 0 and 1 not separated.
[6] From a fit to the total elastic cross section.
[7] Referred to as U or U region by ALSPECTOR 73.

$\pi^- p \to \eta\pi\pi n$

VALUE (MeV)	DOCUMENT ID		TECN	COMMENT
• • • We do not use the following data for averages, fits, limits, etc. • • •				
2330±20±40	AMELIN	00	VES	$37\ \pi^- p \to \eta\pi^+\pi^- n$

pp CENTRAL PRODUCTION

VALUE (MeV)	DOCUMENT ID		COMMENT
2320±60 OUR ESTIMATE			
• • • We do not use the following data for averages, fits, limits, etc. • • •			
2332±15	BARBERIS	00F	$450\ pp \to p_f\omega\omega p_s$

$f_4(2300)$ WIDTH

$\overline{p}p \to \pi\pi$ or $\overline{K}K$

VALUE (MeV)	DOCUMENT ID		TECN	COMMENT
• • • We do not use the following data for averages, fits, limits, etc. • • •				
~ 278	HASAN	94	RVUE	$\overline{p}p \to \pi\pi$
~ 200	[8] MARTIN	80C	RVUE	
~ 150	[9] CARTER	78B	CNTR	0.7–2.4 $\overline{p}p \to K^-K^+$
~ 210	[10] CARTER	77	CNTR	0.7–2.4 $\overline{p}p \to \pi\pi$

[8] $I(J^P) = 0(4^+)$ from simultaneous analysis of $p\overline{p} \to \pi^-\pi^+$ and $\pi^0\pi^0$.
[9] $I(J^P) = 0(4^+)$ from Barrelet-zero analysis.
[10] $I(J^P) = 0(4^+)$ from amplitude analysis.

S-CHANNEL $\overline{p}p$ or $\overline{N}N$

VALUE (MeV)	DOCUMENT ID		TECN	COMMENT
• • • We do not use the following data for averages, fits, limits, etc. • • •				
310± 25	[11] ANISOVICH	00J	SPEC	

Int. J. Mod. Phys. A 2026.41. Downloaded from www.worldscientific.com
by CALIFORNIA @ BERKELEY on 09/16/26. Re-use and distribution is strictly not permitted, except for Open Access articles.

135^{+150}_{-65}	[12,13] COUPLAND	77	CNTR	0.7–2.4 $\overline{p}p \to \overline{p}p$	
165^{+18}_{-8}	[13] ALSPECTOR	73	CNTR	$\overline{p}p$ S channel	
~ 190	ABRAMS	70	CNTR	S channel $\overline{N}N$	

[11] From the combined analysis of ANISOVICH 99C and ANISOVICH 99F on $\overline{p}p \to \eta\pi^0\pi^0$, $\pi^0\pi^0$, $\eta\eta$, $\eta\eta'$, $\pi^+\pi^-$.
[12] From a fit to the total elastic cross section.
[13] Isospins 0 and 1 not separated.

$\pi^- p \to \eta\pi\pi n$

VALUE (MeV)	DOCUMENT ID		TECN	COMMENT
• • • We do not use the following data for averages, fits, limits, etc. • • •				
$235 \pm 50 \pm 40$	AMELIN	00	VES	37 $\pi^- p \to \eta\pi^+\pi^- n$

pp CENTRAL PRODUCTION

VALUE (MeV)	DOCUMENT ID		COMMENT
250±80 OUR ESTIMATE			
• • • We do not use the following data for averages, fits, limits, etc. • • •			
260 ± 57	BARBERIS	00F	450 $pp \to p_f \omega\omega p_s$

$f_4(2300)$ DECAY MODES

	Mode	Fraction (Γ_i/Γ)
Γ_1	$\rho\rho$	seen
Γ_2	$\omega\omega$	seen
Γ_3	$\eta\pi\pi$	seen
Γ_4	$\pi\pi$	seen
Γ_5	$K\overline{K}$	seen
Γ_6	$N\overline{N}$	seen

$f_4(2300)$ BRANCHING RATIOS

$\Gamma(\rho\rho)/\Gamma(\omega\omega)$ — Γ_1/Γ_2

VALUE	DOCUMENT ID		COMMENT
• • • We do not use the following data for averages, fits, limits, etc. • • •			
2.8 ± 0.5	BARBERIS	00F	450 $pp \to p_f \omega\omega p_s$

$f_4(2300)$ REFERENCES

AMELIN	00	NP A668 83	D. Amelin *et al.*	(VES Collab.)
ANISOVICH	00J	PL B491 47	A.V. Anisovich *et al.*	(RAL, LOQM, PNPI+)
BARBERIS	00F	PL B484 198	D. Barberis *et al.*	(WA 102 Collab.)
ANISOVICH	99C	PL B452 173	A.V. Anisovich *et al.*	
ANISOVICH	99F	NP A651 253	A.V. Anisovich *et al.*	
HASAN	94	PL B334 215	A. Hasan, D.V. Bugg	(LOQM)
MARTIN	80B	NP B176 355	B.R. Martin, D. Morgan	(LOUC, RHEL) JP
MARTIN	80C	NP B169 216	A.D. Martin, M.R. Pennington	(DURH) JP
CARTER	78B	NP B141 467	A.A. Carter	(LOQM)
CUTTS	78B	PR D17 16	D. Cutts *et al.*	(STON, WISC)
DULUDE	78B	PL 79B 335	R.S. Dulude *et al.*	(BROW, MIT, BARI) JP
CARTER	77	PL 67B 117	A.A. Carter *et al.*	(LOQM, RHEL) JP
COUPLAND	77	PL 71B 460	M. Coupland *et al.*	(LOQM, RHEL)
ALSPECTOR	73	PRL 30 511	J. Alspector *et al.*	(RUTG, UPNJ)
ABRAMS	70	PR D1 1917	R.J. Abrams *et al.*	(BNL)

$f_0(2330)$

$I^G(J^{PC}) = 0^+(0^{++})$

OMITTED FROM SUMMARY TABLE

$f_0(2330)$ MASS

VALUE (MeV)	DOCUMENT ID		TECN	COMMENT
• • • We do not use the following data for averages, fits, limits, etc. • • •				
$2312 \pm 7^{+7}_{-3}$	[1] ABLIKIM	22AS	BES3	$J/\psi(1S) \to \gamma\eta\eta'$
$2312 \pm 2^{+10}_{-0}$	[2] ABLIKIM	22C	BES3	$J/\psi \to \gamma\eta'\eta' \to 4/5\gamma 2(\pi^+\pi^-)$
2419 ± 64	[3] RODAS	22	RVUE	$J/\psi(1S) \to \gamma(\pi\pi, K\overline{K})$
2340 ± 20	SARANTSEV	21	RVUE	$J/\psi(1S) \to \gamma(\pi\pi, K\overline{K}, \eta\eta, \omega\phi)$
2314 ± 25	[4] BUGG	04A	RVUE	
2337 ± 14	ANISOVICH	00J	SPEC	2.0 $\overline{p}p \to \pi\pi, \eta\eta$
~ 2321	HASAN	94	RVUE	$\overline{p}p \to \pi\pi$

[1] From a Breit-Wigner fit involving 9 resonances and a resonating exotic $\eta_1(1855) \to \eta\eta'$ P-wave.
[2] From a partial wave analysis of the systems (γX), with $X \to \eta'\eta'$, and $(\eta' X)$, with $X \to \gamma\eta'$ in the decay $J/\psi \to \gamma\eta'\eta'$. The intermediate resonance X is parametrized by a constant-width, relativistic Breit-Wigner.
[3] T-matrix pole from coupled channel K-matrix fit to data on $J/\psi \to \gamma\pi^0\pi^0$ (ABLIKIM 15AE) and $J/\psi \to \gamma K^0_S K^0_S$ (ABLIKIM 18AA).
[4] Partial wave analysis of the data on $p\overline{p} \to \overline{\Lambda}\Lambda$ from BARNES 00.

$f_0(2330)$ WIDTH

VALUE (MeV)	DOCUMENT ID		TECN	COMMENT
• • • We do not use the following data for averages, fits, limits, etc. • • •				
$65 \pm 10^{+3}_{-12}$	[1] ABLIKIM	22AS	BES3	$J/\psi(1S) \to \gamma\eta\eta'$
$134 \pm 5^{+30}_{-9}$	[2] ABLIKIM	22C	BES3	$J/\psi \to \gamma\eta'\eta' \to 4/5\gamma 2(\pi^+\pi^-)$
274 ± 94	[3] RODAS	22	RVUE	$J/\psi(1S) \to \gamma(\pi\pi, K\overline{K})$
165 ± 25	SARANTSEV	21	RVUE	$J/\psi(1S) \to \gamma(\pi\pi, K\overline{K}, \eta\eta, \omega\phi)$
144 ± 20	[4] BUGG	04A	RVUE	
217 ± 33	ANISOVICH	00J	SPEC	2.0 $\overline{p}p \to \pi\pi, \eta\eta$
~ 223	HASAN	94	RVUE	$\overline{p}p \to \pi\pi$

[1] From a Breit-Wigner fit involving 9 resonances and a resonating exotic $\eta_1(1855) \to \eta\eta'$ P-wave.
[2] From a partial wave analysis of the systems (γX), with $X \to \eta'\eta'$, and $(\eta' X)$, with $X \to \gamma\eta'$ in the decay $J/\psi \to \gamma\eta'\eta'$. The intermediate resonance X is parametrized by a constant-width, relativistic Breit-Wigner.
[3] T-matrix pole from coupled channel K-matrix fit to data on $J/\psi \to \gamma\pi^0\pi^0$ (ABLIKIM 15AE) and $J/\psi \to \gamma K^0_S K^0_S$ (ABLIKIM 18AA).
[4] Partial wave analysis of the data on $p\overline{p} \to \overline{\Lambda}\Lambda$ from BARNES 00.

$f_0(2330)$ REFERENCES

ABLIKIM	22AS	PR D106 072012	M. Ablikim *et al.*	(BESIII Collab.)
Also		PR D107 079901 (errat.)	M. Ablikim *et al.*	(BESIII Collab.)
ABLIKIM	22C	PR D105 072002	M. Ablikim *et al.*	(BESIII Collab.)
RODAS	22	EPJ C82 80	A. Rodas *et al.*	(JPAC Collab.)
SARANTSEV	21	PL B816 136227	A.V. Sarantsev *et al.*	(BONN, PNPI)
ABLIKIM	18AA	PR D98 072003	M. Ablikim *et al.*	(BESIII Collab.)
ABLIKIM	15AE	PR D92 052003	M. Ablikim *et al.*	(BESIII Collab.)
BUGG	04A	EPJ C36 161	D.V. Bugg	
ANISOVICH	00J	PL B491 47	A.V. Anisovich *et al.*	(RAL, LOQM, PNPI+)
BARNES	00	PR C62 055203	P.D. Barnes *et al.*	
HASAN	94	PL B334 215	A. Hasan, D.V. Bugg	(LOQM)

$f_2(2340)$

$I^G(J^{PC}) = 0^+(2^{++})$

$f_2(2340)$ MASS

VALUE (MeV)	EVTS	DOCUMENT ID		TECN	COMMENT
2346^{+21}_{-10} OUR AVERAGE					
$2346 \pm 8^{+22}_{-6}$		[1] ABLIKIM	22C	BES3	$J/\psi \to \gamma\eta'\eta' \to 4/5\gamma 2(\pi^+\pi^-)$
$2362^{+31+140}_{-30-63}$	5.5k	[2] ABLIKIM	13N	BES3	$e^+e^- \to J/\psi \to \gamma\eta\eta$
2339 ± 55		[3] ETKIN	88	MPS	22 $\pi^- p \to \phi\phi n$
• • • We do not use the following data for averages, fits, limits, etc. • • •					
2350 ± 7	80k	[4] UMAN	06	E835	5.2 $\overline{p}p \to \eta\eta\pi^0$
2412^{+28}_{-32}		[5] LONGACRE	04	RVUE	22 $\pi^- p \to \phi\phi n$, 450 $pp \to p_f 4\pi p_s$
2392 ± 10		BOOTH	86	OMEG	85 π^-Be $\to 2\phi$Be
2360 ± 20		LINDENBAUM	84	RVUE	

[1] From a partial wave analysis of the systems (γX), with $X \to \eta'\eta'$, and $(\eta' X)$, with $X \to \gamma\eta'$ in the decay $J/\psi \to \gamma\eta'\eta'$. The intermediate resonance X is parametrized by a constant-width, relativistic Breit-Wigner.
[2] From partial wave analysis including all possible combinations of 0^{++}, 2^{++}, and 4^{++} resonances.
[3] Includes data of ETKIN 85. The percentage of the resonance going into $\phi\phi$ 2^{++} S_2, D_2, and D_0 is 37 ± 19, 4^{+12}_{-4}, and 59^{+21}_{-19}, respectively.
[4] Statistical error only.
[5] From a four pole K-matrix reanalysis of ETKIN 88 and BARBERIS 00C data.

$f_2(2340)$ WIDTH

VALUE (MeV)	EVTS	DOCUMENT ID		TECN	COMMENT
331^{+27}_{-18} OUR AVERAGE					
$332 \pm 14^{+26}_{-12}$		[1] ABLIKIM	22C	BES3	$J/\psi \to \gamma\eta'\eta' \to 4/5\gamma 2(\pi^+\pi^-)$
$334^{+62+165}_{-54-100}$	5.5k	[2] ABLIKIM	13N	BES3	$e^+e^- \to J/\psi \to \gamma\eta\eta$
319^{+81}_{-69}		[3] ETKIN	88	MPS	22 $\pi^- p \to \phi\phi n$
• • • We do not use the following data for averages, fits, limits, etc. • • •					
218 ± 16	80k	[4] UMAN	06	E835	5.2 $\overline{p}p \to \eta\eta\pi^0$
362^{+100}_{-53}		[5] LONGACRE	04	RVUE	22 $\pi^- p \to \phi\phi n$, 450 $pp \to p_f 4\pi p_s$
198 ± 50		BOOTH	86	OMEG	85 π^-Be $\to 2\phi$Be
150^{+150}_{-50}		LINDENBAUM	84	RVUE	

[1] From a partial wave analysis of the systems (γX), with $X \to \eta'\eta'$, and $(\eta' X)$, with $X \to \gamma\eta'$ in the decay $J/\psi \to \gamma\eta'\eta'$. The intermediate resonance X is parametrized by a constant-width, relativistic Breit-Wigner.

Int. J. Mod. Phys. A 2026.41. Downloaded from www.worldscientific.com by UNIVERSITY OF CALIFORNIA @ BERKELEY on 09/16/26. Re-use and distribution is strictly not permitted, except for Open Access articles.

[2] From partial wave analysis including all possible combinations of 0^{++}, 2^{++}, and 4^{++} resonances.
[3] Includes data of ETKIN 85.
[4] Statistical error only.
[5] From a four pole K-matrix reanalysis of ETKIN 88 and BARBERIS 00C data.

$f_2(2340)$ DECAY MODES

	Mode	Fraction (Γ_i/Γ)
Γ_1	$\phi\phi$	seen
Γ_2	$\eta\eta$	seen
Γ_3	$\eta'\eta'$	seen

$f_2(2340)$ BRANCHING RATIOS

$\Gamma(\eta\eta)/\Gamma_{total}$ — Γ_2/Γ

VALUE	DOCUMENT ID		TECN	COMMENT
seen	UMAN	06	E835	5.2 $\overline{p}p \to \eta\eta\pi^0$

$\Gamma(\eta'\eta')/\Gamma_{total}$ — Γ_3/Γ

VALUE	DOCUMENT ID		TECN	COMMENT
seen	[1] ABLIKIM	22C	BES3	$J/\psi \to \gamma\eta'\eta' \to 4/5\gamma 2(\pi^+\pi^-)$

[1] From a partial wave analysis of the systems (γX), with $X \to \eta'\eta'$, and $(\eta' X)$, with $X \to \gamma\eta'$ in the decay $J/\psi \to \gamma\eta'\eta'$. The intermediate resonance X is parametrized by a constant-width, relativistic Breit-Wigner.

$f_2(2340)$ REFERENCES

ABLIKIM	22C	PR D105 072002	M. Ablikim et al.	(BESIII Collab.)
ABLIKIM	13N	PR D87 092009	M. Ablikim et al.	(BESIII Collab.)
UMAN	06	PR D73 052009	I. Uman et al.	(FNAL E835)
LONGACRE	04	PR D70 094041	R.S. Longacre, S.J. Lindenbaum	(BNL, CUNY)
BARBERIS	00C	PL B471 440	D. Barberis et al.	(WA 102 Collab.)
ETKIN	88	PL B201 568	A. Etkin et al.	(BNL, CUNY)
BOOTH	86	NP B273 677	P.S.L. Booth et al.	(LIVP, GLAS, CERN)
ETKIN	85	PL 165B 217	A. Etkin et al.	(BNL, CUNY)
LINDENBAUM	84	CNPP 13 285	S.J. Lindenbaum	(CUNY)

$\rho_5(2350)$

$I^G(J^{PC}) = 1^+(5^{--})$

OMITTED FROM SUMMARY TABLE

This entry was previously called $U_1(2400)$. See also $\rho(2150)$, $f_2(2150)$, $\rho_3(2250)$, $f_4(2300)$.

$\rho_5(2350)$ MASS

$\pi^- p \to \omega\pi^0 n$

VALUE (MeV)	DOCUMENT ID		TECN	COMMENT
2330±35	ALDE	95	GAM2	38 $\pi^- p \to \omega\pi^0 n$

$\overline{p}p \to \pi\pi$ or $\overline{K}K$

VALUE (MeV)	DOCUMENT ID		TECN	CHG	COMMENT
• • • We do not use the following data for averages, fits, limits, etc. • • •					
~ 2303	HASAN	94	RVUE		$\overline{p}p \to \pi\pi$
~ 2300	[1] MARTIN	80B	RVUE		
~ 2250	[1] MARTIN	80C	RVUE		
~ 2500	[2] CARTER	78B	CNTR	0	0.7–2.4 $\overline{p}p \to K^-K^+$
~ 2480	[3] CARTER	77	CNTR	0	0.7–2.4 $\overline{p}p \to \pi\pi$

S-CHANNEL $\overline{N}N$

VALUE (MeV)	DOCUMENT ID		TECN	CHG	COMMENT
• • • We do not use the following data for averages, fits, limits, etc. • • •					
2300±45	[4] ANISOVICH	02	SPEC		0.6–1.9 $p\overline{p} \to \omega\pi^0$, $\omega\eta\pi^0$, $\pi^+\pi^-$
2295±30	ANISOVICH	00J	SPEC		
~ 2380	[5] CUTTS	78B	CNTR		0.97–3 $\overline{p}p \to \overline{N}N$
2345±15	[5,6] COUPLAND	77	CNTR	0	0.7–2.4 $\overline{p}p \to \overline{p}p$
2359± 2	[5,7] ALSPECTOR	73	CNTR		$\overline{p}p$ S channel
2350±10	[8] ABRAMS	70	CNTR		S channel $\overline{N}N$
2360±25	[9] OH	70B	HDBC	−0	$\overline{p}(pn)$, $K^*K2\pi$

$\pi^- p \to K^+K^- n$

VALUE (MeV)	DOCUMENT ID		TECN	CHG	COMMENT
• • • We do not use the following data for averages, fits, limits, etc. • • •					
2307±6	ALPER	80	CNTR	0	62 $\pi^- p \to K^+K^- n$

[1] $I(J^P) = 1(5^-)$ from simultaneous analysis of $p\overline{p} \to \pi^-\pi^+$ and $\pi^0\pi^0$.
[2] $I = 0(1)$; $J^P = 5^-$ from Barrelet-zero analysis.
[3] $I(J^P) = 1(5^-)$ from amplitude analysis.
[4] From the combined analysis of ANISOVICH 00J, ANISOVICH 01D, ANISOVICH 01E, and ANISOVICH 02.
[5] Isospins 0 and 1 not separated.
[6] From a fit to the total elastic cross section.
[7] Referred to as U or U region by ALSPECTOR 73.
[8] For $I = 1$ $\overline{N}N$.
[9] No evidence for this bump seen in the $\overline{p}p$ data of CHAPMAN 71B. Narrow state not confirmed by OH 73 with more data.

$\rho_5(2350)$ WIDTH

$\pi^- p \to \omega\pi^0 n$

VALUE (MeV)	DOCUMENT ID		TECN	COMMENT
400±100	ALDE	95	GAM2	38 $\pi^- p \to \omega\pi^0 n$

$\overline{p}p \to \pi\pi$ or $\overline{K}K$

VALUE (MeV)	DOCUMENT ID		TECN	CHG	COMMENT
• • • We do not use the following data for averages, fits, limits, etc. • • •					
~ 169	HASAN	94	RVUE		$\overline{p}p \to \pi\pi$
~ 250	[10] MARTIN	80B	RVUE		
~ 300	[10] MARTIN	80C	RVUE		
~ 150	[11] CARTER	78B	CNTR	0	0.7–2.4 $\overline{p}p \to K^-K^+$
~ 210	[12] CARTER	77	CNTR	0	0.7–2.4 $\overline{p}p \to \pi\pi$

S-CHANNEL $\overline{N}N$

VALUE (MeV)	DOCUMENT ID		TECN	CHG	COMMENT
• • • We do not use the following data for averages, fits, limits, etc. • • •					
260± 75	[13] ANISOVICH	02	SPEC		0.6–1.9 $p\overline{p} \to \omega\pi^0$, $\omega\eta\pi^0$, $\pi^+\pi^-$
235^{+65}_{-40}	ANISOVICH	00J	SPEC		
135^{+150}_{-65}	[14,15] COUPLAND	77	CNTR	0	0.7–2.4 $\overline{p}p \to \overline{p}p$
165^{+18}_{-8}	[15] ALSPECTOR	73	CNTR		$\overline{p}p$ S channel
< 60	[16] OH	70B	HDBC	−0	$\overline{p}(pn)$, $K^*K2\pi$
~ 140	ABRAMS	67C	CNTR		S channel $\overline{p}N$

$\pi^- p \to K^+K^- n$

VALUE (MeV)	DOCUMENT ID		TECN	CHG	COMMENT
• • • We do not use the following data for averages, fits, limits, etc. • • •					
245±20	ALPER	80	CNTR	0	62 $\pi^- p \to K^+K^- n$

[10] $I(J^P) = 1(5^-)$ from simultaneous analysis of $p\overline{p} \to \pi^-\pi^+$ and $\pi^0\pi^0$.
[11] $I = 0(1)$; $J^P = 5^-$ from Barrelet-zero analysis.
[12] $I(J^P) = 1(5^-)$ from amplitude analysis.
[13] From the combined analysis of ANISOVICH 00J, ANISOVICH 01D, ANISOVICH 01E, and ANISOVICH 02.
[14] From a fit to the total elastic cross section.
[15] Isospins 0 and 1 not separated.
[16] No evidence for this bump seen in the $\overline{p}p$ data of CHAPMAN 71B. Narrow state not confirmed by OH 73 with more data.

$\rho_5(2350)$ REFERENCES

ANISOVICH	02	PL B542 8	A.V. Anisovich et al.	
ANISOVICH	01D	PL B508 6	A.V. Anisovich et al.	
ANISOVICH	01E	PL B513 281	A.V. Anisovich et al.	
ANISOVICH	00J	PL B491 47	A.V. Anisovich et al.	(RAL, LOQM, PNPI+)
ALDE	95	ZPHY C66 379	D.M. Alde et al.	(GAMS Collab.) JP
HASAN	94	PL B334 215	A. Hasan, D.V. Bugg	(LOQM)
ALPER	80	PL 94B 422	B. Alper et al.	(AMST, CERN, CRAC, MPIM+)
MARTIN	80B	NP B176 355	B.R. Martin, D. Morgan	(LOUC, RHEL) JP
MARTIN	80C	NP B169 216	A.D. Martin, M.R. Pennington	(DURH) JP
CARTER	78B	NP B141 467	A.A. Carter	(LOQM)
CUTTS	78B	PR D17 16	D. Cutts et al.	(STON, WISC)
CARTER	77	PL 67B 117	A.A. Carter et al.	(LOQM, RHEL) JP
COUPLAND	77	PL 71B 460	M. Coupland et al.	(LOQM, RHEL)
ALSPECTOR	73	PRL 30 511	J. Alspector et al.	(RUTG, UPNJ)
OH	73	NP B51 57	B.Y. Oh et al.	(MSU)
CHAPMAN	71B	PR D4 1275	J.W. Chapman et al.	(MICH)
ABRAMS	70	PR D1 1917	R.J. Abrams et al.	(BNL)
OH	70B	PRL 24 1257	B.Y. Oh et al.	(MSU)
ABRAMS	67C	PRL 18 1209	R.J. Abrams et al.	(BNL)

$\eta(2370)$

$I^G(J^{PC}) = 0^+(0^{-+})$

OMITTED FROM SUMMARY TABLE

was $X(2370)$

$J^{PC} = 0^{-+}$ determined by ABLIKIM 24.

$\eta(2370)$ MASS

VALUE (MeV)	EVTS	DOCUMENT ID		TECN	COMMENT
2377 ± 9 OUR AVERAGE					
2395 ±11 $^{+26}_{-94}$		[1] ABLIKIM	24	BES3	$J/\psi \to \gamma K^0_S K^0_S \eta'$
2376.3± 8.7 $^{+3.2}_{-4.3}$	565	ABLIKIM	11C	BES3	$J/\psi \to \gamma\pi^+\pi^-\eta'$
• • • We do not use the following data for averages, fits, limits, etc. • • •					
2341.6± 6.5± 5.7		[2] ABLIKIM	20Q	BES3	$J/\psi \to \gamma K\overline{K}\eta'$

[1] Decaying to $f_0(980)\eta'$, fitted together with $X(1835)$, a 600 MeV broad structure around 2.8 GeV, and the tail of the $\eta_c(1S)$. Supersedes ABLIKIM 20Q.
[2] The state observed by ABLIKIM 11C at 2120 MeV is not observed with 90% CL upper limit of 1.49×10^{-5} for $J/\psi \to \gamma X(2120) \to \gamma K^+K^-\eta'$ and 6.38×10^{-6} for $K^0_S K^0_S \eta'$.

Int. J. Mod. Phys. A 2026.41. Downloaded from www.worldscientific.com by [redacted]LIFORNIA @ BERKELEY on 09/16/26. Re-use and distribution is strictly not permitted, except for Open Access articles.

$\eta(2370)$ WIDTH

VALUE (MeV)	DOCUMENT ID		TECN	COMMENT
148^{+80}_{-28} OUR AVERAGE Error includes scale factor of 1.7.				
$188^{+18+124}_{-17-33}$	[1] ABLIKIM	24	BES3	$J/\psi \to \gamma K^0_S K^0_S \eta'$
$83\pm17^{+44}_{-6}$	ABLIKIM	11C	BES3	$J/\psi \to \gamma\pi^+\pi^-\eta'$
• • • We do not use the following data for averages, fits, limits, etc. • • •				
$117\pm10\pm8$	[2] ABLIKIM	20Q	BES3	$J/\psi \to \gamma K\overline{K}\eta'$

[1] Decaying to $f_0(980)\eta'$, fitted together with $X(1835)$, a 600 MeV broad structure around 2.8 GeV, and the tail of the $\eta_C(1S)$. Supersedes ABLIKIM 20Q.

[2] The state observed by ABLIKIM 11C at 2120 MeV is not observed with 90% CL upper limit of 1.49×10^{-5} for $J/\psi \to \gamma X(2120) \to \gamma K^+K^-\eta'$ and 6.38×10^{-6} for $K^0_S K^0_S \eta'$.

$\eta(2370)$ DECAY MODES

	Mode	Fraction (Γ_i/Γ)
Γ_1	$K^+K^-\eta'$	seen
Γ_2	$K^0_S K^0_S \eta'$	seen
Γ_3	$\pi^+\pi^-\eta'$	seen
Γ_4	$f_0(980)\eta'$	seen
Γ_5	$\eta\eta\eta'$	not seen

$\eta(2370)$ BRANCHING RATIOS

$\Gamma(K^+K^-\eta')/\Gamma_{total}$ — **Γ_1/Γ**

VALUE	DOCUMENT ID		TECN	COMMENT
seen	ABLIKIM	20Q	BES3	$J/\psi \to \gamma K^+K^-\eta'$

$\Gamma(K^0_S K^0_S \eta')/\Gamma_{total}$ — **Γ_2/Γ**

VALUE	DOCUMENT ID		TECN	COMMENT
seen	ABLIKIM	20Q	BES3	$J/\psi \to \gamma K^0_S K^0_S \eta'$

$\Gamma(\pi^+\pi^-\eta')/\Gamma_{total}$ — **Γ_3/Γ**

VALUE	DOCUMENT ID		TECN	COMMENT
seen	ABLIKIM	11C	BES3	$J/\psi \to \gamma\pi^+\pi^-\eta'$

$\Gamma(f_0(980)\eta')/\Gamma_{total}$ — **Γ_4/Γ**

VALUE	DOCUMENT ID		TECN	COMMENT
seen	ABLIKIM	24	BES3	$J/\psi \to \gamma K^0_S K^0_S \eta'$

$\Gamma(\eta\eta\eta')/\Gamma_{total}$ — **Γ_5/Γ**

VALUE	DOCUMENT ID		TECN	COMMENT
not seen	[1] ABLIKIM	21C	BES3	$J/\psi(1S) \to \gamma\eta\eta\eta'$

[1] ABLIKIM 21C measured $B(J/\psi(1S) \to \gamma\eta(2370) \to \gamma\eta\eta\eta') < 9.2\times10^{-6}$.

$\eta(2370)$ REFERENCES

ABLIKIM	24	PRL 132 181901	M. Ablikim *et al.*	(BESIII Collab.) JPC
ABLIKIM	21C	PR D103 012009	M. Ablikim *et al.*	(BESIII Collab.)
ABLIKIM	20Q	EPJ C80 746	M. Ablikim *et al.*	(BESIII Collab.)
ABLIKIM	11C	PRL 106 072002	M. Ablikim *et al.*	(BESIII Collab.)

$f_0(2470)$

$I^G(J^{PC}) = 0^+(0^{++})$

OMITTED FROM SUMMARY TABLE

Seen by ABLIKIM 22C with a significance of 5.2 σ in a partial-wave analysis of the systems (γX), $X \to \eta'\eta'$ and $(\eta' X)$, $X \to \gamma\eta'$ in the decay $J/\psi \to \gamma\eta'\eta'$.

$f_0(2470)$ MASS

VALUE (MeV)	DOCUMENT ID		TECN	COMMENT
$2470\pm4^{+4}_{-6}$	[1] ABLIKIM	22C	BES3	$J/\psi \to \gamma\eta'\eta' \to 4/5\gamma 2(\pi^+\pi^-)$

[1] From a partial wave analysis of the systems (γX), with $X \to \eta'\eta'$, and $(\eta' X)$, with $X \to \gamma\eta'$ in the decay $J/\psi \to \gamma\eta'\eta'$. The intermediate resonance X is parametrized by a constant-width, relativistic Breit-Wigner.

$f_0(2470)$ WIDTH

VALUE (MeV)	DOCUMENT ID		TECN	COMMENT
$75\pm9^{+11}_{-8}$	[1] ABLIKIM	22C	BES3	$J/\psi \to \gamma\eta'\eta' \to 4/5\gamma 2(\pi^+\pi^-)$

[1] From a partial wave analysis of the systems (γX), with $X \to \eta'\eta'$, and $(\eta' X)$, with $X \to \gamma\eta'$ in the decay $J/\psi \to \gamma\eta'\eta'$. The intermediate resonance X is parametrized by a constant-width, relativistic Breit-Wigner.

$f_0(2470)$ DECAY MODES

	Mode	Fraction (Γ_i/Γ)
Γ_1	$\eta'\eta'$	seen

$f_0(2470)$ BRANCHING RATIOS

$\Gamma(\eta'\eta')/\Gamma_{total}$ — **Γ_1/Γ**

VALUE	DOCUMENT ID		TECN	COMMENT
seen	[1] ABLIKIM	22C	BES3	$J/\psi \to \gamma\eta'\eta' \to 4/5\gamma 2(\pi^+\pi^-)$

[1] From a partial wave analysis of the systems (γX), with $X \to \eta'\eta'$, and $(\eta' X)$, with $X \to \gamma\eta'$ in the decay $J/\psi \to \gamma\eta'\eta'$. The intermediate resonance X is parametrized by a constant-width, relativistic Breit-Wigner.

$f_0(2470)$ REFERENCES

ABLIKIM	22C	PR D105 072002	M. Ablikim *et al.*	(BESIII Collab.)

$f_6(2510)$

$I^G(J^{PC}) = 0^+(6^{++})$

OMITTED FROM SUMMARY TABLE

Needs confirmation.

$f_6(2510)$ MASS

VALUE (MeV)	DOCUMENT ID		TECN	COMMENT
2470±50 OUR AVERAGE Error includes scale factor of 2.1.				
2420 ± 30	ALDE	98	GAM4	$100\ \pi^-p \to \pi^0\pi^0 n$
2510 ± 30	BINON	84B	GAM2	$38\ \pi^-p \to n2\pi^0$
• • • We do not use the following data for averages, fits, limits, etc. • • •				
2485 ± 40	[1] ANISOVICH	00J	SPEC	1.92–2.41 $p\overline{p}$

[1] From the combined analysis of ANISOVICH 99C, ANISOVICH 99F, ANISOVICH 99J, ANISOVICH 99K, and ANISOVICH 00B.

$f_6(2510)$ WIDTH

VALUE (MeV)	DOCUMENT ID		TECN	COMMENT
260±40 OUR AVERAGE				
270 ± 60	ALDE	98	GAM4	$100\ \pi^-p \to \pi^0\pi^0 n$
240 ± 60	BINON	84B	GAM2	$38\ \pi^-p \to n2\pi^0$
• • • We do not use the following data for averages, fits, limits, etc. • • •				
410 ± 90	[2] ANISOVICH	00J	SPEC	1.92–2.41 $p\overline{p}$

[2] From the combined analysis of ANISOVICH 99C, ANISOVICH 99F, ANISOVICH 99J, ANISOVICH 99K, and ANISOVICH 00B.

$f_6(2510)$ DECAY MODES

	Mode	Fraction (Γ_i/Γ)
Γ_1	$\pi\pi$	(6.0 ± 1.0) %

$f_6(2510)$ BRANCHING RATIOS

$\Gamma(\pi\pi)/\Gamma_{total}$ — **Γ_1/Γ**

VALUE	DOCUMENT ID		TECN	COMMENT
0.06±0.01	[3] BINON	83C	GAM2	$38\ \pi^-p \to n4\gamma$

[3] Assuming one pion exchange and using data of BOLOTOV 74.

$f_6(2510)$ REFERENCES

ANISOVICH	00B	NP A662 319	A.V. Anisovich *et al.*	
ANISOVICH	00J	PL B491 47	A.V. Anisovich *et al.*	(RAL, LOQM, PNPI+)
ANISOVICH	99C	PL B452 173	A.V. Anisovich *et al.*	
ANISOVICH	99F	NP A651 253	A.V. Anisovich *et al.*	
ANISOVICH	99J	PL B471 271	A.V. Anisovich *et al.*	
ANISOVICH	99K	PL B468 309	A.V. Anisovich *et al.*	
ALDE	98	EPJ A3 361	D. Alde *et al.*	(GAM4 Collab.)
Also		PAN 62 405	D. Alde *et al.*	(GAMS Collab.)
		Translated from YAF 62 446.		
BINON	84B	LNC 39 41	F.G. Binon *et al.*	(SERP, BELG, LAPP) JP
BINON	83C	SJNP 38 723	F.G. Binon *et al.*	(SERP, BRUX+)
		Translated from YAF 38 1199.		
BOLOTOV	74	PL 52B 489	V.N. Bolotov *et al.*	(SERP)

Int. J. Mod. Phys. A 2026.41. Downloaded from www.worldscientific.com
by UNIVERSITY OF CALIFORNIA @ BERKELEY on 09/16/26. Re-use and distribution is strictly not permitted, except for Open Access articles.

STRANGE MESONS
($S = \pm 1$, $C = B = 0$)

$K^+ = u\bar{s}$, $K^0 = d\bar{s}$, $\overline{K}^0 = \bar{d}s$, $K^- = \bar{u}s$, similarly for K^*'s

$K^{\pm}$

$I(J^P) = \frac{1}{2}(0^-)$

CHARGED KAON MASS

Revised 1994 by T.G. Trippe (LBNL).

The average of the six charged kaon mass measurements which we use in the Particle Listings is

$$m_{K^\pm} = 493.677 \pm 0.013 \text{ MeV (S = 2.4)} , \quad (1)$$

where the error has been increased by the scale factor S. The large scale factor indicates a serious disagreement between different input data. The average before scaling the error is

$$m_{K^\pm} = 493.677 \pm 0.005 \text{ MeV} ,$$

$$\chi^2 = 22.9 \text{ for 5 D.F., Prob. } = 0.04\% , \quad (2)$$

where the high χ^2 and correspondingly low χ^2 probability further quantify the disagreement.

The main disagreement is between the two most recent and precise results,

$$m_{K^\pm} = 493.696 \pm 0.007 \text{ MeV} \qquad \text{DENISOV 91}$$

$$m_{K^\pm} = 493.636 \pm 0.011 \text{ MeV (S = 1.5)} \quad \text{GALL 88}$$

$$\text{Average} = 493.679 \pm 0.006 \text{ MeV}$$

$$\chi^2 = 21.2 \text{ for 1 D.F., Prob. } = 0.0004\% , \quad (3)$$

both of which are measurements of x-ray energies from kaonic atoms. Comparing the average in Eq. (3) with the overall average in Eq. (2), it is clear that DENISOV 91 [1] and GALL 88 [2] dominate the overall average, and that their disagreement is responsible for most of the high χ^2.

The GALL 88 measurement was made using four different kaonic atom transitions, K^- Pb $(9 \to 8)$, K^- Pb $(11 \to 10)$, K^- W $(9 \to 8)$, and K^- W $(11 \to 10)$. The $m_{K^\pm}$ values they obtain from each of these transitions is shown in the Particle Listings and in Fig. 1. Their K^- Pb $(9 \to 8)$ $m_{K^\pm}$is below and somewhat inconsistent with their other three transitions. The average of their four measurements is

$$m_{K^\pm} = 493.636 \pm 0.007 ,$$

$$\chi^2 = 7.0 \text{ for 3 D.F., Prob. } = 7.2\% . \quad (4)$$

This is a low but acceptable χ^2 probability so, to be conservative, GALL 88 scaled up the error on their average by S=1.5 to obtain their published error ±0.011 shown in Eq. (3) above and used in the Particle Listings average.

The ideogram in Fig. 1 shows that the DENISOV 91 measurement and the GALL 88 K^- Pb $(9 \to 8)$ measurement yield two well-separated peaks. One might suspect the GALL 88 K^- Pb $(9 \to 8)$ measurement since it is responsible both for the internal inconsistency in the GALL 88 measurements and the disagreement with DENISOV 91.

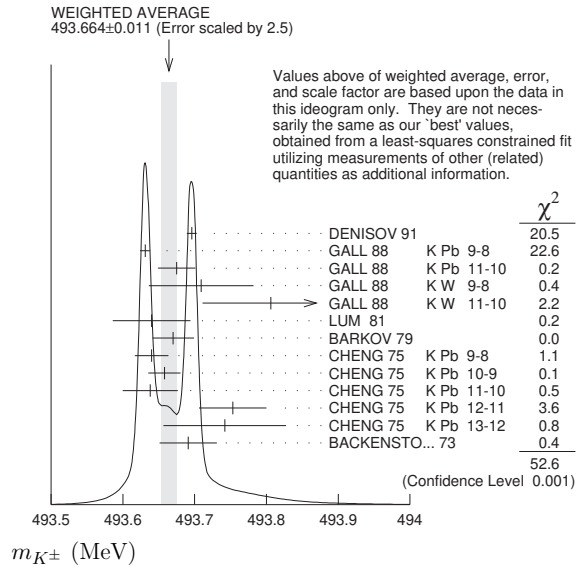

Figure 1: Ideogram of $m_{K^\pm}$ mass measurements. GALL 88 and CHENG 75 measurements are shown separately for each transition they measured.

To see if the disagreement could result from a systematic problem with the K^- Pb $(9 \to 8)$ transition, we have separated the CHENG 75 [3] data, which also used K^- Pb, into its separate transitions. Figure 1 shows that the CHENG 75 and GALL 88 K^- Pb $(9 \to 8)$ values are consistent, suggesting the possibility of a common effect such as contaminant nuclear γ rays near the K^- Pb $(9 \to 8)$ transition energy, although the CHENG 75 errors are too large to make a strong conclusion. The average of all 13 measurements has a χ^2 of 52.6 as shown in Fig. 1 and the first line of Table 1, yielding an unacceptable χ^2 probability of 0.00005%. The second line of Table 1 excludes both the GALL 88 and CHENG 75 measurements of the K^- Pb $(9 \to 8)$ transition and yields a χ^2 probability of 43%. The third [fourth] line of Table 1 excludes only the GALL 88 K^- Pb $(9 \to 8)$ [DENISOV 91] measurement and yields a χ^2 probability of 20% [8.6%]. Table 1 shows that removing both measurements of the K^- Pb $(9 \to 8)$ transition produces the most consistent set of data, but that excluding only the GALL 88 K^- Pb $(9 \to 8)$ transition or DENISOV 91 also produces acceptable probabilities.

Table 1: $m_{K^\pm}$ averages for some combinations of Fig. 1 data.

$m_{K^\pm}$ (MeV)	χ^2	D.F.	Prob. (%)	Measurements used
493.664 ± 0.004	52.6	12	0.00005	all 13 measurements
493.690 ± 0.006	10.1	10	43	no K^- Pb(9→8)
493.687 ± 0.006	14.6	11	20	no GALL 88 K^- Pb(9→8)
493.642 ± 0.006	17.8	11	8.6	no DENISOV 91

Int. J. Mod. Phys. A 2026.41. Downloaded from www.worldscientific.com
by LIFORNIA @ BERKELEY on 09/16/26. Re-use and distribution is strictly not permitted, except for Open Access articles.

Yu.M. Ivanov, representing DENISOV 91, has estimated corrections needed for the older experiments because of improved ^{192}Ir and ^{198}Au calibration γ-ray energies. He estimates that CHENG 75 and BACKENSTOSS 73 [4] $m_{K^{\pm}}$ values could be raised by about 15 keV and 22 keV, respectively. With these estimated corrections, Table 1 becomes Table 2. The last line of Table 2 shows that if such corrections are assumed, then GALL 88 K^- Pb (9 → 8) is inconsistent with the rest of the data even when DENISOV 91 is excluded. Yu.M. Ivanov warns that these are rough estimates. Accordingly, we do not use Table 2 to reject the GALL 88 K^- Pb (9 → 8) transition, but we note that a future reanalysis of the CHENG 75 data could be useful because it might provide supporting evidence for such a rejection.

Table 2: $m_{K^{\pm}}$ averages for some combinations of Fig. 1 data after raising CHENG 75 and BACKENSTOSS 73 values by 0.015 and 0.022 MeV respectively.

$m_{K^{\pm}}$ (MeV)	χ^2	D.F.	Prob. (%)	Measurements used
493.666 ± 0.004	53.9	12	0.00003	all 13 measurements
493.693 ± 0.006	9.0	10	53	no K^- Pb(9→8)
493.690 ± 0.006	11.5	11	40	no GALL 88 K^- Pb(9→8)
493.645 ± 0.006	23.0	11	1.8	no DENISOV 91

The GALL 88 measurement uses a Ge semiconductor spectrometer which has a resolution of about 1 keV, so they run the risk of some contaminant nuclear γ rays. Studies of γ rays following stopped π^- and Σ^- absorption in nuclei (unpublished) do not show any evidence for contaminants according to GALL 88 spokesperson, B.L. Roberts. The DENISOV 91 measurement uses a crystal diffraction spectrometer with a resolution of 6.3 eV for radiation at 22.1 keV to measure the 4f-3d transition in K^- ^{12}C. The high resolution and the light nucleus reduce the probability for overlap by contaminant γ rays, compared with the measurement of GALL 88. The DENISOV 91 measurement is supported by their high-precision measurement of the 4d-2p transition energy in π^- ^{12}C, which is good agreement with the calculated energy.

While we suspect that the GALL 88 K^- Pb (9 → 8) measurements could be the problem, we are unable to find clear grounds for rejecting it. Therefore, we retain their measurement in the average and accept the large scale factor until further information can be obtained from new measurements and/or from reanalysis of GALL 88 and CHENG 75 data.

We thank B.L. Roberts (Boston Univ.) and Yu.M. Ivanov (Petersburg Nuclear Physics Inst.) for their extensive help in understanding this problem.

References

1. A.S. Denisov, *et al.* [DENISOV 91], Sov. Phys. JETP Lett. **54**, 558 (1991).
2. K.P. Gall, *et al.* [GALL 88], Phys. Rev. Lett. **60**, 186 (1988).
3. S.C. Cheng, *et al.* [CHENG 75], Nucl. Phys. **A254**, 381 (1975).
4. G. Backenstoss, *et al.* [BACKENSTOSS 73], Phys. Lett. **43B**, 431 (1973).

$K^{\pm}$ MASS

VALUE (MeV)	DOCUMENT ID		TECN	CHG	COMMENT
493.677±0.015 OUR FIT Error includes scale factor of 2.8.					
493.677±0.013 OUR AVERAGE Error includes scale factor of 2.4. See the ideogram below.					
493.696±0.007	[1] DENISOV	91	CNTR	−	Kaonic atoms
493.636±0.011	[2] GALL	88	CNTR	−	Kaonic atoms
493.640±0.054	LUM	81	CNTR	−	Kaonic atoms
493.670±0.029	BARKOV	79	EMUL	±	$e^+e^- \to K^+K^-$
493.657±0.020	[2] CHENG	75	CNTR	−	Kaonic atoms
493.691±0.040	BACKENSTO...	73	CNTR	−	Kaonic atoms
• • • We do not use the following data for averages, fits, limits, etc. • • •					
493.631±0.007	GALL	88	CNTR	−	K^- Pb (9→ 8)
493.675±0.026	GALL	88	CNTR	−	K^- Pb (11→ 10)
493.709±0.073	GALL	88	CNTR	−	K^- W (9→ 8)
493.806±0.095	GALL	88	CNTR	−	K^- W (11→ 10)
493.640±0.022±0.008	[3] CHENG	75	CNTR	−	K^- Pb (9→ 8)
493.658±0.019±0.012	[3] CHENG	75	CNTR	−	K^- Pb (10→ 9)
493.638±0.035±0.016	[3] CHENG	75	CNTR	−	K^- Pb (11→ 10)
493.753±0.042±0.021	[3] CHENG	75	CNTR	−	K^- Pb (12→ 11)
493.742±0.081±0.027	[3] CHENG	75	CNTR	−	K^- Pb (13→ 12)

[1] Error increased from 0.0059 based on the error analysis in IVANOV 92.
[2] This value is the authors' combination of all of the separate transitions listed for this paper.
[3] The CHENG 75 values for separate transitions were calculated from their Table 7 transition energies. The first error includes a 20% systematic error in the noncircular contaminant shift. The second error is due to a ±5 eV uncertainty in the theoretical transition energies.

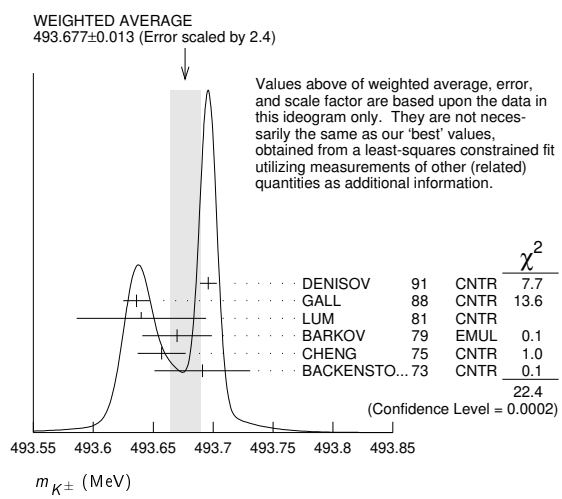

$m_{K^+} - m_{K^-}$

Test of *CPT*.

VALUE (MeV)	EVTS	DOCUMENT ID		TECN	CHG
−0.032±0.090	1.5 M	[1] FORD	72	ASPK	±

[1] FORD 72 uses $m_{\pi^+} - m_{\pi^-} = +28 \pm 70$ keV.

$K^{\pm}$ MEAN LIFE

VALUE (10^{-8} s)	EVTS	DOCUMENT ID		TECN	CHG	COMMENT
1.2380±0.0020 OUR FIT Error includes scale factor of 1.8.						
1.2379±0.0021 OUR AVERAGE Error includes scale factor of 1.9. See the ideogram below.						
1.2347±0.0030	15 M	[1] AMBROSINO	08	KLOE	±	$\phi \to K^+K^-$
1.2451±0.0030	250k	KOPTEV	95	CNTR		K at rest, U target
1.2368±0.0041	150k	KOPTEV	95	CNTR		K at rest, Cu target
1.2380±0.0016	3M	OTT	71	CNTR	+	K at rest
1.2272±0.0036		LOBKOWICZ	69	CNTR	+	K in flight
1.2443±0.0038		FITCH	65B	CNTR	+	K at rest
• • • We do not use the following data for averages, fits, limits, etc. • • •						
1.2415±0.0024	400k	[2] KOPTEV	95	CNTR		K at rest
1.221 ±0.011		FORD	67	CNTR	±	
1.231 ±0.011		BOYARSKI	62	CNTR	+	

Int. J. Mod. Phys. A 2026.41. Downloaded from www.worldscientific.com by UNIVERSITY OF CALIFORNIA @ BERKELEY on 09/16/26. Re-use and distribution is strictly not permitted, except for Open Access articles.

[1] Result obtained by averaging the decay length and decay time analyses taking correlations into account.

[2] KOPTEV 95 report this weighted average of their U-target and Cu-target results, where they have weighted by $1/\sigma$ rather than $1/\sigma^2$.

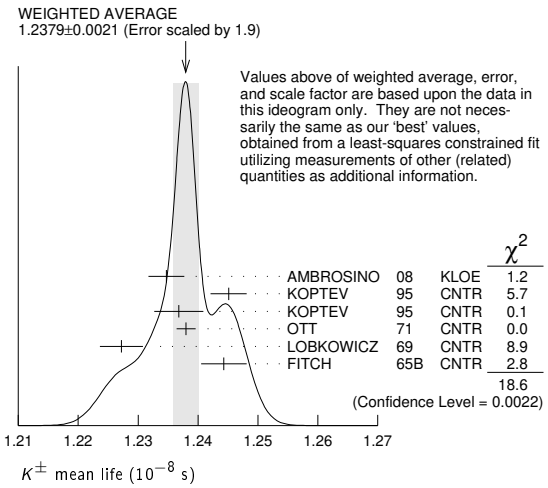

$(\tau_{K^+} - \tau_{K^-}) / \tau_{\text{average}}$

This quantity is a measure of CPT invariance in weak interactions.

VALUE (%)	DOCUMENT ID		TECN
0.10 ±0.09 OUR AVERAGE	Error includes scale factor of 1.2.		
−0.4 ±0.4	AMBROSINO	08	KLOE
0.090±0.078	LOBKOWICZ	69	CNTR
0.47 ±0.30	FORD	67	CNTR

See the related review(s):
Rare Kaon Decays

K^+ DECAY MODES

K^- modes are charge conjugates of the modes below.

	Mode		Fraction (Γ_i/Γ)	Scale factor/ Confidence level
	Leptonic and semileptonic modes			
Γ_1	$e^+\nu_e$		$(1.582\pm0.007)\times10^{-5}$	
Γ_2	$\mu^+\nu_\mu$		(63.56 ± 0.11) %	S=1.2
Γ_3	$\pi^0 e^+\nu_e$		(5.07 ± 0.04) %	S=2.1
	Called K^+_{e3}.			
Γ_4	$\pi^0\mu^+\nu_\mu$		(3.352 ± 0.034) %	S=1.9
	Called $K^+_{\mu3}$.			
Γ_5	$\pi^0\pi^0 e^+\nu_e$		$(2.55\pm0.04)\times10^{-5}$	S=1.1
Γ_6	$\pi^0\pi^0\mu^+\nu_\mu$		$(3.45\pm0.16)\times10^{-6}$	
Γ_7	$\pi^+\pi^- e^+\nu_e$		$(4.247\pm0.024)\times10^{-5}$	
Γ_8	$\pi^+\pi^-\mu^+\nu_\mu$		$(1.4\pm0.9)\times10^{-5}$	
Γ_9	$\pi^0\pi^0\pi^0 e^+\nu_e$		$<5.4\times10^{-8}$	CL=90%
	Hadronic modes			
Γ_{10}	$\pi^+\pi^0$		(20.67 ± 0.08) %	S=1.2
Γ_{11}	$\pi^+\pi^0\pi^0$		(1.760 ± 0.023) %	S=1.1
Γ_{12}	$\pi^+\pi^+\pi^-$		(5.583 ± 0.024) %	
	Leptonic and semileptonic modes with photons			
Γ_{13}	$\mu^+\nu_\mu\gamma$	[a,b]	$(6.2\pm0.8)\times10^{-3}$	
Γ_{14}	$\mu^+\nu_\mu\gamma(\text{SD}^+)$	[c,d]	$(1.33\pm0.22)\times10^{-5}$	
Γ_{15}	$\mu^+\nu_\mu\gamma(\text{SD}^+\text{INT})$	[c,d]	$<2.7\times10^{-5}$	CL=90%
Γ_{16}	$\mu^+\nu_\mu\gamma(\text{SD}^- + \text{SD}^-\text{INT})$	[c,d]	$<2.6\times10^{-4}$	CL=90%
Γ_{17}	$e^+\nu_e\gamma$		$(1.03\pm0.14)\times10^{-5}$	
Γ_{18}	$\pi^0 e^+\nu_e\gamma$	[a,b]	$(2.698\pm0.033)\times10^{-4}$	
Γ_{19}	$\pi^0 e^+\nu_e\gamma(\text{SD})$	[c,d]	$<5.3\times10^{-5}$	CL=90%
Γ_{20}	$\pi^0\mu^+\nu_\mu\gamma$	[a,b]	$(1.25\pm0.25)\times10^{-5}$	
Γ_{21}	$\pi^0\pi^0 e^+\nu_e\gamma$		$<5\times10^{-6}$	CL=90%
	Hadronic modes with photons or $\ell\bar{\ell}$ pairs			
Γ_{22}	$\pi^+\pi^0\gamma(\text{INT})$		$(-4.2\pm0.9)\times10^{-6}$	
Γ_{23}	$\pi^+\pi^0\gamma(\text{DE})$	[a,e]	$(6.0\pm0.4)\times10^{-6}$	
Γ_{24}	$\pi^+\pi^0 e^+ e^-$		$(4.24\pm0.14)\times10^{-6}$	
Γ_{25}	$\pi^+\pi^0\pi^0\gamma$	[a,b]	$(4.0\pm1.1)\times10^{-6}$	
Γ_{26}	$\pi^+\pi^+\pi^-\gamma$	[a,b]	$(7.1\pm0.5)\times10^{-6}$	
Γ_{27}	$\pi^+\gamma\gamma$	[a]	$(9.65\pm0.16)\times10^{-7}$	
Γ_{28}	$\pi^+3\gamma$	[a]	$<1.0\times10^{-4}$	CL=90%
Γ_{29}	$\pi^+ e^+ e^-\gamma$		$(1.19\pm0.13)\times10^{-8}$	
	Leptonic modes with $\ell\bar{\ell}$ pairs			
Γ_{30}	$e^+\nu_e\nu\bar{\nu}$		$<6\times10^{-5}$	CL=90%
Γ_{31}	$\mu^+\nu_\mu\nu\bar{\nu}$		$<1.0\times10^{-6}$	CL=90%
Γ_{32}	$e^+\nu_e e^+ e^-$		$(2.48\pm0.20)\times10^{-8}$	
Γ_{33}	$\mu^+\nu_\mu e^+ e^-$		$(7.06\pm0.31)\times10^{-8}$	
Γ_{34}	$e^+\nu_e\mu^+\mu^-$		$(1.7\pm0.5)\times10^{-8}$	
Γ_{35}	$\mu^+\nu_\mu\mu^+\mu^-$		$<4.1\times10^{-7}$	CL=90%
	Lepton family number (LF), Lepton number (L), $\Delta S = \Delta Q$ (SQ) violating modes, or $\Delta S = 1$ weak neutral current ($S1$) modes			
Γ_{36}	$\pi^+\pi^+ e^-\bar{\nu}_e$	SQ	$<1.3\times10^{-8}$	CL=90%
Γ_{37}	$\pi^+\pi^+\mu^-\bar{\nu}_\mu$	SQ	$<3.0\times10^{-6}$	CL=95%
Γ_{38}	$\pi^+ e^+ e^-$	$S1$	$(3.00\pm0.09)\times10^{-7}$	
Γ_{39}	$\pi^+\mu^+\mu^-$	$S1$	$(9.17\pm0.14)\times10^{-8}$	S=1.8
Γ_{40}	$\pi^+ e^+ e^- e^+ e^-$	$S1$	$<1.4\times10^{-8}$	CL=90%
Γ_{41}	$\pi^+\nu\bar{\nu}$	$S1$	$(1.33\pm0.30)\times10^{-10}$	
Γ_{42}	$\pi^+\pi^0\nu\bar{\nu}$	$S1$	$<4.3\times10^{-5}$	CL=90%
Γ_{43}	$\mu^-\nu e^+ e^+$	LF	$<8.1\times10^{-11}$	CL=90%
Γ_{44}	$\mu^+\nu_e$	LF [f]	$<4\times10^{-3}$	CL=90%
Γ_{45}	$\pi^+\mu^+ e^-$	LF	$<1.3\times10^{-11}$	CL=90%
Γ_{46}	$\pi^0\pi^+\mu^+ e^-$	LF	$<5.0\times10^{-10}$	CL=90%
Γ_{47}	$\pi^+\mu^- e^+$	LF	$<6.6\times10^{-11}$	CL=90%
Γ_{48}	$\pi^0\pi^+\mu^- e^+$	LF	$<3.1\times10^{-10}$	CL=90%
Γ_{49}	$\pi^-\mu^+ e^+$	L	$<4.2\times10^{-11}$	CL=90%
Γ_{50}	$\pi^0\pi^-\mu^+ e^+$	L	$<2.9\times10^{-10}$	CL=90%
Γ_{51}	$\pi^- e^+ e^+$	L	$<5.3\times10^{-11}$	CL=90%
Γ_{52}	$\pi^-\mu^+\mu^+$	L	$<4.2\times10^{-11}$	CL=90%
Γ_{53}	$\pi^-\pi^0 e^+ e^+$	L	$<8.5\times10^{-10}$	CL=90%
Γ_{54}	$\mu^+\bar{\nu}_e$	L [f]	$<3.3\times10^{-3}$	CL=90%
Γ_{55}	$\pi^0 e^+\bar{\nu}_e$	L	$<3\times10^{-3}$	CL=90%
Γ_{56}	$\pi^+\gamma$	[g]	$<2.3\times10^{-9}$	CL=90%

[a] See the Particle Listings below for the energy limits used in this measurement.

[b] Most of this radiative mode, the low-momentum γ part, is also included in the parent mode listed without γ's.

[c] Structure-dependent part.

[d] See the review on "Form Factors for Radiative Pion and Kaon Decays" for definitions and details.

[e] Direct-emission branching fraction.

[f] Derived from an analysis of neutrino-oscillation experiments.

[g] Violates angular-momentum conservation.

CONSTRAINED FIT INFORMATION

An overall fit to the mean life, a decay rate, and 15 branching ratios uses 35 measurements and one constraint to determine 8 parameters. The overall fit has a $\chi^2 = 53.4$ for 28 degrees of freedom.

The following *off-diagonal* array elements are the correlation coefficients $\langle\delta p_i \delta p_j\rangle/(\delta p_i \cdot \delta p_j)$, in percent, from the fit to parameters p_i, including the branching fractions, $x_i \equiv \Gamma_i/\Gamma_{\text{total}}$. The fit constrains the x_i whose labels appear in this array to sum to one.

	x_2	x_3	x_4	x_5	x_{10}	x_{11}	x_{12}
x_3	−66						
x_4	−64	89					
x_5	−12	−5	−5				
x_{10}	−67	0	−1	−6			
x_{11}	−13	−6	−5	91	−6		
x_{12}	−14	−6	−6	2	−7	2	
Γ	3	1	1	0	2	0	−24

	Mode	Rate (10^8 s^{-1})	Scale factor
Γ_2	$\mu^+\nu_\mu$	0.5134 ± 0.0012	1.5
Γ_3	$\pi^0 e^+\nu_e$	0.0410 ± 0.0004	2.1
	Called K^+_{e3}.		
Γ_4	$\pi^0\mu^+\nu_\mu$	0.02707 ± 0.00028	1.9
	Called $K^+_{\mu3}$.		

Γ_5	$\pi^0\pi^0 e^+\nu_e$	$(2.059 \pm 0.029) \times 10^{-5}$	1.1
Γ_{10}	$\pi^+\pi^0$	0.1670 ± 0.0007	1.3
Γ_{11}	$\pi^+\pi^0\pi^0$	0.01421 ± 0.00018	1.1
Γ_{12}	$\pi^+\pi^+\pi^-$	0.04510 ± 0.00019	

$K^{\pm}$ DECAY RATES

$\Gamma(\mu^+\nu_\mu)$ — Γ_2

VALUE (10^6 s^{-1})	DOCUMENT ID		TECN	CHG
51.34±0.12 OUR FIT Error includes scale factor of 1.5.				
• • • We do not use the following data for averages, fits, limits, etc. • • •				
51.2 ±0.8	FORD	67	CNTR	±

$\Gamma(\pi^+\pi^+\pi^-)$ — Γ_{12}

VALUE (10^6 s^{-1})	EVTS	DOCUMENT ID		TECN	CHG
4.510±0.019 OUR FIT					
4.511±0.024		[1] FORD	70	ASPK	
• • • We do not use the following data for averages, fits, limits, etc. • • •					
4.529±0.032	3.2M	[1] FORD	70	ASPK	
4.496±0.030		[1] FORD	67	CNTR	±

[1] First FORD 70 value is second FORD 70 combined with FORD 67.

K^+ BRANCHING RATIOS

Leptonic and semileptonic modes

$\Gamma(e^+\nu_e)/\Gamma(\mu^+\nu_\mu)$ — Γ_1/Γ_2

See the note on "Decay Constants of Charged Pseudoscalar Mesons" in the D_s^+ Listings.

VALUE (units 10^{-5})	EVTS	DOCUMENT ID		TECN	CHG
2.488±0.009 OUR AVERAGE					
2.488±0.007±0.007	150k	[1] LAZZERONI	13	NA62	±
2.493±0.025±0.019	13.8k	[2] AMBROSINO	09E	KLOE	±
• • • We do not use the following data for averages, fits, limits, etc. • • •					
2.487±0.011±0.007	60k	[3] LAZZERONI	11	NA62	+
2.51 ±0.15	404	HEINTZE	76	SPEC	+
2.37 ±0.17	534	HEARD	75B	SPEC	+
2.42 ±0.42	112	CLARK	72	OSPK	+

[1] LAZZERONI 13 uses full data sample collected from 2007 to 2008. This ratio is defined to be fully inclusive, including internal-bremsstrahlung.

[2] The ratio is defined to include internal-bremsstrahlung, ignoring direct-emission contributions. AMBROSINO 09E determined the ratio from the measurement of $\Gamma(K \to e\nu(\gamma), E_\gamma < 10$ MeV$)$ / $\Gamma(K \to \mu\nu(\gamma))$. 89.8% of $K \to e\nu(\gamma)$ events had E_γ <10 MeV.

[3] This ratio is defined to be fully inclusive, including internal-bremsstrahlung.

$\Gamma(\mu^+\nu_\mu)/\Gamma_{total}$ — Γ_2/Γ

See the note on "Decay Constants of Charged Pseudoscalar Mesons" in the D_s^+ Listings.

VALUE (units 10^{-2})	EVTS	DOCUMENT ID		TECN	CHG	COMMENT
63.56±0.11 OUR FIT Error includes scale factor of 1.2.						
63.60±0.16 OUR AVERAGE						
63.66±0.09±0.15	865k	[1] AMBROSINO	06A	KLOE	+	
63.24±0.44	62k	CHIANG	72	OSPK	+	1.84 GeV/c K^+

[1] Fully inclusive. Used tagged kaons from ϕ decays.

$\Gamma(\pi^0 e^+\nu_e)/\Gamma_{total}$ — Γ_3/Γ

VALUE (units 10^{-2})	EVTS	DOCUMENT ID		TECN	CHG	COMMENT
5.07 ±0.04 OUR FIT Error includes scale factor of 2.1.						
4.94 ±0.05 OUR AVERAGE						
4.965±0.038±0.037		[1] AMBROSINO	08A	KLOE	±	
4.86 ±0.10	3516	CHIANG	72	OSPK	+	1.84 GeV/c K^+
• • • We do not use the following data for averages, fits, limits, etc. • • •						
4.7 ±0.3	429	SHAKLEE	64	HLBC	+	
5.0 ±0.5		ROE	61	HLBC	+	

[1] Depends on K^+ lifetime τ. AMBROSINO 08A uses PDG 06 value of $\tau = (1.2385 \pm 0.0024) \times 10^{-8}$ sec. The correlation between K^+_{e3} and $K^+_{\mu3}$ branching fraction measurements is 62.7%.

$\Gamma(\pi^0 e^+\nu_e)/\Gamma(\mu^+\nu_\mu)$ — Γ_3/Γ_2

VALUE	EVTS	DOCUMENT ID		TECN	CHG
0.0798±0.0008 OUR FIT Error includes scale factor of 1.9.					
• • • We do not use the following data for averages, fits, limits, etc. • • •					
0.069 ±0.006	350	ZELLER	69	ASPK	+
0.0775±0.0033	960	BOTTERILL	68C	ASPK	+
0.069 ±0.006	561	GARLAND	68	OSPK	+
0.0791±0.0054	295	[1] AUERBACH	67	OSPK	+

[1] AUERBACH 67 changed from 0.0797 ± 0.0054. See comment with ratio $\Gamma(\pi^0\mu^+\nu_\mu)/\Gamma(\mu^+\nu_\mu)$. The value 0.0785 ± 0.0025 given in AUERBACH 67 is an average of AUERBACH 67 $\Gamma(\pi^0 e^+\nu_e)/\Gamma(\mu^+\nu_\mu)$ and CESTER 66 $\Gamma(\pi^0 e^+\nu_e)/\left[\Gamma(\mu^+\nu_\mu) + \Gamma(\pi^+\pi^0)\right]$.

$\Gamma(\pi^0 e^+\nu_e)/\left[\Gamma(\mu^+\nu_\mu) + \Gamma(\pi^+\pi^0)\right]$ — $\Gamma_3/(\Gamma_2+\Gamma_{10})$

VALUE (units 10^{-2})	EVTS	DOCUMENT ID		TECN	CHG
6.02±0.06 OUR FIT Error includes scale factor of 2.1.					
6.02±0.15 OUR AVERAGE					
6.16±0.22	5110	ESCHSTRUTH	68	OSPK	+
5.89±0.21	1679	CESTER	66	OSPK	+
• • • We do not use the following data for averages, fits, limits, etc. • • •					
5.92±0.65		[1] WEISSENBE...	76	SPEC	+

[1] Value calculated from WEISSENBERG 76 ($\pi^0 e\nu$), ($\mu\nu$), and ($\pi\pi^0$) values to eliminate dependence on our 1974 ($\pi 2\pi^0$) and ($\pi\pi^+\pi^-$) fractions.

$\Gamma(\pi^0 e^+\nu_e)/\left[\Gamma(\pi^0\mu^+\nu_\mu) + \Gamma(\pi^+\pi^0) + \Gamma(\pi^+\pi^0\pi^0)\right]$ — $\Gamma_3/(\Gamma_4+\Gamma_{10}+\Gamma_{11})$

VALUE	EVTS	DOCUMENT ID		TECN	CHG
0.1967±0.0016 OUR FIT Error includes scale factor of 2.5.					
0.1962±0.0008±0.0035	71k	SHER	03	B865	+

$\Gamma(\pi^0 e^+\nu_e)/\Gamma(\pi^+\pi^0)$ — Γ_3/Γ_{10}

VALUE	EVTS	DOCUMENT ID		TECN	CHG	COMMENT
0.2454±0.0023 OUR FIT Error includes scale factor of 2.6.						
0.2467±0.0011 OUR AVERAGE Error includes scale factor of 1.1.						
0.2423±0.0015±0.0037	31k	UVAROV	14	ISTR	−	ISTRA+
0.2470±0.0009±0.0004	87k	BATLEY	07A	NA48	±	
• • • We do not use the following data for averages, fits, limits, etc. • • •						
0.221 ±0.012	786	[1] LUCAS	73B	HBC	−	Dalitz pairs only

[1] LUCAS 73B gives N(K_{e3}) = 786 ± 3.1%, N(2π) = 3564 ± 3.1%. We use these values to obtain quoted result.

$\Gamma(\pi^0 e^+\nu_e)/\Gamma(\pi^+\pi^+\pi^-)$ — Γ_3/Γ_{12}

VALUE	EVTS	DOCUMENT ID		TECN	CHG
0.908±0.009 OUR FIT Error includes scale factor of 1.6.					
• • • We do not use the following data for averages, fits, limits, etc. • • •					
0.867±0.027	2768	BARMIN	87	XEBC	+
0.856±0.040	2827	BRAUN	75	HLBC	+
0.850±0.019	4385	[1] HAIDT	71	HLBC	+
0.846±0.021	4385	[1] EICHTEN	68	HLBC	+
0.94 ±0.09	854	BELLOTTI	67B	HLBC	
0.90 ±0.06	230	BORREANI	64	HBC	+

[1] HAIDT 71 is a reanalysis of EICHTEN 68. Not included in average because of large discrepancy in $\Gamma(\pi^0\mu^+\nu)/\Gamma(\pi^0 e^+\nu)$ with more precise results.

$\Gamma(\pi^0\mu^+\nu_\mu)/\Gamma_{total}$ — Γ_4/Γ

VALUE (units 10^{-2})	EVTS	DOCUMENT ID		TECN	CHG	COMMENT
3.352±0.034 OUR FIT Error includes scale factor of 1.9.						
3.24 ±0.04 OUR AVERAGE						
3.233±0.029±0.026		[1] AMBROSINO	08A	KLOE	±	
3.33 ±0.16	2345	CHIANG	72	OSPK	+	1.84 GeV/c K^+
• • • We do not use the following data for averages, fits, limits, etc. • • •						
2.8 ±0.4		[2] TAYLOR	59	EMUL	+	

[1] Depends on K^+ lifetime τ. AMBROSINO 08A uses PDG 06 value of $\tau = (1.2385 \pm 0.0024) \times 10^{-8}$ sec. The correlation between K^+_{e3} and $K^+_{\mu3}$ branching fraction measurements is 62.7%.

[2] Earlier experiments not averaged.

$\Gamma(\pi^0\mu^+\nu_\mu)/\Gamma(\mu^+\nu_\mu)$ — Γ_4/Γ_2

VALUE	EVTS	DOCUMENT ID		TECN	CHG
0.0527±0.0006 OUR FIT Error includes scale factor of 1.8.					
• • • We do not use the following data for averages, fits, limits, etc. • • •					
0.054 ±0.009	240	ZELLER	69	ASPK	+
0.0480±0.0037	424	[1] GARLAND	68	OSPK	+
0.0486±0.0040	307	[2] AUERBACH	67	OSPK	+

[1] GARLAND 68 changed from 0.055 ± 0.004 in agreement with μ-spectrum calculation of GAILLARD 70 appendix B. L.G.Pondrom, (private communication 73).

[2] AUERBACH 67 changed from 0.0602 ± 0.0046 by erratum which brings the μ-spectrum calculation into agreement with GAILLARD 70 appendix B.

$\Gamma(\pi^0\mu^+\nu_\mu)/\Gamma(\pi^0 e^+\nu_e)$ — Γ_4/Γ_3

VALUE	EVTS	DOCUMENT ID		TECN	CHG	COMMENT
0.6608±0.0031 OUR FIT Error includes scale factor of 1.2.						
0.6618±0.0027 OUR AVERAGE						
0.663 ±0.003 ±0.001	77k	BATLEY	07A	NA48	±	
0.671 ±0.007 ±0.008	24k	HORIE	01	SPEC		
0.670 ±0.014		[1] HEINTZE	77	SPEC	+	
0.667 ±0.017	5601	BOTTERILL	68B	ASPK	+	
• • • We use the following data for averages but not for fits. • • •						
0.6511±0.0064		[2] AMBROSINO	08A	KLOE	±	
• • • We do not use the following data for averages, fits, limits, etc. • • •						
0.608 ±0.014	1585	[3] BRAUN	75	HLBC	+	
0.705 ±0.063	554	[4] LUCAS	73B	HBC	−	Dalitz pairs only
0.698 ±0.025	3480	[5] CHIANG	72	OSPK	+	1.84 GeV/c K^+
0.596 ±0.025		[6] HAIDT	71	HLBC	+	
0.604 ±0.022	1398	[6] EICHTEN	68	HLBC		
0.703 ±0.056	1509	CALLAHAN	66B	HLBC		

Int. J. Mod. Phys. A 2026.41. Downloaded from www.worldscientific.com
by LIFORNIA @ BERKELEY on 09/16/26. Re-use and distribution is strictly not permitted, except for Open Access articles.

Int. J. Mod. Phys. A 2026.41. Downloaded from www.worldscientific.com
by UNIVERSITY OF CALIFORNIA @ BERKELEY on 09/16/26. Re-use and distribution is strictly not permitted, except for Open Access articles.

[1] HEINTZE 77 value from fit to λ_0. Assumes μ-e universality.
[2] Not used in the fit. This result enters the fit via correlation of K^+_{e3} and $K^+_{\mu3}$ branching fraction measurements of AMBROSINO 08A.
[3] BRAUN 75 value is from form factor fit. Assumes μ-e universality.
[4] LUCAS 73B gives $N(K_{\mu3}) = 554 \pm 7.6\%$, $N(K_{e3}) = 786 \pm 3.1\%$. We divide.
[5] CHIANG 72 $\Gamma(\pi^0\mu^+\nu_\mu)/\Gamma(\pi^0 e^+\nu_e)$ is statistically independent of CHIANG 72 $\Gamma(\pi^0\mu^+\nu_\mu)/\Gamma_{total}$ and $\Gamma(\pi^0 e^+\nu_e)/\Gamma_{total}$.
[6] HAIDT 71 is a reanalysis of EICHTEN 68. Not included in average because of large discrepancy with more precise results.

$[\Gamma(\pi^0\mu^+\nu_\mu) + \Gamma(\pi^+\pi^0)]/\Gamma_{total}$ — $(\Gamma_4+\Gamma_{10})/\Gamma$

We combine these two modes for experiments measuring them in xenon bubble chamber because of difficulties of separating them there.

VALUE (units 10^{-2})	EVTS	DOCUMENT ID		TECN	CHG
24.02±0.08 OUR FIT Error includes scale factor of 1.2.					
• • • We do not use the following data for averages, fits, limits, etc. • • •					
25.4 ±0.9	886	SHAKLEE	64	HLBC	+
23.4 ±1.1		ROE	61	HLBC	+

$\Gamma(\pi^0\mu^+\nu_\mu)/\Gamma(\pi^+\pi^0)$ — Γ_4/Γ_{10}

VALUE	EVTS	DOCUMENT ID		TECN	CHG
0.1637±0.0006±0.0003	77k	BATLEY	07A	NA48	±

$\Gamma(\pi^0\mu^+\nu_\mu)/\Gamma(\pi^+\pi^+\pi^-)$ — Γ_4/Γ_{12}

VALUE	EVTS	DOCUMENT ID		TECN	CHG	COMMENT
0.600±0.007 OUR FIT Error includes scale factor of 1.6.						
• • • We do not use the following data for averages, fits, limits, etc. • • •						
0.503±0.019	1505	[1] HAIDT	71	HLBC	+	
0.510±0.017	1505	[1] EICHTEN	68	HLBC	+	
0.63 ±0.07	2845	[2] BISI	65B	BC	+	HBC+HLBC

[1] HAIDT 71 is a reanalysis of EICHTEN 68. Not included in average because of large discrepancy in $\Gamma(\pi^0\mu^+\nu)/\Gamma(\pi^0 e^+\nu)$ with more precise results.
[2] Error enlarged for background problems. See GAILLARD 70.

$\Gamma(\pi^0\pi^0 e^+\nu_e)/\Gamma_{total}$ — Γ_5/Γ

VALUE (units 10^{-5})	EVTS	DOCUMENT ID		TECN	CHG
2.55±0.04 OUR FIT Error includes scale factor of 1.1.					
2.54±0.89	10	BARMIN	88B	HLBC	+

$\Gamma(\pi^0\pi^0\mu^+\nu_\mu)/\Gamma_{total}$ — Γ_6/Γ

VALUE (units 10^{-6})	EVTS	DOCUMENT ID		TECN	CHG	COMMENT
3.45±0.16	2437	[1] BATLEY	24	NA48	±	model extrapolation

[1] BATLEY 24 reported the result extrapolated to the full kinematic space, based on the measurement $B(K^{\pm} \to \pi^0\pi^0\mu^{\pm}\nu) = (0.65 \pm 0.03) \times 10^{-6}$, in the kinematic region where the squared dilepton mass is above 0.03 GeV^2/c^4.

$\Gamma(\pi^0\pi^0 e^+\nu_e)/\Gamma(\pi^+\pi^0\pi^0)$ — Γ_5/Γ_{11}

VALUE (units 10^{-3})	EVTS	DOCUMENT ID		TECN	CHG
1.449±0.008 OUR FIT					
1.449±0.006±0.006	65.2k	[1] BATLEY	14A	NA48	±

[1] Data collected in 2003–2004. This leads to the scalar form factor $(1+\delta_{EM})\ f_s = 6.079 \pm 0.012 \pm 0.027 \pm 0.046$ where the last error is due to the normalizing decay mode uncertainty.

$\Gamma(\pi^0\pi^0 e^+\nu_e)/\Gamma(\pi^0 e^+\nu_e)$ — Γ_5/Γ_3

VALUE (units 10^{-4})	EVTS	DOCUMENT ID		TECN	CHG
5.03±0.09 OUR FIT Error includes scale factor of 1.2.					
4.1 $^{+1.0}_{-0.7}$ OUR AVERAGE					
4.2 $^{+1.0}_{-0.9}$	25	BOLOTOV	86B	CALO	−
3.8 $^{+5.0}_{-1.2}$	2	LJUNG	73	HLBC	+

$\Gamma(\pi^+\pi^- e^+\nu_e)/\Gamma(\pi^+\pi^+\pi^-)$ — Γ_7/Γ_{12}

VALUE (units 10^{-4})	EVTS	DOCUMENT ID		TECN	CHG
7.606±0.029 OUR AVERAGE					
7.615±0.008±0.028	1.1M	[1] BATLEY	12	NA48	±
7.35 ±0.01 ±0.19	388k	[2] PISLAK	01	B865	
7.21 ±0.32	30k	ROSSELET	77	SPEC	+
• • • We do not use the following data for averages, fits, limits, etc. • • •					
7.36 ±0.68	500	BOURQUIN	71	ASPK	
7.0 ±0.9	106	SCHWEINB...	71	HLBC	+
5.83 ±0.63	269	ELY	69	HLBC	+

[1] BATLEY 12 uses data collected in 2003–2004. The result is inclusive of $K^{\pm} \to \pi^+\pi^- e^{\pm}\nu\gamma$ decays. Using PDG 12 value for $\Gamma(\pi^+\pi^-\pi^+)/\Gamma = (5.59 \pm 0.04) \times 10^{-2}$. BATLEY 12 obtains $B(\pi^+\pi^- e\nu) = (4.257 \pm 0.004 \pm 0.035) \times 10^{-5}$ where the syst. error is dominated by the error on the normalization mode.
[2] PISLAK 01 reports $\Gamma(\pi^+\pi^- e^+\nu_e)/\Gamma_{total} = (4.109 \pm 0.008 \pm 0.110) \times 10^{-5}$ using the PDG 00 value $\Gamma(\pi^+\pi^+\pi^-)/\Gamma_{total} = (5.59 \pm 0.05) \times 10^{-2}$. We divide by the PDG value and unfold its error from the systematic error. PISLAK 03 and PISLAK 10A give additional details on the branching ratio measurement and give improved errors on the S-wave π-π scattering length: $a_0^0 = 0.235 \pm 0.013$ and $a_0^2 = -0.0410 \pm 0.0027$.

$\Gamma(\pi^+\pi^-\mu^+\nu_\mu)/\Gamma_{total}$ — Γ_8/Γ

VALUE (units 10^{-5})	EVTS	DOCUMENT ID		TECN	CHG
• • • We do not use the following data for averages, fits, limits, etc. • • •					
$0.77^{+0.54}_{-0.50}$	1	CLINE	65	FBC	+

$\Gamma(\pi^+\pi^-\mu^+\nu_\mu)/\Gamma(\pi^+\pi^+\pi^-)$ — Γ_8/Γ_{12}

VALUE (units 10^{-4})	EVTS	DOCUMENT ID		TECN	CHG
2.57±1.55	7	BISI	67	DBC	+
• • • We do not use the following data for averages, fits, limits, etc. • • •					
~ 2.5	1	GREINER	64	EMUL	+

$\Gamma(\pi^0\pi^0\pi^0 e^+\nu_e)/\Gamma_{total}$ — Γ_9/Γ

VALUE	CL%	DOCUMENT ID		TECN	CHG
<5.4 × 10^{-8}	90	ARTAMONOV	24A	OKA	+
• • • We do not use the following data for averages, fits, limits, etc. • • •					
<9 × 10^{-6}	90	BARMIN	92	XEBC	+
<3.5 × 10^{-6}	90	BOLOTOV	88	SPEC	−

Hadronic modes

$\Gamma(\pi^+\pi^0)/\Gamma_{total}$ — Γ_{10}/Γ

VALUE (units 10^{-2})	EVTS	DOCUMENT ID		TECN	CHG	COMMENT
20.67±0.08 OUR FIT Error includes scale factor of 1.2.						
20.70±0.16 OUR AVERAGE Error includes scale factor of 1.8.						
20.65±0.05±0.08	1.4M	[1] AMBROSINO	08E	KLOE	+	$\phi \to K^+K^-$
21.18±0.28	16k	CHIANG	72	OSPK	+	1.84 GeV/c K^+
• • • We do not use the following data for averages, fits, limits, etc. • • •						
21.0 ±0.6		CALLAHAN	65	HLBC		See Γ_{10}/Γ_{12}

[1] Fully inclusive of final-state radiation. The branching ratio is evaluated using K^+ lifetime, $\tau = 12.385$ ns.

$\Gamma(\pi^+\pi^0)/\Gamma(\mu^+\nu_\mu)$ — Γ_{10}/Γ_2

VALUE	EVTS	DOCUMENT ID		TECN	CHG	COMMENT
0.3252±0.0016 OUR FIT Error includes scale factor of 1.2.						
0.3325±0.0032 OUR AVERAGE						
0.3329±0.0047±0.0010	45k	USHER	92	SPEC	+	$p\overline{p}$ at rest
0.3355±0.0057		[1] WEISSENBE...	76	SPEC	+	
0.3277±0.0065	4517	[2] AUERBACH	67	OSPK	+	
• • • We do not use the following data for averages, fits, limits, etc. • • •						
0.328 ±0.005	25k	[1] WEISSENBE...	74	STRC	+	
0.305 ±0.018	1600	ZELLER	69	ASPK	+	

[1] WEISSENBERG 76 revises WEISSENBERG 74.
[2] AUERBACH 67 changed from 0.3253 ± 0.0065. See comment with ratio $\Gamma(\pi^0\mu^+\nu_\mu)/\Gamma(\mu^+\nu_\mu)$.

$\Gamma(\pi^+\pi^0)/\Gamma(\pi^+\pi^+\pi^-)$ — Γ_{10}/Γ_{12}

VALUE	EVTS	DOCUMENT ID		TECN	CHG
3.702±0.022 OUR FIT Error includes scale factor of 1.1.					
• • • We do not use the following data for averages, fits, limits, etc. • • •					
3.96 ±0.15	1045	CALLAHAN	66	FBC	+

$\Gamma(\pi^+\pi^0\pi^0)/\Gamma_{total}$ — Γ_{11}/Γ

VALUE (units 10^{-2})	EVTS	DOCUMENT ID		TECN	CHG	COMMENT
1.760±0.023 OUR FIT Error includes scale factor of 1.1.						
1.775±0.028 OUR AVERAGE Error includes scale factor of 1.2.						
1.763±0.013±0.022		ALOISIO	04A	KLOE	±	
1.84 ±0.06	1307	CHIANG	72	OSPK	+	1.84 GeV/c K^+
• • • We do not use the following data for averages, fits, limits, etc. • • •						
1.53 ±0.11	198	[1] PANDOULAS	70	EMUL	+	
1.8 ±0.2	108	SHAKLEE	64	HLBC	+	
1.7 ±0.2		ROE	61	HLBC	+	
1.5 ±0.2		[2] TAYLOR	59	EMUL	+	

[1] Includes events of TAYLOR 59.
[2] Earlier experiments not averaged.

$\Gamma(\pi^+\pi^0\pi^0)/\Gamma(\pi^+\pi^0)$ — Γ_{11}/Γ_{10}

VALUE	EVTS	DOCUMENT ID		TECN	CHG	COMMENT
0.0851±0.0012 OUR FIT Error includes scale factor of 1.1.						
• • • We do not use the following data for averages, fits, limits, etc. • • •						
0.081 ±0.005	574	[1] LUCAS	73B	HBC	−	Dalitz pairs only

[1] LUCAS 73B gives $N(\pi 2\pi^0) = 574 \pm 5.9\%$, $N(2\pi) = 3564 \pm 3.1\%$. We quote $0.5N(\pi 2\pi^0)/N(2\pi)$ where 0.5 is because only Dalitz pair π^0's were used.

$\Gamma(\pi^+\pi^0\pi^0)/\Gamma(\pi^+\pi^+\pi^-)$ — Γ_{11}/Γ_{12}

VALUE	EVTS	DOCUMENT ID		TECN	CHG	COMMENT
0.315±0.004 OUR FIT Error includes scale factor of 1.1.						
0.303±0.009	2027	BISI	65	BC	+	HBC+HLBC
• • • We do not use the following data for averages, fits, limits, etc. • • •						
0.393±0.099	17	YOUNG	65	EMUL	+	

Int. J. Mod. Phys. A 2026.41. Downloaded from www.worldscientific.com by LIFORNIA @ BERKELEY on 09/16/26. Re-use and distribution is strictly not permitted, except for Open Access articles.

$\Gamma(\pi^+\pi^+\pi^-)/\Gamma_{total}$ — Γ_{12}/Γ

VALUE (units 10^{-2})	EVTS	DOCUMENT ID		TECN	CHG	COMMENT
5.583±0.024 OUR FIT						
5.565±0.031±0.025	68k	[1] BABUSCI	14B	KLOE	+	
• • • We do not use the following data for averages, fits, limits, etc. • • •						
5.56 ±0.20	2330	[2] CHIANG	72	OSPK	+	1.84 GeV/c K^+
5.34 ±0.21	693	[3] PANDOULAS	70	EMUL	+	
5.71 ±0.15		DEMARCO	65	HBC		
6.0 ±0.4	44	YOUNG	65	EMUL	+	
5.54 ±0.12	2332	CALLAHAN	64	HLBC	+	
5.1 ±0.2	540	SHAKLEE	64	HLBC	+	
5.7 ±0.3		ROE	61	HLBC	+	

[1] Inclusive of final-state radiation. Result obtained from averaging two branching ratios: one from a sample with $K^- \to \mu\nu(\gamma)$ tagging and another with $K^- \to \pi^-\pi^0(\gamma)$ tagging.
[2] Value is not independent of CHIANG 72 $\Gamma(\mu^+\nu_\mu)/\Gamma_{total}$, $\Gamma(\pi^+\pi^0)/\Gamma_{total}$, $\Gamma(\pi^+\pi^0\pi^0)/\Gamma_{total}$, $\Gamma(\pi^0\mu^+\nu_\mu)/\Gamma_{total}$, and $\Gamma(\pi^0 e^+\nu_e)/\Gamma_{total}$.
[3] Includes events of TAYLOR 59.

Leptonic and semileptonic modes with photons

$\Gamma(\mu^+\nu_\mu\gamma)/\Gamma_{total}$ — Γ_{13}/Γ

VALUE (units 10^{-3})	EVTS	DOCUMENT ID		TECN	CHG	COMMENT
6.2±0.8 OUR AVERAGE						
6.6±1.5		[1,2] DEMIDOV	90	XEBC		P(μ) <231.5 MeV/c
6.0±0.9		BARMIN	88	HLBC	+	P(μ) <231.5 MeV/c
• • • We do not use the following data for averages, fits, limits, etc. • • •						
3.5±0.8		[2,3] DEMIDOV	90	XEBC		E(γ) > 20 MeV
3.2±0.5	57	[4] BARMIN	88	HLBC	+	$E(\gamma)$ >20 MeV
5.4±0.3		[5] AKIBA	85	SPEC		P(μ) <231.5 MeV/c

[1] P(μ) cut given in DEMIDOV 90 paper, 235.1 MeV/c, is a misprint according to authors (private communication).
[2] DEMIDOV 90 quotes only inner bremsstrahlung (IB) part.
[3] Not independent of above DEMIDOV 90 value. Cuts differ.
[4] Not independent of above BARMIN 88 value. Cuts differ.
[5] Assumes μ-e universality and uses constraints from $K \to e\nu\gamma$.

$\Gamma(\mu^+\nu_\mu\gamma(SD^+))/\Gamma_{total}$ — Γ_{14}/Γ

Structure-dependent part with $+\gamma$ helicity (SD^+ term). See the "Note on $\pi^\pm \to \ell^\pm\nu\gamma$ and $K^\pm \to \ell^\pm\nu\gamma$ Form Factors" in the $\pi^\pm$ section of the Particle Data Listings above.

VALUE (units 10^{-5})	CL%	EVTS	DOCUMENT ID		TECN
1.33±0.12±0.18		2588	[1] ADLER	00B	B787
• • • We do not use the following data for averages, fits, limits, etc. • • •					
<3.0	90		AKIBA	85	SPEC

[1] ADLER 00B obtains the branching ratio by extrapolating the measurement in the kinematic region $E_\mu > 137$ MeV, $E_\gamma > 90$ MeV to the full SD^+ phase-space. Also reports $|F_V + F_A| = 0.165 \pm 0.007 \pm 0.011$ and $-0.04 < F_V - F_A < 0.24$ at 90% CL.

$\Gamma(\mu^+\nu_\mu\gamma(SD^+INT))/\Gamma_{total}$ — Γ_{15}/Γ

Interference term between internal Bremsstrahlung and SD^+ term. See the "Note on $\pi^\pm \to \ell^\pm\nu\gamma$ and $K^\pm \to \ell^\pm\nu\gamma$ Form Factors" in the $\pi^\pm$ section of the Particle Data Listings above.

VALUE (units 10^{-5})	CL%	DOCUMENT ID		TECN
<2.7	90	AKIBA	85	SPEC

$\Gamma(\mu^+\nu_\mu\gamma(SD^- + SD^-INT))/\Gamma_{total}$ — Γ_{16}/Γ

Sum of structure-dependent part with $-\gamma$ helicity (SD^- term) and interference term between internal Bremsstrahlung and SD^- term. See the "Note on $\pi^\pm \to \ell^\pm\nu\gamma$ and $K^\pm \to \ell^\pm\nu\gamma$ Form Factors" in the $\pi^\pm$ section of the Particle Data Listings above.

VALUE (units 10^{-4})	CL%	DOCUMENT ID		TECN
<2.6	90	[1] AKIBA	85	SPEC

[1] Assumes μ-e universality and uses constraints from $K \to e\nu\gamma$.

$\Gamma(e^+\nu_e\gamma)/\Gamma(\mu^+\nu_\mu)$ — Γ_{17}/Γ_2

VALUE (units 10^{-5})	EVTS	DOCUMENT ID		TECN	CHG	COMMENT
1.62 ±0.22 OUR AVERAGE		Error includes scale factor of 3.9.				
1.98 ±0.11	95	[1] KOBAYASHI	23	E36		E_γ in 10–250 MeV, p_e > 200 MeV/c
1.483±0.066±0.013	1.4k	[2] AMBROSINO	09E	KLOE	±	E_γ in 10–250 MeV, p_e > 200 MeV/c
• • • We do not use the following data for averages, fits, limits, etc. • • •						
1.85 ±0.11 ±0.07	574	[3,4] ITO	22	E36	+	E_γ in 10–250 MeV, p_e > 200 MeV/c

[1] KOBAYASHI 23 observed 95 ± 10 $K^{SD+}_{e2\gamma(\gamma)}$ events and derived $B(K^{SD+}_{e2\gamma(\gamma)})/B(K_{e2(\gamma)}) = 1.25 \pm 0.14 \pm 0.08$. The authors obtained the R_γ value $(1.98 \pm 0.11) \times 10^{-5}$ by averaging KOBAYASHI 23 with ITO 22 after updating the ITO 22 result to include internal bremsstrahlung process in the acceptance calculation.
[2] AMBROSINO 09E measured the differential width $dR_\gamma/dE_\gamma = (1/\Gamma(K \to \mu\nu))(d\Gamma(K \to e\nu\gamma)/dE_\gamma)$. Result obtained by integrating the differential width over E_γ from 10 to 250 MeV.
[3] ITO 22 result derived from $B(K^{SD+}_{e2\gamma})/B(K_{e2(\gamma)}) = 1.12 \pm 0.07 \pm 0.04$.
[4] superseded by KOBAYASHI 2023

$\Gamma(\pi^0 e^+\nu_e\gamma)/\Gamma(\pi^0 e^+\nu_e)$ — Γ_{18}/Γ_3

VALUE (units 10^{-3})	EVTS	DOCUMENT ID		TECN	CHG	COMMENT
5.32±0.05 OUR AVERAGE						
5.33±0.03±0.04	130k	[1] CORTINA-GIL	23D	NA62	+	E_γ > 10 MeV, 0.6 < $\cos(\theta_{e\gamma})$ < 0.9
5.32±0.10±0.12	7248	[2] POLYARUSH	21	OKA	+	E_γ > 10 MeV, 0.6 < $\cos(\theta_{e\gamma})$ < 0.9
4.7 ±0.2 ±0.3	1456	[3] AKIMENKO	07	ISTR	−	E_γ > 10 MeV, 0.6 < $\cos(\theta_{e\gamma})$ < 0.9
4.6 ±0.8	82	[4] BARMIN	91	XEBC		E_γ > 10 MeV, 0.6 < $\cos(\theta_{e\gamma})$ < 0.9
5.6 ±0.4	192	[5] BOLOTOV	86B	CALO	−	E_γ > 10 MeV
• • • We do not use the following data for averages, fits, limits, etc. • • •						
18.1 ±0.3 ±0.7	4476	[3] AKIMENKO	07	ISTR	−	E_γ>10 MeV, $\theta_{e\gamma}$ >10°
6.3 ±0.2 ±0.3		[3] AKIMENKO	07	ISTR	−	E_γ>30 MeV, $\theta_{e\gamma}$ >20°
15.1 ±2.5	82	[4] BARMIN	91	XEBC		E_γ > 10 MeV, $\cos(\theta_{e\gamma})$ < 0.98
4.8 ±2.0	16	[6] LJUNG	73	HLBC	+	E_γ > 30 MeV
$2.2\ ^{+1.5}_{-1.0}$		[6] LJUNG	73	HLBC	+	E_γ > 30 MeV
7.6 ±2.8	13	[7] ROMANO	71	HLBC		E_γ > 10 MeV
5.3 ±2.2		[7] ROMANO	71	HLBC	+	E_γ > 30 MeV
12 ±8		BELLOTTI	67	HLBC		E_γ > 30 MeV

[1] CORTINA-GIL 23D provides values for three kinematic regions. For averaging, we use value with $E_\gamma > 10$ MeV and $0.6 < \cos(\theta_{e\gamma}) < 0.9$.
[2] POLYARUSH 21 provides values for three kinematic regions. For averaging, we use value with $E_\gamma > 10$ MeV and $0.6 < \cos(\theta_{e\gamma}) < 0.9$.
[3] AKIMENKO 07 provides values for three kinematic regions. For averaging, we use value with $E_\gamma > 10$ MeV and $0.6 < \cos(\theta_{e\gamma}) < 0.9$.
[4] BARMIN 91 quotes branching ratio $\Gamma(K \to e\pi^0\nu\gamma)/\Gamma_{all}$. The measured normalization is $[\Gamma(K \to e\pi^0\nu) + \Gamma(K \to \pi^+\pi^+\pi^-)]$. For comparison with other experiments we used $\Gamma(K \to e\pi^0\nu)/\Gamma_{all} = 0.0482$ to calculate the values quoted here.
[5] $\cos(\theta_{e\gamma})$ between 0.6 and 0.9.
[6] First LJUNG 73 value is for $\cos(\theta_{e\gamma})$ <0.9, second value is for $\cos(\theta_{e\gamma})$ between 0.6 and 0.9 for comparison with ROMANO 71.
[7] Both ROMANO 71 values are for $\cos(\theta_{e\gamma})$ between 0.6 and 0.9. Second value is for comparison with second LJUNG 73 value. We use lowest E_γ cut for Summary Table value. See ROMANO 71 for E_γ dependence.

$\Gamma(\pi^0 e^+\nu_e\gamma(SD))/\Gamma_{total}$ — Γ_{19}/Γ

Structure-dependent part.

VALUE (units 10^{-5})	CL%	DOCUMENT ID		TECN	CHG
<5.3	90	BOLOTOV	86B	CALO	−

$\Gamma(\pi^0\mu^+\nu_\mu\gamma)/\Gamma_{total}$ — Γ_{20}/Γ

VALUE (units 10^{-5})	CL%	EVTS	DOCUMENT ID		TECN	CHG	COMMENT
1.25±0.25 OUR AVERAGE							
1.10±0.32±0.05		23	[1] ADLER	10	B787		$30 < E_\gamma < 60$ MeV
1.46±0.22±0.32		153	[2] TCHIKILEV	07	ISTR	−	$30 < E_\gamma < 60$ MeV
• • • We do not use the following data for averages, fits, limits, etc. • • •							
2.4 ±0.5 ±0.6		125	SHIMIZU	06	K470	+	E_γ > 30 MeV; $\Theta_{\mu\gamma}$ >20°
<6.1	90	0	LJUNG	73	HLBC	+	$E(\gamma)$ >30 MeV

[1] Value obtained from $B(K^+ \to \pi^0\mu^+\nu_\mu\gamma) = (2.51 \pm 0.74 \pm 0.12) \times 10^{-5}$ obtained in the kinematic region $E_\gamma > 20$ MeV, and then theoretical $K_{\mu3\gamma}$ spectrum has been used. Also $B(K^+ \to \pi^0\mu^+\nu_\mu\gamma) = (1.58 \pm 0.46 \pm 0.08) \times 10^{-5}$, for $E_\gamma > 30$ MeV and $\theta_{\mu\gamma} > 20°$, was determined.
[2] Obtained from measuring $B(K_{\mu3\gamma}) / B(K_{\mu3})$ and using PDG 02 value $B(K_{\mu3}) = 3.27\%$. $B(K_{\mu3\gamma}) = (8.82 \pm 0.94 \pm 0.86) \times 10^{-5}$ is obtained for 5 MeV < E_γ < 30 MeV.

$\Gamma(\pi^0\pi^0 e^+\nu_e\gamma)/\Gamma_{total}$ — Γ_{21}/Γ

VALUE (units 10^{-6})	CL%	EVTS	DOCUMENT ID		TECN	CHG	COMMENT
<5	90	0	BARMIN	92	XEBC	+	E_γ > 10 MeV

Hadronic modes with photons

$\Gamma(\pi^+\pi^0\gamma(INT))/\Gamma_{total}$ — Γ_{22}/Γ

The $K^+ \to \pi^+\pi^0\gamma$ differential decay rate can be described in terms of T_{π^+}, the charged pion kinetic energy, and $W^2 = (P_K \cdot P_\gamma)(P_{\pi^+} \cdot P_\gamma) / (m_K\, m_{\pi^+})^2$; then we can write $d^2\Gamma(K^+ \to \pi^+\pi^0\gamma) / (dT_{\pi^+}\, dW^2) = d^2\Gamma(K^+ \to \pi^+\pi^0\gamma)_{IB} / (dT_{\pi^+}\, dW^2)\, [1 + 2\cos(\pm\phi + \delta_1^1 - \delta_0^2)\, m_\pi^2\, m_K^2\, W^2\, X_E + m_\pi^4\, m_K^4\, (X_E^2 + X_M^2)\, W^4]$. The IB differential and total branching ratios are expressed in terms of the non-radiative experimental width $\Gamma(K^+ \to \pi^+\pi^0)$ by Low's theorem. Using PDG 10 $B(K^+ \to \pi^+\pi^0) = 0.2066 \pm 0.0008$, one obtains respectively $B(K^+ \to \pi^+\pi^0\gamma)_{IB}$ (55 < T_{π^+} < 90 MeV)= 2.55×10^{-4} and $B(K^+ \to \pi^+\pi^0\gamma)_{IB}$ (0 < T_{π^+} < 80 MeV)= 1.80×10^{-4}. Fitting respectively the piece proportional to W^2 and the piece proportional to W^4, the interference contribution (INT), proportional to X_E, and the direct contribution (DE) proportional to $X_E^2 + X_M^2$ are extracted.

VALUE (units 10^{-6})	EVTS	DOCUMENT ID		TECN	CHG	COMMENT
−4.24±0.63±0.70	600k	[1] BATLEY	10A	NA48	±	T_{π^+} 0–80 MeV

Int. J. Mod. Phys. A 2026.41. Downloaded from www.worldscientific.com
by UNIVERSITY OF CALIFORNIA @ BERKELEY on 09/16/26. Re-use and distribution is strictly not permitted, except for Open Access articles.

[1] The cut on the photon energy implies $W^2 > 0.2$. BATLEY 10A obtains the INT and DE fractional branchings with respect to IB from a simultaneous kinematical fit of INT and DE and then we use the PDG 10 value for $B(K^+ \to \pi^+\pi^0) = 20.66 \pm 0.08$ to determine the IB. The INT and DE correlation coefficients -0.83. Assuming a constant electric amplitude, X_E, this INT value implies $X_E = -24 \pm 6$ GeV^{-4}.

$\Gamma(\pi^+\pi^0\gamma(DE))/\Gamma_{total}$ — Γ_{23}/Γ

Direct emission (DE) part of $\Gamma(\pi^+\pi^0\gamma)/\Gamma_{total}$, assuming that interference (INT) component is zero.

VALUE (units 10^{-6})	EVTS	DOCUMENT ID		TECN	CHG	COMMENT
5.99±0.27±0.25	600k	[1] BATLEY	10A	NA48	±	T_{π^+} 0–80 MeV
• • • We do not use the following data for averages, fits, limits, etc. • • •						
3.8 ±0.8 ±0.7	10k	ALIEV	06	K470	+	T_{π^+} 55–90 MeV
3.7 ±3.9 ±1.0	930	UVAROV	06	ISTR	−	T_{π^-} 55–90 MeV
3.2 ±1.3 ±1.0	4k	ALIEV	03	K470	+	T_{π^+} 55–90 MeV
6.1 ±2.5 ±1.9	4k	ALIEV	03	K470	+	T_{π^+} full range
4.7 ±0.8 ±0.3	20k	[2] ADLER	00C	B787	+	T_{π^+} 55–90 MeV
20.5 ±4.6 $^{+3.9}_{-2.3}$		BOLOTOV	87	WIRE	−	T_{π^-} 55–90 MeV
15.6 ±3.5 ±5.0		ABRAMS	72	ASPK	±	$T_{\pi^\pm}$ 55–90 MeV

[1] The cut on the photon energy implies $W^2 > 0.2$. BATLEY 10A obtains the INT and DE fractional branchings with respect to IB from a simultaneous kinematical fit of INT and DE and then we use the PDG 10 value for $B(K^+ \to \pi^+\pi^0) = 20.66 \pm 0.08$ to determine the IB. The INT and DE correlation coefficients -0.93. Assuming constant electric and magnetic amplitudes, X_E and X_M, these INTand DE values imply $X_E = -24 \pm 6$ GeV^{-4} and $X_M = -254 \pm 9$ GeV^{-4}.

[2] ADLER 00C measures the INT component to be (-0.4 ± 1.6)% of the inner bremsstrahlung (IB) component.

$\Gamma(\pi^+\pi^0 e^+ e^-)/\Gamma_{total}$ — Γ_{24}/Γ

VALUE (units 10^{-6})	EVTS	DOCUMENT ID		TECN
4.24±0.14	4.9k	[1] BATLEY	19	NA48

[1] BATLEY 19 result is obtained from an exposure of 1.7×10^{11} charged kaon decays recorded in 2003–2004. The study of the kinematic space shows evidence for a structure dependent contribution consistent with predictions from chiral perturbation theory.

$\Gamma(\pi^+\pi^0\pi^0\gamma)/\Gamma(\pi^+\pi^0\pi^0)$ — Γ_{25}/Γ_{11}

VALUE (units 10^{-4})	EVTS	DOCUMENT ID		TECN	CHG	COMMENT
2.3±0.6 OUR AVERAGE	Error includes scale factor of 1.2.					
2.1±0.5	60	[1] ARTAMONOV	24	OKA	+	$E(\gamma) > 10$ MeV
4.3 $^{+3.2}_{-1.7}$		BOLOTOV	85	SPEC	−	$E(\gamma) > 10$ MeV

[1] ARTAMONOV 24 obtains the branching ratio $B(K^+ \to \pi^+\pi^0\pi^0\gamma) = (3.7 \pm 0.9 \pm 0.3) \times 10^{-6}$ by normalizing to $B(K^+ \to \pi^+\pi^0\pi^0) = (1.760 \pm 0.023) \times 10^{-2}$.

$\Gamma(\pi^+\pi^+\pi^-\gamma)/\Gamma_{total}$ — Γ_{26}/Γ

VALUE (units 10^{-4})	EVTS	DOCUMENT ID		TECN	CHG	COMMENT
0.071±0.005 OUR AVERAGE						
0.071±0.005	450	SHAPKIN	19	OKA	+	$E(\gamma) > 30$ MeV
1.10 ±0.48	7	BARMIN	89	XEBC		$E(\gamma) > 5$ MeV
1.0 ±0.4		STAMER	65	EMUL	+	$E(\gamma) > 11$ MeV

$\Gamma(\pi^+\gamma\gamma)/\Gamma_{total}$ — Γ_{27}/Γ

VALUE (units 10^{-7})	CL%	EVTS	DOCUMENT ID		TECN	CHG	COMMENT
9.65±0.16 OUR AVERAGE							
9.61±0.15±0.07		3693	[1] CORTINA-GIL	24	NA62	+	ChPT extrapolatioin
10.03±0.51±0.24		215	[2] LAZZERONI	14	NA62	±	
11 ±3 ±1		31	[3] KITCHING	97	B787	+	
• • • We do not use the following data for averages, fits, limits, etc. • • •							
9.10±0.72±0.22		149	[4] BATLEY	14	NA48	±	
< 0.083	90		[5] ARTAMONOV	05	B949	+	$P_\pi > 213$ MeV/c
< 10	90	0	ATIYA	90B	B787	+	T_π117–127 MeV
< 84	90	0	ASANO	82	CNTR	+	T_π 117–127 MeV
−420 ± 520		0	ABRAMS	77	SPEC	+	$T_\pi < 92$ MeV
< 350	90	0	LJUNG	73	HLBC	+	6–102, 114–127 MeV
< 500	90	0	KLEMS	71	OSPK	+	$T_\pi < 117$ MeV
−100 ± 600			CHEN	68	OSPK	+	T_π 60–90 MeV

[1] CORTINA-GIL 24 uses data collected by NA62 at CERN in 2017 to 2018. This result, for the full kinematic range, is extrapolated using $O(p^6)$ ChPT theoretical calculation from the model-independent branching fraction, $B(K^+ \to \pi^+\gamma\gamma)=(9.46 \pm 0.19 \pm 0.07) \times 10^{-7}$, obtained for $0.2<(m_{\gamma\gamma}/m_K)^2 < 0.51$. The ChPT parameter $\hat{c} = 1.144 \pm 0.069 \pm 0.034$ is measured.

[2] LAZZERONI 14 combines NA62 and NA48/2 results. The result for the full kinematic range is extrapolated from the model-independent branching fraction $(9.65 \pm 0.61 \pm 0.14) \times 10^{-7}$ for $(m_{\gamma\gamma}/m_K)^2 > 0.2$. The measured ChPT parameter $\hat{c} = 1.86 \pm 0.25$.

[3] KITCHING 97 is extrapolated from their model-independent branching fraction $(6.0 \pm 1.5 \pm 0.7) \times 10^{-7}$ for 100 MeV/c<P_{π^+} < 180 MeV/c using Chiral Perturbation Theory.

[4] BATLEY 14 uses data collected in 2003 and 2004. Branching ratio is obtained by determining the parameter $\hat{c} = 1.41 \pm 0.38 \pm 0.11$ and integrating the $\mathcal{O}(p^6)$ chiral spectrum. A model independent value for the branching ratio is also obtained $(8.77 \pm 0.87 \pm 0.17) \times 10^{-7}$ for kinematic range $(m_{\gamma\gamma}/m_K)^2 > 0.2$.

[5] ARTAMONOV 05 limit assumes ChPT with $\hat{c}$= 1.8 with unitarity corrections. With $\hat{c}$= 1.6 and no unitarity corrections they obtain < 2.3×10^{-8} at 90% CL. This partial branching ratio is predicted to be 6.10×10^{-9} and 0.49×10^{-9} for the cases with and without unitarity correction.

$\Gamma(\pi^+ 3\gamma)/\Gamma_{total}$ — Γ_{28}/Γ

Values given here assume a phase space pion energy spectrum.

VALUE (units 10^{-4})	CL%	DOCUMENT ID		TECN	CHG	COMMENT
<1.0	90	ASANO	82	CNTR	+	$T(\pi)$ 117–127 MeV
• • • We do not use the following data for averages, fits, limits, etc. • • •						
<3.0	90	KLEMS	71	OSPK	+	$T(\pi)$ >117 MeV

$\Gamma(\pi^+ e^+ e^-\gamma)/\Gamma_{total}$ — Γ_{29}/Γ

VALUE (units 10^{-8})	EVTS	DOCUMENT ID		TECN	COMMENT
1.19±0.12±0.04	113	[1] BATLEY	08	NA48	$m_{ee\gamma} > 260$ MeV

[1] BATLEY 08 also reports the Chiral Perturbation Theory parameter $\hat{c} = 0.9 \pm 0.45$ obtained using the shape of the $e^+e^-\gamma$ invariant mass spectrum. By extrapolating the theoretical amplitude to $m_{ee\gamma} < 260$ MeV, it obtains the inclusive $B(K^+ \to \pi^+e^+e^-\gamma) = (1.29 \pm 0.13 \pm 0.03) \times 10^{-8}$, where the first error is the combined statistical and systematic errors and the second error is from the uncertainty in $\hat{c}$.

Leptonic modes with $\ell\bar{\ell}$ pairs

$\Gamma(e^+\nu_e\nu\overline{\nu})/\Gamma(e^+\nu_e)$ — Γ_{30}/Γ_1

VALUE	CL%	EVTS	DOCUMENT ID		TECN	CHG
<3.8	90	0	HEINTZE	79	SPEC	+

$\Gamma(\mu^+\nu_\mu\nu\overline{\nu})/\Gamma_{total}$ — Γ_{31}/Γ

VALUE	CL%	DOCUMENT ID		TECN	CHG
<1.0 × 10^{-6}	90	[1] CORTINA-GIL	21	NA62	+
• • • We do not use the following data for averages, fits, limits, etc. • • •					
<2.4 × 10^{-6}	90	[2] ARTAMONOV	16	B949	+
<6.0 × 10^{-6}	90	[3] PANG	73	CNTR	+

[1] CORTINA-GIL 21 assumes Standard Model μ spectrum. The search is performed in the reconstructed missing mass interval $m_{miss} > 316$ MeV/c^2.

[2] ARTAMONOV 16 assumes Standard model μ spectrum. The search is performed in the muon momentum region between 130 and 175 MeV/c.

[3] PANG 73 assumes μ spectrum from ν-ν interaction of BARDIN 70.

$\Gamma(e^+\nu_e e^+ e^-)/\Gamma_{total}$ — Γ_{32}/Γ

VALUE (units 10^{-8})	EVTS	DOCUMENT ID		TECN	CHG	COMMENT
2.48± 0.14±0.14	410	POBLAGUEV	02	B865	+	m_{ee} >150 MeV
• • • We do not use the following data for averages, fits, limits, etc. • • •						
20 ±20	4	DIAMANT-...	76	SPEC	+	$m_{e^+e^-}$ >140 MeV

$\Gamma(\mu^+\nu_\mu e^+ e^-)/\Gamma_{total}$ — Γ_{33}/Γ

VALUE (units 10^{-8})	EVTS	DOCUMENT ID		TECN	CHG	COMMENT
7.06± 0.16±0.26	2.7k	POBLAGUEV	02	B865	+	m_{ee} >145 MeV
• • • We do not use the following data for averages, fits, limits, etc. • • •						
100 ±30	14	DIAMANT-...	76	SPEC	+	$m_{e^+e^-}$ >140 MeV

$\Gamma(e^+\nu_e\mu^+\mu^-)/\Gamma_{total}$ — Γ_{34}/Γ

VALUE (units 10^{-8})	CL%	DOCUMENT ID		TECN
1.72±0.45		MA	06	B865
• • • We do not use the following data for averages, fits, limits, etc. • • •				
<50	90	ADLER	98	B787

$\Gamma(\mu^+\nu_\mu\mu^+\mu^-)/\Gamma_{total}$ — Γ_{35}/Γ

VALUE (units 10^{-7})	CL%	DOCUMENT ID		TECN	CHG
<4.1	90	ATIYA	89	B787	+

Lepton Family number (LF), Lepton number (L), $\Delta S = \Delta Q$ (SQ) violating modes, or $\Delta S = 1$ weak neutral current ($S1$) modes

$\Gamma(\pi^+\pi^+e^-\overline{\nu}_e)/\Gamma_{total}$ — Γ_{36}/Γ

Test of $\Delta S = \Delta Q$ rule.

VALUE (units 10^{-7})	CL%	EVTS	DOCUMENT ID		TECN	CHG
• • • We do not use the following data for averages, fits, limits, etc. • • •						
< 9.0	95	0	SCHWEINB...	71	HLBC	+
< 6.9	95	0	ELY	69	HLBC	+
<20.	95		BIRGE	65	FBC	+

$\Gamma(\pi^+\pi^+e^-\overline{\nu}_e)/\Gamma(\pi^+\pi^-e^+\nu_e)$ — Γ_{36}/Γ_7

Test of $\Delta S = \Delta Q$ rule.

VALUE (units 10^{-4})	CL%	EVTS	DOCUMENT ID		TECN
< 3	90	3	[1] BLOCH	76	SPEC
• • • We do not use the following data for averages, fits, limits, etc. • • •					
<130.	95	0	BOURQUIN	71	ASPK

[1] BLOCH 76 quotes 3.6×10^{-4} at CL = 95%, we convert.

$\Gamma(\pi^+\pi^+\mu^-\overline{\nu}_\mu)/\Gamma_{total}$ — Γ_{37}/Γ

Test of $\Delta S = \Delta Q$ rule.

VALUE (units 10^{-6})	CL%	EVTS	DOCUMENT ID		TECN	CHG
<3.0	95	0	BIRGE	65	FBC	+

Int. J. Mod. Phys. A 2026.41. Downloaded from www.worldscientific.com by LIFORNIA @ BERKELEY on 09/16/26. Re-use and distribution is strictly not permitted, except for Open Access articles.

$\Gamma(\pi^+ e^+ e^-)/\Gamma_{total}$ — Γ_{38}/Γ

Test for $\Delta S = 1$ weak neutral current. Allowed by combined first-order weak and electromagnetic interactions.

VALUE (units 10^{-7})	EVTS	DOCUMENT ID		TECN	CHG
3.00±0.09 OUR AVERAGE					
3.11±0.04±0.12	7253	[1] BATLEY	09	NA48	±
2.94±0.05±0.14	10300	[2] APPEL	99	SPEC	+
2.75±0.23±0.13	500	[3] ALLIEGRO	92	SPEC	+
2.7 ±0.5	41	[4] BLOCH	75	SPEC	+

[1] Value extrapolated from a measurement in the region $z = (m_{ee}/m_K)^2 > 0.08$. BATLEY 09 also evaluated the shape of the form factor using four different theoretical models.
[2] APPEL 99 establishes vector nature of this decay and determines form factor $f(Z) = f_0 (1 + \delta Z)$, $Z = M^2_{ee}/m^2_K$, $\delta = 2.14 \pm 0.13 \pm 0.15$. Also reports constraints on scalar and tensor interactions: $|f_S| < 6.6 \times 10^{-5}$, $|f_T| < 3.7 \times 10^{-4}$ at 90% C.L.
[3] ALLIEGRO 92 assumes a vector interaction with a form factor given by $\lambda = 0.105 \pm 0.035 \pm 0.015$ and a correlation coefficient of -0.82.
[4] BLOCH 75 assumes a vector interaction.

$\Gamma(\pi^+ \mu^+ \mu^-)/\Gamma_{total}$ — Γ_{39}/Γ

Test for $\Delta S = 1$ weak neutral current. Allowed by higher-order electroweak interactions.

VALUE (units 10^{-8})	CL%	EVTS	DOCUMENT ID		TECN	CHG	COMMENT
9.17±0.14 OUR AVERAGE Error includes scale factor of 1.8.							
9.15±0.06±0.05		28k	[1] CORTINA-GIL	22A	NA62		2017–18 data
9.62±0.21±0.13		3120	[2] BATLEY	11A	NA48	±	2003–04 data
9.8 ±1.0 ±0.5		110	[3] PARK	02	HYCP	±	
9.22±0.60±0.49		402	[4] MA	00	B865	+	
5.0 ±0.4 ±0.9		207	[5] ADLER	97C	B787	+	
• • • We do not use the following data for averages, fits, limits, etc. • • •							
9.7 ±1.2 ±0.4		65	PARK	02	HYCP	+	
10.0 ±1.9 ±0.7		35	PARK	02	HYCP	−	
<23	90		ATIYA	89	B787	+	

[1] CORTINA-GIL 22A also studies the form factor $f(z)$ dependence of the decay, described via single photon exchange: assuming a linear form factor including π-π rescattering, $W_{\pi\pi}$, as in DAMBROSIO 98A, finding $f(z) = G_F\, m^2_K\, (a_+ + b_+\, z) + W_{\pi\pi}(z)$, $a_+ = -0.575 \pm 0.013$, $b_+ = -0.722 \pm 0.043$.
[2] BATLEY 11A also studies the form factor $f(z)$ dependence of the decay, described via single photon exchange: i) assuming a linear form factor, $f(z) = f_0\, (1 + \delta\, z)$, $z = (M_{\mu\mu}/m_K)^2$, finding $f_0 = 0.470 \pm 0.040$ and $\delta = 3.11 \pm 0.57$ and ii) assuming a linear form factor including π-π rescattering , $W_{\pi\pi}$, as in DAMBROSIO 98A, finding $f(z) = G_F\, m^2_K\, (a_+ + b_+\, z) + W_{\pi\pi}(z)$, $a_+ = -0.575 \pm 0.039$, $b_+ = -0.813 \pm 0.145$.
[3] PARK 02 "±" result comes from combining $K^+ \to \pi^+ \mu^+ \mu^-$ and $K^- \to \pi^- \mu^+ \mu^-$, assuming CP is conserved.
[4] MA 00 establishes vector nature of this decay and determines form factor $f(z) = f_0\, (1 + \delta\, z)$, $z = (M_{\mu\mu}/m_K)^2$, $\delta = 2.45^{+1.30}_{-0.95}$.
[5] ADLER 97C gives systematic error 0.7×10^{-8} and theoretical uncertainty 0.6×10^{-8}, which we combine in quadrature to obtain our second error.

$\Gamma(\pi^+ e^+ e^- e^+ e^-)/\Gamma_{total}$ — Γ_{40}/Γ

VALUE	CL%	DOCUMENT ID		TECN	CHG
$<1.4 \times 10^{-8}$	90	[1] CORTINA-GIL	23B	NA62	+

[1] Quoted limit is obtained using data collected from 2017 to 2018. CORTINA-GIL 23B also reports upper limits at 90% C.L. at the level of 10^{-9} for the branching ratios of two prompt decay chains involving pair-production of hidden-sector mediators: $K^+ \to \pi^+ a a$, $a \to e^+ e^-$ and $K^+ \to \pi^+ S$, $S \to X X$, $X \to e^+ e^-$.

$\Gamma(\pi^+ \nu\overline{\nu})/\Gamma_{total}$ — Γ_{41}/Γ

Test for $\Delta S = 1$ weak neutral current. Allowed by higher-order electroweak interactions. Branching ratio values are extrapolated from the momentum or energy regions shown in the comments assuming Standard Model phase space except for those labeled "Scalar" or "Tensor" to indicate the assumed non-Standard-Model interaction.

VALUE (units 10^{-10})	CL%	EVTS	DOCUMENT ID		TECN	CHG	COMMENT
1.33±0.30 OUR AVERAGE							
$1.30^{+0.33}_{-0.30}$		51	[1] CORTINA-GIL 25		NA62	+	
$1.73^{+1.15}_{-1.05}$		7	[2] ARTAMONOV 08		B949	+	$140<P_\pi<199$ MeV, $211<P_\pi<229$MeV
• • • We do not use the following data for averages, fits, limits, etc. • • •							
$1.06^{+0.41}_{-0.35}$		20	[3] CORTINA-GIL 21B		NA62	+	
$0.48^{+0.72}_{-0.48}$			[4] CORTINA-GIL 20C		NA62	+	
< 11	90	1	[5] CORTINA-GIL 19B		NA62	+	decay-in-flight
$7.89^{+9.26}_{-5.10}$		3	[6] ARTAMONOV 08		B949	+	$140<P_\pi<199$ MeV
< 22	90	1	[7] ADLER 04		B787	+	$211<P_\pi<229$ MeV
< 27	90		ADLER 04		B787	+	Scalar
< 18	90		ADLER 04		B787	+	Tensor
$1.47^{+1.30}_{-0.89}$		3	[8] ANISIMOVSK...04		B949	+	$211<P_\pi<229$ MeV
$1.57^{+1.75}_{-0.82}$		2	ADLER 02		B787	+	$P_\pi>211$ MeV/c
< 42	90	1	ADLER 02C		B787	+	$140<P_\pi<195$ MeV
< 47	90		[9] ADLER 02C		B787	+	Scalar
< 25	90		[9] ADLER 02C		B787	+	Tensor
$1.5^{+3.4}_{-1.2}$		1	ADLER 00		B787		In ADLER 02
$4.2^{+9.7}_{-3.5}$		1	ADLER 97		B787		
< 24	90		ADLER 96		B787		
< 75	90		ATIYA 93		B787	+	$T(\pi)$ 115–127 MeV
< 52	90		[10] ATIYA 93		B787	+	
< 170	90	0	ATIYA 93B		B787	+	$T(\pi)$ 60–100 MeV
< 340	90		ATIYA 90		B787	+	
<1400	90		ASANO 81B		CNTR	+	$T(\pi)$ 116–127 MeV

[1] CORTINA-GIL 25 uses data collected from 2016 to 2022 and observed 51 signal candidates with an expected background of 18^{+3}_{-2} events. The measured $B(K^+ \to \pi^+ \nu\overline{\nu})$ has a signal significance of more than 5σ. Supersedes CORTINA-GIL 21B.
[2] Value obtained combining ANISIMOVSKY 04, ADLER 04, and the present ARTAMONOV 08 results.
[3] CORTINA-GIL 21B analysis of the NA62 data taken in 2016–2018 observed 20 candidate events with an expected background of 7 events. The achieved single event sensitivity is $(0.839 \pm 0.054) \times 10^{-11}$. The quoted branching ratio includes result from CORTINA-GIL 20C which observed two candidate events. This provides evidence for the very rare $K^+ \to \pi^+ \nu\overline{\nu}$ decay, observed with a significance of 3.4 σ. Search for a feebly interacting scalar or pseudo-scalar particle X in the decay $K^+ \to \pi^+ X$ was performed and an upper limit from $< 3 \times 10^{-11}$ to $< 6 \times 10^{-11}$ at the 90% C.L. was set for an invisible particle with a mass of 0–110 MeV/c^2 and $< 1 \times 10^{-11}$ for mass of 160–260 MeV/c^2. Superseded by CORTINA-GIL 25.
[4] CORTINA-GIL 20C analysis of the NA62 data taken in 2017 observed two candidate events with an expected background of 1.5 events. The achieved single event sensitivity is $(0.389 \pm 0.024) \times 10^{-10}$. The quoted branching ratio includes result from CORTINA-GIL 19B which observed one candidate event. The corresponding upper limit $B(K^+ \to \pi^+ \nu\overline{\nu}) < 1.78 \times 10^{-10}$ at 90% C.L. Superseded by CORTINA-GIL 21B.
[5] Based on a sample of 1.21×10^{11} K^+ decays collected in 2016. One signal candidate is observed while the expected background is 0.152 events. The single-event-sensitivity is estimated to be 3.15×10^{-10}.
[6] Observed 3 events with an estimated background of $0.93 \pm 0.17^{+0.32}_{-0.24}$. Signal-to-background ratio for each of these 3 events is 0.20, 0.42, and 0.47.
[7] Value obtained combining the previous result ADLER 02C with 1 event and the present result with 0 events to obtain an expected background 1.22 ± 0.24 events and 1 event observed.
[8] Value obtained combining the previous E787 result ADLER 02 with 2 events and the present E949 with 1 event. The additional event has a signal-to-background ratio 0.9. Superseded by ARTAMONOV 08.
[9] Superseded by ADLER 04.
[10] Combining ATIYA 93 and ATIYA 93B results. Superseded by ADLER 96.

$\Gamma(\pi^+ \pi^0 \nu\overline{\nu})/\Gamma_{total}$ — Γ_{42}/Γ

Test for $\Delta S = 1$ weak neutral current. Allowed by higher-order electroweak interactions.

VALUE (units 10^{-5})	CL%	DOCUMENT ID		TECN
<4.3	90	[1] ADLER	01	SPEC

[1] Search region defined by 90 MeV/$c<P_{\pi^+}<188$ MeV/c and 135 MeV$<E_{\pi^0}<180$ MeV.

$\Gamma(\mu^- \nu e^+ e^+)/\Gamma_{total}$ — Γ_{43}/Γ

VALUE	CL%	DOCUMENT ID		TECN
$<8.1 \times 10^{-11}$	90	[1] CORTINA-GIL	23	NA62

[1] Performed using the dataset collected by the NA62 experiment at CERN from 2016 to 2018.

$\Gamma(\mu^- \nu e^+ e^+)/\Gamma(\pi^+ \pi^- e^+ \nu_e)$ — Γ_{43}/Γ_7

Test of lepton family number conservation.

VALUE (units 10^{-3})	CL%	EVTS	DOCUMENT ID		TECN	CHG
<0.5	90	0	[1] DIAMANT-...	76	SPEC	+

[1] DIAMANT-BERGER 76 quotes this result times our 1975 $\pi^+ \pi^- e \nu$ BR ratio.

$\Gamma(\mu^+ \nu_e)/\Gamma_{total}$ — Γ_{44}/Γ

Forbidden by lepton family number conservation.

VALUE	CL%	EVTS	DOCUMENT ID		TECN	COMMENT
<0.004	90	0	[1] LYONS	81	HLBC	200 GeV K^+ narrow band ν beam
• • • We do not use the following data for averages, fits, limits, etc. • • •						
<0.012	90		[1] COOPER	82	HLBC	Wideband ν beam

[1] COOPER 82 and LYONS 81 limits on ν_e observation are here interpreted as limits on lepton family number violation in the absence of mixing.

$\Gamma(\pi^+ \mu^+ e^-)/\Gamma_{total}$ — Γ_{45}/Γ

Test of lepton family number conservation.

VALUE (units 10^{-10})	CL%	DOCUMENT ID		TECN	CHG
<0.13	90	[1] SHER	05	RVUE	+
• • • We do not use the following data for averages, fits, limits, etc. • • •					
<0.21	90	SHER	05	B865	+
<0.39	90	APPEL	00	B865	+
<2.1	90	LEE	90	SPEC	+

[1] This result combines SHER 05 1998 data, APPEL 00 1996 data, and data from BERGMAN 97 and PISLAK 97 theses, all from BNL-E865, with LEE 90 BNL-E777 data.

$\Gamma(\pi^0 \pi^+ \mu^+ e^-)/\Gamma_{total}$ — Γ_{46}/Γ

VALUE	CL%	DOCUMENT ID		TECN	CHG
$<5.0 \times 10^{-10}$	90	[1] ASHRAF	24	NA62	+

[1] ASHRAF 24 performed the search using a dataset collected by the NA62 experiment from 2016 to 2018.

Int. J. Mod. Phys. A 2026.41. Downloaded from www.worldscientific.com
by UNIVERSITY OF CALIFORNIA @ BERKELEY on 09/16/26. Re-use and distribution is strictly not permitted, except for Open Access articles.

$\Gamma(\pi^+\mu^-e^+)/\Gamma_{total}$ — Γ_{47}/Γ

Test of lepton family number conservation.

VALUE	CL%	DOCUMENT ID		TECN	CHG
$< 6.6\times10^{-11}$	90	ALIBERTI	21	NA62	+
• • • We do not use the following data for averages, fits, limits, etc. • • •					
$< 5.2\times10^{-10}$	90	APPEL	00B	B865	+
$<70\times10^{-10}$	90	[1] DIAMANT-...	76	SPEC	+

[1] Measurement actually applies to the sum of the $\pi^+\mu^-e^+$ and $\pi^-\mu^+e^+$ modes.

$\Gamma(\pi^0\pi^+\mu^-e^+)/\Gamma_{total}$ — Γ_{48}/Γ

VALUE	CL%	DOCUMENT ID		TECN	CHG
$<3.1\times10^{-10}$	90	[1] ASHRAF	24	NA62	+

[1] ASHRAF 24 performed the search using a dataset collected by the NA62 experiment from 2016 to 2018.

$\Gamma(\pi^-\mu^+e^+)/\Gamma_{total}$ — Γ_{49}/Γ

Test of total lepton number conservation.

VALUE	CL%	DOCUMENT ID		TECN	CHG
$< 4.2\times10^{-11}$	90	ALIBERTI	21	NA62	+
• • • We do not use the following data for averages, fits, limits, etc. • • •					
$< 5.0\times10^{-10}$	90	APPEL	00B	B865	+
$<70\times10^{-10}$	90	[1] DIAMANT-...	76	SPEC	+

[1] Measurement actually applies to the sum of the $\pi^+\mu^-e^+$ and $\pi^-\mu^+e^+$ modes.

$\Gamma(\pi^0\pi^-\mu^+e^+)/\Gamma_{total}$ — Γ_{50}/Γ

VALUE	CL%	DOCUMENT ID		TECN	CHG
$<2.9\times10^{-10}$	90	[1] ASHRAF	24	NA62	+

[1] ASHRAF 24 performed the search using a dataset collected by the NA62 experiment from 2016 to 2018.

$\Gamma(\pi^-e^+e^+)/\Gamma_{total}$ — Γ_{51}/Γ

Test of total lepton number conservation.

VALUE	CL%	DOCUMENT ID		TECN	CHG	COMMENT
$<5.3\times10^{-11}$	90	[1] CORTINA-GIL	22	NA62	+	decay-in-flight
• • • We do not use the following data for averages, fits, limits, etc. • • •						
$<2.2\times10^{-10}$	90	[2] CORTINA-GIL	19A	NA62	+	decay-in-flight
$<6.4\times10^{-10}$	90	APPEL	00B	B865	+	
$<9.2\times10^{-9}$	90	DIAMANT-...	76	SPEC	+	
$<1.5\times10^{-5}$		CHANG	68	HBC	−	

[1] CORTINA-GIL 22 uses the complete dataset collected by the NA62 experiment at CERN from 2016 to 2018. Supersedes CORTINA-GIL 19A.
[2] CORTINA-GIL 19A results are obtained with 2017 data. Superseded by CORTINA-GIL 22

$\Gamma(\pi^-\mu^+\mu^+)/\Gamma_{total}$ — Γ_{52}/Γ

Forbidden by total lepton number conservation.

VALUE	CL%	DOCUMENT ID		TECN	CHG	COMMENT
$<4.2\times10^{-11}$	90	[1] CORTINA-GIL	19A	NA62	+	decay-in-flight
• • • We do not use the following data for averages, fits, limits, etc. • • •						
$<8.6\times10^{-11}$	90	[2] BATLEY	17	NA48	±	
$<1.1\times10^{-9}$	90	BATLEY	11A	NA48	±	
$<3.0\times10^{-9}$	90	APPEL	00B	B865	+	
$<1.5\times10^{-4}$	90	[3] LITTENBERG	92	HBC		

[1] CORTINA-GIL 19A results are obtained with 2017 data.
[2] BATLEY 17 result is based on data taken in 2003 to 2004. Limits for two-body resonance X in $K^{\pm}\to\pi\mu\mu$ decays are also reported.
[3] LITTENBERG 92 is from retroactive data analysis of CHANG 68 bubble chamber data.

$\Gamma(\pi^-\pi^0e^+e^+)/\Gamma_{total}$ — Γ_{53}/Γ

Test of total lepton number conservation.

VALUE	CL%	DOCUMENT ID		TECN	CHG	COMMENT
$<8.5\times10^{-10}$	90	[1] CORTINA-GIL	22	NA62	+	decay-in-flight

[1] CORTINA-GIL 22 uses the complete dataset collected by the NA62 experiment at CERN from 2016 to 2018.

$\Gamma(\mu^+\overline{\nu}_e)/\Gamma_{total}$ — Γ_{54}/Γ

Forbidden by total lepton number conservation.

VALUE (units 10^{-3})	CL%	DOCUMENT ID		TECN	COMMENT
<3.3	90	[1] COOPER	82	HLBC	Wideband ν beam

[1] COOPER 82 limit on $\overline{\nu}_e$ observation is here interpreted as a limit on lepton number violation in the absence of mixing.

$\Gamma(\pi^0e^+\overline{\nu}_e)/\Gamma_{total}$ — Γ_{55}/Γ

Forbidden by total lepton number conservation.

VALUE	CL%	DOCUMENT ID		TECN	COMMENT
<0.003	90	[1] COOPER	82	HLBC	Wideband ν beam

[1] COOPER 82 limit on $\overline{\nu}_e$ observation is here interpreted as a limit on lepton number violation in the absence of mixing.

$\Gamma(\pi^+\gamma)/\Gamma_{total}$ — Γ_{56}/Γ

Violates angular momentum conservation and gauge invariance. Current interest in this decay is as a search for non-commutative space-time effects as discussed in ARTAMONOV 05 and for exotic physics such as a vacuum expectation value of a new vector field, non-local Superstring effects, or departures from Lorentz invariance, as discussed in ADLER 02B.

VALUE	CL%	DOCUMENT ID		TECN	CHG
$< 2.3\times10^{-9}$	90	ARTAMONOV	05	B949	+
• • • We do not use the following data for averages, fits, limits, etc. • • •					
$< 360\times10^{-9}$	90	ADLER	02B	B787	+
$<1400\times10^{-9}$	90	ASANO	82	CNTR	+
$<4000\times10^{-9}$	90	[1] KLEMS	71	OSPK	+

[1] Test of model of Selleri, Nuovo Cimento **60A** 291 (1969).

CP VIOLATION TESTS IN $K^{\pm}$ DECAYS

$\Delta = (\Gamma(K^+) - \Gamma(K^-))\ /\ (\Gamma(K^+) + \Gamma(K^-))$

$\Delta(K^{\pm}\to\mu^{\pm}\nu_{\mu})$ RATE DIFFERENCE/SUM

VALUE (%)	DOCUMENT ID		TECN
−0.27±0.21	FORD	67	CNTR

$\Delta(K^{\pm}\to\pi^{\pm}\pi^0)$ RATE DIFFERENCE/SUM

VALUE (%)	DOCUMENT ID		TECN
0.4±0.6	HERZO	69	OSPK

$\Delta(K^{\pm}\to\pi^{\pm}e^+e^-)$ RATE DIFFERENCE/SUM

VALUE (units 10^{-2})	DOCUMENT ID		TECN
−2.2±1.5±0.6	[1] BATLEY	09	NA48

[1] This implies an upper limit of 2.1×10^{-2} at 90% CL.

$\Delta(K^{\pm}\to\pi^{\pm}\mu^+\mu^-)$ RATE DIFFERENCE/SUM

VALUE	DOCUMENT ID		TECN
0.010±0.023 OUR AVERAGE			
0.011±0.023	[1] BATLEY	11A	NA48
−0.02 ±0.11 ±0.04	PARK	02	HYCP

[1] This corresponds to the asymmetry upper limit of $< 2.9\times10^{-2}$ at 90% CL.

$\Delta(K^{\pm}\to\pi^{\pm}\pi^0\gamma)$ RATE DIFFERENCE/SUM

VALUE (units 10^{-3})	EVTS	DOCUMENT ID		TECN	CHG	COMMENT
0.0± 1.2 OUR AVERAGE						
0.0± 1.0±0.6	1M	[1] BATLEY	10A	NA48		
4 ±29	2461	SMITH	76	WIRE	±	E_{π} 55–90 MeV
5 ±20	4000	ABRAMS	73B	ASPK	±	E_{π} 51–100 MeV

[1] This value implies the upper bound for this asymmetry 1.5×10^{-3} at 90% CL.

$\Delta(K^{\pm}\to\pi^{\pm}\pi^+\pi^-)$ RATE DIFFERENCE/SUM

VALUE (%)	EVTS	DOCUMENT ID		TECN	CHG
0.04±0.06		[1] FORD	70	ASPK	
• • • We do not use the following data for averages, fits, limits, etc. • • •					
−0.01±0.08		[2] SMITH	73	ASPK	±
0.05±0.07	3.2M	[1] FORD	70	ASPK	
−0.25±0.45		FLETCHER	67	OSPK	
−0.02±0.11		[1] FORD	67	CNTR	

[1] First FORD 70 value is second FORD 70 combined with FORD 67.
[2] SMITH 73 value of $K^{\pm}\to\pi^{\pm}\pi^+\pi^-$ rate difference is derived from SMITH 73 value of $K^{\pm}\to\pi^{\pm}2\pi^0$ rate difference.

$\Delta(K^{\pm}\to\pi^{\pm}\pi^0\pi^0)$ RATE DIFFERENCE/SUM

VALUE (%)	EVTS	DOCUMENT ID		TECN	CHG
−0.02±0.28 OUR AVERAGE					
0.04±0.29		SMITH	73	ASPK	±
−0.6 ±0.9	1802	HERZO	69	OSPK	

T VIOLATION TESTS IN K^+ AND K^- DECAYS

P_T in $K^+\to\pi^0\mu^+\nu_{\mu}$

T-violating muon polarization. Sensitive to new sources of *CP* violation beyond the Standard Model.

VALUE (units 10^{-3})	EVTS	DOCUMENT ID		TECN	CHG
−1.7±2.3±1.1		[1] ABE	04F	K246	+
• • • We do not use the following data for averages, fits, limits, etc. • • •					
−4.2±4.9±0.9	3.9M	ABE	99S	K246	+

[1] Includes three sets of data: 96-97 (ABE 99S), 98, and 99-00 totaling about three times the ABE 99S data sample. Corresponds to $P_T < 5.0\times10^{-3}$ at 90% CL.

P_T in $K^+\to\mu^+\nu_{\mu}\gamma$

T-violating muon polarization. Sensitive to new sources of *CP* violation beyond the Standard Model.

VALUE (units 10^{-2})	EVTS	DOCUMENT ID		TECN	CHG
−0.64±1.85±0.10	114k	[1] ANISIMOVSK...	03	K246	+

[1] Muons stopped and polarization measured from decay to positrons.

Im(ξ) in $K^+\to\pi^0\mu^+\nu_{\mu}$ DECAY (from transverse μ pol.)

Test of *T* reversal invariance.

VALUE	EVTS	DOCUMENT ID		TECN	CHG	COMMENT
−0.006 ±0.008 OUR AVERAGE						
−0.0053±0.0071±0.0036		[1] ABE	04F	K246	+	
−0.016 ±0.025	20M	CAMPBELL	81	CNTR	+	Pol.
• • • We do not use the following data for averages, fits, limits, etc. • • •						
−0.013 ±0.016 ±0.003	3.9M	ABE	99S	CNTR	+	p_T K^+ at rest

[1] Includes three sets of data: 96-97 (ABE 99s), 98, and 99-00 totaling about three times the ABE 99s data sample. Corresponds to $\mathrm{Im}(\xi) < 0.016$ at 90% CL.

DALITZ PLOT PARAMETERS FOR $K \to 3\pi$ DECAYS

Revised 1999 by T.G. Trippe (LBNL).

The Dalitz plot distribution for $K^{\pm} \to \pi^{\pm}\pi^{\pm}\pi^{\mp}$, $K^{\pm} \to \pi^0\pi^0\pi^{\pm}$, and $K^0_L \to \pi^+\pi^-\pi^0$ can be parameterized by a series expansion such as that introduced by Weinberg [1]. We use the form

$$\left|M\right|^2 \propto 1 + g\frac{(s_3 - s_0)}{m^2_{\pi^+}} + h\left[\frac{s_3 - s_0}{m^2_{\pi^+}}\right]^2 + j\ \frac{(s_2 - s_1)}{m^2_{\pi^+}} + k\left[\frac{s_2 - s_1}{m^2_{\pi^+}}\right]^2 + f\ \frac{(s_2 - s_1)}{m^2_{\pi^+}}\frac{(s_3 - s_0)}{m^2_{\pi^+}} + \cdots\ , \qquad (1)$$

where $m^2_{\pi^+}$ has been introduced to make the coefficients g, h, j, and k dimensionless, and

$$s_i = (P_K - P_i)^2 = (m_K - m_i)^2 - 2m_K T_i\ ,\ i = 1, 2, 3,$$
$$s_0 = \frac{1}{3}\sum_i s_i = \frac{1}{3}(m^2_K + m^2_1 + m^2_2 + m^2_3)\quad .$$

Here the P_i are four-vectors, m_i and T_i are the mass and kinetic energy of the ith pion, and the index 3 is used for the odd pion.

The coefficient g is a measure of the slope in the variable s_3 (or T_3) of the Dalitz plot, while h and k measure the quadratic dependence on s_3 and $(s_2 - s_1)$, respectively. The coefficient j is related to the asymmetry of the plot and must be zero if CP invariance holds. Note also that if CP is good, g, h, and k must be the same for $K^+ \to \pi^+\pi^+\pi^-$ as for $K^- \to \pi^-\pi^-\pi^+$.

Since different experiments use different forms for $\left|M\right|^2$, in order to compare the experiments we have converted to g, h, j, and k whatever coefficients have been measured. Where such conversions have been done, the measured coefficient a_y, a_t, a_u, or a_v is given in the comment at the right. For definitions of these coefficients, details of this conversion, and discussion of the data, see the April 1982 version of this note [2].

References

1. S. Weinberg, Phys. Rev. Lett. **4**, 87 (1960).
2. Particle Data Group, Phys. Lett. **111B**, 69 (1982).

ENERGY DEPENDENCE OF $K^{\pm}$ DALITZ PLOT

$|\text{matrix element}|^2 = 1 + gu + hu^2 + kv^2$
where $u = (s_3 - s_0)\ /\ m^2_{\pi}$ and $v = (s_2 - s_1)\ /\ m^2_{\pi}$

LINEAR COEFFICIENT g FOR $K^{\pm} \to \pi^{\pm}\pi^+\pi^-$

Some experiments use Dalitz variables x and y. In the comments we give a_y = coefficient of y term. See note above on "Dalitz Plot Parameters for $K \to 3\pi$ Decays." For discussion of the conversion of a_y to g, see the earlier version of the same note in the *Review* published in Physics Letters **111B** 70 (1982).

VALUE	EVTS	DOCUMENT ID		TECN	CHG	COMMENT
−0.21134±0.00017	471M	[1] BATLEY	07B	NA48	±	
• • • We do not use the following data for averages, fits, limits, etc. • • •						
−0.2221 ±0.0065	225k	DEVAUX	77	SPEC	+	a_y=.2814±.0082
−0.199 ±0.008	81k	[2] LUCAS	73	HBC	−	a_y=0.252±0.011
−0.2157 ±0.0028	750k	FORD	72	ASPK	+	a_y=.2734±.0035
−0.2186 ±0.0028	750k	FORD	72	ASPK	−	a_y=.2770±.0035
−0.200 ±0.009	39819	[3] HOFFMASTER	72	HLBC	+	
−0.196 ±0.012	17898	[4] GRAUMAN	70	HLBC	+	a_y=0.228±0.030
−0.193 ±0.010	50919	MAST	69	HBC	−	a_y=0.244±0.013
−0.218 ±0.016	9994	[5] BUTLER	68	HBC	+	a_y=0.277±0.020
−0.190 ±0.023	5778	[5,6] MOSCOSO	68	HBC	−	a_y=0.242±0.029
−0.22 ±0.024	5428	[5,6] ZINCHENKO	67	HBC	+	a_y=0.28 ± 0.03
−0.220 ±0.035	1347	[7] FERRO-LUZZI	61	HBC	−	a_y=0.28 ± 0.045

[1] Final state strong interaction and radiative corrections not included in the fit.
[2] Quadratic dependence is required by K^0_L experiments.
[3] HOFFMASTER 72 includes GRAUMAN 70 data.
[4] Emulsion data added — all events included by HOFFMASTER 72.
[5] Experiments with large errors not included in average.
[6] Also includes DBC events.
[7] No radiative corrections included.

QUADRATIC COEFFICIENT h FOR $K^{\pm} \to \pi^{\pm}\pi^+\pi^-$

VALUE (units 10^{-2})	EVTS	DOCUMENT ID		TECN	CHG
1.848±0.040	471M	[1] BATLEY	07B	NA48	±
• • • We do not use the following data for averages, fits, limits, etc. • • •					
−0.06 ±1.43	225k	DEVAUX	77	SPEC	+
1.87 ±0.62	750k	FORD	72	ASPK	+
1.25 ±0.62	750k	FORD	72	ASPK	−
−0.9 ±1.4	39819	HOFFMASTER	72	HLBC	+
−0.1 ±1.2	50919	MAST	69	HBC	−

[1] Final state strong interaction and radiative corrections not included in the fit.

QUADRATIC COEFFICIENT k FOR $K^{\pm} \to \pi^{\pm}\pi^+\pi^-$

VALUE (units 10^{-3})	EVTS	DOCUMENT ID		TECN	CHG
− 4.63± 0.14	471M	[1] BATLEY	07B	NA48	±
• • • We do not use the following data for averages, fits, limits, etc. • • •					
−20.5 ± 3.9	225k	DEVAUX	77	SPEC	+
− 7.5 ± 1.9	750k	FORD	72	ASPK	+
− 8.3 ± 1.9	750k	FORD	72	ASPK	−
−10.5 ± 4.5	39819	HOFFMASTER	72	HLBC	+
−14 ±12	50919	MAST	69	HBC	−

[1] Final state strong interaction and radiative corrections not included in the fit.

$(g_+ - g_-)\ /\ (g_+ + g_-)$ FOR $K^{\pm} \to \pi^{\pm}\pi^+\pi^-$

This is a CP violating asymmetry between linear coefficients g_+ for $K^+ \to \pi^+\pi^+\pi^-$ decay and g_- for $K^- \to \pi^-\pi^+\pi^-$ decay.

VALUE (units 10^{-4})	EVTS	DOCUMENT ID		TECN
− 1.5± 1.5±1.6	3.1G	[1] BATLEY	07E	NA48
• • • We do not use the following data for averages, fits, limits, etc. • • •				
1.7± 2.1±2.0	1.7G	[2] BATLEY	06	NA48
−70.0±53	3.2M	FORD	70	ASPK

[1] BATLEY 07E includes data from BATLEY 06. Uses quadratic parametrization and value $g_+ + g_- = 2g$ from BATLEY 07B. This measurement neglects any possible charge asymmetries in higher order slope parameters h or k.
[2] This measurement neglects any possible charge asymmetries in higher order slope parameters h or k.

LINEAR COEFFICIENT g FOR $K^{\pm} \to \pi^{\pm}\pi^0\pi^0$

Unless otherwise stated, all experiments include terms quadratic in $(s_3 - s_0)\ /\ m^2_{\pi^+}$. See note above on "Dalitz Plot Parameters for $K \to 3\pi$ Decays."

See BATUSOV 98 for a discussion of the discrepancy between their result and others, especially BOLOTOV 86. At this time we have no way to resolve the discrepancy so we depend on the large scale factor as a warning.

VALUE	EVTS	DOCUMENT ID		TECN	CHG	COMMENT
0.626 ±0.007 OUR AVERAGE						
0.6259±0.0043±0.0093	493k	AKOPDZHAN..	05B	TNF	±	
0.627 ±0.004 ±0.010	252k	[1,2] AJINENKO	03B	ISTR	−	
• • • We do not use the following data for averages, fits, limits, etc. • • •						
0.736 ±0.014 ±0.012	33k	BATUSOV	98	SPEC	+	
0.582 ±0.021	43k	BOLOTOV	86	CALO	−	
0.670 ±0.054	3263	BRAUN	76B	HLBC	+	
0.630 ±0.038	5635	SHEAFF	75	HLBC	+	
0.510 ±0.060	27k	SMITH	75	WIRE	+	
0.67 ±0.06	1365	AUBERT	72	HLBC	+	
0.544 ±0.048	4048	DAVISON	69	HLBC	+	Also emulsion

[1] Measured using in-flight decays of the 25 GeV negative secondary beam.
[2] They form new world averages $g_- = (0.617 \pm 0.018)$ and $g_+ = (0.684 \pm 0.033)$ which give $\Delta g_{\tau'} = 0.051 \pm 0.028$.

QUADRATIC COEFFICIENT h FOR $K^{\pm} \to \pi^{\pm}\pi^0\pi^0$

VALUE	EVTS	DOCUMENT ID		TECN	CHG	COMMENT
0.052 ±0.008 OUR AVERAGE						
0.0551±0.0044±0.0086	493k	AKOPDZHAN..	05B	TNF	±	
0.046 ±0.004 ±0.012	252k	[1] AJINENKO	03B	ISTR	−	
• • • We do not use the following data for averages, fits, limits, etc. • • •						
0.128 ±0.015 ±0.024	33k	BATUSOV	98	SPEC	+	
0.037 ±0.024	43k	BOLOTOV	86	CALO	−	
0.152 ±0.082	3263	BRAUN	76B	HLBC	+	

Int. J. Mod. Phys. A 2026.41. Downloaded from www.worldscientific.com
by LIFORNIA @ BERKELEY on 09/16/26. Re-use and distribution is strictly not permitted, except for Open Access articles.

Int. J. Mod. Phys. A 2026.41. Downloaded from www.worldscientific.com by UNIVERSITY OF CALIFORNIA @ BERKELEY on 09/16/26. Re-use and distribution is strictly not permitted, except for Open Access articles.

0.041 ±0.030	5635	SHEAFF	75	HLBC	+	
0.009 ±0.040	27k	SMITH	75	WIRE	+	
−0.01 ±0.08	1365	AUBERT	72	HLBC	+	
0.026 ±0.050	4048	DAVISON	69	HLBC	+	Also emulsion

[1] Measured using in-flight decays of the 25 GeV negative secondary beam.

QUADRATIC COEFFICIENT k FOR $K^{\pm} \to \pi^{\pm}\pi^0\pi^0$

VALUE	EVTS	DOCUMENT ID		TECN	CHG
0.0054±0.0035 OUR AVERAGE	Error includes scale factor of 2.5.				
0.0082±0.0011±0.0014	493k	AKOPDZHAN..	05B	TNF	±
0.001 ±0.001 ±0.002	252k	[1] AJINENKO	03B	ISTR	−
• • • We do not use the following data for averages, fits, limits, etc. • • •					
0.0197±0.0045±0.0029	33k	BATUSOV	98	SPEC	+

[1] Measured using in-flight decays of the 25 GeV negative secondary beam.

$(g_+ - g_-)$ / $(g_+ + g_-)$ FOR $K^{\pm} \to \pi^{\pm}\pi^0\pi^0$

A nonzero value for this quantity indicates *CP* violation.

VALUE (units 10^{-4})	EVTS	DOCUMENT ID		TECN
1.8± 1.8 OUR AVERAGE				
1.8± 1.7±0.6	91.3M	[1] BATLEY	07E	NA48
2 ±18 ±5	619k	[2] AKOPDZHAN..	05	TNF
• • • We do not use the following data for averages, fits, limits, etc. • • •				
1.8± 2.2±1.3	47M	[3] BATLEY	06A	NA48

[1] BATLEY 07E includes data from BATLEY 06A. Uses quadratic parametrization and PDG 06 value $g = 0.626 \pm 0.007$ to obtain $g_+ - g_- = (2.2 \pm 2.1 \pm 0.7) \times 10^{-4}$. Neglects any possible charge asymmetries in higher order slope parameters h or k.

[2] Asymmetry obtained assuming that $g_+ + g_- = 2\times 0.652$ (PDG 02) and that asymmetries in h and k are zero.

[3] Linear and quadratic slopes from PDG 04 are used. Any possible charge asymmetries in higher order slope parameters h or k are neglected.

ALTERNATIVE PARAMETRIZATIONS OF $K^{\pm} \to \pi^{\pm}\pi^0\pi^0$ DALITZ PLOT

The following functional form for the matrix element suggested by $\pi\pi$ rescattering in $K^+ \to \pi^+ \text{“}\pi^+\pi^-\text{”} \to \pi^+\pi^0\pi^0$ is used for this fit (CABIBBO 04A, CABIBBO 05): Matrix element $= M_0 + M_1$ where $M_0 = 1 + (1/2)g_0\, u + (1/2)\, h'\, u^2 + (1/2)k_0\, v^2$ with $u = (s_3 - s_0)/(m_{\pi^+})^2$, $v = (s_2 - s_1)/(m_{\pi^+})^2$ and where M_1 takes into account the non-analytic piece due to pi pi rescattering amplitudes a_0 and a_2; The parameters g_0 and h' are related to the parameters g and h of the matrix element squared given in the previous section by the approximations $g_0 \sim g^{PDG}$ and $h' \sim h^{PDG} - (g/2)^2$ and $k_0 \sim k^{PDG}$.

In addition, we also consider the effective field theory framework of COLANGELO 06A and BISSEGGER 09 to extract g_{BB} and h'_{BB}.

LINEAR COEFFICIENT g_0 FOR $K^{\pm} \to \pi^{\pm}\pi^0\pi^0$

VALUE	EVTS	DOCUMENT ID		TECN	CHG
0.6525±0.0009±0.0033	60M	[1] BATLEY	09A	NA48	±
• • • We do not use the following data for averages, fits, limits, etc. • • •					
0.645 ±0.004 ±0.009	23M	[2] BATLEY	06B	NA48	±

[1] This fit is obtained with the CABIBBO 05 matrix element in the $2\pi^0$ invariant mass squared range $0.074094 < m^2_{2\pi^0} < 0.104244$ GeV^2. Electromagnetic corrections and CHPT constraints for $\pi\pi$ phase shifts (a_0 and a_2) have been used. Also measured $(a_0 - a_2)\, m_{\pi^+} = 0.2646 \pm 0.0021 \pm 0.0023$, where k_0 was kept fixed in the fit at -0.0099.

[2] Superseded by BATLEY 09A. This fit is obtained with the CABIBBO 05 matrix element in the $2\pi^0$ invariant mass squared range 0.074 GeV^2 $< m^2_{2\pi^0} < 0.097$ GeV^2, assuming $k = 0$ (no term proportional to $(s_2 - s_1)^2$) and excluding the kinematic region around the cusp ($m^2_{2\pi^0} = (2m_{\pi^+})^2 \pm 0.000525$ GeV^2). Also π-π phase shifts a_0 and a_2 are measured: $(a_0 - a_2)m_{\pi^+} = 0.268 \pm 0.010 \pm 0.004 \pm 0.013$(external) and $a_2\, m_{\pi^+} = -0.041 \pm 0.022 \pm 0.014$.

QUADRATIC COEFFICIENT h' FOR $K^{\pm} \to \pi^{\pm}\pi^0\pi^0$

VALUE	EVTS	DOCUMENT ID		TECN	CHG
−0.0433±0.0008±0.0026	60M	[1] BATLEY	09A	NA48	±
• • • We do not use the following data for averages, fits, limits, etc. • • •					
−0.047 ±0.012 ±0.011	23M	[2] BATLEY	06B	NA48	±

[1] This fit is obtained with the CABIBBO 05 matrix element in the $2\pi^0$ invariant mass squared range $0.074094 < m^2_{2\pi^0} < 0.104244$ GeV^2. Electromagnetic corrections and CHPT constraints for $\pi\pi$ phase shifts (a_0 and a_2) have been used. Also measured $(a_0 - a_2)\, m_{\pi^+} = 0.2646 \pm 0.0021 \pm 0.0023$, where k_0 was kept fixed in the fit at -0.0099.

[2] Superseded by BATLEY 09A. This fit is obtained with the CABIBBO 05 matrix element in the $2\pi^0$ invariant mass squared range 0.074 GeV^2 $< m^2_{2\pi^0} < 0.097$ GeV^2, assuming $k = 0$ (no term proportional to $(s_2 - s_1)^2$) and excluding the kinematic region around the cusp ($m^2_{2\pi^0} = (2m_{\pi^+})^2 \pm 0.000525$ GeV^2). Also π-π phase shifts a_0 and a_2 are measured: $(a_0 - a_2)m_{\pi^+} = 0.268 \pm 0.010 \pm 0.004 \pm 0.013$(external) and $a_2\, m_{\pi^+} = -0.041 \pm 0.022 \pm 0.014$.

QUADRATIC COEFFICIENT k_0 FOR $K^{\pm} \to \pi^{\pm}\pi^0\pi^0$

VALUE	EVTS	DOCUMENT ID		TECN	CHG
0.0095±0.00017±0.00048	60M	[1] BATLEY	09A	NA48	±

[1] Assumed $a_2\, m_{\pi^+} = -0.0044$ in the fit.

LINEAR COEFFICIENT g_{BB} FOR $K^{\pm} \to \pi^{\pm}\pi^0\pi^0$

VALUE	EVTS	DOCUMENT ID		TECN	CHG
0.6219±0.0009±0.0033	60M	[1] BATLEY	09A	NA48	±

[1] This fit is obtained using parametrizations of COLANGELO 06A and BISSEGGER 09 in the $2\pi^0$ invariant mass squared range $0.074094 < m^2_{2\pi^0} < 0.104244$ GeV^2. Electromagnetic corrections and CHPT constraints for $\pi\pi$ phase shifts (a_0 and a_2) have been used. Also measured $(a_0 - a_2)\, m_{\pi^+} = 0.2633 \pm 0.0024 \pm 0.0024$, where k_0 was kept fixed in the fit at 0.0085.

QUADRATIC COEFFICIENT h'_{BB} FOR $K^{\pm} \to \pi^{\pm}\pi^0\pi^0$

VALUE	EVTS	DOCUMENT ID		TECN	CHG
−0.0520±0.0009±0.0026	60M	[1] BATLEY	09A	NA48	±

[1] This fit is obtained using parametrizations of COLANGELO 06A and BISSEGGER 09 in the $2\pi^0$ invariant mass squared range $0.074094 < m^2_{2\pi^0} < 0.104244$ GeV^2. Electromagnetic corrections and CHPT constraints for $\pi\pi$ phase shifts (a_0 and a_2) have been used. Also measured $(a_0 - a_2)\, m_{\pi^+} = 0.2633 \pm 0.0024 \pm 0.0024$, where k_0 was kept fixed in the fit at 0.0085.

$K^{\pm}_{\ell 3}$ FORM FACTORS

In the form factor comments, the following symbols are used.

f_+ and f_- are form factors for the vector matrix element.

f_S and f_T refer to the scalar and tensor term.

$f_0 = f_+ + f_-\, t/(m^2_{K^+} - m^2_{\pi^0})$.

t = momentum transfer to the π.

λ_+ and λ_0 are the linear expansion coefficients of f_+ and f_0:

$f_+(t) = f_+(0)\,(1 + \lambda_+ t\,/m^2_{\pi^+})$

For quadratic expansion

$f_+(t) = f_+(0)\,(1 + \lambda'_+ t\,/m^2_{\pi^+} + \frac{\lambda''_+}{2}\, t^2/m^4_{\pi^+})$

as used by KTeV. If there is a non-vanishing quadratic term, then λ_+ represents an average slope, which is then different from λ'_+.

NA48/2 and OKA quadratic expansion coefficients are converted with $\lambda'^{PDG}_+ = \lambda'^{NA48/2}_+$ and $\lambda''^{PDG}_+ = 2\,\lambda''^{NA48/2}_+$

$\lambda'^{PDG}_+ = (\frac{m_{\pi^+}}{m_{\pi^0}})^2\, \lambda'^{OKA}_+$ and

$\lambda''^{PDG}_+ = 2\,(\frac{m_{\pi^+}}{m_{\pi^0}})^4\, \lambda''^{OKA}_+$

OKA linear expansion coefficients are converted with

$\lambda_+^{PDG} = (\frac{m_{\pi^+}}{m_{\pi^0}})^2\, \lambda_+^{OKA}$ and $\lambda_0^{PDG} = (\frac{m_{\pi^+}}{m_{\pi^0}})^2\, \lambda_0^{OKA}$

The pole parametrization is

$$f_+(t) = f_+(0)\,(\frac{M_V^2}{M_V^2 - t})$$

$$f_0(t) = f_0(0)\,(\frac{M_S^2}{M_S^2 - t})$$

where M_V and M_S are the vector and scalar pole masses.

The following abbreviations are used:

DP = Dalitz plot analysis.

PI = π spectrum analysis.

MU = μ spectrum analysis.

POL= μ polarization analysis.

BR = $K^{\pm}_{\mu 3}/K^{\pm}_{e3}$ branching ratio analysis.

E = positron or electron spectrum analysis.

RC = radiative corrections.

For previous λ'_+ and λ''_+ parametrizations used by NA48 (e.g. LAI 07A) and ISTRA (e.g. YUSHCHENKO 04B) see PDG 18.

λ_+ (LINEAR ENERGY DEPENDENCE OF f_+ IN $K^{\pm}_{e3}$ DECAY)

These results are for a linear expansion only. See the next section for fits including a quadratic term. For radiative correction of the $K^{\pm}_{e3}$ Dalitz plot, see GINSBERG 67, BECHERRAWY 70, CIRIGLIANO 02, CIRIGLIANO 04, and ANDRE 07. Results labeled OUR FIT are discussed in the review “$K^{\pm}_{\ell 3}$ and $K^0_{\ell 3}$ Form Factors” above. For earlier, lower statistics results, see the 2004 edition of this review, Physics Letters **B592** 1 (2004).

VALUE (units 10^{-2})	EVTS	DOCUMENT ID		TECN	CHG	COMMENT
2.959±0.025 OUR FIT Assuming μ-e universality						
2.956±0.025 OUR AVERAGE						
2.95 ±0.022±0.018	5.25M	YUSHCHENKO	18	OKA	+	
3.044±0.083±0.074	1.1M	AKOPDZANOV	09	TNF	±	
2.966±0.050±0.034	919k	[1] YUSHCHENKO	04B	ISTR	−	DP
2.78 ±0.26 ±0.30	41k	SHIMIZU	00	SPEC	+	DP
2.84 ±0.27 ±0.20	32k	[2] AKIMENKO	91	SPEC		PI, no RC
2.9 ±0.4	62k	[3] BOLOTOV	88	SPEC		PI, no RC
• • • We do not use the following data for averages, fits, limits, etc. • • •						
3.06 ±0.09 ±0.06	550k	[1,4] AJINENKO	03C	ISTR	−	DP
2.93 ±0.15 ±0.2	130k	[4] AJINENKO	02	SPEC		DP

[1] Rescaled to agree with our conventions as noted above.

[2] AKIMENKO 91 state that radiative corrections would raise λ_+ by 0.0013.

[3] BOLOTOV 88 state radiative corrections of GINSBERG 67 would raise λ_+ by 0.002.

[4] Superseded by YUSHCHENKO 04B.

Int. J. Mod. Phys. A 2026.41. Downloaded from www.worldscientific.com by LIFORNIA @ BERKELEY on 09/16/26. Re-use and distribution is strictly not permitted, except for Open Access articles.

λ_+ (LINEAR ENERGY DEPENDENCE OF f_+ IN $K^{\pm}_{\mu3}$ DECAY)

Results labeled OUR FIT are discussed in the review "$K^{\pm}_{\ell3}$ and $K^0_{\ell3}$ Form Factors" above. For earlier, lower statistics results, see the 2004 edition of this review, Physics Letters **B592** 1 (2004).

VALUE (units 10^{-2})	EVTS	DOCUMENT ID		TECN	CHG	COMMENT
2.959±0.025 OUR FIT		Assuming μ-e universality				
3.09 ±0.25 OUR FIT		Error includes scale factor of 1.5. Not assuming μ-e universality				
2.96 ±0.14 ±0.10	540k	[1] YUSHCHENKO	04	ISTR	−	DP
• • • We do not use the following data for averages, fits, limits, etc. • • •						
3.21 ±0.45	112k	[2] AJINENKO	03	ISTR	−	DP

[1] Rescaled to agree with our conventions as noted above.
[2] Superseded by YUSHCHENKO 04.

λ_0 (LINEAR ENERGY DEPENDENCE OF f_0 IN $K^{\pm}_{\mu3}$ DECAY)

Results labeled OUR FIT are discussed in the review "$K^{\pm}_{\ell3}$ and $K^0_{\ell3}$ Form Factors" above. For earlier, lower statistics results, see the 2004 edition of this review, Physics Letters **B592** 1 (2004).

VALUE (units 10^{-2})	$d\lambda_0/d\lambda_+$	EVTS	DOCUMENT ID		TECN	CHG	COMMENT
1.76 ±0.25 OUR FIT			Error includes scale factor of 2.7. Assuming μ-e universality				
1.73 ±0.27 OUR FIT			Error includes scale factor of 2.6. Not assuming μ-e universality				
1.420±0.114±0.107		2.3M	[1] BATLEY	18	NA48	±	
1.96 ±0.12 ±0.06	−0.348	540k	[2] YUSHCHENKO	04	ISTR	−	DP
• • • We do not use the following data for averages, fits, limits, etc. • • •							
2.09 ±0.45	−0.46	112k	[3] AJINENKO	03	ISTR	−	DP
1.9 ±0.64		24k	[4] HORIE	01	SPEC	+	BR
1.9 ±1.0	+0.03	55k	[5] HEINTZE	77	SPEC	+	BR

[1] Data collected in 2004 by NA48/2. Obtained from a fit with a quadratic vector form factor. Correlation coefficient with linear slope is 0.511, with quadratic slope is −0.513. χ^2/NDF = 409.9/381. BATLEY 18 also performed a combined $K^{\pm}_{e3}$ and $K^{\pm}_{\mu3}$ fit assuming $\mu-e$ universality and obtained $(14.47 \pm 0.63 \pm 1.17) \times 10^{-3}$.
[2] Rescaled to agree with our conventions as noted above.
[3] Superseded by YUSHCHENKO 04.
[4] HORIE 01 assumes μ-e universality in $K^{+}_{\ell3}$ decay and uses SHIMIZU 00 value λ=0.0278± 0.0040 from $K^{\pm}_{e3}$ decay.
[5] HEINTZE 77 uses $\lambda_+ = 0.029 \pm 0.003$. $d\lambda_0/d\lambda_+$ estimated by us.

λ'_+ (LINEAR $K^{\pm}_{e3}$ FORM FACTOR FROM QUADRATIC FIT)

VALUE (units 10^{-2})	EVTS	DOCUMENT ID		TECN	CHG	COMMENT
2.59 ±0.04 OUR AVERAGE						
2.426±0.078±0.130	4.4M	[1] BATLEY	18	NA48	±	
2.611±0.035±0.028	5.25M	YUSHCHENKO	18	OKA	+	
2.485±0.163±0.034	919k	[2,3] YUSHCHENKO	04B	ISTR	−	DP
• • • We do not use the following data for averages, fits, limits, etc. • • •						
3.07 ±0.21	550k	[2,4] AJINENKO	03C	ISTR	−	DP

[1] Data collected in 2004 by NA48/2. Correlation coefficient with quadratic slope is −0.929. χ^2/NDF = 569.1/687. BATLEY 18 also performed a combined $K^{\pm}_{e3}$ and $K^{\pm}_{\mu3}$ fit assuming $\mu-e$ universality and obtained $(24.24 \pm 0.75 \pm 1.3) \times 10^{-3}$.
[2] Rescaled to agree with our conventions as noted above.
[3] YUSHCHENKO 04B λ'_+ and λ''_+ are strongly correlated with coefficient $\rho(\lambda'_+, \lambda''_+) = -0.95$.
[4] Superseded by YUSHCHENKO 04B.

λ''_+(QUADRATIC $K^{\pm}_{e3}$ FORM FACTOR)

VALUE (units 10^{-2})	EVTS	DOCUMENT ID		TECN	CHG	COMMENT
0.186±0.021 OUR AVERAGE						
0.164±0.030±0.039	4.4M	[1] BATLEY	18	NA48	±	
0.191±0.019±0.014	5.25M	YUSHCHENKO	18	OKA	+	
0.192±0.062±0.071	919k	[2,3] YUSHCHENKO	04B	ISTR	−	DP
• • • We do not use the following data for averages, fits, limits, etc. • • •						
−0.5 ±0.7 ±1.5	550k	[2,4] AJINENKO	03C	ISTR	−	DP

[1] Data collected in 2004 by NA48/2. Correlation coefficient with quadratic slope is −0.929. χ^2/NDF = 569.1/687. BATLEY 18 also performed a combined $K^{\pm}_{e3}$ and $K^{\pm}_{\mu3}$ fit assuming $\mu-e$ universality and obtained $(1.67 \pm 0.29 \pm 0.41) \times 10^{-3}$.
[2] Rescaled to agree with our conventions as noted above.
[3] YUSHCHENKO 04B λ'_+ and λ''_+ are strongly correlated with coefficient $\rho(\lambda'_+, \lambda''_+) = -0.95$.
[4] Superseded by YUSHCHENKO 04B.

λ'_+ (LINEAR $K^{\pm}_{\mu3}$ FORM FACTOR FROM QUADRATIC FIT)

VALUE (units 10^{-3})	EVTS	DOCUMENT ID		TECN	CHG
24.27±2.88±2.89	2.3M	[1] BATLEY	18	NA48	±

[1] Data collected in 2004 by NA48/2. Correlation coefficient with quadratic slope is −0.974, with scalar slope is 0.511. χ^2/NDF = 409.9/381. BATLEY 18 also performed a combined $K^{\pm}_{e3}$ and $K^{\pm}_{\mu3}$ fit assuming $\mu-e$ universality and obtained $(24.24 \pm 0.75 \pm 1.3) \times 10^{-3}$.

λ''_+ (QUADRATIC $K^{\pm}_{\mu3}$ FORM FACTOR)

VALUE (units 10^{-3})	EVTS	DOCUMENT ID		TECN	CHG
1.83±1.05±1.09	2.3M	[1] BATLEY	18	NA48	±

[1] Data collected in 2004 by NA48/2. Correlation coefficient with linear slope is −0.974, with scalar slope is 0.513. χ^2/NDF = 409.9/381. BATLEY 18 also performed a combined $K^{\pm}_{e3}$ and $K^{\pm}_{\mu3}$ fit assuming $\mu-e$ universality and obtained $(1.67 \pm 0.29 \pm 0.41) \times 10^{-3}$.

M_V (VECTOR POLE MASS FOR $K^{\pm}_{e3}$ DECAY)

See the review on $K^{\pm}_{l3}$ and K^0_{l3} Form Factors for details.

VALUE (MeV)	EVTS	DOCUMENT ID		TECN	CHG
890.3±2.8 OUR AVERAGE					
885.2±3.3±7.2	4.4M	[1] BATLEY	18	NA48	±
891 ±3	5.25M	[2] YUSHCHENKO	18	OKA	+

[1] Data collected in 2004 by NA48/2. χ^2/NDF = 568.9/688. BATLEY 18 also performed a combined $K^{\pm}_{e3}$ and $K^{\pm}_{\mu3}$ fit assuming $\mu-e$ universality and obtained 884.4 ± 3.1 ± 6.7 MeV.
[2] Assumed no scalar or tensor contributions to the form factor.

M_V (VECTOR POLE MASS FOR $K^{\pm}_{\mu3}$ DECAY)

VALUE (MeV)	EVTS	DOCUMENT ID		TECN	CHG
878.4±8.8±8.3	2.3M	[1] BATLEY	18	NA48	±

[1] Data collected in 2004 by NA48/2. χ^2/NDF = 409.9/382. BATLEY 18 also performed a combined $K^{\pm}_{e3}$ and $K^{\pm}_{\mu3}$ fit assuming $\mu-e$ universality and obtained 884.4 ± 3.1 ± 6.7 MeV.

M_S (SCALAR POLE MASS FOR $K^{\pm}_{\mu3}$ DECAY)

VALUE (MeV)	EVTS	DOCUMENT ID		TECN	CHG
1214.8±23.5±49.2	2.3M	[1] BATLEY	18	NA48	±

[1] Data collected in 2004 by NA48/2. χ^2/NDF = 409.9/382. BATLEY 18 also performed a combined $K^{\pm}_{e3}$ and $K^{\pm}_{\mu3}$ fit assuming $\mu-e$ universality and obtained 1208.3±21.2±47.5 MeV.

Λ_+ (DISPERSIVE VECTOR FORM FACTOR IN $K^{\pm}_{e3}$ DECAY)

See the review on $K^{\pm}_{l3}$ and K^0_{l3} Form Factors for details.

VALUE (units 10^{-2})	EVTS	DOCUMENT ID		TECN	CHG
2.460±0.017 OUR AVERAGE					
2.494±0.021±0.064	4.4M	[1] BATLEY	18	NA48	±
2.458±0.018	5.25M	[2] YUSHCHENKO	18	OKA	+

[1] Data collected in 2004 by NA48/2. χ^2/NDF = 569.0/688. BATLEY 18 also performed a combined $K^{\pm}_{e3}$ and $K^{\pm}_{\mu3}$ fit assuming $\mu-e$ universality and obtained $(24.99 \pm 0.20 \pm 0.62) \times 10^{-3}$.
[2] Assumed no scalar or tensor contributions to the form factor.

Λ_+ (DISPERSIVE VECTOR FORM FACTOR IN $K^{\pm}_{\mu3}$ DECAY)

VALUE (units 10^{-3})	EVTS	DOCUMENT ID		TECN	CHG
25.36±0.58±0.72	2.3M	[1] BATLEY	18	NA48	±

[1] Data collected in 2004 by NA48/2. χ^2/NDF = 410.3/382. BATLEY 18 also performed a combined $K^{\pm}_{e3}$ and $K^{\pm}_{\mu3}$ fit assuming $\mu-e$ universality and obtained $(24.99 \pm 0.20 \pm 0.62) \times 10^{-3}$.

ln(C) (DISPERSIVE SCALAR FORM FACTOR in $K^{\pm}_{\mu3}$ decays)

VALUE (units 10^{-3})	EVTS	DOCUMENT ID		TECN	CHG
182.17±6.31±14.45	2.3M	[1] BATLEY	18	NA48	±

[1] Data collected in 2004 by NA48/2. Combined fit with dispersive vector form factor $\Lambda_+ = 25.36 \pm 0.58 \pm 0.72$. Correlation coefficient is 0.104. χ^2/NDF = 410.3/382. BATLEY 18 also performed a combined $K^{\pm}_{e3}$ and $K^{\pm}_{\mu3}$ fit assuming $\mu-e$ universality and obtained $(183.65 \pm 5.92 \pm 14.25) \times 10^{-3}$.

$|f_S/f_+|$ FOR $K^{\pm}_{e3}$ DECAY

Ratio of scalar to f_+ couplings.

VALUE (units 10^{-2})	CL%	EVTS	DOCUMENT ID		TECN	CHG	COMMENT
$-0.08^{+0.34}_{-0.40}$ OUR AVERAGE							
$0.01^{+0.38}_{-0.46}$		5.25M	YUSHCHENKO	18	OKA	+	$\lambda'_+, \lambda''_+, f_S$ fit
$-0.37^{+0.66}_{-0.56}$±0.41		919k	YUSHCHENKO	04B	ISTR	−	$\lambda'_+, \lambda''_+, f_S$ fit
0.2 ±2.6 ±1.4		41k	SHIMIZU	00	SPEC	+	λ_+, f_S, f_T fit
• • • We do not use the following data for averages, fits, limits, etc. • • •							
$0.2^{+2.0}_{-2.2}$ ±0.3		550k	[1] AJINENKO	03C	ISTR	−	λ_+, f_S, f_T fit
$-1.9^{+2.5}_{-1.6}$		130k	[1] AJINENKO	02	SPEC		λ_+, f_S fit
7.0 ±1.6 ±1.6		32k	AKIMENKO	91	SPEC		$\lambda_+, f_S, f_T, \phi$ fit
0 ± 10		2827	[2] BRAUN	75	HLBC	+	
< 13	90	4017	CHIANG	72	OSPK	+	
14^{+3}_{-4}		2707	[2] STEINER	71	HLBC	+	$\lambda_+, f_S, f_T, \phi$ fit
< 23	90		BOTTERILL	68C	ASPK		
< 18	90		BELLOTTI	67B	HLBC		
< 30	95		KALMUS	67	HLBC	+	

[1] Superseded by YUSHCHENKO 04B.
[2] Statistical errors only.

Int. J. Mod. Phys. A 2026.41. Downloaded from www.worldscientific.com
by UNIVERSITY OF CALIFORNIA @ BERKELEY on 09/16/26. Re-use and distribution is strictly not permitted, except for Open Access articles.

$|f_T/f_+|$ FOR $K^{\pm}_{e3}$ DECAY

Ratio of tensor to f_+ couplings.

VALUE (units 10^{-2})	EVTS	DOCUMENT ID		TECN	CHG	COMMENT
$-1.2^{+1.3}_{-1.1}$ OUR AVERAGE						
$-1.24^{+1.6}_{-1.3}$	5.25M	YUSHCHENKO	18	OKA	+	$\lambda'_+, \lambda''_+, f_T$ fit
$-1.2 \pm 2.1 \pm 1.1$	919k	YUSHCHENKO	04B	ISTR	−	$\lambda'_+, \lambda''_+, f_T$ fit
$1 \pm 14 \pm 9$	41k	SHIMIZU	00	SPEC	+	λ_+, f_S, f_T fit
• • • We do not use the following data for averages, fits, limits, etc. • • •						
$2.1^{+6.4}_{-7.5} \pm 2.6$	550k	[1] AJINENKO	03C	ISTR	−	λ_+, f_S, f_T fit
$-4.5^{+6.0}_{-5.7}$	130k	[1] AJINENKO	02	SPEC		λ_+, f_T fit
$53^{+9}_{-10} \pm 10$	32k	AKIMENKO	91	SPEC		λ_+, f_S, f_T, ϕ fit

[1] Superseded by YUSHCHENKO 04B.

f_S/f_+ FOR $K^{\pm}_{\mu3}$ DECAY

Ratio of scalar to f_+ couplings.

VALUE (units 10^{-2})	EVTS	DOCUMENT ID		TECN	CHG	COMMENT
$0.17 \pm 0.14 \pm 0.54$	540k	[1] YUSHCHENKO	04	ISTR	−	DP
• • • We do not use the following data for averages, fits, limits, etc. • • •						
$0.4 \pm 0.5 \pm 0.5$	112k	[2] AJINENKO	03	ISTR	−	DP

[1] The second error is the theoretical error from the uncertainty in the chiral perturbation theory prediction for λ_0, ± 0.0053, combined in quadrature with the systematic error ± 0.0009.

[2] The second error is the theoretical error from the uncertainty in the chiral perturbation theory prediction for λ_0. Superseded by YUSHCHENKO 04.

f_T/f_+ FOR $K^{\pm}_{\mu3}$ DECAY

Ratio of tensor to f_+ couplings.

VALUE (units 10^{-2})	EVTS	DOCUMENT ID		TECN	CHG	COMMENT
$-0.07 \pm 0.71 \pm 0.20$	540k	YUSHCHENKO	04	ISTR	−	DP
• • • We do not use the following data for averages, fits, limits, etc. • • •						
$-2.1 \pm 2.8 \pm 1.4$	112k	[1] AJINENKO	03	ISTR	−	DP
2 ± 12	1585	BRAUN	75	HLBC		

[1] The second error is the theoretical error from the uncertainty in the chiral perturbation theory prediction for λ_0. Superseded by YUSHCHENKO 04.

$K^{\pm}_{\ell4}$ FORM FACTORS

Based on the parametrizations of AMOROS 99, the $K^{\pm}_{\ell4}$ form factors can be expressed as

$$F_s = f_s + f'_s\, q^2 + f''_s\, q^4 + f'_e\, S_e / 4m_\pi^2$$
$$F_p = f_p$$
$$G_p = g_p + g'_p\, q^2$$
$$H_p = h_p$$

where $q^2 = (S_\pi / 4m_\pi^2) - 1$, S_π is the invariant mass squared of the dipion, and S_e is the invariant mass squared of the dilepton.

f_s FOR $K^{\pm} \to \pi^+\pi^- e^{\pm}\nu$ DECAY

VALUE	EVTS	DOCUMENT ID		TECN	CHG
5.712 ± 0.032 OUR AVERAGE					
$5.705 \pm 0.003 \pm 0.035$	1.1M	[1] BATLEY	12	NA48	±
$5.75 \pm 0.02 \pm 0.08$	400k	[2] PISLAK	03	B865	+

[1] BATLEY 12 uses data collected in 2003–2004. The result is obtained from a measurement of $\Gamma(\pi^+\pi^- e\nu)/\Gamma(\pi^+\pi^-\pi^+)$ and assumed PDG 12 value of $\Gamma(\pi^+\pi^-\pi^+)/\Gamma = (5.59 \pm 0.04) \times 10^{-2}$.

[2] Radiative corrections included. Using Roy equations and not including isospin breaking, PISLAK 03 obtains the following $\pi\pi$ scattering lengths $a_0^0 = 0.228 \pm 0.012 \pm 0.004^{+0.012}_{-0.016}$(theor.) and $a_0^2 = -0.0365 \pm 0.0023 \pm 0.0008^{+0.0031}_{-0.0026}$(theor.).

f'_s/f_s FOR $K^{\pm} \to \pi^+\pi^- e^{\pm}\nu$ DECAY

VALUE (units 10^{-2})	EVTS	DOCUMENT ID		TECN	CHG
$15.2 \pm 0.7 \pm 0.5$	1.13M	[1] BATLEY	10C	NA48	±
• • • We do not use the following data for averages, fits, limits, etc. • • •					
$17.2 \pm 0.9 \pm 0.6$	670k	[2] BATLEY	08A	NA48	±

[1] Radiative corrections included. Using Roy equations and including isospin breaking, BATLEY 10C obtains the following scattering lengths $a_0^0 = 0.2220 \pm 0.0128 \pm 0.0050 \pm 0.0037$ (theor.), $a_0^2 = -0.0432 \pm 0.0086 \pm 0.0034 \pm 0.0028$ (theor.). The correlation with $f''_s/f_s = -0.954$ and with $f'_e/f_s = 0.080$. Supersedes BATLEY 08A.

[2] Radiative corrections included. Using Roy equations and not including isospin breaking, BATLEY 08A obtains the following $\pi\pi$ scattering length $a_0^0 = 0.233 \pm 0.016 \pm 0.007$ $a_0^2 = -0.0471 \pm 0.011 \pm 0.004$.

f''_s/f_s FOR $K^{\pm} \to \pi^+\pi^- e^{\pm}\nu$ DECAY

VALUE (units 10^{-2})	EVTS	DOCUMENT ID		TECN	CHG
$-7.3 \pm 0.7 \pm 0.6$	1.13M	[1] BATLEY	10C	NA48	±
• • • We do not use the following data for averages, fits, limits, etc. • • •					
$-9.0 \pm 0.9 \pm 0.7$	670k	[2] BATLEY	08A	NA48	±

[1] Radiative corrections included. Using Roy equations and including isospin breaking, BATLEY 10C obtains the following scattering lengths $a_0^0 = 0.2220 \pm 0.0128 \pm 0.0050 \pm 0.0037$ (theor.), $a_0^2 = -0.0432 \pm 0.0086 \pm 0.0034 \pm 0.0028$ (theor.). The correlation with $f'_s/f_s = -0.954$ and with $f'_e/f_s = 0.019$. Supersedes BATLEY 08A.

[2] Radiative corrections included. Using Roy equations and not including isospin breaking, BATLEY 08A obtains the following $\pi\pi$ scattering length $a_0^0 = 0.233 \pm 0.016 \pm 0.007$ $a_0^2 = -0.0471 \pm 0.011 \pm 0.004$.

f'_e/f_s FOR $K^{\pm} \to \pi^+\pi^- e^{\pm}\nu$ DECAY

VALUE (units 10^{-2})	EVTS	DOCUMENT ID		TECN	CHG
$6.8 \pm 0.6 \pm 0.7$	1.13M	[1] BATLEY	10C	NA48	±
• • • We do not use the following data for averages, fits, limits, etc. • • •					
$8.1 \pm 0.8 \pm 0.9$	670k	[2] BATLEY	08A	NA48	±

[1] Radiative corrections included. Using Roy equations and including isospin breaking, BATLEY 10C obtains the following scattering lengths $a_0^0 = 0.2220 \pm 0.0128 \pm 0.0050 \pm 0.0037$ (theor.), $a_0^2 = -0.0432 \pm 0.0086 \pm 0.0034 \pm 0.0028$ (theor.). The correlation with $f'_s/f_s = 0.080$ and with $f''_s/f_s = 0.019$. Supersedes BATLEY 08A.

[2] Radiative corrections included. Using Roy equations and not including isospin breaking, BATLEY 08A obtains the following $\pi\pi$ scattering length $a_0^0 = 0.233 \pm 0.016 \pm 0.007$ $a_0^2 = -0.0471 \pm 0.011 \pm 0.004$.

f_p/f_s FOR $K^{\pm} \to \pi^+\pi^- e^{\pm}\nu$ DECAY

VALUE (units 10^{-2})	EVTS	DOCUMENT ID		TECN	CHG
$-4.8 \pm 0.3 \pm 0.4$	1.13M	[1] BATLEY	10C	NA48	±
• • • We do not use the following data for averages, fits, limits, etc. • • •					
$-4.8 \pm 0.4 \pm 0.4$	670k	[2] BATLEY	08A	NA48	±

[1] Radiative corrections included. Using Roy equations and including isospin breaking, BATLEY 10C obtains the following scattering lengths $a_0^0 = 0.2220 \pm 0.0128 \pm 0.0050 \pm 0.0037$ (theor.), $a_0^2 = -0.0432 \pm 0.0086 \pm 0.0034 \pm 0.0028$ (theor.). Supersedes BATLEY 08A.

[2] Radiative corrections included. Using Roy equations and not including isospin breaking, BATLEY 08A obtains the following $\pi\pi$ scattering length $a_0^0 = 0.233 \pm 0.016 \pm 0.007$ $a_0^2 = -0.0471 \pm 0.011 \pm 0.004$.

g_p/f_s FOR $K^{\pm} \to \pi^+\pi^- e^{\pm}\nu$ DECAY

VALUE (units 10^{-2})	EVTS	DOCUMENT ID		TECN	CHG
$86.8 \pm 1.0 \pm 1.0$	1.13M	[1] BATLEY	10C	NA48	±
• • • We do not use the following data for averages, fits, limits, etc. • • •					
$87.3 \pm 1.3 \pm 1.2$	670k	[2] BATLEY	08A	NA48	±
$80.9 \pm 0.9 \pm 1.2$	400k	[3] PISLAK	03	B865	±

[1] Radiative corrections included. Using Roy equations and including isospin breaking, BATLEY 10C obtains the following scattering lengths $a_0^0 = 0.2220 \pm 0.0128 \pm 0.0050 \pm 0.0037$ (theor.), $a_0^2 = -0.0432 \pm 0.0086 \pm 0.0034 \pm 0.0028$ (theor.). Supersedes BATLEY 08A. The correlation with $g'_p/f_s = -0.914$. Supersedes BATLEY 08A.

[2] Radiative corrections included. Using Roy equations and not including isospin breaking, BATLEY 08A obtains the following $\pi\pi$ scattering length $a_0^0 = 0.233 \pm 0.016 \pm 0.007$ $a_0^2 = -0.0471 \pm 0.011 \pm 0.004$.

[3] Radiative corrections included. Using Roy equations PISLAK 03 obtains the following scattering lengths $a_0^0 = 0.203 \pm 0.033 \pm 0.004$, $a_0^2 = -0.055 \pm 0.023 \pm 0.003$.

g'_p/f_s FOR $K^{\pm} \to \pi^+\pi^- e^{\pm}\nu$ DECAY

VALUE (units 10^{-2})	EVTS	DOCUMENT ID		TECN	CHG
$8.9 \pm 1.7 \pm 1.3$	1.13M	[1] BATLEY	10C	NA48	±
• • • We do not use the following data for averages, fits, limits, etc. • • •					
$8.1 \pm 2.2 \pm 1.5$	670k	[2] BATLEY	08A	NA48	±
$12.0 \pm 1.9 \pm 0.7$	400k	[3] PISLAK	03	B865	±

[1] Radiative corrections included. Using Roy equations and including isospin breaking, BATLEY 10C obtains the following scattering lengths $a_0^0 = 0.2220 \pm 0.0128 \pm 0.0050 \pm 0.0037$ (theor.), $a_0^2 = -0.0432 \pm 0.0086 \pm 0.0034 \pm 0.0028$ (theor.). The correlation with $g_p/f_s = -0.914$. Supersedes BATLEY 08A.

[2] Radiative corrections included. Using Roy equations and not including isospin breaking, BATLEY 08A obtains the following $\pi\pi$ scattering length $a_0^0 = 0.233 \pm 0.016 \pm 0.007$ $a_0^2 = -0.0471 \pm 0.011 \pm 0.004$.

[3] Radiative corrections included. Using Roy equations PISLAK 03 obtains the following scattering lengths $a_0^0 = 0.203 \pm 0.033 \pm 0.004$, $a_0^2 = -0.055 \pm 0.023 \pm 0.003$.

h_p/f_s FOR $K^{\pm} \to \pi^+\pi^- e^{\pm}\nu$ DECAY

VALUE (units 10^{-2})	EVTS	DOCUMENT ID		TECN	CHG
$-39.8 \pm 1.5 \pm 0.8$	1.13M	[1] BATLEY	10C	NA48	±
• • • We do not use the following data for averages, fits, limits, etc. • • •					
$-41.1 \pm 1.9 \pm 0.8$	670k	[2] BATLEY	08A	NA48	±
$-51.3 \pm 3.3 \pm 3.5$	400k	[3] PISLAK	03	B865	±

[1] Radiative corrections included. Using Roy equations and including isospin breaking, BATLEY 10C obtains the following scattering lengths $a_0^0 = 0.2220 \pm 0.0128 \pm 0.0050 \pm 0.0037$ (theor.), $a_0^2 = -0.0432 \pm 0.0086 \pm 0.0034 \pm 0.0028$ (theor.). Supersedes BATLEY 08A.

[2] Radiative corrections included. Using Roy equations and not including isospin breaking, BATLEY 08A obtains the following $\pi\pi$ scattering length $a_0^0 = 0.233 \pm 0.016 \pm 0.007$ $a_0^2 = -0.0471 \pm 0.011 \pm 0.004$.

[3] Radiative corrections included. Using Roy equations PISLAK 03 obtains the following scattering lengths $a_0^0 = 0.203 \pm 0.033 \pm 0.004$, $a_0^2 = -0.055 \pm 0.023 \pm 0.003$.

DECAY FORM FACTOR FOR $K^{\pm} \to \pi^0\pi^0 e^{\pm}\nu$

Given in BOLOTOV 86B, BARMIN 88B, and SHIMIZU 04.

$K^{\pm} \to \ell^{\pm}\nu\gamma$ FORM FACTORS

For definitions of the axial-vector F_A and vector F_V form factor, see the "Note on $\pi^{\pm} \to \ell^{\pm}\nu\gamma$ and $K^{\pm} \to \ell^{\pm}\nu\gamma$ Form Factors" in the $\pi^{\pm}$ section. In the kaon literature, often different definitions $a_K = F_A/m_K$ and $v_K = F_V/m_K$ are used.

$F_A + F_V$, SUM OF AXIAL-VECTOR AND VECTOR FORM FACTOR FOR $K \to e\nu_e\gamma$

VALUE	EVTS	DOCUMENT ID		TECN	COMMENT
0.133±0.008 OUR AVERAGE		Error includes scale factor of 1.3.			See the ideogram below.
0.125±0.007±0.001	1.4k	[1] AMBROSINO	09E	KLOE	E_γ in 10–250 MeV, $p_e > 200$ MeV/c
0.147±0.011	51	[2] HEINTZE	79	SPEC	
$0.150^{+0.018}_{-0.023}$	56	[3] HEARD	75	SPEC	

[1] AMBROSINO 09E measures the absolute value $|F_A + F_V|$ which is parametrized as $|F_A + F_V| = F_V\ (1 + \lambda(1-x)) + F_A$, $x = 2E_\gamma/m_K$. $(F_A + F_V)$ and λ are fit parameters. The fitted value of $\lambda = 0.38 \pm 0.20 \pm 0.02$ with a correlation of -0.93 between $(F_A + F_V)$ and λ.

[2] HEINTZE 79 quotes absolute value of $|F_A + F_V| \sin\theta_C$. We use $\sin\theta_C = V_{us} = 0.2205$.

[3] HEARD 75 quotes absolute value of $|F_A + F_V| \sin\theta_C$. We use $\sin\theta_C = V_{us} = 0.2205$.

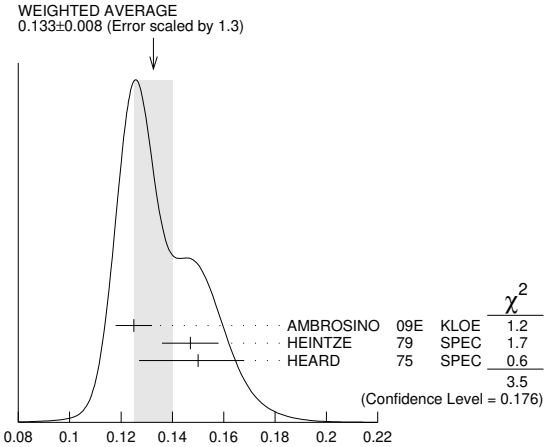

$F_A + F_V$, SUM OF AXIAL-VECTOR AND VECTOR FORM FACTOR FOR $K \to e\nu_e\gamma$

$F_A + F_V$, SUM OF AXIAL-VECTOR AND VECTOR FORM FACTOR FOR $K \to \mu\nu_\mu\gamma$

VALUE	CL%	EVTS	DOCUMENT ID		TECN	CHG
0.165±0.007±0.011		2588	[1] ADLER	00B	B787	+
• • • We do not use the following data for averages, fits, limits, etc. • • •						
−1.2 to 1.1	90		DEMIDOV	90	XEBC	
< 0.23	90		[1] AKIBA	85	SPEC	

[1] Quotes absolute value. Sign not determined.

$F_A - F_V$, DIFFERENCE OF AXIAL-VECTOR AND VECTOR FORM FACTOR FOR $K \to e\nu_e\gamma$

VALUE	CL%	DOCUMENT ID		TECN
<0.49	90	[1] HEINTZE	79	SPEC

[1] HEINTZE 79 quotes $|F_A - F_V| < \sqrt{11}\,|F_A + F_V|$.

$F_A - F_V$, DIFFERENCE OF AXIAL-VECTOR AND VECTOR FORM FACTOR FOR $K \to \mu\nu_\mu\gamma$

VALUE	CL%	EVTS	DOCUMENT ID		TECN	CHG
−0.153±0.033 OUR AVERAGE		Error includes scale factor of 1.1.				
−0.134±0.021±0.027		95k	KRAVTSOV	19	OKA	+
−0.21 ±0.06		22k	DUK	11	ISTR	−
• • • We do not use the following data for averages, fits, limits, etc. • • •						
−0.24 to 0.04	90	2588	ADLER	00B	B787	+
−2.2 to 0.6	90		DEMIDOV	90	XEBC	
−2.5 to 0.3	90		AKIBA	85	SPEC	

$K^{\pm}$ CHARGE RADIUS

VALUE (fm)	DOCUMENT ID		COMMENT
0.560±0.031 OUR AVERAGE			
0.580±0.040	AMENDOLIA	86B	$Ke \to Ke$
0.530±0.050	DALLY	80	$Ke \to Ke$
• • • We do not use the following data for averages, fits, limits, etc. • • •			
0.620±0.037	BLATNIK	79	VMD + dispersion relations

K^+ LONGITUDINAL POLARIZATION OF EMITTED μ^+

VALUE	CL%	DOCUMENT ID		TECN	CHG	COMMENT
<−0.990	90	[1] AOKI	94	SPEC	+	
• • • We do not use the following data for averages, fits, limits, etc. • • •						
<−0.990	90	IMAZATO	92	SPEC	+	Repl. by AOKI 94
−0.970±0.047		[2] YAMANAKA	86	SPEC	+	
−1.0 ±0.1		[2] CUTTS	69	SPRK	+	
−0.96 ±0.12		[2] COOMBES	57	CNTR	+	

[1] AOKI 94 measures $\xi P_\mu = -0.9996 \pm 0.0030 \pm 0.0048$. The above limit is obtained by summing the statistical and systematic errors in quadrature, normalizing to the physically significant region ($|\xi P_\mu| < 1$) and assuming that ξ=1, its maximum value.

[2] Assumes ξ=1.

FORWARD-BACKWARD ASYMMETRY IN $K^{\pm}$ DECAYS

$$A_{FB}(K^{\pm}_{\pi\mu\mu}) = \frac{\Gamma(\cos(\theta_{K\mu})>0) - \Gamma(\cos(\theta_{K\mu})<0)}{\Gamma(\cos(\theta_{K\mu})>0) + \Gamma(\cos(\theta_{K\mu})<0)}$$

VALUE	CL%	DOCUMENT ID		TECN	COMMENT
$<0.9 \times 10^{-2}$	90	[1] CORTINA-GIL	22A	NA62	2017–18 data
• • • We do not use the following data for averages, fits, limits, etc. • • •					
$<2.3 \times 10^{-2}$	90	[2] BATLEY	11A	NA48	

[1] CORTINA-GIL 22A measured the asymmetry $A_{FB} = (0.0 \pm 0.7) \times 10^{-2}$. The quoted 90% C.L. was obtained via private communication and also presented at the Moriond 2023 conference. The authors will publish this limit in an addendum to the publication.

[2] BATLEY 11A gives a corresponding value of the asymmetry $A_{FB} = (-2.4 \pm 1.8) \times 10^{-2}$.

$K^{\pm}$ REFERENCES

CORTINA-GIL 25 JHEP 2502 191 E. Cortina Gil et al. (NA62 Collab.)
ARTAMONOV 24 EPJ C84 345 A.V. Artamonov et al. (OKA Collab.)
ARTAMONOV 24A JETPL 120 554 A.V. Artamonov et al. (OKA Collab.)
ASHRAF 24 PL B859 139122 M.U. Ashraf et al. (NA62 Collab.)
BATLEY 24 JHEP 2403 137 J.R. Batley et al. (NA48/2 Collab.)
CORTINA-GIL 24 PL B850 138513 E. Cortina Gil et al. (NA62 Collab.)
CORTINA-GIL 23 PL B838 137679 E. Cortina Gil et al. (NA62 Collab.)
CORTINA-GIL 23B PL B846 138193 E. Cortina-Gil et al. (NA62 Collab.)
CORTINA-GIL 23D JHEP 2309 040 E. Cortina Gil et al. (NA62 Collab.)
KOBAYASHI 23 PL B843 138020 A. Kobayashi et al. (J-PARC E36 Collab.)
CORTINA-GIL 22 PL B830 137172 E. Cortina Gil et al. (NA62 Collab.)
CORTINA-GIL 22A JHEP 2211 011 E. Cortina Gil et al. (NA62 Collab.)
ITO 22 PL B826 136913 H. Ito et al. (J-PARC E36 Collab.)
ALIBERTI 21 PRL 127 131802 R. Aliberti et al. (NA62 Collab.)
CORTINA-GIL 21 PL B816 136259 E. Cortina Gil et al. (NA62 Collab.)
CORTINA-GIL 21B JHEP 2106 093 E. Cortina Gil et al. (NA62 Collab.)
POLYARUSH 21 EPJ C81 161 A.Yu. Polyarush et al. (OKA Collab.)
CORTINA-GIL 20C JHEP 2011 042 E. Cortina Gil et al. (NA62 Collab.)
BATLEY 19 PL B788 552 J.R. Batley et al. (NA48/2 Collab.)
CORTINA-GIL 19A PL B797 134794 E. Cortina Gil et al. (NA62 Collab.)
CORTINA-GIL 19B PL B791 156 E. Cortina Gil et al. (NA62 Collab.)
KRAVTSOV 19 EPJ C79 635 V.I. Kravtsov et al. (OKA Collab.)
SHAPKIN 19 EPJ C79 296 M.M. Shapkin et al. (OKA Collab.)
BATLEY 18 JHEP 1810 150 J.R. Batley et al. (NA48/2 Collab.)
PDG 18 PR D98 030001 M. Tanabashi et al. (PDG Collab.)
YUSHCHENKO 18 JETPL 107 139 O.P. Yushchenko et al. (OKA Collab.)
BATLEY 17 PL B769 67 J.R. Batley et al. (NA48/2 Collab.)
ARTAMONOV 16 PR D94 032012 A.V. Artamonov et al. (BNL E949 Collab.)
BABUSCI 14B PL B738 128 D. Babusci et al. (KLOE and KLOE-2 Collab.)
BATLEY 14 PL B730 141 J.R. Batley et al. (CERN NA48/2 Collab.)
BATLEY 14A JHEP 1408 159 J.R. Batley et al. (CERN NA48/2 Collab.)
LAZZERONI 14 PL B732 65 C. Lazzeroni et al. (CERN NA62 Collab.)
UVAROV 14 PAN 77 725 V.A. Uvarov et al. (ISTRA+ Collab.)
Translated from YAF 77 765.
LAZZERONI 13 PL B719 326 C. Lazzeroni et al. (CERN NA62 Collab.)
BATLEY 12 PL B715 105 J.R. Batley et al. (CERN NA48/2 Collab.)
PDG 12 PR D86 010001 J. Beringer et al. (PDG Collab.)
BATLEY 11A PL B697 107 J.R. Batley et al. (CERN NA48/2 Collab.)
DUK 11 PL B695 59 V.A. Duk et al. (ISTRA+ Collab.)
LAZZERONI 11 PL B698 105 C. Lazzeroni et al. (CERN NA62 Collab.)
ADLER 10 PR D81 092001 S. Adler et al. (BNL E787 Collab.)
BATLEY 10A EPJ C68 75 J.R. Batley et al. (CERN NA48/2 Collab.)
BATLEY 10C EPJ C70 635 J.R. Batley et al. (CERN NA48/2 Collab.)
PDG 10 JP G37 075021 K. Nakamura et al. (PDG Collab.)
PISLAK 10A PRL 105 019901E S. Pislak et al. (BNL E865 Collab.)
AKOPDZANOV 09 PAN 71 2074 G.A. Akopdzanov et al. (IHEP)
Translated from YAF 71 2108.
AMBROSINO 09E EPJ C64 627 F. Ambrosino et al. (KLOE Collab.)
Also EPJ C65 703 (errat.) F. Ambrosino et al. (KLOE Collab.)
BATLEY 09 PL B677 246 J.R. Batley et al. (CERN NA48/2 Collab.)
BATLEY 09A EPJ C64 589 J.R. Batley et al. (CERN NA48/2 Collab.)
BISSEGGER 09 NP B806 178 M. Bissegger et al.
AMBROSINO 08 JHEP 0801 073 F. Ambrosino et al. (KLOE Collab.)
AMBROSINO 08A JHEP 0802 098 F. Ambrosino et al. (KLOE Collab.)
AMBROSINO 08E PL B666 305 F. Ambrosino et al. (KLOE Collab.)
ARTAMONOV 08 PRL 101 191802 A.V. Artamonov et al. (BNL E949 Collab.)
Also PR D79 092004 A.V. Artamonov et al. (BNL E949 Collab.)
BATLEY 08 PL B659 493 J.R. Batley et al. (CERN NA48/2 Collab.)
BATLEY 08A EPJ C54 411 J.R. Batley et al. (CERN NA48/2 Collab.)
AKIMENKO 07 PAN 70 702 S.A. Akimenko et al. (ISTRA+ Collab.)
Translated from YAF 70 734.
ANDRE 07 ANP 322 2518 T. Andre (EFI)
BATLEY 07A EPJ C50 329 J.R. Batley et al. (CERN NA48/2 Collab.)
Also EPJ C52 1021 (errat.) J.R. Batley et al. (CERN NA48/2 Collab.)
BATLEY 07B PL B649 349 J.R. Batley et al. (CERN NA48/2 Collab.)
BATLEY 07E EPJ C52 875 J.R. Batley et al. (CERN NA48/2 Collab.)

Int. J. Mod. Phys. A 2026.41. Downloaded from www.worldscientific.com by LIFORNIA @ BERKELEY on 09/16/26. Re-use and distribution is strictly not permitted, except for Open Access articles.

Int. J. Mod. Phys. A 2026.41. Downloaded from www.worldscientific.com
by UNIVERSITY OF CALIFORNIA @ BERKELEY on 09/16/26. Re-use and distribution is strictly not permitted, except for Open Access articles.

LAI 07A PL B647 341 A. Lai *et al.* (CERN NA48 Collab.)
TCHIKILEV 07 PAN 70 29 O.G. Tchikilev *et al.* (ISTRA+ Collab.)
ALIEV 06 EPJ C46 61 M.A. Aliev *et al.* (KEK E470 Collab.)
AMBROSINO 06A PL B632 76 F. Ambrosino *et al.* (KLOE Collab.)
BATLEY 06 PL B634 474 J.R. Batley *et al.* (CERN NA48/2 Collab.)
BATLEY 06A PL B638 22 J.R. Batley *et al.* (CERN NA48/2 Collab.)
Also PL B640 297 (errat.) J.R. Batley *et al.* (CERN NA48/2 Collab.)
BATLEY 06B PL B633 173 J.R. Batley *et al.* (CERN NA48/2 Collab.)
COLANGELO 06A PL B638 187 G. Colangelo *et al.*
MA 06 PR D73 037101 H. Ma *et al.* (BNL E865 Collab.)
PDG 06 JP G33 1 W.-M. Yao *et al.* (PDG Collab.)
SHIMIZU 06 PL B633 190 S. Shimizu *et al.* (KEK E470 Collab.)
UVAROV 06 PAN 69 26 V.A. Uvarov *et al.* (ISTRA+ Collab.)
AKOPDZHAN... 05 EPJ C40 343 G.A. Akopdzhanov *et al.* (IHEP)
Also PAN 68 948 G.A. Akopdzhanov *et al.* (IHEP)
Translated from YAF 68 986.
AKOPDZHAN... 05B JETPL 82 675 G.A. Akopdzhanov *et al.* (IHEP)
Translated from ZETFP 82 771.
ARTAMONOV 05 PL B623 192 A.V. Artamonov *et al.* (BNL E949 Collab.)
CABIBBO 05 JHEP 0503 021 N. Cabibbo, G. Isidori (CERN, ROMAI, FRAS)
SHER 05 PR D72 012005 A. Sher *et al.* (BNL E865 Collab.)
ABE 04F PRL 93 131601 M. Abe *et al.* (KEK E246 Collab.)
Also PR D73 072005 M. Abe *et al.* (KEK E246 Collab.)
ADLER 04 PR D70 037102 S. Adler *et al.* (BNL E787 Collab.)
ALOISIO 04A PL B597 139 A. Aloisio *et al.* (KLOE Collab.)
ANISIMOVSK... 04 PRL 93 031801 V.V. Anisimovsky *et al.* (BNL E949 Collab.)
Also PR D77 052003 S. Adler *et al.* (BNL E949 Collab.)
CABIBBO 04A PRL 93 121801 N. Cabibbo (CERN, ROMAI)
CIRIGLIANO 04 EPJ C35 53 V. Cirigliano, H. Neufeld, H. Pichl (CIT, VALE+)
PDG 04 PL B592 1 S. Eidelman *et al.* (PDG Collab.)
SHIMIZU 04 PR D70 037101 S. Shimizu *et al.* (KEK E470 Collab.)
YUSHCHENKO 04 PL B581 31 O.P. Yushchenko *et al.* (INRM, INRM)
YUSHCHENKO 04B PL B589 111 O.P. Yushchenko *et al.* (INRM)
AJINENKO 03 PAN 66 105 I.V. Ajinenko *et al.* (IHEP, INRM)
Translated from YAF 66 107.
AJINENKO 03B PL B567 159 I.V. Ajinenko *et al.* (IHEP, INRM)
AJINENKO 03C PL B574 14 I.V. Ajinenko *et al.* (IHEP, INRM)
ALIEV 03 PL B554 7 M.A. Aliev *et al.* (KEK E470 Collab.)
ANISIMOVSK... 03 PL B562 166 V.V. Anisimovsky *et al.*
PISLAK 03 PR D67 072004 S. Pislak *et al.* (BNL E865 Collab.)
Also PR D81 119903E S. Pislak *et al.* (BNL E865 Collab.)
SHER 03 PRL 91 261802 A. Sher *et al.* (BNL E865 Collab.)
ADLER 02 PRL 88 041803 S. Adler *et al.* (BNL E787 Collab.)
ADLER 02B PR D65 052009 S. Adler *et al.* (BNL E787 Collab.)
ADLER 02C PL B537 211 S. Adler *et al.* (BNL E787 Collab.)
AJINENKO 02 PAN 65 2064 I.V. Ajinenko *et al.* (IHEP, INRM)
Translated from YAF 65 2125.
CIRIGLIANO 02 EPJ C23 121 V. Cirigliano *et al.* (VIEN, VALE, MARS)
PARK 02 PRL 88 111801 H.K. Park *et al.* (FNAL HyperCP Collab.)
PDG 02 PR D66 010001 K. Hagiwara *et al.* (PDG Collab.)
POBLAGUEV 02 PRL 89 061803 A.A. Poblaguev *et al.* (BNL 865 Collab.)
ADLER 01 PR D63 032004 S. Adler *et al.* (BNL E787 Collab.)
HORIE 01 PL B513 311 K. Horie *et al.* (KEK E426 Collab.)
PISLAK 01 PRL 87 221801 S. Pislak *et al.* (BNL E865 Collab.)
Also PR D67 072004 S. Pislak *et al.* (BNL E865 Collab.)
Also PRL 105 019901E S. Pislak *et al.* (BNL E865 Collab.)
ADLER 00 PRL 84 3768 S. Adler *et al.* (BNL E787 Collab.)
ADLER 00B PRL 85 2256 S. Adler *et al.* (BNL E787 Collab.)
ADLER 00C PRL 85 4856 S. Adler *et al.* (BNL E787 Collab.)
APPEL 00 PRL 85 2450 R. Appel *et al.* (BNL 865 Collab.)
Also Thesis, Yale Univ. D.R. Bergman
Also Thesis, Univ. Zurich S. Pislak
APPEL 00B PRL 85 2877 R. Appel *et al.* (BNL 865 Collab.)
MA 00 PRL 84 2580 H. Ma *et al.* (BNL 865 Collab.)
PDG 00 EPJ C15 1 D.E. Groom *et al.* (PDG Collab.)
SHIMIZU 00 PL B495 33 S. Shimizu *et al.* (KEK E246 Collab.)
ABE 99S PRL 83 4253 M. Abe *et al.* (KEK E246 Collab.)
AMOROS 99 JP G25 1607 G. Amoros, J. Bijnens (LUND, HELS)
APPEL 99 PRL 83 4482 R. Appel *et al.* (BNL 865 Collab.)
ADLER 98 PR D58 012003 S. Adler *et al.* (BNL E787 Collab.)
BATUSOV 98 NP B516 3 V.Y. Batusov *et al.*
DAMBROSIO 98A JHEP 9808 004 G. D'Ambrosio *et al.*
ADLER 97 PRL 79 2204 S. Adler *et al.* (BNL E787 Collab.)
ADLER 97C PRL 79 4756 S. Adler *et al.* (BNL E787 Collab.)
BERGMAN 97 Thesis, Yale Univ. D.R. Bergman
KITCHING 97 PRL 79 4079 P. Kitching *et al.* (BNL E787 Collab.)
PISLAK 97 Thesis, Univ. Zurich S. Pislak
ADLER 96 PRL 76 1421 S. Adler *et al.* (BNL E787 Collab.)
KOPTEV 95 JETPL 61 877 V.P. Koptev *et al.* (PNPI)
Translated from ZETFP 61 865.
AOKI 94 PR D50 69 M. Aoki *et al.* (INUS, KEK, TOKMS)
ATIYA 93 PRL 70 2521 M.S. Atiya *et al.* (BNL E787 Collab.)
Also PRL 71 305 (errat.) M.S. Atiya *et al.* (BNL E787 Collab.)
ATIYA 93B PR D48 1 M.S. Atiya *et al.* (BNL E787 Collab.)
ALLIEGRO 92 PRL 68 278 C. Alliegro *et al.* (BNL, FNAL, PSI+)
BARMIN 92 SJNP 55 547 V.V. Barmin *et al.* (ITEP)
Translated from YAF 55 976.
IMAZATO 92 PRL 69 877 J. Imazato *et al.* (KEK, INUS, TOKY+)
IVANOV 92 THESIS Yu.M. Ivanov (PNPI)
LITTENBERG 92 PRL 68 443 L.S. Littenberg, R.E. Shrock (BNL, STON)
USHER 92 PR D45 3961 T. Usher *et al.* (UCI)
AKIMENKO 91 PL B259 225 S.A. Akimenko *et al.* (SERP, JINR, TBIL+)
BARMIN 91 SJNP 53 606 V.V. Barmin *et al.* (ITEP)
Translated from YAF 53 981.
DENISOV 91 JETPL 54 558 A.S. Denisov *et al.* (PNPI)
Translated from ZETFP 54 557.
Also THESIS Yu.M. Ivanov (PNPI)
ATIYA 90 PRL 64 21 M.S. Atiya *et al.* (BNL E787 Collab.)
ATIYA 90B PRL 65 1188 M.S. Atiya *et al.* (BNL E787 Collab.)
DEMIDOV 90 SJNP 52 1006 V.S. Demidov *et al.* (ITEP)
Translated from YAF 52 1595.
LEE 90 PRL 64 165 A.M. Lee *et al.* (BNL, FNAL, VILL, WASH+)
ATIYA 89 PRL 63 2177 M.S. Atiya *et al.* (BNL E787 Collab.)
BARMIN 89 SJNP 50 421 V.V. Barmin *et al.* (ITEP)
Translated from YAF 50 679.
BARMIN 88 SJNP 47 643 V.V. Barmin *et al.* (ITEP)
Translated from YAF 47 1011.
BARMIN 88B SJNP 48 1032 V.V. Barmin *et al.* (ITEP)
Translated from YAF 48 1719.
BOLOTOV 88 JETPL 47 7 V.N. Bolotov *et al.* (ASCI)
Translated from ZETFP 47 8.
GALL 88 PRL 60 186 K.P. Gall *et al.* (BOST, MIT, WILL, CIT+)
BARMIN 87 SJNP 45 62 V.V. Barmin *et al.* (ITEP)
Translated from YAF 45 97.
BOLOTOV 87 SJNP 45 1023 V.N. Bolotov *et al.* (INRM)
Translated from YAF 45 1652.
AMENDOLIA 86B PL B178 435 S.R. Amendolia *et al.* (CERN NA7 Collab.)
BOLOTOV 86 SJNP 44 73 V.N. Bolotov *et al.* (INRM)
Translated from YAF 44 117.
BOLOTOV 86B SJNP 44 68 V.N. Bolotov *et al.* (INRM)
Translated from YAF 44 108.
YAMANAKA 86 PR D34 85 T. Yamanaka *et al.* (KEK, TOKY)
Also PRL 52 329 R.S. Hayano *et al.* (TOKY, KEK)
AKIBA 85 PR D32 2911 Y. Akiba *et al.* (TOKY, TINT, TSUK, KEK)
BOLOTOV 85 JETPL 42 481 V.N. Bolotov *et al.* (INRM)
Translated from ZETFP 42 390.
ASANO 82 PL 113B 195 Y. Asano *et al.* (KEK, TOKY, INUS, OSAK)
COOPER 82 PL 112B 97 A.M. Cooper *et al.* (RL)
PDG 82B PL 111B 70 M. Roos *et al.* (HELS, CIT, CERN)
ASANO 81B PL 107B 159 Y. Asano *et al.* (KEK, TOKY, INUS, OSAK)
CAMPBELL 81 PRL 47 1032 M.K. Campbell *et al.* (YALE, BNL)
Also PR D27 1056 S.R. Blatt *et al.* (YALE, BNL)
LUM 81 PR D23 2522 G.K. Lum *et al.* (LBL, NBS+)
LYONS 81 ZPHY C10 215 L. Lyons, C. Albajar, G. Myatt (OXF)
DALLY 80 PRL 45 232 E.B. Dally *et al.* (UCLA+)
BARKOV 79 NP B148 53 L.M. Barkov *et al.* (NOVO, KIAE)
BLATNIK 79 LNC 24 39 S. Blatnik, J. Stahov, C.B. Lang (TUZL, GRAZ)
HEINTZE 79 NP B149 365 J. Heintze *et al.* (HEIDP, CERN)
ABRAMS 77 PR D15 22 R.J. Abrams *et al.* (BNL)
DEVAUX 77 NP B126 11 B. Devaux *et al.* (SACL, GEVA)
HEINTZE 77 PL 70B 482 J. Heintze *et al.* (HEIDP, CERN)
ROSSELET 77 PR D15 574 L. Rosselet *et al.* (GEVA, SACL)
BLOCH 76 PL 60B 393 P. Bloch *et al.* (GEVA, SACL)
BRAUN 76B LNC 17 521 H.M. Braun *et al.* (AACH3, BARI, BELG+)
DIAMANT-... 76 PL 62B 485 A.M. Diamant-Berger *et al.* (SACL, GEVA)
HEINTZE 76 PL 60B 302 J. Heintze *et al.* (HEIDP)
SMITH 76 NP B109 173 K.M. Smith *et al.* (GLAS, LIVP, OXF+)
WEISSENBE... 76 NP B115 55 A.O. Weissenberg *et al.* (ITEP, LEBD)
BLOCH 75 PL 56B 201 P. Bloch *et al.* (SACL, GEVA)
BRAUN 75 NP B89 210 H.M. Braun *et al.* (AACH3, BARI, BRUX+)
CHENG 75 NP A254 381 S.C. Cheng *et al.* (COLU, YALE)
HEARD 75 PL 55B 324 K.S. Heard *et al.* (CERN, HEIDH)
HEARD 75B PL 55B 327 K.S. Heard *et al.* (CERN, HEIDH)
SHEAFF 75 PR D12 2570 M. Sheaff (WISC)
SMITH 75 NP B91 45 K.M. Smith *et al.* (GLAS, LIVP, OXF+)
WEISSENBE... 74 PL 48B 474 A.O. Weissenberg *et al.* (ITEP, LEBD)
ABRAMS 73B PRL 30 500 R.J. Abrams *et al.* (BNL)
BACKENSTO... 73 PL 43B 431 G. Backenstoss *et al.* (CERN, KARLK, KARLE+)
LJUNG 73 PR D8 1307 D. Ljung, D. Cline (WISC)
Also PRL 28 523 D. Ljung (WISC)
Also PRL 28 1287 D. Cline, D. Ljung (WISC)
Also PRL 23 326 U. Camerini *et al.* (WISC)
LUCAS 73 PR D8 719 P.W. Lucas, H.D. Taft, W.J. Willis (YALE)
LUCAS 73B PR D8 727 P.W. Lucas, H.D. Taft, W.J. Willis (YALE)
PANG 73 PR D8 1989 C.Y. Pang *et al.* (EFI, ARIZ, LBL)
Also PL 40B 699 G.D. Cable *et al.* (EFI, LBL)
SMITH 73 NP B60 411 K.M. Smith *et al.* (GLAS, LIVP, OXF+)
ABRAMS 72 PRL 29 1118 R.J. Abrams *et al.* (BNL)
AUBERT 72 NC 12A 509 B. Aubert *et al.* (ORSAY, BRUX, EPOL)
CHIANG 72 PR D6 1254 I.H. Chiang *et al.* (ROCH, WISC)
CLARK 72 PRL 29 1274 A.R. Clark *et al.* (LBL)
FORD 72 PL 38B 335 W.T. Ford *et al.* (PRIN)
HOFFMASTER 72 NP B36 1 S. Hoffmaster *et al.* (STEV, SETO, LEHI)
BOURQUIN 71 PL 36B 615 M.H. Bourquin *et al.* (GEVA, SACL)
HAIDT 71 PR D3 10 D. Haidt (AACH, BARI, CERN, EPOL, NIJM+)
Also PL 29B 691 D. Haidt *et al.* (AACH, BARI, CERN, EPOL+)
KLEMS 71 PR D4 66 J.H. Klems, R.H. Hildebrand, R. Stiening (CHIC+)
Also PRL 24 1086 J.H. Klems, R.H. Hildebrand, R. Stiening (LRL+)
Also PRL 25 473 J.H. Klems, R.H. Hildebrand, R. Stiening (LRL+)
OTT 71 PR D3 52 R.J. Ott, T.W. Pritchard (LOQM)
ROMANO 71 PL 36B 525 F. Romano *et al.* (BARI, CERN, ORSAY)
SCHWEINB... 71 PL 36B 246 W. Schweinberger (AACH, BELG, CERN, NIJM+)
STEINER 71 PL 36B 521 H.J. Steiner (AACH, BARI, CERN, EPOL, ORSAY+)
BARDIN 70 PL 32B 121 D.Y. Bardin, S.N. Bilenky, B.M. Pontecorvo (JINR)
BECHERRAWY 70 PR D1 1452 T. Becherrawy (ROCH)
FORD 70 PRL 25 1370 W.T. Ford *et al.* (PRIN)
GAILLARD 70 CERN 70-14 J.M. Gaillard, L.M. Chounet (CERN, ORSAY)
GRAUMAN 70 PR D1 1277 J. Grauman *et al.* (STEV, SETO, LEHI)
Also PRL 23 737 J.U. Grauman *et al.* (STEV, SETO, LEHI)
PANDOULAS 70 PR D2 1205 D. Pandoulas *et al.* (STEV, SETO)
CUTTS 69 PR 184 1380 D. Cutts *et al.* (LRL, MIT)
Also PRL 20 955 D. Cutts *et al.* (LRL, MIT)
DAVISON 69 PR 180 1333 D.C. Davison *et al.* (UCR)
ELY 69 PR 180 1319 R.P.J. Ely *et al.* (LOUC, WISC, LRL)
HERZO 69 PR 186 1403 D. Herzo *et al.* (ILL)
LOBKOWICZ 69 PR 185 1676 F. Lobkowicz *et al.* (ROCH, BNL)
Also PRL 17 548 F. Lobkowicz *et al.* (ROCH, BNL)
MAST 69 PR 183 1200 T.S. Mast *et al.* (LRL)
SELLERI 69 NC 60A 291 F. Selleri
ZELLER 69 PR 182 1420 M.E. Zeller *et al.* (UCLA, LRL)
BOTTERILL 68B PRL 21 766 D.R. Botterill *et al.* (OXF)
BOTTERILL 68C PR 174 1661 D.R. Botterill *et al.* (OXF)
BUTLER 68 UCRL 18420 W.D. Butler *et al.* (LRL)
CHANG 68 PRL 20 510 C.Y. Chang *et al.* (UMD, RUTG)
CHEN 68 PRL 20 73 M. Chen *et al.* (LRL, MIT)
EICHTEN 68 PL 27B 586 T. Eichten (AACH, BARI, CERN, EPOL, ORSAY+)
ESCHSTRUTH 68 PR 165 1487 P.T. Eschstruth *et al.* (PRIN, PENN)
GARLAND 68 PR 167 1225 R. Garland *et al.* (COLU, RUTG, WISC)
MOSCOSO 68 Thesis L. Moscoso (ORSAY)
AUERBACH 67 PR 155 1505 L.B. Auerbach *et al.* (PENN, PRIN)
Also PR D9 3216 L.B. Auerbach
Erratum.
BELLOTTI 67 Heidelberg Conf. E. Bellotti, A. Pullia (MILA)
BELLOTTI 67B NC 52A 1287 E. Bellotti, E. Fiorini, A. Pullia (MILA)
Also PL 20 690 E. Bellotti *et al.* (MILA)
BISI 67 PL 25B 572 V. Bisi *et al.* (TORI)
FLETCHER 67 PRL 19 98 C.R. Fletcher *et al.* (ILL)
FORD 67 PRL 18 1214 W.T. Ford *et al.* (PRIN)
GINSBERG 67 PR 162 1570 E.S. Ginsberg (MASB)
KALMUS 67 PR 159 1187 G.E. Kalmus, A. Kernan (LRL)
ZINCHENKO 67 Thesis Rutgers A.I. Zinchenko (RUTG)
CALLAHAN 66 NC 44A 90 A.C. Callahan (WISC)
CALLAHAN 66B PR 150 1153 A.C. Callahan *et al.* (WISC, LRL, UCR+)
CESTER 66 PL 21 343 R. Cester *et al.* (PPA)
See footnote 1 in AUERBACH 67.
Also PR 155 1505 L.B. Auerbach *et al.* (PENN, PRIN)
BIRGE 65 PR 139 B1600 R.W. Birge *et al.* (LRL, WISC)
BISI 65 NC 35 768 V. Bisi *et al.* (TORI)
BISI 65B PR 139 B1068 V. Bisi *et al.* (TORI)
CALLAHAN 65 PRL 15 129 A. Callahan, D. Cline (WISC)
CLINE 65 PL 15 293 D. Cline, W.F. Fry (WISC)
DEMARCO 65 PR 140 B1430 A. de Marco, C. Grosso, G. Rinaudo (TORI, CERN)
FITCH 65B PR 140 B1088 V.L. Fitch, C.A. Quarles, H.C. Wilkins (PRIN+)
STAMER 65 PR 138 B440 P. Stamer *et al.* (STEV)
YOUNG 65 Thesis UCRL 16362 P.S. Young (LRL)
Also PR 156 1464 P.S. Young, W.Z. Osborne, W.H. Barkas (LRL)
BORREANI 64 PL 12 123 G. Borreani, G. Rinaudo, A.E. Werbrouck (TORI)
CALLAHAN 64 PR 136 B1463 A. Callahan, R. March, R. Stark (WISC)
GREINER 64 PRL 13 284 D.E. Greiner, W.Z. Osborne, W.H. Barkas (LRL)
SHAKLEE 64 PR 136 B1423 F.S. Shaklee *et al.* (MICH)
BOYARSKI 62 PR 128 2398 A.M. Boyarski *et al.* (MIT)
FERRO-LUZZI 61 NC 22 1087 M. Ferro-Luzzi *et al.* (LRL)
ROE 61 PRL 7 346 B.P. Roe *et al.* (MICH, LRL)
TAYLOR 59 PR 114 359 S. Taylor *et al.* (COLU)
COOMBES 57 PR 108 1348 C.A. Coombes *et al.* (LBL)

Int. J. Mod. Phys. A 2026.41. Downloaded from www.worldscientific.com by UNIVERSITY OF CALIFORNIA @ BERKELEY on 09/16/26. Re-use and distribution is strictly not permitted, except for Open Access articles.

OTHER RELATED PAPERS

LITTENBERG	93	ARNPS 43 729	L.S. Littenberg, G. Valencia	(BNL, FNAL)
Rare and Radiative Kaon Decays				
RITCHIE	93	RMP 65 1149	J.L. Ritchie, S.G. Wojcicki	
"Rare K Decays"				
BATTISTON	92	PRPL 214 293	R. Battiston *et al.*	(PGIA, CERN, TRSTT)
Status and Perspectives of K Decay Physics				
BRYMAN	89	IJMP A4 79	D.A. Bryman	(TRIU)
"Rare Kaon Decays"				
CHOUNET	72	PRPL 4C 199	L.M. Chounet, J.M. Gaillard, M.K. Gaillard	(ORSAY+)
FEARING	70	PR D2 542	H.W. Fearing, E. Fischbach, J. Smith	(STON, BOHR)
HAIDT	69B	PL 29B 696	D. Haidt *et al.*	(AACH, BARI, CERN, EPOL+)
CRONIN	68B	Vienna Conf. 241	J.W. Cronin	(PRIN)
Rapporteur talk.				
WILLIS	67	Heidelberg Conf. 273	W.J. Willis	(YALE)
Rapporteur talk.				
CABIBBO	66	Berkeley Conf. 33	N. Cabibbo	(CERN)
ADAIR	64	PL 12 67	R.K. Adair, L.B. Leipuner	(YALE, BNL)
CABIBBO	64	PL 9 352	N. Cabibbo, A. Maksymowicz	(CERN)
Also		PL 11 360	N. Cabibbo, A. Maksymowicz	(CERN)
Also		PL 14 72	N. Cabibbo, A. Maksymowicz	(CERN)
BIRGE	63	PRL 11 35	R.W. Birge *et al.*	(LRL, WISC, BARI)
BLOCK	62B	CERN Conf. 371	M.M. Block, L. Lendinara, L. Monari	(NWES, BGNA)
BRENE	61	NP 22 553	N. Brene, L. Egardt, B. Qvist	(NORD)

K^0

$I(J^P) = \frac{1}{2}(0^-)$

K^0 MASS

VALUE (MeV)	EVTS	DOCUMENT ID		TECN	COMMENT
497.611±0.013 OUR FIT Error includes scale factor of 1.2.					
497.611±0.013 OUR AVERAGE Error includes scale factor of 1.2.					
497.607±0.007±0.015	261k	[1] TOMARADZE	14		$\psi(2S) \to K^0_S X$
497.583±0.005±0.020	35k	AMBROSINO	07B	KLOE	$e^+e^- \to K^0_L K^0_S$
497.625±0.001±0.031	655k	LAI	02	NA48	K^0_L beam
497.661±0.033	3713	BARKOV	87B	CMD	$e^+e^- \to K^0_L K^0_S$
497.742±0.085	780	BARKOV	85B	CMD	$e^+e^- \to K^0_L K^0_S$
• • • We do not use the following data for averages, fits, limits, etc. • • •					
497.44 ±0.50		FITCH	67	OSPK	
498.9 ±0.5	4500	BALTAY	66	HBC	K^0 from $\overline{p}p$
497.44 ±0.33	2223	KIM	65B	HBC	K^0 from $\overline{p}p$
498.1 ±0.4		CHRISTENS...	64	OSPK	

[1] Obtained by analyzing CLEO-c data but not authored by the CLEO Collaboration.

$m_{K^0} - m_{K^\pm}$

VALUE (MeV)	EVTS	DOCUMENT ID		TECN	CHG	COMMENT
3.934±0.020 OUR FIT Error includes scale factor of 1.6.						
• • • We do not use the following data for averages, fits, limits, etc. • • •						
3.95 ±0.21	417	HILL	68B	DBC	+	$K^+d \to K^0pp$
3.90 ±0.25	9	BURNSTEIN	65	HBC	−	
3.71 ±0.35	7	KIM	65B	HBC	−	$K^-p \to n\overline{K}^0$
5.4 ±1.1		CRAWFORD	59	HBC	+	
3.9 ±0.6		ROSENFELD	59	HBC	−	

K^0 MEAN SQUARE CHARGE RADIUS

VALUE (fm^2)	EVTS	DOCUMENT ID		TECN	COMMENT
−0.077±0.010 OUR AVERAGE					
−0.077±0.007±0.011	5037	ABOUZAID	06	KTEV	$K^0_L \to \pi^+\pi^-e^+e^-$
−0.090±0.021		LAI	03C	NA48	$K^0_L \to \pi^+\pi^-e^+e^-$
−0.054±0.026		MOLZON	78		K_S regen. by electrons
• • • We do not use the following data for averages, fits, limits, etc. • • •					
−0.087±0.046		BLATNIK	79		VMD + dispersion relations
−0.050±0.130		FOETH	69B		K_S regen. by electrons

T-VIOLATION PARAMETER IN K^0-$\overline{K}^0$ MIXING

The asymmetry $A_T = \frac{\Gamma(\overline{K}^0 \to K^0) - \Gamma(K^0 \to \overline{K}^0)}{\Gamma(\overline{K}^0 \to K^0) + \Gamma(K^0 \to \overline{K}^0)}$ must vanish if T invariance holds.

ASYMMETRY A_T IN K^0-$\overline{K}^0$ MIXING

VALUE (units 10^{-3})	EVTS	DOCUMENT ID		TECN
6.6±1.3±1.0	640k	[1] ANGELOPO...	98E	CPLR

[1] ANGELOPOULOS 98E measures the asymmetry $A_T = [\Gamma(\overline{K}^0_{t=0} \to e^+\pi^-\nu_{t=\tau}) - \Gamma(K^0_{t=0} \to e^-\pi^+\overline{\nu}_{t=\tau})]/[\Gamma(\overline{K}^0_{t=0} \to e^+\pi^-\nu_{t=\tau}) + \Gamma(K^0_{t=0} \to e^-\pi^+\overline{\nu}_{t=\tau})]$ as a function of the neutral-kaon eigentime τ. The initial strangeness of the neutral kaon is tagged by the charge of the accompanying charged kaon in the reactions $p\overline{p} \to K^-\pi^+K^0$ and $p\overline{p} \to K^+\pi^-\overline{K}^0$. The strangeness at the time of the decay is tagged by the lepton charge. The reported result is the average value of A_T over the interval $1\tau_S < \tau < 20\tau_S$. From this value of A_T ANGELOPOULOS 01B, assuming CPT invariance in the $e\pi\nu$ decay amplitude, determine the T-violating as $\Delta S = \Delta S$ conserving parameter (for its definition, see Review below) $4\mathrm{Re}(\epsilon) = (6.2 \pm 1.4 \pm 1.0) \times 10^{-3}$.

See the related review(s):
CPT Invariance Tests in Neutral Kaon Decay

CP-VIOLATION PARAMETERS

Re(ϵ)

VALUE (units 10^{-3})	DOCUMENT ID		TECN
1.596±0.013	[1] AMBROSINO	06H	KLOE
• • • We do not use the following data for averages, fits, limits, etc. • • •			
1.664±0.010	[2] LAI	05A	NA48

[1] AMBROSINO 06H uses Bell-Steinberger relations with the following measurements: $B(K^0_L \to \pi^+\pi^-)$ in AMBROSINO 06F, $B(K^0_S \to \pi^0\pi^0\pi^0)$ in AMBROSINO 05B, the K^0_S-semileptonic charge asymmetry in AMBROSINO 06E, and K^0-semileptonic results in ANGELOPOULOS 98F.
[2] LAI 05A values are obtained through unitarity (Bell-Steinberger relations), improving determination of η_{000} and combining other data from PDG 04 and APOSTOLAKIS 99B.

CPT-VIOLATION PARAMETERS

In K^0-$\overline{K}^0$ mixing, if CP-violating interactions include a T conserving part then

$$|K_S\rangle = [|K_1\rangle + (\epsilon+\delta)|K_2\rangle]/\sqrt{1+|\epsilon+\delta|^2}$$
$$|K_L\rangle = [|K_2\rangle + (\epsilon-\delta)|K_1\rangle]/\sqrt{1+|\epsilon-\delta|^2}$$

where

$$|K_1\rangle = [|K^0\rangle + |\overline{K}^0\rangle]/\sqrt{2}$$
$$|K_2\rangle = [|K^0\rangle - |\overline{K}^0\rangle]/\sqrt{2}$$

and

$$|\overline{K}^0\rangle = CP|K^0\rangle.$$

The parameter δ specifies the CPT-violating part.

Estimates of δ are given below assuming the validity of the $\Delta S = \Delta Q$ rule. See also THOMSON 95 for a test of CPT-symmetry conservation in K^0 decays using the Bell-Steinberger relation.

REAL PART OF δ

A nonzero value violates CPT invariance.

VALUE (units 10^{-4})	EVTS	DOCUMENT ID		TECN	COMMENT
2.51± 2.25		[1] ABOUZAID	11	KTEV	
• • • We do not use the following data for averages, fits, limits, etc. • • •					
2.3 ± 2.7		[2] AMBROSINO	06H	KLOE	
2.4 ± 2.8		[3] APOSTOLA...	99B	RVUE	
2.9 ± 2.6 ±0.6	1.3M	[4] ANGELOPO...	98F	CPLR	
180 ±200	6481	[5] DEMIDOV	95		$K_{\ell 3}$ reanalysis

[1] ABOUZAID 11 uses Bell-Steinberger relations.
[2] AMBROSINO 06H uses Bell-Steinberger relations with the following measurements: $B(K^0_L \to \pi^+\pi^-)$ in AMBROSINO 06F, $B(K^0_S \to \pi^0\pi^0\pi^0)$ in AMBROSINO 05B, the K^0_S-semileptonic charge asymmetry in AMBROSINO 06E, and K^0-semileptonic results in ANGELOPOULOS 98F.
[3] APOSTOLAKIS 99B assumes only unitarity and combines CPLEAR and other results.
[4] ANGELOPOULOS 98F use $\Delta S = \Delta Q$. If $\Delta S = \Delta Q$ is not assumed, they find $\mathrm{Re}\delta = (3.0 \pm 3.3 \pm 0.6) \times 10^{-4}$.
[5] DEMIDOV 95 reanalyzes data from HART 73 and NIEBERGALL 74.

IMAGINARY PART OF δ

A nonzero value violates CPT invariance.

VALUE (units 10^{-5})	EVTS	DOCUMENT ID		TECN	COMMENT
− 1.5± 1.6		[1] ABOUZAID	11	KTEV	
• • • We do not use the following data for averages, fits, limits, etc. • • •					
0.4± 2.1		[2] AMBROSINO	06H	KLOE	
− 0.2± 2.0		[3] LAI	05A	NA48	
2.4± 5.0		[4] APOSTOLA...	99B	RVUE	
− 90 ± 290 ±100	1.3M	[5] ANGELOPO...	98F	CPLR	
2100 ±3700	6481	[6] DEMIDOV	95		$K_{\ell 3}$ reanalysis

[1] ABOUZAID 11 uses Bell-Steinberger relations.
[2] AMBROSINO 06H uses Bell-Steinberger relations with the following measurements: $B(K^0_L \to \pi^+\pi^-)$ in AMBROSINO 06F, $B(K^0_S \to \pi^0\pi^0\pi^0)$ in AMBROSINO 05B, the K^0_S-semileptonic charge asymmetry in AMBROSINO 06E, and K^0-semileptonic results in ANGELOPOULOS 98F.
[3] LAI 05A values are obtained through unitarity (Bell-Steinberger relations), improving determination of η_{000} and combining other data from PDG 04 and APOSTOLAKIS 99B.
[4] APOSTOLAKIS 99B assumes only unitarity and combines CPLEAR and other results.
[5] If $\Delta S = \Delta Q$ is not assumed, ANGELOPOULOS 98F finds $\mathrm{Im}\delta = (-15 \pm 23 \pm 3) \times 10^{-3}$.
[6] DEMIDOV 95 reanalyzes data from HART 73 and NIEBERGALL 74.

Re(y)

A non-zero value would violate CPT invariance in $\Delta S = \Delta Q$ amplitude. Re(y) is the following combination of K_{e3} decay amplitudes:

$$\mathrm{Re(y)} = \mathrm{Re}\left(\frac{A(\overline{K}^0 \to e^-\pi^+\overline{\nu}_e)^* - A(K^0 \to e^+\pi^-\nu_e)}{A(\overline{K}^0 \to e^-\pi^+\overline{\nu}_e)^* + A(K^0 \to e^+\pi^-\nu_e)} \right)$$

VALUE (units 10^{-3})	EVTS	DOCUMENT ID		TECN
0.4±2.5	13k	[1] AMBROSINO	06E	KLOE
• • • We do not use the following data for averages, fits, limits, etc. • • •				
0.3±3.1		[2] APOSTOLA...	99B	CPLR

[1] They use the PDG 04 for the K^0_L semileptonic charge asymmetry and PDG 04 (CP review, CPT NOT ASSUMED) for Re(ϵ).
[2] Constrained by Bell-Steinberger (or unitarity) relation.

Int. J. Mod. Phys. A 2026.41. Downloaded from www.worldscientific.com by UNIVERSITY OF CALIFORNIA @ BERKELEY on 09/16/26. Re-use and distribution is strictly not permitted, except for Open Access articles.

Re(x_)

A non-zero value would violate CPT invariance in decay amplitudes with $\Delta S \neq \Delta Q$. x_, used here to define Re(x_), and x_+, used below in the $\Delta S = \Delta Q$ section are the following combinations of K_{e3} decay amplitudes:

$$x_\pm = \frac{1}{2}\left(\frac{A(\overline{K}^0 \to \pi^- e^+ \nu_e)}{A(K^0 \to \pi^- e^+ \nu_e)} \pm \frac{A(K^0 \to \pi^+ e^- \overline{\nu}_e)^*}{A(\overline{K}^0 \to \pi^+ e^- \overline{\nu}_e)^*} \right).$$

VALUE (units 10^{-3})	EVTS	DOCUMENT ID		TECN	COMMENT
−2.9± 2.0		[1] AMBROSINO	06H	KLOE	
• • • We do not use the following data for averages, fits, limits, etc. • • •					
−0.8± 2.5	13k	[2] AMBROSINO	06E	KLOE	
−0.5± 3.0		[3] APOSTOLA...	99B	CPLR	Strangeness tagged
2 ±13 ±3	650k	ANGELOPO...	98F	CPLR	Strangeness tagged

[1] AMBROSINO 06H uses Bell-Steinberger relations with the following measurements: $B(K^0_L \to \pi^+\pi^-)$ in AMBROSINO 06F, $B(K^0_S \to \pi^0\pi^0\pi^0)$ in AMBROSINO 05B, the K^0_S-semileptonic charge asymmetry in AMBROSINO 06E, and K^0-semileptonic results in ANGELOPOULOS 98F.

[2] Uses PDG 04 for the K^0_L semileptonic charge asymmetry and Re(δ) from CPLEAR, ANGELOPOULOS 98F.

[3] Constrained by Bell-Steinberger (or unitarity) relation.

$|m_{K^0} - m_{\overline{K}^0}| / m_{average}$

A test of CPT invariance. "Our Evaluation" is described in the "Tests of Conservation Laws" section. It assumes CPT invariance in the decay and neglects some contributions from decay channels other than $\pi\pi$.

VALUE	CL%	DOCUMENT ID		TECN
$<6 \times 10^{-19}$	90	PDG	12	
• • • We do not use the following data for averages, fits, limits, etc. • • •				
$(-3 \pm 4) \times 10^{-18}$		[1] ANGELOPO...	99B	RVUE

[1] ANGELOPOULOS 99B assumes only unitarity and combines CPLEAR and other results.

$(\Gamma_{K^0} - \Gamma_{\overline{K}^0})/m_{average}$

A test of CPT invariance.

VALUE	DOCUMENT ID		TECN
$(7.8\pm8.4) \times 10^{-18}$	[1] ANGELOPO...	99B	RVUE

[1] ANGELOPOULOS 99B assumes only unitarity and combines CPLEAR with other results. Correlated with $(m_{K^0} - m_{\overline{K}^0}) / m_{average}$ with a correlation coefficient of −0.95.

TESTS OF $\Delta S = \Delta Q$ RULE

Re(x_+)

A non-zero value would violate the $\Delta S = \Delta Q$ rule in CPT conserving transitions. x_+ is defined above in the Re(x_) section.

VALUE (units 10^{-3})	EVTS	DOCUMENT ID		TECN
−0.9± 3.0 OUR AVERAGE				
−2 ±10		[1] BATLEY	07D	NA48
−0.5± 3.6	13k	[2] AMBROSINO	06E	KLOE
−1.8± 6.1		[3] ANGELOPO...	98D	CPLR

[1] Result obtained from the measurement $\Gamma(K^0_S \to \pi e \nu) / \Gamma(K^0_L \to \pi e \nu) = 0.993 \pm 0.34$, neglecting possible CPT non-invariance and using PDG 06 values of $B(K^0_L \to \pi e \nu) = 0.4053 \pm 0.0015$, $\tau_L = (5.114 \pm 0.021) \times 10^{-8}$ s and $\tau_S = (0.8958 \pm 0.0005) \times 10^{-10}$ s.

[2] Re(x_+) can be shown to be equal to the following combination of rates:

$$\mathrm{Re}(x_+) = \frac{1}{2}\,\frac{\Gamma(K^0_S \to \pi e \nu) - \Gamma(K^0_L \to \pi e \nu)}{\Gamma(K^0_S \to \pi e \nu) + \Gamma(K^0_L \to \pi e \nu)}$$

which is valid up to first order in terms violating CPT and/or the $\Delta S = \Delta Q$ rule.

[3] Obtained neglecting CPT violating amplitudes.

K^0 REFERENCES

TOMARADZE	14	PR D89 031501	A. Tomaradze et al.	(NWES, WAYN)
PDG	12	PR D86 010001	J. Beringer et al.	(PDG Collab.)
ABOUZAID	11	PR D83 092001	E. Abouzaid et al.	(FNAL KTeV Collab.)
AMBROSINO	07B	JHEP 0712 073	F. Ambrosino et al.	(KLOE Collab.)
BATLEY	07D	PL B653 145	J.R. Batley et al.	(CERN NA48 Collab.)
ABOUZAID	06	PRL 96 101801	E. Abouzaid et al.	(KTeV Collab.)
AMBROSINO	06E	PL B636 173	F. Ambrosino et al.	(KLOE Collab.)
AMBROSINO	06F	PL B638 140	F. Ambrosino et al.	(KLOE Collab.)
AMBROSINO	06H	JHEP 0612 011	F. Ambrosino et al.	(KLOE Collab.)
PDG	06	JP G33 1	W.-M. Yao et al.	(PDG Collab.)
AMBROSINO	05B	PL B619 61	F. Ambrosino et al.	(KLOE Collab.)
LAI	05A	PL B610 165	A. Lai et al.	(CERN NA48 Collab.)
PDG	04	PL B592 1	S. Eidelman et al.	(PDG Collab.)
LAI	03C	EPJ C30 33	A. Lai et al.	(CERN NA48 Collab.)
LAI	02	PL B533 196	A. Lai et al.	(CERN NA48 Collab.)
ANGELOPO...	01B	EPJ C22 55	A. Angelopoulos et al.	(CPLEAR Collab.)
ANGELOPO...	99B	PL B471 332	A. Angelopoulos et al.	(CPLEAR Collab.)
APOSTOLA...	99B	PL B456 297	A. Apostolakis et al.	(CPLEAR Collab.)
ANGELOPO...	98D	PL B444 38	A. Angelopoulos et al.	(CPLEAR Collab.)
Also		EPJ C22 55	A. Angelopoulos et al.	(CPLEAR Collab.)
ANGELOPO...	98E	PL B444 43	A. Angelopoulos et al.	(CPLEAR Collab.)
ANGELOPO...	98F	PL B444 52	A. Angelopoulos et al.	(CPLEAR Collab.)
Also		EPJ C22 55	A. Angelopoulos et al.	(CPLEAR Collab.)
DEMIDOV	95	PAN 58 968	V. Demidov, K. Gusev, E. Shabalin	(ITEP)
From YAF 58 1041.				
THOMSON	95	PR D51 1412	G.B. Thomson, Y. Zou	(RUTG)
BARKOV	87B	SJNP 46 630	L.M. Barkov et al.	(NOVO)
		Translated from YAF 46 1088.		
BARKOV	85B	JETPL 42 138	L.M. Barkov et al.	(NOVO)
		Translated from ZETFP 42 113.		
BLATNIK	79	LNC 24 39	S. Blatnik, J. Stahov, C.B. Lang	(TUZL, GRAZ)
MOLZON	78	PRL 41 1213	W.R. Molzon et al.	(EFI+)
NIEBERGALL	74	PL 49B 103	F. Niebergall et al.	(CERN, ORSAY, VIEN)
HART	73	NP B66 317	J.C. Hart et al.	(CAVE, RHEL)
FOETH	69B	PL 30B 276	H. Foeth et al.	(AACH, CERN, TORI)
HILL	68B	PR 168 1534	D.G. Hill et al.	(BNL, CMU)
FITCH	67	PR 164 1711	V.L. Fitch et al.	(PRIN)
BALTAY	66	PR 142 932	C. Baltay et al.	(YALE, BNL)
BURNSTEIN	65	PR 138 B895	R.A. Burnstein, H.A. Rubin	(UMD)
KIM	65B	PR 140 B1334	J.K. Kim, L. Kirsch, D. Miller	(COLU)
CHRISTENS...	64	PRL 13 138	J.H. Christenson et al.	(PRIN)
CRAWFORD	59	PRL 2 112	F.S. Crawford et al.	(LRL)
ROSENFELD	59	PRL 2 110	A.H. Rosenfeld, F.T. Solmitz, R.D. Tripp	(LRL)

K^0_S

$I(J^P) = \frac{1}{2}(0^-)$

K^0_S MEAN LIFE

For earlier measurements, beginning with BOLDT 58B, see our 1986 edition, Physics Letters **170B** 130 (1986).

OUR FIT is described in the note on "CP violation in K_L decays" in the K^0_L Particle Listings. The result labeled "OUR FIT Assuming CPT" ["OUR FIT Not assuming CPT"] includes all measurements except those with the comment "Not assuming CPT" ["Assuming CPT"]. Measurements with neither comment do not assume CPT and enter both fits.

VALUE (10^{-10} s)	EVTS	DOCUMENT ID		TECN	COMMENT
0.8954 ±0.0004 OUR FIT		Error includes scale factor of 1.1. Assuming CPT			
0.89564±0.00033 OUR FIT		Not assuming CPT			
0.89589±0.00070		[1,2] ABOUZAID	11	KTEV	Not assuming CPT
0.89623±0.00047		[1,3] ABOUZAID	11	KTEV	Assuming CPT
0.89562±0.00029±0.00043	20M	[4] AMBROSINO	11	KLOE	Not assuming CPT
0.89598±0.00048±0.00051	16M	LAI	02C	NA48	
0.8971 ±0.0021		BERTANZA	97	NA31	
0.8941 ±0.0014 ±0.0009		SCHWINGEN...	95	E773	Assuming CPT
0.8929 ±0.0016		GIBBONS	93	E731	Assuming CPT
• • • We do not use the following data for averages, fits, limits, etc. • • •					
0.8965 ±0.0007		[5] ALAVI-HARATI	03	KTEV	Assuming CPT
0.8958 ±0.0013		[6] ALAVI-HARATI	03	KTEV	Not assuming CPT
0.8920 ±0.0044	214k	GROSSMAN	87	SPEC	
0.905 ±0.007		[7] ARONSON	82B	SPEC	
0.881 ±0.009	26k	ARONSON	76	SPEC	
0.8926 ±0.0032 ±0.0002		[8] CARITHERS	75	SPEC	
0.8937 ±0.0048	6M	GEWENIGER	74B	ASPK	
0.8958 ±0.0045	50k	[9] SKJEGGEST...	72	HBC	
0.856 ±0.008	19994	[10] DONALD	68B	HBC	
0.872 ±0.009	20000	[9,10] HILL	68	DBC	

[1] The two ABOUZAID 11 values use the same full KTeV dataset from 1996, 1997, and 1999. The first enters the "assuming CPT" fit and the second enters the "not assuming CPT" fit.

[2] ABOUZAID 11 fit has Δm, τ_S, ϕ_ϵ, Re(ϵ'/ϵ), and Im(ϵ'/ϵ) as free parameters. See Im(ϵ'/ϵ) in the "K^0_L CP violation" section for correlation information.

[3] ABOUZAID 11 fit has Δm and τ_S free but constrains ϕ_ϵ to the Superweak value, i.e. assumes CPT. This τ_S value is correlated with their $\Delta m = m_{K^0_L} - m_{K^0_S}$ measurement in the K^0_L listings. The correlation coefficient $\rho(\tau_S, \Delta m) = -0.670$.

[4] Fit to the proper time distribution.

[5] This ALAVI-HARATI 03 fit has Δm and τ_S free but constrains ϕ_{+-} to the Superweak value, i.e. assumes CPT. This τ_S value is correlated with their $\Delta m = m_{K^0_L} - m_{K^0_S}$ measurement in the K^0_L listings. The correlation coefficient $\rho(\tau_S, \Delta m) = -0.396$. Superseded by ABOUZAID 11.

[6] This ALAVI-HARATI 03 fit has Δm, ϕ_{+-}, and τ_{K_S} free. See ϕ_{+-} in the "K_L CP violation" section for correlation information. Superseded by ABOUZAID 11.

[7] ARONSON 82 find that K^0_S mean life may depend on the kaon energy.

[8] CARITHERS 75 measures the Δm dependence of the total decay rate (inverse mean life) to be $\Gamma(K^0_S) = [(1.122 \pm 0.004) + 0.16(\Delta m - 0.5348)/\Delta m] 10^{10}$/s, or, in terms of mean life, CARITHERS 75 measures $\tau_S = (0.8913 \pm 0.0032) - 0.238\,[\Delta m - 0.5348]$ (10^{-10} s). We have adjusted the measurement to use our best values of ($\Delta m = 0.5293 \pm 0.0009$) ($10^{10}$ $\hbar$ s^{-1}). Our first error is their experiment's error and our second error is the systematic error from using our best values.

[9] HILL 68 has been changed by the authors from the published value (0.865 ± 0.009) because of a correction in the shift due to η_{+-}. SKJEGGESTAD 72 and HILL 68 give detailed discussions of systematics encountered in this type of experiment.

[10] Pre-1971 experiments are excluded from the average because of disagreement with later more precise experiments.

K^0_S DECAY MODES

	Mode	Fraction (Γ_i/Γ)	Scale factor/ Confidence level
	Hadronic modes		
Γ_1	$\pi^0\pi^0$	(30.69±0.05) %	
Γ_2	$\pi^+\pi^-$	(69.20±0.05) %	
Γ_3	$\pi^+\pi^-\pi^0$	$(3.5\ ^{+1.1}_{-0.9}) \times 10^{-7}$	

Int. J. Mod. Phys. A 2026.41. Downloaded from www.worldscientific.com by CALIFORNIA @ BERKELEY on 09/16/26. Re-use and distribution is strictly not permitted, except for Open Access articles.

Modes with photons or $\ell\bar{\ell}$ pairs

Γ_4	$\pi^+\pi^-\gamma$	[a,b]	$(1.79\pm0.05)\times10^{-3}$	
Γ_5	$\pi^+\pi^-e^+e^-$		$(4.79\pm0.15)\times10^{-5}$	
Γ_6	$\pi^0\gamma\gamma$	[a]	$(4.9\pm1.8)\times10^{-8}$	
Γ_7	$\gamma\gamma$		$(2.63\pm0.17)\times10^{-6}$	S=3.1
Γ_8	$\mu^+\mu^-\mu^+\mu^-$		$<5.1\times10^{-12}$	CL=90%

Semileptonic modes

Γ_9	$\pi^\pm e^\mp\nu_e$	[c]	$(7.14\pm0.06)\times10^{-4}$	
Γ_{10}	$\pi^\pm\mu^\mp\nu_\mu$	[c,d]	$(4.56\pm0.20)\times10^{-4}$	

CP violating (*CP*) and $\Delta S=1$ weak neutral current (*S1*) modes

Γ_{11}	$3\pi^0$	*CP*	$<2.6\times10^{-8}$	CL=90%
Γ_{12}	$\mu^+\mu^-$	*S1*	$<2.1\times10^{-10}$	CL=90%
Γ_{13}	e^+e^-	*S1*	$<9\times10^{-9}$	CL=90%
Γ_{14}	$\pi^0e^+e^-$	*S1*	[a] $(3.0\,^{+1.5}_{-1.2})\times10^{-9}$	
Γ_{15}	$\pi^0\mu^+\mu^-$	*S1*	$(2.9\,^{+1.5}_{-1.2})\times10^{-9}$	
Γ_{16}	invisible		$<8.4\times10^{-4}$	CL=90%

[a] See the Particle Listings below for the energy limits used in this measurement.

[b] Most of this radiative mode, the low-momentum γ part, is also included in the parent mode listed without γ's.

[c] The value is for the sum of the charge states or particle/antiparticle states indicated.

[d] Not a measurement. Calculated as $0.666\cdot B(\pi^\pm e^\mp\nu_e)$.

CONSTRAINED FIT INFORMATION

An overall fit to 4 branching ratios uses 5 measurements and one constraint to determine 4 parameters. The overall fit has a $\chi^2=0.6$ for 2 degrees of freedom.

The following *off-diagonal* array elements are the correlation coefficients $\langle\delta x_i\delta x_j\rangle/(\delta x_i\cdot\delta x_j)$, in percent, from the fit to the branching fractions, $x_i\equiv\Gamma_i/\Gamma_{total}$. The fit constrains the x_i whose labels appear in this array to sum to one.

	x_1	x_2	x_9
x_2	−100		
x_9	−9	8	
x_{10}	−1	−3	0

K^0_S DECAY RATES

$\Gamma(\pi^\pm e^\mp\nu_e)$ — Γ_9

VALUE (10^6 s^{-1})	EVTS	DOCUMENT ID		TECN	COMMENT
• • • We do not use the following data for averages, fits, limits, etc. • • •					
8.1 ±1.6	75	[1] AKHMETSHIN	99	CMD2	Tagged K^0_S using $\phi\to K^0_LK^0_S$
7.50±0.08		[2] PDG	98		
seen		BURGUN	72	HBC	$K^+p\to K^0p\pi^+$
9.3 ±2.5		AUBERT	65	HLBC	ΔS=ΔQ, *CP* cons. not assumed

[1] AKHMETSHIN 99 is from a measured branching ratio $B(K^0_S\to\pi e\nu_e)=(7.2\pm1.4)\times10^{-4}$ and $\tau_{K^0_S}=(0.8934\pm0.0008)\times10^{-10}$ s. Not independent of measured branching ratio.

[2] PDG 98 from K^0_L measurements, assuming that $\Delta S=\Delta Q$ in K^0 decay so that $\Gamma(K^0_S\to\pi^\pm e^\mp\nu_e)=\Gamma(K^0_L\to\pi^\pm e^\mp\nu_e)$.

$\Gamma(\pi^\pm\mu^\mp\nu_\mu)$ — Γ_{10}

VALUE (10^6 s^{-1})	DOCUMENT ID	
• • • We do not use the following data for averages, fits, limits, etc. • • •		
5.25±0.07	[1] PDG	98

[1] PDG 98 from K^0_L measurements, assuming that $\Delta S=\Delta Q$ in K^0 decay so that $\Gamma(K^0_S\to\pi^\pm\mu^\mp\nu_\mu)=\Gamma(K^0_L\to\pi^\pm\mu^\mp\nu_\mu)$.

K^0_S BRANCHING RATIOS

Hadronic modes

$\Gamma(\pi^0\pi^0)/\Gamma_{total}$ — Γ_1/Γ

VALUE	EVTS	DOCUMENT ID		TECN
0.3069±0.0005 OUR FIT				
• • • We do not use the following data for averages, fits, limits, etc. • • •				
0.335 ±0.014	1066	BROWN	63	HLBC
0.288 ±0.021	198	CHRETIEN	63	HLBC
0.30 ±0.035		BROWN	61	HLBC

$\Gamma(\pi^+\pi^-)/\Gamma_{total}$ — Γ_2/Γ

VALUE	EVTS	DOCUMENT ID		TECN	COMMENT
0.6920±0.0005 OUR FIT					
• • • We do not use the following data for averages, fits, limits, etc. • • •					
0.670 ±0.010	3447	DOYLE	69	HBC	$\pi^-p\to\Lambda K^0$

$\Gamma(\pi^+\pi^-)/\Gamma(\pi^0\pi^0)$ — Γ_2/Γ_1

VALUE	EVTS	DOCUMENT ID		TECN	COMMENT
2.255 ±0.005 OUR FIT					
2.2549±0.0054		[1] AMBROSINO	06C	KLOE	
• • • We do not use the following data for averages, fits, limits, etc. • • •					
2.2555±0.0012±0.0054		[2] AMBROSINO	06C	KLOE	
2.236 ±0.003 ±0.015	766k	[2] ALOISIO	02B	KLOE	
2.11 ±0.09	1315	EVERHART	76	WIRE	$\pi^-p\to\Lambda K^0$
2.169 ±0.094	16k	COWELL	74	OSPK	$\pi^-p\to\Lambda K^0$
2.16 ±0.08	4799	HILL	73	DBC	$K^+d\to K^0pp$
2.22 ±0.10	3068	[3] ALITTI	72	HBC	$K^+p\to\pi^+pK^0$
2.22 ±0.08	6380	MORSE	72B	DBC	$K^+n\to K^0p$
2.10 ±0.11	701	[4] NAGY	72	HLBC	$K^+n\to K^0p$
2.22 ±0.095	6150	[5] BALTAY	71	HBC	$Kp\to K^0$neutrals
2.282 ±0.043	7944	[6] MOFFETT	70	OSPK	$K^+n\to K^0p$
2.12 ±0.17	267	[4] BOZOKI	69	HLBC	
2.285 ±0.055	3016	[6] GOBBI	69	OSPK	$K^+n\to K^0p$
2.10 ±0.06	3700	MORFIN	69	HLBC	$K^+n\to K^0p$

[1] This result combines AMBROSINO 06C KLOE 2001-02 data with ALOISIO 02B KLOE 2000 data. $K^0_S\to\pi^+\pi^-$ fully inclusive.

[2] Includes radiative decays $\pi^+\pi^-\gamma$.

[3] The directly measured quantity is $K^0_S\to\pi^+\pi^-/\text{all }K^0=0.345\pm0.005$.

[4] NAGY 72 is a final result which includes BOZOKI 69.

[5] The directly measured quantity is $K^0_S\to\pi^+\pi^-/\text{all }\overline{K}^0=0.345\pm0.005$.

[6] MOFFETT 70 is a final result which includes GOBBI 69.

$\Gamma(\pi^+\pi^-\pi^0)/\Gamma_{total}$ — Γ_3/Γ

VALUE (units 10^{-7})	EVTS	DOCUMENT ID		TECN	COMMENT
$3.5\,^{+1.1}_{-0.9}$ OUR AVERAGE					
$4.7\,^{+2.2}_{-1.7}\,^{+1.7}_{-1.5}$		[1] BATLEY	05	NA48	
$2.5\,^{+1.3}_{-1.0}\,^{+0.5}_{-0.6}$	500k	[2] ADLER	97B	CPLR	
$4.8\,^{+2.2}_{-1.6}\pm1.1$		[3] ZOU	96	E621	
• • • We do not use the following data for averages, fits, limits, etc. • • •					
$4.1\,^{+2.5}_{-1.9}\,^{+0.5}_{-0.6}$		[4] ADLER	96E	CPLR	Sup. by ADLER 97B
$3.9\,^{+5.4}_{-1.8}\,^{+0.9}_{-0.7}$		[5] THOMSON	94	E621	Sup. by ZOU 96

[1] BATLEY 05 is obtained by measuring the interference parameters in K_S, $K_L\to\pi^+\pi^-\pi^0$: $\mathrm{Re}(\lambda)=0.038\pm0.008\pm0.006$ and $\mathrm{Im}(\lambda)=-0.013\pm0.005\pm0.004$; the correlation coeff. between $\mathrm{Re}(\lambda)$ and $\mathrm{Im}(\lambda)$ is 0.66 (statistical only).

[2] ADLER 97B find the *CP*-conserving parameters $\mathrm{Re}(\lambda)=(28\pm7\pm3)\times10^{-3}$, $\mathrm{Im}(\lambda)=(-10\pm8\pm2)\times10^{-3}$. They estimate $B(K^0_S\to\pi^+\pi^-\pi^0)$ from $\mathrm{Re}(\lambda)$ and the K^0_L decay parameters. See also ANGELOPOULOS 98C.

[3] ZOU 96 is from the the measured quantities $|\rho_{+-0}|=0.039\,^{+0.009}_{-0.006}\pm0.005$ and $\phi_\rho=(-9\pm18)^\circ$.

[4] ADLER 96E is from the measured quantities $\mathrm{Re}(\lambda)=0.036\pm0.010\,^{+0.002}_{-0.003}$ and $\mathrm{Im}(\lambda)$ consistent with zero. Note that the quantity λ is the same as ρ_{+-0} used in other footnotes.

[5] THOMSON 94 calculates this branching ratio from their measurements $|\rho_{+-0}|=0.035\,^{+0.019}_{-0.011}\pm0.004$ and $\phi_\rho=(-59\pm48)^\circ$ where $|\rho_{+-0}|e^{i\phi_\rho}=A(K^0_S\to\pi^+\pi^-\pi^0, l=2)/A(K^0_L\to\pi^+\pi^-\pi^0)$.

Modes with photons or $\ell\bar{\ell}$ pairs

$\Gamma(\pi^+\pi^-\gamma)/\Gamma(\pi^+\pi^-)$ — Γ_4/Γ_2

VALUE (units 10^{-3})	EVTS	DOCUMENT ID		TECN	COMMENT
2.59±0.08 OUR AVERAGE					
2.56±0.09	1286	RAMBERG	93	E731	p_γ >50 MeV/c
2.68±0.15		[1] TAUREG	76	SPEC	p_γ >50 MeV/c
• • • We do not use the following data for averages, fits, limits, etc. • • •					
7.10±0.22	3723	RAMBERG	93	E731	p_γ >20 MeV/c
3.0 ±0.6	29	[2] BOBISUT	74	HLBC	p_γ >40 MeV/c
2.8 ±0.6		[3] BURGUN	73	HBC	p_γ >50 MeV/c

[1] TAUREG 76 find direct emission contribution <0.06, CL = 90%.

[2] BOBISUT 74 not included in average because p_γ cut differs. Estimates direct emission contribution to be 0.5 or less, CL = 95%.

[3] BURGUN 73 estimates that direct emission contribution is 0.3 ± 0.6.

$\Gamma(\pi^+\pi^-e^+e^-)/\Gamma_{total}$ — Γ_5/Γ

VALUE (units 10^{-5})	EVTS	DOCUMENT ID		TECN	COMMENT
4.79±0.15 OUR AVERAGE					
4.83±0.11±0.14	23k	[1] BATLEY	11	NA48	2002 data
4.69±0.30	676	[2] LAI	03C	NA48	1998+1999 data
• • • We do not use the following data for averages, fits, limits, etc. • • •					
4.71±0.23±0.22	620	[2,3] LAI	03C	NA48	1999 data
4.5 ±0.7 ±0.4	56	LAI	00B	NA48	1998 data

[1] BATLEY 11 reports $[\Gamma(K^0_S \to \pi^+\pi^-e^+e^-)/\Gamma_{total}]$ / $[B(K^0_L \to \pi^+\pi^-\pi^0)]$ / $[B(\pi^0 \to e^+e^-\gamma)] = (3.28 \pm 0.06 \pm 0.04) \times 10^{-2}$ which we multiply by our best (shown rounded) values $B(K^0_L \to \pi^+\pi^-\pi^0) = (12.54 \pm 0.05) \times 10^{-2}$, $B(\pi^0 \to e^+e^-\gamma) = (1.174 \pm 0.035) \times 10^{-2}$. Our first error is their experiment's error and our second error is the systematic error from using our best (shown rounded) values. Also a limit on the absolute value of the interference between bremsstrahlung and E1 transition is given : $< 4 \times 10^{-7}$ at 90% C.L.

[2] Uses normalization $BR(K_L \to \pi^+\pi^-\pi^0)*BR(\pi^0 \to e^+e^-) = (1.505 \pm 0.047) \times 10^{-3}$ from our 2000 Edition.

[3] Second error is 0.16(syst) ± 0.15(norm) combined in quadrature.

$\Gamma(\pi^0\gamma\gamma)/\Gamma_{total}$ — Γ_6/Γ

VALUE (units 10^{-8})	CL%	EVTS	DOCUMENT ID		TECN	COMMENT
4.9±1.6±0.9		17	[1] LAI	04	NA48	$m^2_{\gamma\gamma}/m^2_K > 0.2$
• • • We do not use the following data for averages, fits, limits, etc. • • •						
<33	90		LAI	03B	NA48	$m^2_{\gamma\gamma}/m^2_K > 0.2$

[1] Spectrum also measured and found consistent with the one generated by a constant matrix element.

$\Gamma(\gamma\gamma)/\Gamma_{total}$ — Γ_7/Γ

VALUE (units 10^{-6})	CL%	EVTS	DOCUMENT ID		TECN	COMMENT
2.63 ±0.17 OR AVERAGE			Error includes scale factor of 3.1.			
2.26 ±0.12 ±0.06		711	[1] AMBROSINO	08C	KLOE	$\phi \to K^0_S K^0_L$
2.713±0.063±0.005		7.5k	[2] LAI	03	NA48	
• • • We do not use the following data for averages, fits, limits, etc. • • •						
2.58 ±0.36 ±0.22		149	LAI	00	NA48	
2.2 ±1.1		16	[3] BARR	95B	NA31	
2.4 ±0.9		35	[4] BARR	95B	NA31	
< 13	90		BALATS	89	SPEC	
2.4 ±1.2		19	BURKHARDT	87	NA31	
<133	90		BARMIN	86B	XEBC	

[1] AMBROSINO 08C reports $(2.26 \pm 0.12 \pm 0.06) \times 10^{-6}$ from a measurement of $[\Gamma(K^0_S \to \gamma\gamma)/\Gamma_{total}] \times [B(K^0_S \to \pi^0\pi^0)]$ assuming $B(K^0_S \to \pi^0\pi^0) = (30.69 \pm 0.05) \times 10^{-2}$.

[2] LAI 03 reports $[\Gamma(K^0_S \to \gamma\gamma)/\Gamma_{total}]$ / $[B(K^0_S \to \pi^0\pi^0)] = (8.84 \pm 0.18 \pm 0.10) \times 10^{-6}$ which we multiply by our best (shown rounded) value $B(K^0_S \to \pi^0\pi^0) = (30.69 \pm 0.05) \times 10^{-2}$. Our first error is their experiment's error and our second error is the systematic error from using our best (shown rounded) value.

[3] BARR 95B result is calculated using $B(K_L \to \gamma\gamma) = (5.86 \pm 0.17) \times 10^{-4}$.

[4] BARR 95B quotes this as the combined BARR 95B + BURKHARDT 87 result after rescaling BURKHARDT 87 to use same branching ratios and lifetimes as BARR 95B.

$\Gamma(\mu^+\mu^-\mu^+\mu^-)/\Gamma_{total}$ — Γ_8/Γ

VALUE	CL%	DOCUMENT ID		TECN
$<5.1 \times 10^{-12}$	90	[1] AAIJ	23AE	LHCB

[1] AAIJ 23AE uses 5.1 fb^{-1} of LHCb data recorded from 2016 to 2018.

Semileptonic modes

$\Gamma(\pi^\pm e^\mp \nu_e)/\Gamma_{total}$ — Γ_9/Γ

VALUE (units 10^{-4})	EVTS	DOCUMENT ID		TECN	COMMENT
7.14 ±0.06 OR FIT					
7.04 ±0.08 OR AVERAGE					
7.046±0.18±0.16		[1] BATLEY	07D	NA48	$K^0(\overline{K}^0)(t) \to \pi e \nu$
6.91 ±0.34±0.15	624	[2] ALOISIO	02	KLOE	Tagged K^0_S using $\phi \to K^0_L K^0_S$
• • • We use the following data for averages but not for fits. • • •					
7.05 ±0.09	13k	[3] AMBROSINO	06E	KLOE	Not fitted
• • • We use the following data for averages, fits, limits, etc. • • •					
7.2 ±1.4	75	AKHMETSHIN	99	CMD2	Tagged K^0_S using $\phi \to K^0_L K^0_S$

[1] Reconstructed from $K^0(\overline{K}^0)(t) \to \pi e \nu$ distributions using PDG values of $B(K^0_L \to \pi e \nu) = 0.4053 \pm 0.0015$, $\tau_L = (5.114 \pm 0.021) \times 10^{-8}$ s and $\tau_S = (0.8958 \pm 0.0005) \times 10^{-10}$ s.

[2] Uses the PDG 00 value for $B(K^0_S \to \pi^+\pi^-)$.

[3] Obtained by imposing $\Sigma_i B(K^0_S \to i) = 1$, where i runs over all the four branching ratios $\pi^+\pi^-$, $\pi^0\pi^0$, $\pi e \nu$, and $\pi \mu \nu$. Input value of $B(K^0_S \to \pi^+\pi^-)$ / $B(K^0_S \to \pi^0\pi^0)$ from AMBROSINO 06C is used. To derive $\Gamma(K^0_S \to \pi^+\mu\nu)$ / $\Gamma(K^0_S \to \pi^+ e \nu)$, lepton universality is assumed, radiative corrections from ANDRE 07 are used, and phase space integrals are taken from KTeV, ALEXOPOULOS 04A. This branching fraction enters our fit via their $\Gamma(\pi^\pm e^\mp \nu_e)$ / $\Gamma(\pi^+\pi^-)$ branching ratio measurement.

$\Gamma(\pi^\pm \mu^\mp \nu_\mu)/\Gamma_{total}$ — Γ_{10}/Γ

VALUE (units 10^{-4})	EVTS	DOCUMENT ID		TECN	COMMENT
4.56±0.20 OR FIT					
4.56±0.11±0.17	7223	[1] BABUSCI	20	KLOE	direct measurement

[1] Value obtained by normalizing to the KLOE measurement $B(K^0_S \to \pi^+\pi^-) = (69.196 \pm 0.051)\%$. Also comparison with the PDG 18 based derived value leads to a lepton flavor universality test $|V_{us}\ f_+(0)|^2_{K^0_S \to \pi\mu\nu} / |V_{us}\ f_+(0)|^2_{K^0_S \to \pi e \nu} = 0.975 \pm 0.044$.

$\Gamma(\pi^\pm e^\mp \nu_e)/\Gamma(\pi^+\pi^-)$ — Γ_9/Γ_2

VALUE (units 10^{-3})	EVTS	DOCUMENT ID		TECN
1.032 ±0.008 OR FIT				
1.0338±0.0054±0.0064		[1] BABUSCI	23	KLOE
• • • We do not use the following data for averages, fits, limits, etc. • • •				
1.019 ±0.011 ±0.007	13k	[2] AMBROSINO	06E	KLOE

[1] BABUSCI 23 measured $\Gamma(K^0_S \to \pi e \nu)/\Gamma(K^0_S \to \pi^+\pi^-) = (1.0421 \pm 0.0066 \pm 0.0075) \times 10^{-3}$ based on data collected from 2004 to 2005. About 50k signal events were reconstructed from the dataset corresponding to an integrated luminosity of 1.63 fb^{-1}. The quoted value is their combination of this result with the previous measurement of AMBROSINO 06E. The correlation coefficient between the two measurements is 12%.

[2] AMBROSINO 06E result is included in BABUSCI 23.

CP violating (*CP*) and $\Delta S = 1$ weak neutral current (*S1*) modes

$\Gamma(3\pi^0)/\Gamma_{total}$ — Γ_{11}/Γ

Violates *CP* conservation.

VALUE (units 10^{-7})	CL%	EVTS	DOCUMENT ID		TECN	COMMENT
< 0.26	90	590M	[1] BABUSCI	13C	KLOE	$\phi \to K^0_L K^0_S$
• • • We do not use the following data for averages, fits, limits, etc. • • •						
< 1.2	90	37.8M	AMBROSINO	05B	KLOE	
< 7.4	90	4.9M	[2] LAI	05A	NA48	
<140	90	7M	ACHASOV	99D	SND	
<190	90	17300	[3] ANGELOPO...	98B	CPLR	
<370	90		BARMIN	83	HLBC	

[1] BABUSCI 13C uses 1.7 fb^{-1} of data of $\phi \to K^0_L K^0_S$ decays with K^0_L interaction in the calorimeter, collected from 2004 to 2005. No candidate events were found in the data with an expected background of $0.04^{+0.15}_{-0.03}$ events. Upper limit is obtained by normalizing to $K^0_S \to 2\pi^0$ decays.

[2] LAI 05A value is obtained from their bound on $|\eta_{000}|$ (not assuming *CPT*) and $B(K^0_L \to 3\pi^0) = 0.211 \pm 0.003$, and PDG 04 values for K^0_L and K^0_S lifetimes. If *CPT* is assumed then $B(K^0_S \to 3\pi^0)_{CPT} < 2.3 \times 10^{-7}$ at 90% CL

[3] ANGELOPOULOS 98B is from $Im(\eta_{000}) = -0.05 \pm 0.12 \pm 0.05$, assuming $Re(\eta_{000}) = Re(\epsilon) = 1.635 \times 10^{-3}$ and using the value $B(K^0_L \to \pi^0\pi^0\pi^0) = 0.2112 \pm 0.0027$.

$\Gamma(\mu^+\mu^-)/\Gamma_{total}$ — Γ_{12}/Γ

Test for $\Delta S = 1$ weak neutral current. Allowed by first-order weak interaction combined with electromagnetic interaction.

VALUE	CL%	DOCUMENT ID		TECN
$<2.1 \times 10^{-10}$	90	[1] AAIJ	20AE	LHCB
• • • We do not use the following data for averages, fits, limits, etc. • • •				
$<8 \times 10^{-10}$	90	[2] AAIJ	17BQ	LHCB
$<9 \times 10^{-9}$	90	[3] AAIJ	13G	LHCB
$<3.2 \times 10^{-7}$	90	GJESDAL	73	ASPK
$<7 \times 10^{-6}$	90	HYAMS	69B	OSPK

[1] AAIJ 20AE uses 8.6 fb^{-1} of LHCb data from 2011 to 2012 and 2016 to 2018. The result utilizes the normalization mode branching fraction $B(K^0_S \to \pi^+\pi^-) = (69.20 \pm 0.05) \times 10^{-2}$ from PDG 18. Supersedes AAIJ 17BQ.

[2] AAIJ 17BQ uses 3.0 fb^{-1} of pp collisions at $\sqrt{s} = 7$ and 8 TeV. The result utilizes the normalization mode branching fraction $B(K^0_S \to \pi^+\pi^-) = (69.20 \pm 0.05) \times 10^{-2}$ from PDG 16. Supersedes AAIJ 13G.

[3] AAIJ 13G uses 1.0 fb^{-1} of pp collisions at $\sqrt{s} = 7$ TeV. They obtained $B(K^0_S \to \mu^+\mu^-) < 11 \times 10^{-9}$ at 95% C.L.

$\Gamma(e^+e^-)/\Gamma_{total}$ — Γ_{13}/Γ

Test for $\Delta S = 1$ weak neutral current. Allowed by first-order weak interaction combined with electromagnetic interaction.

VALUE (units 10^{-7})	CL%	DOCUMENT ID		TECN	COMMENT
< 0.09	90	[1] AMBROSINO	09A	KLOE	$e^+e^- \to \phi \to K^0_S K^0_L$
• • • We do not use the following data for averages, fits, limits, etc. • • •					
< 1.4	90	ANGELOPO...	97	CPLR	
< 28	90	BLICK	94	CNTR	Hyperon facility
<100	90	BARMIN	86	XEBC	

[1] AMBROSINO 09A reports $< 0.09 \times 10^{-7}$ from a measurement of $[\Gamma(K^0_S \to e^+e^-)/\Gamma_{total}]$ / $[B(K^0_S \to \pi^+\pi^-)]$ assuming $B(K^0_S \to \pi^+\pi^-) = (69.20 \pm 0.05) \times 10^{-2}$.

$\Gamma(\pi^0 e^+e^-)/\Gamma_{total}$ — Γ_{14}/Γ

Test for $\Delta S = 1$ weak neutral current. Allowed by first-order weak interaction combined with electromagnetic interaction.

VALUE (units 10^{-9})	CL%	EVTS	DOCUMENT ID		TECN	COMMENT
$3.0^{+1.5}_{-1.2} \pm 0.2$		7	[1] BATLEY	03	NA48	m_{ee} >0.165 GeV
• • • We do not use the following data for averages, fits, limits, etc. • • •						
< 140	90		LAI	01	NA48	
< 1100	90	0	BARR	93B	NA31	
<45000	90		GIBBONS	88	E731	

[1] BATLEY 03 extrapolate also to the full kinematical region using a constant form factor and a vector matrix element. The resulting branching ratio is $(5.8^{+2.9}_{-2.4}) \times 10^{-9}$.

Int. J. Mod. Phys. A 2026.41. Downloaded from www.worldscientific.com
by UNIVERSITY OF CALIFORNIA @ BERKELEY on 09/16/26. Re-use and distribution is strictly not permitted, except for Open Access articles.

Int. J. Mod. Phys. A 2026.41. Downloaded from www.worldscientific.com by CALIFORNIA @ BERKELEY on 09/16/26. Re-use and distribution is strictly not permitted, except for Open Access articles.

$\Gamma(\pi^0\mu^+\mu^-)/\Gamma_{total}$ — Γ_{15}/Γ

Test for $\Delta S = 1$ weak neutral current. Allowed by first-order weak interaction combined with electromagnetic interaction.

VALUE (units 10^{-9})	EVTS	DOCUMENT ID		TECN	COMMENT
$2.9^{+1.5}_{-1.2}\pm0.2$	6	[1] BATLEY	04A	NA48	NA48/1 K^0_S beam

[1] Background estimate is $0.22^{+0.18}_{-0.11}$ events. Branching ratio assumes a vector matrix element and unit form factor.

$\Gamma(\text{invisible})/\Gamma_{total}$ — Γ_{16}/Γ

VALUE	CL%	DOCUMENT ID		TECN	COMMENT
$<8.4\times10^{-4}$	90	ABLIKIM	25BE	BES3	$J/\psi\to\phi K^0_S K^0_S$

K^0_S FORM FACTORS

For discussion, see note on $K_{\ell3}$ form factors in the $K^\pm$ section of the Particle Listings above. Because the semileptonic branching fraction is smaller in K^0_S than K^0_L by the ratio of the mean lives, the K^0_S semileptonic form factor has so far been measured only in the K_{e3} mode using the linear expansion $f_+(t) = f_+(0)\,(1+\lambda_+ t/m^2_{\pi^+})$, which gives the vector form factor $f_+(t)$ relative to its value at $t=0$.

λ_+ (LINEAR ENERGY DEPENDENCE OF f_+ IN K^0_{e3} DECAY)

VALUE (units 10^{-2})	EVTS	DOCUMENT ID		TECN
3.39 ± 0.41	15k	AMBROSINO	06E	KLOE

CP VIOLATION IN $K_S\to3\pi$

Written 1996 by T. Nakada (Paul Scherrer Institute) and L. Wolfenstein (Carnegie-Mellon University).

The possible final states for the decay $K^0\to\pi^+\pi^-\pi^0$ have isospin $I=0$, 1, 2, and 3. The $I=0$ and $I=2$ states have $CP=+1$ and K_S can decay into them without violating CP symmetry, but they are expected to be strongly suppressed by centrifugal barrier effects. The $I=1$ and $I=3$ states, which have no centrifugal barrier, have $CP=-1$ so that the K_S decay to these requires CP violation.

In order to see CP violation in $K_S\to\pi^+\pi^-\pi^0$, it is necessary to observe the interference between K_S and K_L decay, which determines the amplitude ratio

$$\eta_{+-0} = \frac{A(K_S\to\pi^+\pi^-\pi^0)}{A(K_L\to\pi^+\pi^-\pi^0)}\ . \qquad (1)$$

If η_{+-0} is obtained from an integration over the whole Dalitz plot, there is no contribution from the $I=0$ and $I=2$ final states and a nonzero value of η_{+-0} is entirely due to CP violation.

Only $I=1$ and $I=3$ states, which are $CP=-1$, are allowed for $K^0\to\pi^0\pi^0\pi^0$ decays and the decay of K_S into $3\pi^0$ is an unambiguous sign of CP violation. Similarly to η_{+-0}, η_{000} is defined as

$$\eta_{000} = \frac{A(K_S\to\pi^0\pi^0\pi^0)}{A(K_L\to\pi^0\pi^0\pi^0)}\ . \qquad (2)$$

If one assumes that CPT invariance holds and that there are no transitions to $I=3$ (or to nonsymmetric $I=1$ states), it can be shown that

$$\eta_{+-0} = \eta_{000} = \epsilon + i\frac{\mathrm{Im}\ a_1}{\mathrm{Re}\ a_1}\ . \qquad (3)$$

With the Wu-Yang phase convention, a_1 is the weak decay amplitude for K^0 into $I=1$ final states; ϵ is determined from CP violation in $K_L\to2\pi$ decays. The real parts of η_{+-0} and η_{000} are equal to $\mathrm{Re}(\epsilon)$. Since currently-known upper limits on $|\eta_{+-0}|$ and $|\eta_{000}|$ are much larger than $|\epsilon|$, they can be interpreted as upper limits on $\mathrm{Im}(\eta_{+-0})$ and $\mathrm{Im}(\eta_{000})$ and so as limits on the CP-violating phase of the decay amplitude a_1.

CP-VIOLATION PARAMETERS IN K^0_S DECAY

$A_S = [\,\Gamma(K^0_S\to\pi^-e^+\nu_e) - \Gamma(K^0_S\to\pi^+e^-\overline{\nu}_e)\,]\ /\ \text{SUM}$

Such asymmetry violates CP. If CPT is assumed then $A_S = 2\,\mathrm{Re}(\epsilon)$.

VALUE (units 10^{-3})	EVTS	DOCUMENT ID		TECN
$-3.8\pm5.0\pm2.6$	83k	[1] ANASTASI	18A	KLOE
• • • We do not use the following data for averages, fits, limits, etc. • • •				
$1.5\pm9.6\pm2.9$	13k	AMBROSINO	06E	KLOE

[1] ANASTASI 18A result is a combination of the new measurement and AMBROSINO 06E. The new ANASTASI 18A measurement using data collected from 2004–2005, which corresponds to an integrated luminosity of 1.63 fb^{-1} is $A_S=(-4.9\pm5.7\pm2.6)\times10^{-3}$.

PARAMETERS FOR $K^0_S\to3\pi$ DECAY

$\mathrm{Im}(\eta_{+-0})^2 = \Gamma(K^0_S\to\pi^+\pi^-\pi^0,\ CP\text{-violating})\ /\ \Gamma(K^0_L\to\pi^+\pi^-\pi^0)$

CPT assumed valid (i.e. $\mathrm{Re}(\eta_{+-0})\simeq0$).

VALUE	CL%	EVTS	DOCUMENT ID		TECN
• • • We do not use the following data for averages, fits, limits, etc. • • •					
<0.23	90	601	[1] BARMIN	85	HLBC
<0.12	90	384	METCALF	72	ASPK

[1] BARMIN 85 find $\mathrm{Re}(\eta_{+-0}) = (0.05\pm0.17)$ and $\mathrm{Im}(\eta_{+-0}) = (0.15\pm0.33)$. Includes events of BALDO-CEOLIN 75.

$\mathrm{Im}(\eta_{+-0}) = \mathrm{Im}(A(K^0_S\to\pi^+\pi^-\pi^0,\ CP\text{-violating})\ /\ A(K^0_L\to\pi^+\pi^-\pi^0))$

VALUE	EVTS	DOCUMENT ID		TECN	COMMENT
$-0.002\pm0.009^{+0.002}_{-0.001}$	500k	[1] ADLER	97B	CPLR	
• • • We do not use the following data for averages, fits, limits, etc. • • •					
$-0.002\pm0.018\pm0.003$	137k	[2] ADLER	96D	CPLR	Sup. by ADLER 97B
$-0.015\pm0.017\pm0.025$	272k	[3] ZOU	94	SPEC	

[1] ADLER 97B also find $\mathrm{Re}(\eta_{+-0}) = -0.002\pm0.007^{+0.004}_{-0.001}$. See also ANGELOPOULOS 98C.

[2] The ADLER 96D fit also yields $\mathrm{Re}(\eta_{+-0}) = 0.006\pm0.013\pm0.001$ with a correlation $+0.66$ between real and imaginary parts. Their results correspond to $|\eta_{+-0}|<0.037$ with 90% CL.

[3] ZOU 94 use theoretical constraint $\mathrm{Re}(\eta_{+-0}) = \mathrm{Re}(\epsilon) = 0.0016$. Without this constraint they find $\mathrm{Im}(\eta_{+-0}) = 0.019\pm0.061$ and $\mathrm{Re}(\eta_{+-0}) = 0.019\pm0.027$.

$\mathrm{Im}(\eta_{000})^2 = \Gamma(K^0_S\to3\pi^0)\ /\ \Gamma(K^0_L\to3\pi^0)$

CPT assumed valid (i.e. $\mathrm{Re}(\eta_{000})\simeq0$). This limit determines branching ratio $\Gamma(3\pi^0)/\Gamma_{total}$ above.

VALUE	CL%	EVTS	DOCUMENT ID		TECN	COMMENT
• • • We do not use the following data for averages, fits, limits, etc. • • •						
<0.1	90	632	[1] BARMIN	83	HLBC	
<0.28	90		[2] GJESDAL	74B	SPEC	Indirect meas.

[1] BARMIN 83 find $\mathrm{Re}(\eta_{000}) = (-0.08\pm0.18)$ and $\mathrm{Im}(\eta_{000}) = (-0.05\pm0.27)$. Assuming CPT invariance they obtain the limit quoted above.

[2] GJESDAL 74B uses $K2\pi$, $K_{\mu3}$, and K_{e3} decay results, unitarity, and CPT. Calculates $|(\eta_{000})| = 0.26\pm0.20$. We convert to upper limit.

$\mathrm{Im}(\eta_{000}) = \mathrm{Im}(A(K^0_S\to\pi^0\pi^0\pi^0)/A(K^0_L\to\pi^0\pi^0\pi^0))$

$K^0_S\to\pi^0\pi^0\pi^0$ violates CP conservation, in contrast to $K^0_S\to\pi^+\pi^-\pi^0$ which has a CP-conserving part.

VALUE	EVTS	DOCUMENT ID		TECN	COMMENT
-0.001 ± 0.016 OUR AVERAGE					
$0.000\pm0.009\pm0.013$	4.9M	[1] LAI	05A	NA48	Assumes CPT
$-0.05\ \pm0.12\ \pm0.05$	17300	[2] ANGELOPO...	98B	CPLR	Assumes CPT

[1] LAI 05A assumes $\mathrm{Re}(\eta_{000})=\mathrm{Re}(\epsilon)=1.66\times10^{-3}$. The equivalent limit is $|\eta_{000}|_{CPT}<0.025$ at 90% CL Without assuming CPT invariance, they obtain $\mathrm{Re}(\eta_{000})=-0.002\pm0.011\pm0.015$ and $\mathrm{Im}(\eta_{000})=-0.003\pm0.013\pm0.017$ with a statistical correlation coefficient of 0.77 and an overall correlation coefficient of 0.57 between imaginary and real part. The equivalent limit is $|\eta_{000}|<0.045$ at 90% CL

[2] ANGELOPOULOS 98B assumes $\mathrm{Re}(\eta_{000}) = \mathrm{Re}(\epsilon) = 1.635\times10^{-3}$. Without assuming CPT invariance, they obtain $\mathrm{Re}(\eta_{000}) = 0.18\pm0.14\pm0.06$ and $\mathrm{Im}(\eta_{000}) = 0.15\pm0.20\pm0.03$.

$|\eta_{000}| = |A(K^0_S\to3\pi^0)/A(K^0_L\to3\pi^0)|$

A non-zero value violates CP invariance.

VALUE	CL%	EVTS	DOCUMENT ID		TECN
<0.0088	90	590M	BABUSCI	13C	KLOE
• • • We do not use the following data for averages, fits, limits, etc. • • •					
<0.018	90	37.8M	AMBROSINO	05B	KLOE
<0.045	90	4.9M	LAI	05A	NA48

DECAY-PLANE ASYMMETRY IN $\pi^+\pi^-e^+e^-$ DECAYS

This is the CP-violating asymmetry

$$A = \frac{N_{\sin\phi\cos\phi>0.0} - N_{\sin\phi\cos\phi<0.0}}{N_{\sin\phi\cos\phi>0.0} + N_{\sin\phi\cos\phi<0.0}}$$

Int. J. Mod. Phys. A 2026.41. Downloaded from www.worldscientific.com
by UNIVERSITY OF CALIFORNIA @ BERKELEY on 09/16/26. Re-use and distribution is strictly not permitted, except for Open Access articles.

where ϕ is the angle between the e^+e^- and $\pi^+\pi^-$ planes in the K^0_S rest frame.

CP asymmetry A in $K^0_S \to \pi^+\pi^-e^+e^-$

VALUE (%)	*DOCUMENT ID*		*TECN*	*COMMENT*
−0.4±0.8 OUR AVERAGE				
−0.4±0.8	[1] BATLEY	11	NA48	2002 data
−1.1±4.1	LAI	03C	NA48	1998+1999 data
• • • We do not use the following data for averages, fits, limits, etc. • • •				
0.5±4.0±1.6	LAI	03C	NA48	1999 data

[1] The result is used to set the limit $A < 1.5\%$ at 90% C.L.

K^0_S REFERENCES

ABLIKIM	25BE	JHEP 2505 092	M. Ablikim *et al.*	(BESIII Collab.)
AAIJ	23AE	PR D108 L031102	R. Aaij *et al.*	(LHCb Collab.)
BABUSCI	23	JHEP 2302 098	D. Babusci *et al.*	(KLOE-2 Collab.)
AAIJ	20AE	PRL 125 231801	R. Aaij *et al.*	(LHCb Collab.)
BABUSCI	20	PL B804 135378	D. Babusci *et al.*	(KLOE-2 Collab.)
ANASTASI	18A	JHEP 1809 021	A. Anastasi *et al.*	(KLOE-2 Collab.)
PDG	18	PR D98 030001	M. Tanabashi *et al.*	(PDG Collab.)
AAIJ	17BQ	EPJ C77 678	R. Aaij *et al.*	(LHCb Collab.)
PDG	16	CP C40 100001	C. Patrignani *et al.*	(PDG Collab.)
AAIJ	13G	JHEP 1301 090	R. Aaij *et al.*	(LHCb Collab.)
BABUSCI	13C	PL B723 54	D. Babusci *et al.*	(KLOE-2 Collab.)
ABOUZAID	11	PR D83 092001	E. Abouzaid *et al.*	(FNAL KTeV Collab.)
AMBROSINO	11	EPJ C71 1604	F. Ambrosino *et al.*	(KLOE Collab.)
BATLEY	11	PL B694 301	J.R. Batley *et al.*	(CERN NA48/1 Collab.)
AMBROSINO	09A	PL B672 203	F. Ambrosino *et al.*	(KLOE Collab.)
AMBROSINO	08C	JHEP 0805 051	F. Ambrosino *et al.*	(KLOE Collab.)
ANDRE	07	ANP 322 2518	T. Andre	(EFI)
BATLEY	07D	PL B653 145	J.R. Batley *et al.*	(CERN NA48 Collab.)
AMBROSINO	06C	EPJ C48 767	F. Ambrosino *et al.*	(KLOE Collab.)
AMBROSINO	06E	PL B636 173	F. Ambrosino *et al.*	(KLOE Collab.)
AMBROSINO	05B	PL B619 61	F. Ambrosino *et al.*	(KLOE Collab.)
BATLEY	05	PL B630 31	J.R. Batley *et al.*	(NA48 Collab.)
LAI	05A	PL B610 165	A. Lai *et al.*	(CERN NA48 Collab.)
ALEXOPOU...	04A	PR D70 092007	T. Alexopoulos *et al.*	(FNAL KTeV Collab.)
BATLEY	04A	PL B599 197	J.R. Batley *et al.*	(NA48 Collab.)
LAI	04	PL B578 276	A. Lai *et al.*	(CERN NA48 Collab.)
PDG	04	PL B592 1	S. Eidelman *et al.*	(PDG Collab.)
ALAVI-HARATI	03	PR D67 012005	A. Alavi-Harati *et al.*	(FNAL KTeV Collab.)
Also		PR D70 079904 (errat.)	A. Alavi-Harati *et al.*	(FNAL KTeV Collab.)
BATLEY	03	PL B576 43	J.R. Batley *et al.*	(CERN NA48 Collab.)
LAI	03	PL B551 7	A. Lai *et al.*	(CERN NA48 Collab.)
LAI	03B	PL B556 105	A. Lai *et al.*	(CERN NA48 Collab.)
LAI	03C	EPJ C30 33	A. Lai *et al.*	(CERN NA48 Collab.)
ALOISIO	02	PL B535 37	A. Aloisio *et al.*	(KLOE Collab.)
ALOISIO	02B	PL B538 21	A. Aloisio *et al.*	(KLOE Collab.)
LAI	02C	PL B537 28	A. Lai *et al.*	(CERN NA48 Collab.)
LAI	01	PL B514 253	A. Lai *et al.*	(CERN NA48 Collab.)
LAI	00	PL B493 29	A. Lai *et al.*	(CERN NA48 Collab.)
LAI	00B	PL B496 137	A. Lai *et al.*	(CERN NA48 Collab.)
PDG	00	EPJ C15 1	D.E. Groom *et al.*	(PDG Collab.)
ACHASOV	99D	PL B459 674	M.N. Achasov *et al.*	
AKHMETSHIN	99	PL B456 90	R.R. Akhmetshin *et al.*	(Novosibirsk CMD-2 Collab.)
ANGELOPO...	98B	PL B425 391	A. Angelopoulos *et al.*	(CPLEAR Collab.)
ANGELOPO...	98C	EPJ C5 389	A. Angelopoulos *et al.*	(CPLEAR Collab.)
PDG	98	EPJ C3 1	C. Caso *et al.*	(PDG Collab.)
ADLER	97B	PL B407 193	R. Adler *et al.*	(CPLEAR Collab.)
ANGELOPO...	97	PL B413 232	A. Angelopoulos *et al.*	(CPLEAR Collab.)
BERTANZA	97	ZPHY C73 629	L. Bertanza	(PISA, CERN, EDIN, MAINZ, ORSAY+)
ADLER	96D	PL B370 167	R. Adler *et al.*	(CPLEAR Collab.)
ADLER	96E	PL B374 313	R. Adler *et al.*	(CPLEAR Collab.)
ZOU	96	PL B369 362	Y. Zou *et al.*	(RUTG, MINN, MICH)
BARR	95B	PL B351 579	G.D. Barr *et al.*	(CERN, EDIN, MAINZ, LALO+)
SCHWINGEN...	95	PRL 74 4376	B. Schwingenheuer *et al.*	(EFI, CHIC+)
BLICK	94	PL B334 234	A.M. Blick *et al.*	(SERP, JINR)
THOMSON	94	PL B337 411	G.B. Thomson *et al.*	(RUTG, MINN, MICH)
ZOU	94	PL B329 519	Y. Zou *et al.*	(RUTG, MINN, MICH)
BARR	93B	PL B304 381	G.D. Barr *et al.*	(CERN, EDIN, MAINZ, LALO+)
GIBBONS	93	PRL 70 1199	L.K. Gibbons *et al.*	(FNAL E731 Collab.)
Also		PR D55 6625	L.K. Gibbons *et al.*	(FNAL E731 Collab.)
RAMBERG	93	PRL 70 2525	E. Ramberg *et al.*	(FNAL E731 Collab.)
BALATS	89	SJNP 49 828	M.Y. Balats *et al.*	(ITEP)
		Translated from YAF 49 1332.		
GIBBONS	88	PRL 61 2661	L.K. Gibbons *et al.*	(FNAL E731 Collab.)
BURKHARDT	87	PL B199 139	H. Burkhardt *et al.*	(CERN, EDIN, MAINZ+)
GROSSMAN	87	PRL 59 18	N. Grossman *et al.*	(MINN, MICH, RUTG)
BARMIN	86	SJNP 44 622	V.V. Barmin *et al.*	(ITEP)
		Translated from YAF 44 965.		
BARMIN	86B	NC 96A 159	V.V. Barmin *et al.*	(ITEP, PADO)
PDG	86B	PL 170B 130	M. Aguilar-Benitez *et al.*	(CERN, CIT+)
BARMIN	85	NC 85A 67	V.V. Barmin *et al.*	(ITEP, PADO)
Also		SJNP 41 759	V.V. Barmin *et al.*	(ITEP)
		Translated from YAF 41 1187.		
BARMIN	83	PL 128B 129	V.V. Barmin *et al.*	(ITEP, PADO)
Also		SJNP 39 269	V.V. Barmin *et al.*	(ITEP, PADO)
		Translated from YAF 39 428.		
ARONSON	82	PRL 48 1078	S.H. Aronson *et al.*	(BNL, CHIC, STAN+)
ARONSON	82B	PRL 48 1306	S.H. Aronson *et al.*	(BNL, CHIC, PURD)
Also		PL 116B 73	E. Fischbach *et al.*	(PURD, BNL, CHIC)
Also		PR D28 476	S.H. Aronson *et al.*	(BNL, CHIC, PURD)
Also		PR D28 495	S.H. Aronson *et al.*	(BNL, CHIC, PURD)
ARONSON	76	NC 32A 236	S.H. Aronson *et al.*	(WISC, EFI, UCSD+)
EVERHART	76	PR D14 661	G.C. Everhart *et al.*	(PENN)
TAUREG	76	PL 65B 92	H. Taureg *et al.*	(HEIDH, CERN, DORT)
BALDO-...	75	NC 25A 688	M. Baldo-Ceolin *et al.*	(PADO, WISC)
CARITHERS	75	PRL 34 1244	W.C.J. Carithers *et al.*	(COLU, NYU)
BOBISUT	74	LNC 11 646	F. Bobisut *et al.*	(PADO)
COWELL	74	PR D10 2083	P.L. Cowell *et al.*	(STON, COLU)
GEWENIGER	74B	PL 48B 487	C. Geweniger *et al.*	(CERN, HEIDH)
GJESDAL	74B	PL 52B 119	S. Gjesdal *et al.*	(CERN, HEIDH)
BURGUN	73	PL 46B 481	G. Burgun *et al.*	(SACL, CERN)
GJESDAL	73	PL 44B 217	S. Gjesdal *et al.*	(CERN, HEIDH)
HILL	73	PR D8 1290	D.G. Hill *et al.*	(BNL, CMU)
ALITTI	72	PL 39B 568	J. Alitti, E. Lesquoy, A. Muller	(SACL)
BURGUN	72	NP B50 194	G. Burgun *et al.*	(SACL, CERN, OSLO)
METCALF	72	PL 40B 703	M. Metcalf *et al.*	(CERN, IPN, WIEN)
MORSE	72B	PRL 28 388	R. Morse *et al.*	(COLO, PRIN, UMD)
NAGY	72	NP B47 94	E. Nagy, F. Telbisz, G. Vesztergombi	(BUDA)
Also		PL 30B 498	G. Bozoki *et al.*	(BUDA)
SKJEGGEST...	72	NP B48 343	O. Skjeggestad *et al.*	(OSLO, CERN, SACL)
BALTAY	71	PRL 27 1678	C. Baltay *et al.*	(COLU)
Also		Thesis Nevis 187	W.A. Cooper	(COLU)
MOFFETT	70	BAPS 15 512	R. Moffett *et al.*	(ROCH)
BOZOKI	69	PL 30B 498	G. Bozoki *et al.*	(BUDA)
DOYLE	69	Thesis UCRL 18139	J.C. Doyle	(LRL)
GOBBI	69	PRL 22 682	B. Gobbi *et al.*	(ROCH)
HYAMS	69B	PL 29B 521	B.D. Hyams *et al.*	(CERN, MPIM)
MORFIN	69	PRL 23 660	J.G. Morfin, D. Sinclair	(MICH)
DONALD	68B	PL 27B 58	R.A. Donald *et al.*	(LIVP, CERN, IPNP+)
HILL	68	PR 171 1418	D.G. Hill *et al.*	(BNL, CMU)
AUBERT	65	PL 17 59	B. Aubert *et al.*	(EPOL, ORSAY)
BROWN	63	PR 130 769	J.L. Brown *et al.*	(LRL, MICH)
CHRETIEN	63	PR 131 2208	M. Chretien *et al.*	(BRAN, BROW, HARV+)
BROWN	61	NC 19 1155	J.L. Brown *et al.*	(MICH)
BOLDT	58B	PRL 1 150	E. Boldt, D.O. Caldwell, Y. Pal	(MIT)

OTHER RELATED PAPERS

LITTENBERG	93	ARNPS 43 729	L.S. Littenberg, G. Valencia	(BNL, FNAL)
Rare and Radiative Kaon Decays				
BATTISTON	92	PRPL 214 293	R. Battiston *et al.*	(PGIA, CERN, TRSTT)
Status and Perspectives of K Decay Physics				
TRILLING	65B	UCRL 16473	G.N. Trilling	(LRL)
Updated from 1965 Argonne Conference, page 115.				
CRAWFORD	62	CERN Conf. 827	F.S. Crawford	(LRL)
FITCH	61	NC 22 1160	V.L. Fitch, P.A. Piroue, R.B. Perkins	(PRIN+)
GOOD	61	PR 124 1223	R.H. Good *et al.*	(LRL)
BIRGE	60	Rochester Conf. 601	R.W. Birge *et al.*	(LRL, WISC)
MULLER	60	PRL 4 418	F. Muller *et al.*	(LRL, BNL)

K^0_L

$I(J^P) = \frac{1}{2}(0^-)$

$m_{K^0_L} - m_{K^0_S}$

For earlier measurements, beginning with GOOD 61 and FITCH 61, see our 1986 edition, Physics Letters **170B** 132 (1986).

OUR FIT is described in the note on "*CP* violation in K_L decays" in the K^0_L Particle Listings. The result labeled "OUR FIT Assuming *CPT*" ["OUR FIT Not assuming *CPT*"] includes all measurements except those with the comment "Not assuming *CPT*" ["Assuming *CPT*"]. Measurements with neither comment do not assume *CPT* and enter both fits.

VALUE ($10^{10}\ \hbar\ s^{-1}$)		*DOCUMENT ID*		*TECN*	*COMMENT*
0.5293 ±0.0009	**OUR FIT**	Error includes scale factor of 1.3. Assuming *CPT*			
0.5289 ±0.0010	**OUR FIT**	Not assuming *CPT*			
0.52797±0.00195		[1,2] ABOUZAID	11	KTEV	Not assuming *CPT*
0.52699±0.00123		[1,3] ABOUZAID	11	KTEV	Assuming *CPT*
0.5240 ±0.0044	±0.0033	APOSTOLA...	99C	CPLR	K^0-$\overline{K}^0$ to $\pi^+\pi^-$
0.5297 ±0.0030	±0.0022	[4] SCHWINGEN...	95	E773	20–160 GeV K beams
0.5286 ±0.0028		[5] GIBBONS	93	E731	Assuming *CPT*
0.5257 ±0.0049	±0.0021	[4] GIBBONS	93C	E731	Not assuming *CPT*
0.5340 ±0.00255	±0.0015	[6] GEWENIGER	74C	SPEC	Gap method
0.5334 ±0.0040	±0.0015	[6,7] GJESDAL	74	SPEC	Assuming *CPT*
• • • We do not use the following data for averages, fits, limits, etc. • • •					
0.5261 ±0.0015		[8] ALAVI-HARATI	03	KTEV	Assuming *CPT*
0.5288 ±0.0043		[9] ALAVI-HARATI	03	KTEV	Not assuming *CPT*
0.5343 ±0.0063	±0.0025	[10] ANGELOPO...	01	CPLR	
0.5295 ±0.0020	±0.0003	[11] ANGELOPO...	98D	CPLR	Assuming *CPT*
0.5307 ±0.0013		[12] ADLER	96C	RVUE	
0.5274 ±0.0029	±0.0005	[11] ADLER	95	CPLR	Sup. by ANGELOPOULOS 98D
0.482 ±0.014		[13] ARONSON	82B	SPEC	E=30–110 GeV
0.534 ±0.007		[14] CARNEGIE	71	ASPK	Gap method
0.542 ±0.006		[14] ARONSON	70	ASPK	Gap method
0.542 ±0.006		CULLEN	70	CNTR	

[1] The two ABOUZAID 11 values use the same data. The first enters the "assuming *CPT*" fit and the second enters the "not assuming *CPT*" fit.

[2] ABOUZAID 11 fit has Δm, τ_S, ϕ_ϵ, $\mathrm{Re}(\epsilon'/\epsilon)$, and $\mathrm{Im}(\epsilon'/\epsilon)$ as free parameters. See $\mathrm{Im}(\epsilon'/\epsilon)$ in the "K^0_L *CP* violation" section for correlation information.

[3] ABOUZAID 11 fit has Δm and τ_S free but constrains ϕ_ϵ to the Superweak value, i.e. assumes *CPT*. See "K^0_S Mean Life" section for correlation information.

[4] Fits Δm and ϕ_{+-} simultaneously. GIBBONS 93C systematic error is from B. Winstein via private communication. 20–160 GeV K beams.

[5] GIBBONS 93 value assume $\phi_{+-} = \phi_{00} = \phi_{SW} = (43.7 \pm 0.2)^\circ$, i.e. assumes *CPT*. 20–160 GeV K beams.

[6] These two experiments have a common systematic error due to the uncertainty in the momentum scale, as pointed out in WAHL 89.

[7] GJESDAL 74 uses charge asymmetry in $K^0_{\ell 3}$ decays.

[8] ALAVI-HARATI 03 fit Δm and $\tau_{K^0_S}$ simultaneously. ϕ_{+-} is constrained to the Superweak value, i.e. *CPT* is assumed. See "K^0_S Mean Life" section for correlation information. Superseded by ABOUZAID 11.

[9] ALAVI-HARATI 03 fit Δm, ϕ_{+-}, and τ_{K_S} simultaneously. See ϕ_{+-} in the "K_L *CP* violation" section for correlation information. Superseded by ABOUZAID 11.

[10] ANGELOPOULOS 01 uses strong interactions strangeness tagging at two different times.

[11] Uses $\overline{K}^0_{e3}$ and K^0_{e3} strangeness tagging at production and decay. Assumes *CPT* conservation on $\Delta S = -\Delta Q$ transitions.

[12] ADLER 96C is the result of a fit which includes nearly the same data as entered into the "OUR FIT" value above.

[13] ARONSON 82 find that Δm may depend on the kaon energy.

[14] ARONSON 70 and CARNEGIE 71 use K^0_S mean life = $(0.862 \pm 0.006) \times 10^{-10}$ s. We have not attempted to adjust these values for the subsequent change in the K^0_S mean life or in η_{+-}.

K^0_L MEAN LIFE

VALUE (10^{-8} s)	EVTS	DOCUMENT ID		TECN	COMMENT
5.116±0.021 OUR FIT	Error includes scale factor of 1.1.				
5.099±0.021 OUR AVERAGE					
5.072±0.011±0.035	13M	[1] AMBROSINO	06	KLOE	$\sum_i B_i = 1$
5.092±0.017±0.025	15M	AMBROSINO	05c	KLOE	
5.154±0.044	0.4M	VOSBURGH	72	CNTR	
• • • We do not use the following data for averages, fits, limits, etc. • • •					
5.15 ±0.14		DEVLIN	67	CNTR	

[1] AMBROSINO 06 uses $\phi \to K_L K_S$ with K_L tagged by $K_S \to \pi^+\pi^-$. The four major K_L BR's are measured, the small remainder ($\pi^+\pi^-$,$\pi^0\pi^0$,$\gamma\gamma$) is taken from PDG 04. This KLOE K_L lifetime is obtained by imposing $\sum_i B_i = 1$. The correlation matrix among the four measured K_L BR's and this K_L lifetime is

	K_{e3}	$K_{\mu3}$	$3\pi^0$	$\pi^+\pi^-\pi^0$	τ_{K_L}
K_{e3}	1	−0.25	−0.56	−0.07	0.25
$K_{\mu3}$		1	−0.43	−0.20	0.33
$3\pi^0$			1	−0.39	−0.21
$\pi^+\pi^-\pi^0$				1	−0.39
τ_{K_L}					1

These correlations are taken into account in our fit. The average of this KLOE mean life measurement and the independent KLOE measurement in AMBROSINO 05c is $(5.084 \pm 0.023) \times 10^{-8}$ s.

K^0_L DECAY MODES

	Mode		Fraction (Γ_i/Γ)	Scale factor/ Confidence level
	Semileptonic modes			
Γ_1	$\pi^\pm e^\mp \nu_e$ Called K^0_{e3}.	[a]	(40.55 ±0.11) %	S=1.7
Γ_2	$\pi^\pm \mu^\mp \nu_\mu$ Called $K^0_{\mu3}$.	[a]	(27.04 ±0.07) %	S=1.1
Γ_3	$(\pi\mu\text{atom})\nu$		$(1.05 \pm 0.11) \times 10^{-7}$	
Γ_4	$\pi^0\pi^\pm e^\mp \nu$	[a]	$(5.20 \pm 0.11) \times 10^{-5}$	
Γ_5	$\pi^\pm e^\mp \nu e^+ e^-$	[a]	$(1.26 \pm 0.04) \times 10^{-5}$	
	Hadronic modes, including Charge conjugation×Parity Violating (*CPV*) modes			
Γ_6	$3\pi^0$		(19.52 ±0.12) %	S=1.6
Γ_7	$\pi^+\pi^-\pi^0$		(12.54 ±0.05) %	
Γ_8	$\pi^+\pi^-$	*CPV* [b]	$(1.967 \pm 0.010) \times 10^{-3}$	S=1.5
Γ_9	$\pi^0\pi^0$	*CPV*	$(8.64 \pm 0.06) \times 10^{-4}$	S=1.8
	Semileptonic modes with photons			
Γ_{10}	$\pi^\pm e^\mp \nu_e \gamma$	[a,c,d]	$(3.79 \pm 0.06) \times 10^{-3}$	
Γ_{11}	$\pi^\pm \mu^\mp \nu_\mu \gamma$		$(5.65 \pm 0.23) \times 10^{-4}$	
	Hadronic modes with photons or $\ell\overline{\ell}$ pairs			
Γ_{12}	$\pi^0\pi^0\gamma$		$< 2.43 \times 10^{-7}$	CL=90%
Γ_{13}	$\pi^+\pi^-\gamma$	[c,d]	$(4.15 \pm 0.15) \times 10^{-5}$	S=2.8
Γ_{14}	$\pi^+\pi^-\gamma$(DE)		$(2.84 \pm 0.11) \times 10^{-5}$	S=2.0
Γ_{15}	$\pi^0 2\gamma$	[c]	$(1.273 \pm 0.033) \times 10^{-6}$	
Γ_{16}	$\pi^0\gamma e^+ e^-$		$(1.62 \pm 0.17) \times 10^{-8}$	
	Other modes with photons or $\ell\overline{\ell}$ pairs			
Γ_{17}	2γ		$(5.47 \pm 0.04) \times 10^{-4}$	S=1.1
Γ_{18}	3γ		$< 7.4 \times 10^{-8}$	CL=90%
Γ_{19}	$e^+ e^-\gamma$		$(9.4 \pm 0.4) \times 10^{-6}$	S=2.0
Γ_{20}	$\mu^+\mu^-\gamma$		$(3.59 \pm 0.11) \times 10^{-7}$	S=1.3
Γ_{21}	$\mu^+\mu^-\mu^+\mu^-$		$< 2.3 \times 10^{-9}$	CL=90%
Γ_{22}	$e^+ e^-\gamma\gamma$	[c]	$(5.95 \pm 0.33) \times 10^{-7}$	
Γ_{23}	$\mu^+\mu^-\gamma\gamma$	[c]	$(1.0 {}^{+0.8}_{-0.6}) \times 10^{-8}$	
	Charge conjugation × Parity (*CP*) or Lepton Family number (*LF*) violating modes, or $\Delta S = 1$ weak neutral current (*S1*) modes			
Γ_{24}	$\mu^+\mu^-$	*S1*	$(6.84 \pm 0.11) \times 10^{-9}$	
Γ_{25}	$e^+ e^-$	*S1*	$(9 {}^{+6}_{-4}) \times 10^{-12}$	
Γ_{26}	$\pi^+\pi^- e^+ e^-$	*S1* [c]	$(3.11 \pm 0.19) \times 10^{-7}$	
Γ_{27}	$\pi^0\pi^0 e^+ e^-$	*S1*	$< 6.6 \times 10^{-9}$	CL=90%
Γ_{28}	$\pi^0\pi^0\mu^+\mu^-$	*S1*	$< 9.2 \times 10^{-11}$	CL=90%
Γ_{29}	$\mu^+\mu^- e^+ e^-$	*S1*	$(2.69 \pm 0.27) \times 10^{-9}$	
Γ_{30}	$e^+ e^- e^+ e^-$	*S1*	$(3.56 \pm 0.21) \times 10^{-8}$	
Γ_{31}	$\pi^0\mu^+\mu^-$	*CP,S1* [e]	$< 3.8 \times 10^{-10}$	CL=90%
Γ_{32}	$\pi^0 e^+ e^-$	*CP,S1* [e]	$< 2.8 \times 10^{-10}$	CL=90%
Γ_{33}	$\pi^0\nu\overline{\nu}$	*CP,S1* [f]	$< 2.2 \times 10^{-9}$	CL=90%
Γ_{34}	$\pi^0\pi^0\nu\overline{\nu}$	*S1*	$< 8.1 \times 10^{-7}$	CL=90%
Γ_{35}	$e^\pm\mu^\mp$	*LF* [a]	$< 4.7 \times 10^{-12}$	CL=90%
Γ_{36}	$e^\pm e^\pm\mu^\mp\mu^\mp$	*LF* [a]	$< 4.12 \times 10^{-11}$	CL=90%
Γ_{37}	$\pi^0\mu^\pm e^\mp$	*LF* [a]	$< 7.6 \times 10^{-11}$	CL=90%
Γ_{38}	$\pi^0\pi^0\mu^\pm e^\mp$	*LF*	$< 1.7 \times 10^{-10}$	CL=90%
	Lorentz invariance violating modes			
Γ_{39}	$\pi^0\gamma$		$< 1.7 \times 10^{-7}$	CL=90%

[a] The value is for the sum of the charge states or particle/antiparticle states indicated.

[b] This mode includes gammas from inner bremsstrahlung but not the direct emission mode $K^0_L \to \pi^+\pi^-\gamma$(DE).

[c] See the Particle Listings below for the energy limits used in this measurement.

[d] Most of this radiative mode, the low-momentum γ part, is also included in the parent mode listed without γ's.

[e] Allowed by higher-order electroweak interactions.

[f] Violates *CP* in leading order. Test of direct *CP* violation since the indirect *CP*-violating and *CP*-conserving contributions are expected to be suppressed.

CONSTRAINED FIT INFORMATION

An overall fit to the mean life and 15 branching ratios uses 27 measurements and one constraint to determine 11 parameters. The overall fit has a $\chi^2 = 37.4$ for 17 degrees of freedom.

The following *off-diagonal* array elements are the correlation coefficients $\langle \delta p_i \delta p_j \rangle / (\delta p_i \cdot \delta p_j)$, in percent, from the fit to parameters p_i, including the branching fractions, $x_i \equiv \Gamma_i/\Gamma_{\text{total}}$. The fit constrains the x_i whose labels appear in this array to sum to one.

	x_1	x_2	x_6	x_7	x_8	x_9	x_{13}	x_{14}	x_{17}	x_{19}
x_2	−21									
x_6	−77	−29								
x_7	−15	−20	−18							
x_8	53	−11	−47	4						
x_9	30	−23	−11	−12	64					
x_{13}	6	−1	−6	0	12	8				
x_{14}	6	−1	−6	0	11	7	93			
x_{17}	−46	−22	64	−14	−21	8	−3	−3		
x_{19}	−5	−2	7	−1	−3	−1	0	0	4	
Γ	−27	−9	24	15	−13	−6	−2	−2	15	2

	Mode		Rate (10^8 s^{-1})	Scale factor
Γ_1	$\pi^\pm e^\mp \nu_e$ Called K^0_{e3}.	[a]	0.07927±0.00034	1.1
Γ_2	$\pi^\pm \mu^\mp \nu_\mu$ Called $K^0_{\mu3}$.	[a]	0.05286±0.00025	1.1
Γ_6	$3\pi^0$		0.03815±0.00030	1.5
Γ_7	$\pi^+\pi^-\pi^0$		0.02451±0.00015	
Γ_8	$\pi^+\pi^-$	[b]	$(3.844 \pm 0.023) \times 10^{-4}$	1.2
Γ_9	$\pi^0\pi^0$		$(1.690 \pm 0.013) \times 10^{-4}$	1.4
Γ_{13}	$\pi^+\pi^-\gamma$	[c,d]	$(8.11 \pm 0.29) \times 10^{-6}$	2.7
Γ_{14}	$\pi^+\pi^-\gamma$(DE)		$(5.55 \pm 0.21) \times 10^{-6}$	2.0
Γ_{17}	2γ		$(1.069 \pm 0.010) \times 10^{-4}$	1.2
Γ_{19}	$e^+ e^-\gamma$		$(1.84 \pm 0.08) \times 10^{-6}$	1.9

K^0_L DECAY RATES

$\Gamma(\pi^+\pi^-\pi^0)$ — Γ_7

VALUE (10^6 s^{-1})	EVTS	DOCUMENT ID		TECN	COMMENT
2.451±0.015 OUR FIT					
• • • We do not use the following data for averages, fits, limits, etc. • • •					
2.32 ${}^{+0.13}_{-0.15}$	192	BALDO-...	75	HLBC	Assumes *CP*
2.35 ±0.20	180	[1] JAMES	72	HBC	Assumes *CP*
2.71 ±0.28	99	CHO	71	DBC	Assumes *CP*
2.5 ±0.3	98	[1] JAMES	71	HBC	Assumes *CP*
2.12 ±0.33	50	MEISNER	71	HBC	Assumes *CP*
2.20 ±0.35	53	WEBBER	70	HBC	Assumes *CP*
2.62 ${}^{+0.28}_{-0.27}$	136	BEHR	66	HLBC	Assumes *CP*
3.26 ±0.77	18	ANDERSON	65	HBC	
1.4 ±0.4	14	FRANZINI	65	HBC	

[1] JAMES 72 is a final measurement and includes JAMES 71.

Int. J. Mod. Phys. A 2026.41. Downloaded from www.worldscientific.com
by LIFORNIA @ BERKELEY on 09/16/26. Re-use and distribution is strictly not permitted, except for Open Access articles.

Int. J. Mod. Phys. A 2026.41. Downloaded from www.worldscientific.com
by UNIVERSITY OF CALIFORNIA @ BERKELEY on 09/16/26. Re-use and distribution is strictly not permitted, except for Open Access articles.

$\Gamma(\pi^\pm e^\mp \nu_e)$ — Γ_1

VALUE (10^6 s^{-1})	EVTS	DOCUMENT ID		TECN	COMMENT
7.927±0.034 OUR FIT	Error includes scale factor of 1.1.				
• • • We do not use the following data for averages, fits, limits, etc. • • •					
7.81 ±0.56	620	CHAN	71	HBC	
$7.52\ ^{+0.85}_{-0.72}$		AUBERT	65	HLBC	$\Delta S=\Delta Q, CP$ assumed

$\Gamma(\pi^\pm e^\mp \nu_e) + \Gamma(\pi^\pm \mu^\mp \nu_\mu)$ — $(\Gamma_1+\Gamma_2)$

VALUE (10^6 s^{-1})	EVTS	DOCUMENT ID		TECN	COMMENT
13.21±0.05 OUR FIT					
• • • We do not use the following data for averages, fits, limits, etc. • • •					
12.4 ±0.7	410	[1] BURGUN	72	HBC	$K^+ p \to K^0 p \pi^+$
8.47±1.69	126	[1] MANN	72	HBC	$K^- p \to n \overline{K}^0$
13.1 ±1.3	252	[1] WEBBER	71	HBC	$K^- p \to n \overline{K}^0$
11.6 ±0.9	393	[1,2] CHO	70	DBC	$K^+ n \to K^0 p$
10.3 ±0.8	335	[2] HILL	67	DBC	$K^+ n \to K^0 p$
$9.85\ ^{+1.15}_{-1.05}$	109	[1] FRANZINI	65	HBC	

[1] Assumes $\Delta S = \Delta Q$ rule.
[2] CHO 70 includes events of HILL 67.

K^0_L BRANCHING RATIOS

Semileptonic modes

$\Gamma(\pi^\pm e^\mp \nu_e)/\Gamma_{total}$ — Γ_1/Γ

VALUE	EVTS	DOCUMENT ID		TECN
0.4055±0.0011 OUR FIT	Error includes scale factor of 1.7.			
0.4047±0.0028 OUR AVERAGE	Error includes scale factor of 3.1.			
0.4007±0.0005±0.0015	13M	[1] AMBROSINO	06	KLOE
0.4067±0.0011		[2] ALEXOPOU...	04	KTEV

[1] There are correlations between these five KLOE measurements: $B(K_L \to \pi e \nu)$, $B(K_L \to \pi \mu \nu)$, $B(K_L \to 3\pi^0)$, $B(K_L \to \pi^+\pi^-\pi^0)$, and τ_{K_L} measured in AMBROSINO 06. See the footnote for the τ_{K_L} measurement for the correlation matrix.
[2] ALEXOPOULOS 04 constrains $\sum_i B_i = 0.9993$ for the six major K_L branching fractions. The correlations among these branching fractions are taken into account in our fit. The correlation matrix is

	K_{e3}	$K_{\mu3}$	$3\pi^0$	$\pi^+\pi^-\pi^0$	$\pi^+\pi^-$	$\pi^0\pi^0$
K_{e3}	1					
$K_{\mu3}$	0.15	1				
$3\pi^0$	−0.77	−0.62	1			
$\pi^+\pi^-\pi^0$	0.18	0.08	−0.54	1		
$\pi^+\pi^-$	0.28	0.22	−0.48	0.49	1	
$\pi^0\pi^0$	−0.72	−0.54	0.89	−0.46	−0.39	1

$\Gamma(\pi^\pm \mu^\mp \nu_\mu)/\Gamma_{total}$ — Γ_2/Γ

VALUE	EVTS	DOCUMENT ID		TECN
0.2704±0.0007 OUR FIT	Error includes scale factor of 1.1.			
0.2700±0.0008 OUR AVERAGE				
0.2698±0.0005±0.0015	13M	[1] AMBROSINO	06	KLOE
0.2701±0.0009		[2] ALEXOPOU...	04	KTEV

[1] There are correlations between these five KLOE measurements: $B(K_L \to \pi e \nu)$, $B(K_L \to \pi \mu \nu)$, $B(K_L \to 3\pi^0)$, $B(K_L \to \pi^+\pi^-\pi^0)$, and τ_{K_L} measured in AMBROSINO 06. See the footnote for the τ_{K_L} measurement for the correlation matrix.
[2] For correlations with other ALEXOPOULOS 04 measurements, see the footnote with their $B(K_L \to \pi e \nu)$ measurement.

$[\Gamma(\pi^\pm e^\mp \nu_e) + \Gamma(\pi^\pm \mu^\mp \nu_\mu)]/\Gamma_{total}$ — $(\Gamma_1+\Gamma_2)/\Gamma$

VALUE	DOCUMENT ID
0.6760±0.0012 OUR FIT	Error includes scale factor of 1.6.

$\Gamma(\pi^\pm \mu^\mp \nu_\mu)/\Gamma(\pi^\pm e^\mp \nu_e)$ — Γ_2/Γ_1

VALUE	EVTS	DOCUMENT ID		TECN	COMMENT
0.6669±0.0027 OUR FIT	Error includes scale factor of 1.2.				
0.666 ±0.004 OUR AVERAGE	Error includes scale factor of 1.6.				
• • • We use the following data for averages but not for fits. • • •					
0.6740±0.0059	13M	[1] AMBROSINO	06	KLOE	Not in fit
0.6640±0.0014±0.0022	394k	[2] ALEXOPOU...	04	KTEV	Not in fit
• • • We do not use the following data for averages, fits, limits, etc. • • •					
0.702 ±0.011	33k	CHO	80	HBC	
0.662 ±0.037	10k	WILLIAMS	74	ASPK	
0.741 ±0.044	6700	BRANDENB...	73	HBC	
0.662 ±0.030	1309	EVANS	73	HLBC	
0.68 ±0.08	3548	BASILE	70	OSPK	
0.71 ±0.05	770	BUDAGOV	68	HLBC	

[1] AMBROSINO 06 enters the fit via their separate measurements of these two modes.
[2] ALEXOPOULOS 04 enters the fit via their separate measurements of these two modes.

$\Gamma((\pi\mu\text{atom})\nu)/\Gamma(\pi^\pm \mu^\mp \nu_\mu)$ — Γ_3/Γ_2

VALUE (units 10^{-7})	EVTS	DOCUMENT ID		TECN
3.90±0.39	155	[1] ARONSON	86	SPEC
• • • We do not use the following data for averages, fits, limits, etc. • • •				
seen	18	COOMBES	76	WIRE

[1] ARONSON 86 quote theoretical value of $(4.31 \pm 0.08) \times 10^{-7}$.

$\Gamma(\pi^0 \pi^\pm e^\mp \nu)/\Gamma_{total}$ — Γ_4/Γ

VALUE (units 10^{-5})	CL%	EVTS	DOCUMENT ID		TECN
5.20±0.11 OUR AVERAGE					
5.21±0.07±0.09		5402	BATLEY	04	NA48
5.16±0.20±0.22		729	MAKOFF	93	E731
• • • We do not use the following data for averages, fits, limits, etc. • • •					
6.2 ±2.0		16	CARROLL	80C	SPEC
< 220	90		[1] DONALDSON	74	SPEC

[1] DONALDSON 74 uses $K^0_L \to \pi^+\pi^-\pi^0$/(all K^0_L) decays = 0.126.

$\Gamma(\pi^\pm e^\mp \nu e^+ e^-)/\Gamma(\pi^+\pi^-\pi^0)$ — Γ_5/Γ_7

VALUE (units 10^{-5})	EVTS	DOCUMENT ID		TECN	COMMENT
10.02±0.17±0.29	19k	[1] ABOUZAID	07C	KTEV	M_{ee}> 5 MeV, E^*_{ee} > 30 MeV

[1] E^*_{ee} is the energy of the e^+e^- pair in the kaon rest frame. ABOUZAID 07C reports $[\Gamma(K^0_L \to \pi^\pm e^\mp \nu e^+ e^-)/\Gamma(K^0_L \to \pi^+\pi^-\pi^0)]$ / $[B(\pi^0 \to e^+e^-\gamma)] = (8.54 \pm 0.07 \pm 0.13) \times 10^{-3}$ which we multiply by our best (shown rounded) value $B(\pi^0 \to e^+e^-\gamma) = (1.174 \pm 0.035) \times 10^{-2}$. Our first error is their experiment's error and our second error is the systematic error from using our best (shown rounded) value.

Hadronic modes, including Charge conjugation×Parity Violating (*CPV*) modes

$\Gamma(3\pi^0)/\Gamma_{total}$ — Γ_6/Γ

VALUE	EVTS	DOCUMENT ID		TECN	COMMENT
0.1952±0.0012 OUR FIT	Error includes scale factor of 1.6.				
0.1969±0.0026 OUR AVERAGE	Error includes scale factor of 2.0.				
• • • We use the following data for averages but not for fits. • • •					
0.1997±0.0003±0.0019	13M	[1] AMBROSINO	06	KLOE	Not fitted
0.1945±0.0018		[1] ALEXOPOU...	04	KTEV	Not fitted

[1] We exclude these $B(K_L \to 3\pi^0)$ measurements from our fit because the authors have constrained K_L branching fractions to sum to one. It enters our fit via the other measurements from the experiment and their correlations, along with our constraint that the fitted branching fractions sum to one.

$\Gamma(3\pi^0)/\Gamma(\pi^\pm e^\mp \nu_e)$ — Γ_6/Γ_1

VALUE	EVTS	DOCUMENT ID		TECN	COMMENT
0.481 ±0.004 OUR FIT	Error includes scale factor of 1.8.				
• • • We use the following data for averages but not for fits. • • •					
0.4782±0.0014±0.0053	209k	[1] ALEXOPOU...	04	KTEV	Not in fit
• • • We do not use the following data for averages, fits, limits, etc. • • •					
0.545 ±0.004 ±0.009	38k	KREUTZ	95	NA31	

[1] This measurement enters the fit via their separate measurements of these two modes.

$\Gamma(3\pi^0)/[\Gamma(\pi^\pm e^\mp \nu_e) + \Gamma(\pi^\pm \mu^\mp \nu_\mu) + \Gamma(\pi^+\pi^-\pi^0)]$ — $\Gamma_6/(\Gamma_1+\Gamma_2+\Gamma_7)$

VALUE	EVTS	DOCUMENT ID		TECN	COMMENT
0.2436±0.0018 OUR FIT	Error includes scale factor of 1.6.				
• • • We do not use the following data for averages, fits, limits, etc. • • •					
0.251 ±0.014	549	BUDAGOV	68	HLBC	ORSAY measur.
0.277 ±0.021	444	BUDAGOV	68	HLBC	Ecole polytec.meas
$0.31\ ^{+0.07}_{-0.06}$	29	KULYUKINA	68	CC	
0.24 ±0.08	24	ANIKINA	64	CC	

$\Gamma(3\pi^0)/\Gamma(\pi^+\pi^-\pi^0)$ — Γ_6/Γ_7

VALUE	EVTS	DOCUMENT ID		TECN	COMMENT
1.557±0.012 OUR FIT	Error includes scale factor of 1.3.				
• • • We use the following data for averages but not for fits. • • •					
1.582±0.027	13M	[1] AMBROSINO	06	KLOE	Not in fit
• • • We do not use the following data for averages, fits, limits, etc. • • •					
1.611±0.014±0.034	28k	KREUTZ	95	NA31	
1.65 ±0.07	883	BARMIN	72B	HLBC	Error statistical only
1.80 ±0.13	1010	BUDAGOV	68	HLBC	
2.0 ±0.6	188	ALEKSANYAN	64B	FBC	

[1] AMBROSINO 06 enters the fit via their separate measurements of these two modes.

$\Gamma(\pi^+\pi^-\pi^0)/\Gamma_{total}$ — Γ_7/Γ

VALUE	EVTS	DOCUMENT ID		TECN
0.1254±0.0005 OUR FIT				
0.1255±0.0006 OUR AVERAGE				
0.1263±0.0004±0.0011	13M	[1] AMBROSINO	06	KLOE
0.1252±0.0007		[2] ALEXOPOU...	04	KTEV

[1] There are correlations between these five KLOE measurements: $B(K_L \to \pi e \nu)$, $B(K_L \to \pi \mu \nu)$, $B(K_L \to 3\pi^0)$, $B(K_L \to \pi^+\pi^-\pi^0)$, and τ_{K_L} measured in AMBROSINO 06. See the footnote for the τ_{K_L} measurement for the correlation matrix.
[2] For correlations with other ALEXOPOULOS 04 measurements, see the footnote with their $B(K_L \to \pi e \nu)$ measurement.

$\Gamma(\pi^+\pi^-\pi^0)/\Gamma(\pi^\pm e^\mp \nu_e)$ — Γ_7/Γ_1

VALUE	EVTS	DOCUMENT ID		TECN	COMMENT
0.3092±0.0016 OUR FIT	Error includes scale factor of 1.1.				
• • • We use the following data for averages but not for fits. • • •					
0.3078±0.0005±0.0017	799k	[1] ALEXOPOU...	04	KTEV	Not in fit
• • • We do not use the following data for averages, fits, limits, etc. • • •					
0.336 ±0.003 ±0.007	28k	KREUTZ	95	NA31	

[1] This measurement enters the fit via their separate measurements for the two modes.

Int. J. Mod. Phys. A 2026.41. Downloaded from www.worldscientific.com by CALIFORNIA @ BERKELEY on 09/16/26. Re-use and distribution is strictly not permitted, except for Open Access articles.

$\Gamma(\pi^+\pi^-\pi^0)/[\Gamma(\pi^\pm e^\mp\nu_e)+\Gamma(\pi^\pm\mu^\mp\nu_\mu)+\Gamma(\pi^+\pi^-\pi^0)]$ $\Gamma_7/(\Gamma_1+\Gamma_2+\Gamma_7)$

VALUE	EVTS	DOCUMENT ID		TECN	COMMENT
0.1565±0.0006 OUR FIT		Error includes scale factor of 1.1.			
• • • We do not use the following data for averages, fits, limits, etc. • • •					
0.163 ±0.003	6499	CHO	77	HBC	
0.1605±0.0038	1590	ALEXANDER	73B	HBC	
0.146 ±0.004	3200	BRANDENB...	73	HBC	
0.159 ±0.010	558	EVANS	73	HLBC	
0.167 ±0.016	1402	KULYUKINA	68	CC	
0.161 ±0.005		HOPKINS	67	HBC	
0.162 ±0.015	126	HAWKINS	66	HBC	
0.159 ±0.015	326	ASTBURY	65B	CC	
0.178 ±0.017	566	GUIDONI	65	HBC	
0.144 ±0.004	1729	HOPKINS	65	HBC	See HOPKINS 67

$\Gamma(\pi^+\pi^-)/\Gamma_{total}$ Γ_8/Γ

Violates CP conservation.

VALUE (units 10^{-3})	DOCUMENT ID		TECN
1.967±0.010 OUR FIT	Error includes scale factor of 1.5.		
1.975±0.012	[1] ALEXOPOU...	04	KTEV

[1] For correlations with other ALEXOPOULOS 04 measurements, see the footnote with their $B(K_L \to \pi e\nu)$ measurement.

$\Gamma(\pi^+\pi^-)/\Gamma(\pi^\pm e^\mp\nu_e)$ Γ_8/Γ_1

VALUE (units 10^{-3})	EVTS	DOCUMENT ID		TECN	COMMENT
4.849±0.020 OUR FIT		Error includes scale factor of 1.1.			
4.840±0.020 OUR AVERAGE					
4.826±0.022±0.016	47k	[1] LAI	07	NA48	
• • • We use the following data for averages but not for fits. • • •					
4.856±0.017±0.023	84k	[2] ALEXOPOU...	04	KTEV	Not in fit

[1] The LAI 07 central value of 4.835×10^{-3} has been reduced by 0.19% to 4.826×10^{-3} to subtract the contribution from the direct emission mode $K^0_L \to \pi^+\pi^-\gamma(DE)$.

[2] This measurement enters the fit via their separate measurements for the two modes.

$[\Gamma(\pi^+\pi^-)+\Gamma(\pi^+\pi^-\gamma(DE))]/\Gamma(\pi^\pm\mu^\mp\nu_\mu)$ $(\Gamma_8+\Gamma_{14})/\Gamma_2$

VALUE (units 10^{-3})	EVTS	DOCUMENT ID		TECN
7.38 ±0.04 OUR FIT		Error includes scale factor of 1.4.		
7.275±0.042±0.054	45k	[1] AMBROSINO	06F	KLOE

[1] Fully inclusive. Taking $B(K^0_L \to \pi\mu\nu)$ from KLOE, AMBROSINO 06, $B(K^0_L \to \pi^+\pi^- + \pi^+\pi^-\gamma(DE)) = (1.963 \pm 0.012 \pm 0.017) \times 10^{-3}$ is obtained.

$\Gamma(\pi^+\pi^-)/[\Gamma(\pi^\pm e^\mp\nu_e)+\Gamma(\pi^\pm\mu^\mp\nu_\mu)]$ $\Gamma_8/(\Gamma_1+\Gamma_2)$

Violates CP conservation.

VALUE (units 10^{-3})	EVTS	DOCUMENT ID		TECN	COMMENT
2.909±0.013 OUR FIT		Error includes scale factor of 1.3.			
• • • We do not use the following data for averages, fits, limits, etc. • • •					
3.13 ±0.14	1687	COUPAL	85	SPEC	η_{+-}=2.28 ± 0.06
3.04 ±0.14	2703	DEVOE	77	SPEC	η_{+-}=2.25 ± 0.05
2.51 ±0.23	309	[1] DEBOUARD	67	OSPK	η_{+-}=2.00 ± 0.09
2.35 ±0.19	525	[1] FITCH	67	OSPK	η_{+-}=1.94 ± 0.08

[1] Old experiments excluded from fit. See subsection on η_{+-} in section on "PARAMETERS FOR $K^0_L \to 2\pi$ DECAY" below for average η_{+-} of these experiments and for note on discrepancy.

$\Gamma(\pi^\pm e^\mp\nu_e)/\Gamma(2\text{ tracks})$ $\Gamma_1/(\Gamma_1+\Gamma_2+0.03508\Gamma_6+\Gamma_7+\Gamma_8)$

$\Gamma(2\text{ tracks}) = \Gamma(\pi^\pm e^\mp\nu_e) + \Gamma(\pi^\pm\mu^\mp\nu_\mu) + 0.03508\,\Gamma(3\pi^0) + \Gamma(\pi^+\pi^-\pi^0) + \Gamma(\pi^+\pi^-)$ where 0.03508 is the fraction of $3\pi^0$ events with one Dalitz decay ($\pi^0 \to \gamma e^+e^-$).

VALUE	EVTS	DOCUMENT ID		TECN
0.5006±0.0009 OUR FIT		Error includes scale factor of 1.3.		
0.4978±0.0035	6.8M	LAI	04B	NA48

$\Gamma(\pi^+\pi^-)/[\Gamma(\pi^\pm e^\mp\nu_e)+\Gamma(\pi^\pm\mu^\mp\nu_\mu)+\Gamma(\pi^+\pi^-\pi^0)]$ $\Gamma_8/(\Gamma_1+\Gamma_2+\Gamma_7)$

Violates CP conservation.

VALUE (units 10^{-3})	EVTS	DOCUMENT ID		TECN	COMMENT
2.454±0.011 OUR FIT		Error includes scale factor of 1.3.			
• • • We do not use the following data for averages, fits, limits, etc. • • •					
2.60 ±0.07	4200	[1] MESSNER	73	ASPK	η_{+-} = 2.23 ± 0.05

[1] From same data as $\Gamma(\pi^+\pi^-)/\Gamma(\pi^+\pi^-\pi^0)$ MESSNER 73, but with different normalization.

$\Gamma(\pi^+\pi^-)/\Gamma(\pi^+\pi^-\pi^0)$ Γ_8/Γ_7

Violates CP conservation.

VALUE (units 10^{-2})	EVTS	DOCUMENT ID		TECN	COMMENT
1.568±0.010 OUR FIT		Error includes scale factor of 1.3.			
• • • We do not use the following data for averages, fits, limits, etc. • • •					
1.64 ±0.04	4200	MESSNER	73	ASPK	η_{+-} = 2.23

$\Gamma(\pi^0\pi^0)/\Gamma_{total}$ Γ_9/Γ

Violates CP conservation.

VALUE (units 10^{-3})	DOCUMENT ID		TECN
0.864±0.006 OUR FIT	Error includes scale factor of 1.8.		
0.865±0.012	[1] ALEXOPOU...	04	KTEV

[1] For correlations with other ALEXOPOULOS 04 measurements, see the footnote with their $B(K_L \to \pi e\nu)$ measurement.

$\Gamma(\pi^0\pi^0)/\Gamma(\pi^+\pi^-)$ Γ_9/Γ_8

Violates CP conservation.

VALUE	DOCUMENT ID		
0.4395±0.0023 OUR FIT	Error includes scale factor of 2.0.		
0.4390±0.0012	ETAFIT	16	

$\Gamma(\pi^0\pi^0)/\Gamma(3\pi^0)$ Γ_9/Γ_6

Violates CP conservation.

VALUE (units 10^{-2})	EVTS	DOCUMENT ID		TECN	COMMENT
0.443 ±0.004 OUR FIT		Error includes scale factor of 2.1.			
• • • We use the following data for averages but not for fits. • • •					
0.4446±0.0016±0.0019	100k	[1] ALEXOPOU...	04	KTEV	Not in fit
• • • We do not use the following data for averages, fits, limits, etc. • • •					
0.37 ±0.08	29	BARMIN	70	HLBC	η_{00}=2.02 ± 0.23
0.32 ±0.15	30	BUDAGOV	70	HLBC	η_{00}=1.9 ± 0.5
0.46 ±0.11	57	BANNER	69	OSPK	η_{00}=2.2 ± 0.3

[1] This measurement enters the fit via their separate measurements for the two modes.

Semileptonic modes with photons

$\Gamma(\pi^\pm e^\mp\nu_e\gamma)/\Gamma(\pi^\pm e^\mp\nu_e)$ Γ_{10}/Γ_1

VALUE (units 10^{-2})	EVTS	DOCUMENT ID		TECN	COMMENT
0.935±0.015 OUR AVERAGE		Error includes scale factor of 1.9. See the ideogram below.			
0.924±0.023±0.016	9k	[1] AMBROSINO	08F	KLOE	E^*_γ >30 MeV, $\theta^*_{e\gamma}$ >20°
0.916±0.017	4309	[2] ALEXOPOU...	05	KTEV	E^*_γ >30 MeV, $\theta^*_{e\gamma}$ >20°
0.964±0.008$^{+0.011}_{-0.009}$	19k	LAI	05	NA48	E^*_γ >30 MeV, $\theta^*_{e\gamma}$ >20°
0.908±0.008$^{+0.013}_{-0.012}$	15k	ALAVI-HARATI	01J	KTEV	$E^*_\gamma \geq$ 30 MeV, $\theta^*_{e\gamma} \geq$ 20°
0.934±0.036$^{+0.055}_{-0.039}$	1384	LEBER	96	NA31	$E^*_\gamma \geq$ 30 MeV, $\theta^*_{e\gamma} \geq$ 20°

[1] Direct emission contribution measured $\langle X \rangle = -2.3 \pm 1.3 \pm 1.4$.

[2] Also measured cut E^*_γ >10 MeV, $\theta^*_{e\gamma}$ >0° 14221 evts: $\Gamma(\pi^\pm e^\mp\nu_e\gamma)$ / $\Gamma(\pi^\pm e^\mp\nu_e)$ = (4.942 ± 0.062)%.

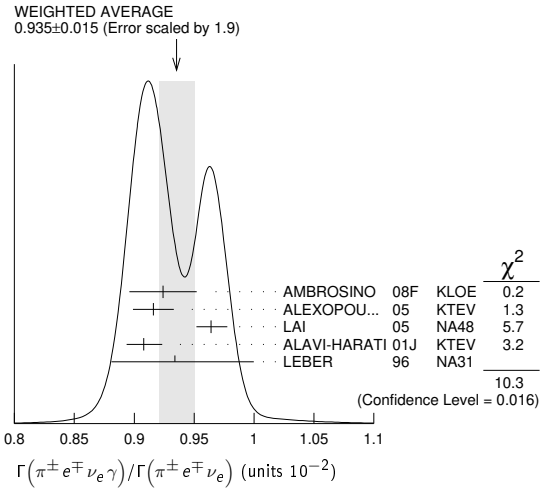

$\Gamma(\pi^\pm\mu^\mp\nu_\mu\gamma)/\Gamma(\pi^\pm\mu^\mp\nu_\mu)$ Γ_{11}/Γ_2

VALUE (units 10^{-3})	EVTS	DOCUMENT ID		TECN	COMMENT
2.09±0.08 OUR AVERAGE					
2.09±0.09		[1] ALEXOPOU...	05	KTEV	E^*_γ > 30 MeV
2.08±0.17$^{+0.16}_{-0.21}$	252	BENDER	98	NA48	$E^*_\gamma \geq$ 30 MeV

[1] Also measured cut E^*_γ >10 MeV, 1385 evts: $\Gamma(\pi^\pm\mu^\mp\nu_\mu\gamma)$ / $\Gamma(\pi^\pm\mu^\mp\nu_\mu)$ = (0.530 ± 0.014 ± 0.012)%.

Hadronic modes with photons or $\ell\bar{\ell}$ pairs

$\Gamma(\pi^0\pi^0\gamma)/\Gamma_{total}$ Γ_{12}/Γ

VALUE (units 10^{-6})	CL%	DOCUMENT ID		TECN	COMMENT
< 0.243	90	ABOUZAID	08B	KTEV	$K^0_L \to \pi^0\pi^0_D\gamma$, $\pi^0_D \to ee\gamma$
• • • We do not use the following data for averages, fits, limits, etc. • • •					
< 5.6	90	BARR	94	NA31	
<230	90	ROBERTS	94	E799	

$\Gamma(\pi^+\pi^-\gamma)/\Gamma(\pi^+\pi^-\pi^0)$ Γ_{13}/Γ_7

For earlier limits see our 1992 edition Physical Review **D45** S1 (1992).

VALUE (units 10^{-4})	EVTS	DOCUMENT ID		TECN	COMMENT
• • • We do not use the following data for averages, fits, limits, etc. • • •					
1.23±0.13	516	[1,2] CARROLL	80B	SPEC	E^*_γ > 20 MeV
2.33±0.23	546	[1,3] CARROLL	80B	SPEC	
3.56±0.26	1062	[1,4] CARROLL	80B	SPEC	E^*_γ > 20 MeV

Int. J. Mod. Phys. A 2026.41. Downloaded from www.worldscientific.com
by UNIVERSITY OF CALIFORNIA @ BERKELEY on 09/16/26. Re-use and distribution is strictly not permitted, except for Open Access articles.

[1] CARROLL 80B quotes $B(\pi^+\pi^-\gamma)$ using normalization $B(\pi^+\pi^-\pi^0) = 0.1239$. We divide by this value to obtain their measured $\Gamma(\pi^+\pi^-\gamma)$ / $\Gamma(\pi^+\pi^-\pi^0)$.
[2] Internal Bremsstrahlung component only.
[3] Direct γ emission component only.
[4] Both IB and DE components.

$\Gamma(\pi^+\pi^-\gamma)/\Gamma(\pi^+\pi^-)$ — Γ_{13}/Γ_8

VALUE (units 10^{-2})	EVTS	DOCUMENT ID		TECN	COMMENT
2.11±0.08 OUR FIT Error includes scale factor of 2.9.					
2.11±0.08 OUR AVERAGE Error includes scale factor of 2.9.					
2.08±0.02±0.02	8669	[1] ALAVI-HARATI	01B	KTEV	$E^*_\gamma > 20$ MeV
2.30±0.07	3136	RAMBERG	93	E731	$E^*_\gamma > 20$ MeV

[1] ALAVI-HARATI 01B includes both Direct Emission (DE) and Inner Bremsstrahlung (IB) processes.

$\Gamma(\pi^+\pi^-\gamma(DE))/\Gamma(\pi^+\pi^-\gamma)$ — Γ_{14}/Γ_{13}

These values assume that $\Gamma(K^0_L \to \pi^+\pi^-\gamma) = \Gamma(K^0_L \to \pi^+\pi^-\gamma(DE)) + \Gamma(K^0_L \to \pi^+\pi^-\gamma(IB))$, the sum of widths for the direct emission (DE) and inner bremsstrahlung (IE) processes, with no IB-DE interference. DE assumes a form factor as described in RAMBERG 93.

VALUE	EVTS	DOCUMENT ID		TECN	COMMENT
0.684±0.009 OUR FIT					
0.684±0.009 OUR AVERAGE					
0.689±0.021	111k	ABOUZAID	06A	KTEV	$E^*_\gamma > 20$ MeV
0.683±0.011	8669	ALAVI-HARATI	01B	KTEV	$E^*_\gamma > 20$ MeV
0.685±0.041	3136	RAMBERG	93	E731	$E^*_\gamma > 20$ MeV

$\Gamma(\pi^0 2\gamma)/\Gamma_{total}$ — Γ_{15}/Γ

VALUE (units 10^{-6})	CL%	EVTS	DOCUMENT ID		TECN	COMMENT
1.273±0.033 OUR AVERAGE						
1.28 ±0.06 ±0.01		1.4k	[1] ABOUZAID	08	KTEV	
1.27 ±0.04 ±0.01		2.5k	[2] LAI	02B	NA48	
• • • We do not use the following data for averages, fits, limits, etc. • • •						
1.68 ±0.07 ±0.08		884	[3] ALAVI-HARATI	99B	KTEV	
1.7 ±0.2 ±0.2		63	[4] BARR	92	NA31	
1.86 ±0.60 ±0.60		60	PAPADIMITR...	91	E731	$m_{\gamma\gamma} > 280$ MeV
<5.1	90		PAPADIMITR...	91	E731	$m_{\gamma\gamma} < 264$ MeV
2.1 ±0.6		14	[5] BARR	90C	NA31	$m_{\gamma\gamma} > 280$ MeV

[1] ABOUZAID 08 reports $(1.29 \pm 0.03 \pm 0.05) \times 10^{-6}$ from a measurement of $[\Gamma(K^0_L \to \pi^0 2\gamma)/\Gamma_{total}]$ / $[B(K^0_L \to \pi^0\pi^0)]$ assuming $B(K^0_L \to \pi^0\pi^0) = (8.69 \pm 0.04) \times 10^{-4}$, which we rescale to our best (shown rounded) value $B(K^0_L \to \pi^0\pi^0) = (8.64 \pm 0.06) \times 10^{-4}$. Our first error is their experiment's error and our second error is the systematic error from using our best (shown rounded) value.
[2] LAI 02B reports $[\Gamma(K^0_L \to \pi^0 2\gamma)/\Gamma_{total}]$ / $[B(K^0_L \to \pi^0\pi^0)] = (1.467 \pm 0.032 \pm 0.032) \times 10^{-3}$ which we multiply by our best (shown rounded) value $B(K^0_L \to \pi^0\pi^0) = (8.64 \pm 0.06) \times 10^{-4}$. Our first error is their experiment's error and our second error is the systematic error from using our best (shown rounded) value. They also find that $B(\pi^0 2\gamma, m_{\gamma\gamma} < 110 \text{ MeV}) < 0.6 \times 10^{-8}$(90% CL).
[3] ALAVI-HARATI 99B finds that $\Gamma(\pi^0 2\gamma, m_{\gamma\gamma} < 240 \text{ MeV}))$ / $\Gamma(\pi^0 2\gamma) = (17.3 \pm 1.3 \pm 1.5)$%. Superseded by ABOUZAID 08.
[4] BARR 92 find that $\Gamma(\pi^0 2\gamma, m_{\gamma\gamma} < 240 \text{ MeV})/\Gamma(\pi^0 2\gamma) < 0.09$ (90% CL).
[5] BARR 90C superseded by BARR 92.

$\Gamma(\pi^0\gamma e^+e^-)/\Gamma_{total}$ — Γ_{16}/Γ

VALUE (units 10^{-8})	CL%	EVTS	DOCUMENT ID		TECN
1.62±0.14±0.09		125	[1] ABOUZAID	07D	KTEV
• • • We do not use the following data for averages, fits, limits, etc. • • •					
2.34±0.35±0.13		44	ALAVI-HARATI	01E	KTEV
<71	90	0	MURAKAMI	99	SPEC

[1] ABOUZAID 07D includes 1997 (ALAVI-HARATI 01E) and 1999 data. It measures the ratio of $B(K^0_L \to \pi^0\gamma e^+e^-)$ / $B(K^0_L \to \pi^0\pi^0_D)$, where π^0_D is the Dalitz decaying π^0, and uses PDG 06 values $B(K^0_L \to \pi^0\pi^0) = (8.69 \pm 0.04) \times 10^{-4}$, and $B(\pi^0_D \to e^+e^-\gamma) = (1.198 \pm 0.032) \times 10^{-2}$. Supersedes ALAVI-HARATI 01E result.

Other modes with photons or $\ell\bar{\ell}$ pairs

$\Gamma(2\gamma)/\Gamma_{total}$ — Γ_{17}/Γ

VALUE (units 10^{-4})	EVTS	DOCUMENT ID		TECN	COMMENT
5.47±0.04 OUR FIT Error includes scale factor of 1.1.					
• • • We do not use the following data for averages, fits, limits, etc. • • •					
4.54±0.84		[1] BANNER	72B	OSPK	
4.5 ±1.0	23	ENSTROM	71	OSPK	K^0_L 1.5–9 GeV/c
5.0 ±1.0		[2] REPELLIN	71	OSPK	
5.5 ±1.1	90	KUNZ	68	OSPK	Norm.to 3 π(C+N)

[1] This value uses $(\eta_{00}/\eta_{+-})^2 = 1.05 \pm 0.14$. In general, $\Gamma(2\gamma)/\Gamma_{total} = [(4.32 \pm 0.55) \times 10^{-4}][(\eta_{00}/\eta_{+-})^2]$.
[2] Assumes regeneration amplitude in copper at 2 GeV is 22 mb. To evaluate for a given regeneration amplitude and error, multiply by (regeneration amplitude/22mb)^2.

$\Gamma(2\gamma)/\Gamma(3\pi^0)$ — Γ_{17}/Γ_6

VALUE (units 10^{-3})	EVTS	DOCUMENT ID		TECN	COMMENT
2.802±0.017 OUR FIT					
2.802±0.018 OUR AVERAGE					
2.79 ±0.02 ±0.02	27k	ADINOLFI	03	KLOE	
2.81 ±0.01 ±0.02		LAI	03	NA48	
• • • We do not use the following data for averages, fits, limits, etc. • • •					
2.13 ±0.43	28	BARMIN	71	HLBC	
2.24 ±0.28	115	BANNER	69	OSPK	
2.5 ±0.7	16	ARNOLD	68B	HLBC	Vacuum decay

$\Gamma(2\gamma)/\Gamma(\pi^0\pi^0)$ — Γ_{17}/Γ_9

VALUE	EVTS	DOCUMENT ID		TECN
0.633±0.006 OUR FIT Error includes scale factor of 1.4.				
0.632±0.004±0.008	110k	BURKHARDT	87	NA31

$\Gamma(3\gamma)/\Gamma_{total}$ — Γ_{18}/Γ

VALUE	CL%	DOCUMENT ID		TECN
<7.4 × 10^{-8}	90	[1] TUNG	11	K391
• • • We do not use the following data for averages, fits, limits, etc. • • •				
<2.4 × 10^{-7}	90	[2] BARR	95C	NA31

[1] TUNG 11 reports the result assuming parity violating interaction and using 2005 data (Run-II and III). Assuming parity conserving or phase space interaction, the 90% upper limits obtained are 7.5×10^{-8} and 8.6×10^{-8}, respectively.
[2] Assumes a phase-space decay distribution.

$\Gamma(e^+e^-\gamma)/\Gamma_{total}$ — Γ_{19}/Γ

VALUE (units 10^{-6})	EVTS	DOCUMENT ID		TECN
9.4±0.4 OUR FIT Error includes scale factor of 2.0.				
10.0±0.5 OUR AVERAGE Error includes scale factor of 1.5. See the ideogram below.				
10.6±0.2±0.4	6864	[1] FANTI	99B	NA48
9.2±0.5±0.5	1053	BARR	90B	NA31
$9.1 \pm 0.4^{+0.6}_{-0.5}$	919	OHL	90B	B845

[1] For FANTI 99B, the ±0.4 systematic error includes for uncertainties in the calculation, primarily uncertainties in the $\pi^0 \to e^+e^-\gamma$ and $K^0_L \to \pi^0\pi^0$ branching ratios, evaluated using our 1999 Web edition values.

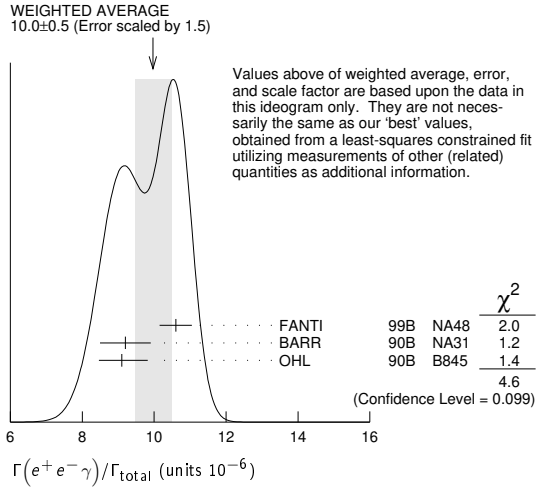

$\Gamma(e^+e^-\gamma)/\Gamma(3\pi^0)$ — Γ_{19}/Γ_6

VALUE (units 10^{-5})	EVTS	DOCUMENT ID		TECN
4.82±0.21 OUR FIT Error includes scale factor of 2.0.				
4.63±0.04±0.13	83k	[1] ABOUZAID	07B	KTEV

[1] ABOUZAID 07B reports $[\Gamma(K^0_L \to e^+e^-\gamma)/\Gamma(K^0_L \to 3\pi^0)]$ / $[3\Gamma(\pi^0 \to 2\gamma)/\Gamma_{total} \times \Gamma(\pi^0 \to e^+e^-\gamma)/\Gamma_{total}] = (1.3302 \pm 0.0046 \pm 0.0103) \times 10^{-3}$ which we multiply by our best (shown rounded) value $3\Gamma(\pi^0 \to 2\gamma)/\Gamma_{total} \times \Gamma(\pi^0 \to e^+e^-\gamma)/\Gamma_{total} = 0.0348 \pm 0.0010$. Our first error is their experiment's error and our second error is the systematic error from using our best (shown rounded) value.

$\Gamma(\mu^+\mu^-\gamma)/\Gamma_{total}$ — Γ_{20}/Γ

VALUE (units 10^{-7})	EVTS	DOCUMENT ID		TECN
3.59±0.11 OUR AVERAGE Error includes scale factor of 1.3.				
3.62±0.04±0.08	9100	ALAVI-HARATI	01G	KTEV
3.4 ±0.6 ±0.4	45	FANTI	97	NA48
3.23±0.23±0.19	197	SPENCER	95	E799

$\Gamma(\mu^+\mu^-\mu^+\mu^-)/\Gamma_{total}$ — Γ_{21}/Γ

VALUE	CL%	DOCUMENT ID		TECN
<2.3 × 10^{-9}	90	[1] AAIJ	23AE	LHCB

[1] AAIJ 23AE uses 5.1 fb^{-1} of LHCb data recorded from 2016 to 2018.

Int. J. Mod. Phys. A 2026.41. Downloaded from www.worldscientific.com by CALIFORNIA @ BERKELEY on 09/16/26. Re-use and distribution is strictly not permitted, except for Open Access articles.

$\Gamma(e^+e^-\gamma\gamma)/\Gamma_{total}$ — Γ_{22}/Γ

VALUE (units 10^{-7})	EVTS	DOCUMENT ID		TECN	COMMENT
5.95±0.33 OUR AVERAGE					
5.84±0.15±0.32	1543	ALAVI-HARATI 01F		KTEV	$E^*_\gamma > 5$ MeV
8.0 ±1.5 $^{+1.4}_{-1.2}$	40	SETZU	98	NA31	$E^*_\gamma > 5$ MeV
6.5 ±1.2 ±0.6	58	NAKAYA	94	E799	$E^*_\gamma > 5$ MeV
6.6 ±3.2		MORSE	92	B845	$E^*_\gamma > 5$ MeV

$\Gamma(\mu^+\mu^-\gamma\gamma)/\Gamma_{total}$ — Γ_{23}/Γ

VALUE (units 10^{-9})	EVTS	DOCUMENT ID	TECN	COMMENT
$10.4^{+7.5}_{-5.9}\pm0.7$	4	ALAVI-HARATI 00E	KTEV	$m_{\gamma\gamma} \geq 1$ MeV/c^2

Charge conjugation × Parity (*CP*) or Lepton Family number (*LF*) violating modes, or $\Delta S = 1$ weak neutral current (*S1*) modes

$\Gamma(\mu^+\mu^-)/\Gamma(\pi^+\pi^-)$ — Γ_{24}/Γ_8

Test for $\Delta S = 1$ weak neutral current. Allowed by higher-order electroweak interaction.

VALUE (units 10^{-6})	EVTS	DOCUMENT ID		TECN	COMMENT
3.48 ±0.05 OUR AVERAGE					
3.474±0.057	6210	AMBROSE	00	B871	
3.87 ±0.30	179	[1] AKAGI	95	SPEC	
3.38 ±0.17	707	HEINSON	95	B791	
• • • We do not use the following data for averages, fits, limits, etc. • • •					
3.9 ±0.3 ±0.1	178	[2] AKAGI	91B	SPEC	In AKAGI 95
3.45 ±0.18 ±0.13	368	[3] HEINSON	91	SPEC	In HEINSON 95
4.1 ±0.5	54	INAGAKI	89	SPEC	In AKAGI 91B
2.8 ±0.3 ±0.2	87	MATHIAZHA...	89B	SPEC	In HEINSON 91

[1] AKAGI 95 gives this number multiplied by the PDG 1992 average for $\Gamma(K_L^0 \to \pi^+\pi^-)/\Gamma(\text{total})$.
[2] AKAGI 91B give this number multiplied by the 1990 PDG average for $\Gamma(K_L^0 \to \pi^+\pi^-)/\Gamma(\text{total})$.
[3] HEINSON 91 give $\Gamma(K_L^0 \to \mu\mu)/\Gamma_{total}$. We divide out the $\Gamma(K_L^0 \to \pi^+\pi^-)/\Gamma_{total}$ PDG average which they used.

$\Gamma(e^+e^-)/\Gamma_{total}$ — Γ_{25}/Γ

Test for $\Delta S = 1$ weak neutral current. Allowed by higher-order electroweak interaction.

VALUE (units 10^{-10})	CL%	EVTS	DOCUMENT ID		TECN
$0.087^{+0.057}_{-0.041}$		4	AMBROSE	98	B871
• • • We do not use the following data for averages, fits, limits, etc. • • •					
<1.6	90	1	AKAGI	95	SPEC
<0.41	90	0	[1] ARISAKA	93B	B791

[1] ARISAKA 93B includes all events with <6 MeV radiated energy.

$\Gamma(\pi^+\pi^-e^+e^-)/\Gamma_{total}$ — Γ_{26}/Γ

Test for $\Delta S = 1$ weak neutral current. Allowed by higher-order electroweak interaction.

VALUE (units 10^{-7})	CL%	EVTS	DOCUMENT ID		TECN	COMMENT
3.11±0.19 OUR AVERAGE						
3.08±0.09±0.18		1125	[1] LAI	03C	NA48	
3.2 ±0.6 ±0.4		37	ADAMS	98	KTEV	
4.4 ±1.3 ±0.5		13	TAKEUCHI	98	SPEC	
• • • We do not use the following data for averages, fits, limits, etc. • • •						
<4.6	90		NOMURA	97	SPEC	$m_{ee} > 4$ MeV

[1] LAI 03C second error is 0.15(syst)±0.10(norm) combined in quadrature. The normalization uses $\text{BR}(K_L \to \pi^+\pi^-\pi^0) * \text{BR}(\pi^0 \to e^+e^-) = (1.505 \pm 0.047) \times 10^{-3}$ from our 2000 Edition.

$\Gamma(\pi^0\pi^0e^+e^-)/\Gamma_{total}$ — Γ_{27}/Γ

Test for $\Delta S = 1$ weak neutral current. Allowed by higher-order electroweak interaction.

VALUE (units 10^{-9})	CL%	EVTS	DOCUMENT ID	TECN
<6.6	90	1	ALAVI-HARATI 02C	E799

$\Gamma(\pi^0\pi^0\mu^+\mu^-)/\Gamma_{total}$ — Γ_{28}/Γ

Test for $\Delta S = 1$ weak neutral current. Allowed by higher-order electroweak interaction.

VALUE	CL%	DOCUMENT ID		TECN
$<9.2 \times 10^{-11}$	90	[1] ABOUZAID	11A	E799

[1] ABOUZAID 11A also reports $\text{B}(K_L^0 \to \pi^0\pi^0X^0 \to \pi^0\pi^0\mu^+\mu^-) < 1.0 \times 10^{-10}$ at 90% C.L., where the X^0 is a possible new neutral boson that was reported by PARK 05 with a mass of 214.3 ± 0.5 MeV/c^2.

$\Gamma(\mu^+\mu^-e^+e^-)/\Gamma_{total}$ — Γ_{29}/Γ

Test for $\Delta S = 1$ weak neutral current. Allowed by higher-order electroweak interaction.

VALUE (units 10^{-9})	CL%	EVTS	DOCUMENT ID		TECN	COMMENT
2.69±0.27 OUR AVERAGE						
2.69±0.24±0.12		131	[1] ALAVI-HARATI 03B		KTEV	
2.9 $^{+6.7}_{-2.4}$		1	GU	96	E799	
• • • We do not use the following data for averages, fits, limits, etc. • • •						
2.62±0.40±0.17		43	ALAVI-HARATI 01H		KTEV	Sup. by ALAVI-HARATI 03B
<4900	90		BALATS	83	SPEC	

[1] ALAVI-HARATI 03B also measures the linear slope $\alpha = -1.59 \pm 0.37$.

$\Gamma(e^+e^-e^+e^-)/\Gamma_{total}$ — Γ_{30}/Γ

Test for $\Delta S = 1$ weak neutral current. Allowed by higher-order electroweak interaction.

VALUE (units 10^{-8})	EVTS	DOCUMENT ID		TECN	COMMENT
3.56±0.21 OUR AVERAGE					
3.30±0.24±0.25	200	[1] LAI	05B	NA48	
3.72±0.18±0.23	441	ALAVI-HARATI 01D		KTEV	
3.96±0.78±0.32	27	GU	94	E799	
3.07±1.25±0.26	6	VAGINS	93	B845	
• • • We do not use the following data for averages, fits, limits, etc. • • •					
6 ±2 ±1	18	[2] AKAGI	95	SPEC	m_{ee} >470 MeV
7 ±3 ±2	6	[2] AKAGI	95	SPEC	m_{ee} >470 MeV
10.4 ±3.7 ±1.1	8	[3] BARR	95	NA31	
6 ±2 ±1	18	AKAGI	93	CNTR	Sup. by AKAGI 95
4 ±3	2	BARR	91	NA31	Sup. by BARR 95

[1] LAI 05B uses 1998 and 1999 data. Data are normalized to the observed events of $K_L^0 \to \pi^+\pi^-\pi^0$ (π^0 into Dalitz pair) and PDG 04 values are used for $\text{B}(K_L^0 \to \pi^+\pi^-\pi^0)$ and $\text{B}(\pi^0 \to e^+e^-\gamma)$. The systematic error includes a normalization error of ±0.10.
[2] Values are for the total branching fraction, acceptance-corrected for the m_{ee} cuts shown.
[3] Distribution of angles between two e^+e^- pair planes favors CP=−1 for K_L^0.

$\Gamma(\pi^0\mu^+\mu^-)/\Gamma_{total}$ — Γ_{31}/Γ

Violates CP in leading order. Test for $\Delta S = 1$ weak neutral current. Allowed by higher-order electroweak interaction.

VALUE (units 10^{-9})	CL%	EVTS	DOCUMENT ID		TECN
<0.38	90		ALAVI-HARATI 00D		KTEV
• • • We do not use the following data for averages, fits, limits, etc. • • •					
<5.1	90	0	HARRIS	93	E799

$\Gamma(\pi^0e^+e^-)/\Gamma_{total}$ — Γ_{32}/Γ

Violates CP in leading order. Direct and indirect CP-violating contributions are expected to be comparable and to dominate the CP-conserving part. LAI 02B result suggests that CP-violation effects dominate. Test for $\Delta S = 1$ weak neutral current. Allowed by higher-order electroweak interaction.

VALUE (units 10^{-10})	CL%	EVTS	DOCUMENT ID		TECN	COMMENT
< 2.8	90		[1] ALAVI-HARATI 04A		KTEV	combined result
• • • We do not use the following data for averages, fits, limits, etc. • • •						
< 3.5	90		ALAVI-HARATI 04A		KTEV	
$0.0047^{+0.0022}_{-0.0018}$			[2] LAI	02B	NA48	CP-conserving part
< 5.1	90	2	ALAVI-HARATI 01		KTEV	
0.01 to 0.02			ALAVI-HARATI 99B		KTEV	CP-conserving part
< 43	90	0	HARRIS	93B	E799	
< 75	90	0	BARKER	90	E731	
< 55	90	0	OHL	90	B845	
< 400	90		BARR	88	NA31	
<3200	90		JASTRZEM...	88	SPEC	

[1] Combined result of ALAVI-HARATI 04A 1999-2000 data set and ALAVI-HARATI 01 1997 data set.
[2] LAI 02B uses the absence of a signal in $K_L^0 \to \pi^0\gamma\gamma$ with $m(\gamma\gamma)<m(\pi^0)$ and their a_V value to predict this value.

$\Gamma(\pi^0\nu\overline{\nu})/\Gamma_{total}$ — Γ_{33}/Γ

Violates CP in leading order. Test of direct CP violation since the indirect CP-violating and CP-conserving contributions are expected to be suppressed. Test of $\Delta S = 1$ weak neutral current.

VALUE (units 10^{-8})	CL%	DOCUMENT ID		TECN
< 0.22	90	[1] AHN	25	KOTO
• • • We do not use the following data for averages, fits, limits, etc. • • •				
< 0.49	90	[2] AHN	21	KOTO
< 0.30	90	[3] AHN	19	KOTO
< 5.1	90	[4] AHN	17	KOTO
< 2.6	90	[5] AHN	10	K391
< 6.7	90	[6] AHN	08	K391
<21	90	[7] AHN	06	K391
<59	90	ALAVI-HARATI 00		KTEV

[1] AHN 25 result is based on data collected in 2021, which corresponds to 3.3×10^{19} protons on target. A single event sensitivity of $(9.33 \pm 0.06 \pm 0.84) \times 10^{-10}$ was achieved with no background events.
[2] AHN 21 result is based on data collected in 2016, 2017 and 2018, which corresponds to 3.05×10^{19} protons on target. A single event sensitivity of $(7.20 \pm 0.05 \pm 0.66) \times 10^{-10}$ was achieved with 3 candidate events observed and total 1.22 ± 0.26 background events.
[3] AHN 19 result is based on data collected in 2015, which corresponds to 2.2×10^{19} protons on target. A single event sensitivity of $(1.30 \pm 0.01 \pm 0.14) \times 10^{-9}$ was achieved with no candidate events observed. An upper limit of $< 2.4 \times 10^{-9}$ at the 90% C.L. for the $K_L \to \pi^0X^0$ decay was also set, where X^0 is an invisible particle with a mass of 135 MeV/c^2.
[4] AHN 17 result is based on the first 100 hours of physics running in 2013. One candidate event was observed with an expected background of 0.34 ± 0.16 events. An upper limit of $< 3.7 \times 10^{-8}$ at the 90% C.L. for the $K_L \to \pi^0X^0$ decay was also set, where X^0 is an invisible particle with a mass of 135 MeV/c^2.
[5] Obtained combining Run-2 (AHN 08) and Run-3 data.
[6] Value obtained using data from February to April 2005.
[7] Value obtained analyzing 10% of data of RUN 1 (performed in 2004).

Int. J. Mod. Phys. A 2026.41. Downloaded from www.worldscientific.com by UNIVERSITY OF CALIFORNIA @ BERKELEY on 09/16/26. Re-use and distribution is strictly not permitted, except for Open Access articles.

$\Gamma(\pi^0\pi^0\nu\overline{\nu})/\Gamma_{total}$ — Γ_{34}/Γ

VALUE	CL%	DOCUMENT ID		TECN
$<8.1\times10^{-7}$	90	[1] OGATA	11	K391
• • • We do not use the following data for averages, fits, limits, etc. • • •				
$<4.7\times10^{-5}$	90	[2] NIX	07	K391

[1] Using 2005 Run-I data. OGATA 11 also sets a limit on the $K^0_L \to \pi^0\pi^0 X \to$ invisible particles process: the limit on the branching fraction varied from 7.0×10^{-7} to 4.0×10^{-5} for the mass of X ranging from 50 to 200 MeV/c^2.

[2] Observed 1 event with expected background of 0.43 ± 0.35 events. NIX 07 also measured $B(K^0_L \to \pi^0\pi^0 P) < 1.2\times10^{-6}$ at 90% CL, where P is the pseudoscalar particle and $m_P < 100$ MeV.

$\Gamma(e^\pm\mu^\mp)/\Gamma_{total}$ — Γ_{35}/Γ

Test of lepton family number conservation.

VALUE (units 10^{-11})	CL%	EVTS	DOCUMENT ID		TECN
<0.47	90		AMBROSE	98B	B871
• • • We do not use the following data for averages, fits, limits, etc. • • •					
<9.4	90	0	AKAGI	95	SPEC
<3.9	90	0	ARISAKA	93	B791
<3.3	90	0	[1] ARISAKA	93	B791

[1] This is the combined result of ARISAKA 93 and MATHIAZHAGAN 89.

$\Gamma(e^\pm e^\pm\mu^\mp\mu^\mp)/\Gamma_{total}$ — Γ_{36}/Γ

Test of lepton family number conservation.

VALUE (units 10^{-11})	CL%	EVTS	DOCUMENT ID		TECN	COMMENT
< 4.12	90	0	ALAVI-HARATI	03B	KTEV	
• • • We do not use the following data for averages, fits, limits, etc. • • •						
< 12.3	90	0	[1] ALAVI-HARATI	01H	KTEV	Sup. by ALAVI-HARATI 03B
<610	90	0	[1] GU	96	E799	

[1] Assuming uniform phase space distribution.

$\Gamma(\pi^0\mu^\pm e^\mp)/\Gamma_{total}$ — Γ_{37}/Γ

Test of lepton family number conservation.

VALUE (units 10^{-10})	CL%	DOCUMENT ID		TECN
< 0.76	90	ABOUZAID	08C	KTEV
• • • We do not use the following data for averages, fits, limits, etc. • • •				
<62	90	ARISAKA	98	E799

$\Gamma(\pi^0\pi^0\mu^\pm e^\mp)/\Gamma_{total}$ — Γ_{38}/Γ

Test of lepton family number conservation.

VALUE (units 10^{-10})	CL%	DOCUMENT ID		TECN
<1.7	90	ABOUZAID	08C	KTEV

Lorentz invariance violating modes

$\Gamma(\pi^0\gamma)/\Gamma_{total}$ — Γ_{39}/Γ

VALUE	CL%	DOCUMENT ID		TECN
$<1.7\times10^{-7}$	90	[1] SHIMIZU	20	KOTO

[1] SHIMIZU 20 uses data collected from 2016 to 2018 at the J-PARC KOTO experiment. The single event sensitivity is $(7.1\pm0.3\pm1.6)\times10^{-8}$. No candidate event was observed.

See the related review(s):
V_{ud}, V_{us} the Cabibbo Angle, and CKM Unitarity

ENERGY DEPENDENCE OF K^0_L DALITZ PLOT

For discussion, see note on Dalitz plot parameters in the $K^\pm$ section of the Particle Listings above. For definitions of a_y, a_t, a_u, and a_y, see the earlier version of the same note in the 1982 edition of this *Review* published in Physics Letters **111B** 70 (1982).

$|\text{matrix element}|^2 = 1 + gu + hu^2 + jv + kv^2 + fuv$
where $u = (s_3 - s_0)\ /\ m^2_\pi$ and $v = (s_2 - s_1)\ /\ m^2_\pi$

LINEAR COEFFICIENT g FOR $K^0_L \to \pi^+\pi^-\pi^0$

VALUE	EVTS	DOCUMENT ID		TECN	COMMENT
0.678 ±0.008 OUR AVERAGE Error includes scale factor of 1.5. See the ideogram below.					
0.6823±0.0044±0.0044	500k	ANGELOPO...	98C	CPLR	
0.681 ±0.024	6499	CHO	77	HBC	
0.620 ±0.023	4709	PEACH	77	HBC	
0.677 ±0.010	509k	MESSNER	74	ASPK	$a_y = -0.917 \pm 0.013$
• • • We do not use the following data for averages, fits, limits, etc. • • •					
0.69 ±0.07	192	[1] BALDO-...	75	HLBC	
0.590 ±0.022	56k	[1] BUCHANAN	75	SPEC	$a_u = -0.277 \pm 0.010$
0.619 ±0.027	20k	[1,2] BISI	74	ASPK	$a_t = -0.282 \pm 0.011$
0.612 ±0.032		[1] ALEXANDER	73B	HBC	
0.73 ±0.04	3200	[1] BRANDENB...	73	HBC	
0.608 ±0.043	1486	[1] KRENZ	72	HLBC	$a_t = -0.277 \pm 0.018$
0.650 ±0.012	29k	[1] ALBROW	70	ASPK	$a_y = -0.858 \pm 0.015$
0.593 ±0.022	36k	[1,3] BUCHANAN	70	SPEC	$a_u = -0.278 \pm 0.010$
0.664 ±0.056	4400	[1] SMITH	70	OSPK	$a_t = -0.306 \pm 0.024$
0.400 ±0.045	2446	[1] BASILE	68B	OSPK	$a_t = -0.188 \pm 0.020$
0.649 ±0.044	1350	[1] HOPKINS	67	HBC	$a_t = -0.294 \pm 0.018$
0.428 ±0.055	1198	[1] NEFKENS	67	OSPK	$a_u = -0.204 \pm 0.025$

[1] Quadratic dependence required by some experiments. (See sections on "QUADRATIC COEFFICIENT h" and "QUADRATIC COEFFICIENT k" below.) Correlations prevent us from averaging results of fits not including g, h, and k terms.

[2] BISI 74 value comes from quadratic fit with quad. term consistent with zero. g error is thus larger than if linear fit were used.

[3] BUCHANAN 70 result revised by BUCHANAN 75 to include radiative correlations and to use more reliable K^0_L momentum spectrum of second experiment (had same beam).

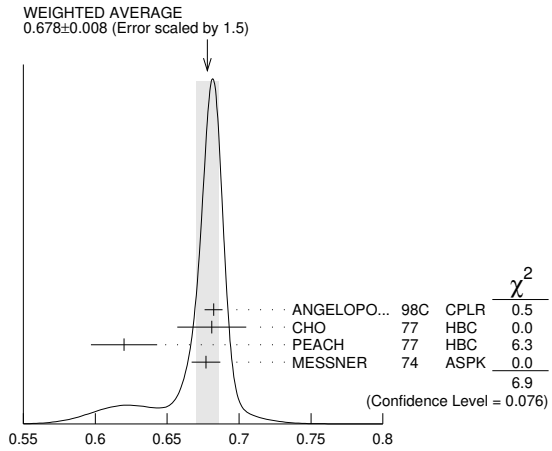

Linear coeff. g for $K^0_L \to \pi^+\pi^-\pi^0$ matrix element squared

QUADRATIC COEFFICIENT h FOR $K^0_L \to \pi^+\pi^-\pi^0$

See notes in section "LINEAR COEFFICIENT g FOR $K^0_L \to \pi^+\pi^-\pi^0$ |MATRIX ELEMENT|^2" above.

VALUE	EVTS	DOCUMENT ID		TECN
0.076±0.006 OUR AVERAGE				
0.061±0.004±0.015	500k	ANGELOPO...	98C	CPLR
0.095±0.032	6499	CHO	77	HBC
0.048±0.036	4709	PEACH	77	HBC
0.079±0.007	509k	MESSNER	74	ASPK
• • • We do not use the following data for averages, fits, limits, etc. • • •				
−0.011±0.018	29k	[1] ALBROW	70	ASPK
0.043±0.052	4400	[1] SMITH	70	OSPK

[1] Quadratic coefficients h and k required by some experiments. (See section on "QUADRATIC COEFFICIENT k" below.) Correlations prevent us from averaging results of fits not including g, h, and k terms.

QUADRATIC COEFFICIENT k FOR $K^0_L \to \pi^+\pi^-\pi^0$

VALUE	EVTS	DOCUMENT ID		TECN
0.0099±0.0015 OUR AVERAGE				
0.0104±0.0017±0.0024	500k	ANGELOPO...	98C	CPLR
0.024 ±0.010	6499	CHO	77	HBC
−0.008 ±0.012	4709	PEACH	77	HBC
0.0097±0.0018	509k	MESSNER	74	ASPK

LINEAR COEFFICIENT j FOR $K^0_L \to \pi^+\pi^-\pi^0$ (CP-VIOLATING TERM)

Listed in CP-violation section below.

QUADRATIC COEFFICIENT f FOR $K^0_L \to \pi^+\pi^-\pi^0$ (CP-VIOLATING TERM)

Listed in CP-violation section below.

QUADRATIC COEFFICIENT h FOR $K^0_L \to \pi^0\pi^0\pi^0$

We do not average measurements that do not account for the effect of final state rescattering.

VALUE (units 10^{-3})	EVTS	DOCUMENT ID		TECN
+0.59±0.20±1.16	68M	[1] ABOUZAID	08A	KTEV
• • • We do not use the following data for averages, fits, limits, etc. • • •				
−6.1 ±0.9 ±0.5	14.7M	[2] LAI	01B	NA48
−3.3 ±1.1 ±0.7	5M	[2,3] SOMALWAR	92	E731

[1] Result obtained using Cl3pl model of CABIBBO 05 to include $\pi\pi$ rescattering effects. The systematic error includes an external error of 1.06×10^{-3} from the parametrization input of $(a_0-a_2)\ m_{\pi^+} = 0.268 \pm 0.017$ from BATLEY 06B.

[2] LAI 01B and SOMALWAR 92 results do not include $\pi\pi$ final state rescattering effects.

[3] SOMALWAR 92 chose m_{π^+} as normalization to make it compatible with the Particle Data Group $K^0_L \to \pi^+\pi^-\pi^0$ definitions.

Int. J. Mod. Phys. A 2026.41. Downloaded from www.worldscientific.com by CALIFORNIA @ BERKELEY on 09/16/26. Re-use and distribution is strictly not permitted, except for Open Access articles.

K^0_L FORM FACTORS

For discussion, see note on form factors in the $K^\pm$ section of the Particle Listings above.

In the form factor comments, the following symbols are used.

f_+ and f_- are form factors for the vector matrix element.

f_S and f_T refer to the scalar and tensor term.

$f_0(t) = f_+(t) + f_-(t)\ t/(m^2_{K^0} - m^2_{\pi^+})$.

t = momentum transfer to the π.

λ_+ and λ_0 are the linear expansion coefficients of f_+ and f_0:

$f_+(t) = f_+(0)\ (1 + \lambda_+ t\ /m^2_{\pi^+})$

For quadratic expansion

$f_+(t) = f_+(0)\ (1 + \lambda'_+ t\ /m^2_{\pi^+} + \frac{\lambda''_+}{2}\ t^2/m^4_{\pi^+}\ )$

as used by KTeV. If there is a non-vanishing quadratic term, then λ_+ represents an average slope, which is then different from λ'_+.

NA48 (K_{e3}) and ISTRA quadratic expansion coefficients are converted with

$\lambda'_+{}^{PDG} = \lambda_+{}^{NA48}$ and $\lambda''_+{}^{PDG} = 2\ \lambda'_+{}^{NA48}$

$\lambda'_+{}^{PDG} = (\frac{m_{\pi^+}}{m_{\pi^0}})^2\ \lambda_+{}^{ISTRA}$ and

$\lambda''_+{}^{PDG} = 2\ (\frac{m_{\pi^+}}{m_{\pi^0}})^4\ \lambda'_+{}^{ISTRA}$

ISTRA linear expansion coefficients are converted with

$\lambda_+{}^{PDG} = (\frac{m_{\pi^+}}{m_{\pi^0}})^2\ \lambda_+{}^{ISTRA}$ and $\lambda_0{}^{PDG} = (\frac{m_{\pi^+}}{m_{\pi^0}})^2\ \lambda_0{}^{ISTRA}$

The pole parametrization is

$f_+(t) = f_+(0)\ (\frac{M^2_V}{M^2_V - t}\ )$

$f_0(t) = f_0(0)\ (\frac{M^2_S}{M^2_S - t}\ )$

where M_V and M_S are the vector and scalar pole masses.

The dispersive parametrization is

$f_+(t) = f_+(0)\ \exp[\ \frac{t}{m^2_\pi}\ (\Lambda_+ + H(t))\ ]$;

$f_0(t) = f_+(0)\ \exp[\ \frac{t}{m^2_K - m^2_\pi}\ (\ln[C] - G(t))\ ]$,

where Λ_+ is the slope parameter and $\ln[C] = \ln[\ f_0\ (m^2_K - m^2_\pi\ )\ ]$ is the logarithm of the scalar form factor at the Callan-Treiman point.

$H(t)$ and $G(t)$ are dispersive integrals.

The following abbreviations are used:

DP = Dalitz plot analysis.

PI = π spectrum analysis.

MU = μ spectrum analysis.

POL= μ polarization analysis.

BR = $K^0_{\mu3}/K^0_{e3}$ branching ratio analysis.

E = positron or electron spectrum analysis.

RC = radiative corrections.

λ_+ (LINEAR ENERGY DEPENDENCE OF f_+ IN K^0_{e3} DECAY)

For radiative correction of K^0_{e3} DP, see GINSBERG 67, BECHERRAWY 70, CIRIGLIANO 02, CIRIGLIANO 04, and ANDRE 07. Results labeled OUR FIT are discussed in the review "$K^\pm_{\ell3}$ and $K^0_{\ell3}$ Form Factors" in the $K^\pm$ Listings. For earlier, lower statistics results, see the 2004 edition of this review, Physics Letters **B592** 1 (2004).

VALUE (units 10^{-2})	EVTS	DOCUMENT ID		TECN	COMMENT
2.82 ±0.04 OUR FIT	Error includes scale factor of 1.1. Assuming μ-e universality				
2.85 ±0.04 OUR AVERAGE					
2.86 ±0.05 ±0.04	2M	AMBROSINO	06D	KLOE	
2.832±0.037±0.043	1.9M	ALEXOPOU...	04A	KTEV	PI, no $\mu = e$
2.88 ±0.04 ±0.11	5.6M	[1] LAI	04C	NA48	DP
• • • We do not use the following data for averages, fits, limits, etc. • • •					
2.84 ±0.07 ±0.13	5.6M	[2] LAI	04C	NA48	DP
2.45 ±0.12 ±0.22	366k	APOSTOLA...	00	CPLR	DP
3.06 ±0.34	74k	BIRULEV	81	SPEC	DP
3.12 ±0.25	500k	GJESDAL	76	SPEC	DP
2.70 ±0.28	25k	BLUMENTHAL	75	SPEC	DP

[1] Results from linear fit and assuming only vector and axial couplings.
[2] Results from linear fit with $|f_S/f_+|$ and $|f_T/f_+|$ free.

λ_+ (LINEAR ENERGY DEPENDENCE OF f_+ IN $K^0_{\mu3}$ DECAY)

Results labeled OUR FIT are discussed in the review "$K^\pm_{\ell3}$ and $K^0_{\ell3}$ Form Factors" in the $K^\pm$ Listings. For earlier, lower statistics results, see the 2004 edition of this review, Physics Letters **B592** 1 (2004).

VALUE (units 10^{-2})	EVTS	DOCUMENT ID		TECN	COMMENT
2.82 ±0.04 OUR FIT	Error includes scale factor of 1.1. Assuming μ-e universality				
2.71 ±0.10 OUR FIT	Error includes scale factor of 1.4. Not assuming μ-e universality				
2.67 ±0.06 ±0.08	2.3M	[1] LAI	07A	NA48	DP
2.745±0.088±0.063	1.5M	ALEXOPOU...	04A	KTEV	DP, no $\mu = e$
2.813±0.051	3.4M	ALEXOPOU...	04A	KTEV	PI, DP, $\mu = e$
3.0 ±0.3	1.6M	DONALDSON	74B	SPEC	DP
• • • We do not use the following data for averages, fits, limits, etc. • • •					
4.27 ±0.44	150k	BIRULEV	81	SPEC	DP

[1] LAI 07A gives a correlation −0.40 between their λ_0 and λ_+ measurements.

λ_0 (LINEAR ENERGY DEPENDENCE OF f_0 IN $K^0_{\mu3}$ DECAY)

Wherever possible, we have converted the above values of $\xi(0)$ into values of λ_0 using the associated λ^μ_+ and $d\xi(0)/d\lambda_+$. Results labeled OUR FIT are discussed in the review "$K^\pm_{\ell3}$ and $K^0_{\ell3}$ Form Factors" in the $K^\pm$ Listings. For earlier, lower statistics results, see the 2004 edition of this review, Physics Letters **B592** 1 (2004).

VALUE (units 10^{-2})	$d\lambda_0/d\lambda_+$	EVTS	DOCUMENT ID		TECN	COMMENT
1.38 ±0.18 OUR FIT	Error includes scale factor of 2.2. Assuming μ-e universality					
1.42 ±0.23 OUR FIT	Error includes scale factor of 2.8. Not assuming μ-e universality					
1.17 ±0.07 ±0.10		2.3M	[1] LAI	07A	NA48	DP
1.657±0.125	−0.44	1.5M	[2] ALEXOPOU...	04A	KTEV	DP, no $\mu = e$
1.635±0.121	−0.85	3.4M	[3] ALEXOPOU...	04A	KTEV	PI, DP, $\mu = e$
+1.9 ±0.4	−0.47	1.6M	[4] DONALDSON	74B	SPEC	DP
• • • We do not use the following data for averages, fits, limits, etc. • • •						
3.41 ±0.67	unknown	150k	[5] BIRULEV	81	SPEC	DP

[1] LAI 07A gives a correlation −0.40 between their λ_0 and λ_+ measurements.
[2] ALEXOPOULOS 04A gives a correlation −0.38 between their λ_0 and λ_+ measurements.
[3] ALEXOPOULOS 04A gives a correlation −0.36 between their λ_0 and λ_+ measurements.
[4] DONALDSON 74B $d\lambda_0/d\lambda_+$ obtained from figure 18.
[5] BIRULEV 81 gives $d\lambda_0/d\lambda_+ = -1.5$, giving an unreasonably narrow error ellipse which dominates all other results. We use $d\lambda_0/d\lambda_+ = 0$.

λ'_+(LINEAR K^0_{e3} FORM FACTOR FROM QUADRATIC FIT)

VALUE (units 10^{-2})	EVTS	DOCUMENT ID		TECN	COMMENT
2.40 ±0.12 OUR FIT	Error includes scale factor of 1.2. Assuming μ-e universality				
2.49 ±0.13 OUR FIT	Error includes scale factor of 1.1. Not assuming μ-e universality				
2.48 ±0.17 OUR AVERAGE	Error includes scale factor of 1.5. See the ideogram below.				
2.55 ±0.15 ±0.10	2M	[1] AMBROSINO	06D	KLOE	
2.167±0.137±0.143	1.9M	[2] ALEXOPOU...	04A	KTEV	PI, no $\mu = e$
2.80 ±0.19 ±0.15	5.6M	[3] LAI	04C	NA48	DP

[1] We use AMBROSINO 06D result in the fit not assuming $\mu-e$ universality. This result enters the fit assuming $\mu-e$ universality via AMBROSINO 07C measurement of λ'_+ in $K_{\mu3}$ decays. AMBROSINO 06D gives a correlation −0.95 between their λ'_+ and λ''_+.
[2] ALEXOPOULOS 04A gives a correlation −0.97 between their λ'_+ and λ''_+.
[3] For LAI 04C we calculate a correlation −0.88 between their λ'_+ and λ''_+.

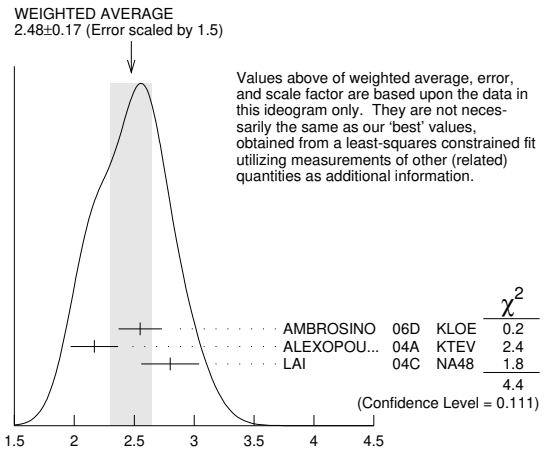

λ'_+(LINEAR K^0_{e3} FORM FACTOR FROM QUADRATIC FIT) (units 10^{-2})

λ''_+(QUADRATIC K^0_{e3} FORM FACTOR)

VALUE (units 10^{-2})	EVTS	DOCUMENT ID		TECN	COMMENT
0.20 ±0.05 OUR FIT	Error includes scale factor of 1.2. Assuming μ-e universality				
0.16 ±0.05 OUR FIT	Error includes scale factor of 1.1. Not assuming μ-e universality				
0.17 ±0.07 OUR AVERAGE	Error includes scale factor of 1.5. See the ideogram below.				
0.14 ±0.07 ±0.04	2M	[1] AMBROSINO	06D	KLOE	
0.287±0.057±0.053	1.9M	[2] ALEXOPOU...	04A	KTEV	PI, no $\mu = e$
0.04 ±0.08 ±0.04	5.6M	[3,4] LAI	04C	NA48	DP

[1] We use AMBROSINO 06D result in the fit not assuming $\mu-e$ universality. This result enters the fit assuming $\mu-e$ universality via AMBROSINO 07C measurement of λ''_+ in $K_{\mu3}$ decays. AMBROSINO 06D gives a correlation −0.95 between their λ'_+ and λ''_+.
[2] ALEXOPOULOS 04A gives a correlation −0.97 between their λ'_+ and λ''_+.
[3] Values doubled to agree with PDG conventions described above.
[4] LAI 04C gives a correlation −0.88 between their λ'_+ and λ''_+.

Int. J. Mod. Phys. A 2026.41. Downloaded from www.worldscientific.com
by UNIVERSITY OF CALIFORNIA @ BERKELEY on 09/16/26. Re-use and distribution is strictly not permitted, except for Open Access articles.

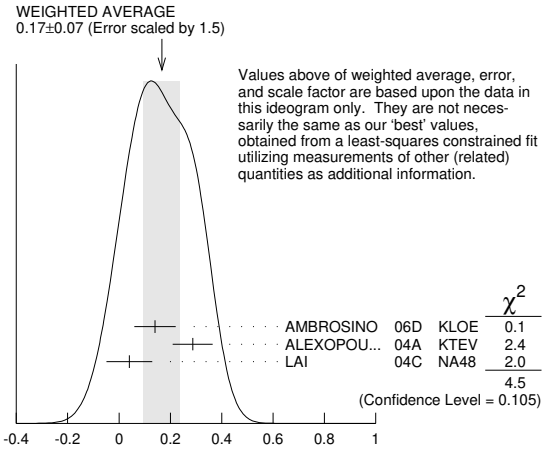

λ''_+(QUADRATIC K^0_{e3} FORM FACTOR) (units 10^{-2})

λ'_+(LINEAR $K^0_{\mu3}$ FORM FACTOR FROM QUADRATIC FIT)

VALUE (units 10^{-2})	EVTS	DOCUMENT ID		TECN	COMMENT
2.40 ±0.12 OUR FIT		Error includes scale factor of 1.2. Assuming μ-e universality			
1.89 ±0.24 OUR FIT		Not assuming μ-e universality			
2.23 ±0.98 ±0.37	1.8M	[1] AMBROSINO	07C	KLOE	no $\mu = e$
2.56 ±0.15 ±0.09	3.8M	[1] AMBROSINO	07C	KLOE	$\mu = e$
2.05 ±0.22 ±0.24	2.3M	[1] LAI	07A	NA48	DP
1.703±0.319±0.177	1.5M	[1] ALEXOPOU...	04A	KTEV	DP, no $\mu = e$
2.064±0.175	3.4M	[1] ALEXOPOU...	04A	KTEV	PI, DP, $\mu = e$

[1] See section λ_0 below for correlations.

λ''_+(QUADRATIC $K^0_{\mu3}$ FORM FACTOR)

VALUE (units 10^{-2})	EVTS	DOCUMENT ID		TECN	COMMENT
0.20 ±0.05 OUR FIT		Error includes scale factor of 1.2. Assuming μ-e universality			
0.37 ±0.12 OUR FIT		Error includes scale factor of 1.3. Not assuming μ-e universality			
0.48 ±0.49 ±0.16	1.8M	[1] AMBROSINO	07C	KLOE	no $\mu = e$
0.15 ±0.07 ±0.04	3.8M	[1] AMBROSINO	07C	KLOE	$\mu = e$
0.26 ±0.09 ±0.10	2.3M	[1] LAI	07A	NA48	DP
0.443±0.131±0.072	1.5M	[1] ALEXOPOU...	04A	KTEV	DP, no $\mu = e$
0.320±0.069	3.4M	[1] ALEXOPOU...	04A	KTEV	PI, DP, $\mu = e$

[1] See section λ_0 below for correlations.

λ_0(LINEAR f_0 $K^0_{\mu3}$ FORM FACTOR FROM QUADRATIC FIT)

VALUE (units 10^{-2})	EVTS	DOCUMENT ID		TECN	COMMENT
1.16 ±0.09 OUR FIT		Error includes scale factor of 1.2. Assuming μ-e universality			
1.07 ±0.14 OUR FIT		Error includes scale factor of 1.3. Not assuming μ-e universality			
0.91 ±0.59 ±0.26	1.8M	[1] AMBROSINO	07C	KLOE	no $\mu = e$
1.54 ±0.18 ±0.13	3.8M	[2] AMBROSINO	07C	KLOE	$\mu = e$
0.95 ±0.11 ±0.08	2.3M	[3] LAI	07A	NA48	DP
1.281±0.136±0.122	1.5M	[4] ALEXOPOU...	04A	KTEV	DP, no $\mu = e$
1.372±0.131	3.4M	[5] ALEXOPOU...	04A	KTEV	PI, DP, $\mu = e$

[1] AMBROSINO 07C, not assuming μ-e universality, gives a correlation matrix

	λ'_+	λ''_+
λ''_+	−0.97	1
λ_0	0.81	−0.91

[2] AMBROSINO 07C, assuming μ-e universality, gives a correlation matrix

	λ'_+	λ''_+
λ''_+	−0.95	1
λ_0	0.29	−0.38

[3] LAI 07A gives a correlation matrix

	λ'_+	λ''_+
λ''_+	−0.96	1
λ_0	0.63	−0.73

[4] ALEXOPOULOS 04A, not assuming μ-e universality, gives a correlation matrix

	λ'_+	λ''_+	λ_0
λ'_+	1		
λ''_+	−0.96	1	
λ_0	0.65	−0.75	1

[5] ALEXOPOULOS 04A, assuming μ-e universality, gives a correlation matrix

	λ'_+	λ''_+	λ_0
λ'_+	1		
λ''_+	−0.97	1	
λ_0	0.34	−0.44	1

M^e_V (POLE MASS FOR K^0_{e3} DECAY)

VALUE (MeV)	EVTS	DOCUMENT ID		TECN	COMMENT
878 ± 6 OUR FIT		Error includes scale factor of 1.1. Assuming μ-e universality			
875 ± 5 OUR AVERAGE					
870 ± 6 ±7	2M	AMBROSINO	06D	KLOE	
881.03± 5.12±4.94	1.9M	ALEXOPOU...	04A	KTEV	PI, no $\mu = e$
859 ±18	5.6M	LAI	04C	NA48	

M^μ_V (POLE MASS FOR $K^0_{\mu3}$ DECAY)

VALUE (MeV)	EVTS	DOCUMENT ID		TECN	COMMENT
878 ± 6 OUR FIT		Error includes scale factor of 1.1. Assuming μ-e universality			
900 ±21 OUR FIT		Error includes scale factor of 1.7. Not assuming μ-e universality			
905 ± 9 ±17	2.3M	[1] LAI	07A	NA48	DP
889.19±12.81± 9.92	1.5M	[1] ALEXOPOU...	04A	KTEV	DP, no $\mu = e$
882.32± 6.54	3.4M	[1] ALEXOPOU...	04A	KTEV	PI, DP, $\mu = e$

[1] See section M^μ_S below for correlations.

M^μ_S (POLE MASS FOR $K^0_{\mu3}$ DECAY)

VALUE (MeV)	EVTS	DOCUMENT ID		TECN	COMMENT
1250 ±90 OUR FIT		Error includes scale factor of 2.6. Assuming μ-e universality			
1220 ±80 OUR FIT		Error includes scale factor of 2.3. Not assuming μ-e universality			
1400 ±46 ±53	2.3M	[1] LAI	07A	NA48	DP
1167.14±28.30±31.04	1.5M	[2] ALEXOPOU...	04A	KTEV	PI, no $\mu = e$
1173.80±39.47	3.4M	[3] ALEXOPOU...	04A	KTEV	PI, DP, $\mu = e$

[1] LAI 07A gives a correlation −0.47 between their M^μ_S and M^μ_V measurements, not assuming μ-e universality.

[2] ALEXOPOULOS 04A gives a correlation −0.46 between their M^μ_S and M^μ_V and measurements, not assuming μ-e universality.

[3] ALEXOPOULOS 04A gives a correlation −0.40 between their M^μ_S and M^μ_V and measurements, assuming μ-e universality.

Λ_+ (DISPERSIVE VECTOR FORM FACTOR FOR $K^0_{\mu3}$ DECAY)

See the review on "$K^\pm_{\ell3}$ and $K^0_{\ell3}$ Form Factors" for details of the dispersive parametrization.

VALUE (units 10^{-2})	EVTS	DOCUMENT ID		TECN	COMMENT
2.51 ±0.06 OUR AVERAGE		Error includes scale factor of 1.5. See the ideogram below.			
2.509±0.035±0.043	3.4M	[1] ABOUZAID	10	KTEV	$\mu = e$
2.57 ±0.04 ±0.04	3.8M	[2] AMBROSINO	07C	KLOE	$\mu = e$
2.33 ±0.05 ±0.08	2.3M	[3] LAI	07A	NA48	DP

[1] Obtained from a sample of 1.9 M K_{e3} and 1.5 M $K_{\mu3}$. The correlation between Λ_+ and ln(C) is −0.269.

[2] AMBROSINO 07C results include 2M K_{e3} events from AMBROSINO 06D. The correlation between Λ_+ and ln(C) is −0.26.

[3] LAI 07A gives a correlation −0.44 between their Λ_+ and ln(C) measurements.

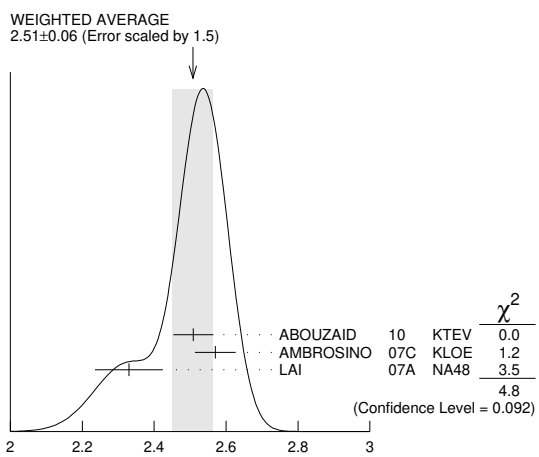

Λ_+ (DISPERSIVE VECTOR FORM FACTOR FOR $K^0_{\mu3}$ DECAY) (units 10^{-2})

ln(C) (DISPERSIVE SCALAR FORM FACTOR FOR $K^0_{\mu3}$ DECAY)

See the review on "$K^\pm_{\ell3}$ and $K^0_{\ell3}$ Form Factors" for details of the dispersive parametrization.

VALUE (units 10^{-1})	EVTS	DOCUMENT ID		TECN	COMMENT
1.75 ±0.18 OUR AVERAGE		Error includes scale factor of 2.0. See the ideogram below.			
1.915±0.078±0.094	3.4M	[1] ABOUZAID	10	KTEV	$\mu = e$
2.04 ±0.19 ±0.15	3.8M	[2] AMBROSINO	07C	KLOE	$\mu = e$
1.438±0.080±0.112	2.3M	[3] LAI	07A	NA48	DP

[1] Obtained from a sample of 1.9 M K_{e3} and 1.5 M $K_{\mu3}$. The correlation between Λ_+ and ln(C) is −0.269.

[2] AMBROSINO 07C results include 2M K_{e3} events from AMBROSINO 06D. We convert (Λ_+, Λ_0) to $(\Lambda_+, \ln(C))$ parametrization using $\ln(C) = (\Lambda_0 \cdot 11.713 + 0.0398) \pm 0.0041$, where the error is due to theory parametrization of the form factor. The correlation between Λ_+ and ln(C) is −0.26.

[3] LAI 07A gives a correlation −0.44 between their Λ_+ and ln(C) measurements.

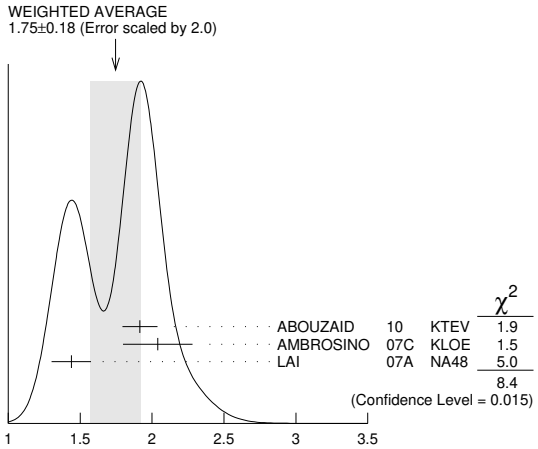

ln(C) (DISPERSIVE SCALAR FORM FACTOR FOR $K^0_{\mu3}$ DECAY) (units 10^{-1})

$a_1(t_0, Q^2)$ FORM FACTOR PARAMETER

See HILL 06 for a definition of this parameter.

VALUE	EVTS	DOCUMENT ID		TECN
1.023±0.028±0.029	2M	[1] ABOUZAID	06C	KTEV

[1] $Q^2 = 2$ GeV^2, $t_0 = 0.49\,(m_K - m_\pi)^2$. Correlation between a_1 and a_2: $\rho_{12} = -0.064$.

$a_2(t_0, Q^2)$ FORM FACTOR PARAMETER

See HILL 06 for a definition of this parameter.

VALUE	EVTS	DOCUMENT ID		TECN
0.75±1.58±1.47	2M	[1] ABOUZAID	06C	KTEV

[1] $Q^2 = 2$ GeV^2, $t_0 = 0.49\,(m_K - m_\pi)^2$. Correlation between a_1 and a_2: $\rho_{12} = -0.064$.

$|f_S/f_+|$ FOR K^0_{e3} DECAY

Ratio of scalar to f_+ couplings.

VALUE (units 10^{-2})	CL%	EVTS	DOCUMENT ID		TECN	COMMENT
$\mathbf{1.5^{+0.7}_{-1.0}\pm1.2}$		5.6M	[1] LAI	04C	NA48	
• • • We do not use the following data for averages, fits, limits, etc. • • •						
<9.5	95	18k	HILL	78	STRC	
<7.	68	48k	BIRULEV	76	SPEC	See also BIRULEV 81
<4.	68	25k	BLUMENTHAL	75	SPEC	

[1] Results from linear fit with $|f_S/f_+|$ and $|f_T/f_+|$ free.

$|f_T/f_+|$ FOR K^0_{e3} DECAY

Ratio of tensor to f_+ couplings.

VALUE (units 10^{-2})	CL%	EVTS	DOCUMENT ID		TECN	COMMENT
$\mathbf{5^{+3}_{-4}\pm3}$		5.6M	[1] LAI	04C	NA48	
• • • We do not use the following data for averages, fits, limits, etc. • • •						
<40.	95	18k	HILL	78	STRC	
<34.	68	48k	BIRULEV	76	SPEC	See also BIRULEV 81
<23.	68	25k	BLUMENTHAL	75	SPEC	

[1] Results from linear fit with $|f_S/f_+|$ and $|f_T/f_+|$ free.

$|f_T/f_+|$ FOR $K^0_{\mu3}$ DECAY

Ratio of tensor to f_+ couplings.

VALUE (units 10^{-2})	DOCUMENT ID		TECN
12.±12.	BIRULEV	81	SPEC

α_{K^*} DECAY FORM FACTOR FOR $K_L \to \ell^+\ell^-\gamma$, $K^0_L \to \ell^+\ell^-\ell'^+\ell'^-$

Average of all α_{K^*} measurements (from each of three datablocks following this one) assuming lepton universality.

VALUE	DOCUMENT ID
−0.205±0.022 OUR AVERAGE Includes data from the 3 datablocks that follow this one. Error includes scale factor of 1.8. See the ideogram below.	

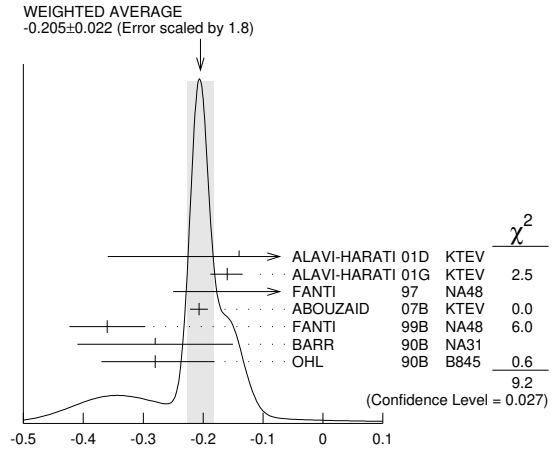

α_{K^*} DECAY FORM FACTOR FOR $K_L \to \ell^+\ell^-\gamma$, $K^0_L \to \ell^+\ell^-\ell'^+\ell'^-$

α_{K^*} DECAY FORM FACTOR FOR $K_L \to e^+e^-\gamma$

α_{K^*} is the constant in the model of BERGSTROM 83 which measures the relative strength of the vector-vector transition $K_L \to K^*\gamma$ with $K^* \to \rho, \omega, \phi \to \gamma^*$ and the pseudoscalar-pseudoscalar transition $K_L \to \pi, \eta, \eta' \to \gamma\gamma^*$.

VALUE	EVTS	DOCUMENT ID		TECN
The data in this block is included in the average printed for a previous datablock.				
−0.217±0.034 OUR AVERAGE Error includes scale factor of 2.4.				
−0.207±0.012±0.009	83k	[1] ABOUZAID	07B	KTEV
−0.36 ±0.06 ±0.02	6864	FANTI	99B	NA48
−0.28 ±0.13		BARR	90B	NA31
$-0.280^{+0.099}_{-0.090}$		OHL	90B	B845

[1] ABOUZAID 07B measures $C\cdot\alpha_{K^*} = -0.517 \pm 0.030 \pm 0.022$. We assume $C = 2.5$, as in all other measurements.

α_{K^*} DECAY FORM FACTOR FOR $K_L \to \mu^+\mu^-\gamma$

α_{K^*} is the constant in the model of BERGSTROM 83 described in the previous section.

VALUE	EVTS	DOCUMENT ID		TECN
The data in this block is included in the average printed for a previous datablock.				
−0.158±0.027 OUR AVERAGE				
$-0.160^{+0.026}_{-0.028}$	9100	ALAVI-HARATI	01G	KTEV
$-0.04\ ^{+0.24}_{-0.21}$		FANTI	97	NA48

$\alpha^{\rm eff}_{K^*}$ DECAY FORM FACTOR FOR $K_L \to e^+e^-e^+e^-$

$\alpha^{\rm eff}_{K^*}$ is the parameter describing the relative strength of an intermediate pseudoscalar decay amplitude and a vector meson decay amplitude in the model of BERGSTROM 83. It takes into account both the radiative effects and the form factor. Since there are two e^+e^- pairs here compared with one in $e^+e^-\gamma$ decays, a factorized expression is used for the $e^+e^-e^+e^-$ decay form factor.

VALUE	EVTS	DOCUMENT ID		TECN
The data in this block is included in the average printed for a previous datablock.				
−0.14±0.16±0.15	441	ALAVI-HARATI	01D	KTEV

α_{DIP} DECAY FORM FACTOR FOR $K^0_L \to \ell^+\ell^-\gamma$, $K^0_L \to \ell^+\ell^-\ell'^+\ell'^-$

Average of all α_{DIP} measurements (from each of three datablocks following this one) assuming lepton universality.

VALUE	DOCUMENT ID
−1.69±0.08 OUR AVERAGE Includes data from the 3 datablocks that follow this one. Error includes scale factor of 1.7.	

α_{DIP} DECAY FORM FACTOR FOR $K^0_L \to e^+e^-\gamma$

α_{DIP} parameter in $K^0_L \to \gamma^*\gamma^*$ form factor by DAMBROSIO 98, motivated by vector meson dominance and a proper short distance behavior.

VALUE	EVTS	DOCUMENT ID		TECN
The data in this block is included in the average printed for a previous datablock.				
−1.729±0.043±0.028	83k	ABOUZAID	07B	KTEV

α_{DIP} DECAY FORM FACTOR FOR $K^0_L \to \mu^+\mu^-\gamma$

α_{DIP} is a constant in the model of DAMBROSIO 98 described in the previous section.

VALUE	EVTS	DOCUMENT ID		TECN
The data in this block is included in the average printed for a previous datablock.				
−1.54±0.10	9100	ALAVI-HARATI	01G	KTEV

α_{DIP} DECAY FORM FACTOR FOR $K^0_L \to e^+e^-\mu^+\mu^-$

α_{DIP} is a constant in the model of DAMBROSIO 98 described in the previous section.

VALUE	EVTS	DOCUMENT ID		TECN
The data in this block is included in the average printed for a previous datablock.				
−1.59±0.37	131	ALAVI-HARATI	03B	KTEV

Int. J. Mod. Phys. A 2026.41. Downloaded from www.worldscientific.com
by [redacted]LIFORNIA @ BERKELEY on 09/16/26. Re-use and distribution is strictly not permitted, except for Open Access articles.

Int. J. Mod. Phys. A 2026.41. Downloaded from www.worldscientific.com
by UNIVERSITY OF CALIFORNIA @ BERKELEY on 09/16/26. Re-use and distribution is strictly not permitted, except for Open Access articles.

a_1/a_2 FORM FACTOR FOR M1 DIRECT EMISSION AMPLITUDE

Form factor $= \tilde{g}_{M1}\left[1+\frac{a_1/a_2}{(M_\rho^2-M_K^2)+2M_K E_\gamma^*}\right]$ as described in ALAVI-HARATI 00B.

VALUE (GeV^2)	EVTS	DOCUMENT ID		TECN	COMMENT
−0.737±0.014 OUR AVERAGE					
−0.744±0.027±0.032	5241	[1] ABOUZAID	06	KTEV	$\pi^+\pi^-e^+e^-$
−0.738±0.007±0.018	111k	[2] ABOUZAID	06A	KTEV	$\pi^+\pi^+\gamma$
$-0.81\ ^{+0.07}_{-0.13}\ \pm0.02$		[3] LAI	03C	NA48	$\pi^+\pi^-e^+e^-$
−0.737±0.026±0.022		[4] ALAVI-HARATI	01B		$\pi^+\pi^-\gamma$
−0.720±0.028±0.009	1766	[5] ALAVI-HARATI	00B	KTEV	$\pi^+\pi^-e^+e^-$

[1] ABOUZAID 06 also measured $|\tilde{g}_{M1}| = 1.11 \pm 0.14$.
[2] ABOUZAID 06A also measured $|\tilde{g}_{M1}| = 1.198 \pm 0.035 \pm 0.086$.
[3] LAI 03C also measured $\tilde{g}_{M1} = 0.99^{+0.28}_{-0.27} \pm 0.07$.
[4] ALAVI-HARATI 01B fit gives χ^2/DOF = 38.8/27. Linear and quadratic fits give χ^2/DOF = 43.2/27 and 37.6/26 respectively.
[5] ALAVI-HARATI 00B also measured $|\tilde{g}_{M1}| = 1.35^{+0.20}_{-0.17} \pm 0.04$.

$\overline{f}_S$ DECAY FORM FACTOR FOR $K^0_L \to \pi^\pm\pi^0e^\mp\nu_e$

VALUE	DOCUMENT ID		TECN
0.049±0.011 OUR AVERAGE Error includes scale factor of 1.7.			
0.052±0.006±0.002	BATLEY	04	NA48
0.010±0.016±0.017	MAKOFF	93	E731

$\overline{f}_P$ DECAY FORM FACTOR FOR $K^0_L \to \pi^\pm\pi^0e^\mp\nu_e$

VALUE	DOCUMENT ID		TECN
−0.052±0.012 OUR AVERAGE			
−0.051±0.011±0.005	BATLEY	04	NA48
−0.079±0.049±0.022	MAKOFF	93	E731

λ_g DECAY FORM FACTOR FOR $K^0_L \to \pi^\pm\pi^0e^\mp\nu_e$

VALUE	DOCUMENT ID		TECN
0.085±0.020 OUR AVERAGE			
0.087±0.019±0.006	BATLEY	04	NA48
0.014±0.087±0.070	MAKOFF	93	E731

$\overline{h}$ DECAY FORM FACTOR FOR $K^0_L \to \pi^\pm\pi^0e^\mp\nu_e$

VALUE	DOCUMENT ID		TECN
−0.30±0.13 OUR AVERAGE			
−0.32±0.12±0.07	BATLEY	04	NA48
−0.07±0.31±0.31	MAKOFF	93	E731

L_3 CHIRAL PERT. THEO. PARAM. FOR $K^0_L \to \pi^\pm\pi^0e^\mp\nu_e$

VALUE (units 10^{-3})	DOCUMENT ID		TECN
−3.96±0.28 OUR AVERAGE Error includes scale factor of 1.6.			
−4.1 ±0.2	BATLEY	04	NA48
−3.4 ±0.4	[1] MAKOFF	93	E731

[1] MAKOFF 93 sign has been changed to negative to agree with the sign convention used in BATLEY 04.

a_V, VECTOR MESON EXCHANGE CONTRIBUTION

VALUE	EVTS	DOCUMENT ID		TECN	COMMENT
−0.43±0.06 OUR AVERAGE Error includes scale factor of 1.5.					
−0.31±0.05±0.07	1.4k	[1] ABOUZAID	08	KTEV	
−0.46±0.03±0.04		LAI	02B	NA48	$K^0_L \to \pi^0 2\gamma$
−0.67±0.21±0.12		ALAVI-HARATI	01E	KTEV	$K^0_L \to \pi^0 e^+e^-\gamma$
• • • We do not use the following data for averages, fits, limits, etc. • • •					
−0.72±0.05±0.06		[2] ALAVI-HARATI	99B	KTEV	$K^0_L \to \pi^0 2\gamma$

[1] Using KTeV dataset collected in 1996, 1997, and 1999.
[2] Superseded by ABOUZAID 08.

See the related review(s):

CP Violation in K^0_L Decays

CP-VIOLATION PARAMETERS IN K^0_L DECAYS

CHARGE ASYMMETRY IN $K^0_{\ell3}$ DECAYS

Such asymmetry violates *CP*. It is related to Re(ϵ).

A_L = weighted average of $A_L(\mu)$ and $A_L(e)$

In previous editions and in the literature the symbol used for this asymmetry was δ_L or δ. We use A_L for consistency with B^0 asymmetry notation and with recent K^0_S notation.

VALUE (%)	EVTS	DOCUMENT ID		TECN	COMMENT
0.332±0.006 OUR AVERAGE Includes data from the 2 datablocks that follow this one.					
0.333±0.050	33M	WILLIAMS	73	ASPK	$K_{\mu3}+K_{e3}$

$A_L(\mu) = [\Gamma(\pi^-\mu^+\nu_\mu) - \Gamma(\pi^+\mu^-\overline{\nu}_\mu)]$/SUM

Only the combined value below is put into the Meson Summary Table.

VALUE (%)	EVTS	DOCUMENT ID		TECN
The data in this block is included in the average printed for a previous datablock.				
0.304±0.025 OUR AVERAGE				
0.313±0.029	15M	GEWENIGER	74	ASPK
0.278±0.051	7.7M	PICCIONI	72	ASPK
• • • We do not use the following data for averages, fits, limits, etc. • • •				
0.60 ±0.14	4.1M	MCCARTHY	73	CNTR
0.57 ±0.17	1M	[1] PACIOTTI	69	OSPK
0.403±0.134	1M	[1] DORFAN	67	OSPK

[1] PACIOTTI 69 is a reanalysis of DORFAN 67 and is corrected for $\mu^+\mu^-$ range difference in MCCARTHY 72.

$A_L(e) = [\Gamma(\pi^-e^+\nu_e) - \Gamma(\pi^+e^-\overline{\nu}_e)]$/SUM

Only the combined value below is put into the Meson Summary Table.

VALUE (%)	EVTS	DOCUMENT ID		TECN
The data in this block is included in the average printed for a previous datablock.				
0.334 ±0.007 OUR AVERAGE				
0.3322±0.0058±0.0047	298M	ALAVI-HARATI	02	
0.341 ±0.018	34M	GEWENIGER	74	ASPK
0.318 ±0.038	40M	FITCH	73	ASPK
0.346 ±0.033	10M	MARX	70	CNTR
• • • We do not use the following data for averages, fits, limits, etc. • • •				
0.36 ±0.18	600k	ASHFORD	72	ASPK
0.246 ±0.059	10M	[1] SAAL	69	CNTR
0.224 ±0.036	10M	[1] BENNETT	67	CNTR

[1] SAAL 69 is a reanalysis of BENNETT 67.

PARAMETERS FOR $K^0_L \to 2\pi$ DECAY

$\eta_{+-} = A(K^0_L \to \pi^+\pi^-)\ /\ A(K^0_S \to \pi^+\pi^-)$
$\eta_{00} = A(K^0_L \to \pi^0\pi^0)\ /\ A(K^0_S \to \pi^0\pi^0)$

The fitted values of $|\eta_{+-}|$ and $|\eta_{00}|$ given below are the results of a fit to $|\eta_{+-}|$, $|\eta_{00}|$, $|\eta_{00}/\eta_{+-}|$, and Re(ϵ'/ϵ). Independent information on $|\eta_{+-}|$ and $|\eta_{00}|$ can be obtained from the fitted values of the $K^0_L \to \pi\pi$ and $K^0_S \to \pi\pi$ branching ratios and the K^0_L and K^0_S lifetimes. This information is included as data in the $|\eta_{+-}|$ and $|\eta_{00}|$ sections with a Document ID "BRFIT." See the note "*CP* violation in K_L decays" above for details.

$|\eta_{00}| = |A(K^0_L \to 2\pi^0)\ /\ A(K^0_S \to 2\pi^0)|$

VALUE (units 10^{-3})	DOCUMENT ID		TECN	COMMENT
2.222±0.012 OUR FIT Error includes scale factor of 1.7.				
2.243±0.014	BRFIT	16		
• • • We do not use the following data for averages, fits, limits, etc. • • •				
2.47 ±0.31 ±0.24	ANGELOPO...	98	CPLR	
2.49 ±0.40	[1] ADLER	96B	CPLR	Sup. by ANGELOPOULOS 98
2.33 ±0.18	CHRISTENS...	79	ASPK	
2.71 ±0.37	[2] WOLFF	71	OSPK	Cu reg., 4γ's
2.95 ±0.63	[2] CHOLLET	70	OSPK	Cu reg., 4γ's

[1] Error is statistical only.
[2] CHOLLET 70 gives $|\eta_{00}| = (1.23 \pm 0.24)\times$(regeneration amplitude, 2 GeV/c Cu)/10000mb. WOLFF 71 gives $|\eta_{00}| = (1.13 \pm 0.12)\times$(regeneration amplitude, 2 GeV/c Cu)/10000mb. We compute both $|\eta_{00}|$ values for (regeneration amplitude, 2 GeV/c Cu) = 24 ± 2mb. This regeneration amplitude results from averaging over FAISSNER 69, extrapolated using optical-model calculations of Bohm et al., Physics Letters **27B** 594 (1968) and the data of BALATS 71. (From H. Faissner, private communication).

$|\eta_{+-}| = |A(K^0_L \to \pi^+\pi^-)\ /\ A(K^0_S \to \pi^+\pi^-)|$

VALUE (units 10^{-3})	EVTS	DOCUMENT ID		TECN	COMMENT
2.233±0.012 OUR FIT Error includes scale factor of 1.7.					
2.226±0.008		BRFIT	16		
• • • We do not use the following data for averages, fits, limits, etc. • • •					
2.223±0.012		[1] LAI	07	NA48	
2.219±0.013		[2] AMBROSINO	06F	KLOE	
2.228±0.010		[3] ALEXOPOU...	04	KTEV	
2.286±0.023±0.026	70M	[4] APOSTOLA...	99C	CPLR	K^0-$\overline{K}^0$ asymmetry
2.310±0.043±0.031		[5] ADLER	95B	CPLR	K^0-$\overline{K}^0$ asymmetry
2.32 ±0.14 ±0.03	10^5	ADLER	92B	CPLR	K^0-$\overline{K}^0$ asymmetry
2.30 ±0.035		GEWENIGER	74B	ASPK	

[1] Value obtained from the NA48 measurements of $\Gamma(K^0_L \to \pi^+\pi^-)/\Gamma(K^0_L \to \pi e\nu_e)$ and $\tau_{K^0_S}$ and KLOE measurements of $B(K^0_S \to \pi^+\pi^-)$ and $\tau_{K^0_L}$. $\Gamma(K^0_L \to \pi^+\pi^-)$ is defined to include the inner bremsstrahlung component $\Gamma(K^0_L \to \pi^+\pi^-\gamma(\text{IB}))$ but exclude the direct emission component $B(K^0_S \to \pi^+\pi^-(\text{DE}))$. Their $|\eta_{+-}|$ value is not directly used in our fit, but enters the fit via their branching ratio and lifetime measurements.
[2] AMBROSINO 06F uses KLOE branching ratios and τ_L together with τ_S from PDG 04. Their $|\eta_{+-}|$ value is not directly used in our fit, but enters the fit via their branching ratio and lifetime measurements.
[3] ALEXOPOULOS 04 $|\eta_{+-}|$ uses their $K^0_L \to \pi\pi$ branching fractions, $\tau_S = (0.8963 \pm 0.0005)\times10^{-10}$ s from the average of KTeV and NA48 τ_S measurements, and assumes that $\Gamma(K^0_S \to \pi\ell\nu_\ell) = \Gamma(K^0_L \to \pi\ell\nu_\ell)$ giving $B(K^0_S \to \pi\ell\nu_\ell) = 0.118\%$. Their η_{+-} is not directly used in our fit, but enters our fit via their branching ratio measurements.
[4] APOSTOLAKIS 99C report $(2.264 \pm 0.023 \pm 0.026 + 9.1[\tau_S - 0.8934])\times10^{-3}$. We evaluate for our 2006 best value $\tau_S = (0.8958 \pm 0.0005)\times10^{-10}$ s.
[5] ADLER 95B report $(2.312 \pm 0.043 \pm 0.030 - 1[\Delta m - 0.5274] + 9.1[\tau_S - 0.8926])\times10^{-3}$. We evaluate for our 1996 best values $\Delta m = (0.5304 \pm 0.0014)\times10^{-10}\ \hbar s^{-1}$ and $\tau_S = (0.8927 \pm 0.0009)\times10^{-10}$ s. Superseded by APOSTOLAKIS 99C.

Int. J. Mod. Phys. A 2026.41. Downloaded from www.worldscientific.com
by [redacted]LIFORNIA @ BERKELEY on 09/16/26. Re-use and distribution is strictly not permitted, except for Open Access articles.

$|\epsilon| = (2|\eta_{+-}| + |\eta_{00}|)/3$

This expression is a very good approximation, good to about one part in 10^{-4} because of the small measured value of $\phi_{00} - \phi_{+-}$ and small theoretical ambiguities.

VALUE (units 10^{-3})	DOCUMENT ID
2.229±0.012 OUR FIT Error includes scale factor of 1.7.	

$|\eta_{00}/\eta_{+-}|$

VALUE	EVTS	DOCUMENT ID		TECN
0.9950±0.0007 OUR FIT Error includes scale factor of 1.6.				
0.9930±0.0020 OUR AVERAGE				
0.9931±0.0020		[1,2] BARR	93D	NA31
0.9904±0.0084±0.0036		[3] WOODS	88	E731
• • • We do not use the following data for averages, fits, limits, etc. • • •				
0.9939±0.0013±0.0015	1M	[1] BARR	93D	NA31
0.9899±0.0020±0.0025		[1] BURKHARDT	88	NA31

[1] This is the square root of the ratio R given by BURKHARDT 88 and BARR 93D.
[2] This is the combined results from BARR 93D and BURKHARDT 88, taking into account a common systematic uncertainty of 0.0014.
[3] We calculate $|\eta_{00}/\eta_{+-}| = 1-3(\epsilon'/\epsilon)$ from WOODS 88 (ϵ'/ϵ) value.

$\mathrm{Re}(\epsilon'/\epsilon) = (1-|\eta_{00}/\eta_{+-}|)/3$

We have neglected terms of order $\omega\cdot\mathrm{Re}(\epsilon'/\epsilon)$, where $\omega = \mathrm{Re}(A_2)/\mathrm{Re}(A_0) \simeq 1/22$. If included, this correction would lower $\mathrm{Re}(\epsilon'/\epsilon)$ by about 0.04×10^{-3}. See SOZZI 04.

VALUE (units 10^{-3})	DOCUMENT ID		TECN	COMMENT
1.67 ±0.23 OUR FIT Error includes scale factor of 1.6.				
1.68 ±0.20 OUR AVERAGE Error includes scale factor of 1.4. See the ideogram below.				
1.92 ±0.21	[1] ABOUZAID	11	KTEV	Assuming CPT
1.47 ±0.22	BATLEY	02	NA48	
0.74 ±0.52 ±0.29	GIBBONS	93B	E731	
• • • We use the following data for averages but not for fits. • • •				
2.3 ±0.65	[2,3] BARR	93D	NA31	
• • • We do not use the following data for averages, fits, limits, etc. • • •				
2.110±0.343	[1,4] ABOUZAID	11	KTEV	Not assuming CPT
2.07 ±0.28	ALAVI-HARATI	03	KTEV	In ABOUZAID 11
1.53 ±0.26	LAI	01C	NA48	Incl. in BATLEY 02
2.80 ±0.30 ±0.28	ALAVI-HARATI	99D	KTEV	In ALAVI-HARATI 03
1.85 ±0.45 ±0.58	FANTI	99C	NA48	In LAI 01C
2.0 ±0.7	[5] BARR	93D	NA31	
−0.4 ±1.4 ±0.6	PATTERSON	90	E731	in GIBBONS 93B
3.3 ±1.1	[5] BURKHARDT	88	NA31	
3.2 ±2.8 ±1.2	[2] WOODS	88	E731	

[1] The two ABOUZAID 11 values use the same data. The fits are performed with and without CPT invariance requirement.
[2] These values are derived from $|\eta_{00}/\eta_{+-}|$ measurements. They enter the average in this section but enter the fit via the $|\eta_{00}/\eta_{+-}|$ only.
[3] This is the combined results from BARR 93D and BURKHARDT 88, taking into account their common systematic uncertainty.
[4] We use ABOUZAID 11 $\mathrm{Re}(\epsilon'/\epsilon)$ value with CPT assumption in our fits for $|\eta_{+-}|$, $|\eta_{00}|$, and $\mathrm{Re}(\epsilon'/\epsilon)$.
[5] These values are derived from $|\eta_{00}/\eta_{+-}|$ measurements.

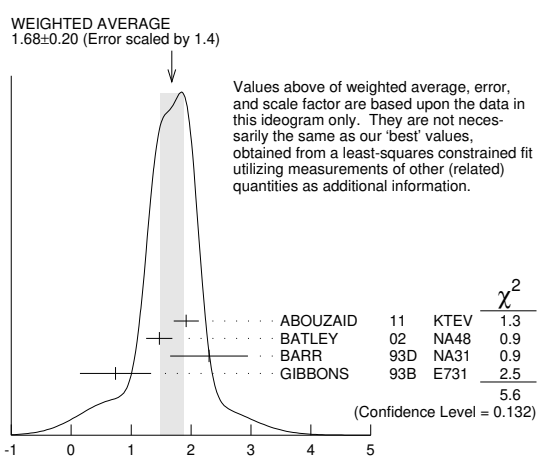

ϕ_{+-}, PHASE of η_{+-}

The dependence of the phase on Δm and τ_S is given for each experiment in the comments below, where Δm is the $K^0_L - K^0_S$ mass difference in units $10^{10}\ \hbar s^{-1}$ and τ_S is the K_S mean life in units 10^{-10} s. We also give the regeneration phase ϕ_f in the comments below.

OUR FIT is described in the note on "CP violation in K_L decays" in the K^0_L Particle Listings. Most experiments in this section are included in both the "Not Assuming CPT" and "Assuming CPT" fits. In the latter fit, they have little direct influence on ϕ_{+-} because their errors are large compared to that assuming CPT, but they influence Δm and τ_S through their dependencies on these parameters, which are given in the footnotes.

VALUE (°)	EVTS	DOCUMENT ID		TECN	COMMENT
43.51±0.05 OUR FIT Error includes scale factor of 1.2. Assuming CPT					
43.4 ±0.5 OUR FIT Error includes scale factor of 1.2. Not assuming CPT					
42.9 ±0.6 ±0.3	70M	[1] APOSTOLA...	99C	CPLR	K^0-$\overline{K}^0$ asymmetry
42.9 ±0.8 ±0.2		[2,3] SCHWINGEN...	95	E773	$CH_{1.1}$ regenerator
41.4 ±0.9 ±0.2		[3,4] GIBBONS	93	E731	B_4C regenerator
44.5 ±1.6 ±0.5		[5] CAROSI	90	NA31	Vacuum regen.
43.3 ±1.0 ±0.5		[6] GEWENIGER	74B	ASPK	Vacuum regen.
• • • We do not use the following data for averages, fits, limits, etc. • • •					
43.76±0.64		[7] ABOUZAID	11	KTEV	Not assuming CPT
44.12±0.72±1.20		[8] ALAVI-HARATI	03	KTEV	Not assuming CPT
42.5 ±0.4 ±0.3		[9,10] ADLER	96C	RVUE	
43.4 ±1.1 ±0.3		[11] ADLER	95B	CPLR	K^0-$\overline{K}^0$ asymmetry
42.3 ±4.4 ±1.4	100k	[12] ADLER	92B	CPLR	K^0-$\overline{K}^0$ asymmetry
47.7 ±2.0 ±0.9		[3,13] KARLSSON	90	E731	
44.3 ±2.8 ±0.2		[14] CARITHERS	75	SPEC	C regenerator

[1] APOSTOLAKIS 99C measures $\phi_{+-} = (43.19 \pm 0.53 \pm 0.28) + 300\,[\Delta m - 0.5301]$ (°). We have adjusted the measurement to use our best values of ($\Delta m = 0.5293 \pm 0.0009$) ($10^{10}\ \hbar\ s^{-1}$). Our first error is their experiment's error and our second error is the systematic error from using our best values.
[2] SCHWINGENHEUER 95 measures $\phi_{+-} = (43.53 \pm 0.76) + 173\,[\Delta m - 0.5282] - 275\,[\tau_S - 0.8926]$ (°). We have adjusted the measurement to use our best values of ($\Delta m = 0.5293 \pm 0.0009$) ($10^{10}\ \hbar\ s^{-1}$), ($\tau_S = 0.8954 \pm 0.0004$) ($10^{-10}$ s). Our first error is their experiment's error and our second error is the systematic error from using our best values.
[3] These experiments measure ϕ_{+-}–ϕ_f and calculate the regeneration phase from the power law momentum dependence of the regeneration amplitude using analyticity and dispersion relations. SCHWINGENHEUER 95 [GIBBONS 93] includes a systematic error of 0.35° [0.5°] for uncertainties in their modeling of the regeneration amplitude.
[4] GIBBONS 93 measures $\phi_{+-} = (42.21 \pm 0.9) + 189\,[\Delta m - 0.5257] - 460\,[\tau_S - 0.8922]$ (°). We have adjusted the measurement to use our best values of ($\Delta m = 0.5293 \pm 0.0009$) ($10^{10}\ \hbar\ s^{-1}$), ($\tau_S = 0.8954 \pm 0.0004$) ($10^{-10}$ s). Our first error is their experiment's error and our second error is the systematic error from using our best values. This is actually reported in SCHWINGENHEUER 95, footnote 8. GIBBONS 93 reports ϕ_{+-} (42.2 ± 1.4)°. They measure ϕ_+–ϕ_f and calculate the regeneration phase ϕ_f from the power law momentum dependence of the regeneration amplitude using analyticity. An error of 0.6° is included for possible uncertainties in the regeneration phase.
[5] CAROSI 90 measures $\phi_{+-} = (46.9 \pm 1.4 \pm 0.7) + 579\,[\Delta m - 0.5351] + 303\,[\tau_S - 0.8922]$ (°). We have adjusted the measurement to use our best values of ($\Delta m = 0.5293 \pm 0.0009$) ($10^{10}\ \hbar\ s^{-1}$), ($\tau_S = 0.8954 \pm 0.0004$) ($10^{-10}$ s). Our first error is their experiment's error and our second error is the systematic error from using our best values.
[6] GEWENIGER 74B measures $\phi_{+-} = (49.4 \pm 1.0) + 565\,[\Delta m - 0.540]$ (°). We have adjusted the measurement to use our best values of ($\Delta m = 0.5293 \pm 0.0009$) ($10^{10}\ \hbar\ s^{-1}$). Our first error is their experiment's error and our second error is the systematic error from using our best values.
[7] Not independent of other phase parameters reported in ABOUZAID 11.
[8] ALAVI-HARATI 03 ϕ_{+-} is correlated with their $\Delta m = m_{K^0_L} - m_{K^0_S}$ and τ_{K_S} measurements in the K^0_L and K^0_S sections respectively. The correlation coefficients are $\rho(\phi_{+-},\Delta m)$=+0.955, $\rho(\phi_{+-},\tau_S)$=−0.871, and $\rho(\tau_S,\Delta m)$=−0.840. CPT is not assumed. Uses scintillator Pb regenerator. Superseded by ABOUZAID 11.
[9] ADLER 96C measures $\phi_{+-} = (43.82 \pm 0.41) + 339\,[\Delta m - 0.5307] - 252\,[\tau_S - 0.8922]$ (°). We have adjusted the measurement to use our best values of ($\Delta m = 0.5293 \pm 0.0009$) ($10^{10}\ \hbar\ s^{-1}$), ($\tau_S = 0.8954 \pm 0.0004$) ($10^{-10}$ s). Our first error is their experiment's error and our second error is the systematic error from using our best values.
[10] ADLER 96C is the result of a fit which includes nearly the same data as entered into the "OUR FIT" value in the 1996 edition of this Review (Physical Review **D54** 1 (1996)).
[11] ADLER 95B measures $\phi_{+-} = (42.7 \pm 0.9 \pm 0.6) + 316\,[\Delta m - 0.5274] + 30\,[\tau_S - 0.8926]$ (°). We have adjusted the measurement to use our best values of ($\Delta m = 0.5293 \pm 0.0009$) ($10^{10}\ \hbar\ s^{-1}$), ($\tau_S = 0.8954 \pm 0.0004$) ($10^{-10}$ s). Our first error is their experiment's error and our second error is the systematic error from using our best values.
[12] ADLER 92B quote separately two systematic errors: ±0.4 from their experiment and ±1.0 degrees due to the uncertainty in the value of Δm.
[13] KARLSSON 90 systematic error does not include regeneration phase uncertainty.
[14] CARITHERS 75 measures $\phi_{+-} = (45.5 \pm 2.8) + 224\,[\Delta m - 0.5348]$ (°). We have adjusted the measurement to use our best values of ($\Delta m = 0.5293 \pm 0.0009$) ($10^{10}\ \hbar\ s^{-1}$). Our first error is their experiment's error and our second error is the systematic error from using our best values. $\phi_f = -40.9 \pm 2.6$°.

ϕ_{00}, PHASE OF η_{00}

See comment in ϕ_{+-} header above for treatment of Δm and τ_S dependence, as well as for the inclusion of data in both the "Assuming CPT" and "Not Assuming CPT" fits.

OUR FIT is described in the note on "CP violation in K_L decays" in the K^0_L Particle Listings.

VALUE (°)	DOCUMENT ID		TECN	COMMENT
43.52±0.05 OUR FIT Error includes scale factor of 1.2. Assuming CPT				
43.7 ±0.6 OUR FIT Error includes scale factor of 1.2. Not assuming CPT				
44.5 ±2.3 ±0.5	[1] CAROSI	90	NA31	
• • • We do not use the following data for averages, fits, limits, etc. • • •				
44.06±0.68	[2] ABOUZAID	11	KTEV	Not assuming CPT
41.7 ±5.9 ±0.2	[3] ANGELOPO...	98	CPLR	

Int. J. Mod. Phys. A 2026.41. Downloaded from www.worldscientific.com by UNIVERSITY OF CALIFORNIA @ BERKELEY on 09/16/26. Re-use and distribution is strictly not permitted, except for Open Access articles.

50.8 ±7.1 ±1.7	[4] ADLER	96B	CPLR	Sup. by ANGELOPOULOS 98
47.4 ±1.4 ±0.9	[5] KARLSSON	90	E731	

[1] CAROSI 90 measures $\phi_{00} = (47.1 \pm 2.1 \pm 1.0) + 579\,[\Delta m - 0.5351] + 252\,[\tau_S - 0.8922]$ (°). We have adjusted the measurement to use our best values of ($\Delta m = 0.5293 \pm 0.0009$) ($10^{10}\ \hbar\ s^{-1}$), ($\tau_S = 0.8954 \pm 0.0004$) ($10^{-10}$ s). Our first error is their experiment's error and our second error is the systematic error from using our best values.

[2] Not independent of other phase parameters reported in ABOUZAID 11.

[3] ANGELOPOULOS 98 measures $\phi_{00} = (42.0 \pm 5.6 \pm 1.9) + 240\,[\Delta m - 0.5307]$ (°). We have adjusted the measurement to use our best values of ($\Delta m = 0.5293 \pm 0.0009$) ($10^{10}\ \hbar\ s^{-1}$). Our first error is their experiment's error and our second error is the systematic error from using our best values. The τ_S dependence is negligible.

[4] ADLER 96B identified initial neutral kaon individually as being a K^0 or a $\overline{K}^0$. The systematic uncertainty is ±1.5° combined in quadrature with ±0.8° due to Δm.

[5] KARLSSON 90 systematic error does not include regeneration phase uncertainty.

$\phi_\epsilon = (2\phi_{+-} + \phi_{00})/3$

This expression is a very good approximation, good to about 10^{-3} degrees because of the small measured values of $\phi_{00} - \phi_{+-}$ and Re ϵ'/ϵ, and small theoretical ambiguities.

VALUE (°)		DOCUMENT ID		TECN	COMMENT
43.52 ±0.04	**OUR FIT**	Error includes scale factor of 1.2. Assuming *CPT*			
43.5 ±0.5	**OUR FIT**	Error includes scale factor of 1.3. Not assuming *CPT*			
43.5164±0.0002±0.0509		[1] SUPERWEAK	16		Assuming *CPT*
43.86 ±0.63		[2] ABOUZAID	11	KTEV	Not assuming *CPT*

[1] SUPERWEAK 16 is a fake measurement used to impose the *CPT* or Superweak constraint $\phi_{+-} = \phi_{SW} = \tan^{-1}[2\,\frac{\Delta m}{\hbar}\,(\frac{\tau_S \tau_L}{\tau_L - \tau_S})]$. This "measurement" is linearized using values near the PDG 04 edition values of Δm, τ_S and τ_L, and then adjusted to our current values as described in the following "measurement". SUPERWEAK 16 measures $\phi_\epsilon = (43.50258 \pm 0.00021) + 54.1\,[\Delta m - 0.5289] + 32.0\,[\tau_S - 0.89564]$ (°). We have adjusted the measurement to use our best values of ($\Delta m = 0.5293 \pm 0.0009$) ($10^{10}\ \hbar\ s^{-1}$), ($\tau_S = 0.8954 \pm 0.0004$) ($10^{-10}$ s). Our first error is their experiment's error and our second error is the systematic error from using our best values.

[2] ABOUZAID 11 uses the full KTeV dataset collected in 1996, 1997, and 1999. See Im(ϵ'/ϵ) section for correlation information.

Im(ϵ'/ϵ) = $-(\phi_{00} - \phi_{+-})/3$

For small $|\epsilon'/\epsilon|$, Im(ϵ'/ϵ) is related to the phases of η_{00} and η_{+-} by the above expression.

VALUE (°)		DOCUMENT ID		TECN	COMMENT
−0.002 ±0.005	**OUR FIT**	Error includes scale factor of 1.7. Assuming *CPT*			
−0.11 ±0.11	**OUR FIT**	Not assuming *CPT*			
−0.0985±0.1157		[1] ABOUZAID	11	KTEV	Not assuming *CPT*

[1] ABOUZAID 11 uses the full KTeV dataset collected in 1996, 1997, and 1999. The fit has Δm, τ_S, ϕ_ϵ, Re(ϵ'/ϵ), and Im(ϵ'/ϵ) as free parameters. The reported value of Im(ϵ'/ϵ) = $(-17.20 \pm 20.20) \times 10^{-4}$ rad. The correlation coefficients are $\rho(\phi_\epsilon, \Delta m) = 0.828$, $\rho(\phi_\epsilon, \tau_S) = -0.765$, $\rho(\Delta m, \tau_S) = -0.858$, ρ(Im(ϵ'/ϵ), ϕ_ϵ) = −0.041, ρ(Im(ϵ'/ϵ), Δm) = 0.026, ρ(Im(ϵ'/ϵ), τ_S) = −0.010.

DECAY-PLANE ASYMMETRY IN $\pi^+\pi^-e^+e^-$ DECAYS

This is the *CP*-violating asymmetry

$$A = \frac{N_{\sin\phi\cos\phi>0.0} - N_{\sin\phi\cos\phi<0.0}}{N_{\sin\phi\cos\phi>0.0} + N_{\sin\phi\cos\phi<0.0}}$$

where ϕ is the angle between the e^+e^- and $\pi^+\pi^-$ planes in the K^0_L rest frame.

CP ASYMMETRY *A* in $K^0_L \to \pi^+\pi^-e^+e^-$

VALUE (%)	DOCUMENT ID		TECN
13.7±1.5 OUR AVERAGE			
13.6±1.4±1.5	ABOUZAID	06	KTEV
14.2±3.0±1.9	LAI	03C	NA48
13.6±2.5±1.2	ALAVI-HARATI	00B	KTEV

PARAMETERS FOR $e^+e^-e^+e^-$ DECAYS

These are the *CP*-violating parameters in the ϕ distribution, where ϕ is the angle between the planes of the two e^+e^- pairs in the kaon rest frame:

$$d\Gamma/d\phi \propto 1 + \beta_{CP}\cos(2\phi) + \gamma_{CP}\sin(2\phi)$$

where $\beta_{CP} = -0.20$ and $\gamma_{CP} = 0$ values correspond to no *CP* violation.

β_{CP} from $K^0_L \to e^+e^-e^+e^-$

VALUE	EVTS	DOCUMENT ID		TECN	COMMENT
−0.19±0.07 OUR AVERAGE					
−0.13±0.10±0.03	200	[1] LAI	05B	NA48	
−0.23±0.09±0.02	441	ALAVI-HARATI	01D	KTEV	M_{ee} >8 MeV/c^2

[1] LAI 05B obtains $\beta_{CP} = -0.13 \pm 0.10$(stat) if $\gamma_{CP} = 0$ is assumed.

γ_{CP} from $K^0_L \to e^+e^-e^+e^-$

VALUE	EVTS	DOCUMENT ID		TECN	COMMENT
0.01±0.11 OUR AVERAGE	Error includes scale factor of 1.6.				
+0.13±0.10±0.03	200	LAI	05B	NA48	
−0.09±0.09±0.02	441	ALAVI-HARATI	01D	KTEV	M_{ee} >8 MeV/c^2

CHARGE ASYMMETRY IN $\pi^+\pi^-\pi^0$ DECAYS

These are *CP*-violating charge-asymmetry parameters, defined at beginning of section "LINEAR COEFFICIENT *g* FOR $K^0_L \to \pi^+\pi^-\pi^0$ above.

See also note on Dalitz plot parameters in $K^\pm$ section and note on "*CP* violation in K_L decays" above.

LINEAR COEFFICIENT *j* FOR $K^0_L \to \pi^+\pi^-\pi^0$

VALUE	EVTS	DOCUMENT ID		TECN
0.0012±0.0008 OUR AVERAGE				
0.0010±0.0024±0.0030	500k	ANGELOPO...	98C	CPLR
−0.001 ±0.011	6499	CHO	77	
0.001 ±0.003	4709	PEACH	77	
0.0013±0.0009	3M	SCRIBANO	70	
0.0 ±0.017	4400	SMITH	70	OSPK
0.001 ±0.004	238k	BLANPIED	68	

QUADRATIC COEFFICIENT *f* FOR $K^0_L \to \pi^+\pi^-\pi^0$

VALUE	EVTS	DOCUMENT ID		TECN
0.0045±0.0024±0.0059	500k	ANGELOPO...	98C	CPLR

PARAMETERS for $K^0_L \to \pi^+\pi^-\gamma$ DECAY

$|\eta_{+-\gamma}| = |A(K^0_L \to \pi^+\pi^-\gamma,\ CP\ \text{violating})/A(K^0_S \to \pi^+\pi^-\gamma)|$

VALUE (units 10^{-3})	EVTS	DOCUMENT ID		TECN
2.35 ±0.07 OUR AVERAGE				
2.359±0.062±0.040	9045	MATTHEWS	95	E773
2.15 ±0.26 ±0.20	3671	RAMBERG	93B	E731

$\phi_{+-\gamma}$ = phase of $\eta_{+-\gamma}$

VALUE (°)	EVTS	DOCUMENT ID		TECN
44 ± 4 OUR AVERAGE				
43.8± 3.5± 1.9	9045	MATTHEWS	95	E773
72 ±23 ±17	3671	RAMBERG	93B	E731

$|\epsilon'_{+-\gamma}|/\epsilon$ for $K^0_L \to \pi^+\pi^-\gamma$

VALUE	CL%	EVTS	DOCUMENT ID		TECN
<0.3	90	3671	[1] RAMBERG	93B	E731

[1] RAMBERG 93B limit on $|\epsilon'_{+-\gamma}|/\epsilon$ assumes than any difference between η_{+-} and $\eta_{+-\gamma}$ is due to direct *CP* violation.

$|g_{E1}|$ for $K^0_L \to \pi^+\pi^-\gamma$

This parameter is the amplitude of the direct emission of a *CP* violating E1 electric dipole photon.

VALUE	CL%	EVTS	DOCUMENT ID		TECN	COMMENT
<0.21	90	111k	ABOUZAID	06A	KTEV	E^*_γ > 20 MeV

T VIOLATION TESTS IN K^0_L DECAYS

Im(ξ) in $K^0_{\mu3}$ DECAY (from transverse μ pol.)

Test of *T* reversal invariance.

VALUE	EVTS	DOCUMENT ID		TECN	COMMENT
−0.007±0.026 OUR AVERAGE					
0.009±0.030	12M	MORSE	80	CNTR	Polarization
0.35 ±0.30	207k	[1] CLARK	77	SPEC	POL, t=0
−0.085±0.064	2.2M	[2] SANDWEISS	73	CNTR	POL, t=0
−0.02 ±0.08		LONGO	69	CNTR	POL, t=3.3
−0.2 ±0.6		ABRAMS	68B	OSPK	Polarization
• • • We do not use the following data for averages, fits, limits, etc. • • •					
0.012±0.026		SCHMIDT	79	CNTR	Repl. by MORSE 80

[1] CLARK 77 value has additional $\xi(0)$ dependence $+0.21\mathrm{Re}[\xi(0)]$.

[2] SANDWEISS 73 value corrected from value quoted in their paper due to new value of Re(ξ). See footnote 4 of SCHMIDT 79.

CPT-INVARIANCE TESTS IN K^0_L DECAYS

PHASE DIFFERENCE $\phi_{00} - \phi_{+-}$

Test of *CPT*.

OUR FIT is described in the note on "*CP* violation in K_L decays" in the K^0_L Particle Listings.

VALUE (°)		DOCUMENT ID		TECN	COMMENT
0.006±0.014 OUR FIT	Error includes scale factor of 1.7. Assuming *CPT*				
0.34 ±0.32 OUR FIT	Not assuming *CPT*				
0.006±0.008		[1] SUPERWEAK	16		Assuming *CPT*
−0.30 ±0.88		[2] SCHWINGEN...	95		Combined E731, E773
• • • We do not use the following data for averages, fits, limits, etc. • • •					
0.30 ±0.35		[3] ABOUZAID	11	KTEV	Not assuming *CPT*
0.39 ±0.22 ±0.45		[4] ALAVI-HARATI	03	KTEV	
0.62 ±0.71 ±0.75		SCHWINGEN...	95	E773	
−1.6 ±1.2		[5] GIBBONS	93	E731	
0.2 ±2.6 ±1.2		[6] CAROSI	90	NA31	
−0.3 ±2.4 ±1.2		KARLSSON	90	E731	

[1] SUPERWEAK 16 is a fake experiment to constrain $\phi_{00} - \phi_{+-}$ to a small value as described in the note "*CP* violation in K_L decays."

[2] This SCHWINGENHEUER 95 values is the combined result of SCHWINGENHEUER 95 and GIBBONS 93, accounting for correlated systematic errors.
[3] Not independent of other phase parameters reported in ABOUZAID 11.
[4] ALAVI-HARATI 03 fit Re(ϵ'/ϵ), Im(ϵ'/ϵ), Δm, τ_S, and ϕ_{+-} simultaneously, not assuming *CPT*. Phase difference is obtained from $\phi_{00} - \phi_{+-} \approx -3\mathrm{Im}(\epsilon'/\epsilon)$ for small $|\epsilon'/\epsilon|$. Superseded by ABOUZAID 11.
[5] GIBBONS 93 give detailed dependence of systematic error on lifetime (see the section on the K^0_S mean life) and mass difference (see the section on $m_{K^0_L} - m_{K^0_S}$).
[6] CAROSI 90 is excluded from the fit because it it is not independent of ϕ_{+-} and ϕ_{00} values.

PHASE DIFFERENCE $\phi_{+-} - \phi_{SW}$

Test of *CPT*. The Superweak phase $\phi_{SW} \equiv \tan^{-1}(2\Delta m/\Delta\Gamma)$ where $\Delta m = m_{K^0_L} - m_{K^0_S}$ and $\Delta\Gamma = \hbar(\tau_L - \tau_S)/(\tau_L\tau_S)$.

VALUE (°)	DOCUMENT ID	TECN
0.61±0.62±1.01	[1] ALAVI-HARATI 03	KTEV

[1] ALAVI-HARATI 03 fit is the same as their ϕ_{+-}, τ_{K_S}, Δm fit, except that the parameter $\phi_{+-} - \phi_{SW}$ is used in place of ϕ.

Re($\frac{2}{3}\eta_{+-} + \frac{1}{3}\eta_{00}$)$-\frac{A_L}{2}$

Test of *CPT*

VALUE (units 10^{-6})	DOCUMENT ID	TECN	COMMENT
−3±35	[1] ALAVI-HARATI 02	E799	Uses A_L from K_{e3} decays

[1] ALAVI-HARATI 02 uses PDG 00 values of η_{+-} and η_{00}.

$\Delta S = \Delta Q$ IN K^0 DECAYS

The relative amount of $\Delta S \neq \Delta Q$ component present is measured by the parameter x, defined as

$$x = A(\overline{K}^0 \to \pi^-\ell^+\nu)/A(K^0 \to \pi^-\ell^+\nu) \ .$$

We list Re{x} and Im{x} for K_{e3} and $K_{\mu3}$ combined.

$x = A(\overline{K}^0 \to \pi^-\ell^+\nu)/A(K^0 \to \pi^-\ell^+\nu) = A(\Delta S{=}{-}\Delta Q)/A(\Delta S{=}\Delta Q)$

REAL PART OF x

VALUE	EVTS	DOCUMENT ID		TECN	COMMENT
−0.0018±0.0041±0.0045		ANGELOPO...	98D	CPLR	K_{e3} from K^0
• • • We do not use the following data for averages, fits, limits, etc. • • •					
$0.10^{+0.18}_{-0.19}$	79	SMITH	75B	WIRE	$\pi^- p \to K^0\Lambda$
0.04 ±0.03	4724	NIEBERGALL	74	ASPK	$K^+ p \to K^0 p\pi^+$
−0.008 ±0.044	1757	FACKLER	73	OSPK	K_{e3} from K^0
−0.03 ±0.07	1367	HART	73	OSPK	K_{e3} from $K^0\Lambda$
−0.070 ±0.036	1079	MALLARY	73	OSPK	K_{e3} from $K^0\Lambda$X
0.03 ±0.06	410	[1] BURGUN	72	HBC	$K^+ p \to K^0 p\pi^+$
$0.04^{+0.10}_{-0.13}$	100	[2] GRAHAM	72	OSPK	$K_{\mu3}$ from $K^0\Lambda$
−0.05 ±0.09	442	[2] GRAHAM	72	OSPK	$\pi^- p \to K^0\Lambda$
$0.26^{+0.10}_{-0.14}$	126	MANN	72	HBC	$K^- p \to n\overline{K}^0$
−0.13 ±0.11	342	[2] MANTSCH	72	OSPK	K_{e3} from $K^0\Lambda$
$0.04^{+0.07}_{-0.08}$	222	[1] BURGUN	71	HBC	$K^+ p \to K^0 p\pi^+$
$0.25^{+0.07}_{-0.09}$	252	WEBBER	71	HBC	$K^- p \to n\overline{K}^0$
0.12 ±0.09	215	[3] CHO	70	DBC	$K^+ d \to K^0 pp$
−0.020 ±0.025		[4] BENNETT	69	CNTR	Charge asym+ Cu regen.
$0.09^{+0.14}_{-0.16}$	686	LITTENBERG	69	OSPK	$K^+ n \to K^0 p$
0.03 ±0.03		[4] BENNETT	68	CNTR	
$0.09^{+0.07}_{-0.09}$	121	JAMES	68	HBC	$\overline{p}p$
$0.17^{+0.16}_{-0.35}$	116	FELDMAN	67B	OSPK	$\pi^- p \to K^0\Lambda$
0.17 ±0.10	335	[3] HILL	67	DBC	$K^+ d \to K^0 pp$
$0.035^{+0.11}_{-0.13}$	196	AUBERT	65	HLBC	K^+ charge exch.
$0.06^{+0.18}_{-0.44}$	152	[5] BALDO-...	65	HLBC	K^+ charge exch.
$-0.08^{+0.16}_{-0.28}$	109	[6] FRANZINI	65	HBC	$\overline{p}p$

[1] BURGUN 72 is a final result which includes BURGUN 71.
[2] First GRAHAM 72 value is second GRAHAM 72 value combined with MANTSCH 72.
[3] CHO 70 is analysis of unambiguous events in new data and HILL 67.
[4] BENNETT 69 is a reanalysis of BENNETT 68.
[5] BALDO-CEOLIN 65 gives x and θ converted by us to Re(x) and Im(x).
[6] FRANZINI 65 gives x and θ for Re(x) and Im(x). See SCHMIDT 67.

IMAGINARY PART OF x

Assumes $m_{K^0_L} - m_{K^0_S}$ positive. See Listings above.

VALUE	EVTS	DOCUMENT ID		TECN	COMMENT
0.0012±0.0019±0.0009	640k	ANGELOPO...	01B	CPLR	K_{e3} from K^0
• • • We do not use the following data for averages, fits, limits, etc. • • •					
0.0012±0.0019	640k	[1] ANGELOPO...	98E	CPLR	K_{e3} from K^0
$-0.10^{+0.16}_{-0.19}$	79	SMITH	75B	WIRE	$\pi^- p \to K^0\Lambda$
−0.06 ±0.05	4724	NIEBERGALL	74	ASPK	$K^+ p \to K^0 p\pi^+$
−0.017 ±0.060	1757	FACKLER	73	OSPK	K_{e3} from K^0
0.09 ±0.07	1367	HART	73	OSPK	K_{e3} from $K^0\Lambda$
$0.107^{+0.092}_{-0.074}$	1079	MALLARY	73	OSPK	K_{e3} from $K^0\Lambda$X
$0.07^{+0.06}_{-0.07}$	410	[2] BURGUN	72	HBC	$K^+ p \to K^0 p\pi^+$
$0.12^{+0.17}_{-0.16}$	100	[3] GRAHAM	72	OSPK	$K_{\mu3}$ from $K^0\Lambda$
0.05 ±0.13	442	[3] GRAHAM	72	OSPK	$\pi^- p \to K^0\Lambda$
$0.21^{+0.15}_{-0.12}$	126	MANN	72	HBC	$K^- p \to n\overline{K}^0$
−0.04 ±0.16	342	[3] MANTSCH	72	OSPK	K_{e3} from $K^0\Lambda$
$0.12^{+0.08}_{-0.09}$	222	[2] BURGUN	71	HBC	$K^+ p \to K^0 p\pi^+$
0.0 ±0.08	252	WEBBER	71	HBC	$K^- p \to n\overline{K}^0$
−0.08 ±0.07	215	[4] CHO	70	DBC	$K^+ d \to K^0 pp$
$-0.11^{+0.10}_{-0.11}$	686	LITTENBERG	69	OSPK	$K^+ n \to K^0 p$
$+0.22^{+0.37}_{-0.29}$	121	JAMES	68	HBC	$\overline{p}p$
0.0 ±0.25	116	FELDMAN	67B	OSPK	$\pi^- p \to K^0\Lambda$
−0.20 ±0.10	335	[4] HILL	67	DBC	$K^+ d \to K^0 pp$
$-0.21^{+0.11}_{-0.15}$	196	AUBERT	65	HLBC	K^+ charge exch.
$-0.44^{+0.32}_{-0.19}$	152	[5] BALDO-...	65	HLBC	K^+ charge exch.
$+0.24^{+0.40}_{-0.30}$	109	[6] FRANZINI	65	HBC	$\overline{p}p$

[1] Superseded by ANGELOPOULOS 01B.
[2] BURGUN 72 is a final result which includes BURGUN 71.
[3] First GRAHAM 72 value is second GRAHAM 72 value combined with MANTSCH 72.
[4] Footnote 10 of HILL 67 should read +0.58, not −0.58 (private communication) CHO 70 is analysis of unambiguous events in new data and HILL 67.
[5] BALDO-CEOLIN 65 gives x and θ converted by us to Re(x) and Im(x).
[6] FRANZINI 65 gives x and θ for Re(x) and Im(x). See SCHMIDT 67.

K^0_L REFERENCES

AHN 25 PRL 134 081802 J.K. Ahn *et al.* (KOTO Collab.)
AAIJ 23AE PR D108 L031102 R. Aaij *et al.* (LHCb Collab.)
AHN 21 PRL 126 121801 J.K. Ahn *et al.* (KOTO Collab.)
SHIMIZU 20 PR D102 051103 N. Shimizu *et al.* (KOTO Collab.)
AHN 19 PRL 122 021802 J.K. Ahn *et al.* (KOTO Collab.)
AHN 17 PTEP 2017 021C01 J.K. Ahn *et al.* (KOTO Collab.)
BRFIT 16 RPP 2016 edition C.-J. Lin (PDG Collab.)
ETAFIT 16 RPP 2016 edition C.-J. Lin (PDG Collab.)
SUPERWEAK 16 RPP 2016 edition C.-J. Lin (PDG Collab.)
ABOUZAID 11 PR D83 092001 E. Abouzaid *et al.* (FNAL KTeV Collab.)
ABOUZAID 11A PRL 107 201803 E. Abouzaid *et al.* (KTeV Collab.)
OGATA 11 PR D84 052009 R. Ogata *et al.* (KEK E391a Collab.)
TUNG 11 PR D83 031101 Y.C. Tung *et al.* (KEK E391a Collab.)
ABOUZAID 10 PR D81 052001 E. Abouzaid *et al.* (FNAL KTeV Collab.)
AHN 10 PR D81 072004 J.K. Ahn *et al.* (KEK E391a Collab.)
ABOUZAID 08 PR D77 112004 E. Abouzaid *et al.* (FNAL KTeV Collab.)
ABOUZAID 08A PR D78 032009 E. Abouzaid *et al.* (FNAL KTeV Collab.)
ABOUZAID 08B PR D78 032014 E. Abouzaid *et al.* (FNAL KTeV Collab.)
ABOUZAID 08C PRL 100 131803 E. Abouzaid *et al.* (FNAL KTeV Collab.)
AHN 08 PRL 100 201802 J.K. Ahn *et al.* (KEK E391a Collab.)
AMBROSINO 08F EPJ C55 539 F. Ambrosino *et al.* (KLOE Collab.)
ABOUZAID 07B PRL 99 051804 E. Abouzaid *et al.* (FNAL KTeV Collab.)
ABOUZAID 07C PRL 99 081803 E. Abouzaid *et al.* (FNAL KTeV Collab.)
ABOUZAID 07D PR D76 052001 E. Abouzaid *et al.* (FNAL KTeV Collab.)
AMBROSINO 07C JHEP 0712 105 F. Ambrosino *et al.* (KLOE Collab.)
ANDRE 07 ANP 322 2518 T. Andre (EFI)
LAI 07 PL B645 26 A. Lai *et al.* (CERN NA48 Collab.)
LAI 07A PL B647 341 A. Lai *et al.* (CERN NA48 Collab.)
NIX 07 PR D76 011101 J. Nix *et al.* (KEK E391a Collab.)
ABOUZAID 06 PRL 96 101801 E. Abouzaid *et al.* (KTeV Collab.)
ABOUZAID 06A PR D74 032004 E. Abouzaid *et al.* (KTeV Collab.)
Also PR D74 039905 (errat.) E. Abouzaid *et al.* (KTeV Collab.)
ABOUZAID 06C PR D74 097101 E. Abouzaid *et al.* (KTeV Collab.)
AHN 06 PR D74 051105 J.K. Ahn *et al.* (KEK E391a Collab.)
Also PR D74 079901 (errat.) J.K. Ahn *et al.* (KEK E391a Collab.)
AMBROSINO 06 PL B632 43 F. Ambrosino *et al.* (KLOE Collab.)
AMBROSINO 06D PL B636 166 F. Ambrosino *et al.* (KLOE Collab.)
AMBROSINO 06F PL B638 140 F. Ambrosino *et al.* (KLOE Collab.)
BATLEY 06B PL B633 173 J.R. Batley *et al.* (CERN NA48/2 Collab.)
HILL 06 PR D74 096006 R.J. Hill (FNAL)
PDG 06 JP G33 1 W.-M. Yao *et al.* (PDG Collab.)
ALEXOPOU... 05 PR D71 012001 T. Alexopoulos *et al.* (FNAL KTeV Collab.)
AMBROSINO 05C PL B626 15 F. Ambrosino *et al.* (KLOE Collab.)
CABIBBO 05 JHEP 0503 021 N. Cabibbo, G. Isidori (CERN, ROMAI, FRAS)
LAI 05 PL B605 247 A. Lai *et al.* (CERN NA48 Collab.)
LAI 05B PL B615 31 A. Lai *et al.* (CERN NA48 Collab.)
PARK 05 PRL 94 021801 H.K. Park *et al.* (FNAL HyperCP Collab.)
ALAVI-HARATI 04A PRL 93 021805 A. Alavi-Harati *et al.* (FNAL KTeV/E799 Collab.)
ALEXOPOU... 04 PR D70 092006 T. Alexopoulos *et al.* (FNAL KTeV Collab.)
ALEXOPOU... 04A PR D70 092007 T. Alexopoulos *et al.* (FNAL KTeV Collab.)
BATLEY 04 PL B595 75 J.R. Batley *et al.* (CERN NA48 Collab.)
CIRIGLIANO 04 EPJ C35 53 V. Cirigliano, H. Neufeld, H. Pichl (CIT, VALE+)
LAI 04B PL B602 41 A. Lai *et al.* (CERN NA48 Collab.)
LAI 04C PL B604 1 A. Lai *et al.* (CERN NA48 Collab.)
PDG 04 PL B592 1 S. Eidelman *et al.* (PDG Collab.)
SOZZI 04 EPJ C36 37 M. Sozzi (PISA)
ADINOLFI 03 PL B566 61 M. Adinolfi *et al.* (KLOE Collab.)
ALAVI-HARATI 03 PR D67 012005 A. Alavi-Harati *et al.* (FNAL KTeV Collab.)
Also PR D70 079904 (errat.) A. Alavi-Harati *et al.* (FNAL KTeV Collab.)
ALAVI-HARATI 03B PRL 90 141801 A. ALavi-Harati *et al.* (FNAL KTeV Collab.)
LAI 03 PL B551 7 A. Lai *et al.* (CERN NA48 Collab.)
LAI 03C EPJ C30 33 A. Lai *et al.* (CERN NA48 Collab.)
ALAVI-HARATI 02 PRL 88 181601 A. Alavi-Harati *et al.* (FNAL KTeV Collab.)
ALAVI-HARATI 02C PRL 89 211801 A. Alavi-Harati *et al.* (FNAL KTeV Collab.)
BATLEY 02 PL B544 97 J.R. Batley *et al.* (CERN NA48 Collab.)

Int. J. Mod. Phys. A 2026.41. Downloaded from www.worldscientific.com
by [redacted]LIFORNIA @ BERKELEY on 09/16/26. Re-use and distribution is strictly not permitted, except for Open Access articles.

Int. J. Mod. Phys. A 2026.41. Downloaded from www.worldscientific.com
by UNIVERSITY OF CALIFORNIA @ BERKELEY on 09/16/26. Re-use and distribution is strictly not permitted, except for Open Access articles.

CIRIGLIANO	02	EPJ C23 121	V. Cirigliano *et al.*	(VIEN, VALE, MARS)
LAI	02B	PL B536 229	A. Lai *et al.*	(CERN NA48 Collab.)
ALAVI-HARATI	01	PRL 86 397	A. Alavi-Harati *et al.*	(FNAL KTeV Collab.)
ALAVI-HARATI	01B	PRL 86 761	A. Alavi-Harati *et al.*	(FNAL KTeV Collab.)
ALAVI-HARATI	01D	PRL 86 5425	A. Alavi-Harati *et al.*	(FNAL KTeV Collab.)
ALAVI-HARATI	01E	PRL 87 021801	A. Alavi-Harati *et al.*	(FNAL KTeV Collab.)
ALAVI-HARATI	01F	PR D64 012003	A. Alavi-Harati *et al.*	(FNAL KTeV Collab.)
ALAVI-HARATI	01G	PRL 87 071801	A. Alavi-Harati *et al.*	(FNAL KTeV Collab.)
ALAVI-HARATI	01H	PRL 87 111802	A. Alavi-Harati *et al.*	(FNAL KTeV Collab.)
ALAVI-HARATI	01J	PR D64 112004	A. Alavi-Harati *et al.*	(FNAL KTeV Collab.)
ANGELOPO...	01	PL B503 49	A. Angelopoulos *et al.*	(CPLEAR Collab.)
ANGELOPO...	01B	EPJ C22 55	A. Angelopoulos *et al.*	(CPLEAR Collab.)
LAI	01B	PL B515 261	A. Lai *et al.*	(CERN NA48 Collab.)
LAI	01C	EPJ C22 231	A. Lai *et al.*	(CERN NA48 Collab.)
ALAVI-HARATI	00	PR D61 072006	A. Alavi-Harati *et al.*	(FNAL KTeV Collab.)
ALAVI-HARATI	00B	PRL 84 408	A. Alavi-Harati *et al.*	(FNAL KTeV Collab.)
ALAVI-HARATI	00D	PRL 84 5279	A. Alavi-Harati *et al.*	(FNAL KTeV Collab.)
ALAVI-HARATI	00E	PR D62 112001	A. Alavi-Harati *et al.*	(FNAL KTeV Collab.)
AMBROSE	00	PRL 84 1389	D. Ambrose *et al.*	(BNL E871 Collab.)
APOSTOLA...	00	PL B473 186	A. Apostolakis *et al.*	(CPLEAR Collab.)
PDG	00	EPJ C15 1	D.E. Groom *et al.*	(PDG Collab.)
ALAVI-HARATI	99B	PRL 83 917	A. Alavi-Harati *et al.*	(FNAL KTeV Collab.)
ALAVI-HARATI	99D	PRL 83 22	A. Alavi-Harati *et al.*	(FNAL KTeV Collab.)
APOSTOLA...	99C	PL B458 545	A. Apostolakis *et al.*	(CPLEAR Collab.)
Also		EPJ C18 41	A. Apostolakis *et al.*	(CPLEAR Collab.)
FANTI	99B	PL B458 553	V. Fanti *et al.*	(CERN NA48 Collab.)
FANTI	99C	PL B465 335	V. Fanti *et al.*	(CERN NA48 Collab.)
MURAKAMI	99	PL B463 333	K. Murakami *et al.*	(KEK E162 Collab.)
ADAMS	98	PRL 80 4123	J. Adams *et al.*	(FNAL KTeV Collab.)
AMBROSE	98	PRL 81 4309	D. Ambrose *et al.*	(BNL E871 Collab.)
AMBROSE	98B	PRL 81 5734	D. Ambrose *et al.*	(BNL E871 Collab.)
ANGELOPO...	98	PL B420 191	A. Angelopoulos *et al.*	(CPLEAR Collab.)
ANGELOPO...	98C	EPJ C5 389	A. Angelopoulos *et al.*	(CPLEAR Collab.)
ANGELOPO...	98D	PL B444 38	A. Angelopoulos *et al.*	(CPLEAR Collab.)
Also		EPJ C22 55	A. Angelopoulos *et al.*	(CPLEAR Collab.)
ANGELOPO...	98E	PL B444 43	A. Angelopoulos *et al.*	(CPLEAR Collab.)
ARISAKA	98	PL B432 230	K. Arisaka *et al.*	(FNAL E799 Collab.)
BENDER	98	PL B418 411	M. Bender *et al.*	(CERN NA48 Collab.)
DAMBROSIO	98	PL B423 385	G. D'Ambrosio, G. Isidori, J. Portoles	
SETZU	98	PL B420 205	M.G. Setzu *et al.*	
TAKEUCHI	98	PL B443 409	Y. Takeuchi *et al.*	(KYOT, KEK, HIRO)
FANTI	97	ZPHY C76 653	V. Fanti *et al.*	(CERN NA48 Collab.)
NOMURA	97	PL B408 445	T. Nomura *et al.*	(KYOT, KEK, HIRO)
ADLER	96B	ZPHY C70 211	R. Adler *et al.*	(CPLEAR Collab.)
ADLER	96C	PL B369 367	R. Adler *et al.*	(CPLEAR Collab.)
GU	96	PRL 76 4312	P. Gu *et al.*	(RUTG, UCLA, EFI, COLO+)
LEBER	96	PL B369 69	F. Leber *et al.*	(MAINZ, CERN, EDIN, ORSAY+)
PDG	96	PR D54 1	R. M. Barnett *et al.*	(PDG Collab.)
ADLER	95	PL B363 237	R. Adler *et al.*	(CPLEAR Collab.)
ADLER	95B	PL B363 243	R. Adler *et al.*	(CPLEAR Collab.)
AKAGI	95	PR D51 2061	T. Akagi *et al.*	(TOHOK, TOKY, KYOT, KEK)
BARR	95	ZPHY C65 361	G.D. Barr *et al.*	(CERN, EDIN, MAINZ, LALO+)
BARR	95C	PL B358 399	G.D. Barr *et al.*	(CERN, EDIN, MAINZ, LALO+)
HEINSON	95	PR D51 985	A.P. Heinson *et al.*	(BNL E791 Collab.)
KREUTZ	95	ZPHY C65 67	A. Kreutz *et al.*	(SIEG, EDIN, MAINZ, ORSAY+)
MATTHEWS	95	PRL 75 2803	J.N. Matthews *et al.*	(RUTG, EFI, ELMT+)
SCHWINGEN...	95	PRL 74 4376	B. Schwingenheuer *et al.*	(EFI, CHIC+)
SPENCER	95	PRL 74 3323	M.B. Spencer *et al.*	(UCLA, EFI, COLO+)
BARR	94	PL B328 528	G.D. Barr *et al.*	(CERN, EDIN, MAINZ, LALO+)
GU	94	PRL 72 3000	P. Gu *et al.*	(RUTG, UCLA, EFI, COLO+)
NAKAYA	94	PRL 73 2169	T. Nakaya *et al.*	(OSAK, UCLA, EFI, COLU+)
ROBERTS	94	PR D50 1874	D. Roberts *et al.*	(UCLA, EFI, COLU+)
AKAGI	93	PR D47 2644	T. Akagi *et al.*	(TOHOK, TOKY, KYOT, KEK)
ARISAKA	93	PRL 70 1049	K. Arisaka *et al.*	(BNL E791 Collab.)
ARISAKA	93B	PRL 71 3910	K. Arisaka *et al.*	(BNL E791 Collab.)
BARR	93D	PL B317 233	G.D. Barr *et al.*	(CERN, EDIN, MAINZ, LALO+)
GIBBONS	93	PRL 70 1199	L.K. Gibbons *et al.*	(FNAL E731 Collab.)
Also		PR D55 6625	L.K. Gibbons *et al.*	(FNAL E731 Collab.)
GIBBONS	93B	PRL 70 1203	L.K. Gibbons *et al.*	(FNAL E731 Collab.)
GIBBONS	93C	Thesis RX-1487	L.K. Gibbons	(CHIC)
Also		PR D55 6625	L.K. Gibbons *et al.*	(FNAL E731 Collab.)
HARRIS	93	PRL 71 3914	D.A. Harris *et al.*	(EFI, UCLA, COLO+)
HARRIS	93B	PRL 71 3918	D.A. Harris *et al.*	(EFI, UCLA, COLO+)
MAKOFF	93	PRL 70 1591	G. Makoff *et al.*	(FNAL E731 Collab.)
Also		PRL 75 2069 (errat.)	G. Makoff *et al.*	
RAMBERG	93	PRL 70 2525	E. Ramberg *et al.*	(FNAL E731 Collab.)
RAMBERG	93B	PRL 70 2529	E.J. Ramberg *et al.*	(FNAL E731 Collab.)
VAGINS	93	PRL 71 35	M.R. Vagins *et al.*	(BNL E845 Collab.)
ADLER	92B	PL B286 180	R. Adler *et al.*	(CPLEAR Collab.)
Also		SJNP 55 840	R. Adler *et al.*	(CPLEAR Collab.)
BARR	92	PL B284 440	G.D. Barr *et al.*	(CERN, EDIN, MAINZ, LALO+)
MORSE	92	PR D45 36	W.M. Morse *et al.*	(BNL, YALE, VASS)
PDG	92	PR D45 S1	K. Hikasa *et al.*	(KEK, LBL, BOST+)
SOMALWAR	92	PRL 68 2580	S.V. Somalwar *et al.*	(FNAL E731 Collab.)
AKAGI	91B	PRL 67 2618	T. Akagi *et al.*	(TOHOK, TOKY, KYOT, KEK)
BARR	91	PL B259 389	G.D. Barr *et al.*	(CERN, EDIN, MAINZ, LALO+)
HEINSON	91	PR D44 1	A.P. Heinson *et al.*	(UCI, UCLA, LANL+)
PAPADIMITR...	91	PR D44 573	V. Papadimitriou *et al.*	(FNAL E731 Collab.)
BARKER	90	PR D41 3546	A.R. Barker *et al.*	(FNAL E731 Collab.)
Also		PRL 61 2661	L.K. Gibbons *et al.*	(FNAL E731 Collab.)
BARR	90B	PL B240 283	G.D. Barr *et al.*	(CERN, EDIN, MAINZ, LALO+)
BARR	90C	PL B242 523	G.D. Barr *et al.*	(CERN, EDIN, MAINZ, LALO+)
CAROSI	90	PL B237 303	R. Carosi *et al.*	(CERN, EDIN, MAINZ, LALO+)
KARLSSON	90	PRL 64 2976	M. Karlsson *et al.*	(FNAL E731 Collab.)
OHL	90	PRL 64 2755	K.E. Ohl *et al.*	(BNL E845 Collab.)
OHL	90B	PRL 65 1407	K.E. Ohl *et al.*	(BNL E845 Collab.)
PATTERSON	90	PRL 64 1491	J.R. Patterson *et al.*	(FNAL E731 Collab.)
INAGAKI	89	PR D40 1712	T. Inagaki *et al.*	(KEK, TOKY, KYOT)
MATHIAZHA...	89	PRL 63 2181	C. Mathiazhagan *et al.*	(UCI, UCLA, LANL+)
MATHIAZHA...	89B	PRL 63 2185	C. Mathiazhagan *et al.*	(UCI, UCLA, LANL+)
WAHL	89	CERN-EP/89-86	H. Wahl	(CERN)
BARR	88	PL B214 303	G.D. Barr *et al.*	(CERN, EDIN, MAINZ, LALO+)
BURKHARDT	88	PL B206 169	H. Burkhardt *et al.*	(CERN, EDIN, MAINZ+)
JASTRZEM...	88	PRL 61 2300	E. Jastrzembski *et al.*	(BNL, YALE)
WOODS	88	PRL 60 1695	M. Woods *et al.*	(FNAL E731 Collab.)
BURKHARDT	87	PL B199 139	H. Burkhardt *et al.*	(CERN, EDIN, MAINZ+)
ARONSON	86	PR D33 3180	S.H. Aronson *et al.*	(BNL, CHIC, STAN+)
Also		PRL 48 1078	S.H. Aronson *et al.*	(BNL, CHIC, STAN+)
PDG	86C	PL 170B 132	M. Aguilar-Benitez *et al.*	(CERN, CIT+)
COUPAL	85	PRL 55 566	D.P. Coupal *et al.*	(CHIC, SACL)
BALATS	83	SJNP 38 556	M.Y. Balats *et al.*	(ITEP)
		Translated from YAF 38 927.		
BERGSTROM	83	PL 131B 229	L. Bergstrom, E. Masso, P. Singer	(CERN)
ARONSON	82	PRL 48 1078	S.H. Aronson *et al.*	(BNL, CHIC, STAN+)
ARONSON	82B	PRL 48 1306	S.H. Aronson *et al.*	(BNL, CHIC, PURD)
Also		PL 116B 73	E. Fischbach *et al.*	(PURD, BNL, CHIC)
Also		PR D28 476	S.H. Aronson *et al.*	(BNL, CHIC, PURD)
Also		PR D28 495	S.H. Aronson *et al.*	(BNL, CHIC, PURD)
PDG	82B	PL 111B 70	M. Roos *et al.*	(HELS, CIT, CERN)
BIRULEV	81	NP B182 1	V.K. Birulev *et al.*	(JINR)
Also		SJNP 31 622	V.K. Birulev *et al.*	(JINR)
		Translated from YAF 31 1204.		
CARROLL	80B	PRL 44 529	A.S. Carroll *et al.*	(BNL, ROCH)
CARROLL	80C	PL 96B 407	A.S. Carroll *et al.*	(BNL, ROCH)
CHO	80	PR D22 2688	Y. Cho *et al.*	(ANL, CMU)
MORSE	80	PR D21 1750	W.M. Morse *et al.*	(BNL, YALE)
CHRISTENS...	79	PRL 43 1209	J.H. Christenson *et al.*	(NYU)
SCHMIDT	79	PRL 43 556	M.P. Schmidt *et al.*	(YALE, BNL)
HILL	78	PL 73B 483	D.G. Hill *et al.*	(BNL, SLAC, SBER)
CHO	77	PR D15 587	Y. Cho *et al.*	(ANL, CMU)
CLARK	77	PR D15 553	A.R. Clark *et al.*	(LBL)
Also		Thesis LBL-4275	G. Shen	(LBL)
DEVOE	77	PR D16 565	R. Devoe *et al.*	(EFI, ANL)
PEACH	77	NP B127 399	K.J. Peach *et al.*	(BGNA, EDIN, GLAS+)
BIRULEV	76	SJNP 24 178	V.K. Birulev *et al.*	(JINR)
		Translated from YAF 24 340.		
COOMBES	76	PRL 37 249	R.W. Coombes *et al.*	(STAN, NYU)
GJESDAL	76	NP B109 118	G. Gjesdal *et al.*	(CERN, HEIDH)
BALDO-...	75	NC 25A 688	M. Baldo-Ceolin *et al.*	(PADO, WISC)
BLUMENTHAL	75	PRL 34 164	R.B. Blumenthal *et al.*	(PENN, CHIC, TEMP)
BUCHANAN	75	PR D11 457	C.D. Buchanan *et al.*	(UCLA, SLAC, JHU)
CARITHERS	75	PRL 34 1244	W.C.J. Carithers *et al.*	(COLU, NYU)
SMITH	75B	Thesis UCSD unpub.	J.G. Smith	(UCSD)
BISI	74	PL 50B 504	V. Bisi, M.I. Ferrero	(TORI)
DONALDSON	74	Thesis SLAC-0184	G. Donaldson	(SLAC)
Also		PR D14 2839	G. Donaldson *et al.*	(SLAC)
DONALDSON	74B	PR D9 2960	G. Donaldson *et al.*	(SLAC, UCSC)
Also		PRL 31 337	G. Donaldson *et al.*	(SLAC, UCSC)
GEWENIGER	74	PL 48B 483	C. Geweniger *et al.*	(CERN, HEIDH)
Also		Thesis CERN Int. 74-4	V. Luth	(CERN)
GEWENIGER	74B	PL 48B 487	C. Geweniger *et al.*	(CERN, HEIDH)
Also		PL 52B 119	S. Gjesdal *et al.*	(CERN, HEIDH)
GEWENIGER	74C	PL 52B 108	C. Geweniger *et al.*	(CERN, HEIDH)
GJESDAL	74	PL 52B 113	S. Gjesdal *et al.*	(CERN, HEIDH)
MESSNER	74	PRL 33 1458	R. Messner *et al.*	(COLO, SLAC, UCSC)
NIEBERGALL	74	PL 49B 103	F. Niebergall *et al.*	(CERN, ORSAY, VIEN)
WILLIAMS	74	PRL 33 240	H.H. Williams *et al.*	(BNL, YALE)
ALEXANDER	73B	NP B65 301	G. Alexander *et al.*	(TELA, HEID)
BRANDENB...	73	PR D8 1978	G.W. Brandenburg *et al.*	(SLAC)
EVANS	73	PR D7 36	G.R. Evans *et al.*	(EDIN, CERN)
Also		PRL 23 427	G.R. Evans *et al.*	(EDIN, CERN)
FACKLER	73	PRL 31 847	O. Fackler *et al.*	(MIT)
FITCH	73	PRL 31 1524	V.L. Fitch *et al.*	(PRIN)
Also		Thesis COO-3072-13	R.C. Webb	(PRIN)
HART	73	NP B66 317	J.C. Hart *et al.*	(CAVE, RHEL)
MALLARY	73	PR D7 1953	M.L. Mallary *et al.*	(CIT)
Also		PRL 25 1214	F.J. Sciulli *et al.*	(CIT)
MCCARTHY	73	PR D7 687	R.L. McCarthy *et al.*	(LBL)
Also		PL 42B 291	R.L. McCarthy *et al.*	(LBL)
Also		Thesis LBL-550	R.L. McCarthy	(LBL)
MESSNER	73	PRL 30 876	R. Messner *et al.*	(COLO, SLAC, UCSC)
SANDWEISS	73	PRL 30 1002	J. Sandweiss *et al.*	(YALE, ANL)
WILLIAMS	73	PRL 31 1521	H.H. Williams *et al.*	(BNL, YALE)
ASHFORD	72	PL 38B 47	V.A. Ashford *et al.*	(UCSD)
BANNER	72B	PRL 29 237	M. Banner *et al.*	(PRIN)
BARMIN	72B	SJNP 15 638	V.V. Barmin *et al.*	(ITEP)
		Translated from YAF 15 1152.		
BURGUN	72	NP B50 194	G. Burgun *et al.*	(SACL, CERN, OSLO)
GRAHAM	72	NC 9A 166	M.F. Graham *et al.*	(ILL, NEAS)
JAMES	72	NP B49 1	F. James *et al.*	(CERN, SACL, OSLO)
KRENZ	72	LNC 4 213	W. Krenz *et al.*	(AACH, CERN, EDIN)
MANN	72	PR D6 137	W.A. Mann *et al.*	(MASA, BNL, YALE)
MANTSCH	72	NC 9A 160	P.M. Mantsch *et al.*	(ILL, NEAS)
MCCARTHY	72	PL 42B 291	R.L. McCarthy *et al.*	(LBL)
PICCIONI	72	PRL 29 1412	R. Piccioni *et al.*	(SLAC)
Also		PR D9 2939	R. Piccioni *et al.*	(SLAC, UCSC, COLO)
VOSBURGH	72	PR D6 1834	K.G. Vosburgh *et al.*	(RUTG, MASA)
Also		PRL 26 866	K.G. Vosburgh *et al.*	(RUTG, MASA)
BALATS	71	SJNP 13 53	M.Y. Balats *et al.*	(ITEP)
		Translated from YAF 13 93.		
BARMIN	71	PL 35B 604	V.V. Barmin *et al.*	(ITEP)
BURGUN	71	LNC 2 1169	G. Burgun *et al.*	(SACL, CERN, OSLO)
CARNEGIE	71	PR D4 1	R.K. Carnegie *et al.*	(PRIN)
CHAN	71	Thesis LBL-350	J.H.S. Chan	(LBL)
CHO	71	PR D3 1557	Y. Cho *et al.*	(CMU, BNL, CASE)
ENSTROM	71	PR D4 2629	J. Enstrom *et al.*	(SLAC, STAN)
Also		Thesis SLAC-0125	J.E. Enstrom	(STAN)
JAMES	71	PL 35B 265	F. James *et al.*	(CERN, SACL, OSLO)
MEISNER	71	PR D3 59	G.W. Meisner *et al.*	(MASA, BNL, YALE)
REPELLIN	71	PL 36B 603	J.P. Repellin *et al.*	(ORSAY, CERN)
WEBBER	71	PR D3 64	B.R. Webber *et al.*	(LRL)
Also		PRL 21 498	B.R. Webber *et al.*	(LRL)
Also		Thesis UCRL 19226	B.R. Webber	(LRL)
WOLFF	71	PL 36B 517	B. Wolff *et al.*	(ORSAY, CERN)
ALBROW	70	PL 33B 516	M.G. Albrow *et al.*	(MCHS, DARE)
ARONSON	70	PRL 25 1057	S.H. Aronson *et al.*	(EFI, ILLC, SLAC)
BARMIN	70	PL 33B 377	V.V. Barmin *et al.*	(ITEP, JINR)
BASILE	70	PR D2 78	P. Basile *et al.*	(SACL)
BECHERRAWY	70	PR D1 1452	T. Becherrawy	(ROCH)
BUCHANAN	70	PL 33B 623	C.D. Buchanan *et al.*	(SLAC, JHU, UCLA)
Also		Private Comm.	A.J. Cox	
BUDAGOV	70	PR D2 815	I.A. Budagov *et al.*	(CERN, ORSAY, EPOL)
Also		PL 28B 215	I.A. Budagov *et al.*	(CERN, ORSAY, EPOL)
CHO	70	PR D1 3031	Y. Cho *et al.*	(CMU, BNL, CASE)
Also		PRL 19 668	D.G. Hill *et al.*	(BNL, CMU)
CHOLLET	70	PL 31B 658	J.C. Chollet *et al.*	(CERN)
CULLEN	70	PL 32B 523	M. Cullen *et al.*	(AACH, CERN, TORI)
MARX	70	PL 32B 219	J. Marx *et al.*	(COLU, HARV, CERN)
Also		Thesis Nevis 179	J. Marx	(COLU)
SCRIBANO	70	PL 32B 224	A. Scribano *et al.*	(PISA, COLU, HARV)
SMITH	70	PL 32B 133	R.C. Smith *et al.*	(UMD, BNL)
WEBBER	70	PR D1 1967	B.R. Webber *et al.*	(LRL)
Also		Thesis UCRL 19226	B.R. Webber	(LRL)
BANNER	69	PR 188 2033	M. Banner *et al.*	(PRIN)
Also		PRL 21 1103	M. Banner *et al.*	(PRIN)
Also		PRL 21 1107	J.W. Cronin, J.K. Liu, J.E. Pilcher	(PRIN)
BENNETT	69	PL 29B 317	S. Bennett *et al.*	(COLU, BNL)
FAISSNER	69	PL 30B 204	H. Faissner *et al.*	(AACH3, CERN, TORI)
LITTENBERG	69	PRL 22 654	L.S. Littenberg *et al.*	(UCSD)
LONGO	69	PR 181 1808	M.J. Longo, K.K. Young, J.A. Helland	(MICH, UCLA)
PACIOTTI	69	Thesis UCRL 19446	M.A. Paciotti	(LRL)
SAAL	69	Thesis	H.J. Saal	(COLU)
ABRAMS	68B	PR 176 1603	R.J. Abrams *et al.*	(ILL)
ARNOLD	68B	PL 28B 56	R.G. Arnold *et al.*	(CERN, ORSAY)
BASILE	68B	PL 28B 58	P. Basile *et al.*	(SACL)
BENNETT	68	PL 27B 244	S. Bennett *et al.*	(COLU, CERN)
BLANPIED	68	PRL 21 1650	W.A. Blanpied *et al.*	(CASE, HARV, MCGI)
BOHM	68B	PL 27B 594	A. Bohm *et al.*	
BUDAGOV	68	NC 57A 182	I.A. Budagov *et al.*	(CERN, ORSAY, IPNP)
Also		PL 28B 215	I.A. Budagov *et al.*	(CERN, ORSAY, EPOL)
JAMES	68	NP B8 365	F. James, H. Briand	(IPNP, CERN)
Also		PRL 21 257	J.A. Helland, M.J. Longo, K.K. Young	(UCLA, MICH)
KULYUKINA	68	JETP 26 20	L.A. Kulyukina *et al.*	(JINR)
		Translated from ZETF 53 29.		

KUNZ	68	Thesis PU-68-46	P.F. Kunz	(PRIN)
BENNETT	67	PRL 19 993	S. Bennett *et al.*	(COLU)
DEBOUARD	67	NC 52A 662	X. de Bouard *et al.*	(CERN)
Also		PL 15 58	X. de Bouard *et al.*	(CERN, ORSAY, MPIM)
DEVLIN	67	PRL 18 54	T.J. Devlin *et al.*	(PRIN, UMD)
Also		PR 169 1045	G.A. Sayer *et al.*	(UMD, PPA, PRIN)
DORFAN	67	PRL 19 987	D.E. Dorfan *et al.*	(SLAC, LRL)
FELDMAN	67B	PR 155 1611	L. Feldman *et al.*	(PENN)
FITCH	67	PR 164 1711	V.L. Fitch *et al.*	(PRIN)
GINSBERG	67	PR 162 1570	E.S. Ginsberg	(MASB)
HILL	67	PRL 19 668	D.G. Hill *et al.*	(BNL, CMU)
HOPKINS	67	PRL 19 185	H.W.K. Hopkins, T.C. Bacon, F.R. Eisler	(BNL)
NEFKENS	67	PR 157 1233	B.M.K. Nefkens *et al.*	(ILL)
SCHMIDT	67	Thesis Nevis 160	P. Schmidt	(COLU)
BEHR	66	PL 22 540	L. Behr *et al.*	(EPOL, MILA, PADO, ORSAY)
HAWKINS	66	PL 21 238	C.J.B. Hawkins	(YALE)
Also		PR 156 1444	C.J.B. Hawkins	(YALE)
ANDERSON	65	PRL 14 475	J.A. Anderson *et al.*	(LRL, WISC)
ASTBURY	65B	PL 18 175	P. Astbury *et al.*	(CERN, ZURI)
AUBERT	65	PL 17 59	B. Aubert *et al.*	(EPOL, ORSAY)
Also		PL 24B 75	J.P. Lowys *et al.*	(EPOL, ORSAY)
BALDO-...	65	NC 38 684	M. Baldo-Ceolin *et al.*	(PADO)
FRANZINI	65	PR 140 B127	P. Franzini *et al.*	(COLU, RUTG)
GUIDONI	65	Argonne Conf. 49	P. Guidoni *et al.*	(BNL, YALE)
HOPKINS	65	Argonne Conf. 67	H.W.K. Hopkins, T.C. Bacon, F. Eisler	(VAND+)
ALEKSANYAN	64B	Dubna Conf. 2 102	A.S. Aleksanyan *et al.*	(YERE)
Also		JETP 19 1019	A.S. Aleksanyan *et al.*	(LEBD, MPEI, YERE)
		Translated from ZETF 46 1504.		
ANIKINA	64	JETP 19 42	M.K. Anikina *et al.*	(GEOR, JINR)
		Translated from ZETF 46 59.		
FITCH	61	NC 22 1160	V.L. Fitch, P.A. Piroue, R.B. Perkins	(PRIN+)
GOOD	61	PR 124 1223	R.H. Good *et al.*	(LRL)

OTHER RELATED PAPERS

HAYAKAWA	93	PR D48 1150	M. Hayakawa, A.I. Sanda	(NAGO)
"Searching for *T*, *CP*, *CPT*, $\Delta S = \Delta Q$ Rule Violations in the Neutral *K* Meson System: A Guide"				
LITTENBERG	93	ARNPS 43 729	L.S. Littenberg, G. Valencia	(BNL, FNAL)
Rare and Radiative Kaon Decays				
RITCHIE	93	RMP 65 1149	J.L. Ritchie, S.G. Wojcicki	
"Rare *K* Decays"				
WINSTEIN	93	RMP 65 1113	B. Winstein, L. Wolfenstein	
"The Search for Direct *CP* Violation"				
BATTISTON	92	PRPL 214 293	R. Battiston *et al.*	(PGIA, CERN, TRSTT)
Status and Perspectives of *K* Decay Physics				
DIB	92	PR D46 2265	C.O. Dib, R.D. Peccei	(UCLA)
Tests of *CPT* conservation in the neutral kaon system.				
KLEINKNECHT	92	CNPP 20 281	K. Kleinknecht	(MAINZ)
New Results on *CP* Violation in Decays of Neutral *K* Mesons.				
KLEINKNECHT	90	ZPHY C46 S57	K. Kleinknecht	(MAINZ)
PEACH	90	JP G16 131	K.J. Peach	(EDIN)
BRYMAN	89	IJMP A4 79	D.A. Bryman	(TRIU)
"Rare Kaon Decays"				
KLEINKNECHT	76	ARNS 26 1	K. Kleinknecht	(DORT)
GINSBERG	73	PR D8 3887	E.S. Ginsberg, J. Smith	(MIT, STON)
GINSBERG	70	PR D1 229	E.S. Ginsberg	(HAIF)
HEUSSE	70	LNC 3 449	P. Heusse *et al.*	(ORSAY)
CRONIN	68C	Vienna Conf. 281	J.W. Cronin	(PRIN)
RUBBIA	67	PL 24B 531	C. Rubbia, J. Steinberger	(CERN, COLU)
Also		PL 23 167	C. Rubbia, J. Steinberger	(CERN, COLU)
Also		PL 20 207	C. Alff-Steinberger *et al.*	(CERN)
Also		PL 21 595	C. Alff-Steinberger *et al.*	(CERN)
AUERBACH	66	PR 149 1052	L.B. Auerbach *et al.*	(PENN)
Also		PRL 14 192	L.B. Auerbach *et al.*	(PENN)
FIRESTONE	66B	PRL 17 116	A. Firestone *et al.*	(YALE, BNL)
BEHR	65	Argonne Conf. 59	L. Behr *et al.*	(EPOL, MILA, PADO)
MESTVIRISH...	65	JINR P 2449	A.N. Mestvirishvili *et al.*	(JINR)
TRILLING	65B	UCRL 16473	G.N. Trilling	(LRL)
Updated from 1965 Argonne Conference, page 115.				
JOVANOV...	63	BNL Conf. 42	J.V. Jovanovich *et al.*	(BNL, UMD)

$K^*_0(700)$

$I(J^P) = \frac{1}{2}(0^+)$

also known as κ; was $K^*_0(800)$

See the related review(s):

Scalar Mesons below 1 GeV

$K^*_0(700)$ T-Matrix Pole $\sqrt{s}$

VALUE (MeV)	DOCUMENT ID		TECN	COMMENT
(630–730) − *i* (260–340) OUR ESTIMATE				(see Fig. 64.1 in the review)
$(702 \pm 12^{+4}_{-5}) - i\,(285 \pm 16^{+8}_{-13})$	[1] DANILKIN	21	RVUE	Compilation
$(648 \pm 7) - i\,(280 \pm 16)$	[2] PELAEZ	20	RVUE	$\pi K \to \pi K$
$(670 \pm 18) - i\,(295 \pm 28)$	[3] PELAEZ	17	RVUE	$\pi K \to \pi K$
$(764 \pm 63^{+71}_{-54}) - i\,(306 \pm 149^{+143}_{-85})$	[4] ABLIKIM	11B	BES2	1.3k $J/\psi \to K^0_S K^0_S \pi^+\pi^-$
$(665 \pm 9) - i\,(268^{+21}_{-6})$	[5] GUO	11B	RVUE	
$(849 \pm 77^{+18}_{-14}) - i\,(256 \pm 40^{+46}_{-22})$	[4] ABLIKIM	10E	BES2	1.4k $J/\psi \to K^\pm K^0_S \pi^\mp \pi^0$
$(663 \pm 8 \pm 34) - i\,(329 \pm 5 \pm 22)$	[6] BUGG	10	RVUE	S-matrix pole
$(706.0 \pm 1.8 \pm 22.8) - i\,(319.4 \pm 2.2 \pm 20.2)$	[7] BONVICINI	08A	CLEO	141k $D^+ \to K^-\pi^+\pi^+$
$(841 \pm 30^{+81}_{-73}) - i\,(309 \pm 45^{+48}_{-72})$	[4] ABLIKIM	06C	BES2	25k $J/\psi \to \overline{K}^*(892)^0 K^+\pi^-$
$(750^{+30}_{-55}) - i\,(342 \pm 60)$	[8] BUGG	06	RVUE	
$(658 \pm 13) - i\,(279 \pm 12)$	[9] DESCOTES-G..	06	RVUE	$\pi K \to \pi K$
$(757 \pm 33) - i\,(279 \pm 41)$	[10] GUO	06	RVUE	
$(694 \pm 53) - i\,(303 \pm 30)$	[11] ZHOU	06	RVUE	$Kp \to K^-\pi^+ n$
$(594 \pm 79) - i\,(362 \pm 166)$	[11] ZHENG	04	RVUE	$K^-p \to K^-\pi^+ n$
$(722 \pm 60) - i\,(386 \pm 50)$	[11] BUGG	03	RVUE	11 $K^-p \to K^-\pi^+ n$
$(875 \pm 75) - i\,(335 \pm 110)$	[12] ISHIDA	97B	RVUE	11 $K^-p \to K^-\pi^+ n$
$727 - i\,263$	[13] VANBEVEREN	86	RVUE	

[1] Data driven analysis using partial-wave dispersion relations.
[2] Extracted employing πK partial wave analysis from ESTABROOKS 78 and ASTON 88, Roy-Steiner equations and once subtracted forward dispersion relations.
[3] Reanalysis of ESTABROOKS 78 and ASTON 88 satisfying Forward Dispersion Relations and using sequences of Pade approximants.
[4] Extracted from Breit-Wigner parameters.
[5] Fit to scattering phase shifts using UChPT amplitudes with explicit resonances.
[6] Supersedes BUGG 06. Combined analysis of ASTON 88, ABLIKIM 06C, AITALA 06, and LINK 09 using an s-dependent width with couplings to $K\pi$ and $K\eta'$, and the Adler zero near thresholds.
[7] From a complex pole included in the fit. Using parameters from the model that fits data best.
[8] Reanalysis of ASTON 88, AITALA 02, and ABLIKIM 06C using for the κ an *s*-dependent width with an Adler zero near threshold.
[9] Using Roy-Steiner equations (ROY 71) consistent with unitarity, analyticity and crossing symmetry constraints.
[10] From UChPT fitted to MERCER 71, BINGHAM 72 and ESTABROOKS 78. Amplitude shown to be consistent with data of ABLIKIM 06C.
[11] Reanalysis of ASTON 88 data.
[12] Reanalysis of ASTON 88 using interfering Breit-Wigner amplitudes. Extracted from Breit-Wigner parameters.
[13] Unitarized Quark Model.

$K^*_0(700)$ Breit-Wigner Mass

VALUE (MeV)	EVTS	DOCUMENT ID		TECN	COMMENT
838 ± 11 OUR AVERAGE					
833 ± 15		[1] ACHARYA	24C	ALCE	$pp \to K^0_S \pi^\pm X$, 13 TeV
826 ± 49 $^{+49}_{-34}$	1.3k	[2] ABLIKIM	11B	BES2	$J/\psi \to K^0_S K^0_S \pi^+\pi^-$
810 ± 68 $^{+15}_{-24}$	1.4k	[3] ABLIKIM	10E	BES2	$J/\psi \to K^\pm K^0_S \pi^\mp \pi^0$
856 ± 17 ± 13	54k	LINK	07B	FOCS	$D^+ \to K^-\pi^+\pi^+$
878 ± 23 $^{+64}_{-55}$	25k	[4] ABLIKIM	06C	BES2	$J/\psi \to \overline{K}^*(892)^0 K^+\pi^-$
797 ± 19 ± 43	15k	[5,6] AITALA	02	E791	$D^+ \to K^-\pi^+\pi^+$
• • • We do not use the following data for averages, fits, limits, etc. • • •					
888.0 ± 1.9	141k	[7] BONVICINI	08A	CLEO	$D^+ \to K^-\pi^+\pi^+$
855 ± 15	0.6k	[8] CAWLFIELD	06A	CLEO	$D^0 \to K^+K^-\pi^0$
905 $^{+65}_{-30}$		[9] ISHIDA	97B	RVUE	11 $K^-p \to K^-\pi^+ n$

[1] Assuming a Gaussian source to the measured two-particle correlation function. Systematic error dominates. For 0–100% multiplicity class.
[2] The Breit-Wigner parameters from a fit with seven intermediate resonances. The S-matrix pole position is $(764 \pm 63^{+71}_{-54}) - i\,(306 \pm 149^{+143}_{-85})$ MeV.
[3] From a fit including ten additional resonances and energy-independent Breit-Wigner width.
[4] A fit in the $K^*_0(700) + K^*(892) + K^*(1410)$ model with mass and width of the $K^*_0(700)$ from ABLIKIM 06C well describes the left slope of the $K^0_S\pi^-$ invariant mass spectrum in $\tau^- \to K^0_S\pi^-\nu_\tau$ decay studied by EPIFANOV 07. Averaged value from different parameterizations.
[5] Not seen by KOPP 01 using 7070 events of $D^0 \to K^-\pi^+\pi^0$. LINK 02E and LINK 05I show clear evidence for a constant non-resonant scalar amplitude rather than $K^*_0(700)$ in their high statistics analysis of $D^+ \to K^-\pi^+\mu^+\nu_\mu$.
[6] AUBERT 07T does not find evidence for the charged $K^*_0(700)$ using 11k events of $D^0 \to K^-K^+\pi^0$.
[7] Using parameters from the model that fits data best.
[8] Breit-Wigner parameters. A significant *S*-wave can be also modeled as a non-resonant contribution.
[9] Reanalysis of ASTON 88 using interfering Breit-Wigner amplitudes.

$K^*_0(700)$ Breit-Wigner Width

VALUE (MeV)	EVTS	DOCUMENT ID		TECN	COMMENT
463 ± 27 OUR AVERAGE					
430 $^{+88}_{-53}$		[1] ACHARYA	24C	ALCE	$pp \to K^0_S \pi^\pm X$, 13 TeV
449 ± 156 $^{+144}_{-81}$	1.3k	[2] ABLIKIM	11B	BES2	$J/\psi \to K^0_S K^0_S \pi^+\pi^-$
536 ± 87 $^{+106}_{-47}$	1.4k	[3] ABLIKIM	10E	BES2	$J/\psi \to K^\pm K^0_S \pi^\mp \pi^0$
464 ± 28 ± 22	54k	LINK	07B	FOCS	$D^+ \to K^-\pi^+\pi^+$
499 ± 52 $^{+55}_{-87}$	25k	[4] ABLIKIM	06C	BES2	$J/\psi \to \overline{K}^*(892)^0 K^+\pi^-$
410 ± 43 ± 87	15k	[5,6] AITALA	02	E791	$D^+ \to K^-\pi^+\pi^+$
• • • We do not use the following data for averages, fits, limits, etc. • • •					
550.4 ± 11.8	141k	[7] BONVICINI	08A	CLEO	$D^+ \to K^-\pi^+\pi^+$
251 ± 48	0.6k	[8] CAWLFIELD	06A	CLEO	$D^0 \to K^+K^-\pi^0$
545 $^{+235}_{-110}$		[9] ISHIDA	97B	RVUE	11 $K^-p \to K^-\pi^+ n$

[1] Assuming a Gaussian source to the measured two-particle correlation function. Systematic error dominates. For 0–100% multiplicity class.
[2] The Breit-Wigner parameters from a fit with seven intermediate resonances. The S-matrix pole position is $(764 \pm 63^{+71}_{-54}) - i\,(306 \pm 149^{+143}_{-85})$ MeV.
[3] From a fit including ten additional resonances and energy-independent Breit-Wigner width.
[4] A fit in the $K^*_0(700) + K^*(892) + K^*(1410)$ model with mass and width of the $K^*_0(700)$ from ABLIKIM 06C well describes the left slope of the $K^0_S\pi^-$ invariant mass spectrum

Int. J. Mod. Phys. A 2026.41. Downloaded from www.worldscientific.com
by UNIVERSITY OF CALIFORNIA @ BERKELEY on 09/16/26. Re-use and distribution is strictly not permitted, except for Open Access articles.

Int. J. Mod. Phys. A 2026.41. Downloaded from www.worldscientific.com by UNIVERSITY OF CALIFORNIA @ BERKELEY on 09/16/26. Re-use and distribution is strictly not permitted, except for Open Access articles.

in $\tau^- \to K_S^0 \pi^- \nu_\tau$ decay studied by EPIFANOV 07. Averaged value from different parameterizations.

[5] Not seen by KOPP 01 using 7070 events of $D^0 \to K^- \pi^+ \pi^0$. LINK 02E and LINK 05I show clear evidence for a constant non-resonant scalar amplitude rather than $K_0^*(700)$ in their high statistics analysis of $D^+ \to K^- \pi^+ \mu^+ \nu_\mu$.

[6] AUBERT 07T does not find evidence for the charged $K_0^*(700)$ using 11k events of $D^0 \to K^- K^+ \pi^0$.

[7] Using parameters from the model that fits data best.

[8] Statistical error only. A fit to the Dalitz plot including the $K_0^*(700)^\pm$, $K^*(892)^\pm$, and ϕ resonances modeled as Breit-Wigners. A significant S-wave can be also modeled as a non-resonant contribution.

[9] Reanalysis of ASTON 88 using interfering Breit-Wigner amplitudes.

$K_0^*(700)$ DECAY MODES

	Mode	Fraction (Γ_i/Γ)
Γ_1	$K\pi$	100 %

$K_0^*(700)$ REFERENCES

ACHARYA	24C	PL B856 138915	S. Acharya *et al.*	(ALICE Collab.)
DANILKIN	21	PR D103 114023	I. Danilkin, O. Deineka, M. Vanderhaeghen	(MAINZ)
PELAEZ	20	PRL 124 172001	J.R. Pelaez *et al.*	
PELAEZ	17	EPJ C77 91	J.R. Pelaez, A.Rodas, J.R. de Elvira	
ABLIKIM	11B	PL B698 183	M. Ablikim *et al.*	(BES II Collab.)
GUO	11B	PR D84 034005	Z.-H. Guo, J.A. Oller	
ABLIKIM	10E	PL B693 88	M. Ablikim *et al.*	(BES II Collab.)
BUGG	10	PR D81 014002	D.V. Bugg	(LOQM)
LINK	09	PL B681 14	J.M. Link *et al.*	(FNAL FOCUS Collab.)
BONVICINI	08A	PR D78 052001	G. Bonvicini *et al.*	(CLEO Collab.)
AUBERT	07T	PR D76 011102	B. Aubert *et al.*	(BABAR Collab.)
EPIFANOV	07	PL B654 65	D. Epifanov *et al.*	(BELLE Collab.)
LINK	07B	PL B653 1	J.M. Link *et al.*	(FNAL FOCUS Collab.)
ABLIKIM	06C	PL B633 681	M. Ablikim *et al.*	(BES Collab.)
AITALA	06	PR D73 032004	E.M. Aitala *et al.*	(FNAL E791 Collab.)
Also		PR D74 059901 (errat.)	E.M. Aitala *et al.*	(FNAL E791 Collab.)
BUGG	06	PL B632 471	D.V. Bugg	(LOQM)
CAWLFIELD	06A	PR D74 031108	C. Cawlfield *et al.*	(CLEO Collab.)
DESCOTES-G...	06	EPJ C48 553	S. Descotes-Genon, B. Moussallam	
GUO	06	NP A773 78	F.K. Guo *et al.*	
ZHOU	06	NP A775 212	Z.Y. Zhou, H.Q. Zheng	
LINK	05I	PL B621 72	J.M. Link *et al.*	(FNAL FOCUS Collab.)
ZHENG	04	NP A733 235	H.Q. Zheng *et al.*	
BUGG	03	PL B572 1	D.V. Bugg	
AITALA	02	PRL 89 121801	E.M. Aitala *et al.*	(FNAL E791 Collab.)
LINK	02E	PL B535 43	J.M. Link *et al.*	(FNAL FOCUS Collab.)
KOPP	01	PR D63 092001	S. Kopp *et al.*	(CLEO Collab.)
ISHIDA	97B	PTP 98 621	S. Ishida *et al.*	
ASTON	88	NP B296 493	D. Aston *et al.*	(SLAC, NAGO, CINC, INUS)
VANBEVEREN	86	ZPHY C30 615	E. van Beveren *et al.*	(NIJM, BIEL)
ESTABROOKS	78	NP B133 490	P.G. Estabrooks *et al.*	(MCGI, CARL, DURH+)
BINGHAM	72	NP B41 1	H.H. Bingham *et al.*	(International K^+ Collab.)
MERCER	71	NP B32 381	R. Mercer *et al.*	(JHU)
ROY	71	PL 36B 353	S.M. Roy	

$K^*(892)$

$I(J^P) = \frac{1}{2}(1^-)$

$K^*(892)$ T-Matrix Pole $\sqrt{s}$

VALUE (MeV)	DOCUMENT ID		TECN	COMMENT
$(890 \pm 14) - i\,(26 \pm 6)$ OUR ESTIMATE				
$(890 \pm 2) - i\,(25.6 \pm 1.2)$	[1] PELAEZ	20	RVUE	$\pi K \to \pi K$
$(892 \pm 1) - i\,(29 \pm 1)$	[2] PELAEZ	17	RVUE	$\pi K \to \pi K$
$(889 \pm 13) - i\,(24 \pm 4)$	[3] PELAEZ	04A	RVUE	$\pi K \to \pi K$

[1] Extracted employing πK partial wave analysis from ESTABROOKS 78 and ASTON 88, Roy-Steiner equations and once subtracted forward dispersion relations.

[2] Reanalysis of ESTABROOKS 78 and ASTON 88 satisfying Forward Dispersion Relations and using sequences of Pade approximants.

[3] Reanalysis of data from ESTABROOKS 78 and ASTON 88 in the unitarized ChPT model.

$K^*(892)$ MASS

CHARGED ONLY, HADROPRODUCED

VALUE (MeV)	EVTS	DOCUMENT ID		TECN	CHG	COMMENT
891.88±0.23 OUR AVERAGE						
892.7 ±0.5 ±0.1	6796	ABLIKIM	25BO	BES3		$D^0 \to \overline{K}^0 \pi^+ \mu^- \nu_\mu$
892.2 ±0.5 ±1.7		ALBRECHT	20	CBAR		$0.9\,\overline{p}p \to K^+ K^- \pi^0$
892.6 ±0.5	5840	BAUBILLIER	84B	HBC	−	$8.25\,K^- p \to \overline{K}^0 \pi^- p$
888 ±3		NAPIER	84	SPEC	+	$200\,\pi^- p \to 2K_S^0 X$
891 ±1		NAPIER	84	SPEC	−	$200\,\pi^- p \to 2K_S^0 X$
891.7 ±2.1	3700	BARTH	83	HBC	+	$70\,K^+ p \to K^0 \pi^+ X$
891 ±1	4100	TOAFF	81	HBC	−	$6.5\,K^- p \to \overline{K}^0 \pi^- p$
892.8 ±1.6		AJINENKO	80	HBC	+	$32\,K^+ p \to K^0 \pi^+ X$
890.7 ±0.9	1800	AGUILAR-...	78B	HBC	±	$0.76\,\overline{p}p \to K^\mp K_S^0 \pi^\pm$
886.6 ±2.4	1225	BALAND	78	HBC	±	$12\,\overline{p}p \to (K\pi)^\pm X$
891.7 ±0.6	6706	COOPER	78	HBC	±	$0.76\,\overline{p}p \to (K\pi)^\pm X$
891.9 ±0.7	9000	[1] PALER	75	HBC	−	$14.3\,K^- p \to (K\pi)^- X$
892.2 ±1.5	4404	AGUILAR-...	71B	HBC	−	$3.9,4.6\,K^- p \to (K\pi)^- p$
891 ±2	1000	CRENNELL	69D	DBC	−	$3.9\,K^- N \to K^0 \pi^- X$
890 ±3.0	720	BARLOW	67	HBC	±	$1.2\,\overline{p}p \to (K^0\pi)^\pm K^\mp$
889 ±3.0	600	BARLOW	67	HBC	±	$1.2\,\overline{p}p \to (K^0\pi)^\pm K\pi$
891 ±2.3	620	[2] DEBAERE	67B	HBC	+	$3.5\,K^+ p \to K^0 \pi^+ p$
891.0 ±1.2	1700	[3] WOJCICKI	64	HBC	−	$1.7\,K^- p \to \overline{K}^0 \pi^- p$
• • • We do not use the following data for averages, fits, limits, etc. • • •						
893.6 ±0.1 $^{+0.2}_{-0.3}$	183k	ABLIKIM	19AQ	BES	±	$J/\psi \to K^+ K^- \pi^0$
895.6 ±0.8	4k	[4] LEES	17C	BABR		$J/\psi \to K_S^0 K^\pm \pi^\mp$
893.2 ±0.1 ±1.0	190k	[5] AAIJ	16N	LHCB		$D^0 \to K_S^0 K^\pm \pi^\mp$
893.5 ±1.1	27k	[6] ABELE	99D	CBAR	±	$0.0\,\overline{p}p \to K^+ K^- \pi^0$
890.4 ±0.2 ±0.5	80k	[7] BIRD	89	LASS	−	$11\,K^- p \to \overline{K}^0 \pi^- p$
890.0 ±2.3	800	[2,3] CLELAND	82	SPEC	+	$30\,K^+ p \to K_S^0 \pi^+ p$
896.0 ±1.1	3200	[2,3] CLELAND	82	SPEC	+	$50\,K^+ p \to K_S^0 \pi^+ p$
893 ±1	3600	[2,3] CLELAND	82	SPEC	−	$50\,K^+ p \to K_S^0 \pi^- p$
896.0 ±1.9	380	DELFOSSE	81	SPEC	+	$50\,K^\pm p \to K^\pm \pi^0 p$
886.0 ±2.3	187	DELFOSSE	81	SPEC	−	$50\,K^\pm p \to K^\pm \pi^0 p$
894.2 ±2.0	765	[2] CLARK	73	HBC	−	$3.13\,K^- p \to \overline{K}^0 \pi^- p$
894.3 ±1.5	1150	[2,3] CLARK	73	HBC	−	$3.3\,K^- p \to \overline{K}^0 \pi^- p$
892.0 ±2.6	341	[2] SCHWEING...	68	HBC	−	$5.5\,K^- p \to \overline{K}^0 \pi^- p$

[1] Inclusive reaction. Complicated background and phase-space effects.

[2] Mass errors enlarged by us to $\Gamma/\sqrt{N}$. See note.

[3] Number of events in peak reevaluated by us.

[4] From a Dalitz plot analysis in an isobar model with charged and neutral $K^*(892)$ masses and widths floating.

[5] Average of fit results with different parametrizations for the $K\pi$ S-wave.

[6] K-matrix pole.

[7] From a partial wave amplitude analysis.

CHARGED ONLY, PRODUCED IN τ LEPTON DECAYS

VALUE (MeV)	EVTS	DOCUMENT ID		TECN	COMMENT
895.47±0.20±0.74	53k	[1] EPIFANOV	07	BELL	$\tau^- \to K_S^0 \pi^- \nu_\tau$
• • • We do not use the following data for averages, fits, limits, etc. • • •					
892.0 ±0.5		[2] BOITO	10	RVUE	$\tau^- \to K_S^0 \pi^- \nu_\tau$
892.0 ±0.9		[3,4] BOITO	09	RVUE	$\tau^- \to K_S^0 \pi^- \nu_\tau$
895.3 ±0.2		[4,5] JAMIN	08	RVUE	$\tau^- \to K_S^0 \pi^- \nu_\tau$
896.4 ±0.9	12k	[6] BONVICINI	02	CLEO	$\tau^- \to K^- \pi^0 \nu_\tau$
895 ±2		[7] BARATE	99R	ALEP	$\tau^- \to K^- \pi^0 \nu_\tau$

[1] From a fit in the $K_0^*(700) + K^*(892) + K^*(1410)$ model.

[2] From the pole position of the $K\pi$ vector form factor using EPIFANOV 07 and constraints from K_{l3} decays in ANTONELLI 10.

[3] From the pole position of the $K\pi$ vector form factor in the complex s-plane and using EPIFANOV 07 data.

[4] Systematic uncertainties not estimated.

[5] Reanalysis of EPIFANOV 07 using resonance chiral theory.

[6] Calculated by us from the shift by 4.7 ± 0.9 MeV (statistical uncertainty only) reported in BONVICINI 02 with respect to the world average value from PDG 00.

[7] With mass and width of the $K^*(1410)$ fixed at 1412 MeV and 227 MeV, respectively.

NEUTRAL ONLY

VALUE (MeV)	EVTS	DOCUMENT ID		TECN	COMMENT
895.56±0.20 OUR AVERAGE		Error includes scale factor of 1.7. See the ideogram below.			
897.3 ±0.3 ±2.2	12k	ABLIKIM	25BP	BES3	$D^+ \to K_S^0 \pi^0 \ell^+ \nu_\ell$
894.68±0.25±0.05		[1] ABLIKIM	16F	BES3	$D^+ \to K^- \pi^+ e^+ \nu_e$
895.4 ±0.2 ±0.2	243k	[2] DEL-AMO-SA...	11I	BABR	$D^+ \to K^- \pi^+ e^+ \nu_e$
895.7 ±0.2 ±0.3	141k	[3] BONVICINI	08A	CLEO	$D^+ \to K^- \pi^+ \pi^+$
895.41±0.32$^{+0.35}_{-0.43}$	18k	[4] LINK	05I	FOCS	$D^+ \to K^- \pi^+ \mu^+ \nu_\mu$
896 ±2		BARBERIS	98E	OMEG	$450\,pp \to p_f p_s K^* \overline{K}^*$
895.9 ±0.5 ±0.2		ASTON	88	LASS	$11\,K^- p \to K^- \pi^+ n$
894.52±0.63	25k	[5] ATKINSON	86	OMEG	20–70 γp
894.63±0.76	20k	[5] ATKINSON	86	OMEG	20–70 γp
897 ±1	28k	EVANGELIS...	80	OMEG	$10\,\pi^- p \to K^+ \pi^- (\Lambda, \Sigma)$
898.4 ±1.4	1180	AGUILAR-...	78B	HBC	$0.76\,\overline{p}p \to K^\mp K_S^0 \pi^\pm$
894.9 ±1.6		WICKLUND	78	ASPK	$3,4,6\,K^\pm N \to (K\pi)^0 N$
897.6 ±0.9		BOWLER	77	DBC	$5.4\,K^+ d \to K^+ \pi^- p p$
895.5 ±1.0	3600	MCCUBBIN	75	HBC	$3.6\,K^- p \to K^- \pi^+ n$
897.1 ±0.7	22k	[5] PALER	75	HBC	$14.3\,K^- p \to (K\pi)^0 X$
896.0 ±0.6	10k	FOX	74	RVUE	$2\,K^- p \to K^- \pi^+ n$
896.0 ±0.6		FOX	74	RVUE	$2\,K^+ n \to K^+ \pi^- p$
896 ±2		[6] MATISON	74	HBC	$12\,K^+ p \to K^+ \pi^- \Delta$
896 ±1	3186	LEWIS	73	HBC	$2.1–2.7\,K^+ p \to K \pi \pi p$
894.0 ±1.3		[6] LINGLIN	73	HBC	$2–13\,K^+ p \to K^+ \pi^- \pi^+ p$
898.4 ±1.3	1700	[7] BUCHNER	72	DBC	$4.6\,K^+ n \to K^+ \pi^- p$
897.9 ±1.1	2934	[7] AGUILAR-...	71B	HBC	$3.9,4.6\,K^- p \to K^- \pi^+ n$
898.0 ±0.7	5362	[7] AGUILAR-...	71B	HBC	$3.9,4.6\,K^- p \to K^- \pi^+ \pi^- p$
895 ±1	4300	[8] HABER	70	DBC	$3\,K^- N \to K^- \pi^+ X$
893.7 ±2.0	10k	DAVIS	69	HBC	$12\,K^+ p \to K^+ \pi^- \pi^+ p$
894.7 ±1.4	1040	[7] DAUBER	67B	HBC	$2.0\,K^- p \to K^- \pi^+ \pi^- p$
• • • We do not use the following data for averages, fits, limits, etc. • • •					
895.50±0.92±2.6		[9] ADUSZKIEW...	20A	NA61	158 pp
898.1 ±1.0	4k	[10] LEES	17C	BABR	$J/\psi \to K_S^0 K^\pm \pi^\mp$

895.53±0.17		LEES	13F	BABR	$D^+ \to K^+ K^- \pi^+$
894.9 ±0.5 ±0.7	14.4k	[11] MITCHELL	09A	CLEO	$D_s^+ \to K^+ K^- \pi^+$
896.2 ±0.3	20k	[12] AUBERT	07AK	BABR	10.6 $e^+ e^- \to K^{*0} K^\pm \pi^\mp \gamma$
900.7 ±1.1	5900	BARTH	83	HBC	70 $K^+ p \to K^+ \pi^- X$

[1] Taking also into account the $K_0^*(1430)^0$ and $K_2^*(1430)^0$.
[2] Taking into account the $K^*(892)^0$, S-wave and P-wave ($K^*(1410)^0$).
[3] From the isobar model with a complex pole for the κ.
[4] Fit to $K\pi$ mass spectrum includes a non-resonant scalar component.
[5] Inclusive reaction. Complicated background and phase-space effects.
[6] From pole extrapolation.
[7] Mass errors enlarged by us to $\Gamma/\sqrt{N}$. See note.
[8] Number of events in peak reevaluated by us.
[9] For transverse momenta between 0.6 and 0.8 GeV/c and rapidity $0 < y < 0.5$.
[10] From a Dalitz plot analysis in an isobar model with charged and neutral $K^*(892)$ masses and widths floating.
[11] This value comes from a fit with χ^2 of 178/117.
[12] Systematic uncertainties not estimated.

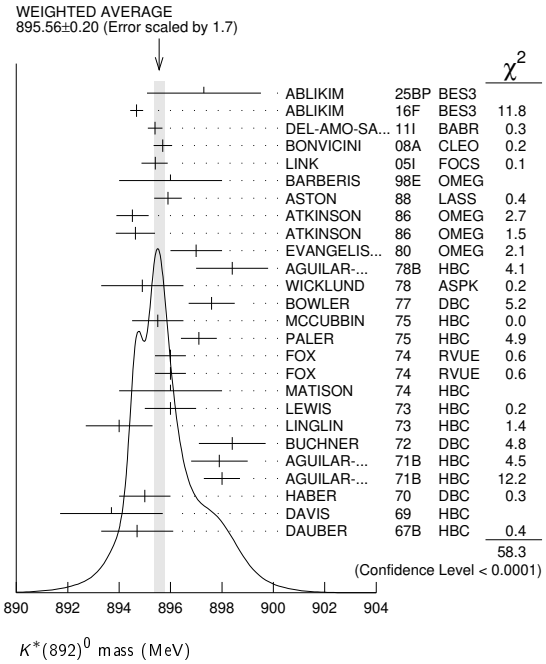

$K^*(892)$ MASSES AND MASS DIFFERENCES

Unrealistically small errors have been reported by some experiments. We use simple "realistic" tests for the minimum errors on the determination of a mass and width from a sample of N events:

$$\delta_{\min}(m) = \frac{\Gamma}{\sqrt{N}}, \quad \delta_{\min}(\Gamma) = 4\frac{\Gamma}{\sqrt{N}} \ . \qquad (1)$$

We consistently increase unrealistic errors before averaging. For a detailed discussion, see the 1971 edition of this Note.

$m_{K^*(892)^0} - m_{K^*(892)^\pm}$

VALUE (MeV)	EVTS	DOCUMENT ID		TECN	CHG	COMMENT
6.7±1.2 OUR AVERAGE						
7.7±1.7	2980	AGUILAR-...	78B	HBC	±0	0.76 $\overline{p}p \to K^\mp K^0_S \pi^\pm$
5.7±1.7	7338	AGUILAR-...	71B	HBC	−0	3.9,4.6 $K^- p$
6.3±4.1	283	[1] BARASH	67B	HBC		0.0 $\overline{p}p$

[1] Number of events in peak reevaluated by us.

$K^*(892)$ RANGE PARAMETER

All from partial wave amplitude analyses.

VALUE (GeV^{-1})	EVTS	DOCUMENT ID		TECN	CHG	COMMENT
2.1 ±0.5 ±0.5	243k	[1] DEL-AMO-SA.	11I	BABR	0	$D^+ \to K^- \pi^+ e^+ \nu_e$
$3.96 \pm 0.54 {}^{+1.31}_{-0.90}$	18k	[2] LINK	05I	FOCS	0	$D^+ \to K^- \pi^+ \mu^+ \nu_\mu$
3.4 ±0.7		ASTON	88	LASS	0	11 $K^- p \to K^- \pi^+ n$
• • • We do not use the following data for averages, fits, limits, etc. • • •						
12.1 ±3.2 ±3.0		BIRD	89	LASS	−	11 $K^- p \to \overline{K}^0 \pi^- p$

[1] Taking into account the $K^*(892)^0$, S-wave and P-wave ($K^*(1410)^0$).
[2] Fit to $K\pi$ mass spectrum includes a non-resonant scalar component.

$K^*(892)$ WIDTH

CHARGED ONLY, HADROPRODUCED

VALUE (MeV)	EVTS	DOCUMENT ID		TECN	CHG	COMMENT
48.5±1.2 OUR FIT Error includes scale factor of 2.1.						
48.5±1.0 OUR AVERAGE Error includes scale factor of 1.8. See the ideogram below.						
45.6±0.8±0.1	6796	ABLIKIM	25BO	BES3		$D^0 \to \overline{K}^0 \pi^+ \mu^- \nu_\mu$
54.4±0.9±1.7		ALBRECHT	20	CBAR		0.9 $\overline{p}p \to K^+ K^- \pi^0$
49 ±2	5840	BAUBILLIER	84B	HBC	−	8.25 $K^- p \to \overline{K}^0 \pi^- p$
56 ±4		NAPIER	84	SPEC	−	200 $\pi^- p \to 2K^0_S X$
51 ±2	4100	TOAFF	81	HBC	−	6.5 $K^- p \to \overline{K}^0 \pi^- p$
50.5±5.6		AJINENKO	80	HBC	+	32 $K^+ p \to K^0 \pi^+ X$
45.8±3.6	1800	AGUILAR-...	78B	HBC	±	0.76 $\overline{p}p \to K^\mp K^0_S \pi^\pm$
52.0±2.5	6706	[1] COOPER	78	HBC	±	0.76 $\overline{p}p \to (K\pi)^\pm X$
52.1±2.2	9000	[2] PALER	75	HBC	−	14.3 $K^- p \to (K\pi)^- X$
46.3±6.7	765	[1] CLARK	73	HBC	−	3.13 $K^- p \to \overline{K}^0 \pi^- p$
48.2±5.7	1150	[1,3] CLARK	73	HBC	−	3.3 $K^- p \to \overline{K}^0 \pi^- p$
54.3±3.3	4404	[1] AGUILAR-...	71B	HBC	−	3.9,4.6 $K^- p \to (K\pi)^- p$
46 ±5	1700	[1,3] WOJCICKI	64	HBC	−	1.7 $K^- p \to \overline{K}^0 \pi^- p$
• • • We do not use the following data for averages, fits, limits, etc. • • •						
$46.7 \pm 0.2 {}^{+0.1}_{-0.2}$	183k	ABLIKIM	19AQ	BES	±	$J/\psi \to K^+ K^- \pi^0$
43.6±1.3	4k	[4] LEES	17C	BABR		$J/\psi \to K^0_S K^\pm \pi^\mp$
47.2±0.3±2.3	190k	[5] AAIJ	16N	LHCB		$D^0 \to K^0_S K^\pm \pi^\mp$
54.8±1.7	27k	[6] ABELE	99D	CBAR	±	0.0 $\overline{p}p \to K^+ K^- \pi^0$
45.2±1 ±2	80k	[7] BIRD	89	LASS	−	11 $K^- p \to \overline{K}^0 \pi^- p$
42.8±7.1	3700	BARTH	83	HBC	+	70 $K^+ p \to K^0 \pi^+ X$
64.0±9.2	800	[1,3] CLELAND	82	SPEC	+	30 $K^+ p \to K^0_S \pi^+ p$
62.0±4.4	3200	[1,3] CLELAND	82	SPEC	+	50 $K^+ p \to K^0_S \pi^+ p$
55 ±4	3600	[1,3] CLELAND	82	SPEC	−	50 $K^+ p \to K^0_S \pi^- p$
62.6±3.8	380	DELFOSSE	81	SPEC	+	50 $K^\pm p \to K^\pm \pi^0 p$
50.5±3.9	187	DELFOSSE	81	SPEC	−	50 $K^\pm p \to K^\pm \pi^0 p$

[1] Width errors enlarged by us to $4 \times \Gamma/\sqrt{N}$; see note.
[2] Inclusive reaction. Complicated background and phase-space effects.
[3] Number of events in peak reevaluated by us.
[4] From a Dalitz plot analysis in an isobar model with charged and neutral $K^*(892)$ masses and widths floating.
[5] Average of fit results with different parametrizations for the $K\pi$ S-wave.
[6] K-matrix pole.
[7] From a partial wave amplitude analysis.

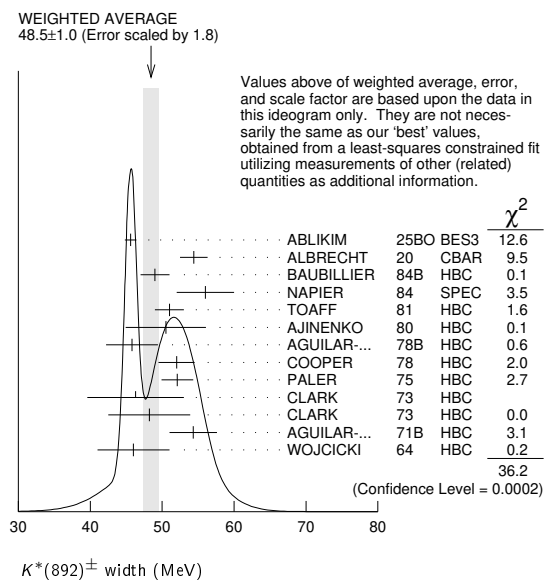

CHARGED ONLY, PRODUCED IN τ LEPTON DECAYS

VALUE (MeV)	EVTS	DOCUMENT ID		TECN	COMMENT
46.2±0.6±1.2	53k	[1] EPIFANOV	07	BELL	$\tau^- \to K^0_S \pi^- \nu_\tau$
• • • We do not use the following data for averages, fits, limits, etc. • • •					
46.5±1.1		[2] BOITO	10	RVUE	$\tau^- \to K^0_S \pi^- \nu_\tau$
46.2±0.4		[3,4] BOITO	09	RVUE	$\tau^- \to K^0_S \pi^- \nu_\tau$
47.5±0.4		[4,5] JAMIN	08	RVUE	$\tau^- \to K^0_S \pi^- \nu_\tau$
55 ±8		[6] BARATE	99R	ALEP	$\tau^- \to K^- \pi^0 \nu_\tau$

[1] From a fit in the $K_0^*(700) + K^*(892) + K^*(1410)$ model.

Int. J. Mod. Phys. A 2026.41. Downloaded from www.worldscientific.com
by CALIFORNIA @ BERKELEY on 09/16/26. Re-use and distribution is strictly not permitted, except for Open Access articles.

[2] From the pole position of the $K\pi$ vector form factor using EPIFANOV 07 and constraints from K_{l3} decays in ANTONELLI 10.
[3] From the pole position of the $K\pi$ vector form factor in the complex s-plane and using EPIFANOV 07 data.
[4] Systematic uncertainties not estimated.
[5] Reanalysis of EPIFANOV 07 using resonance chiral theory.
[6] With mass and width of the $K^*(1410)$ fixed at 1412 MeV and 227 MeV, respectively.

NEUTRAL ONLY

VALUE (MeV)	EVTS	DOCUMENT ID		TECN	COMMENT
47.1 ±0.5 OUR FIT Error includes scale factor of 2.0.					
47.1 ±0.5 OUR AVERAGE Error includes scale factor of 2.0. See the ideogram below.					
45.2 ±0.6 ±0.5	12k	ABLIKIM	25BP	BES3	$D^+ \to K^0_S \pi^0 \ell^+ \nu_\ell$
46.53±0.56±0.31		[1] ABLIKIM	16F	BES3	$D^+ \to K^- \pi^+ e^+ \nu_e$
46.5 ±0.3 ±0.2	243k	[2] DEL-AMO-SA...	11I	BABR	$D^+ \to K^- \pi^+ e^+ \nu_e$
45.3 ±0.5 ±0.6	141k	[3] BONVICINI	08A	CLEO	$D^+ \to K^- \pi^+ \pi^+$
47.79±0.86$^{+1.32}_{-1.06}$	18k	[4] LINK	05I	FOCS	$D^+ \to K^- \pi^+ \mu^+ \nu_\mu$
54 ±3		BARBERIS	98E	OMEG	450 $pp \to p_f p_s K^* \overline{K}^*$
50.8 ±0.8 ±0.9		ASTON	88	LASS	11 $K^- p \to K^- \pi^+ n$
46.5 ±4.3	5900	BARTH	83	HBC	70 $K^+ p \to K^+ \pi^- X$
54 ±2	28k	EVANGELIS...	80	OMEG	10 $\pi^- p \to K^+ \pi^- (\Lambda, \Sigma)$
45.9 ±4.8	1180	AGUILAR-...	78B	HBC	0.76 $\overline{p} p \to K^\mp K^0_S \pi^\pm$
51.2 ±1.7		WICKLUND	78	ASPK	3,4,6 $K^\pm N \to (K\pi)^0 N$
48.9 ±2.5		BOWLER	77	DBC	5.4 $K^+ d \to K^+ \pi^- pp$
48 $^{+3}_{-2}$	3600	MCCUBBIN	75	HBC	3.6 $K^- p \to K^- \pi^+ n$
50.6 ±2.5	22k	[5] PALER	75	HBC	14.3 $K^- p \to (K\pi)^0 X$
47 ±2	10k	FOX	74	RVUE	2 $K^- p \to K^- \pi^+ n$
51 ±2		FOX	74	RVUE	2 $K^+ n \to K^+ \pi^- p$
46.0 ±3.3	3186	[6] LEWIS	73	HBC	2.1–2.7 $K^+ p \to K \pi \pi p$
51.4 ±5.0	1700	[6] BUCHNER	72	DBC	4.6 $K^+ n \to K^+ \pi^- p$
55.8 $^{+4.2}_{-3.4}$	2934	[6] AGUILAR-...	71B	HBC	3.9,4.6 $K^- p \to K^- \pi^+ n$
48.5 ±2.7	5362	AGUILAR-...	71B	HBC	3.9,4.6 $K^- p \to K^- \pi^+ \pi^- p$
54.0 ±3.3	4300	[6,7] HABER	70	DBC	3 $K^- N \to K^- \pi^+ X$
53.2 ±2.1	10k	[6] DAVIS	69	HBC	12 $K^+ p \to K^+ \pi^- \pi^+ p$
44 ±5.5	1040	[6] DAUBER	67B	HBC	2.0 $K^- p \to K^- \pi^+ \pi^- p$
• • • We do not use the following data for averages, fits, limits, etc. • • •					
48.8 ±1.8 ±2.0		[8] ADUSZKIEW...	20A	NA61	158 pp
52.6 ±1.7	4k	[9] LEES	17C	BABR	$J/\psi \to K^0_S K^\pm \pi^\mp$
44.90±0.30		LEES	13F	BABR	$D^+ \to K^+ K^- \pi^+$
45.7 ±1.1 ±0.5	14.4k	[10] MITCHELL	09A	CLEO	$D^+_s \to K^+ K^- \pi^+$
50.6 ±0.9	20k	[11] AUBERT	07AK	BABR	10.6 $e^+ e^- \to K^{*0} K^\pm \pi^\mp \gamma$

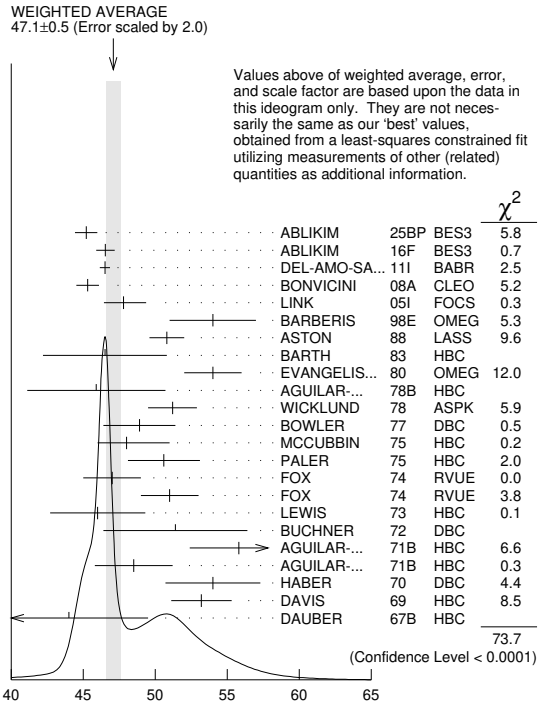

NEUTRAL ONLY (MeV)

[1] Taking also into account the $K^*_0(1430)^0$ and $K^*_2(1430)^0$.
[2] Taking into account the $K^*(892)^0$, S-wave and P-wave ($K^*(1410)^0$).
[3] From the isobar model with a complex pole for the κ.
[4] Fit to $K\pi$ mass spectrum includes a non-resonant scalar component.
[5] Inclusive reaction. Complicated background and phase-space effects.
[6] Width errors enlarged by us to $4 \times \Gamma/\sqrt{N}$; see note.
[7] Number of events in peak reevaluated by us.
[8] For transverse momenta between 0.6 and 0.8 GeV/c and rapidity $0 < y < 0.5$.
[9] From a Dalitz plot analysis in an isobar model with charged and neutral $K^*(892)$ masses and widths floating.
[10] This value comes from a fit with χ^2 of 178/117.
[11] Systematic uncertainties not estimated.

$K^*(892)$ DECAY MODES

	Mode	Fraction (Γ_i/Γ)	Confidence level
Γ_1	$K\pi$	$\sim$ 100 %	
Γ_2	$(K\pi)^\pm$	(99.896±0.010) %	
Γ_3	$(K\pi)^0$	(99.753±0.021) %	
Γ_4	$K^0\gamma$	(2.47 ±0.21) $\times 10^{-3}$	
Γ_5	$K^\pm\gamma$	(1.04 ±0.10) $\times 10^{-3}$	
Γ_6	$K\pi\pi$	< 7 $\times 10^{-4}$	95%

CONSTRAINED FIT INFORMATION

An overall fit to the total width and a partial width uses 15 measurements and one constraint to determine 3 parameters. The overall fit has a $\chi^2 = 36.3$ for 13 degrees of freedom.

The following *off-diagonal* array elements are the correlation coefficients $\langle \delta p_i \delta p_j \rangle / (\delta p_i \cdot \delta p_j)$, in percent, from the fit to parameters p_i, including the branching fractions, $x_i \equiv \Gamma_i/\Gamma_{total}$. The fit constrains the x_i whose labels appear in this array to sum to one.

	x_2	x_5
x_5	−100	
Γ	26	−26

	Mode	Rate (MeV)	Scale factor
Γ_2	$(K\pi)^\pm$	48.4 ±1.2	2.1
Γ_5	$K^\pm\gamma$	0.050±0.005	

CONSTRAINED FIT INFORMATION

An overall fit to the total width and a partial width uses 24 measurements and one constraint to determine 3 parameters. The overall fit has a $\chi^2 = 74.8$ for 22 degrees of freedom.

The following *off-diagonal* array elements are the correlation coefficients $\langle \delta p_i \delta p_j \rangle / (\delta p_i \cdot \delta p_j)$, in percent, from the fit to parameters p_i, including the branching fractions, $x_i \equiv \Gamma_i/\Gamma_{total}$. The fit constrains the x_i whose labels appear in this array to sum to one.

	x_3	x_4
x_4	−100	
Γ	12	−12

	Mode	Rate (MeV)	Scale factor
Γ_3	$(K\pi)^0$	47.0 ±0.5	2.0
Γ_4	$K^0\gamma$	0.117±0.010	

$K^*(892)$ PARTIAL WIDTHS

$\Gamma(K^0\gamma)$ — Γ_4

VALUE (keV)	EVTS	DOCUMENT ID		TECN	CHG	COMMENT
116 ±10 OUR FIT						
116.5± 9.9	584	CARLSMITH	86	SPEC	0	$K^0_L A \to K^0_S \pi^0 A$

$\Gamma(K^\pm\gamma)$ — Γ_5

VALUE (keV)	DOCUMENT ID		TECN	CHG	COMMENT
50± 5 OUR FIT					
50± 5 OUR AVERAGE					
48±11	BERG	83	SPEC	−	156 $K^- A \to \overline{K}\pi A$
51± 5	CHANDLEE	83	SPEC	+	200 $K^+ A \to K\pi A$

$K^*(892)$ BRANCHING RATIOS

$\Gamma(K^0\gamma)/\Gamma_{total}$ — Γ_4/Γ

VALUE (units 10^{-3})	DOCUMENT ID		TECN	CHG	COMMENT
2.47±0.21 OUR FIT					
• • • We do not use the following data for averages, fits, limits, etc. • • •					
1.5 ±0.7	CARITHERS	75B	CNTR	0	8–16 $\overline{K}^0 A$

Int. J. Mod. Phys. A 2026.41. Downloaded from www.worldscientific.com
by UNIVERSITY OF CALIFORNIA @ BERKELEY on 09/16/26. Re-use and distribution is strictly not permitted, except for Open Access articles.

Int. J. Mod. Phys. A 2026.41. Downloaded from www.worldscientific.com by CALIFORNIA @ BERKELEY on 09/16/26. Re-use and distribution is strictly not permitted, except for Open Access articles.

$\Gamma(K^\pm\gamma)/\Gamma_{total}$ — Γ_5/Γ

VALUE (units 10^{-3})	CL%	DOCUMENT ID		TECN	CHG	COMMENT
1.04±0.10 OUR FIT						
• • • We do not use the following data for averages, fits, limits, etc. • • •						
<1.6	95	BEMPORAD	73	CNTR	+	10–16 K^+ A

$\Gamma(K\pi\pi)/\Gamma((K\pi)^\pm)$ — Γ_6/Γ_2

VALUE	CL%	DOCUMENT ID		TECN	CHG	COMMENT
< 7 × 10^{-4}	95	JONGEJANS	78	HBC		4 $K^-p \to p\overline{K}^0 2\pi$
• • • We do not use the following data for averages, fits, limits, etc. • • •						
<20 × 10^{-4}		WOJCICKI	64	HBC	−	1.7 $K^-p \to \overline{K}^0\pi^-p$

$K^*(892)$ REFERENCES

ABLIKIM	25BO	PRL 135 111803	M. Ablikim et al.	(BESIII Collab.)
ABLIKIM	25BP	PRL 135 171801	M. Ablikim et al.	(BESIII Collab.)
ADUSZKIEW...	20A	EPJ C80 460	A. Aduszkiewicz et al.	(CERN NA61 Collab.)
ALBRECHT	20	EPJ C80 453	M. Albrecht et al.	(Crystal Barrel Collab.)
PELAEZ	20	PRL 124 172001	J.R. Pelaez et al.	
ABLIKIM	19AQ	PR D100 032004	M. Ablikim et al.	(BESIII Collab.)
LEES	17C	PR D95 072007	J.P. Lees et al.	(BABAR Collab.)
PELAEZ	17	EPJ C77 91	J.R. Pelaez, A.Rodas, J.R. de Elvira	
AAIJ	16N	PR D93 052018	R. Aaij et al.	(LHCb Collab.)
ABLIKIM	16F	PR D94 032001	M. Ablikim et al.	(BESIII Collab.)
LEES	13F	PR D87 052010	J.P. Lees et al.	(BABAR Collab.)
DEL-AMO-SA...	11I	PR D83 072001	P. del Amo Sanchez et al.	(BABAR Collab.)
ANTONELLI	10	EPJ C69 399	M. Antonelli et al.	(FlaviaNet Working Group)
BOITO	10	JHEP 1009 031	D.R. Boito, R. Escribano, M. Jamin	(BARC)
BOITO	09	EPJ C59 821	D.R. Boito, R. Escribano, M. Jamin	
MITCHELL	09A	PR D79 072008	R.E. Mitchell et al.	(CLEO Collab.)
BONVICINI	08A	PR D78 052001	G. Bonvicini et al.	(CLEO Collab.)
JAMIN	08	PL B664 78	M. Jamin, A. Pich, J. Portoles	
AUBERT	07AK	PR D76 012008	B. Aubert et al.	(BABAR Collab.)
EPIFANOV	07	PL B654 65	D. Epifanov et al.	(BELLE Collab.)
LINK	05I	PL B621 72	J.M. Link et al.	(FNAL FOCUS Collab.)
PELAEZ	04A	MPL A19 2879	J.R. Pelaez	(MADU)
BONVICINI	02	PRL 88 111803	G. Bonvicini et al.	(CLEO Collab.)
PDG	00	EPJ C15 1	D.E. Groom et al.	(PDG Collab.)
ABELE	99D	PL B468 178	A. Abele et al.	(Crystal Barrel Collab.)
BARATE	99R	EPJ C11 599	R. Barate et al.	(ALEPH Collab.)
BARBERIS	98E	PL B436 204	D. Barberis et al.	(Omega Expt.)
BIRD	89	SLAC-332	P.F. Bird	(SLAC)
ASTON	88	NP B296 493	D. Aston et al.	(SLAC, NAGO, CINC, INUS)
ATKINSON	86	ZPHY C30 521	M. Atkinson et al.	(BONN, CERN, GLAS+)
CARLSMITH	86	PRL 56 18	D. Carlsmith et al.	(EFI, SACL)
BAUBILLIER	84B	ZPHY C26 37	M. Baubillier et al.	(BIRM, CERN, GLAS+)
NAPIER	84	PL 149B 514	A. Napier et al.	(TUFTS, ARIZ, FNAL, FLOR+)
BARTH	83	NP B223 296	M. Barth et al.	(BRUX, CERN, GENO, MONS+)
BERG	83	Thesis UMI 83-21652	D.M. Berg	(ROCH)
CHANDLEE	83	PRL 51 168	C. Chandlee et al.	(ROCH, FNAL, MINN)
CLELAND	82	NP B208 189	W.E. Cleland et al.	(DURH, GEVA, LAUS+)
DELFOSSE	81	NP B183 349	A. Delfosse et al.	(GEVA, LAUS)
TOAFF	81	PR D23 1500	S. Toaff et al.	(ANL, KANS)
AJINENKO	80	ZPHY C5 177	I.V. Ajinenko et al.	(SERP, BRUX, MONS+)
EVANGELIS...	80	NP B165 383	C. Evangelista et al.	(BARI, BONN, CERN+)
AGUILAR-...	78B	NP B141 101	M. Aguilar-Benitez et al.	(MADR, TATA+)
BALAND	78	NP B140 220	J.F. Baland et al.	(MONS, BELG, CERN+)
COOPER	78	NP B136 365	A.M. Cooper et al.	(TATA, CERN, CDEF+)
ESTABROOKS	78	NP B133 490	P.G. Estabrooks et al.	(MCGI, CARL, DURH+)
Also		PR D17 658	P.G. Estabrooks et al.	(MCGI, CARL, DURH+)
JONGEJANS	78	NP B139 383	B. Jongejans et al.	(ZEEM, CERN, NIJM+)
WICKLUND	78	PR D17 1197	A.B. Wicklund et al.	(ANL)
BOWLER	77	NP B126 31	M.G. Bowler et al.	(OXF)
CARITHERS	75B	PRL 35 349	W.C.J. Carithers et al.	(ROCH, MCGI)
MCCUBBIN	75	NP B86 13	N.A. McCubbin, L. Lyons	(OXF)
PALER	75	NP B96 1	K. Paler et al.	(RHEL, SACL, EPOL)
FOX	74	NP B80 403	G.C. Fox, M.L. Griss	(CIT)
MATISON	74	PR D9 1872	M.J. Matison et al.	(LBL)
BEMPORAD	73	NP B51 1	C. Bemporad et al.	(CERN, ETH, LOIC)
CLARK	73	NP B54 432	A.G. Clark, L. Lyons, D. Radojicic	(OXF)
LEWIS	73	NP B60 283	P.H. Lewis et al.	(LOWC, LOIC, CDEF)
LINGLIN	73	NP B55 408	D. Linglin	(CERN)
BUCHNER	72	NP B45 333	K. Buchner et al.	(MPIM, CERN, BRUX)
AGUILAR-...	71B	PR D4 2583	M. Aguilar-Benitez, R.L. Eisner, J.B. Kinson	(BNL)
HABER	70	NP B17 289	B. Haber et al.	(REHO, SACL, BGNA, EPOL)
CRENNELL	69D	PRL 22 487	D.J. Crennell et al.	(BNL)
DAVIS	69	PRL 23 1071	P.J. Davis et al.	(LRL)
SCHWEING...	68	PR 166 1317	F. Schweingruber et al.	(ANL, NWES)
BARASH	67B	PR 156 1399	N. Barash et al.	(COLU)
BARLOW	67	NC 50A 701	J. Barlow et al.	(CERN, CDEF, IRAD, LIVP)
DAUBER	67B	PR 153 1403	P.M. Dauber et al.	(UCLA)
DEBAERE	67B	NC 51A 401	W. de Baere et al.	(BRUX, CERN)
WOJCICKI	64	PR 135 B484	S.G. Wojcicki	(LRL)

$K_1(1270)$

$I(J^P) = \frac{1}{2}(1^+)$

$K_1(1270)$ MASS

VALUE (MeV)	DOCUMENT ID
1256±6 OUR AVERAGE Includes data from the 4 datablocks that follow this one. Error includes scale factor of 2.2. See the ideogram below.	

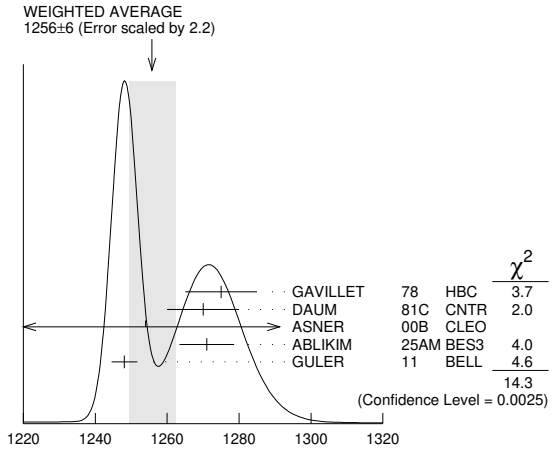

PRODUCED BY K^-, BACKWARD SCATTERING, HYPERON EXCHANGE

VALUE (MeV)	EVTS	DOCUMENT ID		TECN	CHG	COMMENT
The data in this block is included in the average printed for a previous datablock.						
1275±10	700	GAVILLET	78	HBC	+	4.2 $K^-p \to \Xi^-(K\pi\pi)^+$

PRODUCED BY K BEAMS

VALUE (MeV)	DOCUMENT ID		TECN	CHG	COMMENT
The data in this block is included in the average printed for a previous datablock.					
1270±10	[1] DAUM	81C	CNTR	−	63 $K^-p \to K^-2\pi p$
• • • We do not use the following data for averages, fits, limits, etc. • • •					
~ 1276	[2] TORNQVIST	82B	RVUE		
~ 1300	VERGEEST	79	HBC	−	4.2 $K^-p \to (\overline{K}\pi\pi)^-p$
1289±25	[3] CARNEGIE	77	ASPK	±	13 $K^\pm p \to (K\pi\pi)^\pm p$
~ 1300	BRANDENB...	76	ASPK	±	13 $K^\pm p \to (K\pi\pi)^\pm p$
~ 1270	OTTER	76	HBC	−	10,14,16 $K^-p \to (\overline{K}\pi\pi)^-p$
1260	DAVIS	72	HBC	+	12 K^+p
1234±12	FIRESTONE	72B	DBC	+	12 K^+d

[1] Well described in the chiral unitary approach of GENG 07 with two poles at 1195 and 1284 MeV and widths of 246 and 146 MeV, respectively.
[2] From a unitarized quark-model calculation.
[3] From a model-dependent fit with Gaussian background to BRANDENBURG 76 data.

PRODUCED BY BEAMS OTHER THAN K MESONS

VALUE (MeV)	EVTS	DOCUMENT ID		TECN	COMMENT
The data in this block is included in the average printed for a previous datablock.					
1252 ± 9 OUR AVERAGE Error includes scale factor of 2.7.					
1271 ± 3 ±7		[1] ABLIKIM	25AM	BES3	$D^{+(0)} \to K^-\pi^+\pi^{0(-)}e^+\nu_e$
1248.1 ± 3.3 ±1.4		GULER	11	BELL	$B^+ \to J/\psi K^+\pi^+\pi^-$
• • • We do not use the following data for averages, fits, limits, etc. • • •					
1289.81± 0.56±1.66	894k	AAIJ	18AI	LHCB	$D^0 \to K^\mp\pi^\pm\pi^\pm\pi^\mp$
1279 ±10	25k	[2] ABLIKIM	06C	BES2	$J/\psi \to \overline{K}^*(892)^0 K^+\pi^-$
1294 ±10	310	RODEBACK	81	HBC	4 $\pi^-p \to \Lambda K 2\pi$
1300	40	CRENNELL	72	HBC	4.5 $\pi^-p \to \Lambda K 2\pi$
1242 $^{+9}_{-10}$		[3] ASTIER	69	HBC	$\overline{p}p$
1300	45	CRENNELL	67	HBC	6 $\pi^-p \to \Lambda K 2\pi$

[1] Using the relativistic Breit-Wigner parameterization in the amplitude analysis.
[2] Systematic errors not estimated.
[3] This was called the C meson.

PRODUCED IN τ LEPTON DECAYS

VALUE (MeV)	EVTS	DOCUMENT ID		TECN	CHG	COMMENT
The data in this block is included in the average printed for a previous datablock.						
1254±33±34	7k	ASNER	00B	CLEO	±	$\tau^- \to K^-\pi^+\pi^-\nu_\tau$

$K_1(1270)$ WIDTH

VALUE (MeV)	DOCUMENT ID
90±20 OUR ESTIMATE This is only an educated guess; the error given is larger than the error on the average of the published values.	
104±13 OUR AVERAGE Includes data from the 4 datablocks that follow this one. Error includes scale factor of 2.5. See the ideogram below.	

See key on page 1227

Int. J. Mod. Phys. A 2026.41. Downloaded from www.worldscientific.com
by UNIVERSITY OF CALIFORNIA @ BERKELEY on 09/16/26. Re-use and distribution is strictly not permitted, except for Open Access articles.

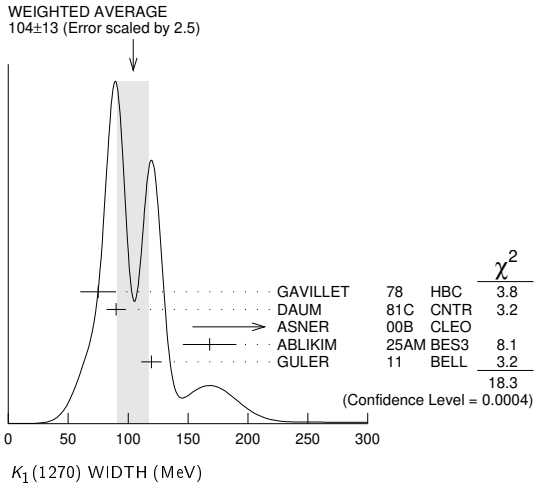

PRODUCED BY K^-, BACKWARD SCATTERING, HYPERON EXCHANGE

VALUE (MeV)	EVTS	DOCUMENT ID		TECN	CHG	COMMENT
The data in this block is included in the average printed for a previous datablock.						
75±15	700	GAVILLET	78	HBC	+	4.2 $K^- p \to \Xi^- K \pi \pi$

PRODUCED BY K BEAMS

VALUE (MeV)	DOCUMENT ID		TECN	CHG	COMMENT
The data in this block is included in the average printed for a previous datablock.					
90± 8	[1] DAUM	81C	CNTR	−	63 $K^- p \to K^- 2\pi p$
• • • We do not use the following data for averages, fits, limits, etc. • • •					
∼ 150	VERGEEST	79	HBC	−	4.2 $K^- p \to (\overline{K}\pi\pi)^- p$
150±71	[2] CARNEGIE	77	ASPK	±	13 $K^\pm p \to (K\pi\pi)^\pm p$
∼ 200	BRANDENB...	76	ASPK	±	13 $K^\pm p \to (K\pi\pi)^\pm p$
120	DAVIS	72	HBC	+	12 $K^+ p$
188±21	FIRESTONE	72B	DBC	+	12 $K^+ d$

[1] Well described in the chiral unitary approach of GENG 07 with two poles at 1195 and 1284 MeV and widths of 246 and 146 MeV, respectively.
[2] From a model-dependent fit with Gaussian background to BRANDENBURG 76 data.

PRODUCED BY BEAMS OTHER THAN K MESONS

VALUE (MeV)	EVTS	DOCUMENT ID		TECN	COMMENT
The data in this block is included in the average printed for a previous datablock.					
126 ±16 OUR AVERAGE Error includes scale factor of 2.0.					
168 ±10 ±20		[1] ABLIKIM	25AM	BES3	$D^{+(0)} \to K^- \pi^+ \pi^{0(-)} e^+ \nu_e$
119.5 ± 5.2 ± 6.7		GULER	11	BELL	$B^+ \to J/\psi K^+ \pi^+ \pi^-$
• • • We do not use the following data for averages, fits, limits, etc. • • •					
116.11± 1.65± 2.96	894k	AAIJ	18AI	LHCB	$D^0 \to K^\mp \pi^\pm \pi^\pm \pi^\mp$
131 ±21	25k	[2] ABLIKIM	06C	BES2	$J/\psi \to \overline{K}^*(892)^0 K^+ \pi^-$
66 ±15	310	RODEBACK	81	HBC	4 $\pi^- p \to \Lambda K 2\pi$
60	40	CRENNELL	72	HBC	4.5 $\pi^- p \to \Lambda K 2\pi$
127 $^{+7}_{-25}$		ASTIER	69	HBC	$\overline{p} p$
60	45	CRENNELL	67	HBC	6 $\pi^- p \to \Lambda K 2\pi$

[1] Using the relativistic Breit-Wigner parameterization in the amplitude analysis.
[2] Systematic errors not estimated.

PRODUCED IN τ LEPTON DECAYS

VALUE (MeV)	EVTS	DOCUMENT ID		TECN	CHG	COMMENT
The data in this block is included in the average printed for a previous datablock.						
260^{+90}_{-70}±80	7k	ASNER	00B	CLEO	±	$\tau^- \to K^- \pi^+ \pi^- \nu_\tau$

$K_1(1270)$ DECAY MODES

	Mode	Fraction (Γ_i/Γ)	Scale factor
Γ_1	$K\rho$	(53 ±8) %	2.1
Γ_2	$K_0^*(1430)\pi$	(14 ±8) %	4.0
Γ_3	$K^*(892)\pi$	(18 ±4) %	1.2
Γ_4	$K\omega$	(9.6±2.1) %	1.3
Γ_5	$K f_0(1370)$	(3.0±2.0) %	
Γ_6	γK^0	seen	

$K_1(1270)$ PARTIAL WIDTHS

$\Gamma(K\rho)$ — Γ_1

VALUE (MeV)	DOCUMENT ID		TECN	CHG	COMMENT
• • • We do not use the following data for averages, fits, limits, etc. • • •					
57±5	MAZZUCATO	79	HBC	+	4.2 $K^- p \to \Xi^- (K\pi\pi)^+$
75±6	CARNEGIE	77B	ASPK	±	13 $K^\pm p \to (K\pi\pi)^\pm p$

$\Gamma(K_0^*(1430)\pi)$ — Γ_2

VALUE (MeV)	DOCUMENT ID		TECN	CHG	COMMENT
• • • We do not use the following data for averages, fits, limits, etc. • • •					
26±6	CARNEGIE	77B	ASPK	±	13 $K^\pm p \to (K\pi\pi)^\pm p$

$\Gamma(K^*(892)\pi)$ — Γ_3

VALUE (MeV)	DOCUMENT ID		TECN	CHG	COMMENT
• • • We do not use the following data for averages, fits, limits, etc. • • •					
14±11	MAZZUCATO	79	HBC	+	4.2 $K^- p \to \Xi^- (K\pi\pi)^+$
2± 2	CARNEGIE	77B	ASPK	±	13 $K^\pm p \to (K\pi\pi)^\pm p$

$\Gamma(K\omega)$ — Γ_4

VALUE (MeV)	DOCUMENT ID		TECN	CHG	COMMENT
• • • We do not use the following data for averages, fits, limits, etc. • • •					
4±4	MAZZUCATO	79	HBC	+	4.2 $K^- p \to \Xi^- (K\pi\pi)^+$
24±3	CARNEGIE	77B	ASPK	±	13 $K^\pm p \to (K\pi\pi)^\pm p$

$\Gamma(K f_0(1370))$ — Γ_5

VALUE (MeV)	DOCUMENT ID		TECN	CHG	COMMENT
• • • We do not use the following data for averages, fits, limits, etc. • • •					
22±5	CARNEGIE	77B	ASPK	±	13 $K^\pm p \to (K\pi\pi)^\pm p$

$\Gamma(\gamma K^0)$ — Γ_6

VALUE (keV)	DOCUMENT ID		TECN	COMMENT
73.2±6.1±28.3	ALAVI-HARATI	02B	KTEV	$K + A \to K^* + A$

$K_1(1270)$ BRANCHING RATIOS

$\Gamma(K\rho)/\Gamma_{total}$ — Γ_1/Γ

VALUE	DOCUMENT ID		TECN	COMMENT
0.53 ±0.08 OUR FIT Error includes scale factor of 2.1.				
0.53 ±0.08 OUR AVERAGE Error includes scale factor of 2.2.				
0.588±0.045	AAIJ	25Q	LHCB	$B^+ \to \psi(2S) K^+ \pi^+ \pi^-$
0.42 ±0.06	[1] DAUM	81C	CNTR	63 $K^- p \to K^- 2\pi p$
• • • We do not use the following data for averages, fits, limits, etc. • • •				
0.584±0.043	[2] GULER	11	BELL	$B^+ \to J/\psi K^+ \pi^+ \pi^-$
dominant	RODEBACK	81	HBC	4 $\pi^- p \to \Lambda K 2\pi$

$\Gamma(K_0^*(1430)\pi)/\Gamma_{total}$ — Γ_2/Γ

VALUE	DOCUMENT ID		TECN	COMMENT
0.14 ±0.08 OUR AVERAGE Error includes scale factor of 4.0.				
0.099 ±0.022	AAIJ	25Q	LHCB	$B^+ \to \psi(2S) K^+ \pi^+ \pi^-$
0.28 ±0.04	[1] DAUM	81C	CNTR	63 $K^- p \to K^- 2\pi p$
• • • We do not use the following data for averages, fits, limits, etc. • • •				
0.0201±0.0064	[2] GULER	11	BELL	$B^+ \to J/\psi K^+ \pi^+ \pi^-$

$\Gamma(K^*(892)\pi)/\Gamma_{total}$ — Γ_3/Γ

VALUE	DOCUMENT ID		TECN	COMMENT
0.18 ±0.04 OUR FIT Error includes scale factor of 1.2.				
0.19 ±0.04 OUR AVERAGE Error includes scale factor of 1.1.				
0.250±0.063	AAIJ	25Q	LHCB	$B^+ \to \psi(2S) K^+ \pi^+ \pi^-$
0.16 ±0.05	[1] DAUM	81C	CNTR	63 $K^- p \to K^- 2\pi p$
• • • We do not use the following data for averages, fits, limits, etc. • • •				
0.171±0.023	[2] GULER	11	BELL	$B^+ \to J/\psi K^+ \pi^+ \pi^-$

$\Gamma(K^*(892)\pi)/\Gamma(K\rho)$ — Γ_3/Γ_1

VALUE	DOCUMENT ID		TECN	COMMENT
0.34 ±0.08 OUR FIT Error includes scale factor of 1.5.				
0.30 ±0.26 OUR AVERAGE Error includes scale factor of 3.1.				
0.203±0.021±0.087	ABLIKIM	25AM	BES3	$D^{+(0)} \to K^- \pi^+ \pi^{0(-)} e^+ \nu_e$
0.99 ±0.15 ±0.18	ABLIKIM	21U	BES3	$D_s^+ \to \overline{K}_1(1270)^0 K^+$

$\Gamma(K\omega)/\Gamma_{total}$ — Γ_4/Γ

VALUE	DOCUMENT ID		TECN	COMMENT
0.096±0.021 OUR AVERAGE Error includes scale factor of 1.3.				
0.063±0.031	AAIJ	25Q	LHCB	$B^+ \to \psi(2S) K^+ \pi^+ \pi^-$
0.11 ±0.02	[1] DAUM	81C	CNTR	63 $K^- p \to K^- 2\pi p$
• • • We do not use the following data for averages, fits, limits, etc. • • •				
0.225±0.052	[2] GULER	11	BELL	$B^+ \to J/\psi K^+ \pi^+ \pi^-$

$\Gamma(K\omega)/\Gamma(K\rho)$ — Γ_4/Γ_1

VALUE	CL%	DOCUMENT ID		TECN	COMMENT
• • • We do not use the following data for averages, fits, limits, etc. • • •					
<0.30	95	RODEBACK	81	HBC	4 $\pi^- p \to \Lambda K 2\pi$

Int. J. Mod. Phys. A 2026.41. Downloaded from www.worldscientific.com
by CALIFORNIA @ BERKELEY on 09/16/26. Re-use and distribution is strictly not permitted, except for Open Access articles.

$\Gamma(K f_0(1370))/\Gamma_{total}$ — Γ_5/Γ

VALUE	DOCUMENT ID		TECN	COMMENT
0.03±0.02	[1] DAUM	81C	CNTR	63 $K^- p \to K^- 2\pi p$

D-wave/S-wave RATIO FOR $K_1(1270) \to K^*(892)\pi$

VALUE	DOCUMENT ID		TECN	COMMENT
1.0±0.7	[1] DAUM	81C	CNTR	63 $K^- p \to K^- 2\pi p$

[1] Average from low and high t data.
[2] Assuming that decays are saturated by the $K\rho$, $K_0^*(1430)\pi$, $K^*(892)\pi$, $K\omega$ decay modes and neglecting interference between them. The values $B(\omega \to \pi^+\pi^-) = (1.53^{+0.11}_{-0.13})\%$ and $B(K_0^*(1430) \to K\pi) = (93 \pm 10)\%$ are used. Systematic uncertainties not estimated.

$K_1(1270)$ REFERENCES

AAIJ	25Q	JHEP 2501 054	R. Aaij et al.	(LHCb Collab.)
ABLIKIM	25AM	PRL 135 091801	M. Ablikim et al.	(BESIII Collab.)
ABLIKIM	21U	PR D104 032011	M. Ablikim et al.	(BESIII Collab.)
AAIJ	18AI	EPJ C78 443	R. Aaij et al.	(LHCb Collab.)
GULER	11	PR D83 032005	H. Guler et al.	(BELLE Collab.)
GENG	07	PR D75 014017	L.S. Geng et al.	
ABLIKIM	06C	PL B633 681	M. Ablikim et al.	(BES Collab.)
ALAVI-HARATI	02B	PRL 89 072001	A. Alavi-Harati et al.	(FNAL KTeV Collab.)
ASNER	00B	PR D62 072006	D.M. Asner et al.	(CLEO Collab.)
TORNQVIST	82B	NP B203 268	N.A. Tornqvist	(HELS)
DAUM	81C	NP B187 1	C. Daum et al.	(AMST, CERN, CRAC, MPIM+)
RODEBACK	81	ZPHY C9 9	S. Rodeback et al.	(CERN, CDEF, MADR+)
MAZZUCATO	79	NP B156 532	M. Mazzucato et al.	(CERN, ZEEM, NIJM+)
VERGEEST	79	NP B158 265	J.S.M. Vergeest et al.	(NIJM, AMST, CERN+)
GAVILLET	78	PL 76B 517	P. Gavillet et al.	(AMST, CERN, NIJM+) JP
CARNEGIE	77	NP B127 509	R.K. Carnegie et al.	(SLAC)
CARNEGIE	77B	PL 68B 287	R.K. Carnegie et al.	(SLAC)
BRANDENB...	76	PRL 36 703	G.W. Brandenburg et al.	(SLAC) JP
OTTER	76	NP B106 77	G. Otter et al.	(AACH3, BERL, CERN, LOIC+) JP
CRENNELL	72	PR D6 1220	D.J. Crennell et al.	(BNL)
DAVIS	72	PR D5 2688	P.J. Davis et al.	(LBL)
FIRESTONE	72B	PR D5 505	A. Firestone et al.	(LBL)
ASTIER	69	NP B10 65	A. Astier et al.	(CDEF, CERN, IPNP, LIVP) IJP
CRENNELL	67	PRL 19 44	D.J. Crennell et al.	(BNL) I

$K_1(1400)$

$I(J^P) = \frac{1}{2}(1^+)$

$K_1(1400)$ MASS

VALUE (MeV)	EVTS	DOCUMENT ID		TECN	CHG	COMMENT
1403± 7 OUR AVERAGE						
1463±64±68	7k	ASNER	00B	CLEO	±	$\tau^- \to K^-\pi^+\pi^-\nu_\tau$
1373±14±18		[1] ASTON	87	LASS	0	11 $K^- p \to \overline{K}^0\pi^+\pi^- n$
1392±18		BAUBILLIER	82B	HBC	0	8.25 $K^- p \to K^0_S\pi^+\pi^- n$
1410±25		DAUM	81C	CNTR	−	63 $K^- p \to K^- 2\pi p$
1415±15		ETKIN	80	MPS	0	6 $K^- p \to \overline{K}^0\pi^+\pi^- n$
1404±10		[2] CARNEGIE	77	ASPK	±	13 $K^\pm p \to (K\pi\pi)^\pm p$
• • • We do not use the following data for averages, fits, limits, etc. • • •						
1418± 8	25k	[3] ABLIKIM	06C	BES2		$J/\psi \to \overline{K}^*(892)^0 K^+\pi^-$
∼ 1350		[4] TORNQVIST	82B	RVUE		
∼ 1400		VERGEEST	79	HBC	−	4.2 $K^- p \to (\overline{K}\pi\pi)^- p$
∼ 1400		BRANDENB...	76	ASPK	±	13 $K^\pm p \to (K\pi\pi)^\pm p$
1420		DAVIS	72	HBC	+	12 $K^+ p$
1368±18		FIRESTONE	72B	DBC	+	12 $K^+ d$

[1] From partial-wave analysis of $K^0\pi^+\pi^-$ system.
[2] From a model-dependent fit with Gaussian background to BRANDENBURG 76 data.
[3] Systematic errors not estimated.
[4] From a unitarized quark-model calculation.

$K_1(1400)$ WIDTH

VALUE (MeV)	EVTS	DOCUMENT ID		TECN	CHG	COMMENT
174± 13 OUR AVERAGE Error includes scale factor of 1.6. See the ideogram below.						
300^{+370}_{-110}±140	7k	ASNER	00B	CLEO	±	$\tau^- \to K^-\pi^+\pi^-\nu_\tau$
188± 54± 60		[1] ASTON	87	LASS	0	11 $K^- p \to \overline{K}^0\pi^+\pi^- n$
276± 65		BAUBILLIER	82B	HBC	0	8.25 $K^- p \to K^0_S\pi^+\pi^- n$
195± 25		DAUM	81C	CNTR	−	63 $K^- p \to K^- 2\pi p$
180± 10		ETKIN	80	MPS	0	6 $K^- p \to \overline{K}^0\pi^+\pi^- n$
142± 16		[2] CARNEGIE	77	ASPK	±	13 $K^\pm p \to (K\pi\pi)^\pm p$
• • • We do not use the following data for averages, fits, limits, etc. • • •						
152± 16	25k	[3] ABLIKIM	06C	BES2		$J/\psi \to \overline{K}^*(892)^0 K^+\pi^-$
∼ 200		VERGEEST	79	HBC	−	4.2 $K^- p \to (\overline{K}\pi\pi)^- p$
∼ 160		BRANDENB...	76	ASPK	±	13 $K^\pm p \to (K\pi\pi)^\pm p$
80		DAVIS	72	HBC	+	12 $K^+ p$
241± 30		FIRESTONE	72B	DBC	+	12 $K^+ d$

[1] From partial-wave analysis of $K^0\pi^+\pi^-$ system.
[2] From a model-dependent fit with Gaussian background to BRANDENBURG 76 data.
[3] Systematic errors not estimated.

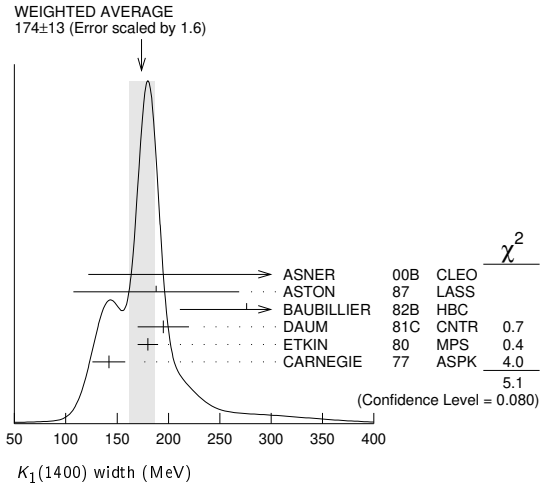

$K_1(1400)$ DECAY MODES

	Mode	Fraction (Γ_i/Γ)
Γ_1	$K^*(892)\pi$	(94 ±6) %
Γ_2	$K\rho$	(3.0±3.0) %
Γ_3	$K f_0(1370)$	(2.0±2.0) %
Γ_4	$K\omega$	(1.0±1.0) %
Γ_5	$K_0^*(1430)\pi$	not seen
Γ_6	γK^0	seen
Γ_7	$K\phi$	seen

$K_1(1400)$ PARTIAL WIDTHS

$\Gamma(K^*(892)\pi)$ — Γ_1

VALUE (MeV)	DOCUMENT ID		TECN	CHG	COMMENT
117±10	CARNEGIE	77	ASPK	±	13 $K^\pm p \to (K\pi\pi)^\pm p$

$\Gamma(K\rho)$ — Γ_2

VALUE (MeV)	DOCUMENT ID		TECN	CHG	COMMENT
2±1	CARNEGIE	77	ASPK	±	13 $K^\pm p \to (K\pi\pi)^\pm p$

$\Gamma(K\omega)$ — Γ_4

VALUE (MeV)	DOCUMENT ID		TECN	CHG	COMMENT
23±12	CARNEGIE	77	ASPK	±	13 $K^\pm p \to (K\pi\pi)^\pm p$

$\Gamma(\gamma K^0)$ — Γ_6

VALUE (keV)	DOCUMENT ID		TECN	COMMENT
280.8±23.2±40.4	ALAVI-HARATI	02B	KTEV	$K + A \to K^* + A$

$K_1(1400)$ BRANCHING RATIOS

$\Gamma(K^*(892)\pi)/\Gamma_{total}$ — Γ_1/Γ

VALUE	DOCUMENT ID		TECN	COMMENT
0.94±0.06	[1] DAUM	81C	CNTR	63 $K^- p \to K^- 2\pi p$

[1] Average from low and high t data.

$\Gamma(K\rho)/\Gamma_{total}$ — Γ_2/Γ

VALUE	DOCUMENT ID		TECN	COMMENT
0.03±0.03	[1] DAUM	81C	CNTR	63 $K^- p \to K^- 2\pi p$

[1] Average from low and high t data.

$\Gamma(K f_0(1370))/\Gamma_{total}$ — Γ_3/Γ

VALUE	DOCUMENT ID		TECN	COMMENT
0.02±0.02	[1] DAUM	81C	CNTR	63 $K^- p \to K^- 2\pi p$

[1] Average from low and high t data.

$\Gamma(K\omega)/\Gamma_{total}$ — Γ_4/Γ

VALUE	DOCUMENT ID		TECN	COMMENT
0.01±0.01	[1] DAUM	81C	CNTR	63 $K^- p \to K^- 2\pi p$

[1] Average from low and high t data.

$\Gamma(K\phi)/\Gamma_{total}$ — Γ_7/Γ

VALUE	EVTS	DOCUMENT ID		TECN	COMMENT
seen	24k	[1] AAIJ	21E	LHCB	$B^+ \to J/\psi\phi K^+$

[1] From an amplitude analysis of the decay $B^+ \to J/\psi\phi K^+$ with a significance of 9.2 σ.

Int. J. Mod. Phys. A 2026.41. Downloaded from www.worldscientific.com by UNIVERSITY OF CALIFORNIA @ BERKELEY on 09/16/26. Re-use and distribution is strictly not permitted, except for Open Access articles.

$\Gamma(K_0^*(1430)\pi)/\Gamma_{total}$ — Γ_5/Γ

VALUE	DOCUMENT ID		TECN	COMMENT
not seen	[1] DAUM	81C	CNTR	63 $K^- p \to K^- 2\pi p$

[1] Average from low and high t data.

D-wave/S-wave RATIO FOR $K_1(1400) \to K^*(892)\pi$

VALUE	DOCUMENT ID		TECN	COMMENT
0.04±0.01	[1] DAUM	81C	CNTR	63 $K^- p \to K^- 2\pi p$

[1] Average from low and high t data.

$K_1(1400)$ REFERENCES

AAIJ	21E	PRL 127 082001	R. Aaij et al.	(LHCb Collab.)
ABLIKIM	06C	PL B633 681	M. Ablikim et al.	(BES Collab.)
ALAVI-HARATI	02B	PRL 89 072001	A. Alavi-Harati et al.	(FNAL KTeV Collab.)
ASNER	00B	PR D62 072006	D.M. Asner et al.	(CLEO Collab.)
ASTON	87	NP B292 693	D. Aston et al.	(SLAC, NAGO, CINC, INUS)
BAUBILLIER	82B	NP B202 21	M. Baubillier et al.	(BIRM, CERN, GLAS+)
TORNQVIST	82B	NP B203 268	N.A. Tornqvist	(HELS)
DAUM	81C	NP B187 1	C. Daum et al.	(AMST, CERN, CRAC, MPIM+)
ETKIN	80	PR D22 42	A. Etkin et al.	(BNL, CUNY) JP
VERGEEST	79	NP B158 265	J.S.M. Vergeest et al.	(NIJM, AMST, CERN+)
CARNEGIE	77	NP B127 509	R.K. Carnegie et al.	(SLAC)
BRANDENB...	76	PRL 36 703	G.W. Brandenburg et al.	(SLAC) JP
DAVIS	72	PR D5 2688	P.J. Davis et al.	(LBL)
FIRESTONE	72B	PR D5 505	A. Firestone et al.	(LBL)

$K^*(1410)$

$I(J^P) = \frac{1}{2}(1^-)$

$K^*(1410)$ T-MATRIX POLE $\sqrt{s}$

Note that $\Gamma = -2\,\mathrm{Im}(\sqrt{s})$.

VALUE (MeV)	DOCUMENT ID		TECN	COMMENT
$(1368 \pm 38) - i\,(106^{+48}_{-59})$ OUR ESTIMATE				
$(1368 \pm 38) - i\,(106^{+48}_{-59})$	[1] PELAEZ	17	RVUE	$\pi K \to \pi K$

[1] Reanalysis of ESTABROOKS 78 and ASTON 88 satisfying Forward Dispersion Relations and using sequences of Pade approximants.

$K^*(1410)$ MASS

VALUE (MeV)	EVTS	DOCUMENT ID		TECN	CHG	COMMENT
1414±15 OUR AVERAGE		Error includes scale factor of 1.3.				
1380±21±19		ASTON	88	LASS	0	11 $K^- p \to K^- \pi^+ n$
1420± 7±10		ASTON	87	LASS	0	11 $K^- p \to \overline{K}^0 \pi^+ \pi^- n$
• • • We do not use the following data for averages, fits, limits, etc. • • •						
1437± 8±16	190k	[1] AAIJ	16N	LHCB		$D^0 \to (K^0_S \pi^\mp) K^\pm$
1426± 8±24	190k	[2] AAIJ	16N	LHCB		$D^0 \to K^0_S (K^\pm \pi^\mp)$
1276^{+72}_{-77}		[3,4] BOITO	09	RVUE		$\tau^- \to K^0_S \pi^- \nu_\tau$
1367±54		BIRD	89	LASS	−	11 $K^- p \to \overline{K}^0 \pi^- p$
1474±25		BAUBILLIER	82B	HBC	0	8.25 $K^- p \to \overline{K}^0 2\pi n$
1500±30		ETKIN	80	MPS	0	6 $K^- p \to \overline{K}^0 \pi^+ \pi^- n$

[1] Using a parametrization for the $K\pi$ S-wave similar to ASTON 88 with fixed resonance width.
[2] Using a $K\pi$ S-wave parametrization with resonant and non-resonant contributions.
[3] From the pole position of the $K\pi$ vector form factor in the complex s-plane and using EPIFANOV 07 data.
[4] Systematic uncertainties not estimated.

$K^*(1410)$ WIDTH

VALUE (MeV)	EVTS	DOCUMENT ID		TECN	CHG	COMMENT
232± 21 OUR AVERAGE		Error includes scale factor of 1.1.				
176± 52±22		ASTON	88	LASS	0	11 $K^- p \to K^- \pi^+ n$
240± 18±12		ASTON	87	LASS	0	11 $K^- p \to \overline{K}^0 \pi^+ \pi^- n$
• • • We do not use the following data for averages, fits, limits, etc. • • •						
210± 20±60	190k	[1] AAIJ	16N	LHCB		$D^0 \to (K^0_S \pi^\mp) K^\pm$
270± 20±40	190k	[1] AAIJ	16N	LHCB		$D^0 \to K^0_S (K^\pm \pi^\mp)$
198^{+61}_{-87}		[2,3] BOITO	09	RVUE		$\tau^- \to K^0_S \pi^- \nu_\tau$
114±101		BIRD	89	LASS	−	11 $K^- p \to \overline{K}^0 \pi^- p$
275± 65		BAUBILLIER	82B	HBC	0	8.25 $K^- p \to \overline{K}^0 2\pi n$
500±100		ETKIN	80	MPS	0	6 $K^- p \to \overline{K}^0 \pi^+ \pi^- n$

[1] Using a $K\pi$ S-wave parametrization with resonant and non-resonant contributions.
[2] From the pole position of the $K\pi$ vector form factor in the complex s-plane and using EPIFANOV 07 data.
[3] Systematic uncertainties not estimated.

$K^*(1410)$ DECAY MODES

	Mode	Fraction (Γ_i/Γ)	Confidence level
Γ_1	$K^*(892)\pi$	> 40 %	95%
Γ_2	$K\pi$	(6.6±1.3) %	
Γ_3	$K\rho$	< 7 %	95%
Γ_4	γK^0	< 2.3 $\times 10^{-4}$	90%
Γ_5	$K\phi$	seen	

$K^*(1410)$ PARTIAL WIDTHS

$\Gamma(\gamma K^0)$ — Γ_4

VALUE (keV)	CL%	DOCUMENT ID		TECN	COMMENT
<52.9	90	ALAVI-HARATI	02B	KTEV	$K + A \to K^* + A$

$K^*(1410)$ BRANCHING RATIOS

$\Gamma(K\rho)/\Gamma(K^*(892)\pi)$ — Γ_3/Γ_1

VALUE	CL%	DOCUMENT ID		TECN	CHG	COMMENT
<0.17	95	ASTON	84	LASS	0	11 $K^- p \to \overline{K}^0 2\pi n$

$\Gamma(K\pi)/\Gamma(K^*(892)\pi)$ — Γ_2/Γ_1

VALUE	CL%	DOCUMENT ID		TECN	CHG	COMMENT
<0.16	95	ASTON	84	LASS	0	11 $K^- p \to \overline{K}^0 2\pi n$

$\Gamma(K\pi)/\Gamma_{total}$ — Γ_2/Γ

VALUE	DOCUMENT ID		TECN	CHG	COMMENT
0.066±0.010±0.008	ASTON	88	LASS	0	11 $K^- p \to K^- \pi^+ n$

$\Gamma(K\phi)/\Gamma_{total}$ — Γ_5/Γ

VALUE	EVTS	DOCUMENT ID		TECN	COMMENT
seen	24k	[1] AAIJ	21E	LHCB	$B^+ \to J/\psi\phi K^+$

[1] From an amplitude analysis of the decay $B^+ \to J/\psi\phi K^+$ with a significance of 7.7 σ.

$K^*(1410)$ REFERENCES

AAIJ	21E	PRL 127 082001	R. Aaij et al.	(LHCb Collab.)
PELAEZ	17	EPJ C77 91	J.R. Pelaez, A.Rodas, J.R. de Elvira	
AAIJ	16N	PR D93 052018	R. Aaij et al.	(LHCb Collab.)
BOITO	09	EPJ C59 821	D.R. Boito, R. Escribano, M. Jamin	
EPIFANOV	07	PL B654 65	D. Epifanov et al.	(BELLE Collab.)
ALAVI-HARATI	02B	PRL 89 072001	A. Alavi-Harati et al.	(FNAL KTeV Collab.)
BIRD	89	SLAC-332	P.F. Bird	(SLAC)
ASTON	88	NP B296 493	D. Aston et al.	(SLAC, NAGO, CINC, INUS)
ASTON	87	NP B292 693	D. Aston et al.	(SLAC, NAGO, CINC, INUS)
ASTON	84	PL 149B 258	D. Aston et al.	(SLAC, CARL, OTTA) JP
BAUBILLIER	82B	NP B202 21	M. Baubillier et al.	(BIRM, CERN, GLAS+)
ETKIN	80	PR D22 42	A. Etkin et al.	(BNL, CUNY) JP
ESTABROOKS	78	NP B133 490	P.G. Estabrooks et al.	(MCGI, CARL, DURH+)

$K_0^*(1430)$

$I(J^P) = \frac{1}{2}(0^+)$

$K_0^*(1430)$ T-MATRIX POLE $\sqrt{s}$

Note that $\Gamma = -2\,\mathrm{Im}(\sqrt{s})$.

VALUE (MeV)	DOCUMENT ID		TECN	COMMENT
$(1431 \pm 6) - i\,(110 \pm 19)$ OUR ESTIMATE				
$(1431 \pm 6) - i\,(110 \pm 19)$	[1] PELAEZ	17	RVUE	$\pi K \to \pi K$

[1] Reanalysis of ESTABROOKS 78 and ASTON 88 satisfying Forward Dispersion Relations and using sequences of Pade approximants.

$K_0^*(1430)$ MASS

VALUE (MeV)	EVTS	DOCUMENT ID		TECN	COMMENT
1425 ±50 OUR ESTIMATE					
• • • We do not use the following data for averages, fits, limits, etc. • • •					
1493 ± 4 ± 7		[1] AAIJ	23AH	LHCB	$B^+ \to K^+ (K^0_S K\pi)$
1449 ±17 ± 2		[2] LEES	21A	BABR	$\eta_c(1S) \to \eta' K^+ K^-$
1438 ± 8 ± 4	5.4k	[3] LEES	14E	BABR	$\eta_c(1S) \to K^+ K^- \eta/\pi^0$
1427 ± 4 ±13		[4] BUGG	10	RVUE	S-matrix pole
1466.6± 0.7± 3.4	141k	[5] BONVICINI	08A	CLEO	$D^+ \to K^- \pi^+ \pi^+$
~ 1412		[6] LINK	07	FOCS	$D^+ \to K^- K^+ \pi^+$
1461.0± 4.0± 2.1	54k	[7] LINK	07B	FOCS	$D^+ \to K^- \pi^+ \pi^+$
1406 ±29		[8] BUGG	06	RVUE	
1435 ± 6		[9] ZHOU	06	RVUE	$Kp \to K^- \pi^+ n$
1455 ±20 ±15		ABLIKIM	05Q	BES2	$\psi(2S) \to \gamma\pi^+\pi^- K^+ K^-$
1456 ± 8		[10] ZHENG	04	RVUE	$K^- p \to K^- \pi^+ n$
~ 1419		[11] BUGG	03	RVUE	11 $K^- p \to K^- \pi^+ n$
~ 1440		[12] LI	03	RVUE	11 $K^- p \to K^- \pi^+ n$
1459 ± 9	15k	[13] AITALA	02	E791	$D^+ \to K^- \pi^+ \pi^+$

~ 1440	[14] JAMIN	00	RVUE	$Kp \to Kp$
1436 ± 8	[15] BARBERIS	98E	OMEG	450 $pp \to p_f p_s K^+ K^- \pi^+ \pi^-$
1415 ± 25	[11] ANISOVICH	97C	RVUE	11 $K^- p \to K^- \pi^+ n$
~ 1450	[16] TORNQVIST	96	RVUE	$\pi\pi \to \pi\pi$, $K\overline{K}$, $K\pi$
1412 ± 6	[17] ASTON	88	LASS	11 $K^- p \to K^- \pi^+ n$
~ 1430	BAUBILLIER	84B	HBC	8.25 $K^- p \to \overline{K}^0 \pi^- p$
~ 1425	[18] ESTABROOKS	78	ASPK	13 $K^\pm p \to K^\pm \pi^\pm (n, \Delta)$
~ 1450.0	MARTIN	78	SPEC	10 $K^\pm p \to K^0_S \pi p$

[1] From Dalitz plot analyses of $\eta_c(1S, 2S) \to K^0_S K^+ \pi^- +$ c.c..
[2] Using a $K\pi - K\eta'$ coupled channel Breit-Wigner function.
[3] Using both $\eta \to \gamma\gamma$ and $\eta \to \pi^+\pi^-\pi^0$. From a likelihood scan in the presence of several interfering scalar-meson resonances with fixed width $\Gamma(K_0^*(1430)) = 210$ MeV.
[4] S-Matrix pole. Supersedes BUGG 06. Combined analysis of ASTON 88, ABLIKIM 06C, AITALA 06, and LINK 09 using an s-dependent width with couplings to $K\pi$ and $K\eta'$, and the Adler zero near thresholds.
[5] From the isobar model with a complex pole for the κ.
[6] From a non-parametric analysis.
[7] A Breit-Wigner mass and width.
[8] S-matrix pole. Reanalysis of ASTON 88, AITALA 02, and ABLIKIM 06C including the κ with an s-dependent width and an Adler zero near threshold.
[9] S-matrix pole. Using ASTON 88 and assuming $K_0^*(700)$, $K_0^*(1950)$.
[10] Using ASTON 88 and assuming $K_0^*(700)$.
[11] T-matrix pole. Reanalysis of ASTON 88 data.
[12] Breit-Wigner fit. Using ASTON 88.
[13] Assuming a low-mass scalar $K\pi$ resonance, $\kappa(700)$.
[14] T-matrix pole. Using data from ESTABROOKS 78 and ASTON 88.
[15] J^P not determined, could be $K_2^*(1430)$.
[16] T-matrix pole.
[17] Uses a model for the background, without this background they get a mass 1340 MeV, where the phase shift passes 90°.
[18] Mass defined by pole position. From elastic $K\pi$ partial-wave analysis.

$K_0^*(1430)$ WIDTH

VALUE (MeV)	EVTS	DOCUMENT ID		TECN	COMMENT
270 ± 80 OUR ESTIMATE					
• • • We do not use the following data for averages, fits, limits, etc. • • •					
215 ± 7 ± 4		[1] AAIJ	23AH	LHCB	$B^+ \to K^+(K^0_S K\pi)$
210 ± 20 ± 12	5.4k	[2] LEES	14E	BABR	$\eta_c(1S) \to K^+ K^- \eta/\pi^0$
270 ± 10 ± 40		[3] BUGG	10	RVUE	S-matrix pole
174.2 ± 1.9 ± 3.2	141k	[4] BONVICINI	08A	CLEO	$D^+ \to K^-\pi^+\pi^+$
~ 500		[5] LINK	07	FOCS	$D^+ \to K^- K^+ \pi^+$
177.0 ± 8.0 ± 3.4	54k	[6] LINK	07B	FOCS	$D^+ \to K^-\pi^+\pi^+$
350 ± 40		[7] BUGG	06	RVUE	
288 ± 22		[8] ZHOU	06	RVUE	$Kp \to K^-\pi^+ n$
270 ± 45 $^{+30}_{-35}$		ABLIKIM	05Q	BES2	$\psi(2S) \to \gamma\pi^+\pi^- K^+ K^-$
217 ± 31		[9] ZHENG	04	RVUE	$K^- p \to K^-\pi^+ n$
~ 316		[10] BUGG	03	RVUE	11 $K^- p \to K^-\pi^+ n$
~ 350		[11] LI	03	RVUE	11 $K^- p \to K^-\pi^+ n$
175 ± 17	15k	[12] AITALA	02	E791	$D^+ \to K^-\pi^+\pi^+$
~ 300		[13] JAMIN	00	RVUE	$Kp \to Kp$
196 ± 45		[14] BARBERIS	98E	OMEG	450 $pp \to p_f p_s K^+ K^- \pi^+ \pi^-$
330 ± 50		[10] ANISOVICH	97C	RVUE	11 $K^- p \to K^-\pi^+ n$
~ 320		[15] TORNQVIST	96	RVUE	$\pi\pi \to \pi\pi$, $K\overline{K}$, $K\pi$
294 ± 23		ASTON	88	LASS	11 $K^- p \to K^-\pi^+ n$
~ 200		BAUBILLIER	84B	HBC	8.25 $K^- p \to \overline{K}^0 \pi^- p$
200 to 300		[16] ESTABROOKS	78	ASPK	13 $K^\pm p \to K^\pm \pi^\pm (n, \Delta)$

[1] From Dalitz plot analyses of $\eta_c(1S, 2S) \to K^0_S K^+ \pi^- +$ c.c..
[2] Using both $\eta \to \gamma\gamma$ and $\eta \to \pi^+\pi^-\pi^0$. From a likelihood scan in the presence of several interfering scalar-meson resonances with fixed mass $M(K_0^*(1430)) = 1435$ MeV.
[3] S-Matrix pole. Supersedes BUGG 06. Combined analysis of ASTON 88, ABLIKIM 06C, AITALA 06, and LINK 09 using an s-dependent width with couplings to $K\pi$ and $K\eta'$, and the Adler zero near thresholds.
[4] From the isobar model with a complex pole for the κ.
[5] From a non-parametric analysis.
[6] A Breit-Wigner mass and width.
[7] S-matrix pole. Reanalysis of ASTON 88, AITALA 02, and ABLIKIM 06C including the κ with an s-dependent width and an Adler zero near threshold.
[8] S-matrix pole. Using ASTON 88 and assuming $K_0^*(700)$, $K_0^*(1950)$.
[9] Using ASTON 88 and assuming $K_0^*(700)$.
[10] T-matrix pole. Reanalysis of ASTON 88 data.
[11] Breit-Wigner fit. Using ASTON 88.
[12] Assuming a low-mass scalar $K\pi$ resonance, $\kappa(700)$.
[13] T-matrix pole. Using data from ESTABROOKS 78 and ASTON 88.
[14] J^P not determined, could be $K_2^*(1430)$.
[15] T-matrix pole.
[16] From elastic $K\pi$ partial-wave analysis.

$K_0^*(1430)$ DECAY MODES

	Mode	Fraction (Γ_i/Γ)
Γ_1	$K\pi$	(93 ± 10) %
Γ_2	$K\eta$	(8.6 $^{+2.7}_{-3.4}$) %
Γ_3	$K\eta'(958)$	seen

$K_0^*(1430)$ BRANCHING RATIOS

$\Gamma(K\pi)/\Gamma_{total}$ — Γ_1/Γ

VALUE	DOCUMENT ID		TECN	CHG	COMMENT
0.93 ± 0.04 ± 0.09	ASTON	88	LASS	0	11 $K^- p \to K^-\pi^+ n$

$\Gamma(K\eta)/\Gamma(K\pi)$ — Γ_2/Γ_1

VALUE (%)	EVTS	DOCUMENT ID		TECN	COMMENT
9.2 ± 2.5 $^{+1.0}_{-2.5}$	5.4k	[1] LEES	14E	BABR	$\eta_c(1S) \to K^+ K^- \eta/\pi^0$

[1] Using both $\eta \to \gamma\gamma$ and $\eta \to \pi^+\pi^-\pi^0$. From a Dalitz analysis in the presence of several interfering scalar-meson resonances.

$\Gamma(K\eta'(958))/\Gamma_{total}$ — Γ_3/Γ

VALUE	DOCUMENT ID		TECN	COMMENT
seen	ABLIKIM	14J	BES3	$\psi(2S) \to \gamma K^+ K^- \eta'(958)$

$\Gamma(K\eta'(958))/\Gamma(K\pi)$ — Γ_3/Γ_1

VALUE	DOCUMENT ID		TECN	COMMENT
0.397 ± 0.064 ± 0.054	[1] LEES	21A	BABR	$\eta_c(1S) \to \eta' K^+ K^-$

[1] Using $K\pi$ data from LEES 14E.

$K_0^*(1430)$ REFERENCES

AAIJ	23AH	PR D108 032010	R. Aaij et al.	(LHCb Collab.)
LEES	21A	PR D104 072002	J.P. Lees et al.	(BABAR Collab.)
PELAEZ	17	EPJ C77 91	J.R. Pelaez, A.Rodas, J.R. de Elvira	
ABLIKIM	14J	PR D89 074030	M. Ablikim et al.	(BESIII Collab.)
LEES	14E	PR D89 112004	J.P. Lees et al.	(BABAR Collab.)
BUGG	10	PR D81 014002	D.V. Bugg	(LOQM)
LINK	09	PL B681 14	J.M. Link et al.	(FNAL FOCUS Collab.)
BONVICINI	08A	PR D78 052001	G. Bonvicini et al.	(CLEO Collab.)
LINK	07	PL B648 156	J.M. Link et al.	(FNAL FOCUS Collab.)
LINK	07B	PL B653 1	J.M. Link et al.	(FNAL FOCUS Collab.)
ABLIKIM	06C	PL B633 681	M. Ablikim et al.	(BES Collab.)
AITALA	06	PR D73 032004	E.M. Aitala et al.	(FNAL E791 Collab.)
Also		PR D74 059901 (errat.)	E.M. Aitala et al.	(FNAL E791 Collab.)
BUGG	06	PL B632 471	D.V. Bugg	(LOQM)
ZHOU	06	NP A775 212	Z.Y. Zhou, H.Q. Zheng	
ABLIKIM	05Q	PR D72 092002	M. Ablikim et al.	(BES Collab.)
ZHENG	04	NP A733 235	H.Q. Zheng et al.	
BUGG	03	PL B572 1	D.V. Bugg	
LI	03	PR D67 034025	L. Li, B. Zou, G. Li	
AITALA	02	PRL 89 121801	E.M. Aitala et al.	(FNAL E791 Collab.)
JAMIN	00	NP B587 331	M. Jamin et al.	
BARBERIS	98E	PL B436 204	D. Barberis et al.	(Omega Expt.)
ANISOVICH	97C	PL B413 137	A.V. Anisovich, A.V. Sarantsev	
TORNQVIST	96	PRL 76 1575	N.A. Tornqvist, M. Roos	(HELS)
ASTON	88	NP B296 493	D. Aston et al.	(SLAC, NAGO, CINC, INUS)
BAUBILLIER	84B	ZPHY C26 37	M. Baubillier et al.	(BIRM, CERN, GLAS+)
ESTABROOKS	78	NP B133 490	P.G. Estabrooks et al.	(MCGI, CARL, DURH+)
MARTIN	78	NP B134 392	A.D. Martin et al.	(DURH, GEVA)

$K_2^*(1430)$

$I(J^P) = \frac{1}{2}(2^+)$

We consider that phase-shift analyses provide more reliable determinations of the mass and width.

$K_2^*(1430)$ T-MATRIX POLE $\sqrt{s}$

Note that $\Gamma = -2\,\mathrm{Im}(\sqrt{s})$.

VALUE (MeV)	DOCUMENT ID		TECN	COMMENT
(1424 ± 4) − i (66 ± 2) OUR ESTIMATE				
(1424 ± 4) − i (66 ± 2)	[1] PELAEZ	17	RVUE	$\pi K \to \pi K$

[1] Reanalysis of ESTABROOKS 78 and ASTON 88 satisfying Forward Dispersion Relations and using sequences of Pade approximants.

$K_2^*(1430)$ MASS

CHARGED ONLY, WITH FINAL STATE $K\pi$

VALUE (MeV)	EVTS	DOCUMENT ID		TECN	CHG	COMMENT
1427.3 ± 1.5 OUR AVERAGE		Error includes scale factor of 1.3. See the ideogram below.				
1432.7 ± 0.7 $^{+2.2}_{-2.3}$	183k	ABLIKIM	19AQ	BES	±	$J/\psi \to K^- K^- \pi^0$
1420 ± 4	1587	BAUBILLIER	84B	HBC	−	8.25 $K^- p \to \overline{K}^0 \pi^- p$
1436 ± 5.5	400	[1,2] CLELAND	82	SPEC	+	30 $K^+ p \to K^0_S \pi^+ p$
1430 ± 3.2	1500	[1,2] CLELAND	82	SPEC	+	50 $K^+ p \to K^0_S \pi^+ p$
1430 ± 3.2	1200	[1,2] CLELAND	82	SPEC	−	50 $K^+ p \to K^0_S \pi^- p$
1423 ± 5	935	TOAFF	81	HBC	−	6.5 $K^- p \to \overline{K}^0 \pi^- p$
1428.0 ± 4.6		[3] MARTIN	78	SPEC	+	10 $K^\pm p \to K^0_S \pi p$

Int. J. Mod. Phys. A 2026.41. Downloaded from www.worldscientific.com
by CALIFORNIA @ BERKELEY on 09/16/26. Re-use and distribution is strictly not permitted, except for Open Access articles.

1423.8 ± 4.6		[3] MARTIN	78	SPEC	−	10 $K^\pm p \to K^0_S \pi p$
1420.0 ± 3.1	1400	AGUILAR-...	71B	HBC	−	3.9,4.6 $K^- p$
1425 ± 8.0	225	[1,2] BARNHAM	71C	HBC	+	$K^+ p \to K^0 \pi^+ p$
1416 ±10	220	CRENNELL	69D	DBC	−	3.9 $K^- N \to \overline{K}^0 \pi^- N$
1414 ±13.0	60	[1] LIND	69	HBC	+	9 $K^+ p \to K^0 \pi^+ p$
1427 ±12	63	[1] SCHWEING...	68	HBC	−	5.5 $K^- p \to \overline{K} \pi N$
1423 ±11.0	39	[1] BASSANO	67	HBC	−	4.6–5.0 $K^- p \to \overline{K}^0 \pi^- p$
• • • We do not use the following data for averages, fits, limits, etc. • • •						
1428 ± 2	4300	[4] ABLIKIM	22L	BES3		2.0–3.08 $e^+ e^- \to K^+ K^- \pi^0$
1423.4 ± 2 ±3	25k	[5] BIRD	89	LASS	−	11 $K^- p \to \overline{K}^0 \pi^- p$

[1] Errors enlarged by us to $\Gamma/\sqrt{N}$; see the note with the $K^*(892)$ mass.
[2] Number of events in peak re-evaluated by us.
[3] Systematic error added by us.
[4] From a partial wave amplitude analysis at $\sqrt{s} = 2.125$ GeV which includes all the possible intermediate states that match J^{PC} conservation in the subsequent two-body decay. The intermediate states are parameterized with the relativistic Breit-Wigner functions. Statistical error only.
[5] From a partial wave amplitude analysis.

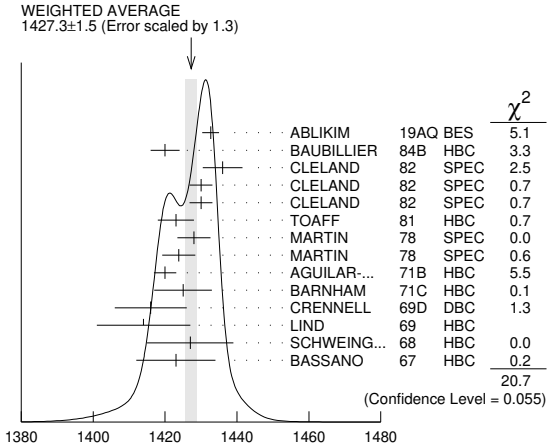

$K_2^*(1430)$ mass, combined neutral and charged (MeV)

NEUTRAL ONLY

VALUE (MeV)	EVTS	DOCUMENT ID		TECN	COMMENT
1432.4 ± 1.3 OUR AVERAGE					
1431.2 ± 1.8 ± 0.7		[1] ASTON	88	LASS	11 $K^- p \to K^- \pi^+ n$
1434 ± 4 ± 6		[1] ASTON	87	LASS	11 $K^- p \to \overline{K}^0 \pi^+ \pi^- n$
1433 ± 6 ±10		[1] ASTON	84B	LASS	11 $K^- p \to \overline{K}^0 2\pi n$
1471 ±12		[1] BAUBILLIER	82B	HBC	8.25 $K^- p \to N K^0_S \pi\pi$
1428 ± 3		[1] ASTON	81C	LASS	11 $K^- p \to K^- \pi^+ n$
1434 ± 2		[1] ESTABROOKS	78	ASPK	13 $K^\pm p \to p K \pi$
1440 ±10		[1] BOWLER	77	DBC	5.5 $K^+ d \to K \pi p p$
• • • We do not use the following data for averages, fits, limits, etc. • • •					
1428.5 ± 3.9	1786 ± 127	[2] AUBERT	07AK	BABR	10.6 $e^+ e^- \to K^{*0} K^\pm \pi^\mp \gamma$
1420 ± 7	300	HENDRICK	76	DBC	8.25 $K^+ N \to K^+ \pi N$
1421.6 ± 4.2	800	MCCUBBIN	75	HBC	3.6 $K^- p \to K^- \pi^+ n$
1420.1 ± 4.3		[3] LINGLIN	73	HBC	2–13 $K^+ p \to K^+ \pi^- X$
1419.1 ± 3.7	1800	AGUILAR-...	71B	HBC	3.9,4.6 $K^- p$
1416 ± 6	600	CORDS	71	DBC	9 $K^+ n \to K^+ \pi^- p$
1421.1 ± 2.6	2200	DAVIS	69	HBC	12 $K^+ p \to K^+ \pi^- X$

[1] From phase shift or partial-wave analysis.
[2] Systematic errors not estimated.
[3] From pole extrapolation, using world $K^+ p$ data summary tape.

$K_2^*(1430)$ WIDTH

CHARGED ONLY, WITH FINAL STATE $K\pi$

VALUE (MeV)	EVTS	DOCUMENT ID		TECN	CHG	COMMENT
100.0 ± 2.2 OUR FIT Error includes scale factor of 1.1.						
100.0 ± 2.2 OUR AVERAGE Error includes scale factor of 1.1.						
102.5 ± 1.6 $^{+3.1}_{-2.8}$	183k	ABLIKIM	19AQ	BES	±	$J/\psi \to K^+ K^- \pi^0$
109 ±22	400	[1,2] CLELAND	82	SPEC	+	30 $K^+ p \to K^0_S \pi^+ p$
124 ±12.8	1500	[1,2] CLELAND	82	SPEC	+	50 $K^+ p \to K^0_S \pi^+ p$
113 ±12.8	1200	[1,2] CLELAND	82	SPEC	−	50 $K^+ p \to K^0_S \pi^- p$
85 ±16	935	TOAFF	81	HBC	−	6.5 $K^- p \to \overline{K}^0 \pi^- p$
96.5 ± 3.8		MARTIN	78	SPEC	+	10 $K^\pm p \to K^0_S \pi p$
97.7 ± 4.0		MARTIN	78	SPEC	−	10 $K^\pm p \to K^0_S \pi p$
94.7 $^{+15.1}_{-12.5}$	1400	AGUILAR-...	71B	HBC	−	3.9,4.6 $K^- p$
• • • We do not use the following data for averages, fits, limits, etc. • • •						
107 ± 4	4300	[3] ABLIKIM	22L	BES3		2.0–3.08 $e^+ e^- \to K^+ K^- \pi^0$
98 ± 4 ±4	25k	[4] BIRD	89	LASS	−	11 $K^- p \to \overline{K}^0 \pi^- p$

[1] Errors enlarged by us to $4\Gamma/\sqrt{N}$; see the note with the $K^*(892)$ mass.
[2] Number of events in peak re-evaluated by us.
[3] From a partial wave amplitude analysis at $\sqrt{s} = 2.125$ GeV which includes all the possible intermediate states that match J^{PC} conservation in the subsequent two-body decay. The intermediate states are parameterized with the relativistic Breit-Wigner functions. Statistical error only.
[4] From a partial wave amplitude analysis.

NEUTRAL ONLY

VALUE (MeV)	EVTS	DOCUMENT ID		TECN	COMMENT
109 ± 5 OUR AVERAGE Error includes scale factor of 1.9. See the ideogram below.					
116.5 ± 3.6 ± 1.7		[1] ASTON	88	LASS	11 $K^- p \to K^- \pi^+ n$
129 ±15 ±15		[1] ASTON	87	LASS	11 $K^- p \to \overline{K}^0 \pi^+ \pi^- n$
131 ±24 ±20		[1] ASTON	84B	LASS	11 $K^- p \to \overline{K}^0 2\pi n$
143 ±34		[1] BAUBILLIER	82B	HBC	8.25 $K^- p \to N K^0_S \pi\pi$
98 ± 8		[1] ASTON	81C	LASS	11 $K^- p \to K^- \pi^+ n$
140 ±30		[1] ETKIN	80	SPEC	6 $K^- p \to \overline{K}^0 \pi^+ \pi^- n$
98 ± 5		[1] ESTABROOKS	78	ASPK	13 $K^\pm p \to p K \pi$
• • • We do not use the following data for averages, fits, limits, etc. • • •					
113.7 ± 9.2	1786 ± 127	[2] AUBERT	07AK	BABR	10.6 $e^+ e^- \to K^{*0} K^\pm \pi^\mp \gamma$
125 ±29	300	[3] HENDRICK	76	DBC	8.25 $K^+ N \to K^+ \pi N$
116 ±18	800	MCCUBBIN	75	HBC	3.6 $K^- p \to K^- \pi^+ n$
61 ±14		[4] LINGLIN	73	HBC	2–13 $K^+ p \to K^+ \pi^- X$
116.6 $^{+10.3}_{-15.5}$	1800	AGUILAR-...	71B	HBC	3.9,4.6 $K^- p$
144 ±24.0	600	[3] CORDS	71	DBC	9 $K^+ n \to K^+ \pi^- p$
101 ±10	2200	DAVIS	69	HBC	12 $K^+ p \to K^+ \pi^- \pi^+ p$

[1] From phase shift or partial-wave analysis.
[2] Systematic errors not estimated.
[3] Errors enlarged by us to $4\Gamma/\sqrt{N}$; see the note with the $K^*(892)$ mass.
[4] From pole extrapolation, using world $K^+ p$ data summary tape.

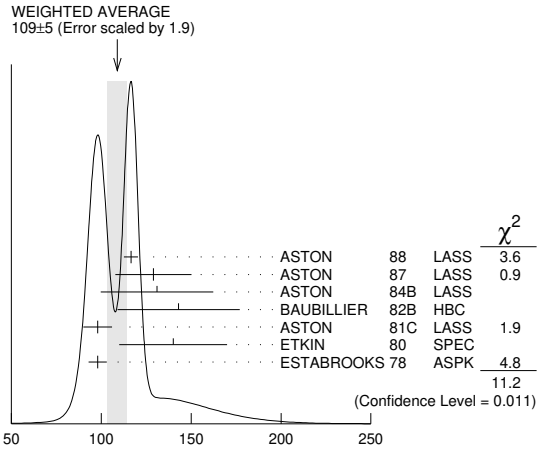

$K_2^*(1430)^0$ width (MeV)

$K_2^*(1430)$ DECAY MODES

	Mode	Fraction (Γ_i/Γ)	Scale factor/ Confidence level
Γ_1	$K\pi$	(49.9 ± 1.2) %	
Γ_2	$K^*(892)\pi$	(24.7 ± 1.5) %	
Γ_3	$K^*(892)\pi\pi$	(13.4 ± 2.2) %	
Γ_4	$K\rho$	(8.7 ± 0.8) %	S=1.2
Γ_5	$K\omega$	(2.9 ± 0.8) %	
Γ_6	$K^+\gamma$	(2.4 ± 0.5) $\times 10^{-3}$	S=1.1
Γ_7	$K\eta$	(1.5 $^{+3.4}_{-1.0}$) $\times 10^{-3}$	S=1.3
Γ_8	$K\omega\pi$	< 7.2 $\times 10^{-4}$	CL=95%
Γ_9	$K^0\gamma$	< 9 $\times 10^{-4}$	CL=90%

CONSTRAINED FIT INFORMATION

An overall fit to the total width, a partial width, and 10 branching ratios uses 32 measurements and one constraint to determine 8 parameters. The overall fit has a χ^2 = 21.1 for 25 degrees of freedom.

Int. J. Mod. Phys. A 2026.41. Downloaded from www.worldscientific.com
by UNIVERSITY OF CALIFORNIA @ BERKELEY on 09/16/26. Re-use and distribution is strictly not permitted, except for Open Access articles.

The following *off-diagonal* array elements are the correlation coefficients $\langle \delta p_i \delta p_j \rangle / (\delta p_i \cdot \delta p_j)$, in percent, from the fit to parameters p_i, including the branching fractions, $x_i \equiv \Gamma_i/\Gamma_{total}$. The fit constrains the x_i whose labels appear in this array to sum to one.

	x_1	x_2	x_3	x_4	x_5	x_6	x_7
x_2	−9						
x_3	−40	−73					
x_4	−8	36	−52				
x_5	−11	−3	−26	−7			
x_6	−1	−1	−1	−1	0		
x_7	−4	−7	−5	−5	−2	0	
Γ	0	0	0	0	0	−11	0

	Mode	Rate (MeV)	Scale factor
Γ_1	$K\pi$	49.9 ±1.6	
Γ_2	$K^*(892)\pi$	24.7 ±1.6	
Γ_3	$K^*(892)\pi\pi$	13.5 ±2.3	
Γ_4	$K\rho$	8.7 ±0.8	1.2
Γ_5	$K\omega$	2.9 ±0.8	
Γ_6	$K^+\gamma$	0.24±0.05	1.1
Γ_7	$K\eta$	$0.15^{+0.34}_{-0.10}$	1.3

$K_2^*(1430)$ PARTIAL WIDTHS

$\Gamma(K^+\gamma)$ — Γ_6

VALUE (keV)	DOCUMENT ID		TECN	CHG	COMMENT
240±50 OUR FIT	Error includes scale factor of 1.1.				
240±45	CIHANGIR	82	SPEC	+	200 $K^+ Z \to Z K^+ \pi^0$, $Z K^0_S \pi^+$

$\Gamma(K^0\gamma)$ — Γ_9

VALUE (keV)	CL%	DOCUMENT ID		TECN	CHG	COMMENT
< 5.4	90	ALAVI-HARATI	02B	KTEV		$K + A \to K^* + A$
• • • We do not use the following data for averages, fits, limits, etc. • • •						
<84	90	CARLSMITH	87	SPEC	0	60–200 $K^0_L A \to K^0_S \pi^0 A$

$K_2^*(1430)$ BRANCHING RATIOS

$\Gamma(K\pi)/\Gamma_{total}$ — Γ_1/Γ

VALUE	DOCUMENT ID		TECN	CHG	COMMENT
0.499±0.012 OUR FIT					
0.488±0.014 OUR AVERAGE					
0.485±0.006±0.020	[1] ASTON	88	LASS	0	11 $K^- p \to K^- \pi^+ n$
0.49 ±0.02	[1] ESTABROOKS	78	ASPK	±	13 $K^\pm p \to p K \pi$

[1] From phase shift analysis.

$\Gamma(K^*(892)\pi)/\Gamma(K\pi)$ — Γ_2/Γ_1

VALUE	DOCUMENT ID		TECN	CHG	COMMENT
0.496±0.034 OUR FIT					
0.47 ±0.04 OUR AVERAGE					
0.44 ±0.09	ASTON	84B	LASS	0	11 $K^- p \to \overline{K}^0 2\pi n$
0.62 ±0.19	LAUSCHER	75	HBC	0	10,16 $K^- p \to K^- \pi^+ n$
0.54 ±0.16	DEHM	74	DBC	0	4.6 $K^+ N$
0.47 ±0.08	AGUILAR-...	71B	HBC		3.9,4.6 $K^- p$
0.47 ±0.10	BASSANO	67	HBC	−0	4.6,5.0 $K^- p$
0.45 ±0.13	BADIER	65C	HBC	−	3 $K^- p$

$\Gamma(K\omega)/\Gamma(K\pi)$ — Γ_5/Γ_1

VALUE	DOCUMENT ID		TECN	CHG	COMMENT
0.059±0.017 OUR FIT					
0.070±0.035 OUR AVERAGE					
0.05 ±0.04	AGUILAR-...	71B	HBC		3.9,4.6 $K^- p$
0.13 ±0.07	BASSOMPIE...	69	HBC	0	5 $K^+ p$

$\Gamma(K\rho)/\Gamma(K\pi)$ — Γ_4/Γ_1

VALUE	DOCUMENT ID		TECN	CHG	COMMENT
0.174±0.017 OUR FIT	Error includes scale factor of 1.2.				
$0.150^{+0.029}_{-0.017}$ OUR AVERAGE					
0.18 ±0.05	ASTON	84B	LASS	0	11 $K^- p \to \overline{K}^0 2\pi n$
$0.02^{+0.10}_{-0.02}$	DEHM	74	DBC	0	4.6 $K^+ N$
0.16 ±0.05	AGUILAR-...	71B	HBC		3.9,4.6 $K^- p$
0.14 ±0.10	BASSANO	67	HBC	−0	4.6,5.0 $K^- p$
0.14 ±0.07	BADIER	65C	HBC	−	3 $K^- p$

$\Gamma(K\rho)/\Gamma(K^*(892)\pi)$ — Γ_4/Γ_2

VALUE	DOCUMENT ID		TECN	CHG	COMMENT
0.350±0.031 OUR FIT	Error includes scale factor of 1.4.				
0.354±0.033 OUR AVERAGE	Error includes scale factor of 1.4. See the ideogram below.				
0.293±0.032±0.020	ASTON	87	LASS	0	11 $K^- p \to \overline{K}^0 \pi^+ \pi^- n$
0.38 ±0.09	BAUBILLIER	82B	HBC	0	8.25 $K^- p \to N K^0_S \pi\pi$
0.39 ±0.03	DAUM	81C	CNTR		63 $K^- p \to K^- 2\pi p$

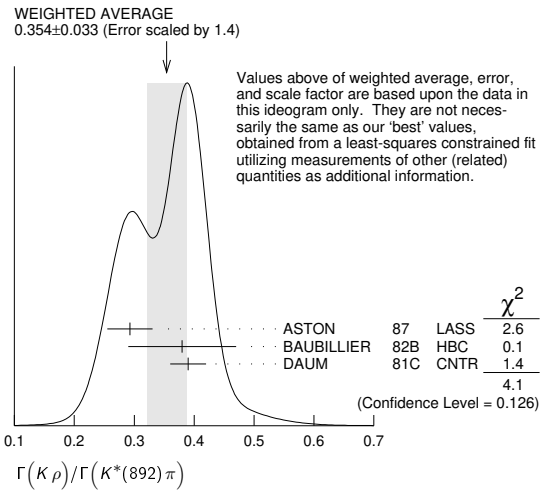

$\Gamma(K\omega)/\Gamma(K^*(892)\pi)$ — Γ_5/Γ_2

VALUE	DOCUMENT ID		TECN	CHG	COMMENT
0.118±0.034 OUR FIT					
0.10 ±0.04	FIELD	67	HBC	−	3.8 $K^- p$

$\Gamma(K\eta)/\Gamma(K^*(892)\pi)$ — Γ_7/Γ_2

VALUE	DOCUMENT ID		TECN	CHG	COMMENT
$0.006^{+0.014}_{-0.004}$ OUR FIT	Error includes scale factor of 1.2.				
0.07 ±0.04	FIELD	67	HBC	−	3.8 $K^- p$

$\Gamma(K\eta)/\Gamma(K\pi)$ — Γ_7/Γ_1

VALUE	CL%	DOCUMENT ID		TECN	CHG	COMMENT
$0.0030^{+0.0070}_{-0.0020}$ OUR FIT		Error includes scale factor of 1.3.				
0 ±0.0056		[1] ASTON	88B	LASS	−	11 $K^- p \to K^- \eta p$
• • • We do not use the following data for averages, fits, limits, etc. • • •						
<0.04	95	AGUILAR-...	71B	HBC		3.9,4.6 $K^- p$
<0.065		[2] BASSOMPIE...	69	HBC		5.0 $K^+ p$
<0.02		BISHOP	69	HBC		3.5 $K^+ p$

[1] ASTON 88B quote < 0.0092 at CL=95%. We convert this to a central value and 1 sigma error in order to be able to use it in our constrained fit.
[2] Restated by us.

$\Gamma(K^*(892)\pi\pi)/\Gamma_{total}$ — Γ_3/Γ

VALUE	DOCUMENT ID		TECN	CHG	COMMENT
0.134±0.022 OUR FIT					
0.12 ±0.04	[1] GOLDBERG	76	HBC	−	3 $K^- p \to p \overline{K}^0 \pi\pi\pi$

[1] Assuming $\pi\pi$ system has isospin 1, which is supported by the data.

$\Gamma(K^*(892)\pi\pi)/\Gamma(K\pi)$ — Γ_3/Γ_1

VALUE	DOCUMENT ID		TECN	CHG	COMMENT
0.27±0.05 OUR FIT					
0.21±0.08	[1,2] JONGEJANS	78	HBC	−	4 $K^- p \to p \overline{K}^0 \pi\pi\pi$

[1] Restated by us.
[2] Assuming $\pi\pi$ system has isospin 1, which is supported by the data.

$\Gamma(K\omega\pi)/\Gamma_{total}$ — Γ_8/Γ

VALUE (units 10^{-3})	CL%	EVTS	DOCUMENT ID		TECN	COMMENT
<0.72	95	0	JONGEJANS	78	HBC	4 $K^- p \to p \overline{K}^0 4\pi$

$K_2^*(1430)$ REFERENCES

ABLIKIM 22L JHEP 2207 045 M. Ablikim et al. (BESIII Collab.)
ABLIKIM 19AQ PR D100 032004 M. Ablikim et al. (BESIII Collab.)
PELAEZ 17 EPJ C77 91 J.R. Pelaez, A.Rodas, J.R. de Elvira
AUBERT 07AK PR D76 012008 B. Aubert et al. (BABAR Collab.)
ALAVI-HARATI 02B PRL 89 072001 A. Alavi-Harati et al. (FNAL KTeV Collab.)
BIRD 89 SLAC-332 P.F. Bird (SLAC)
ASTON 88 NP B296 493 D. Aston et al. (SLAC, NAGO, CINC, INUS)
ASTON 88B PL B201 169 D. Aston et al. (SLAC, NAGO, CINC, INUS)
ASTON 87 NP B292 693 D. Aston et al. (SLAC, NAGO, CINC, INUS)
CARLSMITH 87 PR D36 3502 D. Carlsmith et al. (EFI, SACL)
ASTON 84B NP B247 261 D. Aston et al. (SLAC, CARL, OTTA)
BAUBILLIER 84B ZPHY C26 37 M. Baubillier et al. (BIRM, CERN, GLAS+)
BAUBILLIER 82B NP B202 21 M. Baubillier et al. (BIRM, CERN, GLAS+)
CIHANGIR 82 PL 117B 123 S. Cihangir et al. (FNAL, MINN, ROCH)

Int. J. Mod. Phys. A 2026.41. Downloaded from www.worldscientific.com
by [redacted]LIFORNIA @ BERKELEY on 09/16/26. Re-use and distribution is strictly not permitted, except for Open Access articles.

CLELAND	82	NP B208 189	W.E. Cleland *et al.*	(DURH, GEVA, LAUS+)
ASTON	81C	PL 106B 235	D. Aston *et al.*	(SLAC, CARL, OTTA) JP
DAUM	81C	NP B187 1	C. Daum *et al.*	(AMST, CERN, CRAC, MPIM+)
TOAFF	81	PR D23 1500	S. Toaff *et al.*	(ANL, KANS)
ETKIN	80	PR D22 42	A. Etkin *et al.*	(BNL, CUNY) JP
ESTABROOKS	78	NP B133 490	P.G. Estabrooks *et al.*	(MCGI, CARL, DURH+)
Also		PR D17 658	P.G. Estabrooks *et al.*	(MCGI, CARL, DURH+)
JONGEJANS	78	NP B139 383	B. Jongejans *et al.*	(ZEEM, CERN, NIJM+)
MARTIN	78	NP B134 392	A.D. Martin *et al.*	(DURH, GEVA)
BOWLER	77	NP B126 31	M.G. Bowler *et al.*	(OXF)
GOLDBERG	76	LNC 17 253	J. Goldberg	(HAIF)
HENDRICK	76	NP B112 189	K. Hendrickx *et al.*	(MONS, SACL, PARIS+)
LAUSCHER	75	NP B86 189	P. Lauscher *et al.*	(ABCLV Collab.) JP
MCCUBBIN	75	NP B86 13	N.A. McCubbin, L. Lyons	(OXF)
DEHM	74	NP B75 47	G. Dehm *et al.*	(MPIM, BRUX, MONS, CERN)
LINGLIN	73	NP B55 408	D. Linglin	(CERN)
AGUILAR-...	71B	PR D4 2583	M. Aguilar-Benitez, R.L. Eisner, J.B. Kinson	(BNL)
BARNHAM	71C	NP B28 171	K.W.J. Barnham *et al.*	(BIRM, GLAS)
CORDS	71	PR D4 1974	D. Cords *et al.*	(PURD, UCD, IUPU)
BASSOMPIE...	69	NP B13 189	G. Bassompierre *et al.*	(CERN, BRUX) JP
BISHOP	69	NP B9 403	J.M. Bishop *et al.*	(WISC)
CRENNELL	69D	PRL 22 487	D.J. Crennell *et al.*	(BNL)
DAVIS	69	PRL 23 1071	P.J. Davis *et al.*	(LRL)
LIND	69	NP B14 1	V.G. Lind *et al.*	(LRL) JP
SCHWEING...	68	PR 166 1317	F. Schweingruber *et al.*	(ANL, NWES)
Also		Thesis	F.L. Schweingruber	(NWES, NWES)
BASSANO	67	PRL 19 968	D. Bassano *et al.*	(BNL, SYRA)
FIELD	67	PL 24B 638	J.H. Field *et al.*	(UCSD)
BADIER	65C	PL 19 612	J. Badier *et al.*	(EPOL, SACL, AMST)

$K(1460)$

$I(J^P) = \frac{1}{2}(0^-)$

Observed in $K\pi\pi$ partial-wave analysis.

$K(1460)$ MASS

VALUE (MeV)	EVTS	DOCUMENT ID		TECN	CHG	COMMENT
• • • We do not use the following data for averages, fits, limits, etc. • • •						
$1482.40 \pm 3.58 \pm 15.22$	894k	AAIJ	18AI	LHCB		$D^0 \to K^\mp 2\pi^\pm \pi^\mp$
~ 1460	63	DAUM	81C	CNTR	−	$K^- p \to K^- 2\pi p$
~ 1400	13	[1] BRANDENB...	76B	ASPK	±	$K^\pm p \to K^+ 2\pi p$

[1] Coupled mainly to $K f_0(1370)$. Decay into $K^*(892)\pi$ seen.

$K(1460)$ WIDTH

VALUE (MeV)	EVTS	DOCUMENT ID		TECN	CHG	COMMENT
• • • We do not use the following data for averages, fits, limits, etc. • • •						
$335.60 \pm 6.20 \pm 8.65$	894k	AAIJ	18AI	LHCB		$D^0 \to K^\mp 2\pi^\pm \pi^\mp$
~ 260	63	DAUM	81C	CNTR	−	$K^- p \to K^- 2\pi p$
~ 250	15	[1] BRANDENB...	76B	ASPK	±	$K^\pm p \to K^+ 2\pi p$

[1] Coupled mainly to $K f_0(1370)$. Decay into $K^*(892)\pi$ seen.

$K(1460)$ DECAY MODES

	Mode	Fraction (Γ_i/Γ)
Γ_1	$K^*(892)\pi$	seen
Γ_2	$K\rho$	seen
Γ_3	$K_0^*(1430)\pi$	seen
Γ_4	$K\phi$	seen

$K(1460)$ PARTIAL WIDTHS

$\Gamma(K^*(892)\pi)$ — Γ_1

VALUE (MeV)	DOCUMENT ID		TECN	COMMENT
• • • We do not use the following data for averages, fits, limits, etc. • • •				
~ 109	DAUM	81C	CNTR	63 $K^- p \to K^- 2\pi p$

$\Gamma(K\rho)$ — Γ_2

VALUE (MeV)	DOCUMENT ID		TECN	COMMENT
• • • We do not use the following data for averages, fits, limits, etc. • • •				
~ 34	DAUM	81C	CNTR	63 $K^- p \to K^- 2\pi p$

$\Gamma(K_0^*(1430)\pi)$ — Γ_3

VALUE (MeV)	DOCUMENT ID		TECN	COMMENT
• • • We do not use the following data for averages, fits, limits, etc. • • •				
~ 117	DAUM	81C	CNTR	63 $K^- p \to K^- 2\pi p$

$\Gamma(K\phi)/\Gamma_{total}$ — Γ_4/Γ

VALUE	EVTS	DOCUMENT ID		TECN	COMMENT
seen	24k	[1] AAIJ	21E	LHCB	$B^+ \to J/\psi\phi K^+$

[1] From an amplitude analysis of the decay $B^+ \to J/\psi\phi K^+$ with a significance of 12 σ.

$K(1460)$ REFERENCES

AAIJ	21E	PRL 127 082001	R. Aaij *et al.*	(LHCb Collab.)
AAIJ	18AI	EPJ C78 443	R. Aaij *et al.*	(LHCb Collab.)
DAUM	81C	NP B187 1	C. Daum *et al.*	(AMST, CERN, CRAC, MPIM+)
BRANDENB...	76B	PRL 36 1239	G.W. Brandenburg *et al.*	(SLAC) JP

$K_2(1580)$

$I(J^P) = \frac{1}{2}(2^-)$

OMITTED FROM SUMMARY TABLE

Seen in partial-wave analysis of the $K^-\pi^+\pi^-$ system. Needs confirmation.

$K_2(1580)$ MASS

VALUE (MeV)	DOCUMENT ID		CHG	COMMENT
• • • We do not use the following data for averages, fits, limits, etc. • • •				
~ 1580	OTTER	79	−	10,14,16 $K^- p$

$K_2(1580)$ WIDTH

VALUE (MeV)	DOCUMENT ID		CHG	COMMENT
• • • We do not use the following data for averages, fits, limits, etc. • • •				
~ 110	OTTER	79	−	10,14,16 $K^- p$

$K_2(1580)$ DECAY MODES

	Mode	Fraction (Γ_i/Γ)
Γ_1	$K^*(892)\pi$	seen
Γ_2	$K_2^*(1430)\pi$	possibly seen

$K_2(1580)$ BRANCHING RATIOS

$\Gamma(K^*(892)\pi)/\Gamma_{total}$ — Γ_1/Γ

VALUE	DOCUMENT ID		TECN	CHG	COMMENT
seen	OTTER	79	HBC	−	10,14,16 $K^- p$
• • • We do not use the following data for averages, fits, limits, etc. • • •					
possibly seen	GULER	11	BELL		$B^+ \to J/\psi K^+ \pi^+ \pi^-$

$\Gamma(K_2^*(1430)\pi)/\Gamma_{total}$ — Γ_2/Γ

VALUE	DOCUMENT ID		TECN	CHG	COMMENT
possibly seen	OTTER	79	HBC	−	10,14,16 $K^- p$

$K_2(1580)$ REFERENCES

GULER	11	PR D83 032005	H. Guler *et al.*	(BELLE Collab.)
OTTER	79	NP B147 1	G. Otter *et al.*	(AACH3, BERL, CERN, LOIC+) JP

$K(1630)$

$I(J^P) = \frac{1}{2}(?^?)$

OMITTED FROM SUMMARY TABLE

Seen as a narrow peak, compatible with the experimental resolution, in the invariant mass of the $K_S^0\pi^+\pi^-$ system produced in $\pi^- p$ interactions at high momentum transfers.

$K(1630)$ MASS

VALUE (MeV)	EVTS	DOCUMENT ID	TECN	COMMENT
1629±7	~ 75	KARNAUKHOV98	BC	16.0 $\pi^- p \to (K_S^0\pi^+\pi^-) X^+\pi^- X^0$

$K(1630)$ WIDTH

VALUE (MeV)	EVTS	DOCUMENT ID	TECN	COMMENT
$\mathbf{16^{+19}_{-16}}$	~ 75	[1] KARNAUKHOV98	BC	16.0 $\pi^- p \to (K_S^0\pi^+\pi^-) X^+\pi^- X^0$

[1] Compatible with an experimental resolution of 14 ± 1 MeV.

$K(1630)$ DECAY MODES

	Mode
Γ_1	$K_S^0\pi^+\pi^-$

$K(1630)$ REFERENCES

KARNAUKHOV 98 PAN 61 203 V.M. Karnaukhov, C. Coca, V.I. Moroz
Translated from YAF 61 252.

Int. J. Mod. Phys. A 2026.41. Downloaded from www.worldscientific.com
by UNIVERSITY OF CALIFORNIA @ BERKELEY on 09/16/26. Re-use and distribution is strictly not permitted, except for Open Access articles.

Int. J. Mod. Phys. A 2026.41. Downloaded from www.worldscientific.com by [redacted] LIFORNIA @ BERKELEY on 09/16/26. Re-use and distribution is strictly not permitted, except for Open Access articles.

$K_1(1650)$

$I(J^P) = \frac{1}{2}(1^+)$

This entry contains various peaks in strange meson systems ($K^+\phi$, $K\pi\pi$) reported in partial-wave analysis in the 1600–1900 mass region.

$K_1(1650)$ MASS

VALUE (MeV)	EVTS	DOCUMENT ID		TECN	CHG	COMMENT
1650±50		FRAME	86	OMEG	+	13 $K^+p \to \phi K^+p$
• • • We do not use the following data for averages, fits, limits, etc. • • •						
$1861\pm10^{+16}_{-46}$	24k	[1] AAIJ	21E	LHCB		$B^+ \to J/\psi\phi K^+$
$1911\pm37^{+124}_{-48}$	24k	[1] AAIJ	21E	LHCB		$B^+ \to J/\psi\phi K^+$
$1793\pm59^{+153}_{-101}$	4289	[2,3] AAIJ	17C	LHCB		$B^+ \to J/\psi\phi K^+$
~ 1840		ARMSTRONG	83	OMEG	−	18.5 $K^-p \to 3Kp$
~ 1800		DAUM	81C	CNTR	−	63 $K^-p \to K^-2\pi p$

[1] One of two K_1 states reported by AAIJ 21E. From an amplitude analysis of the decay $B^+ \to J/\psi\phi K^+$ with a significance of 4.5 σ.
[2] From an amplitude analysis of the decay $B^+ \to J/\psi\phi K^+$ with a significance of 7.6 σ.
[3] Superseded by AAIJ 21E.

$K_1(1650)$ WIDTH

VALUE (MeV)	EVTS	DOCUMENT ID		TECN	CHG	COMMENT
150± 50		FRAME	86	OMEG	+	13 $K^+p \to \phi K^+p$
• • • We do not use the following data for averages, fits, limits, etc. • • •						
$149\pm41^{+231}_{-23}$	24k	[1] AAIJ	21E	LHCB		$B^+ \to J/\psi\phi K^+$
$276\pm50^{+319}_{-159}$	24k	[1] AAIJ	21E	LHCB		$B^+ \to J/\psi\phi K^+$
$365\pm157^{+138}_{-215}$	4289	[2,3] AAIJ	17C	LHCB		$B^+ \to J/\psi\phi K^+$
~ 250		DAUM	81C	CNTR	−	63 $K^-p \to K^-2\pi p$

[1] One of two K_1 states reported by AAIJ 21E. From an amplitude analysis of the decay $B^+ \to J/\psi\phi K^+$ with a significance of 4.5 σ.
[2] From an amplitude analysis of the decay $B^+ \to J/\psi\phi K^+$ with a significance of 7.6 σ.
[3] Superseded by AAIJ 21E.

$K_1(1650)$ DECAY MODES

	Mode
Γ_1	$K\pi\pi$
Γ_2	$K\phi$

$K_1(1650)$ REFERENCES

AAIJ	21E	PRL 127 082001	R. Aaij *et al.*	(LHCb Collab.)
AAIJ	17C	PRL 118 022003	R. Aaij *et al.*	(LHCb Collab.)
Also		PR D95 012002	R. Aaij *et al.*	(LHCb Collab.)
FRAME	86	NP B276 667	D. Frame *et al.*	(GLAS)
ARMSTRONG	83	NP B221 1	T.A. Armstrong *et al.*	(BARI, BIRM, CERN+)
DAUM	81C	NP B187 1	C. Daum *et al.*	(AMST, CERN, CRAC, MPIM+)

$K^*(1680)$

$I(J^P) = \frac{1}{2}(1^-)$

$K^*(1680)$ MASS

VALUE (MeV)	EVTS	DOCUMENT ID		TECN	CHG	COMMENT
1718±18 OUR AVERAGE						
$1722\pm20^{+33}_{-109}$	4289	[1] AAIJ	17C	LHCB		$B^+ \to J/\psi\phi K^+$
1677±10± 32		ASTON	88	LASS	0	11 $K^-p \to K^-\pi^+n$
1735±10± 20		ASTON	87	LASS	0	11 $K^-p \to \overline{K}^0\pi^+\pi^-n$
• • • We do not use the following data for averages, fits, limits, etc. • • •						
1678±64		BIRD	89	LASS	−	11 $K^-p \to \overline{K}^0\pi^-p$
1800±70		ETKIN	80	MPS	0	6 $K^-p \to \overline{K}^0\pi^+\pi^-n$
~ 1650		ESTABROOKS	78	ASPK	0	13 $K^\pm p \to K^\pm\pi^\pm n$

[1] From an amplitude analysis of the decay $B^+ \to J/\psi\phi K^+$ with a significance of 8.5 σ.

$K^*(1680)$ WIDTH

VALUE (MeV)	EVTS	DOCUMENT ID		TECN	CHG	COMMENT
320±110 OUR AVERAGE	Error includes scale factor of 4.2.					
$354\pm75^{+140}_{-181}$	4289	[2] AAIJ	17C	LHCB		$B^+ \to J/\psi\phi K^+$
205± 16± 34		ASTON	88	LASS	0	11 $K^-p \to K^-\pi^+n$
423± 18± 30		ASTON	87	LASS	0	11 $K^-p \to \overline{K}^0\pi^+\pi^-n$
• • • We do not use the following data for averages, fits, limits, etc. • • •						
454±270		BIRD	89	LASS	−	11 $K^-p \to \overline{K}^0\pi^-p$
170± 30		ETKIN	80	MPS	0	6 $K^-p \to \overline{K}^0\pi^+\pi^-n$
250 to 300		ESTABROOKS	78	ASPK	0	13 $K^\pm p \to K^\pm\pi^\pm n$

[2] From an amplitude analysis of the decay $B^+ \to J/\psi\phi K^+$ with a significance of 8.5 σ.

$K^*(1680)$ DECAY MODES

	Mode	Fraction (Γ_i/Γ)
Γ_1	$K\pi$	(38.7±2.5) %
Γ_2	$K\rho$	$(31.4^{+5.0}_{-2.1})$ %
Γ_3	$K^*(892)\pi$	$(29.9^{+2.2}_{-5.0})$ %
Γ_4	$K\phi$	seen
Γ_5	$K\eta$	$(1.4^{+1.0}_{-0.8})$ %

CONSTRAINED FIT INFORMATION

An overall fit to 4 branching ratios uses 4 measurements and one constraint to determine 3 parameters. The overall fit has a χ^2 = 2.9 for 2 degrees of freedom.

The following *off-diagonal* array elements are the correlation coefficients $\langle \delta x_i \delta x_j \rangle / (\delta x_i \cdot \delta x_j)$, in percent, from the fit to the branching fractions, $x_i \equiv \Gamma_i/\Gamma_{total}$. The fit constrains the x_i whose labels appear in this array to sum to one.

	x_1	x_2
x_2	−36	
x_3	−39	−72

$K^*(1680)$ BRANCHING RATIOS

$\Gamma(K\pi)/\Gamma_{total}$ — Γ_1/Γ

VALUE	DOCUMENT ID		TECN	CHG	COMMENT
0.387±0.026 OUR FIT					
0.388±0.014±0.022	ASTON	88	LASS	0	11 $K^-p \to K^-\pi^+n$

$\Gamma(K\pi)/\Gamma(K^*(892)\pi)$ — Γ_1/Γ_3

VALUE	DOCUMENT ID		TECN	CHG	COMMENT
$\mathbf{1.30^{+0.23}_{-0.14}}$ **OUR FIT**					
2.8 ±1.1	ASTON	84	LASS	0	11 $K^-p \to \overline{K}^0 2\pi n$

$\Gamma(K\rho)/\Gamma(K\pi)$ — Γ_2/Γ_1

VALUE	DOCUMENT ID		TECN	CHG	COMMENT
$\mathbf{0.81^{+0.14}_{-0.09}}$ **OUR FIT**					
1.2 ±0.4	ASTON	84	LASS	0	11 $K^-p \to \overline{K}^0 2\pi n$

$\Gamma(K\rho)/\Gamma(K^*(892)\pi)$ — Γ_2/Γ_3

VALUE	DOCUMENT ID		TECN	CHG	COMMENT
$\mathbf{1.05^{+0.27}_{-0.11}}$ **OUR FIT**					
$\mathbf{0.97\pm0.09^{+0.30}_{-0.10}}$	ASTON	87	LASS	0	11 $K^-p \to \overline{K}^0\pi^+\pi^-n$

$\Gamma(K\phi)/\Gamma_{total}$ — Γ_4/Γ

VALUE	EVTS	DOCUMENT ID		TECN	COMMENT
seen	24k	[3] AAIJ	21E	LHCB	$B^+ \to J/\psi\phi K^+$
• • • We do not use the following data for averages, fits, limits, etc. • • •					
seen	4289	[4,5] AAIJ	17C	LHCB	$B^+ \to J/\psi\phi K^+$

[3] From an amplitude analysis of the decay $B^+ \to J/\psi\phi K^+$ with a significance of 4.7 σ.
[4] From an amplitude analysis of the decay $B^+ \to J/\psi\phi K^+$ with a significance of 8.5 σ.
[5] Superseded by AAIJ 21E.

$\Gamma(K\eta)/\Gamma(K\pi)$ — Γ_5/Γ_1

VALUE	EVTS	DOCUMENT ID		TECN	COMMENT
$\mathbf{0.037\pm0.007^{+0.024}_{-0.018}}$	116k	[6] CHEN	20A	BELL	$D^0 \to K^-\pi^+\eta$

[6] CHEN 20A quotes the ratio $\Gamma(K^*(1680)^- \to K^-\eta)/\Gamma(K^*(1680)^- \to K^-\pi^0)$ $=0.11 \pm 0.02^{+0.06}_{-0.04} \pm 0.04(B_{PDG})$ where the last uncertainty comes from $B(\eta \to \gamma\gamma) = (39.41 \pm 0.20)$%. We divide it by 3 taking into account that $\Gamma(K^*(1680)^- \to K^-\pi^0)/\Gamma(K^*(1680)^- \to (K\pi)^-) = 1/3$.

$\Gamma(K\eta)/\Gamma_{total}$ — Γ_5/Γ

VALUE (units 10^{-2})	EVTS	DOCUMENT ID		TECN	COMMENT
• • • We do not use the following data for averages, fits, limits, etc. • • •					
$1.44\pm0.21^{+0.96}_{-0.73}$	116k	[7] CHEN	20A	BELL	$D^0 \to K^-\pi^+\eta$

[7] From an amplitude analysis of the decay $D^0 \to K^-\pi^+\eta$ with a significance of 16 σ. Not independent of the CHEN 20A measurement of $\Gamma(K^*(1680) \to K\eta)/\Gamma(K^*(1680) \to K\pi)$.

$K^*(1680)$ REFERENCES

AAIJ	21E	PRL 127 082001	R. Aaij *et al.*	(LHCb Collab.)
CHEN	20A	PR D102 012002	Y.Q. Chen *et al.*	(BELLE Collab.)
AAIJ	17C	PRL 118 022003	R. Aaij *et al.*	(LHCb Collab.)
Also		PR D95 012002	R. Aaij *et al.*	(LHCb Collab.)
BIRD	89	SLAC-332	P.F. Bird	(SLAC)
ASTON	88	NP B296 493	D. Aston *et al.*	(SLAC, NAGO, CINC, INUS)
ASTON	87	NP B292 693	D. Aston *et al.*	(SLAC, NAGO, CINC, INUS)
ASTON	84	PL 149B 258	D. Aston *et al.*	(SLAC, CARL, OTTA) JP
ETKIN	80	PR D22 42	A. Etkin *et al.*	(BNL, CUNY) JP
ESTABROOKS	78	NP B133 490	P.G. Estabrooks *et al.*	(MCGI, CARL, DURH+) JP

$K_2(1770)$

$I(J^P) = \frac{1}{2}(2^-)$

See our mini-review in the 2004 edition of this *Review*, PDG 04.

$K_2(1770)$ MASS

VALUE (MeV)	EVTS	DOCUMENT ID		TECN	CHG	COMMENT
1773± 8 OUR AVERAGE						
$1777\pm35^{+122}_{-77}$	4289	[1] AAIJ	17C	LHCB		$B^+ \to J/\psi\phi K^+$
1773± 8		[2] ASTON	93	LASS		$11 K^-p \to K^-\omega p$
• • • We do not use the following data for averages, fits, limits, etc. • • •						
1743±15		TIKHOMIROV	03	SPEC		$40.0\ \pi^-C \to K^0_S K^0_S K^0_L X$
1810±20		FRAME	86	OMEG	+	$13 K^+p \to \phi K^+p$
~ 1730		ARMSTRONG	83	OMEG	−	$18.5 K^-p \to 3Kp$
~ 1780		[3] DAUM	81C	CNTR	−	$63 K^-p \to K^-2\pi p$
1710±15	60	CHUNG	74	HBC	−	$7.3 K^-p \to K^-\omega p$
1767± 6		BLIEDEN	72	MMS	−	11–$16 K^-p$
1730±20	306	[4] FIRESTONE	72B	DBC	+	$12 K^+d$
1765±40		[5] COLLEY	71	HBC	+	$10 K^+p \to K2\pi N$
1740		DENEGRI	71	DBC	−	$12.6 K^-d \to \overline{K}2\pi d$
1745±20		AGUILAR-...	70C	HBC	−	$4.6 K^-p$
1780±15		BARTSCH	70C	HBC	−	$10.1 K^-p$
1760±15		LUDLAM	70	HBC	−	$12.6 K^-p$

[1] From an amplitude analysis of the decay $B^+ \to J/\psi\phi K^+$ with a significance of 5.0 σ.
[2] From a partial wave analysis of the $K^-\omega$ system.
[3] From a partial wave analysis of the $K^-2\pi$ system.
[4] Produced in conjunction with excited deuteron.
[5] Systematic errors added correspond to spread of different fits.

$K_2(1770)$ WIDTH

VALUE (MeV)	EVTS	DOCUMENT ID		TECN	CHG	COMMENT
186± 14 OUR AVERAGE						
$217\pm116^{+221}_{-154}$	4289	[6] AAIJ	17C	LHCB		$B^+ \to J/\psi\phi K^+$
186± 14		[7] ASTON	93	LASS		$11 K^-p \to K^-\omega p$
• • • We do not use the following data for averages, fits, limits, etc. • • •						
147± 70		TIKHOMIROV	03	SPEC		$40.0\ \pi^-C \to K^0_S K^0_S K^0_L X$
140± 40		FRAME	86	OMEG	+	$13 K^+p \to \phi K^+p$
~ 220		ARMSTRONG	83	OMEG	−	$18.5 K^-p \to 3Kp$
~ 210		[8] DAUM	81C	CNTR	−	$63 K^-p \to K^-2\pi p$
110± 50	60	CHUNG	74	HBC	−	$7.3 K^-p \to K^-\omega p$
100± 26		BLIEDEN	72	MMS	−	11–$16 K^-p$
210± 30	306	[9] FIRESTONE	72B	DBC	+	$12 K^+d$
90± 70		[10] COLLEY	71	HBC	+	$10 K^+p \to K2\pi N$
130		DENEGRI	71	DBC	−	$12.6 K^-d \to \overline{K}2\pi d$
100± 50		AGUILAR-...	70C	HBC	−	$4.6 K^-p$
138± 40		BARTSCH	70C	HBC	−	$10.1 K^-p$
50^{+40}_{-20}		LUDLAM	70	HBC	−	$12.6 K^-p$

[6] From an amplitude analysis of the decay $B^+ \to J/\psi\phi K^+$ with a significance of 5.0 σ.
[7] From a partial wave analysis of the $K^-\omega$ system.
[8] From a partial wave analysis of the $K^-2\pi$ system.
[9] Produced in conjunction with excited deuteron.
[10] Systematic errors added correspond to spread of different fits.

$K_2(1770)$ DECAY MODES

	Mode	Fraction (Γ_i/Γ)
Γ_1	$K\pi\pi$	
Γ_2	$K_2^*(1430)\pi$	seen
Γ_3	$K^*(892)\pi$	seen
Γ_4	$Kf_2(1270)$	seen
Γ_5	$Kf_0(980)$	possibly seen
Γ_6	$K\phi$	seen
Γ_7	$K\omega$	seen

$K_2(1770)$ BRANCHING RATIOS

$\Gamma(K_2^*(1430)\pi)/\Gamma(K\pi\pi)$ — Γ_2/Γ_1

($K_2^*(1430) \to K\pi$)

VALUE	DOCUMENT ID		TECN	CHG	COMMENT
• • • We do not use the following data for averages, fits, limits, etc. • • •					
~ 0.03	DAUM	81C	CNTR		$63 K^-p \to K^-2\pi p$
~ 1.0	[11] FIRESTONE	72B	DBC	+	$12 K^+d$
<1.0	COLLEY	71	HBC		$10 K^+p$
0.2 ±0.2	AGUILAR-...	70C	HBC	−	$4.6 K^-p$
<1.0	BARTSCH	70C	HBC	−	$10.1 K^-p$
1.0	BARBARO-...	69	HBC	+	$12.0 K^+p$

[11] Produced in conjunction with excited deuteron.

$\Gamma(K^*(892)\pi)/\Gamma(K\pi\pi)$ — Γ_3/Γ_1

VALUE	DOCUMENT ID		TECN	COMMENT
• • • We do not use the following data for averages, fits, limits, etc. • • •				
~ 0.23	DAUM	81C	CNTR	$63 K^-p \to K^-2\pi p$

$\Gamma(Kf_2(1270))/\Gamma(K\pi\pi)$ — Γ_4/Γ_1

($f_2(1270) \to \pi\pi$)

VALUE	DOCUMENT ID		TECN	COMMENT
• • • We do not use the following data for averages, fits, limits, etc. • • •				
~ 0.74	DAUM	81C	CNTR	$63 K^-p \to K^-2\pi p$

$\Gamma(Kf_0(980))/\Gamma_{total}$ — Γ_5/Γ

VALUE	DOCUMENT ID		TECN	COMMENT
• • • We do not use the following data for averages, fits, limits, etc. • • •				
possibly seen	TIKHOMIROV	03	SPEC	$40.0\ \pi^-C \to K^0_S K^0_S K^0_L X$

$\Gamma(K\phi)/\Gamma_{total}$ — Γ_6/Γ

VALUE	EVTS	DOCUMENT ID		TECN	CHG	COMMENT
seen	24k	[12] AAIJ	21E	LHCB		$B^+ \to J/\psi\phi K^+$
seen		ARMSTRONG	83	OMEG	−	$18.5 K^-p \to K^-\phi N$
• • • We do not use the following data for averages, fits, limits, etc. • • •						
seen	4289	[13,14] AAIJ	17C	LHCB		$B^+ \to J/\psi\phi K^+$

[12] From an amplitude analysis of the decay $B^+ \to J/\psi\phi K^+$ with a significance of 7.9 σ.
[13] From an amplitude analysis of the decay $B^+ \to J/\psi\phi K^+$ with a significance of 5.0 σ.
[14] Superseded by AAIJ 21E.

$\Gamma(K\omega)/\Gamma_{total}$ — Γ_7/Γ

VALUE	DOCUMENT ID		TECN	CHG	COMMENT
seen	OTTER	81	HBC	±	$8.25,10,16 K^\pm p$
seen	CHUNG	74	HBC	−	$7.3 K^-p \to K^-\omega p$

$K_2(1770)$ REFERENCES

AAIJ	21E	PRL 127 082001	R. Aaij *et al.*	(LHCb Collab.)
AAIJ	17C	PRL 118 022003	R. Aaij *et al.*	(LHCb Collab.)
Also		PR D95 012002	R. Aaij *et al.*	(LHCb Collab.)
PDG	04	PL B592 1	S. Eidelman *et al.*	(PDG Collab.)
TIKHOMIROV	03	PAN 66 828	G.D. Tikhomirov *et al.*	
		Translated from YAF 66 860.		
ASTON	93	PL B308 186	D. Aston *et al.*	(SLAC, NAGO, CINC, INUS)
FRAME	86	NP B276 667	D. Frame *et al.*	(GLAS)
ARMSTRONG	83	NP B221 1	T.A. Armstrong *et al.*	(BARI, BIRM, CERN+)
DAUM	81C	NP B187 1	C. Daum *et al.*	(AMST, CERN, CRAC, MPIM+)
OTTER	81	NP B181 1	G. Otter	(AACH3, BERL, LOIC, VIEN, BIRM+)
CHUNG	74	PL 51B 413	S.U. Chung *et al.*	(BNL)
BLIEDEN	72	PL 39B 668	H.R. Blieden *et al.*	(STON, NEAS)
FIRESTONE	72B	PR D5 505	A. Firestone *et al.*	(LBL)
COLLEY	71	NP B26 71	D.C. Colley *et al.*	(BIRM, GLAS)
DENEGRI	71	NP B28 13	D. Denegri *et al.*	(JHU) JP
AGUILAR-...	70C	PRL 25 54	M. Aguilar-Benitez *et al.*	(BNL)
BARTSCH	70C	PL 33B 186	J. Bartsch *et al.*	(AACH, BERL, CERN+)
LUDLAM	70	PR D2 1234	T. Ludlam, J. Sandweiss, A.J. Slaughter	(YALE)
BARBARO-...	69	PRL 22 1207	A. Barbaro-Galtieri *et al.*	(LRL)

$K_3^*(1780)$

$I(J^P) = \frac{1}{2}(3^-)$

$K_3^*(1780)$ T-MATRIX POLE $\sqrt{s}$

Note that $\Gamma = -2\,\mathrm{Im}(\sqrt{s})$.

VALUE (MeV)	DOCUMENT ID		TECN	COMMENT
(1754 ± 13) − i (119 ± 14) OUR EVALUATION				
(1754 ± 13) − i (119 ± 14)	[1] PELAEZ	17	RVUE	$\pi K \to \pi K$

[1] Reanalysis of ESTABROOKS 78 and ASTON 88 satisfying Forward Dispersion Relations and using sequences of Pade approximants.

$K_3^*(1780)$ MASS

VALUE (MeV)	EVTS	DOCUMENT ID		TECN	CHG	COMMENT
1779± 8 OUR AVERAGE		Error includes scale factor of 1.2.				
$1813\pm15^{+65}_{-16}$	18k	[1] ABLIKIM	20F	BES3		$\psi(2S) \to K^+K^-\eta$
1781± 8± 4		[2] ASTON	88	LASS	0	$11 K^-p \to K^-\pi^+n$
1740±14±15		[2] ASTON	87	LASS	0	$11 K^-p \to \overline{K}^0\pi^+\pi^-n$
1779±11		[3] BALDI	76	SPEC	+	$10 K^+p \to K^0\pi^+p$
1776±26		[4] BRANDENB...	76D	ASPK	0	$13 K^\pm p \to K^\pm\pi^\mp N$

Int. J. Mod. Phys. A 2026.41. Downloaded from www.worldscientific.com
by UNIVERSITY OF CALIFORNIA @ BERKELEY on 09/16/26. Re-use and distribution is strictly not permitted, except for Open Access articles.

Int. J. Mod. Phys. A 2026.41. Downloaded from www.worldscientific.com
by CALIFORNIA @ BERKELEY on 09/16/26. Re-use and distribution is strictly not permitted, except for Open Access articles.

• • • We do not use the following data for averages, fits, limits, etc. • • •

1720±10±15	6111	[5] BIRD	89	LASS	−	11 $K^-p \to \overline{K}^0\pi^-p$
1749±10		ASTON	88B	LASS	−	11 $K^-p \to K^-\eta p$
1780± 9	300	BAUBILLIER	84B	HBC	−	8.25 $K^-p \to \overline{K}^0\pi^-p$
1790±15		BAUBILLIER	82B	HBC	0	8.25 $K^-p \to K^0_S 2\pi N$
1784± 9	2060	CLELAND	82	SPEC	±	50 $K^+p \to K^0_S\pi^\pm p$
1786±15		[6] ASTON	81D	LASS	0	11 $K^-p \to K^-\pi^+n$
1762± 9	190	TOAFF	81	HBC	−	6.5 $K^-p \to \overline{K}^0\pi^-p$
1850±50		ETKIN	80	MPS	0	6 $K^-p \to \overline{K}^0\pi^+\pi^-$
1812±28		BEUSCH	78	OMEG		10 $K^-p \to \overline{K}^0\pi^+\pi^-n$
1786± 8		CHUNG	78	MPS	0	6 $K^-p \to K^-\pi^+n$

[1] Seen in $\psi(2S)$ decay with branching ratio $\psi(2S) \to K^\pm X \to K^+K^-\eta = (2.0 \pm 0.4^{+1.9}_{-0.4}) \times 10^{-6}$.
[2] From energy-independent partial-wave analysis.
[3] From a fit to Y^2_6 moment. $J^P = 3^-$ found.
[4] Confirmed by phase shift analysis of ESTABROOKS 78, yields $J^P = 3^-$.
[5] From a partial wave amplitude analysis.
[6] From a fit to the Y^0_6 moment.

$K_3^*(1780)$ WIDTH

VALUE (MeV)	EVTS	DOCUMENT ID		TECN	CHG	COMMENT
161±17 OUR AVERAGE		Error includes scale factor of 1.1.				
$191^{+43}_{-37}{}^{+3}_{-81}$	1.8k	[1] ABLIKIM	20F	BES3		$\psi(2S) \to K^+K^-\eta$
203±30± 8		[2] ASTON	88	LASS	0	11 $K^-p \to K^-\pi^+n$
171±42±20		[2] ASTON	87	LASS	0	11 $K^-p \to \overline{K}^0\pi^+\pi^-n$
135±22		[3] BALDI	76	SPEC	+	10 $K^+p \to K^0\pi^+p$
• • • We do not use the following data for averages, fits, limits, etc. • • •						
187±31±20	6111	[4] BIRD	89	LASS	−	11 $K^-p \to \overline{K}^0\pi^-p$
193^{+51}_{-37}		ASTON	88B	LASS	−	11 $K^-p \to K^-\eta p$
99±30	300	BAUBILLIER	84B	HBC	−	8.25 $K^-p \to \overline{K}^0\pi^-p$
∼ 130		BAUBILLIER	82B	HBC	0	8.25 $K^-p \to K^0_S 2\pi N$
191±24	2060	CLELAND	82	SPEC	±	50 $K^+p \to K^0_S\pi^\pm p$
225±60		[5] ASTON	81D	LASS	0	11 $K^-p \to K^-\pi^+n$
∼ 80	190	TOAFF	81	HBC	−	6.5 $K^-p \to \overline{K}^0\pi^-p$
240±50		ETKIN	80	MPS	0	6 $K^-p \to \overline{K}^0\pi^+\pi^-$
181±44		[6] BEUSCH	78	OMEG		10 $K^-p \to \overline{K}^0\pi^+\pi^-n$
96±31		CHUNG	78	MPS	0	6 $K^-p \to K^-\pi^+n$
270±70		[7] BRANDENB...	76D	ASPK	0	13 $K^\pm p \to K^\pm\pi^\mp N$

[1] Seen in $\psi(2S)$ decay with branching ratio $\psi(2S) \to K^\pm X \to K^+K^-\eta = (2.0 \pm 0.4^{+1.9}_{-0.4}) \times 10^{-6}$.
[2] From energy-independent partial-wave analysis.
[3] From a fit to Y^2_6 moment. $J^P = 3^-$ found.
[4] From a partial wave amplitude analysis.
[5] From a fit to Y^0_6 moment.
[6] Errors enlarged by us to $4\Gamma/\sqrt{N}$; see the note with the $K^*(892)$ mass.
[7] ESTABROOKS 78 find that BRANDENBURG 76D data are consistent with 175 MeV width. Not averaged.

$K_3^*(1780)$ DECAY MODES

	Mode	Fraction (Γ_i/Γ)	Confidence level
Γ_1	$K\rho$	(31 ± 9) %	
Γ_2	$K^*(892)\pi$	(20 ± 5) %	
Γ_3	$K\pi$	(18.8± 1.0) %	
Γ_4	$K\eta$	(30 ±13) %	
Γ_5	$K^*_2(1430)\pi$	< 16 %	95%

CONSTRAINED FIT INFORMATION

An overall fit to 3 branching ratios uses 4 measurements and one constraint to determine 4 parameters. The overall fit has a $\chi^2 = 0.0$ for 1 degrees of freedom.

The following *off-diagonal* array elements are the correlation coefficients $\langle \delta x_i \delta x_j \rangle / (\delta x_i \cdot \delta x_j)$, in percent, from the fit to the branching fractions, $x_i \equiv \Gamma_i/\Gamma_{\rm total}$. The fit constrains the x_i whose labels appear in this array to sum to one.

	x_1	x_2	x_3
x_2	85		
x_3	18	21	
x_4	−98	−94	−27

$K_3^*(1780)$ BRANCHING RATIOS

$\Gamma(K\rho)/\Gamma(K^*(892)\pi)$ — Γ_1/Γ_2

VALUE	DOCUMENT ID		TECN	CHG	COMMENT
1.52±0.23 OUR FIT					
1.52±0.21±0.10	ASTON	87	LASS	0	11 $K^-p \to \overline{K}^0\pi^+\pi^-n$

$\Gamma(K^*(892)\pi)/\Gamma(K\pi)$ — Γ_2/Γ_3

VALUE	DOCUMENT ID		TECN	CHG	COMMENT
1.09±0.26 OUR FIT					
1.09±0.26	ASTON	84B	LASS	0	11 $K^-p \to \overline{K}^0 2\pi n$

$\Gamma(K\pi)/\Gamma_{\rm total}$ — Γ_3/Γ

VALUE	DOCUMENT ID		TECN	CHG	COMMENT
0.188±0.010 OUR FIT					
0.188±0.010 OUR AVERAGE					
0.187±0.008±0.008	ASTON	88	LASS	0	11 $K^-p \to K^-\pi^+n$
0.19 ±0.02	ESTABROOKS	78	ASPK	0	13 $K^\pm p \to K\pi N$

$\Gamma(K\eta)/\Gamma(K\pi)$ — Γ_4/Γ_3

VALUE	DOCUMENT ID		TECN	CHG	COMMENT
1.6 ±0.7 OUR FIT					
• • • We do not use the following data for averages, fits, limits, etc. • • •					
0.41±0.050	[1] BIRD	89	LASS	−	11 $K^-p \to \overline{K}^0\pi^-p$
0.50±0.18	ASTON	88B	LASS	−	11 $K^-p \to K^-\eta p$

[1] This result supersedes ASTON 88B.

$\Gamma(K^*_2(1430)\pi)/\Gamma(K^*(892)\pi)$ — Γ_5/Γ_2

VALUE	CL%	DOCUMENT ID		TECN	CHG	COMMENT
<0.78	95	ASTON	87	LASS	0	11 $K^-p \to \overline{K}^0\pi^+\pi^-n$

$K_3^*(1780)$ REFERENCES

ABLIKIM	20F	PR D101 032008	M. Ablikim *et al.*	(BESIII Collab.)
PELAEZ	17	EPJ C77 91	J.R. Pelaez, A.Rodas, J.R. de Elvira	
BIRD	89	SLAC-332	P.F. Bird	(SLAC)
ASTON	88	NP B296 493	D. Aston *et al.*	(SLAC, NAGO, CINC, INUS)
ASTON	88B	PL B201 169	D. Aston *et al.*	(SLAC, NAGO, CINC, INUS) JP
ASTON	87	NP B292 693	D. Aston *et al.*	(SLAC, NAGO, CINC, INUS)
ASTON	84B	NP B247 261	D. Aston *et al.*	(SLAC, CARL, OTTA)
BAUBILLIER	84B	ZPHY C26 37	M. Baubillier *et al.*	(BIRM, CERN, GLAS+)
BAUBILLIER	82B	NP B202 21	M. Baubillier *et al.*	(BIRM, CERN, GLAS+)
CLELAND	82	NP B208 189	W.E. Cleland *et al.*	(DURH, GEVA, LAUS+)
ASTON	81D	PL 99B 502	D. Aston *et al.*	(SLAC, CARL, OTTA) JP
TOAFF	81	PR D23 1500	S. Toaff *et al.*	(ANL, KANS)
ETKIN	80	PR D22 42	A. Etkin *et al.*	(BNL, CUNY) JP
BEUSCH	78	PL 74B 282	W. Beusch *et al.*	(CERN, AACH3, ETH) JP
CHUNG	78	PRL 40 355	S.U. Chung *et al.*	(BNL, BRAN, CUNY+) JP
ESTABROOKS	78	NP B133 490	P.G. Estabrooks *et al.*	(MCGI, CARL, DURH+) JP
Also		PR D17 658	P.G. Estabrooks *et al.*	(MCGI, CARL, DURH+)
BALDI	76	PL 63B 344	R. Baldi *et al.*	(GEVA) JP
BRANDENB...	76D	PL 60B 478	G.W. Brandenburg *et al.*	(SLAC) JP

$K_2(1820)$

$I(J^P) = \frac{1}{2}(2^-)$

See our mini-review in the 2004 edition of this *Review* (PDG 04) under $K_2(1770)$.

$K_2(1820)$ MASS

VALUE (MeV)	EVTS	DOCUMENT ID		TECN	COMMENT
1819±12 OUR AVERAGE					
$1853\pm27^{+18}_{-35}$	4289	[1] AAIJ	17C	LHCB	$B^+ \to J/\psi\phi K^+$
1816±13		[2] ASTON	93	LASS	11 $K^-p \to K^-\omega p$
• • • We do not use the following data for averages, fits, limits, etc. • • •					
∼ 1840		[3] DAUM	81C	CNTR	63 $K^-p \to K^-2\pi p$

[1] From an amplitude analysis of the decay $B^+ \to J/\psi\phi K^+$ with a significance of 3.0 σ.
[2] From a partial wave analysis of the $K^-\omega$ system.
[3] From a partial wave analysis of the $K^-2\pi$ system.

$K_2(1820)$ WIDTH

VALUE (MeV)	EVTS	DOCUMENT ID		TECN	COMMENT
264±34 OUR AVERAGE					
$167\pm58^{+82}_{-72}$	4289	[1] AAIJ	17C	LHCB	$B^+ \to J/\psi\phi K^+$
276±35		[2] ASTON	93	LASS	11 $K^-p \to K^-\omega p$
• • • We do not use the following data for averages, fits, limits, etc. • • •					
∼ 230		[3] DAUM	81C	CNTR	63 $K^-p \to K^-2\pi p$

[1] From an amplitude analysis of the decay $B^+ \to J/\psi\phi K^+$ with a significance of 3.0 σ.
[2] From a partial wave analysis of the $K^-\omega$ system.
[3] From a partial wave analysis of the $K^-2\pi$ system.

Int. J. Mod. Phys. A 2026.41. Downloaded from www.worldscientific.com
by UNIVERSITY OF CALIFORNIA @ BERKELEY on 09/16/26. Re-use and distribution is strictly not permitted, except for Open Access articles.

$K_2(1820)$ DECAY MODES

	Mode	Fraction (Γ_i/Γ)
Γ_1	$K\pi\pi$	seen
Γ_2	$K_2^*(1430)\pi$	seen
Γ_3	$K^*(892)\pi$	seen
Γ_4	$Kf_2(1270)$	seen
Γ_5	$K\omega$	seen
Γ_6	$K\phi$	seen

$K_2(1820)$ BRANCHING RATIOS

$\Gamma(K_2^*(1430)\pi)/\Gamma(K\pi\pi)$ — Γ_2/Γ_1

VALUE	DOCUMENT ID		TECN	COMMENT
• • • We do not use the following data for averages, fits, limits, etc. • • •				
~ 0.77	DAUM	81C	CNTR	$63K^-p \to \overline{K}2\pi p$

$\Gamma(K^*(892)\pi)/\Gamma(K\pi\pi)$ — Γ_3/Γ_1

VALUE	DOCUMENT ID		TECN	COMMENT
• • • We do not use the following data for averages, fits, limits, etc. • • •				
~ 0.05	DAUM	81C	CNTR	$63K^-p \to \overline{K}2\pi p$

$\Gamma(Kf_2(1270))/\Gamma(K\pi\pi)$ — Γ_4/Γ_1

VALUE	DOCUMENT ID		TECN	COMMENT
• • • We do not use the following data for averages, fits, limits, etc. • • •				
~ 0.18	DAUM	81C	CNTR	$63K^-p \to \overline{K}2\pi p$

$\Gamma(K\phi)/\Gamma_{total}$ — Γ_6/Γ

VALUE	EVTS	DOCUMENT ID		TECN	COMMENT
seen	24k	[1] AAIJ	21E	LHCB	$B^+ \to J/\psi\phi K^+$
• • • We do not use the following data for averages, fits, limits, etc. • • •					
seen	4289	[2,3] AAIJ	17C	LHCB	$B^+ \to J/\psi\phi K^+$

[1] From an amplitude analysis of the decay $B^+ \to J/\psi\phi K^+$ with a significance of 5.8 σ.
[2] From an amplitude analysis of the decay $B^+ \to J/\psi\phi K^+$ with a significance of 3.0 σ.
[3] Superseded by AAIJ 21E.

$K_2(1820)$ REFERENCES

AAIJ	21E	PRL 127 082001	R. Aaij *et al.*	(LHCb Collab.)
AAIJ	17C	PRL 118 022003	R. Aaij *et al.*	(LHCb Collab.)
Also		PR D95 012002	R. Aaij *et al.*	(LHCb Collab.)
PDG	04	PL B592 1	S. Eidelman *et al.*	(PDG Collab.)
ASTON	93	PL B308 186	D. Aston *et al.*	(SLAC, NAGO, CINC, INUS)
DAUM	81C	NP B187 1	C. Daum *et al.*	(AMST, CERN, CRAC, MPIM+)

$K(1830)$

$I(J^P) = \frac{1}{2}(0^-)$

OMITTED FROM SUMMARY TABLE

Seen in partial-wave analysis of $K\phi$ system. Needs confirmation.

$K(1830)$ MASS

VALUE (MeV)	EVTS	DOCUMENT ID		TECN	CHG	COMMENT
• • • We do not use the following data for averages, fits, limits, etc. • • •						
$1874 \pm 43^{+59}_{-115}$	4289	[1,2] AAIJ	17C	LHCB		$B^+ \to J/\psi\phi K^+$
~ 1830		ARMSTRONG	83	OMEG	−	18.5 $K^-p \to 3Kp$

[1] From an amplitude analysis of the decay $B^+ \to J/\psi\phi K^+$ with a significance of 3.5 σ.
[2] A subsequent amplitude analysis of $B^+ \to J/\psi\phi K^+$ by AAIJ 21E did not confirm this measurement.

$K(1830)$ WIDTH

VALUE (MeV)	EVTS	DOCUMENT ID		TECN	CHG	COMMENT
• • • We do not use the following data for averages, fits, limits, etc. • • •						
$168 \pm 90^{+280}_{-104}$	4289	[3,4] AAIJ	17C	LHCB		$B^+ \to J/\psi\phi K^+$
~ 250		ARMSTRONG	83	OMEG	−	18.5 $K^-p \to 3Kp$

[3] From an amplitude analysis of the decay $B^+ \to J/\psi\phi K^+$ with a significance of 3.5 σ.
[4] A subsequent amplitude analysis of $B^+ \to J/\psi\phi K^+$ by AAIJ 21E did not confirm this measurement.

$K(1830)$ DECAY MODES

	Mode
Γ_1	$K\phi$

$K(1830)$ REFERENCES

AAIJ	21E	PRL 127 082001	R. Aaij *et al.*	(LHCb Collab.)
AAIJ	17C	PRL 118 022003	R. Aaij *et al.*	(LHCb Collab.)
Also		PR D95 012002	R. Aaij *et al.*	(LHCb Collab.)
ARMSTRONG	83	NP B221 1	T.A. Armstrong *et al.*	(BARI, BIRM, CERN+) JP

$K_0^*(1950)$

$I(J^P) = \frac{1}{2}(0^+)$

Seen in partial-wave analysis of the $K^-\pi^+$ system.

$K_0^*(1950)$ MASS

VALUE (MeV)	DOCUMENT ID		TECN	CHG	COMMENT
1957±14 OUR AVERAGE					
$1980 \pm 14 \pm 19$	[1] AAIJ	23AH	LHCB		$B^+ \to K^+(K_S^0 K\pi)$
$1942 \pm 22 \pm 21$	LEES	21A	BABR		$\gamma\gamma \to \eta_c(1S) \to \eta' K^+K^-$
$1945 \pm 10 \pm 20$	[2] ASTON	88	LASS	0	$11\ K^-p \to K^-\pi^+n$
• • • We do not use the following data for averages, fits, limits, etc. • • •					
1917 ± 12	[3] ZHOU	06	RVUE		$Kp \to K^-\pi^+n$
1820 ± 40	[4] ANISOVICH	97C	RVUE		$11\ K^-p \to K^-\pi^+n$

[1] From Dalitz plot analyses of $\eta_c(1S,2S) \to K_S^0 K^+\pi^-$ + c.c..
[2] We take the central value of the two solutions and the larger error given.
[3] S-matrix pole. Using ASTON 88 and assuming $K_0^*(700)$, $K_0^*(1430)$.
[4] T-matrix pole. Reanalysis of ASTON 88 data.

$K_0^*(1950)$ WIDTH

VALUE (MeV)	DOCUMENT ID		TECN	CHG	COMMENT
170± 50 OUR AVERAGE Error includes scale factor of 2.2. See the ideogram below.					
$229 \pm 26 \pm 16$	[1] AAIJ	23AH	LHCB		$B^+ \to K^+(K_S^0 K\pi)$
$80 \pm 32 \pm 20$	LEES	21A	BABR		$\gamma\gamma \to \eta_c(1S) \to \eta' K^+K^-$
$201 \pm 34 \pm 79$	[2] ASTON	88	LASS	0	$11\ K^-p \to K^-\pi^+n$
• • • We do not use the following data for averages, fits, limits, etc. • • •					
145 ± 38	[3] ZHOU	06	RVUE		$Kp \to K^-\pi^+n$
250 ± 100	[4] ANISOVICH	97C	RVUE		$11\ K^-p \to K^-\pi^+n$

[1] From Dalitz plot analyses of $\eta_c(1S,2S) \to K_S^0 K^+\pi^-$ + c.c..
[2] We take the central value of the two solutions and the larger error given.
[3] S-matrix pole. Using ASTON 88 and assuming $K_0^*(700)$, $K_0^*(1430)$.
[4] T-matrix pole. Reanalysis of ASTON 88 data.

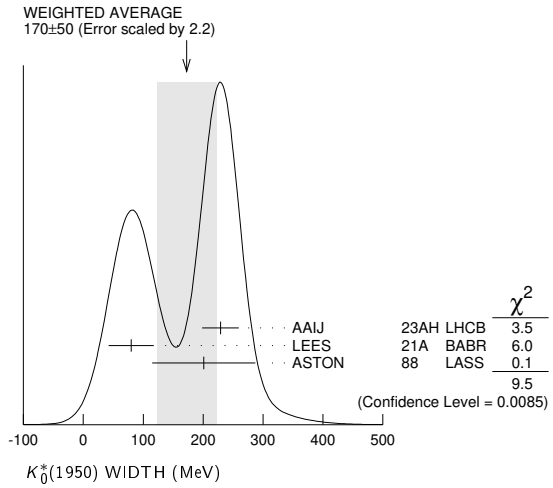

$K_0^*(1950)$ DECAY MODES

	Mode	Fraction (Γ_i/Γ)
Γ_1	$K^-\pi^+$	(52±14) %

$K_0^*(1950)$ BRANCHING RATIOS

$\Gamma(K^-\pi^+)/\Gamma_{total}$ — Γ_1/Γ

VALUE	DOCUMENT ID		TECN	CHG	COMMENT
$0.52 \pm 0.08 \pm 0.12$	[1] ASTON	88	LASS	0	$11\ K^-p \to K^-\pi^+n$
• • • We do not use the following data for averages, fits, limits, etc. • • •					
~ 0.60	[2] ZHOU	06	RVUE		$Kp \to K^-\pi^+n$

[1] We take the central value of the two solutions and the larger error given.
[2] S-matrix pole. Using ASTON 88 and assuming $K_0^*(700)$, $K_0^*(1430)$.

$K_0^*(1950)$ REFERENCES

AAIJ	23AH	PR D108 032010	R. Aaij *et al.*	(LHCb Collab.)
LEES	21A	PR D104 072002	J.P. Lees *et al.*	(BABAR Collab.)
ZHOU	06	NP A775 212	Z.Y. Zhou, H.Q. Zheng	
ANISOVICH	97C	PL B413 137	A.V. Anisovich, A.V. Sarantsev	
ASTON	88	NP B296 493	D. Aston *et al.*	(SLAC, NAGO, CINC, INUS)

Int. J. Mod. Phys. A 2026.41. Downloaded from www.worldscientific.com
by [redacted]LIFORNIA @ BERKELEY on 09/16/26. Re-use and distribution is strictly not permitted, except for Open Access articles.

$K_2^*(1980)$

$I(J^P) = \frac{1}{2}(2^+)$

$K_2^*(1980)$ MASS

VALUE (MeV)	EVTS	DOCUMENT ID		TECN	CHG	COMMENT
1990^{+60}_{-50} OUR AVERAGE	Error includes scale factor of 2.8. See the ideogram below.					
$2046^{+17}_{-16}{}^{+67}_{-15}$	1.8k	[1] ABLIKIM	20F	BES3		$\psi(2S) \to K^+K^-\eta$
$1868 \pm 8^{+40}_{-57}$	183k	ABLIKIM	19AQ	BES	$\pm$	$J/\psi \to K^+K^-\pi^0$
$1973 \pm 8 \pm 25$		ASTON	87	LASS	0	$11\ K^-p \to \overline{K}^0\pi^+\pi^-n$
• • • We do not use the following data for averages, fits, limits, etc. • • •						
$2073 \pm 94^{+245}_{-240}$	4289	[2,3] AAIJ	17C	LHCB		$B^+ \to J/\psi\phi K^+$
2020 ± 20		TIKHOMIROV	03	SPEC		$40.0\ \pi^-C \to K^0_S K^0_S K^0_L X$
1978 ± 40	241	BIRD	89	LASS	$-$	$11\ K^-p \to \overline{K}^0\pi^-p$

[1] Seen in $\psi(2S)$ decay with branching ratio $\psi(2S) \to K^\pm X \to K^+K^-\eta = (7.0 \pm 0.5^{+3.7}_{-0.6}) \times 10^{-6}$.
[2] From an amplitude analysis of the decay $B^+ \to J/\psi\phi K^+$ with a significance of 5.4 σ.
[3] A reanalysis by AAIJ 21E using a larger data sample did not confirm this measurement, the new result having a significance of only 1.6 σ.

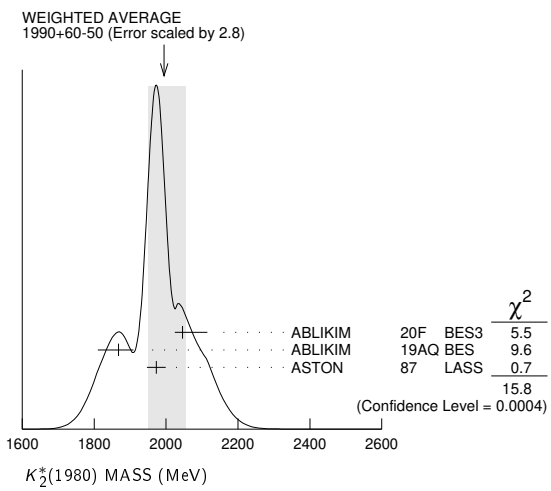

$K_2^*(1980)$ WIDTH

VALUE (MeV)	EVTS	DOCUMENT ID		TECN	CHG	COMMENT
348^{+50}_{-30} OUR AVERAGE	Error includes scale factor of 1.3. See the ideogram below.					
$408^{+38}_{-34}{}^{+72}_{-44}$	1.8k	[1] ABLIKIM	20F	BES3		$\psi(2S) \to K^+K^-\eta$
$272 \pm 24^{+50}_{-15}$	183k	ABLIKIM	19AQ	BES	$\pm$	$J/\psi \to K^+K^-\pi^0$
$373 \pm 33 \pm 60$		ASTON	87	LASS	0	$11\ K^-p \to \overline{K}^0\pi^+\pi^-n$
• • • We do not use the following data for averages, fits, limits, etc. • • •						
$678 \pm 311^{+1153}_{-559}$	4289	[2,3] AAIJ	17C	LHCB		$B^+ \to J/\psi\phi K^+$
180 ± 70		TIKHOMIROV	03	SPEC		$40.0\ \pi^-C \to K^0_S K^0_S K^0_L X$
398 ± 47	241	BIRD	89	LASS	$-$	$11\ K^-p \to \overline{K}^0\pi^-p$

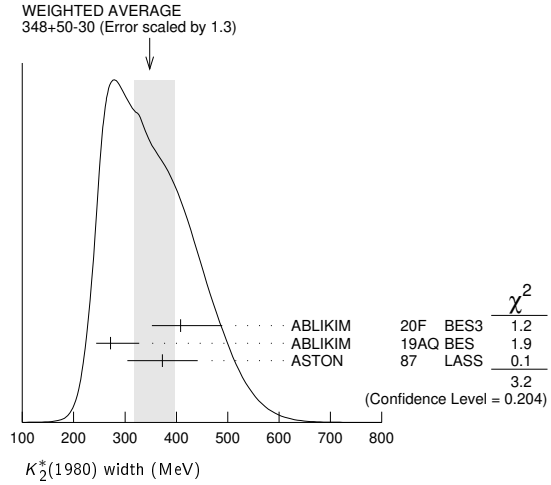

[1] Seen in $\psi(2S)$ decay with branching ratio $\psi(2S) \to K^\pm X \to K^+K^-\eta = (7.0 \pm 0.5^{+3.7}_{-0.6}) \times 10^{-6}$.
[2] From an amplitude analysis of the decay $B^+ \to J/\psi\phi K^+$ with a significance of 5.4 σ.
[3] A reanalysis by AAIJ 21E using a larger data sample did not confirm this measurement, the new result having a significance of only 1.6 σ.

$K_2^*(1980)$ DECAY MODES

	Mode	Fraction (Γ_i/Γ)
Γ_1	$K^*(892)\pi$	possibly seen
Γ_2	$K\rho$	possibly seen
Γ_3	$Kf_2(1270)$	possibly seen
Γ_4	$K\phi$	seen
Γ_5	$K\eta$	seen

$K_2^*(1980)$ BRANCHING RATIOS

$\Gamma(K^*(892)\pi)/\Gamma_{total}$ — Γ_1/Γ

VALUE	DOCUMENT ID		TECN	COMMENT
possibly seen	GULER	11	BELL	$B^+ \to J/\psi K^+\pi^+\pi^-$

$\Gamma(K\rho)/\Gamma_{total}$ — Γ_2/Γ

VALUE	DOCUMENT ID		TECN	COMMENT
possibly seen	GULER	11	BELL	$B^+ \to J/\psi K^+\pi^+\pi^-$

$\Gamma(K\rho)/\Gamma(K^*(892)\pi)$ — Γ_2/Γ_1

VALUE	DOCUMENT ID		TECN	CHG	COMMENT
$1.49 \pm 0.24 \pm 0.09$	ASTON	87	LASS	0	$11\ K^-p \to \overline{K}^0\pi^+\pi^-n$

$\Gamma(Kf_2(1270))/\Gamma_{total}$ — Γ_3/Γ

VALUE	DOCUMENT ID	TECN	COMMENT
possibly seen	TIKHOMIROV 03	SPEC	$40.0\ \pi^-C \to K^0_S K^0_S K^0_L X$

$\Gamma(K\phi)/\Gamma_{total}$ — Γ_4/Γ

VALUE	EVTS	DOCUMENT ID		TECN	COMMENT
seen	4289	[1,2] AAIJ	17C	LHCB	$B^+ \to J/\psi\phi K^+$

[1] From an amplitude analysis of the decay $B^+ \to J/\psi\phi K^+$ with a significance of 5.4 σ.
[2] A reanalysis by AAIJ 21E using a larger data sample did not confirm this measurement, the new result having a significance of only 1.6 σ.

$\Gamma(K\eta)/\Gamma_{total}$ — Γ_5/Γ

VALUE	EVTS	DOCUMENT ID		TECN	COMMENT
seen	1.8k	[1] ABLIKIM	20F	BES3	$\psi(2S) \to K^+K^-\eta$
seen	116k	[2] CHEN	20A	BELL	$D^0 \to K^-\pi^+\eta$

[1] Seen decaying to $K\eta$ in an amplitude analysis of $\psi(2S) \to K^+K^-\eta$.
[2] From an amplitude analysis of the decay $D^0 \to K^-\pi^+\eta$ with a significance of 17 σ.

$K_2^*(1980)$ REFERENCES

AAIJ	21E	PRL 127 082001	R. Aaij *et al.*	(LHCb Collab.)
ABLIKIM	20F	PR D101 032008	M. Ablikim *et al.*	(BESIII Collab.)
CHEN	20A	PR D102 012002	Y.Q. Chen *et al.*	(BELLE Collab.)
ABLIKIM	19AQ	PR D100 032004	M. Ablikim *et al.*	(BESIII Collab.)
AAIJ	17C	PRL 118 022003	R. Aaij *et al.*	(LHCb Collab.)
Also		PR D95 012002	R. Aaij *et al.*	(LHCb Collab.)
GULER	11	PR D83 032005	H. Guler *et al.*	(BELLE Collab.)
TIKHOMIROV	03	PAN 66 828	G.D. Tikhomirov *et al.*	
		Translated from YAF 66 860.		
BIRD	89	SLAC-332	P.F. Bird	(SLAC)
ASTON	87	NP B292 693	D. Aston *et al.*	(SLAC, NAGO, CINC, INUS)

$K_4^*(2045)$

$I(J^P) = \frac{1}{2}(4^+)$

$K_4^*(2045)$ MASS

VALUE (MeV)	EVTS	DOCUMENT ID		TECN	CHG	COMMENT
2048^{+8}_{-9} OUR AVERAGE	Error includes scale factor of 1.1.					
$2090 \pm 9^{+11}_{-29}$	183k	ABLIKIM	19AQ	BES	$\pm$	$J/\psi \to K^+K^-\pi^0$
$2062 \pm 14 \pm 13$		[1] ASTON	86	LASS	0	$11\ K^-p \to K^-\pi^+n$
2039 ± 10	400	[2,3] CLELAND	82	SPEC	$\pm$	$50\ K^+p \to K^0_S\pi^\pm p$
2070^{+100}_{-40}		[4] ASTON	81C	LASS	0	$11\ K^-p \to K^-\pi^+n$
• • • We do not use the following data for averages, fits, limits, etc. • • •						
2079 ± 7	431	TORRES	86	MPSF		$400\ pA \to 4KX$
2088 ± 20	650	BAUBILLIER	82	HBC	$-$	$8.25\ K^-p \to K^0_S\pi^-p$
2115 ± 46	488	CARMONY	77	HBC	0	$9\ K^+d \to K^+\pi$'s X

[1] From a fit to all moments.
[2] From a fit to 8 moments.
[3] Number of events evaluated by us.
[4] From energy-independent partial-wave analysis.

Int. J. Mod. Phys. A 2026.41. Downloaded from www.worldscientific.com by UNIVERSITY OF CALIFORNIA @ BERKELEY on 09/16/26. Re-use and distribution is strictly not permitted, except for Open Access articles.

$K_4^*(2045)$ WIDTH

VALUE (MeV)	EVTS	DOCUMENT ID		TECN	CHG	COMMENT
199^{+27}_{-19} OUR AVERAGE						
$201\pm 19^{+57}_{-17}$	183k	ABLIKIM	19AQ	BES	$\pm$	$J/\psi \to K^+ K^- \pi^0$
$221\pm 48\pm 27$		[5] ASTON	86	LASS	0	$11\ K^- p \to K^- \pi^+ n$
189 ± 35	400	[6,7] CLELAND	82	SPEC	$\pm$	$50\ K^+ p \to K^0_S \pi^\pm p$
• • • We do not use the following data for averages, fits, limits, etc. • • •						
61 ± 58	431	TORRES	86	MPSF		$400\ pA \to 4KX$
170^{+100}_{-50}	650	BAUBILLIER	82	HBC	$-$	$8.25\ K^- p \to K^0_S \pi^- p$
240^{+500}_{-100}		[8] ASTON	81C	LASS	0	$11\ K^- p \to K^- \pi^+ n$
300 ± 200		CARMONY	77	HBC	0	$9\ K^+ d \to K^+ \pi$'s X

[5] From a fit to all moments.
[6] From a fit to 8 moments.
[7] Number of events evaluated by us.
[8] From energy-independent partial-wave analysis.

$K_4^*(2045)$ DECAY MODES

	Mode	Fraction (Γ_i/Γ)
Γ_1	$K\pi$	(9.9 ± 1.2) %
Γ_2	$K^*(892)\pi\pi$	$(9\ \pm 5\ )$ %
Γ_3	$K^*(892)\pi\pi\pi$	$(7\ \pm 5\ )$ %
Γ_4	$\rho K\pi$	(5.7 ± 3.2) %
Γ_5	$\omega K\pi$	(5.0 ± 3.0) %
Γ_6	$\phi K\pi$	(2.8 ± 1.4) %
Γ_7	$\phi K^*(892)$	(1.4 ± 0.7) %

$K_4^*(2045)$ BRANCHING RATIOS

$\Gamma(K\pi)/\Gamma_{total}$ — **Γ_1/Γ**

VALUE	DOCUMENT ID		TECN	CHG	COMMENT
0.099±0.012	ASTON	88	LASS	0	$11\ K^- p \to K^- \pi^+ n$

$\Gamma(K^*(892)\pi\pi)/\Gamma(K\pi)$ — **Γ_2/Γ_1**

VALUE	DOCUMENT ID		TECN	CHG	COMMENT
0.89±0.53	BAUBILLIER	82	HBC	$-$	$8.25\ K^- p \to p K^0_S 3\pi$

$\Gamma(K^*(892)\pi\pi\pi)/\Gamma(K\pi)$ — **Γ_3/Γ_1**

VALUE	DOCUMENT ID		TECN	CHG	COMMENT
0.75±0.49	BAUBILLIER	82	HBC	$-$	$8.25\ K^- p \to p K^0_S 3\pi$

$\Gamma(\rho K\pi)/\Gamma(K\pi)$ — **Γ_4/Γ_1**

VALUE	DOCUMENT ID		TECN	CHG	COMMENT
0.58±0.32	BAUBILLIER	82	HBC	$-$	$8.25\ K^- p \to p K^0_S 3\pi$

$\Gamma(\omega K\pi)/\Gamma(K\pi)$ — **Γ_5/Γ_1**

VALUE	DOCUMENT ID		TECN	CHG	COMMENT
0.50±0.30	BAUBILLIER	82	HBC	$-$	$8.25\ K^- p \to p K^0_S 3\pi$

$\Gamma(\phi K\pi)/\Gamma_{total}$ — **Γ_6/Γ**

VALUE	DOCUMENT ID		TECN	COMMENT
0.028±0.014	[9] TORRES	86	MPSF	$400\ pA \to 4KX$

$\Gamma(\phi K^*(892))/\Gamma_{total}$ — **Γ_7/Γ**

VALUE	DOCUMENT ID		TECN	COMMENT
0.014±0.007	[9] TORRES	86	MPSF	$400\ pA \to 4KX$

[9] Error determination is model dependent.

$K_4^*(2045)$ REFERENCES

ABLIKIM	19AQ	PR D100 032004	M. Ablikim *et al.*	(BESIII Collab.)
ASTON	88	NP B296 493	D. Aston *et al.*	(SLAC, NAGO, CINC, INUS)
ASTON	86	PL B180 308	D. Aston *et al.*	(SLAC, NAGO, CINC, INUS)
TORRES	86	PR D34 707	S. Torres *et al.*	(VPI, ARIZ, FNAL, FSU+)
BAUBILLIER	82	PL 118B 447	M. Baubillier *et al.*	(BIRM, CERN, GLAS+)
CLELAND	82	NP B208 189	W.E. Cleland *et al.*	(DURH, GEVA, LAUS+)
ASTON	81C	PL 106B 235	D. Aston *et al.*	(SLAC, CARL, OTTA) JP
CARMONY	77	PR D16 1251	D.D. Carmony *et al.*	(PURD, UCD, IUPU)

$K_2(2250)$

$I(J^P) = \frac{1}{2}(2^-)$

OMITTED FROM SUMMARY TABLE

This entry contains various peaks in strange meson systems reported in the 2150–2260 MeV region, as well as enhancements seen in the antihyperon-nucleon system, either in the mass spectra or in the $J^P = 2^-$ wave.

$K_2(2250)$ MASS

VALUE (MeV)	EVTS	DOCUMENT ID		TECN	CHG	COMMENT
2247±17 OUR AVERAGE						
2200 ± 40		[1] ARMSTRONG	83C	OMEG	$-$	$18\ K^- p \to \Lambda\overline{p}X$
2235 ± 50		[1] BAUBILLIER	81	HBC	$-$	$8\ K^- p \to \Lambda\overline{p}X$
2260 ± 20		[1] CLELAND	81	SPEC	$\pm$	$50\ K^+ p \to \Lambda\overline{p}X$
• • • We do not use the following data for averages, fits, limits, etc. • • •						
2280 ± 20		TIKHOMIROV	03	SPEC		$40.0\ \pi^- C \to K^0_S K^0_S K^0_L X$
2147 ± 4	37	CHLIAPNIK...	79	HBC	$+$	$32\ K^+ p \to \overline{\Lambda} p X$
2240 ± 20	20	LISSAUER	70	HBC		$9\ K^+ p$

[1] $J^P = 2^-$ from moments analysis.

$K_2(2250)$ WIDTH

VALUE (MeV)	EVTS	DOCUMENT ID		TECN	CHG	COMMENT
180±30 OUR AVERAGE Error includes scale factor of 1.4.						
150 ± 30		[2] ARMSTRONG	83C	OMEG	$-$	$18\ K^- p \to \Lambda\overline{p}X$
210 ± 30		[2] CLELAND	81	SPEC	$\pm$	$50\ K^+ p \to \Lambda\overline{p}X$
• • • We do not use the following data for averages, fits, limits, etc. • • •						
180 ± 60		TIKHOMIROV	03	SPEC		$40.0\ \pi^- C \to K^0_S K^0_S K^0_L X$
~ 200		[2] BAUBILLIER	81	HBC	$-$	$8\ K^- p \to \Lambda\overline{p}X$
~ 40	37	CHLIAPNIK...	79	HBC	$+$	$32\ K^+ p \to \overline{\Lambda} p X$
80 ± 20	20	LISSAUER	70	HBC		$9\ K^+ p$

[2] $J^P = 2^-$ from moments analysis.

$K_2(2250)$ DECAY MODES

	Mode
Γ_1	$K\pi\pi$
Γ_2	$K f_2(1270)$
Γ_3	$K^*(892) f_0(980)$
Γ_4	$p\overline{\Lambda}$

$K_2(2250)$ REFERENCES

TIKHOMIROV	03	PAN 66 828 Translated from YAF 66 860.	G.D. Tikhomirov *et al.*	
ARMSTRONG	83C	NP B227 365	T.A. Armstrong *et al.*	(BARI, BIRM, CERN+)
BAUBILLIER	81	NP B183 1	M. Baubillier *et al.*	(BIRM, CERN, GLAS+) JP
CLELAND	81	NP B184 1	W.E. Cleland *et al.*	(PITT, GEVA, LAUS+) JP
CHLIAPNIK...	79	NP B158 253	P.V. Chliapnikov *et al.*	(CERN, BELG, MONS)
LISSAUER	70	NP B18 491	D. Lissauer *et al.*	(LBL)

$K_3(2320)$

$I(J^P) = \frac{1}{2}(3^+)$

OMITTED FROM SUMMARY TABLE

Seen in the $J^P = 3^+$ wave of the antihyperon-nucleon system. Needs confirmation.

$K_3(2320)$ MASS

VALUE (MeV)	DOCUMENT ID		TECN	CHG	COMMENT
2324±24 OUR AVERAGE					
2330 ± 40	[1] ARMSTRONG	83C	OMEG	$-$	$18\ K^- p \to \Lambda\overline{p}X$
2320 ± 30	[1] CLELAND	81	SPEC	$\pm$	$50\ K^+ p \to \Lambda\overline{p}X$

[1] $J^P = 3^+$ from moments analysis.

$K_3(2320)$ WIDTH

VALUE (MeV)	DOCUMENT ID		TECN	CHG	COMMENT
150±30	[2] ARMSTRONG	83C	OMEG	$-$	$18\ K^- p \to \Lambda\overline{p}X$
• • • We do not use the following data for averages, fits, limits, etc. • • •					
~ 250	[2] CLELAND	81	SPEC	$\pm$	$50\ K^+ p \to \Lambda\overline{p}X$

[2] $J^P = 3^+$ from moments analysis.

$K_3(2320)$ DECAY MODES

	Mode
Γ_1	$p\overline{\Lambda}$

$K_3(2320)$ REFERENCES

ARMSTRONG	83C	NP B227 365	T.A. Armstrong *et al.*	(BARI, BIRM, CERN+)
CLELAND	81	NP B184 1	W.E. Cleland *et al.*	(PITT, GEVA, LAUS+)

Int. J. Mod. Phys. A 2026.41. Downloaded from www.worldscientific.com
by CALIFORNIA @ BERKELEY on 09/16/26. Re-use and distribution is strictly not permitted, except for Open Access articles.

$K_5^*(2380)$

$I(J^P) = \frac{1}{2}(5^-)$

OMITTED FROM SUMMARY TABLE
Needs confirmation.

$K_5^*(2380)$ MASS

VALUE (MeV)	DOCUMENT ID		TECN	CHG	COMMENT
2382±14±19	[1] ASTON	86	LASS	0	11 $K^- p \to K^- \pi^+ n$

[1] From a fit to all the moments.

$K_5^*(2380)$ WIDTH

VALUE (MeV)	DOCUMENT ID		TECN	CHG	COMMENT
178±37±32	[2] ASTON	86	LASS	0	11 $K^- p \to K^- \pi^+ n$

[2] From a fit to all the moments.

$K_5^*(2380)$ DECAY MODES

	Mode	Fraction (Γ_i/Γ)
Γ_1	$K\pi$	(6.1±1.2) %

$K_5^*(2380)$ BRANCHING RATIOS

$\Gamma(K\pi)/\Gamma_{total}$ — Γ_1/Γ

VALUE	DOCUMENT ID		TECN	CHG	COMMENT
0.061±0.012	ASTON	88	LASS	0	11 $K^- p \to K^- \pi^+ n$

$K_5^*(2380)$ REFERENCES

ASTON 88 NP B296 493 D. Aston *et al.* (SLAC, NAGO, CINC, INUS)
ASTON 86 PL B180 308 D. Aston *et al.* (SLAC, NAGO, CINC, INUS)

$K_4(2500)$

$I(J^P) = \frac{1}{2}(4^-)$

OMITTED FROM SUMMARY TABLE
Needs confirmation.

$K_4(2500)$ MASS

VALUE (MeV)	DOCUMENT ID		TECN	CHG	COMMENT
2490±20	[1] CLELAND	81	SPEC	±	50 $K^+ p \to \Lambda\overline{p}$

[1] $J^P = 4^-$ from moments analysis.

$K_4(2500)$ WIDTH

VALUE (MeV)	DOCUMENT ID		TECN	CHG	COMMENT
• • • We do not use the following data for averages, fits, limits, etc. • • •					
~ 250	[2] CLELAND	81	SPEC	±	50 $K^+ p \to \Lambda\overline{p}$

[2] $J^P = 4^-$ from moments analysis.

$K_4(2500)$ DECAY MODES

	Mode
Γ_1	$p\overline{\Lambda}$

$K_4(2500)$ REFERENCES

CLELAND 81 NP B184 1 W.E. Cleland *et al.* (PITT, GEVA, LAUS+)

$K(3100)$

$I^G(J^{PC}) = ?^?(?^{??})$

OMITTED FROM SUMMARY TABLE
also known as $K_J^?(3100)$

Narrow peak observed in several ($\Lambda\overline{p}$ + pions) and ($\overline{\Lambda}p$ + pions) states in Σ^- Be reactions by BOURQUIN 86 and in $n\,p$ and nA reactions by ALEEV 93. Not seen by BOEHNLEIN 91. If due to strong decays, this state has exotic quantum numbers (B=0,Q=+1,S=−1 for $\Lambda\overline{p}\pi^+\pi^+$ and $I \geq 3/2$ for $\Lambda\overline{p}\pi^-$). Needs confirmation.

$K(3100)$ MASS

VALUE (MeV)	DOCUMENT ID
≈ 3100 OUR ESTIMATE	

3-BODY DECAYS

VALUE (MeV)	DOCUMENT ID		TECN	COMMENT
3054±11 OUR AVERAGE				
3060± 7±20	[1] ALEEV	93	BIS2	$K(3100) \to \Lambda\overline{p}\pi^+$
3056± 7±20	[1] ALEEV	93	BIS2	$K(3100) \to \overline{\Lambda}p\pi^-$
3055± 8±20	[1] ALEEV	93	BIS2	$K(3100) \to \Lambda\overline{p}\pi^-$
3045± 8±20	[1] ALEEV	93	BIS2	$K(3100) \to \overline{\Lambda}p\pi^+$

4-BODY DECAYS

VALUE (MeV)	DOCUMENT ID		TECN	COMMENT
3059±11 OUR AVERAGE				
3067± 6±20	[1] ALEEV	93	BIS2	$K(3100) \to \Lambda\overline{p}\pi^+\pi^+$
3060± 8±20	[1] ALEEV	93	BIS2	$K(3100) \to \Lambda\overline{p}\pi^+\pi^-$
3055± 7±20	[1] ALEEV	93	BIS2	$K(3100) \to \overline{\Lambda}p\pi^-\pi^-$
3052± 8±20	[1] ALEEV	93	BIS2	$K(3100) \to \overline{\Lambda}p\pi^-\pi^+$
• • • We do not use the following data for averages, fits, limits, etc. • • •				
3105±30	BOURQUIN	86	SPEC	$K(3100) \to \Lambda\overline{p}\pi^+\pi^+$
3115±30	BOURQUIN	86	SPEC	$K(3100) \to \Lambda\overline{p}\pi^+\pi^-$

5-BODY DECAYS

VALUE (MeV)	DOCUMENT ID		TECN	COMMENT
• • • We do not use the following data for averages, fits, limits, etc. • • •				
3095±30	BOURQUIN	86	SPEC	$K(3100) \to \Lambda\overline{p}\pi^+\pi^+\pi^-$

[1] Supersedes ALEEV 90.

$K(3100)$ WIDTH

3-BODY DECAYS

VALUE (MeV)	DOCUMENT ID		TECN	COMMENT
• • • We do not use the following data for averages, fits, limits, etc. • • •				
42±16	[2] ALEEV	93	BIS2	$K(3100) \to \Lambda\overline{p}\pi^+$
36±15	[2] ALEEV	93	BIS2	$K(3100) \to \overline{\Lambda}p\pi^-$
50±18	[2] ALEEV	93	BIS2	$K(3100) \to \Lambda\overline{p}\pi^-$
30±15	[2] ALEEV	93	BIS2	$K(3100) \to \overline{\Lambda}p\pi^+$

4-BODY DECAYS

VALUE (MeV)	CL%	DOCUMENT ID		TECN	COMMENT
• • • We do not use the following data for averages, fits, limits, etc. • • •					
22± 8		[2] ALEEV	93	BIS2	$K(3100) \to \Lambda\overline{p}\pi^+\pi^+$
28±12		[2] ALEEV	93	BIS2	$K(3100) \to \Lambda\overline{p}\pi^+\pi^-$
32±15		[2] ALEEV	93	BIS2	$K(3100) \to \overline{\Lambda}p\pi^-\pi^-$
30±15		[2] ALEEV	93	BIS2	$K(3100) \to \overline{\Lambda}p\pi^-\pi^+$
<30	90	BOURQUIN	86	SPEC	$K(3100) \to \Lambda\overline{p}\pi^+\pi^+$
<80	90	BOURQUIN	86	SPEC	$K(3100) \to \Lambda\overline{p}\pi^+\pi^-$

5-BODY DECAYS

VALUE (MeV)	CL%	DOCUMENT ID		TECN	COMMENT
• • • We do not use the following data for averages, fits, limits, etc. • • •					
<30	90	BOURQUIN	86	SPEC	$K(3100) \to \Lambda\overline{p}\pi^+\pi^+\pi^-$

[2] Supersedes ALEEV 90.

$K(3100)$ DECAY MODES

	Mode
Γ_1	$K(3100)^0 \to \Lambda\overline{p}\pi^+$
Γ_2	$K(3100)^{--} \to \Lambda\overline{p}\pi^-$
Γ_3	$K(3100)^- \to \Lambda\overline{p}\pi^+\pi^-$
Γ_4	$K(3100)^+ \to \Lambda\overline{p}\pi^+\pi^+$
Γ_5	$K(3100)^0 \to \Lambda\overline{p}\pi^+\pi^+\pi^-$
Γ_6	$K(3100)^0 \to \Sigma(1385)^+\overline{p}$

$\Gamma(\Sigma(1385)^+\overline{p})/\Gamma(\Lambda\overline{p}\pi^+)$ — Γ_6/Γ_1

VALUE	CL%	DOCUMENT ID		TECN	COMMENT
<0.04	90	ALEEV	93	BIS2	$K(3100)^0 \to \Sigma(1385)^+\overline{p}$

$K(3100)$ REFERENCES

ALEEV 93 PAN 56 1358 A.N. Aleev *et al.* (BIS-2 Collab.)
Translated from YAF 56 100.
BOEHNLEIN 91 NPBPS B21 174 A. Boehnlein *et al.* (FLOR, BNL, IND+)
ALEEV 90 ZPHY C47 533 A.N. Aleev *et al.* (BIS-2 Collab.)
BOURQUIN 86 PL B172 113 M.H. Bourquin *et al.* (GEVA, RAL, HEIDP+)

Int. J. Mod. Phys. A 2026.41. Downloaded from www.worldscientific.com
by UNIVERSITY OF CALIFORNIA @ BERKELEY on 09/16/26. Re-use and distribution is strictly not permitted, except for Open Access articles.

CHARMED MESONS
($C = \pm 1$)

$D^+ = c\overline{d}$, $D^0 = c\overline{u}$, $\overline{D}^0 = \overline{c}u$, $D^- = \overline{c}d$, similarly for D^*'s

$D^{\pm}$

$I(J^P) = \frac{1}{2}(0^-)$

$D^{\pm}$ MASS

The fit includes $D^{\pm}$, D^0, $D_s^{\pm}$, $D^{*\pm}$, D^{*0}, $D_s^{*\pm}$, $D_1(2420)^0$, $D_2^*(2460)^0$, and $D_{s1}(2536)^{\pm}$ mass and mass difference measurements.

VALUE (MeV)	EVTS	DOCUMENT ID		TECN	COMMENT
1869.66 ± 0.05 OUR FIT					
1869.55 ± 0.27 OUR AVERAGE					
1869.560 ± 0.288 ± 0.109	0.53k	ANASHIN	25A	KEDR	e^+e^- at $\psi(3770)$
1870.0 ± 0.5 ± 1.0	317	BARLAG	90C	ACCM	π^- Cu 230 GeV
1869.4 ± 0.6		[1] TRILLING	81	RVUE	e^+e^- 3.77 GeV
• • • We do not use the following data for averages, fits, limits, etc. • • •					
1869.560 ± 0.288 ± 0.090	320	ANASHIN	25	KEDR	Superseded by ANASHIN 25A
1869.53 ± 0.49 ± 0.20	110	ANASHIN	10A	KEDR	Superseded by ANASHIN 25
1875 ± 10	9	ADAMOVICH	87	EMUL	Photoproduction
1860 ± 16	6	ADAMOVICH	84	EMUL	Photoproduction
1863 ± 4		DERRICK	84	HRS	e^+e^- 29 GeV
1868.4 ± 0.5		[1] SCHINDLER	81	MRK2	e^+e^- 3.77 GeV
1874 ± 5		GOLDHABER	77	MRK1	D^0, D^+ recoil spectra
1868.3 ± 0.9		[1] PERUZZI	77	LGW	e^+e^- 3.77 GeV
1874 ± 11		PICCOLO	77	MRK1	e^+e^- 4.03, 4.41 GeV
1876 ± 15	50	PERUZZI	76	MRK1	$K^{\mp}\pi^{\pm}\pi^{\pm}$

[1] PERUZZI 77 and SCHINDLER 81 errors do not include the 0.13% uncertainty in the absolute SPEAR energy calibration. TRILLING 81 uses the high precision $J/\psi(1S)$ and $\psi(2S)$ measurements of ZHOLENTZ 80 to determine this uncertainty and combines the PERUZZI 77 and SCHINDLER 81 results to obtain the value quoted.

$D^{\pm}$ MEAN LIFE

Measurements with an error $> 100 \times 10^{-15}$ s have been omitted from the Listings.

VALUE (10^{-15} s)	EVTS	DOCUMENT ID		TECN	COMMENT
1033 ± 5 OUR AVERAGE					
1030.4 ± 4.7 ± 3.1	171k	[1] ABUDINEN	21A	BEL2	e^+e^- at $\Upsilon(4S)$
1039.4 ± 4.3 ± 7.0	110k	LINK	02F	FOCS	γ nucleus, ≈ 180 GeV
• • • We do not use the following data for averages, fits, limits, etc. • • •					
$1033.6 \pm 22.1 ^{+9.9}_{-12.7}$	3.7k	BONVICINI	99	CLEO	$e^+e^- \approx \Upsilon(4S)$
1048 ± 15 ± 11	9k	FRABETTI	94D	E687	$D^+ \to K^-\pi^+\pi^+$
1075 ± 40 ± 18	2.4k	FRABETTI	91	E687	γ Be, $D^+ \to K^-\pi^+\pi^+$
1030 ± 80 ± 60	200	ALVAREZ	90	NA14	γ, $D^+ \to K^-\pi^+\pi^+$
$1050 ^{+77}_{-72}$	317	[2] BARLAG	90C	ACCM	π^- Cu 230 GeV
1050 ± 80 ± 70	363	ALBRECHT	88I	ARG	e^+e^- 10 GeV
1090 ± 30 ± 25	2.9k	RAAB	88	E691	Photoproduction

[1] ABUDINEN 21A determines the lifetime ratio $\tau(D^+)/\tau(D^0) = 2.510 \pm 0.013 \pm 0.007$.
[2] BARLAG 90C estimates the systematic error to be negligible.

D^+ DECAY MODES

Most decay modes (other than the semileptonic modes) that involve a neutral K meson are now given as K^0_S modes, not as $\overline{K}^0$ modes. Nearly always it is a K^0_S that is measured, and interference between Cabibbo-allowed and doubly Cabibbo-suppressed modes can invalidate the assumption that $2\Gamma(K^0_S) = \Gamma(\overline{K}^0)$.

	Mode	Fraction (Γ_i/Γ)	Scale factor/ Confidence level
	Inclusive modes		
Γ_1	e^+ semileptonic	(16.07 ± 0.30) %	
Γ_2	μ^+ anything	(17.6 ± 3.2) %	
Γ_3	K^- anything	(25.7 ± 1.4) %	
Γ_4	K^0_S anything	(33.1 ± 0.4) %	
Γ_5	K^+ anything	(5.9 ± 0.8) %	
Γ_6	$K^*(892)^-$ anything	(6 ± 5) %	
Γ_7	$\overline{K}^*(892)^0$ anything	(23 ± 5) %	
Γ_8	$K^*(892)^0$ anything	< 6.6 %	CL=90%
Γ_9	η anything	(6.3 ± 0.7) %	
Γ_{10}	η' anything	(1.04 ± 0.18) %	
Γ_{11}	ϕ anything	(1.12 ± 0.04) %	
Γ_{12}	$\pi^+\pi^+\pi^-$ anything	(15.25 ± 0.20) %	
	Leptonic and semileptonic modes		
Γ_{13}	$e^+\nu_e$	< 9.7 $\times 10^{-7}$	CL=90%
Γ_{14}	$\gamma e^+\nu_e$	< 1.2 $\times 10^{-5}$	CL=90%
Γ_{15}	$\mu^+\nu_\mu$	(4.02 ± 0.09) $\times 10^{-4}$	
Γ_{16}	$\tau^+\nu_\tau$	(9.9 ± 1.2) $\times 10^{-4}$	
Γ_{17}	$\overline{K}^0 e^+\nu_e$	(8.81 ± 0.07) %	
Γ_{18}	$\overline{K}^0\mu^+\nu_\mu$	(8.68 ± 0.10) %	
Γ_{19}	$K^0_S\pi^0 e^+\nu_e$	(9.43 ± 0.16) $\times 10^{-3}$	
Γ_{20}	$(K^0_S\pi^0)_{S-wave} e^+\nu_e$	(6.03 ± 0.23) $\times 10^{-4}$	
Γ_{21}	$\overline{K}^*(892)^0 e^+\nu_e$, $\overline{K}^{*0} \to K^0_S\pi^0$	(8.82 ± 0.15) $\times 10^{-3}$	
Γ_{22}	$K^-\pi^+ e^+\nu_e$	(4.00 ± 0.17) %	S=3.1
Γ_{23}	$\overline{K}^*(892)^0 e^+\nu_e$, $\overline{K}^*(892)^0 \to K^-\pi^+$	(3.75 ± 0.16) %	
Γ_{24}	$(K^-\pi^+)_{[0.8-1.0]\text{GeV}} e^+\nu_e$	(3.39 ± 0.09) %	
Γ_{25}	$(K^-\pi^+)_{S-wave} e^+\nu_e$	(2.28 ± 0.11) $\times 10^{-3}$	
Γ_{26}	$\overline{K}^*(1410)^0 e^+\nu_e$, $\overline{K}^*(1410)^0 \to K^-\pi^+$	< 6 $\times 10^{-3}$	CL=90%
Γ_{27}	$\overline{K}^*_2(1430)^0 e^+\nu_e$, $\overline{K}^*_2(1430)^0 \to K^-\pi^+$	< 5 $\times 10^{-4}$	CL=90%
Γ_{28}	$K^-\pi^+ e^+\nu_e$ nonresonant	< 7 $\times 10^{-3}$	CL=90%
Γ_{29}	$\overline{K}^*(892)^0 e^+\nu_e$	(5.40 ± 0.10) %	S=1.1
Γ_{30}	$K^0_S\pi^0\mu^+\nu_\mu$	(8.96 ± 0.19) $\times 10^{-3}$	
Γ_{31}	$(K^0_S\pi^0)_{S-wave}\mu^+\nu_\mu$	(6.4 ± 0.7) $\times 10^{-4}$	
Γ_{32}	$\overline{K}^*(892)^0\mu^+\nu_\mu$, $\overline{K}^{*0} \to K^0_S\pi^0$	(8.32 ± 0.19) $\times 10^{-3}$	
Γ_{33}	$K^-\pi^+\mu^+\nu_\mu$	(3.62 ± 0.33) %	
Γ_{34}	$\overline{K}^*(892)^0\mu^+\nu_\mu$, $\overline{K}^*(892)^0 \to K^-\pi^+$	(3.52 ± 0.10) %	
Γ_{35}	$K^-\pi^+\mu^+\nu_\mu$ nonresonant	(1.9 ± 0.5) $\times 10^{-3}$	
Γ_{36}	$\overline{K}^*(892)^0\mu^+\nu_\mu$	(5.26 ± 0.15) %	S=1.1
Γ_{37}	$\overline{K}_1(1270)^0 e^+\nu_e$, $\overline{K}^0_1 \to K^-\pi^+\pi^0$	(1.23 ± 0.08) $\times 10^{-3}$	S=1.3
Γ_{38}	$\overline{K}_1(1270)^0 e^+\nu_e$, $\overline{K}^0_1 \to K^0_S\pi^+\pi^-$	$(1.5 ^{+0.5}_{-0.4}) \times 10^{-4}$	
Γ_{39}	$K^-\pi^+\pi^0\mu^+\nu_\mu$	< 1.5 $\times 10^{-3}$	CL=90%
Γ_{40}	$\overline{K}_1(1270)^0\mu^+\nu_\mu$, $\overline{K}^0_1 \to K^-\pi^+\pi^0$	$(1.09 ^{+0.12}_{-0.16}) \times 10^{-3}$	
Γ_{41}	$\overline{K}_1(1400)^0 e^+\nu_e$	< 1.4 $\times 10^{-4}$	CL=90%
Γ_{42}	$\overline{K}^*_0(1430)^0\mu^+\nu_\mu$	< 2.3 $\times 10^{-4}$	CL=90%
Γ_{43}	$\overline{K}^*(1680)^0\mu^+\nu_\mu$	< 1.4 $\times 10^{-3}$	CL=90%
Γ_{44}	$\pi^0 e^+\nu_e$	(3.72 ± 0.17) $\times 10^{-3}$	S=2.0
Γ_{45}	$\pi^0\mu^+\nu_\mu$	(3.50 ± 0.15) $\times 10^{-3}$	
Γ_{46}	$\eta e^+\nu_e$	(1.11 ± 0.07) $\times 10^{-3}$	
Γ_{47}	$\eta\mu^+\nu_\mu$	(1.04 ± 0.11) $\times 10^{-3}$	
Γ_{48}	$\pi^-\pi^+ e^+\nu_e$	(2.45 ± 0.08) $\times 10^{-3}$	
Γ_{49}	$f_0(500)^0 e^+\nu_e$, $f_0(500)^0 \to \pi^+\pi^-$	(6.2 ± 0.4) $\times 10^{-4}$	
Γ_{50}	$\rho^0 e^+\nu_e$	(1.87 ± 0.06) $\times 10^{-3}$	
Γ_{51}	$\pi^-\pi^+\mu^+\nu_\mu$		
Γ_{52}	$f_0(500)^0\mu^+\nu_\mu$, $f^0_0 \to \pi^+\pi^-$	(7.2 ± 1.5) $\times 10^{-4}$	
Γ_{53}	$\rho^0\mu^+\nu_\mu$	(1.64 ± 0.16) $\times 10^{-3}$	
Γ_{54}	$\omega e^+\nu_e$	(1.69 ± 0.11) $\times 10^{-3}$	
Γ_{55}	$\omega\mu^+\nu_\mu$	(1.77 ± 0.21) $\times 10^{-3}$	
Γ_{56}	$\eta'(958) e^+\nu_e$	(1.84 ± 0.19) $\times 10^{-4}$	
Γ_{57}	$\eta'(958)\mu^+\nu_\mu$	(1.92 ± 0.29) $\times 10^{-4}$	
Γ_{58}	$a(980)^0 e^+\nu_e$, $a(980)^0 \to \eta\pi^0$	$(1.7 ^{+0.8}_{-0.7}) \times 10^{-4}$	
Γ_{59}	$K^0_S K^0_S e^+\nu_e$	< 1.54 $\times 10^{-5}$	CL=90%
Γ_{60}	$K^0_S\eta e^+\nu_e$	< 2.0 $\times 10^{-4}$	CL=90%
Γ_{61}	$\eta\eta e^+\nu_e$	< 1.0 $\times 10^{-4}$	CL=90%
Γ_{62}	$K^+K^- e^+\nu_e$	< 2.10 $\times 10^{-5}$	CL=90%
Γ_{63}	$b_1(1235)^0 e^+\nu_e$, $b^0_1 \to \omega\pi^0$	< 1.75 $\times 10^{-4}$	CL=90%
Γ_{64}	$\phi e^+\nu_e$	< 1.3 $\times 10^{-5}$	CL=90%
Γ_{65}	$D^0 e^+\nu_e$	< 1.0 $\times 10^{-4}$	CL=90%
	Hadronic modes with a $\overline{K}$ or $\overline{K}K\overline{K}$		
Γ_{66}	$K^0_S\pi^+$	(1.554 ± 0.033) %	S=1.8
Γ_{67}	$K^0_L\pi^+$	(1.46 ± 0.05) %	
Γ_{68}	$K^-2\pi^+$ [a]	(9.31 ± 0.14) %	S=1.4

Int. J. Mod. Phys. A 2026.41. Downloaded from www.worldscientific.com
by [redacted] LIFORNIA @ BERKELEY on 09/16/26. Re-use and distribution is strictly not permitted, except for Open Access articles.

Γ_{69}	$(K^-\pi^+)_{S-\text{wave}}\pi^+$		(7.46 ± 0.16) %	
Γ_{70}	$\overline{K}_0^*(700)^0\pi^+$, $\overline{K}_0^* \to K^-\pi^+$			
Γ_{71}	$\overline{K}_0^*(1430)^0\pi^+$, $\overline{K}_0^*(1430)^0 \to K^-\pi^+$	[b]	(1.24 ± 0.06) %	
Γ_{72}	$\overline{K}^*(892)^0\pi^+$, $\overline{K}^*(892)^0 \to K^-\pi^+$		(1.03 ± 0.11) %	
Γ_{73}	$\overline{K}^*(1410)^0\pi^+$, $\overline{K}^{*0} \to K^-\pi^+$		not seen	
Γ_{74}	$\overline{K}_2^*(1430)^0\pi^+$, $\overline{K}_2^*(1430)^0 \to K^-\pi^+$	[b]	$(2.2 \pm 0.7) \times 10^{-4}$	
Γ_{75}	$\overline{K}^*(1680)^0\pi^+$, $\overline{K}^*(1680)^0 \to K^-\pi^+$	[b]	$(2.2 \pm 1.1) \times 10^{-4}$	
Γ_{76}	$K^-(2\pi^+)_{I=2}$		(1.44 ± 0.26) %	
Γ_{77}	$K^-2\pi^+$ nonresonant			
Γ_{78}	$K_S^0\pi^+\pi^0$	[a]	(7.31 ± 0.20) %	
Γ_{79}	$K_S^0\rho^+$		$(6.10 {}^{+0.60}_{-0.35})$ %	
Γ_{80}	$K_S^0\rho(1450)^+$, $\rho^+ \to \pi^+\pi^0$		$(1.5 {}^{+1.2}_{-1.4}) \times 10^{-3}$	
Γ_{81}	$\overline{K}^*(892)^0\pi^+$, $\overline{K}^*(892)^0 \to K_S^0\pi^0$		$(2.62 \pm 0.32) \times 10^{-3}$	
Γ_{82}	$\overline{K}_0^*(1430)^0\pi^+$, $\overline{K}_0^{*0} \to K_S^0\pi^0$		$(2.7 \pm 0.9) \times 10^{-3}$	
Γ_{83}	$\overline{K}_0^*(1680)^0\pi^+$, $\overline{K}_0^{*0} \to K_S^0\pi^0$		$(10 {}^{+7}_{-10}) \times 10^{-4}$	
Γ_{84}	$\overline{\kappa}^0\pi^+$, $\overline{\kappa}^0 \to K_S^0\pi^0$		$(6 {}^{+5}_{-4}) \times 10^{-3}$	
Γ_{85}	$K_S^0\pi^+\pi^0$ nonresonant		$(3 \pm 4) \times 10^{-3}$	
Γ_{86}	$K_S^0\pi^+\pi^0$ nonresonant and $\overline{\kappa}^0\pi^+$		$(1.36 {}^{+0.21}_{-0.40})$ %	
Γ_{87}	$(K_S^0\pi^0)_{S-\text{wave}}\pi^+$		$(1.26 {}^{+0.27}_{-0.33})$ %	
Γ_{88}	$K_S^0\pi^+\omega$		$(7.1 \pm 0.5) \times 10^{-3}$	
Γ_{89}	$K_S^0\pi^+\eta$		(1.27 ± 0.05) %	
Γ_{90}	$K_S^0a_0(980)^+$, $a_0^+ \to \pi^+\eta$		(1.33 ± 0.06) %	
Γ_{91}	$\overline{K}_0^*(1430)^0\pi^+$, $\overline{K}_0^* \to K_S^0\eta$		$(1.38 \pm 0.26) \times 10^{-3}$	
Γ_{92}	$K_S^0\pi^+\eta'(958)$		$(1.90 \pm 0.21) \times 10^{-3}$	
Γ_{93}	$K^-2\pi^+\pi^0$	[c]	(6.35 ± 0.08) %	
Γ_{94}	$\overline{K}^*(892)^0\rho(770)^+$, $\overline{K}^{*0} \to K^-\pi^+$, $\rho^+ \to \pi^0\pi^+$		(4.34 ± 0.19) %	
Γ_{95}	$\overline{K}_1(1270)^0\pi^+$, $\overline{K}_1^0 \to K^-\rho(770)^+$, $\rho^+ \to \pi^+\pi^0$		$(2.41 \pm 0.27) \times 10^{-3}$	
Γ_{96}	$\overline{K}_1(1400)^0\pi^+$, $\overline{K}_1^0 \to \overline{K}^*(892)\pi$, $\overline{K}^* \to K^-\pi$		$(4.64 \pm 0.24) \times 10^{-3}$	
Γ_{97}	$\overline{K}(1460)^0\pi^+$, $\overline{K}(1460)^0 \to \overline{K}^*(892)\pi$, $\overline{K}^* \to K^-\pi$		$(3.24 \pm 0.23) \times 10^{-3}$	
Γ_{98}	$\overline{K}^*(1680)^0\pi^+$, $\overline{K}^{*0} \to \overline{K}^*(892)\pi$, $\overline{K}^* \to K^-\pi$		$(2.4 \pm 0.6) \times 10^{-3}$	
Γ_{99}	$(K^-\pi^+)_{S-wave}\rho(770)^+$, $\rho^+ \to \pi^+\pi^0$		(1.16 ± 0.06) %	
Γ_{100}	$\overline{K}(1460)^0\pi^+$, $\overline{K}(1460)^0 \to K^-(\pi^+\pi^0)_{L=1}$		$(5.5 \pm 0.6) \times 10^{-3}$	
Γ_{101}	$\overline{K}(1460)^0\pi^+$, $\overline{K}(1460)^0 \to (K^-\pi)_{L=1}\pi$		$(2.2 \pm 0.4) \times 10^{-3}$	
Γ_{102}	$(K^-\rho(770)^+)_{L=1}\pi^+$, $\rho^+ \to \pi^+\pi^0$		$(1.14 \pm 0.09) \times 10^{-3}$	
Γ_{103}	$(\overline{K}^*(892)\pi)_{L=1}\pi^+$, $\overline{K}^* \to K^-\pi$		$(5.1 \pm 0.9) \times 10^{-4}$	
Γ_{104}	$(\overline{K}^*(892)^0\pi^+)_{L=1}\pi^0$, $\overline{K}^{*0} \to K^-\pi^+$		$(5.1 \pm 2.8) \times 10^{-4}$	
Γ_{105}	$(K^-(\pi^+\pi^0)_{L=0})_{L=1}\pi^+$		$(5.1 \pm 1.8) \times 10^{-4}$	
Γ_{106}	$(K^-\pi^+)_{L=1}\rho(770)^+$, $\rho^+ \to \pi^+\pi^0$		$(3.2 \pm 0.9) \times 10^{-4}$	
Γ_{107}	$K_S^0 2\pi^+\pi^-$	[c]	(3.08 ± 0.08) %	
Γ_{108}	$K_S^0\pi^+2\pi^0$		(2.89 ± 0.09) %	
Γ_{109}	$K_S^0a_1(1260)^+$, $a_1^+ \to \rho(770)^+\pi^0$		$(8.7 \pm 1.6) \times 10^{-3}$	
Γ_{110}	$K_S^0a_1(1260)^+$, $a_1^+ \to f_0(500)\pi^+$, $f_0 \to \pi^0\pi^0$		$(1.0 \pm 0.6) \times 10^{-3}$	
Γ_{111}	$\overline{K}_1(1400)^0\pi^+$, $\overline{K}_1^0 \to \overline{K}^*(892)^0\pi^0$, $\overline{K}^{*0} \to K_S^0\pi^0$		$(2.3 \pm 0.4) \times 10^{-3}$	
Γ_{112}	$\overline{K}^*(892)^0\rho^+$, $\overline{K}^{*0} \to K_S^0\pi^0$		$(9.7 \pm 0.9) \times 10^{-3}$	
Γ_{113}	$\overline{K}^*(892)^0\pi^+\pi^0$ non-resonant, $\overline{K}^{*0} \to K_S^0\pi^0$		$(2.6 \pm 0.7) \times 10^{-3}$	
Γ_{114}	$K_S^0\rho^+\pi^0$ non-resonant		$(4.8 \pm 0.5) \times 10^{-3}$	
Γ_{115}	$K^-2\pi^+\eta$		$(1.35 \pm 0.12) \times 10^{-3}$	
Γ_{116}	$K_S^0\pi^+\pi^0\eta$		$(1.22 \pm 0.25) \times 10^{-3}$	
Γ_{117}	$K^-3\pi^+\pi^-$	[a]	$(5.7 \pm 0.5) \times 10^{-3}$	S=1.1
Γ_{118}	$\overline{K}^*(892)^0 2\pi^+\pi^-$, $\overline{K}^*(892)^0 \to K^-\pi^+$		$(1.2 \pm 0.4) \times 10^{-3}$	
Γ_{119}	$\overline{K}^*(892)^0\rho^0\pi^+$, $\overline{K}^*(892)^0 \to K^-\pi^+$		$(2.3 \pm 0.4) \times 10^{-3}$	
Γ_{120}	$\overline{K}^*(892)^0a_1(1260)^+$	[d]	$(9.2 \pm 1.8) \times 10^{-3}$	
Γ_{121}	$\overline{K}^*(892)^0 2\pi^+\pi^-$ no-ρ, $\overline{K}^*(892)^0 \to K^-\pi^+$			
Γ_{122}	$K^-\rho^0 2\pi^+$		$(1.70 \pm 0.28) \times 10^{-3}$	
Γ_{123}	$K^-3\pi^+\pi^-$ nonresonant		$(4.0 \pm 2.9) \times 10^{-4}$	
Γ_{124}	$K_S^0 2\pi^+\pi^-\pi^0$		(1.53 ± 0.08) %	
Γ_{125}	$K_S^0\pi^+3\pi^0$		$(5.5 \pm 0.5) \times 10^{-3}$	
Γ_{126}	$K^-2\pi^+2\pi^0$		$(4.95 \pm 0.32) \times 10^{-3}$	
Γ_{127}	$K^-3\pi^+\pi^-\pi^0$		$(6.6 \pm 0.8) \times 10^{-4}$	
Γ_{128}	$K^+2K_S^0$		$(2.54 \pm 0.13) \times 10^{-3}$	
Γ_{129}	$K^+K^-K_S^0\pi^+$		$(2.4 \pm 0.5) \times 10^{-4}$	

Pionic modes

Γ_{130}	$\pi^+\pi^0$		$(1.243 \pm 0.033) \times 10^{-3}$	
Γ_{131}	$2\pi^+\pi^-$		$(3.27 \pm 0.09) \times 10^{-3}$	
Γ_{132}	$\rho^0\pi^+$		$(8.4 \pm 0.8) \times 10^{-4}$	
Γ_{133}	$\pi^+(\pi^+\pi^-)_{S-\text{wave}}$		$(2.01 \pm 0.06) \times 10^{-3}$	
Γ_{134}	$\sigma\pi^+$, $\sigma \to \pi^+\pi^-$		$(1.38 \pm 0.10) \times 10^{-3}$	
Γ_{135}	$f_0(980)\pi^+$, $f_0 \to \pi^+\pi^-$		$(1.57 \pm 0.32) \times 10^{-4}$	
Γ_{136}	$f_0(1370)\pi^+$, $f_0 \to \pi^+\pi^-$		$(8 \pm 4) \times 10^{-5}$	
Γ_{137}	$\omega\pi^+$, $\omega \to \pi^+\pi^-$		$(3.4 \pm 0.5) \times 10^{-6}$	
Γ_{138}	$f_2(1270)\pi^+$, $f_2 \to \pi^+\pi^-$		$(4.58 \pm 0.28) \times 10^{-4}$	
Γ_{139}	$\rho(1450)^0\pi^+$, $\rho^0 \to \pi^+\pi^-$		$(1.8 \pm 0.5) \times 10^{-4}$	
Γ_{140}	$\rho(1700)^0\pi^+$, $\rho^0 \to \pi^+\pi^-$		$(1.9 \pm 0.5) \times 10^{-4}$	
Γ_{141}	$f_0(1500)\pi^+$, $f_0 \to \pi^+\pi^-$		$(1.1 \pm 0.4) \times 10^{-4}$	
Γ_{142}	$f_0(1710)\pi^+$, $f_0 \to \pi^+\pi^-$		$< 5 \times 10^{-5}$	CL=95%
Γ_{143}	$f_0(1790)\pi^+$, $f_0 \to \pi^+\pi^-$		$< 7 \times 10^{-5}$	CL=95%
Γ_{144}	$(\pi^+\pi^+)_{S-\text{wave}}\pi^-$		$< 1.2 \times 10^{-4}$	CL=95%
Γ_{145}	$2\pi^+\pi^-$ nonresonant		$< 1.1 \times 10^{-4}$	CL=95%
Γ_{146}	$\pi^+2\pi^0$		$(4.61 \pm 0.15) \times 10^{-3}$	
Γ_{147}	$2\pi^+\pi^-\pi^0$		(1.165 ± 0.030) %	
Γ_{148}	$\pi^+3\pi^0$		$(4.17 \pm 0.26) \times 10^{-3}$	
Γ_{149}	$\pi^+4\pi^0$		$(1.9 \pm 0.4) \times 10^{-3}$	
Γ_{150}	$2\pi^+\pi^-2\pi^0$		(1.07 ± 0.05) %	
Γ_{151}	$3\pi^+2\pi^-$		$(1.64 \pm 0.16) \times 10^{-3}$	S=1.1
Γ_{152}	$2\pi^+\pi^-3\pi^0$		$(3.42 \pm 0.35) \times 10^{-3}$	
Γ_{153}	$3\pi^+2\pi^-\pi^0$		$(2.34 \pm 0.27) \times 10^{-3}$	
Γ_{154}	$\eta\pi^+$		$(3.75 \pm 0.09) \times 10^{-3}$	
Γ_{155}	$\eta\pi^+\pi^0$		$(2.05 \pm 0.35) \times 10^{-3}$	S=2.2
Γ_{156}	$\rho(770)^+\eta$, $\rho^+ \to \pi^+\pi^0$		$(1.9 \pm 0.8) \times 10^{-4}$	
Γ_{157}	$a_0(980)^+\pi^0$, $a_0^+ \to \pi^+\eta$		$(9.0 \pm 1.9) \times 10^{-4}$	
Γ_{158}	$a_0(980)^0\pi^+$, $a_0^0 \to \pi^0\eta$		$(3.5 \pm 1.1) \times 10^{-4}$	
Γ_{159}	$a_2(1700)^+\pi^0$, $a_2^+ \to \pi^+\eta$		$(9 \pm 5) \times 10^{-5}$	
Γ_{160}	$a_0(1450)^+\pi^0$, $a_0^+ \to \pi^+\eta$		$(1.4 \pm 0.6) \times 10^{-4}$	
Γ_{161}	$\eta 2\pi^+\pi^-$		$(3.41 \pm 0.20) \times 10^{-3}$	
Γ_{162}	$\eta\pi^+2\pi^0$		$(3.20 \pm 0.33) \times 10^{-3}$	
Γ_{163}	$\eta\pi^+3\pi^0$		$(2.9 \pm 0.5) \times 10^{-3}$	
Γ_{164}	$\eta 2\pi^+\pi^-\pi^0$		$(3.88 \pm 0.34) \times 10^{-3}$	
Γ_{165}	$\eta\eta\pi^+$		$(2.96 \pm 0.26) \times 10^{-3}$	
Γ_{166}	$\omega\pi^+$		$(2.8 \pm 0.6) \times 10^{-4}$	
Γ_{167}	$\omega\pi^+\pi^0$		$(3.9 \pm 0.9) \times 10^{-3}$	
Γ_{168}	$\eta'(958)\pi^+$		$(4.96 \pm 0.18) \times 10^{-3}$	
Γ_{169}	$\eta'(958)\pi^+\pi^0$		$(1.6 \pm 0.5) \times 10^{-3}$	

Hadronic modes with a $K\overline{K}$ pair

Γ_{170}	$K_S^0K^+$		$(3.02 \pm 0.09) \times 10^{-3}$	S=2.2
Γ_{171}	$K_L^0K^+$		$(3.21 \pm 0.16) \times 10^{-3}$	
Γ_{172}	$K_S^0K^+\pi^0$		$(5.07 \pm 0.30) \times 10^{-3}$	
Γ_{173}	$K^*(892)^+K_S^0$, $K^{*+} \to K^+\pi^0$		$(2.89 \pm 0.30) \times 10^{-3}$	
Γ_{174}	$\overline{K}^*(892)^0K^+$, $\overline{K}^{*0} \to K_S^0\pi^0$		$(5.2 \pm 1.4) \times 10^{-4}$	
Γ_{175}	$K^*(892)^+K_S^0$			
Γ_{176}	$K_L^0K^+\pi^0$		$(5.24 \pm 0.31) \times 10^{-3}$	
Γ_{177}	$K^+K^-\pi^+$	[a]	$(9.61 \pm 0.17) \times 10^{-3}$	

Int. J. Mod. Phys. A 2026.41. Downloaded from www.worldscientific.com by UNIVERSITY OF CALIFORNIA @ BERKELEY on 09/16/26. Re-use and distribution is strictly not permitted, except for Open Access articles.

Γ_{178}	$K^+\overline{K}^*(892)^0$, $\overline{K}^*(892)^0 \to K^-\pi^+$	$(2.47 \pm^{0.08}_{0.13}) \times 10^{-3}$	
Γ_{179}	$K^+\overline{K}^*_0(1430)^0$, $\overline{K}^*_0(1430)^0 \to K^-\pi^+$	$(1.81 \pm 0.34) \times 10^{-3}$	
Γ_{180}	$K^+\overline{K}^*_2(1430)^0$, $\overline{K}^*_2 \to K^-\pi^+$	$(1.6 \pm^{1.2}_{0.8}) \times 10^{-4}$	
Γ_{181}	$K^+\overline{K}^*_0(700)$, $\overline{K}^*_0 \to K^-\pi^+$	$(6.7 \pm^{3.5}_{2.1}) \times 10^{-4}$	
Γ_{182}	$a_0(1450)^0\pi^+$, $a_0^0 \to K^+K^-$	$(4.4 \pm^{7.0}_{1.8}) \times 10^{-4}$	
Γ_{183}	$\phi(1680)\pi^+$, $\phi \to K^+K^-$	$(4.9 \pm^{4.0}_{1.9}) \times 10^{-5}$	
Γ_{184}	$\phi\pi^+$, $\phi \to K^+K^-$	$(2.67 \pm^{0.06}_{0.08}) \times 10^{-3}$	
Γ_{185}	$\phi\pi^+$	$(5.70 \pm 0.14) \times 10^{-3}$	
Γ_{186}	$K^+K^-\pi^+\pi^0$	$(6.62 \pm 0.32) \times 10^{-3}$	
Γ_{187}	$K^0_S K^0_S \pi^+$	$(2.97 \pm 0.10) \times 10^{-3}$	
Γ_{188}	$K^0_S K^*(892)^+$, $K^{*+} \to K^0_S\pi^+$	$(2.90 \pm 0.11) \times 10^{-3}$	
Γ_{189}	$K^0_S(K^0_S\pi^+) \to K^0_S K^0_S \pi^+$	$(1.31 \pm 0.34) \times 10^{-4}$	
Γ_{190}	$K^0_S K^0_S \pi^+\pi^0$	$(1.34 \pm 0.21) \times 10^{-3}$	
Γ_{191}	$K^0_S K^+\pi^+\pi^-\pi^0$	$(2.5 \pm 0.4) \times 10^{-4}$	
Γ_{192}	$K^0_S K^+\omega$	$(2.0 \pm 0.4) \times 10^{-4}$	
Γ_{193}	$K^0_S K^+\eta$	$(2.27 \pm 0.23) \times 10^{-4}$	
Γ_{194}	$K^+K^0_S\pi^+\pi^-$	$(1.89 \pm 0.13) \times 10^{-3}$	
Γ_{195}	$K^0_S K^+\pi^0\pi^0$	$(5.8 \pm 1.3) \times 10^{-4}$	
Γ_{196}	$K^0_S K^-2\pi^+$	$(2.27 \pm 0.13) \times 10^{-3}$	
Γ_{197}	$K^+K^-2\pi^+\pi^-$	$(6.7 \pm 1.1) \times 10^{-5}$	
Γ_{198}	$\phi 2\pi^+\pi^-$	$(5.4 \pm 1.9) \times 10^{-5}$	
	A few poorly measured branching fractions:		
Γ_{199}	$\phi\pi^+\pi^0$	(2.3 ± 1.0) %	
Γ_{200}	$\phi\rho^+$	< 1.5 %	CL=90%
Γ_{201}	$K^+K^-\pi^+\pi^0$ non-ϕ	$(1.5 \pm^{0.7}_{0.6})$ %	
	Radiative modes		
Γ_{202}	$\rho(770)^+\gamma$	$< 1.3 \times 10^{-5}$	CL=90%
Γ_{203}	$K^*(892)^+\gamma$	$< 1.8 \times 10^{-5}$	CL=90%
	Doubly Cabibbo-suppressed modes		
Γ_{204}	$K^+\pi^0$	$(1.54 \pm 0.13) \times 10^{-4}$	S=1.4
Γ_{205}	$K^+\eta$	$(1.16 \pm 0.09) \times 10^{-4}$	
Γ_{206}	$K^+\eta'(958)$	$(1.88 \pm 0.14) \times 10^{-4}$	
Γ_{207}	$K^+2\pi^0$	$(2.1 \pm 0.4) \times 10^{-4}$	
Γ_{208}	$K^*(892)^+\pi^0$	$(3.4 \pm 1.4) \times 10^{-4}$	
Γ_{209}	$K^+\pi^+\pi^-$	$(4.88 \pm 0.08) \times 10^{-4}$	S=1.4
Γ_{210}	$K^+\rho^0$	$(1.9 \pm 0.4) \times 10^{-4}$	
Γ_{211}	$K^+\eta\pi^0$	$(2.1 \pm 0.5) \times 10^{-4}$	
Γ_{212}	$K^*(892)^+\eta$	$(4.4 \pm^{1.8}_{1.5}) \times 10^{-4}$	
Γ_{213}	$K^*(892)^0\pi^+$, $K^*(892)^0 \to K^+\pi^-$	$(2.3 \pm 0.4) \times 10^{-4}$	
Γ_{214}	$K^+f_0(980)$, $f_0(980) \to \pi^+\pi^-$	$(4.4 \pm 2.6) \times 10^{-5}$	
Γ_{215}	$K^*_2(1430)^0\pi^+$, $K^*_2(1430)^0 \to K^+\pi^-$	$(3.9 \pm 2.6) \times 10^{-5}$	
Γ_{216}	$K^+\pi^+\pi^-$ nonresonant	not seen	
Γ_{217}	$K^+\pi^+\pi^-\pi^0$	$(1.21 \pm 0.09) \times 10^{-3}$	
Γ_{218}	$K^+\pi^+\pi^-\pi^0$ nonresonant	$(1.10 \pm 0.07) \times 10^{-3}$	
Γ_{219}	$K^+\pi^+\pi^-\eta$	$(1.56 \pm 0.22) \times 10^{-4}$	
Γ_{220}	$K^+(\pi^+\pi^-\eta)_{non-\eta'}$	$(6.7 \pm 1.8) \times 10^{-5}$	
Γ_{221}	$K^+\omega$	$(5.7 \pm^{2.5}_{2.1}) \times 10^{-5}$	
Γ_{222}	$K^+\eta\eta$	$(5.9 \pm 2.3) \times 10^{-5}$	
Γ_{223}	$2K^+K^-$	$(6.09 \pm 0.10) \times 10^{-5}$	S=1.3
Γ_{224}	$\phi(1020)^0K^+$	$< 2.1 \times 10^{-5}$	CL=90%
Γ_{225}	$K^+\phi(1020)$, $\phi \to K^+K^-$	$(4.3 \pm 0.6) \times 10^{-6}$	
Γ_{226}	$K^+(K^+K^-)_{S-wave}$	$(5.72 \pm 0.11) \times 10^{-5}$	
	$\Delta C = 1$ weak neutral current ($C1$) modes, or Lepton Family number (LF), or Lepton number (L), or Baryon number (B) violating modes		
Γ_{227}	$\pi^+e^+e^-$	$C1$ $< 1.1 \times 10^{-6}$	CL=90%
Γ_{228}	$\pi^+\pi^0e^+e^-$	$< 1.4 \times 10^{-5}$	CL=90%
Γ_{229}	$\pi^+\phi$, $\phi \to e^+e^-$	[e] $(1.7 \pm^{1.4}_{0.9}) \times 10^{-6}$	
Γ_{230}	$\pi^+\mu^+\mu^-$	$C1$ $< 6.7 \times 10^{-8}$	CL=90%
Γ_{231}	$\pi^+\phi$, $\phi \to \mu^+\mu^-$	[e] $(1.8 \pm 0.8) \times 10^{-6}$	
Γ_{232}	$\rho^+\mu^+\mu^-$	$C1$ $< 5.6 \times 10^{-4}$	CL=90%
Γ_{233}	$K^+e^+e^-$	[f] $< 8.5 \times 10^{-7}$	CL=90%
Γ_{234}	$K^+\pi^0e^+e^-$	$< 1.5 \times 10^{-5}$	CL=90%
Γ_{235}	$K^0_S\pi^+e^+e^-$	$< 2.6 \times 10^{-5}$	CL=90%
Γ_{236}	$K^0_S K^+e^+e^-$	$< 1.1 \times 10^{-5}$	CL=90%
Γ_{237}	$K^+\mu^+\mu^-$	[f] $< 5.4 \times 10^{-8}$	CL=90%
Γ_{238}	$\pi^+e^+\mu^-$	LF $< 2.1 \times 10^{-7}$	CL=90%
Γ_{239}	$\pi^+e^-\mu^+$	LF $< 2.2 \times 10^{-7}$	CL=90%
Γ_{240}	$K^+e^+\mu^-$	LF $< 7.5 \times 10^{-8}$	CL=90%
Γ_{241}	$K^+e^-\mu^+$	LF $< 1.0 \times 10^{-7}$	CL=90%
Γ_{242}	π^-2e^+	L $< 5.3 \times 10^{-7}$	CL=90%
Γ_{243}	$\pi^-2\mu^+$	L $< 1.4 \times 10^{-8}$	CL=90%
Γ_{244}	$\pi^-e^+\mu^+$	L $< 1.3 \times 10^{-7}$	CL=90%
Γ_{245}	$\rho^-2\mu^+$	L $< 5.6 \times 10^{-4}$	CL=90%
Γ_{246}	K^-2e^+	L $< 9 \times 10^{-7}$	CL=90%
Γ_{247}	$K^0_S\pi^-2e^+$	L $< 3.3 \times 10^{-6}$	CL=90%
Γ_{248}	$K^-\pi^02e^+$	L $< 8.5 \times 10^{-6}$	CL=90%
Γ_{249}	$K^-2\mu^+$	L $< 1.0 \times 10^{-5}$	CL=90%
Γ_{250}	$K^-e^+\mu^+$	L $< 1.9 \times 10^{-6}$	CL=90%
Γ_{251}	$K^*(892)^-2\mu^+$	L $< 8.5 \times 10^{-4}$	CL=90%
Γ_{252}	Λe^+	L,B $< 1.1 \times 10^{-6}$	CL=90%
Γ_{253}	$\overline{\Lambda}e^+$	L,B $< 6.5 \times 10^{-7}$	CL=90%
Γ_{254}	Σ^0e^+	L,B $< 1.7 \times 10^{-6}$	CL=90%
Γ_{255}	$\overline{\Sigma}^0e^+$	L,B $< 1.3 \times 10^{-6}$	CL=90%
Γ_{256}	$\overline{n}e^+$	$< 1.43 \times 10^{-5}$	CL=90%
Γ_{257}	ne^+	$< 2.91 \times 10^{-5}$	CL=90%

[a] The branching fraction for this mode may differ from the sum of the submodes that contribute to it, due to interference effects. See the relevant papers.

[b] These subfractions of the $K^-2\pi^+$ mode are uncertain: see the Particle Listings.

[c] See the listings under "$D \to K\pi\pi\pi$ partial wave analyses" and our 2008 Review (Physics Letters **B667** 1 (2008)) for measurements of submodes of this mode.

[d] The unseen decay modes of the resonances are included.

[e] This is *not* a test for the ΔC=1 weak neutral current, but leads to the $\pi^+\ell^+\ell^-$ final state.

[f] This mode is not a useful test for a ΔC=1 weak neutral current because both quarks must change flavor in this decay.

FIT INFORMATION

An overall fit to 41 branching ratios uses 57 measurements to determine 21 parameters. The overall fit has a $\chi^2 = 81.9$ for 36 degrees of freedom.

The following *off-diagonal* array elements are the correlation coefficients $\langle \delta x_i \delta x_j \rangle / (\delta x_i \cdot \delta x_j)$, in percent, from the fit to the branching fractions, $x_i \equiv \Gamma_i/\Gamma_{total}$.

	x_{18}	x_{22}	x_{29}	x_{36}	x_{48}	x_{49}	x_{50}	x_{66}	x_{68}	x_{117}
x_{22}	0									
x_{29}	0	0								
x_{36}	0	1	0							
x_{48}	0	0	0	0						
x_{49}	0	0	0	0	34					
x_{50}	0	0	0	0	73	25				
x_{66}	0	5	0	0	0	0	0			
x_{68}	0	26	0	3	0	0	0	19		
x_{117}	0	5	0	0	0	0	0	3	17	
x_{130}	0	5	0	1	0	0	0	4	20	3
x_{151}	0	4	0	0	0	0	0	3	16	75
x_{154}	0	3	0	0	0	0	0	2	13	2
x_{168}	0	4	0	0	0	0	0	3	17	3
x_{170}	0	8	0	1	0	0	0	30	30	5
x_{197}	0	0	0	0	0	0	0	0	0	0
x_{204}	0	1	0	0	0	0	0	1	3	1
x_{205}	0	0	0	0	0	0	0	0	1	0
x_{206}	0	1	0	0	0	0	0	1	4	1
x_{209}	0	25	0	3	0	0	0	18	95	16
x_{223}	0	24	0	2	0	0	0	17	90	15

	x_{130}	x_{151}	x_{154}	x_{168}	x_{170}	x_{197}	x_{204}	x_{205}	x_{206}	x_{209}
x_{151}	3									
x_{154}	3	2								
x_{168}	3	3	2							
x_{170}	6	5	4	5						
x_{197}	0	0	0	0	0					
x_{204}	1	1	0	1	1	0				
x_{205}	0	0	8	0	0	0	0			
x_{206}	1	1	0	23	1	0	0	0		
x_{209}	19	15	12	16	29	0	3	1	4	
x_{223}	18	14	11	15	27	0	3	1	4	86

D^+ BRANCHING RATIOS

Some now-obsolete measurements have been omitted from these Listings.

c-quark decays

$\Gamma(c \to e^+ \text{anything})/\Gamma(c \to \text{anything})$

For the Summary Table, we only use the average of e^+ and μ^+ measurements from $Z^0 \to c\overline{c}$ decays; see the second data block below.

VALUE	EVTS	DOCUMENT ID		TECN	COMMENT
$0.103 \pm 0.009^{+0.009}_{-0.008}$	378	[1] ABBIENDI	99K	OPAL	$Z^0 \to c\overline{c}$

[1] ABBIENDI 99K uses the excess of right-sign over wrong-sign leptons opposite reconstructed $D^*(2010)^+ \to D^0\pi^+$ decays in $Z^0 \to c\overline{c}$.

$\Gamma(c \to \mu^+ \text{anything})/\Gamma(c \to \text{anything})$

For the Summary Table, we only use the average of e^+ and μ^+ measurements from $Z^0 \to c\overline{c}$ decays; see the next data block.

VALUE	EVTS	DOCUMENT ID		TECN	COMMENT
0.082±0.005 OUR AVERAGE					
$0.073 \pm 0.008 \pm 0.002$	73	KAYIS-TOPAK.	05	CHRS	ν_μ emulsion
$0.095 \pm 0.007^{+0.014}_{-0.013}$	2829	ASTIER	00D	NOMD	$\nu_\mu \text{Fe} \to \mu^-\mu^+ X$
$0.090 \pm 0.007^{+0.007}_{-0.006}$	476	[1] ABBIENDI	99K	OPAL	$Z^0 \to c\overline{c}$
$0.086 \pm 0.017^{+0.008}_{-0.007}$	69	[2] ALBRECHT	92F	ARG	$e^+e^- \approx 10$ GeV
$0.078 \pm 0.009 \pm 0.012$		ONG	88	MRK2	e^+e^- 29 GeV
$0.078 \pm 0.015 \pm 0.02$		BARTEL	87	JADE	e^+e^- 34.6 GeV
$0.082 \pm 0.012^{+0.02}_{-0.01}$		ALTHOFF	84G	TASS	e^+e^- 34.5 GeV
• • • We do not use the following data for averages, fits, limits, etc. • • •					
$0.093 \pm 0.009 \pm 0.009$	88	KAYIS-TOPAK.	02	CHRS	See KAYIS-TOPAKSU 05
$0.089 \pm 0.018 \pm 0.025$		BARTEL	85J	JADE	See BARTEL 87

[1] ABBIENDI 99K uses the excess of right-sign over wrong-sign leptons opposite reconstructed $D^*(2010)^+ \to D^0\pi^+$ decays in $Z^0 \to c\overline{c}$.

[2] ALBRECHT 92F uses the excess of right-sign over wrong-sign leptons in a sample of events tagged by fully reconstructed $D^*(2010)^+ \to D^0\pi^+$ decays.

$\Gamma(c \to \ell^+ \text{anything})/\Gamma(c \to \text{anything})$

This is an average (not a sum) of e^+ and μ^+ measurements.

VALUE	EVTS	DOCUMENT ID		TECN	COMMENT
0.096 ±0.004 OUR AVERAGE					
$0.0958 \pm 0.0042 \pm 0.0028$	1828	[1] ABREU	00O	DLPH	$Z^0 \to c\overline{c}$
$0.095 \pm 0.006 \; ^{+0.007}_{-0.006}$	854	[2] ABBIENDI	99K	OPAL	$Z^0 \to c\overline{c}$

[1] ABREU 00O uses leptons opposite fully reconstructed $D^*(2010)^+$, D^+, or D^0 mesons.

[2] ABBIENDI 99K uses the excess of right-sign over wrong-sign leptons opposite reconstructed $D^*(2010)^+ \to D^0\pi^+$ decays in $Z^0 \to c\overline{c}$.

$\Gamma(c \to D^*(2010)^+ \text{anything})/\Gamma(c \to \text{anything})$

VALUE	EVTS	DOCUMENT ID		TECN	COMMENT
0.255±0.015±0.008	2371	[1] ABREU	00O	DLPH	$Z^0 \to c\overline{c}$

[1] ABREU 00O uses slow pions opposite fully reconstructed $D^*(2010)^+$, D^+, or D^0 mesons as a signal of $D^*(2010)^-$ production.

Inclusive modes

$\Gamma(e^+ \text{semileptonic})/\Gamma_{\text{total}}$ — Γ_1/Γ

The sum of our $\overline{K}^0 e^+\nu_e$, $\overline{K}^*(892)^0 e^+\nu_e$, $\pi^0 e^+\nu_e$, $\eta e^+\nu_e$, $\rho^0 e^+\nu_e$, and $\omega e^+\nu_e$ branching fractions is 15.3 ± 0.3%.

VALUE (%)	EVTS	DOCUMENT ID		TECN	COMMENT
16.07±0.30 OUR AVERAGE					
$16.13 \pm 0.10 \pm 0.29$	26.2 ± 0.2k	[1] ASNER	10	CLEO	e^+e^- at 3774 MeV
$15.2 \pm 0.9 \pm 0.8$	521 ± 32	ABLIKIM	07G	BES2	$e^+e^- \approx \psi(3770)$
• • • We do not use the following data for averages, fits, limits, etc. • • •					
$16.13 \pm 0.20 \pm 0.33$	8798 ± 105	[2] ADAM	06A	CLEO	See ASNER 10
$17.0 \pm 1.9 \pm 0.7$	158	BALTRUSAIT...	85B	MRK3	e^+e^- 3.77 GeV

[1] Using the D^+ and D^0 lifetimes, ASNER 10 finds that the ratio of the D^+ and D^0 semileptonic widths is 0.985 ± 0.015 ± 0.024.

[2] Using the D^+ and D^0 lifetimes, ADAM 06A finds that the ratio of the D^+ and D^0 inclusive e^+ widths is 0.985 ± 0.028 ± 0.015, consistent with the isospin-invariance prediction of 1.

$\Gamma(\mu^+ \text{anything})/\Gamma_{\text{total}}$ — Γ_2/Γ

VALUE (%)	EVTS	DOCUMENT ID		TECN	COMMENT
17.6±2.7±1.8	100 ± 12	[1] ABLIKIM	08L	BES2	$e^+e^- \approx \psi(3772)$

[1] ABLIKIM 08L finds the ratio of $D^+ \to \mu^+ X$ and $D^0 \to \mu^+ X$ branching fractions to be 2.59 ± 0.70 ± 0.25, in accord with the ratio of D^+ and D^0 lifetimes, 2.54 ± 0.02.

$\Gamma(K^- \text{anything})/\Gamma_{\text{total}}$ — Γ_3/Γ

VALUE (%)	EVTS	DOCUMENT ID		TECN	COMMENT
25.7±1.4 OUR AVERAGE					
$24.7 \pm 1.3 \pm 1.2$	631 ± 33	ABLIKIM	07G	BES2	$e^+e^- \approx \psi(3770)$
$27.8^{+3.6}_{-3.1}$		BARLAG	92C	ACCM	π^- Cu 230 GeV
$27.1 \pm 2.3 \pm 2.4$		COFFMAN	91	MRK3	e^+e^- 3.77 GeV

$\Gamma(K^0_S \text{anything})/\Gamma_{\text{total}}$ — Γ_4/Γ

VALUE (%)	EVTS	DOCUMENT ID		TECN	COMMENT
33.11±0.13±0.36	95k	ABLIKIM	23AO	BES3	e^+e^- at 3.773 GeV
• • • We do not use the following data for averages, fits, limits, etc. • • •					
$30.25 \pm 2.75 \pm 1.65$	244	[1] ABLIKIM	06U	BES2	e^+e^- at 3773 MeV
$30.6 \pm 3.25 \pm 2.15$		[2] COFFMAN	91	MRK3	e^+e^- 3.77 GeV

[1] ABLIKIM 06U reports $B(D^0 \to K^0 X \text{ or } \overline{K}^0 X) = (60.5 \pm 5.5 \pm 3.3) \times 10^{-2}$ which we take as twice the branching fraction for $D^+ \to K^0_S X$.

[2] COFFMAN 91 reports $B(D^+ \to K^0 X \text{ or } \overline{K}^0 X) = (61.2 \pm 6.5 \pm 4.3) \times 10^{-2}$ which we take as twice the branching fraction for $D^+ \to K^0_S X$.

$\Gamma(K^+ \text{anything})/\Gamma_{\text{total}}$ — Γ_5/Γ

VALUE (%)	EVTS	DOCUMENT ID		TECN	COMMENT
5.9±0.8 OUR AVERAGE					
$6.1 \pm 0.9 \pm 0.4$	189 ± 27	ABLIKIM	07G	BES2	$e^+e^- \approx \psi(3770)$
$5.5 \pm 1.3 \pm 0.9$		COFFMAN	91	MRK3	e^+e^- 3.77 GeV

$\Gamma(K^*(892)^- \text{anything})/\Gamma_{\text{total}}$ — Γ_6/Γ

VALUE (%)	EVTS	DOCUMENT ID		TECN	COMMENT
5.7±5.2±0.7	7.2 ± 6.5	ABLIKIM	06U	BES2	e^+e^- at 3773 MeV

$\Gamma(\overline{K}^*(892)^0 \text{anything})/\Gamma_{\text{total}}$ — Γ_7/Γ

VALUE (%)	EVTS	DOCUMENT ID		TECN	COMMENT
23.2±4.5±3.0	189 ± 36	ABLIKIM	05P	BES	$e^+e^- \approx 3773$ MeV

$\Gamma(K^*(892)^0 \text{anything})/\Gamma_{\text{total}}$ — Γ_8/Γ

VALUE (%)	CL%	DOCUMENT ID		TECN	COMMENT
<6.6	90	ABLIKIM	05P	BES	$e^+e^- \approx 3773$ MeV

$\Gamma(\eta \text{ anything})/\Gamma_{\text{total}}$ — Γ_9/Γ

This ratio includes η particles from η' decays.

VALUE (%)	EVTS	DOCUMENT ID		TECN	COMMENT
6.3±0.5±0.5	1972 ± 142	HUANG	06B	CLEO	e^+e^- at $\psi(3770)$

$\Gamma(\eta' \text{ anything})/\Gamma_{\text{total}}$ — Γ_{10}/Γ

VALUE (%)	EVTS	DOCUMENT ID		TECN	COMMENT
1.04±0.16±0.09	82 ± 13	HUANG	06B	CLEO	e^+e^- at $\psi(3770)$

$\Gamma(\phi \text{ anything})/\Gamma_{\text{total}}$ — Γ_{11}/Γ

VALUE (%)	EVTS	DOCUMENT ID		TECN	COMMENT
1.12 ±0.04 OUR AVERAGE					
$1.135 \pm 0.034 \pm 0.031$	2.7k	ABLIKIM	19AY	BES3	e^+e^- at 3773 MeV
$1.03 \pm 0.10 \pm 0.07$	248 ± 21	HUANG	06B	CLEO	e^+e^- at $\psi(3770)$

$\Gamma(\pi^+\pi^+\pi^- \text{anything})/\Gamma_{\text{total}}$ — Γ_{12}/Γ

VALUE (%)	EVTS	DOCUMENT ID		TECN	COMMENT
15.25±0.09±0.18	124k	ABLIKIM	23AI	BES3	2.93 fb^{-1}, e^+e^- at $\psi(3770)$

Leptonic and semileptonic modes

$\Gamma(e^+\nu_e)/\Gamma_{\text{total}}$ — Γ_{13}/Γ

VALUE	CL%	DOCUMENT ID		TECN	COMMENT
$<9.7 \times 10^{-7}$	90	ABLIKIM	25BK	BES3	e^+e^- at $\sqrt{s} = 3773$ MeV
• • • We do not use the following data for averages, fits, limits, etc. • • •					
$<8.8 \times 10^{-6}$	90	EISENSTEIN	08	CLEO	e^+e^- at $\psi(3770)$
$<2.4 \times 10^{-5}$	90	ARTUSO	05A	CLEO	See EISENSTEIN 08

$\Gamma(\gamma e^+\nu_e)/\Gamma_{\text{total}}$ — Γ_{14}/Γ

VALUE	CL%	DOCUMENT ID		TECN	COMMENT
$<1.2 \times 10^{-5}$	90	[1] ABLIKIM	25CP	BES3	e^+e^- at 3.773 GeV
• • • We do not use the following data for averages, fits, limits, etc. • • •					
$<3.0 \times 10^{-5}$	90	[1] ABLIKIM	17M	BES3	Superseded by ABLIKIM 25CP

[1] The limit is for photons with energies greater than 10 MeV.

Int. J. Mod. Phys. A 2026.41. Downloaded from www.worldscientific.com
by LIFORNIA @ BERKELEY on 09/16/26. Re-use and distribution is strictly not permitted, except for Open Access articles.

Int. J. Mod. Phys. A 2026.41. Downloaded from www.worldscientific.com
by UNIVERSITY OF CALIFORNIA @ BERKELEY on 09/16/26. Re-use and distribution is strictly not permitted, except for Open Access articles.

$\Gamma(\mu^+\nu_\mu)/\Gamma_{total}$ — Γ_{15}/Γ

See the note on "Decay Constants of Charged Pseudoscalar Mesons" in the D_s^+ Listings.

VALUE (units 10^{-4})	EVTS	DOCUMENT ID		TECN	COMMENT
4.02 ± 0.09 OUR AVERAGE					
4.034 ± 0.080 ± 0.040	2.8k	[1] ABLIKIM	25BM	BES3	$e^+e^- \approx$ 3.773 GeV
3.82 ± 0.32 ± 0.09	150	[2] EISENSTEIN	08	CLEO	e^+e^- at $\psi(3770)$
• • • We do not use the following data for averages, fits, limits, etc. • • •					
3.71 ± 0.19 ± 0.06	409	[3] ABLIKIM	14F	BES3	e^+e^- at $\psi(3770)$
$12.2\ ^{+11.1}_{-5.3}$ ± 1.0	3	[4] ABLIKIM	05D	BES	$e^+e^- \approx$ 3.773 GeV
4.40 ± 0.66 $^{+0.09}_{-0.12}$	47	[5] ARTUSO	05A	CLEO	See EISENSTEIN 08
3.5 ± 1.4 ± 0.6	7	[6] BONVICINI	04A	CLEO	Incl. in ARTUSO 05A
8 $^{+16}_{-5}$ $^{+5}_{-2}$	1	[7] BAI	98B	BES	$e^+e^- \to D^{*+}D^-$

[1] ABLIKIM 25M obtain $|V_{cd}| \cdot f_{D^+} = (48.02 \pm 0.48 \pm 0.24 \pm 0.12 \pm 0.15)$ MeV, where the 3rd and 4th uncertainties are due to the D^+ lifetime and radiative corrections.

[2] EISENSTEIN 08, using the D^+ lifetime and assuming $|V_{cd}| = |V_{us}|$, gets $f_{D^+} = (205.8 \pm 8.5 \pm 2.5)$ MeV from this measurement.

[3] ABLIKIM 14F obtain $|V_{cd}| \cdot f_{D^+} = (45.75 \pm 1.20 \pm 0.39)$ MeV, and using $|V_{cd}| = 0.22520 \pm 0.00065$ gets $f_{D^+} = (203.2 \pm 5.3 \pm 1.8)$ MeV. Superseded by ABLIKIM 25BM.

[4] ABLIKIM 05D finds a background-subtracted 2.67 ± 1.74 $D^+ \to \mu^+\nu_\mu$ events, and from this obtains $f_{D^+} = 371\,^{+129}_{-119} \pm 25$ MeV.

[5] ARTUSO 05A obtains $f_{D^+} = 222.6 \pm 16.7\,^{+2.8}_{-3.4}$ MeV from this measurement.

[6] BONVICINI 04A finds eight events with an estimated background of one, and from the branching fraction obtains $f_{D^+} = 202 \pm 41 \pm 17$ MeV.

[7] BAI 98B obtains $f_{D^+} = (300\,^{+180}_{-150}\,^{+80}_{-40})$ MeV from this measurement.

$\Gamma(\tau^+\nu_\tau)/\Gamma_{total}$ — Γ_{16}/Γ

VALUE (units 10^{-3})	CL%	EVTS	DOCUMENT ID		TECN	COMMENT
0.99±0.11±0.05		283	[1,2] ABLIKIM	25BB	BES3	e^+e^- at 3773 MeV
• • • We do not use the following data for averages, fits, limits, etc. • • •						
1.20±0.24±0.12		137	[1,3] ABLIKIM	19BG	BES3	e^+e^- at 3773 MeV
<1.2	90		EISENSTEIN	08	CLEO	e^+e^- at $\psi(3770)$
<2.1	90		RUBIN	06A	CLEO	See EISENSTEIN 08

[1] Reconstructs the τ via $\tau \to \pi\nu$.

[2] ABLIKIM 25BB obtains $|V_{cd}| \cdot f_{D^+} = 45.9 \pm 2.5 \pm 1.2 \pm 0.1$ MeV, where the 3rd uncertainty is from the D^+ lifetime.

[3] ABLIKIM 19BG observe this mode with a significance of 5.1 σ. Superseded by ABLIKIM 25BB.

$\Gamma(\overline{K}^0 e^+\nu_e)/\Gamma_{total}$ — Γ_{17}/Γ

VALUE (%)	EVTS	DOCUMENT ID		TECN	COMMENT
8.81 ±0.07 OUR AVERAGE					
8.864±0.039±0.082	58k	ABLIKIM	24CN	BES3	e^+e^- at 3.773 GeV
8.68 ±0.14 ±0.16	1172	ABLIKIM	21BA	BES3	e^+e^- at 3.773 GeV
8.59 ±0.14 ±0.21	5013	ABLIKIM	16V	BES3	Using $\overline{K}^0 \to 2\pi^0$
8.83 ±0.10 ±0.20	8.5k	[1] BESSON	09	CLEO	from $D^+ \to K_S e^+\nu_e$
8.95 ±1.59 ±0.67	34	[2] ABLIKIM	05A	BES	from $D^+ \to K_S e^+\nu_e$
• • • We do not use the following data for averages, fits, limits, etc. • • •					
8.60 ±0.06 ±0.15	26k	[3] ABLIKIM	17S	BES3	Using $\overline{K}^0 \to \pi^+\pi^-$
8.962±0.054±0.206	40k	[3,4] ABLIKIM	15AF	BES3	from $D^+ \to K_L e^+\nu_e$
8.53 ±0.13 ±0.23		[5] DOBBS	08	CLEO	See BESSON 09
8.71 ±0.38 ±0.37	545	HUANG	05B	CLEO	See DOBBS 08

[1] See the form-factor parameters near the end of this D^+ Listing.

[2] The ABLIKIM 05A result together with the $D^0 \to K^-e^+\nu_e$ branching fraction of ABLIKIM 04C and Particle Data Group lifetimes gives $\Gamma(D^0 \to K^-e^+\nu_e)\ /\ \Gamma(D^+ \to \overline{K}^0 e^+\nu_e) = 1.08 \pm 0.22 \pm 0.07$; isospin invariance predicts the ratio is 1.0.

[3] Superseded by ABLIKIM 24CN.

[4] ABLIKIM 15AF report $\Gamma(D^+ \to K_L e^+\nu_e)/\Gamma_{total} = (4.481 \pm 0.027 \pm 0.103)\%$. See also the form-factor parameters near the end of this D^+ Listing.

[5] DOBBS 08 establishes $\left|\frac{V_{cd}}{V_{cs}} \cdot \frac{f_+^\pi(0)}{f_+^K(0)}\right| = 0.188 \pm 0.008 \pm 0.002$ from the D^+ and D^0 decays to $\overline{K}e^+\nu_e$ and $\pi e^+\nu_e$. It also finds $\Gamma(D^0 \to K^-e^+\nu_e)\ /\ \Gamma(D^+ \to \overline{K}^0 e^+\nu_e) = 1.06 \pm 0.02 \pm 0.03$; isospin invariance predicts the ratio is 1.0.

$\Gamma(\overline{K}^0\mu^+\nu_\mu)/\Gamma_{total}$ — Γ_{18}/Γ

VALUE (units 10^{-2})	EVTS	DOCUMENT ID		TECN	COMMENT
8.68 ±0.10 OUR FIT					
8.665±0.046±0.084	47k	ABLIKIM	24CN	BES3	e^+e^- at 3.773 GeV
• • • We do not use the following data for averages, fits, limits, etc. • • •					
8.72 ±0.07 ±0.18	21k	[1] ABLIKIM	16G	BES3	e^+e^- at 3773 MeV
10.3 ±2.3 ±0.8	29 ± 6	ABLIKIM	07	BES2	e^+e^- at 3773 MeV

[1] Superseded by ABLIKIM 24CN.

$\Gamma(\overline{K}^0\mu^+\nu_\mu)/\Gamma(K^-2\pi^+)$ — Γ_{18}/Γ_{68}

VALUE	EVTS	DOCUMENT ID		TECN	COMMENT
0.932±0.017 OUR FIT	Error includes scale factor of 1.2.				
1.019±0.076±0.065	555 ± 39	LINK	04E	FOCS	γ nucleus, $\overline{E}_\gamma \approx$ 180 GeV

$\Gamma(K^-\pi^+e^+\nu_e)/\Gamma_{total}$ — Γ_{22}/Γ

VALUE (units 10^{-2})	EVTS	DOCUMENT ID		TECN	COMMENT
4.00±0.17 OUR FIT	Error includes scale factor of 3.1.				
3.77±0.03±0.08	18.3k	ABLIKIM	16F	BES3	e^+e^- at $\psi(3770)$
• • • We do not use the following data for averages, fits, limits, etc. • • •					
3.50±0.75±0.27	29	ABLIKIM	06O	BES2	e^+e^- at 3773 MeV
3.5 $^{+1.2}_{-0.7}$ ±0.4	14	BAI	91	MRK3	$e^+e^- \approx$ 3.77 GeV

$\Gamma(K^-\pi^+e^+\nu_e)/\Gamma(K^-2\pi^+)$ — Γ_{22}/Γ_{68}

VALUE	EVTS	DOCUMENT ID		TECN	COMMENT
0.429 ±0.018 OUR FIT	Error includes scale factor of 3.6.				
0.4380±0.0036±0.0042	70k±363	DEL-AMO-SA...	11I	BABR	$e^+e^- \approx$ 10.6 GeV

$\Gamma(\overline{K}^*(892)^0 e^+\nu_e, \overline{K}^*(892)^0 \to K^-\pi^+)/\Gamma(K^-\pi^+e^+\nu_e)$ — Γ_{23}/Γ_{22}

VALUE (%)	DOCUMENT ID		TECN	COMMENT
93.94±0.27 OUR AVERAGE				
93.93±0.22±0.18	ABLIKIM	16F	BES3	e^+e^- at $\psi(3770)$
94.11±0.74±0.75	DEL-AMO-SA...	11I	BABR	$e^+e^- \approx$ 10.6 GeV

$\Gamma((K^-\pi^+)_{[0.8-1.0]GeV}e^+\nu_e)/\Gamma_{total}$ — Γ_{24}/Γ

VALUE (units 10^{-2})	EVTS	DOCUMENT ID		TECN	COMMENT
3.39±0.03±0.08	16.2k	ABLIKIM	16F	BES3	e^+e^- at $\psi(3770)$

$\Gamma((K^-\pi^+)_{S-wave}e^+\nu_e)/\Gamma_{total}$ — Γ_{25}/Γ

VALUE (units 10^{-3})	DOCUMENT ID		TECN	COMMENT
2.28±0.08±0.08	ABLIKIM	16F	BES3	e^+e^- at $\psi(3770)$

$\Gamma((K^-\pi^+)_{S-wave}e^+\nu_e)/\Gamma(K^-\pi^+e^+\nu_e)$ — Γ_{25}/Γ_{22}

VALUE (%)	DOCUMENT ID		TECN	COMMENT
5.89±0.17 OUR AVERAGE				
6.05±0.22±0.18	ABLIKIM	16F	BES3	e^+e^- at $\psi(3770)$
5.79±0.16±0.15	DEL-AMO-SA...	11I	BABR	$e^+e^- \approx$ 10.6 GeV

$\Gamma(\overline{K}^*(1410)^0 e^+\nu_e, \overline{K}^*(1410)^0 \to K^-\pi^+)/\Gamma_{total}$ — Γ_{26}/Γ

VALUE	CL%	DOCUMENT ID		TECN	COMMENT
<6 × 10^{-3}	90	DEL-AMO-SA...	11I	BABR	$e^+e^- \approx$ 10.6 GeV

$\Gamma(\overline{K}_2^*(1430)^0 e^+\nu_e, \overline{K}_2^*(1430)^0 \to K^-\pi^+)/\Gamma_{total}$ — Γ_{27}/Γ

VALUE	CL%	DOCUMENT ID		TECN	COMMENT
<5 × 10^{-4}	90	DEL-AMO-SA...	11I	BABR	$e^+e^- \approx$ 10.6 GeV

$\Gamma(K^-\pi^+e^+\nu_e$ nonresonant$)/\Gamma_{total}$ — Γ_{28}/Γ

VALUE	CL%	DOCUMENT ID		TECN	COMMENT
<0.007	90	ANJOS	89B	E691	Photoproduction

$\Gamma(K_S^0\pi^0e^+\nu_e)/\Gamma_{total}$ — Γ_{19}/Γ

VALUE (units 10^{-3})	EVTS	DOCUMENT ID		TECN	COMMENT
9.43±0.12±0.10	11k	ABLIKIM	25BP	BES3	e^+e^- at $\sqrt{s}$ = 3.773 GeV
• • • We do not use the following data for averages, fits, limits, etc. • • •					
8.81±0.17±0.16	3.8k	ABLIKIM	24CS	BES3	Superseded by ABLIKIM 25BP

$\Gamma((K_S^0\pi^0)_{S-wave}e^+\nu_e)/\Gamma(K_S^0\pi^0e^+\nu_e)$ — Γ_{20}/Γ_{19}

VALUE (units 10^{-2})	EVTS	DOCUMENT ID		TECN	COMMENT
6.39±0.17±0.14	11k	[1] ABLIKIM	25BP	BES3	e^+e^- at $\sqrt{s}$ = 3.773 GeV
• • • We do not use the following data for averages, fits, limits, etc. • • •					
6.13±0.27±0.30	3.8k	[1,2] ABLIKIM	24CS	BES3	Superseded by ABLIKIM 25BP

[1] Amplitude analysis with two components.

[2] ABLIKIM 24CS reports a branching fraction $B(D^+ \to (K_S^0\pi^0)_{S-wave}e^+\nu_e) = (5.41 \pm 0.35 \pm 0.37) \times 10^{-4}$.

$\Gamma(\overline{K}^*(892)^0 e^+\nu_e, \overline{K}^{*0} \to K_S^0\pi^0)/\Gamma(K_S^0\pi^0e^+\nu_e)$ — Γ_{21}/Γ_{19}

VALUE (units 10^{-2})	EVTS	DOCUMENT ID		TECN	COMMENT
93.50±0.18±0.28	11k	[1] ABLIKIM	25BP	BES3	e^+e^- at $\sqrt{s}$ = 3.773 GeV
• • • We do not use the following data for averages, fits, limits, etc. • • •					
93.88±0.27±0.29	3.8k	[1,2] ABLIKIM	24CS	BES3	Superseded by ABLIKIM 25BP

[1] Amplitude analysis with two components.

[2] ABLIKIM 24CS reports a branching fraction $B(D^+ \to \overline{K}^*(892)^0 e^+\nu_e) = (4.97 \pm 0.11 \pm 0.12) \times 10^{-2}$.

$\Gamma(\overline{K}^*(892)^0 e^+\nu_e)/\Gamma_{total}$ — Γ_{29}/Γ

Unseen decay modes of $\overline{K}^*(892)^0$ are included. See the end of the D^+ Listings for measurements of $D^+ \to \overline{K}^*(892)^0\ell^+\nu_\ell$ form-factor ratios.

VALUE (units 10^{-2})	EVTS	DOCUMENT ID		TECN	COMMENT
5.40±0.10 OUR FIT	Error includes scale factor of 1.1.				
5.40±0.10 OUR AVERAGE	Error includes scale factor of 1.1.				
5.31±0.05±0.12	16.2k	ABLIKIM	16F	BES3	e^+e^- at $\psi(3770)$
5.52±0.07±0.13	≈5k	BRIERE	10	CLEO	e^+e^- at $\psi(3770)$
• • • We do not use the following data for averages, fits, limits, etc. • • •					
5.06±1.21±0.40	28 ± 7	ABLIKIM	06O	BES2	e^+e^- at 3773 MeV
5.56±0.27±0.23	422 ± 21	[1] HUANG	05B	CLEO	e^+e^- at $\psi(3770)$

[1] HUANG 05B finds $\Gamma(D^0 \to K^{*-}e^+\nu_e)\ /\ \Gamma(D^+ \to \overline{K}^{*0}e^+\nu_e) = 0.98 \pm 0.08 \pm 0.04$; isospin invariance predicts the ratio is 1.0.

Int. J. Mod. Phys. A 2026.41. Downloaded from www.worldscientific.com by LIFORNIA @ BERKELEY on 09/16/26. Re-use and distribution is strictly not permitted, except for Open Access articles.

$\Gamma(\overline{K}^*(892)^0 e^+ \nu_e)/\Gamma(K^- 2\pi^+)$ — Γ_{29}/Γ_{68}

Unseen decay modes of the $\overline{K}^*(892)^0$ are included. See the end of the D^+ Listings for measurements of $D^+ \to \overline{K}^*(892)^0 \ell^+ \nu_\ell$ form-factor ratios.

VALUE	EVTS	DOCUMENT ID		TECN	COMMENT
• • • We do not use the following data for averages, fits, limits, etc. • • •					
$0.74 \pm 0.04 \pm 0.05$		BRANDENB...	02	CLEO	$e^+ e^- \approx \Upsilon(4S)$
$0.62 \pm 0.15 \pm 0.09$	35	ADAMOVICH	91	OMEG	π^- 340 GeV
$0.55 \pm 0.08 \pm 0.10$	880	ALBRECHT	91	ARG	$e^+ e^- \approx$ 10.4 GeV
$0.49 \pm 0.04 \pm 0.05$		ANJOS	89B	E691	Photoproduction

$\Gamma(K^0_S \pi^0 \mu^+ \nu_\mu)/\Gamma_{total}$ — Γ_{30}/Γ

VALUE (units 10^{-3})	EVTS	DOCUMENT ID		TECN	COMMENT
$8.96 \pm 0.17 \pm 0.08$	6.8k	ABLIKIM	25BP	BES3	$e^+ e^-$ at $\sqrt{s} = 3.773$ GeV

$\Gamma((K^0_S \pi^0)_{S-wave} \mu^+ \nu_\mu)/\Gamma(K^0_S \pi^0 \mu^+ \nu_\mu)$ — Γ_{31}/Γ_{30}

VALUE (units 10^{-2})	EVTS	DOCUMENT ID		TECN	COMMENT
$7.10 \pm 0.68 \pm 0.41$	6.8k	[1] ABLIKIM	25BP	BES3	$e^+ e^-$ at $\sqrt{s} = 3.773$ GeV

[1] Amplitude analysis with two components.

$\Gamma(\overline{K}^*(892)^0 \mu^+ \nu_\mu, \overline{K}^{*0} \to K^0_S \pi^0)/\Gamma(K^0_S \pi^0 \mu^+ \nu_\mu)$ — Γ_{32}/Γ_{30}

VALUE (units 10^{-2})	EVTS	DOCUMENT ID		TECN	COMMENT
$92.81 \pm 0.67 \pm 0.47$	6.8k	[1] ABLIKIM	25BP	BES3	$e^+ e^-$ at $\sqrt{s} = 3.773$ GeV

[1] Amplitude analysis with two components.

$\Gamma(K^- \pi^+ \mu^+ \nu_\mu)/\Gamma(\overline{K}^0 \mu^+ \nu_\mu)$ — Γ_{33}/Γ_{18}

VALUE	EVTS	DOCUMENT ID		TECN	COMMENT
$0.417 \pm 0.030 \pm 0.023$	555 ± 39	LINK	04E	FOCS	γ nucleus, $\overline{E}_\gamma \approx 180$ GeV

$\Gamma(K^- \pi^+ \mu^+ \nu_\mu \text{ nonresonant})/\Gamma(K^- \pi^+ \mu^+ \nu_\mu)$ — Γ_{35}/Γ_{33}

VALUE	EVTS	DOCUMENT ID		TECN	COMMENT
$0.0530 \pm 0.0074 {}^{+0.0099}_{-0.0096}$	14k	LINK	05I	FOCS	γ nucleus, $\overline{E}_\gamma \approx 180$ GeV

$\Gamma(\overline{K}^*(892)^0 \mu^+ \nu_\mu)/\Gamma_{total}$ — Γ_{36}/Γ

Unseen decay modes of the $\overline{K}^*(892)^0$ are included. See the end of the D^+ Listings for measurements of $D^+ \to \overline{K}^*(892)^0 \ell^+ \nu_\ell$ form-factor ratios.

VALUE (units 10^{-2})	EVTS	DOCUMENT ID		TECN	COMMENT
5.26 ± 0.15 OUR FIT	Error includes scale factor of 1.1.				
$5.27 \pm 0.07 \pm 0.14$	≈ 5k	BRIERE	10	CLEO	$e^+ e^-$ at $\psi(3770)$

$\Gamma(\overline{K}^*(892)^0 \mu^+ \nu_\mu)/\Gamma(\overline{K}^0 \mu^+ \nu_\mu)$ — Γ_{36}/Γ_{18}

Unseen decay modes of the $\overline{K}^*(892)^0$ are included. See the end of the D^+ Listings for measurements of $D^+ \to \overline{K}^*(892)^0 \ell^+ \nu_\ell$ form-factor ratios.

VALUE	EVTS	DOCUMENT ID		TECN	COMMENT
0.607 ± 0.019 OUR FIT	Error includes scale factor of 1.1.				
$0.594 \pm 0.043 \pm 0.033$	555 ± 39	LINK	04E	FOCS	γ nucleus, $\overline{E}_\gamma \approx 180$ GeV

$\Gamma(\overline{K}^*(892)^0 \mu^+ \nu_\mu)/\Gamma(K^- 2\pi^+)$ — Γ_{36}/Γ_{68}

Unseen decay modes of the $\overline{K}^*(892)^0$ are included. See the end of the D^+ Listings for measurements of $D^+ \to \overline{K}^*(892)^0 \ell^+ \nu_\ell$ form-factor ratios.

VALUE	EVTS	DOCUMENT ID		TECN	COMMENT
0.565 ± 0.018 OUR FIT	Error includes scale factor of 1.1.				
0.57 ± 0.06 OUR AVERAGE	Error includes scale factor of 1.2.				
$0.72 \pm 0.10 \pm 0.05$		BRANDENB...	02	CLEO	$e^+ e^- \approx \Upsilon(4S)$
$0.56 \pm 0.04 \pm 0.06$	875	FRABETTI	93E	E687	γBe $\overline{E}_\gamma \approx 200$ GeV
$0.46 \pm 0.07 \pm 0.08$	224	KODAMA	92C	E653	π^- emulsion 600 GeV
• • • We do not use the following data for averages, fits, limits, etc. • • •					
$0.602 \pm 0.010 \pm 0.021$	12k	[1] LINK	02J	FOCS	γ nucleus, ≈ 180 GeV

[1] This LINK 02J result includes the effects of an interference of a small S-wave $K^- \pi^+$ amplitude with the dominant $\overline{K}^{*0}$ amplitude. (The interference effect is reported in LINK 02E.) This result is redundant with results of LINK 04E elsewhere in these Listings.

$\Gamma(K^- \pi^+ \pi^0 \mu^+ \nu_\mu)/\Gamma(K^- \pi^+ \mu^+ \nu_\mu)$ — Γ_{39}/Γ_{33}

VALUE	CL%	DOCUMENT ID		TECN	COMMENT
<0.042	90	FRABETTI	93E	E687	γBe $\overline{E}_\gamma \approx 200$ GeV

$\Gamma(\overline{K}_1(1270)^0 e^+ \nu_e, \overline{K}^0_1 \to K^- \pi^+ \pi^0)/\Gamma_{total}$ — Γ_{37}/Γ

VALUE (units 10^{-3})	EVTS	DOCUMENT ID		TECN	COMMENT
1.23 ± 0.08 OUR AVERAGE	Error includes scale factor of 1.3.				
$1.27 \pm 0.06 \pm 0.04$	1.3k	[1] ABLIKIM	25AM	BES3	$e^+ e^-$ at 3.773 GeV
$1.06 \pm 0.12 {}^{+0.08}_{-0.10}$	120	[2] ABLIKIM	19BH	BES3	$e^+ e^-$ at 3773 MeV

[1] ABLIKIM 25AM quotes $B(D^+ \to \overline{K}_1(1270)^0 e^+ \nu_e) = (2.27 \pm 0.11 \pm 0.07 \pm 0.07) \times 10^{-3}$, where the last uncertainty is due to $B(\overline{K}_1(1270)^0 \to K^- \pi^+ \pi^0) = (56.0 \pm 1.7)\%$. This amplitude analysis with several substructures includes $K_1(1270) \to \rho K^-$ (S-wave) and $K_1(1270) \to \pi \overline{K}^*(892)$ (S- and D-wave).

[2] ABLIKIM 19BH quotes $B(D^+ \to \overline{K}_1(1270)^0 e^+ \nu_e) = (2.30 \pm 0.26 {}^{+0.18}_{-0.21} \pm 0.25) \times 10^{-3}$, where the last uncertainty is due to $B(\overline{K}_1(1270)^0 \to K^- \pi^+ \pi^0) = 0.467 \pm 0.050$.

$\Gamma(\overline{K}_1(1270)^0 e^+ \nu_e, \overline{K}^0_1 \to K^0_S \pi^+ \pi^-)/\Gamma_{total}$ — Γ_{38}/Γ

VALUE (units 10^{-4})	EVTS	DOCUMENT ID		TECN	COMMENT
$1.47 {}^{+0.45}_{-0.40} \pm 0.14$	20	[1] ABLIKIM	24CR	BES3	$e^+ e^-$ at $\sqrt{s} = 3.773$ GeV

[1] ABLIKIM 24CR reconstructs $D^+ \to K^0_S \pi^+ \pi^- e^+ \nu_e$ and assumes that all come from $\overline{K}^0_1 \to K^0_S \pi^+ \pi^-$ decays.

$\Gamma(\overline{K}_1(1270)^0 \mu^+ \nu_\mu, \overline{K}^0_1 \to K^- \pi^+ \pi^0)/\Gamma_{total}$ — Γ_{40}/Γ

VALUE (units 10^{-4})	EVTS	DOCUMENT ID		TECN	COMMENT
$10.92 \pm 0.91 {}^{+0.82}_{-1.26}$	383	ABLIKIM	25AU	BES3	$e^+ e^-$ at 3.773 GeV

$\Gamma(\overline{K}_1(1400)^0 e^+ \nu_e)/\Gamma_{total}$ — Γ_{41}/Γ

VALUE	CL%	DOCUMENT ID		TECN	COMMENT
$<1.4 \times 10^{-4}$	90	ABLIKIM	25AM	BES3	$e^+ e^-$ at 3.773 GeV

$\Gamma(\overline{K}^*_0(1430)^0 \mu^+ \nu_\mu)/\Gamma(K^- \pi^+ \mu^+ \nu_\mu)$ — Γ_{42}/Γ_{33}

Unseen decay modes of the $\overline{K}^*_0(1430)^0$ are included.

VALUE	CL%	DOCUMENT ID		TECN	COMMENT
<0.0064	90	LINK	05I	FOCS	γ A, $\overline{E}_\gamma \approx 180$ GeV

$\Gamma(\overline{K}^*(1680)^0 \mu^+ \nu_\mu)/\Gamma(K^- \pi^+ \mu^+ \nu_\mu)$ — Γ_{43}/Γ_{33}

Unseen decay modes of the $\overline{K}^*(1680)^0$ are included.

VALUE	CL%	DOCUMENT ID		TECN	COMMENT
<0.04	90	LINK	05I	FOCS	γ A, $\overline{E}_\gamma \approx 180$ GeV

$\Gamma(\pi^0 e^+ \nu_e)/\Gamma_{total}$ — Γ_{44}/Γ

VALUE (%)	EVTS	DOCUMENT ID		TECN	COMMENT
0.372 ± 0.017 OUR AVERAGE	Error includes scale factor of 2.0.				
$0.363 \pm 0.008 \pm 0.005$	3.4k	ABLIKIM	17S	BES3	Using $\pi^0 \to 2\gamma$
$0.405 \pm 0.016 \pm 0.009$	838	[1] BESSON	09	CLEO	$e^+ e^-$ at $\psi(3770)$
• • • We do not use the following data for averages, fits, limits, etc. • • •					
$0.373 \pm 0.022 \pm 0.013$		[2] DOBBS	08	CLEO	See BESSON 09
$0.44 \pm 0.06 \pm 0.03$	63 ± 9	HUANG	05B	CLEO	See DOBBS 08

[1] See the form-factor parameters near the end of this D^+ Listing.

[2] DOBBS 08 establishes $\left|\frac{V_{cd}}{V_{cs}} \cdot \frac{f_+^\pi(0)}{f_+^K(0)}\right| = 0.188 \pm 0.008 \pm 0.002$ from the D^+ and D^0 decays to $\overline{K} e^+ \nu_e$ and $\pi e^+ \nu_e$. It finds $\Gamma(D^0 \to \pi^- e^+ \nu_e) / \Gamma(D^+ \to \pi^0 e^+ \nu_e) = 2.03 \pm 0.14 \pm 0.08$; isospin invariance predicts the ratio is 2.0.

$\Gamma(\pi^0 \mu^+ \nu_\mu)/\Gamma_{total}$ — Γ_{45}/Γ

VALUE (%)	EVTS	DOCUMENT ID		TECN	COMMENT
$0.350 \pm 0.011 \pm 0.010$	1.3k	ABLIKIM	18AE	BES3	$e^+ e^-$, 3773 MeV

$\Gamma(\eta e^+ \nu_e)/\Gamma_{total}$ — Γ_{46}/Γ

VALUE (units 10^{-4})	EVTS	DOCUMENT ID		TECN	COMMENT
11.1 ± 0.7 OUR AVERAGE					
$10.74 \pm 0.81 \pm 0.51$	373	ABLIKIM	18R	BES3	$e^+ e^-$, 3773 MeV
$11.4 \pm 0.9 \pm 0.4$		YELTON	11	CLEO	$e^+ e^-$ at $\psi(3770)$
• • • We do not use the following data for averages, fits, limits, etc. • • •					
$13.3 \pm 2.0 \pm 0.6$	46	MITCHELL	09B	CLEO	See YELTON 11

$\Gamma(\eta \mu^+ \nu_\mu)/\Gamma_{total}$ — Γ_{47}/Γ

VALUE (units 10^{-4})	EVTS	DOCUMENT ID		TECN	COMMENT
$10.41 \pm 1.12 \pm 0.05$	234	[1] ABLIKIM	20T	BES3	$e^+ e^-$, 3773 MeV

[1] ABLIKIM 20T reports $(10.4 \pm 1.0 \pm 0.5) \times 10^{-4}$ from a measurement of $[\Gamma(D^+ \to \eta \mu^+ \nu_\mu)/\Gamma_{total}] \times [B(\eta \to 2\gamma)]$ assuming $B(\eta \to 2\gamma) = (39.41 \pm 0.20) \times 10^{-2}$, which we rescale to our best (shown rounded) value $B(\eta \to 2\gamma) = (39.36 \pm 0.18) \times 10^{-2}$. Our first error is their experiment's error and our second error is the systematic error from using our best (shown rounded) value.

$\Gamma(\pi^- \pi^+ e^+ \nu_e)/\Gamma_{total}$ — Γ_{48}/Γ

VALUE (units 10^{-3})	EVTS	DOCUMENT ID		TECN	COMMENT
2.45 ± 0.08 OUR FIT					
$2.449 \pm 0.074 \pm 0.073$	1.7k	ABLIKIM	19C	BES3	$e^+ e^-$ at 3773 MeV

$\Gamma(f_0(500)^0 e^+ \nu_e, f_0(500)^0 \to \pi^+ \pi^-)/\Gamma(\pi^- \pi^+ e^+ \nu_e)$ — Γ_{49}/Γ_{48}

VALUE (units 10^{-2})	EVTS	DOCUMENT ID		TECN	COMMENT
25.4 ± 1.7 OUR FIT					
$25.7 \pm 1.6 \pm 1.1$	1.5k	ABLIKIM	19C	BES3	$\pi^- \pi^+ e^+ \nu_e$ events

$\Gamma(f_0(500)^0 e^+ \nu_e, f_0(500)^0 \to \pi^+ \pi^-)/\Gamma_{total}$ — Γ_{49}/Γ

VALUE (units 10^{-4})	EVTS	DOCUMENT ID		TECN	COMMENT
6.2 ± 0.4 OUR FIT					
$6.0 \pm 0.6 \pm 0.5$	0.4k	ABLIKIM	24CK	BES3	$e^+ e^-$ at 3.773 GeV

$\Gamma(\rho^0 e^+ \nu_e)/\Gamma_{total}$ — Γ_{50}/Γ

VALUE (units 10^{-3})	EVTS	DOCUMENT ID		TECN	COMMENT
1.87 ± 0.06 OUR FIT					
1.88 ± 0.10 OUR AVERAGE	Error includes scale factor of 1.2.				
$1.84 \pm 0.07 \pm 0.06$	1237	ABLIKIM	24CK	BES3	$e^+ e^-$ at 3.773 GeV
$2.17 \pm 0.12 {}^{+0.12}_{-0.22}$	447 ± 25	[1] DOBBS	13	CLEO	$e^+ e^-$ at $\psi(3770)$
• • • We do not use the following data for averages, fits, limits, etc. • • •					
$2.1 \pm 0.4 \pm 0.1$	27 ± 6	[2] HUANG	05B	CLEO	See DOBBS 13

Int. J. Mod. Phys. A 2026.41. Downloaded from www.worldscientific.com by UNIVERSITY OF CALIFORNIA @ BERKELEY on 09/16/26. Re-use and distribution is strictly not permitted, except for Open Access articles.

[1] DOBBS 13 finds $\Gamma(D^0 \to \rho^- e^+ \nu_e)$ / 2 $\Gamma(D^+ \to \rho^0 e^+ \nu_e) = 1.03 \pm 0.09^{+0.08}_{-0.02}$; isospin invariance predicts the ratio is 1.0.

[2] HUANG 05B finds $\Gamma(D^0 \to \rho^- e^+ \nu_e)$ / 2 $\Gamma(D^+ \to \rho^0 e^+ \nu_e) = 1.2^{+0.4}_{-0.3} \pm 0.1$; isospin invariance predicts the ratio is 1.0.

$\Gamma(\rho^0 e^+ \nu_e)/\Gamma(\pi^- \pi^+ e^+ \nu_e)$ — Γ_{50}/Γ_{48}

VALUE (units 10^{-2})	EVTS	DOCUMENT ID		TECN	COMMENT
76.2±1.9 OUR FIT					
76.0±1.7±1.1	1.5k	ABLIKIM	19C	BES3	$\pi^- \pi^+ e^+ \nu_e$ events

$\Gamma(\rho^0 e^+ \nu_e)/\Gamma(\overline{K}^*(892)^0 e^+ \nu_e)$ — Γ_{50}/Γ_{29}

VALUE	EVTS	DOCUMENT ID		TECN	COMMENT
0.0346±0.0013 OUR FIT					
0.045 ±0.014 ±0.009	49	[1] AITALA	97	E791	π^- nucleus, 500 GeV

[1] AITALA 97 explicitly subtracts $D^+ \to \eta' e^+ \nu_e$ and other backgrounds to get this result.

$\Gamma(f_0(500)^0 \mu^+ \nu_\mu,\ f_0^0 \to \pi^+ \pi^-)/\Gamma_{total}$ — Γ_{52}/Γ

VALUE (units 10^{-4})	EVTS	DOCUMENT ID		TECN	COMMENT
7.2±1.3±0.8	0.2k	ABLIKIM	24CK	BES3	$e^+ e^-$ at 3.773 GeV

$\Gamma(\rho^0 \mu^+ \nu_\mu)/\Gamma_{total}$ — Γ_{53}/Γ

VALUE (units 10^{-3})	EVTS	DOCUMENT ID		TECN	COMMENT
1.64±0.13±0.10	0.5k	ABLIKIM	24CK	BES3	$e^+ e^-$ at 3.773 GeV

$\Gamma(\rho^0 \mu^+ \nu_\mu)/\Gamma(\overline{K}^*(892)^0 \mu^+ \nu_\mu)$ — Γ_{53}/Γ_{36}

VALUE	EVTS	DOCUMENT ID		TECN	COMMENT
0.045±0.007 OUR AVERAGE Error includes scale factor of 1.1.					
0.041±0.006±0.004	320 ± 44	LINK	06B	FOCS	γ A, $\overline{E}_\gamma \approx$ 180 GeV
0.051±0.015±0.009	54	[1] AITALA	97	E791	π^- nucleus, 500 GeV
0.079±0.019±0.013	39	[2] FRABETTI	97	E687	γ Be, $\overline{E}_\gamma \approx$ 220 GeV

[1] AITALA 97 explicitly subtracts $D^+ \to \eta' \mu^+ \nu_\mu$ and other backgrounds to get this result.

[2] Because the reconstruction efficiency for photons is low, this FRABETTI 97 result also includes any $D^+ \to \eta' \mu^+ \nu_\mu \to \gamma \rho^0 \mu^+ \nu_\mu$ events in the numerator.

$\Gamma(\omega e^+ \nu_e)/\Gamma_{total}$ — Γ_{54}/Γ

VALUE (units 10^{-3})	EVTS	DOCUMENT ID		TECN	COMMENT
1.69±0.11 OUR AVERAGE					
1.63±0.11±0.08	491 ± 32	ABLIKIM	15W	BES3	292 fb^{-1}, 3773 MeV
1.82±0.18±0.07	129 ± 13	DOBBS	13	CLEO	$e^+ e^-$ at $\psi(3770)$
• • • We do not use the following data for averages, fits, limits, etc. • • •					
1.6 $^{+0.7}_{-0.6}$ ±0.1	7.6$^{+3.3}_{-2.7}$	HUANG	05B	CLEO	See DOBBS 13

$\Gamma(\omega e^+ \nu_e)/\Gamma(\pi^- \pi^+ e^+ \nu_e)$ — Γ_{54}/Γ_{48}

VALUE (units 10^{-2})	EVTS	DOCUMENT ID		TECN	COMMENT
1.28±0.41±0.15	1.5k	ABLIKIM	19C	BES3	$\pi^- \pi^+ e^+ \nu_e$ events

$\Gamma(\omega \mu^+ \nu_\mu)/\Gamma_{total}$ — Γ_{55}/Γ

VALUE (units 10^{-4})	EVTS	DOCUMENT ID		TECN	COMMENT
17.7±2.1±0.1	194	[1] ABLIKIM	20H	BES3	$e^+ e^-$, 3773 MeV

[1] ABLIKIM 20H reports (17.7 ± 1.8 ± 1.1) × 10^{-4} from a measurement of $[\Gamma(D^+ \to \omega \mu^+ \nu_\mu)/\Gamma_{total}] \times [B(\omega(782) \to \pi^+ \pi^- \pi^0)]$ assuming $B(\omega(782) \to \pi^+ \pi^- \pi^0) = (89.3 \pm 0.6) \times 10^{-2}$, which we rescale to our best (shown rounded) value $B(\omega(782) \to \pi^+ \pi^- \pi^0) = (89.2 \pm 0.7) \times 10^{-2}$. Our first error is their experiment's error and our second error is the systematic error from using our best (shown rounded) value.

$\Gamma(\eta'(958) e^+ \nu_e)/\Gamma_{total}$ — Γ_{56}/Γ

VALUE (units 10^{-4})	CL%	EVTS	DOCUMENT ID		TECN	COMMENT
1.84±0.19 OUR AVERAGE						
1.79±0.19±0.07		0.15k	ABLIKIM	25AO	BES3	$e^+ e^-$ at 3.773 GeV
2.16±0.53±0.07			YELTON	11	CLEO	$e^+ e^-$ at $\psi(3770)$
• • • We do not use the following data for averages, fits, limits, etc. • • •						
1.91±0.51±0.13		32	[1] ABLIKIM	18R	BES3	$e^+ e^-$ at 3.773 GeV
<3.5	90		MITCHELL	09B	CLEO	See YELTON 11

[1] Superseded by ABLIKIM 25AO.

$\Gamma(\eta'(958) \mu^+ \nu_\mu)/\Gamma_{total}$ — Γ_{57}/Γ

VALUE (units 10^{-4})	EVTS	DOCUMENT ID		TECN	COMMENT
1.92±0.28±0.08	90	ABLIKIM	25AO	BES3	$e^+ e^-$ at 3.773 GeV

$\Gamma(a(980)^0 e^+ \nu_e,\ a(980)^0 \to \eta \pi^0)/\Gamma_{total}$ — Γ_{58}/Γ

VALUE (units 10^{-4})	EVTS	DOCUMENT ID		TECN	COMMENT
1.66$^{+0.81}_{-0.66}$±0.11	10$^{+5}_{-4}$	[1] ABLIKIM	18F	BES3	$e^+ e^-$ at 3773 MeV

[1] Signal observed at 2.9 σ C.L.

$\Gamma(K_S^0 K_S^0 e^+ \nu_e)/\Gamma_{total}$ — Γ_{59}/Γ

VALUE	CL%	DOCUMENT ID		TECN	COMMENT
<1.54 × 10^{-5}	90	[1] ABLIKIM	24AZ	BES3	7.9 fb^{-1}, $e^+ e^-$ at 3.773 GeV

[1] Includes $D^+ \to a_0(980)^0 e^+ \nu_e$, $a_0(980)^0 \to K_S^0 K_S^0$ resonant contribution.

$\Gamma(K_S^0 \eta e^+ \nu_e)/\Gamma_{total}$ — Γ_{60}/Γ

VALUE	CL%	DOCUMENT ID		TECN	COMMENT
<2.0 × 10^{-4}	90	ABLIKIM	24CM	BES3	$e^+ e^-$ at $\sqrt{s}$ = 3.773 GeV

$\Gamma(\eta \eta e^+ \nu_e)/\Gamma_{total}$ — Γ_{61}/Γ

VALUE	CL%	DOCUMENT ID		TECN	COMMENT
<1.0 × 10^{-4}	90	ABLIKIM	24CM	BES3	$e^+ e^-$ at $\sqrt{s}$ = 3.773 GeV

$\Gamma(K^+ K^- e^+ \nu_e)/\Gamma_{total}$ — Γ_{62}/Γ

VALUE	CL%	DOCUMENT ID		TECN	COMMENT
<2.10 × 10^{-5}	90	[1] ABLIKIM	24AZ	BES3	7.9 fb^{-1}, $e^+ e^-$ at 3.773 GeV

[1] Includes $D^+ \to a_0(980)^0 e^+ \nu_e$, $a_0(980)^0 \to K^+ K^-$ resonant contribution.

$\Gamma(b_1(1235)^0 e^+ \nu_e,\ b_1^0 \to \omega \pi^0)/\Gamma_{total}$ — Γ_{63}/Γ

VALUE	CL%	DOCUMENT ID		TECN	COMMENT
<1.75 × 10^{-4}	90	ABLIKIM	20AF	BES3	$e^+ e^-$, 3773 MeV

$\Gamma(\phi e^+ \nu_e)/\Gamma_{total}$ — Γ_{64}/Γ

Unseen decay modes of the ϕ are included.

VALUE	CL%	DOCUMENT ID		TECN	COMMENT
<1.3 × 10^{-5}	90	ABLIKIM	15W	BES3	292 fb^{-1}, 3773 MeV
• • • We do not use the following data for averages, fits, limits, etc. • • •					
<0.9 × 10^{-4}	90	YELTON	11	CLEO	$e^+ e^-$ at $\psi(3770)$
<1.6 × 10^{-4}	90	MITCHELL	09B	CLEO	See YELTON 11
<0.0201	90	ABLIKIM	06P	BES2	$e^+ e^-$ at 3773 MeV
<0.0209	90	BAI	91	MRK3	$e^+ e^-$ ≈ 3.77 GeV

$\Gamma(D^0 e^+ \nu_e)/\Gamma_{total}$ — Γ_{65}/Γ

VALUE	CL%	DOCUMENT ID		TECN	COMMENT
<1.0 × 10^{-4}	90	ABLIKIM	17AD	BES3	$e^+ e^-$ at 3.773 GeV

Hadronic modes with a $\overline{K}$ or $\overline{K} K \overline{K}$

$\Gamma(K_S^0 \pi^+)/\Gamma_{total}$ — Γ_{66}/Γ

VALUE (units 10^{-2})	EVTS	DOCUMENT ID		TECN	COMMENT
1.554±0.033 OUR FIT Error includes scale factor of 1.8.					
1.591±0.006±0.030	94k	ABLIKIM	18W	BES3	$e^+ e^-$, 3773 MeV
• • • We do not use the following data for averages, fits, limits, etc. • • •					
1.526±0.022±0.038		[1] DOBBS	07	CLEO	See MENDEZ 10
1.55 ±0.05 ±0.06	2.2k	[1] HE	05	CLEO	See DOBBS 07
1.6 ±0.3 ±0.1	161	ADLER	88C	MRK3	$e^+ e^-$ 3.77 GeV

[1] DOBBS 07 and HE 05 use single- and double-tagged events in an overall fit. DOBBS 07 supersedes HE 05.

$\Gamma(K_S^0 \pi^+)/\Gamma(K^- 2\pi^+)$ — Γ_{66}/Γ_{68}

VALUE	EVTS	DOCUMENT ID		TECN	COMMENT
0.167 ±0.004 OUR FIT Error includes scale factor of 2.4.					
0.162 ±0.009 OUR AVERAGE Error includes scale factor of 4.5.					
0.171 ±0.002 ±0.002		BONVICINI	14	CLEO	All CLEO-c runs
0.1530±0.0023±0.0016	10.6k	LINK	02B	FOCS	γ nucleus, $\overline{E}_\gamma \approx$ 180 GeV
• • • We do not use the following data for averages, fits, limits, etc. • • •					
0.1682±0.0012±0.0037	30k	MENDEZ	10	CLEO	See BONVICINI 14
0.174 ±0.012 ±0.011	473	[1] BISHAI	97	CLEO	$e^+ e^- \approx \Upsilon(4S)$
0.137 ±0.015 ±0.016	264	ANJOS	90C	E691	Photoproduction

[1] See BISHAI 97 for an isospin analysis of $D^+ \to \overline{K} \pi$ amplitudes.

$\Gamma(K_L^0 \pi^+)/\Gamma_{total}$ — Γ_{67}/Γ

VALUE (units 10^{-2})	EVTS	DOCUMENT ID		TECN	COMMENT
1.460±0.040±0.035	2023 ± 54	[1] HE	08	CLEO	$e^+ e^-$ at $\psi(3770)$

[1] The difference of CLEO $D^+ \to K_S^0 \pi^+$ and $K_L^0 \pi^+$ branching fractions over the sum (DOBBS 07 and HE 08) is +0.022 ± 0.016 ± 0.018.

$\Gamma(K^- 2\pi^+)/\Gamma_{total}$ — Γ_{68}/Γ

VALUE (units 10^{-2})	EVTS	DOCUMENT ID		TECN	COMMENT
9.31 ±0.14 OUR FIT Error includes scale factor of 1.4.					
9.224±0.059±0.157		BONVICINI	14	CLEO	All CLEO-c runs
• • • We do not use the following data for averages, fits, limits, etc. • • •					
9.14 ±0.10 ±0.17		[1] DOBBS	07	CLEO	See BONVICINI 14
9.5 ±0.2 ±0.3	15.1k	[1] HE	05	CLEO	See DOBBS 07
9.3 ±0.6 ±0.8	1502	[2] BALEST	94	CLEO	$e^+ e^- \approx \Upsilon(4S)$
6.4 $^{+1.5}_{-1.4}$		[3] BARLAG	92C	ACCM	π^- Cu 230 GeV
9.1 ±1.3 ±0.4	1164	ADLER	88C	MRK3	$e^+ e^-$ 3.77 GeV
9.1 ±1.9	239	[4] SCHINDLER	81	MRK2	$e^+ e^-$ 3.771 GeV

[1] DOBBS 07 and HE 05 use single- and double-tagged events in an overall fit. DOBBS 07 supersedes HE 05.

[2] BALEST 94 measures the ratio of $D^+ \to K^- \pi^+ \pi^+$ and $D^0 \to K^- \pi^+$ branching fractions to be 2.35 ± 0.16 ± 0.16 and uses their absolute measurement of the $D^0 \to K^- \pi^+$ fraction (AKERIB 93).

[3] BARLAG 92C computes the branching fraction by topological normalization.

[4] SCHINDLER 81 (MARK-2) measures $\sigma(e^+ e^- \to \psi(3770)) \times$ branching fraction to be 0.38 ± 0.05 nb. We use the MARK-3 (ADLER 88C) value of σ = 4.2 ± 0.6 ± 0.3 nb.

Int. J. Mod. Phys. A 2026.41. Downloaded from www.worldscientific.com
by UNIVERSITY OF CALIFORNIA @ BERKELEY on 09/16/26. Re-use and distribution is strictly not permitted, except for Open Access articles.

See the related review(s):
Multibody Charm Analyses

$\Gamma((K^-\pi^+)_{S\text{-wave}}\pi^+)/\Gamma(K^-2\pi^+)$ — Γ_{69}/Γ_{68}

This is the "fit fraction" from the Dalitz-plot analysis. The $K^-\pi^+$ S-wave includes a broad scalar κ ($\overline{K}^*_0(700)$), the $\overline{K}^*_0(1430)^0$, and non-resonant background.

VALUE	DOCUMENT ID		TECN	COMMENT
0.801 ±0.012 OUR AVERAGE				
0.8024±0.0138±0.0043	[1] LINK	09	FOCS	MIPWA fit, 53k evts
0.838 ±0.038	[2] BONVICINI	08A	CLEO	QMIPWA fit, 141k evts
0.786 ±0.014 ±0.018	AITALA	06	E791	Dalitz fit, 15.1k events
• • • We do not use the following data for averages, fits, limits, etc. • • •				
0.8323±0.0150±0.0008	[3] LINK	07B	FOCS	See LINK 09

[1] This LINK 09 model-independent partial-wave analysis of the $K^-\pi^+$ S-wave slices the $K^-\pi^+$ mass range into 39 bins.

[2] The BONVICINI 08A QMIPWA (quasi-model-independent partial-wave analysis) of the $K^-\pi^+$ S-wave amplitude slices the $K^-\pi^+$ mass range into 26 bins but keeps the Breit-Wigner $\overline{K}^*_0(1430)^0$.

[3] This LINK 07B fit uses a K matrix. The $K^-\pi^+$ S-wave fit fraction given above breaks down into (207.3 ± 25.5 ± 12.4)% isospin-1/2 and (40.5 ± 9.6 ± 3.2)% isospin-3/2 — with large interference between the two. The isospin-1/2 component includes the κ (or $\overline{K}^*_0(700)^0$) and $\overline{K}^*_0(1430)^0$.

$\Gamma(\overline{K}^*_0(700)^0\pi^+, \overline{K}^*_0 \to K^-\pi^+)/\Gamma(K^-2\pi^+)$ — Γ_{70}/Γ_{68}

This is the "fit fraction" from the Dalitz-plot analysis.

VALUE	DOCUMENT ID		TECN	COMMENT
• • • We do not use the following data for averages, fits, limits, etc. • • •				
0.478±0.121±0.053	AITALA	02	E791	See AITALA 06

$\Gamma(\overline{K}^*_0(1430)^0\pi^+, \overline{K}^*_0(1430)^0 \to K^-\pi^+)/\Gamma(K^-2\pi^+)$ — Γ_{71}/Γ_{68}

This is the "fit fraction" from the Dalitz-plot analysis.

VALUE	DOCUMENT ID		TECN	COMMENT
0.1330±0.0062	BONVICINI	08A	CLEO	QMIPWA fit, 141k evts
• • • We do not use the following data for averages, fits, limits, etc. • • •				
0.125 ±0.014 ±0.005	AITALA	02	E791	See AITALA 06
0.284 ±0.022 ±0.059	FRABETTI	94G	E687	Dalitz fit, 8800 evts
0.248 ±0.019 ±0.017	ANJOS	93	E691	γBe 90–260 GeV

$\Gamma(\overline{K}^*(892)^0\pi^+, \overline{K}^*(892)^0 \to K^-\pi^+)/\Gamma(K^-2\pi^+)$ — Γ_{72}/Γ_{68}

This is the "fit fraction" from the Dalitz-plot analysis.

VALUE	DOCUMENT ID		TECN	COMMENT
0.111 ±0.012 OUR AVERAGE Error includes scale factor of 3.7.				
0.1236±0.0034±0.0034	LINK	09	FOCS	MIPWA fit, 53k evts
0.0988±0.0046	BONVICINI	08A	CLEO	QMIPWA fit, 141k evts
0.119 ±0.002 ±0.020	AITALA	06	E791	Dalitz fit, 15.1k events
• • • We do not use the following data for averages, fits, limits, etc. • • •				
0.1361±0.0041±0.0030	[1] LINK	07B	FOCS	See LINK 09
0.123 ±0.010 ±0.009	AITALA	02	E791	See AITALA 06
0.137 ±0.006 ±0.009	FRABETTI	94G	E687	Dalitz fit, 8800 evts
0.170 ±0.009 ±0.034	ANJOS	93	E691	γBe 90–260 GeV
0.14 ±0.04 ±0.04	ALVAREZ	91B	NA14	Photoproduction
0.13 ±0.01 ±0.07	ADLER	87	MRK3	e^+e^- 3.77 GeV

[1] The statistical error on this LINK 07B value is corrected in LINK 09.

$\Gamma(\overline{K}^*(1410)^0\pi^+, \overline{K}^{*0} \to K^-\pi^+)/\Gamma(K^-2\pi^+)$ — Γ_{73}/Γ_{68}

VALUE (units 10^{-3})	DOCUMENT ID		TECN	COMMENT
not seen	LINK	09	FOCS	MIPWA fit, 53k evts
not seen	BONVICINI	08A	CLEO	QMIPWA fit, 141k evts
• • • We do not use the following data for averages, fits, limits, etc. • • •				
4.8±2.1±1.7	LINK	07B	FOCS	See LINK 09

$\Gamma(\overline{K}^*_2(1430)^0\pi^+, \overline{K}^*_2(1430)^0 \to K^-\pi^+)/\Gamma(K^-2\pi^+)$ — Γ_{74}/Γ_{68}

This is the "fit fraction" from the Dalitz-plot analysis.

VALUE (units 10^{-2})	DOCUMENT ID		TECN	COMMENT
0.24 ±0.08 OUR AVERAGE Error includes scale factor of 2.2. See the ideogram below.				
0.58 ±0.10 ±0.06	LINK	09	FOCS	MIPWA fit, 53k evts
0.204±0.040	BONVICINI	08A	CLEO	QMIPWA fit, 141k evts
0.2 ±0.1 ±0.1	AITALA	06	E791	Dalitz fit, 15.1k events
• • • We do not use the following data for averages, fits, limits, etc. • • •				
0.39 ±0.09 ±0.05	LINK	07B	FOCS	See LINK 09
0.5 ±0.1 ±0.2	AITALA	02	E791	See AITALA 06

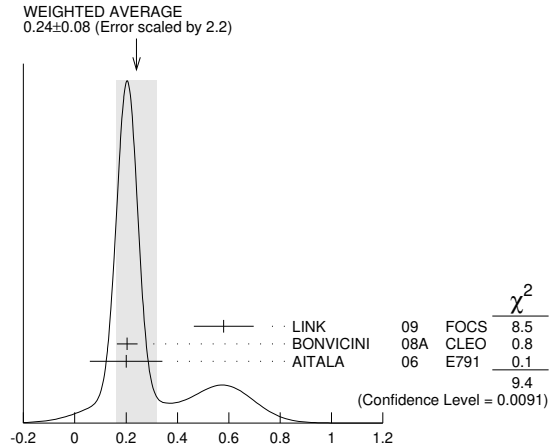

$\Gamma(\overline{K}^*_2(1430)^0\pi^+, \overline{K}^*_2(1430)^0 \to K^-\pi^+)/\Gamma(K^-2\pi^+)$ (units 10^{-2}) — Γ_{74}/Γ_{68}

$\Gamma(\overline{K}^*(1680)^0\pi^+, \overline{K}^*(1680)^0 \to K^-\pi^+)/\Gamma(K^-2\pi^+)$ — Γ_{75}/Γ_{68}

This is the "fit fraction" from the Dalitz-plot analysis.

VALUE (units 10^{-2})	DOCUMENT ID		TECN	COMMENT
0.23 ±0.12 OUR AVERAGE				
1.75 ±0.62 ±0.54	LINK	09	FOCS	MIPWA fit, 53k evts
0.196±0.118	BONVICINI	08A	CLEO	QMIPWA fit, 141k evts
1.2 ±0.6 ±1.2	AITALA	06	E791	Dalitz fit, 15.1k events
• • • We do not use the following data for averages, fits, limits, etc. • • •				
1.90 ±0.63 ±0.43	LINK	07B	FOCS	See LINK 09
2.5 ±0.7 ±0.3	AITALA	02	E791	See AITALA 06
4.7 ±0.6 ±0.7	FRABETTI	94G	E687	Dalitz fit, 8800 evts
3.0 ±0.4 ±1.3	ANJOS	93	E691	γBe 90–260 GeV

$\Gamma(K^-(2\pi^+)_{I=2})/\Gamma(K^-2\pi^+)$ — Γ_{76}/Γ_{68}

VALUE	DOCUMENT ID		TECN	COMMENT
0.155±0.028	BONVICINI	08A	CLEO	QMIPWA fit, 141k evts

$\Gamma(K^-2\pi^+ \text{ nonresonant})/\Gamma(K^-2\pi^+)$ — Γ_{77}/Γ_{68}

This is the "fit fraction" from the Dalitz-plot analysis. Later analyses find little need for this decay mode.

VALUE	DOCUMENT ID		TECN	COMMENT
• • • We do not use the following data for averages, fits, limits, etc. • • •				
0.130±0.058±0.044	AITALA	02	E791	See AITALA 06
0.998±0.037±0.072	FRABETTI	94G	E687	Dalitz fit, 8800 evts
0.838±0.088±0.275	ANJOS	93	E691	γBe 90–260 GeV
0.79 ±0.07 ±0.15	ADLER	87	MRK3	e^+e^- 3.77 GeV

$\Gamma(K^0_S\pi^+\pi^0)/\Gamma_{total}$ — Γ_{78}/Γ

VALUE (units 10^{-2})	EVTS	DOCUMENT ID		TECN	COMMENT
• • • We do not use the following data for averages, fits, limits, etc. • • •					
6.99±0.09±0.25		[1] DOBBS	07	CLEO	See BONVICINI 14
7.2 ±0.2 ±0.4	5.1k	[1] HE	05	CLEO	See DOBBS 07
5.1 ±1.3 ±0.8	159	ADLER	88C	MRK3	e^+e^- 3.77 GeV

[1] DOBBS 07 and HE 05 use single- and double-tagged events in an overall fit. DOBBS 07 supersedes HE 05.

$\Gamma(K^0_S\pi^+\pi^0)/\Gamma(K^-2\pi^+)$ — Γ_{78}/Γ_{68}

VALUE	DOCUMENT ID		TECN	COMMENT
0.785±0.007±0.016	BONVICINI	14	CLEO	All CLEO-c runs

$\Gamma(K^0_S\rho^+)/\Gamma(K^0_S\pi^+\pi^0)$ — Γ_{79}/Γ_{78}

This is the "fit fraction" from the Dalitz-plot analysis.

VALUE (units 10^{-2})	DOCUMENT ID		TECN	COMMENT
$83.4\pm2.2^{+7.1}_{-3.6}$	[1] ABLIKIM	14E	BES3	e^+e^- at $\psi(3770)$

[1] Fit fraction from Dalitz plot analysis of 142k $D^+ \to K^0_S\pi^+\pi^0$ events.

$\Gamma(K^0_S\rho(1450)^+, \rho^+ \to \pi^+\pi^0)/\Gamma(K^0_S\pi^+\pi^0)$ — Γ_{80}/Γ_{78}

This is the "fit fraction" from the Dalitz-plot analysis.

VALUE (%)	DOCUMENT ID		TECN	COMMENT
$2.1\pm0.3^{+1.6}_{-1.9}$	ABLIKIM	14E	BES3	e^+e^- at $\psi(3770)$

$\Gamma(\overline{K}^*(892)^0\pi^+, \overline{K}^*(892)^0 \to K^0_S\pi^0)/\Gamma(K^0_S\pi^+\pi^0)$ — Γ_{81}/Γ_{78}

This is the "fit fraction" from the Dalitz-plot analysis.

VALUE (units 10^{-2})	DOCUMENT ID		TECN	COMMENT
$3.58\pm0.17^{+0.39}_{-0.38}$	[1] ABLIKIM	14E	BES3	e^+e^- at $\psi(3770)$

[1] Fit fraction from Dalitz plot analysis of 142k $D^+ \to K^0_S\pi^+\pi^0$ events.

Int. J. Mod. Phys. A 2026.41. Downloaded from www.worldscientific.com
by UNIVERSITY OF CALIFORNIA @ BERKELEY on 09/16/26. Re-use and distribution is strictly not permitted, except for Open Access articles.

$\Gamma(\overline{K}_0^*(1430)^0\pi^+, \overline{K}_0^{*0} \to K_S^0\pi^0)/\Gamma(K_S^0\pi^+\pi^0)$ — Γ_{82}/Γ_{78}

This is the "fit fraction" from the Dalitz-plot analysis.

VALUE (%)	DOCUMENT ID		TECN	COMMENT
3.7±0.6±1.1	ABLIKIM	14E	BES3	e^+e^- at $\psi(3770)$

$\Gamma(\overline{K}_0^*(1680)^0\pi^+, \overline{K}_0^{*0} \to K_S^0\pi^0)/\Gamma(K_S^0\pi^+\pi^0)$ — Γ_{83}/Γ_{78}

This is the "fit fraction" from the Dalitz-plot analysis.

VALUE (%)	DOCUMENT ID		TECN	COMMENT
$1.3\pm0.2^{+0.9}_{-1.3}$	ABLIKIM	14E	BES3	e^+e^- at $\psi(3770)$

$\Gamma(\overline{\kappa}^0\pi^+, \overline{\kappa}^0 \to K_S^0\pi^0)/\Gamma(K_S^0\pi^+\pi^0)$ — Γ_{84}/Γ_{78}

This is the "fit fraction" from the Dalitz-plot analysis.

VALUE (%)	DOCUMENT ID		TECN	COMMENT
$7.7\pm1.2^{+6.5}_{-4.8}$	ABLIKIM	14E	BES3	e^+e^- at $\psi(3770)$

$\Gamma(K_S^0\pi^+\pi^0 \text{ nonresonant})/\Gamma(K_S^0\pi^+\pi^0)$ — Γ_{85}/Γ_{78}

This is the "fit fraction" from the Dalitz-plot analysis.

VALUE (units 10^{-2})	DOCUMENT ID		TECN	COMMENT
$4.6\pm0.7^{+5.4}_{-5.1}$	[1] ABLIKIM	14E	BES3	e^+e^- at $\psi(3770)$

[1] Fit fraction from Dalitz plot analysis of 142k $D^+ \to K_S^0\pi^+\pi^0$ events.

$\Gamma(K_S^0\pi^+\pi^0 \text{ nonresonant and } \overline{\kappa}^0\pi^+)/\Gamma(K_S^0\pi^+\pi^0)$ — Γ_{86}/Γ_{78}

This is the "fit fraction" from the Dalitz-plot analysis.

VALUE (%)	DOCUMENT ID		TECN	COMMENT
$18.6\pm1.7^{+2.3}_{-4.6}$	ABLIKIM	14E	BES3	e^+e^- at $\psi(3770)$

$\Gamma((K_S^0\pi^0)_{S-\text{wave}}\pi^+)/\Gamma(K_S^0\pi^+\pi^0)$ — Γ_{87}/Γ_{78}

The numerator here is the coherent sum of the $\overline{K}_0^*(1430)^0\pi^+$, $\overline{\kappa}^0\pi^+$, and nonresonant contributions.

VALUE (%)	DOCUMENT ID		TECN	COMMENT
$17.3\pm1.4^{+3.4}_{-4.3}$	ABLIKIM	14E	BES3	e^+e^- at $\psi(3770)$

$\Gamma(K_S^0\pi^+\omega)/\Gamma_{\text{total}}$ — Γ_{88}/Γ

VALUE (units 10^{-2})	EVTS	DOCUMENT ID		TECN	COMMENT
$0.707\pm0.041\pm0.029$	523	[1] ABLIKIM	22U	BES3	e^+e^- at 3.773 GeV

[1] ABLIKIM 22U determines the ratio $B(D^+ \to K_S^0\pi^+\omega)/B(D^0 \to K^-\pi^+\omega) = 0.21 \pm 0.01 \pm 0.01$, in significant tension with statistical isospin model expectation of 0.9.

$\Gamma(K_S^0\pi^+\eta)/\Gamma_{\text{total}}$ — Γ_{89}/Γ

VALUE (units 10^{-3})	EVTS	DOCUMENT ID		TECN	COMMENT
12.7 ±0.4 ±0.3	1.1k	ABLIKIM	24AS	BES3	e^+e^- at 3.773 GeV
• • • We do not use the following data for averages, fits, limits, etc. • • •					
$13.09\pm0.37\pm0.31$	1.3k	ABLIKIM	20V	BES3	e^+e^- at 3773 MeV

$\Gamma(K_S^0a_0(980)^+, a_0^+ \to \pi^+\eta)/\Gamma(K_S^0\pi^+\eta)$ — Γ_{90}/Γ_{89}

VALUE (units 10^{-2})	EVTS	DOCUMENT ID		TECN	COMMENT
$105.00\pm0.94\pm1.04\pm0.07$	1.1k	[1] ABLIKIM	24AS	BES3	e^+e^- at 3.773 GeV

[1] Amplitude analysis with two components. The second and third uncertainties are model and experimental systematic uncertainties, respectively.

$\Gamma(\overline{K}_0^*(1430)^0\pi^+, \overline{K}_0^* \to K_S^0\eta)/\Gamma(K_S^0\pi^+\eta)$ — Γ_{91}/Γ_{89}

VALUE (units 10^{-2})	EVTS	DOCUMENT ID		TECN	COMMENT
$10.83\pm1.50\pm1.27\pm0.08$	1.1k	[1] ABLIKIM	24AS	BES3	e^+e^- at 3.773 GeV

[1] Amplitude analysis with two components. The second and third uncertainties are model and experimental systematic uncertainties, respectively.

$\Gamma(K_S^0\pi^+\eta'(958))/\Gamma_{\text{total}}$ — Γ_{92}/Γ

VALUE (units 10^{-3})	EVTS	DOCUMENT ID		TECN	COMMENT
$1.90\pm0.17\pm0.13$	267	ABLIKIM	18AC	BES3	e^+e^-, 3773 MeV

$\Gamma(K^-2\pi^+\pi^0)/\Gamma_{\text{total}}$ — Γ_{93}/Γ

See the listings under "$D \to K\pi\pi\pi$ partial wave analyses" and our 2008 Review (Physics Letters **B667** 1 (2008)) for measurements of submodes of this mode.

VALUE (units 10^{-2})	EVTS	DOCUMENT ID		TECN	COMMENT
$6.35\pm0.04\pm0.07$	35.5k	ABLIKIM	25BF	BES3	e^+e^- at $\sqrt{s} = 3.773$ GeV
• • • We do not use the following data for averages, fits, limits, etc. • • •					
$5.98\pm0.08\pm0.16$		[1] DOBBS	07	CLEO	See BONVICINI 14
$6.0 \pm0.2 \pm0.2$	4.8k	[1] HE	05	CLEO	See DOBBS 07
$5.8 \pm1.2 \pm1.2$	142	COFFMAN	92B	MRK3	e^+e^- 3.77 GeV
$6.3 \;^{+1.4}_{-1.3} \pm1.2$	175	BALTRUSAIT...86E		MRK3	See COFFMAN 92B

[1] DOBBS 07 and HE 05 use single- and double-tagged events in an overall fit. DOBBS 07 supersedes HE 05.

$\Gamma(\overline{K}^*(892)^0\rho(770)^+, \overline{K}^{*0} \to K^-\pi^+, \rho^+ \to \pi^0\pi^+)/\Gamma(K^-2\pi^+\pi^0)$ — Γ_{94}/Γ_{93}

VALUE (units 10^{-2})	EVTS	DOCUMENT ID		TECN	COMMENT
68.4±1.1±2.6	35.5k	[1] ABLIKIM	25BF	BES3	e^+e^- at $\sqrt{s} = 3.773$ GeV

[1] Amplitude analysis of $D^+ \to K^-2\pi^+\pi^0$ with 15 components.

$\Gamma(\overline{K}_1(1270)^0\pi^+, \overline{K}_1^0 \to K^-\rho(770)^+, \rho^+ \to \pi^+\pi^0)/\Gamma(K^-2\pi^+\pi^0)$ — Γ_{95}/Γ_{93}

VALUE (units 10^{-2})	EVTS	DOCUMENT ID		TECN	COMMENT
3.8±0.3±0.3	35.5k	[1] ABLIKIM	25BF	BES3	e^+e^- at $\sqrt{s} = 3.773$ GeV

[1] Amplitude analysis of $D^+ \to K^-2\pi^+\pi^0$ with 15 components.

$\Gamma(\overline{K}_1(1400)^0\pi^+, \overline{K}_1^0 \to \overline{K}^*(892)\pi, \overline{K}^* \to K^-\pi)/\Gamma(K^-2\pi^+\pi^0)$ — Γ_{96}/Γ_{93}

VALUE (units 10^{-2})	EVTS	DOCUMENT ID		TECN	COMMENT
7.3±0.2±0.3	35.5k	[1] ABLIKIM	25BF	BES3	e^+e^- at $\sqrt{s} = 3.773$ GeV

[1] Amplitude analysis of $D^+ \to K^-2\pi^+\pi^0$ with 15 components.

$\Gamma(\overline{K}(1460)^0\pi^+, \overline{K}(1460)^0 \to \overline{K}^*(892)\pi, \overline{K}^* \to K^-\pi)/\Gamma(K^-2\pi^+\pi^0)$ — Γ_{97}/Γ_{93}

VALUE (units 10^{-2})	EVTS	DOCUMENT ID		TECN	COMMENT
5.1±0.2±0.3	35.5k	[1] ABLIKIM	25BF	BES3	e^+e^- at $\sqrt{s} = 3.773$ GeV

[1] Amplitude analysis of $D^+ \to K^-2\pi^+\pi^0$ with 15 components.

$\Gamma(\overline{K}^*(1680)^0\pi^+, \overline{K}^{*0} \to \overline{K}^*(892)\pi, \overline{K}^* \to K^-\pi)/\Gamma(K^-2\pi^+\pi^0)$ — Γ_{98}/Γ_{93}

VALUE (units 10^{-2})	EVTS	DOCUMENT ID		TECN	COMMENT
3.8±0.4±0.8	35.5k	[1] ABLIKIM	25BF	BES3	e^+e^- at $\sqrt{s} = 3.773$ GeV

[1] Amplitude analysis of $D^+ \to K^-2\pi^+\pi^0$ with 15 components.

$\Gamma((K^-\pi^+)_{S-\text{wave}}\rho(770)^+, \rho^+ \to \pi^+\pi^0)/\Gamma(K^-2\pi^+\pi^0)$ — Γ_{99}/Γ_{93}

VALUE (units 10^{-2})	EVTS	DOCUMENT ID		TECN	COMMENT
18.3±0.7±0.7	35.5k	[1] ABLIKIM	25BF	BES3	e^+e^- at $\sqrt{s} = 3.773$ GeV

[1] Amplitude analysis of $D^+ \to K^-2\pi^+\pi^0$ with 15 components.

$\Gamma(\overline{K}(1460)^0\pi^+, \overline{K}(1460)^0 \to K^-(\pi^+\pi^0)_{L=1})/\Gamma(K^-2\pi^+\pi^0)$ — Γ_{100}/Γ_{93}

VALUE (units 10^{-2})	EVTS	DOCUMENT ID		TECN	COMMENT
8.6±0.8±0.5	35.5k	[1] ABLIKIM	25BF	BES3	e^+e^- at $\sqrt{s} = 3.773$ GeV

[1] Amplitude analysis of $D^+ \to K^-2\pi^+\pi^0$ with 15 components.

$\Gamma(\overline{K}(1460)^0\pi^+, \overline{K}(1460)^0 \to (K^-\pi)_{L=1}\pi)/\Gamma(K^-2\pi^+\pi^0)$ — Γ_{101}/Γ_{93}

VALUE (units 10^{-2})	EVTS	DOCUMENT ID		TECN	COMMENT
3.4±0.5±0.3	35.5k	[1] ABLIKIM	25BF	BES3	e^+e^- at $\sqrt{s} = 3.773$ GeV

[1] Amplitude analysis of $D^+ \to K^-2\pi^+\pi^0$ with 15 components.

$\Gamma((K^-\rho(770)^+)_{L=1}\pi^+, \rho^+ \to \pi^+\pi^0)/\Gamma(K^-2\pi^+\pi^0)$ — Γ_{102}/Γ_{93}

VALUE (units 10^{-2})	EVTS	DOCUMENT ID		TECN	COMMENT
1.8±0.1±0.1	35.5k	[1] ABLIKIM	25BF	BES3	e^+e^- at $\sqrt{s} = 3.773$ GeV

[1] Amplitude analysis of $D^+ \to K^-2\pi^+\pi^0$ with 15 components.

$\Gamma((\overline{K}^*(892)\pi)_{L=1}\pi^+, \overline{K}^* \to K^-\pi)/\Gamma(K^-2\pi^+\pi^0)$ — Γ_{103}/Γ_{93}

VALUE (units 10^{-2})	EVTS	DOCUMENT ID		TECN	COMMENT
0.8±0.1±0.1	35.5k	[1] ABLIKIM	25BF	BES3	e^+e^- at $\sqrt{s} = 3.773$ GeV

[1] Amplitude analysis of $D^+ \to K^-2\pi^+\pi^0$ with 15 components.

$\Gamma((\overline{K}^*(892)^0\pi^+)_{L=1}\pi^0, \overline{K}^{*0} \to K^-\pi^+)/\Gamma(K^-2\pi^+\pi^0)$ — Γ_{104}/Γ_{93}

VALUE (units 10^{-2})	EVTS	DOCUMENT ID		TECN	COMMENT
0.8±0.2±0.4	35.5k	[1] ABLIKIM	25BF	BES3	e^+e^- at $\sqrt{s} = 3.773$ GeV

[1] Amplitude analysis of $D^+ \to K^-2\pi^+\pi^0$ with 15 components.

$\Gamma((K^-(\pi^+\pi^0)_{L=0})_{L=1}\pi^+)/\Gamma(K^-2\pi^+\pi^0)$ — Γ_{105}/Γ_{93}

VALUE (units 10^{-2})	EVTS	DOCUMENT ID		TECN	COMMENT
0.8±0.2±0.2	35.5k	[1] ABLIKIM	25BF	BES3	e^+e^- at $\sqrt{s} = 3.773$ GeV

[1] Amplitude analysis of $D^+ \to K^-2\pi^+\pi^0$ with 15 components.

$\Gamma((K^-\pi^+)_{L=1}\rho(770)^+, \rho^+ \to \pi^+\pi^0)/\Gamma(K^-2\pi^+\pi^0)$ — Γ_{106}/Γ_{93}

VALUE (units 10^{-2})	EVTS	DOCUMENT ID		TECN	COMMENT
0.5±0.1±0.1	35.5k	[1] ABLIKIM	25BF	BES3	e^+e^- at $\sqrt{s} = 3.773$ GeV

[1] Amplitude analysis of $D^+ \to K^-2\pi^+\pi^0$ with 15 components.

$\Gamma(K^-2\pi^+\pi^0)/\Gamma(K^-2\pi^+)$ — Γ_{93}/Γ_{68}

VALUE	DOCUMENT ID		TECN	COMMENT
0.666±0.006±0.014	BONVICINI	14	CLEO	All CLEO-c runs

$\Gamma(K_S^0 2\pi^+\pi^-)/\Gamma_{\text{total}}$ — Γ_{107}/Γ

See the listings under "$D \to K\pi\pi\pi$ partial wave analyses" and our 2008 Review (Physics Letters **B667** 1 (2008)) for measurements of submodes of this mode.

VALUE (units 10^{-2})	EVTS	DOCUMENT ID		TECN	COMMENT
• • • We do not use the following data for averages, fits, limits, etc. • • •					
$3.122\pm0.046\pm0.096$		[1] DOBBS	07	CLEO	See BONVICINI 14
$3.2 \pm0.1 \pm0.2$	3.2k	[1] HE	05	CLEO	See DOBBS 07
$2.1 \;^{+1.0}_{-0.9}$		[2] BARLAG	92C	ACCM	π^- Cu 230 GeV
$3.3 \pm0.8 \pm0.2$	168	ADLER	88C	MRK3	e^+e^- 3.77 GeV

[1] DOBBS 07 and HE 05 use single- and double-tagged events in an overall fit. DOBBS 07 supersedes HE 05.
[2] BARLAG 92C computes the branching fraction by topological normalization.

Int. J. Mod. Phys. A 2026.41. Downloaded from www.worldscientific.com by LIFORNIA @ BERKELEY on 09/16/26. Re-use and distribution is strictly not permitted, except for Open Access articles.

$\Gamma(K^0_S 2\pi^+\pi^-)/\Gamma(K^-2\pi^+)$ — Γ_{107}/Γ_{68}

VALUE	DOCUMENT ID		TECN	COMMENT
0.331±0.004±0.006	BONVICINI	14	CLEO	All CLEO-c runs

$\Gamma(K^0_S\pi^+2\pi^0)/\Gamma_{total}$ — Γ_{108}/Γ

VALUE (units 10^{-3})	EVTS	DOCUMENT ID		TECN	COMMENT
28.88±0.58±0.69	3.7k	ABLIKIM	23BW	BES3	e^+e^- at 3.773 GeV
• • • We do not use the following data for averages, fits, limits, etc. • • •					
29.04±0.62±0.87	3.4k	[1] ABLIKIM	22Y	BES3	e^+e^- at 3.773 GeV

[1] See ABLIKIM 23BW.

$\Gamma(K^0_S a_1(1260)^+,\ a_1^+\to\rho(770)^+\pi^0)/\Gamma(K^0_S\pi^+2\pi^0)$ — $\Gamma_{109}/\Gamma_{108}$

VALUE (units 10^{-2})	DOCUMENT ID		TECN	COMMENT
30.0±3.6±4.2	[1] ABLIKIM	23BW	BES3	$D^+\to K^0_S\pi^+2\pi^0$

[1] Amplitude analysis of 1.4k $D^+\to K^0_S\pi^+2\pi^0$ events.

$\Gamma(K^0_S a_1(1260)^+,\ a_1^+\to f_0(500)\pi^+,\ f_0\to\pi^0\pi^0)/\Gamma(K^0_S\pi^+2\pi^0)$ — $\Gamma_{110}/\Gamma_{108}$

VALUE (units 10^{-2})	DOCUMENT ID		TECN	COMMENT
3.5±1.1±1.9	[1] ABLIKIM	23BW	BES3	$D^+\to K^0_S\pi^+2\pi^0$

[1] Amplitude analysis of 1.4k $D^+\to K^0_S\pi^+2\pi^0$ events.

$\Gamma(\overline{K}_1(1400)^0\pi^+,\ \overline{K}_1^0\to\overline{K}^*(892)^0\pi^0,\ \overline{K}^{*0}\to K^0_S\pi^0)/\Gamma(K^0_S\pi^+2\pi^0)$ — $\Gamma_{111}/\Gamma_{108}$

VALUE (units 10^{-2})	DOCUMENT ID		TECN	COMMENT
8.0±1.2±0.4	[1] ABLIKIM	23BW	BES3	$D^+\to K^0_S\pi^+2\pi^0$

[1] Amplitude analysis of 1.4k $D^+\to K^0_S\pi^+2\pi^0$ events.

$\Gamma(\overline{K}^*(892)^0\rho^+,\ \overline{K}^{*0}\to K^0_S\pi^0)/\Gamma(K^0_S\pi^+2\pi^0)$ — $\Gamma_{112}/\Gamma_{108}$

VALUE (units 10^{-2})	DOCUMENT ID		TECN	COMMENT
33.6±2.7±1.4	[1] ABLIKIM	23BW	BES3	$D^+\to K^0_S\pi^+2\pi^0$

[1] Amplitude analysis of 1.4k $D^+\to K^0_S\pi^+2\pi^0$ events.

$\Gamma(\overline{K}^*(892)^0\pi^+\pi^0$ non-resonant, $\overline{K}^{*0}\to K^0_S\pi^0)/\Gamma(K^0_S\pi^+2\pi^0)$ — $\Gamma_{113}/\Gamma_{108}$

VALUE (units 10^{-2})	DOCUMENT ID		TECN	COMMENT
9.1±2.0±1.0	[1] ABLIKIM	23BW	BES3	$D^+\to K^0_S\pi^+2\pi^0$

[1] Amplitude analysis of 1.4k $D^+\to K^0_S\pi^+2\pi^0$ events.

$\Gamma(K^0_S\rho^+\pi^0$ non-resonant$)/\Gamma(K^0_S\pi^+2\pi^0)$ — $\Gamma_{114}/\Gamma_{108}$

VALUE (units 10^{-2})	DOCUMENT ID		TECN	COMMENT
16.5±1.6±0.3	[1] ABLIKIM	23BW	BES3	$D^+\to K^0_S\pi^+2\pi^0$

[1] Amplitude analysis of 1.4k $D^+\to K^0_S\pi^+2\pi^0$ events.

$\Gamma(K^-2\pi^+\eta)/\Gamma_{total}$ — Γ_{115}/Γ

VALUE (units 10^{-3})	EVTS	DOCUMENT ID		TECN	COMMENT
1.35±0.11±0.04	190	ABLIKIM	20V	BES3	e^+e^-, 3773 MeV

$\Gamma(K^0_S\pi^+\pi^0\eta)/\Gamma_{total}$ — Γ_{116}/Γ

VALUE (units 10^{-3})	EVTS	DOCUMENT ID		TECN	COMMENT
1.22±0.24±0.06	50	ABLIKIM	20V	BES3	e^+e^-, 3773 MeV

$\Gamma(K^-3\pi^+\pi^-)/\Gamma(K^-2\pi^+)$ — Γ_{117}/Γ_{68}

VALUE	EVTS	DOCUMENT ID		TECN	COMMENT
0.061±0.005 OUR FIT Error includes scale factor of 1.1.					
0.062±0.008 OUR AVERAGE Error includes scale factor of 1.3.					
0.058±0.002±0.006	2923	LINK	03D	FOCS	γ A, $\overline{E}_\gamma\approx$ 180 GeV
0.077±0.008±0.010	239	FRABETTI	97C	E687	γBe, $\overline{E}_\gamma\approx$ 200 GeV
• • • We do not use the following data for averages, fits, limits, etc. • • •					
0.09 ±0.01 ±0.01	113	ANJOS	90D	E691	Photoproduction

$\Gamma(\overline{K}^*(892)^0 2\pi^+\pi^-,\overline{K}^*(892)^0\to K^-\pi^+)/\Gamma(K^-3\pi^+\pi^-)$ — $\Gamma_{118}/\Gamma_{117}$

VALUE	DOCUMENT ID		TECN	COMMENT
0.21±0.04±0.06	LINK	03D	FOCS	γ A, $\overline{E}_\gamma\approx$ 180 GeV

$\Gamma(\overline{K}^*(892)^0\rho^0\pi^+,\overline{K}^*(892)^0\to K^-\pi^+)/\Gamma(K^-2\pi^+)$ — Γ_{119}/Γ_{68}

VALUE	DOCUMENT ID		TECN	COMMENT
• • • We do not use the following data for averages, fits, limits, etc. • • •				
0.016±0.007±0.004	FRABETTI	97C	E687	γBe, $\overline{E}_\gamma\approx$ 200 GeV

$\Gamma(\overline{K}^*(892)^0\rho^0\pi^+,\overline{K}^*(892)^0\to K^-\pi^+)/\Gamma(K^-3\pi^+\pi^-)$ — $\Gamma_{119}/\Gamma_{117}$

VALUE	DOCUMENT ID		TECN	COMMENT
0.40±0.03±0.06	LINK	03D	FOCS	γ A, $\overline{E}_\gamma\approx$ 180 GeV

$\Gamma(\overline{K}^*(892)^0 a_1(1260)^+)/\Gamma(K^-2\pi^+)$ — Γ_{120}/Γ_{68}

Unseen decay modes of the $\overline{K}^*(892)^0$ and $a_1(1260)^+$ are included.

VALUE	DOCUMENT ID		TECN	COMMENT
0.099±0.008±0.018	LINK	03D	FOCS	γ A, $\overline{E}_\gamma\approx$ 180 GeV

$\Gamma(\overline{K}^*(892)^0 2\pi^+\pi^-$ no-$\rho,\overline{K}^*(892)^0\to K^-\pi^+)/\Gamma(K^-2\pi^+)$ — Γ_{121}/Γ_{68}

VALUE	DOCUMENT ID		TECN	COMMENT
• • • We do not use the following data for averages, fits, limits, etc. • • •				
0.032±0.010±0.008	FRABETTI	97C	E687	γBe, $\overline{E}_\gamma\approx$ 200 GeV

$\Gamma(K^-\rho^0 2\pi^+)/\Gamma(K^-2\pi^+)$ — Γ_{122}/Γ_{68}

VALUE	DOCUMENT ID		TECN	COMMENT
• • • We do not use the following data for averages, fits, limits, etc. • • •				
0.034±0.009±0.005	FRABETTI	97C	E687	γBe, $\overline{E}_\gamma\approx$ 200 GeV

$\Gamma(K^-\rho^0 2\pi^+)/\Gamma(K^-3\pi^+\pi^-)$ — $\Gamma_{122}/\Gamma_{117}$

VALUE	DOCUMENT ID		TECN	COMMENT
0.30±0.04±0.01	LINK	03D	FOCS	γ A, $\overline{E}_\gamma\approx$ 180 GeV

$\Gamma(K^-3\pi^+\pi^-$ nonresonant$)/\Gamma(K^-3\pi^+\pi^-)$ — $\Gamma_{123}/\Gamma_{117}$

VALUE	CL%	DOCUMENT ID		TECN	COMMENT
0.07 ±0.05±0.01		LINK	03D	FOCS	γ A, $\overline{E}_\gamma\approx$ 180 GeV
• • • We do not use the following data for averages, fits, limits, etc. • • •					
<0.026	90	FRABETTI	97C	E687	γBe, $\overline{E}_\gamma\approx$ 200 GeV

$\Gamma(K^0_S 2\pi^+\pi^-\pi^0)/\Gamma_{total}$ — Γ_{124}/Γ

VALUE (units 10^{-3})	EVTS	DOCUMENT ID		TECN	COMMENT
15.28±0.57±0.60	1k	ABLIKIM	22Y	BES3	e^+e^- at 3.773 GeV

$\Gamma(K^0_S\pi^+3\pi^0)/\Gamma_{total}$ — Γ_{125}/Γ

VALUE (units 10^{-3})	EVTS	DOCUMENT ID		TECN	COMMENT
5.54±0.44±0.32	285	ABLIKIM	22Y	BES3	e^+e^- at 3.773 GeV

$\Gamma(K^-2\pi^+2\pi^0)/\Gamma_{total}$ — Γ_{126}/Γ

VALUE (units 10^{-3})	EVTS	DOCUMENT ID		TECN	COMMENT
4.95±0.26±0.19	756	ABLIKIM	22Y	BES3	e^+e^- at 3.773 GeV

$\Gamma(K^-3\pi^+\pi^-\pi^0)/\Gamma_{total}$ — Γ_{127}/Γ

VALUE (units 10^{-4})	EVTS	DOCUMENT ID		TECN	COMMENT
6.57±0.69±0.33	0.16k	ABLIKIM	25BA	BES3	e^+e^- at 3.773 GeV

$\Gamma(K^+2K^0_S)/\Gamma_{total}$ — Γ_{128}/Γ

VALUE (units 10^{-4})	EVTS	DOCUMENT ID		TECN	COMMENT
25.4±0.5±1.2	3551	ABLIKIM	17A	BES3	$e^+e^-\to\psi(3770)$

$\Gamma(K^+2K^0_S)/\Gamma(K^-2\pi^+)$ — Γ_{128}/Γ_{68}

VALUE	EVTS	DOCUMENT ID		TECN	COMMENT
• • • We do not use the following data for averages, fits, limits, etc. • • •					
0.035±0.010±0.005	39 ± 9	ALBRECHT	94I	ARG	$e^+e^-\approx$ 10 GeV
0.085±0.018	70 ± 12	AMMAR	91	CLEO	$e^+e^-\approx$ 10.5 GeV

$\Gamma(\phi(1020)^0K^+)/\Gamma_{total}$ — Γ_{224}/Γ

VALUE	CL%	DOCUMENT ID		TECN	COMMENT
<2.1 × 10^{-5}	90	ABLIKIM	19BI	BES3	e^+e^- at 3773 MeV

$\Gamma(K^+K^-K^0_S\pi^+)/\Gamma(K^0_S 2\pi^+\pi^-)$ — $\Gamma_{129}/\Gamma_{107}$

VALUE (units 10^{-3})	EVTS	DOCUMENT ID		TECN	COMMENT
7.7±1.5±0.9	35 ± 7	LINK	01C	FOCS	γ nucleus, $\overline{E}_\gamma\approx$ 180 GeV

Pionic modes

$\Gamma(\pi^+\pi^0)/\Gamma_{total}$ — Γ_{130}/Γ

VALUE (units 10^{-3})	EVTS	DOCUMENT ID		TECN	COMMENT
1.243±0.033 OUR FIT					
1.259±0.033±0.023	10k	ABLIKIM	18W	BES3	e^+e^-, 3773 MeV

$\Gamma(\pi^+\pi^0)/\Gamma(K^-2\pi^+)$ — Γ_{130}/Γ_{68}

VALUE (units 10^{-2})	EVTS	DOCUMENT ID		TECN	COMMENT
1.34±0.04 OUR FIT					
1.31±0.06 OUR AVERAGE					
1.29±0.04±0.05	2649 ± 76	MENDEZ	10	CLEO	e^+e^- at 3774 MeV
1.33±0.11±0.09	1229 ± 99	AUBERT,B	06F	BABR	$e^+e^-\approx\Upsilon(4S)$
1.44±0.19±0.10	171 ± 22	ARMS	04	CLEO	$e^+e^-\approx$ 10 GeV
• • • We do not use the following data for averages, fits, limits, etc. • • •					
1.33±0.07±0.06	914 ± 46	RUBIN	06	CLEO	See MENDEZ 10

$\Gamma(2\pi^+\pi^-)/\Gamma_{total}$ — Γ_{131}/Γ

VALUE (units 10^{-4})	EVTS	DOCUMENT ID		TECN	COMMENT
32.7±0.7±0.5	2.6k	ABLIKIM	22BG	BES3	e^+e^- at 3.773 GeV

$\Gamma(2\pi^+\pi^-)/\Gamma(K^-2\pi^+)$ — Γ_{131}/Γ_{68}

VALUE (units 10^{-2})	EVTS	DOCUMENT ID		TECN	COMMENT
3.48±0.19 OUR AVERAGE Error includes scale factor of 1.4. See the ideogram below.					
3.52±0.11±0.12	3303 ± 95	RUBIN	06	CLEO	e^+e^- at $\psi(3770)$
4.1 ±1.1 ±0.3	85 ± 22	ABLIKIM	05F	BES	$e^+e^-\approx\psi(3770)$
$3.11\pm0.18^{+0.16}_{-0.26}$	1172	AITALA	01B	E791	π^- nucleus, 500 GeV
4.3 ±0.3 ±0.3	236	FRABETTI	97D	E687	γ Be $\approx$ 200 GeV
3.5 ±0.7 ±0.3	83	ANJOS	89	E691	Photoproduction

Int. J. Mod. Phys. A 2026.41. Downloaded from www.worldscientific.com
by UNIVERSITY OF CALIFORNIA @ BERKELEY on 09/16/26. Re-use and distribution is strictly not permitted, except for Open Access articles.

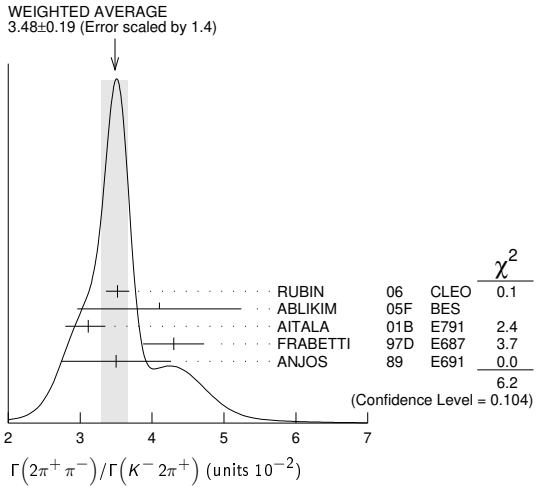

$\Gamma(\rho^0\pi^+)/\Gamma(2\pi^+\pi^-)$ — $\Gamma_{132}/\Gamma_{131}$

This is the "fit fraction" from the Dalitz-plot analysis.

VALUE (units 10^{-2})	EVTS	DOCUMENT ID		TECN	COMMENT
25.8 ±2.4 OUR AVERAGE		Error includes scale factor of 1.9. See the ideogram below.			
26 ±0.3 ±1.6 ±0.3	572k	[1] AAIJ	23H	LHCB	Dalitz plot fit
20.0 ±2.3 ±0.9		BONVICINI	07	CLEO	Dalitz fit, ≈ 2240 evts
30.82±3.14±2.30		LINK	04	FOCS	Dalitz fit, 1527 ± 51 evts
33.6 ±3.2 ±2.2		AITALA	01B	E791	Dalitz fit, 1172 evts

[1] The last error reflects the uncertainty on the amplitude model.

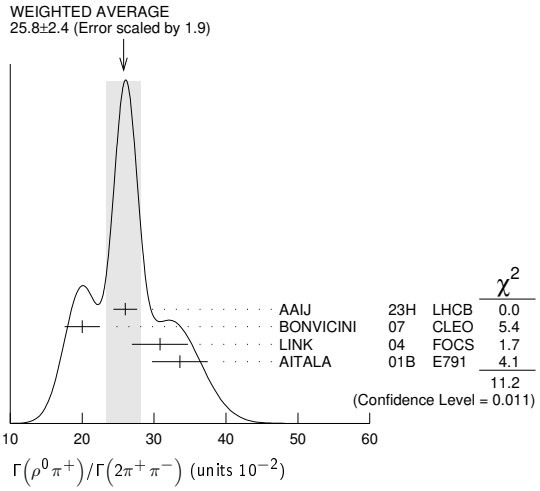

$\Gamma(\pi^+(\pi^+\pi^-)_{S-\text{wave}})/\Gamma(2\pi^+\pi^-)$ — $\Gamma_{133}/\Gamma_{131}$

This is the "fit fraction" from the Dalitz-plot analysis. See also the next three data blocks.

VALUE (units 10^{-2})	EVTS	DOCUMENT ID		TECN	COMMENT
61.5 ±0.9 OUR AVERAGE					
61.8 ±0.5 ±0.6 ±0.5	572k	[1,2] AAIJ	23H	LHCB	Dalitz plot fit
56.00±3.24±2.14		[3] LINK	04	FOCS	Dalitz fit, 1527 ± 51 evts

[1] AAIJ 23H parameterise the $\pi^+\pi^-$ S-wave using one complex number per bin in 50 bins of $\pi^+\pi^-$ invariant mass.
[2] The last error reflects the uncertainty on the amplitude model.
[3] LINK 04 borrows a K-matrix parametrization from ANISOVICH 03 of the full π-π S-wave isoscalar scattering amplitude to describe the $\pi^+\pi^-$ S-wave component of the $\pi^+\pi^+\pi^-$ state. The fit fraction given above is a sum over five f_0 mesons, the $f_0(980)$, $f_0(1300)$, $f_0(1200\text{–}1600)$, $f_0(1500)$, and $f_0(1750)$. See LINK 04 for details and discussion.

$\Gamma(\sigma\pi^+, \sigma\to\pi^+\pi^-)/\Gamma(2\pi^+\pi^-)$ — $\Gamma_{134}/\Gamma_{131}$

This is the "fit fraction" from the Dalitz-plot analysis.

VALUE	DOCUMENT ID		TECN	COMMENT
0.422±0.027 OUR AVERAGE				
0.418±0.014±0.025	BONVICINI	07	CLEO	Dalitz fit, ≈ 2240 evts
0.463±0.090±0.021	AITALA	01B	E791	Dalitz fit, 1172 evts

$\Gamma(f_0(980)\pi^+, f_0\to\pi^+\pi^-)/\Gamma(2\pi^+\pi^-)$ — $\Gamma_{135}/\Gamma_{131}$

This is the "fit fraction" from the Dalitz-plot analysis.

VALUE	DOCUMENT ID		TECN	COMMENT
0.048±0.010 OUR AVERAGE	Error includes scale factor of 1.3.			
0.041±0.009±0.003	BONVICINI	07	CLEO	Dalitz fit, ≈ 2240 evts
0.062±0.013±0.004	AITALA	01B	E791	Dalitz fit, 1172 evts

$\Gamma(f_0(1370)\pi^+, f_0\to\pi^+\pi^-)/\Gamma(2\pi^+\pi^-)$ — $\Gamma_{136}/\Gamma_{131}$

This is the "fit fraction" from the Dalitz-plot analysis.

VALUE	DOCUMENT ID		TECN	COMMENT
0.024±0.013 OUR AVERAGE				
0.026±0.018±0.006	BONVICINI	07	CLEO	Dalitz fit, ≈ 2240 evts
0.023±0.015±0.008	AITALA	01B	E791	Dalitz fit, 1172 evts

$\Gamma(\omega\pi^+, \omega\to\pi^+\pi^-)/\Gamma(2\pi^+\pi^-)$ — $\Gamma_{137}/\Gamma_{131}$

VALUE (units 10^{-3})	EVTS	DOCUMENT ID		TECN	COMMENT
1.03±0.08±0.14±0.02	572k	[1] AAIJ	23H	LHCB	Dalitz plot fit

[1] The last error reflects the uncertainty on the amplitude model.

$\Gamma(f_2(1270)\pi^+, f_2\to\pi^+\pi^-)/\Gamma(2\pi^+\pi^-)$ — $\Gamma_{138}/\Gamma_{131}$

This is the "fit fraction" from the Dalitz-plot analysis.

VALUE (units 10^{-2})	EVTS	DOCUMENT ID		TECN	COMMENT
14.0 ±0.8 OUR AVERAGE		Error includes scale factor of 1.7. See the ideogram below.			
13.8 ±0.2 ±0.4 ±0.2	572k	[1] AAIJ	23H	LHCB	Dalitz plot fit
18.2 ±2.6 ±0.7		BONVICINI	07	CLEO	Dalitz fit, ≈ 2240 evts
11.74±1.90±0.29		LINK	04	FOCS	Dalitz fit, 1527 ± 51 evts
19.4 ±2.5 ±0.4		AITALA	01B	E791	Dalitz fit, 1172 evts

[1] The last error reflects the uncertainty on the amplitude model.

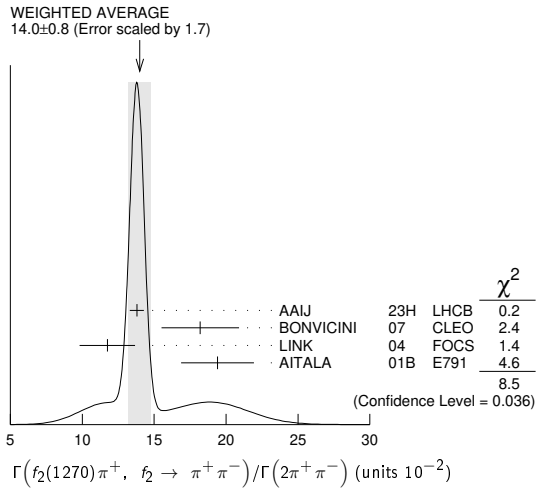

$\Gamma(\rho(1450)^0\pi^+, \rho^0\to\pi^+\pi^-)/\Gamma(2\pi^+\pi^-)$ — $\Gamma_{139}/\Gamma_{131}$

This is the "fit fraction" from the Dalitz-plot analysis.

VALUE (units 10^{-2})	CL%	EVTS	DOCUMENT ID		TECN	COMMENT
5.4±0.4±1.3±0.8		572k	[1] AAIJ	23H	LHCB	Dalitz plot fit
• • • We do not use the following data for averages, fits, limits, etc. • • •						
<2.4	95		BONVICINI	07	CLEO	Dalitz fit, ≈ 2240 evts
0.7±0.7±0.3			AITALA	01B	E791	Dalitz fit, 1172 evts

[1] The last error reflects the uncertainty on the amplitude model.

$\Gamma(\rho(1700)^0\pi^+, \rho^0\to\pi^+\pi^-)/\Gamma(2\pi^+\pi^-)$ — $\Gamma_{140}/\Gamma_{131}$

VALUE (units 10^{-2})	EVTS	DOCUMENT ID		TECN	COMMENT
5.7±0.5±1.0±1.0	572k	[1] AAIJ	23H	LHCB	Dalitz plot fit

[1] The last error reflects the uncertainty on the amplitude model.

$\Gamma(f_0(1500)\pi^+, f_0\to\pi^+\pi^-)/\Gamma(2\pi^+\pi^-)$ — $\Gamma_{141}/\Gamma_{131}$

This is the "fit fraction" from the Dalitz-plot analysis.

VALUE	DOCUMENT ID		TECN	COMMENT
0.034±0.010±0.008	BONVICINI	07	CLEO	Dalitz fit, ≈ 2240 evts

$\Gamma(f_0(1710)\pi^+, f_0\to\pi^+\pi^-)/\Gamma(2\pi^+\pi^-)$ — $\Gamma_{142}/\Gamma_{131}$

This is the "fit fraction" from the Dalitz-plot analysis.

VALUE	CL%	DOCUMENT ID		TECN	COMMENT
<0.016	95	BONVICINI	07	CLEO	Dalitz fit, ≈ 2240 evts

$\Gamma(f_0(1790)\pi^+, f_0\to\pi^+\pi^-)/\Gamma(2\pi^+\pi^-)$ — $\Gamma_{143}/\Gamma_{131}$

This is the "fit fraction" from the Dalitz-plot analysis.

VALUE	CL%	DOCUMENT ID		TECN	COMMENT
<0.02	95	BONVICINI	07	CLEO	Dalitz fit, ≈ 2240 evts

$\Gamma((\pi^+\pi^+)_{S-\text{wave}}\pi^-)/\Gamma(2\pi^+\pi^-)$ — $\Gamma_{144}/\Gamma_{131}$

This is the "fit fraction" from the Dalitz-plot analysis.

VALUE	CL%	DOCUMENT ID		TECN	COMMENT
<0.037	95	BONVICINI	07	CLEO	Dalitz fit, ≈ 2240 evts

$\Gamma(2\pi^+\pi^-\text{ nonresonant})/\Gamma(2\pi^+\pi^-)$ — $\Gamma_{145}/\Gamma_{131}$

This is the "fit fraction" from the Dalitz-plot analysis.

VALUE	CL%	DOCUMENT ID		TECN	COMMENT
<0.035	95	BONVICINI	07	CLEO	Dalitz fit, ≈ 2240 evts
• • • We do not use the following data for averages, fits, limits, etc. • • •					
0.078±0.060±0.027		AITALA	01B	E791	Dalitz fit, 1172 evts

Int. J. Mod. Phys. A 2026.41. Downloaded from www.worldscientific.com
by CALIFORNIA @ BERKELEY on 09/16/26. Re-use and distribution is strictly not permitted, except for Open Access articles.

$\Gamma(\pi^+ 2\pi^0)/\Gamma_{total}$ — Γ_{146}/Γ

VALUE (units 10^{-4})	EVTS	DOCUMENT ID		TECN	COMMENT
46.1±1.2±0.9	2k	ABLIKIM	22BG	BES3	e^+e^- at 3.773 GeV

$\Gamma(\pi^+ 2\pi^0)/\Gamma(K^- 2\pi^+)$ — Γ_{146}/Γ_{68}

VALUE (units 10^{-2})	EVTS	DOCUMENT ID		TECN	COMMENT
5.0±0.3±0.3	1535 ± 89	RUBIN	06	CLEO	e^+e^- at $\psi(3770)$

$\Gamma(\pi^+ 3\pi^0)/\Gamma_{total}$ — Γ_{148}/Γ

VALUE (units 10^{-4})	EVTS	DOCUMENT ID		TECN	COMMENT
41.7±2.2±1.3	570	ABLIKIM	22BG	BES3	e^+e^- at 3.773 GeV

$\Gamma(2\pi^+\pi^-\pi^0)/\Gamma_{total}$ — Γ_{147}/Γ

VALUE (units 10^{-4})	EVTS	DOCUMENT ID		TECN	COMMENT
116.5±2.1±2.1	4.6k	ABLIKIM	22BG	BES3	e^+e^- at 3.773 GeV

$\Gamma(2\pi^+\pi^-\pi^0)/\Gamma(K^- 2\pi^+)$ — Γ_{147}/Γ_{68}

VALUE (units 10^{-2})	EVTS	DOCUMENT ID		TECN	COMMENT
12.4±0.5±0.6	5701 ± 205	RUBIN	06	CLEO	e^+e^- at $\psi(3770)$

$\Gamma(\pi^+ 4\pi^0)/\Gamma_{total}$ — Γ_{149}/Γ

VALUE (units 10^{-4})	EVTS	DOCUMENT ID		TECN	COMMENT
19.5±3.6±2.3	57	ABLIKIM	22BG	BES3	e^+e^- at 3.773 GeV

$\Gamma(2\pi^+\pi^- 2\pi^0)/\Gamma_{total}$ — Γ_{150}/Γ

VALUE (units 10^{-4})	EVTS	DOCUMENT ID		TECN	COMMENT
107.4±4.0±3.0	1.2k	ABLIKIM	22BG	BES3	e^+e^- at 3.773 GeV

$\Gamma(3\pi^+ 2\pi^-)/\Gamma_{total}$ — Γ_{151}/Γ

VALUE (units 10^{-4})	EVTS	DOCUMENT ID		TECN	COMMENT
18.2±1.1±1.0	460	ABLIKIM	22BG	BES3	e^+e^- at 3.773 GeV

$\Gamma(3\pi^+ 2\pi^-)/\Gamma(K^- 2\pi^+)$ — Γ_{151}/Γ_{68}

VALUE (units 10^{-2})	EVTS	DOCUMENT ID		TECN	COMMENT
1.76±0.17 OUR FIT					
1.73±0.20±0.17	732 ± 77	RUBIN	06	CLEO	e^+e^- at $\psi(3770)$
• • • We do not use the following data for averages, fits, limits, etc. • • •					
2.3 ±0.4 ±0.2	58	FRABETTI	97C	E687	γBe, $\overline{E}_\gamma \approx 200$ GeV

$\Gamma(3\pi^+ 2\pi^-)/\Gamma(K^- 3\pi^+\pi^-)$ — $\Gamma_{151}/\Gamma_{117}$

VALUE	EVTS	DOCUMENT ID		TECN	COMMENT
0.289±0.019 OUR FIT					
0.290±0.017±0.011	835	LINK	03D	FOCS	γ A, $\overline{E}_\gamma \approx 180$ GeV

$\Gamma(2\pi^+\pi^- 3\pi^0)/\Gamma_{total}$ — Γ_{152}/Γ

VALUE (units 10^{-4})	EVTS	DOCUMENT ID		TECN	COMMENT
34.2±3.1±1.6	186	ABLIKIM	22BG	BES3	e^+e^- at 3.773 GeV

$\Gamma(3\pi^+ 2\pi^-\pi^0)/\Gamma_{total}$ — Γ_{153}/Γ

VALUE (units 10^{-4})	EVTS	DOCUMENT ID		TECN	COMMENT
23.4±2.2±1.5	183	ABLIKIM	22BG	BES3	e^+e^- at 3.773 GeV

$\Gamma(\eta\pi^+)/\Gamma_{total}$ — Γ_{154}/Γ

Unseen decay modes of the η are included.

VALUE (units 10^{-4})	EVTS	DOCUMENT ID		TECN	COMMENT
37.5 ±0.9 OUR FIT					
37.90±0.70±0.68	12k	ABLIKIM	18W	BES3	e^+e^-, 3773 MeV
• • • We do not use the following data for averages, fits, limits, etc. • • •					
30.7 ±2.2 ±1.3	258	ABLIKIM	16D	BES3	e^+e^- at 3773 MeV
34.3 ±1.4 ±1.7	1033 ± 42	ARTUSO	08	CLEO	See MENDEZ 10

$\Gamma(\eta\pi^+)/\Gamma(K^- 2\pi^+)$ — Γ_{154}/Γ_{68}

Unseen decay modes of the η are included.

VALUE (units 10^{-2})	EVTS	DOCUMENT ID		TECN	COMMENT
4.03±0.10 OUR FIT Error includes scale factor of 1.1.					
3.87±0.09±0.19	2940 ± 68	MENDEZ	10	CLEO	e^+e^- at 3774 MeV
• • • We do not use the following data for averages, fits, limits, etc. • • •					
3.81±0.26±0.21	377 ± 26	RUBIN	06	CLEO	See ARTUSO 08

$\Gamma(\eta\pi^+\pi^0)/\Gamma_{total}$ — Γ_{155}/Γ

VALUE (units 10^{-4})	EVTS	DOCUMENT ID		TECN	COMMENT
20.5±3.5 OUR AVERAGE Error includes scale factor of 2.2.					
22.3±1.5±1.0	381	ABLIKIM	20G	BES3	e^+e^-, 3773 MeV
13.8±3.1±1.6	149 ± 34	ARTUSO	08	CLEO	e^+e^- at $\psi(3770)$
• • • We do not use the following data for averages, fits, limits, etc. • • •					
24.7±9.3±1.6	42	ABLIKIM	20AA	BES3	e^+e^-, 3773 MeV

$\Gamma(\rho(770)^+\eta,\ \rho^+\to\pi^+\pi^0)/\Gamma(\eta\pi^+\pi^0)$ — $\Gamma_{156}/\Gamma_{155}$

VALUE (units 10^{-2})	DOCUMENT ID		TECN	COMMENT
9.3±3.0±2.1	[1] ABLIKIM	24CL	BES3	e^+e^- at 3.773 GeV

[1] Amplitude analysis involving six modes.

$\Gamma(a_0(980)^+\pi^0,\ a_0^+\to\pi^+\eta)/\Gamma(\eta\pi^+\pi^0)$ — $\Gamma_{157}/\Gamma_{155}$

VALUE (units 10^{-2})	DOCUMENT ID		TECN	COMMENT
43.7±5.6±1.9	[1] ABLIKIM	24CL	BES3	e^+e^- at 3.773 GeV

[1] Amplitude analysis involving six modes.

$\Gamma(a_0(980)^0\pi^+,\ a_0^0\to\pi^0\eta)/\Gamma(\eta\pi^+\pi^0)$ — $\Gamma_{158}/\Gamma_{155}$

VALUE (units 10^{-2})	DOCUMENT ID		TECN	COMMENT
17.0±4.4±1.7	[1] ABLIKIM	24CL	BES3	e^+e^- at 3.773 GeV

[1] Amplitude analysis involving six modes.

$\Gamma(a_2(1700)^+\pi^0,\ a_2^+\to\pi^+\eta)/\Gamma(\eta\pi^+\pi^0)$ — $\Gamma_{159}/\Gamma_{155}$

VALUE (units 10^{-2})	DOCUMENT ID		TECN	COMMENT
4.2±2.1±0.7	[1] ABLIKIM	24CL	BES3	e^+e^- at 3.773 GeV

[1] Amplitude analysis involving six modes.

$\Gamma(a_0(1450)^+\pi^0,\ a_0^+\to\pi^+\eta)/\Gamma(\eta\pi^+\pi^0)$ — $\Gamma_{160}/\Gamma_{155}$

VALUE (units 10^{-2})	DOCUMENT ID		TECN	COMMENT
7.0±2.8±0.7	[1] ABLIKIM	24CL	BES3	e^+e^- at 3.773 GeV

[1] Amplitude analysis involving six modes.

$\Gamma(\eta 2\pi^+\pi^-)/\Gamma_{total}$ — Γ_{161}/Γ

VALUE (units 10^{-3})	EVTS	DOCUMENT ID		TECN	COMMENT
3.41±0.17±0.10	515	ABLIKIM	20V	BES3	e^+e^-, 3773 MeV

$\Gamma(\eta\pi^+ 2\pi^0)/\Gamma_{total}$ — Γ_{162}/Γ

VALUE (units 10^{-3})	EVTS	DOCUMENT ID		TECN	COMMENT
3.20±0.28±0.17	190	ABLIKIM	20V	BES3	e^+e^-, 3773 MeV

$\Gamma(\eta\pi^+ 3\pi^0)/\Gamma_{total}$ — Γ_{163}/Γ

VALUE (units 10^{-4})	EVTS	DOCUMENT ID		TECN	COMMENT
28.9±4.0±2.2	80	ABLIKIM	22BG	BES3	e^+e^- at 3.773 GeV

$\Gamma(\eta 2\pi^+\pi^-\pi^0)/\Gamma_{total}$ — Γ_{164}/Γ

VALUE (units 10^{-4})	EVTS	DOCUMENT ID		TECN	COMMENT
38.8±3.2±1.2	190	ABLIKIM	22BG	BES3	e^+e^- at 3.773 GeV

$\Gamma(\eta\eta\pi^+)/\Gamma_{total}$ — Γ_{165}/Γ

VALUE (units 10^{-4})	EVTS	DOCUMENT ID		TECN	COMMENT
29.6±2.4±1.0	179	ABLIKIM	20G	BES3	e^+e^-, 3773 MeV

$\Gamma(\omega\pi^+)/\Gamma_{total}$ — Γ_{166}/Γ

Unseen decay modes of the ω are included.

VALUE (units 10^{-4})	CL%	EVTS	DOCUMENT ID		TECN	COMMENT
2.79±0.57±0.16		79	ABLIKIM	16D	BES3	e^+e^- at 3773 MeV
• • • We do not use the following data for averages, fits, limits, etc. • • •						
<3.4		90	RUBIN	06	CLEO	e^+e^- at $\psi(3770)$

$\Gamma(\omega\pi^+\pi^0)/\Gamma_{total}$ — Γ_{167}/Γ

VALUE (units 10^{-3})	EVTS	DOCUMENT ID		TECN	COMMENT
3.87±0.83±0.25	233	[1] ABLIKIM	20AA	BES3	e^+e^-, 3773 MeV

[1] ABLIKIM 20AA reports a statistical significance of 7.7 σ for this measurement.

$\Gamma(\eta'(958)\pi^+)/\Gamma_{total}$ — Γ_{168}/Γ

Unseen decay modes of the $\eta'(958)$ are included.

VALUE (units 10^{-4})	EVTS	DOCUMENT ID		TECN	COMMENT
49.6±1.8 OUR FIT					
51.2±1.4±2.1	3.1k	ABLIKIM	18W	BES3	e^+e^-, 3773 MeV
• • • We do not use the following data for averages, fits, limits, etc. • • •					
44.2±2.5±2.9	352 ± 20	ARTUSO	08	CLEO	See MENDEZ 10

$\Gamma(\eta'(958)\pi^+)/\Gamma(K^- 2\pi^+)$ — Γ_{168}/Γ_{68}

Unseen decay modes of the $\eta'(958)$ are included.

VALUE (units 10^{-2})	EVTS	DOCUMENT ID		TECN	COMMENT
5.33±0.20 OUR FIT					
5.12±0.17±0.25	1037 ± 35	MENDEZ	10	CLEO	e^+e^- at 3774 MeV

$\Gamma(\eta'(958)\pi^+\pi^0)/\Gamma_{total}$ — Γ_{169}/Γ

Unseen decay modes of the $\eta'(958)$ are included.

VALUE (units 10^{-4})	EVTS	DOCUMENT ID		TECN	COMMENT
15.7±4.3±2.5	33 ± 9	ARTUSO	08	CLEO	e^+e^- at $\psi(3770)$

Hadronic modes with a $K\overline{K}$ pair

$\Gamma(K_S^0 K^+)/\Gamma_{total}$ — Γ_{170}/Γ

VALUE (units 10^{-3})	EVTS	DOCUMENT ID		TECN	COMMENT
3.02 ±0.09 OUR FIT Error includes scale factor of 2.2.					
3.183±0.029±0.060	18k	ABLIKIM	18W	BES3	e^+e^-, 3773 MeV
• • • We do not use the following data for averages, fits, limits, etc. • • •					
3.02 ±0.09 ±0.08	780	ABLIKIM	19M	BES3	See ABLIKIM 18W.
3.14 ±0.09 ±0.08	1971 ± 51	BONVICINI	08	CLEO	See MENDEZ 10

Int. J. Mod. Phys. A 2026.41. Downloaded from www.worldscientific.com
by UNIVERSITY OF CALIFORNIA @ BERKELEY on 09/16/26. Re-use and distribution is strictly not permitted, except for Open Access articles.

$\Gamma(K^0_S K^+)/\Gamma(K^0_S \pi^+)$ — Γ_{170}/Γ_{66}

VALUE	EVTS	DOCUMENT ID		TECN	COMMENT
0.195 ±0.006 OUR FIT Error includes scale factor of 2.8.					
0.1901±0.0024 OUR AVERAGE					
0.1899±0.0011±0.0022	101k±561	WON	09	BELL	e^+e^- at $\Upsilon(4S)$
0.1892±0.0155±0.0073	278 ± 21	ARMS	04	CLEO	$e^+e^- \approx$ 10 GeV
0.1996±0.0119±0.0096	949	LINK	02B	FOCS	γ A, $\overline{E}_\gamma \approx$ 180 GeV
• • • We do not use the following data for averages, fits, limits, etc. • • •					
0.222 ±0.037 ±0.013	63 ± 10	ABLIKIM	05F	BES	$e^+e^- \approx \psi(3770)$
0.222 ±0.041 ±0.019	70	BISHAI	97	CLEO	See ARMS 04
0.25 ±0.04 ±0.02	129	FRABETTI	95	E687	γBe $\overline{E}_\gamma \approx$ 200 GeV
0.271 ±0.065 ±0.039	69	ANJOS	90C	E691	γBe
0.317 ±0.086 ±0.048	31	BALTRUSAIT...	85E	MRK3	e^+e^- 3.77 GeV
0.25 ±0.15	6	SCHINDLER	81	MRK2	e^+e^- 3.771 GeV

$\Gamma(K^0_S K^+)/\Gamma(K^- 2\pi^+)$ — Γ_{170}/Γ_{68}

VALUE (units 10^{-2})	EVTS	DOCUMENT ID		TECN	COMMENT
3.25±0.09 OUR FIT Error includes scale factor of 2.2.					
3.35±0.06±0.07	5161 ± 86	MENDEZ	10	CLEO	e^+e^- at 3774 MeV
• • • We do not use the following data for averages, fits, limits, etc. • • •					
3.02±0.18±0.15	949	[1] LINK	02B	FOCS	γ nucleus, $\overline{E}_\gamma \approx$ 180 GeV

[1] This LINK 02B result is redundant with a result in the previous datablock.

$\Gamma(K^0_L K^+)/\Gamma_{total}$ — Γ_{171}/Γ

VALUE (units 10^{-3})	EVTS	DOCUMENT ID		TECN	COMMENT
3.21±0.11±0.11	650	ABLIKIM	19M	BES3	e^+e^- at 3773 MeV

$\Gamma(K^0_S K^+ \pi^0)/\Gamma_{total}$ — Γ_{172}/Γ

VALUE (units 10^{-3})	EVTS	DOCUMENT ID		TECN	COMMENT
5.07±0.19±0.23	470	ABLIKIM	19M	BES3	e^+e^- at 3773 MeV

$\Gamma(K^*(892)^+ K^0_S,\ K^{*+} \to K^+\pi^0)/\Gamma(K^0_S K^+\pi^0)$ — $\Gamma_{173}/\Gamma_{172}$

VALUE	EVTS	DOCUMENT ID		TECN	COMMENT
0.571±0.026±0.042	692	[1] ABLIKIM	21AD	BES3	e^+e^- at 3.773 GeV

[1] ABLIKIM 21AD value is a fit fraction from an amplitude analysis of $D^+ \to K^+K^0_S\pi^0$ with four components. Reconstructs the $K^*(892)^+$ from its $K^+\pi^0$ final state.

$\Gamma(\overline{K}^*(892)^0 K^+,\ \overline{K}^{*0} \to K^0_S\pi^0)/\Gamma(K^0_S K^+\pi^0)$ — $\Gamma_{174}/\Gamma_{172}$

VALUE	EVTS	DOCUMENT ID		TECN	COMMENT
0.102±0.015±0.022	692	[1] ABLIKIM	21AD	BES3	e^+e^- at 3.773 GeV

[1] ABLIKIM 21AD value is a fit fraction from an amplitude analysis of $D^+ \to K^+K^0_S\pi^0$ with four components. Reconstructs the $\overline{K}^*(892)^0$ from its $K^0_S\pi^0$ final state.

$\Gamma(K^*(892)^+ K^0_S)/\Gamma(K^0_S\pi^+)$ — Γ_{175}/Γ_{66}

Unseen decay modes of the $K^*(892)^+$ are included.

VALUE	EVTS	DOCUMENT ID		TECN	COMMENT
• • • We do not use the following data for averages, fits, limits, etc. • • •					
1.1±0.3±0.4	67	FRABETTI	95	E687	γBe $\overline{E}_\gamma \approx$ 200 GeV

$\Gamma(K^0_L K^+\pi^0)/\Gamma_{total}$ — Γ_{176}/Γ

VALUE (units 10^{-3})	EVTS	DOCUMENT ID		TECN	COMMENT
5.24±0.22±0.22	410	ABLIKIM	19M	BES3	e^+e^- at 3773 MeV

$\Gamma(K^+K^-\pi^+)/\Gamma_{total}$ — Γ_{177}/Γ

VALUE (units 10^{-2})	EVTS	DOCUMENT ID		TECN	COMMENT
• • • We do not use the following data for averages, fits, limits, etc. • • •					
0.935±0.017±0.024		[1] DOBBS	07	CLEO	See BONVICINI 14
0.97 ±0.04 ±0.04	1250 ± 40	[1] HE	05	CLEO	See DOBBS 07

[1] DOBBS 07 and HE 05 use single- and double-tagged events in an overall fit. DOBBS 07 supersedes HE 05.

$\Gamma(K^+K^-\pi^+)/\Gamma(K^-2\pi^+)$ — Γ_{177}/Γ_{68}

VALUE (units 10^{-2})	EVTS	DOCUMENT ID		TECN	COMMENT
10.32 ±0.09 OUR AVERAGE Error includes scale factor of 1.4. See the ideogram below.					
10.282±0.002±0.068	23M	AAIJ	19G	LHCB	pp at 8 TeV
10.6 ±0.2 ±0.3		BONVICINI	14	CLEO	All CLEO-c runs
11.7 ±1.3 ±0.7	181 ± 20	ABLIKIM	05F	BES	$e^+e^- \approx \psi(3770)$
10.7 ±0.1 ±0.2	43k	AUBERT	05S	BABR	$e^+e^- \approx \Upsilon(4S)$
9.3 ±1.0 $^{+0.8}_{-0.6}$		JUN	00	SELX	Σ^- nucleus, 600 GeV
9.76 ±0.42 ±0.46		FRABETTI	95B	E687	γ Be, $\overline{E}_\gamma \approx$ 200 GeV

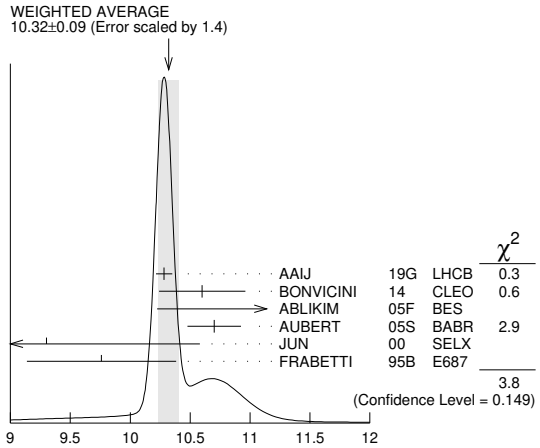

$\Gamma(K^+\overline{K}^*(892)^0,\ \overline{K}^*(892)^0 \to K^-\pi^+)/\Gamma(K^+K^-\pi^+)$ — $\Gamma_{178}/\Gamma_{177}$

This is the "fit fraction" from the Dalitz-plot analysis.

VALUE (%)	DOCUMENT ID		TECN	COMMENT
25.7±0.5 $^{+0.4}_{-1.2}$	RUBIN	08	CLEO	Dalitz fit, 19,458±163 evts
• • • We do not use the following data for averages, fits, limits, etc. • • •				
30.1±2.0±2.5	FRABETTI	95B	E687	Dalitz fit, 915 evts

$\Gamma(K^+\overline{K}^*_0(1430)^0,\ \overline{K}^*_0(1430)^0 \to K^-\pi^+)/\Gamma(K^+K^-\pi^+)$ — $\Gamma_{179}/\Gamma_{177}$

This is the "fit fraction" from the Dalitz-plot analysis.

VALUE (%)	DOCUMENT ID		TECN	COMMENT
18.8±1.2 $^{+3.3}_{-3.4}$	RUBIN	08	CLEO	Dalitz fit, 19,458±163 evts
• • • We do not use the following data for averages, fits, limits, etc. • • •				
37.0±3.5±1.8	FRABETTI	95B	E687	Dalitz fit, 915 evts

$\Gamma(K^+\overline{K}^*_2(1430)^0,\ \overline{K}^*_2 \to K^-\pi^+)/\Gamma(K^+K^-\pi^+)$ — $\Gamma_{180}/\Gamma_{177}$

This is the "fit fraction" from the Dalitz-plot analysis.

VALUE (%)	DOCUMENT ID		TECN	COMMENT
1.7±0.4 $^{+1.2}_{-0.7}$	RUBIN	08	CLEO	Dalitz fit, 19,458±163 evts

$\Gamma(K^+\overline{K}^*_0(700),\ \overline{K}^*_0 \to K^-\pi^+)/\Gamma(K^+K^-\pi^+)$ — $\Gamma_{181}/\Gamma_{177}$

This is the "fit fraction" from the Dalitz-plot analysis.

VALUE (%)	DOCUMENT ID		TECN	COMMENT
7.0±0.8 $^{+3.5}_{-2.0}$	RUBIN	08	CLEO	Dalitz fit, 19,458±163 evts

$\Gamma(a_0(1450)^0\pi^+,\ a^0_0 \to K^+K^-)/\Gamma(K^+K^-\pi^+)$ — $\Gamma_{182}/\Gamma_{177}$

This is the "fit fraction" from the Dalitz-plot analysis.

VALUE (%)	DOCUMENT ID		TECN	COMMENT
4.6±0.6 $^{+7.2}_{-1.8}$	RUBIN	08	CLEO	Dalitz fit, 19,458±163 evts

$\Gamma(\phi(1680)\pi^+,\ \phi \to K^+K^-)/\Gamma(K^+K^-\pi^+)$ — $\Gamma_{183}/\Gamma_{177}$

This is the "fit fraction" from the Dalitz-plot analysis.

VALUE (%)	DOCUMENT ID		TECN	COMMENT
0.51±0.11 $^{+0.37}_{-0.16}$	RUBIN	08	CLEO	Dalitz fit, 19,458±163 evts

$\Gamma(\phi\pi^+,\ \phi \to K^+K^-)/\Gamma(K^+K^-\pi^+)$ — $\Gamma_{184}/\Gamma_{177}$

This is the "fit fraction" from the Dalitz-plot analysis.

VALUE (%)	DOCUMENT ID		TECN	COMMENT
27.8±0.4 $^{+0.2}_{-0.5}$	RUBIN	08	CLEO	Dalitz fit, 19,458±163 evts
• • • We do not use the following data for averages, fits, limits, etc. • • •				
29.2±3.1±3.0	FRABETTI	95B	E687	Dalitz fit, 915 evts

$\Gamma(\phi\pi^+)/\Gamma_{total}$ — Γ_{185}/Γ

VALUE (units 10^{-3})	EVTS	DOCUMENT ID		TECN	COMMENT
5.70±0.05±0.13	18k	ABLIKIM	19BI	BES3	e^+e^- at 3773 MeV

$\Gamma(K^+K^-\pi^+\pi^0)/\Gamma_{total}$ — Γ_{186}/Γ

VALUE (units 10^{-3})	EVTS	DOCUMENT ID		TECN	COMMENT
6.62±0.20±0.25	1.3k	ABLIKIM	20AC	BES3	e^+e^- at 3.773 GeV

$\Gamma(K^+K^-\pi^+\pi^0)/\Gamma(K^-2\pi^+\pi^0)$ — Γ_{186}/Γ_{93}

VALUE (units 10^{-2})	EVTS	DOCUMENT ID		TECN	COMMENT
11.32±0.13±0.26	50k	LI	23G	BELL	e^+e^- at/near Υ(nS), n=1,...,5

Int. J. Mod. Phys. A 2026.41. Downloaded from www.worldscientific.com by CALIFORNIA @ BERKELEY on 09/16/26. Re-use and distribution is strictly not permitted, except for Open Access articles.

$\Gamma(K^0_S K^0_S \pi^+)/\Gamma_{total}$ — Γ_{187}/Γ

VALUE (units 10^{-4})	EVTS	DOCUMENT ID		TECN	COMMENT
29.7±0.9±0.5	1.2k	ABLIKIM	24CJ	BES3	e^+e^- at 3.773 GeV
• • • We do not use the following data for averages, fits, limits, etc. • • •					
27.0±0.5±1.2	4897	ABLIKIM	17A	BES3	$e^+e^- \to \psi(3770)$

$\Gamma(K^0_S K^*(892)^+,\ K^{*+} \to K^0_S \pi^+)/\Gamma(K^0_S K^0_S \pi^+)$ — $\Gamma_{188}/\Gamma_{187}$

VALUE (units 10^{-3})	EVTS	DOCUMENT ID		TECN	COMMENT
978±10±4	1.2k	[1] ABLIKIM	24CJ	BES3	e^+e^- at 3.773 GeV

[1] ABLIKIM 24CJ reports $B(D^+ \to K^0_S K^*(892)^+) = (8.72 \pm 0.28 \pm 0.15) \times 10^{-3}$ from an amplitude analysis of $D^+ \to K^0_S K^0_S \pi^+$ with two modes, assuming that $B(K^*(892)^+ \to K^0_S \pi^+) = 1/3$.

$\Gamma(K^0_S (K^0_S \pi^+) \to K^0_S K^0_S \pi^+)/\Gamma(K^0_S K^0_S \pi^+)$ — $\Gamma_{189}/\Gamma_{187}$

VALUE (units 10^{-2})	EVTS	DOCUMENT ID		TECN	COMMENT
4.4±1.0±0.5	1.2k	[1] ABLIKIM	24CJ	BES3	e^+e^- at 3.773 GeV

[1] From an amplitude analysis of $D^+ \to K^0_S K^0_S \pi^+$ with two modes.

$\Gamma(K^0_S K^0_S \pi^+ \pi^0)/\Gamma_{total}$ — Γ_{190}/Γ

VALUE (units 10^{-3})	EVTS	DOCUMENT ID		TECN	COMMENT
1.34±0.20±0.06	80	ABLIKIM	20AC	BES3	e^+e^- at 3.773 GeV

$\Gamma(K^0_S K^+ \eta)/\Gamma_{total}$ — Γ_{193}/Γ

VALUE (units 10^{-4})	EVTS	DOCUMENT ID		TECN	COMMENT
2.27±0.22±0.05	133	[1] ABLIKIM	25AX	BES3	e^+e^- at 3.773 GeV
• • • We do not use the following data for averages, fits, limits, etc. • • •					
1.85±0.52±0.08	14	[2] ABLIKIM	20V	BES3	e^+e^-, 3773 MeV

[1] ABLIKIM 25AX reconstructs the η via both $\pi^+\pi^-\pi^0$ and $\gamma\gamma$ channels.
[2] Superseded by ABLIKIM 25AX.

$\Gamma(K^+ K^0_S \pi^+ \pi^-)/\Gamma_{total}$ — Γ_{194}/Γ

VALUE (units 10^{-3})	EVTS	DOCUMENT ID		TECN	COMMENT
1.89±0.12±0.05	277	ABLIKIM	20AC	BES3	e^+e^- at 3.773 GeV

$\Gamma(K^+ K^0_S \pi^+ \pi^-)/\Gamma(K^0_S 2\pi^+ \pi^-)$ — $\Gamma_{194}/\Gamma_{107}$

VALUE (units 10^{-2})	EVTS	DOCUMENT ID		TECN	COMMENT
5.62±0.39±0.40	469 ± 32	LINK	01C	FOCS	γ nucleus, $\overline{E}_\gamma \approx$ 180 GeV

$\Gamma(K^0_S K^+ \pi^0 \pi^0)/\Gamma_{total}$ — Γ_{195}/Γ

VALUE (units 10^{-4})	EVTS	DOCUMENT ID		TECN	COMMENT
5.8±1.2±0.4	34	ABLIKIM	20AC	BES3	e^+e^- at 3.773 GeV

$\Gamma(K^0_S K^- 2\pi^+)/\Gamma_{total}$ — Γ_{196}/Γ

VALUE (units 10^{-3})	EVTS	DOCUMENT ID		TECN	COMMENT
2.27±0.12±0.06	467	ABLIKIM	20AC	BES3	e^+e^- at 3.773 GeV

$\Gamma(K^0_S K^- 2\pi^+)/\Gamma(K^0_S 2\pi^+ \pi^-)$ — $\Gamma_{196}/\Gamma_{107}$

VALUE (units 10^{-2})	EVTS	DOCUMENT ID		TECN	COMMENT
7.68±0.41±0.32	670 ± 35	LINK	01C	FOCS	γ nucleus, $\overline{E}_\gamma \approx$ 180 GeV

$\Gamma(K^+ K^- 2\pi^+ \pi^-)/\Gamma_{total}$ — Γ_{197}/Γ

VALUE (units 10^{-4})	EVTS	DOCUMENT ID		TECN	COMMENT
0.67±0.11 OUR FIT					
0.66±0.11±0.03	62	ABLIKIM	25AX	BES3	e^+e^- at 3.773 GeV

$\Gamma(K^+ K^- 2\pi^+ \pi^-)/\Gamma(K^- 3\pi^+ \pi^-)$ — $\Gamma_{197}/\Gamma_{117}$

VALUE (units 10^{-2})	EVTS	DOCUMENT ID		TECN	COMMENT
1.19±0.22 OUR FIT					
4.0 ±0.9 ±1.9	38	LINK	03D	FOCS	γ A, $\overline{E}_\gamma \approx$ 180 GeV

$\Gamma(\phi 2\pi^+ \pi^-)/\Gamma_{total}$ — Γ_{198}/Γ

VALUE (units 10^{-4})	EVTS	DOCUMENT ID		TECN	COMMENT
0.54±0.19±0.02	18	ABLIKIM	25AX	BES3	e^+e^- at 3.773 GeV

$\Gamma(K^0_S K^+ \pi^+ \pi^- \pi^0)/\Gamma_{total}$ — Γ_{191}/Γ

VALUE (units 10^{-4})	EVTS	DOCUMENT ID		TECN	COMMENT
2.51±0.34±0.14	78	ABLIKIM	25AX	BES3	e^+e^- at 3.773 GeV

$\Gamma(K^0_S K^+ \omega)/\Gamma_{total}$ — Γ_{192}/Γ

VALUE (units 10^{-4})	EVTS	DOCUMENT ID		TECN	COMMENT
2.02±0.35±0.10	40	ABLIKIM	25AX	BES3	e^+e^- at 3.773 GeV

$\Gamma(\phi \pi^+ \pi^0)/\Gamma_{total}$ — Γ_{199}/Γ

Unseen decay modes of the ϕ are included.

VALUE	DOCUMENT ID		TECN	COMMENT
0.023±0.010	[1] BARLAG	92C	ACCM	π^- Cu 230 GeV

[1] BARLAG 92C computes the branching fraction using topological normalization.

$\Gamma(\phi \rho^+)/\Gamma(K^- 2\pi^+)$ — Γ_{200}/Γ_{68}

Unseen decay modes of the ϕ are included.

VALUE	CL%	DOCUMENT ID		TECN	COMMENT
<0.16	90	DAOUDI	92	CLEO	$e^+e^- \approx$ 10.5 GeV

$\Gamma(K^+ K^- \pi^+ \pi^0 \text{ non-}\phi)/\Gamma_{total}$ — Γ_{201}/Γ

VALUE	DOCUMENT ID		TECN	COMMENT
$0.015^{+0.007}_{-0.006}$	[1] BARLAG	92C	ACCM	π^- Cu 230 GeV

[1] BARLAG 92C computes the branching fraction using topological normalization.

$\Gamma(\rho(770)^+ \gamma)/\Gamma_{total}$ — Γ_{202}/Γ

VALUE	CL%	DOCUMENT ID		TECN	COMMENT
<1.3 × 10^{-5}	90	ABLIKIM	24CX	BES3	e^+e^- at $\sqrt{s}$ = 3.773 GeV

$\Gamma(K^*(892)^+ \gamma)/\Gamma_{total}$ — Γ_{203}/Γ

VALUE	CL%	DOCUMENT ID		TECN	COMMENT
<1.8 × 10^{-5}	90	ABLIKIM	24CX	BES3	e^+e^- at $\sqrt{s}$ = 3.773 GeV

$\Gamma(K^+ K^- \pi^+ \pi^0 \text{ non-}\phi)/\Gamma(K^- 2\pi^+)$ — Γ_{201}/Γ_{68}

VALUE	CL%	DOCUMENT ID		TECN	COMMENT
• • • We do not use the following data for averages, fits, limits, etc. • • •					
<0.25	90	ANJOS	89E	E691	Photoproduction

Doubly Cabibbo-suppressed modes

$\Gamma(K^+ \pi^0)/\Gamma_{total}$ — Γ_{204}/Γ

VALUE (units 10^{-4})	EVTS	DOCUMENT ID		TECN	COMMENT
1.54±0.13 OUR FIT	Error includes scale factor of 1.4.				
1.49±0.10 OUR AVERAGE					
1.45±0.06±0.08	0.63k	ABLIKIM	25CN	BES3	e^+e^-, 3773 MeV
2.52±0.47±0.26	189 ± 37	AUBERT,B	06F	BABR	$e^+e^- \approx \Upsilon(4S)$
• • • We do not use the following data for averages, fits, limits, etc. • • •					
2.32±0.21±0.06	1.8k	ABLIKIM	18W	BES3	Superseded by ABLIKIM 25CN
2.28±0.36±0.17	148 ± 23	DYTMAN	06	CLEO	See MENDEZ 10

$\Gamma(K^+ \pi^0)/\Gamma(K^- 2\pi^+)$ — Γ_{204}/Γ_{68}

VALUE (units 10^{-3})	EVTS	DOCUMENT ID		TECN	COMMENT
1.65±0.14 OUR FIT	Error includes scale factor of 1.4.				
1.9 ±0.2 ±0.1	343 ± 37	MENDEZ	10	CLEO	e^+e^- at 3774 MeV

$\Gamma(K^+ \eta)/\Gamma_{total}$ — Γ_{205}/Γ

VALUE (units 10^{-3})	EVTS	DOCUMENT ID		TECN	COMMENT
0.116±0.009 OUR FIT					
0.117±0.010±0.003	0.18k	ABLIKIM	25CN	BES3	e^+e^-, 3773 MeV
• • • We do not use the following data for averages, fits, limits, etc. • • •					
0.151±0.025±0.014	439	ABLIKIM	18W	BES3	Superseded by ABLIKIM 25CN

$\Gamma(K^+ \eta)/\Gamma(\eta \pi^+)$ — $\Gamma_{205}/\Gamma_{154}$

VALUE (%)	EVTS	DOCUMENT ID		TECN	COMMENT
3.10±0.24 OUR FIT					
3.06±0.43±0.14	166 ± 23	WON	11	BELL	$e^+e^- \approx \Upsilon(4S)$

$\Gamma(K^+ \eta'(958))/\Gamma_{total}$ — Γ_{206}/Γ

VALUE (units 10^{-3})	EVTS	DOCUMENT ID		TECN	COMMENT
0.188±0.014 OUR FIT					
0.188±0.015±0.011	0.21k	ABLIKIM	25CN	BES3	e^+e^-, 3773 MeV
• • • We do not use the following data for averages, fits, limits, etc. • • •					
0.164±0.051±0.024	87	ABLIKIM	18W	BES3	Superseded by ABLIKIM 25CN

$\Gamma(K^+ \eta'(958))/\Gamma(\eta'(958) \pi^+)$ — $\Gamma_{206}/\Gamma_{168}$

VALUE (%)	EVTS	DOCUMENT ID		TECN	COMMENT
3.78±0.28 OUR FIT					
3.77±0.39±0.10	180 ± 19	WON	11	BELL	$e^+e^- \approx \Upsilon(4S)$

$\Gamma(K^+ 2\pi^0)/\Gamma_{total}$ — Γ_{207}/Γ

VALUE (units 10^{-4})	EVTS	DOCUMENT ID		TECN	COMMENT
2.1±0.4±0.1	43	ABLIKIM	22BK	BES3	e^+e^- at 3.773 GeV

$\Gamma(K^*(892)^+ \pi^0)/\Gamma_{total}$ — Γ_{208}/Γ

VALUE (units 10^{-4})	EVTS	DOCUMENT ID		TECN	COMMENT
$3.4^{+1.4}_{-1.3}$±0.1	17	[1] ABLIKIM	22BK	BES3	e^+e^- at 3.773 GeV

[1] ABLIKIM 22BK report a 2.7 σ significance for the observation of this decay and assign an upper limit for this branching fraction of 5.4×10^{-4} at 90% CL. In their analysis, ABLIKIM 22BK assume negligible interference between $D^+ \to K^{*+}\pi^0 \to K^+\pi^0\pi^0$ and the non-resonant decay to the same final state.

$\Gamma(K^+ \pi^+ \pi^-)/\Gamma_{total}$ — Γ_{209}/Γ

VALUE (units 10^{-4})	EVTS	DOCUMENT ID		TECN	COMMENT
4.88±0.08 OUR FIT	Error includes scale factor of 1.4.				
4.50±0.12±0.35	2k	ABLIKIM	25BI	BES3	e^+e^- at 3.773 GeV

Int. J. Mod. Phys. A 2026.41. Downloaded from www.worldscientific.com
by UNIVERSITY OF CALIFORNIA @ BERKELEY on 09/16/26. Re-use and distribution is strictly not permitted, except for Open Access articles.

$\Gamma(K^+\pi^+\pi^-)/\Gamma(K^-2\pi^+)$ — Γ_{209}/Γ_{68}

VALUE (units 10^{-3})	EVTS	DOCUMENT ID		TECN	COMMENT
5.236±0.025 OUR FIT					
5.238±0.025 OUR AVERAGE					
5.231±0.009±0.023	795k	AAIJ	19G	LHCB	pp at 8 TeV
5.69 ±0.18 ±0.14	2638 ± 84	KO	09	BELL	e^+e^- at $\Upsilon(4S)$
6.5 ±0.8 ±0.4	189 ± 24	LINK	04F	FOCS	γ A, $\overline{E}_\gamma \approx 180$ GeV
7.7 ±1.7 ±0.8	59 ± 13	AITALA	97C	E791	π^- A, 500 GeV
7.2 ±2.3 ±1.7	21	FRABETTI	95E	E687	γBe, $\overline{E}_\gamma$= 220 GeV

$\Gamma(K^+\rho^0)/\Gamma(K^+\pi^+\pi^-)$ — $\Gamma_{210}/\Gamma_{209}$

This is the "fit fraction" from the Dalitz-plot analysis.

VALUE	DOCUMENT ID		TECN	COMMENT
0.39 ±0.09 OUR AVERAGE				
0.3943±0.0787±0.0815	LINK	04F	FOCS	Dalitz fit, 189 evts
0.37 ±0.14 ±0.07	AITALA	97C	E791	Dalitz fit, 59 evts

$\Gamma(K^+\eta\pi^0)/\Gamma_{total}$ — Γ_{211}/Γ

VALUE (units 10^{-4})	EVTS	DOCUMENT ID		TECN	COMMENT
2.1±0.5±0.1	19	ABLIKIM	22BK	BES3	e^+e^- at 3.773 GeV

$\Gamma(K^*(892)^+\eta)/\Gamma_{total}$ — Γ_{212}/Γ

VALUE (units 10^{-4})	EVTS	DOCUMENT ID		TECN	COMMENT
$4.4^{+1.8}_{-1.5}\pm0.2$	11	[1] ABLIKIM	22BK	BES3	e^+e^- at 3.773 GeV

[1] ABLIKIM 22BK report a 3.2 σ significance for the observation of this decay mode. In their analysis, ABLIKIM 22BK assume negligible interference between $D^+ \to K^{*+}\eta \to K^+\eta\pi^0$ and the non-resonant decay to the same final state.

$\Gamma(K^*(892)^0\pi^+, K^*(892)^0 \to K^+\pi^-)/\Gamma(K^+\pi^+\pi^-)$ — $\Gamma_{213}/\Gamma_{209}$

This is the "fit fraction" from the Dalitz-plot analysis.

VALUE	DOCUMENT ID		TECN	COMMENT
0.47 ±0.08 OUR AVERAGE				
0.5220±0.0684±0.0638	LINK	04F	FOCS	Dalitz fit, 189 evts
0.35 ±0.14 ±0.01	AITALA	97C	E791	Dalitz fit, 59 evts

$\Gamma(K^+f_0(980), f_0(980) \to \pi^+\pi^-)/\Gamma(K^+\pi^+\pi^-)$ — $\Gamma_{214}/\Gamma_{209}$

This is the "fit fraction" from the Dalitz-plot analysis.

VALUE	DOCUMENT ID		TECN	COMMENT
0.0892±0.0333±0.0412	LINK	04F	FOCS	Dalitz fit, 189 evts

$\Gamma(K_2^*(1430)^0\pi^+, K_2^*(1430)^0 \to K^+\pi^-)/\Gamma(K^+\pi^+\pi^-)$ — $\Gamma_{215}/\Gamma_{209}$

This is the "fit fraction" from the Dalitz-plot analysis.

VALUE	DOCUMENT ID		TECN	COMMENT
0.0803±0.0372±0.0391	LINK	04F	FOCS	Dalitz fit, 189 evts

$\Gamma(K^+\pi^+\pi^-\text{nonresonant})/\Gamma(K^+\pi^+\pi^-)$ — $\Gamma_{216}/\Gamma_{209}$

This is the "fit fraction" from the Dalitz-plot analysis.

VALUE	DOCUMENT ID		TECN	COMMENT
• • • We do not use the following data for averages, fits, limits, etc. • • •				
0.36±0.14±0.07	[1] AITALA	97C	E791	Dalitz fit, 59 evts

[1] LINK 04F, with three times as many events, finds no need for a nonresonant amplitude.

$\Gamma(K^+\pi^+\pi^-\pi^0)/\Gamma_{total}$ — Γ_{217}/Γ

VALUE (units 10^{-3})	EVTS	DOCUMENT ID		TECN	COMMENT
1.21±0.08±0.03	350	[1] ABLIKIM	20Z	BES3	e^+e^- at 3773 MeV

[1] ABLIKIM 20Z subtracted the known branching fractions of $D^+ \to K^+\eta$, $D^+ \to K^+\phi$, and $D^+ \to K^+\omega$ to obtain an estimate of the non-resonant component (ignoring interference effects and possible additional resonant contributions) B($D^+ \to K^+\pi^+\pi^-\pi^0$ non-resonant) = $(1.13 \pm 0.08 \pm 0.03) \times 10^{-3}$.

$\Gamma(K^+\pi^+\pi^-\pi^0)/\Gamma(K^-2\pi^+\pi^0)$ — Γ_{217}/Γ_{93}

VALUE (units 10^{-2})	EVTS	DOCUMENT ID		TECN	COMMENT
1.68±0.11±0.03	3.6k	LI	23G	BELL	e^+e^- at/near Υ(nS), n=1,...,5

$\Gamma(K^+\pi^+\pi^-\pi^0\text{nonresonant})/\Gamma_{total}$ — Γ_{218}/Γ

VALUE (units 10^{-3})	EVTS	DOCUMENT ID		TECN	COMMENT
1.10±0.07 OUR AVERAGE					
1.03±0.12±0.06	112	[1] ABLIKIM	21BB	BES3	e^+e^- at 3.773 GeV
1.13±0.08±0.03	350	[2] ABLIKIM	20Z	BES3	e^+e^- at 3.773 GeV

[1] ABLIKIM 21BB result has subtracted the known branching fractions of $D^+ \to K^+\eta$, $D^+ \to K^+\phi$, and $D^+ \to K^+\omega$ resonances (ignoring interference effects). The result including these components is measured to be B($D^+ \to K^+\pi^+\pi^-\pi^0$) = $(1.11 \pm 0.12) \times 10^{-3}$, where the uncertainty is statistical only.

[2] ABLIKIM 20Z result has subtracted the known branching fractions of $D^+ \to K^+\eta$, $D^+ \to K^+\phi$, and $D^+ \to K^+\omega$, ignoring interference effects. The result including these components is measured to be $(1.21 \pm 0.08 \pm 0.03) \times 10^{-3}$.

$\Gamma(K^+\pi^+\pi^-\eta)/\Gamma_{total}$ — Γ_{219}/Γ

VALUE (units 10^{-4})	EVTS	DOCUMENT ID		TECN	COMMENT
1.56±0.22±0.04	97	ABLIKIM	25BI	BES3	e^+e^- at 3.773 GeV

$\Gamma(K^+(\pi^+\pi^-\eta)_{non-\eta'})/\Gamma_{total}$ — Γ_{220}/Γ

VALUE (units 10^{-5})	EVTS	DOCUMENT ID		TECN	COMMENT
6.7±1.8±0.2	39	ABLIKIM	25BI	BES3	e^+e^- at 3.773 GeV

$\Gamma(K^+\omega)/\Gamma_{total}$ — Γ_{221}/Γ

VALUE (units 10^{-5})	EVTS	DOCUMENT ID		TECN	COMMENT
$5.7^{+2.5}_{-2.1}\pm0.2$	9	ABLIKIM	20Z	BES3	e^+e^-, 3773 MeV

$\Gamma(K^+\eta\eta)/\Gamma_{total}$ — Γ_{222}/Γ

VALUE (units 10^{-5})	EVTS	DOCUMENT ID		TECN	COMMENT
5.9±2.3±0.2	15	ABLIKIM	25BI	BES3	e^+e^- at 3.773 GeV

$\Gamma(2K^+K^-)/\Gamma_{total}$ — Γ_{223}/Γ

VALUE (units 10^{-5})	EVTS	DOCUMENT ID		TECN	COMMENT
6.09±0.10 OUR FIT Error includes scale factor of 1.3.					
5.1 ±0.5 ±0.1	0.14k	ABLIKIM	25BI	BES3	e^+e^- at 3.773 GeV

$\Gamma(2K^+K^-)/\Gamma(K^-2\pi^+)$ — Γ_{223}/Γ_{68}

VALUE (units 10^{-4})	EVTS	DOCUMENT ID		TECN	COMMENT
6.53 ±0.05 OUR FIT					
6.54 ±0.05 OUR AVERAGE					
6.541±0.025±0.042	134k	AAIJ	19G	LHCB	pp at 8 TeV
9.49 ±2.17 ±0.22	65	[1] LINK	02I	FOCS	γ nucleus, ≈ 180 GeV

[1] LINK 02I finds little evidence for ϕK^+ or $f_0(980)\,K^+$ submodes.

$\Gamma(K^+\phi(1020), \phi \to K^+K^-)/\Gamma(2K^+K^-)$ — $\Gamma_{225}/\Gamma_{223}$

VALUE (%)	DOCUMENT ID		TECN	COMMENT
7.1±0.9	[1] AAIJ	19H	LHCB	pp at 8TeV

[1] Fit fraction from a Dalitz plot analysis of $D^+ \to K^+K^+K^-$ decays. The last uncertainty is due to the amplitude model.

$\Gamma(K^+(K^+K^-)_{S-wave})/\Gamma(2K^+K^-)$ — $\Gamma_{226}/\Gamma_{223}$

VALUE	DOCUMENT ID		TECN	COMMENT
0.94±0.01	[1] AAIJ	19H	LHCB	pp at 8TeV

[1] Fit fraction from a Dalitz plot analysis of $D^+ \to K^+K^+K^-$ decays. The last uncertainty is due to the amplitude model.

Rare or forbidden modes

$\Gamma(\pi^+e^+e^-)/\Gamma_{total}$ — Γ_{227}/Γ

A test for the $\Delta C = 1$ weak neutral current. Allowed by higher-order electroweak interactions.

VALUE	CL%	DOCUMENT ID		TECN	COMMENT
$<1.1 \times 10^{-6}$	90	LEES	11G	BABR	$e^+e^- \approx \Upsilon(4S)$
• • • We do not use the following data for averages, fits, limits, etc. • • •					
$<1.6 \times 10^{-6}$	90	AAIJ	21T	LHCB	1.6 fb^{-1} pp
$<5.9 \times 10^{-6}$	90	[1] RUBIN	10	CLEO	e^+e^- at $\psi(3770)$
$<7.4 \times 10^{-6}$	90	HE	05A	CLEO	See RUBIN 10
$<5.2 \times 10^{-5}$	90	AITALA	99G	E791	π^-N 500 GeV
$<1.1 \times 10^{-4}$	90	FRABETTI	97B	E687	γ Be, $\overline{E}_\gamma \approx 220$ GeV
$<6.6 \times 10^{-5}$	90	AITALA	96	E791	π^-N 500 GeV
$<2.5 \times 10^{-3}$	90	WEIR	90B	MRK2	e^+e^- 29 GeV
$<2.6 \times 10^{-3}$	90	HAAS	88	CLEO	e^+e^- 10 GeV

[1] This RUBIN 10 limit is for the e^+e^- mass in the continuum away from the $\phi(1020)$. See the next data block.

$\Gamma(\pi^+\pi^0e^+e^-)/\Gamma_{total}$ — Γ_{228}/Γ

VALUE	CL%	DOCUMENT ID		TECN	COMMENT
$<1.4 \times 10^{-5}$	90	ABLIKIM	18P	BES3	e^+e^-, 3773 MeV

$\Gamma(\pi^+\phi, \phi \to e^+e^-)/\Gamma_{total}$ — Γ_{229}/Γ

This is *not* a test for the $\Delta C = 1$ weak neutral current, but leads to the $\pi^+e^+e^-$ final state.

VALUE	EVTS	DOCUMENT ID		TECN	COMMENT
$(1.7^{+1.4}_{-0.9}\pm0.1) \times 10^{-6}$	4	[1] RUBIN	10	CLEO	e^+e^- at $\psi(3770)$
• • • We do not use the following data for averages, fits, limits, etc. • • •					
$(2.7^{+3.6}_{-1.8}\pm0.2) \times 10^{-6}$	2	HE	05A	CLEO	See RUBIN 10

[1] This RUBIN 10 result is consistent with the known $D^+ \to \phi\pi^+$ and $\phi \to e^+e^-$ fractions.

$\Gamma(\pi^+\mu^+\mu^-)/\Gamma_{total}$ — Γ_{230}/Γ

A test for the $\Delta C = 1$ weak neutral current. Allowed by higher-order electroweak interactions.

VALUE	CL%	DOCUMENT ID		TECN	COMMENT
$<6.7 \times 10^{-8}$	90	AAIJ	21T	LHCB	1.6 fb^{-1} pp
• • • We do not use the following data for averages, fits, limits, etc. • • •					
$<7.3 \times 10^{-8}$	90	AAIJ	13AF	LHCB	pp at 7 TeV
$<6.5 \times 10^{-6}$	90	LEES	11G	BABR	$e^+e^- \approx \Upsilon(4S)$
$<3.9 \times 10^{-6}$	90	[1] ABAZOV	08D	D0	$p\overline{p}$, E_{cm} = 1.96 TeV
$<8.8 \times 10^{-6}$	90	LINK	03F	FOCS	γ A, $\overline{E}_\gamma \approx 180$ GeV
$<1.5 \times 10^{-5}$	90	AITALA	99G	E791	π^-N 500 GeV

$<8.9\times10^{-5}$	90	FRABETTI	97B	E687	γ Be, $\overline{E}_\gamma \approx$ 220 GeV
$<1.8\times10^{-5}$	90	AITALA	96	E791	π^- N 500 GeV
$<2.2\times10^{-4}$	90	KODAMA	95	E653	π^- emulsion 600 GeV
$<5.9\times10^{-3}$	90	WEIR	90B	MRK2	e^+e^- 29 GeV
$<2.9\times10^{-3}$	90	HAAS	88	CLEO	e^+e^- 10 GeV

[1] This ABAZOV 08D limit is for the $\mu^+\mu^-$ mass in the continuum away from the $\phi(1020)$. See the next data block.

$\Gamma(\pi^+\phi,\ \phi\to\mu^+\mu^-)/\Gamma_{\rm total}$ — Γ_{231}/Γ

This is *not* a test for the $\Delta C=1$ weak neutral current, but leads to the $\pi^+\mu^+\mu^-$ final state.

VALUE	DOCUMENT ID		TECN	COMMENT
$(1.8\pm0.5\pm0.6)\times10^{-6}$	[1] ABAZOV	08D	D0	$p\overline{p}$, $E_{\rm cm}=1.96$ TeV

[1] This ABAZOV 08D value is consistent with the known $D^+\to\phi\pi^+$ and $\phi\to\mu^+\mu^-$ fractions.

$\Gamma(\rho^+\mu^+\mu^-)/\Gamma_{\rm total}$ — Γ_{232}/Γ

A test for the $\Delta C=1$ weak neutral current. Allowed by higher-order electroweak interactions.

VALUE	CL%	DOCUMENT ID		TECN	COMMENT
$<5.6\times10^{-4}$	90	KODAMA	95	E653	π^- emulsion 600 GeV

$\Gamma(K^+e^+e^-)/\Gamma_{\rm total}$ — Γ_{233}/Γ

Both quarks would have to change flavor for this decay to occur.

VALUE	CL%	DOCUMENT ID		TECN	COMMENT
$<8.5\times10^{-7}$	90	AAIJ	21T	LHCB	1.6 fb^{-1} pp
• • • We do not use the following data for averages, fits, limits, etc. • • •					
$<1.0\times10^{-6}$	90	LEES	11G	BABR	$e^+e^-\approx\Upsilon(4S)$
$<3.0\times10^{-6}$	90	RUBIN	10	CLEO	e^+e^- at $\psi(3770)$
$<6.2\times10^{-6}$	90	HE	05A	CLEO	See RUBIN 10
$<2.0\times10^{-4}$	90	AITALA	99G	E791	π^- N 500 GeV
$<2.0\times10^{-4}$	90	FRABETTI	97B	E687	γ Be, $\overline{E}_\gamma\approx$ 220 GeV
$<4.8\times10^{-3}$	90	WEIR	90B	MRK2	e^+e^- 29 GeV

$\Gamma(K^+\pi^0e^+e^-)/\Gamma_{\rm total}$ — Γ_{234}/Γ

VALUE	CL%	DOCUMENT ID		TECN	COMMENT
$<1.5\times10^{-5}$	90	ABLIKIM	18P	BES3	e^+e^-, 3773 MeV

$\Gamma(K^0_S\pi^+e^+e^-)/\Gamma_{\rm total}$ — Γ_{235}/Γ

VALUE	CL%	DOCUMENT ID		TECN	COMMENT
$<2.6\times10^{-5}$	90	ABLIKIM	18P	BES3	e^+e^-, 3773 MeV

$\Gamma(K^0_SK^+e^+e^-)/\Gamma_{\rm total}$ — Γ_{236}/Γ

VALUE	CL%	DOCUMENT ID		TECN	COMMENT
$<1.1\times10^{-5}$	90	ABLIKIM	18P	BES3	e^+e^-, 3773 MeV

$\Gamma(K^+\mu^+\mu^-)/\Gamma_{\rm total}$ — Γ_{237}/Γ

Both quarks would have to change flavor for this decay to occur.

VALUE	CL%	DOCUMENT ID		TECN	COMMENT
$<5.4\times10^{-8}$	90	AAIJ	21T	LHCB	1.6 fb^{-1} pp
• • • We do not use the following data for averages, fits, limits, etc. • • •					
$<4.3\times10^{-6}$	90	LEES	11G	BABR	$e^+e^-\approx\Upsilon(4S)$
$<9.2\times10^{-6}$	90	LINK	03F	FOCS	γ A, $\overline{E}_\gamma\approx$ 180 GeV
$<4.4\times10^{-5}$	90	AITALA	99G	E791	π^- N 500 GeV
$<9.7\times10^{-5}$	90	FRABETTI	97B	E687	γ Be, $\overline{E}_\gamma\approx$ 220 GeV
$<3.2\times10^{-4}$	90	KODAMA	95	E653	π^- emulsion 600 GeV
$<9.2\times10^{-3}$	90	WEIR	90B	MRK2	e^+e^- 29 GeV

$\Gamma(\pi^+e^+\mu^-)/\Gamma_{\rm total}$ — Γ_{238}/Γ

A test of lepton-family-number conservation.

VALUE	CL%	DOCUMENT ID		TECN	COMMENT
$<2.1\times10^{-7}$	90	AAIJ	21T	LHCB	1.6 fb^{-1} pp
• • • We do not use the following data for averages, fits, limits, etc. • • •					
$<2.9\times10^{-6}$	90	LEES	11G	BABR	$e^+e^-\approx\Upsilon(4S)$
$<1.1\times10^{-4}$	90	FRABETTI	97B	E687	γ Be, $\overline{E}_\gamma\approx$ 220 GeV
$<3.3\times10^{-3}$	90	WEIR	90B	MRK2	e^+e^- 29 GeV

$\Gamma(\pi^+e^-\mu^+)/\Gamma_{\rm total}$ — Γ_{239}/Γ

A test of lepton-family-number conservation.

VALUE	CL%	DOCUMENT ID		TECN	COMMENT
$<2.2\times10^{-7}$	90	AAIJ	21T	LHCB	1.6 fb^{-1} pp
• • • We do not use the following data for averages, fits, limits, etc. • • •					
$<3.6\times10^{-6}$	90	LEES	11G	BABR	$e^+e^-\approx\Upsilon(4S)$
$<1.3\times10^{-4}$	90	FRABETTI	97B	E687	γ Be, $\overline{E}_\gamma\approx$ 220 GeV
$<3.3\times10^{-3}$	90	WEIR	90B	MRK2	e^+e^- 29 GeV

$\Gamma(K^+e^+\mu^-)/\Gamma_{\rm total}$ — Γ_{240}/Γ

A test of lepton-family-number conservation.

VALUE	CL%	DOCUMENT ID		TECN	COMMENT
$<7.5\times10^{-8}$	90	AAIJ	21T	LHCB	1.6 fb^{-1} pp
• • • We do not use the following data for averages, fits, limits, etc. • • •					
$<1.2\times10^{-6}$	90	LEES	11G	BABR	$e^+e^-\approx\Upsilon(4S)$
$<1.3\times10^{-4}$	90	FRABETTI	97B	E687	γ Be, $\overline{E}_\gamma\approx$ 220 GeV
$<3.4\times10^{-3}$	90	WEIR	90B	MRK2	e^+e^- 29 GeV

$\Gamma(K^+e^-\mu^+)/\Gamma_{\rm total}$ — Γ_{241}/Γ

A test of lepton-family-number conservation.

VALUE	CL%	DOCUMENT ID		TECN	COMMENT
$<1.0\times10^{-7}$	90	AAIJ	21T	LHCB	1.6 fb^{-1} pp
• • • We do not use the following data for averages, fits, limits, etc. • • •					
$<2.8\times10^{-6}$	90	LEES	11G	BABR	$e^+e^-\approx\Upsilon(4S)$
$<1.2\times10^{-4}$	90	FRABETTI	97B	E687	γ Be, $\overline{E}_\gamma\approx$ 220 GeV
$<3.4\times10^{-3}$	90	WEIR	90B	MRK2	e^+e^- 29 GeV

$\Gamma(\pi^-2e^+)/\Gamma_{\rm total}$ — Γ_{242}/Γ

A test of lepton-number conservation.

VALUE	CL%	DOCUMENT ID		TECN	COMMENT
$<5.3\times10^{-7}$	90	AAIJ	21T	LHCB	1.6 fb^{-1} pp
• • • We do not use the following data for averages, fits, limits, etc. • • •					
$<1.9\times10^{-6}$	90	LEES	11G	BABR	$e^+e^-\approx\Upsilon(4S)$
$<1.1\times10^{-6}$	90	RUBIN	10	CLEO	e^+e^- at $\psi(3770)$
$<3.6\times10^{-6}$	90	HE	05A	CLEO	See RUBIN 10
$<9.6\times10^{-5}$	90	AITALA	99G	E791	π^- N 500 GeV
$<1.1\times10^{-4}$	90	FRABETTI	97B	E687	γ Be, $\overline{E}_\gamma\approx$ 220 GeV
$<4.8\times10^{-3}$	90	WEIR	90B	MRK2	e^+e^- 29 GeV

$\Gamma(\pi^-2\mu^+)/\Gamma_{\rm total}$ — Γ_{243}/Γ

A test of lepton-number conservation.

VALUE	CL%	DOCUMENT ID		TECN	COMMENT
$<1.4\times10^{-8}$	90	AAIJ	21T	LHCB	1.6 fb^{-1} pp
• • • We do not use the following data for averages, fits, limits, etc. • • •					
$<2.2\times10^{-8}$	90	AAIJ	13AF	LHCB	pp at 7 TeV
$<2.0\times10^{-6}$	90	LEES	11G	BABR	$e^+e^-\approx\Upsilon(4S)$
$<4.8\times10^{-6}$	90	LINK	03F	FOCS	γ A, $\overline{E}_\gamma\approx$ 180 GeV
$<1.7\times10^{-5}$	90	AITALA	99G	E791	π^- N 500 GeV
$<8.7\times10^{-5}$	90	FRABETTI	97B	E687	γ Be, $\overline{E}_\gamma\approx$ 220 GeV
$<2.2\times10^{-4}$	90	KODAMA	95	E653	π^- emulsion 600 GeV
$<6.8\times10^{-3}$	90	WEIR	90B	MRK2	e^+e^- 29 GeV

$\Gamma(\pi^-e^+\mu^+)/\Gamma_{\rm total}$ — Γ_{244}/Γ

A test of lepton-number conservation.

VALUE	CL%	DOCUMENT ID		TECN	COMMENT
$<1.3\times10^{-7}$	90	AAIJ	21T	LHCB	1.6 fb^{-1} pp
• • • We do not use the following data for averages, fits, limits, etc. • • •					
$<2.0\times10^{-6}$	90	LEES	11G	BABR	$e^+e^-\approx\Upsilon(4S)$
$<5.0\times10^{-5}$	90	AITALA	99G	E791	π^- N 500 GeV
$<1.1\times10^{-4}$	90	FRABETTI	97B	E687	γ Be, $\overline{E}_\gamma\approx$ 220 GeV
$<3.7\times10^{-3}$	90	WEIR	90B	MRK2	e^+e^- 29 GeV

$\Gamma(\rho^-2\mu^+)/\Gamma_{\rm total}$ — Γ_{245}/Γ

A test of lepton-number conservation.

VALUE	CL%	DOCUMENT ID		TECN	COMMENT
$<5.6\times10^{-4}$	90	KODAMA	95	E653	π^- emulsion 600 GeV

$\Gamma(K^-2e^+)/\Gamma_{\rm total}$ — Γ_{246}/Γ

A test of lepton-number conservation.

VALUE	CL%	DOCUMENT ID		TECN	COMMENT
$<0.9\times10^{-6}$	90	LEES	11G	BABR	$e^+e^-\approx\Upsilon(4S)$
• • • We do not use the following data for averages, fits, limits, etc. • • •					
$<3.5\times10^{-6}$	90	RUBIN	10	CLEO	e^+e^- at $\psi(3770)$
$<4.5\times10^{-6}$	90	HE	05A	CLEO	See RUBIN 10
$<1.2\times10^{-4}$	90	FRABETTI	97B	E687	γ Be, $\overline{E}_\gamma\approx$ 220 GeV
$<9.1\times10^{-3}$	90	WEIR	90B	MRK2	e^+e^- 29 GeV

$\Gamma(K^0_S\pi^-2e^+)/\Gamma_{\rm total}$ — Γ_{247}/Γ

VALUE	CL%	DOCUMENT ID		TECN	COMMENT
$<3.3\times10^{-6}$	90	ABLIKIM	19AL	BES3	e^+e^- at 3773 MeV

$\Gamma(K^-\pi^02e^+)/\Gamma_{\rm total}$ — Γ_{248}/Γ

VALUE	CL%	DOCUMENT ID		TECN	COMMENT
$<8.5\times10^{-6}$	90	ABLIKIM	19AL	BES3	e^+e^- at 3773 MeV

$\Gamma(K^-2\mu^+)/\Gamma_{\rm total}$ — Γ_{249}/Γ

A test of lepton-number conservation.

VALUE	CL%	DOCUMENT ID		TECN	COMMENT
$<10\ \ \times10^{-6}$	90	LEES	11G	BABR	$e^+e^-\approx\Upsilon(4S)$
• • • We do not use the following data for averages, fits, limits, etc. • • •					
$<1.3\times10^{-5}$	90	LINK	03F	FOCS	γ A, $\overline{E}_\gamma\approx$ 180 GeV
$<1.2\times10^{-4}$	90	FRABETTI	97B	E687	γ Be, $\overline{E}_\gamma\approx$ 220 GeV
$<3.2\times10^{-4}$	90	KODAMA	95	E653	π^- emulsion 600 GeV
$<4.3\times10^{-3}$	90	WEIR	90B	MRK2	e^+e^- 29 GeV

$\Gamma(K^-e^+\mu^+)/\Gamma_{\rm total}$ — Γ_{250}/Γ

A test of lepton-number conservation.

VALUE	CL%	DOCUMENT ID		TECN	COMMENT
$<1.9\times10^{-6}$	90	LEES	11G	BABR	$e^+e^-\approx\Upsilon(4S)$
• • • We do not use the following data for averages, fits, limits, etc. • • •					
$<1.3\times10^{-4}$	90	FRABETTI	97B	E687	γ Be, $\overline{E}_\gamma\approx$ 220 GeV
$<4.0\times10^{-3}$	90	WEIR	90B	MRK2	e^+e^- 29 GeV

Int. J. Mod. Phys. A 2026.41. Downloaded from www.worldscientific.com
by LIFORNIA @ BERKELEY on 09/16/26. Re-use and distribution is strictly not permitted, except for Open Access articles.

Int. J. Mod. Phys. A 2026.41. Downloaded from www.worldscientific.com by UNIVERSITY OF CALIFORNIA @ BERKELEY on 09/16/26. Re-use and distribution is strictly not permitted, except for Open Access articles.

$\Gamma(K^*(892)^- 2\mu^+)/\Gamma_{total}$ — Γ_{251}/Γ

A test of lepton-number conservation.

VALUE	CL%	DOCUMENT ID		TECN	COMMENT
$<8.5 \times 10^{-4}$	90	KODAMA	95	E653	π^- emulsion 600 GeV

$\Gamma(\Lambda e^+)/\Gamma_{total}$ — Γ_{252}/Γ

VALUE	CL%	DOCUMENT ID		TECN	COMMENT
$<1.1 \times 10^{-6}$	90	ABLIKIM	20D	BES3	e^+e^-, 3773 MeV

$\Gamma(\overline{\Lambda} e^+)/\Gamma_{total}$ — Γ_{253}/Γ

VALUE	CL%	DOCUMENT ID		TECN	COMMENT
$<6.5 \times 10^{-7}$	90	ABLIKIM	20D	BES3	e^+e^-, 3773 MeV

$\Gamma(\Sigma^0 e^+)/\Gamma_{total}$ — Γ_{254}/Γ

VALUE	CL%	DOCUMENT ID		TECN	COMMENT
$<1.7 \times 10^{-6}$	90	ABLIKIM	20D	BES3	e^+e^-, 3773 MeV

$\Gamma(\overline{\Sigma}^0 e^+)/\Gamma_{total}$ — Γ_{255}/Γ

VALUE	CL%	DOCUMENT ID		TECN	COMMENT
$<1.3 \times 10^{-6}$	90	ABLIKIM	20D	BES3	e^+e^-, 3773 MeV

$\Gamma(\pi e^+)/\Gamma_{total}$ — Γ_{256}/Γ

VALUE	CL%	DOCUMENT ID		TECN	COMMENT
$<1.43 \times 10^{-5}$	90	ABLIKIM	22BJ	BES3	2.93fb^{-1} e^+e^- at 3.773 GeV

$\Gamma(n e^+)/\Gamma_{total}$ — Γ_{257}/Γ

VALUE	CL%	DOCUMENT ID		TECN	COMMENT
$<2.91 \times 10^{-5}$	90	ABLIKIM	22BJ	BES3	2.93fb^{-1} e^+e^- at 3.773 GeV

$D^{\pm}$ CP-VIOLATING DECAY-RATE ASYMMETRIES

This is the difference between D^+ and D^- partial widths for the decay to state f, divided by the sum of the widths:
$A_{CP}(f) = [\Gamma(D^+ \to f) - \Gamma(D^- \to \overline{f})]/[\Gamma(D^+ \to f) + \Gamma(D^- \to \overline{f})]$.

$A_{CP}(\mu^{\pm}\nu)$ in $D^+ \to \mu^+\nu_\mu$, $D^- \to \mu^-\overline{\nu}_\mu$

VALUE (%)	DOCUMENT ID		TECN	COMMENT
$+8\pm8$	EISENSTEIN	08	CLEO	e^+e^- at $\psi(3770)$

$A_{CP}(K^0_L e^{\pm}\nu)$ in $D^+ \to K^0_L e^+\nu_e$, $D^- \to K^0_L e^-\overline{\nu}_e$

VALUE (%)	DOCUMENT ID		TECN	COMMENT
$-0.59\pm0.60\pm1.48$	ABLIKIM	15AF	BES3	e^+e^- 3773 MeV

$A_{CP}(K^0_S\pi^{\pm})$ in $D^{\pm} \to K^0_S\pi^{\pm}$

VALUE (%)	EVTS	DOCUMENT ID		TECN	COMMENT
$-0.41\ \pm0.09$ OUR AVERAGE					
$-1.1\ \pm0.6\ \pm0.2$		BONVICINI	14	CLEO	All CLEO-c runs
$-0.363\pm0.094\pm0.067$	1738k	[1] KO	12A	BELL	$e^+e^- \approx \Upsilon(nS)$
$-0.44\ \pm0.13\ \pm0.10$	807k	DEL-AMO-SA...	11H	BABR	$e^+e^- \approx \Upsilon(4S)$
$-1.6\ \pm1.5\ \pm0.9$	10.6k	[2] LINK	02B	FOCS	γ nucleus, $\overline{E}_\gamma \approx 180$ GeV
• • • We do not use the following data for averages, fits, limits, etc. • • •					
$-0.71\ \pm0.19\ \pm0.20$		KO	10	BELL	See KO 12A
$-1.3\ \pm0.7\ \pm0.3$	30k	MENDEZ	10	CLEO	See BONVICINI 14
$-0.6\ \pm1.0\ \pm0.3$		DOBBS	07	CLEO	See MENDEZ 10

[1] KO 12A finds that after subtracting the contribution due to $K^0 - \overline{K}^0$ mixing, the CP asymmetry due to the change of charm is $(-0.024 \pm 0.094 \pm 0.067)$%, consistent with zero.

[2] LINK 02B measures $N(D^+ \to K^0_S\pi^+)/N(D^+ \to K^-\pi^+\pi^+)$, the ratio of numbers of events observed, and similarly for the D^-.

$A_{CP}(K^0_L K^{\pm})$ in $D^{\pm} \to K^0_L K^{\pm}$

VALUE (units 10^{-2})	EVTS	DOCUMENT ID		TECN	COMMENT
$-4.2\pm3.2\pm1.2$	650	ABLIKIM	19M	BES3	e^+e^- at 3773 MeV

$A_{CP}(K^{\mp}2\pi^{\pm})$ in $D^+ \to K^-2\pi^+$, $D^- \to K^+2\pi^-$

VALUE (%)	EVTS	DOCUMENT ID		TECN	COMMENT
-0.18 ± 0.16 OUR AVERAGE					
$-0.16\pm0.15\pm0.09$	2.3M	ABAZOV	14L	D0	$p\overline{p}$, $\sqrt{s} = 1.96$ TeV
$-0.3\ \pm0.2\ \pm0.4$		BONVICINI	14	CLEO	All CLEO-c runs
• • • We do not use the following data for averages, fits, limits, etc. • • •					
$-0.1\ \pm0.4\ \pm0.9$	231k	MENDEZ	10	CLEO	See BONVICINI 14
$-0.5\ \pm0.4\ \pm0.9$		DOBBS	07	CLEO	See MENDEZ 10

$A_{CP}(K^{\mp}\pi^{\pm}\pi^{\pm}\pi^0)$ in $D^+ \to K^-\pi^+\pi^+\pi^0$, $D^- \to K^+\pi^-\pi^-\pi^0$

VALUE (%)	DOCUMENT ID		TECN	COMMENT
$-0.3\pm0.6\pm0.4$	BONVICINI	14	CLEO	All CLEO-c runs
• • • We do not use the following data for averages, fits, limits, etc. • • •				
$1.0\pm0.9\pm0.9$	DOBBS	07	CLEO	See BONVICINI 14

$A_{CP}(K^0_S\pi^{\pm}\pi^0)$ in $D^+ \to K^0_S\pi^+\pi^0$, $D^- \to K^0_S\pi^-\pi^0$

VALUE (%)	DOCUMENT ID		TECN	COMMENT
$-0.1\pm0.7\pm0.2$	BONVICINI	14	CLEO	All CLEO-c runs
• • • We do not use the following data for averages, fits, limits, etc. • • •				
$0.3\pm0.9\pm0.3$	DOBBS	07	CLEO	See BONVICINI 14

$A_{CP}(K^0_S\pi^{\pm}\eta)$ in $D^{\pm} \to K^0_S\pi^{\pm}\eta$

VALUE (units 10^{-2})	EVTS	DOCUMENT ID		TECN	COMMENT
$-0.9\pm2.9\pm1.0$	1.3k	ABLIKIM	20V	BES3	e^+e^-, 3773 MeV

$A_{CP}(K^0_S\pi^{\pm}\pi^+\pi^-)$ in $D^+ \to K^0_S\pi^+\pi^+\pi^-$, $D^- \to K^0_S\pi^-\pi^-\pi^+$

VALUE (%)	DOCUMENT ID		TECN	COMMENT
$0.0\pm1.2\pm0.3$	BONVICINI	14	CLEO	All CLEO-c runs
• • • We do not use the following data for averages, fits, limits, etc. • • •				
$0.1\pm1.1\pm0.6$	DOBBS	07	CLEO	See BONVICINI 14

$A_{CP}(K^{\pm}\pi^+\pi^-\pi^0)$ in $D^{\pm} \to K^{\pm}\pi^+\pi^-\pi^0$

VALUE	EVTS	DOCUMENT ID		TECN	COMMENT
$-0.04\pm0.06\pm0.01$	350	ABLIKIM	20Z	BES3	e^+e^-, 3773 MeV

$A_{CP}(\pi^{\pm}\pi^0)$ in $D^{\pm} \to \pi^{\pm}\pi^0$

VALUE (%)	EVTS	DOCUMENT ID		TECN	COMMENT
$-0.5\ \pm1.0$ OUR AVERAGE Error includes scale factor of 1.7. See the ideogram below.					
$-1.8\ \pm0.9\ \pm0.1$	23.6k	[1] ADACHI	25Q	BEL2	at/near $\Upsilon(4S)$
$-1.3\ \pm0.9\ \pm0.6$	28.7k	AAIJ	21U	LHCB	pp at 7, 8, 13 TeV
$2.31\pm1.24\pm0.23$	108k	BABU	18	BELL	at/near $\Upsilon(4S)$, $\Upsilon(5S)$
$2.9\ \pm2.9\ \pm0.3$	2.6k	MENDEZ	10	CLEO	e^+e^- at 3774 MeV

[1] D^0 flavour inferred using the information from the charged particles from the rest of the event for 80% of the candidates, and from $D^*(2010)^+ \to D^+\pi^0$ decays for the remaining 20%.

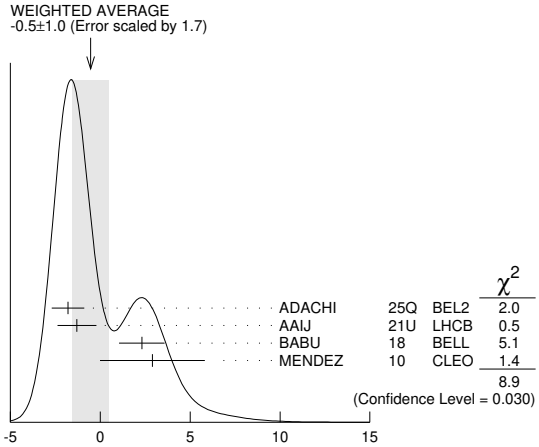

$A_{CP}(\pi^{\pm}\pi^0)$ in $D^{\pm} \to \pi^{\pm}\pi^0$ (%)

$A_{CP}(\pi^{\pm}\eta)$ in $D^{\pm} \to \pi^{\pm}\eta$

VALUE (%)	EVTS	DOCUMENT ID		TECN	COMMENT
$0.3\ \pm0.5$ OUR AVERAGE					
$0.34\pm0.66\pm0.16\pm0.05$	111k	[1] AAIJ	23E	LHCB	6 fb^{-1}, pp at 13 TeV, $\eta \to \gamma\pi\pi$
$-0.2\ \pm0.8\ \pm0.4$	32.7k	AAIJ	21U	LHCB	pp at 13 TeV
$+1.74\pm1.13\pm0.19$		WON	11	BELL	$e^+e^- \approx \Upsilon(4S)$
$-2.0\ \pm2.3\ \pm0.3$	2.9k	MENDEZ	10	CLEO	e^+e^- at 3774 MeV

[1] The last uncertainty is due to the uncertainty on the CP asymmetry of the control channel, $D^+ \to \phi\pi^+$.

$A_{CP}(\pi^{\pm}\pi^0\eta)$ in $D^{\pm} \to \pi^{\pm}\pi^0\eta$

VALUE (units 10^{-2})	EVTS	DOCUMENT ID		TECN	COMMENT
$-5.8\pm6.6\pm1.8$	381	ABLIKIM	20G	BES3	e^+e^- at 3.773 GeV

$A_{CP}(\pi^{\pm}\eta\eta)$ in $D^{\pm} \to \pi^{\pm}\eta\eta$

VALUE (units 10^{-2})	EVTS	DOCUMENT ID		TECN	COMMENT
$8.0\pm8.3\pm1.9$	179	ABLIKIM	20G	BES3	e^+e^- at 3.773 GeV

$A_{CP}(\pi^{\pm}\eta'(958))$ in $D^{\pm} \to \pi^{\pm}\eta'(958)$

VALUE (%)	EVTS	DOCUMENT ID		TECN	COMMENT
0.41 ± 0.23 OUR AVERAGE Error includes scale factor of 1.2.					
$0.49\pm0.18\pm0.06\pm0.05$	555k	[1] AAIJ	23E	LHCB	6 fb^{-1}, pp at 13 TeV, $\eta \to \gamma\pi\pi$
$-0.61\pm0.72\pm0.54$	63k	AAIJ	17AF	LHCB	pp at 7, 8 TeV
$-0.12\pm1.12\pm0.17$		WON	11	BELL	$e^+e^- \approx \Upsilon(4S)$
$-4.0\ \pm3.4\ \pm0.3$	1.0k	MENDEZ	10	CLEO	e^+e^- at 3774 MeV

[1] The last uncertainty is due to the uncertainty on the CP asymmetry of the control channel, $D^+ \to \phi\pi^+$.

$A_{CP}(\overline{K}^0/K^0K^{\pm})$ in $D^+ \to \overline{K}^0K^+$, $D^- \to K^0K^-$

VALUE (%)	EVTS	DOCUMENT ID		TECN	COMMENT
0.11 ± 0.17 OUR AVERAGE					
$0.03\pm0.17\pm0.14$	1.0M	[1] AAIJ	14BD	LHCB	pp at 7, 8 TeV
$0.08\pm0.28\pm0.14$	277k	KO	13	BELL	e^+e^- at $\Upsilon(4S)$
$0.46\pm0.36\pm0.25$	159k	LEES	13E	BABR	e^+e^- at $\Upsilon(4S)$

[1] AAIJ 14BD reports its result as $A_{CP}(D^{\pm} \to K^0_S \pi^{\pm})$ with CP-violation effects in the $K^0 - \overline{K}^0$ system subtracted. It also measures $A_{CP}(D^{\pm} \to \overline{K}^0/K^0 K^{\pm}) + A_{CP}(D^{\pm}_s \to \overline{K}^0/K^0 \pi^{\pm}) = (0.41 \pm 0.49 \pm 0.26)\%$.

$A_{CP}(K^0_S K^{\pm})$ in $D^{\pm} \to K^0_S K^{\pm}$

VALUE (%)	EVTS	DOCUMENT ID		TECN	COMMENT
−0.01 ±0.07 OUR AVERAGE					
−0.004±0.061±0.045	6M	AAIJ	19T	LHCB	pp at 7, 8, 13 TeV
−1.8 ±2.7 ±1.6	780	ABLIKIM	19M	BES3	e^+e^- at 3773 MeV
−0.25 ±0.28 ±0.14	277k	KO	13	BELL	e^+e^- at Υ(nS)
0.13 ±0.36 ±0.25	159k	LEES	13E	BABR	e^+e^- at $\Upsilon(4S)$
−0.2 ±1.5 ±0.9	5.2k	MENDEZ	10	CLEO	e^+e^- at 3774 MeV
7.1 ±6.1 ±1.2	949	[1] LINK	02B	FOCS	γ nucleus, $\overline{E}_\gamma \approx 180$ GeV
• • • We do not use the following data for averages, fits, limits, etc. • • •					
−0.16 ±0.58 ±0.25		KO	10	BELL	$e^+e^- \approx \Upsilon(4S)$
6.9 ±6.0 ±1.5	949	[2] LINK	02B	FOCS	γ nucleus, $\overline{E}_\gamma \approx 180$ GeV

[1] LINK 02B measures $N(D^+ \to K^0_S K^+)/N(D^+ \to K^0_S \pi^+)$, the ratio of numbers of events observed, and similarly for the D^-.
[2] LINK 02B measures $N(D^+ \to K^0_S K^+)/N(D^+ \to K^-\pi^+\pi^+)$, the ratio of numbers of events observed, and similarly for the D^-.

$A_{CP}(K^0_S K^{\pm}\pi^0)$ in $D^{\pm} \to K^0_S K^{\pm}\pi^0$

VALUE (units 10^{-2})	EVTS	DOCUMENT ID		TECN	COMMENT
1.4±3.7±2.4	470	ABLIKIM	19M	BES3	e^+e^- at 3773 MeV

$A_{CP}(K^0_L K^{\pm}\pi^0)$ in $D^{\pm} \to K^0_L K^{\pm}\pi^0$

VALUE (units 10^{-2})	EVTS	DOCUMENT ID		TECN	COMMENT
−0.6±4.1±1.7	410	ABLIKIM	19M	BES3	e^+e^- at 3773 MeV

$A_{CP}(K^+K^-\pi^{\pm})$ in $D^{\pm} \to K^+K^-\pi^{\pm}$

See also AAIJ 11G for a search for CP asymmetry in the $D^{\pm} \to K^+K^-\pi^{\pm}$ Dalitz plots using 370k decays and four different binning schemes. No evidence for CP asymmetry was found.

VALUE (%)	EVTS	DOCUMENT ID		TECN	COMMENT
0.37±0.29 OUR AVERAGE					
0.37±0.30±0.15	224k	[1] LEES	13F	BABR	e^+e^- at $\Upsilon(4S)$
−0.03±0.84±0.29		RUBIN	08	CLEO	e^+e^- at 3774 MeV
1.4 ±1.0 ±0.8	43k	[2] AUBERT	05S	BABR	e^+e^- at $\Upsilon(4S)$
0.6 ±1.1 ±0.5	14k	[3] LINK	00B	FOCS	
−1.4 ±2.9		[3] AITALA	97B	E791	$-0.062 < A_{CP} < +0.034$ (90% CL)
−3.1 ±6.8		[3] FRABETTI	94I	E687	$-0.14 < A_{CP} < +0.081$ (90% CL)
• • • We do not use the following data for averages, fits, limits, etc. • • •					
−0.1 ±0.9 ±0.4		[4] BONVICINI	14	CLEO	See RUBIN 08
−0.1 ±1.5 ±0.8		DOBBS	07	CLEO	See BONVICINI 14 and RUBIN 08

[1] This is the integrated CP asymmetry. LEES 13F also searches for CP asymmetries in four regions of the Dalitz plots (two of which are listed below); in comparisons of binned D^+ and D^- Dalitz plots; in parametrized fits to those plots, including 2-body submodes; and in comparisons of Legendre-polynomial distributions for the K^+K^- and $K^-\pi^+$ systems.
[2] AUBERT 05S measures $N(D^+ \to K^+K^-\pi^+)/N(D^+_s \to K^+K^-\pi^+)$, the ratio of the numbers of events observed, and similarly for the D^-.
[3] FRABETTI 94I, AITALA 98C, and LINK 00B measure $N(D^+ \to K^-K^+\pi^+)/N(D^+ \to K^-\pi^+\pi^+)$, the ratio of numbers of events observed, and similarly for the D^-.
[4] RUBIN 08 performs a dedicated analysis of this decay mode on the same dataset, with slightly better precision. We therefore take it that BONVICINI 14 does not supersede RUBIN 08's A_{CP} result.

$A_{CP}(K^{\pm}K^{*0})$ in $D^+ \to K^+\overline{K}^{*0}$, $D^- \to K^-K^{*0}$

VALUE (%)	EVTS	DOCUMENT ID		TECN	COMMENT
− 0.3± 0.4 OUR AVERAGE					
− 0.3± 0.4±0.2	73k	[1] LEES	13F	BABR	e^+e^- at $\Upsilon(4S)$
− 0.4± 2.0±0.6		RUBIN	08	CLEO	Fit-fraction asymmetry
+ 0.9± 1.7±0.7	11k	[2] AUBERT	05S	BABR	e^+e^- at $\Upsilon(4S)$
− 1.0± 5.0		[3] AITALA	97B	E791	$-0.092 < A_{CP} < +0.072$ (90% CL)
−12 ±13		[3] FRABETTI	94I	E687	$-0.33 < A_{CP} < +0.094$ (90% CL)

[1] This LEES 13F result is for the $K^{\mp}\pi^{\pm}$ mass-squared between 0.4 and 1.0 GeV^2, and does not actually separate out the K^*.
[2] AUBERT 05S measures $N(D^+ \to K^+\overline{K}^{*0})/N(D^+_s \to K^+K^-\pi^+)$, the ratio of the numbers of events observed, and similarly for the D^-.
[3] FRABETTI 94I and AITALA 97B measure $N(D^+ \to K^+\overline{K}^*(892)^0)/N(D^+ \to K^-\pi^+\pi^+)$, the ratio of numbers of events observed, and similarly for the D^-.

$A_{CP|S}(K^+\overline{K}^{*0})$ in $D^{\pm} \to K^-K^+\pi^{\pm}$

The CP asymmetry is measured as $A_{CP|S} = [(\Delta A^{top-left}_{raw} + \Delta A^{bottom-right}_{raw}) - (\Delta A^{top-right}_{raw} + \Delta A^{bottom-left}_{raw})]/2$ where ΔA^{pos}_{raw} is the difference between the signal and control channel raw asymmetries in the pos Dalitz plot bin of the resonance.

VALUE (units 10^{-3})	DOCUMENT ID		TECN	COMMENT
−0.26±0.56±0.18	AAIJ	24AG	LHCB	pp at 13 TeV

$A_{CP}(\phi\pi^{\pm})$ in $D^{\pm} \to \phi\pi^{\pm}$

VALUE (%)	EVTS	DOCUMENT ID		TECN	COMMENT
0.01 ±0.09 OUR AVERAGE		Error includes scale factor of 1.8.			
0.003±0.040±0.029	55M	AAIJ	19T	LHCB	pp at 7, 8, 13 TeV
−0.3 ±0.3 ±0.5	97k	[1] LEES	13F	BABR	e^+e^- at $\Upsilon(4S)$
+0.51 ±0.28 ±0.05	237k	STARIC	12	BELL	Mainly at $\Upsilon(4S)$
−1.8 ±1.6 $^{+0.2}_{-0.4}$		RUBIN	08	CLEO	Fit-fraction asymmetry
+0.2 ±1.5 ±0.6	10k	[2] AUBERT	05S	BABR	e^+e^- at $\Upsilon(4S)$
−2.8 ±3.6		[3] AITALA	97B	E791	$-0.087 < A_{CP} < +0.031$ (90% CL)
+6.6 ±8.6		[3] FRABETTI	94I	E687	$-0.075 < A_{CP} < +0.21$ (90% CL)
• • • We do not use the following data for averages, fits, limits, etc. • • •					
−0.04 ±0.14 ±0.14	1.58M	[4] AAIJ	13W	LHCB	pp at 7 TeV

[1] This LEES 13F result is for the K^+K^- mass-squared less than 1.3 GeV^2 and the $K^{\mp}\pi^{\pm}$ mass-squared above 1.0 GeV^2, and does not actually separate out the ϕ.
[2] AUBERT 05S measures $N(D^+ \to \phi\pi^+)/N(D^+_s \to K^+K^-\pi^+)$, the ratio of the numbers of events observed, and similarly for the D^-.
[3] FRABETTI 94I and AITALA 97B measure $N(D^+ \to \phi\pi^+)/N(D^+ \to K^-\pi^+\pi^+)$, the ratio of numbers of events observed, and similarly for the D^-.
[4] See AAIJ 19T.

$A_{CP|S}(\phi\pi^+)$ in $D^{\pm} \to K^-K^+\pi^{\pm}$

The CP asymmetry is measured as $A_{CP|S} = [(\Delta A^{top-left}_{raw} + \Delta A^{bottom-right}_{raw}) - (\Delta A^{top-right}_{raw} + \Delta A^{bottom-left}_{raw})]/2$ where ΔA^{pos}_{raw} is the difference between the signal and control channel raw asymmetries in the pos Dalitz plot bin of the resonance.

VALUE (units 10^{-3})	DOCUMENT ID		TECN	COMMENT
0.95±0.43±0.26	AAIJ	24AG	LHCB	pp at 13 TeV

$A_{CP}(K^{\pm}K^*_0(1430)^0)$ in $D^+ \to K^+\overline{K}^*_0(1430)^0$, $D^- \to K^-K^*_0(1430)^0$

VALUE (%)	DOCUMENT ID		TECN	COMMENT
$+8\pm6^{+4}_{-2}$	RUBIN	08	CLEO	Fit-fraction asymmetry

$A_{CP}(K^{\pm}K^*_2(1430)^0)$ in $D^+ \to K^+\overline{K}^*_2(1430)^0$, $D^- \to K^-K^*_2(1430)^0$

VALUE (%)	DOCUMENT ID		TECN	COMMENT
$+43\pm19^{+5}_{-18}$	RUBIN	08	CLEO	Fit-fraction asymmetry

$A_{CP}(K^{\pm}K^*_0(700))$ in $D^+ \to K^+\overline{K}^*_0(700)$, $D^- \to K^-K^*_0(700)$

VALUE (%)	DOCUMENT ID		TECN	COMMENT
$-12\pm11^{+14}_{-6}$	RUBIN	08	CLEO	Fit-fraction asymmetry

$A_{CP}(a_0(1450)^0\pi^{\pm})$ in $D^{\pm} \to a_0(1450)^0\pi^{\pm}$

VALUE (%)	DOCUMENT ID		TECN	COMMENT
$-19\pm12^{+8}_{-11}$	RUBIN	08	CLEO	Fit-fraction asymmetry

$A_{CP}(\phi(1680)\pi^{\pm})$ in $D^{\pm} \to \phi(1680)\pi^{\pm}$

VALUE (%)	DOCUMENT ID		TECN	COMMENT
−9±22±14	RUBIN	08	CLEO	Fit-fraction asymmetry

$A_{CP}(\pi^{\pm}2\pi^0)$ in $D^{\pm} \to \pi^{\pm}2\pi^0$

VALUE (%)	EVTS	DOCUMENT ID		TECN	COMMENT
+5.6±2.7±0.5	2k	ABLIKIM	22BG	BES3	e^+e^- at 3.773 GeV

$A_{CP}(\pi^+\pi^-\pi^{\pm})$ in $D^{\pm} \to \pi^+\pi^-\pi^{\pm}$

See also AAIJ 14C for a search for CP violation in $D^{\pm} \to \pi^+\pi^-\pi^{\pm}$ Dalitz plots using model-independent binned and unbinned methods. No evidence was found.

VALUE (%)	EVTS	DOCUMENT ID		TECN	COMMENT
0.5±2.0 OUR AVERAGE					
+1.2±2.2±0.6	2.6k	ABLIKIM	22BG	BES3	e^+e^- at 3.773 GeV
−1.7±4.2		[1] AITALA	97B	E791	$-0.086 < A_{CP} < +0.052$ (90% CL)

[1] AITALA 97B measure $N(D^+ \to \pi^+\pi^-\pi^+)/N(D^+ \to K^-\pi^+\pi^+)$, the ratio of numbers of events observed, and similarly for the D^-.

$A_{CP}(2\pi^{\pm}\pi^{\mp}\pi^0)$ in $D^{\pm} \to 2\pi^{\pm}\pi^{\mp}\pi^0$

VALUE (%)	EVTS	DOCUMENT ID		TECN	COMMENT
+0.3±1.8±0.8	4.6k	ABLIKIM	22BG	BES3	e^+e^- at 3.773 GeV

$A_{CP}(2\pi^{\pm}\pi^{\mp}2\pi^0)$ in $D^{\pm} \to 2\pi^{\pm}\pi^{\mp}2\pi^0$

VALUE (%)	EVTS	DOCUMENT ID		TECN	COMMENT
−4.2±3.8±1.3	1.2k	ABLIKIM	22BG	BES3	e^+e^- at 3.773 GeV

$A_{CP}(\pi^+\pi^-\pi^{\pm}\eta)$ in $D^{\pm} \to \pi^+\pi^-\pi^{\pm}\eta$

VALUE (units 10^{-2})	EVTS	DOCUMENT ID		TECN	COMMENT
2.5±5.0±1.6	510	ABLIKIM	20V	BES3	e^+e^-, 3773 MeV

$A_{CP}(K^0_S K^{\pm}\pi^+\pi^-)$ in $D^{\pm} \to K^0_S K^{\pm}\pi^+\pi^-$

VALUE (%)	EVTS	DOCUMENT ID		TECN	COMMENT
−4.2±6.4±2.2	523 ± 32	LINK	05E	FOCS	γ A, $\overline{E}_\gamma \approx 180$ GeV

Int. J. Mod. Phys. A 2026.41. Downloaded from www.worldscientific.com
by LIFORNIA @ BERKELEY on 09/16/26. Re-use and distribution is strictly not permitted, except for Open Access articles.

Int. J. Mod. Phys. A 2026.41. Downloaded from www.worldscientific.com
by UNIVERSITY OF CALIFORNIA @ BERKELEY on 09/16/26. Re-use and distribution is strictly not permitted, except for Open Access articles.

$A_{CP}(K^{\pm}\pi^0)$ in $D^{\pm} \to K^{\pm}\pi^0$

VALUE (%)	EVTS	DOCUMENT ID		TECN	COMMENT
−3 ± 5 OUR AVERAGE					
−3.2 ± 4.7 ± 2.1	2.5k	AAIJ	21U	LHCB	pp at 7, 8, 13 TeV
−3.5 ± 10.7 ± 0.9	343	MENDEZ	10	CLEO	e^+e^- at 3774 MeV

$A_{CP}(K^{\pm}\eta)$ in $D^{\pm} \to K^{\pm}\eta$

VALUE (units 10^{-2})	EVTS	DOCUMENT ID		TECN	COMMENT
−6 ± 10 ± 4	880	AAIJ	21U	LHCB	pp at 13 TeV

$D^{\pm}$ χ^2 TESTS OF *CP*-VIOLATION (*CPV*)

We list model-independent searches for local *CP* violation in phase-space distributions of multi-body decays.

Most of these searches divide phase space (Dalitz plot for 3-body decays, five-dimensional equivalent for 4-body decays) into bins, and perform a χ^2 test comparing normalised yields N_i, $\overline{N}_i$ in *CP*-conjugate bin pairs i: $\chi^2 = \Sigma_i(N_i - \alpha\,\overline{N}_i)/\sigma(N_i - \alpha\,\overline{N}_i)$. The factor $\alpha = (\Sigma_i N_i)/(\Sigma_i \overline{N}_i)$ removes the dependence on phase-space-integrated rate asymmetries. The result is used to obtain the probability (p-value) to obtain the measured χ^2 or larger under the assumption of CP conservation [AUBERT 08AO, BEDIAGA 09]. Alternative methods obtain p-values from other test variables based on unbinned analyses [WILLIAMS 11, AAIJ 14C]. Results can be combined using Fisher's method [MOSTELLER 48].

Local *CPV* in $D^{\pm} \to \pi^+\pi^-\pi^{\pm}$

p-value (%)	EVTS	DOCUMENT ID		TECN	COMMENT
78.1	3.1M	[1] AAIJ	14C	LHCB	χ^2

[1] AAIJ 14C uses binned and unbinned methods, and finds slightly better sensitivity with the former. We took the first value in the table of results for the binned method.

Local *CPV* in $D^{\pm} \to K^+K^-\pi^{\pm}$

p-value (%)	EVTS	DOCUMENT ID		TECN	COMMENT
31 OUR EVALUATION					
8.1	135M	AAIJ	24AG	LHCB	χ^2
72	224k	LEES	13F	BABR	χ^2
12.7	370k	[1] AAIJ	11G	LHCB	χ^2

[1] AAIJ 11G publishes results for several binning schemes. We picked the first value in their table of results.

Local *CPV* in $D^{\pm} \to K^+K^-K^{\pm}$

VALUE (%)	EVTS	DOCUMENT ID		TECN	COMMENT
31.6	1.27M	AAIJ	23L	LHCB	χ^2

CP VIOLATING ASYMMETRIES OF *P*-ODD (*T*-ODD) MOMENTS

$A_{Tviol}(K^0_S K^{\pm}\pi^+\pi^-)$ in $D^{\pm} \to K^0_S K^{\pm}\pi^+\pi^-$

$C_T \equiv \vec{p}_{K^+} \cdot (\vec{p}_{\pi^+} \times \vec{p}_{\pi^-})$ is a parity-odd correlation of the K^+, π^+, and π^- momenta for the D^+. $\overline{C}_T \equiv \vec{p}_{K^-} \cdot (\vec{p}_{\pi^-} \times \vec{p}_{\pi^+})$ is the corresponding quantity for the D^-. Then
$A_T \equiv [\Gamma(C_T > 0) - \Gamma(C_T < 0)] / [\Gamma(C_T > 0) + \Gamma(C_T < 0)]$, and
$\overline{A}_T \equiv [\Gamma(-\overline{C}_T > 0) - \Gamma(-\overline{C}_T < 0)] / [\Gamma(-\overline{C}_T > 0) + \Gamma(-\overline{C}_T < 0)]$, and
$A_{Tviol} \equiv \frac{1}{2}(A_T - \overline{A}_T)$. C_T and $\overline{C}_T$ are commonly referred to as *T*-odd moments, because they are odd under *T* reversal. However, the *T*-conjugate process $K^0_S K^{\pm}\pi^+\pi^- \to D^{\pm}$ is not accessible, while the *P*-conjugate process is.

VALUE (units 10^{-3})	EVTS	DOCUMENT ID		TECN	COMMENT
− 3 ± 8 OUR AVERAGE Error includes scale factor of 1.1.					
3.4 ± 8.7 ± 3.2	19k	MOON	23	BELL	980 fb^{-1} at $\sim \Upsilon(4S)$
−12.0 ± 10.0 ± 4.6	21k	LEES	11E	BABR	$e^+e^- \approx \Upsilon(4S)$
• • • We do not use the following data for averages, fits, limits, etc. • • •					
23 ± 62 ± 22	523	LINK	05E	FOCS	γ A, $\overline{E}_\gamma \approx$ 180 GeV

$A_{Tviol}(K^0_S K^{\mp}\pi^{\pm}\pi^{\pm})$ in $D^{\pm} \to K^0_S K^{\mp}\pi^{\pm}\pi^{\pm}$

$C_T \equiv \vec{p}_{K^0_S} \cdot (\vec{p}_{K^-} \times \vec{p}_{\pi^+})$ is a parity-odd correlation of the momenta of the K^0_S, K^-, and highest-momenta π^+ for the D^+.$\overline{C}_T \equiv \vec{p}_{K^0_S} \cdot (\vec{p}_{K^+} \times \vec{p}_{\pi^-})$ is the corresponding quantity for the D^-. Then
$A_T \equiv [\Gamma(C_T > 0) - \Gamma(C_T < 0)] / [\Gamma(C_T > 0) + \Gamma(C_T < 0)]$, and
$\overline{A}_T \equiv [\Gamma(-\overline{C}_T > 0) - \Gamma(-\overline{C}_T < 0)] / [\Gamma(-\overline{C}_T > 0) + \Gamma(-\overline{C}_T < 0)]$, and
$A_{Tviol} \equiv \frac{1}{2}(A_T - \overline{A}_T)$. C_T and $\overline{C}_T$ are commonly referred to as *T*-odd moments, because they are odd under *T* reversal. However, the *T*-conjugate process $K^0_S K^{\pm}\pi^+\pi^- \to D^{\pm}$ is not accessible, while the *P*-conjugate process is.

VALUE (units 10^{-3})	EVTS	DOCUMENT ID		TECN	COMMENT
−2.3 ± 4.5 ± 1.5	70.8k	[1] AGGARWAL	25	BEL2	$e^+e^- \approx \Upsilon(4S)$

[1] AGGARWAL 25 measures $C_T \equiv \vec{p}_{K^0_S} \cdot (\vec{p}_{K^-} \times \vec{p}_{\pi^+})$ and other T-odd observables, all compatible with T-conservation, using Belle and Belle II data.

$A_{Tviol}(K^+K^-K^0_S\pi^{\pm})$ in $D^{\pm} \to K^+K^-K^0_S\pi^{\pm}$

$C_T \equiv \vec{p}_{K^+} \cdot (\vec{p}_{\pi^+} \times \vec{p}_{K^-})$ is a parity-odd correlation of the K^+, π^+, and K^- momenta for the D^+. $\overline{C}_T \equiv \vec{p}_{K^-} \cdot (\vec{p}_{\pi^-} \times \vec{p}_{K^+})$ is the corresponding quantity for the D^-. Then
$A_T \equiv [\Gamma(C_T > 0) - \Gamma(C_T < 0)] / [\Gamma(C_T > 0) + \Gamma(C_T < 0)]$, and
$\overline{A}_T \equiv [\Gamma(-\overline{C}_T > 0) - \Gamma(-\overline{C}_T < 0)] / [\Gamma(-\overline{C}_T > 0) + \Gamma(-\overline{C}_T < 0)]$, and
$A_{Tviol} \equiv \frac{1}{2}(A_T - \overline{A}_T)$. C_T and $\overline{C}_T$ are commonly referred to as *T*-odd moments, because they are odd under *T* reversal. However, the *T*-conjugate process $K^+K^-K^0_S\pi^{\pm} \to D^{\pm}$ is not accessible, while the *P*-conjugate process is.

VALUE (%)	EVTS	DOCUMENT ID		TECN	COMMENT
−3.34 ± 2.66 ± 0.35	1.4k	MOON	23	BELL	980 fb^{-1} at $\sim \Upsilon(4S)$

SEMILEPTONIC FORM FACTORS

$f_+(0)|V_{cs}|$ in $D^+ \to \overline{K}^0\ell^+\nu_\ell$

VALUE	EVTS	DOCUMENT ID		TECN	COMMENT
0.7163 ± 0.0033 OUR AVERAGE					
0.7207 ± 0.0027 ± 0.0035	58k	ABLIKIM	24CN	BES3	$\overline{K}^0 e^+\nu_e$ 2-parameter fit
0.7124 ± 0.0035 ± 0.0032	47k	ABLIKIM	24CN	BES3	$\overline{K}^0 \mu^+\nu_\mu$ 2-parameter fit
0.707 ± 0.010 ± 0.009		[1] BESSON	09	CLEO	$K_S e^+\nu_e$ 3-parameter fit
• • • We do not use the following data for averages, fits, limits, etc. • • •					
0.7053 ± 0.0040 ± 0.0112		[2] ABLIKIM	17S	BES3	$K^0_S e^+\nu_e$ 2-parameter fit
0.737 ± 0.006 ± 0.009		[2,3] ABLIKIM	15AF	BES3	$K_L e^+\nu_e$ 3-parameter fit

[1] BESSON 09 finds 0.716 ± 0.007 ± 0.009 for a 2-parameter fit.
[2] Superseded by ABLIKIM 24CN.
[3] ABLIKIM 15AF finds 0.728 ± 0.006 ± 0.011 for a 2-parameter fit.

$r_1 \equiv a_1/a_0$ in $D^+ \to \overline{K}^0\ell^+\nu_\ell$

VALUE	EVTS	DOCUMENT ID		TECN	COMMENT
−2.13 ± 0.14 OUR AVERAGE					
−2.18 ± 0.14 ± 0.05		ABLIKIM	17S	BES3	$K^0_S e^+\nu_e$ 2-parameter fit
−2.23 ± 0.42 ± 0.53	40k	[1] ABLIKIM	15AF	BES3	$K_L e^+\nu_e$ 3-parameter fit
−1.66 ± 0.44 ± 0.10		[2] BESSON	09	CLEO	$K_S e^+\nu_e$ 3-parameter fit

[1] ABLIKIM 15AF finds $r_1 = -1.91 \pm 0.33 \pm 0.28$ for a 2-parameter fit.
[2] BESSON 09 finds $r_1 = -2.10 \pm 0.25 \pm 0.08$ for 2-parameter fit.

$r_2 \equiv a_2/a_0$ in $D^+ \to \overline{K}^0\ell^+\nu_\ell$

VALUE	EVTS	DOCUMENT ID		TECN	COMMENT
− 3 ± 12 OUR AVERAGE Error includes scale factor of 1.5.					
+11 ± 9 ± 9	40k	ABLIKIM	15AF	BES3	$K_L e^+\nu_e$ 3-parameter fit
−14 ± 11 ± 1		BESSON	09	CLEO	$K_S e^+\nu_e$ 3-parameter fit

$f_+(0)|V_{cd}|$ in $D^+ \to \pi^0\ell^+\nu_\ell$

VALUE	DOCUMENT ID		TECN	COMMENT
0.1407 ± 0.0025 OUR AVERAGE				
0.1400 ± 0.0026 ± 0.0007	ABLIKIM	17S	BES3	$\pi^0 e^+\nu_e$ 2-parameter fit
0.146 ± 0.007 ± 0.002	BESSON	09	CLEO	$\pi^0 e^+\nu_e$ 3-parameter fit

$r_1 \equiv a_1/a_0$ in $D^+ \to \pi^0\ell^+\nu_\ell$

VALUE	DOCUMENT ID		TECN	COMMENT
−2.00 ± 0.13 OUR AVERAGE				
−2.01 ± 0.13 ± 0.02	ABLIKIM	17S	BES3	$\pi^0 e^+\nu_e$ 2-parameter fit
−1.37 ± 0.88 ± 0.24	BESSON	09	CLEO	$\pi^0 e^+\nu_e$ 3-parameter fit

$r_2 \equiv a_2/a_0$ in $D^+ \to \pi^0\ell^+\nu_\ell$

VALUE	DOCUMENT ID		TECN	COMMENT
−4 ± 5 ± 1	BESSON	09	CLEO	$\pi^0 e^+\nu_e$ 3-parameter fit

$f_+(0)|V_{cd}|$ in $D^+ \to \eta\ell^+\nu_\ell$ ($\ell = e$ or ν)

VALUE (units 10^{-2})	EVTS	DOCUMENT ID		TECN	COMMENT
8.4 ± 0.4 OUR AVERAGE					
8.7 ± 0.8 ± 0.2	234	ABLIKIM	20T	BES3	$\eta\mu^+\nu_\mu$, z expansion
7.86 ± 0.64 ± 0.21	373	ABLIKIM	18R	BES3	$\eta e^+\nu_e$, z expansion
8.6 ± 0.6 ± 0.1		YELTON	11	CLEO	$\eta e^+\nu_e$, z expansion

$f_+^{\eta'}(0)|V_{cd}|$ in $D^+ \to \eta'\ell^+\nu_\ell$ ($\ell = e, \nu$)

VALUE (units 10^{-2})	EVTS	DOCUMENT ID		TECN	COMMENT
5.92 ± 0.56 ± 0.13	0.24k	[1] ABLIKIM	25AO	BES3	e^+e^- at 3.773 GeV

[1] Uses a two-parameter series expansion for the form factor parametrization .

$r_1 \equiv a_1/a_0$ in $D^+ \to \eta e^+\nu_e$

VALUE	EVTS	DOCUMENT ID		TECN	COMMENT
−5.3 ± 2.7 OUR AVERAGE Error includes scale factor of 1.9.					
−7.33 ± 1.69 ± 0.40	373	ABLIKIM	18R	BES3	z expansion
−1.83 ± 2.23 ± 0.28		YELTON	11	CLEO	z expansion

$r_v \equiv V(0)/A_1(0)$ in $D^+ \to \omega e^+\nu_e$

VALUE	DOCUMENT ID		TECN	COMMENT
1.24 ± 0.09 ± 0.06	ABLIKIM	15W	BES3	292 fb^{-1}, 3773 MeV

$r_2 \equiv A_2(0)/A_1(0)$ in $D^+ \to \omega e^+\nu_e$

VALUE	DOCUMENT ID		TECN	COMMENT
1.06 ± 0.15 ± 0.05	ABLIKIM	15W	BES3	292 fb^{-1}, 3773 MeV

$r_v \equiv V(0)/A_1(0)$ in $D^+, D^0 \to \rho e^+\nu_e$

VALUE	EVTS	DOCUMENT ID		TECN	COMMENT
1.53 ± 0.08 OUR AVERAGE					
1.548 ± 0.079 ± 0.041	3.3k	[1] ABLIKIM	24CP	BES3	e^+e^- at 3.773 GeV

1.48 ±0.15 ±0.05		[2,3] DOBBS	13	CLEO	e^+e^- at $\psi(3770)$
• • • We do not use the following data for averages, fits, limits, etc. • • •					
1.695±0.083±0.051	2.5k	[2,4] ABLIKIM	19C	BES3	e^+e^- at 3773 MeV

[1] $D^0 \to \rho^- e^+ \nu_e$ only, uses a single-pole-dominance parametrization.
[2] Uses both D^+ and D^0 events.
[3] Using PDG 10 values of V_{cd} and lifetimes, DOBBS 13 gets $A_1(0) = 0.56 \pm 0.01^{+0.02}_{-0.03}$, $A_2(0) = 0.47 \pm 0.06 \pm 0.04$, and $V(0) = 0.84 \pm 0.09^{+0.05}_{-0.06}$.
[4] Superseded in part by ABLIKIM 24CP.

$r_2 \equiv A_2(0)/A_1(0)$ in $D^+, D^0 \to \rho e^+ \nu_e$

VALUE	EVTS	DOCUMENT ID		TECN	COMMENT
0.82 ±0.05 OUR AVERAGE					
0.823±0.056±0.026	3.3k	[1] ABLIKIM	24CP	BES3	e^+e^- at 3.773 GeV
0.83 ±0.11 ±0.04		[2,3] DOBBS	13	CLEO	e^+e^- at $\psi(3770)$
• • • We do not use the following data for averages, fits, limits, etc. • • •					
0.845±0.056±0.039	2.5k	[2,4] ABLIKIM	19C	BES3	e^+e^- at 3773 MeV

[1] $D^0 \to \rho^- e^+ \nu_e$ only, uses a single-pole-dominance parametrization.
[2] Uses both D^+ and D^0 events.
[3] Using PDG 10 values of V_{cd} and lifetimes, DOBBS 13 gets $A_1(0) = 0.56 \pm 0.01^{+0.02}_{-0.03}$, $A_2(0) = 0.47 \pm 0.06 \pm 0.04$, and $V(0) = 0.84 \pm 0.09^{+0.05}_{-0.06}$.
[4] Superseded in part by ABLIKIM 24CP.

$r_V \equiv V(0)/A_1(0)$ in $D^+ \to \overline{K}^*(892)^0 \ell^+ \nu_\ell$

See also BRIERE 10 for $\overline{K}^* \ell^+ \nu_\ell$ helicity-basis form-factor measurements.

VALUE	EVTS	DOCUMENT ID		TECN	COMMENT
1.47 ±0.04 OUR AVERAGE		Error includes scale factor of 2.0.			See the ideogram below.
1.42 ±0.03 ±0.02	17.9k	[1] ABLIKIM	25BP	BES3	$\overline{K}^*(892)^0 \ell^+ \nu_\ell$
1.411±0.058±0.007	16.2k	ABLIKIM	16F	BES3	$\overline{K}^*(892)^0 e^+ \nu_e$
1.463±0.017±0.031		[2] DEL-AMO-SA...	11I	BABR	
1.504±0.057±0.039	15k	[3] LINK	02L	FOCS	$\overline{K}^*(892)^0 \mu^+ \nu_\mu$
1.45 ±0.23 ±0.07	763	ADAMOVICH	99	BEAT	$\overline{K}^*(892)^0 \mu^+ \nu_\mu$
1.90 ±0.11 ±0.09	3000	[4] AITALA	98B	E791	$\overline{K}^*(892)^0 e^+ \nu_e$
1.84 ±0.11 ±0.09	3034	AITALA	98F	E791	$\overline{K}^*(892)^0 \mu^+ \nu_\mu$
1.74 ±0.27 ±0.28	874	FRABETTI	93E	E687	$\overline{K}^*(892)^0 \mu^+ \nu_\mu$
2.00 $^{+0.34}_{-0.32}$ ±0.16	305	KODAMA	92	E653	$\overline{K}^*(892)^0 \mu^+ \nu_\mu$
• • • We do not use the following data for averages, fits, limits, etc. • • •					
1.43 ±0.07 ±0.03	3.8k	[1] ABLIKIM	24CS	BES3	Superseded by ABLIKIM 25BP
2.0 ±0.6 ±0.3	183	ANJOS	90E	E691	$\overline{K}^*(892)^0 e^+ \nu_e$

[1] Uses a single-pole dominance parameterization.
[2] DEL-AMO-SANCHEZ 11I finds the pole mass $m_A = (2.63 \pm 0.10 \pm 0.13)$ GeV (m_V is fixed at 2 GeV).
[3] LINK 02L includes the effects of interference with an S-wave background. This much improves the goodness of fit, but does not much shift the values of the form factors.
[4] This is slightly different from the AITALA 98B value: see ref. [5] in AITALA 98F.

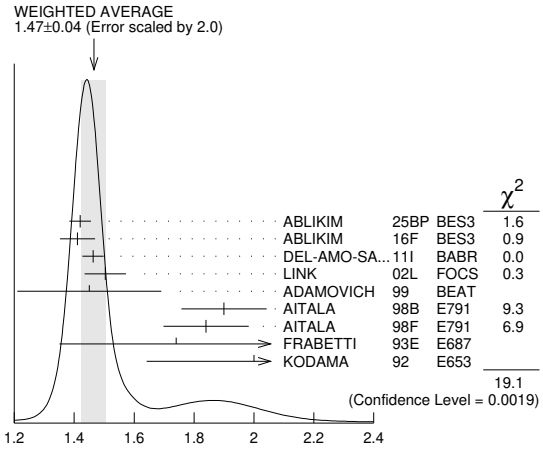

$r_V \equiv V(0)/A_1(0)$ in $D^+ \to \overline{K}^*(892)^0 \ell^+ \nu_\ell$

$r_2 \equiv A_2(0)/A_1(0)$ in $D^+ \to \overline{K}^*(892)^0 \ell^+ \nu_\ell$

See also BRIERE 10 for $\overline{K}^* \ell^+ \nu_\ell$ helicity-basis form-factor measurements.

VALUE	EVTS	DOCUMENT ID		TECN	COMMENT
0.786±0.018 OUR AVERAGE					
0.75 ±0.03 ±0.01	17.9k	[1] ABLIKIM	25BP	BES3	$\overline{K}^*(892)^0 \ell^+ \nu_\ell$
0.788±0.042±0.008	16.2k	ABLIKIM	16F	BES3	$\overline{K}^*(892)^0 e^+ \nu_e$
0.801±0.020±0.020		[2] DEL-AMO-SA...	11I	BABR	
0.875±0.049±0.064	15k	[3] LINK	02L	FOCS	$\overline{K}^*(892)^0 \mu^+ \nu_\mu$
1.00 ±0.15 ±0.03	763	ADAMOVICH	99	BEAT	$\overline{K}^*(892)^0 \mu^+ \nu_\mu$
0.71 ±0.08 ±0.09	3000	AITALA	98B	E791	$\overline{K}^*(892)^0 e^+ \nu_e$
0.75 ±0.08 ±0.09	3034	AITALA	98F	E791	$\overline{K}^*(892)^0 \mu^+ \nu_\mu$
0.78 ±0.18 ±0.10	874	FRABETTI	93E	E687	$\overline{K}^*(892)^0 \mu^+ \nu_\mu$
0.82 $^{+0.22}_{-0.23}$ ±0.11	305	KODAMA	92	E653	$\overline{K}^*(892)^0 \mu^+ \nu_\mu$
• • • We do not use the following data for averages, fits, limits, etc. • • •					
0.72 ±0.06 ±0.02	3.8k	[1] ABLIKIM	24CS	BES3	Superseded by ABLIKIM 25BP
0.0 ±0.5 ±0.2	183	ANJOS	90E	E691	$\overline{K}^*(892)^0 e^+ \nu_e$

[1] Uses a single-pole dominance parameterization.
[2] DEL-AMO-SANCHEZ 11I finds the pole mass $m_A = (2.63 \pm 0.10 \pm 0.13)$ GeV (m_V is fixed at 2 GeV).
[3] LINK 02L includes the effects of interference with an S-wave background. This much improves the goodness of fit, but does not much shift the values of the form factors.

$r_3 \equiv A_3(0)/A_1(0)$ in $D^+ \to \overline{K}^*(892)^0 \ell^+ \nu_\ell$

See also BRIERE 10 for $\overline{K}^* \ell^+ \nu_\ell$ helicity-basis form-factor measurements.

VALUE	EVTS	DOCUMENT ID		TECN	COMMENT
0.04±0.33±0.29	3034	AITALA	98F	E791	$\overline{K}^*(892)^0 \mu^+ \nu_\mu$

Γ_L/Γ_T in $D^+ \to \overline{K}^*(892)^0 \ell^+ \nu_\ell$

See also BRIERE 10 for $\overline{K}^* \ell^+ \nu_\ell$ helicity-basis form-factor measurements.

VALUE	EVTS	DOCUMENT ID		TECN	COMMENT
1.13±0.08 OUR AVERAGE					
1.09±0.10±0.02	763	ADAMOVICH	99	BEAT	$\overline{K}^*(892)^0 \mu^+ \nu_\mu$
1.20±0.13±0.13	874	FRABETTI	93E	E687	$\overline{K}^*(892)^0 \mu^+ \nu_\mu$
1.18±0.18±0.08	305	KODAMA	92	E653	$\overline{K}^*(892)^0 \mu^+ \nu_\mu$
• • • We do not use the following data for averages, fits, limits, etc. • • •					
1.8 $^{+0.6}_{-0.4}$ ±0.3	183	ANJOS	90E	E691	$\overline{K}^*(892)^0 e^+ \nu_e$

Γ_+/Γ_- in $D^+ \to \overline{K}^*(892)^0 \ell^+ \nu_\ell$

See also BRIERE 10 for $\overline{K}^* \ell^+ \nu_\ell$ helicity-basis form-factor measurements.

VALUE	EVTS	DOCUMENT ID		TECN	COMMENT
0.22±0.06 OUR AVERAGE		Error includes scale factor of 1.6.			
0.28±0.05±0.02	763	ADAMOVICH	99	BEAT	$\overline{K}^*(892)^0 \mu^+ \nu_\mu$
0.16±0.05±0.02	305	KODAMA	92	E653	$\overline{K}^*(892)^0 \mu^+ \nu_\mu$
• • • We do not use the following data for averages, fits, limits, etc. • • •					
0.15 $^{+0.07}_{-0.05}$ ±0.03	183	ANJOS	90E	E691	$\overline{K}^*(892)^0 e^+ \nu_e$

$r_V \equiv V_2(0)/V_1(0)$ in $D \to K_1(1270) e^+ \nu_e$

VALUE (units 10^{-2})	EVTS	DOCUMENT ID		TECN	COMMENT
−4.3±1.0±2.5	2k	ABLIKIM	25AM	BES3	e^+e^- at 3.773 GeV

$r_A \equiv A(0)/V_1(0)$ in $D \to K_1(1270) e^+ \nu_e$

VALUE (units 10^{-2})	EVTS	DOCUMENT ID		TECN	COMMENT
−11.2±1.0±0.9	2k	ABLIKIM	25AM	BES3	e^+e^- at 3.773 GeV

Amplitude analyses

$D \to K\pi\pi\pi$ partial wave analyses

Amplitude analyses of D^+ decays to a variety of 4-body kaon or pion final states, fitting simultaneously different partial wave components.

VALUE	DOCUMENT ID		TECN	COMMENT
	ABLIKIM	19AZ	BES3	$D^+ \to K^0_S \pi^+ \pi^+ \pi^-$

$D^+ \to 2\pi^+\pi^-$ partial wave analyses

VALUE	EVTS	DOCUMENT ID		TECN	COMMENT
	572k	[1] AAIJ	23H	LHCB	Dalitz plot fit
	2.2k	BONVICINI	07	CLEO	
	1.5k	LINK	04	FOCS	
	1.2k	AITALA	01B	E791	

[1] The amplitude model has 7 components, including a $\pi^+\pi^\pm$ S-wave parametrised by one complex number per bin in 50 bins of $\pi^+\pi^-$ invariant mass.

$D^+ \to \pi^+\pi^0\eta$ partial wave analyses

VALUE	EVTS	DOCUMENT ID		TECN	COMMENT
	950	[1] ABLIKIM	24CL	BES3	e^+e^- at 3.773 GeV

[1] The amplitude model has six components, including $(\pi^+\pi^0)_V\eta$ with a vector-like mode.

$D^{\pm}$ REFERENCES

ABLIKIM 25AM PRL 135 091801 M. Ablikim et al. (BESIII Collab.)
ABLIKIM 25AO PRL 134 111801 M. Ablikim et al. (BESIII Collab.)
ABLIKIM 25AU PR D111 L071101 M. Ablikim et al. (BESIII Collab.)
ABLIKIM 25AX PR D111 092005 M. Ablikim et al. (BESIII Collab.)
ABLIKIM 25BA PR D112 012001 M. Ablikim et al. (BESIII Collab.)
ABLIKIM 25BB JHEP 2501 089 M. Ablikim et al. (BESIII Collab.)
ABLIKIM 25BF JHEP 2505 195 M. Ablikim et al. (BESIII Collab.)
ABLIKIM 25BI JHEP 2506 220 M. Ablikim et al. (BESIII Collab.)
ABLIKIM 25BK CP C49 063001 M. Ablikim et al. (BESIII Collab.)
ABLIKIM 25BM PRL 135 061801 M. Ablikim et al. (BESIII Collab.)
ABLIKIM 25BP PRL 135 171801 M. Ablikim et al. (BESIII Collab.)
ABLIKIM 25CN JHEP 2510 178 M. Ablikim et al. (BESIII Collab.)
ABLIKIM 25CP CP C49 083001 M. Ablikim et al. (BESIII Collab.)
ABLIKIM 25M PR D111 032011 M. Ablikim et al. (BESIII Collab.)
ADACHI 25Q PR D112 L031101 I. Adachi et al. (BELLE II Collab.)
AGGARWAL 25 JHEP 2504 036 L. Aggarwal et al. (BELLE and BELLE II Collab.)
ANASHIN 25 PPN 56 802 V.V. Anashin et al. (VEPP-4M KEDR Collab.)
ANASHIN 25A JHEP 2511 001 V.V. Anashin et al. (VEPP-4M KEDR Collab.)
AAIJ 24AG PRL 133 251801 R. Aaij et al. (LHCb Collab.)
ABLIKIM 24AS PRL 132 131903 M. Ablikim et al. (BESIII Collab.)
ABLIKIM 24AZ PR D109 072003 M. Ablikim et al. (BESIII Collab.)

Int. J. Mod. Phys. A 2026.41. Downloaded from www.worldscientific.com
by LIFORNIA @ BERKELEY on 09/16/26. Re-use and distribution is strictly not permitted, except for Open Access articles.

Int. J. Mod. Phys. A 2026.41. Downloaded from www.worldscientific.com
by UNIVERSITY OF CALIFORNIA @ BERKELEY on 09/16/26. Re-use and distribution is strictly not permitted, except for Open Access articles.

ABLIKIM	24CJ	PR D110 092006	M. Ablikim *et al.*	(BESIII Collab.)
ABLIKIM	24CK	PR D110 092008	M. Ablikim *et al.*	(BESIII Collab.)
ABLIKIM	24CL	PR D110 L111102	M. Ablikim *et al.*	(BESIII Collab.)
ABLIKIM	24CM	PR D110 112001	M. Ablikim *et al.*	(BESIII Collab.)
ABLIKIM	24CN	PR D110 112006	M. Ablikim *et al.*	(BESIII Collab.)
ABLIKIM	24CP	PR D110 112018	M. Ablikim *et al.*	(BESIII Collab.)
ABLIKIM	24CR	JHEP 2409 089	M. Ablikim *et al.*	(BESIII Collab.)
ABLIKIM	24CS	JHEP 2410 199	M. Ablikim *et al.*	(BESIII Collab.)
ABLIKIM	24CX	JHEP 2412 206	M. Ablikim *et al.*	(BESIII Collab.)
AAIJ	23E	JHEP 2304 081	R. Aaij *et al.*	(LHCb Collab.)
AAIJ	23H	JHEP 2306 044	R. Aaij *et al.*	(LHCb Collab.)
AAIJ	23L	JHEP 2307 067	R. Aaij *et al.*	(LHCb Collab.)
ABLIKIM	23AI	PR D107 032002	M. Ablikim *et al.*	(BESIII Collab.)
ABLIKIM	23AO	PR D107 112005	M. Ablikim *et al.*	(BESIII Collab.)
ABLIKIM	23BW	JHEP 2309 077	M. Ablikim *et al.*	(BESIII Collab.)
LI	23G	PR D107 033003	L.K. Li *et al.*	(BELLE Collab.)
MOON	23	PR D108 L111102	H.K. Moon *et al.*	(BELLE Collab.)
ABLIKIM	22BG	PR D106 092005	M. Ablikim *et al.*	(BESIII Collab.)
ABLIKIM	22BJ	PR D106 112009	M. Ablikim *et al.*	(BESIII Collab.)
ABLIKIM	22BK	JHEP 2209 107	M. Ablikim *et al.*	(BESIII Collab.)
ABLIKIM	22U	PR D105 032009	M. Ablikim *et al.*	(BESIII Collab.)
ABLIKIM	22Y	PR D106 032002	M. Ablikim *et al.*	(BESIII Collab.)
AAIJ	21T	JHEP 2106 044	R. Aaij *et al.*	(LHCb Collab.)
AAIJ	21U	JHEP 2106 019	R. Aaij *et al.*	(LHCb Collab.)
ABLIKIM	21AD	PR D104 012006	M. Ablikim *et al.*	(BESIII Collab.)
ABLIKIM	21BA	PR D104 052008	M. Ablikim *et al.*	(BESIII Collab.)
ABLIKIM	21BB	PR D104 072005	M. Ablikim *et al.*	(BESIII Collab.)
ABUDINEN	21A	PRL 127 211801	F. Abudinen *et al.*	(BELLE II Collab.)
ABLIKIM	20AA	PR D102 052003	M. Ablikim *et al.*	(BESIII Collab.)
ABLIKIM	20AC	PR D102 052006	M. Ablikim *et al.*	(BESIII Collab.)
ABLIKIM	20AF	PR D102 112005	M. Ablikim *et al.*	(BESIII Collab.)
ABLIKIM	20D	PR D101 031102	M. Ablikim *et al.*	(BESIII Collab.)
ABLIKIM	20G	PR D101 052009	M. Ablikim *et al.*	(BESIII Collab.)
ABLIKIM	20H	PR D101 072005	M. Ablikim *et al.*	(BESIII Collab.)
ABLIKIM	20T	PRL 124 231801	M. Ablikim *et al.*	(BESIII Collab.)
ABLIKIM	20V	PRL 124 241803	M. Ablikim *et al.*	(BESIII Collab.)
ABLIKIM	20Z	PRL 125 141802	M. Ablikim *et al.*	(BESIII Collab.)
AAIJ	19G	JHEP 1903 176	R. Aaij *et al.*	(LHCb Collab.)
AAIJ	19H	JHEP 1904 063	R. Aaij *et al.*	(LHCb Collab.)
AAIJ	19T	PRL 122 191803	R. Aaij *et al.*	(LHCb Collab.)
ABLIKIM	19AL	PR D99 112002	M. Ablikim *et al.*	(BESIII Collab.)
ABLIKIM	19AY	PR D100 072006	M. Ablikim *et al.*	(BESIII Collab.)
ABLIKIM	19AZ	PR D100 072008	M. Ablikim *et al.*	(BESIII Collab.)
ABLIKIM	19BG	PRL 123 211802	M. Ablikim *et al.*	(BESIII Collab.)
ABLIKIM	19BH	PRL 123 231801	M. Ablikim *et al.*	(BESIII Collab.)
ABLIKIM	19BI	PL B798 135017	M. Ablikim *et al.*	(BESIII Collab.)
ABLIKIM	19C	PRL 122 062001	M. Ablikim *et al.*	(BESIII Collab.)
ABLIKIM	19M	PR D99 032002	M. Ablikim *et al.*	(BESIII Collab.)
ABLIKIM	18AC	PR D98 092009	M. Ablikim *et al.*	(BESIII Collab.)
ABLIKIM	18AE	PRL 121 171803	M. Ablikim *et al.*	(BESIII Collab.)
ABLIKIM	18F	PRL 121 081802	M. Ablikim *et al.*	(BESIII Collab.)
ABLIKIM	18P	PR D97 072015	M. Ablikim *et al.*	(BESIII Collab.)
ABLIKIM	18R	PR D97 092009	M. Ablikim *et al.*	(BESIII Collab.)
ABLIKIM	18W	PR D97 072004	M. Ablikim *et al.*	(BESIII Collab.)
BABU	18	PR D97 011101	V. Babu *et al.*	(BELLE Collab.)
AAIJ	17AF	PL B771 21	R. Aaij *et al.*	(LHCb Collab.)
ABLIKIM	17A	PL B765 231	M. Ablikim *et al.*	(BESIII Collab.)
ABLIKIM	17AD	PR D96 092002	M. Ablikim *et al.*	(BESIII Collab.)
ABLIKIM	17M	PR D95 071102	M. Ablikim *et al.*	(BESIII Collab.)
ABLIKIM	17S	PR D96 012002	M. Ablikim *et al.*	(BESIII Collab.)
ABLIKIM	16D	PRL 116 082001	M. Ablikim *et al.*	(BESIII Collab.)
ABLIKIM	16F	PR D94 032001	M. Ablikim *et al.*	(BESIII Collab.)
ABLIKIM	16G	EPJ C76 369	M. Ablikim *et al.*	(BESIII Collab.)
ABLIKIM	16V	CP C40 113001	M. Ablikim *et al.*	(BESIII Collab.)
ABLIKIM	15AF	PR D92 112008	M. Ablikim *et al.*	(BESIII Collab.)
ABLIKIM	15W	PR D92 071101	M. Ablikiim *et al.*	(BESIII Collab.)
AAIJ	14BD	JHEP 1410 025	R. Aaij *et al.*	(LHCb Collab.)
AAIJ	14C	PL B728 585	R. Aaij *et al.*	(LHCb Collab.)
ABAZOV	14L	PR D90 111102	V.M. Abazov *et al.*	(D0 Collab.)
ABLIKIM	14E	PR D89 052001	M. Ablikim *et al.*	(BESIII Collab.)
ABLIKIM	14F	PR D89 051104	M. Ablikim *et al.*	(BESIII Collab.)
BONVICINI	14	PR D89 072002	G. Bonvicini *et al.*	(CLEO Collab.)
AAIJ	13AF	PL B724 203	R. Aaij *et al.*	(LHCb Collab.)
AAIJ	13W	JHEP 1306 112	R. Aaij *et al.*	(LHCb Collab.)
DOBBS	13	PRL 110 131802	S. Dobbs *et al.*	(CLEO Collab.)
KO	13	JHEP 1302 098	B.R. Ko *et al.*	(BELLE Collab.)
LEES	13E	PR D87 052012	J.P. Lees *et al.*	(BABAR Collab.)
LEES	13F	PR D87 052010	J.P. Lees *et al.*	(BABAR Collab.)
KO	12A	PRL 109 119903 (errat.)	B.R. Ko *et al.*	(BELLE Collab.)
Also		PRL 109 021601	B.R. Ko *et al.*	(BELLE Collab.)
STARIC	12	PRL 108 071801	M. Staric *et al.*	(BELLE Collab.)
AAIJ	11G	PR D84 112008	R. Aaij *et al.*	(LHCb Collab.)
DEL-AMO-SA...	11H	PR D83 071103	P. del Amo Sanchez *et al.*	(BABAR Collab.)
DEL-AMO-SA...	11I	PR D83 072001	P. del Amo Sanchez *et al.*	(BABAR Collab.)
LEES	11E	PR D84 031103	J.P. Lees *et al.*	(BABAR Collab.)
LEES	11G	PR D84 072006	J.P. Lees *et al.*	(BABAR Collab.)
WILLIAMS	11	PR D84 054015	M. Williams	(LOIC)
WON	11	PRL 107 221801	E. Won *et al.*	(BELLE Collab.)
YELTON	11	PR D84 032001	J. Yelton *et al.*	(CLEO Collab.)
ANASHIN	10A	PL B686 84	V.V. Anashin *et al.*	(VEPP-4M KEDR Collab.)
ASNER	10	PR D81 052007	D.M. Asner *et al.*	(CLEO Collab.)
BRIERE	10	PR D81 112001	R.A. Briere *et al.*	(CLEO Collab.)
KO	10	PRL 104 181602	B.R. Ko *et al.*	(BELLE Collab.)
MENDEZ	10	PR D81 052013	H. Mendez *et al.*	(CLEO Collab.)
PDG	10	JP G37 075021	K. Nakamura *et al.*	(PDG Collab.)
RUBIN	10	PR D82 092007	P. Rubin *et al.*	(CLEO Collab.)
BEDIAGA	09	PR D80 096006	I. Bediaga *et al.*	(CBPF, NDAM)
BESSON	09	PR D80 032005	D. Besson *et al.*	(CLEO Collab.)
Also		PR D79 052010	J.Y. Ge *et al.*	(CLEO Collab.)
KO	09	PRL 102 221802	B.R. Ko *et al.*	(BELLE Collab.)
LINK	09	PL B681 14	J.M. Link *et al.*	(FNAL FOCUS Collab.)
MITCHELL	09B	PRL 102 081801	R.E. Mitchell *et al.*	(CLEO Collab.)
WON	09	PR D80 111101	E. Won *et al.*	(BELLE Collab.)
ABAZOV	08D	PRL 100 101801	V.M. Abazov *et al.*	(D0 Collab.)
ABLIKIM	08L	PL B665 16	M. Ablikim *et al.*	(BES Collab.)
ARTUSO	08	PR D77 092003	M. Artuso *et al.*	(CLEO Collab.)
AUBERT	08AO	PR D78 051102	B. Aubert *et al.*	(BABAR Collab.)
BONVICINI	08	PR D77 091106	G. Bonvicini *et al.*	(CLEO Collab.)
BONVICINI	08A	PR D78 052001	G. Bonvicini *et al.*	(CLEO Collab.)
DOBBS	08	PR D77 112005	S. Dobbs *et al.*	(CLEO Collab.)
Also		PRL 100 251802	D. Cronin-Hennessy *et al.*	(CLEO Collab.)
EISENSTEIN	08	PR D78 052003	B.I. Eisenstein *et al.*	(CLEO Collab.)
HE	08	PRL 100 091801	Q. He *et al.*	(CLEO Collab.)
PDG	08	PL B667 1	C. Amsler *et al.*	(PDG Collab.)
RUBIN	08	PR D78 072003	P. Rubin *et al.*	(CLEO Collab.)
ABLIKIM	07	PL B644 20	M. Ablikim *et al.*	(BES Collab.)
ABLIKIM	07G	PL B658 1	M. Ablikim *et al.*	(BES Collab.)
BONVICINI	07	PR D76 012001	G. Bonvicini *et al.*	(CLEO Collab.)
DOBBS	07	PR D76 112001	S. Dobbs *et al.*	(CLEO Collab.)
LINK	07B	PL B653 1	J.M. Link *et al.*	(FNAL FOCUS Collab.)
ABLIKIM	06O	EPJ C47 31	M. Ablikim *et al.*	(BES Collab.)
ABLIKIM	06P	EPJ C47 39	M. Ablikim *et al.*	(BES Collab.)
ABLIKIM	06U	PL B643 246	M. Ablikim *et al.*	(BES Collab.)
ADAM	06A	PRL 97 251801	N.E. Adam *et al.*	(CLEO Collab.)
AITALA	06	PR D73 032004	E.M. Aitala *et al.*	(FNAL E791 Collab.)
Also		PR D74 059901 (errat.)	E.M. Aitala *et al.*	(FNAL E791 Collab.)
AUBERT,B	06F	PR D74 011107	B. Aubert *et al.*	(BABAR Colla.b)
DYTMAN	06	PR D74 071102	S.A. Dytman *et al.*	(CLEO Collab.)
HUANG	06B	PR D74 112005	G.S. Huang *et al.*	(CLEO Collab.)
LINK	06B	PL B637 32	J.M. Link *et al.*	(FNAL FOCUS Collab.)
RUBIN	06	PRL 96 081802	P. Rubin *et al.*	(CLEO Collab.)
RUBIN	06A	PR D73 112005	P. Rubin *et al.*	(CLEO Collab.)
ABLIKIM	05A	PL B608 24	M. Ablikim *et al.*	(BES Collab.)
ABLIKIM	05D	PL B610 183	M. Ablikim *et al.*	(BES Collab.)
ABLIKIM	05F	PL B622 6	M. Ablikim *et al.*	(BES Collab.)
ABLIKIM	05P	PL B625 196	M. Ablikim *et al.*	(BES Collab.)
ARTUSO	05A	PRL 95 251801	M. Artuso *et al.*	(CLEO Collab.)
AUBERT	05S	PR D71 091101	B. Aubert *et al.*	(BABAR Collab.)
HE	05	PRL 95 121801	Q. He *et al.*	(CLEO Collab.)
Also		PRL 96 199903 (errat.)	Q. He *et al.*	(CLEO Collab.)
HE	05A	PRL 95 221802	Q. He *et al.*	(CLEO Collab.)
HUANG	05B	PRL 95 181801	G.S. Huang *et al.*	(CLEO Collab.)
KAYIS-TOPAK...	05	PL B626 24	A. Kayis-Topaksu *et al.*	(CERN CHORUS Collab.)
LINK	05E	PL B622 239	J.M. Link *et al.*	(FNAL FOCUS Collab.)
LINK	05I	PL B621 72	J.M. Link *et al.*	(FNAL FOCUS Collab.)
ABLIKIM	04C	PL B597 39	M. Ablikim *et al.*	(BEPC BES Collab.)
ARMS	04	PR D69 071102	K. Arms *et al.*	(CLEO Collab.)
BONVICINI	04A	PR D70 112004	G. Bonvicini *et al.*	(CLEO Collab.)
LINK	04	PL B585 200	J.M. Link *et al.*	(FNAL FOCUS Collab.)
LINK	04E	PL B598 33	J.M. Link *et al.*	(FNAL FOCUS Collab.)
LINK	04F	PL B601 10	J.M. Link *et al.*	(FNAL FOCUS Collab.)
ANISOVICH	03	EPJ A16 229	V.V. Anisovich *et al.*	
LINK	03D	PL B561 225	J.M. Link *et al.*	(FNAL FOCUS Collab.)
LINK	03F	PL B572 21	J.M. Link *et al.*	(FNAL FOCUS Collab.)
AITALA	02	PRL 89 121801	E.M. Aitala *et al.*	(FNAL E791 Collab.)
BRANDENB...	02	PRL 89 222001	G. Brandenburg *et al.*	(CLEO Collab.)
KAYIS-TOPAK...	02	PL B549 48	A. Kayis-Topaksu *et al.*	(CERN CHORUS Collab.)
LINK	02B	PRL 88 041602	J.M. Link *et al.*	(FNAL FOCUS Collab.)
Also		PRL 88 159903 (errat.)	J.M. Link *et al.*	(FNAL FOCUS Collab.)
LINK	02E	PL B535 43	J.M. Link *et al.*	(FNAL FOCUS Collab.)
LINK	02F	PL B537 192	J.M. Link *et al.*	(FNAL FOCUS Collab.)
LINK	02I	PL B541 227	J.M. Link *et al.*	(FNAL FOCUS Collab.)
LINK	02J	PL B541 243	J.M. Link *et al.*	(FNAL FOCUS Collab.)
LINK	02L	PL B544 89	J.M. Link *et al.*	(FNAL FOCUS Collab.)
AITALA	01B	PRL 86 770	E.M. Aitala *et al.*	(FNAL E791 Collab.)
LINK	01C	PRL 87 162001	J.M. Link *et al.*	(FNAL FOCUS Collab.)
ABREU	00O	EPJ C12 209	P. Abreu *et al.*	(DELPHI Collab.)
ASTIER	00D	PL B486 35	P. Astier *et al.*	(CERN NOMAD Collab.)
JUN	00	PRL 84 1857	S.Y. Jun *et al.*	(FNAL SELEX Collab.)
LINK	00B	PL B491 232	J.M. Link *et al.*	(FNAL FOCUS Collab.)
Also		PL B495 443 (errat.)	J.M. Link *et al.*	(FNAL FOCUS Collab.)
ABBIENDI	99K	EPJ C8 573	G. Abbiendi *et al.*	(OPAL Collab.)
ADAMOVICH	99	EPJ C6 35	M. Adamovich *et al.*	(CERN BEATRICE Collab.)
AITALA	99G	PL B462 401	E.M. Aitala *et al.*	(FNAL E791 Collab.)
BONVICINI	99	PRL 82 4586	G. Bonvicini *et al.*	(CLEO Collab.)
AITALA	98B	PRL 80 1393	E.M. Aitala *et al.*	(FNAL E791 Collab.)
AITALA	98C	PL B421 405	E.M. Aitala *et al.*	(FNAL E791 Collab.)
AITALA	98F	PL B440 435	E.M. Aitala *et al.*	(FNAL E791 Collab.)
BAI	98B	PL B429 188	J.Z. Bai *et al.*	(BEPC BES Collab.)
AITALA	97	PL B397 325	E.M. Aitala *et al.*	(FNAL E791 Collab.)
AITALA	97B	PL B403 377	E.M. Aitala *et al.*	(FNAL E791 Collab.)
AITALA	97C	PL B404 187	E.M. Aitala *et al.*	(FNAL E791 Collab.)
BISHAI	97	PRL 78 3261	M. Bishai *et al.*	(CLEO Collab.)
FRABETTI	97	PL B391 235	P.L. Frabetti *et al.*	(FNAL E687 Collab.)
FRABETTI	97B	PL B398 239	P.L. Frabetti *et al.*	(FNAL E687 Collab.)
FRABETTI	97C	PL B401 131	P.L. Frabetti *et al.*	(FNAL E687 Collab.)
FRABETTI	97D	PL B407 79	P.L. Frabetti *et al.*	(FNAL E687 Collab.)
AITALA	96	PRL 76 364	E.M. Aitala *et al.*	(FNAL E791 Collab.)
FRABETTI	95	PL B346 199	P.L. Frabetti *et al.*	(FNAL E687 Collab.)
FRABETTI	95B	PL B351 591	P.L. Frabetti *et al.*	(FNAL E687 Collab.)
FRABETTI	95E	PL B359 403	P.L. Frabetti *et al.*	(FNAL E687 Collab.)
KODAMA	95	PL B345 85	K. Kodama *et al.*	(FNAL E653 Collab.)
ALBRECHT	94I	ZPHY C64 375	H. Albrecht *et al.*	(ARGUS Collab.)
BALEST	94	PRL 72 2328	R. Balest *et al.*	(CLEO Collab.)
FRABETTI	94D	PL B323 459	P.L. Frabetti *et al.*	(FNAL E687 Collab.)
FRABETTI	94G	PL B331 217	P.L. Frabetti *et al.*	(FNAL E687 Collab.)
FRABETTI	94I	PR D50 2953	P.L. Frabetti *et al.*	(FNAL E687 Collab.)
AKERIB	93	PRL 71 3070	D.S. Akerib *et al.*	(CLEO Collab.)
ANJOS	93	PR D48 56	J.C. Anjos *et al.*	(FNAL E691 Collab.)
FRABETTI	93E	PL B307 262	P.L. Frabetti *et al.*	(FNAL E687 Collab.)
ALBRECHT	92F	PL B278 202	H. Albrecht *et al.*	(ARGUS Collab.)
BARLAG	92C	ZPHY C55 383	S. Barlag *et al.*	(ACCMOR Collab.)
Also		ZPHY C48 29	S. Barlag *et al.*	(ACCMOR Collab.)
COFFMAN	92B	PR D45 2196	D.M. Coffman *et al.*	(Mark III Collab.)
DAOUDI	92	PR D45 3965	M. Daoudi *et al.*	(CLEO Collab.)
KODAMA	92	PL B274 246	K. Kodama *et al.*	(FNAL E653 Collab.)
KODAMA	92C	PL B286 187	K. Kodama *et al.*	(FNAL E653 Collab.)
ADAMOVICH	91	PL B268 142	M.I. Adamovich *et al.*	(WA82 Collab.)
ALBRECHT	91	PL B255 634	H. Albrecht *et al.*	(ARGUS Collab.)
ALVAREZ	91B	ZPHY C50 11	M.P. Alvarez *et al.*	(CERN NA14/2 Collab.)
AMMAR	91	PR D44 3383	R. Ammar *et al.*	(CLEO Collab.)
BAI	91	PRL 66 1011	Z. Bai *et al.*	(Mark III Collab.)
COFFMAN	91	PL B263 135	D.M. Coffman *et al.*	(Mark III Collab.)
FRABETTI	91	PL B263 584	P.L. Frabetti *et al.*	(FNAL E687 Collab.)
ALVAREZ	90	ZPHY C47 539	M.P. Alvarez *et al.*	(CERN NA14/2 Collab.)
ANJOS	90C	PR D41 2705	J.C. Anjos *et al.*	(FNAL E691 Collab.)
ANJOS	90D	PR D42 2414	J.C. Anjos *et al.*	(FNAL E691 Collab.)
ANJOS	90E	PRL 65 2630	J.C. Anjos *et al.*	(FNAL E691 Collab.)
BARLAG	90C	ZPHY C46 563	S. Barlag *et al.*	(ACCMOR Collab.)
WEIR	90B	PR D41 1384	A.J. Weir *et al.*	(Mark II Collab.)
ANJOS	89	PRL 62 125	J.C. Anjos *et al.*	(FNAL E691 Collab.)
ANJOS	89B	PRL 62 722	J.C. Anjos *et al.*	(FNAL E691 Collab.)
ANJOS	89E	PL B223 267	J.C. Anjos *et al.*	(FNAL E691 Collab.)
ADLER	88C	PRL 60 89	J. Adler *et al.*	(Mark III Collab.)
ALBRECHT	88I	PL B210 267	H. Albrecht *et al.*	(ARGUS Collab.)
HAAS	88	PRL 60 1614	P. Haas *et al.*	(CLEO Collab.)
ONG	88	PRL 60 2587	R.A. Ong *et al.*	(Mark II Collab.)
RAAB	88	PR D37 2391	J.R. Raab *et al.*	(FNAL E691 Collab.)
ADAMOVICH	87	EPL 4 887	M.I. Adamovich *et al.*	(Photon Emulsion Collab.)
ADLER	87	PL B196 107	J. Adler *et al.*	(Mark III Collab.)
BARTEL	87	ZPHY C33 339	W. Bartel *et al.*	(JADE Collab.)
BALTRUSAIT...	86E	PRL 56 2140	R.M. Baltrusaitis *et al.*	(Mark III Collab.)
BALTRUSAIT...	85B	PRL 54 1976	R.M. Baltrusaitis *et al.*	(Mark III Collab.)
BALTRUSAIT...	85E	PRL 55 150	R.M. Baltrusaitis *et al.*	(Mark III Collab.)
BARTEL	85J	PL 163B 277	W. Bartel *et al.*	(JADE Collab.)
ADAMOVICH	84	PL 140B 119	M.I. Adamovich *et al.*	(CERN WA58 Collab.)
ALTHOFF	84G	ZPHY C22 219	M. Althoff *et al.*	(TASSO Collab.)
DERRICK	84	PRL 53 1971	M. Derrick *et al.*	(HRS Collab.)
SCHINDLER	81	PR D24 78	R.H. Schindler *et al.*	(Mark II Collab.)
TRILLING	81	PRPL 75 57	G.H. Trilling	(LBL, UCB) J
ZHOLENTZ	80	PL 96B 214	A.A. Zholents *et al.*	(NOVO)
Also		SJNP 34 814	A.A. Zholents *et al.*	(NOVO)

Translated from YAF 34 1471.

Int. J. Mod. Phys. A 2026.41. Downloaded from www.worldscientific.com by UNIVERSITY OF CALIFORNIA @ BERKELEY on 09/16/26. Re-use and distribution is strictly not permitted, except for Open Access articles.

GOLDHABER	77	PL 69B 503	G. Goldhaber *et al.*	(Mark I Collab.)
PERUZZI	77	PRL 39 1301	I. Peruzzi *et al.*	(LGW Collab.)
PICCOLO	77	PL 70B 260	M. Piccolo *et al.*	(Mark I Collab.)
PERUZZI	76	PRL 37 569	I. Peruzzi *et al.*	(Mark I Collab.)
MOSTELLER	48	AST 2 No.5 30	R.A. Fisher, F. Mosteller	

OTHER RELATED PAPERS

RICHMAN	95	RMP 67 893	J.D. Richman, P.R. Burchat	(UCSB, STAN)
ROSNER	95	CNPP 21 369	J. Rosner	(CHIC)

D^0

$I(J^P) = \frac{1}{2}(0^-)$

D^0 MASS

The fit includes $D^{\pm}$, D^0, $D_s^{\pm}$, $D^{*\pm}$, D^{*0}, $D_s^{*\pm}$, $D_1(2420)^0$, $D_2^*(2460)^0$, and $D_{s1}(2536)^{\pm}$ mass and mass difference measurements.

Given the recent addition of much more precise measurements, we have omitted all those masses published up through 1990. See any Review before 2015 for those earlier results.

VALUE (MeV)	EVTS	DOCUMENT ID		TECN	COMMENT
1864.84 ±0.04 OUR FIT					
1864.85 ±0.04 OUR AVERAGE					
1865.100±0.210±0.046	0.34k	ANASHIN	25A	KEDR	e^+e^- at $\psi(3770)$
1864.845±0.025±0.057	63k	[1] TOMARADZE	14		$D^0 \to K^-2\pi^+\pi^-$
1864.75 ±0.15 ±0.11		AAIJ	13V	LHCB	$D^0 \to K^+2K^-\pi^+$
1864.841±0.048±0.063	4.3k	[2] LEES	13S	BABR	e^+e^- at $\Upsilon(4S)$
1864.847±0.150±0.095	0.3k	CAWLFIELD	07	CLEO	$D^0 \to K^0_S\phi$
• • • We do not use the following data for averages, fits, limits, etc. • • •					
1865.100±0.210±0.039	0.25k	ANASHIN	25	KEDR	Superseded by ANASHIN 25A
1865.30 ±0.33 ±0.23	0.1k	ANASHIN	10A	KEDR	Superseded by ANASHIN 25

[1] Obtained by analyzing CLEO-c data but not authored by the CLEO Collaboration. The largest source of error in the TOMARADZE 14 value is from the uncertainties in the K^- and K^0_S masses. The systematic error given above is the addition in quadrature of $\pm 0.022 \pm 0.053$ MeV, where the second error is from those mass uncertainties.

[2] The largest source of error in the LEES 13S value is from the uncertainty of the K^+ mass. The quoted systematic error is in fact $\pm 0.043 + 3\,(m_{K^+} - 493.677)$, in MeV.

$m_{D^{\pm}} - m_{D^0}$

The fit includes $D^{\pm}$, D^0, $D_s^{\pm}$, $D^{*\pm}$, D^{*0}, $D_s^{*\pm}$, $D_1(2420)^0$, $D_2^*(2460)^0$, and $D_{s1}(2536)^{\pm}$ mass and mass difference measurements.

VALUE (MeV)	DOCUMENT ID		TECN	COMMENT
4.822±0.015 OUR FIT				
4.76 ±0.12 ±0.07	AAIJ	13V	LHCB	$D^+ \to K^+K^-\pi^+$

D^0 MEAN LIFE

Measurements with an error $> 10 \times 10^{-15}$ s have been omitted from the average.

VALUE (10^{-15} s)	EVTS	DOCUMENT ID		TECN	COMMENT
410.3± 1.0 OUR AVERAGE					
410.5± 1.1± 0.8	171k	[1] ABUDINEN	21A	BEL2	e^+e^- at $\Upsilon(4S)$
409.6± 1.1± 1.5	210k	LINK	02F	FOCS	γ nucleus, ≈ 180 GeV
407.9± 6.0± 4.3	10k	KUSHNIR...	01	SELX	$K^-\pi^+$, $K^-\pi^+\pi^+\pi^-$
413 ± 3 ± 4	35k	AITALA	99E	E791	$K^-\pi^+$
408.5± 4.1$^{+3.5}_{-3.4}$	25k	BONVICINI	99	CLE2	$e^+e^- \approx \Upsilon(4S)$
413 ± 4 ± 3	16k	FRABETTI	94D	E687	$K^-\pi^+$, $K^-\pi^+\pi^+\pi^-$
• • • We do not use the following data for averages, fits, limits, etc. • • •					
424 ±11 ± 7	5118	FRABETTI	91	E687	$K^-\pi^+$, $K^-\pi^+\pi^+\pi^-$
417 ±18 ±15	890	ALVAREZ	90	NA14	$K^-\pi^+$, $K^-\pi^+\pi^+\pi^-$
388 $^{+23}_{-21}$	641	[2] BARLAG	90C	ACCM	π^-Cu 230 GeV
480 ±40 ±30	776	ALBRECHT	88I	ARG	e^+e^- 10 GeV
422 ± 8 ±10	4212	RAAB	88	E691	Photoproduction
420 ±50	90	BARLAG	87B	ACCM	K^- and π^- 200 GeV

[1] ABUDINEN 21A determines the lifetime ratio $\tau(D^+)/\tau(D^0) = 2.510 \pm 0.013 \pm 0.007$.

[2] BARLAG 90C estimate systematic error to be negligible.

See the related review(s):

D^0 — $\overline{D}^0$ Mixing

$|m_{D^0_1} - m_{D^0_2}| = x\,\Gamma$

The D^0_1 and D^0_2 are the mass eigenstates of the D^0 meson, as described in the note on "D^0-$\overline{D}^0$ Mixing," above. The experiments usually present $x \equiv \Delta m/\Gamma$. Then $\Delta m = x\,\Gamma = x\,\hbar/\tau$.

VALUE (10^{10} $\hbar$ s^{-1})	CL%	DOCUMENT ID		TECN	COMMENT
0.997±0.116 OUR EVALUATION (Produced by HFLAV)					
0.98 ±0.11 OUR AVERAGE					
		[1] AAIJ	25	LHCB	pp at 13 TeV
2.07 $^{+0.37}_{-0.59}$		[2] AAIJ	25AU	LHCB	pp at 13 TeV, $D^0 \to K^-\pi^+\pi^-\pi^+$
		[3] AAIJ	25U	LHCB	pp at 13 TeV
0.97 ±0.41 ±0.10		[4] ADACHI	25J	BEL2	$e^+e^- \approx \Upsilon(4S)$
1.05 ±0.36 ±0.06		[5] AAIJ	23BC	LHCB	pp at 13 TeV
0.97 $^{+0.14}_{-0.13}$		[6] AAIJ	21AB	LHCB	pp at 13 TeV
0.66 $^{+0.41}_{-0.37}$		[7] AAIJ	19X	LHCB	pp at 7, 8 TeV
		[8] AAIJ	18K	LHCB	pp at 7, 8, 13 TeV
− 2.10 ±1.29 ±0.41		[9] AAIJ	16V	LHCB	pp at 7 TeV
3.7 ±2.9 ±1.5		[10] LEES	16D	BABR	e^+e^-, 10.6 GeV
		[11] KO	14	BELL	$e^+e^- \to \Upsilon(nS)$
1.37 ±0.46 $^{+0.18}_{-0.28}$		[12] PENG	14	BELL	$e^+e^- \to \Upsilon(nS)$
		[13] AALTONEN	13AE	CDF	$p\overline{p}$ at 1.96 TeV
0.39 ±0.56 ±0.35		[14] DEL-AMO-SA...	10D	BABR	e^+e^-, 10.6 GeV
• • • We do not use the following data for averages, fits, limits, etc. • • •					
		[15] AAIJ	17AO	LHCB	Repl. by AAIJ 18K
		[16] AAIJ	13CE	LHCB	Repl. by AAIJ 17AO
		[17] AAIJ	13N	LHCB	Repl. by AAIJ 13CE
6.4 $^{+1.4}_{-1.7}$ ±1.0		[18] AUBERT	09AN	BABR	e^+e^- at 10.58 GeV
− 2 $^{+7}_{-6}$		[19] LOWREY	09	CLEO	e^+e^- at $\psi(3770)$
1.98 ±0.73 $^{+0.32}_{-0.41}$		[20] ZHANG	07B	BELL	Repl. by PENG 14
< 7	95	[21] ZHANG	06	BELL	e^+e^-
−11 to +22		[20] ASNER	05	CLEO	$e^+e^- \approx 10$ GeV
< 11	90	BITENC	05	BELL	
< 30	90	CAWLFIELD	05	CLEO	
< 7	95	[21] LI	05A	BELL	See ZHANG 06
< 22	95	[22] LINK	05H	FOCS	γ nucleus
< 23	95	AUBERT	04Q	BABR	
< 11	95	[21] AUBERT	03Z	BABR	e^+e^-, 10.6 GeV
< 7	95	[23] GODANG	00	CLE2	e^+e^-
< 32	90	[24,25] AITALA	98	E791	π^- nucleus, 500 GeV
< 24	90	[26] AITALA	96C	E791	π^- nucleus, 500 GeV
< 21	90	[25,27] ANJOS	88C	E691	Photoproduction

[1] $D^*(2010)^+$ tag of $D^0 \to K^+\pi^-$.

[2] AAIJ 25AU result based on analysis of 440k events. Measures also the CP violating parameters $\Delta x = (-0.02 \pm 0.04) \times 10^{-2}$ and $\Delta y = (0.02^{+0.04}_{-0.03}) \times 10^{-2}$ taking hadronic parameters as external inputs. And performs an alternative fit extracting the hadronic parameters, fixing the mixing parameters.

[3] Doubly-tagged $D^0 \to K^{\pm}\pi^{\mp}$ from preceding $B \to D^*(2010)^+\mu X$ with $D^*(2010)^+ \to D^0\pi^+$.

[4] ADACHI 25J result is based on $D^0 \to K^0_S\pi^+\pi^-$ decays collected by Belle and Belle II experiments.

[5] AAIJ 23BC analysis of $D^0 \to K^0_S\pi^+\pi^-$ from $B \to D^0\mu\nu X$ events allows for CP violation (none seen).

[6] AAIJ 21AB analysis of $D^0 \to K^0_S\pi^+\pi^-$ decays allows for CP violation (none seen).

[7] AAIJ 19X D^0 come from D^{*+} and $\overline{B} \to D^0\mu^-X$ decays (and c.c.). Analysis of $D^0 \to K^0_S\pi^+\pi^-$ decays allows for CP violation (none seen).

[8] The result was established with D^0 from prompt and secondary D^*. Based on 5 fb^{-1} of data collected at $\sqrt{s} = 7$, 8, 13 TeV. Assumes no CP violation. Reported $x'^2 = (3.9 \pm 2.7) \times 10^{-5}$ and $y' = (5.28 \pm 0.52) \times 10^{-3}$, where $x' = x\cos(\delta) + y\sin(\delta)$, $y' = y$

[9] Model-independent measurement of the charm mixing parameters in the decay $D^0 \to K^0_S\pi^+\pi^-$ using 1.0 fb^{-1} of LHCb data at $\sqrt{s} = 7$ TeV.

[10] Time-dependent amplitude analysis of $D^0 \to \pi^+\pi^-\pi^0$.

[11] Based on 976 fb^{-1} of data collected at $\Upsilon(nS)$ resonances. Assumes no CP violation. Reported $x'^2 = (0.09 \pm 0.22) \times 10^{-3}$ and $y' = (4.6 \pm 3.4) \times 10^{-3}$, where $x' = x\cos(\delta) + y\sin(\delta)$, $y' = y\cos(\delta) - x\sin(\delta)$ and δ is the strong phase between $D^0 \to K^+\pi^-$ and $\overline{D}^0 \to K^+\pi^-$.

[12] The time-dependent Dalitz-plot analysis of $D^0 \to K^0_S\pi^+\pi^-$ is emplored. Decay-time information and interference on the Dalitz plot are used to distinguish doubly Cabibbo-suppressed decays from mixing and to measure the relative phase between $D^0 \to K^{*+}\pi^-$ and $\overline{D}^0 \to K^{*+}\pi^-$. This value allows CP violation and is sensitive to the sign of Δm.

[13] Based on 9.6 fb^{-1} of data collected at the Tevatron. Assumes no CP violation. Reported $x'^2 = (0.08 \pm 0.18) \times 10^{-3}$ and $y' = (4.3 \pm 4.3) \times 10^{-3}$, where $x' = x\cos(\delta) + y\sin(\delta)$, $y' = y\cos(\delta) - x\sin(\delta)$ and δ is the strong phase between the $D^0 \to K^+\pi^-$ and $\overline{D}^0 \to K^+\pi^-$.

[14] DEL-AMO-SANCHEZ 10D uses 540,800±800 $K^0_S\pi^+\pi^-$ and 79,900±300 $K^0_S K^+K^-$ events in a time-dependent amplitude analysis of the D^0 and $\overline{D}^0$ Dalitz plots. No evidence was found for CP violation, and the values here assume no such violation.

[15] The result was established with D^0 from prompt and secondary D^*. Based on 3 fb^{-1} of data collected at $\sqrt{s} = 7$, 8 TeV. Assumes no CP violation. Reported $x'^2 = (3.6 \pm 4.3) \times 10^{-5}$ and $y' = (5.23 \pm 0.84) \times 10^{-3}$, where $x' = x\cos(\delta) + y\sin(\delta)$, $y' = y\cos(\delta) - x\sin(\delta)$ and δ is the strong phase between the $D^0 \to K^+\pi^-$ and $\overline{D}^0 \to K^+\pi^-$.

[16] Based on 3 fb^{-1} of data collected at $\sqrt{s} = 7$, 8 TeV. Assumes no CP violation. Reported $x'^2 = (5.5 \pm 4.9) \times 10^{-4}$ and $y' = (4.8 \pm 1.0) \times 10^{-3}$, where $x' = x\cos(\delta) + y$

Int. J. Mod. Phys. A 2026.41. Downloaded from www.worldscientific.com
by UNIVERSITY OF CALIFORNIA @ BERKELEY on 09/16/26. Re-use and distribution is strictly not permitted, except for Open Access articles.

$\sin(\delta)$, $y' = y\cos(\delta) - x\sin(\delta)$ and δ is the strong phase between the $D^0 \to K^+\pi^-$ and $\overline{D}^0 \to K^+\pi^-$.

[17] Based on 1 fb^{-1} of data collected at $\sqrt{s}$ = 7 TeV in 2011. Assumes no *CP* violation. Reported $x'^2 = (-0.9 \pm 1.3) \times 10^{-4}$ and $y' = (7.2 \pm 2.4) \times 10^{-3}$, where $x' = x\cos(\delta) + y\sin(\delta)$, $y' = y\cos(\delta) - x\sin(\delta)$ and δ is the strong phase between the $D^0 \to K^+\pi^-$ and $\overline{D}^0 \to K^+\pi^-$.

[18] The AUBERT 09AN values are inferred from the branching ratio $\Gamma(D^0 \to K^+\pi^-\pi^0$ via $\overline{D}^0)/\Gamma(D^0 \to K^-\pi^+\pi^0)$ given near the end of this Listings. Mixing is distinguished from DCS decays using decay-time information. Interference between mixing and DCS is allowed. The phase between $D^0 \to K^+\pi^-\pi^0$ and $\overline{D}^0 \to K^+\pi^-\pi^0$ is assumed to be small. The width difference here is y'', which is not the same as y_{CP} in the note on D^0-$\overline{D}^0$ mixing.

[19] LOWREY 09 uses quantum correlations in $e^+e^- \to D^0\overline{D}^0$ at the $\psi(3770)$. See below for coherence factors and average relative strong phases for both $D^0 \to K^-\pi^+\pi^0$ and $D^0 \to K^-\pi^-2\pi^+$. A fit that includes external measurements of charm mixing parameters gets $\Delta m = (2.34 \pm 0.61) \times 10^{10}\ \hbar\,\mathrm{s}^{-1}$.

[20] The ASNER 05 and ZHANG 07B values are from the time-dependent Dalitz-plot analysis of $D^0 \to K^0_S\pi^+\pi^-$. Decay-time information and interference on the Dalitz plot are used to distinguish doubly Cabibbo-suppressed decays from mixing and to measure the relative phase between $D^0 \to K^{*+}\pi^-$ and $\overline{D}^0 \to K^{*+}\pi^-$. This value allows *CP* violation and is sensitive to the sign of Δm.

[21] The AUBERT 03Z, LI 05A, and ZHANG 06 limits are inferred from the D^0-$\overline{D}^0$ mixing ratio $\Gamma(K^+\pi^-$ (via $\overline{D}^0))/\Gamma(K^-\pi^+)$ given near the end of this D^0 Listings. Decay-time information is used to distinguish DCS decays from D^0-$\overline{D}^0$ mixing. The limit allows interference between the DCS and mixing ratios, and also allows *CP* violation. AUBERT 03Z assumes the strong phase between $D^0 \to K^+\pi^-$ and $\overline{D}^0 \to K^+\pi^-$ amplitudes is small; if an arbitrary phase is allowed, the limit degrades by 20%. The LI 05A and ZHANG 06 limits are valid for an arbitrary strong phase.

[22] This LINK 05H limit is inferred from the D^0-$\overline{D}^0$ mixing ratio $\Gamma(K^+\pi^-$ (via $\overline{D}^0))/\Gamma(K^-\pi^+)$ given near the end of this D^0 Listings. Decay-time information is used to distinguish DCS decays from D^0-$\overline{D}^0$ mixing. The limit allows interference between the DCS and mixing ratios, and also allows *CP* violation. The strong phase between $D^0 \to K^+\pi^-$ and $\overline{D}^0 \to K^+\pi^-$ is assumed to be small. If an arbitrary relative strong phase is allowed, the limit degrades by 25%.

[23] This GODANG 00 limit is inferred from the D^0-$\overline{D}^0$ mixing ratio $\Gamma(K^+\pi^-$ (via $\overline{D}^0))/\Gamma(K^-\pi^+)$ given near the end of this D^0 Listings. Decay-time information is used to distinguish DCS decays from D^0-$\overline{D}^0$ mixing. The limit allows interference between the DCS and mixing ratios, and also allows *CP* violation. The strong phase between $D^0 \to K^+\pi^-$ and $\overline{D}^0 \to K^+\pi^-$ is assumed to be small. If an arbitrary relative strong phase is allowed, the limit degrades by a factor of two.

[24] AITALA 98 allows interference between the doubly Cabibbo-suppressed and mixing amplitudes, and also allows *CP* violation in this term, but assumes that $A_D = A_R = 0$. See the note on "D^0-$\overline{D}^0$ Mixing," above.

[25] This limit is inferred from R_M for $f = K^+\pi^-$ and $f = K^+\pi^-\pi^+\pi^-$. See the note on "D^0-$\overline{D}^0$ Mixing," above. Decay-time information is used to distinguish doubly Cabibbo-suppressed decays from D^0-$\overline{D}^0$ mixing.

[26] This limit is inferred from R_M for $f = K^+\ell^-\overline{\nu}_\ell$. See the note on "$D^0$-$\overline{D}^0$ Mixing," above.

[27] ANJOS 88C assumes that $y = 0$. See the note on "D^0-$\overline{D}^0$ Mixing," above. Without this assumption, the limit degrades by about a factor of two.

$(\Gamma_{D^0_1} - \Gamma_{D^0_2})/\Gamma = 2y$

The D^0_1 and D^0_2 are the mass eigenstates of the D^0 meson, as described in the note on "D^0-$\overline{D}^0$ Mixing," above.

Due to the strong phase difference between $D^0 \to K^+\pi^-$ and $\overline{D}^0 \to K^+\pi^-$, we exclude from the average those measurements of y' that are inferred from the D^0-$\overline{D}^0$ mixing ratio $\Gamma(K^+\pi^-$ via $\overline{D}^0)$ / $\Gamma(K^+\pi^-)$ given near the end of this D^0 Listings. OUR AVERAGE assumes *CP* conservation, though this is disfavored by data.

In the absence of *CP* violation, the experimental measurement of the observable y_{CP} corresponds to y. In the presence of *CP* violation, y_{CP} is approximately equal to y up to a *CP*-violating weak phase cosine, that is very close to unity, and higher order *CP*-violating effects. Many experiments measure y_{CP} with respect to a reference channel, such that the quoted results below are often $y_{CP} \pm y_{CP}$(reference). We denote the actual observable and the reference channel below for those experiments with sufficient sensitivity such that y_{CP}(reference) cannot be neglected.

Some early results have been omitted. See our 2006 *Review* (Journal of Physics **G33** 1 (2006)).

VALUE (units 10^{-2})	*EVTS*	*DOCUMENT ID*		*TECN*	*COMMENT*
1.394 ± 0.056 OUR EVALUATION		(Produced by HFLAV)			
1.32 ± 0.09 OUR AVERAGE		Error includes scale factor of 1.7. See the ideogram below.			
		[1] AAIJ	25	LHCB	pp at 13 TeV
$0.42\ ^{+0.58}_{-0.54}$	440k	[2] AAIJ	25AU	LHCB	pp at 13 TeV, $D^0 \to K^-\pi^+\pi^-\pi^+$
		[3] AAIJ	25U	LHCB	pp at 13 TeV
0.58 ± 0.28 ±0.06		[4] ADACHI	25J	BEL2	$e^+e^- \approx \Upsilon(4S)$
2.52 ± 0.62 ±0.17		[5] AAIJ	23BC	LHCB	pp at 13 TeV
1.392± 0.052±0.026		[6] AAIJ	22O	LHCB	pp at 13 TeV
$0.92\ ^{+0.30}_{-0.28}$	30.6M	[7] AAIJ	21AB	LHCB	pp at 13 TeV
$1.92 \pm 1.82\ ^{+1.29}_{-1.24}$	91k	[8] NAYAK	20	BELL	$D^0 \to K^0_S\omega$
1.14 ± 0.26 ±0.18		[9] AAIJ	19	LHCB	pp at 7, 8 TeV
1.48 ± 0.74	2.3M	[10] AAIJ	19X	LHCB	$D^0 \to K^0_S\pi^+\pi^-$
		[11] AAIJ	18K	LHCB	pp at 7, 8, 13 TeV
0.06 ± 0.92 ±0.26		[12] AAIJ	16V	LHCB	pp at 7 TeV
0.4 ± 1.8 ±1.0		[13] LEES	16D	BABR	e^+e^-, 10.6 GeV
2.22 ± 0.44 ±0.18		[14] STARIC	16	BELL	$e^+e^- \to \Upsilon(nS)$
−4.0 ± 2.6 ±1.4		[15] ABLIKIM	15D	BES3	e^+e^- at $\psi(3770)$
		[16] KO	14	BELL	$e^+e^- \to \Upsilon(nS)$
$0.60 \pm 0.30\ ^{+0.10}_{-0.17}$		[17] PENG	14	BELL	$e^+e^- \to \Upsilon(nS)$
		[18] AALTONEN	13AE	CDF	$p\overline{p}$ at 1.96 TeV
1.44 ± 0.36 ±0.24		[19] LEES	13	BABR	$e^+e^- \to \Upsilon(4S)$
0.55 ± 0.63 ±0.41		[20] AAIJ	12K	LHCB	pp at 7 TeV
1.14 ± 0.40 ±0.30		[21] DEL-AMO-SA...	10D	BABR	e^+e^-, 10.6 GeV
0.22 ± 1.22 ±1.04		[22] ZUPANC	09	BELL	$e^+e^- \approx \Upsilon(4S)$
$-1.0 \pm 2.0\ ^{+1.4}_{-1.6}$	18k	[23] ABE	02I	BELL	$e^+e^- \approx \Upsilon(4S)$
−2.4 ± 5.0 ±2.8	3393	[24] CSORNA	02	CLE2	$e^+e^- \approx \Upsilon(4S)$
6.84 ± 2.78 ±1.48	10k	[23] LINK	00	FOCS	γ nucleus
+1.6 ± 5.8 ±2.1		[23] AITALA	99E	E791	$K^-\pi^+$, K^+K^-
• • • We do not use the following data for averages, fits, limits, etc. • • •					
		[25] AAIJ	17AO	LHCB	Repl. by AAIJ 18K
		[26] AAIJ	13CE	LHCB	Repl. by AAIJ 17AO
		[27] AAIJ	13N	LHCB	Repl. by AAIJ 13CE
2.32 ± 0.44 ±0.36		[28] AUBERT	09AI	BABR	See LEES 13
$-0.12\ ^{+1.10}_{-1.28} \pm 0.68$		[29] AUBERT	09AN	BABR	e^+e^- at 10.58 GeV
$1.4\ ^{+4.8}_{-5.4}$		[30] LOWREY	09	CLEO	e^+e^- at $\psi(3770)$
1.70 ± 1.52	13k	[31] AALTONEN	08E	CDF	$p\overline{p}$, $\sqrt{s}$ = 1.96 TeV
2.06 ± 0.66 ±0.38		[32] AUBERT	08U	BABR	See AUBERT 09AI
1.94 ± 0.88 ±0.62	4k	[31] AUBERT	07W	BABR	$e^+e^- \approx$ 10.6 GeV
2.62 ± 0.64 ±0.50	160k	[33] STARIC	07	BELL	Repl. by STARIC 16
$0.74 \pm 0.50\ ^{+0.20}_{-0.31}$	534k	[34] ZHANG	07B	BELL	Repl. by PENG 14
−0.7 ± 4.9	4k	[31,35] ZHANG	06	BELL	e^+e^-
$-3.0\ ^{+5.0}_{-4.8}\ ^{+1.6}_{-0.8}$		[34] ASNER	05	CLEO	$e^+e^- \approx$ 10 GeV
−0.3 ± 5.7		[31,35] LI	05A	BELL	See ZHANG 06
$-5.2\ ^{+18.4}_{-16.8}$		[31,35] LINK	05H	FOCS	γ nucleus
$1.6 \pm 0.8\ ^{+1.0}_{-0.8}$	450k	[36] AUBERT	03P	BABR	See AUBERT 08U
$1.6\ ^{+6.2}_{-12.8}$		[31,35] AUBERT	03Z	BABR	e^+e^-, 10.6 GeV
$-5.0\ ^{+2.8}_{-3.2} \pm 0.6$		[31] GODANG	00	CLE2	e^+e^-

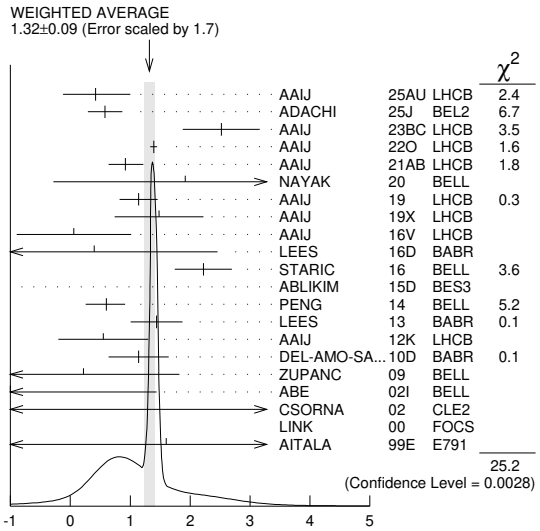

$(\Gamma_1 - \Gamma_2)/\Gamma = 2y$

[1] $D^*(2010)^+$ tag of $D^0 \to K^+\pi^-$.

[2] AAIJ 25AU measures also the *CP* violating parameters $\Delta x = (-0.02 \pm 0.04) \times 10^{-2}$ and $\Delta y = (0.02\ ^{+0.04}_{-0.03}) \times 10^{-2}$ taking hadronic parameters as external inputs. Also performs an alternative fit extracting the hadronic parameters, fixing the mixing parameters.

[3] Doubly-tagged $D^0 \to K^\pm\pi^\mp$ from preceding $B \to D^*(2010)^+\mu X$ with $D^*(2010)^+ \to D^0\pi^+$.

[4] ADACHI 25J result is based on $D^0 \to K^0_S\pi^+\pi^-$ decays collected by Belle and Belle II experiments.

[5] AAIJ 23BC analysis of $D^0 \to K^0_S\pi^+\pi^-$ from $B \to D^0\mu\nu X$ events allows for *CP* violation (none seen).

[6] AAIJ 22O is the combination of the measurement in the $D^0 \to \pi^-\pi^+$ channel and the one in the $D^0 \to K^-K^+$ channel, that are (1.314 ± 0.106 ± 0.032)% and (1.416 ± 0.060 ± 0.028)% respectively, assuming fully correlated systematics except those related to peaking backgrounds. Uses $y_{CP} - y_{CP}(K\pi)$.

Int. J. Mod. Phys. A 2026.41. Downloaded from www.worldscientific.com by LIFORNIA @ BERKELEY on 09/16/26. Re-use and distribution is strictly not permitted, except for Open Access articles.

[7] AAIJ 21AB analysis of $D^0 \to K^0_S \pi^+ \pi^-$ events allows for *CP* violation (none seen).

[8] NAYAK 20 reports $(1.92 \pm 1.82 \pm 1.24^{+0.34}_{-0.00}) \times 10^{-2}$ where the last uncertainty is due to possible presence of *CP*-even decays in the data sample. Extracts $y_{CP}=(\Gamma_{CP+} - \Gamma_{CP-}) / (\Gamma_{CP+} + \Gamma_{CP-})$ in $D^0 \to K^0_S \omega$ versus $\overline{D}^0 \to K^0_S \omega$, by measuring the decay lifetime of $D^0 \to K^0_S \omega$ with $\omega \to \pi^+\pi^-\pi^0$ versus $D^0 \to K^-\pi^+$. We list $2y_{CP} = 2y\ (= \Delta\Gamma/\Gamma)$ in the absence of *CP* violation.

[9] Based on 3 fb^{-1} of data collected at $\sqrt{s}$ = 7, 8 TeV. Measures the lifetime difference between $D^0 \to K^-K^+$ and $D^0 \to \pi^-\pi^+$ (*CP* even) decays and $D^0 \to K^-\pi^+$ (*CP* mixed) decays, or $y_{CP}=(\Gamma_{CP+} - \Gamma_{CP-}) / (\Gamma_{CP+} + \Gamma_{CP-})$. The D^0 mesons are required to originate from semimuonic decays of *B* mesons. We list $2y_{CP} = \Delta\Gamma/\Gamma$.

[10] AAIJ 19X D^0 come from D^{*+} and $\overline{B} \to D^0\mu^-X$ decays (and c.c.) in *pp* collisions at 7 and 8 TeV. Measurement allows for *CP* violation (none seen).

[11] The result was established with D^0 from prompt and secondary D^*. Based on 5 fb^{-1} of data collected at $\sqrt{s}$ = 7, 8, 13 TeV. Assumes no *CP* violation. Reported $x'^2 = (3.9 \pm 2.7) \times 10^{-5}$ and $y' = (5.28 \pm 0.52) \times 10^{-3}$, where $x' = x\cos(\delta) + y\sin(\delta)$, $y' = y\cos(\delta) - x\sin(\delta)$ and δ is the strong phase between the $D^0 \to K^+\pi^-$ and $\overline{D}^0 \to K^+\pi^-$.

[12] Model-independent measurement of the charm mixing parameters in the decay $D^0 \to K^0_S \pi^+\pi^-$ using 1.0 fb^{-1} of LHCb data at $\sqrt{s}$ = 7 TeV.

[13] Time-dependent amplitude analysis of $D^0 \to \pi^+\pi^-\pi^0$.

[14] An improved measurement of $\overline{D}^0 - D^0$ mixing and a search for *CP* violation in D^0 decays to *CP*-even final states K^+K^- and $\pi^+\pi^-$ using the final Belle data sample of 976 fb^{-1}.

[15] ABLIKIM 15D uses quantum correlations in $e^+e^- \to D^0\overline{D}^0$ at the $\psi(3770)$.

[16] Based on 976 fb^{-1} of data collected at $\Upsilon(nS)$ resonances. Assumes no *CP* violation. Reported $x'^2 = (0.09 \pm 0.22) \times 10^{-3}$ and $y' = (4.6 \pm 3.4) \times 10^{-3}$, where $x' = x\cos(\delta) + y\sin(\delta)$, $y' = y\cos(\delta) - x\sin(\delta)$ and δ is the strong phase between $D^0 \to K^+\pi^-$ and $\overline{D}^0 \to K^+\pi^-$.

[17] The time-dependent Dalitz-plot analysis of $D^0 \to K^0_S \pi^+\pi^-$ is emplored. Decay-time information and interference on the Dalitz plot are used to distinguish doubly Cabibbo-suppressed decays from mixing and to measure the relative phase between $D^0 \to K^{*+}\pi^-$ and $\overline{D}^0 \to K^{*+}\pi^-$. This value allows *CP* violation and is sensitive to the sign of Δm.

[18] Based on 9.6 fb^{-1} of data collected at the Tevatron. Assumes no *CP* violation. Reported $x'^2 = (0.08 \pm 0.18) \times 10^{-3}$ and $y' = (4.3 \pm 4.3) \times 10^{-3}$, where $x' = x\cos(\delta) + y\sin(\delta)$, $y' = y\cos(\delta) - x\sin(\delta)$ and δ is the strong phase between the $D^0 \to K^+\pi^-$ and $\overline{D}^0 \to K^+\pi^-$.

[19] Obtained $y_{CP} = (0.72 \pm 0.18 \pm 0.12)\%$ based on three effective D^0 lifetimes measured in $K^\mp\pi^\pm$, K^-K^+, and $\pi^-\pi^+$. We list $2y_{CP} = \Delta\Gamma/\Gamma$.

[20] Compared the lifetimes of D^0 decay to the *CP* eigenstate K^+K^- with D^0 decay to π^+K^-. The values here assume no *CP* violation.

[21] DEL-AMO-SANCHEZ 10D uses 540,800 ± 800 $K^0_S \pi^+\pi^-$ and 79,900 ± 300 $K^0_S K^+K^-$ events in a time-dependent amplitude analyses of the D^0 and $\overline{D}^0$ Dalitz plots. No evidence was found for *CP* violation, and the values here assume no such violation.

[22] ZUPANC 09 uses a method based on measuring the mean decay time of $D^0 \to K^0_S K^+K^-$ events for different K^+K^- mass intervals.

[23] LINK 00, AITALA 99E, and ABE 02I measure the lifetime difference between $D^0 \to K^-K^+$ (*CP* even) decays and $D^0 \to K^-\pi^+$ (*CP* mixed) decays, or $y_{CP}=[\Gamma(CP+)-\Gamma(CP-)]/[\Gamma(CP+)+\Gamma(CP-)]$. We list $2y_{CP}=\Delta\Gamma/\Gamma$.

[24] CSORNA 02 measures the lifetime difference between $D^0 \to K^-K^+$ and $\pi^-\pi^+$ (*CP* even) decays and $D^0 \to K^-\pi^+$ (*CP* mixed) decays, or $y_{CP}=[\Gamma(CP+)-\Gamma(CP-)]/[\Gamma(CP+)+\Gamma(CP-)]$. We list $2y_{CP}=\Delta\Gamma/\Gamma$.

[25] The result was established with D^0 from prompt and secondary D^*. Based on 3 fb^{-1} of data collected at $\sqrt{s}$ = 7, 8 TeV. Assumes no *CP* violation. Reported $x'^2 = (3.6 \pm 4.3) \times 10^{-5}$ and $y' = (5.23 \pm 0.84) \times 10^{-3}$, where $x' = x\cos(\delta) + y\sin(\delta)$, $y' = y\cos(\delta) - x\sin(\delta)$ and δ is the strong phase between the $D^0 \to K^+\pi^-$ and $\overline{D}^0 \to K^+\pi^-$.

[26] Based on 3 fb^{-1} of data collected at $\sqrt{s}$ = 7, 8 TeV. Assumes no *CP* violation. Reported $x'^2 = (5.5 \pm 4.9) \times 10^{-4}$ and $y' = (4.8 \pm 1.0) \times 10^{-3}$, where $x' = x\cos(\delta) + y\sin(\delta)$, $y' = y\cos(\delta) - x\sin(\delta)$ and δ is the strong phase between the $D^0 \to K^+\pi^-$ and $\overline{D}^0 \to K^+\pi^-$.

[27] Based on 1 fb^{-1} of data collected at $\sqrt{s}$ = 7 TeV in 2011. Assumes no *CP* violation. Reported $x'^2 = (-0.9 \pm 1.3) \times 10^{-4}$ and $y' = (7.2 \pm 2.4) \times 10^{-3}$, where $x' = x\cos(\delta) + y\sin(\delta)$, $y' = y\cos(\delta) - x\sin(\delta)$ and δ is the strong phase between the $D^0 \to K^+\pi^-$ and $\overline{D}^0 \to K^+\pi^-$.

[28] This combines the $y_{CP} = (\tau_{K\pi}/\tau_{KK})-1$ using untagged $K^-\pi^+$ and K^-K^+ events of AUBERT 09AI with the disjoint y_{CP} using tagged $K^-\pi^+$, K^-K^+, and $\pi^-\pi^+$ events of AUBERT 08U.

[29] The AUBERT 09AN values are inferred from the branching ratio $\Gamma(D^0 \to K^+\pi^-\pi^0$ via $\overline{D}^0)/\Gamma(D^0 \to K^-\pi^+\pi^0)$ given near the end of this Listings. Mixing is distinguished from DCS decays using decay-time information. Interference between mixing and DCS is allowed. The phase between $D^0 \to K^+\pi^-\pi^0$ and $\overline{D}^0 \to K^+\pi^-\pi^0$ is assumed to be small. The width difference here is y'', which is not the same as y_{CP} in the note on D^0–$\overline{D}^0$ mixing.

[30] LOWREY 09 uses quantum correlations in $e^+e^- \to D^0\overline{D}^0$ at the $\psi(3770)$. See below for coherence factors and average relative strong phases for both $D^0 \to K^-\pi^+\pi^0$ and $D^0 \to K^-\pi^-2\pi^+$. A fit that includes external measurements of charm mixing parameters gets $2y = (1.62 \pm 0.32) \times 10^{-2}$.

[31] The GODANG 00, AUBERT 03Z, LINK 05H, LI 05A, ZHANG 06, AUBERT 07W, and AALTONEN 08E limits are inferred from the D^0-$\overline{D}^0$ mixing ratio $\Gamma(K^+\pi^-$ (via $\overline{D}^0$))/$\Gamma(K^-\pi^+)$ given near the end of this D^0 Listings. Decay-time information is used to distinguish DCS decays from D^0-$\overline{D}^0$ mixing. The limits allow interference between the DCS and mixing ratios, and all except AUBERT 07W and AALTONEN 08E also allow *CP* violation. The phase between $D^0 \to K^+\pi^-$ and $\overline{D}^0 \to K^+\pi^-$ is assumed to be small. This is a measurement of y' and is not the same as the y_{CP} of our note above on "D^0-$\overline{D}^0$ Mixing."

[32] This value combines the results of AUBERT 08U and AUBERT 03P.

[33] STARIC 07 compares the lifetimes of D^0 decay to the *CP* eigenstates K^+K^- and $\pi^+\pi^-$ with D^0 decay to $K^-\pi^+$.

[34] The ASNER 05 and ZHANG 07B values are from the time-dependent Dalitz-plot analysis of $D^0 \to K^0_S \pi^+\pi^-$. Decay-time information and interference on the Dalitz plot are used to distinguish doubly Cabibbo-suppressed decays from mixing and to measure the relative phase between $D^0 \to K^{*+}\pi^-$ and $\overline{D}^0 \to K^{*+}\pi^-$. This limit allows *CP* violation.

[35] The ranges of AUBERT 03Z, LINK 05H, LI 05A, and ZHANG 06 measurements are for 95% confidence level.

[36] AUBERT 03P measures $Y \equiv 2\tau^0 / (\tau^+ + \tau^-) - 1$, where τ^0 is the $D^0 \to K^-\pi^+$ (and $\overline{D}^0 \to K^+\pi^-$) lifetime, and τ^+ and τ^- are the D^0 and $\overline{D}^0$ lifetimes to *CP*-even states (here K^-K^+ and $\pi^-\pi^+$). In the limit of *CP* conservation, $Y = y \equiv \Delta\Gamma / 2\Gamma$ (we list $2y = \Delta\Gamma/\Gamma$). AUBERT 03P also uses $\tau^+ - \tau^-$ to get $\Delta Y = -0.008 \pm 0.006 \pm 0.002$.

|q/p|

The mass eigenstates D^0_1 and D^0_2 are related to the $C = \pm 1$ states by $|D_{1,2}> = p\,|D^0> + q\,|\overline{D}^0>$. See the note on "$D^0$-$\overline{D}^0$ Mixing" above.

VALUE	EVTS	DOCUMENT ID		TECN	COMMENT
0.995±0.016 OUR EVALUATION		(Produced by HFLAV) see the note on "D^0-$\overline{D}^0$ Mixing."			
0.99 ±0.05 OUR AVERAGE					
		[1] AAIJ	25	LHCB	*pp* at 13 TeV
0.996±0.052	30.6M	[2] AAIJ	21AB	LHCB	*pp* at 13 TeV
$1.05\ ^{+0.22}_{-0.17}$	2.3M	[3] AAIJ	19X	LHCB	*pp* at 7, 8 TeV
		[4] AAIJ	18K	LHCB	*pp* at 7, 8, 13 TeV
$0.90\ ^{+0.16}_{-0.15}\ ^{+0.08}_{-0.06}$		[5] PENG	14	BELL	$e^+e^- \to \Upsilon(nS)$
• • • We do not use the following data for averages, fits, limits, etc. • • •					
		[6] AAIJ	13CE	LHCB	Repl. by AAIJ 18K
$0.86\ ^{+0.30}_{-0.29}\ ^{+0.10}_{-0.08}$		[7] ZHANG	07B	BELL	Repl. by PENG 14

[1] $D^*(2010)^+$ tag of $D^0 \to K^+\pi^-$.

[2] AAIJ 21AB result comes form analysis of $D^0 \to K^0_S \pi^+\pi^-$ events.

[3] AAIJ 19X measurement comes form analysis of $D^0 \to K^0_S \pi^+\pi^-$ decays. D^0 come from D^{*+} and $\overline{B} \to D^0\mu^-X$ decays (and c.c.) in *pp* collisions at 7 and 8 TeV.

[4] Based on 5 fb^{-1} of data collected at $\sqrt{s}$ = 7, 8, 13 TeV. Allowing for *CP* violation, the direct *CP* violation in mixing is reported $1.00 < |q/p| < 1.35$ at the 68.3% CL for the $D^0 \to K^+\pi^-$ and $\overline{D}^0 \to K^+\pi^-$.

[5] The time-dependent Dalitz-plot analysis of $D^0 \to K^0_S \pi^+\pi^-$ is employed. Decay-time information and interference on the Dalitz plot are used to distinguish doubly Cabibbo-suppressed decays from mixing and to measure the relative phase between $D^0 \to K^{*+}\pi^-$ and $\overline{D}^0 \to K^{*+}\pi^-$. This value allows *CP* violation and is sensitive to the sign of Δm.

[6] Based on 3 fb^{-1} of data collected at $\sqrt{s}$ = 7, 8 TeV. Allowing for *CP* violation, the direct *CP* violation in mixing is reported $0.75 < |q/p| < 1.24$ at the 68.3% CL for the $D^0 \to K^+\pi^-$ and $\overline{D}^0 \to K^+\pi^-$.

[7] The phase of p/q is $(-14^{+16}_{-18} \pm 5)^\circ$. The ZHANG 07B value is from the time-dependent Dalitz-plot analysis of $D^0 \to K^0_S \pi^+\pi^-$. Decay-time information and interference on the Dalitz plot are used to distinguish doubly Cabibbo-suppressed decays from mixing and to measure the relative phase between $D^0 \to K^{*+}\pi^-$ and $\overline{D}^0 \to K^{*+}\pi^-$. This value allows *CP* violation.

A_Γ

A_Γ is the decay-rate asymmetry for *CP*-even final states $A_\Gamma = (\overline{\tau}_+ - \tau_+) / (\overline{\tau}_+ + \tau_+)$. See the note on "$D^0$-$\overline{D}^0$ Mixing" above.

VALUE (units 10^{-4})	EVTS	DOCUMENT ID		TECN	COMMENT
0.89± 1.13 OUR EVALUATION					
0.9 ± 1.1 OUR AVERAGE					
1.3 ± 6.3 ± 2.4	3.8M	[1] AAIJ	24AF	LHCB	$D^0 \to \pi^+\pi^-\pi^0$
1.0 ± 1.1 ± 0.3		[2] AAIJ	21AI	LHCB	$D^0 \to K^+K^-, \pi^+\pi^-$
− 3 ±20 ± 7		[3] STARIC	16	BELL	$e^+e^- \to \Upsilon(nS)$
−12 ±12	1.8M	[4] AALTONEN	14Q	CDF	$p\overline{p}$, $\sqrt{s}$ = 1.96 TeV
9 ±26 ± 6	0.7M	LEES	13	BABR	$e^+e^- \to \Upsilon(4S)$
−59 ±59 ±21		[5] AAIJ	12K	LHCB	*pp* at 7 TeV, 2010 data.
• • • We do not use the following data for averages, fits, limits, etc. • • •					
2.3 ± 1.5 ± 0.3		[1] AAIJ	21AI	LHCB	$D^0 \to K^+K^-$
4.0 ± 2.8 ± 0.4		[1] AAIJ	21AI	LHCB	$D^0 \to \pi^+\pi^-$
− 4.4 ± 2.3 ± 0.6	21M	[6] AAIJ	20	LHCB	$D^0 \to K^+K^-$
2.5 ± 4.3 ± 0.7	7M	[7] AAIJ	20	LHCB	$D^0 \to \pi^+\pi^-$
− 3.0 ± 3.2 ± 1.0	9.6M	[5] AAIJ	17AK	LHCB	Repl. by AAIJ 20
4.6 ± 5.8 ± 1.2	3.0M	[8] AAIJ	17AK	LHCB	Repl. by AAIJ 20
−13.4 ± 7.7 $^{+2.6}_{-3.4}$	2.3M	[9] AAIJ	15AA	LHCB	Repl. by AAIJ 20
− 9.2 ±14.5 $^{+2.5}_{-3.3}$	0.8M	[10] AAIJ	15AA	LHCB	Repl. by AAIJ 20
− 3.5 ± 6.2 ± 1.2		[5] AAIJ	14AL	LHCB	Repl. by AAIJ 17AK
3.3 ±10.6 ± 1.4		[8] AAIJ	14AL	LHCB	Repl. by AAIJ 17AK
26 ±36 ± 8		AUBERT	08U	BABR	See LEES 13
1 ±30 ±25		STARIC	07	BELL	Repl. by STARIC 16
80 ±60 ±20		AUBERT	03P	BABR	$e^+e^- \approx \Upsilon(4S)$

[1] Requires D^0 to originate from $D^*(2010)^+ \to D^0\pi^+$. Measures the parameter $\Delta Y_f \simeq -A^f_\Gamma$ up to 1% corrections from y^f_{CP}.

Int. J. Mod. Phys. A 2026.41. Downloaded from www.worldscientific.com
by UNIVERSITY OF CALIFORNIA @ BERKELEY on 09/16/26. Re-use and distribution is strictly not permitted, except for Open Access articles.

[2] A combination of $D^0 \to K^+K^-$ and $D^0 \to \pi^+\pi^-$ from AAIJ 21AI, AAIJ 20, AAIJ 17AK and AAIJ 15AA.
[3] An improved measurement of $\overline{D}^0 - D^0$ mixing and a search for CP violation in D^0 decays to CP-even final states K^+K^- and $\pi^+\pi^-$ using the final Belle data sample of 976 fb^{-1}.
[4] Combined result from $D^0 \to K^+K^-$ and $D^0 \to \pi^+\pi^-$, with D^0 from $D^{*+} \to D^0\pi^+$ (and cc).
[5] Measured using $D^{*+} \to D^0\pi^+$, $D^0 \to K^+K^-$ decays (and cc).
[6] Measured using $D^0 \to K^+K^-$ decays, combines measurements with D^0 either from partially reconstructed semileptonic B hadron decays or from $D^{*+} \to D^0\pi^+$.
[7] Measured using $D^0 \to \pi^+\pi^-$ decays, combines measurements with D^0 either from partially reconstructed semileptonic B hadron decays or from $D^{*+} \to D^0\pi^+$.
[8] Measured using $D^{*+} \to D^0\pi^+$, $D^0 \to \pi^+\pi^-$ decays (and cc).
[9] Measured using $D^0 \to K^+K^-$ decays, with D^0 from partially reconstructed semileptonic B hadron decays.
[10] Measured using $D^0 \to \pi^+\pi^-$ decays, with D^0 from partially reconstructed semileptonic B hadron decays.

$\phi^{K^0_S\pi\pi}$

Parametrizes CP violation in the interference between D^0 mixing and decay. The mass eigenstates D^0_1 and D^0_2 are related to the $C = \pm 1$ states by $|D_{1,2}> = p\,|D^0> + q\,|\overline{D}^0>$. In the absence of CP violation in the decay, and using the usual phase convention where CP conservation implies q/p is real, $\phi^{K^0_S\pi\pi}$ is identical to the decay-mode-independent parameter $\phi = \arg(q/p)$.

VALUE	EVTS	DOCUMENT ID		TECN	COMMENT
$0.02^{+0.04}_{-0.05}$ OUR AVERAGE					
$0.056^{+0.047}_{-0.051}$	30.6M	[1] AAIJ	21AB	LHCB	pp at 13 TeV
$-0.09^{+0.11}_{-0.16}$	2.3M	[2] AAIJ	19X	LHCB	pp at 7, 8 TeV
$-0.10 \pm 0.19^{+0.07}_{-0.09}$	1.2M	[3] PENG	14	BELL	e^+e^- at $\Upsilon(4S,5S)$

[1] AAIJ 21AB result comes form analysis of $D^0 \to K^0_S\pi^+\pi^-$ events.
[2] AAIJ 19X result comes form analysis of $D^0 \to K^0_S\pi^+\pi^-$ events. D^0 come from D^{*+} and $\overline{B} \to D^0\mu^-X$ decays (and c.c.) in pp collisions at 7 and 8 TeV.
[3] PENG 14 reports $-0.10 \pm 0.19 \pm 0.05^{+0.05}_{-0.07}$ value where the last uncertainty is due to the amplitude model. We have added the systematic uncertainties in quadrature.

$\delta(K\pi)$ - relative strong phase

$\delta(K\pi)$ is the $D^0 \to K^+\pi^-$ relative strong phase between DCS and CF decays, with the convention $CP\,|D^0> = |\overline{D}^0>$.

VALUE (degrees)	DOCUMENT ID		TECN	COMMENT
191^{+6}_{-7} OUR AVERAGE				
$189.2^{+6.9}_{-7.4}{}^{+3.4}_{-3.8}$	[1] ABLIKIM	25CM	BES3	$e^+e^- \to D^0\overline{D}^0$, 4.13–4.23 GeV and 3.773 GeV
198^{+11}_{-17}	[2,3] ASNER	12	CLEO	$e^+e^- \to D^0\overline{D}^0$, 3.77 GeV
• • • We do not use the following data for averages, fits, limits, etc. • • •				
$192.8^{+11.0}_{-12.4}{}^{+1.9}_{-2.4}$	[4] ABLIKIM	25CM	BES3	$e^+e^- \to D^0\overline{D}^0$, 4.13–4.23 GeV
$187.6^{+8.9}_{-9.7}{}^{+5.4}_{-6.4}$	[5] ABLIKIM	22BM	BES3	$e^+e^- \to D^0\overline{D}^0$, 3.77 GeV
	[3,6] ABLIKIM	14C	BES3	$e^+e^- \to D^0\overline{D}^0$, 3.77 GeV
$202^{+11}_{-12}{}^{+9}_{-11}$	[3,7] ASNER	08	CLEO	Repl. by ASNER 12

[1] The reported value is a combination with that in ABLIKIM 22BM.
[2] Uses quantum correlations in $e^+e^- \to D^0\overline{D}^0$ at the $\psi(3770)$, where decay rates of CP-tagged $K\pi$ final states depend on the strong phases between the decays of $D^0 \to K^+\pi^-$ and $\overline{D}^0 \to K^+\pi^-$. The measurements obtained $\sin(\delta) = -0.01 \pm 0.41 \pm 0.04$ and $|\delta| = (10^{+28}_{-53}{}^{+13}_{-0})^\circ$ as well. A fit that includes external measurements of charm mixing parameters finds $\cos(\delta) = 1.15^{+0.19}_{-0.17}{}^{+0.00}_{-0.08}$, $\sin(\delta) = 0.56^{+0.32}_{-0.31}{}^{+0.21}_{-0.20}$, and $|\delta| = (18^{+11}_{-17})^\circ$.
[3] The value reported here has been rotated by 180 deg with respect to the value quoted in the paper, where the convention $CP\,|D^0> = -|\overline{D}^0>$ is used.
[4] Uses quantum correlations in $D\overline{D}$ produced in $e^+e^- \to D\overline{D}$, $e^+e^- \to D^*\overline{D}$ and $e^+e^- \to D^*\overline{D}^*$ to measure the asymmetry of the branching fraction of $D^0 \to K^-\pi^+$ in CP-odd and CP-even eigenstates. The fit includes external measurements of charm mixing parameters.
[5] Uses quantum correlations in $e^+e^- \to D^0\overline{D}^0$ at the $\psi(3770)$ to measure the asymmetry of the branching fraction of $D^0 \to K^-\pi^+$ in CP-odd and CP-even eigenstates to be $(13.2 \pm 1.1 \pm 0.7)\%$ and $(13.0 \pm 1.2 \pm 0.8)\%$ when using the predominantly CP-even tag $D^0 \to \pi^+\pi^-\pi^0$. A fit that includes external measurements of charm mixing parameters finds the value quoted above.
[6] Uses quantum correlations in $e^+e^- \to D^0\overline{D}^0$ at the $\psi(3770)$ to measure the asymmetry of the branching fraction of $D^0 \to K^-\pi^+$ in CP-odd and CP-even eigenstates to be $(12.7 \pm 1.3 \pm 0.7)\%$. A fit that includes external measurements of charm mixing parameters finds the value of $\cos(\delta) = 1.02 \pm 0.11 \pm 0.06 \pm 0.01$ where the third uncertainty is due to errors introduced by external inputs.
[7] ASNER 08 uses quantum correlations in $e^+e^- \to D^0\overline{D}^0$ at the $\psi(3770)$, where decay rates of CP-tagged $K\pi$ final states depend on $\cos\delta$ because of interfering amplitudes. The above measurement implies $|\delta| < 75^\circ$ with a confidence level of 95%. A fit that includes external measurements of charm mixing parameters finds $\cos\delta = 1.10 \pm 0.35 \pm 0.07$. See also the note on "$D^0$– $\overline{D}^0$ Mixing" p. 783 in our 2008 Review (PDG 08).

$D^0 \to K^-\pi^+\pi^0$ COHERENCE FACTOR $R_{K\pi\pi^0}$

See the note on 'D^0-$\overline{D}^0$ Mixing' for the definition. $R_{K\pi\pi^0}$ can have any value between 0 and 1. A value near 1 indicates the decay is dominated by a few intermediate states with limited interference.

VALUE	EVTS	DOCUMENT ID		TECN	COMMENT
0.792±0.033 OUR AVERAGE					
0.78 ± 0.04	62.4k	[1] ABLIKIM	21AA	BES3	$e^+e^- \to D^0\overline{D}^0$ at $\psi(3770)$
0.82 ± 0.06		[1,2,3] EVANS	16		$e^+e^- \to D^0\overline{D}^0$ at $\psi(3770)$
• • • We do not use the following data for averages, fits, limits, etc. • • •					
0.82 ± 0.07		[1,3] LIBBY	14		Repl. by EVANS 16
$0.78^{+0.11}_{-0.25}$		[4] LOWREY	09	CLEO	Repl. by LIBBY 14

[1] Uses quantum correlations in $e^+e^- \to D^0\overline{D}^0$ at the $\psi(3770)$, where the decay rates of CP-tagged $K^-\pi^+\pi^0$ final states depend on $R_{K\pi\pi^0}$ and $\delta^{K\pi\pi^0}$.
[2] A combined fit with a recent LHCb $D^0\overline{D}^0$ mixing results in AAIJ 16F is also reported to be 0.81 ± 0.06.
[3] Obtained by analyzing CLEO-c data but not authored by the CLEO Collaboration.
[4] LOWREY 09 uses quantum correlations in $e^+e^- \to D^0\overline{D}^0$ at the $\psi(3770)$, where the decay rates of CP-tagged $K^-\pi^+\pi^0$ final states depend on $R_{K\pi\pi^0}$ and $\delta^{K\pi\pi^0}$. A fit that includes external measurements of charm mixing parameters gets $R_{K\pi\pi^0} = 0.84 \pm 0.07$.

$D^0 \to K^-\pi^+\pi^0$ AVERAGE RELATIVE STRONG PHASE $\delta^{K\pi\pi^0}$

The quoted value of δ is based on the same sign CP phase of D^0 and $\overline{D}^0$ convention.

VALUE (°)	EVTS	DOCUMENT ID		TECN	COMMENT
198±10 OUR AVERAGE					
196^{+14}_{-15}	62.4k	[1] ABLIKIM	21AA	BES3	$e^+e^- \to D^0\overline{D}^0$ at $\psi(3770)$
199^{+13}_{-14}		[1,2,3] EVANS	16		$e^+e^- \to D^0\overline{D}^0$ at $\psi(3770)$
• • • We do not use the following data for averages, fits, limits, etc. • • •					
164^{+20}_{-14}		[1,3] LIBBY	14		Repl. by EVANS 16
239^{+32}_{-28}		[4] LOWREY	09	CLEO	Repl. by LIBBY 14

[1] Uses quantum correlations in $e^+e^- \to D^0\overline{D}^0$ at the $\psi(3770)$, where the decay rates of CP-tagged $K^-\pi^+\pi^0$ final states depend on $R_{K\pi\pi^0}$ and $\delta^{K\pi\pi^0}$.
[2] A combined fit with a recent LHCB $D^0\overline{D}^0$ mixing results in AAIJ 16F is also reported to be 198^{+14}_{-15} degree.
[3] Obtained by analyzing CLEO-c data but not authored by the CLEO Collaboration.
[4] LOWREY 09 uses quantum correlations in $e^+e^- \to D^0\overline{D}^0$ at the $\psi(3770)$, where the decay rates of CP-tagged $K^-\pi^+\pi^0$ final states depend on $R_{K\pi\pi^0}$ and $\delta^{K\pi\pi^0}$. A fit that includes external measurements of charm mixing parameters gets $\delta^{K\pi\pi^0} = (227^{+14}_{-17})^\circ$.

$D^0 \to K^-\pi^-2\pi^+$ COHERENCE FACTOR $R_{K3\pi}$

See the note on 'D^0-$\overline{D}^0$ Mixing' for the definition. $R_{K3\pi}$ can have any value between 0 and 1. A value near 1 indicates the decay is dominated by a few intermediate states with limited interference.

VALUE (units 10^{-2})	EVTS	DOCUMENT ID		TECN	COMMENT
45 ± 4 OUR AVERAGE					
$43.0^{+4.3}_{-3.9}$	440k	AAIJ	25AU	LHCB	pp at 13 TeV
52^{+12}_{-10}	8.6k	[1] ABLIKIM	21AA	BES3	$e^+e^- \to D^0\overline{D}^0$ at $\psi(3770)$
53^{+18}_{-21}		[1,2,3] EVANS	16		$e^+e^- \to D^0\overline{D}^0$ at $\psi(3770)$, pp at 7,8 TeV
• • • We do not use the following data for averages, fits, limits, etc. • • •					
$45.8 \pm 1.0 \pm 2.3$	0.9M,3k	[4] AAIJ	18AI	LHCB	amplitude models
32^{+20}_{-28}		[1,3] LIBBY	14		Repl. by EVANS 16
36^{+24}_{-30}		[5] LOWREY	09	CLEO	Repl. by LIBBY 14

[1] Uses quantum correlations in $e^+e^- \to D^0\overline{D}^0$ at the $\psi(3770)$, where the decay rates of CP-tagged $K^-\pi^-2\pi^+$ final states depend on $R_{K3\pi}$ and $\delta^{K3\pi}$.
[2] A combined fit with a recent LHCB $D^0\overline{D}^0$ mixing results in AAIJ 16F is also reported, to be $0.43^{+0.17}_{-0.13}$.
[3] Obtained by analyzing CLEO-c data but not authored by the CLEO Collaboration.
[4] Calculated from amplitude models to $D^0 \to K^-\pi^-2\pi^+$ and $D^0 \to K^+\pi^+2\pi^-$ and cc. Reports $0.458 \pm 0.010 \pm 0.012 \pm 0.020$ value where the 3rd uncertainty is the model uncertainty. We combined both systematic uncertainties in quadrature. Because of the importance of model independence in the practical use of the coherence factor, we do not include model-derived results in the average.
[5] LOWREY 09 uses quantum correlations in $e^+e^- \to D^0\overline{D}^0$ at the $\psi(3770)$, where the decay rates of CP-tagged $K^-\pi^-2\pi^+$ final states depend on $R_{K3\pi}$ and $\delta^{K3\pi}$. A fit that includes external measurements of charm mixing parameters gets $R_{K3\pi} = 0.33^{+0.26}_{-0.23}$.

$D^0 \to K^-\pi^-2\pi^+$ AVERAGE RELATIVE STRONG PHASE $\delta^{K3\pi}$

The quoted value of δ is based on the same sign CP phase of D^0 and $\overline{D}^0$ convention.

VALUE (°)	EVTS	DOCUMENT ID		TECN	COMMENT
156^{+12}_{-10} OUR AVERAGE Error includes scale factor of 1.1.					
$163.3^{+13.8}_{-14.8}$	440k	AAIJ	25AU	LHCB	pp at 13 TeV
167^{+31}_{-19}	8.6k	[1] ABLIKIM	21AA	BES3	$e^+e^- \to D^0\overline{D}^0$ at $\psi(3770)$
125^{+22}_{-14}		[1,2,3] EVANS	16		$e^+e^- \to D^0\overline{D}^0$ at $\psi(3770)$

Int. J. Mod. Phys. A 2026.41. Downloaded from www.worldscientific.com by CALIFORNIA @ BERKELEY on 09/16/26. Re-use and distribution is strictly not permitted, except for Open Access articles.

• • • We do not use the following data for averages, fits, limits, etc. • • •

$255\ ^{+21}_{-78}$	[1,3] LIBBY	14		Repl. by EVANS 16
$118\ ^{+62}_{-53}$	[4] LOWREY	09	CLEO	Repl. by LIBBY 14

[1] Uses quantum correlations in $e^+e^- \to D^0\overline{D}^0$ at the $\psi(3770)$, where the decay rates of CP-tagged $K^-\pi^-2\pi^+$ final states depend on $R_{K3\pi}$ and $\delta^{K3\pi}$.

[2] A combined fit with a recent LHCb $D^0\overline{D}^0$ mixing results in AAIJ 16F is also reported to be $(128^{+28}_{-17})^\circ$.

[3] Obtained by analyzing CLEO-c data but not authored by the CLEO Collaboration.

[4] LOWREY 09 uses quantum correlations in $e^+e^- \to D^0\overline{D}^0$ at the $\psi(3770)$, where the decay rates of CP-tagged $K^-\pi^-2\pi^+$ final states depend on $R_{K3\pi}$ and $\delta^{K3\pi}$. A fit that includes external measurements of charm mixing parameters gets $\delta^{K3\pi} = (114^{+26}_{-23})^\circ$.

$D^0 \to K^-\pi^-2\pi^+$, $R_{K3\pi}$ (y $\cos\delta^{K3\pi}$ − x $\sin\delta^{K3\pi}$)

VALUE (10^{-3} Tev^{-1})	EVTS	DOCUMENT ID		TECN	COMMENT
−3.0±0.7	42.5k	[1] AAIJ	16F	LHCB	pp at 7, 8 TeV

[1] From a time-dependent analysis of D mixing in $D^0 \to K^+\pi^-\pi^+\pi^-$. This result uses external constraints on $R_M = 1/2\ (x^2 + y^2)$. Without such constraints, AAIJ 16F measure $(0.3 \pm 1.8) \times 10^{-3}$, with a large correlation coefficient to R_M.

$D^0 \to K^0_S K^+\pi^-$ COHERENCE FACTOR $R_{K^0_S K\pi}$

VALUE	DOCUMENT ID		TECN	COMMENT
0.70±0.08	[1] INSLER	12	CLEO	$e^+e^- \to D^0\overline{D}^0$ at 3.77 GeV

[1] Uses quantum correlations in $e^+e^- \to D^0\overline{D}^0$ at the $\psi(3770)$, where the signal side D decays to $K^0_S K\pi$ and the tag-side D decays to $K\pi$, $K\pi\pi\pi$, $K\pi\pi^0$, and 10 additional CP-even, CP-odd, and mixed CP modes involving K^0_S or K^0_L.

$D^0 \to K^0_S K^+\pi^-$ AVERAGE RELATIVE STRONG PHASE $\delta^{K^0_S K\pi}$

The quoted value of δ is based on the same sign CP phase of D^0 and $\overline{D}^0$ convention.

VALUE (°)	DOCUMENT ID		TECN	COMMENT
0.1±15.7	[1] INSLER	12	CLEO	$e^+e^- \to D^0\overline{D}^0$ at 3.77 GeV

[1] Uses quantum correlations in $e^+e^- \to D^0\overline{D}^0$ at the $\psi(3770)$, where the signal side D decays to $K^0_S K\pi$ and the tag-side D decays to $K\pi$, $K\pi\pi\pi$, $K\pi\pi^0$, and 10 additional CP-even, CP-odd, and mixed CP modes involving K^0_S or K^0_L.

$D^0 \to K^*K$ COHERENCE FACTOR R_{K^*K}

VALUE	DOCUMENT ID		TECN	COMMENT
0.94±0.12	[1] INSLER	12	CLEO	$e^+e^- \to D^0\overline{D}^0$ at 3.77 GeV

[1] Uses quantum correlations in $e^+e^- \to D^0\overline{D}^0$ at the $\psi(3770)$, where the signal side D decays to $K^0_S K\pi$ and the tag-side D decays to $K\pi$, $K\pi\pi\pi$, $K\pi\pi^0$., and 10 additional CP-even, CP-odd, and mixed CP modes involving K^0_S or K^0_L.

$D^0 \to K^*K$ AVERAGE RELATIVE STRONG PHASE δ^{K^*K}

The quoted value of δ is based on the same sign CP phase of D^0 and $\overline{D}^0$ convention.

VALUE (°)	DOCUMENT ID		TECN	COMMENT
−16.6±18.4	[1] INSLER	12	CLEO	$e^+e^- \to D^0\overline{D}^0$ at 3.77 GeV

[1] Uses quantum correlations in $e^+e^- \to D^0\overline{D}^0$ at the $\psi(3770)$, where the signal side D decays to $K^0_S K\pi$ and the tag-side D decays to $K\pi$, $K\pi\pi\pi$, $K\pi\pi^0$, and 10 additional CP-even, CP-odd, and mixed CP modes involving K^0_S or K^0_L.

D^0 DECAY MODES

Most decay modes (other than the semileptonic modes) that involve a neutral K meson are now given as K^0_S modes, not as $\overline{K}^0$ modes. Nearly always it is a K^0_S that is measured, and interference between Cabibbo-allowed and doubly Cabibbo-suppressed modes can invalidate the assumption that $2\Gamma(K^0_S) = \Gamma(\overline{K}^0)$.

	Mode		Fraction (Γ_i/Γ)	Scale factor/ Confidence level
	Topological modes			
Γ_1	0-prongs	[a]	(15 ± 6) %	
Γ_2	2-prongs		(71 ± 6) %	
Γ_3	4-prongs	[b]	(14.6 ± 0.5) %	
Γ_4	6-prongs	[c]	(6.5 ± 1.3) $\times 10^{-4}$	
	Inclusive modes			
Γ_5	e^+ anything	[d]	(6.49 ± 0.11) %	
Γ_6	μ^+ anything		(6.8 ± 0.6) %	
Γ_7	K^- anything		(54.7 ± 2.8) %	S=1.3
Γ_8	K^0_S anything		(20.75 ± 0.23) %	
Γ_9	K^+ anything		(3.4 ± 0.4) %	
Γ_{10}	$K^*(892)^-$ anything		(15 ± 9) %	
Γ_{11}	$\overline{K}^*(892)^0$ anything		(9 ± 4) %	
Γ_{12}	$K^*(892)^+$ anything		< 3.6 %	CL=90%
Γ_{13}	$K^*(892)^0$ anything		(2.8 ± 1.3) %	
Γ_{14}	η anything		(9.5 ± 0.9) %	
Γ_{15}	η' anything		(2.48 ± 0.27) %	
Γ_{16}	ϕ anything		(1.08 ± 0.04) %	
Γ_{17}	$\pi^+\pi^+\pi^-$ anything		(17.60 ± 0.25) %	
Γ_{18}	invisibles		< 9.4 $\times 10^{-5}$	CL=90%
	Semileptonic modes			
Γ_{19}	$K^-\ell^+\nu_\ell$			
Γ_{20}	$K^-e^+\nu_e$		(3.537 ± 0.017) %	S=1.1
Γ_{21}	$K^-\mu^+\nu_\mu$		(3.418 ± 0.019) %	
Γ_{22}	$K^*(892)^-e^+\nu_e$		(2.16 ± 0.16) %	
Γ_{23}	$K^*(892)^-\mu^+\nu_\mu$		(2.01 ± 0.06) %	S=1.7
Γ_{24}	$K^-\pi^0e^+\nu_e$		$(1.6\ ^{+1.3}_{-0.5})$ %	
Γ_{25}	$\overline{K}^0\pi^-e^+\nu_e$		(1.447 ± 0.033) %	
Γ_{26}	$(\overline{K}^0\pi^-)_{S-wave}e^+\nu_e$		(8.5 ± 0.6) $\times 10^{-4}$	
Γ_{27}	$K^-\pi^0\mu^+\nu_\mu$		(7.10 ± 0.21) $\times 10^{-3}$	S=1.7
Γ_{28}	$(K^-\pi^0)_{S-wave}\mu^+\nu_\mu$		(4.09 ± 0.35) $\times 10^{-4}$	
Γ_{29}	$\overline{K}^0\pi^-\mu^+\nu_\mu$		(1.40 ± 0.04) %	S=1.7
Γ_{30}	$(\overline{K}^0\pi^-)_{S-wave}\mu^+\nu_\mu$		(7.5 ± 1.6) $\times 10^{-4}$	
Γ_{31}	$K^-\eta e^+\nu_e$		(8 ± 4) $\times 10^{-5}$	
Γ_{32}	$K^-\pi^+\pi^-e^+\nu_e$		$(2.8\ ^{+1.4}_{-1.1})\times 10^{-4}$	
Γ_{33}	$K_1(1270)^-e^+\nu_e$, $K_1^- \to K^-\pi^+\pi^-$		(3.23 ± 0.25) $\times 10^{-4}$	
Γ_{34}	$K_1(1270)^-e^+\nu_e$, $K_1^- \to K^0_S\pi^-\pi^0$		$(1.7\ ^{+0.6}_{-0.5})\times 10^{-4}$	
Γ_{35}	$K^-\pi^+\pi^-\mu^+\nu_\mu$		< 1.3 $\times 10^{-3}$	CL=90%
Γ_{36}	$(\overline{K}^*(892)\pi)^-\mu^+\nu_\mu$		< 1.5 $\times 10^{-3}$	CL=90%
Γ_{37}	$K_1(1270)^-\mu^+\nu_\mu$, $K_1^- \to K^-\pi^+\pi^-$		$(2.6\ ^{+0.4}_{-0.5})\times 10^{-4}$	
Γ_{38}	$K_1(1400)^-e^+\nu_e$		< 7 $\times 10^{-5}$	CL=90%
Γ_{39}	$\pi^-e^+\nu_e$		(2.91 ± 0.04) $\times 10^{-3}$	
Γ_{40}	$\pi^-\mu^+\nu_\mu$		(2.67 ± 0.12) $\times 10^{-3}$	S=1.3
Γ_{41}	$\pi^-\pi^0e^+\nu_e$		(1.45 ± 0.07) $\times 10^{-3}$	
Γ_{42}	$\rho^-e^+\nu_e$		(1.46 ± 0.08) $\times 10^{-3}$	S=2.0
Γ_{43}	$\rho^-\mu^+\nu_\mu$		(1.35 ± 0.13) $\times 10^{-3}$	
Γ_{44}	$a(980)^-e^+\nu_e$, $a^- \to \eta\pi^-$		(8.6 ± 1.8) $\times 10^{-5}$	
Γ_{45}	$K^0_S K^-e^+\nu_e$		< 2.13 $\times 10^{-5}$	CL=90%
Γ_{46}	$b_1(1235)^-e^+\nu_e$, $b_1^- \to \omega\pi^-$		< 1.12 $\times 10^{-4}$	CL=90%
	Hadronic modes with one $\overline{K}$			
Γ_{47}	$K^-\pi^+$		(3.936 ± 0.030) %	S=1.3
Γ_{48}	$K^0_S\pi^0$		(1.239 ± 0.022) %	
Γ_{49}	$K^0_L\pi^0$		(9.76 ± 0.32) $\times 10^{-3}$	
Γ_{50}	$K^0_L\eta$		(4.34 ± 0.16) $\times 10^{-3}$	
Γ_{51}	$K^0_L\eta'$		(8.12 ± 0.35) $\times 10^{-3}$	S=1.3
Γ_{52}	$K^0_L\omega$		(1.16 ± 0.04) %	
Γ_{53}	$K^0_S\pi^+\pi^-$	[e]	(2.84 ± 0.16) %	S=1.1
Γ_{54}	$K^0_S\rho^0$		$(6.3\ ^{+0.6}_{-0.8})\times 10^{-3}$	
Γ_{55}	$K^0_S\omega$, $\omega \to \pi^+\pi^-$		(2.1 ± 0.6) $\times 10^{-4}$	
Γ_{56}	$K^0_S(\pi^+\pi^-)_{S-wave}$		(3.4 ± 0.8) $\times 10^{-3}$	
Γ_{57}	$K^0_S f_0(980)$, $f_0 \to \pi^+\pi^-$		$(1.22\ ^{+0.40}_{-0.23})\times 10^{-3}$	
Γ_{58}	$K^0_S f_0(1370)$, $f_0 \to \pi^+\pi^-$		$(2.8\ ^{+0.9}_{-1.3})\times 10^{-3}$	
Γ_{59}	$K^0_S f_2(1270)$, $f_2 \to \pi^+\pi^-$		$(9\ ^{+10}_{-6})\times 10^{-5}$	
Γ_{60}	$K^*(892)^-\pi^+$, $K^{*-} \to K^0_S\pi^-$		$(1.67\ ^{+0.13}_{-0.16})$ %	
Γ_{61}	$K^*_0(1430)^-\pi^+$, $K^{*-}_0 \to K^0_S\pi^-$		$(2.71\ ^{+0.40}_{-0.32})\times 10^{-3}$	
Γ_{62}	$K^*_2(1430)^-\pi^+$, $K^{*-}_2 \to K^0_S\pi^-$		$(3.4\ ^{+1.9}_{-1.0})\times 10^{-4}$	
Γ_{63}	$K^*(1680)^-\pi^+$, $K^{*-} \to K^0_S\pi^-$		(4 ± 4) $\times 10^{-4}$	
Γ_{64}	$K^*(892)^+\pi^-$, $K^{*+} \to K^0_S\pi^+$	[f]	$(1.14\ ^{+0.60}_{-0.34})\times 10^{-4}$	
Γ_{65}	$K^*_0(1430)^+\pi^-$, $K^{*+}_0 \to K^0_S\pi^+$	[f]	< 1.4 $\times 10^{-5}$	CL=95%

Int. J. Mod. Phys. A 2026.41. Downloaded from www.worldscientific.com
by UNIVERSITY OF CALIFORNIA @ BERKELEY on 09/16/26. Re-use and distribution is strictly not permitted, except for Open Access articles.

Γ_{66}	$K_2^*(1430)^+\pi^-$, $K_2^{*+} \to K_S^0\pi^+$	[f]	$< 3.4 \times 10^{-5}$	CL=95%
Γ_{67}	$K_S^0\pi^+\pi^-$ nonresonant		$(2.6 {}^{+6.0}_{-1.6}) \times 10^{-4}$	
Γ_{68}	$K^-\pi^+\pi^0$	[e]	(14.4 ± 0.5) %	S=2.0
Γ_{69}	$K^-\rho^+$		(11.2 ± 0.7) %	
Γ_{70}	$K^-\rho(1700)^+$, $\rho^+ \to \pi^+\pi^0$		$(8.2 \pm 1.8) \times 10^{-3}$	
Γ_{71}	$K^*(892)^-\pi^+$, $K^*(892)^- \to K^-\pi^0$		$(2.30 {}^{+0.40}_{-0.20})$ %	
Γ_{72}	$\overline{K}^*(892)^0\pi^0$, $\overline{K}^*(892)^0 \to K^-\pi^+$		(1.95 ± 0.24) %	
Γ_{73}	$K_0^*(1430)^-\pi^+$, $K_0^{*-} \to K^-\pi^0$		$(4.7 \pm 2.2) \times 10^{-3}$	
Γ_{74}	$\overline{K}_0^*(1430)^0\pi^0$, $\overline{K}_0^{*0} \to K^-\pi^+$		$(5.9 {}^{+5.0}_{-1.6}) \times 10^{-3}$	
Γ_{75}	$K^*(1680)^-\pi^+$, $K^{*-} \to K^-\pi^0$		$(1.9 \pm 0.7) \times 10^{-3}$	
Γ_{76}	$K^-\pi^+\pi^0$ nonresonant		$(1.15 {}^{+0.60}_{-0.20})$ %	
Γ_{77}	$K_S^0 2\pi^0$		$(9.1 \pm 1.1) \times 10^{-3}$	S=2.2
Γ_{78}	$K_L^0\pi^0\pi^0$		(1.26 ± 0.06) %	
Γ_{79}	$K_S^0(2\pi^0)_{S-wave}$		$(2.6 \pm 0.7) \times 10^{-3}$	
Γ_{80}	$\overline{K}^*(892)^0\pi^0$, $\overline{K}^{*0} \to K_S^0\pi^0$		$(6.0 \pm 0.9) \times 10^{-3}$	
Γ_{81}	$\overline{K}^*(1430)^0\pi^0$, $\overline{K}^{*0} \to K_S^0\pi^0$		$(4 \pm 23) \times 10^{-5}$	
Γ_{82}	$\overline{K}^*(1680)^0\pi^0$, $\overline{K}^{*0} \to K_S^0\pi^0$		$(1.0 \pm 0.4) \times 10^{-3}$	
Γ_{83}	$K_S^0 f_2(1270)$, $f_2 \to 2\pi^0$		$(2.3 \pm 1.1) \times 10^{-4}$	
Γ_{84}	$2K_S^0$, one $K_S^0 \to 2\pi^0$		$(3.2 \pm 1.1) \times 10^{-4}$	
Γ_{85}	$K_S^0 2\pi^0$ nonresonant			
Γ_{86}	$K_S^0 3\pi^0$		$(7.6 \pm 0.4) \times 10^{-3}$	
Γ_{87}	$K^-2\pi^+\pi^-$	[e]	(8.20 ± 0.14) %	S=1.2
Γ_{88}	$K^-\pi^+\rho^0$ total		(6.85 ± 0.31) %	
Γ_{89}	$K^-\pi^+\rho^0$ 3-body		$(6.1 \pm 1.6) \times 10^{-3}$	
Γ_{90}	$\overline{K}^*(892)^0\rho^0$, $\overline{K}^{*0} \to K^-\pi^+$		(1.01 ± 0.05) %	
Γ_{91}	$\overline{K}^*(892)^0\rho^0$ transverse, $\overline{K}^{*0} \to K^-\pi^+$		(1.2 ± 0.4) %	
Γ_{92}	$K^-a_1(1260)^+$, $a_1^+ \to \rho^0\pi^+$		(4.31 ± 0.32) %	
Γ_{93}	$K_1(1270)^-\pi^+$, $K_1^- \to K^-\pi^+\pi^-$ total		$(3.9 \pm 0.4) \times 10^{-3}$	
Γ_{94}	$\overline{K}^*(892)^0\pi^+\pi^-$ total, $\overline{K}^*(892)^0 \to K^-\pi^+$			
Γ_{95}	$\overline{K}^*(892)^0\pi^+\pi^-$ 3-body, $\overline{K}^{*0} \to K^-\pi^+$			
Γ_{96}	$K_1(1270)^-\pi^+$, $K_1^- \to \overline{K}^*(892)^0\pi^-$, $\overline{K}^{*0} \to K^-\pi^+$		$(6.6 \pm 2.3) \times 10^{-4}$	
Γ_{97}	$K^-2\pi^+\pi^-$ nonresonant		(1.80 ± 0.07) %	
Γ_{98}	$K_S^0\pi^+\pi^-\pi^0$	[g]	(5.2 ± 0.6) %	
Γ_{99}	$K_S^0\eta$, $\eta \to \pi^+\pi^-\pi^0$		$(1.17 \pm 0.03) \times 10^{-3}$	
Γ_{100}	$K_S^0\omega$, $\omega \to \pi^+\pi^-\pi^0$		$(9.9 \pm 0.6) \times 10^{-3}$	
Γ_{101}	$K^-\pi^+2\pi^0$		(8.86 ± 0.23) %	
Γ_{102}	$K^-\pi^+3\pi^0$		$(9.5 \pm 0.4) \times 10^{-3}$	
Γ_{103}	$K_S^0\pi^+\pi^-2\pi^0$		(1.27 ± 0.06) %	
Γ_{104}	$K^-2\pi^+\pi^-\pi^0$		(4.3 ± 0.4) %	
Γ_{105}	$\overline{K}^*(892)^0\pi^+\pi^-\pi^0$, $\overline{K}^{*0} \to K^-\pi^+$		(1.3 ± 0.6) %	
Γ_{106}	$\overline{K}^*(892)^0\omega$, $\overline{K}^{*0} \to K^-\pi^+$, $\omega \to \pi^+\pi^-\pi^0$		$(6.5 \pm 3.0) \times 10^{-3}$	
Γ_{107}	$K^-\pi^+\omega$		(3.39 ± 0.10) %	
Γ_{108}	$\overline{K}^*(892)^0\omega$		(1.1 ± 0.5) %	
Γ_{109}	$K_S^0\pi^0\omega$		$(8.5 \pm 0.6) \times 10^{-3}$	
Γ_{110}	$K_S^0\eta\pi^0$		(1.01 ± 0.05) %	
Γ_{111}	$K_S^0 a_0(980)$, $a_0 \to \eta\pi^0$		(1.20 ± 0.28) %	
Γ_{112}	$\overline{K}^*(892)^0\eta$, $\overline{K}^{*0} \to K_S^0\pi^0$		$(2.9 \pm 0.7) \times 10^{-3}$	
Γ_{113}	$K^-\pi^+\eta$		(1.88 ± 0.05) %	S=1.4
Γ_{114}	$K^*(892)^0\eta$, $K^{*0} \to K^-\pi^+$		$(8.9 {}^{+0.8}_{-0.6}) \times 10^{-3}$	
Γ_{115}	$a_0(980)^+K^-$, $a_0^+ \to \eta\pi^+$		$(7.4 {}^{+0.9}_{-0.7}) \times 10^{-3}$	
Γ_{116}	$K_2^*(1980)^-\pi^+$, $K_2^{*-} \to K^-\eta$		$(2.2 {}^{+1.7}_{-1.9}) \times 10^{-4}$	
Γ_{117}	$K^-\pi^+\pi^0\eta$		$(4.49 \pm 0.27) \times 10^{-3}$	
Γ_{118}	$K_S^0\pi^+\pi^-\eta$		$(2.80 \pm 0.21) \times 10^{-3}$	
Γ_{119}	$K_S^0 2\pi^0\eta$		$(1.76 \pm 0.26) \times 10^{-3}$	
Γ_{120}	$K_S^0 2\pi^+2\pi^-$		$(2.70 \pm 0.29) \times 10^{-3}$	
Γ_{121}	$K_S^0\rho^0\pi^+\pi^-$, no $K^*(892)^-$		$(1.1 \pm 0.7) \times 10^{-3}$	
Γ_{122}	$K^*(892)^-2\pi^+\pi^-$, $K^*(892)^- \to K_S^0\pi^-$, no ρ^0		$(5 \pm 8) \times 10^{-4}$	
Γ_{123}	$K^*(892)^-\rho^0\pi^+$, $K^*(892)^- \to K_S^0\pi^-$		$(1.6 \pm 0.6) \times 10^{-3}$	
Γ_{124}	$K_S^0 2\pi^+2\pi^-$ nonresonant		$< 1.2 \times 10^{-3}$	CL=90%
Γ_{125}	$\overline{K}^0\pi^+\pi^-2\pi^0(\pi^0)$			
Γ_{126}	$K^-3\pi^+2\pi^-$		$(1.48 \pm 0.32) \times 10^{-4}$	S=1.4
Γ_{127}	$K^-2\pi^+\pi^-2\pi^0$		$(1.90 \pm 0.19) \times 10^{-3}$	

Fractions of some of the following modes with resonances have already appeared above as submodes of particular charged-particle modes. These nine modes below are all corrected for unseen decays of the resonances.

Γ_{128}	$K_S^0\eta$	$(5.08 \pm 0.13) \times 10^{-3}$	
Γ_{129}	$K_S^0\omega$	(1.11 ± 0.06) %	
Γ_{130}	$K_S^0\eta'(958)$	$(9.49 \pm 0.32) \times 10^{-3}$	
Γ_{131}	$\overline{K}^*(892)^0\pi^+\pi^-\pi^0$	(1.9 ± 0.9) %	
Γ_{132}	$\overline{K}^*(892)^0\eta$	(1.41 ± 0.12) %	
Γ_{133}	$K^-\pi^+\eta'(958)$	$(6.43 \pm 0.34) \times 10^{-3}$	
Γ_{134}	$K_S^0\eta'(958)\pi^0$	$(2.52 \pm 0.27) \times 10^{-3}$	
Γ_{135}	$\overline{K}^*(892)^0\eta'(958)$	$< 1.0 \times 10^{-3}$	CL=90%

Hadronic modes with three K's

Γ_{136}	$K_S^0K^+K^-$	$(4.49 \pm 0.29) \times 10^{-3}$	
Γ_{137}	$K_S^0 a_0(980)^0$, $a_0^0 \to K^+K^-$	$(3.0 \pm 0.4) \times 10^{-3}$	
Γ_{138}	$K^-a_0(980)^+$, $a_0^+ \to K^+K_S^0$	$(6.0 \pm 1.8) \times 10^{-4}$	
Γ_{139}	$K^+a_0(980)^-$, $a_0^- \to K^-K_S^0$	$< 1.1 \times 10^{-4}$	CL=95%
Γ_{140}	$K_S^0 f_0(980)$, $f_0 \to K^+K^-$	$< 9 \times 10^{-5}$	CL=95%
Γ_{141}	$K_S^0\phi$, $\phi \to K^+K^-$	$(2.06 \pm 0.14) \times 10^{-3}$	
Γ_{142}	$K_L^0\phi$	$(4.06 \pm 0.23) \times 10^{-3}$	
Γ_{143}	$K_S^0 f_0(1370)$, $f_0 \to K^+K^-$	$(1.7 \pm 1.1) \times 10^{-4}$	
Γ_{144}	$3K_S^0$	$(7.6 \pm 0.7) \times 10^{-4}$	S=1.4
Γ_{145}	$K^+2K^-\pi^+$	$(2.24 \pm 0.32) \times 10^{-4}$	
Γ_{146}	$K^+K^-\overline{K}^*(892)^0$, $\overline{K}^{*0} \to K^-\pi^+$	$(4.5 \pm 1.8) \times 10^{-5}$	
Γ_{147}	$K^-\pi^+\phi$, $\phi \to K^+K^-$	$(4.0 \pm 1.7) \times 10^{-5}$	
Γ_{148}	$\phi\overline{K}^*(892)^0$, $\phi \to K^+K^-$, $\overline{K}^{*0} \to K^-\pi^+$	$(1.08 \pm 0.20) \times 10^{-4}$	
Γ_{149}	$K^+2K^-\pi^+$ nonresonant	$(3.4 \pm 1.5) \times 10^{-5}$	
Γ_{150}	$2K_S^0K^\pm\pi^\mp$	$(6.0 \pm 1.3) \times 10^{-4}$	

Pionic modes

Γ_{151}	$\pi^+\pi^-$	$(1.451 \pm 0.024) \times 10^{-3}$	S=1.4
Γ_{152}	$2\pi^0$	$(8.25 \pm 0.25) \times 10^{-4}$	
Γ_{153}	$\pi^+\pi^-\pi^0$	(1.49 ± 0.06) %	S=2.1
Γ_{154}	$\rho^+\pi^-$	(1.01 ± 0.04) %	
Γ_{155}	$\rho^0\pi^0$	$(3.85 \pm 0.23) \times 10^{-3}$	
Γ_{156}	$\rho^-\pi^+$	$(5.14 \pm 0.25) \times 10^{-3}$	
Γ_{157}	$\rho(1450)^+\pi^-$, $\rho^+ \to \pi^+\pi^0$	$(1.6 \pm 2.1) \times 10^{-5}$	
Γ_{158}	$\rho(1450)^0\pi^0$, $\rho^0 \to \pi^+\pi^-$	$(4.5 \pm 1.9) \times 10^{-5}$	
Γ_{159}	$\rho(1450)^-\pi^+$, $\rho^- \to \pi^-\pi^0$	$(2.7 \pm 0.4) \times 10^{-4}$	
Γ_{160}	$\rho(1700)^+\pi^-$, $\rho^+ \to \pi^+\pi^0$	$(6.1 \pm 1.5) \times 10^{-4}$	
Γ_{161}	$\rho(1700)^0\pi^0$, $\rho^0 \to \pi^+\pi^-$	$(7.4 \pm 1.8) \times 10^{-4}$	
Γ_{162}	$\rho(1700)^-\pi^+$, $\rho^- \to \pi^-\pi^0$	$(4.8 \pm 1.1) \times 10^{-4}$	
Γ_{163}	$f_0(980)\pi^0$, $f_0 \to \pi^+\pi^-$	$(3.7 \pm 0.9) \times 10^{-5}$	
Γ_{164}	$f_0(500)\pi^0$, $f_0 \to \pi^+\pi^-$	$(1.22 \pm 0.22) \times 10^{-4}$	
Γ_{165}	$f_0(1370)\pi^0$, $f_0 \to \pi^+\pi^-$	$(5.5 \pm 2.1) \times 10^{-5}$	
Γ_{166}	$f_0(1500)\pi^0$, $f_0 \to \pi^+\pi^-$	$(5.8 \pm 1.6) \times 10^{-5}$	
Γ_{167}	$f_0(1710)\pi^0$, $f_0 \to \pi^+\pi^-$	$(4.6 \pm 1.6) \times 10^{-5}$	
Γ_{168}	$f_2(1270)\pi^0$, $f_2 \to \pi^+\pi^-$	$(1.96 \pm 0.21) \times 10^{-4}$	
Γ_{169}	$\pi^+\pi^-\pi^0$ nonresonant	$(1.2 \pm 0.4) \times 10^{-4}$	
Γ_{170}	$3\pi^0$	$(2.0 \pm 0.5) \times 10^{-4}$	
Γ_{171}	$2\pi^+2\pi^-$	$(7.15 \pm 0.25) \times 10^{-3}$	S=2.2
Γ_{172}	$a_1(1260)^+\pi^-$, $a_1^+ \to 2\pi^+\pi^-$ total	$(4.37 \pm 0.31) \times 10^{-3}$	
Γ_{173}	$a_1(1260)^+\pi^-$, $a_1^+ \to \rho^0\pi^+$ S-wave	$(2.97 \pm 0.21) \times 10^{-3}$	
Γ_{174}	$a_1(1260)^+\pi^-$, $a_1^+ \to \rho^0\pi^+$ D-wave	$(1.8 \pm 0.5) \times 10^{-4}$	
Γ_{175}	$a_1(1260)^+\pi^-$, $a_1^+ \to \sigma\pi^+$	$(6.0 \pm 0.7) \times 10^{-4}$	
Γ_{176}	$a_1(1260)^-\pi^+$, $a_1^- \to 2\pi^-\pi^+$ total	$(7.4 \pm 2.1) \times 10^{-4}$	
Γ_{177}	$a_1(1260)^-\pi^+$, $a_1^- \to \rho^0\pi^-$ S-wave	$(2.2 \pm 0.8) \times 10^{-4}$	

Γ_{178}	$a_1(1260)^-\pi^+,\ a_1^- \to \sigma\pi^-$	$(5.7 \pm 3.2)\times10^{-5}$	
Γ_{179}	$\pi(1300)^+\pi^-,\ \pi(1300)^+ \to 2\pi^+\pi^-$ total	$(2.3 \pm 0.4)\times10^{-3}$	
Γ_{180}	$\pi(1300)^+\pi^-,\ \pi(1300)^+ \to \sigma\pi^+$	$(4.9 \pm 2.5)\times10^{-4}$	
Γ_{181}	$\pi(1300)^-\pi^+,\ \pi(1300)^- \to 2\pi^-\pi^+$ total	$(1.68 \pm 0.33)\times10^{-3}$	
Γ_{182}	$\pi(1300)^-\pi^+,\ \pi(1300)^- \to \sigma\pi^-$	$(2.1 \pm 2.0)\times10^{-4}$	
Γ_{183}	$a_2(1320)^+\pi^-,\ a_2^+ \to \rho^0\pi^+$ D-wave	$(1.4 \pm 1.0)\times10^{-5}$	
Γ_{184}	$a_2(1320)^-\pi^+,\ a_2^- \to \rho^0\pi^-$ D-wave	$(2.9 \pm 1.0)\times10^{-5}$	
Γ_{185}	$a_1(1420)^+\pi^-,\ a_1^+ \to f_0(980)\pi^+$ P-wave, $f_0 \to \pi^+\pi^-$	$(4.3 \pm 2.0)\times10^{-5}$	
Γ_{186}	$a_1(1640)^+\pi^-,\ a_1^+ \to \rho^0\pi^+$ S-wave	$(1.2 \pm 0.7)\times10^{-4}$	
Γ_{187}	$a_1(1640)^+\pi^-,\ a_1^+ \to \rho^0\pi^+$ D-wave	$(3.0 \pm 1.5)\times10^{-4}$	
Γ_{188}	$a_1(1640)^+\pi^-,\ a_1^+ \to \sigma\pi^+$	$(1.7 \pm 1.3)\times10^{-4}$	
Γ_{189}	$a_1(1640)^-\pi^+,\ a_1^- \to \rho^0\pi^-$ S-wave	$(4 \pm 4)\times10^{-5}$	
Γ_{190}	$\pi_2(1670)^+\pi^-,\ \pi_2^+ \to f_2(1270)^0\pi^+,\ f_2^0 \to \pi^+\pi^-$	$(1.9 \pm 0.9)\times10^{-4}$	
Γ_{191}	$\pi_2(1670)^+\pi^-,\ \pi_2^+ \to \sigma\pi^+$	$(2.5 \pm 1.0)\times10^{-4}$	
Γ_{192}	$2\rho(770)^0$ total	$(1.79 \pm 0.12)\times10^{-3}$	
Γ_{193}	$2\rho^0$, parallel helicities	$(7.9 \pm 3.0)\times10^{-5}$	
Γ_{194}	$2\rho^0$, perpendicular helicities	$(4.6 \pm 0.6)\times10^{-4}$	
Γ_{195}	$2\rho^0$, longitudinal helicities	$(1.20 \pm 0.10)\times10^{-3}$	
Γ_{196}	$2\rho(770)^0$, S-wave	$(1.3 \pm 0.5)\times10^{-4}$	
Γ_{197}	$2\rho(770)^0$, P-wave	$(6.2 \pm 1.0)\times10^{-4}$	
Γ_{198}	$2\rho(770)^0$, D-wave	$(1.2 \pm 0.5)\times10^{-3}$	
Γ_{199}	$\rho(770)^0\rho(1450)^0,\ \rho(1450)^0 \to \pi^+\pi^-$	$(1.8 \pm 1.1)\times10^{-4}$	
Γ_{200}	$\rho(770)^0\rho(1450)^0$ P-wave, $\rho(1450)^0 \to \pi^+\pi^-$	$(7 \pm 5)\times10^{-5}$	
Γ_{201}	$\rho(770)^0\rho(1450)^0$ D-wave, $\rho(1450)^0 \to \pi^+\pi^-$	$(1.1 \pm 1.0)\times10^{-4}$	
Γ_{202}	Resonant $(\pi^+\pi^-)\pi^+\pi^-$ 3-body total	$(1.43 \pm 0.12)\times10^{-3}$	
Γ_{203}	$(\pi^+\pi^-)_{S-wave}(\pi^+\pi^-)_{S-wave}$	$(4.5 \pm 0.8)\times10^{-3}$	
Γ_{204}	$\sigma\pi^+\pi^-$	$(5.9 \pm 0.8)\times10^{-4}$	
Γ_{205}	$f_0(980)\pi^+\pi^-,\ f_0 \to \pi^+\pi^-$	$(1.7 \pm 0.5)\times10^{-4}$	
Γ_{206}	$\rho(770)^0(\pi^+\pi^-)_{S-wave}$	$(1.9 \pm 1.3)\times10^{-4}$	
Γ_{207}	$\sigma\rho(770)^0$	$(4.7 \pm 2.4)\times10^{-4}$	
Γ_{208}	$f_2(1270)\pi^+\pi^-,\ f_2 \to \pi^+\pi^-$	$(3.5 \pm 0.6)\times10^{-4}$	
Γ_{209}	$f_2(1270)^0(\pi^+\pi^-)_{S-wave},\ f_2(1270)^0 \to \pi^+\pi^-$	$(1.3 \pm 1.0)\times10^{-4}$	
Γ_{210}	$f_2(1270)f_2(1270),\ f_2 \to \pi^+\pi^-$	$(1.5 \pm 1.7)\times10^{-4}$	
Γ_{211}	$f_0(1370)\sigma,\ f_0 \to \pi^+\pi^-$	$(1.5 \pm 0.5)\times10^{-3}$	
Γ_{212}	$\pi^+\pi^-2\pi^0$	(1.002 ± 0.031) %	
Γ_{213}	$\pi^+\pi^-2\pi^0$ (non-η)	$(9.51 \pm 0.33)\times10^{-3}$	
Γ_{214}	$a_1(1260)^+\pi^-,\ a_1^+ \to \pi^+2\pi^0$ total	$(5.8 \pm 0.8)\times10^{-3}$	
Γ_{215}	$a_1(1260)^-\pi^+,\ a_1^- \to \pi^-2\pi^0$ total	$(7.2 \pm 2.5)\times10^{-4}$	
Γ_{216}	$a_1(1260)^0\pi^0,\ a_1^0 \to \pi^+\pi^-\pi^0$ total	$(3.3 \pm 0.9)\times10^{-3}$	
Γ_{217}	$a_1(1420)^+\pi^-,\ a_1^+ \to f_0(980)\pi^+$ P-wave, $f_0 \to \pi^0\pi^0$	$(3.0 \pm 1.4)\times10^{-5}$	
Γ_{218}	$a_1(1640)^-\pi^+,\ a_1^- \to \rho^-\pi^0$ S-wave	$(3.0 \pm 2.8)\times10^{-5}$	
Γ_{219}	$a_1(1640)^+\pi^-,\ a_1^+ \to \rho^+\pi^0$ S-wave	$(1.1 \pm 0.7)\times10^{-4}$	
Γ_{220}	$a_2(1320)^+\pi^-,\ a_2^+ \to \rho^+\pi^0$ D-wave	$(2.0 \pm 1.4)\times10^{-5}$	
Γ_{221}	$a_2(1320)^-\pi^+,\ a_2^- \to \rho^-\pi^0$ D-wave	$(3.0 \pm 1.4)\times10^{-5}$	
Γ_{222}	$h_1(1170)^0\pi^0,\ h_1^0 \to \rho\pi$	$(1.3 \pm 1.3)\times10^{-4}$	
Γ_{223}	$\pi(1300)^-\pi^+,\ \pi(1300)^- \to \pi^-2\pi^0$ total	$(1.14 \pm 0.27)\times10^{-3}$	
Γ_{224}	$\pi(1300)^+\pi^-,\ \pi(1300)^+ \to \pi^+2\pi^0$ total	$(1.56 \pm 0.30)\times10^{-3}$	
Γ_{225}	$\pi(1300)^0\pi^0,\ \pi(1300)^0 \to \pi^+\pi^-\pi^0$ total	$(2.3 \pm 0.4)\times10^{-3}$	
Γ_{226}	$\pi_2(1670)^0\pi^0,\ \pi_2(1670)^0 \to \pi^+\pi^-\pi^0$ total	$(1.1 \pm 0.4)\times10^{-4}$	
Γ_{227}	$\rho(770)^+\rho(770)^-$	$(9.1 \pm 0.9)\times10^{-3}$	
Γ_{228}	$\rho(770)^+\rho(770)^-$ S-wave	$(1.3 \pm 0.4)\times10^{-3}$	
Γ_{229}	$\rho(770)^+\rho(770)^-$ P-wave	$(1.96 \pm 0.23)\times10^{-3}$	
Γ_{230}	$\rho(770)^+\rho(770)^-$ D-wave	$(3.6 \pm 0.4)\times10^{-3}$	
Γ_{231}	$\rho(770)^+\rho(1450)^-$ D-wave, $\rho(1450)^- \to \pi^-\pi^0$	$(1.7 \pm 2.0)\times10^{-4}$	
Γ_{232}	$\rho(770)^0(\pi^0\pi^0)_{S-wave}$	$(1.0 \pm 0.4)\times10^{-4}$	
Γ_{233}	$(\pi^+\pi^-)_{S-wave}(\pi^0\pi^0)_{S-wave}$	$(3.7 \pm 0.6)\times10^{-3}$	
Γ_{234}	$f_2(1270)(\pi^0\pi^0)_{S-wave},\ f_2 \to \pi^+\pi^-$		
Γ_{235}	$f_2(1270)(\pi^+\pi^-)_{S-wave},\ f_2 \to \pi^0\pi^0$		
Γ_{236}	$\omega(782)\pi^0,\ \omega \to \pi^+\pi^-\pi^0$	$(9 \pm 4)\times10^{-5}$	
Γ_{237}	$\phi(1020)\pi^0,\ \phi(1020) \to \pi^+\pi^-\pi^0$	$(1.5 \pm 0.5)\times10^{-4}$	
Γ_{238}	$4\pi^0$	$(7.6 \pm 1.1)\times10^{-4}$	
Γ_{239}	$\eta\pi^0$ [h]	$(6.3 \pm 0.5)\times10^{-4}$	S=1.1
Γ_{240}	$\omega\pi^0$ [h]	$(1.17 \pm 0.35)\times10^{-4}$	
Γ_{241}	$\omega\eta$	$(1.98 \pm 0.18)\times10^{-3}$	S=1.1
Γ_{242}	$2\pi^+2\pi^-\pi^0$	$(3.46 \pm 0.21)\times10^{-3}$	
Γ_{243}	$\pi^+\pi^-3\pi^0$	$(1.53 \pm 0.21)\times10^{-3}$	
Γ_{244}	$2\pi^+2\pi^-2\pi^0$	$(4.8 \pm 0.4)\times10^{-3}$	
Γ_{245}	$\eta\pi^+\pi^-$ [h]	$(1.16 \pm 0.07)\times10^{-3}$	
Γ_{246}	$\rho(770)^0\eta,\ \rho^0 \to \pi^+\pi^-$	$(1.77 \pm 0.25)\times10^{-4}$	
Γ_{247}	$a_0(980)^-\pi^+,\ a_0^- \to \pi^-\eta$	$(6.9 \pm 1.9)\times10^{-5}$	
Γ_{248}	$a_0(980)^+\pi^-,\ a_0^+ \to \pi^+\eta$	$(5.1 \pm 0.8)\times10^{-4}$	
Γ_{249}	$a_2(1320)^+\pi^-,\ a_2^+ \to \pi^+\eta$	$(2.4 \pm 1.4)\times10^{-5}$	
Γ_{250}	$a_2(1700)^+\pi^-,\ a_2^+ \to \pi^+\eta$	$(6 \pm 4)\times10^{-5}$	
Γ_{251}	$(\pi^+\pi^-)_{S-wave}\eta$	$(4.5 \pm 3.2)\times10^{-5}$	
Γ_{252}	$\omega\pi^+\pi^-$ [h]	$(1.33 \pm 0.20)\times10^{-3}$	
Γ_{253}	$\omega\pi^0\pi^0$	$< 1.10 \times10^{-3}$	CL=90%
Γ_{254}	$\eta2\pi^0$	$(3.8 \pm 1.3)\times10^{-4}$	
Γ_{255}	$\pi^+\pi^-\pi^0\eta$	$(3.23 \pm 0.22)\times10^{-3}$	
Γ_{256}	$\eta3\pi^0$	$(2.36 \pm 0.28)\times10^{-3}$	
Γ_{257}	$\eta2\pi^+2\pi^-$	$(6.0 \pm 1.2)\times10^{-4}$	
Γ_{258}	$3\pi^+3\pi^-$	$(4.3 \pm 1.2)\times10^{-4}$	
Γ_{259}	$\eta'(958)\pi^0$	$(9.2 \pm 1.0)\times10^{-4}$	
Γ_{260}	$\eta'(958)\pi^+\pi^-$	$(4.5 \pm 1.7)\times10^{-4}$	
Γ_{261}	2η	$(2.11 \pm 0.19)\times10^{-3}$	S=2.3
Γ_{262}	$2\eta\pi^0$	$(7.3 \pm 2.2)\times10^{-4}$	
Γ_{263}	$2\eta\pi^+\pi^-$	$(8.5 \pm 1.4)\times10^{-4}$	
Γ_{264}	3η	$< 1.3 \times10^{-4}$	CL=90%
Γ_{265}	$\eta\eta'(958)$	$(1.01 \pm 0.19)\times10^{-3}$	

Hadronic modes with a $K\overline{K}$ pair

Γ_{266}	K^+K^-	$(4.07 \pm 0.06)\times10^{-3}$	S=1.6
Γ_{267}	$2K^0_S$	$(1.41 \pm 0.05)\times10^{-4}$	S=1.1
Γ_{268}	$K^0_SK^-\pi^+$	$(3.4 \pm 0.5)\times10^{-3}$	S=1.1
Γ_{269}	$\overline{K}^*(892)^0K^0_S,\ \overline{K}^{*0} \to K^-\pi^+$	$(8.3 \pm 1.6)\times10^{-5}$	
Γ_{270}	$K^*(892)^+K^-,\ K^{*+} \to K^0_S\pi^+$	$(1.91 \pm 0.30)\times10^{-3}$	
Γ_{271}	$\overline{K}^*(1410)^0K^0_S,\ \overline{K}^{*0} \to K^-\pi^+$	$(1.3 \pm 1.9)\times10^{-4}$	
Γ_{272}	$K^*(1410)^+K^-,\ K^{*+} \to K^0_S\pi^+$	$(3.2 \pm 1.9)\times10^{-4}$	
Γ_{273}	$(K^-\pi^+)_{S-wave}K^0_S$	$(6.0 \pm 2.9)\times10^{-4}$	
Γ_{274}	$(K^0_S\pi^+)_{S-wave}K^-$	$(3.9 \pm 1.0)\times10^{-4}$	
Γ_{275}	$a_0(980)^-\pi^+,\ a_0^- \to K^0_SK^-$	$(1.3 \pm 1.4)\times10^{-4}$	
Γ_{276}	$a_0(1450)^-\pi^+,\ a_0^- \to K^0_SK^-$	$(2.5 \pm 2.0)\times10^{-5}$	
Γ_{277}	$a_2(1320)^-\pi^+,\ a_2^- \to K^0_SK^-$	$(5 \pm 5)\times10^{-6}$	
Γ_{278}	$\rho(1450)^-\pi^+,\ \rho^- \to K^0_SK^-$	$(4.7 \pm 2.5)\times10^{-5}$	
Γ_{279}	$K^0_SK^+\pi^-$	$(2.19 \pm 0.34)\times10^{-3}$	S=1.1

Int. J. Mod. Phys. A 2026.41. Downloaded from www.worldscientific.com
by LIFORNIA @ BERKELEY on 09/16/26. Re-use and distribution is strictly not permitted, except for Open Access articles.

Int. J. Mod. Phys. A 2026.41. Downloaded from www.worldscientific.com
by UNIVERSITY OF CALIFORNIA @ BERKELEY on 09/16/26. Re-use and distribution is strictly not permitted, except for Open Access articles.

Γ_{280}	$K^*(892)^0 K^0_S$, $K^{*0} \to K^+\pi^-$	$(1.13 \pm 0.21) \times 10^{-4}$		
Γ_{281}	$K^*(892)^- K^+$, $K^{*-} \to K^0_S \pi^-$	$(6.3 \pm 1.0) \times 10^{-4}$		
Γ_{282}	$K^*(1410)^0 K^0_S$, $K^{*0} \to K^+\pi^+$	$(5 \pm 8) \times 10^{-5}$		
Γ_{283}	$K^*(1410)^- K^+$, $K^{*-} \to K^0_S \pi^-$	$(2.6 \pm 2.1) \times 10^{-4}$		
Γ_{284}	$(K^+\pi^-)_{S-wave} K^0_S$	$(3.7 \pm 1.9) \times 10^{-4}$		
Γ_{285}	$(K^0_S\pi^-)_{S-wave} K^+$	$(1.4 \pm 0.6) \times 10^{-4}$		
Γ_{286}	$a_0(980)^+\pi^-$, $a_0^+ \to K^0_S K^+$	$(6 \pm 4) \times 10^{-4}$		
Γ_{287}	$a_0(1450)^+\pi^-$, $a_0^+ \to K^0_S K^+$	$(3.3 \pm 2.6) \times 10^{-5}$		
Γ_{288}	$\rho(1700)^+\pi^-$, $\rho^+ \to K^0_S K^+$	$(1.2 \pm 0.6) \times 10^{-5}$		
Γ_{289}	$K^+K^-\pi^0$	$(3.41 \pm 0.14) \times 10^{-3}$		
Γ_{290}	$K^*(892)^+ K^-$, $K^*(892)^+ \to K^+\pi^0$	$(1.51 \pm 0.07) \times 10^{-3}$		
Γ_{291}	$K^*(892)^- K^+$, $K^*(892)^- \to K^-\pi^0$	$(5.4 \pm 0.4) \times 10^{-4}$		
Γ_{292}	$(K^+\pi^0)_{S-wave} K^-$	$(2.42 \pm 0.17) \times 10^{-3}$		
Γ_{293}	$(K^-\pi^0)_{S-wave} K^+$	$(1.3 \pm 0.5) \times 10^{-4}$		
Γ_{294}	$f_0(980)\pi^0$, $f_0 \to K^+K^-$	$(3.6 \pm 0.6) \times 10^{-4}$		
Γ_{295}	$\phi\pi^0$, $\phi \to K^+K^-$	$(6.6 \pm 0.4) \times 10^{-4}$		
Γ_{296}	$K^+K^-\pi^0$ nonresonant			
Γ_{297}	$2K^0_S\pi^0$	$< 1.45 \times 10^{-4}$	CL=90%	
Γ_{298}	$K^+K^-\eta$	$(5.9 \pm 1.9) \times 10^{-5}$		
Γ_{299}	$\phi(1020)\eta$	$(1.80 \pm 0.12) \times 10^{-4}$		
Γ_{300}	$K^+K^-\eta$ nonresonant	$(9.9 {}^{+0.9}_{-0.8}) \times 10^{-5}$		
Γ_{301}	$2K^0_S\eta$	$(1.3 \pm 0.6) \times 10^{-4}$		
Γ_{302}	$K^+K^-\pi^0\pi^0$	$(6.9 \pm 0.8) \times 10^{-4}$		
Γ_{303}	$K^+K^-\pi^+\pi^-$	$(2.78 \pm 0.17) \times 10^{-3}$	S=3.6	
Γ_{304}	$\phi(\pi^+\pi^-)_{S-wave}$, $\phi \to K^+K^-$	$(1.1 \pm 0.6) \times 10^{-4}$		
Γ_{305}	$(\phi\rho^0)_{S-wave}$, $\phi \to K^+K^-$	$(7.8 \pm 0.8) \times 10^{-4}$		
Γ_{306}	$(\phi\rho^0)_{P-wave}$, $\phi \to K^+K^-$	$(4.4 \pm 2.1) \times 10^{-5}$		
Γ_{307}	$(\phi\rho^0)_{D-wave}$, $\phi \to K^+K^-$	$(4.7 \pm 1.6) \times 10^{-5}$		
Γ_{308}	$K^*(892)^0\overline{K}^*(892)^0$, $K^{*0} \to K^\pm\pi^\mp$			
Γ_{309}	$K^+K^-\rho^0$ 3-body			
Γ_{310}	$f_0(980)\pi^+\pi^-$, $f_0 \to K^+K^-$			
Γ_{311}	$(K^*(892)^0\overline{K}^*(892)^0)_{S-wave}$, $K^{*0} \to K^\pm\pi^\mp$	$(2.52 \pm 0.18) \times 10^{-4}$		
Γ_{312}	$(K^*(892)^0\overline{K}^*(892)^0)_{P-wave}$, $K^* \to K^\pm\pi^\mp$	$(1.35 \pm 0.11) \times 10^{-4}$		
Γ_{313}	$(K^*(892)^0\overline{K}^*(892)^0)_{D-wave}$, $K^* \to K^\pm\pi^\mp$	$(5.3 \pm 0.5) \times 10^{-5}$		
Γ_{314}	$K^*(892)^0 K^\mp\pi^\pm$ 3-body, $K^{*0} \to K^\pm\pi^\mp$			
Γ_{315}	$K^*(892)^0(K^-\pi^+)_{S-wave}$ 3-body, $K^{*0} \to K^+\pi^-$	$(1.6 \pm 0.7) \times 10^{-4}$		
Γ_{316}	$(K^-\pi^+)_{P-wave}$, $(K^+\pi^-)_{S-wave}$			
Γ_{317}	$K_1(1270)^\pm K^\mp$, $K_1^\pm \to K^\pm\pi^+\pi^-$			
Γ_{318}	$K_1(1270)^+ K^-$, $K_1^+ \to K^{*0}\pi^+$	$(1.5 \pm 1.0) \times 10^{-4}$		
Γ_{319}	$K_1(1270)^+ K^-$, $K_1^+ \to K^*(1430)^0\pi^+$, $K^{*0} \to K^+\pi^-$	$(1.7 \pm 0.6) \times 10^{-4}$		
Γ_{320}	$K_1(1270)^+ K^-$, $K_1^+ \to \rho^0 K^+$	$(2.5 \pm 0.7) \times 10^{-4}$		
Γ_{321}	$K_1(1270)^+ K^-$, $K_1^+ \to \omega(782)K^+$, $\omega \to \pi^+\pi^-$	$(1.7 \pm 1.4) \times 10^{-5}$		
Γ_{322}	$K_1(1270)^- K^+$, $K_1^- \to \overline{K}^{*0}\pi^-$			
Γ_{323}	$K_1(1270)^- K^+$, $K_1^- \to \rho^0 K^-$	$(1.5 \pm 0.4) \times 10^{-4}$		
Γ_{324}	$K_1(1400)^\pm K^\mp$, $K_1^\pm \to K^\pm\pi^+\pi^-$			
Γ_{325}	$K_1(1400)^+ K^-$, $K_1^+ \to K^*(892)^0\pi^+$, $K^{*0} \to K^+\pi^-$	$(5.2 \pm 0.5) \times 10^{-4}$		
Γ_{326}	$K^*(1410)^+ K^-$, $K^{*+} \to K^{*0}\pi^+$			
Γ_{327}	$K^*(1410)^- K^+$, $K^{*-} \to \overline{K}^{*0}\pi^-$	$(7.8 \pm 1.3) \times 10^{-5}$		
Γ_{328}	$K_1(1680)^+ K^-$, $K_1^+ \to K^{*0}\pi^+$, $K^{*0} \to K^+\pi^-$	$(1.0 \pm 0.4) \times 10^{-4}$		
Γ_{329}	$K^+K^-\pi^+\pi^-$ non-resonant	$(3.1 \pm 0.7) \times 10^{-4}$		
Γ_{330}	$2K^0_S\pi^+\pi^-$	$(5.3 \pm 0.9) \times 10^{-4}$		
Γ_{331}	$K^0_S K^-\pi^+\pi^0$	$(1.32 \pm 0.16) \times 10^{-3}$		
Γ_{332}	$K^0_S K^+\pi^-\pi^0$	$(6.5 \pm 0.7) \times 10^{-4}$		
Γ_{333}	$K^0_S K^- 2\pi^+\pi^-$	$< 1.5 \times 10^{-4}$	CL=90%	
Γ_{334}	$K^+K^-\pi^+\pi^-\pi^0$	$(3.1 \pm 2.0) \times 10^{-3}$		

Other $K\overline{K}X$ modes. They include all decay modes of the ϕ, η, and ω.

Γ_{335}	$\phi\pi^0$	$(1.17 \pm 0.04) \times 10^{-3}$		
Γ_{336}	$\phi\eta$	$(1.8 \pm 0.5) \times 10^{-4}$		
Γ_{337}	$\phi\omega$	$(6.5 \pm 1.0) \times 10^{-4}$		

Radiative modes

Γ_{338}	$\rho^0\gamma$	$(1.81 \pm 0.31) \times 10^{-5}$		
Γ_{339}	$\omega\gamma$	$< 2.4 \times 10^{-4}$	CL=90%	
Γ_{340}	$\phi\gamma$	$(2.80 \pm 0.19) \times 10^{-5}$		
Γ_{341}	$\overline{K}^*(892)^0\gamma$	$(4.1 \pm 0.7) \times 10^{-4}$		

Doubly Cabibbo suppressed (*DC*) modes or $\Delta C = 2$ forbidden via mixing (*C2M*) modes

Γ_{342}	$K^+\ell^-\overline{\nu}_\ell$ via $\overline{D}^0$		[i] $< 2.2 \times 10^{-5}$	CL=90%	
Γ_{343}	K^+ or $K^*(892)^+ e^-\overline{\nu}_e$ via $\overline{D}^0$		$< 6 \times 10^{-5}$	CL=90%	
Γ_{344}	$K^+\pi^-$	*DC*	$(1.48 \pm 0.07) \times 10^{-4}$	S=3.1	
Γ_{345}	$K^+\pi^-$ via DCS		$(1.359 \pm 0.025) \times 10^{-4}$		
Γ_{346}	$K^+\pi^-$ via $\overline{D}^0$		$< 1.6 \times 10^{-5}$	CL=95%	
Γ_{347}	$K^0_S\pi^+\pi^-$ in $D^0 \to \overline{D}^0$		$< 1.8 \times 10^{-4}$	CL=95%	
Γ_{348}	$K^*(892)^+\pi^-$, $K^{*+} \to K^0_S\pi^+$	*DC*	$(1.14 {}^{+0.60}_{-0.34}) \times 10^{-4}$		
Γ_{349}	$K^*_0(1430)^+\pi^-$, $K^{*+}_0 \to K^0_S\pi^+$	*DC*	$< 1.4 \times 10^{-5}$		
Γ_{350}	$K^*_2(1430)^+\pi^-$, $K^{*+}_2 \to K^0_S\pi^+$	*DC*	$< 3.4 \times 10^{-5}$		
Γ_{351}	$K^+\pi^-\pi^0$	*DC*	$(3.05 \pm 0.13) \times 10^{-4}$	S=1.3	
Γ_{352}	$K^+\pi^-\pi^0$ via $\overline{D}^0$		$(7.6 \pm 0.5) \times 10^{-4}$		
Γ_{353}	$K^+\pi^-\eta$		$(1.04 \pm 0.18) \times 10^{-4}$		
Γ_{354}	$K^+\pi^-2\pi^0$		$(1.40 \pm 0.28) \times 10^{-4}$		
Γ_{355}	$K^+\pi^+2\pi^-$ via DCS		$(2.48 \pm 0.07) \times 10^{-4}$		
Γ_{356}	$K^+\pi^+2\pi^-$	*DC*	$(2.64 \pm 0.06) \times 10^{-4}$	S=1.1	
Γ_{357}	$K^+\pi^+2\pi^-$ via $\overline{D}^0$		$(7.9 \pm 3.0) \times 10^{-6}$		
Γ_{358}	$K^+\pi^-\pi^0\eta$		$< 7 \times 10^{-5}$	CL=90%	
Γ_{359}	$K^+\pi^-$ or $K^+\pi^+2\pi^-$ via $\overline{D}^0$				
Γ_{360}	μ^- anything via $\overline{D}^0$		$< 4 \times 10^{-4}$	CL=90%	

$\Delta C = 1$ weak neutral current (*C1*) modes, Lepton Family number (*LF*) violating modes, Lepton (*L*) or Baryon (*B*) number violating modes

Γ_{361}	$\gamma\gamma$	*C1*	$< 8.5 \times 10^{-7}$	CL=90%	
Γ_{362}	e^+e^-	*C1*	$< 7.9 \times 10^{-8}$	CL=90%	
Γ_{363}	$\mu^+\mu^-$	*C1*	$< 2.1 \times 10^{-9}$	CL=90%	
Γ_{364}	$\pi^0 e^+e^-$	*C1*	$< 4 \times 10^{-6}$	CL=90%	
Γ_{365}	$\pi^0\mu^+\mu^-$	*C1*	$< 1.8 \times 10^{-4}$	CL=90%	
Γ_{366}	$\pi^0\nu\overline{\nu}$		$< 2.1 \times 10^{-4}$	CL=90%	
Γ_{367}	ηe^+e^-	*C1*	$< 3 \times 10^{-6}$	CL=90%	
Γ_{368}	$\eta\mu^+\mu^-$	*C1*	$< 5.3 \times 10^{-4}$	CL=90%	
Γ_{369}	$\pi^+\pi^-e^+e^-$	*C1*	$< 7 \times 10^{-6}$	CL=90%	
Γ_{370}	$\rho^0 e^+e^-$	*C1*	$< 1.0 \times 10^{-4}$	CL=90%	
Γ_{371}	$\pi^+\pi^-\mu^+\mu^-$	*C1*	$(9.6 \pm 1.2) \times 10^{-7}$		
Γ_{372}	$\pi^+\pi^-\mu^+\mu^-$ (non-res)		$< 5.5 \times 10^{-7}$	CL=90%	
Γ_{373}	$\rho^0\mu^+\mu^-$	*C1*	$< 2.2 \times 10^{-5}$	CL=90%	
Γ_{374}	ωe^+e^-	*C1*	$< 6 \times 10^{-6}$	CL=90%	
Γ_{375}	$\omega\mu^+\mu^-$	*C1*	$< 8.3 \times 10^{-4}$	CL=90%	
Γ_{376}	$K^-K^+e^+e^-$	*C1*	$< 1.1 \times 10^{-5}$	CL=90%	
Γ_{377}	ϕe^+e^-	*C1*	$< 5.2 \times 10^{-5}$	CL=90%	
Γ_{378}	$K^-K^+\mu^+\mu^-$	*C1*	$(1.54 \pm 0.32) \times 10^{-7}$		
Γ_{379}	$K^-K^+\mu^+\mu^-$ (non-res)		$< 3.3 \times 10^{-5}$	CL=90%	
Γ_{380}	$\phi\mu^+\mu^-$	*C1*	$< 3.1 \times 10^{-5}$	CL=90%	
Γ_{381}	$\overline{K}^0 e^+e^-$		[j] $< 2.4 \times 10^{-5}$	CL=90%	
Γ_{382}	$\overline{K}^0\mu^+\mu^-$		[j] $< 2.6 \times 10^{-4}$	CL=90%	
Γ_{383}	$K^-\pi^+e^+e^-$				

Γ_{384}	$K^-\pi^+e^+e^-$, 675 < m_{ee} < 875 MeV			$(4.0 \pm 0.4) \times 10^{-6}$	
Γ_{385}	$K^-\pi^+e^+e^-$, 1.005 < m_{ee} < 1.035 GeV			$< 5 \times 10^{-7}$	CL=90%
Γ_{386}	$\overline{K}^*(892)^0 e^+e^-$		[j]	$< 4.7 \times 10^{-5}$	CL=90%
Γ_{387}	$K^-\pi^+\mu^+\mu^-$	C1		$< 3.59 \times 10^{-4}$	CL=90%
Γ_{388}	$K^-\pi^+\mu^+\mu^-$, 675 < $m_{\mu\mu}$ < 875 MeV			$(4.2 \pm 0.4) \times 10^{-6}$	
Γ_{389}	$\overline{K}^*(892)^0 \mu^+\mu^-$		[j]	$< 2.4 \times 10^{-5}$	CL=90%
Γ_{390}	$\pi^+\pi^-\pi^0\mu^+\mu^-$	C1		$< 8.1 \times 10^{-4}$	CL=90%
Γ_{391}	$\mu^\pm e^\mp$	LF	[k]	$< 1.3 \times 10^{-8}$	CL=90%
Γ_{392}	$\pi^0 e^\pm\mu^\mp$	LF	[k]	$< 8.0 \times 10^{-7}$	CL=90%
Γ_{393}	$\eta e^\pm\mu^\mp$	LF	[k]	$< 2.25 \times 10^{-6}$	CL=90%
Γ_{394}	$\pi^+\pi^-e^\pm\mu^\mp$	LF	[k]	$< 1.71 \times 10^{-6}$	CL=90%
Γ_{395}	$\rho^0 e^\pm\mu^\mp$	LF	[k]	$< 5.0 \times 10^{-7}$	CL=90%
Γ_{396}	$\omega e^\pm\mu^\mp$	LF	[k]	$< 1.71 \times 10^{-6}$	CL=90%
Γ_{397}	$K^-K^+e^\pm\mu^\mp$	LF	[k]	$< 1.00 \times 10^{-6}$	CL=90%
Γ_{398}	$\phi e^\pm\mu^\mp$	LF	[k]	$< 5.1 \times 10^{-7}$	CL=90%
Γ_{399}	$\overline{K}^0 e^\pm\mu^\mp$	LF	[k]	$< 1.74 \times 10^{-6}$	CL=90%
Γ_{400}	$K^-\pi^+e^\pm\mu^\mp$	LF	[k]	$< 1.90 \times 10^{-6}$	CL=90%
Γ_{401}	$\overline{K}^*(892)^0 e^\pm\mu^\mp$	LF	[k]	$< 1.25 \times 10^{-6}$	CL=90%
Γ_{402}	$2\pi^-2e^+$	L		$< 9.1 \times 10^{-7}$	CL=90%
Γ_{403}	$2\pi^-2\mu^+$	L		$< 1.52 \times 10^{-6}$	CL=90%
Γ_{404}	$K^-\pi^-2e^+$	L		$< 5.0 \times 10^{-7}$	CL=90%
Γ_{405}	$K^-\pi^-2\mu^+$	L		$< 5.3 \times 10^{-7}$	CL=90%
Γ_{406}	$2K^-2e^+$	L		$< 3.4 \times 10^{-7}$	CL=90%
Γ_{407}	$2K^-2\mu^+$	L		$< 1.0 \times 10^{-7}$	CL=90%
Γ_{408}	$\pi^-\pi^-e^+\mu^+$	L		$< 3.06 \times 10^{-6}$	CL=90%
Γ_{409}	$K^-\pi^-e^+\mu^+$	L		$< 2.10 \times 10^{-6}$	CL=90%
Γ_{410}	$2K^-e^+\mu^+$	L		$< 5.8 \times 10^{-7}$	CL=90%
Γ_{411}	pe^-	L,B		$< 5.5 \times 10^{-7}$	CL=90%
Γ_{412}	$\overline{p}e^+$	L,B		$< 6.9 \times 10^{-7}$	CL=90%
Γ_{413}	$p\mu^-$	L,B		$< 5.1 \times 10^{-7}$	CL=90%
Γ_{414}	$\overline{p}\mu^+$	L,B		$< 6.3 \times 10^{-7}$	CL=90%
	Exotic modes				
Γ_{415}	$\gamma\gamma_D$		[l]	$< 2.0 \times 10^{-6}$	CL=90%
Γ_{416}	$\omega\gamma_D$		[l]	$< 1.1 \times 10^{-5}$	CL=90%

Γ_{417} Unaccounted decay modes

[a] This value is obtained by subtracting the branching fractions for 2-, 4- and 6-prongs from unity.

[b] This is the sum of our $K^-2\pi^+\pi^-$, $K^-2\pi^+\pi^-\pi^0$, $\overline{K}^0 2\pi^+2\pi^-$, $K^+2K^-\pi^+$, $2\pi^+2\pi^-$, $2\pi^+2\pi^-\pi^0$, $K^+K^-\pi^+\pi^-$, and $K^+K^-\pi^+\pi^-\pi^0$, branching fractions.

[c] This is the sum of our $K^-3\pi^+2\pi^-$ and $3\pi^+3\pi^-$ branching fractions.

[d] The branching fractions for the $K^-e^+\nu_e$, $K^*(892)^-e^+\nu_e$, $\pi^-e^+\nu_e$, and $\rho^-e^+\nu_e$ modes add up to 6.17 ± 0.17 %.

[e] The branching fraction for this mode may differ from the sum of the submodes that contribute to it, due to interference effects. See the relevant papers.

[f] This is a doubly Cabibbo-suppressed mode.

[g] Submodes of the $D^0 \to K^0_S\pi^+\pi^-\pi^0$ mode with a K^* and/or ρ were studied by COFFMAN 92B, but with only 140 events. With nothing new for 18 years, we refer to our 2008 edition, Physics Letters **B667** 1 (2008), for those results.

[h] This branching fraction includes all the decay modes of the resonance in the final state.

[i] This limit assumes the average of $B(D^0 \to K^-e^+\nu_e)$ and $B(D^0 \to K^-\mu^+\nu_\mu)$ for the $B(D^0 \to K^-\ell^+\nu_\ell)$ value.

[j] This mode is not a useful test for a ΔC=1 weak neutral current because both quarks must change flavor in this decay.

[k] The value is for the sum of the charge states or particle/antiparticle states indicated.

[l] Here γ_D stands for massless dark photon.

FIT INFORMATION

An overall fit to 81 branching ratios uses 153 measurements to determine 39 parameters. The overall fit has a $\chi^2 = 183.0$ for 114 degrees of freedom.

The following *off-diagonal* array elements are the correlation coefficients $\langle \delta x_i \delta x_j \rangle / (\delta x_i \cdot \delta x_j)$, in percent, from the fit to the branching fractions, $x_i \equiv \Gamma_i/\Gamma_{total}$.

	x_6	x_{20}	x_{21}	x_{22}	x_{23}	x_{27}	x_{29}	x_{39}	x_{40}	x_{47}
x_{20}	0									
x_{21}	3	0								
x_{22}	0	0	0							
x_{23}	0	0	0	2						
x_{27}	0	0	0	2	96					
x_{29}	0	0	0	1	79	76				
x_{39}	0	0	0	0	0	0	0			
x_{40}	0	0	0	0	0	0	0	0		
x_{47}	0	2	0	1	1	1	0	4	0	
x_{48}	0	0	0	1	1	1	1	1	0	15
x_{53}	0	0	0	12	14	13	11	0	0	4
x_{68}	0	0	0	0	0	0	0	1	0	19
x_{87}	0	1	0	0	0	0	0	2	0	44
x_{98}	0	0	0	4	5	4	4	0	0	1
x_{104}	0	0	0	0	0	0	0	0	0	8
x_{113}	0	0	0	0	0	0	0	0	0	6
x_{126}	0	0	0	0	0	0	0	0	0	1
x_{128}	0	0	0	0	0	0	0	0	0	5
x_{129}	0	0	0	1	1	1	1	0	0	0
x_{130}	0	0	0	1	1	1	1	0	0	8
x_{144}	0	0	0	2	2	2	2	0	0	1
x_{151}	0	1	0	0	0	0	0	2	0	40
x_{152}	0	0	0	0	0	0	0	0	0	7
x_{153}	0	0	0	0	0	0	0	1	0	16
x_{171}	0	0	0	0	0	0	0	1	0	17
x_{239}	0	0	0	0	0	0	0	0	0	4
x_{259}	0	0	0	0	0	0	0	0	0	3
x_{261}	0	0	0	0	0	0	0	0	0	2
x_{265}	0	0	0	0	0	0	0	0	0	2
x_{266}	0	1	0	0	0	0	0	2	0	49
x_{267}	0	0	0	0	0	0	0	0	0	7
x_{268}	0	0	0	3	4	4	3	0	0	2
x_{279}	0	0	0	3	4	4	3	0	0	2
x_{303}	0	0	0	0	0	0	0	0	0	2
x_{340}	0	0	0	0	0	0	0	0	0	11
x_{344}	0	0	0	0	0	0	0	1	0	16
x_{351}	0	0	0	0	0	0	0	1	0	13
x_{356}	0	1	0	0	0	0	0	1	0	34

	x_{48}	x_{53}	x_{68}	x_{87}	x_{98}	x_{104}	x_{113}	x_{126}	x_{128}	x_{129}
x_{53}	6									
x_{68}	3	1								
x_{87}	7	2	8							
x_{98}	2	33	0	1						
x_{104}	1	0	1	11	0					
x_{113}	1	0	1	3	0	0				
x_{126}	0	0	0	1	0	0	0			
x_{128}	1	0	1	2	0	0	0	0		
x_{129}	1	8	0	0	13	0	0	0	0	
x_{130}	2	10	2	4	3	1	0	0	0	1
x_{144}	1	18	0	0	6	0	0	0	0	1
x_{151}	6	2	8	18	1	3	2	0	2	0
x_{152}	1	0	1	3	0	1	0	0	0	0
x_{153}	2	1	80	7	0	1	1	0	1	0
x_{171}	2	1	3	24	0	3	1	0	1	0
x_{239}	1	0	1	2	0	0	0	0	0	0
x_{259}	1	0	1	2	0	0	0	0	0	0
x_{261}	0	0	0	1	0	0	0	0	0	0
x_{265}	0	0	0	1	0	0	0	0	0	0
x_{266}	7	2	9	22	1	4	3	0	3	0
x_{267}	47	3	1	3	1	1	0	0	0	0
x_{268}	2	29	0	1	10	0	0	0	0	2
x_{279}	2	29	0	1	10	0	0	0	0	2
x_{303}	0	0	0	5	0	1	0	0	0	0
x_{340}	2	0	2	5	0	1	1	0	1	0
x_{344}	3	1	3	7	0	1	1	0	1	0
x_{351}	2	1	67	6	0	1	1	0	1	0
x_{356}	5	2	6	77	0	9	2	1	2	0

Int. J. Mod. Phys. A 2026.41. Downloaded from www.worldscientific.com
by LIFORNIA @ BERKELEY on 09/16/26. Re-use and distribution is strictly not permitted, except for Open Access articles.

	x_{130}	x_{144}	x_{151}	x_{152}	x_{153}	x_{171}	x_{239}	x_{259}	x_{261}	x_{265}
x_{144}	2									
x_{151}	3	0								
x_{152}	1	0	3							
x_{153}	1	0	6	1						
x_{171}	1	0	7	1	3					
x_{239}	0	0	2	0	1	1				
x_{259}	0	0	1	0	1	1	0			
x_{261}	0	0	1	0	0	0	0	0		
x_{265}	0	0	1	0	0	0	0	0	0	
x_{266}	4	0	20	3	8	8	2	2	1	1
x_{267}	1	1	3	0	1	1	0	0	0	0
x_{268}	3	5	1	0	0	0	0	0	0	0
x_{279}	3	5	1	0	0	0	0	0	0	0
x_{303}	0	0	1	0	0	1	0	0	0	0
x_{340}	1	0	4	1	2	2	0	0	0	0
x_{344}	2	0	7	1	3	3	1	1	0	0
x_{351}	1	0	5	1	53	2	1	0	0	0
x_{356}	3	0	14	2	5	19	1	1	1	1

	x_{266}	x_{267}	x_{268}	x_{279}	x_{303}	x_{340}	x_{344}	x_{351}
x_{267}	3							
x_{268}	1	1						
x_{279}	1	1	100					
x_{303}	1	0	0	0				
x_{340}	18	1	0	0	0			
x_{344}	8	1	0	0	0	2		
x_{351}	6	1	0	0	0	1	2	
x_{356}	17	2	1	1	4	4	5	4

CONSTRAINED FIT INFORMATION

An overall fit to 3 branching ratios uses 3 measurements and one constraint to determine 4 parameters. The overall fit has a $\chi^2 = 0.0$ for 0 degrees of freedom.

The following *off-diagonal* array elements are the correlation coefficients $\langle \delta x_i \delta x_j \rangle / (\delta x_i \cdot \delta x_j)$, in percent, from the fit to the branching fractions, $x_i \equiv \Gamma_i/\Gamma_{total}$. The fit constrains the x_i whose labels appear in this array to sum to one.

	x_1	x_2	x_3
x_2	−100		
x_3	−46	39	
x_4	0	0	0

D^0 BRANCHING RATIOS

Some older now obsolete results have been omitted from these Listings.

Topological modes

Γ(0-prongs)/Γ_{total} — Γ_1/Γ

This value is obtained by subtracting the branching fractions for 2-, 4-, and 6-prongs from unity.

VALUE	DOCUMENT ID
0.15±0.06 OUR FIT	

Γ(4-prongs)/Γ(2-prongs) — Γ_3/Γ_2

VALUE	EVTS	DOCUMENT ID		TECN	COMMENT
0.207±0.016 OUR FIT					
0.207±0.016±0.004	226	ONENGUT	05	CHRS	ν_μ emulsion, $\overline{E}_\nu \approx 27$ GeV

Γ(4-prongs)/Γ_{total} — Γ_3/Γ

This is the sum of our $K^- 2\pi^+ \pi^-$, $K^- 2\pi^+ \pi^- \pi^0$, $\overline{K}^0 2\pi^+ 2\pi^-$, $K^+ 2K^- \pi^+$, $2\pi^+ 2\pi^-$, $2\pi^+ 2\pi^- \pi^0$, $K^+ K^- \pi^+ \pi^-$, and $K^+ K^- \pi^+ \pi^- \pi^0$ branching fractions.

VALUE	DOCUMENT ID	
0.146±0.005 OUR FIT		
0.146±0.005	PDG	19

Γ(6-prongs)/Γ_{total} — Γ_4/Γ

This is the sum of our $K^- 3\pi^+ 2\pi^-$ and $3\pi^+ 3\pi^-$ branching fractions.

VALUE (units 10^{-4})	DOCUMENT ID	
6.5±1.3 OUR FIT		
6.5±1.3	PDG	19

Inclusive modes

$\Gamma(e^+ \text{anything})/\Gamma_{total}$ — Γ_5/Γ

The branching fractions for the $K^- e^+ \nu_e$, $K^*(892)^- e^+ \nu_e$, $\pi^- e^+ \nu_e$, and $\rho^- e^+ \nu_e$ modes add up to 6.17 ± 0.17 %.

VALUE (%)	EVTS	DOCUMENT ID		TECN	COMMENT
6.49±0.11 OUR AVERAGE					
6.46±0.09±0.11	6584 ± 96	[1] ASNER	10	CLEO	$e^+ e^-$ at 3774 MeV
6.3 ±0.7 ±0.4	290 ± 32	ABLIKIM	07G	BES2	$e^+ e^- \approx \psi(3770)$
6.46±0.17±0.13	2246 ± 57	ADAM	06A	CLEO	See ASNER 10
6.9 ±0.3 ±0.5	1670	ALBRECHT	96C	ARG	$e^+ e^- \approx$ 10 GeV
6.64±0.18±0.29	4609	KUBOTA	96B	CLE2	$e^+ e^- \approx \Upsilon(4S)$

[1] Using the D^+ and D^0 lifetimes, ASNER 10 finds that the ratio of the D^+ and D^0 semileptonic widths is 0.985 ± 0.015 ± 0.024.

$\Gamma(\mu^+ \text{anything})/\Gamma_{total}$ — Γ_6/Γ

VALUE (%)	EVTS	DOCUMENT ID		TECN	COMMENT
6.8±0.6 OUR FIT					
6.4±0.8 OUR AVERAGE					
6.8±1.5±0.8	79 ± 10	[1] ABLIKIM	08L	BES2	$e^+ e^- \approx \psi(3772)$
6.5±1.2±0.3	36	KAYIS-TOPAK	05	CHRS	ν_μ emulsion
6.0±0.7±1.2	310	ALBRECHT	96C	ARG	$e^+ e^- \approx$ 10 GeV

[1] ABLIKIM 08L finds the ratio of $D^+ \to \mu^+ X$ and $D^0 \to \mu^+ X$ branching fractions to be 2.59 ± 0.70 ± 0.25, in accord with the ratio of D^+ and D^0 lifetimes, 2.54 ± 0.02.

$\Gamma(K^- \text{anything})/\Gamma_{total}$ — Γ_7/Γ

VALUE	EVTS	DOCUMENT ID		TECN	COMMENT
0.547±0.028 OUR AVERAGE Error includes scale factor of 1.3. See the ideogram below.					
0.578±0.016±0.032	2098 ± 59	ABLIKIM	07G	BES2	$e^+ e^- \approx \psi(3770)$
$0.546^{+0.039}_{-0.038}$		[1] BARLAG	92C	ACCM	π^- Cu 230 GeV
0.609±0.032±0.052		COFFMAN	91	MRK3	$e^+ e^-$ 3.77 GeV
0.42 ±0.08		AGUILAR-...	87E	HYBR	πp, pp 360, 400 GeV
0.55 ±0.11	121	SCHINDLER	81	MRK2	$e^+ e^-$ 3.771 GeV
0.35 ±0.10	19	VUILLEMIN	78	LGW	$e^+ e^-$ 3.772 GeV

[1] BARLAG 92C computes the branching fraction using topological normalization.

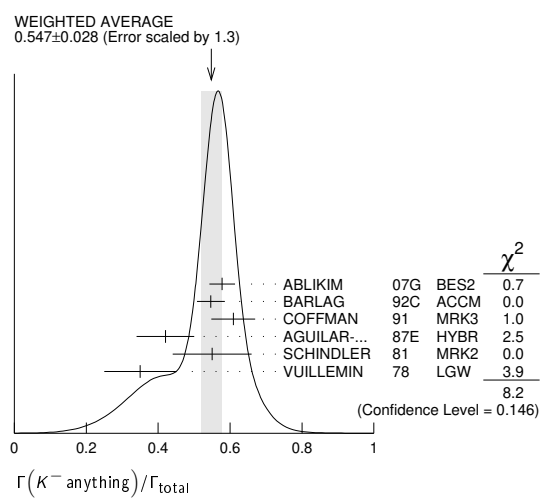

$\Gamma(K^0_S \text{anything})/\Gamma_{total}$ — Γ_8/Γ

VALUE (%)	EVTS	DOCUMENT ID		TECN	COMMENT
20.75±0.12±0.20	37.8k	ABLIKIM	23AO	BES3	$e^+ e^-$ at 3.773 GeV
• • • We do not use the following data for averages, fits, limits, etc. • • •					
23.8 ±2.4 ±1.5	250	[1] ABLIKIM	06U	BES2	$e^+ e^-$ at 3773 MeV
22.8 ±2.5 ±1.6		[2] COFFMAN	91	MRK3	$e^+ e^-$ 3.77 GeV

[1] ABLIKIM 06U reports $B(D^0 \to K^0 X \text{ or } \overline{K}^0 X) = 0.476 \pm 0.048 \pm 0.030$ which we take as twice the branching fraction for $D^0 \to K^0_S X$.

[2] COFFMAN 91 reports $B(D^0 \to K^0 X \text{ or } \overline{K}^0 X) = 0.455 \pm 0.050 \pm 0.032$ which we take as twice the branching fraction for $D^0 \to K^0_S X$.

$\Gamma(K^+ \text{anything})/\Gamma_{total}$ — Γ_9/Γ

VALUE	EVTS	DOCUMENT ID		TECN	COMMENT
0.034±0.004 OUR AVERAGE					
0.035±0.007±0.003	119 ± 23	ABLIKIM	07G	BES2	$e^+ e^- \approx \psi(3770)$
$0.034^{+0.007}_{-0.005}$		[1] BARLAG	92C	ACCM	π^- Cu 230 GeV
0.028±0.009±0.004		COFFMAN	91	MRK3	$e^+ e^-$ 3.77 GeV
$0.03^{+0.05}_{-0.02}$		AGUILAR-...	87E	HYBR	πp, pp 360, 400 GeV
0.08 ±0.03	25	SCHINDLER	81	MRK2	$e^+ e^-$ 3.771 GeV

[1] BARLAG 92C computes the branching fraction using topological normalization.

Int. J. Mod. Phys. A 2026.41. Downloaded from www.worldscientific.com
by UNIVERSITY OF CALIFORNIA @ BERKELEY on 09/16/26. Re-use and distribution is strictly not permitted, except for Open Access articles.

Int. J. Mod. Phys. A 2026.41. Downloaded from www.worldscientific.com by LIFORNIA @ BERKELEY on 09/16/26. Re-use and distribution is strictly not permitted, except for Open Access articles.

$\Gamma(K^*(892)^- \text{anything})/\Gamma_{total}$ — Γ_{10}/Γ

VALUE	EVTS	DOCUMENT ID		TECN	COMMENT
0.153±0.083±0.019	28 ± 15	ABLIKIM	06U	BES2	e^+e^- at 3773 MeV

$\Gamma(\overline{K}^*(892)^0 \text{anything})/\Gamma_{total}$ — Γ_{11}/Γ

VALUE	EVTS	DOCUMENT ID		TECN	COMMENT
0.087±0.040±0.012	96 ± 44	ABLIKIM	05P	BES	$e^+e^- \approx$ 3773 MeV

$\Gamma(K^*(892)^+ \text{anything})/\Gamma_{total}$ — Γ_{12}/Γ

VALUE	CL%	DOCUMENT ID		TECN	COMMENT
<0.036	90	ABLIKIM	06U	BES2	e^+e^- at 3773 MeV

$\Gamma(K^*(892)^0 \text{anything})/\Gamma_{total}$ — Γ_{13}/Γ

VALUE	EVTS	DOCUMENT ID		TECN	COMMENT
0.028±0.012±0.004	31 ± 12	ABLIKIM	05P	BES	$e^+e^- \approx$ 3773 MeV

$\Gamma(\eta \text{ anything})/\Gamma_{total}$ — Γ_{14}/Γ

This ratio includes η particles from η' decays.

VALUE (%)	EVTS	DOCUMENT ID		TECN	COMMENT
9.5±0.4±0.8	4463 ± 197	HUANG	06B	CLEO	e^+e^- at $\psi(3770)$

$\Gamma(\eta' \text{ anything})/\Gamma_{total}$ — Γ_{15}/Γ

VALUE (%)	EVTS	DOCUMENT ID		TECN	COMMENT
2.48±0.17±0.21	299 ± 21	HUANG	06B	CLEO	e^+e^- at $\psi(3770)$

$\Gamma(\phi \text{ anything})/\Gamma_{total}$ — Γ_{16}/Γ

VALUE (%)	EVTS	DOCUMENT ID		TECN	COMMENT
1.08 ±0.04 OUR AVERAGE					
1.091±0.027±0.035	4.1k	ABLIKIM	19AY	BES3	e^+e^- at 3773 MeV
1.05 ±0.08 ±0.07	368 ± 24	HUANG	06B	CLEO	e^+e^- at $\psi(3770)$
• • • We do not use the following data for averages, fits, limits, etc. • • •					
1.71 $^{+0.76}_{-0.71}$ ±0.17	9	BAI	00C	BES	$e^+e^- \to D\overline{D}^*, D^*\overline{D}^*$

$\Gamma(\pi^+\pi^+\pi^- \text{anything})/\Gamma_{total}$ — Γ_{17}/Γ

VALUE (%)	EVTS	DOCUMENT ID		TECN	COMMENT
17.60±0.11±0.22	95k	ABLIKIM	23AI	BES3	2.93 fb^{-1}, e^+e^- at $\psi(3770)$

$\Gamma(\text{invisibles})/\Gamma_{total}$ — Γ_{18}/Γ

VALUE	CL%	DOCUMENT ID		TECN	COMMENT
<9.4 × 10^{-5}	90	LAI	17	BELL	e^+e^- at Υ(nS), n=4,5

Semileptonic modes

$\Gamma(K^- e^+ \nu_e)/\Gamma_{total}$ — Γ_{20}/Γ

VALUE (%)	EVTS	DOCUMENT ID		TECN	COMMENT
3.537±0.017 OUR FIT Error includes scale factor of 1.1.					
3.526±0.016 OUR AVERAGE					
3.521±0.009±0.016	191k	ABLIKIM	24CN	BES3	e^+e^- at 3.773 GeV
3.567±0.031±0.025	4040	ABLIKIM	21BA	BES3	e^+e^- at 3.773 GeV
3.50 ±0.03 ±0.04	14.1k	[1] BESSON	09	CLEO	e^+e^- at $\psi(3770)$
3.45 ±0.10 ±0.19	1.3k	[2] WIDHALM	06	BELL	$e^+e^- \approx \Upsilon(4S)$
3.82 ±0.40 ±0.27	104	ABLIKIM	04C	BES	e^+e^-, 3.773 GeV
3.4 ±0.5 ±0.4	55	ADLER	89	MRK3	e^+e^- 3.77 GeV
• • • We do not use the following data for averages, fits, limits, etc. • • •					
3.505±0.014±0.033	71k	[1,3] ABLIKIM	15X	BES3	2.92 fb^{-1}, 3.773 GeV
3.56 ±0.03 ±0.09		[4] DOBBS	08	CLEO	See BESSON 09
3.44 ±0.10 ±0.10	1.3k	COAN	05	CLEO	See DOBBS 08

[1] See the form-factor parameters near the end of this D^0 Listing.

[2] The $\pi^- e^+ \nu_e$ and $K^- e^+ \nu_e$ results of WIDHALM 06 give $|\frac{V_{cd}}{V_{cs}} \cdot \frac{f_+^\pi(0)}{f_+^K(0)}|^2 = 0.042 \pm 0.003 \pm 0.003$.

[3] Superseded by ABLIKIM 24CN.

[4] DOBBS 08 establishes $|\frac{V_{cd}}{V_{cs}} \cdot \frac{f_+^\pi(0)}{f_+^K(0)}| = 0.188 \pm 0.008 \pm 0.002$ from the D^+ and D^0 decays to $\overline{K} e^+ \nu_e$ and $\pi e^+ \nu_e$.

$\Gamma(K^- e^+ \nu_e)/\Gamma(K^- \pi^+)$ — Γ_{20}/Γ_{47}

VALUE	EVTS	DOCUMENT ID		TECN	COMMENT
0.899±0.008 OUR FIT Error includes scale factor of 1.3.					
0.930±0.013 OUR AVERAGE					
0.927±0.007±0.012	76k±323	[1] AUBERT	07BG	BABR	$e^+e^- \approx \Upsilon(4S)$
0.978±0.027±0.044	2510	[2] BEAN	93C	CLE2	$e^+e^- \approx \Upsilon(4S)$
0.90 ±0.06 ±0.06	584	[3] CRAWFORD	91B	CLEO	$e^+e^- \approx$ 10.5 GeV
0.91 ±0.07 ±0.11	250	[4] ANJOS	89F	E691	Photoproduction

[1] The event samples in this AUBERT 07BG result include radiative photons. The $D^0 \to K^- e^+ \nu_e$ form factor at $q^2 = 0$ is $f_+(0) = 0.727 \pm 0.007 \pm 0.005 \pm 0.007$.

[2] BEAN 93C uses $K^- \mu^+ \nu_\mu$ as well as $K^- e^+ \nu_e$ events and makes a small phase-space adjustment to the number of the μ^+ events to use them as e^+ events. A pole mass of $2.00 \pm 0.12 \pm 0.18$ GeV/c^2 is obtained from the q^2 dependence of the decay rate.

[3] CRAWFORD 91B uses $K^- e^+ \nu_e$ and $K^- \mu^+ \nu_\mu$ candidates to measure a pole mass of $2.1 ^{+0.4}_{-0.2} ^{+0.3}_{-0.2}$ GeV/c^2 from the q^2 dependence of the decay rate.

[4] ANJOS 89F measures a pole mass of $2.1 ^{+0.4}_{-0.2} \pm 0.2$ GeV/c^2 from the q^2 dependence of the decay rate.

$\Gamma(K^- \mu^+ \nu_\mu)/\Gamma_{total}$ — Γ_{21}/Γ

VALUE (%)	EVTS	DOCUMENT ID		TECN	COMMENT
3.418±0.019 OUR FIT					
3.419±0.019 OUR AVERAGE					
3.419±0.011±0.016	148k	ABLIKIM	24CN	BES3	e^+e^- at 3.773 GeV
3.45 ±0.10 ±0.21	1249 ± 43	WIDHALM	06	BELL	$e^+e^- \approx \Upsilon(4S)$
• • • We do not use the following data for averages, fits, limits, etc. • • •					
3.413±0.019±0.035	47k	[1] ABLIKIM	19B	BES3	e^+e^-, 3773 MeV

[1] Superseded by ABLIKIM 24CN.

$\Gamma(K^- \mu^+ \nu_\mu)/\Gamma(\mu^+ \text{anything})$ — Γ_{21}/Γ_6

VALUE	EVTS	DOCUMENT ID		TECN	COMMENT
0.50 ±0.04 OUR FIT					
0.472±0.051±0.040	232	KODAMA	94	E653	π^- emulsion 600 GeV
• • • We do not use the following data for averages, fits, limits, etc. • • •					
0.32 ±0.05 ±0.05	124	KODAMA	91	EMUL	pA 800 GeV

$\Gamma(K^- \mu^+ \nu_\mu)/\Gamma(K^- \pi^+)$ — Γ_{21}/Γ_{47}

VALUE	EVTS	DOCUMENT ID		TECN	COMMENT
0.868±0.008 OUR FIT Error includes scale factor of 1.2.					
0.84 ±0.04 OUR AVERAGE					
0.852±0.034±0.028	1897	[1] FRABETTI	95G	E687	γBe $\overline{E}_\gamma$= 220 GeV
0.82 ±0.13 ±0.13	338	[2] FRABETTI	93I	E687	γBe $\overline{E}_\gamma$= 221 GeV
0.79 ±0.08 ±0.09	231	[3] CRAWFORD	91B	CLEO	$e^+e^- \approx$ 10.5 GeV

[1] FRABETTI 95G extracts the ratio of form factors $f_-(0)/f_+(0) = -1.3 ^{+3.6}_{-3.4} \pm 0.6$, and measures a pole mass of $1.87 ^{+0.11}_{-0.08} ^{+0.07}_{-0.06}$ GeV/c^2 from the q^2 dependence of the decay rate.

[2] FRABETTI 93I measures a pole mass of $2.1 ^{+0.7}_{-0.3} ^{+0.7}_{-0.3}$ GeV/c^2 from the q^2 dependence of the decay rate.

[3] CRAWFORD 91B measures a pole mass of $2.00 \pm 0.12 \pm 0.18$ GeV/c^2 from the q^2 dependence of the decay rate.

$\Gamma(K^*(892)^- e^+ \nu_e)/\Gamma_{total}$ — Γ_{22}/Γ

Both decay modes of the $K^*(892)^-$ are included.

VALUE (%)	EVTS	DOCUMENT ID		TECN	COMMENT
2.16±0.16 OUR FIT					
2.16±0.15±0.08	219 ± 16	[1] COAN	05	CLEO	e^+e^- at $\psi(3770)$

[1] COAN 05 uses both $K^-\pi^0$ and $K^0_S\pi^-$ events.

$\Gamma(K^*(892)^- e^+ \nu_e)/\Gamma(\overline{K}^0 \pi^- e^+ \nu_e)$ — Γ_{22}/Γ_{25}

VALUE (units 10^{-2})	EVTS	DOCUMENT ID		TECN	COMMENT
94.15±0.32±0.16	8.8k	ABLIKIM	25BD	BES3	$K^0_S\pi^- e^+ \nu_e$ events
• • • We do not use the following data for averages, fits, limits, etc. • • •					
94.52±0.97±0.62	3.1k	[1] ABLIKIM	19G	BES3	$K^0_S\pi^- e^+ \nu_e$ events

[1] Superseded by ABLIKIM 25BD.

$\Gamma(K^*(892)^- e^+ \nu_e)/\Gamma(K^0_S \pi^+ \pi^-)$ — Γ_{22}/Γ_{53}

Unseen decay modes of the $K^*(892)^-$ are included.

VALUE	EVTS	DOCUMENT ID		TECN	COMMENT
0.76±0.06 OUR FIT					
0.76±0.12±0.06	152	[1] BEAN	93C	CLE2	$e^+e^- \approx \Upsilon(4S)$

[1] BEAN 93C uses $K^{*-}\mu^+\nu_\mu$ as well as $K^{*-}e^+\nu_e$ events and makes a small phase-space adjustment to the number of the μ^+ events to use them as e^+ events.

$\Gamma(K^*(892)^- \mu^+ \nu_\mu)/\Gamma(K^- \pi^0 \mu^+ \nu_\mu)$ — Γ_{23}/Γ_{27}

VALUE	EVTS	DOCUMENT ID		TECN	COMMENT
2.824 ±0.024 OUR FIT Error includes scale factor of 1.7.					
2.8272±0.0105±0.0087	6.4k	[1] ABLIKIM	25	BES3	e^+e^- at 3.773 GeV

[1] An amplitude analysis of $D^0 \to K^-\pi^0\mu^+\nu_\mu$ with two components. ABLIKIM 25 measures $B(D^0 \to K^*(892)^-\mu^+\nu_\mu,\ K^{*-} \to K^-\pi^0)/B(D^0 \to K^-\pi^0\mu^+\nu_\mu) = (94.24 \pm 0.35 \pm 0.29) \times 10^{-2}$, from which we determine the reported ratio assuming $B(K^{*-} \to K^-\pi^0) = 1/3$. With the same assumption, ABLIKIM 25 reports $B(D^0 \to K^{*-}\mu^+\nu_\mu) = (2.073 \pm 0.039 \pm 0.032) \times 10^{-2}$.

$\Gamma(K^*(892)^- \mu^+ \nu_\mu)/\Gamma(\overline{K}^0 \pi^- \mu^+ \nu_\mu)$ — Γ_{23}/Γ_{29}

VALUE	EVTS	DOCUMENT ID		TECN	COMMENT
1.428±0.027 OUR FIT Error includes scale factor of 1.7.					
1.419±0.013±0.011	6.8k	[1] ABLIKIM	25BO	BES3	e^+e^- at $\sqrt{s}$ = 3.773 GeV

[1] An amplitude analysis of $D^0 \to \overline{K}^0\pi^-\mu^+\nu_\mu$ with two components. ABLIKIM 25BO measures $B(D^0 \to K^*(892)^-\mu^+\nu_\mu,\ K^{*-} \to \overline{K}^0\pi^-)/B(D^0 \to \overline{K}^0\pi^-\mu^+\nu_\mu) = (94.60 \pm 0.87 \pm 0.71) \times 10^{-2}$, from which we determine the reported ratio assuming $B(K^{*-} \to \overline{K}^0\pi^-) = 2/3$. With the same assumption, ABLIKIM 25BO reports $B(D^0 \to K^{*-}\mu^+\nu_\mu) = (1.948 \pm 0.033 \pm 0.036) \times 10^{-2}$.

$\Gamma(K^*(892)^- \mu^+ \nu_\mu)/\Gamma(K^0_S \pi^+ \pi^-)$ — Γ_{23}/Γ_{53}

Unseen decay modes of the $K^*(892)^-$ are included.

VALUE	EVTS	DOCUMENT ID		TECN	COMMENT
0.71 ±0.04 OUR FIT Error includes scale factor of 1.1.					
0.674±0.068±0.026	175 ± 17	[1] LINK	05B	FOCS	γ A, $\overline{E}_\gamma \approx$ 180 GeV

[1] LINK 05B finds that in $D^0 \to \overline{K}^0\pi^-\mu^+\nu_\mu$ the $\overline{K}^0\pi^-$ system is 6% in S-wave.

Int. J. Mod. Phys. A 2026.41. Downloaded from www.worldscientific.com
by UNIVERSITY OF CALIFORNIA @ BERKELEY on 09/16/26. Re-use and distribution is strictly not permitted, except for Open Access articles.

$\Gamma(K^-\pi^0 e^+\nu_e)/\Gamma_{total}$ — Γ_{24}/Γ

VALUE	EVTS	DOCUMENT ID		TECN	COMMENT
$0.016^{+0.013}_{-0.005}\pm0.002$	4	[1] BAI	91	MRK3	$e^+e^-\approx$ 3.77 GeV

[1] BAI 91 finds that a fraction $0.79^{+0.15}_{-0.17}{}^{+0.09}_{-0.03}$ of combined D^+ and D^0 decays to $\overline{K}\pi e^+\nu_e$ (24 events) are $\overline{K}^*(892)e^+\nu_e$. BAI 91 uses 56 $K^-e^+\nu_e$ events to measure a pole mass of $1.8\pm0.3\pm0.2$ GeV/c^2 from the q^2 dependence of the decay rate.

$\Gamma(\overline{K}^0\pi^- e^+\nu_e)/\Gamma_{total}$ — Γ_{25}/Γ

VALUE (%)	EVTS	DOCUMENT ID		TECN	COMMENT
1.447±0.033 OUR AVERAGE					
$1.444\pm0.022\pm0.024$	8.8k	ABLIKIM	25BD	BES3	e^+e^- at 3.773 GeV
$2.61\pm1.04\pm0.28$	9 ± 3	ABLIKIM	06O	BES2	e^+e^- at 3773 MeV
$2.8^{+1.7}_{-0.8}\pm0.3$	6	[1] BAI	91	MRK3	$e^+e^-\approx$ 3.77 GeV
• • • We do not use the following data for averages, fits, limits, etc. • • •					
$1.434\pm0.029\pm0.032$	3.1k	[2] ABLIKIM	19G	BES3	e^+e^- at 3773 MeV

[1] BAI 91 finds that a fraction $0.79^{+0.15}_{-0.17}{}^{+0.09}_{-0.03}$ of combined D^+ and D^0 decays to $\overline{K}\pi e^+\nu_e$ (24 events) are $\overline{K}^*(892)e^+\nu_e$.

[2] Superseded by ABLIKIM 25BD.

$\Gamma((\overline{K}^0\pi^-)_{S-wave}e^+\nu_e)/\Gamma(\overline{K}^0\pi^- e^+\nu_e)$ — Γ_{26}/Γ_{25}

VALUE (units 10^{-2})	EVTS	DOCUMENT ID		TECN	COMMENT
5.87±0.32±0.16	8.8k	ABLIKIM	25BD	BES3	$K^0_S\pi^-e^+\nu_e$ events
• • • We do not use the following data for averages, fits, limits, etc. • • •					
$5.51\pm0.97\pm0.62$	3.1k	[1] ABLIKIM	19G	BES3	$K^0_S\pi^-e^+\nu_e$ events

[1] Superseded by ABLIKIM 25BD.

$\Gamma(K^-\pi^0\mu^+\nu_\mu)/\Gamma_{total}$ — Γ_{27}/Γ

VALUE (units 10^{-3})	EVTS	DOCUMENT ID		TECN	COMMENT
7.10±0.21 OUR FIT Error includes scale factor of 1.7.					
7.33±0.14±0.11	6.4k	ABLIKIM	25	BES3	e^+e^- at 3.773 GeV

$\Gamma((K^-\pi^0)_{S-wave}\mu^+\nu_\mu)/\Gamma(K^-\pi^0\mu^+\nu_\mu)$ — Γ_{28}/Γ_{27}

VALUE (units 10^{-2})	EVTS	DOCUMENT ID		TECN	COMMENT
5.76±0.35±0.29	6.4k	[1] ABLIKIM	25	BES3	e^+e^- at 3.773 GeV

[1] An amplitude analysis of $D^0\to K^-\pi^0\mu^+\nu_\mu$ with two components. ABLIKIM 25 reports $B(D^0\to(K^-\pi^0)_{S-wave}\mu^+\nu_\mu)=(4.223\pm0.268\pm0.222)\times10^{-4}$.

$\Gamma(\overline{K}^0\pi^-\mu^+\nu_\mu)/\Gamma_{total}$ — Γ_{29}/Γ

VALUE (%)	EVTS	DOCUMENT ID		TECN	COMMENT
1.40 ±0.04 OUR FIT Error includes scale factor of 1.7.					
1.373±0.020±0.023	6.8k	ABLIKIM	25BO	BES3	e^+e^- at $\sqrt{s}=$ 3.773 GeV

$\Gamma((\overline{K}^0\pi^-)_{S-wave}\mu^+\nu_\mu)/\Gamma(\overline{K}^0\pi^-\mu^+\nu_\mu)$ — Γ_{30}/Γ_{29}

VALUE (units 10^{-2})	EVTS	DOCUMENT ID		TECN	COMMENT
5.35±0.87±0.71	6.8k	[1] ABLIKIM	25BO	BES3	e^+e^- at $\sqrt{s}=$ 3.773 GeV

[1] An amplitude analysis of $D^0\to\overline{K}^0\pi^-\mu^+\nu_\mu$ with two components. ABLIKIM 25BO reports $B(D^0\to(\overline{K}^0\pi^-)_{S-wave}\mu^+\nu_\mu)=(0.073\pm0.012\pm0.010)\times10^{-2}$.

$\Gamma(K^-\eta e^+\nu_e)/\Gamma_{total}$ — Γ_{31}/Γ

VALUE (units 10^{-4})	EVTS	DOCUMENT ID		TECN	COMMENT
$\mathbf{0.84^{+0.34}_{-0.29}\pm0.22}$	11	ABLIKIM	24CM	BES3	e^+e^- at $\sqrt{s}=$ 3.773 GeV

$\Gamma(K^-\pi^+\pi^- e^+\nu_e)/\Gamma_{total}$ — Γ_{32}/Γ

VALUE (units 10^{-4})	EVTS	DOCUMENT ID		TECN	COMMENT
$\mathbf{2.8^{+1.4}_{-1.1}\pm0.3}$	8	ARTUSO	07A	CLEO	e^+e^- at $\Upsilon(3770)$

$\Gamma(K_1(1270)^-e^+\nu_e,\ K_1^-\to K^-\pi^+\pi^-)/\Gamma_{total}$ — Γ_{33}/Γ

VALUE (units 10^{-4})	EVTS	DOCUMENT ID		TECN	COMMENT
3.23±0.25 OUR AVERAGE					
$3.2\pm0.2\pm0.2$	0.73k	[1] ABLIKIM	25AM	BES3	e^+e^- at 3.773 GeV
$3.59\pm0.41^{+0.31}_{-0.52}$	109	[2] ABLIKIM	21AY	BES3	e^+e^- at 3.773 GeV
$2.5^{+1.3}_{-1.0}\pm0.2$	8	[3] ARTUSO	07A	CLEO	e^+e^- at $\Upsilon(3770)$

[1] ABLIKIM 25AM quotes $B(D^0\to K_1(1270)^-e^+\nu_e)=(1.02\pm0.06\pm0.06\pm0.03)\times10^{-3}$, where the last uncertainty is due to $B(\overline{K}_1(1270)^0\to K^-\pi^+\pi^0)=(31.3\pm0.9)\%$. This amplitude analysis with several substructures includes $K_1(1270)\to\rho K^-$ (S-wave) and $K_1(1270)\to\pi\overline{K}^*(892)$ (S- and D-wave).

[2] ABLIKIM 21AY quotes $B(D^0\to K_1(1270)^-e^+\nu_e)=(1.09\pm0.13^{+0.09}_{-0.16}\pm0.12)\times10^{-3}$ using $B(K_1(1270)^-\to K^-\pi^+\pi^-)=(32.9\pm3.6)\%$, which is the source of the third uncertainty.

[3] ARTUSO 07A quotes $B(D^0\to K_1(1270)^-e^+\nu_e)=(7.6^{+4.1}_{-3.0}\pm0.9)\times10^{-4}$ using $B(K_1(1270)^-\to K^-\pi^+\pi^-)=(33\pm3)\%$, which is the source of the third uncertainty.

$\Gamma(K_1(1270)^-e^+\nu_e,\ K_1^-\to K^0_S\pi^-\pi^0)/\Gamma_{total}$ — Γ_{34}/Γ

VALUE (units 10^{-4})	EVTS	DOCUMENT ID		TECN	COMMENT
$\mathbf{1.69^{+0.53}_{-0.46}\pm0.15}$	17	[1] ABLIKIM	24CR	BES3	e^+e^- at $\sqrt{s}=$ 3.773 GeV

[1] ABLIKIM 24CR reconstructs $D^0\to K^0_S\pi^-\pi^0e^+\nu_e$ and assumes that all come from $\overline{K}_1^-\to K^0_S\pi^-\pi^0$ decays.

$\Gamma(K^-\pi^+\pi^-\mu^+\nu_\mu)/\Gamma(K^-\mu^+\nu_\mu)$ — Γ_{35}/Γ_{21}

VALUE	CL%	DOCUMENT ID		TECN	COMMENT
<0.037	90	KODAMA	93B	E653	π^- emulsion 600 GeV

$\Gamma((\overline{K}^*(892)\pi)^-\mu^+\nu_\mu)/\Gamma(K^-\mu^+\nu_\mu)$ — Γ_{36}/Γ_{21}

VALUE	CL%	DOCUMENT ID		TECN	COMMENT
<0.043	90	[1] KODAMA	93B	E653	π^- emulsion 600 GeV

[1] KODAMA 93B searched in $K^-\pi^+\pi^-\mu^+\nu_\mu$, but the limit includes other $(\overline{K}^*(892)\pi)^-$ charge states.

$\Gamma(K_1(1270)^-\mu^+\nu_\mu,\ K_1^-\to K^-\pi^+\pi^-)/\Gamma_{total}$ — Γ_{37}/Γ

VALUE (units 10^{-4})	EVTS	DOCUMENT ID		TECN	COMMENT
$\mathbf{2.62\pm0.38^{+0.17}_{-0.29}}$	180	ABLIKIM	25AU	BES3	e^+e^- at 3.773 GeV

$\Gamma(K_1(1400)^-e^+\nu_e)/\Gamma_{total}$ — Γ_{38}/Γ

VALUE	CL%	DOCUMENT ID		TECN	COMMENT
$<0.7\times10^{-4}$	90	ABLIKIM	25AM	BES3	e^+e^- at 3.773 GeV

$\Gamma(\pi^-e^+\nu_e)/\Gamma_{total}$ — Γ_{39}/Γ

VALUE (%)	EVTS	DOCUMENT ID		TECN	COMMENT
0.291±0.004 OUR FIT					
0.293±0.004 OUR AVERAGE					
$0.295\pm0.004\pm0.003$	6.3k	[1] ABLIKIM	15X	BES3	2.92 fb^{-1}, 3.773 GeV
$0.288\pm0.008\pm0.003$	1.3k	[1] BESSON	09	CLEO	e^+e^- at $\psi(3770)$
$0.279\pm0.027\pm0.016$	126	[2] WIDHALM	06	BELL	$e^+e^-\approx\Upsilon(4S)$
• • • We do not use the following data for averages, fits, limits, etc. • • •					
$0.299\pm0.011\pm0.009$		[3] DOBBS	08	CLEO	See BESSON 09
$0.262\pm0.025\pm0.008$	117	COAN	05	CLEO	See DOBBS 08

[1] See the form-factor parameters near the end of this D^0 Listing.

[2] The $\pi^-e^+\nu_e$ and $K^-e^+\nu_e$ results of WIDHALM 06 give $|\frac{V_{cd}}{V_{cs}}\cdot\frac{f_+^\pi(0)}{f_+^K(0)}|^2=0.042\pm0.003\pm0.003$.

[3] DOBBS 08 establishes $|\frac{V_{cd}}{V_{cs}}\cdot\frac{f_+^\pi(0)}{f_+^K(0)}|=0.188\pm0.008\pm0.002$ from the D^+ and D^0 decays to $\overline{K}e^+\nu_e$ and $\pi e^+\nu_e$.

$\Gamma(\pi^-e^+\nu_e)/\Gamma(K^-e^+\nu_e)$ — Γ_{39}/Γ_{20}

VALUE	EVTS	DOCUMENT ID		TECN	COMMENT
0.0823±0.0012 OUR FIT Error includes scale factor of 1.1.					
0.085 ±0.007 OUR AVERAGE					
$0.082\pm0.006\pm0.005$		[1] HUANG	05	CLEO	$e^+e^-\approx\Upsilon(4S)$
$0.101\pm0.020\pm0.003$	91	[2] FRABETTI	96B	E687	γ Be, $\overline{E}_\gamma\approx$ 200 GeV
$0.103\pm0.039\pm0.013$	87	[3] BUTLER	95	CLE2	<0.156 (90% CL)

[1] HUANG 05 uses both e and μ events, and makes a small correction to the μ events to make them effectively e events. This result gives $|\frac{V_{cd}}{V_{cs}}\cdot\frac{f_+^\pi(0)}{f_+^K(0)}|^2=0.038^{+0.006}_{-0.007}{}^{+0.005}_{-0.003}$.

[2] FRABETTI 96B uses both e and μ events, and makes a small correction to the μ events to make them effectively e events. This result gives $|\frac{V_{cd}}{V_{cs}}\cdot\frac{f_+^\pi(0)}{f_+^K(0)}|^2=0.050\pm0.011\pm0.002$.

[3] BUTLER 95 has 87 ± 33 $\pi^-e^+\nu_e$ events. The result gives $|\frac{V_{cd}}{V_{cs}}\cdot\frac{f_+^\pi(0)}{f_+^K(0)}|^2=0.052\pm0.020\pm0.007$.

$\Gamma(\pi^-e^+\nu_e)/\Gamma(K^-\pi^+)$ — Γ_{39}/Γ_{47}

VALUE (units 10^{-2})	EVTS	DOCUMENT ID		TECN	COMMENT
7.40±0.12 OUR FIT Error includes scale factor of 1.1.					
7.02±0.17±0.23	375k	[1] LEES	15F	BABR	347 fb^{-1}, 10.58 GeV

[1] See the form-factor parameters near the end of the D^0 Listing.

$\Gamma(\pi^-\mu^+\nu_\mu)/\Gamma_{total}$ — Γ_{40}/Γ

VALUE (%)	EVTS	DOCUMENT ID		TECN	COMMENT
0.267±0.012 OUR FIT Error includes scale factor of 1.3.					
0.268±0.012 OUR AVERAGE Error includes scale factor of 1.2.					
$0.272\pm0.008\pm0.006$	2.3k	ABLIKIM	18AE	BES3	e^+e^-, 3773 MeV
$0.231\pm0.026\pm0.019$	106 ± 13	WIDHALM	06	BELL	$e^+e^-\approx\Upsilon(4S)$

$\Gamma(\pi^-\mu^+\nu_\mu)/\Gamma(K^-\mu^+\nu_\mu)$ — Γ_{40}/Γ_{21}

VALUE	EVTS	DOCUMENT ID		TECN	COMMENT
0.0782±0.0034 OUR FIT Error includes scale factor of 1.3.					
0.074 ±0.008 ±0.007	288 ± 29	[1] LINK	05	FOCS	γ A, $\overline{E}_\gamma\approx$ 180 GeV

[1] LINK 05 finds the form-factor ratio $|f_0^\pi(0)/f_0^K(0)|$ to be $0.85\pm0.04\pm0.04\pm0.01$.

Int. J. Mod. Phys. A 2026.41. Downloaded from www.worldscientific.com by LIFORNIA @ BERKELEY on 09/16/26. Re-use and distribution is strictly not permitted, except for Open Access articles.

$\Gamma(\pi^- \pi^0 e^+ \nu_e)/\Gamma_{total}$ — Γ_{41}/Γ

VALUE (units 10^{-3})	EVTS	DOCUMENT ID		TECN	COMMENT
1.445±0.058±0.039	1.1k	[1] ABLIKIM	19C	BES3	e^+e^- at 3773 MeV

[1] Seen 100% via $D^0 \to \rho(770)^- e^+ \nu_e$, and also reported as the branching fraction for $D^0 \to \rho(770)^- e^+ \nu_e$.

$\Gamma(\rho^- e^+ \nu_e)/\Gamma_{total}$ — Γ_{42}/Γ

VALUE (units 10^{-3})	EVTS	DOCUMENT ID		TECN	COMMENT
1.46 ±0.08 OUR AVERAGE	Error includes scale factor of 2.0.				
1.439±0.033±0.027	3.3k	ABLIKIM	24CP	BES3	e^+e^- at 3.773 GeV
1.77 ±0.12 ±0.10	305	[1,2] DOBBS	13	CLEO	e^+e^- at $\psi(3770)$
• • • We do not use the following data for averages, fits, limits, etc. • • •					
1.445±0.058±0.039	1.1k	[3] ABLIKIM	19C	BES3	e^+e^- at 3773 MeV
1.94 ±0.39 ±0.13	31	COAN	05	CLEO	See DOBBS 13

[1] DOBBS 13 finds $\Gamma(D^0 \to \rho^- e^+ \nu_e)$ / 2 $\Gamma(D^+ \to \rho^0 e^+ \nu_e) = 1.03 \pm 0.09 {}^{+0.08}_{-0.02}$, isospin invariance predicts the ratio is 1.0.

[2] See the D^+ Listings for $D \to \rho e^+ \nu_e$ form factors.

[3] This result is the same as the one reported for $D^0 \to \pi^- \pi^0 e^+ \nu_e$ which ABLIKIM 19C found to proceed 100% via $D^0 \to \rho(770)^- e^+ \nu_e$. Superseded by ABLIKIM 24CP.

$\Gamma(\rho^- \mu^+ \nu_\mu)/\Gamma_{total}$ — Γ_{43}/Γ

VALUE (units 10^{-3})	EVTS	DOCUMENT ID		TECN	COMMENT
1.35±0.09±0.09	570	ABLIKIM	21BC	BES3	e^+e^- at 3.773 GeV

$\Gamma(a(980)^- e^+ \nu_e,\ a^- \to \eta\pi^-)/\Gamma_{total}$ — Γ_{44}/Γ

VALUE (units 10^{-4})	EVTS	DOCUMENT ID		TECN	COMMENT
0.86±0.17±0.05	52	[1] ABLIKIM	25AW	BES3	e^+e^- at 3.773 GeV
• • • We do not use the following data for averages, fits, limits, etc. • • •					
$1.33 {}^{+0.33}_{-0.29} \pm 0.09$	26	[2] ABLIKIM	18F	BES3	e^+e^- at 3.773 GeV

[1] ABLIKIM 25AW obtain $f_+^{a_0}(0)|V_{cd}| = 0.126 \pm 0.013 \pm 0.003$ using a single-pole parametrization for the form factor and a_0 branching fractions deduced from the analysis of ABLIKIM 17K.

[2] ABLIKIM 18F signal observed at 6.4 σ C.L. Superseded by ABLIKIM 25AW.

$\Gamma(K^0_S K^- e^+ \nu_e)/\Gamma_{total}$ — Γ_{45}/Γ

VALUE	CL%	DOCUMENT ID		TECN	COMMENT
$<2.13 \times 10^{-5}$	90	[1] ABLIKIM	24AZ	BES3	7.9 fb^{-1}, e^+e^- at 3.773 GeV

[1] Includes $D^0 \to a_0(980)^- e^+ \nu_e$, $a_0(980)^- \to K^0_S K^-$ resonant contribution.

$\Gamma(b_1(1235)^- e^+ \nu_e,\ b_1^- \to \omega\pi^-)/\Gamma_{total}$ — Γ_{46}/Γ

VALUE	CL%	DOCUMENT ID		TECN	COMMENT
$<1.12 \times 10^{-4}$	90	ABLIKIM	20AF	BES3	e^+e^-, 3773 MeV

Hadronic modes with a single $\overline{K}$

$\Gamma(K^- \pi^+)/\Gamma_{total}$ — Γ_{47}/Γ

VALUE (%)	EVTS	DOCUMENT ID		TECN	COMMENT
3.936±0.030 OUR FIT	Error includes scale factor of 1.3.				
3.909±0.034 OUR AVERAGE					
3.883±0.006±0.051	0.5M	[1] ABLIKIM	18W	BES3	e^+e^-, 3773 MeV
3.934±0.021±0.061		BONVICINI	14	CLEO	All CLEO-c runs
4.007±0.037±0.072	33.8k	AUBERT	08L	BABR	e^+e^- at $\Upsilon(4S)$
3.82 ±0.07 ±0.12		[2] ARTUSO	98	CLE2	CLEO average
3.90 ±0.09 ±0.12	5.4k	[3] BARATE	97C	ALEP	From Z decays
3.41 ±0.12 ±0.28	1.2k	[3] ALBRECHT	94F	ARG	$e^+e^- \approx \Upsilon(4S)$
3.62 ±0.34 ±0.44		[3] DECAMP	91J	ALEP	From Z decays
• • • We do not use the following data for averages, fits, limits, etc. • • •					
3.891±0.035±0.069		[4] DOBBS	07	CLEO	See BONVICINI 14
3.91 ±0.08 ±0.09	10.3k	[4] HE	05	CLEO	See DOBBS 07
3.81 ±0.15 ±0.16	1.2k	[5] ARTUSO	98	CLE2	e^+e^- at $\Upsilon(4S)$
3.69 ±0.11 ±0.16		[6] COAN	98	CLE2	See ARTUSO 98
4.5 ±0.6 ±0.4		[7] ALBRECHT	94	ARG	$e^+e^- \approx \Upsilon(4S)$
3.95 ±0.08 ±0.17	4.2k	[3,8] AKERIB	93	CLE2	See ARTUSO 98
4.5 ±0.8 ±0.5	56	[3] ABACHI	88	HRS	e^+e^- 29 GeV
4.2 ±0.4 ±0.4	0.9k	ADLER	88C	MRK3	e^+e^- 3.77 GeV
4.1 ±0.6	0.3k	[9] SCHINDLER	81	MRK2	e^+e^- 3.771 GeV
4.3 ±1.0	130	[10] PERUZZI	77	LGW	e^+e^- 3.77 GeV

[1] ABLIKIM 18W measured the combined $K^\mp \pi^\pm$ branching fraction to be 3.898%. We have subtracted off the doubly Cabibbo-suppressed branching fraction $B(D^0 \to K^+ \pi^-) = (1.48 \pm 0.07) \times 10^{-4}$, even though it is less than one-third of the uncertainty of the combined measurement, in order to treat this as a measurement of $B(D^0 \to K^- \pi^+)$.

[2] This combines the CLEO results of ARTUSO 98, COAN 98, and AKERIB 93.

[3] ABACHI 88, DECAMP 91J, AKERIB 93, ALBRECHT 94F, and BARATE 97C use $D^*(2010)^+ \to D^0 \pi^+$ decays. The π^+ is both slow and of low p_T with respect to the event thrust axis or nearest jet ($\approx D^{*+}$ direction). The excess number of such π^+'s over background gives the number of $D^*(2010)^+ \to D^0 \pi^+$ events, and the fraction with $D^0 \to K^- \pi^+$ gives the $D^0 \to K^- \pi^+$ branching fraction.

[4] DOBBS 07 and HE 05 use single- and double-tagged events in an overall fit. DOBBS 07 supersedes HE 05.

[5] ARTUSO 98, following ALBRECHT 94, uses D^0 mesons from $\overline{B}^0 \to D^*(2010)^+ X \ell^- \overline{\nu}_\ell$ decays. Our average uses the CLEO average of this value with the values of COAN 98 and AKERIB 93.

[6] COAN 98 assumes that $\Gamma(B \to \overline{D} X \ell^+ \nu)/\Gamma(B \to X \ell^+ \nu) = 1.0 - 3|V_{ub}/V_{cb}|^2 - 0.010 \pm 0.005$, the last term accounting for $\overline{B} \to D_s^+ K X \ell^- \overline{\nu}$. COAN 98 is included in the CLEO average in ARTUSO 98.

[7] ALBRECHT 94 uses D^0 mesons from $\overline{B}^0 \to D^{*+} \ell^- \overline{\nu}_\ell$ decays. This is a different set of events than used by ALBRECHT 94F.

[8] This AKERIB 93 value includes radiative corrections; without them, the value is 0.0391 ± 0.0008 ± 0.0017. AKERIB 93 is included in the CLEO average in ARTUSO 98.

[9] SCHINDLER 81 (MARK-2) measures $\sigma(e^+e^- \to \psi(3770)) \times$ branching fraction to be 0.24 ± 0.02 nb. We use the MARK-3 (ADLER 88C) value of $\sigma = 5.8 \pm 0.5 \pm 0.6$ nb.

[10] PERUZZI 77 (MARK-1) measures $\sigma(e^+e^- \to \psi(3770)) \times$ branching fraction to be 0.25 ± 0.05 nb. We use the MARK-3 (ADLER 88C) value of $\sigma = 5.8 \pm 0.5 \pm 0.6$ nb.

$\Gamma(K^0_S \pi^0)/\Gamma_{total}$ — Γ_{48}/Γ

VALUE (%)	EVTS	DOCUMENT ID		TECN	COMMENT
1.239±0.022 OUR FIT					
1.239±0.006±0.027	67k	ABLIKIM	18W	BES3	e^+e^-, 3773 MeV
• • • We do not use the following data for averages, fits, limits, etc. • • •					
1.240±0.017±0.056	614	HE	08	CLEO	See MENDEZ 10

$\Gamma(K^0_S \pi^0)/[\Gamma(K^- \pi^+) + \Gamma(K^+ \pi^-)]$ — $\Gamma_{48}/(\Gamma_{47}+\Gamma_{344})$

VALUE (units 10^{-2})	EVTS	DOCUMENT ID		TECN	COMMENT
31.4±0.6 OUR FIT					
30.4±0.3±0.9	20k	MENDEZ	10	CLEO	e^+e^- at 3774 MeV

$\Gamma(K^0_S \pi^0)/\Gamma(K^0_S \pi^+ \pi^-)$ — Γ_{48}/Γ_{53}

VALUE	EVTS	DOCUMENT ID		TECN	COMMENT
0.436±0.023 OUR FIT					
0.44 ±0.02 ±0.05	1942 ± 64	PROCARIO	93B	CLE2	e^+e^- 10.36–10.7 GeV
• • • We do not use the following data for averages, fits, limits, etc. • • •					
0.34 ±0.04 ±0.02	92	[1] ALBRECHT	92P	ARG	$e^+e^- \approx$ 10 GeV
0.36 ±0.04 ±0.08	104	KINOSHITA	91	CLEO	$e^+e^- \sim$ 10.7 GeV

[1] This value is calculated from numbers in Table 1 of ALBRECHT 92P.

$\Gamma(K^0_L \pi^0)/\Gamma_{total}$ — Γ_{49}/Γ

VALUE (%)	EVTS	DOCUMENT ID		TECN	COMMENT
0.976±0.032 OUR AVERAGE					
0.97 ±0.03 ±0.02	2590	ABLIKIM	22BM	BES3	e^+e^- at $\psi(3770)$
0.998±0.049±0.048	1116	[1] HE	08	CLEO	e^+e^- at $\psi(3770)$

[1] The difference of HE 08 $D^0 \to K^0_S \pi^0$ and $K^0_L \pi^0$ branching fractions over the sum is 0.108 ± 0.025 ± 0.024. This is consistent with U-spin symmetry and the Cabibbo angle.

$\Gamma(K^0_L \eta)/\Gamma_{total}$ — Γ_{50}/Γ

VALUE (units 10^{-3})	EVTS	DOCUMENT ID		TECN	COMMENT
4.34±0.16 OUR AVERAGE					
4.39±0.24±0.15	543	[1] ABLIKIM	22W	BES3	e^+e^- at 3.773 GeV
4.31±0.14±0.13	2.1k	[2] ABLIKIM	22W	BES3	e^+e^- at 3.773 GeV

[1] Uses $\eta \to \pi^+ \pi^- \pi^0$ with branching fraction (23.02 ± 0.25) $\times 10^{-2}$.

[2] Uses $\eta \to \gamma\gamma$ with branching fraction (39.36 ± 0.18) $\times 10^{-2}$.

$\Gamma(K^0_L \eta')/\Gamma_{total}$ — Γ_{51}/Γ

VALUE (units 10^{-3})	EVTS	DOCUMENT ID		TECN	COMMENT
8.12±0.35 OUR AVERAGE	Error includes scale factor of 1.3.				
8.57±0.37±0.22	684	[1] ABLIKIM	22W	BES3	e^+e^- at 3.773 GeV
7.85±0.24±0.23	2k	[2] ABLIKIM	22W	BES3	e^+e^- at 3.773 GeV

[1] Uses $\eta' \to \pi^+ \pi^- \eta$ with branching fraction 0.425 ± 0.005.

[2] Uses $\eta' \to \rho^0 \gamma$ with branching fraction 0.295 ± 0.004.

$\Gamma(K^0_L \omega)/\Gamma_{total}$ — Γ_{52}/Γ

VALUE (units 10^{-2})	EVTS	DOCUMENT ID		TECN	COMMENT
1.164±0.022±0.028	6.1k	ABLIKIM	22W	BES3	e^+e^- at 3.773 GeV
• • • We do not use the following data for averages, fits, limits, etc. • • •					
1.09 ±0.06 ±0.03	1360	ABLIKIM	22BM	BES3	e^+e^- at $\psi(3770)$

$\Gamma(K^0_S \pi^+ \pi^-)/\Gamma_{total}$ — Γ_{53}/Γ

VALUE (%)	EVTS	DOCUMENT ID		TECN	COMMENT
• • • We do not use the following data for averages, fits, limits, etc. • • •					
2.52±0.20±0.25	284 ± 22	[1] ALBRECHT	94F	ARG	$e^+e^- \approx \Upsilon(4S)$
3.2 ±0.3 ±0.5		ADLER	87	MRK3	e^+e^- 3.77 GeV
2.6 ±0.8	32 ± 8	[2] SCHINDLER	81	MRK2	e^+e^- 3.771 GeV
4.0 ±1.2	28	[3] PERUZZI	77	LGW	e^+e^- 3.77 GeV

[1] See the footnote on the ALBRECHT 94F measurement of $\Gamma(K^- \pi^+)/\Gamma_{total}$ for the method used.

[2] SCHINDLER 81 (MARK-2) measures $\sigma(e^+e^- \to \psi(3770)) \times$ branching fraction to be 0.30 ± 0.08 nb. We use the MARK-3 (ADLER 88C) value of $\sigma = 5.8 \pm 0.5 \pm 0.6$ nb.

[3] PERUZZI 77 (MARK-1) measures $\sigma(e^+e^- \to \psi(3770)) \times$ branching fraction to be 0.46 ± 0.12 nb. We use the MARK-3 (ADLER 88C) value of $\sigma = 5.8 \pm 0.5 \pm 0.6$ nb.

$\Gamma(K^0_S \pi^+ \pi^-)/\Gamma(K^- \pi^+)$ — Γ_{53}/Γ_{47}

VALUE	EVTS	DOCUMENT ID		TECN	COMMENT
0.72±0.04 OUR FIT	Error includes scale factor of 1.1.				
0.81±0.05±0.08	856 ± 35	FRABETTI	94J	E687	γBe $\overline{E}_\gamma$=220 GeV

Int. J. Mod. Phys. A 2026.41. Downloaded from www.worldscientific.com
by UNIVERSITY OF CALIFORNIA @ BERKELEY on 09/16/26. Re-use and distribution is strictly not permitted, except for Open Access articles.

• • • We do not use the following data for averages, fits, limits, etc. • • •

0.85 ± 0.40	35	AVERY	80	SPEC	$\gamma N \to D^{*+}$
1.4 ± 0.5	116	PICCOLO	77	MRK1	e^+e^- 4.03, 4.41 GeV

$\Gamma(K^0_S \rho^0)/\Gamma(K^0_S \pi^+\pi^-)$ — Γ_{54}/Γ_{53}

This is the "fit fraction" from the Dalitz-plot analysis.

VALUE	DOCUMENT ID		TECN	COMMENT
$0.224^{+0.017}_{-0.023}$ OUR AVERAGE	Error includes scale factor of 1.7.			
0.210 ± 0.016	[1] AUBERT	08AL	BABR	Dalitz fit, $\approx$ 487 k evts
$0.264 \pm 0.009^{+0.010}_{-0.026}$	MURAMATSU	02	CLE2	Dalitz fit, 5299 evts
• • • We do not use the following data for averages, fits, limits, etc. • • •				
$0.267 \pm 0.011^{+0.009}_{-0.028}$	ASNER	04A	CLEO	See MURAMATSU 02
$0.350 \pm 0.028 \pm 0.067$	FRABETTI	94G	E687	Dalitz fit, 597 evts
$0.227 \pm 0.032 \pm 0.009$	ALBRECHT	93D	ARG	Dalitz fit, 440 evts
$0.215 \pm 0.051 \pm 0.037$	ANJOS	93	E691	γBe 90–260 GeV
$0.20 \pm 0.06 \pm 0.03$	FRABETTI	92B	E687	γ Be, $\overline{E}_\gamma$ = 221 GeV
$0.12 \pm 0.01 \pm 0.07$	ADLER	87	MRK3	e^+e^- 3.77 GeV

[1] The error on this AUBERT 08AL value includes both statistical and systematic uncertainties; the latter dominates.

$\Gamma(K^0_S \omega, \omega \to \pi^+\pi^-)/\Gamma(K^0_S \pi^+\pi^-)$ — Γ_{55}/Γ_{53}

This is the "fit fraction" from the Dalitz-plot analysis.

VALUE	DOCUMENT ID		TECN	COMMENT
0.0073 ± 0.0020 OUR AVERAGE				
0.009 ± 0.010	[1] AUBERT	08AL	BABR	Dalitz fit, $\approx$ 487 k evts
$0.0072 \pm 0.0018^{+0.0010}_{-0.0009}$	MURAMATSU	02	CLE2	Dalitz fit, 5299 evts
• • • We do not use the following data for averages, fits, limits, etc. • • •				
$0.0081 \pm 0.0019^{+0.0018}_{-0.0010}$	ASNER	04A	CLEO	See MURAMATSU 02

[1] The error on this AUBERT 08AL value includes both statistical and systematic uncertainties; the latter dominates.

$\Gamma(K^0_S(\pi^+\pi^-)_{S-wave})/\Gamma(K^0_S \pi^+\pi^-)$ — Γ_{56}/Γ_{53}

This is the "fit fraction" from the Dalitz-plot analysis. The $(\pi^+\pi^-)_{S-wave}$ includes what in isobar models are the $f_0(980)$ and $f_0(1370)$; see the following two data blocks.

VALUE	DOCUMENT ID		TECN	COMMENT
0.119 ± 0.026	[1] AUBERT	08AL	BABR	Dalitz fit, $\approx$ 487 k evts

[1] The error on this AUBERT 08AL value includes both statistical and systematic uncertainties; the latter dominates.

$\Gamma(K^0_S f_0(980), f_0 \to \pi^+\pi^-)/\Gamma(K^0_S \pi^+\pi^-)$ — Γ_{57}/Γ_{53}

Fit fraction from the Dalitz plot analyses.

VALUE	DOCUMENT ID		TECN	COMMENT
$0.043 \pm 0.005^{+0.012}_{-0.006}$	MURAMATSU	02	CLE2	Dalitz fit, 5299 evts
• • • We do not use the following data for averages, fits, limits, etc. • • •				
$0.042 \pm 0.005^{+0.011}_{-0.005}$	ASNER	04A	CLEO	See MURAMATSU 02
$0.068 \pm 0.016 \pm 0.018$	FRABETTI	94G	E687	Dalitz fit, 597 evts
$0.046 \pm 0.018 \pm 0.006$	ALBRECHT	93D	ARG	Dalitz fit, 440 evts

$\Gamma(K^0_S f_0(1370), f_0 \to \pi^+\pi^-)/\Gamma(K^0_S \pi^+\pi^-)$ — Γ_{58}/Γ_{53}

This is the "fit fraction" from the Dalitz-plot analysis.

VALUE	DOCUMENT ID		TECN	COMMENT
$0.099 \pm 0.011^{+0.028}_{-0.044}$	MURAMATSU	02	CLE2	Dalitz fit, 5299 evts
• • • We do not use the following data for averages, fits, limits, etc. • • •				
$0.098 \pm 0.014^{+0.026}_{-0.036}$	ASNER	04A	CLEO	See MURAMATSU 02
$0.077 \pm 0.022 \pm 0.031$	FRABETTI	94G	E687	Dalitz fit, 597 evts
$0.082 \pm 0.028 \pm 0.013$	ALBRECHT	93D	ARG	Dalitz fit, 440 evts

$\Gamma(K^0_S f_2(1270), f_2 \to \pi^+\pi^-)/\Gamma(K^0_S \pi^+\pi^-)$ — Γ_{59}/Γ_{53}

This is the "fit fraction" from the Dalitz-plot analysis.

VALUE	DOCUMENT ID		TECN	COMMENT
$0.0032^{+0.0035}_{-0.0022}$ OUR AVERAGE				
0.006 ± 0.007	[1] AUBERT	08AL	BABR	Dalitz fit, $\approx$ 487 k evts
$0.0027 \pm 0.0015^{+0.0037}_{-0.0017}$	MURAMATSU	02	CLE2	Dalitz fit, 5299 evts
• • • We do not use the following data for averages, fits, limits, etc. • • •				
$0.0036 \pm 0.0022^{+0.0032}_{-0.0019}$	ASNER	04A	CLEO	See MURAMATSU 02
$0.037 \pm 0.014 \pm 0.017$	FRABETTI	94G	E687	Dalitz fit, 597 evts
$0.050 \pm 0.021 \pm 0.008$	ALBRECHT	93D	ARG	Dalitz fit, 440 evts

[1] The error on this AUBERT 08AL value includes both statistical and systematic uncertainties; the latter dominates.

$\Gamma(K^*(892)^-\pi^+, K^{*-} \to K^0_S \pi^-)/\Gamma(K^0_S \pi^+\pi^-)$ — Γ_{60}/Γ_{53}

This is the "fit fraction" from the Dalitz-plot analysis.

VALUE	DOCUMENT ID		TECN	COMMENT
$0.588^{+0.034}_{-0.050}$ OUR AVERAGE	Error includes scale factor of 2.0.			
0.557 ± 0.028	[1] AUBERT	08AL	BABR	Dalitz fit, $\approx$ 487 k evts
$0.657 \pm 0.013^{+0.018}_{-0.040}$	MURAMATSU	02	CLE2	Dalitz fit, 5299 evts
• • • We do not use the following data for averages, fits, limits, etc. • • •				
$0.663 \pm 0.013^{+0.024}_{-0.043}$	ASNER	04A	CLEO	See MURAMATSU 02
$0.625 \pm 0.036 \pm 0.026$	FRABETTI	94G	E687	Dalitz fit, 597 evts
$0.718 \pm 0.042 \pm 0.030$	ALBRECHT	93D	ARG	Dalitz fit, 440 evts
0.480 ± 0.097	ANJOS	93	E691	γBe 90–260 GeV
$0.56 \pm 0.04 \pm 0.05$	ADLER	87	MRK3	e^+e^- 3.77 GeV

[1] The error on this AUBERT 08AL value includes both statistical and systematic uncertainties; the latter dominates.

$\Gamma(K^*_0(1430)^-\pi^+, K^{*-}_0 \to K^0_S \pi^-)/\Gamma(K^0_S \pi^+\pi^-)$ — Γ_{61}/Γ_{53}

This is the "fit fraction" from the Dalitz-plot analysis.

VALUE	DOCUMENT ID		TECN	COMMENT
$0.095^{+0.014}_{-0.010}$ OUR AVERAGE				
0.102 ± 0.015	[1] AUBERT	08AL	BABR	Dalitz fit, $\approx$ 487 k evts
$0.073 \pm 0.007^{+0.031}_{-0.011}$	MURAMATSU	02	CLE2	Dalitz fit, 5299 evts
• • • We do not use the following data for averages, fits, limits, etc. • • •				
$0.072 \pm 0.007^{+0.014}_{-0.013}$	ASNER	04A	CLEO	See MURAMATSU 02
$0.109 \pm 0.027 \pm 0.029$	FRABETTI	94G	E687	Dalitz fit, 597 evts
$0.129 \pm 0.034 \pm 0.021$	ALBRECHT	93D	ARG	Dalitz fit, 440 evts

[1] The error on this AUBERT 08AL value includes both statistical and systematic uncertainties; the latter dominates.

$\Gamma(K^*_2(1430)^-\pi^+, K^{*-}_2 \to K^0_S \pi^-)/\Gamma(K^0_S \pi^+\pi^-)$ — Γ_{62}/Γ_{53}

This is the "fit fraction" from the Dalitz-plot analysis.

VALUE	DOCUMENT ID		TECN	COMMENT
$0.0120^{+0.0070}_{-0.0035}$ OUR AVERAGE				
0.022 ± 0.016	[1] AUBERT	08AL	BABR	Dalitz fit, $\approx$ 487 k evts
$0.011 \pm 0.002 \; ^{+0.007}_{-0.003}$	MURAMATSU	02	CLE2	Dalitz fit, 5299 evts
• • • We do not use the following data for averages, fits, limits, etc. • • •				
$0.011 \pm 0.002 \; ^{+0.005}_{-0.003}$	ASNER	04A	CLEO	See MURAMATSU 02

[1] The error on this AUBERT 08AL value includes both statistical and systematic uncertainties; the latter dominates.

$\Gamma(K^*(1680)^-\pi^+, K^{*-} \to K^0_S \pi^-)/\Gamma(K^0_S \pi^+\pi^-)$ — Γ_{63}/Γ_{53}

This is the "fit fraction" from the Dalitz-plot analysis.

VALUE	DOCUMENT ID		TECN	COMMENT
0.016 ± 0.013 OUR AVERAGE				
0.007 ± 0.019	[1] AUBERT	08AL	BABR	Dalitz fit, $\approx$ 487 k evts
$0.022 \pm 0.004^{+0.018}_{-0.015}$	MURAMATSU	02	CLE2	Dalitz fit, 5299 evts
• • • We do not use the following data for averages, fits, limits, etc. • • •				
$0.023 \pm 0.005^{+0.007}_{-0.014}$	ASNER	04A	CLEO	See MURAMATSU 02

[1] The error on this AUBERT 08AL value includes both statistical and systematic uncertainties; the latter dominates.

$\Gamma(K^*(892)^+\pi^-, K^{*+} \to K^0_S \pi^+)/\Gamma(K^0_S \pi^+\pi^-)$ — Γ_{64}/Γ_{53}

This is the "fit fraction" from the Dalitz-plot analysis. This is a doubly Cabibbo-suppressed mode.

VALUE (units 10^{-3})	DOCUMENT ID		TECN	COMMENT
$4.0^{+2.0}_{-1.2}$ OUR AVERAGE				
4.6 ± 2.3	[1] AUBERT	08AL	BABR	Dalitz fit, $\approx$ 487 k evts
$3.4 \pm 1.3^{+4.1}_{-0.4}$	MURAMATSU	02	CLE2	Dalitz fit, 5299 evts
• • • We do not use the following data for averages, fits, limits, etc. • • •				
$3.4 \pm 1.3^{+3.6}_{-0.5}$	ASNER	04A	CLEO	See MURAMATSU 02

[1] The error on this AUBERT 08AL value includes both statistical and systematic uncertainties; the latter dominates.

$\Gamma(K^*_0(1430)^+\pi^-, K^{*+}_0 \to K^0_S \pi^+)/\Gamma(K^0_S \pi^+\pi^-)$ — Γ_{65}/Γ_{53}

This is the "fit fraction" from the Dalitz-plot analysis. This is a doubly Cabibbo-suppressed mode.

VALUE	CL%	DOCUMENT ID		TECN	COMMENT
$<5 \times 10^{-4}$	95	AUBERT	08AL	BABR	Dalitz fit, $\approx$ 487 k evts

$\Gamma(K^*_2(1430)^+\pi^-, K^{*+}_2 \to K^0_S \pi^+)/\Gamma(K^0_S \pi^+\pi^-)$ — Γ_{66}/Γ_{53}

This is the "fit fraction" from the Dalitz-plot analysis. This is a doubly Cabibbo-suppressed mode.

VALUE	CL%	DOCUMENT ID		TECN	COMMENT
$<1.2 \times 10^{-3}$	95	AUBERT	08AL	BABR	Dalitz fit, $\approx$ 487 k evts

$\Gamma(K^0_S \pi^+\pi^-$ nonresonant$)/\Gamma(K^0_S \pi^+\pi^-)$ — Γ_{67}/Γ_{53}

This is the "fit fraction" from the Dalitz-plot analysis. Neither FRABETTI 94G nor ALBRECHT 93D (quoted in many of the earlier submodes of $K^0_S \pi^+\pi^-$) sees evidence for a nonresonant component.

VALUE	DOCUMENT ID		TECN	COMMENT
$0.009 \pm 0.004^{+0.020}_{-0.004}$	MURAMATSU	02	CLE2	Dalitz fit, 5299 evts
• • • We do not use the following data for averages, fits, limits, etc. • • •				
$0.007 \pm 0.007^{+0.021}_{-0.006}$	ASNER	04A	CLEO	See MURAMATSU 02
$0.263 \pm 0.024 \pm 0.041$	ANJOS	93	E691	γBe 90–260 GeV
$0.26 \pm 0.08 \pm 0.05$	FRABETTI	92B	E687	γ Be, $\overline{E}_\gamma$ = 221 GeV
$0.33 \pm 0.05 \pm 0.10$	ADLER	87	MRK3	e^+e^- 3.77 GeV

Int. J. Mod. Phys. A 2026.41. Downloaded from www.worldscientific.com by LIFORNIA @ BERKELEY on 09/16/26. Re-use and distribution is strictly not permitted, except for Open Access articles.

$\Gamma(K^-\pi^+\pi^0)/\Gamma_{total}$ — Γ_{68}/Γ

VALUE (%)	EVTS	DOCUMENT ID		TECN	COMMENT
• • • We do not use the following data for averages, fits, limits, etc. • • •					
14.57±0.12±0.38		[1] DOBBS	07	CLEO	See BONVICINI 14
14.9 ±0.3 ±0.5	19k ±150	[1] HE	05	CLEO	See DOBBS 07
13.3 ±1.2 ±1.3	931	ADLER	88C	MRK3	e^+e^- 3.77 GeV
11.7 ±4.3	37	[2] SCHINDLER	81	MRK2	e^+e^- 3.771 GeV

[1] DOBBS 07 and HE 05 use single- and double-tagged events in an overall fit. DOBBS 07 supersedes HE 05.
[2] SCHINDLER 81 (MARK-2) measures $\sigma(e^+e^- \to \psi(3770)) \times$ branching fraction to be 0.68 ± 0.23 nb. We use the MARK-3 (ADLER 88C) value of $\sigma = 5.8 \pm 0.5 \pm 0.6$ nb.

$\Gamma(K^-\pi^+\pi^0)/\Gamma(K^-\pi^+)$ — Γ_{68}/Γ_{47}

VALUE	EVTS	DOCUMENT ID		TECN	COMMENT
3.66 ±0.12 OUR FIT Error includes scale factor of 2.0.					
3.76 ±0.10 OUR AVERAGE Error includes scale factor of 1.4. See the ideogram below.					
3.802±0.022±0.073		BONVICINI	14	CLEO	All CLEO-c runs
3.81 ±0.07 ±0.26	10k	BARISH	96	CLE2	$e^+e^- \approx \Upsilon(4S)$
3.04 ±0.16 ±0.34	931	[1] ALBRECHT	92P	ARG	$e^+e^- \approx$ 10 GeV
2.8 ±0.14 ±0.52	1050	KINOSHITA	91	CLEO	$e^+e^- \sim$ 10.7 GeV

[1] This value is calculated from numbers in Table 1 of ALBRECHT 92P.

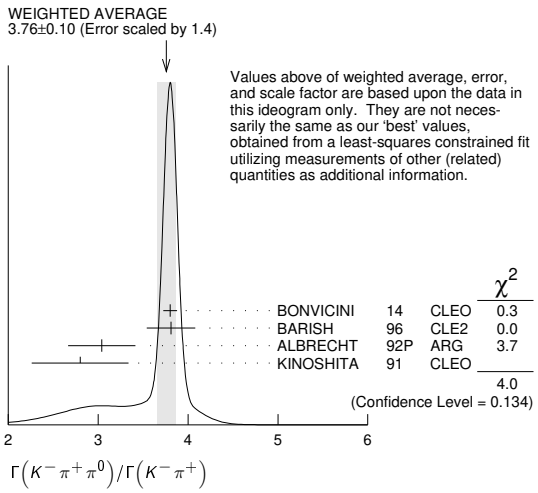

$\Gamma(K^-\rho^+)/\Gamma(K^-\pi^+\pi^0)$ — Γ_{69}/Γ_{68}

This is the "fit fraction" from the Dalitz-plot analysis.

VALUE	DOCUMENT ID		TECN	COMMENT
0.78 ±0.04 OUR AVERAGE				
0.788±0.019±0.048	KOPP	01	CLE2	Dalitz fit, ≈ 7,000 evts
0.765±0.041±0.054	FRABETTI	94G	E687	Dalitz fit, 530 evts
• • • We do not use the following data for averages, fits, limits, etc. • • •				
0.647±0.039±0.150	ANJOS	93	E691	γBe 90–260 GeV
0.81 ±0.03 ±0.06	ADLER	87	MRK3	e^+e^- 3.77 GeV

$\Gamma(K^-\rho(1700)^+,\ \rho^+ \to \pi^+\pi^0)/\Gamma(K^-\pi^+\pi^0)$ — Γ_{70}/Γ_{68}

This is the "fit fraction" from the Dalitz-plot analysis.

VALUE	DOCUMENT ID		TECN	COMMENT
0.057±0.008±0.009	KOPP	01	CLE2	Dalitz fit, ≈ 7,000 evts

$\Gamma(K^*(892)^-\pi^+,\ K^*(892)^- \to K^-\pi^0)/\Gamma(K^-\pi^+\pi^0)$ — Γ_{71}/Γ_{68}

This is the "fit fraction" from the Dalitz-plot analysis.

VALUE	DOCUMENT ID		TECN	COMMENT
$0.160^{+0.025}_{-0.013}$ OUR AVERAGE				
$0.161\pm0.007^{+0.027}_{-0.011}$	KOPP	01	CLE2	Dalitz fit, ≈ 7,000 evts
0.148±0.028±0.049	FRABETTI	94G	E687	Dalitz fit, 530 evts
• • • We do not use the following data for averages, fits, limits, etc. • • •				
0.084±0.011±0.012	ANJOS	93	E691	γBe 90–260 GeV
0.12 ±0.02 ±0.03	ADLER	87	MRK3	e^+e^- 3.77 GeV

$\Gamma(\overline{K}^*(892)^0\pi^0,\ \overline{K}^*(892)^0 \to K^-\pi^+)/\Gamma(K^-\pi^+\pi^0)$ — Γ_{72}/Γ_{68}

This is the "fit fraction" from the Dalitz-plot analysis.

VALUE	DOCUMENT ID		TECN	COMMENT
0.135±0.016 OUR AVERAGE				
0.127±0.009±0.016	KOPP	01	CLE2	Dalitz fit, ≈ 7,000 evts
0.165±0.031±0.015	FRABETTI	94G	E687	Dalitz fit, 530 evts
• • • We do not use the following data for averages, fits, limits, etc. • • •				
0.142±0.018±0.024	ANJOS	93	E691	γBe 90–260 GeV
0.13 ±0.02 ±0.03	ADLER	87	MRK3	e^+e^- 3.77 GeV

$\Gamma(K_0^*(1430)^-\pi^+,\ K_0^{*-} \to K^-\pi^0)/\Gamma(K^-\pi^+\pi^0)$ — Γ_{73}/Γ_{68}

This is the "fit fraction" from the Dalitz-plot analysis.

VALUE	DOCUMENT ID		TECN	COMMENT
0.033±0.006±0.014	KOPP	01	CLE2	Dalitz fit, ≈ 7,000 evts

$\Gamma(\overline{K}_0^*(1430)^0\pi^0,\ \overline{K}_0^{*0} \to K^-\pi^+)/\Gamma(K^-\pi^+\pi^0)$ — Γ_{74}/Γ_{68}

This is the "fit fraction" from the Dalitz-plot analysis.

VALUE	DOCUMENT ID		TECN	COMMENT
$0.041\pm0.006^{+0.032}_{-0.009}$	KOPP	01	CLE2	Dalitz fit, ≈ 7,000 evts

$\Gamma(K^*(1680)^-\pi^+,\ K^{*-} \to K^-\pi^0)/\Gamma(K^-\pi^+\pi^0)$ — Γ_{75}/Γ_{68}

This is the "fit fraction" from the Dalitz-plot analysis.

VALUE	DOCUMENT ID		TECN	COMMENT
0.013±0.003±0.004	KOPP	01	CLE2	Dalitz fit, ≈ 7,000 evts

$\Gamma(K^-\pi^+\pi^0$ nonresonant$)/\Gamma(K^-\pi^+\pi^0)$ — Γ_{76}/Γ_{68}

This is the "fit fraction" from the Dalitz-plot analysis.

VALUE	EVTS	DOCUMENT ID		TECN	COMMENT
$0.080^{+0.040}_{-0.014}$ OUR AVERAGE					
$0.075\pm0.009^{+0.056}_{-0.011}$		KOPP	01	CLE2	Dalitz fit, ≈ 7,000 evts
0.101±0.033±0.040		FRABETTI	94G	E687	Dalitz fit, 530 evts
• • • We do not use the following data for averages, fits, limits, etc. • • •					
0.036±0.004±0.018		ANJOS	93	E691	γBe 90–260 GeV
0.09 ±0.02 ±0.04		ADLER	87	MRK3	e^+e^- 3.77 GeV
0.51 ±0.22	21	SUMMERS	84	E691	Photoproduction

$\Gamma(K_S^0 2\pi^0)/\Gamma_{total}$ — Γ_{77}/Γ

VALUE (units 10^{-3})	EVTS	DOCUMENT ID		TECN	COMMENT
9.1 ±1.1 OUR AVERAGE Error includes scale factor of 2.2.					
10.58±0.38±0.73	1259	LOWREY	11	CLEO	$e^+e^- \approx$ 3.77 GeV
8.34±0.45±0.42		ASNER	08	CLEO	$e^+e^- \to D^0\overline{D}^0$, 3.77 GeV

$\Gamma(K_L^0\pi^0\pi^0)/\Gamma_{total}$ — Γ_{78}/Γ

VALUE (%)	EVTS	DOCUMENT ID		TECN	COMMENT
1.26±0.05±0.03	1300	ABLIKIM	22BM	BES3	e^+e^- at $\psi(3770)$

$\Gamma(K_S^0(2\pi^0)_{S-wave})/\Gamma(K_S^0 2\pi^0)$ — Γ_{79}/Γ_{77}

This is the "fit fraction" from the Dalitz-plot analysis.

VALUE (units 10^{-2})	DOCUMENT ID		TECN	COMMENT
28.9±6.3±3.1	LOWREY	11	CLEO	Dalitz analysis, 1259 evts

$\Gamma(\overline{K}^*(892)^0\pi^0,\ \overline{K}^{*0} \to K_S^0\pi^0)/\Gamma(K_S^0 2\pi^0)$ — Γ_{80}/Γ_{77}

VALUE (units 10^{-2})	EVTS	DOCUMENT ID		TECN	COMMENT
65.6±5.3±2.5	1259	LOWREY	11	CLEO	Dalitz analysis

$\Gamma(\overline{K}^*(892)^0\pi^0,\ \overline{K}^{*0} \to K_S^0\pi^0)/\Gamma(K_S^0\pi^0)$ — Γ_{80}/Γ_{48}

This is the "fit fraction" from the Dalitz-plot analysis.

VALUE (units 10^{-2})	DOCUMENT ID		TECN	COMMENT
$55^{+13}_{-10}\pm7$	PROCARIO	93B	CLE2	Dalitz plot fit, 122 evts

$\Gamma(\overline{K}^*(1430)^0\pi^0,\ \overline{K}^{*0} \to K_S^0\pi^0)/\Gamma(K_S^0 2\pi^0)$ — Γ_{81}/Γ_{77}

This is the "fit fraction" from the Dalitz-plot analysis.

VALUE (units 10^{-2})	DOCUMENT ID		TECN	COMMENT
0.49±0.45±2.51	LOWREY	11	CLEO	Dalitz analysis, 1259 evts

$\Gamma(\overline{K}^*(1680)^0\pi^0,\ \overline{K}^{*0} \to K_S^0\pi^0)/\Gamma(K_S^0 2\pi^0)$ — Γ_{82}/Γ_{77}

This is the "fit fraction" from the Dalitz-plot analysis.

VALUE (units 10^{-2})	DOCUMENT ID		TECN	COMMENT
11.2±2.7±2.5	LOWREY	11	CLEO	Dalitz analysis, 1259 evts

$\Gamma(K_S^0 f_2(1270),\ f_2 \to 2\pi^0)/\Gamma(K_S^0 2\pi^0)$ — Γ_{83}/Γ_{77}

This is the "fit fraction" from the Dalitz-plot analysis.

VALUE (units 10^{-2})	DOCUMENT ID		TECN	COMMENT
2.48±0.91±0.78	LOWREY	11	CLEO	Dalitz analysis, 1259 evts

$\Gamma(2K_S^0$, one $K_S^0 \to 2\pi^0)/\Gamma(K_S^0 2\pi^0)$ — Γ_{84}/Γ_{77}

This is the "fit fraction" from the Dalitz-plot analysis.

VALUE (units 10^{-2})	DOCUMENT ID		TECN	COMMENT
3.46±0.92±0.66	LOWREY	11	CLEO	Dalitz analysis, 1259 evts

$\Gamma(K_S^0 2\pi^0$ nonresonant$)/\Gamma(K_S^0\pi^0)$ — Γ_{85}/Γ_{48}

This is the "fit fraction" from the Dalitz-plot analysis.

VALUE	DOCUMENT ID		TECN	COMMENT
• • • We do not use the following data for averages, fits, limits, etc. • • •				
0.37±0.08±0.04	PROCARIO	93B	CLE2	Dalitz plot fit, 122 evts

$\Gamma(K_S^0 3\pi^0)/\Gamma_{total}$ — Γ_{86}/Γ

VALUE (units 10^{-3})	EVTS	DOCUMENT ID		TECN	COMMENT
7.64±0.30±0.29	870	ABLIKIM	22Y	BES3	e^+e^- at 3.773 GeV

$\Gamma(K^-2\pi^+\pi^-)/\Gamma_{total}$ — Γ_{87}/Γ

VALUE (%)	EVTS	DOCUMENT ID		TECN	COMMENT
• • • We do not use the following data for averages, fits, limits, etc. • • •					
8.30±0.07±0.20		[1] DOBBS	07	CLEO	See BONVICINI 14
8.3 ±0.2 ±0.3	15k	[1] HE	05	CLEO	See DOBBS 07

Int. J. Mod. Phys. A 2026.41. Downloaded from www.worldscientific.com
by UNIVERSITY OF CALIFORNIA @ BERKELEY on 09/16/26. Re-use and distribution is strictly not permitted, except for Open Access articles.

7.9 ±1.5 ±0.9		[2] ALBRECHT	94	ARG	$e^+e^- \approx \Upsilon(4S)$
6.80±0.27±0.57	1.4k	[3] ALBRECHT	94F	ARG	$e^+e^- \approx \Upsilon(4S)$
9.1 ±0.8 ±0.8	992	ADLER	88C	MRK3	e^+e^- 3.77 GeV
11.7 ±2.5	185	[4] SCHINDLER	81	MRK2	e^+e^- 3.771 GeV
6.2 ±1.9	44	[5] PERUZZI	77	LGW	e^+e^- 3.77 GeV

[1] DOBBS 07 and HE 05 use single- and double-tagged events in an overall fit. DOBBS 07 supersedes HE 05.
[2] ALBRECHT 94 uses D^0 mesons from $\overline{B}^0 \to D^{*+}\ell^-\overline{\nu}_\ell$ decays. This is a different set of events than used by ALBRECHT 94F.
[3] See the footnote on the ALBRECHT 94F measurement of $\Gamma(K^-\pi^+)/\Gamma_{total}$ for the method used.
[4] SCHINDLER 81 (MARK-2) measures $\sigma(e^+e^- \to \psi(3770)) \times$ branching fraction to be 0.68 ± 0.11 nb. We use the MARK-3 (ADLER 88C) value of σ = 5.8 ± 0.5 ± 0.6 nb.
[5] PERUZZI 77 (MARK-1) measures $\sigma(e^+e^- \to \psi(3770)) \times$ branching fraction to be 0.36 ± 0.10 nb. We use the MARK-3 (ADLER 88C) value of σ = 5.8 ± 0.5 ± 0.6 nb.

$\Gamma(K^-2\pi^+\pi^-)/\Gamma(K^-\pi^+)$ — Γ_{87}/Γ_{47}

VALUE	EVTS	DOCUMENT ID		TECN	COMMENT
2.084±0.031 OUR FIT	Error includes scale factor of 1.1.				
2.087±0.032 OUR AVERAGE					
2.106±0.013±0.032		BONVICINI	14	CLEO	All CLEO-c runs
1.94 ±0.07 $^{+0.09}_{-0.11}$		JUN	00	SELX	Σ^- nucleus, 600 GeV
1.7 ±0.2 ±0.2	1745	ANJOS	92C	E691	γBe 90–260 GeV
1.90 ±0.25 ±0.20	337	ALVAREZ	91B	NA14	Photoproduction
2.12 ±0.16 ±0.09		BORTOLETTO	88	CLEO	e^+e^- 10.55 GeV
2.17 ±0.28 ±0.23		ALBRECHT	85F	ARG	e^+e^- 10 GeV
• • • We do not use the following data for averages, fits, limits, etc. • • •					
2.0 ±0.9	48	BAILEY	86	ACCM	π^-Be fixed target
2.0 ±1.0	10	BAILEY	83B	SPEC	π^-Be $\to D^0$
2.2 ±0.8	214	PICCOLO	77	MRK1	e^+e^- 4.03, 4.41 GeV

$\Gamma(K^-\pi^+\rho^0\text{total})/\Gamma(K^-2\pi^+\pi^-)$ — Γ_{88}/Γ_{87}

VALUE (units 10^{-2})	DOCUMENT ID		TECN	COMMENT
83.5±3.5 OUR AVERAGE				
80 ±3 ±5	ANJOS	92C	E691	1745 $K^-2\pi^+\pi^-$ evts
85.5±3.2±3.0	COFFMAN	92B	MRK3	1281 ±45 $K^-2\pi^+\pi^-$ evts

$\Gamma(K^-\pi^+\rho^0\text{3-body})/\Gamma(K^-2\pi^+\pi^-)$ — Γ_{89}/Γ_{87}

VALUE (units 10^{-2})	EVTS	DOCUMENT ID		TECN	COMMENT
7.4±2.0 OUR AVERAGE					
8.4±1.1±2.5	16k	ABLIKIM	17O	BES3	$D^0 \to K^-2\pi^+\pi^-$
5 ±3 ±2		ANJOS	92C	E691	1745 $K^-2\pi^+\pi^-$ evts
8.4±2.2±4.0		COFFMAN	92B	MRK3	1281 ±45 $K^-2\pi^+\pi^-$ evts

$\Gamma(\overline{K}^*(892)^0\rho^0, \overline{K}^{*0} \to K^-\pi^+)/\Gamma(K^-2\pi^+\pi^-)$ — Γ_{90}/Γ_{87}

VALUE (units 10^{-2})	EVTS	DOCUMENT ID		TECN	COMMENT
12.3±0.6 OUR AVERAGE					
12.3±0.4±0.5	16k	ABLIKIM	17O	BES3	$D^0 \to K^-2\pi^+\pi^-$
13 ±2 ±2		ANJOS	92C	E691	1745 $K^-2\pi^+\pi^-$ evts

$\Gamma(\overline{K}^*(892)^0\rho^0\text{transverse}, \overline{K}^{*0} \to K^-\pi^+)/\Gamma(K^-2\pi^+\pi^-)$ — Γ_{91}/Γ_{87}

VALUE	EVTS	DOCUMENT ID		TECN	COMMENT
0.142±0.016±0.05	1281	COFFMAN	92B	MRK3	$K^-2\pi^+\pi^-$ evts

$\Gamma(K^-a_1(1260)^+, a_1^+ \to \rho^0\pi^+)/\Gamma(K^-2\pi^+\pi^-)$ — Γ_{92}/Γ_{87}

VALUE (units 10^{-2})	EVTS	DOCUMENT ID		TECN	COMMENT
53 ±4 OUR AVERAGE					
54.6±2.8± 3.7	16k	ABLIKIM	17O	BES3	$D^0 \to K^-2\pi^+\pi^-$
47 ±5 ±10	1745	ANJOS	92C	E691	$K^-2\pi^+\pi^-$ evts
49.2±2.4± 8.0	1281	COFFMAN	92B	MRK3	$K^-2\pi^+\pi^-$ evts

$\Gamma(K_1(1270)^-\pi^+, K_1^- \to K^-\pi^+\pi^-\text{total})/\Gamma(K^-2\pi^+\pi^-)$ — Γ_{93}/Γ_{87}

VALUE (units 10^{-2})	EVTS	DOCUMENT ID		TECN	COMMENT
4.8 ±0.4 OUR AVERAGE					
4.66±0.05±0.39±0.24	891k	[1] AAIJ	18AI	LHCB	$D^0 \to K^-2\pi^+\pi^-$
6.6 ±1.9 ±0.3	1281	COFFMAN	92B	MRK3	$K^-2\pi^+\pi^-$ evts

[1] The 3rd error is due to the uncertainty in the amplitude model composition.

$\Gamma(K_1(1270)^-\pi^+, K_1^- \to \overline{K}^*(892)^0\pi^-, \overline{K}^{*0} \to K^-\pi^+)/\Gamma(K^-2\pi^+\pi^-)$ — Γ_{96}/Γ_{87}

VALUE (units 10^{-2})	EVTS	DOCUMENT ID		TECN	COMMENT
0.8±0.2±0.2	16k	ABLIKIM	17O	BES3	$D^0 \to K^-2\pi^+\pi^-$

$\Gamma(K^-2\pi^+\pi^-\text{nonresonant})/\Gamma(K^-2\pi^+\pi^-)$ — Γ_{97}/Γ_{87}

VALUE (units 10^{-2})	EVTS	DOCUMENT ID		TECN	COMMENT
22.0 ±0.8 OUR AVERAGE					
22.04±0.28±2.09±1.51	891k	[1] AAIJ	18AI	LHCB	$D^0 \to K^-2\pi^+\pi^-$
21.9 ±0.6 ±0.6	16k	[2] ABLIKIM	17O	BES3	$D^0 \to K^-2\pi^+\pi^-$
23 ±2 ±3	1.7k	ANJOS	92C	E691	$D^0 \to K^-2\pi^+\pi^-$
24.2 ±2.5 ±6.0	1.2k	COFFMAN	92B	MRK3	$D^0 \to K^-2\pi^+\pi^-$

[1] The 3rd error is due to the uncertainty in the amplitude model composition.
[2] In addition to the 14 ABLIKIM 17O branching ratios we have listed, the paper gives 15 more ratios for mostly non-resonant modes. Four of the 15 have less than 2-standard-deviation significance. Here are some of the omitted modes, with S, P, V, A, and T for scalar, pseudo-scalar, vector, axial-vector, and tensor spin sub-structures: $\pi^+(K^-\rho^0)_P$, $\pi^+(K^-\rho^0)_V$, $\pi^+(\overline{K}^{*0}\pi^-)_P$, $\pi^+(\overline{K}^{*0}\pi^-)_V$, $\pi^+(\pi^-(K^-\pi^+)_{S-wave})_A$, $(K^-\pi^+)_V(\pi^+\pi^-)_S$, $(K^-\pi^+)_T(\pi^+\pi^-)_S \cdots$

$\Gamma(K_S^0\pi^+\pi^-\pi^0)/\Gamma_{total}$ — Γ_{98}/Γ

VALUE (%)	EVTS	DOCUMENT ID		TECN	COMMENT
5.2±0.6 OUR FIT					
5.2±1.1±1.2	140	COFFMAN	92B	MRK3	e^+e^- 3.77 GeV
• • • We do not use the following data for averages, fits, limits, etc. • • •					
6.7 $^{+1.6}_{-1.7}$		[1] BARLAG	92C	ACCM	π^- Cu 230 GeV

[1] BARLAG 92C computes the branching fraction using topological normalization.

$\Gamma(K_S^0\pi^+\pi^-\pi^0)/\Gamma(K_S^0\pi^+\pi^-)$ — Γ_{98}/Γ_{53}

Branching fractions for submodes of this mode with narrow resonances (the η, ω, η') are fairly well determined (see below). COFFMAN 92B gives fractions of K^* and ρ submodes, but with only 140 ± 28 events above background could not determine them with much accuracy. We omit those measurements here; they are in our 2008 Review (Physics Letters **B667** 1 (2008)).

VALUE	EVTS	DOCUMENT ID		TECN	COMMENT
1.84±0.20 OUR FIT					
1.86±0.23 OUR AVERAGE					
1.80±0.20±0.21	190	[1] ALBRECHT	92P	ARG	$e^+e^- \approx$ 10 GeV
2.8 ±0.8 ±0.8	46	ANJOS	92C	E691	γBe 90–260 GeV
1.85±0.26±0.30	158	KINOSHITA	91	CLEO	$e^+e^- \sim$ 10.7 GeV

[1] This value is calculated from numbers in Table 1 of ALBRECHT 92P.

$\Gamma(K^-\pi^+2\pi^0)/\Gamma_{total}$ — Γ_{101}/Γ

VALUE (%)	EVTS	DOCUMENT ID		TECN	COMMENT
8.86±0.13±0.19	6.1k	ABLIKIM	19AK	BES3	e^+e^- at 3773 MeV
• • • We do not use the following data for averages, fits, limits, etc. • • •					
17.7 ±2.9		[1] BARLAG	92C	ACCM	π^- Cu 230 GeV
14.9 ±3.7 ±3.0	24	[2] ADLER	88C	MRK3	e^+e^- 3.77 GeV
20.9 $^{+7.4}_{-4.3}$ ±1.2	9	[1] AGUILAR-...	87F	HYBR	πp, pp 360, 400 GeV

[1] AGUILAR-BENITEZ 87F and BARLAG 92C compute the branching fraction using topological normalization. They do not distinguish the presence of a third π^0, and thus are not included in the average.
[2] ADLER 88C uses an absolute normalization method finding this decay channel opposite a detected $\overline{D}^0 \to K^+\pi^-$ in pure $D\overline{D}$ events.

$\Gamma(K^-\pi^+3\pi^0)/\Gamma_{total}$ — Γ_{102}/Γ

VALUE (units 10^{-3})	EVTS	DOCUMENT ID		TECN	COMMENT
9.54±0.30±0.31	1.6k	ABLIKIM	22Y	BES3	e^+e^- at 3.773 GeV

$\Gamma(K_S^0\pi^+\pi^-2\pi^0)/\Gamma_{total}$ — Γ_{103}/Γ

VALUE (units 10^{-3})	EVTS	DOCUMENT ID		TECN	COMMENT
12.66±0.45±0.43	1.2k	ABLIKIM	22Y	BES3	e^+e^- at 3.773 GeV

$\Gamma(K^-2\pi^+\pi^-\pi^0)/\Gamma(K^-\pi^+)$ — Γ_{104}/Γ_{47}

VALUE	EVTS	DOCUMENT ID		TECN	COMMENT
1.09±0.10 OUR FIT					
0.98±0.11±0.11	225	[1] ALBRECHT	92P	ARG	$e^+e^- \approx$ 10 GeV

[1] This value is calculated from numbers in Table 1 of ALBRECHT 92P.

$\Gamma(K^-2\pi^+\pi^-\pi^0)/\Gamma(K^-2\pi^+\pi^-)$ — Γ_{104}/Γ_{87}

VALUE	EVTS	DOCUMENT ID		TECN	COMMENT
0.52±0.05 OUR FIT					
0.56±0.07 OUR AVERAGE					
0.55±0.07 $^{+0.12}_{-0.09}$	167	KINOSHITA	91	CLEO	$e^+e^- \sim$ 10.7 GeV
0.57±0.06±0.05	180	ANJOS	90D	E691	Photoproduction

$\Gamma(\overline{K}^*(892)^0\pi^+\pi^-\pi^0, \overline{K}^{*0} \to K^-\pi^+)/\Gamma_{total}$ — Γ_{105}/Γ

VALUE (units 10^{-2})	DOCUMENT ID		TECN	COMMENT
1.3±0.6 OUR EVALUATION				
seen	ALBRECHT	92P	ARG	$e^+e^- \approx$ 10 GeV

$\Gamma(\overline{K}^*(892)^0\omega, \overline{K}^{*0} \to K^-\pi^+, \omega \to \pi^+\pi^-\pi^0)/\Gamma_{total}$ — Γ_{106}/Γ

VALUE (units 10^{-3})	DOCUMENT ID		TECN	COMMENT
6.5±3.0	[1] ALBRECHT	92P	ARG	$e^+e^- \approx$ 10 GeV

[1] This value is calculated from numbers in Table 2 of ALBRECHT 92P.

$\Gamma(K^-\pi^+\omega)/\Gamma_{total}$ — Γ_{107}/Γ

VALUE (units 10^{-2})	EVTS	DOCUMENT ID		TECN	COMMENT
3.392±0.044±0.085	10.1k	[1] ABLIKIM	22U	BES3	e^+e^- at 3.773 GeV

[1] ABLIKIM 22U determines the ratios $B(D^0 \to K_S^0\pi^0\omega)/B(D^0 \to K^-\pi^+\omega)$ = 0.23 ± 0.01 ± 0.01 and $B(D^+ \to K_S^0\pi^+\omega)/B(D^0 \to K^-\pi^+\omega)$ = 0.21 ± 0.01 ± 0.01, in significant tension with statistical isospin model expectations of 0.4 and 0.9 respectively.

$\Gamma(K^-\pi^+\omega)/\Gamma(K^-\pi^+)$ — Γ_{107}/Γ_{47}

Unseen decay modes of the ω are included.

VALUE	EVTS	DOCUMENT ID		TECN	COMMENT
• • • We do not use the following data for averages, fits, limits, etc. • • •					
0.78±0.12±0.10	99	[1] ALBRECHT	92P	ARG	$e^+e^- \approx$ 10 GeV

[1] This value is calculated from numbers in Table 1 of ALBRECHT 92P.

Int. J. Mod. Phys. A 2026.41. Downloaded from www.worldscientific.com by LIFORNIA @ BERKELEY on 09/16/26. Re-use and distribution is strictly not permitted, except for Open Access articles.

$\Gamma(\overline{K}^*(892)^0\omega)/\Gamma(K^-\pi^+)$ — Γ_{108}/Γ_{47}

Unseen decay modes of the $\overline{K}^*(892)^0$ and ω are included.

VALUE	EVTS	DOCUMENT ID		TECN	COMMENT
0.28±0.11±0.04	17	[1] ALBRECHT	92P	ARG	$e^+e^- \approx$ 10 GeV

[1] This value is calculated from numbers in Table 1 of ALBRECHT 92P.

$\Gamma(K^0_S\pi^0\omega)/\Gamma_{total}$ — Γ_{109}/Γ

VALUE (units 10^{-2})	EVTS	DOCUMENT ID		TECN	COMMENT
0.848±0.046±0.031	697	[1] ABLIKIM	22U	BES3	e^+e^- at 3.773 GeV

[1] ABLIKIM 22U determines the ratio $B(D^0 \to K^0_S\pi^0\omega)/B(D^0 \to K^-\pi^+\omega) = 0.23 \pm 0.01 \pm 0.01$, in significant tension with statistical isospin model expectation of 0.4.

$\Gamma(K^0_S\eta\pi^0)/\Gamma_{total}$ — Γ_{110}/Γ

VALUE (units 10^{-3})	EVTS	DOCUMENT ID		TECN	COMMENT
10.06±0.34±0.30	1.1k	ABLIKIM	20V	BES3	e^+e^-, 3773 MeV

$\Gamma(K^0_S\eta\pi^0)/\Gamma(K^0_S\pi^0)$ — Γ_{110}/Γ_{48}

VALUE	EVTS	DOCUMENT ID		TECN	COMMENT
0.46±0.07±0.06	155 ± 22	[1] RUBIN	04	CLEO	$e^+e^- \approx$ 10 GeV

[1] The η here is detected in its $\gamma\gamma$ mode, but other η modes are included in the value given.

$\Gamma(K^0_S a_0(980),\ a_0 \to \eta\pi^0)/\Gamma(K^0_S\eta\pi^0)$ — $\Gamma_{111}/\Gamma_{110}$

This is the "fit fraction" from the Dalitz-plot analysis, with interference.

VALUE	DOCUMENT ID		TECN	COMMENT
1.19±0.09±0.26	[1] RUBIN	04	CLEO	Dalitz fit, 155 evts

[1] In addition to $K^0_S a_0(980)$ and $\overline{K}^*(892)^0\eta$ modes, RUBIN 04 finds a fit fraction of 0.246 ± 0.092 ± 0.091 for other, undetermined modes.

$\Gamma(\overline{K}^*(892)^0\eta,\ \overline{K}^{*0} \to K^0_S\pi^0)/\Gamma(K^0_S\eta\pi^0)$ — $\Gamma_{112}/\Gamma_{110}$

This is the "fit fraction" from the Dalitz-plot analysis, with interference.

VALUE	DOCUMENT ID		TECN	COMMENT
0.293±0.062±0.035	[1] RUBIN	04	CLEO	Dalitz fit, 155 evts

[1] See the note on RUBIN 04 in the preceding data block.

$\Gamma(K^-\pi^+\eta)/\Gamma_{total}$ — Γ_{113}/Γ

VALUE (units 10^{-2})	EVTS	DOCUMENT ID		TECN	COMMENT
1.88 ±0.05 OUR FIT	Error includes scale factor of 1.4.				
1.853±0.025±0.031	6.1k	ABLIKIM	20V	BES3	e^+e^-, 3773 MeV

$\Gamma(K^-\pi^+\eta)/\Gamma(K^-\pi^+)$ — Γ_{113}/Γ_{47}

VALUE (units 10^{-2})	EVTS	DOCUMENT ID		TECN	COMMENT
47.7±1.3 OUR FIT	Error includes scale factor of 1.4.				
50.1±2.0±0.2	116k	[1] CHEN	20A	BELL	e^+e^- at $\Upsilon(4S)$

[1] CHEN 20A reports 0.500 ± 0.002 ± 0.020 ± 0.003 from a measurement of $[\Gamma(D^0 \to K^-\pi^+\eta)/\Gamma(D^0 \to K^-\pi^+)] \times [B(\eta \to 2\gamma)]$ assuming $B(\eta \to 2\gamma) = (39.41 \pm 0.20) \times 10^{-2}$, which we rescale to our best (shown rounded) value $B(\eta \to 2\gamma) = (39.36 \pm 0.18) \times 10^{-2}$. Our first error is their experiment's error and our second error is the systematic error from using our best (shown rounded) value. The third reported uncertainty is the uncertainty from $B(\eta \to \gamma\gamma)$.

$\Gamma(K^*(892)^0\eta,\ K^{*0} \to K^-\pi^+)/\Gamma(K^-\pi^+\eta)$ — $\Gamma_{114}/\Gamma_{113}$

VALUE (units 10^{-2})	DOCUMENT ID		TECN	COMMENT
$47.61 \pm 1.32^{+0.24}_{-0.49}{}^{+3.64}_{-2.71}$	[1] CHEN	20A	BELL	e^+e^- at $\Upsilon(4S)$

[1] The third uncertainty is due to the uncertainty from the Dalitz model.

$\Gamma(a_0(980)^+K^-,\ a_0^+ \to \eta\pi^+)/\Gamma(K^-\pi^+\eta)$ — $\Gamma_{115}/\Gamma_{113}$

VALUE (units 10^{-2})	DOCUMENT ID		TECN	COMMENT
$39.28 \pm 1.50^{+1.58}_{-0.51}{}^{+4.38}_{-3.30}$	[1] CHEN	20A	BELL	e^+e^- at $\Upsilon(4S)$

[1] The third uncertainty is due to the uncertainty from the Dalitz model.

$\Gamma(K^*_2(1980)^-\pi^+,\ K^{*-}_2 \to K^-\eta)/\Gamma_{total}$ — Γ_{116}/Γ

VALUE (units 10^{-4})	DOCUMENT ID		TECN	COMMENT
$2.2^{+1.7}_{-1.9}$	CHEN	20A	BELL	e^+e^- at $\Upsilon(4S)$

$\Gamma(K^-\pi^+\pi^0\eta)/\Gamma_{total}$ — Γ_{117}/Γ

VALUE (units 10^{-3})	EVTS	DOCUMENT ID		TECN	COMMENT
4.49±0.22±0.15	580	ABLIKIM	20V	BES3	e^+e^-, 3773 MeV

$\Gamma(K^0_S\pi^+\pi^-\eta)/\Gamma_{total}$ — Γ_{118}/Γ

VALUE (units 10^{-3})	EVTS	DOCUMENT ID		TECN	COMMENT
2.80±0.19±0.10	250	ABLIKIM	20V	BES3	e^+e^-, 3773 MeV

$\Gamma(K^0_S 2\pi^0\eta)/\Gamma_{total}$ — Γ_{119}/Γ

VALUE (units 10^{-3})	EVTS	DOCUMENT ID		TECN	COMMENT
1.76±0.23±0.13	65	ABLIKIM	20V	BES3	e^+e^-, 3773 MeV

$\Gamma(K^0_S 2\pi^+2\pi^-)/\Gamma(K^0_S\pi^+\pi^-)$ — Γ_{120}/Γ_{53}

VALUE	EVTS	DOCUMENT ID		TECN	COMMENT
0.095±0.005±0.007	1283 ± 57	LINK	04D	FOCS	γ A, $\overline{E}_\gamma \approx 180$ GeV
• • • We do not use the following data for averages, fits, limits, etc. • • •					
0.07 ±0.02 ±0.01	11	[1] ALBRECHT	92P	ARG	$e^+e^- \approx$ 10 GeV
0.149±0.026	56	AMMAR	91	CLEO	$e^+e^- \approx$ 10.5 GeV
0.18 ±0.07 ±0.04	6	ANJOS	90D	E691	Photoproduction

[1] This value is calculated from numbers in Table 1 of ALBRECHT 92P.

$\Gamma(K^0_S\rho^0\pi^+\pi^-,\ \text{no}\,K^*(892)^-)/\Gamma(K^0_S 2\pi^+2\pi^-)$ — $\Gamma_{121}/\Gamma_{120}$

VALUE	DOCUMENT ID		TECN	COMMENT
0.40±0.24±0.07	LINK	04D	FOCS	γ A, $\overline{E}_\gamma \approx 180$ GeV

$\Gamma(K^*(892)^-2\pi^+\pi^-,\ K^*(892)^- \to K^0_S\pi^-,\ \text{no}\,\rho^0)/\Gamma(K^0_S 2\pi^+2\pi^-)$ — $\Gamma_{122}/\Gamma_{120}$

VALUE	DOCUMENT ID		TECN	COMMENT
0.17±0.28±0.02	LINK	04D	FOCS	γ A, $\overline{E}_\gamma \approx 180$ GeV

$\Gamma(K^*(892)^-\rho^0\pi^+,\ K^*(892)^- \to K^0_S\pi^-)/\Gamma(K^0_S 2\pi^+2\pi^-)$ — $\Gamma_{123}/\Gamma_{120}$

VALUE	DOCUMENT ID		TECN	COMMENT
0.60±0.21±0.09	LINK	04D	FOCS	γ A, $\overline{E}_\gamma \approx 180$ GeV

$\Gamma(K^0_S 2\pi^+2\pi^-\ \text{nonresonant})/\Gamma(K^0_S 2\pi^+2\pi^-)$ — $\Gamma_{124}/\Gamma_{120}$

VALUE	CL%	DOCUMENT ID		TECN	COMMENT
<0.46	90	LINK	04D	FOCS	γ A, $\overline{E}_\gamma \approx 180$ GeV

$\Gamma(K^-3\pi^+2\pi^-)/\Gamma_{total}$ — Γ_{126}/Γ

VALUE (units 10^{-4})	EVTS	DOCUMENT ID		TECN	COMMENT
1.48±0.32 OUR FIT	Error includes scale factor of 1.4.				
1.35±0.23±0.08	64	ABLIKIM	25BA	BES3	e^+e^- at 3.773 GeV

$\Gamma(K^-3\pi^+2\pi^-)/\Gamma(K^-2\pi^+\pi^-)$ — Γ_{126}/Γ_{87}

VALUE (units 10^{-3})	EVTS	DOCUMENT ID		TECN	COMMENT
1.8 ±0.4 OUR FIT	Error includes scale factor of 1.4.				
2.70±0.58±0.38	48 ± 10	LINK	04B	FOCS	γA, $\overline{E}_\gamma \approx 180$ GeV

$\Gamma(K^-2\pi^+\pi^-2\pi^0)/\Gamma_{total}$ — Γ_{127}/Γ

VALUE (units 10^{-4})	EVTS	DOCUMENT ID		TECN	COMMENT
19.0±1.1±1.5	0.44k	ABLIKIM	25BA	BES3	e^+e^- at 3.773 GeV

$\Gamma(K^0_S\eta)/\Gamma_{total}$ — Γ_{128}/Γ

Unseen decay modes of the η are included.

VALUE (units 10^{-3})	EVTS	DOCUMENT ID		TECN	COMMENT
5.08±0.13 OUR FIT					
5.13±0.07±0.12	9.5k	ABLIKIM	18W	BES3	e^+e^-, 3773 MeV
• • • We do not use the following data for averages, fits, limits, etc. • • •					
4.42±0.15±0.28		ASNER	08	CLEO	See MENDEZ 10

$\Gamma(K^0_S\eta)/[\Gamma(K^-\pi^+)+\Gamma(K^+\pi^-)]$ — $\Gamma_{128}/(\Gamma_{47}+\Gamma_{344})$

Unseen decay modes of the η are included.

VALUE (units 10^{-2})	EVTS	DOCUMENT ID		TECN	COMMENT
12.86±0.33 OUR FIT					
12.3 ±0.3 ±0.7	2864 ± 65	MENDEZ	10	CLEO	e^+e^- at 3774 MeV

$\Gamma(K^0_S\eta)/\Gamma(K^0_S\pi^0)$ — Γ_{128}/Γ_{48}

Unseen decay modes of the η are included.

VALUE	EVTS	DOCUMENT ID		TECN	COMMENT
• • • We do not use the following data for averages, fits, limits, etc. • • •					
0.32±0.04±0.03	225 ± 30	PROCARIO	93B	CLE2	$\eta \to \gamma\gamma$

$\Gamma(K^0_S\eta)/\Gamma(K^0_S\pi^+\pi^-)$ — Γ_{128}/Γ_{53}

Unseen decay modes of the η are included.

VALUE	EVTS	DOCUMENT ID		TECN	COMMENT
• • • We do not use the following data for averages, fits, limits, etc. • • •					
0.14±0.02±0.02	80 ± 12	PROCARIO	93B	CLE2	$\eta \to \pi^+\pi^-\pi^0$

$\Gamma(K^0_S\omega)/\Gamma_{total}$ — Γ_{129}/Γ

Unseen decay modes of the ω are included.

VALUE (%)	DOCUMENT ID		TECN	COMMENT
1.11±0.06 OUR FIT				
1.12±0.04±0.05	ASNER	08	CLEO	$e^+e^- \to D^0\overline{D}^0$, 3.77 GeV

$\Gamma(K^0_S\omega)/\Gamma(K^-\pi^+)$ — Γ_{129}/Γ_{47}

Unseen decay modes of the ω are included.

VALUE	DOCUMENT ID		TECN	COMMENT
• • • We do not use the following data for averages, fits, limits, etc. • • •				
0.50±0.18±0.10	ALBRECHT	89D	ARG	e^+e^- 10 GeV

$\Gamma(K^0_S\omega)/\Gamma(K^0_S\pi^+\pi^-)$ — Γ_{129}/Γ_{53}

Unseen decay modes of the ω are included.

VALUE	EVTS	DOCUMENT ID		TECN	COMMENT
0.391±0.028 OUR FIT					
0.33 ±0.09 OUR AVERAGE	Error includes scale factor of 1.1.				
0.29 ±0.08 ±0.05	16	[1] ALBRECHT	92P	ARG	$e^+e^- \approx$ 10 GeV
0.54 ±0.14 ±0.16	40	KINOSHITA	91	CLEO	$e^+e^- \sim$ 10.7 GeV

[1] This value is calculated from numbers in Table 1 of ALBRECHT 92P.

Int. J. Mod. Phys. A 2026.41. Downloaded from www.worldscientific.com
by UNIVERSITY OF CALIFORNIA @ BERKELEY on 09/16/26. Re-use and distribution is strictly not permitted, except for Open Access articles.

$\Gamma(K^0_S\omega)/\Gamma(K^0_S\pi^+\pi^-\pi^0)$ — Γ_{129}/Γ_{98}

Unseen decay modes of the ω are included.

VALUE	DOCUMENT ID		TECN	COMMENT
0.213±0.025 OUR FIT				
0.220±0.048±0.0116	COFFMAN	92B	MRK3	1281 ± 45 $K^-2\pi^+\pi^-$ evts

$\Gamma(K^0_S\eta'(958))/\Gamma_{total}$ — Γ_{130}/Γ

VALUE (units 10^{-3})	EVTS	DOCUMENT ID		TECN	COMMENT
9.49±0.32 OUR FIT					
9.49±0.20±0.36	3k	ABLIKIM	18W	BES3	e^+e^-, 3773 MeV

$\Gamma(K^0_S\eta'(958))/[\Gamma(K^-\pi^+)+\Gamma(K^+\pi^-)]$ — $\Gamma_{130}/(\Gamma_{47}+\Gamma_{344})$

Unseen decay modes of the $\eta'(958)$ are included.

VALUE (units 10^{-2})	EVTS	DOCUMENT ID		TECN	COMMENT
24.0±0.8 OUR FIT					
24.3±0.8±1.1	1321 ± 42	MENDEZ	10	CLEO	e^+e^- at 3774 MeV

$\Gamma(K^0_S\eta'(958))/\Gamma(K^0_S\pi^+\pi^-)$ — Γ_{130}/Γ_{53}

Unseen decay modes of the $\eta'(958)$ are included.

VALUE	EVTS	DOCUMENT ID		TECN	COMMENT
0.334±0.020 OUR FIT					
0.32 ±0.04 OUR AVERAGE					
0.31 ±0.02 ±0.04	594	PROCARIO	93B	CLE2	$\eta' \to \eta\pi^+\pi^-, \rho^0\gamma$
0.37 ±0.13 ±0.06	18	[1] ALBRECHT	92P	ARG	$e^+e^- \approx$ 10 GeV

[1] This value is calculated from numbers in Table 1 of ALBRECHT 92P.

$\Gamma(\overline{K}^*(892)^0\pi^+\pi^-\pi^0)/\Gamma(K^-2\pi^+\pi^-\pi^0)$ — $\Gamma_{131}/\Gamma_{104}$

Unseen decay modes of the $\overline{K}^*(892)^0$ are included.

VALUE	DOCUMENT ID		TECN	COMMENT
0.45±0.15±0.15	ANJOS	90D	E691	Photoproduction

$\Gamma(\overline{K}^*(892)^0\eta)/\Gamma_{total}$ — Γ_{132}/Γ

VALUE (units 10^{-2})	DOCUMENT ID		TECN	COMMENT
$1.41^{+0.13}_{-0.12}\pm0.01$	[1] CHEN	20A	BELL	e^+e^- at $\Upsilon(4S)$

[1] CHEN 20A reports $(1.41 \pm 0.04^{+0.12}_{-0.11} \pm 0.01)\times10^{-2}$ from a measurement of $[\Gamma(D^0 \to \overline{K}^*(892)^0\eta)/\Gamma_{total}] \times [B(\eta \to 2\gamma)]$ assuming $B(\eta \to 2\gamma) = (39.41 \pm 0.20)\times10^{-2}$, which we rescale to our best (shown rounded) value $B(\eta \to 2\gamma) = (39.36\pm0.18)\times10^{-2}$. Our first error is their experiment's error and our second error is the systematic error from using our best (shown rounded) value. The third reported uncertainty is the uncertainty from $B(\eta \to \gamma\gamma)$.

$\Gamma(\overline{K}^*(892)^0\eta)/\Gamma(K^-\pi^+)$ — Γ_{132}/Γ_{47}

Unseen decay modes of the $\overline{K}^*(892)^0$ and η are included.

VALUE	EVTS	DOCUMENT ID		TECN	COMMENT
• • • We do not use the following data for averages, fits, limits, etc. • • •					
$0.58\pm0.19^{+0.24}_{-0.28}$	46	KINOSHITA	91	CLEO	$e^+e^- \sim$ 10.7 GeV

$\Gamma(\overline{K}^*(892)^0\eta)/\Gamma(K^-\pi^+\pi^0)$ — Γ_{132}/Γ_{68}

Unseen decay modes of the $\overline{K}^*(892)^0$ and η are included.

VALUE	EVTS	DOCUMENT ID		TECN	COMMENT
• • • We do not use the following data for averages, fits, limits, etc. • • •					
0.13±0.02±0.03	214	PROCARIO	93B	CLE2	$\overline{K}^{*0}\eta \to K^-\pi^+/\gamma\gamma$

$\Gamma(K^-\pi^+\eta'(958))/\Gamma_{total}$ — Γ_{133}/Γ

VALUE (units 10^{-3})	EVTS	DOCUMENT ID		TECN	COMMENT
6.43±0.15±0.31	2.5k	ABLIKIM	18AC	BES3	e^+e^-, 3773 MeV

$\Gamma(K^-\pi^+\eta'(958))/\Gamma(K^-2\pi^+\pi^-)$ — Γ_{133}/Γ_{87}

Unseen decay modes of the $\eta'(958)$ are included.

VALUE	EVTS	DOCUMENT ID		TECN	COMMENT
0.093±0.014±0.019	286	PROCARIO	93B	CLE2	$\eta' \to \eta\pi^+\pi^-, \rho^0\gamma$

$\Gamma(K^0_S\eta'(958)\pi^0)/\Gamma_{total}$ — Γ_{134}/Γ

VALUE (units 10^{-3})	EVTS	DOCUMENT ID		TECN	COMMENT
2.52±0.22±0.15	289	ABLIKIM	18AC	BES3	e^+e^-, 3773 MeV

$\Gamma(\overline{K}^*(892)^0\eta'(958))/\Gamma(K^-\pi^+\eta'(958))$ — $\Gamma_{135}/\Gamma_{133}$

Unseen decay modes of the $\overline{K}^*(892)^0$ are included.

VALUE	CL%	DOCUMENT ID		TECN
<0.15	90	PROCARIO	93B	CLE2

Hadronic modes with three K's

$\Gamma(K^0_S K^+K^-)/\Gamma(K^0_S\pi^+\pi^-)$ — Γ_{136}/Γ_{53}

VALUE	EVTS	DOCUMENT ID		TECN	COMMENT
0.158±0.001±0.005	14k±116	AUBERT,B	05J	BABR	$e^+e^- \approx \Upsilon(4S)$
• • • We do not use the following data for averages, fits, limits, etc. • • •					
0.20 ±0.05 ±0.04	47	FRABETTI	92B	E687	γ Be, $\overline{E}_\gamma$= 221 GeV
0.170±0.022	136	AMMAR	91	CLEO	$e^+e^- \approx$ 10.5 GeV
0.24 ±0.08		BEBEK	86	CLEO	e^+e^- near $\Upsilon(4S)$
0.185±0.055	52	ALBRECHT	85B	ARG	e^+e^- 10 GeV

$\Gamma(K^0_S a_0(980)^0,\ a^0_0 \to K^+K^-)/\Gamma(K^0_S K^+K^-)$ — $\Gamma_{137}/\Gamma_{136}$

This is the "fit fraction" from the Dalitz-plot analysis, with interference.

VALUE	DOCUMENT ID		TECN	COMMENT
0.664±0.016±0.070	AUBERT,B	05J	BABR	Dalitz fit, 12540 ± 112 evts

$\Gamma(K^- a_0(980)^+,\ a^+_0 \to K^+K^0_S)/\Gamma(K^0_S K^+K^-)$ — $\Gamma_{138}/\Gamma_{136}$

This is the "fit fraction" from the Dalitz-plot analysis, with interference.

VALUE	DOCUMENT ID		TECN	COMMENT
0.134±0.011±0.037	AUBERT,B	05J	BABR	Dalitz fit, 12540 ± 112 evts

$\Gamma(K^+ a_0(980)^-,\ a^-_0 \to K^-K^0_S)/\Gamma(K^0_S K^+K^-)$ — $\Gamma_{139}/\Gamma_{136}$

This is a doubly Cabibbo-suppressed mode.

VALUE	CL%	DOCUMENT ID		TECN	COMMENT
<0.025	95	AUBERT,B	05J	BABR	Dalitz fit, 12540 ± 112 evts

$\Gamma(K^0_S f_0(980),\ f_0 \to K^+K^-)/\Gamma(K^0_S K^+K^-)$ — $\Gamma_{140}/\Gamma_{136}$

VALUE	CL%	DOCUMENT ID		TECN	COMMENT
<0.021	95	AUBERT,B	05J	BABR	Dalitz fit, 12540 ± 112 evts

$\Gamma(K^0_S\phi,\ \phi \to K^+K^-)/\Gamma(K^0_S K^+K^-)$ — $\Gamma_{141}/\Gamma_{136}$

This is the "fit fraction" from the Dalitz-plot analysis, with interference.

VALUE	DOCUMENT ID		TECN	COMMENT
0.459±0.007±0.007	AUBERT,B	05J	BABR	Dalitz fit, 12540 ± 112 evts

$\Gamma(K^0_L\phi)/\Gamma_{total}$ — Γ_{142}/Γ

VALUE (units 10^{-3})	EVTS	DOCUMENT ID		TECN	COMMENT
4.06±0.22±0.04	904	[1] ABLIKIM	22W	BES3	e^+e^- at 3.773 GeV

[1] ABLIKIM 22W reports $(0.414 \pm 0.021 \pm 0.010)\times10^{-2}$ from a measurement of $[\Gamma(D^0 \to K^0_L\phi)/\Gamma_{total}] \times [B(\phi(1020) \to K^+K^-)]$ assuming $B(\phi(1020) \to K^+K^-) = 0.491 \pm 0.005$, which we rescale to our best (shown rounded) value $B(\phi(1020) \to K^+K^-) = (50.1 \pm 0.6)\times10^{-2}$. Our first error is their experiment's error and our second error is the systematic error from using our best (shown rounded) value.

$\Gamma(K^0_S f_0(1370),\ f_0 \to K^+K^-)/\Gamma(K^0_S K^+K^-)$ — $\Gamma_{143}/\Gamma_{136}$

This is the "fit fraction" from the Dalitz-plot analysis, with interference.

VALUE	DOCUMENT ID		TECN	COMMENT
0.038±0.007±0.023	[1] AUBERT,B	05J	BABR	Dalitz fit, 12540 ± 112 evts

[1] AUBERT,B 05J calls the mode $K^0_S f_0(1400)$, but insofar as it is seen here at all, it is certainly the same as $f_0(1370)$.

$\Gamma(3K^0_S)/\Gamma_{total}$ — Γ_{144}/Γ

VALUE (units 10^{-4})	EVTS	DOCUMENT ID		TECN	COMMENT
7.6 ±0.7 OUR FIT	Error includes scale factor of 1.4.				
7.21±0.33±0.44	597	ABLIKIM	17A	BES3	$e^+e^- \to \psi(3770)$

$\Gamma(3K^0_S)/\Gamma(K^0_S\pi^+\pi^-)$ — Γ_{144}/Γ_{53}

VALUE (units 10^{-2})	EVTS	DOCUMENT ID		TECN	COMMENT
2.66±0.25 OUR FIT	Error includes scale factor of 1.2.				
3.2 ±0.4 OUR AVERAGE					
3.58±0.54±0.52	170 ± 26	LINK	05A	FOCS	γBe, $\overline{E}_\gamma \approx$ 180 GeV
2.78±0.38±0.48	61	ASNER	96B	CLE2	$e^+e^- \approx \Upsilon(4S)$
7.0 ±2.4 ±1.2	10 ± 3	FRABETTI	94J	E687	γBe, $\overline{E}_\gamma$=220 GeV
3.2 ±1.0	22	AMMAR	91	CLEO	$e^+e^- \approx$ 10.5 GeV
3.4 ±1.4 ±1.0	5	ALBRECHT	90C	ARG	$e^+e^- \approx$ 10 GeV

$\Gamma(K^+2K^-\pi^+)/\Gamma(K^-2\pi^+\pi^-)$ — Γ_{145}/Γ_{87}

VALUE	EVTS	DOCUMENT ID		TECN	COMMENT
0.0027 ±0.0004 OUR AVERAGE	Error includes scale factor of 1.1.				
0.00257±0.00034±0.00024	143	LINK	03G	FOCS	γ A, $\overline{E}_\gamma \approx$ 180 GeV
0.0054 ±0.0016 ±0.0008	18	AITALA	01D	E791	π^- A, 500 GeV
0.0028 ±0.0007 ±0.0001	20	FRABETTI	95C	E687	γ Be, $\overline{E}_\gamma \approx$ 200 GeV

$\Gamma(K^+K^-\overline{K}^*(892)^0,\ \overline{K}^{*0} \to K^-\pi^+)/\Gamma(K^+2K^-\pi^+)$ — $\Gamma_{146}/\Gamma_{145}$

VALUE	DOCUMENT ID		TECN	COMMENT
0.20±0.07±0.02	LINK	03G	FOCS	γ A, $\overline{E}_\gamma \approx$ 180 GeV

$\Gamma(K^-\pi^+\phi,\ \phi \to K^+K^-)/\Gamma(K^+2K^-\pi^+)$ — $\Gamma_{147}/\Gamma_{145}$

VALUE	DOCUMENT ID		TECN	COMMENT
0.18±0.06±0.04	LINK	03G	FOCS	γ A, $\overline{E}_\gamma \approx$ 180 GeV

$\Gamma(\phi\overline{K}^*(892)^0,\ \phi \to K^+K^-,\ \overline{K}^{*0} \to K^-\pi^+)/\Gamma(K^+2K^-\pi^+)$ — $\Gamma_{148}/\Gamma_{145}$

VALUE	DOCUMENT ID		TECN	COMMENT
0.48±0.06±0.01	LINK	03G	FOCS	γ A, $\overline{E}_\gamma \approx$ 180 GeV

$\Gamma(K^+2K^-\pi^+\text{nonresonant})/\Gamma(K^+2K^-\pi^+)$ — $\Gamma_{149}/\Gamma_{145}$

VALUE	DOCUMENT ID		TECN	COMMENT
0.15±0.06±0.02	LINK	03G	FOCS	γ A, $\overline{E}_\gamma \approx$ 180 GeV

$\Gamma(2K^0_S K^\pm\pi^\mp)/\Gamma(K^0_S\pi^+\pi^-)$ — Γ_{150}/Γ_{53}

VALUE (units 10^{-2})	EVTS	DOCUMENT ID		TECN	COMMENT
2.12±0.38±0.20	57 ± 10	LINK	05A	FOCS	γ Be, $\overline{E}_\gamma \approx$ 180 GeV

Int. J. Mod. Phys. A 2026.41. Downloaded from www.worldscientific.com by LIFORNIA @ BERKELEY on 09/16/26. Re-use and distribution is strictly not permitted, except for Open Access articles.

Pionic modes

$\Gamma(\pi^+\pi^-)/\Gamma_{total}$ — Γ_{151}/Γ

VALUE (units 10^{-3})	EVTS	DOCUMENT ID		TECN	COMMENT
1.451±0.024 OUR FIT	Error includes scale factor of 1.4.				
1.508±0.018±0.022	21k	ABLIKIM	18W	BES3	e^+e^-, 3773 MeV

$\Gamma(\pi^+\pi^-)/\Gamma(K^-\pi^+)$ — Γ_{151}/Γ_{47}

VALUE (units 10^{-2})	EVTS	DOCUMENT ID		TECN	COMMENT
3.69 ±0.06 OUR FIT	Error includes scale factor of 1.3.				
3.59 ±0.06 OUR AVERAGE					
3.594±0.054±0.040	7334 ± 97	ACOSTA	05C	CDF	$p\overline{p}$, $\sqrt{s}$ = 1.96 TeV
3.53 ±0.12 ±0.06	3453	LINK	03	FOCS	γ A, $\overline{E}_\gamma \approx$ 180 GeV
3.51 ±0.16 ±0.17	710	CSORNA	02	CLE2	$e^+e^- \approx \Upsilon(4S)$
4.0 ±0.2 ±0.3	2043	AITALA	98C	E791	π^- A, 500 GeV
• • • We do not use the following data for averages, fits, limits, etc. • • •					
3.62 ±0.10 ±0.08	2085 ± 54	RUBIN	06	CLEO	See MENDEZ 10
3.4 ±0.7 ±0.1	76 ± 15	ABLIKIM	05F	BES	$e^+e^- \approx \psi(3770)$
4.3 ±0.7 ±0.3	177	FRABETTI	94C	E687	γBe $\overline{E}_\gamma$= 220 GeV
3.48 ±0.30 ±0.23	227	SELEN	93	CLE2	$e^+e^- \approx \Upsilon(4S)$
5.5 ±0.8 ±0.5	120	ANJOS	91D	E691	Photoproduction
5.0 ±0.7 ±0.5	110	ALEXANDER	90	CLEO	e^+e^- 10.5–11 GeV

$\Gamma(\pi^+\pi^-)/[\Gamma(K^-\pi^+)+\Gamma(K^+\pi^-)]$ — $\Gamma_{151}/(\Gamma_{47}+\Gamma_{344})$

VALUE (units 10^{-2})	EVTS	DOCUMENT ID		TECN	COMMENT
3.67±0.06 OUR FIT	Error includes scale factor of 1.3.				
3.70±0.06±0.09	6210 ± 93	MENDEZ	10	CLEO	e^+e^- at 3774 MeV

$\Gamma(2\pi^0)/\Gamma_{total}$ — Γ_{152}/Γ

VALUE (units 10^{-4})	EVTS	DOCUMENT ID		TECN	COMMENT
8.25±0.25 OUR FIT					
8.29±0.30 OUR AVERAGE					
8.24±0.21±0.30	6k	ABLIKIM	15F	BES3	e^+e^- at 3.773GeV
8.4 ±0.1 ±0.5	26k	LEES	12L	BABR	$e^+e^- \approx$ 10.58 GeV

$\Gamma(2\pi^0)/\Gamma(K^-\pi^+)$ — Γ_{152}/Γ_{47}

VALUE (units 10^{-2})	EVTS	DOCUMENT ID		TECN	COMMENT
• • • We do not use the following data for averages, fits, limits, etc. • • •					
2.05±0.13±0.16	499 ± 32	RUBIN	06	CLEO	See MENDEZ 10
2.2 ±0.4 ±0.4	40	SELEN	93	CLE2	$e^+e^- \to \Upsilon(4S)$

$\Gamma(2\pi^0)/[\Gamma(K^-\pi^+)+\Gamma(K^+\pi^-)]$ — $\Gamma_{152}/(\Gamma_{47}+\Gamma_{344})$

VALUE (units 10^{-2})	EVTS	DOCUMENT ID		TECN	COMMENT
2.09±0.07 OUR FIT					
2.06±0.07±0.10	1567 ± 54	MENDEZ	10	CLEO	e^+e^- at 3774 MeV

$\Gamma(\pi^+\pi^-\pi^0)/\Gamma(K^-\pi^+)$ — Γ_{153}/Γ_{47}

VALUE (units 10^{-2})	EVTS	DOCUMENT ID		TECN	COMMENT
37.7±1.6 OUR FIT	Error includes scale factor of 2.2.				
34.4±0.5±1.2	11k±164	RUBIN	06	CLEO	e^+e^- at $\psi(3770)$

$\Gamma(\pi^+\pi^-\pi^0)/\Gamma(K^-\pi^+\pi^0)$ — Γ_{153}/Γ_{68}

VALUE (units 10^{-2})	EVTS	DOCUMENT ID		TECN	COMMENT
10.32±0.25 OUR FIT	Error includes scale factor of 2.3.				
10.41±0.23 OUR AVERAGE	Error includes scale factor of 2.0.				
10.12±0.04±0.18	123k±490	ARINSTEIN	08	BELL	$e^+e^- \approx \Upsilon(4S)$
10.59±0.06±0.13	60k±343	AUBERT,B	06X	BABR	$e^+e^- \approx \Upsilon(4S)$

$\Gamma(\pi^+\pi^-\pi^0)/\Gamma_{total}$ — Γ_{153}/Γ

VALUE (units 10^{-4})	EVTS	DOCUMENT ID		TECN	COMMENT
134.3±1.3±1.6	12.8k	ABLIKIM	22BG	BES3	e^+e^- at 3.773 GeV

$\Gamma(\rho^+\pi^-)/\Gamma(\pi^+\pi^-\pi^0)$ — $\Gamma_{154}/\Gamma_{153}$

This is the "fit fraction" from the Dalitz-plot analysis, with interference. See GASPERO 08 and BHATTACHARYA 10A for isospin decompositions of the $D^0 \to \pi^+\pi^0\pi^-$ Dalitz plot, both based on the amplitudes of AUBERT 07BJ. They quantify the conclusion that the final state is dominantly isospin 0.

VALUE (units 10^{-2})	DOCUMENT ID		TECN	COMMENT
68.1±0.6 OUR AVERAGE				
67.8±0.0±0.6	AUBERT	07BJ	BABR	Dalitz fit, 45k events
76.3±1.9±2.5	CRONIN-HEN...	05	CLEO	$e^+e^- \approx$ 10 GeV

$\Gamma(\rho^0\pi^0)/\Gamma(\pi^+\pi^-\pi^0)$ — $\Gamma_{155}/\Gamma_{153}$

This is the "fit fraction" from the Dalitz-plot analysis, with interference.

VALUE (units 10^{-2})	DOCUMENT ID		TECN	COMMENT
25.9±1.1 OUR AVERAGE				
26.2±0.5±1.1	AUBERT	07BJ	BABR	Dalitz fit, 45k events
24.4±2.0±2.1	CRONIN-HEN...	05	CLEO	$e^+e^- \approx$ 10 GeV

$\Gamma(\rho^-\pi^+)/\Gamma(\pi^+\pi^-\pi^0)$ — $\Gamma_{156}/\Gamma_{153}$

This is the "fit fraction" from the Dalitz-plot analysis, with interference.

VALUE (units 10^{-2})	DOCUMENT ID		TECN	COMMENT
34.6±0.8 OUR AVERAGE				
34.6±0.8±0.3	AUBERT	07BJ	BABR	Dalitz fit, 45k events
34.5±2.4±1.3	CRONIN-HEN...	05	CLEO	$e^+e^- \approx$ 10 GeV

$\Gamma(\rho(1450)^+\pi^-,\ \rho^+\to\pi^+\pi^0)/\Gamma(\pi^+\pi^-\pi^0)$ — $\Gamma_{157}/\Gamma_{153}$

This is the "fit fraction" from the Dalitz-plot analysis.

VALUE (units 10^{-2})	DOCUMENT ID		TECN	COMMENT
0.11±0.07±0.12	AUBERT	07BJ	BABR	Dalitz fit, 45k events

$\Gamma(\rho(1450)^0\pi^0,\ \rho^0\to\pi^+\pi^-)/\Gamma(\pi^+\pi^-\pi^0)$ — $\Gamma_{158}/\Gamma_{153}$

This is the "fit fraction" from the Dalitz-plot analysis.

VALUE (units 10^{-2})	DOCUMENT ID		TECN	COMMENT
0.30±0.11±0.07	AUBERT	07BJ	BABR	Dalitz fit, 45k events

$\Gamma(\rho(1450)^-\pi^+,\ \rho^-\to\pi^-\pi^0)/\Gamma(\pi^+\pi^-\pi^0)$ — $\Gamma_{159}/\Gamma_{153}$

This is the "fit fraction" from the Dalitz-plot analysis.

VALUE (units 10^{-2})	DOCUMENT ID		TECN	COMMENT
1.79±0.22±0.12	AUBERT	07BJ	BABR	Dalitz fit, 45k events

$\Gamma(\rho(1700)^+\pi^-,\ \rho^+\to\pi^+\pi^0)/\Gamma(\pi^+\pi^-\pi^0)$ — $\Gamma_{160}/\Gamma_{153}$

This is the "fit fraction" from the Dalitz-plot analysis.

VALUE (units 10^{-2})	DOCUMENT ID		TECN	COMMENT
4.1±0.7±0.7	AUBERT	07BJ	BABR	Dalitz fit, 45k events

$\Gamma(\rho(1700)^0\pi^0,\ \rho^0\to\pi^+\pi^-)/\Gamma(\pi^+\pi^-\pi^0)$ — $\Gamma_{161}/\Gamma_{153}$

This is the "fit fraction" from the Dalitz-plot analysis.

VALUE (units 10^{-2})	DOCUMENT ID		TECN	COMMENT
5.0±0.6±1.0	AUBERT	07BJ	BABR	Dalitz fit, 45k events

$\Gamma(\rho(1700)^-\pi^+,\ \rho^-\to\pi^-\pi^0)/\Gamma(\pi^+\pi^-\pi^0)$ — $\Gamma_{162}/\Gamma_{153}$

This is the "fit fraction" from the Dalitz-plot analysis.

VALUE (units 10^{-2})	DOCUMENT ID		TECN	COMMENT
3.2±0.4±0.6	AUBERT	07BJ	BABR	Dalitz fit, 45k events

$\Gamma(f_0(980)\pi^0,\ f_0\to\pi^+\pi^-)/\Gamma(\pi^+\pi^-\pi^0)$ — $\Gamma_{163}/\Gamma_{153}$

This is the "fit fraction" from the Dalitz-plot analysis.

VALUE (units 10^{-2})	DOCUMENT ID		TECN	COMMENT
0.25±0.04±0.04	AUBERT	07BJ	BABR	Dalitz fit, 45k events

$\Gamma(f_0(500)\pi^0,\ f_0\to\pi^+\pi^-)/\Gamma(\pi^+\pi^-\pi^0)$ — $\Gamma_{164}/\Gamma_{153}$

The $f_0(500)$ is the σ. This is the "fit fraction" from the Dalitz-plot analysis.

VALUE (units 10^{-2})	DOCUMENT ID		TECN	COMMENT
0.82±0.10±0.10	AUBERT	07BJ	BABR	Dalitz fit, 45k events

$\Gamma(f_0(1370)\pi^0,\ f_0\to\pi^+\pi^-)/\Gamma(\pi^+\pi^-\pi^0)$ — $\Gamma_{165}/\Gamma_{153}$

This is the "fit fraction" from the Dalitz-plot analysis.

VALUE (units 10^{-2})	DOCUMENT ID		TECN	COMMENT
0.37±0.11±0.09	AUBERT	07BJ	BABR	Dalitz fit, 45k events

$\Gamma(f_0(1500)\pi^0,\ f_0\to\pi^+\pi^-)/\Gamma(\pi^+\pi^-\pi^0)$ — $\Gamma_{166}/\Gamma_{153}$

This is the "fit fraction" from the Dalitz-plot analysis.

VALUE (units 10^{-2})	DOCUMENT ID		TECN	COMMENT
0.39±0.08±0.07	AUBERT	07BJ	BABR	Dalitz fit, 45k events

$\Gamma(f_0(1710)\pi^0,\ f_0\to\pi^+\pi^-)/\Gamma(\pi^+\pi^-\pi^0)$ — $\Gamma_{167}/\Gamma_{153}$

This is the "fit fraction" from the Dalitz-plot analysis.

VALUE (units 10^{-2})	DOCUMENT ID		TECN	COMMENT
0.31±0.07±0.08	AUBERT	07BJ	BABR	Dalitz fit, 45k events

$\Gamma(f_2(1270)\pi^0,\ f_2\to\pi^+\pi^-)/\Gamma(\pi^+\pi^-\pi^0)$ — $\Gamma_{168}/\Gamma_{153}$

This is the "fit fraction" from the Dalitz-plot analysis.

VALUE (units 10^{-2})	DOCUMENT ID		TECN	COMMENT
1.32±0.08±0.10	AUBERT	07BJ	BABR	Dalitz fit, 45k events

$\Gamma(\pi^+\pi^-\pi^0\,\text{nonresonant})/\Gamma(\pi^+\pi^-\pi^0)$ — $\Gamma_{169}/\Gamma_{153}$

This is the "fit fraction" from the Dalitz-plot analysis.

VALUE (units 10^{-2})	DOCUMENT ID		TECN	COMMENT
0.84±0.21±0.12	AUBERT	07BJ	BABR	Dalitz fit, 45k events

$\Gamma(3\pi^0)/\Gamma_{total}$ — Γ_{170}/Γ

VALUE (units 10^{-4})	CL%	EVTS	DOCUMENT ID		TECN	COMMENT
2.0±0.4±0.3		60	[1] ABLIKIM	18X	BES3	e^+e^-, 3773 MeV
• • • We do not use the following data for averages, fits, limits, etc. • • •						
<3.5		90	RUBIN	06	CLEO	e^+e^- at $\psi(3770)$

[1] Significance of signal reported by ABLIKIM 18X is 4.8σ.

$\Gamma(2\pi^+2\pi^-)/\Gamma_{total}$ — Γ_{171}/Γ

VALUE (units 10^{-2})	EVTS	DOCUMENT ID		TECN	COMMENT
0.715±0.025 OUR FIT	Error includes scale factor of 2.2.				
0.688±0.010±0.010	5.8k	ABLIKIM	24BG	BES3	e^+e^- at 3.773 GeV

$\Gamma(2\pi^+2\pi^-)/\Gamma(K^-\pi^+)$ — Γ_{171}/Γ_{47}

VALUE (units 10^{-2})	EVTS	DOCUMENT ID		TECN	COMMENT
18.2±0.6 OUR FIT	Error includes scale factor of 2.1.				
19.1±0.4±0.6	7331 ± 130	RUBIN	06	CLEO	e^+e^- at $\psi(3770)$

Int. J. Mod. Phys. A 2026.41. Downloaded from www.worldscientific.com
by UNIVERSITY OF CALIFORNIA @ BERKELEY on 09/16/26. Re-use and distribution is strictly not permitted, except for Open Access articles.

$\Gamma(2\pi^+2\pi^-)/\Gamma(K^-2\pi^+\pi^-)$ — Γ_{171}/Γ_{87}

VALUE (units 10^{-2})	EVTS	DOCUMENT ID		TECN	COMMENT
8.72±0.30 OUR FIT Error includes scale factor of 1.9.					
9.20±0.26 OUR AVERAGE					
9.14±0.18±0.22	6360±115	LINK	07A	FOCS	γBe, $\overline{E}_\gamma \approx 180$ GeV
7.9 ±1.8 ±0.5	162	ABLIKIM	05F	BES	$e^+e^- \approx \psi(3770)$
9.5 ±0.7 ±0.2	814	FRABETTI	95C	E687	γBe, $\overline{E}_\gamma \approx 200$ GeV
10.2 ±1.3	345	AMMAR	91	CLEO	$e^+e^- \approx 10.5$ GeV
• • • We do not use the following data for averages, fits, limits, etc. • • •					
11.5 ±2.3 ±1.6	64	ADAMOVICH	92	OMEG	π^- 340 GeV
10.8 ±2.4 ±0.8	79	FRABETTI	92	E687	γBe
9.6 ±1.8 ±0.7	66	ANJOS	91	E691	γBe 80–240 GeV

$\Gamma(a_1(1260)^+\pi^-,\ a_1^+ \to 2\pi^+\pi^-\text{total})/\Gamma(2\pi^+2\pi^-)$ — $\Gamma_{172}/\Gamma_{171}$

This is the fit fraction from the coherent amplitude analysis.

VALUE (units 10^{-2})	EVTS	DOCUMENT ID		TECN	COMMENT
61 ±4 OUR AVERAGE					
82.2±3.3±16.0	5.8k	ABLIKIM	24BG	BES3	e^+e^- at 3.773 GeV
60.0±3.0± 2.4	5.7k	LINK	07A	FOCS	$D^0 \to 4\pi$

$\Gamma(a_1(1260)^+\pi^-,\ a_1^+ \to \rho^0\pi^+ S\text{-wave})/\Gamma(2\pi^+2\pi^-)$ — $\Gamma_{173}/\Gamma_{171}$

This is the fit fraction from the coherent amplitude analysis.

VALUE (units 10^{-2})		DOCUMENT ID		TECN	COMMENT
41.5±2.5 OUR AVERAGE					
38.1±2.3±3.6	[1,2]	DARGENT	17		4-body fit, 7.3k 4π evts
43.3±2.5±1.9	[2]	LINK	07A	FOCS	4-body fit, ≈ 5.7k evts

[1] Obtained by analyzing CLEO-c data but not authored by the CLEO Collaboration.
[2] See also ABLIKIM 24BG.

$\Gamma(a_1(1260)^+\pi^-,\ a_1^+ \to \rho^0\pi^+ D\text{-wave})/\Gamma(2\pi^+2\pi^-)$ — $\Gamma_{174}/\Gamma_{171}$

This is the fit fraction from the coherent amplitude analysis.

VALUE (units 10^{-2})		DOCUMENT ID		TECN	COMMENT
2.5±0.5±0.4	[1,2]	LINK	07A	FOCS	4-body fit, ≈ 5.7k evts

[1] DARGENT 17 using 7.3k events find this contribution negligible.
[2] See also ABLIKIM 24BG.

$\Gamma(a_1(1260)^+\pi^-,\ a_1^+ \to \sigma\pi^+)/\Gamma(2\pi^+2\pi^-)$ — $\Gamma_{175}/\Gamma_{171}$

This is the fit fraction from the coherent amplitude analysis.

VALUE (units 10^{-2})		DOCUMENT ID		TECN	COMMENT
8.4±0.9 OUR AVERAGE					
10.2±1.4±3.3	[1,2]	DARGENT	17		7.3k 4-body fit, 4π evts
8.3±0.7±0.6	[2]	LINK	07A	FOCS	4-body fit, ≈ 5.7k evts

[1] Obtained by analyzing CLEO-c data but not authored by the CLEO Collaboration.
[2] See also ABLIKIM 24BG.

$\Gamma(a_1(1260)^-\pi^+,\ a_1^- \to 2\pi^-\pi^+\text{total})/\Gamma(2\pi^+2\pi^-)$ — $\Gamma_{176}/\Gamma_{171}$

VALUE (units 10^{-2})	EVTS	DOCUMENT ID		TECN	COMMENT
10.3±1.5±2.5	5.8k	[1] ABLIKIM	24BG	BES3	e^+e^- at 3.773 GeV

[1] See also DARGENT 17.

$\Gamma(a_1(1260)^-\pi^+,\ a_1^- \to \rho^0\pi^- S\text{-wave})/\Gamma(2\pi^+2\pi^-)$ — $\Gamma_{177}/\Gamma_{171}$

This is the fit fraction from a coherent amplitude analysis.

VALUE (units 10^{-2})	EVTS	DOCUMENT ID		COMMENT
3.1±0.6±1.0	7.3k	[1,2] DARGENT	17	4-body fit, 4π evts

[1] Obtained by analyzing CLEO-c data but not authored by the CLEO Collaboration.
[2] See also ABLIKIM 24BG.

$\Gamma(a_1(1260)^-\pi^+,\ a_1^- \to \sigma\pi^-)/\Gamma(2\pi^+2\pi^-)$ — $\Gamma_{178}/\Gamma_{171}$

This is the fit fraction from a coherent amplitude analysis.

VALUE (units 10^{-2})	EVTS	DOCUMENT ID		COMMENT
0.8±0.2±0.4	7.3k	[1,2] DARGENT	17	4-body fit, 4π evts

[1] Obtained by analyzing CLEO-c data but not authored by the CLEO Collaboration.
[2] See also ABLIKIM 24BG.

$\Gamma(\pi(1300)^+\pi^-,\ \pi(1300)^+ \to 2\pi^+\pi^-\text{total})/\Gamma(2\pi^+2\pi^-)$ — $\Gamma_{179}/\Gamma_{171}$

VALUE (units 10^{-2})	EVTS	DOCUMENT ID		TECN	COMMENT
32.3±2.6±4.5	5.8k	[1] ABLIKIM	24BG	BES3	e^+e^- at 3.773 GeV

[1] See also DARGENT 17.

$\Gamma(\pi(1300)^+\pi^-,\ \pi(1300)^+ \to \sigma\pi^+)/\Gamma(2\pi^+2\pi^-)$ — $\Gamma_{180}/\Gamma_{171}$

This is the fit fraction from a coherent amplitude analysis.

VALUE (units 10^{-2})	EVTS	DOCUMENT ID		COMMENT
6.8±0.9±3.4	7.3k	[1,2] DARGENT	17	4-body fit, 4π evts

[1] Obtained by analyzing CLEO-c data but not authored by the CLEO Collaboration.
[2] See also ABLIKIM 24BG.

$\Gamma(\pi(1300)^-\pi^+,\ \pi(1300)^- \to 2\pi^-\pi^+\text{total})/\Gamma(2\pi^+2\pi^-)$ — $\Gamma_{181}/\Gamma_{171}$

VALUE (units 10^{-2})	EVTS	DOCUMENT ID		TECN	COMMENT
23.5±2.3±3.9	5.8k	[1] ABLIKIM	24BG	BES3	e^+e^- at 3.773 GeV

[1] See also DARGENT 17.

$\Gamma(\pi(1300)^-\pi^+,\ \pi(1300)^- \to \sigma\pi^-)/\Gamma(2\pi^+2\pi^-)$ — $\Gamma_{182}/\Gamma_{171}$

This is the fit fraction from a coherent amplitude analysis.

VALUE (units 10^{-2})	EVTS	DOCUMENT ID		COMMENT
3.0±0.6±2.8	7.3k	[1,2] DARGENT	17	4-body fit, 4π evts

[1] Obtained by analyzing CLEO-c data but not authored by the CLEO Collaboration.
[2] See also ABLIKIM 24BG.

$\Gamma(a_2(1320)^+\pi^-,\ a_2^+ \to \rho^0\pi^+ D\text{-wave})/\Gamma(2\pi^+2\pi^-)$ — $\Gamma_{183}/\Gamma_{171}$

VALUE (units 10^{-2})	EVTS	DOCUMENT ID		TECN	COMMENT
0.2±0.1±0.1	5.8k	[1] ABLIKIM	24BG	BES3	e^+e^- at 3.773 GeV

[1] Evidence with 4.6 σ significance.

$\Gamma(a_2(1320)^-\pi^+,\ a_2^- \to \rho^0\pi^- D\text{-wave})/\Gamma(2\pi^+2\pi^-)$ — $\Gamma_{184}/\Gamma_{171}$

VALUE (units 10^{-2})	EVTS	DOCUMENT ID		TECN	COMMENT
0.4±0.1±0.1	5.8k	ABLIKIM	24BG	BES3	e^+e^- at 3.773 GeV

$\Gamma(a_1(1420)^+\pi^-,\ a_1^+ \to f_0(980)\pi^+ P\text{-wave},\ f_0 \to \pi^+\pi^-)/\Gamma(2\pi^+2\pi^-)$ — $\Gamma_{185}/\Gamma_{171}$

VALUE (units 10^{-2})	EVTS	DOCUMENT ID		TECN	COMMENT
0.6±0.2±0.2	5.8k	ABLIKIM	24BG	BES3	e^+e^- at 3.773 GeV

$\Gamma(a_1(1640)^+\pi^-,\ a_1^+ \to \rho^0\pi^+ S\text{-wave})/\Gamma(2\pi^+2\pi^-)$ — $\Gamma_{186}/\Gamma_{171}$

VALUE (units 10^{-2})	EVTS	DOCUMENT ID		TECN	COMMENT
1.7±0.5±0.9	5.8k	ABLIKIM	24BG	BES3	e^+e^- at 3.773 GeV

$\Gamma(a_1(1640)^+\pi^-,\ a_1^+ \to \rho^0\pi^+ D\text{-wave})/\Gamma(2\pi^+2\pi^-)$ — $\Gamma_{187}/\Gamma_{171}$

This is the fit fraction from a coherent amplitude analysis.

VALUE (units 10^{-2})	EVTS	DOCUMENT ID		COMMENT
4.2±0.6±2.0	7.3k	[1,2] DARGENT	17	4-body fit, 4π evts

[1] Obtained by analyzing CLEO-c data but not authored by the CLEO Collaboration.
[2] See also ABLIKIM 24BG.

$\Gamma(a_1(1640)^+\pi^-,\ a_1^+ \to \sigma\pi^+)/\Gamma(2\pi^+2\pi^-)$ — $\Gamma_{188}/\Gamma_{171}$

This is the fit fraction from a coherent amplitude analysis.

VALUE (units 10^{-2})	EVTS	DOCUMENT ID		COMMENT
2.4±0.7±1.7	7.3k	[1,2] DARGENT	17	4-body fit, 4π evts

[1] Obtained by analyzing CLEO-c data but not authored by the CLEO Collaboration.
[2] See also ABLIKIM 24BG.

$\Gamma(a_1(1640)^-\pi^+,\ a_1^- \to \rho^0\pi^- S\text{-wave})/\Gamma(2\pi^+2\pi^-)$ — $\Gamma_{189}/\Gamma_{171}$

VALUE (units 10^{-2})	EVTS	DOCUMENT ID		TECN	COMMENT
0.5±0.3±0.4	5.8k	ABLIKIM	24BG	BES3	e^+e^- at 3.773 GeV

$\Gamma(\pi_2(1670)^+\pi^-,\ \pi_2^+ \to f_2(1270)^0\pi^+,\ f_2^0 \to \pi^+\pi^-)/\Gamma(2\pi^+2\pi^-)$ — $\Gamma_{190}/\Gamma_{171}$

This is the fit fraction from a coherent amplitude analysis.

VALUE (units 10^{-2})	EVTS	DOCUMENT ID		COMMENT
2.7±0.6±1.1	7.3k	[1] DARGENT	17	4-body fit, 4π evts

[1] Obtained by analyzing CLEO-c data but not authored by the CLEO Collaboration.

$\Gamma(\pi_2(1670)^+\pi^-,\ \pi_2^+ \to \sigma\pi^+)/\Gamma(2\pi^+2\pi^-)$ — $\Gamma_{191}/\Gamma_{171}$

This is the fit fraction from a coherent amplitude analysis.

VALUE (units 10^{-2})	EVTS	DOCUMENT ID		COMMENT
3.5±0.6±1.2	7.3k	[1] DARGENT	17	4-body fit, 4π evts

[1] Obtained by analyzing CLEO-c data but not authored by the CLEO Collaboration.

$\Gamma(2\rho(770)^0\text{total})/\Gamma(2\pi^+2\pi^-)$ — $\Gamma_{192}/\Gamma_{171}$

This is the fit fraction from the coherent amplitude analysis.

VALUE (units 10^{-2})	EVTS	DOCUMENT ID		TECN	COMMENT
25.1±1.5 OUR AVERAGE					
28.0±1.9±3.1	5.8k	ABLIKIM	24BG	BES3	e^+e^- at 3.773 GeV
24.5±1.3±1.0		LINK	07A	FOCS	4-body fit, ≈ 5.7k evts

$\Gamma(2\rho^0,\text{parallel helicities})/\Gamma(2\pi^+2\pi^-)$ — $\Gamma_{193}/\Gamma_{171}$

This is the fit fraction from the coherent amplitude analysis.

VALUE (units 10^{-2})	DOCUMENT ID		TECN	COMMENT
1.1±0.3±0.3	LINK	07A	FOCS	4-body fit, ≈ 5.7k evts

$\Gamma(2\rho^0,\text{perpendicular helicities})/\Gamma(2\pi^+2\pi^-)$ — $\Gamma_{194}/\Gamma_{171}$

This is the fit fraction from the coherent amplitude analysis.

VALUE (units 10^{-2})	DOCUMENT ID		TECN	COMMENT
6.4±0.6±0.5	LINK	07A	FOCS	4-body fit, ≈ 5.7k evts

$\Gamma(2\rho^0,\text{longitudinal helicities})/\Gamma(2\pi^+2\pi^-)$ — $\Gamma_{195}/\Gamma_{171}$

This is the fit fraction from the coherent amplitude analysis.

VALUE (units 10^{-2})	DOCUMENT ID		TECN	COMMENT
16.8±1.0±0.8	LINK	07A	FOCS	4-body fit, ≈ 5.7k evts

Int. J. Mod. Phys. A 2026.41. Downloaded from www.worldscientific.com
by LIFORNIA @ BERKELEY on 09/16/26. Re-use and distribution is strictly not permitted, except for Open Access articles.

$\Gamma(2\rho(770)^0,\ S\text{-wave})/\Gamma(2\pi^+2\pi^-)$ — $\Gamma_{196}/\Gamma_{171}$

This is the fit fraction from a coherent amplitude analysis.

VALUE (units 10^{-2})	EVTS	DOCUMENT ID		TECN	COMMENT
1.8±0.7 OUR AVERAGE					
1.7±0.6±0.5	5.8k	ABLIKIM	24BG	BES3	e^+e^- at 3.773 GeV
2.4±0.7±1.5	7.3k	[1] DARGENT	17		4-body fit, 4π evts

[1] Obtained by analyzing CLEO-c data but not authored by the CLEO Collaboration.

$\Gamma(2\rho(770)^0,\ P\text{-wave})/\Gamma(2\pi^+2\pi^-)$ — $\Gamma_{197}/\Gamma_{171}$

This is the fit fraction from a coherent amplitude analysis.

VALUE (units 10^{-2})	EVTS	DOCUMENT ID		TECN	COMMENT
8.7±1.4 OUR AVERAGE Error includes scale factor of 1.3.					
9.8±1.0±0.9	5.8k	ABLIKIM	24BG	BES3	e^+e^- at 3.773 GeV
7.0±0.5±1.6	7.3k	[1] DARGENT	17		4-body fit, 4π evts

[1] Obtained by analyzing CLEO-c data but not authored by the CLEO Collaboration.

$\Gamma(2\rho(770)^0,\ D\text{-wave})/\Gamma(2\pi^+2\pi^-)$ — $\Gamma_{198}/\Gamma_{171}$

This is the fit fraction from a coherent amplitude analysis.

VALUE (units 10^{-2})	EVTS	DOCUMENT ID		TECN	COMMENT
17 ±7 OUR AVERAGE Error includes scale factor of 2.9.					
23.1±2.1±2.4	5.8k	ABLIKIM	24BG	BES3	e^+e^- at 3.773 GeV
8.2±1.0±3.9	7.3k	[1] DARGENT	17		4-body fit, 4π evts

[1] Obtained by analyzing CLEO-c data but not authored by the CLEO Collaboration.

$\Gamma(\rho(770)^0\rho(1450)^0,\ \rho(1450)^0\to\pi^+\pi^-)/\Gamma(2\pi^+2\pi^-)$ — $\Gamma_{199}/\Gamma_{171}$

VALUE (units 10^{-2})	EVTS	DOCUMENT ID		TECN	COMMENT
2.5±0.9±1.2	5.8k	ABLIKIM	24BG	BES3	e^+e^- at 3.773 GeV

$\Gamma(\rho(770)^0\rho(1450)^0\ P\text{-wave},\ \rho(1450)^0\to\pi^+\pi^-)/\Gamma(2\pi^+2\pi^-)$ — $\Gamma_{200}/\Gamma_{171}$

VALUE (units 10^{-2})	EVTS	DOCUMENT ID		TECN	COMMENT
1.0±0.4±0.6	5.8k	ABLIKIM	24BG	BES3	e^+e^- at 3.773 GeV

$\Gamma(\rho(770)^0\rho(1450)^0\ D\text{-wave},\ \rho(1450)^0\to\pi^+\pi^-)/\Gamma(2\pi^+2\pi^-)$ — $\Gamma_{201}/\Gamma_{171}$

VALUE (units 10^{-2})	EVTS	DOCUMENT ID		TECN	COMMENT
1.5±0.9±1.1	5.8k	ABLIKIM	24BG	BES3	e^+e^- at 3.773 GeV

$\Gamma(\text{Resonant }(\pi^+\pi^-)\pi^+\pi^-\text{ 3-body total})/\Gamma(2\pi^+2\pi^-)$ — $\Gamma_{202}/\Gamma_{171}$

This is the fit fraction from the coherent amplitude analysis.

VALUE (units 10^{-2})	DOCUMENT ID		TECN	COMMENT
20.0±1.2±1.0	LINK	07A	FOCS	4-body fit, ≈ 5.7k evts

$\Gamma((\pi^+\pi^-)_{S-wave}(\pi^+\pi^-)_{S-wave})/\Gamma(2\pi^+2\pi^-)$ — $\Gamma_{203}/\Gamma_{171}$

VALUE (units 10^{-2})	EVTS	DOCUMENT ID		TECN	COMMENT
62.8±4.6±9.7	5.8k	[1] ABLIKIM	24BG	BES3	e^+e^- at 3.773 GeV

[1] The $\pi\pi$ S-wave is parametrized by a K-matrix with five coupled channels (2π, $2K$, 4π, 2η, $\eta\eta'$) and five poles, as in DEANDREA 08.

$\Gamma(\sigma\pi^+\pi^-)/\Gamma(2\pi^+2\pi^-)$ — $\Gamma_{204}/\Gamma_{171}$

This is the fit fraction from the coherent amplitude analysis.

VALUE (units 10^{-2})	DOCUMENT ID		TECN	COMMENT
8.2±0.9±0.7	LINK	07A	FOCS	4-body fit, ≈ 5.7k evts

$\Gamma(f_0(980)\pi^+\pi^-,\ f_0\to\pi^+\pi^-)/\Gamma(2\pi^+2\pi^-)$ — $\Gamma_{205}/\Gamma_{171}$

This is the fit fraction from the coherent amplitude analysis.

VALUE (units 10^{-2})	DOCUMENT ID		TECN	COMMENT
2.4±0.5±0.4	LINK	07A	FOCS	4-body fit, ≈ 5.7k evts

$\Gamma(\rho(770)^0(\pi^+\pi^-)_{S-wave})/\Gamma(2\pi^+2\pi^-)$ — $\Gamma_{206}/\Gamma_{171}$

VALUE (units 10^{-2})	EVTS	DOCUMENT ID		TECN	COMMENT
2.7±0.6±1.7	5.8k	[1] ABLIKIM	24BG	BES3	e^+e^- at 3.773 GeV

[1] The $\pi\pi$ S-wave is parametrized by a K-matrix with five coupled channels (2π, $2K$, 4π, 2η, $\eta\eta'$) and five poles, as in DEANDREA 08.

$\Gamma(\sigma\rho(770)^0)/\Gamma(2\pi^+2\pi^-)$ — $\Gamma_{207}/\Gamma_{171}$

This is the fit fraction from a coherent amplitude analysis.

VALUE (units 10^{-2})	EVTS	DOCUMENT ID		COMMENT
6.6±1.0±3.2	7.3k	[1] DARGENT	17	4-body fit, 4π evts

[1] Obtained by analyzing CLEO-c data but not authored by the CLEO Collaboration.

$\Gamma(f_2(1270)\pi^+\pi^-,\ f_2\to\pi^+\pi^-)/\Gamma(2\pi^+2\pi^-)$ — $\Gamma_{208}/\Gamma_{171}$

This is the fit fraction from the coherent amplitude analysis.

VALUE (units 10^{-2})	DOCUMENT ID		TECN	COMMENT
4.9±0.6±0.5	LINK	07A	FOCS	4-body fit, ≈ 5.7k evts

$\Gamma(f_2(1270)^0(\pi^+\pi^-)_{S-wave},\ f_2(1270)^0\to\pi^+\pi^-)/\Gamma(2\pi^+2\pi^-)$ — $\Gamma_{209}/\Gamma_{171}$

VALUE (units 10^{-2})	EVTS	DOCUMENT ID		TECN	COMMENT
1.8±0.4±1.3	5.8k	[1] ABLIKIM	24BG	BES3	e^+e^- at 3.773 GeV

[1] The $\pi\pi$ S-wave is parametrized by a K-matrix with five coupled channels (2π, $2K$, 4π, 2η, $\eta\eta'$) and five poles, as in DEANDREA 08.

$\Gamma(f_2(1270)f_2(1270),\ f_2\to\pi^+\pi^-)/\Gamma(2\pi^+2\pi^-)$ — $\Gamma_{210}/\Gamma_{171}$

This is the fit fraction from a coherent amplitude analysis.

VALUE (units 10^{-2})	EVTS	DOCUMENT ID		COMMENT
2.1±0.5±2.3	7.3k	[1] DARGENT	17	4-body fit, 4π evts

[1] Obtained by analyzing CLEO-c data but not authored by the CLEO Collaboration.

$\Gamma(f_0(1370)\sigma,\ f_0\to\pi^+\pi^-)/\Gamma(2\pi^+2\pi^-)$ — $\Gamma_{211}/\Gamma_{171}$

This is the fit fraction from a coherent amplitude analysis.

VALUE (units 10^{-2})	EVTS	DOCUMENT ID		COMMENT
21.2±1.8±6.7	7.3k	[1] DARGENT	17	4-body fit, 4π evts

[1] Obtained by analyzing CLEO-c data but not authored by the CLEO Collaboration.

$\Gamma(\pi^+\pi^-2\pi^0)/\Gamma_{total}$ — Γ_{212}/Γ

VALUE (units 10^{-3})	EVTS	DOCUMENT ID		TECN	COMMENT
10.02±0.19±0.24	3.8k	ABLIKIM	22BG	BES3	e^+e^- at 3.773 GeV

$\Gamma(\pi^+\pi^-2\pi^0)/\Gamma(K^-\pi^+)$ — Γ_{212}/Γ_{47}

VALUE (units 10^{-2})	EVTS	DOCUMENT ID		TECN	COMMENT
25.8±1.5±1.8	2724 ± 166	RUBIN	06	CLEO	e^+e^- at $\psi(3770)$

$\Gamma(\pi^+\pi^-2\pi^0(\text{non-}\eta))/\Gamma_{total}$ — Γ_{213}/Γ

VALUE (units 10^{-2})	EVTS	DOCUMENT ID		TECN	COMMENT
0.951±0.025±0.021	2.2k	ABLIKIM	24BG	BES3	e^+e^- at 3.773 GeV

$\Gamma(a_1(1260)^+\pi^-,\ a_1^+\to\pi^+2\pi^0\text{total})/\Gamma(\pi^+\pi^-2\pi^0)$ — $\Gamma_{214}/\Gamma_{212}$

VALUE (units 10^{-2})	EVTS	DOCUMENT ID		TECN	COMMENT
57.4±2.7±7.2	2.2k	ABLIKIM	24BG	BES3	e^+e^- at 3.773 GeV

$\Gamma(a_1(1260)^-\pi^+,\ a_1^-\to\pi^-2\pi^0\text{total})/\Gamma(\pi^+\pi^-2\pi^0)$ — $\Gamma_{215}/\Gamma_{212}$

VALUE (units 10^{-2})	EVTS	DOCUMENT ID		TECN	COMMENT
7.2±1.1±2.2	2.2k	ABLIKIM	24BG	BES3	e^+e^- at 3.773 GeV

$\Gamma(a_1(1260)^0\pi^0,\ a_1^0\to\pi^+\pi^-\pi^0\text{total})/\Gamma(\pi^+\pi^-2\pi^0)$ — $\Gamma_{216}/\Gamma_{212}$

VALUE (units 10^{-2})	EVTS	DOCUMENT ID		TECN	COMMENT
32.9±3.2±8.5	2.2k	ABLIKIM	24BG	BES3	e^+e^- at 3.773 GeV

$\Gamma(a_1(1420)^+\pi^-,\ a_1^+\to f_0(980)\pi^+\ P\text{-wave},\ f_0\to\pi^0\pi^0)/\Gamma(\pi^+\pi^-2\pi^0)$ — $\Gamma_{217}/\Gamma_{212}$

VALUE (units 10^{-2})	EVTS	DOCUMENT ID		TECN	COMMENT
0.3±0.1±0.1	2.2k	ABLIKIM	24BG	BES3	e^+e^- at 3.773 GeV

$\Gamma(a_1(1640)^-\pi^+,\ a_1^-\to\rho^-\pi^0\ S\text{-wave})/\Gamma(\pi^+\pi^-2\pi^0)$ — $\Gamma_{218}/\Gamma_{212}$

VALUE (units 10^{-2})	EVTS	DOCUMENT ID		TECN	COMMENT
0.3±0.2±0.2	2.2k	ABLIKIM	24BG	BES3	e^+e^- at 3.773 GeV

$\Gamma(a_1(1640)^+\pi^-,\ a_1^+\to\rho^+\pi^0\ S\text{-wave})/\Gamma(\pi^+\pi^-2\pi^0)$ — $\Gamma_{219}/\Gamma_{212}$

VALUE (units 10^{-2})	EVTS	DOCUMENT ID		TECN	COMMENT
1.1±0.3±0.6	2.2k	ABLIKIM	24BG	BES3	e^+e^- at 3.773 GeV

$\Gamma(a_2(1320)^+\pi^-,\ a_2^+\to\rho^+\pi^0\ D\text{-wave})/\Gamma(\pi^+\pi^-2\pi^0)$ — $\Gamma_{220}/\Gamma_{212}$

VALUE (units 10^{-2})	EVTS	DOCUMENT ID		TECN	COMMENT
0.2±0.1±0.1	8k	[1] ABLIKIM	24BG	BES3	e^+e^- at 3.773 GeV

[1] Seen with 4.6 σ significance in a combined fit to 2.2k $D^0\to\pi^+\pi^-2\pi^0$ and 5.8k $D^0\to 2\pi^+2\pi^-$ events.

$\Gamma(a_2(1320)^-\pi^+,\ a_2^-\to\rho^-\pi^0\ D\text{-wave})/\Gamma(\pi^+\pi^-2\pi^0)$ — $\Gamma_{221}/\Gamma_{212}$

VALUE (units 10^{-2})	EVTS	DOCUMENT ID		TECN	COMMENT
0.3±0.1±0.1	2.2k	ABLIKIM	24BG	BES3	e^+e^- at 3.773 GeV

$\Gamma(h_1(1170)^0\pi^0,\ h_1^0\to\rho\pi)/\Gamma(\pi^+\pi^-2\pi^0)$ — $\Gamma_{222}/\Gamma_{212}$

VALUE (units 10^{-2})	EVTS	DOCUMENT ID		TECN	COMMENT
1.3±0.6±1.1	2.2k	[1] ABLIKIM	24BG	BES3	e^+e^- at 3.773 GeV

[1] This comprises h_1^0 decays to $\rho^+\pi^-$, $\rho^0\pi^0$, and $\rho^-\pi^+$, with relative rates constrained to obey isospin symmetry.

$\Gamma(\pi(1300)^-\pi^+,\ \pi(1300)^-\to\pi^-2\pi^0\text{total})/\Gamma(\pi^+\pi^-2\pi^0)$ — $\Gamma_{223}/\Gamma_{212}$

VALUE (units 10^{-2})	EVTS	DOCUMENT ID		TECN	COMMENT
11.4±1.1±2.4	2.2k	ABLIKIM	24BG	BES3	e^+e^- at 3.773 GeV

$\Gamma(\pi(1300)^+\pi^-,\ \pi(1300)^+\to\pi^+2\pi^0\text{total})/\Gamma(\pi^+\pi^-2\pi^0)$ — $\Gamma_{224}/\Gamma_{212}$

VALUE (units 10^{-2})	EVTS	DOCUMENT ID		TECN	COMMENT
15.6±1.4±2.6	2.2k	ABLIKIM	24BG	BES3	e^+e^- at 3.773 GeV

$\Gamma(\pi(1300)^0\pi^0,\ \pi(1300)^0\to\pi^+\pi^-\pi^0\text{total})/\Gamma(\pi^+\pi^-2\pi^0)$ — $\Gamma_{225}/\Gamma_{212}$

VALUE (units 10^{-2})	EVTS	DOCUMENT ID		TECN	COMMENT
23.2±2.8±3.4	2.2k	ABLIKIM	24BG	BES3	e^+e^- at 3.773 GeV

Int. J. Mod. Phys. A 2026.41. Downloaded from www.worldscientific.com
by UNIVERSITY OF CALIFORNIA @ BERKELEY on 09/16/26. Re-use and distribution is strictly not permitted, except for Open Access articles.

$\Gamma(\pi_2(1670)^0\pi^0,\ \pi_2(1670)^0 \to \pi^+\pi^-\pi^0\text{total})/\Gamma(\pi^+\pi^-2\pi^0)$ — $\Gamma_{226}/\Gamma_{212}$

VALUE (units 10^{-2})	EVTS	DOCUMENT ID		TECN	COMMENT
1.1±0.2±0.4	2.2k	ABLIKIM	24BG	BES3	e^+e^- at 3.773 GeV

$\Gamma(\rho(770)^+\rho(770)^-)/\Gamma(\pi^+\pi^-2\pi^0)$ — $\Gamma_{227}/\Gamma_{212}$

VALUE (units 10^{-2})	EVTS	DOCUMENT ID		TECN	COMMENT
90.9±3.9±7.5	2.2k	ABLIKIM	24BG	BES3	e^+e^- at 3.773 GeV

$\Gamma(\rho(770)^+\rho(770)^-\ S\text{-wave})/\Gamma(\pi^+\pi^-2\pi^0)$ — $\Gamma_{228}/\Gamma_{212}$

VALUE (units 10^{-2})	EVTS	DOCUMENT ID		TECN	COMMENT
13.0±2.0±3.4	2.2k	ABLIKIM	24BG	BES3	e^+e^- at 3.773 GeV

$\Gamma(\rho(770)^+\rho(770)^-\ P\text{-wave})/\Gamma(\pi^+\pi^-2\pi^0)$ — $\Gamma_{229}/\Gamma_{212}$

VALUE (units 10^{-2})	EVTS	DOCUMENT ID		TECN	COMMENT
19.6±1.3±1.8	2.2k	ABLIKIM	24BG	BES3	e^+e^- at 3.773 GeV

$\Gamma(\rho(770)^+\rho(770)^-\ D\text{-wave})/\Gamma(\pi^+\pi^-2\pi^0)$ — $\Gamma_{230}/\Gamma_{212}$

VALUE (units 10^{-2})	EVTS	DOCUMENT ID		TECN	COMMENT
36.0±3.0±2.5	2.2k	ABLIKIM	24BG	BES3	e^+e^- at 3.773 GeV

$\Gamma(\rho(770)^+\rho(1450)^-\ D\text{-wave},\ \rho(1450)^- \to \pi^-\pi^0)/\Gamma(\pi^+\pi^-2\pi^0)$ — $\Gamma_{231}/\Gamma_{212}$

VALUE (units 10^{-2})	EVTS	DOCUMENT ID		TECN	COMMENT
1.7±0.8±1.8	2.2k	ABLIKIM	24BG	BES3	e^+e^- at 3.773 GeV

$\Gamma(\rho(770)^0(\pi^0\pi^0)_{S-wave})/\Gamma(\pi^+\pi^-2\pi^0)$ — $\Gamma_{232}/\Gamma_{212}$

VALUE (units 10^{-2})	EVTS	DOCUMENT ID		TECN	COMMENT
1.0±0.2±0.4	2.2k	[1] ABLIKIM	24BG	BES3	e^+e^- at 3.773 GeV

[1] The $\pi\pi$ S-wave is parametrized by a K-matrix with five coupled channels (2π, $2K$, 4π, 2η, $\eta\eta'$) and five poles, as in DEANDREA 08.

$\Gamma((\pi^+\pi^-)_{S-wave}(\pi^0\pi^0)_{S-wave})/\Gamma(\pi^+\pi^-2\pi^0)$ — $\Gamma_{233}/\Gamma_{212}$

VALUE (units 10^{-2})	EVTS	DOCUMENT ID		TECN	COMMENT
37.4±3.0±5.2	2.2k	[1] ABLIKIM	24BG	BES3	e^+e^- at 3.773 GeV

[1] The $\pi\pi$ S-wave is parametrized by a K-matrix with five coupled channels (2π, $2K$, 4π, 2η, $\eta\eta'$) and five poles, as in DEANDREA 08.

$[\Gamma(f_2(1270)(\pi^0\pi^0)_{S-wave},\ f_2 \to \pi^+\pi^-) + \Gamma(f_2(1270)(\pi^+\pi^-)_{S-wave},\ f_2 \to \pi^0\pi^0)]/\Gamma(\pi^+\pi^-2\pi^0)$ — $(\Gamma_{234}+\Gamma_{235})/\Gamma_{212}$

VALUE (units 10^{-2})	EVTS	DOCUMENT ID		TECN	COMMENT
1.1±0.2±0.7	2.2k	[1] ABLIKIM	24BG	BES3	e^+e^- at 3.773 GeV

[1] The relative size of the $D^0 \to f_2(\pi^+\pi^-)$, $f_2 \to \pi^0\pi^0$ and $D^0 \to f_2(\pi^0\pi^0)$, $f_2 \to \pi^+\pi^-$ amplitudes is constrained to obey isospin symmetry.

$\Gamma(\omega(782)\pi^0,\ \omega \to \pi^+\pi^-\pi^0)/\Gamma(\pi^+\pi^-2\pi^0)$ — $\Gamma_{236}/\Gamma_{212}$

VALUE (units 10^{-2})	EVTS	DOCUMENT ID		TECN	COMMENT
0.9±0.4±0.2	2.2k	ABLIKIM	24BG	BES3	e^+e^- at 3.773 GeV

$\Gamma(\phi(1020)\pi^0,\ \phi(1020) \to \pi^+\pi^-\pi^0)/\Gamma(\pi^+\pi^-2\pi^0)$ — $\Gamma_{237}/\Gamma_{212}$

VALUE (units 10^{-2})	EVTS	DOCUMENT ID		TECN	COMMENT
1.5±0.4±0.3	2.2k	ABLIKIM	24BG	BES3	e^+e^- at 3.773 GeV

$\Gamma(4\pi^0)/\Gamma_{total}$ — Γ_{238}/Γ

VALUE (units 10^{-4})	EVTS	DOCUMENT ID		TECN	COMMENT
7.6±0.9±0.7	96	ABLIKIM	22BG	BES3	e^+e^- at 3.773 GeV

$\Gamma(\eta\pi^0)/\Gamma_{total}$ — Γ_{239}/Γ

Unseen decay modes of the η are included.

VALUE (units 10^{-4})	EVTS	DOCUMENT ID		TECN	COMMENT
6.3±0.5 OUR FIT	Error includes scale factor of 1.1.				
5.8±0.5±0.5	1.7k	ABLIKIM	18L	BES3	e^+e^-, 3773 MeV
• • • We do not use the following data for averages, fits, limits, etc. • • •					
6.5±0.9±0.4	75	ABLIKIM	16D	BES3	See ABLIKIM 18L
6.4±1.0±0.4	156 ± 24	ARTUSO	08	CLEO	See MENDEZ 10

$\Gamma(\eta\pi^0)/\Gamma(K^-\pi^+)$ — Γ_{239}/Γ_{47}

Unseen decay modes of the η are included.

VALUE (units 10^{-2})	EVTS	DOCUMENT ID		TECN	COMMENT
• • • We do not use the following data for averages, fits, limits, etc. • • •					
1.47±0.34±0.11	62 ± 14	RUBIN	06	CLEO	See ARTUSO 08

$\Gamma(\eta\pi^0)/[\Gamma(K^-\pi^+) + \Gamma(K^+\pi^-)]$ — $\Gamma_{239}/(\Gamma_{47}+\Gamma_{344})$

Unseen decay modes of the η are included.

VALUE (units 10^{-2})	EVTS	DOCUMENT ID		TECN	COMMENT
1.60±0.14 OUR FIT	Error includes scale factor of 1.1.				
1.74±0.15±0.11	481 ± 40	MENDEZ	10	CLEO	e^+e^- at 3774 MeV

$\Gamma(\omega\pi^0)/\Gamma_{total}$ — Γ_{240}/Γ

Unseen decay modes of the ω are included.

VALUE (units 10^{-4})	EVTS	DOCUMENT ID		TECN	COMMENT
1.17±0.34±0.07	45	ABLIKIM	16D	BES3	e^+e^-, 3773 MeV

$\Gamma(\omega\eta)/\Gamma_{total}$ — Γ_{241}/Γ

VALUE (units 10^{-3})	EVTS	DOCUMENT ID		TECN	COMMENT
1.98±0.18 OUR AVERAGE	Error includes scale factor of 1.1.				
2.15±0.17±0.15	2.2k	ABLIKIM	18L	BES3	e^+e^-, 3773 MeV
1.78±0.19±0.15	600	[1] SMITH	18		e^+e^-, 3773 MeV

[1] Obtained by analyzing CLEO-c data but not authored by the CLEO Collaboration.

$\Gamma(2\pi^+2\pi^-\pi^0)/\Gamma_{total}$ — Γ_{242}/Γ

VALUE (units 10^{-4})	EVTS	DOCUMENT ID		TECN	COMMENT
34.6±1.5±1.5	940	ABLIKIM	22BG	BES3	e^+e^- at 3.773 GeV

$\Gamma(2\pi^+2\pi^-\pi^0)/\Gamma(K^-\pi^+)$ — Γ_{242}/Γ_{47}

VALUE (units 10^{-2})	EVTS	DOCUMENT ID		TECN	COMMENT
10.7±1.2±0.5	1614 ± 171	RUBIN	06	CLEO	e^+e^- at $\psi(3770)$

$\Gamma(\pi^+\pi^-3\pi^0)/\Gamma_{total}$ — Γ_{243}/Γ

VALUE (units 10^{-4})	EVTS	DOCUMENT ID		TECN	COMMENT
15.3±1.7±1.3	180	ABLIKIM	22BG	BES3	e^+e^- at 3.773 GeV

$\Gamma(2\pi^+2\pi^-2\pi^0)/\Gamma_{total}$ — Γ_{244}/Γ

VALUE (units 10^{-4})	EVTS	DOCUMENT ID		TECN	COMMENT
47.7±3.1±2.1	350	ABLIKIM	22BG	BES3	e^+e^- at 3.773 GeV

$\Gamma(\eta\pi^+\pi^-)/\Gamma_{total}$ — Γ_{245}/Γ

Unseen decay modes of the η are included.

VALUE (units 10^{-4})	EVTS	DOCUMENT ID		TECN	COMMENT
11.6±0.7 OUR AVERAGE					
10.6±1.8±0.7	96	ABLIKIM	20AA	BES3	e^+e^-, 3773 MeV
12.0±0.7±0.4	450	ABLIKIM	20G	BES3	e^+e^-, 3773 MeV
10.9±1.3±0.9	257	ARTUSO	08	CLEO	e^+e^- at $\psi(3770)$

$\Gamma(\eta\pi^+\pi^-)/\Gamma(K^-\pi^+\eta)$ — $\Gamma_{245}/\Gamma_{113}$

VALUE (units 10^{-2})	EVTS	DOCUMENT ID		TECN	COMMENT
6.49±0.09±0.12	13k	LI	21G	BELL	e^+e^- at $\Upsilon(nS)$

$\Gamma(\rho(770)^0\eta,\ \rho^0 \to \pi^+\pi^-)/\Gamma(\eta\pi^+\pi^-)$ — $\Gamma_{246}/\Gamma_{245}$

VALUE (units 10^{-2})	DOCUMENT ID		TECN	COMMENT
15.2±1.7±1.0	[1] ABLIKIM	24CL	BES3	e^+e^- at 3.773 GeV

[1] Amplitude analysis involving six modes.

$\Gamma(a_0(980)^-\pi^+,\ a_0^- \to \pi^-\eta)/\Gamma(\eta\pi^+\pi^-)$ — $\Gamma_{247}/\Gamma_{245}$

VALUE (units 10^{-2})	DOCUMENT ID		TECN	COMMENT
5.9±1.3±1.0	[1] ABLIKIM	24CL	BES3	e^+e^- at 3.773 GeV

[1] Amplitude analysis involving six modes.

$\Gamma(a_0(980)^+\pi^-,\ a_0^+ \to \pi^+\eta)/\Gamma(\eta\pi^+\pi^-)$ — $\Gamma_{248}/\Gamma_{245}$

VALUE (units 10^{-2})	DOCUMENT ID		TECN	COMMENT
44.0±4.0±5.3	[1] ABLIKIM	24CL	BES3	e^+e^- at 3.773 GeV

[1] Amplitude analysis involving six modes.

$\Gamma(a_2(1320)^+\pi^-,\ a_2^+ \to \pi^+\eta)/\Gamma(\eta\pi^+\pi^-)$ — $\Gamma_{249}/\Gamma_{245}$

VALUE (units 10^{-2})	DOCUMENT ID		TECN	COMMENT
2.1±0.9±0.8	[1] ABLIKIM	24CL	BES3	e^+e^- at 3.773 GeV

[1] Amplitude analysis involving six modes.

$\Gamma(a_2(1700)^+\pi^-,\ a_2^+ \to \pi^+\eta)/\Gamma(\eta\pi^+\pi^-)$ — $\Gamma_{250}/\Gamma_{245}$

VALUE (units 10^{-2})	DOCUMENT ID		TECN	COMMENT
5.5±1.8±2.7	[1] ABLIKIM	24CL	BES3	e^+e^- at 3.773 GeV

[1] Amplitude analysis involving six modes.

$\Gamma((\pi^+\pi^-)_{S-wave}\eta)/\Gamma(\eta\pi^+\pi^-)$ — $\Gamma_{251}/\Gamma_{245}$

VALUE (units 10^{-2})	DOCUMENT ID		TECN	COMMENT
3.9±1.8±2.1	[1] ABLIKIM	24CL	BES3	e^+e^- at 3.773 GeV

[1] Amplitude analysis involving six modes.

$\Gamma(\omega\pi^+\pi^-)/\Gamma_{total}$ — Γ_{252}/Γ

VALUE (units 10^{-3})	EVTS	DOCUMENT ID		TECN	COMMENT
1.33±0.16±0.12	411	ABLIKIM	20AA	BES3	e^+e^-, 3773 MeV

$\Gamma(\omega\pi^+\pi^-)/\Gamma(K^-\pi^+)$ — Γ_{252}/Γ_{47}

Unseen decay modes of the ω are included.

VALUE (units 10^{-2})	EVTS	DOCUMENT ID		TECN	COMMENT
4.1±1.2±0.4	472 ± 132	RUBIN	06	CLEO	e^+e^- at $\psi(3770)$

$\Gamma(\omega\pi^0\pi^0)/\Gamma_{total}$ — Γ_{253}/Γ

VALUE	CL%	DOCUMENT ID		TECN	COMMENT
<1.10 × 10^{-3}	90	ABLIKIM	20AA	BES3	e^+e^-, 3773 MeV

Int. J. Mod. Phys. A 2026.41. Downloaded from www.worldscientific.com
by LIFORNIA @ BERKELEY on 09/16/26. Re-use and distribution is strictly not permitted, except for Open Access articles.

$\Gamma(\eta 2\pi^0)/\Gamma_{total}$ — Γ_{254}/Γ

VALUE (units 10^{-4})	CL%	EVTS	DOCUMENT ID		TECN	COMMENT
3.8±1.1±0.7		42	[1] ABLIKIM	18X	BES3	e^+e^-, 3773 MeV
• • • We do not use the following data for averages, fits, limits, etc. • • •						
<23.8	90		ABLIKIM	20AA	BES3	e^+e^-, 3773 MeV

[1] Significance of signal reported by ABLIKIM 18X is 3.8σ.

$\Gamma(\pi^+\pi^-\pi^0\eta)/\Gamma_{total}$ — Γ_{255}/Γ

VALUE (units 10^{-3})	EVTS	DOCUMENT ID		TECN	COMMENT
3.23±0.17±0.14	510	ABLIKIM	20V	BES3	e^+e^-, 3773 MeV

$\Gamma(\eta 3\pi^0)/\Gamma_{total}$ — Γ_{256}/Γ

VALUE (units 10^{-4})	EVTS	DOCUMENT ID		TECN	COMMENT
23.6±2.2±1.7	155	ABLIKIM	22BG	BES3	e^+e^- at 3.773 GeV

$\Gamma(\eta 2\pi^+2\pi^-)/\Gamma_{total}$ — Γ_{257}/Γ

VALUE (units 10^{-4})	EVTS	DOCUMENT ID		TECN	COMMENT
6.0±1.0±0.6	49	ABLIKIM	22BG	BES3	e^+e^- at 3.773 GeV

$\Gamma(3\pi^+3\pi^-)/\Gamma(K^-2\pi^+\pi^-)$ — Γ_{258}/Γ_{87}

VALUE (units 10^{-3})	EVTS	DOCUMENT ID		TECN	COMMENT
5.23±0.59±1.35	149 ± 17	LINK	04B	FOCS	γA, $\overline{E}_\gamma \approx$ 180 GeV

$\Gamma(3\pi^+3\pi^-)/\Gamma(K^-3\pi^+2\pi^-)$ — $\Gamma_{258}/\Gamma_{126}$

VALUE	DOCUMENT ID		TECN	COMMENT
• • • We do not use the following data for averages, fits, limits, etc. • • •				
1.93±047±0.48	[1] LINK	04B	FOCS	γA, $\overline{E}_\gamma \approx$ 180 GeV

[1] This LINK 04B result is not independent of other results in these Listings.

$\Gamma(\eta'(958)\pi^0)/\Gamma_{total}$ — Γ_{259}/Γ

Unseen decay modes of the $\eta'(958)$ are included.

VALUE (units 10^{-4})	EVTS	DOCUMENT ID		TECN	COMMENT
9.2±1.0 OUR FIT					
9.3±1.1±0.9	469 ± 56	ABLIKIM	18L	BES3	e^+e^-, 3773 MeV
• • • We do not use the following data for averages, fits, limits, etc. • • •					
8.1±1.5±0.6	50 ± 9	ARTUSO	08	CLEO	See MENDEZ 10

$\Gamma(\eta'(958)\pi^0)/[\Gamma(K^-\pi^+)+\Gamma(K^+\pi^-)]$ — $\Gamma_{259}/(\Gamma_{47}+\Gamma_{344})$

Unseen decay modes of the $\eta'(958)$ are included.

VALUE (units 10^{-2})	EVTS	DOCUMENT ID		TECN	COMMENT
2.33±0.26 OUR FIT					
2.3 ±0.3 ±0.2	159 ± 19	MENDEZ	10	CLEO	e^+e^- at 3774 MeV

$\Gamma(\eta'(958)\pi^+\pi^-)/\Gamma_{total}$ — Γ_{260}/Γ

Unseen decay modes of the $\eta'(958)$ are included.

VALUE (units 10^{-4})	EVTS	DOCUMENT ID		TECN	COMMENT
4.5±1.6±0.5	21 ± 8	ARTUSO	08	CLEO	e^+e^- at $\psi(3770)$

$\Gamma(2\eta)/\Gamma_{total}$ — Γ_{261}/Γ

Unseen decay modes of the η are included.

VALUE (units 10^{-4})	EVTS	DOCUMENT ID		TECN	COMMENT
21.1±1.9 OUR FIT	Error includes scale factor of 2.3.				
22.0±0.7±0.6	3.4k	ABLIKIM	18L	BES3	e^+e^-, 3773 MeV
• • • We do not use the following data for averages, fits, limits, etc. • • •					
16.7±1.4±1.3	255 ± 22	ARTUSO	08	CLEO	See MENDEZ 10

$\Gamma(2\eta)/[\Gamma(K^-\pi^+)+\Gamma(K^+\pi^-)]$ — $\Gamma_{261}/(\Gamma_{47}+\Gamma_{344})$

Unseen decay modes of the η are included.

VALUE (units 10^{-2})	EVTS	DOCUMENT ID		TECN	COMMENT
5.3±0.5 OUR FIT	Error includes scale factor of 2.3.				
4.3±0.3±0.4	430 ± 29	MENDEZ	10	CLEO	e^+e^- at 3774 MeV

$\Gamma(2\eta\pi^0)/\Gamma_{total}$ — Γ_{262}/Γ

VALUE (units 10^{-4})	EVTS	DOCUMENT ID		TECN	COMMENT
7.3±1.6±1.5	27	[1] ABLIKIM	18X	BES3	e^+e^-, 3773 MeV

[1] Significance of signal reported by ABLIKIM 18X is 5.5σ.

$\Gamma(2\eta\pi^+\pi^-)/\Gamma_{total}$ — Γ_{263}/Γ

VALUE (units 10^{-4})	EVTS	DOCUMENT ID		TECN	COMMENT
8.5±1.3±0.4	43	ABLIKIM	22BG	BES3	e^+e^- at 3.773 GeV

$\Gamma(3\eta)/\Gamma_{total}$ — Γ_{264}/Γ

VALUE	CL%	DOCUMENT ID		TECN	COMMENT
<1.3 × 10^{-4}	90	ABLIKIM	18X	BES3	e^+e^-, 3773 MeV

$\Gamma(\eta\eta'(958))/\Gamma_{total}$ — Γ_{265}/Γ

Unseen decay modes of the η and $\eta'(958)$ are included.

VALUE (units 10^{-4})	EVTS	DOCUMENT ID		TECN	COMMENT
10.1±1.9 OUR FIT					
9.4±2.5±1.1	158 ± 41	ABLIKIM	18L	BES3	e^+e^-, 3773 MeV
• • • We do not use the following data for averages, fits, limits, etc. • • •					
12.6±2.5±1.1	46 ± 9	ARTUSO	08	CLEO	See MENDEZ 10

$\Gamma(\eta\eta'(958))/[\Gamma(K^-\pi^+)+\Gamma(K^+\pi^-)]$ — $\Gamma_{265}/(\Gamma_{47}+\Gamma_{344})$

Unseen decay modes of the η and $\eta'(958)$ are included.

VALUE (units 10^{-2})	EVTS	DOCUMENT ID		TECN	COMMENT
2.5±0.5 OUR FIT					
2.7±0.6±0.3	66 ± 15	MENDEZ	10	CLEO	e^+e^- at 3774 MeV

Hadronic modes with a $K\overline{K}$ pair

$\Gamma(K^+K^-)/\Gamma_{total}$ — Γ_{266}/Γ

VALUE (units 10^{-3})	EVTS	DOCUMENT ID		TECN	COMMENT
4.07 ±0.06 OUR FIT	Error includes scale factor of 1.6.				
4.233±0.021±0.064	56k	ABLIKIM	18W	BES3	e^+e^-, 3773 MeV
• • • We do not use the following data for averages, fits, limits, etc. • • •					
4.08 ±0.08 ±0.09	4.7k	BONVICINI	08	CLEO	See MENDEZ 10

$\Gamma(K^+K^-)/\Gamma(K^-\pi^+)$ — Γ_{266}/Γ_{47}

VALUE	EVTS	DOCUMENT ID		TECN	COMMENT
0.1034±0.0013 OUR FIT	Error includes scale factor of 1.6.				
0.1010±0.0016 OUR AVERAGE	Error includes scale factor of 1.4. See the ideogram below.				
0.122 ±0.011 ±0.004	242 ± 20	ABLIKIM	05F	BES	$e^+e^- \approx \psi(3770)$
0.0992±0.0011±0.0012	16k±200	ACOSTA	05C	CDF	$p\overline{p}$, $\sqrt{s}$=1.96 TeV
0.0993±0.0014±0.0014	11k	LINK	03	FOCS	γ nucleus, $\overline{E}_\gamma \approx$ 180 GeV
0.1040±0.0033±0.0027	1900	CSORNA	02	CLE2	$e^+e^- \approx \Upsilon(4S)$
0.109 ±0.003 ±0.003	3317	AITALA	98C	E791	π^- nucleus, 500 GeV
0.116 ±0.007 ±0.007	1102	ASNER	96B	CLE2	$e^+e^- \approx \Upsilon(4S)$
0.109 ±0.007 ±0.009	581	FRABETTI	94C	E687	γBe $\overline{E}_\gamma$= 220 GeV
0.107 ±0.010 ±0.009	193	ANJOS	91D	E691	Photoproduction
0.117 ±0.010 ±0.007	249	ALEXANDER	90	CLEO	e^+e^- 10.5–11 GeV
• • • We do not use the following data for averages, fits, limits, etc. • • •					
0.107 ±0.029 ±0.015	103	ADAMOVICH	92	OMEG	π^- 340 GeV
0.138 ±0.027 ±0.010	155	FRABETTI	92	E687	γBe
0.16 ±0.05	34	ALVAREZ	91B	NA14	Photoproduction
0.10 ±0.02 ±0.01	131	ALBRECHT	90C	ARG	$e^+e^- \approx$ 10 GeV
0.122 ±0.018 ±0.012	118	BALTRUSAIT...	85E	MRK3	e^+e^- 3.77 GeV
0.113 ±0.030		ABRAMS	79D	MRK2	e^+e^- 3.77 GeV

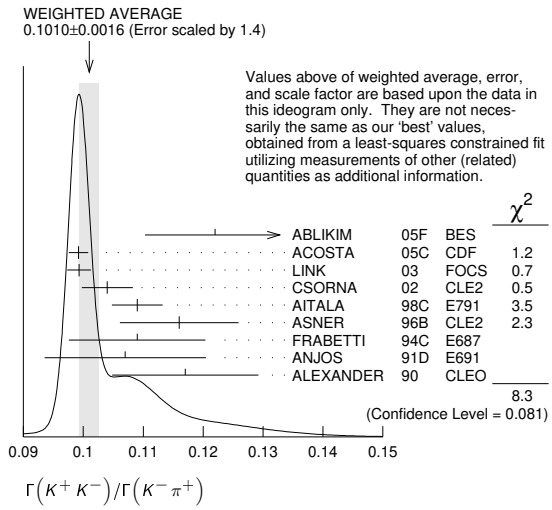

$\Gamma(K^+K^-)/[\Gamma(K^-\pi^+)+\Gamma(K^+\pi^-)]$ — $\Gamma_{266}/(\Gamma_{47}+\Gamma_{344})$

VALUE (units 10^{-2})	EVTS	DOCUMENT ID		TECN	COMMENT
10.30±0.13 OUR FIT	Error includes scale factor of 1.6.				
10.41±0.11±0.12	13.8k	MENDEZ	10	CLEO	e^+e^- at 3774 MeV

$\Gamma(K^+K^-)/\Gamma(\pi^+\pi^-)$ — $\Gamma_{266}/\Gamma_{151}$

The unused results here are redundant with $\Gamma(K^+K^-)/\Gamma(K^-\pi^+)$ and $\Gamma(\pi^+\pi^-)/\Gamma(K^-\pi^+)$ measurements by the same experiments.

VALUE	EVTS	DOCUMENT ID		TECN	COMMENT
• • • We do not use the following data for averages, fits, limits, etc. • • •					
2.760±0.040±0.034	7334	ACOSTA	05C	CDF	$p\overline{p}$, $\sqrt{s}$=1.96 TeV
2.81 ±0.10 ±0.06		LINK	03	FOCS	γ nucleus, $\overline{E}_\gamma \approx$ 180 GeV
2.96 ±0.16 ±0.15	710	CSORNA	02	CLE2	$e^+e^- \approx \Upsilon(4S)$
2.75 ±0.15 ±0.16		AITALA	98C	E791	π^- nucleus, 500 GeV
2.53 ±0.46 ±0.19		FRABETTI	94C	E687	γBe $\overline{E}_\gamma$= 220 GeV
2.23 ±0.81 ±0.46		ADAMOVICH	92	OMEG	π^- 340 GeV
1.95 ±0.34 ±0.22		ANJOS	91D	E691	Photoproduction
2.5 ±0.7		ALBRECHT	90C	ARG	$e^+e^- \approx$ 10 GeV
2.35 ±0.37 ±0.28		ALEXANDER	90	CLEO	e^+e^- 10.5–11 GeV

Int. J. Mod. Phys. A 2026.41. Downloaded from www.worldscientific.com
by UNIVERSITY OF CALIFORNIA @ BERKELEY on 09/16/26. Re-use and distribution is strictly not permitted, except for Open Access articles.

$\Gamma(2K^0_S)/\Gamma_{total}$ — Γ_{267}/Γ

VALUE (units 10^{-4})	EVTS	DOCUMENT ID		TECN	COMMENT
1.41±0.05 OUR FIT	Error includes scale factor of 1.1.				
1.67±0.11±0.11	576	ABLIKIM	17A	BES3	$e^+e^- \to \psi(3770)$
• • • We do not use the following data for averages, fits, limits, etc. • • •					
1.46±0.32±0.09	68 ± 15	BONVICINI	08	CLEO	See MENDEZ 10

$\Gamma(2K^0_S)/[\Gamma(K^-\pi^+)+\Gamma(K^+\pi^-)]$ — $\Gamma_{267}/(\Gamma_{47}+\Gamma_{344})$

VALUE (units 10^{-2})	EVTS	DOCUMENT ID		TECN	COMMENT
0.358±0.013 OUR FIT	Error includes scale factor of 1.1.				
0.41 ±0.04 ±0.02	215 ± 23	MENDEZ	10	CLEO	e^+e^- at 3774 MeV

$\Gamma(2K^0_S)/\Gamma(K^0_S\pi^0)$ — Γ_{267}/Γ_{48}

VALUE (units 10^{-2})	EVTS	DOCUMENT ID		TECN	COMMENT
1.14 ±0.04 OUR FIT	Error includes scale factor of 1.1.				
1.101±0.023±0.030	4.8k	DASH	17	BELL	At/near $\Upsilon(4S)$, $\Upsilon(5S)$

$\Gamma(2K^0_S)/\Gamma(K^0_S\pi^+\pi^-)$ — Γ_{267}/Γ_{53}

This is the same as $\Gamma(K^0\overline{K}^0)$ / $\Gamma(\overline{K}^0\pi^+\pi^-)$ because $D^0 \to K^0_S K^0_L$ is forbidden by CP conservation.

VALUE (units 10^{-2})	EVTS	DOCUMENT ID		TECN	COMMENT
0.498±0.030 OUR FIT					
1.20 ±0.22 OUR AVERAGE					
1.44 ±0.32 ±0.16	79 ± 17	LINK	05A	FOCS	γ Be, $\overline{E}_\gamma \approx$ 180 GeV
1.01 ±0.22 ±0.16	26	ASNER	96B	CLE2	$e^+e^- \approx \Upsilon(4S)$
3.9 ±1.3 ±1.3	20 ± 7	FRABETTI	94J	E687	γ Be $\overline{E}_\gamma$=220 GeV
• • • We do not use the following data for averages, fits, limits, etc. • • •					
2.1 $^{+1.1}_{-0.8}$ ±0.2	5	ALEXANDER	90	CLEO	e^+e^- 10.5–11 GeV

$\Gamma(K^0_S K^-\pi^+)/\Gamma(K^-\pi^+)$ — Γ_{268}/Γ_{47}

VALUE	DOCUMENT ID		TECN	COMMENT
0.085±0.013 OUR FIT Error includes scale factor of 1.1.				
0.08 ±0.03	[1] ANJOS	91	E691	γBe 80–240 GeV

[1] The factor 100 at the top of column 2 of Table I of ANJOS 91 should be omitted.

$\Gamma(K^0_S K^-\pi^+)/\Gamma(K^0_S\pi^+\pi^-)$ — Γ_{268}/Γ_{53}

VALUE	EVTS	DOCUMENT ID		TECN	COMMENT
0.118±0.017 OUR FIT Error includes scale factor of 1.1.					
0.119±0.021 OUR AVERAGE Error includes scale factor of 1.3.					
0.108±0.019	61	AMMAR	91	CLEO	$e^+e^- \approx$ 10.5 GeV
0.16 ±0.03 ±0.02	39	ALBRECHT	90C	ARG	$e^+e^- \approx$ 10 GeV

$\Gamma(\overline{K}^*(892)^0 K^0_S,\ \overline{K}^{*0} \to K^-\pi^+)/\Gamma(K^0_S K^-\pi^+)$ — $\Gamma_{269}/\Gamma_{268}$

Fit fraction from Dalitz plot analyses. The fraction for the $K^0_S\pi^+$ mass between 792 and 992 MeV is 0.370 ± 0.003 ± 0.012.

VALUE (units 10^{-2})	EVTS	DOCUMENT ID		TECN	COMMENT
2.47±0.15±0.23	113k	[1] AAIJ	16N	LHCB	Dalitz plot fit

[1] AAIJ 16N gives results for two S-wave parameterisations. We take the values from the model with LASS parametrization, and the difference as a systematic uncertainty.

$\Gamma(K^*(892)^+ K^-,\ K^{*+} \to K^0_S\pi^+)/\Gamma(K^0_S K^-\pi^+)$ — $\Gamma_{270}/\Gamma_{268}$

Fit fraction from Dalitz plot analyses.

VALUE (units 10^{-2})	EVTS	DOCUMENT ID		TECN	COMMENT
56.9±0.6±1.1	113k	[1] AAIJ	16N	LHCB	Dalitz plot fit

[1] AAIJ 16N gives results for two S-wave parameterisations. We take the values from the model with LASS parametrization, and the difference as a systematic uncertainty.

$\Gamma(\overline{K}^*(1410)^0 K^0_S,\ \overline{K}^{*0} \to K^-\pi^+)/\Gamma(K^0_S K^-\pi^+)$ — $\Gamma_{271}/\Gamma_{268}$

Fit fraction from Dalitz plot analyses.

VALUE (units 10^{-2})	EVTS	DOCUMENT ID		TECN	COMMENT
3.8±0.5±5.6	113k	[1] AAIJ	16N	LHCB	Dalitz plot fit

[1] AAIJ 16N gives results for two S-wave parameterisations. We take the values from the model with LASS parametrization, and the difference as a uncertainty (which in this case dominates)

$\Gamma(K^*(1410)^+ K^-,\ K^{*+} \to K^0_S\pi^+)/\Gamma(K^0_S K^-\pi^+)$ — $\Gamma_{272}/\Gamma_{268}$

Fit fraction from Dalitz plot analyses.

VALUE (units 10^{-2})	EVTS	DOCUMENT ID		TECN	COMMENT
9.6±1.1±5.4	113k	[1] AAIJ	16N	LHCB	Dalitz plot fit

[1] AAIJ 16N gives results for two S-wave parameterisations. We take the values from the model with LASS parametrization, and the difference as a systematic uncertainty (which in this case dominates).

$\Gamma((K^-\pi^+)_{S-wave} K^0_S)/\Gamma(K^0_S K^-\pi^+)$ — $\Gamma_{273}/\Gamma_{268}$

Fit fraction from Dalitz plot analyses.

VALUE (units 10^{-2})	EVTS	DOCUMENT ID		TECN	COMMENT
18±2±8	113k	[1] AAIJ	16N	LHCB	Dalitz plot fit

[1] AAIJ 16N gives results for two S-wave parameterisations. We take the values from the model with LASS parametrization, and the difference as a systematic uncertainty (which in this case dominates).

$\Gamma((K^0_S\pi^+)_{S-wave} K^-)/\Gamma(K^0_S K^-\pi^+)$ — $\Gamma_{274}/\Gamma_{268}$

Fit fraction from Dalitz plot analyses.

VALUE (units 10^{-2})	EVTS	DOCUMENT ID		TECN	COMMENT
11.7±1.0±2.3	113k	[1] AAIJ	16N	LHCB	Dalitz plot fit

[1] AAIJ 16N gives results for two S-wave parameterisations. We take the values from the model with LASS parametrization, and the difference as a systematic uncertainty.

$\Gamma(a_0(980)^-\pi^+,\ a_0^- \to K^0_S K^-)/\Gamma(K^0_S K^-\pi^+)$ — $\Gamma_{275}/\Gamma_{268}$

Fit fraction from Dalitz plot analyses.

VALUE (units 10^{-2})	EVTS	DOCUMENT ID		TECN	COMMENT
4.0±0.7±4.1	113k	[1] AAIJ	16N	LHCB	Dalitz plot fit

[1] AAIJ 16N gives results for two S-wave parameterisations. We take the values from the model with LASS parametrization, and the difference as a systematic uncertainty (which in this case dominates).

$\Gamma(a_0(1450)^-\pi^+,\ a_0^- \to K^0_S K^-)/\Gamma(K^0_S K^-\pi^+)$ — $\Gamma_{276}/\Gamma_{268}$

Fit fraction from Dalitz plot analyses.

VALUE (units 10^{-2})	EVTS	DOCUMENT ID		TECN	COMMENT
0.74±0.15±0.57	113k	[1] AAIJ	16N	LHCB	Dalitz plot fit

[1] AAIJ 16N gives results for two S-wave parameterisations. We take the values from the model with LASS parametrization, and the difference as a systematic uncertainty (which in this case dominates).

$\Gamma(a_2(1320)^-\pi^+,\ a_2^- \to K^0_S K^-)/\Gamma(K^0_S K^-\pi^+)$ — $\Gamma_{277}/\Gamma_{268}$

VALUE (units 10^{-2})	EVTS	DOCUMENT ID		TECN	COMMENT
0.15±0.06±0.14	113k	[1] AAIJ	16N	LHCB	Dalitz plot fit

[1] AAIJ 16N gives results for two S-wave parameterisations. We take the values from the model with LASS parametrization, and the difference as a systematic uncertainty.

$\Gamma(\rho(1450)^-\pi^+,\ \rho^- \to K^0_S K^-)/\Gamma(K^0_S K^-\pi^+)$ — $\Gamma_{278}/\Gamma_{268}$

Fit fraction from Dalitz plot analyses.

VALUE (units 10^{-2})	EVTS	DOCUMENT ID		TECN	COMMENT
1.4±0.2±0.7	113k	[1] AAIJ	16N	LHCB	Dalitz plot fit

[1] AAIJ 16N gives results for two S-wave parameterisations. We take the values from the model with LASS parametrization, and the difference as a systematic uncertainty.

$\Gamma(K^0_S K^+\pi^-)/\Gamma(K^-\pi^+)$ — Γ_{279}/Γ_{47}

VALUE	DOCUMENT ID		TECN	COMMENT
• • • We do not use the following data for averages, fits, limits, etc. • • •				
0.05±0.025	[1] ANJOS	91	E691	γBe 80–240 GeV

[1] The factor 100 at the top of column 2 of Table I of ANJOS 91 should be omitted.

$\Gamma(K^0_S K^+\pi^-)/\Gamma(K^0_S\pi^+\pi^-)$ — Γ_{279}/Γ_{53}

VALUE	EVTS	DOCUMENT ID		TECN	COMMENT
• • • We do not use the following data for averages, fits, limits, etc. • • •					
0.098±0.020	55	AMMAR	91	CLEO	$e^+e^- \approx$ 10.5 GeV

$\Gamma(K^0_S K^+\pi^-)/\Gamma(K^0_S K^-\pi^+)$ — $\Gamma_{279}/\Gamma_{268}$

VALUE	EVTS	DOCUMENT ID		TECN	COMMENT
0.654±0.007 OUR FIT					
0.654±0.007 OUR AVERAGE					
0.655±0.004±0.006	76k,113k	AAIJ	16N	LHCB	pp at 7, 8 TeV
0.592±0.044±0.018		INSLER	12	CLEO	$e^+e^- \to D^0\overline{D}^0$ at 3.77 GeV

$\Gamma(K^*(892)^0 K^0_S,\ K^{*0} \to K^+\pi^-)/\Gamma(\overline{K}^*(892)^0 K^0_S,\ \overline{K}^{*0} \to K^-\pi^+)$ — $\Gamma_{280}/\Gamma_{269}$

VALUE	CL%	DOCUMENT ID		TECN	COMMENT
0.356±0.034±0.007		[1] INSLER	12	CLEO	$e^+e^- \to D^0\overline{D}^0$, 3.77 GeV
• • • We do not use the following data for averages, fits, limits, etc. • • •					
<0.010	90	AMMAR	91	CLEO	$e^+e^- \approx$ 10.5 GeV

[1] Uses quantum correlations in $e^+e^- \to D^0\overline{D}^0$ at the $\psi(3770)$, where the signal side D decays to $K^0_S K\pi$ and the tag-side D decays to $K\pi$, $K\pi\pi\pi$, $K\pi\pi^0$, and 10 additional CP-even, CP-odd, and mixed CP modes involving K^0_S or K^0_L.

$\Gamma(K^*(892)^0 K^0_S,\ K^{*0} \to K^+\pi^-)/\Gamma(K^0_S K^+\pi^-)$ — $\Gamma_{280}/\Gamma_{279}$

Fit fraction from Dalitz plot analyses.

VALUE (units 10^{-2})	EVTS	DOCUMENT ID		TECN	COMMENT
5.17±0.21±0.47	76k	[1] AAIJ	16N	LHCB	Dalitz plot fit

[1] AAIJ 16N gives results for two S-wave parameterisations. We take the values from the model with LASS parametrization, and the difference as a systematic uncertainty.

$\Gamma(K^*(892)^- K^+,\ K^{*-} \to K^0_S\pi^-)/\Gamma(K^0_S K^+\pi^-)$ — $\Gamma_{281}/\Gamma_{279}$

Fit fraction from Dalitz plot analyses.

VALUE (units 10^{-2})	EVTS	DOCUMENT ID		TECN	COMMENT
28.8±0.4±1.5	76k	[1] AAIJ	16N	LHCB	Dalitz plot fit

[1] AAIJ 16N gives results for two S-wave parameterisations. We take the values from the model with LASS parametrization, and the difference as a systematic uncertainty.

Int. J. Mod. Phys. A 2026.41. Downloaded from www.worldscientific.com by LIFORNIA @ BERKELEY on 09/16/26. Re-use and distribution is strictly not permitted, except for Open Access articles.

$\Gamma(K^*(1410)^0 K^0_S,\ K^{*0} \to K^+\pi^+)/\Gamma(K^0_S K^+\pi^-)$ — $\Gamma_{282}/\Gamma_{279}$

Fit fraction from Dalitz plot analyses.

VALUE (units 10^{-2})	EVTS	DOCUMENT ID		TECN	COMMENT
2.2±0.6±3.7	76k	[1] AAIJ	16N	LHCB	Dalitz plot fit

[1] AAIJ 16N gives results for two S-wave parameterisations. We take the values from the model with LASS parametrization, and the difference as a systematic uncertainty (which in this case dominates).

$\Gamma(K^*(1410)^- K^+,\ K^{*-} \to K^0_S\pi^-)/\Gamma(K^0_S K^+\pi^-)$ — $\Gamma_{283}/\Gamma_{279}$

Fit fraction from Dalitz plot analyses.

VALUE (units 10^{-2})	EVTS	DOCUMENT ID		TECN	COMMENT
11.9±1.5±9.1	76k	[1] AAIJ	16N	LHCB	Dalitz plot fit

[1] AAIJ 16N gives results for two S-wave parameterisations. We take the values from the model with LASS parametrization, and the difference as a systematic uncertainty (which in this case dominates).

$\Gamma((K^+\pi^-)_{S-wave} K^0_S)/\Gamma(K^0_S K^+\pi^-)$ — $\Gamma_{284}/\Gamma_{279}$

Fit fraction from Dalitz plot analyses.

VALUE (units 10^{-2})	EVTS	DOCUMENT ID		TECN	COMMENT
17±2±8	76k	[1] AAIJ	16N	LHCB	Dalitz plot fit

[1] AAIJ 16N gives results for two S-wave parameterisations. We take the values from the model with LASS parametrization, and the difference as a systematic uncertainty.

$\Gamma((K^0_S\pi^-)_{S-wave} K^+)/\Gamma(K^0_S K^+\pi^-)$ — $\Gamma_{285}/\Gamma_{279}$

Fit fraction from Dalitz plot analyses.

VALUE (units 10^{-2})	EVTS	DOCUMENT ID		TECN	COMMENT
6.3±0.9±2.3	76k	[1] AAIJ	16N	LHCB	Dalitz plot fit

[1] AAIJ 16N gives results for two S-wave parameterisations. We take the values from the model with LASS parametrization, and the difference as a systematic uncertainty.

$\Gamma(a_0(980)^+\pi^-,\ a_0^+ \to K^0_S K^+)/\Gamma(K^0_S K^+\pi^-)$ — $\Gamma_{286}/\Gamma_{279}$

Fit fraction from Dalitz plot analyses.

VALUE (units 10^{-2})	EVTS	DOCUMENT ID		TECN	COMMENT
26±2±18	76k	[1] AAIJ	16N	LHCB	Dalitz plot fit

[1] AAIJ 16N gives results for two S-wave parameterisations. We take the values from the model with LASS parametrization, and the difference as a systematic uncertainty (which in this case dominates).

$\Gamma(a_0(1450)^+\pi^-,\ a_0^+ \to K^0_S K^+)/\Gamma(K^0_S K^+\pi^-)$ — $\Gamma_{287}/\Gamma_{279}$

Fit fraction from Dalitz plot analyses.

VALUE (units 10^{-2})	EVTS	DOCUMENT ID		TECN	COMMENT
1.5±0.3±1.1	76k	[1] AAIJ	16N	LHCB	Dalitz plot fit

[1] AAIJ 16N gives results for two S-wave parameterisations. We take the values from the model with LASS parametrization, and the difference as a systematic uncertainty (which in this case dominates).

$\Gamma(\rho(1700)^+\pi^-,\ \rho^+ \to K^0_S K^+)/\Gamma(K^0_S K^+\pi^-)$ — $\Gamma_{288}/\Gamma_{279}$

Fit fraction from Dalitz plot analyses.

VALUE (units 10^{-2})	EVTS	DOCUMENT ID		TECN	COMMENT
0.53±0.11±0.23	76k	[1] AAIJ	16N	LHCB	Dalitz plot fit

[1] AAIJ 16N gives results for two S-wave parameterisations. We take the values from the model with LASS parametrization, and the difference as a systematic uncertainty.

$\Gamma(K^+K^-\pi^0)/\Gamma(K^-\pi^+\pi^0)$ — Γ_{289}/Γ_{68}

VALUE (units 10^{-2})	EVTS	DOCUMENT ID		TECN	COMMENT
2.37±0.03±0.04	11k±122	AUBERT,B	06X	BABR	$e^+e^- \approx \Upsilon(4S)$
• • • We do not use the following data for averages, fits, limits, etc. • • •					
0.95±0.26	151	ASNER	96B	CLE2	$e^+e^- \approx \Upsilon(4S)$

$\Gamma(K^*(892)^+K^-,\ K^*(892)^+ \to K^+\pi^0)/\Gamma(K^+K^-\pi^0)$ — $\Gamma_{290}/\Gamma_{289}$

This is the "fit fraction" from the Dalitz-plot analysis with interference.

VALUE (units 10^{-2})	DOCUMENT ID		TECN	COMMENT
44.4±0.8±0.6	AUBERT	07T	BABR	Dalitz fit II, 11k evts
• • • We do not use the following data for averages, fits, limits, etc. • • •				
46.1±3.1	[1] CAWLFIELD	06A	CLEO	Dalitz fit, 627 ± 30 evts

[1] The error on this CAWLFIELD 06A result is statistical only.

$\Gamma(K^*(892)^-K^+,\ K^*(892)^- \to K^-\pi^0)/\Gamma(K^+K^-\pi^0)$ — $\Gamma_{291}/\Gamma_{289}$

This is the "fit fraction" from the Dalitz-plot analysis with interference.

VALUE (units 10^{-2})	DOCUMENT ID		TECN	COMMENT
15.9±0.7±0.6	AUBERT	07T	BABR	Dalitz fit II, 11k evts
• • • We do not use the following data for averages, fits, limits, etc. • • •				
12.3±2.2	[1] CAWLFIELD	06A	CLEO	Dalitz fit, 627 ± 30 evts

[1] The error on this CAWLFIELD 06A result is statistical only.

$\Gamma((K^+\pi^0)_{S-wave} K^-)/\Gamma(K^+K^-\pi^0)$ — $\Gamma_{292}/\Gamma_{289}$

This is the "fit fraction" from the Dalitz-plot analysis with interference.

VALUE (units 10^{-2})	DOCUMENT ID		TECN	COMMENT
71.1±3.7±1.9	[1] AUBERT	07T	BABR	Dalitz fit II, 11k evts

[1] The only major difference between fits I and II in the AUBERT 07T analysis is in this mode, where the fit-I fraction is (16.3 ± 3.4 ± 2.1)%.

$\Gamma((K^-\pi^0)_{S-wave} K^+)/\Gamma(K^+K^-\pi^0)$ — $\Gamma_{293}/\Gamma_{289}$

This is the "fit fraction" from the Dalitz-plot analysis with interference.

VALUE (units 10^{-2})	DOCUMENT ID		TECN	COMMENT
3.9±0.9±1.0	AUBERT	07T	BABR	Dalitz fit II, 11k evts

$\Gamma(f_0(980)\pi^0,\ f_0 \to K^+K^-)/\Gamma(K^+K^-\pi^0)$ — $\Gamma_{294}/\Gamma_{289}$

This is the "fit fraction" from the Dalitz-plot analysis with interference.

VALUE (units 10^{-2})	DOCUMENT ID		TECN	COMMENT
10.5±1.1±1.2	[1] AUBERT	07T	BABR	Dalitz fit II, 11k evts

[1] When AUBERT 07T replace the $f_0(980)\pi^0$ mode with $a_0(980)\pi^0$, the fit fraction is a negligibly different (11.0 ± 1.5 ± 1.2)%.

$\Gamma(\phi\pi^0,\ \phi \to K^+K^-)/\Gamma(K^+K^-\pi^0)$ — $\Gamma_{295}/\Gamma_{289}$

This is the "fit fraction" from the Dalitz-plot analysis with interference.

VALUE (units 10^{-2})	DOCUMENT ID		TECN	COMMENT
19.4±0.6±0.5	AUBERT	07T	BABR	Dalitz fit II, 11k evts
• • • We do not use the following data for averages, fits, limits, etc. • • •				
14.9±1.6	[1] CAWLFIELD	06A	CLEO	Dalitz fit, 627 ± 30 evts

[1] The error on this CAWLFIELD 06A result is statistical only.

$\Gamma(K^+K^-\pi^0\ \text{nonresonant})/\Gamma(K^+K^-\pi^0)$ — $\Gamma_{296}/\Gamma_{289}$

This is the "fit fraction" from the Dalitz-plot analysis with interference.

VALUE	DOCUMENT ID		TECN	COMMENT
• • • We do not use the following data for averages, fits, limits, etc. • • •				
0.360±0.037	[1] CAWLFIELD	06A	CLEO	Dalitz fit, 627 ± 30 evts

[1] The error is statistical only. CAWLFIELD 06A also fits the Dalitz plot replacing this flat nonresonant background with broad S−wave $\kappa^\pm \to K^\pm\pi^0$ resonances. There is no significant improvement in the fit, and $K^{*\pm}K^\mp$ and $\phi\pi^0$ results are not much changed.

$\Gamma(2K^0_S\pi^0)/\Gamma_{total}$ — Γ_{297}/Γ

VALUE	CL%	DOCUMENT ID		TECN	COMMENT
<1.45 × 10^{-4}	90	ABLIKIM	22Y	BES3	e^+e^- at 3.773 GeV
<5.9 × 10^{-4}	90	ASNER	96B	CLE2	$e^+e^- \approx \Upsilon(4S)$

$\Gamma(K^+K^-\eta)/\Gamma_{total}$ — Γ_{298}/Γ

VALUE (units 10^{-4})	EVTS	DOCUMENT ID		TECN	COMMENT
0.59±0.18±0.05	13	ABLIKIM	20V	BES3	e^+e^-, 3773 MeV

$\Gamma(K^+K^-\eta)/\Gamma(K^-\pi^+\eta)$ — $\Gamma_{298}/\Gamma_{113}$

VALUE (units 10^{-3})	EVTS	DOCUMENT ID		TECN	COMMENT
$9.57^{+0.36}_{-0.33}$±0.20	1.4k	LI	21G	BELL	e^+e^- at $\Upsilon(nS)$

$\Gamma(\phi(1020)\eta)/\Gamma(K^-\pi^+\eta)$ — $\Gamma_{299}/\Gamma_{113}$

VALUE (units 10^{-3})	EVTS	DOCUMENT ID		TECN	COMMENT
9.6±0.6±0.1	1.4k	[1] LI	21G	BELL	e^+e^- at $\Upsilon(nS)$

[1] LI 21G reports $[\Gamma(D^0 \to \phi(1020)\eta)/\Gamma(D^0 \to K^-\pi^+\eta)] \times [B(\phi(1020) \to K^+K^-)] = (4.82 \pm 0.23 \pm 0.16) \times 10^{-3}$ which we divide by our best (shown rounded) value $B(\phi(1020) \to K^+K^-) = (50.1 \pm 0.6) \times 10^{-2}$. Our first error is their experiment's error and our second error is the systematic error from using our best (shown rounded) value.

$\Gamma(K^+K^-\eta\ \text{nonresonant})/\Gamma(K^-\pi^+\eta)$ — $\Gamma_{300}/\Gamma_{113}$

VALUE (units 10^{-3})	EVTS	DOCUMENT ID		TECN	COMMENT
$5.26^{+0.45}_{-0.38}$±0.11	1.4k	LI	21G	BELL	e^+e^- at $\Upsilon(nS)$

$\Gamma(2K^0_S\eta)/\Gamma_{total}$ — Γ_{301}/Γ

VALUE (units 10^{-4})	EVTS	DOCUMENT ID		TECN	COMMENT
1.33±0.59±0.18	7	ABLIKIM	20V	BES3	e^+e^-, 3773 MeV

$\Gamma(K^+K^-\pi^0\pi^0)/\Gamma_{total}$ — Γ_{302}/Γ

VALUE (units 10^{-4})	EVTS	DOCUMENT ID		TECN	COMMENT
6.9±0.7±0.4	132	ABLIKIM	20AC	BES3	e^+e^- at 3.773 GeV

$\Gamma(K^+K^-\pi^+\pi^-)/\Gamma_{total}$ — Γ_{303}/Γ

VALUE (units 10^{-3})	DOCUMENT ID		TECN	COMMENT
2.78 ±0.17 OUR FIT Error includes scale factor of 3.6.				
2.863±0.028±0.045	ABLIKIM	25AZ	BES3	e^+e^- at 3.770 GeV

$\Gamma(K^+K^-\pi^+\pi^-)/\Gamma(K^-2\pi^+\pi^-)$ — Γ_{303}/Γ_{87}

VALUE (units 10^{-2})	EVTS	DOCUMENT ID		TECN	COMMENT
3.39±0.21 OUR FIT Error includes scale factor of 3.1.					
3.00±0.13 OUR AVERAGE					
2.95±0.11±0.08	2669 ± 101	[1] LINK	05G	FOCS	γBe, $\overline{E}_\gamma \approx 180$ GeV
3.13±0.37±0.36	136 ± 15	AITALA	98D	E791	π^- nucleus, 500 GeV
3.5 ±0.4 ±0.2	244 ± 26	FRABETTI	95C	E687	γBe, $\overline{E}_\gamma \approx 200$ GeV
• • • We do not use the following data for averages, fits, limits, etc. • • •					
4.4 ±1.8 ±0.5	19 ± 8	ABLIKIM	05F	BES	$e^+e^- \approx \psi(3770)$
4.1 ±0.7 ±0.5	114 ± 20	ALBRECHT	94I	ARG	$e^+e^- \approx 10$ GeV
3.14±1.0	89 ± 29	AMMAR	91	CLEO	$e^+e^- \approx 10.5$ GeV
2.8 $^{+0.8}_{-0.7}$		ANJOS	91	E691	γBe 80–240 GeV

[1] LINK 05G uses a smaller, cleaner subset of 1279 ± 48 events for the amplitude analysis that gives the results in the next data blocks.

Int. J. Mod. Phys. A 2026.41. Downloaded from www.worldscientific.com
by UNIVERSITY OF CALIFORNIA @ BERKELEY on 09/16/26. Re-use and distribution is strictly not permitted, except for Open Access articles.

$\Gamma(\phi(\pi^+\pi^-)_{S-wave}, \phi \to K^+K^-)/\Gamma(K^+K^-\pi^+\pi^-)$ — $\Gamma_{304}/\Gamma_{303}$

This is the fraction from a coherent amplitude analysis.

VALUE (units 10^{-2})	EVTS	DOCUMENT ID		TECN	COMMENT
4.0±0.6±2.1	3k	[1] DARGENT	17		4-body fit, $KK\pi\pi$ events
• • • We do not use the following data for averages, fits, limits, etc. • • •					
10.3±1.0±0.8	3k	[2] ARTUSO	12	CLEO	4-body fit, $KK\pi\pi$ events
1 ±1	1.3k	LINK	05G	FOCS	4-body fit, $KK\pi\pi$ events

[1] Obtained by analyzing CLEO data but not authored by the CLEO Collaboration.
[2] See DARGENT 17

$\Gamma((\phi\rho^0)_{S-wave}, \phi \to K^+K^-)/\Gamma(K^+K^-\pi^+\pi^-)$ — $\Gamma_{305}/\Gamma_{303}$

This is the fraction from a coherent amplitude analysis.

VALUE (units 10^{-2})	EVTS	DOCUMENT ID		TECN	COMMENT
28.1±1.3±1.7	2.9k	[1,2] DARGENT	17		4-body fit, $KK\pi\pi$ evts
• • • We do not use the following data for averages, fits, limits, etc. • • •					
38.3±2.5±3.8		[1,3] ARTUSO	12	CLEO	Fitting 2959 evts.
29 ±2 ±1		LINK	05G	FOCS	Fits 1279 ± 48 evts.

[1] ARTUSO 12 and DARGENT 17 use the same dataset, but ARTUSO 12 uses a formulation for the D-wave component that is in fact a mix of S- and D-wave, while DARGENT 17 uses a pure D-wave. This explains the discrepancy in their $\rho\phi$ S- and D-wave components.
[2] Obtained by analyzing CLEO data but not authored by the CLEO Collaboration.
[3] See DARGENT 17

$\Gamma((\phi\rho^0)_{P-wave}, \phi \to K^+K^-)/\Gamma(K^+K^-\pi^+\pi^-)$ — $\Gamma_{306}/\Gamma_{303}$

This is the fit fraction from a coherent amplitude analysis.

VALUE (units 10^{-2})	EVTS	DOCUMENT ID		COMMENT
1.6±0.3±0.7	2.9k	[1] DARGENT	17	4-body fit, $KK\pi\pi$ evts

[1] Obtained by analyzing CLEO data but not authored by the CLEO Collaboration.

$\Gamma((\phi\rho^0)_{D-wave}, \phi \to K^+K^-)/\Gamma(K^+K^-\pi^+\pi^-)$ — $\Gamma_{307}/\Gamma_{303}$

VALUE (units 10^{-2})	EVTS	DOCUMENT ID		TECN	COMMENT
1.7±0.4±0.4	2.9k	[1,2] DARGENT	17		4-body fit, $KK\pi\pi$ evts
• • • We do not use the following data for averages, fits, limits, etc. • • •					
3.4±0.7±0.6		[1,3] ARTUSO	12	CLEO	Fitting 2959 evts.

[1] ARTUSO 12 use a formulation for the D-wave component that is in fact a mix of S- and D-wave, while DARGENT 17 uses a pure D-wave.
[2] Obtained by analyzing CLEO data but not authored by the CLEO Collaboration.
[3] See DARGENT 17

$\Gamma(K^*(892)^0\overline{K}^*(892)^0, K^{*0} \to K^\pm\pi^\mp)/\Gamma(K^+K^-\pi^+\pi^-)$ — $\Gamma_{308}/\Gamma_{303}$

This is the fraction from a coherent amplitude analysis.

VALUE (units 10^{-2})	DOCUMENT ID		TECN	COMMENT
• • • We do not use the following data for averages, fits, limits, etc. • • •				
3±2±1	LINK	05G	FOCS	Fits 1279 ± 48 evts.

$\Gamma(K^+K^-\rho^0$ 3-body$)/\Gamma(K^+K^-\pi^+\pi^-)$ — $\Gamma_{309}/\Gamma_{303}$

This is the fraction from a coherent amplitude analysis.

VALUE (units 10^{-2})	DOCUMENT ID		TECN	COMMENT
• • • We do not use the following data for averages, fits, limits, etc. • • •				
2±2±2	LINK	05G	FOCS	Fits 1279 ± 48 evts.

$\Gamma(f_0(980)\pi^+\pi^-, f_0 \to K^+K^-)/\Gamma(K^+K^-\pi^+\pi^-)$ — $\Gamma_{310}/\Gamma_{303}$

This is the fraction from a coherent amplitude analysis.

VALUE (units 10^{-2})	DOCUMENT ID		TECN	COMMENT
• • • We do not use the following data for averages, fits, limits, etc. • • •				
15±3±2	LINK	05G	FOCS	Fits 1279 ± 48 evts.

$\Gamma((K^*(892)^0\overline{K}^*(892)^0)_{S-wave}, K^{*0} \to K^\pm\pi^\mp)/\Gamma(K^+K^-\pi^+\pi^-)$ — $\Gamma_{311}/\Gamma_{303}$

VALUE (units 10^{-2})	EVTS	DOCUMENT ID		TECN	COMMENT
9.06±0.35 OUR AVERAGE					
9.18±0.21±0.28	163k	AAIJ	19C	LHCB	4-body fit, $KK\pi\pi$ evts
4.5 ±0.8 ±2.0	3k	[1] DARGENT	17		4-body fit, $KK\pi\pi$ evts
• • • We do not use the following data for averages, fits, limits, etc. • • •					
6.1 ±0.8 ±0.9	3k	[2] ARTUSO	12	CLEO	4-body fit, $KK\pi\pi$ evts

[1] Obtained by analyzing CLEO data but not authored by the CLEO Collaboration.
[2] See DARGENT 17

$\Gamma((K^*(892)^0\overline{K}^*(892)^0)_{P-wave}, K^* \to K^\pm\pi^\mp)/\Gamma(K^+K^-\pi^+\pi^-)$ — $\Gamma_{312}/\Gamma_{303}$

This is the fit fraction from a coherent amplitude analysis.

VALUE (units 10^{-2})	EVTS	DOCUMENT ID		TECN	COMMENT
4.87±0.24 OUR AVERAGE					
4.90±0.16±0.18	163k	AAIJ	19C	LHCB	4-body fit, $KK\pi\pi$ evts
3.6 ±0.7 ±1.5	2.9k	[1] DARGENT	17		4-body fit, $KK\pi\pi$ evts

[1] Obtained by analyzing CLEO data but not authored by the CLEO Collaboration.

$\Gamma((K^*(892)^0\overline{K}^*(892)^0)_{D-wave}, K^* \to K^\pm\pi^\mp)/\Gamma(K^+K^-\pi^+\pi^-)$ — $\Gamma_{313}/\Gamma_{303}$

This is the fit fraction from a coherent amplitude analysis.

VALUE (units 10^{-2})	EVTS	DOCUMENT ID		TECN	COMMENT
1.89±0.13 OUR AVERAGE					
1.85±0.09±0.10	163k	AAIJ	19C	LHCB	4-body fit, $KK\pi\pi$ evts
4.0 ±0.6 ±0.7	2.9k	[1] DARGENT	17		4-body fit, $KK\pi\pi$ evts

[1] Obtained by analyzing CLEO data but not authored by the CLEO Collaboration.

$\Gamma(K^*(892)^0K^\mp\pi^\pm$ 3-body, $K^{*0} \to K^\pm\pi^\mp)/\Gamma(K^+K^-\pi^+\pi^-)$ — $\Gamma_{314}/\Gamma_{303}$

This is the fraction from a coherent amplitude analysis.

VALUE (units 10^{-2})	DOCUMENT ID		TECN	COMMENT
• • • We do not use the following data for averages, fits, limits, etc. • • •				
11±2±1	LINK	05G	FOCS	Fits 1279 ± 48 evts.

$\Gamma(K^*(892)^0(K^-\pi^+)_{S-wave}$ 3-body, $K^{*0} \to K^+\pi^-)/\Gamma(K^+K^-\pi^+\pi^-)$ — $\Gamma_{315}/\Gamma_{303}$

This is the fit fraction from a coherent amplitude analysis.

VALUE (units 10^{-2})	EVTS	DOCUMENT ID		COMMENT
5.8±1.2±2.1	2.9k	[1] DARGENT	17	4-body fit, $KK\pi\pi$ evts

[1] Obtained by analyzing CLEO data but not authored by the CLEO Collaboration.

$\Gamma((K^-\pi^+)_{P-wave}, (K^+\pi^-)_{S-wave})/\Gamma(K^+K^-\pi^+\pi^-)$ — $\Gamma_{316}/\Gamma_{303}$

VALUE (units 10^{-2})	DOCUMENT ID		TECN	COMMENT
• • • We do not use the following data for averages, fits, limits, etc. • • •				
10.9±1.2±1.7	[1] ARTUSO	12	CLEO	Fitting 2959 evts.

[1] See DARGENT 17

$\Gamma(K_1(1270)^\pm K^\mp, K_1^\pm \to K^\pm\pi^+\pi^-)/\Gamma(K^+K^-\pi^+\pi^-)$ — $\Gamma_{317}/\Gamma_{303}$

This is the fraction from a coherent amplitude analysis.

VALUE (units 10^{-2})	DOCUMENT ID		TECN	COMMENT
• • • We do not use the following data for averages, fits, limits, etc. • • •				
33±6±4	[1] LINK	05G	FOCS	Fits 1279 ± 48 evts.

[1] This LINK 05G value includes $K_1(1270)^\pm \to \rho^0K^\pm$, $\to K_0^*(1430)^0\pi^\pm$, and $K^*(892)^0\pi^\pm$.

$\Gamma(K_1(1270)^+K^-, K_1^+ \to K^{*0}\pi^+)/\Gamma(K^+K^-\pi^+\pi^-)$ — $\Gamma_{318}/\Gamma_{303}$

VALUE (units 10^{-2})	EVTS	DOCUMENT ID		TECN	COMMENT
5.5±1.4±3.4	3k	[1] DARGENT	17		4-body fit, $KK\pi\pi$ evts
• • • We do not use the following data for averages, fits, limits, etc. • • •					
7.3±0.8±1.9	3k	[2] ARTUSO	12	CLEO	4-body fit, $KK\pi\pi$ events

[1] Obtained by analyzing CLEO data but not authored by the CLEO Collaboration.
[2] See DARGENT 17

$\Gamma(K_1(1270)^+K^-, K_1^+ \to K^*(1430)^0\pi^+, K^{*0} \to K^+\pi^-)/\Gamma(K^+K^-\pi^+\pi^-)$ — $\Gamma_{319}/\Gamma_{303}$

This is the fit fraction from a coherent amplitude analysis.

VALUE (units 10^{-2})	EVTS	DOCUMENT ID		COMMENT
6.1±1.2±1.8	2.9k	[1] DARGENT	17	4-body fit, $KK\pi\pi$ evts

[1] Obtained by analyzing CLEO data but not authored by the CLEO Collaboration.

$\Gamma(K_1(1270)^+K^-, K_1^+ \to \rho^0K^+)/\Gamma(K^+K^-\pi^+\pi^-)$ — $\Gamma_{320}/\Gamma_{303}$

VALUE (units 10^{-2})	EVTS	DOCUMENT ID		TECN	COMMENT
9.1±1.5±1.9	2.9k	[1] DARGENT	17		4-body fit, $KK\pi\pi$ evts
• • • We do not use the following data for averages, fits, limits, etc. • • •					
4.7±0.7±0.8		[2] ARTUSO	12	CLEO	Fitting 2959 evts.

[1] Obtained by analyzing CLEO data but not authored by the CLEO Collaboration.
[2] see DARGENT 17

$\Gamma(K_1(1270)^+K^-, K_1^+ \to \omega(782)K^+, \omega \to \pi^+\pi^-)/\Gamma(K^+K^-\pi^+\pi^-)$ — $\Gamma_{321}/\Gamma_{303}$

This is the fit fraction from a coherent amplitude analysis.

VALUE (units 10^{-2})	EVTS	DOCUMENT ID		COMMENT
0.6±0.3±0.4	2.9k	[1] DARGENT	17	4-body fit, $KK\pi\pi$ evts

[1] Obtained by analyzing CLEO data but not authored by the CLEO Collaboration.

$\Gamma(K_1(1270)^-K^+, K_1^- \to \overline{K}^{*0}\pi^-)/\Gamma(K^+K^-\pi^+\pi^-)$ — $\Gamma_{322}/\Gamma_{303}$

VALUE (units 10^{-2})	DOCUMENT ID		TECN	COMMENT
• • • We do not use the following data for averages, fits, limits, etc. • • •				
0.9±0.3±0.4	[1] ARTUSO	12	CLEO	Fitting 2959 evts.

[1] See DARGENT 17

$\Gamma(K_1(1270)^-K^+, K_1^- \to \rho^0K^-)/\Gamma(K^+K^-\pi^+\pi^-)$ — $\Gamma_{323}/\Gamma_{303}$

VALUE (units 10^{-2})	EVTS	DOCUMENT ID		TECN	COMMENT
5.4±0.7±1.3	2.9k	[1] DARGENT	17		4-body fit, $KK\pi\pi$ evts
• • • We do not use the following data for averages, fits, limits, etc. • • •					
6.0±0.8±0.6		[2] ARTUSO	12	CLEO	Fitting 2959 evts.

[1] Obtained by analyzing CLEO data but not authored by the CLEO Collaboration.
[2] See DARGENT 17

Int. J. Mod. Phys. A 2026.41. Downloaded from www.worldscientific.com by CALIFORNIA @ BERKELEY on 09/16/26. Re-use and distribution is strictly not permitted, except for Open Access articles.

$\Gamma(K_1(1400)^\pm K^\mp, K_1^\pm \to K^\pm\pi^+\pi^-)/\Gamma(K^+K^-\pi^+\pi^-)$ — $\Gamma_{324}/\Gamma_{303}$

This is the fraction from a coherent amplitude analysis.

VALUE (units 10^{-2})	DOCUMENT ID		TECN	COMMENT
• • • We do not use the following data for averages, fits, limits, etc. • • •				
22±3±4	LINK	05G	FOCS	Fits 1279 ± 48 evts.

$\Gamma(K_1(1400)^+ K^-, K_1^+ \to K^*(892)^0\pi^+, K^{*0} \to K^+\pi^-)/\Gamma(K^+K^-\pi^+\pi^-)$ — $\Gamma_{325}/\Gamma_{303}$

This is the fit fraction from a coherent amplitude analysis.

VALUE (units 10^{-2})	EVTS	DOCUMENT ID		TECN	COMMENT
18.7 ±1.5 OUR AVERAGE					
19.08±0.60±1.46	163k	AAIJ	19C	LHCB	4-body fit, $KK\pi\pi$ evts
12.4 ±2.6 ±6.3	2.9k	[1] DARGENT	17		4-body fit, $KK\pi\pi$ evts

[1] Obtained by analyzing CLEO data but not authored by the CLEO Collaboration.

$\Gamma(K^*(1410)^+ K^-, K^{*+} \to K^{*0}\pi^+)/\Gamma(K^+K^-\pi^+\pi^-)$ — $\Gamma_{326}/\Gamma_{303}$

VALUE (units 10^{-2})	DOCUMENT ID		TECN	COMMENT
• • • We do not use the following data for averages, fits, limits, etc. • • •				
4.2±0.7±0.8	[1,2] ARTUSO	12	CLEO	Fitting 2959 evts.

[1] DARGENT 17 find $K^*(1410)^+\pi^-$ and $K^*(1680)^+\pi^-$, which both peak outside the $D^0 \to KK\pi\pi$ kinematic range, effectively indistinguishable; we list their result under $K^*(1680)^+\pi^-$.
[2] See DARGENT 17

$\Gamma(K^*(1410)^- K^+, K^{*-} \to \overline{K}^{*0}\pi^-)/\Gamma(K^+K^-\pi^+\pi^-)$ — $\Gamma_{327}/\Gamma_{303}$

VALUE (units 10^{-2})	EVTS	DOCUMENT ID		TECN	COMMENT
2.82±0.19±0.39	163k	AAIJ	19C	LHCB	4-body fit, $KK\pi\pi$ evts
• • • We do not use the following data for averages, fits, limits, etc. • • •					
4.7 ±0.7 ±0.7	3k	[1] ARTUSO	12	CLEO	4-body fit, $KK\pi\pi$ evts

[1] See DARGENT 17.

$\Gamma(K_1(1680)^+ K^-, K_1^+ \to K^{*0}\pi^+, K^{*0} \to K^+\pi^-)/\Gamma(K^+K^-\pi^+\pi^-)$ — $\Gamma_{328}/\Gamma_{303}$

This is the fit fraction from a coherent amplitude analysis.

VALUE (units 10^{-2})	EVTS	DOCUMENT ID		COMMENT
3.6±0.8±1.0	2.9k	[1,2] DARGENT	17	4-body fit, $KK\pi\pi$ evts

[1] DARGENT 17 find $K^*(1410)^+\pi^-$ and $K^*(1680)^+\pi^-$, which both peak outside the $D^0 \to KK\pi\pi$ kinematic range, effectively indistinguishable.
[2] Obtained by analyzing CLEO data but not authored by the CLEO Collaboration.

$\Gamma(K^+K^-\pi^+\pi^-\text{ non-resonant})/\Gamma(K^+K^-\pi^+\pi^-)$ — $\Gamma_{329}/\Gamma_{303}$

This is the fit fraction from a coherent amplitude analysis.

VALUE (units 10^{-2})	EVTS	DOCUMENT ID		COMMENT
11.1±1.2±2.2	2.9k	[1] DARGENT	17	4-body fit, $KK\pi\pi$ evts

[1] Obtained by analyzing CLEO data but not authored by the CLEO Collaboration.

$\Gamma(2K_S^0\pi^+\pi^-)/\Gamma_{total}$ — Γ_{330}/Γ

VALUE (units 10^{-4})	EVTS	DOCUMENT ID		TECN	COMMENT
5.3±0.9±0.3	63	ABLIKIM	20AC	BES3	e^+e^- at 3.773 GeV

$\Gamma(2K_S^0\pi^+\pi^-)/\Gamma(K_S^0\pi^+\pi^-)$ — Γ_{330}/Γ_{53}

VALUE (units 10^{-2})	EVTS	DOCUMENT ID		TECN	COMMENT
1.72±0.05 OUR AVERAGE					
1.71±0.03±0.04	6095	SANGAL	23	BELL	e^+e at $\Upsilon(4S,5S)$, 10.520 GeV
4.16±0.70±0.42	113	LINK	05A	FOCS	γ Be, $\overline{E}_\gamma \approx$ 180 GeV
6.2 ±2.0 ±1.6	25	ALBRECHT	94I	ARG	$e^+e^- \approx$ 10 GeV

$\Gamma(K_S^0 K^-\pi^+\pi^0)/\Gamma_{total}$ — Γ_{331}/Γ

VALUE (units 10^{-3})	EVTS	DOCUMENT ID		TECN	COMMENT
1.32±0.14±0.07	195	ABLIKIM	20AC	BES3	e^+e^- at 3.773 GeV

$\Gamma(K_S^0 K^+\pi^-\pi^0)/\Gamma_{total}$ — Γ_{332}/Γ

VALUE (units 10^{-4})	EVTS	DOCUMENT ID		TECN	COMMENT
6.5±0.7±0.2	119	ABLIKIM	20AC	BES3	e^+e^- at 3.773 GeV

$\Gamma(K_S^0 K^-2\pi^+\pi^-)/\Gamma(K_S^0 2\pi^+2\pi^-)$ — $\Gamma_{333}/\Gamma_{120}$

VALUE	CL%	DOCUMENT ID		TECN	COMMENT
<0.054	90	LINK	04D	FOCS	γ A, $\overline{E}_\gamma \approx$ 180 GeV

$\Gamma(K^+K^-\pi^+\pi^-\pi^0)/\Gamma_{total}$ — Γ_{334}/Γ

VALUE	DOCUMENT ID		TECN	COMMENT
0.0031±0.0020	[1] BARLAG	92C	ACCM	π^- Cu 230 GeV

[1] BARLAG 92C computes the branching fraction using topological normalization.

$\Gamma(\phi\pi^0)/\Gamma_{total}$ — Γ_{335}/Γ

VALUE (units 10^{-3})	EVTS	DOCUMENT ID		TECN	COMMENT
1.168±0.028±0.028	3.3k	ABLIKIM	19BI	BES3	e^+e^- at 3.773 MeV

$\Gamma(\phi\pi^0)/\Gamma(K^+K^-)$ — $\Gamma_{335}/\Gamma_{266}$

VALUE	EVTS	DOCUMENT ID		TECN	COMMENT
• • • We do not use the following data for averages, fits, limits, etc. • • •					
0.194±0.006±0.009	1254	TAJIMA	04	BELL	e^+e^- at $\Upsilon(4S)$

$\Gamma(\phi\eta)/\Gamma_{total}$ — Γ_{336}/Γ

VALUE (units 10^{-4})	EVTS	DOCUMENT ID		TECN	COMMENT
1.81±0.46±0.06	102	ABLIKIM	19BI	BES3	e^+e^- at 3773 MeV

$\Gamma(\phi\eta)/\Gamma(K^+K^-)$ — $\Gamma_{336}/\Gamma_{266}$

VALUE (units 10^{-2})	EVTS	DOCUMENT ID		TECN	COMMENT
3.59±1.14±0.18	31	TAJIMA	04	BELL	e^+e^- at $\Upsilon(4S)$

$\Gamma(\phi\omega)/\Gamma_{total}$ — Γ_{337}/Γ

VALUE (units 10^{-4})	CL%	EVTS	DOCUMENT ID		TECN	COMMENT
6.48±0.96±0.40		196	[1] ABLIKIM	22	BES3	e^+e^- at 3.773 GeV
• • • We do not use the following data for averages, fits, limits, etc. • • •						
<21	90		ALBRECHT	94I	ARG	$e^+e^- \approx$ 10 GeV

[1] ABLIKIM 22 determines the longitudinal polarization fraction of the ϕ and ω, f_L = 0.00 ± 0.10 ± 0.08, corresponding to f_L < 0.24 at 95% CL.

Radiative modes

$\Gamma(\rho^0\gamma)/\Gamma(\pi^+\pi^-)$ — $\Gamma_{338}/\Gamma_{151}$

VALUE (units 10^{-2})	EVTS	DOCUMENT ID		TECN	COMMENT
1.25±0.21±0.05	500	NANUT	17	BELL	e^+e^- at Υ(nS), n=2,3,4,5

$\Gamma(\omega\gamma)/\Gamma_{total}$ — Γ_{339}/Γ

VALUE	CL%	DOCUMENT ID		TECN
<2.4 × 10^{-4}	90	ASNER	98	CLE2

$\Gamma(\phi\gamma)/\Gamma(K^-\pi^+)$ — Γ_{340}/Γ_{47}

VALUE (units 10^{-4})	EVTS	DOCUMENT ID		TECN	COMMENT
7.1 ±0.5 OUR FIT					
7.15±0.78±0.69	243 ± 25	AUBERT	08AZ	BABR	$e^+e^- \approx$ 10.6 GeV

$\Gamma(\phi\gamma)/\Gamma(K^+K^-)$ — $\Gamma_{340}/\Gamma_{266}$

VALUE (units 10^{-3})	EVTS	DOCUMENT ID		TECN	COMMENT
6.9 ±0.5 OUR FIT					
6.88±0.47±0.21	524	NANUT	17	BELL	e^+e^- at Υ(nS), n=2,3,4,5
• • • We do not use the following data for averages, fits, limits, etc. • • •					
$6.31^{+1.70+0.30}_{-1.48-0.36}$	28	TAJIMA	04	BELL	See NANUT 17

$\Gamma(\overline{K}^*(892)^0\gamma)/\Gamma(K^-\pi^+)$ — Γ_{341}/Γ_{47}

VALUE (units 10^{-3})	EVTS	DOCUMENT ID		TECN	COMMENT
10.5 ±1.7 OUR AVERAGE Error includes scale factor of 3.1.					
11.9 ±0.5 ±0.5	9.1k	NANUT	17	BELL	e^+e^- at Υ(nS), n=2,3,4,5
8.43±0.51±0.70	2.2k	AUBERT	08AZ	BABR	$e^+e^- \approx$ 10.6 GeV

Doubly Cabibbo-suppressed / Mixing modes

$\Gamma(K^+\ell^-\overline{\nu}_\ell \text{ via } \overline{D}^0)/\Gamma(K^-\ell^+\nu_\ell)$ — Γ_{342}/Γ_{19}

This is a limit on R_M without the complications of possible doubly Cabibbo-suppressed decays that occur when using hadronic modes. For the limits on $|m_1 - m_2|$ and $(\Gamma_1 - \Gamma_2)/\Gamma$ that come from the best mixing limit, see near the beginning of these D^0 Listings.

VALUE	CL%	DOCUMENT ID		TECN	COMMENT
< 6.1 × 10^{-4}	90	[1] BITENC	08	BELL	e^+e^-, 10.58 GeV
• • • We do not use the following data for averages, fits, limits, etc. • • •					
<50 × 10^{-4}	90	[2] AITALA	96C	E791	π^- nucleus, 500 GeV

[1] The BITENC 08 right-sign sample includes about 15% of $D^0 \to K^-\pi^0\ell^+\nu_\ell$ and other decays.
[2] AITALA 96C uses $D^{*+} \to D^0\pi^+$ (and charge conjugate) decays to identify the charm at production and $D^0 \to K^-\ell^+\nu_\ell$ (and charge conjugate) decays to identify the charm at decay.

$\Gamma(K^+ \text{ or } K^*(892)^+ e^-\overline{\nu}_e \text{ via } \overline{D}^0)/[\Gamma(K^-e^+\nu_e) + \Gamma(K^*(892)^- e^+\nu_e)]$ — $\Gamma_{343}/(\Gamma_{20}+\Gamma_{22})$

This is a limit on R_M without the complications of possible doubly Cabibbo-suppressed decays that occur when using hadronic modes. The experiments use $D^{*+} \to D^0\pi^+$ (and charge conjugate) decays to identify the charm at production and the charge of the e to identify the charm at decay. These limits do not allow CP violation. For the limits on $|m_1 - m_2|$ and $(\Gamma_1 - \Gamma_2)/\Gamma$ that come from the best mixing limit, see near the beginning of these D^0 Listings.

VALUE	CL%	DOCUMENT ID		TECN	COMMENT
<0.001	90	BITENC	05	BELL	$e^+e^- \approx$ 10.6 GeV
• • • We do not use the following data for averages, fits, limits, etc. • • •					
−0.0013 <R< +0.0012	90	AUBERT	07AB	BABR	$e^+e^- \approx$ 10.58 GeV
<0.0078	90	CAWLFIELD	05	CLEO	$e^+e^- \approx$ 10.6 GeV
<0.0042	90	AUBERT,B	04Q	BABR	See AUBERT 07AB

Int. J. Mod. Phys. A 2026.41. Downloaded from www.worldscientific.com by UNIVERSITY OF CALIFORNIA @ BERKELEY on 09/16/26. Re-use and distribution is strictly not permitted, except for Open Access articles.

$\Gamma(K^+\pi^-)/\Gamma_{total}$ — Γ_{344}/Γ

VALUE (units 10^{-4})	EVTS	DOCUMENT ID		TECN	COMMENT
1.48±0.07 OUR FIT	Error includes scale factor of 3.1.				
1.30±0.09±0.04	0.38k	ABLIKIM	25BI	BES3	e^+e^- at 3.773 GeV

$\Gamma(K^+\pi^-)/\Gamma(K^-\pi^+)$ — Γ_{344}/Γ_{47}

This is R, the time-integrated wrong-sign rate compared to the right-sign rate. See the note on "D^0-$\overline{D}^0$ Mixing," near the start of the D^0 Listings.

The experiments here use the charge of the pion in $D^*(2010)^\pm \to (D^0 \text{ or } \overline{D}^0)\ \pi^\pm$ decay to tell whether a D^0 or a $\overline{D}^0$ was born. The $D^0 \to K^+\pi^-$ decay can occur directly by doubly Cabibbo-suppressed (DCS) decay, or indirectly by $D^0 \to \overline{D}^0$ mixing followed by $\overline{D}^0 \to K^+\pi^-$ decay. Some of the experiments can use the decay-time information to disentangle the two mechanisms. Here, we list the experimental branching ratio, which if there is no mixing is the DCS ratio. See the next data block for values of the DCS ratio R_D, and the following data block for limits on the mixing ratio R_M. See the section on CP-violating asymmetries near the end of this D^0 Listing for values of A_D, and the note on "D^0-$\overline{D}^0$ Mixing" for limits on x' and y'.

Some early limits have been omitted from this Listing; see our 1998 edition (The European Physical Journal **C3** 1 (1998)) and our 2006 edition (Journal of Physics **G33** 1 (2006)).

VALUE (units 10^{-3})	EVTS	DOCUMENT ID		TECN	COMMENT
3.77±0.18 OUR FIT	Error includes scale factor of 3.3.				
3.79±0.18 OUR AVERAGE	Error includes scale factor of 3.3. See the ideogram below.				
4.15 ± 0.10	12.7 ± 0.3k	[1] AALTONEN	08E	CDF	$p\overline{p}$, $\sqrt{s} = 1.96$ TeV
$3.53 \pm 0.08 \pm 0.04$	4030 ± 90	[2] AUBERT	07W	BABR	$e^+e^- \approx 10.6$ GeV
$3.77 \pm 0.08 \pm 0.05$	4024 ± 88	[1] ZHANG	06	BELL	e^+e^-
• • • We do not use the following data for averages, fits, limits, etc. • • •					
$4.05 \pm 0.21 \pm 0.11$	2.0 ± 0.1k	[3] ABULENCIA	06X	CDF	See AALTONEN 08E
$3.81 \pm 0.17 {}^{+0.08}_{-0.16}$	845 ± 40	[2] LI	05A	BELL	See ZHANG 06
$4.29 {}^{+0.63}_{-0.61} \pm 0.27$	234	[4] LINK	05H	FOCS	γ nucleus
$3.57 \pm 0.22 \pm 0.27$		[5] AUBERT	03Z	BABR	See AUBERT 07W
$4.04 \pm 0.85 \pm 0.25$	149	[6] LINK	01	FOCS	γ nucleus
$3.32 {}^{+0.63}_{-0.65} \pm 0.40$	45	[1] GODANG	00	CLE2	e^+e^-
$6.8\ {}^{+3.4}_{-3.3} \pm 0.7$	34	[2] AITALA	98	E791	π^- nucl., 500 GeV

[1] GODANG 00, ZHANG 06, and AALTONEN 08E allow CP violation.
[2] AITALA 98, LI 05A, and AUBERT 07W assume no CP violation.
[3] This ABULENCIA 06X result assumes no mixing.
[4] This LINK 05H result assumes no mixing but allows CP violation. If neither mixing nor CP violation is allowed, $R = (4.29 \pm 0.63 \pm 0.28) \times 10^{-3}$.
[5] This AUBERT 03Z result allows CP violation. If CP violation is not allowed, $R = 0.00359 \pm 0.00020 \pm 0.00027$.
[6] This LINK 01 result assumes no mixing or CP violation.

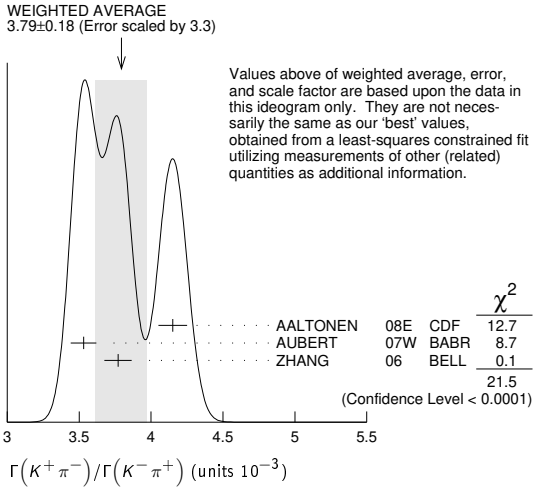

$\Gamma(K^+\pi^- \text{via DCS})/\Gamma(K^-\pi^+)$ — Γ_{345}/Γ_{47}

This is R_D, the doubly Cabibbo-suppressed ratio when mixing is allowed.

VALUE (units 10^{-3})	EVTS	DOCUMENT ID		TECN	COMMENT
3.45 ±0.06 OUR AVERAGE	Error includes scale factor of 1.5. See the ideogram below.				
$3.454 \pm 0.040 \pm 0.020$	722k	[1] AAIJ	18K	LHCB	pp at 7, 8, 13 TeV
3.53 ± 0.13		[2] KO	14	BELL	$e^+e^- \to \Upsilon(nS)$
3.51 ± 0.35		[3] AALTONEN	13AE	CDF	$p\overline{p}$ at 1.96 TeV
3.04 ± 0.55	13k	AALTONEN	08E	CDF	$p\overline{p}$, $\sqrt{s} = 1.96$ TeV
$3.03 \pm 0.16 \pm 0.10$	4.0k	[4] AUBERT	07W	BABR	$e^+e^- \approx 10.6$ GeV
3.64 ± 0.17	4.0k	[5] ZHANG	06	BELL	e^+e^-
$5.17\ {}^{+1.47}_{-1.58} \pm 0.76$	234	[6] LINK	05H	FOCS	γ nucleus
$4.8 \pm 1.2 \pm 0.4$	45	[7] GODANG	00	CLE2	e^+e^-
• • • We do not use the following data for averages, fits, limits, etc. • • •					
3.533 ± 0.054	236k	[8] AAIJ	17AO	LHCB	See AAIJ 18K
3.568 ± 0.066		[9] AAIJ	13CE	LHCB	pp at 7, 8 TeV
3.52 ± 0.15		[10] AAIJ	13N	LHCB	Repl. by AAIJ 13CE
2.87 ± 0.37	0.8k	LI	05A	BELL	See ZHANG 06

[1] This AAIJ 18K value is for direct and indirect CP violation allowed. The value is the same if either one or the other is not allowed, but in each case the error then is $(0.028 \pm 0.014) \times 10^{-3}$.
[2] Based on 976 fb^{-1} of data collected at $\Upsilon(nS)$ resonances. Assumes no CP violation.
[3] Based on 9.6 fb^{-1} of data collected at the Tevatron. Assumes no CP violation.
[4] Result is the same whether or not CP violation is allowed.
[5] This ZHANG 06 assumes no CP violation.
[6] This LINK 05H result allows CP violation. Allowing mixing but not CP violation, $R_D = (3.81 {}^{+1.67}_{-1.63} \pm 0.92) \times 10^{-3}$.
[7] This GODANG 00 result allows CP violation.
[8] The result was established with D^0 from prompt and secondary D^* assuming no CPV or no direct CPV.
[9] Based on 3 fb^{-1} of data collected at $\sqrt{s} = 7$, 8 TeV. Assumes no CP violation.
[10] Based on 1 fb^{-1} of data collected at $\sqrt{s} = 7$ TeV in 2011. Assumes no CP violation.

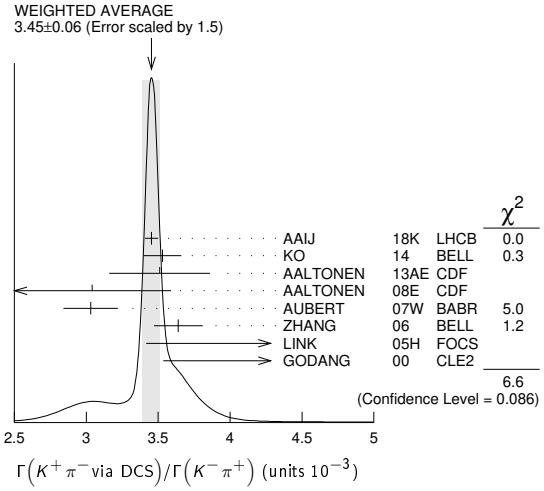

$\Gamma(K^+\pi^- \text{via } \overline{D}^0)/\Gamma(K^-\pi^+)$ — Γ_{346}/Γ_{47}

This is R_M in the note on "D^0-$\overline{D}^0$ Mixing" near the start of the D^0 Listings. The experiments here (1) use the charge of the pion in $D^*(2010)^\pm \to (D^0 \text{ or } \overline{D}^0)\ \pi^\pm$ decay to tell whether a D^0 or a $\overline{D}^0$ was born; and (2) use the decay-time distribution to disentangle doubly Cabibbo-suppressed decay and mixing. For the limits on $|m_1 - m_2|$ and $(\Gamma_1 - \Gamma_2)/\Gamma$ that come from the best mixing limit, see near the beginning of these D^0 Listings.

VALUE	CL%	DOCUMENT ID		TECN	COMMENT
<0.00040	95	[1] ZHANG	06	BELL	e^+e^-
• • • We do not use the following data for averages, fits, limits, etc. • • •					
<0.00046	95	[2] LI	05A	BELL	See ZHANG 06
<0.0063	95	[3] LINK	05H	FOCS	γ nucleus
<0.0013	95	[4] AUBERT	03Z	BABR	e^+e^-, 10.6 GeV
<0.00041	95	[5] GODANG	00	CLE2	e^+e^-
<0.0092	95	[6] BARATE	98W	ALEP	e^+e^- at Z^0
<0.005	90	[7] ANJOS	88C	E691	Photoproduction

[1] This ZHANG 06 result allows CP violation, but the result does not change if CP violation is not allowed.
[2] This LI 05A result allows CP violation. The limit becomes < 0.00042 (95% CL) if CP violation is not allowed.
[3] LINK 05H obtains the same result whether or not CP violation is allowed.
[4] This AUBERT 03Z result allows CP violation and assumes that the strong phase between $D^0 \to K^+\pi^-$ and $\overline{D}^0 \to K^+\pi^-$ is small, and limits only $D^0 \to \overline{D}^0$ transitions via off-shell intermediate states. The limit on transitions via on-shell intermediate states is 0.0016.
[5] This GODANG 00 result allows CP violation and assumes that the strong phase between $D^0 \to K^+\pi^-$ and $\overline{D}^0 \to K^+\pi^-$ is small, and limits only $D^0 \to \overline{D}^0$ transitions via off-shell intermediate states. The limit on transitions via on-shell intermediate states is 0.0017.
[6] This BARATE 98W result assumes no interference between the DCS and mixing amplitudes ($y' = 0$ in the note on "D^0-$\overline{D}^0$ Mixing" near the start of the D^0 Listings). When interference is allowed, the limit degrades to 0.036 (95%CL).
[7] This ANJOS 88C result assumes no interference between the DCS and mixing amplitudes ($y' = 0$ in the note on "D^0-$\overline{D}^0$ Mixing" near the start of the D^0 Listings). When interference is allowed, the limit degrades to 0.019.

Int. J. Mod. Phys. A 2026.41. Downloaded from www.worldscientific.com by CALIFORNIA @ BERKELEY on 09/16/26. Re-use and distribution is strictly not permitted, except for Open Access articles.

$\Gamma(K^0_S\pi^+\pi^-$ in $D^0\to\overline{D}^0)/\Gamma(K^0_S\pi^+\pi^-)$ — Γ_{347}/Γ_{53}

This is R_M in the note on "D^0-$\overline{D}^0$ Mixing" near the start of the D^0 Listings. The experiments here (1) use the charge of the pion in $D^*(2010)^\pm\to(D^0$ or $\overline{D}^0)\,\pi^\pm$ decay to tell whether a D^0 or a $\overline{D}^0$ was born; and (2) use the decay-time distribution to disentangle doubly Cabibbo-suppressed decay and mixing. For the limits on $|m_1-m_2|$ and $(\Gamma_1-\Gamma_2)/\Gamma$ that come from the best mixing limit, see near the beginning of these D^0 Listings.

VALUE	CL%	DOCUMENT ID		TECN	COMMENT
<0.0063	95	[1] ASNER	05	CLEO	$e^+e^-\approx$ 10 GeV

[1] This ASNER 05 limit allows *CP* violation. If *CP* violation is not allowed, the limit is 0.0042 at 95% CL.

$\Gamma(K^+\pi^-\pi^0)/\Gamma_{total}$ — Γ_{351}/Γ

VALUE (units 10^{-4})	EVTS	DOCUMENT ID		TECN	COMMENT
3.05±0.13 OUR FIT	Error includes scale factor of 1.3.				
3.07±0.22 OUR AVERAGE					
3.06±0.21±0.10	0.46k	ABLIKIM	25BI	BES3	e^+e^- at 3.773 GeV
$3.13^{+0.60}_{-0.56}\pm0.15$	46	[1] ABLIKIM	22X	BES3	e^+e^- at 3.773 GeV

[1] Uses the semileptonic tag method of ABLIKIM 21BB.

$\Gamma(K^+\pi^-\pi^0)/\Gamma(K^-\pi^+\pi^0)$ — Γ_{351}/Γ_{68}

The experiments here use the charge of the pion in $D^*(2010)^\pm\to(D^0$ or $\overline{D}^0)\,\pi^\pm$ decay to tell whether a D^0 or a $\overline{D}^0$ was born. The $D^0\to K^+\pi^-\pi^0$ decay can occur directly by doubly Cabibbo-suppressed (DCS) decay, or indirectly by $D^0\to\overline{D}^0$ mixing followed by $\overline{D}^0\to K^+\pi^-\pi^0$ decay.

VALUE (units 10^{-3})	EVTS	DOCUMENT ID		TECN	COMMENT
2.12±0.07 OUR FIT					
2.12±0.07 OUR AVERAGE					
2.01±0.11		[1] EVANS	16	CLEO	$e^+e^-\to D^0\overline{D}^0$ at $\psi(3770)$
2.14±0.08±0.08	763	[2] AUBERT,B	06N	BABR	$e^+e^-\approx\Upsilon(4S)$
$2.29\pm0.15^{+0.13}_{-0.09}$	1.9k	TIAN	05	BELL	$e^+e^-\approx\Upsilon(4S)$
$4.3\ ^{+1.1}_{-1.0}\pm0.7$	38	BRANDENB...	01	CLE2	$e^+e^-\approx\Upsilon(4S)$

[1] A combined fit with a recent LHCb $D^0\overline{D}^0$ mixing results in AAIJ 16F is also reported to be $(2.00\pm0.11)\times10^{-3}$.
[2] This AUBERT,B 06N result assumes no mixing.

$\Gamma(K^+\pi^-\pi^0$ via $\overline{D}^0)/\Gamma(K^-\pi^+\pi^0)$ — Γ_{352}/Γ_{68}

This is R_M in the note on "D^0-$\overline{D}^0$ Mixing" near the start of the D^0 Listings. The experiments here (1) use the charge of the pion in $D^*(2010)^\pm\to(D^0$ or $\overline{D}^0)\,\pi^\pm$ decay to tell whether a D^0 or a $\overline{D}^0$ was born; and (2) use the decay-time distribution to disentangle doubly Cabibbo-suppressed decay and mixing. For the limits on $|m_1-m_2|$ and $(\Gamma_1-\Gamma_2)/\Gamma$ that come from the best mixing limit, see near the beginning of these D^0 Listings.

VALUE (units 10^{-3})	CL%	DOCUMENT ID		TECN	COMMENT
$\mathbf{5.25^{+0.25}_{-0.31}\pm0.12}$		AUBERT	09AN	BABR	e^+e^- at 10.58 GeV
• • • We do not use the following data for averages, fits, limits, etc. • • •					
<0.54	95	[1] AUBERT,B	06N	BABR	$e^+e^-\approx\Upsilon(4S)$

[1] This AUBERT,B 06N limit assumes no *CP* violation. The measured value corresponding to the limit is $(2.3^{+1.8}_{-1.4}\pm0.4)\times10^{-4}$. If *CP* violation is allowed, this becomes $(1.0^{+2.2}_{-0.7}\pm0.3)\times10^{-4}$.

$\Gamma(K^+\pi^-\eta)/\Gamma_{total}$ — Γ_{353}/Γ

VALUE (units 10^{-4})	EVTS	DOCUMENT ID		TECN	COMMENT
1.04±0.16±0.08	62	ABLIKIM	25BI	BES3	e^+e^- at 3.773 GeV

$\Gamma(K^+\pi^-2\pi^0)/\Gamma_{total}$ — Γ_{354}/Γ

VALUE (units 10^{-4})	CL%	EVTS	DOCUMENT ID		TECN	COMMENT
1.40±0.27±0.09		85	ABLIKIM	25BI	BES3	e^+e^- at 3.773 GeV
• • • We do not use the following data for averages, fits, limits, etc. • • •						
<3.6	90		[1] ABLIKIM	22X	BES3	e^+e^- at 3.773 GeV

[1] Uses the semileptonic tag method of ABLIKIM 21BB.

$\Gamma(K^+\pi^+2\pi^-$ via DCS$)/\Gamma(K^-2\pi^+\pi^-)$ — Γ_{355}/Γ_{87}

VALUE (units 10^{-3})	EVTS	DOCUMENT ID		TECN	COMMENT
3.03 ±0.07 OUR AVERAGE					
3.025±0.077	42k,11M	[1] AAIJ	16F	LHCB	pp at 7, 8 TeV
3.03 ±0.13		[2] EVANS	16	CLEO	$e^+e^-\to D^0\overline{D}^0$ at $\psi(3770)$

[1] This result uses external input on the mixing parameters x, y. Without this input, the result is $(3.215\pm0.136)\times10^{-3}$.
[2] A combined fit with a recent LHCb $D^0\overline{D}^0$ mixing results in AAIJ 16F is also reported to be $(3.01\pm0.07)\times10^{-3}$.

$\Gamma(K^+\pi^+2\pi^-)/\Gamma_{total}$ — Γ_{356}/Γ

VALUE (units 10^{-4})	EVTS	DOCUMENT ID		TECN	COMMENT
2.64±0.06 OUR FIT	Error includes scale factor of 1.1.				
2.38±0.19±0.12	0.34k	ABLIKIM	25BI	BES3	e^+e^- at 3.773 GeV

$\Gamma(K^+\pi^+2\pi^-)/\Gamma(K^-2\pi^+\pi^-)$ — Γ_{356}/Γ_{87}

The experiments here use the charge of the pion in $D^*(2010)^\pm\to(D^0$ or $\overline{D}^0)\,\pi^\pm$ decay to tell whether a D^0 or a $\overline{D}^0$ was born. The $D^0\to K^+\pi^-\pi^+\pi^-$ decay can occur directly by doubly Cabibbo-suppressed (DCS) decay, or indirectly by $D^0\to\overline{D}^0$ mixing followed by $\overline{D}^0\to K^+\pi^-\pi^+\pi^-$ decay. Some of the experiments can use the decay-time information to disentangle the two mechanisms. Here, we list the experimental branching ratio, which if there is no mixing is the DCS ratio; in the next data block we give the limits on the mixing ratio.

Some early limits have been omitted from this Listing; see our 1998 edition (EPJ **C3** 1).

VALUE (units 10^{-3})	CL%	EVTS	DOCUMENT ID		TECN	COMMENT
3.22±0.05 OUR FIT						
3.22±0.05 OUR AVERAGE						
3.22±0.05		42k,11M	[1] AAIJ	16F	LHCB	pp at 7, 8 TeV
3.24±0.08±0.07		3.3k	[2] WHITE	13	BELL	$e^+e^-\approx\Upsilon(4S)$
$4.4\ ^{+1.3}_{-1.2}\pm0.4$		54	[2] DYTMAN	01	CLE2	$e^+e^-\approx\Upsilon(4S)$
$2.5\ ^{+3.6}_{-3.4}\pm0.3$			[3] AITALA	98	E791	π^- nucl., 500 GeV
• • • We do not use the following data for averages, fits, limits, etc. • • •						
$3.20\pm0.18^{+0.18}_{-0.13}$		1.7k	[2] TIAN	05	BELL	See WHITE 13
<18	90		[2] AMMAR	91	CLEO	$e^+e^-\approx$ 10.5 GeV
<18	90		[4] ANJOS	88C	E691	Photoproduction

[1] AAIJ 16F result comes from time-dependent analysis that uses external input on the mixing parameters x, y. Without this input, the result is $(3.29\pm0.08)\times10^{-3}$.
[2] AMMAR 91 cannot and DYTMAN 01, TIAN 05 do not distinguish between doublyCabibbo-suppressed decay and D^0-$\overline{D}^0$ mixing.
[3] This AITALA 98result assumes no D^0-$\overline{D}^0$ mixing (R_M in the note on "D^0-$\overline{D}^0$ Mixing").It becomes $-0.0020^{+0.0117}_{-0.0106}\pm0.0035$ whenmixing is allowed and decay-time information is used todistinguish doubly Cabibbo-suppressed decays from mixing.
[4] ANJOS 88C uses decay-time information to distinguish doubly Cabibbo-suppressed (DCS) decays from D^0-$\overline{D}^0$ mixing. However, the result assumes no interference between the DCS and mixing amplitudes ($y'=0$ in the note on "D^0-$\overline{D}^0$ Mixing" near the start of the D^0 Listings). When interference is allowed, the limit degrades to 0.033.

$\Gamma(K^+\pi^+2\pi^-$ via $\overline{D}^0)/\Gamma(K^-2\pi^+\pi^-)$ — Γ_{357}/Γ_{87}

This is a D^0-$\overline{D}^0$ mixing limit. The experiments here (1) use the charge of the pion in $D^*(2010)^\pm\to(D^0$ or $\overline{D}^0)\,\pi^\pm$ decay to tell whether a D^0 or a $\overline{D}^0$ was born; and (2) use the decay-time distribution to disentangle doubly Cabibbo-suppressed decay and mixing. For the limits on $|m_{D^0_1}-m_{D^0_2}|$ and $(\Gamma_{D^0_1}-\Gamma_{D^0_2})/\Gamma_{D^0}$ that come from the best mixing limit, see near the beginning of these D^0 Listings.

VALUE (units 10^{-5})	CL%	DOCUMENT ID		TECN	COMMENT
9.6±3.6		[1] AAIJ	16F	LHCB	pp at 7, 8 TeV
• • • We do not use the following data for averages, fits, limits, etc. • • •					
<500	90	[2] ANJOS	88C	E691	Photoproduction

[1] AAIJ 16F result comes from an unconstrained decay-time dependent fit to the wrong-sign to right-sign decay rates ratio as $(x^2+y^2)/2$.
[2] ANJOS 88C uses decay-time information to distinguish doubly Cabibbo-suppressed (DCS) decays from D^0-$\overline{D}^0$ mixing. However, the result assumes no interference between the DCS and mixing amplitudes ($y'=0$ in the note on "D^0-$\overline{D}^0$ Mixing" near the start of the D^0 Listings). When interference is allowed, the limit degrades to 0.007.

$\Gamma(K^+\pi^-\pi^0\eta)/\Gamma_{total}$ — Γ_{358}/Γ

VALUE	CL%	DOCUMENT ID		TECN	COMMENT
$\mathbf{<7\times10^{-5}}$	90	ABLIKIM	25BI	BES3	e^+e^- at 3.773 GeV

$\Gamma(K^+\pi^-$ or $K^+\pi^+2\pi^-$ via $\overline{D}^0)/\Gamma(K^-\pi^+$ or $K^-2\pi^+\pi^-)$ — Γ_{359}/Γ_0

This is a D^0-$\overline{D}^0$ mixing limit. For the limits on $|m_{D^0_1}-m_{D^0_2}|$ and $(\Gamma_{D^0_1}-\Gamma_{D^0_2})/\Gamma_{D^0}$ that come from the best mixing limit, see near the beginning of these D^0 Listings.

VALUE	CL%	DOCUMENT ID		TECN	COMMENT
• • • We do not use the following data for averages, fits, limits, etc. • • •					
<0.0085	90	[1] AITALA	98	E791	π^- nucleus, 500 GeV
<0.0037	90	[2] ANJOS	88C	E691	Photoproduction

[1] AITALA 98 uses decay-time information to distinguish doubly Cabibbo-suppressed decays from D^0-$\overline{D}^0$ mixing. The fit allows interference between the two amplitudes, and also allows *CP* violation in this term. The central value obtained is $0.0039^{+0.0036}_{-0.0032}\pm0.0016$. When interference is disallowed, the result becomes $0.0021\pm0.0009\pm0.0002$.
[2] This combines results of ANJOS 88C on $K^+\pi^-$ and $K^+\pi^-\pi^+\pi^-$ (via $\overline{D}^0$) reported in the data block above (see footnotes there). It assumes no interference.

$\Gamma(\mu^-$ anything via $\overline{D}^0)/\Gamma(\mu^+$ anything$)$ — Γ_{360}/Γ_6

This is a D^0-$\overline{D}^0$ mixing limit. See the somewhat better limits above.

VALUE	CL%	DOCUMENT ID		TECN	COMMENT
<0.0056	90	LOUIS	86	SPEC	π^-W 225 GeV
• • • We do not use the following data for averages, fits, limits, etc. • • •					
<0.012	90	BENVENUTI	85	CNTR	μC, 200 GeV
<0.044	90	BODEK	82	SPEC	π^-, pFe $\to D^0$

Int. J. Mod. Phys. A 2026.41. Downloaded from www.worldscientific.com
by UNIVERSITY OF CALIFORNIA @ BERKELEY on 09/16/26. Re-use and distribution is strictly not permitted, except for Open Access articles.

Rare or forbidden modes

$\Gamma(\gamma\gamma)/\Gamma_{total}$ — Γ_{361}/Γ

$D^0 \to \gamma\gamma$ is a flavor-changing neutral-current decay, forbidden in the Standard Model at the tree level.

VALUE	CL%	DOCUMENT ID		TECN	COMMENT
< 8.5 × 10⁻⁷	90	NISAR	16	BELL	e^+e^- at $\Upsilon(4S)$, $\Upsilon(5S)$
• • • We do not use the following data for averages, fits, limits, etc. • • •					
$< 3.8 \times 10^{-6}$	90	ABLIKIM	15F	BES3	e^+e^- at 3.773 GeV
$< 2.2 \times 10^{-6}$	90	LEES	12L	BABR	$e^+e^- \approx$ 10.58 GeV
$<29 \times 10^{-6}$	90	COAN	03	CLE2	$e^+e^- \approx \Upsilon(4S)$

$\Gamma(e^+e^-)/\Gamma_{total}$ — Γ_{362}/Γ

A test for the $\Delta C = 1$ weak neutral current. Allowed by first-order weak interaction combined with electromagnetic interaction.

VALUE	CL%	DOCUMENT ID		TECN	COMMENT
<7.9 × 10⁻⁸	90	PETRIC	10	BELL	$e^+e^- \approx \Upsilon(4S)$
• • • We do not use the following data for averages, fits, limits, etc. • • •					
$<1.7 \times 10^{-7}$	90	LEES	12Q	BABR	$e^+e^- \approx$ 10.58 GeV
$<1.2 \times 10^{-6}$	90	AUBERT,B	04Y	BABR	$e^+e^- \approx \Upsilon(4S)$
$<8.19 \times 10^{-6}$	90	PRIPSTEIN	00	E789	p nucleus, 800 GeV
$<6.2 \times 10^{-6}$	90	AITALA	99G	E791	$\pi^- N$ 500 GeV
$<1.3 \times 10^{-5}$	90	FREYBERGER	96	CLE2	$e^+e^- \approx \Upsilon(4S)$
$<1.3 \times 10^{-4}$	90	ADLER	88	MRK3	e^+e^- 3.77 GeV
$<1.7 \times 10^{-4}$	90	ALBRECHT	88G	ARG	e^+e^- 10 GeV
$<2.2 \times 10^{-4}$	90	HAAS	88	CLEO	e^+e^- 10 GeV

$\Gamma(\mu^+\mu^-)/\Gamma_{total}$ — Γ_{363}/Γ

A test for the $\Delta C = 1$ weak neutral current. Allowed by first-order weak interaction combined with electromagnetic interaction.

VALUE	CL%	DOCUMENT ID		TECN	COMMENT
<2.1 × 10⁻⁹	90	[1] CHEKHOVSKY	25F	CMS	pp at 13.6 TeV
• • • We do not use the following data for averages, fits, limits, etc. • • •					
$<3.1 \times 10^{-9}$	90	[2] AAIJ	23R	LHCB	pp at 7, 8, 13 TeV
$<6.2 \times 10^{-9}$	90	[3] AAIJ	13AI	LHCB	pp at 7 TeV
$0.6–8.1 \times 10^{-7}$	90	[4] LEES	12Q	BABR	$e^+e^- \approx$ 10.58 GeV
$<2.1 \times 10^{-7}$	90	AALTONEN	10X	CDF	$p\overline{p}$, $\sqrt{s}$ = 1.96 TeV
$<1.4 \times 10^{-7}$	90	PETRIC	10	BELL	$e^+e^- \approx \Upsilon(4S)$
$<2.0 \times 10^{-6}$	90	ABT	04	HERB	pA, 920 GeV
$<1.3 \times 10^{-6}$	90	AUBERT,B	04Y	BABR	$e^+e^- \approx \Upsilon(4S)$
$<2.5 \times 10^{-6}$	90	ACOSTA	03F	CDF	See AALTONEN 10X
$<1.56 \times 10^{-5}$	90	PRIPSTEIN	00	E789	p nucleus, 800 GeV
$<5.2 \times 10^{-6}$	90	AITALA	99G	E791	$\pi^- N$ 500 GeV
$<4.1 \times 10^{-6}$	90	ADAMOVICH	97	BEAT	π^- Cu, W 350 GeV
$<4.2 \times 10^{-6}$	90	ALEXOPOU...	96	E771	p Si, 800 GeV
$<3.4 \times 10^{-5}$	90	FREYBERGER	96	CLE2	$e^+e^- \approx \Upsilon(4S)$
$<7.6 \times 10^{-6}$	90	ADAMOVICH	95	BEAT	See ADAMOVICH 97
$<4.4 \times 10^{-5}$	90	KODAMA	95	E653	π^- emulsion 600 GeV
$<3.1 \times 10^{-5}$	90	[5] MISHRA	94	E789	-4.1 ± 4.8 events
$<7.0 \times 10^{-5}$	90	ALBRECHT	88G	ARG	e^+e^- 10 GeV
$<1.1 \times 10^{-5}$	90	LOUIS	86	SPEC	π^- W 225 GeV
$<3.4 \times 10^{-4}$	90	AUBERT	85	EMC	Deep inelast. $\mu^- N$

[1] CHEKHOVSKY 25F reports a 95% CL limit of $< 2.4 \times 10^{-9}$.
[2] AAIJ 23R reports a 95% CL limit of $< 3.5 \times 10^{-9}$.
[3] Superseded by AAIJ 23R.
[4] LEES 12Q gives a 2-sided range.
[5] Here MISHRA 94 uses "the statistical approach advocated by the PDG." For an alternate approach, giving a limit of 9×10^{-6} at 90% confidence level, see the paper.

$\Gamma(\pi^0 e^+e^-)/\Gamma_{total}$ — Γ_{364}/Γ

A test for the $\Delta C = 1$ weak neutral current. Allowed by higher-order electroweak interactions.

VALUE	CL%	DOCUMENT ID		TECN	COMMENT
<4 × 10⁻⁶	90	ABLIKIM	18P	BES3	e^+e^-, 3773 MeV
• • • We do not use the following data for averages, fits, limits, etc. • • •					
$<4.5 \times 10^{-5}$	90	FREYBERGER	96	CLE2	$e^+e^- \approx \Upsilon(4S)$

$\Gamma(\pi^0\mu^+\mu^-)/\Gamma_{total}$ — Γ_{365}/Γ

A test for the ΔC=1 weak neutral current. Allowed by higher-order electroweak interactions.

VALUE	CL%	DOCUMENT ID		TECN	COMMENT
<1.8 × 10⁻⁴	90	KODAMA	95	E653	π^- emulsion 600 GeV
• • • We do not use the following data for averages, fits, limits, etc. • • •					
$<5.4 \times 10^{-4}$	90	FREYBERGER	96	CLE2	$e^+e^- \approx \Upsilon(4S)$

$\Gamma(\pi^0\nu\overline{\nu})/\Gamma_{total}$ — Γ_{366}/Γ

VALUE	CL%	DOCUMENT ID		TECN	COMMENT
<2.1 × 10⁻⁴	90	[1] ABLIKIM	22V	BES3	e^+e^- at 3773 MeV

[1] ABLIKIM 22V easurement comes from a sample of 10.6×10^6 $D^0\overline{D}^0$ pairs .

$\Gamma(\eta e^+e^-)/\Gamma_{total}$ — Γ_{367}/Γ

A test for the $\Delta C = 1$ weak neutral current. Allowed by higher-order electroweak interactions.

VALUE	CL%	DOCUMENT ID		TECN	COMMENT
<3 × 10⁻⁶	90	ABLIKIM	18P	BES3	e^+e^-, 3773 MeV
• • • We do not use the following data for averages, fits, limits, etc. • • •					
$<1.1 \times 10^{-4}$	90	FREYBERGER	96	CLE2	$e^+e^- \approx \Upsilon(4S)$

$\Gamma(\eta\mu^+\mu^-)/\Gamma_{total}$ — Γ_{368}/Γ

A test for the $\Delta C = 1$ weak neutral current. Allowed by higher-order electroweak interactions.

VALUE	CL%	DOCUMENT ID		TECN	COMMENT
<5.3 × 10⁻⁴	90	FREYBERGER	96	CLE2	$e^+e^- \approx \Upsilon(4S)$

$\Gamma(\pi^+\pi^-e^+e^-)/\Gamma_{total}$ — Γ_{369}/Γ

A test for the $\Delta C = 1$ weak neutral current. Allowed by higher-order electroweak interactions.

VALUE (units 10^{-6})	CL%	DOCUMENT ID		TECN	COMMENT
< 7	90	ABLIKIM	18P	BES3	e^+e^-, 3773 MeV
• • • We do not use the following data for averages, fits, limits, etc. • • •					
$1.33 \pm 0.17 \pm 0.25$		[1] AAIJ	25M	LHCB	pp at 13 TeV
not seen		[2] ADACHI	25W	BELL	e^+e^- near $\Upsilon(4S)$
<373	90	AITALA	01C	E791	π^- nucleus, 500 GeV

[1] AAIJ 25M value measured only in the region $m(e^+e^-) > 2m_\mu$, for five different dielectron mass intervals. The systematic uncertainty includes a 13.7% relative uncertainty from the normalization mode $D^0 \to K^-\pi^+(e^+e^-)_{\rho/\omega}$.
[2] ADACHI 25W sets limits at 90% CL of order 10^{-7} to 10^{-6} for four different dielectron mass ranges, $520 < m(e^+e^-) < 560$ MeV, $675 < m(e^+e^-) < 875$ MeV, $995 < m(e^+e^-) < 1035$ MeV, and $m(e^+e^-) > 200$ MeV excluding resonance regions.

$\Gamma(\rho^0 e^+e^-)/\Gamma_{total}$ — Γ_{370}/Γ

A test for the $\Delta C = 1$ weak neutral current. Allowed by higher-order electroweak interactions.

VALUE	CL%	DOCUMENT ID		TECN	COMMENT
<1.0 × 10⁻⁴	90	[1] FREYBERGER	96	CLE2	$e^+e^- \approx \Upsilon(4S)$
• • • We do not use the following data for averages, fits, limits, etc. • • •					
$<1.24 \times 10^{-4}$	90	AITALA	01C	E791	π^- nucleus, 500 GeV
$<4.5 \times 10^{-4}$	90	HAAS	88	CLEO	e^+e^- 10 GeV

[1] This FREYBERGER 96 limit is obtained using a phase-space model. The limit changes to $< 1.8 \times 10^{-4}$ using a photon pole amplitude model.

$\Gamma(\pi^+\pi^-\mu^+\mu^-)/\Gamma_{total}$ — Γ_{371}/Γ

A test for the $\Delta C = 1$ weak neutral current. Allowed by higher-order electroweak interactions.

VALUE (units 10^{-7})	EVTS	DOCUMENT ID		TECN	COMMENT
9.64±0.48±1.10	561	[1] AAIJ	17BG	LHCB	pp at 8 TeV

[1] The second AAIJ 17BG error is the systematic 0.51×10^{-7} and normalization 0.97×10^{-7} mode errors added in quadrature.

$\Gamma(\pi^+\pi^-\mu^+\mu^-(\text{non-res}))/\Gamma_{total}$ — Γ_{372}/Γ

VALUE	CL%	DOCUMENT ID		TECN	COMMENT
<5.5 × 10⁻⁷	90	[1] AAIJ	14B	LHCB	pp at 7 TeV
• • • We do not use the following data for averages, fits, limits, etc. • • •					
$<3.0 \times 10^{-5}$	90	AITALA	01C	E791	π^- nucleus, 500 GeV

[1] AAIJ 14B measures this branching-fraction limit relative to the $\pi^+\pi^-\phi$, $\phi \to \mu^+\mu^-$ fraction. The above limit excludes the resonant ϕ, ω, and ρ regions, and then fills those gaps with a phase-space model.

$\Gamma(\rho^0\mu^+\mu^-)/\Gamma_{total}$ — Γ_{373}/Γ

A test for the $\Delta C = 1$ weak neutral current. Allowed by higher-order electroweak interactions.

VALUE	CL%	DOCUMENT ID		TECN	COMMENT
<2.2 × 10⁻⁵	90	AITALA	01C	E791	π^- nucleus, 500 GeV
• • • We do not use the following data for averages, fits, limits, etc. • • •					
$<4.9 \times 10^{-4}$	90	[1] FREYBERGER	96	CLE2	$e^+e^- \approx \Upsilon(4S)$
$<2.3 \times 10^{-4}$	90	KODAMA	95	E653	π^- emulsion 600 GeV
$<8.1 \times 10^{-4}$	90	HAAS	88	CLEO	e^+e^- 10 GeV

[1] This FREYBERGER 96 limit is obtained using a phase-space model. The limit changes to $< 4.5 \times 10^{-4}$ using a photon pole amplitude model.

$\Gamma(\omega e^+e^-)/\Gamma_{total}$ — Γ_{374}/Γ

A test for the $\Delta C = 1$ weak neutral current. Allowed by higher-order electroweak interactions.

VALUE	CL%	DOCUMENT ID		TECN	COMMENT
<6 × 10⁻⁶	90	ABLIKIM	18P	BES3	e^+e^-, 3773 MeV
• • • We do not use the following data for averages, fits, limits, etc. • • •					
$<1.8 \times 10^{-4}$	90	[1] FREYBERGER	96	CLE2	$e^+e^- \approx \Upsilon(4S)$

[1] This FREYBERGER 96 limit is obtained using a phase-space model. The limit changes to $< 2.7 \times 10^{-4}$ using a photon pole amplitude model.

$\Gamma(\omega\mu^+\mu^-)/\Gamma_{total}$ — Γ_{375}/Γ

A test for the $\Delta C = 1$ weak neutral current. Allowed by higher-order electroweak interactions.

VALUE	CL%	DOCUMENT ID		TECN	COMMENT
<8.3 × 10⁻⁴	90	[1] FREYBERGER	96	CLE2	$e^+e^- \approx \Upsilon(4S)$

[1] This FREYBERGER 96 limit is obtained using a phase-space model. The limit changes to $< 6.5 \times 10^{-4}$ using a photon pole amplitude model.

Int. J. Mod. Phys. A 2026.41. Downloaded from www.worldscientific.com by LIFORNIA @ BERKELEY on 09/16/26. Re-use and distribution is strictly not permitted, except for Open Access articles.

$\Gamma(K^- K^+ e^+ e^-)/\Gamma_{total}$ — Γ_{376}/Γ

A test for the $\Delta C = 1$ weak neutral current. Allowed by higher-order electroweak interactions.

VALUE	CL%	DOCUMENT ID		TECN	COMMENT
<1.1 × 10⁻⁵	90	ABLIKIM	18P	BES3	e^+e^-, 3773 MeV
• • • We do not use the following data for averages, fits, limits, etc. • • •					
not seen		[1] AAIJ	25M	LHCB	pp at 13 TeV
not seen		[2] ADACHI	25W	BELL	e^+e^- near $\Upsilon(4S)$
$<3.15 \times 10^{-4}$	90	AITALA	01C	E791	π^- nucleus, 500 GeV

[1] AAIJ 25M sets limits for three different dielectron mass ranges, $2m_\mu < m(e^+e^-) <$ 525 MeV, 525 MeV $< m(e^+e^-) <$ 565 MeV, and $m(e^+e^-) >$ 565 MeV.

[2] ADACHI 25W sets limits at 90% CL of order 10^{-7} to 10^{-6} for three different dielectron mass ranges, 520 $< m(e^+e^-) <$ 560 MeV, $m(e^+e^-) >$ 675 MeV, and $m(e^+e^-) >$ 200 MeV excluding resonance regions.

$\Gamma(\phi e^+ e^-)/\Gamma_{total}$ — Γ_{377}/Γ

A test for the $\Delta C = 1$ weak neutral current. Allowed by higher-order electroweak interactions.

VALUE	CL%	DOCUMENT ID		TECN	COMMENT
<5.2 × 10⁻⁵	90	[1] FREYBERGER	96	CLE2	$e^+e^- \approx \Upsilon(4S)$
• • • We do not use the following data for averages, fits, limits, etc. • • •					
$<5.9 \times 10^{-5}$	90	AITALA	01C	E791	π^- nucleus, 500 GeV

[1] This FREYBERGER 96 limit is obtained using a phase-space model. The limit changes to $< 7.6 \times 10^{-5}$ using a photon pole amplitude model.

$\Gamma(K^- K^+ \mu^+ \mu^-)/\Gamma_{total}$ — Γ_{378}/Γ

A test for the $\Delta C = 1$ weak neutral current. Allowed by higher-order electroweak interactions.

VALUE (units 10^{-7})	EVTS	DOCUMENT ID		TECN	COMMENT
1.54±0.27±0.18	34	[1] AAIJ	17BG	LHCB	pp at 8 TeV

[1] The second AAIJ 17BG error is the systematic 0.09×10^{-7} and normalization 0.16×10^{-7} mode errors added in quadrature.

$\Gamma(K^- K^+ \mu^+ \mu^-$ (non-res))$/\Gamma_{total}$ — Γ_{379}/Γ

VALUE	CL%	DOCUMENT ID		TECN	COMMENT
<3.3 × 10⁻⁵	90	AITALA	01C	E791	π^- nucleus, 500 GeV

$\Gamma(\phi \mu^+ \mu^-)/\Gamma_{total}$ — Γ_{380}/Γ

A test for the $\Delta C = 1$ weak neutral current. Allowed by higher-order electroweak interactions.

VALUE	CL%	DOCUMENT ID		TECN	COMMENT
<3.1 × 10⁻⁵	90	AITALA	01C	E791	π^- nucleus, 500 GeV
• • • We do not use the following data for averages, fits, limits, etc. • • •					
$<4.1 \times 10^{-4}$	90	[1] FREYBERGER	96	CLE2	$e^+e^- \approx \Upsilon(4S)$

[1] This FREYBERGER 96 limit is obtained using a phase-space model. The limit changes to $< 2.4 \times 10^{-4}$ using a photon pole amplitude model.

$\Gamma(\overline{K}^0 e^+ e^-)/\Gamma_{total}$ — Γ_{381}/Γ

Not a useful test for $\Delta C = 1$ weak neutral current because both quarks must change flavor.

VALUE	CL%	DOCUMENT ID		TECN	COMMENT
<2.4 × 10⁻⁵	90	[1] ABLIKIM	18P	BES3	e^+e^-, 3773 MeV
• • • We do not use the following data for averages, fits, limits, etc. • • •					
$<1.1 \times 10^{-4}$	90	FREYBERGER	96	CLE2	$e^+e^- \approx \Upsilon(4S)$
$<1.7 \times 10^{-3}$	90	ADLER	89C	MRK3	e^+e^- 3.77 GeV

[1] ABLIKIM 18P report a 90% C.L. limit on $D^0 \to K^0_S e^+e^-$ of 1.2×10^{-5} which is here interpreted in terms of $D^0 \to \overline{K}^0 e^+e^-$.

$\Gamma(\overline{K}^0 \mu^+ \mu^-)/\Gamma_{total}$ — Γ_{382}/Γ

Not a useful test for $\Delta C = 1$ weak neutral current because both quarks must change flavor.

VALUE	CL%	DOCUMENT ID		TECN	COMMENT
<2.6 × 10⁻⁴	90	KODAMA	95	E653	π^- emulsion 600 GeV
• • • We do not use the following data for averages, fits, limits, etc. • • •					
$<6.7 \times 10^{-4}$	90	FREYBERGER	96	CLE2	$e^+e^- \approx \Upsilon(4S)$

$\Gamma(K^- \pi^+ e^+ e^-)/\Gamma_{total}$ — Γ_{383}/Γ

A test for the $\Delta C = 1$ weak neutral current. Allowed by higher-order electroweak interactions.

VALUE	CL%	DOCUMENT ID		TECN	COMMENT
• • • We do not use the following data for averages, fits, limits, etc. • • •					
$<4.1 \times 10^{-5}$	90	ABLIKIM	18P	BES3	see LEES 19A
$<3.85 \times 10^{-4}$	90	AITALA	01C	E791	π^- nucleus, 500 GeV

$\Gamma(K^- \pi^+ e^+ e^-, 675 < m_{ee} < 875\,\text{MeV})/\Gamma_{total}$ — Γ_{384}/Γ

VALUE (units 10^{-6})	EVTS	DOCUMENT ID		TECN	COMMENT
4.0 ±0.4 OUR AVERAGE					
3.96±0.45±0.29	110	[1] ADACHI	25W	BELL	e^+e^- near $\Upsilon(4S)$
4.0 ±0.5 ±0.2 ±0.1	68	[2,3] LEES	19A	BABR	e^+e^- near $\Upsilon(4S)$

[1] ADACHI 25W also sets upper limits at 90% CL for the $m_{e^+e^-}$ resonant regions around the m_η and m_ϕ, $< 5.6\times10^{-7}$ and $< 2.9\times10^{-7}$, respectively.

[2] Observation with 9.7 σ significance. The last uncertainty is due to the uncertainty on the branching fraction of the normalization mode, $D^0 \to K^-\pi^+\pi^+\pi^-$. The second uncertainty is other systematic and is dominated by the model parameterization.

[3] LEES 19A also sets an upper limit for non-resonant regions, where long-distance effects are expected to be small: $< 3.1\times10^{-6}$ at 90% CL.

$\Gamma(K^- \pi^+ e^+ e^-, 1.005 < m_{ee} < 1.035\,\text{GeV})/\Gamma_{total}$ — Γ_{385}/Γ

VALUE	CL%	DOCUMENT ID		TECN	COMMENT
<5 × 10⁻⁷	90	[1] LEES	19A	BABR	e^+e^- near $\Upsilon(4S)$

[1] LEES 19A also sets an upper limit for non-resonant regions, where long-distance effects are expected to be small: $< 3.1\times10^{-6}$ at 90% CL.

$\Gamma(\overline{K}^*(892)^0 e^+ e^-)/\Gamma_{total}$ — Γ_{386}/Γ

Not a useful test for $\Delta C = 1$ weak neutral current because both quarks must change flavor.

VALUE	CL%	DOCUMENT ID		TECN	COMMENT
<4.7 × 10⁻⁵	90	AITALA	01C	E791	π^- nucleus, 500 GeV
• • • We do not use the following data for averages, fits, limits, etc. • • •					
$<1.4 \times 10^{-4}$	90	[1] FREYBERGER	96	CLE2	$e^+e^- \approx \Upsilon(4S)$

[1] This FREYBERGER 96 limit is obtained using a phase-space model. The limit changes to $< 2.0\times10^{-4}$ using a photon pole amplitude model.

$\Gamma(K^- \pi^+ \mu^+ \mu^-)/\Gamma_{total}$ — Γ_{387}/Γ

A test for the $\Delta C = 1$ weak neutral current. Allowed by higher-order electroweak interactions.

VALUE	CL%	DOCUMENT ID		TECN	COMMENT
<3.59 × 10⁻⁴	90	AITALA	01C	E791	π^- nucleus, 500 GeV

$\Gamma(K^- \pi^+ \mu^+ \mu^-, 675 < m_{\mu\mu} < 875\,\text{MeV})/\Gamma_{total}$ — Γ_{388}/Γ

VALUE (units 10^{-6})	EVTS	DOCUMENT ID		TECN	COMMENT
4.17±0.12±0.40	2.4k	[1] AAIJ	16I	LHCB	pp at 8 TeV

[1] AAIJ 16I uses $B(D^0 \to K^-\pi^+\pi^+\pi^-) = (8.287 \pm 0.043 \pm 0.200)\times10^{-2}$ value for the normalization mode.

$\Gamma(\overline{K}^*(892)^0 \mu^+ \mu^-)/\Gamma_{total}$ — Γ_{389}/Γ

Not a useful test for $\Delta C = 1$ weak neutral current because both quarks must change flavor.

VALUE	CL%	DOCUMENT ID		TECN	COMMENT
<2.4 × 10⁻⁵	90	AITALA	01C	E791	π^- nucleus, 500 GeV
• • • We do not use the following data for averages, fits, limits, etc. • • •					
$<1.18 \times 10^{-3}$	90	[1] FREYBERGER	96	CLE2	$e^+e^- \approx \Upsilon(4S)$

[1] This FREYBERGER 96 limit is obtained using a phase-space model. The limit changes to $< 1.0\times10^{-3}$ using a photon pole amplitude model.

$\Gamma(\pi^+ \pi^- \pi^0 \mu^+ \mu^-)/\Gamma_{total}$ — Γ_{390}/Γ

A test for the ΔC=1 weak neutral current. Allowed by higher-order electroweak interactions.

VALUE	CL%	DOCUMENT ID		TECN	COMMENT
<8.1 × 10⁻⁴	90	KODAMA	95	E653	π^- emulsion 600 GeV

$\Gamma(\mu^\pm e^\mp)/\Gamma_{total}$ — Γ_{391}/Γ

A test of lepton family number conservation.

VALUE	CL%	DOCUMENT ID		TECN	COMMENT
< 1.3 × 10⁻⁸	90	AAIJ	16H	LHCB	pp at 7, 8 GeV
• • • We do not use the following data for averages, fits, limits, etc. • • •					
$< 3.3 \times 10^{-7}$	90	LEES	12Q	BABR	$e^+e^- \approx$ 10.58 GeV
$< 2.6 \times 10^{-7}$	90	PETRIC	10	BELL	$e^+e^- \approx \Upsilon(4S)$
$< 8.1 \times 10^{-7}$	90	AUBERT,B	04Y	BABR	$e^+e^- \approx \Upsilon(4S)$
$< 1.72 \times 10^{-5}$	90	PRIPSTEIN	00	E789	p nucleus, 800 GeV
$< 8.1 \times 10^{-6}$	90	AITALA	99G	E791	$\pi^- N$ 500 GeV
$< 1.9 \times 10^{-5}$	90	[1] FREYBERGER	96	CLE2	$e^+e^- \approx \Upsilon(4S)$
$< 1.0 \times 10^{-4}$	90	ALBRECHT	88G	ARG	e^+e^- 10 GeV
$< 2.7 \times 10^{-4}$	90	HAAS	88	CLEO	e^+e^- 10 GeV
$< 1.2 \times 10^{-4}$	90	BECKER	87C	MRK3	e^+e^- 3.77 GeV
$< 9 \times 10^{-4}$	90	PALKA	87	SILI	200 GeV πp
$<21 \times 10^{-4}$	90	[2] RILES	87	MRK2	e^+e^- 29 GeV

[1] This is the corrected result given in the erratum to FREYBERGER 96.

[2] RILES 87 assumes $B(D \to K\pi) = 3.0\%$ and has production model dependency.

$\Gamma(\pi^0 e^\pm \mu^\mp)/\Gamma_{total}$ — Γ_{392}/Γ

A test of lepton family number conservation. The value is for the sum of the two charge states.

VALUE	CL%	DOCUMENT ID		TECN	COMMENT
<8.0 × 10⁻⁷	90	LEES	20A	BABR	e^+e^- at $\Upsilon(4S)$
• • • We do not use the following data for averages, fits, limits, etc. • • •					
$<8.6 \times 10^{-5}$	90	FREYBERGER	96	CLE2	$e^+e^- \approx \Upsilon(4S)$

$\Gamma(\eta e^\pm \mu^\mp)/\Gamma_{total}$ — Γ_{393}/Γ

A test of lepton family number conservation. The value is for the sum of the two charge states.

VALUE	CL%	DOCUMENT ID		TECN	COMMENT
<22.5 × 10⁻⁷	90	[1] LEES	20A	BABR	e^+e^- at $\Upsilon(4S)$
• • • We do not use the following data for averages, fits, limits, etc. • • •					
$< 1.0 \times 10^{-4}$	90	FREYBERGER	96	CLE2	$e^+e^- \approx \Upsilon(4S)$

[1] LEES 20A quotes separate limits $B(D^0 \to \eta e^\pm\mu^\mp,\ \eta \to \gamma\gamma) < 24.0\times10^{-7}$ and $B(D^0 \to \eta e^\pm\mu^\mp,\ \eta \to \pi^+\pi^-\pi^0) < 43.0\times10^{-7}$.

Int. J. Mod. Phys. A 2026.41. Downloaded from www.worldscientific.com
by UNIVERSITY OF CALIFORNIA @ BERKELEY on 09/16/26. Re-use and distribution is strictly not permitted, except for Open Access articles.

$\Gamma(\pi^+\pi^- e^\pm\mu^\mp)/\Gamma_{total}$ — Γ_{394}/Γ

A test of lepton family-number conservation.

VALUE	CL%	DOCUMENT ID		TECN	COMMENT
$<1.71\times10^{-6}$	90	LEES	20B	BABR	e^+e^- at $\Upsilon(4S)$
• • • We do not use the following data for averages, fits, limits, etc. • • •					
$<1.5\ \times10^{-5}$	90	AITALA	01C	E791	π^- nucleus, 500 GeV

$\Gamma(\rho^0 e^\pm\mu^\mp)/\Gamma_{total}$ — Γ_{395}/Γ

A test of lepton family number conservation. The value is for the sum of the two charge states.

VALUE	CL%	DOCUMENT ID		TECN	COMMENT
$<5.0\times10^{-7}$	90	LEES	20A	BABR	e^+e^- at $\Upsilon(4S)$
• • • We do not use the following data for averages, fits, limits, etc. • • •					
$<6.6\times10^{-5}$	90	AITALA	01C	E791	π^- nucleus, 500 GeV
$<4.9\times10^{-5}$	90	[1] FREYBERGER	96	CLE2	$e^+e^-\approx\Upsilon(4S)$

[1] This FREYBERGER 96 limit is obtained using a phase-space model. The limit changes to $<5.0\times10^{-5}$ using a photon pole amplitude model.

$\Gamma(\omega e^\pm\mu^\mp)/\Gamma_{total}$ — Γ_{396}/Γ

A test of lepton family number conservation. The value is for the sum of the two charge states.

VALUE	CL%	DOCUMENT ID		TECN	COMMENT
$<17.1\times10^{-7}$	90	LEES	20A	BABR	e^+e^- at $\Upsilon(4S)$
• • • We do not use the following data for averages, fits, limits, etc. • • •					
$<1.2\times10^{-4}$	90	[1] FREYBERGER	96	CLE2	$e^+e^-\approx\Upsilon(4S)$

[1] This FREYBERGER 96 limit is obtained using a phase-space model. The same limit is obtained using a photon pole amplitude model.

$\Gamma(K^- K^+ e^\pm\mu^\mp)/\Gamma_{total}$ — Γ_{397}/Γ

A test of lepton family-number conservation.

VALUE	CL%	DOCUMENT ID		TECN	COMMENT
$<1.00\times10^{-6}$	90	LEES	20B	BABR	e^+e^- at $\Upsilon(4S)$
• • • We do not use the following data for averages, fits, limits, etc. • • •					
$<1.8\ \times10^{-4}$	90	AITALA	01C	E791	π^- nucleus, 500 GeV

$\Gamma(\phi e^\pm\mu^\mp)/\Gamma_{total}$ — Γ_{398}/Γ

A test of lepton family number conservation. The value is for the sum of the two charge states.

VALUE	CL%	DOCUMENT ID		TECN	COMMENT
$<5.1\times10^{-7}$	90	LEES	20A	BABR	e^+e^- at $\Upsilon(4S)$
• • • We do not use the following data for averages, fits, limits, etc. • • •					
$<4.7\times10^{-5}$	90	AITALA	01C	E791	π^- nucleus, 500 GeV
$<3.4\times10^{-5}$	90	[1] FREYBERGER	96	CLE2	$e^+e^-\approx\Upsilon(4S)$

[1] This FREYBERGER 96 limit is obtained using a phase-space model. The limit changes to $<3.3\times10^{-5}$ using a photon pole amplitude model.

$\Gamma(\overline{K}^0 e^\pm\mu^\mp)/\Gamma_{total}$ — Γ_{399}/Γ

A test of lepton family number conservation. The value is for the sum of the two charge states.

VALUE	CL%	DOCUMENT ID		TECN	COMMENT
$<17.4\times10^{-7}$	90	[1] LEES	20A	BABR	e^+e^- at $\Upsilon(4S)$
• • • We do not use the following data for averages, fits, limits, etc. • • •					
$<1.0\times10^{-4}$	90	FREYBERGER	96	CLE2	$e^+e^-\approx\Upsilon(4S)$

[1] LEES 20A quotes $B(D^0\to K^0_S e^\pm\mu^\mp)<8.7\times10^{-7}$ at 90% CL.

$\Gamma(K^-\pi^+ e^\pm\mu^\mp)/\Gamma_{total}$ — Γ_{400}/Γ

A test of lepton family-number conservation.

VALUE	CL%	DOCUMENT ID		TECN	COMMENT
$<1.90\times10^{-6}$	90	LEES	20B	BABR	e^+e^- at $\Upsilon(4S)$
• • • We do not use the following data for averages, fits, limits, etc. • • •					
$<5.53\times10^{-4}$	90	AITALA	01C	E791	π^- nucleus, 500 GeV

$\Gamma(\overline{K}^*(892)^0 e^\pm\mu^\mp)/\Gamma_{total}$ — Γ_{401}/Γ

A test of lepton family number conservation. The value is for the sum of the two charge states.

VALUE	CL%	DOCUMENT ID		TECN	COMMENT
$<12.5\times10^{-7}$	90	LEES	20A	BABR	e^+e^- at $\Upsilon(4S)$
• • • We do not use the following data for averages, fits, limits, etc. • • •					
$<8.3\times10^{-5}$	90	AITALA	01C	E791	π^- nucleus, 500 GeV
$<1.0\times10^{-4}$	90	[1] FREYBERGER	96	CLE2	$e^+e^-\approx\Upsilon(4S)$

[1] This FREYBERGER 96 limit is obtained using a phase-space model. The same limit is obtained using a photon pole amplitude model.

$\Gamma(2\pi^- 2e^+)/\Gamma_{total}$ — Γ_{402}/Γ

A test of lepton-number conservation.

VALUE	CL%	DOCUMENT ID		TECN	COMMENT
$<9.1\ \times10^{-7}$	90	LEES	20B	BABR	e^+e^- at $\Upsilon(4S)$
• • • We do not use the following data for averages, fits, limits, etc. • • •					
$<1.12\times10^{-4}$	90	[1] AITALA	01C	E791	π^- nucleus, 500 GeV

[1] Value includes decay to the charge conjugate state.

$\Gamma(2\pi^- 2\mu^+)/\Gamma_{total}$ — Γ_{403}/Γ

A test of lepton-number conservation.

VALUE	CL%	DOCUMENT ID		TECN	COMMENT
$<1.52\times10^{-6}$	90	LEES	20B	BABR	e^+e^- at $\Upsilon(4S)$
• • • We do not use the following data for averages, fits, limits, etc. • • •					
$<2.9\ \times10^{-5}$	90	[1] AITALA	01C	E791	π^- nucleus, 500 GeV

[1] Value includes decay to the charge conjugate state.

$\Gamma(K^-\pi^- 2e^+)/\Gamma_{total}$ — Γ_{404}/Γ

A test of lepton-number conservation.

VALUE	CL%	DOCUMENT ID		TECN	COMMENT
$<5.0\ \times10^{-7}$	90	LEES	20B	BABR	e^+e^- at $\Upsilon(4S)$
• • • We do not use the following data for averages, fits, limits, etc. • • •					
$<2.8\ \times10^{-6}$	90	ABLIKIM	19AL	BES3	e^+e^- at 3773 MeV
$<2.06\times10^{-4}$	90	[1] AITALA	01C	E791	π^- nucleus, 500 GeV

[1] Value includes decay to the charge conjugate state.

$\Gamma(K^-\pi^- 2\mu^+)/\Gamma_{total}$ — Γ_{405}/Γ

A test of lepton-number conservation.

VALUE	CL%	DOCUMENT ID		TECN	COMMENT
$<5.3\times10^{-7}$	90	LEES	20B	BABR	e^+e^- at $\Upsilon(4S)$
• • • We do not use the following data for averages, fits, limits, etc. • • •					
$<3.9\times10^{-4}$	90	[1] AITALA	01C	E791	π^- nucleus, 500 GeV

[1] Value includes decay to the charge conjugate state.

$\Gamma(2K^- 2e^+)/\Gamma_{total}$ — Γ_{406}/Γ

A test of lepton-number conservation.

VALUE	CL%	DOCUMENT ID		TECN	COMMENT
$<3.4\ \times10^{-7}$	90	LEES	20B	BABR	e^+e^- at $\Upsilon(4S)$
• • • We do not use the following data for averages, fits, limits, etc. • • •					
$<1.52\times10^{-4}$	90	[1] AITALA	01C	E791	π^- nucleus, 500 GeV

[1] Value includes decay to the charge conjugate state.

$\Gamma(2K^- 2\mu^+)/\Gamma_{total}$ — Γ_{407}/Γ

A test of lepton-number conservation.

VALUE	CL%	DOCUMENT ID		TECN	COMMENT
$<1.0\times10^{-7}$	90	LEES	20B	BABR	e^+e^- at $\Upsilon(4S)$
• • • We do not use the following data for averages, fits, limits, etc. • • •					
$<9.4\times10^{-5}$	90	[1] AITALA	01C	E791	π^- nucleus, 500 GeV

[1] Value includes decay to the charge conjugate state.

$\Gamma(\pi^-\pi^- e^+\mu^+)/\Gamma_{total}$ — Γ_{408}/Γ

A test of lepton-number conservation.

VALUE	CL%	DOCUMENT ID		TECN	COMMENT
$<3.06\times10^{-6}$	90	LEES	20B	BABR	e^+e^- at $\Upsilon(4S)$
• • • We do not use the following data for averages, fits, limits, etc. • • •					
$<7.9\ \times10^{-5}$	90	[1] AITALA	01C	E791	π^- nucleus, 500 GeV

[1] Value includes decay to the charge conjugate state.

$\Gamma(K^-\pi^- e^+\mu^+)/\Gamma_{total}$ — Γ_{409}/Γ

A test of lepton-number conservation.

VALUE	CL%	DOCUMENT ID		TECN	COMMENT
$<2.10\times10^{-6}$	90	LEES	20B	BABR	e^+e^- at $\Upsilon(4S)$
• • • We do not use the following data for averages, fits, limits, etc. • • •					
$<2.18\times10^{-4}$	90	[1] AITALA	01C	E791	π^- nucleus, 500 GeV

[1] Value includes decay to the charge conjugate state.

$\Gamma(2K^- e^+\mu^+)/\Gamma_{total}$ — Γ_{410}/Γ

A test of lepton-number conservation.

VALUE	CL%	DOCUMENT ID		TECN	COMMENT
$<5.8\times10^{-7}$	90	LEES	20B	BABR	e^+e^- at $\Upsilon(4S)$
• • • We do not use the following data for averages, fits, limits, etc. • • •					
$<5.7\times10^{-5}$	90	[1] AITALA	01C	E791	π^- nucleus, 500 GeV

[1] Value includes decay to the charge conjugate state.

$\Gamma(pe^-)/\Gamma_{total}$ — Γ_{411}/Γ

A test of baryon- and lepton-number conservation.

VALUE	CL%	DOCUMENT ID		TECN	COMMENT
$<5.5\times10^{-7}$	90	MAITY	24	BELL	e^+e^- at $\Upsilon(4S)$ to $\Upsilon(5S)$
• • • We do not use the following data for averages, fits, limits, etc. • • •					
$<7.6\times10^{-7}$	90	[1] MAITY	24	BELL	e^+e^- at $\Upsilon(4S)$ to $\Upsilon(5S)$
$<2.2\times10^{-6}$	90	ABLIKIM	22T	BES3	e^+e^- at 3.773 GeV
$<1.0\times10^{-5}$	90	[2] RUBIN	09	CLEO	e^+e^- at $\psi(3770)$

[1] Limit from measurement of the conjugate decay mode $\overline{D}^0\to\overline{p}e^+$.
[2] This RUBIN 09 limit is for either $D^0\to pe^-$ or $\overline{D}^0\to pe^-$ decay.

$\Gamma(\overline{p}e^+)/\Gamma_{total}$ — Γ_{412}/Γ

A test of baryon- and lepton-number conservation.

VALUE	CL%	DOCUMENT ID		TECN	COMMENT
$<6.9\times10^{-7}$	90	[1] MAITY	24	BELL	e^+e^- at $\Upsilon(4S)$ to $\Upsilon(5S)$
• • • We do not use the following data for averages, fits, limits, etc. • • •					
$<7.2\times10^{-7}$	90	MAITY	24	BELL	e^+e^- at $\Upsilon(4S)$ to $\Upsilon(5S)$
$<1.2\times10^{-6}$	90	ABLIKIM	22T	BES3	e^+e^- at 3.773 GeV
$<1.1\times10^{-5}$	90	[2] RUBIN	09	CLEO	e^+e^- at $\psi(3770)$

[1] Limit from measurement of the conjugate decay mode $\overline{D}^0\to pe^-$.
[2] This RUBIN 09 limit is for either $D^0\to\overline{p}e^+$ or $\overline{D}^0\to\overline{p}e^+$ decay.

Int. J. Mod. Phys. A 2026.41. Downloaded from www.worldscientific.com by CALIFORNIA @ BERKELEY on 09/16/26. Re-use and distribution is strictly not permitted, except for Open Access articles.

$\Gamma(p\mu^-)/\Gamma_{total}$ — Γ_{413}/Γ

VALUE	CL%	DOCUMENT ID		TECN	COMMENT
$<5.1\times10^{-7}$	90	MAITY	24	BELL	e^+e^- at $\Upsilon(4S)$ to $\Upsilon(5S)$
• • • We do not use the following data for averages, fits, limits, etc. • • •					
$<6.5\times10^{-7}$	90	[1] MAITY	24	BELL	e^+e^- at $\Upsilon(4S)$ to $\Upsilon(5S)$

[1] Limit from measurement of the conjugate decay mode $\overline{D}^0 \to \overline{p}\mu^+$.

$\Gamma(\overline{p}\mu^+)/\Gamma_{total}$ — Γ_{414}/Γ

VALUE	CL%	DOCUMENT ID		TECN	COMMENT
$<6.3\times10^{-7}$	90	MAITY	24	BELL	e^+e^- at $\Upsilon(4S)$ to $\Upsilon(5S)$
• • • We do not use the following data for averages, fits, limits, etc. • • •					
$<6.5\times10^{-7}$	90	[1] MAITY	24	BELL	e^+e^- at $\Upsilon(4S)$ to $\Upsilon(5S)$

[1] Limit from measurement of the conjugate decay mode $\overline{D}^0 \to p\mu^-$.

Exotic modes

$\Gamma(\gamma\gamma_D)/\Gamma_{total}$ — Γ_{415}/Γ

VALUE	CL%	DOCUMENT ID		TECN	COMMENT
$<2.0\times10^{-6}$	90	ABLIKIM	25AP	BES3	e^+e^- at 3.773 GeV

$\Gamma(\omega\gamma_D)/\Gamma_{total}$ — Γ_{416}/Γ

VALUE	CL%	DOCUMENT ID		TECN	COMMENT
$<1.1\times10^{-5}$	90	ABLIKIM	25AP	BES3	e^+e^- at 3.773 GeV

D^0 CP-EVEN FRACTIONS

The CP-even fraction F_+, defined for self-conjugate final states, like the coherence factor is useful for measuring the unitary triangle angle γ in $B \to DK$ decays. A purely CP-even state has $F_+ = 1$, a CP-odd one has $F_+ = 0$. For details, see NAYAK 15.

CP-even fraction in $D^0 \to K^0_S\pi^+\pi^-\pi^0$ decays

VALUE (%)	DOCUMENT ID		COMMENT
23.6±0.9 OUR AVERAGE			
23.5±1.0±0.2	ABLIKIM	23AW	e^+e^- at $\psi(3770)$, 2.93 fb^{-1}
23.8±1.2±1.2	[1] RESMI	18	Uses CLEO-c data

[1] Obtained by analyzing CLEO-c data but not authored by the CLEO Collaboration.

CP-even fraction in $D^0 \to \pi^+\pi^-\pi^0$ decays

VALUE (%)	DOCUMENT ID		TECN	COMMENT
94.2 ±0.7 OUR AVERAGE Error includes scale factor of 1.9.				
94.06±0.36±0.21	ABLIKIM	25AQ	BES3	e^+e^- at 3.773 GeV
97.3 ±1.7	MALDE	15		Uses CLEO data
• • • We do not use the following data for averages, fits, limits, etc. • • •				
96.8 ±1.7 ±0.6	NAYAK	15		see MALDE 15

CP-even fraction in $D^0 \to \pi^+\pi^-\pi^+\pi^-$ decays

VALUE (%)	DOCUMENT ID		TECN	COMMENT
74.6±0.8 OUR AVERAGE				
74.6±1.0±0.4	[1] ABLIKIM	24CO	BES3	e^+e^- at $\sqrt{s}$ = 3.773 GeV
73.5±1.5±0.5	[2] ABLIKIM	22BF	BES	2.93 fb^{-1} in e^+e^- at 3.773 GeV
76.9±2.1±1.0	[3] HARNEW	18		Uses CLEO-c data
• • • We do not use the following data for averages, fits, limits, etc. • • •				
72.9±0.9±1.8	[3,4] DARGENT	17		from amplitude model
73.7±2.8	MALDE	15	CLEO	amplitude model independent

[1] ABLIKIM 24CO also reports the measurement of the strong phase difference between D^0 and $\overline{D}^0$ decays in bins of the phase space.
[2] A combination of three consistent measurements with CP-eigenstate, quasi-CP-eigenstate and CP-mixed tags.
[3] Obtained by analyzing CLEO-c data but not authored by the CLEO Collaboration.
[4] MALDE 15 and DARGENT 17 use different CLEO data sets, so in principle their results could be averaged. However, given the importance that model-independence has in the use of this value, we exclude the amplitude model-derived result from the average.

CP-even fraction in $D^0 \to \pi^+\pi^-2\pi^0$ decays

VALUE	EVTS	DOCUMENT ID		TECN	COMMENT
0.682±0.077	236	ABLIKIM	22BG	BES3	e^+e^- at 3.773 GeV

CP-even fraction in $D^0 \to 2\pi^+2\pi^-\pi^0$ decays

VALUE	EVTS	DOCUMENT ID		TECN	COMMENT
0.438±0.104	73	ABLIKIM	22BG	BES3	e^+e^- at 3.773 GeV

CP-even fraction in $D^0 \to \pi^+\pi^-3\pi^0$ decays

VALUE	EVTS	DOCUMENT ID		TECN	COMMENT
$0.520^{+0.338}_{-0.269}$	$12^{+4.9}_{-3.9}$	ABLIKIM	22BG	BES3	e^+e^- at 3.773 GeV

CP-even fraction in $D^0 \to 2\pi^+2\pi^-2\pi^0$ decays

VALUE	EVTS	DOCUMENT ID		TECN	COMMENT
$0.790^{+0.269}_{-0.255}$	19	ABLIKIM	22BG	BES3	e^+e^- at 3.773 GeV

CP-even fraction in $D^0 \to K^+K^-\pi^0$ decays

VALUE (%)	DOCUMENT ID		TECN	COMMENT
64.1±3.0 OUR AVERAGE Error includes scale factor of 1.7.				
63.1±1.4±1.1	ABLIKIM	25AQ	BES3	e^+e^- at 3.773 GeV
73.2±5.5	MALDE	15		Uses CLEO data
• • • We do not use the following data for averages, fits, limits, etc. • • •				
73.1±5.8±2.1	NAYAK	15		see MALDE 15

CP-even fraction in $D^0 \to K^+K^-\pi^+\pi^-$ decays

VALUE (%)	DOCUMENT ID		TECN	COMMENT
74.1±3.0 OUR AVERAGE				
73.0±3.7±2.1	[1] ABLIKIM	23AJ	BES3	2.93 fb^{-1}, e^+e^- at $\psi(3770)$
75.3±1.8±3.9	[2] DARGENT	17		from amplitude model

[1] A combined measurement of the CP-even fraction using both CP tags and $K^0_{S,L}\pi^+\pi^-$ tags. ABLIKIM 23AJ reports CP-even fractions 0.704 ± 0.042 ± 0.028 and 0.798 ± 0.077 ± 0.019 for the former and latter tags, respectively.
[2] Obtained by analyzing CLEO data but not authored by the CLEO Collaboration.

D^0 CP-VIOLATING DECAY-RATE ASYMMETRIES

This is the difference between D^0 and $\overline{D}^0$ partial widths for the decay to state f, divided by the sum of the widths:
$A_{CP}(f) = [\Gamma(D^0 \to f) - \Gamma(\overline{D}^0 \to \overline{f})] / [\Gamma(D^0 \to f) + \Gamma(\overline{D}^0 \to \overline{f})]$.

$A_{CP}(K^+K^-)$ in $D^0, \overline{D}^0 \to K^+K^-$

VALUE (units 10^{-4})	EVTS	DOCUMENT ID		TECN	COMMENT
4 ± 5 OUR AVERAGE					
6.8± 5.4± 1.6	37M	[1] AAIJ	23AC	LHCB	pp at 13 TeV
4 ± 12 ± 10	4.56M	AAIJ	17M	LHCB	pp 7, 8 TeV
− 24 ± 22 ± 9	476k	[2] AALTONEN	12B	CDF	$p\overline{p}$, $\sqrt{s}$=1.96 TeV
0 ± 34 ± 13	129k	[3] AUBERT	08M	BABR	$e^+e^- \approx \Upsilon(4S)$
− 43 ± 30 ± 11	120k	[4] STARIC	08	BELL	$e^+e^- \approx \Upsilon(4S)$
200 ±120 ± 60		[5] ACOSTA	05C	CDF	$p\overline{p}$, $\sqrt{s}$=1.96 TeV
0 ±220 ± 80	3023	[5] CSORNA	02	CLE2	$e^+e^- \approx \Upsilon(4S)$
− 10 ±220 ±150	3330	[5] LINK	00B	FOCS	
−100 ±490 ±120	609	[5] AITALA	98C	E791	$-0.093 < A_{CP} < +0.073$ (90% CL)
• • • We do not use the following data for averages, fits, limits, etc. • • •					
− 6 ± 15 ± 10	1.8M	[2] AAIJ	14AK	LHCB	See AAIJ 17M

[1] AAIJ 23AC result comes from 5.7 fb^{-1} of data. Also reports the values of the direct CP asymmetries, $a^{CP}_{\pi\pi} = (23.2 \pm 6.1) \times 10^{-4}$ and $a^{CP}_{KK} = (7.7 \pm 5.7) \times 10^{-4}$, with a correlation of 88%, obtained using previous determinations of $A_{CP}(KK)$, ΔA_{CP}, ΔY, the reconstructed mean decay times of $D^0 \to \pi\pi$ and $D^0 \to KK$ in the aforementioned measurements, and the world average of the D^0 lifetime (PDG 22).
[2] See also "D^0 CP-violating asymmetry differences" at the end of the CP-violating asymmetries.
[3] AUBERT 08M uses corrected numbers of events directly, not ratios with $K^\mp\pi^\pm$ events.
[4] STARIC 08 uses $D^0 \to K^-\pi^+$ and $\overline{D}^0 \to K^+\pi^-$ decays to correct for detector-induced asymmetries.
[5] AITALA 98C, LINK 00B, CSORNA 02, and ACOSTA 05C measure $N(D^0 \to K^+K^-)/N(D^0 \to K^-\pi^+)$, the ratio of numbers of events observed, and similarly for the $\overline{D}^0$.

$A_{CP}(K^0_SK^0_S)$ in $D^0, \overline{D}^0 \to K^0_SK^0_S$

VALUE (%)	EVTS	DOCUMENT ID		TECN	COMMENT
− 0.9 ± 1.2 OUR AVERAGE Error includes scale factor of 1.7. See the ideogram below.					
− 0.6 ± 1.1 ±0.1		[1] ADACHI	25M	BEL2	e^+e^- at/near $\Upsilon(4S)$
6.2 ± 3.0 ±0.8	2k	[2] HAYRAPETY...	24BB	CMS	pp at 13 TeV
− 3.1 ± 1.2 ±0.5	8.1k	[3] AAIJ	21X	LHCB	pp at 13 TeV
− 0.02± 1.53±0.17	5.4k	[4] DASH	17	BELL	at/near $\Upsilon(4S)$, $\Upsilon(5S)$
− 2.9 ± 5.2 ±2.2	630	AAIJ	15AT	LHCB	pp at 7, 8 TeV
• • • We do not use the following data for averages, fits, limits, etc. • • •					
− 1.4 ± 1.3 ±0.1	7.1k	[5] ADACHI	25D	BEL2	e^+e^- at/near $\Upsilon(4S)$
1.3 ± 2.0 ±0.2	19.7k	[6] ADACHI	25M	BEL2	e^+e^- at/near $\Upsilon(4S)$
2.3 ± 2.8 ±0.9	1.7k	AAIJ	18AV	LHCB	see AAIJ 21X
−23 ±19	65	BONVICINI	01	CLE2	$e^+e^- \approx$ 10.6 GeV

[1] Combination of ADACHI 25M and ADACHI 25D results.
[2] HAYRAPETYAN 24BB reports a value of $(6.3 \pm 3.0 \pm 0.2 \pm 0.8) \times 10^{-2}$ where the third uncertainty is from the world-average value of $A_{CP}(K^0_S\pi^+\pi^-) = 0.1 \pm 0.8\%$. We have added the systematic uncertainties in quadrature.
[3] AAIJ 21X reports a value of $(-3.1 \pm 1.2 \pm 0.4 \pm 0.2) \times 10^{-2}$ where the third uncertainty is from $A_{CP}(K^+K^-) = 0.04 \pm 0.12 \pm 0.10\%$, as measured by LHCb. We have added the systematic uncertainties in quadrature. Supersedes AAIJ 18AV.
[4] The systematic uncertainty is dominated by the uncertainty on A_{CP} in the control channel $D^0 \to K^0_S\pi^0$.
[5] Based on data collected by Belle and Belle II. D^0 flavor determined using $D^*(2010)^+ \to D^0\pi^+$ decays.
[6] Based on data collected by Belle and Belle II. D^0 flavor inferred using the information from the charged particles of the rest of the event.

Int. J. Mod. Phys. A 2026.41. Downloaded from www.worldscientific.com
by UNIVERSITY OF CALIFORNIA @ BERKELEY on 09/16/26. Re-use and distribution is strictly not permitted, except for Open Access articles.

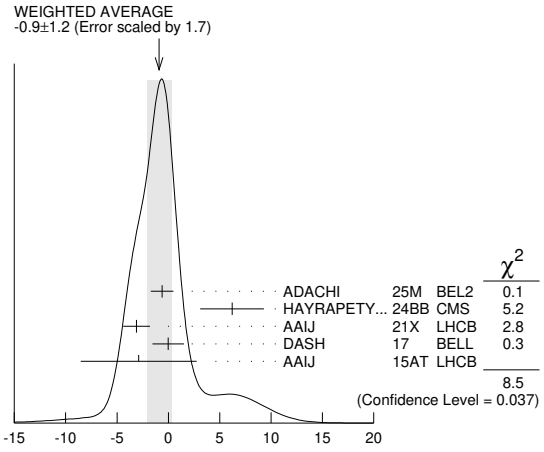

$A_{CP}(K^0_S K^0_S)$ in $D^0, \overline{D}^0 \to K^0_S K^0_S$ (%)

$A_{CP}(\pi^+\pi^-)$ in $D^0, \overline{D}^0 \to \pi^+\pi^-$

VALUE (%)	EVTS	DOCUMENT ID		TECN	COMMENT
0.13±0.14 OUR AVERAGE					
0.07±0.14±0.11		[1] AAIJ	17M	LHCB	pp 7, 8 TeV
0.22±0.24±0.11	215k	[2] AALTONEN	12B	CDF	$p\overline{p}$, $\sqrt{s}$=1.96 TeV
−0.24±0.52±0.22	63.7k	[3] AUBERT	08M	BABR	$e^+e^- \approx$ 10.6 GeV
0.43±0.52±0.12	51k	[4] STARIC	08	BELL	$e^+e^- \approx \Upsilon(4S)$
1.0 ±1.3 ±0.6		[5] ACOSTA	05C	CDF	$p\overline{p}$, $\sqrt{s}$=1.96 TeV
1.9 ±3.2 ±0.8	1136	[5] CSORNA	02	CLE2	$e^+e^- \approx \Upsilon(4S)$
4.8 ±3.9 ±2.5	1177	[5] LINK	00B	FOCS	
−4.9 ±7.8 ±3.0	343	[5] AITALA	98C	E791	$-0.186 < A_{CP} < +0.088$ (90% CL)
• • • We do not use the following data for averages, fits, limits, etc. • • •					
−0.20±0.19±0.10	774k	[2,6] AAIJ	14AK	LHCB	See AAIJ 17M

[1] AAIJ 17M value combines $\Delta A_{CP}(\pi\pi, KK)$ from AAIJ 16D, $A_{CP}(KK)$ from AAIJ 17M, and $A_{CP}(\pi\pi)$ from AAIJ 14AK.
[2] See also "D^0 CP-violating asymmetry differences" at the end of the CP-violating asymmetries.
[3] AUBERT 08M uses corrected numbers of events directly, not ratios with $K^\mp\pi^\pm$ events.
[4] STARIC 08 uses $D^0 \to K^-\pi^+$ and $\overline{D}^0 \to K^+\pi^-$ decays to correct for detector-induced asymmetries.
[5] AITALA 98C, LINK 00B, CSORNA 02, and ACOSTA 05C measure $N(D^0 \to \pi^+\pi^-)/N(D^0 \to K^-\pi^+)$, the ratio of numbers of events observed, and similarly for the $\overline{D}^0$.
[6] AAIJ 14AK uses $\Delta A_{CP}(\pi\pi, KK)$ and $A_{CP}(KK)$ reported in the same paper.

$A_{CP}(\pi^0\pi^0)$ in $D^0, \overline{D}^0 \to \pi^0\pi^0$

VALUE (%)	EVTS	DOCUMENT ID		TECN	COMMENT
0.1 ±0.5 OUR AVERAGE					
0.30±0.72±0.20	25.7k	ADACHI	25K	BEL2	e^+e^- at/near $\Upsilon(4S)$
−0.03±0.64±0.10	34k	NISAR	14	BELL	e^+e^- at/near Υ's
0.1 ±4.8	810	BONVICINI	01	CLE2	$e^+e^- \approx$ 10.6 GeV

$A_{CP}(\rho\gamma)$ in $D^0, \overline{D}^0 \to \rho\gamma$

VALUE (units 10^{-2})	DOCUMENT ID		TECN	COMMENT
5.6±15.2±0.6	NANUT	17	BELL	e^+e^- at Υ(nS), n=2,3,4,5

$A_{CP}(\phi\gamma)$ in $D^0, \overline{D}^0 \to \phi\gamma$

VALUE (units 10^{-2})	DOCUMENT ID		TECN	COMMENT
−9.4±6.6±0.1	NANUT	17	BELL	e^+e^- at Υ(nS), n=2,3,4,5

$A_{CP}(\overline{K}^*(892)^0\gamma)$ in $D^0, \overline{D}^0 \to \overline{K}^*(892)^0\gamma$

VALUE (units 10^{-2})	DOCUMENT ID		TECN	COMMENT
−0.3±2.0±0.0	NANUT	17	BELL	e^+e^- at Υ(nS), n=2,3,4,5

$A_{CP}(\pi^+\pi^-\pi^0)$ in $D^0, \overline{D}^0 \to \pi^+\pi^-\pi^0$

VALUE (%)	EVTS	DOCUMENT ID		TECN	COMMENT
0.4 ±0.4 OUR AVERAGE					
+0.6 ±0.9 ±0.4	12.8k	ABLIKIM	22BG	BES3	e^+e^- at 3.773 GeV
0.43±1.30	123k	ARINSTEIN	08	BELL	$e^+e^- \approx \Upsilon(4S)$
0.31±0.41±0.17	80k	[1] AUBERT	08AO	BABR	$e^+e^- \approx$ 10.6 GeV
1^{+9}_{-7} ±5		CRONIN-HEN...	05	CLEO	$e^+e^- \approx$ 10 GeV

[1] AUBERT 08AO report their result using a different sign convention.

$A_{CP}(\eta\pi^+\pi^-)$ in $D^0, \overline{D}^0 \to \eta\pi^+\pi^-$

VALUE (units 10^{-2})	EVTS	DOCUMENT ID		TECN	COMMENT
0.9±1.2±0.5	13k	LI	21G	BELL	e^+e^- at Υ(nS)
• • • We do not use the following data for averages, fits, limits, etc. • • •					
9.6±5.4±1.8	450	ABLIKIM	20G	BES3	e^+e^- at 3.773 GeV

$A_{CP}(\rho(770)^+\pi^- \to \pi^+\pi^-\pi^0)$ in $D^0 \to \rho^+\pi^-, \overline{D}^0 \to \rho^-\pi^+$

VALUE (%)	DOCUMENT ID		TECN	COMMENT
+1.2±0.8±0.3	AUBERT	08AO	BABR	Table 1, −Col.5/2×Col.2

$A_{CP}(\rho(770)^0\pi^0 \to \pi^+\pi^-\pi^0)$ in $D^0, \overline{D}^0 \to \rho^0\pi^0$

VALUE (%)	DOCUMENT ID		TECN	COMMENT
−3.1±2.7±1.2	AUBERT	08AO	BABR	Table 1, −Col.5/2×Col.2

$A_{CP}(\rho(770)^-\pi^+ \to \pi^+\pi^-\pi^0)$ in $D^0 \to \rho^-\pi^+, \overline{D}^0 \to \rho^+\pi^-$

VALUE (%)	DOCUMENT ID		TECN	COMMENT
−1.0±1.6±0.7	AUBERT	08AO	BABR	Table 1, −Col.5/2×Col.2

$A_{CP}(\rho(1450)^+\pi^- \to \pi^+\pi^-\pi^0)$ in $D^0 \to \rho(1450)^+\pi^-, \overline{D}^0 \to$ c.c.

VALUE (%)	DOCUMENT ID		TECN	COMMENT
0±50±50	AUBERT	08AO	BABR	Table 1, −Col.5/2×Col.2

$A_{CP}(\rho(1450)^0\pi^0 \to \pi^+\pi^-\pi^0)$ in $D^0, \overline{D}^0 \to \rho(1450)^0\pi^0$

VALUE (%)	DOCUMENT ID		TECN	COMMENT
−17±33±17	AUBERT	08AO	BABR	Table 1, −Col.5/2×Col.2

$A_{CP}(\rho(1450)^-\pi^+ \to \pi^+\pi^-\pi^0)$ in $D^0 \to \rho(1450)^-\pi^+, \overline{D}^0 \to$ c.c.

VALUE (%)	DOCUMENT ID		TECN	COMMENT
+6±8±3	AUBERT	08AO	BABR	Table 1, −Col.5/2×Col.2

$A_{CP}(\rho(1700)^+\pi^- \to \pi^+\pi^-\pi^0)$ in $D^0 \to \rho(1700)^+\pi^-, \overline{D}^0 \to$ c.c.

VALUE (%)	DOCUMENT ID		TECN	COMMENT
−5±13±5	AUBERT	08AO	BABR	Table 1, −Col.5/2×Col.2

$A_{CP}(\rho(1700)^0\pi^0 \to \pi^+\pi^-\pi^0)$ in $D^0, \overline{D}^0 \to \rho(1700)^0\pi^0$

VALUE (%)	DOCUMENT ID		TECN	COMMENT
+13±8±3	AUBERT	08AO	BABR	Table 1, −Col.5/2×Col.2

$A_{CP}(\rho(1700)^-\pi^+ \to \pi^+\pi^-\pi^0)$ in $D^0 \to \rho(1700)^-\pi^+, \overline{D}^0 \to$ c.c.

VALUE (%)	DOCUMENT ID		TECN	COMMENT
+8±10±5	AUBERT	08AO	BABR	Table 1, −Col.5/2×Col.2

$A_{CP}(f_0(980)\pi^0 \to \pi^+\pi^-\pi^0)$ in $D^0, \overline{D}^0 \to f_0(980)\pi^0$

VALUE (%)	DOCUMENT ID		TECN	COMMENT
0±25±25	AUBERT	08AO	BABR	Table 1, −Col.5/2×Col.2

$A_{CP}(f_0(1370)\pi^0 \to \pi^+\pi^-\pi^0)$ in $D^0, \overline{D}^0 \to f_0(1370)\pi^0$

VALUE (%)	DOCUMENT ID		TECN	COMMENT
+25±13±13	AUBERT	08AO	BABR	Table 1, −Col.5/2×Col.2

$A_{CP}(f_0(1500)\pi^0 \to \pi^+\pi^-\pi^0)$ in $D^0, \overline{D}^0 \to f_0(1500)\pi^0$

VALUE (%)	DOCUMENT ID		TECN	COMMENT
0±13±13	AUBERT	08AO	BABR	Table 1, −Col.5/2×Col.2

$A_{CP}(f_0(1710)\pi^0 \to \pi^+\pi^-\pi^0)$ in $D^0, \overline{D}^0 \to f_0(1710)\pi^0$

VALUE (%)	DOCUMENT ID		TECN	COMMENT
0±17±17	AUBERT	08AO	BABR	Table 1, −Col.5/2×Col.2

$A_{CP}(f_2(1270)\pi^0 \to \pi^+\pi^-\pi^0)$ in $D^0, \overline{D}^0 \to f_2(1270)\pi^0$

VALUE (%)	DOCUMENT ID		TECN	COMMENT
−4±4±4	AUBERT	08AO	BABR	Table 1, −Col.5/2×Col.2

$A_{CP}(\sigma(400)\pi^0 \to \pi^+\pi^-\pi^0)$ in $D^0, \overline{D}^0 \to \sigma(400)\pi^0$

VALUE (%)	DOCUMENT ID		TECN	COMMENT
+6±6±6	AUBERT	08AO	BABR	Table 1, −Col.5/2×Col.2

A_{CP}(nonresonant $\pi^+\pi^-\pi^0$) in $D^0, \overline{D}^0 \to$ nonresonant $\pi^+\pi^-\pi^0$

VALUE (%)	DOCUMENT ID		TECN	COMMENT
−13±19±13	AUBERT	08AO	BABR	Table 1, −Col.5/2×Col.2

$A_{CP}(\pi^+\pi^-2\pi^0)$ in $D^0, \overline{D}^0 \to \pi^+\pi^-2\pi^0$

VALUE (%)	EVTS	DOCUMENT ID		TECN	COMMENT
−2.5±1.9±0.7	3.8k	ABLIKIM	22BG	BES3	e^+e^- at 3.773 GeV

$A_{CP}(2\pi^+2\pi^-)$ in $D^0, \overline{D}^0 \to 2\pi^+2\pi^-$

VALUE (%)	EVTS	DOCUMENT ID		COMMENT
0.54±1.04±0.51	7.3k	[1,2] DARGENT	17	e^+e^- at $\psi(3770)$

[1] Decay rate asymmetry integrated in decay time and across full 4π phase space.
[2] Obtained by analyzing CLEO-c data but not authored by the CLEO Collaboration.

$A_{CP}(a_1(1260)^+\pi^- \to 2\pi^+2\pi^-)$ in $D^0 \to a_1(1260)^+\pi^-, \overline{D}^0 \to$ c.c.

VALUE (%)	EVTS	DOCUMENT ID		COMMENT
4.7±2.6±4.9	7.3k	[1] DARGENT	17	4-body fit, 4π evts

[1] Obtained by analyzing CLEO-c data but not authored by the CLEO Collaboration.

$A_{CP}(a_1(1260)^-\pi^+ \to 2\pi^+2\pi^-)$ in $D^0 \to a_1(1260)^-\pi^+, \overline{D}^0 \to$ c.c.

VALUE (%)	EVTS	DOCUMENT ID		COMMENT
13.7±13.8±11.4	7.3k	[1] DARGENT	17	4-body fit, 4π evts

[1] Obtained by analyzing CLEO-c data but not authored by the CLEO Collaboration.

Int. J. Mod. Phys. A 2026.41. Downloaded from www.worldscientific.com by LIFORNIA @ BERKELEY on 09/16/26. Re-use and distribution is strictly not permitted, except for Open Access articles.

$A_{CP}(\pi(1300)^+\pi^- \to 2\pi^+2\pi^-)$ in $D^0 \to \pi(1300)^+\pi^-, \overline{D}^0 \to$ c.c.

VALUE (%)	EVTS	DOCUMENT ID		COMMENT
−1.6±12.9±6.7	7.3k	[1] DARGENT	17	4-body fit, 4π evts

[1] Obtained by analyzing CLEO-c data but not authored by the CLEO Collaboration.

$A_{CP}(\pi(1300)^-\pi^+ \to 2\pi^+2\pi^-)$ in $D^0 \to \pi(1300)^-\pi^+, \overline{D}^0 \to$ c.c.

VALUE (%)	EVTS	DOCUMENT ID		COMMENT
−5.6±11.9±27.7	7.3k	[1] DARGENT	17	4-body fit, 4π evts

[1] Obtained by analyzing CLEO-c data but not authored by the CLEO Collaboration.

$A_{CP}(a_1(1640)^+\pi^- \to 2\pi^+2\pi^-)$ in $D^0 \to a_1(1640)^+\pi^-, \overline{D}^0 \to$ c.c.

VALUE (%)	EVTS	DOCUMENT ID		COMMENT
8.6±17.8±19.3	7.3k	[1] DARGENT	17	4-body fit, 4π evts

[1] Obtained by analyzing CLEO-c data but not authored by the CLEO Collaboration.

$A_{CP}(\pi_2(1670)^+\pi^- \to 2\pi^+2\pi^-)$ in $D^0 \to \pi_2(1670)^+\pi^-, \overline{D}^0 \to$ c.c.

VALUE (%)	EVTS	DOCUMENT ID		COMMENT
7.3±15.1±10.4	7.3k	[1] DARGENT	17	4-body fit, 4π evts

[1] Obtained by analyzing CLEO-c data but not authored by the CLEO Collaboration.

$A_{CP}(\sigma f_0(1370) \to 2\pi^+2\pi^-)$ in $D^0, \overline{D}^0 \to \sigma f_0(1370)$

VALUE (%)	EVTS	DOCUMENT ID		COMMENT
−14.6±16.5±9.4	7.3k	[1] DARGENT	17	4-body fit, 4π evts

[1] Obtained by analyzing CLEO-c data but not authored by the CLEO Collaboration.

$A_{CP}(\sigma\rho(770)^0 \to 2\pi^+2\pi^-)$ in $D^0, \overline{D}^0 \to \sigma\rho(770)^0$

VALUE (%)	EVTS	DOCUMENT ID		COMMENT
2.5±16.8±20.8	7.3k	[1] DARGENT	17	4-body fit, 4π evts

[1] Obtained by analyzing CLEO-c data but not authored by the CLEO Collaboration.

$A_{CP}(2\rho(770)^0 \to 2\pi^+2\pi^-)$ in $D^0, \overline{D}^0 \to 2\rho(770)^0$

VALUE (%)	EVTS	DOCUMENT ID		COMMENT
−5.6±5.0±2.9	7.3k	[1] DARGENT	17	4-body fit, 4π evts

[1] Obtained by analyzing CLEO-c data but not authored by the CLEO Collaboration.

$A_{CP}(2f_2(1270) \to 2\pi^+2\pi^-)$ in $D^0, \overline{D}^0 \to 2f_2(1270)$

VALUE (%)	EVTS	DOCUMENT ID		COMMENT
−28.3±12.3±20.9	7.3k	[1] DARGENT	17	4-body fit, 4π evts

[1] Obtained by analyzing CLEO-c data but not authored by the CLEO Collaboration.

$A_{CP}(\pi^+\pi^-\pi^0\eta)$ in $D^0, \overline{D}^0 \to \pi^+\pi^-\pi^0\eta$

VALUE (units 10^{-2})	EVTS	DOCUMENT ID		TECN	COMMENT
−5.5±5.2±2.4	510	ABLIKIM	20V	BES3	e^+e^-, 3773 MeV

$A_{CP}(K^+K^-\pi^0)$ in $D^0, \overline{D}^0 \to K^+K^-\pi^0$

VALUE (%)	EVTS	DOCUMENT ID		TECN	COMMENT
−1.00±1.67±0.25	11 ± 0.11k	AUBERT	08AO	BABR	$e^+e^- \approx$ 10.6 GeV

$A_{CP}(K^*(892)^+K^- \to K^+K^-\pi^0)$ in $D^0 \to K^*(892)^+K^-, \overline{D}^0 \to$ c.c.

VALUE (%)	DOCUMENT ID		TECN	COMMENT
−0.9±1.2±0.4	[1] AUBERT	08AO	BABR	Table 1, −Col.5/2×Col.2

[1] AUBERT 08AO report their result using a different sign convention.

$A_{CP}(K^*(1410)^+K^- \to K^+K^-\pi^0)$ in $D^0 \to K^*(1410)^+K^-, \overline{D}^0 \to$ c.c.

VALUE (%)	DOCUMENT ID		TECN	COMMENT
−21±23±8	AUBERT	08AO	BABR	Table 1, −Col.5/2×Col.2

$A_{CP}((K^+\pi^0)_{S-wave}K^- \to K^+K^-\pi^0)$ in $D^0 \to (K^+\pi^0)_S K^-, \overline{D}^0 \to$ c.c.

VALUE (%)	DOCUMENT ID		TECN	COMMENT
+7±15±3	AUBERT	08AO	BABR	Table 1, −Col.5/2×Col.2

$A_{CP}(\phi(1020)\pi^0 \to K^+K^-\pi^0)$ in $D^0, \overline{D}^0 \to \phi(1020)\pi^0$

VALUE (%)	DOCUMENT ID		TECN	COMMENT
+1.1±2.1±0.5	AUBERT	08AO	BABR	Table 1, −Col.5/2×Col.2

$A_{CP}(f_0(980)\pi^0 \to K^+K^-\pi^0)$ in $D^0, \overline{D}^0 \to f_0(980)\pi^0$

VALUE (%)	DOCUMENT ID		TECN	COMMENT
−3±19±1	AUBERT	08AO	BABR	Table 1, −Col.5/2×Col.2

$A_{CP}(a_0(980)^0\pi^0 \to K^+K^-\pi^0)$ in $D^0, \overline{D}^0 \to a_0(980)^0\pi^0$

VALUE (%)	DOCUMENT ID		TECN	COMMENT
−5±16±2	[1] AUBERT	08AO	BABR	Table 1, −Col.5/2×Col.2

[1] This AUBERT 08AO value is obtained when the $a_0(980)^0$ replaces the $f_0(980)$ in the fit.

$A_{CP}(f_2'(1525)\pi^0 \to K^+K^-\pi^0)$ in $D^0, \overline{D}^0 \to f_2'(1525)\pi^0$

VALUE (%)	DOCUMENT ID		TECN	COMMENT
0±50±150	AUBERT	08AO	BABR	Table 1, −Col.5/2×Col.2

$A_{CP}(K^*(892)^-K^+ \to K^+K^-\pi^0)$ in $D^0 \to K^*(892)^-K^+, \overline{D}^0 \to$ c.c.

VALUE (%)	DOCUMENT ID		TECN	COMMENT
−5±4±1	AUBERT	08AO	BABR	Table 1, −Col.5/2×Col.2

$A_{CP}(K^*(1410)^-K^+ \to K^+K^-\pi^0)$ in $D^0 \to K^*(1410)^-K^+, \overline{D}^0 \to$ c.c.

VALUE (%)	DOCUMENT ID		TECN	COMMENT
−17±28±7	AUBERT	08AO	BABR	Table 1, −Col.5/2×Col.2

$A_{CP}((K^-\pi^0)_{S-wave}K^+ \to K^+K^-\pi^0)$ in $D^0 \to (K^-\pi^0)_S K^+, \overline{D}^0 \to$ c.c.

VALUE (%)	DOCUMENT ID		TECN	COMMENT
−7±40±8	AUBERT	08AO	BABR	Table 1, −Col.5/2×Col.2

$A_{CP}(K^+K^-\eta)$ in $D^0, \overline{D}^0 \to K^+K^-\eta$

VALUE (units 10^{-2})	EVTS	DOCUMENT ID		TECN	COMMENT
−1.4±3.3±1.1	1.4k	LI	21G	BELL	e^+e^- at $\Upsilon(nS)$

$A_{CP}(\phi(1020)\eta \to K^+K^-\eta)$ in $D^0, \overline{D}^0 \to \phi(1020)\eta$

VALUE (units 10^{-2})	EVTS	DOCUMENT ID		TECN	COMMENT
−1.9±4.4±0.6	1.4k	LI	21G	BELL	e^+e^- at $\Upsilon(nS)$

$A_{CP}(K^0_S\pi^0)$ in $D^0, \overline{D}^0 \to K^0_S\pi^0$

VALUE (%)	EVTS	DOCUMENT ID		TECN	COMMENT
−0.20±0.17 OUR AVERAGE					
−0.21±0.16±0.07	467k	[1] NISAR	14	BELL	e^+e^- at/near Υ's
0.1 ±1.3	9099	BONVICINI	01	CLE2	$e^+e^- \approx$ 10.6 GeV
• • • We do not use the following data for averages, fits, limits, etc. • • •					
−0.28±0.19±0.10	326k	KO	11	BELL	See NISAR 14
−1.8 ±3.0		BARTELT	95	CLE2	See BONVICINI 01

[1] After subtracting CPV in $K^0 - \overline{K}^0$ mixing, NISAR 14 gets $A_{CP} = (+0.12 \pm 0.16 \pm 0.07)$%.

$A_{CP}(K^0_S\eta)$ in $D^0, \overline{D}^0 \to K^0_S\eta$

VALUE (%)	EVTS	DOCUMENT ID		TECN	COMMENT
+0.54±0.51±0.16	46k	KO	11	BELL	$e^+e^- \approx \Upsilon(4S)$

$A_{CP}(K^0_S\eta')$ in $D^0, \overline{D}^0 \to K^0_S\eta'$

VALUE (%)	EVTS	DOCUMENT ID		TECN	COMMENT
+0.98±0.67±0.14	27k	KO	11	BELL	$e^+e^- \approx \Upsilon(4S)$

$A_{CP}(K^0_S\phi)$ in $D^0, \overline{D}^0 \to K^0_S\phi$

VALUE (%)	DOCUMENT ID		TECN	COMMENT
−2.8±9.4	BARTELT	95	CLE2	$-18.2 < A_{CP} < +12.6\%$ (90%CL)

$A_{CP}(K^\mp\pi^\pm)$ in $D^0 \to K^-\pi^+, \overline{D}^0 \to K^+\pi^-$

VALUE (%)	EVTS	DOCUMENT ID		TECN	COMMENT
0.2 ±0.5 OUR AVERAGE					
−0.01±0.91		AAIJ	18K	LHCB	pp at 7, 8, 13 TeV
0.3 ±0.3 ±0.6		BONVICINI	14	CLEO	All CLEO-c runs
• • • We do not use the following data for averages, fits, limits, etc. • • •					
+0.5 ±0.4 ±0.9	150k	MENDEZ	10	CLEO	See BONVICINI 14
−0.4 ±0.5 ±0.9		DOBBS	07	CLEO	See BONVICINI 14

$A_{CP}(K^\pm\pi^\mp)$ in $D^0 \to K^+\pi^-, \overline{D}^0 \to K^-\pi^+$

VALUE (%)	EVTS	DOCUMENT ID		TECN	COMMENT
− 0.4 ± 0.7 OUR AVERAGE Error includes scale factor of 1.3. See the ideogram below.					
− 0.66± 0.57		[1,2] AAIJ	25	LHCB	pp at 7, 8, 13 TeV
2.3 ± 1.7	20k	[1,3] AAIJ	25U	LHCB	pp at 13 TeV
− 1.7 ± 1.6		[1,3,4] AAIJ	17AO	LHCB	pp at 7,8 TeV
− 2.1 ± 5.2 ±1.5	4.0k	AUBERT	07W	BABR	$e^+e^- \approx$ 10.6 GeV
+ 2.3 ± 4.7	4.0k	[5] ZHANG	06	BELL	e^+e^-
+18 ±14 ±4		[6] LINK	05H	FOCS	γ nucleus
+ 9.5 ± 6.1 ±8.3		[7] AUBERT	03Z	BABR	e^+e^-, 10.6 GeV
+ 2 $^{+19}_{-20}$ ±1	45	[8] GODANG	00	CLE2	e^+e^-
• • • We do not use the following data for averages, fits, limits, etc. • • •					
− 0.71± 0.60	1.6M	[1] AAIJ	25	LHCB	pp at 13 TeV
− 0.7 ± 1.9		[4] AAIJ	13CE	LHCB	Repl. by AAIJ 17AO
− 8.0 ± 7.7	0.8k	[9] LI	05A	BELL	See ZHANG 06

[1] The CPV is derived from $A_{CP} = (R^+_D - R^-_D)/(R^+_D + R^-_D)$.
[2] $D^*(2010)^+$ tag of $D^0 \to K^+\pi^-$.
[3] Doubly-tagged $D^0 \to K^\pm\pi^\mp$ from preceding $B \to D^*(2010)^+\mu X$ with $D^*(2010)^+ \to D^0\pi^+$.
[4] Based on 3 fb^{-1} of data collected at $\sqrt{s}$ = 7, 8 TeV.
[5] This ZHANG 06 result allows mixing.
[6] This LINK 05H result assumes no mixing. If mixing is allowed, it becomes $0.13^{+0.33}_{-0.25} \pm 0.10$.
[7] This AUBERT 03Z limit assumes no mixing. If mixing is allowed, the 95% confidence-level interval is $(-2.8 < A_D < 4.9)\times10^{-3}$.
[8] This GODANG 00 result assumes no D^0-$\overline{D}^0$ mixing and becomes $-0.43 < A_{CP} < +0.34$ at 95% CL. If mixing is allowd $A_{CP} = -0.01^{+0.16}_{-0.17} \pm 0.01$.
[9] This LI 05A result allows mixing.

Int. J. Mod. Phys. A 2026.41. Downloaded from www.worldscientific.com
by UNIVERSITY OF CALIFORNIA @ BERKELEY on 09/16/26. Re-use and distribution is strictly not permitted, except for Open Access articles.

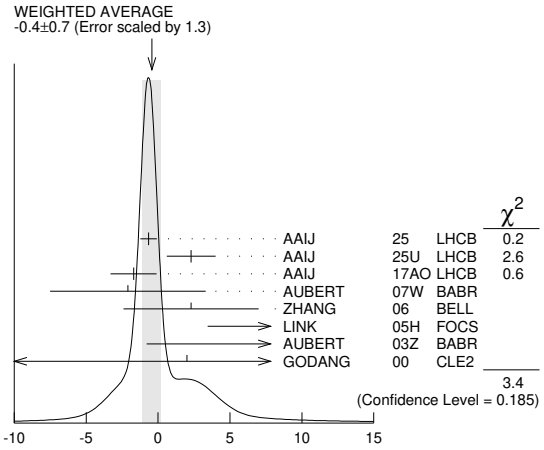

$A_{CP}(K^{\pm}\pi^{\mp})$ in $D^0 \to K^+\pi^-$, $\overline{D}^0 \to K^-\pi^+$ (%)

$A_{CP}(K^-\pi^+)$ in $D_{CP(\pm1)} \to K^{\mp}\pi^{\pm}$

$A_{CP}(K^-\pi^+) = [B(D_{CP(-)} \to K^-\pi^+) - B(D_{CP(+)} \to K^-\pi^+)]$ / Sum

VALUE (%)	DOCUMENT ID		TECN	COMMENT
13.1±1.0 OUR AVERAGE				
13.2±1.1±0.7	[1] ABLIKIM	22BM	BES3	e^+e^- at $\psi(3770)$
13.0±1.2±0.8	[2] ABLIKIM	22BM	BES3	$D^0 \to \pi^+\pi^-\pi^0$ reference
• • • We do not use the following data for averages, fits, limits, etc. • • •				
12.7±1.3±0.7	[3] ABLIKIM	14C	BES3	$e^+e^- \to D^0\overline{D}^0$, 3.77 GeV

[1] ABLIKIM 22B uses quantum correlations in $e^+e^- \to D^0\overline{D}^0$ at the $\psi(3770)$ to measure the asymmetry of the branching fraction of $D^0 \to K^-\pi^+$ in *CP*-odd and *CP*-even eigenstates. It then extracts the strong-phase difference $\delta_{K\pi}$.

[2] ABLIKIM 22B uses quantum correlations in $e^+e^- \to D^0\overline{D}^0$ at the $\psi(3770)$ to measure the asymmetry of the branching fraction of $D^0 \to K^-\pi^+$ in *CP*-odd and *CP*-even eigenstates, using the predominantly CP-even decay $D^0 \to \pi^+\pi^-\pi^0$ mode as reference. It then extracts the strong-phase difference $\delta_{K\pi}$.

[3] ABLIKIM 14C uses quantum correlations in $e^+e^- \to D^0\overline{D}^0$ at the $\psi(3770)$ to measure the asymmetry of the branching fraction of $D^0 \to K^-\pi^+$ in *CP*-odd and *CP*-even eigenstates. It then extracts the strong-phase difference $\delta_{K\pi}$. Superseded by ABLIKIM 22BM.

$A_{CP}(K^{\mp}\pi^{\pm}\pi^0)$ in $D^0 \to K^-\pi^+\pi^0$, $\overline{D}^0 \to K^+\pi^-\pi^0$

VALUE (%)	DOCUMENT ID		TECN	COMMENT
0.1±0.5 OUR AVERAGE				
0.1±0.3±0.4	BONVICINI	14	CLEO	All CLEO-c runs
−3.1±8.6	[1] KOPP	01	CLE2	$e^+e^- \approx$ 10.6 GeV
• • • We do not use the following data for averages, fits, limits, etc. • • •				
0.2±0.4±0.8	DOBBS	07	CLEO	See BONVICINI 14

[1] KOPP 01 fits separately the D^0 and $\overline{D}^0$ Dalitz plots and then calculates the integrated difference of normalized densities divided by the integrated sum.

$A_{CP}(K^{\pm}\pi^{\mp}\pi^0)$ in $D^0 \to K^+\pi^-\pi^0$, $\overline{D}^0 \to K^-\pi^+\pi^0$

VALUE (%)	EVTS	DOCUMENT ID		TECN	COMMENT
0 ± 5 OUR AVERAGE					
−0.6± 5.3	1978 ± 104	TIAN	05	BELL	$e^+e^- \approx \Upsilon(4S)$
$+9\ ^{+25}_{-22}$	38	BRANDENB...	01	CLE2	$e^+e^- \approx \Upsilon(4S)$

$A_{CP}(K^0_S\pi^+\pi^-)$ in $D^0, \overline{D}^0 \to K^0_S\pi^+\pi^-$

VALUE (%)	EVTS	DOCUMENT ID		TECN	COMMENT
−0.1 ±0.8 OUR AVERAGE					
−0.05±0.57±0.54	350k	[1] AALTONEN	12AD	CDF	
$-0.9\ \pm2.1\ ^{+1.6}_{-5.7}$	4854	[2] ASNER	04A	CLEO	$e^+e^- \approx$ 10 GeV

[1] This is the overall result of AALTONEN 12AD. Following are the 15 *CP* fit-fraction asymmetries from the amplitude analysis of the D^0 and $\overline{D}^0 \to K^0_S\pi^+\pi^-$ Dalitz plots.

[2] This is the overall result of ASNER 04A; *CP*-violating limits are also given below for each of the 10 resonant submodes found in an amplitude analysis of the D^0 and $\overline{D}^0 \to K^0_S\pi^+\pi^-$ Dalitz plots.

$A_{CP}(K^{\mp}\pi^{\pm}\eta)$ in $D^0, \overline{D}^0 \to K^{\mp}\pi^{\pm}\eta$

VALUE (units 10^{-2})	EVTS	DOCUMENT ID		TECN	COMMENT
−1.9±1.3±1.0	6.1k	ABLIKIM	20V	BES3	e^+e^-, 3773 MeV

$A_{CP}(K^0_S\pi^0\eta)$ in $D^0, \overline{D}^0 \to K^0_S\pi^0\eta$

VALUE (units 10^{-2})	EVTS	DOCUMENT ID		TECN	COMMENT
−3.9±3.2±0.8	1.1k	ABLIKIM	20V	BES3	e^+e^-, 3773 MeV

$A_{CP}(K^{\mp}\pi^{\pm}\pi^0\eta)$ in $D^0, \overline{D}^0 \to K^{\mp}\pi^{\pm}\pi^0\eta$

VALUE (units 10^{-2})	EVTS	DOCUMENT ID		TECN	COMMENT
−7.9±4.8±2.5	580	ABLIKIM	20V	BES3	e^+e^-, 3773 MeV

$A_{CP}(K^*(892)^{\mp}\pi^{\pm} \to K^0_S\pi^+\pi^-)$ in $D^0 \to K^{*-}\pi^+$, $\overline{D}^0 \to K^{*+}\pi^-$

VALUE (%)	DOCUMENT ID		TECN	COMMENT
+0.36±0.33±0.40	AALTONEN	12AD	CDF	Dalitz fit, ∼ 350k evts
• • • We do not use the following data for averages, fits, limits, etc. • • •				
$+2.5\ \pm1.9\ ^{+3.3}_{-0.8}$	ASNER	04A	CLEO	Dalitz fit, 4854 evts

$A_{CP}(K^*(892)^{\pm}\pi^{\mp} \to K^0_S\pi^+\pi^-)$ in $D^0 \to K^{*+}\pi^-$, $\overline{D}^0 \to K^{*-}\pi^+$

This is a doubly Cabibbo-suppressed mode.

VALUE (%)	DOCUMENT ID		TECN	COMMENT
+ 1.0± 5.7± 2.1	AALTONEN	12AD	CDF	Dalitz fit, ∼ 350k evts
• • • We do not use the following data for averages, fits, limits, etc. • • •				
−21 ±42 ±28	ASNER	04A	CLEO	Dalitz fit, 4854 evts

$A_{CP}(K^0_S\rho^0 \to K^0_S\pi^+\pi^-)$ in $D^0 \to \overline{K}^0\rho^0$, $\overline{D}^0 \to K^0\rho^0$

VALUE (%)	DOCUMENT ID		TECN	COMMENT
−0.05±0.50±0.08	AALTONEN	12AD	CDF	Dalitz fit, ∼ 350k evts
• • • We do not use the following data for averages, fits, limits, etc. • • •				
$+3.1\ \pm3.8\ ^{+2.7}_{-2.2}$	ASNER	04A	CLEO	Dalitz fit, 4854 evts

$A_{CP}(K^0_S\omega \to K^0_S\pi^+\pi^-)$ in $D^0 \to \overline{K}^0\omega$, $\overline{D}^0 \to K^0\omega$

VALUE (%)	DOCUMENT ID		TECN	COMMENT
−12.6± 6.0± 2.6	AALTONEN	12AD	CDF	Dalitz fit, ∼ 350k evts
• • • We do not use the following data for averages, fits, limits, etc. • • •				
$-26\ \pm24\ ^{+22}_{-4}$	ASNER	04A	CLEO	Dalitz fit, 4854 evts

$A_{CP}(K^0_S f_0(980) \to K^0_S\pi^+\pi^-)$ in $D^0 \to \overline{K}^0 f_0(980)$, $\overline{D}^0 \to K^0 f_0(980)$

VALUE (%)	DOCUMENT ID		TECN	COMMENT
−0.4± 2.2± 1.6	AALTONEN	12AD	CDF	Dalitz fit, ∼ 350k evts
• • • We do not use the following data for averages, fits, limits, etc. • • •				
$-4.7\pm11.0^{+24.9}_{-8.8}$	ASNER	04A	CLEO	Dalitz fit, 4854 evts

$A_{CP}(K^0_S f_2(1270) \to K^0_S\pi^+\pi^-)$ in $D^0 \to \overline{K}^0 f_2(1270)$, $\overline{D}^0 \to K^0 f_2(1270)$

VALUE (%)	DOCUMENT ID		TECN	COMMENT
− 4.0± 3.4± 3.0	AALTONEN	12AD	CDF	Dalitz fit, ∼ 350k evts
• • • We do not use the following data for averages, fits, limits, etc. • • •				
$+34\ \pm51\ ^{+33}_{-79}$	ASNER	04A	CLEO	Dalitz fit, 4854 evts

$A_{CP}(K^0_S f_0(1370) \to K^0_S\pi^+\pi^-)$ in $D^0 \to \overline{K}^0 f_0(1370)$, $\overline{D}^0 \to K^0 f_0(1370)$

VALUE (%)	DOCUMENT ID		TECN	COMMENT
− 0.5± 4.6± 7.7	AALTONEN	12AD	CDF	Dalitz fit, ∼ 350k evts
• • • We do not use the following data for averages, fits, limits, etc. • • •				
$+18\ \pm10\ ^{+13}_{-22}$	ASNER	04A	CLEO	Dalitz fit, 4854 evts

$A_{CP}(K^0_S\rho^0(1450))$ in $D^0 \to \overline{K}^0\rho^0(1450)$, $\overline{D}^0 \to K^0\rho^0(1450)$

VALUE (%)	DOCUMENT ID		TECN	COMMENT
−4.1±5.2±8.1	AALTONEN	12AD	CDF	Dalitz fit, ∼ 350k evts

$A_{CP}(K^0_S f_0(600))$ in $D^0 \to \overline{K}^0 f_0(600)$, $\overline{D}^0 \to K^0 f_0(600)$

VALUE (%)	DOCUMENT ID		TECN	COMMENT
−2.7±2.7±3.6	AALTONEN	12AD	CDF	Dalitz fit, ∼ 350k evts

$A_{CP}(K^*(1410)^{\mp}\pi^{\pm})$ in $D^0 \to K^*(1410)^-\pi^+$, $\overline{D}^0 \to K^*(1410)^+\pi^-$

VALUE (%)	DOCUMENT ID		TECN	COMMENT
−2.3±5.7±6.4	AALTONEN	12AD	CDF	Dalitz fit, ∼ 350k evts

$A_{CP}(K^*_0(1430)^{\mp}\pi^{\pm} \to K^0_S\pi^+\pi^-)$ in $D^0 \to K^*_0(1430)^-\pi^+$, $\overline{D}^0 \to$ c.c.

VALUE (%)	DOCUMENT ID		TECN	COMMENT
4.0± 2.4±3.8	AALTONEN	12AD	CDF	Dalitz fit, ∼ 350k evts
• • • We do not use the following data for averages, fits, limits, etc. • • •				
$-0.2\pm11.3^{+8.8}_{-5.0}$	ASNER	04A	CLEO	Dalitz fit, 4854 evts

$A_{CP}(K^*_0(1430)^{\pm}\pi^{\mp})$ in $D^0 \to K^*_0(1430)^+\pi^-$, $\overline{D}^0 \to K^*_0(1430)^-\pi^+$

This is a doubly Cabibbo-suppressed mode.

VALUE (%)	DOCUMENT ID		TECN	COMMENT
+12±11±10	AALTONEN	12AD	CDF	Dalitz fit, ∼ 350k evts

$A_{CP}(K^*_2(1430)^{\mp}\pi^{\pm} \to K^0_S\pi^+\pi^-)$ in $D^0 \to K^*_2(1430)^-\pi^+$, $\overline{D}^0 \to$ c.c.

VALUE (%)	DOCUMENT ID		TECN	COMMENT
+2.9± 4.0± 4.1	AALTONEN	12AD	CDF	Dalitz fit, ∼ 350k evts
• • • We do not use the following data for averages, fits, limits, etc. • • •				
$-7\ \pm25\ ^{+13}_{-26}$	ASNER	04A	CLEO	Dalitz fit, 4854 evts

$A_{CP}(K^*_2(1430)^{\pm}\pi^{\mp})$ in $D^0 \to K^*_2(1430)^+\pi^-$, $\overline{D}^0 \to K^*_2(1430)^-\pi^+$

This is a doubly Cabibbo-suppressed mode.

VALUE (%)	DOCUMENT ID		TECN	COMMENT
−10±14±29	AALTONEN	12AD	CDF	Dalitz fit, ∼ 350k evts

Int. J. Mod. Phys. A 2026.41. Downloaded from www.worldscientific.com by LIFORNIA @ BERKELEY on 09/16/26. Re-use and distribution is strictly not permitted, except for Open Access articles.

$A_{CP}(K^*(1680)^{\mp}\pi^{\pm} \to K^0_S\pi^+\pi^-)$ in $D^0 \to K^*(1680)^-\pi^+$, $\overline{D}^0 \to$ c.c.

VALUE (%)	DOCUMENT ID		TECN	COMMENT
• • • We do not use the following data for averages, fits, limits, etc. • • •				
$-36\pm19^{+10}_{-35}$	ASNER	04A	CLEO	Dalitz fit, 4854 evts

$A_{CP}(K^-\pi^+\pi^+\pi^-)$ in $D^0 \to K^-\pi^+\pi^+\pi^-$, $\overline{D}^0 \to K^+\pi^-\pi^-\pi^+$

VALUE (%)	DOCUMENT ID		TECN	COMMENT
0.2±0.3±0.4	BONVICINI	14	CLEO	All CLEO-c runs
• • • We do not use the following data for averages, fits, limits, etc. • • •				
$+0.7\pm0.5\pm0.9$	DOBBS	07	CLEO	See BONVICINI 14

$A_{CP}(K^{\pm}\pi^{\mp}\pi^+\pi^-)$ in $D^0 \to K^+\pi^-\pi^+\pi^-$, $\overline{D}^0 \to K^-\pi^+\pi^+\pi^-$

VALUE (%)	EVTS	DOCUMENT ID		TECN	COMMENT
−1.8±4.4	1721 ± 75	TIAN	05	BELL	$e^+e^- \approx \Upsilon(4S)$

$A_{CP}(K^+K^-\pi^+\pi^-)$ in D^0, $\overline{D}^0 \to K^+K^-\pi^+\pi^-$

See also AAIJ 13BR for a search for CP violation in $D^0 \to K^+K^-\pi^+\pi^-$ in binned phase space. No evidence of CP violation was found.

VALUE (%)	EVTS	DOCUMENT ID		TECN	COMMENT
1.3 ±1.7 OUR AVERAGE					
$1.84\pm1.74\pm0.3$	2.9k	[1] DARGENT	17		e^+e^-
$-8.2\pm5.6\pm4.7$	828 ± 46	LINK	05E	FOCS	γ A, $\overline{E}_\gamma \approx 180$ GeV

[1] Obtained by analyzing CLEO data but not authored by the CLEO Collaboration.

$A_{CP}(2K^0_S\pi^+\pi^-)$ in D^0, $\overline{D}^0 \to 2K^0_S\pi^+\pi^-$

VALUE (units 10^{-2})	EVTS	DOCUMENT ID		TECN	COMMENT
$\mathbf{-2.54\pm1.44^{+0.11}_{-0.10}}$	6095	[1] SANGAL	23	BELL	e^+e at $\Upsilon(4S,5S)$, 10.520 GeV

[1] SANGAL 23 also measures the parity asymmetry A_T in the sign of the triple product of momenta between one K^0_S (the one with higher momentum) and the two charged pions, and reports the resulting CP asymmetry between the CP conjugate modes $(A_T - \overline{A}_T)/2 = (-1.95 \pm 1.42^{+0.14}_{-0.12}) \times 10^{-2}$.

$A_{CP}(K^*_1(1270)^+K^- \to K^+K^-\pi^+\pi^-)$ in $D^0 \to K^*_1(1270)^+K^-$, $\overline{D}^0 \to$ c.c.

Including the full $K^*_1(1270)^+$ phase space accessible in this decay chain, with its various resonance contributions.

VALUE (%)	EVTS	DOCUMENT ID		TECN	COMMENT
− 2.3±1.7 OUR AVERAGE					
$-2.6\pm1.7\pm0.2$	163k	AAIJ	19C	LHCB	4-body fit, $KK\pi\pi$ evts
$25.3\pm9.7\pm12.7$	2.9k	[1] DARGENT	17		4-body fit, $KK\pi\pi$ evts

[1] Obtained by analyzing CLEO data but not authored by the CLEO Collaboration.

$A_{CP}(K^*_1(1270)^+K^- \to K^{*0}\pi^+K^-)$ in $D^0 \to K^*_1(1270)^+K^-$, $\overline{D}^0 \to$ c.c.

VALUE (%)	DOCUMENT ID		TECN	COMMENT
−0.7±10.4	ARTUSO	12	CLEO	Amplitude fit, 2959 evts.

$A_{CP}(K^*_1(1270)^-K^+ \to \overline{K}^{*0}\pi^-K^+)$ in $D^0 \to K^*_1(1270)^-K^+$, $\overline{D}^0 \to$ c.c.

VALUE (%)	DOCUMENT ID		TECN	COMMENT
−10.0±31.5	ARTUSO	12	CLEO	Amplitude fit, 2959 evts.

$A_{CP}(K^*_1(1270)^-K^+ \to K^+K^-\pi^+\pi^-)$ in $D^0 \to K^*_1(1270)^-K^+$, $\overline{D}^0 \to$ c.c.

Including the full $K^*_1(1270)^-$ phase space accessible in this decay chain, with its various resonance contributions.

VALUE (%)	EVTS	DOCUMENT ID		TECN	COMMENT
1.7± 3.5 OUR AVERAGE					
$3.3\pm3.5\pm0.5$	163k	AAIJ	19C	LHCB	4-body fit, $KK\pi\pi$ evts
$-50.4\pm12.0\pm16.1$	2.9k	[1] DARGENT	17		4-body fit, $KK\pi\pi$ evts

[1] Obtained by analyzing CLEO data but not authored by the CLEO Collaboration.

$A_{CP}(K^*_1(1270)^+K^- \to \rho^0K^+K^-)$ in $D^0 \to K^*_1(1270)^+K^-$, $\overline{D}^0 \to$ c.c.

VALUE (%)	DOCUMENT ID		TECN	COMMENT
−6.5±16.9	ARTUSO	12	CLEO	Amplitude fit, 2959 evts.

$A_{CP}(K^*_1(1270)^-K^+ \to \rho^0K^-K^+)$ in $D^0 \to K^*_1(1270)^-K^+$, $\overline{D}^0 \to$ c.c.

VALUE (%)	DOCUMENT ID		TECN	COMMENT
+9.6±12.9	ARTUSO	12	CLEO	Amplitude fit, 2959 evts.

$A_{CP}(K_1(1400)^+K^- \to K^+K^-\pi^+\pi^-)$ in $D^0 \to K_1(1400)^+K^-$, $\overline{D}^0 \to$ c.c.

Including the full $K_1(1400)^+$ phase space accessible in this decay chain, with its various resonance contributions.

VALUE (%)	EVTS	DOCUMENT ID		TECN	COMMENT
−4.4± 2.1 OUR AVERAGE					
$-4.5\pm2.1\pm0.3$	163k	AAIJ	19C	LHCB	4-body fit, $KK\pi\pi$ evts
$9.2\pm15.2\pm20.3$	2.9k	[1] DARGENT	17		4-body fit, $KK\pi\pi$ evts

[1] Obtained by analyzing CLEO data but not authored by the CLEO Collaboration.

$A_{CP}(K^*(1410)^+K^- \to K^{*0}\pi^+K^-)$ in $D^0 \to K^*(1410)^+K^-$, $\overline{D}^0 \to$ c.c.

VALUE (%)	DOCUMENT ID		TECN	COMMENT
−20.0±16.8	ARTUSO	12	CLEO	Amplitude fit, 2959 evts.

$A_{CP}(K^*(1410)^-K^+ \to \overline{K}^{*0}\pi^-K^+)$ in $D^0 \to K^*(1410)^-K^+$, $\overline{D}^0 \to$ c.c.

VALUE (%)	DOCUMENT ID		TECN	COMMENT
−1.1±13.7	ARTUSO	12	CLEO	Amplitude fit, 2959 evts.

$A_{CP}(K^*(1680)^+K^- \to K^+K^-\pi^+\pi^-)$ in $D^0 \to K^*(1680)^+K^-$, $\overline{D}^0 \to$ c.c.

Including the full $K^*(1680)^+$ phase space accessible in this decay chain, with its various resonance contributions.

VALUE (%)	EVTS	DOCUMENT ID		COMMENT
−17.1±21.8±18.5	2.9k	[1] DARGENT	17	4-body fit, $KK\pi\pi$ evts

[1] Obtained by analyzing CLEO data but not authored by the CLEO Collaboration.

$A_{CP}(K^{*0}\overline{K}^{*0})$ in D^0, $\overline{D}^0 \to K^{*0}\overline{K}^{*0}$

Including S, P, D wave

VALUE (%)	EVTS	DOCUMENT ID		COMMENT
−4.6±9.0±11.3	2.9k	[1] DARGENT	17	4-body fit, $KK\pi\pi$ evts

[1] Obtained by analyzing CLEO data but not authored by the CLEO Collaboration.

$A_{CP}(K^{*0}\overline{K}^{*0}$ S-wave) in D^0, $\overline{D}^0 \to K^{*0}\overline{K}^{*0}$ S-wave

VALUE (%)	EVTS	DOCUMENT ID		TECN	COMMENT
−3.9± 2.2 OUR AVERAGE					
$-4.3\pm2.2\pm0.5$	163k	AAIJ	19C	LHCB	4-body fit, $KK\pi\pi$ evts
$+9.5\pm13.5$	3k	ARTUSO	12	CLEO	4-body fit, $KK\pi\pi$ evts

$A_{CP}(\phi\rho^0)$ in D^0, $\overline{D}^0 \to \phi\rho^0$

Including S, P, D wave

VALUE (%)	EVTS	DOCUMENT ID		COMMENT
1.5±4.6±8.0	2.9k	[1] DARGENT	17	4-body fit, $KK\pi\pi$ evts

[1] Obtained by analyzing CLEO data but not authored by the CLEO Collaboration.

$A_{CP}(\phi\rho^0$ S-wave) in D^0, $\overline{D}^0 \to \phi\rho^0$ S-wave

VALUE (%)	DOCUMENT ID		TECN	COMMENT
−2.7±5.3	ARTUSO	12	CLEO	Amplitude fit, 2959 evts.

$A_{CP}(\phi\rho^0$ D-wave) in D^0, $\overline{D}^0 \to \phi\rho^0$ D-wave

VALUE (%)	DOCUMENT ID		TECN	COMMENT
−37.1±19.0	ARTUSO	12	CLEO	Amplitude fit, 2959 evts.

$A_{CP}(\phi(\pi^+\pi^-)_{S-wave})$ in D^0, $\overline{D}^0 \to \phi(\pi^+\pi^-)_{S-wave}$

VALUE (%)	EVTS	DOCUMENT ID		TECN	COMMENT
6 ± 6 OUR AVERAGE					
$5.8\pm6.1\pm0.8$	163k	AAIJ	19C	LHCB	4-body fit, $KK\pi\pi$ evts
$-4.0\pm18.0\pm44.6$	3k	[1] DARGENT	17		4-body fit, $KK\pi\pi$ evts
• • • We do not use the following data for averages, fits, limits, etc. • • •					
-8.6 ± 10.4	3k	[2] ARTUSO	12	CLEO	4-body fit, $KK\pi\pi$ evts

[1] Obtained by analyzing CLEO data but not authored by the CLEO Collaboration.
[2] see DARGENT 17

$A_{CP}(K^*(892)^0(K^-\pi^+)_{S-wave})$ in D^0, $\overline{D}^0 \to K^*(892)^0(K^-\pi^+)_{S-wave}$

VALUE (%)	EVTS	DOCUMENT ID		COMMENT
−13.1±17.9±31.2	2.9k	[1] DARGENT	17	4-body fit, $KK\pi\pi$ evts

[1] Obtained by analyzing CLEO data but not authored by the CLEO Collaboration.

$A_{CP}(K^+K^-\pi^+\pi^-$ non-resonant) in D^0, $\overline{D}^0 \to K^+K^-\pi^+\pi^-$ non-resonant

VALUE (%)	DOCUMENT ID		COMMENT
+8.2±10.9±17.1	[1] DARGENT	17	4-body fit, 2.9k $KK\pi\pi$ evts

[1] Obtained by analyzing CLEO data but not authored by the CLEO Collaboration.

$A_{CP}((K^-\pi^+)_{P-wave}(K^+\pi^-)_{S-wave})$ in $D^0 \to (K^-\pi^+)_{P-wave}(K^+\pi^-)_{S-wave}$, $\overline{D}^0 \to$ c.c.

VALUE (%)	DOCUMENT ID		TECN	COMMENT
+2.7±10.6	ARTUSO	12	CLEO	Amplitude fit, 2959 evts.

$A_{CP}(K^+K^-\mu^+\mu^-)$ in D^0, $\overline{D}^0 \to K^+K^-\mu^+\mu^-$

VALUE (%)	EVTS	DOCUMENT ID		TECN	COMMENT
−2.3± 6.3±0.6	318	[1] AAIJ	22L	LHCB	pp at 7, 8, 13TeV
• • • We do not use the following data for averages, fits, limits, etc. • • •					
$0\pm11\pm2$	110	AAIJ	18I	LHCB	pp at 7, 8, 13TeV

[1] Supersedes AAIJ 18I. This analysis provides the first complete angular analysis of $D^0 \to K^+K^-\mu^+\mu^-$, and measures angular moments for several bins in the dimuon invariant mass. The mass of the dihadron system is required to be less than 1200 MeV.

$A_{CP}(\pi^+\pi^-\mu^+\mu^-)$ in D^0, $\overline{D}^0 \to \pi^+\pi^-\mu^+\mu^-$

VALUE (%)	EVTS	DOCUMENT ID		TECN	COMMENT
2.9±2.1±0.4	3.6k	[1] AAIJ	22L	LHCB	pp at 7, 8, 13 TeV
• • • We do not use the following data for averages, fits, limits, etc. • • •					
$4.9\pm3.8\pm0.7$	1.1k	AAIJ	18I	LHCB	pp at 7, 8, 13TeV

[1] Supersedes AAIJ 18I. This analysis provides the first complete angular analysis of $D^0 \to \pi^+\pi^-\mu^+\mu^-$, and measures angular moments for several bins in the dimuon invariant mass. The mass of the dihadron system is required to be less than 1200 MeV.

Int. J. Mod. Phys. A 2026.41. Downloaded from www.worldscientific.com by UNIVERSITY OF CALIFORNIA @ BERKELEY on 09/16/26. Re-use and distribution is strictly not permitted, except for Open Access articles.

D^0 CP-VIOLATING ASYMMETRY DIFFERENCES

$\Delta A_{CP} = A_{CP}(K^+K^-) - A_{CP}(\pi^+\pi^-)$

CP violation in these modes can come from the decay amplitudes (direct) and/or from mixing or interference of mixing and decay (indirect). The difference ΔA_{CP} is primarily sensitive to the direct component, and only retains a second-order dependence on the indirect component for measurements where the mean decay time of the K^+K^- and $\pi^+\pi^-$ samples are not identical. The results below are averaged assuming the indirect component can be neglected.

VALUE (%)	EVTS	DOCUMENT ID		TECN	COMMENT
−0.154±0.029	53M,17M	AAIJ	19D	LHCB	Time-integrated
• • • We do not use the following data for averages, fits, limits, etc. • • •					
−0.10 ±0.08 ±0.03	6.5M,2.2M	AAIJ	16D	LHCB	See AAIJ 19D
0.14 ±0.16 ±0.08	2.2M,0.8M	AAIJ	14AK	LHCB	See AAIJ 19D
0.49 ±0.30 ±0.14	0.56M,0.22M	AAIJ	13AD	LHCB	See AAIJ 14AK
−0.82 ±0.21 ±0.11	1.4M,0.4M	AAIJ	12G	LHCB	See AAIJ 16D
−0.46 ±0.31 ±0.12		AALTONEN	12B	CDF	See AALTONEN 12O
−0.62 ±0.21 ±0.10		AALTONEN	12O	CDF	Time-integrated
0.24 ±0.62 ±0.26		[1] AUBERT	08M	BABR	Time-integrated
−0.86 ±0.60 ±0.07	120k	STARIC	08	BELL	Time-integrated

[1] Calculated from the AUBERT 08M values of $A_{CP}(K^+K^-)$ and $A_{CP}(\pi^+\pi^-)$. The systematic error here combines the systematic errors in quadrature, and therefore somewhat over-estimates it.

D^0 TESTS OF LOCAL CP-VIOLATION (CPV)

We list model-independent searches for local CP violation in phase-space distributions of multi-body decays.

Most of these searches divide phase space (Dalitz plot for 3-body decays, five-dimensional equivalent for 4-body decays) into bins, and perform a χ^2 test comparing normalised yields N_i, $\overline{N}_i$ in CP-conjugate bin pairs i: $\chi^2 = \Sigma_i(N_i - \alpha\,\overline{N}_i)/\sigma(N_i - \alpha\,\overline{N}_i)$. The factor $\alpha = (\Sigma_i N_i)/(\Sigma_i \overline{N}_i)$ removes the dependence on phase-space-integrated rate asymmetries. The result is used to obtain the probability (p-value) to obtain the measured χ^2 or larger under the assumption of CP conservation [AUBERT 08AO, BEDIAGA 09]. Alternative methods obtain p-values from other test variables based on unbinned analyses [WILLIAMS 11, AAIJ 14C]. Results can be combined using Fisher's method [MOSTELLER 48].

Local CPV in $D^0, \overline{D}^0 \to \pi^+\pi^-\pi^0$

p-value (%)	EVTS	DOCUMENT ID		TECN	COMMENT
10.6 OUR EVALUATION					
62	2.5M	AAIJ	23AW	LHCB	unbinned method
2.6	566k	[1] AAIJ	15A	LHCB	unbinned method
32.8	82k	AUBERT	08AO	BABR	χ^2

[1] Unusually, AAIJ 15A assigns an uncertainty on the p value of ±0.5%. This results from limited test statistics.

Local CPV in $D^0, \overline{D}^0 \to \pi^+\pi^-\pi^+\pi^-$

p-value (%)	EVTS	DOCUMENT ID		TECN	COMMENT
0.6±0.2	1.0M	[1] AAIJ	17AE	LHCB	unbinned, P-odd
• • • We do not use the following data for averages, fits, limits, etc. • • •					
4.6±0.5	1.0M	[2,3] AAIJ	17AE	LHCB	unbinned, P-even
41	330k	[2,4] AAIJ	13BR	LHCB	χ^2, P-even

[1] This AAIJ 17AE value tests CP Violation in P-odd variables.
[2] This value tests CP Violation in P-even variables.
[3] Not included in average as correlation to P-odd measurement using the same data is unclear.
[4] See AAIJ 17AE.

Local CPV in $D^0, \overline{D}^0 \to K^0_S\pi^+\pi^-$

p-value (%)	EVTS	DOCUMENT ID		TECN	COMMENT
96	350k	AALTONEN	12AD	CDF	χ^2

Local CPV in $D^0, \overline{D}^0 \to K^+K^-\pi^0$

p-value (%)	EVTS	DOCUMENT ID		TECN	COMMENT
16.6	11k	AUBERT	08AO	BABR	χ^2

Local CPV in $D^0, \overline{D}^0 \to K^+K^-\pi^+\pi^-$

p-value (%)	EVTS	DOCUMENT ID		TECN	COMMENT
9.1	57k	AAIJ	13BR	LHCB	χ^2

Local CPV in $D^0, \overline{D}^0 \to K^0_S K^+\pi^-$

p-value (%)	EVTS	DOCUMENT ID		TECN	COMMENT
66	620k	AAIJ	24J	LHCB	5.4fb^{-1}, pp at 13 TeV

Local CPV in $D^0, \overline{D}^0 \to K^0_S K^-\pi^+$

p-value (%)	EVTS	DOCUMENT ID		TECN	COMMENT
70	950k	AAIJ	24J	LHCB	5.4fb^{-1}, pp at 13 TeV

CP VIOLATING ASYMMETRIES OF P-ODD (T-ODD) MOMENTS

The CP-sensitive P-odd (T-odd) correlation in D^0, $\overline{D}^0$ decays. The D^0 and $\overline{D}^0$ are distinguished by the charge of the parent D^*: $D^{*+} \to D^0\pi^+$ and $D^{*-} \to \overline{D}^0\pi^-$.

$A_{Tviol}(K^+K^-\pi^+\pi^-)$ in $D^0, \overline{D}^0 \to K^+K^-\pi^+\pi^-$

$C_T \equiv \vec{p}_{K^+} \cdot (\vec{p}_{\pi^+} \times \vec{p}_{\pi^-})$ is a parity-odd correlation of the K^+, π^+, and π^- momenta (evaluated in the D^0 rest frame) for the D^0. $\overline{C}_T \equiv \vec{p}_{K^-} \cdot (\vec{p}_{\pi^-} \times \vec{p}_{\pi^+})$ is the corresponding quantity for the $\overline{D}^0$. Then
$A_T \equiv [\Gamma(C_T > 0) - \Gamma(C_T \le 0)] / [\Gamma(C_T > 0) + \Gamma(C_T < 0)]$, and
$\overline{A}_T \equiv [\Gamma(-\overline{C}_T > 0) - \Gamma(-\overline{C}_T < 0)] / [\Gamma(-\overline{C}_T > 0) + \Gamma(-\overline{C}_T < 0)]$, and
$A_{Tviol} \equiv \frac{1}{2}(A_T - \overline{A}_T)$. C_T and $\overline{C}_T$ are commonly referred to as T-odd moments, because they are odd under T reversal. However, the T-conjugate process $K^+K^-\pi^+\pi^- \to D^0$ is not accessible, while the CP-conjugate process is.

VALUE (units 10^{-3})	EVTS	DOCUMENT ID		TECN	COMMENT
2.9± 2.2 OUR AVERAGE					
5.2± 3.7± 0.7	110k	[1] KIM	19	BELL	e^+e^- at $\Upsilon(1S)-\Upsilon(6S)$
1.8± 2.9± 0.4	171k	AAIJ	14BC	LHCB	$B \to D^0\mu^-X$
1.0± 5.1± 4.4	47k	DEL-AMO-SA...10		BABR	$e^+e^- \approx$ 10.6 GeV
• • • We do not use the following data for averages, fits, limits, etc. • • •					
10 ±57 ±37	0.8k	LINK	05E	FOCS	γ A, $\overline{E}_\gamma \approx$ 180 GeV

[1] KIM 19 also study CP-violating asymmetries in several other kinematic variables. No evidence for CP violation is found in any of them.

$A_{Tviol}(2K^0_S\pi^+\pi^-)$ in $D^0, \overline{D}^0 \to 2K^0_S\pi^+\pi^-$

$C_T \equiv \vec{p}_{K^0_S} \cdot (\vec{p}_{\pi^+} \times \vec{p}_{\pi^-})$ is a parity-odd correlation of the K^0_S (with higher momentum), π^+, and π^- momenta (evaluated in the D^0 rest frame) for the D^0. $\overline{C}_T \equiv \vec{p}_{K^0_S} \cdot (\vec{p}_{\pi^-} \times \vec{p}_{\pi^+})$ is the corresponding quantity for the $\overline{D}^0$. Then
$A_T \equiv [\Gamma(C_T > 0) - \Gamma(C_T \le 0)] / [\Gamma(C_T > 0) + \Gamma(C_T < 0)]$, and
$\overline{A}_T \equiv [\Gamma(-\overline{C}_T > 0) - \Gamma(-\overline{C}_T < 0)] / [\Gamma(-\overline{C}_T > 0) + \Gamma(-\overline{C}_T < 0)]$, and
$A_{Tviol} \equiv \frac{1}{2}(A_T - \overline{A}_T)$. C_T and $\overline{C}_T$ are commonly referred to as T-odd moments, because they are odd under T reversal. However, the T-conjugate process $K^0_S K^0_S \pi^+\pi^- \to D^0$ is not accessible, while the CP-conjugate process is.

VALUE (units 10^{-2})	EVTS	DOCUMENT ID		TECN	COMMENT
$-1.95 \pm 1.42^{+0.14}_{-0.12}$	6095	SANGAL	23	BELL	e^+e at Υ(4S,5S), 10.520 GeV

$A_{Tviol}(K^0_S\pi^+\pi^-\pi^0)$ in $D^0, \overline{D}^0 \to K^0_S\pi^+\pi^-\pi^0$

$C_T \equiv \vec{p}_{K^0_S} \cdot (\vec{p}_{\pi^+} \times \vec{p}_{\pi^-})$ is a parity-odd correlation evaluated in the D^0 rest frame. $\overline{C}_T$ is defined as the CP-conjugate observable with $\overline{D}^0$ daughter particles. Then
$A_T \equiv [\Gamma(C_T > 0) - \Gamma(C_T \le 0)] / [\Gamma(C_T > 0) + \Gamma(C_T < 0)]$, and
$\overline{A}_T \equiv [\Gamma(-\overline{C}_T > 0) - \Gamma(-\overline{C}_T < 0)] / [\Gamma(-\overline{C}_T > 0) + \Gamma(-\overline{C}_T < 0)]$, and
$A_{Tviol} \equiv \frac{1}{2}(A_T - \overline{A}_T)$. C_T and $\overline{C}_T$ are commonly referred to as T-odd moments, because they are odd under T reversal. However, the T-conjugate process $K^0_S\pi^+\pi^-\pi^0 \to D^0$ is not accessible, while the CP-conjugate process is.

VALUE (units 10^{-3})	EVTS	DOCUMENT ID		TECN	COMMENT
$-0.28 \pm 1.38^{+0.23}_{-0.76}$	745k	[1] PRASANTH	17	BELL	e^+e^- at Υ(nS)'s

[1] PRASANTH 17 also measures A_{Tviol} in sub-regions of the $D^0 \to K^0_S\pi^+\pi^-\pi^0$ phase-space. No evidence of T violation is found.

D^0 CPT-VIOLATING DECAY-RATE ASYMMETRIES

$A_{CPT}(K^\mp\pi^\pm)$ in $D^0 \to K^-\pi^+$, $\overline{D}^0 \to K^+\pi^-$

$A_{CPT}(t)$ is defined in terms of the time-dependent decay probabilities $P(D^0 \to K^-\pi^+)$ and $\overline{P}(\overline{D}^0 \to K^+\pi^-)$ by $A_{CPT}(t) = (\overline{P} - P)/(\overline{P} + P)$. For small mixing parameters $x \equiv \Delta m/\Gamma$ and $y \equiv \Delta\Gamma/2\Gamma$ (as is the case), and times t, $A_{CPT}(t)$ reduces to $[y\,Re(z) - x\,Im(z)]\,\Gamma t$, where z is the CPT-violating parameter. The following is actually $y\,Re(z) - x\,Im(z)$.

VALUE	CL%	DOCUMENT ID		TECN	COMMENT
-14.6×10^{-5} to 6.6×10^{-5}	95	[1] KRZEMIEN	24	RVUE	from LHCb data
• • • We do not use the following data for averages, fits, limits, etc. • • •					
$(8.3 \pm 6.5 \pm 4.1) \times 10^{-3}$		LINK	03B	FOCS	γ nucleus, $\overline{E}_\gamma \approx$ 180 GeV

[1] The constraints are derived by reinterpreting the LHCb measurement of the time-dependent asymmetry in the Cabibbo-favored $D^0 \to K^-\pi^+$ and $\overline{D}^0 \to K^+\pi^-$ decay rates. These constraints can be directly translated into the flavor eigenstate decay width difference $\delta\Gamma = \Gamma_{D^0} - \Gamma_{\overline{D}^0}$ by the relation $\delta\Gamma = (y\,Re(z) - x\,Im(z)) \times 2\Gamma$, yielding $(-4.7 < \delta\Gamma < 2.1) \times 10^{-16}$ GeV at 95% CL.

SEMILEPTONIC FORM FACTORS

$r_V \equiv V(0)/A_1(0)$ in $D^0 \to K^*(892)^-\ell^+\nu_\ell$

VALUE	EVTS	DOCUMENT ID		TECN	COMMENT
1.45±0.04 OUR AVERAGE					
1.37±0.09±0.03	6.4k	ABLIKIM	25	BES3	$K^*(892)^-\mu^+\nu_\mu$, $K^{*-} \to K^-\pi^0$
1.48±0.05±0.02	8.8k	ABLIKIM	25BD	BES3	$K^*(892)^-e^+\nu_e$, $K^{*-} \to \overline{K}^0\pi^-$

1.46±0.11±0.04	6.8k	ABLIKIM	25BO	BES3	$K^*(892)^-\mu^+\nu_\mu$, $K^{*-}\to\overline{K}^0\pi^-$
1.71±0.68±0.34		LINK	05B	FOCS	$K^*(892)^-\mu^+\nu_\mu$
• • • We do not use the following data for averages, fits, limits, etc. • • •					
1.46±0.07±0.02	3k	[1] ABLIKIM	19G	BES3	$K^*(892)^-e^+\nu_e$

[1] Superseded by ABLIKIM 25BD.

$r_2 \equiv A_2(0)/A_1(0)$ in $D^0 \to K^*(892)^-\ell^+\nu_\ell$

VALUE	EVTS	DOCUMENT ID		TECN	COMMENT
0.720±0.033 OUR AVERAGE					
0.76 ±0.06 ±0.02	6.4k	ABLIKIM	25	BES3	$K^*(892)^-\mu^+\nu_\mu$, $K^{*-}\to K^-\pi^0$
0.70 ±0.04 ±0.02	8.8k	ABLIKIM	25BD	BES3	$K^*(892)^-e^+\nu_e$, $K^{*-}\to\overline{K}^0\pi^-$
0.71 ±0.08 ±0.03	6.8k	ABLIKIM	25BO	BES3	$K^*(892)^-\mu^+\nu_\mu$, $K^{*-}\to\overline{K}^0\pi^-$
0.91 ±0.37 ±0.10		LINK	05B	FOCS	$K^*(892)^-\mu^+\nu_\mu$
• • • We do not use the following data for averages, fits, limits, etc. • • •					
0.67 ±0.06 ±0.01	3k	[1] ABLIKIM	19G	BES3	$K^*(892)^-e^+\nu_e$

[1] Superseded by ABLIKIM 25BD.

$r_V \equiv V(0)/A_1(0)$ in $D^0 \to \rho^-\ell^+\nu_\ell$

See the D^+ listings for combinations of $D^0 \to \rho^-e^+\nu_e$ and $D^+ \to \rho^0e^+\nu_e$ measurements.

VALUE	EVTS	DOCUMENT ID		TECN	COMMENT
1.548±0.079±0.041	3.3k	[1] ABLIKIM	24CP	BES3	$D^0\to\rho^-e^+\nu_e$

[1] Fit to a single-pole-dominance parametrization.

$r_2 \equiv A_2(0)/A_1(0)$ in $D^0 \to \rho^-\ell^+\nu_\ell$

See the D^+ listings for combinations of $D^0 \to \rho^-e^+\nu_e$ and $D^+ \to \rho^0e^+\nu_e$ measurements.

VALUE	EVTS	DOCUMENT ID		TECN	COMMENT
0.823±0.056±0.026	3.3k	[1] ABLIKIM	24CP	BES3	$D^0\to\rho^-e^+\nu_e$

[1] Fit to a single-pole-dominance parametrization.

$f_+(0)$ in $D^0 \to K^-\ell^+\nu_\ell$

VALUE	EVTS	DOCUMENT ID		TECN	COMMENT
0.736 ±0.004 OUR AVERAGE					
0.7368±0.0026±0.0036	71k	ABLIKIM	15X	BES3	$\ell=e$, 2-parameter fit
0.727 ±0.007 ±0.009		AUBERT	07BG	BABR	$\ell=e$, 2-parameter fit

$f_+(0)|V_{cs}|$ in $D^0 \to K^-\ell^+\nu_\ell$

VALUE	EVTS	DOCUMENT ID		TECN	COMMENT
0.7176±0.0018 OUR AVERAGE					
0.7179±0.0016±0.0017	191k	ABLIKIM	24CN	BES3	$\ell=e$, 2-parameter fit
0.7162±0.0022±0.0019	148k	ABLIKIM	24CN	BES3	$\ell=\mu$, 2-parameter fit
0.726 ±0.008 ±0.004		BESSON	09	CLEO	$\ell=e$, 2-parameter fit
• • • We do not use the following data for averages, fits, limits, etc. • • •					
0.7133±0.0038±0.0029	47k	[1] ABLIKIM	19B	BES3	$\ell=\mu$, 2-parameter fit
0.7172±0.0025±0.0035	71k	[1,2] ABLIKIM	15X	BES3	$\ell=e$, 2-parameter fit

[1] Superseded by ABLIKIM 24CN.
[2] The 3-parameter fit yields 0.7195 ± 0.0035 ± 0.0041.

$r_1 \equiv a_1/a_0$ in $D^0 \to K^-\ell^+\nu_\ell$

VALUE	EVTS	DOCUMENT ID		TECN	COMMENT
−2.40±0.16 OUR AVERAGE					
−2.33±0.16±0.08	71k	[1] ABLIKIM	15X	BES3	$\ell=e$, 3-parameter fit
−2.65±0.34±0.08		BESSON	09	CLEO	$\ell=e$, 3-parameter fit

[1] The 2-parameter fit yields −2.23 ± 0.09 ± 0.06.

$r_2 \equiv a_2/a_0$ in $D^0 \to K^-\ell^+\nu_\ell$

VALUE	EVTS	DOCUMENT ID		TECN	COMMENT
5 ±4 OUR AVERAGE					
3.4±3.9±2.4	71k	ABLIKIM	15X	BES3	$\ell=e$, 3-parameter fit
13 ±9 ±1		BESSON	09	CLEO	$\ell=e$, 3-parameter fit

$f_+(0)$ in $D^0 \to \pi^-\ell^+\nu_\ell$

VALUE	EVTS	DOCUMENT ID		TECN	COMMENT
0.6372±0.0080±0.0044	6.3k	ABLIKIM	15X	BES3	$\ell=e$, 2-parameter fit

$f_+(0)|V_{cd}|$ in $D^0 \to \pi^-\ell^+\nu_\ell$

VALUE	EVTS	DOCUMENT ID		TECN	COMMENT
0.1436±0.0026 OUR AVERAGE Error includes scale factor of 1.5. See the ideogram below.					
0.1435±0.0018±0.0009	6.3k	[1] ABLIKIM	15X	BES3	$\ell=e$, 2-parameter fit
0.1374±0.0038±0.0024	5.3k	[2] LEES	15F	BABR	$\ell=e$, 3-parameter fit
0.152 ±0.005 ±0.001		BESSON	09	CLEO	$\ell=e$, 3-parameter fit

[1] The 3-parameter fit yields 0.1420 ± 0.0024 ± 0.0010.
[2] LEES 15F reports a value 0.1374 ± 0.0038 ± 0.0022 ± 0.0009, where the last uncertainty is due to the uncertainties of the $D^0 \to K^-\pi^+$ branching fraction.

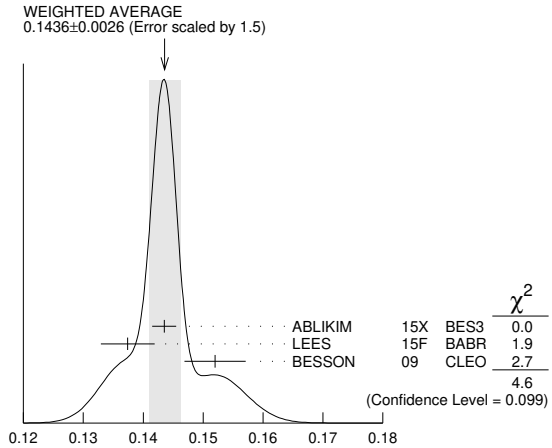

$f_+(0)|V_{cd}|$ in $D^0 \to \pi^-\ell^+\nu_\ell$

$r_1 \equiv a_1/a_0$ in $D^0 \to \pi^-\ell^+\nu_\ell$

VALUE	EVTS	DOCUMENT ID		TECN	COMMENT
−1.97±0.28 OUR AVERAGE Error includes scale factor of 1.4. See the ideogram below.					
−1.84±0.22±0.07	6.3k	[1] ABLIKIM	15X	BES3	$\ell=e$, 3-parameter fit
−1.31±0.70±0.43	5.3k	LEES	15F	BABR	$\ell=e$, 3-parameter fit
−2.80±0.49±0.04		BESSON	09	CLEO	$\ell=e$, 3-parameter fit

[1] The 2-parameter fit yields −2.04 ± 0.08 ± 0.03.

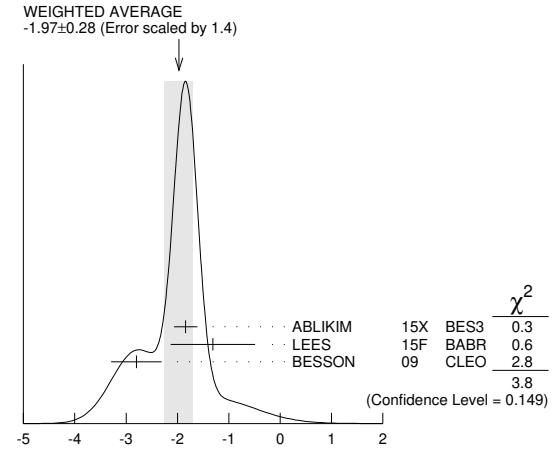

$r_1 \equiv a_1/a_0$ in $D^0 \to \pi^-\ell^+\nu_\ell$

$r_2 \equiv a_1/a_0$ in $D^0 \to \pi^-\ell^+\nu_\ell$

VALUE	EVTS	DOCUMENT ID		TECN	COMMENT
−0.2±2.2 OUR AVERAGE Error includes scale factor of 1.7. See the ideogram below.					
−1.4±1.5±0.5	6.3k	ABLIKIM	15X	BES3	$\ell=e$, 3-parameter fit
−4.2±4.0±1.9	5.3k	LEES	15F	BABR	$\ell=e$, 3-parameter fit
6 ±3 ±0		BESSON	09	CLEO	$\ell=e$, 3-parameter fit

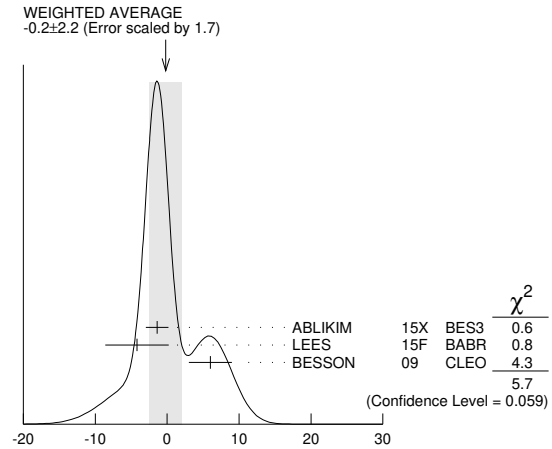

$r_2 \equiv a_1/a_0$ in $D^0 \to \pi^-\ell^+\nu_\ell$

Int. J. Mod. Phys. A 2026.41. Downloaded from www.worldscientific.com
by [redacted] LIFORNIA @ BERKELEY on 09/16/26. Re-use and distribution is strictly not permitted, except for Open Access articles.

Int. J. Mod. Phys. A 2026.41. Downloaded from www.worldscientific.com
by UNIVERSITY OF CALIFORNIA @ BERKELEY on 09/16/26. Re-use and distribution is strictly not permitted, except for Open Access articles.

$f_+^{a_0}(0)|V_{cd}|$ in $D^0 \to a_0(980)^- e^+ \nu_e$

VALUE	EVTS	DOCUMENT ID		TECN	COMMENT
0.126±0.013±0.003	52	[1] ABLIKIM	25AW	BES3	e^+e^- at 3.773 GeV

[1] ABLIKIM 25AW uses a single-pole parametrization for the form factor and a_0 branching fractions deduced from the analysis of ABLIKIM 17K.

Amplitude analyses

$D \to K\pi\pi\pi$, $D \to KK\pi\pi$ partial wave analyses

Amplitude analyses of D^0 decays to a variety of 4-body kaon or pion final states, fitting simultaneously different partial wave components.

VALUE	DOCUMENT ID		TECN	COMMENT
	[1] AAIJ	19C	LHCB	$D^0 \to K^+K^-\pi^+\pi^-$
	ABLIKIM	19AK	BES3	$D^0 \to K^-\pi^+\pi^0\pi^0$
	AAIJ	18AI	LHCB	$D^0 \to K^+\pi^-\pi^+\pi^-$ and $D^0 \to K^-\pi^+\pi^+\pi^-$
	ABLIKIM	17O	BES3	$D^0 \to K^-\pi^+\pi^+\pi^-$

[1] AAIJ 19C also provides measurements of CP violation in $D^0 \to K^+K^-\pi^+\pi^-$, with results compatible with CP symmetry.

$D^0 \to \pi^+\pi^-\eta$ partial wave analyses

VALUE	EVTS	DOCUMENT ID		TECN	COMMENT
	1.4k	[1] ABLIKIM	24CL	BES3	e^+e^- at 3.773 GeV

[1] The amplitude model has six components, including $(\pi^+\pi^-)_{S-wave}\eta$.

$D^0 \to 4\pi$ partial wave analyses

Including $D^0 \to 2\pi^+2\pi^-$, $D^0 \to \pi^+\pi^-2\pi^0$, $D^0 \to 4\pi^0$.

VALUE	EVTS	DOCUMENT ID		TECN	COMMENT
	8k	[1] ABLIKIM	24BG	BES3	e^+e^- at 3.773 GeV

[1] Joint amplitude analysis of $D^0 \to 2\pi^+2\pi^-$ and $D^0 \to \pi^+\pi^-2\pi^0$.

D^0 REFERENCES

AAIJ	25	PR D111 012001	R. Aaij et al.	(LHCb Collab.)
AAIJ	25AU	JHEP 2512 153	R. Aaij et al.	(LHCb Collab.)
AAIJ	25M	PR D111 L091101	R. Aaij et al.	(LHCb Collab.)
AAIJ	25U	JHEP 2503 149	R. Aaij et al.	(LHCb Collab.)
ABLIKIM	25	PRL 134 011803	M. Ablikim et al.	(BESIII Collab.)
ABLIKIM	25AM	PRL 135 091801	M. Ablikim et al.	(BESIII Collab.)
ABLIKIM	25AP	PR D111 L011103	M. Ablikim et al.	(BESIII Collab.)
ABLIKIM	25AQ	PR D111 012007	M. Ablikim et al.	(BESIII Collab.)
ABLIKIM	25AU	PR D111 L071101	M. Ablikim et al.	(BESIII Collab.)
ABLIKIM	25AW	PR D111 L091501	M. Ablikim et al.	(BESIII Collab.)
ABLIKIM	25AZ	PR D112 012015	M. Ablikim et al.	(BESIII Collab.)
ABLIKIM	25BA	PR D112 012001	M. Ablikim et al.	(BESIII Collab.)
ABLIKIM	25BD	JHEP 2503 197	M. Ablikim et al.	(BESIII Collab.)
ABLIKIM	25BI	JHEP 2506 220	M. Ablikim et al.	(BESIII Collab.)
ABLIKIM	25BO	PRL 135 111803	M. Ablikim et al.	(BESIII Collab.)
ABLIKIM	25CM	PR D112 072006	M. Ablikim et al.	(BESIII Collab.)
ADACHI	25D	PR D111 012015	I. Adachi et al.	(BELLE and BELLE II Collab.)
ADACHI	25J	PR D111 112011	I. Adachi et al.	(BELLE and BELLE II Collab.)
ADACHI	25K	PR D112 012006	I. Adachi et al.	(BELLE II Collab.)
ADACHI	25M	PR D112 012017	I. Adachi et al.	(BELLE II Collab.)
ADACHI	25W	PR D112 L071101	I. Adachi et al.	(BELLE and BELLE II Collab.)
ANASHIN	25	PPN 56 802	V.V. Anashin et al.	(VEPP-4M KEDR Collab.)
ANASHIN	25A	JHEP 2511 001	V.V. Anashin et al.	(VEPP-4M KEDR Collab.)
CHEKHOVSKY	25F	PRL 135 151803	V. Chekhovsky et al.	(CMS Collab.)
AAIJ	24AF	PRL 133 101803	R. Aaij et al.	(LHCb Collab.)
AAIJ	24J	JHEP 2403 107	R. Aaij et al.	(LHCb Collab.)
ABLIKIM	24AZ	PR D109 072003	M. Ablikim et al.	(BESIII Collab.)
ABLIKIM	24BG	CP C48 083001	M. Ablikim et al.	(BESIII Collab.)
ABLIKIM	24CL	PR D110 L111102	M. Ablikim et al.	(BESIII Collab.)
ABLIKIM	24CM	PR D110 112001	M. Ablikim et al.	(BESIII Collab.)
ABLIKIM	24CN	PR D110 112006	M. Ablikim et al.	(BESIII Collab.)
ABLIKIM	24CO	PR D110 112008	M. Ablikim et al.	(BESIII Collab.)
ABLIKIM	24CP	PR D110 112018	M. Ablikim et al.	(BESIII Collab.)
ABLIKIM	24CR	JHEP 2409 089	M. Ablikim et al.	(BESIII Collab.)
HAYRAPETY...	24BB	EPJ C84 1264	A. Hayrapetyan et al.	(CMS Collab.)
KRZEMIEN	24	PR D110 055021	W. Krzemien et al.	(NCBJ)
MAITY	24	PR D109 L031101	S. Maity	(BELLE Collab.)
AAIJ	23AC	PRL 131 091802	R. Aaij et al.	(LHCb Collab.)
AAIJ	23AW	JHEP 2309 129	R. Aaij et al.	(LHCb Collab.)
AAIJ	23BC	PR D108 052005	R. Aaij et al.	(LHCb Collab.)
AAIJ	23R	PRL 131 041804	R. Aaij et al.	(LHCb Collab.)
ABLIKIM	23AI	PR D107 032002	M. Ablikim et al.	(BESIII Collab.)
ABLIKIM	23AJ	PR D107 032009	M. Ablikim et al.	(BESIII Collab.)
ABLIKIM	23AO	PR D107 112005	M. Ablikim et al.	(BESIII Collab.)
ABLIKIM	23AW	PR D108 032003	M. Ablikim et al.	(BESIII Collab.)
SANGAL	23	PR D107 052001	A. Sangal et al.	(BELLE Collab.)
AAIJ	22L	PRL 128 221801	R. Aaij et al.	(LHCb Collab.)
AAIJ	22O	PR D105 092013	R. Aaij et al.	(LHCb Collab.)
ABLIKIM	22	PRL 128 011803	M. Ablikim et al.	(BESIII Collab.)
ABLIKIM	22B	PRL 129 022002	M. Ablikim et al.	(BESIII Collab.)
ABLIKIM	22BF	PR D106 092004	M. Ablikim et al.	(BESIII Collab.)
ABLIKIM	22BG	PR D106 092005	M. Ablikim et al.	(BESIII Collab.)
ABLIKIM	22BM	EPJ C82 1009	M. Ablikim et al.	(BESIII Collab.)
ABLIKIM	22T	PR D105 032006	M. Ablikim et al.	(BESIII Collab.)
ABLIKIM	22U	PR D105 032009	M. Ablikim et al.	(BESIII Collab.)
ABLIKIM	22V	PR D105 L071102	M. Ablikim et al.	(BESIII Collab.)
ABLIKIM	22W	PR D105 092010	M. Ablikim et al.	(BESIII Collab.)
ABLIKIM	22X	PR D105 112001	M. Ablikim et al.	(BESIII Collab.)
ABLIKIM	22Y	PR D106 032002	M. Ablikim et al.	(BESIII Collab.)
PDG	22	PTEP 2022 083C01	R.L. Workman et al.	(PDG Collab.)
AAIJ	21AB	PRL 127 111801	R. Aaij et al.	(LHCb Collab.)
AAIJ	21AI	PR D104 072010	R. Aaij et al.	(LHCb Collab.)
AAIJ	21X	PR D104 L031102	R. Aaij et al.	(LHCb Collab.)
ABLIKIM	21AA	JHEP 2105 164	M. Ablikim et al.	(BESIII Collab.)
ABLIKIM	21AY	PRL 127 131801	M. Ablikim et al.	(BESIII Collab.)
ABLIKIM	21BA	PR D104 052008	M. Ablikim et al.	(BESIII Collab.)
ABLIKIM	21BB	PR D104 072005	M. Ablikim et al.	(BESIII Collab.)
ABLIKIM	21BC	PR D104 L091103	M. Ablikim et al.	(BESIII Collab.)
ABUDINEN	21A	PRL 127 211801	F. Abudinen et al.	(BELLE II Collab.)
LI	21G	JHEP 2109 075	L.K. Li et al.	(BELLE Collab.)
AAIJ	20	PR D101 012005	R. Aaij et al.	(LHCb Collab.)
ABLIKIM	20AA	PR D102 052003	M. Ablikim et al.	(BESIII Collab.)
ABLIKIM	20AC	PR D102 052006	M. Ablikim et al.	(BESIII Collab.)
ABLIKIM	20AF	PR D102 112005	M. Ablikim et al.	(BESIII Collab.)
ABLIKIM	20G	PR D101 052009	M. Ablikim et al.	(BESIII Collab.)
ABLIKIM	20V	PRL 124 241803	M. Ablikim et al.	(BESIII Collab.)
CHEN	20A	PR D102 012002	Y.Q. Chen et al.	(BELLE Collab.)
LEES	20A	PR D101 112003	J.P. Lees et al.	(BABAR Collab.)
LEES	20B	PRL 124 071802	J.P. Lees et al.	(BABAR Collab.)
NAYAK	20	PR D102 071102	M. Nayak et al.	(BELLE Collab.)
AAIJ	19	PRL 122 011802	R. Aaij et al.	(LHCb Collab.)
AAIJ	19C	JHEP 1902 126	R. Aaij et al.	(LHCb Collab.)
AAIJ	19D	PRL 122 211803	R. Aaij et al.	(LHCb Collab.)
AAIJ	19X	PRL 122 231802	R. Aaij et al.	(LHCb Collab.)
ABLIKIM	19AK	PR D99 092008	M. Ablikim et al.	(BESIII Collab.)
ABLIKIM	19AL	PR D99 112002	M. Ablikim et al.	(BESIII Collab.)
ABLIKIM	19AY	PR D100 072006	M. Ablikim et al.	(BESIII Collab.)
ABLIKIM	19B	PRL 122 011804	M. Ablikim et al.	(BESIII Collab.)
ABLIKIM	19BI	PL B798 135017	M. Ablikim et al.	(BESIII Collab.)
ABLIKIM	19C	PRL 122 062001	M. Ablikim et al.	(BESIII Collab.)
ABLIKIM	19G	PR D99 011103	M. Ablikim et al.	(BESIII Collab.)
KIM	19	PR D99 011104	J.B. Kim et al.	(BELLE Collab.)
LEES	19A	PRL 122 081802	J.P. Lees et al.	(BABAR Collab.)
PDG	19	RPP 2019 at pdg.lbl.gov	M. Tanabashi et al.	(PDG Collab.)
AAIJ	18AI	EPJ C78 443	R. Aaij et al.	(LHCb Collab.)
AAIJ	18AV	JHEP 1811 048	R. Aaij et al.	(LHCb Collab.)
AAIJ	18I	PRL 121 091801	R. Aaij et al.	(LHCb Collab.)
AAIJ	18K	PR D97 031101	R. Aaij et al.	(LHCb Collab.)
ABLIKIM	18AC	PR D98 092009	M. Ablikim et al.	(BESIII Collab.)
ABLIKIM	18AE	PRL 121 171803	M. Ablikim et al.	(BESIII Collab.)
ABLIKIM	18F	PRL 121 081802	M. Ablikim et al.	(BESIII Collab.)
ABLIKIM	18L	PR D97 052005	M. Ablikim et al.	(BESIII Collab.)
ABLIKIM	18P	PR D97 072015	M. Ablikim et al.	(BESIII Collab.)
ABLIKIM	18W	PR D97 072004	M. Ablikim et al.	(BESIII Collab.)
ABLIKIM	18X	PL B781 368	M. Ablikim et al.	(BESIII Collab.)
HARNEW	18	JHEP 1801 144	S. Harnew et al.	(BRIS, PNNL)
RESMI	18	JHEP 1801 082	P.K. Resmi et al.	
SMITH	18	PR D98 051101	M.J. Smith, D. Cinabro, P. Naik	(LTU, WAYN+)
AAIJ	17AE	PL B769 345	R. Aaij et al.	(LHCb Collab.)
AAIJ	17AK	PRL 118 261803	R. Aaij et al.	(LHCb Collab.)
AAIJ	17AO	PR D95 052004	R. Aaij et al.	(LHCb Collab.)
Also		PR D96 099907 (errat.)	R. Aaij et al.	(LHCb Collab.)
AAIJ	17BG	PRL 119 181805	R. Aaij et al.	(LHCb Collab.)
AAIJ	17M	PL B767 177	R. Aaij et al.	(LHCb Collab.)
ABLIKIM	17A	PL B765 231	M. Ablikim et al.	(BESIII Collab.)
ABLIKIM	17K	PR D95 032002	M. Ablikim et al.	(BESIII Collab.)
ABLIKIM	17O	PR D95 072010	M. Ablikim et al.	(BESIII Collab.)
DARGENT	17	JHEP 1705 143	P. dArgent et al.	(HEID, BRIS)
DASH	17	PRL 119 171801	N. Dash et al.	(BELLE Collab.)
LAI	17	PR D95 011102	Y.-T. Lai et al.	(BELLE Collab.)
NANUT	17	PRL 118 051801	T. Nanut et al.	(BELLE Collab.)
PRASANTH	17	PR D95 091101	K. Prasanth et al.	(BELLE Collab.)
AAIJ	16D	PRL 116 191601	R. Aaij et al.	(LHCb Collab.)
AAIJ	16F	PRL 116 241801	R. Aaij et al.	(LHCb Collab.)
AAIJ	16H	PL B754 167	R. Aaij et al.	(LHCb Collab.)
AAIJ	16I	PL B757 558	R. Aaij et al.	(LHCb Collab.)
AAIJ	16N	PR D93 052018	R. Aaij et al.	(LHCb Collab.)
AAIJ	16V	JHEP 1604 033	R. Aaij et al.	(LHCb Collab.)
ABLIKIM	16D	PRL 116 082001	M. Ablikim et al.	(BESIII Collab.)
EVANS	16	PL B757 520	T. Evans et al.	(OXF, BRIS, MDRA)
Also		PL B765 402 (errat.)	T. Evans et al.	(OXF, BRIS, MDRA)
LEES	16D	PR D93 112014	J.P. Lees et al.	(BABAR Collab.)
NISAR	16	PR D93 051102	N.K. Nisar et al.	(BELLE Collab.)
STARIC	16	PL B753 412	M. Staric et al.	(BELLE Collab.)
AAIJ	15A	PL B740 158	R. Aaij et al.	(LHCb Collab.)
AAIJ	15AA	JHEP 1504 043	R. Aaij et al.	(LHCb Collab.)
AAIJ	15AT	JHEP 1510 055	R. Aaij et al.	(LHCb Collab.)
ABLIKIM	15D	PL B744 339	M. Ablikim et al.	(BESIII Collab.)
ABLIKIM	15F	PR D91 112015	M. Ablikim et al.	(BESIII Collab.)
ABLIKIM	15X	PR D92 072012	M. Ablikim et al.	(BESIII Collab.)
LEES	15F	PR D91 052022	J.P. Lees et al.	(BABAR Collab.)
MALDE	15	PL B747 9	S. Malde et al.	(BRIS, CERN, MDRA, OXF+)
NAYAK	15	PL B740 1	M. Nayak et al.	(MDRA, OXF, CERN, CMU+)
AAIJ	14AK	JHEP 1407 041	R. Aaij et al.	(LHCb Collab.)
AAIJ	14AL	PRL 112 041801	R. Aaij et al.	(LHCb Collab.)
AAIJ	14B	PL B728 234	R. Aaij et al.	(LHCb Collab.)
AAIJ	14BC	JHEP 1410 005	R. Aaij et al.	(LHCb Collab.)
AAIJ	14C	PL B728 585	R. Aaij et al.	(LHCb Collab.)
AALTONEN	14Q	PR D90 111103	T. Aaltonen et al.	(CDF Collab.)
ABLIKIM	14C	PL B734 227	M. Ablikim et al.	(BESIII Collab.)
BONVICINI	14	PR D89 072002	G. Bonvicini et al.	(CLEO Collab.)
KO	14	PRL 112 111801	B.R. Ko et al.	(BELLE Collab.)
LIBBY	14	PL B731 197	J. Libby et al.	(MDRA, OXF, PNL, +)
NISAR	14	PRL 112 211601	N.K. Nisar et al.	(BELLE Collab.)
PENG	14	PR D89 091103	T. Peng et al.	(BELLE Collab.)
TOMARADZE	14	PR D89 031501	A. Tomaradze et al.	(NWES, WAYN)
AAIJ	13AD	PL B723 33	R. Aaij et al.	(LHCb Collab.)
AAIJ	13AI	PL B725 15	R. Aaij et al.	(LHCb Collab.)
AAIJ	13BR	PL B726 623	R. Aaij et al.	(LHCb Collab.)
AAIJ	13CE	PRL 111 251801	R. Aaij et al.	(LHCb Collab.)
AAIJ	13N	PRL 110 101802	R. Aaij et al.	(LHCb Collab.)
AAIJ	13V	JHEP 1306 065	R. Aaij et al.	(LHCb Collab.)
AALTONEN	13AE	PRL 111 231802	T. Aaltonen et al.	(CDF Collab.)
DOBBS	13	PRL 110 131802	S. Dobbs et al.	(CLEO Collab.)
LEES	13	PR D87 012004	J.P. Lees et al.	(BABAR Collab.)
LEES	13S	PR D88 071104	J.P. Lees et al.	(BABAR Collab.)
WHITE	13	PR D88 051101	E. White et al.	(BELLE Collab.)
AAIJ	12G	PRL 108 111602	R. Aaij et al.	(LHCb Collab.)
AAIJ	12K	JHEP 1204 129	R. Aaij et al.	(LHCb Collab.)
AALTONEN	12AD	PR D86 032007	T. Aaltonen et al.	(CDF Collab.)
AALTONEN	12B	PR D85 012009	T. Aaltonen et al.	(CDF Collab.)
AALTONEN	12O	PRL 109 111801	T. Aaltonen et al.	(CDF Collab.)
ARTUSO	12	PR D85 122002	M. Artuso et al.	(CLEO Collab.)
ASNER	12	PR D86 112001	D.M. Asner	(CLEO Collab.)
INSLER	12	PR D85 092016	J. Insler et al.	(CLEO Collab.)
Also		PR D94 099905 (errat.)	J. Insler et al.	(CLEO Collab.)
LEES	12L	PR D85 091107	J.P. Lees et al.	(BABAR Collab.)
LEES	12Q	PR D86 032001	J.P. Lees et al.	(BABAR Collab.)
KO	11	PRL 106 211801	B.R. Ko et al.	(BELLE Collab.)
LOWREY	11	PR D84 092005	N. Lowrey et al.	(CLEO Collab.)
WILLIAMS	11	PR D84 054015	M. Williams	(LOIC)
AALTONEN	10X	PR D82 091105	T. Aaltonen et al.	(CDF Collab.)
ANASHIN	10A	PL B686 84	V.V. Anashin et al.	(VEPP-4M KEDR Collab.)
ASNER	10	PR D81 052007	D.M. Asner et al.	(CLEO Collab.)
BHATTACHAR..	10A	PR D81 096008	B. Bhattacharya, C.-W. Chiang, J.L. Rosner	(CHIC+)
DEL-AMO-SA...	10	PR D81 111103	P. del Amo Sanchez et al.	(BABAR Collab.)
DEL-AMO-SA...	10D	PRL 105 081803	P. del Amo Sanchez et al.	(BABAR Collab.)
MENDEZ	10	PR D81 052013	H. Mendez et al.	(CLEO Collab.)
PETRIC	10	PR D81 091102	M. Petric et al.	(BELLE Collab.)
AUBERT	09AI	PR D80 071103	B. Aubert et al.	(BABAR Collab.)
AUBERT	09AN	PRL 103 211801	B. Aubert et al.	(BABAR Collab.)
BEDIAGA	09	PR D80 096006	I. Bediaga et al.	(CBPF, NDAM)
BESSON	09	PR D80 032005	D. Besson et al.	(CLEO Collab.)
Also		PR D79 052010	J.Y. Ge et al.	(CLEO Collab.)
LOWREY	09	PR D80 031105	N. Lowrey et al.	(CLEO Collab.)
RUBIN	09	PR D79 097101	P. Rubin et al.	(CLEO Collab.)

ZUPANC	09	PR D80 052006	A. Zupanc *et al.*	(BELLE Collab.)
AALTONEN	08E	PRL 100 121802	T. Aaltonen *et al.*	(CDF Collab.)
ABLIKIM	08L	PL B665 16	M. Ablikim *et al.*	(BES Collab.)
ARINSTEIN	08	PL B662 102	K. Arinstein *et al.*	(BELLE Collab.)
ARTUSO	08	PR D77 092003	M. Artuso *et al.*	(CLEO Collab.)
ASNER	08	PR D78 012001	D.M. Asner *et al.*	(CLEO Collab.)
AUBERT	08AL	PR D78 034023	B. Aubert *et al.*	(BABAR Collab.)
AUBERT	08AO	PR D78 051102	B. Aubert *et al.*	(BABAR Collab.)
AUBERT	08AZ	PR D78 071101	B. Aubert *et al.*	(BABAR Collab.)
AUBERT	08L	PRL 100 051802	B. Aubert *et al.*	(BABAR Collab.)
AUBERT	08M	PRL 100 061803	B. Aubert *et al.*	(BABAR Collab.)
AUBERT	08U	PR D78 011105	B. Aubert *et al.*	(BABAR Collab.)
BITENC	08	PR D77 112003	U. Bitenc *et al.*	(BELLE Collab.)
BONVICINI	08	PR D77 091106	G. Bonvicini *et al.*	(CLEO Collab.)
DEANDREA	08	PR D78 034032	A. Deandrea, A. Nehme, P. Talavera	
DOBBS	08	PR D77 112005	S. Dobbs *et al.*	(CLEO Collab.)
Also		PRL 100 251802	D. Cronin-Hennessy *et al.*	(CLEO Collab.)
GASPERO	08	PR D78 014015	M. Gaspero *et al.*	(ROMA, CINN, TELA)
HE	08	PRL 100 091801	Q. He *et al.*	(CLEO Collab.)
PDG	08	PL B667 1	C. Amsler *et al.*	(PDG Collab.)
STARIC	08	PL B670 190	M. Staric *et al.*	(BELLE Collab.)
ABLIKIM	07G	PL B658 1	M. Ablikim *et al.*	(BES Collab.)
ARTUSO	07A	PRL 99 191801	M. Artuso *et al.*	(CLEO Collab.)
AUBERT	07AB	PR D76 014018	B. Aubert *et al.*	(BABAR Collab.)
AUBERT	07BG	PR D76 052005	B. Aubert *et al.*	(BABAR Collab.)
AUBERT	07BJ	PRL 99 251801	B. Aubert *et al.*	(BABAR Collab.)
AUBERT	07T	PR D76 011102	B. Aubert *et al.*	(BABAR Collab.)
AUBERT	07W	PRL 98 211802	B. Aubert *et al.*	(BABAR Collab.)
CAWLFIELD	07	PRL 98 092002	C. Cawlfield *et al.*	(CLEO Collab.)
DOBBS	07	PR D76 112001	S. Dobbs *et al.*	(CLEO Collab.)
LINK	07A	PR D75 052003	J.M. Link *et al.*	(FNAL FOCUS Collab.)
STARIC	07	PRL 98 211803	M. Staric *et al.*	(BELLE Collab.)
ZHANG	07B	PRL 99 131803	L.M. Zhang *et al.*	(BELLE Collab.)
ABLIKIM	06O	EPJ C47 31	M. Ablikim *et al.*	(BES Collab.)
ABLIKIM	06U	PL B643 246	M. Ablikim *et al.*	(BES Collab.)
ABULENCIA	06X	PR D74 031109	A. Abulencia *et al.*	(CDF Collab.)
ADAM	06A	PRL 97 251801	N.E. Adam *et al.*	(CLEO Collab.)
AUBERT,B	06N	PRL 97 221803	B. Aubert *et al.*	(BABAR Collab.)
AUBERT,B	06X	PR D74 091102	B. Aubert *et al.*	(BABAR Collab.)
CAWLFIELD	06A	PR D74 031108	C. Cawlfield *et al.*	(CLEO Collab.)
HUANG	06B	PR D74 112005	G.S. Huang *et al.*	(CLEO Collab.)
PDG	06	JP G33 1	W.-M. Yao *et al.*	(PDG Collab.)
RUBIN	06	PRL 96 081802	P. Rubin *et al.*	(CLEO Collab.)
WIDHALM	06	PRL 97 061804	L. Widhalm *et al.*	(BELLE Collab.)
ZHANG	06	PRL 96 151801	L.M. Zhang *et al.*	(BELLE Collab.)
ABLIKIM	05F	PL B622 6	M. Ablikim *et al.*	(BES Collab.)
ABLIKIM	05P	PL B625 196	M. Ablikim *et al.*	(BES Collab.)
ACOSTA	05C	PRL 94 122001	D. Acosta *et al.*	(FNAL CDF Collab.)
ASNER	05	PR D72 012001	D.M. Asner *et al.*	(CLEO Collab.)
AUBERT,B	05J	PR D72 052008	B. Aubert *et al.*	(BABAR Collab.)
BITENC	05	PR D72 071101	U. Bitenc *et al.*	(BELLE Collab.)
CAWLFIELD	05	PR D71 077101	C. Cawlfield *et al.*	(CLEO Collab.)
COAN	05	PRL 95 181802	T.E. Coan *et al.*	(CLEO Collab.)
CRONIN-HEN...	05	PR D72 031102	D. Cronin-Hennessy *et al.*	(CLEO Collab.)
HE	05	PRL 95 121801	Q. He *et al.*	(CLEO Collab.)
Also		PRL 96 199903 (errat.)	Q. He *et al.*	(CLEO Collab.)
HUANG	05	PRL 94 011802	G.S. Huang *et al.*	(CLEO Collab.)
KAYIS-TOPAK...	05	PL B626 24	A. Kayis-Topaksu *et al.*	(CERN CHORUS Collab.)
LI	05A	PRL 94 071801	J. Li *et al.*	(BELLE Collab.)
LINK	05	PL B607 51	J.M. Link *et al.*	(FNAL FOCUS Collab.)
LINK	05A	PL B607 59	J.M. Link *et al.*	(FNAL FOCUS Collab.)
LINK	05B	PL B607 67	J.M. Link *et al.*	(FNAL FOCUS Collab.)
LINK	05E	PL B622 239	J.M. Link *et al.*	(FNAL FOCUS Collab.)
LINK	05G	PL B610 225	J.M. Link *et al.*	(FNAL FOCUS Collab.)
LINK	05H	PL B618 23	J.M. Link *et al.*	(FNAL FOCUS Collab.)
ONENGUT	05	PL B613 105	G. Onengut *et al.*	(CERN CHORUS Collab.)
TIAN	05	PRL 95 231801	X.C. Tian *et al.*	(BELLE Collab.)
ABLIKIM	04C	PL B597 39	M. Ablikim *et al.*	(BEPC BES Collab.)
ABT	04	PL B596 173	I. Abt *et al.*	(HERA B Collab.)
ASNER	04A	PR D70 091101	D.M. Asner *et al.*	(CLEO Collab.)
AUBERT	04Q	PR D69 051101	B. Aubert *et al.*	(BABAR Collab.)
AUBERT,B	04Q	PR D70 091102	B. Aubert *et al.*	(BABAR Collab.)
AUBERT,B	04Y	PRL 93 191801	B. Aubert *et al.*	(BABAR Collab.)
LINK	04B	PL B586 21	J.M. Link *et al.*	(FNAL FOCUS Collab.)
LINK	04D	PL B586 191	J.M. Link *et al.*	(FNAL FOCUS Collab.)
RUBIN	04	PRL 93 111801	P. Rubin *et al.*	(CLEO Collab.)
TAJIMA	04	PRL 92 101803	O. Tajima *et al.*	(BELLE Collab.)
ACOSTA	03F	PR D68 091101	D. Acosta *et al.*	(CDF Collab.)
AUBERT	03P	PRL 91 121801	B. Aubert *et al.*	(BABAR Collab.)
AUBERT	03Z	PRL 91 171801	B. Aubert *et al.*	(BABAR Collab.)
COAN	03	PRL 90 101801	T.E. Coan *et al.*	(CLEO Collab.)
LINK	03	PL B555 167	J.M. Link *et al.*	(FNAL FOCUS Collab.)
LINK	03B	PL B556 7	J.M. Link *et al.*	(FNAL FOCUS Collab.)
LINK	03G	PL B575 190	J.M. Link *et al.*	(FNAL FOCUS Collab.)
ABE	02I	PRL 88 162001	K. Abe *et al.*	(KEK BELLE Collab.)
CSORNA	02	PR D65 092001	S.E. Csorna *et al.*	(CLEO Collab.)
LINK	02F	PL B537 192	J.M. Link *et al.*	(FNAL FOCUS Collab.)
MURAMATSU	02	PRL 89 251802	H. Muramatsu *et al.*	(CLEO Collab.)
Also		PRL 90 059901 (errat.)	H. Muramatsu *et al.*	(CLEO Collab.)
AITALA	01C	PRL 86 3969	E.M. Aitala *et al.*	(FNAL E791 Collab.)
AITALA	01D	PR D64 112003	E.M. Aitala *et al.*	(FNAL E791 Collab.)
BONVICINI	01	PR D63 071101	G. Bonvicini *et al.*	(CLEO Collab.)
BRANDENB...	01	PRL 87 071802	G. Brandenburg *et al.*	(CLEO Collab.)
DYTMAN	01	PR D64 111101	S.A. Dytman *et al.*	(CLEO Collab.)
KOPP	01	PR D63 092001	S. Kopp *et al.*	(CLEO Collab.)
KUSHNIR...	01	PRL 86 5243	A. Kushnirenko *et al.*	(FNAL SELEX Collab.)
LINK	01	PRL 86 2955	J.M. Link *et al.*	(FNAL FOCUS Collab.)
BAI	00C	PR D62 052001	J.Z. Bai *et al.*	(BEPC BES Collab.)
GODANG	00	PRL 84 5038	R. Godang *et al.*	(CLEO Collab.)
JUN	00	PRL 84 1857	S.Y. Jun *et al.*	(FNAL SELEX Collab.)
LINK	00	PL B485 62	J.M. Link *et al.*	(FNAL FOCUS Collab.)
LINK	00B	PL B491 232	J.M. Link *et al.*	(FNAL FOCUS Collab.)
Also		PL B495 443 (errat.)	J.M. Link *et al.*	(FNAL FOCUS Collab.)
PRIPSTEIN	00	PR D61 032005	D. Pripstein *et al.*	(FNAL E789 Collab.)
AITALA	99E	PRL 83 32	E.M. Aitala *et al.*	(FNAL E791 Collab.)
AITALA	99G	PL B462 401	E.M. Aitala *et al.*	(FNAL E791 Collab.)
BONVICINI	99	PRL 82 4586	G. Bonvicini *et al.*	(CLEO Collab.)
AITALA	98	PR D57 13	E.M. Aitala *et al.*	(FNAL E791 Collab.)
AITALA	98C	PL B421 405	E.M. Aitala *et al.*	(FNAL E791 Collab.)
AITALA	98D	PL B423 185	E.M. Aitala *et al.*	(FNAL E791 Collab.)
ARTUSO	98	PRL 80 3193	M. Artuso *et al.*	(CLEO Collab.)
ASNER	98	PR D58 092001	D.M. Asner *et al.*	(CLEO Collab.)
BARATE	98W	PL B436 211	R. Barate *et al.*	(ALEPH Collab.)
COAN	98	PRL 80 1150	T.E. Coan *et al.*	(CLEO Collab.)
PDG	98	EPJ C3 1	C. Caso *et al.*	(PDG Collab.)
ADAMOVICH	97	PL B408 469	M.I. Adamovich *et al.*	(CERN BEATRICE Collab.)
BARATE	97C	PL B403 367	R. Barate *et al.*	(ALEPH Collab.)
AITALA	96C	PRL 77 2384	E.M. Aitala *et al.*	(FNAL E791 Collab.)
ALBRECHT	96C	PL B374 249	H. Albrecht *et al.*	(ARGUS Collab.)
ALEXOPOU...	96	PRL 77 2380	T. Alexopoulos *et al.*	(FNAL E771 Collab.)
ASNER	96B	PR D54 4211	D.M. Asner *et al.*	(CLEO Collab.)
BARISH	96	PL B373 334	B.C. Barish *et al.*	(CLEO Collab.)
FRABETTI	96B	PL B382 312	P.L. Frabetti *et al.*	(FNAL E687 Collab.)
FREYBERGER	96	PRL 76 3065	A. Freyberger *et al.*	(CLEO Collab.)
Also		PRL 77 2147 (errat.)	A. Freyberger *et al.*	(CLEO Collab.)
KUBOTA	96B	PR D54 2994	Y. Kubota *et al.*	(CLEO Collab.)
ADAMOVICH	95	PL B353 563	M.I. Adamovich *et al.*	(CERN BEATRICE Collab.)
BARTELT	95	PR D52 4860	J.E. Bartelt *et al.*	(CLEO Collab.)
BUTLER	95	PR D52 2656	F. Butler *et al.*	(CLEO Collab.)
FRABETTI	95C	PL B354 486	P.L. Frabetti *et al.*	(FNAL E687 Collab.)
FRABETTI	95G	PL B364 127	P.L. Frabetti *et al.*	(FNAL E687 Collab.)
KODAMA	95	PL B345 85	K. Kodama *et al.*	(FNAL E653 Collab.)
ALBRECHT	94	PL B324 249	H. Albrecht *et al.*	(ARGUS Collab.)
ALBRECHT	94F	PL B340 125	H. Albrecht *et al.*	(ARGUS Collab.)
ALBRECHT	94I	ZPHY C64 375	H. Albrecht *et al.*	(ARGUS Collab.)
FRABETTI	94C	PL B321 295	P.L. Frabetti *et al.*	(FNAL E687 Collab.)
FRABETTI	94D	PL B323 459	P.L. Frabetti *et al.*	(FNAL E687 Collab.)
FRABETTI	94G	PL B331 217	P.L. Frabetti *et al.*	(FNAL E687 Collab.)
FRABETTI	94J	PL B340 254	P.L. Frabetti *et al.*	(FNAL E687 Collab.)
KODAMA	94	PL B336 605	K. Kodama *et al.*	(FNAL E653 Collab.)
MISHRA	94	PR D50 9	C.S. Mishra *et al.*	(FNAL E789 Collab.)
AKERIB	93	PRL 71 3070	D.S. Akerib *et al.*	(CLEO Collab.)
ALBRECHT	93D	PL B308 435	H. Albrecht *et al.*	(ARGUS Collab.)
ANJOS	93	PR D48 56	J.C. Anjos *et al.*	(FNAL E691 Collab.)
BEAN	93C	PL B317 647	A. Bean *et al.*	(CLEO Collab.)
FRABETTI	93I	PL B315 203	P.L. Frabetti *et al.*	(FNAL E687 Collab.)
KODAMA	93B	PL B313 260	K. Kodama *et al.*	(FNAL E653 Collab.)
PROCARIO	93B	PR D48 4007	M. Procario *et al.*	(CLEO Collab.)
SELEN	93	PRL 71 1973	M.A. Selen *et al.*	(CLEO Collab.)
ADAMOVICH	92	PL B280 163	M.I. Adamovich *et al.*	(CERN WA82 Collab.)
ALBRECHT	92P	ZPHY C56 7	H. Albrecht *et al.*	(ARGUS Collab.)
ANJOS	92C	PR D46 1941	J.C. Anjos *et al.*	(FNAL E691 Collab.)
BARLAG	92C	ZPHY C55 383	S. Barlag *et al.*	(ACCMOR Collab.)
Also		ZPHY C48 29	S. Barlag *et al.*	(ACCMOR Collab.)
COFFMAN	92B	PR D45 2196	D.M. Coffman *et al.*	(Mark III Collab.)
Also		PRL 64 2615	J. Adler *et al.*	(Mark III Collab.)
FRABETTI	92	PL B281 167	P.L. Frabetti *et al.*	(FNAL E687 Collab.)
FRABETTI	92B	PL B286 195	P.L. Frabetti *et al.*	(FNAL E687 Collab.)
ALVAREZ	91B	ZPHY C50 11	M.P. Alvarez *et al.*	(CERN NA14/2 Collab.)
AMMAR	91	PR D44 3383	R. Ammar *et al.*	(CLEO Collab.)
ANJOS	91	PR D43 635	J.C. Anjos *et al.*	(FNAL-TPS Collab.)
ANJOS	91D	PR D44 3371	J.C. Anjos *et al.*	(FNAL-TPS Collab.)
BAI	91	PRL 66 1011	Z. Bai *et al.*	(Mark III Collab.)
COFFMAN	91	PL B263 135	D.M. Coffman *et al.*	(Mark III Collab.)
CRAWFORD	91B	PR D44 3394	G. Crawford *et al.*	(CLEO Collab.)
DECAMP	91J	PL B266 218	D. Decamp *et al.*	(ALEPH Collab.)
FRABETTI	91	PL B263 584	P.L. Frabetti *et al.*	(FNAL E687 Collab.)
KINOSHITA	91	PR D43 2836	K. Kinoshita *et al.*	(CLEO Collab.)
KODAMA	91	PRL 66 1819	K. Kodama *et al.*	(FNAL E653 Collab.)
ALBRECHT	90C	ZPHY C46 9	H. Albrecht *et al.*	(ARGUS Collab.)
ALEXANDER	90	PRL 65 1184	J. Alexander *et al.*	(CLEO Collab.)
ALVAREZ	90	ZPHY C47 539	M.P. Alvarez *et al.*	(CERN NA14/2 Collab.)
ANJOS	90D	PR D42 2414	J.C. Anjos *et al.*	(FNAL E691 Collab.)
BARLAG	90C	ZPHY C46 563	S. Barlag *et al.*	(ACCMOR Collab.)
ADLER	89	PRL 62 1821	J. Adler *et al.*	(Mark III Collab.)
ADLER	89C	PR D40 906	J. Adler *et al.*	(Mark III Collab.)
ALBRECHT	89D	ZPHY C43 181	H. Albrecht *et al.*	(ARGUS Collab.)
ANJOS	89F	PRL 62 1587	J.C. Anjos *et al.*	(FNAL E691 Collab.)
ABACHI	88	PL B205 411	S. Abachi *et al.*	(HRS Collab.)
ADLER	88	PR D37 2023	J. Adler *et al.*	(Mark III Collab.)
ADLER	88C	PRL 60 89	J. Adler *et al.*	(Mark III Collab.)
ALBRECHT	88G	PL B209 380	H. Albrecht *et al.*	(ARGUS Collab.)
ALBRECHT	88I	PL B210 267	H. Albrecht *et al.*	(ARGUS Collab.)
ANJOS	88C	PRL 60 1239	J.C. Anjos *et al.*	(FNAL E691 Collab.)
BORTOLETTO	88	PR D37 1719	D. Bortoletto *et al.*	(CLEO Collab.)
Also		PR D39 1471 (errat.)	D. Bortoletto *et al.*	(CLEO Collab.)
HAAS	88	PRL 60 1614	P. Haas *et al.*	(CLEO Collab.)
RAAB	88	PR D37 2391	J.R. Raab *et al.*	(FNAL E691 Collab.)
ADLER	87	PL B196 107	J. Adler *et al.*	(Mark III Collab.)
AGUILAR-...	87E	ZPHY C36 551	M. Aguilar-Benitez *et al.*	(LEBC-EHS Collab.)
Also		ZPHY C40 321	M. Aguilar-Benitez *et al.*	(LEBC-EHS Collab.)
AGUILAR-...	87F	ZPHY C36 559	M. Aguilar-Benitez *et al.*	(LEBC-EHS Collab.)
Also		ZPHY C38 520 (errat.)	M. Aguilar-Benitez *et al.*	(LEBC-EHS Collab.)
BARLAG	87B	ZPHY C37 17	S. Barlag *et al.*	(ACCMOR Collab.)
BECKER	87C	PL B193 147	J.J. Becker *et al.*	(Mark III Collab.)
Also		PL B198 590 (errat.)	J.J. Becker *et al.*	(Mark III Collab.)
PALKA	87	PL B189 238	H. Palka *et al.*	(ACCMOR Collab.)
RILES	87	PR D35 2914	K. Riles *et al.*	(Mark II Collab.)
BAILEY	86	ZPHY C30 51	R. Bailey *et al.*	(ACCMOR Collab.)
BEBEK	86	PRL 56 1893	C. Bebek *et al.*	(CLEO Collab.)
LOUIS	86	PRL 56 1027	W.C. Louis *et al.*	(PRIN, CHIC, ISU)
ALBRECHT	85B	PL 158B 525	H. Albrecht *et al.*	(ARGUS Collab.)
ALBRECHT	85F	PL 150B 235	H. Albrecht *et al.*	(ARGUS Collab.)
AUBERT	85	PL 155B 461	J.J. Aubert *et al.*	(EMC Collab.)
BALTRUSAIT...	85E	PRL 55 150	R.M. Baltrusaitis *et al.*	(Mark III Collab.)
BENVENUTI	85	PL 158B 531	A.C. Benvenuti *et al.*	(BCDMS Collab.)
SUMMERS	84	PRL 52 410	D.J. Summers *et al.*	(UCSB, CARL, COLO+)
BAILEY	83B	PL 132B 237	R. Bailey *et al.*	(ACCMOR Collab.)
BODEK	82	PL 113B 82	A. Bodek *et al.*	(ROCH, CIT, CHIC, FNAL+)
SCHINDLER	81	PR D24 78	R.H. Schindler *et al.*	(Mark II Collab.)
AVERY	80	PRL 44 1309	P. Avery *et al.*	(ILL, FNAL, COLU)
ABRAMS	79D	PRL 43 481	G.S. Abrams *et al.*	(Mark II Collab.)
VUILLEMIN	78	PRL 41 1149	V. Vuillemin *et al.*	(LGW Collab.)
PERUZZI	77	PRL 39 1301	I. Peruzzi *et al.*	(LGW Collab.)
PICCOLO	77	PL 70B 260	M. Piccolo *et al.*	(Mark I Collab.)
MOSTELLER	48	AST 2 No.5 30	R.A. Fisher, F. Mosteller	

OTHER RELATED PAPERS

RICHMAN	95	RMP 67 893	J.D. Richman, P.R. Burchat	(UCSB, STAN)
ROSNER	95	CNPP 21 369	J. Rosner	(CHIC)

$D^*(2007)^0$

$I(J^P) = \frac{1}{2}(1^-)$

$J^P = 1^-$ established by ABLIKIM 23AZ.

$D^*(2007)^0$ MASS

The fit includes $D^\pm$, D^0, $D_s^\pm$, $D^{*\pm}$, D^{*0}, $D_s^{*\pm}$, $D_1(2420)^0$, $D_2^*(2460)^0$, and $D_{s1}(2536)^\pm$ mass and mass difference measurements.

VALUE (MeV)	DOCUMENT ID	TECN	COMMENT
2006.86 ± 0.05 OUR FIT Error includes scale factor of 1.1.			
• • • We do not use the following data for averages, fits, limits, etc. • • •			
2006 ±1.5	[1] GOLDHABER 77	MRK1	e^+e^-

Int. J. Mod. Phys. A 2026.41. Downloaded from www.worldscientific.com
by CALIFORNIA @ BERKELEY on 09/16/26. Re-use and distribution is strictly not permitted, except for Open Access articles.

Int. J. Mod. Phys. A 2026.41. Downloaded from www.worldscientific.com by UNIVERSITY OF CALIFORNIA @ BERKELEY on 09/16/26. Re-use and distribution is strictly not permitted, except for Open Access articles.

[1] From simultaneous fit to $D^*(2010)^+$, $D^*(2007)^0$, D^+, and D^0.

$m_{D^*(2007)^0} - m_{D^0}$

The fit includes $D^\pm$, D^0, $D_s^\pm$, $D^{*\pm}$, D^{*0}, $D_s^{*\pm}$, $D_1(2420)^0$, $D_2^*(2460)^0$, and $D_{s1}(2536)^\pm$ mass and mass difference measurements.

VALUE (MeV)	EVTS	DOCUMENT ID		TECN	COMMENT
142.014±0.030 OUR FIT Error includes scale factor of 1.5.					
142.016±0.030 OUR AVERAGE Error includes scale factor of 1.5.					
142.007±0.015±0.014	10k	[1] TOMARADZE	15	CLEO	$e^+e^- \to$ hadrons
142.2 ±0.3 ±0.2	145	ALBRECHT	95F	ARG	$e^+e^- \to$ hadrons
142.12 ±0.05 ±0.05	1176	BORTOLETTO	92B	CLE2	$e^+e^- \to$ hadrons
• • • We do not use the following data for averages, fits, limits, etc. • • •					
142.2 ±2.0		SADROZINSKI	80	CBAL	$D^{*0} \to D^0\pi^0$
142.7 ±1.7		[2] GOLDHABER	77	MRK1	e^+e^-

[1] Obtained by analyzing CLEO-c data but not authored by the CLEO Collaboration. This value comes from the average of the results for two decay modes, $D^0 \to K^-\pi^+$ and $D^0 \to K^-\pi^+\pi^-\pi^+$.
[2] From simultaneous fit to $D^*(2010)^+$, $D^*(2007)^0$, D^+, and D^0.

$D^*(2007)^0$ WIDTH

VALUE (MeV)	CL%	DOCUMENT ID		TECN	COMMENT
<2.1	90	[1] ABACHI	88B	HRS	$D^{*0} \to D^+\pi^-$

[1] Assuming $m_{D^{*0}} = 2007.2 \pm 2.1$ MeV/c^2.

$D^*(2007)^0$ DECAY MODES

$\overline{D}^*(2007)^0$ modes are charge conjugates of modes below.

	Mode	Fraction (Γ_i/Γ)	Confidence level
Γ_1	$D^0\pi^0$	(64.7 ±0.9) %	
Γ_2	$D^0\gamma$	(35.3 ±0.9) %	
Γ_3	$D^0e^+e^-$	(3.91±0.33) $\times 10^{-3}$	
Γ_4	$\mu^+\mu^-$	< 2.5 $\times 10^{-8}$	90%
Γ_5	e^+e^-	< 1.7 $\times 10^{-6}$	90%

CONSTRAINED FIT INFORMATION

An overall fit to 2 branching ratios uses 5 measurements and one constraint to determine 2 parameters. The overall fit has a $\chi^2 =$ 2.5 for 4 degrees of freedom.

The following *off-diagonal* array elements are the correlation coefficients $\langle \delta x_i \delta x_j \rangle / (\delta x_i \cdot \delta x_j)$, in percent, from the fit to the branching fractions, $x_i \equiv \Gamma_i/\Gamma_{total}$. The fit constrains the x_i whose labels appear in this array to sum to one.

	x_1
x_2	−100

$D^*(2007)^0$ BRANCHING RATIOS

$\Gamma(D^0\pi^0)/\Gamma_{total}$ — Γ_1/Γ

VALUE	EVTS	DOCUMENT ID		TECN	COMMENT
0.647±0.009 OUR FIT					
• • • We do not use the following data for averages, fits, limits, etc. • • •					
0.655±0.008±0.005	3.2k	[1] ABLIKIM	15B	BES3	$e^+e^- \to$ hadrons
0.635±0.003±0.017	69k	[1] AUBERT,BE	05G	BABR	10.6 $e^+e^- \to$ hadrons
0.596±0.035±0.028	858	[2] ALBRECHT	95F	ARG	$e^+e^- \to$ hadrons
0.636±0.023±0.033	1097	[2] BUTLER	92	CLE2	$e^+e^- \to$ hadrons

[1] Derived from the ratio $\Gamma(D^0\pi^0)$ / $\Gamma(D^0\gamma)$ assuming that the branching fractions of $D^{*0} \to D^0\pi^0$ and $D^{*0} \to D^0\gamma$ decays sum to 100%.
[2] The BUTLER 92 and ALBRECHT 95F branching ratios are not independent, they have been constrained by the authors to sum to 100%.

$\Gamma(D^0\gamma)/\Gamma_{total}$ — Γ_2/Γ

VALUE	EVTS	DOCUMENT ID		TECN	COMMENT
0.353±0.009 OUR FIT					
0.381±0.029 OUR AVERAGE					
0.404±0.035±0.028	456	[1] ALBRECHT	95F	ARG	$e^+e^- \to$ hadrons
0.364±0.023±0.033	621	[1] BUTLER	92	CLE2	$e^+e^- \to$ hadrons
0.37 ±0.08 ±0.08		ADLER	88D	MRK3	e^+e^-
• • • We do not use the following data for averages, fits, limits, etc. • • •					
0.345±0.008±0.005	1.8k	[2] ABLIKIM	15B	BES3	$e^+e^- \to$ hadrons
0.365±0.003±0.017	68k	[2] AUBERT,BE	05G	BABR	10.6 $e^+e^- \to$ hadrons
0.47 ±0.23		LOW	87	HRS	29 GeV e^+e^-
0.53 ±0.13		BARTEL	85G	JADE	e^+e^-, hadrons
0.47 ±0.12		COLES	82	MRK2	e^+e^-
0.45 ±0.15		GOLDHABER	77	MRK1	e^+e^-

[1] The BUTLER 92 and ALBRECHT 95F branching ratios are not independent, they have been constrained by the authors to sum to 100%.
[2] Derived from the ratio $\Gamma(D^0\pi^0)$ / $\Gamma(D^0\gamma)$ assuming that the branching fractions of $D^{*0} \to D^0\pi^0$ and $D^{*0} \to D^0\gamma$ decays sum to 100%.

$\Gamma(D^0\pi^0)/\Gamma(D^0\gamma)$ — Γ_1/Γ_2

VALUE	EVTS	DOCUMENT ID		TECN	COMMENT
1.83 ±0.07 OUR FIT					
1.85 ±0.07 OUR AVERAGE					
1.90 ±0.07 ±0.05	4.9k	ABLIKIM	15B	BES3	10.6 $e^+e^- \to$ hadrons
1.74 ±0.02 ±0.13		AUBERT,BE	05G	BABR	10.6 $e^+e^- \to$ hadrons
• • • We do not use the following data for averages, fits, limits, etc. • • •					
1.789±0.082		[1] AAIJ	22N	LHCB	$B^0, B_s^0 \to \overline{D}^{*0}(K\pi,\ \pi\pi)$

[1] Statistical error only.

$\Gamma(D^0e^+e^-)/\Gamma(D^0\gamma)$ — Γ_3/Γ_2

VALUE (units 10^{-3})	EVTS	DOCUMENT ID		TECN	COMMENT
11.08±0.76±0.49	421	ABLIKIM	21BD	BES3	4.178 GeV e^+e^-

$\Gamma(\mu^+\mu^-)/\Gamma_{total}$ — Γ_4/Γ

VALUE	CL%	DOCUMENT ID		TECN	COMMENT
<2.5 × 10^{-8}	90	[1] AAIJ	23D	LHCB	$B^- \to \pi^-\mu^+\mu^-$

[1] AAIJ 23D reports < 2.6 × 10^{-8} from a measurement of $[\Gamma(D^*(2007)^0 \to \mu^+\mu^-)/\Gamma_{total}] \times [B(B^+ \to \overline{D}^*(2007)^0\pi^+)]$ assuming $B(B^+ \to \overline{D}^*(2007)^0\pi^+) = (4.90 \pm 0.17) \times 10^{-3}$, which we rescale to our best (shown rounded) value $B(B^+ \to \overline{D}^*(2007)^0\pi^+) = 5.17 \times 10^{-3}$. The reported value also assumes $B(B^- \to J/\psi(1S)K^-) = (10.20 \pm 0.19) \times 10^{-4}$ and $B(J/\psi(1S) \to \mu^+\mu^-) = (59.61 \pm 0.33) \times 10^{-3}$ for the normalization mode $B^- \to J/\psi(1S)K^-$.

$\Gamma(e^+e^-)/\Gamma_{total}$ — Γ_5/Γ

VALUE	CL%	DOCUMENT ID		TECN	COMMENT
<1.7 × 10^{-6}	90	SHEMYAKIN	20	CMD3	$e^+e^- \to D^0\pi^0,\ D^0\gamma$

$D^*(2007)^0$ REFERENCES

AAIJ	23D	EPJ C83 666	R. Aaij *et al.*	(LHCb Collab.)
ABLIKIM	23AZ	PL B846 138245	M. Ablikim *et al.*	(BESIII Collab.) JP
AAIJ	22N	PR D105 072005	R. Aaij *et al.*	(LHCb Collab.)
ABLIKIM	21BD	PR D104 112012	M. Ablikim *et al.*	(BESIII Collab.)
SHEMYAKIN	20	PAN 83 954	D.N. Shemyakin	(CMD-3 Collab.)
ABLIKIM	15B	PR D91 031101	M. Ablikim *et al.*	(BESIII Collab.)
TOMARADZE	15	PR D91 011102	A. Tomaradze *et al.*	(NWES)
AUBERT,BE	05G	PR D72 091101	B. Aubert *et al.*	(BABAR Collab.)
ALBRECHT	95F	ZPHY C66 63	H. Albrecht *et al.*	(ARGUS Collab.)
BORTOLETTO	92B	PRL 69 2046	D. Bortoletto *et al.*	(CLEO Collab.)
BUTLER	92	PRL 69 2041	F. Butler *et al.*	(CLEO Collab.)
ABACHI	88B	PL B212 533	S. Abachi *et al.*	(ANL, IND, MICH, PURD+)
ADLER	88D	PL B208 152	J. Adler *et al.*	(Mark III Collab.)
LOW	87	PL B183 232	E.H. Low *et al.*	(HRS Collab.)
BARTEL	85G	PL 161B 197	W. Bartel *et al.*	(JADE Collab.)
COLES	82	PR D26 2190	M.W. Coles *et al.*	(LBL, SLAC)
SADROZINSKI	80	Madison Conf. 681	H.F.W. Sadrozinski *et al.*	(PRIN, CIT+)
GOLDHABER	77	PL 69B 503	G. Goldhaber *et al.*	(Mark I Collab.)

$D^*(2010)^\pm$

$I(J^P) = \frac{1}{2}(1^-)$

$J^P = 1^-$ established by ABLIKIM 23AZ.

$D^*(2010)^\pm$ MASS

The fit includes $D^\pm$, D^0, $D_s^\pm$, $D^{*\pm}$, D^{*0}, $D_s^{*\pm}$, $D_1(2420)^0$, $D_2^*(2460)^0$, and $D_{s1}(2536)^\pm$ mass and mass difference measurements.

VALUE (MeV)	DOCUMENT ID		TECN	CHG	COMMENT
2010.27±0.04 OUR FIT					
• • • We do not use the following data for averages, fits, limits, etc. • • •					
2008 ±3	[1] GOLDHABER	77	MRK1	±	e^+e^-
2008.6 ±1.0	[2] PERUZZI	77	LGW	±	e^+e^-

[1] From simultaneous fit to $D^*(2010)^+$, $D^*(2007)^0$, D^+, and D^0; not independent of FELDMAN 77B mass difference below.
[2] PERUZZI 77 mass not independent of FELDMAN 77B mass difference below and PERUZZI 77 D^0 mass value.

$m_{D^*(2010)^+} - m_{D^+}$

The fit includes $D^\pm$, D^0, $D_s^\pm$, $D^{*\pm}$, D^{*0}, $D_s^{*\pm}$, $D_1(2420)^0$, $D_2^*(2460)^0$, and $D_{s1}(2536)^\pm$ mass and mass difference measurements.

VALUE (MeV)	EVTS	DOCUMENT ID		TECN	COMMENT
140.603 ±0.015 OUR FIT					
140.602 ±0.014 OUR AVERAGE					
140.6010±0.0068±0.0129	151k	LEES	17F	BABR	$e^+e^- \to$ hadrons
140.64 ±0.08 ±0.06	620	BORTOLETTO	92B	CLE2	$e^+e^- \to$ hadrons

Int. J. Mod. Phys. A 2026.41. Downloaded from www.worldscientific.com
by LIFORNIA @ BERKELEY on 09/16/26. Re-use and distribution is strictly not permitted, except for Open Access articles.

$m_{D^*(2010)^+} - m_{D^0}$

The fit includes $D^\pm$, D^0, $D_s^\pm$, $D^{*\pm}$, D^{*0}, $D_s^{*\pm}$, $D_1(2420)^0$, $D_2^*(2460)^0$, and $D_{s1}(2536)^\pm$ mass and mass difference measurements.

VALUE (MeV)	EVTS	DOCUMENT ID		TECN	COMMENT
145.4257±0.0017 OUR FIT					
145.4258±0.0020 OUR AVERAGE		Error includes scale factor of 1.2.			
145.4259±0.0004±0.0017	312.8k	LEES	13X	BABR	$D^{*\pm} \to D^0\pi^\pm \to (K\pi, K3\pi)\pi^\pm$
145.412 ±0.002 ±0.012		ANASTASSOV	02	CLE2	$D^{*\pm} \to D^0\pi^\pm \to (K\pi)\pi^\pm$
145.54 ±0.08	611	[1] ADINOLFI	99	BEAT	$D^{*\pm} \to D^0\pi^\pm$
145.45 ±0.02		[1] BREITWEG	99	ZEUS	$D^{*\pm} \to D^0\pi^\pm \to (K\pi)\pi^\pm$
145.42 ±0.05		[1] BREITWEG	99	ZEUS	$D^{*\pm} \to D^0\pi^\pm \to (K^-3\pi)\pi^\pm$
145.5 ±0.15	103	[2] ADLOFF	97B	H1	$D^{*\pm} \to D^0\pi^\pm$
145.44 ±0.08	152	[2] BREITWEG	97	ZEUS	$D^{*\pm} \to D^0\pi^\pm$, $D^0 \to K^-3\pi$
145.42 ±0.11	199	[2] BREITWEG	97	ZEUS	$D^{*\pm} \to D^0\pi^\pm$, $D^0 \to K^-\pi^+$
145.4 ±0.2	48	[2] DERRICK	95	ZEUS	$D^{*\pm} \to D^0\pi^\pm$
145.39 ±0.06 ±0.03		BARLAG	92B	ACCM	π^- 230 GeV
145.5 ±0.2	115	[2] ALEXANDER	91B	OPAL	$D^{*\pm} \to D^0\pi^\pm$
145.30 ±0.06		[2] DECAMP	91J	ALEP	$D^{*\pm} \to D^0\pi^\pm$
145.40 ±0.05 ±0.10		ABACHI	88B	HRS	$D^{*\pm} \to D^0\pi^\pm$
145.46 ±0.07 ±0.03		ALBRECHT	85F	ARG	$D^{*\pm} \to D^0\pi^+$
145.5 ±0.3	28	BAILEY	83	SPEC	$D^{*\pm} \to D^0\pi^\pm$
145.5 ±0.3	60	FITCH	81	SPEC	π^-A
145.3 ±0.5	30	FELDMAN	77B	MRK1	$D^{*+} \to D^0\pi^+$
• • • We do not use the following data for averages, fits, limits, etc. • • •					
145.4256±0.0006±0.0017	138.5k	LEES	13X	BABR	$D^{*\pm} \to D^0\pi^\pm \to (K^-\pi^+)\pi^\pm$
145.4266±0.0005±0.0019	174.3k	LEES	13X	BABR	$D^{*\pm} \to D^0\pi^\pm \to (K^-2\pi^+\pi^-)\pi^\pm$
145.44 ±0.09	122	[2] BREITWEG	97B	ZEUS	$D^{*\pm} \to D^0\pi^\pm$, $D^0 \to K^-\pi^+$
145.8 ±1.5	16	AHLEN	83	HRS	$D^{*+} \to D^0\pi^+$
145.1 ±1.8	12	BAILEY	83	SPEC	$D^{*\pm} \to D^0\pi^\pm$
145.1 ±0.5	14	BAILEY	83	SPEC	$D^{*\pm} \to D^0\pi^\pm$
145.5 ±0.5	14	YELTON	82	MRK2	29 $e^+e^- \to K^-\pi^+$
~ 145.5		AVERY	80	SPEC	γA
145.2 ±0.6	2	BLIETSCHAU	79	BEBC	νp

[1] Statistical errors only.
[2] Systematic error not evaluated.

$m_{D^*(2010)^+} - m_{D^*(2007)^0}$

VALUE (MeV)	DOCUMENT ID		TECN	COMMENT
• • • We do not use the following data for averages, fits, limits, etc. • • •				
2.6±1.8	[1] PERUZZI	77	LGW	e^+e^-

[1] Not independent of FELDMAN 77B mass difference above, PERUZZI 77 D^0 mass, and GOLDHABER 77 $D^*(2007)^0$ mass.

$D^*(2010)^\pm$ WIDTH

VALUE (keV)	CL%	EVTS	DOCUMENT ID		TECN	COMMENT
83.4±1.8 OUR AVERAGE						
83.3±1.2± 1.4		312.8k	[1] LEES	13X	BABR	$D^{*\pm} \to D^0\pi^\pm \to (K\pi, K3\pi)\pi^\pm$
96 ±4 ±22			[1] ANASTASSOV	02	CLE2	$D^{*\pm} \to D^0\pi^\pm \to (K\pi)\pi^\pm$
• • • We do not use the following data for averages, fits, limits, etc. • • •						
83.4±1.7± 1.5		138.5k	[1] LEES	13X	BABR	$D^{*\pm} \to D^0\pi^\pm \to (K^-\pi^+)\pi^\pm$
83.2±1.5± 2.6		174.3k	[1] LEES	13X	BABR	$D^{*\pm} \to D^0\pi^\pm \to (K^-2\pi^+\pi^-)\pi^\pm$
<131	90	110	BARLAG	92B	ACCM	π^- 230 GeV

[1] Ignoring the electromagnetic contribution from $D^{*\pm} \to D^\pm\gamma$.

$D^*(2010)^\pm$ DECAY MODES

$D^*(2010)^-$ modes are charge conjugates of the modes below.

	Mode	Fraction (Γ_i/Γ)	Confidence level
Γ_1	$D^0\pi^+$	(67.7±0.5) %	
Γ_2	$D^+\pi^0$	(30.7±0.5) %	
Γ_3	$D^+\gamma$	(1.6±0.4) %	
Γ_4	$e^+\nu_e$	$< 1.1 \times 10^{-5}$	90%
Γ_5	$\mu^+\nu_\mu$	$< 4.3 \times 10^{-6}$	90%

CONSTRAINED FIT INFORMATION

An overall fit to 3 branching ratios uses 6 measurements and one constraint to determine 3 parameters. The overall fit has a χ^2 = 0.3 for 4 degrees of freedom.

The following *off-diagonal* array elements are the correlation coefficients $\langle \delta x_i \delta x_j \rangle / (\delta x_i \cdot \delta x_j)$, in percent, from the fit to the branching fractions, $x_i \equiv \Gamma_i/\Gamma_{total}$. The fit constrains the x_i whose labels appear in this array to sum to one.

	x_1	x_2
x_2	−62	
x_3	−43	−44

$D^*(2010)^+$ BRANCHING RATIOS

$\Gamma(D^0\pi^+)/\Gamma_{total}$ — Γ_1/Γ

VALUE	DOCUMENT ID		TECN	COMMENT
0.677 ±0.005 OUR FIT				
0.677 ±0.006 OUR AVERAGE				
0.6759±0.0029±0.0064	[1,2,3] BARTELT	98	CLE2	e^+e^-
0.688 ±0.024 ±0.013	ALBRECHT	95F	ARG	$e^+e^- \to$ hadrons
0.681 ±0.010 ±0.013	[1] BUTLER	92	CLE2	$e^+e^- \to$ hadrons
• • • We do not use the following data for averages, fits, limits, etc. • • •				
0.57 ±0.04 ±0.04	ADLER	88D	MRK3	e^+e^-
0.44 ±0.10	COLES	82	MRK2	e^+e^-
0.6 ±0.15	[3] GOLDHABER	77	MRK1	e^+e^-

[1] The branching ratios are not independent, they have been constrained by the authors to sum to 100%.
[2] Systematic error includes theoretical error on the prediction of the ratio of hadronic modes.
[3] Assuming that isospin is conserved in the decay.

$\Gamma(D^+\pi^0)/\Gamma_{total}$ — Γ_2/Γ

VALUE	EVTS	DOCUMENT ID		TECN	COMMENT
0.307 ±0.005 OUR FIT					
0.3073±0.0013±0.0062		[1,2,3] BARTELT	98	CLE2	e^+e^-
• • • We do not use the following data for averages, fits, limits, etc. • • •					
0.312 ±0.011 ±0.008	1404	ALBRECHT	95F	ARG	$e^+e^- \to$ hadrons
0.308 ±0.004 ±0.008	410	[1] BUTLER	92	CLE2	$e^+e^- \to$ hadrons
0.26 ±0.02 ±0.02		ADLER	88D	MRK3	e^+e^-
0.34 ±0.07		COLES	82	MRK2	e^+e^-

[1] The branching ratios are not independent, they have been constrained by the authors to sum to 100%.
[2] Systematic error includes theoretical error on the prediction of the ratio of hadronic modes.
[3] Assuming that isospin is conserved in the decay.

$\Gamma(D^+\gamma)/\Gamma_{total}$ — Γ_3/Γ

VALUE	CL%	EVTS	DOCUMENT ID		TECN	COMMENT
0.016 ±0.004 OUR FIT						
0.016 ±0.005 OUR AVERAGE						
0.0168±0.0042±0.0029			[1,2] BARTELT	98	CLE2	e^+e^-
0.011 ±0.014 ±0.016		12	[1] BUTLER	92	CLE2	$e^+e^- \to$ hadrons
• • • We do not use the following data for averages, fits, limits, etc. • • •						
<0.052		90	ALBRECHT	95F	ARG	$e^+e^- \to$ hadrons
0.17 ±0.05 ±0.05			ADLER	88D	MRK3	e^+e^-
0.22 ±0.12			[3] COLES	82	MRK2	e^+e^-

[1] The branching ratios are not independent, they have been constrained by the authors to sum to 100%.
[2] Systematic error includes theoretical error on the prediction of the ratio of hadronic modes.
[3] Not independent of $\Gamma(D^0\pi^+)/\Gamma_{total}$ and $\Gamma(D^+\pi^0)/\Gamma_{total}$ measurement.

$\Gamma(e^+\nu_e)/\Gamma_{total}$ — Γ_4/Γ

VALUE	CL%	DOCUMENT ID		TECN	COMMENT
$<1.1 \times 10^{-5}$	90	ABLIKIM	24AO	BES3	e^+e^- at 4.178–4.226 GeV

$\Gamma(\mu^+\nu_\mu)/\Gamma_{total}$ — Γ_5/Γ

VALUE	CL%	DOCUMENT ID		TECN	COMMENT
$<4.3 \times 10^{-6}$	90	ABLIKIM	24AO	BES3	e^+e^- at 4.178–4.226 GeV

$D^*(2010)^\pm$ REFERENCES

ABLIKIM	24AO	PR D110 012003	M. Ablikim *et al.*	(BESIII Collab.)
ABLIKIM	23AZ	PL B846 138245	M. Ablikim *et al.*	(BESIII Collab.) JP
LEES	17F	PRL 119 202003	J.P. Lees *et al.*	(BABAR Collab.)
LEES	13X	PRL 111 111801	J.P. Lees *et al.*	(BABAR Collab.)
Also		PR D88 052003	J.P. Lees *et al.*	(BABAR Collab.)
Also		PR D88 079902 (errat.)	J.P. Lees *et al.*	(BABAR Collab.)
ANASTASSOV	02	PR D65 032003	A. Anastassov *et al.*	(CLEO Collab.)
ADINOLFI	99	NP B547 3	M. Adinolfi *et al.*	(Beatrice Collab.)
BREITWEG	99	EPJ C6 67	J. Breitweg *et al.*	(ZEUS Collab.)
BARTELT	98	PRL 80 3919	J. Bartelt *et al.*	(CLEO Collab.)
ADLOFF	97B	ZPHY C72 593	C. Adloff *et al.*	(H1 Collab.)
BREITWEG	97	PL B401 192	J. Breitweg *et al.*	(ZEUS Collab.)

BREITWEG	97B	PL B407 402	J. Breitweg *et al.*	(ZEUS Collab.)
ALBRECHT	95F	ZPHY C66 63	H. Albrecht *et al.*	(ARGUS Collab.)
DERRICK	95	PL B349 225	M. Derrick *et al.*	(ZEUS Collab.)
BARLAG	92B	PL B278 480	S. Barlag *et al.*	(ACCMOR Collab.)
BORTOLETTO	92B	PRL 69 2046	D. Bortoletto *et al.*	(CLEO Collab.)
BUTLER	92	PRL 69 2041	F. Butler *et al.*	(CLEO Collab.)
ALEXANDER	91B	PL B262 341	G. Alexander *et al.*	(OPAL Collab.)
DECAMP	91J	PL B266 218	D. Decamp *et al.*	(ALEPH Collab.)
ABACHI	88B	PL B212 533	S. Abachi *et al.*	(ANL, IND, MICH, PURD+)
ADLER	88D	PL B208 152	J. Adler *et al.*	(Mark III Collab.)
ALBRECHT	85F	PL 150B 235	H. Albrecht *et al.*	(ARGUS Collab.)
AHLEN	83	PRL 51 1147	S.P. Ahlen *et al.*	(ANL, IND, LBL+)
BAILEY	83	PL 132B 230	R. Bailey *et al.*	(AMST, BRIS, CERN, CRAC+)
COLES	82	PR D26 2190	M.W. Coles *et al.*	(LBL, SLAC)
YELTON	82	PRL 49 430	J.M. Yelton *et al.*	(SLAC, LBL, UCB+)
FITCH	81	PRL 46 761	V.L. Fitch *et al.*	(PRIN, SACL, TORI+)
AVERY	80	PRL 44 1309	P. Avery *et al.*	(ILL, FNAL, COLU)
BLIETSCHAU	79	PL 86B 108	J. Blietschau *et al.*	(AACH3, BONN, CERN+)
FELDMAN	77B	PRL 38 1313	G.J. Feldman *et al.*	(Mark I Collab.)
GOLDHABER	77	PL 69B 503	G. Goldhaber *et al.*	(Mark I Collab.)
PERUZZI	77	PRL 39 1301	I. Peruzzi *et al.*	(LGW Collab.)

$D_0^*(2300)$

$I(J^P) = \frac{1}{2}(0^+)$

was $D_0^*(2400)$

There is a strong evidence that recent data on $B \to D\pi\pi$ (AAIJ 15Y, AAIJ 16AH) and $B \to D\pi K$ (AAIJ 14BH, AAIJ 15V, AAIJ 15X) call for two poles in the scalar $I = 1/2$ πD amplitude in this mass range. The data are consistent with a lower pole at $(2105^{+6}_{-8}) - i(102^{+10}_{-11})$ MeV and a higher pole at $(2451^{+35}_{-26}) - i(134^{+7}_{-8})$ MeV (DU 18A, DU 19, DU 21). For details see review on "Heavy Non-$q\overline{q}$ Mesons."

$D_0^*(2300)$ MASS

VALUE (MeV)	EVTS	DOCUMENT ID		TECN	CHG	COMMENT
2343±10 OUR AVERAGE		Error includes scale factor of 1.5. See the ideogram below.				
2360±15±30		[1] AAIJ	15X	LHCB	+	$B^0 \to \overline{D}^0 K^+ \pi^-$
2349± 6± 4		[2] AAIJ	15Y	LHCB	+	$B^0 \to \overline{D}^0 \pi^+ \pi^-$
2297± 8±20	3.4k	AUBERT	09AB	BABR	0	$B^- \to D^+ \pi^- \pi^-$
2308±17±32		ABE	04D	BELL	0	$B^- \to D^+ \pi^- \pi^-$
• • • We do not use the following data for averages, fits, limits, etc. • • •						
2354± 7±11		[3] AAIJ	15Y	LHCB	+	$B^0 \to \overline{D}^0 \pi^+ \pi^-$
2403±14±35	18.8k	[4] LINK	04A	FOCS	+	γ A
2407±21±35	9.8k	[4] LINK	04A	FOCS	0	γ A

[1] From the Dalitz plot analysis including various K^* and D^{**} mesons as well as broad structures in the $K\pi$ S-wave and the $D\pi$ S- and P-waves.
[2] Modeling the $\pi^+\pi^-$ S-wave with the Isobar formalism.
[3] Modeling the $\pi^+\pi^-$ S-wave with the K-matrix formalism.
[4] Possibly the feed-down from another state.

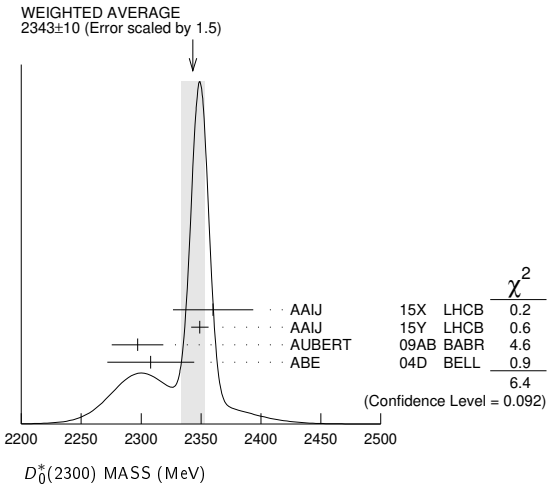

$D_0^*(2300)$ WIDTH

VALUE (MeV)	EVTS	DOCUMENT ID		TECN	CHG	COMMENT
229±16 OUR AVERAGE						
255±26±51		[1] AAIJ	15X	LHCB	+	$B^0 \to \overline{D}^0 K^+ \pi^-$
217±13±13		[2] AAIJ	15Y	LHCB	+	$B^0 \to \overline{D}^0 \pi^+ \pi^-$
273±12±48	3.4k	AUBERT	09AB	BABR	0	$B^- \to D^+ \pi^- \pi^-$
276±21±63		ABE	04D	BELL	0	$B^- \to D^+ \pi^- \pi^-$
• • • We do not use the following data for averages, fits, limits, etc. • • •						
230±15±21		[3] AAIJ	15Y	LHCB	+	$B^0 \to \overline{D}^0 \pi^+ \pi^-$
283±24±34	18.8k	[4] LINK	04A	FOCS	+	γ A
240±55±59	9.8k	[4] LINK	04A	FOCS	0	γ A

[1] From the Dalitz plot analysis including various K^* and D^{**} mesons as well as broad structures in the $K\pi$ S-wave and the $D\pi$ S- and P-waves.
[2] Modeling the $\pi^+\pi^-$ S-wave with the Isobar formalism.
[3] Modeling the $\pi^+\pi^-$ S-wave with the K-matrix formalism.
[4] Possibly the feed-down from another state.

$D_0^*(2300)$ DECAY MODES

	Mode	Fraction (Γ_i/Γ)
Γ_1	$D\pi^\pm$	seen

$D_0^*(2300)$ BRANCHING RATIOS

$\Gamma(D\pi^\pm)/\Gamma_{total}$ — Γ_1/Γ

VALUE	EVTS	DOCUMENT ID		TECN	CHG	COMMENT
seen		AAIJ	15X	LHCB	+	$D^*(2300)^+ \to D^0\pi^+$
seen		AAIJ	15Y	LHCB	+	$D^*(2300)^+ \to D^0\pi^+$
seen	3.4k	AUBERT	09AB	BABR	0	$D^*(2300)^0 \to D^+\pi^-$
seen		ABE	04D	BELL	0	$D^*(2300)^0 \to D^+\pi^-$
seen	18.8k	LINK	04A	FOCS	+	$D^*(2300)^+ \to D^0\pi^+$

$D_0^*(2300)$ REFERENCES

DU	21	PRL 126 192001	M.-L. Du *et al.*	
DU	19	PR D99 114002	M.-L. Du, F.-K. Guo, U.-G. Meissner	
DU	18A	PR D98 094018	M.-L. Du *et al.*	
AAIJ	16AH	PR D94 072001	R. Aaij *et al.*	(LHCb Collab.)
AAIJ	15V	PR D91 092002	R. Aaij *et al.*	(LHCb Collab.)
Also		PR D93 119901 (errat.)	R. Aaij *et al.*	(LHCb Collab.)
AAIJ	15X	PR D92 012012	R. Aaij *et al.*	(LHCb Collab.)
AAIJ	15Y	PR D92 032002	R. Aaij *et al.*	(LHCb Collab.)
AAIJ	14BH	PR D90 072003	R. Aaij *et al.*	(LHCb Collab.)
AUBERT	09AB	PR D79 112004	B. Aubert *et al.*	(BABAR Collab.)
ABE	04D	PR D69 112002	K. Abe *et al.*	(BELLE Collab.)
LINK	04A	PL B586 11	J.M. Link *et al.*	(FOCUS Collab.)

$D_1(2420)$

$I(J^P) = \frac{1}{2}(1^+)$

$D_1(2420)$ MASS

The fit includes $D^\pm$, D^0, $D_s^\pm$, $D^{*\pm}$, D^{*0}, $D_s^{*\pm}$, $D_1(2420)^0$, $D_2^*(2460)^0$, and $D_{s1}(2536)^\pm$ mass and mass difference measurements.

VALUE (MeV)	EVTS	DOCUMENT ID		TECN	CHG	COMMENT
2422.1±0.6 OUR FIT		Error includes scale factor of 1.7.				
2422.1±0.8 OUR AVERAGE		Error includes scale factor of 2.1. See the ideogram below.				
2424.8±0.1±0.7	79k	[1] AAIJ	20D	LHCB	0	$B^- \to D^{*+}\pi^-\pi^-$
2427.2±1.0±1.2	4207	ABLIKIM	20P	BES3	+	$e^+e^- \to D^+D^-\pi^+\pi^-$
2419.6±0.1±0.7	210k	AAIJ	13CC	LHCB	0	$pp \to D^{*+}\pi^- X$
2423.1±1.5$^{+0.4}_{-1.0}$	2.7k	[2] ABRAMOWICZ	13	ZEUS	0	$e^\pm p \to D^{(*)+}\pi^- X$
2421.9±4.7$^{+3.4}_{-1.2}$	759	[3] ABRAMOWICZ	13	ZEUS	+	$e^\pm p \to D^{(*)0}\pi^+ X$
2420.1±0.1±0.8	103k	DEL-AMO-SA...	10P	BABR	0	$e^+e^- \to D^{*+}\pi^- X$
2426 ±3 ±1	151	ABE	05A	BELL	0	$B^- \to D^0\pi^+\pi^-\pi^-$
2421 ±2 ±1	124	ABE	05A	BELL	+	$\overline{B}^0 \to D^+\pi^+\pi^-\pi^-$
2421.4±1.5±0.9		[4] ABE	04D	BELL	0	$B^- \to D^{*+}\pi^-\pi^-$
2421 $^{+1}_{-2}$ ±2	286	AVERY	94C	CLE2	0	$e^+e^- \to D^{*+}\pi^- X$
2425 ±2 ±2	146	BERGFELD	94B	CLE2	+	$e^+e^- \to D^{*0}\pi^+ X$
2422 ±2 ±2	51	FRABETTI	94B	E687	0	γBe $\to D^{*+}\pi^- X$
2428 ±3 ±2	279	AVERY	90	CLEO	0	$e^+e^- \to D^{*+}\pi^- X$
2414 ±2 ±5	171	ALBRECHT	89H	ARG	0	$e^+e^- \to D^{*+}\pi^- X$
2428 ±8 ±5	171	ANJOS	89C	TPS	0	$\gamma N \to D^{*+}\pi^- X$
2443 ±7 ±5	190	ANJOS	89C	TPS	+	$\gamma N \to D^0\pi^+ X^0$
• • • We do not use the following data for averages, fits, limits, etc. • • •						
2420.5±2.1±0.9	3.1k	[5] CHEKANOV	09	ZEUS	0	$e^\pm p \to D^{*+}\pi^- X$
2421.7±0.7±0.6	7.5k	ABULENCIA	06A	CDF	0	1900 $p\overline{p} \to D^{*+}\pi^- X$
2425 ±3	235	[6] ABREU	98M	DLPH	0	e^+e^-

[1] From a full four-body amplitude analysis of the $B^- \to D^{*+}\pi^-\pi^-$ decay.
[2] From the combined fit of the $M(D^+\pi^-)$ and $M(D^{*+}\pi^-)$ distributions. and A_{D_2} fixed to the theoretical prediction of -1.
[3] From the fit of the $M(D^0\pi^+)$ distribution. The widths of the D_1^+ and D_2^{*+} are fixed to 25 MeV and 37 MeV, and A_{D_1} and A_{D_2} are fixed to the theoretical predictions of 3 and -1, respectively.
[4] Fit includes the contribution from $D_1^*(2430)^0$.
[5] Calculated using the mass difference $m(D_1^0) - m(D^{*+})_{PDG}$ reported below and $m(D^{*+})_{PDG} = 2010.27 \pm 0.17$ MeV. The 0.17 MeV uncertainty of the PDG mass value should be added to the experimental uncertainty of 0.9 MeV.
[6] No systematic error given.

Int. J. Mod. Phys. A 2026.41. Downloaded from www.worldscientific.com
by UNIVERSITY OF CALIFORNIA @ BERKELEY on 09/16/26. Re-use and distribution is strictly not permitted, except for Open Access articles.

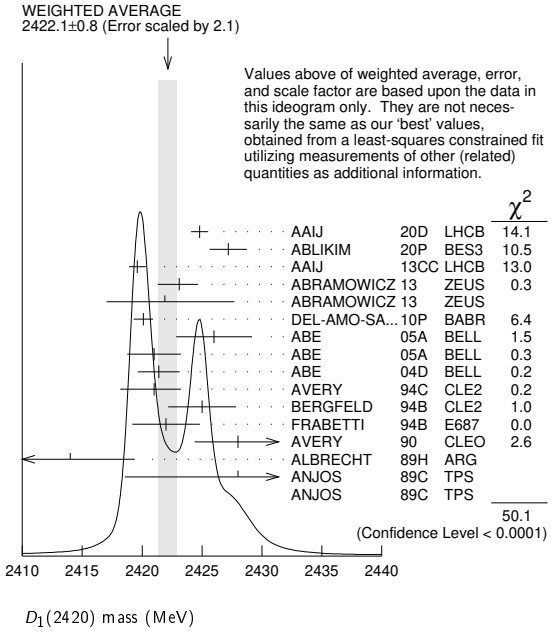

$m_{D_1(2420)^0} - m_{D^{*+}}$

The fit includes $D^\pm$, D^0, $D_s^\pm$, $D^{*\pm}$, D^{*0}, $D_s^{*\pm}$, $D_1(2420)^0$, $D_2^*(2460)^0$, and $D_{s1}(2536)^\pm$ mass and mass difference measurements.

VALUE (MeV)	EVTS	DOCUMENT ID		TECN	COMMENT
411.8±0.6 OUR FIT	Error includes scale factor of 1.7.				
411.5±0.8 OUR AVERAGE					
410.2±2.1±0.9	3.1k	CHEKANOV	09	ZEUS	$e^\pm p \to D^{*+}\pi^- X$
411.7±0.7±0.4	7.5k	ABULENCIA	06A	CDF	1900 $p\overline{p} \to D^{*+}\pi^- X$

$m_{D_1(2420)^\pm} - m_{D_1(2420)^0}$

VALUE (MeV)	DOCUMENT ID		TECN	COMMENT
$4^{+2}_{-3}\pm3$	BERGFELD	94B	CLE2	$e^+e^- \to$ hadrons

$D_1(2420)$ WIDTH

VALUE (MeV)	EVTS	DOCUMENT ID		TECN	CHG	COMMENT
31.3± 1.9 OUR AVERAGE	Error includes scale factor of 2.8. See the ideogram below.					
33.6± 0.3± 2.7	79k	[1] AAIJ	20D	LHCB	0	$B^- \to D^{*+}\pi^-\pi^-$
23.2± 2.3± 2.3	4207	ABLIKIM	20P	BES3	+	$e^+e^- \to D^+D^-\pi^+\pi^-$
35.2± 0.4± 0.9	210k	AAIJ	13CC	LHCB	0	$pp \to D^{*+}\pi^- X$
38.8± $5.0^{+1.9}_{-5.4}$	2.7k	[2] ABRAMOWICZ13		ZEUS	0	$e^\pm p \to D^{(*)+}\pi^- X$
31.4± 0.5± 1.3	103k	DEL-AMO-SA...	10P	BABR	0	$e^+e^- \to D^{*+}\pi^- X$
20.0± 1.7± 1.3	7.5k	ABULENCIA	06A	CDF	0	1900 $p\overline{p} \to D^{*+}\pi^- X$
24 ± 7 ± 8	151	ABE	05A	BELL	0	$B^- \to D^0\pi^+\pi^-\pi^-$
21 ± 5 ± 8	124	ABE	05A	BELL	+	$\overline{B}^0 \to D^+\pi^+\pi^-\pi^-$
23.7± 2.7± 4.0		[3] ABE	04D	BELL	0	$B^- \to D^{*+}\pi^-\pi^-$
20 $^{+6}_{-5}$ ± 3	286	AVERY	94C	CLE2	0	$e^+e^- \to D^{*+}\pi^- X$
26 $^{+8}_{-7}$ ± 4	146	BERGFELD	94B	CLE2	+	$e^+e^- \to D^0\pi^+ X$
15 ± 8 ± 4	51	FRABETTI	94B	E687	0	γBe $\to D^{*+}\pi^- X$
23 $^{+8}_{-6}$ $^{+10}_{-3}$	279	AVERY	90	CLEO	0	$e^+e^- \to D^{*+}\pi^- X$
13 ± 6 $^{+10}_{-5}$	171	ALBRECHT	89H	ARG	0	$e^+e^- \to D^{*+}\pi^- X$
41 ±19 ± 8	190	ANJOS	89C	TPS	+	$\gamma N \to D^0\pi^+ X^0$
• • • We do not use the following data for averages, fits, limits, etc. • • •						
53.2± $7.2^{+3.3}_{-4.9}$	3.1k	CHEKANOV	09	ZEUS	0	$e^\pm p \to D^{*+}\pi^- X$
58 ±14 ±10	171	ANJOS	89C	TPS	0	$\gamma N \to D^{*+}\pi^- X$

[1] From a full four-body amplitude analysis of the $B^- \to D^{*+}\pi^-\pi^-$ decay.
[2] From the combined fit of the $M(D^+\pi^-)$ and $M(D^{*+}\pi^-)$ distributions. and A_{D_2} fixed to the theoretical prediction of −1.
[3] Fit includes the contribution from $D_1^*(2430)^0$.

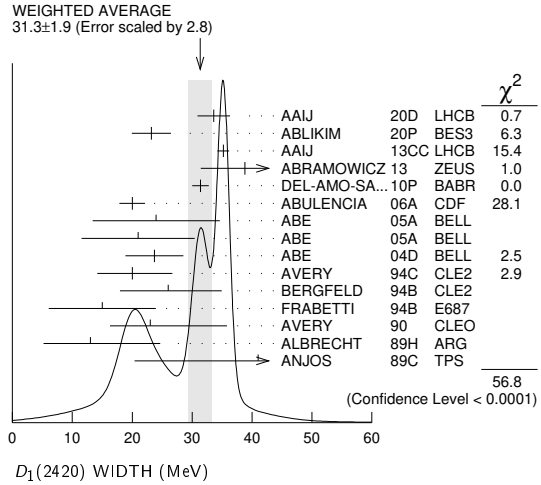

$D_1(2420)$ DECAY MODES

$\overline{D}_1(2420)$ modes are charge conjugates of modes below.

	Mode	Fraction (Γ_i/Γ)
Γ_1	$D^*(2007)^0\pi$	seen
Γ_2	$D\pi^+\pi^-$	
Γ_3	$D\rho^0$	
Γ_4	$Df_0(500)$	
Γ_5	$D_0^*(2300)^0\pi$	
Γ_6	$D^0\pi$	
Γ_7	$D^*\pi^+\pi^-$	

$D_1(2420)$ BRANCHING RATIOS

$\Gamma(D^*(2007)^0\pi)/\Gamma_{total}$ — Γ_1/Γ

VALUE	DOCUMENT ID		TECN	CHG	COMMENT
seen	ACKERSTAFF	97W	OPAL	0	$e^+e^- \to D^{*+}\pi^- X$
seen	AVERY	90	CLEO	0	$e^+e^- \to D^{*+}\pi^- X$
seen	ALBRECHT	89H	ARG	0	$e^+e^- \to D^*\pi^- X$
seen	ANJOS	89C	TPS	0	$\gamma N \to D^{*+}\pi^- X$
seen	ANJOS	89C	TPS	+	$\gamma N \to D^0\pi^+ X^0$

$\Gamma(D^0\pi)/\Gamma(D^*(2007)^0\pi)$ — Γ_6/Γ_1

VALUE	CL%	DOCUMENT ID		TECN	CHG	COMMENT
<0.18	90	BERGFELD	94B	CLE2	+	$e^+e^- \to$ hadrons
• • • We do not use the following data for averages, fits, limits, etc. • • •						
<0.24	90	AVERY	90	CLEO	0	$e^+e^- \to D^+\pi^- X$

$D_1(2420)$ POLARIZATION AMPLITUDE A_{D_1}

A polarization amplitude A_{D_1} is a parameter that depends on the initial polarization of the D_1 and is sensitive to a possible S-wave contribution to its decay. For D_1 decays the helicity angle, θ_h, distribution varies like $1 + A_{D_1}\cos^2\theta_h$, where θ_h is the angle in the D^* rest frame between the two pions emitted by the $D_1 \to D^*\pi$ and the $D^* \to D\pi$.

Unpolarized D_1 decaying purely via D-wave is predicted to give $A_{D_1} = 3$.

VALUE	EVTS	DOCUMENT ID		TECN	CHG	COMMENT
5.73±0.25 OUR AVERAGE						
7.8 $^{+6.7}_{-2.7}$ $^{+4.6}_{-1.8}$	2.7k	[1] ABRAMOWICZ13		ZEUS	0	$e^\pm p \to D^{(*)+}\pi^- X$
5.72±0.25	103k	DEL-AMO-SA...	10P	BABR	0	$e^+e^- \to D^{*+}\pi^- X$
5.9 $^{+3.0}_{-1.7}$ $^{+2.4}_{-1.0}$		CHEKANOV	09	ZEUS	0	$e^\pm p \to D^{*+}\pi^- X$
• • • We do not use the following data for averages, fits, limits, etc. • • •						
3.30±0.48	210k	[2] AAIJ	13CC	LHCB	0	$pp \to D^{*+}\pi^- X$
3.8 ±0.6 ±0.8		[3] AUBERT	09Y	BABR	0	$B^+ \to D_1^0\ell^+\nu_\ell$
3.8 ±0.6 ±0.8		[3] AUBERT	09Y	BABR	+	$B^0 \to D_1^-\ell^+\nu_\ell$
2.74 $^{+1.40}_{-0.93}$		[4] AVERY	94C	CLE2	0	$e^+e^- \to D^{*+}\pi^- X$

[1] From the combined fit of the $M(D^+\pi^-)$ and $M(D^{*+}\pi^-)$ distributions. and A_{D_2} fixed to the theoretical prediction of −1. A pure D-wave not excluded although some S-wave mixing possible.
[2] Systematic uncertainty not estimated. Resonance parameters fixed.
[3] Assuming $\Gamma(\Upsilon(4S) \to B^+B^-) / \Gamma(\Upsilon(4S) \to B^0\overline{B}^0) = 1.065 \pm 0.026$ and equal partial widths and helicity angle distributions for charged and neutral D_1 mesons.
[4] Systematic uncertainties not estimated.

Int. J. Mod. Phys. A 2026.41. Downloaded from www.worldscientific.com
by [redacted]LIFORNIA @ BERKELEY on 09/16/26. Re-use and distribution is strictly not permitted, except for Open Access articles.

Int. J. Mod. Phys. A 2026.41. Downloaded from www.worldscientific.com
by UNIVERSITY OF CALIFORNIA @ BERKELEY on 09/16/26. Re-use and distribution is strictly not permitted, except for Open Access articles.

$D_1(2420)$ REFERENCES

AAIJ	20D	PR D101 032005	R. Aaij *et al.*	(LHCb Collab.)
ABLIKIM	20P	PL B804 135395	M. Ablikim *et al.*	(BESIII Collab.)
AAIJ	13CC	JHEP 1309 145	R. Aaij *et al.*	(LHCb Collab.)
ABRAMOWICZ	13	NP B866 229	H. Abramowicz *et al.*	(ZEUS Collab.)
DEL-AMO-SA...	10P	PR D82 111101	P. del Amo Sanchez *et al.*	(BABAR Collab.)
AUBERT	09Y	PRL 103 051803	B. Aubert *et al.*	(BABAR Collab.)
CHEKANOV	09	EPJ C60 25	S. Chekanov *et al.*	(ZEUS Collab.)
ABULENCIA	06A	PR D73 051104	A. Abulencia *et al.*	(CDF Collab.)
ABE	05A	PRL 94 221805	K. Abe *et al.*	(BELLE Collab.)
ABE	04D	PR D69 112002	K. Abe *et al.*	(BELLE Collab.)
ABREU	98M	PL B426 231	P. Abreu *et al.*	(DELPHI Collab.)
ACKERSTAFF	97W	ZPHY C76 425	K. Ackerstaff *et al.*	(OPAL Collab.)
AVERY	94C	PL B331 236	P. Avery *et al.*	(CLEO Collab.)
BERGFELD	94B	PL B340 194	T. Bergfeld *et al.*	(CLEO Collab.)
FRABETTI	94B	PRL 72 324	P.L. Frabetti *et al.*	(FNAL E687 Collab.)
AVERY	90	PR D41 774	P. Avery, D. Besson	(CLEO Collab.)
ALBRECHT	89H	PL B232 398	H. Albrecht *et al.*	(ARGUS Collab.) JP
ANJOS	89C	PRL 62 1717	J.C. Anjos *et al.*	(FNAL E691 Collab.)

$D_1(2430)^0$

$I(J^P) = \frac{1}{2}(1^+)$

$J^P = 1^+$ determined by AAIJ 20D.

$D_1(2430)^0$ MASS

VALUE (MeV)	EVTS	DOCUMENT ID		TECN	COMMENT
2412± 9 OUR AVERAGE					
2411± 3± 9	79k	[1] AAIJ	20D	LHCB	$B^- \to D^{*+}\pi^-\pi^-$
2427±26±25		ABE	04D	BELL	$B^- \to D^{*+}\pi^-\pi^-$
• • • We do not use the following data for averages, fits, limits, etc. • • •					
2477±28		[2] AUBERT	06L	BABR	$\overline{B}^0 \to D^{*+}\omega\pi^-$

[1] From a full four-body amplitude analysis of the $B^- \to D^{*+}\pi^-\pi^-$ decay.
[2] Systematic errors not estimated.

$D_1(2430)^0$ WIDTH

VALUE (MeV)	EVTS	DOCUMENT ID		TECN	COMMENT
314± 29 OUR AVERAGE					
309± 9±28	79k	[1] AAIJ	20D	LHCB	$B^- \to D^{*+}\pi^-\pi^-$
$384^{+107}_{-75}\pm74$		ABE	04D	BELL	$B^- \to D^{*+}\pi^-\pi^-$
• • • We do not use the following data for averages, fits, limits, etc. • • •					
266± 97		[2] AUBERT	06L	BABR	$\overline{B}^0 \to D^{*+}\omega\pi^-$

[1] From a full four-body amplitude analysis of the $B^- \to D^{*+}\pi^-\pi^-$ decay.
[2] Systematic errors not estimated.

$D_1(2430)^0$ DECAY MODES

	Mode	Fraction (Γ_i/Γ)
Γ_1	$D^*(2010)^+\pi^-$	seen

$D_1(2430)^0$ REFERENCES

AAIJ	20D	PR D101 032005	R. Aaij *et al.*	(LHCb Collab.) JP
AUBERT	06L	PR D74 012001	B. Aubert *et al.*	(BABAR Collab.)
ABE	04D	PR D69 112002	K. Abe *et al.*	(BELLE Collab.)

$D_2^*(2460)$

$I(J^P) = \frac{1}{2}(2^+)$

$D_2^*(2460)$ MASS

The fit includes $D^\pm$, D^0, $D_s^\pm$, $D^{*\pm}$, D^{*0}, $D_s^{*\pm}$, $D_1(2420)^0$, $D_2^*(2460)^0$, and $D_{s1}(2536)^\pm$ mass and mass difference measurements.

VALUE (MeV)	EVTS	DOCUMENT ID		TECN	CHG	COMMENT
2461.1±0.8 OUR FIT Error includes scale factor of 6.3.						
2461.1±0.7 OUR AVERAGE Error includes scale factor of 5.2. See the ideogram below.						
2463.7±0.4±0.7	28k	[1] AAIJ	16AH	LHCB	0	$B^- \to D^+\pi^-\pi^-$
2464.0±1.4±0.5	2k	[2] AAIJ	15V	LHCB	0	$B^- \to D^+K^-\pi^-$
2465.6±1.8±1.3		[3] AAIJ	15X	LHCB	+	$B^0 \to \overline{D}^0K^+\pi^-$
2468.6±0.6±0.3		[4] AAIJ	15Y	LHCB	+	$B^0 \to \overline{D}^0\pi^+\pi^-$
2460.4±0.4±1.2	82k	AAIJ	13CC	LHCB	0	$pp \to D^{*+}\pi^-X$
2460.4±0.1±0.1	675k	AAIJ	13CC	LHCB	0	$pp \to D^+\pi^-X$
2463.1±0.2±0.6	342k	AAIJ	13CC	LHCB	+	$pp \to D^0\pi^+X$
$2462.5\pm2.4^{+1.3}_{-1.1}$	2.3k	[5] ABRAMOWICZ	13	ZEUS	0	$e^\pm p \to D^{(*)+}\pi^-X$
$2460.6\pm4.4^{+3.6}_{-0.8}$	1371	[6] ABRAMOWICZ	13	ZEUS	+	$e^\pm p \to D^{(*)0}\pi^+X$
2462.2±0.1±0.8	243k	DEL-AMO-SA...	10P	BABR	0	$e^+e^- \to D^+\pi^-X$
2465.4±0.2±1.1	111k	[7] DEL-AMO-SA...	10P	BABR	+	$e^+e^- \to D^0\pi^+X$
2460.4±1.2±2.2	3.4k	AUBERT	09AB	BABR	0	$B^- \to D^+\pi^-\pi^-$
$2465.7\pm1.8^{+1.4}_{-4.8}$	2909	KUZMIN	07	BELL	+	$e^+e^- \to$ hadrons
2461.6±2.1±3.3		[8] ABE	04D	BELL	0	$B^- \to D^+\pi^-\pi^-$
2464.5±1.1±1.9	5.8k	[8] LINK	04A	FOCS	0	γ A
2465 ±3 ±3	486	AVERY	94C	CLE2	0	$e^+e^- \to D^+\pi^-X$
2463 ±3 ±3	310	BERGFELD	94B	CLE2	+	$e^+e^- \to D^0\pi^+X$
2453 ±3 ±2	128	FRABETTI	94B	E687	0	γBe $\to D^+\pi^-X$
2453 ±3 ±2	185	FRABETTI	94B	E687	+	γBe $\to D^0\pi^+X$
2461 ±3 ±1	440	AVERY	90	CLEO	0	$e^+e^- \to D^{*+}\pi^-X$
2455 ±3 ±5	337	ALBRECHT	89B	ARG	0	$e^+e^- \to D^+\pi^-X$
2469 ±4 ±6		ALBRECHT	89F	ARG	+	$e^+e^- \to D^0\pi^+X$
2459 ±3 ±2	153	ANJOS	89C	TPS	0	$\gamma N \to D^+\pi^-X$
• • • We do not use the following data for averages, fits, limits, etc. • • •						
2468.1±0.6±0.5		[9] AAIJ	15Y	LHCB	+	$B^0 \to \overline{D}^0\pi^+\pi^-$
$2469.1\pm3.7^{+1.2}_{-1.3}$	1.5k	[10] CHEKANOV	09	ZEUS	0	$e^\pm p \to D^{(*)+}\pi^-X$
2463.3±0.6±0.8	20k	ABULENCIA	06A	CDF	0	1900 $p\overline{p} \to D^+\pi^-X$
2467.6±1.5±0.8	3.5k	[11] LINK	04A	FOCS	+	γ A
2461 ±6	126	[12] ABREU	98M	DLPH	0	e^+e^-
2466 ±7	1	ASRATYAN	95	BEBC	0	53,40 $\nu(\overline{\nu}) \to pX,dX$

[1] From the amplitude analysis in the model describing the $D^+\pi^-$ wave together with virtual contributions from the $D^*(2007)^0$ and B^{*0} states, and components corresponding to the $D_2^*(2460)^0$, $D_1^*(2680)^0$, $D_3^*(2760)^0$, and $D_2^*(3000)^0$ resonances.
[2] From the amplitude analysis in the model describing the $D^+\pi^-$ wave together with virtual contributions from the $D^*(2007)^0$ and B^{*0} states, nonresonant spin-0 and spin-1 components as well as the $D_0^*(2400)^0$, $D_2^*(2460)^0$ and $D_1^*(2760)^0$ resonances.
[3] From the Dalitz plot analysis including various K^* and D^{**} mesons as well as broad structures in the $K\pi$ S-wave and the $D\pi$ S- and P-waves.
[4] Modeling the $\pi^+\pi^-$ S-wave with the Isobar formalism.
[5] From the combined fit of the $M(D^+\pi^-)$ and $M(D^{*+}\pi^-)$ distributions. and A_{D_2} fixed to the theoretical prediction of -1.
[6] From the fit of the $M(D^0\pi^+)$ distribution. The widths of the D_1^+ and D_2^{*+} are fixed to 25 MeV and 37 MeV, and A_{D_1} and A_{D_2} are fixed to the theoretical predictions of 3 and -1, respectively.
[7] At a fixed width of 50.5 MeV.
[8] Fit includes the contribution from $D_0^*(2400)^0$.
[9] Modeling the $\pi^+\pi^-$ S-wave with the K-matrix formalism.
[10] Calculated using the mass difference $m(D_2^{*0}) - m(D^{*+})_{PDG}$ reported below and $m(D^{*+})_{PDG} = 2010.27 \pm 0.17$ MeV. The 0.17 MeV uncertainty of the PDG mass value should be added to the experimental uncertainty of $^{+1.2}_{-1.3}$ MeV.
[11] Fit includes the contribution from $D_0^*(2400)^\pm$. Not independent of the corresponding mass difference measurement, $(m_{D_2^*(2460)^\pm}) - (m_{D_2^*(2460)^0})$.
[12] No systematic error given.

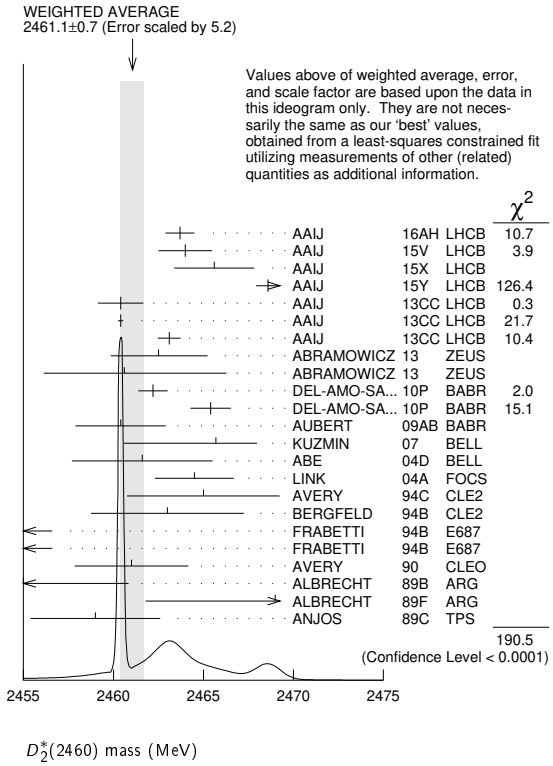

Int. J. Mod. Phys. A 2026.41. Downloaded from www.worldscientific.com
by CALIFORNIA @ BERKELEY on 09/16/26. Re-use and distribution is strictly not permitted, except for Open Access articles.

$m_{D_2^*(2460)^0} - m_{D^+}$

The fit includes $D^\pm$, D^0, $D_s^\pm$, $D^{*\pm}$, D^{*0}, $D_s^{*\pm}$, $D_1(2420)^0$, $D_2^*(2460)^0$, and $D_{s1}(2536)^\pm$ mass and mass difference measurements.

VALUE (MeV)	EVTS	DOCUMENT ID		TECN	COMMENT
591.5±0.8 OUR FIT	Error includes scale factor of 6.0.				
593.9±0.6±0.5	20k	ABULENCIA	06A	CDF	1900 $p\overline{p} \to D^+\pi^- X$

$m_{D_2^*(2460)^0} - m_{D^{*+}}$

The fit includes $D^\pm$, D^0, $D_s^\pm$, $D^{*\pm}$, D^{*0}, $D_s^{*\pm}$, $D_1(2420)^0$, $D_2^*(2460)^0$, and $D_{s1}(2536)^\pm$ mass and mass difference measurements.

VALUE (MeV)	EVTS	DOCUMENT ID		TECN	COMMENT
450.9±0.8 OUR FIT	Error includes scale factor of 6.0.				
458.8±3.7$^{+1.2}_{-1.3}$	1.5k	CHEKANOV	09	ZEUS	$e^\pm p \to D^{(*)+}\pi^- X$

$m_{D_2^*(2460)^\pm} - m_{D_2^*(2460)^0}$

VALUE (MeV)	DOCUMENT ID		TECN	COMMENT
2.4±1.7 OUR AVERAGE				
3.1±1.9±0.9	LINK	04A	FOCS	γ A
− 2 ±4 ±4	BERGFELD	94B	CLE2	$e^+e^- \to$ hadrons
0 ±4	FRABETTI	94B	E687	γBe $\to D\pi$X
14 ±5 ±8	ALBRECHT	89F	ARG	$e^+e^- \to D^0\pi^+$X

$D_2^*(2460)$ WIDTH

VALUE (MeV)	EVTS	DOCUMENT ID		TECN	CHG	COMMENT
47.3± 0.8 OUR AVERAGE	Error includes scale factor of 1.5. See the ideogram below.					
47.0± 0.8± 1.0	28k	[1] AAIJ	16AH	LHCB	0	$B^- \to D^+\pi^-\pi^-$
43.8± 2.9± 1.8	2k	[2] AAIJ	15V	LHCB	0	$B^- \to D^+K^-\pi^-$
46.0± 3.4± 3.2		[3] AAIJ	15X	LHCB	+	$B^0 \to \overline{D}^0K^+\pi^-$
47.3± 1.5± 0.7		[4] AAIJ	15Y	LHCB	+	$B^0 \to \overline{D}^0\pi^+\pi^-$
43.2± 1.2± 3.0	82k	AAIJ	13CC	LHCB	0	$pp \to D^{*+}\pi^- X$
45.6± 0.4± 1.1	675k	AAIJ	13CC	LHCB	0	$pp \to D^+\pi^- X$
48.6± 1.3± 1.9	342k	AAIJ	13CC	LHCB	+	$pp \to D^0\pi^+ X$
46.6± 8.1$^{+5.9}_{-3.8}$	2.3k	[5] ABRAMOWICZ	13	ZEUS	0	$e^\pm p \to D^{(*)+}\pi^- X$
50.5± 0.6± 0.7	243k	DEL-AMO-SA...	10P	BABR	0	$e^+e^- \to D^+\pi^- X$
41.8± 2.5± 2.9	3.4k	AUBERT	09AB	BABR	0	$B^- \to D^+\pi^-\pi^-$
49.7± 3.8± 6.4	2909	KUZMIN	07	BELL	+	$e^+e^- \to$ hadrons
49.2± 2.3± 1.3	20k	ABULENCIA	06A	CDF	0	1900 $p\overline{p} \to D^+\pi^- X$
45.6± 4.4± 6.7		[6] ABE	04D	BELL	0	$B^- \to D^+\pi^-\pi^-$
38.7± 5.3± 2.9	5.8k	[6] LINK	04A	FOCS	0	γ A
34.1± 6.5± 4.2	3.5k	[7] LINK	04A	FOCS	+	γ A
28 $^{+8}_{-7}$ ± 6	486	AVERY	94C	CLE2	0	$e^+e^- \to D^+\pi^-$X
27 $^{+11}_{-8}$ ± 5	310	BERGFELD	94B	CLE2	+	$e^+e^- \to D^0\pi^+$X
25 ±10 ± 5	128	FRABETTI	94B	E687	0	γBe $\to D^+\pi^-$X
23 ± 9 ± 5	185	FRABETTI	94B	E687	+	γBe $\to D^0\pi^+$X
20 $^{+9}_{-12}$ $^{+9}_{-10}$	440	AVERY	90	CLEO	0	$e^+e^- \to D^{*+}\pi^-$X
15 $^{+13}_{-10}$ $^{+5}_{-10}$	337	ALBRECHT	89B	ARG	0	$e^+e^- \to D^+\pi^-$X
20 ±10 ± 5	153	ANJOS	89C	TPS	0	$\gamma N \to D^+\pi^-$X
• • • We do not use the following data for averages, fits, limits, etc. • • •						
46.0± 1.4± 1.8		[8] AAIJ	15Y	LHCB	+	$B^0 \to \overline{D}^0\pi^+\pi^-$

[1] From the amplitude analysis in the model describing the $D^+\pi^-$ wave together with virtual contributions from the $D^*(2007)^0$ and B^{*0} states, and components corresponding to the $D_2^*(2460)^0$, $D_1^*(2680)^0$, $D_3^*(2760)^0$, and $D_2^*(3000)^0$ resonances.

[2] From the amplitude analysis in the model describing the $D^+\pi^-$ wave together with virtual contributions from the $D^*(2007)^0$ and B^{*0} states, nonresonant spin-0 and spin-1 components as well as the $D_0^*(2400)^0$, $D_2^*(2460)^0$ and $D_1^*(2760)^0$ resonances.

[3] From the Dalitz plot analysis including various K^* and D^{**} mesons as well as broad structures in the $K\pi$ S-wave and the $D\pi$ S- and P-waves.

[4] Modeling the $\pi^+\pi^-$ S-wave with the Isobar formalism.

[5] From the combined fit of the $M(D^+\pi^-)$ and $M(D^{*+}\pi^-)$ distributions. and A_{D_2} fixed to the theoretical prediction of −1.

[6] Fit includes the contribution from $D_0^*(2400)^0$.

[7] Fit includes the contribution from $D_0^*(2400)^\pm$.

[8] Modeling the $\pi^+\pi^-$ S-wave with the K-matrix formalism.

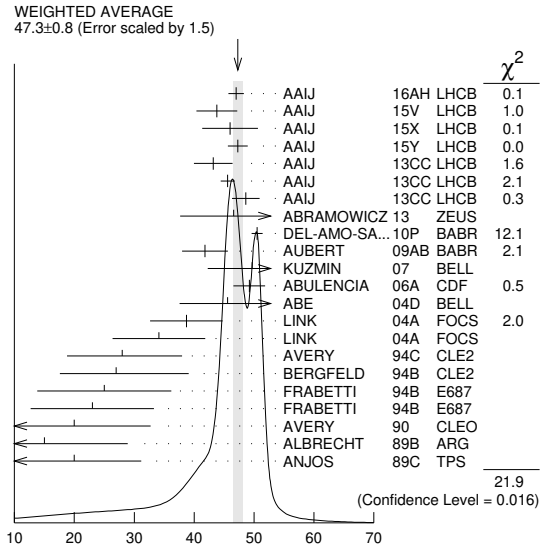

$D_2^*(2460)$ DECAY MODES

$\overline{D}_2^*(2460)$ modes are charge conjugates of modes below.

	Mode	Fraction (Γ_i/Γ)
Γ_1	$D\pi^-$	seen
Γ_2	$D^*(2010)\pi^-$	seen
Γ_3	$D\pi^+\pi^-$	
Γ_4	$D^*\pi^+\pi^-$	

$D_2^*(2460)$ BRANCHING RATIOS

$\Gamma(D\pi^-)/\Gamma_{total}$ — Γ_1/Γ

VALUE	EVTS	DOCUMENT ID		TECN	CHG	COMMENT
seen	3.4k	AUBERT	09AB	BABR	0	$B^- \to D^+\pi^-\pi^-$
seen	337	ALBRECHT	89B	ARG	0	$e^+e^- \to D^+\pi^-$X
seen		ALBRECHT	89F	ARG	+	$e^+e^- \to D^0\pi^+$X
seen		ANJOS	89C	TPS	0	$\gamma N \to D^+\pi^-$X

$\Gamma(D^*(2010)\pi^-)/\Gamma_{total}$ — Γ_2/Γ

VALUE	DOCUMENT ID		TECN	CHG	COMMENT
seen	ACKERSTAFF	97W	OPAL	0	$e^+e^- \to D^{*+}\pi^-$X
seen	AVERY	90	CLEO	0	$e^+e^- \to D^{*+}\pi^-$X
seen	ALBRECHT	89H	ARG	0	$e^+e^- \to D^*\pi^-$X

$\Gamma(D\pi^-)/\Gamma(D^*(2010)\pi^-)$ — Γ_1/Γ_2

VALUE	EVTS	DOCUMENT ID		TECN	CHG	COMMENT
1.52±0.14 OUR AVERAGE						
1.4 ±0.3 ±0.3	2.3k	[1] ABRAMOWICZ	13	ZEUS	0	$e^\pm p \to D^{(*)+}\pi^- X$
1.1 ±0.4 $^{+0.3}_{-0.2}$	1371	[2] ABRAMOWICZ	13	ZEUS	+	$e^\pm p \to D^{(*)0}\pi^+ X$
1.47±0.03±0.16	379k	DEL-AMO-SA...	10P	BABR	0	$e^+e^- \to D^{(*)+}\pi^- X$
2.8 ±0.8 $^{+0.5}_{-0.6}$	1.5k	CHEKANOV	09	ZEUS	0	$e^\pm p \to D^{(*)+}\pi^- X$
2.2 ±0.7 ±0.6		AVERY	94C	CLE2	0	$e^+e^- \to D^{*+}\pi^-$X
1.9 ±1.1 ±0.3		BERGFELD	94B	CLE2	+	$e^+e^- \to$ hadrons
2.3 ±0.8		AVERY	90	CLEO	0	e^+e^-
3.0 ±1.1 ±1.5		ALBRECHT	89H	ARG	0	$e^+e^- \to D^*\pi^-$X
• • • We do not use the following data for averages, fits, limits, etc. • • •						
1.9 ±0.5		ABE	04D	BELL	0	$B^- \to D^{(*)+}\pi^-\pi^-$

[1] From the combined fit of the $M(D^+\pi^-)$ and $M(D^{*+}\pi^-)$ distributions. and A_{D_2} fixed to the theoretical prediction of −1.

[2] From the fit of the $M(D^0\pi^+)$ distribution. The widths of the D_1^+ and D_2^{*+} are fixed to 25 MeV and 37 MeV, and A_{D_1} and A_{D_2} are fixed to the theoretical predictions of 3 and −1, respectively.

$\Gamma(D\pi^-)/[\Gamma(D\pi^-)+\Gamma(D^*(2010)\pi^-)]$ — $\Gamma_1/(\Gamma_1+\Gamma_2)$

VALUE	EVTS	DOCUMENT ID		TECN	CHG	COMMENT
• • • We do not use the following data for averages, fits, limits, etc. • • •						
0.62±0.03±0.02	8414	[1] AUBERT	09Y	BABR	0	$B^+ \to D_2^{*0}\ell^+\nu_\ell$
0.62±0.03±0.02	3361	[1] AUBERT	09Y	BABR	+	$\overline{B}^0 \to D_2^{*+}\ell^-\nu_\ell$

[1] Assuming $\Gamma(\Upsilon(4S) \to B^+B^-) / \Gamma(\Upsilon(4S) \to B^0\overline{B}^0) = 1.065 \pm 0.026$ and equal partial widths for charged and neutral D_2^* mesons.

$D_2^*(2460)$ POLARIZATION AMPLITUDE A_{D_2}

A polarization amplitude A_{D_2} is a parameter that depends on the initial polarization of the D_2. For D_2 decays the helicity angle, θ_H, distribution varies like $1 + A_{D_2} \cos^2(\theta_H)$, where θ_H is the angle in the D^* rest frame between the two pions emitted by the $D_2 \to D^*\pi$ and $D^* \to D\pi$.

VALUE	EVTS	DOCUMENT ID		TECN	CHG	COMMENT
• • • We do not use the following data for averages, fits, limits, etc. • • •						
-1.16 ± 0.35	2.3k	[1] ABRAMOWICZ	13	ZEUS	0	$e^\pm p \to D^{(*)+}\pi^- X$
consistent with -1	243k	DEL-AMO-SA...	10P	BABR	0	$e^+e^- \to D^+\pi^- X$
$-0.74^{+0.49}_{-0.38}$		[2] AVERY	94C	CLE2	0	$e^+e^- \to D^{*+}\pi^- X$

[1] From the combined fit of the $M(D^+\pi^-)$ and $M(D^{*+}\pi^-)$ distributions.
[2] Systematic uncertainties not estimated.

$D_2^*(2460)$ REFERENCES

AAIJ	16AH	PR D94 072001	R. Aaij et al.	(LHCb Collab.)
AAIJ	15V	PR D91 092002	R. Aaij et al.	(LHCb Collab.)
Also		PR D93 119901 (errat.)	R. Aaij et al.	(LHCb Collab.)
AAIJ	15X	PR D92 012012	R. Aaij et al.	(LHCb Collab.)
AAIJ	15Y	PR D92 032002	R. Aaij et al.	(LHCb Collab.)
AAIJ	13CC	JHEP 1309 145	R. Aaij et al.	(LHCb Collab.)
ABRAMOWICZ	13	NP B866 229	H. Abramowicz et al.	(ZEUS Collab.)
DEL-AMO-SA...	10P	PR D82 111101	P. del Amo Sanchez et al.	(BABAR Collab.)
AUBERT	09AB	PR D79 112004	B. Aubert et al.	(BABAR Collab.)
AUBERT	09Y	PRL 103 051803	B. Aubert et al.	(BABAR Collab.)
CHEKANOV	09	EPJ C60 25	S. Chekanov et al.	(ZEUS Collab.)
KUZMIN	07	PR D76 012006	A. Kuzmin et al.	(BELLE Collab.)
ABULENCIA	06A	PR D73 051104	A. Abulencia et al.	(CDF Collab.)
ABE	04D	PR D69 112002	K. Abe et al.	(BELLE Collab.)
LINK	04A	PL B586 11	J.M. Link et al.	(FOCUS Collab.)
ABREU	98M	PL B426 231	P. Abreu et al.	(DELPHI Collab.)
ACKERSTAFF	97W	ZPHY C76 425	K. Ackerstaff et al.	(OPAL Collab.)
ASRATYAN	95	ZPHY C68 43	A.E. Asratyan et al.	(BIRM, BELG, CERN+)
AVERY	94C	PL B331 236	P. Avery et al.	(CLEO Collab.)
BERGFELD	94B	PL B340 194	T. Bergfeld et al.	(CLEO Collab.)
FRABETTI	94B	PRL 72 324	P.L. Frabetti et al.	(FNAL E687 Collab.)
AVERY	90	PR D41 774	P. Avery, D. Besson	(CLEO Collab.)
ALBRECHT	89B	PL B221 422	H. Albrecht et al.	(ARGUS Collab.) JP
ALBRECHT	89F	PL B231 208	H. Albrecht et al.	(ARGUS Collab.)
ALBRECHT	89H	PL B232 398	H. Albrecht et al.	(ARGUS Collab.) JP
ANJOS	89C	PRL 62 1717	J.C. Anjos et al.	(FNAL E691 Collab.)

$D_0(2550)^0$

$I(J^P) = \frac{1}{2}(0^-)$

OMITTED FROM SUMMARY TABLE

$J^P = 0^-$ determined by AAIJ 20D.

$D_0(2550)^0$ MASS

VALUE (MeV)	EVTS	DOCUMENT ID		TECN	COMMENT
2549 ±19 OUR AVERAGE		Error includes scale factor of 4.6.			See the ideogram below.
2518 ± 2 ±7	79k	[1] AAIJ	20D	LHCB	$B^- \to D^{*+}\pi^-\pi^-$
2579.5 ± 3.4 ± 5.5	60k	AAIJ	13CC	LHCB	$pp \to D^{*+}\pi^- X$
2539.4 ± 4.5 ± 6.8	34k	DEL-AMO-SA...	10P	BABR	$e^+e^- \to D^{*+}\pi^- X$

[1] From a full four-body amplitude analysis of the $B^- \to D^{*+}\pi^-\pi^-$ decay.

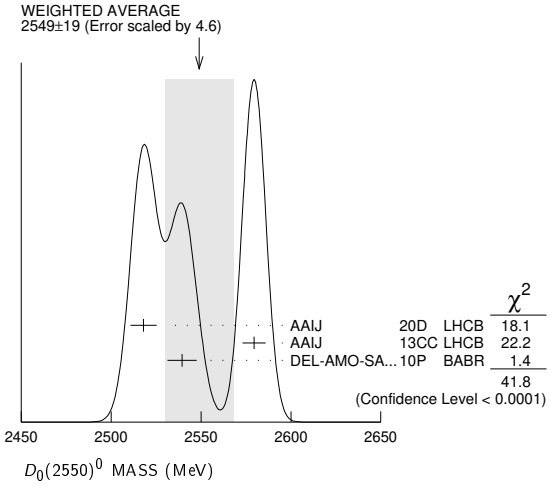

$D_0(2550)^0$ WIDTH

VALUE (MeV)	EVTS	DOCUMENT ID		TECN	COMMENT
165 ±24 OUR AVERAGE		Error includes scale factor of 2.0.			See the ideogram below.
199 ± 5 ±17	79k	[1] AAIJ	20D	LHCB	$B^- \to D^{*+}\pi^-\pi^-$
177.5 ± 17.8 ± 46.0	60k	AAIJ	13CC	LHCB	$pp \to D^{*+}\pi^- X$
130 ±12 ±13	34k	DEL-AMO-SA...	10P	BABR	$e^+e^- \to D^{*+}\pi^- X$

[1] From a full four-body amplitude analysis of the $B^- \to D^{*+}\pi^-\pi^-$ decay.

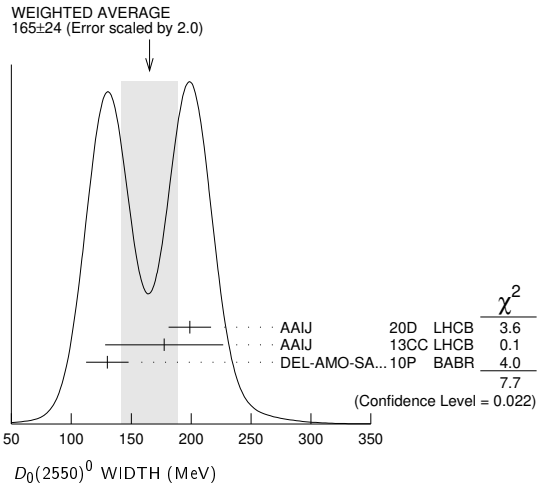

$D_0(2550)^0$ DECAY MODES

	Mode	Fraction (Γ_i/Γ)
Γ_1	$D^{*+}\pi^-$	seen

$D_0(2550)^0$ POLARIZATION AMPLITUDE A_{D_J}

A polarization amplitude A_{D_J} is a parameter that depends on the initial polarization of the D_J. For D_J decays the helicity angle, θ_H, distribution varies like $1 + A_{D_J} \cos^2(\theta_H)$, where θ_H is the angle in the D_J rest frame between the two pions emitted in the $D_J \to D^*\pi$ and $D^* \to D\pi$ decays.

VALUE	EVTS	DOCUMENT ID		TECN	COMMENT
• • • We do not use the following data for averages, fits, limits, etc. • • •					
4.2 ± 1.3	60k	[1] AAIJ	13CC	LHCB	$pp \to D^{*+}\pi^- X$

[1] Systematic uncertainty not estimated.

$D_0(2550)^0$ REFERENCES

AAIJ	20D	PR D101 032005	R. Aaij et al.	(LHCb Collab.) JP
AAIJ	13CC	JHEP 1309 145	R. Aaij et al.	(LHCb Collab.)
DEL-AMO-SA...	10P	PR D82 111101	P. del Amo Sanchez et al.	(BABAR Collab.)

$D_1^*(2600)^0$

$I(J^P) = \frac{1}{2}(1^-)$

OMITTED FROM SUMMARY TABLE

was $D_J^*(2600)$

$J^P = 1^-$ determined by AAIJ 20D.

$D_1^*(2600)^0$ MASS

VALUE (MeV)	EVTS	DOCUMENT ID		TECN	CHG	COMMENT
2627 ±10 OUR AVERAGE		Error includes scale factor of 4.4.				See the ideogram below.
2641.9 ± 1.8 ± 4.5	79k	[1] AAIJ	20D	LHCB		$B^- \to D^{*+}\pi^-\pi^-$
2681.1 ± 5.6 ± 14.0	28k	[2] AAIJ	16AH	LHCB		$B^- \to D^+\pi^-\pi^-$
2649.2 ± 3.5 ± 3.5	51k	AAIJ	13CC	LHCB		$pp \to D^{*+}\pi^- X$
2608.7 ± 2.4 ± 2.5	26k	DEL-AMO-SA...	10P	BABR	0	$e^+e^- \to D^+\pi^- X$
2621.3 ± 3.7 ± 4.2	13k	[3] DEL-AMO-SA...	10P	BABR	+	$e^+e^- \to D^0\pi^+ X$

[1] From a full four-body amplitude analysis of the $B^- \to D^{*+}\pi^-\pi^-$ decay.
[2] From the amplitude analysis in the model describing the $D^+\pi^-$ wave together with virtual contributions from the $D^*(2007)^0$ and B^{*0} states, and components corresponding to the $D_2^*(2460)^0$, $D_1^*(2680)^0$, $D_3^*(2760)^0$, and $D_2^*(3000)^0$ resonances.
[3] At a fixed width of 93 MeV.

Int. J. Mod. Phys. A 2026.41. Downloaded from www.worldscientific.com
by UNIVERSITY OF CALIFORNIA @ BERKELEY on 09/16/26. Re-use and distribution is strictly not permitted, except for Open Access articles.

Int. J. Mod. Phys. A 2026.41. Downloaded from www.worldscientific.com
by [redacted]LIFORNIA @ BERKELEY on 09/16/26. Re-use and distribution is strictly not permitted, except for Open Access articles.

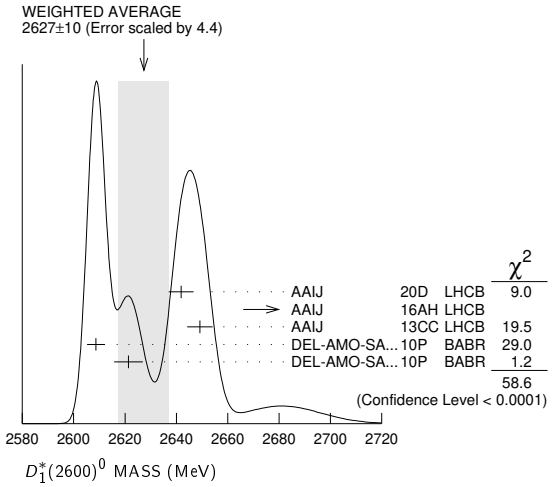

$D_1^*(2600)^0$ WIDTH

VALUE (MeV)	EVTS	DOCUMENT ID		TECN	COMMENT
141 ±23 OUR AVERAGE		Error includes scale factor of 2.7. See the ideogram below.			
149 ± 4 ±20	79k	[1] AAIJ	20D	LHCB	$B^- \to D^{*+}\pi^-\pi^-$
186.7± 8.5±11.9	28k	[2] AAIJ	16AH	LHCB	$B^- \to D^+\pi^-\pi^-$
140.2±17.1±18.6	51k	AAIJ	13CC	LHCB	$pp \to D^{*+}\pi^- X$
93 ± 6 ±13	26k	DEL-AMO-SA...	10P	BABR	$e^+e^- \to D^+\pi^- X$

[1] From a full four-body amplitude analysis of the $B^- \to D^{*+}\pi^-\pi^-$ decay.
[2] From the amplitude analysis in the model describing the $D^+\pi^-$ wave together with virtual contributions from the $D^*(2007)^0$ and B^{*0} states, and components corresponding to the $D_2^*(2460)^0$, $D_1^*(2680)^0$, $D_3^*(2760)^0$, and $D_2^*(3000)^0$ resonances.

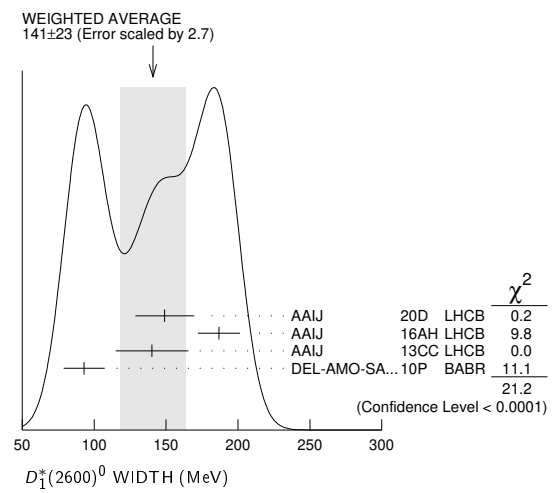

$D_1^*(2600)^0$ DECAY MODES

	Mode	Fraction (Γ_i/Γ)
Γ_1	$D\pi$	seen
Γ_2	$D^+\pi^-$	seen
Γ_3	$D^0\pi^\pm$	seen
Γ_4	$D^*\pi$	seen
Γ_5	$D^{*+}\pi^-$	seen

$D_1^*(2600)^0$ BRANCHING RATIOS

$\Gamma(D^+\pi^-)/\Gamma(D^{*+}\pi^-)$ — Γ_2/Γ_5

VALUE	EVTS	DOCUMENT ID		TECN	COMMENT
0.32±0.02±0.09	76k	DEL-AMO-SA...	10P	BABR	$e^+e^- \to D^{(*)+}\pi^- X$

$D_1^*(2600)^0$ REFERENCES

AAIJ	20D	PR D101 032005	R. Aaij *et al.*	(LHCb Collab.) JP
AAIJ	16AH	PR D94 072001	R. Aaij *et al.*	(LHCb Collab.)
AAIJ	13CC	JHEP 1309 145	R. Aaij *et al.*	(LHCb Collab.)
DEL-AMO-SA...	10P	PR D82 111101	P. del Amo Sanchez *et al.*	(BABAR Collab.)

$D^*(2640)^\pm$

$I(J^P) = \frac{1}{2}(?^?)$

OMITTED FROM SUMMARY TABLE
Seen in Z decays by ABREU 98M. Not seen by ABBIENDI 01N and CHEKANOV 09. Needs confirmation.

$D^*(2640)^\pm$ MASS

VALUE (MeV)	EVTS	DOCUMENT ID		TECN	COMMENT
2637±2±6	66 ± 14	ABREU	98M	DLPH	$e^+e^- \to D^{*+}\pi^+\pi^- X$

$D^*(2640)^\pm$ WIDTH

VALUE (MeV)	CL%	DOCUMENT ID		TECN	COMMENT
<15	95	ABREU	98M	DLPH	$e^+e^- \to D^{*+}\pi^+\pi^- X$

$D^*(2640)^+$ DECAY MODES

$D^*(2640)^-$ modes are charge conjugates of modes below.

	Mode	Fraction (Γ_i/Γ)
Γ_1	$D^*(2010)^+\pi^+\pi^-$	seen

$D^*(2640)^\pm$ REFERENCES

CHEKANOV	09	EPJ C60 25	S. Chekanov *et al.*	(ZEUS Collab.)
ABBIENDI	01N	EPJ C20 445	G. Abbiendi *et al.*	(OPAL Collab.)
ABREU	98M	PL B426 231	P. Abreu *et al.*	(DELPHI Collab.)

$D_2(2740)^0$

$I(J^P) = \frac{1}{2}(2^-)$

OMITTED FROM SUMMARY TABLE
was $D(2740)^0$
$J^P = 2^-$ determined by (AAIJ 20D).

$D_2(2740)^0$ MASS

VALUE (MeV)	EVTS	DOCUMENT ID		TECN	COMMENT
2747 ±6 OUR AVERAGE					
2751 ±3 ± 7	79k	[1] AAIJ	20D	LHCB	$B^- \to D^{*+}\pi^-\pi^-$
2737.0±3.5±11.2	7.7k	AAIJ	13CC	LHCB	$pp \to D^{*+}\pi^- X$

[1] From a full four-body amplitude analysis of the $B^- \to D^{*+}\pi^-\pi^-$ decay.

$D_2(2740)^0$ WIDTH

VALUE (MeV)	EVTS	DOCUMENT ID		TECN	COMMENT
88 ±19 OUR AVERAGE					
102 ± 6 ±26	79k	[1] AAIJ	20D	LHCB	$B^- \to D^{*+}\pi^-\pi^-$
73.2±13.4±25.0	7.7k	AAIJ	13CC	LHCB	$pp \to D^{*+}\pi^- X$

[1] From a full four-body amplitude analysis of the $B^- \to D^{*+}\pi^-\pi^-$ decay.

$D_2(2740)^0$ DECAY MODES

	Mode	Fraction (Γ_i/Γ)
Γ_1	$D^{*+}\pi^-$	seen

$D_2(2740)^0$ POLARIZATION AMPLITUDE A_{D_J}

A polarization amplitude A_{D_J} is a parameter that depends on the initial polarization of the D_J. For D_J decays the helicity angle, θ_H, distribution varies like $1 + A_{D_J}\cos^2(\theta_H)$, where θ_H is the angle in the D_J rest frame between the two pions emitted in the $D_J \to D^*\pi$ and $D^* \to D\pi$ decays.

VALUE	EVTS	DOCUMENT ID		TECN	COMMENT
• • • We do not use the following data for averages, fits, limits, etc. • • •					
3.1±2.2	7.7k	[1] AAIJ	13CC	LHCB	$pp \to D^{*+}\pi^- X$

[1] Systematic uncertainty not estimated.

$D_2(2740)^0$ REFERENCES

AAIJ	20D	PR D101 032005	R. Aaij *et al.*	(LHCb Collab.) JP
AAIJ	13CC	JHEP 1309 145	R. Aaij *et al.*	(LHCb Collab.)

Int. J. Mod. Phys. A 2026.41. Downloaded from www.worldscientific.com by UNIVERSITY OF CALIFORNIA @ BERKELEY on 09/16/26. Re-use and distribution is strictly not permitted, except for Open Access articles.

$D_3^*(2750)$

$I(J^P) = \frac{1}{2}(3^-)$

J^P determined by AAIJ 15Y from the Dalitz plot analysis of $B^0 \to \overline{D}^0 \pi^+ \pi^-$ decays.

$D_3^*(2750)$ MASS

VALUE (MeV)	EVTS	DOCUMENT ID		TECN	CHG	COMMENT
2763.1 ± 3.2 OUR AVERAGE		Error includes scale factor of 2.1. See the ideogram below.				
2753 ± 4 ± 6	79k	[1] AAIJ	20D	LHCB		$B^- \to D^{*+} \pi^- \pi^-$
2775.5 ± 4.5 ± 6.5	28k	[2] AAIJ	16AH	LHCB		$B^- \to D^+ \pi^- \pi^-$
2798 ± 7 ± 7		[3] AAIJ	15Y	LHCB		$B^0 \to \overline{D}^0 \pi^+ \pi^-$
2761.1 ± 5.1 ± 6.5	14k	AAIJ	13CC	LHCB	0	$pp \to D^{*+} \pi^- X$
2760.1 ± 1.1 ± 3.7	56k	AAIJ	13CC	LHCB	0	$pp \to D^+ \pi^- X$
2771.7 ± 1.7 ± 3.8	20k	AAIJ	13CC	LHCB	+	$pp \to D^0 \pi^+ X$
2752.4 ± 1.7 ± 2.7	23.5k	[4] DEL-AMO-SA...	10P	BABR	0	$e^+ e^- \to D^{*+} \pi^- X$
2763.3 ± 2.3 ± 2.3	11.3k	[4] DEL-AMO-SA...	10P	BABR	0	$e^+ e^- \to D^+ \pi^- X$
2769.7 ± 3.8 ± 1.5	5.7k	[4,5] DEL-AMO-SA...	10P	BABR	+	$e^+ e^- \to D^0 \pi^+ X$
• • • We do not use the following data for averages, fits, limits, etc. • • •						
2802 ± 11 ± 10		[6] AAIJ	15Y	LHCB		$B^0 \to \overline{D}^0 \pi^+ \pi^-$

[1] From a full four-body amplitude analysis of the $B^- \to D^{*+} \pi^- \pi^-$ decay.
[2] From the amplitude analysis in the model describing the $D^+ \pi^-$ wave together with virtual contributions from the $D^*(2007)^0$ and B^{*0} states, and components corresponding to the $D_2^*(2460)^0$, $D_1^*(2680)^0$, $D_3^*(2760)^0$, and $D_2^*(3000)^0$ resonances.
[3] Modeling the $\pi^+ \pi^-$ S-wave with the Isobar formalism.
[4] The states observed in the $D^* \pi$ and $D \pi$ final states are not necessarily the same.
[5] At a fixed width of 60.9 MeV.
[6] Modeling the $\pi^+ \pi^-$ S-wave with the K-matrix formalism.

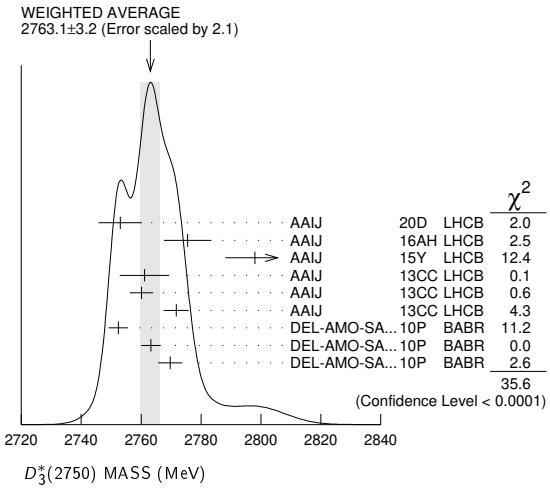

$D_3^*(2750)$ WIDTH

VALUE (MeV)	EVTS	DOCUMENT ID		TECN	CHG	COMMENT
66 ± 5 OUR AVERAGE						
66 ± 10 ± 14	79k	[1] AAIJ	20D	LHCB		$B^- \to D^{*+} \pi^- \pi^-$
95.3 ± 9.6 ± 34.0	28k	[2] AAIJ	16AH	LHCB		$B^- \to D^+ \pi^- \pi^-$
105 ± 18 ± 24		[3] AAIJ	15Y	LHCB		$B^0 \to \overline{D}^0 \pi^+ \pi^-$
74.4 ± 3.4 ± 37.0	14k	AAIJ	13CC	LHCB	0	$pp \to D^{*+} \pi^- X$
74.4 ± 3.4 ± 19.1	56k	AAIJ	13CC	LHCB	0	$pp \to D^+ \pi^- X$
66.7 ± 6.6 ± 10.5	20k	AAIJ	13CC	LHCB	+	$pp \to D^0 \pi^+ X$
71 ± 6 ± 11	23.5k	[4] DEL-AMO-SA...	10P	BABR		$e^+ e^- \to D^{*+} \pi^- X$
60.9 ± 5.1 ± 3.6	11.3k	[4] DEL-AMO-SA...	10P	BABR		$e^+ e^- \to D^+ \pi^- X$
• • • We do not use the following data for averages, fits, limits, etc. • • •						
154 ± 27 ± 16		[5] AAIJ	15Y	LHCB		$B^0 \to \overline{D}^0 \pi^+ \pi^-$

[1] From a full four-body amplitude analysis of the $B^- \to D^{*+} \pi^- \pi^-$ decay.
[2] From the amplitude analysis in the model describing the $D^+ \pi^-$ wave together with virtual contributions from the $D^*(2007)^0$ and B^{*0} states, and components corresponding to the $D_2^*(2460)^0$, $D_1^*(2680)^0$, $D_3^*(2760)^0$, and $D_2^*(3000)^0$ resonances.
[3] Modeling the $\pi^+ \pi^-$ S-wave with the Isobar formalism.
[4] The states observed in the $D^* \pi$ and $D \pi$ final states are not necessarily the same.
[5] Modeling the $\pi^+ \pi^-$ S-wave with the K-matrix formalism.

$D_3^*(2750)$ DECAY MODES

	Mode	Fraction (Γ_i/Γ)
Γ_1	$D \pi$	seen
Γ_2	$D^+ \pi^-$	seen
Γ_3	$D^0 \pi^\pm$	seen
Γ_4	$D^* \pi$	seen
Γ_5	$D^{*+} \pi^-$	seen

$D_3^*(2750)$ BRANCHING RATIOS

$\Gamma(D^+ \pi^-)/\Gamma(D^{*+} \pi^-)$ — Γ_2/Γ_5

VALUE	EVTS	DOCUMENT ID		TECN	COMMENT
0.42 ± 0.05 ± 0.11	34.8k	[1] DEL-AMO-SA...	10P	BABR	$e^+ e^- \to D^{(*)+} \pi^- X$

[1] The states observed in the $D^* \pi$ and $D \pi$ final states are not necessarily the same.

$D_3^*(2750)$ POLARIZATION AMPLITUDE A_D

A polarization amplitude A_D is a parameter that depends on the initial polarization of the $D_3^*(2750)$. For $D_3^*(2750)$ decays the helicity angle, θ_H, distribution varies like $1 + A_D \cos(\theta_H)$, where θ_H is the angle in the D^* rest frame between the two pions emitted by the $D_3^*(2750) \to D^* \pi$ and $D^* \to D \pi$.

VALUE	EVTS	DOCUMENT ID		TECN	COMMENT
• • • We do not use the following data for averages, fits, limits, etc. • • •					
−0.33 ± 0.28	23.5k	[1] DEL-AMO-SA...	10P	BABR	$e^+ e^- \to D^{*+} \pi^- X$

[1] Systematic uncertainties not estimated. The states observed in the $D^* \pi$ and $D \pi$ final states are not necessarily the same.

$D_3^*(2750)$ REFERENCES

AAIJ 20D PR D101 032005 R. Aaij et al. (LHCb Collab.)
AAIJ 16AH PR D94 072001 R. Aaij et al. (LHCb Collab.)
AAIJ 15Y PR D92 032002 R. Aaij et al. (LHCb Collab.) JP
AAIJ 13CC JHEP 1309 145 R. Aaij et al. (LHCb Collab.)
DEL-AMO-SA... 10P PR D82 111101 P. del Amo Sanchez et al. (BABAR Collab.)

$D_1^*(2760)^0$

$I(J^P) = \frac{1}{2}(1^-)$

OMITTED FROM SUMMARY TABLE

J^P determined by AAIJ 15V from the Dalitz plot analysis of $B^- \to D^+ K^- \pi^-$ decays.

$D_1^*(2760)^0$ MASS

VALUE (MeV)	EVTS	DOCUMENT ID		TECN	COMMENT
2781 ± 18 ± 13	2k	[1] AAIJ	15V	LHCB	$B^- \to D^+ K^- \pi^-$

[1] From the amplitude analysis in the model describing the $D^+ \pi^-$ wave together with virtual contributions from the $D^*(2007)^0$ and B^{*0} states, nonresonant spin-0 and spin-1 components as well as the $D_0^*(2400)^0$, $D_2^*(2460)^0$ and $D_1^*(2760)^0$ resonances.

$D_1^*(2760)^0$ WIDTH

VALUE (MeV)	EVTS	DOCUMENT ID		TECN	COMMENT
177 ± 32 ± 21	2k	[1] AAIJ	15V	LHCB	$B^- \to D^+ K^- \pi^-$

[1] From the amplitude analysis in the model describing the $D^+ \pi^-$ wave together with virtual contributions from the $D^*(2007)^0$ and B^{*0} states, nonresonant spin-0 and spin-1 components as well as the $D_0^*(2400)^0$, $D_2^*(2460)^0$ and $D_1^*(2760)^0$ resonances.

$D_1^*(2760)^0$ DECAY MODES

	Mode	Fraction (Γ_i/Γ)
Γ_1	$D^+ \pi^-$	seen

$D_1^*(2760)^0$ BRANCHING RATIOS

$\Gamma(D^+ \pi^-)/\Gamma_{total}$ — Γ_1/Γ

VALUE	DOCUMENT ID		TECN	COMMENT
seen	[1] AAIJ	15V	LHCB	$B^- \to D^+ K^- \pi^-$

[1] From the amplitude analysis in the model describing the $D^+ \pi^-$ wave together with virtual contributions from the $D^*(2007)^0$ and B^{*0} states, nonresonant spin-0 and spin-1 components as well as the $D_0^*(2400)^0$, $D_2^*(2460)^0$ and $D_1^*(2760)^0$ resonances.

$D_1^*(2760)^0$ REFERENCES

AAIJ 15V PR D91 092002 R. Aaij et al. (LHCb Collab.) JP
Also PR D93 119901 (errat.) R. Aaij et al. (LHCb Collab.)

$D_2^*(3000)^0$

$I(J^P) = \frac{1}{2}(2^+)$

OMITTED FROM SUMMARY TABLE

$D_2^*(3000)^0$ MASS

VALUE (MeV)	EVTS	DOCUMENT ID		TECN	COMMENT
3214 ±29 ±49	28k	[1] AAIJ	16AH	LHCB	$B^- \to D^+\pi^-\pi^-$
• • • We do not use the following data for averages, fits, limits, etc. • • •					
2971.8± 8.7	9.5k	[2,3] AAIJ	13CC	LHCB	$pp \to D^{*+}\pi^- X$
3008.1± 4.0	17.6k	[2,4] AAIJ	13CC	LHCB	$pp \to D^+\pi^- X$

[1] From the amplitude analysis in the model describing the $D^+\pi^-$ wave together with virtual contributions from the $D^*(2007)^0$ and B^{*0} states, and components corresponding to the $D_2^*(2460)^0$, $D_1^*(2680)^0$, $D_3^*(2760)^0$, and $D_2^*(3000)^0$ resonances.
[2] Systematic uncertainty not estimated.
[3] Unnatural parity preferred.
[4] Natural parity state. A state $D(3000)^+$ is possibly seen in $D^0\pi^+$ final state.

$D_2^*(3000)^0$ WIDTH

VALUE (MeV)	EVTS	DOCUMENT ID		TECN	COMMENT
186 ±38 ±72	28k	[1] AAIJ	16AH	LHCB	$B^- \to D^+\pi^-\pi^-$
• • • We do not use the following data for averages, fits, limits, etc. • • •					
188.1±44.8	9.5k	[2,3] AAIJ	13CC	LHCB	$pp \to D^{*+}\pi^- X$
110.5±11.5	17.6k	[2,4] AAIJ	13CC	LHCB	$pp \to D^+\pi^- X$

[1] From the amplitude analysis in the model describing the $D^+\pi^-$ wave together with virtual contributions from the $D^*(2007)^0$ and B^{*0} states, and components corresponding to the $D_2^*(2460)^0$, $D_1^*(2680)^0$, $D_3^*(2760)^0$, and $D_2^*(3000)^0$ resonances.
[2] Systematic uncertainty not estimated.
[3] Unnatural parity preferred.
[4] Natural parity state. A state $D(3000)^+$ is possibly seen in $D^0\pi^+$ final state.

$D_2^*(3000)^0$ DECAY MODES

	Mode	Fraction (Γ_i/Γ)
Γ_1	$D^{*+}\pi^-$	seen

$D_2^*(3000)^0$ POLARIZATION AMPLITUDE A_{D_J}

A polarization amplitude A_{D_J} is a parameter that depends on the initial polarization of the D_J. For D_J decays the helicity angle, θ_H, distribution varies like $1 + A_{D_J}\cos^2(\theta_H)$, where θ_H is the angle in the D_J rest frame between the two pions emitted in the $D_J \to D^*\pi$ and $D^* \to D\pi$ decays.

VALUE	EVTS	DOCUMENT ID		TECN	COMMENT
• • • We do not use the following data for averages, fits, limits, etc. • • •					
1.5±0.9	9.5k	[1] AAIJ	13CC	LHCB	$pp \to D^{*+}\pi^- X$

[1] Systematic uncertainty not estimated.

$D_2^*(3000)^0$ REFERENCES

AAIJ 16AH PR D94 072001 R. Aaij *et al.* (LHCb Collab.)
AAIJ 13CC JHEP 1309 145 R. Aaij *et al.* (LHCb Collab.)

Int. J. Mod. Phys. A 2026.41. Downloaded from www.worldscientific.com
by [redacted]LIFORNIA @ BERKELEY on 09/16/26. Re-use and distribution is strictly not permitted, except for Open Access articles.

Int. J. Mod. Phys. A 2026.41. Downloaded from www.worldscientific.com
by UNIVERSITY OF CALIFORNIA @ BERKELEY on 09/16/26. Re-use and distribution is strictly not permitted, except for Open Access articles.

CHARMED, STRANGE MESONS ($C = \pm1$, $S = \pm1$) (including possibly non-$q\overline{q}$ states)

$D_s^+ = c\overline{s}$, $D_s^- = \overline{c}s$, similarly for D_s^*'s

$D_s^\pm$

$I(J^P) = 0(0^-)$

The angular distributions of the decays of the ϕ and $\overline{K}^*(892)^0$ in the $\phi\pi^+$ and $K^+\overline{K}^*(892)^0$ modes strongly indicate that the spin is zero. The parity given is that expected of a $c\overline{s}$ ground state.

$D_s^\pm$ MASS

The fit includes $D^\pm$, D^0, $D_s^\pm$, $D^{*\pm}$, D^{*0}, $D_s^{*\pm}$, $D_1(2420)^0$, $D_2^*(2460)^0$, and $D_{s1}(2536)^\pm$ mass and mass difference measurements. Measurements of the $D_s^\pm$ mass with an error greater than 10 MeV are omitted from the fit and average. A number of early measurements have been omitted altogether.

VALUE (MeV)	EVTS	DOCUMENT ID		TECN	COMMENT
1968.35 ± 0.07 OUR FIT					
1969.0 ± 1.4 OUR AVERAGE Error includes scale factor of 1.5. See the ideogram below.					
1967.0 ± 1.0 ± 1.0	54	BARLAG	90C	ACCM	π^- Cu 230 GeV
1969.3 ± 1.4 ± 1.4		ALBRECHT	88	ARG	e^+e^- 9.4–10.6 GeV
1972.7 ± 1.5 ± 1.0	21	BECKER	87B	SILI	200 GeV π, K, p
1972.4 ± 3.7 ± 3.7	27	BLAYLOCK	87	MRK3	e^+e^- 4.14 GeV
1963 ± 3 ± 3	30	DERRICK	85B	HRS	e^+e^- 29 GeV
1970 ± 5 ± 5	104	CHEN	83C	CLEO	e^+e^- 10.5 GeV
• • • We do not use the following data for averages, fits, limits, etc. • • •					
1968.3 ± 0.7 ± 0.7	290	[1] ANJOS	88	E691	Photoproduction
1980 ±15	6	USHIDA	86	EMUL	ν wideband
1973.6 ± 2.6 ± 3.0	163	ALBRECHT	85D	ARG	e^+e^- 10 GeV
1948 ±28 ±10	65	AIHARA	84D	TPC	e^+e^- 29 GeV
1975 ± 9 ±10	49	ALTHOFF	84	TASS	e^+e^- 14–25 GeV
1975 ± 4	3	BAILEY	84	ACCM	hadron$^+$ Be $\to \phi\pi^+$ X

[1] ANJOS 88 enters the fit via $m_{D_s^\pm} - m_{D^\pm}$ (see below).

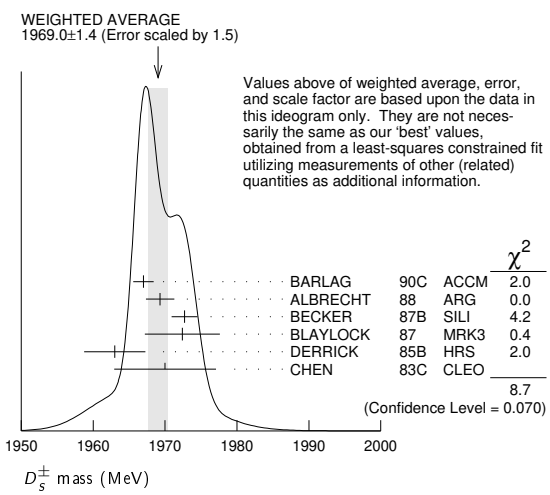

$m_{D_s^\pm} - m_{D^\pm}$

The fit includes $D^\pm$, D^0, $D_s^\pm$, $D^{*\pm}$, D^{*0}, $D_s^{*\pm}$, $D_1(2420)^0$, $D_2^*(2460)^0$, and $D_{s1}(2536)^\pm$ mass and mass difference measurements.

VALUE (MeV)	EVTS	DOCUMENT ID		TECN	COMMENT
98.69±0.05 OUR FIT					
98.69±0.05 OUR AVERAGE					
98.68±0.03±0.04		AAIJ	13V	LHCB	$D_s^+ \to K^+K^-\pi^+$
99.41±0.38±0.21		ACOSTA	03D	CDF2	$\overline{p}p$, $\sqrt{s}$= 1.96 TeV
98.4 ±0.1 ±0.3	48k	AUBERT	02G	BABR	$e^+e^- \approx \Upsilon(4S)$
99.5 ±0.6 ±0.3		BROWN	94	CLE2	$e^+e^- \approx \Upsilon(4S)$
98.5 ±1.5	555	CHEN	89	CLEO	e^+e^- 10.5 GeV
99.0 ±0.8	290	ANJOS	88	E691	Photoproduction

$D_s^\pm$ MEAN LIFE

Measurements with an error greater than 100×10^{-15} s or with fewer than 100 events have been omitted from the Listings.

VALUE (10^{-15} s)	EVTS	DOCUMENT ID		TECN	COMMENT
501.2± 2.2 OUR AVERAGE Error includes scale factor of 1.3. See the ideogram below.					
499.5± 1.7± 0.9	116k	ADACHI	23G	BEL2	$D_s^+ \to \phi\pi^+$
506.4± 3.0± 1.7±1.7		[1] AAIJ	17AN	LHCB	pp at 7, 8 TeV
507.4± 5.5± 5.1	13.6k	LINK	05J	FOCS	$\Phi\pi^+$ and $\overline{K}^{*0}K^+$
• • • We do not use the following data for averages, fits, limits, etc. • • •					
472.5±17.2± 6.6	760	IORI	01	SELX	600 GeV Σ^-, π^-, p
518 ±14 ± 7	1662	AITALA	99	E791	π^- nucleus, 500 GeV
486.3±15.0$^{+4.9}_{-5.1}$	2167	[2] BONVICINI	99	CLE2	$e^+e^- \approx \Upsilon(4S)$
475 ±20 ± 7	900	FRABETTI	93F	E687	γBe, $\phi\pi^+$
500 ±60 ±30	104	FRABETTI	90	E687	γBe, $\phi\pi^+$
470 ±40 ±20	228	RAAB	88	E691	Photoproduction

[1] This AAIJ 17AN value is derived from the difference between the D_s^- and D^- widths. The 3rd uncertainty, $\pm1.7 \times 10^{-15}$ s, arises from the uncertainty of the D^- width.
[2] BONVICINI 99 obtains 1.19 ± 0.04 for the ratio of D_s^+ to D^0 lifetimes.

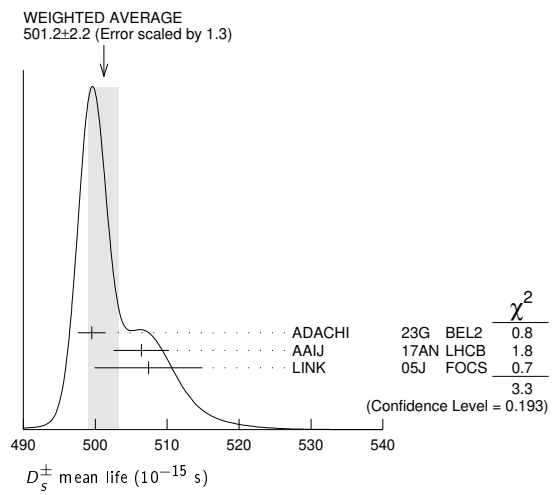

D_s^+ DECAY MODES

Unless otherwise noted, the branching fractions for modes with a resonance in the final state include all the decay modes of the resonance. D_s^- modes are charge conjugates of the modes below.

	Mode		Fraction (Γ_i/Γ)	Scale factor/ Confidence level
	Inclusive modes			
Γ_1	e^+ semileptonic	[a]	(6.33 ±0.15) %	
Γ_2	π^+ anything		(119.3 ±1.4) %	
Γ_3	π^- anything		(43.2 ±0.9) %	
Γ_4	π^0 anything		(123 ±7) %	
Γ_5	K^- anything		(18.7 ±0.5) %	
Γ_6	K^+ anything		(28.9 ±0.7) %	
Γ_7	K^0_S anything		(19.0 ±1.1) %	
Γ_8	η anything	[b]	(29.9 ±2.8) %	
Γ_9	ω anything		(6.1 ±1.4) %	
Γ_{10}	η' anything	[c]	(10.3 ±1.4) %	S=1.1
Γ_{11}	$f_0(980)$ anything, $f_0 \to \pi^+\pi^-$		< 1.3 %	CL=90%
Γ_{12}	ϕ anything		(15.7 ±1.0) %	
Γ_{13}	K^+K^- anything		(15.8 ±0.7) %	
Γ_{14}	$K^0_S K^+$ anything		(5.8 ±0.5) %	
Γ_{15}	$K^0_S K^-$ anything		(1.9 ±0.4) %	
Γ_{16}	$2K^0_S$ anything		(1.70 ±0.32) %	
Γ_{17}	$2K^+$ anything		< 2.6 $\times 10^{-3}$	CL=90%
Γ_{18}	$2K^-$ anything		< 6 $\times 10^{-4}$	CL=90%
Γ_{19}	$2\pi^+\pi^-$ + anything		(32.8 ±0.7) %	
	Leptonic and semileptonic modes			
Γ_{20}	$e^+\nu_e$		< 8.3 $\times 10^{-5}$	CL=90%
Γ_{21}	$\mu^+\nu_\mu$		(5.37 ±0.11) $\times 10^{-3}$	
Γ_{22}	$\tau^+\nu_\tau$		(5.39 ±0.09) %	
Γ_{23}	$\gamma e^+\nu_e$		< 1.3 $\times 10^{-4}$	CL=90%
Γ_{24}	$K^+K^-e^+\nu_e$		—	

Int. J. Mod. Phys. A 2026.41. Downloaded from www.worldscientific.com
by CALIFORNIA @ BERKELEY on 09/16/26. Re-use and distribution is strictly not permitted, except for Open Access articles.

Γ_{25}	$K^0_S K^0_S e^+ \nu_e$		< 3.8	$\times 10^{-4}$	CL=90%
Γ_{26}	$\phi e^+ \nu_e$	[d]	(2.34 ± 0.12) %		S=1.2
Γ_{27}	$K_1(1270)^0 e^+ \nu_e$		< 4.1	$\times 10^{-4}$	CL=90%
Γ_{28}	$b_1(1235)^0 e^+ \nu_e$, $b_1^0 \to \omega \pi^0$		< 6.4	$\times 10^{-4}$	CL=90%
Γ_{29}	$\phi \mu^+ \nu_\mu$		(2.24 ± 0.11) %		
Γ_{30}	$\eta e^+ \nu_e$	[d]	(2.27 ± 0.06) %		
Γ_{31}	$\eta'(958) e^+ \nu_e$	[d]	(8.1 ± 0.4)	$\times 10^{-3}$	
Γ_{32}	$\eta \mu^+ \nu_\mu$		(2.24 ± 0.07) %		
Γ_{33}	$\eta'(958) \mu^+ \nu_\mu$		(8.0 ± 0.6)	$\times 10^{-3}$	
Γ_{34}	$\omega e^+ \nu_e$	[e]	< 2.0	$\times 10^{-3}$	CL=90%
Γ_{35}	$K^0 e^+ \nu_e$		(2.88 ± 0.26)	$\times 10^{-3}$	S=1.2
Γ_{36}	$K^*(892)^0 e^+ \nu_e$	[d]	(2.05 ± 0.20)	$\times 10^{-3}$	
Γ_{37}	$f_0(500) e^+ \nu_e$, $f_0 \to \pi^0 \pi^0$		< 7.3	$\times 10^{-4}$	CL=90%
Γ_{38}	$f_0(500) e^+ \nu_e$, $f_0 \to \pi^+ \pi^-$		< 3.3	$\times 10^{-4}$	CL=90%
Γ_{39}	$f_0(980) e^+ \nu_e$, $f_0 \to \pi^0 \pi^0$		(7.9 ± 1.5)	$\times 10^{-4}$	
Γ_{40}	$f_0(980) e^+ \nu_e$, $f_0 \to \pi^+ \pi^-$		(1.64 ± 0.13)	$\times 10^{-3}$	
Γ_{41}	$f_0(980) \mu^+ \nu_\mu$, $f_0 \to K^+ K^-$		< 5.45	$\times 10^{-4}$	CL=90%
Γ_{42}	$a_0(980)^0 e^+ \nu_e$, $a_0^0 \to \pi^0 \eta$		< 1.2	$\times 10^{-4}$	CL=90%
Γ_{43}	$\pi^0 e^+ \nu_e$		< 6.4	$\times 10^{-5}$	CL=90%

Hadronic modes with a $K\overline{K}$ pair

Γ_{44}	$K^+ K^0_S$		(1.500 ± 0.014) %		
Γ_{45}	$K^+ K^0_L$		(1.49 ± 0.06) %		
Γ_{46}	$K^0_S K^0_L \pi^+$		(1.86 ± 0.07) %		
Γ_{47}	$\phi(1020) \pi^+$, $\phi \to K^0_L K^0_S$		(1.31 ± 0.06) %		
Γ_{48}	$K^0_L K^*(892)^+$, $K^{*+} \to K^0_S \pi^+$		(3.59 ± 0.32)	$\times 10^{-3}$	
Γ_{49}	$K^0_S K^*(892)^+$, $K^{*+} \to K^0_L \pi^+$		(2.68 ± 0.33)	$\times 10^{-3}$	
Γ_{50}	$\phi(1680) \pi^+$, $\phi \to K^0_L K^0_S$		(6.1 ± 2.1)	$\times 10^{-4}$	
Γ_{51}	$K^+ \overline{K}^0$		(2.95 ± 0.14) %		
Γ_{52}	$K^+ K^- \pi^+$	[f]	(5.45 ± 0.08) %		S=1.3
Γ_{53}	$\phi \pi^+$	[d,g]	(4.5 ± 0.4) %		
Γ_{54}	$\phi \pi^+$, $\phi \to K^+ K^-$	[g]	(2.25 ± 0.05) %		
Γ_{55}	$K^+ \overline{K}^*(892)^0$		(12.7 $^{+4.0}_{-3.1}$) %		
Γ_{56}	$K^+ \overline{K}^*(892)^0$, $\overline{K}^{*0} \to K^- \pi^+$		(2.61 ± 0.05) %		
Γ_{57}	$K^+ \overline{K}^*(892)^0$, $\overline{K}^{*0} \to K^0_S \pi^0$		(4.8 ± 0.4)	$\times 10^{-3}$	
Γ_{58}	$f_0(980) \pi^+$, $f_0 \to K^+ K^-$		(1.12 ± 0.19) %		
Γ_{59}	$f_0(1370) \pi^+$, $f_0 \to K^+ K^-$		(7.2 ± 3.0)	$\times 10^{-4}$	
Γ_{60}	$f_0(1710) \pi^+$, $f_0 \to K^+ K^-$		(6.8 ± 2.8)	$\times 10^{-4}$	
Γ_{61}	$a_0(980)^+ \pi^0$, $a_0^+ \to K^+ K^0_S$		(1.1 ± 0.4)	$\times 10^{-3}$	
Γ_{62}	$a_0(1710)^+ \pi^0$, $a_0^+ \to K^+ K^0_S$		(3.5 ± 0.6)	$\times 10^{-3}$	
Γ_{63}	$K^+ \overline{K}^*_0(1430)^0$, $\overline{K}^*_0 \to K^- \pi^+$		(1.79 ± 0.26)	$\times 10^{-3}$	
Γ_{64}	$K^+ \overline{K}^*(1410)^0$, $\overline{K}^*_0 \to K^0_S \pi^0$		(8.8 ± 2.8)	$\times 10^{-4}$	
Γ_{65}	$K^+ K^0_S \pi^0$		(1.471 ± 0.028) %		
Γ_{66}	$K^*(892)^+ K^0_S$, $K^{*+} \to K^+ \pi^0$		(2.04 ± 0.32)	$\times 10^{-3}$	
Γ_{67}	$2K^0_S \pi^+$		(7.32 ± 0.14)	$\times 10^{-3}$	
Γ_{68}	$f_0(980) \pi^+$, $f_0 \to K^0_S K^0_S$		< 1.8	$\times 10^{-4}$	CL=90%
Γ_{69}	$f_0(1710) \pi^+$, $f_0 \to K^0_S K^0_S$		(3.39 ± 0.31)	$\times 10^{-3}$	
Γ_{70}	$K^*(892)^+ K^0_S$, $K^{*+} \to K^0_S \pi^+$		(3.19 ± 0.29)	$\times 10^{-3}$	
Γ_{71}	$K^0 \overline{K}^0 \pi^+$		—		
Γ_{72}	$K^*(892)^+ \overline{K}^0$	[d]	(5.4 ± 1.2) %		
Γ_{73}	$\phi \rho^+$		(4.9 ± 0.8) %		S=3.0
Γ_{74}	$K^+ K^- \pi^+ \pi^0$		(5.53 ± 0.15) %		S=1.3
Γ_{75}	$\overline{K}_1(1270)^0 K^+$, $\overline{K}_1(1270)^0 \to K^- \rho^+$		(5.7 ± 0.6)	$\times 10^{-3}$	
Γ_{76}	$\overline{K}_1(1270)^0 K^+$, $\overline{K}_1(1270)^0 \to K^*(892) \pi$		(1.31 ± 0.25) %		
Γ_{77}	$\overline{K}_1(1400)^0 K^+$, $\overline{K}_1(1400)^0 \to K^*(892) \pi$		(2.0 ± 0.4) %		
Γ_{78}	$a_0(980)^0 \rho^+$, $a_0^0 \to K^+ K^-$		(1.9 ± 0.4)	$\times 10^{-3}$	
Γ_{79}	$f_1(1420)^0 \pi^+$, $f_1(1420)^0 \to K^*(892)^\mp K^\pm$		(3.9 ± 0.7)	$\times 10^{-3}$	
Γ_{80}	$f_1(1420)^0 \pi^+$, $f_1^0 \to a_0(980)^0 \pi^0$, $a_0^0 \to K^+ K^-$		(4.0 ± 1.4)	$\times 10^{-4}$	
Γ_{81}	$\eta(1475) \pi^+$, $\eta \to a_0(980)^0 \pi^0$, $a_0^0 \to K^+ K^-$		(7.0 ± 2.8)	$\times 10^{-4}$	
Γ_{82}	$K^0_S K^- 2\pi^+$		(1.569 ± 0.028) %		
Γ_{83}	$K^+ K^- K^0_S \pi^+$		(1.27 ± 0.15)	$\times 10^{-4}$	
Γ_{84}	$K^*(892)^+ \overline{K}^*(892)^0$	[d]	(5.64 ± 0.35) %		
Γ_{85}	$\eta(1475) K^0_S$, $\eta \to K^*(892)^0 \pi^+$, $K^{*0} \to K^- \pi^+$		(3.5 ± 1.0)	$\times 10^{-4}$	
Γ_{86}	$\eta(1475) \pi^+$, $\eta \to \overline{K}^*(892)^+ K^-$, $\overline{K}^{*+} \to K^0_S \pi^+$		(3.5 ± 1.0)	$\times 10^{-4}$	
Γ_{87}	$\eta(1475) \pi^+$, $\eta \to a_0(980)^- \pi^+$, $a_0^- \to K^0_S K^-$		(1.7 ± 0.9)	$\times 10^{-3}$	
Γ_{88}	$f_1(1285) \pi^+$, $f_1 \to a_0(980)^- \pi^+$, $a_0^- \to K^0_S K^-$		(3.5 ± 0.8)	$\times 10^{-4}$	
Γ_{89}	$K^+ K^0_S \pi^+ \pi^-$		(9.34 ± 0.22)	$\times 10^{-3}$	
Γ_{90}	$K^+ K^- 2\pi^+ \pi^-$		(6.6 ± 0.6)	$\times 10^{-3}$	
Γ_{91}	$\phi 2\pi^+ \pi^-$	[d]	(1.21 ± 0.16) %		
Γ_{92}	$\phi \rho^0 \pi^+$, $\phi \to K^+ K^-$		(4.9 ± 0.7)	$\times 10^{-3}$	
Γ_{93}	$\phi a_1(1260)^+$, $\phi \to K^+ K^-$, $a_1^+ \to \rho^0 \pi^+$		(7.5 ± 1.2)	$\times 10^{-3}$	
Γ_{94}	$\phi 2\pi^+ \pi^-$ non-ρ, $\phi \to K^+ K^-$		(1.4 ± 0.5)	$\times 10^{-3}$	
Γ_{95}	$K^+ K^- \rho^0 \pi^+$ non-ϕ		< 2.0	$\times 10^{-4}$	CL=90%
Γ_{96}	$K^+ K^- 2\pi^+ \pi^-$ nonresonant		(1.0 ± 0.4)	$\times 10^{-3}$	
Γ_{97}	$2K^0_S 2\pi^+ \pi^-$		(8.0 ± 3.3)	$\times 10^{-4}$	

Hadronic modes without K's

Γ_{98}	$\pi^+ \pi^0$		< 1.2	$\times 10^{-4}$	CL=90%
Γ_{99}	$2\pi^+ \pi^-$		(1.090 ± 0.014) %		
Γ_{100}	$\rho^0 \pi^+$		(1.14 ± 0.16)	$\times 10^{-4}$	
Γ_{101}	$\omega \pi^+$, $\omega \to \pi^+ \pi^-$		(3.9 ± 0.4)	$\times 10^{-5}$	
Γ_{102}	$\pi^+ (\pi^+ \pi^-)_{S-\text{wave}}$	[h]	(9.23 ± 0.13)	$\times 10^{-3}$	
Γ_{103}	$f_0(980) \pi^+$, $f_0 \to \pi^+ \pi^-$				
Γ_{104}	$f_0(1370) \pi^+$, $f_0 \to \pi^+ \pi^-$				
Γ_{105}	$f_0(1500) \pi^+$, $f_0 \to \pi^+ \pi^-$				
Γ_{106}	$f_2(1270) \pi^+$, $f_2 \to \pi^+ \pi^-$		(1.42 ± 0.10)	$\times 10^{-3}$	
Γ_{107}	$f'_2(1525)^0 \pi^+$, $f'_2 \to \pi^+ \pi^-$		(5.8 ± 2.0)	$\times 10^{-6}$	
Γ_{108}	$\rho(1450)^0 \pi^+$, $\rho^0 \to \pi^+ \pi^-$		(1.8 ± 0.6)	$\times 10^{-4}$	
Γ_{109}	$\rho(1700)^0 \pi^+$, $\rho^0 \to \pi^+ \pi^-$		(4 ± 4)	$\times 10^{-5}$	
Γ_{110}	$\pi^+ 2\pi^0$		(5.2 ± 0.5)	$\times 10^{-3}$	S=1.1
Γ_{111}	$f_0(980) \pi^+$, $f_0 \to \pi^0 \pi^0$		(2.9 ± 0.6)	$\times 10^{-3}$	
Γ_{112}	$f_0(1370) \pi^+$, $f_0 \to \pi^0 \pi^0$		(1.3 ± 0.6)	$\times 10^{-3}$	
Γ_{113}	$f_2(1270) \pi^+$, $f_2 \to \pi^0 \pi^0$		(5.0 ± 3.5)	$\times 10^{-4}$	
Γ_{114}	$2\pi^+ \pi^- \pi^0$		—		
Γ_{115}	$\omega \pi^+$	[d]	(1.93 ± 0.30)	$\times 10^{-3}$	
Γ_{116}	$\eta \pi^+$	[d]	(1.686 ± 0.027) %		
Γ_{117}	$(2\pi^+ \pi^- \pi^0)_{\text{non}-\eta}$		(2.04 ± 0.09) %		
Γ_{118}	$f_0(1370) \rho^+$, $f_0 \rho^+ \to 2\pi^+ \pi^- \pi^0$		(5.1 ± 0.9)	$\times 10^{-3}$	
Γ_{119}	$f_0(980)^0 \rho^+$, $f_0^0 \rho^+ \to 2\pi^+ \pi^- \pi^0$		(2.6 ± 0.5)	$\times 10^{-3}$	
Γ_{120}	$f_2(1270)^0 \rho^+$, $f_2(1270)^0 \rho^+ \to 2\pi^+ \pi^- \pi^0$		(1.9 ± 0.4)	$\times 10^{-3}$	
Γ_{121}	$(\rho^+ \rho^0)_{S-wave} \to 2\pi^+ \pi^- \pi^0$		(7.1 ± 2.8)	$\times 10^{-4}$	
Γ_{122}	$(\rho(1450)^+ \rho^0)_{S-wave} \to 2\pi^+ \pi^- \pi^0$		(9.4 ± 3.1)	$\times 10^{-4}$	
Γ_{123}	$(\rho^+ \rho(1450)^0)_{P-wave} \to 2\pi^+ \pi^- \pi^0$		(1.75 ± 0.29)	$\times 10^{-3}$	
Γ_{124}	$\phi \pi^+$, $\phi \to \rho \pi$		(5.08 ± 0.35)	$\times 10^{-3}$	
Γ_{125}	$\omega \pi^+$, $\omega \to \rho \pi$		(1.41 ± 0.19)	$\times 10^{-3}$	
Γ_{126}	$a_1(1260)^+ \pi^0$, $a_1^+ \to (\rho^0 \pi^+)_{S-wave}$		(2.6 ± 0.4)	$\times 10^{-3}$	
Γ_{127}	$a_1(1260)^0 \pi^+$, $a_1^0 \to (\rho \pi)_{S-wave}$		(1.3 ± 0.5)	$\times 10^{-3}$	
Γ_{128}	$\pi(1300)^0 \pi^+$, $\pi^0 \to (\rho \pi)_{P-wave}$		(2.4 ± 0.7)	$\times 10^{-3}$	
Γ_{129}	$3\pi^+ 2\pi^-$		(8.0 ± 0.8)	$\times 10^{-3}$	
Γ_{130}	$2\pi^+ \pi^- 2\pi^0$		(4.41 ± 0.20) %		
Γ_{131}	$\omega \rho^+$, $\omega \to \pi^+ \pi^- \pi^0$		(8.8 ± 0.9)	$\times 10^{-3}$	

Int. J. Mod. Phys. A 2026.41. Downloaded from www.worldscientific.com
by UNIVERSITY OF CALIFORNIA @ BERKELEY on 09/16/26. Re-use and distribution is strictly not permitted, except for Open Access articles.

Γ_{132}	$\phi\rho^+$, $\phi \to \pi^+\pi^-\pi^0$		$(6.1 \pm 0.6) \times 10^{-3}$	
Γ_{133}	$\rho(1450)^+\pi^0$, $\rho(1450)^+ \to \omega\pi^+$, $\omega \to \pi^+\pi^-\pi^0$		$(3.5 \pm 0.5) \times 10^{-3}$	
Γ_{134}	$a_1(1260)^0\rho^+$, $a_1(1260)^0 \to \rho^+\pi^-$		$(5.0 \pm 0.4) \times 10^{-3}$	
Γ_{135}	$a_1(1260)^0\rho^+$, $a_1(1260)^0 \to \rho^-\pi^+$		$(3.26 \pm 0.27) \times 10^{-3}$	
Γ_{136}	$a_1(1260)^+\rho^0$, $a_1(1260)^+ \to \rho^+\pi^0$		$(7.3 \pm 1.0) \times 10^{-3}$	
Γ_{137}	$b_1(1235)^+\pi^0$, $b_1(1235)^+ \to \omega\pi^+$, $\omega \to \pi^+\pi^-\pi^0$		$(4.8 \pm 0.6) \times 10^{-3}$	
Γ_{138}	$b_1(1235)^0\pi^+$, $b_1(1235)^0 \to \omega\pi^0$, $\omega \to \pi^+\pi^-\pi^0$		$(6.4 \pm 0.6) \times 10^{-3}$	
Γ_{139}	$\eta\rho^+$	[d]	(8.9 ± 0.8) %	
Γ_{140}	$\eta\pi^+\pi^0$		(9.10 ± 0.17) %	
Γ_{141}	$\eta(\pi^+\pi^0)_{P-wave}$		$(4.9 \pm 3.0) \times 10^{-3}$	
Γ_{142}	$a_0(980)^{+0}\pi^{0+}$, $a_0(980)^{+0} \to \eta\pi^{+0}$		(2.1 ± 0.4) %	
Γ_{143}	$\omega\pi^+\pi^0$	[d]	(2.8 ± 0.7) %	
Γ_{144}	$2\pi^+\pi^-\eta$		(3.08 ± 0.08) %	
Γ_{145}	$a_1(1260)^+\eta$, $a_1^+ \to \rho(770)^0\pi^+$, $\rho^0 \to \pi^+\pi^-$		(1.71 ± 0.14) %	
Γ_{146}	$a_1(1260)^+\eta$, $a_1^+ \to f_0(500)\pi^+$, $f_0 \to \pi^+\pi^-$		$(2.5 \pm 0.9) \times 10^{-3}$	
Γ_{147}	$a_0(980)^+\rho(770)^0$, $a_0^+ \to \eta\pi^+$		$(2.1 \pm 0.9) \times 10^{-3}$	
Γ_{148}	$\eta(1405)\pi^+$, $\eta \to a_0(980)^-\pi^+$, $a_0^- \to \eta\pi^-$		$(2.2 \pm 0.7) \times 10^{-4}$	
Γ_{149}	$\eta(1405)\pi^+$, $\eta \to a_0(980)^+\pi^-$, $a_0^+ \to \eta\pi^+$		$(2.2 \pm 0.7) \times 10^{-4}$	
Γ_{150}	$f_1(1420)\pi^+$, $f_1 \to a_0(980)^-\pi^+$, $a_0^- \to \eta\pi^-$		$(5.9 \pm 1.8) \times 10^{-4}$	
Γ_{151}	$f_1(1420)\pi^+$, $f_1 \to a_0(980)^+\pi^-$, $a_0^+ \to \eta\pi^+$		$(5.2 \pm 1.8) \times 10^{-4}$	
Γ_{152}	$3\pi^+2\pi^-\pi^0$		(4.9 ± 3.2) %	
Γ_{153}	$\omega 2\pi^+\pi^-$	[d]	(1.6 ± 0.5) %	
Γ_{154}	$\eta'(958)\pi^+$	[c,d]	(3.95 ± 0.08) %	
Γ_{155}	$3\pi^+2\pi^-2\pi^0$		—	
Γ_{156}	$\omega\eta\pi^+$	[d]	$(5.4 \pm 1.3) \times 10^{-3}$	
Γ_{157}	$\eta'(958)\rho^+$	[c,d]	(5.8 ± 1.5) %	
Γ_{158}	$\eta'(958)\pi^+\pi^0$		(6.14 ± 0.18) %	
Γ_{159}	$\eta'(958)\pi^+\pi^0$ nonresonant		< 5.1 %	CL=90%

Modes with one or three K's

Γ_{160}	$K^+\pi^0$		$(7.5 \pm 0.5) \times 10^{-4}$	
Γ_{161}	$K_S^0\pi^+$		$(1.22 \pm 0.04) \times 10^{-3}$	
Γ_{162}	$K^+\eta$	[d]	$(1.76 \pm 0.08) \times 10^{-3}$	
Γ_{163}	$K^+\omega$	[d]	$(9.9 \pm 1.5) \times 10^{-4}$	
Γ_{164}	$K^+\eta'(958)$	[d]	$(2.68 \pm 0.24) \times 10^{-3}$	
Γ_{165}	$K^+\pi^+\pi^-$		$(6.23 \pm 0.10) \times 10^{-3}$	
Γ_{166}	$K^+\rho^0$		$(2.18 \pm 0.25) \times 10^{-3}$	
Γ_{167}	$K^+\rho(1450)^0$, $\rho^0 \to \pi^+\pi^-$		$(7.3 \pm 1.7) \times 10^{-4}$	
Γ_{168}	$K^+f_0(500)$, $f_0 \to \pi^+\pi^-$		$(4.5 \pm 3.0) \times 10^{-4}$	
Γ_{169}	$K^+f_0(980)$, $f_0 \to \pi^+\pi^-$		$(2.8 \pm 1.1) \times 10^{-4}$	
Γ_{170}	$K^+f_0(1370)$, $f_0 \to \pi^+\pi^-$		$(1.2 \pm 0.6) \times 10^{-3}$	
Γ_{171}	$K^*(892)^0\pi^+$, $K^{*0} \to K^+\pi^-$		$(1.68 \pm 0.26) \times 10^{-3}$	
Γ_{172}	$K^*(1410)^0\pi^+$, $K^{*0} \to K^+\pi^-$		$(6 \pm 4) \times 10^{-4}$	
Γ_{173}	$K^*(1430)^0\pi^+$, $K^{*0} \to K^+\pi^-$		$(9.4 \pm 3.2) \times 10^{-4}$	
Γ_{174}	$K^+\pi^+\pi^-$ nonresonant		$(9.9 \pm 3.2) \times 10^{-4}$	
Γ_{175}	$K^0\pi^+\pi^0$			
Γ_{176}	$K_S^0\pi^+\pi^0$		$(5.09 \pm 0.22) \times 10^{-3}$	
Γ_{177}	$K_S^0\rho(770)^+$, $\rho^+ \to \pi^+\pi^0$		$(2.6 \pm 0.4) \times 10^{-3}$	
Γ_{178}	$K_S^0\rho(1450)^+$, $\rho^+ \to \pi^+\pi^0$		$(1.04 \pm 0.32) \times 10^{-3}$	
Γ_{179}	$K^*(892)^0\pi^+$, $K^{*0} \to K_S^0\pi^0$		$(4.3 \pm 1.2) \times 10^{-4}$	
Γ_{180}	$K^*(892)^+\pi^0$, $K^{*+} \to K_S^0\pi^+$		$(2.3 \pm 0.7) \times 10^{-4}$	
Γ_{181}	$K^*(1410)^0\pi^+$, $K^{*0} \to K_S^0\pi^0$		$(1.7 \pm 0.9) \times 10^{-4}$	
Γ_{182}	$K_S^0 2\pi^+\pi^-$		$(2.8 \pm 1.0) \times 10^{-3}$	
Γ_{183}	$K^+\pi^+\pi^-\pi^0$		$(9.7 \pm 0.6) \times 10^{-3}$	
Γ_{184}	$K^*(892)^0\rho^+$, $K^{*0} \to K^+\pi^-$		$(3.9 \pm 0.4) \times 10^{-3}$	
Γ_{185}	$K^*(892)^+\rho^0$, $K^{*+} \to K^+\pi^0$		$(4.2 \pm 1.2) \times 10^{-4}$	
Γ_{186}	$K_1(1270)^0\pi^+$, $K_1^0 \to K^+\rho^-$		$(3.9 \pm 1.3) \times 10^{-4}$	
Γ_{187}	$K_1(1400)^0\pi^+$, $K_1^0 \to K^*(890)^+\pi^-$, $K^{*+} \to K^+\pi^0$		$(5.4 \pm 0.9) \times 10^{-4}$	
Γ_{188}	$K_1(1400)^0\pi^+$, $K_1^0 \to K^*(890)^0\pi^0$, $K^{*0} \to K^+\pi^-$		$(5.9 \pm 1.0) \times 10^{-4}$	
Γ_{189}	$K^+a_1(1260)^0$, $a_1 \to \rho^+\pi^-$		$(1.8 \pm 1.1) \times 10^{-4}$	
Γ_{190}	$K^+a_1(1260)^0$, $a_1 \to \rho^-\pi^+$		$(1.8 \pm 1.1) \times 10^{-4}$	
Γ_{191}	$K^+\pi^+\pi^-\pi^0$ nonresonant		$(9.2 \pm 2.4) \times 10^{-4}$	
Γ_{192}	$(K^+\pi^0)_{P-wave}\rho^0$		$(1.01 \pm 0.21) \times 10^{-3}$	
Γ_{193}	$K^+\omega\pi^0$	[d]	$< 8.2 \times 10^{-3}$	CL=90%
Γ_{194}	$K^+\omega\pi^+\pi^-$	[d]	$< 5.4 \times 10^{-3}$	CL=90%
Γ_{195}	$K^+\omega\eta$	[d]	$< 7.9 \times 10^{-3}$	CL=90%
Γ_{196}	$2K^+K^-$		$(2.18 \pm 0.20) \times 10^{-4}$	
Γ_{197}	ϕK^+, $\phi \to K^+K^-$		$(8.9 \pm 2.0) \times 10^{-5}$	

Radiative decays

Γ_{198}	$\rho(770)^+\gamma$		$< 6.1 \times 10^{-4}$	CL=90%

Doubly Cabibbo-suppressed modes

Γ_{199}	$2K^+\pi^-$		$(1.293 \pm 0.027) \times 10^{-4}$	S=1.1
Γ_{200}	$K^+K^*(892)^0$, $K^{*0} \to K^+\pi^-$		$(6.1 \pm 3.4) \times 10^{-5}$	
Γ_{201}	$2K^+\pi^-\pi^0$		$< 1.7 \times 10^{-4}$	CL=90%

Baryon-antibaryon mode

Γ_{202}	$p\overline{n}$		$(1.22 \pm 0.11) \times 10^{-3}$	
Γ_{203}	$p\overline{p}e^+\nu_e$		$< 2.0 \times 10^{-4}$	CL=90%

$\Delta C = 1$ weak neutral current ($C1$) modes, Lepton family number (LF), or Lepton number (L) violating modes

Γ_{204}	$\pi^+e^+e^-$	[i]	$< 5.5 \times 10^{-6}$	CL=90%
Γ_{205}	$\pi^+\phi$, $\phi \to e^+e^-$	[j]	$(1.17 \pm 0.22) \times 10^{-5}$	
Γ_{206}	$\pi^+\pi^0e^+e^-$		$< 7.0 \times 10^{-5}$	CL=90%
Γ_{207}	$\rho^+\phi$, $\phi \to e^+e^-$		$(2.4 \pm 0.7) \times 10^{-5}$	
Γ_{208}	$\pi^+\mu^+\mu^-$	[i]	$< 1.8 \times 10^{-7}$	CL=90%
Γ_{209}	$K^+e^+e^-$	$C1$	$< 3.7 \times 10^{-6}$	CL=90%
Γ_{210}	$K^+\pi^0e^+e^-$		$< 7.1 \times 10^{-5}$	CL=90%
Γ_{211}	$K_S^0\pi^+e^+e^-$		$< 8.1 \times 10^{-5}$	CL=90%
Γ_{212}	$K^+\mu^+\mu^-$	$C1$	$< 1.4 \times 10^{-7}$	CL=90%
Γ_{213}	$K^*(892)^+\mu^+\mu^-$	$C1$	$< 1.4 \times 10^{-3}$	CL=90%
Γ_{214}	$\pi^+e^+\mu^-$	LF	$< 1.1 \times 10^{-6}$	CL=90%
Γ_{215}	$\pi^+e^-\mu^+$	LF	$< 9.4 \times 10^{-7}$	CL=90%
Γ_{216}	$K^+e^+\mu^-$	LF	$< 7.9 \times 10^{-7}$	CL=90%
Γ_{217}	$K^+e^-\mu^+$	LF	$< 5.6 \times 10^{-7}$	CL=90%
Γ_{218}	π^-2e^+	L	$< 1.4 \times 10^{-6}$	CL=90%
Γ_{219}	$\pi^-2\mu^+$	L	$< 8.6 \times 10^{-8}$	CL=90%
Γ_{220}	$\pi^-e^+\mu^+$	L	$< 6.3 \times 10^{-7}$	CL=90%
Γ_{221}	K^-2e^+	L	$< 7.7 \times 10^{-7}$	CL=90%
Γ_{222}	$\pi^-\pi^0e^+e^+$		$< 2.9 \times 10^{-5}$	CL=90%
Γ_{223}	$K^-\pi^0e^+e^+$		$< 3.4 \times 10^{-5}$	CL=90%
Γ_{224}	$K_S^0\pi^-e^+e^+$		$< 1.3 \times 10^{-5}$	CL=90%
Γ_{225}	$K_S^0K^-e^+e^+$		$< 2.9 \times 10^{-5}$	CL=90%
Γ_{226}	$\phi\pi^-e^+e^+$		$< 6.9 \times 10^{-5}$	CL=90%
Γ_{227}	$\phi K^-e^+e^+$		$< 9.9 \times 10^{-5}$	CL=90%
Γ_{228}	$K^-2\mu^+$	L	$< 2.6 \times 10^{-8}$	CL=90%
Γ_{229}	$K^-e^+\mu^+$	L	$< 2.6 \times 10^{-7}$	CL=90%
Γ_{230}	$K^*(892)^-2\mu^+$	L	$< 1.4 \times 10^{-3}$	CL=90%

[a] This is the purely e^+ semileptonic branching fraction: the e^+ fraction from τ^+ decays has been subtracted off. The sum of our (non-τ) e^+ exclusive fractions — an $e^+\nu_e$ with an η, η', ϕ, K^0, or K^{*0} — is 5.99 ± 0.31 %.

[b] This fraction includes η from η' decays.

[c] The sum of our exclusive η' fractions — $\eta' e^+\nu_e$, $\eta'\mu^+\nu_\mu$, $\eta'\pi^+$, $\eta'\rho^+$, and $\eta' K^+$ — is 11.8 ± 1.6%.

[d] This branching fraction includes all the decay modes of the final-state resonance.

[e] A test for $u\overline{u}$ or $d\overline{d}$ content in the D_s^+. Neither Cabibbo-favored nor Cabibbo-suppressed decays can contribute, and $\omega-\phi$ mixing is an unlikely explanation for any fraction above about 2×10^{-4}.

[f] The branching fraction for this mode may differ from the sum of the submodes that contribute to it, due to interference effects. See the relevant papers.

[g] We decouple the $D_s^+ \to \phi\pi^+$ branching fraction obtained from mass projections (and used to get some of the other branching fractions) from the $D_s^+ \to \phi\pi^+$, $\phi \to K^+K^-$ branching fraction obtained from the Dalitz-plot analysis of $D_s^+ \to K^+K^-\pi^+$. That is, the ratio of these two branching fractions is not exactly the $\phi \to K^+K^-$ branching fraction 0.491.

[h] This is the average of a model-independent and a K-matrix parametrization of the $\pi^+\pi^-$ S-wave and is a sum over several f_0 mesons.

[i] This mode is not a useful test for a ΔC=1 weak neutral current because both quarks must change flavor in this decay.

[j] This is *not* a test for the ΔC=1 weak neutral current, but leads to the $\pi^+\ell^+\ell^-$ final state.

FIT INFORMATION

An overall fit to 18 branching ratios uses 32 measurements to determine 12 parameters. The overall fit has a $\chi^2 = 12.1$ for 20 degrees of freedom.

The following *off-diagonal* array elements are the correlation coefficients $\langle \delta x_i \delta x_j \rangle / (\delta x_i \cdot \delta x_j)$, in percent, from the fit to the branching fractions, $x_i \equiv \Gamma_i/\Gamma_{total}$.

x_{52}	11									
x_{74}	−1	1								
x_{82}	1	2	2							
x_{89}	0	1	1	1						
x_{99}	1	1	0	1	0					
x_{115}	0	0	0	0	0	0				
x_{116}	2	2	−1	0	0	0	1			
x_{163}	0	0	0	0	0	0	0	0		
x_{165}	0	2	1	1	1	0	0	0	0	
x_{183}	0	0	0	0	0	0	0	0	26	0
x_{199}	8	72	1	2	0	1	0	1	0	1
	x_{44}	x_{52}	x_{74}	x_{82}	x_{89}	x_{99}	x_{115}	x_{116}	x_{163}	x_{165}

x_{199}	0
	x_{183}

D_s^+ BRANCHING RATIOS

A number of older, now obsolete results have been omitted. They may be found in earlier editions.

Inclusive modes

$\Gamma(e^+ \text{semileptonic})/\Gamma_{total}$ — Γ_1/Γ

This is the purely e^+ semileptonic branching fraction: the e^+ fraction from τ^+ decays has been subtracted off.

VALUE (%)	EVTS	DOCUMENT ID		TECN	COMMENT
6.33±0.15 OUR AVERAGE					
6.30±0.13±0.10	17k	[1,2] ABLIKIM	21AC	BES3	e^+e^- at 4.178–4.230 GeV
6.52±0.39±0.15	0.5k	[3] ASNER	10	CLEO	e^+e^- at 3774 MeV

[1] ABLIKIM 21AC finds that the ratio of the D_s^+ and D^0 semielectronic widths is 0.790 ± 0.016 ± 0.020.

[2] ABLIKIM 21AC reports a value of (6.30 ± 0.13 ± 0.09 ± 0.04) × 10^{-2}, where the last uncertainty is an external systematic from $B(D_s^+ \to \tau\nu)$. We have added the systematic uncertainties in quadrature.

[3] Using the D_s^+ and D^0 lifetimes, ASNER 10 finds that the ratio of the D_s^+ and D^0 semileptonic widths is 0.828 ± 0.051 ± 0.025.

$\Gamma(\pi^+ \text{anything})/\Gamma_{total}$ — Γ_2/Γ

Events with two π^+'s count twice, etc. But π^+'s from $K_S^0 \to \pi^+\pi^-$ are not included.

VALUE (%)	DOCUMENT ID		TECN	COMMENT
119.3±1.2±0.7	DOBBS	09	CLEO	e^+e^- at 4170 MeV

$\Gamma(\pi^- \text{anything})/\Gamma_{total}$ — Γ_3/Γ

Events with two π^-'s count twice, etc. But π^-'s from $K_S^0 \to \pi^+\pi^-$ are not included.

VALUE (%)	DOCUMENT ID		TECN	COMMENT
43.2±0.9±0.3	DOBBS	09	CLEO	e^+e^- at 4170 MeV

$\Gamma(\pi^0 \text{anything})/\Gamma_{total}$ — Γ_4/Γ

Events with two π^0's count twice, etc. But π^0's from $K_S^0 \to 2\pi^0$ are not included.

VALUE (%)	DOCUMENT ID		TECN	COMMENT
123.4±3.8±5.3	DOBBS	09	CLEO	e^+e^- at 4170 MeV

$\Gamma(K^- \text{anything})/\Gamma_{total}$ — Γ_5/Γ

VALUE (%)	DOCUMENT ID		TECN	COMMENT
18.7±0.5±0.2	DOBBS	09	CLEO	e^+e^- at 4170 MeV

$\Gamma(K^+ \text{anything})/\Gamma_{total}$ — Γ_6/Γ

VALUE (%)	DOCUMENT ID		TECN	COMMENT
28.9±0.6±0.3	DOBBS	09	CLEO	e^+e^- at 4170 MeV

$\Gamma(K_S^0 \text{anything})/\Gamma_{total}$ — Γ_7/Γ

VALUE (%)	DOCUMENT ID		TECN	COMMENT
19.0±1.0±0.4	DOBBS	09	CLEO	e^+e^- at 4170 MeV

$\Gamma(\eta \text{anything})/\Gamma_{total}$ — Γ_8/Γ

This ratio includes η particles from η' decays.

VALUE (%)	EVTS	DOCUMENT ID		TECN	COMMENT
29.9±2.2±1.7		DOBBS	09	CLEO	e^+e^- at 4170 MeV
• • • We do not use the following data for averages, fits, limits, etc. • • •					
23.5±3.1±2.0	674 ± 91	HUANG	06B	CLEO	See DOBBS 09

$\Gamma(\omega \text{anything})/\Gamma_{total}$ — Γ_9/Γ

VALUE (%)	DOCUMENT ID		TECN	COMMENT
6.1±1.4±0.3	DOBBS	09	CLEO	e^+e^- at 4170 MeV

$\Gamma(\eta' \text{anything})/\Gamma_{total}$ — Γ_{10}/Γ

VALUE (%)	EVTS	DOCUMENT ID		TECN	COMMENT
10.3±1.4 OUR AVERAGE Error includes scale factor of 1.1.					
8.8±1.8±0.5	68	ABLIKIM	15Z	BES3	482 pb^{-1}, 4009 MeV
11.7±1.7±0.7		DOBBS	09	CLEO	e^+e^- at 4170 MeV
• • • We do not use the following data for averages, fits, limits, etc. • • •					
8.7±1.9±0.8	68	HUANG	06B	CLEO	See DOBBS 09

$\Gamma(f_0(980) \text{ anything}, f_0 \to \pi^+\pi^-)/\Gamma_{total}$ — Γ_{11}/Γ

VALUE (%)	CL%	DOCUMENT ID		TECN	COMMENT
<1.3	90	DOBBS	09	CLEO	e^+e^- at 4170 MeV

$\Gamma(\phi \text{ anything})/\Gamma_{total}$ — Γ_{12}/Γ

VALUE (%)	EVTS	DOCUMENT ID		TECN	COMMENT
15.7±0.8±0.6		DOBBS	09	CLEO	e^+e^- at 4170 MeV
• • • We do not use the following data for averages, fits, limits, etc. • • •					
16.1±1.2±1.1	398 ± 27	HUANG	06B	CLEO	See DOBBS 09

$\Gamma(K^+K^- \text{anything})/\Gamma_{total}$ — Γ_{13}/Γ

VALUE (%)	DOCUMENT ID		TECN	COMMENT
15.8±0.6±0.3	DOBBS	09	CLEO	e^+e^- at 4170 MeV

$\Gamma(K_S^0 K^+ \text{anything})/\Gamma_{total}$ — Γ_{14}/Γ

VALUE (%)	DOCUMENT ID		TECN	COMMENT
5.8±0.5±0.1	DOBBS	09	CLEO	e^+e^- at 4170 MeV

$\Gamma(K_S^0 K^- \text{anything})/\Gamma_{total}$ — Γ_{15}/Γ

VALUE (%)	DOCUMENT ID		TECN	COMMENT
1.9±0.4±0.1	DOBBS	09	CLEO	e^+e^- at 4170 MeV

$\Gamma(K_S^0 K_L^0 \pi^+)/\Gamma_{total}$ — Γ_{46}/Γ

VALUE (%)	EVTS	DOCUMENT ID		TECN	COMMENT
1.86±0.06±0.03	2.35k	ABLIKIM	25BR	BES3	e^+e^- at 4.128–4.226 GeV

$\Gamma(\phi(1020)\pi^+, \phi \to K_L^0 K_S^0)/\Gamma(K_S^0 K_L^0 \pi^+)$ — Γ_{47}/Γ_{46}

VALUE (units 10^{-2})	EVTS	DOCUMENT ID		TECN	COMMENT
70.2±1.4±1.2	2.35k	ABLIKIM	25BR	BES3	e^+e^- at 4.128–4.226 GeV

$\Gamma(K_L^0 K^*(892)^+, K^{*+} \to K_S^0 \pi^+)/\Gamma(K_S^0 K_L^0 \pi^+)$ — Γ_{48}/Γ_{46}

VALUE (units 10^{-2})	EVTS	DOCUMENT ID		TECN	COMMENT
19.3±1.2±1.0	2.35k	ABLIKIM	25BR	BES3	e^+e^- at 4.128–4.226 GeV

$\Gamma(K_S^0 K^*(892)^+, K^{*+} \to K_L^0 \pi^+)/\Gamma(K_S^0 K_L^0 \pi^+)$ — Γ_{49}/Γ_{46}

VALUE (units 10^{-2})	EVTS	DOCUMENT ID		TECN	COMMENT
14.4±1.2±1.2	2.35k	ABLIKIM	25BR	BES3	e^+e^- at 4.128–4.226 GeV

$\Gamma(\phi(1680)\pi^+, \phi \to K_L^0 K_S^0)/\Gamma(K_S^0 K_L^0 \pi^+)$ — Γ_{50}/Γ_{46}

VALUE (units 10^{-2})	EVTS	DOCUMENT ID		TECN	COMMENT
3.3±0.9±0.7	2.35k	ABLIKIM	25BR	BES3	e^+e^- at 4.128–4.226 GeV

$\Gamma(2K_S^0 \text{ anything})/\Gamma_{total}$ — Γ_{16}/Γ

VALUE (%)	DOCUMENT ID		TECN	COMMENT
1.7±0.3±0.1	DOBBS	09	CLEO	e^+e^- at 4170 MeV

$\Gamma(2K^+ \text{anything})/\Gamma_{total}$ — Γ_{17}/Γ

VALUE (%)	CL%	DOCUMENT ID		TECN	COMMENT
<0.26	90	DOBBS	09	CLEO	e^+e^- at 4170 MeV

Int. J. Mod. Phys. A 2026.41. Downloaded from www.worldscientific.com
by CALIFORNIA @ BERKELEY on 09/16/26. Re-use and distribution is strictly not permitted, except for Open Access articles.

Int. J. Mod. Phys. A 2026.41. Downloaded from www.worldscientific.com by UNIVERSITY OF CALIFORNIA @ BERKELEY on 09/16/26. Re-use and distribution is strictly not permitted, except for Open Access articles.

$\Gamma(2K^- \text{anything})/\Gamma_{\text{total}}$ — Γ_{18}/Γ

VALUE (%)	CL%	DOCUMENT ID		TECN	COMMENT
<0.06	90	DOBBS	09	CLEO	e^+e^- at 4170 MeV

$\Gamma(2\pi^+\pi^- + \text{anything})/\Gamma_{\text{total}}$ — Γ_{19}/Γ

VALUE (%)	EVTS	DOCUMENT ID		TECN	COMMENT
32.81±0.35±0.63	25k	[1] ABLIKIM	23AV	BES3	e^+e^- at 4.178 GeV

[1] Charged pions from K^0_S meson decays are excluded from this measurement

Leptonic and semileptonic modes

See the related review(s):

Leptonic Decays of Charged Pseudoscalar Mesons

$\Gamma(e^+\nu_e)/\Gamma_{\text{total}}$ — Γ_{20}/Γ

VALUE	CL%	DOCUMENT ID		TECN	COMMENT
$<0.83\times10^{-4}$	90	[1] ZUPANC	13	BELL	e^+e^- at $\Upsilon(4S), \Upsilon(5S)$
• • • We do not use the following data for averages, fits, limits, etc. • • •					
$<2.3\ \times10^{-4}$	90	DEL-AMO-SA...	10J	BABR	e^+e^-, 10.58 GeV
$<1.2\ \times10^{-4}$	90	ALEXANDER	09	CLEO	e^+e^- at 4170 MeV
$<1.3\ \times10^{-4}$	90	PEDLAR	07A	CLEO	See ALEXANDER 09

[1] ZUPANC 13 also gives the limit as $<1.0\times10^{-4}$ at 95% CL.

$\Gamma(\mu^+\nu_\mu)/\Gamma_{\text{total}}$ — Γ_{21}/Γ

See the note on "Decay Constants of Charged Pseudoscalar Mesons."

VALUE (units 10^{-3})	EVTS	DOCUMENT ID		TECN	COMMENT
5.37 ±0.11 OUR AVERAGE					
5.47 ±0.26 ±0.16	0.5k	ABLIKIM	24CG	BES3	e^+e^- at 4.237–4.699 GeV
5.294±0.108±0.085	2.5k	ABLIKIM	23BR	BES3	e^+e^- at 4.128–4.226 GeV
5.17 ±0.75 ±0.21	69	[1] ABLIKIM	16O	BES3	e^+e^- at 4.009 GeV
5.31 ±0.28 ±0.20	490	[2] ZUPANC	13	BELL	e^+e^- at $\Upsilon(4S), \Upsilon(5S)$
6.02 ±0.38 ±0.34	270	[3] DEL-AMO-SA...	10J	BABR	e^+e^-, 10.58 GeV
5.65 ±0.45 ±0.17	230	ALEXANDER	09	CLEO	e^+e^- at 4.170 GeV
• • • We do not use the following data for averages, fits, limits, etc. • • •					
5.35 ±0.13 ±0.16	2.2k	[4] ABLIKIM	21BE	BES3	e^+e^-,4.178,4.226 GeV
5.49 ±0.16 ±0.15	1.1k	[4] ABLIKIM	19E	BES3	e^+e^- at 4.178 GeV
6.44 ±0.76 ±0.57	170	[5] WIDHALM	08	BELL	See ZUPANC 13
5.94 ±0.66 ±0.31	88	[6] PEDLAR	07A	CLEO	See ALEXANDER 09
6.8 ±1.1 ±1.8	553	[7] HEISTER	02I	ALEP	Z decays

[1] ABLIKIM 16O also reports that when constrained by the Standard Model ratio of $\Gamma(D_s^+ \to \tau^+\nu_\tau)/\Gamma(D_s^+ \to \mu^+\nu_\mu) = 9.76$, the branching fraction is found to be $(0.495 \pm 0.067 \pm 0.026)$%. The constrained value is used to obtain the decay constant, $f_{D_s^+} = (241.0 \pm 16.3 \pm 6.6)$ MeV.

[2] ZUPANC 13 uses both $\mu^+\nu$ and $\tau^+\nu$ events to get $f_{D_s} = (255.5 \pm 4.2 \pm 5.1)$ MeV.

[3] DEL-AMO-SANCHEZ 10J uses $\mu^+\nu_\mu$ and $\tau^+\nu_\tau$ events together to get $f_{D_s} = (258.6 \pm 6.4 \pm 7.5)$ MeV.

[4] Superseded by ABLIKIM 23BR.

[5] WIDHALM 08 gets $f_{D_s} = (275 \pm 16 \pm 12)$ MeV from the branching fraction.

[6] PEDLAR 07A also fits μ^+ and τ^+ events together and gets an effective $\mu^+\nu_\mu$ branching fraction of $(6.38 \pm 0.59 \pm 0.33)\times10^{-3}$

[7] This HEISTER 02I result is not actually an independent measurement of the absolute $\mu^+\nu_\mu$ branching fraction, but is in fact based on our $\phi\pi^+$ branching fraction of 3.6 ± 0.9%, so it cannot be included in our overall fit. HEISTER 02I combines its $D_s^+ \to \tau^+\nu_\tau$ and $\mu^+\nu_\mu$ branching fractions to get $f_{D_s} = (285 \pm 19 \pm 40)$ MeV.

$\Gamma(\mu^+\nu_\mu)/\Gamma(\phi\pi^+)$ — Γ_{21}/Γ_{53}

See the note on "Decay Constants of Charged Pseudoscalar Mesons" above.

VALUE	EVTS	DOCUMENT ID		TECN	COMMENT
• • • We do not use the following data for averages, fits, limits, etc. • • •					
0.143±0.018±0.006	489 ± 55	[1] AUBERT	07V	BABR	$e^+e^- \approx \Upsilon(4S)$
0.23 ±0.06 ±0.04	18	[2] ALEXANDROV	00	BEAT	π^- nucleus, 350 GeV
0.173±0.023±0.035	182	[3] CHADHA	98	CLE2	$e^+e^- \approx \Upsilon(4S)$
0.245±0.052±0.074	39	[4] ACOSTA	94	CLE2	See CHADHA 98

[1] AUBERT 07V gets $f_{D_s^+} = (283 \pm 17 \pm 16)$ MeV, using $\Gamma(D_s^+ \to \phi\pi^+)/\Gamma(\text{total}) = (4.71 \pm 0.46)$%.

[2] ALEXANDROV 00 uses $f_D^2/f_{D_s}^2 = 0.82 \pm 0.09$ from a lattice-gauge-theory calculation to get the relative numbers of $D^+ \to \mu^+\nu_\mu$ and $D_s^+ \to \mu^+\nu_\mu$ events. The present result leads to $f_{D_s} = (323 \pm 44 \pm 36)$ MeV.

[3] CHADHA 98 obtains $f_{D_s} = (280 \pm 19 \pm 28 \pm 34)$ MeV from this measurement, using $\Gamma(D_s^+ \to \phi\pi^+)/\Gamma(\text{total}) = 0.036 \pm 0.009$.

[4] ACOSTA 94 obtains $f_{D_s} = (344 \pm 37 \pm 52 \pm 42)$ MeV from this measurement, using $\Gamma(D_s^+ \to \phi\pi^+)/\Gamma(\text{total}) = 0.037 \pm 0.009$.

$\Gamma(\tau^+\nu_\tau)/\Gamma_{\text{total}}$ — Γ_{22}/Γ

See the note on "Decay Constants of Charged Pseudoscalar Mesons" above.

VALUE (%)	EVTS	DOCUMENT ID		TECN	COMMENT
5.39±0.09 OUR AVERAGE					
5.60±0.16±0.20	2.8k	[1] ABLIKIM	24CG	BES3	e^+e^- at 4.237–4.699 GeV
5.44±0.17±0.13	2.4k	[2] ABLIKIM	23BP	BES3	e^+e^- at 4.128–4.226 GeV
5.37±0.17±0.15	2.3k	[3] ABLIKIM	23BX	BES3	e^+e^- at 4.128–4.226 GeV
5.29±0.25±0.20	1.7k	[4] ABLIKIM	21AF	BES3	e^+e^- at 4.178, 4.226 GeV
5.27±0.10±0.12	4.9k	[5] ABLIKIM	21AZ	BES3	e^+e^- at 4.178, 4.226 GeV
3.28±1.83±0.37	33	[6] ABLIKIM	16O	BES3	e^+e^- at 4.009 GeV
5.70±0.21$^{+0.31}_{-0.30}$	2.2k	[7] ZUPANC	13	BELL	e^+e^- at $\Upsilon(4S), \Upsilon(5S)$
4.96±0.37±0.57	748	[8] DEL-AMO-SA...	10J	BABR	$e^-\overline{\nu}_e\nu_\tau, \mu^-\overline{\nu}_\mu\nu_\tau$
6.42±0.81±0.18	126	[9] ALEXANDER	09	CLEO	$\tau^+ \to \pi^+\overline{\nu}_\tau$
5.52±0.57±0.21	155	[9] NAIK	09A	CLEO	$\tau^+ \to \rho^+\overline{\nu}_\tau$
5.30±0.47±0.22	181	[9] ONYISI	09	CLEO	$\tau^+ \to e^+\nu_e\overline{\nu}_\tau$
• • • We do not use the following data for averages, fits, limits, etc. • • •					
5.21±0.25±0.17	950	[10] ABLIKIM	21BE	BES3	e^+e^- at 4.178, 4.226 GeV
6.17±0.71±0.34	102	[11] ECKLUND	08	CLEO	See ONYISI 09
8.0 ±1.3 ±0.4	47	[11] PEDLAR	07A	CLEO	See ALEXANDER 09
5.79±0.77±1.84	881	[12] HEISTER	02I	ALEP	Z decays
7.0 ±2.1 ±2.0	22	[13] ABBIENDI	01L	OPAL	$D_s^{*+} \to \gamma D_s^+$ from Z's
7.4 ±2.8 ±2.4	16	[14] ACCIARRI	97F	L3	$D_s^{*+} \to \gamma D_s^+$ from Z's

[1] ABLIKIM 24CG uses $\tau^+ \to (e^+\nu_e,\ \mu^+\nu_\nu,\ \pi^+,\ \rho^+)\overline{\nu}_\tau$ decays.

[2] ABLIKIM 23BP uses $\tau^+ \to \pi^+\overline{\nu}_\tau$ decays.

[3] ABLIKIM 23BX uses $\tau^+ \to \mu^+\nu_\mu\overline{\nu}_\tau$ decays.

[4] ABLIKIM 21AF uses $\tau^+ \to \pi^+\pi^0\overline{\nu}$ decays.

[5] ABLIKIM 21AZ uses $\tau^+ \to e^+\nu_e\overline{\nu}_\tau$ decays.

[6] ABLIKIM 16O also reports that when constrained by the Standard Model ratio of $\Gamma(D_s^+ \to \tau^+\nu_\tau)/\Gamma(D_s^+ \to \mu^+\nu_\mu) = 9.76$; the branching fraction is found to be $(4.83 \pm 0.65 \pm 0.26)$%.

[7] ZUPANC 13 uses both $\mu^+\nu$ and $\tau^+\nu$ events to get $f_{D_s} = (255.5 \pm 4.2 \pm 5.1)$ MeV.

[8] DEL-AMO-SANCHEZ 10J (with a small correction; see LEES 15D) uses $\mu^+\nu_\mu$ and $\tau^+\nu_\tau$ events together to get $f_{D_s} = (259.9 \pm 6.6 \pm 7.6)$ MeV.

[9] ALEXANDER 09, NAIK 09A, and ONYISI 09 use different τ decay modes and are independent. The three papers combined give $f_{D_s} = (259.7 \pm 7.8 \pm 3.4)$ MeV.

[10] ABLIKIM 21BE uses $\tau^+ \to \pi^+\overline{\nu}_\tau$ decays. When constrained by the Standard Model ratio of $\Gamma(D_s^+ \to \tau^+\nu_\tau)/\Gamma(D_s^+ \to \mu^+\nu_\mu) = 9.75$, the branching fraction is found to be $(5.22 \pm 0.10 \pm 0.14)$%. Superseded by ABLIKIM 23BP.

[11] ECKLUND 08 and PEDLAR 07A are independent: ECKLUND 08 uses $\tau^+ \to e^+\nu_e\overline{\nu}_\tau$ events, PEDLAR 07A uses $\tau^+ \to \pi^+\overline{\nu}_\tau$ events.

[12] HEISTER 02I combines its $D_s^+ \to \tau^+\nu_\tau$ and $\mu^+\nu_\mu$ branching fractions to get $f_{D_s} = (285 \pm 19 \pm 40)$ MeV.

[13] This ABBIENDI 01L value gives a decay constant f_{D_s} of $(286 \pm 44 \pm 41)$ MeV.

[14] The second ACCIARRI 97F error here combines in quadrature systematic (0.016) and normalization (0.018) errors. The branching fraction gives $f_{D_s} = (309 \pm 58 \pm 33 \pm 38)$ MeV.

$\Gamma(\tau^+\nu_\tau)/\Gamma(\mu^+\nu_\mu)$ — Γ_{22}/Γ_{21}

VALUE	EVTS	DOCUMENT ID		TECN	COMMENT
• • • We do not use the following data for averages, fits, limits, etc. • • •					
10.73±0.69$^{+0.56}_{-0.53}$	2.2k/492	[1] ZUPANC	13	BELL	e^+e^- at $\Upsilon(4S), \Upsilon(5S)$
11.0 ±1.4 ±0.6	102	[2] ECKLUND	08	CLEO	See ONYISI 09

[1] This ZUPANC 13 ratio is not independent of the separate $\tau\nu$ and $\mu\nu$ fractions listed above.

[2] This ECKLUND 08 value also uses results from PEDLAR 07A, and it is not independent of other results in these Listings. Combined with earlier CLEO results, the decay constant f_{D_s} is 274 ± 10 ± 5 MeV.

$\Gamma(\gamma e^+\nu_e)/\Gamma_{\text{total}}$ — Γ_{23}/Γ

VALUE	CL%	DOCUMENT ID		TECN	COMMENT
$<1.3\times10^{-4}$	90	ABLIKIM	19AD	BES3	for $E_\gamma > 10$ MeV

$\Gamma(K^+K^-e^+\nu_e)/\Gamma(K^+K^-\pi^+)$ — Γ_{24}/Γ_{52}

VALUE	DOCUMENT ID		TECN	COMMENT
• • • We do not use the following data for averages, fits, limits, etc. • • •				
0.558±0.007±0.016	[1] AUBERT	08AN	BABR	e^+e^- at $\Upsilon(4S)$

[1] This AUBERT 08AN ratio is only for the K^+K^- mass in the range 1.01–to–1.03 GeV in the numerator and 1.0095–to–1.0295 GeV in the denominator.

$\Gamma(K^0_S K^0_S e^+\nu_e)/\Gamma_{\text{total}}$ — Γ_{25}/Γ

VALUE	CL%	DOCUMENT ID		TECN	COMMENT
$<3.8\times10^{-4}$	90	ABLIKIM	22J	BES3	e^+e^- at 4.178-4.226 GeV

$\Gamma(\phi e^+\nu_e)/\Gamma_{\text{total}}$ — Γ_{26}/Γ

See the end of the D_s^+ Listings for measurements of $D_s^+ \to \phi e^+\nu_e$ form factors. Unseen decay modes of the ϕ are included.

VALUE (%)	EVTS	DOCUMENT ID		TECN	COMMENT
2.34±0.12 OUR AVERAGE	Error includes scale factor of 1.2.				
2.21±0.16±0.11	350	ABLIKIM	24CI	BES3	e^+e^- at 4237–4699 MeV
2.26±0.45±0.09	26	ABLIKIM	18A	BES3	e^+e^- at 4009 MeV
2.14±0.17±0.08	207	HIETALA	15		Uses CLEO data
2.61±0.03±0.17	25k	AUBERT	08AN	BABR	e^+e^- at $\Upsilon(4S)$
• • • We do not use the following data for averages, fits, limits, etc. • • •					
2.36±0.23±0.13	106	ECKLUND	09	CLEO	See HIETALA 15
2.29±0.37±0.11	45	YELTON	09	CLEO	See ECKLUND 09

Int. J. Mod. Phys. A 2026.41. Downloaded from www.worldscientific.com
by LIFORNIA @ BERKELEY on 09/16/26. Re-use and distribution is strictly not permitted, except for Open Access articles.

$\Gamma(\phi e^+\nu_e)/\Gamma(\phi\pi^+)$ — Γ_{26}/Γ_{53}

As noted in the comment column, most of these measurements use $\phi\mu^+\nu_\mu$ events in addition to or instead of $\phi e^+\nu_e$ events.

VALUE	EVTS	DOCUMENT ID	TECN	COMMENT
• • • We do not use the following data for averages, fits, limits, etc. • • •				
$0.540\pm0.033\pm0.048$	793	LINK 02J	FOCS	Uses $\phi\mu^+\nu_\mu$
$0.54\pm0.05\pm0.04$	367	BUTLER 94	CLE2	Uses $\phi e^+\nu_e$ and $\phi\mu^+\nu_\mu$
$0.58\pm0.17\pm0.07$	97	FRABETTI 93G	E687	Uses $\phi\mu^+\nu_\mu$
$0.57\pm0.15\pm0.15$	104	ALBRECHT 91	ARG	Uses $\phi e^+\nu_e$
$0.49\pm0.10\ ^{+0.10}_{-0.14}$	54	ALEXANDER 90B	CLEO	Uses $\phi e^+\nu_e$ and $\phi\mu^+\nu_\mu$

$\Gamma(\phi\mu^+\nu_\mu)/\Gamma_{total}$ — Γ_{29}/Γ

VALUE (%)	EVTS	DOCUMENT ID	TECN	COMMENT
2.24±0.11 OUR AVERAGE				
$2.25\pm0.09\pm0.07$	1.7k	ABLIKIM 23BZ	BES3	e^+e^- at 4.128-4.226 GeV
$1.94\pm0.53\pm0.09$	22	ABLIKIM 18A	BES3	e^+e^- at 4.009 GeV

$\Gamma(\eta e^+\nu_e)/\Gamma_{total}$ — Γ_{30}/Γ

Unseen decay modes of the η are included.

VALUE (%)	EVTS	DOCUMENT ID	TECN	COMMENT
2.27 ±0.06 OUR AVERAGE				
$2.35\pm0.11\pm0.10$	716	ABLIKIM 24CI	BES3	e^+e^- at 4237–4699 MeV
$2.255\pm0.039\pm0.051$	4k	ABLIKIM 23BO	BES3	e^+e^- at 4128–4226 MeV
$2.30\pm0.31\pm0.08$	63	ABLIKIM 16T	BES3	e^+e^- at 4009 MeV
$2.28\pm0.14\pm0.19$	358	[1] HIETALA 15		Uses CLEO data
• • • We do not use the following data for averages, fits, limits, etc. • • •				
$2.323\pm0.063\pm0.063$	1.8k	[2] ABLIKIM 19S	BES3	e^+e^- at 4178 MeV
$2.48\pm0.29\pm0.13$	82	YELTON 09	CLEO	See HIETALA 15

[1] Obtained by analyzing CLEO-c data but not authored by the CLEO Collaboration.
[2] Superseded by ABLIKIM 23BO

$\Gamma(\eta e^+\nu_e)/\Gamma(\phi e^+\nu_e)$ — Γ_{30}/Γ_{26}

Unseen decay modes of the η and the ϕ are included.

VALUE	EVTS	DOCUMENT ID	TECN	COMMENT
• • • We do not use the following data for averages, fits, limits, etc. • • •				
$1.24\pm0.12\pm0.15$	440	[1] BRANDENB... 95	CLE2	See HIETALA 15

[1] BRANDENBURG 95 uses both e^+ and μ^+ events and makes a phase-space adjustment to use the μ^+ events as e^+ events.

$\Gamma(\eta'(958)e^+\nu_e)/\Gamma_{total}$ — Γ_{31}/Γ

Unseen decay modes of the $\eta'(958)$ are included.

VALUE (%)	EVTS	DOCUMENT ID	TECN	COMMENT
0.81 ±0.04 OUR AVERAGE				
$0.82\pm0.09\pm0.04$	134	ABLIKIM 24CI	BES3	e^+e^- at 4237–4699 MeV
$0.810\pm0.038\pm0.024$	675	ABLIKIM 23BO	BES3	e^+e^- at 4128–4226 MeV
$0.93\pm0.30\pm0.05$	14	ABLIKIM 16T	BES3	e^+e^- at 4009 MeV
$0.68\pm0.15\pm0.06$	20	[1] HIETALA 15		Uses CLEO data
• • • We do not use the following data for averages, fits, limits, etc. • • •				
$0.824\pm0.073\pm0.027$	261	[2] ABLIKIM 19S	BES3	e^+e^- at 4178 MeV
$0.91\pm0.33\pm0.05$	7.5	YELTON 09	CLEO	See HIETALA 15

[1] Obtained by analyzing CLEO-c data but not authored by the CLEO Collaboration.
[2] Superseded by ABLIKIM 23BO

$\Gamma(\eta'(958)e^+\nu_e)/\Gamma(\phi e^+\nu_e)$ — Γ_{31}/Γ_{26}

Unseen decay modes of the resonances are included.

VALUE	EVTS	DOCUMENT ID	TECN	COMMENT
• • • We do not use the following data for averages, fits, limits, etc. • • •				
$0.43\pm0.11\pm0.07$	29	[1] BRANDENB... 95	CLE2	See HIETALA 15

[1] BRANDENBURG 95 uses both e^+ and μ^+ events and makes a phase-space adjustment to use the μ^+ events as e^+ events.

$\Gamma(\eta\mu^+\nu_\mu)/\Gamma_{total}$ — Γ_{32}/Γ

VALUE (%)	EVTS	DOCUMENT ID	TECN	COMMENT
2.24 ±0.07 OUR AVERAGE				
$2.235\pm0.051\pm0.052$	3.1k	ABLIKIM 24AQ	BES3	e^+e^-, 4.128–4.266 GeV
$2.42\pm0.46\pm0.11$	44	ABLIKIM 18A	BES3	e^+e^- at 4.009 GeV

$\Gamma(\eta'(958)\mu^+\nu_\mu)/\Gamma_{total}$ — Γ_{33}/Γ

VALUE (%)	EVTS	DOCUMENT ID	TECN	COMMENT
0.80 ±0.06 OUR AVERAGE				
$0.801\pm0.055\pm0.028$	390	ABLIKIM 24AQ	BES3	e^+e^-, 4.128–4.266 GeV
$1.06\pm0.54\pm0.07$	10	ABLIKIM 18A	BES3	e^+e^- at 4.009 GeV

$\Gamma(\omega e^+\nu_e)/\Gamma_{total}$ — Γ_{34}/Γ

A test for $u\overline{u}$ or $d\overline{d}$ content in the D_s^+. Neither Cabibbo-favored nor Cabibbo-suppressed decays can contribute, and $\omega-\phi$ mixing is an unlikely explanation for any fraction above about 2×10^{-4}.

VALUE (%)	CL%	DOCUMENT ID	TECN	COMMENT
<0.20	90	MARTIN 11	CLEO	e^+e^- at 4170 MeV

$\Gamma(K^0 e^+\nu_e)/\Gamma_{total}$ — Γ_{35}/Γ

VALUE (%)	EVTS	DOCUMENT ID	TECN	COMMENT
0.288±0.026 OUR AVERAGE		Error includes scale factor of 1.2.		
$0.298\pm0.023\pm0.012$	228	[1] ABLIKIM 24CH	BES3	e^+e^- at 4128–4226 MeV
$0.24\pm0.04\pm0.01$	51	ABLIKIM 24CI	BES3	e^+e^- at 4237–4699 MeV
$0.39\pm0.08\pm0.03$	42	HIETALA 15		Uses CLEO data
• • • We do not use the following data for averages, fits, limits, etc. • • •				
$0.325\pm0.038\pm0.016$	117	[1,2] ABLIKIM 19D	BES3	e^+e^- at 4178 MeV
$0.37\pm0.10\pm0.02$	14	YELTON 09	CLEO	See HIETALA 15

[1] K^0 reconstructed via $K^0\to K^0_S\to\pi^+\pi^-$ decays.
[2] Superseded by ABLIKIM 24CH.

$\Gamma(K_1(1270)^0 e^+\nu_e)/\Gamma_{total}$ — Γ_{27}/Γ

VALUE	CL%	DOCUMENT ID	TECN	COMMENT
<4.1 × 10^{-4}	90	[1] ABLIKIM 23BS	BES3	e^+e^- at 4.128–4.226 GeV

[1] ABLIKIM 23BS uses $K_1(1270)^0\to K^-\pi^+\pi^0$ decays.

$\Gamma(K^*(892)^0 e^+\nu_e)/\Gamma_{total}$ — Γ_{36}/Γ

Unseen decay modes of the $K^*(892)^0$ are included.

VALUE (%)	EVTS	DOCUMENT ID	TECN	COMMENT
0.205±0.020 OUR AVERAGE				
$0.19\pm0.03\pm0.01$	65	ABLIKIM 24CI	BES3	e^+e^- at 4237–4699 MeV
$0.237\pm0.026\pm0.020$	155	ABLIKIM 19D	BES3	e^+e^- at 4178 MeV
$0.18\pm0.04\pm0.01$	32	[1] HIETALA 15		e^+e^- at 4170 MeV
• • • We do not use the following data for averages, fits, limits, etc. • • •				
$0.18\pm0.07\pm0.01$	7.5	YELTON 09	CLEO	See HIETALA 15

[1] Uses CLEO data, but not authored by the CLEO collaboration

$\Gamma(f_0(500)e^+\nu_e,\ f_0\to\pi^0\pi^0)/\Gamma_{total}$ — Γ_{37}/Γ

VALUE	CL%	DOCUMENT ID	TECN	COMMENT
<7.3 × 10^{-4}	90	ABLIKIM 22J	BES3	e^+e^- at 4.178-4.226 GeV

$\Gamma(f_0(500)e^+\nu_e,\ f_0\to\pi^+\pi^-)/\Gamma_{total}$ — Γ_{38}/Γ

VALUE	CL%	DOCUMENT ID	TECN	COMMENT
<3.3 × 10^{-4}	90	ABLIKIM 24AT	BES3	e^+e^- at 4.128–4.226 GeV

$\Gamma(f_0(980)e^+\nu_e,\ f_0\to\pi^0\pi^0)/\Gamma_{total}$ — Γ_{39}/Γ

VALUE (units 10^{-4})	EVTS	DOCUMENT ID	TECN	COMMENT
7.9±1.4±0.4	55	[1] ABLIKIM 22J	BES3	e^+e^- at 4.178-4.226 GeV

[1] Assuming $B(f_0\to\pi^0\pi^0)=1/3$ via the isospin limit, this result implies $B(D_s^+\to f_0(980)e^+\nu_e)=(2.4\pm0.4)\times10^{-3}$.

$\Gamma(f_0(980)e^+\nu_e,\ f_0\to\pi^+\pi^-)/\Gamma_{total}$ — Γ_{40}/Γ

VALUE (units 10^{-3})	EVTS	DOCUMENT ID	TECN	COMMENT
1.64±0.13 OUR AVERAGE				
$1.72\pm0.13\pm0.10$	0.4k	ABLIKIM 24AT	BES3	e^+e^- at 4128–4226 MeV
$1.5\pm0.2\pm0.1$	91	ABLIKIM 24CI	BES3	e^+e^- at 4237–4699 MeV
• • • We do not use the following data for averages, fits, limits, etc. • • •				
$1.3\pm0.3\pm0.1$	42	[1] HIETALA 15		Uses CLEO data
$2.0\pm0.3\pm0.1$	44	ECKLUND 09	CLEO	See HIETALA 15
$1.3\pm0.4\pm0.1$	13	YELTON 09	CLEO	See ECKLUND 09

[1] HIETALA 15 uses a tighter cut on the reconstructed $\pi^+\pi^-$ mass (±60 MeV around the f^0) than ECKLUND 09. It finds that applying the same tight cut to both analyses gives consistent results.

$\Gamma(f_0(980)\mu^+\nu_\mu,\ f_0\to K^+K^-)/\Gamma_{total}$ — Γ_{41}/Γ

VALUE	CL%	DOCUMENT ID	TECN	COMMENT
<5.45 × 10^{-4}	90	[1] ABLIKIM 23BZ	BES3	e^+e^- at 4.128-4.226 GeV

[1] Partial wave analysis of 939 $D_s^+\to K^+K^-\mu^+\nu_\mu$ events, assuming K^+K^- S-wave is 100% $f_0(980)$.

$\Gamma(a_0(980)^0 e^+\nu_e,\ a_0^0\to\pi^0\eta)/\Gamma_{total}$ — Γ_{42}/Γ

VALUE	CL%	DOCUMENT ID	TECN	COMMENT
<1.2 × 10^{-4}	90	ABLIKIM 21Y	BES3	e^+e^- at 4.178–4.226 GeV

$\Gamma(\pi^0 e^+\nu_e)/\Gamma_{total}$ — Γ_{43}/Γ

VALUE	CL%	DOCUMENT ID	TECN	COMMENT
<6.4 × 10^{-5}	90	ABLIKIM 22BH	BES3	6.32 fb^{-1} of e^+e^- at 4.178–4.226 GeV

$\Gamma(b_1(1235)^0 e^+\nu_e,\ b_1^0\to\omega\pi^0)/\Gamma_{total}$ — Γ_{28}/Γ

VALUE	CL%	DOCUMENT ID	TECN	COMMENT
<6.4 × 10^{-4}	90	ABLIKIM 23BS	BES3	e^+e^- at 4.128–4.226 GeV

Hadronic modes with a $K\overline{K}$ pair

$\Gamma(K^+K^0_S)/\Gamma_{total}$ — Γ_{44}/Γ

VALUE (%)	EVTS	DOCUMENT ID	TECN	COMMENT
1.500±0.014 OUR FIT				
1.503±0.015 OUR AVERAGE				
$1.502\pm0.012\pm0.009$		ABLIKIM 24BD	BES3	e^+e^-, 4.128–4.226 GeV
$1.52\pm0.05\pm0.03$		ONYISI 13	CLEO	e^+e^- at 4.17 GeV
• • • We do not use the following data for averages, fits, limits, etc. • • •				
$1.425\pm0.038\pm0.031$	1.8k	[1] ABLIKIM 19AM	BES3	e^+e^- at 4178 MeV
$1.49\pm0.07\pm0.05$		[2] ALEXANDER 08	CLEO	See ONYISI 13

Int. J. Mod. Phys. A 2026.41. Downloaded from www.worldscientific.com
by UNIVERSITY OF CALIFORNIA @ BERKELEY on 09/16/26. Re-use and distribution is strictly not permitted, except for Open Access articles.

[1] Superseded by ABLIKIM 24BD.
[2] ALEXANDER 08 uses single- and double-tagged events in an overall fit.

$\Gamma(K^+ K_S^0)/\Gamma(K^+ K^- \pi^+)$ — Γ_{44}/Γ_{52}

VALUE (units 10^{-2})	EVTS	DOCUMENT ID		TECN	COMMENT
27.55±0.18±0.50	40k	ABLIKIM	20R	BES3	e^+e^-, 4178 ∼ 4226 MeV

$\Gamma(K^+ K_L^0)/\Gamma_{total}$ — Γ_{45}/Γ

VALUE (%)	EVTS	DOCUMENT ID		TECN	COMMENT
1.485±0.039±0.046	2.3k	ABLIKIM	19AM	BES3	e^+e^- at 4178 MeV

$\Gamma(K^+ \overline{K}^0)/\Gamma_{total}$ — Γ_{51}/Γ

VALUE (%)	EVTS	DOCUMENT ID		TECN	COMMENT
2.95±0.11±0.09	2.0k	[1] ZUPANC	13	BELL	e^+e^- at $\Upsilon(4S), \Upsilon(5S)$

[1] ZUPANC 13 finds the $\overline{K}^0$ from its missing-mass squared, not from $K_S^0 \to \pi^+\pi^-$. The DCS ($D_s^+ \to K^+K^0$) contribution to this fraction is estimated to be an order of magnitude below the statistical uncertainty.

$\Gamma(K^+ K^- \pi^+)/\Gamma_{total}$ — Γ_{52}/Γ

VALUE (%)	EVTS	DOCUMENT ID		TECN	COMMENT
5.45±0.08 OUR FIT Error includes scale factor of 1.3.					
5.48±0.08 OUR AVERAGE Error includes scale factor of 1.1.					
5.49±0.04±0.07		ABLIKIM	24BD	BES3	e^+e^-, 4.128–4.226 GeV
5.55±0.14±0.13		ONYISI	13	CLEO	e^+e^- at 4.17 GeV
5.06±0.15±0.21	4.1k	ZUPANC	13	BELL	e^+e^- at $\Upsilon(4S), \Upsilon(5S)$
5.78±0.20±0.30		DEL-AMO-SA...	10J	BABR	e^+e^-, 10.58 GeV
• • • We do not use the following data for averages, fits, limits, etc. • • •					
5.47±0.08±0.13	5.1k	[1] ABLIKIM	21AE	BES3	e^+e^- at 4.178 GeV
5.50±0.23±0.16		[2] ALEXANDER	08	CLEO	See ONYISI 13

[1] Superseded by ABLIKIM 24BD.
[2] ALEXANDER 08 uses single- and double-tagged events in an overall fit.

$\Gamma(\phi\pi^+)/\Gamma_{total}$ — Γ_{53}/Γ

The results here are model-independent. For earlier, model-dependent results, see our PDG 06 edition. We decouple the $D_s^+ \to \phi\pi^+$ branching fraction obtained from mass projections (and used to get some of the other branching fractions) from the $D_s^+ \to \phi\pi^+, \phi \to K^+K^-$ branching fraction obtained from the Dalitz-plot analysis of $D_s^+ \to K^+K^-\pi^+$. That is, the ratio of these two branching fractions is not exactly the $\phi \to K^+K^-$ branching fraction 0.491.

VALUE (%)	EVTS	DOCUMENT ID		TECN	COMMENT
4.5 ±0.4 OUR AVERAGE					
4.62±0.36±0.51		[1] AUBERT	06N	BABR	e^+e^- at $\Upsilon(4S)$
4.81±0.52±0.38	212 ± 19	[2] AUBERT	05V	BABR	$e^+e^- \approx \Upsilon(4S)$
3.59±0.77±0.48		[3] ARTUSO	96	CLE2	e^+e^- at $\Upsilon(4S)$
• • • We do not use the following data for averages, fits, limits, etc. • • •					
$3.9\ ^{+5.1}_{-1.9}\ ^{+1.8}_{-1.1}$		[4] BAI	95C	BES	e^+e^- 4.03 GeV

[1] This AUBERT 06N measurement uses $\overline{B}^0 \to D_s^{(*)-} D^{(*)+}$ and $B^- \to D_s^{(*)-} D^{(*)0}$ decays, including some from other papers. However, the result is independent of AUBERT 05V.
[2] AUBERT 05V uses the ratio of $B^0 \to D^{*-} D_s^{*+}$ events seen in two different ways, in both of which the $D^{*-} \to \overline{D}^0\pi^-$ decay is fully reconstructed: (1) The $D_s^{*+} \to D_s^+\gamma$, $D_s^+ \to \phi\pi^+$ decay is fully reconstructed. (2) The number of events in the D_s^+ peak in the missing mass spectrum against the $D^{*-}\gamma$ is measured.
[3] ARTUSO 96 uses partially reconstructed $\overline{B}^0 \to D^{*+} D_s^{*-}$ decays to get a model-independent value for $\Gamma(D_s^- \to \phi\pi^-)/\Gamma(D^0 \to K^-\pi^+)$ of 0.92 ± 0.20 ± 0.11.
[4] BAI 95C uses $e^+e^- \to D_s^+ D_s^-$ events in which one or both of the $D_s^\pm$ are observed to obtain the first model-independent measurement of the $D_s^+ \to \phi\pi^+$ branching fraction, without assumptions about $\sigma(D_s^\pm)$. However, with only two "doubly-tagged" events, the statistical error is very large.

$\Gamma(\phi\pi^+, \phi \to K^+K^-)/\Gamma(K^+K^-\pi^+)$ — Γ_{54}/Γ_{52}

This is the "fit fraction" from the Dalitz-plot analysis. We decouple the $D_s^+ \to \phi\pi^+$ branching fraction obtained from mass projections (and used to get some of the other branching fractions) from the $D_s^+ \to \phi\pi^+, \phi \to K^+K^-$ branching fraction obtained from the Dalitz-plot analysis of $D_s^+ \to K^+K^-\pi^+$. That is, the ratio of these two branching fractions is not exactly the $\phi \to K^+K^-$ branching fraction 0.491.

VALUE (units 10^{-2})	EVTS	DOCUMENT ID		TECN	COMMENT
41.2±0.7 OUR AVERAGE					
40.5±0.7±0.9	18.6k	ABLIKIM	21AE	BES3	e^+e^- at 4.178 GeV
41.4±0.8±0.5		DEL-AMO-SA...	11G	BABR	Dalitz fit, 96k evts
42.2±1.6±0.3		MITCHELL	09A	CLEO	Dalitz fit, 12k evts
• • • We do not use the following data for averages, fits, limits, etc. • • •					
39.6±3.3±4.7		FRABETTI	95B	E687	Dalitz fit, 701 evts

$\Gamma(K^+\overline{K}^*(892)^0)/\Gamma(K^*(892)^+\overline{K}^0)$ — Γ_{55}/Γ_{72}

VALUE	DOCUMENT ID		TECN	COMMENT
$\mathbf{2.35^{+0.42}_{-0.23}\pm0.10}$	ABLIKIM	22AH	BES3	Dalitz plot fit to 990 $D_s^\pm \to K^\pm K_S \pi^0$ evts

$\Gamma(K^+\overline{K}^*(892)^0, \overline{K}^{*0} \to K^-\pi^+)/\Gamma(K^+K^-\pi^+)$ — Γ_{56}/Γ_{52}

This is the "fit fraction" from the Dalitz-plot analysis.

VALUE (units 10^{-2})	EVTS	DOCUMENT ID		TECN	COMMENT
47.9±0.6 OUR AVERAGE					
48.3±0.9±0.6	18.6k	ABLIKIM	21AE	BES3	e^+e^- at 4.178 GeV
47.9±0.5±0.5		DEL-AMO-SA...	11G	BABR	Dalitz fit, 96k evts
47.4±1.5±0.4		MITCHELL	09A	CLEO	Dalitz fit, 12k evts
• • • We do not use the following data for averages, fits, limits, etc. • • •					
47.8±4.6±4.0		FRABETTI	95B	E687	Dalitz fit, 701 evts

$\Gamma(K^+\overline{K}^*(892)^0, \overline{K}^{*0} \to K_S^0\pi^0)/\Gamma(K^+K_S^0\pi^0)$ — Γ_{57}/Γ_{65}

VALUE (units 10^{-2})	DOCUMENT ID		TECN	COMMENT
32.7±2.2±1.9	ABLIKIM	22AH	BES3	Dalitz plot fit, 990 evts

$\Gamma(f_0(980)\pi^+, f_0 \to K^+K^-)/\Gamma(K^+K^-\pi^+)$ — Γ_{58}/Γ_{52}

This is the "fit fraction" from the Dalitz-plot analysis. This is likely a superposition of $D_s^+ \to f_0(980)\pi$ and $D_s^+ \to a_0(980)\pi$ which are indistinguishable in such an analysis.

VALUE (units 10^{-2})	EVTS	DOCUMENT ID		TECN	COMMENT
20.6±3.5 OUR AVERAGE Error includes scale factor of 2.5. See the ideogram below.					
19.3±1.7±2.0	18.6k	ABLIKIM	21AE	BES3	e^+e^- at 4.178 GeV
16.4±0.7±2.0		DEL-AMO-SA...	11G	BABR	Dalitz fit, 96k evts
28.2±1.9±1.8		MITCHELL	09A	CLEO	Dalitz fit, 12k evts
• • • We do not use the following data for averages, fits, limits, etc. • • •					
11.0±3.5±2.6		FRABETTI	95B	E687	Dalitz fit, 701 evts

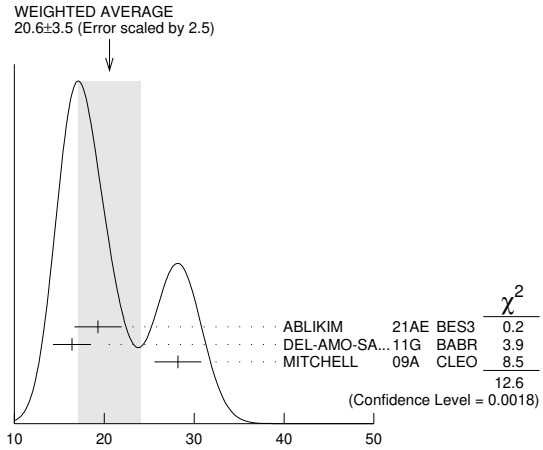

$\Gamma(f_0(980)\pi^+, f_0 \to K^+K^-)/\Gamma(K^+K^-\pi^+)$ (units 10^{-2})

$\Gamma(f_0(1370)\pi^+, f_0 \to K^+K^-)/\Gamma(K^+K^-\pi^+)$ — Γ_{59}/Γ_{52}

This is the "fit fraction" from the Dalitz-plot analysis.

VALUE (units 10^{-2})	EVTS	DOCUMENT ID		TECN	COMMENT
1.3±0.5 OUR AVERAGE Error includes scale factor of 2.8. See the ideogram below.					
1.2±0.4±0.2	18.6k	ABLIKIM	21AE	BES3	e^+e^- at 4.178 GeV
1.1±0.1±0.2		DEL-AMO-SA...	11G	BABR	Dalitz fit, 96k evts
4.3±0.6±0.5		MITCHELL	09A	CLEO	Dalitz fit, 12k evts

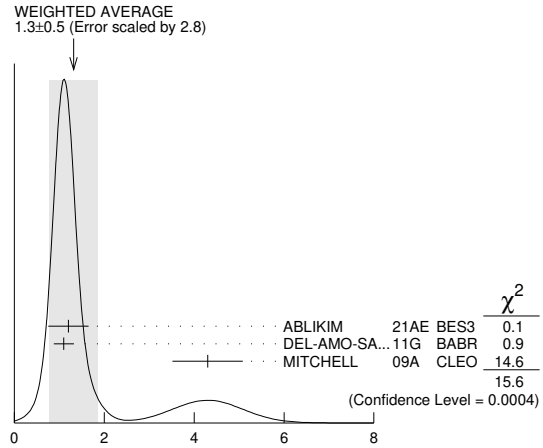

$\Gamma(f_0(1370)\pi^+, f_0 \to K^+K^-)/\Gamma(K^+K^-\pi^+)$ (units 10^{-2})

Int. J. Mod. Phys. A 2026.41. Downloaded from www.worldscientific.com
by CALIFORNIA @ BERKELEY on 09/16/26. Re-use and distribution is strictly not permitted, except for Open Access articles.

$\Gamma(f_0(1710)\pi^+,\ f_0 \to K^+K^-)/\Gamma(K^+K^-\pi^+)$ — Γ_{60}/Γ_{52}

This is the "fit fraction" from the Dalitz-plot analysis. This is likely a superposition of $D_s^+ \to f_0(1710)\pi$ and $D_s^+ \to a_0(1710)\pi$ which are indistinguishable in such an analysis.

VALUE (units 10^{-2})	EVTS	DOCUMENT ID		TECN	COMMENT
1.3±0.5 OUR AVERAGE	Error includes scale factor of 3.8.				
1.9±0.4±0.6	18.6k	ABLIKIM	21AE	BES3	e^+e^- at 4.178 GeV
1.1±0.1±0.1		DEL-AMO-SA...	11G	BABR	Dalitz fit, 96k evts
3.4±0.5±0.3		MITCHELL	09A	CLEO	Dalitz fit, 12k evts
• • • We do not use the following data for averages, fits, limits, etc. • • •					
3.4±2.3±3.5		FRABETTI	95B	E687	Dalitz fit, 701 evts

$\Gamma(a_0(980)^+\pi^0,\ a_0^+ \to K^+K_S^0)/\Gamma(K^+K_S^0\pi^0)$ — Γ_{61}/Γ_{65}

VALUE (units 10^{-2})	DOCUMENT ID		TECN	COMMENT
7.7±1.7±1.8	ABLIKIM	22AH	BES3	Dalitz plot fit, 990 evts

$\Gamma(a_0(1710)^+\pi^0,\ a_0^+ \to K^+K_S^0)/\Gamma(K^+K_S^0\pi^0)$ — Γ_{62}/Γ_{65}

VALUE (units 10^{-2})	DOCUMENT ID		TECN	COMMENT
23.6±3.4±2.0	[1] ABLIKIM	22AH	BES3	Dalitz plot fit, 990 evts

[1] ABLIKIM 22AH observe an a_0-like state with mass $m_{a_0} = 1.817 \pm 0.008 \pm 0.020$ GeV, and name the intermediate resonance $a_0(1817)$. We interpret this as the $a_0(1710)$ observed by LEES 21A.

$\Gamma(K^+\overline{K}_0^*(1430)^0,\ \overline{K}_0^* \to K^-\pi^+)/\Gamma(K^+K^-\pi^+)$ — Γ_{63}/Γ_{52}

This is the "fit fraction" from the Dalitz-plot analysis.

VALUE (units 10^{-2})	EVTS	DOCUMENT ID		TECN	COMMENT
3.3±0.5 OUR AVERAGE					
3.0±0.6±0.5	18.6k	ABLIKIM	21AE	BES3	e^+e^- at 4.178 GeV
2.4±0.3±1.0		DEL-AMO-SA...	11G	BABR	Dalitz fit, 96k evts
3.9±0.5±0.5		MITCHELL	09A	CLEO	Dalitz fit, 12k evts
• • • We do not use the following data for averages, fits, limits, etc. • • •					
9.3±3.2±3.2		FRABETTI	95B	E687	Dalitz fit, 701 evts

$\Gamma(K^+\overline{K}^*(1410)^0,\ \overline{K}_0^* \to K_S^0\pi^0)/\Gamma(K^+K_S^0\pi^0)$ — Γ_{64}/Γ_{65}

VALUE (units 10^{-2})	DOCUMENT ID		TECN	COMMENT
6.0±1.4±1.3	ABLIKIM	22AH	BES3	Dalitz plot fit, 990 evts

$\Gamma(K^+K_S^0\pi^0)/\Gamma_{total}$ — Γ_{65}/Γ

VALUE (%)	EVTS	DOCUMENT ID		TECN	COMMENT
1.471±0.028 OUR AVERAGE					
1.47 ±0.02 ±0.02		ABLIKIM	24BD	BES3	e^+e^-, 4.128–4.226 GeV
1.52 ±0.09 ±0.20		ONYISI	13	CLEO	e^+e^- at 4.17 GeV
• • • We do not use the following data for averages, fits, limits, etc. • • •					
1.46 ±0.06 ±0.05	990	[1] ABLIKIM	22AH	BES3	e^+e^- at 4.178–4.226 GeV

[1] Superseded by ABLIKIM 24BD.

$\Gamma(K^*(892)^+K_S^0,\ K^{*+} \to K^+\pi^0)/\Gamma(K^+K_S^0\pi^0)$ — Γ_{66}/Γ_{65}

VALUE (units 10^{-2})	DOCUMENT ID		TECN	COMMENT
13.9±1.7±1.3	ABLIKIM	22AH	BES3	Dalitz plot fit, 990 evts

$\Gamma(2K_S^0\pi^+)/\Gamma_{total}$ — Γ_{67}/Γ

VALUE (%)	EVTS	DOCUMENT ID		TECN	COMMENT
0.732±0.014 OUR AVERAGE					
0.73 ±0.01 ±0.01		ABLIKIM	24BD	BES3	e^+e^-, 4.128–4.226 GeV
0.77 ±0.05 ±0.03		ONYISI	13	CLEO	e^+e^- at 4.17 GeV
• • • We do not use the following data for averages, fits, limits, etc. • • •					
0.68 ±0.04 ±0.01	370	[1] ABLIKIM	22F	BES3	e^+e^-, 4.178–4.226 GeV

[1] Superseded by ABLIKIM 24BD.

$\Gamma(f_0(980)\pi^+,\ f_0 \to K_S^0K_S^0)/\Gamma_{total}$ — Γ_{68}/Γ

This is the "fit fraction" from the Dalitz-plot analysis. This is likely a superposition of $D_s^+ \to f_0(980)\pi$ and $D_s^+ \to a_0(980)\pi$ which are indistinguishable in such an analysis.

VALUE	CL%	DOCUMENT ID		TECN	COMMENT
<1.8 × 10^{-4}	90	[1] ABLIKIM	22F	BES3	Dalitz plot fit

[1] Based on isospin considerations, the authors interpret the suppression in the observed rate of this mode compared to $D_S^+ \to f_0(980)\pi^+$, $f_0 \to K^+K^-$ as likely due to the destructive interference between $a_0(980)$ and $f_0(980)$ in decays to $K_S^0K_S^0$.

$\Gamma(f_0(1710)\pi^+,\ f_0 \to K_S^0K_S^0)/\Gamma(2K_S^0\pi^+)$ — Γ_{69}/Γ_{67}

This is the "fit fraction" from the Dalitz-plot analysis. This is likely a superposition of $D_s^+ \to f_0(1710)\pi$ and $D_s^+ \to a_0(1700)\pi$ which are indistinguishable in such an analysis.

VALUE (units 10^{-2})	DOCUMENT ID		TECN	COMMENT
46.3±4.0±1.2	ABLIKIM	22F	BES3	Dalitz plot fit, 400 evts

$\Gamma(K^*(892)^+K_S^0,\ K^{*+} \to K_S^0\pi^+)/\Gamma(2K_S^0\pi^+)$ — Γ_{70}/Γ_{67}

VALUE (units 10^{-2})	DOCUMENT ID		TECN	COMMENT
43.5±3.9±0.5	ABLIKIM	22F	BES3	Dalitz plot fit, 400 evts

$\Gamma(K^*(892)^+\overline{K}^0)/\Gamma(\phi\pi^+)$ — Γ_{72}/Γ_{53}

Unseen decay modes of the resonances are included.

VALUE	DOCUMENT ID		TECN	COMMENT
1.20±0.21±0.13	CHEN	89	CLEO	e^+e^- 10 GeV

$\Gamma(\phi\rho^+)/\Gamma_{total}$ — Γ_{73}/Γ

VALUE (units 10^{-2})	EVTS	DOCUMENT ID		TECN	COMMENT
4.9 ±0.8 OUR AVERAGE	Error includes scale factor of 3.0.				
4.0 ±0.4 ±0.1	2k	[1,2] ABLIKIM	25F	BES3	e^+e^- at 4.128–4.226 GeV, $\phi \to \pi^+\pi^-\pi^0$
5.59±0.15±0.30	3k	[3] ABLIKIM	21U	BES3	e^+e^- at 4.178–4.226 GeV, $\phi \to K^+K^-$

[1] See $\Gamma(D_s^+ \to \phi\rho^+,\ \phi \to \pi^+\pi^-\pi^0)/\Gamma(D_s^+ \to 2\pi^+\pi^-2\pi^0)$, $\Gamma_{132}/\Gamma_{130}$. ABLIKIM 25F reports $(3.98 \pm 0.33^{+0.21}_{-0.19}) \times 10^{-2}$ from a measurement of $[\Gamma(D_s^+ \to \phi\rho^+)/\Gamma_{total}] \times [B(\phi(1020) \to \rho\pi + \pi^+\pi^-\pi^0)]$ assuming $B(\phi(1020) \to \rho\pi + \pi^+\pi^-\pi^0) = (14.9 \pm 0.4) \times 10^{-2}$, which we rescale to our best (shown rounded) value $B(\phi(1020) \to \rho\pi + \pi^+\pi^-\pi^0) = (14.7 \pm 0.4) \times 10^{-2}$. Our first error is their experiment's error and our second error is the systematic error from using our best (shown rounded) value.

[2] Amplitude analysis of $D_s^+ \to 2\pi^+\pi^-2\pi^0$ with 14 components.

[3] ABLIKIM 21U uses an amplitude analysis of $D_s^+ \to K^+K^-\pi^+\pi^0$ with 9 components.

$\Gamma(\phi\rho^+)/\Gamma(\phi\pi^+)$ — Γ_{73}/Γ_{53}

VALUE	EVTS	DOCUMENT ID		TECN	COMMENT
1.86±0.26$^{+0.29}_{-0.40}$	253	AVERY	92	CLE2	$e^+e^- \simeq$ 10.5 GeV

$\Gamma(K^+K^-\pi^+\pi^0)/\Gamma_{total}$ — Γ_{74}/Γ

VALUE (%)	EVTS	DOCUMENT ID		TECN	COMMENT
5.53±0.15 OUR FIT	Error includes scale factor of 1.3.				
5.53±0.12 OUR AVERAGE					
5.50±0.05±0.11		ABLIKIM	24BD	BES3	e^+e^-, 4.128–4.226 GeV
6.37±0.21±0.56		ONYISI	13	CLEO	e^+e^- at 4.17 GeV
• • • We do not use the following data for averages, fits, limits, etc. • • •					
5.42±0.10±0.17	3k	[1] ABLIKIM	21U	BES3	e^+e^-, 4.178–4.226 GeV
5.65±0.29±0.40		[2] ALEXANDER	08	CLEO	See ONYISI 13

[1] ABLIKIM 21U uses an amplitude analysis of $D_s^+ \to K^+K^-\pi^+\pi^0$ with 9 components. Superseded by ABLIKIM 24BD.

[2] ALEXANDER 08 uses single- and double-tagged events in an overall fit.

$\Gamma(\overline{K}_1(1270)^0K^+,\ \overline{K}_1(1270)^0 \to K^-\rho^+)/\Gamma_{total}$ — Γ_{75}/Γ

VALUE (units 10^{-2})	EVTS	DOCUMENT ID		TECN	COMMENT
0.57±0.05±0.04	3k	[1] ABLIKIM	21U	BES3	e^+e^- at 4.178–4.226 GeV

[1] ABLIKIM 21U uses an amplitude analysis of $D_s^+ \to K^+K^-\pi^+\pi^0$ with 9 components.

$\Gamma(\overline{K}_1(1270)^0K^+,\ \overline{K}_1(1270)^0 \to K^*(892)\pi)/\Gamma_{total}$ — Γ_{76}/Γ

VALUE (units 10^{-2})	EVTS	DOCUMENT ID		TECN	COMMENT
1.31±0.18±0.18	3k	[1,2] ABLIKIM	21U	BES3	e^+e^- at 4.178–4.226 GeV

[1] ABLIKIM 21U uses an amplitude analysis of $D_s^+ \to K^+K^-\pi^+\pi^0$ with 9 components.

[2] $\overline{K}_1(1270)^0 \to K^*(892)\pi$ denotes a sum over $\overline{K}(892)^0\pi^0$ and $K(892)^-\pi^+$ final states, which are assumed to have relative branching ratio 1/2, as per isospin.

$\Gamma(\overline{K}_1(1400)^0K^+,\ \overline{K}_1(1400)^0 \to K^*(892)\pi)/\Gamma_{total}$ — Γ_{77}/Γ

VALUE (units 10^{-2})	EVTS	DOCUMENT ID		TECN	COMMENT
1.98±0.27±0.32	3k	[1] ABLIKIM	21U	BES3	e^+e^- at 4.178–4.226 GeV

[1] $\overline{K}_1(1400)^0 \to K^*(892)\pi$ denotes a sum over $\overline{K}(892)^0\pi^0$ and $K(892)^-\pi^+$ final states, which are assumed to have relative branching ratio 1/2, as per isospin.

$\Gamma(a_0(980)^0\rho^+,\ a_0^0 \to K^+K^-)/\Gamma_{total}$ — Γ_{78}/Γ

VALUE (units 10^{-2})	EVTS	DOCUMENT ID		TECN	COMMENT
0.19±0.03±0.03	3k	[1] ABLIKIM	21U	BES3	e^+e^- at 4.178–4.226 GeV

[1] ABLIKIM 21U uses an amplitude analysis of $D_s^+ \to K^+K^-\pi^+\pi^0$ with 9 components.

$\Gamma(f_1(1420)^0\pi^+,\ f_1(1420)^0 \to K^*(892)^\mp K^\pm)/\Gamma_{total}$ — Γ_{79}/Γ

VALUE (units 10^{-2})	EVTS	DOCUMENT ID		TECN	COMMENT
0.39±0.06±0.03	3k	[1] ABLIKIM	21U	BES3	e^+e^- at 4.178–4.226 GeV

[1] ABLIKIM 21U uses an amplitude analysis of $D_s^+ \to K^+K^-\pi^+\pi^0$ with 9 components.

$\Gamma(f_1(1420)^0\pi^+,\ f_1^0 \to a_0(980)^0\pi^0,\ a_0^0 \to K^+K^-)/\Gamma_{total}$ — Γ_{80}/Γ

VALUE (units 10^{-2})	EVTS	DOCUMENT ID		TECN	COMMENT
0.04±0.01±0.01	3k	[1] ABLIKIM	21U	BES3	e^+e^- at 4.178–4.226 GeV

[1] ABLIKIM 21U uses an amplitude analysis of $D_s^+ \to K^+K^-\pi^+\pi^0$ with 9 components.

$\Gamma(\eta(1475)\pi^+,\ \eta \to a_0(980)^0\pi^0,\ a_0^0 \to K^+K^-)/\Gamma_{total}$ — Γ_{81}/Γ

VALUE (units 10^{-2})	EVTS	DOCUMENT ID		TECN	COMMENT
0.07±0.02±0.02	3k	[1] ABLIKIM	21U	BES3	e^+e^- at 4.178–4.226 GeV

[1] ABLIKIM 21U uses an amplitude analysis of $D_s^+ \to K^+K^-\pi^+\pi^0$ with 9 components.

Int. J. Mod. Phys. A 2026.41. Downloaded from www.worldscientific.com
by UNIVERSITY OF CALIFORNIA @ BERKELEY on 09/16/26. Re-use and distribution is strictly not permitted, except for Open Access articles.

$\Gamma(K_S^0 K^- 2\pi^+)/\Gamma_{total}$ — Γ_{82}/Γ

VALUE (%)	EVTS	DOCUMENT ID		TECN	COMMENT
1.569±0.028 OUR FIT					
1.569±0.032 OUR AVERAGE					Error includes scale factor of 1.2.
1.56 ±0.02 ±0.02		ABLIKIM	24BD	BES3	e^+e^-, 4.128–4.226 GeV
1.69 ±0.07 ±0.08		ONYISI	13	CLEO	e^+e^- at 4.17 GeV
• • • We do not use the following data for averages, fits, limits, etc. • • •					
1.46 ±0.05 ±0.05	1.3k	[1] ABLIKIM	21K	BES3	e^+e^-, 4.178–4.226 GeV
1.64 ±0.10 ±0.07		[2] ALEXANDER	08	CLEO	See ONYISI 13

[1] Superseded by ABLIKIM 24BD.
[2] ALEXANDER 08 uses single- and double-tagged events in an overall fit.

$\Gamma(K^+K^-K_S^0\pi^+)/\Gamma(K^+K_S^0\pi^+\pi^-)$ — Γ_{83}/Γ_{89}

VALUE (%)	EVTS	DOCUMENT ID		TECN	COMMENT
1.36±0.15±0.04	645	MOON	23	BELL	980 fb^{-1} at $\sim \Upsilon(4S)$

$\Gamma(K^*(892)^+\overline{K}^*(892)^0)/\Gamma_{total}$ — Γ_{84}/Γ

VALUE (units 10^{-2})	EVTS	DOCUMENT ID		TECN	COMMENT
5.64±0.23±0.27	3k	[1] ABLIKIM	21U	BES3	e^+e^- at 4.178–4.226 GeV

[1] ABLIKIM 21U uses an amplitude analysis of $D_s^+ \to K^+K^-\pi^+\pi^0$ with 9 components.

$\Gamma(K^*(892)^+\overline{K}^*(892)^0)/\Gamma(\phi\pi^+)$ — Γ_{84}/Γ_{53}

Unseen decay modes of the resonances are included.

VALUE	DOCUMENT ID		TECN	COMMENT
1.6±0.4±0.4	ALBRECHT	92B	ARG	$e^+e^- \simeq$ 10.4 GeV

$\Gamma(K^*(892)^+\overline{K}^*(892)^0)/\Gamma(K_S^0K^-2\pi^+)$ — Γ_{84}/Γ_{82}

VALUE (units 10^{-2})	EVTS	DOCUMENT ID		TECN	COMMENT
40.6±2.9±4.9	1.3k	[1,2] ABLIKIM	21K	BES3	e^+e^- at 4.178–4.226 GeV

[1] Predominantly S-wave, with a significant D-wave component.
[2] $D_s^+ \to K_S^0K^-2\pi^+$ amplitude analysis with 13 components.

$\Gamma(\eta(1475)K_S^0,\ \eta\to K^*(892)^0\pi^+,\ K^{*0}\to K^-\pi^+)/\Gamma(K_S^0K^-2\pi^+)$ — Γ_{85}/Γ_{82}

VALUE (units 10^{-2})	EVTS	DOCUMENT ID		TECN	COMMENT
2.2±0.6±0.2	1.3k	[1] ABLIKIM	21K	BES3	e^+e^- at 4.178–4.226 GeV

[1] $D_s^+ \to K_S^0K^-2\pi^+$ amplitude analysis with 13 components.

$\Gamma(\eta(1475)\pi^+,\ \eta\to\overline{K}^*(892)^+K^-,\ \overline{K}^{*+}\to K_S^0\pi^+)/\Gamma(K_S^0K^-2\pi^+)$ — Γ_{86}/Γ_{82}

VALUE (units 10^{-2})	EVTS	DOCUMENT ID		TECN	COMMENT
2.2±0.6±0.2	1.3k	[1] ABLIKIM	21K	BES3	e^+e^- at 4.178–4.226 GeV

[1] $D_s^+ \to K_S^0K^-2\pi^+$ amplitude analysis with 13 components.

$\Gamma(\eta(1475)\pi^+,\ \eta\to a_0(980)^-\pi^+,\ a_0^-\to K_S^0K^-)/\Gamma(K_S^0K^-2\pi^+)$ — Γ_{87}/Γ_{82}

VALUE (units 10^{-2})	EVTS	DOCUMENT ID		TECN	COMMENT
10.8±2.6±5.2	1.3k	[1] ABLIKIM	21K	BES3	e^+e^- at 4.178–4.226 GeV

[1] $D_s^+ \to K_S^0K^-2\pi^+$ amplitude analysis with 13 components.

$\Gamma(f_1(1285)\pi^+,\ f_1\to a_0(980)^-\pi^+,\ a_0^-\to K_S^0K^-)/\Gamma(K_S^0K^-2\pi^+)$ — Γ_{88}/Γ_{82}

VALUE (units 10^{-2})	EVTS	DOCUMENT ID		TECN	COMMENT
2.2±0.5±0.2	1.3k	[1] ABLIKIM	21K	BES3	e^+e^- at 4.178–4.226 GeV

[1] $D_s^+ \to K_S^0K^-2\pi^+$ amplitude analysis with 13 components.

$\Gamma(K^+K_S^0\pi^+\pi^-)/\Gamma_{total}$ — Γ_{89}/Γ

VALUE (%)	DOCUMENT ID		TECN	COMMENT
0.934±0.022 OUR FIT				
0.935±0.022 OUR AVERAGE				
0.93 ±0.02 ±0.01	ABLIKIM	24BD	BES3	e^+e^-, 4.128–4.226 GeV
1.03 ±0.06 ±0.08	ONYISI	13	CLEO	e^+e^- at 4.17 GeV

$\Gamma(K^+K_S^0\pi^+\pi^-)/\Gamma(K_S^0K^-2\pi^+)$ — Γ_{89}/Γ_{82}

VALUE	EVTS	DOCUMENT ID		TECN	COMMENT
0.595±0.017 OUR FIT					
0.586±0.052±0.043	476	LINK	01C	FOCS	γ A, $\overline{E}_\gamma \approx$ 180 GeV

$\Gamma(K^+K^-2\pi^+\pi^-)/\Gamma_{total}$ — Γ_{90}/Γ

VALUE (units 10^{-3})	EVTS	DOCUMENT ID		TECN	COMMENT
6.60±0.47±0.38	309	ABLIKIM	22AB	BES3	e^+e^- at 4.178–4.226 GeV

$\Gamma(K^+K^-2\pi^+\pi^-)/\Gamma(K^+K^-\pi^+)$ — Γ_{90}/Γ_{52}

VALUE	EVTS	DOCUMENT ID		TECN	COMMENT
0.160±0.027 OUR AVERAGE					
0.150±0.019±0.025	240	LINK	03D	FOCS	γ A, $\overline{E}_\gamma \approx$ 180 GeV
0.188±0.036±0.040	75	FRABETTI	97C	E687	γBe, $\overline{E}_\gamma \approx$ 200 GeV

$\Gamma(\phi 2\pi^+\pi^-)/\Gamma(\phi\pi^+)$ — Γ_{91}/Γ_{53}

VALUE	EVTS	DOCUMENT ID		TECN	COMMENT
0.269±0.027 OUR AVERAGE					
0.249±0.024±0.021	136	LINK	03D	FOCS	γ A, $\overline{E}_\gamma \approx$ 180 GeV
0.28 ±0.06 ±0.01	40	FRABETTI	97C	E687	γBe, $\overline{E}_\gamma \approx$ 200 GeV
0.58 ±0.21 ±0.10	21	FRABETTI	92	E687	γBe
0.42 ±0.13 ±0.07	19	ANJOS	88	E691	Photoproduction
1.11 ±0.37 ±0.28	62	ALBRECHT	85D	ARG	e^+e^- 10 GeV

$\Gamma(\phi\rho^0\pi^+,\ \phi\to K^+K^-)/\Gamma(K^+K^-2\pi^+\pi^-)$ — Γ_{92}/Γ_{90}

VALUE	DOCUMENT ID		TECN	COMMENT
0.75±0.06±0.04	LINK	03D	FOCS	γ A, $\overline{E}_\gamma \approx$ 180 GeV

$\Gamma(\phi a_1(1260)^+,\ \phi\to K^+K^-,\ a_1^+\to\rho^0\pi^+)/\Gamma(K^+K^-\pi^+)$ — Γ_{93}/Γ_{52}

VALUE	DOCUMENT ID		TECN	COMMENT
0.137±0.019±0.011	LINK	03D	FOCS	γ A, $\overline{E}_\gamma \approx$ 180 GeV

$\Gamma(\phi a_1(1260)^+,\ \phi\to K^+K^-,\ a_1^+\to\rho^0\pi^+)/\Gamma(K^+K^-2\pi^+\pi^-)$ — Γ_{93}/Γ_{90}

VALUE	EVTS	DOCUMENT ID		TECN	COMMENT
0.781±0.029±0.016	235	ABLIKIM	22AB	BES3	e^+e^- at 4.178–4.226 GeV

$\Gamma(\phi 2\pi^+\pi^-\text{ non-}\rho,\ \phi\to K^+K^-)/\Gamma(K^+K^-2\pi^+\pi^-)$ — Γ_{94}/Γ_{90}

VALUE	DOCUMENT ID		TECN	COMMENT
0.21±0.05±0.06	LINK	03D	FOCS	γ A, $\overline{E}_\gamma \approx$ 180 GeV

$\Gamma(K^+K^-\rho^0\pi^+\text{ non-}\phi)/\Gamma(K^+K^-2\pi^+\pi^-)$ — Γ_{95}/Γ_{90}

VALUE	CL%	DOCUMENT ID		TECN	COMMENT
<0.03	90	LINK	03D	FOCS	γ A, $\overline{E}_\gamma \approx$ 180 GeV

$\Gamma(K^+K^-2\pi^+\pi^-\text{ nonresonant})/\Gamma(K^+K^-2\pi^+\pi^-)$ — Γ_{96}/Γ_{90}

VALUE	EVTS	DOCUMENT ID		TECN	COMMENT
0.15 ±0.06 OUR AVERAGE					
0.218±0.029±0.08	235	ABLIKIM	22AB	BES3	e^+e^- at 4.178–4.226 GeV
0.10 ±0.06 ±0.05		LINK	03D	FOCS	γ A, $\overline{E}_\gamma \approx$ 180 GeV

$\Gamma(2K_S^0 2\pi^+\pi^-)/\Gamma(K_S^0K^-2\pi^+)$ — Γ_{97}/Γ_{82}

VALUE	EVTS	DOCUMENT ID		TECN	COMMENT
0.051±0.015±0.015	37 ± 10	LINK	04D	FOCS	γ A, $\overline{E}_\gamma \approx$ 180 GeV

Pionic modes

$\Gamma(\pi^+\pi^0)/\Gamma_{total}$ — Γ_{98}/Γ

VALUE	CL%	DOCUMENT ID		TECN	COMMENT
<1.2 × 10^{-4}	90	[1] GUAN	21	BELL	$e^+e^- \approx \Upsilon(4,5S)$

[1] Uses B($D_s^+ \to \pi^+\phi,\ \phi\to K^+K^-$) = (2.24 ± 0.08)%.

$\Gamma(\pi^+\pi^0)/\Gamma(K^+K_S^0)$ — Γ_{98}/Γ_{44}

VALUE (units 10^{-2})	CL%	DOCUMENT ID		TECN	COMMENT
<2.3	90	MENDEZ	10	CLEO	e^+e^- at 4170 MeV
• • • We do not use the following data for averages, fits, limits, etc. • • •					
<4.1	90	ADAMS	07A	CLEO	See MENDEZ 10

$\Gamma(2\pi^+\pi^-)/\Gamma_{total}$ — Γ_{99}/Γ

VALUE (%)	DOCUMENT ID		TECN	COMMENT
1.090±0.014 OUR FIT				
1.091±0.014 OUR AVERAGE				
1.09 ±0.01 ±0.01	ABLIKIM	24BD	BES3	e^+e^-, 4.128–4.226 GeV
1.11 ±0.04 ±0.04	ONYISI	13	CLEO	e^+e^- at 4.17 GeV
• • • We do not use the following data for averages, fits, limits, etc. • • •				
1.11 ±0.07 ±0.04	[1] ALEXANDER	08	CLEO	See ONYISI 13

[1] ALEXANDER 08 uses single- and double-tagged events in an overall fit.

$\Gamma(2\pi^+\pi^-)/\Gamma(K^+K^-\pi^+)$ — Γ_{99}/Γ_{52}

VALUE	EVTS	DOCUMENT ID		TECN	COMMENT
0.200±0.004 OUR FIT	Error includes scale factor of 1.2.				
0.199±0.004±0.009	≈ 10.5k	AUBERT	09O	BABR	$e^+e^- \approx$ 10.6 GeV
• • • We do not use the following data for averages, fits, limits, etc. • • •					
0.265±0.041±0.031	98	FRABETTI	97D	E687	γ Be ≈ 200 GeV

$\Gamma(\rho^0\pi^+)/\Gamma(2\pi^+\pi^-)$ — Γ_{100}/Γ_{99}

VALUE (units 10^{-2})	DOCUMENT ID		TECN	COMMENT
1.04 ±0.15 OUR AVERAGE				
1.038±0.054±0.097±0.11	[1] AAIJ	23AN	LHCB	Dalitz fit, 0.7M events
0.9 ±0.4 ±0.5	ABLIKIM	22BI	BES3	Dalitz fit, 11.1k events
1.8 ±0.5 ±1.0	AUBERT	09O	BABR	Dalitz fit, ≈ 10.5k evts
• • • We do not use the following data for averages, fits, limits, etc. • • •				
not seen	LINK	04	FOCS	Dalitz fit, 1475 ± 50 evts
5.8 ±2.3 ±3.7	AITALA	01A	E791	Dalitz fit, 848 evts

[1] The last error reflects the uncertainty on the amplitude model.

$\Gamma(\omega\pi^+,\ \omega\to\pi^+\pi^-)/\Gamma(2\pi^+\pi^-)$ — Γ_{101}/Γ_{99}

VALUE (units 10^{-3})	DOCUMENT ID		TECN	COMMENT
3.60±0.16±0.34±0.16	[1] AAIJ	23AN	LHCB	Dalitz fit, 0.7M events

[1] The last error reflects the uncertainty on the amplitude model.

Int. J. Mod. Phys. A 2026.41. Downloaded from www.worldscientific.com
by CALIFORNIA @ BERKELEY on 09/16/26. Re-use and distribution is strictly not permitted, except for Open Access articles.

$\Gamma(\pi^+(\pi^+\pi^-)_{S-\text{wave}})/\Gamma(2\pi^+\pi^-)$ — Γ_{102}/Γ_{99}

This is the "fit fraction" from the Dalitz-plot analysis. See also KLEMPT 08, which uses 568 $D_s^+ \to 3\pi$ decays (over 280 background events) from FNAL E791 to study various parametrizations of the decay amplitudes. The emphasis there is more on S-wave $\pi\pi$ decay products — 20 different solutions are given — than on D_s^+ fit fractions.

VALUE (units 10^{-2})	DOCUMENT ID		TECN	COMMENT
84.7 ±0.6 OUR AVERAGE				
84.97±0.14±0.30±0.63	[1,2] AAIJ	23AN	LHCB	Dalitz fit, 0.7M events
84.2 ±0.8 ±1.2	[2] ABLIKIM	22BI	BES3	Dalitz fit, 11.1k events
83.0 ±0.9 ±1.9	[2] AUBERT	09O	BABR	Dalitz fit, ≈ 10.5k evts
87.04±5.60±4.38	[3] LINK	04	FOCS	Dalitz fit, 1475 ± 50 evts

[1] The last error reflects the uncertainty due to the amplitude model.
[2] AAIJ 23AN, ABLIKIM 22BI, and AUBERT 09O give the amplitude and phase of the $\pi^+\pi^-$ S-wave in bins of $\pi^+\pi^-$ invariant-mass. (50 bins for AAIJ 23AN, 29 for ABLIKIM 22BI and AUBERT 09O.)
[3] LINK 04 borrows a K-matrix parametrization from ANISOVICH 03 of the full π-π S-wave isoscalar scattering amplitude to describe the $\pi^+\pi^-$ S-wave component of the $\pi^+\pi^+\pi^-$ state. The fit fraction given above is a sum over five f_0 mesons, the $f_0(980)$, $f_0(1300)$, $f_0(1200\text{–}1600)$, $f_0(1500)$, and $f_0(1750)$. See LINK 04 for details and discussion.

$\Gamma(f_0(980)\pi^+,\ f_0 \to \pi^+\pi^-)/\Gamma(2\pi^+\pi^-)$ — Γ_{103}/Γ_{99}

This is the "fit fraction" from the Dalitz-plot analysis. See above for the full $\pi^+(\pi^+\pi^-)_{S-wave}$ fit fraction.

VALUE	DOCUMENT ID		TECN	COMMENT
• • • We do not use the following data for averages, fits, limits, etc. • • •				
0.565±0.043±0.047	AITALA	01A	E791	Dalitz fit, 848 evts
1.074±0.140±0.043	FRABETTI	97D	E687	γ Be ≈ 200 GeV

$\Gamma(f_0(1370)\pi^+,\ f_0 \to \pi^+\pi^-)/\Gamma(2\pi^+\pi^-)$ — Γ_{104}/Γ_{99}

This is the "fit fraction" from the Dalitz-plot analysis. See above for the full $\pi^+(\pi^+\pi^-)_{S-wave}$ fit fraction.

VALUE	DOCUMENT ID		TECN	COMMENT
• • • We do not use the following data for averages, fits, limits, etc. • • •				
0.324±0.077±0.017	AITALA	01A	E791	Dalitz fit, 848 evts

$\Gamma(f_0(1500)\pi^+,\ f_0 \to \pi^+\pi^-)/\Gamma(2\pi^+\pi^-)$ — Γ_{105}/Γ_{99}

This is the "fit fraction" from the Dalitz-plot analysis. See above for the full $\pi^+(\pi^+\pi^-)_{S-wave}$ fit fraction.

VALUE	DOCUMENT ID		TECN	COMMENT
• • • We do not use the following data for averages, fits, limits, etc. • • •				
0.274±0.114±0.019	[1] FRABETTI	97D	E687	γ Be ≈ 200 GeV

[1] FRABETTI 97D calls this mode $S(1475)\,\pi^+$, but finds the mass and width of this $S(1475)$ to be in excellent agreement with those of the $f_0(1500)$.

$\Gamma(f_2(1270)\pi^+,\ f_2 \to \pi^+\pi^-)/\Gamma(2\pi^+\pi^-)$ — Γ_{106}/Γ_{99}

This is the "fit fraction" from the Dalitz-plot analysis.

VALUE (units 10^{-2})	DOCUMENT ID		TECN	COMMENT
13.0 ±0.9 OUR AVERAGE	Error includes scale factor of 1.9. See the ideogram below.			
13.69±0.14±0.22±0.49	[1] AAIJ	23AN	LHCB	Dalitz fit, 0.7M events
10.5 ±0.8 ±1.1	ABLIKIM	22BI	BES3	Dalitz fit, 11.1k events
10.1 ±1.5 ±1.1	AUBERT	09O	BABR	Dalitz fit, ≈ 10.5k evts
9.74±4.49±2.94	LINK	04	FOCS	Dalitz fit, 1475 ± 50 evts
• • • We do not use the following data for averages, fits, limits, etc. • • •				
19.7 ±3.3 ±0.6	AITALA	01A	E791	Dalitz fit, 848 evts
12.3 ±5.6 ±1.8	FRABETTI	97D	E687	γ Be ≈ 200 GeV

[1] The last error reflects the uncertainty on the amplitude model.

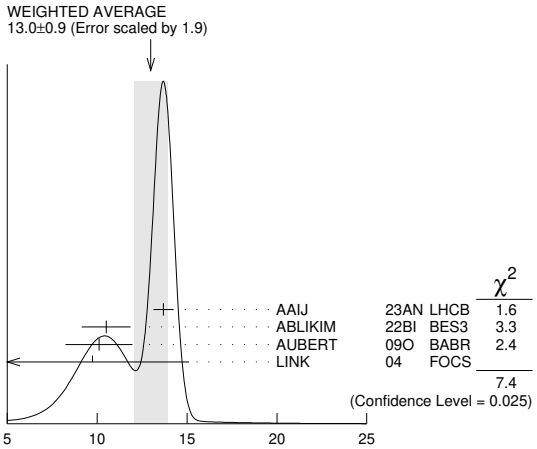

$\Gamma(f_2(1270)\pi^+,\ f_2 \to \pi^+\pi^-)/\Gamma(2\pi^+\pi^-)$ (units 10^{-2})

$\Gamma(f_2'(1525)^0\pi^+,\ f_2' \to \pi^+\pi^-)/\Gamma(2\pi^+\pi^-)$ — Γ_{107}/Γ_{99}

VALUE (units 10^{-4})	DOCUMENT ID		TECN	COMMENT
5.28±0.70±1.50±0.87	[1] AAIJ	23AN	LHCB	Dalitz fit, 0.7M events

[1] The last error reflects the uncertainty on the amplitude model.

$\Gamma(\rho(1450)^0\pi^+,\ \rho^0 \to \pi^+\pi^-)/\Gamma(2\pi^+\pi^-)$ — Γ_{108}/Γ_{99}

This is the "fit fraction" from the Dalitz-plot analysis.

VALUE (units 10^{-2})	DOCUMENT ID		TECN	COMMENT
1.7 ±0.6 OUR AVERAGE				
3.86±0.15±0.14±2.0	[1] AAIJ	23AN	LHCB	Dalitz fit, 0.7M events
1.3 ±0.4 ±0.5	ABLIKIM	22BI	BES3	Dalitz fit, 11.1k events
2.3 ±0.8 ±1.7	AUBERT	09O	BABR	Dalitz fit, ≈ 10.5k evts
6.56±3.43±4.40	LINK	04	FOCS	Dalitz fit, 1475 ± 50 evts
• • • We do not use the following data for averages, fits, limits, etc. • • •				
4.4 ±2.1 ±0.2	AITALA	01A	E791	Dalitz fit, 848 evts

[1] The last error reflects the uncertainty on the amplitude model.

$\Gamma(\rho(1700)^0\pi^+,\ \rho^0 \to \pi^+\pi^-)/\Gamma(2\pi^+\pi^-)$ — Γ_{109}/Γ_{99}

VALUE (units 10^{-3})	DOCUMENT ID		TECN	COMMENT
3.65±0.50±0.45±3.40	[1] AAIJ	23AN	LHCB	Dalitz fit, 0.7M events

[1] The last error reflects the uncertainty on the amplitude model.

$\Gamma(\pi^+2\pi^0)/\Gamma_{\text{total}}$ — Γ_{110}/Γ

VALUE (%)	EVTS	DOCUMENT ID		TECN	COMMENT
0.52±0.05 OUR AVERAGE		Error includes scale factor of 1.1.			
0.50±0.04±0.02	590	ABLIKIM	22Z	BES3	e^+e^- at 4.178–4.226 GeV
0.65±0.13±0.03	72 ± 16	NAIK	09A	CLEO	e^+e^- at 4170 MeV

$\Gamma(f_0(980)\pi^+,\ f_0 \to \pi^0\pi^0)/\Gamma(\pi^+2\pi^0)$ — $\Gamma_{111}/\Gamma_{110}$

This is a "fit fraction" from an amplitude analysis.

VALUE (units 10^{-2})	DOCUMENT ID		TECN	COMMENT
55.4±6.8±7.3	ABLIKIM	22Z	BES3	Dalitz plot fit, 440 evts

$\Gamma(f_0(1370)\pi^+,\ f_0 \to \pi^0\pi^0)/\Gamma(\pi^+2\pi^0)$ — $\Gamma_{112}/\Gamma_{110}$

This is a "fit fraction" from an amplitude analysis.

VALUE (units 10^{-2})	DOCUMENT ID		TECN	COMMENT
25.5±5.1±9.3	ABLIKIM	22Z	BES3	Dalitz plot fit, 440 evts

$\Gamma(f_2(1270)\pi^+,\ f_2 \to \pi^0\pi^0)/\Gamma(\pi^+2\pi^0)$ — $\Gamma_{113}/\Gamma_{110}$

This is a "fit fraction" from an amplitude analysis.

VALUE (units 10^{-2})	DOCUMENT ID		TECN	COMMENT
9.7±2.9±6.0	ABLIKIM	22Z	BES3	Dalitz plot fit, 440 evts

$\Gamma(2\pi^+\pi^-\pi^0)/\Gamma(\phi\pi^+)$ — Γ_{114}/Γ_{53}

VALUE	CL%	DOCUMENT ID		TECN	COMMENT
• • • We do not use the following data for averages, fits, limits, etc. • • •					
<3.3	90	ANJOS	89E	E691	Photoproduction

$\Gamma(\omega\pi^+)/\Gamma_{\text{total}}$ — Γ_{115}/Γ

Unseen decay modes of the ω are included.

VALUE (%)	EVTS	DOCUMENT ID		TECN	COMMENT
0.193±0.030 OUR FIT					
0.181±0.032 OUR AVERAGE					
0.177±0.032±0.013	65 ± 12	ABLIKIM	19AH	BES3	e^+e^- at 4.178 GeV
0.21 ±0.09 ±0.01	6 ± 2.4	GE	09A	CLEO	e^+e^- at 4170 MeV

$\Gamma(\omega\pi^+)/\Gamma(\eta\pi^+)$ — $\Gamma_{115}/\Gamma_{116}$

Unseen decay modes of the resonances are included.

VALUE	DOCUMENT ID		TECN	COMMENT
0.114±0.018 OUR FIT				
0.16 ±0.04 ±0.03	BALEST	97	CLE2	$e^+e^- \approx \Upsilon(4S)$

$\Gamma(\eta\pi^+)/\Gamma_{\text{total}}$ — Γ_{116}/Γ

Unseen decay modes of the η are included.

VALUE (%)	EVTS	DOCUMENT ID		TECN	COMMENT
1.686±0.027 OUR FIT					
1.689±0.027 OUR AVERAGE					
1.69 ±0.02 ±0.02		ABLIKIM	24BD	BES3	e^+e^-, 4.128–4.226 GeV
1.67 ±0.08 ±0.06		ONYISI	13	CLEO	e^+e^- at 4.17 GeV
• • • We do not use the following data for averages, fits, limits, etc. • • •					
1.56 ±0.09 ±0.02	0.4k	[1,2] ABLIKIM	25A	BES3	e^+e^-, 4.128–4.226 GeV
1.82 ±0.14 ±0.07	0.8k	ZUPANC	13	BELL	e^+e^- at $\Upsilon(4S), \Upsilon(5S)$
1.58 ±0.11 ±0.18		[3] ALEXANDER	08	CLEO	See ONYISI 13

[1] Subsumed by ABLIKIM 24BD which uses both $\eta \to \pi^+\pi^-\pi^0$ and $\eta \to 2\gamma$ modes.
[2] ABLIKIM 25A reports $[\Gamma(D_s^+ \to \eta\pi^+)/\Gamma_{\text{total}}] \times [B(\eta \to \pi^+\pi^-\pi^0)] = (3.58 \pm 0.21 \pm 0.06) \times 10^{-3}$ which we divide by our best (shown rounded) value $B(\eta \to \pi^+\pi^-\pi^0) = (23.02 \pm 0.25) \times 10^{-2}$. Our first error is their experiment's error and our second error is the systematic error from using our best (shown rounded) value.
[3] ALEXANDER 08 uses single- and double-tagged events in an overall fit.

$\Gamma(\eta\pi^+)/\Gamma(K^+K_S^0)$ — Γ_{116}/Γ_{44}

Unseen decay modes of the η are included.

VALUE	EVTS	DOCUMENT ID		TECN	COMMENT
1.124±0.021 OUR FIT					
• • • We do not use the following data for averages, fits, limits, etc. • • •					
1.236±0.043±0.063	2587 ± 89	MENDEZ	10	CLEO	See ONYISI 13

Int. J. Mod. Phys. A 2026.41. Downloaded from www.worldscientific.com
by UNIVERSITY OF CALIFORNIA @ BERKELEY on 09/16/26. Re-use and distribution is strictly not permitted, except for Open Access articles.

$\Gamma(\eta\pi^+)/\Gamma(K^+K^-\pi^+)$ — Γ_{116}/Γ_{52}

VALUE (units 10^{-2})	EVTS	DOCUMENT ID		TECN	COMMENT
31.94±0.33±0.49	19.5k	ABLIKIM	20R	BES3	e^+e^-, 4178 ∼ 4226 MeV

$\Gamma(\eta\pi^+)/\Gamma(\phi\pi^+)$ — Γ_{116}/Γ_{53}

Unseen decay modes of the resonances are included.

VALUE	EVTS	DOCUMENT ID		TECN	COMMENT
• • • We do not use the following data for averages, fits, limits, etc. • • •					
0.48±0.03±0.04	920	JESSOP	98	CLE2	$e^+e^- \approx \Upsilon(4S)$
0.54±0.09±0.06	165	ALEXANDER	92	CLE2	See JESSOP 98

$\Gamma(\eta\pi^+)/\Gamma(\phi\pi^+, \phi\to K^+K^-)$ — Γ_{116}/Γ_{54}

VALUE (%)	EVTS	DOCUMENT ID		TECN	COMMENT
84.80±0.47±2.64	22k	GUAN	21	BELL	$e^+e^- \approx \Upsilon(4,5S)$

$\Gamma((2\pi^+\pi^-\pi^0)_{non-\eta})/\Gamma_{total}$ — Γ_{117}/Γ

VALUE (%)	EVTS	DOCUMENT ID		TECN	COMMENT
2.04±0.08±0.05	2.5k	ABLIKIM	25A	BES3	e^+e^- at 4.128–4.226 GeV

$\Gamma(f_0(1370)\rho^+, f_0\rho^+\to 2\pi^+\pi^-\pi^0)/\Gamma((2\pi^+\pi^-\pi^0)_{non-\eta})$ — $\Gamma_{118}/\Gamma_{117}$

VALUE (units 10^{-2})	EVTS	DOCUMENT ID		TECN	COMMENT
24.9±3.8±2.1	2.5k	[1] ABLIKIM	25A	BES3	e^+e^- at 4.128–4.226 GeV

[1] Amplitude analysis with 11 components.

$\Gamma(f_0(980)^0\rho^+, f_0^0\rho^+\to 2\pi^+\pi^-\pi^0)/\Gamma((2\pi^+\pi^-\pi^0)_{non-\eta})$ — $\Gamma_{119}/\Gamma_{117}$

VALUE (units 10^{-2})	EVTS	DOCUMENT ID		TECN	COMMENT
12.6±2.1±1.0	2.5k	[1] ABLIKIM	25A	BES3	e^+e^- at 4.128–4.226 GeV

[1] Amplitude analysis with 11 components.

$\Gamma(f_2(1270)^0\rho^+, f_2(1270)^0\rho^+\to 2\pi^+\pi^-\pi^0)/\Gamma((2\pi^+\pi^-\pi^0)_{non-\eta})$ — $\Gamma_{120}/\Gamma_{117}$

VALUE (units 10^{-2})	EVTS	DOCUMENT ID		TECN	COMMENT
9.5±1.7±0.6	2.5k	[1] ABLIKIM	25A	BES3	e^+e^- at 4.128–4.226 GeV

[1] Amplitude analysis with 11 components.

$\Gamma((\rho^+\rho^0)_{S-wave}\to 2\pi^+\pi^-\pi^0)/\Gamma((2\pi^+\pi^-\pi^0)_{non-\eta})$ — $\Gamma_{121}/\Gamma_{117}$

VALUE (units 10^{-2})	EVTS	DOCUMENT ID		TECN	COMMENT
3.5±1.2±0.6	2.5k	[1] ABLIKIM	25A	BES3	e^+e^- at 4.128–4.226 GeV

[1] Amplitude analysis with 11 components.

$\Gamma((\rho(1450)^+\rho^0)_{S-wave}\to 2\pi^+\pi^-\pi^0)/\Gamma((2\pi^+\pi^-\pi^0)_{non-\eta})$ — $\Gamma_{122}/\Gamma_{117}$

VALUE (units 10^{-2})	EVTS	DOCUMENT ID		TECN	COMMENT
4.6±1.3±0.8	2.5k	[1] ABLIKIM	25A	BES3	e^+e^- at 4.128–4.226 GeV

[1] Amplitude analysis with 11 components.

$\Gamma((\rho^+\rho(1450)^0)_{P-wave}\to 2\pi^+\pi^-\pi^0)/\Gamma((2\pi^+\pi^-\pi^0)_{non-\eta})$ — $\Gamma_{123}/\Gamma_{117}$

VALUE (units 10^{-2})	EVTS	DOCUMENT ID		TECN	COMMENT
8.6±1.3±0.4	2.5k	[1] ABLIKIM	25A	BES3	e^+e^- at 4.128–4.226 GeV

[1] Amplitude analysis with 11 components.

$\Gamma(\phi\pi^+, \phi\to\rho\pi)/\Gamma((2\pi^+\pi^-\pi^0)_{non-\eta})$ — $\Gamma_{124}/\Gamma_{117}$

VALUE (units 10^{-2})	EVTS	DOCUMENT ID		TECN	COMMENT
24.9±1.2±0.4	2.5k	[1] ABLIKIM	25A	BES3	e^+e^- at 4.128–4.226 GeV

[1] Amplitude analysis with 11 components.

$\Gamma(\omega\pi^+, \omega\to\rho\pi)/\Gamma((2\pi^+\pi^-\pi^0)_{non-\eta})$ — $\Gamma_{125}/\Gamma_{117}$

VALUE (units 10^{-2})	EVTS	DOCUMENT ID		TECN	COMMENT
6.9±0.8±0.3	2.5k	[1] ABLIKIM	25A	BES3	e^+e^- at 4.128–4.226 GeV

[1] Amplitude analysis with 11 components.

$\Gamma(a_1(1260)^+\pi^0, a_1^+\to(\rho^0\pi^+)_{S-wave})/\Gamma((2\pi^+\pi^-\pi^0)_{non-\eta})$ — $\Gamma_{126}/\Gamma_{117}$

VALUE (units 10^{-2})	EVTS	DOCUMENT ID		TECN	COMMENT
12.5±1.6±1.0	2.5k	[1] ABLIKIM	25A	BES3	e^+e^- at 4.128–4.226 GeV

[1] Amplitude analysis with 11 components.

$\Gamma(a_1(1260)^0\pi^+, a_1^0\to(\rho\pi)_{S-wave})/\Gamma((2\pi^+\pi^-\pi^0)_{non-\eta})$ — $\Gamma_{127}/\Gamma_{117}$

VALUE (units 10^{-2})	EVTS	DOCUMENT ID		TECN	COMMENT
6.3±1.9±1.2	2.5k	[1] ABLIKIM	25A	BES3	e^+e^- at 4.128–4.226 GeV

[1] Amplitude analysis with 11 components.

$\Gamma(\pi(1300)^0\pi^+, \pi^0\to(\rho\pi)_{P-wave})/\Gamma((2\pi^+\pi^-\pi^0)_{non-\eta})$ — $\Gamma_{128}/\Gamma_{117}$

VALUE (units 10^{-2})	EVTS	DOCUMENT ID		TECN	COMMENT
11.7±2.3±2.2	2.5k	[1] ABLIKIM	25A	BES3	e^+e^- at 4.128–4.226 GeV

[1] Amplitude analysis with 11 components.

$\Gamma(3\pi^+2\pi^-)/\Gamma(K^+K^-\pi^+)$ — Γ_{129}/Γ_{52}

VALUE	EVTS	DOCUMENT ID		TECN	COMMENT
0.146±0.014 OUR AVERAGE					
0.145±0.011±0.010	671	LINK	03D	FOCS	γ A, $\overline{E}_\gamma \approx$ 180 GeV
0.158±0.042±0.031	37	FRABETTI	97C	E687	γBe, $\overline{E}_\gamma \approx$ 200 GeV

$\Gamma(2\pi^+\pi^-2\pi^0)/\Gamma_{total}$ — Γ_{130}/Γ

VALUE (units 10^{-2})	EVTS	DOCUMENT ID		TECN	COMMENT
4.41±0.15±0.13	2k	ABLIKIM	25F	BES3	e^+e^- at 4.128–4.226 GeV

$\Gamma(\omega\rho^+, \omega\to\pi^+\pi^-\pi^0)/\Gamma(2\pi^+\pi^-2\pi^0)$ — $\Gamma_{131}/\Gamma_{130}$

VALUE (units 10^{-2})	EVTS	DOCUMENT ID		TECN	COMMENT
$19.98\pm1.40^{+0.92}_{-1.20}$	2k	[1] ABLIKIM	25F	BES3	e^+e^- at 4.128–4.226 GeV

[1] Amplitude analysis of 2.0k $D_s^+\to 2\pi^+\pi^-2\pi^0$ events, with 14 components. The value quoted here includes an $\omega\rho^+$ S-, P-, and D-wave, where the D-wave component dominates.

$\Gamma(\phi\rho^+, \phi\to\pi^+\pi^-\pi^0)/\Gamma(2\pi^+\pi^-2\pi^0)$ — $\Gamma_{132}/\Gamma_{130}$

VALUE (units 10^{-2})	EVTS	DOCUMENT ID		TECN	COMMENT
$13.86\pm1.03^{+0.47}_{-0.35}$	2k	[1] ABLIKIM	25F	BES3	e^+e^- at 4.128–4.226 GeV

[1] Amplitude analysis of 2.0k $D_s^+\to 2\pi^+\pi^-2\pi^0$ events, with 14 components. The value quoted here includes a $\phi\rho^+$ S- and P-wave components.

$\Gamma(\rho(1450)^+\pi^0, \rho(1450)^+\to\omega\pi^+, \omega\to\pi^+\pi^-\pi^0)/\Gamma(2\pi^+\pi^-2\pi^0)$ — $\Gamma_{133}/\Gamma_{130}$

VALUE (units 10^{-2})	EVTS	DOCUMENT ID		TECN	COMMENT
$7.84\pm0.83^{+0.49}_{-0.58}$	2k	[1] ABLIKIM	25F	BES3	e^+e^- at 4.128–4.226 GeV

[1] Amplitude analysis of 2.0k $D_s^+\to 2\pi^+\pi^-2\pi^0$ events, with 14 components.

$\Gamma(a_1(1260)^0\rho^+, a_1(1260)^0\to\rho^+\pi^-)/\Gamma(2\pi^+\pi^-2\pi^0)$ — $\Gamma_{134}/\Gamma_{130}$

VALUE (units 10^{-2})	EVTS	DOCUMENT ID		TECN	COMMENT
11.43±0.67±0.35	2k	[1] ABLIKIM	25F	BES3	e^+e^- at 4.128–4.226 GeV

[1] Amplitude analysis of 2.0k $D_s^+\to 2\pi^+\pi^-2\pi^0$ events, with 14 components. The value quoted here includes an $a_1\rho$ S- and P-wave components.

$\Gamma(a_1(1260)^0\rho^+, a_1(1260)^0\to\rho^-\pi^+)/\Gamma(2\pi^+\pi^-2\pi^0)$ — $\Gamma_{135}/\Gamma_{130}$

VALUE (units 10^{-2})	EVTS	DOCUMENT ID		TECN	COMMENT
7.39±0.44±0.26	2k	[1] ABLIKIM	25F	BES3	e^+e^- at 4.128–4.226 GeV

[1] Amplitude analysis of 2.0k $D_s^+\to 2\pi^+\pi^-2\pi^0$ events, with 14 components. The value quoted here includes an $a_1\rho$ S- and P-wave components.

$\Gamma(a_1(1260)^+\rho^0, a_1(1260)^+\to\rho^+\pi^0)/\Gamma(2\pi^+\pi^-2\pi^0)$ — $\Gamma_{136}/\Gamma_{130}$

VALUE (units 10^{-2})	EVTS	DOCUMENT ID		TECN	COMMENT
16.53±1.37±1.52	2k	[1] ABLIKIM	25F	BES3	e^+e^- at 4.128–4.226 GeV

[1] Amplitude analysis of 2.0k $D_s^+\to 2\pi^+\pi^-2\pi^0$ events, with 14 components. The value quoted here includes an $a_1\rho$ S- and P-wave components.

$\Gamma(b_1(1235)^+\pi^0, b_1(1235)^+\to\omega\pi^+, \omega\to\pi^+\pi^-\pi^0)/\Gamma(2\pi^+\pi^-2\pi^0)$ — $\Gamma_{137}/\Gamma_{130}$

VALUE (units 10^{-2})	EVTS	DOCUMENT ID		TECN	COMMENT
10.79±0.98±0.68	2k	[1] ABLIKIM	25F	BES3	e^+e^- at 4.128–4.226 GeV

[1] Amplitude analysis of 2.0k $D_s^+\to 2\pi^+\pi^-2\pi^0$ events, with 14 components.

$\Gamma(b_1(1235)^0\pi^+, b_1(1235)^0\to\omega\pi^0, \omega\to\pi^+\pi^-\pi^0)/\Gamma(2\pi^+\pi^-2\pi^0)$ — $\Gamma_{138}/\Gamma_{130}$

VALUE (units 10^{-2})	EVTS	DOCUMENT ID		TECN	COMMENT
$14.60\pm1.20^{+0.52}_{-0.49}$	2k	[1] ABLIKIM	25F	BES3	e^+e^- at 4.128–4.226 GeV

[1] Amplitude analysis of 2.0k $D_s^+\to 2\pi^+\pi^-2\pi^0$ events, with 14 components.

$\Gamma(\eta\rho^+)/\Gamma_{total}$ — Γ_{139}/Γ

Unseen decay modes of the η are included.

VALUE (%)	EVTS	DOCUMENT ID		TECN	COMMENT
8.9±0.6±0.5	328 ± 22	NAIK	09A	CLEO	$\eta\to 2\gamma$

Int. J. Mod. Phys. A 2026.41. Downloaded from www.worldscientific.com by CALIFORNIA @ BERKELEY on 09/16/26. Re-use and distribution is strictly not permitted, except for Open Access articles.

$\Gamma(\eta\rho^+)/\Gamma(\phi\pi^+)$ — Γ_{139}/Γ_{53}

Unseen decay modes of the resonances are included.

VALUE	EVTS	DOCUMENT ID		TECN	COMMENT
• • • We do not use the following data for averages, fits, limits, etc. • • •					
$2.98\pm0.20\pm0.39$	447	JESSOP	98	CLE2	$e^+e^-\approx\Upsilon(4S)$
$2.86\pm0.38^{+0.36}_{-0.38}$	217	AVERY	92	CLE2	See JESSOP 98

$\Gamma(\eta\rho^+)/\Gamma(\eta\pi^+\pi^0)$ — $\Gamma_{139}/\Gamma_{140}$

VALUE (units 10^{-2})	EVTS	DOCUMENT ID		TECN	COMMENT
78.3±5.0±2.1	1.2k	ABLIKIM	19BE	BES3	$\eta\pi^+\pi^0$ amplitude analysis

$\Gamma(\eta\pi^+\pi^0)/\Gamma_{total}$ — Γ_{140}/Γ

VALUE (%)	EVTS	DOCUMENT ID		TECN	COMMENT
9.10±0.17 OUR AVERAGE					
$9.10\pm0.09\pm0.15$		ABLIKIM	24BD	BES3	e^+e^-, 4.128–4.226 GeV
$9.2\ \pm0.4\ \pm1.1$		ONYISI	13	CLEO	e^+e^- at 4.17 GeV
• • • We do not use the following data for averages, fits, limits, etc. • • •					
$9.50\pm0.28\pm0.41$	2.6k	[1] ABLIKIM	19BE	BES3	e^+e^- at 4.178 GeV

[1] Superseded by ABLIKIM 24BD.

$\Gamma(\eta(\pi^+\pi^0)_{P-wave})/\Gamma(\eta\pi^+\pi^0)$ — $\Gamma_{141}/\Gamma_{140}$

VALUE (units 10^{-2})	EVTS	DOCUMENT ID		TECN	COMMENT
5.4±2.1±2.5	1.2k	ABLIKIM	19BE	BES3	$\eta\pi^+\pi^0$ amplitude analysis

$\Gamma(a_0(980)^{+0}\pi^{0+},\ a_0(980)^{+0}\to\eta\pi^{+0})/\Gamma(\eta\pi^+\pi^0)$ — $\Gamma_{142}/\Gamma_{140}$

VALUE (units 10^{-2})	EVTS	DOCUMENT ID		TECN	COMMENT
23.2±2.3±3.3	1.2k	[1] ABLIKIM	19BE	BES3	$\eta\pi^+\pi^0$ amplitude analysis

[1] Coherent sum of $D_s^+\to a_0^+\pi^0\to\eta\pi^+\pi^0$ and $D_s^+\to a_0^0\pi^+\to\eta\pi^+\pi^0$. ABLIKIM 19BE find $a_0(980)^0-f(980)$ mixing effects negligibly small in this $D_s^+\to\eta\pi^+\pi^0$ Dalitz plot analysis.

$\Gamma(\omega\pi^+\pi^0)/\Gamma_{total}$ — Γ_{143}/Γ

Unseen decay modes of the ω are included.

VALUE (%)	EVTS	DOCUMENT ID		TECN	COMMENT
2.78±0.65±0.25	34 ± 7.9	GE	09A	CLEO	e^+e^- at 4170 MeV

$\Gamma(2\pi^+\pi^-\eta)/\Gamma_{total}$ — Γ_{144}/Γ

VALUE (units 10^{-2})	EVTS	DOCUMENT ID		TECN	COMMENT
3.08±0.06±0.05		ABLIKIM	24BD	BES3	e^+e^-, 4.128–4.226 GeV
• • • We do not use the following data for averages, fits, limits, etc. • • •					
$3.12\pm0.13\pm0.09$	2.1k	[1] ABLIKIM	21AR	BES3	e^+e^-, 4.178–4.226 GeV

[1] Superseded by ABLIKIM 24BD.

$\Gamma(a_1(1260)^+\eta,\ a_1^+\to\rho(770)^0\pi^+,\ \rho^0\to\pi^+\pi^-)/\Gamma(2\pi^+\pi^-\eta)$ — $\Gamma_{145}/\Gamma_{144}$

VALUE (units 10^{-2})	DOCUMENT ID		TECN	COMMENT
55.4±3.9±2.0	[1] ABLIKIM	21AR	BES3	e^+e^- at 4.178–4.226 GeV

[1] $D_s^+\to2\pi^+\pi^-\eta$ amplitude analysis with 11 components.

$\Gamma(a_1(1260)^+\eta,\ a_1^+\to f_0(500)\pi^+,\ f_0\to\pi^+\pi^-)/\Gamma(2\pi^+\pi^-\eta)$ — $\Gamma_{146}/\Gamma_{144}$

VALUE (units 10^{-2})	DOCUMENT ID		TECN	COMMENT
8.1±1.9±2.1	[1] ABLIKIM	21AR	BES3	e^+e^- at 4.178–4.226 GeV

[1] $D_s^+\to2\pi^+\pi^-\eta$ amplitude analysis with 11 components.

$\Gamma(a_0(980)^+\rho(770)^0,\ a_0^+\to\eta\pi^+)/\Gamma(2\pi^+\pi^-\eta)$ — $\Gamma_{147}/\Gamma_{144}$

VALUE (units 10^{-2})	DOCUMENT ID		TECN	COMMENT
6.7±2.5±1.5	[1] ABLIKIM	21AR	BES3	e^+e^- at 4.178–4.226 GeV

[1] $D_s^+\to2\pi^+\pi^-\eta$ amplitude analysis with 11 components.

$\Gamma(\eta(1405)\pi^+,\ \eta\to a_0(980)^-\pi^+,\ a_0^-\to\eta\pi^-)/\Gamma(2\pi^+\pi^-\eta)$ — $\Gamma_{148}/\Gamma_{144}$

VALUE (units 10^{-2})	DOCUMENT ID		TECN	COMMENT
0.7±0.2±0.1	[1] ABLIKIM	21AR	BES3	e^+e^- at 4.178–4.226 GeV

[1] $D_s^+\to2\pi^+\pi^-\eta$ amplitude analysis with 11 components.

$\Gamma(\eta(1405)\pi^+,\ \eta\to a_0(980)^+\pi^-,\ a_0^+\to\eta\pi^+)/\Gamma(2\pi^+\pi^-\eta)$ — $\Gamma_{149}/\Gamma_{144}$

VALUE (units 10^{-2})	DOCUMENT ID		TECN	COMMENT
0.7±0.2±0.1	[1] ABLIKIM	21AR	BES3	e^+e^- at 4.178–4.226 GeV

[1] $D_s^+\to2\pi^+\pi^-\eta$ amplitude analysis with 11 components.

$\Gamma(f_1(1420)\pi^+,\ f_1\to a_0(980)^-\pi^+,\ a_0^-\to\eta\pi^-)/\Gamma(2\pi^+\pi^-\eta)$ — $\Gamma_{150}/\Gamma_{144}$

VALUE (units 10^{-2})	DOCUMENT ID		TECN	COMMENT
1.9±0.5±0.3	[1] ABLIKIM	21AR	BES3	e^+e^- at 4.178–4.226 GeV

[1] $D_s^+\to2\pi^+\pi^-\eta$ amplitude analysis with 11 components.

$\Gamma(f_1(1420)\pi^+,\ f_1\to a_0(980)^+\pi^-,\ a_0^+\to\eta\pi^+)/\Gamma(2\pi^+\pi^-\eta)$ — $\Gamma_{151}/\Gamma_{144}$

VALUE (units 10^{-2})	DOCUMENT ID		TECN	COMMENT
1.7±0.5±0.3	[1] ABLIKIM	21AR	BES3	e^+e^- at 4.178–4.226 GeV

[1] $D_s^+\to2\pi^+\pi^-\eta$ amplitude analysis with 11 components.

$\Gamma(3\pi^+2\pi^-\pi^0)/\Gamma_{total}$ — Γ_{152}/Γ

VALUE	DOCUMENT ID		TECN	COMMENT
$\mathbf{0.049^{+0.033}_{-0.030}}$	BARLAG	92C	ACCM	π^- 230 GeV

$\Gamma(\omega2\pi^+\pi^-)/\Gamma_{total}$ — Γ_{153}/Γ

Unseen decay modes of the ω are included.

VALUE (%)	EVTS	DOCUMENT ID		TECN	COMMENT
1.58±0.45±0.09	29 ± 8.2	GE	09A	CLEO	e^+e^- at 4170 MeV

$\Gamma(\eta'(958)\pi^+)/\Gamma_{total}$ — Γ_{154}/Γ

Unseen decay modes of the $\eta'(958)$ are included.

VALUE (%)	DOCUMENT ID		TECN	COMMENT
3.95±0.08 OUR AVERAGE				
$3.95\pm0.04\pm0.07$	ABLIKIM	24BD	BES3	e^+e^-, 4.128–4.226 GeV
$3.94\pm0.15\pm0.20$	ONYISI	13	CLEO	e^+e^- at 4.17 GeV
• • • We do not use the following data for averages, fits, limits, etc. • • •				
$3.77\pm0.25\pm0.30$	[1] ALEXANDER	08	CLEO	See ONYISI 13

[1] ALEXANDER 08 uses single- and double-tagged events in an overall fit.

$\Gamma(\eta'(958)\pi^+)/\Gamma(K^+K_S^0)$ — Γ_{154}/Γ_{44}

Unseen decay modes of the $\eta'(958)$ are included.

VALUE	EVTS	DOCUMENT ID		TECN	COMMENT
• • • We do not use the following data for averages, fits, limits, etc. • • •					
$2.654\pm0.088\pm0.139$	1436 ± 47	MENDEZ	10	CLEO	See ONYISI 13

$\Gamma(\eta'(958)\pi^+)/\Gamma(K^+K^-\pi^+)$ — Γ_{154}/Γ_{52}

VALUE (units 10^{-2})	EVTS	DOCUMENT ID		TECN	COMMENT
69.4±0.8±3.8	9.9k	ABLIKIM	20R	BES3	e^+e^-, 4178 ∼ 4226 MeV

$\Gamma(\eta'(958)\pi^+)/\Gamma(\phi\pi^+)$ — Γ_{154}/Γ_{53}

Unseen decay modes of the resonances are included.

VALUE	EVTS	DOCUMENT ID		TECN	COMMENT
• • • We do not use the following data for averages, fits, limits, etc. • • •					
$1.03\pm0.06\pm0.07$	537	JESSOP	98	CLE2	$e^+e^-\approx\Upsilon(4S)$
$1.20\pm0.15\pm0.11$	281	ALEXANDER	92	CLE2	See JESSOP 98
$2.5\ \pm1.0\ ^{+1.5}_{-0.4}$	22	ALVAREZ	91	NA14	Photoproduction
$2.5\ \pm0.5\ \pm0.3$	215	ALBRECHT	90D	ARG	$e^+e^-\approx10.4$ GeV

$\Gamma(\omega\eta\pi^+)/\Gamma_{total}$ — Γ_{156}/Γ

Unseen decay modes of the ω and η are included.

VALUE (units 10^{-3})	CL%	EVTS	DOCUMENT ID		TECN	COMMENT
5.4±1.2±0.4		78	ABLIKIM	23AL	BES3	e^+e^- at 4.128–4.226 GeV
• • • We do not use the following data for averages, fits, limits, etc. • • •						
<21.3	90		GE	09A	CLEO	e^+e^- at 4170 MeV

$\Gamma(\eta'(958)\rho^+)/\Gamma_{total}$ — Γ_{157}/Γ

VALUE (%)	DOCUMENT ID		TECN	COMMENT
5.8±1.4±0.4	ABLIKIM	15Z	BES3	482 pb^{-1}, 4009 MeV

$\Gamma(\eta'(958)\rho^+)/\Gamma(\phi\pi^+)$ — Γ_{157}/Γ_{53}

Unseen decay modes of the resonances are included.

VALUE	EVTS	DOCUMENT ID		TECN	COMMENT
• • • We do not use the following data for averages, fits, limits, etc. • • •					
$2.78\pm0.28\pm0.30$	137	[1] JESSOP	98	CLE2	$e^+e^-\approx\Upsilon(4S)$
$3.44\pm0.62^{+0.44}_{-0.46}$	68	AVERY	92	CLE2	See JESSOP 98

[1] This JESSOP 98 fraction, when combined with other η' fractions, greatly overshoots the inclusive η' fraction. See the measurement just above, which fits nicely.

$\Gamma(\eta'(958)\rho^+)/\Gamma(\eta'(958)\pi^+\pi^0)$ — $\Gamma_{157}/\Gamma_{158}$

VALUE	EVTS	DOCUMENT ID		TECN	COMMENT
• • • We do not use the following data for averages, fits, limits, etc. • • •					
≈1	395	[1] ABLIKIM	22AA	BES3	e^+e^- at 4.178–4.226 GeV

[1] Result of an amplitude analysis of $D_s^+\to\pi^+\pi^0\eta'$ which found that $D_s^+\to\rho^+\eta'$ is the dominant decay mode, with other contributions negligible. No uncertainty is assigned to this 100% fit fraction; however, the fit fractions of non-resonant contributions are shown to be below 1%.

$\Gamma(\eta'(958)\pi^+\pi^0)/\Gamma_{total}$ — Γ_{158}/Γ

VALUE (%)	EVTS	DOCUMENT ID		TECN	COMMENT
6.14±0.18 OUR AVERAGE					
$6.17\pm0.12\pm0.14$		ABLIKIM	24BD	BES3	e^+e^-, 4.128–4.226 GeV
$5.6\ \pm0.5\ \pm0.6$		ONYISI	13	CLEO	e^+e^- at 4.17 GeV
• • • We do not use the following data for averages, fits, limits, etc. • • •					
$6.15\pm0.25\pm0.18$	837	[1] ABLIKIM	22AA	BES3	e^+e^-, 4.178–4.226 GeV

[1] An amplitude analysis in the same publication finds that $D_s^+\to\rho^+\eta'$ is the only statistically significant contribution to this decay. Superseded by ABLIKIM 24BD.

$\Gamma(\eta'(958)\pi^+\pi^0\text{nonresonant})/\Gamma_{total}$ — Γ_{159}/Γ

VALUE	CL%	DOCUMENT ID		TECN	COMMENT
$\mathbf{<5.1\times10^{-2}}$	90	ABLIKIM	15Z	BES3	482 pb^{-1}, 4009 MeV

Int. J. Mod. Phys. A 2026.41. Downloaded from www.worldscientific.com by UNIVERSITY OF CALIFORNIA @ BERKELEY on 09/16/26. Re-use and distribution is strictly not permitted, except for Open Access articles.

Modes with one or three K's

$\Gamma(K^+\pi^0)/\Gamma(K^+K^0_S)$ — Γ_{160}/Γ_{44}

VALUE (units 10^{-2})	EVTS	DOCUMENT ID		TECN	COMMENT
4.2±1.4±0.2	202 ± 70	MENDEZ	10	CLEO	e^+e^- at 4170 MeV
• • • We do not use the following data for averages, fits, limits, etc. • • •					
5.5±1.3±0.7	141 ± 34	ADAMS	07A	CLEO	See MENDEZ 10

$\Gamma(K^+\pi^0)/\Gamma(K^+K^-\pi^+)$ — Γ_{160}/Γ_{52}

VALUE (units 10^{-3})	EVTS	DOCUMENT ID		TECN	COMMENT
13.73±0.90±0.33	2.3k	ABLIKIM	20R	BES3	e^+e^-, 4178 ∼ 4226 MeV

$\Gamma(K^+\pi^0)/\Gamma(\phi\pi^+,\ \phi\to K^+K^-)$ — Γ_{160}/Γ_{54}

VALUE (%)	EVTS	DOCUMENT ID		TECN	COMMENT
3.28±0.23±0.13	12k	GUAN	21	BELL	$e^+e^-\approx\ \Upsilon(4,5S)$

$\Gamma(K^0_S\pi^+)/\Gamma(K^+K^0_S)$ — Γ_{161}/Γ_{44}

VALUE (units 10^{-2})	EVTS	DOCUMENT ID		TECN	COMMENT
8.12±0.28 OUR AVERAGE					
8.5 ±0.7 ±0.2	393 ± 33	MENDEZ	10	CLEO	e^+e^- at 4170 MeV
8.03±0.24±0.19	17.6k±481	WON	09	BELL	e^+e^- at $\Upsilon(4S)$
10.4 ±2.4 ±1.4	113 ± 26	LINK	08	FOCS	γ A, $\overline{E}_\gamma\approx$ 180 GeV
• • • We do not use the following data for averages, fits, limits, etc. • • •					
8.2 ±0.9 ±0.2	206 ± 22	ADAMS	07A	CLEO	See MENDEZ 10

$\Gamma(K^0_S\pi^+)/\Gamma(K^+K^-\pi^+)$ — Γ_{161}/Γ_{52}

VALUE (units 10^{-3})	EVTS	DOCUMENT ID		TECN	COMMENT
20.35±0.62±0.42	2.7k	ABLIKIM	20R	BES3	e^+e^-, 4178 ∼ 4226 MeV

$\Gamma(K^+\eta)/\Gamma(K^+K^0_S)$ — Γ_{162}/Γ_{44}

Unseen decay modes of the η are included.

VALUE (units 10^{-2})	EVTS	DOCUMENT ID		TECN	COMMENT
11.8±2.2±0.6	222 ± 41	MENDEZ	10	CLEO	e^+e^- at 4170 MeV

$\Gamma(K^+\eta)/\Gamma(K^+K^-\pi^+)$ — Γ_{162}/Γ_{52}

VALUE (units 10^{-2})	EVTS	DOCUMENT ID		TECN	COMMENT
2.97±0.18±0.06	1.8k	ABLIKIM	20R	BES3	e^+e^-, 4178 ∼ 4226 MeV

$\Gamma(K^+\eta)/\Gamma(\phi\pi^+,\ \phi\to K^+K^-)$ — Γ_{162}/Γ_{54}

VALUE (%)	EVTS	DOCUMENT ID		TECN	COMMENT
7.81±0.22±0.24	14k	GUAN	21	BELL	$e^+e^-\approx\ \Upsilon(4,5S)$

$\Gamma(K^+\eta)/\Gamma(\eta\pi^+)$ — $\Gamma_{162}/\Gamma_{116}$

VALUE (units 10^{-2})	EVTS	DOCUMENT ID		TECN	COMMENT
• • • We do not use the following data for averages, fits, limits, etc. • • •					
8.9±1.5±0.4	113 ± 18	ADAMS	07A	CLEO	See MENDEZ 10

$\Gamma(K^+\omega)/\Gamma_{total}$ — Γ_{163}/Γ

Unseen decay modes of the ω are included.

VALUE (units 10^{-4})	CL%	EVTS	DOCUMENT ID		TECN	COMMENT
9.9±1.5 OUR FIT						
8.7±2.4±0.8		29	[1] ABLIKIM	19AH	BES3	e^+e^- at 4.178 GeV
• • • We do not use the following data for averages, fits, limits, etc. • • •						
<24		90	GE	09A	CLEO	e^+e^- at 4170 MeV

[1] Evidence for mode at 4.4σ.

$\Gamma(K^+\omega)/\Gamma(K^+\pi^+\pi^-\pi^0)$ — $\Gamma_{163}/\Gamma_{183}$

VALUE (units 10^{-2})	DOCUMENT ID		TECN	COMMENT
10.3±1.5 OUR FIT				
10.9±1.8±0.1	[1] ABLIKIM	22BL	BES3	PWA, 550 $D_s^\pm\to K^\pm\pi^\pm\pi^\mp\pi^0$

[1] ABLIKIM 22BL reports $[\Gamma(D_s^+\to K^+\omega)/\Gamma(D_s^+\to K^+\pi^+\pi^-\pi^0)]\times[B(\omega(782)\to\pi^+\pi^-\pi^0)] = (9.7\pm1.5\pm0.6)\times10^{-2}$ which we divide by our best (shown rounded) value $B(\omega(782)\to\pi^+\pi^-\pi^0) = (89.2\pm0.7)\times10^{-2}$. Our first error is their experiment's error and our second error is the systematic error from using our best (shown rounded) value.

$\Gamma(K^+\eta'(958))/\Gamma(K^+K^0_S)$ — Γ_{164}/Γ_{44}

Unseen decay modes of the $\eta'(958)$ are included.

VALUE (units 10^{-2})	EVTS	DOCUMENT ID		TECN	COMMENT
11.8±3.6±0.7	56 ± 17	MENDEZ	10	CLEO	e^+e^- at 4170 MeV

$\Gamma(K^+\eta'(958))/\Gamma(K^+K^-\pi^+)$ — Γ_{164}/Γ_{52}

VALUE (units 10^{-2})	EVTS	DOCUMENT ID		TECN	COMMENT
4.91±0.31±0.31	675	ABLIKIM	20R	BES3	e^+e^-, 4178 ∼ 4226 MeV

$\Gamma(K^+\eta'(958))/\Gamma(\eta'(958)\pi^+)$ — $\Gamma_{164}/\Gamma_{154}$

VALUE (units 10^{-2})	EVTS	DOCUMENT ID		TECN	COMMENT
• • • We do not use the following data for averages, fits, limits, etc. • • •					
4.2±1.3±0.3	28 ± 9	ADAMS	07A	CLEO	See MENDEZ 10

$\Gamma(K^+\pi^+\pi^-)/\Gamma_{total}$ — Γ_{165}/Γ

VALUE (units 10^{-3})	EVTS	DOCUMENT ID		TECN	COMMENT
6.23±0.10 OUR FIT					
6.22±0.10 OUR AVERAGE					
6.20±0.09±0.06		ABLIKIM	24BD	BES3	e^+e^-, 4.128–4.226 GeV
6.54±0.33±0.25		ONYISI	13	CLEO	e^+e^- at 4.17 GeV
• • • We do not use the following data for averages, fits, limits, etc. • • •					
6.11±0.18±0.11	1.3k	[1] ABLIKIM	22AC	BES3	e^+e^-, 4.178–4.226 GeV
6.9 ±0.5 ±0.3		[2] ALEXANDER	08	CLEO	See ONYISI 13

[1] Superseded by ABLIKIM 24BD.

[2] ALEXANDER 08 uses single- and double-tagged events in an overall fit.

$\Gamma(K^+\pi^+\pi^-)/\Gamma(K^+K^-\pi^+)$ — Γ_{165}/Γ_{52}

VALUE	EVTS	DOCUMENT ID		TECN	COMMENT
0.1142±0.0025 OUR FIT Error includes scale factor of 1.1.					
0.127 ±0.007 ±0.014	567 ± 31	LINK	04F	FOCS	γ A, $\overline{E}_\gamma\approx$ 180 GeV

$\Gamma(K^+\rho^0)/\Gamma(K^+\pi^+\pi^-)$ — $\Gamma_{166}/\Gamma_{165}$

This is the "fit fraction" from the Dalitz-plot analysis.

VALUE	DOCUMENT ID		TECN	COMMENT
0.35 ±0.04 OUR AVERAGE				
0.321±0.037±0.037	ABLIKIM	22AC	BES3	Dalitz plot fit, 1.3k evts
0.388±0.053±0.026	LINK	04F	FOCS	Dalitz plot fit, 567 evts

$\Gamma(K^+\rho(1450)^0,\ \rho^0\to\pi^+\pi^-)/\Gamma(K^+\pi^+\pi^-)$ — $\Gamma_{167}/\Gamma_{165}$

This is the "fit fraction" from the Dalitz-plot analysis.

VALUE	DOCUMENT ID		TECN	COMMENT
0.117±0.028 OUR AVERAGE				
0.131±0.031±0.029	ABLIKIM	22AC	BES3	Dalitz plot fit, 1.3k evts
0.106±0.035±0.010	LINK	04F	FOCS	Dalitz plot fit, 567 evts

$\Gamma(K^+f_0(500),\ f_0\to\pi^+\pi^-)/\Gamma(K^+\pi^+\pi^-)$ — $\Gamma_{168}/\Gamma_{165}$

VALUE (units 10^{-2})	DOCUMENT ID		TECN	COMMENT
7.2±2.1±4.4	ABLIKIM	22AC	BES3	Dalitz plot fit, 1.3k evts

$\Gamma(K^+f_0(980),\ f_0\to\pi^+\pi^-)/\Gamma(K^+\pi^+\pi^-)$ — $\Gamma_{169}/\Gamma_{165}$

VALUE (units 10^{-2})	DOCUMENT ID		TECN	COMMENT
4.5±1.3±1.2	ABLIKIM	22AC	BES3	Dalitz plot fit, 1.3k evts

$\Gamma(K^+f_0(1370),\ f_0\to\pi^+\pi^-)/\Gamma(K^+\pi^+\pi^-)$ — $\Gamma_{170}/\Gamma_{165}$

VALUE (units 10^{-2})	DOCUMENT ID		TECN	COMMENT
19.9±2.9±9.3	ABLIKIM	22AC	BES3	Dalitz plot fit, 1.3k evts

$\Gamma(K^*(892)^0\pi^+,\ K^{*0}\to K^+\pi^-)/\Gamma(K^+\pi^+\pi^-)$ — $\Gamma_{171}/\Gamma_{165}$

This is the "fit fraction" from the Dalitz-plot analysis.

VALUE	DOCUMENT ID		TECN	COMMENT
0.27 ±0.04 OUR AVERAGE Error includes scale factor of 2.0.				
0.302 ±0.018 ±0.020	ABLIKIM	22AC	BES3	Dalitz plot fit, 1.3k evts
0.2164±0.0321±0.0114	LINK	04F	FOCS	Dalitz plot fit, 567 evts

$\Gamma(K^*(1410)^0\pi^+,\ K^{*0}\to K^+\pi^-)/\Gamma(K^+\pi^+\pi^-)$ — $\Gamma_{172}/\Gamma_{165}$

This is the "fit fraction" from the Dalitz-plot analysis.

VALUE	DOCUMENT ID		TECN	COMMENT
0.10 ±0.07 OUR AVERAGE Error includes scale factor of 2.7.				
0.045 ±0.021 ±0.025	ABLIKIM	22AC	BES3	Dalitz plot fit, 1.3k evts
0.1882±0.0403±0.0122	LINK	04F	FOCS	Dalitz plot fit, 567 evts

$\Gamma(K^*(1430)^0\pi^+,\ K^{*0}\to K^+\pi^-)/\Gamma(K^+\pi^+\pi^-)$ — $\Gamma_{173}/\Gamma_{165}$

This is the "fit fraction" from the Dalitz-plot analysis.

VALUE	DOCUMENT ID		TECN	COMMENT
0.15 ±0.05 OUR AVERAGE Error includes scale factor of 1.7.				
0.185 ±0.025 ±0.026	ABLIKIM	22AC	BES3	Dalitz plot fit, 1.3k evts
0.0765±0.0500±0.0170	LINK	04F	FOCS	Dalitz plot fit, 567 evts

$\Gamma(K^+\pi^+\pi^-\text{nonresonant})/\Gamma(K^+\pi^+\pi^-)$ — $\Gamma_{174}/\Gamma_{165}$

This is the "fit fraction" from the Dalitz-plot analysis.

VALUE	DOCUMENT ID		TECN	COMMENT
0.1588±0.0492±0.0153	LINK	04F	FOCS	Dalitz fit, 567 evts

$\Gamma(K^0_S\pi^+\pi^0)/\Gamma_{total}$ — Γ_{176}/Γ

VALUE (units 10^{-3})	EVTS	DOCUMENT ID		TECN	COMMENT
5.09±0.22 OUR AVERAGE					
5.1 ±0.2 ±0.1		ABLIKIM	24BD	BES3	e^+e^-, 4.128–4.226 GeV
5.0 ±0.9 ±0.2	44	[1] NAIK	09A	CLEO	e^+e^- at 4170 MeV
• • • We do not use the following data for averages, fits, limits, etc. • • •					
5.43±0.30±0.15	666	[2] ABLIKIM	21AB	BES3	e^+e^-, 4.178–4.226 GeV

[1] NAIK 09A reports $B(D_s^+\to K^0\pi^+\pi^-) = (1.00\pm0.18\pm0.04)\times10^{-2}$ which we have divided by 2.

[2] ABLIKIM 21AB uses an amplitude analysis with 5 resonant modes plus one background component. Superseded by ABLIKIM 24BD.

$\Gamma(K^0_S\rho(770)^+,\ \rho^+\to\pi^+\pi^0)/\Gamma(K^0_S\pi^+\pi^0)$ — $\Gamma_{177}/\Gamma_{176}$

VALUE (units 10^{-2})	EVTS	DOCUMENT ID		TECN	COMMENT
50.2±7.2±3.9	666	[1] ABLIKIM	21AB	BES3	e^+e^- at 4.178–4.226 GeV

[1] ABLIKIM 21AB uses an amplitude analysis with 5 resonant modes plus one background component.

Int. J. Mod. Phys. A 2026.41. Downloaded from www.worldscientific.com
by CALIFORNIA @ BERKELEY on 09/16/26. Re-use and distribution is strictly not permitted, except for Open Access articles.

$\Gamma(K^0_S\rho(1450)^+,\ \rho^+\to\pi^+\pi^0)/\Gamma(K^0_S\pi^+\pi^0)$ — $\Gamma_{178}/\Gamma_{176}$

VALUE (units 10^{-2})	EVTS	DOCUMENT ID	TECN	COMMENT
20.4±4.3±4.4	666	[1] ABLIKIM 21AB	BES3	e^+e^- at 4.178–4.226 GeV

[1] ABLIKIM 21AB uses an amplitude analysis with 5 resonant modes plus one background component.

$\Gamma(K^*(892)^0\pi^+,\ K^{*0}\to K^0_S\pi^0)/\Gamma(K^0_S\pi^+\pi^0)$ — $\Gamma_{179}/\Gamma_{176}$

VALUE (units 10^{-2})	EVTS	DOCUMENT ID	TECN	COMMENT
8.4±2.2±0.9	666	[1] ABLIKIM 21AB	BES3	e^+e^- at 4.178–4.226 GeV

[1] ABLIKIM 21AB uses an amplitude analysis with 5 resonant modes plus one background component.

$\Gamma(K^*(892)^+\pi^0,\ K^{*+}\to K^0_S\pi^+)/\Gamma(K^0_S\pi^+\pi^0)$ — $\Gamma_{180}/\Gamma_{176}$

VALUE (units 10^{-2})	EVTS	DOCUMENT ID	TECN	COMMENT
4.6±1.4±0.4	666	[1] ABLIKIM 21AB	BES3	e^+e^- at 4.178–4.226 GeV

[1] ABLIKIM 21AB uses an amplitude analysis with 5 resonant modes plus one background component.

$\Gamma(K^*(1410)^0\pi^+,\ K^{*0}\to K^0_S\pi^0)/\Gamma(K^0_S\pi^+\pi^0)$ — $\Gamma_{181}/\Gamma_{176}$

VALUE (units 10^{-2})	EVTS	DOCUMENT ID	TECN	COMMENT
3.3±1.6±0.5	666	[1] ABLIKIM 21AB	BES3	e^+e^- at 4.178–4.226 GeV

[1] ABLIKIM 21AB uses an amplitude analysis with 5 resonant modes plus one background component.

$\Gamma(K^0_S2\pi^+\pi^-)/\Gamma(K^0_SK^-2\pi^+)$ — Γ_{182}/Γ_{82}

VALUE	EVTS	DOCUMENT ID	TECN	COMMENT
0.18±0.04±0.05	179 ± 36	LINK 08	FOCS	γ A, $\overline{E}_\gamma\approx$ 180 GeV

$\Gamma(K^+\pi^+\pi^-\pi^0)/\Gamma(K^+K^-\pi^+\pi^0)$ — Γ_{183}/Γ_{74}

VALUE (units 10^{-2})	EVTS	DOCUMENT ID	TECN	COMMENT
17.13±0.62±0.51	26k	LI 23G	BELL	e^+e^- at/near Υ(nS), n=1,...,5

$\Gamma(K^+\pi^+\pi^-\pi^0)/\Gamma_{total}$ — Γ_{183}/Γ

VALUE (units 10^{-3})	EVTS	DOCUMENT ID	TECN	COMMENT
9.7 ±0.6 OUR FIT				
9.75±0.54±0.17	776	ABLIKIM 22BL	BES3	e^+e^- at 4.178–4.226 GeV

$\Gamma(K^*(892)^0\rho^+,\ K^{*0}\to K^+\pi^-)/\Gamma(K^+\pi^+\pi^-\pi^0)$ — $\Gamma_{184}/\Gamma_{183}$

VALUE (units 10^{-2})	DOCUMENT ID	TECN	COMMENT
40.5±2.8±1.5	ABLIKIM 22BL	BES3	PWA, 550 $D_s^\pm\to K^\pm\pi^\pm\pi^\mp\pi^0$

$\Gamma(K^*(892)^+\rho^0,\ K^{*+}\to K^+\pi^0)/\Gamma(K^+\pi^+\pi^-\pi^0)$ — $\Gamma_{185}/\Gamma_{183}$

VALUE (units 10^{-2})	DOCUMENT ID	TECN	COMMENT
4.3±1.1±0.6	ABLIKIM 22BL	BES3	PWA, 550 $D_s^\pm\to K^\pm\pi^\pm\pi^\mp\pi^0$

$\Gamma(K_1(1270)^0\pi^+,\ K_1^0\to K^+\rho^-)/\Gamma(K^+\pi^+\pi^-\pi^0)$ — $\Gamma_{186}/\Gamma_{183}$

VALUE (units 10^{-2})	DOCUMENT ID	TECN	COMMENT
4.0±1.2±0.6	ABLIKIM 22BL	BES3	PWA, 550 $D_s^\pm\to K^\pm\pi^\pm\pi^\mp\pi^0$

$\Gamma(K_1(1400)^0\pi^+,\ K_1^0\to K^*(890)^+\pi^-,\ K^{*+}\to K^+\pi^0)/\Gamma(K^+\pi^+\pi^-\pi^0)$ — $\Gamma_{187}/\Gamma_{183}$

VALUE (units 10^{-2})	DOCUMENT ID	TECN	COMMENT
5.6±0.9±0.2	ABLIKIM 22BL	BES3	PWA, 550 $D_s^\pm\to K^\pm\pi^\pm\pi^\mp\pi^0$

$\Gamma(K_1(1400)^0\pi^+,\ K_1^0\to K^*(890)^0\pi^0,\ K^{*0}\to K^+\pi^-)/\Gamma(K^+\pi^+\pi^-\pi^0)$ — $\Gamma_{188}/\Gamma_{183}$

VALUE (units 10^{-2})	DOCUMENT ID	TECN	COMMENT
6.1±0.9±0.2	ABLIKIM 22BL	BES3	PWA, 550 $D_s^\pm\to K^\pm\pi^\pm\pi^\mp\pi^0$

$\Gamma(K^+a_1(1260)^0,\ a_1\to\rho^+\pi^-)/\Gamma(K^+\pi^+\pi^-\pi^0)$ — $\Gamma_{189}/\Gamma_{183}$

VALUE (units 10^{-2})	DOCUMENT ID	TECN	COMMENT
1.9±0.7±0.9	ABLIKIM 22BL	BES3	PWA, 550 $D_s^\pm\to K^\pm\pi^\pm\pi^\mp\pi^0$

$\Gamma(K^+a_1(1260)^0,\ a_1\to\rho^-\pi^+)/\Gamma(K^+\pi^+\pi^-\pi^0)$ — $\Gamma_{190}/\Gamma_{183}$

VALUE (units 10^{-2})	DOCUMENT ID	TECN	COMMENT
1.9±0.7±0.9	ABLIKIM 22BL	BES3	PWA, 550 $D_s^\pm\to K^\pm\pi^\pm\pi^\mp\pi^0$

$\Gamma(K^+\pi^+\pi^-\pi^0\,\text{nonresonant})/\Gamma(K^+\pi^+\pi^-\pi^0)$ — $\Gamma_{191}/\Gamma_{183}$

VALUE (units 10^{-2})	DOCUMENT ID	TECN	COMMENT
9.5±2.2±0.9	ABLIKIM 22BL	BES3	PWA, 550 $D_s^\pm\to K^\pm\pi^\pm\pi^\mp\pi^0$

$\Gamma((K^+\pi^0)_{P-wave}\rho^0)/\Gamma(K^+\pi^+\pi^-\pi^0)$ — $\Gamma_{192}/\Gamma_{183}$

VALUE (units 10^{-2})	DOCUMENT ID	TECN	COMMENT
10.4±2.0±0.6	ABLIKIM 22BL	BES3	PWA, 550 $D_s^\pm\to K^\pm\pi^\pm\pi^\mp\pi^0$

$\Gamma(K^+\omega\pi^0)/\Gamma_{total}$ — Γ_{193}/Γ

Unseen decay modes of the ω are included.

VALUE (%)	CL%	DOCUMENT ID	TECN	COMMENT
<0.82	90	GE 09A	CLEO	e^+e^- at 4170 MeV

$\Gamma(K^+\omega\pi^+\pi^-)/\Gamma_{total}$ — Γ_{194}/Γ

Unseen decay modes of the ω are included.

VALUE (%)	CL%	DOCUMENT ID	TECN	COMMENT
<0.54	90	GE 09A	CLEO	e^+e^- at 4170 MeV

$\Gamma(K^+\omega\eta)/\Gamma_{total}$ — Γ_{195}/Γ

Unseen decay modes of the ω and η are included.

VALUE (%)	CL%	DOCUMENT ID	TECN	COMMENT
<0.79	90	GE 09A	CLEO	e^+e^- at 4170 MeV

$\Gamma(2K^+K^-)/\Gamma(K^+K^-\pi^+)$ — Γ_{196}/Γ_{52}

VALUE (units 10^{-3})	EVTS	DOCUMENT ID	TECN	COMMENT
4.0 ±0.3 ±0.2	748 ± 60	DEL-AMO-SA...11G	BABR	$e^+e^-\approx\Upsilon(4S)$
• • • We do not use the following data for averages, fits, limits, etc. • • •				
$8.95\pm2.12^{+2.24}_{-2.31}$	31	LINK 02I	FOCS	γ A, $\approx$ 180 GeV

$\Gamma(\phi K^+,\ \phi\to K^+K^-)/\Gamma(2K^+K^-)$ — $\Gamma_{197}/\Gamma_{196}$

VALUE	DOCUMENT ID	TECN	COMMENT
0.41±0.08±0.03	DEL-AMO-SA...11G	BABR	$e^+e^-\approx\Upsilon(4S)$

Radiative decays

$\Gamma(\rho(770)^+\gamma)/\Gamma_{total}$ — Γ_{198}/Γ

VALUE	CL%	DOCUMENT ID	TECN	COMMENT
<6.1 × 10^{-4}	90	[1] ABLIKIM 24CT	BES3	e^+e^- at 4.128–4.226 GeV

[1] ABLIKIM 24CT reports an absolute branching fraction $(2.2\pm0.9\pm0.2)\times10^{-4}$ at 2.5σ significance.

Doubly Cabibbo-suppressed modes

$\Gamma(2K^+\pi^-)/\Gamma_{total}$ — Γ_{199}/Γ

VALUE (units 10^{-4})	EVTS	DOCUMENT ID	TECN	COMMENT
1.293±0.027 OUR FIT Error includes scale factor of 1.1.				
1.24 $^{+0.28}_{-0.26}$ ±0.06	33^{+8}_{-7}	ABLIKIM 24AV	BES3	e^+e^- at 4.128–4.266 GeV

$\Gamma(2K^+\pi^-)/\Gamma(K^+K^-\pi^+)$ — Γ_{199}/Γ_{52}

VALUE (units 10^{-3})	EVTS	DOCUMENT ID	TECN	COMMENT
2.371±0.035 OUR FIT				
2.371±0.034 OUR AVERAGE				
2.372±0.024±0.025	67k	AAIJ 19G	LHCB	pp at 8 TeV
2.3 ±0.3 ±0.2	356 ± 52	DEL-AMO-SA...11G	BABR	$e^+e^-\approx\Upsilon(4S)$
2.29 ±0.28 ±0.12	281 ± 34	KO 09	BELL	e^+e^- at $\Upsilon(4S)$
5.2 ±1.7 ±1.1	27 ± 9	LINK 05K	FOCS	<0.78%, CL = 90%

$\Gamma(K^+K^*(892)^0,\ K^{*0}\to K^+\pi^-)/\Gamma(2K^+\pi^-)$ — $\Gamma_{200}/\Gamma_{199}$

VALUE	DOCUMENT ID	TECN	COMMENT
0.47±0.22±0.15	DEL-AMO-SA...11G	BABR	$e^+e^-\approx\Upsilon(4S)$

$\Gamma(2K^+\pi^-\pi^0)/\Gamma_{total}$ — Γ_{201}/Γ

VALUE	CL%	DOCUMENT ID	TECN	COMMENT
<1.7 × 10^{-4}	90	ABLIKIM 24AV	BES3	e^+e^- at 4.128–4.266 GeV

Baryon-antibaryon mode

$\Gamma(p\overline{n})/\Gamma_{total}$ — Γ_{202}/Γ

This is the only baryonic mode allowed kinematically.

VALUE (units 10^{-3})	EVTS	DOCUMENT ID	TECN	COMMENT
1.22±0.11 OUR AVERAGE				
1.21±0.10±0.05	193 ± 17	ABLIKIM 19O	BES3	e^+e^-, E_{cm} = 4178 MeV
$1.30\pm0.36^{+0.12}_{-0.16}$	13.0 ± 3.6	ATHAR 08	CLEO	e^+e^-, $E_{cm}\approx$ 4170 MeV

$\Gamma(p\overline{p}e^+\nu_e)/\Gamma_{total}$ — Γ_{203}/Γ

VALUE	CL%	DOCUMENT ID	TECN	COMMENT
<2.0 × 10^{-4}	90	ABLIKIM 19BD	BES3	e^+e^- at 4178 MeV

Rare or forbidden modes

$\Gamma(\pi^+e^+e^-)/\Gamma_{total}$ — Γ_{204}/Γ

This mode is not a useful test for a ΔC=1 weak neutral current because both quarks must change flavor in this decay.

VALUE	CL%	DOCUMENT ID	TECN	COMMENT
< 5.5 × 10^{-6}	90	AAIJ 21T	LHCB	1.6 fb^{-1} pp
• • • We do not use the following data for averages, fits, limits, etc. • • •				
<13 × 10^{-6}	90	LEES 11G	BABR	$e^+e^-\approx\Upsilon(4S)$
< 2.2 × 10^{-5}	90	[1] RUBIN 10	CLEO	e^+e^- at 4170 MeV
<27 × 10^{-5}	90	AITALA 99G	E791	π^-N 500 GeV

[1] This RUBIN 10 limit is for the e^+e^- mass in the continuum away from the $\phi(1020)$. See the next data block.

Int. J. Mod. Phys. A 2026.41. Downloaded from www.worldscientific.com
by UNIVERSITY OF CALIFORNIA @ BERKELEY on 09/16/26. Re-use and distribution is strictly not permitted, except for Open Access articles.

$\Gamma(\pi^+\phi,\ \phi\to e^+e^-)/\Gamma_{total}$ — Γ_{205}/Γ

This is *not* a test for the $\Delta C = 1$ weak neutral current, but leads to the $\pi^+e^+e^-$ final state.

VALUE (units 10^{-5})	EVTS	DOCUMENT ID		TECN	COMMENT
$1.17^{+0.23}_{-0.21}\pm0.03$	38	ABLIKIM	24CF	BES3	e^+e^- at 4.128–4.226 GeV
• • • We do not use the following data for averages, fits, limits, etc. • • •					
$0.6\ ^{+0.8}_{-0.4}\ \pm0.1$	3	RUBIN	10	CLEO	e^+e^- at 4.170 GeV

$\Gamma(\pi^+\pi^0e^+e^-)/\Gamma_{total}$ — Γ_{206}/Γ

VALUE	CL%	DOCUMENT ID		TECN	COMMENT
$<7.0\times10^{-5}$	90	ABLIKIM	24CF	BES3	e^+e^- at 4.128–4.226 GeV

$\Gamma(\rho^+\phi,\ \phi\to e^+e^-)/\Gamma_{total}$ — Γ_{207}/Γ

VALUE (units 10^{-5})	EVTS	DOCUMENT ID		TECN	COMMENT
$2.44^{+0.67}_{-0.62}\pm0.16$	38	ABLIKIM	24CF	BES3	e^+e^- at 4.128–4.226 GeV

$\Gamma(\pi^+\mu^+\mu^-)/\Gamma_{total}$ — Γ_{208}/Γ

This mode is not a useful test for a ΔC=1 weak neutral current because both quarks must change flavor in this decay.

VALUE	CL%	DOCUMENT ID		TECN	COMMENT
$<1.8\times10^{-7}$	90	AAIJ	21T	LHCB	1.6 fb^{-1} pp
• • • We do not use the following data for averages, fits, limits, etc. • • •					
$<4.1\times10^{-7}$	90	AAIJ	13AF	LHCB	pp at 7 TeV
$<4.3\times10^{-5}$	90	LEES	11G	BABR	$e^+e^-\approx\ \Upsilon(4S)$
$<2.6\times10^{-5}$	90	LINK	03F	FOCS	γ A, $\overline{E}_\gamma\approx$ 180 GeV
$<1.4\times10^{-4}$	90	AITALA	99G	E791	π^-N 500 GeV
$<4.3\times10^{-4}$	90	KODAMA	95	E653	π^- emulsion 600 GeV

$\Gamma(K^+e^+e^-)/\Gamma_{total}$ — Γ_{209}/Γ

A test for the ΔC=1 weak neutral current. Allowed by higher-order electroweak interactions.

VALUE	CL%	DOCUMENT ID		TECN	COMMENT
$<3.7\times10^{-6}$	90	LEES	11G	BABR	$e^+e^-\approx\ \Upsilon(4S)$
• • • We do not use the following data for averages, fits, limits, etc. • • •					
$<4.9\times10^{-6}$	90	AAIJ	21T	LHCB	1.6 fb^{-1} pp
$<5.2\times10^{-5}$	90	RUBIN	10	CLEO	e^+e^- at 4170 MeV
$<1.6\times10^{-3}$	90	AITALA	99G	E791	π^-N 500 GeV

$\Gamma(K^+\pi^0e^+e^-)/\Gamma_{total}$ — Γ_{210}/Γ

VALUE	CL%	DOCUMENT ID		TECN	COMMENT
$<7.1\times10^{-5}$	90	ABLIKIM	24CF	BES3	e^+e^- at 4.128–4.226 GeV

$\Gamma(K^0_S\pi^+e^+e^-)/\Gamma_{total}$ — Γ_{211}/Γ

VALUE	CL%	DOCUMENT ID		TECN	COMMENT
$<8.1\times10^{-5}$	90	ABLIKIM	24CF	BES3	e^+e^- at 4.128–4.226 GeV

$\Gamma(K^+\mu^+\mu^-)/\Gamma_{total}$ — Γ_{212}/Γ

A test for the ΔC=1 weak neutral current. Allowed by higher-order electroweak interactions.

VALUE	CL%	DOCUMENT ID		TECN	COMMENT
$<1.4\times10^{-7}$	90	AAIJ	21T	LHCB	1.6 fb^{-1} pp
• • • We do not use the following data for averages, fits, limits, etc. • • •					
$<21\ \times10^{-6}$	90	LEES	11G	BABR	$e^+e^-\approx\ \Upsilon(4S)$
$<3.6\times10^{-5}$	90	LINK	03F	FOCS	γ A, $\overline{E}_\gamma\approx$ 180 GeV
$<1.4\times10^{-4}$	90	AITALA	99G	E791	π^-N 500 GeV
$<5.9\times10^{-4}$	90	KODAMA	95	E653	π^- emulsion 600 GeV

$\Gamma(K^*(892)^+\mu^+\mu^-)/\Gamma_{total}$ — Γ_{213}/Γ

A test for the ΔC=1 weak neutral current. Allowed by higher-order electroweak interactions.

VALUE	CL%	DOCUMENT ID		TECN	COMMENT
$<1.4\times10^{-3}$	90	KODAMA	95	E653	π^- emulsion 600 GeV

$\Gamma(\pi^+e^+\mu^-)/\Gamma_{total}$ — Γ_{214}/Γ

A test of lepton-family-number conservation.

VALUE	CL%	DOCUMENT ID		TECN	COMMENT
$<1.1\times10^{-6}$	90	AAIJ	21T	LHCB	1.6 fb^{-1} pp
• • • We do not use the following data for averages, fits, limits, etc. • • •					
$<12\ \times10^{-6}$	90	LEES	11G	BABR	$e^+e^-\approx\ \Upsilon(4S)$

$\Gamma(\pi^+e^-\mu^+)/\Gamma_{total}$ — Γ_{215}/Γ

A test of lepton-family-number conservation.

VALUE	CL%	DOCUMENT ID		TECN	COMMENT
$<9.4\times10^{-7}$	90	AAIJ	21T	LHCB	1.6 fb^{-1} pp
• • • We do not use the following data for averages, fits, limits, etc. • • •					
$<20\ \times10^{-6}$	90	LEES	11G	BABR	$e^+e^-\approx\ \Upsilon(4S)$

$\Gamma(K^+e^+\mu^-)/\Gamma_{total}$ — Γ_{216}/Γ

A test of lepton-family-number conservation.

VALUE	CL%	DOCUMENT ID		TECN	COMMENT
$<7.9\times10^{-7}$	90	AAIJ	21T	LHCB	1.6 fb^{-1} pp
• • • We do not use the following data for averages, fits, limits, etc. • • •					
$<14\ \times10^{-6}$	90	LEES	11G	BABR	$e^+e^-\approx\ \Upsilon(4S)$

$\Gamma(K^+e^-\mu^+)/\Gamma_{total}$ — Γ_{217}/Γ

A test of lepton-family-number conservation.

VALUE	CL%	DOCUMENT ID		TECN	COMMENT
$<5.6\times10^{-7}$	90	AAIJ	21T	LHCB	1.6 fb^{-1} pp
• • • We do not use the following data for averages, fits, limits, etc. • • •					
$<9.7\times10^{-6}$	90	LEES	11G	BABR	$e^+e^-\approx\ \Upsilon(4S)$

$\Gamma(\pi^-2e^+)/\Gamma_{total}$ — Γ_{218}/Γ

A test of lepton-number conservation.

VALUE	CL%	DOCUMENT ID		TECN	COMMENT
$<1.4\times10^{-6}$	90	AAIJ	21T	LHCB	1.6 fb^{-1} pp
• • • We do not use the following data for averages, fits, limits, etc. • • •					
$<4.1\times10^{-6}$	90	LEES	11G	BABR	$e^+e^-\approx\ \Upsilon(4S)$
$<1.8\times10^{-5}$	90	RUBIN	10	CLEO	e^+e^- at 4170 MeV
$<69\ \times10^{-5}$	90	AITALA	99G	E791	π^-N 500 GeV

$\Gamma(\pi^-2\mu^+)/\Gamma_{total}$ — Γ_{219}/Γ

A test of lepton-number conservation.

VALUE	CL%	DOCUMENT ID		TECN	COMMENT
$<8.6\times10^{-8}$	90	AAIJ	21T	LHCB	1.6 fb^{-1} pp
• • • We do not use the following data for averages, fits, limits, etc. • • •					
$<1.2\times10^{-7}$	90	AAIJ	13AF	LHCB	pp at 7 TeV
$<1.4\times10^{-5}$	90	LEES	11G	BABR	$e^+e^-\approx\ \Upsilon(4S)$
$<2.9\times10^{-5}$	90	LINK	03F	FOCS	γ A, $\overline{E}_\gamma\approx$ 180 GeV
$<8.2\times10^{-5}$	90	AITALA	99G	E791	π^-N 500 GeV
$<4.3\times10^{-4}$	90	KODAMA	95	E653	π^- emulsion 600 GeV

$\Gamma(\pi^-e^+\mu^+)/\Gamma_{total}$ — Γ_{220}/Γ

A test of lepton-number conservation.

VALUE	CL%	DOCUMENT ID		TECN	COMMENT
$<6.3\times10^{-7}$	90	AAIJ	21T	LHCB	1.6 fb^{-1} pp
• • • We do not use the following data for averages, fits, limits, etc. • • •					
$<8.4\times10^{-6}$	90	LEES	11G	BABR	$e^+e^-\approx\ \Upsilon(4S)$
$<7.3\times10^{-4}$	90	AITALA	99G	E791	π^-N 500 GeV

$\Gamma(K^-2e^+)/\Gamma_{total}$ — Γ_{221}/Γ

A test of lepton-number conservation.

VALUE	CL%	DOCUMENT ID		TECN	COMMENT
$<7.7\times10^{-7}$	90	AAIJ	21T	LHCB	1.6 fb^{-1} pp
• • • We do not use the following data for averages, fits, limits, etc. • • •					
$<5.2\times10^{-6}$	90	LEES	11G	BABR	$e^+e^-\approx\ \Upsilon(4S)$
$<1.7\times10^{-5}$	90	RUBIN	10	CLEO	e^+e^- at 4170 MeV
$<63\ \times10^{-5}$	90	AITALA	99G	E791	π^-N 500 GeV

$\Gamma(\pi^-\pi^0e^+e^+)/\Gamma_{total}$ — Γ_{222}/Γ

VALUE	CL%	DOCUMENT ID		TECN	COMMENT
$<2.9\times10^{-5}$	90	ABLIKIM	25BC	BES3	e^+e^- at 4.128–4.266 GeV

$\Gamma(K^-\pi^0e^+e^+)/\Gamma_{total}$ — Γ_{223}/Γ

VALUE	CL%	DOCUMENT ID		TECN	COMMENT
$<3.4\times10^{-5}$	90	ABLIKIM	25BC	BES3	e^+e^- at 4.128–4.266 GeV

$\Gamma(K^0_S\pi^-e^+e^+)/\Gamma_{total}$ — Γ_{224}/Γ

VALUE	CL%	DOCUMENT ID		TECN	COMMENT
$<1.3\times10^{-5}$	90	ABLIKIM	25BC	BES3	e^+e^- at 4.128–4.266 GeV

$\Gamma(K^0_SK^-e^+e^+)/\Gamma_{total}$ — Γ_{225}/Γ

VALUE	CL%	DOCUMENT ID		TECN	COMMENT
$<2.9\times10^{-5}$	90	ABLIKIM	25BC	BES3	e^+e^- at 4.128–4.266 GeV

$\Gamma(\phi\pi^-e^+e^+)/\Gamma_{total}$ — Γ_{226}/Γ

VALUE	CL%	DOCUMENT ID		TECN	COMMENT
$<6.9\times10^{-5}$	90	ABLIKIM	25BC	BES3	e^+e^- at 4.128–4.266 GeV

$\Gamma(\phi K^-e^+e^+)/\Gamma_{total}$ — Γ_{227}/Γ

VALUE	CL%	DOCUMENT ID		TECN	COMMENT
$<9.9\times10^{-5}$	90	ABLIKIM	25BC	BES3	e^+e^- at 4.128–4.266 GeV

$\Gamma(K^-2\mu^+)/\Gamma_{total}$ — Γ_{228}/Γ

A test of lepton-number conservation.

VALUE	CL%	DOCUMENT ID		TECN	COMMENT
$<2.6\times10^{-8}$	90	AAIJ	21T	LHCB	1.6 fb^{-1} pp

Int. J. Mod. Phys. A 2026.41. Downloaded from www.worldscientific.com
by CALIFORNIA @ BERKELEY on 09/16/26. Re-use and distribution is strictly not permitted, except for Open Access articles.

• • • We do not use the following data for averages, fits, limits, etc. • • •

$<1.3\times10^{-5}$	90	LEES	11G	BABR	$e^+e^-\approx\Upsilon(4S)$
$<1.3\times10^{-5}$	90	LINK	03F	FOCS	γ A, $E_\gamma\approx$ 180 GeV
$<1.8\times10^{-4}$	90	AITALA	99G	E791	π^-N 500 GeV
$<5.9\times10^{-4}$	90	KODAMA	95	E653	π^- emulsion 600 GeV

$\Gamma(K^-e^+\mu^+)/\Gamma_{total}$ — Γ_{229}/Γ

A test of lepton-number conservation.

VALUE	CL%	DOCUMENT ID		TECN	COMMENT
$<2.6\times10^{-7}$	90	AAIJ	21T	LHCB	1.6 fb^{-1} pp

• • • We do not use the following data for averages, fits, limits, etc. • • •

$<6.1\times10^{-6}$	90	LEES	11G	BABR	$e^+e^-\approx\Upsilon(4S)$
$<6.8\times10^{-4}$	90	AITALA	99G	E791	π^-N 500 GeV

$\Gamma(K^*(892)^-2\mu^+)/\Gamma_{total}$ — Γ_{230}/Γ

A test of lepton-number conservation.

VALUE	CL%	DOCUMENT ID		TECN	COMMENT
$<1.4\times10^{-3}$	90	KODAMA	95	E653	π^- emulsion 600 GeV

$D_s^\pm$ Amplitude analyses

$D_s^+\to K^+K^-\pi^+$ partial wave analyses

Amplitude analyses of D_s^+ decays to the $K^+K^-\pi^+$ final state, fitting simultaneously different partial wave components.

VALUE	EVTS	DOCUMENT ID		TECN	COMMENT
seen	18.6k	[1] ABLIKIM	21AE	BES3	e^+e^- at 4.178 GeV
seen	96k	[1] DEL-AMO-SA...	11G	BABR	e^+e^- at $\Upsilon(4S)$
seen	12k	[1] MITCHELL	09A	CLEO	e^+e^- at 4.17 GeV
seen	701	[2] FRABETTI	95B	E687	

[1] Amplitude analysis with 6 components.
[2] Amplitude analysis with 5 components.

$D_s^+\to K^+K_S\pi^0$ partial wave analyses

VALUE	EVTS	DOCUMENT ID		TECN	COMMENT
	990	[1] ABLIKIM	22AH	BES3	e^+e^- at 4.178–4.226 GeV

[1] Amplitude analysis with 5 components.

$D_s^+\to 2\pi^+\pi^-$ partial wave analyses

VALUE	EVTS	DOCUMENT ID		TECN	COMMENT
	0.7M	[1] AAIJ	23AN	LHCB	Dalitz fit, 0.7M events
	11.1k	[2] ABLIKIM	22BI	BES3	Dalitz fit
	10.5k	[2] AUBERT	09O	BABR	Dalitz fit
	1.5k	[3] LINK	04	FOCS	Dalitz fit
	848	[4] AITALA	01A	E791	Dalitz fit

[1] Amplitude analysis with 7 components, one of which is a model-independent $\pi^+\pi^-$ S-wave parametrisation as complex numbers in 50 $\pi^+\pi^-$ mass bins.
[2] Amplitude analysis with 4 components, one of which is a model-independent $\pi^+\pi^-$ S-wave parametrisation as complex numbers in 29 $\pi^+\pi^-$ mass bins.
[3] Amplitude analysis with 5 components.
[4] Amplitude analysis with 6 components.

$D_s^+\to 2\pi^+\pi^-\pi^0$ partial wave analyses

VALUE	EVTS	DOCUMENT ID		TECN	COMMENT
	2.5k	[1] ABLIKIM	25A	BES3	e^+e^- at 4.128–4.226 GeV

[1] Amplitude analysis with 11 components contributing to the $2\pi^+\pi^-\pi^0{}_{non-\eta}$ final state.

$D_s^+\to 2\pi^+\pi^-\eta$ partial wave analyses

Amplitude analyses of D_s^+ decays to the $\pi^+\pi^+\pi^-\eta$ final state, fitting simultaneously different partial wave components.

VALUE	EVTS	DOCUMENT ID		TECN	COMMENT
seen	2.1k	[1] ABLIKIM	21AR	BES3	e^+e^- at 4.178–4.226 GeV

[1] Amplitude analysis with 11 components.

$D_s^+\to\pi^+\pi^0\eta'$ partial wave analyses.

VALUE	EVTS	DOCUMENT ID		TECN	COMMENT
	395	[1] ABLIKIM	22AA	BES3	e^+e^- at 4.178–4.226 GeV

[1] The only significant contribution found in this analysis is $D_s^+\to\rho^+\eta'$.

$D_s^+\to\pi^+2\pi^0$ partial wave analyses.

VALUE	EVTS	DOCUMENT ID		TECN	COMMENT
	440	ABLIKIM	22Z	BES3	e^+e^- at 4.178–4.226 GeV

$D_s^+\to 2\pi^+\pi^-2\pi^0$ partial wave analyses

VALUE	EVTS	DOCUMENT ID		TECN	COMMENT
	2k	[1] ABLIKIM	25F	BES3	e^+e^- at 4.128–4.226 GeV

[1] Amplitude analysis with 14 components.

$D_s^+\to K^+\pi^+\pi^-$ partial wave analyses

VALUE	EVTS	DOCUMENT ID		TECN	COMMENT
	1.3k	[1] ABLIKIM	22AC	BES3	e^+e^- at 4.178–4.226 GeV

[1] ABLIKIM 22AC uses an amplitude analysis with 8 components.

$D_s^+\to K_S^0\pi^+\pi^0$ partial wave analyses

VALUE	EVTS	DOCUMENT ID		TECN	COMMENT
	666	[1] ABLIKIM	21AB	BES3	e^+e^- at 4.178–4.226 GeV

[1] ABLIKIM 21AB uses an amplitude analysis with 5 resonant modes plus one background component.

$D_s^+\to K^+\pi^+\pi^-\pi^0$ partial wave analyses

VALUE	EVTS	DOCUMENT ID		TECN	COMMENT
seen	550	[1] ABLIKIM	22BL	BES3	e^+e^- at 4.178–4.226 GeV

[1] Amplitude analysis with 11 components.

$D_s^+\to 2K_S^0\pi^+$ partial wave analyses

VALUE	EVTS	DOCUMENT ID		TECN	COMMENT
	400	[1] ABLIKIM	22F	BES3	e^+e^- at 4.178–4.226 GeV

[1] Amplitude analysis with 2 components.

$D_s^+\to (KS)^0K^-2\pi^+$ partial wave analyses

Amplitude analyses of D_s^+ decays to the $K_S^0K^-2\pi^+$ final state, fitting simultaneously different partial wave components.

VALUE	EVTS	DOCUMENT ID		TECN	COMMENT
seen	1.3k	[1] ABLIKIM	21K	BES3	e^+e^- at 4.178–4.226 GeV

[1] Amplitude analysis with 13 components.

$D_s^+\to K^-K^+\pi^+\pi^0$ partial wave analyses

Amplitude analyses of D_s^+ decays to the $K^-K^+\pi^+\pi^0$ final state, fitting simultaneously different partial wave components.

VALUE	EVTS	DOCUMENT ID		TECN	COMMENT
seen	3k	[1] ABLIKIM	21U	BES3	e^+e^- at 4.178–4.226 GeV

[1] ABLIKIM 21U uses an amplitude analysis with 9 components.

$D_s^+\to K^-K^+2\pi^+\pi^-$ partial wave analyses

VALUE	EVTS	DOCUMENT ID		TECN	COMMENT
	309	ABLIKIM	22AB	BES3	e^+e^- at 4.178–4.226 GeV

$D_s^+\to K_S^0K_L^0\pi^+$ partial wave analyses

VALUE	EVTS	DOCUMENT ID	
	2.35k	[1] ABLIKIM	25BR

[1] ABLIKIM 25BR amplitude analysis with 4 resonant modes plus one background component measures the asymmetry of the branching fractions of $D_s^+\to K_S^0K^*(892)^+$ and $D_s^+\to K_L^0K^*(892)^+$.

$D_s^+-D_s^-$ CP-VIOLATING DECAY-RATE ASYMMETRIES

This is the difference between D_s^+ and D_s^- partial widths for the decay to state f, divided by the sum of the widths:
$A_{CP}(f)=[\Gamma(D_s^+\to f)-\Gamma(D_s^-\to\overline{f})]/[\Gamma(D_s^+\to f)+\Gamma(D_s^-\to\overline{f})]$.

$A_{CP}(\mu^\pm\nu)$ in $D_s^+\to\mu^+\nu$, $D_s^-\to\mu^-\overline{\nu}_\mu$

VALUE (%)	EVTS	DOCUMENT ID		TECN	COMMENT
-0.2 ± 2.5 OUR AVERAGE					
$-1.2\pm2.5\pm1.0$	2.2k	ABLIKIM	21BE	BES3	e^+e^- at 4.178, 4.226 GeV
4.8 ± 6.1		ALEXANDER	09	CLEO	e^+e^- at 4170 MeV

$A_{CP}(\tau^\pm\nu)$ in $D_s^+\to\tau^+\nu_\tau$, $D_s^-\to\tau^-\overline{\nu}_\tau$

VALUE (%)	EVTS	DOCUMENT ID		TECN	COMMENT
$2.9\pm4.8\pm1.0$	950	[1] ABLIKIM	21BE	BES3	e^+e^- at 4.178, 4.226 GeV

[1] ABLIKIM 21BE also reports that when constrained by the Standard Model ratio of $\Gamma(D_s^+\to\tau^+\nu_\tau)/\Gamma(D_s^+\to\mu^+\nu_\mu)=9.75$, the result is $(-0.1\pm1.9\pm1.0)$%.

$A_{CP}(K^\pm K_S^0)$ in $D_s^\pm\to K^\pm K_S^0$

VALUE (%)	EVTS	DOCUMENT ID		TECN	COMMENT
0.07±0.24 OUR AVERAGE					
$0.29\pm0.50\pm0.21$		ABLIKIM	24BD	BES3	e^+e^-, 4.128–4.226 GeV
$-0.05\pm0.23\pm0.24$	288k	[1] LEES	13E	BABR	e^+e^- at $\Upsilon(4S)$
$0.12\pm0.36\pm0.22$		KO	10	BELL	$e^+e^-\approx\Upsilon(4S)$

• • • We do not use the following data for averages, fits, limits, etc. • • •

$0.6\pm2.8\pm0.6$	1.8k	[2] ABLIKIM	19AM	BES3	e^+e^- at 4178 MeV
$2.6\pm1.5\pm0.6$		ONYISI	13	CLEO	e^+e^- at 4.17 GeV
$4.7\pm1.8\pm0.9$	4.0k	MENDEZ	10	CLEO	See ONYISI 13
$4.9\pm2.1\pm0.9$		ALEXANDER	08	CLEO	See MENDEZ 10

[1] LEES 13E finds that after subtracting the contribution due to $K^0-\overline{K}^0$ mixing, the CP asymmetry is $(+0.28\pm0.23\pm0.24)$%.
[2] Superseded by ABLIKIM 24BD.

$A_{CP}(K^\pm K_L^0)$ in $D_s^\pm\to K^\pm K_L^0$

VALUE (units 10^{-2})	EVTS	DOCUMENT ID		TECN	COMMENT
$-1.1\pm2.6\pm0.6$	2.3k	ABLIKIM	19AM	BES3	e^+e^- at 4178 MeV

Int. J. Mod. Phys. A 2026.41. Downloaded from www.worldscientific.com
by UNIVERSITY OF CALIFORNIA @ BERKELEY on 09/16/26. Re-use and distribution is strictly not permitted, except for Open Access articles.

$A_{CP}(K^+K^-\pi^\pm)$ in $D_s^\pm \to K^+K^-\pi^\pm$

VALUE (%)	DOCUMENT ID		TECN	COMMENT
0.35±0.34 OUR AVERAGE				
0.48±0.26±0.24	ABLIKIM	24BD	BES3	e^+e^-, 4.128–4.226 GeV
−0.5 ±0.8 ±0.4	ONYISI	13	CLEO	e^+e^- at 4.17 GeV
• • • We do not use the following data for averages, fits, limits, etc. • • •				
0.3 ±1.1 ±0.8	ALEXANDER	08	CLEO	See ONYISI 13

$A_{CP}(\phi\pi^\pm)$ in $D_s^\pm \to \phi\pi^\pm$

VALUE (%)	DOCUMENT ID		TECN	COMMENT
−0.38±0.26±0.08	ABAZOV	14B	D0	$p\overline{p}$ at 1.96 TeV

$A_{CP}(K^\pm K^0_S\pi^0)$ in $D_s^\pm \to K^\pm K^0_S\pi^0$

VALUE (%)	DOCUMENT ID		TECN	COMMENT
−0.9 ±1.9 OUR AVERAGE				
−0.85±1.97±0.46	ABLIKIM	24BD	BES3	e^+e^-, 4.128–4.226 GeV
−1.6 ±6.0 ±1.1	ONYISI	13	CLEO	e^+e^- at 4.17 GeV

$A_{CP}(2K^0_S\pi^\pm)$ in $D_s^\pm \to 2K^0_S\pi^\pm$

VALUE (%)	DOCUMENT ID		TECN	COMMENT
1.3 ±1.6 OUR AVERAGE				
1.14±1.58±0.44	ABLIKIM	24BD	BES3	e^+e^-, 4.128–4.226 GeV
3.1 ±5.2 ±0.6	ONYISI	13	CLEO	e^+e^- at 4.17 GeV

$A_{CP}(K^+K^-\pi^\pm\pi^0)$ in $D_s^\pm \to K^+K^-\pi^\pm\pi^0$

VALUE (%)	DOCUMENT ID		TECN	COMMENT
−0.6 ±0.9 OUR AVERAGE				
−0.66±0.91±0.33	ABLIKIM	24BD	BES3	e^+e^-, 4.128–4.226 GeV
0.0 ±2.7 ±1.2	ONYISI	13	CLEO	e^+e^- at 4.17 GeV
• • • We do not use the following data for averages, fits, limits, etc. • • •				
−5.9 ±4.2 ±1.2	ALEXANDER	08	CLEO	See ONYISI 13

$A_{CP}(K^\pm K^0_S\pi^+\pi^-)$ in $D_s^\pm \to K^\pm K^0_S\pi^+\pi^-$

VALUE (%)	DOCUMENT ID		TECN	COMMENT
0.7 ±2.9 OUR AVERAGE Error includes scale factor of 1.3.				
2.00±2.37±0.70	ABLIKIM	24BD	BES3	e^+e^-, 4.128–4.226 GeV
−5.7 ±5.3 ±0.9	ONYISI	13	CLEO	e^+e^- at 4.17 GeV

$A_{CP}(K^0_S K^\mp 2\pi^\pm)$ in $D_s^+ \to K^0_S K^\mp 2\pi^\pm$

VALUE (%)	DOCUMENT ID		TECN	COMMENT
0.7 ±1.8 OUR AVERAGE Error includes scale factor of 1.3.				
−0.24±1.05±1.07	ABLIKIM	24BD	BES3	e^+e^-, 4.128–4.226 GeV
4.1 ±2.7 ±0.9	ONYISI	13	CLEO	e^+e^- at 4.17 GeV
• • • We do not use the following data for averages, fits, limits, etc. • • •				
−0.7 ±3.6 ±1.1	ALEXANDER	08	CLEO	See ONYISI 13

$A_{CP}(\pi^+\pi^-\pi^\pm)$ in $D_s^\pm \to \pi^+\pi^-\pi^\pm$

VALUE (%)	DOCUMENT ID		TECN	COMMENT
−0.9 ±1.1 OUR AVERAGE				
−0.88±1.17±0.38	ABLIKIM	24BD	BES3	e^+e^-, 4.128–4.226 GeV
−0.7 ±3.0 ±0.6	ONYISI	13	CLEO	e^+e^- at 4.17 GeV
• • • We do not use the following data for averages, fits, limits, etc. • • •				
2.0 ±4.6 ±0.7	ALEXANDER	08	CLEO	See ONYISI 13

$A_{CP}(\pi^\pm\eta)$ in $D_s^\pm \to \pi^\pm\eta$

VALUE (%)	EVTS	DOCUMENT ID		TECN	COMMENT
0.24±0.29 OUR AVERAGE					
−0.44±0.89±0.19		ABLIKIM	24BD	BES3	e^+e^-, 4.128–4.226 GeV
0.32±0.51±0.12	136k	AAIJ	23E	LHCB	6 fb^{-1}, pp at 13 TeV, $\eta \to \gamma\pi\pi$
0.8 ±0.7 ±0.5	38k	AAIJ	21U	LHCB	pp at 13 TeV
0.2 ±0.3 ±0.3	22k	GUAN	21	BELL	$e^+e^- \approx \Upsilon(4,5S)$
• • • We do not use the following data for averages, fits, limits, etc. • • •					
1.1 ±3.0 ±0.8		ONYISI	13	CLEO	e^+e^- at 4.17 GeV
−4.6 ±2.9 ±0.3	2.5k	MENDEZ	10	CLEO	See ONYISI 13
−8.2 ±5.2 ±0.8		ALEXANDER	08	CLEO	See MENDEZ 10

$A_{CP}(\pi^\pm\pi^+\pi^-\eta)$ in $D_s^\pm \to \pi^\pm\pi^+\pi^-\eta$

VALUE (%)	DOCUMENT ID		TECN	COMMENT
2.42±2.85±0.78	ABLIKIM	24BD	BES3	e^+e^-, 4.128–4.226 GeV

$A_{CP}(\pi^\pm\eta')$ in $D_s^\pm \to \pi^\pm\eta'$

VALUE (%)	EVTS	DOCUMENT ID		TECN	COMMENT
−0.08±0.17 OUR AVERAGE Error includes scale factor of 1.2.					
−0.59±0.76±0.20		ABLIKIM	24BD	BES3	e^+e^-, 4.128–4.226 GeV
0.01±0.12±0.08	1M	AAIJ	23E	LHCB	6 fb^{-1}, pp at 13 TeV, $\eta \to \gamma\pi\pi$
−0.82±0.36±0.35	152k	AAIJ	17AF	LHCB	pp at 7, 8 TeV
−2.2 ±2.2 ±0.6		ONYISI	13	CLEO	e^+e^- at 4.17 GeV
• • • We do not use the following data for averages, fits, limits, etc. • • •					
−6.1 ±3.0 ±0.3	1.4k	MENDEZ	10	CLEO	See ONYISI 13
−5.5 ±3.7 ±1.2		ALEXANDER	08	CLEO	See MENDEZ 10

$A_{CP}(\eta\pi^\pm\pi^0)$ in $D_s^\pm \to \eta\pi^\pm\pi^0$

VALUE (%)	DOCUMENT ID		TECN	COMMENT
0.9 ±1.5 OUR AVERAGE				
1.05±1.45±0.62	ABLIKIM	24BD	BES3	e^+e^-, 4.128–4.226 GeV
−0.5 ±3.9 ±2.0	ONYISI	13	CLEO	e^+e^- at 4.17 GeV

$A_{CP}(\eta'\pi^\pm\pi^0)$ in $D_s^\pm \to \eta'\pi^\pm\pi^0$

VALUE (%)	DOCUMENT ID		TECN	COMMENT
−1.5 ±2.5 OUR AVERAGE				
−1.60±2.57±0.64	ABLIKIM	24BD	BES3	e^+e^-, 4.128–4.226 GeV
−0.4 ±7.4 ±1.9	ONYISI	13	CLEO	e^+e^- at 4.17 GeV

$A_{CP}(K^\pm\pi^0)$ in $D_s^\pm \to K^\pm\pi^0$

VALUE (%)	EVTS	DOCUMENT ID		TECN	COMMENT
2 ± 4 OUR AVERAGE Error includes scale factor of 1.2.					
− 0.8± 3.9±1.2	2.8k	AAIJ	21U	LHCB	pp at 7, 8, 13 TeV
6.4± 4.4±1.1	12k	GUAN	21	BELL	$e^+e^- \approx \Upsilon(4,5S)$
• • • We do not use the following data for averages, fits, limits, etc. • • •					
−26.6±23.8±0.9	202	MENDEZ	10	CLEO	e^+e^- at 4170 MeV
2 ±29		ADAMS	07A	CLEO	See MENDEZ 10

$A_{CP}(\overline{K}^0/K^0\pi^\pm)$ in $D_s^+ \to \overline{K}^0\pi^+$, $D_s^- \to K^0\pi^-$

VALUE (%)	EVTS	DOCUMENT ID		TECN	COMMENT
0.4 ±0.5 OUR AVERAGE					
0.38±0.46±0.17	121k	[1] AAIJ	14BD	LHCB	pp at 7, 8 TeV
0.3 ±2.0 ±0.3	14k	LEES	13E	BABR	e^+e^- at $\Upsilon(4S)$
• • • We do not use the following data for averages, fits, limits, etc. • • •					
0.61±0.83±0.14	26k	AAIJ	13W	LHCB	See AAIJ 14BD

[1] AAIJ 14BD reports its result as $A_{CP}(D_s^\pm \to K^0_S K^\pm)$ with CP-violation effects in the $K^0 - \overline{K}^0$ system subtracted. It also measures $A_{CP}(D^\pm \to \overline{K}^0/K^0K^\pm) + A_{CP}(D_s^\pm \to \overline{K}^0/K^0\pi^\pm) = (0.41 \pm 0.49 \pm 0.26)\%$.

$A_{CP}(K^0_S\pi^\pm)$ in $D_s^\pm \to K^0_S\pi^\pm$

VALUE (%)	EVTS	DOCUMENT ID		TECN	COMMENT
0.20± 0.18 OUR AVERAGE					
0.16± 0.17±0.05	721k	AAIJ	19T	LHCB	pp at 7, 8, 13 TeV
0.6 ± 2.0 ±0.3	14k	LEES	13E	BABR	e^+e^- at $\Upsilon(4S)$
5.45± 2.50±0.33		KO	10	BELL	$e^+e^- \approx \Upsilon(4S)$
16.3 ± 7.3 ±0.3	0.4k	MENDEZ	10	CLEO	e^+e^- at 4170 MeV
• • • We do not use the following data for averages, fits, limits, etc. • • •					
27 ±11		ADAMS	07A	CLEO	See MENDEZ 10

$A_{CP}(K^\pm\pi^+\pi^-)$ in $D_s^\pm \to K^\pm\pi^+\pi^-$

VALUE (%)	EVTS	DOCUMENT ID		TECN	COMMENT
2.2 ±1.9 OUR AVERAGE					
1.81±2.01±0.45		ABLIKIM	24BD	BES3	e^+e^-, 4.128–4.226 GeV
4.5 ±4.8 ±0.6		ONYISI	13	CLEO	e^+e^- at 4.17 GeV
• • • We do not use the following data for averages, fits, limits, etc. • • •					
3.3 ±3.0 ±1.3	1.3k	[1] ABLIKIM	22AC	BES3	e^+e^-, 4.178–4.226 GeV
11.2 ±7.0 ±0.9		ALEXANDER	08	CLEO	See ONYISI 13

[1] Superseded by ABLIKIM 24BD.

$A_{CP}(K^0_S\pi^+\pi^0)$ in $D_s^\pm \to K^0_S\pi^\pm\pi^0$

VALUE (%)	EVTS	DOCUMENT ID		TECN	COMMENT
−2.17±4.65±1.10		ABLIKIM	24BD	BES3	e^+e^-, 4.128–4.226 GeV
• • • We do not use the following data for averages, fits, limits, etc. • • •					
2.7 ±5.5 ±0.9	666	[1] ABLIKIM	21AB	BES3	e^+e^-, 4.178–4.226 GeV

[1] ABLIKIM 21AB uses an amplitude analysis with 5 resonant modes plus one background component. Superseded by ABLIKIM 24BD.

$A_{CP}(K^\pm\pi^+\pi^-\pi^0)$ in $D_s^\pm \to K^\pm\pi^+\pi^-\pi^0$

VALUE (units 10^{-2})	EVTS	DOCUMENT ID		TECN	COMMENT
6.6±5.4±0.7	776	ABLIKIM	22BL	BES3	e^+e^- at 4.178–4.226 GeV

$A_{CP}(K^\pm\eta)$ in $D_s^\pm \to K^\pm\eta$

VALUE (%)	EVTS	DOCUMENT ID		TECN	COMMENT
1.8± 1.9 OUR AVERAGE					
0.9± 3.7±1.1	2.5k	AAIJ	21U	LHCB	pp at 13 TeV
2.1± 2.1±0.4	14k	GUAN	21	BELL	$e^+e^- \approx \Upsilon(4,5S)$
• • • We do not use the following data for averages, fits, limits, etc. • • •					
9.3±15.2±0.9	222	MENDEZ	10	CLEO	e^+e^- at 4170 MeV
−20 ±18		ADAMS	07A	CLEO	See MENDEZ 10

$A_{CP}(K^\pm\eta'(958))$ in $D_s^\pm \to K^\pm\eta'(958)$

VALUE (%)	EVTS	DOCUMENT ID		TECN	COMMENT
6.0±18.9±0.9	56 ± 17	MENDEZ	10	CLEO	e^+e^- at 4170 MeV
• • • We do not use the following data for averages, fits, limits, etc. • • •					
−17 ±37		ADAMS	07A	CLEO	See MENDEZ 10

Int. J. Mod. Phys. A 2026.41. Downloaded from www.worldscientific.com
by CALIFORNIA @ BERKELEY on 09/16/26. Re-use and distribution is strictly not permitted, except for Open Access articles.

$D_s^\pm$ χ^2 TESTS OF *CP*-VIOLATION (*CPV*)

We list model-independent searches for local *CP* violation in phase-space distributions of multi-body decays.

Most of these searches divide phase space (Dalitz plot for 3-body decays, five-dimensional equivalent for 4-body decays) into bins, and perform a χ^2 test comparing normalised yields N_i, $\overline{N}_i$ in *CP*-conjugate bin pairs i: $\chi^2 = \Sigma_i(N_i - \alpha\,\overline{N}_i)/\sigma(N_i - \alpha\,\overline{N}_i)$. The factor $\alpha = (\Sigma_i N_i)/(\Sigma_i \overline{N}_i)$ removes the dependence on phase-space-integrated rate asymmetries. The result is used to obtain the probability (p-value) to obtain the measured χ^2 or larger under the assumption of CP conservation [AUBERT 08AO, BEDIAGA 09]. Alternative methods obtain p-values from other test variables based on unbinned analyses [WILLIAMS 11, AAIJ 14C]. Results can be combined using Fisher's method [MOSTELLER 48].

Local *CPV* in $D_s^\pm \to K^+K^-K^\pm$

VALUE	EVTS	DOCUMENT ID		TECN	COMMENT
0.133	970k	AAIJ	23L	LHCB	χ^2

CP VIOLATING ASYMMETRIES OF *P*-ODD (*T*-ODD) MOMENTS

$A_{Tviol}(K_S^0 K^\pm\pi^+\pi^-)$ in $D_s^\pm \to K_S^0 K^\pm\pi^+\pi^-$

$C_T \equiv \vec{p}_{K^+}\cdot(\vec{p}_{\pi^+}\times\vec{p}_{\pi^-})$ is a parity-odd correlation of the K^+, π^+, and π^- momenta for the D_s^+. $\overline{C}_T \equiv \vec{p}_{K^-}\cdot(\vec{p}_{\pi^-}\times\vec{p}_{\pi^+})$ is the corresponding quantity for the D_s^-. Then
$A_T \equiv [\Gamma(C_T>0)-\Gamma(C_T<0)]\,/\,[\Gamma(C_T>0)+\Gamma(C_T<0)]$, and
$\overline{A}_T \equiv [\Gamma(-\overline{C}_T>0)-\Gamma(-\overline{C}_T<0)]\,/\,[\Gamma(-\overline{C}_T>0)+\Gamma(-\overline{C}_T<0)]$, and
$A_{Tviol} \equiv \frac{1}{2}(A_T - \overline{A}_T)$. C_T and $\overline{C}_T$ are commonly referred to as *T*-odd moments, because they are odd under *T* reversal. However, the *T*-conjugate process $K_S^0 K^\pm\pi^+\pi^- \to D_s^\pm$ is not accessible, while the *P*-conjugate process is.

VALUE (units 10^{-3})	EVTS	DOCUMENT ID		TECN	COMMENT
− 8 ± 6 OUR AVERAGE					
− 4.6± 6.3± 3.8	70k	MOON	23	BELL	980 fb^{-1} at $\sim\Upsilon(4S)$
−13.6± 7.7± 3.4	29.8k	LEES	11E	BABR	$e^+e^-\approx\Upsilon(4S)$
• • • We do not use the following data for averages, fits, limits, etc. • • •					
−36 ±67 ±23	508	LINK	05E	FOCS	γ A, $\overline{E}_\gamma\approx$180 GeV

$A_{Tviol}(K_S^0 K^\mp\pi^\pm\pi^\pm)$ in $D_s^\pm \to K_S^0 K^\mp\pi^\pm\pi^\pm$

$C_T \equiv \vec{p}_{K_S^0}\cdot(\vec{p}_{K^-}\times\vec{p}_{\pi^+})$ is a parity-odd correlation of the momenta of the K_S^0, K^-, and highest-momenta π^+ fortheD_s^+.$\overline{C}_T \equiv \vec{p}_{K_S^0}\cdot(\vec{p}_{K^+}\times\vec{p}_{\pi^-})$ is the corresponding quantity for the D_s^-. Then
$A_T \equiv [\Gamma(C_T>0)-\Gamma(C_T<0)]\,/\,[\Gamma(C_T>0)+\Gamma(C_T<0)]$, and
$\overline{A}_T \equiv [\Gamma(-\overline{C}_T>0)-\Gamma(-\overline{C}_T<0)]\,/\,[\Gamma(-\overline{C}_T>0)+\Gamma(-\overline{C}_T<0)]$,and
$A_{Tviol} \equiv \frac{1}{2}(A_T - \overline{A}_T)$. C_T and $\overline{C}_T$ are commonly referred to as *T*-odd moments, because they are odd under *T* reversal.However,the *T*-conjugate process $K_S^0 K^\pm\pi^+\pi^- \to D_s^\pm$ is not accessible, while the *P*-conjugate process is.

VALUE (units 10^{-3})	EVTS	DOCUMENT ID		TECN	COMMENT
0.2±2.4±0.8	303k	[1] AGGARWAL	25	BEL2	$e^+e^-\approx\Upsilon(4S)$

[1] AGGARWAL 25 measures $C_T \equiv \vec{p}_{K_S^0}\cdot(\vec{p}_{K^-}\times\vec{p}_{\pi^+})$ and other T-odd observables, all compatible with T-conservation, using Belle and Belle II data.

D_s^+ Semileptonic Form Factors and Decay Constants

$r_2 \equiv A_2(0)/A_1(0)$ in $D_s^+ \to \phi\ell^+\nu_\ell$

VALUE	EVTS	DOCUMENT ID		TECN	COMMENT
0.83 ±0.08 OUR AVERAGE		Error includes scale factor of 1.8. See the ideogram below.			
0.71 ±0.14 ±0.02		[1] ABLIKIM	23BZ	BES3	$D_s^+ \to K^+K^-\mu^+\nu_\mu$
0.816±0.036±0.030	25k	[2] AUBERT	08AN	BABR	$\phi e^+\nu_e$
0.713±0.202±0.284	793	LINK	04C	FOCS	$\phi\mu^+\nu_\mu$
1.57 ±0.25 ±0.19	271	AITALA	99D	E791	$\phi e^+\nu_e$, $\phi\mu^+\nu_\mu$
1.4 ±0.5 ±0.3	308	AVERY	94B	CLE2	$\phi e^+\nu_e$
1.1 ±0.8 ±0.1	90	FRABETTI	94F	E687	$\phi\mu^+\nu_\mu$
2.1 $^{+0.6}_{-0.5}$ ±0.2	19	KODAMA	93	E653	$\phi\mu^+\nu_\mu$

[1] Partial wave analysis of 939 $D_s^+ \to K^+K^-\mu^+\nu_\mu$ events.
[2] To compare with previous measurements, this AUBERT 08AN value is from a fit that fixes the pole masses at m_A = 2.5 GeV/c^2 and m_V = 2.1 GeV/c^2. A simultaneous fit to r_2, r_V, r_0 (a significant *s*-wave contribution) and m_A, gives r_2 = 0.763 ± 0.071 ± 0.065.

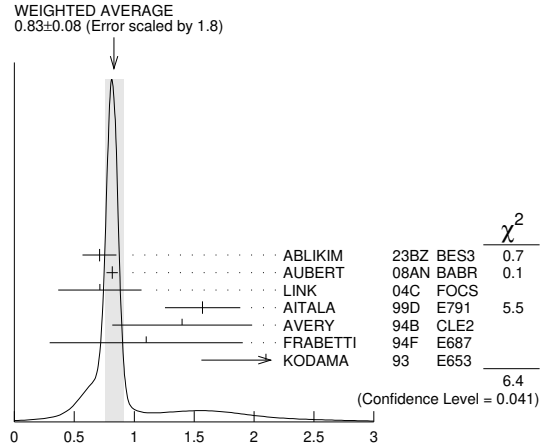

$r_2 \equiv A_2(0)/A_1(0)$ in $D_s^+ \to \phi\ell^+\nu_\ell$

$r_V \equiv V(0)/A_1(0)$ in $D_s^+ \to \phi\ell^+\nu_\ell$

VALUE	EVTS	DOCUMENT ID		TECN	COMMENT
1.76 ±0.07 OUR AVERAGE		Error includes scale factor of 1.1.			
1.58 ±0.17 ±0.02		[1] ABLIKIM	23BZ	BES3	$D_s^+ \to K^+K^-\mu^+\nu_\mu$
1.807±0.046±0.065	25k	[2] AUBERT	08AN	BABR	$\phi e^+\nu_e$
1.549±0.250±0.148	793	LINK	04C	FOCS	$\phi\mu^+\nu_\mu$
2.27 ±0.35 ±0.22	271	AITALA	99D	E791	$\phi e^+\nu_e$, $\phi\mu^+\nu_\mu$
0.9 ±0.6 ±0.3	308	AVERY	94B	CLE2	$\phi e^+\nu_e$
1.8 ±0.9 ±0.2	90	FRABETTI	94F	E687	$\phi\mu^+\nu_\mu$
2.3 $^{+1.1}_{-0.9}$ ±0.4	19	KODAMA	93	E653	$\phi\mu^+\nu_\mu$

[1] Partial wave analysis of 939 $D_s^+ \to K^+K^-\mu^+\nu_\mu$ events.
[2] To compare with previous measurements, this AUBERT 08AN value is from a fit that fixes the pole masses at m_A = 2.5 GeV/c^2 and m_V = 2.1 GeV/c^2. A simultaneous fit to r_2, r_V, r_0 (a significant *s*-wave contribution) and m_A, gives r_V = 1.849 ± 0.060 ± 0.095.

Γ_L/Γ_T in $D_s^+ \to \phi\ell^+\nu_\ell$

VALUE	EVTS	DOCUMENT ID		TECN	COMMENT
0.72±0.18 OUR AVERAGE					
1.0 ±0.3 ±0.2	308	AVERY	94B	CLE2	$\phi e^+\nu_e$
1.0 ±0.5 ±0.1	90	[1] FRABETTI	94F	E687	$\phi\mu^+\nu_\mu$
0.54±0.21±0.10	19	[1] KODAMA	93	E653	$\phi\mu^+\nu_\mu$

[1] FRABETTI 94F and KODAMA 93 evaluate Γ_L/Γ_T for a lepton mass of zero.

$f_+(0)\,|V_{cs}|$ in $D_s^+ \to \eta e^+\nu_e$

VALUE	EVTS	DOCUMENT ID		TECN	COMMENT
0.449 ±0.009 OUR AVERAGE					
0.430 ±0.021 ±0.016	716	[1] ABLIKIM	24CI	BES3	e^+e^- at 4237–4699 MeV
0.4519±0.0071±0.0065	4k	ABLIKIM	23BO	BES3	e^+e^- at 4128–4226 MeV
• • • We do not use the following data for averages, fits, limits, etc. • • •					
0.4455±0.0053±0.0044	1.8k	[2] ABLIKIM	19S	BES3	e^+e^- at 4178 MeV

[1] Using a two parameter fit in the *z* expansion .
[2] Superseded by ABLIKIM 23BO

$f_+(0)\,|V_{cs}|$ in $D_s^+ \to \eta\mu^+\nu_\mu$

VALUE	EVTS	DOCUMENT ID		TECN	COMMENT
0.452±0.010±0.007	3.1k	ABLIKIM	24AQ	BES3	e^+e^-, 4.128–4.266 GeV

$r_1 \equiv a_1/a_0$ in $D_s^+ \to \eta\mu^+\nu_\mu$

VALUE	EVTS	DOCUMENT ID		TECN	COMMENT
−2.9±0.6±0.2	3.1k	ABLIKIM	24AQ	BES3	e^+e^-, 4.128–4.266 GeV

$\langle A_{FB}^\eta\rangle$ in $D_s^+ \to \eta\mu^+\nu_\mu$

VALUE (units 10^{-2})	EVTS	DOCUMENT ID		TECN	COMMENT
−5.9±3.1±0.5	3.1k	ABLIKIM	24AQ	BES3	e^+e^-, 4.128–4.266 GeV

$f_+(0)\,|V_{cs}|$ in $D_s^+ \to \eta' e^+\nu_e$

VALUE	EVTS	DOCUMENT ID		TECN	COMMENT
0.527±0.024 OUR AVERAGE					
0.542±0.062±0.023	134	[1] ABLIKIM	24CI	BES3	e^+e^- at 4237–4699 MeV
0.525±0.024±0.009	675	ABLIKIM	23BO	BES3	e^+e^- at 4128–4226 MeV
• • • We do not use the following data for averages, fits, limits, etc. • • •					
0.477±0.049±0.011	261	[2] ABLIKIM	19S	BES3	e^+e^- at 4178 MeV

[1] Using a two parameter fit in the *z* expansion.
[2] Superseded by ABLIKIM 23BO

$r_1 \equiv a_1/a_0$ in $D_s^+ \to \eta'\mu^+\nu_\mu$

VALUE	EVTS	DOCUMENT ID		TECN	COMMENT
−10.8±5.3±1.4	390	ABLIKIM	24AQ	BES3	e^+e^-, 4.128–4.266 GeV

Int. J. Mod. Phys. A 2026.41. Downloaded from www.worldscientific.com
by UNIVERSITY OF CALIFORNIA @ BERKELEY on 09/16/26. Re-use and distribution is strictly not permitted, except for Open Access articles.

$\langle A_{FB}^{\eta'} \rangle$ in $D_s^+ \to \eta' \mu^+ \nu_\mu$

VALUE (units 10^{-2})	EVTS	DOCUMENT ID		TECN	COMMENT
−6.4±7.9±0.6	390	ABLIKIM	24AQ	BES3	e^+e^-, 4.128–4.266 GeV

$f_+(0)\,|V_{cs}|$ in $D_s^+ \to \eta' \mu^+ \nu_\mu$

VALUE	EVTS	DOCUMENT ID		TECN	COMMENT
0.504±0.037±0.012	390	ABLIKIM	24AQ	BES3	e^+e^-, 4.128–4.266 GeV

$f_+(0)\,|V_{cs}|$ in $D_s^+ \to f_0(980) e^+ \nu_e$

VALUE	EVTS	DOCUMENT ID		TECN	COMMENT
0.504±0.017±0.035	0.4k	[1] ABLIKIM	24AT	BES3	e^+e^- at 4128–4226 MeV

[1] From an analysis of $D_s^+ \to \pi^+\pi^- e^+ \mu_e$ decays. ABLIKIM 24AT uses a simple pole parametrization of the hadronic form factor and the Flatte' formula for describing the $f_0(980)$ decay.

$f_+(0)|V_{cd}|$ in $D_s^+ \to K^0 e^+ \nu_e$

VALUE	EVTS	DOCUMENT ID		TECN	COMMENT
0.145±0.010 OUR AVERAGE					
0.143±0.011±0.003	228	[1] ABLIKIM	24CH	BES3	e^+e^- at 4128–4226 MeV
0.152±0.022±0.005	51	[1] ABLIKIM	24CI	BES3	e^+e^- at 4237–4699 MeV
• • • We do not use the following data for averages, fits, limits, etc. • • •					
0.162±0.019±0.003	117	[1,2] ABLIKIM	19D	BES3	$K_S^0 e^+ \nu_e$

[1] Using a two parameter fit in the z expansion.
[2] Superseded by ABLIKIM 24CH.

$r_V \equiv V(0)/A_1(0)$ in $D_s^+ \to K^*(892)^0 e^+ \nu_e$

VALUE	EVTS	DOCUMENT ID		TECN	COMMENT
1.67±0.34±0.16	155	ABLIKIM	19D	BES3	e^+e^- at 4178 MeV

$r_2 \equiv A_2(0)/A_1(0)$ in $D_s^+ \to K^*(892)^0 e^+ \nu_e$

VALUE	EVTS	DOCUMENT ID		TECN	COMMENT
0.77±0.28±0.07	155	ABLIKIM	19D	BES3	e^+e^- at 4178 MeV

$f_{D_s^+}\,|V_{cs}|$ in $D_s^+ \to \mu^+ \nu_\mu$

VALUE (MeV)	EVTS	DOCUMENT ID		TECN	COMMENT
242.7±3.0 OUR AVERAGE					
246.5±5.9±3.6±0.5	0.5k	[1] ABLIKIM	24CG	BES3	e^+e^- at 4.237–4.699 GeV
241.8±2.5±2.2	2.5k	ABLIKIM	23BR	BES3	e^+e^- at 4.128–4.226 GeV
• • • We do not use the following data for averages, fits, limits, etc. • • •					
243.1±3.0±3.6±1.0	2.2K	[2,3] ABLIKIM	21BE	BES3	e^+e^- at 4.178, 4.226 GeV
246.2±3.6±3.5	1.1k	[3] ABLIKIM	19E	BES3	e^+e^- at 4.178 GeV

[1] The third uncertainty is due to the uncertainty of the D_s^+ lifetime.
[2] The third uncertainty is dominated by the uncertainty of the D_s^+ lifetime.
[3] Superseded by ABLIKIM 23BR.

$f_{D_s^+}\,|V_{cs}|$ in $D_s^+ \to \tau^+ \nu_\tau$

VALUE (MeV)	EVTS	DOCUMENT ID		TECN	COMMENT
247.5±2.3 OUR AVERAGE					
252.7±3.6±4.5±0.6	2.8k	[1] ABLIKIM	24CG	BES3	e^+e^- at 4.237–4.699 GeV
248.3±3.9±3.1±1.0	2.4k	[2] ABLIKIM	23BP	BES3	e^+e^- at 4.128–4.226 GeV
246.7±3.9±3.6	2.3k	[3] ABLIKIM	23BX	BES3	e^+e^- at 4.128–4.226 GeV
251.6±5.9±4.9	1.7k	[4] ABLIKIM	21AF	BES3	e^+e^- at 4.178, 4.226 GeV
244.4±2.3±2.9	4.9k	[5] ABLIKIM	21AZ	BES3	e^+e^- at 4.178, 4.226 GeV
• • • We do not use the following data for averages, fits, limits, etc. • • •					
243.0±5.8±4.0±1.0	950	[6,7] ABLIKIM	21BE	BES3	e^+e^- at 4.178, 4.226 GeV

[1] ABLIKIM 24CG uses $\tau^+ \to (e^+\nu_e,\ \mu^+\nu_\mu,\ \pi^+,\ \rho^+)\overline{\nu}_\tau$ decays. The third uncertainty is due to the uncertainty of the D_s^+ lifetime.
[2] ABLIKIM 23BP uses $\tau^+ \to \pi^+\overline{\nu}_\tau$ decays. The third uncertainty is due to the input parameters, mainly the D_s^+ lifetime.
[3] ABLIKIM 23BX uses $\tau^+ \to \mu^+\nu_\mu\overline{\nu}_\tau$ decays.
[4] ABLIKIM 21AF uses $\tau^+ \to \pi^+\pi^0\overline{\nu}$ decays.
[5] ABLIKIM 21AZ uses $\tau^+ \to e^+\nu_e\overline{\nu}_\tau$ decays.
[6] ABLIKIM 21BE uses $\tau^+ \to \pi^+\overline{\nu}_\tau$ decays. When constrained by the Standard Model ratio of $\Gamma(D_s^+ \to \tau^+\nu_\tau)/\Gamma(D_s^+ \to \mu^+\nu_\mu) = 9.75$, the result is $243.2 \pm 2.3 \pm 3.3 \pm 1.0$.
[7] The third uncertainty is dominated by the uncertainty of the D_s^+ lifetime. Superseded by ABLIKIM 23BP.

$D_s^\pm$ REFERENCES

ABLIKIM 25A PRL 134 011904 M. Ablikim et al. (BESIII Collab.)
ABLIKIM 25BC JHEP 2501 109 M. Ablikim et al. (BESIII Collab.)
ABLIKIM 25BR PRL 135 161902 M. Ablikim et al. (BESIII Collab.)
ABLIKIM 25F PRL 134 201902 M. Ablikim et al. (BESIII Collab.)
AGGARWAL 25 JHEP 2504 036 L. Aggarwal et al. (BELLE and BELLE II Collab.)
ABLIKIM 24AQ PRL 132 091802 M. Ablikim et al. (BESIII Collab.)
ABLIKIM 24AT PRL 132 141901 M. Ablikim et al. (BESIII Collab.)
ABLIKIM 24AV PR D109 032011 M. Ablikim et al. (BESIII Collab.)
ABLIKIM 24BD JHEP 2405 335 M. Ablikim et al. (BESIII Collab.)
ABLIKIM 24CF PRL 133 121801 M. Ablikim (BESIII Collab.)
ABLIKIM 24CG PR D110 052002 M. Ablikim et al. (BESIII Collab.)
ABLIKIM 24CH PR D110 052012 M. Ablikim (BESIII Collab.)
ABLIKIM 24CI PR D110 072017 M. Ablikim et al. (BESIII Collab.)
ABLIKIM 24CT JHEP 2411 119 M. Ablikim et al. (BESIII Collab.)
AAIJ 23AN JHEP 2307 204 R. Aaij et al. (LHCb Collab.)
AAIJ 23E JHEP 2304 081 R. Aaij et al. (LHCb Collab.)
AAIJ 23L JHEP 2307 067 R. Aaij et al. (LHCb Collab.)
ABLIKIM 23AL PR D107 052010 M. Ablikim et al. (BESIII Collab.)
ABLIKIM 23AV PR D108 032001 M. Ablikim et al. (BESIII Collab.)
ABLIKIM 23BO PR D108 092003 M. Ablikim et al. (BESIII Collab.)
ABLIKIM 23BP PR D108 092014 M. Ablikim et al. (BESIII Collab.)
ABLIKIM 23BR PR D108 112001 M. Ablikim et al. (BESIII Collab.)
ABLIKIM 23BS PR D108 112002 M. Ablikim et al. (BESIII Collab.)
ABLIKIM 23BX JHEP 2309 124 M. Ablikim et al. (BESIII Collab.)
ABLIKIM 23BZ JHEP 2312 072 M. Ablikim et al. (BESIII Collab.)
ADACHI 23G PRL 131 171803 I. Adachi et al. (BELLE II Collab.)
LI 23G PR D107 033003 L.K. Li et al. (BELLE Collab.)
MOON 23 PR D108 L111102 H.K. Moon et al. (BELLE Collab.)
ABLIKIM 22AA JHEP 2204 058 M. Ablikim et al. (BESIII Collab.)
ABLIKIM 22AB JHEP 2207 051 M. Ablikim et al. (BESIII Collab.)
ABLIKIM 22AC JHEP 2208 196 M. Ablikim et al. (BESIII Collab.)
ABLIKIM 22AH PRL 129 182001 M. Ablikim et al. (BESIII Collab.)
ABLIKIM 22BH PR D106 112004 M. Ablikim et al. (BESIII Collab.)
ABLIKIM 22BI PR D106 112006 M. Ablikim et al. (BESIII Collab.)
ABLIKIM 22BL JHEP 2209 242 M. Ablikim et al. (BESIII Collab.)
ABLIKIM 22F PR D105 L051103 M. Ablikim et al. (BESIII Collab.)
ABLIKIM 22J PR D105 L031101 M. Ablikim et al. (BESIII Collab.)
ABLIKIM 22Z JHEP 2201 052 M. Ablikim et al. (BESIII Collab.)
AAIJ 21T JHEP 2106 044 R. Aaij et al. (LHCb Collab.)
AAIJ 21U JHEP 2106 019 R. Aaij et al. (LHCb Collab.)
ABLIKIM 21AB JHEP 2106 181 M. Ablikim et al. (BESIII Collab.)
ABLIKIM 21AC PR D104 012003 M. Ablikim et al. (BESIII Collab.)
ABLIKIM 21AE PR D104 012016 M. Ablikim et al. (BESIII Collab.)
ABLIKIM 21AF PR D104 032001 M. Ablikim et al. (BESIII Collab.)
ABLIKIM 21AR PR D104 L071101 M. Ablikim et al. (BESIII Collab.)
ABLIKIM 21AZ PRL 127 171801 M. Ablikim et al. (BESIII Collab.)
ABLIKIM 21BE PR D104 052009 M. Ablikim et al. (BESIII Collab.)
ABLIKIM 21K PR D103 092006 M. Ablikim et al. (BESIII Collab.)
ABLIKIM 21U PR D104 032011 M. Ablikim et al. (BESIII Collab.)
ABLIKIM 21Y PR D103 092004 M. Ablikim et al. (BESIII Collab.)
GUAN 21 PR D103 112005 Y. Guan et al. (BELLE Collab.)
LEES 21A PR D104 072002 J.P. Lees et al. (BABAR Collab.)
ABLIKIM 20R JHEP 2008 146 M. Ablikim et al. (BESIII Collab.)
AAIJ 19G JHEP 1903 176 R. Aaij et al. (LHCb Collab.)
AAIJ 19T PRL 122 191803 R. Aaij et al. (LHCb Collab.)
ABLIKIM 19AD PR D99 072002 M. Ablikim et al. (BESIII Collab.)
ABLIKIM 19AH PR D99 091101 M. Ablikim et al. (BESIII Collab.)
ABLIKIM 19AM PR D99 112005 M. Ablikim et al. (BESIII Collab.)
ABLIKIM 19BD PR D100 112008 M. Ablikim et al. (BESIII Collab.)
ABLIKIM 19BE PRL 123 112001 M. Ablikim et al. (BESIII Collab.)
ABLIKIM 19D PRL 122 061801 M. Ablikim et al. (BESIII Collab.)
ABLIKIM 19E PRL 122 071802 M. Ablikim et al. (BESIII Collab.)
ABLIKIM 19O PR D99 031101 M. Ablikim et al. (BESIII Collab.)
ABLIKIM 19S PRL 122 121801 M. Ablikim et al. (BESIII Collab.)
ABLIKIM 18A PR D97 012006 M. Ablikim et al. (BESIII Collab.)
AAIJ 17AF PL B771 21 R. Aaij et al. (LHCb Collab.)
AAIJ 17AN PRL 119 101801 R. Aaij et al. (LHCb Collab.)
ABLIKIM 16O PR D94 072004 M. Ablikim et al. (BESIII Collab.)
ABLIKIM 16T PR D94 112003 M. Ablikim et al. (BESIII Collab.)
ABLIKIM 15Z PL B750 466 M. Ablikim et al. (BESIII Collab.)
HIETALA 15 PR D92 012009 J. Hietala et al. (MINN, LUTH, OXF)
LEES 15D PR D91 019901 (errat.) J.P. Lees et al. (BABAR Collab.)
AAIJ 14BD JHEP 1410 025 R. Aaij et al. (LHCb Collab.)
AAIJ 14C PL B728 585 R. Aaij et al. (LHCb Collab.)
ABAZOV 14B PRL 112 111804 V.M. Abazov et al. (D0 Collab.)
AAIJ 13AF PL B724 203 R. Aaij et al. (LHCb Collab.)
AAIJ 13V JHEP 1306 065 R. Aaij et al. (LHCb Collab.)
AAIJ 13W JHEP 1306 112 R. Aaij et al. (LHCb Collab.)
LEES 13E PR D87 052012 J.P. Lees et al. (BABAR Collab.)
ONYISI 13 PR D88 032009 P.U.E. Onyisi et al. (CLEO Collab.)
ZUPANC 13 JHEP 1309 139 A. Zupanc et al. (BELLE Collab.)
DEL-AMO-SA... 11G PR D83 052001 P. del Amo Sanchez et al. (BABAR Collab.)
LEES 11E PR D84 031103 J.P. Lees et al. (BABAR Collab.)
LEES 11G PR D84 072006 J.P. Lees et al. (BABAR Collab.)
MARTIN 11 PR D84 012005 L. Martin et al. (CLEO Collab.)
WILLIAMS 11 PR D84 054015 M. Williams (LOIC)
ASNER 10 PR D81 052007 D.M. Asner et al. (CLEO Collab.)
DEL-AMO-SA... 10J PR D82 091103 P. del Amo Sanchez et al. (BABAR Collab.)
Also PR D91 019901 (errat.) J.P. Lees et al. (BABAR Collab.)
KO 10 PRL 104 181602 B.R. Ko et al. (BELLE Collab.)
MENDEZ 10 PR D81 052013 H. Mendez et al. (CLEO Collab.)
RUBIN 10 PR D82 092007 P. Rubin et al. (CLEO Collab.)
ALEXANDER 09 PR D79 052001 J.P. Alexander et al. (CLEO Collab.)
AUBERT 09O PR D79 032003 B. Aubert et al. (BABAR Collab.)
BEDIAGA 09 PR D80 096006 I. Bediaga et al. (CBPF, NDAM)
DOBBS 09 PR D79 112008 S. Dobbs et al. (CLEO Collab.)
ECKLUND 09 PR D80 052009 K.M. Ecklund et al. (CLEO Collab.)
GE 09A PR D80 051102 J.Y. Ge et al. (CLEO Collab.)
KO 09 PRL 102 221802 B.R. Ko et al. (BELLE Collab.)
MITCHELL 09A PR D79 072008 R.E. Mitchell et al. (CLEO Collab.)
NAIK 09A PR D80 112004 P. Naik et al. (CLEO Collab.)
ONYISI 09 PR D79 052002 P.U.E. Onyisi et al. (CLEO Collab.)
WON 09 PR D80 111101 E. Won et al. (BELLE Collab.)
YELTON 09 PR D80 052007 J. Yelton et al. (CLEO Collab.)
ALEXANDER 08 PRL 100 161804 J.P. Alexander et al. (CLEO Collab.)
ATHAR 08 PRL 100 181802 S.B. Athar et al. (CLEO Collab.)
AUBERT 08AN PR D78 051101 B. Aubert et al. (BABAR Collab.)
AUBERT 08AO PR D78 051102 B. Aubert et al. (BABAR Collab.)
ECKLUND 08 PRL 100 161801 K.M. Ecklund et al. (CLEO Collab.)
KLEMPT 08 EPJ C55 39 E. Klempt, M. Matveev, A.V. Sarantsev (BONN+)
LINK 08 PL B660 147 J.M. Link et al. (FNAL FOCUS Collab.)
WIDHALM 08 PRL 100 241801 L. Widhalm et al. (BELLE Collab.)
ADAMS 07A PRL 99 191805 G.S. Adams et al. (CLEO Collab.)
AUBERT 07V PRL 98 141801 B. Aubert et al. (BABAR Collab.)
PEDLAR 07A PR D76 072002 T.K. Pedlar et al. (CLEO Collab.)
Also PRL 99 071802 M. Artuso et al. (CLEO Collab.)
AUBERT 06N PR D74 031103 B. Aubert et al. (BABAR Collab.)
HUANG 06B PR D74 112005 G.S. Huang et al. (CLEO Collab.)
PDG 06 JP G33 1 W.-M. Yao et al. (PDG Collab.)
AUBERT 05V PR D71 091104 B. Aubert et al. (BABAR Collab.)
LINK 05E PL B622 239 J.M. Link et al. (FNAL FOCUS Collab.)
LINK 05J PRL 95 052003 J.M. Link et al. (FNAL FOCUS Collab.)
LINK 05K PL B624 166 J.M. Link et al. (FNAL FOCUS Collab.)
LINK 04 PL B585 200 J.M. Link et al. (FNAL FOCUS Collab.)
LINK 04C PL B586 183 J.M. Link et al. (FNAL FOCUS Collab.)
LINK 04D PL B586 191 J.M. Link et al. (FNAL FOCUS Collab.)
LINK 04F PL B601 10 J.M. Link et al. (FNAL FOCUS Collab.)
ACOSTA 03D PR D68 072004 D. Acosta et al. (FNAL CDF-II Collab.)
ANISOVICH 03 EPJ A16 229 V.V. Anisovich et al.
LINK 03D PL B561 225 J.M. Link et al. (FNAL FOCUS Collab.)
LINK 03F PL B572 21 J.M. Link et al. (FNAL FOCUS Collab.)
AUBERT 02G PR D65 091104 B. Aubert et al. (BABAR Collab.)
HEISTER 02I PL B528 1 A. Heister et al. (ALEPH Collab.)
LINK 02I PL B541 227 J.M. Link et al. (FNAL FOCUS Collab.)
LINK 02J PL B541 243 J.M. Link et al. (FNAL FOCUS Collab.)
ABBIENDI 01L PL B516 236 G. Abbiendi et al. (OPAL Collab.)

AITALA	01A	PRL 86 765	E.M. Aitala *et al.*	(FNAL E791 Collab.)
IORI	01	PL B523 22	M. Iori *et al.*	(FNAL SELEX Collab.)
LINK	01C	PRL 87 162001	J.M. Link *et al.*	(FNAL FOCUS Collab.)
ALEXANDROV	00	PL B478 31	Y. Alexandrov *et al.*	(CERN BEATRICE Collab.)
AITALA	99	PL B445 449	E.M. Aitala *et al.*	(FNAL E791 Collab.)
AITALA	99D	PL B450 294	E.M. Aitala *et al.*	(FNAL E791 Collab.)
AITALA	99G	PL B462 401	E.M. Aitala *et al.*	(FNAL E791 Collab.)
BONVICINI	99	PRL 82 4586	G. Bonvicini *et al.*	(CLEO Collab.)
CHADHA	98	PR D58 032002	M. Chada *et al.*	(CLEO Collab.)
JESSOP	98	PR D58 052002	C.P. Jessop *et al.*	(CLEO Collab.)
ACCIARRI	97F	PL B396 327	M. Acciarri *et al.*	(L3 Collab.)
BALEST	97	PRL 79 1436	R. Balest *et al.*	(CLEO Collab.)
FRABETTI	97C	PL B401 131	P.L. Frabetti *et al.*	(FNAL E687 Collab.)
FRABETTI	97D	PL B407 79	P.L. Frabetti *et al.*	(FNAL E687 Collab.)
ARTUSO	96	PL B378 364	M. Artuso *et al.*	(CLEO Collab.)
BAI	95C	PR D52 3781	J.Z. Bai *et al.*	(BES Collab.)
BRANDENB...	95	PRL 75 3804	G.W. Brandenburg *et al.*	(CLEO Collab.)
FRABETTI	95B	PL B351 591	P.L. Frabetti *et al.*	(FNAL E687 Collab.)
KODAMA	95	PL B345 85	K. Kodama *et al.*	(FNAL E653 Collab.)
ACOSTA	94	PR D49 5690	D. Acosta *et al.*	(CLEO Collab.)
AVERY	94B	PL B337 405	P. Avery *et al.*	(CLEO Collab.)
BROWN	94	PR D50 1884	D. Brown *et al.*	(CLEO Collab.)
BUTLER	94	PL B324 255	F. Butler *et al.*	(CLEO Collab.)
FRABETTI	94F	PL B328 187	P.L. Frabetti *et al.*	(FNAL E687 Collab.)
FRABETTI	93F	PRL 71 827	P.L. Frabetti *et al.*	(FNAL E687 Collab.)
FRABETTI	93G	PL B313 253	P.L. Frabetti *et al.*	(FNAL E687 Collab.)
KODAMA	93	PL B309 483	K. Kodama *et al.*	(FNAL E653 Collab.)
ALBRECHT	92B	ZPHY C53 361	H. Albrecht *et al.*	(ARGUS Collab.)
ALEXANDER	92	PRL 68 1275	J. Alexander *et al.*	(CLEO Collab.)
AVERY	92	PRL 68 1279	P. Avery *et al.*	(CLEO Collab.)
BARLAG	92C	ZPHY C55 383	S. Barlag *et al.*	(ACCMOR Collab.)
Also		ZPHY C48 29	S. Barlag *et al.*	(ACCMOR Collab.)
FRABETTI	92	PL B281 167	P.L. Frabetti *et al.*	(FNAL E687 Collab.)
ALBRECHT	91	PL B255 634	H. Albrecht *et al.*	(ARGUS Collab.)
ALVAREZ	91	PL B255 639	M.P. Alvarez *et al.*	(CERN NA14/2 Collab.)
ALBRECHT	90D	PL B245 315	H. Albrecht *et al.*	(ARGUS Collab.)
ALEXANDER	90B	PRL 65 1531	J. Alexander *et al.*	(CLEO Collab.)
BARLAG	90C	ZPHY C46 563	S. Barlag *et al.*	(ACCMOR Collab.)
FRABETTI	90	PL B251 639	P.L. Frabetti *et al.*	(FNAL E687 Collab.)
ANJOS	89E	PL B223 267	J.C. Anjos *et al.*	(FNAL E691 Collab.)
CHEN	89	PL B226 192	W.Y. Chen *et al.*	(CLEO Collab.)
ALBRECHT	88	PL B207 349	H. Albrecht *et al.*	(ARGUS Collab.)
ANJOS	88	PRL 60 897	J.C. Anjos *et al.*	(FNAL E691 Collab.)
RAAB	88	PR D37 2391	J.R. Raab *et al.*	(FNAL E691 Collab.)
BECKER	87B	PL B184 277	H. Becker *et al.*	(NA11 and NA32 Collabs.)
BLAYLOCK	87	PRL 58 2171	G.T. Blaylock *et al.*	(Mark III Collab.)
USHIDA	86	PRL 56 1767	N. Ushida *et al.*	(FNAL E531 Collab.)
ALBRECHT	85D	PL 153B 343	H. Albrecht *et al.*	(ARGUS Collab.)
DERRICK	85B	PRL 54 2568	M. Derrick *et al.*	(HRS Collab.)
AIHARA	84D	PRL 53 2465	H. Aihara *et al.*	(TPC Collab.)
ALTHOFF	84	PL 136B 130	M. Althoff *et al.*	(TASSO Collab.)
BAILEY	84	PL 139B 320	R. Bailey *et al.*	(ACCMOR Collab.)
CHEN	83C	PRL 51 634	A. Chen *et al.*	(CLEO Collab.)
MOSTELLER	48	AST 2 No.5 30	R.A. Fisher, F. Mosteller	

OTHER RELATED PAPERS

RICHMAN	95	RMP 67 893	J.D. Richman, P.R. Burchat	(UCSB, STAN)

$D_s^{*\pm}$

$I(J^P) = 0(1^-)$

$J^P = 1^-$ established by ABLIKIM 23AZ.

$D_s^{*\pm}$ MASS

The fit includes $D^{\pm}$, D^0, $D_s^{\pm}$, $D^{*\pm}$, D^{*0}, $D_s^{*\pm}$, $D_1(2420)^0$, $D_2^*(2460)^0$, and $D_{s1}(2536)^{\pm}$ mass and mass difference measurements.

VALUE (MeV)	DOCUMENT ID		TECN	COMMENT
2112.2±0.4 OUR FIT				
2106.6±2.1±2.7	[1] BLAYLOCK	87	MRK3	$e^+e^- \to D_s^{\pm}\gamma X$

[1] Assuming $D_s^{\pm}$ mass = 1968.7 ± 0.9 MeV.

$m_{D_s^{*\pm}} - m_{D_s^{\pm}}$

The fit includes $D^{\pm}$, D^0, $D_s^{\pm}$, $D^{*\pm}$, D^{*0}, $D_s^{*\pm}$, $D_1(2420)^0$, $D_2^*(2460)^0$, and $D_{s1}(2536)^{\pm}$ mass and mass difference measurements.

VALUE (MeV)	EVTS	DOCUMENT ID		TECN	COMMENT
143.8 ± 0.4 OUR FIT					
143.9 ± 0.4 OUR AVERAGE					
143.76± 0.39±0.40		GRONBERG	95	CLE2	e^+e^-
144.22± 0.47±0.37		BROWN	94	CLE2	e^+e^-
142.5 ± 0.8 ±1.5		[2] ALBRECHT	88	ARG	$e^+e^- \to D_s^{\pm}\gamma X$
139.5 ± 8.3 ±9.7	60	AIHARA	84D	TPC	$e^+e^- \to$ hadrons
• • • We do not use the following data for averages, fits, limits, etc. • • •					
143.0 ±18.0	8	ASRATYAN	85	HLBC	FNAL 15-ft, ν-^{2}H
110 ±46		BRANDELIK	79	DASP	$e^+e^- \to D_s^{\pm}\gamma X$

[2] Result includes data of ALBRECHT 84B.

$D_s^{*\pm}$ WIDTH

VALUE (MeV)	CL%	DOCUMENT ID		TECN	COMMENT
< 1.9	90	GRONBERG	95	CLE2	e^+e^-
< 4.5	90	ALBRECHT	88	ARG	E_{cm}^{ee} = 10.2 GeV
• • • We do not use the following data for averages, fits, limits, etc. • • •					
< 4.9	90	BROWN	94	CLE2	e^+e^-
<22	90	BLAYLOCK	87	MRK3	$e^+e^- \to D_s^{\pm}\gamma X$

D_s^{*+} DECAY MODES

D_s^{*-} modes are charge conjugates of the modes below.

	Mode	Fraction (Γ_i/Γ)
Γ_1	$D_s^+\gamma$	(93.6 ±0.4) %
Γ_2	$D_s^+\pi^0$	(5.77±0.35) %
Γ_3	$D_s^+e^+e^-$	(6.7 ±1.6) × 10^{-3}
Γ_4	$e^+\nu_e$	(2.1 $^{+1.2}_{-0.9}$) × 10^{-5}

CONSTRAINED FIT INFORMATION

An overall fit to 2 branching ratios uses 4 measurements and one constraint to determine 3 parameters. The overall fit has a χ^2 = 0.0 for 2 degrees of freedom.

The following *off-diagonal* array elements are the correlation coefficients $\langle \delta x_i \delta x_j \rangle / (\delta x_i \cdot \delta x_j)$, in percent, from the fit to the branching fractions, $x_i \equiv \Gamma_i/\Gamma_{total}$. The fit constrains the x_i whose labels appear in this array to sum to one.

	x_1	x_2
x_2	−91	
x_3	−38	−4

D_s^{*+} BRANCHING RATIOS

$\Gamma(D_s^+\gamma)/\Gamma_{total}$ — Γ_1/Γ

VALUE (%)	DOCUMENT ID		TECN	COMMENT
• • • We do not use the following data for averages, fits, limits, etc. • • •				
seen	ASRATYAN	91	HLBC	$\bar{\nu}_\mu$ Ne
seen	ALBRECHT	88	ARG	$e^+e^- \to D_s^{\pm}\gamma X$
seen	AIHARA	84D		
seen	ALBRECHT	84B		
seen	BRANDELIK	79		

$\Gamma(D_s^+\pi^0)/\Gamma(D_s^+\gamma)$ — Γ_2/Γ_1

VALUE (units 10^{-2})	DOCUMENT ID		TECN	COMMENT
6.2 ±0.4 OUR FIT				
6.2 ±0.4 OUR AVERAGE				
6.16±0.43±0.18	ABLIKIM	23P	BES3	e^+e^-
6.2 ±0.5 ±0.6	AUBERT,BE	05G	BABR	10.6 $e^+e^- \to$ hadrons
6.2 $^{+2.0}_{-1.8}$ ±2.2	GRONBERG	95	CLE2	e^+e^-

$\Gamma(D_s^+e^+e^-)/\Gamma(D_s^+\gamma)$ — Γ_3/Γ_1

VALUE (units 10^{-3})	EVTS	DOCUMENT ID		TECN	COMMENT
7.2±1.7 OUR FIT					
7.2$^{+1.5}_{-1.3}$±1.0	38	CRONIN-HEN..	12	CLEO	4.17 $e^+e^- \to$ hadrons

$\Gamma(e^+\nu_e)/\Gamma_{total}$ — Γ_4/Γ

VALUE (units 10^{-5})	DOCUMENT ID		TECN	COMMENT
2.1$^{+1.2}_{-0.9}$±0.2	ABLIKIM	23BF	BES3	$e^+e^- \to D_s^- D_s^{*+}$

$D_s^{*\pm}$ REFERENCES

ABLIKIM	23AZ	PL B846 138245	M. Ablikim *et al.*	(BESIII Collab.) JP
ABLIKIM	23BF	PRL 131 141802	M. Ablikim *et al.*	(BESIII Collab.)
ABLIKIM	23P	PR D107 032011	M. Ablikim *et al.*	(BESIII Collab.)
CRONIN-HEN...	12	PR D86 072005	D. Cronin-Hennessey *et al.*	(CLEO Collab.)
AUBERT,BE	05G	PR D72 091101	B. Aubert *et al.*	(BABAR Collab.)
GRONBERG	95	PRL 75 3232	J. Gronberg *et al.*	(CLEO Collab.)
BROWN	94	PR D50 1884	D. Brown *et al.*	(CLEO Collab.)
ASRATYAN	91	PL B257 525	A.E. Asratyan *et al.*	(ITEP, BELG, SACL+)
ALBRECHT	88	PL B207 349	H. Albrecht *et al.*	(ARGUS Collab.)
BLAYLOCK	87	PRL 58 2171	G.T. Blaylock *et al.*	(Mark III Collab.)
ASRATYAN	85	PL 156B 441	A.E. Asratyan *et al.*	(ITEP, SERP)
AIHARA	84D	PRL 53 2465	H. Aihara *et al.*	(TPC Collab.)
ALBRECHT	84B	PL 146B 111	H. Albrecht *et al.*	(ARGUS Collab.)
BRANDELIK	79	PL 80B 412	R. Brandelik *et al.*	(DASP Collab.)

Int. J. Mod. Phys. A 2026.41. Downloaded from www.worldscientific.com
by CALIFORNIA @ BERKELEY on 09/16/26. Re-use and distribution is strictly not permitted, except for Open Access articles.

Int. J. Mod. Phys. A 2026.41. Downloaded from www.worldscientific.com by UNIVERSITY OF CALIFORNIA @ BERKELEY on 09/16/26. Re-use and distribution is strictly not permitted, except for Open Access articles.

$D_{s0}^*(2317)^\pm$

$I(J^P) = 0(0^+)$
J, P need confirmation.

AUBERT 06P and CHOI 15A do not observe neutral and doubly charged partners of the $D_{s0}^*(2317)^+$. See the review on "Heavy Non-$q\overline{q}$ Mesons."

$D_{s0}^*(2317)^\pm$ MASS

The fit includes $D^\pm$, D^0, $D_s^\pm$, $D^{*\pm}$, D^{*0}, $D_s^{*\pm}$, $D_1(2420)^0$, $D_2^*(2460)^0$, and $D_{s1}(2536)^\pm$ mass and mass difference measurements.

VALUE (MeV)	EVTS	DOCUMENT ID		TECN	COMMENT
2317.8±0.5 OUR FIT					
2318.0±0.7 OUR AVERAGE					
2318.3±1.2±1.2	115	[1] ABLIKIM	18J	BES3	4.6 $e^+e^- \to D_s^{*\pm} D_{s0}^*(2317)^\mp$
2319.6±0.2±1.4	3.1k	AUBERT	06P	BABR	10.6 $e^+e^- \to D_s^+ \pi^0 X$
2317.3±0.4±0.8	1.0k	[2] AUBERT	04E	BABR	10.6 e^+e^-
• • • We do not use the following data for averages, fits, limits, etc. • • •					
2317.2±1.3	88	[3] AUBERT,B	04S	BABR	$B \to D_{s0}^{(*)}(2317)^+ \overline{D}^{(*)}$
2317.2±0.5±0.9	761	[4] MIKAMI	04	BELL	10.6 e^+e^-
2316.8±0.4±3.0	1.2k	[4,5] AUBERT	03G	BABR	10.6 e^+e^-
2317.6±1.3	273	[4,6] AUBERT	03G	BABR	10.6 e^+e^-
2319.8±2.1±2.0	24	[4] KROKOVNY	03B	BELL	10.6 e^+e^-

[1] From a fit of the D_s^* recoil mass where the $D_{s0}^*(2317)$ signal is described with a Crystal Ball function convolved with a Gaussian function.
[2] Supersedes AUBERT 03G.
[3] Systematic errors not evaluated.
[4] Not independent of the corresponding $m_{D_{s0}^*(2317)} - m_{D_s}$.
[5] From $D_s^+ \to K^+K^-\pi^+$ decay.
[6] From $D_s^+ \to K^+K^-\pi^+\pi^0$ decay.

$m_{D_{s0}^*(2317)^\pm} - m_{D_s^\pm}$

The fit includes $D^\pm$, D^0, $D_s^\pm$, $D^{*\pm}$, D^{*0}, $D_s^{*\pm}$, $D_1(2420)^0$, $D_2^*(2460)^0$, and $D_{s1}(2536)^\pm$ mass and mass difference measurements.

VALUE (MeV)	EVTS	DOCUMENT ID		TECN	COMMENT
349.4±0.5 OUR FIT					
349.2±0.7 OUR AVERAGE					
348.7±0.5±0.7	761	MIKAMI	04	BELL	10.6 e^+e^-
350.0±1.2±1.0	135	BESSON	03	CLE2	10.6 e^+e^-
351.3±2.1±1.9	24	[7] KROKOVNY	03B	BELL	10.6 e^+e^-
• • • We do not use the following data for averages, fits, limits, etc. • • •					
349.6±0.4±3.0	1267	[8,9] AUBERT	03G	BABR	10.6 e^+e^-
350.2±1.3	273	[10,11] AUBERT	03G	BABR	10.6 e^+e^-

[7] Recalculated by us using $m_{D_s^+} = 1968.5 \pm 0.6$ MeV.
[8] From $D_s^+ \to K^+K^-\pi^+$ decay.
[9] Recalculated by us using $m_{D_s^+} = 1967.20 \pm 0.03$ MeV.
[10] From $D_s^+ \to K^+K^-\pi^+\pi^0$ decay.
[11] Recalculated by us using $m_{D_s^+} = 1967.4 \pm 0.2$ MeV. Systematic errors not estimated.

$D_{s0}^*(2317)^\pm$ WIDTH

VALUE (MeV)	CL%	EVTS	DOCUMENT ID		TECN	COMMENT
< 3.8	95	3180	AUBERT	06P	BABR	10.6 $e^+e^- \to D_s^+ \pi^0 X$
• • • We do not use the following data for averages, fits, limits, etc. • • •						
< 4.6	90	761	MIKAMI	04	BELL	10.6 e^+e^-
<10			AUBERT	03G	BABR	10.6 e^+e^-
< 7	90	135	BESSON	03	CLE2	10.6 e^+e^-

$D_{s0}^*(2317)^\pm$ DECAY MODES

$D_{s0}^*(2317)^-$ modes are charge conjugates of modes below.

	Mode	Fraction (Γ_i/Γ)	Confidence level
Γ_1	$D_s^+\pi^0$	$(100^+_{-20}{}^0)$ %	
Γ_2	$D_s^+\gamma$	< 5 %	90%
Γ_3	$D_s^*(2112)^+\gamma$	< 6 %	90%
Γ_4	$D_s^+\gamma\gamma$	< 18 %	95%
Γ_5	$D_s^*(2112)^+\pi^0$	< 11 %	90%
Γ_6	$D_s^+\pi^+\pi^-$	< 4 $\times 10^{-3}$	90%
Γ_7	$D_s^+\pi^0\pi^0$	not seen	

$D_{s0}^*(2317)^\pm$ BRANCHING RATIOS

$\Gamma(D_s^+\pi^0)/\Gamma_{total}$ — Γ_1/Γ

VALUE	EVTS	DOCUMENT ID		TECN	COMMENT
$\mathbf{1.00^{+0.00}_{-0.14}{}^{+0.00}_{-0.14}}$	47	ABLIKIM	18J	BES3	4.6 $e^+e^- \to D_s^{*\pm} D_{s0}^*(2317)^\mp$
• • • We do not use the following data for averages, fits, limits, etc. • • •					
seen	1.5k	AUBERT	03G	BABR	10.6 e^+e^-

$\Gamma(D_s^+\gamma)/\Gamma(D_s^+\pi^0)$ — Γ_2/Γ_1

VALUE	CL%	DOCUMENT ID		TECN	COMMENT
<0.05	90	MIKAMI	04	BELL	10.6 e^+e^-
• • • We do not use the following data for averages, fits, limits, etc. • • •					
<0.14	95	AUBERT	06P	BABR	10.6 e^+e^-
<0.052	90	BESSON	03	CLE2	10.6 e^+e^-

$\Gamma(D_s^*(2112)^+\gamma)/\Gamma(D_s^+\pi^0)$ — Γ_3/Γ_1

VALUE	CL%	DOCUMENT ID		TECN	COMMENT
<0.059	90	BESSON	03	CLE2	10.6 e^+e^-
• • • We do not use the following data for averages, fits, limits, etc. • • •					
<0.16	95	AUBERT	06P	BABR	10.6 e^+e^-
<0.18	90	MIKAMI	04	BELL	10.6 e^+e^-

$\Gamma(D_s^+\gamma\gamma)/\Gamma(D_s^+\pi^0)$ — Γ_4/Γ_1

VALUE	CL%	DOCUMENT ID		TECN	COMMENT
<0.18	95	AUBERT	06P	BABR	10.6 e^+e^-
• • • We do not use the following data for averages, fits, limits, etc. • • •					
not seen		AUBERT	03G	BABR	10.6 e^+e^-

$\Gamma(D_s^*(2112)^+\pi^0)/\Gamma(D_s^+\pi^0)$ — Γ_5/Γ_1

VALUE	CL%	DOCUMENT ID		TECN	COMMENT
<0.11	90	BESSON	03	CLE2	10.6 e^+e^-

$\Gamma(D_s^+\pi^+\pi^-)/\Gamma(D_s^+\pi^0)$ — Γ_6/Γ_1

VALUE	CL%	DOCUMENT ID		TECN	COMMENT
<0.004	90	MIKAMI	04	BELL	10.6 e^+e^-
• • • We do not use the following data for averages, fits, limits, etc. • • •					
<0.005	95	AUBERT	06P	BABR	10.6 e^+e^-
<0.019	90	BESSON	03	CLE2	10.6 e^+e^-

$\Gamma(D_s^+\pi^0\pi^0)/\Gamma(D_s^+\pi^0)$ — Γ_7/Γ_1

VALUE	CL%	DOCUMENT ID		TECN	COMMENT
<0.25	95	AUBERT	06P	BABR	10.6 e^+e^-

$D_{s0}^*(2317)^\pm$ REFERENCES

ABLIKIM	18J	PR D97 051103	M. Ablikim *et al.*	(BESIII Collab.)
CHOI	15A	PR D91 092011	S.-K. Choi *et al.*	(BELLE Collab.)
AUBERT	06P	PR D74 032007	B. Aubert *et al.*	(BABAR Collab.)
AUBERT	04E	PR D69 031101	B. Aubert *et al.*	(BABAR Collab.)
AUBERT,B	04S	PRL 93 181801	B. Aubert *et al.*	(BABAR Collab.)
MIKAMI	04	PRL 92 012002	Y. Mikami *et al.*	(BELLE Collab.)
AUBERT	03G	PRL 90 242001	B. Aubert *et al.*	(BABAR Collab.)
BESSON	03	PR D68 032002	D. Besson *et al.*	(CLEO Collab.)
KROKOVNY	03B	PRL 91 262002	P. Krokovny *et al.*	(BELLE Collab.)

$D_{s1}(2460)^\pm$

$I(J^P) = 0(1^+)$

See the review on "Heavy Non-$q\overline{q}$ Mesons."

$D_{s1}(2460)^\pm$ MASS

The fit includes $D^\pm$, D^0, $D_s^\pm$, $D^{*\pm}$, D^{*0}, $D_s^{*\pm}$, $D_1(2420)^0$, $D_2^*(2460)^0$, and $D_{s1}(2536)^\pm$ mass and mass difference measurements.

VALUE (MeV)	EVTS	DOCUMENT ID		TECN	COMMENT
2459.5±0.6 OUR FIT Error includes scale factor of 1.1.					
2459.6±0.9 OUR AVERAGE Error includes scale factor of 1.3.					
2460.1±0.2±0.8		[1] AUBERT	06P	BABR	10.6 e^+e^-
2458.0±1.0±1.0	195	AUBERT	04E	BABR	10.6 e^+e^-
• • • We do not use the following data for averages, fits, limits, etc. • • •					
2459.5±1.2±3.7	920	AUBERT	06P	BABR	10.6 $e^+e^- \to D_s^+\gamma X$
2458.6±1.0±2.5	560	AUBERT	06P	BABR	10.6 $e^+e^- \to D_s^+\pi^0\gamma X$
2460.2±0.2±0.8	123	AUBERT	06P	BABR	10.6 $e^+e^- \to D_s^+\pi^+\pi^- X$
2458.9±1.5	112	[2] AUBERT,B	04S	BABR	$B \to D_{s1}(2460)^+ \overline{D}^{(*)}$
2461.1±1.6	139	[3] AUBERT,B	04S	BABR	$B \to D_{s1}(2460)^+ \overline{D}^{(*)}$
2456.5±1.3±1.3	126	[4,5] MIKAMI	04	BELL	10.6 e^+e^-
2459.5±1.3±2.0	152	[6,7] MIKAMI	04	BELL	10.6 e^+e^-
2459.9±0.9±1.6	60	[6,7] MIKAMI	04	BELL	10.6 e^+e^-
2459.2±1.6±2.0	57	KROKOVNY	03B	BELL	10.6 e^+e^-

[1] The average of the values obtained from the $D_s^+\gamma$, $D_s^+\pi^0\gamma$, $D_s^+\pi^+\pi^-$ final state.
[2] Systematic errors not evaluated. From the decay to $D_s^{*+}\pi^0$.
[3] Systematic errors not evaluated. From the decay to $D_s^+\gamma$.
[4] Not independent of the corresponding $m_{D_{s1}(2460)^{\pm}} - m_{D_s^{*\pm}}$.
[5] Using $m_{D_s^{*+}} = 2112.4 \pm 0.7$ MeV.
[6] Not independent of the corresponding $m_{D_{s1}(2460)^{\pm}} - m_{D_s^{\pm}}$.
[7] Using $m_{D_s^+} = 1968.5 \pm 0.6$ MeV.

$m_{D_{s1}(2460)^{\pm}} - m_{D_s^{*\pm}}$

The fit includes $D^{\pm}$, D^0, $D_s^{\pm}$, $D^{*\pm}$, D^{*0}, $D_s^{*\pm}$, $D_1(2420)^0$, $D_2^*(2460)^0$, and $D_{s1}(2536)^{\pm}$ mass and mass difference measurements.

VALUE (MeV)	EVTS	DOCUMENT ID		TECN	COMMENT
347.3±0.7 OUR FIT Error includes scale factor of 1.2.					
347.1±2.2 OUR AVERAGE Error includes scale factor of 1.9. See the ideogram below.					
344.1±1.3±1.1	126	MIKAMI	04	BELL	10.6 e^+e^-
351.2±1.7±1.0	41	BESSON	03	CLE2	10.6 e^+e^-
346.8±1.6±1.9	57	[8] KROKOVNY	03B	BELL	10.6 e^+e^-

[8] Recalculated by us using $m_{D_s^{*+}} = 2112.4 \pm 0.7$ MeV.

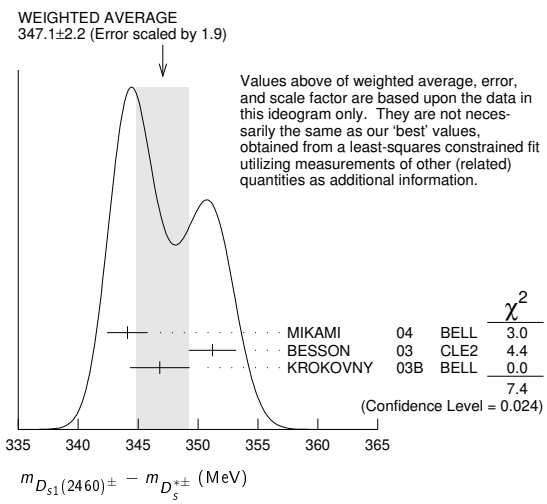

$m_{D_{s1}(2460)^{\pm}} - m_{D_s^{\pm}}$

The fit includes $D^{\pm}$, D^0, $D_s^{\pm}$, $D^{*\pm}$, D^{*0}, $D_s^{*\pm}$, $D_1(2420)^0$, $D_2^*(2460)^0$, and $D_{s1}(2536)^{\pm}$ mass and mass difference measurements.

VALUE (MeV)	EVTS	DOCUMENT ID		TECN	COMMENT
491.1±0.6 OUR FIT Error includes scale factor of 1.1.					
491.3±1.4 OUR AVERAGE					
491.0±1.3±1.9	152	[9] MIKAMI	04	BELL	10.6 e^+e^-
491.4±0.9±1.5	60	[10] MIKAMI	04	BELL	10.6 e^+e^-

[9] From the decay to $D_s^{\pm}\gamma$.
[10] From the decay to $D_s^{\pm}\pi^+\pi^-$.

$D_{s1}(2460)^{\pm}$ WIDTH

VALUE (MeV)	CL%	EVTS	DOCUMENT ID		TECN	COMMENT
< 3.5	95	123	AUBERT	06P	BABR	10.6 $e^+e^- \to D_s^+\pi^+\pi^-X$
• • • We do not use the following data for averages, fits, limits, etc. • • •						
< 6.3	95	560	AUBERT	06P	BABR	10.6 $e^+e^- \to D_s^+\pi^0\gamma X$
<10		195	AUBERT	04E	BABR	10.6 e^+e^-
< 5.5	90	126	MIKAMI	04	BELL	10.6 e^+e^-
< 7	90	41	BESSON	03	CLE2	10.6 e^+e^-

$D_{s1}(2460)^+$ DECAY MODES

$D_{s1}(2460)^-$ modes are charge conjugates of the modes below.

	Mode	Fraction (Γ_i/Γ)	Scale factor/ Confidence level
Γ_1	$D_s^{*+}\pi^0$	(48 ±11) %	
Γ_2	$D_s^+\gamma$	(18 ± 4) %	
Γ_3	$D_s^+\pi^+\pi^-$	(4.3± 1.3) %	S=1.1
Γ_4	$D_s^{*+}\gamma$	< 8 %	CL=90%
Γ_5	$D_{s0}^*(2317)^+\gamma$	$(3.7^{+5.0}_{-2.4})$ %	
Γ_6	$D_s^+\pi^0$		
Γ_7	$D_s^+\pi^0\pi^0$		
Γ_8	$D_s^+\gamma\gamma$		

CONSTRAINED FIT INFORMATION

An overall fit to 7 branching ratios uses 8 measurements and one constraint to determine 5 parameters. The overall fit has a χ^2 = 3.4 for 4 degrees of freedom.

The following *off-diagonal* array elements are the correlation coefficients $\langle \delta x_i \delta x_j \rangle / (\delta x_i \cdot \delta x_j)$, in percent, from the fit to the branching fractions, $x_i \equiv \Gamma_i/\Gamma_{total}$. The fit constrains the x_i whose labels appear in this array to sum to one.

x_2	80		
x_3	68	62	
x_5	−3	25	26
	x_1	x_2	x_3

$D_{s1}(2460)^{\pm}$ BRANCHING RATIOS

$\Gamma(D_s^{*+}\pi^0)/\Gamma_{total}$ — Γ_1/Γ

VALUE	EVTS	DOCUMENT ID		TECN	COMMENT
0.48±0.11 OUR FIT					
0.56±0.13±0.09		[11] AUBERT	06N	BABR	$B \to D_{s1}(2460)^- \overline{D}^{(*)}$
• • • We do not use the following data for averages, fits, limits, etc. • • •					
seen	41	BESSON	03	CLE2	10.6 e^+e^-

[11] Evaluated in AUBERT 06N including measurements from AUBERT,B 04S.

$\Gamma(D_s^+\gamma)/\Gamma_{total}$ — Γ_2/Γ

VALUE	DOCUMENT ID		TECN	COMMENT
0.18±0.04 OUR FIT				
0.16±0.04±0.03	[12] AUBERT	06N	BABR	$B \to D_{s1}(2460)^- \overline{D}^{(*)}$

[12] Evaluated in AUBERT 06N including measurements from AUBERT,B 04S.

$\Gamma(D_s^+\gamma)/\Gamma(D_s^{*+}\pi^0)$ — Γ_2/Γ_1

VALUE	CL%	EVTS	DOCUMENT ID		TECN	COMMENT
0.38 ±0.05 OUR FIT						
0.44 ±0.09 OUR AVERAGE						
0.55 ±0.13 ±0.08		152	MIKAMI	04	BELL	10.6 e^+e^-
0.38 ±0.11 ±0.04		38	KROKOVNY	03B	BELL	10.6 e^+e^-
• • • We do not use the following data for averages, fits, limits, etc. • • •						
0.274±0.045±0.020		251	[13] AUBERT,B	04S	BABR	$B \to D_{s1}(2460)^+ \overline{D}^{(*)}$
< 0.49	90		BESSON	03	CLE2	10.6 e^+e^-

[13] Used by AUBERT 06N in their measurement of $B(D_s^{*-}\pi^0)$ and $B(D_s^-\gamma)$.

$\Gamma(D_s^+\pi^+\pi^-)/\Gamma(D_s^{*+}\pi^0)$ — Γ_3/Γ_1

VALUE	CL%	EVTS	DOCUMENT ID		TECN	COMMENT
0.090±0.020 OUR FIT Error includes scale factor of 1.2.						
0.14 ±0.04 ±0.02		60	MIKAMI	04	BELL	10.6 e^+e^-
• • • We do not use the following data for averages, fits, limits, etc. • • •						
<0.08		90	BESSON	03	CLE2	10.6 e^+e^-

$\Gamma(D_s^{*+}\gamma)/\Gamma(D_s^{*+}\pi^0)$ — Γ_4/Γ_1

VALUE	CL%	DOCUMENT ID		TECN	COMMENT
<0.16	90	BESSON	03	CLE2	10.6 e^+e^-
• • • We do not use the following data for averages, fits, limits, etc. • • •					
<0.31	90	MIKAMI	04	BELL	10.6 e^+e^-

$\Gamma(D_{s0}^*(2317)^+\gamma)/\Gamma(D_s^{*+}\pi^0)$ — Γ_5/Γ_1

VALUE	CL%	DOCUMENT ID		TECN	COMMENT
<0.22	95	AUBERT	04E	BABR	10.6 e^+e^-
• • • We do not use the following data for averages, fits, limits, etc. • • •					
<0.58	90	BESSON	03	CLE2	10.6 e^+e^-

$\Gamma(D_s^{*+}\pi^0)/[\Gamma(D_s^{*+}\pi^0)+\Gamma(D_{s0}^*(2317)^+\gamma)]$ — $\Gamma_1/(\Gamma_1+\Gamma_5)$

VALUE	DOCUMENT ID		TECN	COMMENT
0.93±0.09 OUR FIT				
0.97±0.09±0.05	AUBERT	06P	BABR	10.6 e^+e^-

$\Gamma(D_s^+\gamma)/[\Gamma(D_s^{*+}\pi^0)+\Gamma(D_{s0}^*(2317)^+\gamma)]$ — $\Gamma_2/(\Gamma_1+\Gamma_5)$

VALUE	DOCUMENT ID		TECN	COMMENT
0.35 ±0.04 OUR FIT				
0.337±0.036±0.038	AUBERT	06P	BABR	10.6 e^+e^-

Int. J. Mod. Phys. A 2026.41. Downloaded from www.worldscientific.com
by [redacted]LIFORNIA @ BERKELEY on 09/16/26. Re-use and distribution is strictly not permitted, except for Open Access articles.

Int. J. Mod. Phys. A 2026.41. Downloaded from www.worldscientific.com
by UNIVERSITY OF CALIFORNIA @ BERKELEY on 09/16/26. Re-use and distribution is strictly not permitted, except for Open Access articles.

$\Gamma(D_s^+\pi^+\pi^-)/[\Gamma(D_s^{*+}\pi^0)+\Gamma(D_{s0}^*(2317)^+\gamma)]$ — $\Gamma_3/(\Gamma_1+\Gamma_5)$

VALUE	DOCUMENT ID		TECN	COMMENT
0.083±0.017 OUR FIT	Error includes scale factor of 1.2.			
0.077±0.013±0.008	AUBERT	06P	BABR	10.6 e^+e^-

$\Gamma(D_s^{*+}\gamma)/[\Gamma(D_s^{*+}\pi^0)+\Gamma(D_{s0}^*(2317)^+\gamma)]$ — $\Gamma_4/(\Gamma_1+\Gamma_5)$

VALUE	CL%	DOCUMENT ID		TECN	COMMENT
<0.24	95	AUBERT	06P	BABR	10.6 e^+e^-

$\Gamma(D_{s0}^*(2317)^+\gamma)/[\Gamma(D_s^{*+}\pi^0)+\Gamma(D_{s0}^*(2317)^+\gamma)]$ — $\Gamma_5/(\Gamma_1+\Gamma_5)$

VALUE	CL%	DOCUMENT ID		TECN	COMMENT
<0.25	95	AUBERT	06P	BABR	10.6 e^+e^-

$\Gamma(D_s^+\pi^0)/[\Gamma(D_s^{*+}\pi^0)+\Gamma(D_{s0}^*(2317)^+\gamma)]$ — $\Gamma_6/(\Gamma_1+\Gamma_5)$

VALUE	CL%	DOCUMENT ID		TECN	COMMENT
<0.042	95	AUBERT	06P	BABR	10.6 e^+e^-

$\Gamma(D_s^+\pi^0\pi^0)/[\Gamma(D_s^{*+}\pi^0)+\Gamma(D_{s0}^*(2317)^+\gamma)]$ — $\Gamma_7/(\Gamma_1+\Gamma_5)$

VALUE	CL%	DOCUMENT ID		TECN	COMMENT
<0.68	95	AUBERT	06P	BABR	10.6 e^+e^-

$\Gamma(D_s^+\gamma\gamma)/[\Gamma(D_s^{*+}\pi^0)+\Gamma(D_{s0}^*(2317)^+\gamma)]$ — $\Gamma_8/(\Gamma_1+\Gamma_5)$

VALUE	CL%	DOCUMENT ID		TECN	COMMENT
<0.33	95	AUBERT	06P	BABR	10.6 e^+e^-

$D_{s1}(2460)^{\pm}$ REFERENCES

AUBERT	06N	PR D74 031103	B. Aubert *et al.*	(BABAR Collab.)
AUBERT	06P	PR D74 032007	B. Aubert *et al.*	(BABAR Collab.)
AUBERT	04E	PR D69 031101	B. Aubert *et al.*	(BABAR Collab.)
AUBERT,B	04S	PRL 93 181801	B. Aubert *et al.*	(BABAR Collab.)
MIKAMI	04	PRL 92 012002	Y. Mikami *et al.*	(BELLE Collab.)
BESSON	03	PR D68 032002	D. Besson *et al.*	(CLEO Collab.)
KROKOVNY	03B	PRL 91 262002	P. Krokovny *et al.*	(BELLE Collab.)

$D_{s1}(2536)^{\pm}$

$I(J^P) = 0(1^+)$
J, P need confirmation.

Seen in $D^*(2010)^+K^0$, $D^*(2007)^0K^+$, and $D_s^+\pi^+\pi^-$. Not seen in D^+K^0 or D^0K^+. $J^P = 1^+$ assignment strongly favored.

$D_{s1}(2536)^{\pm}$ MASS

The fit includes $D^{\pm}$, D^0, $D_s^{\pm}$, $D^{*\pm}$, D^{*0}, $D_s^{*\pm}$, $D_1(2420)^0$, $D_2^*(2460)^0$, and $D_{s1}(2536)^{\pm}$ mass and mass difference measurements.

VALUE (MeV)	EVTS	DOCUMENT ID		TECN	COMMENT
2535.12±0.06 OUR FIT					
2535.21±0.28 OUR AVERAGE					
2537.7 ±0.5 ±3.1	24	[1] ABLIKIM	19P	BES3	4.6 $e^+e^-\to D_s^+\overline{D}^0K^-$
2535.7 ±0.6 ±0.5	46	[2] ABAZOV	09G	D0	$B_s^0\to D_{s1}^-\mu^+\nu_\mu X$
2534.78±0.31±0.40	182	AUBERT	08B	BABR	$B\to\overline{D}^{(*)}D^*K$
2534.6 ±0.3 ±0.7	193	AUBERT	06P	BABR	10.6 $e^+e^-\to D_s^+\pi^+\pi^-X$
2535.3 ±0.7	92	[3] HEISTER	02B	ALEP	$e^+e^-\to D^{*+}K^0X$, $D^{*0}K^+X$
2534.2 ±1.2	9	ASRATYAN	94	BEBC	$\nu N\to D^*K^0X, D^*K^{\pm}X$
2535 ±0.6 ±1	75	FRABETTI	94B	E687	γBe $\to D^{*+}K^0X$, $D^{*0}K^+X$
2535.2 ±0.5 ±1.5	28	ALBRECHT	92R	ARG	10.4 $e^+e^-\to D^{*0}K^+X$
2536.6 ±0.7 ±0.4		AVERY	90	CLEO	$e^+e^-\to D^{*+}K^0X$
2535.9 ±0.6 ±2.0		ALBRECHT	89E	ARG	$D_{s1}^*\to D^*(2010)K^0$
• • • We do not use the following data for averages, fits, limits, etc. • • •					
2534.1 ±0.6	116	[4] AUSHEV	11	BELL	$B\to D_{s1}(2536)^+D^{(*)}$
2535.08±0.01±0.15	8038	[5] LEES	11B	BABR	10.6 $e^+e^-\to D^{*+}K_S^0X$
2535.57$^{+0.44}_{-0.41}$±0.10	236	[6] CHEKANOV	09	ZEUS	$e^{\pm}p\to D^{*+}K_S^0X$, $D^{*0}K^+X$
2535.3 ±0.2 ±0.5	134	[7] ALEXANDER	93	CLE2	$e^+e^-\to D^{*0}K^+X$
2534.8 ±0.6 ±0.6	44	[8] ALEXANDER	93	CLE2	$e^+e^-\to D^{*+}K^0X$
2535 ± 28		[9] ASRATYAN	88	HLBC	$\nu N\to D_s\gamma\gamma X$

[1] From a fit of the D_s^+ recoil mass distribution with an incoherent sum of the S-wave and D-wave Breit-Wigner line shapes.
[2] Using the $D^*(2010)^{\pm}$ mass of 2010.0 ± 0.4 MeV from PDG 06.
[3] Calculated using $m(D^*(2010)^{\pm})$ = 2010.0 ± 0.5 MeV, $m(D^*(2007)^0)$ = 2006.7 ± 0.5 MeV, and the mass difference below.
[4] Systematic uncertainties not evaluated.
[5] Calculated using the mass difference $m(D_{s1}^+) - m(D^{*+})_{PDG}$ below and $m(D^{*+})_{PDG}$ = 2010.25 ± 0.14 MeV. Assuming S-wave decay of the $D_{s1}(2536)$ to $D^{*+}K_S^0$, using a Breit-Wigner line shape corresponding to L=0.
[6] Calculated using the mass difference $m(D_{s1}^+) - m(D^{*+})_{PDG}$ reported below and $m(D^{*+})_{PDG}$ = 2010.27 ± 0.17 MeV.
[7] Calculated using $m(D^*(2007)^0)$=2006.6 ± 0.5 MeV and the mass difference below.
[8] Calculated using $m(D^*(2010)^{\pm})$=2010.1 ± 0.6 MeV and the mass difference below.
[9] Not seen in D^*K.

$m_{D_{s1}(2536)^{\pm}} - m_{D_s^*(2111)}$

The fit includes $D^{\pm}$, D^0, $D_s^{\pm}$, $D^{*\pm}$, D^{*0}, $D_s^{*\pm}$, $D_1(2420)^0$, $D_2^*(2460)^0$, and $D_{s1}(2536)^{\pm}$ mass and mass difference measurements.

VALUE (MeV)	DOCUMENT ID		TECN	COMMENT
422.9± 0.4 OUR FIT				
424 ±28	ASRATYAN	88	HLBC	$D_s^{*\pm}\gamma$

$m_{D_{s1}(2536)^{\pm}} - m_{D^*(2010)^{\pm}}$

The fit includes $D^{\pm}$, D^0, $D_s^{\pm}$, $D^{*\pm}$, D^{*0}, $D_s^{*\pm}$, $D_1(2420)^0$, $D_2^*(2460)^0$, and $D_{s1}(2536)^{\pm}$ mass and mass difference measurements.

VALUE (MeV)	EVTS	DOCUMENT ID		TECN	COMMENT
524.85±0.04 OUR FIT					
524.84±0.04 OUR AVERAGE					
524.83±0.01±0.04	8038	[10] LEES	11B	BABR	10.6 $e^+e^-\to D^{*+}K_S^0X$
525.30$^{+0.44}_{-0.41}$±0.10	236 ± 30	CHEKANOV	09	ZEUS	$e^{\pm}p\to D^{*+}K_S^0X$, $D^{*0}K^+X$
525.3 ±0.6 ±0.1	41	HEISTER	02B	ALEP	$e^+e^-\to D^{*+}K^0X$
524.7 ±0.6 ±0.2	44	ALEXANDER	93	CLE2	$e^+e^-\to D^{*+}K_S^0X$

[10] Assuming S-wave decay of the $D_{s1}(2536)$ to $D^{*+}K_S^0$, using a Breit-Wigner line shape corresponding to L=0.

$m_{D_{s1}(2536)^{\pm}} - m_{D^*(2007)^0}$

The fit includes $D^{\pm}$, D^0, $D_s^{\pm}$, $D^{*\pm}$, D^{*0}, $D_s^{*\pm}$, $D_1(2420)^0$, $D_2^*(2460)^0$, and $D_{s1}(2536)^{\pm}$ mass and mass difference measurements.

VALUE (MeV)	EVTS	DOCUMENT ID		TECN	COMMENT
528.26±0.05 OUR FIT	Error includes scale factor of 1.1.				
528.68±0.28 OUR AVERAGE					
528.7 ±1.9 ±0.5	51	HEISTER	02B	ALEP	$e^+e^-\to D^{*0}K^+X$
527.3 ±2.2	29	ACKERSTAFF	97W	OPAL	$e^+e^-\to D^{*0}K^+X$
528.7 ±0.2 ±0.2	134	ALEXANDER	93	CLE2	$e^+e^-\to D^{*0}K^+X$

$D_{s1}(2536)^{\pm}$ WIDTH

VALUE (MeV)	CL%	EVTS	DOCUMENT ID		TECN	COMMENT
0.92±0.05 OUR AVERAGE						
1.7 ±1.2 ±0.6		24	[11] ABLIKIM	19P	BES3	4.6 $e^+e^-\to D_s^+\overline{D}^0K^-$
0.92±0.03±0.04		8038	[12] LEES	11B	BABR	10.6 $e^+e^-\to D^{*+}K_S^0X$
• • • We do not use the following data for averages, fits, limits, etc. • • •						
0.75±0.23		116	[13] AUSHEV	11	BELL	$B\to D_{s1}(2536)^+D^{(*)}$
< 2.5	95	193	AUBERT	06P	BABR	10.6 $e^+e^-\to D_s^+\pi^+\pi^-X$
< 3.2	90	75	FRABETTI	94B	E687	γBe $\to D^{*+}K^0X$, $D^{*0}K^+X$
< 2.3	90		ALEXANDER	93	CLEO	$e^+e^-\to D^{*0}K^+X$
< 3.9	90		ALBRECHT	92R	ARG	10.4 $e^+e^-\to D^{*0}K^+X$
< 5.44	90		AVERY	90	CLEO	$e^+e^-\to D^{*+}K^0X$
< 4.6	90		ALBRECHT	89E	ARG	$D_{s1}^*\to D^*(2010)K^0$

[11] From a fit of the D_s^+ recoil mass distribution with an incoherent sum of the S-wave and S-wave Breit-Wigner line shapes.
[12] Assuming S-wave decay of the $D_{s1}(2536)$ to $D^{*+}K_S^0$, using a Breit-Wigner line shape corresponding to L=0.
[13] Systematic uncertainties not evaluated.

$D_{s1}(2536)^+$ DECAY MODES

Branching fractions are given relative to the one **DEFINED AS 1**.
$D_{s1}(2536)^-$ modes are charge conjugates of the modes below.

	Mode	Fraction (Γ_i/Γ)	Confidence level
Γ_1	$D^*(2010)^+K^0$	(31 ±7) %	
Γ_2	$(D^*(2010)^+K^0)_{S-wave}$	(22 ±5) %	
Γ_3	$(D^*(2010)^+K^0)_{D-wave}$		
Γ_4	$K_S^0D^*(2010)^+$	(17 ±4) %	
Γ_5	$D^+\pi^-K^+$	(10.0±2.5) × 10^{-3}	
Γ_6	$D^*(2007)^0K^+$	(36 ±6) %	
Γ_7	D^+K^0	< 12 %	90%
Γ_8	D^0K^+	< 4 %	90%
Γ_9	$D_s^{*+}\gamma$	possibly seen	
Γ_{10}	$D_s^+\pi^+\pi^-$	seen	

Int. J. Mod. Phys. A 2026.41. Downloaded from www.worldscientific.com
by LIFORNIA @ BERKELEY on 09/16/26. Re-use and distribution is strictly not permitted, except for Open Access articles.

$D_{s1}(2536)^+$ BRANCHING RATIOS

$\Gamma((D^*(2010)^+K^0)_{S-wave})/\Gamma(D^*(2010)^+K^0)$ — Γ_2/Γ_1

VALUE	EVTS	DOCUMENT ID		TECN	COMMENT
0.72±0.05±0.01	5485	BALAGURA	08	BELL	10.6 $e^+e^- \to D^{*+}K^0X$

$\Gamma(K^0_S D^*(2010)^+)/\Gamma(D^*(2007)^0K^+)$ — Γ_4/Γ_6

VALUE	DOCUMENT ID		TECN	COMMENT
0.48±0.07±0.02	GAO	23	BELL	e^+e^- at 10.52 GeV

$\Gamma(D^+\pi^-K^+)/\Gamma(D^*(2010)^+K^0)$ — Γ_5/Γ_1

VALUE (units 10^{-2})	EVTS	DOCUMENT ID		TECN	COMMENT
3.27±0.18±0.37	1264	BALAGURA	08	BELL	10.6 $e^+e^- \to D^+\pi^-K^+X$

$\Gamma(D^*(2007)^0K^+)/\Gamma_{total}$ — Γ_6/Γ

VALUE (%)	DOCUMENT ID		TECN	COMMENT
35.9±4.8±3.5	[14] ABLIKIM	24BN	BES3	$e^+e^- \to D^+_s D_{s1}(2536)^-$

[14] Determined as ratio of exclusive $e^+e^- \to D^+_s[\overline{D}^{*0}K^-]$ and inclusive $e^+e^- \to D^+_s X$ measurements.

$\Gamma(D^*(2007)^0K^+)/\Gamma(D^*(2010)^+K^0)$ — Γ_6/Γ_1

VALUE	EVTS	DOCUMENT ID		TECN	COMMENT
1.18±0.16 OUR AVERAGE					
0.88±0.24±0.08	116	AUSHEV	11	BELL	$B \to D_{s1}(2536)^+D^{(*)}$
2.3 ±0.6 ±0.3	236 ± 30	CHEKANOV	09	ZEUS	$e^\pm p \to D^{*+}K^0_S X$, $D^{*0}K^+X$
1.32±0.47±0.23	92	[15] HEISTER	02B	ALEP	$e^+e^- \to D^{*+}K^0X$, $D^{*0}K^+X$
1.9 $^{+1.1}_{-0.9}$ ±0.4	35	[15] ACKERSTAFF	97W	OPAL	$e^+e^- \to D^{*0}K^+X$, $D^{*+}K^0X$
1.1 ±0.3		ALEXANDER	93	CLEO	$e^+e^- \to D^{*0}K^+X, D^{*+}K^0X$
1.4 ±0.3 ±0.2		[16] ALBRECHT	92R	ARG	10.4 $e^+e^- \to D^{*0}K^+X, D^{*+}K^0X$

[15] Ratio of the production rates measured in Z^0 decays.
[16] Evaluated by us from published inclusive cross-sections.

$\Gamma(D^+K^0)/\Gamma(D^*(2010)^+K^0)$ — Γ_7/Γ_1

VALUE	CL%	DOCUMENT ID		TECN	COMMENT
<0.40	90	ALEXANDER	93	CLEO	$e^+e^- \to D^{*+}K^0X$
• • • We do not use the following data for averages, fits, limits, etc. • • •					
<0.43	90	ALBRECHT	89E	ARG	$D^*_{s1} \to D^*(2010)K^0$

$\Gamma(D^0K^+)/\Gamma(D^*(2007)^0K^+)$ — Γ_8/Γ_6

VALUE	CL%	DOCUMENT ID		TECN	COMMENT
<0.12	90	ALEXANDER	93	CLEO	$e^+e^- \to D^{*0}K^+X$

$\Gamma(D^{*+}_s\gamma)/\Gamma_{total}$ — Γ_9/Γ

VALUE	DOCUMENT ID		TECN	COMMENT
possibly seen	ASRATYAN	88	HLBC	$\nu N \to D_s\gamma\gamma X$

$\Gamma(D^{*+}_s\gamma)/\Gamma(D^*(2007)^0K^+)$ — Γ_9/Γ_6

VALUE	CL%	DOCUMENT ID		TECN	COMMENT
<0.42	90	ALEXANDER	93	CLEO	$e^+e^- \to D^{*0}K^+X$

$\Gamma(D^+_s\pi^+\pi^-)/\Gamma_{total}$ — Γ_{10}/Γ

VALUE	DOCUMENT ID		TECN	COMMENT
seen	AUBERT	06P	BABR	10.6 $e^+e^- \to D^+_s\pi^+\pi^-X$

$D_{s1}(2536)^{\pm}$ REFERENCES

ABLIKIM	24BN	PRL 133 171903	M. Ablikim *et al.*	(BESIII Collab.)
GAO	23	PR D108 112015	B.S. Gao *et al.*	(BELLE Collab.)
ABLIKIM	19P	CP C43 031001	M. Ablikim *et al.*	(BESIII Collab.)
AUSHEV	11	PR D83 051102	T. Aushev *et al.*	(BELLE Collab.)
LEES	11B	PR D83 072003	J.P. Lees *et al.*	(BABAR Collab.)
ABAZOV	09G	PRL 102 051801	V.M. Abazov *et al.*	(D0 Collab.)
CHEKANOV	09	EPJ C60 25	S. Chekanov *et al.*	(ZEUS Collab.)
AUBERT	08B	PR D77 011102	B. Aubert *et al.*	(BABAR Collab.)
BALAGURA	08	PR D77 032001	V. Balagura *et al.*	(BELLE Collab.)
AUBERT	06P	PR D74 032007	B. Aubert *et al.*	(BABAR Collab.)
PDG	06	JP G33 1	W.-M. Yao *et al.*	(PDG Collab.)
HEISTER	02B	PL B526 34	A. Heister *et al.*	(ALEPH Collab.)
ACKERSTAFF	97W	ZPHY C76 425	K. Ackerstaff *et al.*	(OPAL Collab.)
ASRATYAN	94	ZPHY C61 563	A.E. Asratyan *et al.*	(BIRM, BELG, CERN+)
FRABETTI	94B	PRL 72 324	P.L. Frabetti *et al.*	(FNAL E687 Collab.)
ALEXANDER	93	PL B303 377	J. Alexander *et al.*	(CLEO Collab.)
ALBRECHT	92R	PL B297 425	H. Albrecht *et al.*	(ARGUS Collab.)
AVERY	90	PR D41 774	P. Avery, D. Besson	(CLEO Collab.)
ALBRECHT	89E	PL B230 162	H. Albrecht *et al.*	(ARGUS Collab.)
ASRATYAN	88	ZPHY C40 483	A.E. Asratyan *et al.*	(ITEP, SERP)

$D^*_{s2}(2573)$

$I(J^P) = 0(2^+)$

$D^*_{s2}(2573)$ MASS

VALUE (MeV)	EVTS	DOCUMENT ID		TECN	COMMENT
2569.1 ±0.8 OUR AVERAGE		Error includes scale factor of 2.4. See the ideogram below.			
2570.7 ±2.0 ±1.7	62	[1] ABLIKIM	19P	BES3	4.6 $e^+e^- \to D^+_s\overline{D}^0K^-$
2568.39±0.29±0.26		AAIJ	14AW	LHCB	$B^0_s \to \overline{D}^0K^-\pi^+$
2569.4 ±1.6 ±0.5	82	AAIJ	11A	LHCB	$B_s \to D^*_{s2}(2573)\mu\overline{\nu}X$
2572.2 ±0.3 ±1.0		AUBERT,BE	06E	BABR	$e^+e^- \to DKX$
2574.5 ±3.3 ±1.6		ALBRECHT	96	ARG	$e^+e^- \to D^0K^+X$
2573.2 $^{+1.7}_{-1.6}$ ±0.9	217	KUBOTA	94	CLE2	$e^+e^- \sim$ 10.5 GeV
• • • We do not use the following data for averages, fits, limits, etc. • • •					
2570.0 ±4.3	25	[2] EVDOKIMOV	04	SELX	600 $\Sigma^-A \to D^0K^+X$
2568.6 ±3.2	64	[3] HEISTER	02B	ALEP	$e^+e^- \to D^0K^+X$

[1] From a fit of the D^+_s recoil mass distribution.
[2] Not independent of the mass difference below.
[3] Calculated using m_{D^0}= 1864.5 ± 0.5 MeV and the mass difference below.

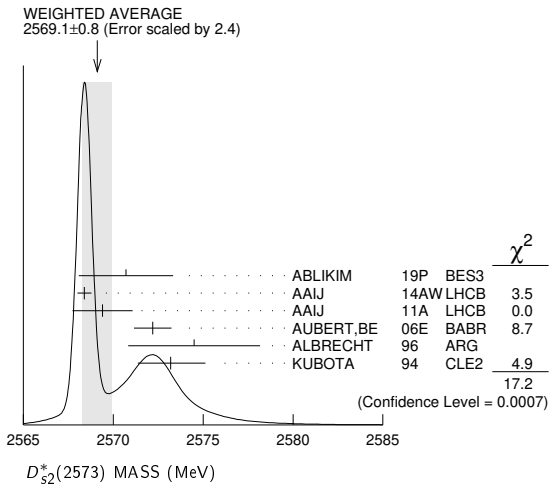

$m_{D^*_{s2}(2573)} - m_{D^0}$

VALUE (MeV)	EVTS	DOCUMENT ID		TECN	COMMENT
704 ±3 ±1	64	HEISTER	02B	ALEP	$e^+e^- \to D^0K^+X$
• • • We do not use the following data for averages, fits, limits, etc. • • •					
705.4±4.3	25	[1] EVDOKIMOV	04	SELX	600 $\Sigma^-A \to D^0K^+X$

[1] Systematic errors not estimated.

$D^*_{s2}(2573)$ WIDTH

VALUE (MeV)	EVTS	DOCUMENT ID		TECN	COMMENT
16.9±0.7 OUR AVERAGE					
17.2±3.6±1.1	62	[1] ABLIKIM	19P	BES3	4.6 $e^+e^- \to D^+_s\overline{D}^0K^-$
16.9±0.5±0.6		AAIJ	14AW	LHCB	$B^0_s \to \overline{D}^0K^-\pi^+$
12.1±4.5±1.6	82	AAIJ	11A	LHCB	$B_s \to D^*_{s2}(2573)\mu\overline{\nu}X$
27.1±0.6±5.6		AUBERT,BE	06E	BABR	$e^+e^- \to DKX$
10.4±8.3±3.0		ALBRECHT	96	ARG	$e^+e^- \to D^0K^+X$
16 $^{+5}_{-4}$ ±3	217	KUBOTA	94	CLE2	$e^+e^- \sim$ 10.5 GeV
• • • We do not use the following data for averages, fits, limits, etc. • • •					
14 $^{+9}_{-6}$	25	[2] EVDOKIMOV	04	SELX	600 $\Sigma^-A \to D^0K^+X$

[1] From a fit of the D^+_s recoil mass distribution.
[2] Systematic errors not estimated.

$D^*_{s2}(2573)^+$ DECAY MODES

$D^*_{s2}(2573)^-$ modes are charge conjugates of the modes below.

	Mode	Fraction (Γ_i/Γ)
Γ_1	D^0K^+	(37±6) %
Γ_2	$D^*(2007)^0K^+$	not seen
Γ_3	$D^+K^0_S$	seen
Γ_4	$D^{*+}K^0_S$	seen

Int. J. Mod. Phys. A 2026.41. Downloaded from www.worldscientific.com by UNIVERSITY OF CALIFORNIA @ BERKELEY on 09/16/26. Re-use and distribution is strictly not permitted, except for Open Access articles.

$D_{s2}^*(2573)^+$ BRANCHING RATIOS

$\Gamma(D^0 K^+)/\Gamma_{total}$ — Γ_1/Γ

VALUE (%)	EVTS	DOCUMENT ID		TECN	CHG	COMMENT
37.4±3.1±4.6		[1] ABLIKIM	24BN	BES3		$e^+e^- \to D_s^+ D_{s2}^*(2573)^-$
• • • We do not use the following data for averages, fits, limits, etc. • • •						
seen	217	KUBOTA	94	CLE2	±	$e^+e^- \sim$ 10.5 GeV

[1] Determined as ratio of exclusive $e^+e^- \to D_s^+ [\overline{D}^0 K^-]$ and inclusive $e^+e^- \to D_s^+ X$ measurements.

$\Gamma(D^*(2007)^0 K^+)/\Gamma(D^0 K^+)$ — Γ_2/Γ_1

VALUE	CL%	DOCUMENT ID		TECN	CHG	COMMENT
<0.33	90	KUBOTA	94	CLE2	+	$e^+e^- \sim$ 10.5 GeV

$\Gamma(D^+ K_S^0)/\Gamma(D^0 K^+)$ — Γ_3/Γ_1

VALUE	DOCUMENT ID		TECN	COMMENT
0.49±0.10±0.02	GAO	23	BELL	e^+e^- at 10.52 GeV

$\Gamma(D^{*+} K_S^0)/\Gamma(D^+ K_S^0)$ — Γ_4/Γ_3

VALUE	EVTS	DOCUMENT ID		TECN	COMMENT
0.044±0.005±0.011	2000	[1] AAIJ	16AW	LHCB	$pp \to D^{*+} K_S^0 X$ at 7, 8 TeV

[1] First observation of the $D_{s2}^*(2573)^+ \to D^{*+} K_S^0$ decay with a significance of 6.9 σ.

$D_{s2}^*(2573)$ REFERENCES

ABLIKIM	24BN	PRL 133 171903	M. Ablikim *et al.*	(BESIII Collab.)
GAO	23	PR D108 112015	B.S. Gao *et al.*	(BELLE Collab.)
ABLIKIM	19P	CP C43 031001	M. Ablikim *et al.*	(BESIII Collab.)
AAIJ	16AW	JHEP 1602 133	R. Aaij *et al.*	(LHCb Collab.)
AAIJ	14AW	PRL 113 162001	R. Aaij *et al.*	(LHCb Collab.) JP
AAIJ	11A	PL B698 14	R. Aaij *et al.*	(LHCb Collab.)
AUBERT,BE	06E	PRL 97 222001	B. Aubert *et al.*	(BABAR Collab.)
EVDOKIMOV	04	PRL 93 242001	A.V. Evdokimov *et al.*	(SELEX Collab.)
HEISTER	02B	PL B526 34	A. Heister *et al.*	(ALEPH Collab.)
ALBRECHT	96	ZPHY C69 405	H. Albrecht *et al.*	(ARGUS Collab.)
KUBOTA	94	PRL 72 1972	Y. Kubota *et al.*	(CLEO Collab.)

$D_{s0}(2590)^+$

$I(J^P) = 0(0^-)$

OMITTED FROM SUMMARY TABLE

$D_{s0}(2590)^+$ MASS

VALUE (MeV)	EVTS	DOCUMENT ID		TECN	COMMENT
2591±6±7	444	[1] AAIJ	21A	LHCB	$B^0 \to D^-(D^+K^+\pi^-)$

[1] The mass is calculated from the position of the T-matrix pole

$D_{s0}(2590)^+$ WIDTH

VALUE (MeV)	EVTS	DOCUMENT ID		TECN	COMMENT
89±16±12	444	[1] AAIJ	21A	LHCB	$B^0 \to D^-(D^+K^+\pi^-)$

[1] The width is calculated from the position of the T-matrix pole

$D_{s0}(2590)^+$ DECAY MODES

	Mode	Fraction (Γ_i/Γ)
Γ_1	$D^+K^+\pi^-$	seen

$D_{s0}(2590)^+$ BRANCHING RATIOS

$\Gamma(D^+K^+\pi^-)/\Gamma_{total}$ — Γ_1/Γ

VALUE	EVTS	DOCUMENT ID		TECN	COMMENT
seen	444	AAIJ	21A	LHCB	$B^0 \to D^-(D^+K^+\pi^-)$

$D_{s0}(2590)^+$ REFERENCES

AAIJ	21A	PRL 126 122002	R. Aaij *et al.*	(LHCb Collab.)

$D_{s1}^*(2700)^\pm$

$I(J^P) = 0(1^-)$

$D_{s1}^*(2700)^+$ MASS

VALUE (MeV)	EVTS	DOCUMENT ID		TECN	COMMENT
2714 ± 5 OUR AVERAGE		Error includes scale factor of 1.5. See the ideogram below.			
2732.3± 4.3± 5.8	15.7k	AAIJ	16AW	LHCB	$pp \to D^{*+} K_S^0 X$ at 7, 8 TeV
2699 $^{+14}_{-7}$		[1] LEES	15C	BABR	$B \to D D^0 K^+$
2709.2± 1.9± 4.5	52k	[2] AAIJ	12AU	LHCB	$pp \to (DK)^+ X$ at 7 TeV
2710 ± 2 $^{+12}_{-7}$	10.4k	[3] AUBERT	09AR	BABR	$e^+e^- \to D^{(*)} K X$
2708 ± 9 $^{+11}_{-10}$	182	BRODZICKA	08	BELL	$B^+ \to D^0 \overline{D}^0 K^+$
• • • We do not use the following data for averages, fits, limits, etc. • • •					
2694 ± 8 $^{+13}_{-3}$		LEES	15C	BABR	$B^0 \to D^- D^0 K^+$
2707 ± 8 ± 8		LEES	15C	BABR	$B^+ \to \overline{D}^0 D^0 K^+$
2688 ± 4 ± 3		[4] AUBERT,BE	06E	BABR	10.6 $e^+e^- \to D K X$

[1] From a combined analysis of $B^0 \to D^- D^0 K^+$ and $B^+ \to \overline{D}^0 D^0 K^+$.
[2] From the combined fit of the $D^+ K_S^0$ and $D^0 K^+$ modes in the model including the $D_{s2}^*(2573)^+$, $D_{s1}^*(2700)^+$ and spin-0 $D_{sJ}^*(2860)^+$.
[3] From simultaneous fits to the two DK mass spectra and to the total D^*K mass spectrum.
[4] Superseded by AUBERT 09AR.

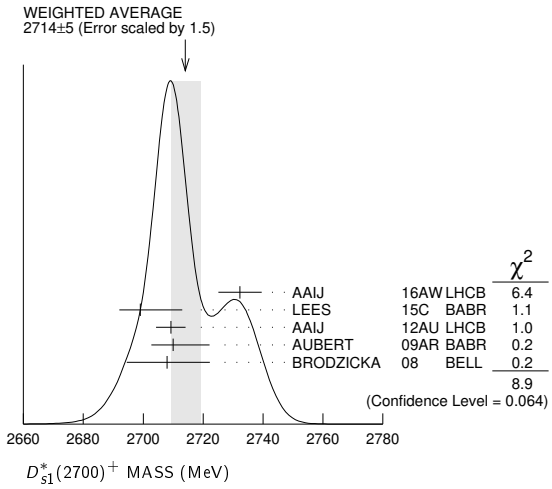

$D_{s1}^*(2700)^+$ WIDTH

VALUE (MeV)	EVTS	DOCUMENT ID		TECN	COMMENT
122 ±10 OUR AVERAGE					
136 ±19 ±24	15.7k	AAIJ	16AW	LHCB	$pp \to D^{*+} K_S^0 X$ at 7, 8 TeV
127 $^{+24}_{-19}$		[1] LEES	15C	BABR	$B \to D D^0 K^+$
115.8± 7.3±12.1	52k	[2] AAIJ	12AU	LHCB	$pp \to (DK)^+ X$ at 7 TeV
149 ± 7 $^{+39}_{-52}$	10.4k	[3] AUBERT	09AR	BABR	$e^+e^- \to D^{(*)} K X$
108 ±23 $^{+36}_{-31}$	182	BRODZICKA	08	BELL	$B^+ \to D^0 \overline{D}^0 K^+$
• • • We do not use the following data for averages, fits, limits, etc. • • •					
145 ±24 $^{+22}_{-14}$		LEES	15C	BABR	$B^0 \to D^- D^0 K^+$
113 ±21 $^{+20}_{-16}$		LEES	15C	BABR	$B^+ \to \overline{D}^0 D^0 K^+$
112 ± 7 ±36		[4] AUBERT,BE	06E	BABR	10.6 $e^+e^- \to D K X$

[1] From a combined analysis of $B^0 \to D^- D^0 K^+$ and $B^+ \to \overline{D}^0 D^0 K^+$.
[2] From the combined fit of the $D^+ K_S^0$ and $D^0 K^+$ modes in the model including the $D_{s2}^*(2573)^+$, $D_{s1}^*(2700)^+$ and spin-0 $D_{sJ}^*(2860)^+$.
[3] From simultaneous fits to the two DK mass spectra and to the total D^*K mass spectrum.
[4] Superseded by AUBERT 09AR.

$D_{s1}^*(2700)^\pm$ DECAY MODES

	Mode	Fraction (Γ_i/Γ)
Γ_1	DK	
Γ_2	D^0K^+	seen
Γ_3	$D^+K_S^0$	seen
Γ_4	D^*K	
Γ_5	$D^{*0}K^+$	seen
Γ_6	$D^{*+}K_S^0$	seen

$D_{s1}^*(2700)^\pm$ BRANCHING RATIOS

$\Gamma(D^*K)/\Gamma(DK)$ — Γ_4/Γ_1

VALUE	EVTS	DOCUMENT ID		TECN	COMMENT
0.91±0.13±0.12	10.4k	[1] AUBERT	09AR	BABR	$e^+e^- \to D^{(*)} K X$

[1] From the average of the corresponding ratios with $D^{(*)0}K^+$ and $D^{(*)+}K_S^0$.

$\Gamma(D^{*0}K^+)/\Gamma(D^0K^+)$ — Γ_5/Γ_2

VALUE	EVTS	DOCUMENT ID		TECN	COMMENT
0.88±0.14±0.14	7716	[1] AUBERT	09AR	BABR	$e^+e^- \to D^{(*)} K X$

[1] From the $D^{*0}K^+$ and D^0K^+, where $D^{*0} \to D^0\pi^0$.

$\Gamma(D^{*+}K_S^0)/\Gamma(D^+K_S^0)$ — Γ_6/Γ_3

VALUE	EVTS	DOCUMENT ID		TECN	COMMENT
1.14±0.39±0.23	2700	[1] AUBERT	09AR	BABR	$e^+e^- \to D^{(*)}KX$

[1] From the $D^{*+}K_S^0$ and $D^+K_S^0$, where $D^{*+} \to D^+\pi^0$.

$D_{s1}^*(2700)^\pm$ REFERENCES

AAIJ	16AW	JHEP 1602 133	R. Aaij *et al.*	(LHCb Collab.)
LEES	15C	PR D91 052002	J.P. Lees *et al.*	(BABAR Collab.)
AAIJ	12AU	JHEP 1210 151	R. Aaij *et al.*	(LHCb Collab.)
AUBERT	09AR	PR D80 092003	B. Aubert *et al.*	(BABAR Collab.)
BRODZICKA	08	PRL 100 092001	J. Brodzicka *et al.*	(BELLE Collab.)
AUBERT,BE	06E	PRL 97 222001	B. Aubert *et al.*	(BABAR Collab.)

$D_{s1}^*(2860)^\pm$

$I(J^P) = 0(1^-)$

OMITTED FROM SUMMARY TABLE
was $D_{sJ}^*(2860)$

J^P consistent with 1^- from angular analysis of AAIJ 14AW.

$D_{s1}^*(2860)^+$ MASS

VALUE (MeV)	DOCUMENT ID		TECN	COMMENT
2859±12±24	[1] AAIJ	14AW	LHCB	$B_s^0 \to \overline{D}^0K^-\pi^+$

[1] Separated from the spin-3 component $D_{s3}^*(2860)^-$ by a fit of the helicity angle of the $\overline{D}^0K^-$ system, with a statistical significance of the spin-3 and spin-1 components in excess of 10 σ.

$D_{s1}^*(2860)^+$ WIDTH

VALUE (MeV)	DOCUMENT ID		TECN	COMMENT
159±23±77	[1] AAIJ	14AW	LHCB	$B_s^0 \to \overline{D}^0K^-\pi^+$

[1] Separated from the spin-3 component $D_{s3}^*(2860)^-$ by a fit of the helicity angle of the $\overline{D}^0K^-$ system, with a statistical significance of the spin-3 and spin-1 components in excess of 10 σ.

$D_{s1}^*(2860)^\pm$ REFERENCES

AAIJ	14AW	PRL 113 162001	R. Aaij *et al.*	(LHCb Collab.) JP

$D_{s3}^*(2860)^\pm$

$I(J^P) = 0(3^-)$

J^P consistent with 3^- from angular analysis of AAIJ 14AW. Observed by AUBERT,BE 06E and AUBERT 09AR in inclusive production of DK and D^*K in e^+e^- annihilation.

$D_{s3}^*(2860)^+$ MASS

VALUE (MeV)	EVTS	DOCUMENT ID		TECN	COMMENT
2860.5±2.6±6.5		[1] AAIJ	14AW	LHCB	$B_s^0 \to \overline{D}^0K^-\pi^+$
• • • We do not use the following data for averages, fits, limits, etc. • • •					
2867.1±4.3±1.9	3.1k	AAIJ	16AW	LHCB	$pp \to D^{*+}K_S^0X$ at 7, 8 TeV
2866.1±1.0±6.3	36k	[2,3] AAIJ	12AU	LHCB	$pp \to (DK)^+X$ at 7 TeV
2862 ±2 $^{+5}_{-2}$	3122	[2,4] AUBERT	09AR	BABR	$e^+e^- \to D^{(*)}KX$
2856.6±1.5±5.0		[5] AUBERT,BE	06E	BABR	$e^+e^- \to DKX$

[1] Separated from the spin-1 component $D_{s1}^*(2860)^-$ by a fit of the helicity angle of the $\overline{D}^0K^-$ system, with a statistical significance of the spin-3 and spin-1 components in excess of 10 σ.
[2] Possible contribution from the $D_{s1}^*(2860)$ state.
[3] From the combined fit of the $D^+K_S^0$ and D^0K^+ modes in the model including the $D_{s2}^*(2573)^+$, $D_{s1}^*(2700)^+$ and spin-0 $D_{sJ}^*(2860)^+$.
[4] From simultaneous fits to the two DK mass spectra and to the total D^*K mass spectrum.
[5] Superseded by AUBERT 09AR.

$D_{s3}^*(2860)^+$ WIDTH

VALUE (MeV)	EVTS	DOCUMENT ID		TECN	COMMENT
53 ± 7 ± 7		[1] AAIJ	14AW	LHCB	$B_s^0 \to \overline{D}^0K^-\pi^+$
• • • We do not use the following data for averages, fits, limits, etc. • • •					
50 ±11 ±13	3.1k	AAIJ	16AW	LHCB	$pp \to D^{*+}K_S^0X$ at 7, 8 TeV
69.9± 3.2± 6.6	36k	[2,3] AAIJ	12AU	LHCB	$pp \to (DK)^+X$ at 7 TeV
48 ± 3 ± 6	3122	[2,4] AUBERT	09AR	BABR	$e^+e^- \to D^{(*)}KX$
47 ± 7 ±10		[5] AUBERT,BE	06E	BABR	$e^+e^- \to DKX$

[1] Separated from the spin-1 component $D_{s1}^*(2860)^-$ by a fit of the helicity angle of the $\overline{D}^0K^-$ system, with a statistical significance of the spin-3 and spin-1 components in excess of 10 σ.
[2] Possible contribution from the $D_{s1}^*(2860)$ state.
[3] From the combined fit of the $D^+K_S^0$ and D^0K^+ modes in the model including the $D_{s2}^*(2573)^+$, $D_{s1}^*(2700)^+$ and spin-0 $D_{sJ}^*(2860)^+$.
[4] From simultaneous fits to the two DK mass spectra and to the total D^*K mass spectrum.
[5] Superseded by AUBERT 09AR.

$D_{s3}^*(2860)^\pm$ DECAY MODES

	Mode	Fraction (Γ_i/Γ)
Γ_1	DK	
Γ_2	D^0K^+	seen
Γ_3	$D^+K_S^0$	seen
Γ_4	D^*K	
Γ_5	$D^{*0}K^+$	seen
Γ_6	$D^{*+}K_S^0$	seen

$D_{s3}^*(2860)^\pm$ BRANCHING RATIOS

$\Gamma(D^*K)/\Gamma(DK)$ — Γ_4/Γ_1

VALUE	EVTS	DOCUMENT ID		TECN	COMMENT
1.10±0.15±0.19	3122	[1] AUBERT	09AR	BABR	$e^+e^- \to D^{(*)}KX$

[1] From the average of the corresponding ratios with $D^{(*)0}K^+$ and $D^{(*)+}K_S^0$.

$\Gamma(D^{*0}K^+)/\Gamma(D^0K^+)$ — Γ_5/Γ_2

VALUE	EVTS	DOCUMENT ID		TECN	COMMENT
1.04±0.17±0.20	2241	[1] AUBERT	09AR	BABR	$e^+e^- \to D^{(*)}KX$

[1] From the $D^{*0}K^+$ and D^0K^+, where $D^{*0} \to D^0\pi^0$.

$\Gamma(D^{*+}K_S^0)/\Gamma(D^+K_S^0)$ — Γ_6/Γ_3

VALUE	EVTS	DOCUMENT ID		TECN	COMMENT
1.38±0.35±0.49	881	[1] AUBERT	09AR	BABR	$e^+e^- \to D^{(*)}KX$

[1] From the $D^{*+}K_S^0$ and $D^+K_S^0$, where $D^{*+} \to D^+\pi^0$.

$D_{s3}^*(2860)^\pm$ REFERENCES

AAIJ	16AW	JHEP 1602 133	R. Aaij *et al.*	(LHCb Collab.)
AAIJ	14AW	PRL 113 162001	R. Aaij *et al.*	(LHCb Collab.) JP
AAIJ	12AU	JHEP 1210 151	R. Aaij *et al.*	(LHCb Collab.)
AUBERT	09AR	PR D80 092003	B. Aubert *et al.*	(BABAR Collab.)
AUBERT,BE	06E	PRL 97 222001	B. Aubert *et al.*	(BABAR Collab.)

$D_{sJ}(3040)^\pm$

$I(J^P) = 0(?^?)$

OMITTED FROM SUMMARY TABLE

Observed by AUBERT 09AR in inclusive production of D^*K in e^+e^- annihilation.

$D_{sJ}(3040)^+$ MASS

VALUE (MeV)	DOCUMENT ID		TECN	COMMENT
3044±8$^{+30}_{-5}$	AUBERT	09AR	BABR	$e^+e^- \to D^*KX$

$D_{sJ}(3040)^+$ WIDTH

VALUE (MeV)	DOCUMENT ID		TECN	COMMENT
239±35$^{+46}_{-42}$	AUBERT	09AR	BABR	$e^+e^- \to D^*KX$

$D_{sJ}(3040)^\pm$ DECAY MODES

	Mode
Γ_1	D^*K
Γ_2	$D^{*0}K^+$
Γ_3	$D^{*+}K_S^0$

$D_{sJ}(3040)^\pm$ REFERENCES

AUBERT	09AR	PR D80 092003	B. Aubert *et al.*	(BABAR Collab.)

Int. J. Mod. Phys. A 2026.41. Downloaded from www.worldscientific.com
by CALIFORNIA @ BERKELEY on 09/16/26. Re-use and distribution is strictly not permitted, except for Open Access articles.

Int. J. Mod. Phys. A 2026.41. Downloaded from www.worldscientific.com by UNIVERSITY OF CALIFORNIA @ BERKELEY on 09/16/26. Re-use and distribution is strictly not permitted, except for Open Access articles.

BOTTOM MESONS ($B = \pm 1$)

$B^+ = u\overline{b}$, $B^0 = d\overline{b}$, $\overline{B}^0 = \overline{d}b$, $B^- = \overline{u}b$, similarly for B^*'s

B-particle organization

Many measurements of B decays involve admixtures of B hadrons. Previously we arbitrarily included such admixtures in the $B^\pm$ section, but because of their importance we have created two new sections: "$B^\pm/B^0$ Admixture" for $\Upsilon(4S)$ results and "$B^\pm/B^0/B^0_s/b$-baryon Admixture" for results at higher energies. Most inclusive decay branching fractions and χ_b at high energy are found in the Admixture sections. B^0-$\overline{B}^0$ mixing data are found in the B^0 section, while B^0_s-$\overline{B}^0_s$ mixing data and B-$\overline{B}$ mixing data for a B^0/B^0_s admixture are found in the B^0_s section. CP-violation data are found in the $B^\pm$, B^0, and $B^\pm$ B^0 Admixture sections. b-baryons are found near the end of the Baryon section. Recently, we also created a new section: "V_{cb} and V_{ub} CKM Matrix Elements."

The organization of the B sections is now as follows, where bullets indicate particle sections and brackets indicate reviews.

[Production and Decay of b-flavored Hadrons]
[A Short Note on HFLAV Activities]
- $B^\pm$
  - mass, mean life
  - branching fractions
  - polarization in $B^\pm$ decay
  - CP violation
- B^0
  - mass, mean life
  - branching fractions
  - [Polarization in B decay]
  - polarization in B^0 decay
  - [B-$\overline{B}$ Mixing]
  - B^0-$\overline{B}^0$ mixing
  - CP violation
- $B^\pm$ B^0 Admixture
  - branching fractions, CP violation
  - CP violation
- $B^\pm/B^0/B^0_s/b$-baryon Admixture
  - mean life
  - production fractions
  - branching fractions
  - χ_b at high energy
  - production fractions in hadronic Z decay
- V_{cb} and V_{ub} CKM Matrix Elements
  - [Determination of V_{cb} and V_{ub}]
- B^*, $B_1(5721)$, $B^*_J(5732)$, $B^*_2(5747)$, $B_J(5840)$, $B_J(5970)$
  - mass, width, branching fracions
- B^0_s
  - mass, mean life
  - branching fractions
  - polarization in B^0_s decay
  - B^0_s-$\overline{B}^0_s$ mixing
- B^*_s, $B_{s1}(5830)^0$, $B^*_{s2}(5840)^0$, $B^*_{sJ}(5850)$, $B_{sJ}(6063)^0$, $B_{sJ}(6114)^0$
  - mass, width, branching fractions
- $B^\pm_c$
  - mass, mean life
  - branching fractions
- $B_c(2S)^\pm$
  - mass, branching fractions

At the end of Baryon Listings:
- Λ_b
  - mass, mean life
  - branching fractions
- $\Lambda_b(5912)^0$, $\Lambda_b(5920)^0$, $\Lambda_b(6070)^0$, $\Lambda_b(6146)^0$, $\Lambda_b(6152)^0$
  - mass, width, branchibg fractions
- Σ_b
  - mass, width, branching fractions
- Σ^*_b, $\Sigma_b(6097)^+$, $\Sigma_b(6097)^-$
  - mass, width, branching fractions
- Ξ^0_b, Ξ^-_b
  - mass, mean life
  - branching fractions, P, CP violation
- $\Xi'_b(5935)^-$, $\Xi_b(5945)^0$, $\Xi_b(5955)^-$, $\Xi_b(6100)^-$, $\Xi_b(6227)^-$, $\Xi_b(6227)^0$, $\Xi_b(6327)^0$, $\Xi_b(6333)^0$
  - mass, width, branching fractions
- Ω^-_b
  - mass, mean life
  - branching fractions
- $\Omega_b(6316)^-$, $\Omega_b(6330)^-$, $\Omega_b(6340)^-$, $\Omega_b(6350)^-$
  - mass, width, branching fractions
- b-baryon Admixture
  - mean life
  - branching fractions

See the related review(s):
Production and Decay of b-flavored Hadrons

HEAVY FLAVOR AVERAGING GROUP

Revised March 2026 by M. Dorigo (INFN Trieste) and U. Egede (Monash University)

The Heavy Flavor Averaging Group (HFLAV) is an international collaboration of physicists from experiments measuring properties of heavy flavored particles, *i.e.*, hadrons containing b and c quarks, and τ leptons. HFLAV calculates and publishes [1] world average values of quantities such as lifetimes, branching fractions, form factors, mixing parameters, and CP-violating asymmetries. Most parameters concern decays of B and D mesons, and many are related to elements of the Cabibbo-Kobayashi-Maskawa (CKM) quark mixing matrix [2], [3].

A special subset of HFLAV averages are included in the PDG listings; for these averages, only measurements that are published or accepted for publication are used. The averages provided by HFLAV are listed by the PDG as "Produced by HFLAV" and are linked to an immutable record in Zenodo with a DOI. This record specifies exactly which measurements were used in the average. An example is the $R(D^{(*)})$ average, which is used in the review of Semileptonic B Hadron Decays [4] and is available at `doi:10.5281/zenodo.19102822` [5]. See the reference here for how the result should be cited.

HFLAV was originally formed in 2002 to continue the activities of the LEP Heavy Flavor Steering group. Since its inception, a wide range of results have become available from increasingly larger data sets. Consequently, HFLAV has expanded to include eight subgroups:

- b-hadron lifetimes and oscillations, including parameters of CP violation in b mixing;
- decay-time-dependent CP violation in B decays, and angles of the CKM Unitarity Triangle;
- semileptonic decays of b-hadrons ($B \to X\ell\nu$, $\ell = e, \mu, \tau$), including determinations of the CKM matrix elements $|V_{cb}|$ and $|V_{ub}|$;
- b-hadron decays to hadronic final states containing c-quarks (open charm and charmonium);

Int. J. Mod. Phys. A 2026.41. Downloaded from www.worldscientific.com
by LIFORNIA @ BERKELEY on 09/16/26. Re-use and distribution is strictly not permitted, except for Open Access articles.

- (rarer) b-hadron decays to final states not containing c-quarks, including fully hadronic, semileptonic ($B \to X\ell\ell, X\nu\bar{\nu}$), leptonic, and radiative decays;
- CP- and T-violating asymmetries of D mesons and D^0–$\bar{D}^0$ mixing;
- c-hadron decays (hadronic, semileptonic, leptonic), properties of excited D states and charm baryons and determination of $|V_{cs}|$ and $|V_{cd}|$;
- τ-lepton physics including branching fractions, tests of lepton universality, determination of $|V_{us}|$, and searches for lepton flavor violation.

Each subgroup has one or two conveners and typically a half-dozen members representing experiments that conduct measurements in that area. Most groups contain representatives from the Belle II and LHCb experiments, and some groups have representatives from the ATLAS, BABAR, Belle, BESIII and CMS experiments. Members of HFLAV are appointed by their respective experimental collaborations. HFLAV has two co-leaders, who are appointed by the managements of Belle II and LHCb.

The averaging procedures used by HFLAV are similar to those of the PDG [6]. When sufficient information is available in publications when calculating world averages, common parameters used for different input measurements are adjusted (rescaled) to common values. The p-value of the fit is provided to indicate the consistency of the measurements included in the average. However, unlike the PDG, when obtaining a world average with a low p-value (*i.e.*, a large χ^2 per degree of freedom), HFLAV does not usually scale the resulting uncertainty. Rather, the systematic uncertainties of the measurements are reviewed with experts from the experiments to understand the discrepancy. Unless inconsistencies among measurements are found, no correction is made to the calculated uncertainty. Close communication between representatives of the experiments and HFLAV members who perform averages helps ensure that measurement uncertainties, known correlations, and systematic effects are properly accounted for. If a special treatment is needed to calculate an average, or if an approximation used in an average calculation might not be sufficiently accurate (*e.g.*, assuming Gaussian uncertainties when the likelihood function is non-Gaussian), a note is included in the HFLAV publication and online documentation to describe this.

In general, HFLAV uses all publicly available results that have written documentation such as a journal publication, preprint, or conference note. These include preliminary results presented at conferences and workshops. However, preliminary results that remain unpublished for an extended period of time, or for which no publication is planned, are not included.

All HFLAV averages and input measurements are documented in an approximately biennial journal paper or preprint; the most recent version is Ref. [1]. The latest results and plots are posted on an extensive set of webpages that are updated several times per year; these are available at `https://hflav.web.cern.ch`.

References:

1. S. Banerjee *et al.* (Heavy Flavor Averaging Group), accepted by Phys. Rev. D (2025), Phys. Rev. **D113**, 012008 (2026), doi:10.1103/x87q-tld5 [arXiv:2411.18639], updated results and plots available at `https://hflav.web.cern.ch/`.
2. N. Cabibbo, Phys. Rev. Lett. **10**, 531 (1963).
3. M. Kobayashi and T. Maskawa, Prog. Theor. Phys. **49**, 652 (1973).
4. See Section 75, "Semileptonic B Hadron Decays, Determination of V_{cb} and V_{ub}", of this *Review*.
5. S. Banerjee *et al.* (Heavy Flavor Averaging Group), Phys. Rev. **D113**, 012008 (2026), doi:10.1103/x87q-tld5 [arXiv:2411.18639], with specific result from `doi:10.5281/zenodo.19102822`..
6. See Section 5 of the "Introduction" to this *Review*.

$B^{\pm}$

$I(J^P) = \frac{1}{2}(0^-)$

Quantum numbers not measured. Values shown are quark-model predictions.

See also the $B^{\pm}/B^0$ ADMIXTURE and $B^{\pm}/B^0/B^0_s/b$-baryon ADMIXTURE sections.

$B^{\pm}$ MASS

The fit uses m_{B^+}, $(m_{B^0} - m_{B^+})$, and m_{B^0} to determine m_{B^+}, m_{B^0}, and the mass difference.

VALUE (MeV)	EVTS	DOCUMENT ID		TECN	COMMENT
5279.41±0.07 OUR FIT					
5279.42±0.08 OUR AVERAGE					
5279.44±0.05±0.07		[1] AAIJ	23Q	LHCB	pp at 7, 8, 13 TeV
5279.38±0.11±0.33		[2] AAIJ	12E	LHCB	pp at 7 TeV
5279.10±0.41±0.36		[3] ACOSTA	06	CDF	$p\overline{p}$ at 1.96 TeV
5279.1 ±0.4 ±0.4	526	[4] CSORNA	00	CLE2	$e^+e^- \to \Upsilon(4S)$
5279.1 ±1.7 ±1.4	147	ABE	96B	CDF	$p\overline{p}$ at 1.8 TeV
• • • We do not use the following data for averages, fits, limits, etc. • • •					
5278.8 ±0.54±2.0	362	ALAM	94	CLE2	$e^+e^- \to \Upsilon(4S)$
5278.3 ±0.4 ±2.0		BORTOLETTO	92	CLEO	$e^+e^- \to \Upsilon(4S)$
5280.5 ±1.0 ±2.0		[5] ALBRECHT	90J	ARG	$e^+e^- \to \Upsilon(4S)$
5275.8 ±1.3 ±3.0	32	ALBRECHT	87C	ARG	$e^+e^- \to \Upsilon(4S)$
5278.2 ±1.8 ±3.0	12	[6] ALBRECHT	87D	ARG	$e^+e^- \to \Upsilon(4S)$
5278.6 ±0.8 ±2.0		BEBEK	87	CLEO	$e^+e^- \to \Upsilon(4S)$

[1] Uses $B^+ \to J/\psi\overline{\Lambda}p$ decays.
[2] Uses $B^+ \to J/\psi K^+$ fully reconstructed decays.
[3] Uses exclusively reconstructed final states containing a $J/\psi \to \mu^+\mu^-$ decays.
[4] CSORNA 00 uses fully reconstructed 526 $B^+ \to J/\psi^{(\prime)} K^+$ events and invariant masses without beam constraint.
[5] ALBRECHT 90J assumes 10580 for $\Upsilon(4S)$ mass. Supersedes ALBRECHT 87C and ALBRECHT 87D.
[6] Found using fully reconstructed decays with $J/\psi(1S)$. ALBRECHT 87D assume $m_{\Upsilon(4S)}$ = 10577 MeV.

$B^{\pm}$ MEAN LIFE

See $B^{\pm}/B^0/B^0_s/b$-baryon ADMIXTURE section for data on B-hadron mean life averaged over species of bottom particles.

VALUE (10^{-12} s)	EVTS	DOCUMENT ID		TECN	COMMENT
1.637±0.004 OUR EVALUATION		(Produced by HFLAV)			
1.637±0.004±0.003		AAIJ	14E	LHCB	pp at 7 TeV
1.639±0.009±0.009		[1] AALTONEN	11	CDF	$p\overline{p}$ at 1.96 TeV
1.663±0.023±0.015		[2] AALTONEN	11B	CDF	$p\overline{p}$ at 1.96 TeV
1.635±0.011±0.011		[3] ABE	05B	BELL	$e^+e^- \to \Upsilon(4S)$
1.624±0.014±0.018		[4] ABDALLAH	04E	DLPH	$e^+e^- \to Z$
1.636±0.058±0.025		[5] ACOSTA	02C	CDF	$p\overline{p}$ at 1.8 TeV
1.673±0.032±0.023		[6] AUBERT	01F	BABR	$e^+e^- \to \Upsilon(4S)$
1.648±0.049±0.035		[7] BARATE	00R	ALEP	$e^+e^- \to Z$
1.643±0.037±0.025		[8] ABBIENDI	99J	OPAL	$e^+e^- \to Z$
$1.637 \pm 0.058 {}^{+0.045}_{-0.043}$		[7] ABE	98Q	CDF	$p\overline{p}$ at 1.8 TeV
1.66 ±0.06 ±0.03		[8] ACCIARRI	98S	L3	$e^+e^- \to Z$
1.66 ±0.06 ±0.05		[8] ABE	97J	SLD	$e^+e^- \to Z$
$1.58\ {}^{+0.21}_{-0.18}\ {}^{+0.04}_{-0.03}$	94	[5] BUSKULIC	96J	ALEP	$e^+e^- \to Z$
1.61 ±0.16 ±0.12		[7,9] ABREU	95Q	DLPH	$e^+e^- \to Z$
1.72 ±0.08 ±0.06		[10] ADAM	95	DLPH	$e^+e^- \to Z$
1.52 ±0.14 ±0.09		[7] AKERS	95T	OPAL	$e^+e^- \to Z$

Int. J. Mod. Phys. A 2026.41. Downloaded from www.worldscientific.com
by UNIVERSITY OF CALIFORNIA @ BERKELEY on 09/16/26. Re-use and distribution is strictly not permitted, except for Open Access articles.

• • • We do not use the following data for averages, fits, limits, etc. • • •

$1.695 \pm 0.026 \pm 0.015$			[6] ABE	02H	BELL	Repl. by ABE 05B
$1.68 \pm 0.07 \pm 0.02$			[5] ABE	98B	CDF	Repl. by ACOSTA 02C
$1.56 \pm 0.13 \pm 0.06$			[7] ABE	96C	CDF	Repl. by ABE 98Q
$1.58 \pm 0.09 \pm 0.03$			[11] BUSKULIC	96J	ALEP	$e^+ e^- \to Z$
$1.58 \pm 0.09 \pm 0.04$			[7] BUSKULIC	96J	ALEP	Repl. by BARATE 00R
1.70 ± 0.09			[12] ADAM	95	DLPH	$e^+ e^- \to Z$
$1.61 \pm 0.16 \pm 0.05$		148	[5] ABE	94D	CDF	Repl. by ABE 98B
$1.30 {}^{+0.33}_{-0.29} \pm 0.16$		92	[7] ABREU	93D	DLPH	Sup. by ABREU 95Q
$1.56 \pm 0.19 \pm 0.13$		134	[10] ABREU	93G	DLPH	Sup. by ADAM 95
$1.51 {}^{+0.30}_{-0.28} {}^{+0.12}_{-0.14}$		59	[7] ACTON	93C	OPAL	Sup. by AKERS 95T
$1.47 {}^{+0.22}_{-0.19} {}^{+0.15}_{-0.14}$		77	[7] BUSKULIC	93D	ALEP	Sup. by BUSKULIC 96J

[1] Measured mean life using fully reconstructed decays ($J/\psi K^{(*)}$).
[2] Measured using $B^- \to D^0 \pi^-$ with $D^0 \to K^- \pi^+$ events that were selected using a silicon vertex trigger.
[3] Measurement performed using a combined fit of *CP*-violation, mixing and lifetimes.
[4] Measurement performed using an inclusive reconstruction and B flavor identification technique.
[5] Measured mean life using fully reconstructed decays.
[6] Events are selected in which one B meson is fully reconstructed while the second B meson is reconstructed inclusively.
[7] Data analyzed using $D/D^* \ell X$ event vertices.
[8] Data analyzed using charge of secondary vertex.
[9] ABREU 95Q assumes $B(B^0 \to D^{**-} \ell^+ \nu_\ell) = 3.2 \pm 1.7\%$.
[10] Data analyzed using vertex-charge technique to tag B charge.
[11] Combined result of $D/D^* \ell X$ analysis and fully reconstructed B analysis.
[12] Combined ABREU 95Q and ADAM 95 result.

τ_{B^+}/τ_{B^-}

VALUE	DOCUMENT ID		TECN	COMMENT
$1.002 \pm 0.004 \pm 0.002$	[1] AAIJ	14E	LHCB	pp at 7 TeV

[1] Measured using $B^{\pm} \to J/\psi K^{\pm}$ decays.

B^+ DECAY MODES

B^- modes are charge conjugates of the modes below. Modes which do not identify the charge state of the B are listed in the $B^{\pm}/B^0$ ADMIXTURE section.

The branching fractions listed below assume 50% $B^0 \overline{B}^0$ and 50% $B^+ B^-$ production at the $\Upsilon(4S)$. We have attempted to bring older measurements up to date by rescaling their assumed $\Upsilon(4S)$ production ratio to 50:50 and their assumed D, D_s, D^*, and ψ branching ratios to current values whenever this would affect our averages and best limits significantly.

Indentation is used to indicate a subchannel of a previous reaction. All resonant subchannels have been corrected for resonance branching fractions to the final state so the sum of the subchannel branching fractions can exceed that of the final state.

For inclusive branching fractions, *e.g.*, $B \to D^{\pm} X$, the values usually are multiplicities, not branching fractions. They can be greater than one.

	Mode		Fraction (Γ_i/Γ)	Scale factor/ Confidence level
	Semileptonic and leptonic modes			
Γ_1	$\ell^+ \nu_\ell X$	[a]	(10.99 ± 0.28) %	
Γ_2	$e^+ \nu_e X_c$		(10.8 ± 0.4) %	
Γ_3	$e^+ \nu_e X$		(10.8 ± 2.7) %	
Γ_4	$\mu^+ \nu_\mu X$		(11.3 ± 3.5) %	
Γ_5	$\ell^+ \nu_\ell X_u$	[a]	$(1.65 \pm 0.21) \times 10^{-3}$	
Γ_6	$D \ell^+ \nu_\ell X$	[a]	(9.5 ± 0.7) %	
Γ_7	$\overline{D}^0 \ell^+ \nu_\ell$	[a]	(2.21 ± 0.06) %	
Γ_8	$\tau^+ \nu_\tau X$		(2.5 ± 0.4) %	
Γ_9	$\overline{D}^0 \tau^+ \nu_\tau$		$(7.7 \pm 2.5) \times 10^{-3}$	
Γ_{10}	$\overline{D}^*(2007)^0 \ell^+ \nu_\ell$	[a]	(5.53 ± 0.22) %	
Γ_{11}	$\overline{D}^*(2007)^0 e^+ \nu_e$			
Γ_{12}	$\overline{D}^*(2007)^0 \mu^+ \nu_\mu$			
Γ_{13}	$\overline{D}^*(2007)^0 \tau^+ \nu_\tau$		(1.88 ± 0.20) %	
Γ_{14}	$D^{(*)} n \pi \ell^+ \nu_\ell (n \geq 1)$	[a]	(1.83 ± 0.25) %	
Γ_{15}	$D^- \pi^+ \ell^+ \nu_\ell$	[a]	$(3.82 \pm 0.20) \times 10^{-3}$	
Γ_{16}	$\overline{D}_2^*(2460)^0 \ell^+ \nu_\ell$, $\overline{D}_2^{*0} \to D^- \pi^+$	[a]	$(1.59 \pm 0.10) \times 10^{-3}$	
Γ_{17}	$\overline{D}_0^*(2420)^0 \ell^+ \nu_\ell$, $\overline{D}_0^{*0} \to D^- \pi^+$	[a]	$(9 \pm 5) \times 10^{-4}$	S=2.6
Γ_{18}	$D^{*-} \pi^+ \ell^+ \nu_\ell$	[a]	$(5.42 \pm 0.28) \times 10^{-3}$	
Γ_{19}	$\overline{D}_1(2420)^0 \ell^+ \nu_\ell$, $\overline{D}_1^0 \to D^{*-} \pi^+$	[a]	$(2.84 \pm 0.17) \times 10^{-3}$	S=1.1
Γ_{20}	$\overline{D}_1'(2430)^0 \ell^+ \nu_\ell$, $\overline{D}_1'^0 \to D^{*-} \pi^+$	[a]	$(1.7 \pm 0.6) \times 10^{-3}$	S=1.8
Γ_{21}	$\overline{D}_2^*(2460)^0 \ell^+ \nu_\ell$, $\overline{D}_2^{*0} \to D^{*-} \pi^+$	[a]	$(1.06 \pm 0.18) \times 10^{-3}$	S=1.7
Γ_{22}	$\overline{D}_1(2420)^0 \tau^+ \nu_\tau$			
Γ_{23}	$\overline{D}_2^*(2460)^0 \tau^+ \nu_\tau$			
Γ_{24}	$\overline{D}^0 \pi^+ \pi^- \ell^+ \nu_\ell$	[a]	$(1.73 \pm 0.19) \times 10^{-3}$	
Γ_{25}	$\overline{D}_1(2420)^0 \ell^+ \nu_\ell$, $\overline{D}_1^0 \to \overline{D}^0 \pi^+ \pi^-$	[a]	$(1.05 \pm 0.14) \times 10^{-3}$	
Γ_{26}	$\overline{D}^{*0} \pi^+ \pi^- \ell^+ \nu_\ell$	[a]	$(7.0 \pm 1.7) \times 10^{-4}$	
Γ_{27}	$D_s^{(*)-} K^+ \ell^+ \nu_\ell$	[a]	$(6.1 \pm 1.0) \times 10^{-4}$	
Γ_{28}	$D_s^- K^+ \ell^+ \nu_\ell$	[a]	$(3.0 {}^{+1.4}_{-1.2}) \times 10^{-4}$	
Γ_{29}	$D_s^{*-} K^+ \ell^+ \nu_\ell$	[a]	$(2.9 \pm 1.9) \times 10^{-4}$	
Γ_{30}	$\pi^0 \ell^+ \nu_\ell$	[a]	$(7.80 \pm 0.27) \times 10^{-5}$	
Γ_{31}	$\pi^0 e^+ \nu_e$			
Γ_{32}	$\eta \ell^+ \nu_\ell$	[a]	$(3.5 \pm 0.4) \times 10^{-5}$	
Γ_{33}	$\eta' \ell^+ \nu_\ell$	[a]	$(2.4 \pm 0.7) \times 10^{-5}$	
Γ_{34}	$\omega \ell^+ \nu_\ell$	[a]	$(1.19 \pm 0.09) \times 10^{-4}$	
Γ_{35}	$\omega \mu^+ \nu_\mu$			
Γ_{36}	$\rho^0 \ell^+ \nu_\ell$	[a]	$(1.58 \pm 0.11) \times 10^{-4}$	
Γ_{37}	$\pi^+ \pi^- \ell^+ \nu_\ell$	[a]	$(2.3 \pm 0.4) \times 10^{-4}$	
Γ_{38}	$p \overline{p} \ell^+ \nu_\ell$	[a]	$(5.8 {}^{+2.6}_{-2.3}) \times 10^{-6}$	
Γ_{39}	$p \overline{p} \mu^+ \nu_\mu$		$(5.32 \pm 0.33) \times 10^{-6}$	
Γ_{40}	$p \overline{p} e^+ \nu_e$		$(8.2 {}^{+4.0}_{-3.3}) \times 10^{-6}$	
Γ_{41}	$e^+ \nu_e$		$< 9.8 \times 10^{-7}$	CL=90%
Γ_{42}	$\mu^+ \nu_\mu$		$< 8.6 \times 10^{-7}$	CL=90%
Γ_{43}	$\tau^+ \nu_\tau$		$(1.12 \pm 0.19) \times 10^{-4}$	
Γ_{44}	$\ell^+ \nu_\ell \gamma$	[a]	$< 3.0 \times 10^{-6}$	CL=90%
Γ_{45}	$e^+ \nu_e \gamma$		$< 4.3 \times 10^{-6}$	CL=90%
Γ_{46}	$\mu^+ \nu_\mu \gamma$		$< 3.4 \times 10^{-6}$	CL=90%
Γ_{47}	$\mu^+ \mu^- \mu^+ \nu_\mu$		$< 1.6 \times 10^{-8}$	CL=95%
	Inclusive modes			
Γ_{48}	$D^0 X$		(8.6 ± 0.7) %	
Γ_{49}	$\overline{D}^0 X$		(79 ± 4) %	
Γ_{50}	$D^+ X$		(2.5 ± 0.5) %	
Γ_{51}	$D^- X$		(9.9 ± 1.2) %	
Γ_{52}	$D_s^+ X$		$(7.9 {}^{+1.4}_{-1.3})$ %	
Γ_{53}	$D_s^- X$		$(1.10 {}^{+0.40}_{-0.32})$ %	
Γ_{54}	$\Lambda_c^+ X$		$(2.1 {}^{+0.9}_{-0.6})$ %	
Γ_{55}	$\overline{\Lambda}_c^- X$		$(2.8 {}^{+1.1}_{-0.9})$ %	
Γ_{56}	$\overline{c} X$		(97 ± 4) %	
Γ_{57}	$c X$		$(23.4 {}^{+2.2}_{-1.8})$ %	
Γ_{58}	$c/\overline{c} X$		(120 ± 6) %	
	D, D^*, or D_s modes			
Γ_{59}	$\overline{D}^0 \pi^+$		$(4.61 \pm 0.10) \times 10^{-3}$	
Γ_{60}	$D_{CP(+1)} \pi^+$	[b]	$(2.04 \pm 0.20) \times 10^{-3}$	
Γ_{61}	$D_{CP(-1)} \pi^+$	[b]	$(2.1 \pm 0.4) \times 10^{-3}$	
Γ_{62}	$\overline{D}^0 \rho^+$		$(9.7 \pm 1.1) \times 10^{-3}$	S=2.1
Γ_{63}	$\overline{D}^0 K^+$		$(3.64 \pm 0.15) \times 10^{-4}$	
Γ_{64}	$D_{CP(+1)} K^+$	[b]	$(1.81 \pm 0.08) \times 10^{-4}$	
Γ_{65}	$D_{CP(-1)} K^+$	[b]	$(2.04 \pm 0.13) \times 10^{-4}$	
Γ_{66}	$D^0 K^+$		$(3.60 \pm 0.24) \times 10^{-6}$	
Γ_{67}	$[K^- \pi^+]_D K^+$	[c]	$< 2.8 \times 10^{-7}$	CL=90%
Γ_{68}	$[K^+ \pi^-]_D K^+$	[c]	$< 1.6 \times 10^{-5}$	CL=90%
Γ_{69}	$[K^- \pi^+ \pi^0]_D K^+$		seen	
Γ_{70}	$[K^+ \pi^- \pi^0]_D K^+$		seen	
Γ_{71}	$[K^- \pi^+ \pi^+ \pi^-]_D K^+$		seen	
Γ_{72}	$[K^+ \pi^- \pi^+ \pi^-]_D K^+$		seen	
Γ_{73}	$[\pi^+ \pi^+ \pi^- \pi^-] K^+$			
Γ_{74}	$[\pi^+ \pi^- \pi^+ \pi^-]_D K^*(892)^+$			
Γ_{75}	$[K^- \pi^+]_D K^*(892)^+$	[c]		
Γ_{76}	$[K^+ \pi^-]_D K^*(892)^+$	[c]		
Γ_{77}	$[K^- \pi^+ \pi^- \pi^+]_D K^*(892)^+$			
Γ_{78}	$[K^+ \pi^- \pi^+ \pi^-]_D K^*(892)^+$			
Γ_{79}	$[K^- \pi^+]_D \pi^+$	[c]	$(6.3 \pm 1.1) \times 10^{-7}$	
Γ_{80}	$[K^+ \pi^-]_D \pi^+$		$(1.72 \pm 0.30) \times 10^{-4}$	
Γ_{81}	$[K^- \pi^+ \pi^0]_D \pi^+$		seen	
Γ_{82}	$[K^+ \pi^- \pi^0]_D \pi^+$		seen	
Γ_{83}	$[K^- \pi^+ \pi^+ \pi^-]_D \pi^+$		seen	
Γ_{84}	$[K^+ \pi^- \pi^+ \pi^-]_D \pi^+$		seen	

Int. J. Mod. Phys. A 2026.41. Downloaded from www.worldscientific.com
by LIFORNIA @ BERKELEY on 09/16/26. Re-use and distribution is strictly not permitted, except for Open Access articles.

Γ_{85}	$([K^-\pi^+]_D\pi^0)_{D^*}\pi^+$				
Γ_{86}	$([K^+\pi^-]_D\pi^0)_{D^*}\pi^+$				
Γ_{87}	$([K^-\pi^+]_D\gamma)_{D^*}\pi^+$				
Γ_{88}	$([K^+\pi^-]_D\gamma)_{D^*}\pi^+$				
Γ_{89}	$([K^-\pi^+]_D\pi^0)_{D^*}K^+$				
Γ_{90}	$([K^+\pi^-]_D\pi^0)_{D^*}K^+$				
Γ_{91}	$([K^-\pi^+]_D\gamma)_{D^*}K^+$				
Γ_{92}	$([K^+\pi^-]_D\gamma)_{D^*}K^+$				
Γ_{93}	$[\pi^+\pi^-\pi^0]_D K^-$		$(4.6 \pm 0.9)\times10^{-6}$		
Γ_{94}	$[K^0_S K^+\pi^-]_D K^+$		seen		
Γ_{95}	$[K^*(892)^- K^+]_D K^+$				
Γ_{96}	$[K^0_S K^-\pi^+]_D K^+$		seen		
Γ_{97}	$[K^*(892)^+ K^-]_D K^+$		seen		
Γ_{98}	$[K^0_S K^-\pi^+]_D \pi^+$		seen		
Γ_{99}	$[K^*(892)^+ K^-]_D \pi^+$		seen		
Γ_{100}	$[K^0_S K^+\pi^-]_D \pi^+$		seen		
Γ_{101}	$[K^*(892)^- K^+]_D \pi^+$		seen		
Γ_{102}	$[K^+K^-\pi^0]_D K^+$				
Γ_{103}	$[K^+K^-\pi^0]_D \pi^+$				
Γ_{104}	$[\pi^+\pi^-\pi^0]_D K^+$				
Γ_{105}	$[\pi^+\pi^-\pi^0]_D \pi^+$				
Γ_{106}	$\overline{D}^0 K^*(892)^+$		$(5.3 \pm 0.4)\times10^{-4}$		
Γ_{107}	$D_{CP(-1)} K^*(892)^+$	[b]	$(2.7 \pm 0.8)\times10^{-4}$		
Γ_{108}	$D_{CP(+1)} K^*(892)^+$	[b]	$(6.2 \pm 0.7)\times10^{-4}$		
Γ_{109}	$D^0 K^*(892)^+$		$(5.4 {}^{+1.8}_{-4.0})\times10^{-6}$		
Γ_{110}	$\overline{D}^0 K^+\pi^+\pi^-$		$(5.2 \pm 2.1)\times10^{-4}$		
Γ_{111}	$[K^+\pi^-]_D K^+\pi^-\pi^+$				
Γ_{112}	$[K^-\pi^+]_D K^+\pi^-\pi^+$				
Γ_{113}	$D_{CP(+1)} K^+\pi^-\pi^+$				
Γ_{114}	$\overline{D}^0 K^+\overline{K}^0$		$(3.75 \pm 0.35)\times10^{-4}$		
Γ_{115}	$\overline{D}^0 K^+\overline{K}^*(892)^0$		$(7.2 \pm 0.5)\times10^{-4}$		
Γ_{116}	$\overline{D}^0\pi^+\pi^+\pi^-$		$(5.5 \pm 2.0)\times10^{-3}$		S=3.6
Γ_{117}	$[K^-\pi^+]_D\pi^+\pi^-\pi^+$				
Γ_{118}	$\overline{D}^0\pi^+\pi^+\pi^-$ nonresonant		$(5 \pm 4)\times10^{-3}$		
Γ_{119}	$\overline{D}^0\pi^+\rho^0$		$(4.2 \pm 3.0)\times10^{-3}$		
Γ_{120}	$\overline{D}^0 a_1(1260)^+$		$(4 \pm 4)\times10^{-3}$		
Γ_{121}	$\overline{D}^0\omega\pi^+$		$(4.1 \pm 0.9)\times10^{-3}$		
Γ_{122}	$D^*(2010)^-\pi^+\pi^+$		$(1.35 \pm 0.22)\times10^{-3}$		
Γ_{123}	$D^*(2010)^- K^+\pi^+$		$(8.2 \pm 1.4)\times10^{-5}$		
Γ_{124}	$\overline{D}_1(2420)^0\pi^+,\ \overline{D}^0_1 \to D^*(2010)^-\pi^+$		$(8.4 \pm 1.5)\times10^{-4}$		
Γ_{125}	$D^-\pi^+\pi^+$		$(1.07 \pm 0.05)\times10^{-3}$		
Γ_{126}	$D^- K^+\pi^+$		$(7.7 \pm 0.5)\times10^{-5}$		
Γ_{127}	$D^*_0(2300)^0 K^+,\ D^{*0}_0 \to D^-\pi^+$		$(6.1 \pm 2.4)\times10^{-6}$		
Γ_{128}	$D^*_2(2460)^0 K^+,\ D^{*0}_2 \to D^-\pi^+$		$(2.32 \pm 0.23)\times10^{-5}$		
Γ_{129}	$D^*_1(2760)^0 K^+,\ D^{*0}_1 \to D^-\pi^+$		$(3.6 \pm 1.2)\times10^{-6}$		
Γ_{130}	$D^+ K^0$		$< 2 \times10^{-6}$		CL=90%
Γ_{131}	$D^+ K^+\pi^-$		$(5.6 \pm 1.1)\times10^{-6}$		
Γ_{132}	$D^+\eta$		$< 1.2 \times10^{-5}$		CL=90%
Γ_{133}	$D^*_2(2460)^0 K^+,\ D^{*0}_2 \to D^+\pi^-$		$< 6.3 \times10^{-7}$		CL=90%
Γ_{134}	$D^+ K^{*0}$		$< 4.9 \times10^{-7}$		CL=90%
Γ_{135}	$D^+\overline{K}^{*0}$		$< 1.4 \times10^{-6}$		CL=90%
Γ_{136}	$\overline{D}^*(2007)^0\pi^+$		$(5.17 \pm 0.15)\times10^{-3}$		
Γ_{137}	$\overline{D}^{*0}_{CP(+1)}\pi^+$	[d]	$(2.9 \pm 0.6)\times10^{-3}$		
Γ_{138}	$D^{*0}_{CP(-1)}\pi^+$	[d]	$(2.6 \pm 1.0)\times10^{-3}$		
Γ_{139}	$\overline{D}^*(2007)^0\omega\pi^+$		$(4.5 \pm 1.2)\times10^{-3}$		
Γ_{140}	$\overline{D}^*(2007)^0\rho^+$		$(9.8 \pm 1.7)\times10^{-3}$		
Γ_{141}	$\overline{D}^*(2007)^0 K^+$		$(4.19 {}^{+0.31}_{-0.28})\times10^{-4}$		
Γ_{142}	$\overline{D}^{*0}_{CP(+1)} K^+$	[d]	$(2.75 \pm 0.35)\times10^{-4}$		
Γ_{143}	$\overline{D}^{*0}_{CP(-1)} K^+$	[d]	$(2.31 \pm 0.31)\times10^{-4}$		
Γ_{144}	$D^*(2007)^0 K^+$		$(4.5 \pm 1.2)\times10^{-6}$		
Γ_{145}	$\overline{D}^*(2007)^0 K^*(892)^+$		$(8.1 \pm 1.4)\times10^{-4}$		
Γ_{146}	$\overline{D}^*(2007)^0 K^+\overline{K}^0$		$(2.9 \pm 0.6)\times10^{-4}$		
Γ_{147}	$\overline{D}^*(2007)^0 K^+\overline{K}^*(892)^0$		$(1.23 \pm 0.14)\times10^{-3}$		
Γ_{148}	$\overline{D}^*(2007)^0\pi^+\pi^+\pi^-$		(1.03 ± 0.12) %		
Γ_{149}	$\overline{D}^*(2007)^0 a_1(1260)^+$		(1.9 ± 0.5) %		
Γ_{150}	$\overline{D}^*(2007)^0\pi^-\pi^+\pi^+\pi^0$		(1.8 ± 0.4) %		
Γ_{151}	$\overline{D}^{*0} 3\pi^+ 2\pi^-$		$(5.7 \pm 1.2)\times10^{-3}$		
Γ_{152}	$D^*(2010)^+\pi^0$		$< 3.6 \times10^{-6}$		
Γ_{153}	$D^*(2010)^+ K^0$		$< 9.0 \times10^{-6}$		CL=90%
Γ_{154}	$D^*(2010)^-\pi^+\pi^+\pi^0$		(1.5 ± 0.7) %		
Γ_{155}	$D^*(2010)^-\pi^+\pi^+\pi^+\pi^-$		$(2.6 \pm 0.4)\times10^{-3}$		
Γ_{156}	$\overline{D}^{**0}\pi^+$	[e]	$(5.6 \pm 1.2)\times10^{-3}$		
Γ_{157}	$\overline{D}^*_1(2420)^0\pi^+$		$(1.5 \pm 0.6)\times10^{-3}$		S=1.3
Γ_{158}	$\overline{D}_1(2420)^0\pi^+ \times B(\overline{D}^0_1 \to \overline{D}^0\pi^+\pi^-)$		$(2.5 {}^{+1.6}_{-1.4})\times10^{-4}$		S=3.8
Γ_{159}	$\overline{D}_1(2420)^0\pi^+ \times B(\overline{D}^0_1 \to \overline{D}^0\pi^+\pi^-$ (nonresonant))		$(2.2 \pm 0.9)\times10^{-4}$		
Γ_{160}	$\overline{D}_1(2430)^0\pi^+,\ \overline{D}^0_1 \to D^*(2010)^-\pi^+$		$(3.5 \pm 0.6)\times10^{-4}$		
Γ_{161}	$\overline{D}(2550)^0\pi^+,\ \overline{D}^0 \to D^*(2010)^-\pi^+$		$(7.2 \pm 1.4)\times10^{-5}$		
Γ_{162}	$\overline{D}^*_J(2600)^0\pi^+,\ \overline{D}^{*0}_J \to D^*(2010)^-\pi^+$		$(6.8 \pm 1.3)\times10^{-5}$		
Γ_{163}	$\overline{D}^*_2(2462)^0\pi^+,\ \overline{D}^{*0}_2 \to D^-\pi^+$		$(3.56 \pm 0.24)\times10^{-4}$		
Γ_{164}	$\overline{D}^*_2(2462)^0\pi^+,\ \overline{D}^{*0}_2 \to \overline{D}^0\pi^-\pi^+$		$(2.2 \pm 1.0)\times10^{-4}$		
Γ_{165}	$\overline{D}^*_2(2462)^0\pi^+,\ \overline{D}^{*0}_2 \to \overline{D}^0\pi^-\pi^+$ (nonresonant)		$< 1.6 \times10^{-4}$		CL=90%
Γ_{166}	$\overline{D}^*_2(2462)^0\pi^+,\ \overline{D}^{*0}_2 \to D^*(2010)^-\pi^+$		$(2.1 \pm 1.0)\times10^{-4}$		
Γ_{167}	$\overline{D}^*_0(2400)^0\pi^+ \times B(\overline{D}^*_0(2400)^0 \to D^-\pi^+)$		$(6.4 \pm 1.4)\times10^{-4}$		
Γ_{168}	$\overline{D}_1(2421)^0\pi^+,\ \overline{D}^0_1 \to D^{*-}\pi^+$		$(7.4 \pm 1.0)\times10^{-4}$		
Γ_{169}	$\overline{D}^*_2(2462)^0\pi^+,\ \overline{D}^{*0}_2 \to D^{*-}\pi^+$		$(1.98 \pm 0.30)\times10^{-4}$		
Γ_{170}	$\overline{D}'_1(2427)^0\pi^+,\ \overline{D}'^0_1 \to D^{*-}\pi^+$		$(3.5 \pm 0.9)\times10^{-4}$		S=1.5
Γ_{171}	$\overline{D}_1(2420)^0\pi^+ \times B(\overline{D}^0_1 \to \overline{D}^{*0}\pi^+\pi^-)$		$< 6 \times10^{-6}$		CL=90%
Γ_{172}	$\overline{D}^*_1(2420)^0\rho^+$		$< 1.4 \times10^{-3}$		CL=90%
Γ_{173}	$\overline{D}^*_2(2460)^0\pi^+$		$< 1.3 \times10^{-3}$		CL=90%
Γ_{174}	$\overline{D}^*_2(2460)^0\pi^+ \times B(\overline{D}^{*0}_2 \to \overline{D}^{*0}\pi^+\pi^-)$		$< 2.2 \times10^{-5}$		CL=90%
Γ_{175}	$\overline{D}^*_1(2680)^0\pi^+,\ \overline{D}^*_1(2680)^0 \to D^-\pi^+$		$(8.4 \pm 2.1)\times10^{-5}$		
Γ_{176}	$\overline{D}(2740)^0\pi^+,\ \overline{D}^0 \to D^*(2010)^-\pi^+$		$(3.3 \pm 1.5)\times10^{-5}$		
Γ_{177}	$\overline{D}^*_3(2750)^0\pi^+,\ \overline{D}^{*0}_3 \to D^*(2010)^-\pi^+$		$(1.10 \pm 0.32)\times10^{-5}$		
Γ_{178}	$\overline{D}^*_3(2760)^0\pi^+,\ \overline{D}^*_3(2760)^0\pi^+ \to D^-\pi^+$		$(1.00 \pm 0.22)\times10^{-5}$		
Γ_{179}	$\overline{D}^*_2(3000)^0\pi^+,\ \overline{D}^*_2(3000)^0\pi^+ \to D^-\pi^+$		$(2.0 \pm 1.4)\times10^{-6}$		
Γ_{180}	$\overline{D}^*_2(2460)^0\rho^+$		$< 4.7 \times10^{-3}$		CL=90%
Γ_{181}	$\overline{D}^0 D^+_s$		$(9.3 \pm 0.6)\times10^{-3}$		
Γ_{182}	$D^*_{s0}(2317)^+\overline{D}^0,\ D^{*+}_{s0} \to D^+_s\pi^0$		$(7.9 {}^{+1.5}_{-1.3})\times10^{-4}$		
Γ_{183}	$D_{s0}(2317)^+\overline{D}^0 \times B(D_{s0}(2317)^+ \to D^{*+}_s\gamma)$		$< 7.6 \times10^{-4}$		CL=90%
Γ_{184}	$D_{s0}(2317)^+\overline{D}^*(2007)^0 \times B(D_{s0}(2317)^+ \to D^+_s\pi^0)$		$(9 \pm 7)\times10^{-4}$		
Γ_{185}	$D_{sJ}(2457)^+\overline{D}^0$		$(3.1 {}^{+1.0}_{-0.9})\times10^{-3}$		
Γ_{186}	$D_{sJ}(2457)^+\overline{D}^0 \times B(D_{sJ}(2457)^+ \to D^+_s\gamma)$		$(4.6 {}^{+1.3}_{-1.1})\times10^{-4}$		
Γ_{187}	$D_{sJ}(2457)^+\overline{D}^0 \times B(D_{sJ}(2457)^+ \to D^+_s\pi^+\pi^-)$		$< 2.2 \times10^{-4}$		CL=90%
Γ_{188}	$D_{sJ}(2457)^+\overline{D}^0 \times B(D_{sJ}(2457)^+ \to D^+_s\pi^0)$		$< 2.7 \times10^{-4}$		CL=90%
Γ_{189}	$D_{sJ}(2457)^+\overline{D}^0 \times B(D_{sJ}(2457)^+ \to D^{*+}_s\gamma)$		$< 9.8 \times10^{-4}$		CL=90%
Γ_{190}	$D_{sJ}(2457)^+\overline{D}^*(2007)^0$		(1.20 ± 0.30) %		
Γ_{191}	$D_{sJ}(2457)^+\overline{D}^*(2007)^0 \times B(D_{sJ}(2457)^+ \to D^+_s\gamma)$		$(1.4 {}^{+0.7}_{-0.6})\times10^{-3}$		
Γ_{192}	$\overline{D}^0 D_{s1}(2536)^+ \times B(D_{s1}(2536)^+ \to D^*(2007)^0 K^+ + D^*(2010)^+ K^0)$		$(4.0 \pm 1.0)\times10^{-4}$		

Int. J. Mod. Phys. A 2026.41. Downloaded from www.worldscientific.com
by UNIVERSITY OF CALIFORNIA @ BERKELEY on 09/16/26. Re-use and distribution is strictly not permitted, except for Open Access articles.

Γ_{193}	$\overline{D}^0 D_{s1}(2536)^+ \times B(D_{s1}(2536)^+ \to D^*(2007)^0 K^+)$	$(2.2 \pm 0.7) \times 10^{-4}$		
Γ_{194}	$\overline{D}^*(2007)^0 D_{s1}(2536)^+ \times B(D_{s1}(2536)^+ \to D^*(2007)^0 K^+)$	$(5.5 \pm 1.6) \times 10^{-4}$		
Γ_{195}	$\overline{D}^0 D_{s1}(2536)^+ \times B(D_{s1}(2536)^+ \to D^{*+} K^0)$	$(2.3 \pm 1.1) \times 10^{-4}$		
Γ_{196}	$\overline{D}^0 D_{sJ}(2700)^+ \times B(D_{sJ}(2700)^+ \to D^0 K^+)$	$(5.6 \pm 1.8) \times 10^{-4}$	S=1.7	
Γ_{197}	$\overline{D}^{*0} D_{s1}(2536)^+,\ D_{s1}^+ \to D^{*+} K^0$	$(3.9 \pm 2.6) \times 10^{-4}$		
Γ_{198}	$\overline{D}^0 D_{sJ}(2573)^+,\ D_{sJ}^+ \to D^0 K^+$	$(8 \pm 15) \times 10^{-6}$		
Γ_{199}	$\overline{D}^{*0} D_{sJ}(2573),\ D_{sJ}^+ \to D^0 K^+$	$< 2 \times 10^{-4}$	CL=90%	
Γ_{200}	$\overline{D}^*(2007)^0 D_{sJ}(2573),\ D_{sJ}^+ \to D^0 K^+$	$< 5 \times 10^{-4}$	CL=90%	
Γ_{201}	$\overline{D}^0 D_s^{*+}$	$(7.6 \pm 1.6) \times 10^{-3}$		
Γ_{202}	$D^- D_s^+ \pi^+$			
Γ_{203}	$\overline{D}^*(2007)^0 D_s^+$	$(7.0 \pm 1.0) \times 10^{-3}$		
Γ_{204}	$\overline{D}^*(2007)^0 D_s^+,\ \overline{D}^{*0} \to D^- \pi^+$			
Γ_{205}	$\overline{D}^*(2007)^0 D_s^{*+}$	(1.71 ± 0.24) %		
Γ_{206}	$\overline{D}_2^*(2460)^0 D_s^+,\ \overline{D}_2^{*0} \to D^- \pi^+$			
Γ_{207}	$\overline{D}_1(2420)^0 D_s^{(*)+}$			
Γ_{208}	$\overline{D}_2^*(2460)^0 D_s^{(*)+}$			
Γ_{209}	$\overline{D}_1^*(2600)^0 D_s^+,\ \overline{D}_1^{*0} \to D^- \pi^+$			
Γ_{210}	$\overline{D}_3^*(2750)^0 D_s^+,\ \overline{D}_3^{*0} \to D^- \pi^+$			
Γ_{211}	$\overline{D}_1^*(2760)^0 D_s^+,\ \overline{D}_1^{*0} \to D^- \pi^+$			
Γ_{212}	$\overline{D}_J^*(3000)^0 D_s^+,\ \overline{D}_J^{*0} \to D^- \pi^+$			
Γ_{213}	$T_{cs0}^*(2900)^{++} D^-,\ T_{cs0}^{*++} \to D_s^+ \pi^+$			
Γ_{214}	$D_s^{(*)+} \overline{D}^{**0}$	(2.7 ± 1.2) %		
Γ_{215}	$\overline{D}^*(2007)^0 D^*(2010)^+$	$(8.1 \pm 1.7) \times 10^{-4}$		
Γ_{216}	$\overline{D}^0 D^*(2010)^+ + \overline{D}^*(2007)^0 D^+$	< 1.30 %	CL=90%	
Γ_{217}	$\overline{D}^0 D^*(2010)^+$	$(3.9 \pm 0.5) \times 10^{-4}$		
Γ_{218}	$\overline{D}^0 D^+$	$(3.8 \pm 0.4) \times 10^{-4}$		
Γ_{219}	$\overline{D}^0 D^+ K^0$	$(1.55 \pm 0.21) \times 10^{-3}$		
Γ_{220}	$D^+ \overline{D}^*(2007)^0$	$(6.3 \pm 1.7) \times 10^{-4}$		
Γ_{221}	$\overline{D}^*(2007)^0 D^+ K^0$	$(2.1 \pm 0.5) \times 10^{-3}$		
Γ_{222}	$\overline{D}^0 D^*(2010)^+ K^0$	$(3.8 \pm 0.4) \times 10^{-3}$		
Γ_{223}	$\overline{D}^*(2007)^0 D^*(2010)^+ K^0$	$(9.2 \pm 1.2) \times 10^{-3}$		
Γ_{224}	$\overline{D}^0 D^0 K^+$	$(1.45 \pm 0.33) \times 10^{-3}$	S=2.6	
Γ_{225}	$\overline{D}^*(2007)^0 D^0 K^+$	$(2.26 \pm 0.23) \times 10^{-3}$		
Γ_{226}	$\overline{D}^0 D^*(2007)^0 K^+$	$(6.3 \pm 0.5) \times 10^{-3}$		
Γ_{227}	$\overline{D}^*(2007)^0 D^*(2007)^0 K^+$	(1.12 ± 0.13) %		
Γ_{228}	$D^- D^+ K^+$	$(2.2 \pm 0.7) \times 10^{-4}$		
Γ_{229}	$T_{cs0}^*(2870)^0 D^+,\ T_{cs0}^{*0} \to D^- K^+$	$(1.2 \pm 0.5) \times 10^{-5}$		
Γ_{230}	$T_{cs1}^*(2900)^0 D^+,\ T_{cs1}^{*0} \to D^- K^+$	$(6.7 \pm 2.3) \times 10^{-5}$		
Γ_{231}	$D^- D^+ K^+$ nonresonant	$(5.3 \pm 1.8) \times 10^{-5}$		
Γ_{232}	$D^- D^*(2010)^+ K^+$	$(6.3 \pm 1.1) \times 10^{-4}$		
Γ_{233}	$D^*(2010)^- D^+ K^+$	$(6.0 \pm 1.3) \times 10^{-4}$		
Γ_{234}	EFF$K+$, EFF $\to D^*(2010)^{\mp} D^{\pm}$	$(1.5 \pm 0.4) \times 10^{-4}$		
Γ_{235}	$\eta_c(3945) K^+,\ \eta_c \to D^*(2010)^{\mp} D^{\pm}$	$(4.6 {}^{+2.7}_{-1.7}) \times 10^{-5}$		
Γ_{236}	$\chi_{c2}(3930) K^+,\ \chi_{c2} \to D^*(2010)^{\mp} D^{\pm}$	$(2.4 {}^{+1.0}_{-1.7}) \times 10^{-5}$		
Γ_{237}	$h_c(4000) K^+,\ h_c \to D^*(2010)^{\mp} D^{\pm}$	$(7.0 {}^{+2.5}_{-1.6}) \times 10^{-5}$		
Γ_{238}	$\chi_{c1}(4010) K^+,\ \chi_{c1} \to D^*(2010)^{\mp} D^{\pm}$	$(1.38 {}^{+0.31}_{-0.28}) \times 10^{-4}$		
Γ_{239}	$\psi(4040) K^+,\ \psi \to D^*(2010)^{\mp} D^{\pm}$	$(3.8 {}^{+1.1}_{-0.9}) \times 10^{-5}$		
Γ_{240}	$h_c(4300) K^+,\ h_c \to D^*(2010)^{\mp} D^{\pm}$	$(1.6 {}^{+0.4}_{-0.7}) \times 10^{-5}$		
Γ_{241}	$T_{\overline{c}s0}^*(2870)^0 K^+,\ T_{\overline{c}s0}^{*0} \to D^*(2010)^{\mp} D^{\pm}$	$(4.5 {}^{+1.2}_{-1.4}) \times 10^{-5}$		
Γ_{242}	$T_{\overline{c}s1}^*(2900)^0 K^+,\ T_{\overline{c}s1}^{*0} \to D^*(2010)^{\mp} D^{\pm}$	$(3.8 {}^{+1.7}_{-1.6}) \times 10^{-5}$		
Γ_{243}	NR K^+, NR $\to D^*(2010)^{\mp} D^{\pm}$	$(2.8 {}^{+0.5}_{-0.4}) \times 10^{-4}$		
Γ_{244}	NR K^+, NR $\to D^*(2010)^{\mp} D^{\pm}$	$(1.6 {}^{+1.3}_{-0.8}) \times 10^{-5}$		
Γ_{245}	NR K^+, NR $\to D^*(2010)^{\mp} D^{\pm}$	$(2.4 {}^{+0.6}_{-0.4}) \times 10^{-4}$		
Γ_{246}	NR K^+, NR $\to D^*(2010)^{\mp} D^{\pm}$	$(2.2 {}^{+0.7}_{-0.5}) \times 10^{-4}$		
Γ_{247}	$D^*(2010)^- D^*(2010)^+ K^+$	$(1.32 \pm 0.18) \times 10^{-3}$		
Γ_{248}	$(\overline{D} + \overline{D}^*)(D + D^*) K$	(4.05 ± 0.30) %		
Γ_{249}	$D_s^- D_s^+ K^+$	$(1.2 \pm 0.4) \times 10^{-4}$		
Γ_{250}	$D_s^+ \pi^0$	$(1.6 \pm 0.5) \times 10^{-5}$		
Γ_{251}	$D_s^{*+} \pi^0$	$< 2.6 \times 10^{-4}$	CL=90%	
Γ_{252}	$D_s^+ \eta$	$< 1.4 \times 10^{-5}$	CL=90%	
Γ_{253}	$D_s^{*+} \eta$	$< 1.7 \times 10^{-5}$	CL=90%	
Γ_{254}	$D_s^+ \rho^0$	$< 3.0 \times 10^{-4}$	CL=90%	
Γ_{255}	$D_s^{*+} \rho^0$	$< 4 \times 10^{-4}$	CL=90%	
Γ_{256}	$D_s^+ \omega$	$< 4 \times 10^{-4}$	CL=90%	
Γ_{257}	$D_s^{*+} \omega$	$< 6 \times 10^{-4}$	CL=90%	
Γ_{258}	$D_s^+ a_1(1260)^0$	$< 1.8 \times 10^{-3}$	CL=90%	
Γ_{259}	$D_s^{*+} a_1(1260)^0$	$< 1.3 \times 10^{-3}$	CL=90%	
Γ_{260}	$D_s^+ K^+ K^-$	$(7.5 \pm 1.0) \times 10^{-6}$		
Γ_{261}	$D_s^+ \phi$	$< 4.2 \times 10^{-7}$	CL=90%	
Γ_{262}	$D_s^{*+} \phi$	$< 1.2 \times 10^{-5}$	CL=90%	
Γ_{263}	$D_s^+ \overline{K}^0$	$< 3 \times 10^{-6}$	CL=90%	
Γ_{264}	$D_s^{*+} \overline{K}^0$	$< 6 \times 10^{-6}$	CL=90%	
Γ_{265}	$D_s^+ \overline{K}^*(892)^0$	$< 4.4 \times 10^{-6}$	CL=90%	
Γ_{266}	$D_s^+ K^{*0}$	$< 3.5 \times 10^{-6}$	CL=90%	
Γ_{267}	$D_s^{*+} \overline{K}^*(892)^0$	$< 3.5 \times 10^{-4}$	CL=90%	
Γ_{268}	$D_s^- \pi^+ K^+$	$(1.80 \pm 0.22) \times 10^{-4}$		
Γ_{269}	$D_s^{*-} \pi^+ K^+$	$(1.45 \pm 0.24) \times 10^{-4}$		
Γ_{270}	$D_s^- \pi^+ K^*(892)^+$	$< 5 \times 10^{-3}$	CL=90%	
Γ_{271}	$D_s^{*-} \pi^+ K^*(892)^+$	$< 7 \times 10^{-3}$	CL=90%	
Γ_{272}	$D_s^- K^+ K^+$	$(9.7 \pm 2.1) \times 10^{-6}$		
Γ_{273}	$D_s^{*-} K^+ K^+$	$< 1.5 \times 10^{-5}$	CL=90%	

Charmonium modes

Γ_{274}	$\eta_c K^+$	$(1.20 \pm 0.08) \times 10^{-3}$	S=1.3	
Γ_{275}	$\eta_c K^*(892)^+$	$(1.4 {}^{+0.7}_{-0.5}) \times 10^{-3}$		
Γ_{276}	$\eta_c K^+ \pi^+ \pi^-$	$< 3.9 \times 10^{-4}$	CL=90%	
Γ_{277}	$\eta_c K^+ \omega(782)$	$< 5.3 \times 10^{-4}$	CL=90%	
Γ_{278}	$\eta_c K^+ \eta$	$< 2.2 \times 10^{-4}$	CL=90%	
Γ_{279}	$\eta_c K^+ \pi^0$	$< 6.2 \times 10^{-5}$	CL=90%	
Γ_{280}	$\eta_c(2S) K^+$	$(4.4 \pm 1.0) \times 10^{-4}$		
Γ_{281}	$\eta_c(2S) K^+,\ \eta_c \to p\overline{p}$	$(3.5 \pm 0.8) \times 10^{-8}$		
Γ_{282}	$\eta_c(2S) K^+,\ \eta_c \to K_S^0 K^{\mp} \pi^{\pm}$	$(3.4 {}^{+2.3}_{-1.6}) \times 10^{-6}$		
Γ_{283}	$\eta_c(2S) K^+,\ \eta_c \to p\overline{p} \pi^+ \pi^-$	$(1.12 \pm 0.18) \times 10^{-6}$		
Γ_{284}	$h_c(1P) K^+,\ h_c \to J/\psi \pi^+ \pi^-$	$< 3.4 \times 10^{-6}$	CL=90%	
Γ_{285}	$X(3730)^0 K^+,\ X^0 \to \eta_c \eta$	$< 4.6 \times 10^{-5}$	CL=90%	
Γ_{286}	$X(3730)^0 K^+,\ X^0 \to \eta_c \pi^0$	$< 5.7 \times 10^{-6}$	CL=90%	
Γ_{287}	$\eta_{c2}(1D) K^+,\ \eta_{c2} \to h_c \gamma$	$< 3.7 \times 10^{-5}$	CL=90%	
Γ_{288}	$\eta_{c2}(1D) \pi^+ K_S^0,\ \eta_{c2} \to h_c \gamma$	$< 1.1 \times 10^{-4}$	CL=90%	
Γ_{289}	$\psi_2(3823) K^+,\ \psi_2 \to J/\psi \pi^+ \pi^-$	$(2.8 \pm 0.6) \times 10^{-7}$		
Γ_{290}	$\psi_2(3823) K^+,\ \psi_2 \to J/\psi \eta$	$(1.2 {}^{+0.7}_{-0.5}) \times 10^{-6}$		
Γ_{291}	$\psi_3(3842) K^+,\ \psi_3 \to J/\psi \eta$	$< 6.1 \times 10^{-7}$	CL=90%	
Γ_{292}	$\chi_{c1}(3872) K^+$	$(1.9 \pm 0.6) \times 10^{-4}$		
Γ_{293}	$\chi_{c0}(3915) K^+$	$< 2.8 \times 10^{-4}$	CL=90%	
Γ_{294}	$\chi_{c0}(3915) K^+,\ \chi_{c0} \to D^+ D^-$	$(8.1 \pm 3.3) \times 10^{-6}$		
Γ_{295}	$\chi_{c0}(3915) K^+,\ \chi_{c0} \to \eta_c \eta$	$< 4.7 \times 10^{-5}$	CL=90%	
Γ_{296}	$\chi_{c0}(3915) K^+,\ \chi_{c0} \to \eta_c \pi^0$	$< 1.7 \times 10^{-5}$	CL=90%	
Γ_{297}	$X(4014)^0 K^+,\ X^0 \to \eta_c \eta$	$< 3.9 \times 10^{-5}$	CL=90%	
Γ_{298}	$X(4014)^0 K^+,\ X^0 \to \eta_c \pi^0$	$< 1.2 \times 10^{-5}$	CL=90%	
Γ_{299}	$T_{c\overline{c}1}(3900)^0 K^+,\ T_{c\overline{c}1}^0 \to \eta_c \pi^+ \pi^-$	$< 4.7 \times 10^{-5}$	CL=90%	
Γ_{300}	$T_{c\overline{c}1}(3900)^0 K^+,\ T_{c\overline{c}1}^0 \to J/\psi \eta$	$< 4.3 \times 10^{-7}$	CL=90%	

Int. J. Mod. Phys. A 2026.41. Downloaded from www.worldscientific.com
by LIFORNIA @ BERKELEY on 09/16/26. Re-use and distribution is strictly not permitted, except for Open Access articles.

Γ_{301}	$T_{c\overline{c}}(4020)^0 K^+$, $T^0_{c\overline{c}} \to \eta_c \pi^+ \pi^-$		< 1.6	$\times 10^{-5}$	CL=90%
Γ_{302}	$\chi_{c1}(3872) K^*(892)^+$		< 5	$\times 10^{-4}$	CL=90%
Γ_{303}	$\chi_{c1}(3872)^+ K^0$, $\chi^+_{c1} \to J/\psi(1S) \pi^+ \pi^0$	[f]	< 6.1	$\times 10^{-6}$	CL=90%
Γ_{304}	$\chi_{c1}(3872) K^0 \pi^+$		(2.4 ± 1.1)	$\times 10^{-4}$	
Γ_{305}	$T_{c\overline{c}1}(4430)^+ K^0$, $T^+_{c\overline{c}1} \to J/\psi \pi^+$		< 1.5	$\times 10^{-5}$	CL=95%
Γ_{306}	$T_{c\overline{c}1}(4430)^+ K^0$, $T^+_{c\overline{c}1} \to \psi(2S) \pi^+$		< 4.7	$\times 10^{-5}$	CL=95%
Γ_{307}	$T_{c\overline{c}1}(4430)^0 K^+$, $T^0_{c\overline{c}1} \to J/\psi \eta$		< 1.27	$\times 10^{-6}$	CL=90%
Γ_{308}	$\psi(4230)^0 K^+$, $\psi^0 \to J/\psi \pi^+ \pi^-$		< 1.56	$\times 10^{-5}$	CL=95%
Γ_{309}	$\psi(4230) K^+$, $\psi \to J/\psi \eta$		< 3.9	$\times 10^{-7}$	CL=90%
Γ_{310}	$\psi(4360) K^+$, $\psi \to J/\psi \eta$		< 1.24	$\times 10^{-6}$	CL=90%
Γ_{311}	$\psi(4360) K^+$, $\psi(4360) \to \psi(2S) \pi^+ \pi^-$		(2.8 ± 0.9)	$\times 10^{-6}$	
Γ_{312}	$\psi(4390) K^+$, $\psi \to J/\psi \eta$		< 2.41	$\times 10^{-6}$	CL=90%
Γ_{313}	$\chi_{c0}(3915) K^+$, $\chi_{c0} \to J/\psi \gamma$		< 1.4	$\times 10^{-5}$	CL=90%
Γ_{314}	$\chi_{c0}(3915) K^+$, $\chi_{c0} \to \chi_{c1}(1P) \pi^0$		< 3.8	$\times 10^{-5}$	CL=90%
Γ_{315}	$X(3930)^0 K^+$, $X^0 \to J/\psi \gamma$		< 2.5	$\times 10^{-6}$	CL=90%
Γ_{316}	$J/\psi(1S) K^+$		(1.019 ± 0.019)	$\times 10^{-3}$	
Γ_{317}	$J/\psi(1S) K^0 \pi^+$		(1.13 ± 0.11)	$\times 10^{-3}$	
Γ_{318}	$J/\psi(1S) K^+ \pi^+ \pi^-$		(8.1 ± 1.3)	$\times 10^{-4}$	S=2.5
Γ_{319}	$J/\psi(1S) K^+ K^- K^+$		(3.37 ± 0.29)	$\times 10^{-5}$	
Γ_{320}	$\chi_{c0}(3915) K^+$, $\chi_{c0} \to p \overline{p}$		< 7.1	$\times 10^{-8}$	CL=95%
Γ_{321}	$J/\psi(1S) K^*(892)^+$		(1.43 ± 0.08)	$\times 10^{-3}$	
Γ_{322}	$J/\psi(1S) K(1270)^+$		(1.8 ± 0.5)	$\times 10^{-3}$	
Γ_{323}	$J/\psi(1S) K(1400)^+$		< 5	$\times 10^{-4}$	CL=90%
Γ_{324}	$J/\psi(1S) \eta K^+$		(1.24 ± 0.14)	$\times 10^{-4}$	
Γ_{325}	$\chi_{c1-odd}(3872) K^+$, $\chi_{c1-odd} \to J/\psi \eta$		< 3.8	$\times 10^{-6}$	CL=90%
Γ_{326}	$\psi(4160) K^+$, $\psi \to J/\psi \eta$		< 8.7	$\times 10^{-7}$	CL=90%
Γ_{327}	$J/\psi(1S) \eta' K^+$		(3.1 ± 0.4)	$\times 10^{-5}$	
Γ_{328}	$J/\psi(1S) \phi K^+$		(5.0 ± 0.4)	$\times 10^{-5}$	
Γ_{329}	$J/\psi(1S) K_1(1650)$, $K_1 \to \phi K^+$		$(6 {}^{+10}_{-6})$	$\times 10^{-6}$	
Γ_{330}	$J/\psi(1S) K^*(1680)^+$, $K^* \to \phi K^+$		$(3.4 {}^{+1.9}_{-2.2})$	$\times 10^{-6}$	
Γ_{331}	$J/\psi(1S) K^*_2(1980)$, $K^*_2 \to \phi K^+$		$(1.5 {}^{+0.9}_{-0.5})$	$\times 10^{-6}$	
Γ_{332}	$J/\psi(1S) K(1830)^+$, $K(1830)^+ \to \phi K^+$		$(1.3 {}^{+1.3}_{-1.1})$	$\times 10^{-6}$	
Γ_{333}	$\chi_{c1}(4140) K^+$, $\chi_{c1} \to J/\psi(1S) \phi$		(10 ± 4)	$\times 10^{-6}$	
Γ_{334}	$\chi_{c1}(4274) K^+$, $\chi_{c1} \to J/\psi(1S) \phi$		$(3.6 {}^{+2.2}_{-1.8})$	$\times 10^{-6}$	
Γ_{335}	$\chi_{c0}(4500) K^+$, $\chi_{c0} \to J/\psi(1S) \phi$		$(3.3 {}^{+2.1}_{-1.7})$	$\times 10^{-6}$	
Γ_{336}	$\chi_{c0}(4700) K^+$, $\chi_{c0} \to J/\psi(1S) \phi$		$(6 {}^{+5}_{-4})$	$\times 10^{-6}$	
Γ_{337}	$J/\psi(1S) \omega K^+$		$(3.20 {}^{+0.60}_{-0.32})$	$\times 10^{-4}$	
Γ_{338}	$\chi_{c0}(3915) K^+$, $\chi_{c0} \to J/\psi \omega$		$(3.0 {}^{+0.9}_{-0.7})$	$\times 10^{-5}$	
Γ_{339}	$J/\psi(1S) \pi^+$		(4.1 ± 0.4)	$\times 10^{-5}$	S=2.5
Γ_{340}	$J/\psi(1S) \pi^+ \pi^+ \pi^+ \pi^- \pi^-$		(1.17 ± 0.13)	$\times 10^{-5}$	
Γ_{341}	$\psi(2S) \pi^+ \pi^+ \pi^-$		(1.9 ± 0.4)	$\times 10^{-5}$	
Γ_{342}	$J/\psi(1S) \rho^+$		(4.1 ± 0.5)	$\times 10^{-5}$	S=1.4
Γ_{343}	$J/\psi(1S) \pi^+ \pi^0$ nonresonant		< 7.3	$\times 10^{-6}$	CL=90%
Γ_{344}	$J/\psi(1S) a_1(1260)^+$		< 1.2	$\times 10^{-3}$	CL=90%
Γ_{345}	$J/\psi(1S) p \overline{p} \pi^+$		< 5.0	$\times 10^{-7}$	CL=90%
Γ_{346}	$J/\psi(1S) p \overline{\Lambda}$		(1.46 ± 0.12)	$\times 10^{-5}$	
Γ_{347}	$J/\psi(1S) \overline{\Sigma}^0 p$		< 1.1	$\times 10^{-5}$	CL=90%
Γ_{348}	$J/\psi(1S) D^+$		< 1.2	$\times 10^{-4}$	CL=90%
Γ_{349}	$J/\psi(1S) \overline{D}^0 \pi^+$		< 2.5	$\times 10^{-5}$	CL=90%
Γ_{350}	$J/\psi(1S) D^+_s$		< 2.8	$\times 10^{-7}$	CL=90%
Γ_{351}	$\psi(2S) \pi^+$		(2.44 ± 0.30)	$\times 10^{-5}$	
Γ_{352}	$\psi(2S) K^+$		(6.25 ± 0.21)	$\times 10^{-4}$	
Γ_{353}	$\psi(2S) K^*(892)^+$		(6.7 ± 1.4)	$\times 10^{-4}$	S=1.3
Γ_{354}	$\psi(2S) K^0 \pi^+$				
Γ_{355}	$\psi(2S) K^+ \pi^+ \pi^-$		(4.3 ± 0.5)	$\times 10^{-4}$	
Γ_{356}	$\chi_{c0}(4500) K^+$, $\chi_{c0}(4500) \to \psi(2S) \pi^+ \pi^-$		(8.0 ± 1.7)	$\times 10^{-5}$	
Γ_{357}	$\chi_{c1}(4685) K^+$, $\chi_{c1}(4685) \to \psi(2S) \pi^+ \pi^-$		(1.25 ± 0.32)	$\times 10^{-5}$	
Γ_{358}	$\chi_{c0}(4700) K^+$, $\chi_{c0}(4700) \to \psi(2S) \pi^+ \pi^-$		(7.5 ± 2.3)	$\times 10^{-6}$	
Γ_{359}	$\psi(2S) K^*(1410)^+$, $K^*(1410)^+ \to K^+ \pi^+ \pi^-$		(8 ± 4)	$\times 10^{-6}$	
Γ_{360}	$\psi(2S) K^*(1680)^+$, $K^*(1680)^+ \to K^+ \pi^+ \pi^-$		(3.5 ± 1.7)	$\times 10^{-5}$	
Γ_{361}	$\psi(2S) K_1(1270)^+$, $K_1(1270)^+ \to K^+ \pi^+ \pi^-$		(3.3 ± 0.8)	$\times 10^{-5}$	
Γ_{362}	$[\psi(2S) K_1(1270)^+$, $K_1(1270)^+ \to K^+ \pi^+ \pi^-]_{P-wave}$		(3.3 ± 0.7)	$\times 10^{-5}$	
Γ_{363}	$[\psi(2S) K_1(1270)^+$, $K_1(1270)^+ \to K^+ \pi^+ \pi^-]_{D-wave}$		(3.0 ± 0.7)	$\times 10^{-5}$	
Γ_{364}	$\psi(2S) K_1(1400)^+$, $K_1(1400)^+ \to K^+ \pi^+ \pi^-$		(2.5 ± 0.6)	$\times 10^{-5}$	
Γ_{365}	$[\psi(2S) K_1(1400)^+$, $K_1(1400)^+ \to K^+ \pi^+ \pi^-]_{P-wave}$		(2.1 ± 1.9)	$\times 10^{-6}$	
Γ_{366}	$\psi(2S) K_1(1460)^+$, $K_1(1460)^+ \to K^+ \pi^+ \pi^-$		(2.3 ± 0.5)	$\times 10^{-5}$	
Γ_{367}	$\psi(2S) K^*_2(1430)^+$, $K^*_2(1430)^+ \to K^+ \pi^+ \pi^-$		(1.89 ± 0.29)	$\times 10^{-5}$	
Γ_{368}	$T_{c\overline{c}1}(4200)^+ K^*(892)^0 \to \psi(2S) K^+ \pi^+ \pi^-$		(1.7 ± 0.6)	$\times 10^{-5}$	
Γ_{369}	$[T_{c\overline{c}1}(4200)^+ K^*(892)^0 \to \psi(2S) K^+ \pi^+ \pi^-]_{P-wave}$		(2.0 ± 1.0)	$\times 10^{-5}$	
Γ_{370}	$[T_{c\overline{c}1}(4200)^+ K^*(892)^0 \to \psi(2S) K^+ \pi^+ \pi^-]_{D-wave}$		(1.21 ± 0.34)	$\times 10^{-5}$	
Γ_{371}	$T_{c\overline{c}1}(4430)^+ K^*(892)^0 \to \psi(2S) K^+ \pi^+ \pi^-$		(3 ± 10)	$\times 10^{-6}$	
Γ_{372}	$T_{c\overline{c}1}(4430)^+ [K^+ \pi^-]_{S-wave} \to \psi(2S) K^+ \pi^+ \pi^-$		(1.5 ± 0.5)	$\times 10^{-5}$	
Γ_{373}	$T_{c\overline{c}s1}(4600)^0 \pi^+$, $T_{c\overline{c}s1}(4600)^0 \to \psi(2S) K^+ \pi^-$		(1.9 ± 1.1)	$\times 10^{-5}$	
Γ_{374}	$T_{c\overline{c}s1}(4900)^0 \pi^+$, $T_{c\overline{c}s1}(4900)^0 \to \psi(2S) K^+ \pi^-$		(1.1 ± 0.9)	$\times 10^{-5}$	
Γ_{375}	$\psi(2S) \phi(1020) K^+$		(3.4 ± 0.5)	$\times 10^{-6}$	
Γ_{376}	$\psi(3770) K^+$		(4.3 ± 1.1)	$\times 10^{-4}$	
Γ_{377}	$\psi(3770) K+, \psi \to D^0 \overline{D}^0$		(1.5 ± 0.5)	$\times 10^{-4}$	S=1.4
Γ_{378}	$\psi(3770) K+, \psi \to D^+ D^-$		(9.4 ± 3.5)	$\times 10^{-5}$	
Γ_{379}	$\psi(3770) K^+$, $\psi \to p \overline{p}$		< 2	$\times 10^{-7}$	CL=95%
Γ_{380}	$\psi(3770) K^+$, $\psi \to J/\psi \eta$		< 4.6	$\times 10^{-7}$	CL=90%
Γ_{381}	$\psi(4040) K^+$		(1.6 ± 0.5)	$\times 10^{-3}$	
Γ_{382}	$\psi(4040) K^+$, $\psi \to D^+ D^-$		(1.1 ± 0.5)	$\times 10^{-5}$	
Γ_{383}	$\psi(4160) K^+$		(5.1 ± 2.7)	$\times 10^{-4}$	
Γ_{384}	$\psi(4160) K^+$, $\psi \to \overline{D}^0 D^0$		(8 ± 5)	$\times 10^{-5}$	
Γ_{385}	$\psi(4160) K^+$, $\psi \to D^+ D^-$		(1.5 ± 0.6)	$\times 10^{-5}$	
Γ_{386}	$\psi(4415) K^+$, $\psi \to D^+ D^-$		(2.0 ± 0.8)	$\times 10^{-5}$	
Γ_{387}	$\psi(4415) K^+$, $\psi \to J/\psi \eta$		< 9.6	$\times 10^{-7}$	CL=90%
Γ_{388}	$\chi_{c0} \pi^+$, $\chi_{c0} \to \pi^+ \pi^-$		< 1	$\times 10^{-7}$	CL=90%
Γ_{389}	$\chi_{c0} \pi^+$, $\chi_{c0} \to \pi^0 \pi^0$		< 5	$\times 10^{-7}$	CL=90%
Γ_{390}	$\chi_{c0} K^+$		$(1.49 {}^{+0.15}_{-0.14})$	$\times 10^{-4}$	
Γ_{391}	$\chi_{c0} K^0 \pi^+$		(1.45 ± 0.21)	$\times 10^{-3}$	
Γ_{392}	$\chi_{c0} K^*(892)^+$		< 2.1	$\times 10^{-4}$	CL=90%
Γ_{393}	$\chi_{c1}(1P) \pi^+$		(2.2 ± 0.5)	$\times 10^{-5}$	
Γ_{394}	$\chi_{c1}(1P) K^+$		(4.74 ± 0.22)	$\times 10^{-4}$	
Γ_{395}	$\chi_{c1}(1P) K^*(892)^+$		(3.0 ± 0.6)	$\times 10^{-4}$	S=1.1
Γ_{396}	$\chi_{c1}(1P) K^0 \pi^+$		(5.8 ± 0.4)	$\times 10^{-4}$	
Γ_{397}	$\chi_{c1}(1P) K^+ \pi^0$		(3.29 ± 0.35)	$\times 10^{-4}$	
Γ_{398}	$\chi_{c1}(1P) K^+ \pi^+ \pi^-$		(3.74 ± 0.30)	$\times 10^{-4}$	
Γ_{399}	$\chi_{c1}(2P) K^+$, $\chi_{c1}(2P) \to \pi^+ \pi^- \chi_{c1}(1P)$		< 1.1	$\times 10^{-5}$	CL=90%
Γ_{400}	$\chi_{c2} \pi^+$, $\chi_{c2} \to \pi^0 \pi^0$		< 7	$\times 10^{-7}$	CL=90%
Γ_{401}	$\chi_{c2} K^+$		(1.1 ± 0.4)	$\times 10^{-5}$	
Γ_{402}	$\chi_{c2} K^+$, $\chi_{c2} \to p \overline{p} \pi^+ \pi^-$		< 1.9	$\times 10^{-7}$	
Γ_{403}	$\chi_{c2} K^*(892)^+$		< 1.2	$\times 10^{-4}$	CL=90%

Int. J. Mod. Phys. A 2026.41. Downloaded from www.worldscientific.com
by UNIVERSITY OF CALIFORNIA @ BERKELEY on 09/16/26. Re-use and distribution is strictly not permitted, except for Open Access articles.

Γ_{404}	$\chi_{c2} K^0 \pi^+$	$(1.24 \pm 0.25) \times 10^{-4}$	
Γ_{405}	$\chi_{c2} K^+ \pi^0$	$< 6.2 \times 10^{-5}$	CL=90%
Γ_{406}	$\chi_{c2} K^+ \pi^+ \pi^-$	$(1.34 \pm 0.19) \times 10^{-4}$	
Γ_{407}	$\chi_{c2}(3930) K^+,\ \chi_{c2} \to D^+ D^-$	$(1.6 \pm 0.6) \times 10^{-5}$	
Γ_{408}	$\chi_{c2}(3930) \pi^+,\ \chi_{c2} \to \pi^+ \pi^-$	$< 1 \times 10^{-7}$	CL=90%
Γ_{409}	$h_c(1P) K^+$	$(3.7 \pm 1.2) \times 10^{-5}$	
Γ_{410}	$h_c(1P) K^+,\ h_c \to p\overline{p}$	$< 6.4 \times 10^{-8}$	CL=95%

K or K^* modes

Γ_{411}	$K^0 \pi^+$	$(2.39 \pm 0.06) \times 10^{-5}$	
Γ_{412}	$K^+ \pi^0$	$(1.32 \pm 0.04) \times 10^{-5}$	
Γ_{413}	$\eta' K^+$	$(7.04 \pm 0.25) \times 10^{-5}$	
Γ_{414}	$\eta' K^*(892)^+$	$(4.8 {}^{+1.8}_{-1.6}) \times 10^{-6}$	
Γ_{415}	$\eta' K_0^*(1430)^+$	$(5.2 \pm 2.1) \times 10^{-6}$	
Γ_{416}	$\eta' K_2^*(1430)^+$	$(2.8 \pm 0.5) \times 10^{-5}$	
Γ_{417}	ηK^+	$(2.4 \pm 0.4) \times 10^{-6}$	S=1.7
Γ_{418}	$\eta K^*(892)^+$	$(1.93 \pm 0.16) \times 10^{-5}$	
Γ_{419}	$\eta K_0^*(1430)^+$	$(1.8 \pm 0.4) \times 10^{-5}$	
Γ_{420}	$\eta K_2^*(1430)^+$	$(9.1 \pm 3.0) \times 10^{-6}$	
Γ_{421}	$\eta(1295) K^+,\ \eta \to \eta\pi\pi$	$(2.9 {}^{+0.8}_{-0.7}) \times 10^{-6}$	
Γ_{422}	$\eta(1405) K^+,\ \eta \to \eta\pi\pi$	$< 1.3 \times 10^{-6}$	CL=90%
Γ_{423}	$\eta(1405) K^+,\ \eta \to K^* K$	$< 1.2 \times 10^{-6}$	CL=90%
Γ_{424}	$\eta(1405) K^+,\ \eta \to K^0 K\pi$	$(8.0 \pm 1.1) \times 10^{-6}$	
Γ_{425}	$\eta(1475) K^+,\ \eta \to K^* K$	$(1.42 \pm 0.13) \times 10^{-5}$	
Γ_{426}	$\eta(1475) K^+,\ \eta \to a_0(980)\pi$	$(2.2 \pm 0.5) \times 10^{-6}$	
Γ_{427}	$\eta(1475) K^+,\ \eta \to K^0 K\pi$	$(1.51 \pm 0.31) \times 10^{-5}$	
Γ_{428}	$\eta(1760) K^+,\ \eta \to K^* \overline{K}$	$(3.4 \pm 0.6) \times 10^{-6}$	
Γ_{429}	$\eta(1760) K^+,\ \eta \to a_0(980)\pi$	$(2.6 \pm 0.5) \times 10^{-6}$	
Γ_{430}	$\eta(1760) K^+,\ \eta \to K^0 K\pi$	$(2.2 \pm 0.4) \times 10^{-5}$	
Γ_{431}	$f_1(1285) K^+$	$< 2.0 \times 10^{-6}$	CL=90%
Γ_{432}	$f_1(1285) K^+,\ f_1 \to a_0(980)\pi$	$(2.8 \pm 0.4) \times 10^{-6}$	
Γ_{433}	$f_1(1420) K^+,\ f_1 \to \eta\pi\pi$	$< 2.9 \times 10^{-6}$	CL=90%
Γ_{434}	$f_1(1420) K^+,\ f_1 \to K^* K$	$< 4.1 \times 10^{-6}$	CL=90%
Γ_{435}	$f_1(1510) K^+,\ f_1 \to K^* \overline{K}$	$(3.8 \pm 1.5) \times 10^{-6}$	
Γ_{436}	$h_1(1415) K^+,\ h_1 \to K^* \overline{K}$	$(2.22 \pm 0.27) \times 10^{-5}$	
Γ_{437}	$h_1(1595) K^+,\ h_1 \to K^* \overline{K}$	$(1.04 \pm 0.16) \times 10^{-5}$	
Γ_{438}	$\eta_2(1645) K^+,\ \eta_2 \to K^* \overline{K}$	$(1.50 \pm 0.28) \times 10^{-6}$	
Γ_{439}	$\phi(1680) K^+,\ \phi \to K^* K$	$< 3.4 \times 10^{-6}$	CL=90%
Γ_{440}	$f_0(1500) K^+$	$(3.7 \pm 2.2) \times 10^{-6}$	
Γ_{441}	ωK^+	$(6.5 \pm 0.4) \times 10^{-6}$	
Γ_{442}	$\omega K^*(892)^+$	$< 7.4 \times 10^{-6}$	CL=90%
Γ_{443}	$\omega (K\pi)_0^{*+}$	$(2.8 \pm 0.4) \times 10^{-5}$	
Γ_{444}	$\omega K_0^*(1430)^+$	$(2.4 \pm 0.5) \times 10^{-5}$	
Γ_{445}	$\omega K_2^*(1430)^+$	$(2.1 \pm 0.4) \times 10^{-5}$	
Γ_{446}	$a_0(980)^+ K^0,\ a_0^+ \to \eta\pi^+$	$< 3.9 \times 10^{-6}$	CL=90%
Γ_{447}	$a_0(980)^0 K^+,\ a_0^0 \to \eta\pi^0$	$< 2.5 \times 10^{-6}$	CL=90%
Γ_{448}	$K^*(892)^0 \pi^+$	$(1.01 \pm 0.08) \times 10^{-5}$	
Γ_{449}	$K^*(892)^+ \pi^0$	$(6.8 \pm 0.9) \times 10^{-6}$	
Γ_{450}	$K^+ \pi^- \pi^+$	$(5.10 \pm 0.29) \times 10^{-5}$	
Γ_{451}	$K^+ \pi^- \pi^+$ nonresonant	$(1.63 {}^{+0.21}_{-0.15}) \times 10^{-5}$	
Γ_{452}	$\omega(782) K^+$	$(6 \pm 9) \times 10^{-6}$	
Γ_{453}	$K^+ f_0(980) \times B(f_0(980) \to \pi^+\pi^-)$	$(9.4 {}^{+1.0}_{-1.2}) \times 10^{-6}$	
Γ_{454}	$f_2(1270)^0 K^+$	$(1.07 \pm 0.27) \times 10^{-6}$	
Γ_{455}	$f_0(1370)^0 K^+ \times B(f_0(1370)^0 \to \pi^+\pi^-)$	$< 1.07 \times 10^{-5}$	CL=90%
Γ_{456}	$\rho(14500) K^+ \times B(\rho(1450)^0 \to \pi^+\pi^-)$	$< 1.17 \times 10^{-5}$	CL=90%
Γ_{457}	$f_2'(1525) K^+ \times B(f_2'(1525) \to \pi^+\pi^-)$	$< 3.4 \times 10^{-6}$	CL=90%
Γ_{458}	$K^+ \rho^0$	$(3.7 \pm 0.5) \times 10^{-6}$	
Γ_{459}	$K_0^*(1430)^0 \pi^+$	$(3.9 {}^{+0.6}_{-0.5}) \times 10^{-5}$	S=1.4
Γ_{460}	$K_2^*(1430)^0 \pi^+$	$(5.6 {}^{+2.2}_{-1.5}) \times 10^{-6}$	
Γ_{461}	$K^*(1410)^0 \pi^+$	$< 4.5 \times 10^{-5}$	CL=90%
Γ_{462}	$K^*(1680)^0 \pi^+$	$< 1.2 \times 10^{-5}$	CL=90%
Γ_{463}	$K^+ \pi^0 \pi^0$	$(1.62 \pm 0.19) \times 10^{-5}$	
Γ_{464}	$f_0(980) K^+ \times B(f_0 \to \pi^0\pi^0)$	$(2.8 \pm 0.8) \times 10^{-6}$	
Γ_{465}	$K^- \pi^+ \pi^+$	$< 4.6 \times 10^{-8}$	CL=90%
Γ_{466}	$K^- \pi^+ \pi^+$ nonresonant	$< 5.6 \times 10^{-5}$	CL=90%
Γ_{467}	$K_1(1270)^0 \pi^+$	$< 4.0 \times 10^{-5}$	CL=90%
Γ_{468}	$K_1(1400)^0 \pi^+$	$< 3.9 \times 10^{-5}$	CL=90%
Γ_{469}	$K^0 \pi^+ \pi^0$	$< 6.6 \times 10^{-5}$	CL=90%
Γ_{470}	$K_0^*(1430)^+ \pi^0$	$(1.19 {}^{+0.20}_{-0.23}) \times 10^{-5}$	
Γ_{471}	$K^0 \rho^+$	$(7.3 {}^{+1.0}_{-1.2}) \times 10^{-6}$	
Γ_{472}	$K^*(892)^+ \pi^+ \pi^-$	$(7.5 \pm 1.0) \times 10^{-5}$	
Γ_{473}	$K^*(892)^+ \rho^0$	$(4.6 \pm 1.1) \times 10^{-6}$	
Γ_{474}	$K^*(892)^+ f_0(980)$	$(4.2 \pm 0.7) \times 10^{-6}$	
Γ_{475}	$a_1^+ K^0$	$(3.5 \pm 0.7) \times 10^{-5}$	
Γ_{476}	$b_1^+ K^0 \times B(b_1^+ \to \omega\pi^+)$	$(9.6 \pm 1.9) \times 10^{-6}$	
Γ_{477}	$K^*(892)^0 \rho^+$	$(9.2 \pm 1.5) \times 10^{-6}$	
Γ_{478}	$K_1(1400)^+ \rho^0$	$< 7.8 \times 10^{-4}$	CL=90%
Γ_{479}	$K_2^*(1430)^+ \rho^0$	$< 1.5 \times 10^{-3}$	CL=90%
Γ_{480}	$b_1^0 K^+ \times B(b_1^0 \to \omega\pi^0)$	$(9.1 \pm 2.0) \times 10^{-6}$	
Γ_{481}	$b_1^+ K^{*0} \times B(b_1^+ \to \omega\pi^+)$	$< 5.9 \times 10^{-6}$	CL=90%
Γ_{482}	$b_1^0 K^{*+} \times B(b_1^0 \to \omega\pi^0)$	$< 6.7 \times 10^{-6}$	CL=90%
Γ_{483}	$K^+ \overline{K}^0$	$(1.32 \pm 0.17) \times 10^{-6}$	S=1.2
Γ_{484}	$\overline{K}^0 K^+ \pi^0$	$< 2.4 \times 10^{-5}$	CL=90%
Γ_{485}	$K^+ K_S^0 K_S^0$	$(1.05 \pm 0.04) \times 10^{-5}$	
Γ_{486}	$f_0(980) K^+,\ f_0 \to K_S^0 K_S^0$	$(1.47 \pm 0.33) \times 10^{-5}$	
Γ_{487}	$f_0(1710) K^+,\ f_0 \to K_S^0 K_S^0$	$(4.8 {}^{+4.0}_{-2.6}) \times 10^{-7}$	
Γ_{488}	$K^+ K_S^0 K_S^0$ nonresonant	$(2.0 \pm 0.4) \times 10^{-5}$	
Γ_{489}	$K_S^0 K_S^0 \pi^+$	$< 5.1 \times 10^{-7}$	CL=90%
Γ_{490}	$K^+ K^- \pi^+$	$(5.2 \pm 0.4) \times 10^{-6}$	
Γ_{491}	$K^+ K^- \pi^+$ nonresonant	$(1.68 \pm 0.26) \times 10^{-6}$	
Γ_{492}	$K^+ \overline{K}^*(892)^0$	$(5.9 \pm 0.8) \times 10^{-7}$	
Γ_{493}	$K^+ \overline{K}_0^*(1430)^0$	$(3.8 \pm 1.3) \times 10^{-7}$	
Γ_{494}	$\pi^+ (K^+ K^-)_{S-wave}$	$(8.5 \pm 0.9) \times 10^{-7}$	
Γ_{495}	$\pi^+ K^+ K^-$, $m_{K^+K^-} < 1.1$ GeV	$(5.4 \pm 0.5) \times 10^{-6}$	
Γ_{496}	$K^+ K^+ \pi^-$	$< 1.1 \times 10^{-8}$	CL=90%
Γ_{497}	$K^+ K^+ \pi^-$ nonresonant	$< 8.79 \times 10^{-5}$	CL=90%
Γ_{498}	$f_2'(1525) K^+$	$(1.8 \pm 0.5) \times 10^{-6}$	S=1.1
Γ_{499}	$K^+ f_J(2220)$		
Γ_{500}	$K^{*+} \pi^+ K^-$	$< 1.18 \times 10^{-5}$	CL=90%
Γ_{501}	$K^*(892)^+ K^*(892)^0$	$(9.1 \pm 2.9) \times 10^{-7}$	
Γ_{502}	$K^{*+} K^+ \pi^-$	$< 6.1 \times 10^{-6}$	CL=90%
Γ_{503}	$K^+ K^- K^+$	$(3.40 \pm 0.14) \times 10^{-5}$	S=1.4
Γ_{504}	$K^+ \phi$	$(8.8 {}^{+0.7}_{-0.6}) \times 10^{-6}$	S=1.1
Γ_{505}	$f_0(980) K^+ \times B(f_0(980) \to K^+ K^-)$	$(9.4 \pm 3.2) \times 10^{-6}$	
Γ_{506}	$a_2(1320) K^+ \times B(a_2(1320) \to K^+ K^-)$	$< 1.1 \times 10^{-6}$	CL=90%
Γ_{507}	$X_0(1550) K^+ \times B(X_0(1550) \to K^+ K^-)$	$(4.3 \pm 0.7) \times 10^{-6}$	
Γ_{508}	$\phi(1680) K^+ \times B(\phi(1680) \to K^+ K^-)$	$< 8 \times 10^{-7}$	CL=90%
Γ_{509}	$f_0(1710) K^+ \times B(f_0(1710) \to K^+ K^-)$	$(1.1 \pm 0.6) \times 10^{-6}$	
Γ_{510}	$K^+ K^- K^+$ nonresonant	$(2.38 {}^{+0.28}_{-0.50}) \times 10^{-5}$	
Γ_{511}	$K^*(892)^+ K^+ K^-$	$(3.6 \pm 0.5) \times 10^{-5}$	
Γ_{512}	$K^*(892)^+ \phi$	$(10.0 \pm 2.0) \times 10^{-6}$	S=1.7
Γ_{513}	$K^0 K^+ K^- \pi^+$	$(3.40 \pm 0.33) \times 10^{-4}$	
Γ_{514}	$J/\psi K^+,\ J/\psi \to K^0 K^- \pi^+$	$(5.4 \pm 1.2) \times 10^{-6}$	
Γ_{515}	$\chi_{c1} K^+,\ \chi_{c1} \to K^0 K^- \pi^+$	$(2.25 \pm 0.25) \times 10^{-6}$	
Γ_{516}	$\eta_c K^+,\ \eta_c \to K^0 K^- \pi^+$	$(2.83 \pm 0.30) \times 10^{-5}$	
Γ_{517}	$\eta_c(2S) K^+,\ \eta_c(2S) \to K^0 K^- \pi^+$	$(3.3 \pm 0.4) \times 10^{-6}$	
Γ_{518}	$K^0 K^+ K^+ \pi^-$	$(2.80 \pm 0.30) \times 10^{-4}$	
Γ_{519}	$J/\psi K^+,\ J/\psi \to K^0 K^+ \pi^-$	$(5.4 \pm 1.3) \times 10^{-6}$	
Γ_{520}	$\chi_{c1} K^+,\ \chi_{c1} \to K^0 K^+ \pi^-$	$(2.06 \pm 0.32) \times 10^{-6}$	
Γ_{521}	$\eta_c K^+,\ \eta_c \to K^0 K^+ \pi^-$	$(3.00 \pm 0.34) \times 10^{-5}$	
Γ_{522}	$\eta_c(2S) K^+,\ \eta_c(2S) \to K^0 K^+ \pi^-$	$(3.1 \pm 0.6) \times 10^{-6}$	
Γ_{523}	$\phi (K\pi)_0^{*+}$	$(8.3 \pm 1.6) \times 10^{-6}$	
Γ_{524}	$\phi K_1(1270)^+$	$(6.1 \pm 1.9) \times 10^{-6}$	
Γ_{525}	$\phi K_1(1400)^+$	$< 3.2 \times 10^{-6}$	CL=90%
Γ_{526}	$\phi K^*(1410)^+$	$< 4.3 \times 10^{-6}$	CL=90%
Γ_{527}	$\phi K_0^*(1430)^+$	$(7.0 \pm 1.6) \times 10^{-6}$	
Γ_{528}	$\phi K_2^*(1430)^+$	$(8.4 \pm 2.1) \times 10^{-6}$	
Γ_{529}	$\phi K_2^*(1770)^+$	$< 1.50 \times 10^{-5}$	CL=90%
Γ_{530}	$\phi K_2^*(1820)^+$	$< 1.63 \times 10^{-5}$	CL=90%
Γ_{531}	$a_1^+ K^{*0}$	$< 3.6 \times 10^{-6}$	CL=90%
Γ_{532}	$K^+ \phi\phi$	$(4.2 \pm 0.8) \times 10^{-6}$	S=2.2

Int. J. Mod. Phys. A 2026.41. Downloaded from www.worldscientific.com
by [redacted] LIFORNIA @ BERKELEY on 09/16/26. Re-use and distribution is strictly not permitted, except for Open Access articles.

Γ_{533}	$\eta' \eta' K^+$	$< 2.5 \times 10^{-5}$	CL=90%	
Γ_{534}	$\omega \phi K^+$	$< 1.9 \times 10^{-6}$	CL=90%	
Γ_{535}	$X(1812) K^+ \times B(X \to \omega\phi)$	$< 3.2 \times 10^{-7}$	CL=90%	
Γ_{536}	$K^*(892)^+ \gamma$	$(3.95 \pm 0.13) \times 10^{-5}$		S=1.3
Γ_{537}	$K_1(1270)^+ \gamma$	$(4.4 {}^{+0.7}_{-0.6}) \times 10^{-5}$		
Γ_{538}	$\eta K^+ \gamma$	$(7.9 \pm 0.9) \times 10^{-6}$		
Γ_{539}	$\eta' K^+ \gamma$	$(2.9 {}^{+1.0}_{-0.9}) \times 10^{-6}$		
Γ_{540}	$\phi K^+ \gamma$	$(2.7 \pm 0.4) \times 10^{-6}$		S=1.2
Γ_{541}	$K^+ \pi^- \pi^+ \gamma$	$(2.58 \pm 0.15) \times 10^{-5}$		S=1.3
Γ_{542}	$K^*(892)^0 \pi^+ \gamma$	$(2.33 \pm 0.12) \times 10^{-5}$		
Γ_{543}	$K^+ \rho^0 \gamma$	$(8.2 \pm 0.9) \times 10^{-6}$		
Γ_{544}	$(K^+ \pi^-)_{NR} \pi^+ \gamma$	$(9.9 {}^{+1.7}_{-2.0}) \times 10^{-6}$		
Γ_{545}	$K^0 \pi^+ \pi^0 \gamma$	$(4.6 \pm 0.5) \times 10^{-5}$		
Γ_{546}	$K_1(1400)^+ \gamma$	$(10 {}^{+5}_{-4}) \times 10^{-6}$		
Γ_{547}	$K^*(1410)^+ \gamma$	$(2.7 {}^{+0.8}_{-0.6}) \times 10^{-5}$		
Γ_{548}	$K_0^*(1430)^0 \pi^+ \gamma$	$(1.32 {}^{+0.26}_{-0.32}) \times 10^{-6}$		
Γ_{549}	$K_2^*(1430)^+ \gamma$	$(1.4 \pm 0.4) \times 10^{-5}$		
Γ_{550}	$K^*(1680)^+ \gamma$	$(6.7 {}^{+1.7}_{-1.4}) \times 10^{-5}$		
Γ_{551}	$K_3^*(1780)^+ \gamma$	$< 3.9 \times 10^{-5}$	CL=90%	
Γ_{552}	$K_4^*(2045)^+ \gamma$	$< 9.9 \times 10^{-3}$	CL=90%	

Light unflavored meson modes

Γ_{553}	$\rho^+ \gamma$	$(1.16 \pm 0.17) \times 10^{-6}$		
Γ_{554}	$\pi^+ \pi^0$	$(5.31 \pm 0.26) \times 10^{-6}$		
Γ_{555}	$\pi^+ \pi^+ \pi^-$	$(1.52 \pm 0.14) \times 10^{-5}$		
Γ_{556}	$\rho^0 \pi^+$	$(8.3 \pm 1.2) \times 10^{-6}$		
Γ_{557}	$\pi^+ f_0(980)$, $f_0 \to \pi^+ \pi^-$	$< 1.5 \times 10^{-6}$	CL=90%	
Γ_{558}	$\pi^+ f_2(1270)$	$(2.2 {}^{+0.7}_{-0.4}) \times 10^{-6}$		
Γ_{559}	$\rho(1450)^0 \pi^+$, $\rho^0 \to \pi^+ \pi^-$	$(1.4 {}^{+0.6}_{-0.9}) \times 10^{-6}$		
Γ_{560}	$\rho(1450)^0 \pi^+$, $\rho^0 \to K^+ K^-$	$(1.60 \pm 0.14) \times 10^{-6}$		
Γ_{561}	$f_0(1370) \pi^+$, $f_0 \to \pi^+ \pi^-$	$< 4.0 \times 10^{-6}$	CL=90%	
Γ_{562}	$f_0(1370) \pi^+$, $f_0 \to \pi^0 \pi^0$	$< 1.1 \times 10^{-6}$	CL=90%	
Γ_{563}	$f_0(500) \pi^+$, $f_0 \to \pi^+ \pi^-$	$< 4.1 \times 10^{-6}$	CL=90%	
Γ_{564}	$\pi^+ \pi^- \pi^+$ nonresonant	$(5.3 {}^{+1.5}_{-1.1}) \times 10^{-6}$		
Γ_{565}	$\pi^+ \pi^0 \pi^0$	$(1.90 \pm 0.21) \times 10^{-5}$		
Γ_{566}	$\rho^+ \pi^0$	$(1.06 {}^{+0.12}_{-0.13}) \times 10^{-5}$		
Γ_{567}	$\rho(1450)^+ \pi^0$, $\rho^+ \to \pi^+ \pi^0$	$(1.2 \pm 0.6) \times 10^{-6}$		
Γ_{568}	$\pi^+ \pi^0 \pi^0$ nonresonant	$< 6 \times 10^{-7}$	CL=90%	
Γ_{569}	$X pi+, X \to \pi^0 \pi^0$	$(6.9 \pm 1.1) \times 10^{-6}$		
Γ_{570}	$\pi^+ \pi^- \pi^+ \pi^0$	$< 4.0 \times 10^{-3}$	CL=90%	
Γ_{571}	$\rho^+ \rho^0$	$(2.40 \pm 0.19) \times 10^{-5}$		
Γ_{572}	$\rho^+ f_0(980)$, $f_0 \to \pi^+ \pi^-$	$< 2.0 \times 10^{-6}$	CL=90%	
Γ_{573}	$a_1(1260)^+ \pi^0$	$(2.6 \pm 0.7) \times 10^{-5}$		
Γ_{574}	$a_1(1260)^0 \pi^+$	$(2.0 \pm 0.6) \times 10^{-5}$		
Γ_{575}	$\omega \pi^+$	$(6.9 \pm 0.5) \times 10^{-6}$		
Γ_{576}	$\omega \rho^+$	$(1.59 \pm 0.21) \times 10^{-5}$		
Γ_{577}	$\eta \pi^+$	$(4.02 \pm 0.27) \times 10^{-6}$		
Γ_{578}	$\eta \rho^+$	$(7.0 \pm 2.9) \times 10^{-6}$		S=2.8
Γ_{579}	$\eta' \pi^+$	$(2.7 \pm 0.9) \times 10^{-6}$		S=1.9
Γ_{580}	$\eta' \rho^+$	$(9.7 \pm 2.2) \times 10^{-6}$		
Γ_{581}	$\phi \pi^+$	$(3.2 \pm 1.5) \times 10^{-8}$		
Γ_{582}	$\phi \rho^+$	$< 3.0 \times 10^{-6}$	CL=90%	
Γ_{583}	$a_0(980)^0 \pi^+$, $a_0^0 \to \eta \pi^0$	$< 5.8 \times 10^{-6}$	CL=90%	
Γ_{584}	$a_0(980)^+ \pi^0$, $a_0^+ \to \eta \pi^+$	$< 1.4 \times 10^{-6}$	CL=90%	
Γ_{585}	$\pi^+ \pi^+ \pi^+ \pi^- \pi^-$	$< 8.6 \times 10^{-4}$	CL=90%	
Γ_{586}	$\rho^0 a_1(1260)^+$	$< 6.2 \times 10^{-4}$	CL=90%	
Γ_{587}	$\rho^0 a_2(1320)^+$	$< 7.2 \times 10^{-4}$	CL=90%	
Γ_{588}	$b_1^0 \pi^+$, $b_1^0 \to \omega \pi^0$	$(6.7 \pm 2.0) \times 10^{-6}$		
Γ_{589}	$b_1^+ \pi^0$, $b_1^+ \to \omega \pi^+$	$< 3.3 \times 10^{-6}$	CL=90%	
Γ_{590}	$\pi^+ \pi^+ \pi^+ \pi^- \pi^- \pi^0$	$< 6.3 \times 10^{-3}$	CL=90%	
Γ_{591}	$b_1^+ \rho^0$, $b_1^+ \to \omega \pi^+$	$< 5.2 \times 10^{-6}$	CL=90%	
Γ_{592}	$a_1(1260)^+ a_1(1260)^0$	< 1.3 %	CL=90%	
Γ_{593}	$b_1^0 \rho^+$, $b_1^0 \to \omega \pi^0$	$< 3.3 \times 10^{-6}$	CL=90%	

Charged particle ($h^{\pm}$) modes

$h^{\pm} = K^{\pm}$ or $\pi^{\pm}$

Γ_{594}	$h^+ \pi^0$	$(1.6 {}^{+0.7}_{-0.6}) \times 10^{-5}$		
Γ_{595}	ωh^+	$(1.38 {}^{+0.27}_{-0.24}) \times 10^{-5}$		
Γ_{596}	$h^+ X^0$ (Familon)	$< 4.9 \times 10^{-5}$	CL=90%	
Γ_{597}	$K^+ X^0$, $X^0 \to \mu^+ \mu^-$	$< 1 \times 10^{-7}$	CL=95%	

Baryon modes

Γ_{598}	$p \overline{p} \pi^+$	$(1.62 \pm 0.20) \times 10^{-6}$		
Γ_{599}	$p \overline{p} \pi^+$ nonresonant	$< 5.3 \times 10^{-5}$	CL=90%	
Γ_{600}	$p \overline{p} \pi^+ \pi^0$	$(4.6 \pm 1.3) \times 10^{-6}$		
Γ_{601}	$p \overline{p} \pi^+ \pi^+ \pi^-$			
Γ_{602}	$p \overline{p} K^+$	$(5.9 \pm 0.5) \times 10^{-6}$		S=1.5
Γ_{603}	$\Theta(1710)^{++} \overline{p}$, $\Theta^{++} \to p K^+$	[g] $< 9.1 \times 10^{-8}$	CL=90%	
Γ_{604}	$f_J(2220) K^+$, $f_J \to p \overline{p}$	[g] $< 4.1 \times 10^{-7}$	CL=90%	
Γ_{605}	$p \overline{n} \pi^0$	$< 6.3 \times 10^{-6}$	CL=90%	
Γ_{606}	$p \overline{\Lambda}(1520)$	$(3.1 \pm 0.6) \times 10^{-7}$		
Γ_{607}	$p \overline{p} K^+$ nonresonant	$< 8.9 \times 10^{-5}$	CL=90%	
Γ_{608}	$p \overline{p} K^*(892)^+$	$(3.6 {}^{+0.8}_{-0.7}) \times 10^{-6}$		
Γ_{609}	$f_J(2220) K^{*+}$, $f_J \to p \overline{p}$	$< 7.7 \times 10^{-7}$	CL=90%	
Γ_{610}	$p \overline{\Lambda}$	$(2.4 {}^{+1.0}_{-0.9}) \times 10^{-7}$		
Γ_{611}	$p \overline{\Lambda} \gamma$	$(2.4 {}^{+0.5}_{-0.4}) \times 10^{-6}$		
Γ_{612}	$p \overline{\Lambda} \pi^0$	$(3.0 {}^{+0.7}_{-0.6}) \times 10^{-6}$		
Γ_{613}	$p \overline{\Sigma}(1385)^0$	$< 4.7 \times 10^{-7}$	CL=90%	
Γ_{614}	$\Delta^+ \overline{\Lambda}$	$< 8.2 \times 10^{-7}$	CL=90%	
Γ_{615}	$p \overline{\Sigma} \gamma$	$< 4.6 \times 10^{-6}$	CL=90%	
Γ_{616}	$p \overline{\Lambda} \pi^+ \pi^-$	$(1.13 \pm 0.13) \times 10^{-5}$		
Γ_{617}	$p \overline{\Lambda} \pi^+ \pi^-$ nonresonant	$(5.9 \pm 1.1) \times 10^{-6}$		
Γ_{618}	$p \overline{\Lambda} \rho^0$, $\rho^0 \to \pi^+ \pi^-$	$(4.8 \pm 0.9) \times 10^{-6}$		
Γ_{619}	$p \overline{\Lambda} f_2(1270)$, $f_2 \to \pi^+ \pi^-$	$(2.0 \pm 0.8) \times 10^{-6}$		
Γ_{620}	$p \overline{\Lambda} K^+ K^-$	$(4.1 \pm 0.7) \times 10^{-6}$		
Γ_{621}	$p \overline{\Lambda} \phi$	$(8.0 \pm 2.2) \times 10^{-7}$		
Γ_{622}	$\overline{p} \Lambda K^+ K^-$	$(3.7 \pm 0.6) \times 10^{-6}$		
Γ_{623}	$\Lambda \overline{\Lambda} \pi^+$	$< 9.4 \times 10^{-7}$	CL=90%	
Γ_{624}	$\Lambda \overline{\Lambda} K^+$	$(3.4 \pm 0.6) \times 10^{-6}$		
Γ_{625}	$\Lambda \overline{\Lambda} K^{*+}$	$(2.2 {}^{+1.2}_{-0.9}) \times 10^{-6}$		
Γ_{626}	$\Lambda(1520) \overline{\Lambda} K^+$	$(2.2 \pm 0.7) \times 10^{-6}$		
Γ_{627}	$\Lambda \overline{\Lambda}(1520) K^+$	$< 2.08 \times 10^{-6}$		
Γ_{628}	$\overline{\Delta}^0 p$	$< 1.38 \times 10^{-6}$	CL=90%	
Γ_{629}	$\Delta^{++} \overline{p}$	$< 1.4 \times 10^{-7}$	CL=90%	
Γ_{630}	$\overline{\Lambda} p \overline{p} p$	$(2.1 \pm 0.5) \times 10^{-7}$		
Γ_{631}	$\overline{\Lambda} p \eta_c$	$< 1.9 \times 10^{-5}$	CL=90%	
Γ_{632}	$D^+ p \overline{p}$	$< 1.5 \times 10^{-5}$	CL=90%	
Γ_{633}	$D^*(2010)^+ p \overline{p}$	$< 1.5 \times 10^{-5}$	CL=90%	
Γ_{634}	$\overline{D}^0 p \overline{p} \pi^+$	$(3.72 \pm 0.27) \times 10^{-4}$		
Γ_{635}	$\overline{D}^{*0} p \overline{p} \pi^+$	$(3.73 \pm 0.32) \times 10^{-4}$		
Γ_{636}	$D^- p \overline{p} \pi^+ \pi^-$	$(1.66 \pm 0.30) \times 10^{-4}$		
Γ_{637}	$D^{*-} p \overline{p} \pi^+ \pi^-$	$(1.86 \pm 0.25) \times 10^{-4}$		
Γ_{638}	$p \overline{\Lambda}^0 \overline{D}^0$	$(1.43 \pm 0.32) \times 10^{-5}$		
Γ_{639}	$p \overline{\Lambda}^0 \overline{D}^*(2007)^0$	$< 5 \times 10^{-5}$	CL=90%	
Γ_{640}	$\overline{\Lambda}_c^- p \pi^+$	$(2.2 \pm 0.4) \times 10^{-4}$		S=2.7
Γ_{641}	$\overline{\Lambda}_c^- p K^+$	$(8.8 \pm 1.6) \times 10^{-6}$		
Γ_{642}	$\overline{\Lambda}_c^- \Delta(1232)^{++}$	$< 1.9 \times 10^{-5}$	CL=90%	
Γ_{643}	$\overline{\Lambda}_c^- \Delta_X(1600)^{++}$	$(4.6 \pm 0.9) \times 10^{-5}$		
Γ_{644}	$\overline{\Lambda}_c^- \Delta_X(2420)^{++}$	$(3.7 \pm 0.8) \times 10^{-5}$		
Γ_{645}	$(\overline{\Lambda}_c^- p)_s \pi^+$	[h] $(3.1 {}^{+0.7}_{-0.6}) \times 10^{-5}$		
Γ_{646}	$\overline{\Sigma}_c(2520)^0 p$	$< 3 \times 10^{-6}$	CL=90%	
Γ_{647}	$\overline{\Sigma}_c(2800)^0 p$	$(2.6 \pm 0.9) \times 10^{-5}$		
Γ_{648}	$\overline{\Lambda}_c^- p \pi^+ \pi^0$	$(1.8 \pm 0.6) \times 10^{-3}$		
Γ_{649}	$\overline{\Lambda}_c^- p \pi^+ \pi^+ \pi^-$	$(2.2 \pm 0.7) \times 10^{-3}$		
Γ_{650}	$\overline{\Lambda}_c^- p \pi^+ \pi^+ \pi^- \pi^0$	< 1.34 %	CL=90%	
Γ_{651}	$\Lambda_c^+ \Lambda_c^- K^+$	$(4.9 \pm 0.7) \times 10^{-4}$		
Γ_{652}	$\Xi_c(2930) \Lambda_c^+$, $\Xi_c \to K^+ \Lambda_c^-$	$(1.7 \pm 0.5) \times 10^{-4}$		
Γ_{653}	$\overline{\Sigma}_c(2455)^0 p$	$(2.9 \pm 0.6) \times 10^{-5}$		
Γ_{654}	$\overline{\Sigma}_c(2455)^0 p \pi^0$	$(3.5 \pm 1.1) \times 10^{-4}$		
Γ_{655}	$\overline{\Sigma}_c(2455)^0 p \pi^- \pi^+$	$(3.5 \pm 1.0) \times 10^{-4}$		
Γ_{656}	$\overline{\Sigma}_c(2455)^{--} p \pi^+ \pi^+$	$(2.33 \pm 0.17) \times 10^{-4}$		
Γ_{657}	$\Sigma_c(2455)^{++} \overline{\Xi}_c^-$	$(5.7 {}^{+2.7}_{-1.9}) \times 10^{-4}$		
Γ_{658}	$\overline{\Lambda}_c(2593)^- / \overline{\Lambda}_c(2625)^- p \pi^+$	$< 1.9 \times 10^{-4}$	CL=90%	
Γ_{659}	$\overline{\Xi}_c^0 \Lambda_c^+$	$(9.5 \pm 2.3) \times 10^{-4}$		
Γ_{660}	$\Xi_c^0 \Lambda_c^+$	$< 2.6 \times 10^{-5}$	CL=95%	
Γ_{661}	$\overline{\Xi}_c^0 \Lambda_c^+$, $\overline{\Xi}_c^0 \to \overline{\Xi}^+ \pi^-$	$(1.76 \pm 0.29) \times 10^{-5}$		
Γ_{662}	$\overline{\Xi}_c^0 \Lambda_c^+$, $\overline{\Xi}_c^0 \to \Lambda K^+ \pi^-$	$(1.14 \pm 0.26) \times 10^{-5}$		

Int. J. Mod. Phys. A 2026.41. Downloaded from www.worldscientific.com
by UNIVERSITY OF CALIFORNIA @ BERKELEY on 09/16/26. Re-use and distribution is strictly not permitted, except for Open Access articles.

Γ_{663}	$\Xi_c^0 \Lambda_c^+$, $\Xi_c^0 \to p K^- K^- \pi^+$		$(5.5 \pm 1.9) \times 10^{-6}$	
Γ_{664}	$\Lambda_c^+ \Xi_c'^0$		$< 6.5 \times 10^{-4}$	CL=90%
Γ_{665}	$\Lambda_c^+ \Xi_c(2645)^0$		$< 7.9 \times 10^{-4}$	CL=90%
Γ_{666}	$\Lambda_c^+ \Xi_c(2790)^0$		$(1.1 \pm 0.4) \times 10^{-3}$	
Γ_{667}	$\Lambda_c^+ \psi_{DS}$			
Γ_{668}	$p \psi_{DS}$			

Lepton Family number (*LF*) or Lepton number (*L*) or Baryon number (*B*) violating modes, or/and $\Delta B = 1$ weak neutral current (*B1*) modes

Γ_{669}	$\pi^+ \ell^+ \ell^-$	*B1*	[a]	$< 4.9 \times 10^{-8}$	CL=90%
Γ_{670}	$\pi^+ e^+ e^-$	*B1*		$< 5.4 \times 10^{-8}$	CL=90%
Γ_{671}	$\pi^+ \mu^+ \mu^-$	*B1*		$(1.78 \pm 0.22) \times 10^{-8}$	
Γ_{672}	$\rho(770)^+ e^+ e^-$	*B1*		$< 4.67 \times 10^{-7}$	CL=90%
Γ_{673}	$\rho(770)^+ \mu^+ \mu^-$	*B1*		$< 3.81 \times 10^{-7}$	CL=90%
Γ_{674}	$\rho(770)^+ \ell^+ \ell^-$	*B1*		$< 1.89 \times 10^{-7}$	CL=90%
Γ_{675}	$\pi^+ \nu \overline{\nu}$	*B1*		$< 1.4 \times 10^{-5}$	CL=90%
Γ_{676}	$K^+ \ell^+ \ell^-$	*B1*	[a]	$(4.7 \pm 0.5) \times 10^{-7}$	S=2.3
Γ_{677}	$K^+ e^+ e^-$	*B1*		$(5.6 \pm 0.6) \times 10^{-7}$	
Γ_{678}	$K^+ \mu^+ \mu^-$	*B1*		$(4.53 \pm 0.35) \times 10^{-7}$	S=1.8
Γ_{679}	$K^+ \mu^+ \mu^-$ nonresonant	*B1*		$(4.37 \pm 0.27) \times 10^{-7}$	
Γ_{680}	$K^+ \tau^+ \tau^-$	*B1*		$< 2.25 \times 10^{-3}$	CL=90%
Γ_{681}	$K^+ \overline{\nu} \nu$	*B1*		$(2.3 \pm 0.7) \times 10^{-5}$	
Γ_{682}	$\rho^+ \nu \overline{\nu}$	*B1*		$< 3.0 \times 10^{-5}$	CL=90%
Γ_{683}	$K^*(892)^+ \ell^+ \ell^-$	*B1*	[a]	$(1.01 \pm 0.11) \times 10^{-6}$	S=1.1
Γ_{684}	$K^*(892)^+ e^+ e^-$	*B1*		$(1.55 {}^{+0.40}_{-0.31}) \times 10^{-6}$	
Γ_{685}	$K^*(892)^+ \mu^+ \mu^-$	*B1*		$(9.6 \pm 1.0) \times 10^{-7}$	
Γ_{686}	$K^*(892)^+ \nu \overline{\nu}$	*B1*		$< 4.0 \times 10^{-5}$	CL=90%
Γ_{687}	$K^+ \pi^+ \pi^- \mu^+ \mu^-$	*B1*		$(4.3 \pm 0.4) \times 10^{-7}$	
Γ_{688}	$D_s^+ \mu^+ \mu^-$	*B1*		$< 2.4 \times 10^{-8}$	CL=90%
Γ_{689}	$\phi K^+ \mu^+ \mu^-$	*B1*		$(7.9 {}^{+2.1}_{-1.7}) \times 10^{-8}$	
Γ_{690}	$\overline{\Lambda} p \nu \overline{\nu}$	*B1*		$< 3.0 \times 10^{-5}$	CL=90%
Γ_{691}	$\pi^+ e^+ \mu^-$	*LF*		$< 6.4 \times 10^{-3}$	CL=90%
Γ_{692}	$\pi^+ e^- \mu^+$	*LF*		$< 6.4 \times 10^{-3}$	CL=90%
Γ_{693}	$\pi^+ e^\pm \mu^\mp$	*LF*		$< 1.7 \times 10^{-7}$	CL=90%
Γ_{694}	$\pi^+ e^+ \tau^-$	*LF*		$< 7.4 \times 10^{-5}$	CL=90%
Γ_{695}	$\pi^+ e^- \tau^+$	*LF*		$< 2.0 \times 10^{-5}$	CL=90%
Γ_{696}	$\pi^+ e^\pm \tau^\mp$	*LF*		$< 7.5 \times 10^{-5}$	CL=90%
Γ_{697}	$\pi^+ \mu^+ \tau^-$	*LF*		$< 6.2 \times 10^{-5}$	CL=90%
Γ_{698}	$\pi^+ \mu^- \tau^+$	*LF*		$< 4.5 \times 10^{-5}$	CL=90%
Γ_{699}	$\pi^+ \mu^\pm \tau^\mp$	*LF*		$< 7.2 \times 10^{-5}$	CL=90%
Γ_{700}	$K^+ e^+ \mu^-$	*LF*		$< 7.0 \times 10^{-9}$	CL=90%
Γ_{701}	$K^+ e^- \mu^+$	*LF*		$< 6.4 \times 10^{-9}$	CL=90%
Γ_{702}	$K^+ e^\pm \mu^\mp$	*LF*		$< 9.1 \times 10^{-8}$	CL=90%
Γ_{703}	$K^+ e^+ \tau^-$	*LF*		$< 1.53 \times 10^{-5}$	CL=90%
Γ_{704}	$K^+ e^- \tau^+$	*LF*		$< 1.5 \times 10^{-5}$	CL=90%
Γ_{705}	$K^+ e^\pm \tau^\mp$	*LF*		$< 3.0 \times 10^{-5}$	CL=90%
Γ_{706}	$K^+ \mu^+ \tau^-$	*LF*		$< 2.45 \times 10^{-5}$	CL=90%
Γ_{707}	$K^+ \mu^- \tau^+$	*LF*		$< 5.9 \times 10^{-6}$	CL=90%
Γ_{708}	$K^+ \mu^\pm \tau^\mp$	*LF*		$< 4.8 \times 10^{-5}$	CL=90%
Γ_{709}	$K^*(892)^+ e^+ \mu^-$	*LF*		$< 1.3 \times 10^{-6}$	CL=90%
Γ_{710}	$K^*(892)^+ e^- \mu^+$	*LF*		$< 9.9 \times 10^{-7}$	CL=90%
Γ_{711}	$K^*(892)^+ e^\pm \mu^\mp$	*LF*		$< 1.4 \times 10^{-6}$	CL=90%
Γ_{712}	$\pi^- e^+ e^+$	*L*		$< 2.3 \times 10^{-8}$	CL=90%
Γ_{713}	$\pi^- \mu^+ \mu^+$	*L*		$< 4.0 \times 10^{-9}$	CL=95%
Γ_{714}	$\pi^- e^+ \mu^+$	*L*		$< 1.5 \times 10^{-7}$	CL=90%
Γ_{715}	$\rho^- e^+ e^+$	*L*		$< 1.7 \times 10^{-7}$	CL=90%
Γ_{716}	$\rho^- \mu^+ \mu^+$	*L*		$< 4.2 \times 10^{-7}$	CL=90%
Γ_{717}	$\rho^- e^+ \mu^+$	*L*		$< 4.7 \times 10^{-7}$	CL=90%
Γ_{718}	$K^- e^+ e^+$	*L*		$< 3.0 \times 10^{-8}$	CL=90%
Γ_{719}	$K^- \mu^+ \mu^+$	*L*		$< 4.1 \times 10^{-8}$	CL=90%
Γ_{720}	$K^- e^+ \mu^+$	*L*		$< 1.6 \times 10^{-7}$	CL=90%
Γ_{721}	$K^*(892)^- e^+ e^+$	*L*		$< 4.0 \times 10^{-7}$	CL=90%
Γ_{722}	$K^*(892)^- \mu^+ \mu^+$	*L*		$< 5.9 \times 10^{-7}$	CL=90%
Γ_{723}	$K^*(892)^- e^+ \mu^+$	*L*		$< 3.0 \times 10^{-7}$	CL=90%
Γ_{724}	$D^- e^+ e^+$	*L*		$< 2.6 \times 10^{-6}$	CL=90%
Γ_{725}	$D^- e^+ \mu^+$	*L*		$< 1.8 \times 10^{-6}$	CL=90%
Γ_{726}	$D^- \mu^+ \mu^+$	*L*		$< 6.9 \times 10^{-7}$	CL=95%
Γ_{727}	$D^{*-} \mu^+ \mu^+$	*L*		$< 2.4 \times 10^{-6}$	CL=95%
Γ_{728}	$D_s^- \mu^+ \mu^+$	*L*		$< 5.8 \times 10^{-7}$	CL=95%
Γ_{729}	$\overline{D}^0 \pi^- \mu^+ \mu^+$	*L*		$< 1.5 \times 10^{-6}$	CL=95%
Γ_{730}	$\Lambda^0 \mu^+$	*L,B*		$< 6 \times 10^{-8}$	CL=90%
Γ_{731}	$\Lambda^0 e^+$	*L,B*		$< 3.2 \times 10^{-8}$	CL=90%
Γ_{732}	$\overline{\Lambda}^0 \mu^+$	*L,B*		$< 6 \times 10^{-8}$	CL=90%
Γ_{733}	$\overline{\Lambda}^0 e^+$	*L,B*		$< 8 \times 10^{-8}$	CL=90%

[a] An ℓ indicates an e or a μ mode, not a sum over these modes.

[b] An $CP(\pm 1)$ indicates the $CP=+1$ and $CP=-1$ eigenstates of the D^0-$\overline{D}^0$ system.

[c] D denotes D^0 or $\overline{D}^0$.

[d] D^{*0}_{CP+} decays into $D^0 \pi^0$ with the D^0 reconstructed in CP-even eigenstates $K^+ K^-$ and $\pi^+ \pi^-$.

[e] $\overline{D}^{**}$ represents an excited state with mass $2.2 < M < 2.8$ GeV/c^2.

[f] $\chi_{c1}(3872)^+$ is a hypothetical charged partner of the $\chi_{c1}(3872)$.

[g] $\Theta(1710)^{++}$ is a possible narrow pentaquark state and $G(2220)$ is a possible glueball resonance.

[h] $(\overline{\Lambda}_c^- p)_s$ denotes a low-mass enhancement near 3.35 GeV/c^2.

FIT INFORMATION

An overall fit to 21 branching ratios uses 66 measurements to determine 13 parameters. The overall fit has a $\chi^2 = 66.7$ for 53 degrees of freedom.

The following *off-diagonal* array elements are the correlation coefficients $\langle \delta x_i \delta x_j \rangle / (\delta x_i \cdot \delta x_j)$, in percent, from the fit to the branching fractions, $x_i \equiv \Gamma_i / \Gamma_{total}$.

	x_{10}	x_{13}	x_{59}	x_{116}	x_{158}	x_{316}	x_{321}	x_{339}	x_{352}	x_{411}
x_{13}	33									
x_{59}	0	0								
x_{116}	0	0	5							
x_{158}	0	0	1	14						
x_{316}	0	0	0	0	0					
x_{321}	0	0	0	0	0	0				
x_{339}	0	0	0	0	0	18	0			
x_{352}	0	0	0	0	0	38	0	7		
x_{411}	0	0	0	0	0	0	0	0	0	
x_{483}	0	0	0	0	0	0	0	0	0	8
x_{678}	0	0	0	0	0	14	0	3	5	0
x_{685}	0	0	0	0	0	0	5	0	0	0

	x_{483}	x_{678}
x_{678}	0	
x_{685}	0	0

FIT INFORMATION

A multiparticle fit to $\eta_c(1S)$, $J/\psi(1S)$, $\psi(2S)$, $h_c(1P)$, and $B^\pm$ with the total width, 10 combinations of partial widths obtained from integrated cross section, and 38 branching ratios uses 115 measurements to determine 19 parameters. The overall fit has a $\chi^2 = 215.4$ for 96 degrees of freedom.

B^+ BRANCHING RATIOS

$\Gamma(\ell^+ \nu_\ell X)/\Gamma_{total}$ — Γ_1/Γ

VALUE (units 10^{-2})	DOCUMENT ID		TECN	COMMENT
10.99±0.28 OUR EVALUATION	(Produced by HFLAV)			
10.76±0.32 OUR AVERAGE	Error includes scale factor of 1.1.			
11.17±0.25±0.28	[1] URQUIJO	07	BELL	$e^+e^- \to \Upsilon(4S)$
10.28±0.26±0.39	[2] AUBERT,B	06Y	BABR	$e^+e^- \to \Upsilon(4S)$
10.25±0.57±0.65	[3] ARTUSO	97	CLE2	$e^+e^- \to \Upsilon(4S)$
• • • We do not use the following data for averages, fits, limits, etc. • • •				
11.15±0.26±0.41	[4] OKABE	05	BELL	Repl. by URQUIJO 07
10.1 ±1.8 ±1.5	ATHANAS	94	CLE2	Sup. by ARTUSO 97

[1] URQUIJO 07 report a measurement of (10.34 ± 023 ± 0.25)% for the partial branching fraction of $B^+ \to e^+ \nu_e X_c$ decay with electron energy above 0.6 GeV. We converted the result to $B^+ \to e^+ \nu_e X$ branching fraction.

[2] The measurements are obtained for charged and neutral B mesons partial rates of semileptonic decay to electrons with momentum above 0.6 GeV/c in the B rest frame. The best precision on the ratio is achieved for a momentum threshold of 1.0 GeV: $B(B^+ \to e^+ \nu_e X) / B(B^0 \to e^+ \nu_e X) = 1.074 \pm 0.041 \pm 0.026$.

[3] ARTUSO 97 uses partial reconstruction of $B \to D^* \ell \nu_\ell$ and inclusive semileptonic branching ratio from BARISH 96B (0.1049 ± 0.0017 ± 0.0043).

[4] The measurements are obtained for charged and neutral B mesons partial rates of semileptonic decay to electrons with momentum above 0.6 GeV/c in the B rest frame, and their ratio of $B(B^+ \to e^+ \nu_e X)/B(B^0 \to e^+ \nu_e X) = 1.08 \pm 0.05 \pm 0.02$.

$\Gamma(e^+ \nu_e X_c)/\Gamma_{total}$ — Γ_2/Γ

VALUE (units 10^{-2})	DOCUMENT ID		TECN	COMMENT
10.79±0.25±0.27	[1] URQUIJO	07	BELL	$e^+e^- \to \Upsilon(4S)$

[1] Measure the independent B^+ and B^0 partial branching fractions with electron threshold energies of 0.4 GeV.

Int. J. Mod. Phys. A 2026.41. Downloaded from www.worldscientific.com by CALIFORNIA @ BERKELEY on 09/16/26. Re-use and distribution is strictly not permitted, except for Open Access articles.

$\Gamma(\ell^+ \nu_\ell X_u)/\Gamma_{total}$ — Γ_5/Γ

Requires $E^*_\ell > 1$ GeV, where E^*_ℓ is letpon energy in B rest frame.

VALUE (units 10^{-3})	DOCUMENT ID		TECN	COMMENT
1.65±0.10±0.18	[1] CAO	21A	BELL	$e^+e^- \to \Upsilon(4S)$

[1] The correlation of 50% with $B(B^0 \to \ell^+ \nu_\ell X_u)$(letpon energy in B rest frame $E^*_\ell >$ 1 GeV) was reported.

$\Gamma(\overline{D}^0 \ell^+ \nu_\ell)/\Gamma_{total}$ — Γ_7/Γ

$\ell = e$ or μ, not sum over e and μ modes.

VALUE (%)	DOCUMENT ID		TECN	COMMENT
2.21±0.06 OUR EVALUATION	(Produced by HFLAV)			
2.30±0.06 OUR AVERAGE				
2.31±0.04±0.09	[1] ADACHI	25Y	BELL	$e^+e^- \to \Upsilon(4S)$
2.29±0.08±0.09	[2] AUBERT	10	BABR	$e^+e^- \to \Upsilon(4S)$
2.34±0.03±0.13	AUBERT	09A	BABR	$e^+e^- \to \Upsilon(4S)$
2.21±0.13±0.19	[3] BARTELT	99	CLE2	$e^+e^- \to \Upsilon(4S)$
1.6 ±0.6 ±0.3	[4] FULTON	91	CLEO	$e^+e^- \to \Upsilon(4S)$
• • • We do not use the following data for averages, fits, limits, etc. • • •				
2.33±0.09±0.09	[2] AUBERT	08Q	BABR	Repl. by AUBERT 09A
1.94±0.15±0.34	[5] ATHANAS	97	CLE2	Repl. by BARTELT 99

[1] The second B meson from the $\Upsilon(4S)$ decay is not explicitly reconstructed.
[2] Uses a fully reconstructed B meson as a tag on the recoil side.
[3] Assumes equal production of B^+ and B^0 at the $\Upsilon(4S)$.
[4] FULTON 91 assumes equal production of $B^0\overline{B}^0$ and B^+B^- at the $\Upsilon(4S)$.
[5] ATHANAS 97 uses missing energy and missing momentum to reconstruct neutrino.

$\Gamma(\overline{D}^0 \ell^+ \nu_\ell)/\Gamma(\ell^+ \nu_\ell X)$ — Γ_7/Γ_1

VALUE	DOCUMENT ID		TECN	COMMENT
0.255±0.009±0.009	[1] AUBERT	10	BABR	$e^+e^- \to \Upsilon(4S)$

[1] Uses a fully reconstructed B meson on the recoil side.

$\Gamma(\overline{D}^0 \ell^+ \nu_\ell)/\Gamma(D \ell^+ \nu_\ell X)$ — Γ_7/Γ_6

VALUE	DOCUMENT ID		TECN	COMMENT
0.230±0.020 OUR AVERAGE				
0.25 ±0.06	[1] AAIJ	19AC	LHCB	pp at 7 and 8 TeV
0.227±0.014±0.016	[2] AUBERT	07AN	BABR	$e^+e^- \to \Upsilon(4S)$

[1] The relative branching fractions of $B^- \to D^0$, D^{*0}, D^{**0} in the $B^- \to D^0 X \mu^- \overline{\nu}$ channel are determined by fitting the distribution of the missing mass in $\overline{B}^{*0}_{s2} \to B^- K^+$ decays.
[2] Uses a fully reconstructed B meson on the recoil side.

$\Gamma(\tau^+ \nu_\tau X)/\Gamma(\ell^+ \nu_\ell X)$ — Γ_8/Γ_1

VALUE	DOCUMENT ID		TECN	COMMENT
0.228±0.016±0.036	[1] ADACHI	24B	BELL	$e^+e^- \to \Upsilon(4S)$

[1] Measures the lepton in a primary decay of the signal B meson, while tagging the partner B in fully reconstructed hadronic decay modes.

$\Gamma(\tau^+ \nu_\tau X)/\Gamma(e^+ \nu_e X)$ — Γ_8/Γ_3

VALUE	DOCUMENT ID		TECN	COMMENT
0.232±0.020±0.037	[1] ADACHI	24B	BELL	$e^+e^- \to \Upsilon(4S)$

[1] Measures the lepton in a primary decay of the signal B meson, while tagging the partner B in fully reconstructed hadronic decay modes.

$\Gamma(\tau^+ \nu_\tau X)/\Gamma(\mu^+ \nu_\mu X)$ — Γ_8/Γ_4

VALUE	DOCUMENT ID		TECN	COMMENT
0.222±0.027±0.050	[1] ADACHI	24B	BELL	$e^+e^- \to \Upsilon(4S)$

[1] Measures the lepton in a primary decay of the signal B meson, while tagging the partner B in fully reconstructed hadronic decay modes.

$\Gamma(\overline{D}^0 \tau^+ \nu_\tau)/\Gamma_{total}$ — Γ_9/Γ

VALUE (units 10^{-2})	DOCUMENT ID		TECN	COMMENT
0.77±0.22±0.12	[1] BOZEK	10	BELL	$e^+e^- \to \Upsilon(4S)$
• • • We do not use the following data for averages, fits, limits, etc. • • •				
0.67±0.37±0.13	[2] AUBERT	08N	BABR	Repl. by AUBERT 09S

[1] Assumes equal production of B^+ and B^0 at the $\Upsilon(4S)$.
[2] Uses a fully reconstructed B meson as a tag on the recoil side.

$\Gamma(\overline{D}^0 \tau^+ \nu_\tau)/\Gamma(\overline{D}^0 \ell^+ \nu_\ell)$ — Γ_9/Γ_7

VALUE	DOCUMENT ID		TECN	COMMENT
0.44 ±0.07 OUR AVERAGE				
0.441±0.060±0.066	[1] AAIJ	23AR	LHCB	pp at 7 and 8 TeV
0.429±0.082±0.052	[2,3] LEES	12D	BABR	$e^+e^- \to \Upsilon(4S)$
• • • We do not use the following data for averages, fits, limits, etc. • • •				
0.314±0.170±0.049	[2] AUBERT	09S	BABR	Repl. by LEES 12D

[1] Uses $\tau^+ \to \mu^+ \nu_\mu \overline{\nu}_\tau$ and μ^+ as ℓ^+.
[2] Uses a fully reconstructed B meson as a tag on the recoil side.
[3] Uses $\tau^+ \to e^+ \nu_e \overline{\nu}_\tau$ and $\tau^+ \to \mu^+ \nu_\mu \overline{\nu}_\tau$ and e^+ or μ^+ as ℓ^+.

$\Gamma(\overline{D}^*(2007)^0 \ell^+ \nu_\ell)/\Gamma_{total}$ — Γ_{10}/Γ

$\ell = e$ or μ, not sum over e and μ modes.

VALUE (%)	EVTS	DOCUMENT ID		TECN	COMMENT
5.53±0.22 OUR EVALUATION		(Produced by HFLAV)			
5.60±0.26 OUR FIT		Error includes scale factor of 1.5.			
5.58±0.26 OUR AVERAGE		Error includes scale factor of 1.5. See the ideogram below.			
5.40±0.02±0.21		AUBERT	09A	BABR	$e^+e^- \to \Upsilon(4S)$
5.56±0.08±0.41		[1] AUBERT	08AT	BABR	$e^+e^- \to \Upsilon(4S)$
6.50±0.20±0.43		[2] ADAM	03	CLE2	$e^+e^- \to \Upsilon(4S)$
6.6 ±1.6 ±1.5		[3] ALBRECHT	92C	ARG	$e^+e^- \to \Upsilon(4S)$
• • • We do not use the following data for averages, fits, limits, etc. • • •					
5.83±0.15±0.30		[4] AUBERT	08Q	BABR	Repl. by AUBERT 09A
6.50±0.20±0.43		[5] BRIERE	02	CLE2	$e^+e^- \to \Upsilon(4S)$
5.13±0.54±0.64	302	[6] BARISH	95	CLE2	Repl. by ADAM 03
seen	398	[7] SANGHERA	93	CLE2	$e^+e^- \to \Upsilon(4S)$
4.1 ±0.8 $^{+0.8}_{-0.9}$		[8] FULTON	91	CLEO	$e^+e^- \to \Upsilon(4S)$
7.0 ±1.8 ±1.4		[9] ANTREASYAN	90B	CBAL	$e^+e^- \to \Upsilon(4S)$

[1] Measured using the dependence of $B^- \to D^{*0} e^- \overline{\nu}_e$ decay differential rate and the form factor description by CAPRINI 98.
[2] Simultaneous measurements of both $B^0 \to D^*(2010)^- \ell\nu$ and $B^+ \to \overline{D}(2007)^0 \ell\nu$.
[3] ALBRECHT 92C reports 0.058±0.014±0.013. We rescale using the method described in STONE 94 but with the updated PDG 94 $B(D^0 \to K^-\pi^+)$. Assumes equal production of $B^0\overline{B}^0$ and B^+B^- at the $\Upsilon(4S)$.
[4] Uses a fully reconstructed B meson as a tag on the recoil side.
[5] The results are based on the same analysis and data sample reported in ADAM 03.
[6] BARISH 95 use $B(D^0 \to K^-\pi^+)$ = (3.91 ± 0.08 ± 0.17)% and $B(D^{*0} \to D^0\pi^0)$ = (63.6 ± 2.3 ± 3.3)%.
[7] Combining $\overline{D}^{*0}\ell^+\nu_\ell$ and $\overline{D}^{*-}\ell^+\nu_\ell$ SANGHERA 93 test $V-A$ structure and fit the decay angular distributions to obtain $A_{FB} = 3/4*(\Gamma^- - \Gamma^+)/\Gamma = 0.14 \pm 0.06 \pm 0.03$. Assuming a value of V_{cb}, they measure V, A_1, and A_2, the three form factors for the $D^*\ell\nu_\ell$ decay, where results are slightly dependent on model assumptions.
[8] Assumes equal production of $B^0\overline{B}^0$ and B^+B^- at the $\Upsilon(4S)$. Uncorrected for D and D^* branching ratio assumptions.
[9] ANTREASYAN 90B is average over B and $\overline{D}^*(2010)$ charge states.

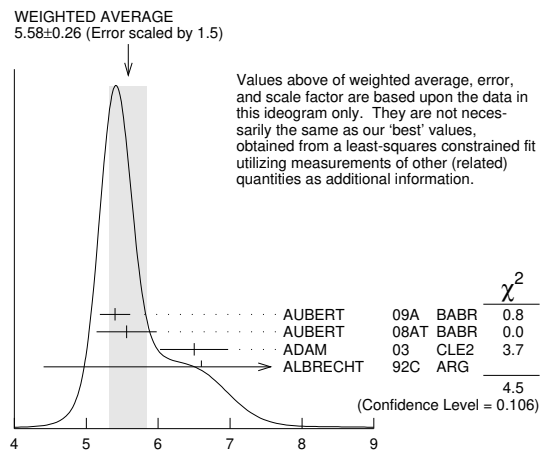

$\Gamma(\overline{D}^*(2007)^0 \ell^+ \nu_\ell)/\Gamma_{total}$ — Γ_{10}/Γ

$\Gamma(\overline{D}^*(2007)^0 \ell^+ \nu_\ell)/\Gamma(D \ell^+ \nu_\ell X)$ — Γ_{10}/Γ_6

VALUE	DOCUMENT ID		TECN	COMMENT
0.582±0.018±0.030	[1] AUBERT	07AN	BABR	$e^+e^- \to \Upsilon(4S)$

[1] Uses a fully reconstructed B meson on the recoil side.

$\Gamma(\overline{D}^*(2007)^0 e^+ \nu_e)/\Gamma(\overline{D}^*(2007)^0 \mu^+ \nu_\mu)$ — Γ_{11}/Γ_{12}

VALUE	DOCUMENT ID		TECN	COMMENT
0.976±0.029±0.023	PRIM	23	BELL	$e^+e^- \to \Upsilon(4S)$

$\Gamma(\overline{D}^*(2007)^0 \tau^+ \nu_\tau)/\Gamma_{total}$ — Γ_{13}/Γ

VALUE (units 10^{-2})	DOCUMENT ID		TECN	COMMENT
1.88±0.20 OUR FIT				
$2.12^{+0.28}_{-0.27}$±0.29	[1] BOZEK	10	BELL	$e^+e^- \to \Upsilon(4S)$
• • • We do not use the following data for averages, fits, limits, etc. • • •				
2.25±0.48±0.28	[2] AUBERT	08N	BABR	Repl. by AUBERT 09S

[1] Assumes equal production of B^+ and B^0 at the $\Upsilon(4S)$.
[2] Uses a fully reconstructed B meson as a tag on the recoil side.

$\Gamma(\overline{D}^*(2007)^0 \tau^+ \nu_\tau)/\Gamma(\overline{D}^*(2007)^0 \ell^+ \nu_\ell)$ — Γ_{13}/Γ_{10}

VALUE	DOCUMENT ID		TECN	COMMENT
0.335±0.034 OUR FIT				
0.322±0.032±0.022	[1,2] LEES	12D	BABR	$e^+e^- \to \Upsilon(4S)$
• • • We do not use the following data for averages, fits, limits, etc. • • •				
0.346±0.073±0.034	[1] AUBERT	09S	BABR	Repl. by LEES 12D

[1] Uses a fully reconstructed B meson as a tag on the recoil side.
[2] Uses $\tau^+ \to e^+ \nu_e \overline{\nu}_\tau$ and $\tau^+ \to \mu^+ \nu_\mu \overline{\nu}_\tau$ and e^+ or μ^+ as ℓ^+.

$\Gamma(D^{(*)} n\pi \ell^+ \nu_\ell (n \geq 1))/\Gamma(D \ell^+ \nu_\ell X)$ — Γ_{14}/Γ_6

VALUE	DOCUMENT ID		TECN	COMMENT
0.193±0.022 OUR AVERAGE				
0.21 ±0.07	[1,2] AAIJ	19AC	LHCB	pp at 7 and 8 TeV
0.191±0.013±0.019	[3] AUBERT	07AN	BABR	$e^+e^- \to \Upsilon(4S)$

[1] The relative branching fractions of $B^- \to D^0$, D^{*0}, D^{**0} in the $B^- \to D^0 X \mu^- \overline{\nu}$ channel are determined by fitting the distribution of the missing mass in $\overline{B}^{*0}_{s2} \to B^- K^+$ decays.

[2] In this measurement of $f_{D^{**0}} = B(B^- \to (D^{**0} \to D^0 X)\mu^- \overline{\nu})/B(B^- \to D^0 X \mu^- \overline{\nu})$, D^{**0} refers collectively to L = 1 states $D_0^*(2400)$, $D_1(2420)$, $D_1(2430)$, and $D_2^*(2460)$, as well as other resonances such as radially excited D mesons, and to nonresonant contributions with additional pions.

[3] Uses a fully reconstructed B meson on the recoil side.

$\Gamma(D^- \pi^+ \ell^+ \nu_\ell)/\Gamma_{total}$ — Γ_{15}/Γ

VALUE (units 10^{-3})	DOCUMENT ID		TECN	COMMENT
3.82±0.20 OUR AVERAGE				
3.78±0.13±0.17	MEIER	23	BELL	$e^+e^- \to \Upsilon(4S)$
4.2 ±0.6 ±0.3	[1] AUBERT	08Q	BABR	$e^+e^- \to \Upsilon(4S)$
• • • We do not use the following data for averages, fits, limits, etc. • • •				
4.55±0.27±0.39	VOSSEN	18	BELL	Repl. by MEIER 23
4.1 ±0.6 ±0.1	[1,2] LIVENTSEV	08	BELL	Repl. by VOSSEN 18
5.3 ±0.9 ±0.1	[3] LIVENTSEV	05	BELL	Repl. by LIVENTSEV 08

[1] Uses a fully reconstructed B meson as a tag on the recoil side.

[2] LIVENTSEV 08 reports $(4.0 \pm 0.4 \pm 0.6) \times 10^{-3}$ from a measurement of $[\Gamma(B^+ \to D^- \pi^+ \ell^+ \nu_\ell)/\Gamma_{total}] / [B(B^+ \to \overline{D}^0 \ell^+ \nu_\ell)]$ assuming $B(B^+ \to \overline{D}^0 \ell^+ \nu_\ell) = (2.15 \pm 0.22) \times 10^{-2}$, which we rescale to our best (shown rounded) value $B(B^+ \to \overline{D}^0 \ell^+ \nu_\ell) = (2.21 \pm 0.06) \times 10^{-2}$. Our first error is their experiment's error and our second error is the systematic error from using our best (shown rounded) value.

[3] LIVENTSEV 05 reports $[\Gamma(B^+ \to D^- \pi^+ \ell^+ \nu_\ell)/\Gamma_{total}] / [B(B^0 \to D^- \ell^+ \nu_\ell)] = 0.25 \pm 0.03 \pm 0.03$ which we multiply by our best (shown rounded) value $B(B^0 \to D^- \ell^+ \nu_\ell) = (2.12 \pm 0.06) \times 10^{-2}$. Our first error is their experiment's error and our second error is the systematic error from using our best (shown rounded) value.

$\Gamma(\overline{D}_2^*(2460)^0 \ell^+ \nu_\ell, \overline{D}_2^{*0} \to D^- \pi^+)/\Gamma_{total}$ — Γ_{16}/Γ

VALUE (units 10^{-3})	DOCUMENT ID		TECN	COMMENT
1.59±0.10 OUR AVERAGE				
1.63±0.11±0.07	MEIER	23	BELL	$e^+e^- \to \Upsilon(4S)$
1.42±0.15±0.15	[1] AUBERT	09Y	BABR	$e^+e^- \to \Upsilon(4S)$
1.5 ±0.2 ±0.2	[2] AUBERT	08BL	BABR	$e^+e^- \to \Upsilon(4S)$
2.2 ±0.3 ±0.4	[2] LIVENTSEV	08	BELL	$e^+e^- \to \Upsilon(4S)$

[1] Uses a simultaneous fit of all B semileptonic decays without full reconstruction of events. AUBERT 09Y reports $B(B^+ \to \overline{D}_2^*(2460)^0 \ell^+ \nu_\ell) \cdot B(\overline{D}_2^*(2460)^0 \to D^{(*)-} \pi^+) = (2.29 \pm 0.23 \pm 0.21) \times 10^{-3}$ and the authors have provided us the individual measurement.

[2] Uses a fully reconstructed B meson as a tag on the recoil side.

$\Gamma(\overline{D}_0^*(2420)^0 \ell^+ \nu_\ell, \overline{D}_0^{*0} \to D^- \pi^+)/\Gamma_{total}$ — Γ_{17}/Γ

VALUE (units 10^{-3})	DOCUMENT ID		TECN	COMMENT
0.9 ±0.5 OUR AVERAGE Error includes scale factor of 2.6. See the ideogram below.				
0.54±0.22±0.05	MEIER	23	BELL	$e^+e^- \to \Upsilon(4S)$
2.6 ±0.5 ±0.4	[1] AUBERT	08BL	BABR	$e^+e^- \to \Upsilon(4S)$
2.4 ±0.4 ±0.6	[1] LIVENTSEV	08	BELL	$e^+e^- \to \Upsilon(4S)$

[1] Uses a fully reconstructed B meson as a tag on the recoil side.

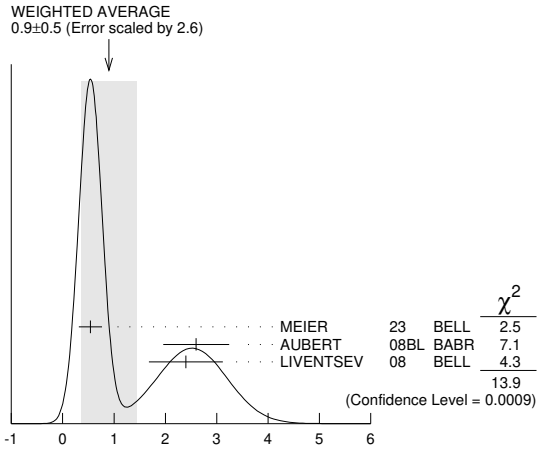

$\Gamma(D^{*-} \pi^+ \ell^+ \nu_\ell)/\Gamma_{total}$ — Γ_{18}/Γ

VALUE (units 10^{-3})	DOCUMENT ID		TECN	COMMENT
5.42±0.28 OUR AVERAGE				
5.30±0.19±0.25	MEIER	23	BELL	$e^+e^- \to \Upsilon(4S)$
5.9 ±0.5 ±0.4	[1] AUBERT	08Q	BABR	$e^+e^- \to \Upsilon(4S)$
• • • We do not use the following data for averages, fits, limits, etc. • • •				
6.03±0.43±0.38	VOSSEN	18	BELL	Repl. by MEIER 23
6.6 ±1.0 ±0.2	[1,2] LIVENTSEV	08	BELL	Repl. by VOSSEN 18
5.9 ±1.4 ±0.1	[3,4] LIVENTSEV	05	BELL	Repl. by LIVENTSEV 08

[1] Uses a fully reconstructed B meson as a tag on the recoil side.

[2] LIVENTSEV 08 reports $(6.4 \pm 0.8 \pm 0.9) \times 10^{-3}$ from a measurement of $[\Gamma(B^+ \to D^{*-} \pi^+ \ell^+ \nu_\ell)/\Gamma_{total}] / [B(B^+ \to \overline{D}^0 \ell^+ \nu_\ell)]$ assuming $B(B^+ \to \overline{D}^0 \ell^+ \nu_\ell) = (2.15 \pm 0.22) \times 10^{-2}$, which we rescale to our best (shown rounded) value $B(B^+ \to \overline{D}^0 \ell^+ \nu_\ell) = (2.21 \pm 0.06) \times 10^{-2}$. Our first error is their experiment's error and our second error is the systematic error from using our best (shown rounded) value.

[3] Excludes D^{*+} contribution to $D\pi$ modes.

[4] LIVENTSEV 05 reports $[\Gamma(B^+ \to D^{*-} \pi^+ \ell^+ \nu_\ell)/\Gamma_{total}] / [B(B^0 \to D^*(2010)^- \ell^+ \nu_\ell)] = 0.12 \pm 0.02 \pm 0.02$ which we multiply by our best (shown rounded) value $B(B^0 \to D^*(2010)^- \ell^+ \nu_\ell) = (4.90 \pm 0.12) \times 10^{-2}$. Our first error is their experiment's error and our second error is the systematic error from using our best (shown rounded) value.

$\Gamma(\overline{D}_1(2420)^0 \ell^+ \nu_\ell, \overline{D}_1^0 \to D^{*-} \pi^+)/\Gamma_{total}$ — Γ_{19}/Γ

VALUE (units 10^{-3})	DOCUMENT ID		TECN	COMMENT
2.84±0.17 OUR AVERAGE Error includes scale factor of 1.1.				
2.49±0.23±0.14	MEIER	23	BELL	$e^+e^- \to \Upsilon(4S)$
2.97±0.17±0.17	[1] AUBERT	09Y	BABR	$e^+e^- \to \Upsilon(4S)$
2.9 ±0.3 ±0.3	[2] AUBERT	08BL	BABR	$e^+e^- \to \Upsilon(4S)$
4.2 ±0.7 ±0.7	[2] LIVENTSEV	08	BELL	$e^+e^- \to \Upsilon(4S)$
3.73±0.85±0.57	[3] ANASTASSOV	98	CLE2	$e^+e^- \to \Upsilon(4S)$

[1] Uses a simultaneous measurement of all B semileptonic decays without full reconstruction of events.

[2] Uses a fully reconstructed B meson as a tag on the recoil side.

[3] Assumes equal production of B^+ and B^0 at the $\Upsilon(4S)$.

$\Gamma(\overline{D}_1'(2430)^0 \ell^+ \nu_\ell, \overline{D}_1'^0 \to D^{*-} \pi^+)/\Gamma_{total}$ — Γ_{20}/Γ

VALUE (units 10^{-3})	CL%	DOCUMENT ID		TECN	COMMENT
1.7 ±0.6 OUR AVERAGE Error includes scale factor of 1.8.					
1.38±0.36±0.08		MEIER	23	BELL	$e^+e^- \to \Upsilon(4S)$
2.7 ±0.4 ±0.5		[1] AUBERT	08BL	BABR	$e^+e^- \to \Upsilon(4S)$
• • • We do not use the following data for averages, fits, limits, etc. • • •					
<0.7	90	[1] LIVENTSEV	08	BELL	$e^+e^- \to \Upsilon(4S)$

[1] Uses a fully reconstructed B meson as a tag on the recoil side.

$\Gamma(\overline{D}_2^*(2460)^0 \ell^+ \nu_\ell, \overline{D}_2^{*0} \to D^{*-} \pi^+)/\Gamma_{total}$ — Γ_{21}/Γ

VALUE (units 10^{-3})	CL%	DOCUMENT ID		TECN	COMMENT
1.06±0.18 OUR AVERAGE Error includes scale factor of 1.7. See the ideogram below.					
1.37±0.26±0.09		MEIER	23	BELL	$e^+e^- \to \Upsilon(4S)$
0.87±0.11±0.07		[1] AUBERT	09Y	BABR	$e^+e^- \to \Upsilon(4S)$
1.5 ±0.2 ±0.2		[2] AUBERT	08BL	BABR	$e^+e^- \to \Upsilon(4S)$
1.8 ±0.6 ±0.3		[2] LIVENTSEV	08	BELL	$e^+e^- \to \Upsilon(4S)$
• • • We do not use the following data for averages, fits, limits, etc. • • •					
<1.6	90	[3] ANASTASSOV	98	CLE2	$e^+e^- \to \Upsilon(4S)$

[1] Uses a simultaneous fit of all B semileptonic decays without full reconstruction of events. AUBERT 09Y reports $B(B^+ \to \overline{D}_2^*(2460)^0 \ell^+ \nu_\ell) \cdot B(\overline{D}_2^*(2460)^0 \to D^{(*)-} \pi^+) = (2.29 \pm 0.23 \pm 0.21) \times 10^{-3}$ and the authors have provided us the individual measurement.

[2] Uses a fully reconstructed B meson as a tag on the recoil side.

[3] Assumes equal production of B^+ and B^0 at the $\Upsilon(4S)$.

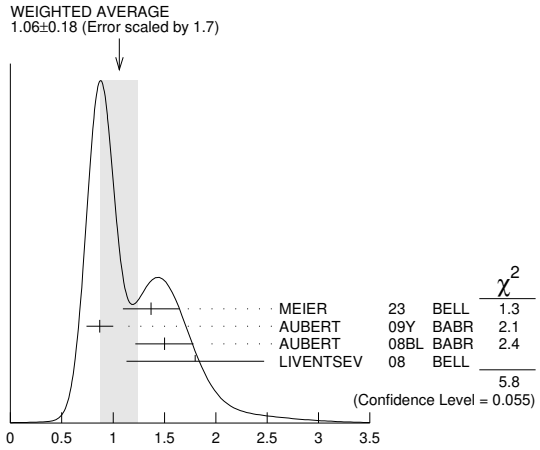

$[\Gamma(\overline{D}_1(2420)^0 \tau^+ \nu_\tau) + \Gamma(\overline{D}_2^*(2460)^0 \tau^+ \nu_\tau)] / [\Gamma(\overline{D}_1(2420)^0 D_s^{(*)+}) + \Gamma(\overline{D}_2^*(2460)^0 D_s^{(*)+})]$ — $(\Gamma_{22}+\Gamma_{23})/(\Gamma_{207}+\Gamma_{208})$

VALUE	DOCUMENT ID		TECN	COMMENT
0.19±0.04±0.02	[1] AAIJ	25E	LHCB	pp at 7, 8, 13 TeV

[1] Uses $\tau^+ \to \pi^+ \pi^- \pi^+ (\pi^0) \overline{\nu}_\tau$ with π^0 not reconstructed.

$\Gamma(\overline{D}^0 \pi^+ \pi^- \ell^+ \nu_\ell)/\Gamma_{total}$ — Γ_{24}/Γ

VALUE (units 10^{-3})	DOCUMENT ID		TECN	COMMENT
1.73±0.14±0.13	MEIER	23	BELL	$e^+e^- \to \Upsilon(4S)$

Int. J. Mod. Phys. A 2026.41. Downloaded from www.worldscientific.com
by UNIVERSITY OF CALIFORNIA @ BERKELEY on 09/16/26. Re-use and distribution is strictly not permitted, except for Open Access articles.

Int. J. Mod. Phys. A 2026.41. Downloaded from www.worldscientific.com by CALIFORNIA @ BERKELEY on 09/16/26. Re-use and distribution is strictly not permitted, except for Open Access articles.

$\Gamma(\overline{D}^0\pi^+\pi^-\ell^+\nu_\ell)/\Gamma(\overline{D}^0\ell^+\nu_\ell)$ — Γ_{24}/Γ_7

VALUE (units 10^{-2})	DOCUMENT ID		TECN	COMMENT
7.1±1.3±0.8	[1] LEES	16	BABR	$e^+e^- \to \Upsilon(4S)$

[1] Measurement used electrons and muons as leptons.

$\Gamma(\overline{D}_1(2420)^0\ell^+\nu_\ell, \overline{D}_1^0 \to \overline{D}^0\pi^+\pi^-)/\Gamma_{total}$ — Γ_{25}/Γ

VALUE (units 10^{-3})	DOCUMENT ID		TECN	COMMENT
1.05±0.11±0.08	MEIER	23	BELL	$e^+e^- \to \Upsilon(4S)$

$\Gamma(\overline{D}^{*0}\pi^+\pi^-\ell^+\nu_\ell)/\Gamma(\overline{D}^*(2007)^0\ell^+\nu_\ell)$ — Γ_{26}/Γ_{10}

VALUE (units 10^{-2})	DOCUMENT ID		TECN	COMMENT
1.4±0.7±0.4	[1] LEES	16	BABR	$e^+e^- \to \Upsilon(4S)$

[1] Measurement used electrons and muons as leptons.

$\Gamma(\overline{D}^{*0}\pi^+\pi^-\ell^+\nu_\ell)/\Gamma_{total}$ — Γ_{26}/Γ

VALUE (units 10^{-4})	DOCUMENT ID		TECN	COMMENT
7.0±1.5±0.8	MEIER	23	BELL	$e^+e^- \to \Upsilon(4S)$

$\Gamma(D_s^{(*)-}K^+\ell^+\nu_\ell)/\Gamma_{total}$ — Γ_{27}/Γ

VALUE (units 10^{-4})	DOCUMENT ID		TECN	COMMENT
6.1 ±1.0 OUR AVERAGE				
5.9 ±1.2 ±1.5	[1] STYPULA	12	BELL	$e^+e^- \to \Upsilon(4S)$
$6.13^{+1.04}_{-1.03}\pm0.67$	[1] DEL-AMO-SA...	11L	BABR	$e^+e^- \to \Upsilon(4S)$

[1] Assumes equal production of B^+ and B^0 at the $\Upsilon(4S)$.

$\Gamma(D_s^- K^+\ell^+\nu_\ell)/\Gamma_{total}$ — Γ_{28}/Γ

VALUE (units 10^{-4})	DOCUMENT ID		TECN	COMMENT
$\mathbf{3.0\pm0.9^{+1.1}_{-0.8}}$	[1] STYPULA	12	BELL	$e^+e^- \to \Upsilon(4S)$

[1] Assumes equal production of B^+ and B^0 at the $\Upsilon(4S)$.

$\Gamma(D_s^{*-} K^+\ell^+\nu_\ell)/\Gamma_{total}$ — Γ_{29}/Γ

VALUE (units 10^{-4})	DOCUMENT ID		TECN	COMMENT
$\mathbf{2.9\pm1.6^{+1.1}_{-1.0}}$	[1,2] STYPULA	12	BELL	$e^+e^- \to \Upsilon(4S)$

[1] Assumes equal production of B^+ and B^0 at the $\Upsilon(4S)$.
[2] STYPULA 12 provides also an upper limit of 0.56×10^{-3} at 90% CL for the same data. Also measures branching fraction of the combined modes of $D_s^- K^+\ell^+\nu_\ell$ and $D_s^{*-} K^+\ell^+\nu_\ell$ as $B(B^+ \to D_s^{(*)-} K^+\ell^+\nu_\ell) = (5.9\pm1.2\pm1.5)\times10^{-4}$.

$\Gamma(\pi^0\ell^+\nu_\ell)/\Gamma_{total}$ — Γ_{30}/Γ

VALUE (units 10^{-4})	DOCUMENT ID		TECN	COMMENT
0.780±0.027 OUR EVALUATION	(Produced by HFLAV)			
0.748±0.029 OUR AVERAGE				
0.80 ±0.08 ±0.04	[1] SIBIDANOV	13	BELL	$e^+e^- \to \Upsilon(4S)$
0.77 ±0.04 ±0.03	[2] LEES	12AA	BABR	$e^+e^- \to \Upsilon(4S)$
0.705±0.025±0.035	[3] DEL-AMO-SA...	11C	BABR	$e^+e^- \to \Upsilon(4S)$
0.82 ±0.09 ±0.05	[3] AUBERT	08AV	BABR	$e^+e^- \to \Upsilon(4S)$
0.77 ±0.14 ±0.08	[4] HOKUUE	07	BELL	$e^+e^- \to \Upsilon(4S)$
• • • We do not use the following data for averages, fits, limits, etc. • • •				
0.74 ±0.05 ±0.10	[5] AUBERT,B	05O	BABR	Repl. by DEL-AMO-SANCHEZ 11C

[1] The signal events are tagged by a second B meson reconstructed in the fully hadronic decays.
[2] Uses loose neutrino reconstruction technique. Assumes $B(\Upsilon(4S) \to B^+B^-) = (51.6\pm0.6)\%$ and $B(\Upsilon(4S) \to B^0\overline{B}^0) = (48.4\pm0.6)\%$.
[3] Using the isospin symmetry relation, B^+ and B^0 branching fractions are combined.
[4] The signal events are tagged by a second B meson reconstructed in the semileptonic mode $B \to D^{(*)}\ell\nu_\ell$.
[5] B^+ and B^0 decays combined assuming isospin symmetry. Systematic errors include both experimental and form-factor uncertainties.

$\Gamma(\pi^0 e^+\nu_e)/\Gamma_{total}$ — Γ_{31}/Γ

VALUE (units 10^{-4})	CL%	DOCUMENT ID		TECN	COMMENT
• • • We do not use the following data for averages, fits, limits, etc. • • •					
0.9±0.2±0.2		[1] ALEXANDER	96T	CLE2	$e^+e^- \to \Upsilon(4S)$
<22	90	ANTREASYAN	90B	CBAL	$e^+e^- \to \Upsilon(4S)$

[1] Derived based in the reported B^0 result by assuming isospin symmetry: $\Gamma(B^0 \to \pi^-\ell^+\nu) = 2\Gamma(B^+ \to \pi^0\ell^+\nu)$.

$\Gamma(\eta\ell^+\nu_\ell)/\Gamma_{total}$ — Γ_{32}/Γ

VALUE (units 10^{-4})	CL%	DOCUMENT ID		TECN	COMMENT
0.35 ±0.04 OUR AVERAGE					
0.283±0.055±0.034		[1] GEBAUER	22	BELL	$e^+e^- \to \Upsilon(4S)$
0.42 ±0.11 ±0.03		[2] BELENO	17	BELL	$e^+e^- \to \Upsilon(4S)$
0.38 ±0.05 ±0.05		[3] LEES	12AA	BABR	$e^+e^- \to \Upsilon(4S)$
0.31 ±0.06 ±0.08		[3] AUBERT	09Q	BABR	$e^+e^- \to \Upsilon(4S)$
0.64 ±0.20 ±0.03		[4] AUBERT	08AV	BABR	$e^+e^- \to \Upsilon(4S)$
• • • We do not use the following data for averages, fits, limits, etc. • • •					
0.36 ±0.05 ±0.04		[3] DEL-AMO-SA...	11F	BABR	Repl. by LEES 12AA
<1.01	90	[5] ADAM	07	CLE2	$e^+e^- \to \Upsilon(4S)$
0.84 ±0.31 ±0.18		[6] ATHAR	03	CLE2	Repl. by ADAM 07

[1] Assumes $B(\Upsilon(4S) \to B^+B^-) = (51.3\pm0.6)\%$.
[2] Uses missing-mass technique by fully reconstructing the hadronic decay chain of the accompanying B.
[3] Uses loose neutrino reconstruction technique. Assumes $B(\Upsilon(4S) \to B^+B^-) = (51.6\pm0.6)\%$ and $B(\Upsilon(4S) \to B^0\overline{B}^0) = (48.4\pm0.6)\%$.
[4] Assumes equal production of B^+ and B^0 at the $\Upsilon(4S)$.
[5] The B^0 and B^+ results are combined assuming the isospin, B lifetimes, and relative charged/neutral B production at the $\Upsilon(4S)$.
[6] ATHAR 03 reports systematic errors 0.16 ± 0.09, which are experimental systematic and systematic due to model dependence. We combine these in quadrature.

$\Gamma(\eta'\ell^+\nu_\ell)/\Gamma_{total}$ — Γ_{33}/Γ

VALUE (units 10^{-4})	CL%	DOCUMENT ID		TECN	COMMENT
0.24 ±0.07 OUR AVERAGE					
0.279±0.129±0.030		[1] GEBAUER	22	BELL	$e^+e^- \to \Upsilon(4S)$
0.24 ±0.08 ±0.03		[2] LEES	12AA	BABR	$e^+e^- \to \Upsilon(4S)$
$0.04 \pm0.22 ^{+0.05}_{-0.02}$		[3] AUBERT	08AV	BABR	$e^+e^- \to \Upsilon(4S)$
2.66 ±0.80 ±0.56		[4] ADAM	07	CLE2	$e^+e^- \to \Upsilon(4S)$
• • • We do not use the following data for averages, fits, limits, etc. • • •					
<0.72	90	[5] BELENO	17	BELL	$e^+e^- \to \Upsilon(4S)$
0.24 ±0.08 ±0.03		[2] DEL-AMO-SA...	11F	BABR	Repl. by LEES 12AA

[1] Assumes $B(\Upsilon(4S) \to B^+B^-) = (51.3\pm0.6)\%$.
[2] Uses loose neutrino reconstruction technique. Assumes $B(Y(4S) \to B^+B^-) = (51.6\pm0.6)\%$ and $B(Y(4S) \to B^0\overline{B}^0) = (48.4\pm0.6)\%$.
[3] Assumes equal production of B^+ and B^0 at the $\Upsilon(4S)$.
[4] The B^0 and B^+ results are combined assuming the isospin, B lifetimes, and relative charged/neutral B production at the $\Upsilon(4S)$. Corresponds to 90% CL interval $(1.20\text{–}4.46)\times10^{-4}$.
[5] Uses missing-mass technique by fully reconstructing the hadronic decay chain of the accompanying B.

$\Gamma(\omega\ell^+\nu_\ell)/\Gamma_{total}$ — Γ_{34}/Γ

$\ell = e$ or μ, not sum over e and μ modes.

VALUE (units 10^{-4})	CL%	DOCUMENT ID		TECN	COMMENT
1.19±0.09 OUR AVERAGE					
1.21±0.14±0.08		[1,2] LEES	13A	BABR	$e^+e^- \to \Upsilon(4S)$
1.35±0.21±0.11		[3] LEES	13T	BABR	$e^+e^- \to \Upsilon(4S)$
1.07±0.16±0.07		[4] SIBIDANOV	13	BELL	$e^+e^- \to \Upsilon(4S)$
1.19±0.16±0.09		[2,5] LEES	12AA	BABR	$e^+e^- \to \Upsilon(4S)$
1.3 ±0.4 ±0.4		[6] SCHWANDA	04	BELL	$e^+e^- \to \Upsilon(4S)$
• • • We do not use the following data for averages, fits, limits, etc. • • •					
1.14±0.16±0.08		[2] AUBERT	09Q	BABR	Repl. by LEES 13A
<2.1	90	[7] BEAN	93B	CLE2	$e^+e^- \to \Upsilon(4S)$

[1] LEES 13A reports $(1.21\pm0.14\pm0.08)\times10^{-4}$ from a measurement of $[\Gamma(B^+ \to \omega\ell^+\nu_\ell)/\Gamma_{total}] \times [B(\omega(782) \to \pi^+\pi^-\pi^0)]$ assuming $B(\omega(782) \to \pi^+\pi^-\pi^0) = (89.2\pm0.7)\times10^{-2}$.
[2] Uses $B(\Upsilon(4S) \to B^+B^-) = (51.6\pm0.6)\%$ and $B(\Upsilon(4S) \to B^0\overline{B}^0) = (48.4\pm0.6)\%$.
[3] Uses semileptonic tagging. Assumes $B(\omega \to \pi^+\pi^-\pi^0) = (89.2\pm0.7)\%$ and that the production ratio of B^+B^- to $B^0\overline{B}^0$ from $\Upsilon(4S)$ is 1.056 ± 0.028. The partial branching fractions in three bins of q^2 are also reported.
[4] The signal events are tagged by a second B meson reconstructed in the fully hadronic decays.
[5] Uses loose neutrino reconstruction technique.
[6] Assumes equal production of B^+ and B^0 at the $\Upsilon(4S)$.
[7] BEAN 93B limit set using ISGW Model. Using isospin and the quark model to combine $\Gamma(\rho^0\ell^+\nu_\ell)$ and $\Gamma(\rho^-\ell^+\nu_\ell)$ with this result, they obtain a limit $<(1.6\text{–}2.7)\times10^{-4}$ at 90% CL for $B^+ \to \omega\ell^+\nu_\ell$. The range corresponds to the ISGW, WSB, and KS models. An upper limit on $|V_{ub}/V_{cb}| < 0.8\text{–}0.13$ at 90% CL is derived as well.

$\Gamma(\omega\mu^+\nu_\mu)/\Gamma_{total}$ — Γ_{35}/Γ

VALUE	DOCUMENT ID		TECN
• • • We do not use the following data for averages, fits, limits, etc. • • •			
seen	[1] ALBRECHT	91C	ARG

[1] In ALBRECHT 91C, one event is fully reconstructed providing evidence for the $b \to u$ transition.

$\Gamma(\rho^0\ell^+\nu_\ell)/\Gamma_{total}$ — Γ_{36}/Γ

$\ell = e$ or μ, not sum over e and μ modes.

VALUE (units 10^{-4})	CL%	DOCUMENT ID		TECN	COMMENT
1.58 ±0.11 OUR EVALUATION	(Produced by HFLAV)				
1.46 ±0.18 OUR AVERAGE Error includes scale factor of 2.1. See the ideogram below.					
1.625±0.079±0.180		[1] ADACHI	25I	BELL	$e^+e^- \to \Upsilon(4S)$
1.83 ±0.10 ±0.10		[2] SIBIDANOV	13	BELL	$e^+e^- \to \Upsilon(4S)$
0.94 ±0.08 ±0.14		[3] DEL-AMO-SA...	11C	BABR	$e^+e^- \to \Upsilon(4S)$
1.33 ±0.23 ±0.18		[4] HOKUUE	07	BELL	$e^+e^- \to \Upsilon(4S)$
$1.34 \pm0.15 ^{+0.28}_{-0.32}$		[5] BEHRENS	00	CLE2	$e^+e^- \to \Upsilon(4S)$
• • • We do not use the following data for averages, fits, limits, etc. • • •					
1.16 ±0.11 ±0.30		[3] AUBERT,B	05O	BABR	Repl. by DEL-AMO-SANCHEZ 11C
$1.40 \pm0.21 ^{+0.32}_{-0.33}$		[5] BEHRENS	00	CLE2	$e^+e^- \to \Upsilon(4S)$
$1.2 \pm0.2 ^{+0.3}_{-0.4}$		[5] ALEXANDER	96T	CLE2	$e^+e^- \to \Upsilon(4S)$

Int. J. Mod. Phys. A 2026.41. Downloaded from www.worldscientific.com
by UNIVERSITY OF CALIFORNIA @ BERKELEY on 09/16/26. Re-use and distribution is strictly not permitted, except for Open Access articles.

<2.1	90	[6] BEAN	93B	CLE2	$e^+e^- \to \Upsilon(4S)$

[1] Uses $B(\Upsilon(4S) \to B^+B^-)/B(\Upsilon(4S) \to B^0\overline{B}^0) = 1.065 \pm 0.052$.
[2] The signal events are tagged by a second B meson reconstructed in the fully hadronic decays.
[3] B^+ and B^0 decays combined assuming isospin symmetry. Systematic errors include both experimental and form-factor uncertainties.
[4] The signal events are tagged by a second B meson reconstructed in the semileptonic mode $B \to D^{(*)}\ell\nu_\ell$.
[5] Derived based in the reported B^0 result by assuming isospin symmetry: $\Gamma(B^0 \to \rho^-\ell^+\nu) = 2\Gamma(B^+ \to \rho^0\ell^+\nu) \approx 2\Gamma(B^+ \to \omega\ell^+\nu)$.
[6] BEAN 93B limit set using ISGW Model. Using isospin and the quark model to combine $\Gamma(\omega^0\ell^+\nu_\ell)$ and $\Gamma(\rho^-\ell^+\nu_\ell)$ with this result, they obtain a limit $<(1.6\text{–}2.7)\times10^{-4}$ at 90% CL for $B^+ \to \rho^0\ell^+\nu_\ell$. The range corresponds to the ISGW, WSB, and KS models. An upper limit on $|V_{ub}/V_{cb}| < 0.8\text{–}0.13$ at 90% CL is derived as well.

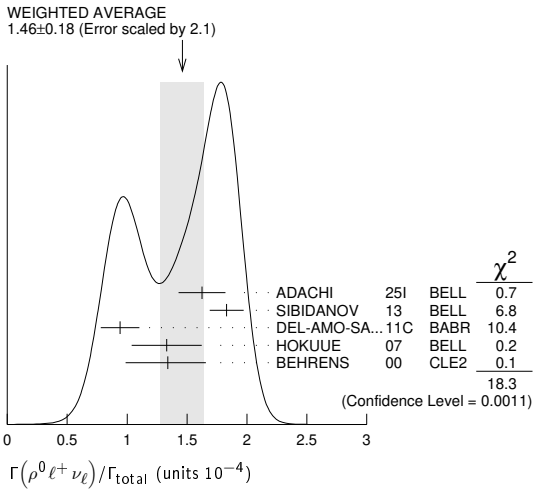

$\Gamma(\pi^+\pi^-\ell^+\nu_\ell)/\Gamma_{total}$ — Γ_{37}/Γ

VALUE (units 10^{-5})	DOCUMENT ID		TECN	COMMENT
$\mathbf{22.7^{+1.9}_{-1.6}\pm3.5}$	BELENO	21	BELL	$e^+e^- \to \Upsilon(4S)$

$\Gamma(p\overline{p}\ell^+\nu_\ell)/\Gamma_{total}$ — Γ_{38}/Γ

VALUE (units 10^{-6})	DOCUMENT ID		TECN	COMMENT
$\mathbf{5.8^{+2.4}_{-2.1}\pm0.9}$	[1] TIEN	14	BELL	$e^+e^- \to \Upsilon(4S)$

[1] Assumes equal production of B^+ and B^0 at the $\Upsilon(4S)$.

$\Gamma(p\overline{p}\mu^+\nu_\mu)/\Gamma_{total}$ — Γ_{39}/Γ

VALUE (units 10^{-6})	CL%	DOCUMENT ID		TECN	COMMENT
• • • We do not use the following data for averages, fits, limits, etc. • • •					
<8.5	90	[1] TIEN	14	BELL	$e^+e^- \to \Upsilon(4S)$

[1] Assumes equal production of B^+ and B^0 at the $\Upsilon(4S)$.

$\Gamma(p\overline{p}\mu^+\nu_\mu)/\Gamma(J/\psi(1S)K^+)$ — Γ_{39}/Γ_{316}

VALUE (units 10^{-3})	DOCUMENT ID		TECN	COMMENT
$\mathbf{5.22\pm0.31\pm0.03}$	[1] AAIJ	20K	LHCB	pp at 7, 8 and 13 TeV

[1] AAIJ 20K reports $[\Gamma(B^+ \to p\overline{p}\mu^+\nu_\mu)/\Gamma(B^+ \to J/\psi(1S)K^+)] / [B(J/\psi(1S) \to \mu^+\mu^-)] = (8.75 \pm 0.39 \pm 0.35)\times10^{-2}$ which we multiply by our best (shown rounded) value $B(J/\psi(1S) \to \mu^+\mu^-) = (5.961 \pm 0.033)\times10^{-2}$. Our first error is their experiment's error and our second error is the systematic error from using our best (shown rounded) value.

$\Gamma(p\overline{p}e^+\nu_e)/\Gamma_{total}$ — Γ_{40}/Γ

VALUE (units 10^{-6})	CL%	DOCUMENT ID		TECN	COMMENT
$\mathbf{8.2^{+3.7}_{-3.2}\pm0.6}$		[1] TIEN	14	BELL	$e^+e^- \to \Upsilon(4S)$
• • • We do not use the following data for averages, fits, limits, etc. • • •					
<5200	90	[2] ADAM	03B	CLE2	$e^+e^- \to \Upsilon(4S)$

[1] Assumes equal production of B^+ and B^0 at the $\Upsilon(4S)$.
[2] Based on phase-space model; if $V-A$ model is used, the 90% CL upper limit becomes $< 1.2\times10^{-3}$.

$\Gamma(e^+\nu_e)/\Gamma_{total}$ — Γ_{41}/Γ

VALUE (units 10^{-6})	CL%	DOCUMENT ID		TECN	COMMENT
< 0.98	90	[1] SATOYAMA	07	BELL	$e^+e^- \to \Upsilon(4S)$
• • • We do not use the following data for averages, fits, limits, etc. • • •					
< 3.5	90	[2] YOOK	15	BELL	$e^+e^- \to \Upsilon(4S)$
< 8	90	[1] AUBERT	10E	BABR	$e^+e^- \to \Upsilon(4S)$
< 1.9	90	[1] AUBERT	09V	BABR	$e^+e^- \to \Upsilon(4S)$
< 5.2	90	[1] AUBERT	08AD	BABR	$e^+e^- \to \Upsilon(4S)$
<15	90	ARTUSO	95	CLE2	$e^+e^- \to \Upsilon(4S)$

[1] Assumes equal production of B^+ and B^0 at the $\Upsilon(4S)$.
[2] Assumes $B(\Upsilon(4S) \to B^+B^-) = 0.513 \pm 0.006$.

$\Gamma(\mu^+\nu_\mu)/\Gamma_{total}$ — Γ_{42}/Γ

VALUE (units 10^{-6})	CL%	DOCUMENT ID		TECN	COMMENT
< 0.86	90	[1] PRIM	20	BELL	$e^+e^- \to \Upsilon(4S)$
• • • We do not use the following data for averages, fits, limits, etc. • • •					
0.29 to 1.07	90	[2] SIBIDANOV	18	BELL	$e^+e^- \to \Upsilon(4S)$
< 2.7	90	[3] YOOK	15	BELL	$e^+e^- \to \Upsilon(4S)$
<11	90	[4] AUBERT	10E	BABR	$e^+e^- \to \Upsilon(4S)$
< 1.0	90	[4] AUBERT	09V	BABR	$e^+e^- \to \Upsilon(4S)$
< 5.6	90	[4] AUBERT	08AD	BABR	$e^+e^- \to \Upsilon(4S)$
< 1.7	90	[4,5] SATOYAMA	07	BELL	$e^+e^- \to \Upsilon(4S)$
< 6.6	90	AUBERT	04O	BABR	Repl. by AUBERT 09V
<21	90	ARTUSO	95	CLE2	$e^+e^- \to \Upsilon(4S)$

[1] This is a 90% C.L. upper limit in the frequentist approach. The corresponding upper limit in the Bayesian approach is $< 8.9\times10^{-7}$. A 2.8 standard deviation signal above the background is found, with a measured branching fraction $(5.3 \pm 2.0 \pm 0.9)\times10^{-7}$.
[2] This is a 90% confidence interval in the frequentist approach. A 2.4 standard deviation signal above the background is found, with a measured branching fraction $(6.46 \pm 2.22 \pm 1.60)\times10^{-7}$.
[3] Assumes $B(\Upsilon(4S) \to B^+B^-) = 0.513 \pm 0.006$.
[4] Assumes equal production of B^+ and B^0 at the $\Upsilon(4S)$.
[5] Superseded by SIBIDANOV 18.

$\Gamma(\tau^+\nu_\tau)/\Gamma_{total}$ — Γ_{43}/Γ

See the note on "Decay Constants of Charged Pseudoscalar Mesons" in the D_s^+ Listings.

VALUE (units 10^{-4})	CL%	DOCUMENT ID		TECN	COMMENT
1.12±0.19 OUR AVERAGE					
$1.24\pm0.41\pm0.19$		[1] ADACHI	25X	BEL2	$e^+e^- \to \Upsilon(4S)$
$1.25\pm0.28\pm0.27$		[2,3] KRONENBIT...	15	BELL	$e^+e^- \to \Upsilon(4S)$
$0.72^{+0.27}_{-0.25}\pm0.11$		[4] HARA	13	BELL	$e^+e^- \to \Upsilon(4S)$
$1.83^{+0.53}_{-0.49}\pm0.24$		[3,5] LEES	13K	BABR	$e^+e^- \to \Upsilon(4S)$
$1.7\ \pm0.8\ \pm0.2$		[3,6] AUBERT	10E	BABR	$e^+e^- \to \Upsilon(4S)$
• • • We do not use the following data for averages, fits, limits, etc. • • •					
$1.54^{+0.38+0.29}_{-0.37-0.31}$		[3,7] HARA	10	BELL	Repl. by KRONENBIT-TER 15
$1.8\ ^{+0.9}_{-0.8}\ \pm0.45$		[3,8] AUBERT	08D	BABR	Repl. by LEES 13K
$0.9\ \pm0.6\ \pm0.1$		[3,6] AUBERT	07AL	BABR	Repl. by AUBERT 10E
< 2.6	90	[3] AUBERT	06K	BABR	$e^+e^- \to \Upsilon(4S)$
$1.79^{+0.56+0.46}_{-0.49-0.51}$		[3,8] IKADO	06	BELL	Repl. by HARA 13
< 4.2	90	[3] AUBERT,B	05B	BABR	Repl. by AUBERT 06K
< 8.3	90	[9] BARATE	01E	ALEP	$e^+e^- \to Z$
< 8.4	90	[3] BROWDER	01	CLE2	$e^+e^- \to \Upsilon(4S)$
< 5.7	90	[10] ACCIARRI	97F	L3	$e^+e^- \to Z$
<104	90	[11] ALBRECHT	95D	ARG	$e^+e^- \to \Upsilon(4S)$
< 22	90	ARTUSO	95	CLE2	$e^+e^- \to \Upsilon(4S)$
< 18	90	[12] BUSKULIC	95	ALEP	$e^+e^- \to Z$

[1] ADACHI 25X evidence for the $B^+ \to \tau^+\nu_\tau$ decay is found at 3.0 standard deviations, including systematic uncertainties. The accompanying B^- mesons are fully reconstructed in exclusive hadronic decays, while the signal in the recoil side is identified in $\tau \to \rho^+\overline{\nu}_\tau$ with a single charged particle plus a neutral particle final state.
[2] Requires one reconstructed semileptonic B decay $B^- \to D^{(*)0}\ell^-\overline{\nu}_\ell$ in the recoil.
[3] Assumes equal production of B^+ and B^0 at the $\Upsilon(4S)$.
[4] The authors combine their result with that from HARA 10 obtaining $B(B^- \to \tau^-\overline{\nu}_\tau) = (0.96 \pm 0.26)\times10^{-4}$ and deriving $f_B\ |V_{ub}| = (7.4 \pm 0.8 \pm 0.5)\times10^{-4}$ GeV.
[5] Requires a fully reconstructed hadronic B-decay in the recoil. Reports that this result combined with AUBERT 10E value gives $B(B^- \to \tau^-\overline{\nu}_\tau) = (1.79 \pm 0.48)\times10^{-4}$.
[6] Requires one reconstructed semileptonic B decay $B^- \to D^0\ell^-\overline{\nu}_\ell X$ in the recoil.
[7] Requires one reconstructed semileptonic B decay $B^- \to D^{(*)0}\ell^-\overline{\nu}_\ell X$ in the recoil.
[8] The analysis is based on a sample of events with one fully reconstructed tag B in a hadronic decay mode $B^- \to D^{(*)0}X^-$.
[9] The energy-flow and b-tagging algorithms were used.
[10] ACCIARRI 97F uses missing-energy technique and $f(b \to B^-) = (38.2 \pm 2.5)\%$.
[11] ALBRECHT 95D uses full reconstruction of one B decay as tag.
[12] BUSKULIC 95 uses same missing-energy technique as in $\overline{b} \to \tau^+\nu_\tau X$, but analysis is restricted to endpoint region of missing-energy distribution.

$\Gamma(\ell^+\nu_\ell\gamma)/\Gamma_{total}$ — Γ_{44}/Γ

VALUE	CL%	DOCUMENT ID		TECN	COMMENT
$\mathbf{< 3.0\times10^{-6}}$	90	[1,2] GELB	18	BELL	$e^+e^- \to \Upsilon(4S)$
• • • We do not use the following data for averages, fits, limits, etc. • • •					
$< 3.5\times10^{-6}$	90	[2,3] HELLER	15	BELL	$e^+e^- \to \Upsilon(4S)$
$<15.6\times10^{-6}$	90	[2] AUBERT	09AT	BABR	$e^+e^- \to \Upsilon(4S)$

[1] Supersedes HELLER 15.
[2] Assumes equal production of B^+ and B^0 at the $\Upsilon(4S)$.
[3] Superseded by GELB 18.

Int. J. Mod. Phys. A 2026.41. Downloaded from www.worldscientific.com by [redacted] LIFORNIA @ BERKELEY on 09/16/26. Re-use and distribution is strictly not permitted, except for Open Access articles.

$\Gamma(e^+\nu_e\gamma)/\Gamma_{total}$ — Γ_{45}/Γ

VALUE	CL%	DOCUMENT ID		TECN	COMMENT
< 4.3 × 10⁻⁶	90	[1,2] GELB	18	BELL	$e^+e^- \to \Upsilon(4S)$
• • • We do not use the following data for averages, fits, limits, etc. • • •					
< 6.1 × 10⁻⁶	90	[2,3] HELLER	15	BELL	$e^+e^- \to \Upsilon(4S)$
< 17 × 10⁻⁶	90	[2] AUBERT	09AT	BABR	$e^+e^- \to \Upsilon(4S)$
<200 × 10⁻⁶	90	[4] BROWDER	97	CLE2	$e^+e^- \to \Upsilon(4S)$

[1] Supersedes HELLER 15.
[2] Assumes equal production of B^+ and B^0 at the $\Upsilon(4S)$.
[3] Superseded by GELB 18.
[4] BROWDER 97 uses the hermiticity of the CLEO II detector to reconstruct the neutrino energy and momentum.

$\Gamma(\mu^+\nu_\mu\gamma)/\Gamma_{total}$ — Γ_{46}/Γ

VALUE	CL%	DOCUMENT ID		TECN	COMMENT
< 3.4 × 10⁻⁶	90	[1,2] GELB	18	BELL	$e^+e^- \to \Upsilon(4S)$
• • • We do not use the following data for averages, fits, limits, etc. • • •					
< 3.4 × 10⁻⁶	90	[2,3] HELLER	15	BELL	$e^+e^- \to \Upsilon(4S)$
<24 × 10⁻⁶	90	[2,4] AUBERT	09AT	BABR	$e^+e^- \to \Upsilon(4S)$
<52 × 10⁻⁶	90	[5] BROWDER	97	CLE2	$e^+e^- \to \Upsilon(4S)$

[1] Supersedes HELLER 15.
[2] Assumes equal production of B^+ and B^0 at the $\Upsilon(4S)$.
[3] Superseded by GELB 18.
[4] Note that the value given by AUBERT 09AT is 24×10^{-6} in the paper abstract, and 26×10^{-6} in the paper itself (Table I).
[5] BROWDER 97 uses the hermiticity of the CLEO II detector to reconstruct the neutrino energy and momentum.

$\Gamma(\mu^+\mu^-\mu^+\nu_\mu)/\Gamma_{total}$ — Γ_{47}/Γ

VALUE	CL%	DOCUMENT ID		TECN	COMMENT
<1.6 × 10⁻⁸	95	[1] AAIJ	19P	LHCB	pp at 7, 8, 13 TeV

[1] AAIJ 19P limit established for the kinematic region where the lower of the two $M(\mu^+\mu^-)$ is less than 980 MeV/c^2.

$\Gamma(D^0X)/\Gamma_{total}$ — Γ_{48}/Γ

VALUE	DOCUMENT ID		TECN	COMMENT
0.086±0.006±0.004	[1] AUBERT	07N	BABR	$e^+e^- \to \Upsilon(4S)$
• • • We do not use the following data for averages, fits, limits, etc. • • •				
0.098±0.009±0.006	[1] AUBERT,BE	04B	BABR	Repl. by AUBERT 07N

[1] Events are selected by completely reconstructing one B and searching for a reconstructed charmed particle in the rest of the event. The last error includes systematic and charm branching ratio uncertainties.

$\Gamma(\overline{D}^0X)/\Gamma_{total}$ — Γ_{49}/Γ

VALUE	DOCUMENT ID		TECN	COMMENT
0.786±0.016$^{+0.034}_{-0.033}$	[1] AUBERT	07N	BABR	$e^+e^- \to \Upsilon(4S)$
• • • We do not use the following data for averages, fits, limits, etc. • • •				
0.793±0.025$^{+0.045}_{-0.044}$	[1] AUBERT,BE	04B	BABR	Repl. by AUBERT 07N

[1] Events are selected by completely reconstructing one B and searching for a reconstructed charmed particle in the rest of the event. The last error includes systematic and charm branching ratio uncertainties.

$\Gamma(D^0X)/[\Gamma(D^0X)+\Gamma(\overline{D}^0X)]$ — $\Gamma_{48}/(\Gamma_{48}+\Gamma_{49})$

VALUE	DOCUMENT ID		TECN	COMMENT
0.098±0.007±0.001	AUBERT	07N	BABR	$e^+e^- \to \Upsilon(4S)$
• • • We do not use the following data for averages, fits, limits, etc. • • •				
0.110±0.010±0.003	AUBERT,BE	04B	BABR	Repl. by AUBERT 07N

$\Gamma(D^+X)/\Gamma_{total}$ — Γ_{50}/Γ

VALUE	DOCUMENT ID		TECN	COMMENT
0.025±0.005±0.002	[1] AUBERT	07N	BABR	$e^+e^- \to \Upsilon(4S)$
• • • We do not use the following data for averages, fits, limits, etc. • • •				
0.038±0.009±0.005	[1] AUBERT,BE	04B	BABR	Repl. by AUBERT 07N

[1] Events are selected by completely reconstructing one B and searching for a reconstructed charmed particle in the rest of the event. The last error includes systematic and charm branching ratio uncertainties.

$\Gamma(D^-X)/\Gamma_{total}$ — Γ_{51}/Γ

VALUE	DOCUMENT ID		TECN	COMMENT
0.099±0.008±0.009	[1] AUBERT	07N	BABR	$e^+e^- \to \Upsilon(4S)$
• • • We do not use the following data for averages, fits, limits, etc. • • •				
0.098±0.012±0.014	[1] AUBERT,BE	04B	BABR	Repl. by AUBERT 07N

[1] Events are selected by completely reconstructing one B and searching for a reconstructed charmed particle in the rest of the event. The last error includes systematic and charm branching ratio uncertainties.

$\Gamma(D^+X)/[\Gamma(D^+X)+\Gamma(D^-X)]$ — $\Gamma_{50}/(\Gamma_{50}+\Gamma_{51})$

VALUE	DOCUMENT ID		TECN	COMMENT
0.204±0.035±0.001	AUBERT	07N	BABR	$e^+e^- \to \Upsilon(4S)$
• • • We do not use the following data for averages, fits, limits, etc. • • •				
0.278±0.052±0.009	AUBERT,BE	04B	BABR	Repl. by AUBERT 07N

$\Gamma(D_s^+X)/\Gamma_{total}$ — Γ_{52}/Γ

VALUE	DOCUMENT ID		TECN	COMMENT
0.079±0.006$^{+0.013}_{-0.011}$	[1] AUBERT	07N	BABR	$e^+e^- \to \Upsilon(4S)$
• • • We do not use the following data for averages, fits, limits, etc. • • •				
0.143±0.016$^{+0.051}_{-0.034}$	[1] AUBERT,BE	04B	BABR	Repl. by AUBERT 07N

[1] Events are selected by completely reconstructing one B and searching for a reconstructed charmed particle in the rest of the event. The last error includes systematic and charm branching ratio uncertainties.

$\Gamma(D_s^-X)/\Gamma_{total}$ — Γ_{53}/Γ

VALUE	CL%	DOCUMENT ID		TECN	COMMENT
0.011$^{+0.004+0.002}_{-0.003-0.001}$		[1] AUBERT	07N	BABR	$e^+e^- \to \Upsilon(4S)$
• • • We do not use the following data for averages, fits, limits, etc. • • •					
<0.022	90	[1] AUBERT,BE	04B	BABR	Repl. by AUBERT 07N

[1] Events are selected by completely reconstructing one B and searching for a reconstructed charmed particle in the rest of the event. The last error includes systematic and charm branching ratio uncertainties.

$\Gamma(D_s^+X)/[\Gamma(D_s^+X)+\Gamma(D_s^-X)]$ — $\Gamma_{52}/(\Gamma_{52}+\Gamma_{53})$

VALUE	DOCUMENT ID		TECN	COMMENT
0.884±0.038±0.002	AUBERT	07N	BABR	$e^+e^- \to \Upsilon(4S)$
• • • We do not use the following data for averages, fits, limits, etc. • • •				
0.966±0.039±0.012	AUBERT,BE	04B	BABR	Repl. by AUBERT 07N

$\Gamma(D_s^-X)/[\Gamma(D_s^+X)+\Gamma(D_s^-X)]$ — $\Gamma_{53}/(\Gamma_{52}+\Gamma_{53})$

VALUE	CL%	DOCUMENT ID		TECN	COMMENT
<0.126	90	AUBERT,BE	04B	BABR	$e^+e^- \to \Upsilon(4S)$

$\Gamma(\Lambda_c^+X)/\Gamma_{total}$ — Γ_{54}/Γ

VALUE	DOCUMENT ID		TECN	COMMENT
0.021±0.005$^{+0.008}_{-0.004}$	[1] AUBERT	07N	BABR	$e^+e^- \to \Upsilon(4S)$
• • • We do not use the following data for averages, fits, limits, etc. • • •				
0.029±0.008$^{+0.011}_{-0.007}$	[1] AUBERT,BE	04B	BABR	Repl. by AUBERT 07N

[1] Events are selected by completely reconstructing one B and searching for a reconstructed charmed particle in the rest of the event. The last error includes systematic and charm branching ratio uncertainties.

$\Gamma(\overline{\Lambda}_c^-X)/\Gamma_{total}$ — Γ_{55}/Γ

VALUE	DOCUMENT ID		TECN	COMMENT
0.028±0.005$^{+0.010}_{-0.007}$	[1] AUBERT	07N	BABR	$e^+e^- \to \Upsilon(4S)$
• • • We do not use the following data for averages, fits, limits, etc. • • •				
0.035±0.008$^{+0.013}_{-0.009}$	[1] AUBERT,BE	04B	BABR	Repl. by AUBERT 07N

[1] Events are selected by completely reconstructing one B and searching for a reconstructed charmed particle in the rest of the event. The last error includes systematic and charm branching ratio uncertainties.

$\Gamma(\Lambda_c^+X)/[\Gamma(\Lambda_c^+X)+\Gamma(\overline{\Lambda}_c^-X)]$ — $\Gamma_{54}/(\Gamma_{54}+\Gamma_{55})$

VALUE	DOCUMENT ID		TECN	COMMENT
0.427±0.071±0.001	AUBERT	07N	BABR	$e^+e^- \to \Upsilon(4S)$
• • • We do not use the following data for averages, fits, limits, etc. • • •				
0.452±0.090±0.003	AUBERT,BE	04B	BABR	Repl. by AUBERT 07N

$\Gamma(\overline{c}X)/\Gamma_{total}$ — Γ_{56}/Γ

VALUE	DOCUMENT ID		TECN	COMMENT
0.968±0.019$^{+0.041}_{-0.039}$	[1] AUBERT	07N	BABR	$e^+e^- \to \Upsilon(4S)$
• • • We do not use the following data for averages, fits, limits, etc. • • •				
0.983±0.030$^{+0.054}_{-0.051}$	[1] AUBERT,BE	04B	BABR	Repl. by AUBERT 07N

[1] Events are selected by completely reconstructing one B and searching for a reconstructed charmed particle in the rest of the event. The last error includes systematic and charm branching ratio uncertainties.

$\Gamma(cX)/\Gamma_{total}$ — Γ_{57}/Γ

VALUE	DOCUMENT ID		TECN	COMMENT
0.234±0.012$^{+0.018}_{-0.014}$	[1] AUBERT	07N	BABR	$e^+e^- \to \Upsilon(4S)$
• • • We do not use the following data for averages, fits, limits, etc. • • •				
0.330±0.022$^{+0.055}_{-0.037}$	[1] AUBERT,BE	04B	BABR	Repl. by AUBERT 07N

[1] Events are selected by completely reconstructing one B and searching for a reconstructed charmed particle in the rest of the event. The last error includes systematic and charm branching ratio uncertainties.

$\Gamma(c/\overline{c}X)/\Gamma_{total}$ — Γ_{58}/Γ

VALUE	DOCUMENT ID		TECN	COMMENT
1.202±0.023$^{+0.053}_{-0.049}$	[1] AUBERT	07N	BABR	$e^+e^- \to \Upsilon(4S)$
• • • We do not use the following data for averages, fits, limits, etc. • • •				
1.313±0.037$^{+0.088}_{-0.075}$	[1] AUBERT,BE	04B	BABR	Repl. by AUBERT 07N

[1] Events are selected by completely reconstructing one B and searching for a reconstructed charmed particle in the rest of the event. The last error includes systematic and charm branching ratio uncertainties.

Int. J. Mod. Phys. A 2026.41. Downloaded from www.worldscientific.com
by UNIVERSITY OF CALIFORNIA @ BERKELEY on 09/16/26. Re-use and distribution is strictly not permitted, except for Open Access articles.

$\Gamma(\overline{D}^0\pi^+)/\Gamma_{total}$ — Γ_{59}/Γ

VALUE (units 10^{-3})	EVTS	DOCUMENT ID		TECN	COMMENT
4.61±0.10 OUR FIT					
4.63±0.10 OUR AVERAGE					
4.53±0.02±0.15		BLOOMFIELD	22	BELL	$e^+e^- \to \Upsilon(4S)$
4.34±0.10±0.23		[1] KATO	18	BELL	$e^+e^- \to \Upsilon(4S)$
4.90±0.07±0.22		[2] AUBERT	07H	BABR	$e^+e^- \to \Upsilon(4S)$
4.9 ±0.6 ±0.2		[3] ABULENCIA	06J	CDF	$p\overline{p}$ at 1.96 TeV
4.49±0.21±0.23		[4] AUBERT,BE	06J	BABR	$e^+e^- \to \Upsilon(4S)$
4.97±0.12±0.29		[2,5] AHMED	02B	CLE2	$e^+e^- \to \Upsilon(4S)$
5.0 ±0.7 ±0.6	54	[6] BORTOLETTO	92	CLEO	$e^+e^- \to \Upsilon(4S)$
5.4 $^{+1.8}_{-1.5}$ $^{+1.2}_{-0.9}$	14	[7] BEBEK	87	CLEO	$e^+e^- \to \Upsilon(4S)$
• • • We do not use the following data for averages, fits, limits, etc. • • •					
4.69±0.26±0.04		[8] AUBERT,B	04P	BABR	Repl. by AUBERT 07H
5.5 ±0.4 ±0.5	304	[9] ALAM	94	CLE2	Repl. by AHMED 02B
2.0 ±0.8 ±0.6	12	[6] ALBRECHT	90J	ARG	$e^+e^- \to \Upsilon(4S)$
1.9 ±1.0 ±0.6	7	[10] ALBRECHT	88K	ARG	$e^+e^- \to \Upsilon(4S)$

[1] Measures absolute branching fractions using a missing-mass technique.
[2] Assumes equal production of B^+ and B^0 at the $\Upsilon(4S)$.
[3] ABULENCIA 06J reports $[\Gamma(B^+ \to \overline{D}^0\pi^+)/\Gamma_{total}]$ / $[B(B^0 \to D^-\pi^+)] = 1.97 \pm 0.10 \pm 0.21$ which we multiply by our best (shown rounded) value $B(B^0 \to D^-\pi^+) = (2.51 \pm 0.08) \times 10^{-3}$. Our first error is their experiment's error and our second error is the systematic error from using our best (shown rounded) value.
[4] Uses a missing-mass method. Does not depend on D branching fractions or B^+/B^0 production rates.
[5] AHMED 02B reports an additional uncertainty on the branching ratios to account for 4.5% uncertainty on relative production of B^0 and B^+, which is not included here.
[6] Assumes equal production of B^+ and B^0 at the $\Upsilon(4S)$ and uses the Mark III branching fractions for the D.
[7] BEBEK 87 value has been updated in BERKELMAN 91 to use same assumptions as noted for BORTOLETTO 92.
[8] AUBERT,B 04P reports $[\Gamma(B^+ \to \overline{D}^0\pi^+)/\Gamma_{total}] \times [B(D^0 \to K^-\pi^+)] = (1.846 \pm 0.032 \pm 0.097) \times 10^{-4}$ which we divide by our best (shown rounded) value $B(D^0 \to K^-\pi^+) = (3.936 \pm 0.030) \times 10^{-2}$. Our first error is their experiment's error and our second error is the systematic error from using our best (shown rounded) value.
[9] ALAM 94 assume equal production of B^+ and B^0 at the $\Upsilon(4S)$ and use the CLEO II absolute $B(D^0 \to K^-\pi^+)$ and the PDG 1992 $B(D^0 \to K^-\pi^+\pi^0)/B(D^0 \to K^-\pi^+)$ and $B(D^0 \to K^-2\pi^+\pi^-)/B(D^0 \to K^-\pi^+)$.
[10] ALBRECHT 88K assumes $B^0\overline{B}^0$:B^+B^- ratio is 45:55. Superseded by ALBRECHT 90J.

$\Gamma(\overline{D}^0\rho^+)/\Gamma_{total}$ — Γ_{62}/Γ

VALUE (units 10^{-2})	EVTS	DOCUMENT ID		TECN	COMMENT
0.97 ±0.11 OUR AVERAGE		Error includes scale factor of 2.1.			
0.939±0.021±0.050		[1] ADACHI	24D	BELL	$e^+e^- \to \Upsilon(4S)$
1.35 ±0.12 ±0.15	212	[2] ALAM	94	CLE2	$e^+e^- \to \Upsilon(4S)$
1.3 ±0.4 ±0.4	19	[3] ALBRECHT	90J	ARG	$e^+e^- \to \Upsilon(4S)$
• • • We do not use the following data for averages, fits, limits, etc. • • •					
2.1 ±0.8 ±0.9	10	[4] ALBRECHT	88K	ARG	$e^+e^- \to \Upsilon(4S)$

[1] ADACHI 24D uses $B(\Upsilon(4S) \to B^+B^-) = 0.516 \pm 0.012$.
[2] ALAM 94 assume equal production of B^+ and B^0 at the $\Upsilon(4S)$ and use the CLEO II absolute $B(D^0 \to K^-\pi^+)$ and the PDG 1992 $B(D^0 \to K^-\pi^+\pi^0)/B(D^0 \to K^-\pi^+)$ and $B(D^0 \to K^-2\pi^+\pi^-)/B(D^0 \to K^-\pi^+)$.
[3] Assumes equal production of B^+ and B^0 at the $\Upsilon(4S)$ and uses the Mark III branching fractions for the D.
[4] ALBRECHT 88K assumes $B^0\overline{B}^0$:B^+B^- ratio is 45:55.

$\Gamma(\overline{D}^0K^+)/\Gamma(\overline{D}^0\pi^+)$ — Γ_{63}/Γ_{59}

VALUE (units 10^{-2})	DOCUMENT ID		TECN	COMMENT
7.89 ±0.27 OUR AVERAGE	Error includes scale factor of 2.3. See the ideogram below.			
7.96 ±0.03 ±0.13	AAIJ	21Q	LHCB	pp at 7, 8, 13 TeV
6.77 ±0.23 ±0.30	HORII	08	BELL	$e^+e^- \to \Upsilon(4S)$
8.31 ±0.35 ±0.20	AUBERT	04N	BABR	$e^+e^- \to \Upsilon(4S)$
9.9 $^{+1.4}_{-1.2}$ $^{+0.7}_{-0.6}$	BORNHEIM	03	CLE2	$e^+e^- \to \Upsilon(4S)$
• • • We do not use the following data for averages, fits, limits, etc. • • •				
7.768±0.038±0.066	[1,2] AAIJ	18A	LHCB	pp at 7, 8, 13 TeV
7.79 ±0.06 ±0.19	AAIJ	16L	LHCB	pp at 7, 8 TeV
7.93 ±0.10 ±0.18	[3] AAIJ	16L	LHCB	pp at 7, 8 TeV
7.71 ±0.17 ±0.26	[3] AAIJ	13AE	LHCB	Repl. by AAIJ 16L
7.74 ±0.12 ±0.19	AAIJ	12M	LHCB	Repl. by AAIJ 16L
9.4 ±0.9 ±0.7	ABE	03D	BELL	Repl. by SWAIN 03
7.7 ±0.5 ±0.6	SWAIN	03	BELL	Repl. by HORII 08
7.9 ±0.9 ±0.6	ABE	01I	BELL	Repl. by ABE 03D
5.5 ±1.4 ±0.5	ATHANAS	98	CLE2	Repl. by BORNHEIM 03

[1] Supersedes AAIJ 16L.
[2] Superseded by AAIJ 21Q.
[3] Uses $B^{\pm} \to [K^{\pm}\pi^{\mp}\pi^+\pi^-]_D h^{\pm}$ mode.

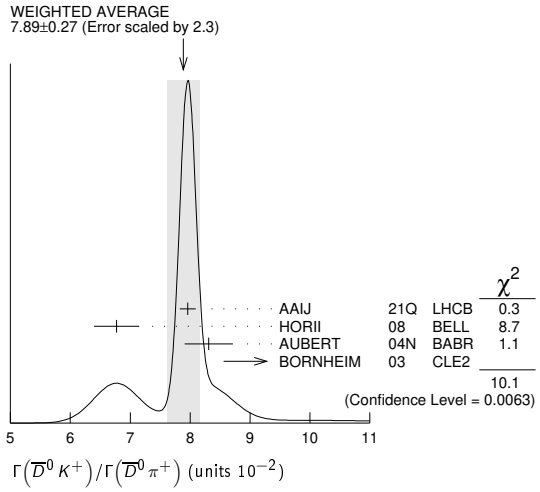

$\Gamma(D_{CP(+1)}K^+)/\Gamma(D_{CP(+1)}\pi^+)$ — Γ_{64}/Γ_{60}

VALUE	DOCUMENT ID		TECN	COMMENT
0.089±0.008 OUR AVERAGE				
0.089±0.008±0.003	[1,2] ABE	06	BELL	$e^+e^- \to \Upsilon(4S)$
0.088±0.016±0.005	[3] AUBERT	04N	BABR	$e^+e^- \to \Upsilon(4S)$
• • • We do not use the following data for averages, fits, limits, etc. • • •				
0.125±0.036±0.010	[3] ABE	03D	BELL	Repl. by SWAIN 03
0.093±0.018±0.008	[3] SWAIN	03	BELL	Repl. by ABE 06

[1] Reports a double ratio of $B(B^+ \to D_{CP(+1)}K^+)/B(B^+ \to D_{CP(+1)}\pi^+)$ and $B(B^+ \to \overline{D}^0K^+)/B(B^+ \to \overline{D}^0\pi^+)$, $1.13 \pm 0.16 \pm 0.08$. We multiply by our best value of $B(B^+ \to \overline{D}^0K^+)/B(B^+ \to \overline{D}^0\pi^+) = 0.083 \pm 0.006$. Our first error is their experiment's error and the second error is systematic error from using our best value.
[2] ABE 06 reports $[\Gamma(B^+ \to D_{CP(+1)}K^+)/\Gamma(B^+ \to D_{CP(+1)}\pi^+)]$ / $[\Gamma(B^+ \to \overline{D}^0K^+)/\Gamma(B^+ \to \overline{D}^0\pi^+)] = 1.13 \pm 0.06 \pm 0.08$ which we multiply by our best (shown rounded) value $\Gamma(B^+ \to \overline{D}^0K^+)/\Gamma(B^+ \to \overline{D}^0\pi^+) = 0.0789 \pm 0.0027$. Our first error is their experiment's error and our second error is the systematic error from using our best (shown rounded) value.
[3] $CP=+1$ eigenstate of $D^0\overline{D}^0$ system is reconstructed via K^+K^- and $\pi^+\pi^-$.

$\Gamma(D_{CP(+1)}K^+)/\Gamma(\overline{D}^0K^+)$ — Γ_{64}/Γ_{63}

VALUE	DOCUMENT ID		TECN	COMMENT
0.497±0.009 OUR AVERAGE	Error includes scale factor of 1.4. See the ideogram below.			
0.582±0.041±0.018	[1] ADACHI	24I	BELL	$e^+e^- \to \Upsilon(4S)$
0.494±0.008±0.006	[2] AAIJ	18A	LHCB	pp at 7, 8, 13 TeV
0.496±0.014±0.008	[3] AAIJ	18A	LHCB	pp at 7, 8, 13 TeV
0.489±0.010±0.009	[4] AAIJ	16L	LHCB	pp at 7, 8 TeV
0.65 ±0.12 ±0.06	[5] AALTONEN	10A	CDF	$p\overline{p}$ at 1.96 TeV
0.590±0.045±0.025	[6] DEL-AMO-SA...	10G	BABR	$e^+e^- \to \Upsilon(4S)$
• • • We do not use the following data for averages, fits, limits, etc. • • •				
0.504±0.019±0.006	[7] AAIJ	12M	LHCB	Repl. by AAIJ 16L
0.53 ±0.05 ±0.025	AUBERT	08AA	BABR	Repl. by DEL-AMO-SANCHEZ 10G
0.45 ±0.06 ±0.02	AUBERT	06J	BABR	Repl. by AUBERT 08AA

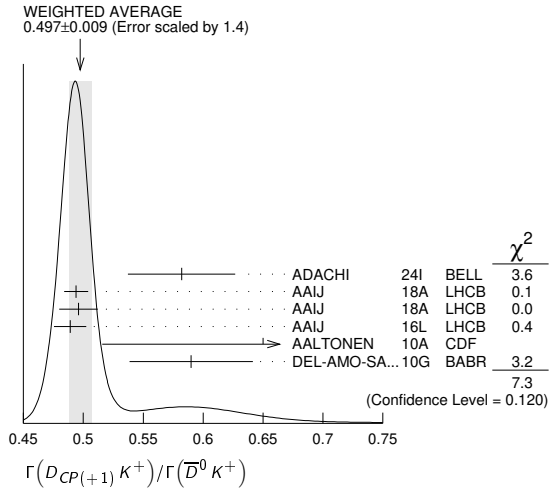

[1] Reports $R_{CP+} = 1.164 \pm 0.081 \pm 0.036$ that we have divided by 2.
[2] Uses $D \to K^+K^-$ decay mode and reports $R_{CP+} = 0.988 \pm 0.015 \pm 0.011$ which we have divided by 2.

[3] Uses $D \to \pi^+\pi^-$ decay mode and reports $R_{CP+} = 0.992 \pm 0.027 \pm 0.015$ which we have divided by 2.
[4] AAIJ 16L reports $R_{CP+} = 0.978 \pm 0.019 \pm 0.018$ which we have divided by 2.
[5] Reports $R_{CP+} = 2\ (B(B^- \to D_{CP(+1)} K^-) + B(B^+ \to D_{CP(+1)} K^+))\ /\ (B(B^- \to D^0 K^-) + B(B^+ \to \overline{D}^0 K^+)) = 1.30 \pm 0.24 \pm 0.12$ that we have divided by 2.
[6] Reports $R_{CP+} = 1.18 \pm 0.09 \pm 0.05$ that we have divided by 2.
[7] AAIJ 12M reports $R_{CP+} = 1.007 \pm 0.038 \pm 0.012$ which we have divided by 2.

$\Gamma(D_{CP(-1)} K^+)/\Gamma(D_{CP(-1)} \pi^+)$ — Γ_{65}/Γ_{61}

VALUE	DOCUMENT ID		TECN	COMMENT
0.097±0.016±0.007	[1] ABE	06	BELL	$e^+e^- \to \Upsilon(4S)$
• • • We do not use the following data for averages, fits, limits, etc. • • •				
0.119±0.028±0.006	[2] ABE	03D	BELL	Repl. by SWAIN 03
0.108±0.019±0.007	[2] SWAIN	03	BELL	Repl. by ABE 06

[1] Reports a double ratio of $B(B^+ \to D_{CP(-1)} K^+)/B(B^+ \to D_{CP(-1)} \pi^+)$ and $B(B^+ \to \overline{D}^0 K^+)/B(B^+ \to \overline{D}^0 \pi^+)$, 1.17 ± 0.14 ± 0.14. We multiply by our best value of $B(B^+ \to \overline{D}^0 K^+)/B(B^+ \to \overline{D}^0 \pi^+) = 0.083 \pm 0.006$. Our first error is their experiment's error and the second error is systematic error from using our best value.
[2] $CP=-1$ eigenstate of $D^0\overline{D}^0$ system is reconstructed via $K^0_S\pi^0$, $K^0_S\omega$, $K^0_S\phi$, $K^0_S\eta$, and $K^0_S\eta'$.

$\Gamma(D_{CP(-1)} K^+)/\Gamma(\overline{D}^0 K^+)$ — Γ_{65}/Γ_{63}

VALUE	DOCUMENT ID		TECN	COMMENT
0.561±0.029 OUR AVERAGE				
0.576±0.037±0.010	[1] ADACHI	24I	BELL	$e^+e^- \to \Upsilon(4S)$
0.54 ±0.04 ±0.02	[2] DEL-AMO-SA...	10G	BABR	$e^+e^- \to \Upsilon(4S)$
• • • We do not use the following data for averages, fits, limits, etc. • • •				
0.515±0.05 ±0.025	AUBERT	08AA	BABR	Repl. by DEL-AMO-SANCHEZ 10G
0.43 ±0.05 ±0.02	AUBERT	06J	BABR	Repl. by AUBERT 08AA

[1] Reports $R_{CP+} = 1.151 \pm 0.074 \pm 0.019$ that we have divided by 2.
[2] Reports $R_{CP+} = 1.07 \pm 0.08 \pm 0.04$ that we have divided by 2.

$\Gamma(D^0 K^+)/\Gamma(\overline{D}^0 K^+)$ — Γ_{66}/Γ_{63}

VALUE (units 10^{-3})	DOCUMENT ID
9.88±0.52 OUR EVALUATION	(Produced by HFLAV)

$\Gamma([K^-\pi^+]_D K^+)/\Gamma_{total}$ — Γ_{67}/Γ

VALUE	CL%	DOCUMENT ID		TECN	COMMENT
$<2.8 \times 10^{-7}$	90	HORII	08	BELL	$e^+e^- \to \Upsilon(4S)$
• • • We do not use the following data for averages, fits, limits, etc. • • •					
$<6.3 \times 10^{-7}$	90	SAIGO	05	BELL	$e^+e^- \to \Upsilon(4S)$

$\Gamma([K^-\pi^+]_D K^+)/\Gamma([K^+\pi^-]_D K^+)$ — Γ_{67}/Γ_{68}

VALUE (units 10^{-3})	CL%	DOCUMENT ID		TECN	COMMENT
17.2±0.6 OUR AVERAGE					
17.3±0.6		[1] AAIJ	21Q	LHCB	pp at 7, 8, 13 TeV
22.0±8.6±2.6		[2] AALTONEN	11AJ	CDF	$p\overline{p}$ at 1.96 TeV
$16.3^{+4.4+0.7}_{-4.1-1.3}$		HORII	11	BELL	$e^+e^- \to \Upsilon(4S)$
11 ±6 ±2		DEL-AMO-SA...	10H	BABR	$e^+e^- \to \Upsilon(4S)$
• • • We do not use the following data for averages, fits, limits, etc. • • •					
18.8±1.1±1.0		[3] AAIJ	16L	LHCB	pp at 7, 8 TeV
15.2±2.0±0.4		AAIJ	12M	LHCB	Repl. by AAIJ 16L
$7.8^{+6.2+2.0}_{-5.7-2.8}$		HORII	08	BELL	Repl. by HORII 11
<29	90	[4] AUBERT	05G	BABR	Repl. by DEL-AMO-SANCHEZ 10H
<44	90	[5] SAIGO	05	BELL	$e^+e^- \to \Upsilon(4S)$
<26	90	[6] AUBERT,B	04L	BABR	Repl. by AUBERT 05G

[1] AAIJ 21Q reports the charge-averaged rate, where the statistical and systematic uncertainties have been combined according to the correlations between the observables. The individual ratio of $B^- \to [K^+\pi^-]_D K^-$ and $B^- \to [K^-\pi^+]_D K^-$ and the ratio of $B^+ \to [K^-\pi^+]_D K^+$ and $B^+ \to [K^+\pi^-]_D K^+$ are also reported to be $(9.5 \pm 0.5 \pm 0.3) \times 10^{-3}$ and $(25.2 \pm 0.8 \pm 0.4) \times 10^{-3}$, respectively.
[2] AALTONEN 11AJ also measures the ratio separately for B^+ ($R^+(K)$) and B^- ($R^-(K)$) and obtains: $R^+(K) = (42.6 \pm 13.7 \pm 2.8) \times 10^{-3}$, $R^-(K) = (3.8 \pm 10.3 \pm 2.7) \times 10^{-3}$.
[3] Superseded by AAIJ 21Q.
[4] AUBERT 05G extract a constraint on the magnitude of the ratio of amplitudes $|A(B^+ \to D^0 K^+)\ /\ A(B^+ \to \overline{D}^0 K^+)| < 0.23$ at 90% CL (Bayesian). Similar measurements from $B^+ \to D^{*0} K^+$ are also reported.
[5] SAIGO 05 extract a constraint on the magnitude of the ratio of amplitudes $|A(B^+ \to D^0 K^+)\ /\ A(B^+ \to \overline{D}^0 K^+)| < 0.27$ at 90% CL.
[6] AUBERT,B 04L extract a constraint on the magnitude of the ratio of amplitudes $|A(B^+ \to D^0 K^+)/A(B^+ \to \overline{D}^0 K^+)| < 0.22$ at 90% CL.

$\Gamma([K^-\pi^+\pi^0]_D K^+)/\Gamma([K^+\pi^-\pi^0]_D K^+)$ — Γ_{69}/Γ_{70}

VALUE (units 10^{-3})	CL%	DOCUMENT ID		TECN	COMMENT
13.1±1.6 OUR AVERAGE					
12.7±1.6±0.2		AAIJ	22T	LHCB	pp at 7, 8, 13 TeV
19.8±6.2±2.4		NAYAK	13	BELL	$e^+e^- \to \Upsilon(4S)$
• • • We do not use the following data for averages, fits, limits, etc. • • •					
14.0±4.7±2.1		[1] AAIJ	15W	LHCB	Repl. by AAIJ 22T
<21	90	[2] LEES	11D	BABR	$e^+e^- \to \Upsilon(4S)$
<39	95	[3] AUBERT	07BN	BABR	Repl. by LEES 11D

[1] Uses $D^0 \to K^-\pi^+\pi^0$ for the favored mode, and $D^0 \to K^+\pi^-\pi^0$ for the suppressed mode.
[2] Extracts a constraint on the magnitude of the ratio of amplitudes $|A(B^+ \to D^0 K^+)/A(B^+ \to \overline{D}^0 K^+)| < 0.13$ at 95% CL.
[3] Extracts a constraint on the magnitude of the ratio of amplitudes $|A(B^+ \to D^0 K^+)/A(B^+ \to \overline{D}^0 K^+)| < 0.19$ at 95% CL.

$\Gamma([K^-\pi^+\pi^+\pi^-]_D K^+)/\Gamma([K^+\pi^-\pi^+\pi^-]_D K^+)$ — Γ_{71}/Γ_{72}

VALUE (units 10^{-2})	DOCUMENT ID		TECN	COMMENT
1.333±0.055±0.008	AAIJ	23I	LHCB	pp at 7, 8, 13 TeV
• • • We do not use the following data for averages, fits, limits, etc. • • •				
1.40 ±0.15 ±0.06	[1] AAIJ	16L	LHCB	pp at 7, 8 TeV
1.24 ±0.27	AAIJ	13AE	LHCB	Repl. by AAIJ 16L

[1] Superseded by AAIJ 23I.

$\Gamma([\pi^+\pi^+\pi^-\pi^-] K^+)/\Gamma([K^+\pi^-\pi^+\pi^-]_D K^+)$ — Γ_{73}/Γ_{72}

VALUE	DOCUMENT ID		TECN	COMMENT
0.975±0.037±0.019	AAIJ	16L	LHCB	pp at 7, 8 TeV

$\Gamma([K^-\pi^+]_D K^*(892)^+)/\Gamma([K^+\pi^-]_D K^*(892)^+)$ — Γ_{75}/Γ_{76}

VALUE	DOCUMENT ID		TECN	COMMENT
0.012±0.004 OUR AVERAGE				
0.011±0.004±0.001	AAIJ	17BO	LHCB	pp at 7, 8, 13 TeV
0.066±0.031±0.010	AUBERT	09AJ	BABR	$e^+e^- \to \Upsilon(4S)$
• • • We do not use the following data for averages, fits, limits, etc. • • •				
0.046±0.031±0.008	AUBERT,B	05V	BABR	Repl. by AUBERT 09AJ

$\Gamma([K^-\pi^+\pi^-\pi^+]_D K^*(892)^+)/\Gamma([K^+\pi^-\pi^+\pi^-]_D K^*(892)^+)$ — Γ_{77}/Γ_{78}

VALUE	DOCUMENT ID		TECN	COMMENT
0.011±0.005±0.003	AAIJ	17BO	LHCB	pp at 7, 8, 13 TeV

$\Gamma([\pi^+\pi^-\pi^+\pi^-]_D K^*(892)^+)/\Gamma([K^+\pi^-\pi^+\pi^-]_D K^*(892)^+)$ — Γ_{74}/Γ_{78}

VALUE	DOCUMENT ID		TECN	COMMENT
1.08±0.13±0.03	AAIJ	17BO	LHCB	pp at 7, 8, 13 TeV

$\Gamma([K^-\pi^+]_D \pi^+)/\Gamma_{total}$ — Γ_{79}/Γ

VALUE (units 10^{-7})	DOCUMENT ID		TECN	COMMENT
$6.29^{+1.02+0.37}_{-0.98-0.48}$	HORII	08	BELL	$e^+e^- \to \Upsilon(4S)$
• • • We do not use the following data for averages, fits, limits, etc. • • •				
$6.6\ ^{+1.9}_{-1.7} \pm 0.5$	SAIGO	05	BELL	Repl. by HORII 08

$\Gamma([K^-\pi^+]_D \pi^+)/\Gamma([K^+\pi^-]_D \pi^+)$ — Γ_{79}/Γ_{80}

VALUE (units 10^{-3})	DOCUMENT ID		TECN	COMMENT
3.66±0.07 OUR AVERAGE				
3.68±0.07	[1] AAIJ	21Q	LHCB	pp at 7, 8, 13 TeV
2.8 ±0.7 ±0.4	[2] AALTONEN	11AJ	CDF	$p\overline{p}$ at 1.96 TeV
$3.28^{+0.38+0.12}_{-0.36-0.18}$	HORII	11	BELL	$e^+e^- \to \Upsilon(4S)$
3.3 ±0.6 ±0.4	DEL-AMO-SA...	10H	BABR	$e^+e^- \to \Upsilon(4S)$
• • • We do not use the following data for averages, fits, limits, etc. • • •				
3.60±0.12±0.09	[3] AAIJ	16L	LHCB	pp at 7, 8 TeV
4.10±0.25±0.05	AAIJ	12M	LHCB	Repl. by AAIJ 16L
$3.40^{+0.55+0.15}_{-0.53-0.22}$	HORII	08	BELL	Repl. by HORII 11
$3.5\ ^{+1.0}_{-0.9} \pm 0.2$	SAIGO	05	BELL	Repl. by HORII 08

[1] AAIJ 21Q gives the charge-averaged rate, where the statistical and systematic uncertainties have been combined according to the correlations between the observables. The individual ratio of $B^- \to [K^+\pi^-]_D K^-$ and $B^- \to [K^-\pi^+]_D K^-$ and the ratio of $B^+ \to [K^-\pi^+]_D \pi^+$ and $B^+ \to [K^+\pi^-]_D \pi^+$ are also reported to be $(4.15 \pm 0.08 \pm 0.04) \times 10^{-3}$ and $(3.20 \pm 0.07 \pm 0.04) \times 10^{-3}$, respectively.
[2] AALTONEN 11AJ also measures the ratio separately for B^+ ($R^+(\pi)$) and B^- ($R^-(\pi)$) and obtains: $R^+(\pi) = (2.4 \pm 1.0 \pm 0.4) \times 10^{-3}$, $R^-(K) = (3.1 \pm 1.1 \pm 0.4) \times 10^{-3}$.
[3] Superseded by AAIJ 21Q.

$\Gamma([K^-\pi^+\pi^0]_D \pi^+)/\Gamma([K^+\pi^-\pi^0]_D \pi^+)$ — Γ_{81}/Γ_{82}

VALUE (units 10^{-3})	DOCUMENT ID		TECN	COMMENT
2.05±0.19 OUR AVERAGE				
2.07±0.20±0.03	AAIJ	22T	LHCB	pp at 7, 8, 13 TeV
$1.89 \pm 0.54\ ^{+0.22}_{-0.25}$	NAYAK	13	BELL	$e^+e^- \to \Upsilon(4S)$
• • • We do not use the following data for averages, fits, limits, etc. • • •				
2.35±0.49±0.06	[1] AAIJ	15W	LHCB	Repl. by AAIJ 22T

[1] Uses $D^0 \to K^-\pi^+\pi^0$ for the favored mode, and $D^0 \to K^+\pi^-\pi^0$ for the suppressed mode.

$\Gamma([K^-\pi^+\pi^+\pi^-]_D \pi^+)/\Gamma([K^+\pi^-\pi^+\pi^-]_D \pi^+)$ — Γ_{83}/Γ_{84}

VALUE (units 10^{-3})	DOCUMENT ID		TECN	COMMENT
3.45±0.07±0.01	AAIJ	23I	LHCB	pp at 7, 8, 13 TeV

Int. J. Mod. Phys. A 2026.41. Downloaded from www.worldscientific.com
by LIFORNIA @ BERKELEY on 09/16/26. Re-use and distribution is strictly not permitted, except for Open Access articles.

Int. J. Mod. Phys. A 2026.41. Downloaded from www.worldscientific.com
by UNIVERSITY OF CALIFORNIA @ BERKELEY on 09/16/26. Re-use and distribution is strictly not permitted, except for Open Access articles.

• • • We do not use the following data for averages, fits, limits, etc. • • •

3.77±0.18±0.06	[1] AAIJ	16L	LHCB	pp at 7, 8 TeV
3.7 ±0.4	AAIJ	13AE	LHCB	Repl. by AAIJ 16L

[1] Superseded by AAIJ 23I.

$\Gamma(([K^-\pi^+]_D\pi^0)_{D^*}\pi^+)/\Gamma(([K^+\pi^-]_D\pi^0)_{D^*}\pi^+)$ — Γ_{85}/Γ_{86}

VALUE (units 10^{-3})	DOCUMENT ID		TECN	COMMENT
4.3 ±0.7 OUR AVERAGE Error includes scale factor of 1.1.				
4.71±0.77	[1] AAIJ	21Q	LHCB	pp at 7, 8, 13 TeV
3.2 ±0.9 ±0.8	DEL-AMO-SA...	10H	BABR	$e^+e^- \to \Upsilon(4S)$

[1] AAIJ 21Q gives the charge-averaged rate, where the statistical and systematic uncertainties have been combined according to the correlations between the observables. The individual ratio of $B^- \to ([K^+\pi^-]_D\pi^0)_{D^*}\pi^-$ to $B^- \to ([K^-\pi^+]_D\pi^0)_{D^*}\pi^-$ and the ratio of $B^+ \to ([K^-\pi^+]_D\pi^0)_{D^*}\pi^+$ to $B^+ \to ([K^+\pi^-]_D\pi^0)_{D^*}\pi^+$, without inclusion of the neutral pion in the reconstruction, are also reported to be $(4.05 \pm 0.56 \pm 0.59) \times 10^{-3}$ and $(5.36 \pm 0.56 \pm 0.58) \times 10^{-3}$, respectively.

$\Gamma(([K^-\pi^+]_D\gamma)_{D^*}\pi^+)/\Gamma(([K^+\pi^-]_D\gamma)_{D^*}\pi^+)$ — Γ_{87}/Γ_{88}

VALUE (units 10^{-3})	DOCUMENT ID		TECN	COMMENT
3.9 ±1.2 OUR AVERAGE				
4.20±1.38	[1] AAIJ	21Q	LHCB	pp at 7, 8, 13 TeV
2.7 ±1.4 ±2.2	DEL-AMO-SA...	10H	BABR	$e^+e^- \to \Upsilon(4S)$

[1] AAIJ 21Q gives the charge-averaged rate, where the statistical and systematic uncertainties have been combined according to the correlations between the observables. The individual the ratio of $B^- \to ([K^+\pi^-]_D\gamma)_{D^*}\pi^-$ to $B^- \to ([K^-\pi^+]_D\gamma)_{D^*}\pi^-$ and the ratio of $B^+ \to ([K^-\pi^+]_D\gamma)_{D^*}\pi^+$ to $B^+ \to ([K^+\pi^-]_D\gamma)_{D^*}\pi^+$, without inclusion of the photon in the reconstruction, are also reported to be $(4.72 \pm 0.92 \pm 1.18) \times 10^{-3}$ and $(4.03 \pm 0.91 \pm 1.14) \times 10^{-3}$, respectively.

$\Gamma(([K^-\pi^+]_D\pi^0)_{D^*}K^+)/\Gamma(([K^+\pi^-]_D\pi^0)_{D^*}K^+)$ — Γ_{89}/Γ_{90}

VALUE (units 10^{-3})	DOCUMENT ID		TECN	COMMENT
2.6±2.7 OUR AVERAGE Error includes scale factor of 2.8.				
11.8±3.4	[1] AAIJ	21Q	LHCB	pp at 7, 8, 13 TeV
1.8±0.9±0.4	DEL-AMO-SA...	10H	BABR	$e^+e^- \to \Upsilon(4S)$

[1] AAIJ 21Q gives the charge-averaged rate, where the statistical and systematic uncertainties have been combined according to the correlations between the observables. The individual ratio of $B^- \to ([K^+\pi^-]_D\pi^0)_{D^*}K^-$ to $B^- \to ([K^-\pi^+]_D\pi^0)_{D^*}K^-$ and the ratio of $B^+ \to ([K^-\pi^+]_D\pi^0)_{D^*}K^+$ to $B^+ \to ([K^+\pi^-]_D\pi^0)_{D^*}K^+$, without inclusion of the neutral pion in the reconstruction, are also reported to be $(20.2 \pm 3.5 \pm 2.3) \times 10^{-3}$ and $(3.3 \pm 3.5 \pm 2.2) \times 10^{-3}$, respectively.

$\Gamma(([K^-\pi^+]_D\gamma)_{D^*}K^+)/\Gamma(([K^+\pi^-]_D\gamma)_{D^*}K^+)$ — Γ_{91}/Γ_{92}

VALUE (units 10^{-3})	DOCUMENT ID		TECN	COMMENT
1.3± 1.6 OUR AVERAGE				
16.3±37.3	[1] AAIJ	21Q	LHCB	pp at 7, 8, 13 TeV
1.3± 1.4±0.8	DEL-AMO-SA...	10H	BABR	$e^+e^- \to \Upsilon(4S)$

[1] AAIJ 21Q gives the charge-averaged rate, where the statistical and systematic uncertainties have been combined according to the correlations between the observables. The individual ratio of $B^- \to ([K^+\pi^-]_D\gamma)_{D^*}K^-$ to $B^- \to ([K^-\pi^+]_D\gamma)_{D^*}K^-$ and the ratio of $B^+ \to ([K^-\pi^+]_D\gamma)_{D^*}K^+$ to $B^+ \to ([K^+\pi^-]_D\gamma)_{D^*}K^+$, without inclusion of the photon in the reconstruction, are also reported to be $(11.7 \pm 21.5 \pm 31.3) \times 10^{-3}$ and $(29.2 \pm 21.4 \pm 31.2) \times 10^{-3}$, respectively.

$\Gamma([\pi^+\pi^-\pi^0]_D K^-)/\Gamma_{total}$ — Γ_{93}/Γ

VALUE (units 10^{-6})	DOCUMENT ID		TECN	COMMENT
4.6±0.8±0.4	[1] AUBERT	07BJ	BABR	$e^+e^- \to \Upsilon(4S)$
• • • We do not use the following data for averages, fits, limits, etc. • • •				
5.5±1.0±0.7	[1] AUBERT,B	05T	BABR	Repl. by AUBERT 07BJ

[1] Assumes equal production of B^+ and B^0 at the $\Upsilon(4S)$.

$\Gamma([K^0_S K^+\pi^-]_D K^+)/\Gamma([K^0_S K^+\pi^-]_D\pi^+)$ — Γ_{94}/Γ_{100}

VALUE	DOCUMENT ID		TECN	COMMENT
0.103±0.015 OUR AVERAGE Error includes scale factor of 1.9.				
0.122±0.012±0.004	[1] ADACHI	23L	BELL	$e^+e^- \to \Upsilon(4S)$
0.092±0.009±0.004	[1] AAIJ	14V	LHCB	pp at 7, 8 TeV
• • • We do not use the following data for averages, fits, limits, etc. • • •				
0.081±0.008±0.004	[2] AAIJ	20N	LHCB	pp at 7, 8, 13 TeV

[1] The anaysis uses all of $D \to K^0_S K\pi$ Dalitz decays.

[2] The analysis uses $D \to K^0_S K\pi$ Dalitz decays with $K^{*-}K^+$ region excluded.

$\Gamma([K^0_S K^-\pi^+]_D K^+)/\Gamma([K^0_S K^-\pi^+]_D\pi^+)$ — Γ_{96}/Γ_{98}

VALUE	DOCUMENT ID		TECN	COMMENT
0.075±0.013 OUR AVERAGE Error includes scale factor of 1.7.				
0.093±0.013±0.003	[1] ADACHI	23L	BELL	$e^+e^- \to \Upsilon(4S)$
0.066±0.009±0.002	[1] AAIJ	14V	LHCB	pp at 7, 8 TeV
• • • We do not use the following data for averages, fits, limits, etc. • • •				
0.073±0.006±0.002	[2] AAIJ	20N	LHCB	pp at 7, 8, 13 TeV

[1] The anaysis uses all of $D \to K^0_S K\pi$ Dalitz decays.

[2] The analysis uses $D \to K^0_S K\pi$ Dalitz decays with $K^{*-}K^+$ region excluded.

$\Gamma([K^*(892)^- K^+]_D K^+)/\Gamma([K^*(892)^- K^+]_D\pi^+)$ — Γ_{95}/Γ_{101}

VALUE	DOCUMENT ID		TECN	COMMENT
0.080±0.004 OUR AVERAGE				
0.093±0.012±0.005	[1] ADACHI	23L	BELL	$e^+e^- \to \Upsilon(4S)$
0.079±0.004±0.002	[1] AAIJ	20N	LHCB	pp at 7, 8, 13 TeV
• • • We do not use the following data for averages, fits, limits, etc. • • •				
0.084±0.011±0.003	[1] AAIJ	14V	LHCB	Repl. by AAIJ 20N

[1] The Analysis uses $D \to K^*(892)K \to K^0_S K\pi$ decays.

$\Gamma([K^*(892)^+ K^-]_D K^+)/\Gamma([K^*(892)^+ K^-]_D\pi^+)$ — Γ_{97}/Γ_{99}

VALUE	DOCUMENT ID		TECN	COMMENT
0.066±0.012 OUR AVERAGE Error includes scale factor of 1.9.				
0.103±0.020±0.006	[1] ADACHI	23L	BELL	$e^+e^- \to \Upsilon(4S)$
0.062±0.006±0.003	[1] AAIJ	20N	LHCB	pp at 7, 8, 13 TeV
• • • We do not use the following data for averages, fits, limits, etc. • • •				
0.056±0.013±0.002	[1] AAIJ	14V	LHCB	Repl. by AAIJ 20N

[1] The Analysis uses $D \to K^*(892)K \to K^0_S K\pi$ decays.

$\Gamma([K^0_S K^+\pi^-]_D\pi^+)/\Gamma([K^0_S K^-\pi^+]_D\pi^+)$ — Γ_{100}/Γ_{98}

VALUE	DOCUMENT ID		TECN	COMMENT
1.47 ±0.05 OUR AVERAGE Error includes scale factor of 1.2.				
1.428±0.057±0.002	[1] ADACHI	23L	BELL	$e^+e^- \to \Upsilon(4S)$
1.528±0.058±0.025	[1] AAIJ	14V	LHCB	pp at 7, 8 TeV
• • • We do not use the following data for averages, fits, limits, etc. • • •				
0.706±0.019±0.009	[2] AAIJ	20N	LHCB	pp at 7, 8, 13 TeV

[1] The anaysis uses all of $D \to K^0_S K\pi$ Dalitz decays.

[2] The analysis uses $D \to K^0_S K\pi$ Dalitz decays with $K^{*-}K^+$ region excluded.

$\Gamma([K^+K^-\pi^0]_D K^+)/\Gamma([K^+K^-\pi^0]_D\pi^+)$ — $\Gamma_{102}/\Gamma_{103}$

VALUE	DOCUMENT ID		TECN	COMMENT
0.95±0.22±0.05	[1] AAIJ	15W	LHCB	pp at 7, 8 TeV

[1] Uses $D \to K^+K^-\pi^0$ mode.

$\Gamma([\pi^+\pi^-\pi^0]_D K^+)/\Gamma([\pi^+\pi^-\pi^0]_D\pi^+)$ — $\Gamma_{104}/\Gamma_{105}$

VALUE	DOCUMENT ID		TECN	COMMENT
0.98±0.11±0.05	[1] AAIJ	15W	LHCB	pp at 7, 8 TeV

[1] Uses $D \to \pi^+\pi^-\pi^0$ mode.

$\Gamma([K^*(892)^- K^+]_D\pi^+)/\Gamma([K^*(892)^+ K^-]_D\pi^+)$ — Γ_{101}/Γ_{99}

VALUE	DOCUMENT ID		TECN	COMMENT
2.56 ±0.06 OUR AVERAGE Error includes scale factor of 1.2.				
2.412±0.132±0.019	[1] ADACHI	23L	BELL	$e^+e^- \to \Upsilon(4S)$
2.585±0.057±0.019	[1] AAIJ	20N	LHCB	pp at 7, 8, 13 TeV
• • • We do not use the following data for averages, fits, limits, etc. • • •				
2.57 ±0.13 ±0.06	[1] AAIJ	14V	LHCB	Repl. by AAIJ 20N

[1] The Analysis uses $D \to K^*(892)K \to K^0_S K\pi$ decays.

$\Gamma(\overline{D}^0 K^*(892)^+)/\Gamma_{total}$ — Γ_{106}/Γ

VALUE (units 10^{-4})	DOCUMENT ID		TECN	COMMENT
5.3 ±0.4 OUR AVERAGE				
5.29±0.30±0.34	[1] AUBERT	06Z	BABR	$e^+e^- \to \Upsilon(4S)$
6.1 ±1.6 ±1.7	[1] MAHAPATRA	02	CLE2	$e^+e^- \to \Upsilon(4S)$
• • • We do not use the following data for averages, fits, limits, etc. • • •				
6.3 ±0.7 ±0.5	[1] AUBERT	04Q	BABR	Repl. by AUBERT 06Z

[1] Assumes equal production of B^+ and B^0 at the $\Upsilon(4S)$.

$\Gamma(D_{CP(-1)} K^*(892)^+)/\Gamma(\overline{D}^0 K^*(892)^+)$ — $\Gamma_{107}/\Gamma_{106}$

VALUE	DOCUMENT ID		TECN	COMMENT
0.515±0.135±0.065	[1] AUBERT	09AJ	BABR	$e^+e^- \to \Upsilon(4S)$
• • • We do not use the following data for averages, fits, limits, etc. • • •				
0.325±0.13 ±0.04	[2] AUBERT,B	05U	BABR	Repl. by AUBERT 09AJ

[1] The authors report $R_{CP-} = 1.03 \pm 0.27 \pm 0.13$ which is, assuming CP conservation, twice the value of the quoted above branching ratio,

[2] The authors report $R_{CP-} = 0.65 \pm 0.26 \pm 0.08$ which is, assuming CP conservation, twice the value of the quoted above branching ratio.

$\Gamma(D_{CP(+1)} K^*(892)^+)/\Gamma(\overline{D}^0 K^*(892)^+)$ — $\Gamma_{108}/\Gamma_{106}$

VALUE	DOCUMENT ID		TECN	COMMENT
1.16 ±0.08 OUR AVERAGE				
1.18 ±0.08 ±0.02	[1] AAIJ	18X	LHCB	pp at 7, 8, 13 TeV
1.085±0.175±0.045	[2] AUBERT	09AJ	BABR	$e^+e^- \to \Upsilon(4S)$
• • • We do not use the following data for averages, fits, limits, etc. • • •				
1.18 ±0.08 ±0.01	[3] AAIJ	17BO	LHCB	Repl. by AAIJ 18X
0.98 ±0.20 ±0.055	[4] AUBERT,B	05U	BABR	Repl. by AUBERT 09AJ

[1] Measures the ratio separately for K^+K^- and $\pi^+\pi^-$ final states, $R_{KK} = 1.22 \pm 0.09 \pm 0.02$ and $R_{\pi\pi} = 1.08 \pm 0.14 \pm 0.03$, and combines the two results.

[2] The authors report $R_{CP+} = 2.17 \pm 0.35 \pm 0.09$ which is, assuming CP conservation, twice the value of the quoted above branching ratio,

[3] Measures the ratio separately for K^+K^- and $\pi^+\pi^-$ final states, $R_{KK} = 1.22 \pm 0.09 \pm 0.01$ and $R_{\pi\pi} = 1.08 \pm 0.14 \pm 0.03$, and combines the two results.

[4] The authors report $R_{CP+} = 1.96 \pm 0.40 \pm 0.11$ which is, assuming CP conservation, twice the value of the quoted above branching ratio.

Int. J. Mod. Phys. A 2026.41. Downloaded from www.worldscientific.com by LIFORNIA @ BERKELEY on 09/16/26. Re-use and distribution is strictly not permitted, except for Open Access articles.

$\Gamma(D^0 K^*(892)^+)/\Gamma(\overline{D}^0 K^*(892)^+)$ — $\Gamma_{109}/\Gamma_{106}$

VALUE (units 10^{-3})	DOCUMENT ID
$10.2^{+3.2}_{-6.9}$ OUR EVALUATION	(Produced by HFLAV)

$\Gamma(\overline{D}^0 K^+\pi^+\pi^-)/\Gamma(\overline{D}^0\pi^+\pi^+\pi^-)$ — $\Gamma_{110}/\Gamma_{116}$

VALUE (units 10^{-2})	DOCUMENT ID		TECN	COMMENT
9.4±1.3±0.9	AAIJ	12T	LHCB	pp at 7 TeV

$\Gamma(D_{CP(+1)} K^+\pi^-\pi^+)/\Gamma([K^+\pi^-]_D K^+\pi^-\pi^+)$ — $\Gamma_{113}/\Gamma_{111}$

VALUE	DOCUMENT ID		TECN	COMMENT
1.040±0.064	AAIJ	15BC	LHCB	pp at 7, 8 TeV

$\Gamma([K^-\pi^+]_D K^+\pi^-\pi^+)/\Gamma([K^+\pi^-]_D K^+\pi^-\pi^+)$ — $\Gamma_{112}/\Gamma_{111}$

VALUE (units 10^{-4})	DOCUMENT ID		TECN	COMMENT
85^{+36}_{-33}	AAIJ	15BC	LHCB	pp at 7, 8 TeV

$\Gamma(\overline{D}^0 K^+\overline{K}^0)/\Gamma_{total}$ — Γ_{114}/Γ

VALUE (units 10^{-4})	DOCUMENT ID		TECN	COMMENT
3.75±0.35 OUR AVERAGE				
$3.67\pm0.35^{+0.08}_{-0.05}$	[1] ADACHI	24L	BEL2	362 fb^{-1}, $e^+e^-\to\Upsilon(4S)$
5.4 ±1.6 ±0.1	[2] DRUTSKOY	02	BELL	$e^+e^-\to\Upsilon(4S)$

[1] ADACHI 24L reports $(3.64\pm0.32\pm0.16)\times10^{-4}$ from a measurement of $[\Gamma(B^+\to\overline{D}^0K^+\overline{K}^0)/\Gamma_{total}]\times[B(\Upsilon(4S)\to B^+B^-)]$ assuming $B(\Upsilon(4S)\to B^+B^-)=(51.6\pm1.2)\times10^{-2}$, which we rescale to our best (shown rounded) value $B(\Upsilon(4S)\to B^+B^-)=(51.1^{+0.7}_{-1.1})\times10^{-2}$. Our first error is their experiment's error and our second error is the systematic error from using our best (shown rounded) value.

[2] DRUTSKOY 02 reports $(5.5\pm1.4\pm0.8)\times10^{-4}$ from a measurement of $[\Gamma(B^+\to\overline{D}^0K^+\overline{K}^0)/\Gamma_{total}]\times[B(\Upsilon(4S)\to B^+B^-)]$ assuming $B(\Upsilon(4S)\to B^+B^-)=(50\pm0)\times10^{-2}$, which we rescale to our best (shown rounded) value $B(\Upsilon(4S)\to B^+B^-)=(51.1^{+0.7}_{-1.1})\times10^{-2}$. Our first error is their experiment's error and our second error is the systematic error from using our best (shown rounded) value.

$\Gamma(\overline{D}^0 K^+\overline{K}^*(892)^0)/\Gamma_{total}$ — Γ_{115}/Γ

VALUE (units 10^{-4})	DOCUMENT ID		TECN	COMMENT
7.2 ±0.5 OUR AVERAGE				
7.19±0.45±0.33	[1] ADACHI	24L	BEL2	$e^+e^-\to\Upsilon(4S)$
7.5 ±1.3 ±1.1	[2] DRUTSKOY	02	BELL	$e^+e^-\to\Upsilon(4S)$

[1] Used 362 fb^{-1} Belle II data and $B(\Upsilon(4S)\to B^0\overline{B}^0)=0.484\pm0.012$.

[2] Assumes equal production of B^+ and B^0 at the $\Upsilon(4S)$.

$\Gamma(\overline{D}^0\pi^+\pi^+\pi^-)/\Gamma_{total}$ — Γ_{116}/Γ

VALUE	DOCUMENT ID		TECN	COMMENT
0.0055±0.0020 OUR FIT Error includes scale factor of 3.6.				
0.0115±0.0029±0.0021	[1] BORTOLETTO	92	CLEO	$e^+e^-\to\Upsilon(4S)$

[1] BORTOLETTO 92 assumes equal production of B^+ and B^0 at the $\Upsilon(4S)$ and uses Mark III branching fractions for the D.

$\Gamma(\overline{D}^0\pi^+\pi^+\pi^-)/\Gamma(\overline{D}^0\pi^+)$ — Γ_{116}/Γ_{59}

VALUE	DOCUMENT ID		TECN	COMMENT
1.2 ±0.4 OUR FIT Error includes scale factor of 3.6.				
1.27±0.06±0.11	AAIJ	11E	LHCB	pp at 7 TeV

$\Gamma([K^-\pi^+]_D\pi^+\pi^-\pi^+)/\Gamma([K^+\pi^-]_D K^+\pi^-\pi^+)$ — $\Gamma_{117}/\Gamma_{111}$

VALUE (units 10^{-4})	DOCUMENT ID		TECN	COMMENT
42.7±5.6	AAIJ	15BC	LHCB	pp at 7, 8 TeV

$\Gamma(\overline{D}^0\pi^+\pi^+\pi^-\text{nonresonant})/\Gamma_{total}$ — Γ_{118}/Γ

VALUE	DOCUMENT ID		TECN	COMMENT
0.0051±0.0034±0.0023	[1] BORTOLETTO	92	CLEO	$e^+e^-\to\Upsilon(4S)$

[1] BORTOLETTO 92 assumes equal production of B^+ and B^0 at the $\Upsilon(4S)$ and uses Mark III branching fractions for the D.

$\Gamma(\overline{D}^0\pi^+\rho^0)/\Gamma_{total}$ — Γ_{119}/Γ

VALUE	DOCUMENT ID		TECN	COMMENT
0.0042±0.0023±0.0020	[1] BORTOLETTO	92	CLEO	$e^+e^-\to\Upsilon(4S)$

[1] BORTOLETTO 92 assumes equal production of B^+ and B^0 at the $\Upsilon(4S)$ and uses Mark III branching fractions for the D.

$\Gamma(\overline{D}^0 a_1(1260)^+)/\Gamma_{total}$ — Γ_{120}/Γ

VALUE	DOCUMENT ID		TECN	COMMENT
0.0045±0.0019±0.0031	[1] BORTOLETTO	92	CLEO	$e^+e^-\to\Upsilon(4S)$

[1] BORTOLETTO 92 assumes equal production of B^+ and B^0 at the $\Upsilon(4S)$ and uses Mark III branching fractions for the D.

$\Gamma(\overline{D}^0\omega\pi^+)/\Gamma_{total}$ — Γ_{121}/Γ

VALUE	DOCUMENT ID		TECN	COMMENT
0.0041±0.0007±0.0006	[1] ALEXANDER	01B	CLE2	$e^+e^-\to\Upsilon(4S)$

[1] Assumes equal production of B^+ and B^0 at the $\Upsilon(4S)$. The signal is consistent with all observed $\omega\pi^+$ having proceeded through the ρ'^+ resonance at mass $1349\pm25^{+10}_{-5}$ MeV and width $547\pm86^{+46}_{-45}$ MeV.

$\Gamma(D^*(2010)^-\pi^+\pi^+)/\Gamma_{total}$ — Γ_{122}/Γ

VALUE (units 10^{-3})	CL%	EVTS	DOCUMENT ID		TECN	COMMENT
1.35±0.22 OUR AVERAGE						
1.25±0.08±0.22			[1] ABE	04D	BELL	$e^+e^-\to\Upsilon(4S)$
1.9 ±0.7 ±0.3		14	[2] ALAM	94	CLE2	$e^+e^-\to\Upsilon(4S)$
2.6 ±1.4 ±0.7		11	[3] ALBRECHT	90J	ARG	$e^+e^-\to\Upsilon(4S)$
$2.4^{+1.7}_{-1.6}\ ^{+1.0}_{-0.6}$		3	[4] BEBEK	87	CLEO	$e^+e^-\to\Upsilon(4S)$
• • • We do not use the following data for averages, fits, limits, etc. • • •						
<4.		90	[5] BORTOLETTO	92	CLEO	$e^+e^-\to\Upsilon(4S)$
5. ±2. ±3.		7	[6] ALBRECHT	87C	ARG	$e^+e^-\to\Upsilon(4S)$

[1] Assumes equal production of B^+ and B^0 at the $\Upsilon(4S)$.

[2] ALAM 94 assume equal production of B^+ and B^0 at the $\Upsilon(4S)$ and use the CLEO II $B(D^*(2010)^+\to D^0\pi^+)$ and absolute $B(D^0\to K^-\pi^+)$ and the PDG 1992 $B(D^0\to K^-\pi^+\pi^0)/B(D^0\to K^-\pi^+)$ and $B(D^0\to K^-2\pi^+\pi^-)/B(D^0\to K^-\pi^+)$.

[3] Assumes equal production of B^+ and B^0 at the $\Upsilon(4S)$ and uses the Mark III branching fractions for the D.

[4] BEBEK 87 value has been updated in BERKELMAN 91 to use same assumptions as noted for BORTOLETTO 92.

[5] BORTOLETTO 92 assumes equal production of B^+ and B^0 at the $\Upsilon(4S)$ and uses Mark III branching fractions for the D and $D^*(2010)$. The authors also find the product branching fraction into $D^{**}\pi$ followed by $D^{**}\to D^*(2010)\pi$ to be $0.0014^{+0.0008}_{-0.0006}\pm0.0003$ where D^{**} represents all orbitally excited D mesons.

[6] ALBRECHT 87C use PDG 86 branching ratios for D and $D^*(2010)$ and assume $B(\Upsilon(4S)\to B^+B^-)=55\%$ and $B(\Upsilon(4S)\to B^0\overline{B}^0)=45\%$. Superseded by ALBRECHT 90J.

$\Gamma(D^*(2010)^-K^+\pi^+)/\Gamma_{total}$ — Γ_{123}/Γ

VALUE (units 10^{-5})	DOCUMENT ID		TECN	COMMENT
8.2±0.3±1.4	[1] AAIJ	17AR	LHCB	pp at 7 , 8 TeV

[1] The branching fraction of the normalization mode $B^+\to D^{*-}\pi^+\pi^+$ is rescaled to the updated ratio of $\Upsilon(4S)\to B^+B^-$ to $\Upsilon(4S)\to B^0\overline{B}^0$ decay rates of 1.058 ± 0.024.

$\Gamma(D^*(2010)^-K^+\pi^+)/\Gamma(D^*(2010)^-\pi^+\pi^+)$ — $\Gamma_{123}/\Gamma_{122}$

VALUE (units 10^{-2})	DOCUMENT ID		TECN	COMMENT
6.39±0.27±0.48	[1] AAIJ	17AR	LHCB	pp at 7, 8 TeV

[1] Uses $D^{*-}\to\overline{D}^0\pi^-$ and $\overline{D}^0\to K^+\pi^-$ decays.

$\Gamma(\overline{D}_1(2420)^0\pi^+,\ \overline{D}_1^0\to D^*(2010)^-\pi^+)/\Gamma_{total}$ — Γ_{124}/Γ

VALUE (units 10^{-4})	DOCUMENT ID		TECN	COMMENT
8.42±0.08±1.46	[1] AAIJ	20D	LHCB	pp at 7, 8, 13 TeV

[1] AAIJ 20D used a 4-body amplitude analysis of $B^-\to D^{*+}\pi^-\pi^-$ decays.

$\Gamma(\overline{D}_1(2420)^0\pi^+,\ \overline{D}_1^0\to D^*(2010)^-\pi^+)/\Gamma(\overline{D}^0\pi^+\pi^+\pi^-)$ — $\Gamma_{124}/\Gamma_{116}$

VALUE (units 10^{-2})	DOCUMENT ID		TECN	COMMENT
9.3±1.6±0.9	[1] AAIJ	11E	LHCB	pp at 7 TeV

[1] AAIJ 11E reports $(9.3\pm1.6\pm0.9)\times10^{-2}$ from a measurement of $[\Gamma(B^+\to\overline{D}_1(2420)^0\pi^+,\ \overline{D}_1^0\to D^*(2010)^-\pi^+)/\Gamma(B^+\to\overline{D}^0\pi^+\pi^+\pi^-)]\times[B(D^*(2010)^+\to D^0\pi^+)]$ assuming $B(D^*(2010)^+\to D^0\pi^+)=(67.7\pm0.5)\times10^{-2}$.

$\Gamma(D^-\pi^+\pi^+)/\Gamma_{total}$ — Γ_{125}/Γ

VALUE (units 10^{-3})	CL%	EVTS	DOCUMENT ID		TECN	COMMENT
1.07±0.05 OUR AVERAGE						
1.08±0.03±0.05			[1] AUBERT	09AB	BABR	$e^+e^-\to\Upsilon(4S)$
1.02±0.04±0.15			[1] ABE	04D	BELL	$e^+e^-\to\Upsilon(4S)$
• • • We do not use the following data for averages, fits, limits, etc. • • •						
<1.4		90	[2] ALAM	94	CLE2	$e^+e^-\to\Upsilon(4S)$
<7		90	[3] BORTOLETTO	92	CLEO	$e^+e^-\to\Upsilon(4S)$
$2.5\ ^{+4.1}_{-2.3}\ ^{+2.4}_{-0.8}$		1	[4] BEBEK	87	CLEO	$e^+e^-\to\Upsilon(4S)$

[1] Assumes equal production of B^+ and B^0 at the $\Upsilon(4S)$.

[2] ALAM 94 assume equal production of B^+ and B^0 at the $\Upsilon(4S)$ and use the Mark III $B(D^+\to K^-2\pi^+)$.

[3] BORTOLETTO 92 assumes equal production of B^+ and B^0 at the $\Upsilon(4S)$ and uses Mark III branching fractions for the D. The product branching fraction into $D_0^*(2340)\pi$ followed by $D_0^*(2340)\to D\pi$ is <0.005 at 90%CL and into $D_2^*(2460)$ followed by $D_2^*(2460)\to D\pi$ is <0.004 at 90%CL.

[4] BEBEK 87 assume the $\Upsilon(4S)$ decays 43% to $B^0\overline{B}^0$. $B(D^-\to K^+\pi^-\pi^-)=(9.1\pm1.3\pm0.4)\%$ is assumed.

$\Gamma(D^-K^+\pi^+)/\Gamma(D^-\pi^+\pi^+)$ — $\Gamma_{126}/\Gamma_{125}$

VALUE (units 10^{-2})	DOCUMENT ID		TECN	COMMENT
7.20±0.19±0.21	AAIJ	15V	LHCB	pp at 7, 8 TeV

$\Gamma(D_0^*(2300)^0K^+,\ D_0^{*0}\to D^-\pi^+)/\Gamma_{total}$ — Γ_{127}/Γ

VALUE (units 10^{-6})	DOCUMENT ID		TECN	COMMENT
6.1±1.9±1.5	[1] AAIJ	15V	LHCB	pp at 7, 8 TeV

[1] Performs the amplitude analysis by fitting the square-Dalitz-plot distribution.

$\Gamma(D_2^*(2460)^0K^+,\ D_2^{*0}\to D^-\pi^+)/\Gamma_{total}$ — Γ_{128}/Γ

VALUE (units 10^{-6})	DOCUMENT ID		TECN	COMMENT
23.2±1.1±2.0	[1] AAIJ	15V	LHCB	pp at 7, 8 TeV

[1] Performs the amplitude analysis by fitting the square-Dalitz-plot distribution.

Int. J. Mod. Phys. A 2026.41. Downloaded from www.worldscientific.com by UNIVERSITY OF CALIFORNIA @ BERKELEY on 09/16/26. Re-use and distribution is strictly not permitted, except for Open Access articles.

$\Gamma(D_1^*(2760)^0 K^+,\ D_1^{*0} \to D^-\pi^+)/\Gamma_{total}$ — Γ_{129}/Γ

VALUE (units 10^{-6})	DOCUMENT ID		TECN	COMMENT
3.6±0.9±0.8	[1] AAIJ	15V	LHCB	pp at 7, 8 TeV

[1] Performs the amplitude analysis by fitting the square-Dalitz-plot distribution.

$\Gamma(D^+ K^0)/\Gamma_{total}$ — Γ_{130}/Γ

VALUE	CL%	DOCUMENT ID		TECN	COMMENT
<2 $\times 10^{-6}$	90	KUMAR	23	BELL	$e^+e^- \to \Upsilon(4S)$
• • • We do not use the following data for averages, fits, limits, etc. • • •					
$<2.9 \times 10^{-6}$	90	[1] DEL-AMO-SA...	10K	BABR	$e^+e^- \to \Upsilon(4S)$
$<5.0 \times 10^{-6}$	90	[1] AUBERT,B	05E	BABR	Repl. by DEL-AMO-SANCHEZ 10K

[1] Assumes equal production of B^+ and B^0 at the $\Upsilon(4S)$.

$\Gamma(D^+ K^+\pi^-)/\Gamma(D^- K^+\pi^+)$ — $\Gamma_{131}/\Gamma_{126}$

VALUE (units 10^{-2})	DOCUMENT ID		TECN	COMMENT
7.3±1.2±0.7	AAIJ	16M	LHCB	pp at 7, 8 TeV

$\Gamma(D^+\eta)/\Gamma_{total}$ — Γ_{132}/Γ

VALUE	CL%	DOCUMENT ID		TECN	COMMENT
<1.2 $\times 10^{-5}$	90	KUMAR	23	BELL	$e^+e^- \to \Upsilon(4S)$

$\Gamma(D_2^*(2460)^0 K^+,\ D_2^{*0} \to D^+\pi^-)/\Gamma_{total}$ — Γ_{133}/Γ

VALUE	CL%	DOCUMENT ID		TECN	COMMENT
<6.3 $\times 10^{-7}$	90	AAIJ	16R	LHCB	pp at 7, 8 TeV

$\Gamma(D^+ K^{*0})/\Gamma_{total}$ — Γ_{134}/Γ

VALUE	CL%	DOCUMENT ID		TECN	COMMENT
<4.9 $\times 10^{-7}$	90	AAIJ	16M	LHCB	pp at 7, 8 TeV
• • • We do not use the following data for averages, fits, limits, etc. • • •					
$<1.8 \times 10^{-6}$	90	AAIJ	13R	LHCB	Repl. by AAIJ 16M
$<3.0 \times 10^{-6}$	90	[1] DEL-AMO-SA...	10K	BABR	$e^+e^- \to \Upsilon(4S)$

[1] Assumes equal production of B^+ and B^0 at the $\Upsilon(4S)$.

$\Gamma(D^+ \overline{K}^{*0})/\Gamma_{total}$ — Γ_{135}/Γ

VALUE (units 10^{-6})	CL%	DOCUMENT ID		TECN	COMMENT
<1.4	90	AAIJ	13R	LHCB	pp at 7 TeV

$\Gamma(\overline{D}^*(2007)^0\pi^+)/\Gamma_{total}$ — Γ_{136}/Γ

VALUE (units 10^{-3})	EVTS	DOCUMENT ID		TECN	COMMENT
5.17 ±0.15 OUR AVERAGE					
5.35 ±0.04 ±0.22		AAIJ	21Q	LHCB	pp at 7, 8, 13 TeV
4.82 ±0.12 ±0.35		[1] KATO	18	BELL	$e^+e^- \to \Upsilon(4S)$
5.52 ±0.17 ±0.42		[2] AUBERT	07H	BABR	$e^+e^- \to \Upsilon(4S)$
5.3 ±0.4 ±0.1		[3,4] AUBERT,BE	06J	BABR	$e^+e^- \to \Upsilon(4S)$
4.34 ±0.47 ±0.18		[5] BRANDENB...	98	CLE2	$e^+e^- \to \Upsilon(4S)$
5.2 ±0.7 ±0.7	71	[6] ALAM	94	CLE2	$e^+e^- \to \Upsilon(4S)$
7.2 ±1.8 ±1.6		[7] BORTOLETTO	92	CLEO	$e^+e^- \to \Upsilon(4S)$
4.0 ±1.4 ±1.2	9	[7] ALBRECHT	90J	ARG	$e^+e^- \to \Upsilon(4S)$
• • • We do not use the following data for averages, fits, limits, etc. • • •					
4.664±0.029±0.268		[8] AAIJ	18A	LHCB	pp at 7, 8, 13 TeV
2.7 ±4.4		[9] BEBEK	87	CLEO	$e^+e^- \to \Upsilon(4S)$

[1] Measures absolute branching fractions using a missing-mass technique.

[2] Assumes equal production of B^+ and B^0 at the $\Upsilon(4S)$.

[3] AUBERT,BE 06J reports $[\Gamma(B^+ \to \overline{D}^*(2007)^0\pi^+)/\Gamma_{total}]$ / $[B(B^+ \to \overline{D}^0\pi^+)]$ = 1.14 ± 0.07 ± 0.04 which we multiply by our best (shown rounded) value $B(B^+ \to \overline{D}^0\pi^+) = (4.61 \pm 0.10) \times 10^{-3}$. Our first error is their experiment's error and our second error is the systematic error from using our best (shown rounded) value.

[4] Uses a missing-mass method. Does not depend on D branching fractions or B^+/B^0 production rates.

[5] BRANDENBURG 98 assume equal production of B^+ and B^0 at $\Upsilon(4S)$ and use the D^* reconstruction technique. The first error is their experiment's error and the second error is the systematic error from the PDG 96 value of $B(D^* \to D\pi)$.

[6] ALAM 94 assume equal production of B^+ and B^0 at the $\Upsilon(4S)$ and use the CLEO II $B(D^*(2007)^0 \to D^0\pi^0)$ and absolute $B(D^0 \to K^-\pi^+)$ and the PDG 1992 $B(D^0 \to K^-\pi^+\pi^0)/B(D^0 \to K^-\pi^+)$ and $B(D^0 \to K^-2\pi^+\pi^-)/B(D^0 \to K^-\pi^+)$.

[7] Assumes equal production of B^+ and B^0 at the $\Upsilon(4S)$ and uses Mark III branching fractions for the D and $D^*(2010)$.

[8] Superseded by AAIJ 21Q.

[9] This is a derived branching ratio, using the inclusive pion spectrum and other two-body B decays. BEBEK 87 assume the $\Upsilon(4S)$ decays 43% to $B^0\overline{B}^0$.

$\Gamma(\overline{D}^*(2007)^0\omega\pi^+)/\Gamma_{total}$ — Γ_{139}/Γ

VALUE	DOCUMENT ID		TECN	COMMENT
0.0045±0.0010±0.0007	[1] ALEXANDER	01B	CLE2	$e^+e^- \to \Upsilon(4S)$

[1] Assumes equal production of B^+ and B^0 at the $\Upsilon(4S)$. The signal is consistent with all observed $\omega\pi^+$ having proceeded through the ρ'^+ resonance at mass $1349 \pm 25^{+10}_{-5}$ MeV and width $547 \pm 86^{+46}_{-45}$ MeV.

$\Gamma(\overline{D}^*(2007)^0\rho^+)/\Gamma_{total}$ — Γ_{140}/Γ

VALUE	EVTS	DOCUMENT ID		TECN	COMMENT
0.0098±0.0017 OUR AVERAGE					
0.0098±0.0006±0.0017		[1] CSORNA	03	CLE2	$e^+e^- \to \Upsilon(4S)$
0.010 ±0.006 ±0.004	7	[2] ALBRECHT	90J	ARG	$e^+e^- \to \Upsilon(4S)$
• • • We do not use the following data for averages, fits, limits, etc. • • •					
0.0168±0.0021±0.0028	86	[3] ALAM	94	CLE2	$e^+e^- \to \Upsilon(4S)$

[1] Assumes equal production of B^0 and B^+ at the $\Upsilon(4S)$ resonance. The second error combines the systematic and theoretical uncertainties in quadrature. CSORNA 03 includes data used in ALAM 94. A full angular fit to three complex helicity amplitudes is performed.

[2] Assumes equal production of B^+ and B^0 at the $\Upsilon(4S)$ and uses Mark III branching fractions for the D and $D^*(2010)$.

[3] ALAM 94 assume equal production of B^+ and B^0 at the $\Upsilon(4S)$ and use the CLEO II $B(D^*(2007)^0 \to D^0\pi^0)$ and absolute $B(D^0 \to K^-\pi^+)$ and the PDG 1992 $B(D^0 \to K^-\pi^+\pi^0)/B(D^0 \to K^-\pi^+)$ and $B(D^0 \to K^-2\pi^+\pi^-)/B(D^0 \to K^-\pi^+)$. The nonresonant $\pi^+\pi^0$ contribution under the ρ^+ is negligible.

$\Gamma(\overline{D}^*(2007)^0 K^+)/\Gamma_{total}$ — Γ_{141}/Γ

VALUE (units 10^{-4})	DOCUMENT ID		TECN	COMMENT
$4.19^{+0.31}_{-0.28}$ OUR AVERAGE				
$4.21^{+0.30}_{-0.26} \pm 0.12$	[1] AUBERT	05N	BABR	$e^+e^- \to \Upsilon(4S)$
4.0 ±1.1 ±0.1	[2] ABE	01I	BELL	$e^+e^- \to \Upsilon(4S)$

[1] AUBERT 05N reports $[\Gamma(B^+ \to \overline{D}^*(2007)^0 K^+)/\Gamma_{total}]$ / $[B(B^+ \to \overline{D}^*(2007)^0\pi^+)]$ = $0.0813 \pm 0.0040^{+0.0042}_{-0.0031}$ which we multiply by our best (shown rounded) value $B(B^+ \to \overline{D}^*(2007)^0\pi^+) = (5.17 \pm 0.15) \times 10^{-3}$. Our first error is their experiment's error and our second error is the systematic error from using our best (shown rounded) value.

[2] ABE 01I reports $[\Gamma(B^+ \to \overline{D}^*(2007)^0 K^+)/\Gamma_{total}]$ / $[B(B^+ \to \overline{D}^*(2007)^0\pi^+)]$ = 0.078 ± 0.019 ± 0.009 which we multiply by our best (shown rounded) value $B(B^+ \to \overline{D}^*(2007)^0\pi^+) = (5.17 \pm 0.15) \times 10^{-3}$. Our first error is their experiment's error and our second error is the systematic error from using our best (shown rounded) value.

$\Gamma(\overline{D}^{*0}_{CP(+1)} K^+)/\Gamma_{total}$ — Γ_{142}/Γ

VALUE (units 10^{-4})	DOCUMENT ID		TECN	COMMENT
$2.75 \pm 0.29^{+0.21}_{-0.18}$	[1] AUBERT	08BF	BABR	$e^+e^- \to \Upsilon(4S)$

[1] AUBERT 08BF reports $[\Gamma(B^+ \to \overline{D}^{*0}_{CP(+1)} K^+)/\Gamma_{total}]$ / $[B(B^+ \to \overline{D}^*(2007)^0 K^+)]$ = 0.655 ± 0.065 ± 0.020 which we multiply by our best (shown rounded) value $B(B^+ \to \overline{D}^*(2007)^0 K^+) = (4.19^{+0.31}_{-0.28}) \times 10^{-4}$. Our first error is their experiment's error and our second error is the systematic error from using our best (shown rounded) value.

$\Gamma(\overline{D}^*(2007)^0 K^+)/\Gamma(\overline{D}^*(2007)^0\pi^+)$ — $\Gamma_{141}/\Gamma_{136}$

VALUE (units 10^{-2})	DOCUMENT ID		TECN	COMMENT
8.51 ±0.12 ±0.48	[1] AAIJ	21Q	LHCB	pp at 7, 8, 13 TeV
• • • We do not use the following data for averages, fits, limits, etc. • • •				
7.930±0.110±0.560	[2] AAIJ	18A	LHCB	pp at 7, 8, 13 TeV

[1] Uses semi-inclusive reconstruction of $B^+ \to ([K^+\pi^-]_D\gamma/\pi^0)_{D^*} K^+/\pi^+$. Decays of $D^* \to D\gamma/\pi^0$ are reconstructed without inclusion of π^0 or γ.

[2] Superseded by AAIJ 21Q.

$\Gamma(\overline{D}^{*0}_{CP(+1)} K^+)/\Gamma(\overline{D}^{*0}_{CP(+1)}\pi^+)$ — $\Gamma_{142}/\Gamma_{137}$

VALUE	DOCUMENT ID		TECN	COMMENT
0.095±0.017 OUR AVERAGE				
0.11 ±0.02 ±0.02	[1] ABE	06	BELL	$e^+e^- \to \Upsilon(4S)$
0.086±0.021±0.007	[2] AUBERT	05N	BABR	$e^+e^- \to \Upsilon(4S)$

[1] Reports a double ratio of $B(B^+ \to D^{*0}_{CP(+1)} K^+)/B(B^+ \to D^{*0}_{CP(+1)}\pi^+)$ and $B(B^+ \to \overline{D}^{*0} K^+)/B(B^+ \to \overline{D}^{*0}\pi^+)$, 1.41 ± 0.25 ± 0.06. We multiply by our best value of $B(B^+ \to \overline{D}^{*0} K^+)/B(B^+ \to \overline{D}^{*0}\pi^+)$ = 0.080 ± 0.011. Our first error is their experiment's error and the second error is systematic error from using our best value.

[2] Uses $D^{*0} \to D^0\pi^0$ with D^0 reconstructed in the CP-even eigenstates K^+K^- and $\pi^+\pi^-$.

$\Gamma(\overline{D}^{*0}_{CP(-1)} K^+)/\Gamma_{total}$ — Γ_{143}/Γ

VALUE (units 10^{-4})	DOCUMENT ID		TECN	COMMENT
$2.31 \pm 0.27^{+0.17}_{-0.16}$	[1] AUBERT	08BF	BABR	$e^+e^- \to \Upsilon(4S)$

[1] AUBERT 08BF reports $[\Gamma(B^+ \to \overline{D}^{*0}_{CP(-1)} K^+)/\Gamma_{total}]$ / $[B(B^+ \to \overline{D}^*(2007)^0 K^+)]$ = 0.55 ± 0.06 ± 0.02 which we multiply by our best (shown rounded) value $B(B^+ \to \overline{D}^*(2007)^0 K^+) = (4.19^{+0.31}_{-0.28}) \times 10^{-4}$. Our first error is their experiment's error and our second error is the systematic error from using our best (shown rounded) value.

$\Gamma(\overline{D}^{*0}_{CP(-1)} K^+)/\Gamma(D^{*0}_{CP(-1)}\pi^+)$ — $\Gamma_{143}/\Gamma_{138}$

VALUE	DOCUMENT ID		TECN	COMMENT
0.09±0.03±0.01	[1] ABE	06	BELL	$e^+e^- \to \Upsilon(4S)$

[1] Reports a double ratio of $B(B^+ \to D^{*0}_{CP(-1)} K^+)/B(B^+ \to D^{*0}_{CP(-1)}\pi^+)$ and $B(B^+ \to \overline{D}^{*0} K^+)/B(B^+ \to \overline{D}^{*0}\pi^+)$, 1.15 ± 0.31 ± 0.12. We multiply by our best value of $B(B^+ \to \overline{D}^{*0} K^+)/B(B^+ \to \overline{D}^{*0}\pi^+)$ = 0.080 ± 0.011. Our first error is their experiment's error and the second error is systematic error from using our best value.

Int. J. Mod. Phys. A 2026.41. Downloaded from www.worldscientific.com by CALIFORNIA @ BERKELEY on 09/16/26. Re-use and distribution is strictly not permitted, except for Open Access articles.

$\Gamma(D^*(2007)^0 K^+)/\Gamma(\overline{D}^*(2007)^0 K^+)$ — $\Gamma_{144}/\Gamma_{141}$

VALUE (units 10^{-2})	DOCUMENT ID
$1.08^{+0.27}_{-0.29}$ OUR EVALUATION	(Produced by HFLAV)

$\Gamma(\overline{D}^*(2007)^0 K^*(892)^+)/\Gamma_{total}$ — Γ_{145}/Γ

VALUE (units 10^{-4})	DOCUMENT ID		TECN	COMMENT
8.1±1.4 OUR AVERAGE				
8.3±1.1±1.0	[1] AUBERT	04K	BABR	$e^+e^- \to \Upsilon(4S)$
7.2±2.2±2.6	[2] MAHAPATRA	02	CLE2	$e^+e^- \to \Upsilon(4S)$

[1] Assumes equal production of B^+ and B^0 at the $\Upsilon(4S)$.
[2] Assumes equal production of B^+ and B^0 at the $\Upsilon(4S)$ and an unpolarized final state.

$\Gamma(\overline{D}^*(2007)^0 K^+ \overline{K}^0)/\Gamma_{total}$ — Γ_{146}/Γ

VALUE (units 10^{-4})	CL%	DOCUMENT ID		TECN	COMMENT
2.94±0.54±0.20		[1] ADACHI	24L	BEL2	$e^+e^- \to \Upsilon(4S)$
• • • We do not use the following data for averages, fits, limits, etc. • • •					
<10.6	90	[2] DRUTSKOY	02	BELL	$e^+e^- \to \Upsilon(4S)$

[1] Used 362 fb^{-1} Belle II data and B($\Upsilon(4S) \to B^0\overline{B}^0$)=0.484 ± 0.012.
[2] Assumes equal production of B^+ and B^0 at the $\Upsilon(4S)$.

$\Gamma(\overline{D}^*(2007)^0 K^+ \overline{K}^*(892)^0)/\Gamma_{total}$ — Γ_{147}/Γ

VALUE (units 10^{-4})	DOCUMENT ID		TECN	COMMENT
12.3 ±1.4 OUR AVERAGE				
11.93±1.14±0.93	[1] ADACHI	24L	BEL2	$e^+e^- \to \Upsilon(4S)$
15.3 ±3.1 ±2.9	[2] DRUTSKOY	02	BELL	$e^+e^- \to \Upsilon(4S)$

[1] Used 362 fb^{-1} Belle II data and B($\Upsilon(4S) \to B^0\overline{B}^0$)=0.484 ± 0.012.
[2] Assumes equal production of B^+ and B^0 at the $\Upsilon(4S)$.

$\Gamma(\overline{D}^*(2007)^0 \pi^+\pi^+\pi^-)/\Gamma_{total}$ — Γ_{148}/Γ

VALUE (units 10^{-2})	EVTS	DOCUMENT ID		TECN	COMMENT
1.03 ±0.12 OUR AVERAGE					
1.055±0.047±0.129		[1] MAJUMDER	04	BELL	$e^+e^- \to \Upsilon(4S)$
0.94 ±0.20 ±0.17	48	[2,3] ALAM	94	CLE2	$e^+e^- \to \Upsilon(4S)$

[1] Assumes equal production of B^+ and B^0 at the $\Upsilon(4S)$.
[2] ALAM 94 assume equal production of B^+ and B^0 at the $\Upsilon(4S)$ and use the CLEO II B($D^*(2007)^0 \to D^0\pi^0$) and absolute B($D^0 \to K^-\pi^+$) and the PDG 1992 B($D^0 \to K^-\pi^+\pi^0$)/B($D^0 \to K^-\pi^+$) and B($D^0 \to K^-2\pi^+\pi^-$)/B($D^0 \to K^-\pi^+$).
[3] The three pion mass is required to be between 1.0 and 1.6 GeV consistent with an a_1 meson. (If this channel is dominated by a_1^+, the branching ratio for $\overline{D}^{*0}a_1^+$ is twice that for $\overline{D}^{*0}\pi^+\pi^+\pi^-$.)

$\Gamma(\overline{D}^*(2007)^0 a_1(1260)^+)/\Gamma_{total}$ — Γ_{149}/Γ

VALUE	DOCUMENT ID		TECN	COMMENT
0.0188±0.0040±0.0034	[1,2] ALAM	94	CLE2	$e^+e^- \to \Upsilon(4S)$

[1] ALAM 94 value is twice their $\Gamma(\overline{D}^*(2007)^0\pi^+\pi^+\pi^-)/\Gamma_{total}$ value based on their observation that the three pions are dominantly in the $a_1(1260)$ mass range 1.0 to 1.6 GeV.
[2] ALAM 94 assume equal production of B^+ and B^0 at the $\Upsilon(4S)$ and use the CLEO II B($D^*(2007)^0 \to D^0\pi^0$) and absolute B($D^0 \to K^-\pi^+$) and the PDG 1992 B($D^0 \to K^-\pi^+\pi^0$)/B($D^0 \to K^-\pi^+$) and B($D^0 \to K^-2\pi^+\pi^-$)/B($D^0 \to K^-\pi^+$).

$\Gamma(\overline{D}^*(2007)^0 \pi^-\pi^+\pi^+\pi^0)/\Gamma_{total}$ — Γ_{150}/Γ

VALUE	DOCUMENT ID		TECN	COMMENT
0.0180±0.0024±0.0027	[1] ALEXANDER	01B	CLE2	$e^+e^- \to \Upsilon(4S)$

[1] Assumes equal production of B^+ and B^0 at the $\Upsilon(4S)$. The signal is consistent with all observed $\omega\pi^+$ having proceeded through the ρ'^+ resonance at mass $1349 \pm 25^{+10}_{-5}$ MeV and width $547 \pm 86^{+46}_{-45}$ MeV.

$\Gamma(\overline{D}^{*0} 3\pi^+ 2\pi^-)/\Gamma_{total}$ — Γ_{151}/Γ

VALUE (units 10^{-3})	DOCUMENT ID		TECN	COMMENT
5.67±0.91±0.85	[1] MAJUMDER	04	BELL	$e^+e^- \to \Upsilon(4S)$

[1] Assumes equal production of B^+ and B^0 at the $\Upsilon(4S)$.

$\Gamma(D^*(2010)^+\pi^0)/\Gamma_{total}$ — Γ_{152}/Γ

VALUE	CL%	DOCUMENT ID		TECN	COMMENT
$<3.6 \times 10^{-6}$		[1] IWABUCHI	08	BELL	$e^+e^- \to \Upsilon(4S)$
• • • We do not use the following data for averages, fits, limits, etc. • • •					
$<1.7 \times 10^{-4}$	90	[2] BRANDENB...	98	CLE2	$e^+e^- \to \Upsilon(4S)$

[1] Assumes equal production of B^+ and B^0 at the $\Upsilon(4S)$.
[2] BRANDENBURG 98 assume equal production of B^+ and B^0 at $\Upsilon(4S)$ and use the D^* partial reconstruction technique. The first error is their experiment's error and the second error is the systematic error from the PDG 96 value of B($D^* \to D\pi$).

$\Gamma(D^*(2010)^+ K^0)/\Gamma_{total}$ — Γ_{153}/Γ

VALUE	CL%	DOCUMENT ID		TECN	COMMENT
$<9.0 \times 10^{-6}$	90	[1] AUBERT,B	05E	BABR	$e^+e^- \to \Upsilon(4S)$
• • • We do not use the following data for averages, fits, limits, etc. • • •					
$<9.5 \times 10^{-5}$	90	[1] GRITSAN	01	CLE2	$e^+e^- \to \Upsilon(4S)$

[1] Assumes equal production of B^+ and B^0 at the $\Upsilon(4S)$.

$\Gamma(D^*(2010)^-\pi^+\pi^+\pi^0)/\Gamma_{total}$ — Γ_{154}/Γ

VALUE	EVTS	DOCUMENT ID		TECN	COMMENT
0.0152±0.0071±0.0001	26	[1] ALBRECHT	90J	ARG	$e^+e^- \to \Upsilon(4S)$
• • • We do not use the following data for averages, fits, limits, etc. • • •					
0.043 ±0.013 ±0.026	24	[2] ALBRECHT	87C	ARG	$e^+e^- \to \Upsilon(4S)$

[1] ALBRECHT 90J reports 0.018 ± 0.007 ± 0.005 from a measurement of $[\Gamma(B^+ \to D^*(2010)^-\pi^+\pi^+\pi^0)/\Gamma_{total}] \times [B(D^*(2010)^+ \to D^0\pi^+)]$ assuming $B(D^*(2010)^+ \to D^0\pi^+) = 0.57 \pm 0.06$, which we rescale to our best (shown rounded) value $B(D^*(2010)^+ \to D^0\pi^+) = (67.7 \pm 0.5) \times 10^{-2}$. Our first error is their experiment's error and our second error is the systematic error from using our best (shown rounded) value. Assumes equal production of B^+ and B^0 at the $\Upsilon(4S)$ and uses Mark III branching fractions for the D.
[2] ALBRECHT 87C use PDG 86 branching ratios for D and $D^*(2010)$ and assume B($\Upsilon(4S) \to B^+B^-$) = 55% and B($\Upsilon(4S) \to B^0\overline{B}^0$) = 45%. Superseded by ALBRECHT 90J.

$\Gamma(D^*(2010)^-\pi^+\pi^+\pi^+\pi^-)/\Gamma_{total}$ — Γ_{155}/Γ

VALUE (units 10^{-3})	CL%	DOCUMENT ID		TECN	COMMENT
2.56±0.26±0.33		[1] MAJUMDER	04	BELL	$e^+e^- \to \Upsilon(4S)$
• • • We do not use the following data for averages, fits, limits, etc. • • •					
<10	90	[2] ALBRECHT	90J	ARG	$e^+e^- \to \Upsilon(4S)$

[1] Assumes equal production of B^+ and B^0 at the $\Upsilon(4S)$.
[2] Assumes equal production of B^+ and B^0 at the $\Upsilon(4S)$ and uses Mark III branching fractions for the D and $D^*(2010)$.

$\Gamma(\overline{D}^{**0}\pi^+)/\Gamma_{total}$ — Γ_{156}/Γ

D^{**0} represents an excited state with mass $2.2 < M < 2.8$ GeV/c^2.

VALUE (units 10^{-3})	DOCUMENT ID		TECN	COMMENT
5.6±1.2±0.1	[1,2] AUBERT,BE	06J	BABR	$e^+e^- \to \Upsilon(4S)$

[1] AUBERT,BE 06J reports $[\Gamma(B^+ \to \overline{D}^{**0}\pi^+)/\Gamma_{total}] / [B(B^+ \to \overline{D}^0\pi^+)] = 1.22 \pm 0.13 \pm 0.23$ which we multiply by our best (shown rounded) value $B(B^+ \to \overline{D}^0\pi^+) = (4.61 \pm 0.10) \times 10^{-3}$. Our first error is their experiment's error and our second error is the systematic error from using our best (shown rounded) value.
[2] Uses a missing-mass method. Does not depend on D branching fractions or B^+/B^0 production rates.

$\Gamma(\overline{D}_1^*(2420)^0\pi^+)/\Gamma_{total}$ — Γ_{157}/Γ

VALUE	EVTS	DOCUMENT ID		TECN	COMMENT
0.0015±0.0006 OUR AVERAGE Error includes scale factor of 1.3.					
0.0011±0.0005±0.0002	8	[1] ALAM	94	CLE2	$e^+e^- \to \Upsilon(4S)$
0.0025±0.0007±0.0006		[2] ALBRECHT	94D	ARG	$e^+e^- \to \Upsilon(4S)$

[1] ALAM 94 assume equal production of B^+ and B^0 at the $\Upsilon(4S)$ and use the CLEO II B($D^*(2010)^+ \to D^0\pi^+$) and absolute B($D^0 \to K^-\pi^+$) and the PDG 1992 B($D^0 \to K^-\pi^+\pi^0$)/B($D^0 \to K^-\pi^+$) and assuming B($D_1(2420)^0 \to D^*(2010)^+\pi^-$) = 67%.
[2] ALBRECHT 94D assume equal production of B^+ and B^0 at the $\Upsilon(4S)$ and use the CLEO II B($D^*(2010)^+ \to D^0\pi^+$) assuming B($D_1(2420)^0 \to D^*(2010)^+\pi^-$) = 67%.

$\Gamma(\overline{D}_1(2420)^0\pi^+ \times B(\overline{D}_1^0 \to \overline{D}^0\pi^+\pi^-))/\Gamma_{total}$ — Γ_{158}/Γ

VALUE (units 10^{-4})	DOCUMENT ID		TECN	COMMENT
$2.5\ ^{+1.6}_{-1.4}$ OUR FIT Error includes scale factor of 3.8.				
$1.85 \pm 0.29^{+0.35}_{-0.55}$	[1] ABE	05A	BELL	$e^+e^- \to \Upsilon(4S)$

[1] Assumes equal production of B^+ and B^0 at the $\Upsilon(4S)$.

$\Gamma(\overline{D}_1(2420)^0\pi^+ \times B(\overline{D}_1^0 \to \overline{D}^0\pi^+\pi^-))/\Gamma(\overline{D}^0\pi^+\pi^+\pi^-)$ — $\Gamma_{158}/\Gamma_{116}$

VALUE (units 10^{-2})	DOCUMENT ID		TECN	COMMENT
$4.6^{+3.3}_{-2.7}$ OUR FIT Error includes scale factor of 3.9.				
10.3±1.5±0.9	AAIJ	11E	LHCB	pp at 7 TeV

$\Gamma(\overline{D}_1(2420)^0\pi^+ \times B(\overline{D}_1^0 \to \overline{D}^0\pi^+\pi^- \text{(nonresonant)}))/\Gamma(\overline{D}^0\pi^+\pi^+\pi^-)$ — $\Gamma_{159}/\Gamma_{116}$

VALUE (units 10^{-2})	DOCUMENT ID		TECN	COMMENT
4.0±0.7±0.5	[1] AAIJ	11E	LHCB	pp at 7 TeV

[1] Excludes decays where $\overline{D}_1(2420)^0 \to D*(2010)^-\pi^+$.

$\Gamma(\overline{D}_1(2430)^0\pi^+, \overline{D}_1^0 \to D^*(2010)^-\pi^+)/\Gamma_{total}$ — Γ_{160}/Γ

VALUE (units 10^{-4})	DOCUMENT ID		TECN	COMMENT
3.51±0.06±0.61	[1] AAIJ	20D	LHCB	pp at 7, 8, 13 TeV

[1] AAIJ 20D used a 4-body amplitude analysis of $B^- \to D^{*+}\pi^-\pi^-$ decays.

$\Gamma(\overline{D}_2^*(2462)^0\pi^+, \overline{D}_2^{*0} \to D^-\pi^+)/\Gamma_{total}$ — Γ_{163}/Γ

VALUE (units 10^{-4})	DOCUMENT ID		TECN	COMMENT
3.56±0.24 OUR AVERAGE				
3.62±0.06±0.30	[1] AAIJ	16AH	LHCB	pp at 7, 8 TeV
3.5 ±0.2 ±0.4	[2] AUBERT	09AB	BABR	$e^+e^- \to \Upsilon(4S)$
3.4 ±0.3 ±0.72	[2] ABE	04D	BELL	$e^+e^- \to \Upsilon(4S)$

[1] Measured using a Dalitz plot analysis of $B^- \to D^+\pi^-\pi^-$ decays.
[2] Assumes equal production of B^+ and B^0 at the $\Upsilon(4S)$.

Int. J. Mod. Phys. A 2026.41. Downloaded from www.worldscientific.com
by UNIVERSITY OF CALIFORNIA @ BERKELEY on 09/16/26. Re-use and distribution is strictly not permitted, except for Open Access articles.

$\Gamma(\overline{D}_2^*(2462)^0\pi^+, \overline{D}_2^{*0} \to \overline{D}^0\pi^-\pi^+)/\Gamma(\overline{D}^0\pi^+\pi^+\pi^-)$ — $\Gamma_{164}/\Gamma_{116}$

VALUE (units 10^{-2})	DOCUMENT ID		TECN	COMMENT
4.0±1.0±0.4	AAIJ	11E	LHCB	pp at 7 TeV

$\Gamma(\overline{D}_2^*(2462)^0\pi^+, \overline{D}_2^{*0} \to \overline{D}^0\pi^-\pi^+(\text{nonresonant}))/\Gamma(\overline{D}^0\pi^+\pi^+\pi^-)$ — $\Gamma_{165}/\Gamma_{116}$

VALUE	CL%	DOCUMENT ID		TECN	COMMENT
<3.0 × 10^{-2}	90	[1] AAIJ	11E	LHCB	pp at 7 TeV

[1] Excludes decays where $\overline{D}_2^*(2462)^0 \to D^*(2010)^-\pi^+$.

$\Gamma(\overline{D}_2^*(2462)^0\pi^+, \overline{D}_2^{*0} \to D^*(2010)^-\pi^+)/\Gamma(\overline{D}^0\pi^+\pi^+\pi^-)$ — $\Gamma_{166}/\Gamma_{116}$

VALUE (units 10^{-2})	DOCUMENT ID		TECN	COMMENT
3.9±1.2±0.4	[1] AAIJ	11E	LHCB	pp at 7 TeV

[1] Uses $B(D^*(2010)^+ \to D^0\pi^+) = (67.7 +- 0.5)\%$.

$\Gamma(\overline{D}_0^*(2400)^0\pi^+ \times B(\overline{D}_0^*(2400)^0 \to D^-\pi^+))/\Gamma_{total}$ — Γ_{167}/Γ

VALUE (units 10^{-4})	DOCUMENT ID		TECN	COMMENT
6.4±1.4 OUR AVERAGE				
6.8±0.3±2.0	[1] AUBERT	09AB	BABR	$e^+e^- \to \Upsilon(4S)$
6.1±0.6±1.8	[1] ABE	04D	BELL	$e^+e^- \to \Upsilon(4S)$

[1] Assumes equal production of B^+ and B^0 at the $\Upsilon(4S)$.

$\Gamma(\overline{D}_1(2421)^0\pi^+, \overline{D}_1^0 \to D^{*-}\pi^+)/\Gamma_{total}$ — Γ_{168}/Γ

VALUE (units 10^{-4})	DOCUMENT ID		TECN	COMMENT
7.4 ±1.0 OUR AVERAGE				
7.95±0.09±1.34	[1] AAIJ	20D	LHCB	pp at 7, 8, 13 TeV
6.8 ±0.7 ±1.3	[2] ABE	04D	BELL	$e^+e^- \to \Upsilon(4S)$

[1] AAIJ 20D used a 4-body amplitude analysis of $B^- \to D^{*+}\pi^-\pi^-$ decays.
[2] Assumes equal production of B^+ and B^0 at the $\Upsilon(4S)$.

$\Gamma(\overline{D}_2^*(2462)^0\pi^+, \overline{D}_2^{*0} \to D^{*-}\pi^+)/\Gamma_{total}$ — Γ_{169}/Γ

VALUE (units 10^{-4})	DOCUMENT ID		TECN	COMMENT
1.98±0.30 OUR AVERAGE				
2.08±0.03±0.37	[1] AAIJ	20D	LHCB	pp at 7, 8, 13 TeV
1.8 ±0.3 ±0.4	[2] ABE	04D	BELL	$e^+e^- \to \Upsilon(4S)$

[1] AAIJ 20D used a 4-body amplitude analysis of $B^- \to D^{*+}\pi^-\pi^-$ decays.
[2] Assumes equal production of B^+ and B^0 at the $\Upsilon(4S)$.

$\Gamma(\overline{D}_1'(2427)^0\pi^+, \overline{D}_1'^0 \to D^{*-}\pi^+)/\Gamma_{total}$ — Γ_{170}/Γ

VALUE (units 10^{-4})	DOCUMENT ID		TECN	COMMENT
3.5 ±0.9 OUR AVERAGE Error includes scale factor of 1.5.				
2.96±0.30±0.63	[1] AAIJ	20D	LHCB	pp at 7, 8, 13 TeV
5.0 ±0.4 ±1.1	[2] ABE	04D	BELL	$e^+e^- \to \Upsilon(4S)$

[1] AAIJ 20D used a 4-body amplitude analysis of $B^- \to D^{*+}\pi^-\pi^-$ decays.
[2] Assumes equal production of B^+ and B^0 at the $\Upsilon(4S)$.

$\Gamma(\overline{D}_1(2420)^0\pi^+ \times B(\overline{D}_1^0 \to \overline{D}^{*0}\pi^+\pi^-))/\Gamma_{total}$ — Γ_{171}/Γ

VALUE (units 10^{-4})	CL%	DOCUMENT ID		TECN	COMMENT
<0.06	90	[1] ABE	05A	BELL	$e^+e^- \to \Upsilon(4S)$

[1] Assumes equal production of B^+ and B^0 at the $\Upsilon(4S)$.

$\Gamma(\overline{D}_1^*(2420)^0\rho^+)/\Gamma_{total}$ — Γ_{172}/Γ

VALUE	CL%	DOCUMENT ID		TECN	COMMENT
<0.0014	90	[1] ALAM	94	CLE2	$e^+e^- \to \Upsilon(4S)$

[1] ALAM 94 assume equal production of B^+ and B^0 at the $\Upsilon(4S)$ and use the CLEO II $B(D^*(2010)^+ \to D^0\pi^+)$ assuming $B(D_1(2420)^0 \to D^*(2010)^+\pi^-) = 67\%$.

$\Gamma(\overline{D}_2^*(2460)^0\pi^+)/\Gamma_{total}$ — Γ_{173}/Γ

VALUE	CL%	DOCUMENT ID		TECN	COMMENT
<0.0013	90	[1] ALAM	94	CLE2	$e^+e^- \to \Upsilon(4S)$
• • • We do not use the following data for averages, fits, limits, etc. • • •					
<0.0028	90	[2] ALAM	94	CLE2	$e^+e^- \to \Upsilon(4S)$
<0.0023	90	[3] ALBRECHT	94D	ARG	$e^+e^- \to \Upsilon(4S)$

[1] ALAM 94 assume equal production of B^+ and B^0 at the $\Upsilon(4S)$ and use the Mark III $B(D^+ \to K^-2\pi^+)$ and $B(D_2^*(2460)^0 \to D^+\pi^-) = 30\%$.
[2] ALAM 94 assume equal production of B^+ and B^0 at the $\Upsilon(4S)$ and use the Mark III $B(D^+ \to K^-2\pi^+)$, the CLEO II $B(D^*(2010)^+ \to D^0\pi^+)$ and $B(D_2^*(2460)^0 \to D^*(2010)^+\pi^-) = 20\%$.
[3] ALBRECHT 94D assume equal production of B^+ and B^0 at the $\Upsilon(4S)$ and use the CLEO II $B(D^*(2010)^+ \to D^0\pi^+)$ and $B(D_2^*(2460)^0 \to D^*(2010)^+\pi^-) = 30\%$.

$\Gamma(\overline{D}_2^*(2460)^0\pi^+ \times B(\overline{D}_2^{*0} \to \overline{D}^{*0}\pi^+\pi^-))/\Gamma_{total}$ — Γ_{174}/Γ

VALUE (units 10^{-4})	CL%	DOCUMENT ID		TECN	COMMENT
<0.22	90	[1] ABE	05A	BELL	$e^+e^- \to \Upsilon(4S)$

[1] Assumes equal production of B^+ and B^0 at the $\Upsilon(4S)$.

$\Gamma(\overline{D}_2^*(2460)^0\rho^+)/\Gamma_{total}$ — Γ_{180}/Γ

VALUE	CL%	DOCUMENT ID		TECN	COMMENT
<0.0047	90	[1] ALAM	94	CLE2	$e^+e^- \to \Upsilon(4S)$
<0.005	90	[2] ALAM	94	CLE2	$e^+e^- \to \Upsilon(4S)$

[1] ALAM 94 assume equal production of B^+ and B^0 at the $\Upsilon(4S)$ and use the Mark III $B(D^+ \to K^-2\pi^+)$ and $B(D_2^*(2460)^0 \to D^+\pi^-) = 30\%$.
[2] ALAM 94 assume equal production of B^+ and B^0 at the $\Upsilon(4S)$ and use the Mark III $B(D^+ \to K^-2\pi^+)$, the CLEO II $B(D^*(2010)^+ \to D^0\pi^+)$ and $B(D_2^*(2460)^0 \to D^*(2010)^+\pi^-) = 20\%$.

$\Gamma(\overline{D}(2550)^0\pi^+, \overline{D}^0 \to D^*(2010)^-\pi^+)/\Gamma_{total}$ — Γ_{161}/Γ

VALUE (units 10^{-4})	DOCUMENT ID		TECN	COMMENT
0.72±0.01±0.14	[1] AAIJ	20D	LHCB	pp at 7, 8, 13 TeV

[1] AAIJ 20D used a 4-body amplitude analysis of $B^- \to D^{*+}\pi^-\pi^-$ decays.

$\Gamma(\overline{D}_J^*(2600)^0\pi^+, \overline{D}_J^{*0} \to D^*(2010)^-\pi^+)/\Gamma_{total}$ — Γ_{162}/Γ

VALUE (units 10^{-4})	DOCUMENT ID		TECN	COMMENT
0.68±0.01±0.13	[1] AAIJ	20D	LHCB	pp at 7, 8, 13 TeV

[1] AAIJ 20D used a 4-body amplitude analysis of $B^- \to D^{*+}\pi^-\pi^-$ decays.

$\Gamma(\overline{D}_1^*(2680)^0\pi^+, \overline{D}_1^*(2680)^0 \to D^-\pi^+)/\Gamma_{total}$ — Γ_{175}/Γ

VALUE (units 10^{-4})	DOCUMENT ID		TECN	COMMENT
0.84±0.06±0.20	[1] AAIJ	16AH	LHCB	pp at 7, 8 TeV

[1] Measured using a Dalitz plot analysis of $B^+ \to D^-\pi^+\pi^+$ decays.

$\Gamma(\overline{D}(2740)^0\pi^+, \overline{D}^0 \to D^*(2010)^-\pi^+)/\Gamma_{total}$ — Γ_{176}/Γ

VALUE (units 10^{-4})	DOCUMENT ID		TECN	COMMENT
0.33±0.02±0.15	[1] AAIJ	20D	LHCB	pp at 7, 8, 13 TeV

[1] AAIJ 20D used a 4-body amplitude analysis of $B^- \to D^{*+}\pi^-\pi^-$ decays.

$\Gamma(\overline{D}_3^*(2750)^0\pi^+, \overline{D}_3^{*0} \to D^*(2010)^-\pi^+)/\Gamma_{total}$ — Γ_{177}/Γ

VALUE (units 10^{-4})	DOCUMENT ID		TECN	COMMENT
0.11±0.01±0.03	[1] AAIJ	20D	LHCB	pp at 7, 8, 13 TeV

[1] AAIJ 20D used a 4-body amplitude analysis of $B^- \to D^{*+}\pi^-\pi^-$ decays.

$\Gamma(\overline{D}_3^*(2760)^0\pi^+, \overline{D}_3^*(2760)^0\pi^+ \to D^-\pi^+)/\Gamma_{total}$ — Γ_{178}/Γ

VALUE (units 10^{-5})	DOCUMENT ID		TECN	COMMENT
1.0±0.1±0.2	[1] AAIJ	16AH	LHCB	pp at 7, 8 TeV

[1] Measured using a Dalitz plot analysis of $B^+ \to D^-\pi^+\pi^+$ decays.

$\Gamma(\overline{D}_2^*(3000)^0\pi^+, \overline{D}_2^*(3000)^0\pi^+ \to D^-\pi^+)/\Gamma_{total}$ — Γ_{179}/Γ

VALUE (units 10^{-6})	DOCUMENT ID		TECN	COMMENT
2±1±1	[1] AAIJ	16AH	LHCB	pp at 7, 8 TeV

[1] Measured using a Dalitz plot analysis of $B^+ \to D^-\pi^+\pi^+$ decays.

$\Gamma(\overline{D}^0 D_s^+)/\Gamma_{total}$ — Γ_{181}/Γ

VALUE (units 10^{-3})	DOCUMENT ID		TECN	COMMENT
9.3±0.6 OUR AVERAGE				
9.5±0.6±0.5	[1] ADACHI	24L	BEL2	$e^+e^- \to \Upsilon(4S)$
8.6±0.2±1.1	[2] AAIJ	13AP	LHCB	pp at 7 TeV
9.5±2.0±0.8	[3] AUBERT	06N	BABR	$e^+e^- \to \Upsilon(4S)$
9.8±2.6±0.9	[4] GIBAUT	96	CLE2	$e^+e^- \to \Upsilon(4S)$
14 ±8 ±1	[5] ALBRECHT	92G	ARG	$e^+e^- \to \Upsilon(4S)$
13 ±6 ±1	[6] BORTOLETTO	90	CLEO	$e^+e^- \to \Upsilon(4S)$

[1] Used 362 fb^{-1} Belle II data and $B(\Upsilon(4S) \to B^0\overline{B}^0)$=0.484 ± 0.012.
[2] Uses $B(B^0 \to D^-D_s^+) = (7.2 \pm 0.8) \times 10^{-3}$.
[3] AUBERT 06N reports $(0.92 \pm 0.14 \pm 0.18) \times 10^{-2}$ from a measurement of $[\Gamma(B^+ \to \overline{D}^0 D_s^+)/\Gamma_{total}] \times [B(D_s^+ \to \phi\pi^+)]$ assuming $B(D_s^+ \to \phi\pi^+) = 0.0462 \pm 0.0062$, which we rescale to our best (shown rounded) value $B(D_s^+ \to \phi\pi^+) = (4.5 \pm 0.4) \times 10^{-2}$. Our first error is their experiment's error and our second error is the systematic error from using our best (shown rounded) value.
[4] GIBAUT 96 reports $0.0126 \pm 0.0022 \pm 0.0025$ from a measurement of $[\Gamma(B^+ \to \overline{D}^0 D_s^+)/\Gamma_{total}] \times [B(D_s^+ \to \phi\pi^+)]$ assuming $B(D_s^+ \to \phi\pi^+) = 0.035$, which we rescale to our best (shown rounded) value $B(D_s^+ \to \phi\pi^+) = (4.5 \pm 0.4) \times 10^{-2}$. Our first error is their experiment's error and our second error is the systematic error from using our best (shown rounded) value.
[5] ALBRECHT 92G reports $0.024 \pm 0.012 \pm 0.004$ from a measurement of $[\Gamma(B^+ \to \overline{D}^0 D_s^+)/\Gamma_{total}] \times [B(D_s^+ \to \phi\pi^+)]$ assuming $B(D_s^+ \to \phi\pi^+) = 0.027$, which we rescale to our best (shown rounded) value $B(D_s^+ \to \phi\pi^+) = (4.5 \pm 0.4) \times 10^{-2}$. Our first error is their experiment's error and our second error is the systematic error from using our best (shown rounded) value. Assumes PDG 1990 D^0 branching ratios, e.g., $B(D^0 \to K^-\pi^+) = 3.71 \pm 0.25\%$.
[6] BORTOLETTO 90 reports 0.029 ± 0.013 from a measurement of $[\Gamma(B^+ \to \overline{D}^0 D_s^+)/\Gamma_{total}] \times [B(D_s^+ \to \phi\pi^+)]$ assuming $B(D_s^+ \to \phi\pi^+) = 0.02$, which we rescale to our best (shown rounded) value $B(D_s^+ \to \phi\pi^+) = (4.5 \pm 0.4) \times 10^{-2}$. Our first error is their experiment's error and our second error is the systematic error from using our best (shown rounded) value.

$\Gamma(\overline{D}^0 D^+)/\Gamma(\overline{D}^0 D_s^+)$ — $\Gamma_{218}/\Gamma_{181}$

VALUE (units 10^{-2})	DOCUMENT ID		TECN	COMMENT
7.25±0.09±0.09	AAIJ	23AX	LHCB	pp at 7, 8, 13 TeV

Int. J. Mod. Phys. A 2026.41. Downloaded from www.worldscientific.com by LIFORNIA @ BERKELEY on 09/16/26. Re-use and distribution is strictly not permitted, except for Open Access articles.

$\Gamma(D_{s0}^*(2317)^+\overline{D}^0,\ D_{s0}^{*+} \to D_s^+\pi^0)/\Gamma_{total}$ — Γ_{182}/Γ

VALUE (units 10^{-3})	DOCUMENT ID		TECN	COMMENT
$0.79^{+0.15}_{-0.13}$ OUR AVERAGE				
$0.79^{+0.17}_{-0.16}\pm0.01$	[1,2] CHOI	15A	BELL	$e^+e^- \to \Upsilon(4S)$
$0.80^{+0.35}_{-0.21}\pm0.07$	[2,3] AUBERT,B	04S	BABR	$e^+e^- \to \Upsilon(4S)$
• • • We do not use the following data for averages, fits, limits, etc. • • •				
$0.65^{+0.26}_{-0.24}\pm0.06$	[2,4] KROKOVNY	03B	BELL	Repl. by CHOI 15A

[1] CHOI 15A reports $(8.0^{+1.3}_{-1.2}\pm1.1\pm0.4)\times10^{-4}$ from a measurement of $[\Gamma(B^+ \to D_{s0}^*(2317)^+\overline{D}^0,\ D_{s0}^{*+} \to D_s^+\pi^0)/\Gamma_{total}]\times[B(D_s^+ \to K^+K^-\pi^+)]$ assuming $B(D_s^+ \to K^+K^-\pi^+) = (5.39\pm0.21)\times10^{-2}$, which we rescale to our best (shown rounded) value $B(D_s^+ \to K^+K^-\pi^+) = (5.45\pm0.08)\times10^{-2}$. Our first error is their experiment's error and our second error is the systematic error from using our best (shown rounded) value.

[2] Assumes equal production of B^+ and B^0 at the $\Upsilon(4S)$.

[3] AUBERT,B 04S reports $(1.0\pm0.3^{+0.4}_{-0.2})\times10^{-3}$ from a measurement of $[\Gamma(B^+ \to D_{s0}^*(2317)^+\overline{D}^0,\ D_{s0}^{*+} \to D_s^+\pi^0)/\Gamma_{total}]\times[B(D_s^+ \to \phi\pi^+)]$ assuming $B(D_s^+ \to \phi\pi^+) = 0.036\pm0.009$, which we rescale to our best (shown rounded) value $B(D_s^+ \to \phi\pi^+) = (4.5\pm0.4)\times10^{-2}$. Our first error is their experiment's error and our second error is the systematic error from using our best (shown rounded) value.

[4] KROKOVNY 03B reports $(0.81^{+0.30}_{-0.27}\pm0.24)\times10^{-3}$ from a measurement of $[\Gamma(B^+ \to D_{s0}^*(2317)^+\overline{D}^0,\ D_{s0}^{*+} \to D_s^+\pi^0)/\Gamma_{total}]\times[B(D_s^+ \to \phi\pi^+)]$ assuming $B(D_s^+ \to \phi\pi^+) = 0.036\pm0.009$, which we rescale to our best (shown rounded) value $B(D_s^+ \to \phi\pi^+) = (4.5\pm0.4)\times10^{-2}$. Our first error is their experiment's error and our second error is the systematic error from using our best (shown rounded) value.

$\Gamma(D_{s0}(2317)^+\overline{D}^0\times B(D_{s0}(2317)^+ \to D_s^{*+}\gamma))/\Gamma_{total}$ — Γ_{183}/Γ

VALUE (units 10^{-3})	CL%	DOCUMENT ID		TECN	COMMENT
<0.76	90	[1] KROKOVNY	03B	BELL	$e^+e^- \to \Upsilon(4S)$

[1] Assumes equal production of B^+ and B^0 at the $\Upsilon(4S)$.

$\Gamma(D_{s0}(2317)^+\overline{D}^*(2007)^0\times B(D_{s0}(2317)^+ \to D_s^+\pi^0))/\Gamma_{total}$ — Γ_{184}/Γ

VALUE (units 10^{-3})	DOCUMENT ID		TECN	COMMENT
$0.9\pm0.6^{+0.4}_{-0.3}$	[1] AUBERT,B	04S	BABR	$e^+e^- \to \Upsilon(4S)$

[1] Assumes equal production of B^+ and B^0 at the $\Upsilon(4S)$.

$\Gamma(D_{sJ}(2457)^+\overline{D}^0)/\Gamma_{total}$ — Γ_{185}/Γ

VALUE (units 10^{-3})	DOCUMENT ID		TECN	COMMENT
$3.1^{+1.0}_{-0.9}$ OUR AVERAGE				
$4.3\pm1.6\pm1.3$	[1] AUBERT	06N	BABR	$e^+e^- \to \Upsilon(4S)$
$4.6^{+1.8}_{-1.6}\pm1.0$	[2,3] AUBERT,B	04S	BABR	$e^+e^- \to \Upsilon(4S)$
$2.1^{+1.1}_{-0.9}\pm0.5$	[2,4] KROKOVNY	03B	BELL	$e^+e^- \to \Upsilon(4S)$

[1] Uses a missing-mass method in the events that one of the B mesons is fully reconstructed.

[2] Assumes equal production of B^+ and B^0 at the $\Upsilon(4S)$.

[3] AUBERT,B 04S reports $[\Gamma(B^+ \to D_{sJ}(2457)^+\overline{D}^0)/\Gamma_{total}]\times[B(D_{s1}(2460)^+ \to D_s^{*+}\pi^0)] = (2.2^{+0.8}_{-0.7}\pm0.3)\times10^{-3}$ which we divide by our best (shown rounded) value $B(D_{s1}(2460)^+ \to D_s^{*+}\pi^0) = (48\pm11)\times10^{-2}$. Our first error is their experiment's error and our second error is the systematic error from using our best (shown rounded) value.

[4] KROKOVNY 03B reports $[\Gamma(B^+ \to D_{sJ}(2457)^+\overline{D}^0)/\Gamma_{total}]\times[B(D_{s1}(2460)^+ \to D_s^{*+}\pi^0)] = (1.0^{+0.5}_{-0.4}\pm0.1)\times10^{-3}$ which we divide by our best (shown rounded) value $B(D_{s1}(2460)^+ \to D_s^{*+}\pi^0) = (48\pm11)\times10^{-2}$. Our first error is their experiment's error and our second error is the systematic error from using our best (shown rounded) value.

$\Gamma(D_{sJ}(2457)^+\overline{D}^0\times B(D_{sJ}(2457)^+ \to D_s^+\gamma))/\Gamma_{total}$ — Γ_{186}/Γ

VALUE (units 10^{-3})	DOCUMENT ID		TECN	COMMENT
$0.46^{+0.13}_{-0.11}$ OUR AVERAGE				
$0.48^{+0.19}_{-0.13}\pm0.04$	[1,2] AUBERT,B	04S	BABR	$e^+e^- \to \Upsilon(4S)$
$0.45^{+0.15}_{-0.14}\pm0.04$	[1,3] KROKOVNY	03B	BELL	$e^+e^- \to \Upsilon(4S)$

[1] Assumes equal production of B^+ and B^0 at the $\Upsilon(4S)$.

[2] AUBERT,B 04S reports $(0.6\pm0.2^{+0.2}_{-0.1})\times10^{-3}$ from a measurement of $[\Gamma(B^+ \to D_{sJ}(2457)^+\overline{D}^0\times B(D_{sJ}(2457)^+ \to D_s^+\gamma))/\Gamma_{total}]\times[B(D_s^+ \to \phi\pi^+)]$ assuming $B(D_s^+ \to \phi\pi^+) = 0.036\pm0.009$, which we rescale to our best (shown rounded) value $B(D_s^+ \to \phi\pi^+) = (4.5\pm0.4)\times10^{-2}$. Our first error is their experiment's error and our second error is the systematic error from using our best (shown rounded) value.

[3] KROKOVNY 03B reports $(0.56^{+0.16}_{-0.15}\pm0.17)\times10^{-3}$ from a measurement of $[\Gamma(B^+ \to D_{sJ}(2457)^+\overline{D}^0\times B(D_{sJ}(2457)^+ \to D_s^+\gamma))/\Gamma_{total}]\times[B(D_s^+ \to \phi\pi^+)]$ assuming $B(D_s^+ \to \phi\pi^+) = 0.036\pm0.009$, which we rescale to our best (shown rounded) value $B(D_s^+ \to \phi\pi^+) = (4.5\pm0.4)\times10^{-2}$. Our first error is their experiment's error and our second error is the systematic error from using our best (shown rounded) value.

$\Gamma(D_{sJ}(2457)^+\overline{D}^0\times B(D_{sJ}(2457)^+ \to D_s^+\pi^+\pi^-))/\Gamma_{total}$ — Γ_{187}/Γ

VALUE (units 10^{-3})	CL%	DOCUMENT ID		TECN	COMMENT
<0.22	90	[1] KROKOVNY	03B	BELL	$e^+e^- \to \Upsilon(4S)$

[1] Assumes equal production of B^+ and B^0 at the $\Upsilon(4S)$.

$\Gamma(D_{sJ}(2457)^+\overline{D}^0\times B(D_{sJ}(2457)^+ \to D_s^+\pi^0))/\Gamma_{total}$ — Γ_{188}/Γ

VALUE (units 10^{-3})	CL%	DOCUMENT ID		TECN	COMMENT
<0.27	90	[1] KROKOVNY	03B	BELL	$e^+e^- \to \Upsilon(4S)$

[1] Assumes equal production of B^+ and B^0 at the $\Upsilon(4S)$.

$\Gamma(D_{sJ}(2457)^+\overline{D}^0\times B(D_{sJ}(2457)^+ \to D_s^{*+}\gamma))/\Gamma_{total}$ — Γ_{189}/Γ

VALUE (units 10^{-3})	CL%	DOCUMENT ID		TECN	COMMENT
<0.98	90	[1] KROKOVNY	03B	BELL	$e^+e^- \to \Upsilon(4S)$

[1] Assumes equal production of B^+ and B^0 at the $\Upsilon(4S)$.

$\Gamma(D_{sJ}(2457)^+\overline{D}^*(2007)^0)/\Gamma_{total}$ — Γ_{190}/Γ

VALUE (units 10^{-3})	DOCUMENT ID		TECN	COMMENT
12.0 ± 3.0 OUR AVERAGE				
$11.2\pm2.6\pm2.0$	[1] AUBERT	06N	BABR	$e^+e^- \to \Upsilon(4S)$
$16\ ^{+8}_{-6}\ \pm4$	[2,3] AUBERT,B	04S	BABR	$e^+e^- \to \Upsilon(4S)$

[1] Uses a missing-mass method in the events that one of the B mesons is fully reconstructed.

[2] AUBERT,B 04S reports $[\Gamma(B^+ \to D_{sJ}(2457)^+\overline{D}^*(2007)^0)/\Gamma_{total}]\times[B(D_{s1}(2460)^+ \to D_s^{*+}\pi^0)] = (7.6\pm1.7^{+3.2}_{-2.4})\times10^{-3}$ which we divide by our best (shown rounded) value $B(D_{s1}(2460)^+ \to D_s^{*+}\pi^0) = (48\pm11)\times10^{-2}$. Our first error is their experiment's error and our second error is the systematic error from using our best (shown rounded) value.

[3] Assumes equal production of B^+ and B^0 at the $\Upsilon(4S)$.

$\Gamma(D_{sJ}(2457)^+\overline{D}^*(2007)^0\times B(D_{sJ}(2457)^+ \to D_s^+\gamma))/\Gamma_{total}$ — Γ_{191}/Γ

VALUE (units 10^{-3})	DOCUMENT ID		TECN	COMMENT
$1.4\pm0.4^{+0.6}_{-0.4}$	[1] AUBERT,B	04S	BABR	$e^+e^- \to \Upsilon(4S)$

[1] Assumes equal production of B^+ and B^0 at the $\Upsilon(4S)$.

$\Gamma(\overline{D}^0 D_{s1}(2536)^+\times B(D_{s1}(2536)^+ \to D^*(2007)^0K^+))/\Gamma_{total}$ — Γ_{193}/Γ

VALUE (units 10^{-4})	CL%	DOCUMENT ID		TECN	COMMENT
$2.16\pm0.52\pm0.45$		[1] AUBERT	08B	BABR	$e^+e^- \to \Upsilon(4S)$
• • • We do not use the following data for averages, fits, limits, etc. • • •					
<2	90	AUBERT	03X	BABR	Repl. by AUBERT 08B

[1] Assumes equal production of B^+ and B^0 at the $\Upsilon(4S)$.

$\Gamma(\overline{D}^0 D_{s1}(2536)^+\times B(D_{s1}(2536)^+ \to D^*(2007)^0K^+ + D^*(2010)^+K^0))/\Gamma_{total}$ — Γ_{192}/Γ

VALUE (units 10^{-4})	DOCUMENT ID		TECN	COMMENT
$3.97\pm0.85\pm0.56$	[1,2] AUSHEV	11	BELL	$e^+e^- \to \Upsilon(4S)$

[1] Uses $\Gamma(D^*(2007)^0 \to D^0\pi^0)\ /\ \Gamma(D^*(2007)^0 \to D^0\gamma) = 1.74\pm0.13$ and $\Gamma(D_{s1}(2536)^+ \to D^*(2007)^0K^+)\ /\ \Gamma(D_{s1}(2536)^+ \to D^*(2010)^+K^0) = 1.36\pm0.2$.

[2] Assumes equal production of B^+ and B^0 at the $\Upsilon(4S)$.

$\Gamma(\overline{D}^*(2007)^0 D_{s1}(2536)^+\times B(D_{s1}(2536)^+ \to D^*(2007)^0K^+))/\Gamma_{total}$ — Γ_{194}/Γ

VALUE (units 10^{-4})	CL%	DOCUMENT ID		TECN	COMMENT
$5.46\pm1.17\pm1.04$		[1] AUBERT	08B	BABR	$e^+e^- \to \Upsilon(4S)$
• • • We do not use the following data for averages, fits, limits, etc. • • •					
<7	90	AUBERT	03X	BABR	Repl. by AUBERT 08B

[1] Assumes equal production of B^+ and B^0 at the $\Upsilon(4S)$.

$\Gamma(\overline{D}^0 D_{s1}(2536)^+\times B(D_{s1}(2536)^+ \to D^{*+}K^0))/\Gamma_{total}$ — Γ_{195}/Γ

VALUE (units 10^{-4})	DOCUMENT ID		TECN	COMMENT
$2.30\pm0.98\pm0.43$	[1] AUBERT	08B	BABR	$e^+e^- \to \Upsilon(4S)$

[1] Assumes equal production of B^+ and B^0 at the $\Upsilon(4S)$.

$\Gamma(\overline{D}^0 D_{sJ}(2700)^+\times B(D_{sJ}(2700)^+ \to D^0K^+))/\Gamma_{total}$ — Γ_{196}/Γ

VALUE (units 10^{-4})	DOCUMENT ID		TECN	COMMENT
5.6 ±1.8 OUR AVERAGE Error includes scale factor of 1.7.				
$5.02\pm0.71\pm0.93$	[1] LEES	15C	BABR	$e^+e^- \to \Upsilon(4S)$
$11.3\ \pm2.2\ ^{+1.4}_{-2.8}$	[1] BRODZICKA	08	BELL	$e^+e^- \to \Upsilon(4S)$

[1] Assumes equal production of B^+ and B^0 at the $\Upsilon(4S)$.

$\Gamma(\overline{D}^{*0} D_{s1}(2536)^+,\ D_{s1}^+ \to D^{*+}K^0)/\Gamma_{total}$ — Γ_{197}/Γ

VALUE (units 10^{-4})	DOCUMENT ID		TECN	COMMENT
$3.92\pm2.46\pm0.83$	[1] AUBERT	08B	BABR	$e^+e^- \to \Upsilon(4S)$

[1] Assumes equal production of B^+ and B^0 at the $\Upsilon(4S)$.

$\Gamma(\overline{D}^0 D_{sJ}(2573)^+,\ D_{sJ}^+ \to D^0K^+)/\Gamma_{total}$ — Γ_{198}/Γ

VALUE (units 10^{-4})	DOCUMENT ID		TECN	COMMENT
$0.08\pm0.14\pm0.05$	[1] LEES	15C	BABR	$e^+e^- \to \Upsilon(4S)$

[1] Assumes equal production of B^+ and B^0 at the $\Upsilon(4S)$.

Int. J. Mod. Phys. A 2026.41. Downloaded from www.worldscientific.com
by UNIVERSITY OF CALIFORNIA @ BERKELEY on 09/16/26. Re-use and distribution is strictly not permitted, except for Open Access articles.

$\Gamma(\overline{D}^{*0} D_{sJ}(2573),\ D_{sJ}^{+} \to D^0 K^+)/\Gamma_{total}$ — Γ_{199}/Γ

VALUE (units 10^{-4})	CL%	DOCUMENT ID		TECN	COMMENT
<2	90	AUBERT	03X	BABR	$e^+e^- \to \Upsilon(4S)$

$\Gamma(\overline{D}^{*}(2007)^0 D_{sJ}(2573),\ D_{sJ}^{+} \to D^0 K^+)/\Gamma_{total}$ — Γ_{200}/Γ

VALUE (units 10^{-4})	CL%	DOCUMENT ID		TECN	COMMENT
<5	90	AUBERT	03X	BABR	$e^+e^- \to \Upsilon(4S)$

$\Gamma(\overline{D}^0 D_s^{*+})/\Gamma_{total}$ — Γ_{201}/Γ

VALUE	DOCUMENT ID		TECN	COMMENT
0.0076±0.0016 OUR AVERAGE				
0.0079±0.0017±0.0007	[1] AUBERT	06N	BABR	$e^+e^- \to \Upsilon(4S)$
0.0068±0.0025±0.0006	[2] GIBAUT	96	CLE2	$e^+e^- \to \Upsilon(4S)$
0.010 ±0.007 ±0.001	[3] ALBRECHT	92G	ARG	$e^+e^- \to \Upsilon(4S)$

[1] AUBERT 06N reports $(0.77 \pm 0.15 \pm 0.13) \times 10^{-2}$ from a measurement of $[\Gamma(B^+ \to \overline{D}^0 D_s^{*+})/\Gamma_{total}] \times [B(D_s^+ \to \phi\pi^+)]$ assuming $B(D_s^+ \to \phi\pi^+) = 0.0462 \pm 0.0062$, which we rescale to our best (shown rounded) value $B(D_s^+ \to \phi\pi^+) = (4.5 \pm 0.4) \times 10^{-2}$. Our first error is their experiment's error and our second error is the systematic error from using our best (shown rounded) value.

[2] GIBAUT 96 reports $0.0087 \pm 0.0027 \pm 0.0017$ from a measurement of $[\Gamma(B^+ \to \overline{D}^0 D_s^{*+})/\Gamma_{total}] \times [B(D_s^+ \to \phi\pi^+)]$ assuming $B(D_s^+ \to \phi\pi^+) = 0.035$, which we rescale to our best (shown rounded) value $B(D_s^+ \to \phi\pi^+) = (4.5 \pm 0.4) \times 10^{-2}$. Our first error is their experiment's error and our second error is the systematic error from using our best (shown rounded) value.

[3] ALBRECHT 92G reports $0.016 \pm 0.012 \pm 0.003$ from a measurement of $[\Gamma(B^+ \to \overline{D}^0 D_s^{*+})/\Gamma_{total}] \times [B(D_s^+ \to \phi\pi^+)]$ assuming $B(D_s^+ \to \phi\pi^+) = 0.027$, which we rescale to our best (shown rounded) value $B(D_s^+ \to \phi\pi^+) = (4.5 \pm 0.4) \times 10^{-2}$. Our first error is their experiment's error and our second error is the systematic error from using our best (shown rounded) value. Assumes PDG 1990 D^0 branching ratios, e.g., $B(D^0 \to K^-\pi^+) = 3.71 \pm 0.25\%$.

$\Gamma(\overline{D}^{*}(2007)^0 D_s^+,\ \overline{D}^{*0} \to D^-\pi^+)/\Gamma(D^- D_s^+ \pi^+)$ — $\Gamma_{204}/\Gamma_{202}$

VALUE (units 10^{-2})	DOCUMENT ID		TECN	COMMENT
14.7±1.3±2.7	[1] AAIJ	23B	LHCB	pp at 7, 8, 13 TeV

[1] Uses simultaneous fits of $\overline{B}^0 \to \overline{D}^0 D_s^+ \pi^-$ and $B^+ \to D^- D_s^+ \pi^+$ amplitudes assuming isospin symmetry.

$\Gamma(\overline{D}^{*}(2007)^0 D_s^+)/\Gamma_{total}$ — Γ_{203}/Γ

VALUE (units 10^{-3})	DOCUMENT ID		TECN	COMMENT
7.0±1.0 OUR AVERAGE				
6.5±1.0±0.6	[1] ADACHI	24L	BEL2	$e^+e^- \to \Upsilon(4S)$
7.8±1.8±0.7	[2] AUBERT	06N	BABR	$e^+e^- \to \Upsilon(4S)$
11 ±4 ±1	[3] GIBAUT	96	CLE2	$e^+e^- \to \Upsilon(4S)$
8 ±6 ±1	[4] ALBRECHT	92G	ARG	$e^+e^- \to \Upsilon(4S)$

[1] Used 362 fb^{-1} Belle II data and $B(\Upsilon(4S) \to B^0\overline{B}^0)$=0.484 ± 0.012.

[2] AUBERT 06N reports $(0.76 \pm 0.15 \pm 0.13) \times 10^{-2}$ from a measurement of $[\Gamma(B^+ \to \overline{D}^*(2007)^0 D_s^+)/\Gamma_{total}] \times [B(D_s^+ \to \phi\pi^+)]$ assuming $B(D_s^+ \to \phi\pi^+) = 0.0462 \pm 0.0062$, which we rescale to our best (shown rounded) value $B(D_s^+ \to \phi\pi^+) = (4.5 \pm 0.4) \times 10^{-2}$. Our first error is their experiment's error and our second error is the systematic error from using our best (shown rounded) value.

[3] GIBAUT 96 reports $0.0140 \pm 0.0043 \pm 0.0035$ from a measurement of $[\Gamma(B^+ \to \overline{D}^*(2007)^0 D_s^+)/\Gamma_{total}] \times [B(D_s^+ \to \phi\pi^+)]$ assuming $B(D_s^+ \to \phi\pi^+) = 0.035$, which we rescale to our best (shown rounded) value $B(D_s^+ \to \phi\pi^+) = (4.5 \pm 0.4) \times 10^{-2}$. Our first error is their experiment's error and our second error is the systematic error from using our best (shown rounded) value.

[4] ALBRECHT 92G reports $0.013 \pm 0.009 \pm 0.002$ from a measurement of $[\Gamma(B^+ \to \overline{D}^*(2007)^0 D_s^+)/\Gamma_{total}] \times [B(D_s^+ \to \phi\pi^+)]$ assuming $B(D_s^+ \to \phi\pi^+) = 0.027$, which we rescale to our best (shown rounded) value $B(D_s^+ \to \phi\pi^+) = (4.5 \pm 0.4) \times 10^{-2}$. Our first error is their experiment's error and our second error is the systematic error from using our best (shown rounded) value. Assumes PDG 1990 D^0 and $D^*(2007)^0$ branching ratios, e.g., $B(D^0 \to K^-\pi^+) = 3.71 \pm 0.25\%$ and $B(D^*(2007)^0 \to D^0\pi^0) = 55 \pm 6\%$.

$\Gamma(\overline{D}^{*}(2007)^0 D_s^{*+})/\Gamma_{total}$ — Γ_{205}/Γ

VALUE	DOCUMENT ID		TECN	COMMENT
0.0171±0.0024 OUR AVERAGE				
0.0167±0.0019±0.0015	[1] AUBERT	06N	BABR	$e^+e^- \to \Upsilon(4S)$
0.024 ±0.009 ±0.002	[2] GIBAUT	96	CLE2	$e^+e^- \to \Upsilon(4S)$
0.019 ±0.010 ±0.002	[3] ALBRECHT	92G	ARG	$e^+e^- \to \Upsilon(4S)$

[1] AUBERT 06N reports $(1.62 \pm 0.22 \pm 0.18) \times 10^{-2}$ from a measurement of $[\Gamma(B^+ \to \overline{D}^*(2007)^0 D_s^{*+})/\Gamma_{total}] \times [B(D_s^+ \to \phi\pi^+)]$ assuming $B(D_s^+ \to \phi\pi^+) = 0.0462 \pm 0.0062$, which we rescale to our best (shown rounded) value $B(D_s^+ \to \phi\pi^+) = (4.5 \pm 0.4) \times 10^{-2}$. Our first error is their experiment's error and our second error is the systematic error from using our best (shown rounded) value.

[2] GIBAUT 96 reports $0.0310 \pm 0.0088 \pm 0.0065$ from a measurement of $[\Gamma(B^+ \to \overline{D}^*(2007)^0 D_s^{*+})/\Gamma_{total}] \times [B(D_s^+ \to \phi\pi^+)]$ assuming $B(D_s^+ \to \phi\pi^+) = 0.035$, which we rescale to our best (shown rounded) value $B(D_s^+ \to \phi\pi^+) = (4.5 \pm 0.4) \times 10^{-2}$. Our first error is their experiment's error and our second error is the systematic error from using our best (shown rounded) value.

[3] ALBRECHT 92G reports $0.031 \pm 0.016 \pm 0.005$ from a measurement of $[\Gamma(B^+ \to \overline{D}^*(2007)^0 D_s^{*+})/\Gamma_{total}] \times [B(D_s^+ \to \phi\pi^+)]$ assuming $B(D_s^+ \to \phi\pi^+) = 0.027$, which we rescale to our best (shown rounded) value $B(D_s^+ \to \phi\pi^+) = (4.5 \pm 0.4) \times 10^{-2}$. Our first error is their experiment's error and our second error is the systematic error from using our best (shown rounded) value. Assumes PDG 1990 D^0 and $D^*(2007)^0$ branching ratios, e.g., $B(D^0 \to K^-\pi^+) = 3.71 \pm 0.25\%$ and $B(D^*(2007)^0 \to D^0\pi^0) = 55 \pm 6\%$.

$\Gamma(\overline{D}_2^{*}(2460)^0 D_s^+,\ \overline{D}_2^{*0} \to D^-\pi^+)/\Gamma(D^- D_s^+ \pi^+)$ — $\Gamma_{206}/\Gamma_{202}$

VALUE (units 10^{-2})	DOCUMENT ID		TECN	COMMENT
22.35±0.91±0.71	[1] AAIJ	23B	LHCB	pp at 7, 8, 13 TeV

[1] Uses simultaneous fits of $\overline{B}^0 \to \overline{D}^0 D_s^+ \pi^-$ and $B^+ \to D^- D_s^+ \pi^+$ amplitudes assuming isospin symmetry.

$\Gamma(\overline{D}_1^{*}(2600)^0 D_s^+,\ \overline{D}_1^{*0} \to D^-\pi^+)/\Gamma(D^- D_s^+ \pi^+)$ — $\Gamma_{209}/\Gamma_{202}$

VALUE (units 10^{-2})	DOCUMENT ID		TECN	COMMENT
1.37±0.42±0.62	[1] AAIJ	23B	LHCB	pp at 7, 8, 13 TeV

[1] Uses simultaneous fits of $\overline{B}^0 \to \overline{D}^0 D_s^+ \pi^-$ and $B^+ \to D^- D_s^+ \pi^+$ amplitudes assuming isospin symmetry.

$\Gamma(\overline{D}_3^{*}(2750)^0 D_s^+,\ \overline{D}_3^{*0} \to D^-\pi^+)/\Gamma(D^- D_s^+ \pi^+)$ — $\Gamma_{210}/\Gamma_{202}$

VALUE (units 10^{-2})	DOCUMENT ID		TECN	COMMENT
0.31±0.15±0.17	[1] AAIJ	23B	LHCB	pp at 7, 8, 13 TeV

[1] Uses simultaneous fits of $\overline{B}^0 \to \overline{D}^0 D_s^+ \pi^-$ and $B^+ \to D^- D_s^+ \pi^+$ amplitudes assuming isospin symmetry.

$\Gamma(\overline{D}_1^{*}(2760)^0 D_s^+,\ \overline{D}_1^{*0} \to D^-\pi^+)/\Gamma(D^- D_s^+ \pi^+)$ — $\Gamma_{211}/\Gamma_{202}$

VALUE (units 10^{-2})	DOCUMENT ID		TECN	COMMENT
0.28±0.26±1.53	[1] AAIJ	23B	LHCB	pp at 7, 8, 13 TeV

[1] Uses simultaneous fits of $\overline{B}^0 \to \overline{D}^0 D_s^+ \pi^-$ and $B^+ \to D^- D_s^+ \pi^+$ amplitudes assuming isospin symmetry.

$\Gamma(\overline{D}_J^{*}(3000)^0 D_s^+,\ \overline{D}_J^{*0} \to D^-\pi^+)/\Gamma(D^- D_s^+ \pi^+)$ — $\Gamma_{212}/\Gamma_{202}$

VALUE (units 10^{-2})	DOCUMENT ID		TECN	COMMENT
0.45±0.16±0.37	[1] AAIJ	23B	LHCB	pp at 7, 8, 13 TeV

[1] Uses simultaneous fits of $\overline{B}^0 \to \overline{D}^0 D_s^+ \pi^-$ and $B^+ \to D^- D_s^+ \pi^+$ amplitudes assuming isospin symmetry.

$\Gamma(T_{cs0}^{*}(2900)^{++} D^-,\ T_{cs0}^{*++} \to D_s^+\pi^+)/\Gamma(D^- D_s^+ \pi^+)$ — $\Gamma_{213}/\Gamma_{202}$

VALUE (units 10^{-2})	DOCUMENT ID		TECN	COMMENT
2.25±0.67±0.77	[1] AAIJ	23B	LHCB	pp at 7, 8, 13 TeV

[1] Uses simultaneous fits of $\overline{B}^0 \to \overline{D}^0 D_s^+ \pi^-$ and $B^+ \to D^- D_s^+ \pi^+$ amplitudes assuming isospin symmetry.

$\Gamma(D_s^{(*)+}\overline{D}^{**0})/\Gamma_{total}$ — Γ_{214}/Γ

VALUE	DOCUMENT ID		TECN	COMMENT
(2.73±0.93±0.68) × 10^{-2}	[1] AHMED	00B	CLE2	$e^+e^- \to \Upsilon(4S)$

[1] AHMED 00B reports their experiment's uncertainties (±0.78 ± 0.48 ± 0.68)%, where the first error is statistical, the second is systematic, and the third is the uncertainty in the $D_S \to \phi\pi$ branching fraction. We combine the first two in quadrature.

$\Gamma(\overline{D}^{*}(2007)^0 D^{*}(2010)^+)/\Gamma_{total}$ — Γ_{215}/Γ

VALUE (units 10^{-4})	CL%	DOCUMENT ID		TECN	COMMENT
8.1±1.2±1.2		[1] AUBERT,B	06A	BABR	$e^+e^- \to \Upsilon(4S)$
• • • We do not use the following data for averages, fits, limits, etc. • • •					
<110	90	BARATE	98Q	ALEP	$e^+e^- \to Z$

[1] Assumes equal production of B^+ and B^0 at the $\Upsilon(4S)$.

$[\Gamma(\overline{D}^0 D^{*}(2010)^+) + \Gamma(\overline{D}^{*}(2007)^0 D^+)]/\Gamma_{total}$ — Γ_{216}/Γ

VALUE (units 10^{-4})	CL%	DOCUMENT ID		TECN	COMMENT
<130	90	BARATE	98Q	ALEP	$e^+e^- \to Z$

$\Gamma(\overline{D}^0 D^{*}(2010)^+)/\Gamma_{total}$ — Γ_{217}/Γ

VALUE (units 10^{-4})	DOCUMENT ID		TECN	COMMENT
3.9 ±0.5 OUR AVERAGE				
3.6 ±0.5 ±0.4	[1] AUBERT,B	06A	BABR	$e^+e^- \to \Upsilon(4S)$
4.57±0.71±0.56	[1] MAJUMDER	05	BELL	$e^+e^- \to \Upsilon(4S)$

[1] Assumes equal production of B^+ and B^0 at the $\Upsilon(4S)$.

$\Gamma(\overline{D}^0 D^+)/\Gamma_{total}$ — Γ_{218}/Γ

VALUE (units 10^{-4})	CL%	DOCUMENT ID		TECN	COMMENT
3.8 ±0.4 OUR AVERAGE					
3.85±0.31±0.38		[1] ADACHI	08	BELL	$e^+e^- \to \Upsilon(4S)$
3.8 ±0.6 ±0.5		[1] AUBERT,B	06A	BABR	$e^+e^- \to \Upsilon(4S)$
• • • We do not use the following data for averages, fits, limits, etc. • • •					
4.83±0.78±0.58		[1] MAJUMDER	05	BELL	Repl. by ADACHI 08
<67	90	BARATE	98Q	ALEP	$e^+e^- \to Z$

[1] Assumes equal production of B^+ and B^0 at the $\Upsilon(4S)$.

Int. J. Mod. Phys. A 2026.41. Downloaded from www.worldscientific.com by LIFORNIA @ BERKELEY on 09/16/26. Re-use and distribution is strictly not permitted, except for Open Access articles.

$\Gamma(\overline{D}^0 D^*(2010)^+)/\Gamma(\overline{D}^0 D^+)$ — $\Gamma_{217}/\Gamma_{218}$

VALUE	DOCUMENT ID		TECN	COMMENT
0.271±0.007±0.005	AAIJ	23AX	LHCB	pp at 7, 8, 13 TeV

$\Gamma(\overline{D}^0 D^+ K^0)/\Gamma_{total}$ — Γ_{219}/Γ

VALUE (units 10^{-3})	CL%	DOCUMENT ID		TECN	COMMENT
1.55±0.17±0.13		[1] DEL-AMO-SA...	11B	BABR	$e^+e^- \to \Upsilon(4S)$
• • • We do not use the following data for averages, fits, limits, etc. • • •					
<2.8	90	[1] AUBERT	03X	BABR	Repl. by DEL-AMO-SANCHEZ 11B

[1] Assumes equal production of B^+ and B^0 at the $\Upsilon(4S)$.

$\Gamma(D^+ \overline{D}^*(2007)^0)/\Gamma_{total}$ — Γ_{220}/Γ

VALUE (units 10^{-4})	DOCUMENT ID		TECN	COMMENT
6.3±1.4±1.0	[1] AUBERT,B	06A	BABR	$e^+e^- \to \Upsilon(4S)$

[1] Assumes equal production of B^+ and B^0 at the $\Upsilon(4S)$.

$\Gamma(\overline{D}^*(2007)^0 D^+ K^0)/\Gamma_{total}$ — Γ_{221}/Γ

VALUE (units 10^{-3})	CL%	DOCUMENT ID		TECN	COMMENT
2.06±0.38±0.30		[1] DEL-AMO-SA...	11B	BABR	$e^+e^- \to \Upsilon(4S)$
• • • We do not use the following data for averages, fits, limits, etc. • • •					
<6.1	90	[1] AUBERT	03X	BABR	Repl. by DEL-AMO-SANCHEZ 11B

[1] Assumes equal production of B^+ and B^0 at the $\Upsilon(4S)$.

$\Gamma(\overline{D}^0 D^*(2010)^+ K^0)/\Gamma_{total}$ — Γ_{222}/Γ

VALUE (units 10^{-3})	DOCUMENT ID		TECN	COMMENT
3.81±0.31±0.23	[1] DEL-AMO-SA...	11B	BABR	$e^+e^- \to \Upsilon(4S)$
• • • We do not use the following data for averages, fits, limits, etc. • • •				
$5.2\ ^{+1.0}_{-0.9}\ \pm0.7$	[1] AUBERT	03X	BABR	Repl. by DEL-AMO-SANCHEZ 11B

[1] Assumes equal production of B^+ and B^0 at the $\Upsilon(4S)$.

$\Gamma(\overline{D}^*(2007)^0 D^*(2010)^+ K^0)/\Gamma_{total}$ — Γ_{223}/Γ

VALUE (units 10^{-3})	DOCUMENT ID		TECN	COMMENT
9.17±0.83±0.90	[1] DEL-AMO-SA...	11B	BABR	$e^+e^- \to \Upsilon(4S)$
• • • We do not use the following data for averages, fits, limits, etc. • • •				
$7.8\ ^{+2.3}_{-2.1}\ \pm1.4$	[1] AUBERT	03X	BABR	Repl. by DEL-AMO-SANCHEZ 11B

[1] Assumes equal production of B^+ and B^0 at the $\Upsilon(4S)$.

$\Gamma(\overline{D}^0 D^0 K^+)/\Gamma_{total}$ — Γ_{224}/Γ

VALUE (units 10^{-3})	DOCUMENT ID		TECN	COMMENT
1.45±0.33 OUR AVERAGE	Error includes scale factor of 2.6.			
1.31±0.07±0.12	[1] DEL-AMO-SA...	11B	BABR	$e^+e^- \to \Upsilon(4S)$
$2.22\pm0.22\ ^{+0.26}_{-0.24}$	[1] BRODZICKA	08	BELL	$e^+e^- \to \Upsilon(4S)$
• • • We do not use the following data for averages, fits, limits, etc. • • •				
1.17±0.21±0.15	[1] CHISTOV	04	BELL	Repl. by BRODZICKA 08
1.9 ±0.3 ±0.3	[1] AUBERT	03X	BABR	Repl. by DEL-AMO-SANCHEZ 11B

[1] Assumes equal production of B^+ and B^0 at the $\Upsilon(4S)$.

$\Gamma(\overline{D}^*(2007)^0 D^0 K^+)/\Gamma_{total}$ — Γ_{225}/Γ

VALUE (units 10^{-3})	CL%	DOCUMENT ID		TECN	COMMENT
2.26±0.16±0.17		[1] DEL-AMO-SA...	11B	BABR	$e^+e^- \to \Upsilon(4S)$
• • • We do not use the following data for averages, fits, limits, etc. • • •					
<3.8	90	[1] AUBERT	03X	BABR	Repl. by DEL-AMO-SANCHEZ 11B

[1] Assumes equal production of B^+ and B^0 at the $\Upsilon(4S)$.

$\Gamma(\overline{D}^0 D^*(2007)^0 K^+)/\Gamma_{total}$ — Γ_{226}/Γ

VALUE (units 10^{-3})	DOCUMENT ID		TECN	COMMENT
6.32±0.19±0.45	[1] DEL-AMO-SA...	11B	BABR	$e^+e^- \to \Upsilon(4S)$
• • • We do not use the following data for averages, fits, limits, etc. • • •				
4.7 ±0.7 ±0.7	[1] AUBERT	03X	BABR	Repl. by DEL-AMO-SANCHEZ 11B

[1] Assumes equal production of B^+ and B^0 at the $\Upsilon(4S)$.

$\Gamma(\overline{D}^*(2007)^0 D^*(2007)^0 K^+)/\Gamma_{total}$ — Γ_{227}/Γ

VALUE (units 10^{-3})	DOCUMENT ID		TECN	COMMENT
11.23±0.36±1.26	[1] DEL-AMO-SA...	11B	BABR	$e^+e^- \to \Upsilon(4S)$
• • • We do not use the following data for averages, fits, limits, etc. • • •				
$5.3\ ^{+1.1}_{-1.0}\ \pm1.2$	[1] AUBERT	03X	BABR	Repl. by DEL-AMO-SANCHEZ 11B

[1] Assumes equal production of B^+ and B^0 at the $\Upsilon(4S)$.

$\Gamma(D^- D^+ K^+)/\Gamma_{total}$ — Γ_{228}/Γ

VALUE (units 10^{-3})	CL%	DOCUMENT ID		TECN	COMMENT
0.22±0.05±0.05		[1] DEL-AMO-SA...	11B	BABR	$e^+e^- \to \Upsilon(4S)$
• • • We do not use the following data for averages, fits, limits, etc. • • •					
<0.90	90	[1] CHISTOV	04	BELL	$e^+e^- \to \Upsilon(4S)$
<0.4	90	[1] AUBERT	03X	BABR	Repl. by DEL-AMO-SANCHEZ 11B

[1] Assumes equal production of B^+ and B^0 at the $\Upsilon(4S)$.

$\Gamma(T^*_{cs0}(2870)^0 D^+,\ T^{*0}_{cs0} \to D^- K^+)/\Gamma(D^- D^+ K^+)$ — $\Gamma_{229}/\Gamma_{228}$

VALUE (units 10^{-2})	DOCUMENT ID		TECN	COMMENT
5.6±1.4±0.5	[1] AAIJ	20AI	LHCB	pp at 7, 8, 13 TeV

[1] Measured in Dalitz plot analysis of $B^+ \to D^- D^+ K^+$ decays.

$\Gamma(T^*_{cs1}(2900)^0 D^+,\ T^{*0}_{cs1} \to D^- K^+)/\Gamma(D^- D^+ K^+)$ — $\Gamma_{230}/\Gamma_{228}$

VALUE (units 10^{-2})	DOCUMENT ID		TECN	COMMENT
30.6±2.4±2.1	[1] AAIJ	20AI	LHCB	pp at 7, 8, 13 TeV

[1] Measured in Dalitz plot analysis of $B^+ \to D^- D^+ K^+$ decays.

$\Gamma(D^- D^+ K^+ \text{nonresonant})/\Gamma(D^- D^+ K^+)$ — $\Gamma_{231}/\Gamma_{228}$

VALUE (units 10^{-2})	DOCUMENT ID		TECN	COMMENT
24.2±2.2±0.5	[1] AAIJ	20AI	LHCB	pp at 7, 8, 13 TeV

[1] Measured in Dalitz plot analysis of $B^+ \to D^- D^+ K^+$ decays.

$\Gamma(D^- D^*(2010)^+ K^+)/\Gamma_{total}$ — Γ_{232}/Γ

VALUE (units 10^{-3})	CL%	DOCUMENT ID		TECN	COMMENT
0.63±0.09±0.06		[1] DEL-AMO-SA...	11B	BABR	$e^+e^- \to \Upsilon(4S)$
• • • We do not use the following data for averages, fits, limits, etc. • • •					
<0.7	90	[1] AUBERT	03X	BABR	Repl. by DEL-AMO-SANCHEZ 11B

[1] Assumes equal production of B^+ and B^0 at the $\Upsilon(4S)$.

$\Gamma(D^- D^*(2010)^+ K^+)/\Gamma(\overline{D}^0 D^0 K^+)$ — $\Gamma_{232}/\Gamma_{224}$

VALUE	DOCUMENT ID		TECN	COMMENT
0.517±0.015±0.017	[1] AAIJ	20AN	LHCB	pp at 7, 8, 13 TeV

[1] Uses $D^+ \to K^-\pi^+\pi^+$, $D^0 \to K^-\pi^+$ and $D^0 \to K^-\pi^+\pi^+\pi^-$ decays.

$\Gamma(D^*(2010)^- D^+ K^+)/\Gamma_{total}$ — Γ_{233}/Γ

VALUE (units 10^{-3})	DOCUMENT ID		TECN	COMMENT
0.60±0.10±0.08	[1] DEL-AMO-SA...	11B	BABR	$e^+e^- \to \Upsilon(4S)$
• • • We do not use the following data for averages, fits, limits, etc. • • •				
1.5 ±0.3 ±0.2	[1] AUBERT	03X	BABR	Repl. by DEL-AMO-SANCHEZ 11B

[1] Assumes equal production of B^+ and B^0 at the $\Upsilon(4S)$.

$\Gamma(D^*(2010)^- D^+ K^+)/\Gamma(\overline{D}^0 D^0 K^+)$ — $\Gamma_{233}/\Gamma_{224}$

VALUE	DOCUMENT ID		TECN	COMMENT
0.577±0.016±0.018	[1] AAIJ	20AN	LHCB	pp at 7, 8, 13 TeV

[1] Uses $D^+ \to K^-\pi^+\pi^+$, $D^0 \to K^-\pi^+$ and $D^0 \to K^-\pi^+\pi^+\pi^-$ decays.

$\Gamma(D^- D^*(2010)^+ K^+)/\Gamma(D^*(2010)^- D^+ K^+)$ — $\Gamma_{232}/\Gamma_{233}$

VALUE	DOCUMENT ID		TECN	COMMENT
0.907±0.033±0.014	[1] AAIJ	20AN	LHCB	pp at 7, 8, 13 TeV

[1] Uses $D^+ \to K^-\pi^+\pi^+$, $D^0 \to K^-\pi^+$ and $D^0 \to K^-\pi^+\pi^+\pi^-$ decays.

$\Gamma(\text{EFF}\,K+, \text{EFF} \to D^*(2010)^{\mp} D^{\pm})/\Gamma_{total}$ — Γ_{234}/Γ

VALUE (units 10^{-4})	DOCUMENT ID		TECN	COMMENT
$\mathbf{1.48^{+0.32+0.26}_{-0.16-0.32}}$	AAIJ	24AB	LHCB	pp at 7, 8, and 13 TeV

$\Gamma(\eta_c(3945) K^+,\ \eta_c \to D^*(2010)^{\mp} D^{\pm})/\Gamma_{total}$ — Γ_{235}/Γ

VALUE (units 10^{-4})	DOCUMENT ID		TECN	COMMENT
$\mathbf{0.46^{+0.08+0.26}_{-0.14-0.10}}$	AAIJ	24AB	LHCB	pp at 7, 8, and 13 TeV

$\Gamma(h_c(4000) K^+,\ h_c \to D^*(2010)^{\mp} D^{\pm})/\Gamma_{total}$ — Γ_{237}/Γ

VALUE (units 10^{-4})	DOCUMENT ID		TECN	COMMENT
$\mathbf{0.70^{+0.14+0.21}_{-0.10-0.12}}$	AAIJ	24AB	LHCB	pp at 7, 8, and 13 TeV

$\Gamma(\chi_{c2}(3930) K^+,\ \chi_{c2} \to D^*(2010)^{\mp} D^{\pm})/\Gamma_{total}$ — Γ_{236}/Γ

VALUE (units 10^{-4})	DOCUMENT ID		TECN	COMMENT
$\mathbf{0.24\pm0.06^{+0.08}_{-0.16}}$	AAIJ	24AB	LHCB	pp at 7, 8, and 13 TeV

$\Gamma(\chi_{c1}(4010) K^+,\ \chi_{c1} \to D^*(2010)^{\mp} D^{\pm})/\Gamma_{total}$ — Γ_{238}/Γ

VALUE (units 10^{-4})	DOCUMENT ID		TECN	COMMENT
$\mathbf{1.38^{+0.22+0.22}_{-0.12-0.25}}$	AAIJ	24AB	LHCB	pp at 7, 8, and 13 TeV

$\Gamma(\psi(4040) K^+,\ \psi \to D^*(2010)^{\mp} D^{\pm})/\Gamma_{total}$ — Γ_{239}/Γ

VALUE (units 10^{-4})	DOCUMENT ID		TECN	COMMENT
$\mathbf{0.38^{+0.08}_{-0.06}\pm0.07}$	AAIJ	24AB	LHCB	pp at 7, 8, and 13 TeV

Int. J. Mod. Phys. A 2026.41. Downloaded from www.worldscientific.com
by UNIVERSITY OF CALIFORNIA @ BERKELEY on 09/16/26. Re-use and distribution is strictly not permitted, except for Open Access articles.

$\Gamma(h_c(4300)K^+,\ h_c \to D^*(2010)^{\mp} D^{\pm})/\Gamma_{total}$ — Γ_{240}/Γ

VALUE (units 10^{-4})	DOCUMENT ID		TECN	COMMENT
$0.16^{+0.02+0.04}_{-0.06-0.03}$	AAIJ	24AB	LHCB	pp at 7, 8, and 13 TeV

$\Gamma(T^*_{\overline{c}s0}(2870)^0 K^+,\ T^{*0}_{\overline{c}s0} \to D^*(2010)^{\mp} D^{\pm})/\Gamma_{total}$ — Γ_{241}/Γ

VALUE (units 10^{-4})	DOCUMENT ID		TECN	COMMENT
$0.45^{+0.06+0.10}_{-0.08-0.11}$	AAIJ	24AB	LHCB	pp at 7, 8, and 13 TeV

$\Gamma(T^*_{\overline{c}s1}(2900)^0 K^+,\ T^{*0}_{\overline{c}s1} \to D^*(2010)^{\mp} D^{\pm})/\Gamma_{total}$ — Γ_{242}/Γ

VALUE (units 10^{-4})	DOCUMENT ID		TECN	COMMENT
$0.38^{+0.07+0.16}_{-0.10-0.12}$	AAIJ	24AB	LHCB	pp at 7, 8, and 13 TeV

$\Gamma(\mathrm{NR}K^+,\ \mathrm{NR} \to D^*(2010)^{\mp} D^{\pm})/\Gamma_{total}$ — Γ_{243}/Γ

VALUE (units 10^{-4})	DOCUMENT ID		TECN	COMMENT
$2.78^{+0.32+0.37}_{-0.08-0.42}$	[1] AAIJ	24AB	LHCB	pp at 7, 8, and 13 TeV

[1] The NR_{1--} line shape is described by $f_R(m) = 1$.

$\Gamma(\mathrm{NR}K^+,\ \mathrm{NR} \to D^*(2010)^{\mp} D^{\pm})/\Gamma_{total}$ — Γ_{244}/Γ

VALUE (units 10^{-4})	DOCUMENT ID		TECN	COMMENT
$0.16^{+0.08+0.10}_{-0.02-0.08}$	[1] AAIJ	24AB	LHCB	pp at 7, 8, and 13 TeV

[1] The NR_{0--} line shape is described by $f_R(m) = 1$.

$\Gamma(\mathrm{NR}K^+,\ \mathrm{NR} \to D^*(2010)^{\mp} D^{\pm})/\Gamma_{total}$ — Γ_{245}/Γ

VALUE (units 10^{-4})	DOCUMENT ID		TECN	COMMENT
$2.42^{+0.26+0.53}_{-0.20-0.40}$	[1] AAIJ	24AB	LHCB	pp at 7, 8, and 13 TeV

[1] Only the S-wave component is considered, and the line shape is described by $f_R(m) = 1$.

$\Gamma(\mathrm{NR}K^+,\ \mathrm{NR} \to D^*(2010)^{\mp} D^{\pm})/\Gamma_{total}$ — Γ_{246}/Γ

VALUE (units 10^{-4})	DOCUMENT ID		TECN	COMMENT
$2.18^{+0.46+0.48}_{-0.16-0.49}$	[1] AAIJ	24AB	LHCB	pp at 7, 8, and 13 TeV

[1] The NR_{0-+} line shapes is described by $f_R(m) = e^{(\alpha+\beta i)/(m^2-m_0^2)}$ with $m_0 = 4.35$ GeV. The parameters α and β are determined from the fit to the data.

$\Gamma(D^*(2010)^- D^*(2010)^+ K^+)/\Gamma_{total}$ — Γ_{247}/Γ

VALUE (units 10^{-3})	CL%	DOCUMENT ID		TECN	COMMENT
$1.32 \pm 0.13 \pm 0.12$		[1] DEL-AMO-SA...	11B	BABR	$e^+e^- \to \Upsilon(4S)$
• • • We do not use the following data for averages, fits, limits, etc. • • •					
<1.8	90	[1] AUBERT	03X	BABR	Repl. by DEL-AMO-SANCHEZ 11B

[1] Assumes equal production of B^+ and B^0 at the $\Upsilon(4S)$.

$\Gamma((\overline{D}+\overline{D}^*)(D+D^*)K)/\Gamma_{total}$ — Γ_{248}/Γ

VALUE (units 10^{-2})	DOCUMENT ID		TECN	COMMENT
$4.05 \pm 0.11 \pm 0.28$	[1] DEL-AMO-SA...	11B	BABR	$e^+e^- \to \Upsilon(4S)$
• • • We do not use the following data for averages, fits, limits, etc. • • •				
$3.5 \pm 0.3 \pm 0.5$	[1] AUBERT	03X	BABR	Repl. by DEL-AMO-SANCHEZ 11B

[1] Assumes equal production of B^+ and B^0 at the $\Upsilon(4S)$.

$\Gamma(D_s^- D_s^+ K^+)/\Gamma(D^- D^+ K^+)$ — $\Gamma_{249}/\Gamma_{228}$

VALUE	DOCUMENT ID		TECN	COMMENT
$0.525 \pm 0.033 \pm 0.027 \pm 0.034$	[1] AAIJ	23AI	LHCB	pp at 7, 8, 13 TeV

[1] AAIJ 23AI report that the last error is due to the uncertainties on the branching fractions of the $D_s^{\pm} \to K^{\mp}K^{\pm}\pi^{\pm}$ and $D^{\pm} \to K^{\mp}\pi^{\pm}\pi^{\pm}$ decays.

$\Gamma(D_s^+ \pi^0)/\Gamma_{total}$ — Γ_{250}/Γ

VALUE (units 10^{-5})	CL%	DOCUMENT ID		TECN	COMMENT
$1.6^{+0.6}_{-0.5} \pm 0.1$		[1] AUBERT	07M	BABR	$e^+e^- \to \Upsilon(4S)$
• • • We do not use the following data for averages, fits, limits, etc. • • •					
<16	90	[2] ALEXANDER	93B	CLE2	$e^+e^- \to \Upsilon(4S)$

[1] AUBERT 07M reports $[\Gamma(B^+ \to D_s^+\pi^0)/\Gamma_{total}] \times [B(D_s^+ \to \phi\pi^+)] = (7.0^{+2.4+0.6}_{-2.1-0.8}) \times 10^{-7}$ which we divide by our best (shown rounded) value $B(D_s^+ \to \phi\pi^+) = (4.5 \pm 0.4) \times 10^{-2}$. Our first error is their experiment's error and our second error is the systematic error from using our best (shown rounded) value.

[2] ALEXANDER 93B reports $< 2.0 \times 10^{-4}$ from a measurement of $[\Gamma(B^+ \to D_s^+\pi^0)/\Gamma_{total}] \times [B(D_s^+ \to \phi\pi^+)]$ assuming $B(D_s^+ \to \phi\pi^+) = 0.037$, which we rescale to our best (shown rounded) value $B(D_s^+ \to \phi\pi^+) = 4.5 \times 10^{-2}$.

$[\Gamma(D_s^+\pi^0) + \Gamma(D_s^{*+}\pi^0)]/\Gamma_{total}$ — $(\Gamma_{250}+\Gamma_{251})/\Gamma$

VALUE	CL%	DOCUMENT ID		TECN	COMMENT
$<5 \times 10^{-4}$	90	[1] ALBRECHT	93E	ARG	$e^+e^- \to \Upsilon(4S)$

[1] ALBRECHT 93E reports $< 0.9 \times 10^{-3}$ from a measurement of $[\left[\Gamma(B^+ \to D_s^+\pi^0) + \Gamma(B^+ \to D_s^{*+}\pi^0)\right]/\Gamma_{total}] \times [B(D_s^+ \to \phi\pi^+)]$ assuming $B(D_s^+ \to \phi\pi^+) = 0.027$, which we rescale to our best (shown rounded) value $B(D_s^+ \to \phi\pi^+) = 4.5 \times 10^{-2}$.

$\Gamma(D_s^{*+}\pi^0)/\Gamma_{total}$ — Γ_{251}/Γ

VALUE	CL%	DOCUMENT ID		TECN	COMMENT
$<2.6 \times 10^{-4}$	90	[1] ALEXANDER	93B	CLE2	$e^+e^- \to \Upsilon(4S)$

[1] ALEXANDER 93B reports $< 3.2 \times 10^{-4}$ from a measurement of $[\Gamma(B^+ \to D_s^{*+}\pi^0)/\Gamma_{total}] \times [B(D_s^+ \to \phi\pi^+)]$ assuming $B(D_s^+ \to \phi\pi^+) = 0.037$, which we rescale to our best (shown rounded) value $B(D_s^+ \to \phi\pi^+) = 4.5 \times 10^{-2}$.

$\Gamma(D_s^+\eta)/\Gamma_{total}$ — Γ_{252}/Γ

VALUE	CL%	DOCUMENT ID		TECN	COMMENT
$<1.4 \times 10^{-5}$	90	KUMAR	23	BELL	$e^+e^- \to \Upsilon(4S)$
• • • We do not use the following data for averages, fits, limits, etc. • • •					
$<4 \times 10^{-4}$	90	[1] ALEXANDER	93B	CLE2	$e^+e^- \to \Upsilon(4S)$

[1] ALEXANDER 93B reports $< 4.6 \times 10^{-4}$ from a measurement of $[\Gamma(B^+ \to D_s^+\eta)/\Gamma_{total}] \times [B(D_s^+ \to \phi\pi^+)]$ assuming $B(D_s^+ \to \phi\pi^+) = 0.037$, which we rescale to our best (shown rounded) value $B(D_s^+ \to \phi\pi^+) = 4.5 \times 10^{-2}$.

$\Gamma(D_s^{*+}\eta)/\Gamma_{total}$ — Γ_{253}/Γ

VALUE	CL%	DOCUMENT ID		TECN	COMMENT
$<1.7 \times 10^{-5}$	90	KUMAR	23	BELL	$e^+e^- \to \Upsilon(4S)$
• • • We do not use the following data for averages, fits, limits, etc. • • •					
$<6 \times 10^{-4}$	90	[1] ALEXANDER	93B	CLE2	$e^+e^- \to \Upsilon(4S)$

[1] ALEXANDER 93B reports $< 7.5 \times 10^{-4}$ from a measurement of $[\Gamma(B^+ \to D_s^{*+}\eta)/\Gamma_{total}] \times [B(D_s^+ \to \phi\pi^+)]$ assuming $B(D_s^+ \to \phi\pi^+) = 0.037$, which we rescale to our best (shown rounded) value $B(D_s^+ \to \phi\pi^+) = 4.5 \times 10^{-2}$.

$\Gamma(D_s^+\rho^0)/\Gamma_{total}$ — Γ_{254}/Γ

VALUE	CL%	DOCUMENT ID		TECN	COMMENT
$<3.0 \times 10^{-4}$	90	[1] ALEXANDER	93B	CLE2	$e^+e^- \to \Upsilon(4S)$

[1] ALEXANDER 93B reports $< 3.7 \times 10^{-4}$ from a measurement of $[\Gamma(B^+ \to D_s^+\rho^0)/\Gamma_{total}] \times [B(D_s^+ \to \phi\pi^+)]$ assuming $B(D_s^+ \to \phi\pi^+) = 0.037$, which we rescale to our best (shown rounded) value $B(D_s^+ \to \phi\pi^+) = 4.5 \times 10^{-2}$.

$[\Gamma(D_s^+\rho^0) + \Gamma(D_s^+\overline{K}^*(892)^0)]/\Gamma_{total}$ — $(\Gamma_{254}+\Gamma_{265})/\Gamma$

VALUE	CL%	DOCUMENT ID		TECN	COMMENT
$<2.0 \times 10^{-3}$	90	[1] ALBRECHT	93E	ARG	$e^+e^- \to \Upsilon(4S)$

[1] ALBRECHT 93E reports $< 3.4 \times 10^{-3}$ from a measurement of $[\left[\Gamma(B^+ \to D_s^+\rho^0) + \Gamma(B^+ \to D_s^+\overline{K}^*(892)^0)\right]/\Gamma_{total}] \times [B(D_s^+ \to \phi\pi^+)]$ assuming $B(D_s^+ \to \phi\pi^+) = 0.027$, which we rescale to our best (shown rounded) value $B(D_s^+ \to \phi\pi^+) = 4.5 \times 10^{-2}$.

$\Gamma(D_s^{*+}\rho^0)/\Gamma_{total}$ — Γ_{255}/Γ

VALUE	CL%	DOCUMENT ID		TECN	COMMENT
$<4 \times 10^{-4}$	90	[1] ALEXANDER	93B	CLE2	$e^+e^- \to \Upsilon(4S)$

[1] ALEXANDER 93B reports $< 4.8 \times 10^{-4}$ from a measurement of $[\Gamma(B^+ \to D_s^{*+}\rho^0)/\Gamma_{total}] \times [B(D_s^+ \to \phi\pi^+)]$ assuming $B(D_s^+ \to \phi\pi^+) = 0.037$, which we rescale to our best (shown rounded) value $B(D_s^+ \to \phi\pi^+) = 4.5 \times 10^{-2}$.

$[\Gamma(D_s^{*+}\rho^0) + \Gamma(D_s^{*+}\overline{K}^*(892)^0)]/\Gamma_{total}$ — $(\Gamma_{255}+\Gamma_{267})/\Gamma$

VALUE	CL%	DOCUMENT ID		TECN	COMMENT
$<1.2 \times 10^{-3}$	90	[1] ALBRECHT	93E	ARG	$e^+e^- \to \Upsilon(4S)$

[1] ALBRECHT 93E reports $< 2.0 \times 10^{-3}$ from a measurement of $[\left[\Gamma(B^+ \to D_s^{*+}\rho^0) + \Gamma(B^+ \to D_s^{*+}\overline{K}^*(892)^0)\right]/\Gamma_{total}] \times [B(D_s^+ \to \phi\pi^+)]$ assuming $B(D_s^+ \to \phi\pi^+) = 0.027$, which we rescale to our best (shown rounded) value $B(D_s^+ \to \phi\pi^+) = 4.5 \times 10^{-2}$.

$\Gamma(D_s^+\omega)/\Gamma_{total}$ — Γ_{256}/Γ

VALUE	CL%	DOCUMENT ID		TECN	COMMENT
$<4 \times 10^{-4}$	90	[1] ALEXANDER	93B	CLE2	$e^+e^- \to \Upsilon(4S)$
• • • We do not use the following data for averages, fits, limits, etc. • • •					
$<2.0 \times 10^{-3}$	90	[2] ALBRECHT	93E	ARG	$e^+e^- \to \Upsilon(4S)$

[1] ALEXANDER 93B reports $< 4.8 \times 10^{-4}$ from a measurement of $[\Gamma(B^+ \to D_s^+\omega)/\Gamma_{total}] \times [B(D_s^+ \to \phi\pi^+)]$ assuming $B(D_s^+ \to \phi\pi^+) = 0.037$, which we rescale to our best (shown rounded) value $B(D_s^+ \to \phi\pi^+) = 4.5 \times 10^{-2}$.

[2] ALBRECHT 93E reports $< 3.4 \times 10^{-3}$ from a measurement of $[\Gamma(B^+ \to D_s^+\omega)/\Gamma_{total}] \times [B(D_s^+ \to \phi\pi^+)]$ assuming $B(D_s^+ \to \phi\pi^+) = 0.027$, which we rescale to our best (shown rounded) value $B(D_s^+ \to \phi\pi^+) = 4.5 \times 10^{-2}$.

Int. J. Mod. Phys. A 2026.41. Downloaded from www.worldscientific.com by LIFORNIA @ BERKELEY on 09/16/26. Re-use and distribution is strictly not permitted, except for Open Access articles.

$\Gamma(D_s^{*+}\omega)/\Gamma_{total}$ — Γ_{257}/Γ

VALUE	CL%	DOCUMENT ID		TECN	COMMENT
<6 × 10⁻⁴	90	[1] ALEXANDER	93B	CLE2	$e^+e^- \to \Upsilon(4S)$
• • • We do not use the following data for averages, fits, limits, etc. • • •					
$<1.1\times10^{-3}$	90	[2] ALBRECHT	93E	ARG	$e^+e^- \to \Upsilon(4S)$

[1] ALEXANDER 93B reports $<6.8\times10^{-4}$ from a measurement of $[\Gamma(B^+\to D_s^{*+}\omega)/\Gamma_{total}]\times[B(D_s^+\to\phi\pi^+)]$ assuming $B(D_s^+\to\phi\pi^+)=0.037$, which we rescale to our best (shown rounded) value $B(D_s^+\to\phi\pi^+)=4.5\times10^{-2}$.

[2] ALBRECHT 93E reports $<1.9\times10^{-3}$ from a measurement of $[\Gamma(B^+\to D_s^{*+}\omega)/\Gamma_{total}]\times[B(D_s^+\to\phi\pi^+)]$ assuming $B(D_s^+\to\phi\pi^+)=0.037$, which we rescale to our best (shown rounded) value $B(D_s^+\to\phi\pi^+)=4.5\times10^{-2}$.

$\Gamma(D_s^+ a_1(1260)^0)/\Gamma_{total}$ — Γ_{258}/Γ

VALUE	CL%	DOCUMENT ID		TECN	COMMENT
<1.8 × 10⁻³	90	[1] ALBRECHT	93E	ARG	$e^+e^- \to \Upsilon(4S)$

[1] ALBRECHT 93E reports $<3.0\times10^{-3}$ from a measurement of $[\Gamma(B^+\to D_s^+a_1(1260)^0)/\Gamma_{total}]\times[B(D_s^+\to\phi\pi^+)]$ assuming $B(D_s^+\to\phi\pi^+)=0.027$, which we rescale to our best (shown rounded) value $B(D_s^+\to\phi\pi^+)=4.5\times10^{-2}$.

$\Gamma(D_s^{*+} a_1(1260)^0)/\Gamma_{total}$ — Γ_{259}/Γ

VALUE	CL%	DOCUMENT ID		TECN	COMMENT
<1.3 × 10⁻³	90	[1] ALBRECHT	93E	ARG	$e^+e^- \to \Upsilon(4S)$

[1] ALBRECHT 93E reports $<2.2\times10^{-3}$ from a measurement of $[\Gamma(B^+\to D_s^{*+}a_1(1260)^0)/\Gamma_{total}]\times[B(D_s^+\to\phi\pi^+)]$ assuming $B(D_s^+\to\phi\pi^+)=0.027$, which we rescale to our best (shown rounded) value $B(D_s^+\to\phi\pi^+)=4.5\times10^{-2}$.

$\Gamma(D_s^+K^+K^-)/\Gamma(\overline{D}^0D_s^+)$ — $\Gamma_{260}/\Gamma_{181}$

VALUE (units 10^{-4})	DOCUMENT ID		TECN	COMMENT
8.0±0.9±0.1	[1] AAIJ	18B	LHCB	pp at 7, 8, 13 TeV

[1] AAIJ 18B reports $[\Gamma(B^+\to D_s^+K^+K^-)/\Gamma(B^+\to\overline{D}^0D_s^+)]\,/\,[B(D^0\to K^+K^-)]=0.197\pm0.015\pm0.017$ which we multiply by our best (shown rounded) value $B(D^0\to K^+K^-)=(4.07\pm0.06)\times10^{-3}$. Our first error is their experiment's error and our second error is the systematic error from using our best (shown rounded) value.

$\Gamma(D_s^+\phi)/\Gamma_{total}$ — Γ_{261}/Γ

VALUE (units 10^{-6})	CL%	DOCUMENT ID		TECN	COMMENT
< 0.42	90	[1] AAIJ	18B	LHCB	pp at 7, 8, 13 TeV
• • • We do not use the following data for averages, fits, limits, etc. • • •					
$1.7\ ^{+1.2}_{-0.7}\pm0.1$		[2] AAIJ	13R	LHCB	Repl. by AAIJ 18B
< 1.9	90	[3] AUBERT	06F	BABR	$e^+e^- \to \Upsilon(4S)$
<1000	90	[4] ALBRECHT	93E	ARG	$e^+e^- \to \Upsilon(4S)$
< 260	90	[5] ALEXANDER	93B	CLE2	$e^+e^- \to \Upsilon(4S)$

[1] AAIJ 18B uses $B^+\to D_s^+\overline{D}^0$ decays for normalization.

[2] AAIJ 13R reports $(1.87^{+1.25}_{-0.73}\pm0.19\pm0.32)\times10^{-6}$ from a measurement of $[\Gamma(B^+\to D_s^+\phi)/\Gamma_{total}]\,/\,[B(B^+\to\overline{D}^0D_s^+)]$ assuming $B(B^+\to\overline{D}^0D_s^+)=(10.0\pm1.7)\times10^{-3}$, which we rescale to our best (shown rounded) value $B(B^+\to\overline{D}^0D_s^+)=(9.3\pm0.6)\times10^{-3}$. Our first error is their experiment's error and our second error is the systematic error from using our best (shown rounded) value.

[3] Assumes equal production of B^+ and B^0 at the $\Upsilon(4S)$.

[4] ALBRECHT 93E reports $<1.7\times10^{-3}$ from a measurement of $[\Gamma(B^+\to D_s^+\phi)/\Gamma_{total}]\times[B(D_s^+\to\phi\pi^+)]$ assuming $B(D_s^+\to\phi\pi^+)=0.027$, which we rescale to our best (shown rounded) value $B(D_s^+\to\phi\pi^+)=4.5\times10^{-2}$.

[5] ALEXANDER 93B reports $<3.1\times10^{-4}$ from a measurement of $[\Gamma(B^+\to D_s^+\phi)/\Gamma_{total}]\times[B(D_s^+\to\phi\pi^+)]$ assuming $B(D_s^+\to\phi\pi^+)=0.037$, which we rescale to our best (shown rounded) value $B(D_s^+\to\phi\pi^+)=4.5\times10^{-2}$.

$\Gamma(D_s^{*+}\phi)/\Gamma_{total}$ — Γ_{262}/Γ

VALUE	CL%	DOCUMENT ID		TECN	COMMENT
<1.2 × 10⁻⁵	90	[1] AUBERT	06F	BABR	$e^+e^- \to \Upsilon(4S)$
• • • We do not use the following data for averages, fits, limits, etc. • • •					
$<1.3\times10^{-3}$	90	[2] ALBRECHT	93E	ARG	$e^+e^- \to \Upsilon(4S)$
$<3.5\times10^{-4}$	90	[3] ALEXANDER	93B	CLE2	$e^+e^- \to \Upsilon(4S)$

[1] Assumes equal production of B^+ and B^0 at the $\Upsilon(4S)$.

[2] ALBRECHT 93E reports $<2.1\times10^{-3}$ from a measurement of $[\Gamma(B^+\to D_s^{*+}\phi)/\Gamma_{total}]\times[B(D_s^+\to\phi\pi^+)]$ assuming $B(D_s^+\to\phi\pi^+)=0.027$, which we rescale to our best (shown rounded) value $B(D_s^+\to\phi\pi^+)=4.5\times10^{-2}$.

[3] ALEXANDER 93B reports $<4.2\times10^{-4}$ from a measurement of $[\Gamma(B^+\to D_s^{*+}\phi)/\Gamma_{total}]\times[B(D_s^+\to\phi\pi^+)]$ assuming $B(D_s^+\to\phi\pi^+)=0.037$, which we rescale to our best (shown rounded) value $B(D_s^+\to\phi\pi^+)=4.5\times10^{-2}$.

$\Gamma(D_s^+\overline{K}^0)/\Gamma_{total}$ — Γ_{263}/Γ

VALUE	CL%	DOCUMENT ID		TECN	COMMENT
<3 × 10⁻⁶	90	KUMAR	23	BELL	$e^+e^- \to \Upsilon(4S)$
• • • We do not use the following data for averages, fits, limits, etc. • • •					
$<1.5\times10^{-3}$	90	[1] ALBRECHT	93E	ARG	$e^+e^- \to \Upsilon(4S)$
$<8\times10^{-4}$	90	[2] ALEXANDER	93B	CLE2	$e^+e^- \to \Upsilon(4S)$

[1] ALBRECHT 93E reports $<2.5\times10^{-3}$ from a measurement of $[\Gamma(B^+\to D_s^+\overline{K}^0)/\Gamma_{total}]\times[B(D_s^+\to\phi\pi^+)]$ assuming $B(D_s^+\to\phi\pi^+)=0.027$, which we rescale to our best (shown rounded) value $B(D_s^+\to\phi\pi^+)=4.5\times10^{-2}$.

[2] ALEXANDER 93B reports $<10.3\times10^{-4}$ from a measurement of $[\Gamma(B^+\to D_s^+\overline{K}^0)/\Gamma_{total}]\times[B(D_s^+\to\phi\pi^+)]$ assuming $B(D_s^+\to\phi\pi^+)=0.037$, which we rescale to our best (shown rounded) value $B(D_s^+\to\phi\pi^+)=4.5\times10^{-2}$.

$\Gamma(D_s^{*+}\overline{K}^0)/\Gamma_{total}$ — Γ_{264}/Γ

VALUE	CL%	DOCUMENT ID		TECN	COMMENT
<6 × 10⁻⁶	90	KUMAR	23	BELL	$e^+e^- \to \Upsilon(4S)$
• • • We do not use the following data for averages, fits, limits, etc. • • •					
$<1.9\times10^{-3}$	90	[1] ALBRECHT	93E	ARG	$e^+e^- \to \Upsilon(4S)$
$<9\times10^{-4}$	90	[2] ALEXANDER	93B	CLE2	$e^+e^- \to \Upsilon(4S)$

[1] ALBRECHT 93E reports $<3.1\times10^{-3}$ from a measurement of $[\Gamma(B^+\to D_s^{*+}\overline{K}^0)/\Gamma_{total}]\times[B(D_s^+\to\phi\pi^+)]$ assuming $B(D_s^+\to\phi\pi^+)=0.027$, which we rescale to our best (shown rounded) value $B(D_s^+\to\phi\pi^+)=4.5\times10^{-2}$.

[2] ALEXANDER 93B reports $<10.9\times10^{-4}$ from a measurement of $[\Gamma(B^+\to D_s^{*+}\overline{K}^0)/\Gamma_{total}]\times[B(D_s^+\to\phi\pi^+)]$ assuming $B(D_s^+\to\phi\pi^+)=0.037$, which we rescale to our best (shown rounded) value $B(D_s^+\to\phi\pi^+)=4.5\times10^{-2}$.

$\Gamma(D_s^+\overline{K}^*(892)^0)/\Gamma_{total}$ — Γ_{265}/Γ

VALUE	CL%	DOCUMENT ID		TECN	COMMENT
<4.4 × 10⁻⁶	90	AAIJ	13R	LHCB	pp at 7 TeV
• • • We do not use the following data for averages, fits, limits, etc. • • •					
$<4\times10^{-4}$	90	[1] ALEXANDER	93B	CLE2	$e^+e^- \to \Upsilon(4S)$

[1] ALEXANDER 93B reports $<4.4\times10^{-4}$ from a measurement of $[\Gamma(B^+\to D_s^+\overline{K}^*(892)^0)/\Gamma_{total}]\times[B(D_s^+\to\phi\pi^+)]$ assuming $B(D_s^+\to\phi\pi^+)=0.037$, which we rescale to our best (shown rounded) value $B(D_s^+\to\phi\pi^+)=4.5\times10^{-2}$.

$\Gamma(D_s^+K^{*0})/\Gamma_{total}$ — Γ_{266}/Γ

VALUE (units 10^{-6})	CL%	DOCUMENT ID		TECN	COMMENT
<3.5	90	AAIJ	13R	LHCB	pp at 7 TeV

$\Gamma(D_s^{*+}\overline{K}^*(892)^0)/\Gamma_{total}$ — Γ_{267}/Γ

VALUE	CL%	DOCUMENT ID		TECN	COMMENT
<3.5 × 10⁻⁴	90	[1] ALEXANDER	93B	CLE2	$e^+e^- \to \Upsilon(4S)$

[1] ALEXANDER 93B reports $<4.3\times10^{-4}$ from a measurement of $[\Gamma(B^+\to D_s^{*+}\overline{K}^*(892)^0)/\Gamma_{total}]\times[B(D_s^+\to\phi\pi^+)]$ assuming $B(D_s^+\to\phi\pi^+)=0.037$, which we rescale to our best (shown rounded) value $B(D_s^+\to\phi\pi^+)=4.5\times10^{-2}$.

$\Gamma(D_s^-\pi^+K^+)/\Gamma_{total}$ — Γ_{268}/Γ

VALUE (units 10^{-4})	CL%	DOCUMENT ID		TECN	COMMENT
1.80±0.22 OUR AVERAGE					
$1.71\ ^{+0.08}_{-0.07}\pm0.25$		[1] WIECHCZYN...	09	BELL	$e^+e^- \to \Upsilon(4S)$
$2.02\pm0.13\pm0.38$		[1] AUBERT	08G	BABR	$e^+e^- \to \Upsilon(4S)$
• • • We do not use the following data for averages, fits, limits, etc. • • •					
<7	90	[2] ALBRECHT	93E	ARG	$e^+e^- \to \Upsilon(4S)$

[1] Assumes equal production of B^+ and B^0 at the $\Upsilon(4S)$.

[2] ALBRECHT 93E reports $<1.1\times10^{-3}$ from a measurement of $[\Gamma(B^+\to D_s^-\pi^+K^+)/\Gamma_{total}]\times[B(D_s^+\to\phi\pi^+)]$ assuming $B(D_s^+\to\phi\pi^+)=0.027$, which we rescale to our best (shown rounded) value $B(D_s^+\to\phi\pi^+)=4.5\times10^{-2}$.

$\Gamma(D_s^{*-}\pi^+K^+)/\Gamma_{total}$ — Γ_{269}/Γ

VALUE (units 10^{-4})	CL%	DOCUMENT ID		TECN	COMMENT
1.45±0.24 OUR AVERAGE					
$1.31\ ^{+0.13}_{-0.12}\pm0.28$		[1] WIECHCZYN...	09	BELL	$e^+e^- \to \Upsilon(4S)$
$1.67\pm0.16\pm0.35$		[1] AUBERT	08G	BABR	$e^+e^- \to \Upsilon(4S)$
• • • We do not use the following data for averages, fits, limits, etc. • • •					
<10	90	[2] ALBRECHT	93E	ARG	$e^+e^- \to \Upsilon(4S)$

[1] Assumes equal production of B^+ and B^0 at the $\Upsilon(4S)$.

[2] ALBRECHT 93E reports $<1.6\times10^{-3}$ from a measurement of $[\Gamma(B^+\to D_s^{*-}\pi^+K^+)/\Gamma_{total}]\times[B(D_s^+\to\phi\pi^+)]$ assuming $B(D_s^+\to\phi\pi^+)=0.027$, which we rescale to our best (shown rounded) value $B(D_s^+\to\phi\pi^+)=4.5\times10^{-2}$.

$\Gamma(D_s^-\pi^+K^*(892)^+)/\Gamma_{total}$ — Γ_{270}/Γ

VALUE	CL%	DOCUMENT ID		TECN	COMMENT
<5 × 10⁻³	90	[1] ALBRECHT	93E	ARG	$e^+e^- \to \Upsilon(4S)$

[1] ALBRECHT 93E reports $<8.6\times10^{-3}$ from a measurement of $[\Gamma(B^+\to D_s^-\pi^+K^*(892)^+)/\Gamma_{total}]\times[B(D_s^+\to\phi\pi^+)]$ assuming $B(D_s^+\to\phi\pi^+)=0.027$, which we rescale to our best (shown rounded) value $B(D_s^+\to\phi\pi^+)=4.5\times10^{-2}$.

Int. J. Mod. Phys. A 2026.41. Downloaded from www.worldscientific.com
by UNIVERSITY OF CALIFORNIA @ BERKELEY on 09/16/26. Re-use and distribution is strictly not permitted, except for Open Access articles.

$\Gamma(D_s^{*-}\pi^+K^*(892)^+)/\Gamma_{total}$ — Γ_{271}/Γ

VALUE	CL%	DOCUMENT ID		TECN	COMMENT
$<7\times10^{-3}$	90	[1] ALBRECHT	93E	ARG	$e^+e^-\to\Upsilon(4S)$

[1] ALBRECHT 93E reports $<1.1\times10^{-2}$ from a measurement of $[\Gamma(B^+\to D_s^{*-}\pi^+K^*(892)^+)/\Gamma_{total}]\times[B(D_s^+\to\phi\pi^+)]$ assuming $B(D_s^+\to\phi\pi^+)=0.027$, which we rescale to our best (shown rounded) value $B(D_s^+\to\phi\pi^+)=4.5\times10^{-2}$.

$\Gamma(D_s^-K^+K^+)/\Gamma_{total}$ — Γ_{272}/Γ

VALUE (units 10^{-5})	DOCUMENT ID		TECN	COMMENT
0.97±0.21 OUR AVERAGE				
0.93±0.22±0.10	[1] WIECHCZYN...	15	BELL	$e^+e^-\to\Upsilon(4S)$
1.1 ±0.4 ±0.2	[1] AUBERT	08G	BABR	$e^+e^-\to\Upsilon(4S)$

[1] Assumes equal production of B^+ and B^0 at the $\Upsilon(4S)$.

$\Gamma(D_s^-K^+K^+)/\Gamma(D_s^-\pi^+K^+)$ — $\Gamma_{272}/\Gamma_{268}$

VALUE	DOCUMENT ID		TECN	COMMENT
0.054±0.013±0.006	WIECHCZYN...	15	BELL	$e^+e^-\to\Upsilon(4S)$

$\Gamma(D_s^{*-}K^+K^+)/\Gamma_{total}$ — Γ_{273}/Γ

VALUE (units 10^{-4})	CL%	DOCUMENT ID		TECN	COMMENT
<0.15	90	[1] AUBERT	08G	BABR	$e^+e^-\to\Upsilon(4S)$

[1] Assumes equal production of B^+ and B^0 at the $\Upsilon(4S)$.

$\Gamma(\eta_c K^+)/\Gamma_{total}$ — Γ_{274}/Γ

VALUE (units 10^{-3})	DOCUMENT ID		TECN	COMMENT
1.20±0.08 OUR FIT Error includes scale factor of 1.3.				
1.11±0.12 OUR AVERAGE Error includes scale factor of 1.4.				
0.96±0.12±0.06±0.03	[1,2] LEES	20C	BABR	$e^+e^-\to\Upsilon(4S)$
1.20±0.08±0.07	[1] KATO	18	BELL	$e^+e^-\to\Upsilon(4S)$
• • • We do not use the following data for averages, fits, limits, etc. • • •				
$1.17^{+0.14}_{-0.13}\pm0.17$	[3] CHILIKIN	19	BELL	$e^+e^-\to\Upsilon(4S)$
0.87±0.15	[1,4] AUBERT	06E	BABR	Repl. by LEES 20C
$1.62^{+0.32}_{-0.25}\pm0.17$	[5] AUBERT,B	05L	BABR	$e^+e^-\to\Upsilon(4S)$
1.26±0.15±0.11	[4,6] AUBERT,B	04B	BABR	$e^+e^-\to\Upsilon(4S)$
$1.25\pm0.14^{+0.39}_{-0.40}$	[7] FANG	03	BELL	$e^+e^-\to\Upsilon(4S)$
$0.69^{+0.26}_{-0.21}\pm0.22$	[8] EDWARDS	01	CLE2	$e^+e^-\to\Upsilon(4S)$

[1] Measures absolute branching fractions using a missing-mass technique.
[2] LEES 20C measurement's last uncertainty is due to the used $B(B^\pm\to K^\pm J/\psi)$ value.
[3] CHILIKIN 19 reports $[\Gamma(B^+\to\eta_c K^+)/\Gamma_{total}]\times[B(\eta_c(1S)\to p\overline{p}\pi^+\pi^-)]=(39.4^{+4.1+2.2}_{-3.9-1.8})\times10^{-7}$ which we divide by our best (shown rounded) value $B(\eta_c(1S)\to p\overline{p}\pi^+\pi^-)=(3.4\pm0.5)\times10^{-3}$. Our first error is their experiment's error and our second error is the systematic error from using our best (shown rounded) value.
[4] The ratio of $B(B^\pm\to K^\pm\eta_c)\,B(\eta_c\to K\overline{K}\pi)=(7.4\pm0.5\pm0.7)\times10^{-5}$ reported in AUBERT,B 04B and $B(B^\pm\to K^\pm\eta_c)=(8.7\pm1.5)\times10^{-3}$ reported in AUBERT 06E contribute to the determination of $B(\eta_c\to K\overline{K}\pi)$, which is used by others for normalization.
[5] AUBERT,B 05L reports $[\Gamma(B^+\to\eta_c K^+)/\Gamma_{total}]\times[B(\eta_c(1S)\to p\overline{p})]=(1.8^{+0.3}_{-0.2}\pm0.2)\times10^{-6}$ which we divide by our best (shown rounded) value $B(\eta_c(1S)\to p\overline{p})=(1.11\pm0.12)\times10^{-3}$. Our first error is their experiment's error and our second error is the systematic error from using our best (shown rounded) value.
[6] AUBERT,B 04B reports $[\Gamma(B^+\to\eta_c K^+)/\Gamma_{total}]\times[B(\eta_c(1S)\to K\overline{K}\pi)]=(0.074\pm0.005\pm0.007)\times10^{-3}$ which we divide by our best (shown rounded) value $B(\eta_c(1S)\to K\overline{K}\pi)=(5.9\pm0.5)\times10^{-2}$. Our first error is their experiment's error and our second error is the systematic error from using our best (shown rounded) value.
[7] Assumes equal production of B^+ and B^0 at the $\Upsilon(4S)$.
[8] EDWARDS 01 assumes equal production of B^0 and B^+ at the $\Upsilon(4S)$. The correlated uncertainties (28.3)% from $B(J/\psi(1S)\to\gamma\eta_c)$ in those modes have been accounted for.

$\Gamma(B^+\to\eta_c K^+)/\Gamma_{total}\times\Gamma(\eta_c(1S)\to\gamma\gamma)/\Gamma_{total}$ — $\Gamma_{274}/\Gamma\times\Gamma_{60}^{\eta_c(1S)}/\Gamma^{\eta_c(1S)}$

VALUE (units 10^{-6})	DOCUMENT ID		TECN	COMMENT
$\mathbf{0.22^{+0.09+0.04}_{-0.07-0.02}}$	[1] WICHT	08	BELL	$e^+e^-\to\Upsilon(4S)$

[1] Assumes equal production of B^+ and B^0 at the $\Upsilon(4S)$.

$\Gamma(\eta_c K^*(892)^+)/\Gamma_{total}$ — Γ_{275}/Γ

VALUE (units 10^{-3})	DOCUMENT ID		TECN	COMMENT
$\mathbf{1.4^{+0.6}_{-0.5}\pm0.1}$	[1,2] AUBERT	07AV	BABR	$e^+e^-\to\Upsilon(4S)$

[1] AUBERT 07AV reports $[\Gamma(B^+\to\eta_c K^*(892)^+)/\Gamma_{total}]\times[B(\eta_c(1S)\to p\overline{p})]=(1.57^{+0.56+0.45}_{-0.46-0.36})\times10^{-6}$ which we divide by our best (shown rounded) value $B(\eta_c(1S)\to p\overline{p})=(1.11\pm0.12)\times10^{-3}$. Our first error is their experiment's error and our second error is the systematic error from using our best (shown rounded) value.
[2] Assumes equal production of B^+ and B^0 at the $\Upsilon(4S)$.

$\Gamma(\eta_c K^+\pi^+\pi^-)/\Gamma_{total}$ — Γ_{276}/Γ

VALUE	CL%	DOCUMENT ID		TECN	COMMENT
$<3.9\times10^{-4}$	90	VINOKUROVA	15	BELL	$e^+e^-\to\Upsilon(4S)$

$\Gamma(\eta_c K^+\omega(782))/\Gamma_{total}$ — Γ_{277}/Γ

VALUE	CL%	DOCUMENT ID		TECN	COMMENT
$<5.3\times10^{-4}$	90	VINOKUROVA	15	BELL	$e^+e^-\to\Upsilon(4S)$

$\Gamma(\eta_c K^+\eta)/\Gamma_{total}$ — Γ_{278}/Γ

VALUE	CL%	DOCUMENT ID		TECN	COMMENT
$<2.2\times10^{-4}$	90	VINOKUROVA	15	BELL	$e^+e^-\to\Upsilon(4S)$

$\Gamma(\eta_c K^+\pi^0)/\Gamma_{total}$ — Γ_{279}/Γ

VALUE	CL%	DOCUMENT ID		TECN	COMMENT
$<6.2\times10^{-5}$	90	VINOKUROVA	15	BELL	$e^+e^-\to\Upsilon(4S)$

$\Gamma(\eta_c(2S)K^+)/\Gamma_{total}$ — Γ_{280}/Γ

VALUE (units 10^{-4})	DOCUMENT ID		TECN	COMMENT
4.4±1.0 OUR AVERAGE				
3.5±1.7±0.5±0.1	[1,2] LEES	20C	BABR	$e^+e^-\to\Upsilon(4S)$
4.8±1.1±0.3	[2] KATO	18	BELL	$e^+e^-\to\Upsilon(4S)$
• • • We do not use the following data for averages, fits, limits, etc. • • •				
3.4±1.8±0.3	[2] AUBERT	06E	BABR	Repl. by LEES 20C

[1] LEES 20C measurement's last uncertainty is due to the used $B(B^\pm\to K^\pm J/\psi)$ value.
[2] Measures absolute branching fractions using a missing-mass technique.

$\Gamma(\eta_c(2S)K^+,\ \eta_c\to p\overline{p})/\Gamma_{total}$ — Γ_{281}/Γ

VALUE (units 10^{-8})	CL%	DOCUMENT ID		TECN	COMMENT
3.47±0.72±0.26		[1] AAIJ	17AD	LHCB	pp at 7 and 8 TeV
• • • We do not use the following data for averages, fits, limits, etc. • • •					
<10.6	95	[2] AAIJ	13S	LHCB	Repl. by AAIJ 17AD

[1] Measured relative to $B^+\to J/\psi K^+$ decay with charmonia reconstructed in $p\overline{p}$ final state and using $B(B^+\to J/\psi K^+)\times B(J/\psi\to p\overline{p})=(2.17\pm0.08)\times10^{-6}$. The last uncertainty includes the uncertainty of $B(B^+\to J/\psi K^+)\times B(J/\psi\to p\overline{p})$.
[2] Measured relative to $B^+\to J/\psi K^+$ decay with charmonia reconstructed in $p\overline{p}$ final state and using $B(B^+\to J/\psi K^+)=(1.013\pm0.034)\times10^{-3}$ and $B(J/\psi\to p\overline{p})=(2.17\pm0.07)\times10^{-3}$.

$\Gamma(\eta_c(2S)K^+,\ \eta_c\to p\overline{p}\pi^+\pi^-)/\Gamma_{total}$ — Γ_{283}/Γ

VALUE (units 10^{-7})	DOCUMENT ID		TECN	COMMENT
$\mathbf{11.2^{+1.8+0.5}_{-1.6-0.7}}$	CHILIKIN	19	BELL	$e^+e^-\to\Upsilon(4S)$

$\Gamma(B^+\to h_c(1P)K^+)/\Gamma_{total}\times\Gamma(h_c(1P)\to\gamma\eta_c(1S))/\Gamma_{total}$ — $\Gamma_{409}/\Gamma\times\Gamma_{30}^{h_c(1P)}/\Gamma^{h_c(1P)}$

VALUE (units 10^{-4})	CL%	DOCUMENT ID		TECN	COMMENT
<0.48	90	[1] AUBERT	08AB	BABR	$e^+e^-\to\Upsilon(4S)$

[1] Uses the production ratio of $(B^+B^-)/(B^0\overline{B}^0)=1.026\pm0.032$ at $\Upsilon(4S)$.

$\Gamma(B^+\to\eta_c(2S)K^+)/\Gamma_{total}\times\Gamma(\eta_c(2S)\to\gamma\gamma)/\Gamma_{total}$ — $\Gamma_{280}/\Gamma\times\Gamma_{26}^{\eta_c(2S)}/\Gamma^{\eta_c(2S)}$

VALUE (units 10^{-6})	CL%	DOCUMENT ID		TECN	COMMENT
<0.18	90	[1] WICHT	08	BELL	$e^+e^-\to\Upsilon(4S)$

[1] Assumes equal production of B^+ and B^0 at the $\Upsilon(4S)$.

$\Gamma(\eta_c(2S)K^+,\ \eta_c\to K_S^0K^\mp\pi^\pm)/\Gamma_{total}$ — Γ_{282}/Γ

VALUE (units 10^{-6})	DOCUMENT ID		TECN	COMMENT
$\mathbf{3.4^{+2.2+0.5}_{-1.5-0.4}}$	[1,2] VINOKUROVA	11	BELL	$e^+e^-\to\Upsilon(4S)$

[1] Assumes equal production of B^0 and B^+ from Upsilon(4S) decays.
[2] The first uncertainty includes both statistical and interference effects while the second is due to systematics.

$\Gamma(J/\psi(1S)K^+)/\Gamma_{total}$ — Γ_{316}/Γ

VALUE (units 10^{-4})	EVTS	DOCUMENT ID		TECN	COMMENT
10.19± 0.19 OUR FIT					
10.18± 0.20 OUR AVERAGE					
10.32± 0.07±0.24		[1] CHOUDHURY	21	BELL	$e^+e^-\to\Upsilon(4S)$
9.4 ± 0.7 ±0.8		[2] CHILIKIN	19	BELL	$e^+e^-\to\Upsilon(4S)$
8.9 ± 0.6 ±0.5		[3] KATO	18	BELL	$e^+e^-\to\Upsilon(4S)$
8.1 ± 1.3 ±0.7		[3] AUBERT	06E	BABR	$e^+e^-\to\Upsilon(4S)$
10.61± 0.15±0.48		[4] AUBERT	05J	BABR	$e^+e^-\to\Upsilon(4S)$
10.4 ± 1.1 ±0.1		[5] AUBERT,B	05L	BABR	$e^+e^-\to\Upsilon(4S)$
10.2 ± 0.8 ±0.7		[4] JESSOP	97	CLE2	$e^+e^-\to\Upsilon(4S)$
9.24± 3.04±0.05		[6] BORTOLETTO	92	CLEO	$e^+e^-\to\Upsilon(4S)$
8.09± 3.50±0.04	6	[7] ALBRECHT	90J	ARG	$e^+e^-\to\Upsilon(4S)$
• • • We do not use the following data for averages, fits, limits, etc. • • •					
10.1 ± 0.2 ±0.7		[4] ABE	03B	BELL	Repl. by CHOUDHURY 21
10.1 ± 0.3 ±0.5		[4] AUBERT	02	BABR	Repl. by AUBERT 05J
11.0 ± 1.5 ±0.9	59	[4] ALAM	94	CLE2	Repl. by JESSOP 97
22 ±10 ±2		BUSKULIC	92G	ALEP	$e^+e^-\to Z$
7 ± 4	3	[8] ALBRECHT	87D	ARG	$e^+e^-\to\Upsilon(4S)$
10 ± 7 ±2	3	[9] BEBEK	87	CLEO	$e^+e^-\to\Upsilon(4S)$
9 ± 5	3	[10] ALAM	86	CLEO	$e^+e^-\to\Upsilon(4S)$

[1] CHOUDHURY 21 uses the relative production fraction of charged (f^{+-}) to neutral (f^{00}) B mesons at $\Upsilon(4S)$ value of $f^{+-}/f^{00} = 1.058 \pm 0.024$.

[2] CHILIKIN 19 reports $[\Gamma(B^+ \to J/\psi(1S)K^+)/\Gamma_{total}] \times [B(J/\psi(1S) \to p\overline{p}\pi^+\pi^-)] = (56.4^{+3.3+2.7}_{-3.2-2.5}) \times 10^{-7}$ which we divide by our best (shown rounded) value $B(J/\psi(1S) \to p\overline{p}\pi^+\pi^-) = (6.0 \pm 0.5) \times 10^{-3}$. Our first error is their experiment's error and our second error is the systematic error from using our best (shown rounded) value.

[3] Measures absolute branching fractions using a missing-mass technique.

[4] Assumes equal production of B^+ and B^0 at the $\Upsilon(4S)$.

[5] AUBERT,B 05L reports $[\Gamma(B^+ \to J/\psi(1S)K^+)/\Gamma_{total}] \times [B(J/\psi(1S) \to p\overline{p})] = (2.2 \pm 0.2 \pm 0.1) \times 10^{-6}$ which we divide by our best (shown rounded) value $B(J/\psi(1S) \to p\overline{p}) = (2.121 \pm 0.029) \times 10^{-3}$. Our first error is their experiment's error and our second error is the systematic error from using our best (shown rounded) value.

[6] BORTOLETTO 92 reports $(8 \pm 2 \pm 2) \times 10^{-4}$ from a measurement of $[\Gamma(B^+ \to J/\psi(1S)K^+)/\Gamma_{total}] \times [B(J/\psi(1S) \to e^+e^-)]$ assuming $B(J/\psi(1S) \to e^+e^-) = 0.069 \pm 0.009$, which we rescale to our best (shown rounded) value $B(J/\psi(1S) \to e^+e^-) = (5.971 \pm 0.032) \times 10^{-2}$. Our first error is their experiment's error and our second error is the systematic error from using our best (shown rounded) value. Assumes equal production of B^+ and B^0 at the $\Upsilon(4S)$.

[7] ALBRECHT 90J reports $(7 \pm 3 \pm 1) \times 10^{-4}$ from a measurement of $[\Gamma(B^+ \to J/\psi(1S)K^+)/\Gamma_{total}] \times [B(J/\psi(1S) \to e^+e^-)]$ assuming $B(J/\psi(1S) \to e^+e^-) = 0.069 \pm 0.009$, which we rescale to our best (shown rounded) value $B(J/\psi(1S) \to e^+e^-) = (5.971 \pm 0.032) \times 10^{-2}$. Our first error is their experiment's error and our second error is the systematic error from using our best (shown rounded) value. Assumes equal production of B^+ and B^0 at the $\Upsilon(4S)$.

[8] ALBRECHT 87D assume $B^+B^-/B^0\overline{B}^0$ ratio is 55/45. Superseded by ALBRECHT 90J.

[9] BEBEK 87 value has been updated in BERKELMAN 91 to use same assumptions as noted for BORTOLETTO 92.

[10] ALAM 86 assumes $B^{\pm}/B^0$ ratio is 60/40.

$\Gamma(\eta_c K^+)/\Gamma(J/\psi(1S)K^+)$ — $\Gamma_{274}/\Gamma_{316}$

VALUE	DOCUMENT ID		TECN	COMMENT
1.12±0.14 OUR AVERAGE				
1.10±0.08±0.12	[1] AAIJ	13S	LHCB	pp at 7 TeV
1.33±0.10±0.43	[2] AUBERT,B	04B	BABR	$e^+e^- \to \Upsilon(4S)$

[1] AAIJ 13S reports $[\Gamma(B^+ \to \eta_c K^+)/\Gamma(B^+ \to J/\psi(1S)K^+)] \times [B(\eta_c(1S) \to p\overline{p})] / [B(J/\psi(1S) \to p\overline{p})] = 0.578 \pm 0.035 \pm 0.026$ which we multiply or divide by our best (shown rounded) values $B(\eta_c(1S) \to p\overline{p}) = (1.11 \pm 0.12) \times 10^{-3}$, $B(J/\psi(1S) \to p\overline{p}) = (2.121 \pm 0.029) \times 10^{-3}$. Our first error is their experiment's error and our second error is the systematic error from using our best (shown rounded) values.

[2] Uses BABAR measurement of $B(B^+ \to J/\psi K^+) = (10.1 \pm 0.3 \pm 0.5) \times 10^{-4}$.

$\Gamma(B^+ \to J/\psi(1S)K^+)/\Gamma_{total} \times \Gamma(J/\psi(1S) \to \gamma\gamma)/\Gamma_{total}$ — $\Gamma_{316}/\Gamma \times \Gamma^{J/\psi(1S)}_{413}/\Gamma^{J/\psi(1S)}$

VALUE (units 10^{-6})	CL%	DOCUMENT ID		TECN	COMMENT
<0.16	90	[1] WICHT	08	BELL	$e^+e^- \to \Upsilon(4S)$

[1] Assumes equal production of B^+ and B^0 at the $\Upsilon(4S)$.

$\Gamma(J/\psi(1S)K^+\pi^+\pi^-)/\Gamma_{total}$ — Γ_{318}/Γ

VALUE (units 10^{-3})	CL%	EVTS	DOCUMENT ID		TECN	COMMENT
0.81 ±0.13 OUR AVERAGE Error includes scale factor of 2.5. See the ideogram below.						
0.716±0.010±0.060			[1] GULER	11	BELL	$e^+e^- \to \Upsilon(4S)$
1.16 ±0.07 ±0.09			[1] AUBERT	05R	BABR	$e^+e^- \to \Upsilon(4S)$
0.69 ±0.18 ±0.12			[2] ACOSTA	02F	CDF	$p\overline{p}$ 1.8 TeV
1.39 ±0.81 ±0.01			[3] BORTOLETTO	92	CLEO	$e^+e^- \to \Upsilon(4S)$
1.39 ±0.91 ±0.01		6	[4] ALBRECHT	87D	ARG	$e^+e^- \to \Upsilon(4S)$
• • • We do not use the following data for averages, fits, limits, etc. • • •						
<1.8	90		[5] ALBRECHT	90J	ARG	$e^+e^- \to \Upsilon(4S)$

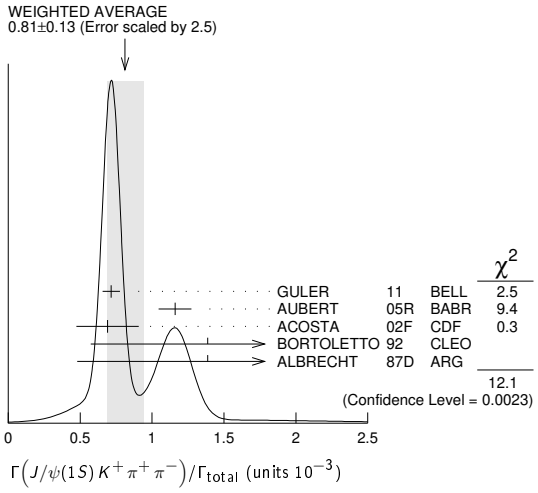

[1] Assumes equal production of B^+ and B^0 at the $\Upsilon(4S)$.

[2] ACOSTA 02F uses as reference of $B(B \to J/\psi(1S)K^+) = (10.1 \pm 0.6) \times 10^{-4}$. The second error includes the systematic error and the uncertainties of the branching ratio.

[3] BORTOLETTO 92 reports $(1.2 \pm 0.6 \pm 0.4) \times 10^{-3}$ from a measurement of $[\Gamma(B^+ \to J/\psi(1S)K^+\pi^+\pi^-)/\Gamma_{total}] \times [B(J/\psi(1S) \to e^+e^-)]$ assuming $B(J/\psi(1S) \to e^+e^-) = 0.069 \pm 0.009$, which we rescale to our best (shown rounded) value $B(J/\psi(1S) \to e^+e^-) = (5.971 \pm 0.032) \times 10^{-2}$. Our first error is their experiment's error and our second error is the systematic error from using our best (shown rounded) value. Assumes equal production of B^+ and B^0 at the $\Upsilon(4S)$.

[4] ALBRECHT 87D reports $(1.2 \pm 0.8) \times 10^{-3}$ from a measurement of $[\Gamma(B^+ \to J/\psi(1S)K^+\pi^+\pi^-)/\Gamma_{total}] \times [B(J/\psi(1S) \to e^+e^-)]$ assuming $B(J/\psi(1S) \to e^+e^-) = 0.069 \pm 0.009$, which we rescale to our best (shown rounded) value $B(J/\psi(1S) \to e^+e^-) = (5.971 \pm 0.032) \times 10^{-2}$. Our first error is their experiment's error and our second error is the systematic error from using our best (shown rounded) value. They actually report 0.0011 ± 0.0007 assuming $B^+B^-/B^0\overline{B}^0$ ratio is 55/45. We rescale to 50/50. Analysis explicitly removes $B^+ \to \psi(2S)K^+$.

[5] ALBRECHT 90J reports $< 1.6 \times 10^{-3}$ from a measurement of $[\Gamma(B^+ \to J/\psi(1S)K^+\pi^+\pi^-)/\Gamma_{total}] \times [B(J/\psi(1S) \to e^+e^-)]$ assuming $B(J/\psi(1S) \to e^+e^-) = 0.069$, which we rescale to our best (shown rounded) value $B(J/\psi(1S) \to e^+e^-) = 5.971 \times 10^{-2}$. Assumes equal production of B^+ and B^0 at the $\Upsilon(4S)$.

$\Gamma(J/\psi(1S)K^+K^-K^+)/\Gamma_{total}$ — Γ_{319}/Γ

VALUE (units 10^{-6})	DOCUMENT ID		TECN	COMMENT
33.7±2.5±1.4	LEES	15	BABR	$e^+e^- \to \Upsilon(4S)$

$\Gamma(h_c(1P)K^+,\ h_c \to J/\psi\pi^+\pi^-)/\Gamma_{total}$ — Γ_{284}/Γ

VALUE	CL%	DOCUMENT ID		TECN	COMMENT
<3.4 × 10⁻⁶	90	[1] AUBERT	05R	BABR	$e^+e^- \to \Upsilon(4S)$

[1] Assumes equal production of B^+ and B^0 at the $\Upsilon(4S)$.

$\Gamma(X(3730)^0K^+,\ X^0 \to \eta_c\eta)/\Gamma_{total}$ — Γ_{285}/Γ

VALUE	CL%	DOCUMENT ID		TECN	COMMENT
<4.6 × 10⁻⁵	90	VINOKUROVA	15	BELL	$e^+e^- \to \Upsilon(4S)$

$\Gamma(X(3730)^0K^+,\ X^0 \to \eta_c\pi^0)/\Gamma_{total}$ — Γ_{286}/Γ

VALUE	CL%	DOCUMENT ID		TECN	COMMENT
<5.7 × 10⁻⁶	90	VINOKUROVA	15	BELL	$e^+e^- \to \Upsilon(4S)$

$\Gamma(\eta_{c2}(1D)K^+,\ \eta_{c2} \to h_c\gamma)/\Gamma_{total}$ — Γ_{287}/Γ

VALUE	CL%	DOCUMENT ID		TECN	COMMENT
<3.7 × 10⁻⁵	90	CHILIKIN	20	BELL	$e^+e^- \to \Upsilon(4S)$

$\Gamma(\eta_{c2}(1D)\pi^+K^0_S,\ \eta_{c2} \to h_c\gamma)/\Gamma_{total}$ — Γ_{288}/Γ

VALUE	CL%	DOCUMENT ID		TECN	COMMENT
<1.1 × 10⁻⁴	90	CHILIKIN	20	BELL	$e^+e^- \to \Upsilon(4S)$

$\Gamma(\psi_2(3823)K^+,\ \psi_2 \to J/\psi\pi^+\pi^-)/\Gamma_{total}$ — Γ_{289}/Γ

VALUE (units 10^{-7})	DOCUMENT ID		TECN	COMMENT
2.82±0.54±0.13	[1] AAIJ	20S	LHCB	pp at 7, 8, 13 TeV

[1] The first error is statistic; the second error is the total systematic error.

$\Gamma(\psi_2(3823)K^+,\ \psi_2 \to J/\psi\eta)/\Gamma_{total}$ — Γ_{290}/Γ

VALUE (units 10^{-6})	DOCUMENT ID		TECN	COMMENT
$1.25^{+0.71}_{-0.53} \pm 0.04$	AAIJ	22D	LHCB	pp at 7, 8, 13 TeV

$\Gamma(\psi_3(3842)K^+,\ \psi_3 \to J/\psi\eta)/\Gamma_{total}$ — Γ_{291}/Γ

VALUE	CL%	DOCUMENT ID		TECN	COMMENT
<6.1 × 10⁻⁷	90	AAIJ	22D	LHCB	pp at 7, 8, 13 TeV

$\Gamma(\chi_{c1}(3872)K^+)/\Gamma_{total}$ — Γ_{292}/Γ

VALUE (units 10^{-4})	CL%	DOCUMENT ID		TECN	COMMENT
1.9±0.6 OUR AVERAGE					
2.1±0.6±0.3±0.1		[1,2] LEES	20C	BABR	$e^+e^- \to \Upsilon(4S)$
1.2±1.1±0.1		[1,3] KATO	18	BELL	$e^+e^- \to \Upsilon(4S)$
• • • We do not use the following data for averages, fits, limits, etc. • • •					
2.3±0.6±0.7		[4,5] AUBERT	06	BABR	Repl. by AUBERT 08Y
<3.2	90	[1] AUBERT	06E	BABR	$e^+e^- \to \Upsilon(4S)$
2.9±0.9±0.9		[4,6] AUBERT	05R	BABR	Repl. by AUBERT 06
3.1±0.7±1.0		[7] CHOI	03	BELL	Repl. by CHOI 11

[1] Measures absolute branching fractions using a missing-mass technique.

[2] LEES 20C measurement's last uncertainty is due to the used $B(B^{\pm} \to K^{\pm}J/\psi)$ value.

[3] KATO 18 value corresponds to upper limit of $< 2.6 \times 10^{-4}$ at 90% CL.

[4] Assumes equal production of B^+ and B^0 at the $\Upsilon(4S)$.

[5] AUBERT 06 reports $[\Gamma(B^+ \to \chi_{c1}(3872)K^+)/\Gamma_{total}] \times [B(\chi_{c1}(3872) \to \pi^+\pi^-J/\psi(1S))] = (10.1 \pm 2.5 \pm 1.0) \times 10^{-6}$ which we divide by our best (shown rounded) value $B(\chi_{c1}(3872) \to \pi^+\pi^-J/\psi(1S)) = (4.3 \pm 1.4) \times 10^{-2}$. Our first error is their experiment's error and our second error is the systematic error from using our best (shown rounded) value.

[6] AUBERT 05R reports $[\Gamma(B^+ \to \chi_{c1}(3872)K^+)/\Gamma_{total}] \times [B(\chi_{c1}(3872) \to \pi^+\pi^-J/\psi(1S))] = (12.8 \pm 4.1) \times 10^{-6}$ which we divide by our best (shown rounded) value $B(\chi_{c1}(3872) \to \pi^+\pi^-J/\psi(1S)) = (4.3 \pm 1.4) \times 10^{-2}$. Our first error is their experiment's error and our second error is the systematic error from using our best (shown rounded) value.

Int. J. Mod. Phys. A 2026.41. Downloaded from www.worldscientific.com
by LIFORNIA @ BERKELEY on 09/16/26. Re-use and distribution is strictly not permitted, except for Open Access articles.

Int. J. Mod. Phys. A 2026.41. Downloaded from www.worldscientific.com by UNIVERSITY OF CALIFORNIA @ BERKELEY on 09/16/26. Re-use and distribution is strictly not permitted, except for Open Access articles.

[7] CHOI 03 reports $[\Gamma(B^+ \to \chi_{c1}(3872) K^+)/\Gamma_{total}] \times [B(\chi_{c1}(3872) \to \pi^+\pi^- J/\psi(1S))] = (13.6 \pm 3.0 \pm 0.5) \times 10^{-6}$ which we divide by our best (shown rounded) value $B(\chi_{c1}(3872) \to \pi^+\pi^- J/\psi(1S)) = (4.3 \pm 1.4) \times 10^{-2}$. Our first error is their experiment's error and our second error is the systematic error from using our best (shown rounded) value.

$\Gamma(\chi_{c0}(3915) K^+)/\Gamma_{total}$ — Γ_{293}/Γ

VALUE	CL%	DOCUMENT ID		TECN	COMMENT
$<2.8 \times 10^{-4}$	90	[1] KATO	18	BELL	$e^+e^- \to \Upsilon(4S)$

[1] Measures absolute branching fractions using a missing-mass technique.

$\Gamma(\chi_{c0}(3915) K^+, \chi_{c0} \to D^+D^-)/\Gamma(D^-D^+K^+)$ — $\Gamma_{294}/\Gamma_{228}$

VALUE (units 10^{-2})	DOCUMENT ID		TECN	COMMENT
3.7±0.9±0.2	[1] AAIJ	20AI	LHCB	pp at 7, 8, 13 TeV

[1] Measured in Dalitz plot analysis of $B^+ \to D^-D^+K^+$ decays.

$\Gamma(\chi_{c0}(3915) K^+, \chi_{c0} \to \eta_c \eta)/\Gamma_{total}$ — Γ_{295}/Γ

VALUE	CL%	DOCUMENT ID		TECN	COMMENT
$<4.7 \times 10^{-5}$	90	[1] VINOKUROVA	15	BELL	$e^+e^- \to \Upsilon(4S)$

[1] Upper limit is corrected in the Erratum.

$\Gamma(\chi_{c0}(3915) K^+, \chi_{c0} \to \eta_c \pi^0)/\Gamma_{total}$ — Γ_{296}/Γ

VALUE	CL%	DOCUMENT ID		TECN	COMMENT
$<1.7 \times 10^{-5}$	90	[1] VINOKUROVA	15	BELL	$e^+e^- \to \Upsilon(4S)$

[1] Upper limit is corrected in the Erratum.

$\Gamma(X(4014)^0 K^+, X^0 \to \eta_c \eta)/\Gamma_{total}$ — Γ_{297}/Γ

VALUE	CL%	DOCUMENT ID		TECN	COMMENT
$<3.9 \times 10^{-5}$	90	VINOKUROVA	15	BELL	$e^+e^- \to \Upsilon(4S)$

$\Gamma(X(4014)^0 K^+, X^0 \to \eta_c \pi^0)/\Gamma_{total}$ — Γ_{298}/Γ

VALUE	CL%	DOCUMENT ID		TECN	COMMENT
$<1.2 \times 10^{-5}$	90	VINOKUROVA	15	BELL	$e^+e^- \to \Upsilon(4S)$

$\Gamma(T_{c\overline{c}1}(3900)^0 K^+, T^0_{c\overline{c}1} \to \eta_c \pi^+\pi^-)/\Gamma_{total}$ — Γ_{299}/Γ

VALUE	CL%	DOCUMENT ID		TECN	COMMENT
$<4.7 \times 10^{-5}$	90	VINOKUROVA	15	BELL	$e^+e^- \to \Upsilon(4S)$

$\Gamma(T_{c\overline{c}1}(3900)^0 K^+, T^0_{c\overline{c}1} \to J/\psi \eta)/\Gamma_{total}$ — Γ_{300}/Γ

VALUE	CL%	DOCUMENT ID		TECN	COMMENT
$<4.3 \times 10^{-7}$	90	AAIJ	22D	LHCB	pp at 7, 8, 13 TeV

$\Gamma(T_{c\overline{c}}(4020)^0 K^+, T^0_{c\overline{c}} \to \eta_c \pi^+\pi^-)/\Gamma_{total}$ — Γ_{301}/Γ

VALUE	CL%	DOCUMENT ID		TECN	COMMENT
$<1.6 \times 10^{-5}$	90	VINOKUROVA	15	BELL	$e^+e^- \to \Upsilon(4S)$

$\Gamma(\chi_{c1}(3872) K^*(892)^+)/\Gamma_{total}$ — Γ_{302}/Γ

VALUE	CL%	DOCUMENT ID		TECN	COMMENT
$<5 \times 10^{-4}$	90	[1,2] AUBERT	09B	BABR	$e^+e^- \to \Upsilon(4S)$
• • • We do not use the following data for averages, fits, limits, etc. • • •					
5×10^{-4}	90	[2,3] AUBERT	09B	BABR	$e^+e^- \to \Upsilon(4S)$

[1] AUBERT 09B reports $[\Gamma(B^+ \to \chi_{c1}(3872) K^*(892)^+)/\Gamma_{total}] \times [B(\chi_{c1}(3872) \to \gamma J/\psi)] < 4.8 \times 10^{-6}$ which we divide by our best (shown rounded) value $B(\chi_{c1}(3872) \to \gamma J/\psi) = 10 \times 10^{-3}$.

[2] Uses $B(\Upsilon(4S) \to B^+B^-) = (51.6 \pm 0.6)\%$ and $B(\Upsilon(4S) \to B^0\overline{B}^0) = (48.4 \pm 0.6)\%$.

[3] AUBERT 09B reports $[\Gamma(B^+ \to \chi_{c1}(3872) K^*(892)^+)/\Gamma_{total}] \times [B(\chi_{c1}(3872) \to \gamma\psi(2S))] < 28 \times 10^{-6}$ which we divide by our best (shown rounded) value $B(\chi_{c1}(3872) \to \gamma\psi(2S)) = 0 \times 10^{-2}$.

$\Gamma(\chi_{c1}(3872)^+ K^0, \chi^+_{c1} \to J/\psi(1S)\pi^+\pi^0)/\Gamma_{total}$ — Γ_{303}/Γ

VALUE (units 10^{-6})	CL%	DOCUMENT ID		TECN	COMMENT
< 6.1	90	[1,2] CHOI	11	BELL	$e^+e^- \to \Upsilon(4S)$
• • • We do not use the following data for averages, fits, limits, etc. • • •					
<22	90	[3] AUBERT	05B	BABR	$e^+e^- \to \Upsilon(4S)$

[1] Assumes $\pi^+\pi^0$ originates from ρ^+.

[2] Assumes equal production of B^+ and B^0 at the $\Upsilon(4S)$.

[3] Assumes equal production of B^+ and B^0 at the $\Upsilon(4S)$. The isovector-X hypothesis is excluded with a likelihood test at 1×10^{-4} level.

$\Gamma(\chi_{c1}(3872) K^0 \pi^+)/\Gamma_{total}$ — Γ_{304}/Γ

VALUE (units 10^{-4})	DOCUMENT ID		TECN	COMMENT
2.4±0.7±0.8	[1] BALA	15	BELL	$e^+e^- \to \Upsilon(4S)$

[1] BALA 15 reports $[\Gamma(B^+ \to \chi_{c1}(3872) K^0\pi^+)/\Gamma_{total}] \times [B(\chi_{c1}(3872) \to \pi^+\pi^- J/\psi(1S))] = (10.6 \pm 3.0 \pm 0.9) \times 10^{-6}$ which we divide by our best (shown rounded) value $B(\chi_{c1}(3872) \to \pi^+\pi^- J/\psi(1S)) = (4.3 \pm 1.4) \times 10^{-2}$. Our first error is their experiment's error and our second error is the systematic error from using our best (shown rounded) value.

$\Gamma(T_{c\overline{c}1}(4430)^+ K^0, T^+_{c\overline{c}1} \to J/\psi\pi^+)/\Gamma_{total}$ — Γ_{305}/Γ

VALUE (units 10^{-5})	CL%	DOCUMENT ID		TECN	COMMENT
<1.5	95	[1] AUBERT	09AA	BABR	$e^+e^- \to \Upsilon(4S)$

[1] Assumes equal production of B^+ and B^0 at the $\Upsilon(4S)$.

$\Gamma(T_{c\overline{c}1}(4430)^+ K^0, T^+_{c\overline{c}1} \to \psi(2S)\pi^+)/\Gamma_{total}$ — Γ_{306}/Γ

VALUE (units 10^{-5})	CL%	DOCUMENT ID		TECN	COMMENT
<4.7	95	[1] AUBERT	09AA	BABR	$e^+e^- \to \Upsilon(4S)$

[1] Assumes equal production of B^+ and B^0 at the $\Upsilon(4S)$.

$\Gamma(T_{c\overline{c}1}(4430)^0 K^+, T^0_{c\overline{c}1} \to J/\psi\eta)/\Gamma_{total}$ — Γ_{307}/Γ

VALUE	CL%	DOCUMENT ID		TECN	COMMENT
$<12.7 \times 10^{-7}$	90	AAIJ	22D	LHCB	pp at 7, 8, 13 TeV

$\Gamma(\psi(4230)^0 K^+, \psi^0 \to J/\psi\pi^+\pi^-)/\Gamma_{total}$ — Γ_{308}/Γ

VALUE (units 10^{-6})	CL%	DOCUMENT ID		TECN	COMMENT
<15.6	95	[1,2] GARG	19	BELL	$e^+e^- \to \Upsilon(4S)$
• • • We do not use the following data for averages, fits, limits, etc. • • •					
<29	95	[2] AUBERT	06	BABR	$e^+e^- \to \Upsilon(4S)$

[1] Corresponds to a 90% CL upper limit of $< 14 \times 10^{-6}$.

[2] Assumes equal production of B^+ and B^0 at the $\Upsilon(4S)$.

$\Gamma(\psi(4230) K^+, \psi \to J/\psi\eta)/\Gamma_{total}$ — Γ_{309}/Γ

VALUE	CL%	DOCUMENT ID		TECN	COMMENT
$<3.9 \times 10^{-7}$	90	AAIJ	22D	LHCB	pp at 7, 8, 13 TeV

$\Gamma(\psi(4360) K^+, \psi \to J/\psi\eta)/\Gamma_{total}$ — Γ_{310}/Γ

VALUE	CL%	DOCUMENT ID		TECN	COMMENT
$<12.4 \times 10^{-7}$	90	AAIJ	22D	LHCB	pp at 7, 8, 13 TeV

$\Gamma(\psi(4360) K^+, \psi(4360) \to \psi(2S)\pi^+\pi^-)/\Gamma(\psi(2S) K^+\pi^+\pi^-)$ — $\Gamma_{311}/\Gamma_{355}$

VALUE	DOCUMENT ID		TECN	COMMENT
0.0064±0.0014±0.0012	[1] AAIJ	25Q	LHCB	pp at 7, 8 and 13 TeV

[1] Measured in amplitude analysis of $B^+ \to \psi(2S) K^+\pi^+\pi^-$.

$\Gamma(\psi(4390) K^+, \psi \to J/\psi\eta)/\Gamma_{total}$ — Γ_{312}/Γ

VALUE	CL%	DOCUMENT ID		TECN	COMMENT
$<24.1 \times 10^{-7}$	90	AAIJ	22D	LHCB	pp at 7, 8, 13 TeV

$\Gamma(\chi_{c0}(3915) K^+, \chi_{c0} \to J/\psi\gamma)/\Gamma_{total}$ — Γ_{313}/Γ

VALUE (units 10^{-6})	CL%	DOCUMENT ID		TECN	COMMENT
<14	90	[1] AUBERT,BE	06M	BABR	$e^+e^- \to \Upsilon(4S)$

[1] Assumes equal production of B^+ and B^0 at the $\Upsilon(4S)$.

$\Gamma(\chi_{c0}(3915) K^+, \chi_{c0} \to \chi_{c1}(1P)\pi^0)/\Gamma_{total}$ — Γ_{314}/Γ

VALUE	CL%	DOCUMENT ID		TECN	COMMENT
$<3.8 \times 10^{-5}$	90	[1] BHARDWAJ	19	BELL	$e^+e^- \to \Upsilon(4S)$

[1] Assumes equal production of B^+ and B^0 at the $\Upsilon(4S)$.

$\Gamma(X(3930)^0 K^+, X^0 \to J/\psi\gamma)/\Gamma_{total}$ — Γ_{315}/Γ

VALUE (units 10^{-6})	CL%	DOCUMENT ID		TECN	COMMENT
<2.5	90	[1] AUBERT,BE	06M	BABR	$e^+e^- \to \Upsilon(4S)$

[1] Assumes equal production of B^+ and B^0 at the $\Upsilon(4S)$.

$\Gamma(J/\psi(1S) K^0\pi^+)/\Gamma_{total}$ — Γ_{317}/Γ

VALUE (units 10^{-3})	DOCUMENT ID		TECN	COMMENT
• • • We do not use the following data for averages, fits, limits, etc. • • •				
1.101±0.021	[1] AUBERT	09AA	BABR	$e^+e^- \to \Upsilon(4S)$

[1] Does not report systematic uncertainties.

$\Gamma(J/\psi(1S) K^*(892)^+)/\Gamma_{total}$ — Γ_{321}/Γ

For polarization information see the Listings at the end of the "B^0 Branching Ratios" section.

VALUE (units 10^{-3})	EVTS	DOCUMENT ID		TECN	COMMENT
1.43 ±0.08 OUR FIT					
1.43 ±0.08 OUR AVERAGE					
$1.78\ ^{+0.36}_{-0.32} \pm 0.02$		[1,2] AUBERT	07AV	BABR	$e^+e^- \to \Upsilon(4S)$
1.454±0.047±0.097		[2] AUBERT	05J	BABR	$e^+e^- \to \Upsilon(4S)$
1.28 ±0.07 ±0.14		[2] ABE	02N	BELL	$e^+e^- \to \Upsilon(4S)$
1.41 ±0.23 ±0.24		[2] JESSOP	97	CLE2	$e^+e^- \to \Upsilon(4S)$
1.58 ±0.47 ±0.27		[3] ABE	96H	CDF	$p\overline{p}$ at 1.8 TeV
1.50 ±1.08 ±0.01		[4] BORTOLETTO	92	CLEO	$e^+e^- \to \Upsilon(4S)$
1.85 ±1.30 ±0.01	2	[5] ALBRECHT	90J	ARG	$e^+e^- \to \Upsilon(4S)$
• • • We do not use the following data for averages, fits, limits, etc. • • •					
1.37 ±0.09 ±0.11		[2] AUBERT	02	BABR	Repl. by AUBERT 05J
1.78 ±0.51 ±0.23	13	[2] ALAM	94	CLE2	Sup. by JESSOP 97

[1] AUBERT 07AV reports $[\Gamma(B^+ \to J/\psi(1S) K^*(892)^+)/\Gamma_{total}] \times [B(J/\psi(1S) \to p\overline{p})] = (3.78\ ^{+0.72+0.28}_{-0.64-0.23}) \times 10^{-6}$ which we divide by our best (shown rounded) value $B(J/\psi(1S) \to p\overline{p}) = (2.121 \pm 0.029) \times 10^{-3}$. Our first error is their experiment's error and our second error is the systematic error from using our best (shown rounded) value.

[2] Assumes equal production of B^+ and B^0 at the $\Upsilon(4S)$.

[3] ABE 96H assumes that $B(B^+ \to J/\psi K^+) = (1.02 \pm 0.14) \times 10^{-3}$.

[4] BORTOLETTO 92 reports $(1.3 \pm 0.9 \pm 0.3) \times 10^{-3}$ from a measurement of $[\Gamma(B^+ \to J/\psi(1S) K^*(892)^+)/\Gamma_{total}] \times [B(J/\psi(1S) \to e^+e^-)]$ assuming $B(J/\psi(1S) \to$

$e^+e^-) = 0.069 \pm 0.009$, which we rescale to our best (shown rounded) value $B(J/\psi(1S) \to e^+e^-) = (5.971 \pm 0.032) \times 10^{-2}$. Our first error is their experiment's error and our second error is the systematic error from using our best (shown rounded) value. Assumes equal production of B^+ and B^0 at the $\Upsilon(4S)$.

[5] ALBRECHT 90J reports $(1.6 \pm 1.1 \pm 0.3) \times 10^{-3}$ from a measurement of $[\Gamma(B^+ \to J/\psi(1S) K^*(892)^+)/\Gamma_{total}] \times [B(J/\psi(1S) \to e^+e^-)]$ assuming $B(J/\psi(1S) \to e^+e^-) = 0.069 \pm 0.009$, which we rescale to our best (shown rounded) value $B(J/\psi(1S) \to e^+e^-) = (5.971 \pm 0.032) \times 10^{-2}$. Our first error is their experiment's error and our second error is the systematic error from using our best (shown rounded) value. Assumes equal production of B^+ and B^0 at the $\Upsilon(4S)$.

$\Gamma(J/\psi(1S) K^*(892)^+)/\Gamma(J/\psi(1S) K^+)$ — $\Gamma_{321}/\Gamma_{316}$

VALUE	DOCUMENT ID		TECN	COMMENT
1.39±0.09 OUR AVERAGE				
1.37±0.05±0.08	AUBERT	05J	BABR	$e^+e^- \to \Upsilon(4S)$
1.45±0.20±0.17	[1] JESSOP	97	CLE2	$e^+e^- \to \Upsilon(4S)$
1.92±0.60±0.17	ABE	96Q	CDF	$p\overline{p}$
• • • We do not use the following data for averages, fits, limits, etc. • • •				
1.37±0.10±0.08	[2] AUBERT	02	BABR	Repl. by AUBERT 05J

[1] JESSOP 97 assumes equal production of B^+ and B^0 at the $\Upsilon(4S)$. The measurement is actually measured as an average over kaon charged and neutral states.
[2] Assumes equal production of B^+ and B^0 at the $\Upsilon(4S)$.

$\Gamma(J/\psi(1S) K(1270)^+)/\Gamma_{total}$ — Γ_{322}/Γ

VALUE (units 10^{-3})	DOCUMENT ID		TECN	COMMENT
1.80±0.34±0.39	[1] ABE	01L	BELL	$e^+e^- \to \Upsilon(4S)$

[1] Uses the PDG value of $B(B^+ \to J/\psi(1S) K^+) = (1.00 \pm 0.10) \times 10^{-3}$.

$\Gamma(J/\psi(1S) K(1400)^+)/\Gamma(J/\psi(1S) K(1270)^+)$ — $\Gamma_{323}/\Gamma_{322}$

VALUE	CL%	DOCUMENT ID		TECN	COMMENT
<0.30	90	ABE	01L	BELL	$e^+e^- \to \Upsilon(4S)$

$\Gamma(J/\psi(1S) \eta K^+)/\Gamma_{total}$ — Γ_{324}/Γ

VALUE (units 10^{-5})	DOCUMENT ID		TECN	COMMENT
12.4±1.4 OUR AVERAGE				
12.7±1.1±1.1	[1] IWASHITA	14	BELL	$e^+e^- \to \Upsilon(4S)$
10.8±2.3±2.4	[1] AUBERT	04Y	BABR	$e^+e^- \to \Upsilon(4S)$

[1] Assumes equal production of B^+ and B^0 at the $\Upsilon(4S)$.

$\Gamma(\chi_{c1-odd}(3872) K^+, \chi_{c1-odd} \to J/\psi\eta)/\Gamma_{total}$ — Γ_{325}/Γ

VALUE	CL%	DOCUMENT ID		TECN	COMMENT
<3.8 × 10^{-6}	90	IWASHITA	14	BELL	$e^+e^- \to \Upsilon(4S)$

$\Gamma(\psi(4160) K^+, \psi \to J/\psi\eta)/\Gamma_{total}$ — Γ_{326}/Γ

VALUE	CL%	DOCUMENT ID		TECN	COMMENT
<8.7 × 10^{-7}	90	AAIJ	22D	LHCB	pp at 7, 8, 13 TeV
• • • We do not use the following data for averages, fits, limits, etc. • • •					
<7.4 × 10^{-6}	90	IWASHITA	14	BELL	$e^+e^- \to \Upsilon(4S)$

$\Gamma(J/\psi(1S) \eta' K^+)/\Gamma_{total}$ — Γ_{327}/Γ

VALUE (units 10^{-5})	CL%	DOCUMENT ID		TECN	COMMENT
• • • We do not use the following data for averages, fits, limits, etc. • • •					
<8.8	90	[1] XIE	07	BELL	$e^+e^- \to \Upsilon(4S)$

[1] Assumes equal production of B^+ and B^0 at the $\Upsilon(4S)$.

$\Gamma(J/\psi(1S) \eta' K^+)/\Gamma(\psi(2S) K^+)$ — $\Gamma_{327}/\Gamma_{352}$

VALUE (units 10^{-2})	DOCUMENT ID		TECN	COMMENT
4.91±0.47±0.30	[1] AAIJ	23AK	LHCB	pp at 7, 8 and 13 TeV

[1] AAIJ 23AK measurements last uncertainty includes ±0.07 uncertainties on the branching fractions of the intermediate resonances.

$\Gamma(J/\psi(1S) \phi K^+)/\Gamma_{total}$ — Γ_{328}/Γ

VALUE (units 10^{-5})	DOCUMENT ID		TECN	COMMENT
5.0 ±0.4 OUR AVERAGE				
5.00±0.37±0.15	LEES	15	BABR	$e^+e^- \to \Upsilon(4S)$
4.4 ±1.4 ±0.5	[1] AUBERT	03O	BABR	$e^+e^- \to \Upsilon(4S)$
8.8 $^{+3.5}_{-3.0}$ ±1.3	[2] ANASTASSOV	00	CLE2	$e^+e^- \to \Upsilon(4S)$

[1] Assumes equal production of B^+ and B^0 at the $\Upsilon(4S)$.
[2] ANASTASSOV 00 finds 10 events on a background of 0.5 ± 0.2. Assumes equal production of B^0 and B^+ at the $\Upsilon(4S)$, a uniform Dalitz plot distribution, isotropic $J/\psi(1S)$ and ϕ decays, and $B(B^+ \to J/\psi(1S)\phi K^+) = B(B^0 \to J/\psi(1S)\phi K^0)$.

$\Gamma(J/\psi(1S) K_1(1650), K_1 \to \phi K^+)/\Gamma(J/\psi(1S)\phi K^+)$ — $\Gamma_{329}/\Gamma_{328}$

VALUE	DOCUMENT ID		TECN	COMMENT
0.12±0.10$^{+0.17}_{-0.06}$	[1] AAIJ	17	LHCB	pp at 7, 8 TeV

[1] Measured in amplitude analysis of $B^+ \to J/\psi(1S)\phi K^+$.

$\Gamma(J/\psi(1S) K^*(1680)^+, K^* \to \phi K^+)/\Gamma(J/\psi(1S)\phi K^+)$ — $\Gamma_{330}/\Gamma_{328}$

VALUE (units 10^{-2})	DOCUMENT ID		TECN	COMMENT
6.7±1.9$^{+3.2}_{-3.9}$	[1] AAIJ	17	LHCB	pp at 7, 8 TeV

[1] Measured in amplitude analysis of $B^+ \to J/\psi(1S)\phi K^+$.

$\Gamma(J/\psi(1S) K_2^*(1980), K_2^* \to \phi K^+)/\Gamma(J/\psi(1S)\phi K^+)$ — $\Gamma_{331}/\Gamma_{328}$

VALUE (units 10^{-2})	DOCUMENT ID		TECN	COMMENT
2.9±0.8$^{+1.7}_{-0.7}$	[1] AAIJ	17	LHCB	pp at 7, 8 TeV

[1] Measured in amplitude analysis of $B^+ \to J/\psi(1S)\phi K^+$.

$\Gamma(J/\psi(1S) K(1830)^+, K(1830)^+ \to \phi K^+)/\Gamma(J/\psi(1S)\phi K^+)$ — $\Gamma_{332}/\Gamma_{328}$

VALUE (units 10^{-2})	DOCUMENT ID		TECN	COMMENT
2.6±1.1$^{+2.3}_{-1.8}$	[1] AAIJ	17	LHCB	pp at 7, 8 TeV

[1] Measured in amplitude analysis of $B^+ \to J/\psi(1S)\phi K^+$.

$\Gamma(\chi_{c1}(4140) K^+, \chi_{c1} \to J/\psi(1S)\phi)/\Gamma(J/\psi(1S)\phi K^+)$ — $\Gamma_{333}/\Gamma_{328}$

VALUE	CL%	DOCUMENT ID		TECN	COMMENT
0.19 ±0.08 OUR AVERAGE					
0.13 ±0.032$^{+4.8}_{-2.0}$		[1] AAIJ	17	LHCB	pp at 7, 8 TeV
0.19 ±0.07 ±0.04		[2] ABAZOV	14A	D0	$p\overline{p}$ at 1.96 TeV
• • • We do not use the following data for averages, fits, limits, etc. • • •					
<0.133	90	LEES	15	BABR	$e^+e^- \to \Upsilon(4S)$
<0.07	90	[3] AAIJ	12AA	LHCB	pp at 7 TeV

[1] Measured in amplitude analysis of $B^+ \to J/\psi(1S)\phi K^+$.
[2] Reported a threshold enhancement in the $J/\psi\phi$ mass distribution consistent with the $\chi_{c1}(4140)$ state with a statistical significance of 3.1 standard deviations.
[3] Branching fractions are normalized to 382 ± 22 events of $B^+ \to J/\psi\phi K^+$.

$\Gamma(\chi_{c1}(4274) K^+, \chi_{c1} \to J/\psi(1S)\phi)/\Gamma(J/\psi(1S)\phi K^+)$ — $\Gamma_{334}/\Gamma_{328}$

VALUE (units 10^{-2})	CL%	DOCUMENT ID		TECN	COMMENT
7.1±2.5$^{+3.5}_{-2.4}$		[1] AAIJ	17	LHCB	pp at 7, 8 TeV
• • • We do not use the following data for averages, fits, limits, etc. • • •					
<18.1	90	LEES	15	BABR	$e^+e^- \to \Upsilon(4S)$
< 8	90	[2] AAIJ	12AA	LHCB	Repl. by AAIJ 17

[1] Measured in amplitude analysis of $B^+ \to J/\psi(1S)\phi K^+$.
[2] Branching fractions are normalized to 382 ± 22 events of $B^+ \to J/\psi\phi K^+$.

$\Gamma(\chi_{c0}(4500) K^+, \chi_{c0} \to J/\psi(1S)\phi)/\Gamma(J/\psi(1S)\phi K^+)$ — $\Gamma_{335}/\Gamma_{328}$

VALUE (units 10^{-2})	DOCUMENT ID		TECN	COMMENT
6.6±2.4$^{+3.5}_{-2.3}$	[1] AAIJ	17	LHCB	pp at 7, 8 TeV

[1] Measured in amplitude analysis of $B^+ \to J/\psi(1S)\phi K^+$.

$\Gamma(\chi_{c0}(4700) K^+, \chi_{c0} \to J/\psi(1S)\phi)/\Gamma(J/\psi(1S)\phi K^+)$ — $\Gamma_{336}/\Gamma_{328}$

VALUE	DOCUMENT ID		TECN	COMMENT
0.12±0.05$^{+0.09}_{-0.05}$	[1] AAIJ	17	LHCB	pp at 7, 8 TeV

[1] Measured in amplitude analysis of $B^+ \to J/\psi(1S)\phi K^+$.

$\Gamma(J/\psi(1S)\omega K^+)/\Gamma_{total}$ — Γ_{337}/Γ

VALUE (units 10^{-4})	DOCUMENT ID		TECN	COMMENT
3.2±0.1$^{+0.6}_{-0.3}$	[1] DEL-AMO-SA...10B		BABR	$e^+e^- \to \Upsilon(4S)$
• • • We do not use the following data for averages, fits, limits, etc. • • •				
3.5±0.2±0.4	[1] AUBERT	08W	BABR	Repl. by DEL-AMO-SANCHEZ 10B

[1] Assumes equal production of B^+ and B^0 at the $\Upsilon(4S)$.

$\Gamma(\chi_{c0}(3915) K^+, \chi_{c0} \to J/\psi\omega)/\Gamma_{total}$ — Γ_{338}/Γ

VALUE (units 10^{-5})	DOCUMENT ID		TECN	COMMENT
3.0$^{+0.7}_{-0.6}$$^{+0.5}_{-0.3}$	[1] DEL-AMO-SA...10B		BABR	$e^+e^- \to \Upsilon(4S)$
• • • We do not use the following data for averages, fits, limits, etc. • • •				
4.9$^{+1.0}_{-0.9}$±0.5	[1] AUBERT	08W	BABR	Repl. by DEL-AMO-SANCHEZ 10B

[1] Assumes equal production of B^+ and B^0 at the $\Upsilon(4S)$.

$\Gamma(\chi_{c0}(3915) K^+, \chi_{c0} \to p\overline{p})/\Gamma_{total}$ — Γ_{320}/Γ

VALUE	CL%	DOCUMENT ID		TECN	COMMENT
<7.1 × 10^{-8}	95	[1] AAIJ	13S	LHCB	pp at 7 TeV

[1] Measured relative to $B^+ \to J/\psi K^+$ decay with charmonia reconstructed in $p\overline{p}$ final state and using $B(B^+ \to J/\psi K^+) = (1.013 \pm 0.034) \times 10^{-3}$ and $B(J/\psi \to p\overline{p}) = (2.17 \pm 0.07) \times 10^{-3}$.

$\Gamma(J/\psi(1S)\pi^+)/\Gamma_{total}$ — Γ_{339}/Γ

VALUE	DOCUMENT ID		TECN	COMMENT
(4.1±0.4) × 10^{-5} OUR FIT	Error includes scale factor of 2.5.			
(3.8±0.6±0.3) × 10^{-5}	[1] ABE	03B	BELL	$e^+e^- \to \Upsilon(4S)$

[1] Assumes equal production of B^+ and B^0 at the $\Upsilon(4S)$.

$\Gamma(J/\psi(1S)\pi^+)/\Gamma(J/\psi(1S) K^+)$ — $\Gamma_{339}/\Gamma_{316}$

VALUE (units 10^{-2})	EVTS	DOCUMENT ID		TECN	COMMENT
4.1 ±0.4 OUR FIT	Error includes scale factor of 2.7.				
4.1 ±0.4 OUR AVERAGE	Error includes scale factor of 2.3. See the ideogram below.				
3.846±0.18 ±0.018		[1] AAIJ	25I	LHCB	pp at 7, 8, 13 TeV

Int. J. Mod. Phys. A 2026.41. Downloaded from www.worldscientific.com
by LIFORNIA @ BERKELEY on 09/16/26. Re-use and distribution is strictly not permitted, except for Open Access articles.

Int. J. Mod. Phys. A 2026.41. Downloaded from www.worldscientific.com
by UNIVERSITY OF CALIFORNIA @ BERKELEY on 09/16/26. Re-use and distribution is strictly not permitted, except for Open Access articles.

3.5 ±0.3 ±1.2	AABOUD	16L	ATLS	pp at 7, 8 TeV
4.86 ±0.82 ±0.15	ABULENCIA	09	CDF	$p\overline{p}$ at 1.96 TeV
5.37 ±0.45 ±0.11	AUBERT	04P	BABR	$e^+e^- \to \Upsilon(4S)$
5.0 $^{+1.9}_{-1.7}$ ±0.1	ABE	96R	CDF	$p\overline{p}$ 1.8 TeV
5.2 ±2.4	BISHAI	96	CLE2	$e^+e^- \to \Upsilon(4S)$

• • • We do not use the following data for averages, fits, limits, etc. • • •

3.852±0.022±0.018	AAIJ	25I	LHCB	pp at 13 TeV
3.83 ±0.03 ±0.03	AAIJ	17O	LHCB	Repl. by AAIJ 25I
3.83 ±0.11 ±0.07	AAIJ	12AC	LHCB	Repl. by AAIJ 17O
3.91 ±0.78 ±0.19	AUBERT	02F	BABR	Repl. by AUBERT 04P
4.3 ±2.3 5	[2] ALEXANDER	95	CLE2	Sup. by BISHAI 96

[1] AAIJ 25I measurement combined with the one referred in AAIJ 17O.
[2] Assumes equal production of B^+B^- and $B^0\overline{B}^0$ on $\Upsilon(4S)$.

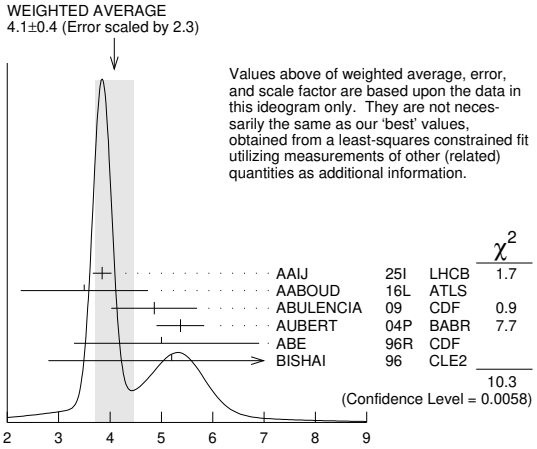

$\Gamma(J/\psi(1S)\pi^+\pi^+\pi^+\pi^-\pi^-)/\Gamma(\psi(2S)K^+)$ — $\Gamma_{340}/\Gamma_{352}$

VALUE (units 10^{-2})	DOCUMENT ID		TECN	COMMENT
1.88±0.17±0.09	[1] AAIJ	17K	LHCB	pp at 7 and 8 TeV

[1] Contains also the contribution from $B^+ \to \psi(2S)[\to J/\psi\pi^+\pi^-]\pi^+\pi^+\pi^-$ decays.

$\Gamma(\psi(2S)\pi^+\pi^+\pi^-)/\Gamma(\psi(2S)K^+)$ — $\Gamma_{341}/\Gamma_{352}$

VALUE (units 10^{-2})	DOCUMENT ID		TECN	COMMENT
3.04±0.50±0.26	AAIJ	17K	LHCB	pp at 7 and 8 TeV

$\Gamma(J/\psi(1S)\rho^+)/\Gamma_{total}$ — Γ_{342}/Γ

VALUE (units 10^{-5})	CL%	DOCUMENT ID		TECN	COMMENT
4.1 ±0.5 OUR AVERAGE		Error includes scale factor of 1.4.			
$3.81^{+0.25}_{-0.24}$ ±0.35		AAIJ	19O	LHCB	pp at 7 and 8 TeV
5.0 ±0.7 ±0.3		[1] AUBERT	07AC	BABR	$e^+e^- \to \Upsilon(4S)$
• • • We do not use the following data for averages, fits, limits, etc. • • •					
<77	90	BISHAI	96	CLE2	$e^+e^- \to \Upsilon(4S)$

[1] Assumes equal production of B^+ and B^0 at the $\Upsilon(4S)$.

$\Gamma(J/\psi(1S)\pi^+\pi^0 \text{nonresonant})/\Gamma_{total}$ — Γ_{343}/Γ

VALUE (units 10^{-5})	CL%	DOCUMENT ID		TECN	COMMENT
<0.73	90	[1] AUBERT	07AC	BABR	$e^+e^- \to \Upsilon(4S)$

[1] Assumes equal production of B^+ and B^0 at the $\Upsilon(4S)$.

$\Gamma(J/\psi(1S)a_1(1260)^+)/\Gamma_{total}$ — Γ_{344}/Γ

VALUE	CL%	DOCUMENT ID		TECN	COMMENT
$<1.2\times10^{-3}$	90	BISHAI	96	CLE2	$e^+e^- \to \Upsilon(4S)$

$\Gamma(J/\psi(1S)p\overline{p}\pi^+)/\Gamma_{total}$ — Γ_{345}/Γ

VALUE	CL%	DOCUMENT ID		TECN	COMMENT
$<5.0\times10^{-7}$	90	[1] AAIJ	13Z	LHCB	pp at 7 TeV

[1] Uses $B(B^0_s \to J/\psi(1S)\pi^+\pi^-) = (1.98 \pm 0.20)\times10^{-4}$.

$\Gamma(J/\psi(1S)p\overline{\Lambda})/\Gamma_{total}$ — Γ_{346}/Γ

VALUE (units 10^{-6})	CL%	DOCUMENT ID		TECN	COMMENT
14.6±1.2 OUR AVERAGE					
15.1±0.8±1.0		[1] SIRUNYAN	19CM	CMS	pp at 8 TeV
11.7±2.8$^{+1.8}_{-2.3}$		[2] XIE	05	BELL	$e^+e^- \to \Upsilon(4S)$
12 $^{+9}_{-6}$		[2] AUBERT	03K	BABR	$e^+e^- \to \Upsilon(4S)$
• • • We do not use the following data for averages, fits, limits, etc. • • •					
<41	90	ZANG	04	BELL	$e^+e^- \to \Upsilon(4S)$

[1] SIRUNYAN 19CM reports $B(B^+ \to J/\psi\overline{\Lambda}p)/B(B^+ \to J/\psi K^*(892)) = (1.054 \pm 0.057 \pm 0.035 \pm 0.011)\times10^{-2}$ and rescaled with the best value of $B(B^+ \to J/\psi K^*(892)) = (1.43 \pm 0.08)\times10^{-3}$, where the last uncertainty is the uncertainty from the branching fractions of $\overline{\Lambda}$ and $K^*(892)$ to reconstructed final states.
[2] Assumes equal production of B^+ and B^0 at the $\Upsilon(4S)$.

$\Gamma(J/\psi(1S)\overline{\Sigma}^0p)/\Gamma_{total}$ — Γ_{347}/Γ

VALUE	CL%	DOCUMENT ID		TECN	COMMENT
$<1.1\times10^{-5}$	90	[1] XIE	05	BELL	$e^+e^- \to \Upsilon(4S)$

[1] Assumes equal production of B^+ and B^0 at the $\Upsilon(4S)$.

$\Gamma(J/\psi(1S)D^+)/\Gamma_{total}$ — Γ_{348}/Γ

VALUE	CL%	DOCUMENT ID		TECN	COMMENT
$<12\times10^{-5}$	90	[1] AUBERT	05U	BABR	$e^+e^- \to \Upsilon(4S)$

[1] Assumes equal production of B^+ and B^0 at the $\Upsilon(4S)$.

$\Gamma(J/\psi(1S)\overline{D}^0\pi^+)/\Gamma_{total}$ — Γ_{349}/Γ

VALUE (units 10^{-5})	CL%	DOCUMENT ID		TECN	COMMENT
<2.5	90	[1] ZHANG	05B	BELL	$e^+e^- \to \Upsilon(4S)$
• • • We do not use the following data for averages, fits, limits, etc. • • •					
<5.2	90	[1] AUBERT	05R	BABR	$e^+e^- \to \Upsilon(4S)$

[1] Assumes equal production of B^+ and B^0 at the $\Upsilon(4S)$.

$\Gamma(J/\psi(1S)D_s^+)/\Gamma_{total}$ — Γ_{350}/Γ

VALUE	CL%	DOCUMENT ID		TECN	COMMENT
$<2.8\times10^{-7}$	90	AAIJ	24F	LHCB	pp at 7, 8, and 13 TeV

$\Gamma(\psi(2S)\pi^+)/\Gamma_{total}$ — Γ_{351}/Γ

VALUE (units 10^{-5})	DOCUMENT ID		TECN	COMMENT
2.44±0.22±0.20	[1] BHARDWAJ	08	BELL	$e^+e^- \to \Upsilon(4S)$

[1] Assumes equal production of B^+ and B^0 at the $\Upsilon(4S)$.

$\Gamma(\psi(2S)\pi^+)/\Gamma(\psi(2S)K^+)$ — $\Gamma_{351}/\Gamma_{352}$

VALUE (units 10^{-2})	DOCUMENT ID		TECN	COMMENT
3.97±0.29 OUR AVERAGE				
3.95±0.40±0.12	AAIJ	12AC	LHCB	pp at 7 TeV
3.99±0.36±0.17	BHARDWAJ	08	BELL	$e^+e^- \to \Upsilon(4S)$

$\Gamma(\psi(2S)K^+)/\Gamma_{total}$ — Γ_{352}/Γ

VALUE (units 10^{-4})	EVTS	DOCUMENT ID		TECN	COMMENT
6.25± 0.21 OUR FIT					
6.40± 0.34 OUR AVERAGE					
4.6 ± 1.0 ±0.7		[1] LEES	20C	BABR	$e^+e^- \to \Upsilon(4S)$
6.4 ± 1.0 ±0.4		[1] KATO	18	BELL	$e^+e^- \to \Upsilon(4S)$
6.65± 0.17±0.55		[2] GULER	11	BELL	$e^+e^- \to \Upsilon(4S)$
6.17± 0.32±0.44		[2] AUBERT	05J	BABR	$e^+e^- \to \Upsilon(4S)$
7.8 ± 0.7 ±0.9		[2] RICHICHI	01	CLE2	$e^+e^- \to \Upsilon(4S)$
18 ± 8 ±4	5	[2] ALBRECHT	90J	ARG	$e^+e^- \to \Upsilon(4S)$
• • • We do not use the following data for averages, fits, limits, etc. • • •					
4.9 ± 1.6 ±0.4		[1] AUBERT	06E	BABR	Repl. by LEES 20C
6.9 ± 0.6		[2] ABE	03B	BELL	Repl. by GULER 11
6.4 ± 0.5 ±0.8		[2] AUBERT	02	BABR	Repl. by AUBERT 05J
6.1 ± 2.3 ±0.9	7	[2] ALAM	94	CLE2	Repl. by RICHICHI 01
<5 at 90% CL		[2] BORTOLETTO	92	CLEO	$e^+e^- \to \Upsilon(4S)$
22 ±17	3	[3] ALBRECHT	87D	ARG	$e^+e^- \to \Upsilon(4S)$

[1] Measures absolute branching fractions using a missing-mass technique.
[2] Assumes equal production of B^+ and B^0 at the $\Upsilon(4S)$.
[3] ALBRECHT 87D assume $B^+B^-/B^0\overline{B}^0$ ratio is 55/45. Superseded by ALBRECHT 90J.

$\Gamma(\psi(2S)K^+)/\Gamma(J/\psi(1S)K^+)$ — $\Gamma_{352}/\Gamma_{316}$

VALUE	DOCUMENT ID		TECN	COMMENT
0.613±0.019 OUR FIT				
0.606±0.023 OUR AVERAGE				
0.58 ±0.11 ±0.02	[1] AAIJ	13S	LHCB	pp at 7 TeV
0.609±0.018±0.017	[2,3] AAIJ	12L	LHCB	pp at 7 TeV
0.63 ±0.05 ±0.08	ABAZOV	09Y	D0	$p\overline{p}$ at 1.96 TeV
0.558±0.082±0.056	ABE	98O	CDF	$p\overline{p}$ 1.8 TeV
• • • We do not use the following data for averages, fits, limits, etc. • • •				
0.64 ±0.06 ±0.07	[4] AUBERT	02	BABR	$e^+e^- \to \Upsilon(4S)$

[1] AAIJ 13S reports $[\Gamma(B^+ \to \psi(2S)K^+)/\Gamma(B^+ \to J/\psi(1S)K^+)] \times [B(\psi(2S) \to p\overline{p})] / [B(J/\psi(1S) \to p\overline{p})] = 0.080 \pm 0.012 \pm 0.009$ which we multiply or divide by our best (shown rounded) values $B(\psi(2S) \to p\overline{p}) = (2.95 \pm 0.09)\times10^{-4}$, $B(J/\psi(1S) \to p\overline{p}) = (2.121 \pm 0.029)\times10^{-3}$. Our first error is their experiment's error and our second error is the systematic error from using our best (shown rounded) values.
[2] AAIJ 12L reports $0.594 \pm 0.006 \pm 0.016 \pm 0.015$ from a measurement of $[\Gamma(B^+ \to \psi(2S)K^+)/\Gamma(B^+ \to J/\psi(1S)K^+)] \times [B(J/\psi(1S) \to e^+e^-)] / [B(\psi(2S) \to e^+e^-)]$ assuming $B(J/\psi(1S) \to e^+e^-) = (5.94 \pm 0.06)\times10^{-2}$, $B(\psi(2S) \to e^+e^-) = (7.72 \pm 0.17)\times10^{-3}$, which we rescale to our best (shown rounded) values $B(J/\psi(1S) \to e^+e^-) = (5.971 \pm 0.032)\times10^{-2}$, $B(\psi(2S) \to e^+e^-) = (7.95 \pm 0.22)\times10^{-3}$. Our first error is their experiment's error and our second error is the systematic error from using our best (shown rounded) values.
[3] Assumes $B(J/\psi \to \mu^+\mu^-) / B(\psi(2S) \to \mu^+\mu^-) = B(J/\psi \to e^+e^-) / B(\psi(2S) \to e^+e^-) = 7.69 \pm 0.19$.
[4] Assumes equal production of B^+ and B^0 at the $\Upsilon(4S)$.

Int. J. Mod. Phys. A 2026.41. Downloaded from www.worldscientific.com by LIFORNIA @ BERKELEY on 09/16/26. Re-use and distribution is strictly not permitted, except for Open Access articles.

$\Gamma(\psi(2S)K^*(892)^+)/\Gamma_{total}$ — Γ_{353}/Γ

VALUE (units 10^{-4})	CL%	DOCUMENT ID		TECN	COMMENT
6.7 ±1.4 OUR AVERAGE		Error includes scale factor of 1.3.			
5.92±0.85±0.89		[1] AUBERT	05J	BABR	$e^+e^- \to \Upsilon(4S)$
9.2 ±1.9 ±1.2		[1] RICHICHI	01	CLE2	$e^+e^- \to \Upsilon(4S)$
• • • We do not use the following data for averages, fits, limits, etc. • • •					
<30	90	[1] ALAM	94	CLE2	Repl. by RICHICHI 01
<35	90	[1] BORTOLETTO	92	CLEO	$e^+e^- \to \Upsilon(4S)$
<49	90	[1] ALBRECHT	90J	ARG	$e^+e^- \to \Upsilon(4S)$

[1] Assumes equal production of B^+ and B^0 at the $\Upsilon(4S)$.

$\Gamma(\psi(2S)K^*(892)^+)/\Gamma(\psi(2S)K^+)$ — $\Gamma_{353}/\Gamma_{352}$

VALUE	DOCUMENT ID		TECN	COMMENT
0.96±0.15±0.09	AUBERT	05J	BABR	$e^+e^- \to \Upsilon(4S)$

$\Gamma(\psi(2S)K^0\pi^+)/\Gamma_{total}$ — Γ_{354}/Γ

VALUE (units 10^{-3})	DOCUMENT ID		TECN	COMMENT
• • • We do not use the following data for averages, fits, limits, etc. • • •				
0.588±0.034	[1] AUBERT	09AA	BABR	$e^+e^- \to \Upsilon(4S)$

[1] Does not report systematic uncertainties.

$\Gamma(\psi(2S)K^+\pi^+\pi^-)/\Gamma_{total}$ — Γ_{355}/Γ

VALUE (units 10^{-4})	EVTS	DOCUMENT ID		TECN	COMMENT
4.3 ± 0.5 OUR AVERAGE					
4.31± 0.20±0.50		[1] GULER	11	BELL	$e^+e^- \to \Upsilon(4S)$
19 ±11 ±4	3	[1] ALBRECHT	90J	ARG	$e^+e^- \to \Upsilon(4S)$

[1] Assumes equal production of B^+ and B^0 at the $\Upsilon(4S)$.

$\Gamma(\chi_{c0}(4500)K^+, \chi_{c0}(4500) \to \psi(2S)\pi^+\pi^-)/\Gamma(\psi(2S)K^+\pi^+\pi^-)$ — $\Gamma_{356}/\Gamma_{355}$

VALUE	DOCUMENT ID		TECN	COMMENT
0.1845±0.0131±0.0292	[1,2] AAIJ	25Q	LHCB	pp at 7, 8 and 13 TeV

[1] Measured in amplitude analysis of $B^+ \to \psi(2S)K^+\pi^+\pi^-$.
[2] AAIJ 25Q identifies $T^*_{c\bar{c}0}(4475)$ as $\chi_{c0}(4500)$.

$\Gamma(\chi_{c1}(4685)K^+, \chi_{c1}(4685) \to \psi(2S)\pi^+\pi^-)/\Gamma(\psi(2S)K^+\pi^+\pi^-)$ — $\Gamma_{357}/\Gamma_{355}$

VALUE	DOCUMENT ID		TECN	COMMENT
0.0289±0.0045±0.0045	[1,2] AAIJ	25Q	LHCB	pp at 7, 8 and 13 TeV

[1] Measured in amplitude analysis of $B^+ \to \psi(2S)K^+\pi^+\pi^-$.
[2] AAIJ 25Q identifies $T_{c\bar{c}1}(4650)$ as $\chi_{c1}(4685)$.

$\Gamma(\chi_{c0}(4700)K^+, \chi_{c0}(4700) \to \psi(2S)\pi^+\pi^-)/\Gamma(\psi(2S)K^+\pi^+\pi^-)$ — $\Gamma_{358}/\Gamma_{355}$

VALUE	DOCUMENT ID		TECN	COMMENT
0.0173±0.0028±0.0040	[1,2] AAIJ	25Q	LHCB	pp at 7, 8 and 13 TeV

[1] Measured in amplitude analysis of $B^+ \to \psi(2S)K^+\pi^+\pi^-$.
[2] AAIJ 25Q identifies $T^*_{c\bar{c}0}(4710)$ as $\chi_{c0}(4700)$.

$\Gamma(\psi(2S)K^*(1410)^+, K^*(1410)^+ \to K^+\pi^+\pi^-)/\Gamma(\psi(2S)K^+\pi^+\pi^-)$ — $\Gamma_{359}/\Gamma_{355}$

VALUE	DOCUMENT ID		TECN	COMMENT
0.0179±0.0035±0.0074	[1] AAIJ	25Q	LHCB	pp at 7, 8 and 13 TeV

[1] Measured in amplitude analysis of $B^+ \to \psi(2S)K^+\pi^+\pi^-$.

$\Gamma(\psi(2S)K^*(1680)^+, K^*(1680)^+ \to K^+\pi^+\pi^-)/\Gamma(\psi(2S)K^+\pi^+\pi^-)$ — $\Gamma_{360}/\Gamma_{355}$

VALUE	DOCUMENT ID		TECN	COMMENT
0.0815±0.0131±0.0351	[1] AAIJ	25Q	LHCB	pp at 7, 8 and 13 TeV

[1] Measured in amplitude analysis of $B^+ \to \psi(2S)K^+\pi^+\pi^-$.

$\Gamma(\psi(2S)K_1(1270)^+, K_1(1270)^+ \to K^+\pi^+\pi^-)/\Gamma(\psi(2S)K^+\pi^+\pi^-)$ — $\Gamma_{361}/\Gamma_{355}$

VALUE	DOCUMENT ID		TECN	COMMENT
0.0760±0.0085±0.0135	[1] AAIJ	25Q	LHCB	pp at 7, 8 and 13 TeV

[1] Measured the S-wave fraction in amplitude analysis of $B^+ \to \psi(2S)K^+\pi^+\pi^-$.

$\Gamma([\psi(2S)K_1(1270)^+, K_1(1270)^+ \to K^+\pi^+\pi^-]_{P-wave})/\Gamma(\psi(2S)K^+\pi^+\pi^-)$ — $\Gamma_{362}/\Gamma_{355}$

VALUE	DOCUMENT ID		TECN	COMMENT
0.0752±0.0060±0.0108	[1] AAIJ	25Q	LHCB	pp at 7, 8 and 13 TeV

[1] Measured in amplitude analysis of $B^+ \to \psi(2S)K^+\pi^+\pi^-$.

$\Gamma([\psi(2S)K_1(1270)^+, K_1(1270)^+ \to K^+\pi^+\pi^-]_{D-wave})/\Gamma(\psi(2S)K^+\pi^+\pi^-)$ — $\Gamma_{363}/\Gamma_{355}$

VALUE	DOCUMENT ID		TECN	COMMENT
0.0681±0.0045±0.0118	[1] AAIJ	25Q	LHCB	pp at 7, 8 and 13 TeV

[1] Measured in amplitude analysis of $B^+ \to \psi(2S)K^+\pi^+\pi^-$.

$\Gamma(\psi(2S)K_1(1400)^+, K_1(1400)^+ \to K^+\pi^+\pi^-)/\Gamma(\psi(2S)K^+\pi^+\pi^-)$ — $\Gamma_{364}/\Gamma_{355}$

VALUE	DOCUMENT ID		TECN	COMMENT
0.0578±0.0062±0.0092	[1] AAIJ	25Q	LHCB	pp at 7, 8 and 13 TeV

[1] Measured the S-wave fraction in amplitude analysis of $B^+ \to \psi(2S)K^+\pi^+\pi^-$.

$\Gamma([\psi(2S)K_1(1400)^+, K_1(1400)^+ \to K^+\pi^+\pi^-]_{P-wave})/\Gamma(\psi(2S)K^+\pi^+\pi^-)$ — $\Gamma_{365}/\Gamma_{355}$

VALUE	DOCUMENT ID		TECN	COMMENT
0.0048±0.0018±0.0040	[1] AAIJ	25Q	LHCB	pp at 7, 8 and 13 TeV

[1] Measured in amplitude analysis of $B^+ \to \psi(2S)K^+\pi^+\pi^-$.

$\Gamma(\psi(2S)K_1(1460)^+, K_1(1460)^+ \to K^+\pi^+\pi^-)/\Gamma(\psi(2S)K^+\pi^+\pi^-)$ — $\Gamma_{366}/\Gamma_{355}$

VALUE	DOCUMENT ID		TECN	COMMENT
0.0526±0.0048±0.0087	[1] AAIJ	25Q	LHCB	pp at 7, 8 and 13 TeV

[1] Measured in amplitude analysis of $B^+ \to \psi(2S)K^+\pi^+\pi^-$.

$\Gamma(\psi(2S)K_2^*(1430)^+, K_2^*(1430)^+ \to K^+\pi^+\pi^-)/\Gamma(\psi(2S)K^+\pi^+\pi^-)$ — $\Gamma_{367}/\Gamma_{355}$

VALUE	DOCUMENT ID		TECN	COMMENT
0.0435±0.0029±0.0026	[1] AAIJ	25Q	LHCB	pp at 7, 8 and 13 TeV

[1] Measured in amplitude analysis of $B^+ \to \psi(2S)K^+\pi^+\pi^-$.

$\Gamma(T_{c\bar{c}1}(4200)^+K^*(892)^0 \to \psi(2S)K^+\pi^+\pi^-)/\Gamma(\psi(2S)K^+\pi^+\pi^-)$ — $\Gamma_{368}/\Gamma_{355}$

VALUE	DOCUMENT ID		TECN	COMMENT
0.0402±0.0088±0.0101	[1] AAIJ	25Q	LHCB	pp at 7, 8 and 13 TeV

[1] Measured the S-wave fraction in amplitude analysis of $B^+ \to \psi(2S)K^+\pi^+\pi^-$.

$\Gamma([T_{c\bar{c}1}(4200)^+K^*(892)^0 \to \psi(2S)K^+\pi^+\pi^-]_{P-wave})/\Gamma(\psi(2S)K^+\pi^+\pi^-)$ — $\Gamma_{369}/\Gamma_{355}$

VALUE	DOCUMENT ID		TECN	COMMENT
0.0460±0.0054±0.0217	[1] AAIJ	25Q	LHCB	pp at 7, 8 and 13 TeV

[1] Measured in amplitude analysis of $B^+ \to \psi(2S)K^+\pi^+\pi^-$.

$\Gamma([T_{c\bar{c}1}(4200)^+K^*(892)^0 \to \psi(2S)K^+\pi^+\pi^-]_{D-wave})/\Gamma(\psi(2S)K^+\pi^+\pi^-)$ — $\Gamma_{370}/\Gamma_{355}$

VALUE	DOCUMENT ID		TECN	COMMENT
0.0278±0.0033±0.0061	[1] AAIJ	25Q	LHCB	pp at 7, 8 and 13 TeV

[1] Measured in amplitude analysis of $B^+ \to \psi(2S)K^+\pi^+\pi^-$.

$\Gamma(T_{c\bar{c}1}(4430)^+K^*(892)^0 \to \psi(2S)K^+\pi^+\pi^-)/\Gamma(\psi(2S)K^+\pi^+\pi^-)$ — $\Gamma_{371}/\Gamma_{355}$

VALUE	DOCUMENT ID		TECN	COMMENT
0.0075±0.0043±0.0224	[1] AAIJ	25Q	LHCB	pp at 7, 8 and 13 TeV

[1] Measured in amplitude analysis of $B^+ \to \psi(2S)K^+\pi^+\pi^-$.

$\Gamma(T_{c\bar{c}1}(4430)^+[K^+\pi^-]_{S-wave} \to \psi(2S)K^+\pi^+\pi^-)/\Gamma(\psi(2S)K^+\pi^+\pi^-)$ — $\Gamma_{372}/\Gamma_{355}$

VALUE	DOCUMENT ID		TECN	COMMENT
0.0341±0.0054±0.0078	[1] AAIJ	25Q	LHCB	pp at 7, 8 and 13 TeV

[1] Measured in amplitude analysis of $B^+ \to \psi(2S)K^+\pi^+\pi^-$.

$\Gamma(T_{c\bar{c}s1}(4600)^0\pi^+, T_{c\bar{c}s1}(4600)^0 \to \psi(2S)K^+\pi^-)/\Gamma(\psi(2S)K^+\pi^+\pi^-)$ — $\Gamma_{373}/\Gamma_{355}$

VALUE	DOCUMENT ID		TECN	COMMENT
0.0442±0.0098±0.0217	[1] AAIJ	25Q	LHCB	pp at 7, 8 and 13 TeV

[1] Measured in amplitude analysis of $B^+ \to \psi(2S)K^+\pi^+\pi^-$.

$\Gamma(T_{c\bar{c}s1}(4900)^0\pi^+, T_{c\bar{c}s1}(4900)^0 \to \psi(2S)K^+\pi^-)/\Gamma(\psi(2S)K^+\pi^+\pi^-)$ — $\Gamma_{374}/\Gamma_{355}$

VALUE	DOCUMENT ID		TECN	COMMENT
0.0260±0.0066±0.0194	[1] AAIJ	25Q	LHCB	pp at 7, 8 and 13 TeV

[1] Measured in amplitude analysis of $B^+ \to \psi(2S)K^+\pi^+\pi^-$.

$\Gamma(\psi(2S)\phi(1020)K^+)/\Gamma_{total}$ — Γ_{375}/Γ

VALUE (units 10^{-6})	DOCUMENT ID		TECN	COMMENT
3.4±0.5 OUR AVERAGE				
3.1±0.5±0.2	[1] AAIJ	25P	LHCB	pp at 7, 8, 13 TeV
4.0±0.4±0.6	[2,3] KHACHATRY...	17C	CMS	pp at 8 TeV

[1] AAIJ 25P reports $[\Gamma(B^+ \to \psi(2S)\phi(1020)K^+)/\Gamma_{total}] / [B(B^+ \to J/\psi(1S)\phi K^+)] = 0.061 \pm 0.004 \pm 0.009$ which we multiply by our best (shown rounded) value $B(B^+ \to J/\psi(1S)\phi K^+) = (5.0 \pm 0.4) \times 10^{-5}$. Our first error is their experiment's error and our second error is the systematic error from using our best (shown rounded) value.
[2] Measured using $B^+ \to \psi(2S)K^+$ as a normalization channel. The second error represents total systematic uncertainties including those from branching fractions which were taken from PDG 16 as $B(\phi \to K^+K^-) = 0.489 \pm 0.005$ and $B(B^+ \to \psi(2S)K^+) = (6.26 \pm 0.24) \times 10^{-4}$.
[3] An upper limit on the fraction of the non-ϕ component in $B^+ \to \psi(2S)K^+K^-K^+$ decays is set as 0.26 at the 95% confidence level.

Int. J. Mod. Phys. A 2026.41. Downloaded from www.worldscientific.com
by UNIVERSITY OF CALIFORNIA @ BERKELEY on 09/16/26. Re-use and distribution is strictly not permitted, except for Open Access articles.

$\Gamma(\psi(3770)K^+)/\Gamma_{total}$ — Γ_{376}/Γ

VALUE (units 10^{-3})	CL%	DOCUMENT ID		TECN	COMMENT
0.43±0.11 OUR AVERAGE					
0.32±0.20±0.05±0.01		[1,2] LEES	20C	BABR	$e^+e^- \to \Upsilon(4S)$
0.48±0.11±0.07		[3] CHISTOV	04	BELL	$e^+e^- \to \Upsilon(4S)$
• • • We do not use the following data for averages, fits, limits, etc. • • •					
<0.23	90	[2] KATO	18	BELL	$e^+e^- \to \Upsilon(4S)$
3.5 ±2.5 ±0.3		[2] AUBERT	06E	BABR	Repl. by LEES 20C

[1] LEES 20C measurement's last uncertainty is due to the used $B(B^{\pm} \to K^{\pm}J/\psi)$ value.
[2] Measures absolute branching fractions using a missing-mass technique.
[3] Assumes equal production of B^+ and B^0 at the $\Upsilon(4S)$.

$\Gamma(\psi(3770)K^+)/\Gamma(D^-D^+K^+)$ — $\Gamma_{376}/\Gamma_{228}$

VALUE	DOCUMENT ID		TECN	COMMENT
$0.352\pm0.035^{+0.034}_{-0.031}$	[1,2] AAIJ	20AI	LHCB	pp at 7, 8, 13 TeV

[1] AAIJ 20AI reports $[\Gamma(B^+ \to \psi(3770)K^+)/\Gamma(B^+ \to D^-D^+K^+)] \times [B(\psi(3770) \to D^+D^-)] = (14.5 \pm 1.2 \pm 0.8) \times 10^{-2}$ which we divide by our best (shown rounded) value $B(\psi(3770) \to D^+D^-) = (41 \pm 4) \times 10^{-2}$. Our first error is their experiment's error and our second error is the systematic error from using our best (shown rounded) value.
[2] Measured in Dalitz plot analysis of $B^+ \to D^-D^+K^+$ decays.

$\Gamma(\psi(3770)K+, \psi \to D^0\overline{D}^0)/\Gamma_{total}$ — Γ_{377}/Γ

VALUE (units 10^{-4})	DOCUMENT ID		TECN	COMMENT
1.5 ±0.5 OUR AVERAGE	Error includes scale factor of 1.4.			
1.18±0.41±0.15	[1] LEES	15C	BABR	$e^+e^- \to \Upsilon(4S)$
2.2 ±0.5 ±0.3	[1] BRODZICKA	08	BELL	$e^+e^- \to \Upsilon(4S)$
• • • We do not use the following data for averages, fits, limits, etc. • • •				
1.41±0.30±0.22	[1] AUBERT	08B	BABR	Repl. by LEES 15C
3.4 ±0.8 ±0.5	[1] CHISTOV	04	BELL	Repl. by BRODZICKA 08

[1] Assumes equal production of B^+ and B^0 at the $\Upsilon(4S)$.

$\Gamma(\psi(3770)K+, \psi \to D^+D^-)/\Gamma_{total}$ — Γ_{378}/Γ

VALUE (units 10^{-4})	DOCUMENT ID		TECN	COMMENT
0.94±0.35 OUR AVERAGE				
0.84±0.32±0.21	[1] AUBERT	08B	BABR	$e^+e^- \to \Upsilon(4S)$
1.4 ±0.8 ±0.2	[1] CHISTOV	04	BELL	$e^+e^- \to \Upsilon(4S)$

[1] Assumes equal production of B^+ and B^0 at the $\Upsilon(4S)$.

$\Gamma(\psi(3770)K^+, \psi \to p\overline{p})/\Gamma_{total}$ — Γ_{379}/Γ

VALUE	CL%	DOCUMENT ID		TECN	COMMENT
$<2\times10^{-7}$	95	[1] AAIJ	17AD	LHCB	pp at 7 and 8 TeV

[1] Measured relative to $B^+ \to J/\psi K^+$ decay with charmonia reconstructed in $p\overline{p}$ final state and using $B(B^+ \to J/\psi K^+) \times B(J/\psi \to p\overline{p}) = (2.17 \pm 0.08) \times 10^{-6}$.

$\Gamma(\psi(3770)K^+, \psi \to J/\psi\eta)/\Gamma_{total}$ — Γ_{380}/Γ

VALUE	CL%	DOCUMENT ID		TECN	COMMENT
$<4.6\times10^{-7}$	90	AAIJ	22D	LHCB	pp at 7, 8, 13 TeV

$\Gamma(\psi(4040)K^+)/\Gamma_{total}$ — Γ_{381}/Γ

VALUE (units 10^{-3})	CL%	DOCUMENT ID		TECN	COMMENT
1.6 ±0.5±0.2		[1] AAIJ	22D	LHCB	pp at 7, 8, 13 TeV
• • • We do not use the following data for averages, fits, limits, etc. • • •					
<3.0	90	[2] IWASHITA	14	BELL	$e^+e^- \to \Upsilon(4S)$
<0.13	90	AAIJ	13BC	LHCB	pp at 7, 8 TeV

[1] AAIJ 22D reports $[\Gamma(B^+ \to \psi(4040)K^+)/\Gamma_{total}] \times [B(\psi(4040) \to J/\psi\eta)] = (8.53 \pm 2.35 \pm 0.30) \times 10^{-6}$ which we divide by our best (shown rounded) value $B(\psi(4040) \to J/\psi\eta) = (5.2 \pm 0.7) \times 10^{-3}$. Our first error is their experiment's error and our second error is the systematic error from using our best (shown rounded) value.
[2] IWASHITA 14 reports $[\Gamma(B^+ \to \psi(4040)K^+)/\Gamma_{total}] \times [B(\psi(4040) \to J/\psi\eta)] < 15.5 \times 10^{-6}$ which we divide by our best (shown rounded) value $B(\psi(4040) \to J/\psi\eta) = 5.2 \times 10^{-3}$.

$\Gamma(\psi(4040)K^+, \psi \to D^+D^-)/\Gamma(D^-D^+K^+)$ — $\Gamma_{382}/\Gamma_{228}$

VALUE (units 10^{-2})	DOCUMENT ID		TECN	COMMENT
5.0±1.3±0.4	[1] AAIJ	20AI	LHCB	pp at 7, 8, 13 TeV

[1] Measured in Dalitz plot analysis of $B^+ \to D^-D^+K^+$ decays.

$\Gamma(\psi(4160)K^+)/\Gamma_{total}$ — Γ_{383}/Γ

VALUE (units 10^{-4})	DOCUMENT ID		TECN	COMMENT
$5.1^{+1.3}_{-1.2}\pm2.4$	[1] AAIJ	13BC	LHCB	pp at 7, 8 TeV

[1] AAIJ 13BC reports $[\Gamma(B^+ \to \psi(4160)K^+)]/\Gamma_{total}] \times B(\psi(4160) \to \mu^+\mu^-) = (3.5^{+0.9}_{-0.8}) \times 10^{-9}$ which we devide by our best value $B(\psi(4160) \to e^+e^-) = (6.9 \pm 3.3) \times 10^{-6}$ assuming lepton universality. Our first error is their experiment's error and our second error is the systematic error from using our best value.

$\Gamma(\psi(4160)K^+, \psi \to \overline{D}^0D^0)/\Gamma_{total}$ — Γ_{384}/Γ

VALUE (units 10^{-4})	DOCUMENT ID		TECN	COMMENT
0.84±0.41±0.33	[1] LEES	15C	BABR	$e^+e^- \to \Upsilon(4S)$

[1] Assumes equal production of B^+ and B^0 at the $\Upsilon(4S)$.

$\Gamma(\psi(4160)K^+, \psi \to D^+D^-)/\Gamma(D^-D^+K^+)$ — $\Gamma_{385}/\Gamma_{228}$

VALUE (units 10^{-2})	DOCUMENT ID		TECN	COMMENT
6.6±1.5±1.2	[1] AAIJ	20AI	LHCB	pp at 7, 8, 13 TeV

[1] Measured in Dalitz plot analysis of $B^+ \to D^-D^+K^+$ decays.

$\Gamma(\psi(4415)K^+, \psi \to D^+D^-)/\Gamma(D^-D^+K^+)$ — $\Gamma_{386}/\Gamma_{228}$

VALUE (units 10^{-2})	DOCUMENT ID		TECN	COMMENT
9.2±1.4±1.5	[1] AAIJ	20AI	LHCB	pp at 7, 8, 13 TeV

[1] Measured in Dalitz plot analysis of $B^+ \to D^-D^+K^+$ decays.

$\Gamma(\psi(4415)K^+, \psi \to J/\psi\eta)/\Gamma_{total}$ — Γ_{387}/Γ

VALUE	CL%	DOCUMENT ID		TECN	COMMENT
$<9.6\times10^{-7}$	90	AAIJ	22D	LHCB	pp at 7, 8, 13 TeV

$\Gamma(\chi_{c0}\pi^+, \chi_{c0} \to \pi^+\pi^-)/\Gamma_{total}$ — Γ_{388}/Γ

VALUE (units 10^{-6})	CL%	DOCUMENT ID		TECN	COMMENT
<0.1	90	[1] AUBERT	09L	BABR	$e^+e^- \to \Upsilon(4S)$
• • • We do not use the following data for averages, fits, limits, etc. • • •					
<0.3	90	[1] AUBERT,B	05G	BABR	Repl. by AUBERT 09L

[1] Assumes equal production of B^+ and B^0 at the $\Upsilon(4S)$.

$\Gamma(\chi_{c0}\pi^+, \chi_{c0} \to \pi^0\pi^0)/\Gamma_{total}$ — Γ_{389}/Γ

VALUE	CL%	DOCUMENT ID		TECN	COMMENT
$<5\times10^{-7}$	90	LAI	23	BELL	$e^+e^- \to \Upsilon(4S)$

$\Gamma(\chi_{c0}K^+)/\Gamma_{total}$ — Γ_{390}/Γ

VALUE (units 10^{-4})	CL%	DOCUMENT ID		TECN	COMMENT
$1.49^{+0.15}_{-0.14}$ **OUR AVERAGE**					
2.0 ±1.3 ±0.3 ±0.1		[1,2] LEES	20C	BABR	$e^+e^- \to \Upsilon(4S)$
$1.9^{+0.6}_{-0.5}$ ±1.1		[3] CHILIKIN	19	BELL	$e^+e^- \to \Upsilon(4S)$
1.84±0.25±0.14		[4,5] LEES	12O	BABR	$e^+e^- \to \Upsilon(4S)$
1.68±0.32±0.16		[4,6] LEES	12O	BABR	$e^+e^- \to \Upsilon(4S)$
1.7 ±0.8 ±0.1		[7] LEES	11I	BABR	$e^+e^- \to \Upsilon(4S)$
$1.20^{+0.27}_{-0.24}\pm0.04$		[4,8] AUBERT	08AI	BABR	$e^+e^- \to \Upsilon(4S)$
4.5 ±2.1 ±0.3		[9] AUBERT,BE	06M	BABR	$e^+e^- \to \Upsilon(4S)$
$1.12\pm0.12^{+0.30}_{-0.20}$		[4] GARMASH	06	BELL	$e^+e^- \to \Upsilon(4S)$
• • • We do not use the following data for averages, fits, limits, etc. • • •					
<3.3	90	[2] KATO	18	BELL	$e^+e^- \to \Upsilon(4S)$
<2.6	95	[10] AAIJ	13S	LHCB	pp at 7 TeV
<6	90	[4,11] WICHT	08	BELL	$e^+e^- \to \Upsilon(4S)$
<1.8	90	[2] AUBERT	06E	BABR	$e^+e^- \to \Upsilon(4S)$
1.84±0.32±0.31		[4,12] AUBERT	06O	BABR	Repl. by LEES 12O
<8.9	90	[4] AUBERT	05K	BABR	$e^+e^- \to \Upsilon(4S)$
1.39±0.49±0.11		[13] AUBERT,B	05N	BABR	Repl. by AUBERT 08AI
$1.96\pm0.35^{+2.00}_{-0.42}$		[4] GARMASH	05	BELL	Repl. by GARMASH 06
2.7 ±0.7		[14] AUBERT	04T	BABR	Repl. by AUBERT,B 04P
3.0 ±0.8 ±0.3		[15] AUBERT,B	04P	BABR	Repl. by AUBERT,B 05N
$6.0^{+2.1}_{-1.8}$ ±1.1		[16] ABE	02B	BELL	Repl. by GARMASH 05
<4.8	90	[17] EDWARDS	01	CLE2	$e^+e^- \to \Upsilon(4S)$

[1] LEES 20C measurement's last uncertainty is due to the used $B(B^{\pm} \to K^{\pm}J/\psi)$ value.
[2] Measures absolute branching fractions using a missing-mass technique.
[3] CHILIKIN 19 reports $[\Gamma(B^+ \to \chi_{c0}K^+)/\Gamma_{total}] \times [B(\chi_{c0}(1P) \to p\overline{p}\pi^+\pi^-)] = (3.7^{+1.2}_{-1.0}{}^{+0.2}_{-0.3}) \times 10^{-7}$ which we divide by our best (shown rounded) value $B(\chi_{c0}(1P) \to p\overline{p}\pi^+\pi^-) = (1.9 \pm 1.1) \times 10^{-3}$. Our first error is their experiment's error and our second error is the systematic error from using our best (shown rounded) value.
[4] Assumes equal production of B^+ and B^0 at the $\Upsilon(4S)$.
[5] Measured in the $B^+ \to K^+K^-K^+$ decay.
[6] Measured in the $B^+ \to K^+K^0_SK^0_S$ decay.
[7] LEES 11I reports $[\Gamma(B^+ \to \chi_{c0}K^+)/\Gamma_{total}] \times [B(\chi_{c0}(1P) \to \pi\pi)] = (1.53 \pm 0.66 \pm 0.27) \times 10^{-6}$ which we divide by our best (shown rounded) value $B(\chi_{c0}(1P) \to \pi\pi) = (8.76 \pm 0.26) \times 10^{-3}$. Our first error is their experiment's error and our second error is the systematic error from using our best (shown rounded) value.
[8] AUBERT 08AI reports $(0.70 \pm 0.10^{+0.12}_{-0.10}) \times 10^{-6}$ for $B(B^+ \to \chi_{c0}K^+) \times B(\chi_{c0} \to \pi^+\pi^-)$. We compute $B(B^+ \to \chi_{c0}K^+)$ using the PDG value $B(\chi_{c0} \to \pi\pi)=(8.76 \pm 0.26) \times 10^{-3}$ and 2/3 for the $\pi^+\pi^-$ fraction. Our first error is their experiment's error and the second error is systematic error from using our best value.
[9] AUBERT,BE 06M reports $[\Gamma(B^+ \to \chi_{c0}K^+)/\Gamma_{total}] \times [B(\chi_{c0}(1P) \to \gamma J/\psi(1S))] = (6.1 \pm 2.6 \pm 1.1) \times 10^{-6}$ which we divide by our best (shown rounded) value $B(\chi_{c0}(1P) \to \gamma J/\psi(1S)) = (1.35 \pm 0.09) \times 10^{-2}$. Our first error is their experiment's error and our second error is the systematic error from using our best (shown rounded) value. The significance of the observed signal is 2.4 σ.
[10] AAIJ 13S reports $[\Gamma(B^+ \to \chi_{c0}K^+)/\Gamma_{total}] \times [B(\chi_{c0}(1P) \to p\overline{p})] < 6 \times 10^{-8}$ which we divide by our best (shown rounded) value $B(\chi_{c0}(1P) \to p\overline{p}) = 2.35 \times 10^{-4}$.
[11] WICHT 08 reports $[\Gamma(B^+ \to \chi_{c0}K^+)/\Gamma_{total}] \times [B(\chi_{c0}(1P) \to \gamma\gamma)] < 0.11 \times 10^{-6}$ which we divide by our best (shown rounded) value $B(\chi_{c0}(1P) \to \gamma\gamma) = 1.96 \times 10^{-4}$.
[12] Measured in the $B^+ \to K^+K^-K^+$ decay.

[13] AUBERT,B 05N reports $(0.66 \pm 0.22 \pm 0.08) \times 10^{-6}$ for $B(B^+ \to \chi_c^0 K^+) \times B(\chi_c^0 \to \pi^+\pi^-)$. We compute $B(B^+ \to \chi_c^0 K^+)$ using the PDG value $B(\chi_c^0 \to \pi^+\pi^-) = (7.1 \pm 0.6) \times 10^{-3}$ and 2/3 for the $\pi^+\pi^-$ fraction.

[14] The measurement performed using decay channels $\chi_{c0} \to \pi^+\pi^-$ and $\chi_{c0} \to K^+K^-$. The ratio of the branching ratios for these channels is found to be consistent with world average.

[15] AUBERT 04P reports $B(B^+ \to \chi_{c0} K^+) \times B(\chi_{c0} \to \pi^+\pi^-) = (1.5 \pm 0.4 \pm 0.1) \times 10^{-6}$ and used PDG value of $B(\chi_{c0} \to \pi\pi) = (7.4 \pm 0.8) \times 10^{-3}$ and Clebsh-Gordan coefficient to compute $B(B^{\pm} -> \chi_{c0} K^+)$.

[16] ABE 02B measures the ratio of $B(B^+ \to \chi_{c0} K^+)/B(B^+ \to J/\psi(1S) K^+) = 0.60 + 0.21 - 0.18 \pm 0.05 \pm 0.08$, where the third error is due to the uncertainty in the $B(\chi_{c0} \to \pi^+\pi^-)$, and uses $B(B^+ \to J/\psi(1S) K^+) = (10.0 \pm 1.0) \times 10^{-4}$ to obtain the result.

[17] EDWARDS 01 assumes equal production of B^0 and B^+ at the $\Upsilon(4S)$. The correlated uncertainties (28.3)% from $B(J/\psi(1S) \to \gamma\eta_c)$ in those modes have been accounted for.

$\Gamma(\chi_{c0} K^0 \pi^+)/\Gamma_{total}$ — Γ_{391}/Γ

VALUE (units 10^{-3})	DOCUMENT ID		TECN	COMMENT
1.45±0.08±0.19	[1] AAIJ	23AH	LHCB	pp at 7, 8 and 13 TeV

[1] The second uncertainty includes systematic and reference branching reaction of $B^+ \to J/\psi K^+$ uncertainties.

$\Gamma(\chi_{c0} K^*(892)^+)/\Gamma_{total}$ — Γ_{392}/Γ

VALUE (units 10^{-4})	CL%	DOCUMENT ID		TECN	COMMENT
< 2.1	90	[1] AUBERT	08BD	BABR	$e^+e^- \to \Upsilon(4S)$
• • • We do not use the following data for averages, fits, limits, etc. • • •					
<28.6	90	[1] AUBERT	05K	BABR	Repl. by AUBERT 08BD

[1] Assumes equal production of B^+ and B^0 at the $\Upsilon(4S)$.

$\Gamma(\chi_{c1}(1P)\pi^+)/\Gamma_{total}$ — Γ_{393}/Γ

VALUE (units 10^{-5})	DOCUMENT ID		TECN	COMMENT
2.2±0.4±0.3	[1] KUMAR	06	BELL	$e^+e^- \to \Upsilon(4S)$

[1] Assumes equal production of B^+ and B^0 at the $\Upsilon(4S)$.

$\Gamma(\chi_{c1}(1P) K^+)/\Gamma_{total}$ — Γ_{394}/Γ

VALUE (units 10^{-4})	DOCUMENT ID		TECN	COMMENT
4.74± 0.22 OUR AVERAGE				
4.0 ± 0.8 ±0.6 ±0.1	[1,2] LEES	20C	BABR	$e^+e^- \to \Upsilon(4S)$
9^{+3}_{-2} ±4	[3] CHILIKIN	19	BELL	$e^+e^- \to \Upsilon(4S)$
5.8 ± 0.9 ±0.5	[1] KATO	18	BELL	$e^+e^- \to \Upsilon(4S)$
4.94± 0.11±0.33	[4] BHARDWAJ	11	BELL	$e^+e^- \to \Upsilon(4S)$
4.5 ± 0.1 ±0.3	[5] AUBERT	09B	BABR	$e^+e^- \to \Upsilon(4S)$
15.5 ± 5.4 ±2.0	[6] ACOSTA	02F	CDF	$p\overline{p}$ 1.8 TeV
• • • We do not use the following data for averages, fits, limits, etc. • • •				
8.1 ± 1.4 ±0.7	[1] AUBERT	06E	BABR	Repl. by LEES 20C
5.2 ± 0.4 ±0.2	[7] AUBERT,BE	06M	BABR	Repl. by AUBERT 09B
4.49± 0.19±0.53	[4] SONI	06	BELL	Repl. by BHARDWAJ 11
5.79± 0.26±0.65	[4] AUBERT	05J	BABR	Repl. by AUBERT,BE 06M
6.0 ± 0.9 ±0.2	[8] AUBERT	02	BABR	Repl. by AUBERT 05J
9.7 ± 4.0 ±0.9	[4] ALAM	94	CLE2	$e^+e^- \to \Upsilon(4S)$
19 ±13 ±6	[9] ALBRECHT	92E	ARG	$e^+e^- \to \Upsilon(4S)$

[1] Measures absolute branching fractions using a missing-mass technique.

[2] LEES 20C measurement's last uncertainty is due to the used $B(B^{\pm} \to K^{\pm} J/\psi)$ value.

[3] CHILIKIN 19 reports $[\Gamma(B^+ \to \chi_{c1}(1P) K^+)/\Gamma_{total}] \times [B(\chi_{c1}(1P) \to p\overline{p}\pi^+\pi^-)] = (4.7^{+1.3+0.4}_{-1.2-0.2}) \times 10^{-7}$ which we divide by our best (shown rounded) value $B(\chi_{c1}(1P) \to p\overline{p}\pi^+\pi^-) = (5.0 \pm 1.9) \times 10^{-4}$. Our first error is their experiment's error and our second error is the systematic error from using our best (shown rounded) value.

[4] Assumes equal production of B^+ and B^0 at the $\Upsilon(4S)$.

[5] Uses $\chi_{c1,2} \to J/\psi\gamma$. Assumes $B(\Upsilon(4S) \to B^+B^-) = (51.6 \pm 0.6)$% and $B(\Upsilon(4S) \to B^0\overline{B}^0) = (48.4 \pm 0.6)$%.

[6] ACOSTA 02F uses as reference of $B(B \to J/\psi(1S) K^+) = (10.1 \pm 0.6) \times 10^{-4}$. The second error includes the systematic error and the uncertainties of the branching ratio.

[7] AUBERT,BE 06M reports $[\Gamma(B^+ \to \chi_{c1}(1P) K^+)/\Gamma_{total}] \times [B(\chi_{c1}(1P) \to \gamma J/\psi(1S))] = (1.76 \pm 0.07 \pm 0.12) \times 10^{-4}$ which we divide by our best (shown rounded) value $B(\chi_{c1}(1P) \to \gamma J/\psi(1S)) = (33.9 \pm 1.2) \times 10^{-2}$. Our first error is their experiment's error and our second error is the systematic error from using our best (shown rounded) value.

[8] AUBERT 02 reports $(7.5 \pm 0.9 \pm 0.8) \times 10^{-4}$ from a measurement of $[\Gamma(B^+ \to \chi_{c1}(1P) K^+)/\Gamma_{total}] \times [B(\chi_{c1}(1P) \to \gamma J/\psi(1S))]$ assuming $B(\chi_{c1}(1P) \to \gamma J/\psi(1S)) = 0.273 \pm 0.016$, which we rescale to our best (shown rounded) value $B(\chi_{c1}(1P) \to \gamma J/\psi(1S)) = (33.9 \pm 1.2) \times 10^{-2}$. Our first error is their experiment's error and our second error is the systematic error from using our best (shown rounded) value. Assumes equal production of B^+ and B^0 at the $\Upsilon(4S)$.

[9] ALBRECHT 92E assumes no $\chi_{c2}(1P)$ production and $B(\Upsilon(4S) \to B^+B^-) = 50$%.

$\Gamma(\chi_{c1}(1P) K^+)/\Gamma(J/\psi(1S) K^+)$ — $\Gamma_{394}/\Gamma_{316}$

VALUE	DOCUMENT ID		TECN	COMMENT
0.60±0.07±0.02	[1] AUBERT	02	BABR	$e^+e^- \to \Upsilon(4S)$

[1] AUBERT 02 reports $0.75 \pm 0.08 \pm 0.05$ from a measurement of $[\Gamma(B^+ \to \chi_{c1}(1P) K^+)/\Gamma(B^+ \to J/\psi(1S) K^+)] \times [B(\chi_{c1}(1P) \to \gamma J/\psi(1S))]$ assuming $B(\chi_{c1}(1P) \to \gamma J/\psi(1S)) = 0.273 \pm 0.016$, which we rescale to our best (shown rounded) value $B(\chi_{c1}(1P) \to \gamma J/\psi(1S)) = (33.9 \pm 1.2) \times 10^{-2}$. Our first error is their experiment's error and our second error is the systematic error from using our best (shown rounded) value. Assumes equal production of B^+ and B^0 at the $\Upsilon(4S)$.

$\Gamma(\chi_{c1}(1P)\pi^+)/\Gamma(\chi_{c1}(1P) K^+)$ — $\Gamma_{393}/\Gamma_{394}$

VALUE	DOCUMENT ID		TECN	COMMENT
0.043±0.008±0.003	[1] KUMAR	06	BELL	$e^+e^- \to \Upsilon(4S)$

[1] Assumes equal production of B^+ and B^0 at the $\Upsilon(4S)$.

$\Gamma(\chi_{c1}(1P) K^*(892)^+)/\Gamma_{total}$ — Γ_{395}/Γ

VALUE (units 10^{-4})	CL%	DOCUMENT ID		TECN	COMMENT
3.0 ±0.6 OUR AVERAGE		Error includes scale factor of 1.1.			
2.6 ±0.5 ±0.4		[1] AUBERT	09B	BABR	$e^+e^- \to \Upsilon(4S)$
4.05±0.59±0.95		[2] SONI	06	BELL	$e^+e^- \to \Upsilon(4S)$
• • • We do not use the following data for averages, fits, limits, etc. • • •					
2.94±0.95±0.98		[2] AUBERT	05J	BABR	Repl. by AUBERT 09B
<21	90	[2] ALAM	94	CLE2	$e^+e^- \to \Upsilon(4S)$

[1] Uses $\chi_{c1,2} \to J/\psi\gamma$. Assumes $B(\Upsilon(4S) \to B^+B^-) = (51.6 \pm 0.6)$% and $B(\Upsilon(4S) \to B^0\overline{B}^0) = (48.4 \pm 0.6)$%.

[2] Assumes equal production of B^+ and B^0 at the $\Upsilon(4S)$.

$\Gamma(\chi_{c1}(1P) K^*(892)^+)/\Gamma(\chi_{c1}(1P) K^+)$ — $\Gamma_{395}/\Gamma_{394}$

VALUE	DOCUMENT ID		TECN	COMMENT
0.51±0.17±0.16	AUBERT	05J	BABR	$e^+e^- \to \Upsilon(4S)$

$\Gamma(\chi_{c1}(1P) K^0\pi^+)/\Gamma_{total}$ — Γ_{396}/Γ

VALUE (units 10^{-4})	DOCUMENT ID		TECN	COMMENT
5.75±0.26±0.32	[1] BHARDWAJ	16	BELL	$e^+e^- \to \Upsilon(4S)$

[1] Assumes equal production of B^+ and B^0 at the $\Upsilon(4S)$.

$\Gamma(\chi_{c1}(1P) K^0\pi^+)/\Gamma(J/\psi(1S) K^0\pi^+)$ — $\Gamma_{396}/\Gamma_{317}$

VALUE	DOCUMENT ID		TECN	COMMENT
0.509±0.030±0.018	[1] LEES	12B	BABR	$e^+e^- \to \Upsilon(4S)$

[1] LEES 12B reports $0.501 \pm 0.024 \pm 0.028$ from a measurement of $[\Gamma(B^+ \to \chi_{c1}(1P) K^0\pi^+)/\Gamma(B^+ \to J/\psi(1S) K^0\pi^+)] \times [B(\chi_{c1}(1P) \to \gamma J/\psi(1S))]$ assuming $B(\chi_{c1}(1P) \to \gamma J/\psi(1S)) = (34.4 \pm 1.5) \times 10^{-2}$, which we rescale to our best (shown rounded) value $B(\chi_{c1}(1P) \to \gamma J/\psi(1S)) = (33.9 \pm 1.2) \times 10^{-2}$. Our first error is their experiment's error and our second error is the systematic error from using our best (shown rounded) value.

$\Gamma(\chi_{c1}(1P) K^+\pi^0)/\Gamma_{total}$ — Γ_{397}/Γ

VALUE (units 10^{-4})	DOCUMENT ID		TECN	COMMENT
3.29±0.29±0.19	[1] BHARDWAJ	16	BELL	$e^+e^- \to \Upsilon(4S)$

[1] Assumes equal production of B^+ and B^0 at the $\Upsilon(4S)$.

$\Gamma(\chi_{c1}(1P) K^+\pi^+\pi^-)/\Gamma_{total}$ — Γ_{398}/Γ

VALUE (units 10^{-4})	DOCUMENT ID		TECN	COMMENT
3.74±0.18±0.24	[1] BHARDWAJ	16	BELL	$e^+e^- \to \Upsilon(4S)$

[1] Assumes equal production of B^+ and B^0 at the $\Upsilon(4S)$.

$\Gamma(\chi_{c1}(2P) K^+, \chi_{c1}(2P) \to \pi^+\pi^-\chi_{c1}(1P))/\Gamma_{total}$ — Γ_{399}/Γ

VALUE	CL%	DOCUMENT ID		TECN	COMMENT
<1.1 × 10^{-5}	90	[1,2] BHARDWAJ	16	BELL	$e^+e^- \to \Upsilon(4S)$

[1] BHARDWAJ 16 analysis fixes mass and width of the $\chi_{c1}(2P)$ state to 3920 MeV and 20 MeV.

[2] Assumes equal production of B^+ and B^0 at the $\Upsilon(4S)$.

$\Gamma(\chi_{c2}\pi^+, \chi_{c2} \to \pi^0\pi^0)/\Gamma_{total}$ — Γ_{400}/Γ

VALUE	CL%	DOCUMENT ID		TECN	COMMENT
<7 × 10^{-7}	90	LAI	23	BELL	$e^+e^- \to \Upsilon(4S)$

$\Gamma(\chi_{c2} K^+)/\Gamma_{total}$ — Γ_{401}/Γ

VALUE (units 10^{-5})	CL%	DOCUMENT ID		TECN	COMMENT
$1.11^{+0.36}_{-0.34}$±0.09		[1] BHARDWAJ	11	BELL	$e^+e^- \to \Upsilon(4S)$
• • • We do not use the following data for averages, fits, limits, etc. • • •					
< 1.8	90	[2] AUBERT	09B	BABR	$e^+e^- \to \Upsilon(4S)$
<20	90	[3] AUBERT	06E	BABR	$e^+e^- \to \Upsilon(4S)$
< 2.9	90	[1] SONI	06	BELL	Repl. by BHARDWAJ 11
< 3.0	90	[1] AUBERT	05K	BABR	Repl. by AUBERT 06E

[1] Assumes equal production of B^+ and B^0 at the $\Upsilon(4S)$.

[2] Uses $\chi_{c1,2} \to J/\psi\gamma$. Assumes $B(\Upsilon(4S) \to B^+B^-) = (51.6 \pm 0.6)$% and $B(\Upsilon(4S) \to B^0\overline{B}^0) = (48.4 \pm 0.6)$%.

[3] Perform measurements of absolute branching fractions using a missing mass technique.

$\Gamma(\chi_{c2} K^+, \chi_{c2} \to p\overline{p}\pi^+\pi^-)/\Gamma_{total}$ — Γ_{402}/Γ

VALUE	DOCUMENT ID		TECN	COMMENT
<1.9 × 10^{-7}	CHILIKIN	19	BELL	$e^+e^- \to \Upsilon(4S)$

$\Gamma(B^+ \to \chi_{c2} K^+)/\Gamma_{total} \times \Gamma(\chi_{c2}(1P) \to \gamma\gamma)/\Gamma_{total}$ — $\Gamma_{401}/\Gamma \times \Gamma^{\chi_{c2}(1P)}_{111}/\Gamma^{\chi_{c2}(1P)}$

VALUE (units 10^{-6})	CL%	DOCUMENT ID		TECN	COMMENT
<0.09	90	[1] WICHT	08	BELL	$e^+e^- \to \Upsilon(4S)$

[1] Assumes equal production of B^+ and B^0 at the $\Upsilon(4S)$.

Int. J. Mod. Phys. A 2026.41. Downloaded from www.worldscientific.com by LIFORNIA @ BERKELEY on 09/16/26. Re-use and distribution is strictly not permitted, except for Open Access articles.

Int. J. Mod. Phys. A 2026.41. Downloaded from www.worldscientific.com
by UNIVERSITY OF CALIFORNIA @ BERKELEY on 09/16/26. Re-use and distribution is strictly not permitted, except for Open Access articles.

$\Gamma(\chi_{c2} K^*(892)^+)/\Gamma_{total}$ — Γ_{403}/Γ

VALUE	CL%	DOCUMENT ID		TECN	COMMENT
$<12 \times 10^{-5}$	90	[1] AUBERT	09B	BABR	$e^+e^- \to \Upsilon(4S)$
• • • We do not use the following data for averages, fits, limits, etc. • • •					
$<12.7 \times 10^{-5}$	90	[2] SONI	06	BELL	$e^+e^- \to \Upsilon(4S)$
$< 1.2 \times 10^{-5}$	90	[2] AUBERT	05K	BABR	Repl. by AUBERT 09B

[1] Uses $\chi_{c1,2} \to J/\psi\gamma$. Assumes $B(\Upsilon(4S) \to B^+B^-) = (51.6 \pm 0.6)\%$ and $B(\Upsilon(4S) \to B^0\overline{B}^0) = (48.4 \pm 0.6)\%$.
[2] Assumes equal production of B^+ and B^0 at the $\Upsilon(4S)$.

$\Gamma(\chi_{c2} K^0\pi^+)/\Gamma_{total}$ — Γ_{404}/Γ

VALUE (units 10^{-4})	DOCUMENT ID		TECN	COMMENT
1.24±0.25 OUR AVERAGE				
9.2 ±2.1 ±1.3	[1] AAIJ	23AH	LHCB	pp at 7, 8 and 13 TeV
1.16±0.22±0.12	[2] BHARDWAJ	16	BELL	$e^+e^- \to \Upsilon(4S)$

[1] The second uncertainty includes systematic and reference branching reaction of $B^+ \to J/\psi K^+$ uncertainties.
[2] Assumes equal production of B^+ and B^0 at the $\Upsilon(4S)$.

$\Gamma(\chi_{c2} K^+\pi^0)/\Gamma_{total}$ — Γ_{405}/Γ

VALUE	CL%	DOCUMENT ID		TECN	COMMENT
$<0.62 \times 10^{-4}$	90	[1] BHARDWAJ	16	BELL	$e^+e^- \to \Upsilon(4S)$

[1] Assumes equal production of B^+ and B^0 at the $\Upsilon(4S)$.

$\Gamma(\chi_{c2} K^+\pi^+\pi^-)/\Gamma_{total}$ — Γ_{406}/Γ

VALUE (units 10^{-4})	DOCUMENT ID		TECN	COMMENT
1.34±0.17±0.09	[1] BHARDWAJ	16	BELL	$e^+e^- \to \Upsilon(4S)$

[1] Assumes equal production of B^+ and B^0 at the $\Upsilon(4S)$.

$\Gamma(\chi_{c2}(3930) K^+, \chi_{c2} \to D^+D^-)/\Gamma(D^-D^+K^+)$ — $\Gamma_{407}/\Gamma_{228}$

VALUE (units 10^{-2})	DOCUMENT ID		TECN	COMMENT
7.2±1.2±0.3	[1] AAIJ	20AI	LHCB	pp at 7, 8, 13 TeV

[1] Measured in Dalitz plot analysis of $B^+ \to D^-D^+K^+$ decays.

$\Gamma(\chi_{c2}(3930)\pi^+, \chi_{c2} \to \pi^+\pi^-)/\Gamma_{total}$ — Γ_{408}/Γ

VALUE (units 10^{-6})	CL%	DOCUMENT ID		TECN	COMMENT
<0.1	90	[1] AUBERT	09L	BABR	$e^+e^- \to \Upsilon(4S)$

[1] Assumes equal production of B^+ and B^0 at the $\Upsilon(4S)$.

$\Gamma(h_c(1P) K^+)/\Gamma_{total}$ — Γ_{409}/Γ

VALUE (units 10^{-5})	CL%	DOCUMENT ID		TECN	COMMENT
$3.7^{+1.0}_{-0.9}{}^{+0.8}_{-0.8}$		CHILIKIN	19	BELL	$e^+e^- \to \Upsilon(4S)$
• • • We do not use the following data for averages, fits, limits, etc. • • •					
<3.8	90	[1] FANG	06	BELL	$e^+e^- \to \Upsilon(4S)$

[1] Assumes equal production of B^+ and B^0 at the $\Upsilon(4S)$ and $B(h_c \to \eta_c\gamma) = 50\%$.

$\Gamma(h_c(1P) K^+, h_c \to p\overline{p})/\Gamma_{total}$ — Γ_{410}/Γ

VALUE	CL%	DOCUMENT ID		TECN	COMMENT
$<6.4 \times 10^{-8}$	95	[1] AAIJ	13S	LHCB	pp at 7 TeV

[1] Measured relative to $B^+ \to J/\psi K^+$ decay with charmonia reconstructed in $p\overline{p}$ final state and using $B(B^+ \to J/\psi K^+) = (1.013 \pm 0.034) \times 10^{-3}$ and $B(J/\psi \to p\overline{p}) = (2.17 \pm 0.07) \times 10^{-3}$.

$\Gamma(K^0\pi^+)/\Gamma_{total}$ — Γ_{411}/Γ

VALUE (units 10^{-6})	CL%	DOCUMENT ID		TECN	COMMENT
23.9 ± 0.6 OUR FIT					
24.0 ± 0.6 OUR AVERAGE					
24.37± 0.71±0.86		ADACHI	24	BELL	$e^+e^- \to \Upsilon(4S)$
23.97± 0.53±0.71		[1] DUH	13	BELL	$e^+e^- \to \Upsilon(4S)$
23.9 ± 1.1 ±1.0		[1] AUBERT,BE	06C	BABR	$e^+e^- \to \Upsilon(4S)$
18.8 $^{+3.7}_{-3.3}$ $^{+2.1}_{-1.8}$		[1] BORNHEIM	03	CLE2	$e^+e^- \to \Upsilon(4S)$
• • • We do not use the following data for averages, fits, limits, etc. • • •					
22.8 $^{+0.8}_{-0.7}$ ±1.3		[1] LIN	07	BELL	Repl. by DUH 13
26.0 ± 1.3 ±1.0		[1] AUBERT,BE	05E	BABR	Repl. by AUBERT,BE 06C
22.3 ± 1.7 ±1.1		[1] AUBERT	04M	BABR	Repl. by AUBERT,BE 05E
22.0 ± 1.9 ±1.1		[1] CHAO	04	BELL	Repl. by LIN 07
19.4 $^{+3.1}_{-3.0}$ ±1.6		[1] CASEY	02	BELL	Repl. by CHAO 04
13.7 $^{+5.7}_{-4.8}$ $^{+1.9}_{-1.8}$		[1] ABE	01H	BELL	Repl. by CASEY 02
18.2 $^{+3.3}_{-3.0}$ ±2.0		[1] AUBERT	01E	BABR	Repl. by AUBERT 04M
18.2 $^{+4.6}_{-4.0}$ ±1.6		[1] CRONIN-HEN...	00	CLE2	Repl. by BORNHEIM 03
23 $^{+11}_{-10}$ ±3.6		GODANG	98	CLE2	Repl. by CRONIN-HENNESSY 00
< 48	90	ASNER	96	CLE2	Repl. by GODANG 98
<190	90	ALBRECHT	91B	ARG	$e^+e^- \to \Upsilon(4S)$
<100	90	[2] AVERY	89B	CLEO	$e^+e^- \to \Upsilon(4S)$
<680	90	AVERY	87	CLEO	$e^+e^- \to \Upsilon(4S)$

[1] Assumes equal production of B^+ and B^0 at the $\Upsilon(4S)$.
[2] AVERY 89B reports $< 9 \times 10^{-5}$ assuming the $\Upsilon(4S)$ decays 43% to $B^0\overline{B}^0$. We rescale to 50%.

$\Gamma(K^+\pi^0)/\Gamma_{total}$ — Γ_{412}/Γ

VALUE (units 10^{-6})	CL%	DOCUMENT ID		TECN	COMMENT
13.2 ±0.4 OUR AVERAGE					
13.93±0.38±0.71		ADACHI	24	BELL	$e^+e^- \to \Upsilon(4S)$
12.62±0.31±0.56		[1] DUH	13	BELL	$e^+e^- \to \Upsilon(4S)$
13.6 ±0.6 ±0.7		[1] AUBERT	07BC	BABR	$e^+e^- \to \Upsilon(4S)$
12.9 $^{+2.4}_{-2.2}$ $^{+1.2}_{-1.1}$		[1] BORNHEIM	03	CLE2	$e^+e^- \to \Upsilon(4S)$
• • • We do not use the following data for averages, fits, limits, etc. • • •					
12.4 ±0.5 ±0.6		[1] LIN	07A	BELL	Repl. by DUH 13
12.0 ±0.7 ±0.6		[1] AUBERT	05L	BABR	Repl. by AUBERT 07BC
12.0 ±1.3 $^{+1.3}_{-0.9}$		[1] CHAO	04	BELL	Repl. by LIN 07A
12.8 $^{+1.2}_{-1.1}$ ±1.0		[1] AUBERT	03L	BABR	Repl. by AUBERT 05L
13.0 $^{+2.5}_{-2.4}$ ±1.3		[1] CASEY	02	BELL	Repl. by CHAO 04
16.3 $^{+3.5}_{-3.3}$ $^{+1.6}_{-1.8}$		[1] ABE	01H	BELL	Repl. by CASEY 02
10.8 $^{+2.1}_{-1.9}$ ±1.0		[1] AUBERT	01E	BABR	Repl. by AUBERT 03L
11.6 $^{+3.0}_{-2.7}$ $^{+1.4}_{-1.3}$		[1] CRONIN-HEN...	00	CLE2	Repl. by BORNHEIM 03
<16	90	GODANG	98	CLE2	Repl. by CRONIN-HENNESSY 00
<14	90	ASNER	96	CLE2	Repl. by GODANG 98

[1] Assumes equal production of B^+ and B^0 at the $\Upsilon(4S)$.

$\Gamma(K^+\pi^0)/\Gamma(K^0\pi^+)$ — $\Gamma_{412}/\Gamma_{411}$

VALUE	DOCUMENT ID		TECN	COMMENT
0.54±0.03±0.04	LIN	07A	BELL	$e^+e^- \to \Upsilon(4S)$
• • • We do not use the following data for averages, fits, limits, etc. • • •				
$2.38^{+0.98}_{-1.10}{}^{+0.39}_{-0.26}$	ABE	01H	BELL	Repl. by LIN 07A

$\Gamma(\eta' K^+)/\Gamma_{total}$ — Γ_{413}/Γ

VALUE (units 10^{-6})	DOCUMENT ID		TECN	COMMENT
70.4± 2.5 OUR AVERAGE				
71.5± 1.3±3.2	[1] AUBERT	09AV	BABR	$e^+e^- \to \Upsilon(4S)$
61 $^{+10}_{-8}$ ±1	[1,2] WICHT	08	BELL	$e^+e^- \to \Upsilon(4S)$
69.2± 2.2±3.7	[1] SCHUEMANN	06	BELL	$e^+e^- \to \Upsilon(4S)$
80 $^{+10}_{-9}$ ±7	[1] RICHICHI	00	CLE2	$e^+e^- \to \Upsilon(4S)$
• • • We do not use the following data for averages, fits, limits, etc. • • •				
70.0± 1.5±2.8	[1] AUBERT	07AE	BABR	Repl. by AUBERT 09AV
68.9± 2.0±3.2	[1] AUBERT	05M	BABR	Repl. by AUBERT 07AE
76.9± 3.5±4.4	[1] AUBERT	03W	BABR	Repl. by AUBERT 05M
79 $^{+12}_{-11}$ ±9	[1] ABE	01M	BELL	Repl. by SCHUEMANN 06
70 ± 8 ±5	[1] AUBERT	01G	BABR	Repl. by AUBERT 03W
65 $^{+15}_{-14}$ ±9	BEHRENS	98	CLE2	Repl. by RICHICHI 00

[1] Assumes equal production of B^+ and B^0 at the $\Upsilon(4S)$.
[2] WICHT 08 reports $[\Gamma(B^+ \to \eta' K^+)/\Gamma_{total}] \times [B(\eta'(958) \to \gamma\gamma)] = (1.40^{+0.16}_{-0.15}{}^{+0.15}_{-0.12}) \times 10^{-6}$ which we divide by our best (shown rounded) value $B(\eta'(958) \to \gamma\gamma) = (2.307 \pm 0.033) \times 10^{-2}$. Our first error is their experiment's error and our second error is the systematic error from using our best (shown rounded) value.

$\Gamma(\eta' K^*(892)^+)/\Gamma_{total}$ — Γ_{414}/Γ

VALUE (units 10^{-6})	CL%	DOCUMENT ID		TECN	COMMENT
$4.8^{+1.6}_{-1.4}$±0.8		[1] DEL-AMO-SA...	10A	BABR	$e^+e^- \to \Upsilon(4S)$
• • • We do not use the following data for averages, fits, limits, etc. • • •					
$4.9^{+1.9}_{-1.7}$±0.8		[1] AUBERT	07E	BABR	Repl. by DEL-AMO-SANCHEZ 10A
< 2.9	90	[1] SCHUEMANN	07	BELL	$e^+e^- \to \Upsilon(4S)$
<14	90	[1] AUBERT,B	04D	BABR	Repl. by AUBERT 07E
<35	90	[1] RICHICHI	00	CLE2	$e^+e^- \to \Upsilon(4S)$
<13	90	BEHRENS	98	CLE2	Repl. by RICHICHI 00

[1] Assumes equal production of B^+ and B^0 at the $\Upsilon(4S)$.

$\Gamma(\eta' K_0^*(1430)^+)/\Gamma_{total}$ — Γ_{415}/Γ

VALUE (units 10^{-6})	DOCUMENT ID		TECN	COMMENT
5.2±1.9±1.0	[1] DEL-AMO-SA...	10A	BABR	$e^+e^- \to \Upsilon(4S)$

[1] Assumes equal production of B^+ and B^0 at the $\Upsilon(4S)$.

$\Gamma(\eta' K_2^*(1430)^+)/\Gamma_{total}$ — Γ_{416}/Γ

VALUE (units 10^{-6})	DOCUMENT ID		TECN	COMMENT
$28.0^{+4.6}_{-4.3}$±2.6	[1] DEL-AMO-SA...	10A	BABR	$e^+e^- \to \Upsilon(4S)$

[1] Assumes equal production of B^+ and B^0 at the $\Upsilon(4S)$.

$\Gamma(\eta K^+)/\Gamma_{total}$ — Γ_{417}/Γ

VALUE (units 10^{-6})	CL%	DOCUMENT ID		TECN	COMMENT
2.4 ±0.4 OUR AVERAGE		Error includes scale factor of 1.7.			
2.12±0.23±0.11		[1] HOI	12	BELL	$e^+e^- \to \Upsilon(4S)$

Int. J. Mod. Phys. A 2026.41. Downloaded from www.worldscientific.com by LIFORNIA @ BERKELEY on 09/16/26. Re-use and distribution is strictly not permitted, except for Open Access articles.

$2.94^{+0.39}_{-0.34}\pm0.21$	[1] AUBERT	09AV	BABR	$e^+e^-\to\Upsilon(4S)$
$2.2\ ^{+2.8}_{-2.2}$	[1] RICHICHI	00	CLE2	$e^+e^-\to\Upsilon(4S)$

• • • We do not use the following data for averages, fits, limits, etc. • • •

$2.21^{+0.48}_{-0.42}\pm0.01$	[1,2] WICHT	08	BELL	Repl. by HOI 12
$3.7\ \pm0.4\ \pm0.1$	[1] AUBERT	07AE	BABR	Repl. by AUBERT 09AV
$1.9\ \pm0.3\ ^{+0.2}_{-0.1}$	[1] CHANG	07B	BELL	Repl. by HOI 12
$3.3\ \pm0.6\ \pm0.3$	[1] AUBERT,B	05K	BABR	Repl. by AUBERT 07AE
$2.1\ \pm0.6\ \pm0.2$	[1] CHANG	05A	BELL	Repl. by CHANG 07B
$3.4\ \pm0.8\ \pm0.2$	[1] AUBERT	04H	BABR	Repl. by AUBERT,B 05K
<14 90	BEHRENS	98	CLE2	Repl. by RICHICHI 00

[1] Assumes equal production of B^+ and B^0 at the $\Upsilon(4S)$.

[2] WICHT 08 reports $[\Gamma(B^+\to\eta K^+)/\Gamma_{total}]\times[B(\eta\to2\gamma)]=(0.87^{+0.16}_{-0.15}{}^{+0.10}_{-0.07})\times10^{-6}$ which we divide by our best (shown rounded) value $B(\eta\to2\gamma)=(39.36\pm0.18)\times10^{-2}$. Our first error is their experiment's error and our second error is the systematic error from using our best (shown rounded) value.

$\Gamma(\eta K^*(892)^+)/\Gamma_{total}$ — Γ_{418}/Γ

VALUE (units 10^{-6})	CL%	DOCUMENT ID		TECN	COMMENT
19.3±1.6 OUR AVERAGE					
$19.3^{+2.0}_{-1.9}\pm1.5$		[1] WANG	07B	BELL	$e^+e^-\to\Upsilon(4S)$
$18.9\pm1.8\pm1.3$		[1] AUBERT,B	06H	BABR	$e^+e^-\to\Upsilon(4S)$
$26.4^{+9.6}_{-8.2}\pm3.3$		[1] RICHICHI	00	CLE2	$e^+e^-\to\Upsilon(4S)$

• • • We do not use the following data for averages, fits, limits, etc. • • •

$25.6\pm4.0\pm2.4$		[1] AUBERT,B	04D	BABR	Repl. by AUBERT,B 06H
<30	90	BEHRENS	98	CLE2	Repl. by RICHICHI 00

[1] Assumes equal production of B^+ and B^0 at the $\Upsilon(4S)$.

$\Gamma(\eta K_0^*(1430)^+)/\Gamma_{total}$ — Γ_{419}/Γ

VALUE (units 10^{-6})	DOCUMENT ID		TECN	COMMENT
18.2±2.6±2.6	[1] AUBERT,B	06H	BABR	$e^+e^-\to\Upsilon(4S)$

[1] Assumes equal production of B^+ and B^0 at the $\Upsilon(4S)$.

$\Gamma(\eta K_2^*(1430)^+)/\Gamma_{total}$ — Γ_{420}/Γ

VALUE (units 10^{-6})	DOCUMENT ID		TECN	COMMENT
9.1±2.7±1.4	[1] AUBERT,B	06H	BABR	$e^+e^-\to\Upsilon(4S)$

[1] Assumes equal production of B^+ and B^0 at the $\Upsilon(4S)$.

$\Gamma(\eta(1295)K^+,\ \eta\to\eta\pi\pi)/\Gamma_{total}$ — Γ_{421}/Γ

VALUE (units 10^{-6})	DOCUMENT ID		TECN	COMMENT
$\mathbf{2.9^{+0.8}_{-0.7}\pm0.2}$	[1] AUBERT	08X	BABR	$e^+e^-\to\Upsilon(4S)$

[1] Assumes equal production of B^+ and B^0 at the $\Upsilon(4S)$.

$\Gamma(\eta(1405)K^+,\ \eta\to\eta\pi\pi)/\Gamma_{total}$ — Γ_{422}/Γ

VALUE (units 10^{-6})	CL%	DOCUMENT ID		TECN	COMMENT
<1.3	90	[1] AUBERT	08X	BABR	$e^+e^-\to\Upsilon(4S)$

[1] Assumes equal production of B^+ and B^0 at the $\Upsilon(4S)$.

$\Gamma(\eta(1405)K^+,\ \eta\to K^*K)/\Gamma_{total}$ — Γ_{423}/Γ

VALUE (units 10^{-6})	CL%	DOCUMENT ID		TECN	COMMENT
3.8±0.5±0.9		[1,2] AAIJ	25F	LHCB	pp at 7, 8 and 13 TeV
<1.2	90	[3] AUBERT	08X	BABR	$e^+e^-\to\Upsilon(4S)$

[1] The second uncertainty includes the systematic and the uncertainties on the known branching fractions.

[2] This is the inverse-variance weighted average of the branching fraction measurements $B^+\to K^0K^-\pi^+K^+$ and $B^+\to\overline{K}^0K^+\pi^-K^+$ decays. AAIJ 25F also lists the two measurements separately and finds that the resulting fractions are consistent among the two channels when including the systematic uncertainties.

[3] Assumes equal production of B^+ and B^0 at the $\Upsilon(4S)$.

$\Gamma(\eta(1405)K^+,\ \eta\to K^0K\pi)/\Gamma_{total}$ — Γ_{424}/Γ

VALUE (units 10^{-5})	DOCUMENT ID		TECN	COMMENT
0.80±0.05±0.10	[1,2] AAIJ	25F	LHCB	pp at 7, 8 and 13 TeV

[1] The second uncertainty includes the systematic and the uncertainties on the known branching fractions.

[2] This is the inverse-variance weighted average of the branching fraction measurements $B^+\to K^0K^-\pi^+K^+$ and $B^+\to\overline{K}^0K^+\pi^-K^+$ decays. AAIJ 25F also lists the two measurements separately and finds that the resulting fractions are consistent among the two channels when including the systematic uncertainties.

$\Gamma(\eta(1475)K^+,\ \eta\to K^*K)/\Gamma_{total}$ — Γ_{425}/Γ

VALUE (units 10^{-6})	DOCUMENT ID		TECN	COMMENT
14.2±1.3 OUR AVERAGE				
$14.5\pm1.1\pm1.5$	[1,2] AAIJ	25F	LHCB	pp at 7, 8 and 13 TeV
$13.8^{+1.8}_{-1.7}{}^{+1.0}_{-0.6}$	[3] AUBERT	08X	BABR	$e^+e^-\to\Upsilon(4S)$

[1] The second uncertainty includes the systematic and the uncertainties on the known branching fractions.

[2] This is the inverse-variance weighted average of the branching fraction measurements $B^+\to K^0K^-\pi^+K^+$ and $B^+\to\overline{K}^0K^+\pi^-K^+$ decays. AAIJ 25F also lists the two measurements separately and finds that the resulting fractions are consistent among the two channels when including the systematic uncertainties.

[3] Assumes equal production of B^+ and B^0 at the $\Upsilon(4S)$.

$\Gamma(\eta(1475)K^+,\ \eta\to a_0(980)\pi)/\Gamma_{total}$ — Γ_{426}/Γ

VALUE (units 10^{-5})	DOCUMENT ID		TECN	COMMENT
0.22±0.04±0.03	[1,2] AAIJ	25F	LHCB	pp at 7, 8 and 13 TeV

[1] The second uncertainty includes the systematic and the uncertainties on the known branching fractions.

[2] This is the inverse-variance weighted average of the branching fraction measurements from $B^+\to K^0K^-\pi^+K^+$ and $B^+\to\overline{K}^0K^+\pi^-K^+$ decays. AAIJ 25F also lists the two measurements separately and finds that the resulting fractions are consistent among the two channels when including the systematic uncertainties.

$\Gamma(\eta(1475)K^+,\ \eta\to K^0K\pi)/\Gamma_{total}$ — Γ_{427}/Γ

VALUE (units 10^{-5})	DOCUMENT ID		TECN	COMMENT
1.51±0.16±0.26	[1,2] AAIJ	25F	LHCB	pp at 7, 8 and 13 TeV

[1] The second uncertainty includes the systematic and the uncertainties on the known branching fractions.

[2] This is the inverse-variance weighted average of the branching fraction measurements $B^+\to K^0K^-\pi^+K^+$ and $B^+\to\overline{K}^0K^+\pi^-K^+$ decays. AAIJ 25F also lists the two measurements separately and finds that the resulting fractions are consistent among the two channels when including the systematic uncertainties.

$\Gamma(\eta(1760)K^+,\ \eta\to K^*\overline{K})/\Gamma_{total}$ — Γ_{428}/Γ

VALUE (units 10^{-5})	DOCUMENT ID		TECN	COMMENT
0.34±0.04±0.045	[1,2] AAIJ	25F	LHCB	pp at 7, 8 and 13 TeV

[1] The second uncertainty includes the systematic and the uncertainties on the known branching fractions.

[2] This is the inverse-variance weighted average of the branching fraction measurements $B^+\to K^0K^-\pi^+K^+$ and $B^+\to\overline{K}^0K^+\pi^-K^+$ decays. AAIJ 25F also lists the two measurements separately and finds that the resulting fractions are consistent among the two channels when including the systematic uncertainties.

$\Gamma(\eta(1760)K^+,\ \eta\to a_0(980)\pi)/\Gamma_{total}$ — Γ_{429}/Γ

VALUE (units 10^{-5})	DOCUMENT ID		TECN	COMMENT
0.26±0.04±0.03	[1,2] AAIJ	25F	LHCB	pp at 7, 8 and 13 TeV

[1] The second uncertainty includes the systematic and the uncertainties on the known branching fractions.

[2] This is the inverse-variance weighted average of the branching fraction measurements $B^+\to K^0K^-\pi^+K^+$ and $B^+\to\overline{K}^0K^+\pi^-K^+$ decays. AAIJ 25F also lists the two measurements separately and finds that the resulting fractions are consistent among the two channels when including the systematic uncertainties.

$\Gamma(\eta(1760)K^+,\ \eta\to K^0K\pi)/\Gamma_{total}$ — Γ_{430}/Γ

VALUE (units 10^{-5})	DOCUMENT ID		TECN	COMMENT
2.21±0.20±0.35	[1,2] AAIJ	25F	LHCB	pp at 7, 8 and 13 TeV

[1] This is the inverse-variance weighted average of the branching fraction measurements $B^+\to K^0K^-\pi^+K^+$ and $B^+\to\overline{K}^0K^+\pi^-K^+$ decays. AAIJ 25F also lists the two measurements separately and finds that the resulting fractions are consistent among the two channels when including the systematic uncertainties.

[2] The second uncertainty includes the systematic and the uncertainties on the known branching fractions.

$\Gamma(f_1(1285)K^+)/\Gamma_{total}$ — Γ_{431}/Γ

VALUE (units 10^{-6})	CL%	DOCUMENT ID		TECN	COMMENT
<2.0	90	[1] AUBERT	08X	BABR	$e^+e^-\to\Upsilon(4S)$

[1] Assumes equal production of B^+ and B^0 at the $\Upsilon(4S)$.

$\Gamma(f_1(1285)K^+,\ f_1\to a_0(980)\pi)/\Gamma_{total}$ — Γ_{432}/Γ

VALUE (units 10^{-5})	DOCUMENT ID		TECN	COMMENT
0.28±0.02±0.03	[1,2] AAIJ	25F	LHCB	pp at 7, 8 and 13 TeV

[1] The second uncertainty includes the systematic and the uncertainties on the known branching fractions.

[2] This is the inverse-variance weighted average of the branching fraction measurements $B^+\to K^0K^-\pi^+K^+$ and $B^+\to\overline{K}^0K^+\pi^-K^+$ decays. AAIJ 25F also lists the two measurements separately and finds that the resulting fractions are consistent among the two channels when including the systematic uncertainties.

$\Gamma(f_1(1420)K^+,\ f_1\to\eta\pi\pi)/\Gamma_{total}$ — Γ_{433}/Γ

VALUE (units 10^{-6})	CL%	DOCUMENT ID		TECN	COMMENT
<2.9	90	[1] AUBERT	08X	BABR	$e^+e^-\to\Upsilon(4S)$

[1] Assumes equal production of B^+ and B^0 at the $\Upsilon(4S)$.

$\Gamma(f_1(1420)K^+,\ f_1\to K^*K)/\Gamma_{total}$ — Γ_{434}/Γ

VALUE (units 10^{-6})	CL%	DOCUMENT ID		TECN	COMMENT
11.4±0.6±2.0		[1,2] AAIJ	25F	LHCB	pp at 7, 8 and 13 TeV
< 4.1	90	[3] AUBERT	08X	BABR	$e^+e^-\to\Upsilon(4S)$

[1] The second uncertainty includes the systematic and the uncertainties on the known branching fractions.

Int. J. Mod. Phys. A 2026.41. Downloaded from www.worldscientific.com
by UNIVERSITY OF CALIFORNIA @ BERKELEY on 09/16/26. Re-use and distribution is strictly not permitted, except for Open Access articles.

[2] This is the inverse-variance weighted average of the branching fraction measurements $B^+ \to K^0 K^- \pi^+ K^+$ and $B^+ \to \overline{K}^0 K^+ \pi^- K^+$ decays. AAIJ 25F also lists the two measurements separately and finds that the resulting fractions are consistent among the two channels when including the systematic uncertainties.
[3] Assumes equal production of B^+ and B^0 at the $\Upsilon(4S)$.

$\Gamma(f_1(1510) K^+, f_1 \to K^* \overline{K})/\Gamma_{total}$ — Γ_{435}/Γ

VALUE (units 10^{-5})	DOCUMENT ID		TECN	COMMENT
0.38±0.03±0.15	[1,2] AAIJ	25F	LHCB	pp at 7, 8 and 13 TeV

[1] The second uncertainty includes the systematic and the uncertainties on the known branching fractions.
[2] This is the inverse-variance weighted average of the branching fraction measurements $B^+ \to K^0 K^- \pi^+ K^+$ and $B^+ \to \overline{K}^0 K^+ \pi^- K^+$ decays. AAIJ 25F also lists the two measurements separately and finds that the resulting fractions are consistent among the two channels when including the systematic uncertainties.

$\Gamma(h_1(1415) K^+, h_1 \to K^* \overline{K})/\Gamma_{total}$ — Γ_{436}/Γ

VALUE (units 10^{-5})	DOCUMENT ID		TECN	COMMENT
2.22±0.10±0.25	[1,2] AAIJ	25F	LHCB	pp at 7, 8 and 13 TeV

[1] The second uncertainty includes the systematic and the uncertainties on the known branching fractions.
[2] This is the inverse-variance weighted average of the branching fraction measurements $B^+ \to K^0 K^- \pi^+ K^+$ and $B^+ \to \overline{K}^0 K^+ \pi^- K^+$ decays. AAIJ 25F also lists the two measurements separately and finds that the resulting fractions are consistent among the two channels when including the systematic uncertainties.

$\Gamma(h_1(1595) K^+, h_1 \to K^* \overline{K})/\Gamma_{total}$ — Γ_{437}/Γ

VALUE (units 10^{-5})	DOCUMENT ID		TECN	COMMENT
1.04±0.10±0.13	[1,2] AAIJ	25F	LHCB	pp at 7, 8 and 13 TeV

[1] The second uncertainty includes the systematic and the uncertainties on the known branching fractions.
[2] This is the inverse-variance weighted average of the branching fraction measurements $B^+ \to K^0 K^- \pi^+ K^+$ and $B^+ \to \overline{K}^0 K^+ \pi^- K^+$ decays. AAIJ 25F also lists the two measurements separately and finds that the resulting fractions are consistent among the two channels when including the systematic uncertainties.

$\Gamma(\eta_2(1645) K^+, \eta_2 \to K^* \overline{K})/\Gamma_{total}$ — Γ_{438}/Γ

VALUE (units 10^{-5})	DOCUMENT ID		TECN	COMMENT
0.15±0.02±0.02	[1,2] AAIJ	25F	LHCB	pp at 7, 8 and 13 TeV

[1] The second uncertainty includes the systematic and the uncertainties on the known branching fractions.
[2] This is the inverse-variance weighted average of the branching fraction measurements $B^+ \to K^0 K^- \pi^+ K^+$ and $B^+ \to \overline{K}^0 K^+ \pi^- K^+$ decays. AAIJ 25F also lists the two measurements separately and finds that the resulting fractions are consistent among the two channels when including the systematic uncertainties.

$\Gamma(\phi(1680) K^+, \phi \to K^* K)/\Gamma_{total}$ — Γ_{439}/Γ

VALUE (units 10^{-6})	CL%	DOCUMENT ID		TECN	COMMENT
<3.4	90	[1] AUBERT	08X	BABR	$e^+e^- \to \Upsilon(4S)$

[1] Assumes equal production of B^+ and B^0 at the $\Upsilon(4S)$.

$\Gamma(f_0(1500) K^+)/\Gamma_{total}$ — Γ_{440}/Γ

VALUE (units 10^{-6})	CL%	DOCUMENT ID		TECN	COMMENT
3.7± 2.2 OUR AVERAGE					
17 ± 4 ±12		[1] LEES	12O	BABR	$e^+e^- \to \Upsilon(4S)$
20 ±10 ±27		[2] LEES	12O	BABR	$e^+e^- \to \Upsilon(4S)$
$3.2^{+2.2}_{-2.3}$± 0.2		[3,4] AUBERT	08AI	BABR	$e^+e^- \to \Upsilon(4S)$
• • • We do not use the following data for averages, fits, limits, etc. • • •					
<19	90	[4,5] AUBERT,B	05N	BABR	Repl. by AUBERT 08AI

[1] Measured in the $B^+ \to K^+ K^- K^+$ decay.
[2] Measured in the $B^+ \to K^+ K^0_S K^0_S$ decay.
[3] AUBERT 08AI reports $B(B^+ \to f_0(1500) K^+) \cdot B(f_0(1500) \to \pi^+\pi^-) = (0.73 \pm 0.21^{+0.47}_{-0.48}) \times 10^{-6}$. We divide this result by our best value of $B(f_0(1500) \to \pi\pi) = (34.5 \pm 2.2) \times 10^{-2}$ multiplied by 2/3 to account for the $\pi^+\pi^-$ fraction. Our first quoted uncertainty is the combined experiment's uncertainty and our second is the systematic uncertainty from using out best value.
[4] Assumes equal production of B^+ and B^0 at the $\Upsilon(4S)$.
[5] AUBERT,B 05N reports $B(B^+ \to f_0(1500) K^+) \cdot B(f_0(1500) \to \pi^+\pi^-) < 4.4 \times 10^{-6}$. We divide this result by our best value of $B(f_0(1500) \to \pi\pi) = (34.5 \pm 2.2) \times 10^{-2}$ multiplied by 2/3 to account for the $\pi^+\pi^-$ fraction. Our first quoted uncertainty is the combined experiment's uncertainty and our second is the systematic uncertainty from using out best value.

$\Gamma(\omega K^+)/\Gamma_{total}$ — Γ_{441}/Γ

VALUE (units 10^{-6})	CL%	DOCUMENT ID		TECN	COMMENT
6.5±0.4 OUR AVERAGE					
6.8±0.4±0.4		[1] CHOBANOVA	14	BELL	$e^+e^- \to \Upsilon(4S)$
6.3±0.5±0.3		[1] AUBERT	07AE	BABR	$e^+e^- \to \Upsilon(4S)$
$3.2^{+2.4}_{-1.9}$±0.8		[1] JESSOP	00	CLE2	$e^+e^- \to \Upsilon(4S)$
• • • We do not use the following data for averages, fits, limits, etc. • • •					
6.1±0.6±0.4		[1] AUBERT,B	06E	BABR	AUBERT 07AE
8.1±0.6±0.6		[1] JEN	06	BELL	Repl. by CHOBANOVA 14
4.8±0.8±0.4		[1] AUBERT	04H	BABR	Repl. by AUBERT,B 06E
$6.5^{+1.3}_{-1.2}$±0.6		[1] WANG	04A	BELL	Repl. by JEN 06
$9.2^{+2.6}_{-2.3}$±1.0		[1] LU	02	BELL	Repl. by WANG 04A
<4	90	[1] AUBERT	01G	BABR	$e^+e^- \to \Upsilon(4S)$
1.5^{+7}_{-6} ±2		[1] BERGFELD	98	CLE2	Repl. by JESSOP 00

[1] Assumes equal production of B^+ and B^0 at the $\Upsilon(4S)$.

$\Gamma(\omega K^*(892)^+)/\Gamma_{total}$ — Γ_{442}/Γ

VALUE (units 10^{-6})	CL%	DOCUMENT ID		TECN	COMMENT
< 7.4	90	[1] AUBERT	09H	BABR	$e^+e^- \to \Upsilon(4S)$
• • • We do not use the following data for averages, fits, limits, etc. • • •					
< 3.4	90	[1] AUBERT,B	06T	BABR	Repl. by AUBERT 09H
< 7.4	90	[1] AUBERT	05O	BABR	Repl. by AUBERT,B 06T
<87	90	[1] BERGFELD	98	CLE2	

[1] Assumes equal production of B^+ and B^0 at the $\Upsilon(4S)$.

$\Gamma(\omega (K\pi)^{*+}_0)/\Gamma_{total}$ — Γ_{443}/Γ

$(K\pi)^{*+}_0$ is the total S-wave composed of $K^*_0(1430)$ and nonresonant that are described using LASS shape.

VALUE (units 10^{-6})	DOCUMENT ID		TECN	COMMENT
27.5±3.0±2.6	[1] AUBERT	09H	BABR	$e^+e^- \to \Upsilon(4S)$

[1] Assumes equal production of B^+ and B^0 at the $\Upsilon(4S)$.

$\Gamma(\omega K^*_0(1430)^+)/\Gamma_{total}$ — Γ_{444}/Γ

VALUE (units 10^{-6})	DOCUMENT ID		TECN	COMMENT
24.0±2.6±4.4	[1] AUBERT	09H	BABR	$e^+e^- \to \Upsilon(4S)$

[1] Assumes equal production of B^+ and B^0 at the $\Upsilon(4S)$.

$\Gamma(\omega K^*_2(1430)^+)/\Gamma_{total}$ — Γ_{445}/Γ

VALUE (units 10^{-6})	DOCUMENT ID		TECN	COMMENT
21.5±3.6±2.4	[1] AUBERT	09H	BABR	$e^+e^- \to \Upsilon(4S)$

[1] Assumes equal production of B^+ and B^0 at the $\Upsilon(4S)$.

$\Gamma(a_0(980)^0 K^+, a^0_0 \to \eta\pi^0)/\Gamma_{total}$ — Γ_{447}/Γ

VALUE (units 10^{-6})	CL%	DOCUMENT ID		TECN	COMMENT
<2.5	90	[1] AUBERT,BE	04	BABR	$e^+e^- \to \Upsilon(4S)$

[1] Assumes equal production of charged and neutral B mesons from $\Upsilon(4S)$ decays.

$\Gamma(a_0(980)^+ K^0, a^+_0 \to \eta\pi^+)/\Gamma_{total}$ — Γ_{446}/Γ

VALUE (units 10^{-6})	CL%	DOCUMENT ID		TECN	COMMENT
<3.9	90	[1] AUBERT,BE	04	BABR	$e^+e^- \to \Upsilon(4S)$

[1] Assumes equal production of charged and neutral B mesons from $\Upsilon(4S)$ decays.

$\Gamma(K^*(892)^0 \pi^+)/\Gamma_{total}$ — Γ_{448}/Γ

VALUE (units 10^{-6})	CL%	DOCUMENT ID		TECN	COMMENT
10.1 ±0.8 OUR AVERAGE					
10.1 ±1.7 ±1.0		[1] LEES	17G	BABR	$e^+e^- \to \Upsilon(4S)$
10.8 ±0.6 $^{+1.2}_{-1.4}$		[2] AUBERT	08AI	BABR	$e^+e^- \to \Upsilon(4S)$
9.67±0.64$^{+0.81}_{-0.89}$		[2] GARMASH	06	BELL	$e^+e^- \to \Upsilon(4S)$
• • • We do not use the following data for averages, fits, limits, etc. • • •					
13.5 ±1.2 $^{+0.8}_{-0.9}$		[2] AUBERT,B	05N	BABR	Repl. by AUBERT 08AI
9.8 ±0.9 $^{+1.1}_{-1.2}$		[2] GARMASH	05	BELL	Repl. by GARMASH 06
15.5 ±1.8 $^{+1.5}_{-4.0}$		[2,3] AUBERT,B	04P	BABR	Repl. by AUBERT,B 05N
19.4 $^{+4.2}_{-3.9}$ $^{+4.1}_{-7.1}$		[4] GARMASH	02	BELL	Repl. by GARMASH 05
<119	90	[5] ABE	00C	SLD	$e^+e^- \to Z$
< 16	90	[2] JESSOP	00	CLE2	$e^+e^- \to \Upsilon(4S)$
<390	90	[6] ADAM	96D	DLPH	$e^+e^- \to Z$
< 41	90	ASNER	96	CLE2	Repl. by JESSOP 00
<480	90	[6] ABREU	95N	DLPH	Sup. by ADAM 96D
<170	90	ALBRECHT	91B	ARG	$e^+e^- \to \Upsilon(4S)$
<150	90	[7] AVERY	89B	CLEO	$e^+e^- \to \Upsilon(4S)$
<260	90	AVERY	87	CLEO	$e^+e^- \to \Upsilon(4S)$

[1] Obtains the result from a Dalitz analysis of $B^+ \to K^0_S \pi^+ \pi^0$ decays. The first error is statistical, the second combines all the systematic uncertainties reported in the paper, including signal modelling.
[2] Assumes equal production of B^+ and B^0 at the $\Upsilon(4S)$.
[3] AUBERT 04P also report a branching ratio for $B^+ \to$ "higher K^* resonances" π^+, $K^* \to K^+\pi^-$, $(25.1 \pm 2.0^{+11.0}_{-5.7}) \times 10^{-6}$.
[4] Uses a reference decay mode $B^+ \to \overline{D}^0 \pi^+$ and $\overline{D}^0 \to K^+\pi^-$ with $B(B^+ \to \overline{D}^0\pi^+) \cdot B(\overline{D}^0 \to K^+\pi^-) = (20.3 \pm 2.0) \times 10^{-5}$.
[5] ABE 00C assumes $B(Z \to b\overline{b})$=(21.7 ± 0.1)% and the B fractions $f_{B^0} = f_{B^+} = (39.7^{+1.8}_{-2.2})$% and $f_{B_s} = (10.5^{+1.8}_{-2.2})$%.
[6] Assumes a B^0, B^- production fraction of 0.39 and a B_s production fraction of 0.12.
[7] AVERY 89B reports $< 1.3 \times 10^{-4}$ assuming the $\Upsilon(4S)$ decays 43% to $B^0\overline{B}^0$. We rescale to 50%.

Int. J. Mod. Phys. A 2026.41. Downloaded from www.worldscientific.com
by LIFORNIA @ BERKELEY on 09/16/26. Re-use and distribution is strictly not permitted, except for Open Access articles.

$\Gamma(K^*(892)^+\pi^0)/\Gamma_{total}$ — Γ_{449}/Γ

VALUE (units 10^{-6})	CL%	DOCUMENT ID		TECN	COMMENT
6.8±0.9 OUR AVERAGE					
$6.4\pm0.9^{+0.4}_{-0.5}$		[1] LEES	17G	BABR	$e^+e^-\to\Upsilon(4S)$
$8.2\pm1.5\pm1.1$		[2] LEES	11I	BABR	$e^+e^-\to\Upsilon(4S)$
• • • We do not use the following data for averages, fits, limits, etc. • • •					
$6.9\pm2.0\pm1.3$		[2] AUBERT	05X	BABR	Repl. by LEES 11I
<31	90	[2] JESSOP	00	CLE2	$e^+e^-\to\Upsilon(4S)$
<99	90	ASNER	96	CLE2	Repl. by JESSOP 00

[1] Obtains the result from a Dalitz analysis of $B^+\to K^0_S\pi^+\pi^0$ decays. The first error is statistical, the second combines all the systematic uncertainties reported in the paper, including signal modelling.
[2] Assumes equal production of B^+ and B^0 at the $\Upsilon(4S)$.

$\Gamma(K^+\pi^-\pi^+)/\Gamma(K^+K^-K^+)$ — $\Gamma_{450}/\Gamma_{503}$

VALUE	DOCUMENT ID		TECN	COMMENT
1.703±0.011±0.022	AAIJ	20AJ	LHCB	pp at 7 and 8 TeV

$\Gamma(K^+\pi^-\pi^+)/\Gamma_{total}$ — Γ_{450}/Γ

VALUE (units 10^{-6})	DOCUMENT ID		TECN	COMMENT
51.0±2.9 OUR AVERAGE				
54.4±1.1±4.6	[1] AUBERT	08AI	BABR	$e^+e^-\to\Upsilon(4S)$
48.8±1.1±3.6	[1] GARMASH	06	BELL	$e^+e^-\to\Upsilon(4S)$
• • • We do not use the following data for averages, fits, limits, etc. • • •				
64.1±2.4±4.0	[1] AUBERT,B	05N	BABR	Repl. by AUBERT 08AI
46.6±2.1±4.3	[1] GARMASH	05	BELL	Repl. by GARMASH 06
53.6±3.1±5.1	[1] GARMASH	04	BELL	Repl. by GARMASH 05
59.1±3.8±3.2	[2] AUBERT	03M	BABR	Repl. by AUBERT,B 05N
55.6±5.8±7.7	[3] GARMASH	02	BELL	Repl. by GARMASH 04

[1] Assumes equal production of B^+ and B^0 at the $\Upsilon(4S)$.
[2] Assumes equal production of B^0 and B^+ at the $\Upsilon(4S)$; charm and charmonium contributions are subtracted, otherwise no assumptions about intermediate resonances.
[3] Uses a reference decay mode $B^+\to\overline{D}^0\pi^+$ and $\overline{D}^0\to K^+\pi^-$ with $B(B^+\to\overline{D}^0\pi^+)\cdot B(\overline{D}^0\to K^+\pi^-)=(20.3\pm2.0)\times10^{-5}$.

$\Gamma(K^+\pi^-\pi^+\text{nonresonant})/\Gamma_{total}$ — Γ_{451}/Γ

VALUE (units 10^{-6})	CL%	DOCUMENT ID		TECN	COMMENT
$16.3^{+2.1}_{-1.5}$ OUR AVERAGE					
$9.3\pm1.0^{+6.9}_{-1.7}$		[1,2] AUBERT	08AI	BABR	$e^+e^-\to\Upsilon(4S)$
$16.9\pm1.3^{+1.7}_{-1.6}$		[1] GARMASH	06	BELL	$e^+e^-\to\Upsilon(4S)$
• • • We do not use the following data for averages, fits, limits, etc. • • •					
$2.9\pm0.6^{+0.8}_{-0.5}$		[1] AUBERT,B	05N	BABR	Repl. by AUBERT 08AI
$17.3\pm1.7^{+17.2}_{-8.0}$		[1] GARMASH	05	BELL	Repl. by GARMASH 06
< 17	90	[1] AUBERT,B	04P	BABR	Repl. by AUBERT,B 05N
<330	90	[3] ADAM	96D	DLPH	$e^+e^-\to Z$
< 28	90	BERGFELD	96B	CLE2	$e^+e^-\to\Upsilon(4S)$
<400	90	[3] ABREU	95N	DLPH	Sup. by ADAM 96D
<330	90	ALBRECHT	91E	ARG	$e^+e^-\to\Upsilon(4S)$
<190	90	[4] AVERY	89B	CLEO	$e^+e^-\to\Upsilon(4S)$

[1] Assumes equal production of B^+ and B^0 at the $\Upsilon(4S)$.
[2] Calculate the total nonresonant contribution by combining the S-wave composed of $K^*_0(1430)$ and nonresonant that are described using LASS shape.
[3] Assumes a B^0, B^- production fraction of 0.39 and a B_s production fraction of 0.12.
[4] AVERY 89B reports $<1.7\times10^{-4}$ assuming the $\Upsilon(4S)$ decays 43% to $B^0\overline{B}^0$. We rescale to 50%.

$\Gamma(\omega(782)K^+)/\Gamma_{total}$ — Γ_{452}/Γ

VALUE (units 10^{-6})	DOCUMENT ID		TECN	COMMENT
$5.9^{+8.8}_{-9.0}\pm0.5$	[1,2] AUBERT	08AI	BABR	$e^+e^-\to\Upsilon(4S)$

[1] Assumes equal production of B^+ and B^0 at the $\Upsilon(4S)$.
[2] AUBERT 08AI reports $[\Gamma(B^+\to\omega(782)K^+)/\Gamma_{total}]\times[B(\omega(782)\to\pi^+\pi^-)]=(0.09\pm0.13^{+0.036}_{-0.045})\times10^{-6}$ which we divide by our best (shown rounded) value $B(\omega(782)\to\pi^+\pi^-)=(1.53\pm0.12)\times10^{-2}$. Our first error is their experiment's error and our second error is the systematic error from using our best (shown rounded) value.

$\Gamma(K^+f_0(980)\times B(f_0(980)\to\pi^+\pi^-))/\Gamma_{total}$ — Γ_{453}/Γ

VALUE (units 10^{-6})	CL%	DOCUMENT ID		TECN	COMMENT
$9.4^{+1.0}_{-1.2}$ OUR AVERAGE					
$10.3\pm0.5^{+2.0}_{-1.4}$		[1] AUBERT	08AI	BABR	$e^+e^-\to\Upsilon(4S)$
$8.78\pm0.82^{+0.85}_{-1.76}$		[1] GARMASH	06	BELL	$e^+e^-\to\Upsilon(4S)$
• • • We do not use the following data for averages, fits, limits, etc. • • •					
$9.47\pm0.97^{+0.62}_{-0.88}$		[1] AUBERT,B	05N	BABR	Repl. by AUBERT 08AI
$7.55\pm1.24^{+1.63}_{-1.18}$		[1] GARMASH	05	BELL	Repl. by GARMASH 06
$9.2\pm1.2^{+2.1}_{-2.6}$		[2] AUBERT,B	04P	BABR	Repl. by AUBERT,B 05N
$9.6^{+2.5}_{-2.3}{}^{+3.7}_{-1.7}$		[3] GARMASH	02	BELL	Repl. by GARMASH 05
<80	90	[4] AVERY	89B	CLEO	$e^+e^-\to\Upsilon(4S)$

[1] Assumes equal production of B^+ and B^0 at the $\Upsilon(4S)$.
[2] AUBERT,B 04P also reports $B(B^+\to$ "higher f^0 resonances" π^+, $f(980)^0\to\pi^+\pi^-)=(3.2\pm1.2^{+6.0}_{-2.9})\times10^{-6}$.
[3] Uses a reference decay mode $B^+\to\overline{D}^0\pi^+$ and $\overline{D}^0\to K^+\pi^-$ with $B(B^+\to\overline{D}^0\pi^+)\times B(\overline{D}^0\to K^+\pi^-)=(20.3\pm2.0)\times10^{-5}$. Only charged pions from the $f_0(980)$ are used.
[4] AVERY 89B reports $<7\times10^{-5}$ assuming the $\Upsilon(4S)$ decays 43% to $B^0\overline{B}^0$. We rescale to 50%.

$\Gamma(f_2(1270)^0K^+)/\Gamma_{total}$ — Γ_{454}/Γ

VALUE (units 10^{-6})	CL%	DOCUMENT ID		TECN	COMMENT
1.07±0.27 OUR AVERAGE					
$0.89^{+0.38}_{-0.33}{}^{+0.01}_{-0.03}$		[1,2] AUBERT	08AI	BABR	$e^+e^-\to\Upsilon(4S)$
$1.33\pm0.30^{+0.23}_{-0.34}$		[1] GARMASH	06	BELL	$e^+e^-\to\Upsilon(4S)$
• • • We do not use the following data for averages, fits, limits, etc. • • •					
<16	90	[3] AUBERT,B	05N	BABR	Repl. by AUBERT 08AI
< 2.3	90	[4] GARMASH	05	BELL	Repl. by GARMASH 06

[1] Assumes equal production of B^+ and B^0 at the $\Upsilon(4S)$.
[2] AUBERT 08AI reports $(0.50\pm0.15^{+0.15}_{-0.11})\times10^{-6}$ for $B(B^+\to f_2(1270)K^+)\times B(f_2\to\pi^+\pi^-)$. We compute $B(B^+\to f_2(1270)K^+)$ using the PDG value $B(f_2(1270)\to\pi\pi)=(84.3^{+2.8}_{-1.0})\times10^{-2}$ and 2/3 for the $\pi^+\pi^-$ fraction. Our first error is their experiment's error and the second error is systematic error from using our best value.
[3] AUBERT,B 05N reports 8.9×10^{-6} at 90% CL for $B(B^+\to f_2(1270)K^+)\times B(f_2(1270)\to\pi^+\pi^-)$. We rescaled it using the PDG value $B(f_2(1270)\to\pi\pi)=84.7\%$ and 2/3 for the $\pi^+\pi^-$ fraction.
[4] GARMASH 05 reports 1.3×10^{-6} at 90% CL for $B(B^+\to f_2(1270)K^+)\times B(f_2(1270)\to\pi^+\pi^-)$. We rescaled it using the PDG value $B(f_2(1270)\to\pi\pi)=84.7\%$ and 2/3 for the $\pi^+\pi^-$ fraction.

$\Gamma(f_0(1370)^0K^+\times B(f_0(1370)^0\to\pi^+\pi^-))/\Gamma_{total}$ — Γ_{455}/Γ

VALUE	CL%	DOCUMENT ID		TECN	COMMENT
$<10.7\times10^{-6}$	90	[1] AUBERT,B	05N	BABR	$e^+e^-\to\Upsilon(4S)$

[1] Assumes equal production of B^+ and B^0 at the $\Upsilon(4S)$.

$\Gamma(\rho(14500)K^+\times B(\rho(1450)^0\to\pi^+\pi^-))/\Gamma_{total}$ — Γ_{456}/Γ

VALUE	CL%	DOCUMENT ID		TECN	COMMENT
$<11.7\times10^{-6}$	90	[1] AUBERT,B	05N	BABR	$e^+e^-\to\Upsilon(4S)$

[1] Assumes equal production of B^+ and B^0 at the $\Upsilon(4S)$.

$\Gamma(f'_2(1525)K^+\times B(f'_2(1525)\to\pi^+\pi^-))/\Gamma_{total}$ — Γ_{457}/Γ

VALUE	CL%	DOCUMENT ID		TECN	COMMENT
$<3.4\times10^{-6}$	90	[1] AUBERT,B	05N	BABR	$e^+e^-\to\Upsilon(4S)$

[1] Assumes equal production of B^+ and B^0 at the $\Upsilon(4S)$.

$\Gamma(K^+\rho^0)/\Gamma_{total}$ — Γ_{458}/Γ

VALUE (units 10^{-6})	CL%	DOCUMENT ID		TECN	COMMENT
3.7 ±0.5 OUR AVERAGE					
$3.56\pm0.45^{+0.57}_{-0.46}$		[1] AUBERT	08AI	BABR	$e^+e^-\to\Upsilon(4S)$
$3.89\pm0.47^{+0.43}_{-0.41}$		[1] GARMASH	06	BELL	$e^+e^-\to\Upsilon(4S)$
• • • We do not use the following data for averages, fits, limits, etc. • • •					
$5.07\pm0.75^{+0.55}_{-0.88}$		[1] AUBERT,B	05N	BABR	Repl. by AUBERT 08AI
$4.78\pm0.75^{+1.01}_{-0.97}$		[1] GARMASH	05	BELL	Repl. by GARMASH 06
< 6.2	90	[2] AUBERT,B	04P	BABR	Repl. by AUBERT,B 05N
< 12	90	[3] GARMASH	02	BELL	$e^+e^-\to\Upsilon(4S)$
< 86	90	[4] ABE	00C	SLD	$e^+e^-\to Z$
< 17	90	[1] JESSOP	00	CLE2	$e^+e^-\to\Upsilon(4S)$
<120	90	[5] ADAM	96D	DLPH	$e^+e^-\to Z$
< 19	90	ASNER	96	CLE2	Repl. by JESSOP 00
<190	90	[5] ABREU	95N	DLPH	Sup. by ADAM 96D
<180	90	ALBRECHT	91B	ARG	$e^+e^-\to\Upsilon(4S)$
< 80	90	[6] AVERY	89B	CLEO	$e^+e^-\to\Upsilon(4S)$
<260	90	AVERY	87	CLEO	$e^+e^-\to\Upsilon(4S)$

[1] Assumes equal production of B^+ and B^0 at the $\Upsilon(4S)$.
[2] AUBERT 04P reports a central value of $(3.9\pm1.2^{+1.3}_{-3.5})\times10^{-6}$ for this branching ratio.
[3] Uses a reference decay mode $B^+\to\overline{D}^0\pi^+$ and $\overline{D}^0\to K^+\pi^-$ with $B(B^+\to\overline{D}^0\pi^+)\cdot B(\overline{D}^0\to K^+\pi^-)=(20.3\pm2.0)\times10^{-5}$.
[4] ABE 00C assumes $B(Z\to b\overline{b})=(21.7\pm0.1)\%$ and the B fractions $f_{B^0}=f_{B^+}=(39.7^{+1.8}_{-2.2})\%$ and $f_{B_s}=(10.5^{+1.8}_{-2.2})\%$.
[5] Assumes production fractions $f_{B^0}=f_{B^-}=0.39$ and $f_{B_s}=0.12$.
[6] AVERY 89B reports $<7\times10^{-5}$ assuming the $\Upsilon(4S)$ decays 43% to $B^0\overline{B}^0$. We rescale to 50%.

Int. J. Mod. Phys. A 2026.41. Downloaded from www.worldscientific.com
by UNIVERSITY OF CALIFORNIA @ BERKELEY on 09/16/26. Re-use and distribution is strictly not permitted, except for Open Access articles.

$\Gamma(K_0^*(1430)^0\pi^+)/\Gamma_{total}$ — Γ_{459}/Γ

VALUE (units 10^{-6})	DOCUMENT ID		TECN	COMMENT
39^{+6}_{-5} OUR AVERAGE Error includes scale factor of 1.4. See the ideogram below.				
$34.6\pm3.3\pm4.6$	[1] LEES	17G	BABR	$e^+e^-\to\Upsilon(4S)$
$32.0\pm1.2^{+10.8}_{-6.0}$	[2] AUBERT	08AI	BABR	$e^+e^-\to\Upsilon(4S)$
$51.6\pm1.7^{+7.0}_{-7.5}$	[2] GARMASH	06	BELL	$e^+e^-\to\Upsilon(4S)$
• • • We do not use the following data for averages, fits, limits, etc. • • •				
$44.4\pm2.2\pm5.3$	[2,3] AUBERT,B	05N	BABR	Repl. by AUBERT 08AI
$45.0\pm2.9^{+15.0}_{-10.7}$	[2] GARMASH	05	BELL	Repl. by GARMASH 06

[1] Obtains the result from a Dalitz analysis of $B^+\to K^0_S\pi^+\pi^0$ decays. The first error is statistical, the second combines all the systematic uncertainties reported in the paper, including signal modelling.
[2] Assumes equal production of B^+ and B^0 at the $\Upsilon(4S)$.
[3] See erratum: AUBERT,BE 06A.

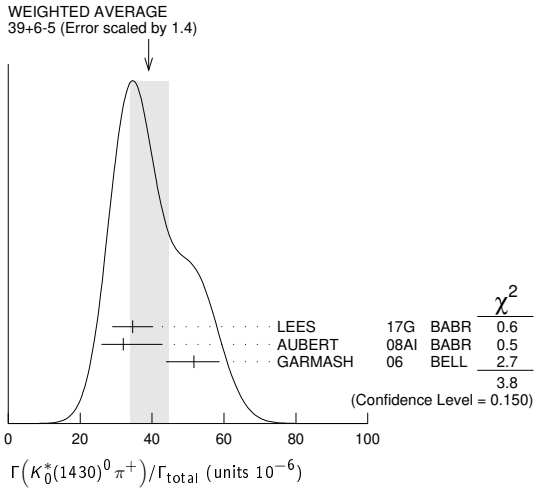

$\Gamma(K_2^*(1430)^0\pi^+)/\Gamma_{total}$ — Γ_{460}/Γ

VALUE (units 10^{-6})	CL%	DOCUMENT ID		TECN	COMMENT
$\mathbf{5.6^{+2.2}_{-1.5}\pm0.1}$		[1,2] AUBERT	08AI	BABR	$e^+e^-\to\Upsilon(4S)$
• • • We do not use the following data for averages, fits, limits, etc. • • •					
<23	90	[3] AUBERT,B	05N	BABR	Repl. by AUBERT 08AI
<6.9	90	[4] GARMASH	05	BELL	$e^+e^-\to\Upsilon(4S)$
<680	90	ALBRECHT	91B	ARG	$e^+e^-\to\Upsilon(4S)$

[1] Assumes equal production of B^+ and B^0 at the $\Upsilon(4S)$.
[2] AUBERT 08AI reports $(1.85\pm0.41^{+0.61}_{-0.29})\times10^{-6}$ for $B(B^+\to K_2^*(1430)^0\pi^+)\times B(K_2^*(1430)^0\to K^+\pi^-)$. We compute $B(B^+\to K_2^*(1430)^0\pi^+)$ using the PDG value $B(K_2^*(1430)^0\to K\pi)=(49.9\pm1.2)\times10^{-2}$ and 2/3 for the $K^+\pi^-$ fraction. Our first error is their experiment's error and the second error is systematic error from using our best value.
[3] AUBERT,B 05N reports 7.7×10^{-6} at 90% CL for $B(B^+\to K_2^*(1430)^0\pi^+)\times B(K_2^*(1430)^0\to K^+\pi^-)$. We rescaled it using the PDG value $B(K_2^*(1430)^0\to K\pi)=49.9\%$ and 2/3 for the $K^+\pi^-$ fraction.
[4] GARMASH 05 reports 2.3×10^{-6} at 90% CL for $B(B^+\to K_2^*(1430)^0\pi^+)\times B(K_2^*(1430)^0\to K^+\pi^-)$. We rescaled it using the PDG value $B(K_2^*(1430)^0\to K\pi)=49.9\%$ and 2/3 for the $K^+\pi^-$ mode.

$\Gamma(K^*(1410)^0\pi^+)/\Gamma_{total}$ — Γ_{461}/Γ

VALUE (units 10^{-6})	CL%	DOCUMENT ID		TECN	COMMENT
<45	90	[1] GARMASH	05	BELL	$e^+e^-\to\Upsilon(4S)$

[1] GARMASH 05 reports 2.0×10^{-6} at 90% CL for $B(B^+\to K^*(1410)^0\pi^+)\times B(K^*(1410)^0\to K^+\pi^-)$. We rescaled it using the PDG value $B(K^*(1410)^0\to K\pi)=6.6\%$ and 2/3 for the $K^+\pi^-$ mode.

$\Gamma(K^*(1680)^0\pi^+)/\Gamma_{total}$ — Γ_{462}/Γ

VALUE (units 10^{-6})	CL%	DOCUMENT ID		TECN	COMMENT
<12	90	[1] GARMASH	05	BELL	$e^+e^-\to\Upsilon(4S)$
• • • We do not use the following data for averages, fits, limits, etc. • • •					
<15	90	[2] AUBERT,B	05N	BABR	$e^+e^-\to\Upsilon(4S)$

[1] GARMASH 05 reports 3.1×10^{-6} at 90% CL for $B(B^+\to K^*(1680)^0\pi^+)\times B(K^*(1680)^0\to K^+\pi^-)$. We rescaled it using the PDG value $B(K^*(1680)^0\to K\pi)=38.7\%$ and 2/3 for the $K^+\pi^-$ mode.
[2] AUBERT,B 05N reports 3.8×10^{-6} at 90% CL for $B(B^+\to K^*(1680)^0\pi^+)\times B(K^*(1680)^0\to K^+\pi^-)$. We rescaled it using the PDG value $B(K^*(1680)^0\to K\pi)=38.7\%$ and 2/3 for the $K^+\pi^-$ fraction.

$\Gamma(K^+\pi^0\pi^0)/\Gamma_{total}$ — Γ_{463}/Γ

VALUE (units 10^{-6})	DOCUMENT ID		TECN	COMMENT
$16.2\pm1.2\pm1.5$	[1] LEES	11I	BABR	$e^+e^-\to\Upsilon(4S)$

[1] Assumes equal production of B^+ and B^0 at the $\Upsilon(4S)$.

$\Gamma(f_0(980)K^+\times B(f_0\to\pi^0\pi^0))/\Gamma_{total}$ — Γ_{464}/Γ

VALUE (units 10^{-6})	DOCUMENT ID		TECN	COMMENT
$2.8\pm0.6\pm0.5$	[1] LEES	11I	BABR	$e^+e^-\to\Upsilon(4S)$

[1] Assumes equal production of B^+ and B^0 at the $\Upsilon(4S)$.

$\Gamma(K^-\pi^+\pi^+)/\Gamma_{total}$ — Γ_{465}/Γ

VALUE	CL%	DOCUMENT ID		TECN	COMMENT
$<4.6\times10^{-8}$	90	AAIJ	17E	LHCB	pp at 7, 8 TeV
• • • We do not use the following data for averages, fits, limits, etc. • • •					
$<9.5\times10^{-7}$	90	[1] AUBERT	08BE	BABR	$e^+e^-\to\Upsilon(4S)$
$<4.5\times10^{-6}$	90	[1] GARMASH	04	BELL	$e^+e^-\to\Upsilon(4S)$
$<1.8\times10^{-6}$	90	[2] AUBERT	03M	BABR	Repl. by AUBERT 08BE
$<7.0\times10^{-6}$	90	[3] GARMASH	02	BELL	$e^+e^-\to\Upsilon(4S)$

[1] Assumes equal production of B^+ and B^0 at the $\Upsilon(4S)$.
[2] Assumes equal production of B^0 and B^+ at the $\Upsilon(4S)$; charm and charmonium contributions are subtracted, otherwise no assumptions about intermediate resonances.
[3] Uses a reference decay mode $B^+\to\overline{D}^0\pi^+$ and $\overline{D}^0\to K^+\pi^-$ with $B(B^+\to\overline{D}^0\pi^+)\cdot B(\overline{D}^0\to K^+\pi^-)=(20.3\pm2.0)\times10^{-5}$.

$\Gamma(K^-\pi^+\pi^+\text{ nonresonant})/\Gamma_{total}$ — Γ_{466}/Γ

VALUE (units 10^{-6})	CL%	DOCUMENT ID		TECN	COMMENT
<56	90	BERGFELD	96B	CLE2	$e^+e^-\to\Upsilon(4S)$

$\Gamma(K_1(1270)^0\pi^+)/\Gamma_{total}$ — Γ_{467}/Γ

VALUE	CL%	DOCUMENT ID		TECN	COMMENT
$<4.0\times10^{-5}$	90	[1] AUBERT	10D	BABR	$e^+e^-\to\Upsilon(4S)$

[1] Assumes equal production of B^+ and B^0 at the $\Upsilon(4S)$.

$\Gamma(K_1(1400)^0\pi^+)/\Gamma_{total}$ — Γ_{468}/Γ

VALUE	CL%	DOCUMENT ID		TECN	COMMENT
$<3.9\times10^{-5}$	90	[1] AUBERT	10D	BABR	$e^+e^-\to\Upsilon(4S)$
• • • We do not use the following data for averages, fits, limits, etc. • • •					
$<2.6\times10^{-3}$	90	ALBRECHT	91B	ARG	$e^+e^-\to\Upsilon(4S)$

[1] Assumes equal production of B^+ and B^0 at the $\Upsilon(4S)$.

$\Gamma(K^0\pi^+\pi^0)/\Gamma_{total}$ — Γ_{469}/Γ

VALUE (units 10^{-6})	CL%	DOCUMENT ID		TECN	COMMENT
$31.8\pm1.8^{+6.3}_{-2.1}$		[1] LEES	17G	BABR	$e^+e^-\to\Upsilon(4S)$
<66	90	[2] ECKHART	02	CLE2	$e^+e^-\to\Upsilon(4S)$

[1] Obtains the result from a Dalitz analysis of $B^+\to K^0_S\pi^+\pi^0$ decays. The first error is statistical, the second combines all the systematic uncertainties reported in the paper, including signal modelling.
[2] Assumes equal production of B^+ and B^0 at the $\Upsilon(4S)$.

$\Gamma(K^0\rho^+)/\Gamma_{total}$ — Γ_{471}/Γ

VALUE (units 10^{-6})	CL%	DOCUMENT ID		TECN	COMMENT
$7.3^{+1.0}_{-1.2}$ OUR AVERAGE					
$6.5\pm1.1^{+0.8}_{-1.9}$		[1] LEES	17G	BABR	$e^+e^-\to\Upsilon(4S)$
$8.0^{+1.4}_{-1.3}\pm0.6$		AUBERT	07Z	BABR	$e^+e^-\to\Upsilon(4S)$
• • • We do not use the following data for averages, fits, limits, etc. • • •					
<48	90	ASNER	96	CLE2	$e^+e^-\to\Upsilon(4S)$

[1] Obtains the result from a Dalitz analysis of $B^+\to K^0_S\pi^+\pi^0$ decays. The first error is statistical, the second combines all the systematic uncertainties reported in the paper, including signal modelling.

$\Gamma(K_0^*(1430)^+\pi^0)/\Gamma_{total}$ — Γ_{470}/Γ

VALUE (units 10^{-6})	DOCUMENT ID		TECN	COMMENT
$11.9\pm1.7^{+1.0}_{-1.6}$	[1] LEES	17G	BABR	$e^+e^-\to\Upsilon(4S)$

[1] Obtains the result from a Dalitz analysis of $B^+\to K^0_S\pi^+\pi^0$ decays. The first error is statistical, the second combines all the systematic uncertainties reported in the paper, including signal modelling.

$\Gamma(K^*(892)^+\pi^+\pi^-)/\Gamma_{total}$ — Γ_{472}/Γ

VALUE (units 10^{-6})	CL%	DOCUMENT ID		TECN	COMMENT
$75.3\pm6.0\pm8.1$		[1] AUBERT,B	06U	BABR	$e^+e^-\to\Upsilon(4S)$
• • • We do not use the following data for averages, fits, limits, etc. • • •					
<1100	90	ALBRECHT	91E	ARG	$e^+e^-\to\Upsilon(4S)$

[1] Assumes equal production of B^+ and B^0 at the $\Upsilon(4S)$.

$\Gamma(K^*(892)^+\rho^0)/\Gamma_{total}$ — Γ_{473}/Γ

VALUE (units 10^{-6})	CL%	DOCUMENT ID		TECN	COMMENT
$4.6\pm1.0\pm0.4$		[1] DEL-AMO-SA...11D		BABR	$e^+e^-\to\Upsilon(4S)$

Int. J. Mod. Phys. A 2026.41. Downloaded from www.worldscientific.com by LIFORNIA @ BERKELEY on 09/16/26. Re-use and distribution is strictly not permitted, except for Open Access articles.

• • • We do not use the following data for averages, fits, limits, etc. • • •

$<$ 6.1	90	[1] AUBERT,B	06G	BABR	Repl. by DEL-AMO-SANCHEZ 11D
$10.6^{+3.0}_{-2.6}\pm2.4$		[1] AUBERT	03V	BABR	Repl. by AUBERT,B 06G
$<$ 74	90	[2] GODANG	02	CLE2	$e^+e^- \to \Upsilon(4S)$
$<$900	90	ALBRECHT	91B	ARG	$e^+e^- \to \Upsilon(4S)$

[1] Assumes equal production of B^+ and B^0 at the $\Upsilon(4S)$.
[2] Assumes a helicity 00 configuration. For a helicity 11 configuration, the limit decreases to 4.9×10^{-5}.

$\Gamma(K^*(892)^+ f_0(980))/\Gamma_{total}$ — Γ_{474}/Γ

VALUE (units 10^{-6})	DOCUMENT ID		TECN	COMMENT
4.2±0.6±0.3	[1] DEL-AMO-SA...11D		BABR	$e^+e^- \to \Upsilon(4S)$

• • • We do not use the following data for averages, fits, limits, etc. • • •

5.2±1.2±0.5	[1] AUBERT,B	06G	BABR	Repl. by DEL-AMO-SANCHEZ 11D

[1] Assumes equal production of B^+ and B^0 at the $\Upsilon(4S)$.

$\Gamma(a_1^+ K^0)/\Gamma_{total}$ — Γ_{475}/Γ

VALUE (units 10^{-6})	DOCUMENT ID		TECN	COMMENT
34.9±5.0±4.4	[1,2] AUBERT	08F	BABR	$e^+e^- \to \Upsilon(4S)$

[1] Assumes equal production of B^+ and B^0 at the $\Upsilon(4S)$.
[2] Assumes $a_1^{\pm}$ decays only to 3π and $B(a_1^{\pm} \to \pi^{\pm}\pi^{\mp}\pi^{\pm}) = 0.5$.

$\Gamma(b_1^+ K^0 \times B(b_1^+ \to \omega\pi^+))/\Gamma_{total}$ — Γ_{476}/Γ

VALUE (units 10^{-6})	DOCUMENT ID		TECN	COMMENT
9.6±1.7±0.9	[1] AUBERT	08AG	BABR	$e^+e^- \to \Upsilon(4S)$

[1] Assumes equal production of B^+ and B^0 at the $\Upsilon(4S)$.

$\Gamma(K^*(892)^0 \rho^+)/\Gamma_{total}$ — Γ_{477}/Γ

VALUE (units 10^{-6})	DOCUMENT ID		TECN	COMMENT
9.2±1.5 OUR AVERAGE				
9.6±1.7±1.5	[1] AUBERT,B	06G	BABR	$e^+e^- \to \Upsilon(4S)$
8.9±1.7±1.2	[1] ZHANG	05D	BELL	$e^+e^- \to \Upsilon(4S)$

[1] Assumes equal production of B^+ and B^0 at the $\Upsilon(4S)$.

$\Gamma(K_1(1400)^+ \rho^0)/\Gamma_{total}$ — Γ_{478}/Γ

VALUE	CL%	DOCUMENT ID		TECN	COMMENT
$<7.8\times10^{-4}$	90	ALBRECHT	91B	ARG	$e^+e^- \to \Upsilon(4S)$

$\Gamma(K_2^*(1430)^+ \rho^0)/\Gamma_{total}$ — Γ_{479}/Γ

VALUE	CL%	DOCUMENT ID		TECN	COMMENT
$<1.5\times10^{-3}$	90	ALBRECHT	91B	ARG	$e^+e^- \to \Upsilon(4S)$

$\Gamma(b_1^0 K^+ \times B(b_1^0 \to \omega\pi^0))/\Gamma_{total}$ — Γ_{480}/Γ

VALUE (units 10^{-6})	DOCUMENT ID		TECN	COMMENT
9.1±1.7±1.0	[1] AUBERT	07BI	BABR	$e^+e^- \to \Upsilon(4S)$

[1] Assumes equal production of B^+ and B^0 at the $\Upsilon(4S)$.

$\Gamma(b_1^+ K^{*0} \times B(b_1^+ \to \omega\pi^+))/\Gamma_{total}$ — Γ_{481}/Γ

VALUE	CL%	DOCUMENT ID		TECN	COMMENT
$<5.9\times10^{-6}$	90	[1] AUBERT	09AF	BABR	$e^+e^- \to \Upsilon(4S)$

[1] Assumes equal production of B^+ and B^0 at the $\Upsilon(4S)$.

$\Gamma(b_1^0 K^{*+} \times B(b_1^0 \to \omega\pi^0))/\Gamma_{total}$ — Γ_{482}/Γ

VALUE	CL%	DOCUMENT ID		TECN	COMMENT
$<6.7\times10^{-6}$	90	[1] AUBERT	09AF	BABR	$e^+e^- \to \Upsilon(4S)$

[1] Assumes equal production of B^+ and B^0 at the $\Upsilon(4S)$.

$\Gamma(K^+\overline{K}^0)/\Gamma_{total}$ — Γ_{483}/Γ

VALUE (units 10^{-6})	CL%	DOCUMENT ID		TECN	COMMENT
1.32±0.17 OUR FIT Error includes scale factor of 1.2.					
1.19±0.18 OUR AVERAGE					
1.11±0.19±0.05		[1] DUH	13	BELL	$e^+e^- \to \Upsilon(4S)$
1.61±0.44±0.09		[1] AUBERT,BE	06C	BABR	$e^+e^- \to \Upsilon(4S)$

• • • We do not use the following data for averages, fits, limits, etc. • • •

$1.22^{+0.32+0.13}_{-0.28-0.16}$		[1] LIN	07	BELL	Repl. by DUH 13
1.0 ±0.4 ±0.1		[1] ABE	05G	BELL	Repl. by LIN 07
1.5 ±0.5 ±0.1		[1] AUBERT,BE	05E	BABR	Repl. by AUBERT,BE 06C
$<$ 2.5	90	[1] AUBERT	04M	BABR	Repl. by AUBERT,BE 05E
$<$ 3.3	90	[1] CHAO	04	BELL	$e^+e^- \to \Upsilon(4S)$
$<$ 3.3	90	[1] BORNHEIM	03	CLE2	$e^+e^- \to \Upsilon(4S)$
$<$ 2.0	90	[1] CASEY	02	BELL	Repl. by CHAO 04
$<$ 5.0	90	[1] ABE	01H	BELL	$e^+e^- \to \Upsilon(4S)$
$<$ 2.4	90	[1] AUBERT	01E	BABR	$e^+e^- \to \Upsilon(4S)$
$<$ 5.1	90	[1] CRONIN-HEN..00		CLE2	$e^+e^- \to \Upsilon(4S)$
$<$21	90	GODANG	98	CLE2	Repl. by CRONIN-HENNESSY 00

[1] Assumes equal production of B^+ and B^0 at the $\Upsilon(4S)$.

$\Gamma(K^+\overline{K}^0)/\Gamma(K^0\pi^+)$ — $\Gamma_{483}/\Gamma_{411}$

VALUE	DOCUMENT ID		TECN	COMMENT
0.055±0.007 OUR FIT Error includes scale factor of 1.2.				
0.064±0.009±0.004	AAIJ	13BS	LHCB	pp at 7 TeV

$\Gamma(\overline{K}^0 K^+\pi^-)/\Gamma_{total}$ — Γ_{484}/Γ

VALUE	CL%	DOCUMENT ID		TECN	COMMENT
$<24\times10^{-6}$	90	[1] ECKHART	02	CLE2	$e^+e^- \to \Upsilon(4S)$

[1] Assumes equal production of B^+ and B^0 at the $\Upsilon(4S)$.

$\Gamma(K^+ K_S^0 K_S^0)/\Gamma_{total}$ — Γ_{485}/Γ

VALUE (units 10^{-6})	DOCUMENT ID		TECN	COMMENT
10.5 ±0.4 OUR AVERAGE				
10.42±0.43±0.22	[1] KALIYAR	19	BELL	$e^+e^- \to \Upsilon(4S)$
10.6 ±0.5 ±0.3	[1,2] LEES	12O	BABR	$e^+e^- \to \Upsilon(4S)$

• • • We do not use the following data for averages, fits, limits, etc. • • •

10.7 ±1.2 ±1.0	[1] AUBERT,B	04V	BABR	Repl. by LEES 12O
13.4 ±1.9 ±1.5	[1] GARMASH	04	BELL	Repl. by KALIYAR 19

[1] Assumes equal production of B^+ and B^0 at the $\Upsilon(4S)$.
[2] All intermediate charmonium and charm resonances are removed, except of χ_{c0}.

$\Gamma(f_0(980) K^+,\ f_0 \to K_S^0 K_S^0)/\Gamma_{total}$ — Γ_{486}/Γ

VALUE (units 10^{-6})	DOCUMENT ID		TECN	COMMENT
14.7±2.8±1.8	[1] LEES	12O	BABR	$e^+e^- \to \Upsilon(4S)$

[1] Assumes equal production of B^+ and B^0 at the $\Upsilon(4S)$.

$\Gamma(f_0(1710) K^+,\ f_0 \to K_S^0 K_S^0)/\Gamma_{total}$ — Γ_{487}/Γ

VALUE (units 10^{-6})	DOCUMENT ID		TECN	COMMENT
$0.48^{+0.40}_{-0.24}\pm0.11$	[1] LEES	12O	BABR	$e^+e^- \to \Upsilon(4S)$

[1] Assumes equal production of B^+ and B^0 at the $\Upsilon(4S)$.

$\Gamma(K^+ K_S^0 K_S^0 \text{ nonresonant})/\Gamma_{total}$ — Γ_{488}/Γ

VALUE (units 10^{-6})	DOCUMENT ID		TECN	COMMENT
19.8±3.7±2.5	[1] LEES	12O	BABR	$e^+e^- \to \Upsilon(4S)$

[1] Assumes equal production of B^+ and B^0 at the $\Upsilon(4S)$.

$\Gamma(K_S^0 K_S^0 \pi^+)/\Gamma_{total}$ — Γ_{489}/Γ

VALUE	CL%	DOCUMENT ID		TECN	COMMENT
$<5.1\times10^{-7}$	90	[1] AUBERT	09J	BABR	$e^+e^- \to \Upsilon(4S)$

• • • We do not use the following data for averages, fits, limits, etc. • • •

$<8.7\times10^{-7}$		[1] KALIYAR	19	BELL	$e^+e^- \to \Upsilon(4S)$
$<3.2\times10^{-6}$	90	[1] GARMASH	04	BELL	$e^+e^- \to \Upsilon(4S)$

[1] Assumes equal production of B^+ and B^0 at the $\Upsilon(4S)$.

$\Gamma(K^+K^-\pi^+)/\Gamma(K^+K^-K^+)$ — $\Gamma_{490}/\Gamma_{503}$

VALUE	DOCUMENT ID		TECN	COMMENT
0.151±0.004±0.008	AAIJ	20AJ	LHCB	pp at 7 and 8 TeV

$\Gamma(K^+K^-\pi^+)/\Gamma_{total}$ — Γ_{490}/Γ

VALUE (units 10^{-6})	CL%	DOCUMENT ID		TECN	COMMENT
5.2 ±0.4 OUR AVERAGE					
5.38±0.40±0.35		[1,2] HSU	17	BELL	$e^+e^- \to \Upsilon(4S)$
5.0 ±0.5 ±0.5		[2] AUBERT	07BB	BABR	$e^+e^- \to \Upsilon(4S)$

• • • We do not use the following data for averages, fits, limits, etc. • • •

$<$13	90	[2] GARMASH	04	BELL	$e^+e^- \to \Upsilon(4S)$
$<$ 6.3	90	[2,3] AUBERT	03M	BABR	Repl. by AUBERT 07BB
$<$12	90	[4] GARMASH	02	BELL	$e^+e^- \to \Upsilon(4S)$

[1] HSU 17 provides also measurement as a function of K^+K^- invariant mass.
[2] Assumes equal production of B^+ and B^0 at the $\Upsilon(4S)$.
[3] Charm and charmonium contributions are subtracted, otherwise no assumptions about intermediate resonances.
[4] Uses a reference decay mode $B^+ \to \overline{D}^0\pi^+$ and $\overline{D}^0 \to K^+\pi^-$ with $B(B^+ \to \overline{D}^0\pi^+)\cdot B(\overline{D}^0 \to K^+\pi^-) = (20.3\pm2.0)\times10^{-5}$.

$\Gamma(K^+K^-\pi^+ \text{ nonresonant})/\Gamma_{total}$ — Γ_{491}/Γ

VALUE (units 10^{-6})	CL%	DOCUMENT ID		TECN	COMMENT
1.68±0.23±0.13		[1] AAIJ	19AL	LHCB	pp at 7, 8 TeV

• • • We do not use the following data for averages, fits, limits, etc. • • •

$<$75	90	BERGFELD	96B	CLE2	$e^+e^- \to \Upsilon(4S)$

[1] AAIJ 19AL reports $0.323\pm0.015\pm0.041$ fit fraction for $B^+ \to K^+K^-\pi^+$ nonresonant from the amplitude analysis of $B^{\pm} \to \pi^{\pm}K^+K^-$ decays. We use the PDG 19 value $B(B^+ \to K^+K^-\pi^+) = (5.2\pm0.4)\times10^{-6}$ to obtain $B(B^+ \to K^+K^-\pi^+$ nonresonant). Our first error is the experiment's error and the second error is systematic error from using our best value.

$\Gamma(K^+\overline{K}^*(892)^0)/\Gamma_{total}$ — Γ_{492}/Γ

VALUE (units 10^{-7})	CL%	DOCUMENT ID		TECN	COMMENT
5.9±0.6±0.5		[1] AAIJ	19AL	LHCB	pp at 7, 8 TeV

Int. J. Mod. Phys. A 2026.41. Downloaded from www.worldscientific.com
by UNIVERSITY OF CALIFORNIA @ BERKELEY on 09/16/26. Re-use and distribution is strictly not permitted, except for Open Access articles.

• • • We do not use the following data for averages, fits, limits, etc. • • •

< 11	90	[2] AUBERT	07AR	BABR	$e^+e^- \to \Upsilon(4S)$
<1290	90	ABBIENDI	00B	OPAL	$e^+e^- \to Z$
<1380	90	[3] ABE	00C	SLD	$e^+e^- \to Z$
< 53	90	[2] JESSOP	00	CLE2	$e^+e^- \to \Upsilon(4S)$

[1] AAIJ 19AL reports $(7.5 \pm 0.6 \pm 0.5) \times 10^{-2}$ fit fraction for $B^+ \to K^+ \overline{K}^*(892)^0$ from the amplitude analysis of $B^{\pm} \to \pi^{\pm} K^+ K^-$ decays. We use the PDG 19 value $B(B^+ \to K^+ K^- \pi^+) = (5.2 \pm 0.4) \times 10^{-6}$ to obtain $B(B^+ \to K^+ \overline{K}^*(892)^0, \overline{K}^*(892)^0 \to K^+ \pi^-)$. We compute $B(B^+ \to K^+ \overline{K}^*(892)^0)$ using 2/3 of $B(\overline{K}^*(892)^0 \to (K\pi)^0) = (99.754 \pm 0.021)\%$ for the $K^+\pi^-$ fraction. Our first error is the experiment's error and the second error is systematic error from using our best value.
[2] Assumes equal production of B^+ and B^0 at the $\Upsilon(4S)$.
[3] ABE 00C assumes $B(Z \to b\overline{b}) = (21.7 \pm 0.1)\%$ and the B fractions $f_{B^0} = f_{B^+} = (39.7^{+1.8}_{-2.2})\%$ and $f_{B_s} = (10.5^{+1.8}_{-2.2})\%$.

$\Gamma(K^+ \overline{K}_0^*(1430)^0)/\Gamma_{total}$ — Γ_{493}/Γ

VALUE (units 10^{-6})	CL%	DOCUMENT ID		TECN	COMMENT
0.38±0.12±0.05		[1] AAIJ	19AL	LHCB	pp at 7, 8 TeV

• • • We do not use the following data for averages, fits, limits, etc. • • •

<2.2	90	[2] AUBERT	07AR	BABR	$e^+e^- \to \Upsilon(4S)$

[1] AAIJ 19AL reports $(4.5 \pm 0.7 \pm 1.2) \times 10^{-2}$ for fit fraction for $B^+ \to K^+ \overline{K}_0^*(1430)^0$ from the amplitude analysis of $B^{\pm} \to \pi^{\pm} K^+ K^-$ decays. We use the PDG 19 value $B(B^+ \to K^+ K^- \pi^+) = (5.2 \pm 0.4) \times 10^{-6}$ to obtain $B(B^+ \to K^+ \overline{K}_0^*(1430)^0, \overline{K}_0^*(1430)^0 \to K^+\pi^-)$. We compute $B(B^+ \to K^+ \overline{K}_0^*(1430)^0)$ using 2/3 of PDG 19 value $B(K_0^*(1430)^0 \to K\pi) = (93 \pm 10)\%$ for the $K^+\pi^-$ fraction. Our first error is the experiment's error and the second error is systematic error from using our best value.
[2] Assumes equal production of B^+ and B^0 at the $\Upsilon(4S)$.

$\Gamma(\rho(1450)^0 \pi^+, \rho^0 \to K^+ K^-)/\Gamma_{total}$ — Γ_{560}/Γ

VALUE (units 10^{-6})	DOCUMENT ID		TECN	COMMENT
1.60±0.08±0.12	[1] AAIJ	19AL	LHCB	pp at 7, 8 TeV

[1] AAIJ 19AL reports $0.307 \pm 0.012 \pm 0.009$ fit fraction for $B^+ \to \rho(1450)\pi^+$ from the amplitude analysis of $B^{\pm} \to \pi^{\pm} K^+ K^-$ decays. We use the PDG 19 value $B(B^+ \to K^+ K^- \pi^+) = (5.2 \pm 0.4) \times 10^{-6}$ to obtain $B(B^+ \to \rho(1450)\pi^+, \rho(1450) \to K^+ K^-)$. Our first error is the experiment's error and the second error is systematic error from using our best value.

$\Gamma(\pi^+ (K^+ K^-)_{S-wave})/\Gamma_{total}$ — Γ_{494}/Γ

VALUE (units 10^{-7})	DOCUMENT ID		TECN	COMMENT
8.53±0.67±0.66	[1] AAIJ	19AL	LHCB	pp at 7, 8 TeV

[1] AAIJ 19AL reports $0.164 \pm 0.008 \pm 0.01$ fit fraction for $B^+ \to \pi^+ (K^+ K^-)_{S-wave}$ in the region of $0.95 < m(K^+K^-) < 1.42$ GeV/c^2 from the amplitude analysis of $B^{\pm} \to \pi^{\pm} K^+ K^-$ decays. We use the PDG 19 value $B(B^+ \to K^+ K^- \pi^+) = (5.2 \pm 0.4) \times 10^{-6}$ to obtain $B(B^+ \to \pi^+ (K^+ K^-)_{S-wave})$. Our first error is the experiment's error and the second error is systematic error from using our best value.

$\Gamma(\pi^+ K^+ K^-, m_{K^+K^-} < 1.1\ \text{GeV})/\Gamma_{total}$ — Γ_{495}/Γ

VALUE (units 10^{-6})	DOCUMENT ID		TECN	COMMENT
5.38±0.40±0.35	[1] HSU	23	BELL	$e^+e^- \to \Upsilon(4S)$

[1] Investigated the angular distribution of K^+K^- pairs with invariant mass below 1.1 GeV/c^2, which exhibits both a strong enhancement in signal and very large direct CP violation.

$\Gamma(K^+ K^+ \pi^-)/\Gamma_{total}$ — Γ_{496}/Γ

VALUE	CL%	DOCUMENT ID		TECN	COMMENT
<1.1 × 10^{-8}	90	AAIJ	17E	LHCB	pp at 7, 8 TeV

• • • We do not use the following data for averages, fits, limits, etc. • • •

$<1.6 \times 10^{-7}$	90	[1] AUBERT	08BE	BABR	$e^+e^- \to \Upsilon(4S)$
$<2.4 \times 10^{-6}$	90	[1] GARMASH	04	BELL	$e^+e^- \to \Upsilon(4S)$
$<1.3 \times 10^{-6}$	90	[2] AUBERT	03M	BABR	Repl. by AUBERT 08BE
$<3.2 \times 10^{-6}$	90	[3] GARMASH	02	BELL	$e^+e^- \to \Upsilon(4S)$

[1] Assumes equal production of B^+ and B^0 at the $\Upsilon(4S)$.
[2] Assumes equal production of B^0 and B^+ at the $\Upsilon(4S)$; charm and charmonium contributions are subtracted, otherwise no assumptions about intermediate resonances.
[3] Uses a reference decay mode $B^+ \to \overline{D}^0 \pi^+$ and $\overline{D}^0 \to K^+\pi^-$ with $B(B^+ \to \overline{D}^0\pi^+) \cdot B(\overline{D}^0 \to K^+\pi^-) = (20.3 \pm 2.0) \times 10^{-5}$.

$\Gamma(K^+ K^+ \pi^- \text{nonresonant})/\Gamma_{total}$ — Γ_{497}/Γ

VALUE (units 10^{-6})	CL%	DOCUMENT ID		TECN	COMMENT
<87.9	90	ABBIENDI	00B	OPAL	$e^+e^- \to Z$

$\Gamma(f_2'(1525) K^+)/\Gamma_{total}$ — Γ_{498}/Γ

VALUE (units 10^{-6})	CL%	DOCUMENT ID		TECN	COMMENT
1.8 ±0.5 OUR AVERAGE		Error includes scale factor of 1.1.			
1.56±0.36±0.30		[1,2] LEES	12O	BABR	$e^+e^- \to \Upsilon(4S)$
2.8 ±0.9 $^{+0.5}_{-0.4}$		[1,3] LEES	12O	BABR	$e^+e^- \to \Upsilon(4S)$

• • • We do not use the following data for averages, fits, limits, etc. • • •

<8	90	[1,4] GARMASH	05	BELL	$e^+e^- \to \Upsilon(4S)$

[1] Assumes equal production of B^+ and B^0 at the $\Upsilon(4S)$.
[2] Measured in the $B^+ \to K^+K^-K^+$ decay.
[3] Measured in the $B^+ \to K^+ K_S^0 K_S^0$ decay.
[4] GARMASH 05 reports $B(B^+ \to f_2'(1525) K^+) \cdot B(f_2'(1525) \to K^+K^-) < 4.9 \times 10^{-6}$ at 90% CL. We divide this result by our best value of $B(f_2'(1525) \to K\overline{K}) = 88.8 \times 10^{-2}$ multiplied by 2/3 to account for the K^+K^- fraction.

$\Gamma(K^+ f_J(2220))/\Gamma_{total}$ — Γ_{499}/Γ

VALUE (units 10^{-6})	DOCUMENT ID		TECN	COMMENT
not seen	[1] HUANG	03	BELL	$e^+e^- \to \Upsilon(4S)$

[1] No evidence is found for such decay and set a limit on $B(B^+ \to f_J(2220)) \times B(f_J(2220) \to \phi\phi) < 1.2 \times 10^{-6}$ at 90%CL where the $f_J(2220)$ is a possible glueball state.

$\Gamma(K^{*+} \pi^+ K^-)/\Gamma_{total}$ — Γ_{500}/Γ

VALUE (units 10^{-6})	CL%	DOCUMENT ID		TECN	COMMENT
<11.8	90	[1] AUBERT,B	06U	BABR	$e^+e^- \to \Upsilon(4S)$

[1] Assumes equal production of B^+ and B^0 at the $\Upsilon(4S)$.

$\Gamma(K^*(892)^+ K^*(892)^0)/\Gamma_{total}$ — Γ_{501}/Γ

VALUE (units 10^{-6})	CL%	DOCUMENT ID		TECN	COMMENT
0.91±0.29 OUR AVERAGE					
$0.77^{+0.35}_{-0.30} \pm 0.12$		[1] GOH	15	BELL	$e^+e^- \to \Upsilon(4S)$
1.2 ±0.5 ±0.1		[2] AUBERT	09F	BABR	$e^+e^- \to \Upsilon(4S)$

• • • We do not use the following data for averages, fits, limits, etc. • • •

<71	90	[3] GODANG	02	CLE2	$e^+e^- \to \Upsilon(4S)$

[1] Signal significance is 2.7 standard deviations. This measurement corresponds to an upper limit of $< 1.31 \times 10^{-6}$ at 90% CL.
[2] Signal signicance is 3.7 standard deviations.
[3] Assumes a helicity 00 configuration. For a helicity 11 configuration, the limit decreases to 4.8×10^{-5}.

$\Gamma(K^{*+} K^+ \pi^-)/\Gamma_{total}$ — Γ_{502}/Γ

VALUE (units 10^{-6})	CL%	DOCUMENT ID		TECN	COMMENT
<6.1	90	[1] AUBERT,B	06U	BABR	$e^+e^- \to \Upsilon(4S)$

[1] Assumes equal production of B^+ and B^0 at the $\Upsilon(4S)$.

$\Gamma(K^+ K^- K^+)/\Gamma_{total}$ — Γ_{503}/Γ

VALUE (units 10^{-6})	CL%	DOCUMENT ID		TECN	COMMENT
34.0±1.4 OUR AVERAGE		Error includes scale factor of 1.4.			
34.6±0.6±0.9		[1,2] LEES	12O	BABR	$e^+e^- \to \Upsilon(4S)$
30.6±1.2±2.3		[1] GARMASH	05	BELL	$e^+e^- \to \Upsilon(4S)$

• • • We do not use the following data for averages, fits, limits, etc. • • •

35.2±0.9±1.6		[1] AUBERT	06O	BABR	Repl. by LEES 12O
32.8±1.8±2.8		[1] GARMASH	04	BELL	Repl. by GARMASH 05
29.6±2.1±1.6		[3] AUBERT	03M	BABR	Repl. by AUBERT 06O
35.3±3.7±4.5		[4] GARMASH	02	BELL	Repl. by GARMASH 04
<200	90	[5] ADAM	96D	DLPH	$e^+e^- \to Z$
<320	90	[5] ABREU	95N	DLPH	Sup. by ADAM 96D
<350	90	ALBRECHT	91E	ARG	$e^+e^- \to \Upsilon(4S)$

[1] Assumes equal production of B^+ and B^0 at the $\Upsilon(4S)$.
[2] All intermediate charmonium and charm resonances are removed, except of χ_{c0}.
[3] Assumes equal production of B^0 and B^+ at the $\Upsilon(4S)$; charm and charmonium contributions are subtracted, otherwise no assumptions about intermediate resonances.
[4] Uses a reference decay mode $B^+ \to \overline{D}^0 \pi^+$ and $\overline{D}^0 \to K^+\pi^-$ with $B(B^+ \to \overline{D}^0\pi^+) \cdot B(\overline{D}^0 \to K^+\pi^-) = (20.3 \pm 2.0) \times 10^{-5}$.
[5] Assumes B^0 and B^- production fractions of 0.39, and B_s production fraction of 0.12.

$\Gamma(K^+ \phi)/\Gamma_{total}$ — Γ_{504}/Γ

VALUE (units 10^{-6})	CL%	DOCUMENT ID		TECN	COMMENT
8.8 $^{+0.7}_{-0.6}$ OUR AVERAGE		Error includes scale factor of 1.1.			
9.2 ±0.4 $^{+0.7}_{-0.5}$		[1] LEES	12O	BABR	$e^+e^- \to \Upsilon(4S)$
7.6 ±1.3 ±0.6		[2] ACOSTA	05J	CDF	$p\overline{p}$ at 1.96 TeV
$9.60 \pm 0.92^{+1.05}_{-0.85}$		[1] GARMASH	05	BELL	$e^+e^- \to \Upsilon(4S)$
5.5 $^{+2.1}_{-1.8}$ ±0.6		[1] BRIERE	01	CLE2	$e^+e^- \to \Upsilon(4S)$

• • • We do not use the following data for averages, fits, limits, etc. • • •

8.4 ±0.7 ±0.7		[1] AUBERT	06O	BABR	Repl. by LEES 12O
10.0 $^{+0.9}_{-0.8}$ ±0.5		[1] AUBERT	04A	BABR	Repl. by AUBERT 06O
9.4 ±1.1 ±0.7		[1] CHEN	03B	BELL	Repl. by GARMASH 05
14.6 $^{+3.0}_{-2.8}$ ±2.0		[3] GARMASH	02	BELL	Repl. by CHEN 03B
7.7 $^{+1.6}_{-1.4}$ ±0.8		[1] AUBERT	01D	BABR	$e^+e^- \to \Upsilon(4S)$
<144	90	[4] ABE	00C	SLD	$e^+e^- \to Z$
< 5	90	[1] BERGFELD	98	CLE2	
<280	90	[5] ADAM	96D	DLPH	$e^+e^- \to Z$
< 12	90	ASNER	96	CLE2	$e^+e^- \to \Upsilon(4S)$
<440	90	[6] ABREU	95N	DLPH	Sup. by ADAM 96D
<180	90	ALBRECHT	91B	ARG	$e^+e^- \to \Upsilon(4S)$
< 90	90	[7] AVERY	89B	CLEO	$e^+e^- \to \Upsilon(4S)$
<210	90	AVERY	87	CLEO	$e^+e^- \to \Upsilon(4S)$

[1] Assumes equal production of B^+ and B^0 at the $\Upsilon(4S)$.
[2] Uses $B(B^+ \to J/\psi K^+) = (1.00 \pm 0.04) \times 10^{-3}$ and $B(J/\psi \to \mu^+\mu^-) = 0.0588 \pm 0.0010$.
[3] Uses a reference decay mode $B^+ \to \overline{D}^0\pi^+$ and $\overline{D}^0 \to K^+\pi^-$ with $B(B^+ \to \overline{D}^0\pi^+)\cdot B(\overline{D}^0 \to K^+\pi^-) = (20.3 \pm 2.0) \times 10^{-5}$.
[4] ABE 00C assumes $B(Z \to b\overline{b}) = (21.7 \pm 0.1)\%$ and the B fractions $f_{B^0} = f_{B^+} = (39.7^{+1.8}_{-2.2})\%$ and $f_{B_s} = (10.5^{+1.8}_{-2.2})\%$.
[5] ADAM 96D assumes $f_{B^0} = f_{B^-} = 0.39$ and $f_{B_s} = 0.12$.
[6] Assumes a B^0, B^- production fraction of 0.39 and a B_s production fraction of 0.12.
[7] AVERY 89B reports $< 8 \times 10^{-5}$ assuming the $\Upsilon(4S)$ decays 43% to $B^0\overline{B}^0$. We rescale to 50%.

$\Gamma(f_0(980) K^+ \times B(f_0(980) \to K^+K^-))/\Gamma_{total}$ — Γ_{505}/Γ

VALUE (units 10^{-6})	CL%	DOCUMENT ID		TECN	COMMENT
9.4±1.6±2.8		[1] LEES	12O	BABR	$e^+e^- \to \Upsilon(4S)$
• • • We do not use the following data for averages, fits, limits, etc. • • •					
6.5±2.5±1.6		[1] AUBERT	06O	BABR	$e^+e^- \to \Upsilon(4S)$
<2.9	90	[1] GARMASH	05	BELL	$e^+e^- \to \Upsilon(4S)$

[1] Assumes equal production of B^+ and B^0 at the $\Upsilon(4S)$.

$\Gamma(a_2(1320) K^+ \times B(a_2(1320) \to K^+K^-))/\Gamma_{total}$ — Γ_{506}/Γ

VALUE	CL%	DOCUMENT ID		TECN	COMMENT
$<1.1 \times 10^{-6}$	90	[1] GARMASH	05	BELL	$e^+e^- \to \Upsilon(4S)$

[1] Assumes equal production of B^+ and B^0 at the $\Upsilon(4S)$.

$\Gamma(X_0(1550) K^+ \times B(X_0(1550) \to K^+K^-))/\Gamma_{total}$ — Γ_{507}/Γ

$X_0(1550)$ is a possible spin zero state near 1.55 GeV/c^2 invariant mass of K^+K^-.

VALUE (units 10^{-6})	DOCUMENT ID		TECN	COMMENT
4.3±0.6±0.3	[1] AUBERT	06O	BABR	$e^+e^- \to \Upsilon(4S)$

[1] Assumes equal production of B^+ and B^0 at the $\Upsilon(4S)$.

$\Gamma(\phi(1680) K^+ \times B(\phi(1680) \to K^+K^-))/\Gamma_{total}$ — Γ_{508}/Γ

VALUE	CL%	DOCUMENT ID		TECN	COMMENT
$<0.8 \times 10^{-6}$	90	[1] GARMASH	05	BELL	$e^+e^- \to \Upsilon(4S)$

[1] Assumes equal production of B^+ and B^0 at the $\Upsilon(4S)$.

$\Gamma(f_0(1710) K^+ \times B(f_0(1710) \to K^+K^-))/\Gamma_{total}$ — Γ_{509}/Γ

VALUE (units 10^{-6})	DOCUMENT ID		TECN	COMMENT
1.12±0.25±0.50	[1] LEES	12O	BABR	$e^+e^- \to \Upsilon(4S)$
• • • We do not use the following data for averages, fits, limits, etc. • • •				
1.7 ±1.0 ±0.3	[1] AUBERT	06O	BABR	Repl. by LEES 12O

[1] Assumes equal production of B^+ and B^0 at the $\Upsilon(4S)$.

$\Gamma(K^+K^-K^+ \text{nonresonant})/\Gamma_{total}$ — Γ_{510}/Γ

VALUE (units 10^{-6})	CL%	DOCUMENT ID		TECN	COMMENT
$23.8^{+2.8}_{-5.0}$ OUR AVERAGE					
22.8±2.7±7.6		[1] LEES	12O	BABR	$e^+e^- \to \Upsilon(4S)$
$24.0 \pm 1.5^{+2.6}_{-6.0}$		[1] GARMASH	05	BELL	$e^+e^- \to \Upsilon(4S)$
• • • We do not use the following data for averages, fits, limits, etc. • • •					
50.0±6.0±4.0		[1] AUBERT	06O	BABR	Repl. by LEES 12O
<38	90	BERGFELD	96B	CLE2	$e^+e^- \to \Upsilon(4S)$

[1] Assumes equal production of B^+ and B^0 at the $\Upsilon(4S)$.

$\Gamma(K^*(892)^+ K^+K^-)/\Gamma_{total}$ — Γ_{511}/Γ

VALUE (units 10^{-6})	CL%	DOCUMENT ID		TECN	COMMENT
36.2±3.3±3.6		[1] AUBERT,B	06U	BABR	$e^+e^- \to \Upsilon(4S)$
• • • We do not use the following data for averages, fits, limits, etc. • • •					
<1600	90	ALBRECHT	91E	ARG	$e^+e^- \to \Upsilon(4S)$

[1] Assumes equal production of B^+ and B^0 at the $\Upsilon(4S)$.

$\Gamma(K^*(892)^+ \phi)/\Gamma_{total}$ — Γ_{512}/Γ

VALUE (units 10^{-6})	CL%	DOCUMENT ID		TECN	COMMENT
10.0±2.0 OUR AVERAGE	Error includes scale factor of 1.7.				
11.2±1.0±0.9		[1] AUBERT	07BA	BABR	$e^+e^- \to \Upsilon(4S)$
$6.7^{+2.1}_{-1.9}{}^{+0.7}_{-1.0}$		[1] CHEN	03B	BELL	$e^+e^- \to \Upsilon(4S)$
• • • We do not use the following data for averages, fits, limits, etc. • • •					
$12.7^{+2.2}_{-2.0} \pm 1.1$		[1] AUBERT	03V	BABR	Repl. by AUBERT 07BA
$9.7^{+4.2}_{-3.4} \pm 1.7$		[1] AUBERT	01D	BABR	Repl. by AUBERT 03V
< 22.5	90	[1] BRIERE	01	CLE2	$e^+e^- \to \Upsilon(4S)$
< 41	90	[1] BERGFELD	98	CLE2	
< 70	90	ASNER	96	CLE2	$e^+e^- \to \Upsilon(4S)$
<1300	90	ALBRECHT	91B	ARG	$e^+e^- \to \Upsilon(4S)$

[1] Assumes equal production of B^+ and B^0 at the $\Upsilon(4S)$.

$\Gamma(K^0K^+K^-\pi^+)/\Gamma_{total}$ — Γ_{513}/Γ

VALUE (units 10^{-5})	DOCUMENT ID		TECN	COMMENT
34.01±0.74±3.23	[1] AAIJ	23AH	LHCB	pp at 7, 8 and 13 TeV

[1] The second uncertainty includes systematic and reference branching reaction of $B^+ \to J/\psi K^+$ uncertainties.

$\Gamma(J/\psi K^+, J/\psi \to K^0K^-\pi^+)/\Gamma_{total}$ — Γ_{514}/Γ

VALUE (units 10^{-6})	DOCUMENT ID		TECN	COMMENT
5.43±0.12±1.23	[1] AAIJ	23AH	LHCB	pp at 7, 8 and 13 TeV

[1] The second uncertainty includes systematic and reference branching reaction of $B^+ \to \eta_c K^+$ uncertainties.

$\Gamma(\chi_{c1} K^+, \chi_{c1} \to K^0K^-\pi^+)/\Gamma_{total}$ — Γ_{515}/Γ

VALUE (units 10^{-6})	DOCUMENT ID		TECN	COMMENT
2.25±0.11±0.22	[1] AAIJ	23AH	LHCB	pp at 7, 8 and 13 TeV

[1] The second uncertainty includes systematic and reference branching reaction of $B^+ \to J/\psi K^+$ uncertainties.

$\Gamma(\eta_c K^+, \eta_c \to K^0K^-\pi^+)/\Gamma_{total}$ — Γ_{516}/Γ

VALUE (units 10^{-5})	DOCUMENT ID		TECN	COMMENT
2.83±0.07±0.29	[1] AAIJ	23AH	LHCB	pp at 7, 8 and 13 TeV

[1] The second uncertainty includes systematic and reference branching reaction of $B^+ \to J/\psi K^+$ uncertainties.

$\Gamma(\eta_c(2S) K^+, \eta_c(2S) \to K^0K^-\pi^+)/\Gamma_{total}$ — Γ_{517}/Γ

VALUE (units 10^{-6})	DOCUMENT ID		TECN	COMMENT
3.27±0.17±0.34	[1] AAIJ	23AH	LHCB	pp at 7, 8 and 13 TeV

[1] The second uncertainty includes systematic and reference branching reaction of $B^+ \to J/\psi K^+$ uncertainties.

$\Gamma(K^0K^+K^+\pi^-)/\Gamma_{total}$ — Γ_{518}/Γ

VALUE (units 10^{-5})	DOCUMENT ID		TECN	COMMENT
28.01±0.68±2.89	[1] AAIJ	23AH	LHCB	pp at 7, 8 and 13 TeV

[1] The second uncertainty includes systematic and reference branching reaction of $B^+ \to J/\psi K^+$ uncertainties.

$\Gamma(J/\psi K^+, J/\psi \to K^0K^+\pi^-)/\Gamma_{total}$ — Γ_{519}/Γ

VALUE (units 10^{-6})	DOCUMENT ID		TECN	COMMENT
5.41±0.14±1.25	[1] AAIJ	23AH	LHCB	pp at 7, 8 and 13 TeV

[1] The second uncertainty includes systematic and reference branching reaction of $B^+ \to \eta_c K^+$ uncertainties.

$\Gamma(\chi_{c1} K^+, \chi_{c1} \to K^0K^+\pi^-)/\Gamma_{total}$ — Γ_{520}/Γ

VALUE (units 10^{-6})	DOCUMENT ID		TECN	COMMENT
2.06±0.12±0.30	[1] AAIJ	23AH	LHCB	pp at 7, 8 and 13 TeV

[1] The second uncertainty includes systematic and reference branching reaction of $B^+ \to J/\psi K^+$ uncertainties.

$\Gamma(\eta_c K^+, \eta_c \to K^0K^+\pi^-)/\Gamma_{total}$ — Γ_{521}/Γ

VALUE (units 10^{-5})	DOCUMENT ID		TECN	COMMENT
3.00±0.14±0.31	[1] AAIJ	23AH	LHCB	pp at 7, 8 and 13 TeV

[1] The second uncertainty includes systematic and reference branching reaction of $B^+ \to J/\psi K^+$ uncertainties.

$\Gamma(\eta_c(2S) K^+, \eta_c(2S) \to K^0K^+\pi^-)/\Gamma_{total}$ — Γ_{522}/Γ

VALUE (units 10^{-6})	DOCUMENT ID		TECN	COMMENT
3.13±0.21±0.52	[1] AAIJ	23AH	LHCB	pp at 7, 8 and 13 TeV

[1] The second uncertainty includes systematic and reference branching reaction of $B^+ \to J/\psi K^+$ uncertainties.

$\Gamma(\phi(K\pi)_0^{*+})/\Gamma_{total}$ — Γ_{523}/Γ

$(K\pi)_0^{*+}$ is the total S-wave composed of $K_0^*(1430)$ and nonresonant that are described using LASS shape.

VALUE (units 10^{-6})	DOCUMENT ID		TECN	COMMENT
8.3±1.4±0.8	[1] AUBERT	08BI	BABR	$e^+e^- \to \Upsilon(4S)$

[1] Assumes equal production of B^+ and B^0 at the $\Upsilon(4S)$.

$\Gamma(\phi K_1(1270)^+)/\Gamma_{total}$ — Γ_{524}/Γ

VALUE (units 10^{-6})	DOCUMENT ID		TECN	COMMENT
6.1±1.6±1.1	[1] AUBERT	08BI	BABR	$e^+e^- \to \Upsilon(4S)$

[1] Assumes equal production of B^+ and B^0 at the $\Upsilon(4S)$.

$\Gamma(\phi K_1(1400)^+)/\Gamma_{total}$ — Γ_{525}/Γ

VALUE (units 10^{-6})	CL%	DOCUMENT ID		TECN	COMMENT
< 3.2	90	[1] AUBERT	08BI	BABR	$e^+e^- \to \Upsilon(4S)$
• • • We do not use the following data for averages, fits, limits, etc. • • •					
<1100	90	ALBRECHT	91B	ARG	$e^+e^- \to \Upsilon(4S)$

[1] Assumes equal production of B^+ and B^0 at the $\Upsilon(4S)$.

Int. J. Mod. Phys. A 2026.41. Downloaded from www.worldscientific.com
by LIFORNIA @ BERKELEY on 09/16/26. Re-use and distribution is strictly not permitted, except for Open Access articles.

Int. J. Mod. Phys. A 2026.41. Downloaded from www.worldscientific.com
by UNIVERSITY OF CALIFORNIA @ BERKELEY on 09/16/26. Re-use and distribution is strictly not permitted, except for Open Access articles.

$\Gamma(\phi K^*(1410)^+)/\Gamma_{total}$ — Γ_{526}/Γ

VALUE (units 10^{-6})	CL%	DOCUMENT ID		TECN	COMMENT
<4.3	90	[1] AUBERT	08BI	BABR	$e^+e^- \to \Upsilon(4S)$

[1] Assumes equal production of B^+ and B^0 at the $\Upsilon(4S)$.

$\Gamma(\phi K_0^*(1430)^+)/\Gamma_{total}$ — Γ_{527}/Γ

VALUE (units 10^{-6})		DOCUMENT ID		TECN	COMMENT
7.0±1.3±0.9		[1] AUBERT	08BI	BABR	$e^+e^- \to \Upsilon(4S)$

[1] Assumes equal production of B^+ and B^0 at the $\Upsilon(4S)$.

$\Gamma(\phi K_2^*(1430)^+)/\Gamma_{total}$ — Γ_{528}/Γ

VALUE (units 10^{-6})	CL%	DOCUMENT ID		TECN	COMMENT
8.4±1.8±1.0		[1] AUBERT	08BI	BABR	$e^+e^- \to \Upsilon(4S)$
• • • We do not use the following data for averages, fits, limits, etc. • • •					
<3400	90	ALBRECHT	91B	ARG	$e^+e^- \to \Upsilon(4S)$

[1] Assumes equal production of B^+ and B^0 at the $\Upsilon(4S)$.

$\Gamma(\phi K_2^*(1770)^+)/\Gamma_{total}$ — Γ_{529}/Γ

VALUE (units 10^{-6})	CL%	DOCUMENT ID		TECN	COMMENT
<15.0	90	[1] AUBERT	08BI	BABR	$e^+e^- \to \Upsilon(4S)$

[1] Assumes equal production of B^+ and B^0 at the $\Upsilon(4S)$.

$\Gamma(\phi K_2^*(1820)^+)/\Gamma_{total}$ — Γ_{530}/Γ

VALUE (units 10^{-6})	CL%	DOCUMENT ID		TECN	COMMENT
<16.3	90	[1] AUBERT	08BI	BABR	$e^+e^- \to \Upsilon(4S)$

[1] Assumes equal production of B^+ and B^0 at the $\Upsilon(4S)$.

$\Gamma(a_1^+ K^{*0})/\Gamma_{total}$ — Γ_{531}/Γ

VALUE (units 10^{-6})	CL%	DOCUMENT ID		TECN	COMMENT
<3.6	90	[1,2] DEL-AMO-SA...10I		BABR	$e^+e^- \to \Upsilon(4S)$

[1] Assumes $B(a_1^{\pm} \to \pi^{\pm}\pi^{\mp}\pi^{\pm}) = 0.5$

[2] Assumes equal production of B^+ and B^0 at the $\Upsilon(4S)$.

$\Gamma(K^+\phi\phi)/\Gamma_{total}$ — Γ_{532}/Γ

VALUE (units 10^{-6})	DOCUMENT ID		TECN	COMMENT
4.2 ±0.8 OUR AVERAGE Error includes scale factor of 2.2. See the ideogram below.				
$3.43^{+0.48}_{-0.46} \pm 0.22$	[1] MOHANTY	21	BELL	$e^+e^- \to \Upsilon(4S)$
5.6 ±0.5 ±0.3	[1] LEES	11A	BABR	$e^+e^- \to \Upsilon(4S)$
$2.6\ ^{+1.1}_{-0.9} \pm 0.3$	[1] HUANG	03	BELL	$e^+e^- \to \Upsilon(4S)$
• • • We do not use the following data for averages, fits, limits, etc. • • •				
7.5 ±1.0 ±0.7	[1] AUBERT,BE	06H	BABR	Repl. by LEES 11A

[1] Assumes equal production of B^0 and B^+ at the $\Upsilon(4S)$ and the $\phi\phi$ invariant mass below 2.85 GeV/c^2.

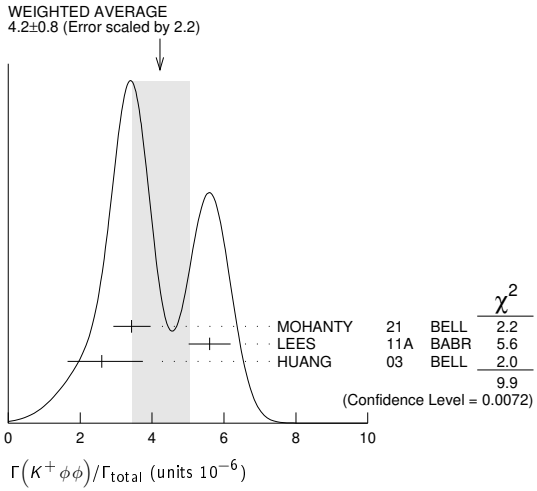

$\Gamma(\eta'\eta' K^+)/\Gamma_{total}$ — Γ_{533}/Γ

VALUE (units 10^{-6})	CL%	DOCUMENT ID		TECN	COMMENT
<25	90	[1] AUBERT,B	06P	BABR	$e^+e^- \to \Upsilon(4S)$

[1] Assumes equal production of B^+ and B^0 at the $\Upsilon(4S)$.

$\Gamma(\omega\phi K^+)/\Gamma_{total}$ — Γ_{534}/Γ

VALUE (units 10^{-6})	CL%	DOCUMENT ID		TECN	COMMENT
<1.9	90	[1] LIU	09	BELL	$e^+e^- \to \Upsilon(4S)$

[1] Assumes equal production of B^+ and B^0 at the $\Upsilon(4S)$.

$\Gamma(X(1812)K^+ \times B(X \to \omega\phi))/\Gamma_{total}$ — Γ_{535}/Γ

VALUE (units 10^{-6})	CL%	DOCUMENT ID		TECN	COMMENT
<0.32	90	[1] LIU	09	BELL	$e^+e^- \to \Upsilon(4S)$

[1] Assumes equal production of B^+ and B^0 at the $\Upsilon(4S)$.

$\Gamma(K^*(892)^+\gamma)/\Gamma_{total}$ — Γ_{536}/Γ

VALUE (units 10^{-5})	CL%	DOCUMENT ID		TECN	COMMENT
3.95±0.13 OUR AVERAGE Error includes scale factor of 1.3. See the ideogram below.					
$4.04^{+0.16}_{-0.19} \pm^{+0.09}_{-0.06}$		[1] ADACHI	25Z	BELL	$e^+e^- \to \Upsilon(4S)$
3.76±0.10±0.12		[2] HORIGUCHI	17	BELL	$e^+e^- \to \Upsilon(4S)$
4.22±0.14±0.16		[3] AUBERT	09AO	BABR	$e^+e^- \to \Upsilon(4S)$
$3.76^{+0.89}_{-0.83} \pm 0.28$		[4] COAN	00	CLE2	$e^+e^- \to \Upsilon(4S)$
• • • We do not use the following data for averages, fits, limits, etc. • • •					
3.87±0.28±0.26		[5] AUBERT,BE	04A	BABR	Repl. by AUBERT 09AO
4.25±0.31±0.24		[4] NAKAO	04	BELL	Repl. by HORIGUCHI 17
3.83±0.62±0.22		[4] AUBERT	02C	BABR	Repl. by AUBERT,BE 04A
5.7 ±3.1 ±1.1		[6] AMMAR	93	CLE2	Repl. by COAN 00
< 55	90	[7] ALBRECHT	89G	ARG	$e^+e^- \to \Upsilon(4S)$
< 55	90	[7] AVERY	89B	CLEO	$e^+e^- \to \Upsilon(4S)$
<180	90	AVERY	87	CLEO	$e^+e^- \to \Upsilon(4S)$

[1] ADACHI 25Z reports $(4.04 \pm 0.13^{+0.13}_{-0.15}) \times 10^{-5}$ from a measurement of $[\Gamma(B^+ \to K^*(892)^+\gamma)/\Gamma_{total}] \times [B(\Upsilon(4S) \to B^+B^-)]$ assuming $B(\Upsilon(4S) \to B^+B^-) = (51.13^{+0.73}_{-1.08}) \times 10^{-2}$, which we rescale to our best (shown rounded) value $B(\Upsilon(4S) \to B^+B^-) = (51.1^{+0.7}_{-1.1}) \times 10^{-2}$. Our first error is their experiment's error and our second error is the systematic error from using our best (shown rounded) value.

[2] Uses $B(\Upsilon(4S) \to B^+B^-) = (51.4 \pm 0.6)\%$ and $B(\Upsilon(4S) \to B^0\overline{B}^0) = (48.6 \pm 0.6)\%$.

[3] Uses $B(\Upsilon(4S) \to B^+B^-) = (51.6 \pm 0.6)\%$ and $B(\Upsilon(4S) \to B^0\overline{B}^0) = (48.4 \pm 0.6)\%$.

[4] Assumes equal production of B^+ and B^0 at the $\Upsilon(4S)$.

[5] Uses the production ratio of charged and neutral B from $\Upsilon(4S)$ decays $R^{+/0} = 1.006 \pm 0.048$.

[6] AMMAR 93 observed 4.1 ± 2.3 events above background.

[7] Assumes the $\Upsilon(4S)$ decays 43% to $B^0\overline{B}^0$.

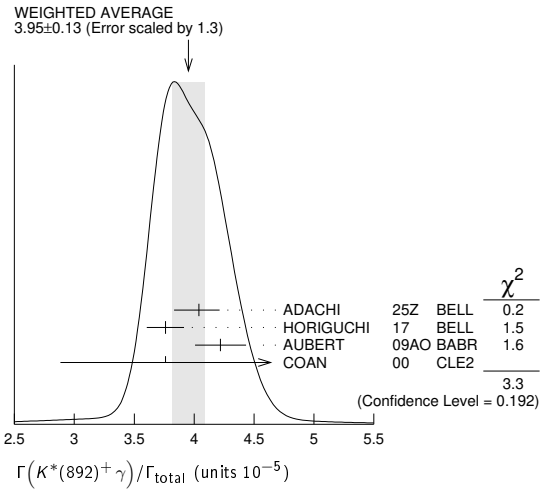

$\Gamma(K_1(1270)^+\gamma)/\Gamma_{total}$ — Γ_{537}/Γ

VALUE (units 10^{-5})	CL%	DOCUMENT ID		TECN	COMMENT
$4.4\ ^{+0.7}_{-0.6}$ OUR AVERAGE					
$4.41^{+0.63}_{-0.44} \pm 0.58$		[1,2] DEL-AMO-SA...16		BABR	$e^+e^- \to \Upsilon(4S)$
4.3 ±0.9 ±0.9		[3] YANG	05	BELL	$e^+e^- \to \Upsilon(4S)$
• • • We do not use the following data for averages, fits, limits, etc. • • •					
< 9.9	90	[3] NISHIDA	02	BELL	Repl. by YANG 05
<730	90	[4] ALBRECHT	89G	ARG	$e^+e^- \to \Upsilon(4S)$

[1] Requires $M_{K\pi\pi} < 1.8$ GeV/c^2.

[2] Uses $B(\Upsilon(4S) \to B^+B^-) = 0.513 \pm 0.006$.

[3] Assumes equal production of B^+ and B^0 at the $\Upsilon(4S)$.

[4] ALBRECHT 89G reports < 0.0066 assuming the $\Upsilon(4S)$ decays 45% to $B^0\overline{B}^0$. We rescale to 50%.

$\Gamma(\eta K^+\gamma)/\Gamma_{total}$ — Γ_{538}/Γ

VALUE (units 10^{-6})	DOCUMENT ID		TECN	COMMENT
7.9±0.9 OUR AVERAGE				
7.7±1.0±0.4	[1,2] AUBERT	09	BABR	$e^+e^- \to \Upsilon(4S)$
$8.4 \pm 1.5\ ^{+1.2}_{-0.9}$	[2,3] NISHIDA	05	BELL	$e^+e^- \to \Upsilon(4S)$
• • • We do not use the following data for averages, fits, limits, etc. • • •				
10.0±1.3±0.5	[1,2] AUBERT,B	06M	BABR	Repl. by AUBERT 09

[1] $m_{\eta K} < 3.25$ GeV/c^2.
[2] Assumes equal production of B^+ and B^0 at the $\Upsilon(4S)$.
[3] $m_{\eta K} < 2.4$ GeV/c^2

$\Gamma(\eta' K^+\gamma)/\Gamma_{total}$ — Γ_{539}/Γ

VALUE (units 10^{-6})	DOCUMENT ID		TECN	COMMENT
$2.9^{+1.0}_{-0.9}$ OUR AVERAGE				
$3.6\pm1.2\pm0.4$	[1,2] WEDD	10	BELL	$e^+e^- \to \Upsilon(4S)$
$1.9^{+1.5}_{-1.2}\pm0.1$	[1,3] AUBERT,B	06M	BABR	$e^+e^- \to \Upsilon(4S)$

[1] Assumes equal production of B^+ and B^0 at the $\Upsilon(4S)$.
[2] $m_{\eta' K} < 3.4$ GeV/c^2.
[3] Set the upper limit of 4.2×10^{-6} at 90% CL with $m_{\eta' K} < 3.25$ GeV/c^2.

$\Gamma(\phi K^+\gamma)/\Gamma_{total}$ — Γ_{540}/Γ

VALUE (units 10^{-6})	DOCUMENT ID		TECN	COMMENT
2.7 ±0.4 OUR AVERAGE Error includes scale factor of 1.2.				
$2.48\pm0.30\pm0.24$	[1] SAHOO	11A	BELL	$e^+e^- \to \Upsilon(4S)$
$3.5\ \pm0.6\ \pm0.4$	[1] AUBERT	07Q	BABR	$e^+e^- \to \Upsilon(4S)$
• • • We do not use the following data for averages, fits, limits, etc. • • •				
$3.4\ \pm0.9\ \pm0.4$	[1] DRUTSKOY	04	BELL	Repl. by SAHOO 11A

[1] Assumes equal production of B^+ and B^0 at $\Upsilon(4S)$.

$\Gamma(K^+\pi^-\pi^+\gamma)/\Gamma_{total}$ — Γ_{541}/Γ

VALUE (units 10^{-5})	DOCUMENT ID		TECN	COMMENT
2.58±0.15 OUR AVERAGE Error includes scale factor of 1.3. See the ideogram below.				
$2.45\pm0.09\pm0.12$	[1,2] DEL-AMO-SA...16		BABR	$e^+e^- \to \Upsilon(4S)$
$2.95\pm0.13\pm0.20$	[1,3] AUBERT	07R	BABR	$e^+e^- \to \Upsilon(4S)$
$2.50\pm0.18\pm0.22$	[3,4] YANG	05	BELL	$e^+e^- \to \Upsilon(4S)$
• • • We do not use the following data for averages, fits, limits, etc. • • •				
$2.4\ \pm0.5\ ^{+0.4}_{-0.2}$	[3,5] NISHIDA	02	BELL	Repl. by YANG 05

[1] $M_{K\pi\pi} < 1.8$ GeV/c^2.
[2] Uses B($\Upsilon(4S) \to B^+B^-$) = 0.513 ± 0.006.
[3] Assumes equal production of B^+ and B^0 at the $\Upsilon(4S)$.
[4] $M_{K\pi\pi} < 2.0$ GeV/c^2.
[5] $M_{K\pi\pi} < 2.4$ GeV/c^2.

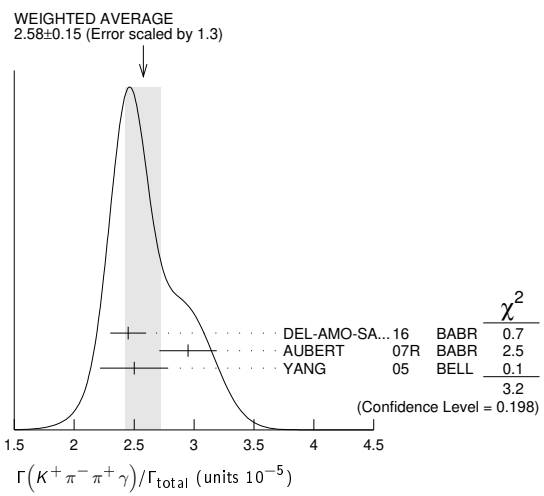

$\Gamma(K^*(892)^0\pi^+\gamma)/\Gamma_{total}$ — Γ_{542}/Γ

VALUE (units 10^{-5})	DOCUMENT ID		TECN	COMMENT
2.33±0.12 OUR AVERAGE				
$2.34\pm0.09^{+0.08}_{-0.07}$	[1,2] DEL-AMO-SA...16		BABR	$e^+e^- \to \Upsilon(4S)$
$2.0\ ^{+0.7}_{-0.6}\ \pm0.2$	[3,4] NISHIDA	02	BELL	$e^+e^- \to \Upsilon(4S)$

[1] Requires $M_{K\pi\pi} < 1.8$ GeV/c^2.
[2] Uses B($\Upsilon(4S) \to B^+B^-$) = 0.513 ± 0.006.
[3] Assumes equal production of B^+ and B^0 at the $\Upsilon(4S)$.
[4] $M_{K\pi\pi} < 2.4$ GeV/c^2.

$\Gamma(K^+\rho^0\gamma)/\Gamma_{total}$ — Γ_{543}/Γ

VALUE (units 10^{-6})	CL%	DOCUMENT ID		TECN	COMMENT
8.2±0.4±0.8		[1,2] DEL-AMO-SA...16		BABR	$e^+e^- \to \Upsilon(4S)$
• • • We do not use the following data for averages, fits, limits, etc. • • •					
<20	90	[3,4] NISHIDA	02	BELL	$e^+e^- \to \Upsilon(4S)$

[1] Requires $M_{K\pi\pi} < 1.8$ GeV/c^2.
[2] Uses B($\Upsilon(4S) \to B^+B^-$) = 0.513 ± 0.006.
[3] Assumes equal production of B^+ and B^0 at the $\Upsilon(4S)$.
[4] $M_{K\pi\pi} < 2.4$ GeV/c^2.

$\Gamma((K^+\pi^-)_{NR}\pi^+\gamma)/\Gamma_{total}$ — Γ_{544}/Γ

VALUE (units 10^{-6})	CL%	DOCUMENT ID		TECN	COMMENT
$9.9\pm0.7^{+1.5}_{-1.9}$		[1,2] DEL-AMO-SA...16		BABR	$e^+e^- \to \Upsilon(4S)$
• • • We do not use the following data for averages, fits, limits, etc. • • •					
<9.2	90	[3,4] NISHIDA	02	BELL	$e^+e^- \to \Upsilon(4S)$

[1] Requires $M_{K\pi\pi} < 1.8$ GeV/c^2.
[2] Uses B($\Upsilon(4S) \to B^+B^-$) = 0.513 ± 0.006.
[3] Assumes equal production of B^+ and B^0 at the $\Upsilon(4S)$.
[4] $M_{K\pi\pi} < 2.4$ GeV/c^2.

$\Gamma(K^0\pi^+\pi^0\gamma)/\Gamma_{total}$ — Γ_{545}/Γ

VALUE (units 10^{-5})	DOCUMENT ID		TECN	COMMENT
4.56±0.42±0.31	[1,2] AUBERT	07R	BABR	$e^+e^- \to \Upsilon(4S)$

[1] $M_{K\pi\pi} < 1.8$ GeV/c^2.
[2] Assumes equal production of B^+ and B^0 at the $\Upsilon(4S)$.

$\Gamma(K_1(1400)^+\gamma)/\Gamma_{total}$ — Γ_{546}/Γ

VALUE (units 10^{-6})	CL%	DOCUMENT ID		TECN	COMMENT
$9.7^{+4.6+2.9}_{-2.9-2.4}$		[1,2] DEL-AMO-SA...16		BABR	$e^+e^- \to \Upsilon(4S)$
• • • We do not use the following data for averages, fits, limits, etc. • • •					
< 15	90	[3] YANG	05	BELL	$e^+e^- \to \Upsilon(4S)$
< 50	90	[3] NISHIDA	02	BELL	Repl. by YANG 05
<2200	90	[4] ALBRECHT	89G	ARG	$e^+e^- \to \Upsilon(4S)$

[1] Requires $M_{K\pi\pi} < 1.8$ GeV/c^2.
[2] Uses B($\Upsilon(4S) \to B^+B^-$) = 0.513 ± 0.006.
[3] Assumes equal production of B^+ and B^0 at the $\Upsilon(4S)$.
[4] ALBRECHT 89G reports < 0.0020 assuming the $\Upsilon(4S)$ decays 45% to $B^0\overline{B}^0$. We rescale to 50%.

$\Gamma(K^*(1410)^+\gamma)/\Gamma_{total}$ — Γ_{547}/Γ

VALUE (units 10^{-5})	DOCUMENT ID		TECN	COMMENT
$2.71^{+0.54+0.59}_{-0.48-0.37}$	[1,2] DEL-AMO-SA...16		BABR	$e^+e^- \to \Upsilon(4S)$

[1] Requires $M_{K\pi\pi} < 1.8$ GeV/c^2.
[2] Uses B($\Upsilon(4S) \to B^+B^-$) = 0.513 ± 0.006.

$\Gamma(K_0^*(1430)^0\pi^+\gamma)/\Gamma_{total}$ — Γ_{548}/Γ

VALUE (units 10^{-6})	DOCUMENT ID		TECN	COMMENT
$1.32^{+0.09+0.24}_{-0.10-0.30}$	[1,2] DEL-AMO-SA...16		BABR	$e^+e^- \to \Upsilon(4S)$

[1] Requires $M_{K\pi\pi} < 1.8$ GeV/c^2.
[2] Uses B($\Upsilon(4S) \to B^+B^-$) = 0.513 ± 0.006.

$\Gamma(K_2^*(1430)^+\gamma)/\Gamma_{total}$ — Γ_{549}/Γ

VALUE (units 10^{-5})	CL%	DOCUMENT ID		TECN	COMMENT
1.4 ±0.4 OUR AVERAGE					
$0.87^{+0.70+0.87}_{-0.53-1.04}$		[1,2] DEL-AMO-SA...16		BABR	$e^+e^- \to \Upsilon(4S)$
$1.45\pm0.40\pm0.15$		[3] AUBERT,B	04U	BABR	$e^+e^- \to \Upsilon(4S)$
• • • We do not use the following data for averages, fits, limits, etc. • • •					
<140	90	[4] ALBRECHT	89G	ARG	$e^+e^- \to \Upsilon(4S)$

[1] Requires $M_{K\pi\pi} < 1.8$ GeV/c^2.
[2] Uses B($\Upsilon(4S) \to B^+B^-$) = 0.513 ± 0.006.
[3] Assumes equal production of B^+ and B^0 at the $\Upsilon(4S)$.
[4] ALBRECHT 89G reports < 0.0013 assuming the $\Upsilon(4S)$ decays 45% to $B^0\overline{B}^0$. We rescale to 50%.

$\Gamma(K^*(1680)^+\gamma)/\Gamma_{total}$ — Γ_{550}/Γ

VALUE (units 10^{-5})	CL%	DOCUMENT ID		TECN	COMMENT
$6.67^{+0.93+1.44}_{-0.78-1.14}$		[1,2] DEL-AMO-SA...16		BABR	$e^+e^- \to \Upsilon(4S)$
• • • We do not use the following data for averages, fits, limits, etc. • • •					
<190	90	[3] ALBRECHT	89G	ARG	$e^+e^- \to \Upsilon(4S)$

[1] Requires $M_{K\pi\pi} < 1.8$ GeV/c^2.
[2] Uses B($\Upsilon(4S) \to B^+B^-$) = 0.513 ± 0.006.
[3] ALBRECHT 89G reports < 0.0017 assuming the $\Upsilon(4S)$ decays 45% to $B^0\overline{B}^0$. We rescale to 50%.

$\Gamma(K_3^*(1780)^+\gamma)/\Gamma_{total}$ — Γ_{551}/Γ

VALUE (units 10^{-6})	CL%	DOCUMENT ID		TECN	COMMENT
< 39	90	[1,2] NISHIDA	05	BELL	$e^+e^- \to \Upsilon(4S)$
• • • We do not use the following data for averages, fits, limits, etc. • • •					
<5500	90	[3] ALBRECHT	89G	ARG	$e^+e^- \to \Upsilon(4S)$

[1] Assumes equal production of B^+ and B^0 at the $\Upsilon(4S)$.
[2] Uses B($K_3^*(1780) \to \eta K$) = $0.11^{+0.05}_{-0.04}$.
[3] ALBRECHT 89G reports < 0.005 assuming the $\Upsilon(4S)$ decays 45% to $B^0\overline{B}^0$. We rescale to 50%.

Int. J. Mod. Phys. A 2026.41. Downloaded from www.worldscientific.com
by [redacted]LIFORNIA @ BERKELEY on 09/16/26. Re-use and distribution is strictly not permitted, except for Open Access articles.

Int. J. Mod. Phys. A 2026.41. Downloaded from www.worldscientific.com
by UNIVERSITY OF CALIFORNIA @ BERKELEY on 09/16/26. Re-use and distribution is strictly not permitted, except for Open Access articles.

$\Gamma(K_4^*(2045)^+\gamma)/\Gamma_{total}$ — Γ_{552}/Γ

VALUE	CL%	DOCUMENT ID		TECN	COMMENT
<0.0099	90	[1] ALBRECHT	89G	ARG	$e^+e^- \to \Upsilon(4S)$

[1] ALBRECHT 89G reports < 0.0090 assuming the $\Upsilon(4S)$ decays 45% to $B^0\overline{B}^0$. We rescale to 50%.

$\Gamma(\rho^+\gamma)/\Gamma_{total}$ — Γ_{553}/Γ

VALUE (units 10^{-6})	CL%	DOCUMENT ID		TECN	COMMENT
1.16±0.17 OUR AVERAGE					
$1.31^{+0.20}_{-0.19}{}^{+0.13}_{-0.12}$		ADACHI	25G	BELL	$e^+e^- \to \Upsilon(4S)$
$1.20^{+0.42}_{-0.37}\pm0.20$		[1] AUBERT	08BH	BABR	$e^+e^- \to \Upsilon(4S)$
$0.87^{+0.29}_{-0.27}{}^{+0.09}_{-0.11}$		[1] TANIGUCHI	08	BELL	$e^+e^- \to \Upsilon(4S)$
• • • We do not use the following data for averages, fits, limits, etc. • • •					
$1.10^{+0.37}_{-0.33}\pm0.09$		[1] AUBERT	07L	BABR	Repl. by AUBERT 08BH
$0.55^{+0.42}_{-0.36}{}^{+0.09}_{-0.08}$		[1] MOHAPATRA	06	BELL	Repl. by TANIGUCHI 08
$0.9\ ^{+0.6}_{-0.5}\ \pm0.1$	90	[1] AUBERT	05	BABR	Repl. by AUBERT 07L
< 2.2	90	[1] MOHAPATRA	05	BELL	$e^+e^- \to \Upsilon(4S)$
< 2.1	90	[1] AUBERT	04C	BABR	$e^+e^- \to \Upsilon(4S)$
<13	90	[1,2] COAN	00	CLE2	$e^+e^- \to \Upsilon(4S)$

[1] Assumes equal production of B^+ and B^0 at $\Upsilon(4S)$.
[2] No evidence for a nonresonant $K\pi\gamma$ contamination was seen; the central value assumes no contamination.

$\Gamma(\pi^+\pi^0)/\Gamma_{total}$ — Γ_{554}/Γ

VALUE (units 10^{-6})	CL%	DOCUMENT ID		TECN	COMMENT
5.31±0.26 OUR AVERAGE					
5.10±0.29±0.27		ADACHI	24	BELL	$e^+e^- \to \Upsilon(4S)$
5.86±0.26±0.38		[1] DUH	13	BELL	$e^+e^- \to \Upsilon(4S)$
5.02±0.46±0.29		[1] AUBERT	07BC	BABR	$e^+e^- \to \Upsilon(4S)$
$4.6\ ^{+1.8}_{-1.6}\ ^{+0.6}_{-0.7}$		[1] BORNHEIM	03	CLE2	$e^+e^- \to \Upsilon(4S)$
• • • We do not use the following data for averages, fits, limits, etc. • • •					
$6.5\ \pm0.4\ \pm0.4$		[1] LIN	07A	BELL	Repl. by DUH 13
$5.8\ \pm0.6\ \pm0.4$		[1] AUBERT	05L	BABR	Repl. by AUBERT 07BC
$5.0\ \pm1.2\ \pm0.5$		[1] CHAO	04	BELL	Repl. by LIN 07A
$5.5\ ^{+1.0}_{-1.9}\ \pm0.6$		[1] AUBERT	03L	BABR	Repl. by AUBERT 05L
$7.4\ ^{+2.3}_{-2.2}\ \pm0.9$		[1] CASEY	02	BELL	Repl. by CHAO 04
< 13.4	90	[1] ABE	01H	BELL	$e^+e^- \to \Upsilon(4S)$
< 9.6	90	[1] AUBERT	01E	BABR	$e^+e^- \to \Upsilon(4S)$
< 12.7	90	[1] CRONIN-HEN..	00	CLE2	$e^+e^- \to \Upsilon(4S)$
< 20	90	GODANG	98	CLE2	Repl. by CRONIN-HENNESSY 00
< 17	90	ASNER	96	CLE2	Repl. by GODANG 98
< 240	90	[1] ALBRECHT	90B	ARG	$e^+e^- \to \Upsilon(4S)$
<2300	90	[2] BEBEK	87	CLEO	$e^+e^- \to \Upsilon(4S)$

[1] Assumes equal production of B^+ and B^0 at the $\Upsilon(4S)$.
[2] BEBEK 87 assume the $\Upsilon(4S)$ decays 43% to $B^0\overline{B}^0$.

$\Gamma(\pi^+\pi^0)/\Gamma(K^0\pi^+)$ — $\Gamma_{554}/\Gamma_{411}$

VALUE	DOCUMENT ID		TECN	COMMENT
0.285±0.02±0.02	LIN	07A	BELL	$e^+e^- \to \Upsilon(4S)$

$\Gamma(\pi^+\pi^+\pi^-)/\Gamma(K^+K^-K^+)$ — $\Gamma_{555}/\Gamma_{503}$

VALUE	DOCUMENT ID		TECN	COMMENT
0.488±0.005±0.009	AAIJ	20AJ	LHCB	pp at 7 and 8 TeV

$\Gamma(\pi^+\pi^+\pi^-)/\Gamma_{total}$ — Γ_{555}/Γ

VALUE (units 10^{-6})	CL%	DOCUMENT ID		TECN	COMMENT
$\mathbf{15.2\pm0.6^{+1.3}_{-1.2}}$		[1] AUBERT	09L	BABR	$e^+e^- \to \Upsilon(4S)$
• • • We do not use the following data for averages, fits, limits, etc. • • •					
16.2±1.2±0.9		[1] AUBERT,B	05G	BABR	Repl. by AUBERT 09L
10.9±3.3±1.6		[1] AUBERT	03M	BABR	Repl. by AUBERT 05G
<130	90	[2] ADAM	96D	DLPH	$e^+e^- \to Z$
<220	90	[3] ABREU	95N	DLPH	Sup. by ADAM 96D
<450	90	[4] ALBRECHT	90B	ARG	$e^+e^- \to \Upsilon(4S)$
<190	90	[5] BORTOLETTO	89	CLEO	$e^+e^- \to \Upsilon(4S)$

[1] Assumes equal production of B^0 and B^+ at the $\Upsilon(4S)$; charm and charmonium contributions are subtracted, otherwise no assumptions about intermediate resonances.
[2] ADAM 96D assumes $f_{B^0} = f_{B^-} = 0.39$ and $f_{B_s} = 0.12$.
[3] Assumes a B^0, B^- production fraction of 0.39 and a B_s production fraction of 0.12.
[4] ALBRECHT 90B limit assumes equal production of $B^0\overline{B}^0$ and B^+B^- at $\Upsilon(4S)$.
[5] BORTOLETTO 89 reports $< 1.7\times10^{-4}$ assuming the $\Upsilon(4S)$ decays 43% to $B^0\overline{B}^0$. We rescale to 50%.

$\Gamma(\rho^0\pi^+)/\Gamma_{total}$ — Γ_{556}/Γ

VALUE (units 10^{-6})	CL%	DOCUMENT ID		TECN	COMMENT
8.3±1.2 OUR AVERAGE					
$8.1\pm0.7^{+1.3}_{-1.6}$		[1] AUBERT	09L	BABR	$e^+e^- \to \Upsilon(4S)$
$8.0^{+2.3}_{-2.0}\pm0.7$		[1] GORDON	02	BELL	$e^+e^- \to \Upsilon(4S)$
$10.4^{+3.3}_{-3.4}\pm2.1$		[1] JESSOP	00	CLE2	$e^+e^- \to \Upsilon(4S)$
• • • We do not use the following data for averages, fits, limits, etc. • • •					
$8.8\pm1.0^{+0.6}_{-0.9}$		[1] AUBERT,B	05G	BABR	Repl. by AUBERT 09L
9.5±1.1±0.9		[1] AUBERT	04Z	BABR	Repl. by AUBERT 05G
< 83	90	[2] ABE	00C	SLD	$e^+e^- \to Z$
<160	90	[3] ADAM	96D	DLPH	$e^+e^- \to Z$
< 43	90	ASNER	96	CLE2	Repl. by JESSOP 00
<260	90	[4] ABREU	95N	DLPH	Sup. by ADAM 96D
<150	90	[1] ALBRECHT	90B	ARG	$e^+e^- \to \Upsilon(4S)$
<170	90	[5] BORTOLETTO	89	CLEO	$e^+e^- \to \Upsilon(4S)$
<230	90	[5] BEBEK	87	CLEO	$e^+e^- \to \Upsilon(4S)$
<600	90	GILES	84	CLEO	Repl. by BEBEK 87

[1] Assumes equal production of B^+ and B^0 at the $\Upsilon(4S)$.
[2] ABE 00C assumes $B(Z \to b\overline{b})=(21.7\pm0.1)\%$ and the B fractions $f_{B^0}=f_{B^+}=(39.7^{+1.8}_{-2.2})\%$ and $f_{B_s}=(10.5^{+1.8}_{-2.2})\%$.
[3] ADAM 96D assumes $f_{B^0} = f_{B^-} = 0.39$ and $f_{B_s} = 0.12$.
[4] Assumes a B^0, B^- production fraction of 0.39 and a B_s production fraction of 0.12.
[5] Papers assume the $\Upsilon(4S)$ decays 43% to $B^0\overline{B}^0$. We rescale to 50%.

$[\Gamma(K^*(892)^0\pi^+) + \Gamma(\rho^0\pi^+)]/\Gamma_{total}$ — $(\Gamma_{448}+\Gamma_{556})/\Gamma$

VALUE (units 10^{-6})	DOCUMENT ID		TECN	COMMENT
$\mathbf{170^{+120}_{-80}\pm20}$	[1] ADAM	96D	DLPH	$e^+e^- \to Z$

[1] ADAM 96D assumes $f_{B^0} = f_{B^-} = 0.39$ and $f_{B_s} = 0.12$.

$\Gamma(\pi^+ f_0(980),\ f_0 \to \pi^+\pi^-)/\Gamma_{total}$ — Γ_{557}/Γ

VALUE (units 10^{-6})	CL%	DOCUMENT ID		TECN	COMMENT
< 1.5	90	[1] AUBERT	09L	BABR	$e^+e^- \to \Upsilon(4S)$
• • • We do not use the following data for averages, fits, limits, etc. • • •					
< 3.0	90	[1] AUBERT,B	05G	BABR	Repl. by AUBERT 09L
<140	90	[2] BORTOLETTO	89	CLEO	$e^+e^- \to \Upsilon(4S)$

[1] Assumes equal production of B^+ and B^0 at the $\Upsilon(4S)$.
[2] BORTOLETTO 89 reports $< 1.2\times10^{-4}$ assuming the $\Upsilon(4S)$ decays 43% to $B^0\overline{B}^0$. We rescale to 50%.

$\Gamma(\pi^+ f_2(1270))/\Gamma_{total}$ — Γ_{558}/Γ

VALUE (units 10^{-6})	CL%	DOCUMENT ID		TECN	COMMENT
$2.2\ ^{+0.7}_{-0.4}$ OUR AVERAGE					
$17.0\ \pm2.4\ \pm2.1$		[1] AAIJ	19AL	LHCB	pp at 7, 8 TeV
$1.60^{+0.67}_{-0.44}{}^{+0.02}_{-0.05}$		[2,3] AUBERT	09L	BABR	$e^+e^- \to \Upsilon(4S)$
• • • We do not use the following data for averages, fits, limits, etc. • • •					
$4.09\pm1.28^{+0.05}_{-0.14}$		[3,4] AUBERT,B	05G	BABR	Repl. by AUBERT 09L
<240	90	[5] BORTOLETTO	89	CLEO	$e^+e^- \to \Upsilon(4S)$

[1] AAIJ 19AL reports 0.075 ± 0.008 ± 0.007 fit fraction for $B^+ \to f_2(1270)\pi^+$ from the amplitude analysis of $B^\pm \to \pi^\pm K^+K^-$ decays. We use the PDG 19 value $B(B^+ \to K^+K^-\pi^+) = (5.2\pm0.4)\times10^{-6}$ to obtain $B(B^+ \to f_2(1270)\pi^+,\ f_2(1270) \to K^+K^-)$. We compute $B(B^+ \to f_2(1270)\pi^+)$ using 1/2 of PDG 19 value of $B(f_2(1270) \to K\overline{K}) = (4.6^{+0.5}_{-0.4})\%$ for K^+K^- fraction. Our first error is the experiment's error and the second error is systematic error from using our best value.
[2] AUBERT 09L reports $[\Gamma(B^+ \to \pi^+ f_2(1270))/\Gamma_{total}] \times [B(f_2(1270) \to \pi^+\pi^-)] = (0.9\pm0.2\pm0.1^{+0.3}_{-0.1})\times10^{-6}$ which we divide by our best (shown rounded) value $B(f_2(1270) \to \pi^+\pi^-) = (56.2^{+1.9}_{-0.6})\times10^{-2}$. Our first error is their experiment's error and our second error is the systematic error from using our best (shown rounded) value.
[3] Assumes equal production of B^+ and B^0 at the $\Upsilon(4S)$.
[4] AUBERT,B 05G reports $[\Gamma(B^+ \to \pi^+ f_2(1270))/\Gamma_{total}] \times [B(f_2(1270) \to \pi^+\pi^-)] = (2.3\pm0.6\pm0.4)\times10^{-6}$ which we divide by our best (shown rounded) value $B(f_2(1270) \to \pi^+\pi^-) = (56.2^{+1.9}_{-0.6})\times10^{-2}$. Our first error is their experiment's error and our second error is the systematic error from using our best (shown rounded) value.
[5] BORTOLETTO 89 reports $< 2.1\times10^{-4}$ assuming the $\Upsilon(4S)$ decays 43% to $B^0\overline{B}^0$. We rescale to 50%.

$\Gamma(\rho(1450)^0\pi^+,\ \rho^0 \to \pi^+\pi^-)/\Gamma_{total}$ — Γ_{559}/Γ

VALUE (units 10^{-6})	CL%	DOCUMENT ID		TECN	COMMENT
$\mathbf{1.4\pm0.4^{+0.5}_{-0.8}}$		[1] AUBERT	09L	BABR	$e^+e^- \to \Upsilon(4S)$
• • • We do not use the following data for averages, fits, limits, etc. • • •					
<2.3	90	[1] AUBERT,B	05G	BABR	Repl. by AUBERT 09L

[1] Assumes equal production of B^+ and B^0 at the $\Upsilon(4S)$.

$\Gamma(f_0(1370)\pi^+,\ f_0 \to \pi^+\pi^-)/\Gamma_{total}$ — Γ_{561}/Γ

VALUE (units 10^{-6})	CL%	DOCUMENT ID		TECN	COMMENT
<4.0	90	[1] AUBERT	09L	BABR	$e^+e^- \to \Upsilon(4S)$
• • • We do not use the following data for averages, fits, limits, etc. • • •					
<3.0	90	[1] AUBERT,B	05G	BABR	Repl. by AUBERT 09L

[1] Assumes equal production of B^+ and B^0 at the $\Upsilon(4S)$.

Int. J. Mod. Phys. A 2026.41. Downloaded from www.worldscientific.com by LIFORNIA @ BERKELEY on 09/16/26. Re-use and distribution is strictly not permitted, except for Open Access articles.

$\Gamma(f_0(1370)\pi^+,\ f_0 \to \pi^0\pi^0)/\Gamma_{total}$ — Γ_{562}/Γ

VALUE	CL%	DOCUMENT ID		TECN	COMMENT
$<1.1 \times 10^{-6}$	90	LAI	23	BELL	$e^+e^- \to \Upsilon(4S)$

$\Gamma(f_0(500)\pi^+,\ f_0 \to \pi^+\pi^-)/\Gamma_{total}$ — Γ_{563}/Γ

VALUE (units 10^{-6})	CL%	DOCUMENT ID		TECN	COMMENT
<4.1	90	[1] AUBERT,B	05G	BABR	$e^+e^- \to \Upsilon(4S)$

[1] Assumes equal production of B^+ and B^0 at the $\Upsilon(4S)$.

$\Gamma(\pi^+\pi^-\pi^+ \text{nonresonant})/\Gamma_{total}$ — Γ_{564}/Γ

VALUE (units 10^{-6})	CL%	DOCUMENT ID		TECN	COMMENT
$5.3 \pm 0.7^{+1.3}_{-0.8}$		[1] AUBERT	09L	BABR	$e^+e^- \to \Upsilon(4S)$
• • • We do not use the following data for averages, fits, limits, etc. • • •					
<4.6	90	[1] AUBERT,B	05G	BABR	Repl. by AUBERT 09L
<41	90	BERGFELD	96B	CLE2	$e^+e^- \to \Upsilon(4S)$

[1] Assumes equal production of B^+ and B^0 at the $\Upsilon(4S)$.

$\Gamma(\pi^+\pi^0\pi^0)/\Gamma_{total}$ — Γ_{565}/Γ

VALUE (units 10^{-5})	CL%	DOCUMENT ID		TECN	COMMENT
$1.90 \pm 0.15 \pm 0.14$		LAI	23	BELL	$e^+e^- \to \Upsilon(4S)$
• • • We do not use the following data for averages, fits, limits, etc. • • •					
<89	90	[1] ALBRECHT	90B	ARG	$e^+e^- \to \Upsilon(4S)$

[1] ALBRECHT 90B limit assumes equal production of $B^0\overline{B}^0$ and B^+B^- at $\Upsilon(4S)$.

$\Gamma(\rho^+\pi^0)/\Gamma_{total}$ — Γ_{566}/Γ

VALUE (units 10^{-5})	CL%	DOCUMENT ID		TECN	COMMENT
$1.06^{+0.12}_{-0.13}$ OUR AVERAGE					
$1.12 \pm 0.11^{+0.12}_{-0.18}$		[1] LAI	23	BELL	$e^+e^- \to \Upsilon(4S)$
$1.02 \pm 0.14 \pm 0.09$		[2] AUBERT	07X	BABR	$e^+e^- \to \Upsilon(4S)$
• • • We do not use the following data for averages, fits, limits, etc. • • •					
$1.32 \pm 0.23^{+0.14}_{-0.19}$		[2] ZHANG	05A	BELL	Repl. by LAI 23
$1.09 \pm 0.19 \pm 0.19$		[2] AUBERT	04Z	BABR	Repl. by AUBERT 07X
<4.3	90	[2,3] JESSOP	00	CLE2	$e^+e^- \to \Upsilon(4S)$
<7.7	90	ASNER	96	CLE2	Repl. by JESSOP 00
<55	90	[2] ALBRECHT	90B	ARG	$e^+e^- \to \Upsilon(4S)$

[1] The second uncertainty includes both systematics ($(\pm 0.09) \times 10^{-5}$) and possible interference with $B^+ \to \rho(1450)^+\pi^0$ ($(^{+0.08}_{-0.16}) \times 10^{-5}$).
[2] Assumes equal production of B^+ and B^0 at the $\Upsilon(4S)$.
[3] Assumes no nonresonant contributions of $B^+ \to \pi^+\pi^0\pi^0$.

$\Gamma(\rho(1450)^+\pi^0,\ \rho^+ \to \pi^+\pi^0)/\Gamma_{total}$ — Γ_{567}/Γ

VALUE (units 10^{-6})	DOCUMENT ID		TECN	COMMENT
$1.2 \pm 0.6 \pm 0.2$	LAI	23	BELL	$e^+e^- \to \Upsilon(4S)$

$\Gamma(\pi^+\pi^0\pi^0 \text{nonresonant})/\Gamma_{total}$ — Γ_{568}/Γ

VALUE	CL%	DOCUMENT ID		TECN	COMMENT
$<6 \times 10^{-7}$	90	LAI	23	BELL	$e^+e^- \to \Upsilon(4S)$

$\Gamma(X pi+, X \to \pi^0\pi^0)/\Gamma_{total}$ — Γ_{569}/Γ

VALUE (units 10^{-6})	DOCUMENT ID		TECN	COMMENT
$6.9 \pm 0.9 \pm 0.6$	LAI	23	BELL	$e^+e^- \to \Upsilon(4S)$

$\Gamma(\pi^+\pi^-\pi^+\pi^0)/\Gamma_{total}$ — Γ_{570}/Γ

VALUE	CL%	DOCUMENT ID		TECN	COMMENT
$<4.0 \times 10^{-3}$	90	[1] ALBRECHT	90B	ARG	$e^+e^- \to \Upsilon(4S)$

[1] ALBRECHT 90B limit assumes equal production of $B^0\overline{B}^0$ and B^+B^- at $\Upsilon(4S)$.

$\Gamma(\rho^+\rho^0)/\Gamma_{total}$ — Γ_{571}/Γ

VALUE (units 10^{-6})	CL%	DOCUMENT ID		TECN	COMMENT
24.0 ± 1.9 OUR AVERAGE					
$23.7 \pm 1.4 \pm 1.4$		[1] AUBERT	09G	BABR	$e^+e^- \to \Upsilon(4S)$
$31.7 \pm 7.1^{+3.8}_{-6.7}$		[1,2] ZHANG	03B	BELL	$e^+e^- \to \Upsilon(4S)$
• • • We do not use the following data for averages, fits, limits, etc. • • •					
$16.8 \pm 2.2 \pm 2.3$		[1] AUBERT,BE	06G	BABR	Repl. by AUBERT 09G
$22.5^{+5.7}_{-5.4} \pm 5.8$		[1] AUBERT	03V	BABR	Repl. by AUBERT,BE 06G
<1000	90	[1] ALBRECHT	90B	ARG	$e^+e^- \to \Upsilon(4S)$

[1] Assumes equal production of B^+ and B^0 at the $\Upsilon(4S)$.
[2] The systematic error includes the error associated with the helicity-mix uncertainty.

$\Gamma(\rho^+ f_0(980),\ f_0 \to \pi^+\pi^-)/\Gamma_{total}$ — Γ_{572}/Γ

VALUE (units 10^{-6})	CL%	DOCUMENT ID		TECN	COMMENT
<2.0	90	[1] AUBERT	09G	BABR	$e^+e^- \to \Upsilon(4S)$
• • • We do not use the following data for averages, fits, limits, etc. • • •					
<1.9	90	[1] AUBERT,BE	06G	BABR	Repl. by AUBERT 09G

[1] Assumes equal production of B^+ and B^0 at the $\Upsilon(4S)$.

$\Gamma(a_1(1260)^+\pi^0)/\Gamma_{total}$ — Γ_{573}/Γ

VALUE (units 10^{-6})	CL%	DOCUMENT ID		TECN	COMMENT
$26.4 \pm 5.4 \pm 4.1$		[1,2] AUBERT	07BL	BABR	$e^+e^- \to \Upsilon(4S)$
• • • We do not use the following data for averages, fits, limits, etc. • • •					
<1700	90	[1] ALBRECHT	90B	ARG	$e^+e^- \to \Upsilon(4S)$

[1] Assumes equal production of B^+ and B^0 at the $\Upsilon(4S)$.
[2] Assumes a_1^+ decays only to 3π and $B(a_1^+ \to \pi^\pm\pi^\mp\pi^+) = 0.5$.

$\Gamma(a_1(1260)^0\pi^+)/\Gamma_{total}$ — Γ_{574}/Γ

VALUE (units 10^{-6})	CL%	DOCUMENT ID		TECN	COMMENT
$20.4 \pm 4.7 \pm 3.4$		[1,2] AUBERT	07BL	BABR	$e^+e^- \to \Upsilon(4S)$
• • • We do not use the following data for averages, fits, limits, etc. • • •					
<900	90	[1] ALBRECHT	90B	ARG	$e^+e^- \to \Upsilon(4S)$

[1] Assumes equal production of B^+ and B^0 at the $\Upsilon(4S)$.
[2] Assumes a_1^0 decays only to 3π and $B(a_1^+ \to \pi^\pm\pi^\mp\pi^0) = 1.0$.

$\Gamma(\omega\pi^+)/\Gamma_{total}$ — Γ_{575}/Γ

VALUE (units 10^{-6})	CL%	DOCUMENT ID		TECN	COMMENT
6.9 ± 0.5 OUR AVERAGE					
$6.7 \pm 0.5 \pm 0.4$		[1] AUBERT	07AE	BABR	$e^+e^- \to \Upsilon(4S)$
$6.9 \pm 0.6 \pm 0.5$		[1] JEN	06	BELL	$e^+e^- \to \Upsilon(4S)$
$11.3^{+3.3}_{-2.9} \pm 1.4$		[1] JESSOP	00	CLE2	$e^+e^- \to \Upsilon(4S)$
• • • We do not use the following data for averages, fits, limits, etc. • • •					
$6.1 \pm 0.7 \pm 0.4$		[1] AUBERT,B	06E	BABR	Repl. by AUBERT 07AE
$5.5 \pm 0.9 \pm 0.5$		[1] AUBERT	04H	BABR	Repl. by AUBERT,B 06E
$5.7^{+1.4}_{-1.3} \pm 0.6$		[1] WANG	04A	BELL	Repl. by JEN 06
$4.2^{+2.0}_{-1.8} \pm 0.5$		[1] LU	02	BELL	Repl. by WANG 04A
$6.6^{+2.1}_{-1.8} \pm 0.7$		[1] AUBERT	01G	BABR	Repl. by AUBERT 04H
<23	90	[1] BERGFELD	98	CLE2	Repl. by JESSOP 00
<400	90	[1] ALBRECHT	90B	ARG	$e^+e^- \to \Upsilon(4S)$

[1] Assumes equal production of B^+ and B^0 at the $\Upsilon(4S)$.

$\Gamma(\omega\rho^+)/\Gamma_{total}$ — Γ_{576}/Γ

VALUE (units 10^{-6})	CL%	DOCUMENT ID		TECN	COMMENT
$15.9 \pm 1.6 \pm 1.4$		[1] AUBERT	09H	BABR	$e^+e^- \to \Upsilon(4S)$
• • • We do not use the following data for averages, fits, limits, etc. • • •					
$10.6 \pm 2.1^{+1.6}_{-1.0}$		[1] AUBERT,B	06T	BABR	Repl. by AUBERT 09H
$12.6^{+3.7}_{-3.3} \pm 1.6$		[1] AUBERT	05O	BABR	Repl. by AUBERT,B 06T
<61	90	[1] BERGFELD	98	CLE2	

[1] Assumes equal production of B^+ and B^0 at the $\Upsilon(4S)$.

$\Gamma(\eta\pi^+)/\Gamma_{total}$ — Γ_{577}/Γ

VALUE (units 10^{-6})	CL%	DOCUMENT ID		TECN	COMMENT
4.02 ± 0.27 OUR AVERAGE					
$4.07 \pm 0.26 \pm 0.21$		[1] HOI	12	BELL	$e^+e^- \to \Upsilon(4S)$
$4.00 \pm 0.40 \pm 0.24$		[1] AUBERT	09AV	BABR	$e^+e^- \to \Upsilon(4S)$
$1.2\ ^{+2.8}_{-1.2}$		[1] RICHICHI	00	CLE2	$e^+e^- \to \Upsilon(4S)$
• • • We do not use the following data for averages, fits, limits, etc. • • •					
$5.0\ \pm 0.5\ \pm 0.3$		[1] AUBERT	07AE	BABR	Repl. by AUBERT 09AV
$4.2\ \pm 0.4\ \pm 0.2$		[1] CHANG	07B	BELL	Repl. by HOI 12
$5.1\ \pm 0.6\ \pm 0.3$		[1] AUBERT,B	05K	BABR	Repl. by AUBERT 07AE
$4.8\ \pm 0.7\ \pm 0.3$		[1] CHANG	05A	BELL	Repl. by CHANG 07B
$5.3\ \pm 1.0\ \pm 0.3$		[1] AUBERT	04H	BABR	Repl. by AUBERT,B 05K
<15	90	BEHRENS	98	CLE2	Repl. by RICHICHI 00
<700	90	[1] ALBRECHT	90B	ARG	$e^+e^- \to \Upsilon(4S)$

[1] Assumes equal production of B^+ and B^0 at the $\Upsilon(4S)$.

$\Gamma(\eta\rho^+)/\Gamma_{total}$ — Γ_{578}/Γ

VALUE (units 10^{-6})	CL%	DOCUMENT ID		TECN	COMMENT
7.0 ± 2.9 OUR AVERAGE Error includes scale factor of 2.8.					
$9.9 \pm 1.2 \pm 0.8$		[1] AUBERT	08AH	BABR	$e^+e^- \to \Upsilon(4S)$
$4.1^{+1.4}_{-1.3} \pm 0.4$		[1] WANG	07B	BELL	$e^+e^- \to \Upsilon(4S)$
• • • We do not use the following data for averages, fits, limits, etc. • • •					
$8.4 \pm 1.9 \pm 1.1$		[1] AUBERT,B	05K	BABR	Repl. by AUBERT 08AH
<14	90	[1] AUBERT,B	04D	BABR	Repl. by AUBERT,B 05K
<15	90	[1] RICHICHI	00	CLE2	$e^+e^- \to \Upsilon(4S)$
<32	90	BEHRENS	98	CLE2	Repl. by RICHICHI 00

[1] Assumes equal production of B^+ and B^0 at the $\Upsilon(4S)$.

$\Gamma(\eta'\pi^+)/\Gamma_{total}$ — Γ_{579}/Γ

VALUE (units 10^{-6})	CL%	DOCUMENT ID		TECN	COMMENT
$2.7\ \pm 0.9$ OUR AVERAGE Error includes scale factor of 1.9.					
$3.5\ \pm 0.6\ \pm 0.2$		[1] AUBERT	09AV	BABR	$e^+e^- \to \Upsilon(4S)$
$1.76^{+0.67}_{-0.62}{}^{+0.15}_{-0.14}$		[1] SCHUEMANN	06	BELL	$e^+e^- \to \Upsilon(4S)$

Int. J. Mod. Phys. A 2026.41. Downloaded from www.worldscientific.com
by UNIVERSITY OF CALIFORNIA @ BERKELEY on 09/16/26. Re-use and distribution is strictly not permitted, except for Open Access articles.

• • • We do not use the following data for averages, fits, limits, etc. • • •

3.9 ±0.7 ±0.3		[1] AUBERT	07AE	BABR	Repl. by AUBERT 09AV
4.0 ±0.8 ±0.4		[1] AUBERT,B	05K	BABR	Repl. by AUBERT 07AE
< 4.5	90	[1] AUBERT	04H	BABR	Repl. by AUBERT,B 05K
< 7.0	90	[1] ABE	01M	BELL	$e^+e^- \to \Upsilon(4S)$
<12	90	[1] AUBERT	01G	BABR	$e^+e^- \to \Upsilon(4S)$
<12	90	[1] RICHICHI	00	CLE2	$e^+e^- \to \Upsilon(4S)$
<31	90	BEHRENS	98	CLE2	Repl. by RICHICHI 00

[1] Assumes equal production of B^+ and B^0 at the $\Upsilon(4S)$.

$\Gamma(\eta'\rho^+)/\Gamma_{total}$ — Γ_{580}/Γ

VALUE (units 10^{-6})	CL%	DOCUMENT ID		TECN	COMMENT
$9.7^{+1.9}_{-1.8}\pm1.1$		[1] DEL-AMO-SA...10A		BABR	$e^+e^- \to \Upsilon(4S)$

• • • We do not use the following data for averages, fits, limits, etc. • • •

$8.7^{+3.1+2.3}_{-2.8-1.3}$		[1] AUBERT	07E	BABR	Repl. by DEL-AMO-SANCHEZ 10A
< 5.8	90	[1] SCHUEMANN	07	BELL	$e^+e^- \to \Upsilon(4S)$
<22	90	[1] AUBERT,B	04D	BABR	Repl. by AUBERT 07E
<33	90	[1] RICHICHI	00	CLE2	$e^+e^- \to \Upsilon(4S)$
<47	90	BEHRENS	98	CLE2	Repl. by RICHICHI 00

[1] Assumes equal production of B^+ and B^0 at the $\Upsilon(4S)$.

$\Gamma(\phi\pi^+)/\Gamma_{total}$ — Γ_{581}/Γ

VALUE (units 10^{-8})	CL%	DOCUMENT ID		TECN	COMMENT
$3.2\pm1.5\pm0.3$		[1] AAIJ	19AL	LHCB	pp at 7, 8 TeV

• • • We do not use the following data for averages, fits, limits, etc. • • •

< 15	90	[2] AAIJ	14A	LHCB	Repl. by AAIJ 19AL
< 33	90	[3] KIM	12A	BELL	$e^+e^- \to \Upsilon(4S)$
< 24	90	[3] AUBERT,B	06C	BABR	$e^+e^- \to \Upsilon(4S)$
< 41	90	[3] AUBERT	04A	BABR	Repl. by AUBERT,B 06C
< 140	90	[3] AUBERT	01D	BABR	$e^+e^- \to \Upsilon(4S)$
<15300	90	[4] ABE	00C	SLD	$e^+e^- \to Z$
< 500	90	[3] BERGFELD	98	CLE2	

[1] AAIJ 19AL reports $(0.3\pm0.1\pm0.1)\times10^{-2}$ fit fraction for $B^+ \to \phi(1020)\pi^+$ from the amplitude analysis of $B^\pm \to \pi^\pm K^+K^-$ decays. We use the PDG 19 value $B(B^+ \to K^+K^-\pi^+) = (5.2\pm0.4)\times10^{-6}$ to obtain $B(B^+ \to \phi(1020)\pi^+,\ \phi(1020) \to K^+K^-)$. We compute $B(B^+ \to \phi(1020)\pi^+)$ using the PDG 19 value of $B(\phi(1020) \to K^+K^-) = (49.2\pm0.5)\%$. Our first error is the experiment's error and the second error is systematic error from using our best value.

[2] Measures $B(B^+ \to \phi\pi^+)/B(B^+ \to \phi K^+) < 0.018$ at 90% C.L. and assumes $B(B^+ \to \phi K^+) = (8.8^{+0.7}_{-0.6})\times10^{-6}$.

[3] Assumes equal production of B^+ and B^0 at the $\Upsilon(4S)$.

[4] ABE 00C assumes $B(Z \to b\overline{b}) = (21.7\pm0.1)\%$ and the B fractions $f_{B^0} = f_{B^+} = (39.7^{+1.8}_{-2.2})\%$ and $f_{B_s} = (10.5^{+1.8}_{-2.2})\%$.

$\Gamma(\phi\rho^+)/\Gamma_{total}$ — Γ_{582}/Γ

VALUE (units 10^{-6})	CL%	DOCUMENT ID		TECN	COMMENT
< 3.0	90	[1] AUBERT	08BK	BABR	$e^+e^- \to \Upsilon(4S)$

• • • We do not use the following data for averages, fits, limits, etc. • • •

<16		[1] BERGFELD	98	CLE2	

[1] Assumes equal production of B^+ and B^0 at the $\Upsilon(4S)$.

$\Gamma(a_0(980)^0\pi^+,\ a_0^0 \to \eta\pi^0)/\Gamma_{total}$ — Γ_{583}/Γ

VALUE (units 10^{-6})	CL%	DOCUMENT ID		TECN	COMMENT
<5.8	90	[1] AUBERT,BE	04	BABR	$e^+e^- \to \Upsilon(4S)$

[1] Assumes equal production of charged and neutral B mesons from $\Upsilon(4S)$ decays.

$\Gamma(a_0(980)^+\pi^0,\ a_0^+ \to \eta\pi^+)/\Gamma_{total}$ — Γ_{584}/Γ

VALUE (units 10^{-6})	CL%	DOCUMENT ID		TECN	COMMENT
<1.4	90	[1] AUBERT	08A	BABR	$e^+e^- \to \Upsilon(4S)$

[1] Assumes equal production of B^+ and B^0 at the $\Upsilon(4S)$.

$\Gamma(\pi^+\pi^+\pi^+\pi^-\pi^-)/\Gamma_{total}$ — Γ_{585}/Γ

VALUE	CL%	DOCUMENT ID		TECN	COMMENT
$<8.6\times10^{-4}$	90	[1] ALBRECHT	90B	ARG	$e^+e^- \to \Upsilon(4S)$

[1] ALBRECHT 90B limit assumes equal production of $B^0\overline{B}^0$ and B^+B^- at $\Upsilon(4S)$.

$\Gamma(\rho^0 a_1(1260)^+)/\Gamma_{total}$ — Γ_{586}/Γ

VALUE	CL%	DOCUMENT ID		TECN	COMMENT
$<6.2\times10^{-4}$	90	[1] BORTOLETTO	89	CLEO	$e^+e^- \to \Upsilon(4S)$

• • • We do not use the following data for averages, fits, limits, etc. • • •

$<6.0\times10^{-4}$	90	[2] ALBRECHT	90B	ARG	$e^+e^- \to \Upsilon(4S)$
$<3.2\times10^{-3}$	90	[1] BEBEK	87	CLEO	$e^+e^- \to \Upsilon(4S)$

[1] BORTOLETTO 89 reports $< 5.4\times10^{-4}$ assuming the $\Upsilon(4S)$ decays 43% to $B^0\overline{B}^0$. We rescale to 50%.

[2] ALBRECHT 90B limit assumes equal production of $B^0\overline{B}^0$ and B^+B^- at $\Upsilon(4S)$.

$\Gamma(\rho^0 a_2(1320)^+)/\Gamma_{total}$ — Γ_{587}/Γ

VALUE	CL%	DOCUMENT ID		TECN	COMMENT
$<7.2\times10^{-4}$	90	[1] BORTOLETTO	89	CLEO	$e^+e^- \to \Upsilon(4S)$

• • • We do not use the following data for averages, fits, limits, etc. • • •

$<2.6\times10^{-3}$	90	[2] BEBEK	87	CLEO	$e^+e^- \to \Upsilon(4S)$

[1] BORTOLETTO 89 reports $< 6.3\times10^{-4}$ assuming the $\Upsilon(4S)$ decays 43% to $B^0\overline{B}^0$. We rescale to 50%.

[2] BEBEK 87reports $< 2.3\times10^{-3}$ assuming the $\Upsilon(4S)$ decays 43% to $B^0\overline{B}^0$. We rescale to 50%.

$\Gamma(b_1^0\pi^+,\ b_1^0 \to \omega\pi^0)/\Gamma_{total}$ — Γ_{588}/Γ

VALUE (units 10^{-6})	DOCUMENT ID		TECN	COMMENT
$6.7\pm1.7\pm1.0$	[1] AUBERT	07BI	BABR	$e^+e^- \to \Upsilon(4S)$

[1] Assumes equal production of B^+ and B^0 at the $\Upsilon(4S)$.

$\Gamma(b_1^+\pi^0,\ b_1^+ \to \omega\pi^+)/\Gamma_{total}$ — Γ_{589}/Γ

VALUE (units 10^{-6})	CL%	DOCUMENT ID		TECN	COMMENT
<3.3	90	[1] AUBERT	08AG	BABR	$e^+e^- \to \Upsilon(4S)$

[1] Assumes equal production of B^+ and B^0 at the $\Upsilon(4S)$.

$\Gamma(\pi^+\pi^+\pi^+\pi^-\pi^-\pi^0)/\Gamma_{total}$ — Γ_{590}/Γ

VALUE	CL%	DOCUMENT ID		TECN	COMMENT
$<6.3\times10^{-3}$	90	[1] ALBRECHT	90B	ARG	$e^+e^- \to \Upsilon(4S)$

[1] ALBRECHT 90B limit assumes equal production of $B^0\overline{B}^0$ and B^+B^- at $\Upsilon(4S)$.

$\Gamma(b_1^+\rho^0,\ b_1^+ \to \omega\pi^+)/\Gamma_{total}$ — Γ_{591}/Γ

VALUE	CL%	DOCUMENT ID		TECN	COMMENT
$<5.2\times10^{-6}$	90	[1] AUBERT	09AF	BABR	$e^+e^- \to \Upsilon(4S)$

[1] Assumes equal production of B^+ and B^0 at the $\Upsilon(4S)$.

$\Gamma(b_1^0\rho^+,\ b_1^0 \to \omega\pi^0)/\Gamma_{total}$ — Γ_{593}/Γ

VALUE	CL%	DOCUMENT ID		TECN	COMMENT
$<3.3\times10^{-6}$	90	[1] AUBERT	09AF	BABR	$e^+e^- \to \Upsilon(4S)$

[1] Assumes equal production of B^+ and B^0 at the $\Upsilon(4S)$.

$\Gamma(a_1(1260)^+ a_1(1260)^0)/\Gamma_{total}$ — Γ_{592}/Γ

VALUE	CL%	DOCUMENT ID		TECN	COMMENT
$<1.3\times10^{-2}$	90	[1] ALBRECHT	90B	ARG	$e^+e^- \to \Upsilon(4S)$

[1] ALBRECHT 90B limit assumes equal production of $B^0\overline{B}^0$ and B^+B^- at $\Upsilon(4S)$.

$\Gamma(h^+\pi^0)/\Gamma_{total}$ — Γ_{594}/Γ

$h^+ = K^+$ or π^+

VALUE (units 10^{-6})	DOCUMENT ID		TECN	COMMENT
$16^{+6}_{-5}\pm3.6$	GODANG	98	CLE2	$e^+e^- \to \Upsilon(4S)$

$\Gamma(\omega h^+)/\Gamma_{total}$ — Γ_{595}/Γ

$h^+ = K^+$ or π^+

VALUE (units 10^{-6})	DOCUMENT ID		TECN	COMMENT
$13.8^{+2.7}_{-2.4}$ OUR AVERAGE				
$13.4^{+3.3}_{-2.9}\pm1.1$	[1] LU	02	BELL	$e^+e^- \to \Upsilon(4S)$
$14.3^{+3.6}_{-3.2}\pm2.0$	[1] JESSOP	00	CLE2	$e^+e^- \to \Upsilon(4S)$

• • • We do not use the following data for averages, fits, limits, etc. • • •

$25\ ^{+8}_{-7}\ \pm3$	[1] BERGFELD	98	CLE2	Repl. by JESSOP 00

[1] Assumes equal production of B^+ and B^0 at the $\Upsilon(4S)$.

$\Gamma(h^+X^0(\text{Familon}))/\Gamma_{total}$ — Γ_{596}/Γ

VALUE (units 10^{-6})	CL%	DOCUMENT ID		TECN	COMMENT
<49	90	[1] AMMAR	01B	CLE2	$e^+e^- \to \Upsilon(4S)$

[1] AMMAR 01B searched for the two-body decay of the B meson to a massless neutral feebly-interacting particle X^0 such as the familon, the Nambu-Goldstone boson associated with a spontaneously broken global family symmetry.

$\Gamma(K^+X^0,\ X^0 \to \mu^+\mu^-)/\Gamma_{total}$ — Γ_{597}/Γ

X^0 stands here for a long-lived scalar particle.

VALUE	CL%	DOCUMENT ID		TECN	COMMENT
$<1\times10^{-7}$	95	[1] AAIJ	17AQ	LHCB	pp at 7, 8 TeV

[1] AAIJ 17AQ searched for a long-lived scalar particle $X^0 \to \mu^+\mu^-$ in the mass range 250–4700 MeV and lifetime range 0.1–1000 ps. The limit is between 10^{-7} and 2×10^{-10} in these ranges except in vetoed mass regions around K^0_S, J/ψ, $\psi(2S)$, and $\psi(3770)$.

$\Gamma(p\overline{p}\pi^+)/\Gamma_{total}$ — Γ_{598}/Γ

VALUE (units 10^{-6})	CL%	DOCUMENT ID		TECN	COMMENT
$1.62\pm\ 0.20$ OUR AVERAGE					
$1.60^{+0.22}_{-0.19}\pm0.12$		[1,2,3] WEI	08	BELL	$e^+e^- \to \Upsilon(4S)$
$1.69\pm0.29\pm0.26$		[1] AUBERT	07AV	BABR	$e^+e^- \to \Upsilon(4S)$

• • • We do not use the following data for averages, fits, limits, etc. • • •

$1.07\pm0.11\pm0.11$		[4] AAIJ	14AF	LHCB	pp at 7, 8 TeV
$3.06^{+0.73}_{-0.62}\pm0.37$		[1,3] WANG	04	BELL	Repl. by WEI 08

$<$ 3.7	90	[1,2] ABE	02K	BELL	Repl. by WANG 04
$<$500	90	[5] ABREU	95N	DLPH	Repl. by ADAM 96D
$<$160	90	[6] BEBEK	89	CLEO	$e^+e^- \to \Upsilon(4S)$
570 $\pm$150 $\pm$210		[7] ALBRECHT	88F	ARG	$e^+e^- \to \Upsilon(4S)$

[1] Assumes equal production of B^+ and B^0 at the $\Upsilon(4S)$.
[2] Explicitly vetoes resonant production of $p\overline{p}$ from Charmonium states.
[3] Also provides results with $m_{p\overline{p}} < 2.85$ GeV/c^2 and angular asymmetry of $p\overline{p}$ system.
[4] Requires $m_{p\overline{p}} < 2.85$ GeV/c^2.
[5] Assumes a B^0, B^- production fraction of 0.39 and a B_s production fraction of 0.12.
[6] BEBEK 89 reports $< 1.4\times10^{-4}$ assuming the $\Upsilon(4S)$ decays 43% to $B^0\overline{B}^0$. We rescale to 50%.
[7] ALBRECHT 88F reports $(5.2 \pm 1.4 \pm 1.9)\times10^{-4}$ assuming the $\Upsilon(4S)$ decays 45% to $B^0\overline{B}^0$. We rescale to 50%.

$\Gamma(p\overline{p}\pi^+ \text{nonresonant})/\Gamma_{\text{total}}$ — Γ_{599}/Γ

VALUE (units 10^{-6})	CL%	DOCUMENT ID		TECN	COMMENT
<53	90	BERGFELD	96B	CLE2	$e^+e^- \to \Upsilon(4S)$

$\Gamma(p\overline{p}\pi^+\pi^0)/\Gamma_{\text{total}}$ — Γ_{600}/Γ

VALUE (units 10^{-6})	DOCUMENT ID		TECN	COMMENT
4.58$\pm$1.17$\pm$0.67	[1] CHU	20	BELL	$e^+e^- \to \Upsilon(4S)$

[1] Assumes equal production of B^0 and B^+ from $\Upsilon(4S)$ decays. This measurement is quoted for $M(\pi^+\pi^0) < 1.3$ GeV.

$\Gamma(p\overline{p}\pi^+\pi^+\pi^-)/\Gamma_{\text{total}}$ — Γ_{601}/Γ

VALUE	CL%	DOCUMENT ID		TECN	COMMENT
• • • We do not use the following data for averages, fits, limits, etc. • • •					
$<5.2\times10^{-4}$	90	[1] ALBRECHT	88F	ARG	$e^+e^- \to \Upsilon(4S)$

[1] ALBRECHT 88F reports $< 4.7\times10^{-4}$ assuming the $\Upsilon(4S)$ decays 45% to $B^0\overline{B}^0$. We rescale to 50%.

$\Gamma(p\overline{p}K^+)/\Gamma_{\text{total}}$ — Γ_{602}/Γ

VALUE (units 10^{-6})	DOCUMENT ID		TECN	COMMENT
5.9 $\pm$0.5 OUR AVERAGE Error includes scale factor of 1.5.				
$5.54^{+0.27}_{-0.25}\pm0.36$	[1,2,3] WEI	08	BELL	$e^+e^- \to \Upsilon(4S)$
6.7 $\pm$0.5 $\pm$0.4	[1,3] AUBERT,B	05L	BABR	$e^+e^- \to \Upsilon(4S)$
• • • We do not use the following data for averages, fits, limits, etc. • • •				
$4.59^{+0.38}_{-0.34}\pm0.50$	[1,2,3] WANG	05A	BELL	Repl. by WEI 08
$5.66^{+0.67}_{-0.57}\pm0.62$	[1,2,3] WANG	04	BELL	Repl. by WANG 05A
4.3 $^{+1.1}_{-0.9}$ $\pm$0.5	[1,2] ABE	02K	BELL	Repl. by WANG 04

[1] Assumes equal production of B^+ and B^0 at the $\Upsilon(4S)$.
[2] Explicitly vetoes resonant production of $p\overline{p}$ from Charmonium states.
[3] Provides also results with $m_{p\overline{p}} < 2.85$ GeV/c^2 and angular asymmetry of $p\overline{p}$ system.

$\Gamma(p\overline{p}K^+)/\Gamma(J/\psi(1S)K^+)$ — $\Gamma_{602}/\Gamma_{316}$

VALUE	DOCUMENT ID		TECN	COMMENT
0.0104$\pm$0.0005$\pm$0.0001	[1,2] AAIJ	13S	LHCB	pp at 7 TeV

[1] AAIJ 13S reports $[\Gamma(B^+ \to p\overline{p}K^+)/\Gamma(B^+ \to J/\psi(1S)K^+)]$ / $[B(J/\psi(1S) \to p\overline{p})] = 4.91\pm0.19\pm0.14$ which we multiply by our best (shown rounded) value $B(J/\psi(1S) \to p\overline{p}) = (2.121\pm0.029)\times10^{-3}$. Our first error is their experiment's error and our second error is the systematic error from using our best (shown rounded) value.
[2] Measurement includes contribution where $p\overline{p}$ is produced in charmonia decays.

$\Gamma(\Theta(1710)^{++}\overline{p},\ \Theta^{++} \to pK^+)/\Gamma_{\text{total}}$ — Γ_{603}/Γ

VALUE (units 10^{-6})	CL%	DOCUMENT ID		TECN	COMMENT
<0.091	90	[1] WANG	05A	BELL	$e^+e^- \to \Upsilon(4S)$
• • • We do not use the following data for averages, fits, limits, etc. • • •					
$<$0.1	90	[1,2] AUBERT,B	05L	BABR	$e^+e^- \to \Upsilon(4S)$

[1] Assumes equal production of B^+ and B^0 at the $\Upsilon(4S)$.
[2] Provides upper limits depending on the pentaquark masses between 1.43 to 2.0 GeV/c^2.

$\Gamma(f_J(2220)K^+,\ f_J \to p\overline{p})/\Gamma_{\text{total}}$ — Γ_{604}/Γ

VALUE (units 10^{-6})	CL%	DOCUMENT ID		TECN	COMMENT
<0.41	90	[1] WANG	05A	BELL	$e^+e^- \to \Upsilon(4S)$

[1] Assumes equal production of B^+ and B^0 at the $\Upsilon(4S)$.

$\Gamma(p\overline{n}\pi^0)/\Gamma_{\text{total}}$ — Γ_{605}/Γ

VALUE	CL%	DOCUMENT ID		TECN	COMMENT
<6.3 $\times10^{-6}$	90	CHU	23	BELL	$e^+e^- \to \Upsilon(4S)$

$\Gamma(p\overline{\Lambda}(1520))/\Gamma_{\text{total}}$ — Γ_{606}/Γ

VALUE (units 10^{-7})	CL%	DOCUMENT ID		TECN	COMMENT
3.15$\pm$0.48$\pm$0.27		[1] AAIJ	14AF	LHCB	pp at 7, 8 TeV
• • • We do not use the following data for averages, fits, limits, etc. • • •					
3.9 $^{+1.0}_{-0.9}$ $\pm$0.3		[1] AAIJ	13AU	LHCB	Repl. by AAIJ 14AF
$<$15	90	[2] AUBERT,B	05L	BABR	$e^+e^- \to \Upsilon(4S)$

[1] Uses $B(B^+ \to J/\psi K^+) = (1.016\pm0.033)\times10^{-3}$, $B(J/\psi \to p\overline{p}) = (2.17\pm0.07)\times10^{-3}$ and $B(\Lambda(1520) \to K^-p) = 0.234\pm0.016$.
[2] Assumes equal production of B^+ and B^0 at the $\Upsilon(4S)$.

$\Gamma(p\overline{p}K^+ \text{nonresonant})/\Gamma_{\text{total}}$ — Γ_{607}/Γ

VALUE (units 10^{-6})	CL%	DOCUMENT ID		TECN	COMMENT
<89	90	BERGFELD	96B	CLE2	$e^+e^- \to \Upsilon(4S)$

$\Gamma(p\overline{p}K^*(892)^+)/\Gamma_{\text{total}}$ — Γ_{608}/Γ

VALUE (units 10^{-6})	DOCUMENT ID		TECN	COMMENT
3.6 $^{+0.8}_{-0.7}$ OUR AVERAGE				
$3.38^{+0.73}_{-0.60}\pm0.39$	[1,2] CHEN	08C	BELL	$e^+e^- \to \Upsilon(4S)$
5.3 $\pm$1.5 $\pm$1.3	[2] AUBERT	07AV	BABR	$e^+e^- \to \Upsilon(4S)$
• • • We do not use the following data for averages, fits, limits, etc. • • •				
10.3 $^{+3.6}_{-2.8}$ $^{+1.3}_{-1.7}$	[2,3] WANG	04	BELL	Repl. by CHEN 08C

[1] Explicitly vetoes resonant production of $p\overline{p}$ from charmonium states.
[2] Assumes equal production of B^+ and B^0 at the $\Upsilon(4S)$.
[3] Explicitly vetoes resonant production of $p\overline{p}$ from charmonium states. The branching fraction for $M_{p\overline{p}} < 2.85$ GeV/c^2 is also reported.

$\Gamma(f_J(2220)K^{*+},\ f_J \to p\overline{p})/\Gamma_{\text{total}}$ — Γ_{609}/Γ

VALUE (units 10^{-6})	CL%	DOCUMENT ID		TECN	COMMENT
<0.77	90	[1] AUBERT	07AV	BABR	$e^+e^- \to \Upsilon(4S)$

[1] Assumes equal production of B^+ and B^0 at the $\Upsilon(4S)$.

$\Gamma(p\overline{\Lambda})/\Gamma_{\text{total}}$ — Γ_{610}/Γ

VALUE (units 10^{-6})	CL%	DOCUMENT ID		TECN	COMMENT
0.24$^{+0.10}_{-0.08}\pm0.03$		[1] AAIJ	17R	LHCB	pp at 7, 8 TeV
• • • We do not use the following data for averages, fits, limits, etc. • • •					
$<$ 0.32	90	[2] TSAI	07	BELL	$e^+e^- \to \Upsilon(4S)$
$<$ 0.49	90	[2] CHANG	05	BELL	Repl. by TSAI 07
$<$ 1.5	90	[2] BORNHEIM	03	CLE2	$e^+e^- \to \Upsilon(4S)$
$<$ 2.2	90	[2] ABE	02O	BELL	$e^+e^- \to \Upsilon(4S)$
$<$ 2.6	90	[2] COAN	99	CLE2	$e^+e^- \to \Upsilon(4S)$
$<$60	90	[3] AVERY	89B	CLEO	$e^+e^- \to \Upsilon(4S)$
$<$93	90	[4] ALBRECHT	88F	ARG	$e^+e^- \to \Upsilon(4S)$

[1] Statistical significance of the signal is 4.1 standard deviations where the the normalisation is based on $B(B^+ \to K^0_S\pi^+) = (11.895\pm0.375)\times10^{-06}$.
[2] Assumes equal production of B^+ and B^0 at the $\Upsilon(4S)$.
[3] AVERY 89B reports $< 5\times10^{-5}$ assuming the $\Upsilon(4S)$ decays 43% to $B^0\overline{B}^0$. We rescale to 50%.
[4] ALBRECHT 88F reports $< 8.5\times10^{-5}$ assuming the $\Upsilon(4S)$ decays 45% to $B^0\overline{B}^0$. We rescale to 50%.

$\Gamma(p\overline{\Lambda}\gamma)/\Gamma_{\text{total}}$ — Γ_{611}/Γ

VALUE (units 10^{-6})	CL%	DOCUMENT ID		TECN	COMMENT
2.45$^{+0.44}_{-0.38}\pm0.22$		[1] WANG	07C	BELL	$e^+e^- \to \Upsilon(4S)$
• • • We do not use the following data for averages, fits, limits, etc. • • •					
$2.16^{+0.58}_{-0.53}\pm0.20$		[1] LEE	05	BELL	Repl. by WANG 07C
$<$3.9	90	[2] EDWARDS	03	CLE2	$e^+e^- \to \Upsilon(4S)$

[1] Assumes equal production of B^+ and B^0 at the $\Upsilon(4S)$.
[2] Corresponds to $E_\gamma > 1.5$ GeV. The limit changes to 3.3×10^{-6} for $E_\gamma > 2.0$ GeV.

$\Gamma(p\overline{\Lambda}\pi^0)/\Gamma_{\text{total}}$ — Γ_{612}/Γ

VALUE (units 10^{-6})	DOCUMENT ID		TECN	COMMENT
3.00$^{+0.61}_{-0.53}\pm0.33$	[1] WANG	07C	BELL	$e^+e^- \to \Upsilon(4S)$

[1] Assumes equal production of B^+ and B^0 at the $\Upsilon(4S)$.

$\Gamma(p\overline{\Sigma}(1385)^0)/\Gamma_{\text{total}}$ — Γ_{613}/Γ

VALUE (units 10^{-6})	CL%	DOCUMENT ID		TECN	COMMENT
<0.47	90	[1] WANG	07C	BELL	$e^+e^- \to \Upsilon(4S)$

[1] Assumes equal production of B^+ and B^0 at the $\Upsilon(4S)$.

$\Gamma(\Delta^+\overline{\Lambda})/\Gamma_{\text{total}}$ — Γ_{614}/Γ

VALUE (units 10^{-6})	CL%	DOCUMENT ID		TECN	COMMENT
<0.82	90	[1] WANG	07C	BELL	$e^+e^- \to \Upsilon(4S)$

[1] Assumes equal production of B^+ and B^0 at the $\Upsilon(4S)$.

$\Gamma(p\overline{\Sigma}\gamma)/\Gamma_{\text{total}}$ — Γ_{615}/Γ

VALUE (units 10^{-6})	CL%	DOCUMENT ID		TECN	COMMENT
<4.6	90	[1] LEE	05	BELL	$e^+e^- \to \Upsilon(4S)$
• • • We do not use the following data for averages, fits, limits, etc. • • •					
$<$7.9	90	[2] EDWARDS	03	CLE2	$e^+e^- \to \Upsilon(4S)$

[1] Assumes equal production of B^+ and B^0 at the $\Upsilon(4S)$.
[2] Corresponds to $E_\gamma > 1.5$ GeV. The limit changes to 6.4×10^{-6} for $E_\gamma > 2.0$ GeV.

$\Gamma(p\overline{\Lambda}\pi^+\pi^-)/\Gamma_{\text{total}}$ — Γ_{616}/Γ

VALUE (units 10^{-6})	CL%	DOCUMENT ID		TECN	COMMENT
11.28$^{+0.91}_{-0.72}\pm1.03$		[1] CHEN	09C	BELL	$e^+e^- \to \Upsilon(4S)$

Int. J. Mod. Phys. A 2026.41. Downloaded from www.worldscientific.com
by LIFORNIA @ BERKELEY on 09/16/26. Re-use and distribution is strictly not permitted, except for Open Access articles.

Int. J. Mod. Phys. A 2026.41. Downloaded from www.worldscientific.com
by UNIVERSITY OF CALIFORNIA @ BERKELEY on 09/16/26. Re-use and distribution is strictly not permitted, except for Open Access articles.

• • • We do not use the following data for averages, fits, limits, etc. • • •

<200	90	[2] ALBRECHT	88F	ARG	$e^+e^- \to \Upsilon(4S)$

[1] Assumes equal production of B^+ and B^0 at the $\Upsilon(4S)$.
[2] ALBRECHT 88F reports $< 1.8 \times 10^{-4}$ assuming the $\Upsilon(4S)$ decays 45% to $B^0\overline{B}^0$. We rescale to 50%.

$\Gamma(p\overline{\Lambda}\pi^+\pi^-$ nonresonant$)/\Gamma_{total}$ — Γ_{617}/Γ

VALUE (units 10^{-6})	DOCUMENT ID		TECN	COMMENT
$5.92^{+0.88}_{-0.84} \pm 0.69$	[1] CHEN	09C	BELL	$e^+e^- \to \Upsilon(4S)$

[1] Assumes equal production of B^+ and B^0 at the $\Upsilon(4S)$.

$\Gamma(p\overline{\Lambda}\rho^0,\ \rho^0 \to \pi^+\pi^-)/\Gamma_{total}$ — Γ_{618}/Γ

VALUE (units 10^{-6})	DOCUMENT ID		TECN	COMMENT
$4.78^{+0.67}_{-0.64} \pm 0.60$	[1] CHEN	09C	BELL	$e^+e^- \to \Upsilon(4S)$

[1] Assumes equal production of B^+ and B^0 at the $\Upsilon(4S)$.

$\Gamma(p\overline{\Lambda}f_2(1270),\ f_2 \to \pi^+\pi^-)/\Gamma_{total}$ — Γ_{619}/Γ

VALUE (units 10^{-6})	DOCUMENT ID		TECN	COMMENT
$2.03^{+0.77}_{-0.72} \pm 0.27$	[1] CHEN	09C	BELL	$e^+e^- \to \Upsilon(4S)$

[1] Assumes equal production of B^+ and B^0 at the $\Upsilon(4S)$.

$\Gamma(p\overline{\Lambda}K^+K^-)/\Gamma_{total}$ — Γ_{620}/Γ

VALUE (units 10^{-6})	DOCUMENT ID		TECN	COMMENT
$4.10^{+0.45}_{-0.43} \pm 0.50$	[1] LU	19	BELL	$e^+e^- \to \Upsilon(4S)$

[1] Assumes equal production of B^+ and B^0 at the $\Upsilon(4S)$.

$\Gamma(p\overline{\Lambda}\phi)/\Gamma_{total}$ — Γ_{621}/Γ

VALUE (units 10^{-6})	DOCUMENT ID		TECN	COMMENT
$0.795 \pm 0.209 \pm 0.077$	[1] LU	19	BELL	$e^+e^- \to \Upsilon(4S)$

[1] Assumes equal production of B^+ and B^0 at the $\Upsilon(4S)$.

$\Gamma(\overline{p}\Lambda K^+K^-)/\Gamma_{total}$ — Γ_{622}/Γ

VALUE (units 10^{-6})	DOCUMENT ID		TECN	COMMENT
$3.70^{+0.39}_{-0.37} \pm 0.44$	[1] LU	19	BELL	$e^+e^- \to \Upsilon(4S)$

[1] Assumes equal production of B^+ and B^0 at the $\Upsilon(4S)$.

$\Gamma(\Lambda\overline{\Lambda}\pi^+)/\Gamma_{total}$ — Γ_{623}/Γ

VALUE (units 10^{-6})	CL%	DOCUMENT ID		TECN	COMMENT
<0.94	90	[1,2] CHANG	09	BELL	Repl. by CHANG 09

• • • We do not use the following data for averages, fits, limits, etc. • • •

<2.8	90	[2] LEE	04	BELL	$e^+e^- \to \Upsilon(4S)$

[1] For $m_{\Lambda\overline{\Lambda}} < 2.85$ GeV/c^2.
[2] Assumes equal production of B^+ and B^0 at the $\Upsilon(4S)$.

$\Gamma(\Lambda\overline{\Lambda}K^+)/\Gamma_{total}$ — Γ_{624}/Γ

VALUE (units 10^{-6})	DOCUMENT ID		TECN	COMMENT
$3.38^{+0.41}_{-0.36} \pm 0.41$	[1,2] CHANG	09	BELL	$e^+e^- \to \Upsilon(4S)$

• • • We do not use the following data for averages, fits, limits, etc. • • •

$2.91^{+0.9}_{-0.70} \pm 0.38$	[2] LEE	04	BELL	Repl. by CHANG 09

[1] Excluding charmonium events in $2.85 < m_{\Lambda\overline{\Lambda}} < 3.128$ GeV/c^2 and $3.315 < m_{\Lambda\overline{\Lambda}} < 3.735$ GeV/c^2. Measurements in various $m_{\Lambda\overline{\Lambda}}$ bins are also reported.
[2] Assumes equal production of B^+ and B^0 at the $\Upsilon(4S)$.

$\Gamma(\Lambda\overline{\Lambda}K^{*+})/\Gamma_{total}$ — Γ_{625}/Γ

VALUE (units 10^{-6})	DOCUMENT ID		TECN	COMMENT
$2.19^{+1.13}_{-0.88} \pm 0.33$	[1,2] CHANG	09	BELL	$e^+e^- \to \Upsilon(4S)$

[1] For $m_{\Lambda\overline{\Lambda}} < 2.85$ GeV/c^2.
[2] Assumes equal production of B^+ and B^0 at the $\Upsilon(4S)$.

$\Gamma(\Lambda(1520)\overline{\Lambda}K^+)/\Gamma_{total}$ — Γ_{626}/Γ

VALUE (units 10^{-6})	DOCUMENT ID		TECN	COMMENT
$2.23 \pm 0.63 \pm 0.25$	[1] LU	19	BELL	$e^+e^- \to \Upsilon(4S)$

[1] Assumes equal production of B^+ and B^0 at the $\Upsilon(4S)$.

$\Gamma(\Lambda\overline{\Lambda}(1520)K^+)/\Gamma_{total}$ — Γ_{627}/Γ

VALUE	DOCUMENT ID		TECN	COMMENT
$<2.08 \times 10^{-6}$	[1] LU	19	BELL	$e^+e^- \to \Upsilon(4S)$

[1] Assumes equal production of B^+ and B^0 at the $\Upsilon(4S)$.

$\Gamma(\overline{\Delta}^0 p)/\Gamma_{total}$ — Γ_{628}/Γ

VALUE (units 10^{-6})	CL%	DOCUMENT ID		TECN	COMMENT
< 1.38	90	[1] WEI	08	BELL	$e^+e^- \to \Upsilon(4S)$

• • • We do not use the following data for averages, fits, limits, etc. • • •

<380	90	[2] BORTOLETTO	89	CLEO	$e^+e^- \to \Upsilon(4S)$

[1] Assumes equal production of B^+ and B^0 at the $\Upsilon(4S)$.
[2] BORTOLETTO 89 reports $< 3.3 \times 10^{-4}$ assuming the $\Upsilon(4S)$ decays 43% to $B^0\overline{B}^0$. We rescale to 50%.

$\Gamma(\Delta^{++}\overline{p})/\Gamma_{total}$ — Γ_{629}/Γ

VALUE (units 10^{-6})	CL%	DOCUMENT ID		TECN	COMMENT
< 0.14	90	[1] WEI	08	BELL	$e^+e^- \to \Upsilon(4S)$

• • • We do not use the following data for averages, fits, limits, etc. • • •

<150	90	[2] BORTOLETTO	89	CLEO	$e^+e^- \to \Upsilon(4S)$

[1] Assumes equal production of B^+ and B^0 at the $\Upsilon(4S)$.
[2] BORTOLETTO 89 reports $< 1.3 \times 10^{-4}$ assuming the $\Upsilon(4S)$ decays 43% to $B^0\overline{B}^0$. We rescale to 50%.

$\Gamma(\overline{\Lambda}p\overline{p}p)/\Gamma_{total}$ — Γ_{630}/Γ

VALUE (units 10^{-7})	DOCUMENT ID		TECN	COMMENT
$2.15 \pm 0.35 \pm 0.30$	AAIJ	25AT	LHCB	pp at 13 TeV

$\Gamma(\overline{\Lambda}p\eta_c)/\Gamma_{total}$ — Γ_{631}/Γ

VALUE	CL%	DOCUMENT ID		TECN	COMMENT
$<1.9 \times 10^{-5}$	90	[1] AAIJ	25AT	LHCB	pp at 13 TeV

[1] AAIJ 25AT reports $[\Gamma(B^+ \to \overline{\Lambda}p\eta_c)/\Gamma_{total}] \times [B(\eta_c(1S) \to p\overline{p})] < 2.1 \times 10^{-8}$ which we divide by our best (shown rounded) value $B(\eta_c(1S) \to p\overline{p}) = 1.11 \times 10^{-3}$.

$\Gamma(D^+p\overline{p})/\Gamma_{total}$ — Γ_{632}/Γ

VALUE	CL%	DOCUMENT ID		TECN	COMMENT
$<1.5 \times 10^{-5}$	90	[1] ABE	02W	BELL	$e^+e^- \to \Upsilon(4S)$

[1] Assumes equal production of B^+ and B^0 at the $\Upsilon(4S)$.

$\Gamma(D^*(2010)^+p\overline{p})/\Gamma_{total}$ — Γ_{633}/Γ

VALUE	CL%	DOCUMENT ID		TECN	COMMENT
$<1.5 \times 10^{-5}$	90	[1] ABE	02W	BELL	$e^+e^- \to \Upsilon(4S)$

[1] Assumes equal production of B^+ and B^0 at the $\Upsilon(4S)$.

$\Gamma(\overline{D}^0p\overline{p}\pi^+)/\Gamma_{total}$ — Γ_{634}/Γ

VALUE (units 10^{-4})	DOCUMENT ID		TECN	COMMENT
$3.72 \pm 0.11 \pm 0.25$	[1,2] DEL-AMO-SA...12		BABR	$e^+e^- \to \Upsilon(4S)$

[1] Uses the values of D and D^* branching fractions from PDG 08.
[2] Assumes equal production of B^+ and B^0 at the $\Upsilon(4S)$.

$\Gamma(\overline{D}^{*0}p\overline{p}\pi^+)/\Gamma_{total}$ — Γ_{635}/Γ

VALUE (units 10^{-4})	DOCUMENT ID		TECN	COMMENT
$3.73 \pm 0.17 \pm 0.27$	[1,2] DEL-AMO-SA...12		BABR	$e^+e^- \to \Upsilon(4S)$

[1] Uses the values of D and D^* branching fractions from PDG 08.
[2] Assumes equal production of B^+ and B^0 at the $\Upsilon(4S)$.

$\Gamma(D^-p\overline{p}\pi^+\pi^-)/\Gamma_{total}$ — Γ_{636}/Γ

VALUE (units 10^{-4})	DOCUMENT ID		TECN	COMMENT
$1.66 \pm 0.13 \pm 0.27$	[1,2] DEL-AMO-SA...12		BABR	$e^+e^- \to \Upsilon(4S)$

[1] Uses the values of D and D^* branching fractions from PDG 08.
[2] Assumes equal production of B^+ and B^0 at the $\Upsilon(4S)$.

$\Gamma(D^{*-}p\overline{p}\pi^+\pi^-)/\Gamma_{total}$ — Γ_{637}/Γ

VALUE (units 10^{-4})	DOCUMENT ID		TECN	COMMENT
$1.86 \pm 0.16 \pm 0.19$	[1,2] DEL-AMO-SA...12		BABR	$e^+e^- \to \Upsilon(4S)$

[1] Uses the values of D and D^* branching fractions from PDG 08.
[2] Assumes equal production of B^+ and B^0 at the $\Upsilon(4S)$.

$\Gamma(p\overline{\Lambda}^0\overline{D}^0)/\Gamma_{total}$ — Γ_{638}/Γ

VALUE (units 10^{-5})	DOCUMENT ID		TECN	COMMENT
$1.43^{+0.28}_{-0.25} \pm 0.18$	[1,2] CHEN	11F	BELL	$e^+e^- \to \Upsilon(4S)$

[1] Uses $B(\Lambda \to p\pi^-) = 63.9 \pm 0.5\%$, $B(D^0 \to K^-\pi^+) = 3.89 \pm 0.05\%$, and $B(D^0 \to K^-\pi^+\pi^0) = 13.9 \pm 0.5\%$.
[2] Assumes equal production of B^0 and B^+ from Upsilon(4S) decays.

$\Gamma(p\overline{\Lambda}^0\overline{D}^*(2007)^0)/\Gamma_{total}$ — Γ_{639}/Γ

VALUE (units 10^{-5})	CL%	DOCUMENT ID		TECN	COMMENT
<5	90	[1,2,3] CHEN	11F	BELL	$e^+e^- \to \Upsilon(4S)$

[1] CHEN 11F reports $< 4.8 \times 10^{-5}$ from a measurement of $[\Gamma(B^+ \to p\overline{\Lambda}^0\overline{D}^*(2007)^0)/\Gamma_{total}]/[B(D^*(2007)^0 \to D^0\pi^0)]$ assuming $B(D^*(2007)^0 \to D^0\pi^0) = (61.9 \pm 2.9) \times 10^{-2}$, which we rescale to our best (shown rounded) value $B(D^*(2007)^0 \to D^0\pi^0) = 64.7 \times 10^{-2}$.
[2] Uses $B(\Lambda \to p\pi^-) = 63.9 \pm 0.5\%$ and $B(D^0 \to K^-\pi^+) = 3.89 \pm 0.05\%$.
[3] Assumes equal production of B^0 and B^+ from Upsilon(4S) decays.

$\Gamma(\overline{\Lambda}_c^-p\pi^+)/\Gamma_{total}$ — Γ_{640}/Γ

VALUE (units 10^{-4})	DOCUMENT ID		TECN	COMMENT
2.2 ±0.4 OUR AVERAGE	Error includes scale factor of 2.7. See the ideogram below.			
$2.67 \pm 0.15 \pm 0.09$	[1,2] AUBERT	08BN	BABR	$e^+e^- \to \Upsilon(4S)$

$1.58 \pm 0.20 \pm 0.05$	[1,3] GABYSHEV	06A	BELL	$e^+e^- \to \Upsilon(4S)$
$1.9 \pm 0.5 \pm 0.1$	[1,4] DYTMAN	02	CLE2	$e^+e^- \to \Upsilon(4S)$
• • • We do not use the following data for averages, fits, limits, etc. • • •				
$1.47^{+0.40}_{-0.38} \pm 0.05$	[1,5] GABYSHEV	02	BELL	Repl. by GABYSHEV 06A
$6.2 \ ^{+2.3}_{-2.0} \pm 1.6$	[1,6] FU	97	CLE2	Repl. by DYTMAN 02

[1] Assumes equal production of B^+ and B^0 at the $\Upsilon(4S)$.

[2] AUBERT 08BN reports $(3.4 \pm 0.1 \pm 0.9) \times 10^{-4}$ from a measurement of $[\Gamma(B^+ \to \overline{\Lambda}_c^- p\pi^+)/\Gamma_{total}] \times [B(\Lambda_c^+ \to pK^-\pi^+)]$ assuming $B(\Lambda_c^+ \to pK^-\pi^+) = (5.0 \pm 1.3) \times 10^{-2}$, which we rescale to our best (shown rounded) value $B(\Lambda_c^+ \to pK^-\pi^+) = (6.37 \pm 0.21) \times 10^{-2}$. Our first error is their experiment's error and our second error is the systematic error from using our best (shown rounded) value.

[3] GABYSHEV 06A reports $(2.01 \pm 0.15 \pm 0.20) \times 10^{-4}$ from a measurement of $[\Gamma(B^+ \to \overline{\Lambda}_c^- p\pi^+)/\Gamma_{total}] \times [B(\Lambda_c^+ \to pK^-\pi^+)]$ assuming $B(\Lambda_c^+ \to pK^-\pi^+) = 0.05$, which we rescale to our best (shown rounded) value $B(\Lambda_c^+ \to pK^-\pi^+) = (6.37 \pm 0.21) \times 10^{-2}$. Our first error is their experiment's error and our second error is the systematic error from using our best (shown rounded) value.

[4] DYTMAN 02 reports $(2.4^{+0.63}_{-0.62}) \times 10^{-4}$ from a measurement of $[\Gamma(B^+ \to \overline{\Lambda}_c^- p\pi^+)/\Gamma_{total}] \times [B(\Lambda_c^+ \to pK^-\pi^+)]$ assuming $B(\Lambda_c^+ \to pK^-\pi^+) = 0.05$, which we rescale to our best (shown rounded) value $B(\Lambda_c^+ \to pK^-\pi^+) = (6.37 \pm 0.21) \times 10^{-2}$. Our first error is their experiment's error and our second error is the systematic error from using our best (shown rounded) value.

[5] GABYSHEV 02 reports $(1.87^{+0.51}_{-0.49}) \times 10^{-4}$ from a measurement of $[\Gamma(B^+ \to \overline{\Lambda}_c^- p\pi^+)/\Gamma_{total}] \times [B(\Lambda_c^+ \to pK^-\pi^+)]$ assuming $B(\Lambda_c^+ \to pK^-\pi^+) = 0.05$, which we rescale to our best (shown rounded) value $B(\Lambda_c^+ \to pK^-\pi^+) = (6.37 \pm 0.21) \times 10^{-2}$. Our first error is their experiment's error and our second error is the systematic error from using our best (shown rounded) value.

[6] FU 97 uses PDG 96 values of Λ_c branching fraction.

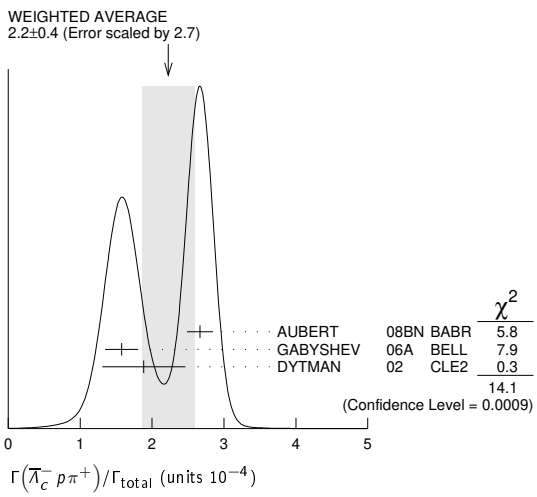

$\Gamma(\overline{\Lambda}_c^- pK^+)/\Gamma(\overline{\Lambda}_c^- p\pi^+)$ — $\Gamma_{641}/\Gamma_{640}$

VALUE (units 10^{-2})	DOCUMENT ID		TECN	COMMENT
$3.97 \pm 0.23 \pm 0.12$	AAIJ	24T	LHCB	pp at 7, 8, 13 TeV

$\Gamma(\overline{\Lambda}_c^- \Delta(1232)^{++})/\Gamma_{total}$ — Γ_{642}/Γ

VALUE (units 10^{-5})	CL%	DOCUMENT ID		TECN	COMMENT
<1.9	90	GABYSHEV	06A	BELL	$e^+e^- \to \Upsilon(4S)$

$\Gamma(\overline{\Lambda}_c^- \Delta_X(1600)^{++})/\Gamma_{total}$ — Γ_{643}/Γ

VALUE (units 10^{-5})	DOCUMENT ID		TECN	COMMENT
$4.6 \pm 0.9 \pm 0.2$	[1] GABYSHEV	06A	BELL	$e^+e^- \to \Upsilon(4S)$

[1] GABYSHEV 06A reports $(5.9 \pm 1.0 \pm 0.6) \times 10^{-5}$ from a measurement of $[\Gamma(B^+ \to \overline{\Lambda}_c^- \Delta_X(1600)^{++})/\Gamma_{total}] \times [B(\Lambda_c^+ \to pK^-\pi^+)]$ assuming $B(\Lambda_c^+ \to pK^-\pi^+) = 0.05$, which we rescale to our best (shown rounded) value $B(\Lambda_c^+ \to pK^-\pi^+) = (6.37 \pm 0.21) \times 10^{-2}$. Our first error is their experiment's error and our second error is the systematic error from using our best (shown rounded) value.

$\Gamma(\overline{\Lambda}_c^- \Delta_X(2420)^{++})/\Gamma_{total}$ — Γ_{644}/Γ

VALUE (units 10^{-5})	DOCUMENT ID		TECN	COMMENT
$3.7 \pm 0.8 \pm 0.1$	[1] GABYSHEV	06A	BELL	$e^+e^- \to \Upsilon(4S)$

[1] GABYSHEV 06A reports $(4.7^{+1.0}_{-0.9} \pm 0.4) \times 10^{-5}$ from a measurement of $[\Gamma(B^+ \to \overline{\Lambda}_c^- \Delta_X(2420)^{++})/\Gamma_{total}] \times [B(\Lambda_c^+ \to pK^-\pi^+)]$ assuming $B(\Lambda_c^+ \to pK^-\pi^+) = 0.05$, which we rescale to our best (shown rounded) value $B(\Lambda_c^+ \to pK^-\pi^+) = (6.37 \pm 0.21) \times 10^{-2}$. Our first error is their experiment's error and our second error is the systematic error from using our best (shown rounded) value.

$\Gamma((\overline{\Lambda}_c^- p)_s \pi^+)/\Gamma_{total}$ — Γ_{645}/Γ

$(\overline{\Lambda}_c^- p)_s$ denotes a low-mass enhancement near 3.35 GeV/c^2.

VALUE (units 10^{-5})	DOCUMENT ID		TECN	COMMENT
$3.1^{+0.7}_{-0.6} \pm 0.1$	[1] GABYSHEV	06A	BELL	$e^+e^- \to \Upsilon(4S)$

[1] GABYSHEV 06A reports $(3.9^{+0.8}_{-0.7} \pm 0.4) \times 10^{-5}$ from a measurement of $[\Gamma(B^+ \to (\overline{\Lambda}_c^- p)_s \pi^+)/\Gamma_{total}] \times [B(\Lambda_c^+ \to pK^-\pi^+)]$ assuming $B(\Lambda_c^+ \to pK^-\pi^+) = 0.05$, which we rescale to our best (shown rounded) value $B(\Lambda_c^+ \to pK^-\pi^+) = (6.37 \pm 0.21) \times 10^{-2}$. Our first error is their experiment's error and our second error is the systematic error from using our best (shown rounded) value.

$\Gamma(\overline{\Sigma}_c(2520)^0 p)/\Gamma_{total}$ — Γ_{646}/Γ

VALUE (units 10^{-5})	CL%	DOCUMENT ID		TECN	COMMENT
<0.3	90	[1,2] AUBERT	08BN	BABR	$e^+e^- \to \Upsilon(4S)$
• • • We do not use the following data for averages, fits, limits, etc. • • •					
<2.7	90	[1,2] GABYSHEV	06A	BELL	$e^+e^- \to \Upsilon(4S)$
<4.6	90	[1,2] GABYSHEV	02	BELL	Repl. by GABYSHEV 06A

[1] Assumes equal production of B^+ and B^0 at the $\Upsilon(4S)$.

[2] Uses the value for $\Lambda_c \to pK^-\pi^+$ branching ratio $(5.0 \pm 1.3)\%$.

$\Gamma(\overline{\Sigma}_c(2520)^0 p)/\Gamma(\overline{\Lambda}_c^- p\pi^+)$ — $\Gamma_{646}/\Gamma_{640}$

VALUE (units 10^{-3})	CL%	DOCUMENT ID		TECN	COMMENT
<9	90	AUBERT	08BN	BABR	$e^+e^- \to \Upsilon(4S)$

$\Gamma(\overline{\Sigma}_c(2800)^0 p)/\Gamma_{total}$ — Γ_{647}/Γ

VALUE (units 10^{-5})	DOCUMENT ID		TECN	COMMENT
$2.6 \pm 0.7 \pm 0.4$	[1] AUBERT	08BN	BABR	$e^+e^- \to \Upsilon(4S)$

[1] AUBERT 08BN reports $[\Gamma(B^+ \to \overline{\Sigma}_c(2800)^0 p)/\Gamma_{total}] / [B(B^+ \to \overline{\Lambda}_c^- p\pi^+)] = 0.117 \pm 0.023 \pm 0.024$ which we multiply by our best (shown rounded) value $B(B^+ \to \overline{\Lambda}_c^- p\pi^+) = (2.2 \pm 0.4) \times 10^{-4}$. Our first error is their experiment's error and our second error is the systematic error from using our best (shown rounded) value.

$\Gamma(\overline{\Lambda}_c^- p\pi^+\pi^0)/\Gamma_{total}$ — Γ_{648}/Γ

VALUE (units 10^{-3})	CL%	DOCUMENT ID		TECN	COMMENT
$1.81 \pm 0.29^{+0.52}_{-0.50}$		[1,2] DYTMAN	02	CLE2	$e^+e^- \to \Upsilon(4S)$
• • • We do not use the following data for averages, fits, limits, etc. • • •					
<3.12	90	[3] FU	97	CLE2	$e^+e^- \to \Upsilon(4S)$

[1] Assumes equal production of B^+ and B^0 at the $\Upsilon(4S)$.

[2] DYTMAN 02 measurement uses $B(\Lambda_c^- \to \overline{p}K^+\pi^-) = 5.0 \pm 1.3\%$. The second error includes the systematic and the uncertainty of the branching ratio.

[3] FU 97 uses PDG 96 values of Λ_c branching ratio.

$\Gamma(\overline{\Lambda}_c^- p\pi^+\pi^+\pi^-)/\Gamma_{total}$ — Γ_{649}/Γ

VALUE (units 10^{-3})	CL%	DOCUMENT ID		TECN	COMMENT
$2.25 \pm 0.25^{+0.63}_{-0.61}$		[1,2] DYTMAN	02	CLE2	$e^+e^- \to \Upsilon(4S)$
• • • We do not use the following data for averages, fits, limits, etc. • • •					
<1.46	90	[3] FU	97	CLE2	$e^+e^- \to \Upsilon(4S)$

[1] Assumes equal production of B^+ and B^0 at the $\Upsilon(4S)$.

[2] DYTMAN 02 measurement uses $B(\Lambda_c^- \to \overline{p}K^+\pi^-) = 5.0 \pm 1.3\%$. The second error includes the systematic and the uncertainty of the branching ratio.

[3] FU 97 uses PDG 96 values of Λ_c branching ratio.

$\Gamma(\overline{\Lambda}_c^- p\pi^+\pi^+\pi^-\pi^0)/\Gamma_{total}$ — Γ_{650}/Γ

VALUE	CL%	DOCUMENT ID		TECN	COMMENT
$<1.34 \times 10^{-2}$	90	[1] FU	97	CLE2	$e^+e^- \to \Upsilon(4S)$

[1] FU 97 uses PDG 96 values of Λ_c branching ratio.

$\Gamma(\Lambda_c^+ \Lambda_c^- K^+)/\Gamma_{total}$ — Γ_{651}/Γ

VALUE (units 10^{-4})	DOCUMENT ID		TECN	COMMENT
4.9 ± 0.7 OUR AVERAGE				
$4.80 \pm 0.43 \pm 0.60$	LI	18A	BELL	$e^+e^- \to \Upsilon(4S)$
$8.9 \pm 4.4 \pm 0.3$	[1,2] AUBERT	08H	BABR	$e^+e^- \to \Upsilon(4S)$
• • • We do not use the following data for averages, fits, limits, etc. • • •				
$6.2 \pm 2.4 \pm 0.2$	[2,3] GABYSHEV	06	BELL	Repl. by LI 18A.

[1] AUBERT 08H reports $(1.14 \pm 0.15 \pm 0.62) \times 10^{-3}$ from a measurement of $[\Gamma(B^+ \to \Lambda_c^+ \Lambda_c^- K^+)/\Gamma_{total}] \times [B(\Lambda_c^+ \to pK^-\pi^+)]$ assuming $B(\Lambda_c^+ \to pK^-\pi^+) = (5.0 \pm 1.3) \times 10^{-2}$, which we rescale to our best (shown rounded) value $B(\Lambda_c^+ \to pK^-\pi^+) = (6.37 \pm 0.21) \times 10^{-2}$. Our first error is their experiment's error and our second error is the systematic error from using our best (shown rounded) value.

[2] Assumes equal production of B^+ and B^0 at the $\Upsilon(4S)$.

[3] GABYSHEV 06 reports $(7.9^{+1.0}_{-0.9} \pm 3.6) \times 10^{-4}$ from a measurement of $[\Gamma(B^+ \to \Lambda_c^+ \Lambda_c^- K^+)/\Gamma_{total}] \times [B(\Lambda_c^+ \to pK^-\pi^+)]$ assuming $B(\Lambda_c^+ \to pK^-\pi^+) = (5.0 \pm 1.3) \times 10^{-2}$, which we rescale to our best (shown rounded) value $B(\Lambda_c^+ \to pK^-\pi^+) = (6.37 \pm 0.21) \times 10^{-2}$. Our first error is their experiment's error and our second error is the systematic error from using our best (shown rounded) value.

Int. J. Mod. Phys. A 2026.41. Downloaded from www.worldscientific.com
by LIFORNIA @ BERKELEY on 09/16/26. Re-use and distribution is strictly not permitted, except for Open Access articles.

Int. J. Mod. Phys. A 2026.41. Downloaded from www.worldscientific.com
by UNIVERSITY OF CALIFORNIA @ BERKELEY on 09/16/26. Re-use and distribution is strictly not permitted, except for Open Access articles.

$\Gamma(\Lambda_c^+ \Lambda_c^- K^+)/\Gamma(D^- D^+ K^+)$ — $\Gamma_{651}/\Gamma_{228}$

VALUE	DOCUMENT ID		TECN	COMMENT
2.36±0.11±0.33	[1] AAIJ	23X	LHCB	pp at 13 TeV

[1] The second uncertainty includes both systematic (±0.22) and the charm decay branching fraction (±0.25).

$\Gamma(\Xi_c(2930)\Lambda_c^+,\ \Xi_c \to K^+\Lambda_c^-)/\Gamma_{total}$ — Γ_{652}/Γ

VALUE (units 10^{-4})	DOCUMENT ID		TECN	COMMENT
1.73±0.45±0.21	[1] LI	18A	BELL	$e^+e^- \to \Upsilon(4S)$

[1] The $\Xi_c(2930)$ is found in its decay to $K^-\Lambda_c^+$ in $B^- \to K^-\Lambda_c^-\Lambda_c^+$ with a significance more than 5 sigma.

$\Gamma(\Sigma_c(2455)^0 p)/\Gamma_{total}$ — Γ_{653}/Γ

VALUE (units 10^{-5})	CL%	DOCUMENT ID		TECN	COMMENT
2.9±0.6±0.1		[1,2] GABYSHEV	06A	BELL	$e^+e^- \to \Upsilon(4S)$
• • • We do not use the following data for averages, fits, limits, etc. • • •					
<8	90	[1,3] DYTMAN	02	CLE2	$e^+e^- \to \Upsilon(4S)$
<9.3	90	[1,4] GABYSHEV	02	BELL	Repl. by GABYSHEV 06A

[1] Assumes equal production of B^+ and B^0 at the $\Upsilon(4S)$.
[2] GABYSHEV 06A reports $(3.7 \pm 0.7 \pm 0.4) \times 10^{-5}$ from a measurement of $[\Gamma(B^+ \to \overline{\Sigma}_c(2455)^0 p)/\Gamma_{total}] \times [B(\Lambda_c^+ \to pK^-\pi^+)]$ assuming $B(\Lambda_c^+ \to pK^-\pi^+) = 0.05$, which we rescale to our best (shown rounded) value $B(\Lambda_c^+ \to pK^-\pi^+) = (6.37 \pm 0.21) \times 10^{-2}$. Our first error is their experiment's error and our second error is the systematic error from using our best (shown rounded) value.
[3] DYTMAN 02 measurement uses $B(\Lambda_c^- \to \overline{p}K^+\pi^-) = 5.0 \pm 1.3\%$. The second error includes the systematic and the uncertainty of the branching ratio.
[4] Uses the value for $\Lambda_c \to pK^-\pi^+$ branching ratio (5.0 ± 1.3)%.

$\Gamma(\Sigma_c(2455)^0 p)/\Gamma(\Lambda_c^- p\pi^+)$ — $\Gamma_{653}/\Gamma_{640}$

VALUE	DOCUMENT ID		TECN	COMMENT
0.123±0.012±0.008	[1] AUBERT	08BN	BABR	$e^+e^- \to \Upsilon(4S)$

[1] Assumes equal production of B^+ and B^0 at the $\Upsilon(4S)$.

$\Gamma(\Sigma_c(2455)^0 p\pi^0)/\Gamma_{total}$ — Γ_{654}/Γ

VALUE (units 10^{-4})	DOCUMENT ID		TECN	COMMENT
3.5±1.1±0.1	[1,2] DYTMAN	02	CLE2	$e^+e^- \to \Upsilon(4S)$

[1] DYTMAN 02 reports $(4.4 \pm 1.4) \times 10^{-4}$ from a measurement of $[\Gamma(B^+ \to \overline{\Sigma}_c(2455)^0 p\pi^0)/\Gamma_{total}] \times [B(\Lambda_c^+ \to pK^-\pi^+)]$ assuming $B(\Lambda_c^+ \to pK^-\pi^+) = 0.05$, which we rescale to our best (shown rounded) value $B(\Lambda_c^+ \to pK^-\pi^+) = (6.37 \pm 0.21) \times 10^{-2}$. Our first error is their experiment's error and our second error is the systematic error from using our best (shown rounded) value.
[2] Assumes equal production of B^+ and B^0 at the $\Upsilon(4S)$.

$\Gamma(\Sigma_c(2455)^0 p\pi^-\pi^+)/\Gamma_{total}$ — Γ_{655}/Γ

VALUE (units 10^{-4})	DOCUMENT ID		TECN	COMMENT
3.5±1.0±0.1	[1,2] DYTMAN	02	CLE2	$e^+e^- \to \Upsilon(4S)$

[1] DYTMAN 02 reports $(4.4 \pm 1.3) \times 10^{-4}$ from a measurement of $[\Gamma(B^+ \to \overline{\Sigma}_c(2455)^0 p\pi^-\pi^+)/\Gamma_{total}] \times [B(\Lambda_c^+ \to pK^-\pi^+)]$ assuming $B(\Lambda_c^+ \to pK^-\pi^+) = 0.05$, which we rescale to our best (shown rounded) value $B(\Lambda_c^+ \to pK^-\pi^+) = (6.37 \pm 0.21) \times 10^{-2}$. Our first error is their experiment's error and our second error is the systematic error from using our best (shown rounded) value.
[2] Assumes equal production of B^+ and B^0 at the $\Upsilon(4S)$.

$\Gamma(\Sigma_c(2455)^{--} p\pi^+\pi^+)/\Gamma_{total}$ — Γ_{656}/Γ

VALUE (units 10^{-4})	DOCUMENT ID		TECN	COMMENT
2.33±0.17 OUR AVERAGE				
2.34±0.16±0.08	[1,2] LEES	12Z	BABR	$e^+e^- \to \Upsilon(4S)$
2.2 ±0.8 ±0.1	[1,3] DYTMAN	02	CLE2	$e^+e^- \to \Upsilon(4S)$

[1] Assumes equal production of B^+ and B^0 at the $\Upsilon(4S)$.
[2] LEES 12Z reports $(2.98 \pm 0.16 \pm 0.15 \pm 0.77) \times 10^{-4}$ from a measurement of $[\Gamma(B^+ \to \overline{\Sigma}_c(2455)^{--} p\pi^+\pi^+)/\Gamma_{total}] \times [B(\Lambda_c^+ \to pK^-\pi^+)]$ assuming $B(\Lambda_c^+ \to pK^-\pi^+) = (5.0 \pm 1.3) \times 10^{-2}$, which we rescale to our best (shown rounded) value $B(\Lambda_c^+ \to pK^-\pi^+) = (6.37 \pm 0.21) \times 10^{-2}$. Our first error is their experiment's error and our second error is the systematic error from using our best (shown rounded) value.
[3] DYTMAN 02 reports $(2.8 \pm 0.9 \pm 0.5 \pm 0.7) \times 10^{-4}$ from a measurement of $[\Gamma(B^+ \to \overline{\Sigma}_c(2455)^{--} p\pi^+\pi^+)/\Gamma_{total}] \times [B(\Lambda_c^+ \to pK^-\pi^+)]$ assuming $B(\Lambda_c^+ \to pK^-\pi^+) = (5.0 \pm 1.3) \times 10^{-2}$, which we rescale to our best (shown rounded) value $B(\Lambda_c^+ \to pK^-\pi^+) = (6.37 \pm 0.21) \times 10^{-2}$. Our first error is their experiment's error and our second error is the systematic error from using our best (shown rounded) value.

$\Gamma(\Sigma_c(2455)^{++}\overline{\Xi}_c^-)/\Gamma_{total}$ — Γ_{657}/Γ

VALUE (units 10^{-4})	DOCUMENT ID		TECN	COMMENT
$5.74 \pm 1.11 {}^{+2.51}_{-1.59}$	[1] ABUMUSABH	25	BELL	$e^+e^- \to \Upsilon(4S)$

[1] Uses $\Sigma_c(2455)^{++} \to \Lambda_c^+\pi^+$ and $\overline{\Xi}_c^- \to \overline{\Xi}^+\pi^-\pi^-$ and $\overline{p}K^+\pi^-$ decays.

$\Gamma(\overline{\Lambda}_c(2593)^-/\overline{\Lambda}_c(2625)^- p\pi^+)/\Gamma_{total}$ — Γ_{658}/Γ

VALUE	CL%	DOCUMENT ID		TECN	COMMENT
<1.9 × 10^{-4}	90	[1,2] DYTMAN	02	CLE2	$e^+e^- \to \Upsilon(4S)$

[1] Assumes equal production of B^+ and B^0 at the $\Upsilon(4S)$.
[2] DYTMAN 02 measurement uses $B(\Lambda_c^- \to \overline{p}K^+\pi^-) = 5.0 \pm 1.3\%$. The second error includes the systematic and the uncertainty of the branching ratio.

$\Gamma(\overline{\Xi}_c^0\Lambda_c^+)/\Gamma_{total}$ — Γ_{659}/Γ

VALUE (units 10^{-4})	DOCUMENT ID		TECN	COMMENT
9.51±2.10±0.88	[1] LI	19A	BELL	$e^+e^- \to \Upsilon(4S)$

[1] First measured the absolute branching fraction using a missing-mass technique.

$\Gamma(\overline{\Xi}_c^0\Lambda_c^+,\ \overline{\Xi}_c^0 \to \overline{\Xi}^+\pi^-)/\Gamma_{total}$ — Γ_{661}/Γ

VALUE (units 10^{-5})	DOCUMENT ID		TECN	COMMENT
1.76±0.29 OUR AVERAGE				
1.71±0.28±0.15	[1] LI	19A	BELL	$e^+e^- \to \Upsilon(4S)$
2.0 ±0.7 ±0.1	[2,3] AUBERT	08H	BABR	$e^+e^- \to \Upsilon(4S)$
• • • We do not use the following data for averages, fits, limits, etc. • • •				
4.4 $^{+1.8}_{-1.5}$ ±0.1	[3,4] CHISTOV	06A	BELL	Repl. by LI 19A

[1] Using a hadronic B-tagging method based on a full reconstruction.
[2] AUBERT 08H reports $(2.51 \pm 0.89 \pm 0.61) \times 10^{-5}$ from a measurement of $[\Gamma(B^+ \to \overline{\Xi}_c^0\Lambda_c^+,\ \overline{\Xi}_c^0 \to \overline{\Xi}^+\pi^-)/\Gamma_{total}] \times [B(\Lambda_c^+ \to pK^-\pi^+)]$ assuming $B(\Lambda_c^+ \to pK^-\pi^+) = (5.0 \pm 1.3) \times 10^{-2}$, which we rescale to our best (shown rounded) value $B(\Lambda_c^+ \to pK^-\pi^+) = (6.37 \pm 0.21) \times 10^{-2}$. Our first error is their experiment's error and our second error is the systematic error from using our best (shown rounded) value.
[3] Assumes equal production of B^+ and B^0 at the $\Upsilon(4S)$.
[4] CHISTOV 06A reports $(5.6 {}^{+1.9}_{-1.5} \pm 1.9) \times 10^{-5}$ from a measurement of $[\Gamma(B^+ \to \overline{\Xi}_c^0\Lambda_c^+,\ \overline{\Xi}_c^0 \to \overline{\Xi}^+\pi^-)/\Gamma_{total}] \times [B(\Lambda_c^+ \to pK^-\pi^+)]$ assuming $B(\Lambda_c^+ \to pK^-\pi^+) = (5.0 \pm 1.3) \times 10^{-2}$, which we rescale to our best (shown rounded) value $B(\Lambda_c^+ \to pK^-\pi^+) = (6.37 \pm 0.21) \times 10^{-2}$. Our first error is their experiment's error and our second error is the systematic error from using our best (shown rounded) value.

$\Gamma(\overline{\Xi}_c^0\Lambda_c^+,\ \overline{\Xi}_c^0 \to \Lambda K^+\pi^-)/\Gamma_{total}$ — Γ_{662}/Γ

VALUE (units 10^{-5})	DOCUMENT ID		TECN	COMMENT
1.14±0.26 OUR AVERAGE				
1.11±0.26±0.10	[1] LI	19A	BELL	$e^+e^- \to \Upsilon(4S)$
1.33±0.76±0.04	[2,3] AUBERT	08H	BABR	$e^+e^- \to \Upsilon(4S)$
• • • We do not use the following data for averages, fits, limits, etc. • • •				
3.1 $^{+1.1}_{-0.9}$ ±0.1	[3,4] CHISTOV	06A	BELL	Repl. by LI 19A

[1] Using a hadronic B-tagging method based on a full reconstruction.
[2] AUBERT 08H reports $(1.70 \pm 0.93 \pm 0.53) \times 10^{-5}$ from a measurement of $[\Gamma(B^+ \to \overline{\Xi}_c^0\Lambda_c^+,\ \overline{\Xi}_c^0 \to \Lambda K^+\pi^-)/\Gamma_{total}] \times [B(\Lambda_c^+ \to pK^-\pi^+)]$ assuming $B(\Lambda_c^+ \to pK^-\pi^+) = (5.0 \pm 1.3) \times 10^{-2}$, which we rescale to our best (shown rounded) value $B(\Lambda_c^+ \to pK^-\pi^+) = (6.37 \pm 0.21) \times 10^{-2}$. Our first error is their experiment's error and our second error is the systematic error from using our best (shown rounded) value.
[3] Assumes equal production of B^+ and B^0 at the $\Upsilon(4S)$.
[4] CHISTOV 06A reports $(4.0 {}^{+1.1}_{-0.9} \pm 1.3) \times 10^{-5}$ from a measurement of $[\Gamma(B^+ \to \overline{\Xi}_c^0\Lambda_c^+,\ \overline{\Xi}_c^0 \to \Lambda K^+\pi^-)/\Gamma_{total}] \times [B(\Lambda_c^+ \to pK^-\pi^+)]$ assuming $B(\Lambda_c^+ \to pK^-\pi^+) = (5.0 \pm 1.3) \times 10^{-2}$, which we rescale to our best (shown rounded) value $B(\Lambda_c^+ \to pK^-\pi^+) = (6.37 \pm 0.21) \times 10^{-2}$. Our first error is their experiment's error and our second error is the systematic error from using our best (shown rounded) value.

$\Gamma(\overline{\Xi}_c^0\Lambda_c^+,\ \overline{\Xi}_c^0 \to pK^-K^-\pi^+)/\Gamma_{total}$ — Γ_{663}/Γ

VALUE (units 10^{-6})	DOCUMENT ID		TECN	COMMENT
5.47±1.78±0.57	[1] LI	19A	BELL	$e^+e^- \to \Upsilon(4S)$

[1] Using a hadronic B-tagging method based on a full reconstruction.

$\Gamma(\Lambda_c^+\overline{\Xi}_c'^0)/\Gamma_{total}$ — Γ_{664}/Γ

VALUE	CL%	DOCUMENT ID		TECN	COMMENT
<6.5 × 10^{-4}	90	[1] LI	19G	BELL	$e^+e^- \to \Upsilon(4S)$

[1] Uses fully reconstructed B^+ meson on tag side and recoil against Λ_c^+ on signal side.

$\Gamma(\Lambda_c^+\overline{\Xi}_c(2645)^0)/\Gamma_{total}$ — Γ_{665}/Γ

VALUE	CL%	DOCUMENT ID		TECN	COMMENT
<7.9 × 10^{-4}	90	[1] LI	19G	BELL	$e^+e^- \to \Upsilon(4S)$

[1] Uses fully reconstructed B^+ meson on tag side and recoil against Λ_c^+ on signal side.

$\Gamma(\Lambda_c^+\overline{\Xi}_c(2790)^0)/\Gamma_{total}$ — Γ_{666}/Γ

VALUE (units 10^{-3})	DOCUMENT ID		TECN	COMMENT
1.1±0.4±0.2	[1] LI	19G	BELL	$e^+e^- \to \Upsilon(4S)$

[1] Uses fully reconstructed B^+ meson on tag side and recoil against Λ_c^+ on signal side.

$\Gamma(\Lambda_c^+\psi_{DS})/\Gamma_{total}$ — Γ_{667}/Γ

VALUE	DOCUMENT ID		TECN	COMMENT
< 1.6–1.7 × 10^{-4}	[1] LEES	25	BABR	$e^+e^- \to \Upsilon(4S)$

[1] LEES 25 searched for ψ_{DS} in the recoil mass against Λ_c^+ and the fully reconstructed accompanying B meson. The cited upper limit is for $m(\psi_{DS})$ between 0.94 and 2.99 GeV/c^2.

Int. J. Mod. Phys. A 2026.41. Downloaded from www.worldscientific.com
by LIFORNIA @ BERKELEY on 09/16/26. Re-use and distribution is strictly not permitted, except for Open Access articles.

$\Gamma(p\psi_{DS})/\Gamma_{total}$ — Γ_{668}/Γ

VALUE	CL%	DOCUMENT ID		TECN	COMMENT
< 10^{-7}–10^{-5}	90	[1] LEES	23C	BABR	$e^+e^- \to \Upsilon(4S)$

[1] LEES 23C searched for ψ_{DS}, where ψ_{DS} is a dark sector antibaryon, in the recoil mass against p and the fully reconstructed accompanying B meson. The cited upper limit is for $m_{\psi_{DS}}$ between 1 and 4.3 GeV/c^2.

$\Gamma(\pi^+\ell^+\ell^-)/\Gamma_{total}$ — Γ_{669}/Γ

VALUE	CL%	DOCUMENT ID		TECN	COMMENT
$<4.9\times10^{-8}$	90	[1] WEI	08A	BELL	$e^+e^- \to \Upsilon(4S)$
• • • We do not use the following data for averages, fits, limits, etc. • • •					
$<6.6\times10^{-8}$	90	[1] LEES	13M	BABR	$e^+e^- \to \Upsilon(4S)$
$<1.2\times10^{-7}$	90	[1] AUBERT	07AG	BABR	$e^+e^- \to \Upsilon(4S)$

[1] Assumes equal production of B^+ and B^0 at the $\Upsilon(4S)$.

$\Gamma(\pi^+e^+e^-)/\Gamma_{total}$ — Γ_{670}/Γ

Test for ΔB=1 weak neutral current. Allowed by higher-order electroweak interactions.

VALUE	CL%	DOCUMENT ID		TECN	COMMENT
$<5.4\times10^{-8}$	90	ADACHI	24N	BELL	$e^+e^- \to \Upsilon(4S)$
• • • We do not use the following data for averages, fits, limits, etc. • • •					
$<12.5\times10^{-8}$	90	[1] LEES	13M	BABR	$e^+e^- \to \Upsilon(4S)$
$<8.0\times10^{-8}$	90	[1] WEI	08A	BELL	$e^+e^- \to \Upsilon(4S)$
$<18\times10^{-8}$	90	[1] AUBERT	07AG	BABR	$e^+e^- \to \Upsilon(4S)$
$<3.9\times10^{-3}$	90	[2] WEIR	90B	MRK2	e^+e^- 29 GeV

[1] Assumes equal production of B^+ and B^0 at the $\Upsilon(4S)$.
[2] WEIR 90B assumes B^+ production cross section from LUND.

$\Gamma(\pi^+\mu^+\mu^-)/\Gamma_{total}$ — Γ_{671}/Γ

Test for ΔB=1 weak neutral current. Allowed by higher-order electroweak interactions.

VALUE (units 10^{-8})	CL%	DOCUMENT ID		TECN	COMMENT
1.78±0.22±0.03		[1] AAIJ	15AR	LHCB	pp at 7, 8 TeV
• • • We do not use the following data for averages, fits, limits, etc. • • •					
< 5.5	90	[2] LEES	13M	BABR	$e^+e^- \to \Upsilon(4S)$
2.3 ±0.6 ±0.1		AAIJ	12AY	LHCB	Repl. by AAIJ 15AR
< 6.9	90	[2] WEI	08A	BELL	$e^+e^- \to \Upsilon(4S)$
<28	90	[2] AUBERT	07AG	BABR	$e^+e^- \to \Upsilon(4S)$

[1] AAIJ 15AR reports $(1.83 \pm 0.24 \pm 0.05)\times10^{-8}$ from a measurement of $[\Gamma(B^+ \to \pi^+\mu^+\mu^-)/\Gamma_{total}]$ / $[B(B^+ \to J/\psi(1S)K^+)]$ / $[B(J/\psi(1S) \to \mu^+\mu^-)]$ assuming $B(B^+ \to J/\psi(1S)K^+) = (1.05 \pm 0.05)\times10^{-3}$, $B(J/\psi(1S) \to \mu^+\mu^-) = (5.961 \pm 0.033)\times10^{-2}$, which we rescale to our best (shown rounded) values $B(B^+ \to J/\psi(1S)K^+) = (1.019 \pm 0.019)\times10^{-3}$, $B(J/\psi(1S) \to \mu^+\mu^-) = (5.961 \pm 0.033)\times10^{-2}$. Our first error is their experiment's error and our second error is the systematic error from using our best (shown rounded) values.
[2] Assumes equal production of B^+ and B^0 at the $\Upsilon(4S)$.

$\Gamma(\pi^+\mu^+\mu^-)/\Gamma(K^+\mu^+\mu^-)$ — $\Gamma_{671}/\Gamma_{678}$

VALUE	DOCUMENT ID		TECN	COMMENT
• • • We do not use the following data for averages, fits, limits, etc. • • •				
0.053±0.014±0.001	AAIJ	12AY	LHCB	Repl. by AAIJ 15AR

$\Gamma(\rho(770)^+e^+e^-)/\Gamma_{total}$ — Γ_{672}/Γ

VALUE	CL%	DOCUMENT ID		TECN	COMMENT
$<46.7\times10^{-8}$	90	ADACHI	24N	BELL	$e^+e^- \to \Upsilon(4S)$

$\Gamma(\rho(770)^+\mu^+\mu^-)/\Gamma_{total}$ — Γ_{673}/Γ

VALUE	CL%	DOCUMENT ID		TECN	COMMENT
$<38.1\times10^{-8}$	90	ADACHI	24N	BELL	$e^+e^- \to \Upsilon(4S)$

$\Gamma(\rho(770)^+\ell^+\ell^-)/\Gamma_{total}$ — Γ_{674}/Γ

VALUE	CL%	DOCUMENT ID		TECN	COMMENT
$<18.9\times10^{-8}$	90	[1] ADACHI	24N	BELL	$e^+e^- \to \Upsilon(4S)$

[1] Where $\ell = e,\ \mu$.

$\Gamma(\pi^+\nu\overline{\nu})/\Gamma_{total}$ — Γ_{675}/Γ

Test for ΔB=1 weak neutral current. Allowed by higher-order electroweak interactions.

VALUE	CL%	DOCUMENT ID		TECN	COMMENT
$<1.4\times10^{-5}$	90	[1] GRYGIER	17	BELL	$e^+e^- \to \Upsilon(4S)$
• • • We do not use the following data for averages, fits, limits, etc. • • •					
$<9.8\times10^{-5}$	90	[1] LUTZ	13	BELL	$e^+e^- \to \Upsilon(4S)$
$<1.7\times10^{-4}$	90	[1] CHEN	07D	BELL	$e^+e^- \to \Upsilon(4S)$
$<1.0\times10^{-4}$	90	[1] AUBERT	05H	BABR	$e^+e^- \to \Upsilon(4S)$

[1] Assumes equal production of B^+ and B^0 at the $\Upsilon(4S)$.

$\Gamma(K^+\ell^+\ell^-)/\Gamma_{total}$ — Γ_{676}/Γ

Test for ΔB=1 weak neutral current. Allowed by higher-order electroweak interactions.

VALUE (units 10^{-7})	DOCUMENT ID		TECN	COMMENT
4.7 ±0.5 OUR AVERAGE Error includes scale factor of 2.3. See the ideogram below.				
$5.99^{+0.45}_{-0.43}\pm0.14$	CHOUDHURY	21	BELL	$e^+e^- \to \Upsilon(4S)$
4.36±0.15±0.18	[1] AAIJ	13H	LHCB	pp at 7 TeV
4.8 ±0.9 ±0.2	[2] AUBERT	09T	BABR	$e^+e^- \to \Upsilon(4S)$
• • • We do not use the following data for averages, fits, limits, etc. • • •				
$5.3^{+0.6}_{-0.5}\pm0.3$	[2,3] WEI	09A	BELL	$e^+e^- \to \Upsilon(4S)$
$3.8^{+0.9}_{-0.8}\pm0.2$	[2] AUBERT,B	06J	BABR	Repl. by AUBERT 09T
$5.3^{+1.1}_{-1.0}\pm0.3$	[2] ISHIKAWA	03	BELL	Repl. by WEI 09A

[1] Uses $B(B^+ \to J/\psi K^+ \to \mu^+\mu^- K^+) = (6.01 \pm 0.21)\times10^{-5}$.
[2] Assumes equal production of B^+ and B^0 at the $\Upsilon(4S)$.
[3] Superseded by CHOUDHURY 21.

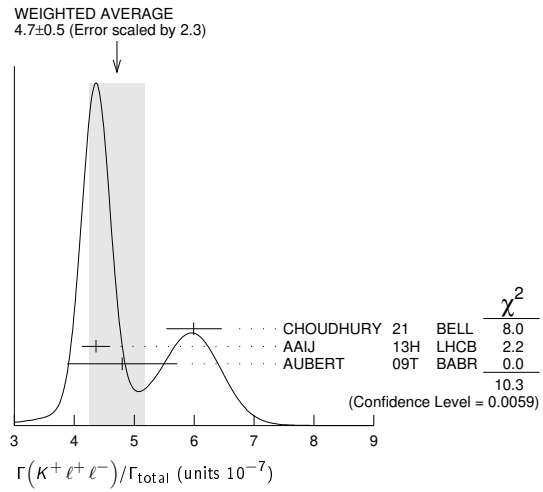

$\Gamma(K^+e^+e^-)/\Gamma_{total}$ — Γ_{677}/Γ

Test for ΔB=1 weak neutral current. Allowed by higher-order electroweak interactions.

VALUE (units 10^{-7})	CL%	DOCUMENT ID		TECN	COMMENT
5.6 ±0.6 OUR AVERAGE					
$5.75^{+0.64}_{-0.61}\pm0.15$		CHOUDHURY	21	BELL	$e^+e^- \to \Upsilon(4S)$
$5.1^{+1.2}_{-1.1}\pm0.2$		[1] AUBERT	09T	BABR	$e^+e^- \to \Upsilon(4S)$
• • • We do not use the following data for averages, fits, limits, etc. • • •					
$5.7^{+0.9}_{-0.8}\pm0.3$		[1,2] WEI	09A	BELL	$e^+e^- \to \Upsilon(4S)$
$4.2^{+1.2}_{-1.1}\pm0.2$		[1] AUBERT,B	06J	BABR	Repl. by AUBERT 09T
$10.5^{+2.5}_{-2.2}\pm0.7$		[1] AUBERT	03U	BABR	Repl. by AUBERT,B 06J
$6.3^{+1.9}_{-1.7}\pm0.3$		[3] ISHIKAWA	03	BELL	Repl. by WEI 09A
<14	90	[1] ABE	02	BELL	$e^+e^- \to \Upsilon(4S)$
< 9	90	[1] AUBERT	02L	BABR	$e^+e^- \to \Upsilon(4S)$
<24	90	[4] ANDERSON	01B	CLE2	$e^+e^- \to \Upsilon(4S)$

[1] Assumes equal production of B^+ and B^0 at the $\Upsilon(4S)$.
[2] Superseded by CHOUDHURY 21.
[3] Assumes equal production of B^0 and B^+ at $\Upsilon(4S)$. The second error is a total of systematic uncertainties including model dependence.
[4] The result is for di-lepton masses above 0.5 GeV.

$\Gamma(K^+\mu^+\mu^-)/\Gamma_{total}$ — Γ_{678}/Γ

Test for ΔB=1 weak neutral current. Allowed by higher-order electroweak interactions.

VALUE (units 10^{-7})	CL%	DOCUMENT ID		TECN	COMMENT
4.53±0.35 OUR FIT Error includes scale factor of 1.8.					
4.5 ±0.6 OUR AVERAGE Error includes scale factor of 2.9.					
$6.24^{+0.65}_{-0.61}\pm0.16$		CHOUDHURY	21	BELL	$e^+e^- \to \Upsilon(4S)$
4.29±0.07±0.21		[1] AAIJ	14M	LHCB	pp at 7, 8 TeV
$4.1^{+1.6}_{-1.5}\pm0.2$		[2] AUBERT	09T	BABR	$e^+e^- \to \Upsilon(4S)$
• • • We do not use the following data for averages, fits, limits, etc. • • •					
4.36±0.15±0.18		[3] AAIJ	13H	LHCB	Repl. by AAIJ 14M
$5.3^{+0.8}_{-0.7}\pm0.3$		[2,4] WEI	09A	BELL	$e^+e^- \to \Upsilon(4S)$
$3.1^{+1.5}_{-1.2}\pm0.3$		[2] AUBERT,B	06J	BABR	Repl. by AUBERT 09T
$0.7^{+1.9}_{-1.1}\pm0.2$		[2] AUBERT	03U	BABR	Repl. by AUBERT,B 06J
$4.5^{+1.4}_{-1.2}\pm0.3$		[5] ISHIKAWA	03	BELL	Repl. by WEI 09A
$9.8^{+4.6}_{-3.6}\pm1.6$		[2] ABE	02	BELL	Repl. by ISHIKAWA 03
< 12	90	[2] AUBERT	02L	BABR	$e^+e^- \to \Upsilon(4S)$
< 36.8	90	[6] ANDERSON	01B	CLE2	$e^+e^- \to \Upsilon(4S)$
< 52	90	[7] AFFOLDER	99B	CDF	$p\overline{p}$ at 1.8 TeV
< 100	90	[8] ABE	96L	CDF	Repl. by AFFOLDER 99B
< 2400	90	[9] ALBRECHT	91E	ARG	$e^+e^- \to \Upsilon(4S)$
<64000	90	[10] WEIR	90B	MRK2	e^+e^- 29 GeV
< 1700	90	[11] AVERY	89B	CLEO	$e^+e^- \to \Upsilon(4S)$
< 3800	90	[12] AVERY	87	CLEO	$e^+e^- \to \Upsilon(4S)$

Int. J. Mod. Phys. A 2026.41. Downloaded from www.worldscientific.com by UNIVERSITY OF CALIFORNIA @ BERKELEY on 09/16/26. Re-use and distribution is strictly not permitted, except for Open Access articles.

[1] Uses B($B^+ \to J/\psi(1S) K^+$) = (0.998 ± 0.014 ± 0.040) × 10^{-3} for normalization.
[2] Assumes equal production of B^+ and B^0 at the $\Upsilon(4S)$.
[3] Uses B($B^+ \to J/\psi K^+ \to \mu^+\mu^- K^+$) = (6.01 ± 0.21) × 10^{-5}.
[4] Superseded by CHOUDHURY 21.
[5] Assumes equal production of B^0 and B^+ at $\Upsilon(4S)$. The second error is a total of systematic uncertainties including model dependence.
[6] The result is for di-lepton masses above 0.5 GeV.
[7] AFFOLDER 99B measured relative to $B^+ \to J/\psi(1S) K^+$.
[8] ABE 96L measured relative to $B^+ \to J/\psi(1S) K^+$ using PDG 94 branching ratios.
[9] ALBRECHT 91E reports < 2.2 × 10^{-4} assuming the $\Upsilon(4S)$ decays 45% to $B^0\overline{B}^0$. We rescale to 50%.
[10] WEIR 90B assumes B^+ production cross section from LUND.
[11] AVERY 89B reports < 1.5 × 10^{-4} assuming the $\Upsilon(4S)$ decays 43% to $B^0\overline{B}^0$. We rescale to 50%.
[12] AVERY 87 reports < 3.2 × 10^{-4} assuming the $\Upsilon(4S)$ decays 40% to $B^0\overline{B}^0$. We rescale to 50%.

$\Gamma(K^+\mu^+\mu^-$ nonresonant$)/\Gamma_{total}$ — Γ_{679}/Γ

VALUE (units 10^{-7})	DOCUMENT ID		TECN	COMMENT
4.37±0.15±0.23	[1] AAIJ	17Y	LHCB	pp at 7, 8 TeV

[1] Measured in amplitude analysis using model including short-distance $K^+\mu^+\mu^-$ and $\rho(770)$, $\omega(782)$, $\phi(1020)$, J/ψ, $\psi(2S)$, $\psi(3770)$, $\psi(4040)$, $\psi(4160)$, and $\psi(4415)$ contributions.

$\Gamma(K^+\tau^+\tau^-)/\Gamma_{total}$ — Γ_{680}/Γ

VALUE	CL%	DOCUMENT ID		TECN	COMMENT
<2.25 × 10^{-3}	90	[1,2] LEES	17	BABR	$e^+e^- \to \Upsilon(4S)$

[1] Uses only leptonic decays of τ and the quoted limit combines the final states $K^+e^+e^-$, $K^+\mu^+\mu^-$, and $K^+e^\pm\mu^\mp$.
[2] If observed events are interpreted as a signal the branching fraction measurement becomes $(1.31^{+0.66}_{-0.61}{}^{+0.35}_{-0.25}) \times 10^{-3}$.

$\Gamma(K^+\mu^+\mu^-)/\Gamma(J/\psi(1S)K^+)$ — $\Gamma_{678}/\Gamma_{316}$

VALUE (units 10^{-3})	DOCUMENT ID		TECN	COMMENT
0.444±0.034 OUR FIT	Error includes scale factor of 1.7.			
0.46 ±0.04 ±0.02	AALTONEN	11AI	CDF	$p\overline{p}$ at 1.96 TeV
• • • We do not use the following data for averages, fits, limits, etc. • • •				
0.38 ±0.05 ±0.02	AALTONEN	11L	CDF	Repl. by AALTONEN 11AI
0.59 ±0.15 ±0.03	AALTONEN	09B	CDF	Repl. by AALTONEN 11L

$\Gamma(K^+\overline{\nu}\nu)/\Gamma_{total}$ — Γ_{681}/Γ

Test for ΔB=1 weak neutral current. Allowed by higher-order electroweak interactions.

VALUE (units 10^{-5})	CL%	DOCUMENT ID		TECN	COMMENT
2.3±0.5$^{+0.5}_{-0.4}$		[1] ADACHI	24E	BELL	$e^+e^- \to \Upsilon(4S)$
• • • We do not use the following data for averages, fits, limits, etc. • • •					
< 4.1	90	[2] ABUDINEN	21	BEL2	$e^+e^- \to \Upsilon(4S)$
< 1.9	90	[3,4] GRYGIER	17	BELL	$e^+e^- \to \Upsilon(4S)$
< 1.6	90	[4,5] LEES	13I	BABR	$e^+e^- \to \Upsilon(4S)$
< 5.5	90	[4] LUTZ	13	BELL	$e^+e^- \to \Upsilon(4S)$
< 1.3	90	[4] DEL-AMO-SA...	10Q	BABR	Repl. by LEES 13I
< 1.4	90	[4] CHEN	07D	BELL	$e^+e^- \to \Upsilon(4S)$
< 5.2	90	[4] AUBERT	05H	BABR	$e^+e^- \to \Upsilon(4S)$
<24	90	[4] BROWDER	01	CLE2	$e^+e^- \to \Upsilon(4S)$

[1] Taking an average value from two methods, using (1) a hadronic tagging of the other B meson in the event, and (2) an inclusive tagging method that exploits the inclusive properties of the other B meson in the event.
[2] Using an inclusive tagging method that exploits not only the properties of the $B^+ \to K^+\nu\overline{\nu}$ decay, but also the inclusive properties of the other B meson in the event.
[3] The result was reported in arXiv:1702.03224, but missing from the publication by mistake.
[4] Assumes equal production of B^+ and B^0 at the $\Upsilon(4S)$.
[5] Also reported a limit < 3.7 × 10^{-5} at 90% CL obtained using a fully reconstructed hadronic B-tag evnets.

$\Gamma(\rho^+\nu\overline{\nu})/\Gamma_{total}$ — Γ_{682}/Γ

Test for ΔB = 1 weak neutral current. Allowed by higher-order electroweak interaction.

VALUE	CL%	DOCUMENT ID		TECN	COMMENT
<3.0 × 10^{-5}	90	[1] GRYGIER	17	BELL	$e^+e^- \to \Upsilon(4S)$
• • • We do not use the following data for averages, fits, limits, etc. • • •					
<2.13 × 10^{-4}	90	[1] LUTZ	13	BELL	$e^+e^- \to \Upsilon(4S)$
<1.5 × 10^{-4}	90	[1] CHEN	07D	BELL	Repl. by LUTZ 13

[1] Assumes equal production of B^+ and B^0 at the $\Upsilon(4S)$.

$\Gamma(K^*(892)^+\ell^+\ell^-)/\Gamma_{total}$ — Γ_{683}/Γ

Test for ΔB=1 weak neutral current. Allowed by higher-order electroweak interactions.

VALUE (units 10^{-7})	CL%	DOCUMENT ID		TECN	COMMENT
10.1 ±1.1 OUR AVERAGE	Error includes scale factor of 1.1.				
9.24±0.93±0.67		AAIJ	14M	LHCB	pp at 7, 8 TeV
14.0 $^{+4.0}_{-3.7}$ ±0.9		[1] AUBERT	09T	BABR	$e^+e^- \to \Upsilon(4S)$
12.4 $^{+2.3}_{-2.1}$ ±1.3		[1] WEI	09A	BELL	$e^+e^- \to \Upsilon(4S)$
• • • We do not use the following data for averages, fits, limits, etc. • • •					
11.6 ±1.9		[2] AAIJ	12AH	LHCB	Repl. by AAIJ 14M
7.3 $^{+5.0}_{-4.2}$ ±2.1		[1] AUBERT,B	06J	BABR	Repl. by AUBERT 09T
<22	90	[1] ISHIKAWA	03	BELL	$e^+e^- \to \Upsilon(4S)$

[1] Assumes equal production of B^+ and B^0 at the $\Upsilon(4S)$.
[2] Measured in $B^+ \to K^*(892)^+\mu^+\mu^-$ decays.

$\Gamma(K^*(892)^+e^+e^-)/\Gamma_{total}$ — Γ_{684}/Γ

Test for ΔB=1 weak neutral current. Allowed by higher-order electroweak interactions.

VALUE (units 10^{-7})	CL%	DOCUMENT ID		TECN	COMMENT
15.5 $^{+4.0}_{-3.1}$ OUR AVERAGE					
13.8 $^{+4.7}_{-4.2}$ ±0.8		[1] AUBERT	09T	BABR	$e^+e^- \to \Upsilon(4S)$
17.3 $^{+5.0}_{-4.2}$ ±2.0		[1] WEI	09A	BELL	$e^+e^- \to \Upsilon(4S)$
• • • We do not use the following data for averages, fits, limits, etc. • • •					
7.5 $^{+7.6}_{-6.5}$ ±3.8		[1] AUBERT,B	06J	BABR	Repl. by AUBERT 09T
2.0 $^{+13.4}_{-8.7}$ ±2.8		[1] AUBERT	03U	BABR	$e^+e^- \to \Upsilon(4S)$
< 46	90	[2] ISHIKAWA	03	BELL	$e^+e^- \to \Upsilon(4S)$
< 89	90	[1] ABE	02	BELL	Repl. by ISHIKAWA 03
< 95	90	[1] AUBERT	02L	BABR	$e^+e^- \to \Upsilon(4S)$
<6900	90	[3] ALBRECHT	91E	ARG	$e^+e^- \to \Upsilon(4S)$

[1] Assumes equal production of B^+ and B^0 at the $\Upsilon(4S)$.
[2] Assumes equal production of B^0 and B^+ at $\Upsilon(4S)$. The second error is a total of systematic uncertainties including model dependence.
[3] ALBRECHT 91E reports < 6.3 × 10^{-4} assuming the $\Upsilon(4S)$ decays 45% to $B^0\overline{B}^0$. We rescale to 50%.

$\Gamma(K^*(892)^+\mu^+\mu^-)/\Gamma_{total}$ — Γ_{685}/Γ

Test for ΔB=1 weak neutral current. Allowed by higher-order electroweak interactions.

VALUE (units 10^{-7})	CL%	DOCUMENT ID		TECN	COMMENT
9.6 ± 1.0 OUR FIT					
9.6 ± 1.1 OUR AVERAGE					
9.24± 0.93±0.67		[1] AAIJ	14M	LHCB	pp at 7, 8 TeV
14.6 $^{+7.9}_{-7.5}$ ±1.2		[2] AUBERT	09T	BABR	$e^+e^- \to \Upsilon(4S)$
11.1 $^{+3.2}_{-2.7}$ ±1.0		[2] WEI	09A	BELL	$e^+e^- \to \Upsilon(4S)$
• • • We do not use the following data for averages, fits, limits, etc. • • •					
11.6 ± 1.9		AAIJ	12AH	LHCB	Repl. by AAIJ 14M
9.7 $^{+9.4}_{-6.9}$ ±1.4		[2] AUBERT,B	06J	BABR	Repl. by AUBERT 09T
30.7 $^{+25.8}_{-17.8}$ ±4.2		[2] AUBERT	03U	BABR	$e^+e^- \to \Upsilon(4S)$
6.5 $^{+6.9}_{-5.3}$ $^{+1.5}_{-1.6}$		[3] ISHIKAWA	03	BELL	Repl. by WEI 09A
< 39	90	[2] ABE	02	BELL	Repl. by ISHIKAWA 03
<170	90	[2] AUBERT	02L	BABR	$e^+e^- \to \Upsilon(4S)$

[1] Uses B($B^+ \to J/\psi(1S) K^*(892)^+$) = (1.431±0.027±0.090)×$10^{-3}$ for normalization.
[2] Assumes equal production of B^+ and B^0 at the $\Upsilon(4S)$.
[3] Assumes equal production of B^0 and B^+ at $\Upsilon(4S)$. The second error is a total of systematic uncertainties including model dependence. The 90% C.L. upper limit is 2.2 × 10^{-6}.

$\Gamma(K^*(892)^+\mu^+\mu^-)/\Gamma(J/\psi(1S)K^*(892)^+)$ — $\Gamma_{685}/\Gamma_{321}$

VALUE (units 10^{-3})	DOCUMENT ID		TECN	COMMENT
0.67±0.08 OUR FIT				
0.67±0.22±0.04	AALTONEN	11AI	CDF	$p\overline{p}$ at 1.96 TeV

$\Gamma(K^*(892)^+\nu\overline{\nu})/\Gamma_{total}$ — Γ_{686}/Γ

Test for ΔB = 1 weak neutral current. Allowed by higher-order electroweak interaction.

VALUE	CL%	DOCUMENT ID		TECN	COMMENT
<4.0 × 10^{-5}	90	[1] LUTZ	13	BELL	$e^+e^- \to \Upsilon(4S)$
• • • We do not use the following data for averages, fits, limits, etc. • • •					
<6.1 × 10^{-5}	90	[1] GRYGIER	17	BELL	$e^+e^- \to \Upsilon(4S)$
<6.4 × 10^{-5}	90	[1,2] LEES	13I	BABR	$e^+e^- \to \Upsilon(4S)$
<8 × 10^{-5}	90	AUBERT	08BC	BABR	Repl. by LEES 13I
<1.4 × 10^{-4}	90	[1] CHEN	07D	BELL	$e^+e^- \to \Upsilon(4S)$

[1] Assumes equal production of B^+ and B^0 at the $\Upsilon(4S)$.
[2] Also reported a limit < 11.6 × 10^{-5} at 90% CL obtained using a fully reconstructed hadronic B-tag evnets.

$\Gamma(K^+\pi^+\pi^-\mu^+\mu^-)/\Gamma(\psi(2S)K^+)$ — $\Gamma_{687}/\Gamma_{352}$

VALUE (units 10^{-4})	DOCUMENT ID		TECN	COMMENT
6.95$^{+0.46}_{-0.43}$±0.34	AAIJ	14AZ	LHCB	pp at 7, 8 TeV

$\Gamma(\phi K^+\mu^+\mu^-)/\Gamma(J/\psi(1S)\phi K^+)$ — $\Gamma_{689}/\Gamma_{328}$

VALUE (units 10^{-3})	DOCUMENT ID		TECN	COMMENT
1.58$^{+0.36}_{-0.32}$$^{+0.19}_{-0.07}$	AAIJ	14AZ	LHCB	pp at 7, 8 TeV

$\Gamma(\overline{\Lambda}p\nu\overline{\nu})/\Gamma_{total}$ — Γ_{690}/Γ

VALUE	CL%	DOCUMENT ID		TECN	COMMENT
<3.0 × 10^{-5}	90	[1] LEES	19C	BABR	$e^+e^- \to \Upsilon(4S)$

[1] Signal candidates are identified by first fully reconstructing B^+ in one of many possible exclusive decays to hadronic final states.

$\Gamma(\pi^+e^+\mu^-)/\Gamma_{total}$ — Γ_{691}/Γ

Test of lepton family number conservation.

VALUE	CL%	DOCUMENT ID		TECN	COMMENT
<0.0064	90	[1] WEIR	90B	MRK2	e^+e^- 29 GeV

[1] WEIR 90B assumes B^+ production cross section from LUND.

Int. J. Mod. Phys. A 2026.41. Downloaded from www.worldscientific.com by LIFORNIA @ BERKELEY on 09/16/26. Re-use and distribution is strictly not permitted, except for Open Access articles.

$\Gamma(\pi^+ e^- \mu^+)/\Gamma_{total}$ — Γ_{692}/Γ

Test of lepton family number conservation.

VALUE	CL%	DOCUMENT ID		TECN	COMMENT
<0.0064	90	[1] WEIR	90B	MRK2	e^+e^- 29 GeV

[1] WEIR 90B assumes B^+ production cross section from LUND.

$\Gamma(\pi^+ e^\pm \mu^\mp)/\Gamma_{total}$ — Γ_{693}/Γ

VALUE	CL%	DOCUMENT ID		TECN	COMMENT
$<1.7 \times 10^{-7}$	90	[1] AUBERT	07AG	BABR	$e^+e^- \to \Upsilon(4S)$

[1] Assumes equal production of B^+ and B^0 at the $\Upsilon(4S)$.

$\Gamma(\pi^+ e^+ \tau^-)/\Gamma_{total}$ — Γ_{694}/Γ

Test of lepton family number conservation.

VALUE (units 10^{-6})	CL%	DOCUMENT ID		TECN	COMMENT
<74	90	[1] LEES	12P	BABR	$e^+e^- \to \Upsilon(4S)$

[1] Uses a fully reconstructed hadronic B decay as a tag on the recoil side.

$\Gamma(\pi^+ e^- \tau^+)/\Gamma_{total}$ — Γ_{695}/Γ

Test of lepton family number conservation.

VALUE (units 10^{-6})	CL%	DOCUMENT ID		TECN	COMMENT
<20	90	[1] LEES	12P	BABR	$e^+e^- \to \Upsilon(4S)$

[1] Uses a fully reconstructed hadronic B decay as a tag on the recoil side.

$\Gamma(\pi^+ e^\pm \tau^\mp)/\Gamma_{total}$ — Γ_{696}/Γ

Test of lepton family number conservation.

VALUE (units 10^{-6})	CL%	DOCUMENT ID		TECN	COMMENT
<75	90	[1,2] LEES	12P	BABR	$e^+e^- \to \Upsilon(4S)$

[1] Assumes $B(B^+ \to h^+\ell^+\tau^-) = B(B^+ \to h^+\ell^-\tau^+)$.
[2] Uses a fully reconstructed hadronic B decay as a tag on the recoil side.

$\Gamma(\pi^+ \mu^+ \tau^-)/\Gamma_{total}$ — Γ_{697}/Γ

Test of lepton family number conservation.

VALUE (units 10^{-6})	CL%	DOCUMENT ID		TECN	COMMENT
<62	90	[1] LEES	12P	BABR	$e^+e^- \to \Upsilon(4S)$

[1] Uses a fully reconstructed hadronic B decay as a tag on the recoil side.

$\Gamma(\pi^+ \mu^- \tau^+)/\Gamma_{total}$ — Γ_{698}/Γ

Test of lepton family number conservation.

VALUE (units 10^{-6})	CL%	DOCUMENT ID		TECN	COMMENT
<45	90	[1] LEES	12P	BABR	$e^+e^- \to \Upsilon(4S)$

[1] Uses a fully reconstructed hadronic B decay as a tag on the recoil side.

$\Gamma(\pi^+ \mu^\pm \tau^\mp)/\Gamma_{total}$ — Γ_{699}/Γ

Test of lepton family number conservation.

VALUE (units 10^{-6})	CL%	DOCUMENT ID		TECN	COMMENT
<72	90	[1,2] LEES	12P	BABR	$e^+e^- \to \Upsilon(4S)$

[1] Assumes $B(B^+ \to h^+\ell^+\tau^-) = B(B^+ \to h^+\ell^-\tau^+)$.
[2] Uses a fully reconstructed hadronic B decay as a tag on the recoil side.

$\Gamma(K^+ e^+ \mu^-)/\Gamma_{total}$ — Γ_{700}/Γ

Test of lepton family number conservation.

VALUE	CL%	DOCUMENT ID		TECN	COMMENT
$<7.0 \times 10^{-9}$	90	AAIJ	19AM	LHCB	pp at 7, 8 TeV
• • • We do not use the following data for averages, fits, limits, etc. • • •					
$<3.0 \times 10^{-8}$	90	CHOUDHURY	21	BELL	$e^+e^- \to \Upsilon(4S)$
$<0.91 \times 10^{-7}$	90	[1] AUBERT,B	06J	BABR	$e^+e^- \to \Upsilon(4S)$
$<8 \times 10^{-7}$	90	[1] AUBERT	02L	BABR	Repl. by AUBERT,B 06J
$<6.4 \times 10^{-3}$	90	[2] WEIR	90B	MRK2	e^+e^- 29 GeV

[1] Assumes equal production of B^+ and B^0 at the $\Upsilon(4S)$.
[2] WEIR 90B assumes B^+ production cross section from LUND.

$\Gamma(K^+ e^- \mu^+)/\Gamma_{total}$ — Γ_{701}/Γ

Test of lepton family number conservation.

VALUE	CL%	DOCUMENT ID		TECN	COMMENT
$<6.4 \times 10^{-9}$	90	AAIJ	19AM	LHCB	pp at 7, 8 TeV
• • • We do not use the following data for averages, fits, limits, etc. • • •					
$<8.5 \times 10^{-8}$	90	CHOUDHURY	21	BELL	$e^+e^- \to \Upsilon(4S)$
$<1.3 \times 10^{-7}$	90	[1] AUBERT,B	06J	BABR	$e^+e^- \to \Upsilon(4S)$
$<6.4 \times 10^{-3}$	90	[2] WEIR	90B	MRK2	e^+e^- 29 GeV

[1] Assumes equal production of B^+ and B^0 at the $\Upsilon(4S)$.
[2] WEIR 90B assumes B^+ production cross section from LUND.

$\Gamma(K^+ e^\pm \mu^\mp)/\Gamma_{total}$ — Γ_{702}/Γ

VALUE (units 10^{-7})	CL%	DOCUMENT ID		TECN	COMMENT
<0.91	90	[1] AUBERT,B	06J	BABR	$e^+e^- \to \Upsilon(4S)$

[1] Assumes equal production of B^+ and B^0 at the $\Upsilon(4S)$.

$\Gamma(K^+ e^+ \tau^-)/\Gamma_{total}$ — Γ_{703}/Γ

Test of lepton family number conservation.

VALUE	CL%	DOCUMENT ID		TECN	COMMENT
$<1.53 \times 10^{-5}$	90	[1] WATANUKI	23	BELL	$e^+e^- \to \Upsilon(4S)$
• • • We do not use the following data for averages, fits, limits, etc. • • •					
$<4.3 \times 10^{-5}$	90	[2] LEES	12P	BABR	$e^+e^- \to \Upsilon(4S)$

[1] Uses a fully reconstructed hadronic B^- decay as a tag on the recoil side.
[2] Uses a fully reconstructed hadronic B decay as a tag on the recoil side.

$\Gamma(K^+ e^- \tau^+)/\Gamma_{total}$ — Γ_{704}/Γ

Test of lepton family number conservation.

VALUE	CL%	DOCUMENT ID		TECN	COMMENT
$<1.51 \times 10^{-5}$	90	[1] WATANUKI	23	BELL	$e^+e^- \to \Upsilon(4S)$
$<1.5 \times 10^{-5}$	90	[2] LEES	12P	BABR	$e^+e^- \to \Upsilon(4S)$

[1] Uses a fully reconstructed hadronic B^- decay as a tag on the recoil side.
[2] Uses a fully reconstructed hadronic B decay as a tag on the recoil side.

$\Gamma(K^+ e^\pm \tau^\mp)/\Gamma_{total}$ — Γ_{705}/Γ

Test of lepton family number conservation.

VALUE (units 10^{-6})	CL%	DOCUMENT ID		TECN	COMMENT
<30	90	[1,2] LEES	12P	BABR	$e^+e^- \to \Upsilon(4S)$

[1] Assumes $B(B^+ \to h^+\ell^+\tau^-) = B(B^+ \to h^+\ell^-\tau^+)$.
[2] Uses a fully reconstructed hadronic B decay as a tag on the recoil side.

$\Gamma(K^+ \mu^+ \tau^-)/\Gamma_{total}$ — Γ_{706}/Γ

Test of lepton family number conservation.

VALUE	CL%	DOCUMENT ID		TECN	COMMENT
$<2.45 \times 10^{-5}$	90	[1] WATANUKI	23	BELL	$e^+e^- \to \Upsilon(4S)$
• • • We do not use the following data for averages, fits, limits, etc. • • •					
$<4.5 \times 10^{-5}$	90	[2] LEES	12P	BABR	$e^+e^- \to \Upsilon(4S)$

[1] Uses a fully reconstructed hadronic B^- decay as a tag on the recoil side.
[2] Uses a fully reconstructed hadronic B decay as a tag on the recoil side.

$\Gamma(K^+ \mu^- \tau^+)/\Gamma_{total}$ — Γ_{707}/Γ

Test of lepton family number conservation.

VALUE	CL%	DOCUMENT ID		TECN	COMMENT
$<0.59 \times 10^{-5}$	90	[1] WATANUKI	23	BELL	$e^+e^- \to \Upsilon(4S)$
• • • We do not use the following data for averages, fits, limits, etc. • • •					
$<3.9 \times 10^{-5}$	90	[2] AAIJ	20P	LHCB	pp at 7, 8, 13 TeV
$<2.8 \times 10^{-5}$	90	[3] LEES	12P	BABR	$e^+e^- \to \Upsilon(4S)$

[1] Uses a fully reconstructed hadronic B^- decay as a tag on the recoil side.
[2] Uses the $B^*_{s2}{}^0 \to B^+K^-$ decays for kinematic constraints.
[3] Uses a fully reconstructed hadronic B decay as a tag on the recoil side.

$\Gamma(K^+ \mu^\pm \tau^\mp)/\Gamma_{total}$ — Γ_{708}/Γ

Test of lepton family number conservation.

VALUE (units 10^{-6})	CL%	DOCUMENT ID		TECN	COMMENT
<48	90	[1,2] LEES	12P	BABR	$e^+e^- \to \Upsilon(4S)$
• • • We do not use the following data for averages, fits, limits, etc. • • •					
<77	90	[1] AUBERT	07AZ	BABR	Repl. by LEES 12P

[1] Uses a fully reconstructed hadronic B decay as a tag on the recoil side.
[2] Assumes $B(B^+ \to h^+\ell^+\tau^-) = B(B^+ \to h^+\ell^-\tau^+)$.

$\Gamma(K^*(892)^+ e^+ \mu^-)/\Gamma_{total}$ — Γ_{709}/Γ

VALUE (units 10^{-7})	CL%	DOCUMENT ID		TECN	COMMENT
<13	90	[1] AUBERT,B	06J	BABR	$e^+e^- \to \Upsilon(4S)$

[1] Assumes equal production of B^+ and B^0 at the $\Upsilon(4S)$.

$\Gamma(K^*(892)^+ e^- \mu^+)/\Gamma_{total}$ — Γ_{710}/Γ

VALUE (units 10^{-7})	CL%	DOCUMENT ID		TECN	COMMENT
<9.9	90	[1] AUBERT,B	06J	BABR	$e^+e^- \to \Upsilon(4S)$

[1] Assumes equal production of B^+ and B^0 at the $\Upsilon(4S)$.

$\Gamma(K^*(892)^+ e^\pm \mu^\mp)/\Gamma_{total}$ — Γ_{711}/Γ

Test of lepton family number conservation.

VALUE	CL%	DOCUMENT ID		TECN	COMMENT
$<1.4 \times 10^{-6}$	90	[1] AUBERT,B	06J	BABR	$e^+e^- \to \Upsilon(4S)$
• • • We do not use the following data for averages, fits, limits, etc. • • •					
$<7.9 \times 10^{-6}$	90	[1] AUBERT	02L	BABR	Repl. by AUBERT,B 06J

[1] Assumes equal production of B^+ and B^0 at the $\Upsilon(4S)$.

$\Gamma(\pi^- e^+ e^+)/\Gamma_{total}$ — Γ_{712}/Γ

Test of total lepton number conservation.

VALUE	CL%	DOCUMENT ID		TECN	COMMENT
$<2.3 \times 10^{-8}$	90	[1] LEES	12J	BABR	$e^+e^- \to \Upsilon(4S)$
• • • We do not use the following data for averages, fits, limits, etc. • • •					
$<1.6 \times 10^{-6}$	90	[1] EDWARDS	02B	CLE2	$e^+e^- \to \Upsilon(4S)$
<0.0039	90	[2] WEIR	90B	MRK2	e^+e^- 29 GeV

[1] Assumes equal production of B^+ and B^0 at the $\Upsilon(4S)$.
[2] WEIR 90B assumes B^+ production cross section from LUND.

$\Gamma(\pi^- \mu^+ \mu^+)/\Gamma_{total}$ — Γ_{713}/Γ

Test of total lepton number conservation.

VALUE	CL%	DOCUMENT ID		TECN	COMMENT
$< 4.0 \times 10^{-9}$	95	[1] AAIJ	14AC	LHCB	pp at 7, 8 TeV
• • • We do not use the following data for averages, fits, limits, etc. • • •					
$< 1.3 \times 10^{-8}$	95	[2] AAIJ	12AD	LHCB	Repl. by AAIJ 14AC
$< 4.4 \times 10^{-8}$	90	AAIJ	12C	LHCB	pp at 7 TeV
$<10.7 \times 10^{-8}$	90	[3] LEES	12J	BABR	$e^+e^- \to \Upsilon(4S)$
$< 1.4 \times 10^{-6}$	90	[3] EDWARDS	02B	CLE2	$e^+e^- \to \Upsilon(4S)$
$< 9.1 \times 10^{-3}$	90	[4] WEIR	90B	MRK2	e^+e^- 29 GeV

Int. J. Mod. Phys. A 2026.41. Downloaded from www.worldscientific.com by UNIVERSITY OF CALIFORNIA @ BERKELEY on 09/16/26. Re-use and distribution is strictly not permitted, except for Open Access articles.

[1] Uses $B^+ \to J/\psi K^+$, $J/\psi \to \mu^+\mu^-$ mode for normalization. Obtains neutrino-mass-dependent upper limits in the range 0.4–4.0 $\times 10^{-9}$. This limit is applicable for Majorana neutrino lifetime < 1 ps.

[2] Uses $B^+ \to J/\psi K^+$, $J/\psi \to \mu^+\mu^-$ mode for normalization. Obtains neutrino-mass-dependent upper limits in the range 0.4–1.0 $\times 10^{-8}$.

[3] Assumes equal production of B^+ and B^0 at the $\Upsilon(4S)$.

[4] WEIR 90B assumes B^+ production cross section from LUND.

$\Gamma(\pi^- e^+ \mu^+)/\Gamma_{total}$ — Γ_{714}/Γ

Test of total lepton number conservation.

VALUE	CL%	DOCUMENT ID		TECN	COMMENT
<1.5 $\times 10^{-7}$	90	[1] LEES	14A	BABR	$e^+e^- \to \Upsilon(4S)$
• • • We do not use the following data for averages, fits, limits, etc. • • •					
<1.3 $\times 10^{-6}$	90	[1] EDWARDS	02B	CLE2	$e^+e^- \to \Upsilon(4S)$
<0.0064	90	[2] WEIR	90B	MRK2	e^+e^- 29 GeV

[1] Assumes equal production of B^+ and B^0 at the $\Upsilon(4S)$.

[2] WEIR 90B assumes B^+ production cross section from LUND.

$\Gamma(\rho^- e^+ e^+)/\Gamma_{total}$ — Γ_{715}/Γ

Test of total lepton number conservation.

VALUE (units 10^{-6})	CL%	DOCUMENT ID		TECN	COMMENT
<0.17	90	[1] LEES	14A	BABR	$e^+e^- \to \Upsilon(4S)$
• • • We do not use the following data for averages, fits, limits, etc. • • •					
<2.6	90	[1] EDWARDS	02B	CLE2	$e^+e^- \to \Upsilon(4S)$

[1] Assumes equal production of B^+ and B^0 at the $\Upsilon(4S)$.

$\Gamma(\rho^- \mu^+ \mu^+)/\Gamma_{total}$ — Γ_{716}/Γ

Test of total lepton number conservation.

VALUE (units 10^{-6})	CL%	DOCUMENT ID		TECN	COMMENT
<0.42	90	LEES	14A	BABR	$e^+e^- \to \Upsilon(4S)$
• • • We do not use the following data for averages, fits, limits, etc. • • •					
<5.0	90	[1] EDWARDS	02B	CLE2	$e^+e^- \to \Upsilon(4S)$

[1] Assumes equal production of B^+ and B^0 at the $\Upsilon(4S)$.

$\Gamma(\rho^- e^+ \mu^+)/\Gamma_{total}$ — Γ_{717}/Γ

Test of total lepton number conservation.

VALUE (units 10^{-6})	CL%	DOCUMENT ID		TECN	COMMENT
<0.47	90	[1] LEES	14A	BABR	$e^+e^- \to \Upsilon(4S)$
• • • We do not use the following data for averages, fits, limits, etc. • • •					
<3.3	90	[1] EDWARDS	02B	CLE2	$e^+e^- \to \Upsilon(4S)$

[1] Assumes equal production of B^+ and B^0 at the $\Upsilon(4S)$.

$\Gamma(K^- e^+ e^+)/\Gamma_{total}$ — Γ_{718}/Γ

Test of total lepton number conservation.

VALUE	CL%	DOCUMENT ID		TECN	COMMENT
<3.0 $\times 10^{-8}$	90	[1] LEES	12J	BABR	$e^+e^- \to \Upsilon(4S)$
• • • We do not use the following data for averages, fits, limits, etc. • • •					
<1.0 $\times 10^{-6}$	90	[1] EDWARDS	02B	CLE2	$e^+e^- \to \Upsilon(4S)$
<0.0039	90	[2] WEIR	90B	MRK2	e^+e^- 29 GeV

[1] Assumes equal production of B^+ and B^0 at the $\Upsilon(4S)$.

[2] WEIR 90B assumes B^+ production cross section from LUND.

$\Gamma(K^- \mu^+ \mu^+)/\Gamma_{total}$ — Γ_{719}/Γ

Test of total lepton number conservation.

VALUE	CL%	DOCUMENT ID		TECN	COMMENT
<4.1 $\times 10^{-8}$	90	AAIJ	12C	LHCB	pp at 7 TeV
• • • We do not use the following data for averages, fits, limits, etc. • • •					
<6.7 $\times 10^{-8}$	90	[1] LEES	12J	BABR	$e^+e^- \to \Upsilon(4S)$
<1.8 $\times 10^{-6}$	90	[1] EDWARDS	02B	CLE2	$e^+e^- \to \Upsilon(4S)$
<9.1 $\times 10^{-3}$	90	[2] WEIR	90B	MRK2	e^+e^- 29 GeV

[1] Assumes equal production of B^+ and B^0 at the $\Upsilon(4S)$.

[2] WEIR 90B assumes B^+ production cross section from LUND.

$\Gamma(K^- e^+ \mu^+)/\Gamma_{total}$ — Γ_{720}/Γ

Test of total lepton number conservation.

VALUE	CL%	DOCUMENT ID		TECN	COMMENT
<1.6 $\times 10^{-7}$	90	[1] LEES	14A	BABR	$e^+e^- \to \Upsilon(4S)$
• • • We do not use the following data for averages, fits, limits, etc. • • •					
<2.0 $\times 10^{-6}$	90	[1] EDWARDS	02B	CLE2	$e^+e^- \to \Upsilon(4S)$
<0.0064	90	[2] WEIR	90B	MRK2	e^+e^- 29 GeV

[1] Assumes equal production of B^+ and B^0 at the $\Upsilon(4S)$.

[2] WEIR 90B assumes B^+ production cross section from LUND.

$\Gamma(K^*(892)^- e^+ e^+)/\Gamma_{total}$ — Γ_{721}/Γ

Test of total lepton number conservation.

VALUE (units 10^{-6})	CL%	DOCUMENT ID		TECN	COMMENT
<0.40	90	[1] LEES	14A	BABR	$e^+e^- \to \Upsilon(4S)$
• • • We do not use the following data for averages, fits, limits, etc. • • •					
<2.8	90	[1] EDWARDS	02B	CLE2	$e^+e^- \to \Upsilon(4S)$

[1] Assumes equal production of B^+ and B^0 at the $\Upsilon(4S)$.

$\Gamma(K^*(892)^- \mu^+ \mu^+)/\Gamma_{total}$ — Γ_{722}/Γ

Test of total lepton number conservation.

VALUE (units 10^{-6})	CL%	DOCUMENT ID		TECN	COMMENT
<0.59	90	[1] LEES	14A	BABR	$e^+e^- \to \Upsilon(4S)$
• • • We do not use the following data for averages, fits, limits, etc. • • •					
<8.3	90	[1] EDWARDS	02B	CLE2	$e^+e^- \to \Upsilon(4S)$

[1] Assumes equal production of B^+ and B^0 at the $\Upsilon(4S)$.

$\Gamma(K^*(892)^- e^+ \mu^+)/\Gamma_{total}$ — Γ_{723}/Γ

Test of total lepton number conservation.

VALUE (units 10^{-6})	CL%	DOCUMENT ID		TECN	COMMENT
<0.30	90	[1] LEES	14A	BABR	$e^+e^- \to \Upsilon(4S)$
• • • We do not use the following data for averages, fits, limits, etc. • • •					
<4.4	90	[1] EDWARDS	02B	CLE2	$e^+e^- \to \Upsilon(4S)$

[1] Assumes equal production of B^+ and B^0 at the $\Upsilon(4S)$.

$\Gamma(D_s^+ \mu^+ \mu^-)/\Gamma_{total}$ — Γ_{688}/Γ

VALUE	CL%	DOCUMENT ID		TECN	COMMENT
<2.4 $\times 10^{-8}$	90	AAIJ	24F	LHCB	pp at 7, 8, 13 TeV

$\Gamma(D^- e^+ e^+)/\Gamma_{total}$ — Γ_{724}/Γ

VALUE	CL%	DOCUMENT ID		TECN	COMMENT
<2.6 $\times 10^{-6}$	90	[1] LEES	14A	BABR	$e^+e^- \to \Upsilon(4S)$
<2.6 $\times 10^{-6}$	90	[1,2] SEON	11	BELL	$e^+e^- \to \Upsilon(4S)$

[1] Assumes equal production of B^0 and B^+ from Upsilon(4S) decays.

[2] Uses $D^- \to K^+\pi^-\pi^-$ mode and 3-body phase-space hypothesis for the signal decays.

$\Gamma(D^- e^+ \mu^+)/\Gamma_{total}$ — Γ_{725}/Γ

VALUE	CL%	DOCUMENT ID		TECN	COMMENT
<1.8 $\times 10^{-6}$	90	[1,2] SEON	11	BELL	$e^+e^- \to \Upsilon(4S)$
• • • We do not use the following data for averages, fits, limits, etc. • • •					
<2.1 $\times 10^{-6}$	90	[1] LEES	14A	BABR	$e^+e^- \to \Upsilon(4S)$

[1] Assumes equal production of B^0 and B^+ from Upsilon(4S) decays.

[2] Uses $D^- \to K^+\pi^-\pi^-$ mode and 3-body phase-space hypothesis for the signal decays.

$\Gamma(D^- \mu^+ \mu^+)/\Gamma_{total}$ — Γ_{726}/Γ

VALUE	CL%	DOCUMENT ID		TECN	COMMENT
< 6.9 $\times 10^{-7}$	95	[1] AAIJ	12AD	LHCB	pp at 7 TeV
• • • We do not use the following data for averages, fits, limits, etc. • • •					
<17 $\times 10^{-7}$	90	[2] LEES	14A	BABR	$e^+e^- \to \Upsilon(4S)$
< 1.1 $\times 10^{-6}$	90	[2,3] SEON	11	BELL	$e^+e^- \to \Upsilon(4S)$

[1] Uses $B^+ \to \psi(2S)K^+$, $\psi(2S) \to J/\psi\pi^+\pi^-$ mode for normalization.

[2] Assumes equal production of B^0 and B^+ from Upsilon(4S) decays.

[3] Uses $D^- \to K^+\pi^-\pi^-$ mode and 3-body phase-space hypothesis for the signal decays.

$\Gamma(D^{*-} \mu^+ \mu^+)/\Gamma_{total}$ — Γ_{727}/Γ

VALUE	CL%	DOCUMENT ID		TECN	COMMENT
<2.4 $\times 10^{-6}$	95	[1] AAIJ	12AD	LHCB	pp at 7 TeV

[1] Uses $B^+ \to \psi(2S)K^+$, $\psi(2S) \to J/\psi\pi^+\pi^-$ mode for normalization.

$\Gamma(D_s^- \mu^+ \mu^+)/\Gamma_{total}$ — Γ_{728}/Γ

VALUE	CL%	DOCUMENT ID		TECN	COMMENT
<5.8 $\times 10^{-7}$	95	[1] AAIJ	12AD	LHCB	pp at 7 TeV

[1] Uses $B^+ \to \psi(2S)K^+$, $\psi(2S) \to J/\psi\pi^+\pi^-$ mode for normalization. Obtains neutrino-mass-dependent upper limits in the range 1.5–8.0 $\times 10^{-7}$.

$\Gamma(\overline{D}^0 \pi^- \mu^+ \mu^+)/\Gamma_{total}$ — Γ_{729}/Γ

VALUE	CL%	DOCUMENT ID		TECN	COMMENT
<1.5 $\times 10^{-6}$	95	[1] AAIJ	12AD	LHCB	pp at 7 TeV

[1] Uses $B^+ \to \psi(2S)K^+$, $\psi(2S) \to J/\psi\pi^+\pi^-$ mode for normalization. Obtains neutrino-mass-dependent upper limits in the range 0.3–1.5 $\times 10^{-6}$.

$\Gamma(\Lambda^0 \mu^+)/\Gamma_{total}$ — Γ_{730}/Γ

VALUE	CL%	DOCUMENT ID		TECN	COMMENT
<6 $\times 10^{-8}$	90	[1,2] DEL-AMO-SA...11K		BABR	$e^+e^- \to \Upsilon(4S)$

[1] DEL-AMO-SANCHEZ 11K reports $< 6.1 \times 10^{-8}$ from a measurement of $[\Gamma(B^+ \to \Lambda^0\mu^+)/\Gamma_{total}] \times [B(\Lambda \to p\pi^-)]$ assuming $B(\Lambda \to p\pi^-) = (63.9 \pm 0.5) \times 10^{-2}$, which we rescale to our best (shown rounded) value $B(\Lambda \to p\pi^-) = 64.1 \times 10^{-2}$.

[2] Uses $B(\Upsilon(4S) \to B^0\overline{B}^0) = (51.6 \pm 0.6)\%$ and $B(\Upsilon(4S) \to B^+B^-) = (48.4 \pm 0.6)\%$.

$\Gamma(\Lambda^0 e^+)/\Gamma_{total}$ — Γ_{731}/Γ

VALUE	CL%	DOCUMENT ID		TECN	COMMENT
<3.2 $\times 10^{-8}$	90	[1,2] DEL-AMO-SA...11K		BABR	$e^+e^- \to \Upsilon(4S)$

[1] DEL-AMO-SANCHEZ 11K reports $< 3.2 \times 10^{-8}$ from a measurement of $[\Gamma(B^+ \to \Lambda^0 e^+)/\Gamma_{total}] \times [B(\Lambda \to p\pi^-)]$ assuming $B(\Lambda \to p\pi^-) = (63.9 \pm 0.5) \times 10^{-2}$, which we rescale to our best (shown rounded) value $B(\Lambda \to p\pi^-) = 64.1 \times 10^{-2}$.

[2] Uses $B(\Upsilon(4S) \to B^0\overline{B}^0) = (51.6 \pm 0.6)\%$ and $B(\Upsilon(4S) \to B^+B^-) = (48.4 \pm 0.6)\%$.

$\Gamma(\overline{\Lambda}^0 \mu^+)/\Gamma_{total}$ — Γ_{732}/Γ

VALUE	CL%	DOCUMENT ID		TECN	COMMENT
<6 $\times 10^{-8}$	90	[1,2] DEL-AMO-SA...11K		BABR	$e^+e^- \to \Upsilon(4S)$

[1] DEL-AMO-SANCHEZ 11K reports $< 6.2 \times 10^{-8}$ from a measurement of $[\Gamma(B^+ \to \overline{\Lambda}^0 \mu^+)/\Gamma_{total}] \times [B(\Lambda \to p\pi^-)]$ assuming $B(\Lambda \to p\pi^-) = (63.9 \pm 0.5) \times 10^{-2}$, which we rescale to our best (shown rounded) value $B(\Lambda \to p\pi^-) = 64.1 \times 10^{-2}$.
[2] Uses $B(\Upsilon(4S) \to B^0\overline{B}^0) = (51.6 \pm 0.6)\%$ and $B(\Upsilon(4S) \to B^+B^-) = (48.4 \pm 0.6)\%$.

$\Gamma(\overline{\Lambda}^0 e^+)/\Gamma_{total}$ — Γ_{733}/Γ

VALUE	CL%	DOCUMENT ID		TECN	COMMENT
$<8 \times 10^{-8}$	90	[1,2] DEL-AMO-SA...11K		BABR	$e^+e^- \to \Upsilon(4S)$

[1] DEL-AMO-SANCHEZ 11K reports $< 8.1 \times 10^{-8}$ from a measurement of $[\Gamma(B^+ \to \overline{\Lambda}^0 e^+)/\Gamma_{total}] \times [B(\Lambda \to p\pi^-)]$ assuming $B(\Lambda \to p\pi^-) = (63.9 \pm 0.5) \times 10^{-2}$, which we rescale to our best (shown rounded) value $B(\Lambda \to p\pi^-) = 64.1 \times 10^{-2}$.
[2] Uses $B(\Upsilon(4S) \to B^0\overline{B}^0) = (51.6 \pm 0.6)\%$ and $B(\Upsilon(4S) \to B^+B^-) = (48.4 \pm 0.6)\%$.

$\Gamma(\Xi_c^0 \Lambda_c^+)/\Gamma(\overline{\Xi}_c^0 \Lambda_c^+)$ — $\Gamma_{660}/\Gamma_{659}$

VALUE	CL%	DOCUMENT ID		TECN	COMMENT
$<2.7 \times 10^{-2}$	95	[1] GU	24	BELL	$e^+e^- \to \Upsilon(4S)$

[1] The signals are reconstructed in decay chains: $\Xi_c^0 \to \Xi^-\pi^+$, $\Lambda^0 K^-\pi^+$, $pK^-K^-\pi^+$, and $\Lambda_c^- \to \overline{p}K_S^0$, $\overline{p}K^+\pi^-$.

POLARIZATION IN B^+ DECAY

In decays involving two vector mesons, one can distinguish among the states in which meson polarizations are both longitudinal (L) or both are transverse and parallel ($\|$) or perpendicular ($\perp$) to each other with the parameters Γ_L/Γ, $\Gamma_\perp/\Gamma$, and the relative phases $\phi_\|$ and $\phi_\perp$. See the definitions in the note on "Polarization in B Decays" review in the B^0 Particle Listings.

Γ_L/Γ in $B^+ \to \overline{D}^{*0}\rho^+$

VALUE	DOCUMENT ID		TECN	COMMENT
0.892±0.018±0.016	CSORNA	03	CLE2	$e^+e^- \to \Upsilon(4S)$

Γ_L/Γ in $B^+ \to \overline{D}^{*0}K^{*+}$

VALUE	DOCUMENT ID		TECN	COMMENT
0.86±0.06±0.03	AUBERT	04K	BABR	$e^+e^- \to \Upsilon(4S)$

Γ_L/Γ in $B^+ \to \overline{D}^{*0}\ell^+\nu_\ell$

VALUE	DOCUMENT ID		TECN	COMMENT
0.514±0.018±0.005	PRIM	23	BELL	$e^+e^- \to \Upsilon(4S)$

Γ_L/Γ in $B^+ \to \overline{D}^{*0}e^+\nu_e$

VALUE	DOCUMENT ID		TECN	COMMENT
0.505±0.027±0.006	PRIM	23	BELL	$e^+e^- \to \Upsilon(4S)$

Γ_L/Γ in $B^+ \to \overline{D}^{*0}\mu^+\nu_\mu$

VALUE	DOCUMENT ID		TECN	COMMENT
0.522±0.025±0.007	PRIM	23	BELL	$e^+e^- \to \Upsilon(4S)$

$\Delta(\Gamma_L/\Gamma)$ in $B^+ \to \overline{D}^{*0}\ell^+\nu_\ell$

$\Delta(\Gamma_L/\Gamma) = (\Gamma_L/\Gamma)^\mu - (\Gamma_L/\Gamma)^e$

VALUE	DOCUMENT ID		TECN	COMMENT
0.017±0.037±0.009	PRIM	23	BELL	$e^+e^- \to \Upsilon(4S)$

Γ_L/Γ in $B^+ \to J/\psi K^{*+}$

VALUE	DOCUMENT ID		TECN	COMMENT
0.604±0.015±0.018	ITOH	05	BELL	$e^+e^- \to \Upsilon(4S)$

$\Gamma_\perp/\Gamma$ in $B^+ \to J/\psi K^{*+}$

VALUE	DOCUMENT ID		TECN	COMMENT
0.180±0.014±0.010	ITOH	05	BELL	$e^+e^- \to \Upsilon(4S)$

Γ_L/Γ in $B^+ \to \omega K^{*+}$

VALUE	DOCUMENT ID		TECN	COMMENT
0.41±0.18±0.05	AUBERT	09H	BABR	$e^+e^- \to \Upsilon(4S)$

Γ_L/Γ in $B^+ \to \omega K_2^*(1430)^+$

VALUE	DOCUMENT ID		TECN	COMMENT
0.56±0.10±0.04	AUBERT	09H	BABR	$e^+e^- \to \Upsilon(4S)$

Γ_L/Γ in $B^+ \to K^{*+}\overline{K}^{*0}$

VALUE	DOCUMENT ID		TECN	COMMENT
$0.82^{+0.15}_{-0.21}$ OUR AVERAGE				
1.06±0.30±0.14	[1] GOH	15	BELL	$e^+e^- \to \Upsilon(4S)$
$0.75^{+0.16}_{-0.26}$±0.03	[2,3] AUBERT	09F	BABR	$e^+e^- \to \Upsilon(4S)$

[1] Signal significance 2.7 standard deviations.
[2] Signal significance 3.7 standard deviations.
[3] Assumes equal production of B^+ and B^0 at the $\Upsilon(4S)$.

Γ_L/Γ in $B^+ \to \phi K^*(892)^+$

VALUE	DOCUMENT ID		TECN	COMMENT
0.50±0.05 OUR AVERAGE				
0.49±0.05±0.03	AUBERT	07BA	BABR	$e^+e^- \to \Upsilon(4S)$
0.52±0.08±0.03	CHEN	05A	BELL	$e^+e^- \to \Upsilon(4S)$
• • • We do not use the following data for averages, fits, limits, etc. • • •				
0.46±0.12±0.03	AUBERT	03V	BABR	Repl. by AUBERT 07BA

$\Gamma_\perp/\Gamma$ in $B^+ \to \phi K^{*+}$

VALUE	DOCUMENT ID		TECN	COMMENT
0.20±0.05 OUR AVERAGE				
0.21±0.05±0.02	AUBERT	07BA	BABR	$e^+e^- \to \Upsilon(4S)$
0.19±0.08±0.02	CHEN	05A	BELL	$e^+e^- \to \Upsilon(4S)$

$\phi_\|$ in $B^+ \to \phi K^{*+}$

VALUE (°)	DOCUMENT ID		TECN	COMMENT
2.34±0.18 OUR AVERAGE				
2.47±0.20±0.07	AUBERT	07BA	BABR	$e^+e^- \to \Upsilon(4S)$
2.10±0.28±0.04	CHEN	05A	BELL	$e^+e^- \to \Upsilon(4S)$

$\phi_\perp$ in $B^+ \to \phi K^{*+}$

VALUE (°)	DOCUMENT ID		TECN	COMMENT
2.58±0.17 OUR AVERAGE				
2.69±0.20±0.03	AUBERT	07BA	BABR	$e^+e^- \to \Upsilon(4S)$
2.31±0.30±0.07	CHEN	05A	BELL	$e^+e^- \to \Upsilon(4S)$

$\delta_0(B^+ \to \phi K^{*+})$

VALUE (rad)	DOCUMENT ID		TECN	COMMENT
3.07±0.18±0.06	AUBERT	07BA	BABR	$e^+e^- \to \Upsilon(4S)$

$A_{CP}^0(B^+ \to \phi K^{*+})$

VALUE	DOCUMENT ID		TECN	COMMENT
0.17±0.11±0.02	AUBERT	07BA	BABR	$e^+e^- \to \Upsilon(4S)$

$A_{CP}^\perp(B^+ \to \phi K^{*+})$

VALUE	DOCUMENT ID		TECN	COMMENT
0.22±0.24±0.08	AUBERT	07BA	BABR	$e^+e^- \to \Upsilon(4S)$

$\Delta\phi_\|(B^+ \to \phi K^{*+})$

VALUE (rad)	DOCUMENT ID		TECN	COMMENT
0.07±0.20±0.05	AUBERT	07BA	BABR	$e^+e^- \to \Upsilon(4S)$

$\Delta\phi_\perp(B^+ \to \phi K^{*+})$

VALUE (rad)	DOCUMENT ID		TECN	COMMENT
0.19±0.20±0.07	AUBERT	07BA	BABR	$e^+e^- \to \Upsilon(4S)$

$\Delta\delta_0(B^+ \to \phi K^{*+})$

VALUE (rad)	DOCUMENT ID		TECN	COMMENT
0.20±0.18±0.03	AUBERT	07BA	BABR	$e^+e^- \to \Upsilon(4S)$

Γ_L/Γ in $B^+ \to \phi K_1(1270)^+$

VALUE	DOCUMENT ID		TECN	COMMENT
$0.46^{+0.12}_{-0.13}{}^{+0.06}_{-0.07}$	AUBERT	08BI	BABR	$e^+e^- \to \Upsilon(4S)$

Γ_L/Γ in $B^+ \to \phi K_2^*(1430)^+$

VALUE	DOCUMENT ID		TECN	COMMENT
$0.80^{+0.09}_{-0.10}$±0.03	AUBERT	08BI	BABR	$e^+e^- \to \Upsilon(4S)$

$\delta_0(B^+ \to \phi K_2^*(1430)^+)$

VALUE (rad)	DOCUMENT ID		TECN	COMMENT
3.59±0.19±0.12	AUBERT	08BI	BABR	$e^+e^- \to \Upsilon(4S)$

$\Delta\delta_0(B^+ \to \phi K_2^*(1430)^+)$

VALUE (rad)	DOCUMENT ID		TECN	COMMENT
−0.05±0.19±0.06	AUBERT	08BI	BABR	$e^+e^- \to \Upsilon(4S)$

Γ_L/Γ in $B^+ \to \rho^0 K^*(892)^+$

VALUE	DOCUMENT ID		TECN	COMMENT
0.78±0.12±0.03	DEL-AMO-SA...11D		BABR	$e^+e^- \to \Upsilon(4S)$
• • • We do not use the following data for averages, fits, limits, etc. • • •				
$0.96^{+0.04}_{-0.15}$±0.04	AUBERT	03V	BABR	Repl. by DEL-AMO-SANCHEZ 11D

$\Gamma_L/\Gamma(B^+ \to K^*(892)^0\rho^+)$

VALUE	DOCUMENT ID		TECN	COMMENT
0.48±0.08 OUR AVERAGE				
0.52±0.10±0.04	AUBERT,B	06G	BABR	$e^+e^- \to \Upsilon(4S)$
$0.43 \pm 0.11^{+0.05}_{-0.02}$	ZHANG	05D	BELL	$e^+e^- \to \Upsilon(4S)$

Γ_L/Γ in $B^+ \to \mu^+\mu^- K^*(892)^+$ ($1.0 < q^2 < 8.68$ GeV$^2/c^4$)

VALUE	DOCUMENT ID		TECN	COMMENT
$0.60^{+0.31}_{-0.25}$±0.13	[1] SIRUNYAN	21AC	CMS	pp at 8 TeV

[1] SIRUNYAN 21AC measurement is performed in $1.0 < q^2 < 8.68$ GeV$^2/c^4$. Reports also measurements in several other q^2 intervals.

Γ_L/Γ in $B^+ \to \mu^+\mu^- K^*(892)^+$ ($1.1 < q^2 < 6.0$ GeV$^2/c^4$)

VALUE	DOCUMENT ID		TECN	COMMENT
0.59±0.09±0.03	[1] AAIJ	21J	LHCB	pp at 7, 8, 13 TeV

Int. J. Mod. Phys. A 2026.41. Downloaded from www.worldscientific.com
by LIFORNIA @ BERKELEY on 09/16/26. Re-use and distribution is strictly not permitted, except for Open Access articles.

Int. J. Mod. Phys. A 2026.41. Downloaded from www.worldscientific.com
by UNIVERSITY OF CALIFORNIA @ BERKELEY on 09/16/26. Re-use and distribution is strictly not permitted, except for Open Access articles.

[1] The full set of CP-averaged angular observables is measured as a function of the q^2. The measured Γ_L is related to the polarisation of the $K^*(892)^+$.

Γ_L/Γ in $B^+ \to \mu^+\mu^- K^*(892)^+$ ($10.09 < q^2 < 12.86$ GeV^2/c^4)

VALUE	DOCUMENT ID		TECN	COMMENT
$\mathbf{0.88^{+0.10}_{-0.13} \pm 0.05}$	[1] SIRUNYAN	21AC	CMS	pp at 8 TeV

[1] SIRUNYAN 21AC measurement is performed in $10.09 < q^2 < 12.86$ GeV^2/c^4. Reports also measurements in several other q^2 intervals.

Γ_L/Γ in $B^+ \to \mu^+\mu^- K^*(892)^+$ ($14.18 < q^2 < 19.0$ GeV^2/c^4)

VALUE	DOCUMENT ID		TECN	COMMENT
$\mathbf{0.55^{+0.13}_{-0.10} \pm 0.06}$	[1] SIRUNYAN	21AC	CMS	pp at 8 TeV

[1] SIRUNYAN 21AC measurement is performed in $14.18 < q^2 < 19.0$ GeV^2/c^4. Reports also measurements in several other q^2 intervals.

Γ_L/Γ in $B^+ \to \mu^+\mu^- K^*(892)^+$ ($15.0 < q^2 < 19.0$ GeV^2/c^4)

VALUE	DOCUMENT ID		TECN	COMMENT
$\mathbf{0.40^{+0.13}_{-0.11} \pm 0.03}$	[1] AAIJ	21J	LHCB	pp at 7, 8, 13 TeV

[1] The full set of CP-averaged angular observables is measured as a function of the q^2. The measured Γ_L is related to the polarisation of the $K^*(892)^+$.

Γ_L/Γ in $B^+ \to \rho^+\rho^0$

VALUE	DOCUMENT ID		TECN	COMMENT
0.950±0.016 OUR AVERAGE				
$0.950 \pm 0.015 \pm 0.006$	AUBERT	09G	BABR	$e^+e^- \to \Upsilon(4S)$
$0.948 \pm 0.106 \pm 0.021$	ZHANG	03B	BELL	$e^+e^- \to \Upsilon(4S)$
• • • We do not use the following data for averages, fits, limits, etc. • • •				
$0.905 \pm 0.042^{+0.023}_{-0.027}$	AUBERT,BE	06G	BABR	Repl. by AUBERT 09G
$0.97\ ^{+0.03}_{-0.07} \pm 0.04$	AUBERT	03V	BABR	Repl. by AUBERT,BE 06G

Γ_L/Γ in $B^+ \to \omega\rho^+$

VALUE	DOCUMENT ID		TECN	COMMENT
0.90±0.05±0.03	AUBERT	09H	BABR	$e^+e^- \to \Upsilon(4S)$
• • • We do not use the following data for averages, fits, limits, etc. • • •				
$0.82 \pm 0.11 \pm 0.02$	AUBERT,B	06T	BABR	Repl. by AUBERT 09H
$0.88^{+0.12}_{-0.15} \pm 0.03$	AUBERT	05O	BABR	Repl. by AUBERT,B 06T

Γ_L/Γ in $B^+ \to p\overline{p}K^*(892)^+$

VALUE	DOCUMENT ID		TECN	COMMENT
0.32±0.17±0.09	CHEN	08C	BELL	$e^+e^- \to \Upsilon(4S)$

CP VIOLATION

A_{CP} is defined as

$$\frac{B(B^- \to \overline{f}) - B(B^+ \to f)}{B(B^- \to \overline{f}) + B(B^+ \to f)},$$

the CP-violation charge asymmetry of exclusive B^- and B^+ decay.

$A_{CP}(B^+ \to J/\psi(1S)K^+)$

VALUE (units 10^{-3})	DOCUMENT ID		TECN	COMMENT
1.8± 3.0 OUR AVERAGE	Error includes scale factor of 1.5. See the ideogram below.			
$0.9 \pm 2.7 \pm 0.7$	AAIJ	17AP	LHCB	pp at 7, 8 TeV
$5.9 \pm 3.6 \pm 0.7$	ABAZOV	13M	D0	$p\overline{p}$ at 1.96 TeV
$-7.6 \pm 5.0 \pm 2.2$	SAKAI	10	BELL	$e^+e^- \to \Upsilon(4S)$
$90 \pm 70 \pm 20$	[1] WEI	08	BELL	$e^+e^- \to \Upsilon(4S)$
$30 \pm 14 \pm 10$	[2] AUBERT	05J	BABR	$e^+e^- \to \Upsilon(4S)$
$18 \pm 43 \pm 4$	[3] BONVICINI	00	CLE2	$e^+e^- \to \Upsilon(4S)$
• • • We do not use the following data for averages, fits, limits, etc. • • •				
$7.5 \pm 6.1 \pm 3.0$	[4] ABAZOV	08O	D0	Repl. by ABAZOV 13M
$30 \pm 15 \pm 6$	AUBERT	04P	BABR	Repl. by AUBERT 05J
$-26 \pm 22 \pm 17$	ABE	03B	BELL	Repl. by SAKAI 10
$3 \pm 30 \pm 4$	AUBERT	02F	BABR	Repl. by AUBERT 04P

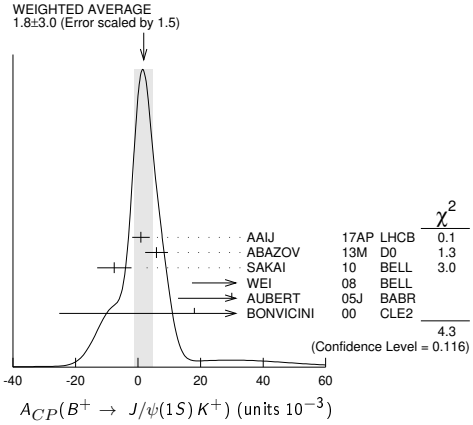

[1] Uses $B^+ \to J/\psi K^+$, where $J/\psi \to p\overline{p}$.
[2] The result reported corresponds to $-A_{CP}$.
[3] A +0.3% correction is applied due to a slightly higher reconstruction efficiency for the positive kaons.
[4] Uses $J/\psi \to \mu^+\mu^-$ decay.

$A_{CP}(B^+ \to J/\psi(1S)\pi^+)$

VALUE (units 10^{-2})	DOCUMENT ID		TECN	COMMENT
1.5 ± 0.5 OUR AVERAGE				
$1.51 \pm 0.50 \pm 0.08$	[1] AAIJ	25I	LHCB	pp at 7, 8, 13 TeV
$-4.2 \pm 4.4 \pm 0.9$	ABAZOV	13M	D0	$p\overline{p}$ at 1.96 TeV
$12.3 \pm 8.5 \pm 0.4$	AUBERT	04P	BABR	$e^+e^- \to \Upsilon(4S)$
$-2.3 \pm 16.4 \pm 1.5$	ABE	03B	BELL	$e^+e^- \to \Upsilon(4S)$
• • • We do not use the following data for averages, fits, limits, etc. • • •				
$1.91 \pm 0.89 \pm 0.16$	[1] AAIJ	17O	LHCB	Repl. by AAIJ 25I
$0.5 \pm 2.7 \pm 1.1$	[2] AAIJ	12AC	LHCB	Repl. by AAIJ 17O
$-9 \pm 8 \pm 3$	[3] ABAZOV	08O	D0	Repl. by ABAZOV 13M
$1 \pm 22 \pm 1$	AUBERT	02F	BABR	Repl. by AUBERT 04P

[1] Obtained by using LHCb measurement of $A_{CP}(B^+ \to J/\psi K^+) = (0.09 \pm 0.27 \pm 0.07) \times 10^{-2}$ of AAIJ 17AP.
[2] Uses $A_{CP}(B^+ \to J/\psi K^+) = 0.001 \pm 0.007$ to extract production asymmetry.
[3] Uses $J/\psi \to \mu^+\mu^-$ decay.

$A_{CP}(B^+ \to J/\psi\rho^+)$

VALUE	DOCUMENT ID		TECN	COMMENT
−0.05 ±0.05 OUR AVERAGE				
$-0.045^{+0.056}_{-0.057} \pm 0.008$	AAIJ	19O	LHCB	pp at 7 and 8 TeV
$-0.11 \pm 0.12 \pm 0.08$	AUBERT	07AC	BABR	$e^+e^- \to \Upsilon(4S)$

$A_{CP}(B^+ \to J/\psi K^*(892)^+)$

VALUE	DOCUMENT ID		TECN	COMMENT
−0.048±0.029±0.016	[1] AUBERT	05J	BABR	$e^+e^- \to \Upsilon(4S)$

[1] The result reported corresponds to $-A_{CP}$.

$A_{CP}(B^+ \to \eta_c K^+)$

VALUE	DOCUMENT ID		TECN	COMMENT
−0.05 ±0.05 OUR AVERAGE	Error includes scale factor of 1.5.			
$-0.027 \pm 0.034 \pm 0.004$	[1] AAIJ	14AF	LHCB	pp at 7, 8 TeV
$-0.16 \pm 0.08 \pm 0.02$	[1] WEI	08	BELL	$e^+e^- \to \Upsilon(4S)$
• • • We do not use the following data for averages, fits, limits, etc. • • •				
$0.046 \pm 0.057 \pm 0.007$	[1] AAIJ	13AU	LHCB	Repl. by AAIJ 14AF

[1] Uses $B^+ \to \eta_c K^+$, where $\eta_c \to p\overline{p}$.

$A_{CP}(B^+ \to \psi(2S)\pi^+)$

VALUE	DOCUMENT ID		TECN	COMMENT
0.03 ±0.06 OUR AVERAGE				
$0.048 \pm 0.090 \pm 0.011$	[1] AAIJ	12AC	LHCB	pp at 7 TeV
$0.022 \pm 0.085 \pm 0.016$	BHARDWAJ	08	BELL	$e^+e^- \to \Upsilon(4S)$

[1] Uses $A_{CP}(B^+ \to J/\psi K^+) = 0.001 \pm 0.007$ to extract production asymmetry.

$A_{CP}(B^+ \to \psi(2S)K^+)$

VALUE	DOCUMENT ID		TECN	COMMENT
0.004±0.020 OUR AVERAGE	Error includes scale factor of 1.5. See the ideogram below.			
$-0.079 \pm 0.059 \pm 0.004$	[1] AAIJ	14AF	LHCB	pp at 7, 8 TeV
$0.024 \pm 0.014 \pm 0.008$	[2] AAIJ	12AC	LHCB	pp at 7 TeV
$0.052 \pm 0.059 \pm 0.020$	AUBERT	05J	BABR	$e^+e^- \to \Upsilon(4S)$
$-0.042 \pm 0.020 \pm 0.017$	ABE	03B	BELL	$e^+e^- \to \Upsilon(4S)$
$0.02 \pm 0.091 \pm 0.01$	[3] BONVICINI	00	CLE2	$e^+e^- \to \Upsilon(4S)$
• • • We do not use the following data for averages, fits, limits, etc. • • •				
$-0.002 \pm 0.123 \pm 0.012$	[1,2] AAIJ	13AU	LHCB	Repl. by AAIJ 14AF

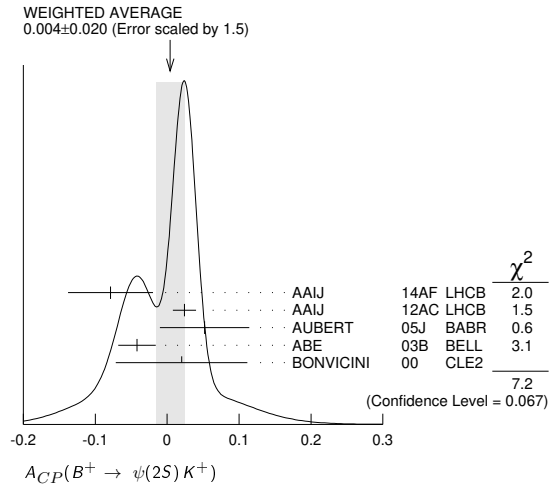

[1] Uses $\psi(2S) \to p\overline{p}$ decays.
[2] Uses $A_{CP}(B^+ \to J/\psi K^+) = 0.001 \pm 0.007$ to extract production asymmetry.
[3] A $+0.3\%$ correction is applied due to a slightly higher reconstruction efficiency for the positive kaons.

$A_{CP}(B^+ \to \psi(2S) K^*(892)^+)$

VALUE	DOCUMENT ID		TECN	COMMENT
0.077±0.207±0.051	[1] AUBERT	05J	BABR	$e^+e^- \to \Upsilon(4S)$

[1] The result reported corresponds to $-A_{CP}$.

$A_{CP}(B^+ \to \chi_{c1}(1P)\pi^+)$

VALUE	DOCUMENT ID		TECN	COMMENT
0.07±0.18±0.02	KUMAR	06	BELL	$e^+e^- \to \Upsilon(4S)$

$A_{CP}(B^+ \to \chi_{c0} K^+)$

VALUE	DOCUMENT ID		TECN	COMMENT
−0.20 ±0.18 OUR AVERAGE Error includes scale factor of 1.5. See the ideogram below.				
−0.96 ±0.37±0.04	LEES	11I	BABR	$e^+e^- \to \Upsilon(4S)$
−0.14 ±0.15 $^{+0.03}_{-0.06}$	AUBERT	08AI	BABR	$e^+e^- \to \Upsilon(4S)$
−0.065 ± 0.20 $^{+0.035}_{-0.024}$	GARMASH	06	BELL	$e^+e^- \to \Upsilon(4S)$

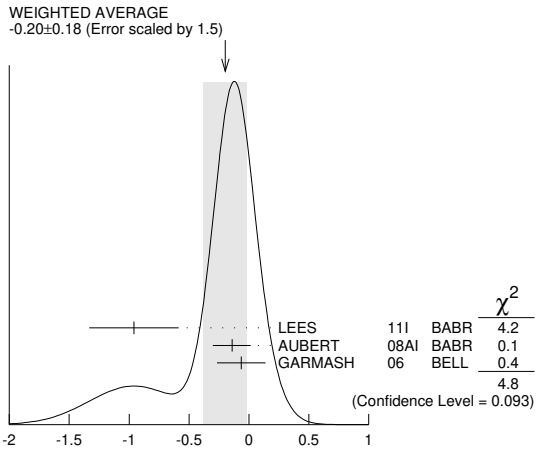

$A_{CP}(B^+ \to \chi_{c0} K^+)$

$A_{CP}(B^+ \to \chi_{c1} K^+)$

VALUE	DOCUMENT ID		TECN	COMMENT
−0.009±0.033 OUR AVERAGE				
−0.01 ±0.03 ±0.02	KUMAR	06	BELL	$e^+e^- \to \Upsilon(4S)$
−0.003±0.076±0.017	[1] AUBERT	05J	BABR	$e^+e^- \to \Upsilon(4S)$

[1] The result reported corresponds to $-A_{CP}$.

$A_{CP}(B^+ \to \chi_{c1} K^*(892)^+)$

VALUE	DOCUMENT ID		TECN	COMMENT
0.471±0.378±0.268	[1] AUBERT	05J	BABR	$e^+e^- \to \Upsilon(4S)$

[1] The result reported corresponds to $-A_{CP}$.

$A_{CP}(B^+ \to D^0 \ell^+ \nu_\ell)$

VALUE (units 10^{-2})	DOCUMENT ID		TECN	COMMENT
−0.14±0.14±0.14	[1] ABAZOV	17A	D0	$p\overline{p}$ at 1.96 TeV

[1] Uses $D^0 \to K^-\pi^+$ decays and $f(B^+) = 0.56 \pm 0.01$ from 10.4 fb^{-1} of Run II data.

$A_{CP}(B^+ \to \overline{D}^0\pi^+)$

VALUE (units 10^{-3})	DOCUMENT ID		TECN	COMMENT
−3.2±3.5 OUR AVERAGE				
−5 ±4 ± 2	ADACHI	24I	BELL	$e^+e^- \to \Upsilon(4S)$
1.9±3.6± 5.7	BLOOMFIELD	22	BELL	$e^+e^- \to \Upsilon(4S)$
−6 ±5 ±10	[1] AAIJ	13AE	LHCB	pp at 7 TeV
• • • We do not use the following data for averages, fits, limits, etc. • • •				
−8 ±8	ABE	06	BELL	Repl. by ADACHI 24I

[1] Uses $B^{\pm} \to [K^{\pm}\pi^{\mp}\pi^+\pi^-]_D h^{\pm}$ mode.

$A_{CP}(B^+ \to D_{CP(+1)}\pi^+)$

VALUE	DOCUMENT ID		TECN	COMMENT
−0.0088±0.0024 OUR AVERAGE				
−0.02 ±0.014 ±0.002	ADACHI	24I	BELL	$e^+e^- \to \Upsilon(4S)$
−0.008 ±0.002 ±0.002	[1] AAIJ	21Q	LHCB	pp at 7, 8, 13 TeV
−0.0098±0.0043±0.0021	AAIJ	16L	LHCB	pp at 7, 8 TeV
• • • We do not use the following data for averages, fits, limits, etc. • • •				
−0.008 ±0.003 ±0.002	[2,3] AAIJ	18A	LHCB	pp at 7, 8, 13 TeV
−0.008 ±0.006 ±0.002	[3,4] AAIJ	18A	LHCB	pp at 7, 8, 13 TeV
0.035 ±0.024	ABE	06	BELL	Repl. by ADACHI 24I

[1] Uses $D \to K^+K^-$ and $D \to \pi^+\pi^-$ decay modes.
[2] Uses $D \to K^+K^-$ decay mode.
[3] Superseded by AAIJ 21Q.
[4] Uses $D \to \pi^+\pi^-$ decay mode.

$A_{CP}(B^+ \to D_{CP(-1)}\pi^+)$

VALUE	DOCUMENT ID		TECN	COMMENT
−0.003±0.012±0.002	ADACHI	24I	BELL	$e^+e^- \to \Upsilon(4S)$
• • • We do not use the following data for averages, fits, limits, etc. • • •				
0.017±0.026	ABE	06	BELL	Repl. by ADACHI 24I

$A_{CP}([K^{\mp}\pi^{\pm}\pi^+\pi^-]_D\pi^+)$

VALUE	DOCUMENT ID		TECN	COMMENT
0.070±0.019±0.006	AAIJ	23I	LHCB	pp at 7, 8, 13 TeV
• • • We do not use the following data for averages, fits, limits, etc. • • •				
0.023±0.048±0.005	[1] AAIJ	16L	LHCB	pp at 7, 8 TeV
0.13 ±0.10	AAIJ	13AE	LHCB	Repl. by AAIJ 16L

[1] Superseded by AAIJ 23I.

$A_{CP}(B^+ \to [\pi^+\pi^+\pi^-\pi^-]_D K^+)$

VALUE	DOCUMENT ID		TECN	COMMENT
0.061±0.013±0.002	AAIJ	23N	LHCB	pp at 7, 8, 13 TeV
• • • We do not use the following data for averages, fits, limits, etc. • • •				
0.100±0.034±0.018	[1] AAIJ	16L	LHCB	pp at 7, 8 TeV

[1] Supersended by AAIJ 23N.

$A_{CP}(B^+ \to [\pi^+\pi^-\pi^+\pi^-]_D K^*(892)^+)$

VALUE	DOCUMENT ID		TECN	COMMENT
0.02±0.11±0.01	AAIJ	17BO	LHCB	pp at 7, 8, 13 TeV

$A_{CP}(B^+ \to [K^+K^-\pi^+\pi^-]_D K^+)$

VALUE	DOCUMENT ID		TECN	COMMENT
0.095±0.023±0.002	AAIJ	23N	LHCB	pp at 7, 8, 13 TeV

$A_{CP}(B^+ \to [K^+K^-\pi^+\pi^-]_D \pi^+)$

VALUE	DOCUMENT ID		TECN	COMMENT
−0.009±0.006±0.001	AAIJ	23N	LHCB	pp at 7, 8, 13 TeV

$A_{CP}(B^+ \to \overline{D}^0 K^+)$

VALUE	DOCUMENT ID		TECN	COMMENT
−0.018 ±0.004 OUR AVERAGE				
−0.014 ±0.017 ±0.001	ADACHI	24I	BELL	$e^+e^- \to \Upsilon(4S)$
−0.019 ±0.005 ±0.002	[1] AAIJ	18A	LHCB	pp at 7, 8, 13 TeV
−0.0194±0.0072±0.0060	AAIJ	16L	LHCB	pp at 7, 8 TeV
0.010 ±0.026 ±0.005	[2] AAIJ	15W	LHCB	pp at 7, 8 TeV
• • • We do not use the following data for averages, fits, limits, etc. • • •				
0.000 ±0.012 ±0.002	[3] AAIJ	16L	LHCB	pp at 7, 8 TeV
−0.029 ±0.020 ±0.018	[3] AAIJ	13AE	LHCB	Repl. by AAIJ 16L
0.066 ±0.036	ABE	06	BELL	Repl. by ADACHI 24I
0.003 ±0.080 ±0.037	[4] ABE	03D	BELL	Repl. by SWAIN 03
0.04 ±0.06 ±0.03	[5] SWAIN	03	BELL	Repl. by ABE 06

[1] Supersedes AAIJ 16L.
[2] Uses $D^0 \to K^-\pi^+\pi^0$ for the favored mode, and $D^0 \to K^+\pi^-\pi^0$ for the suppressed mode.
[3] Uses $B^{\pm} \to [K^{\pm}\pi^{\mp}\pi^+\pi^-]_D h^{\pm}$ mode.
[4] Corresponds to 90% confidence range $-0.15 < A_{CP} < 0.16$.
[5] Corresponds to 90% confidence range $-0.07 < A_{CP} < 0.15$.

$A_{CP}([K^{\mp}\pi^{\pm}\pi^+\pi^-]_D K^+)$

VALUE	DOCUMENT ID		TECN	COMMENT
−0.321±0.039±0.005	AAIJ	23I	LHCB	pp at 7, 8, 13 TeV
• • • We do not use the following data for averages, fits, limits, etc. • • •				
−0.313±0.102±0.038	[1] AAIJ	16L	LHCB	pp at 7, 8 TeV
−0.42 ±0.22	AAIJ	13AE	LHCB	Repl. by AAIJ 16L

[1] Superseded by AAIJ 23I.

$A_{CP}(B^+ \to [\pi^+\pi^+\pi^-\pi^-]_D \pi^+)$

VALUE (units 10^{-3})	DOCUMENT ID		TECN	COMMENT
−8.2±3.1±0.7	AAIJ	23N	LHCB	pp at 7, 8, 13 TeV
• • • We do not use the following data for averages, fits, limits, etc. • • •				
−4.1±7.9±2.4	[1] AAIJ	16L	LHCB	pp at 7, 8 TeV

[1] Superseded by AAIJ 23N.

$A_{CP}(B^+ \to [K^-\pi^+]_D K^+)$

VALUE	DOCUMENT ID		TECN	COMMENT
−0.58±0.21 OUR AVERAGE				
−0.82±0.44±0.09	AALTONEN	11AJ	CDF	$p\overline{p}$ at 1.96 TeV
−0.39 $^{+0.26}_{-0.28}$ $^{+0.04}_{-0.03}$	HORII	11	BELL	$e^+e^- \to \Upsilon(4S)$
−0.86±0.47 $^{+0.12}_{-0.16}$	DEL-AMO-SA...	10H	BABR	$e^+e^- \to \Upsilon(4S)$
• • • We do not use the following data for averages, fits, limits, etc. • • •				
−0.1 $^{+0.8}_{-1.0}$ ±0.4	HORII	08	BELL	Repl. by HORII 11
+0.88 $^{+0.77}_{-0.62}$ ±0.06	SAIGO	05	BELL	Repl. by HORII 08

Int. J. Mod. Phys. A 2026.41. Downloaded from www.worldscientific.com
by [redacted]LIFORNIA @ BERKELEY on 09/16/26. Re-use and distribution is strictly not permitted, except for Open Access articles.

Int. J. Mod. Phys. A 2026.41. Downloaded from www.worldscientific.com
by UNIVERSITY OF CALIFORNIA @ BERKELEY on 09/16/26. Re-use and distribution is strictly not permitted, except for Open Access articles.

$A_{CP}(B^+ \to [K^-\pi^+\pi^0]_D K^+)$

VALUE	DOCUMENT ID		TECN	COMMENT
−0.27±0.27 OUR AVERAGE	Error includes scale factor of 2.4.			
−0.38±0.12±0.02	AAIJ	22T	LHCB	pp at 7, 8, 13 TeV
0.41±0.30±0.05	NAYAK	13	BELL	$e^+e^- \to \Upsilon(4S)$
• • • We do not use the following data for averages, fits, limits, etc. • • •				
−0.20±0.27±0.04	[1] AAIJ	15W	LHCB	Repl. by AAIJ 22T

[1] Uses $D^0 \to K^-\pi^+\pi^0$ for the favored mode, and $D^0 \to K^+\pi^-\pi^0$ for the suppressed mode.

$A_{CP}(B^+ \to [K^+\pi^-\pi^0]_D K^+)$

VALUE	DOCUMENT ID		TECN	COMMENT
−0.024±0.013±0.002	AAIJ	22T	LHCB	pp at 7, 8, 13 TeV

$A_{CP}(B^+ \to [K^+K^-\pi^0]_D K^+)$

VALUE	DOCUMENT ID		TECN	COMMENT
0.067±0.073±0.003	AAIJ	22T	LHCB	pp at 7, 8, 13 TeV
• • • We do not use the following data for averages, fits, limits, etc. • • •				
0.30 ±0.20 ±0.02	[1] AAIJ	15W	LHCB	Repl. by AAIJ 22T

[1] Uses $D \to K^+K^-\pi^0$ mode.

$A_{CP}(B^+ \to [\pi^+\pi^-\pi^0]_D K^+)$

VALUE	DOCUMENT ID		TECN	COMMENT
0.109±0.043±0.003	AAIJ	22T	LHCB	pp at 7, 8, 13 TeV
• • • We do not use the following data for averages, fits, limits, etc. • • •				
0.054±0.091±0.011	[1] AAIJ	15W	LHCB	Repl. by AAIJ 22T

[1] Uses $D \to \pi^+\pi^-\pi^0$ mode.

$A_{CP}(B^+ \to \overline{D}^0 K^*(892)^+)$

VALUE	DOCUMENT ID		TECN	COMMENT
−0.007±0.019 OUR AVERAGE				
−0.004±0.023±0.008	[1] AAIJ	17BO	LHCB	pp at 7, 8, 13 TeV
−0.013±0.031±0.009	[2] AAIJ	17BO	LHCB	pp at 7, 8, 13 TeV

[1] Uses $B^{\pm} \to [K^{\pm}\pi^{\mp}]_D K^*(892)^{\pm}$ decay mode.
[2] Uses $B^{\pm} \to [K^{\pm}\pi^{\mp}\pi^+\pi^-]_D K^*(892)^{\pm}$ decay mode.

$A_{CP}(B^+ \to [K^-\pi^+]_{\overline{D}} K^*(892)^+)$

VALUE	DOCUMENT ID		TECN	COMMENT
−0.75±0.16 OUR AVERAGE				
−0.81±0.17±0.04	AAIJ	17BO	LHCB	pp at 7, 8, 13 TeV
−0.34±0.43±0.16	AUBERT	09AJ	BABR	$e^+e^- \to \Upsilon(4S)$
• • • We do not use the following data for averages, fits, limits, etc. • • •				
−0.22±0.61±0.17	AUBERT,B	05V	BABR	Repl. by AUBERT 09AJ

$A_{CP}(B^+ \to [K^-\pi^+\pi^-\pi^+]_{\overline{D}} K^*(892)^+)$

VALUE	DOCUMENT ID		TECN	COMMENT
−0.45±0.21±0.14	AAIJ	17BO	LHCB	pp at 7, 8, 13 TeV

$A_{CP}(B^+ \to [K^-\pi^+]_D \pi^+)$

VALUE	DOCUMENT ID		TECN	COMMENT
0.00±0.09 OUR AVERAGE				
0.13±0.25±0.02	AALTONEN	11AJ	CDF	$p\overline{p}$ at 1.96 TeV
$-0.04\pm0.11^{+0.02}_{-0.01}$	HORII	11	BELL	$e^+e^- \to \Upsilon(4S)$
0.03±0.17±0.04	DEL-AMO-SA...	10H	BABR	$e^+e^- \to \Upsilon(4S)$
• • • We do not use the following data for averages, fits, limits, etc. • • •				
$-0.02^{+0.15}_{-0.16}\pm0.04$	HORII	08	BELL	Repl. by HORII 11
$+0.30^{+0.29}_{-0.25}\pm0.06$	SAIGO	05	BELL	Repl. by HORII 08

$A_{CP}(B^+ \to [K^-\pi^+\pi^0]_D \pi^+)$

VALUE	DOCUMENT ID		TECN	COMMENT
0.08 ±0.09 OUR AVERAGE				
0.069±0.094±0.016	AAIJ	22T	LHCB	pp at 7, 8, 13 TeV
$0.16 \pm0.27\ ^{+0.03}_{-0.04}$	NAYAK	13	BELL	$e^+e^- \to \Upsilon(4S)$
• • • We do not use the following data for averages, fits, limits, etc. • • •				
0.438±0.190±0.011	[1] AAIJ	15W	LHCB	Repl. by AAIJ 22T

[1] Uses $D^0 \to K^-\pi^+\pi^0$ for the favored mode, and $D^0 \to K^+\pi^-\pi^0$ for the suppressed mode.

$A_{CP}(B^+ \to [K^+K^-\pi^0]_D \pi^+)$

VALUE	DOCUMENT ID		TECN	COMMENT
−0.001±0.019±0.002	AAIJ	22T	LHCB	pp at 7, 8, 13 TeV
• • • We do not use the following data for averages, fits, limits, etc. • • •				
−0.030±0.040±0.005	[1] AAIJ	15W	LHCB	Repl. by AAIJ 22T

[1] Uses $D \to K^+K^-$ mode.

$A_{CP}(B^+ \to [\pi^+\pi^-\pi^0]_D \pi^+)$

VALUE	DOCUMENT ID		TECN	COMMENT
0.001±0.010±0.002	AAIJ	22T	LHCB	pp at 7, 8, 13 TeV
• • • We do not use the following data for averages, fits, limits, etc. • • •				
−0.016±0.020±0.004	[1] AAIJ	15W	LHCB	Repl. by AAIJ 22T

[1] Uses $D \to \pi^+\pi^-$ mode.

$A_{CP}(B^+ \to [K^-\pi^+]_{(D\pi)} \pi^+)$

VALUE	DOCUMENT ID		TECN	COMMENT
−0.09±0.27±0.05	DEL-AMO-SA...	10H	BABR	$e^+e^- \to \Upsilon(4S)$

$A_{CP}(B^+ \to [K^-\pi^+]_{(D\gamma)} \pi^+)$

VALUE	DOCUMENT ID		TECN	COMMENT
−0.65±0.55±0.22	DEL-AMO-SA...	10H	BABR	$e^+e^- \to \Upsilon(4S)$

$A_{CP}(B^+ \to [K^-\pi^+]_{(D\pi)} K^+)$

VALUE	DOCUMENT ID		TECN	COMMENT
0.77±0.35±0.12	DEL-AMO-SA...	10H	BABR	$e^+e^- \to \Upsilon(4S)$

$A_{CP}(B^+ \to [K^-\pi^+]_{(D\gamma)} K^+)$

VALUE	DOCUMENT ID		TECN	COMMENT
$\mathbf{0.36\pm0.94^{+0.25}_{-0.41}}$	DEL-AMO-SA...	10H	BABR	$e^+e^- \to \Upsilon(4S)$

$A_{CP}(B^+ \to [\pi^+\pi^-\pi^0]_D K^+)$

VALUE	DOCUMENT ID		TECN	COMMENT
−0.02±0.15±0.03	[1] AUBERT	07BJ	BABR	$e^+e^- \to \Upsilon(4S)$
• • • We do not use the following data for averages, fits, limits, etc. • • •				
−0.02±0.16±0.03	AUBERT,B	05T	BABR	Repl. by AUBERT 07BJ

[1] Uses a Dalitz plot analysis of $D^0 \to \pi^+\pi^-\pi^0$. Also reports the one-sigma regions: $0.06 < r_B < 0.78$, $-30^\circ < \gamma < 76^\circ$, and $-27^\circ < \delta < 78^\circ$.

$A_{CP}(B^+ \to [K^0_S K^+\pi^-]_D K^+)$

VALUE	DOCUMENT ID		TECN	COMMENT
0.00 ±0.09 OUR AVERAGE	Error includes scale factor of 1.4.			
−0.089±0.091±0.011	[1] ADACHI	23L	BELL	$e^+e^- \to \Upsilon(4S)$
0.095±0.089±0.018	[2] AAIJ	20N	LHCB	pp at 7, 8, 13 TeV
• • • We do not use the following data for averages, fits, limits, etc. • • •				
0.040±0.091±0.018	[1] AAIJ	14V	LHCB	Repl. by AAIJ 20N

[1] The analysis uses all of $D \to K^0_S K\pi$ Dalitz decays.
[2] The analysis uses $D \to K^0_S K\pi$ Dalitz decays with $K^{*-}K^+$ region excluded.

$A_{CP}(B^+ \to [K^0_S K^-\pi^+]_D K^+)$

VALUE	DOCUMENT ID		TECN	COMMENT
0.00 ±0.07 OUR AVERAGE				
0.109±0.133±0.013	[1] ADACHI	23L	BELL	$e^+e^- \to \Upsilon(4S)$
−0.038±0.075±0.011	[2] AAIJ	20N	LHCB	pp at 7, 8, 13 TeV
• • • We do not use the following data for averages, fits, limits, etc. • • •				
0.233±0.129±0.024	[1] AAIJ	14V	LHCB	Repl. by AAIJ 20N

[1] The anaysis uses all of $D \to K^0_S K\pi$ Dalitz decays.
[2] The analysis uses $D \to K^0_S K\pi$ Dalitz decays with $K^{*-}K^+$ region excluded.

$A_{CP}(B^+ \to [K^0_S K^-\pi^+]_D \pi^+)$

VALUE	DOCUMENT ID		TECN	COMMENT
−0.003±0.014 OUR AVERAGE				
−0.028±0.031±0.009	[1] ADACHI	23L	BELL	$e^+e^- \to \Upsilon(4S)$
0.003±0.015±0.003	[2] AAIJ	20N	LHCB	pp at 7, 8, 13 TeV
• • • We do not use the following data for averages, fits, limits, etc. • • •				
−0.052±0.029±0.017	[1] AAIJ	14V	LHCB	Repl. by AAIJ 20N

[1] The anaysis uses all of $D \to K^0_S K\pi$ Dalitz decays.
[2] The analysis uses $D \to K^0_S K\pi$ Dalitz decays with $K^{*-}K^+$ region excluded.

$A_{CP}(B^+ \to [K^0_S K^+\pi^-]_D \pi^+)$

VALUE	DOCUMENT ID		TECN	COMMENT
−0.016±0.025 OUR AVERAGE	Error includes scale factor of 1.5.			
0.018±0.026±0.009	[1] ADACHI	23L	BELL	$e^+e^- \to \Upsilon(4S)$
−0.034±0.020±0.003	[2] AAIJ	20N	LHCB	pp at 7, 8, 13 TeV
• • • We do not use the following data for averages, fits, limits, etc. • • •				
−0.025±0.024±0.010	[1] AAIJ	14V	LHCB	Repl. by AAIJ 20N

[1] The anaysis uses all of $D \to K^0_S K\pi$ Dalitz decays.
[2] The analysis uses $D \to K^0_S K\pi$ Dalitz decays with $K^{*-}K^+$ region excluded.

$A_{CP}(B^+ \to [K^*(892)^-K^+]_D K^+)$

VALUE	DOCUMENT ID		TECN	COMMENT
0.08 ±0.05 OUR AVERAGE				
0.055±0.119±0.020	[1] ADACHI	23L	BELL	$e^+e^- \to \Upsilon(4S)$
0.084±0.049±0.008	[1] AAIJ	20N	LHCB	pp at 7, 8, 13 TeV
• • • We do not use the following data for averages, fits, limits, etc. • • •				
0.026±0.109±0.029	[1] AAIJ	14V	LHCB	Repl. by AAIJ 20N

[1] The Analysis uses $D \to K^*(892)K \to K^0_S K\pi$ decays.

$A_{CP}(B^+ \to [K^*(892)^+K^-]_D K^+)$

VALUE	DOCUMENT ID		TECN	COMMENT
0.07 ±0.09 OUR AVERAGE				
0.231±0.184±0.014	[1] ADACHI	23L	BELL	$e^+e^- \to \Upsilon(4S)$
0.021±0.094±0.017	[1] AAIJ	20N	LHCB	pp at 7, 8, 13 TeV
• • • We do not use the following data for averages, fits, limits, etc. • • •				
0.336±0.208±0.026	[1] AAIJ	14V	LHCB	Repl. by AAIJ 20N

[1] The Analysis uses $D \to K^*(892)K \to K^0_S K\pi$ decays.

Int. J. Mod. Phys. A 2026.41. Downloaded from www.worldscientific.com by LIFORNIA @ BERKELEY on 09/16/26. Re-use and distribution is strictly not permitted, except for Open Access articles.

$A_{CP}(B^+ \to [K^*(892)^+ K^-]_D \pi^+)$

VALUE	DOCUMENT ID		TECN	COMMENT
0.007±0.016 OUR AVERAGE				
0.009±0.046±0.009	[1] ADACHI	23L	BELL	$e^+e^- \to \Upsilon(4S)$
0.007±0.017±0.003	[1] AAIJ	20N	LHCB	pp at 7, 8, 13 TeV
• • • We do not use the following data for averages, fits, limits, etc. • • •				
−0.054±0.043±0.017	[1] AAIJ	14V	LHCB	Repl. by AAIJ 20N

[1] The Analysis uses $D \to K^*(892) K \to K^0_S K \pi$ decays.

$A_{CP}(B^+ \to [K^*(892)^- K^+]_D \pi^+)$

VALUE	DOCUMENT ID		TECN	COMMENT
−0.013±0.020 OUR AVERAGE Error includes scale factor of 1.9.				
0.046±0.029±0.016	[1] ADACHI	23L	BELL	$e^+e^- \to \Upsilon(4S)$
−0.020±0.011±0.003	[1] AAIJ	20N	LHCB	pp at 7, 8, 13 TeV
• • • We do not use the following data for averages, fits, limits, etc. • • •				
−0.012±0.028±0.010	[1] AAIJ	14V	LHCB	Repl. by AAIJ 20N

[1] The Analysis uses $D \to K^*(892) K \to K^0_S K \pi$ decays.

$A_{CP}(B^+ \to D_{CP(+1)} K^+)$

VALUE	DOCUMENT ID		TECN	COMMENT
0.132±0.015 OUR AVERAGE Error includes scale factor of 1.8.				
0.125±0.058±0.014	ADACHI	24I	BELL	$e^+e^- \to \Upsilon(4S)$
0.136±0.009±0.001	[1] AAIJ	21Q	LHCB	pp at 7, 8, 13 TeV
0.097±0.018±0.009	AAIJ	16L	LHCB	pp at 7, 8 TeV
0.39 ±0.17 ±0.04	AALTONEN	10A	CDF	$p\overline{p}$ at 1.96 TeV
0.25 ±0.06 ±0.02	[2] DEL-AMO-SA...10G		BABR	$e^+e^- \to \Upsilon(4S)$
• • • We do not use the following data for averages, fits, limits, etc. • • •				
0.126±0.014±0.002	[3,4] AAIJ	18A	LHCB	pp at 7, 8, 13 TeV
0.115±0.025±0.007	[4,5] AAIJ	18A	LHCB	pp at 7, 8, 13 TeV
0.145±0.032±0.010	[6] AAIJ	12M	LHCB	Repl. by AAIJ 16L
0.27 ±0.09 ±0.04	AUBERT	08AA	BABR	Repl. by DEL-AMO-SANCHEZ 10G
0.06 ±0.14 ±0.05	ABE	06	BELL	Repl. by ADACHI 24I
0.35 ±0.13 ±0.04	AUBERT	06J	BABR	Repl. by AUBERT 08AA
0.07 ±0.17 ±0.06	AUBERT	04N	BABR	Repl. by AUBERT 06J
0.29 ±0.26 ±0.05	[7] ABE	03D	BELL	Repl. by SWAIN 03
0.06 ±0.19 ±0.04	[8] SWAIN	03	BELL	Repl. by ABE 06

[1] Uses $D \to K^+K^-$ and $D \to \pi^+\pi^-$ decay modes.
[2] Reports the first evidence for direct CP violation in $B \to D K$ decays with 3.6 standard deviations.
[3] Uses $D \to K^+K^-$ decay mode.
[4] Superseded by AAIJ 21Q.
[5] Uses $D \to \pi^+\pi^-$ decay mode.
[6] AAIJ 12M reports an evidence of direct CP violation in $B^\pm \to D K^\pm$ decays with a total significance of 5.8 σ.
[7] Corresponds to 90% confidence range $-0.14 < A_{CP} < 0.73$.
[8] Corresponds to 90% confidence range $-0.26 < A_{CP} < 0.38$.

$A_{ADS}(B^+ \to D K^+)$

$A_{ADS}(B^+ \to D K^+) = \frac{(R^-_K - R^+_K)}{(R^-_K + R^+_K)}$ where

$R^-_K = \Gamma(B^- \to [K^+\pi^-]_D K^-) / \Gamma(B^- \to [K^-\pi^+]_D K^-)$ and

$R^+_K = \Gamma(B^+ \to [K^-\pi^+]_D K^+) / \Gamma(B^+ \to [K^+\pi^-]_D K^+)$

VALUE	DOCUMENT ID		TECN	COMMENT
−0.451±0.026	[1] AAIJ	21Q	LHCB	pp at 7, 8, 13 TeV
• • • We do not use the following data for averages, fits, limits, etc. • • •				
−0.403±0.056±0.011	[2] AAIJ	16L	LHCB	pp at 7, 8 TeV
−0.52 ±0.15 ±0.02	AAIJ	12M	LHCB	Repl. by AAIJ 16L

[1] The statistical and systematic uncertainties have been combined according to the correlations between the R^-_K and R^+_K observables.
[2] Superseded by AAIJ 21Q.

$A_{ADS}(B^+ \to D \pi^+)$

$A_{ADS}(B^+ \to D \pi^+) = \frac{(R^-_\pi - R^+_\pi)}{(R^-_\pi + R^+_\pi)}$ where

$R^-_\pi = \Gamma(B^- \to [K^+\pi^-]_D \pi^-) / \Gamma(B^- \to [K^-\pi^+]_D \pi^-)$ and

$R^+_\pi = \Gamma(B^+ \to [K^-\pi^+]_D \pi^+) / \Gamma(B^+ \to [K^+\pi^-]_D \pi^+)$

VALUE	DOCUMENT ID		TECN	COMMENT
0.129±0.014	[1] AAIJ	21Q	LHCB	pp at 7, 8, 13 TeV
• • • We do not use the following data for averages, fits, limits, etc. • • •				
0.100±0.031±0.009	[2] AAIJ	16L	LHCB	pp at 7, 8 TeV
0.143±0.062±0.011	AAIJ	12M	LHCB	Repl. by AAIJ 16L

[1] The statistical and systematic uncertainties have been combined according to the correlations between the R^-_π and R^+_π observables.
[2] Superseded by AAIJ 21Q.

$A_{ADS}(B^+ \to [D\gamma]_{D^*} K^+)$

$A_{ADS}(B^+ \to D^*(D\gamma) K^+) = (R^-_K - R^+_K) / (R^-_K + R^+_K)$, where

$R^-_K = \Gamma(B^- \to (\gamma[K^+\pi^-]_D)_{D^*} K^-) / \Gamma(B^- \to (\gamma[K^-\pi^+]_D)_{D^*} K^-)$ and

$R^+_K = \Gamma(B^+ \to (\gamma[K^-\pi^+]_D)_{D^*} K^+) / \Gamma(B^+ \to (\gamma[K^+\pi^-]_D)_{D^*} K^+)$

VALUE	DOCUMENT ID		TECN	COMMENT
−0.558±1.349	[1] AAIJ	21Q	LHCB	pp at 7, 8, 13 TeV

[1] The statistical and systematic uncertainties have been combined according to the correlations between the R^-_K and R^+_K observables.

$A_{ADS}(B^+ \to [D\pi^0]_{D^*} K^+)$

$A_{ADS}(B^+ \to D^*(D\pi^0) K^+) = (R^-_K - R^+_K) / (R^-_K + R^+_K)$, where

$R^-_K = \Gamma(B^- \to ([K^+\pi^-]_D \pi^0)_{D^*} K^-) / \Gamma(B^- \to ([K^-\pi^+]_D \pi^0)_{D^*} K^-)$ and

$R^+_K = \Gamma(B^+ \to ([K^-\pi^+]_D \pi^0)_{D^*} K^+) / \Gamma(B^+ \to ([K^+\pi^-]_D \pi^0)_{D^*} K^+)$

VALUE	DOCUMENT ID		TECN	COMMENT
0.717±0.286	[1] AAIJ	21Q	LHCB	pp at 7, 8, 13 TeV

[1] The statistical and systematic uncertainties have been combined according to the correlations between the R^-_K and R^+_K observables.

$A_{ADS}(B^+ \to [D\gamma]_{D^*} \pi^+)$

$A_{ADS}(B^+ \to D^*(D\gamma) \pi^+) = (R^-_\pi - R^+_\pi) / (R^-_\pi + R^+_\pi)$, where

$R^-_\pi = \Gamma(B^- \to (\gamma[K^+\pi^-]_D)_{D^*} \pi^-) / \Gamma(B^- \to (\gamma[K^-\pi^+]_D)_{D^*} \pi^-)$ and

$R^+_\pi = \Gamma(B^+ \to (\gamma[K^-\pi^+]_D)_{D^*} \pi^+) / \Gamma(B^+ \to (\gamma[K^+\pi^-]_D)_{D^*} \pi^+)$

VALUE	DOCUMENT ID		TECN	COMMENT
0.079±0.128	[1] AAIJ	21Q	LHCB	pp at 7, 8, 13 TeV

[1] The statistical and systematic uncertainties have been combined according to the correlations between the R^-_π and R^+_π observables.

$A_{ADS}(B^+ \to [D\pi^0]_{D^*} \pi^+)$

$A_{ADS}(B^+ \to D^*(D\pi^0) \pi^+) = (R^-_\pi - R^+_\pi) / (R^-_\pi + R^+_\pi)$, where

$R^-_\pi = \Gamma(B^- \to ([K^+\pi^-]_D \pi^0)_{D^*} \pi^-) / \Gamma(B^- \to ([K^-\pi^+]_D \pi^0)_{D^*} \pi^-)$ and

$R^+_\pi = \Gamma(B^+ \to ([K^-\pi^+]_D \pi^0)_{D^*} \pi^+) / \Gamma(B^+ \to ([K^+\pi^-]_D \pi^0)_{D^*} \pi^+)$

VALUE	DOCUMENT ID		TECN	COMMENT
−0.140±0.059	[1] AAIJ	21Q	LHCB	pp at 7, 8, 13 TeV

[1] The statistical and systematic uncertainties have been combined according to the correlations between the R^-_π and R^+_π observables.

$A_{ADS}(B^+ \to [K^-\pi^+]_D K^+\pi^-\pi^+)$

VALUE	DOCUMENT ID		TECN	COMMENT
$-0.33^{+0.36}_{-0.34}$	AAIJ	15BC	LHCB	pp at 7, 8 TeV

$A_{ADS}(B^+ \to [K^-\pi^+]_D \pi^+\pi^-\pi^+)$

VALUE	DOCUMENT ID		TECN	COMMENT
−0.013±0.087	AAIJ	15BC	LHCB	pp at 7, 8 TeV

$A_{CP}(B^+ \to D_{CP(-1)} K^+)$

VALUE	DOCUMENT ID		TECN	COMMENT
−0.14 ±0.05 OUR AVERAGE				
−0.167±0.057±0.006	ADACHI	24I	BELL	$e^+e^- \to \Upsilon(4S)$
−0.09 ±0.07 ±0.02	DEL-AMO-SA...10G		BABR	$e^+e^- \to \Upsilon(4S)$
• • • We do not use the following data for averages, fits, limits, etc. • • •				
−0.09 ±0.09 ±0.02	AUBERT	08AA	BABR	Repl. by DEL-AMO-SANCHEZ 10G
−0.12 ±0.14 ±0.05	ABE	06	BELL	Repl. by ADACHI 24I
−0.06 ±0.13 ±0.04	AUBERT	06J	BABR	Repl. by AUBERT 08AA
−0.22 ±0.24 ±0.04	[1] ABE	03D	BELL	Repl. by SWAIN 03
−0.19 ±0.17 ±0.05	[2] SWAIN	03	BELL	Repl. by ABE 06

[1] Corresponds to 90% confidence range $-0.62 < A_{CP} < 0.18$.
[2] Corresponds to 90% confidence range $-0.47 < A_{CP} < 0.11$.

$A_{CP}(B^+ \to [K^+K^-]_D K^+\pi^-\pi^+)$

VALUE	DOCUMENT ID		TECN	COMMENT
−0.045±0.064±0.011	AAIJ	15BC	LHCB	pp at 7, 8 TeV

$A_{CP}(B^+ \to [\pi^+\pi^-]_D K^+\pi^-\pi^+)$

VALUE	DOCUMENT ID		TECN	COMMENT
−0.054±0.101±0.011	AAIJ	15BC	LHCB	pp at 7, 8 TeV

$A_{CP}(B^+ \to [K^-\pi^+]_D K^+\pi^-\pi^+)$

VALUE	DOCUMENT ID		TECN	COMMENT
0.013±0.019±0.013	AAIJ	15BC	LHCB	pp at 7, 8 TeV

$A_{CP}(B^+ \to [K^+K^-]_D \pi^+\pi^-\pi^+)$

VALUE	DOCUMENT ID		TECN	COMMENT
−0.019±0.011±0.010	AAIJ	15BC	LHCB	pp at 7, 8 TeV

$A_{CP}(B^+ \to [\pi^+\pi^-]_D \pi^+\pi^-\pi^+)$

VALUE	DOCUMENT ID		TECN	COMMENT
−0.013±0.016±0.010	AAIJ	15BC	LHCB	pp at 7, 8 TeV

$A_{CP}(B^+ \to [K^-\pi^+]_D \pi^+\pi^-\pi^+)$

VALUE	DOCUMENT ID		TECN	COMMENT
−0.002±0.003±0.011	AAIJ	15BC	LHCB	pp at 7, 8 TeV

$A_{CP}(B^+ \to [\overline{D}^0\gamma]_{\overline{D}^*} \pi^+)$

VALUE	DOCUMENT ID		TECN	COMMENT
−0.004±0.004±0.001	AAIJ	21Q	LHCB	pp at 7, 8, 13 TeV

Int. J. Mod. Phys. A 2026.41. Downloaded from www.worldscientific.com
by UNIVERSITY OF CALIFORNIA @ BERKELEY on 09/16/26. Re-use and distribution is strictly not permitted, except for Open Access articles.

• • • We do not use the following data for averages, fits, limits, etc. • • •

0.000±0.006±0.001	[1] AAIJ	18A	LHCB	pp at 7, 8, 13 TeV

[1] Superseded by AAIJ 21Q.

$A_{CP}(B^+ \to [\overline{D}^0\pi^0]_{\overline{D}^*}\pi^+)$

VALUE	DOCUMENT ID		TECN	COMMENT
0.0007±0.0022 OUR AVERAGE				
0.001 ±0.002 ±0.001	AAIJ	21Q	LHCB	pp at 7, 8, 13 TeV
−0.014 ±0.015	ABE	06	BELL	$e^+e^- \to \Upsilon(4S)$
• • • We do not use the following data for averages, fits, limits, etc. • • •				
0.002 ±0.003 ±0.001	[1] AAIJ	18A	LHCB	pp at 7, 8, 13 TeV

[1] Superseded by AAIJ 21Q.

$A_{CP}(B^+ \to [\overline{D}^0\gamma]_{\overline{D}^{*0}_{CP(-1)}}\pi^+)$

VALUE	DOCUMENT ID		TECN	COMMENT
0.000±0.014±0.006	AAIJ	21Q	LHCB	pp at 7, 8, 13 TeV
• • • We do not use the following data for averages, fits, limits, etc. • • •				
−0.003±0.017±0.002	[1] AAIJ	18A	LHCB	pp at 7, 8, 13 TeV

[1] Superseded by AAIJ 21Q.

$A_{CP}(B^+ \to [\overline{D}^0\pi^0]_{D^{*0}_{CP(+1)}}\pi^+)$

VALUE	DOCUMENT ID		TECN	COMMENT
0.012±0.008 OUR AVERAGE				
0.013±0.007±0.003	AAIJ	21Q	LHCB	pp at 7, 8, 13 TeV
−0.021±0.045	ABE	06	BELL	$e^+e^- \to \Upsilon(4S)$
• • • We do not use the following data for averages, fits, limits, etc. • • •				
0.025±0.010±0.003	[1] AAIJ	18A	LHCB	pp at 7, 8, 13 TeV

[1] Superseded by AAIJ 21Q.

$A_{CP}(B^+ \to [\overline{D}^0\pi^0]_{D^{*0}_{CP(-1)}}\pi^+)$

VALUE	DOCUMENT ID		TECN	COMMENT
−0.090±0.051	ABE	06	BELL	$e^+e^- \to \Upsilon(4S)$

$A_{CP}(B^+ \to [\overline{D}^0\gamma]_{\overline{D}^{*0}}K^+)$

VALUE	DOCUMENT ID		TECN	COMMENT
−0.004±0.014±0.003	[1] AAIJ	21Q	LHCB	pp at 7, 8, 13 TeV
• • • We do not use the following data for averages, fits, limits, etc. • • •				
0.001±0.021±0.007	[2] AAIJ	18A	LHCB	pp at 7, 8, 13 TeV

[1] The $\overline{D}^0 \to K^+\pi^-$ decay is used.
[2] Superseded by AAIJ 21Q.

$A_{CP}(B^+ \to [\overline{D}^0\pi^0]_{\overline{D}^{*0}}K^+)$

VALUE	DOCUMENT ID		TECN	COMMENT
0.017±0.007 OUR AVERAGE				
0.020±0.007±0.003	[1] AAIJ	21Q	LHCB	pp at 7, 8, 13 TeV
−0.06 ±0.04 ±0.01	AUBERT	08BF	BABR	$e^+e^- \to \Upsilon(4S)$
−0.089±0.086	ABE	06	BELL	$e^+e^- \to \Upsilon(4S)$
• • • We do not use the following data for averages, fits, limits, etc. • • •				
0.006±0.012±0.004	[2] AAIJ	18A	LHCB	pp at 7, 8, 13 TeV

[1] The $\overline{D}^0 \to K^+\pi^-$ decay is used.
[2] Superseded by AAIJ 21Q.

$A_{CP}(B^+ \to [\overline{D}^0\gamma]_{\overline{D}^{*0}_{CP(-1)}}K^+)$

VALUE	DOCUMENT ID		TECN	COMMENT
0.123±0.054±0.031	AAIJ	21Q	LHCB	pp at 7, 8, 13 TeV
• • • We do not use the following data for averages, fits, limits, etc. • • •				
0.276±0.094±0.047	[1] AAIJ	18A	LHCB	pp at 7, 8, 13 TeV

[1] Superseded by AAIJ 21Q.

$A_{CP}(B^+ \to [D^0\pi^0]_{D^{*0}_{CP(+1)}}K^+)$

VALUE	DOCUMENT ID		TECN	COMMENT
−0.115±0.020 OUR AVERAGE				
−0.115±0.019±0.009	AAIJ	21Q	LHCB	pp at 7, 8, 13 TeV
−0.11 ±0.09 ±0.01	AUBERT	08BF	BABR	$e^+e^- \to \Upsilon(4S)$
−0.20 ±0.22 ±0.04	ABE	06	BELL	$e^+e^- \to \Upsilon(4S)$
• • • We do not use the following data for averages, fits, limits, etc. • • •				
−0.151±0.033±0.011	[1] AAIJ	18A	LHCB	pp at 7, 8, 13 TeV
$-0.10 \pm 0.23\ ^{+0.03}_{-0.04}$	AUBERT	05N	BABR	Repl. by AUBERT 08BF

[1] Superseded by AAIJ 21Q.

$A_{CP}(B^+ \to [D^0\pi^0]_{D^{*0}_{CP(-1)}}K^+)$

VALUE	DOCUMENT ID		TECN	COMMENT
0.07±0.10 OUR AVERAGE				
+0.06±0.10±0.02	AUBERT	08BF	BABR	$e^+e^- \to \Upsilon(4S)$
+0.13±0.30±0.08	ABE	06	BELL	$e^+e^- \to \Upsilon(4S)$

$A_{CP}(B^+ \to D_{CP(+1)}K^*(892)^+)$

VALUE	DOCUMENT ID		TECN	COMMENT
0.08±0.06 OUR AVERAGE				
0.08±0.06±0.01	[1] AAIJ	17BO	LHCB	pp at 7, 8, 13 TeV
0.09±0.13±0.06	AUBERT	09AJ	BABR	$e^+e^- \to \Upsilon(4S)$
• • • We do not use the following data for averages, fits, limits, etc. • • •				
−0.08±0.19±0.08	AUBERT,B	05U	BABR	Repl. by AUBERT 09AJ

[1] Measures the asymmetry separately for K^+K^- and $\pi^+\pi^-$ final states, $A(KK) = 0.06 \pm 0.07 \pm 0.01$and $A(\pi\pi) = 0.15 \pm 0.13 \pm 0.01$, and combines the two results. The value of $A(\pi\pi)$ was updated in AAIJ 18X.

$A_{CP}(B^+ \to D_{CP(-1)}K^*(892)^+)$

VALUE	DOCUMENT ID		TECN	COMMENT
−0.23±0.21±0.07	AUBERT	09AJ	BABR	$e^+e^- \to \Upsilon(4S)$
• • • We do not use the following data for averages, fits, limits, etc. • • •				
−0.26±0.40±0.12	AUBERT,B	05U	BABR	Repl. by AUBERT 09AJ

$A_{CP}(B^+ \to D_s^+\phi)$

VALUE	DOCUMENT ID		TECN	COMMENT
−0.01±0.41±0.03	AAIJ	13R	LHCB	pp at 7 TeV

$A_{CP}(B^+ \to D_s^+\overline{D}^0)$

VALUE (%)	DOCUMENT ID		TECN	COMMENT
0.5±0.2±0.6	[1] AAIJ	23AX	LHCB	pp at 7, 8, 13 TeV
• • • We do not use the following data for averages, fits, limits, etc. • • •				
−0.4±0.5±0.5	AAIJ	18W	LHCB	Repl. by AAIJ 23AX

[1] The last error includes the uncertainty from $A_{CP}(B^+ \to J/\psi K^+)$.

$A_{CP}(B^+ \to D_s^{*+}\overline{D}^0)$

VALUE (units 10^{-2})	DOCUMENT ID		TECN	COMMENT
−0.5±1.1±1.0	[1] AAIJ	23AX	LHCB	pp at 7, 8, 13 TeV

[1] The last error includes the uncertainty from $A_{CP}(B^+ \to J/\psi K^+)$.

$A_{CP}(B^+ \to D_s^+\overline{D}^{*0})$

VALUE (units 10^{-2})	DOCUMENT ID		TECN	COMMENT
1.1±0.8±0.7	[1] AAIJ	23AX	LHCB	pp at 7, 8, 13 TeV

[1] The last error includes the uncertainty from $A_{CP}(B^+ \to J/\psi K^+)$.

$A_{CP}(B^+ \to D^{*+}\overline{D}^{*0})$

VALUE (units 10^{-2})	DOCUMENT ID		TECN	COMMENT
1.3± 2.6 OUR AVERAGE				
2.3± 2.1±1.7	[1] AAIJ	23AX	LHCB	pp at 7, 8, 13 TeV
−15 ±11 ±2	AUBERT,B	06A	BABR	$e^+e^- \to \Upsilon(4S)$

[1] The last error includes the uncertainty from $A_{CP}(B^+ \to J/\psi K^+)$.

$A_{CP}(B^+ \to D^{*+}\overline{D}^0)$

VALUE (units 10^{-2})	DOCUMENT ID		TECN	COMMENT
3.1± 1.7 OUR AVERAGE				
3.3± 1.6±0.7	[1] AAIJ	23AX	LHCB	pp at 7, 8, 13 TeV
−6 ±13 ±2	AUBERT,B	06A	BABR	$e^+e^- \to \Upsilon(4S)$

[1] The last error includes the uncertainty from $A_{CP}(B^+ \to J/\psi K^+)$.

$A_{CP}(B^+ \to D^+\overline{D}^{*0})$

VALUE (units 10^{-2})	DOCUMENT ID		TECN	COMMENT
0.0± 2.4 OUR AVERAGE				
− 0.2± 2.0±1.4	[1] AAIJ	23AX	LHCB	pp at 7, 8, 13 TeV
13 ±18 ±4	AUBERT,B	06A	BABR	$e^+e^- \to \Upsilon(4S)$

[1] The last error includes the uncertainty from $A_{CP}(B^+ \to J/\psi K^+)$.

$A_{CP}(B^+ \to D^+\overline{D}^0)$

VALUE (units 10^{-2})	DOCUMENT ID		TECN	COMMENT
2.4± 1.1 OUR AVERAGE				
2.5± 1.0±0.5	[1] AAIJ	23AX	LHCB	pp at 7, 8, 13 TeV
0 ± 8 ±2	ADACHI	08	BELL	$e^+e^- \to \Upsilon(4S)$
−13 ±14 ±2	AUBERT,B	06A	BABR	$e^+e^- \to \Upsilon(4S)$
• • • We do not use the following data for averages, fits, limits, etc. • • •				
2.3± 2.7±0.4	AAIJ	18W	LHCB	Repl. by AAIJ 23AX

[1] The last error includes the uncertainty from $A_{CP}(B^+ \to J/\psi K^+)$.

$A_{CP}(B^+ \to K_S^0\pi^+)$

VALUE	DOCUMENT ID		TECN	COMMENT
−0.003±0.015 OUR AVERAGE	Error includes scale factor of 1.1.			
0.046±0.029±0.007	ADACHI	24	BELL	$e^+e^- \to \Upsilon(4S)$
−0.022±0.025±0.010	AAIJ	13BS	LHCB	pp at 7 TeV
−0.011±0.021±0.006	DUH	13	BELL	$e^+e^- \to \Upsilon(4S)$
−0.029±0.039±0.010	[1] AUBERT,BE	06C	BABR	$e^+e^- \to \Upsilon(4S)$
0.18 ±0.24	[2] CHEN	00	CLE2	$e^+e^- \to \Upsilon(4S)$
• • • We do not use the following data for averages, fits, limits, etc. • • •				
0.03 ±0.03 ±0.01	LIN	07	BELL	Repl. by DUH 13
−0.09 ±0.05 ±0.01	[3] AUBERT,BE	05E	BABR	Repl. by AUBERT,BE 06C
0.05 ±0.05 ±0.01	[4] CHAO	05A	BELL	Repl. by LIN 07
−0.05 ±0.08 ±0.01	[5] AUBERT	04M	BABR	Repl. by AUBERT,BE 05E
$0.07\ ^{+0.09}_{-0.08}\ ^{+0.01}_{-0.03}$	[6] UNNO	03	BELL	Repl. by CHAO 05A
0.46 ±0.15 ±0.02	[7] CASEY	02	BELL	Repl. by UNNO 03
$0.098^{+0.430}_{-0.343}{}^{+0.020}_{-0.063}$	[8] ABE	01K	BELL	Repl. by CASEY 02
−0.21 ±0.18 ±0.03	[9] AUBERT	01E	BABR	Repl. by AUBERT 04M

[1] Corresponds to 90% confidence range $-0.092 < A_{CP} < 0.036$.
[2] Corresponds to 90% confidence range $-0.22 < A_{CP} < 0.56$.
[3] Corresponds to 90% confidence range $-0.16 < A_{CP} < -0.02$.
[4] Corresponds to 90% confidence range $-0.04 < A_{CP} < 0.13$.
[5] Corresponds to 90% confidence range $-0.18 < A_{CP} < 0.08$.
[6] Corresponds to 90% confidence range $-0.10 < A_{CP} < +0.22$.
[7] Corresponds to 90% confidence range $+0.19 < A_{CP} < +0.72$.
[8] Corresponds to 90% confidence range $-0.53 < A_{CP} < 0.82$.
[9] Corresponds to 90% confidence range $-0.51 < A_{CP} < 0.09$.

$A_{CP}(B^+ \to K^+\pi^0)$

VALUE	DOCUMENT ID		TECN	COMMENT
0.027±0.012 OUR AVERAGE				
0.013±0.027±0.005	ADACHI	24	BELL	$e^+e^- \to \Upsilon(4S)$
0.025±0.015±0.007	AAIJ	21H	LHCB	pp at 13 TeV
0.043±0.024±0.002	DUH	13	BELL	$e^+e^- \to \Upsilon(4S)$
0.030±0.039±0.010	AUBERT	07BC	BABR	$e^+e^- \to \Upsilon(4S)$
−0.29 ±0.23	[1] CHEN	00	CLE2	$e^+e^- \to \Upsilon(4S)$
• • • We do not use the following data for averages, fits, limits, etc. • • •				
0.07 ±0.03 ±0.01	LIN	08	BELL	Repl. by DUH 13
0.06 ±0.06 ±0.01	[2] AUBERT	05L	BABR	Repl. by AUBERT 07BC
0.06 ±0.06 ±0.02	[2] CHAO	05A	BELL	Repl. by CHAO 04B
0.04 ±0.05 ±0.02	[3] CHAO	04B	BELL	Repl. by LIN 08
−0.09 ±0.09 ±0.01	[4] AUBERT	03L	BABR	Repl. by AUBERT 05L
−0.02 ±0.19 ±0.02	[5] CASEY	02	BELL	Repl. by CHAO 04B
$-0.059^{+0.222+0.055}_{-0.196-0.017}$	[6] ABE	01K	BELL	Repl. by CASEY 02
0.00 ±0.18 ±0.04	[7] AUBERT	01E	BABR	Repl. by AUBERT 03L

[1] Corresponds to 90% confidence range $-0.67 < A_{CP} < 0.09$.
[2] Corresponds to a 90% CL interval of $-0.06 < A_{CP} < 0.18$.
[3] Corresponds to 90% CL interval of $-0.05 < A_{CP} < 0.13$.
[4] Corresponds to 90% confidence range $-0.24 < A_{CP} < 0.06$.
[5] Corresponds to 90% confidence range $-0.35 < A_{CP} < +0.30$.
[6] Corresponds to 90% confidence range $-0.40 < A_{CP} < 0.36$.
[7] Corresponds to 90% confidence range $-0.30 < A_{CP} < +0.30$.

$A_{CP}(B^+ \to \eta' K^+)$

VALUE	DOCUMENT ID		TECN	COMMENT
0.004±0.011 OUR AVERAGE				
−0.002±0.012±0.006	[1] AAIJ	15O	LHCB	pp at 7, 8 TeV
$0.008^{+0.017}_{-0.018}\pm0.009$	AUBERT	09AV	BABR	$e^+e^- \to \Upsilon(4S)$
0.028±0.028±0.021	SCHUEMANN	06	BELL	$e^+e^- \to \Upsilon(4S)$
0.03 ±0.12	[2] CHEN	00	CLE2	$e^+e^- \to \Upsilon(4S)$
• • • We do not use the following data for averages, fits, limits, etc. • • •				
0.010±0.022±0.006	AUBERT	07AE	BABR	Repl. by AUBERT 09AV
0.033±0.028±0.005	[3] AUBERT	05M	BABR	Repl. by AUBERT 07AE
0.037±0.045±0.011	[4] AUBERT	03W	BABR	Repl. by AUBERT 05M
−0.11 ±0.11 ±0.02	[5] AUBERT	02E	BABR	Repl. by AUBERT 05M
−0.015±0.070±0.009	[6] CHEN	02B	BELL	Repl. by SCHUEMANN 06
0.06 ±0.15 ±0.01	[7] ABE	01M	BELL	Repl. by CHEN 02B

[1] Obtained using $A_{CP}(B^\pm \to J/\psi K^\pm) = (0.3 \pm 0.6) \times 10^{-2}$.
[2] Corresponds to 90% confidence range $-0.17 < A_{CP} < 0.23$.
[3] Corresponds to 90% confidence range $-0.012 < A_{CP} < 0.078$.
[4] Corresponds to 90% confidence range $-0.04 < A_{CP} < 0.11$.
[5] Corresponds to 90% confidence range $-0.28 < A_{CP} < 0.07$.
[6] Corresponds to 90% confidence range $-0.13 < A_{CP} < 0.10$.
[7] Corresponds to 90% confidence range $-0.20 < A_{CP} < 0.32$.

$A_{CP}(B^+ \to \eta' K^*(892)^+)$

VALUE	DOCUMENT ID		TECN	COMMENT
−0.26±0.27±0.02	DEL-AMO-SA...	10A	BABR	$e^+e^- \to \Upsilon(4S)$
• • • We do not use the following data for averages, fits, limits, etc. • • •				
$-0.30^{+0.33}_{-0.37}\pm0.02$	[1] AUBERT	07E	BABR	Repl. by DEL-AMO-SANCHEZ 10A

[1] Reports A_{CP} with the opposite sign convention.

$A_{CP}(B^+ \to \eta' K_0^*(1430)^+)$

VALUE	DOCUMENT ID		TECN	COMMENT
0.06±0.20±0.02	DEL-AMO-SA...	10A	BABR	$e^+e^- \to \Upsilon(4S)$

$A_{CP}(B^+ \to \eta' K_2^*(1430)^+)$

VALUE	DOCUMENT ID		TECN	COMMENT
0.15±0.13±0.02	DEL-AMO-SA...	10A	BABR	$e^+e^- \to \Upsilon(4S)$

$A_{CP}(B^+ \to \eta K^+)$

VALUE	DOCUMENT ID		TECN	COMMENT
−0.37±0.08 OUR AVERAGE				
−0.38±0.11±0.01	HOI	12	BELL	$e^+e^- \to \Upsilon(4S)$
−0.36±0.11±0.03	AUBERT	09AV	BABR	$e^+e^- \to \Upsilon(4S)$
• • • We do not use the following data for averages, fits, limits, etc. • • •				
−0.22±0.11±0.01	AUBERT	07AE	BABR	Repl. by AUBERT 09AV
−0.39±0.16±0.03	CHANG	07B	BELL	Repl. by HOI 12
−0.20±0.15±0.01	AUBERT,B	05K	BABR	Repl. by AUBERT 07AE
−0.49±0.31±0.07	CHANG	05A	BELL	Repl. by CHANG 07B
−0.52±0.24±0.01	AUBERT	04H	BABR	Repl. by AUBERT,B 05K

$A_{CP}(B^+ \to \eta K^*(892)^+)$

VALUE	DOCUMENT ID		TECN	COMMENT
0.02±0.06 OUR AVERAGE				
0.03±0.10±0.01	WANG	07B	BELL	$e^+e^- \to \Upsilon(4S)$
0.01±0.08±0.02	AUBERT,B	06H	BABR	$e^+e^- \to \Upsilon(4S)$
• • • We do not use the following data for averages, fits, limits, etc. • • •				
0.13±0.14±0.02	AUBERT,B	04D	BABR	Repl. by AUBERT,B 06H

$A_{CP}(B^+ \to \eta K_0^*(1430)^+)$

VALUE	DOCUMENT ID		TECN	COMMENT
0.05±0.13±0.02	AUBERT,B	06H	BABR	$e^+e^- \to \Upsilon(4S)$

$A_{CP}(B^+ \to \eta K_2^*(1430)^+)$

VALUE	DOCUMENT ID		TECN	COMMENT
−0.45±0.30±0.02	AUBERT,B	06H	BABR	$e^+e^- \to \Upsilon(4S)$

$A_{CP}(B^+ \to \omega K^+)$

VALUE	DOCUMENT ID		TECN	COMMENT
−0.02±0.04 OUR AVERAGE				
−0.03±0.04±0.01	CHOBANOVA	14	BELL	$e^+e^- \to \Upsilon(4S)$
−0.01±0.07±0.01	AUBERT	07AE	BABR	$e^+e^- \to \Upsilon(4S)$
• • • We do not use the following data for averages, fits, limits, etc. • • •				
0.05±0.09±0.01	AUBERT,B	06E	BABR	Repl. by AUBERT 07AE
$0.05^{+0.08}_{-0.07}\pm0.01$	JEN	06	BELL	Repl. by CHOBANOVA 14
−0.09±0.17±0.01	AUBERT	04H	BABR	Repl. by AUBERT,B 06E
$0.06^{+0.21}_{-0.18}\pm0.01$	[1] WANG	04A	BELL	Repl. by JEN 06
−0.21±0.28±0.03	[2] LU	02	BELL	Repl. by WANG 04A

[1] Corresponds to 90% CL interval $0.15 < A_{CP} < 0.90$
[2] Corresponds to 90% confidence range $-0.70 < A_{CP} < +0.38$.

$A_{CP}(B^+ \to \omega K^{*+})$

VALUE	DOCUMENT ID		TECN	COMMENT
+0.29±0.35±0.02	AUBERT	09H	BABR	$e^+e^- \to \Upsilon(4S)$

$A_{CP}(B^+ \to \omega(K\pi)_0^{*+})$

VALUE	DOCUMENT ID		TECN	COMMENT
−0.10±0.09±0.02	AUBERT	09H	BABR	$e^+e^- \to \Upsilon(4S)$

$A_{CP}(B^+ \to \omega K_2^*(1430)^+)$

VALUE	DOCUMENT ID		TECN	COMMENT
+0.14±0.15±0.02	AUBERT	09H	BABR	$e^+e^- \to \Upsilon(4S)$

$A_{CP}(B^+ \to K^{*0}\pi^+)$

VALUE	DOCUMENT ID		TECN	COMMENT
−0.021±0.032 OUR AVERAGE Error includes scale factor of 1.5. See the ideogram below.				
−0.015±0.021±0.012	AAIJ	23V	LHCB	pp at 13 TeV
$-0.12 \pm0.21\ ^{+0.08}_{-0.14}$	[1] LEES	17G	BABR	$e^+e^- \to \Upsilon(4S)$
$0.032\pm0.052^{+0.016}_{-0.013}$	AUBERT	08AI	BABR	$e^+e^- \to \Upsilon(4S)$
−0.149±0.064±0.022	GARMASH	06	BELL	$e^+e^- \to \Upsilon(4S)$
• • • We do not use the following data for averages, fits, limits, etc. • • •				
$0.068\pm0.078^{+0.070}_{-0.067}$	AUBERT,B	05N	BABR	Repl. by AUBERT 08AI

[1] Obtains the result from a Dalitz analysis of $B^+ \to K_S^0\pi^+\pi^0$ decays. The first error is statistical, the second combines all the systematic uncertainties reported in the paper, including signal modelling.

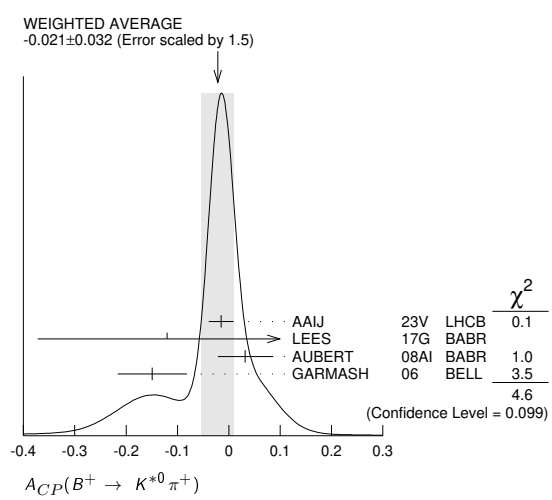

Int. J. Mod. Phys. A 2026.41. Downloaded from www.worldscientific.com
by CALIFORNIA @ BERKELEY on 09/16/26. Re-use and distribution is strictly not permitted, except for Open Access articles.

Int. J. Mod. Phys. A 2026.41. Downloaded from www.worldscientific.com
by UNIVERSITY OF CALIFORNIA @ BERKELEY on 09/16/26. Re-use and distribution is strictly not permitted, except for Open Access articles.

$A_{CP}(B^+ \to K^*(892)^+\pi^0)$

VALUE	DOCUMENT ID		TECN	COMMENT
-0.39 ± 0.21 OUR AVERAGE	Error includes scale factor of 1.6.			
$-0.52\pm0.14^{+0.06}_{-0.05}$	[1] LEES	17G	BABR	$e^+e^- \to \Upsilon(4S)$
$-0.06\pm0.24\pm0.04$	LEES	11I	BABR	$e^+e^- \to \Upsilon(4S)$
• • • We do not use the following data for averages, fits, limits, etc. • • •				
$0.04\pm0.29\pm0.05$	AUBERT	05X	BABR	Repl. by LEES 11I

[1] Obtains the result from a Dalitz analysis of $B^+ \to K^0_S\pi^+\pi^0$ decays. The first error is statistical, the second combines all the systematic uncertainties reported in the paper, including signal modelling.

$A_{CP}(B^+ \to K^+\pi^-\pi^+)$

VALUE	DOCUMENT ID		TECN	COMMENT
0.015 ± 0.006 OUR AVERAGE	Error includes scale factor of 1.4.			
$0.011\pm0.002\pm0.004$	[1] AAIJ	23U	LHCB	pp at 13 TeV
$0.025\pm0.004\pm0.008$	[1] AAIJ	14BO	LHCB	pp at 7, 8 TeV
$0.028\pm0.020\pm0.023$	AUBERT	08AI	BABR	$e^+e^- \to \Upsilon(4S)$
$0.049\pm0.026\pm0.020$	GARMASH	06	BELL	$e^+e^- \to \Upsilon(4S)$
• • • We do not use the following data for averages, fits, limits, etc. • • •				
$0.032\pm0.008\pm0.008$	AAIJ	13AZ	LHCB	Repl. by AAIJ 14BO
$-0.013\pm0.037\pm0.011$	AUBERT,B	05N	BABR	Repl. by AUBERT 08AI
$0.01\ \pm0.07\ \pm0.03$	AUBERT	03M	BABR	Repl. by AUBERT,B 05N

[1] The second error includes both systematics and the uncertainties from CP asymmetries in restricted regions of phase space.

$A_{CP}(B^+ \to K^+K^-K^+$ nonresonant$)$

VALUE	DOCUMENT ID		TECN	COMMENT
$0.060\pm0.044\pm0.019$	LEES	12O	BABR	$e^+e^- \to \Upsilon(4S)$

$A_{CP}(B^+ \to f(980)^0K^+)$

VALUE	DOCUMENT ID		TECN	COMMENT
$-0.08\pm0.08\pm0.04$	[1] LEES	12O	BABR	$e^+e^- \to \Upsilon(4S)$

[1] Measured in the $B^+ \to K^+K^-K^+$ decay.

$A_{CP}(B^+ \to f_2(1270)K^+)$

VALUE	DOCUMENT ID		TECN	COMMENT
$-0.68^{+0.19}_{-0.17}$ OUR AVERAGE				
$-0.85\pm0.22^{+0.26}_{-0.13}$	AUBERT	08AI	BABR	$e^+e^- \to \Upsilon(4S)$
$-0.59\pm0.22\pm0.036$	GARMASH	06	BELL	$e^+e^- \to \Upsilon(4S)$

$A_{CP}(B^+ \to f_0(1500)K^+)$

VALUE	DOCUMENT ID		TECN	COMMENT
$0.28\pm0.26^{+0.15}_{-0.14}$	AUBERT	08AI	BABR	$e^+e^- \to \Upsilon(4S)$

$A_{CP}(B^+ \to f'_2(1525)^0K^+)$

VALUE	DOCUMENT ID		TECN	COMMENT
$-0.08\ ^{+0.05}_{-0.04}$ OUR AVERAGE				
$0.18\ \pm0.18\ \pm0.04$	[1] LEES	11I	BABR	$e^+e^- \to \Upsilon(4S)$
$-0.106\pm0.050^{+0.036}_{-0.015}$	AUBERT	08AI	BABR	$e^+e^- \to \Upsilon(4S)$
$-0.077\pm0.065^{+0.046}_{-0.026}$	GARMASH	06	BELL	$e^+e^- \to \Upsilon(4S)$
• • • We do not use the following data for averages, fits, limits, etc. • • •				
$0.14\ \pm0.10\ \pm0.04$	[2] LEES	12O	BABR	$e^+e^- \to \Upsilon(4S)$
$-0.31\ \pm0.25\ \pm0.08$	[3] AUBERT	06O	BABR	Repl. by LEES 12O
$0.088\pm0.095^{+0.097}_{-0.056}$	AUBERT,B	05N	BABR	Repl. by AUBERT 08AI

[1] Measured in $B^+ \to f_0K^+$ with $f_0 \to \pi^0\pi^0$ decay.
[2] Measured in the $B^+ \to K^+K^-K^+$ decay assuming $A_{CP}(B^+ \to f'_2(1525)^0K^+) = A_{CP}(B^+ \to f_0(1500)^0K^+) = A_{CP}(B^+ \to f_0(1710)^0K^+)$
[3] Measured in the $B^+ \to K^+K^-K^+$ decay.

$A_{CP}(B^+ \to \rho^0K^+)$

VALUE	DOCUMENT ID		TECN	COMMENT
0.160 ± 0.021 OUR AVERAGE				
$0.150\pm0.019\pm0.011$	AAIJ	23V	LHCB	pp at 13 TeV
$0.44\ \pm0.10\ ^{+0.06}_{-0.14}$	AUBERT	08AI	BABR	$e^+e^- \to \Upsilon(4S)$
$0.30\ \pm0.11\ ^{+0.11}_{-0.04}$	GARMASH	06	BELL	$e^+e^- \to \Upsilon(4S)$
• • • We do not use the following data for averages, fits, limits, etc. • • •				
$0.32\ \pm0.13\ ^{+0.10}_{-0.08}$	AUBERT,B	05N	BABR	Repl. by AUBERT 08AI

$A_{CP}(B^+ \to K^0\pi^+\pi^0)$

VALUE	DOCUMENT ID		TECN	COMMENT
$0.07\pm0.05\pm0.04$	[1] LEES	17G	BABR	$e^+e^- \to \Upsilon(4S)$

[1] Obtains the result from a Dalitz analysis of $B^+ \to K^0_S\pi^+\pi^0$ decays. The first error is statistical, the second combines all the systematic uncertainties reported in the paper, including signal modelling.

$A_{CP}(B^+ \to K^*_0(1430)^0\pi^+)$

VALUE	DOCUMENT ID		TECN	COMMENT
0.061 ± 0.032 OUR AVERAGE				
$0.14\ \pm0.10\ ^{+0.14}_{-0.06}$	[1] LEES	17G	BABR	$e^+e^- \to \Upsilon(4S)$
$0.032\pm0.035^{+0.034}_{-0.028}$	AUBERT	08AI	BABR	$e^+e^- \to \Upsilon(4S)$
$0.076\pm0.038^{+0.028}_{-0.022}$	GARMASH	06	BELL	$e^+e^- \to \Upsilon(4S)$
• • • We do not use the following data for averages, fits, limits, etc. • • •				
$-0.064\pm0.032^{+0.023}_{-0.026}$	AUBERT,B	05N	BABR	Repl. by AUBERT 08AI

[1] Obtains the result from a Dalitz analysis of $B^+ \to K^0_S\pi^+\pi^0$ decays. The first error is statistical, the second combines all the systematic uncertainties reported in the paper, including signal modelling.

$A_{CP}(B^+ \to K^*_0(1430)^+\pi^0)$

VALUE	DOCUMENT ID		TECN	COMMENT
$0.26\pm0.12^{+0.14}_{-0.08}$	[1] LEES	17G	BABR	$e^+e^- \to \Upsilon(4S)$

[1] Obtains the result from a Dalitz analysis of $B^+ \to K^0_S\pi^+\pi^0$ decays. The first error is statistical, the second combines all the systematic uncertainties reported in the paper, including signal modelling.

$A_{CP}(B^+ \to K^*_2(1430)^0\pi^+)$

VALUE	DOCUMENT ID		TECN	COMMENT
$0.05\pm0.23^{+0.18}_{-0.08}$	AUBERT	08AI	BABR	$e^+e^- \to \Upsilon(4S)$

$A_{CP}(B^+ \to K^+\pi^0\pi^0)$

VALUE	DOCUMENT ID		TECN	COMMENT
$-0.06\pm0.06\pm0.04$	LEES	11I	BABR	$e^+e^- \to \Upsilon(4S)$

$A_{CP}(B^+ \to K^0\rho^+)$

VALUE	DOCUMENT ID		TECN	COMMENT
-0.03 ± 0.15 OUR AVERAGE				
$0.21\pm0.19^{+0.24}_{-0.20}$	[1] LEES	17G	BABR	$e^+e^- \to \Upsilon(4S)$
$-0.12\pm0.17\pm0.02$	AUBERT	07Z	BABR	$e^+e^- \to \Upsilon(4S)$

[1] Obtains the result from a Dalitz analysis of$B^+ \to K^0_S\pi^+\pi^0$ decays. The first error is statistical, the second combines all the systematic uncertainties reported in the paper, including signal modelling.

$A_{CP}(B^+ \to K^{*+}\pi^+\pi^-)$

VALUE	DOCUMENT ID		TECN	COMMENT
$0.07\pm0.07\pm0.04$	AUBERT,B	06U	BABR	$e^+e^- \to \Upsilon(4S)$

$A_{CP}(B^+ \to \rho^0K^*(892)^+)$

VALUE	DOCUMENT ID		TECN	COMMENT
$0.31\pm0.13\pm0.03$	DEL-AMO-SA...11D		BABR	$e^+e^- \to \Upsilon(4S)$
• • • We do not use the following data for averages, fits, limits, etc. • • •				
$0.20^{+0.32}_{-0.29}\pm0.04$	AUBERT	03V	BABR	Repl. by DEL-AMO-SANCHEZ 11D

$A_{CP}(B^+ \to K^*(892)^+f_0(980))$

VALUE	DOCUMENT ID		TECN	COMMENT
$-0.15\pm0.12\pm0.03$	DEL-AMO-SA...11D		BABR	$e^+e^- \to \Upsilon(4S)$
• • • We do not use the following data for averages, fits, limits, etc. • • •				
$-0.34\pm0.21\pm0.03$	AUBERT,B	06G	BABR	Repl. by DEL-AMO-SANCHEZ 11D

$A_{CP}(B^+ \to a_1^+K^0)$

VALUE	DOCUMENT ID		TECN	COMMENT
$+0.12\pm0.11\pm0.02$	AUBERT	08F	BABR	$e^+e^- \to \Upsilon(4S)$

$A_{CP}(B^+ \to b_1^+K^0)$

VALUE	DOCUMENT ID		TECN	COMMENT
$-0.03\pm0.15\pm0.02$	AUBERT	08AG	BABR	$e^+e^- \to \Upsilon(4S)$

$A_{CP}(B^+ \to K^*(892)^0\rho^+)$

VALUE	DOCUMENT ID		TECN	COMMENT
$-0.01\pm0.16\pm0.02$	AUBERT,B	06G	BABR	$e^+e^- \to \Upsilon(4S)$

$A_{CP}(B^+ \to b_1^0K^+)$

VALUE	DOCUMENT ID		TECN	COMMENT
$-0.46\pm0.20\pm0.02$	AUBERT	07BI	BABR	$e^+e^- \to \Upsilon(4S)$

$A_{CP}(B^+ \to K^0K^+)$

VALUE	DOCUMENT ID		TECN	COMMENT
$0.04\ \pm0.14$ OUR AVERAGE				
$0.014\pm0.168\pm0.002$	DUH	13	BELL	$e^+e^- \to \Upsilon(4S)$
$0.10\ \pm0.26\ \pm0.03$	[1] AUBERT,BE	06C	BABR	$e^+e^- \to \Upsilon(4S)$
• • • We do not use the following data for averages, fits, limits, etc. • • •				
$0.13\ ^{+0.23}_{-0.24}\ \pm0.02$	LIN	07	BELL	Repl. by DUH 13
$0.15\ \pm0.33\ \pm0.03$	[2] AUBERT,BE	05E	BABR	Repl. by AUBERT,BE 06C

[1] Corresponds to 90% confidence range $-0.31 < A_{CP} < 0.54$.
[2] Corresponds to 90% confidence range $-0.43 < A_{CP} < 0.68$.

Int. J. Mod. Phys. A 2026.41. Downloaded from www.worldscientific.com by LIFORNIA @ BERKELEY on 09/16/26. Re-use and distribution is strictly not permitted, except for Open Access articles.

$A_{CP}(B^+ \to K^0_S K^+)$

VALUE	DOCUMENT ID		TECN	COMMENT
$-0.21 \pm 0.14 \pm 0.01$	AAIJ	13BS	LHCB	pp at 7 TeV

$A_{CP}(B^+ \to K^+ K^0_S K^0_S)$

VALUE	DOCUMENT ID		TECN	COMMENT
0.025 ± 0.031 OUR AVERAGE				
$0.016 \pm 0.039 \pm 0.009$	KALIYAR	19	BELL	$e^+e^- \to \Upsilon(4S)$
$0.04\ ^{+0.04}_{-0.05}\ \pm 0.02$	LEES	12O	BABR	$e^+e^- \to \Upsilon(4S)$
• • • We do not use the following data for averages, fits, limits, etc. • • •				
$-0.04\ \pm 0.11\ \pm 0.02$	[1] AUBERT,B	04V	BABR	Repl. by LEES 12O

[1] Corresponds to 90% confidence range $-0.23 < A_{CP} < 0.15$.

$A_{CP}(B^+ \to K^+ K^- \pi^+)$

VALUE	DOCUMENT ID		TECN	COMMENT
-0.115 ± 0.008 OUR AVERAGE				
$-0.114 \pm 0.007 \pm 0.004$	[1] AAIJ	23U	LHCB	pp at 13 TeV
$-0.170 \pm 0.073 \pm 0.017$	[2] HSU	17	BELL	$e^+e^- \to \Upsilon(4S)$
$-0.123 \pm 0.017 \pm 0.014$	[1] AAIJ	14BO	LHCB	pp at 7, 8 TeV
$0.00\ \pm 0.10\ \pm 0.03$	AUBERT	07BB	BABR	$e^+e^- \to \Upsilon(4S)$
• • • We do not use the following data for averages, fits, limits, etc. • • •				
$-0.141 \pm 0.040 \pm 0.019$	[3] AAIJ	14	LHCB	Repl. by AAIJ 14BO

[1] The second error includes both systematics and the uncertainties from CP asymmetries in restricted regions of phase space.
[2] HSU 17 provides also measurement as a function of K^+K^- invariant mass.
[3] AAIJ 14 reports $A_{CP}(B^+ \to K^+K^-\pi^+) = -0.648 \pm 0.070 \pm 0.013 \pm 0.007$ in the Dalitz plot region of $m^2_{K^+K^-} < 1.5$ GeV^2/c^4. The third uncertainty is due to the CP asymmetry of the $B^{\pm} \to J/\psi K^{\pm}$ reference mode uncertainty.

$A_{CP}(B^+ \to K^+ K^- \pi^+$ nonresonant$)$

VALUE	DOCUMENT ID		TECN	COMMENT
$-0.107 \pm 0.053 \pm 0.035$	[1] AAIJ	19AL	LHCB	pp at 7, 8 TeV

[1] Uses amplitude analysis of $B^{\pm} \to \pi^{\pm} K^+ K^-$ decays.

$A_{CP}(B^+ \to \pi^+ K^+ K^-, m_{K^+K^-} < 1.1$ GeV$)$

VALUE	DOCUMENT ID		TECN	COMMENT
$-0.170 \pm 0.073 \pm 0.017$	[1] HSU	23	BELL	$e^+e^- \to \Upsilon(4S)$

[1] Investigated the angular distribution of K^+K^- pairs with invariant mass below 1.1 GeV/c^2, which exhibits both a strong enhancement in signal and very large direct CP violation.

$A_{CP}(B^+ \to K^+ \overline{K}^*(892)^0)$

VALUE	DOCUMENT ID		TECN	COMMENT
$0.04\ \pm 0.05$ OUR AVERAGE				
$0.007 \pm 0.054 \pm 0.032$	AAIJ	23V	LHCB	pp at 13 TeV
$0.123 \pm 0.087 \pm 0.045$	[1] AAIJ	19AL	LHCB	pp at 7, 8 TeV

[1] Uses amplitude analysis of $B^{\pm} \to \pi^{\pm} K^+ K^-$ decays.

$A_{CP}(B^+ \to K^+ \overline{K}^*_0(1430)^0)$

VALUE	DOCUMENT ID		TECN	COMMENT
$0.104 \pm 0.149 \pm 0.088$	[1] AAIJ	19AL	LHCB	pp at 7, 8 TeV

[1] Uses amplitude analysis of $B^{\pm} \to \pi^{\pm} K^+ K^-$ decays.

$A_{CP}(B^+ \to \phi \pi^+)$

VALUE	DOCUMENT ID		TECN	COMMENT
$0.098 \pm 0.436 \pm 0.266$	[1] AAIJ	19AL	LHCB	pp at 7, 8 TeV

[1] Uses amplitude analysis of $B^{\pm} \to \pi^{\pm} K^+ K^-$ decays.

$A_{CP}(B^+ \to \pi^+ (K^+K^-)_{S-wave})$

VALUE	DOCUMENT ID		TECN	COMMENT
$-0.664 \pm 0.038 \pm 0.019$	[1] AAIJ	19AL	LHCB	pp at 7, 8 TeV

[1] Uses amplitude analysis of $B^{\pm} \to \pi^{\pm} K^+ K^-$ decays in the $\pi\pi - KK$ rescattering mass region of $0.95 < m(K^+K^-) < 1.42$ GeV/c^2.

$A_{CP}(B^+ \to K^+ K^- K^+)$

VALUE	DOCUMENT ID		TECN	COMMENT
-0.036 ± 0.004 OUR AVERAGE				
$-0.037 \pm 0.002 \pm 0.004$	[1] AAIJ	23U	LHCB	pp at 13 TeV
$-0.036 \pm 0.004 \pm 0.007$	[1] AAIJ	14BO	LHCB	pp at 7, 8 TeV
$-0.017\ ^{+0.019}_{-0.014} \pm 0.014$	[2] LEES	12O	BABR	$e^+e^- \to \Upsilon(4S)$
• • • We do not use the following data for averages, fits, limits, etc. • • •				
$-0.043 \pm 0.009 \pm 0.008$	AAIJ	13AZ	LHCB	Repl. by AAIJ 14BO
$-0.017 \pm 0.026 \pm 0.015$	AUBERT	06O	BABR	Repl. by LEES 12O
$0.02\ \pm 0.07\ \pm 0.03$	AUBERT	03M	BABR	Repl. by AUBERT 06O

[1] The second error includes both systematics and the uncertainties from CP asymmetries in restricted regions of phase space.
[2] All intermediate charmonium and charm resonances are removed, except of χ_{c0}.

$A_{CP}(B^+ \to \phi K^+)$

VALUE	DOCUMENT ID		TECN	COMMENT
0.017 ± 0.017 OUR AVERAGE	Error includes scale factor of 1.8. See the ideogram below.			
$0.004 \pm 0.014 \pm 0.007$	AAIJ	23V	LHCB	pp at 13 TeV
$0.017 \pm 0.011 \pm 0.006$	[1] AAIJ	15O	LHCB	pp at 7, 8 TeV
$0.128 \pm 0.044 \pm 0.013$	LEES	12O	BABR	$e^+e^- \to \Upsilon(4S)$
$-0.07\ \pm 0.17\ ^{+0.03}_{-0.02}$	ACOSTA	05J	CDF	$p\overline{p}$ at 1.96 TeV
$0.01\ \pm 0.12\ \pm 0.05$	[2] CHEN	03B	BELL	$e^+e^- \to \Upsilon(4S)$
• • • We do not use the following data for averages, fits, limits, etc. • • •				
$0.022 \pm 0.021 \pm 0.009$	AAIJ	14A	LHCB	Repl. by AAIJ 15O
$0.00\ \pm 0.08\ \pm 0.02$	AUBERT	06O	BABR	Repl. by LEES 12O
$0.04\ \pm 0.09\ \pm 0.01$	[3] AUBERT	04A	BABR	Repl. by AUBERT 06O
$-0.05\ \pm 0.20\ \pm 0.03$	[4] AUBERT	02E	BABR	$e^+e^- \to \Upsilon(4S)$

[1] Obtained using $A_{CP}(B^{\pm} \to J/\psi K^{\pm}) = (0.3 \pm 0.6) \times 10^{-2}$.
[2] Corresponds to 90% confidence range $-0.20 < A_{CP} < 0.22$.
[3] Corresponds to 90% confidence range $-0.10 < A_{CP} < 0.18$.
[4] Corresponds to 90% confidence range $-0.37 < A_{CP} < 0.28$.

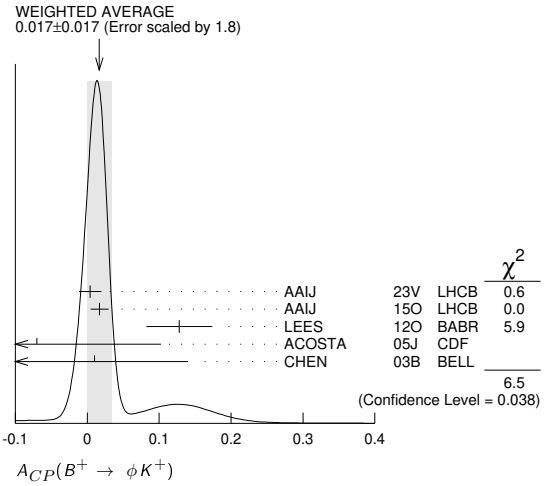

$A_{CP}(B^+ \to X_0(1550) K^+)$

VALUE	DOCUMENT ID		TECN	COMMENT
$-0.04 \pm 0.07 \pm 0.02$	[1] AUBERT	06O	BABR	$e^+e^- \to \Upsilon(4S)$

[1] Measured in the $B^+ \to K^+K^-K^+$ decay.

$A_{CP}(B^+ \to K^{*+} K^+ K^-)$

VALUE	DOCUMENT ID		TECN	COMMENT
$0.11 \pm 0.08 \pm 0.03$	AUBERT,B	06U	BABR	$e^+e^- \to \Upsilon(4S)$

$A_{CP}(B^+ \to \phi K^*(892)^+)$

VALUE	DOCUMENT ID		TECN	COMMENT
-0.01 ± 0.08 OUR AVERAGE				
$0.00 \pm 0.09 \pm 0.04$	AUBERT	07BA	BABR	$e^+e^- \to \Upsilon(4S)$
$-0.02 \pm 0.14 \pm 0.03$	[1] CHEN	05A	BELL	$e^+e^- \to \Upsilon(4S)$
• • • We do not use the following data for averages, fits, limits, etc. • • •				
$0.16 \pm 0.17 \pm 0.03$	AUBERT	03V	BABR	Repl. by AUBERT 07BA
$-0.13 \pm 0.29\ ^{+0.08}_{-0.11}$	[2] CHEN	03B	BELL	Repl. by CHEN 05A
$-0.43\ ^{+0.36}_{-0.30} \pm 0.06$	[3] AUBERT	02E	BABR	Repl. by AUBERT 03V

[1] Corresponds to 90% confidence range $-0.25 < A_{CP} < 0.22$.
[2] Corresponds to 90% confidence range $-0.64 < A_{CP} < 0.36$.
[3] Corresponds to 90% confidence range $-0.88 < A_{CP} < 0.18$.

$A_{CP}(B^+ \to \phi (K\pi)^{*+}_0)$

VALUE	DOCUMENT ID		TECN	COMMENT
$0.04 \pm 0.15 \pm 0.04$	AUBERT	08BI	BABR	$e^+e^- \to \Upsilon(4S)$

$A_{CP}(B^+ \to \phi K_1(1270)^+)$

VALUE	DOCUMENT ID		TECN	COMMENT
$0.15 \pm 0.19 \pm 0.05$	AUBERT	08BI	BABR	$e^+e^- \to \Upsilon(4S)$

$A_{CP}(B^+ \to \phi K^*_2(1430)^+)$

VALUE	DOCUMENT ID		TECN	COMMENT
$-0.23 \pm 0.19 \pm 0.06$	AUBERT	08BI	BABR	$e^+e^- \to \Upsilon(4S)$

$A_{CP}(B^+ \to K^+ \phi\phi)$

VALUE	DOCUMENT ID		TECN	COMMENT
-0.08 ± 0.07 OUR AVERAGE				
$-0.02 \pm 0.11 \pm 0.11$	[1] MOHANTY	21	BELL	$e^+e^- \to \Upsilon(4S)$
$-0.10 \pm 0.08 \pm 0.02$	[1] LEES	11A	BABR	$e^+e^- \to \Upsilon(4S)$

[1] Assumes $m_{\phi\phi} < 2.85$ GeV/c^2.

$A_{CP}(B^+ \to K^+ [\phi\phi]_{\eta_c})$

VALUE	DOCUMENT ID		TECN	COMMENT
0.10 ± 0.08 OUR AVERAGE				
$0.12 \pm 0.12 \pm 0.01$	[1] MOHANTY	21	BELL	$e^+e^- \to \Upsilon(4S)$
$0.09 \pm 0.10 \pm 0.02$	[1] LEES	11A	BABR	$e^+e^- \to \Upsilon(4S)$

[1] $m_{\phi\phi}$ is consistent with η_c mass in [2.94, 3.02] GeV/c^2.

Int. J. Mod. Phys. A 2026.41. Downloaded from www.worldscientific.com
by UNIVERSITY OF CALIFORNIA @ BERKELEY on 09/16/26. Re-use and distribution is strictly not permitted, except for Open Access articles.

$A_{CP}(B^+ \to K^*(892)^+\gamma)$

VALUE	DOCUMENT ID		TECN	COMMENT
0.008±0.015 OUR AVERAGE				
−0.007±0.029±0.005	ADACHI	25Z	BELL	$e^+e^- \to \Upsilon(4S)$
0.011±0.023±0.003	[1] HORIGUCHI	17	BELL	$e^+e^- \to \Upsilon(4S)$
0.018±0.028±0.007	AUBERT	09AO	BABR	$e^+e^- \to \Upsilon(4S)$

[1] Uses B($\Upsilon(4S) \to B^+B^-$) = (51.4 ± 0.6)% and B($\Upsilon(4S) \to B^0\overline{B}^0$) = (48.6 ± 0.6)%.

$A_{CP}(B^+ \to X_s\gamma)$

VALUE	DOCUMENT ID		TECN	COMMENT
0.0275±0.0184±0.0032	[1] WATANUKI	19	BELL	$e^+e^- \to \Upsilon(4S)$

[1] Using a sum-of-exclusive technique with $m_{X_s} < 2.8$ GeV/c^2.

$A_{CP}(B^+ \to \eta K^+\gamma)$

VALUE	DOCUMENT ID		TECN	COMMENT
−0.12±0.07 OUR AVERAGE				
−0.09±0.10±0.01	[1] AUBERT	09	BABR	$e^+e^- \to \Upsilon(4S)$
−0.16±0.09±0.06	[2] NISHIDA	05	BELL	$e^+e^- \to \Upsilon(4S)$
• • • We do not use the following data for averages, fits, limits, etc. • • •				
−0.09±0.12±0.01	[1] AUBERT,B	06M	BABR	Repl. by AUBERT 09

[1] $m_{\eta K} < 3.25$ GeV/c^2.
[2] $m_{\eta K} < 2.4$ GeV/c^2

$A_{CP}(B^+ \to \phi K^+\gamma)$

VALUE	DOCUMENT ID		TECN	COMMENT
−0.13±0.11 OUR AVERAGE Error includes scale factor of 1.1.				
−0.03±0.11±0.08	SAHOO	11A	BELL	$e^+e^- \to \Upsilon(4S)$
−0.26±0.14±0.05	AUBERT	07Q	BABR	$e^+e^- \to \Upsilon(4S)$

$A_{CP}(B^+ \to \rho^+\gamma)$

VALUE (units 10^{-2})	DOCUMENT ID		TECN	COMMENT
− 9 ±14 OUR AVERAGE				
− 8.2±15.2$^{+2.0}_{-1.3}$	ADACHI	25G	BELL	$e^+e^- \to \Upsilon(4S)$
−11 ±32 ±9	TANIGUCHI	08	BELL	$e^+e^- \to \Upsilon(4S)$

$A_{CP}(B^+ \to \pi^+\pi^0)$

VALUE	DOCUMENT ID		TECN	COMMENT
−0.01 ±0.04 OUR AVERAGE Error includes scale factor of 1.1.				
−0.081±0.054±0.008	ADACHI	24	BELL	$e^+e^- \to \Upsilon(4S)$
0.025±0.043±0.007	DUH	13	BELL	$e^+e^- \to \Upsilon(4S)$
0.03 ±0.08 ±0.01	AUBERT	07BC	BABR	$e^+e^- \to \Upsilon(4S)$
• • • We do not use the following data for averages, fits, limits, etc. • • •				
0.07 ±0.06 ±0.01	LIN	08	BELL	Repl. by DUH 13
−0.01 ±0.10 ±0.02	[1] AUBERT	05L	BABR	Repl. by AUBERT 07BC
0.00 ±0.10 ±0.02	[2] CHAO	05A	BELL	Repl. by CHAO 04B
−0.02 ±0.10 ±0.01	[3] CHAO	04B	BELL	Repl. by LIN 08
−0.03 $^{+0.18}_{-0.17}$ ±0.02	[4] AUBERT	03L	BABR	Repl. by AUBERT 05L
0.30 ±0.30 $^{+0.06}_{-0.04}$	[5] CASEY	02	BELL	Repl. by CHAO 04B

[1] Corresponds to a 90% CL interval of $-0.19 < A_{CP} < 0.21$.
[2] Corresponds to a 90% CL interval of $-0.17 < A_{CP} < 0.16$.
[3] This corresponds to 90% CL interval of $-0.18 < A_{CP} < 0.14$.
[4] Corresponds to 90% confidence range $-0.32 < A_{CP} < 0.27$.
[5] Corresponds to 90% confidence range $-0.23 < A_{CP} < +0.86$.

$A_{CP}(B^+ \to \pi^+\pi^-\pi^+)$

VALUE	DOCUMENT ID		TECN	COMMENT
0.076±0.008 OUR AVERAGE Error includes scale factor of 1.5.				
0.080±0.004±0.004	[1] AAIJ	23U	LHCB	pp at 13 TeV
0.058±0.008±0.011	[1] AAIJ	14BO	LHCB	pp at 7, 8 TeV
0.032±0.044$^{+0.040}_{-0.037}$	AUBERT	09L	BABR	$e^+e^- \to \Upsilon(4S)$
• • • We do not use the following data for averages, fits, limits, etc. • • •				
0.117±0.021±0.011	[2] AAIJ	14	LHCB	Repl. by AAIJ 14BO
−0.007±0.077±0.025	AUBERT,B	05G	BABR	Repl. by AUBERT 09L
−0.39 ±0.33 ±0.12	AUBERT	03M	BABR	Repl. by AUBERT 05G

[1] The second error includes both systematics and the uncertainties from CP asymmetries in restricted regions of phase space.
[2] AAIJ 14 reports $A_{CP}(B^+ \to \pi^+\pi^-\pi^+) = 0.584 \pm 0.082 \pm 0.027 \pm 0.007$ in the Dalitz plot region of $m^2_{\pi^+\pi^-} > 15$ GeV^2/c^4 or $m^2_{\pi^+\pi^-} < 0.4$ GeV^2/c^4. The third uncertainty is due to the CP asymmetry of the $B^{\pm} \to J/\psi K^{\pm}$ reference mode uncertainty.

$A_{CP}(B^+ \to \pi^+\pi^0\pi^0)$

VALUE (units 10^{-2})	DOCUMENT ID		TECN	COMMENT
9.2±6.8±0.7	LAI	23	BELL	$e^+e^- \to \Upsilon(4S)$

$A_{CP}(B^+ \to \rho^0\pi^+)$

VALUE	DOCUMENT ID		TECN	COMMENT
0.003±0.014 OUR AVERAGE				
−0.004±0.017±0.009	AAIJ	23V	LHCB	pp at 13 TeV
0.007±0.011±0.016	[1] AAIJ	20A	LHCB	pp at 7, 8 TeV
0.18 ±0.07 $^{+0.05}_{-0.15}$	AUBERT	09L	BABR	$e^+e^- \to \Upsilon(4S)$
• • • We do not use the following data for averages, fits, limits, etc. • • •				
−0.074±0.120$^{+0.035}_{-0.055}$	AUBERT,B	05G	BABR	Repl. by AUBERT 09L
−0.19 ±0.11 ±0.02	AUBERT	04Z	BABR	Repl. by AUBERT,B 05G

[1] This result is obtained with an amplitude analysis of $B^+ \to \pi^+\pi^+\pi^-$ decays, using the isobar model within the mass range $1.0 < m(\pi^+\pi^-) < 1.5$ GeV to describe the $\pi^+\pi^-$ S-wave contribution.

$A_{CP}(B^+ \to f_2(1270)\pi^+)$

VALUE	DOCUMENT ID		TECN	COMMENT
0.40 ±0.06 OUR AVERAGE				
0.468±0.061±0.046	[1] AAIJ	20A	LHCB	pp at 7, 8 TeV
0.267±0.102±0.048	[2] AAIJ	19AL	LHCB	pp at 7, 8 TeV
0.41 ±0.25 $^{+0.18}_{-0.15}$	AUBERT	09L	BABR	$e^+e^- \to \Upsilon(4S)$
• • • We do not use the following data for averages, fits, limits, etc. • • •				
−0.004±0.247$^{+0.028}_{-0.032}$	AUBERT,B	05G	BABR	Repl. by AUBERT 09L

[1] This result is obtained with an amplitude analysis of $B^+ \to \pi^+\pi^+\pi^-$ decays, using the isobar model within the mass range $1.0 < m(\pi^+\pi^-) < 1.5$ GeV to describe the $\pi^+\pi^-$ S-wave contribution.
[2] Uses amplitude analysis of $B^{\pm} \to \pi^{\pm}K^+K^-$ decays.

$A_{CP}(B^+ \to \rho^0(1450)\pi^+)$

VALUE	DOCUMENT ID		TECN	COMMENT
−0.11 ±0.05 OUR AVERAGE				
−0.129±0.033±0.359	[1] AAIJ	20A	LHCB	pp at 7, 8 TeV
−0.109±0.044±0.024	[2] AAIJ	19AL	LHCB	pp at 7, 8 TeV
−0.06 ±0.28 $^{+0.23}_{-0.40}$	AUBERT	09L	BABR	$e^+e^- \to \Upsilon(4S)$

[1] This result is obtained with an amplitude analysis of $B^+ \to \pi^+\pi^+\pi^-$ decays, using the isobar model within the mass range $1.0 < m(\pi^+\pi^-) < 1.5$ GeV to describe the $\pi^+\pi^-$ S-wave contribution.
[2] Uses amplitude analysis of $B^{\pm} \to \pi^{\pm}K^+K^-$ decays.

$A_{CP}(B^+ \to \rho_3(1690)\pi^+)$

VALUE	DOCUMENT ID		TECN	COMMENT
−0.801±0.114±0.253	[1] AAIJ	20A	LHCB	pp at 7, 8 TeV

[1] This result is obtained with an amplitude analysis of $B^+ \to \pi^+\pi^+\pi^-$ decays, using the isobar model within the mass range $1.0 < m(\pi^+\pi^-) < 1.5$ GeV to describe the $\pi^+\pi^-$ S-wave contribution.

$A_{CP}(B^+ \to f_0(1370)\pi^+)$

VALUE	DOCUMENT ID		TECN	COMMENT
0.72±0.15±0.16	AUBERT	09L	BABR	$e^+e^- \to \Upsilon(4S)$

$A_{CP}(B^+ \to \pi^+\pi^-\pi^+$ nonresonant)

VALUE	DOCUMENT ID		TECN	COMMENT
−0.14±0.14$^{+0.18}_{-0.08}$	AUBERT	09L	BABR	$e^+e^- \to \Upsilon(4S)$

$A_{CP}(B^+ \to \rho^+\pi^0)$

VALUE	DOCUMENT ID		TECN	COMMENT
0.03 ±0.10 OUR AVERAGE				
0.080±0.150$^{+0.023}_{-0.075}$	LAI	23	BELL	$e^+e^- \to \Upsilon(4S)$
−0.01 ±0.13 ±0.02	AUBERT	07X	BABR	$e^+e^- \to \Upsilon(4S)$
• • • We do not use the following data for averages, fits, limits, etc. • • •				
0.06 ±0.17 $^{+0.04}_{-0.05}$	ZHANG	05A	BELL	Repl. by LAI 23
0.24 ±0.16 ±0.06	AUBERT	04Z	BABR	Repl. by AUBERT 07X

$A_{CP}(B^+ \to X\pi^+,\ X \to \pi^0\pi^0)$

VALUE	DOCUMENT ID		TECN	COMMENT
0.182±0.116±0.007	LAI	23	BELL	$e^+e^- \to \Upsilon(4S)$

$A_{CP}(B^+ \to \rho^+\rho^0)$

VALUE	DOCUMENT ID		TECN	COMMENT
−0.05 ±0.05 OUR AVERAGE				
−0.054±0.055±0.010	AUBERT	09G	BABR	$e^+e^- \to \Upsilon(4S)$
0.00 ±0.22 ±0.03	ZHANG	03B	BELL	$e^+e^- \to \Upsilon(4S)$
• • • We do not use the following data for averages, fits, limits, etc. • • •				
−0.12 ±0.13 ±0.10	AUBERT,BE	06G	BABR	Repl. by AUBERT 09G
−0.19 ±0.23 ±0.03	AUBERT	03V	BABR	Repl. by AUBERT,BE 06G

$A_{CP}(B^+ \to \omega\pi^+)$

VALUE	DOCUMENT ID		TECN	COMMENT
−0.04 ±0.05 OUR AVERAGE				
−0.048±0.065±0.038	[1] AAIJ	20A	LHCB	pp at 7, 8 TeV
−0.02 ±0.08 ±0.01	AUBERT	07AE	BABR	$e^+e^- \to \Upsilon(4S)$
−0.02 ±0.09 ±0.01	JEN	06	BELL	$e^+e^- \to \Upsilon(4S)$
−0.34 ±0.25	[2] CHEN	00	CLE2	$e^+e^- \to \Upsilon(4S)$
• • • We do not use the following data for averages, fits, limits, etc. • • •				
−0.01 ±0.10 ±0.01	AUBERT,B	06E	BABR	Repl. by AUBERT 07AE
0.03 ±0.16 ±0.01	AUBERT	04H	BABR	Repl. by AUBERT,B 06E
0.50 $^{+0.23}_{-0.20}$ ±0.02	[3] WANG	04A	BELL	Repl. by JEN 06
−0.01 $^{+0.29}_{-0.31}$ ±0.03	[4] AUBERT	02E	BABR	Repl. by AUBERT 04H

[1] This result is obtained with an amplitude analysis of $B^+ \to \pi^+\pi^+\pi^-$ decays, using the isobar model within the mass range $1.0 < m(\pi^+\pi^-) < 1.5$ GeV to describe the $\pi^+\pi^-$ S-wave contribution.
[2] Corresponds to 90% confidence range $-0.75 < A_{CP} < 0.07$.
[3] Corresponds to 90% CL interval $-0.25 < A_{CP} < 0.41$
[4] Corresponds to 90% confidence range $-0.50 < A_{CP} < 0.46$.

$A_{CP}(B^+ \to \omega\rho^+)$

VALUE	DOCUMENT ID		TECN	COMMENT
−0.20±0.09±0.02	AUBERT	09H	BABR	$e^+e^- \to \Upsilon(4S)$
• • • We do not use the following data for averages, fits, limits, etc. • • •				
0.04±0.18±0.02	AUBERT,B	06T	BABR	Repl. by AUBERT 09H
0.05±0.26±0.02	AUBERT	05O	BABR	Repl. by AUBERT,B 06T

$A_{CP}(B^+ \to \eta\pi^+)$

VALUE	DOCUMENT ID		TECN	COMMENT
−0.14±0.07 OUR AVERAGE	Error includes scale factor of 1.4.			
−0.19±0.06±0.01	HOI	12	BELL	$e^+e^- \to \Upsilon(4S)$
−0.03±0.09±0.03	AUBERT	09AV	BABR	$e^+e^- \to \Upsilon(4S)$
• • • We do not use the following data for averages, fits, limits, etc. • • •				
−0.08±0.10±0.01	AUBERT	07AE	BABR	Repl. by AUBERT 09AV
−0.23±0.09±0.02	CHANG	07B	BELL	Repl. by HOI 12
−0.13±0.12±0.01	AUBERT,B	05K	BABR	Repl. by AUBERT 07AE
0.07±0.15±0.03	CHANG	05A	BELL	Repl. by CHANG 07B
−0.44±0.18±0.01	AUBERT	04H	BABR	Repl. by AUBERT,B 05K

$A_{CP}(B^+ \to \eta\rho^+)$

VALUE	DOCUMENT ID		TECN	COMMENT
0.11±0.11 OUR AVERAGE				
0.13±0.11±0.02	AUBERT	08AH	BABR	$e^+e^- \to \Upsilon(4S)$
$-0.04^{+0.34}_{-0.32}\pm0.01$	WANG	07B	BELL	$e^+e^- \to \Upsilon(4S)$
• • • We do not use the following data for averages, fits, limits, etc. • • •				
0.02±0.18±0.02	AUBERT,B	05K	BABR	Repl. by AUBERT 08AH

$A_{CP}(B^+ \to \eta'\pi^+)$

VALUE	DOCUMENT ID		TECN	COMMENT
0.06±0.16 OUR AVERAGE				
0.03±0.17±0.02	AUBERT	09AV	BABR	$e^+e^- \to \Upsilon(4S)$
$0.20^{+0.37}_{-0.36}\pm0.04$	SCHUEMANN	06	BELL	$e^+e^- \to \Upsilon(4S)$
• • • We do not use the following data for averages, fits, limits, etc. • • •				
0.21±0.17±0.01	AUBERT	07AE	BABR	Repl. by AUBERT 09AV
0.14±0.16±0.01	AUBERT,B	05K	BABR	Repl. by AUBERT 07AE

$A_{CP}(B^+ \to \eta'\rho^+)$

VALUE	DOCUMENT ID		TECN	COMMENT
0.26±0.17±0.02	DEL-AMO-SA...10A		BABR	$e^+e^- \to \Upsilon(4S)$
• • • We do not use the following data for averages, fits, limits, etc. • • •				
0.04±0.28±0.02	[1] AUBERT	07E	BABR	Repl. by DEL-AMO-SANCHEZ 10A

[1] Reports A_{CP} with the opposite sign convention.

$A_{CP}(B^+ \to b_1^0\pi^+)$

VALUE	DOCUMENT ID		TECN	COMMENT
+0.05±0.16±0.02	AUBERT	07BI	BABR	$e^+e^- \to \Upsilon(4S)$

$A_{CP}(B^+ \to p\overline{p}\pi^+)$

VALUE	DOCUMENT ID		TECN	COMMENT
0.021±0.030 OUR AVERAGE				
0.039±0.039±0.005	[1] AAIJ	14AF	LHCB	pp at 7, 8 TeV
−0.02 ±0.05 ±0.02	[1] WEI	08	BELL	$e^+e^- \to \Upsilon(4S)$
+0.04 ±0.07 ±0.04	AUBERT	07AV	BABR	$e^+e^- \to \Upsilon(4S)$
• • • We do not use the following data for averages, fits, limits, etc. • • •				
−0.16 ±0.22 ±0.01	WANG	04	BELL	Repl. by WEI 08

[1] Requires $m_{p\overline{p}} < 2.85$ GeV/c^2.

$A_{CP}(B^+ \to p\overline{p}K^+)$

VALUE	DOCUMENT ID		TECN	COMMENT
−0.02 ±0.04 OUR AVERAGE	Error includes scale factor of 1.9.			
−0.006±0.020±0.004	[1] AAIJ	14AF	LHCB	pp at 7, 8 TeV
−0.17 ±0.10 ±0.02	[1] WEI	08	BELL	$e^+e^- \to \Upsilon(4S)$
$-0.16\ ^{+0.07}_{-0.08}\ \pm0.04$	[1] AUBERT,B	05L	BABR	$e^+e^- \to \Upsilon(4S)$
• • • We do not use the following data for averages, fits, limits, etc. • • •				
−0.047±0.036±0.007	[1] AAIJ	13AU	LHCB	Repl. by AAIJ 14AF
−0.05 ±0.11 ±0.01	WANG	04	BELL	Repl. by WEI 08

[1] Requires $m_{p\overline{p}} < 2.85$ GeV/c^2.

$A_{CP}(B^+ \to p\overline{p}K^*(892)^+)$

VALUE	DOCUMENT ID		TECN	COMMENT
0.21±0.16 OUR AVERAGE	Error includes scale factor of 1.4.			
−0.01±0.19±0.02	CHEN	08C	BELL	$e^+e^- \to \Upsilon(4S)$
+0.32±0.13±0.05	AUBERT	07AV	BABR	$e^+e^- \to \Upsilon(4S)$

$A_{CP}(B^+ \to p\overline{\Lambda}\gamma)$

VALUE	DOCUMENT ID		TECN	COMMENT
+0.17±0.16±0.05	WANG	07C	BELL	$e^+e^- \to \Upsilon(4S)$

$A_{CP}(B^+ \to p\overline{\Lambda}\pi^0)$

VALUE	DOCUMENT ID		TECN	COMMENT
+0.01±0.17±0.04	WANG	07C	BELL	$e^+e^- \to \Upsilon(4S)$

$A_{CP}(B^+ \to \overline{\Lambda}p\overline{p}p)$

VALUE (%)	DOCUMENT ID		TECN	COMMENT
5.4±15.6±2.4	AAIJ	25AT	LHCB	pp at 13 TeV

$A_{CP}(B^+ \to K^+\ell^+\ell^-)$

VALUE	DOCUMENT ID		TECN	COMMENT
−0.02±0.08 OUR AVERAGE				
−0.03±0.14±0.01	[1] LEES	12S	BABR	$e^+e^- \to \Upsilon(4S)$
−0.18±0.18±0.01	AUBERT	09T	BABR	$e^+e^- \to \Upsilon(4S)$
+0.04±0.10±0.02	WEI	09A	BELL	$e^+e^- \to \Upsilon(4S)$
• • • We do not use the following data for averages, fits, limits, etc. • • •				
−0.07±0.22±0.02	AUBERT,B	06J	BABR	Repl. by AUBERT 09T

[1] Measured in the union of $0.10 < q^2 < 8.12$ GeV^2/c^4 and $q^2 > 10.11$ GeV^2/c^4. LEES 12S reports also individual measurements $A_{CP}(B^+ \to K^+\ell^+\ell^-) = 0.02 \pm 0.18 \pm 0.01$ for $0.10 < q^2 < 8.12$ GeV^2/c^4 and $A_{CP}(B^+ \to K^+\ell^+\ell^-) = -0.06^{+0.22}_{-0.21} \pm 0.01$ for $q^2 > 10.11$ GeV^2/c^4.

$A_{CP}(B^+ \to K^+e^+e^-)$

VALUE	DOCUMENT ID		TECN	COMMENT
+0.14±0.14±0.03	WEI	09A	BELL	$e^+e^- \to \Upsilon(4S)$

$A_{CP}(B^+ \to K^+\mu^+\mu^-)$

VALUE	DOCUMENT ID		TECN	COMMENT
0.011±0.017 OUR AVERAGE				
0.012±0.017±0.001	AAIJ	14AN	LHCB	pp at 7, 8 TeV
−0.05 ±0.13 ±0.03	WEI	09A	BELL	$e^+e^- \to \Upsilon(4S)$
• • • We do not use the following data for averages, fits, limits, etc. • • •				
0.000±0.033±0.009	AAIJ	13BN	LHCB	Repl. by AAIJ 14AN

$A_{CP}(B^+ \to \pi^+\mu^+\mu^-)$

VALUE	DOCUMENT ID		TECN	COMMENT
−0.11±0.12±0.01	AAIJ	15AR	LHCB	pp at 7, 8 TeV

$A_{CP}(B^+ \to K^{*+}\ell^+\ell^-)$

VALUE	DOCUMENT ID		TECN	COMMENT
−0.09±0.14 OUR AVERAGE				
$0.01^{+0.26}_{-0.24}\pm0.02$	AUBERT	09T	BABR	$e^+e^- \to \Upsilon(4S)$
$-0.13^{+0.17}_{-0.16}\pm0.01$	WEI	09A	BELL	$e^+e^- \to \Upsilon(4S)$
• • • We do not use the following data for averages, fits, limits, etc. • • •				
0.03±0.23±0.03	AUBERT,B	06J	BABR	Repl. by AUBERT 09T

$A_{CP}(B^+ \to K^*e^+e^-)$

VALUE	DOCUMENT ID		TECN	COMMENT
$\mathbf{-0.14^{+0.23}_{-0.22}\pm0.02}$	WEI	09A	BELL	$e^+e^- \to \Upsilon(4S)$

$A_{CP}(B^+ \to K^*\mu^+\mu^-)$

VALUE	DOCUMENT ID		TECN	COMMENT
−0.12±0.24±0.02	WEI	09A	BELL	$e^+e^- \to \Upsilon(4S)$

− CP VIOLATION PARAMETERS IN $B^+ \to DK^+$ AND SIMILAR DECAYS −

The parameters r_{B^+} and δ_{B^+} are the magnitude ratio and strong phase difference between the amplitudes of $A(B^+ \to \overline{D}^{(*)0}K^{(*)+})$ and $A(B^- \to D^{(*)0}K^{(*)-})$. The measured observables are defined as $x_\pm = r_{B^+}\cos(\delta_{B^+} \pm \gamma)$ and $y_\pm = r_{B^+}\sin(\delta_{B^+} \pm \gamma)$, and can be used to measure the CKM angle γ.

"OUR EVALUATION" is provided by the Heavy Flavor Averaging Group (HFLAV). It is derived from combinations of their results on $B^+ \to DK^+$ and related processes.

γ

For angle $\gamma(\phi_3)$ of the CKM unitarity triangle, see the review on "*CP* Violation" in the Reviews section.

VALUE (°)	CL%	DOCUMENT ID		TECN	COMMENT
$\mathbf{66.4^{+2.7}_{-2.8}}$ **OUR EVALUATION**	(Produced by HFLAV)				
74 ± 6 OUR AVERAGE					
63 ±13		[1] AAIJ	25R	LHCB	pp at 7, 8, 13 TeV
$81\ ^{+12}_{-11}$		[2,3] AAIJ	25T	LHCB	pp at 7, 8, 13 TeV
75.2± 7.6		[4] ADACHI	24T	BELL	$e^+e^- \to \Upsilon(4S)$)
• • • We do not use the following data for averages, fits, limits, etc. • • •					
74 ±12		[2] AAIJ	25T	LHCB	pp at 13 TeV
$92\ ^{+21}_{-17}$		[5] AAIJ	24H	LHCB	pp at 7, 8, 13 TeV

Int. J. Mod. Phys. A 2026.41. Downloaded from www.worldscientific.com
by LIFORNIA @ BERKELEY on 09/16/26. Re-use and distribution is strictly not permitted, except for Open Access articles.

Int. J. Mod. Phys. A 2026.41. Downloaded from www.worldscientific.com
by UNIVERSITY OF CALIFORNIA @ BERKELEY on 09/16/26. Re-use and distribution is strictly not permitted, except for Open Access articles.

$49\ ^{+22}_{-19}$	[6] AAIJ	24U	LHCB	pp at 7, 8, 13 TeV	
$69\ ^{+13}_{-14}$	[7] AAIJ	23BA	LHCB	pp at 7, 8, 13 TeV	
$54.8^{+\ 6.0}_{-\ 5.8}{}^{+\ 6.7}_{-\ 4.3}$	[8] AAIJ	23I	LHCB	pp at 7, 8, 13 TeV	
$116\ ^{+12}_{-14}$	[9] AAIJ	23N	LHCB	pp at 7, 8, 13 TeV	
$78.4 \pm 11.4 \pm 1.1$	[10,11] ABUDINEN	22	BELL	$e^+e^- \to \Upsilon(4S)$	
$65.4^{+\ 3.8}_{-\ 4.2}$	[12] AAIJ	21AM	LHCB	pp at 7, 8, 13 TeV	
$68.7^{+\ 5.2}_{-\ 5.1}$	[10] AAIJ	21L	LHCB	pp at 7, 8, 13 TeV	
44 ± 12	[13,14] AAIJ	21M	LHCB	pp at 7, 8, 13 TeV	
$5.7^{+10.2}_{-\ 8.8} \pm 6.7$	[15] RESMI	19	BELL	$e^+e^- \to \Upsilon(4S)$	
$87\ ^{+11}_{-12}$	[16] AAIJ	18AD	LHCB	Repl. by AAIJ 21L	
$128\ ^{+17}_{-22}$	[17] AAIJ	18U	LHCB	pp at 7, 8 TeV	
5–86 or 185–266	[18] AAIJ	18Z	LHCB	pp at 7, 8 TeV	
$80\ ^{+21}_{-22}$	[19] AAIJ	16AA	LHCB	Repl. by AAIJ 16Z	
$72.2^{+\ 6.8}_{-\ 7.3}$	[20] AAIJ	16AQ	LHCB	Repl. by AAIJ 21AM	
71 ± 20	[21,22,23] AAIJ	16Z	LHCB	Repl. by AAIJ 24U	
$74\ ^{+20}_{-19}$	AAIJ	15BC	LHCB	pp at 7, 8 TeV	
$63.5^{+\ 7.2}_{-\ 6.7}$	[24,25] AAIJ	15K	LHCB	pp at 7, 8 TeV	
$62\ ^{+15}_{-14}$	[26] AAIJ	14BA	LHCB	Repl. by AAIJ 21L	
$84\ ^{+49}_{-42}$	[27] AAIJ	14BE	LHCB	Repl. by AAIJ 14BA	
$115\ ^{+28}_{-43}$	[28] AAIJ	14BF	LHCB	Repl. by AAIJ 18U	
$72.6^{+\ 9.7}_{-17.2}$	[29] AAIJ	13AK	LHCB	Repl. by AAIJ 21AM	
$69\ ^{+17}_{-16}$	[30] LEES	13B	BABR	$e^+e^- \to \Upsilon(4S)$	
$44\ ^{+43}_{-38}$	[31,32] AAIJ	12AQ	LHCB	Repl. by AAIJ 13AK	
$77.3^{+15.1}_{-14.9} \pm 5.9$	[32,33] AIHARA	12	BELL	$e^+e^- \to \Upsilon(4S)$.	
$68 \pm 14 \pm 5$	[34] DEL-AMO-SA...	10F	BABR	Repl. by LEES 13B	
7 to 173	95 [35] DEL-AMO-SA...	10G	BABR	$e^+e^- \to \Upsilon(4S)$	
$78.4^{+10.8}_{-11.6} \pm 9.6$	[36] POLUEKTOV	10	BELL	$e^+e^- \to \Upsilon(4S)$	
162 ± 56	[37] AUBERT	09R	BABR	$e^+e^- \to \Upsilon(4S)$	
$76\ ^{+22}_{-23} \pm 7.1$	[38] AUBERT	08AL	BABR	Repl. by DEL-AMO-SANCHEZ 10F	
$53\ ^{+15}_{-18} \pm 10$	[39] POLUEKTOV	06	BELL	Repl. by POLUEKTOV 10	
$70 \pm 31\ ^{+18}_{-15}$	[40] AUBERT,B	05Y	BABR	Repl. by AUBERT 08AL	
$77\ ^{+17}_{-19} \pm 17$	[41] POLUEKTOV	04	BELL	Repl. by POLUEKTOV 06	

[1] Extracted from $B^{\pm} \to D K^{*\pm}$ decays, using the D decays: $D \to K^{\pm}\pi^{\mp}$, K^+K^-, $\pi^+\pi^-$, $K^{\pm}\pi^{\mp}\pi^{\pm}\pi^{\mp}$, $\pi^+\pi^-\pi^+\pi^-$, $K^0_S\pi^+\pi^-$, and $K^0_S K^+K^-$.

[2] Measured in $B^0_s \to D^{\mp}_s K^{\pm}$ decays, constraining $-2\beta_s$ by the measurement of $\phi_s = -0.031 \pm 0.018$ rad. The value is modulo 180°.

[3] Combines the result with that of AAIJ 18U, for which the values of the nuisance parameters Δm_s, Γ_s and $\Delta\Gamma_s$ have been re-evaluated and the related systematic uncertainties updated.

[4] Uses combined sample of Belle and Belle II experiments in B^+ decays to $D K^+$, $D^* K^+$, and $D\pi^+$ final states.

[5] Extracted from yields of partially reconstructed $B^{\pm} \to D^* K^{\pm}$, $D^* \to D\pi^0/\gamma$, $D \to K^0_S\pi^+\pi^-/K^0_S K^+K^-$ decays. The uncertainty is predominantly statistical. Its correlation with the AAIJ 23BA result is found to be less than 3%.

[6] A model-independent binned Dalitz plot analysis of the decays $B^0 \to D K^{*0}$, with $D \to K^0_S h^+h^-$, $h = \pi, K$. Angle γ is required to satisfy $0 < \gamma < 180$ degrees.

[7] Measured using $B^{\pm} \to D^* K^{\pm}$ and $B^{\pm} \to D^*\pi^{\pm}$ decays analysing the signal yield variation with the fully reconstructed $D^* \to D\pi^0/\gamma$, $D \to K^0_S\pi^+\pi^-/K^0_S K^+K^-$ decays. The model-independent approach uses external strong phase input from BESIII and CLEO collaborations.

[8] Measured using $B^{\pm} \to D[K^{\mp}\pi^{\pm}\pi^{\pm}\pi^{\mp}]h^{\pm}$ decays in bins of the phase space of the D decay. The third uncertainty includes systematic and finite knowledge of the D-meson decay parameters.

[9] A model-dependent binned analysis of the decays $B^{\pm} \to [K^+K^-\pi^+\pi^-]_D h^{\pm}$ is used.

[10] Uses binned Dalitz plot analysis of $D \to K^0_S\pi^+\pi^-$ and $K^0_S K^+K^-$ from $B^{\pm} \to D K^{\pm}$ modes. Strong phase measurements from CLEO-c and BES-III of the D decay over the Dalitz plot are used as input. Value is modulo 180°.

[11] Supersedes AIHARA 12.

[12] AAIJ 21AM presents a combination of existing measurements from LHCb collaboration. It includes also charm mixing parameters.

[13] Measured in $B^0_s \to D^{\pm}_s K^{\mp}\pi^{\pm}\pi^{\mp}$ decays in restricted phase space with $m(K^+\pi^+\pi^-) < 1950$ MeV, $m(K^+\pi^-) < 1200$ MeV and $m(\pi^+\pi^-) < 1200$ MeV. The value is modulo 180°.

[14] A model-independent coherence factor for the decay $B_s \to D_s K\pi\pi$ (in the restricted phase space region) is also reported.

[15] Uses binned analysis of $D \to K^0_S\pi^+\pi^-\pi^0$ from $B^{\pm} \to D K^{\pm}$ modes over the phase space. Strong phase measurements from RESMI 18 analysis of CLEO-c data of the D decay over the phase space binning are used as input.

[16] Uses binned Dalitz plot analysis of $D \to K^0_S\pi^+\pi^-$ and $K^0_S K^+K^-$ from $B^{\pm} \to D K^{\pm}$ modes. Strong phase measurements from CLEO-c of the D decay over the Dalitz plot are used as input.

[17] Measured in $B^0_s \to D^{\mp}_s K^{\pm}$ decays, constraining $-2\beta_s$ by the measurement of $\phi_s = 0.030 \pm 0.033$ from HFLAV. The value is modulo 180°.

[18] AAIJ 18Z reports the intervals (5–86)° or (185–266)° at 68% C.L. The extraction uses the time dependent CP violation measurement in $B^0 \to D^{\mp}\pi^{\pm}$ decays with external input and some theoretical assumptions.

[19] Uses Dalitz plot analysis of $D \to K^0_S\pi^+\pi^-$ decays coming from $B^0 \to D K^*(892)^0$ modes. Measures $r_{B^0} = 0.39 \pm 0.13$, and $\delta_{B^0} = 197^{+24}_{-20}$ degrees.

[20] A combination of measurements from analyses of time-integrated $B^+ \to D K^+$, $B^0 \to D K^{(*)0}$, $B^0 \to D K^+\pi^-$, and $B^+ \to D K^+\pi^+\pi^-$ tree-level decays. In addition, results from a time-dependent analysis of $B^0_s \to D_s K$ decays are included.

[21] A model-independent binned Dalitz plot analysis of the decays $B^0 \to D K^{*0}$, with $D \to K^0_S\pi^+\pi^-$ and $D \to K^0_S K^+K^-$. The results cannot be combined with the model-dependent analysis of the same dataset reported in AAIJ 16AA.

[22] Angle γ required to satisfy $0 < \gamma < 180$ degrees.

[23] Uses Dalitz plot analysis of $D \to K^0_S\pi^+\pi^-$, $K^0_S K^+K^-$ decays coming from $B^0 \to D K^*(892)^0$ modes.

[24] Obtained by measuring time-dependent CP asymmetry in $B^0_s \to K^+K^-$ and using a U-spin relation between $B^0_s \to K^+K^-$ and $B^0 \to \pi^+\pi^-$.

[25] Results are also presented using additional inputs on $B^0 \to \pi^0\pi^0$ and $B^+ \to \pi^+\pi^0$ decays from other experiments and isospin symmetry assumptions. The dependence of the results on the maximum allowed amount of U-spin breaking up to 50% is also included.

[26] Uses binned Dalitz plot analysis of $B^+ \to D K^+$ decays, with $D \to K^0_S\pi^+\pi^-$ and $D \to K^0_S K^+K^-$. Strong phase measurements from CLEO-c (LIBBY 10) of the D decay over the Dalitz plot are used as input. Solution that satisfies $0 < \gamma < 180$ is chosen.

[27] AAIJ 14BE uses model-dependent analysis of $D \to K^0_S\pi^+\pi^-$ amplitudes. The model is the same as in DEL-AMO-SANCHEZ 10F.

[28] Measured in $B^0_s \to D^{\mp}_s K^{\pm}$ decays, constraining $-2\beta_s$ by the measurement of $\phi_s = 0.01 \pm 0.07 \pm 0.0$ from AAIJ 13AR. The value is modulo 180° at 68% CL.

[29] Presents a confidence region $55.4° < \gamma < 82.3°$ at 68% CL with best fit value 72.6° and includes both statistical and systematic uncertainties. The corresponding 95% CL is $40.2° < \gamma < 92.7°$. The value is determined from combination of measuremets using D meson decaying to K^+K^-, $\pi^+\pi^-$, $K^{\pm}\pi^{\mp}$, $K^0_S\pi^+\pi^-$, $K^0_S K^+K^-$, and $K^{\pm}\pi^{\mp}\pi^{\pm}\pi^{\mp}$. Combines $B^{\pm} \to D K^{\pm}$ and $B^{\pm} \to D\pi^{\pm}$.

[30] Reports combination of published measurements using GGSZ, GLW, and ADS methods. Reports also 2σ range of 41–102° and a 5.9σ significance for $\gamma(B^+ \to D^{(*)0} K^{(*)+}) \neq 0$ hypothesis.

[31] Reports combined statistical and systematic uncertainties.

[32] Uses binned Dalitz plot of $\overline{D}^0 \to K^0_S\pi^+\pi^-$ decays from $B^+ \to \overline{D}^0 K^+$. Measurement of strong phases in $\overline{D}^0 \to K^0_S\pi^+\pi^-$ Dalitz plot from LIBBY 10 is used as input.

[33] We combined the systematics in quadrature. The authors report separately the contribution to the systematic uncertainty due to the uncertainty on the bin-averaged strong phase difference between D^0 and $\overline{D}^0$ amplitudes. Superseded by ABUDINEN 22.

[34] Uses Dalitz plot analysis of $\overline{D}^0 \to K^0_S\pi^+\pi^-$, $K^0_S K^+K^-$ decays from $B^+ \to D^{(*)} K^+$, $D K^{*+}$ modes. The corresponding two standard deviation interval for γ is $39° < \gamma < 98°$. CP conservation in the combined result is ruled out with a significance of 3.5 standard deviations.

[35] Reports confidence intervals for the CKM angle γ from the measured values of the GLW parameters using $B^{\pm} \to D K^{\pm}$ decays with D mesons decaying to non-$CP(K\pi)$, CP-even (K^+K^-, $\pi^+\pi^-$), and CP-odd ($K^0_S\pi^0$, $K^0_S\omega$) states.

[36] Uses Dalitz plot analysis of $\overline{D}^0 \to K^0_S\pi^+\pi^-$ decays from $B^+ \to D^{(*)} K^+$ modes. The corresponding two standard deviation interval for γ is $54.2° < \gamma < 100.5°$. CP conservation in the combined result is ruled out with a significance of 3.5 standard deviations.

[37] Uses Dalitz plot analysis of $D^0 \to K^0_S\pi^+\pi^-$ decays coming from $B^0 \to D^0 K^{*0}$ modes. The corresponding 95% CL interval is $77° < \gamma < 247°$. A 180 degree ambiguity is implied.

[38] Uses Dalitz plot analysis of $\overline{D}^0 \to K^0_S\pi^+\pi^-$ and $\overline{D}^0 \to K^0_S K^+K^-$ decays coming from $B^{\pm} \to D^{(*)} K^{(*)\pm}$ modes. The corresponding two standard deviation interval is $29° < \gamma < 122°$.

[39] Uses a Dalitz plot analysis of the $\overline{D}^0 \to K^0_S\pi^+\pi^-$ decays; Combines the $D K^+$, $D^* K^+$ and $D K^{*+}$ modes. The corresponding two standard deviations interval for gamma is $8° < \gamma < 111°$.

[40] Uses a Dalitz plot analysis of neutral $D \to K^0_S\pi^+\pi^-$ decays coming from $B^{\pm} \to D K^{\pm}$ and $B^{\pm} \to D^{*0} K^{\pm}$ followed by $D^{*0} \to D\pi^0$, $D\gamma$. The corresponding two standard deviations interval for gamma is $12° < \gamma < 137°$. AUBERT,B 05Y also reports the amplitude ratios and the strong phases.

[41] Uses a Dalitz plot analysis of the 3-body $D \to K^0_S\pi^+\pi^-$ decays coming from $B^{\pm} \to D K^{\pm}$ and $B^{\pm} \to D^* K^{\pm}$ followed by $D^* \to D\pi^0$; here we use D to denote that the neutral D meson produced in the decay is an admixture of D^0 and $\overline{D}^0$. The corresponding two standard deviations interval for γ is $26° < \gamma < 126°$. POLUEKTOV 04 also reports the amplitude ratios and the strong phases.

$r_B(B^+ \to D^0 K^+)$

r_B and δ_B are the amplitude ratio and relative strong phase between the amplitudes of $A(B^+ \to D^0 K^+)$ and $A(B^+ \to \overline{D}^0 K^+)$,

VALUE (units 10^{-2})	CL%	DOCUMENT ID		TECN	COMMENT
$\mathbf{9.88^{+\ 0.22}_{-\ 0.21}}$ **OUR EVALUATION**		(Produced by HFLAV)			
$\mathbf{11.5\ ^{+\ 1.2}_{-\ 1.3}}$		[1] ADACHI	24T	BELL	$e^+e^- \to \Upsilon(4S)$

Int. J. Mod. Phys. A 2026.41. Downloaded from www.worldscientific.com by CALIFORNIA @ BERKELEY on 09/16/26. Re-use and distribution is strictly not permitted, except for Open Access articles.

• • • We do not use the following data for averages, fits, limits, etc. • • •

$9.46 \pm 0.31^{+0.30}_{-0.24}$	[2] AAIJ	23I	LHCB	pp at 7, 8, 13 TeV	
11.0 ± 2.0	[3] AAIJ	23N	LHCB	pp at 7, 8, 13 TeV	
$12.9 \pm 2.4 \pm 0.2$	[4] ABUDINEN	22	BELL	$e^+e^- \to \Upsilon(4S)$	
$9.04^{+0.77}_{-0.75}$	[5] AAIJ	21L	LHCB	pp at 7, 8, 13 TeV	
$32.3 \pm 14.7 \pm 5.6$	[6] RESMI	19	BELL	$e^+e^- \to \Upsilon(4S)$	
$8.6^{+1.3}_{-1.4}$	[7] AAIJ	18AD	LHCB	Repl. by AAIJ 21L	
$8.0^{+1.9}_{-2.1}$	[4] AAIJ	14BA	LHCB	Repl. by AAIJ 21L	
6 ± 4	[8] AAIJ	14BE	LHCB	Repl. by AAIJ 14BA	
9.7 ± 1.1	[9] AAIJ	13AE	LHCB	pp at 7 TeV	
$9.2^{+1.3}_{-1.2}$	[10] LEES	13B	BABR	$e^+e^- \to \Upsilon(4S)$	
7 ± 4	[11,12] AAIJ	12AQ	LHCB	pp at 7 TeV	
$14.5 \pm 3.0 \pm 1.5$	[12,13] AIHARA	12	BELL	$e^+e^- \to \Upsilon(4S)$.	
<13 90	[14] LEES	11D	BABR	$e^+e^- \to \Upsilon(4S)$	
$9.6 \pm 2.9 \pm 0.6$	[15] DEL-AMO-SA...	10F	BABR	Repl. by LEES 13B	
$9.5^{+5.1}_{-4.1}$	[16] DEL-AMO-SA...	10H	BABR	Repl. by LEES 13B	
$16.0^{+4.0}_{-3.8} {}^{+5.1}_{-1.5}$	[17] POLUEKTOV	10	BELL	$e^+e^- \to \Upsilon(4S)$	
$8.6 \pm 3.2 \pm 1.5$	[18] AUBERT	08AL	BABR	Repl. by DEL-AMO-SANCHEZ 10F	
<19 90	HORII	08	BELL	$e^+e^- \to \Upsilon(4S)$	
$15.9^{+5.4}_{-5.0} \pm 5.0$	[19] POLUEKTOV	06	BELL	Repl. by POLUEKTOV 10	
$12 \pm 8 \pm 5$	[20] AUBERT,B	05Y	BABR	Repl. by AUBERT 08AL	

[1] Uses combined sample of Belle and Belle II experiments in B^+ decays to DK^+, D^*K^+, and $D\pi^+$ final states.
[2] Measured using $B^{\pm} \to D[K^{\mp}\pi^{\pm}\pi^{\pm}\pi^{\mp}]h^{\pm}$ decays in bins of the phase space of the D decay. The third uncertainty includes systematic and finite knowledge of the D-meson decay parameters.
[3] A model-dependent binned analysis of the decays $B^{\pm} \to [K^+K^-\pi^+\pi^-]_D h^{\pm}$ is used.
[4] Uses binned Dalitz plot analysis of $B^+ \to DK^+$ decays, with $D \to K^0_S\pi^+\pi^-$ and $D \to K^0_S K^+K^-$. Strong phase measurements from CLEO-c (LIBBY 10) of the D decay over the Dalitz plot are used as input. Supersedes AIHARA 12.
[5] Uses binned analysis of $D \to K^0_S\pi^+\pi^-\pi^0$ from $B^{\pm} \to DK^{\pm}$ modes over the phase space. Strong phase measurements from CLEO-c and BES-III data of the D decay over the phase space binning are used as input.
[6] Uses binned analysis of $D \to K^0_S\pi^+\pi^-\pi^0$ from $B^{\pm} \to DK^{\pm}$ modes over the phase space. Strong phase measurements from RESMI 18 analysis of CLEO-c data of the D decay over the phase space binning are used as input.
[7] Uses binned Dalitz plot analysis of $D \to K^0_S\pi^+\pi^-$ and $K^0_S K^+K^-$ from $B^{\pm} \to DK^{\pm}$ modes. Strong phase measurements from CLEO-c of the D decay over the Dalitz plot are used as input.
[8] AAIJ 14BE uses model-dependent analysis of $D \to K^0_S\pi^+\pi^-$ amplitudes. The model is the same as in DEL-AMO-SANCHEZ 10F.
[9] Uses $B^{\pm} \to [K^{\pm}\pi^{\mp}\pi^+\pi^-]_D h^{\pm}$ mode.
[10] Reports combination of published measurements using GGSZ, GLW, and ADS methods.
[11] Reports combined statistical and systematic uncertainties.
[12] Uses binned Dalitz plot of $\overline{D}^0 \to K^0_S\pi^+\pi^-$ decays from $B^+ \to \overline{D}^0K^+$. Measurement of strong phases in $\overline{D}^0 \to K^0_S\pi^+\pi^-$ Dalitz plot from LIBBY 10 is used as input.
[13] We combined the systematics in quadrature. The authors report separately the contribution to the systematic uncertainty due to the uncertainty on the bin-averaged strong phase difference between D^0 and $\overline{D}^0$ amplitudes. Superseded by ABUDINEN 22.
[14] Uses decays of neutral D to $K^-\pi^+\pi^0$.
[15] Uses Dalitz plot analysis of $\overline{D}^0 \to K^0_S\pi^+\pi^-$, $K^0_S K^+K^-$ decays from $B^+ \to D^{(*)}K^{(*)+}$ modes. The corresponding two standard deviation interval is $0.037 < r_B < 0.155$.
[16] Uses the Cabibbo suppressed decay of $B^+ \to \overline{D}K^+$ followed by $\overline{D} \to K^-\pi^+$.
[17] Uses Dalitz plot analysis of $\overline{D}^0 \to K^0_S\pi^+\pi^-$ decays from $B^+ \to D^0K^+$ modes. The corresponding two standard deviation interval is $0.084 < r_B < 0.239$.
[18] Uses Dalitz plot analysis of $\overline{D}^0 \to K^0_S\pi^+\pi^-$ and $\overline{D}^0 \to K^0_S K^+K^-$ decays coming from $B^{\pm} \to D^{(*)}K^{(*)\pm}$ modes.
[19] Uses a Dalitz plot analysis of the $\overline{D}^0 \to K^0_S\pi^+\pi^-$ decays; Combines the DK^+, D^*K^+ and DK^{*+} modes.
[20] Uses a Dalitz analysis of neutral D decays to $K^0_S\pi^+\pi^-$ in the processes $B^{\pm} \to D^{(*)}K^{\pm}$, $D^* \to D\pi^0$, $D\gamma$.

$\delta_B(B^+ \to D^0K^+)$

VALUE (°)	DOCUMENT ID		TECN	COMMENT
$128.5^{+2.8}_{-3.0}$ OUR EVALUATION	(Produced by HFLAV)			
$137.8^{+8.5}_{-9.8}$	[1] ADACHI	24T	BELL	$e^+e^- \to \Upsilon(4S)$)
• • • We do not use the following data for averages, fits, limits, etc. • • •				
$134.6 \pm 6.0^{+8.6}_{-8.7}$	[2] AAIJ	23I	LHCB	pp at 7, 8, 13 TeV
81^{+14}_{-13}	[3] AAIJ	23N	LHCB	pp at 7, 8, 13 TeV
$124.8 \pm 12.9 \pm 1.8$	[4,5] ABUDINEN	22	BELL	$e^+e^- \to \Upsilon(4S)$
$118.3^{+5.5}_{-5.6}$	[6] AAIJ	21L	LHCB	pp at 7, 8, 13 TeV
$83.4^{+18.3}_{-16.6} \pm 5.1$	[7] RESMI	19	BELL	$e^+e^- \to \Upsilon(4S)$
101 ± 11	[8] AAIJ	18AD	LHCB	Repl. by AAIJ 21L
134^{+14}_{-15}	[4] AAIJ	14BA	LHCB	Repl. by AAIJ 21L
115^{+41}_{-51}	[9] AAIJ	14BE	LHCB	Repl. by AAIJ 14BA
105^{+16}_{-17}	[10] LEES	13B	BABR	$e^+e^- \to \Upsilon(4S)$
137^{+35}_{-46}	[11,12] AAIJ	12AQ	LHCB	pp at 7 TeV
$129.9 \pm 15.0 \pm 6.0$	[12,13] AIHARA	12	BELL	$e^+e^- \to \Upsilon(4S)$
$119^{+19}_{-20} \pm 4$	[14] DEL-AMO-SA...	10F	BABR	Repl. by LEES 13B
$136.7^{+13.0}_{-15.8} \pm 23.2$	[15] POLUEKTOV	10	BELL	$e^+e^- \to \Upsilon(4S)$
$109^{+27}_{-30} \pm 8$	[16] AUBERT	08AL	BABR	Repl. by DEL-AMO-SANCHEZ 10F
$145.7^{+19.0}_{-19.7} \pm 23.1$	[17] POLUEKTOV	06	BELL	Repl. by POLUEKTOV 10
$104 \pm 45^{+23}_{-32}$	[18] AUBERT,B	05Y	BABR	Repl. by AUBERT 08AL

[1] Uses combined sample of Belle and Belle II experiments in B^+ decays to DK^+, D^*K^+, and $D\pi^+$ final states.
[2] Measured using $B^{\pm} \to D[K^{\mp}\pi^{\pm}\pi^{\pm}\pi^{\mp}]h^{\pm}$ decays in bins of the phase space of the D decay. The third uncertainty includes systematic and finite knowledge of the D-meson decay parameters.
[3] A model-dependent binned analysis of the decays $B^{\pm} \to [K^+K^-\pi^+\pi^-]_D h^{\pm}$ is used.
[4] Uses binned Dalitz plot analysis of $B^+ \to DK^+$ decays, with $D \to K^0_S\pi^+\pi^-$ and $D \to K^0_S K^+K^-$. Strong phase measurements from CLEO-c (LIBBY 10) of the D decay over the Dalitz plot are used as input.
[5] Supersedes AIHARA 12.
[6] Uses binned Dalitz plot analysis of $D \to K^0_S\pi^+\pi^-$ and $K^0_S K^+K^-$ from $B^{\pm} \to DK^{\pm}$ modes. Strong phase measurements from CLEO-c and BES-III of the D decay over the Dalitz plot are used as input. Value is modulo 180°.
[7] Uses binned analysis of $D \to K^0_S\pi^+\pi^-\pi^0$ from $B^{\pm} \to DK^{\pm}$ modes over the phase space. Strong phase measurements from RESMI 18 analysis of CLEO-c data of the D decay over the phase space binning are used as input.
[8] Uses binned Dalitz plot analysis of $D \to K^0_S\pi^+\pi^-$ and $K^0_S K^+K^-$ from $B^{\pm} \to DK^{\pm}$ modes. Strong phase measurements from CLEO-c of the D decay over the Dalitz plot are used as input.
[9] AAIJ 14BE uses model-dependent analysis of $D \to K^0_S\pi^+\pi^-$ amplitudes. The model is the same as in DEL-AMO-SANCHEZ 10F.
[10] Reports combination of published measurements using GGSZ, GLW, and ADS methods.
[11] Reports combined statistical and systematic uncertainties.
[12] Uses binned Dalitz plot of $\overline{D}^0 \to K^0_S\pi^+\pi^-$ decays from $B^+ \to \overline{D}^0K^+$. Measurement of strong phases in $\overline{D}^0 \to K^0_S\pi^+\pi^-$ Dalitz plot from LIBBY 10 is used as input.
[13] We combined the systematics in quadrature. The authors report separately the contribution to the systematic uncertainty due to the uncertainty on the bin-averaged strong phase difference between D^0 and $\overline{D}^0$ amplitudes. Superseded by ABUDINEN 22.
[14] Uses Dalitz plot analysis of $\overline{D}^0 \to K^0_S\pi^+\pi^-$, $K^0_S K^+K^-$ decays from $B^+ \to D^{(*)}K^{(*)+}$ modes. The corresponding two standard deviation interval is $75° < \delta_B < 157°$.
[15] Uses Dalitz plot analysis of $\overline{D}^0 \to K^0_S\pi^+\pi^-$ decays from $B^+ \to \overline{D}^0K^+$ modes. The corresponding two standard deviation interval is $102.2° < \delta_B < 162.3°$.
[16] Uses Dalitz plot analysis of $\overline{D}^0 \to K^0_S\pi^+\pi^-$ and $\overline{D}^0 \to K^0_S K^+K^-$ decays coming from $B^{\pm} \to D^{(*)}K^{(*)\pm}$ modes.
[17] Uses a Dalitz plot analysis of the $\overline{D}^0 \to K^0_S\pi^+\pi^-$ decays; Combines the DK^+, D^*K^+ and DK^{*+} modes.
[18] Uses a Dalitz analysis of neutral D decays to $K^0_S\pi^+\pi^-$ in the processes $B^{\pm} \to D^{(*)}K^{\pm}$, $D^* \to D\pi^0$, $D\gamma$.

$r_B(B^+ \to D^0\pi^+)$

VALUE (units 10^{-3})	DOCUMENT ID		TECN	COMMENT
$16.5^{+5.5}_{-5.2}$	[1] ADACHI	24T	BELL	$e^+e^- \to \Upsilon(4S)$)
• • • We do not use the following data for averages, fits, limits, etc. • • •				
$4.5^{+1.1}_{-1.0} {}^{+0.5}_{-0.4}$	[2] AAIJ	23I	LHCB	pp at 7, 8, 13 TeV
$4.1^{+5.4}_{-4.1}$	[3] AAIJ	23N	LHCB	pp at 7, 8, 13 TeV
$17 \pm 6 \pm 1$	[4] ABUDINEN	22	BELL	$e^+e^- \to \Upsilon(4S)$
5.0 ± 1.7	[4] AAIJ	21L	LHCB	pp at 7, 8, 13 TeV

[1] Uses combined sample of Belle and Belle II experiments in B^+ decays to DK^+, D^*K^+, and $D\pi^+$ final states.
[2] Measured using $B^{\pm} \to D[K^{\mp}\pi^{\pm}\pi^{\pm}\pi^{\mp}]h^{\pm}$ decays in bins of the phase space of the D decay. The third uncertainty includes systematic and finite knowledge of the D-meson decay parameters.
[3] A model-dependent binned analysis of the decays $B^{\pm} \to [K^+K^-\pi^+\pi^-]_D h^{\pm}$ is used.
[4] Uses binned Dalitz plot analysis of $D \to K^0_S\pi^+\pi^-$ and $K^0_S K^+K^-$ from $B^{\pm} \to D\pi^{\pm}$ modes. Strong phase measurements from CLEO-c and BES-III of the D decay over the Dalitz plot are used as input.

$\delta_B(B^+ \to D^0\pi^+)$

VALUE (°)	DOCUMENT ID		TECN	COMMENT
$347.0^{+8.7}_{-9.6}$	[1] ADACHI	24T	BELL	$e^+e^- \to \Upsilon(4S)$)
• • • We do not use the following data for averages, fits, limits, etc. • • •				
$311.8^{+14.7}_{-15.0} {}^{+15.0}_{-15.2}$	[2] AAIJ	23I	LHCB	pp at 7, 8, 13 TeV
298^{+62}_{-118}	[3] AAIJ	23N	LHCB	pp at 7, 8, 13 TeV
$341.0 \pm 17.0 \pm 2.9$	[4] ABUDINEN	22	BELL	$e^+e^- \to \Upsilon(4S)$
291^{+24}_{-26}	[4] AAIJ	21L	LHCB	pp at 7, 8, 13 TeV

[1] Uses combined sample of Belle and Belle II experiments in B^+ decays to $D K^+$, $D^* K^+$, and $D \pi^+$ final states.
[2] Measured using $B^{\pm} \to D[K^{\mp}\pi^{\pm}\pi^{\pm}\pi^{\mp}]h^{\pm}$ decays in bins of the phase space of the D decay. The third uncertainty includes systematic and finite knowledge of the D-meson decay parameters.
[3] A model-dependent binned analysis of the decays $B^{\pm} \to [K^+K^-\pi^+\pi^-]_D h^{\pm}$ is used.
[4] Uses binned Dalitz plot analysis of $D \to K^0_S \pi^+\pi^-$ and $K^0_S K^+K^-$ from $B^{\pm} \to D\pi^{\pm}$ modes. Strong phase measurements from CLEO-c and BES-III of the D decay over the Dalitz plot are used as input. Value is modulo 180°.

$r_B(B^+ \to D^0 K^{*+})$

r_B and δ_B are the amplitude ratio and relative strong phase between the amplitudes of $A_{CP}(B^+ \to D^0 K^{*+})$ and $A_{CP}(B^+ \to \overline{D}^0 K^{*+})$,

VALUE	DOCUMENT ID		TECN	COMMENT
$0.101^{+0.016}_{-0.036}$ OUR EVALUATION	(Produced by HFLAV)			
0.103 ± 0.010	[1] AAIJ	25R	LHCB	pp at 7, 8, 13 TeV
• • • We do not use the following data for averages, fits, limits, etc. • • •				
$0.143^{+0.048}_{-0.049}$	[2] LEES	13B	BABR	$e^+e^- \to \Upsilon(4S)$
$0.166^{+0.073}_{-0.069}$	[3] DEL-AMO-SA...	10F	BABR	Repl. by LEES 13B
0.31 ± 0.07	[4] AUBERT	09AJ	BABR	Repl. by LEES 13B
$0.181^{+0.088}_{-0.108} \pm 0.042$	[5] AUBERT	08AL	BABR	Repl. by AUBERT 09AJ
$0.564^{+0.216}_{-0.155} \pm 0.093$	[6] POLUEKTOV	06	BELL	$e^+e^- \to \Upsilon(4S)$

[1] Extracted from $B^{\pm} \to D K^{*\pm}$ decays, using the D decays: $D \to K^{\pm}\pi^{\mp}$, K^+K^-, $\pi^+\pi^-$, $K^{\pm}\pi^{\mp}\pi^{\pm}\pi^{\mp}$, $\pi^+\pi^-\pi^+\pi^-$, $K^0_S\pi^+\pi^-$, and $K^0_S K^+K^-$.
[2] Reports combination of published measurements using GGSZ, GLW, and ADS methods.
[3] DEL-AMO-SANCHEZ 10F reports $r_B \cdot k = 0.149^{+0.066}_{-0.062}$ for k = 0.9.
[4] Obtained by combining the GLW and ADS methods. The 2-sigma range corresponds to [0.17, 0.43].
[5] Uses Dalitz plot analysis of $\overline{D}^0 \to K^0_S\pi^+\pi^-$ and $\overline{D}^0 \to K^0_S K^+K^-$ decays coming from $B^{\pm} \to D^{(*)} K^{(*)\pm}$ modes.
[6] Uses a Dalitz plot analysis of the $\overline{D}^0 \to K^0_S\pi^+\pi^-$ decays; Combines the $D K^+$, $D^* K^+$ and $D K^{*+}$ modes.

$\delta_B(B^+ \to D^0 K^{*+})$

VALUE (°)	DOCUMENT ID		TECN	COMMENT
47^{+61}_{-16} OUR EVALUATION	(Produced by HFLAV)			
47^{+14}_{-12}	[1] AAIJ	25R	LHCB	pp at 7, 8, 13 TeV
• • • We do not use the following data for averages, fits, limits, etc. • • •				
101 ± 43	[2] LEES	13B	BABR	$e^+e^- \to \Upsilon(4S)$
111 ± 32	DEL-AMO-SA...	10F	BABR	Repl. by LEES 13B
$104^{+39}_{-37} \pm 18$	[3] AUBERT	08AL	BABR	Repl. by LEES 13B
$242.6^{+20.2}_{-23.2} \pm 49.4$	[4] POLUEKTOV	06	BELL	$e^+e^- \to \Upsilon(4S)$

[1] Extracted from $B^{\pm} \to D K^{*\pm}$ decays, using the D decays: $D \to K^{\pm}\pi^{\mp}$, K^+K^-, $\pi^+\pi^-$, $K^{\pm}\pi^{\mp}\pi^{\pm}\pi^{\mp}$, $\pi^+\pi^-\pi^+\pi^-$, $K^0_S\pi^+\pi^-$, and $K^0_S K^+K^-$.
[2] Reports combination of published measurements using GGSZ, GLW, and ADS methods.
[3] Uses Dalitz plot analysis of $\overline{D}^0 \to K^0_S\pi^+\pi^-$ and $\overline{D}^0 \to K^0_S K^+K^-$ decays coming from $B^{\pm} \to D^{(*)} K^{(*)\pm}$ modes.
[4] Uses a Dalitz plot analysis of the $\overline{D}^0 \to K^0_S\pi^+\pi^-$ decays; Combines the $D K^+$, $D^* K^+$ and $D K^{*+}$ modes.

$r_B(B^+ \to D^{*0} K^+)$

r_B and δ_B are the amplitude ratio and relative strong phase between the amplitudes of $A(B^+ \to D^{*0} K^+)$ and $A(B^+ \to \overline{D}^{*0} K^+)$,

VALUE	DOCUMENT ID		TECN	COMMENT
$0.103^{+0.010}_{-0.011}$ OUR EVALUATION	(Produced by HFLAV)			
$0.229^{+0.068}_{-0.067}$	[1] ADACHI	24T	BELL	$e^+e^- \to \Upsilon(4S)$)
• • • We do not use the following data for averages, fits, limits, etc. • • •				
$0.080^{+0.022}_{-0.023}$	[2] AAIJ	24H	LHCB	pp at 7, 8, 13 TeV
0.15 ± 0.03	[3] AAIJ	23BA	LHCB	pp at 7, 8, 13 TeV
$0.106^{+0.019}_{-0.036}$	[4] LEES	13B	BABR	$e^+e^- \to \Upsilon(4S)$
$0.133^{+0.042}_{-0.039} \pm 0.013$	[5] DEL-AMO-SA...	10F	BABR	Repl. by LEES 13B
$0.096^{+0.035}_{-0.051}$	[6] DEL-AMO-SA...	10H	BABR	Repl. by LEES 13B
$0.196^{+0.072}_{-0.069} {}^{+0.064}_{-0.017}$	[7] POLUEKTOV	10	BELL	$e^+e^- \to \Upsilon(4S)$
$0.135 \pm 0.050 \pm 0.012$	[8] AUBERT	08AL	BABR	Repl. by DEL-AMO-SANCHEZ 10F
$0.175^{+0.108}_{-0.099} \pm 0.050$	[9] POLUEKTOV	06	BELL	Repl. by POLUEKTOV 10
$0.17 \pm 0.10 \pm 0.04$	[10] AUBERT,B	05Y	BABR	Repl. by AUBERT 08AL

[1] Uses combined sample of Belle and Belle II experiments in B^+ decays to $D K^+$, $D^* K^+$, and $D \pi^+$ final states.
[2] Extracted from yields of partially reconstructed $B^{\pm} \to D^* K^{\pm}$, $D^* \to D\pi^0/\gamma$, $D \to K^0_S\pi^+\pi^-/K^0_S K^+K^-$ decays. The uncertainty is predominantly statistical. Its correlation with the AAIJ 23BA result is found to be less than 3%.
[3] Measured using $B^{\pm} \to D^* K^{\pm}$ decays analysing the signal yield variation with the fully reconstructed $D^* \to D\pi^0/\gamma$, $D \to K^0_S\pi^+\pi^-/K^0_S K^+K^-$ decays. The model-independent approach uses external strong phase input from BESIII and CLEO collaborations.
[4] Reports combination of published measurements using GGSZ, GLW, and ADS methods.
[5] Uses Dalitz plot analysis of $\overline{D}^0 \to K^0_S\pi^+\pi^-$, $K^0_S K^+K^-$ decays from $B^+ \to D^{(*)} K^{(*)+}$ modes. The corresponding two standard deviation interval is $0.049 < r^*_B < 0.215$.
[6] Uses the Cabibbo suppressed decay of $B^+ \to \overline{D}^* K^+$ followed by $\overline{D}^* \to \overline{D}\pi^0$ or $\overline{D}\gamma$, and $\overline{D} \to K^-\pi^+$.
[7] Uses Dalitz plot analysis of $\overline{D}^0 \to K^0_S\pi^+\pi^-$ decays from $B^+ \to D^{*0} K^+$ modes. The corresponding two standard deviation interval is $0.061 < r^*_B < 0.271$.
[8] Uses Dalitz plot analysis of $\overline{D}^0 \to K^0_S\pi^+\pi^-$ and $\overline{D}^0 \to K^0_S K^+K^-$ decays coming from $B^{\pm} \to D^{(*)} K^{(*)\pm}$ modes.
[9] Uses a Dalitz plot analysis of the $\overline{D}^0 \to K^0_S\pi^+\pi^-$ decays; Combines the $D K^+$, $D^* K^+$ and $D K^{*+}$ modes.
[10] Uses a Dalitz analysis of neutral D decays to $K^0_S\pi^+\pi^-$ in the processes $B^{\pm} \to D^{(*)} K^{\pm}$, $D^* \to D\pi^0$, $D\gamma$.

$\delta_B(B^+ \to D^{*0} K^+)$

VALUE (°)	DOCUMENT ID		TECN	COMMENT
$312.2^{+6.3}_{-7.1}$ OUR EVALUATION	(Produced by HFLAV)			
342^{+14}_{-16}	[1] ADACHI	24T	BELL	$e^+e^- \to \Upsilon(4S)$)
• • • We do not use the following data for averages, fits, limits, etc. • • •				
310^{+15}_{-20}	[2] AAIJ	24H	LHCB	pp at 7, 8, 13 TeV
311 ± 14	[3] AAIJ	23BA	LHCB	pp at 7, 8, 13 TeV
294^{+21}_{-31}	[4] LEES	13B	BABR	$e^+e^- \to \Upsilon(4S)$
$278 \pm 21 \pm 6$	[5] DEL-AMO-SA...	10F	BABR	Repl. by LEES 13B
$341.9^{+18.0}_{-19.6} \pm 23.1$	[6] POLUEKTOV	10	BELL	$e^+e^- \to \Upsilon(4S)$
$297^{+27}_{-29} \pm 6.4$	[7] AUBERT	08AL	BABR	Repl. by DEL-AMO-SANCHEZ 10F
$302.0^{+33.8}_{-35.1} \pm 23.7$	[8] POLUEKTOV	06	BELL	Repl. by POLUEKTOV 10
$296 \pm 41^{+20}_{-19}$	[9] AUBERT,B	05Y	BABR	Repl. by AUBERT 08AL

[1] Uses combined sample of Belle and Belle II experiments in B^+ decays to $D K^+$, $D^* K^+$, and $D \pi^+$ final states.
[2] Extracted from yields of partially reconstructed $B^{\pm} \to D^* K^{\pm}$, $D^* \to D\pi^0/\gamma$, $D \to K^0_S\pi^+\pi^-/K^0_S K^+K^-$ decays. The uncertainty is predominantly statistical. Its correlation with the AAIJ 23BA result is found to be less than 3%.
[3] Measured using $B^{\pm} \to D^* K^{\pm}$ decays analysing the signal yield variation with the fully reconstructed $D^* \to D\pi^0/\gamma$, $D \to K^0_S\pi^+\pi^-/K^0_S K^+K^-$ decays. The model-independent approach uses external strong phase input from BESIII and CLEO collaborations.
[4] Reports combination of published measurements using GGSZ, GLW, and ADS methods. We added 360° to the value of $(-66^{+21}_{-31})°$ quoted by LEES 13B.
[5] Uses Dalitz plot analysis of $\overline{D}^0 \to K^0_S\pi^+\pi^-$, $K^0_S K^+K^-$ decays from $B^+ \to D^{(*)} K^{(*)+}$ modes. The corresponding two standard deviation interval is $236° < \delta^*_B < 322°$.
[6] Uses Dalitz plot analysis of $\overline{D}^0 \to K^0_S\pi^+\pi^-$ decays from $B^+ \to D^* K^+$ modes. The corresponding two standard deviation interval is $296.5° < \delta^*_B < 382.7°$.
[7] Uses Dalitz plot analysis of $\overline{D}^0 \to K^0_S\pi^+\pi^-$ and $\overline{D}^0 \to K^0_S K^+K^-$ decays coming from $B^{\pm} \to D^{(*)} K^{(*)\pm}$ modes.
[8] Uses a Dalitz plot analysis of the $\overline{D}^0 \to K^0_S\pi^+\pi^-$ decays; Combines the $D K^+$, $D^* K^+$ and $D K^{*+}$ modes.
[9] Uses a Dalitz analysis of neutral D decays to $K^0_S\pi^+\pi^-$ in the processes $B^{\pm} \to D^{(*)} K^{\pm}$, $D^* \to D\pi^0$, $D\gamma$.

$r_B(B^+ \to D^{*0} \pi^+)$

r_B and δ_B are the amplitude ratio and relative strong phase between the amplitudes of $A(B^+ \to D^{*0}\pi^+)$ and $A(B^+ \to \overline{D}^{*0}\pi^+)$.

VALUE	DOCUMENT ID		TECN	COMMENT
• • • We do not use the following data for averages, fits, limits, etc. • • •				
$0.009^{+0.005}_{-0.007}$	[1] AAIJ	24H	LHCB	pp at 7, 8, 13 TeV
0.01 ± 0.01	[2] AAIJ	23BA	LHCB	pp at 7, 8, 13 TeV

[1] Extracted from yields of partially reconstructed $B^{\pm} \to D^* K^{\pm}$, $D^* \to D\pi^0/\gamma$, $D \to K^0_S\pi^+\pi^-/K^0_S K^+K^-$ decays. The uncertainty is predominantly statistical. Its correlation with the AAIJ 23BA result is found to be less than 3%.
[2] Measured using $B^{\pm} \to D^*\pi^{\pm}$ decays analysing the signal yield variation with the fully reconstructed $D^* \to D\pi^0/\gamma$, $D \to K^0_S\pi^+\pi^-/K^0_S K^+K^-$ decays. The model-independent approach uses external strong phase input from BESIII and CLEO collaborations.

$\delta_B(B^+ \to D^{*0} \pi^+)$

VALUE (°)	DOCUMENT ID		TECN	COMMENT
• • • We do not use the following data for averages, fits, limits, etc. • • •				
304^{+37}_{-38}	[1] AAIJ	24H	LHCB	pp at 7, 8, 13 TeV
37 ± 37	[2] AAIJ	23BA	LHCB	pp at 7, 8, 13 TeV

Int. J. Mod. Phys. A 2026.41. Downloaded from www.worldscientific.com
by UNIVERSITY OF CALIFORNIA @ BERKELEY on 09/16/26. Re-use and distribution is strictly not permitted, except for Open Access articles.

[1] Extracted from yields of partially reconstructed $B^{\pm} \to D^* K^{\pm}$, $D^* \to D\pi^0/\gamma$, $D \to K^0_S \pi^+\pi^-/K^0_S K^+K^-$ decays. The uncertainty is predominantly statistical. Its correlation with the AAIJ 23BA result is found to be less than 3%.
[2] Measured using $B^{\pm} \to D^*\pi^{\pm}$ decays analysing the signal yield variation with the fully reconstructed $D^* \to D\pi^0/\gamma$, $D \to K^0_S\pi^+\pi^-/K^0_S K^+K^-$ decays. The model-independent approach uses external strong phase input from BESIII and CLEO collaborations.

PARTIAL BRANCHING FRACTIONS

B($B^+ \to K^{*+}\ell^+\ell^-$) ($q^2$ < 2.0 GeV^2/c^4)

VALUE (units 10^{-7})	DOCUMENT ID		TECN	COMMENT
1.4 ±0.5 OUR AVERAGE				
$1.37^{+0.60}_{-0.58}$	AAIJ	12AH	LHCB	pp at 7 TeV
1.30±0.98±0.14	AALTONEN	11AI	CDF	$p\overline{p}$ at 1.96 TeV

B($B^+ \to K^{*+}\ell^+\ell^-$) (2.0 < q^2 < 4.3 GeV^2/c^4)

VALUE (units 10^{-7})	DOCUMENT ID		TECN	COMMENT
1.1 ±0.5 OUR AVERAGE				
$1.24^{+0.60}_{-0.55}$	AAIJ	12AH	LHCB	pp at 7 TeV
0.71±1.00±0.15	AALTONEN	11AI	CDF	$p\overline{p}$ at 1.96 TeV

B($B^+ \to K^{*+}\ell^+\ell^-$) (4.3 < q^2 < 8.68 GeV^2/c^4)

VALUE (units 10^{-7})	DOCUMENT ID		TECN	COMMENT
$2.4^{+0.8}_{-0.7}$ OUR AVERAGE				
$2.50^{+0.88}_{-0.74}$	AAIJ	12AH	LHCB	pp at 7 TeV
1.71±1.58±0.49	AALTONEN	11AI	CDF	$p\overline{p}$ at 1.96 TeV

B($B^+ \to K^{*+}\ell^+\ell^-$) (10.09 < q^2 < 12.86 GeV^2/c^4)

VALUE (units 10^{-7})	DOCUMENT ID		TECN	COMMENT
2.1 ±0.6 OUR AVERAGE				
$2.13^{+0.72}_{-0.66}$	AAIJ	12AH	LHCB	pp at 7 TeV
1.97±0.99±0.22	AALTONEN	11AI	CDF	$p\overline{p}$ at 1.96 TeV

B($B^+ \to K^{*+}\ell^+\ell^-$) (14.18 < q^2 < 16.0 GeV^2/c^4)

VALUE (units 10^{-7})	DOCUMENT ID		TECN	COMMENT
$0.86^{+0.40}_{-0.32}$ OUR AVERAGE				
$1.00^{+0.47}_{-0.38}$	AAIJ	12AH	LHCB	pp at 7 TeV
0.52±0.61±0.09	AALTONEN	11AI	CDF	$p\overline{p}$ at 1.96 TeV

B($B^+ \to K^{*+}\ell^+\ell^-$) (15.0 < q^2 < 19.0 GeV^2/c^4)

VALUE (units 10^{-7})	DOCUMENT ID		TECN	COMMENT
$1.78^{+0.32}_{-0.29}$ OUR AVERAGE				
$2.9\ ^{+1.0}_{-0.8}\ \pm0.3$	[1] WEHLE	21	BELL	$e^+e^- \to \Upsilon(4S)$
$2.1\ ^{+1.2}_{-1.0}\ \pm0.2$	[2] WEHLE	21	BELL	$e^+e^- \to \Upsilon(4S)$
$1.58^{+0.32}_{-0.29}\pm0.11$	[3] AAIJ	14M	LHCB	pp at 7, 8 TeV

[1] Measured with $\mu^+\mu^-$ as lepton pair.
[2] Measured with e^+e^- as lepton pair.
[3] Uses B($B^+ \to J/\psi(1S)K^*(892)^+$) = (1.431 ± 0.027 ± 0.090)×10^{-3} for normalization and $\mu^+\mu^-$ as a lepton pair.

B($B^+ \to K^{*+}\ell^+\ell^-$) ($q^2$ > 16.0 GeV^2/c^4)

VALUE (units 10^{-7})	DOCUMENT ID		TECN	COMMENT
1.3 ±0.4 OUR AVERAGE				
1.25±0.46	AAIJ	12AH	LHCB	pp at 7 TeV
1.57±0.96±0.17	AALTONEN	11AI	CDF	$p\overline{p}$ at 1.96 TeV

B($B^+ \to K^{*+}\ell^+\ell^-$) (1.0 < q^2 < 6.0 GeV^2/c^4)

VALUE (units 10^{-7})	DOCUMENT ID		TECN	COMMENT
$1.72^{+0.40}_{-0.32}$ OUR AVERAGE				
$1.2\ ^{+0.9}_{-0.7}\ \pm0.2$	[1,2] WEHLE	21	BELL	$e^+e^- \to \Upsilon(4S)$
$1.7\ ^{+1.0}_{-1.0}\ \pm0.2$	[2,3] WEHLE	21	BELL	$e^+e^- \to \Upsilon(4S)$
$1.79^{+0.41}_{-0.37}\pm0.13$	[4] AAIJ	14M	LHCB	pp at 7, 8 TeV
2.57±1.61±0.40	AALTONEN	11AI	CDF	$p\overline{p}$ at 1.96 TeV
• • • We do not use the following data for averages, fits, limits, etc. • • •				
$2.90^{+0.90}_{-0.85}$	AAIJ	12AH	LHCB	Repl. by AAIJ 14M

[1] Measured with $\mu^+\mu^-$ as lepton pair.
[2] Result is determined for the range 1.1 < q^2 < 6.0 GeV^4/c^2.
[3] Measured with e^+e^- as lepton pair.
[4] Uses B($B^+ \to J/\psi(1S)K^*(892)^+$) = (1.431 ± 0.027 ± 0.090)×10^{-3} for normalization and $\mu^+\mu^-$ as a lepton pair. Measured in 1.1 < q^2 < 6.0 GeV^2/c^4.

B($B^+ \to K^{*+}\ell^+\ell^-$) (0.0 < q^2 < 4.3 GeV^2/c^4)

VALUE (units 10^{-7})	DOCUMENT ID		TECN	COMMENT
2.01±1.39±0.27	AALTONEN	11AI	CDF	$p\overline{p}$ at 1.96 TeV

B($B^+ \to K^{*+}e^+e^-$) (0.045 < q^2 < 6.0 GeV^2/c^4)

VALUE (units 10^{-8})	DOCUMENT ID		TECN	COMMENT
$55\pm11^{+5}_{-4}$	[1] AAIJ	22J	LHCB	pp at 7, 8, 13 TeV

[1] The reported value is converted from the measured $dB/dq^2 = (9.2^{+1.9+0.8}_{-1.8-0.6})\times10^{-8}$ (GeV^2/c^4)$^{-1}$ by multiplying by the Δq^2 = 5.955 GeV^2/c^4 range.

B($B^+ \to K^{*+}\mu^+\mu^-$) / B($B^+ \to K^{*+}e^+e^-$) (0.045 < q^2 < 1.1 GeV^2/c^4)

VALUE	DOCUMENT ID		TECN	COMMENT
$0.62^{+0.60}_{-0.36}\pm0.07$	WEHLE	21	BELL	$e^+e^- \to \Upsilon(4S)$

B($B^+ \to K^{*+}\mu^+\mu^-$) / B($B^+ \to K^{*+}e^+e^-$) (1.1 < q^2 < 6.0 GeV^2/c^4)

VALUE	DOCUMENT ID		TECN	COMMENT
$0.72^{+0.99}_{-0.44}\pm0.14$	WEHLE	21	BELL	$e^+e^- \to \Upsilon(4S)$

B($B^+ \to K^{*+}\mu^+\mu^-$) / B($B^+ \to K^{*+}e^+e^-$) (0.045 < q^2 < 6.0 GeV^2/c^4)

VALUE	DOCUMENT ID		TECN	COMMENT
$0.70^{+0.18+0.03}_{-0.13-0.04}$	AAIJ	22J	LHCB	pp at 7, 8, 13 TeV

B($B^+ \to K^{*+}\mu^+\mu^-$)/B($B^+ \to K^{*+}e^+e^-$) (15.0 < q^2 < 19.0 GeV^2/c^4)

VALUE	DOCUMENT ID		TECN	COMMENT
$1.40^{+1.99}_{-0.68}\pm0.11$	WEHLE	21	BELL	$e^+e^- \to \Upsilon(4S)$

B($B^+ \to K^+\ell^+\ell^-$) (q^2 < 2.0 GeV^2/c^4)

VALUE (units 10^{-7})	DOCUMENT ID		TECN	COMMENT
0.51 ±0.08 OUR AVERAGE	Error includes scale factor of 1.5.			
0.556±0.053±0.027	[1] AAIJ	13H	LHCB	pp at 7 TeV
0.36 ±0.11 ±0.03	AALTONEN	11AI	CDF	$p\overline{p}$ at 1.96 TeV

[1] Measured in 0.05 < q^2 < 2.0 GeV^2/c^4 range.

B($B^+ \to K^+\ell^+\ell^-$) (2.0 < q^2 < 4.3 GeV^2/c^4)

VALUE (units 10^{-7})	DOCUMENT ID		TECN	COMMENT
0.60 ±0.07 OUR AVERAGE	Error includes scale factor of 1.3.			
0.573±0.053±0.023	AAIJ	13H	LHCB	pp at 7 TeV
0.80 ±0.15 ±0.05	AALTONEN	11AI	CDF	$p\overline{p}$ at 1.96 TeV

B($B^+ \to K^+\ell^+\ell^-$) (4.3 < q^2 < 8.68 GeV^2/c^4)

VALUE (units 10^{-7})	DOCUMENT ID		TECN	COMMENT
1.03 ±0.07 OUR AVERAGE				
1.003±0.070±0.039	AAIJ	13H	LHCB	pp at 7 TeV
1.18 ±0.19 ±0.09	AALTONEN	11AI	CDF	$p\overline{p}$ at 1.96 TeV

B($B^+ \to K^+\ell^+\ell^-$) (10.09 < q^2 < 12.86 GeV^2/c^4)

VALUE (units 10^{-7})	DOCUMENT ID		TECN	COMMENT
0.58 ±0.05 OUR AVERAGE				
0.565±0.050±0.022	AAIJ	13H	LHCB	pp at 7 TeV
0.68 ±0.12 ±0.05	AALTONEN	11AI	CDF	$p\overline{p}$ at 1.96 TeV

B($B^+ \to K^+\ell^+\ell^-$) (14.18 < q^2 < 16.0 GeV^2/c^4)

VALUE (units 10^{-7})	DOCUMENT ID		TECN	COMMENT
0.40 ±0.05 OUR AVERAGE	Error includes scale factor of 1.4.			
0.377±0.036±0.015	AAIJ	13H	LHCB	pp at 7 TeV
0.53 ±0.10 ±0.03	AALTONEN	11AI	CDF	$p\overline{p}$ at 1.96 TeV

B($B^+ \to K^+\ell^+\ell^-$) (16.0 < q^2 < 18.0 GeV^2/c^4)

VALUE (units 10^{-7})	DOCUMENT ID		TECN	COMMENT
0.354±0.036±0.018	AAIJ	13H	LHCB	pp at 7 TeV

B($B^+ \to K^+\ell^+\ell^-$) (18.0 < q^2 < 22.0 GeV^2/c^4)

F_H is a fractional contribution of (pseudo) scalar and tensor amplitudes to the decay width in the massless muon approximation.

VALUE (units 10^{-7})	DOCUMENT ID		TECN	COMMENT
0.312±0.040±0.016	AAIJ	13H	LHCB	pp at 7 TeV

B($B^+ \to K^+\ell^+\ell^-$) (15.0 < q^2 < 22.0 GeV^2/c^4)

VALUE (units 10^{-7})	DOCUMENT ID		TECN	COMMENT
0.85±0.03±0.04	[1] AAIJ	14M	LHCB	pp at 7, 8 TeV

[1] Uses B($B^+ \to J/\psi(1S)K^+$) = (0.998 ± 0.014 ± 0.040)×10^{-3} for normalization and $\mu^+\mu^-$ as a lepton pair.

B($B^+ \to K^+\ell^+\ell^-$) (16.0 < q^2 GeV^2/c^4)

VALUE (units 10^{-7})	DOCUMENT ID		TECN	COMMENT
0.48±0.11±0.03	AALTONEN	11AI	CDF	$p\overline{p}$ at 1.96 TeV

Int. J. Mod. Phys. A 2026.41. Downloaded from www.worldscientific.com
by LIFORNIA @ BERKELEY on 09/16/26. Re-use and distribution is strictly not permitted, except for Open Access articles.

Int. J. Mod. Phys. A 2026.41. Downloaded from www.worldscientific.com
by UNIVERSITY OF CALIFORNIA @ BERKELEY on 09/16/26. Re-use and distribution is strictly not permitted, except for Open Access articles.

$B(B^+ \to K^+\ell^+\ell^-)$ $(1.0 < q^2 < 6.0\ \mathrm{GeV}^2/c^4)$

VALUE (units 10^{-7})	DOCUMENT ID	TECN	COMMENT
1.26 ±0.12 OUR AVERAGE	Error includes scale factor of 1.9.		See the ideogram below.
$2.30\ ^{+0.41}_{-0.38} \pm 0.05$	[1] CHOUDHURY 21	BELL	$e^+e^- \to \Upsilon(4S)$
$1.66\ ^{+0.32}_{-0.29} \pm 0.04$	[2] CHOUDHURY 21	BELL	$e^+e^- \to \Upsilon(4S)$
$1.40\ ^{+0.98}_{-0.34} \pm 0.69$	[3] AAIJ 19S	LHCB	pp at 7, 8, 13 TeV
$1.19 \pm 0.034 \pm 0.059$	[4] AAIJ 14M	LHCB	pp at 7, 8 TeV
$1.41 \pm 0.20 \pm 0.10$	AALTONEN 11AI	CDF	$p\overline{p}$ at 1.96 TeV
• • • We do not use the following data for averages, fits, limits, etc. • • •			
$1.56\ ^{+0.19}_{-0.15}\ ^{+0.06}_{-0.04}$	[5] AAIJ 14AR	LHCB	pp at 7, 8 TeV
$1.205 \pm 0.085 \pm 0.070$	AAIJ 13H	LHCB	Repl. by AAIJ 14M

[1] Measured for $B^+ \to K^+\mu^+\mu^-$ decays. Measurements in other q^2 bins are also reported.
[2] Measured for $B^+ \to K^+e^+e^-$ decays. Measurements in other q^2 bins are also reported.
[3] Measured by taking the ratio of the branching fraction from $B^+ \to K^+e^+e^-$ and $B^+ \to J/\psi(e^+e^-)K^+$ decays and multiplying it by the measured value of $B^+ \to J/\psi K^+$ and $J/\psi \to e^+e^-$ as in PDG 18. The branching fraction of $B^+ \to K^+e^+e^-$ is determined in the region $1.1 < q^2 < 6\ \mathrm{GeV}^2/c^4$.
[4] Uses $B(B^+ \to J/\psi(1S)K^+) = (0.998 \pm 0.014 \pm 0.040) \times 10^{-3}$ for normalization and $\mu^+\mu^-$ for leptons. Measured for $1.1 < q^2 < 6.0\ \mathrm{GeV}^2/c^4$.
[5] Measured by taking the ratio of the branching fraction from $B^+ \to K^+e^+e^-$ and $B^+ \to J/\psi(e^+e^-)K^+$decays and multiplying it by the measured value of $B^+ \to J/\psi K^+$ and $J/\psi \to e^+e^-$ as in PDG 12.The branching fraction of $B^+ \to K^+e^+e^-$ is determined in the region $1 < q^2 < 6\ \mathrm{GeV}^2/c^4$.

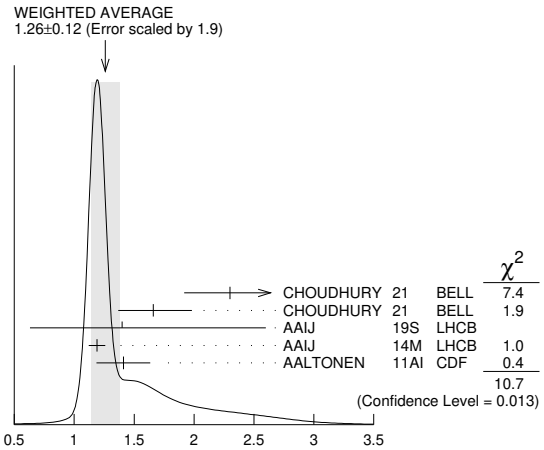

$B(B^+ \to K^+\ell^+\ell^-)$ $(1.0 < q^2 < 6.0\ \mathrm{GeV}^2/c^4)$ (units 10^{-7})

$B(B^+ \to K^+\mu^+\mu^-)$ / $B(B^+ \to K^+e^+e^-)$ $(0.1 < q^2 < 1.1\ \mathrm{GeV}^2/c^4)$

VALUE	DOCUMENT ID	TECN	COMMENT
$\mathbf{0.994\ ^{+0.090}_{-0.082} \pm 0.029}$	AAIJ 23AB	LHCB	pp at 7, 8, 13 TeV

$B(B^+ \to K^+\mu^+\mu^-)$ / $B(B^+ \to K^+e^+e^-)$ $(1.0 < q^2 < 6.0\ \mathrm{GeV}^2/c^4)$

VALUE	DOCUMENT ID	TECN	COMMENT
0.96 ±0.05 OUR AVERAGE			
$0.949\ ^{+0.042}_{-0.041} \pm 0.022$	[1] AAIJ 23AB	LHCB	pp at 7, 8, 13 TeV
$1.39\ ^{+0.36}_{-0.33} \pm 0.02$	[2] CHOUDHURY 21	BELL	$e^+e^- \to \Upsilon(4S)$
• • • We do not use the following data for averages, fits, limits, etc. • • •			
$0.846\ ^{+0.042}_{-0.039} \pm 0.013 \pm 0.012$	[3,4] AAIJ 22V	LHCB	pp at 7, 8, 13 TeV
$0.846\ ^{+0.060}_{-0.054} \pm 0.016 \pm 0.014$	[3,5] AAIJ 19S	LHCB	pp at 7, 8, 13 TeV
$0.745\ ^{+0.090}_{-0.074} \pm 0.036$	[3] AAIJ 14AR	LHCB	pp at 7, 8 TeV

[1] Measured for the region $1.1 < q^2 < 6.0\ \mathrm{GeV}^2/c^4$.
[2] Measurements in other q^2 bins are also reported.
[3] The ratio is determined using the relative branching fractions of the decays $B^+ \to K^+\ell^+\ell^-$ and $B^+ \to J/\psi(\to \ell^+\ell^-)K^+$, with $\ell = e, \mu$. Measured for the region $1.1 < q^2 < 6.0\ \mathrm{GeV}^2/c^4$.
[4] Superseded by AAIJ 23AB.
[5] Superseded by AAIJ 22V.

$B(B^+ \to K^+\mu^+\mu^-)$ / $B(B^+ \to K^+e^+e^-)$ $(q^2 > 14.3\ \mathrm{GeV}^2/c^4)$

VALUE	DOCUMENT ID	TECN	COMMENT
$\mathbf{1.08\ ^{+0.11}_{-0.09} \pm 0.04}$	AAIJ 25Y	LHCB	pp at 7, 8 and 13 TeV

$B(B^+ \to K^+\ell^+\ell^-)$ $(0.0 < q^2 < 4.3\ \mathrm{GeV}^2/c^4)$

VALUE (units 10^{-7})	DOCUMENT ID	TECN	COMMENT
1.13±0.19±0.08	AALTONEN 11AI	CDF	$p\overline{p}$ at 1.96 TeV

$B(B^+ \to K^+\pi^+\pi^-\mu^+\mu^-)$ $(1.00 < q^2 < 6.00\ \mathrm{GeV}^2/c^4)$

VALUE (units 10^{-7})	DOCUMENT ID	TECN	COMMENT
$\mathbf{1.38\ ^{+0.15}_{-0.14} \pm 0.08}$	AAIJ 14AZ	LHCB	pp at 7, 8 TeV

$B(B^+ \to K^+\pi^+\pi^-\mu^+\mu^-)$ $(0.10 < q^2 < 2.00\ \mathrm{GeV}^2/c^4)$

VALUE (units 10^{-7})	DOCUMENT ID	TECN	COMMENT
$\mathbf{1.33\ ^{+0.13}_{-0.12} \pm 0.09}$	AAIJ 14AZ	LHCB	pp at 7, 8 TeV

$B(B^+ \to K^+\pi^+\pi^-\mu^+\mu^-)$ $(2.00 < q^2 < 4.30\ \mathrm{GeV}^2/c^4)$

VALUE (units 10^{-8})	DOCUMENT ID	TECN	COMMENT
$\mathbf{5.38\ ^{+0.94}_{-0.87} \pm 0.35}$	AAIJ 14AZ	LHCB	pp at 7, 8 TeV

$B(B^+ \to K^+\pi^+\pi^-\mu^+\mu^-)$ $(4.30 < q^2 < 8.68\ \mathrm{GeV}^2/c^4)$

VALUE (units 10^{-7})	DOCUMENT ID	TECN	COMMENT
$\mathbf{1.01\ ^{+0.12}_{-0.13} \pm 0.09}$	AAIJ 14AZ	LHCB	pp at 7, 8 TeV

$B(B^+ \to K^+\pi^+\pi^-\mu^+\mu^-)$ $(10.09 < q^2 < 12.86\ \mathrm{GeV}^2/c^4)$

VALUE (units 10^{-8})	DOCUMENT ID	TECN	COMMENT
$\mathbf{5.07\ ^{+0.94}_{-0.89} \pm 0.47}$	AAIJ 14AZ	LHCB	pp at 7, 8 TeV

$B(B^+ \to K^+\pi^+\pi^-\mu^+\mu^-)$ $(14.18 < q^2 < 19.00\ \mathrm{GeV}^2/c^4)$

VALUE (units 10^{-8})	DOCUMENT ID	TECN	COMMENT
$\mathbf{0.48\ ^{+0.39}_{-0.29} \pm 0.05}$	AAIJ 14AZ	LHCB	pp at 7, 8 TeV

$B(B^+ \to K^+\pi^+\pi^-e^+e^-)$ / $B(B^+ \to K^+\pi^+\pi^-\mu^+\mu^-)$ $(1.1 < q^2 < 7.0\ \mathrm{GeV}^2/c^4)$

VALUE	DOCUMENT ID	TECN	COMMENT
$\mathbf{1.31\ ^{+0.18}_{-0.17}\ ^{+0.12}_{-0.09}}$	AAIJ 25L	LHCB	pp at 7, 8 and 13 TeV

$B(B^+ \to \pi^+\mu^+\mu^-)/B(B^+ \to K^+\mu^+\mu^-)$ $(1.00 < q^2 < 6.00\ \mathrm{GeV}^2/c^4)$

VALUE (units 10^{-2})	DOCUMENT ID	TECN	COMMENT
3.8±0.9±0.1	AAIJ 15AR	LHCB	pp at 7, 8 TeV

$B(B^+ \to \pi^+\mu^+\mu^-)$ $(1.00 < q^2 < 6.00\ \mathrm{GeV}^2/c^4)$

VALUE (units 10^{-9})	DOCUMENT ID	TECN	COMMENT
$\mathbf{4.55\ ^{+1.05}_{-1.00} \pm 0.15}$	AAIJ 15AR	LHCB	pp at 7, 8 TeV

$B(B^+ \to \pi^+\mu^+\mu^-)$ $(15.00 < q^2 < 22.00\ \mathrm{GeV}^2/c^4)$

VALUE (units 10^{-9})	DOCUMENT ID	TECN	COMMENT
$\mathbf{3.29\ ^{+0.84}_{-0.70} \pm 0.07}$	AAIJ 15AR	LHCB	pp at 7, 8 TeV

$B(B^+ \to \pi^+\mu^+\mu^-)/B(B^+ \to K^+\mu^+\mu^-)$ $(15.0 < q^2 < 22.0\ \mathrm{GeV}^2/c^4)$

VALUE (units 10^{-2})	DOCUMENT ID	TECN	COMMENT
3.7±0.8±0.1	AAIJ 15AR	LHCB	pp at 7, 8 TeV

$A_{FB}(B^+ \to K^+\mu^+\mu^-)$ $(1.1 < q^2 < 6.0\ \mathrm{GeV}^2/c^4)$

A_{FB} is the forward-backward angular asymmetry of the lepton pair in $B \to K^{(*)}\ell^+\ell^-$ decay as defined in B^+, B^0 admixture particle listings.

VALUE	DOCUMENT ID	TECN	COMMENT
−0.003±0.017 OUR AVERAGE			
$-0.14\ ^{+0.07}_{-0.06} \pm 0.03$	[1] SIRUNYAN 18DX	CMS	pp at 8 TeV
$0.005 \pm 0.015 \pm 0.010$	[2] AAIJ 14O	LHCB	pp at 7,8 TeV
• • • We do not use the following data for averages, fits, limits, etc. • • •			
$0.02\ ^{+0.05}_{-0.03}\ ^{+0.02}_{-0.01}$	AAIJ 13H	LHCB	Repl. by AAIJ 14O

[1] Measurement is performed in $1.0 < q^2 < 6.0\ \mathrm{GeV}^2/c^4$. SIRUNYAN 18DX reports also measurements in several other q^2 intervals.
[2] AAIJ 14O reports 68% C.L. interval, which we encode as midpoint with uncertainty as half of the width of interval.

$A_{FB}(B^+ \to K^+\mu^+\mu^-)$ $(15.0 < q^2 < 22.0\ \mathrm{GeV}^2/c^4)$

VALUE	DOCUMENT ID	TECN	COMMENT
−0.015±0.015±0.01	[1] AAIJ 14O	LHCB	pp at 7, 8 TeV

[1] AAIJ 14O reports 68% C.L. interval, which we encode as midpoint with uncertainty as half of the width of interval.

$F_H(B^+ \to K^+\mu^+\mu^-)$ $(1.1 < q^2 < 6.0\ \mathrm{GeV}^2/c^4)$

F_H is a fractional contribution of (pseudo) scalar and tensor amplitudes to the decay width in the massless muon approximation.

VALUE	DOCUMENT ID	TECN	COMMENT
0.04±0.04 OUR AVERAGE			
$0.38\ ^{+0.17}_{-0.21} \pm 0.09$	[1] SIRUNYAN 18DX	CMS	pp at 8 TeV
$0.03 \pm 0.03 \pm 0.02$	[2] AAIJ 14O	LHCB	pp at 7, 8 TeV
• • • We do not use the following data for averages, fits, limits, etc. • • •			
$0.05\ ^{+0.08}_{-0.05}\ ^{+0.04}_{-0.02}$	AAIJ 13H	LHCB	Repl. by AAIJ 14O

[1] Measurement is performed in $1.0 < q^2 < 6.0$ GeV^2/c^4. SIRUNYAN 18DX reports also measurements in several other q^2 intervals.
[2] AAIJ 14O reports 68% C.L. interval, which we encode as midpoint with uncertainty as half of the width of interval.

$F_H(B^+ \to K^+\mu^+\mu^-)$ ($15.0 < q^2 < 22.0$ GeV^2/c^4)

F_H is a fractional contribution of (pseudo) scalar and tensor amplitudes to the decay width in the massless muon approximation.

VALUE	DOCUMENT ID		TECN	COMMENT
0.035±0.035±0.02	[1] AAIJ	14O	LHCB	pp at 7, 8 TeV

[1] AAIJ 14O reports 68% C.L. interval, which we encode as midpoint with uncertainty as half of the width of interval.

FORWARD-BACKWARD ASYMMETRIES

The forward-backward assymmetry is defined as A_{FB} = [N(q_{FB} > 0) − N(q_{FB} < 0)] / [N(q_{FB} > 0) + N(q_{FB} < 0)], where q_{FB} = − q_B · sgn(η_B) with q_B as the B hadron electric charge, η_B as its pseudorapidity, and sgn(η_B) as a sign function of η_B.

$A_{FB}(B^{\pm} \to J/\psi K^{\pm})$

VALUE (units 10^{-2})	DOCUMENT ID		TECN	COMMENT
−0.24±0.41±0.19	ABAZOV	15	D0	$p\overline{p}$ at 1.96 TeV

A_{FB} in $B^+ \to \overline{D}^{*0} e^+ \nu_e$

VALUE	DOCUMENT ID		TECN	COMMENT
0.234±0.026±0.006	PRIM	23	BELL	$e^+e^- \to \Upsilon(4S)$

A_{FB} in $B^+ \to \overline{D}^{*0} \mu^+ \nu_\mu$

VALUE	DOCUMENT ID		TECN	COMMENT
0.243±0.026±0.006	PRIM	23	BELL	$e^+e^- \to \Upsilon(4S)$

$\Delta(A_{FB}) = (A^{\mu}_{FB} - A^{e}_{FB})$ in $B^+ \to \overline{D}^{*0} \ell^+ \nu_\ell$

VALUE	DOCUMENT ID		TECN	COMMENT
0.008±0.037±0.009	PRIM	23	BELL	$e^+e^- \to \Upsilon(4S)$

$A_{FB}(B^{\pm} \to K^*(892)^+ \mu^+\mu^-)$ ($1.0 < q^2 < 8.68$ GeV^2/c^4)

VALUE	DOCUMENT ID		TECN	COMMENT
$-0.14^{+0.32}_{-0.35}\pm0.17$	[1,2] SIRUNYAN	21AC	CMS	pp at 8 TeV

[1] SIRUNYAN 21AC measurement is performed in $1.0 < q^2 < 8.68$ GeV^2/c^4. Reports also measurements in several other q^2 intervals.
[2] A_{FB} is defined with respect to $\mu^+\mu^-$ direction and not the B direction.

$A_{FB}(B^{\pm} \to K^*(892)^+ \mu^+\mu^-)$ ($1.1 < q^2 < 6.0$ GeV^2/c^4)

VALUE	DOCUMENT ID		TECN	COMMENT
$-0.08^{+0.07}_{-0.08}\pm0.02$	[1] AAIJ	21J	LHCB	pp at 7, 8, 13 TeV

[1] The full set of CP-averaged angular observables is measured as a function of the q^2. The A_{FB} is measured related to the dimuon system.

$A_{FB}(B^{\pm} \to K^*(892)^+ \mu^+\mu^-)$ ($10.09 < q^2 < 12.86$ GeV^2/c^4)

VALUE	DOCUMENT ID		TECN	COMMENT
$0.09^{+0.16}_{-0.11}\pm0.04$	[1,2] SIRUNYAN	21AC	CMS	pp at 8 TeV

[1] SIRUNYAN 21AC measurement is performed in $10.09 < q^2 < 12.86$ GeV^2/c^4. Reports also measurements in several other q^2 intervals.
[2] A_{FB} is defined with respect to $\mu^+\mu^-$ direction and not the B direction.

$A_{FB}(B^{\pm} \to K^*(892)^+ \mu^+\mu^-)$ ($14.18 < q^2 < 19.0$ GeV^2/c^4)

VALUE	DOCUMENT ID		TECN	COMMENT
$0.33^{+0.11}_{-0.07}\pm0.05$	[1,2] SIRUNYAN	21AC	CMS	pp at 8 TeV

[1] SIRUNYAN 21AC measurement is performed in $14.18 < q^2 < 19.0$ GeV^2/c^4. Reports also measurements in several other q^2 intervals.
[2] A_{FB} is defined with respect to $\mu^+\mu^-$ direction and not the B direction.

$A_{FB}(B^{\pm} \to K^*(892)^+ \mu^+\mu^-)$ ($15.0 < q^2 < 19.0$ GeV^2/c^4)

VALUE	DOCUMENT ID		TECN	COMMENT
0.31±0.06±0.04	[1] AAIJ	21J	LHCB	pp at 7, 8, 13 TeV

[1] The full set of CP-averaged angular observables is measured as a function of the q^2. The A_{FB} is measured related to the dimuon system.

$A_P(B^+) = [\sigma(B^-) - \sigma(B^+)] / [\sigma(B^-) + \sigma(B^+)]$

Production asymmetries

VALUE (units 10^{-3})	DOCUMENT ID		TECN	COMMENT
−5.7±1.7 OUR AVERAGE				
−7.0±0.8±3.1	[1] AAIJ	23U	LHCB	pp at 13 TeV
−4.1±4.9±1.0	[2] AAIJ	17AP	LHCB	pp at 7 TeV
−5.3±3.1±1.0	[2] AAIJ	17AP	LHCB	pp at 8 TeV
−2.3±2.4±3.7	[3] AAIJ	17BF	LHCB	pp at 7 TeV
−7.4±1.5±3.2	[3] AAIJ	17BF	LHCB	pp at 8 TeV

[1] The second error includes the uncertainties from $A_{CP}(B^+ \to J/\psi K^+) = 0.0018 \pm 0.0030$.
[2] AAIJ 17AP uses $B^+ \to \overline{D}^0\pi^+$ decays with B^+ transverse momenta p_T and rapidities y in the region of $2 < p_T < 30$ GeV/c and $2.1 < y < 4.5$.
[3] AAIJ 17BF uses $B^+ \to J/\psi K^+$ decays with B^+ transverse momenta p_T and rapidities y in the region of $0 < p_T < 30$ GeV/c and $2.1 < y < 4.5$.

$B^{\pm}$ REFERENCES

AAIJ	25AT	PRL 135 261901	R. Aaij *et al.*	(LHCb Collab.)
AAIJ	25E	PRL 135 021802	R. Aaij *et al.*	(LHCb Collab.)
AAIJ	25F	PR D111 092009	R. Aaij *et al.*	(LHCb Collab.)
AAIJ	25I	PRL 134 101801	R. Aaij *et al.*	(LHCb Collab.)
AAIJ	25L	PRL 134 181803	R. Aaij *et al.*	(LHCb Collab.)
AAIJ	25P	PR D111 092008	R. Aaij *et al.*	(LHCb Collab.)
AAIJ	25Q	JHEP 2501 054	R. Aaij *et al.*	(LHCb Collab.)
AAIJ	25R	JHEP 2502 113	R. Aaij *et al.*	(LHCb Collab.)
AAIJ	25T	JHEP 2503 139	R. Aaij *et al.*	(LHCb Collab.)
AAIJ	25Y	JHEP 2507 198	R. Aaij *et al.*	(LHCb Collab.)
ABUMUSABH	25	PR D112 L051101	M. Abumusabh *et al.*	(BELLE and BELLE II Collabs.)
ADACHI	25G	PR D111 L071103	I. Adachi *et al.*	(BELLE and BELLE II Collab.)
ADACHI	25I	PR D111 112009	I. Adachi *et al.*	(BELLE II Collab.)
ADACHI	25X	PR D112 072002	I. Adachi *et al.*	(BELLE II Collab.)
ADACHI	25Y	PR D112 112009	I. Adachi *et al.*	(BELLE II Collab.)
ADACHI	25Z	JHEP 2509 024	I. Adachi *et al.*	(BELLE II Collab.)
LEES	25	PR D111 L031101	J.P. Lees *et al.*	(BABAR Collab.)
AAIJ	24AB	PRL 133 131902	R. Aaij *et al.*	(LHCb Collab.)
AAIJ	24F	JHEP 2402 032	R. Aaij *et al.*	(LHCb Collab.)
AAIJ	24H	JHEP 2402 118	R. Aaij *et al.*	(LHCb Collab.)
AAIJ	24T	JHEP 2408 132	R. Aaij	(LHCb Collab.)
AAIJ	24U	EPJ C84 206	R. Aaij *et al.*	(LHCb Collab.)
ADACHI	24	PR D109 012001	I. Adachi *et al.*	(BELLE II Collab.)
ADACHI	24B	PRL 132 211804	I. Adachi *et al.*	(BELLE II Collab.)
ADACHI	24D	PR D109 L111103	I. Adachi *et al.*	(BELLE II Collab.)
ADACHI	24E	PR D109 112006	I. Adachi *et al.*	(BELLE II Collab.)
ADACHI	24I	JHEP 2405 212	I. Adachi *et al.*	(BELLE II, BELLE Collab.)
ADACHI	24L	JHEP 2408 206	I. Adachi *et al.*	(BELLE II Collab.)
ADACHI	24N	PRL 133 101804	I. Adachi *et al.*	(BELLE and BELLE II Collab.)
ADACHI	24T	JHEP 2410 143	I. Adachi *et al.*	(BELLE II Collab.)
GU	24	PRL 133 071802	T. Gu *et al.*	(BELLE Collab.)
AAIJ	23AB	PRL 131 051803	R. Aaij *et al.*	(LHCb Collab.)
Also		PR D108 032002	R. Aaij *et al.*	(LHCb Collab.)
AAIJ	23AH	PR D108 032010	R. Aaij *et al.*	(LHCb Collab.)
AAIJ	23AI	PR D108 034012	R. Aaij *et al.*	(LHCb Collab.)
AAIJ	23AK	JHEP 2308 174	R. Aaij *et al.*	(LHCb Collab.)
Also		JHEP 2308 174	R. Aaij *et al.*	(LHCb Collab.)
AAIJ	23AR	PRL 131 111802	R. Aaij *et al.*	(LHCb Collab.)
AAIJ	23AX	JHEP 2309 202	R. Aaij *et al.*	(LHCb Collab.)
AAIJ	23B	PR D108 012017	R. Aaij *et al.*	(LHCb Collab.)
AAIJ	23BA	JHEP 2312 013	R. Aaij *et al.*	(LHCb Collab.)
AAIJ	23I	JHEP 2307 138	R. Aaij *et al.*	(LHCb Collab.)
AAIJ	23N	EPJ C83 547	R. Aaij *et al.*	(LHCb Collab.)
Also		EPJ C83 672 (errat.)	R. Aaij *et al.*	(LHCb Collab.)
AAIJ	23Q	PRL 131 031901	R. Aaij *et al.*	(LHCb Collab.)
AAIJ	23U	PR D108 012008	R. Aaij *et al.*	(LHCb Collab.)
AAIJ	23V	PR D108 012013	R. Aaij *et al.*	(LHCb Collab.)
AAIJ	23X	PR D108 012020	R. Aaij *et al.*	(LHCb Collab.)
ADACHI	23L	JHEP 2309 146	I. Adachi *et al.*	(BELLE II Collab.)
CHU	23	PR D108 112007	K.-N. Chu *et al.*	(BELLE Collab.)
HSU	23	PR D107 032013	C.-L. Hsu *et al.*	(BELLE Collab.)
KUMAR	23	PR D107 L031101	M. Kumar *et al.*	(BELLE Collab.)
LAI	23	PRL 130 181804	Y.-T. Lai *et al.*	(BELLE Collab.)
LEES	23C	PRL 131 201801	J.P. Lees *et al.*	(BABAR Collab.)
MEIER	23	PR D107 092003	F. Meier *et al.*	(BELLE Collab.)
PRIM	23	PR D108 012002	M.T. Prim *et al.*	(BELLE Collab.)
WATANUKI	23	PRL 130 261802	S. Watanuki *et al.*	(BELLE Collab.)
AAIJ	22D	JHEP 2204 046	R. Aaij *et al.*	(LHCb Collab.)
AAIJ	22J	PRL 128 191802	R. Aaij *et al.*	(LHCb Collab.)
AAIJ	22T	JHEP 2207 099	R. Aaij *et al.*	(LHCb Collab.)
AAIJ	22V	NATP 18 277	R. Aaij *et al.*	(LHCb Collab.)
ABUDINEN	22	JHEP 2202 063	F. Abudinen *et al.*	(BELLE and BELLE II Collab.)
BLOOMFIELD	22	PR D105 072007	T. Bloomfield *et al.*	(BELLE Collab.)
GEBAUER	22	PR D106 032013	U. Gebauer *et al.*	(BELLE Collab.)
AAIJ	21AM	JHEP 2112 141	R. Aaij *et al.*	(LHCb Collab.)
AAIJ	21H	PRL 126 091802	R. Aaij *et al.*	(LHCb Collab.)
AAIJ	21J	PRL 126 161802	R. Aaij *et al.*	(LHCb Collab.)
AAIJ	21L	JHEP 2102 169	R. Aaij *et al.*	(LHCb Collab.)
AAIJ	21M	JHEP 2103 137	R. Aaij *et al.*	(LHCb Collab.)
AAIJ	21Q	JHEP 2104 081	R. Aaij *et al.*	(LHCb Collab.)
ABUDINEN	21	PRL 127 181802	F. Abudinen *et al.*	(BELLE II Collab.)
BELENO	21	PR D103 112001	C. Beleno *et al.*	(BELLE Collab.)
CAO	21A	PR D104 012008	L. Cao *et al.*	(BELLE Collab.)
CHOUDHURY	21	JHEP 2103 105	S. Choudhury *et al.*	(BELLE Collab.)
MOHANTY	21	PR D103 052013	S. Mohanty *et al.*	(BELLE Collab.)
SIRUNYAN	21AC	JHEP 2104 124	A.M. Sirunyan *et al.*	(CMS Collab.)
WEHLE	21	PRL 126 161801	S. Wehle *et al.*	(BELLE Collab.)
AAIJ	20A	PRL 124 031801	R. Aaij *et al.*	(LHCb Collab.)
Also		PR D101 012006	R. Aaij *et al.*	(LHCb Collab.)
AAIJ	20AI	PR D102 112003	R. Aaij *et al.*	(LHCb Collab.)
AAIJ	20AJ	PR D102 112010	R. Aaij *et al.*	(LHCb Collab.)
AAIJ	20AN	JHEP 2012 139	R. Aaij *et al.*	(LHCb Collab.)
AAIJ	20D	PR D101 032005	R. Aaij *et al.*	(LHCb Collab.)
AAIJ	20K	JHEP 2003 146	R. Aaij *et al.*	(LHCb Collab.)
AAIJ	20N	JHEP 2006 058	R. Aaij *et al.*	(LHCb Collab.)
AAIJ	20P	JHEP 2006 129	R. Aaij *et al.*	(LHCb Collab.)
AAIJ	20S	JHEP 2008 123	R. Aaij *et al.*	(LHCb Collab.)
CHILIKIN	20	JHEP 2005 034	K. Chilikin *et al.*	(BELLE Collab.)
CHU	20	PR D101 052012	K. Chu *et al.*	(BELLE Collab.)
LEES	20C	PRL 124 152001	J.P. Lees *et al.*	(BABAR Collab.)
PRIM	20	PR D101 032007	M.T. Prim *et al.*	(BELLE Collab.)
AAIJ	19AC	PR D99 092009	R. Aaij *et al.*	(LHCb Collab.)
AAIJ	19AL	PRL 123 231802	R. Aaij *et al.*	(LHCb Collab.)
AAIJ	19AM	PRL 123 241802	R. Aaij *et al.*	(LHCb Collab.)
AAIJ	19O	EPJ C79 537	R. Aaij *et al.*	(LHCb Collab.)
AAIJ	19P	EPJ C79 675	R. Aaij *et al.*	(LHCb Collab.)
AAIJ	19S	PRL 122 191801	R. Aaij *et al.*	(LHCb Collab.)
BHARDWAJ	19	PR D99 111101	V. Bhardwaj *et al.*	(BELLE Collab.)
CHILIKIN	19	PR D100 012001	K. Chilikin *et al.*	(BELLE Collab.)
GARG	19	PR D99 071102	R. Garg *et al.*	(BELLE Collab.)
KALIYAR	19	PR D99 031102	A.B. Kaliyar *et al.*	(BELLE Collab.)
LEES	19C	PR D100 111101	J.P. Lees *et al.*	(BABAR Collab.)
LI	19A	PRL 122 082001	Y.B. Li *et al.*	(BELLE Collab.)
LI	19G	PR D100 112010	Y. Li *et al.*	(BELLE Collab.)
LU	19	PR D99 032003	P.-C. Lu *et al.*	(BELLE Collab.)
PDG	19	RPP 2019 at pdg.lbl.gov	M. Tanabashi *et al.*	(PDG Collab.)
RESMI	19	JHEP 1910 178	P.K. Resmi *et al.*	(BELLE Collab.)
SIRUNYAN	19CM	JHEP 1912 100	A.M. Sirunyan *et al.*	(CMS Collab.)
WATANUKI	19	PR D99 032012	S. Watanuki *et al.*	(BELLE Collab.)
AAIJ	18A	PL B777 16	R. Aaij *et al.*	(LHCb Collab.)
AAIJ	18AD	JHEP 1808 176	R. Aaij *et al.*	(LHCb Collab.)
Also		JHEP 1810 107 (errat.)	R. Aaij *et al.*	(LHCb Collab.)
AAIJ	18B	JHEP 1801 131	R. Aaij *et al.*	(LHCb Collab.)
AAIJ	18U	JHEP 1803 059	R. Aaij *et al.*	(LHCb Collab.)
AAIJ	18W	JHEP 1805 160	R. Aaij *et al.*	(LHCb Collab.)
AAIJ	18X	JHEP 1805 067	R. Aaij *et al.*	(LHCb Collab.)
AAIJ	18Z	JHEP 1806 084	R. Aaij *et al.*	(LHCb Collab.)
GELB	18	PR D98 112016	M. Gelb *et al.*	(BELLE Collab.)
KATO	18	PR D97 012005	Y. Kato *et al.*	(BELLE Collab.)
LI	18A	EPJ C78 252	Y.B. Li *et al.*	(BELLE Collab.)

Int. J. Mod. Phys. A 2026.41. Downloaded from www.worldscientific.com
by LIFORNIA @ BERKELEY on 09/16/26. Re-use and distribution is strictly not permitted, except for Open Access articles.

Int. J. Mod. Phys. A 2026.41. Downloaded from www.worldscientific.com
by UNIVERSITY OF CALIFORNIA @ BERKELEY on 09/16/26. Re-use and distribution is strictly not permitted, except for Open Access articles.

PDG	18	PR D98 030001	M. Tanabashi *et al.*	(PDG Collab.)
RESMI	18	JHEP 1801 082	P.K. Resmi *et al.*	
SIBIDANOV	18	PRL 121 031801	A. Sibidanov *et al.*	(BELLE Collab.)
SIRUNYAN	18DX	PR D98 112011	A.M. Sirunyan *et al.*	(CMS Collab.)
VOSSEN	18	PR D98 012005	A. Vossen *et al.*	(BELLE Collab.)
AAIJ	17	PR D95 012002	R. Aaij *et al.*	(LHCb Collab.)
AAIJ	17AD	PL B769 305	R. Aaij *et al.*	(LHCb Collab.)
AAIJ	17AP	PR D95 052005	R. Aaij *et al.*	(LHCb Collab.)
AAIJ	17AQ	PR D95 071101	R. Aaij *et al.*	(LHCb Collab.)
AAIJ	17AR	PR D96 011101	R. Aaij *et al.*	(LHCb Collab.)
AAIJ	17BF	PL B774 139	R. Aaij *et al.*	(LHCb Collab.)
AAIJ	17BO	JHEP 1711 156	R. Aaij *et al.*	(LHCb Collab.)
AAIJ	17E	PL B765 307	R. Aaij *et al.*	(LHCb Collab.)
AAIJ	17K	EPJ C77 72	R. Aaij *et al.*	(LHCb Collab.)
AAIJ	17O	JHEP 1703 036	R. Aaij *et al.*	(LHCb Collab.)
AAIJ	17R	JHEP 1704 162	R. Aaij *et al.*	(LHCb Collab.)
AAIJ	17Y	EPJ C77 161	R. Aaij *et al.*	(LHCb Collab.)
ABAZOV	17A	PR D95 031101	V.M. Abazov *et al.*	(D0 Collab.)
BELENO	17	PR D96 091102	C. Beleno *et al.*	(BELLE Collab.)
GRYGIER	17	PR D96 091101	J. Grygier *et al.*	(BELLE Collab.)
HORIGUCHI	17	PRL 119 191802	T. Horiguchi *et al.*	(BELLE Collab.)
HSU	17	PR D96 031101	C.-L. Hsu *et al.*	(BELLE Collab.)
KHACHATRY...	17C	PL B764 66	V. Khachatryan *et al.*	(CMS Collab.)
LEES	17	PRL 118 031802	J.P. Lees *et al.*	(BABAR Collab.)
LEES	17G	PR D96 072001	J.P. Lees *et al.*	(BABAR Collab.)
AABOUD	16L	EPJ C76 513	M. Aaboud *et al.*	(ATLAS Collab.)
AAIJ	16AA	JHEP 1608 137	R. Aaij *et al.*	(LHCb Collab.)
AAIJ	16AH	PR D94 072001	R. Aaij *et al.*	(LHCb Collab.)
AAIJ	16AQ	JHEP 1612 087	R. Aaij *et al.*	(LHCb Collab.)
AAIJ	16L	PL B760 117	R. Aaij *et al.*	(LHCb Collab.)
AAIJ	16M	PR D93 051101	R. Aaij *et al.*	(LHCb Collab.)
AAIJ	16R	PR D93 119902	R. Aaij *et al.*	(LHCb Collab.)
AAIJ	16Z	JHEP 1606 131	R. Aaij *et al.*	(LHCb Collab.)
BHARDWAJ	16	PR D93 052016	V. Bhardwaj *et al.*	(BELLE Collab.)
DEL-AMO-SA...	16	PR D93 052013	P. del Amo Sanchez *et al.*	(BABAR Collab.)
LEES	16	PRL 116 041801	J.P. Lees *et al.*	(BABAR Collab.)
PDG	16	CP C40 100001	C. Patrignani *et al.*	(PDG Collab.)
AAIJ	15AR	JHEP 1510 034	R. Aaij *et al.*	(LHCb Collab.)
AAIJ	15BC	PR D92 112005	R. Aaij *et al.*	(LHCb Collab.)
AAIJ	15K	PL B741 1	R. Aaij *et al.*	(LHCb Collab.)
AAIJ	15O	PRL 115 051801	R. Aaij *et al.*	(LHCb Collab.)
AAIJ	15V	PR D91 092002	R. Aaij *et al.*	(LHCb Collab.)
Also		PR D93 119901 (errat.)	R. Aaij *et al.*	(LHCb Collab.)
AAIJ	15W	PR D91 112014	R. Aaij *et al.*	(LHCb Collab.)
ABAZOV	15	PRL 114 051803	V.M. Abazov *et al.*	(D0 Collab.)
BALA	15	PR D91 051101	A. Bala *et al.*	(BELLE Collab.)
CHOI	15A	PR D91 092011	S.-K. Choi *et al.*	(BELLE Collab.)
GOH	15	PR D91 071101	Y.M. Goh *et al.*	(BELLE Collab.)
HELLER	15	PR D91 112009	A. Heller *et al.*	(BELLE Collab.)
KRONENBIT...	15	PR D92 051102	B. Kronenbitter *et al.*	(BELLE Collab.)
LEES	15	PR D91 012003	J.P. Lees *et al.*	(BABAR Collab.)
LEES	15C	PR D91 052002	J.P. Lees *et al.*	(BABAR Collab.)
VINOKUROVA	15	JHEP 1506 132	A. Vinokurova *et al.*	(BELLE Collab.)
Also		JHEP 1702 088 (errat.)	A. Vinokurava *et al.*	(BELLE Collab.)
WIECHCZYN...	15	PR D91 032008	J. Wiechczynski *et al.*	(BELLE Collab.)
YOOK	15	PR D91 052016	Y. Yook *et al.*	(BELLE Collab.)
AAIJ	14	PRL 112 011801	R. Aaij *et al.*	(LHCb Collab.)
AAIJ	14A	PL B728 85	R. Aaij *et al.*	(LHCb Collab.)
AAIJ	14AC	PRL 112 131802	R. Aaij *et al.*	(LHCb Collab.)
AAIJ	14AF	PRL 113 141801	R. Aaij *et al.*	(LHCb Collab.)
Also		PRL 134 179901 (errat.)	R. Aaij *et al.*	(LHCb Collab.)
AAIJ	14AN	JHEP 1409 177	R. Aaij *et al.*	(LHCb Collab.)
AAIJ	14AR	PRL 113 151601	R. Aaij *et al.*	(LHCb Collab.)
AAIJ	14AZ	JHEP 1410 064	R. Aaij *et al.*	(LHCb Collab.)
AAIJ	14BA	JHEP 1410 097	R. Aaij *et al.*	(LHCb Collab.)
AAIJ	14BE	NP B888 169	R. Aaij *et al.*	(LHCb Collab.)
AAIJ	14BF	JHEP 1411 060	R. Aaij *et al.*	(LHCb Collab.)
AAIJ	14BO	PR D90 112004	R. Aaij *et al.*	(LHCb Collab.)
AAIJ	14E	JHEP 1404 114	R. Aaij *et al.*	(LHCb Collab.)
AAIJ	14M	JHEP 1406 133	R. Aaij *et al.*	(LHCb Collab.)
AAIJ	14O	JHEP 1405 082	R. Aaij *et al.*	(LHCb Collab.)
AAIJ	14V	PL B733 36	R. Aaij *et al.*	(LHCb Collab.)
ABAZOV	14A	PR D89 012004	V.M. Abazov *et al.*	(D0 Collab.)
CHOBANOVA	14	PR D90 012002	V. Chobanova *et al.*	(BELLE Collab.)
IWASHITA	14	PTEP 2014 043C01	T. Iwashita *et al.*	(BELLE Collab.)
LEES	14A	PR D89 011102	J.P. Lees *et al.*	(BABAR Collab.)
TIEN	14	PR D89 011101	K.-J. Tien *et al.*	(BELLE Collab.)
AAIJ	13AE	PL B723 44	R. Aaij *et al.*	(LHCb Collab.)
AAIJ	13AK	PL B726 151	R. Aaij *et al.*	(LHCb Collab.)
AAIJ	13AP	PR D87 092007	R. Aaij *et al.*	(LHCb Collab.)
AAIJ	13AR	PR D87 112010	R. Aaij *et al.*	(LHCb Collab.)
AAIJ	13AU	PR D88 052015	R. Aaij *et al.*	(LHCb Collab.)
AAIJ	13AZ	PRL 111 101801	R. Aaij *et al.*	(LHCb Collab.)
AAIJ	13BC	PRL 111 112003	R. Aaij *et al.*	(LHCb Collab.)
AAIJ	13BN	PRL 111 151801	R. Aaij *et al.*	(LHCb Collab.)
AAIJ	13BS	PL B726 646	R. Aaij *et al.*	(LHCb Collab.)
AAIJ	13H	JHEP 1302 105	R. Aaij *et al.*	(LHCb Collab.)
AAIJ	13R	JHEP 1302 043	R. Aaij *et al.*	(LHCb Collab.)
AAIJ	13S	EPJ C73 2462	R. Aaij *et al.*	(LHCb Collab.)
AAIJ	13Z	JHEP 1309 006	R. Aaij *et al.*	(LHCb Collab.)
ABAZOV	13M	PRL 110 241801	V.M. Abazov *et al.*	(D0 Collab.)
DUH	13	PR D87 031103	Y. T. Duh *et al.*	(BELLE Collab.)
HARA	13	PRL 110 131801	K. Hara *et al.*	(BELLE Collab.)
LEES	13A	PR D87 032004	J.P. Lees *et al.*	(BABAR Collab.)
LEES	13B	PR D87 052015	J.P. Lees *et al.*	(BABAR Collab.)
LEES	13I	PR D87 112005	J.P. Lees *et al.*	(BABAR Collab.)
LEES	13K	PR D88 031102	J.P. Lees *et al.*	(BABAR Collab.)
LEES	13M	PR D88 032012	J.P. Lees *et al.*	(BABAR Collab.)
LEES	13T	PR D88 072006	J.P. Lees *et al.*	(BABAR Collab.)
LUTZ	13	PR D87 111103	O. Lutz *et al.*	(BELLE Collab.)
NAYAK	13	PR D88 091104	M. Nayak *et al.*	(BELLE Collab.)
SIBIDANOV	13	PR D88 032005	A. Sibidanov *et al.*	(BELLE Collab.)
AAIJ	12AA	PR D85 091103	R. Aaij *et al.*	(LHCb Collab.)
AAIJ	12AC	PR D85 091105	R. Aaij *et al.*	(LHCb Collab.)
AAIJ	12AD	PR D85 112004	R. Aaij *et al.*	(LHCb Collab.)
AAIJ	12AH	JHEP 1207 133	R. Aaij *et al.*	(LHCb Collab.)
AAIJ	12AQ	PL B718 43	R. Aaij *et al.*	(LHCb Collab.)
AAIJ	12AY	JHEP 1212 125	R. Aaij *et al.*	(LHCb Collab.)
AAIJ	12C	PRL 108 101601	R. Aaij *et al.*	(LHCb Collab.)
AAIJ	12E	PL B708 241	R. Aaij *et al.*	(LHCb Collab.)
AAIJ	12L	EPJ C72 2118	R. Aaij *et al.*	(LHCb Collab.)
AAIJ	12M	PL B712 203	R. Aaij *et al.*	(LHCb Collab.)
Also		PL B713 351 (errat.)	R. Aaij *et al.*	(LHCb Collab.)
AAIJ	12T	PRL 108 161801	R. Aaij *et al.*	(LHCb Collab.)
AIHARA	12	PR D85 112014	H. Aihara *et al.*	(BELLE Collab.)
DEL-AMO-SA...	12	PR D85 092017	P. del Amo Sanchez *et al.*	(BABAR Collab.)
HOI	12	PRL 108 031801	C.-T. Hoi *et al.*	(BELLE Collab.)
KIM	12A	PR D86 031101	J.H. Kim *et al.*	(BELLE Collab.)
LEES	12AA	PR D86 092004	J.P. Lees *et al.*	(BABAR Collab.)
LEES	12B	PR D85 052003	J.P. Lees *et al.*	(BABAR Collab.)
LEES	12D	PRL 109 101802	J.P. Lees *et al.*	(BABAR Collab.)
Also		PR D88 072012	J.P. Lees *et al.*	(BABAR Collab.)
LEES	12J	PR D85 071103	J.P. Lees *et al.*	(BABAR Collab.)
LEES	12O	PR D85 112010	J.P. Lees *et al.*	(BABAR Collab.)
LEES	12P	PR D86 012004	J.P. Lees *et al.*	(BABAR Collab.)
LEES	12S	PR D86 032012	J.P. Lees *et al.*	(BABAR Collab.)
LEES	12Z	PR D86 091102	J.P. Lees *et al.*	(BABAR Collab.)
PDG	12	PR D86 010001	J. Beringer *et al.*	(PDG Collab.)
STYPULA	12	PR D86 072007	J. Stypula *et al.*	(BELLE Collab.)
AAIJ	11E	PR D84 092001	R. Aaij *et al.*	(LHCb Collab.)
Also		PR D85 039904 (errat.)	R. Aaij *et al.*	(LHCb Collab.)
AALTONEN	11	PRL 106 121804	T. Aaltonen *et al.*	(CDF Collab.)
AALTONEN	11AI	PRL 107 201802	T. Aaltonen *et al.*	(CDF Collab.)
AALTONEN	11AJ	PR D84 091504	T. Aaltonen *et al.*	(CDF Collab.)
AALTONEN	11B	PR D83 032008	T. Aaltonen *et al.*	(CDF Collab.)
AALTONEN	11L	PRL 106 161801	T. Aaltonen *et al.*	(CDF Collab.)
AUSHEV	11	PR D83 051102	T. Aushev *et al.*	(BELLE Collab.)
BHARDWAJ	11	PRL 107 091803	V. Bhardwaj *et al.*	(BELLE Collab.)
CHEN	11F	PR D84 071501	P. Chen *et al.*	(BELLE Collab.)
CHOI	11	PR D84 052004	S.-K. Choi *et al.*	(BELLE Collab.)
DEL-AMO-SA...	11B	PR D83 032004	P. del Amo Sanchez *et al.*	(BABAR Collab.)
DEL-AMO-SA...	11C	PR D83 032007	P. del Amo Sanchez *et al.*	(BABAR Collab.)
DEL-AMO-SA...	11D	PR D83 051101	P. del Amo Sanchez *et al.*	(BABAR Collab.)
DEL-AMO-SA...	11F	PR D83 052011	P. del Amo Sanchez *et al.*	(BABAR Collab.)
DEL-AMO-SA...	11K	PR D83 091101	P. del Amo Sanchez *et al.*	(BABAR Collab.)
DEL-AMO-SA...	11L	PRL 107 041804	P. del Amo Sanchez *et al.*	(BABAR Collab.)
GULER	11	PR D83 032005	H. Guler *et al.*	(BELLE Collab.)
HORII	11	PRL 106 231803	Y. Horii *et al.*	(BELLE Collab.)
LEES	11A	PR D84 012001	J.P. Lees *et al.*	(BABAR Collab.)
LEES	11D	PR D84 012002	J.P. Lees *et al.*	(BABAR Collab.)
LEES	11I	PR D84 092007	J.P. Lees *et al.*	(BABAR Collab.)
SAHOO	11A	PR D84 071101	H. Sahoo *et al.*	(BELLE Collab.)
SEON	11	PR D84 071106	O. Seon *et al.*	(BELLE Collab.)
VINOKUROVA	11	PL B706 139	A. Vinokurova *et al.*	(BELLE Collab.)
AALTONEN	10A	PR D81 031105	T. Aaltonen *et al.*	(CDF Collab.)
AUBERT	10	PRL 104 011802	B. Aubert *et al.*	(BABAR Collab.)
AUBERT	10D	PR D81 052009	B. Aubert *et al.*	(BABAR Collab.)
AUBERT	10E	PR D81 051101	B. Aubert *et al.*	(BABAR Collab.)
BOZEK	10	PR D82 072005	A. BOZEK *et al.*	(BELLE Collab.)
DEL-AMO-SA...	10A	PR D82 011502	P. del Amo Sanchez *et al.*	(BABAR Collab.)
DEL-AMO-SA...	10B	PR D82 011101	P. del Amo Sanchez *et al.*	(BABAR Collab.)
DEL-AMO-SA...	10F	PRL 105 121801	P. del Amo Sanchez *et al.*	(BABAR Collab.)
DEL-AMO-SA...	10G	PR D82 072004	P. del Amo Sanchez *et al.*	(BABAR Collab.)
DEL-AMO-SA...	10H	PR D82 072006	P. del Amo Sanchez *et al.*	(BABAR Collab.)
DEL-AMO-SA...	10I	PR D82 091101	P. del Amo Sanchez *et al.*	(BABAR Collab.)
DEL-AMO-SA...	10K	PR D82 092006	P. del Amo Sanchez *et al.*	(BABAR Collab.)
DEL-AMO-SA...	10Q	PR D82 112002	P. del Amo Sanchez *et al.*	(BABAR Collab.)
HARA	10	PR D82 071101	K. Hara *et al.*	(BELLE Collab.)
LIBBY	10	PR D82 112006	J. Libby *et al.*	(CLEO Collab.)
POLUEKTOV	10	PR D81 112002	A. Poluektov *et al.*	(BELLE Collab.)
SAKAI	10	PR D82 091104	K. Sakai *et al.*	(BELLE Collab.)
WEDD	10	PR D81 111104	R. Wedd *et al.*	(BELLE Collab.)
AALTONEN	09B	PR D79 011104	T. Aaltonen *et al.*	(CDF Collab.)
ABAZOV	09Y	PR D79 111102	V.M. Abazov *et al.*	(D0 Collab.)
ABULENCIA	09	PR D79 112003	A. Abulencia *et al.*	(CDF Collab.)
AUBERT	09	PR D79 011102	B. Aubert *et al.*	(BABAR Collab.)
AUBERT	09A	PR D79 012002	B. Aubert *et al.*	(BABAR Collab.)
AUBERT	09AA	PR D79 112001	B. Aubert *et al.*	(BABAR Collab.)
AUBERT	09AB	PR D79 112004	B. Aubert *et al.*	(BABAR Collab.)
AUBERT	09AF	PR D80 051101	B. Aubert *et al.*	(BABAR Collab.)
AUBERT	09AJ	PR D80 092001	B. Aubert *et al.*	(BABAR Collab.)
AUBERT	09AO	PRL 103 211802	B. Aubert *et al.*	(BABAR Collab.)
AUBERT	09AT	PR D80 111105	B. Aubert *et al.*	(BABAR Collab.)
AUBERT	09AV	PR D80 112002	B. Aubert *et al.*	(BABAR Collab.)
AUBERT	09B	PRL 102 132001	B. Aubert *et al.*	(BABAR Collab.)
AUBERT	09F	PR D79 051102	B. Aubert *et al.*	(BABAR Collab.)
AUBERT	09G	PRL 102 141802	B. Aubert *et al.*	(BABAR Collab.)
AUBERT	09H	PR D79 052005	B. Aubert *et al.*	(BABAR Collab.)
AUBERT	09J	PR D79 051101	B. Aubert *et al.*	(BABAR Collab.)
AUBERT	09L	PR D79 072006	B. Aubert *et al.*	(BABAR Collab.)
AUBERT	09Q	PR D79 052011	B. Aubert *et al.*	(BABAR Collab.)
AUBERT	09R	PR D79 072003	B. Aubert *et al.*	(BABAR Collab.)
AUBERT	09S	PR D79 092002	B. Aubert *et al.*	(BABAR Collab.)
AUBERT	09T	PRL 102 091803	B. Aubert *et al.*	(BABAR Collab.)
Also		EPAPS Document No. E-PRLTAO-102-060910		(BABAR Collab.)
AUBERT	09V	PR D79 091101	B. Aubert *et al.*	(BABAR Collab.)
AUBERT	09Y	PRL 103 051803	B. Aubert *et al.*	(BABAR Collab.)
CHANG	09	PR D79 052006	Y.-W. Chang *et al.*	(BELLE Collab.)
CHEN	09C	PR D80 111103	P. Chen *et al.*	(BELLE Collab.)
LIU	09	PR D79 071102	C. Liu *et al.*	(BELLE Collab.)
WEI	09A	PRL 103 171801	J.-T. Wei *et al.*	(BELLE Collab.)
Also		EPAPS Supplement	J.-T. Wei *et al.*	(BELLE Collab.)
WIECHCZYN...	09	PR D80 052005	J. Wiechczynski *et al.*	(BELLE Collab.)
ABAZOV	08O	PRL 100 211802	V.M. Abazov *et al.*	(D0 Collab.)
ADACHI	08	PR D77 091101	I. Adachi *et al.*	(BELLE Collab.)
AUBERT	08A	PR D77 011101	B. Aubert *et al.*	(BABAR Collab.)
AUBERT	08AA	PR D77 111102	B. Aubert *et al.*	(BABAR Collab.)
AUBERT	08AB	PR D78 012006	B. Aubert *et al.*	(BABAR Collab.)
AUBERT	08AD	PR D77 091104	B. Aubert *et al.*	(BABAR Collab.)
AUBERT	08AG	PR D78 011104	B. Aubert *et al.*	(BABAR Collab.)
AUBERT	08AH	PR D78 011107	B. Aubert *et al.*	(BABAR Collab.)
AUBERT	08AI	PR D78 012004	B. Aubert *et al.*	(BABAR Collab.)
AUBERT	08AL	PR D78 034023	B. Aubert *et al.*	(BABAR Collab.)
AUBERT	08AT	PRL 100 231803	B. Aubert *et al.*	(BABAR Collab.)
AUBERT	08AV	PRL 101 081801	B. Aubert *et al.*	(BABAR Collab.)
AUBERT	08B	PR D77 011102	B. Aubert *et al.*	(BABAR Collab.)
AUBERT	08BC	PR D78 072007	B. Aubert *et al.*	(BABAR Collab.)
AUBERT	08BD	PR D78 091101	B. Aubert *et al.*	(BABAR Collab.)
AUBERT	08BE	PR D78 091102	B. Aubert *et al.*	(BABAR Collab.)
AUBERT	08BF	PR D78 092002	B. Aubert *et al.*	(BABAR Collab.)
AUBERT	08BH	PR D78 112001	B. Aubert *et al.*	(BABAR Collab.)
AUBERT	08BI	PRL 101 161801	B. Aubert *et al.*	(BABAR Collab.)
AUBERT	08BK	PRL 101 201801	B. Aubert *et al.*	(BABAR Collab.)
AUBERT	08BL	PRL 101 261802	B. Aubert *et al.*	(BABAR Collab.)
AUBERT	08BN	PR D78 112003	B. Aubert *et al.*	(BABAR Collab.)
AUBERT	08D	PR D77 011107	B. Aubert *et al.*	(BABAR Collab.)
AUBERT	08F	PRL 100 051803	B. Aubert *et al.*	(BABAR Collab.)
AUBERT	08G	PRL 100 171803	B. Aubert *et al.*	(BABAR Collab.)
AUBERT	08H	PR D77 031101	B. Aubert *et al.*	(BABAR Collab.)
AUBERT	08N	PRL 100 021801	B. Aubert *et al.*	(BABAR Collab.)
Also		PR D79 092002	B. Aubert *et al.*	(BABAR Collab.)
AUBERT	08Q	PRL 100 151802	B. Aubert *et al.*	(BABAR Collab.)
AUBERT	08W	PRL 101 082001	B. Aubert *et al.*	(BABAR Collab.)
AUBERT	08X	PRL 101 091801	B. Aubert *et al.*	(BABAR Collab.)
AUBERT	08Y	PR D77 111101	B. Aubert *et al.*	(BABAR Collab.)
BHARDWAJ	08	PR D78 051104	V. Bhardwaj *et al.*	(BELLE Collab.)
BRODZICKA	08	PRL 100 092001	J. Brodzicka *et al.*	(BELLE Collab.)
CHEN	08C	PRL 100 251801	J.-H. Chen *et al.*	(BELLE Collab.)
HORII	08	PR D78 071901	Y. Horii *et al.*	(BELLE Collab.)
IWABUCHI	08	PRL 101 041601	M. Iwabuchi *et al.*	(BELLE Collab.)
LIN	08	NAT 452 332	S.-W. Lin *et al.*	(BELLE Collab.)
LIVENTSEV	08	PR D77 091503	D. Liventsev *et al.*	(BELLE Collab.)
PDG	08	PL B667 1	C. Amsler *et al.*	(PDG Collab.)
TANIGUCHI	08	PRL 101 111801	N. Taniguchi *et al.*	(BELLE Collab.)

Int. J. Mod. Phys. A 2026.41. Downloaded from www.worldscientific.com
by [redacted] LIFORNIA @ BERKELEY on 09/16/26. Re-use and distribution is strictly not permitted, except for Open Access articles.

WEI	08	PL B659 80	J.-T. Wei *et al.*	(BELLE Collab.)
WEI	08A	PR D78 011101	J.-T. Wei *et al.*	(BELLE Collab.)
WICHT	08	PL B662 323	J. Wicht *et al.*	(BELLE Collab.)
ADAM	07	PRL 99 041802	N.E. Adam *et al.*	(CLEO Collab.)
Also		PR D76 012007	D.M. Asner *et al.*	(CLEO Collab.)
AUBERT	07AC	PR D76 031101	B. Aubert *et al.*	(BABAR Collab.)
AUBERT	07AE	PR D76 031103	B. Aubert *et al.*	(BABAR Collab.)
AUBERT	07AG	PRL 99 051801	B. Aubert *et al.*	(BABAR Collab.)
AUBERT	07AL	PR D76 052002	B. Aubert *et al.*	(BABAR Collab.)
AUBERT	07AN	PR D76 051101	B. Aubert *et al.*	(BABAR Collab.)
AUBERT	07AR	PR D76 071103	B. Aubert *et al.*	(BABAR Collab.)
AUBERT	07AV	PR D76 092004	B. Aubert *et al.*	(BABAR Collab.)
AUBERT	07AZ	PRL 99 201801	B. Aubert *et al.*	(BABAR Collab.)
AUBERT	07BA	PRL 99 201802	B. Aubert *et al.*	(BABAR Collab.)
AUBERT	07BB	PRL 99 221801	B. Aubert *et al.*	(BABAR Collab.)
AUBERT	07BC	PR D76 091102	B. Aubert *et al.*	(BABAR Collab.)
AUBERT	07BI	PRL 99 241803	B. Aubert *et al.*	(BABAR Collab.)
AUBERT	07BJ	PRL 99 251801	B. Aubert *et al.*	(BABAR Collab.)
AUBERT	07BL	PRL 99 261801	B. Aubert *et al.*	(BABAR Collab.)
AUBERT	07BN	PR D76 111101	B. Aubert *et al.*	(BABAR Collab.)
AUBERT	07E	PRL 98 051802	B. Aubert *et al.*	(BABAR Collab.)
AUBERT	07H	PR D75 031101	B. Aubert *et al.*	(BABAR Collab.)
AUBERT	07L	PRL 98 151802	B. Aubert *et al.*	(BABAR Collab.)
AUBERT	07M	PRL 98 171801	B. Aubert *et al.*	(BABAR Collab.)
AUBERT	07N	PR D75 072002	B. Aubert *et al.*	(BABAR Collab.)
AUBERT	07Q	PR D75 051102	B. Aubert *et al.*	(BABAR Collab.)
AUBERT	07R	PRL 98 211804	B. Aubert *et al.*	(BABAR Collab.)
Also		PRL 100 189903E	B. Aubert *et al.*	(BABAR Collab.)
Also		PRL 100 199905E	B. Aubert *et al.*	(BABAR Collab.)
AUBERT	07X	PR D75 091103	B. Aubert *et al.*	(BABAR Collab.)
AUBERT	07Z	PR D76 011103	B. Aubert *et al.*	(BABAR Collab.)
CHANG	07B	PR D75 071104	P. Chang *et al.*	(BELLE Collab.)
CHEN	07D	PRL 99 221802	K.-F. Chen *et al.*	(BELLE Collab.)
HOKUUE	07	PL B648 139	T. Hokuue *et al.*	(BELLE Collab.)
LIN	07	PRL 98 181804	S.-W. Lin *et al.*	(BELLE Collab.)
LIN	07A	PRL 99 121601	S.-W. Lin *et al.*	(BELLE Collab.)
SATOYAMA	07	PL B647 67	N. Satoyama *et al.*	(BELLE Collab.)
SCHUEMANN	07	PR D75 092002	J. Schuemann *et al.*	(BELLE Collab.)
TSAI	07	PR D75 111101	Y.-T. Tsai *et al.*	(BELLE Collab.)
URQUIJO	07	PR D75 032001	P. Urquijo *et al.*	(BELLE Collab.)
WANG	07B	PR D75 092005	C.H. Wang *et al.*	(BELLE Collab.)
WANG	07C	PR D76 052004	M.-Z. Wang *et al.*	(BELLE Collab.)
XIE	07	PR D75 017101	Q.L. Xie *et al.*	(BELLE Collab.)
ABE	06	PR D73 051106	K. Abe *et al.*	(BELLE Collab.)
ABULENCIA	06J	PRL 96 191801	A. Abulencia *et al.*	(CDF Collab.)
ACOSTA	06	PRL 96 202001	D. Acosta *et al.*	(CDF Collab.)
AUBERT	06	PR D73 011101	B. Aubert *et al.*	(BABAR Collab.)
AUBERT	06E	PRL 96 052002	B. Aubert *et al.*	(BABAR Collab.)
AUBERT	06F	PR D73 011103	B. Aubert *et al.*	(BABAR Collab.)
AUBERT	06J	PR D73 051105	B. Aubert *et al.*	(BABAR Collab.)
AUBERT	06K	PR D73 057101	B. Aubert *et al.*	(BABAR Collab.)
AUBERT	06N	PR D74 031103	B. Aubert *et al.*	(BABAR Collab.)
AUBERT	06O	PR D74 032003	B. Aubert *et al.*	(BABAR Collab.)
AUBERT	06Z	PR D73 111104	B. Aubert *et al.*	(BABAR Collab.)
AUBERT,B	06A	PR D73 112004	B. Aubert *et al.*	(BABAR Collab.)
AUBERT,B	06C	PR D74 011102	B. Aubert *et al.*	(BABAR Collab.)
AUBERT,B	06E	PR D74 011106	B. Aubert *et al.*	(BABAR Collab.)
AUBERT,B	06G	PRL 97 201801	B. Aubert *et al.*	(BABAR Collab.)
AUBERT,B	06H	PRL 97 201802	B. Aubert *et al.*	(BABAR Collab.)
AUBERT,B	06J	PR D73 092001	B. Aubert *et al.*	(BABAR Collab.)
AUBERT,B	06M	PR D74 031102	B. Aubert *et al.*	(BABAR Collab.)
AUBERT,B	06P	PR D74 031105	B. Aubert *et al.*	(BABAR Collab.)
AUBERT,B	06T	PR D74 051102	B. Aubert *et al.*	(BABAR Collab.)
AUBERT,B	06U	PR D74 051104	B. Aubert *et al.*	(BABAR Collab.)
AUBERT,B	06Y	PR D74 091105	B. Aubert *et al.*	(BABAR Collab.)
AUBERT,BE	06A	PR D74 099903 (errat.)	B. Aubert *et al.*	(BABAR Collab.)
AUBERT,BE	06C	PRL 97 171805	B. Aubert *et al.*	(BABAR Collab.)
AUBERT,BE	06G	PRL 97 261801	B. Aubert *et al.*	(BABAR Collab.)
AUBERT,BE	06H	PRL 97 261803	B. Aubert *et al.*	(BABAR Collab.)
AUBERT,BE	06J	PR D74 111102	B. Aubert *et al.*	(BABAR Collab.)
AUBERT,BE	06M	PR D74 071101	B. Aubert *et al.*	(BABAR Collab.)
CHISTOV	06A	PR D74 111105	R. Chistov *et al.*	(BELLE Collab.)
FANG	06	PR D74 012007	F. Fang *et al.*	(BELLE Collab.)
GABYSHEV	06	PRL 97 202003	N. Gabyshev *et al.*	(BELLE Collab.)
GABYSHEV	06A	PRL 97 242001	N. Gabyshev *et al.*	(BELLE Collab.)
GARMASH	06	PRL 96 251803	A. Garmash *et al.*	(BELLE Collab.)
IKADO	06	PRL 97 251802	K. Ikado *et al.*	(BELLE Collab.)
JEN	06	PR D74 111101	C.-M. Jen *et al.*	(BELLE Collab.)
KUMAR	06	PR D74 051103	R. Kumar *et al.*	(BELLE Collab.)
MOHAPATRA	06	PRL 96 221601	D. Mohapatra *et al.*	(BELLE Collab.)
POLUEKTOV	06	PR D73 112009	A. Poluektov *et al.*	(BELLE Collab.)
SCHUEMANN	06	PRL 97 061802	J. Schuemann *et al.*	(BELLE Collab.)
SONI	06	PL B634 155	N. Soni *et al.*	(BELLE Collab.)
ABE	05A	PRL 94 221805	K. Abe *et al.*	(BELLE Collab.)
ABE	05B	PR D71 072003	K. Abe *et al.*	(BELLE Collab.)
Also		PR D71 079903 (errat.)	K. Abe *et al.*	(BELLE Collab.)
ABE	05G	PRL 95 231802	K. Abe *et al.*	(BELLE Collab.)
ACOSTA	05J	PRL 95 031801	D. Acosta *et al.*	(CDF Collab.)
AUBERT	05	PRL 94 011801	B. Aubert *et al.*	(BABAR Collab.)
AUBERT	05B	PR D71 031501	B. Aubert *et al.*	(BABAR Collab.)
AUBERT	05G	PR D72 032004	B. Aubert *et al.*	(BABAR Collab.)
AUBERT	05H	PRL 94 101801	B. Aubert *et al.*	(BABAR Collab.)
AUBERT	05J	PRL 94 141801	B. Aubert *et al.*	(BABAR Collab.)
AUBERT	05K	PRL 94 171801	B. Aubert *et al.*	(BABAR Collab.)
AUBERT	05L	PRL 94 181802	B. Aubert *et al.*	(BABAR Collab.)
AUBERT	05M	PRL 94 191802	B. Aubert *et al.*	(BABAR Collab.)
AUBERT	05N	PR D71 031102	B. Aubert *et al.*	(BABAR Collab.)
AUBERT	05O	PR D71 031103	B. Aubert *et al.*	(BABAR Collab.)
AUBERT	05R	PR D71 071103	B. Aubert *et al.*	(BABAR Collab.)
AUBERT	05U	PR D71 091103	B. Aubert *et al.*	(BABAR Collab.)
AUBERT	05X	PR D71 111101	B. Aubert *et al.*	(BABAR Collab.)
AUBERT,B	05B	PRL 95 041804	B. Aubert *et al.*	(BABAR Collab.)
AUBERT,B	05E	PR D72 011102	B. Aubert *et al.*	(BABAR Collab.)
AUBERT,B	05G	PR D72 052002	B. Aubert *et al.*	(BABAR Collab.)
AUBERT,B	05K	PRL 95 131803	B. Aubert *et al.*	(BABAR Collab.)
AUBERT,B	05L	PR D72 051101	B. Aubert *et al.*	(BABAR Collab.)
AUBERT,B	05N	PR D72 072003	B. Aubert *et al.*	(BABAR Collab.)
Also		PR D74 099903 (errat.)	B. Aubert *et al.*	(BABAR Collab.)
AUBERT,B	05O	PR D72 051102	B. Aubert *et al.*	(BABAR Collab.)
AUBERT,B	05T	PR D72 071102	B. Aubert *et al.*	(BABAR Collab.)
AUBERT,B	05U	PR D72 071103	B. Aubert *et al.*	(BABAR Collab.)
AUBERT,B	05V	PR D72 071104	B. Aubert *et al.*	(BABAR Collab.)
AUBERT,B	05Y	PRL 95 121802	B. Aubert *et al.*	(BABAR Collab.)
AUBERT,BE	05E	PRL 95 221801	B. Aubert *et al.*	(BABAR Collab.)
CHANG	05	PR D71 072007	M.-C. Chang *et al.*	(BELLE Collab.)
CHANG	05A	PR D71 091106	P. Chang *et al.*	(BELLE Collab.)
CHAO	05A	PR D71 031502	Y. Chao *et al.*	(BELLE Collab.)
CHEN	05A	PRL 94 221804	K.-F. Chen *et al.*	(BELLE Collab.)
GARMASH	05	PR D71 092003	A. Garmash *et al.*	(BELLE Collab.)
ITOH	05	PRL 95 091601	R. Itoh *et al.*	(BELLE Collab.)
LEE	05	PRL 95 061802	Y.-J. Lee *et al.*	(BELLE Collab.)
LIVENTSEV	05	PR D72 051109	D. Liventsev *et al.*	(BELLE Collab.)
MAJUMDER	05	PRL 95 041803	G. Majumder *et al.*	(BELLE Collab.)
MOHAPATRA	05	PR D72 011101	D. Mohapatra *et al.*	(BELLE Collab.)
NISHIDA	05	PL B610 23	S. Nishida *et al.*	(BELLE Collab.)
OKABE	05	PL B614 27	T. Okabe *et al.*	(BELLE Collab.)
SAIGO	05	PRL 94 091601	M. Saigo *et al.*	(BELLE Collab.)
WANG	05A	PL B617 141	M.-Z. Wang *et al.*	(BELLE Collab.)
XIE	05	PR D72 051105	Q.L. Xie *et al.*	(BELLE Collab.)
YANG	05	PRL 94 111802	H. Yang *et al.*	(BELLE Collab.)
ZHANG	05A	PRL 94 031801	J. Zhang *et al.*	(BELLE Collab.)
ZHANG	05B	PR D71 091107	L.M. Zhang *et al.*	(BELLE Collab.)
ZHANG	05D	PRL 95 141801	J. Zhang *et al.*	(BELLE Collab.)
ABDALLAH	04E	EPJ C33 307	J. Abdallah *et al.*	(DELPHI Collab.)
ABE	04D	PR D69 112002	K. Abe *et al.*	(BELLE Collab.)
AUBERT	04A	PR D69 011102	B. Aubert *et al.*	(BABAR Collab.)
AUBERT	04C	PRL 92 111801	B. Aubert *et al.*	(BABAR Collab.)
AUBERT	04H	PRL 92 061801	B. Aubert *et al.*	(BABAR Collab.)
AUBERT	04K	PRL 92 141801	B. Aubert *et al.*	(BABAR Collab.)
AUBERT	04M	PRL 92 201802	B. Aubert *et al.*	(BABAR Collab.)
AUBERT	04N	PRL 92 202002	B. Aubert *et al.*	(BABAR Collab.)
AUBERT	04O	PRL 92 221803	B. Aubert *et al.*	(BABAR Collab.)
AUBERT	04P	PRL 92 241802	B. Aubert *et al.*	(BABAR Collab.)
AUBERT	04Q	PR D69 051101	B. Aubert *et al.*	(BABAR Collab.)
AUBERT	04T	PR D69 071103	B. Aubert *et al.*	(BABAR Collab.)
AUBERT	04Y	PRL 93 041801	B. Aubert *et al.*	(BABAR Collab.)
AUBERT	04Z	PRL 93 051802	B. Aubert *et al.*	(BABAR Collab.)
AUBERT,B	04B	PR D70 011101	B. Aubert *et al.*	(BABAR Collab.)
AUBERT,B	04D	PR D70 032006	B. Aubert *et al.*	(BABAR Collab.)
AUBERT,B	04L	PRL 93 131804	B. Aubert *et al.*	(BABAR Collab.)
AUBERT,B	04P	PR D70 092001	B. Aubert *et al.*	(BABAR Collab.)
AUBERT,B	04S	PRL 93 181801	B. Aubert *et al.*	(BABAR Collab.)
AUBERT,B	04U	PR D70 091105	B. Aubert *et al.*	(BABAR Collab.)
AUBERT,B	04V	PRL 93 181805	B. Aubert *et al.*	(BABAR Collab.)
AUBERT,BE	04	PR D70 111102	B. Aubert *et al.*	(BABAR Collab.)
AUBERT,BE	04A	PR D70 112006	B. Aubert *et al.*	(BABAR Collab.)
AUBERT,BE	04B	PR D70 091106	B. Aubert *et al.*	(BABAR Collab.)
CHAO	04	PR D69 111102	Y. Chao *et al.*	(BELLE Collab.)
CHAO	04B	PRL 93 191802	Y. Chao *et al.*	(BELLE Collab.)
CHISTOV	04	PRL 93 051803	R. Chistov *et al.*	(BELLE Collab.)
DRUTSKOY	04	PRL 92 051801	A. Drutskoy *et al.*	(BELLE Collab.)
GARMASH	04	PR D69 012001	A. Garmash *et al.*	(BELLE Collab.)
LEE	04	PRL 93 211801	Y.-J. Lee *et al.*	(BELLE Collab.)
MAJUMDER	04	PR D70 111103	G. Majumder *et al.*	(BELLE Collab.)
NAKAO	04	PR D69 112001	M. Nakao *et al.*	(BELLE Collab.)
POLUEKTOV	04	PR D70 072003	A. Poluektov *et al.*	(BELLE Collab.)
SCHWANDA	04	PRL 93 131803	C. Schwanda *et al.*	(BELLE Collab.)
WANG	04	PRL 92 131801	M.Z. Wang *et al.*	(BELLE Collab.)
WANG	04A	PR D70 012001	C.H. Wang *et al.*	(BELLE Collab.)
ZANG	04	PR D69 017101	S.L. Zang *et al.*	(BELLE Collab.)
ABE	03B	PR D67 032003	K. Abe *et al.*	(BELLE Collab.)
ABE	03D	PRL 90 131803	K. Abe *et al.*	(BELLE Collab.)
ADAM	03	PR D67 032001	N.E. Adam *et al.*	(CLEO Collab.)
ADAM	03B	PR D68 012004	N.E. Adam *et al.*	(CLEO Collab.)
ATHAR	03	PR D68 072003	S.B. Athar *et al.*	(CLEO Collab.)
AUBERT	03K	PRL 90 231801	B. Aubert *et al.*	(BABAR Collab.)
AUBERT	03L	PRL 91 021801	B. Aubert *et al.*	(BABAR Collab.)
AUBERT	03M	PRL 91 051801	B. Aubert *et al.*	(BABAR Collab.)
AUBERT	03O	PRL 91 071801	B. Aubert *et al.*	(BABAR Collab.)
AUBERT	03U	PRL 91 221802	B. Aubert *et al.*	(BABAR Collab.)
AUBERT	03V	PRL 91 171802	B. Aubert *et al.*	(BABAR Collab.)
AUBERT	03W	PRL 91 161801	B. Aubert *et al.*	(BABAR Collab.)
AUBERT	03X	PR D68 092001	B. Aubert *et al.*	(BABAR Collab.)
BORNHEIM	03	PR D68 052002	A. Bornheim *et al.*	(CLEO Collab.)
CHEN	03B	PRL 91 201801	K.-F. Chen *et al.*	(BELLE Collab.)
CHOI	03	PRL 91 262001	S.-K. Choi *et al.*	(BELLE Collab.)
CSORNA	03	PR D67 112002	S.E. Csorna *et al.*	(CLEO Collab.)
EDWARDS	03	PR D68 011102	K.W. Edwards *et al.*	(CLEO Collab.)
FANG	03	PRL 90 071801	F. Fang *et al.*	(BELLE Collab.)
HUANG	03	PRL 91 241802	H.-C. Huang *et al.*	(BELLE Collab.)
ISHIKAWA	03	PRL 91 261601	A. Ishikawa *et al.*	(BELLE Collab.)
KROKOVNY	03B	PRL 91 262002	P. Krokovny *et al.*	(BELLE Collab.)
SWAIN	03	PR D68 051101	S.K. Swain *et al.*	(BELLE Collab.)
UNNO	03	PR D68 011103	Y. Unno *et al.*	(BELLE Collab.)
ZHANG	03B	PRL 91 221801	J. Zhang *et al.*	(BELLE Collab.)
ABE	02	PRL 88 021801	K. Abe *et al.*	(BELLE Collab.)
ABE	02B	PRL 88 031802	K. Abe *et al.*	(BELLE Collab.)
ABE	02H	PRL 88 171801	K. Abe *et al.*	(BELLE Collab.)
ABE	02K	PRL 88 181803	K. Abe *et al.*	(BELLE Collab.)
ABE	02N	PL B538 11	K. Abe *et al.*	(BELLE Collab.)
ABE	02O	PR D65 091103	K. Abe *et al.*	(BELLE Collab.)
ABE	02W	PRL 89 151802	K. Abe *et al.*	(BELLE Collab.)
ACOSTA	02C	PR D65 092009	D. Acosta *et al.*	(CDF Collab.)
ACOSTA	02F	PR D66 052005	D. Acosta *et al.*	(CDF Collab.)
AHMED	02B	PR D66 031101	S. Ahmed *et al.*	(CLEO Collab.)
AUBERT	02	PR D65 032001	B. Aubert *et al.*	(BABAR Collab.)
AUBERT	02C	PRL 88 101805	B. Aubert *et al.*	(BABAR Collab.)
AUBERT	02E	PR D65 051101	B. Aubert *et al.*	(BABAR Collab.)
AUBERT	02F	PR D65 091101	B. Aubert *et al.*	(BABAR Collab.)
AUBERT	02L	PRL 88 241801	B. Aubert *et al.*	(BABAR Collab.)
BRIERE	02	PRL 89 081803	R. Briere *et al.*	(CLEO Collab.)
CASEY	02	PR D66 092002	B.C.K. Casey *et al.*	(BELLE Collab.)
CHEN	02B	PL B546 196	K.-F. Chen *et al.*	(BELLE Collab.)
DRUTSKOY	02	PL B542 171	A. Drutskoy *et al.*	(BELLE Collab.)
DYTMAN	02	PR D66 091101	S.A. Dytman *et al.*	(CLEO Collab.)
ECKHART	02	PRL 89 251801	E. Eckhart *et al.*	(CLEO Collab.)
EDWARDS	02B	PR D65 111102	K.W. Edwards *et al.*	(CLEO Collab.)
GABYSHEV	02	PR D66 091102	N. Gabyshev *et al.*	(BELLE Collab.)
GARMASH	02	PR D65 092005	A. Garmash *et al.*	(BELLE Collab.)
GODANG	02	PRL 88 021802	R. Godang *et al.*	(CLEO Collab.)
GORDON	02	PL B542 183	A. Gordon *et al.*	(BELLE Collab.)
LU	02	PRL 89 191801	R.-S. Lu *et al.*	(BELLE Collab.)
MAHAPATRA	02	PRL 88 101803	R. Mahapatra *et al.*	(CLEO Collab.)
NISHIDA	02	PRL 89 231801	S. Nishida *et al.*	(BELLE Collab.)
ABE	01H	PRL 87 101801	K. Abe *et al.*	(BELLE Collab.)
ABE	01I	PRL 87 111801	K. Abe *et al.*	(BELLE Collab.)
ABE	01K	PR D64 071101	K. Abe *et al.*	(BELLE Collab.)
ABE	01L	PRL 87 161601	K. Abe *et al.*	(BELLE Collab.)
ABE	01M	PL B517 309	K. Abe *et al.*	(BELLE Collab.)
ALEXANDER	01B	PR D64 092001	J.P. Alexander *et al.*	(CLEO Collab.)
AMMAR	01B	PRL 87 271801	R. Ammar *et al.*	(CLEO Collab.)
ANDERSON	01B	PRL 87 181803	S. Anderson *et al.*	(CLEO Collab.)
AUBERT	01D	PRL 87 151801	B. Aubert *et al.*	(BABAR Collab.)
AUBERT	01E	PRL 87 151802	B. Aubert *et al.*	(BABAR Collab.)
AUBERT	01F	PRL 87 201803	B. Aubert *et al.*	(BABAR Collab.)
AUBERT	01G	PRL 87 221802	B. Aubert *et al.*	(BABAR Collab.)
BARATE	01E	EPJ C19 213	R. Barate *et al.*	(ALEPH Collab.)
BRIERE	01	PRL 86 3718	R.A. Briere *et al.*	(CLEO Collab.)
BROWDER	01	PRL 86 2950	T.E. Browder *et al.*	(CLEO Collab.)
EDWARDS	01	PRL 86 30	K.W. Edwards *et al.*	(CLEO Collab.)
GRITSAN	01	PR D64 077501	A. Gritsan *et al.*	(CLEO Collab.)
RICHICHI	01	PR D63 031103	S.J. Richichi *et al.*	(CLEO Collab.)
ABBIENDI	00B	PL B476 233	G. Abbiendi *et al.*	(OPAL Collab.)
ABE	00C	PR D62 071101	K. Abe *et al.*	(SLD Collab.)

Int. J. Mod. Phys. A 2026.41. Downloaded from www.worldscientific.com
by UNIVERSITY OF CALIFORNIA @ BERKELEY on 09/16/26. Re-use and distribution is strictly not permitted, except for Open Access articles.

AHMED	00B	PR D62 112003	S. Ahmed *et al.*	(CLEO Collab.)
ANASTASSOV	00	PRL 84 1393	A. Anastassov *et al.*	(CLEO Collab.)
BARATE	00R	PL B492 275	R. Barate *et al.*	(ALEPH Collab.)
BEHRENS	00	PR D61 052001	B.H. Behrens *et al.*	(CLEO Collab.)
BONVICINI	00	PRL 84 5940	G. Bonvicini *et al.*	(CLEO Collab.)
CHEN	00	PRL 85 525	S. Chen *et al.*	(CLEO Collab.)
COAN	00	PRL 84 5283	T.E. Coan *et al.*	(CLEO Collab.)
CRONIN-HEN...	00	PRL 85 515	D. Cronin-Hennessy *et al.*	(CLEO Collab.)
CSORNA	00	PR D61 111101	S.E. Csorna *et al.*	(CLEO Collab.)
JESSOP	00	PRL 85 2881	C.P. Jessop *et al.*	(CLEO Collab.)
RICHICHI	00	PRL 85 520	S.J. Richichi *et al.*	(CLEO Collab.)
ABBIENDI	99J	EPJ C12 609	G. Abbiendi *et al.*	(OPAL Collab.)
AFFOLDER	99B	PRL 83 3378	T. Affolder *et al.*	(CDF Collab.)
BARTELT	99	PRL 82 3746	J. Bartelt *et al.*	(CLEO Collab.)
COAN	99	PR D59 111101	T.E. Coan *et al.*	(CLEO Collab.)
ABE	98B	PR D57 5382	F. Abe *et al.*	(CDF Collab.)
ABE	98O	PR D58 072001	F. Abe *et al.*	(CDF Collab.)
ABE	98Q	PR D58 092002	F. Abe *et al.*	(CDF Collab.)
ACCIARRI	98S	PL B438 417	M. Acciarri *et al.*	(L3 Collab.)
ANASTASSOV	98	PRL 80 4127	A. Anastassov *et al.*	(CLEO Collab.)
ATHANAS	98	PRL 80 5493	M. Athanas *et al.*	(CLEO Collab.)
BARATE	98Q	EPJ C4 387	R. Barate *et al.*	(ALEPH Collab.)
BEHRENS	98	PRL 80 3710	B.H. Behrens *et al.*	(CLEO Collab.)
BERGFELD	98	PRL 81 272	T. Bergfeld *et al.*	(CLEO Collab.)
BRANDENB...	98	PRL 80 2762	G. Brandenbrug *et al.*	(CLEO Collab.)
CAPRINI	98	NP B530 153	I. Caprini, L. Lellouch, M. Neubert	(BCIP, CERN)
GODANG	98	PRL 80 3456	R. Godang *et al.*	(CLEO Collab.)
ABE	97J	PRL 79 590	K. Abe *et al.*	(SLD Collab.)
ACCIARRI	97F	PL B396 327	M. Acciarri *et al.*	(L3 Collab.)
ARTUSO	97	PL B399 321	M. Artuso *et al.*	(CLEO Collab.)
ATHANAS	97	PRL 79 2208	M. Athanas *et al.*	(CLEO Collab.)
BROWDER	97	PR D56 11	T. Browder *et al.*	(CLEO Collab.)
FU	97	PRL 79 3125	X. Fu *et al.*	(CLEO Collab.)
JESSOP	97	PRL 79 4533	C.P. Jessop *et al.*	(CLEO Collab.)
ABE	96B	PR D53 3496	F. Abe *et al.*	(CDF Collab.)
ABE	96C	PRL 76 4462	F. Abe *et al.*	(CDF Collab.)
ABE	96H	PRL 76 2015	F. Abe *et al.*	(CDF Collab.)
ABE	96L	PRL 76 4675	F. Abe *et al.*	(CDF Collab.)
ABE	96Q	PR D54 6596	F. Abe *et al.*	(CDF Collab.)
ABE	96R	PRL 77 5176	F. Abe *et al.*	(CDF Collab.)
ADAM	96D	ZPHY C72 207	W. Adam *et al.*	(DELPHI Collab.)
ALEXANDER	96T	PRL 77 5000	J.P. Alexander *et al.*	(CLEO Collab.)
ASNER	96	PR D53 1039	D.M. Asner *et al.*	(CLEO Collab.)
BARISH	96B	PRL 76 1570	B.C. Barish *et al.*	(CLEO Collab.)
BERGFELD	96B	PRL 77 4503	T. Bergfeld *et al.*	(CLEO Collab.)
BISHAI	96	PL B369 186	M. Bishai *et al.*	(CLEO Collab.)
BUSKULIC	96J	ZPHY C71 31	D. Buskulic *et al.*	(ALEPH Collab.)
GIBAUT	96	PR D53 4734	D. Gibaut *et al.*	(CLEO Collab.)
PDG	96	PR D54 1	R. M. Barnett *et al.*	(PDG Collab.)
ABREU	95N	PL B357 255	P. Abreu *et al.*	(DELPHI Collab.)
ABREU	95Q	ZPHY C68 13	P. Abreu *et al.*	(DELPHI Collab.)
ADAM	95	ZPHY C68 363	W. Adam *et al.*	(DELPHI Collab.)
AKERS	95T	ZPHY C67 379	R. Akers *et al.*	(OPAL Collab.)
ALBRECHT	95D	PL B353 554	H. Albrecht *et al.*	(ARGUS Collab.)
ALEXANDER	95	PL B341 435	J. Alexander *et al.*	(CLEO Collab.)
Also		PL B347 469 (errat.)	J. Alexander *et al.*	(CLEO Collab.)
ARTUSO	95	PRL 75 785	M. Artuso *et al.*	(CLEO Collab.)
BARISH	95	PR D51 1014	B.C. Barish *et al.*	(CLEO Collab.)
BUSKULIC	95	PL B343 444	D. Buskulic *et al.*	(ALEPH Collab.)
ABE	94D	PRL 72 3456	F. Abe *et al.*	(CDF Collab.)
ALAM	94	PR D50 43	M.S. Alam *et al.*	(CLEO Collab.)
ALBRECHT	94D	PL B335 526	H. Albrecht *et al.*	(ARGUS Collab.)
ATHANAS	94	PRL 73 3503	M. Athanas *et al.*	(CLEO Collab.)
Also		PRL 74 3090 (errat.)	M. Athanas *et al.*	(CLEO Collab.)
PDG	94	PR D50 1173	L. Montanet *et al.*	(CERN, LBL, BOST+)
STONE	94	HEPSY 93-11	S. Stone	
Published in B Decays, 2nd Edition, World Scientific, Singapore				
ABREU	93D	ZPHY C57 181	P. Abreu *et al.*	(DELPHI Collab.)
ABREU	93G	PL B312 253	P. Abreu *et al.*	(DELPHI Collab.)
ACTON	93C	PL B307 247	P.D. Acton *et al.*	(OPAL Collab.)
ALBRECHT	93E	ZPHY C60 11	H. Albrecht *et al.*	(ARGUS Collab.)
ALEXANDER	93B	PL B319 365	J. Alexander *et al.*	(CLEO Collab.)
AMMAR	93	PRL 71 674	R. Ammar *et al.*	(CLEO Collab.)
BEAN	93B	PRL 70 2681	A. Bean *et al.*	(CLEO Collab.)
BUSKULIC	93D	PL B307 194	D. Buskulic *et al.*	(ALEPH Collab.)
Also		PL B325 537 (errat.)	D. Buskulic *et al.*	(ALEPH Collab.)
SANGHERA	93	PR D47 791	S. Sanghera *et al.*	(CLEO Collab.)
ALBRECHT	92C	PL B275 195	H. Albrecht *et al.*	(ARGUS Collab.)
ALBRECHT	92E	PL B277 209	H. Albrecht *et al.*	(ARGUS Collab.)
ALBRECHT	92G	ZPHY C54 1	H. Albrecht *et al.*	(ARGUS Collab.)
BORTOLETTO	92	PR D45 21	D. Bortoletto *et al.*	(CLEO Collab.)
BUSKULIC	92G	PL B295 396	D. Buskulic *et al.*	(ALEPH Collab.)
ALBRECHT	91B	PL B254 288	H. Albrecht *et al.*	(ARGUS Collab.)
ALBRECHT	91C	PL B255 297	H. Albrecht *et al.*	(ARGUS Collab.)
ALBRECHT	91E	PL B262 148	H. Albrecht *et al.*	(ARGUS Collab.)
BERKELMAN	91	ARNPS 41 1	K. Berkelman, S. Stone	(CORN, SYRA)
"Decays of B Mesons"				
FULTON	91	PR D43 651	R. Fulton *et al.*	(CLEO Collab.)
ALBRECHT	90B	PL B241 278	H. Albrecht *et al.*	(ARGUS Collab.)
ALBRECHT	90J	ZPHY C48 543	H. Albrecht *et al.*	(ARGUS Collab.)
ANTREASYAN	90B	ZPHY C48 553	D. Antreasyan *et al.*	(Crystal Ball Collab.)
BORTOLETTO	90	PRL 64 2117	D. Bortoletto *et al.*	(CLEO Collab.)
Also		PR D45 21	D. Bortoletto *et al.*	(CLEO Collab.)
WEIR	90B	PR D41 1384	A.J. Weir *et al.*	(Mark II Collab.)
ALBRECHT	89G	PL B229 304	H. Albrecht *et al.*	(ARGUS Collab.)
AVERY	89B	PL B223 470	P. Avery *et al.*	(CLEO Collab.)
BEBEK	89	PRL 62 8	C. Bebek *et al.*	(CLEO Collab.)
BORTOLETTO	89	PRL 62 2436	D. Bortoletto *et al.*	(CLEO Collab.)
ALBRECHT	88F	PL B209 119	H. Albrecht *et al.*	(ARGUS Collab.)
ALBRECHT	88K	PL B215 424	H. Albrecht *et al.*	(ARGUS Collab.)
ALBRECHT	87C	PL B185 218	H. Albrecht *et al.*	(ARGUS Collab.)
ALBRECHT	87D	PL B199 451	H. Albrecht *et al.*	(ARGUS Collab.)
AVERY	87	PL B183 429	P. Avery *et al.*	(CLEO Collab.)
BEBEK	87	PR D36 1289	C. Bebek *et al.*	(CLEO Collab.)
ALAM	86	PR D34 3279	M.S. Alam *et al.*	(CLEO Collab.)
PDG	86	PL 170B 1	M. Aguilar-Benitez *et al.*	(CERN, CIT+)
GILES	84	PR D30 2279	R. Giles *et al.*	(CLEO Collab.)

B^0

$I(J^P) = \frac{1}{2}(0^-)$

Quantum numbers not measured. Values shown are quark-model predictions.

See also the $B^{\pm}/B^0$ ADMIXTURE and $B^{\pm}/B^0/B^0_s/b$-baryon ADMIXTURE sections.

See the Note "Production and Decay of b-flavored Hadrons" at the beginning of the $B^{\pm}$ Particle Listings and the Note on "B^0-$\overline{B}^0$ Mixing" near the end of the B^0 Particle Listings.

B^0 MASS

The fit uses m_{B^+}, $(m_{B^0} - m_{B^+})$, and m_{B^0} to determine m_{B^+}, m_{B^0}, and the mass difference.

VALUE (MeV)	EVTS	DOCUMENT ID		TECN	COMMENT
5279.72±0.08 OUR FIT					
5279.63±0.20 OUR AVERAGE					
5279.74±0.30±0.10		[1] AAIJ	19U	LHCB	pp at 7, 8, 13 TeV
5279.6 ±0.2 ±1.0		[2] AAD	13U	ATLS	pp at 7 TeV
5279.58±0.15±0.28		[3] AAIJ	12E	LHCB	pp at 7 TeV
5279.63±0.53±0.33		[4] ACOSTA	06	CDF	$p\overline{p}$ at 1.96 TeV
5279.1 ±0.7 ±0.3	135	[5] CSORNA	00	CLE2	$e^+e^- \to \Upsilon(4S)$
5281.3 ±2.2 ±1.4	51	ABE	96B	CDF	$p\overline{p}$ at 1.8 TeV
• • • We do not use the following data for averages, fits, limits, etc. • • •					
5279.2 ±0.54±2.0	340	ALAM	94	CLE2	$e^+e^- \to \Upsilon(4S)$
5278.0 ±0.4 ±2.0		BORTOLETTO	92	CLEO	$e^+e^- \to \Upsilon(4S)$
5279.6 ±0.7 ±2.0	40	[6] ALBRECHT	90J	ARG	$e^+e^- \to \Upsilon(4S)$
5278.2 ±1.0 ±3.0	40	ALBRECHT	87C	ARG	$e^+e^- \to \Upsilon(4S)$
5279.5 ±1.6 ±3.0	7	[7] ALBRECHT	87D	ARG	$e^+e^- \to \Upsilon(4S)$
5280.6 ±0.8 ±2.0		BEBEK	87	CLEO	$e^+e^- \to \Upsilon(4S)$

[1] Uses $B^0 \to J/\psi p\overline{p}$ decays.
[2] Measured with $B^0_d \to J/\psi(\mu^+\mu^-)\, K^0_S(\pi^+\pi^-)$ decays.
[3] Uses $B^0 \to J/\psi K^0$ fully reconstructed decays.
[4] Uses exclusively reconstructed final states containing a $J/\psi \to \mu^+\mu^-$ decays.
[5] CSORNA 00 uses fully reconstructed 135 $B^0 \to J/\psi^{(\prime)} K^0_S$ events and invariant masses without beam constraint.
[6] ALBRECHT 90J assumes 10580 for $\Upsilon(4S)$ mass. Supersedes ALBRECHT 87C and ALBRECHT 87D.
[7] Found using fully reconstructed decays with J/ψ. ALBRECHT 87D assume $m_{\Upsilon(4S)}$ = 10577 MeV.

$m_{B^0} - m_{B^+}$

VALUE (MeV)	DOCUMENT ID		TECN	COMMENT
0.31±0.05 OUR FIT				
0.33±0.05 OUR AVERAGE				
0.57±0.49±0.10	[1] SIRUNYAN	18DF	CMS	pp at 8 TeV
0.20±0.17±0.11	[1] AAIJ	12E	LHCB	pp at 7 TeV
0.33±0.05±0.03	[2] AUBERT	08AF	BABR	$e^+e^- \to \Upsilon(4S)$
0.53±0.67±0.14	[1] ACOSTA	06	CDF	$p\overline{p}$ at 1.96 TeV
0.41±0.25±0.19	ALAM	94	CLE2	$e^+e^- \to \Upsilon(4S)$
−0.4 ±0.6 ±0.5	BORTOLETTO	92	CLEO	$e^+e^- \to \Upsilon(4S)$
−0.9 ±1.2 ±0.5	ALBRECHT	90J	ARG	$e^+e^- \to \Upsilon(4S)$
2.0 ±1.1 ±0.3	[3] BEBEK	87	CLEO	$e^+e^- \to \Upsilon(4S)$

[1] Uses exclusively reconstructed final states containing a $J/\psi \to \mu^+\mu^-$ decay.
[2] Uses the B-momentum distributions in the e^+e^- rest frame.
[3] BEBEK 87 actually measure the difference between half of E_{cm} and the $B^{\pm}$ or B^0 mass, so the $m_{B^0} - m_{B^{\pm}}$ is more accurate. Assume $m_{\Upsilon(4S)}$ = 10580 MeV.

$m_{B^0_H} - m_{B^0_L}$

See the B^0-$\overline{B}^0$ MIXING PARAMETERS section near the end of these B^0 Listings.

B^0 MEAN LIFE

The B^0 mean life is defined and computed as $1/\Gamma_{B^0}$, where Γ_{B^0} is the average decay width of the B^0 mass eigenstates.

VALUE (10^{-12} s)	DOCUMENT ID		TECN	COMMENT
1.5113±0.0027 OUR EVALUATION (Produced by HFLAV)				
1.5053±0.0012±0.0035	[1] AAD	25AM	ATLS	pp at 13 TeV
1.499 ±0.013 ±0.008	[2] ABUDINEN	23D	BELL	$e^+e^- \to \Upsilon(4S)$
1.511 ±0.005 ±0.006	[1] SIRUNYAN	18BY	CMS	pp at 8 TeV
1.527 ±0.009 ±0.009	[3] SIRUNYAN	18BY	CMS	pp at 8 TeV
1.534 ±0.019 ±0.021	[4] ABAZOV	15A	D0	$p\overline{p}$ at 1.96 TeV
1.499 ±0.013 ±0.005	[3] AAIJ	14E	LHCB	pp at 7 TeV
1.524 ±0.006 ±0.004	[1] AAIJ	14E	LHCB	pp at 7 TeV
1.524 ±0.011 ±0.004	[5] AAIJ	14R	LHCB	pp at 7 TeV
1.509 ±0.012 ±0.018	[6] AAD	13U	ATLS	pp at 7 TeV

1.508	±0.025	±0.043	[3] ABAZOV	12U	D0	$p\overline{p}$ at 1.96 TeV
1.414	±0.018	±0.034	[7] ABAZOV	09E	D0	$p\overline{p}$ at 1.96 TeV
1.504	±0.013	$^{+0.018}_{-0.013}$	[8] AUBERT	06G	BABR	$e^+e^- \to \Upsilon(4S)$
1.534	±0.008	±0.010	[9] ABE	05B	BELL	$e^+e^- \to \Upsilon(4S)$
1.523	$^{+0.024}_{-0.023}$	±0.022	[10] AUBERT	03C	BABR	$e^+e^- \to \Upsilon(4S)$
1.533	±0.034	±0.038	[11] AUBERT	03H	BABR	$e^+e^- \to \Upsilon(4S)$
1.497	±0.073	±0.032	[12] ACOSTA	02C	CDF	$p\overline{p}$ at 1.8 TeV
1.529	±0.012	±0.029	[13] AUBERT	02H	BABR	$e^+e^- \to \Upsilon(4S)$
1.546	±0.032	±0.022	[14] AUBERT	01F	BABR	$e^+e^- \to \Upsilon(4S)$
1.541	±0.028	±0.023	[13] ABBIENDI,G	00B	OPAL	$e^+e^- \to Z$
1.518	±0.053	±0.034	[15] BARATE	00R	ALEP	$e^+e^- \to Z$
1.474	±0.039	$^{+0.052}_{-0.051}$	[15] ABE	98Q	CDF	$p\overline{p}$ at 1.8 TeV
1.56	$^{+0.14}_{-0.13}$	±0.10	[16,17] ABE	97J	SLD	$e^+e^- \to Z$
1.532	±0.041	±0.040	[18] ABREU	97F	DLPH	$e^+e^- \to Z$
1.49	$^{+0.17}_{-0.15}$	$^{+0.08}_{-0.06}$	[19] BUSKULIC	96J	ALEP	$e^+e^- \to Z$
1.61	$^{+0.14}_{-0.13}$	±0.08	[15,20] ABREU	95Q	DLPH	$e^+e^- \to Z$
1.53	±0.12	±0.08	[15,21] AKERS	95T	OPAL	$e^+e^- \to Z$
• • • We do not use the following data for averages, fits, limits, etc. • • •						
1.515	±0.005	±0.006	[22] SIRUNYAN	18BY	CMS	pp at 8 TeV
1.507	±0.010	±0.008	[23] AALTONEN	11	CDF	$p\overline{p}$ at 1.96 TeV
1.501	$^{+0.078}_{-0.074}$	±0.050	[3] ABAZOV	07S	D0	Repl. by ABAZOV 12U
1.524	±0.030	±0.016	[3] ABULENCIA	07A	CDF	Repl. by AALTONEN 11
1.473	$^{+0.052}_{-0.050}$	±0.023	[7] ABAZOV	05B	D0	Repl. by ABAZOV 05W
1.40	$^{+0.11}_{-0.10}$	±0.03	[3] ABAZOV	05C	D0	Repl. by ABAZOV 07S
1.530	±0.043	±0.023	[7] ABAZOV	05W	D0	Repl. by ABAZOV 09E
1.54	±0.05	±0.02	[24] ACOSTA	05	CDF	Repl. by AALTONEN 11
1.531	±0.021	±0.031	[25] ABDALLAH	04E	DLPH	$e^+e^- \to Z$
1.554	±0.030	±0.019	[14] ABE	02H	BELL	Repl. by ABE 05B
1.523	±0.057	±0.053	[16] ABBIENDI	99J	OPAL	$e^+e^- \to Z$
1.58	±0.09	±0.02	[12] ABE	98B	CDF	Repl. by ACOSTA 02C
1.52	±0.06	±0.04	[16] ACCIARRI	98S	L3	$e^+e^- \to Z$
1.54	±0.08	±0.06	[15] ABE	96C	CDF	Repl. by ABE 98Q
1.55	±0.06	±0.03	[26] BUSKULIC	96J	ALEP	$e^+e^- \to Z$
1.61	±0.07	±0.04	[15] BUSKULIC	96J	ALEP	Repl. by BARATE 00R
1.25	$^{+0.15}_{-0.13}$	±0.05	[12] BUSKULIC	96J	ALEP	$e^+e^- \to Z$
1.63	±0.14	±0.13	[27] ADAM	95	DLPH	$e^+e^- \to Z$
1.62	±0.12		[28] ADAM	95	DLPH	$e^+e^- \to Z$
1.57	±0.18	±0.08	[12] ABE	94D	CDF	Repl. by ABE 98B
1.17	$^{+0.29}_{-0.23}$	±0.16	[15] ABREU	93D	DLPH	Sup. by ABREU 95Q
1.55	±0.25	±0.18	[27] ABREU	93G	DLPH	Sup. by ADAM 95
1.51	$^{+0.24}_{-0.23}$	$^{+0.12}_{-0.14}$	[15] ACTON	93C	OPAL	Sup. by AKERS 95T
1.52	$^{+0.20}_{-0.18}$	$^{+0.07}_{-0.13}$	[15] BUSKULIC	93D	ALEP	Sup. by BUSKULIC 96J
1.20	$^{+0.52}_{-0.36}$	$^{+0.16}_{-0.14}$	[29] WAGNER	90	MRK2	E^{ee}_{cm}= 29 GeV
0.82	$^{+0.57}_{-0.37}$	±0.27	[30] AVERILL	89	HRS	E^{ee}_{cm}= 29 GeV

[1] Measured using $B^0 \to J/\psi K^{*0}$ decays.
[2] Measured using $B^0 \to D^{(*)-}\pi^+$ decays.
[3] Measured using $B^0 \to J/\psi K^0_S$ decays.
[4] Measured using $B^0 \to D^-\mu^+\nu X$ decays.
[5] Measured using $B^0 \to K^+\pi^-$ decays.
[6] Measured with $B^0_d \to J/\psi(\mu^+\mu^-)\ K^0_S(\pi^+\pi^-)$ decays.
[7] Measured mean life using $B^0 \to J/\psi K^{*0}$ decays.
[8] Measured using a simultaneous fit of the B^0 lifetime and $\overline{B}^0 B^0$ oscillation frequency Δm_d in the partially reconstructed $B^0 \to D^{*-}\ell\nu$ decays.
[9] Measurement performed using a combined fit of *CP*-violation, mixing and lifetimes.
[10] AUBERT 03C uses a sample of approximately 14,000 exclusively reconstructed $B^0 \to D^*(2010)^-\ell\nu$ and simultaneously measures the lifetime and oscillation frequency.
[11] Measurement performed with decays $B^0 \to D^{*-}\pi^+$ and $B^0 \to D^{*-}\rho^+$ using a partial reconstruction technique.
[12] Measured mean life using fully reconstructed decays.
[13] Data analyzed using partially reconstructed $\overline{B}^0 \to D^{*+}\ell^-\overline{\nu}$ decays.
[14] Events are selected in which one B meson is fully reconstructed while the second B meson is reconstructed inclusively.
[15] Data analyzed using $D/D^*\ell X$ event vertices.
[16] Data analyzed using charge of secondary vertex.
[17] Reported the combined measurement of $1.64 \pm 0.08 \pm 0.08$ ps^{-1} using the charge of the secondary vertex with the lepton and without. Only the flavor-specific measurement with the lepton is reported and used.
[18] Data analyzed using inclusive $D/D^*\ell X$.
[19] Measured mean life using partially reconstructed $D^{*-}\pi^+X$ vertices.
[20] ABREU 95Q assumes $B(B^0 \to D^{**-}\ell^+\nu_\ell) = 3.2 \pm 1.7\%$.
[21] AKERS 95T assumes $B(B^0 \to D_s{}^{(*)}D^{0(*)}) = 5.0 \pm 0.9\%$ to find B^+/B^0 yield.
[22] Measured using $B^0 \to J/\psi K^*(892)^0$ and $B^0 \to J/\psi K^0_S$ decays.
[23] Measured mean life using fully reconstructed decays ($J/\psi K^{(*)}$).
[24] Measured using the time-dependent angular analysis of $B^0_d \to J/\psi K^{*0}$ decays.
[25] Measurement performed using an inclusive reconstruction and B flavor identification technique.
[26] Combined result of $D/D^*\ell x$ analysis, fully reconstructed B analysis, and partially reconstructed $D^{*-}\pi^+X$ analysis.
[27] Data analyzed using vertex-charge technique to tag B charge.
[28] Combined ABREU 95Q and ADAM 95 result.
[29] WAGNER 90 tagged B^0 mesons by their decays into $D^{*-}e^+\nu$ and $D^{*-}\mu^+\nu$ where the D^{*-} is tagged by its decay into $\pi^-\overline{D}^0$.
[30] AVERILL 89 is an estimate of the B^0 mean lifetime assuming that $B^0 \to D^{*+} + X$ always.

$\tau_{B^0}/\tau_{\overline{B}^0}$

VALUE	DOCUMENT ID		TECN	COMMENT
1.000±0.008±0.009	[1] AAIJ	14E	LHCB	pp at 7 TeV

[1] Measured using $B^0 \to J/\psi K^{*0}$ decays.

MEAN LIFE RATIO τ_{B^+}/τ_{B^0}

τ_{B^+}/τ_{B^0} (direct measurements)

VALUE		EVTS	DOCUMENT ID		TECN	COMMENT
1.0832±0.0034 OUR EVALUATION			(Produced by HFLAV)			
1.074	±0.005	±0.003	[1] AAIJ	14E	LHCB	pp at 7 TeV
1.080	±0.016	±0.014	[2] ABAZOV	05D	D0	$p\overline{p}$ at 1.96 TeV
1.066	±0.008	±0.008	[3] ABE	05B	BELL	$e^+e^- \to \Upsilon(4S)$
1.093	±0.066	±0.028	[4] ACOSTA	02C	CDF	$p\overline{p}$ at 1.8 TeV
1.082	±0.026	±0.012	[5] AUBERT	01F	BABR	$e^+e^- \to \Upsilon(4S)$
1.085	±0.059	±0.018	[2] BARATE	00R	ALEP	$e^+e^- \to Z$
1.110	±0.056	$^{+0.033}_{-0.030}$	[2] ABE	98Q	CDF	$p\overline{p}$ at 1.8 TeV
1.03	$^{+0.16}_{-0.14}$	±0.09	[6] ABE	97J	SLD	$e^+e^- \to Z$
1.00	$^{+0.17}_{-0.15}$	±0.10	[2,7] ABREU	95Q	DLPH	$e^+e^- \to Z$
0.99	±0.14	$^{+0.05}_{-0.04}$	[2,8] AKERS	95T	OPAL	$e^+e^- \to Z$
• • • We do not use the following data for averages, fits, limits, etc. • • •						
1.088	±0.009	±0.004	[9] AALTONEN	11	CDF	$p\overline{p}$ at 1.96 TeV
1.060	±0.021	±0.024	[10] ABDALLAH	04E	DLPH	$e^+e^- \to Z$
1.091	±0.023	±0.014	[5] ABE	02H	BELL	Repl. by ABE 05B
1.079	±0.064	±0.041	[11] ABBIENDI	99J	OPAL	$e^+e^- \to Z$
1.06	±0.07	±0.02	[4] ABE	98B	CDF	Repl. by ACOSTA 02C
1.09	±0.07	±0.03	[11] ACCIARRI	98S	L3	$e^+e^- \to Z$
1.01	$^{+0.09}_{-0.08}$	±0.05	[11] ABE	97J	SLD	$e^+e^- \to Z$
1.01	±0.11	±0.02	[2] ABE	96C	CDF	Repl. by ABE 98Q
1.03	±0.08	±0.02	[12] BUSKULIC	96J	ALEP	$e^+e^- \to Z$
0.98	±0.08	±0.03	[2] BUSKULIC	96J	ALEP	Repl. by BARATE 00R
1.27	$^{+0.23}_{-0.19}$	$^{+0.03}_{-0.02}$	[4] BUSKULIC	96J	ALEP	$e^+e^- \to Z$
1.06	$^{+0.13}_{-0.11}$	±0.10	[13] ADAM	95	DLPH	$e^+e^- \to Z$
1.02	±0.16	±0.05 269	[4] ABE	94D	CDF	Repl. by ABE 98B
1.11	$^{+0.51}_{-0.39}$	±0.11 188	[2] ABREU	93D	DLPH	Sup. by ABREU 95Q
1.01	$^{+0.29}_{-0.22}$	±0.12 253	[13] ABREU	93G	DLPH	Sup. by ADAM 95
1.0	$^{+0.33}_{-0.25}$	±0.08 130	ACTON	93C	OPAL	Sup. by AKERS 95T
0.96	$^{+0.19}_{-0.15}$	$^{+0.18}_{-0.12}$ 154	[2] BUSKULIC	93D	ALEP	Sup. by BUSKULIC 96J

[1] Measured using $B \to J/\psi K^{(*)}$ decays.
[2] Data analyzed using $D/D^*\mu X$ vertices.
[3] Measurement performed using a combined fit of *CP*-violation, mixing and lifetimes.
[4] Measured using fully reconstructed decays.
[5] Events are selected in which one B meson is fully reconstructed while the second B meson is reconstructed inclusively.
[6] Data analyzed using charge of secondary vertex with a lepton.
[7] ABREU 95Q assumes $B(B^0 \to D^{**-}\ell^+\nu_\ell) = 3.2 \pm 1.7\%$.
[8] AKERS 95T assumes $B(B^0 \to D_s{}^{(*)}D^{0(*)}) = 5.0 \pm 0.9\%$ to find B^+/B^0 yield.
[9] Measured mean life using fully reconstructed decays ($J/\psi K^{(*)}$).
[10] Measurement performed using an inclusive reconstruction and B flavor identification technique.
[11] Data analyzed using charge of secondary vertex.
[12] Combined result of $D/D^*\ell X$ analysis and fully reconstructed B analysis.
[13] Data analyzed using vertex-charge technique to tag B charge.

τ_{B^+}/τ_{B^0} (inferred from branching fractions)

These measurements are inferred from the branching fractions for semileptonic decay or other spectator-dominated decays by assuming that the rates for such decays are equal for B^0 and B^+. We do not use measurements which assume equal production of B^0 and B^+ because of the large uncertainty in the production ratio.

VALUE	CL%	EVTS	DOCUMENT ID		TECN	COMMENT
1.07 ±0.04 OUR AVERAGE						
1.07 ±0.04 ±0.03			URQUIJO	07	BELL	$e^+e^- \to \Upsilon(4S)$
1.067$\pm0.041\pm0.033$			AUBERT,B	06Y	BABR	$e^+e^- \to \Upsilon(4S)$
• • • We do not use the following data for averages, fits, limits, etc. • • •						
0.95 $^{+0.117}_{-0.080}\pm0.091$			[1] ARTUSO	97	CLE2	$e^+e^- \to \Upsilon(4S)$
1.15 ±0.17 ±0.06			[2] JESSOP	97	CLE2	$e^+e^- \to \Upsilon(4S)$

Int. J. Mod. Phys. A 2026.41. Downloaded from www.worldscientific.com
by LIFORNIA @ BERKELEY on 09/16/26. Re-use and distribution is strictly not permitted, except for Open Access articles.

Int. J. Mod. Phys. A 2026.41. Downloaded from www.worldscientific.com
by UNIVERSITY OF CALIFORNIA @ BERKELEY on 09/16/26. Re-use and distribution is strictly not permitted, except for Open Access articles.

0.93 ±0.18 ±0.12		[3] ATHANAS	94	CLE2	Sup. by ARTUSO 97
0.91 ±0.27 ±0.21		[4] ALBRECHT	92C	ARG	$e^+e^- \to \Upsilon(4S)$
1.0 ±0.4	29	[4,5] ALBRECHT	92G	ARG	$e^+e^- \to \Upsilon(4S)$
0.89 ±0.19 ±0.13		[4] FULTON	91	CLEO	$e^+e^- \to \Upsilon(4S)$
1.00 ±0.23 ±0.14		[4] ALBRECHT	89L	ARG	$e^+e^- \to \Upsilon(4S)$
0.49 to 2.3	90	[6] BEAN	87B	CLEO	$e^+e^- \to \Upsilon(4S)$

[1] ARTUSO 97 uses partial reconstruction of $B \to D^* \ell \nu_\ell$ and independent of B^0 and B^+ production fraction.
[2] Assumes equal production of B^+ and B^0 at the $\Upsilon(4S)$.
[3] ATHANAS 94 uses events tagged by fully reconstructed B^- decays and partially or fully reconstructed B^0 decays.
[4] Assumes equal production of B^0 and B^+.
[5] ALBRECHT 92G data analyzed using $B \to D_s \overline{D}$, $D_s \overline{D}^*$, $D_s^* \overline{D}$, $D_s^* \overline{D}^*$ events.
[6] BEAN 87B assume the fraction of $B^0 \overline{B}^0$ events at the $\Upsilon(4S)$ is 0.41.

$\Delta\Gamma_{B^0_d} / \Gamma_{B^0_d}$

$\Gamma_{B^0_d}$ and $\Delta\Gamma_{B^0_d}$ are the decay rate average and difference between the two B^0_d mass eignstates (light-heavy). These are inferred by comparing the effective lifetimes measured using B^0_d decays to a CP-odd state ($B^0 \to J/\psi K^0_S$), a CP-even state ($B^0 \to J/\psi K^0_L$), or flavour-specific states.

VALUE (units 10^{-2})	CL%	DOCUMENT ID		TECN	COMMENT
0.5 ±1.0 OUR EVALUATION (Produced by HFLAV)					
0.1 ±1.0 OUR AVERAGE					
3.4 ±2.3 ±2.4		[1] SIRUNYAN	18BY	CMS	pp at 8 TeV
− 0.1 ±1.1 ±0.9		[2] AABOUD	16G	ATLS	pp at 7, 8 TeV
− 4.4 ±2.5 ±1.1		[3] AAIJ	14E	LHCB	pp at 7 TeV
1.7 ±1.8 ±1.1		[4] HIGUCHI	12	BELL	$e^+e^- \to \Upsilon(4S)$
0.8 ±3.7 ±1.8		[5] AUBERT,B	04C	BABR	$e^+e^- \to \Upsilon(4S)$
• • • We do not use the following data for averages, fits, limits, etc. • • •					
0.50±1.38		ABAZOV	14	D0	$p\overline{p}$ at 1.96 TeV
0 ±9		[6] ABDALLAH	03B	DLPH	$e^+e^- \to Z$
< 80	95	[7] BEHRENS	00B	CLE2	$e^+e^- \to \Upsilon(4S)$

[1] Measured using $B^0 \to J/\psi K^*(892)^0$ and $B^0 \to J/\psi K^0_S$ decays, and assuming $\beta = 21.9 \pm 0.7$ degrees.
[2] Measured from the ratio of decay time distributions of $B^0 \to J/\psi K^0_S$ and $B^0 \to J/\psi K^{*0}$ decays.
[3] Measured using the effective lifetimes of $B^0 \to J/\psi K^0_S$ and $B^0 \to J/\psi K^{*0}$ decays.
[4] Reports $-\Delta\Gamma_d/\Gamma_d$ using $B^0 \to J/\psi K^0_S$, $J/\psi K^0_L$, $D^-\pi^+$, $D^{*-}\pi^+$, $D^{*-}\rho^+$, and $D^{*-}\ell^+\nu$ decays.
[5] Corresponds to 90% confidence range [−0.084, 0.068].
[6] Used the measured $\tau_{B^0} = 1.55 \pm 0.03$ ps. Corresponds to an upper limit of < 0.18 at 95% C.L.
[7] BEHRENS 00B uses high-momentum lepton tags and partially reconstructed $\overline{B}^0 \to D^{*+}\pi^-$, ρ^- decays to determine the flavor of the B meson. Assumes Δ_{md}=0.478 ± 0.018 ps^{-1} and τ_{B^0}=1.548 ± 0.032 ps.

B^0 DECAY MODES

$\overline{B}^0$ modes are charge conjugates of the modes below. Reactions indicate the weak decay vertex and do not include mixing. Modes which do not identify the charge state of the B are listed in the $B^\pm/B^0$ ADMIXTURE section.

The branching fractions listed below assume 50% $B^0\overline{B}^0$ and 50% B^+B^- production at the $\Upsilon(4S)$. We have attempted to bring older measurements up to date by rescaling their assumed $\Upsilon(4S)$ production ratio to 50:50 and their assumed D, D_s, D^*, and ψ branching ratios to current values whenever this would affect our averages and best limits significantly.

Indentation is used to indicate a subchannel of a previous reaction. All resonant subchannels have been corrected for resonance branching fractions to the final state so the sum of the subchannel branching fractions can exceed that of the final state.

For inclusive branching fractions, *e.g.*, $B \to D^\pm X$, the values usually are multiplicities, not branching fractions. They can be greater than one.

	Mode		Fraction (Γ_i/Γ)	Scale factor/ Confidence level
Γ_1	$\ell^+\nu_\ell X$	[a]	(10.33± 0.28) %	
Γ_2	$e^+\nu_e X_c$		(10.1 ± 0.4) %	
Γ_3	$\ell^+\nu_\ell X_u$	[a]	(1.51± 0.19) $\times 10^{-3}$	
Γ_4	$D\ell^+\nu_\ell X$	[a]	(9.1 ± 0.8) %	
Γ_5	$D^-\ell^+\nu_\ell$	[a]	(2.12± 0.06) %	
Γ_6	$D^-\tau^+\nu_\tau$		(7.2 ± 1.5) $\times 10^{-3}$	
Γ_7	$D^*(2010)^-\ell^+\nu_\ell$	[a]	(4.90± 0.12) %	
Γ_8	$D^*(2010)^- e^+\nu_e$			
Γ_9	$D^*(2010)^-\mu^+\nu_\mu$			
Γ_{10}	$D^*(2010)^-\tau^+\nu_\tau$		(1.50± 0.08) %	S=1.1
Γ_{11}	$\overline{D}^{(*)} n\pi\ell^+\nu_\ell (n \geq 1)$	[a]	(2.3 ± 0.5) %	
Γ_{12}	$\overline{D}^0\pi^-\ell^+\nu_\ell$	[a]	(3.64± 0.20) $\times 10^{-3}$	
Γ_{13}	$D_0^*(2300)^-\ell^+\nu_\ell$, $D_0^{*-} \to \overline{D}^0\pi^-$	[a]	< 4.4 $\times 10^{-4}$	CL=90%
Γ_{14}	$D_2^*(2460)^-\ell^+\nu_\ell$, $D_2^{*-} \to \overline{D}^0\pi^-$	[a]	(1.41± 0.20) $\times 10^{-3}$	S=1.7
Γ_{15}	$\overline{D}^{*0}\pi^-\ell^+\nu_\ell$	[a]	(5.44± 0.28) $\times 10^{-3}$	
Γ_{16}	$D_1(2420)^-\ell^+\nu_\ell$, $D_1^- \to \overline{D}^{*0}\pi^-$	[a]	(2.85± 0.25) $\times 10^{-3}$	
Γ_{17}	$D_1(2420)^-\ell^+\nu_\ell$, $D_1^- \to D^-\pi^+\pi^-$	[a]	(1.02± 0.16) $\times 10^{-3}$	
Γ_{18}	$D_1'(2430)^-\ell^+\nu_\ell$, $D_1'^- \to \overline{D}^{*0}\pi^-$	[a]	(2.5 ± 0.6) $\times 10^{-3}$	
Γ_{19}	$D_2^*(2460)^-\ell^+\nu_\ell$, $D_2^{*-} \to \overline{D}^{*0}\pi^-$	[a]	(6.6 ± 1.1) $\times 10^{-4}$	
Γ_{20}	$D^-\pi^+\pi^-\ell^+\nu_\ell$	[a]	(1.45± 0.22) $\times 10^{-3}$	
Γ_{21}	$D^{*-}\pi^+\pi^-\ell^+\nu_\ell$	[a]	(5.1 ± 2.3) $\times 10^{-4}$	
Γ_{22}	$\rho^-\ell^+\nu_\ell$	[a]	(2.94± 0.21) $\times 10^{-4}$	
Γ_{23}	$\pi^-\ell^+\nu_\ell$	[a]	(1.50± 0.05) $\times 10^{-4}$	
Γ_{24}	$\pi^-\mu^+\nu_\mu$			
Γ_{25}	$\pi^-\tau^+\nu_\tau$		< 2.5 $\times 10^{-4}$	CL=90%
	Inclusive modes			
Γ_{26}	$K^\pm X$		(78 ± 8) %	
Γ_{27}	$D^0 X$		(8.1 ± 1.5) %	
Γ_{28}	$\overline{D}^0 X$		(47.4 ± 2.8) %	
Γ_{29}	$D^+ X$		< 3.9 %	CL=90%
Γ_{30}	$D^- X$		(36.9 ± 3.3) %	
Γ_{31}	$D_s^+ X$		(10.3 $^{+2.1}_{-1.8}$) %	
Γ_{32}	$D_s^- X$		< 2.6 %	CL=90%
Γ_{33}	$\Lambda_c^+ X$		< 3.1 %	CL=90%
Γ_{34}	$\overline{\Lambda}_c^- X$		(5.0 $^{+2.1}_{-1.5}$) %	
Γ_{35}	$\overline{c} X$		(95 ± 5) %	
Γ_{36}	$c X$		(24.6 ± 3.1) %	
Γ_{37}	$\overline{c}/c X$		(119 ± 6) %	
	D, D^*, or D_s modes			
Γ_{38}	$D^-\pi^+$		(2.51± 0.08) $\times 10^{-3}$	
Γ_{39}	$D^-\rho^+$		(7.6 ± 1.3) $\times 10^{-3}$	
Γ_{40}	$D^- K^0\pi^+$		(4.9 ± 0.9) $\times 10^{-4}$	
Γ_{41}	$D^- K^*(892)^+$		(4.5 ± 0.7) $\times 10^{-4}$	
Γ_{42}	$D^-\omega\pi^+$		(2.8 ± 0.6) $\times 10^{-3}$	
Γ_{43}	$D^- K^+$		(2.05± 0.08) $\times 10^{-4}$	
Γ_{44}	$D^- K^+\pi^+\pi^-$		(3.5 ± 0.8) $\times 10^{-4}$	
Γ_{45}	$D^- K^+\overline{K}^0$		(1.64± 0.26) $\times 10^{-4}$	
Γ_{46}	$D^- K^+\overline{K}^*(892)^0$		(7.7 ± 0.6) $\times 10^{-4}$	
Γ_{47}	$\overline{D}^0\pi^+\pi^-$		(8.8 ± 0.5) $\times 10^{-4}$	
Γ_{48}	$D^*(2010)^-\pi^+$		(2.66± 0.07) $\times 10^{-3}$	
Γ_{49}	$\overline{D}^0 K^+ K^-$		(6.1 ± 0.5) $\times 10^{-5}$	
Γ_{50}	$D^-\pi^+\pi^+\pi^-$		(6.0 ± 0.6) $\times 10^{-3}$	
Γ_{51}	$(D^-\pi^+\pi^+\pi^-)$ nonresonant		(3.9 ± 1.9) $\times 10^{-3}$	
Γ_{52}	$D^-\pi^+\rho^0$		(1.1 ± 1.0) $\times 10^{-3}$	
Γ_{53}	$D^- a_1(1260)^+$		(6.0 ± 3.3) $\times 10^{-3}$	
Γ_{54}	$D^*(2010)^-\pi^+\pi^0$		(1.5 ± 0.5) %	
Γ_{55}	$D^*(2010)^-\rho^+$		(6.8 ± 0.9) $\times 10^{-3}$	
Γ_{56}	$D^*(2010)^- K^+$		(2.16± 0.08) $\times 10^{-4}$	
Γ_{57}	$D^*(2010)^- K^0\pi^+$		(3.0 ± 0.8) $\times 10^{-4}$	
Γ_{58}	$D^*(2010)^- K^*(892)^+$		(3.3 ± 0.6) $\times 10^{-4}$	
Γ_{59}	$D^*(2010)^- K^+\overline{K}^0$		(1.8 ± 0.4) $\times 10^{-4}$	
Γ_{60}	$D^*(2010)^- K^+\overline{K}^*(892)^0$		(1.31± 0.13) $\times 10^{-3}$	
Γ_{61}	$D^*(2010)^-\pi^+\pi^+\pi^-$		(7.21± 0.29) $\times 10^{-3}$	
Γ_{62}	$(D^*(2010)^-\pi^+\pi^+\pi^-)$ nonresonant		(0.0 ± 2.5) $\times 10^{-3}$	
Γ_{63}	$D^*(2010)^-\pi^+\rho^0$		(5.7 ± 3.2) $\times 10^{-3}$	
Γ_{64}	$D^*(2010)^- a_1(1260)^+$		(1.30± 0.27) %	
Γ_{65}	$\overline{D}_1(2420)^0\pi^-\pi^+$, $\overline{D}_1^0 \to D^{*-}\pi^+$		(1.47± 0.35) $\times 10^{-4}$	
Γ_{66}	$D^*(2010)^- K^+\pi^-\pi^+$		(4.7 ± 0.4) $\times 10^{-4}$	
Γ_{67}	$D^*(2010)^-\pi^+\pi^+\pi^-\pi^0$		(1.76± 0.27) %	
Γ_{68}	$D^{*-} 3\pi^+ 2\pi^-$		(4.7 ± 0.9) $\times 10^{-3}$	
Γ_{69}	$D^*(2010)^-\omega\pi^+$		(2.46± 0.18) $\times 10^{-3}$	S=1.2
Γ_{70}	$\overline{D}_1(2430)^0\omega$, $\overline{D}_1^0 \to D^{*-}\pi^+$		(2.7 $^{+0.8}_{-0.4}$) $\times 10^{-4}$	
Γ_{71}	$D^{*-}\rho(1450)^+$, $\rho^+ \to \omega\pi^+$		(1.07$^{+0.40}_{-0.34}$) $\times 10^{-3}$	
Γ_{72}	$\overline{D}_1(2420)^0\omega$, $\overline{D}_1^0 \to D^{*-}\pi^+$		(7.0 ± 2.2) $\times 10^{-5}$	

Γ_{73}	$\overline{D}_2^*(2460)^0\omega$, $\overline{D}_2^0 \to D^{*-}\pi^+$		$(4.0 \pm 1.4) \times 10^{-5}$	
Γ_{74}	$D^{*-}b_1(1235)^+$, $b_1^+ \to \omega\pi^+$		$< 7 \times 10^{-5}$	CL=90%
Γ_{75}	$\overline{D}^{**-}\pi^+$	[b]	$(1.9 \pm 0.9) \times 10^{-3}$	
Γ_{76}	$D_1(2420)^-\pi^+$, $D_1^- \to D^-\pi^+\pi^-$		$(9.9 {}^{+2.0}_{-2.5}) \times 10^{-5}$	
Γ_{77}	$D_1(2420)^-\pi^+$, $D_1^- \to D^{*-}\pi^+\pi^-$		$< 3.3 \times 10^{-5}$	CL=90%
Γ_{78}	$\overline{D}_2^*(2460)^-\pi^+$, $D_2^{*-} \to D^0\pi^-$		$(2.38 \pm 0.16) \times 10^{-4}$	
Γ_{79}	$\overline{D}_0^*(2400)^-\pi^+$, $D_0^{*-} \to D^0\pi^-$		$(7.6 \pm 0.8) \times 10^{-5}$	
Γ_{80}	$D_2^*(2460)^-\pi^+$, $D_2^{*-} \to D^{*-}\pi^+\pi^-$		$< 2.4 \times 10^{-5}$	CL=90%
Γ_{81}	$\overline{D}_2^*(2460)^-\rho^+$		$< 4.9 \times 10^{-3}$	CL=90%
Γ_{82}	$D^0\overline{D}^0$		$(1.4 \pm 0.7) \times 10^{-5}$	
Γ_{83}	$D^{*0}\overline{D}^0$		$< 2.9 \times 10^{-4}$	CL=90%
Γ_{84}	D^-D^+		$(2.11 \pm 0.18) \times 10^{-4}$	
Γ_{85}	$D^\pm D^{*\mp}$ (CP-averaged)		$(6.1 \pm 0.6) \times 10^{-4}$	
Γ_{86}	$D^-D_s^+$		$(8.1 \pm 0.6) \times 10^{-3}$	S=1.1
Γ_{87}	$\overline{D}^0 D_s^+\pi^-$, $m(\overline{D}^0\pi^-)>2.05$ GeV			
Γ_{88}	$D^*(2010)^-D_s^+$		$(8.2 \pm 0.8) \times 10^{-3}$	
Γ_{89}	$D^*(2010)^-D_s^+$, $D^{*-} \to \overline{D}^0\pi^-$, $m(\overline{D}^0\pi^-)>2.05$ GeV			
Γ_{90}	$D_2^*(2460)^-D_s^+$, $D_2^{*-} \to \overline{D}^0\pi^-$			
Γ_{91}	$D_1^*(2600)^-D_s^+$, $D_1^{*-} \to \overline{D}^0\pi^-$			
Γ_{92}	$D_3^*(2750)^-D_s^+$, $D_3^{*-} \to \overline{D}^0\pi^-$			
Γ_{93}	$D_1^*(2760)^-D_s^+$, $D_1^{*-} \to \overline{D}^0\pi^-$			
Γ_{94}	$D_J^*(3000)^-D_s^+$, $D_J^{*-} \to \overline{D}^0\pi^-$			
Γ_{95}	$T_{cs0}^*(2870)^0\overline{D}^0$, $T_{cs0}^{*0} \to D_s^+\pi^-$			
Γ_{96}	$D^-D_s^{*+}$		$(7.4 \pm 1.6) \times 10^{-3}$	
Γ_{97}	$D^*(2010)^-D_s^{*+}$		(1.77 ± 0.14) %	
Γ_{98}	$D_{s0}(2317)^-K^+$, $D_{s0}^- \to D_s^-\pi^0$		$(4.2 \pm 1.4) \times 10^{-5}$	
Γ_{99}	$D_{s0}(2317)^-\pi^+$, $D_{s0}^- \to D_s^-\pi^0$		$< 2.5 \times 10^{-5}$	CL=90%
Γ_{100}	$D_{sJ}(2457)^-K^+$, $D_{sJ}^- \to D_s^-\pi^0$		$< 9.4 \times 10^{-6}$	CL=90%
Γ_{101}	$D_{sJ}(2457)^-\pi^+$, $D_{sJ}^- \to D_s^-\pi^0$		$< 4.0 \times 10^{-6}$	CL=90%
Γ_{102}	$D_s^-D_s^+$		$< 3.6 \times 10^{-5}$	CL=90%
Γ_{103}	$D_s^{*-}D_s^+$		$< 1.3 \times 10^{-4}$	CL=90%
Γ_{104}	$D_s^{*-}D_s^{*+}$		$< 2.4 \times 10^{-4}$	CL=90%
Γ_{105}	$D_{s0}^*(2317)^+D^-$, $D_{s0}^{*+} \to D_s^+\pi^0$		$(1.05 \pm 0.16) \times 10^{-3}$	S=1.1
Γ_{106}	$D_{s0}(2317)^+D^-$, $D_{s0}^+ \to D_s^{*+}\gamma$		$< 9.5 \times 10^{-4}$	CL=90%
Γ_{107}	$D_{s0}(2317)^+D^*(2010)^-$, $D_{s0}^+ \to D_s^+\pi^0$		$(1.5 \pm 0.6) \times 10^{-3}$	
Γ_{108}	$D_{sJ}(2457)^+D^-$		$(3.5 \pm 1.1) \times 10^{-3}$	
Γ_{109}	$D_{sJ}(2457)^+D^-$, $D_{sJ}^+ \to D_s^+\gamma$		$(6.5 {}^{+1.7}_{-1.4}) \times 10^{-4}$	
Γ_{110}	$D_{sJ}(2457)^+D^-$, $D_{sJ}^+ \to D_s^{*+}\gamma$		$< 6.0 \times 10^{-4}$	CL=90%
Γ_{111}	$D_{sJ}(2457)^+D^-$, $D_{sJ}^+ \to D_s^+\pi^+\pi^-$		$< 2.0 \times 10^{-4}$	CL=90%
Γ_{112}	$D_{sJ}(2457)^+D^-$, $D_{sJ}^+ \to D_s^+\pi^0$		$< 3.6 \times 10^{-4}$	CL=90%
Γ_{113}	$D^*(2010)^-D_{sJ}(2457)^+$		$(9.3 \pm 2.2) \times 10^{-3}$	
Γ_{114}	$D_{sJ}(2457)^+D^*(2010)$, $D_{sJ}^+ \to D_s^+\gamma$		$(2.3 {}^{+0.9}_{-0.7}) \times 10^{-3}$	
Γ_{115}	$D^-D_{s1}(2536)^+$, $D_{s1}^+ \to D^{*0}K^+ + D^{*+}K^0$		$(2.8 \pm 0.7) \times 10^{-4}$	
Γ_{116}	$D^-D_{s1}(2536)^+$, $D_{s1}^+ \to D^{*0}K^+$		$(1.7 \pm 0.6) \times 10^{-4}$	
Γ_{117}	$D^-D_{s1}(2536)^+$, $D_{s1}^+ \to D^{*+}K^0$		$(2.6 \pm 1.1) \times 10^{-4}$	
Γ_{118}	$D^*(2010)^-D_{s1}(2536)^+$, $D_{s1}^+ \to D^{*0}K^+ + D^{*+}K^0$		$(5.0 \pm 1.4) \times 10^{-4}$	
Γ_{119}	$D^*(2010)^-D_{s1}(2536)^+$, $D_{s1}^+ \to D^{*0}K^+$		$(3.3 \pm 1.1) \times 10^{-4}$	
Γ_{120}	$D^{*-}D_{s1}(2536)^+$, $D_{s1}^+ \to D^{*+}K^0$		$(5.0 \pm 1.7) \times 10^{-4}$	
Γ_{121}	$D^-D_{sJ}(2573)^+$, $D_{sJ}^+ \to D^0K^+$		$(3.4 \pm 1.8) \times 10^{-5}$	
Γ_{122}	$D^*(2010)^-D_{sJ}(2573)^+$, $D_{sJ}^+ \to D^0K^+$		$< 2 \times 10^{-4}$	CL=90%
Γ_{123}	$D^-D_{sJ}(2700)^+$, $D_{sJ}^+ \to D^0K^+$		$(7.1 \pm 1.2) \times 10^{-4}$	
Γ_{124}	$D^+\pi^-$		$(7.3 \pm 1.2) \times 10^{-7}$	
Γ_{125}	$D_s^+\pi^-$		$(2.03 \pm 0.18) \times 10^{-5}$	
Γ_{126}	$D_s^{*+}\pi^-$		$(2.1 \pm 0.4) \times 10^{-5}$	S=1.4
Γ_{127}	$D_s^+\rho^-$		$< 2.4 \times 10^{-5}$	CL=90%
Γ_{128}	$D_s^{*+}\rho^-$		$(4.1 \pm 1.3) \times 10^{-5}$	
Γ_{129}	$D_s^+a_0^-$		$< 1.9 \times 10^{-5}$	CL=90%
Γ_{130}	$D_s^{*+}a_0^-$		$< 3.6 \times 10^{-5}$	CL=90%
Γ_{131}	$D_s^+a_1(1260)^-$		$< 2.1 \times 10^{-3}$	CL=90%
Γ_{132}	$D_s^{*+}a_1(1260)^-$		$< 1.7 \times 10^{-3}$	CL=90%
Γ_{133}	$D_s^+a_2^-$		$< 1.9 \times 10^{-4}$	CL=90%
Γ_{134}	$D_s^{*+}a_2^-$		$< 2.0 \times 10^{-4}$	CL=90%
Γ_{135}	$D_s^-K^+$		$(2.7 \pm 0.5) \times 10^{-5}$	S=2.7
Γ_{136}	$D_s^{*-}K^+$		$(2.19 \pm 0.30) \times 10^{-5}$	
Γ_{137}	$D_{s1}(2536)^\mp K^\pm$, $D_{s1}^- \to \overline{D}^*(2007)^0K^-$		$(5.1 \pm 0.6) \times 10^{-6}$	
Γ_{138}	$D_s^-K^*(892)^+$		$(3.5 \pm 1.0) \times 10^{-5}$	
Γ_{139}	$D_s^{*-}K^*(892)^+$		$(3.2 {}^{+1.5}_{-1.3}) \times 10^{-5}$	
Γ_{140}	$D_s^-\pi^+K^0$		$(9.7 \pm 1.4) \times 10^{-5}$	
Γ_{141}	$D_s^{*-}\pi^+K^0$		$< 1.10 \times 10^{-4}$	CL=90%
Γ_{142}	$D_s^-K^+\pi^+\pi^-$		$(1.7 \pm 0.5) \times 10^{-4}$	
Γ_{143}	$D_s^-\pi^+K^*(892)^0$		$< 3.0 \times 10^{-3}$	CL=90%
Γ_{144}	$D_s^{*-}\pi^+K^*(892)^0$		$< 1.6 \times 10^{-3}$	CL=90%
Γ_{145}	$\overline{D}^0K^0$		$(5.5 \pm 0.4) \times 10^{-5}$	
Γ_{146}	$\overline{D}^0K^+\pi^-$		$(8.8 \pm 1.7) \times 10^{-5}$	
Γ_{147}	$\overline{D}^0K^*(892)^0$		$(4.5 \pm 0.6) \times 10^{-5}$	
Γ_{148}	$\overline{D}^0K^*(1410)^0$		$< 6.7 \times 10^{-5}$	CL=90%
Γ_{149}	$\overline{D}^0K_0^*(1430)^0$		$(7 \pm 7) \times 10^{-6}$	
Γ_{150}	$\overline{D}^0K_2^*(1430)^0$		$(2.1 \pm 0.9) \times 10^{-5}$	
Γ_{151}	$D_0^*(2300)^-K^+$, $D_0^{*-} \to \overline{D}^0\pi^-$		$(1.9 \pm 0.9) \times 10^{-5}$	
Γ_{152}	$D_2^*(2460)^-K^+$, $D_2^{*-} \to \overline{D}^0\pi^-$		$(2.03 \pm 0.35) \times 10^{-5}$	
Γ_{153}	$D_3^*(2760)^-K^+$, $D_3^{*-} \to \overline{D}^0\pi^-$		$< 1.0 \times 10^{-6}$	CL=90%
Γ_{154}	$\overline{D}^0K^+\pi^-$ nonresonant		$< 3.7 \times 10^{-5}$	CL=90%
Γ_{155}	$[K^+K^-]_DK^*(892)^0$		$(3.7 \pm 0.5) \times 10^{-5}$	
Γ_{156}	$[\pi^+\pi^-]_DK^*(892)^0$		$(5.0 \pm 0.8) \times 10^{-5}$	
Γ_{157}	$[\pi^+K^-]_DK^*(892)^0$			
Γ_{158}	$[K^+\pi^-]_DK^*(892)^0$			
Γ_{159}	$[\pi^+\pi^-\pi^+\pi^-]_DK^{*0}$		$(4.0 \pm 0.6) \times 10^{-5}$	
Γ_{160}	$[\pi^+K^-\pi^+\pi^-]_DK^{*0}$			
Γ_{161}	$[K^+\pi^-\pi^+\pi^-]_DK^{*0}$			
Γ_{162}	$\overline{D}^0\pi^0$		$(2.67 \pm 0.09) \times 10^{-4}$	
Γ_{163}	$\overline{D}^0\rho^0$		$(3.21 \pm 0.21) \times 10^{-4}$	
Γ_{164}	$\overline{D}^0f_2$		$(1.56 \pm 0.21) \times 10^{-4}$	
Γ_{165}	$\overline{D}^0\eta$		$(2.56 \pm 0.12) \times 10^{-4}$	
Γ_{166}	$\overline{D}^0\eta'$		$(1.38 \pm 0.16) \times 10^{-4}$	S=1.3
Γ_{167}	$\overline{D}^0\omega$		$(2.54 \pm 0.16) \times 10^{-4}$	
Γ_{168}	$\overline{D}^0\phi$		$(7.7 \pm 2.3) \times 10^{-7}$	
Γ_{169}	$D^0K^+\pi^-$		$(5.3 \pm 3.2) \times 10^{-6}$	
Γ_{170}	$D^0K^*(892)^0$		$(3.0 \pm 0.6) \times 10^{-6}$	
Γ_{171}	$\overline{D}^{*0}\gamma$		$< 2.5 \times 10^{-5}$	CL=90%
Γ_{172}	$\overline{D}^*(2007)^0\pi^0$		$(2.2 \pm 0.6) \times 10^{-4}$	S=2.6
Γ_{173}	$\overline{D}^*(2007)^0\rho^0$		$< 5.1 \times 10^{-4}$	CL=90%
Γ_{174}	$\overline{D}^*(2007)^0\eta$		$(2.3 \pm 0.6) \times 10^{-4}$	S=2.8
Γ_{175}	$\overline{D}^*(2007)^0\eta'$		$(1.40 \pm 0.22) \times 10^{-4}$	
Γ_{176}	$\overline{D}^*(2007)^0\pi^+\pi^-$		$(6.2 \pm 2.2) \times 10^{-4}$	
Γ_{177}	$\overline{D}^*(2007)^0K^+\pi^-$		$(5.2 \pm 1.9) \times 10^{-5}$	
Γ_{178}	$\overline{D}^*(2007)^0K^0$		$(3.6 \pm 1.2) \times 10^{-5}$	
Γ_{179}	$\overline{D}^*(2007)^0K^*(892)^0$		$< 6.9 \times 10^{-5}$	CL=90%
Γ_{180}	$\overline{D}^*(2007)^0\phi$		$(2.2 \pm 0.6) \times 10^{-6}$	
Γ_{181}	$D^*(2007)^0K^*(892)^0$		$< 4.0 \times 10^{-5}$	CL=90%
Γ_{182}	$D^*(2007)^0\pi^+\pi^+\pi^-\pi^-$		$(2.7 \pm 0.5) \times 10^{-3}$	
Γ_{183}	$D^*(2010)^+D^*(2010)^-$		$(8.0 \pm 0.6) \times 10^{-4}$	
Γ_{184}	$\overline{D}^*(2007)^0\omega$		$(3.6 \pm 1.1) \times 10^{-4}$	S=3.1
Γ_{185}	$D^*(2010)^+D^-$		$(6.1 \pm 1.5) \times 10^{-4}$	S=1.6

Int. J. Mod. Phys. A 2026.41. Downloaded from www.worldscientific.com
by [redacted] LIFORNIA @ BERKELEY on 09/16/26. Re-use and distribution is strictly not permitted, except for Open Access articles.

Int. J. Mod. Phys. A 2026.41. Downloaded from www.worldscientific.com
by UNIVERSITY OF CALIFORNIA @ BERKELEY on 09/16/26. Re-use and distribution is strictly not permitted, except for Open Access articles.

Γ_{186}	$D^*(2007)^0 \overline{D}^*(2007)^0$	$<$ 9	$\times 10^{-5}$	CL=90%
Γ_{187}	$D^- D^0 K^+$	(1.07 ± 0.11)	$\times 10^{-3}$	
Γ_{188}	$D^- D^*(2007)^0 K^+$	(3.5 ± 0.4)	$\times 10^{-3}$	
Γ_{189}	$D^*(2010)^- D^0 K^+$	(2.47 ± 0.21)	$\times 10^{-3}$	
Γ_{190}	$D^*(2010)^- D^*(2007)^0 K^+$	(1.06 ± 0.09)	%	
Γ_{191}	$D^- D^+ K^0$	(7.5 ± 1.7)	$\times 10^{-4}$	
Γ_{192}	$D^*(2010)^- D^+ K^0 + D^- D^*(2010)^+ K^0$	(6.4 ± 0.5)	$\times 10^{-3}$	
Γ_{193}	$D^*(2010)^- D^*(2010)^+ K^0$	(8.1 ± 0.7)	$\times 10^{-3}$	
Γ_{194}	$D^{*-} D_{s1}(2536)^+$, $D_{s1}^+ \to D^{*+} K^0$	(8.0 ± 2.4)	$\times 10^{-4}$	
Γ_{195}	$\overline{D}^0 D^0 K^0$	(2.7 ± 1.1)	$\times 10^{-4}$	
Γ_{196}	$D^0 \overline{D}^0 K^+ \pi^-$	(3.5 ± 0.5)	$\times 10^{-4}$	
Γ_{197}	$\overline{D}^0 D^*(2007)^0 K^0 + \overline{D}^*(2007)^0 D^0 K^0$	(1.1 ± 0.5)	$\times 10^{-3}$	
Γ_{198}	$\overline{D}^*(2007)^0 D^*(2007)^0 K^0$	(2.4 ± 0.9)	$\times 10^{-3}$	
Γ_{199}	$(\overline{D}+\overline{D}^*)(D+D^*)K$	(3.68 ± 0.26)	%	

Charmonium modes

Γ_{200}	$\eta_c K^0$	(1.04 ± 0.13)	$\times 10^{-3}$	
Γ_{201}	$\eta_c(1S) K^+ \pi^-$	(7.8 ± 1.0)	$\times 10^{-4}$	
Γ_{202}	$\eta_c(1S) K^+ \pi^-$ (NR)	(8.1 ± 1.7)	$\times 10^{-5}$	
Γ_{203}	$T_{c\overline{c}}(4100)^- K^+$, $T_{c\overline{c}}^- \to \eta_c \pi^-$	(2.6 ± 1.3)	$\times 10^{-5}$	
Γ_{204}	$\eta_c(1S) K^*(1410)^0$	(2.5 ± 1.9)	$\times 10^{-4}$	
Γ_{205}	$\eta_c(1S) K_0^*(1430)^0$	(2.1 ± 0.5)	$\times 10^{-4}$	
Γ_{206}	$\eta_c(1S) K_2^*(1430)^0$	(6.4 $^{+2.9}_{-3.5}$)	$\times 10^{-5}$	
Γ_{207}	$\eta_c(1S) K^*(1680)^0$	(4 ± 5)	$\times 10^{-5}$	
Γ_{208}	$\eta_c(1S) K_0^*(1950)^0$	(6 $^{+4}_{-5}$)	$\times 10^{-5}$	
Γ_{209}	$\eta_c K^*(892)^0$	(5.3 $^{+1.0}_{-1.2}$)	$\times 10^{-4}$	S=2.0
Γ_{210}	$\eta_c(2S) K_S^0$, $\eta_c \to p\overline{p}\pi^+\pi^-$	(4.2 $^{+1.4}_{-1.2}$)	$\times 10^{-7}$	
Γ_{211}	$\eta_c(2S) K^{*0}$	$<$ 3.9	$\times 10^{-4}$	CL=90%
Γ_{212}	$h_c(1P) K_S^0$	$<$ 1.4	$\times 10^{-5}$	
Γ_{213}	$h_c(1P) K^{*0}$	$<$ 3.4	$\times 10^{-4}$	CL=90%
Γ_{214}	$J/\psi(1S) K^0$	(8.91 ± 0.21)	$\times 10^{-4}$	
Γ_{215}	$J/\psi(1S) K^+ \pi^-$	(1.15 ± 0.05)	$\times 10^{-3}$	
Γ_{216}	$J/\psi(1S) K^*(892)^0$	(1.27 ± 0.05)	$\times 10^{-3}$	
Γ_{217}	$J/\psi(1S) \eta K_S^0$	(5.4 ± 0.9)	$\times 10^{-5}$	
Γ_{218}	$J/\psi(1S) \eta' K_S^0$	$<$ 2.5	$\times 10^{-5}$	CL=90%
Γ_{219}	$J/\psi(1S) \phi K^0$	(4.9 ± 1.0)	$\times 10^{-5}$	S=1.3
Γ_{220}	$J/\psi(1S) \omega K^0$	(2.3 ± 0.4)	$\times 10^{-4}$	
Γ_{221}	$\chi_{c0}(3915)$, $\chi_{c0} \to J/\psi\omega$	(2.1 ± 0.9)	$\times 10^{-5}$	
Γ_{222}	$J/\psi(1S) K(1270)^0$	(1.3 ± 0.5)	$\times 10^{-3}$	
Γ_{223}	$J/\psi(1S) \pi^0$	(1.73 ± 0.09)	$\times 10^{-5}$	S=1.2
Γ_{224}	$J/\psi(1S) \eta$	(1.23 ± 0.19)	$\times 10^{-5}$	
Γ_{225}	$J/\psi(1S) \pi^+\pi^-$	(3.99 ± 0.15)	$\times 10^{-5}$	
Γ_{226}	$J/\psi(1S) \pi^+\pi^-$ nonresonant	$<$ 1.2	$\times 10^{-5}$	CL=90%
Γ_{227}	$J/\psi(1S) f_0(500)$, $f_0 \to \pi\pi$	(8.8 $^{+1.2}_{-1.6}$)	$\times 10^{-6}$	
Γ_{228}	$J/\psi(1S) f_2$	(3.3 $^{+0.5}_{-0.6}$)	$\times 10^{-6}$	S=1.5
Γ_{229}	$J/\psi(1S) \rho^0$	(2.55 $^{+0.18}_{-0.16}$)	$\times 10^{-5}$	
Γ_{230}	$J/\psi(1S) f_0(980)$, $f_0 \to \pi^+\pi^-$	$<$ 1.1	$\times 10^{-6}$	CL=90%
Γ_{231}	$J/\psi(1S) \rho(1450)^0$, $\rho^0 \to \pi\pi$	(2.9 $^{+1.6}_{-0.7}$)	$\times 10^{-6}$	
Γ_{232}	$J/\psi \rho(1700)^0$, $\rho^0 \to \pi^+\pi^-$	(2.0 ± 1.3)	$\times 10^{-6}$	
Γ_{233}	$J/\psi(1S) \omega$	(2.08 ± 0.29)	$\times 10^{-5}$	
Γ_{234}	$J/\psi(1S) K^+ K^-$	(2.53 ± 0.35)	$\times 10^{-6}$	
Γ_{235}	$J/\psi(1S) a_0(980)$, $a_0 \to K^+ K^-$	(4.7 ± 3.4)	$\times 10^{-7}$	
Γ_{236}	$J/\psi(1S) \phi$	$<$ 1.1	$\times 10^{-7}$	CL=90%
Γ_{237}	$J/\psi(1S) \eta'(958)$	(5.9 ± 1.2)	$\times 10^{-6}$	
Γ_{238}	$J/\psi(1S) K^0 \pi^+\pi^-$	(4.5 ± 0.4)	$\times 10^{-4}$	
Γ_{239}	$J/\psi(1S) K^0 K^- \pi^+ +$ c.c.	$<$ 2.1	$\times 10^{-5}$	CL=90%
Γ_{240}	$J/\psi(1S) K^0 K^+ K^-$	(2.5 ± 0.7)	$\times 10^{-5}$	S=1.8
Γ_{241}	$J/\psi(1S) K^0 K^\pm \pi^\mp$			
Γ_{242}	$J/\psi(1S) K^0 \rho^0$	(5.4 ± 3.0)	$\times 10^{-4}$	
Γ_{243}	$J/\psi(1S) K^*(892)^+ \pi^-$	(8 ± 4)	$\times 10^{-4}$	
Γ_{244}	$J/\psi(1S) \pi^+\pi^-\pi^+\pi^-$	(1.44 ± 0.12)	$\times 10^{-5}$	
Γ_{245}	$J/\psi(1S) f_1(1285)$	(8.4 ± 2.1)	$\times 10^{-6}$	
Γ_{246}	$J/\psi(1S) K^*(892)^0 \pi^+\pi^-$	(6.6 ± 2.2)	$\times 10^{-4}$	
Γ_{247}	$\eta_{c2}(1D) K_S^0$, $\eta_{c2} \to h_c\gamma$	$<$ 3.5	$\times 10^{-5}$	CL=90%
Γ_{248}	$\eta_{c2}(1D) \pi^- K^+$, $\eta_{c2} \to h_c\gamma$	$<$ 1.0	$\times 10^{-4}$	CL=90%
Γ_{249}	$\chi_{c1}(3872)^- K^+$	$<$ 5	$\times 10^{-4}$	CL=90%
Γ_{250}	$\chi_{c1}(3872)^- K^+$, $\chi_{c1}(3872)^- \to J/\psi(1S)\pi^-\pi^0$	[c] $<$ 4.2	$\times 10^{-6}$	CL=90%
Γ_{251}	$\chi_{c1}(3872) K^0$	(1.1 ± 0.4)	$\times 10^{-4}$	
Γ_{252}	$\chi_{c1}(3872) K^*(892)^0$	(9 ± 5)	$\times 10^{-5}$	
Γ_{253}	$\chi_{c1}(3872) K^+ \pi^-$	(1.8 ± 0.7)	$\times 10^{-4}$	
Γ_{254}	$\chi_{c1}(3872) \gamma$	$<$ 1.2	$\times 10^{-5}$	CL=90%
Γ_{255}	$T_{c\overline{c}1}(4430)^\pm K^\mp$, $T_{c\overline{c}1}^\pm \to \psi(2S)\pi^\pm$	(6.0 $^{+3.0}_{-2.4}$)	$\times 10^{-5}$	
Γ_{256}	$T_{c\overline{c}1}(4430)^\pm K^\mp$, $T_{c\overline{c}1}^\pm \to J/\psi\pi^\pm$	(5.4 $^{+4.0}_{-1.2}$)	$\times 10^{-6}$	
Γ_{257}	$T_{c\overline{c}1}(3900)^\pm K^\mp$, $T_{c\overline{c}1}^\pm \to J/\psi\pi^\pm$	$<$ 9	$\times 10^{-7}$	
Γ_{258}	$T_{c\overline{c}1}(4200)^\pm K^\mp$, $T_{c\overline{c}1}^\pm \to J/\psi\pi^\pm$	(2.2 $^{+1.3}_{-0.8}$)	$\times 10^{-5}$	
Γ_{259}	$J/\psi(1S) p\overline{p}$	(4.5 ± 0.6)	$\times 10^{-7}$	
Γ_{260}	$J/\psi(1S)\gamma$	$<$ 1.5	$\times 10^{-6}$	CL=90%
Γ_{261}	$J/\psi\mu^+\mu^-$, $J/\psi \to \mu^+\mu^-$	$<$ 1.0	$\times 10^{-9}$	CL=95%
Γ_{262}	$J/\psi(1S) \overline{D}^0$	$<$ 9.6	$\times 10^{-7}$	CL=90%
Γ_{263}	$\psi(2S)\pi^0$	(1.17 ± 0.19)	$\times 10^{-5}$	
Γ_{264}	$\psi(2S) K^0$	(5.8 ± 0.5)	$\times 10^{-4}$	
Γ_{265}	$\psi(2S) K^0 \pi^+\pi^-$	(2.81 ± 0.30)	$\times 10^{-4}$	
Γ_{266}	$\psi(3770) K^0$, $\psi \to \overline{D}^0 D^0$	$<$ 1.23	$\times 10^{-4}$	CL=90%
Γ_{267}	$\psi(3770) K^0$, $\psi \to D^- D^+$	$<$ 1.88	$\times 10^{-4}$	CL=90%
Γ_{268}	$\psi(2S)\pi^+\pi^-$	(2.24 ± 0.35)	$\times 10^{-5}$	
Γ_{269}	$\psi(2S) K^+ \pi^-$	(5.8 ± 0.4)	$\times 10^{-4}$	
Γ_{270}	$\psi(2S) K^*(892)^0$	(5.9 ± 0.4)	$\times 10^{-4}$	
Γ_{271}	$\chi_{c0} K^0$	(1.9 ± 0.4)	$\times 10^{-4}$	
Γ_{272}	$\chi_{c0} K^*(892)^0$	(1.7 ± 0.4)	$\times 10^{-4}$	
Γ_{273}	$\chi_{c1}\pi^0$	(1.12 ± 0.28)	$\times 10^{-5}$	
Γ_{274}	$\chi_{c1} K^0$	(3.95 ± 0.27)	$\times 10^{-4}$	
Γ_{275}	$\chi_{c1}\pi^- K^+$	(4.97 ± 0.30)	$\times 10^{-4}$	
Γ_{276}	$\chi_{c1} K^*(892)^0$	(2.38 ± 0.19)	$\times 10^{-4}$	S=1.2
Γ_{277}	$T_{c\overline{c}}(4050)^- K^+$, $T_{c\overline{c}}^- \to \chi_{c1}\pi^-$	(3.0 $^{+4.0}_{-1.8}$)	$\times 10^{-5}$	
Γ_{278}	$T_{c\overline{c}}(4250)^- K^+$, $T_{c\overline{c}}^- \to \chi_{c1}\pi^-$	(4.0 $^{+20.0}_{-1.0}$)	$\times 10^{-5}$	
Γ_{279}	$\chi_{c1}\pi^+\pi^- K^0$	(3.2 ± 0.5)	$\times 10^{-4}$	
Γ_{280}	$\chi_{c1}\pi^-\pi^0 K^+$	(3.5 ± 0.6)	$\times 10^{-4}$	
Γ_{281}	$\chi_{c2} K^0$	$<$ 1.5	$\times 10^{-5}$	CL=90%
Γ_{282}	$\chi_{c2} K^*(892)^0$	(4.9 ± 1.2)	$\times 10^{-5}$	S=1.1
Γ_{283}	$\chi_{c2}\pi^- K^+$	(7.2 ± 1.0)	$\times 10^{-5}$	
Γ_{284}	$\chi_{c2}\pi^+\pi^- K^0$	$<$ 1.70	$\times 10^{-4}$	CL=90%
Γ_{285}	$\chi_{c2}\pi^-\pi^0 K^+$	$<$ 7.4	$\times 10^{-5}$	CL=90%
Γ_{286}	$\psi(4660) K^0$, $\psi \to \Lambda_c^+ \Lambda_c^-$	$<$ 2.3	$\times 10^{-4}$	CL=90%
Γ_{287}	$\psi(4230)^0 K^0$, $\psi^0 \to J/\psi\pi^+\pi^-$	$<$ 1.7	$\times 10^{-5}$	CL=90%

K* or *K modes

Γ_{288}	$K^+\pi^-$	(2.00 ± 0.04)	$\times 10^{-5}$	
Γ_{289}	$K^0\pi^0$	(1.01 ± 0.04)	$\times 10^{-5}$	
Γ_{290}	$\eta' K^0$	(6.6 ± 0.4)	$\times 10^{-5}$	S=1.4
Γ_{291}	$\eta' K^*(892)^0$	(2.8 ± 0.6)	$\times 10^{-6}$	
Γ_{292}	$\eta' K_0^*(1430)^0$	(6.3 ± 1.6)	$\times 10^{-6}$	
Γ_{293}	$\eta' K_2^*(1430)^0$	(1.37 ± 0.32)	$\times 10^{-5}$	
Γ_{294}	ηK^0	(1.23 $^{+0.27}_{-0.24}$)	$\times 10^{-6}$	
Γ_{295}	$\eta K^*(892)^0$	(1.59 ± 0.10)	$\times 10^{-5}$	
Γ_{296}	$\eta K_0^*(1430)^0$	(1.10 ± 0.22)	$\times 10^{-5}$	
Γ_{297}	$\eta K_2^*(1430)^0$	(9.6 ± 2.1)	$\times 10^{-6}$	
Γ_{298}	ωK^0	(4.8 ± 0.4)	$\times 10^{-6}$	
Γ_{299}	$a_0(980)^0 K^0$, $a_0^0 \to \eta\pi^0$	$<$ 7.8	$\times 10^{-6}$	CL=90%
Γ_{300}	$b_1^0 K^0$, $b_1^0 \to \omega\pi^0$	$<$ 7.8	$\times 10^{-6}$	CL=90%
Γ_{301}	$a_0(980)^\pm K^\mp$, $a_0^\pm \to \eta\pi^\pm$	$<$ 1.9	$\times 10^{-6}$	CL=90%
Γ_{302}	$b_1^- K^+$, $b_1^- \to \omega\pi^-$	(7.4 ± 1.4)	$\times 10^{-6}$	
Γ_{303}	$b_1^0 K^{*0}$, $b_1^0 \to \omega\pi^0$	$<$ 8.0	$\times 10^{-6}$	CL=90%
Γ_{304}	$b_1^- K^{*+}$, $b_1^- \to \omega\pi^-$	$<$ 5.0	$\times 10^{-6}$	CL=90%
Γ_{305}	$a_0(1450)^\pm K^\mp$, $a_0^\pm \to \eta\pi^\pm$	$<$ 3.1	$\times 10^{-6}$	CL=90%
Γ_{306}	$K_S^0 X^0$ (Familon)	$<$ 5.3	$\times 10^{-5}$	CL=90%
Γ_{307}	$\omega K^*(892)^0$	(2.0 ± 0.5)	$\times 10^{-6}$	
Γ_{308}	$\omega(K\pi)_0^{*0}$	(1.84 ± 0.25)	$\times 10^{-5}$	
Γ_{309}	$\omega K_0^*(1430)^0$	(1.60 ± 0.34)	$\times 10^{-5}$	

Int. J. Mod. Phys. A 2026.41. Downloaded from www.worldscientific.com
by LIFORNIA @ BERKELEY on 09/16/26. Re-use and distribution is strictly not permitted, except for Open Access articles.

Γ_{310}	$\omega K_2^*(1430)^0$		$(1.01 \pm 0.23) \times 10^{-5}$		
Γ_{311}	$\omega K^+\pi^-$ nonresonant		$(5.1 \pm 1.0) \times 10^{-6}$		
Γ_{312}	$K^+\pi^-\pi^0$		$(3.78 \pm 0.32) \times 10^{-5}$		
Γ_{313}	$K^+\rho^-$		$(7.0 \pm 0.9) \times 10^{-6}$		
Γ_{314}	$K^+\rho(1450)^-$		$(2.4 \pm 1.2) \times 10^{-6}$		
Γ_{315}	$K^+\rho(1700)^-$		$(6 \pm 7) \times 10^{-7}$		
Γ_{316}	$(K^+\pi^-\pi^0)$ nonresonant		$(2.8 \pm 0.6) \times 10^{-6}$		
Γ_{317}	$(K\pi)_0^{*+}\pi^-$, $(K\pi)_0^{*+} \to K^+\pi^0$		$(3.4 \pm 0.5) \times 10^{-5}$		
Γ_{318}	$(K\pi)_0^{*0}\pi^0$, $(K\pi)_0^{*0} \to K^+\pi^-$		$(8.6 \pm 1.7) \times 10^{-6}$		
Γ_{319}	$K_2^*(1430)^0\pi^0$		$< 4.0 \times 10^{-6}$	CL=90%	
Γ_{320}	$K^*(1680)^0\pi^0$		$< 7.5 \times 10^{-6}$	CL=90%	
Γ_{321}	$K_x^{*0}\pi^0$	[d]	$(6.1 \pm 1.6) \times 10^{-6}$		
Γ_{322}	$K^0\pi^+\pi^-$		$(4.97 \pm 0.18) \times 10^{-5}$		
Γ_{323}	$K^0\pi^+\pi^-$ nonresonant		$(1.39 {}^{+0.26}_{-0.18}) \times 10^{-5}$		S=1.6
Γ_{324}	$K^0\rho^0$		$(3.4 \pm 1.1) \times 10^{-6}$		S=2.3
Γ_{325}	$K^*(892)^+\pi^-$		$(7.5 \pm 0.4) \times 10^{-6}$		
Γ_{326}	$K_0^*(1430)^+\pi^-$		$(3.3 \pm 0.7) \times 10^{-5}$		S=2.0
Γ_{327}	$K_x^{*+}\pi^-$	[d]	$(5.1 \pm 1.6) \times 10^{-6}$		
Γ_{328}	$K^*(1410)^+\pi^-$, $K^{*+} \to K^0\pi^+$		$< 3.8 \times 10^{-6}$	CL=90%	
Γ_{329}	$(K\pi)_0^{*+}\pi^-$, $(K\pi)_0^{*+} \to K^0\pi^+$		$(1.62 \pm 0.13) \times 10^{-5}$		
Γ_{330}	$f_0(980)K^0$, $f_0 \to \pi^+\pi^-$		$(8.1 \pm 0.8) \times 10^{-6}$		S=1.3
Γ_{331}	$K^0 f_0(500)$		$(1.6 {}^{+2.5}_{-1.6}) \times 10^{-7}$		
Γ_{332}	$K^0 f_0(1500)$		$(1.3 \pm 0.8) \times 10^{-6}$		
Γ_{333}	$f_2(1270)K^0$		$(2.7 {}^{+1.3}_{-1.2}) \times 10^{-6}$		
Γ_{334}	$f_x(1300)K0, f_x \to \pi^+\pi^-$		$(1.8 \pm 0.7) \times 10^{-6}$		
Γ_{335}	$K^*(892)^0\pi^0$		$(3.3 \pm 0.6) \times 10^{-6}$		
Γ_{336}	$K_2^*(1430)^+\pi^-$		$(3.65 \pm 0.34) \times 10^{-6}$		
Γ_{337}	$K^*(1680)^+\pi^-$		$(1.41 \pm 0.10) \times 10^{-5}$		
Γ_{338}	$K^+\pi^-\pi^+\pi^-$	[e]	$< 2.3 \times 10^{-4}$	CL=90%	
Γ_{339}	$\rho^0 K^+\pi^-$		$(2.8 \pm 0.7) \times 10^{-6}$		
Γ_{340}	$f_0(980)K^+\pi^-$, $f_0 \to \pi\pi$		$(1.4 {}^{+0.5}_{-0.6}) \times 10^{-6}$		
Γ_{341}	$K^+\pi^-\pi^+\pi^-$ nonresonant		$< 2.1 \times 10^{-6}$	CL=90%	
Γ_{342}	$K^*(892)^0\pi^+\pi^-$		$(5.5 \pm 0.5) \times 10^{-5}$		
Γ_{343}	$K^*(892)^0\rho^0$		$(3.9 \pm 1.3) \times 10^{-6}$		S=1.9
Γ_{344}	$K^*(892)^0 f_0(980)$, $f_0 \to \pi\pi$		$(3.9 {}^{+2.1}_{-1.8}) \times 10^{-6}$		S=3.9
Γ_{345}	$K_1(1270)^+\pi^-$		$< 3.0 \times 10^{-5}$	CL=90%	
Γ_{346}	$K_1(1400)^+\pi^-$		$< 2.7 \times 10^{-5}$	CL=90%	
Γ_{347}	$a_1(1260)^- K^+$	[e]	$(1.6 \pm 0.4) \times 10^{-5}$		
Γ_{348}	$K^*(892)^+\rho^-$		$(1.03 \pm 0.26) \times 10^{-5}$		
Γ_{349}	$K_0^*(1430)^+\rho^-$		$(2.8 \pm 1.2) \times 10^{-5}$		
Γ_{350}	$K_1(1400)^0\rho^0$		$< 3.0 \times 10^{-3}$	CL=90%	
Γ_{351}	$K_0^*(1430)^0\rho^0$		$(2.7 \pm 0.6) \times 10^{-5}$		
Γ_{352}	$K_0^*(1430)^0 f_0(980)$, $f_0 \to \pi\pi$		$(2.7 \pm 0.9) \times 10^{-6}$		
Γ_{353}	$K_2^*(1430)^0 f_0(980)$, $f_0 \to \pi\pi$		$(8.6 \pm 2.0) \times 10^{-6}$		
Γ_{354}	K^+K^-		$(7.8 \pm 1.5) \times 10^{-8}$		
Γ_{355}	$K^0\overline{K}^0$		$(1.21 \pm 0.16) \times 10^{-6}$		
Γ_{356}	$K^0K^-\pi^+$		$(6.7 \pm 0.5) \times 10^{-6}$		
Γ_{357}	$K^*(892)^\pm K^\mp$		$< 4 \times 10^{-7}$	CL=90%	
Γ_{358}	$\overline{K}^{*0}K^0 + K^{*0}\overline{K}^0$		$< 9.6 \times 10^{-7}$	CL=90%	
Γ_{359}	$K^+K^-\pi^0$		$(2.2 \pm 0.6) \times 10^{-6}$		
Γ_{360}	$K_S^0K_S^0\pi^0$		$< 9 \times 10^{-7}$	CL=90%	
Γ_{361}	$K_S^0K_S^0\eta$		$< 1.0 \times 10^{-6}$	CL=90%	
Γ_{362}	$K_S^0K_S^0\eta'$		$< 2.0 \times 10^{-6}$	CL=90%	
Γ_{363}	$K^0K^+K^-$		$(2.68 \pm 0.11) \times 10^{-5}$		
Γ_{364}	$K^0\phi$		$(7.3 \pm 0.7) \times 10^{-6}$		
Γ_{365}	$f_0(980)K^0$, $f_0 \to K^+K^-$		$(7.0 {}^{+3.5}_{-3.0}) \times 10^{-6}$		
Γ_{366}	$f_0(1500)K^0$		$(1.3 {}^{+0.7}_{-0.5}) \times 10^{-5}$		
Γ_{367}	$f_2'(1525)^0K^0$		$(3 {}^{+5}_{-4}) \times 10^{-7}$		
Γ_{368}	$f_0(1710)K^0$, $f_0 \to K^+K^-$		$(4.4 \pm 0.9) \times 10^{-6}$		
Γ_{369}	$K^0K^+K^-$ nonresonant		$(3.3 \pm 1.0) \times 10^{-5}$		
Γ_{370}	$K_S^0K_S^0K_S^0$		$(6.0 \pm 0.5) \times 10^{-6}$		S=1.1
Γ_{371}	$f_0(980)K^0$, $f_0 \to K_S^0K_S^0$		$(2.7 \pm 1.8) \times 10^{-6}$		
Γ_{372}	$f_0(1710)K^0$, $f_0 \to K_S^0K_S^0$		$(5.0 {}^{+5.0}_{-2.6}) \times 10^{-7}$		
Γ_{373}	$f_2(2010)K^0$, $f_2 \to K_S^0K_S^0$		$(5 \pm 6) \times 10^{-7}$		
Γ_{374}	$K_S^0K_S^0K_S^0$ nonresonant		$(1.33 \pm 0.31) \times 10^{-5}$		
Γ_{375}	$K_S^0K_S^0K_L^0$		$< 1.6 \times 10^{-5}$	CL=90%	
Γ_{376}	$K^*(892)^0K^+K^-$		$(2.75 \pm 0.26) \times 10^{-5}$		
Γ_{377}	$K^*(892)^0\phi$		$(1.00 \pm 0.05) \times 10^{-5}$		
Γ_{378}	$K^+K^-\pi^+\pi^-$ nonresonant		$< 7.17 \times 10^{-5}$	CL=90%	
Γ_{379}	$K^*(892)^0K^-\pi^+$		$(4.5 \pm 1.3) \times 10^{-6}$		
Γ_{380}	$K^*(892)^0\overline{K}^*(892)^0$		$(8.3 \pm 2.4) \times 10^{-7}$		S=1.5
Γ_{381}	$K^+K^+\pi^-\pi^-$ nonresonant		$< 6.0 \times 10^{-6}$	CL=90%	
Γ_{382}	$K^*(892)^0K^+\pi^-$		$< 2.2 \times 10^{-6}$	CL=90%	
Γ_{383}	$K^*(892)^0K^*(892)^0$		$< 2 \times 10^{-7}$	CL=90%	
Γ_{384}	$K^*(892)^+K^*(892)^-$		$< 2.0 \times 10^{-6}$	CL=90%	
Γ_{385}	$K_1(1400)^0\phi$		$< 5.0 \times 10^{-3}$	CL=90%	
Γ_{386}	$\phi(K\pi)_0^{*0}$		$(4.3 \pm 0.4) \times 10^{-6}$		
Γ_{387}	$\phi(K\pi)_0^{*0}$ $(1.60 < m_{K\pi} < 2.15)$	[f]	$< 1.7 \times 10^{-6}$	CL=90%	
Γ_{388}	$K_0^*(1430)^0K^-\pi^+$		$< 3.18 \times 10^{-5}$	CL=90%	
Γ_{389}	$K_0^*(1430)^0\overline{K}^*(892)^0$		$< 3.3 \times 10^{-6}$	CL=90%	
Γ_{390}	$K_0^*(1430)^0\overline{K}_0^*(1430)^0$		$< 8.4 \times 10^{-6}$	CL=90%	
Γ_{391}	$K_0^*(1430)^0\phi$		$(3.9 \pm 0.8) \times 10^{-6}$		
Γ_{392}	$K_0^*(1430)^0K^*(892)^0$		$< 1.7 \times 10^{-6}$	CL=90%	
Γ_{393}	$K_0^*(1430)^0K_0^*(1430)^0$		$< 4.7 \times 10^{-6}$	CL=90%	
Γ_{394}	$K^*(1680)^0\phi$		$< 3.5 \times 10^{-6}$	CL=90%	
Γ_{395}	$K^*(1780)^0\phi$		$< 2.7 \times 10^{-6}$	CL=90%	
Γ_{396}	$K^*(2045)^0\phi$		$< 1.53 \times 10^{-5}$	CL=90%	
Γ_{397}	$K_2^*(1430)^0\rho^0$		$< 1.1 \times 10^{-3}$	CL=90%	
Γ_{398}	$K_2^*(1430)^0\phi$		$(6.8 \pm 0.9) \times 10^{-6}$		S=1.2
Γ_{399}	$K^0\phi\phi$		$(3.7 \pm 0.7) \times 10^{-6}$		S=1.3
Γ_{400}	$\eta'\eta'K^0$		$< 3.1 \times 10^{-5}$	CL=90%	
Γ_{401}	$\eta K^0\gamma$		$(7.6 \pm 1.8) \times 10^{-6}$		
Γ_{402}	$\eta' K^0\gamma$		$< 6.4 \times 10^{-6}$	CL=90%	
Γ_{403}	$K^0\phi\gamma$		$(2.7 \pm 0.7) \times 10^{-6}$		
Γ_{404}	$K^+\pi^-\gamma$		$(4.6 \pm 1.4) \times 10^{-6}$		
Γ_{405}	$K^*(892)^0\gamma$		$(4.21 \pm 0.24) \times 10^{-5}$		S=2.0
Γ_{406}	$K^*(1410)\gamma$		$< 1.3 \times 10^{-4}$	CL=90%	
Γ_{407}	$K^+\pi^-\gamma$ nonresonant		$< 2.6 \times 10^{-6}$	CL=90%	
Γ_{408}	$K^*(892)^0X(214)$, $X \to \mu^+\mu^-$	[g]	$< 2.26 \times 10^{-8}$	CL=90%	
Γ_{409}	$K^0\pi^+\pi^-\gamma$		$(1.99 \pm 0.18) \times 10^{-5}$		
Γ_{410}	$K^+\pi^-\pi^0\gamma$		$(4.1 \pm 0.4) \times 10^{-5}$		
Γ_{411}	$K_1(1270)^0\gamma$		$< 5.8 \times 10^{-5}$	CL=90%	
Γ_{412}	$K_1(1400)^0\gamma$		$< 1.2 \times 10^{-5}$	CL=90%	
Γ_{413}	$K_2^*(1430)^0\gamma$		$(1.24 \pm 0.24) \times 10^{-5}$		
Γ_{414}	$K^*(1680)^0\gamma$		$< 2.0 \times 10^{-3}$	CL=90%	
Γ_{415}	$K_3^*(1780)^0\gamma$		$< 8.3 \times 10^{-5}$	CL=90%	
Γ_{416}	$K_4^*(2045)^0\gamma$		$< 4.3 \times 10^{-3}$	CL=90%	

Light unflavored meson modes

Γ_{417}	$\rho^0\gamma$		$(8.0 \pm 0.6) \times 10^{-7}$		S=1.4
Γ_{418}	$\rho^0X(214)$, $X \to \mu^+\mu^-$	[g]	$< 1.73 \times 10^{-8}$	CL=90%	
Γ_{419}	$\omega\gamma$		$(4.4 {}^{+1.8}_{-1.6}) \times 10^{-7}$		
Γ_{420}	$\phi\gamma$		$< 1.0 \times 10^{-7}$	CL=90%	
Γ_{421}	$f_2(1270)\gamma$, $f_2 \to (KS)^0(KS)^0$		$< 3.1 \times 10^{-7}$		
Γ_{422}	$f_2'(1525)\gamma$, $f_2' \to (KS)^0(KS)^0$		$< 2.1 \times 10^{-7}$		
Γ_{423}	$\pi^+\pi^-$		$(5.37 \pm 0.20) \times 10^{-6}$		S=1.3
Γ_{424}	$\pi^0\pi^0$		$(1.46 \pm 0.19) \times 10^{-6}$		S=1.3
Γ_{425}	$\eta\pi^0$		$(4.1 \pm 1.7) \times 10^{-7}$		
Γ_{426}	$\eta\eta$		$< 1.0 \times 10^{-6}$	CL=90%	
Γ_{427}	$\eta'\pi^0$		$(1.2 \pm 0.6) \times 10^{-6}$		S=1.7
Γ_{428}	$\eta'\eta'$		$< 1.7 \times 10^{-6}$	CL=90%	
Γ_{429}	$\eta'\eta$		$< 1.2 \times 10^{-6}$	CL=90%	
Γ_{430}	$\eta'\rho^0$		$< 1.3 \times 10^{-6}$	CL=90%	
Γ_{431}	$\eta' f_0(980)$, $f_0 \to \pi^+\pi^-$		$< 9 \times 10^{-7}$	CL=90%	
Γ_{432}	$\eta\rho^0$		$< 1.5 \times 10^{-6}$	CL=90%	
Γ_{433}	$\eta f_0(980)$, $f_0 \to \pi^+\pi^-$		$< 4 \times 10^{-7}$	CL=90%	
Γ_{434}	$\omega\eta$		$(9.4 {}^{+4.0}_{-3.1}) \times 10^{-7}$		
Γ_{435}	$\omega\eta'$		$(1.0 {}^{+0.5}_{-0.4}) \times 10^{-6}$		
Γ_{436}	$\omega\rho^0$		$< 1.6 \times 10^{-6}$	CL=90%	
Γ_{437}	$\omega f_0(980)$, $f_0 \to \pi^+\pi^-$		$< 1.5 \times 10^{-6}$	CL=90%	
Γ_{438}	$\omega\omega$		$(1.40 \pm 0.25) \times 10^{-6}$		
Γ_{439}	$\phi\pi^0$		$< 1.5 \times 10^{-7}$	CL=90%	
Γ_{440}	$\phi\eta$		$< 5 \times 10^{-7}$	CL=90%	
Γ_{441}	$\phi\eta'$		$< 5 \times 10^{-7}$	CL=90%	
Γ_{442}	$\phi\pi^+\pi^-$		$(1.8 \pm 0.5) \times 10^{-7}$		
Γ_{443}	$\phi\rho^0$		$< 3.3 \times 10^{-7}$	CL=90%	
Γ_{444}	$\phi f_0(980)$, $f_0 \to \pi^+\pi^-$		$< 3.8 \times 10^{-7}$	CL=90%	

Int. J. Mod. Phys. A 2026.41. Downloaded from www.worldscientific.com
by UNIVERSITY OF CALIFORNIA @ BERKELEY on 09/16/26. Re-use and distribution is strictly not permitted, except for Open Access articles.

Γ_{445}	$\phi\omega$		$<$ 7	$\times 10^{-7}$	CL=90%
Γ_{446}	$\phi\phi$		$<$ 1.3	$\times 10^{-8}$	CL=90%
Γ_{447}	$a_0(980)^{\pm}\pi^{\mp},\ a_0^{\pm} \to \eta\pi^{\pm}$		$<$ 3.1	$\times 10^{-6}$	CL=90%
Γ_{448}	$a_0(1450)^{\pm}\pi^{\mp},\ a_0^{\pm} \to \eta\pi^{\pm}$		$<$ 2.3	$\times 10^{-6}$	CL=90%
Γ_{449}	$\pi^+\pi^-\pi^0$		$<$ 7.2	$\times 10^{-4}$	CL=90%
Γ_{450}	$\rho^0\pi^0$		(2.0 ± 0.5)	$\times 10^{-6}$	
Γ_{451}	$\rho^{\mp}\pi^{\pm}$	[h]	(2.30 ± 0.23)	$\times 10^{-5}$	
Γ_{452}	$\pi^+\pi^-\pi^+\pi^-$		$<$ 1.12	$\times 10^{-5}$	CL=90%
Γ_{453}	$\rho^0\pi^+\pi^-$		$<$ 8.8	$\times 10^{-6}$	CL=90%
Γ_{454}	$\rho^0\rho^0$		(9.6 ± 1.5)	$\times 10^{-7}$	
Γ_{455}	$f_0(980)\pi^+\pi^-,\ f_0 \to \pi^+\pi^-$		$<$ 3.0	$\times 10^{-6}$	CL=90%
Γ_{456}	$\rho^0 f_0(980),\ f_0 \to \pi^+\pi^-$		(7.8 ± 2.5)	$\times 10^{-7}$	
Γ_{457}	$f_0(980) f_0(980),\ f_0 \to \pi^+\pi^-,\ f_0 \to \pi^+\pi^-$		$<$ 1.9	$\times 10^{-7}$	CL=90%
Γ_{458}	$f_0(980) f_0(980),\ f_0 \to \pi^+\pi^-,\ f_0 \to K^+K^-$		$<$ 2.3	$\times 10^{-7}$	CL=90%
Γ_{459}	$a_1(1260)^{\mp}\pi^{\pm}$	[h]	(2.6 ± 0.5)	$\times 10^{-5}$	S=1.9
Γ_{460}	$a_2(1320)^{\mp}\pi^{\pm}$	[h]	$<$ 6.3	$\times 10^{-6}$	CL=90%
Γ_{461}	$\pi^+\pi^-\pi^0\pi^0$		$<$ 3.1	$\times 10^{-3}$	CL=90%
Γ_{462}	$\rho^+\rho^-$		(2.80 ± 0.17)	$\times 10^{-5}$	
Γ_{463}	$a_1(1260)^0\pi^0$		$<$ 1.1	$\times 10^{-3}$	CL=90%
Γ_{464}	$\omega\pi^0$		$<$ 5	$\times 10^{-7}$	CL=90%
Γ_{465}	$\pi^+\pi^+\pi^-\pi^-\pi^0$		$<$ 9.0	$\times 10^{-3}$	CL=90%
Γ_{466}	$a_1(1260)^+\rho^-$		$<$ 6.1	$\times 10^{-5}$	CL=90%
Γ_{467}	$a_1(1260)^0\rho^0$		$<$ 2.4	$\times 10^{-3}$	CL=90%
Γ_{468}	$b_1^{\mp}\pi^{\pm},\ b_1^{\mp} \to \omega\pi^{\mp}$		(1.09 ± 0.15)	$\times 10^{-5}$	
Γ_{469}	$b_1^0\pi^0,\ b_1^0 \to \omega\pi^0$		$<$ 1.9	$\times 10^{-6}$	CL=90%
Γ_{470}	$b_1^-\rho^+,\ b_1^- \to \omega\pi^-$		$<$ 1.4	$\times 10^{-6}$	CL=90%
Γ_{471}	$b_1^0\rho^0,\ b_1^0 \to \omega\pi^0$		$<$ 3.4	$\times 10^{-6}$	CL=90%
Γ_{472}	$\pi^+\pi^+\pi^+\pi^-\pi^-\pi^-$		$<$ 3.0	$\times 10^{-3}$	CL=90%
Γ_{473}	$a_1(1260)^+ a_1(1260)^-,\ a_1^+ \to 2\pi^+\pi^-,\ a_1^- \to 2\pi^-\pi^+$		(1.18 ± 0.31)	$\times 10^{-5}$	
Γ_{474}	$\pi^+\pi^+\pi^+\pi^-\pi^-\pi^-\pi^0$		$<$ 1.1	%	CL=90%

Baryon modes

Γ_{475}	$p\overline{p}$		(1.27 ± 0.14)	$\times 10^{-8}$	
Γ_{476}	$p\overline{p}\pi^+\pi^-$		(2.87 ± 0.19)	$\times 10^{-6}$	
Γ_{477}	$p\overline{p}K^+\pi^-$		(6.3 ± 0.5)	$\times 10^{-6}$	
Γ_{478}	$p\overline{p}K^0$		(2.79 ± 0.16)	$\times 10^{-6}$	
Γ_{479}	$\Theta(1540)^+\overline{p},\ \Theta^+ \to pK^0_S$	[i]	$<$ 5	$\times 10^{-8}$	CL=90%
Γ_{480}	$f_J(2220)K^0,\ f_J \to p\overline{p}$		$<$ 4.5	$\times 10^{-7}$	CL=90%
Γ_{481}	$p\overline{p}K^*(892)^0$		($1.24^{+0.28}_{-0.25}$)	$\times 10^{-6}$	
Γ_{482}	$f_J(2220)K^*_0,\ f_J \to p\overline{p}$		$<$ 1.5	$\times 10^{-7}$	CL=90%
Γ_{483}	$p\overline{p}K^+K^-$		(1.21 ± 0.32)	$\times 10^{-7}$	
Γ_{484}	$p\overline{p}\pi^0$		(5.0 ± 1.9)	$\times 10^{-7}$	
Γ_{485}	$p\overline{p}p\overline{p}$		(2.2 ± 0.4)	$\times 10^{-8}$	
Γ_{486}	$p\overline{\Lambda}\pi^-$		(3.16 ± 0.24)	$\times 10^{-6}$	
Γ_{487}	$p\overline{\Lambda}\pi^-\gamma$		$<$ 6.5	$\times 10^{-7}$	CL=90%
Γ_{488}	$p\overline{\Sigma}(1385)^-$		$<$ 2.6	$\times 10^{-7}$	CL=90%
Γ_{489}	$\Delta(1232)^+\overline{p} + \Delta(1232)^- p$		$<$ 1.6	$\times 10^{-6}$	
Γ_{490}	$\Delta^0\overline{\Lambda}$		$<$ 9.3	$\times 10^{-7}$	CL=90%
Γ_{491}	$p\overline{\Lambda}K^-$		$<$ 8.2	$\times 10^{-7}$	CL=90%
Γ_{492}	$p\overline{\Lambda}D^-$		(2.5 ± 0.4)	$\times 10^{-5}$	
Γ_{493}	$p\overline{\Lambda}D^{*-}$		(3.4 ± 0.8)	$\times 10^{-5}$	
Γ_{494}	$p\overline{\Sigma}^0\pi^-$		(1.2 ± 0.4)	$\times 10^{-6}$	
Γ_{495}	$\overline{\Lambda}\Lambda$		$<$ 3.2	$\times 10^{-7}$	CL=90%
Γ_{496}	$\overline{\Lambda}\Lambda K^0$		($4.8^{+1.0}_{-0.9}$)	$\times 10^{-6}$	
Γ_{497}	$\overline{\Lambda}\Lambda K^{*0}$		($2.5^{+0.9}_{-0.8}$)	$\times 10^{-6}$	
Γ_{498}	$\overline{\Lambda}\Lambda D^0$		($1.00^{+0.30}_{-0.26}$)	$\times 10^{-5}$	
Γ_{499}	$D^0\Sigma^0\overline{\Lambda}$ + c.c.		$<$ 3.1	$\times 10^{-5}$	CL=90%
Γ_{500}	$\Delta^0\overline{\Delta}^0$		$<$ 1.5	$\times 10^{-3}$	CL=90%
Γ_{501}	$\Delta^{++}\overline{\Delta}^{--}$		$<$ 1.1	$\times 10^{-4}$	CL=90%
Γ_{502}	$\overline{D}^0 p\overline{p}$		(1.04 ± 0.07)	$\times 10^{-4}$	
Γ_{503}	$D^-_s\overline{\Lambda}p$		(2.8 ± 0.9)	$\times 10^{-5}$	
Γ_{504}	$\overline{D}^*(2007)^0 p\overline{p}$		(9.9 ± 1.1)	$\times 10^{-5}$	
Γ_{505}	$D^*(2010)^- p\overline{n}$		(1.4 ± 0.4)	$\times 10^{-3}$	
Γ_{506}	$D^- p\overline{p}\pi^+$		(3.32 ± 0.31)	$\times 10^{-4}$	
Γ_{507}	$D^*(2010)^- p\overline{p}\pi^+$		(4.7 ± 0.5)	$\times 10^{-4}$	S=1.2
Γ_{508}	$\overline{D}^0 p\overline{p}\pi^+\pi^-$		(3.0 ± 0.5)	$\times 10^{-4}$	
Γ_{509}	$\overline{D}^{*0} p\overline{p}\pi^+\pi^-$		(1.9 ± 0.5)	$\times 10^{-4}$	
Γ_{510}	$\Theta_c\overline{p}\pi^+,\ \Theta_c \to D^- p$		$<$ 9	$\times 10^{-6}$	CL=90%
Γ_{511}	$\Theta_c\overline{p}\pi^+,\ \Theta_c \to D^{*-} p$		$<$ 1.4	$\times 10^{-5}$	CL=90%
Γ_{512}	$\overline{\Sigma}_c^{--}\Delta^{++}$		$<$ 8	$\times 10^{-4}$	CL=90%
Γ_{513}	$\overline{\Lambda}_c^- p\pi^+\pi^-$		(1.00 ± 0.14)	$\times 10^{-3}$	S=1.4
Γ_{514}	$\overline{\Lambda}_c^- p$		(1.51 ± 0.17)	$\times 10^{-5}$	
Γ_{515}	$\overline{\Lambda}_c^- p\pi^0$		(1.52 ± 0.17)	$\times 10^{-4}$	
Γ_{516}	$\Sigma_c(2455)^- p$		$<$ 2.4	$\times 10^{-5}$	
Γ_{517}	$\overline{\Lambda}_c^- p\pi^+\pi^-\pi^0$		$<$ 5.07	$\times 10^{-3}$	CL=90%
Γ_{518}	$\overline{\Lambda}_c^- p\pi^+\pi^-\pi^+\pi^-$		$<$ 2.74	$\times 10^{-3}$	CL=90%
Γ_{519}	$\overline{\Lambda}_c^- p\pi^+\pi^-$ (nonresonant)		(5.4 ± 1.0)	$\times 10^{-4}$	S=1.3
Γ_{520}	$\overline{\Sigma}_c(2520)^{--} p\pi^+$		(1.01 ± 0.18)	$\times 10^{-4}$	
Γ_{521}	$\overline{\Sigma}_c(2520)^0 p\pi^-$		$<$ 3.1	$\times 10^{-5}$	CL=90%
Γ_{522}	$\overline{\Sigma}_c(2455)^0 p\pi^-$		(1.08 ± 0.09)	$\times 10^{-4}$	
Γ_{523}	$\overline{\Sigma}_c(2455)^0 N^0,\ N^0 \to p\pi^-$		(6.3 ± 1.6)	$\times 10^{-5}$	
Γ_{524}	$\overline{\Sigma}_c(2455)^{--} p\pi^+$		(1.89 ± 0.15)	$\times 10^{-4}$	
Γ_{525}	$\Lambda_c^- pK^+\pi^-$		(3.4 ± 0.7)	$\times 10^{-5}$	
Γ_{526}	$\overline{\Sigma}_c(2455)^{--} pK^+,\ \overline{\Sigma}_c^{--} \to \overline{\Lambda}_c^-\pi^-$		(8.7 ± 2.5)	$\times 10^{-6}$	
Γ_{527}	$\Sigma_c(2455)^0\overline{\Xi}_c^0$		(4.8 ± 1.4)	$\times 10^{-4}$	
Γ_{528}	$\Lambda_c^- pK^*(892)^0$		$<$ 2.42	$\times 10^{-5}$	CL=90%
Γ_{529}	$\Lambda_c^- pK^+K^-$		(2.0 ± 0.4)	$\times 10^{-5}$	
Γ_{530}	$\Lambda_c^- p\phi$		$<$ 9	$\times 10^{-6}$	CL=90%
Γ_{531}	$\Lambda_c^- p\overline{p}p$		$<$ 2.8	$\times 10^{-6}$	
Γ_{532}	$\overline{\Lambda}_c^-\Lambda K^+$		(4.9 ± 1.1)	$\times 10^{-5}$	
Γ_{533}	$\overline{\Lambda}_c^-\Lambda_c^+$		$<$ 1.6	$\times 10^{-5}$	CL=95%
Γ_{534}	$\overline{\Lambda}_c(2593)^- / \overline{\Lambda}_c(2625)^- p$		$<$ 1.1	$\times 10^{-4}$	CL=90%
Γ_{535}	$\overline{\Xi}_c^-\Lambda_c^+$		(1.1 ± 0.8)	$\times 10^{-3}$	
Γ_{536}	$\overline{\Xi}_c^-\Lambda_c^+,\ \overline{\Xi}_c^- \to \overline{\Xi}^+\pi^-\pi^-$		(2.3 ± 1.0)	$\times 10^{-5}$	S=1.8
Γ_{537}	$\overline{\Xi}_c^-\Lambda_c^+,\ \overline{\Xi}_c^- \to \overline{p}K^+\pi^-$		(5.2 ± 1.6)	$\times 10^{-6}$	
Γ_{538}	$\Lambda_c^+\Lambda_c^- K^0$		(4.0 ± 0.9)	$\times 10^{-4}$	
Γ_{539}	$\overline{\Lambda}_c(2910)^- p,\ \overline{\Lambda}_c^- \to \overline{\Sigma}_c(2455)^{--}\pi^+$		(1.2 ± 0.4)	$\times 10^{-5}$	
Γ_{540}	$\overline{\Lambda}_c(2910)^- p,\ \overline{\Lambda}_c^- \to \overline{\Sigma}_c(2455)^0\pi^-$		(9 ± 4)	$\times 10^{-6}$	
Γ_{541}	$\overline{\Xi}_c(2930)^-\Lambda_c^+,\ \overline{\Xi}_c^- \to \Lambda_c^- K^0$		(2.4 ± 0.6)	$\times 10^{-4}$	
Γ_{542}	$\Omega_c^0\overline{\Lambda},\ \Omega_c^0 \to \Omega^-\pi^+$		$<$ 9.7	$\times 10^{-8}$	CL=95%
Γ_{543}	$\Omega_c(2770)^0\overline{\Lambda},\ \Omega_c^0 \to \Omega^-\pi^+$		$<$ 3.12	$\times 10^{-7}$	CL=95%
Γ_{544}	$\Omega_c^0\Lambda,\ \Omega_c^0 \to \Omega^-\pi^+$		$<$ 9.5	$\times 10^{-8}$	CL=95%
Γ_{545}	$\Omega_c(2770)^0\Lambda,\ \Omega_c^0 \to \Omega^-\pi^+$		$<$ 1.00	$\times 10^{-7}$	CL=95%
Γ_{546}	$\Lambda\psi_{DS}$	[j]	$<$ 0.13–5.2	$\times 10^{-5}$	

Lepton Family number (*LF*) or Lepton number (*L*) or Baryon number (*B*) violating modes, or/and $\Delta B = 1$ weak neutral current (*B1*) modes

Γ_{547}	$\gamma\gamma$	*B1*		$<$ 6.4	$\times 10^{-8}$	CL=90%
Γ_{548}	e^+e^-	*B1*		$<$ 2.5	$\times 10^{-9}$	CL=90%
Γ_{549}	$e^+e^-\gamma$	*B1*		$<$ 1.2	$\times 10^{-7}$	CL=90%
Γ_{550}	$\mu^+\mu^-$	*B1*		$<$ 1.5	$\times 10^{-10}$	CL=90%
Γ_{551}	$\mu^+\mu^-\gamma$	*B1*				
Γ_{552}	$\mu^+\mu^-\mu^+\mu^-$	*B1*		$<$ 1.8	$\times 10^{-10}$	CL=95%
Γ_{553}	$SP,\ S \to \mu^+\mu^-,\ P \to \mu^+\mu^-$	*B1*	[k]	$<$ 6.0	$\times 10^{-10}$	CL=95%
Γ_{554}	$aa,\ a \to \mu^+\mu^-$	*B1*		$<$ 2.3	$\times 10^{-10}$	CL=95%
Γ_{555}	$\tau^+\tau^-$	*B1*		$<$ 2.1	$\times 10^{-3}$	CL=95%
Γ_{556}	$\pi^0\ell^+\ell^-$	*B1*	[a]	$<$ 3.8	$\times 10^{-8}$	CL=90%
Γ_{557}	$\pi^0 e^+e^-$	*B1*		$<$ 7.9	$\times 10^{-8}$	CL=90%
Γ_{558}	$\pi^0\mu^+\mu^-$	*B1*		$<$ 5.9	$\times 10^{-8}$	CL=90%
Γ_{559}	$\eta\ell^+\ell^-$	*B1*	[a]	$<$ 4.8	$\times 10^{-8}$	CL=90%
Γ_{560}	ηe^+e^-	*B1*		$<$ 1.05	$\times 10^{-7}$	CL=90%
Γ_{561}	$\eta\mu^+\mu^-$	*B1*		$<$ 9.4	$\times 10^{-8}$	CL=90%
Γ_{562}	$\rho(770)^0 e^+e^-$	*B1*		$<$ 4.55	$\times 10^{-7}$	CL=90%
Γ_{563}	ωe^+e^-	*B1*		$<$ 3.07	$\times 10^{-7}$	CL=90%
Γ_{564}	$\omega\mu^+\mu^-$	*B1*		$<$ 2.49	$\times 10^{-7}$	CL=90%
Γ_{565}	$\omega\ell^+\ell^-$	*B1*		$<$ 2.20	$\times 10^{-7}$	CL=90%
Γ_{566}	$\pi^0\nu\overline{\nu}$	*B1*		$<$ 9	$\times 10^{-6}$	CL=90%
Γ_{567}	$K^0\ell^+\ell^-$	*B1*	[a]	(3.3 ± 0.6)	$\times 10^{-7}$	
Γ_{568}	$K^0 e^+e^-$	*B1*		($2.5^{+1.1}_{-0.9}$)	$\times 10^{-7}$	S=1.3
Γ_{569}	$K^0\mu^+\mu^-$	*B1*		(3.39 ± 0.35)	$\times 10^{-7}$	S=1.1
Γ_{570}	$K^0\nu\overline{\nu}$	*B1*		$<$ 2.6	$\times 10^{-5}$	CL=90%
Γ_{571}	$\rho^0\nu\overline{\nu}$	*B1*		$<$ 4.0	$\times 10^{-5}$	CL=90%
Γ_{572}	$K^*(892)^0\ell^+\ell^-$	*B1*	[a]	($9.9^{+1.2}_{-1.1}$)	$\times 10^{-7}$	
Γ_{573}	$K^*(892)^0 e^+e^-$	*B1*		($1.03^{+0.19}_{-0.17}$)	$\times 10^{-6}$	
Γ_{574}	$K^*(892)^0\mu^+\mu^-$	*B1*		(9.4 ± 0.5)	$\times 10^{-7}$	

Γ_{575}	$K^*(892)^0\chi,\ \chi\to\mu^+\mu^-$	B1				
Γ_{576}	$K^*(892)^0\tau^+\tau^-$	B1	<	1.8	$\times10^{-3}$	CL=90%
Γ_{577}	$\overline{D}^0\mu^+\mu^-$	B1	<	4.0	$\times10^{-8}$	CL=90%
Γ_{578}	$\pi^+\pi^-\mu^+\mu^-$	B1	(	2.1 ± 0.5)	$\times10^{-8}$	
Γ_{579}	$K^*(892)^0\nu\overline{\nu}$	B1	<	1.8	$\times10^{-5}$	CL=90%
Γ_{580}	invisible	B1	<	2.4	$\times10^{-5}$	CL=90%
Γ_{581}	$\nu\overline{\nu}\gamma$	B1	<	1.6	$\times10^{-5}$	CL=90%
Γ_{582}	$\phi\mu^+\mu^-$	B1	<	3.2	$\times10^{-9}$	CL=90%
Γ_{583}	$\phi\nu\overline{\nu}$	B1	<	1.27	$\times10^{-4}$	CL=90%
Γ_{584}	$e^\pm\mu^\mp$	LF	[h] <	1.0	$\times10^{-9}$	CL=90%
Γ_{585}	$\pi^0e^\pm\mu^\mp$	LF	<	1.4	$\times10^{-7}$	CL=90%
Γ_{586}	$K^0e^\pm\mu^\mp$	LF	<	3.8	$\times10^{-8}$	CL=90%
Γ_{587}	$K^0_S\tau^+e^-$		<	1.5	$\times10^{-5}$	CL=90%
Γ_{588}	$K^0_S\tau^-e^+$		<	8	$\times10^{-6}$	CL=90%
Γ_{589}	$K^0_S\tau^+\mu^-$		<	1.1	$\times10^{-5}$	CL=90%
Γ_{590}	$K^0_S\tau^-\mu^+$		<	3.6	$\times10^{-5}$	CL=90%
Γ_{591}	$K^*(892)^0e^+\mu^-$	LF	<	6.8	$\times10^{-9}$	CL=90%
Γ_{592}	$K^*(892)^0e^-\mu^+$	LF	<	5.7	$\times10^{-9}$	CL=90%
Γ_{593}	$K^*(892)^0e^\pm\mu^\mp$	LF	<	1.01	$\times10^{-8}$	CL=90%
Γ_{594}	$K^*(892)^0\tau^+e^-$		<	4.9	$\times10^{-6}$	CL=90%
Γ_{595}	$K^*(892)^0\tau^-e^+$		<	5.9	$\times10^{-6}$	CL=90%
Γ_{596}	$K^*(892)^0\tau^+\mu^-$	LF	<	1.0	$\times10^{-5}$	CL=90%
Γ_{597}	$K^*(892)^0\tau^-\mu^+$	LF	<	8.2	$\times10^{-6}$	CL=90%
Γ_{598}	$e^\pm\tau^\mp$	LF	[h] <	1.6	$\times10^{-5}$	CL=90%
Γ_{599}	$\mu^\pm\tau^\mp$	LF	[h] <	1.4	$\times10^{-5}$	CL=95%
Γ_{600}	$p\mu^-$	L,B	<	2.6	$\times10^{-9}$	CL=90%
Γ_{601}	$\Lambda_c^+\mu^-$	L,B	<	1.4	$\times10^{-6}$	CL=90%
Γ_{602}	$\Lambda_c^+e^-$	L,B	<	4	$\times10^{-6}$	CL=90%

[a] An ℓ indicates an e or a μ mode, not a sum over these modes.

[b] $\overline{D}^{**}$ represents an excited state with mass $2.2 < M < 2.8$ GeV/c^2.

[c] $\chi_{c1}(3872)^+$ is a hypothetical charged partner of the $\chi_{c1}(3872)$.

[d] Stands for the possible candidates of $K^*(1410)$, $K^*_0(1430)$ and $K^*_2(1430)$.

[e] B^0 and B^0_s contributions not separated. Limit is on weighted average of the two decay rates.

[f] This decay refers to the coherent sum of resonant and nonresonant $J^P = 0^+$ $K\pi$ components with $1.60 < m_{K\pi} < 2.15$ GeV/c^2.

[g] $X(214)$ is a hypothetical particle of mass 214 MeV/c^2 reported by the HyperCP experiment, Physical Review Letters **94** 021801 (2005)

[h] The value is for the sum of the charge states or particle/antiparticle states indicated.

[i] $\Theta(1540)^+$ denotes a possible narrow pentaquark state.

[j] ψ_{DS} is a GeV-scale dark sector antibaryon (mass range 1–4 GeV/c^2).

[k] Here S and P are the hypothetical scalar and pseudoscalar particles with masses of 2.5 GeV/c^2 and 214.3 MeV/c^2, respectively.

FIT INFORMATION

An overall fit to 39 branching ratios uses 105 measurements to determine 24 parameters. The overall fit has a $\chi^2 = 814.8$ for 81 degrees of freedom.

The following *off-diagonal* array elements are the correlation coefficients $\langle\delta x_i\delta x_j\rangle/(\delta x_i\cdot\delta x_j)$, in percent, from the fit to the branching fractions, $x_i \equiv \Gamma_i/\Gamma_{total}$.

x_{10}	40									
x_{38}	0	0								
x_{50}	0	0	28							
x_{76}	0	0	4	13						
x_{125}	0	0	19	6	1					
x_{135}	0	0	7	2	0	1				
x_{214}	0	0	0	0	0	0	0			
x_{216}	0	0	0	0	0	0	0	0		
x_{264}	0	0	0	0	0	0	0	0	0	
x_{270}	0	0	0	0	0	0	0	0	0	19
x_{276}	0	0	0	0	0	0	0	0	29	0
x_{282}	0	0	0	0	0	0	0	0	6	0
x_{288}	0	0	0	0	0	0	0	0	0	0
x_{322}	0	0	0	0	0	0	0	0	0	0
x_{356}	0	0	0	0	0	0	0	0	0	0
x_{363}	0	0	0	0	0	0	0	0	0	0
x_{377}	0	0	0	0	0	0	0	0	0	0
x_{405}	0	0	0	0	0	0	0	0	0	0
x_{417}	0	0	0	0	0	0	0	0	0	0
x_{423}	0	0	0	0	0	0	0	0	0	0
x_{454}	0	0	0	0	0	0	0	0	0	0
x_{569}	0	0	0	0	0	0	0	0	0	0
x_{574}	0	0	0	0	0	0	0	0	15	0
	x_7	x_{10}	x_{38}	x_{50}	x_{76}	x_{125}	x_{135}	x_{214}	x_{216}	x_{264}

x_{276}	0									
x_{282}	0	22								
x_{288}	0	0	0							
x_{322}	0	0	0	0						
x_{356}	0	0	0	0	16					
x_{363}	0	0	0	0	27	4				
x_{377}	0	0	0	0	0	0	0			
x_{405}	0	0	0	0	0	0	0	0		
x_{417}	0	0	0	0	0	0	0	0	77	
x_{423}	0	0	0	24	0	0	0	0	0	0
x_{454}	0	0	0	0	0	0	0	20	0	0
x_{569}	0	0	0	0	0	0	0	0	0	0
x_{574}	0	4	1	0	0	0	0	0	0	0
	x_{270}	x_{276}	x_{282}	x_{288}	x_{322}	x_{356}	x_{363}	x_{377}	x_{405}	x_{417}

x_{454}	0		
x_{569}	0	0	
x_{574}	0	0	0
	x_{423}	x_{454}	x_{569}

B^0 BRANCHING RATIOS

For branching ratios in which the charge of the decaying B is not determined, see the $B^\pm$ section.

$\Gamma(\ell^+\nu_\ell X)/\Gamma_{total}$ — Γ_1/Γ

VALUE (units 10^{-2})	DOCUMENT ID		TECN	COMMENT
10.33±0.28 OUR EVALUATION	(Produced by HFLAV)			
10.14±0.30 OUR AVERAGE	Error includes scale factor of 1.1.			
10.46±0.30±0.23	[1] URQUIJO	07	BELL	$e^+e^-\to\Upsilon(4S)$
9.64±0.27±0.33	[2] AUBERT,B	06Y	BABR	$e^+e^-\to\Upsilon(4S)$
10.78±0.60±0.69	[3] ARTUSO	97	CLE2	$e^+e^-\to\Upsilon(4S)$
9.3 ±1.1 ±1.5	ALBRECHT	94	ARG	$e^+e^-\to\Upsilon(4S)$
9.9 ±3.0 ±0.9	HENDERSON	92	CLEO	$e^+e^-\to\Upsilon(4S)$
• • • We do not use the following data for averages, fits, limits, etc. • • •				
10.32±0.36±0.35	[4] OKABE	05	BELL	Repl. by URQUIJO 07
10.9 ±0.7 ±1.1	ATHANAS	94	CLE2	Sup. by ARTUSO 97

[1] URQUIJO 07 report a measurement of (9.80 ± 0.29 ± 0.21)% for the partial branching fraction of $B\to e\nu_e X_c$ decay with electron energy above 0.6 GeV. We converted the result to $B\to e\nu_e X$ branching fraction.

[2] The measurements are obtained for charged and neutral B mesons partial rates of semileptonic decay to electrons with momentum above 0.6 GeV/c in the B rest frame. The best precision on the ratio is achieved for a momentum threshold of 1.0 GeV: $B(B^+\to e^+\nu_e X)$ / $B(B^0\to e^+\nu_e X) = 1.074 \pm 0.041 \pm 0.026$.

[3] ARTUSO 97 uses partial reconstruction of $B\to D^*\ell\nu_\ell$ and inclusive semileptonic branching ratio from BARISH 96B (0.1049 ± 0.0017 ± 0.0043).

[4] The measurements are obtained for charged and neutral B mesons partial rates of semileptonic decay to electrons with momentum above 0.6 GeV/c in the B rest frame, and their ratio of $B(B^+\to e^+\nu_e X)/B(B^0\to e^+\nu_e X) = 1.08 \pm 0.05 \pm 0.02$.

Int. J. Mod. Phys. A 2026.41. Downloaded from www.worldscientific.com
by LIFORNIA @ BERKELEY on 09/16/26. Re-use and distribution is strictly not permitted, except for Open Access articles.

Int. J. Mod. Phys. A 2026.41. Downloaded from www.worldscientific.com
by UNIVERSITY OF CALIFORNIA @ BERKELEY on 09/16/26. Re-use and distribution is strictly not permitted, except for Open Access articles.

$\Gamma(e^+\nu_e X_c)/\Gamma_{total}$ — Γ_2/Γ

VALUE (units 10^{-2})	DOCUMENT ID		TECN	COMMENT
10.08±0.30±0.22	[1] URQUIJO	07	BELL	$e^+e^- \to \Upsilon(4S)$

[1] Measure the independent B^+ and B^0 partial branching fractions with electron threshold energies of 0.4 GeV.

$\Gamma(\ell^+\nu_\ell X_u)/\Gamma_{total}$ — Γ_3/Γ

Requires $E^*_\ell > 1$ GeV, where E^*_ℓ is letpon energy in B rest frame.

VALUE (units 10^{-3})	DOCUMENT ID		TECN	COMMENT
1.51±0.10±0.16	[1] CAO	21A	BELL	$e^+e^- \to \Upsilon(4S)$

[1] The correlation of 50% with $B(B^+ \to \ell^+\nu_\ell X_u)$(letpon energy in B rest frame $E^*_\ell >$ 1 GeV) was reported.

$\Gamma(D^-\ell^+\nu_\ell)/\Gamma_{total}$ — Γ_5/Γ

ℓ denotes e or μ, not the sum.

VALUE (%)	DOCUMENT ID		TECN	COMMENT
2.12±0.06 OUR EVALUATION	(Produced by HFLAV)			
2.18±0.07 OUR AVERAGE				
2.06±0.05±0.10	[1] ADACHI	25Y	BELL	$e^+e^- \to \Upsilon(4S)$
2.31±0.03±0.11	[2] GLATTAUER	16	BELL	$e^+e^- \to \Upsilon(4S)$
2.21±0.11±0.11	[3] AUBERT	10	BABR	$e^+e^- \to \Upsilon(4S)$
2.09±0.13±0.18	[4] BARTELT	99	CLE2	$e^+e^- \to \Upsilon(4S)$
2.35±0.20±0.44	[5] BUSKULIC	97	ALEP	$e^+e^- \to Z$
• • • We do not use the following data for averages, fits, limits, etc. • • •				
2.21±0.11±0.12	[3] AUBERT	08Q	BABR	Repl. by AUBERT 10
2.13±0.12±0.39	ABE	02E	BELL	Repl. by GLATTAUER 16
1.87±0.15±0.32	[6] ATHANAS	97	CLE2	Repl. by BARTELT 99
1.8 ±0.6 ±0.3	[7] FULTON	91	CLEO	$e^+e^- \to \Upsilon(4S)$
2.0 ±0.7 ±0.6	[8] ALBRECHT	89J	ARG	$e^+e^- \to \Upsilon(4S)$

[1] The second B meson from the $\Upsilon(4S)$ decay is not explicitly reconstructed.
[2] Uses a fully reconstructed B meson as a tag on the recoil side while the other, on the signal side, is partially reconstructed from $B \to D\ell\nu$.
[3] Uses a fully reconstructed B meson as a tag on the recoil side.
[4] Assumes equal production of B^+ and B^0 at the $\Upsilon(4S)$.
[5] BUSKULIC 97 assumes fraction (B^+) = fraction (B^0) = (37.8 ± 2.2)% and PDG 96 values for B lifetime and branching ratio of D^* and D decays.
[6] ATHANAS 97 uses missing energy and missing momentum to reconstruct neutrino.
[7] FULTON 91 assumes assuming equal production of B^0 and B^+ at the $\Upsilon(4S)$ and uses Mark III D and D^* branching ratios.
[8] ALBRECHT 89J reports 0.018 ± 0.006 ± 0.005. We rescale using the method described in STONE 94 but with the updated PDG 94 $B(D^0 \to K^-\pi^+)$.

$\Gamma(D^-\ell^+\nu_\ell)/\Gamma(\ell^+\nu_\ell X)$ — Γ_5/Γ_1

VALUE	DOCUMENT ID		TECN	COMMENT
0.230±0.011±0.011	[1] AUBERT	10	BABR	$e^+e^- \to \Upsilon(4S)$

[1] Uses a fully reconstructed B meson on the recoil side.

$\Gamma(D^-\ell^+\nu_\ell)/\Gamma(D\ell^+\nu_\ell X)$ — Γ_5/Γ_4

VALUE	DOCUMENT ID		TECN	COMMENT
0.215±0.016±0.013	[1] AUBERT	07AN	BABR	$e^+e^- \to \Upsilon(4S)$

[1] Uses a fully reconstructed B meson on the recoil side.

$\Gamma(D^-\tau^+\nu_\tau)/\Gamma_{total}$ — Γ_6/Γ

VALUE (units 10^{-2})	DOCUMENT ID		TECN	COMMENT
• • • We do not use the following data for averages, fits, limits, etc. • • •				
1.04±0.35±0.18	[1] AUBERT	08N	BABR	Repl. by AUBERT 09S

[1] Uses a fully reconstructed B meson as a tag on the recoil side.

$\Gamma(D^-\tau^+\nu_\tau)/\Gamma(D^-\ell^+\nu_\ell)$ — Γ_6/Γ_5

VALUE	DOCUMENT ID		TECN	COMMENT
0.34 ±0.07 OUR AVERAGE	Error includes scale factor of 1.5. See the ideogram below.			
0.249±0.043±0.047	[1,2] AAIJ	25G	LHCB	pp at 13 TeV
$0.418^{+0.075}_{-0.073}{}^{+0.049}_{-0.056}$	[3] ADACHI	25R	BELL	$e^+e^- \to \Upsilon(4S)$
0.469±0.084±0.053	[4,5] LEES	12D	BABR	$e^+e^- \to \Upsilon(4S)$
• • • We do not use the following data for averages, fits, limits, etc. • • •				
0.489±0.165±0.069	[4] AUBERT	09S	BABR	Repl. by LEES 12D

[1] Uses $\tau^+ \to \mu^-\overline{\nu}_\mu\nu_\tau$ and μ^+ as ℓ^+.
[2] AAIJ 25G simultaneously measures also $B(B^0 \to D^*(2010)^-\tau^+\nu_\tau)/B(B^0 \to D^*(2010)^-\mu^+\nu_\mu)$ and reports correlation factor -0.39.
[3] Uses leptonic decay modes of τ^+ and reconstruction of the companion B meson in semileptonic decay modes.
[4] Uses a fully reconstructed B meson as a tag on the recoil side.
[5] Uses $\tau^+ \to e^+\nu_e\overline{\nu}_\tau$ and $\tau^+ \to \mu^+\nu_\mu\overline{\nu}_\tau$ and e^+ or μ^+ as ℓ^+.

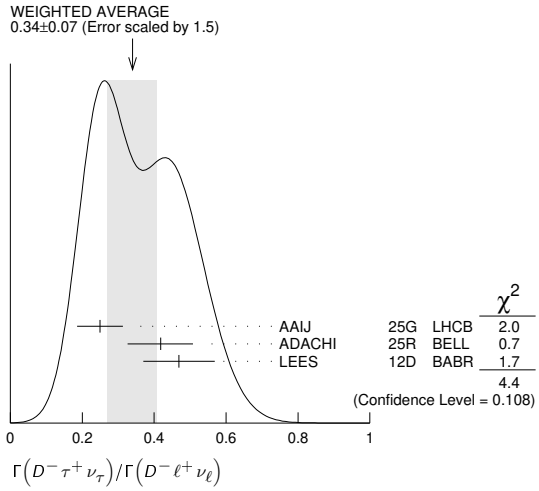

$\Gamma(D^*(2010)^-\ell^+\nu_\ell)/\Gamma_{total}$ — Γ_7/Γ

VALUE (%)	EVTS	DOCUMENT ID		TECN	COMMENT
4.90 ±0.12 OUR EVALUATION		(Produced by HFLAV) This value assumes isospin symmetry.			
5.10 ±0.14 OUR FIT		Error includes scale factor of 1.4.			
5.11 ±0.15 OUR AVERAGE		Error includes scale factor of 1.4. See the ideogram below.			
4.922±0.023±0.220		[1] ADACHI	23J	BELL	$e^+e^- \to \Upsilon(4S)$
5.02 ±0.02 ±0.16		[2] WAHEED	21	BELL	$e^+e^- \to \Upsilon(4S)$
5.49 ±0.16 ±0.25		[3] AUBERT	08Q	BABR	$e^+e^- \to \Upsilon(4S)$
4.69 ±0.04 ±0.34		[4] AUBERT	08R	BABR	$e^+e^- \to \Upsilon(4S)$
5.90 ±0.22 ±0.50		[5] ABDALLAH	04D	DLPH	$e^+e^- \to Z^0$
6.09 ±0.19 ±0.40		[6] ADAM	03	CLE2	$e^+e^- \to \Upsilon(4S)$
4.70 ±0.13 $^{+0.36}_{-0.31}$		[7] ABREU	01H	DLPH	$e^+e^- \to Z$
5.26 ±0.20 ±0.46		[8] ABBIENDI	00Q	OPAL	$e^+e^- \to Z$
5.53 ±0.26 ±0.52		[9] BUSKULIC	97	ALEP	$e^+e^- \to Z$
• • • We do not use the following data for averages, fits, limits, etc. • • •					
4.917±0.032±0.216		[10] ADACHI	23J	BELL	$e^+e^- \to \Upsilon(4S)$
4.926±0.032±0.231		[11] ADACHI	23J	BELL	$e^+e^- \to \Upsilon(4S)$
4.90 ±0.02 ±0.16		[2] WAHEED	19	BELL	Repl. by WAHEED 21
4.58 ±0.03 ±0.26		[2] DUNGEL	10	BELL	Repl. by WAHEED 19
4.90 ±0.07 $^{+0.36}_{-0.35}$		[5] AUBERT	05E	BABR	Repl. by AUBERT 08R
5.39 ±0.11 ±0.34		[12] ABDALLAH	04D	DLPH	$e^+e^- \to Z^0$
4.59 ±0.23 ±0.40		[13] ABE	02F	BELL	Repl. by DUNGEL 10
6.09 ±0.19 ±0.40		[14] BRIERE	02	CLE2	$e^+e^- \to \Upsilon(4S)$
5.08 ±0.21 ±0.66		[15] ACKERSTAFF	97G	OPAL	Repl. by ABBIENDI 00Q
5.52 ±0.17 ±0.68		[16] ABREU	96P	DLPH	Repl. by ABREU 01H
4.49 ±0.32 ±0.39	376	[17] BARISH	95	CLE2	Repl. by ADAM 03
5.18 ±0.30 ±0.62	410	[18] BUSKULIC	95N	ALEP	Sup. by BUSKULIC 97
4.5 ±0.3 ±0.4		[19] ALBRECHT	94	ARG	$e^+e^- \to \Upsilon(4S)$
4.7 ±0.5 ±0.5	235	[20] ALBRECHT	93	ARG	$e^+e^- \to \Upsilon(4S)$
seen	398	[21] SANGHERA	93	CLE2	$e^+e^- \to \Upsilon(4S)$
7.0 ±1.8 ±1.4		[22] ANTREASYAN	90B	CBAL	$e^+e^- \to \Upsilon(4S)$
		[23] ALBRECHT	89C	ARG	$e^+e^- \to \Upsilon(4S)$
6.0 ±1.0 ±1.4		[24] ALBRECHT	89J	ARG	$e^+e^- \to \Upsilon(4S)$
4.0 ±0.4 ±0.6		[25] BORTOLETTO	89B	CLEO	$e^+e^- \to \Upsilon(4S)$
7.0 ±1.2 ±1.9	47	[26] ALBRECHT	87J	ARG	$e^+e^- \to \Upsilon(4S)$

[1] Uses fully reconstructed $D^{*-}\ell^+\nu$ events with $\ell = e$ or μ.
[2] WAHEED 21 uses fully reconstructed $D^{*-}\ell^+\nu$ events ($\ell = e$ or μ).
[3] Uses a fully reconstructed B meson as a tag on the recoil side.
[4] Measured using fully reconstructed D^* sample and a simultaneous fit to the Caprini-Lellouch-Neubert form factor parameters: $\rho^2 = 1.191 \pm 0.048 \pm 0.028$, $R_1(1) = 1.429 \pm 0.061 \pm 0.044$, and $R_2(1) = 0.827 \pm 0.038 \pm 0.022$.
[5] Measured using fully reconstructed D^* sample.
[6] Uses the combined fit of both $B^0 \to D^*(2010)^-\ell\nu$ and $B^+ \to \overline{D}(2007)^0\ell\nu$ samples.
[7] ABREU 01H measured using about 5000 partial reconstructed D^* sample.
[8] ABBIENDI 00Q assumes the fraction $B(b \to B^0)$= $(39.7^{+1.8}_{-2.2})$%. This result is an average of two methods using exclusive and partial D^* reconstruction.
[9] BUSKULIC 97 assumes fraction (B^+) = fraction (B^0) = (37.8 ± 2.2)% and PDG 96 values for B lifetime and D^* and D branching fractions.
[10] Uses fully reconstructed $D^{*-}e^+\nu$ events.
[11] Uses fully reconstructed $D^{*-}\mu^+\nu$ events.
[12] Combines with previous partial reconstructed D^* measurement.
[13] Assumes equal production of B^+ and B^0 at the $\Upsilon(4S)$.
[14] The results are based on the same analysis and data sample reported in ADAM 03.
[15] ACKERSTAFF 97G assumes fraction (B^+) = fraction (B^0) = (37.8 ± 2.2)% and PDG 96 values for B lifetime and branching ratio of D^* and D decays.
[16] ABREU 96P result is the average of two methods using exclusive and partial D^* reconstruction.
[17] BARISH 95 use $B(D^0 \to K^-\pi^+)$ = (3.91 ± 0.08 ± 0.17)% and $B(D^{*+} \to D^0\pi^+)$ = (68.1 ± 1.0 ± 1.3)%.

[18] BUSKULIC 95N assumes fraction (B^+) = fraction $(B^0) = 38.2 \pm 1.3 \pm 2.2\%$ and $\tau_{B^0} = 1.58 \pm 0.06$ ps. $\Gamma(D^{*-}\ell^+\nu_\ell)$/total = [5.18 − 0.13(fraction(B^0)−38.2)−1.5(τ_{B^0} − 1.58)]%.

[19] ALBRECHT 94 assumes $B(D^{*+} \to D^0\pi^+) = 68.1 \pm 1.0 \pm 1.3\%$. Uses partial reconstruction of D^{*+} and is independent of D^0 branching ratios.

[20] ALBRECHT 93 reports $0.052 \pm 0.005 \pm 0.006$. We rescale using the method described in STONE 94 but with the updated PDG 94 $B(D^0 \to K^-\pi^+)$. We have taken their average e and μ value. They also obtain $\alpha = 2*\Gamma^0/(\Gamma^- + \Gamma^+) - 1 = 1.1 \pm 0.4 \pm 0.2$, $A_{AF} = 3/4*(\Gamma^- - \Gamma^+)/\Gamma = 0.2 \pm 0.08 \pm 0.06$ and a value of $|V_{cb}| = 0.036$–0.045 depending on model assumptions.

[21] Combining $\overline{D}^{*0}\ell^+\nu_\ell$ and $\overline{D}^{*-}\ell^+\nu_\ell$ SANGHERA 93 test $V-A$ structure and fit the decay angular distributions to obtain $A_{FB} = 3/4*(\Gamma^- - \Gamma^+)/\Gamma = 0.14 \pm 0.06 \pm 0.03$. Assuming a value of V_{cb}, they measure V, A_1, and A_2, the three form factors for the $D^*\ell\nu_\ell$ decay, where results are slightly dependent on model assumptions.

[22] ANTREASYAN 90B is average over B and $\overline{D}^*(2010)$ charge states.

[23] The measurement of ALBRECHT 89C suggests a D^* polarization γ_L/γ_T of 0.85 ± 0.45. or $\alpha = 0.7 \pm 0.9$.

[24] ALBRECHT 89J is ALBRECHT 87J value rescaled using $B(D^*(2010)^- \to D^0\pi^-) = 0.57 \pm 0.04 \pm 0.04$. Superseded by ALBRECHT 93.

[25] We have taken average of the the BORTOLETTO 89B values for electrons and muons, $0.046 \pm 0.005 \pm 0.007$. We rescale using the method described in STONE 94 but with the updated PDG 94 $B(D^0 \to K^-\pi^+)$. The measurement suggests a D^* polarization parameter value $\alpha = 0.65 \pm 0.66 \pm 0.25$.

[26] ALBRECHT 87J assume μ-e universality, the $B(\Upsilon(4S) \to B^0\overline{B}^0) = 0.45$, the $B(D^0 \to K^-\pi^+) = (0.042 \pm 0.004 \pm 0.004)$, and the $B(D^*(2010)^- \to D^0\pi^-) = 0.49 \pm 0.08$. Superseded by ALBRECHT 89J.

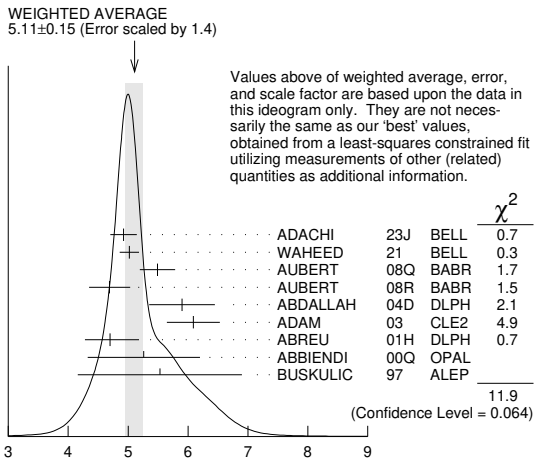

$\Gamma\left(D^*(2010)^-\ell^+\nu_\ell\right)/\Gamma_{\rm total}$ (%)

$\Gamma(D^*(2010)^-\ell^+\nu_\ell)/\Gamma(D\ell^+\nu_\ell X)$ — Γ_7/Γ_4

VALUE	DOCUMENT ID		TECN	COMMENT
0.537±0.031±0.036	[1] AUBERT	07AN	BABR	$e^+e^- \to \Upsilon(4S)$

[1] Uses a fully reconstructed B meson on the recoil side.

$\Gamma(D^*(2010)^-e^+\nu_e)/\Gamma(D^*(2010)^-\mu^+\nu_\mu)$ — Γ_8/Γ_9

VALUE	DOCUMENT ID		TECN	COMMENT
1.001±0.019 OUR AVERAGE				
0.998±0.009±0.020	ADACHI	23J	BELL	$e^+e^- \to \Upsilon(4S)$
1.011±0.035±0.024	PRIM	23	BELL	$e^+e^- \to \Upsilon(4S)$

$\Gamma(D^*(2010)^-\tau^+\nu_\tau)/\Gamma_{\rm total}$ — Γ_{10}/Γ

VALUE (units 10^{-2})	DOCUMENT ID		TECN	COMMENT
1.50±0.08 OUR FIT Error includes scale factor of 1.1.				
1.48±0.18 OUR AVERAGE Error includes scale factor of 1.1.				
1.42±0.094±0.140	[1] AAIJ	18D	LHCB	pp at 7, 8 TeV
$2.02^{+0.40}_{-0.37}$ ±0.37	[2] MATYJA	07	BELL	$e^+e^- \to \Upsilon(4S)$
• • • We do not use the following data for averages, fits, limits, etc. • • •				
1.11±0.51 ±0.06	[3] AUBERT	08N	BABR	Repl. by AUBERT 09S

[1] Noramlizes to $B(B^0 \to D^*(2010)^-\pi^+\pi^-\pi^+) = (7.214 \pm 0.28) \times 10^{-3}$.
[2] Observed in the recoil of the accompanying B meson.
[3] Uses a fully reconstructed B meson as a tag on the recoil side.

$\Gamma(D^*(2010)^-\tau^+\nu_\tau)/\Gamma(D^*(2010)^-\ell^+\nu_\ell)$ — Γ_{10}/Γ_7

VALUE	DOCUMENT ID		TECN	COMMENT
0.294±0.015 OUR FIT Error includes scale factor of 1.1.				
0.295±0.017 OUR AVERAGE Error includes scale factor of 1.1.				
0.402±0.081±0.085	[1,2] AAIJ	25G	LHCB	pp at 13 TeV
$0.306^{+0.035}_{-0.033}{}^{+0.016}_{-0.018}$	[3] ADACHI	25R	BELL	$e^+e^- \to \Upsilon(4S)$
0.267±0.012±0.020	[4,5] AAIJ	23W	LHCB	pp at 13 TeV
0.302±0.030±0.011	[6] SATO	16B	BELL	$e^+e^- \to \Upsilon(4S)$
0.355±0.039±0.021	[7,8] LEES	12D	BABR	$e^+e^- \to \Upsilon(4S)$
• • • We do not use the following data for averages, fits, limits, etc. • • •				
0.260±0.015±0.019	[4] AAIJ	23W	LHCB	pp at 13 TeV
0.291±0.019±0.029	[4] AAIJ	18D	LHCB	Repl. by AAIJ 23W
0.336±0.027±0.030	[9] AAIJ	15Q	LHCB	Repl. by AAIJ 23AR
0.207±0.095±0.008	[7] AUBERT	09S	BABR	Repl. by LEES 12D

[1] Uses $\tau^+ \to \mu^-\overline{\nu}_\mu\nu_\tau$ and μ^+ as ℓ^+.
[2] AAIJ 25G simultaneously measures also $B(B^0 \to D^-\tau^+\nu_\tau)/B(B^0 \to D^-\mu^+\nu_\mu)$ and reports correlation factor -0.39.
[3] Uses leptonic decay modes of τ^+ and reconstruction of the companion B meson in semileptonic decay modes.
[4] Uses $\tau^+ \to \pi^+\pi^-\pi^+\overline{\nu}_\tau$ and $\tau^+ \to \pi^+\pi^-\pi^+\pi^0\overline{\nu}_\tau$, and μ^+ as ℓ^+.
[5] Combination with measurement from AAIJ 18D.
[6] Uses semileptonic B decay events for tagging and $\tau^+ \to \ell^+\nu_\ell\overline{\nu}_\tau$ mode.
[7] Uses a fully reconstructed B meson as a tag on the recoil side.
[8] Uses $\tau^+ \to e^+\nu_e\overline{\nu}_\tau$ and $\tau^+ \to \mu^+\nu_\mu\overline{\nu}_\tau$ and e^+ or μ^+ as ℓ^+.
[9] Uses $\tau^+ \to \mu^+\nu_\mu\overline{\nu}_\tau$ and μ^+ as ℓ^+.

$\Gamma(D^*(2010)^-\tau^+\nu_\tau)/\Gamma(D^*(2010)^-\pi^+\pi^+\pi^-)$ — Γ_{10}/Γ_{61}

VALUE	DOCUMENT ID		TECN	COMMENT
1.84±0.08±0.10	[1,2] AAIJ	23W	LHCB	pp at 7, 8, 13 TeV
• • • We do not use the following data for averages, fits, limits, etc. • • •				
1.79±0.11±0.11	[1] AAIJ	23W	LHCB	pp at 13 TeV
1.97±0.13±0.18	[1] AAIJ	18D	LHCB	Repl. by AAIJ 23W

[1] Uses $\tau^+ \to \pi^+\pi^-\pi^+\overline{\nu}_\tau$ and $\tau^+ \to \pi^+\pi^-\pi^+\pi^0\overline{\nu}_\tau$ modes.
[2] Combination with result from AAIJ 18D.

$\Gamma(\overline{D}^{(*)}n\pi\ell^+\nu_\ell(n \geq 1))/\Gamma(D\ell^+\nu_\ell X)$ — Γ_{11}/Γ_4

VALUE	DOCUMENT ID		TECN	COMMENT
0.248±0.032±0.030	[1] AUBERT	07AN	BABR	$e^+e^- \to \Upsilon(4S)$

[1] Uses a fully reconstructed B meson on the recoil side.

$\Gamma(\overline{D}^0\pi^-\ell^+\nu_\ell)/\Gamma_{\rm total}$ — Γ_{12}/Γ

VALUE (units 10^{-3})	DOCUMENT ID		TECN	COMMENT
3.64±0.20 OUR AVERAGE				
3.60±0.18±0.11	MEIER	23	BELL	$e^+e^- \to \Upsilon(4S)$
4.3 ±0.8 ±0.3	[1] AUBERT	08Q	BABR	$e^+e^- \to \Upsilon(4S)$
• • • We do not use the following data for averages, fits, limits, etc. • • •				
4.05±0.36±0.41	VOSSEN	18	BELL	Repl. by MEIER 23
4.2 ±0.8 ±0.1	[1,2] LIVENTSEV	08	BELL	Repl. by VOSSEN 18
3.3 ±0.9 ±0.1	[3] LIVENTSEV	05	BELL	Repl. by LIVENTSEV 08

[1] Uses a fully reconstructed B meson as a tag on the recoil side.
[2] LIVENTSEV 08 reports $(4.2 \pm 0.7 \pm 0.6) \times 10^{-3}$ from a measurement of $[\Gamma(B^0 \to \overline{D}^0\pi^-\ell^+\nu_\ell)/\Gamma_{\rm total}]$ / $[B(B^0 \to D^-\ell^+\nu_\ell)]$ assuming $B(B^0 \to D^-\ell^+\nu_\ell) = (2.12 \pm 0.20) \times 10^{-2}$, which we rescale to our best (shown rounded) value $B(B^0 \to D^-\ell^+\nu_\ell) = (2.12 \pm 0.06) \times 10^{-2}$. Our first error is their experiment's error and our second error is the systematic error from using our best (shown rounded) value.
[3] LIVENTSEV 05 reports $[\Gamma(B^0 \to \overline{D}^0\pi^-\ell^+\nu_\ell)/\Gamma_{\rm total}]$ / $[B(B^+ \to \overline{D}^0\ell^+\nu_\ell)] = 0.15 \pm 0.03 \pm 0.03$ which we multiply by our best (shown rounded) value $B(B^+ \to \overline{D}^0\ell^+\nu_\ell) = (2.21 \pm 0.06) \times 10^{-2}$. Our first error is their experiment's error and our second error is the systematic error from using our best (shown rounded) value.

$\Gamma(D_0^*(2300)^-\ell^+\nu_\ell,\ D_0^{*-} \to \overline{D}^0\pi^-)/\Gamma_{\rm total}$ — Γ_{13}/Γ

VALUE (units 10^{-4})	CL%	DOCUMENT ID		TECN	COMMENT
< 4.4	90	MEIER	23	BELL	$e^+e^- \to \Upsilon(4S)$
• • • We do not use the following data for averages, fits, limits, etc. • • •					
44 ±8±6		[1] AUBERT	08BL	BABR	$e^+e^- \to \Upsilon(4S)$
20 ±7±5		[1] LIVENTSEV	08	BELL	$e^+e^- \to \Upsilon(4S)$

[1] Uses a fully reconstructed B meson as a tag on the recoil side.

$\Gamma(D_2^*(2460)^-\ell^+\nu_\ell,\ D_2^{*-} \to \overline{D}^0\pi^-)/\Gamma_{\rm total}$ — Γ_{14}/Γ

VALUE (units 10^{-3})	DOCUMENT ID		TECN	COMMENT
1.41±0.20 OUR AVERAGE Error includes scale factor of 1.7. See the ideogram below.				
1.57±0.15±0.05	MEIER	23	BELL	$e^+e^- \to \Upsilon(4S)$
1.10±0.17±0.08	[1] AUBERT	09Y	BABR	$e^+e^- \to \Upsilon(4S)$
2.2 ±0.4 ±0.4	[2] LIVENTSEV	08	BELL	$e^+e^- \to \Upsilon(4S)$

[1] Uses a simultaneous fit of all B semileptonic decays without full reconstruction of events. AUBERT 09Y reports $B(B^0 \to \overline{D}_2^*(2460)^-\ell^+\nu_\ell) \cdot B(\overline{D}_2^*(2460)^- \to \overline{D}^{(*)0}\pi^-) = (1.77 \pm 0.26 \pm 0.11) \times 10^{-3}$ and the authors have provided us the individual measurement.
[2] Uses a fully reconstructed B meson as a tag on the recoil side.

Int. J. Mod. Phys. A 2026.41. Downloaded from www.worldscientific.com
by LIFORNIA @ BERKELEY on 09/16/26. Re-use and distribution is strictly not permitted, except for Open Access articles.

Int. J. Mod. Phys. A 2026.41. Downloaded from www.worldscientific.com
by UNIVERSITY OF CALIFORNIA @ BERKELEY on 09/16/26. Re-use and distribution is strictly not permitted, except for Open Access articles.

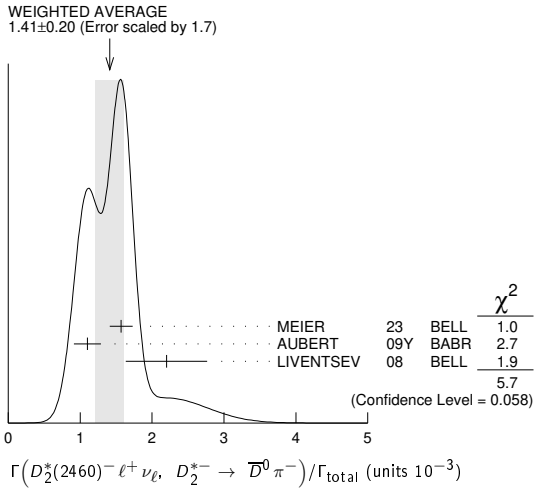

$\Gamma(\overline{D}^{*0}\pi^-\ell^+\nu_\ell)/\Gamma_{total}$ — Γ_{15}/Γ

VALUE (units 10^{-3})	DOCUMENT ID		TECN	COMMENT
5.44±0.28 OUR AVERAGE				
5.51±0.24±0.17	MEIER	23	BELL	$e^+e^- \to \Upsilon(4S)$
4.8 ±0.8 ±0.4	[1] AUBERT	08Q	BABR	$e^+e^- \to \Upsilon(4S)$
• • • We do not use the following data for averages, fits, limits, etc. • • •				
6.46±0.53±0.52	VOSSEN	18	BELL	Repl. by MEIER 23
5.6 ±2.2 ±0.2	[1,2] LIVENTSEV	08	BELL	Repl. by VOSSEN 18
5.5 ±1.2 ±0.2	[3,4] LIVENTSEV	05	BELL	Repl. by LIVENTSEV 08

[1] Uses a fully reconstructed B meson as a tag on the recoil side.
[2] LIVENTSEV 08 reports $(5.6 \pm 2.1 \pm 0.8) \times 10^{-3}$ from a measurement of $[\Gamma(B^0 \to \overline{D}^{*0}\pi^-\ell^+\nu_\ell)/\Gamma_{total}] / [B(B^0 \to D^-\ell^+\nu_\ell)]$ assuming $B(B^0 \to D^-\ell^+\nu_\ell) = (2.12 \pm 0.20) \times 10^{-2}$, which we rescale to our best (shown rounded) value $B(B^0 \to D^-\ell^+\nu_\ell) = (2.12 \pm 0.06) \times 10^{-2}$. Our first error is their experiment's error and our second error is the systematic error from using our best (shown rounded) value.
[3] Excludes D^{*+} contribution to $D\pi$ modes.
[4] LIVENTSEV 05 reports $[\Gamma(B^0 \to \overline{D}^{*0}\pi^-\ell^+\nu_\ell)/\Gamma_{total}] / [B(B^+ \to \overline{D}^*(2007)^0\ell^+\nu_\ell)] = 0.10 \pm 0.02 \pm 0.01$ which we multiply by our best (shown rounded) value $B(B^+ \to \overline{D}^*(2007)^0\ell^+\nu_\ell) = (5.53 \pm 0.22) \times 10^{-2}$. Our first error is their experiment's error and our second error is the systematic error from using our best (shown rounded) value.

$\Gamma(D_1(2420)^-\ell^+\nu_\ell, D_1^- \to \overline{D}^{*0}\pi^-)/\Gamma_{total}$ — Γ_{16}/Γ

VALUE (units 10^{-3})	DOCUMENT ID		TECN	COMMENT
2.85±0.25 OUR AVERAGE				
3.06±0.50±0.28	MEIER	23	BELL	$e^+e^- \to \Upsilon(4S)$
2.78±0.24±0.25	[1] AUBERT	09Y	BABR	$e^+e^- \to \Upsilon(4S)$
2.7 ±0.4 ±0.3	[2] AUBERT	08BL	BABR	$e^+e^- \to \Upsilon(4S)$
5.4 ±1.9 ±0.9	[2] LIVENTSEV	08	BELL	$e^+e^- \to \Upsilon(4S)$

[1] Uses a simultaneous measurement of all B semileptonic decays without full reconstruction of events.
[2] Uses a fully reconstructed B meson as a tag on the recoil side.

$\Gamma(D_1(2420)^-\ell^+\nu_\ell, D_1^- \to D^-\pi^+\pi^-)/\Gamma_{total}$ — Γ_{17}/Γ

VALUE (units 10^{-3})	DOCUMENT ID		TECN	COMMENT
1.02±0.13±0.09	MEIER	23	BELL	$e^+e^- \to \Upsilon(4S)$

$\Gamma(D_1'(2430)^-\ell^+\nu_\ell, D_1'^- \to \overline{D}^{*0}\pi^-)/\Gamma_{total}$ — Γ_{18}/Γ

VALUE (units 10^{-3})	CL%	DOCUMENT ID		TECN	COMMENT
2.5 ±0.6 OUR AVERAGE					
2.06±0.68±0.25		MEIER	23	BELL	$e^+e^- \to \Upsilon(4S)$
3.1 ±0.7 ±0.5		[1] AUBERT	08BL	BABR	$e^+e^- \to \Upsilon(4S)$
• • • We do not use the following data for averages, fits, limits, etc. • • •					
<5.0	90	[1] LIVENTSEV	08	BELL	$e^+e^- \to \Upsilon(4S)$

[1] Uses a fully reconstructed B meson as a tag on the recoil side.

$\Gamma(D_2^*(2460)^-\ell^+\nu_\ell, D_2^{*-} \to \overline{D}^{*0}\pi^-)/\Gamma_{total}$ — Γ_{19}/Γ

VALUE (units 10^{-4})	CL%	DOCUMENT ID		TECN	COMMENT
6.6±1.1 OUR AVERAGE					
5.1±4.0±1.0		MEIER	23	BELL	$e^+e^- \to \Upsilon(4S)$
6.7±1.2±0.5		[1] AUBERT	09Y	BABR	$e^+e^- \to \Upsilon(4S)$
7 ±2 ±2		[2] AUBERT	08BL	BABR	$e^+e^- \to \Upsilon(4S)$
• • • We do not use the following data for averages, fits, limits, etc. • • •					
<30	90	[2] LIVENTSEV	08	BELL	$e^+e^- \to \Upsilon(4S)$

[1] Uses a simultaneous fit of all B semileptonic decays without full reconstruction of events. AUBERT 09Y reports $B(B^0 \to \overline{D}_2^*(2460)^-\ell^+\nu_\ell) \cdot B(\overline{D}_2^*(2460)^- \to \overline{D}^{(*)0}\pi^-) = (1.77 \pm 0.26 \pm 0.11) \times 10^{-3}$ and the authors have provided us the individual measurement.
[2] Uses a fully reconstructed B meson as a tag on the recoil side.

$\Gamma(D^-\pi^+\pi^-\ell^+\nu_\ell)/\Gamma_{total}$ — Γ_{20}/Γ

VALUE (units 10^{-3})	DOCUMENT ID		TECN	COMMENT
1.45±0.18±0.13	MEIER	23	BELL	$e^+e^- \to \Upsilon(4S)$

$\Gamma(D^-\pi^+\pi^-\ell^+\nu_\ell)/\Gamma(D^-\ell^+\nu_\ell)$ — Γ_{20}/Γ_5

VALUE (units 10^{-2})	DOCUMENT ID		TECN	COMMENT
5.8±1.8±1.2	[1] LEES	16	BABR	$e^+e^- \to \Upsilon(4S)$

[1] Measurement used electrons and muons as leptons.

$\Gamma(D^{*-}\pi^+\pi^-\ell^+\nu_\ell)/\Gamma_{total}$ — Γ_{21}/Γ

VALUE (units 10^{-4})	DOCUMENT ID		TECN	COMMENT
5.1±2.1±0.9	MEIER	23	BELL	$e^+e^- \to \Upsilon(4S)$

$\Gamma(D^{*-}\pi^+\pi^-\ell^+\nu_\ell)/\Gamma(D^*(2010)^-\ell^+\nu_\ell)$ — Γ_{21}/Γ_7

VALUE (units 10^{-2})	DOCUMENT ID		TECN	COMMENT
2.8±0.8±0.6	[1] LEES	16	BABR	$e^+e^- \to \Upsilon(4S)$

[1] Measurement used electrons and muons as leptons.

$\Gamma(\rho^-\ell^+\nu_\ell)/\Gamma_{total}$ — Γ_{22}/Γ

$\ell = e$ or μ, not sum over e and μ modes.

"OUR EVALUATION" includes both B^0 and B^+ decays. The average assumes equality of the semileptonic decay width for these isospin conjugate states.

VALUE (units 10^{-4})	CL%	DOCUMENT ID		TECN	COMMENT
2.94±0.11±0.18 OUR EVALUATION (Produced by HFLAV)					
2.45±0.32 OUR AVERAGE Error includes scale factor of 1.6. See the ideogram below.					
3.22±0.27±0.24		[1] SIBIDANOV	13	BELL	$e^+e^- \to \Upsilon(4S)$
1.75±0.15±0.27		[2] DEL-AMO-SA...	11C	BABR	$e^+e^- \to \Upsilon(4S)$
2.93±0.37±0.37		[3] ADAM	07	CLE2	$e^+e^- \to \Upsilon(4S)$
2.17±0.54±0.32		[4] HOKUUE	07	BELL	$e^+e^- \to \Upsilon(4S)$
$2.57 \pm 0.29^{+0.53}_{-0.62}$		[5] BEHRENS	00	CLE2	$e^+e^- \to \Upsilon(4S)$
• • • We do not use the following data for averages, fits, limits, etc. • • •					
2.14±0.21±0.56		[2] AUBERT,B	05O	BABR	Repl. by DEL-AMO-SANCHEZ 11C
$2.17 \pm 0.34^{+0.62}_{-0.68}$		[6] ATHAR	03	CLE2	Repl. by ADAM 07
3.29±0.42±0.72		[7] AUBERT	03E	BABR	Repl. by AUBERT,B 05O
$2.69 \pm 0.41^{+0.61}_{-0.64}$		[8] BEHRENS	00	CLE2	$e^+e^- \to \Upsilon(4S)$
$2.5 \pm 0.4^{+0.7}_{-0.9}$		[9] ALEXANDER	96T	CLE2	Repl. by BEHRENS 00
<4.1	90	[10] BEAN	93B	CLE2	$e^+e^- \to \Upsilon(4S)$

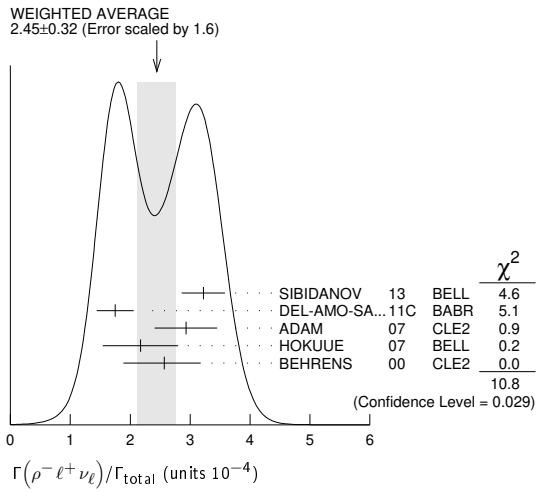

[1] The signal events are tagged by a second B meson reconstructed in the fully hadronic decays.
[2] B^+ and B^0 decays combined assuming isospin symmetry. Systematic errors include both experimental and form-factor uncertainties.
[3] The B^0 and B^+ results are combined assuming the isospin, B lifetimes, and relative charged/neutral B production at the $\Upsilon(4S)$.
[4] The signal events are tagged by a second B meson reconstructed in the semileptonic mode $B \to D^{(*)}\ell\nu_\ell$.
[5] Averaging with ALEXANDER 96T results including experimental and theoretical correlations considered, BEHRENS 00 reports systematic errors $^{+0.33}_{-0.46} \pm 0.41$, where the second error is theoretical model dependence. We combine these in quadrature.
[6] ATHAR 03 reports systematic errors $^{+0.47}_{-0.50} \pm 0.41 \pm 0.01$, which are experimental systematic, systematic due to residual form-factor uncertainties in the signal, and systematic due to residual form-factor uncertainties in the cross-feed modes, respectively. We combine these in quadrature.
[7] Uses isospin constraints and extrapolation to all electron energies according to five different form-factor calculations. The second error combines the systematic and theoretical uncertainties in quadrature.

[8] BEHRENS 00 reports $^{+0.35}_{-0.40} \pm 0.50$, where the second error is the theoretical model dependence. We combine these in quadrature. B^+ and B^0 decays combined using isospin symmetry: $\Gamma(B^0 \to \rho^- \ell^+ \nu) = 2\Gamma(B^+ \to \rho^0 \ell^+ \nu) \approx 2\Gamma(B^+ \to \omega \ell^+ \nu)$. No evidence for $\omega \ell \nu$ is reported.

[9] ALEXANDER 96T reports $^{+0.5}_{-0.7} \pm 0.5$ where the second error is the theoretical model dependence. We combine these in quadrature. B^+ and B^0 decays combined using isospin symmetry: $\Gamma(B^0 \to \rho^- \ell^+ \nu) = 2\Gamma(B^+ \to \rho^0 \ell^+ \nu) \approx 2\Gamma(B^+ \to \omega \ell^+ \nu)$. No evidence for $\omega \ell \nu$ is reported.

[10] BEAN 93B limit set using ISGW Model. Using isospin and the quark model to combine $\Gamma(\rho^0 \ell^+ \nu_\ell)$ and $\Gamma(\omega \ell^+ \nu_\ell)$ with this result, they obtain a limit $<(1.6\text{–}2.7) \times 10^{-4}$ at 90% CL for $B^+ \to (\omega \text{or } \rho^0) \ell^+ \nu_\ell$. The range corresponds to the ISGW, WSB, and KS models. An upper limit on $|V_{ub}/V_{cb}| < 0.08\text{–}0.13$ at 90% CL is derived as well.

$\Gamma(\pi^- \ell^+ \nu_\ell)/\Gamma_{\text{total}}$ — Γ_{23}/Γ

VALUE (units 10^{-4})	DOCUMENT ID		TECN	COMMENT
1.50 ±0.05 OUR EVALUATION	(Produced by HFLAV)			
1.473±0.035 OUR AVERAGE				
1.516±0.042±0.059	[1] ADACHI	25I	BELL	$e^+e^- \to \Upsilon(4S)$
1.49 ±0.09 ±0.07	[2] SIBIDANOV	13	BELL	$e^+e^- \to \Upsilon(4S)$
1.47 ±0.05 ±0.06	[3,4] LEES	12AA	BABR	$e^+e^- \to \Upsilon(4S)$
1.41 ±0.05 ±0.07	[5] DEL-AMO-SA...	11C	BABR	$e^+e^- \to \Upsilon(4S)$
1.49 ±0.04 ±0.07	[3] HA	11	BELL	$e^+e^- \to \Upsilon(4S)$
1.54 ±0.17 ±0.09	[5] AUBERT	08AV	BABR	$e^+e^- \to \Upsilon(4S)$
1.37 ±0.15 ±0.11	[6,7] ADAM	07	CLE2	$e^+e^- \to \Upsilon(4S)$
1.38 ±0.19 ±0.14	[8] HOKUUE	07	BELL	$e^+e^- \to \Upsilon(4S)$
• • • We do not use the following data for averages, fits, limits, etc. • • •				
1.53 ±0.18 ±0.12	[2,9] CAO	23	BELL	$e^+e^- \to \Upsilon(4S)$
1.42 ±0.05 ±0.08	[3] DEL-AMO-SA...	11F	BABR	Repl. by LEES 12AA
1.46 ±0.07 ±0.08	[10] AUBERT	07J	BABR	Repl. by DEL-AMO-SANCHEZ 11F
1.33 ±0.17 ±0.11	[11] AUBERT,B	06K	BABR	Repl. by AUBERT 08AV
1.38 ±0.10 ±0.18	[12] AUBERT,B	05O	BABR	Repl. by DEL-AMO-SANCHEZ 11C
1.33 ±0.18 ±0.13	[13] ATHAR	03	CLE2	Repl. by ADAM 07
1.8 ±0.4 ±0.4	[14] ALEXANDER	96T	CLE2	Repl. by ATHAR 03

[1] Uses $B(\Upsilon(4S) \to B^+B^-)/B(\Upsilon(4S) \to B^0\overline{B}^0) = 1.065 \pm 0.052$.

[2] The signal events are tagged by a second B meson reconstructed in the fully hadronic decays.

[3] Uses loose neutrino reconstruction technique. Assumes $B(\Upsilon(4S) \to B^+B^-) = (51.6 \pm 0.6)\%$ and $B(\Upsilon(4S) \to B^0\overline{B}^0) = (48.4 \pm 0.6)\%$.

[4] Reports also a branching fraction value $B(B^0 \to \pi^- \ell^+ \nu) = (1.45 \pm 0.04 \pm 0.06) \times 10^{-4}$ from the decays of B^+ and B^0 that are combined using the isospin symmetry relation.

[5] Using the isospin symmetry relation, B^+ and B^0 branching fractions are combined.

[6] The B^0 and B^+ results are combined assuming the isospin, B lifetimes, and relative charged/neutral B production at the $\Upsilon(4S)$.

[7] Also report the rate for $q^2 > 16$ GeV^2 of $(0.41 \pm 0.08 \pm 0.04) \times 10^{-4}$ from which they obtain $|V_{ub}| = 3.6 \pm 0.4 \pm 0.2^{+0.6}_{-0.4}$ (last error is from theory).

[8] The signal events are tagged by a second B meson reconstructed in the semileptonic mode $B \to D^{(*)} \ell \nu_\ell$.

[9] This analysis provides the inclusive and exclusive measurement of $|V_{ub}|$.

[10] The analysis uses events in which the signal B decays are reconstructed with an innovative loose neutrino reconstruction technique.

[11] The signals are tagged by a second B meson reconstructed in a semileptonic or hadronic decay. The B^0 and B^+ results are combined assuming the isospin symmetry.

[12] B^+ and B^0 decays combined assuming isospin symmetry. Systematic errors include both experimental and form-factor uncertainties.

[13] ATHAR 03 reports systematic errors $0.11 \pm 0.01 \pm 0.07$, which are experimental systematic, systematic due to residual form-factor uncertainties in the signal, and systematic due to residual form-factor uncertainties in the cross-feed modes, respectively. We combine these in quadrature.

[14] ALEXANDER 96T gives systematic errors $\pm 0.3 \pm 0.2$ where the second error reflects the estimated model dependence. We combine these in quadrature. Assumes isospin symmetry: $\Gamma(B^0 \to \pi^- \ell^+ \nu) = 2 \times \Gamma(B^+ \to \pi^0 \ell^+ \nu)$.

$\Gamma(\pi^- \mu^+ \nu_\mu)/\Gamma_{\text{total}}$ — Γ_{24}/Γ

VALUE	DOCUMENT ID		TECN
• • • We do not use the following data for averages, fits, limits, etc. • • •			
seen	[1] ALBRECHT	91C	ARG

[1] In ALBRECHT 91C, one event is fully reconstructed providing evidence for the $b \to u$ transition.

$\Gamma(\pi^- \tau^+ \nu_\tau)/\Gamma_{\text{total}}$ — Γ_{25}/Γ

VALUE	CL%	DOCUMENT ID		TECN	COMMENT
$<2.5 \times 10^{-4}$	90	[1] HAMER	16	BELL	$e^+e^- \to \Upsilon(4S)$

[1] Assumes equal production of B^+ and B^0 at the $\Upsilon(4S)$.

$\Gamma(K^\pm X)/\Gamma_{\text{total}}$ — Γ_{26}/Γ

VALUE	DOCUMENT ID		TECN	COMMENT
0.78±0.08	[1] ALBRECHT	96D	ARG	$e^+e^- \to \Upsilon(4S)$

[1] Average multiplicity.

$\Gamma(D^0 X)/\Gamma_{\text{total}}$ — Γ_{27}/Γ

VALUE	DOCUMENT ID		TECN	COMMENT
0.081±0.014±0.005	[1] AUBERT	07N	BABR	$e^+e^- \to \Upsilon(4S)$
• • • We do not use the following data for averages, fits, limits, etc. • • •				
0.063±0.019±0.005	[1] AUBERT,BE	04B	BABR	Repl. by AUBERT 07N

[1] Events are selected by completely reconstructing one B and searching for a reconstructed charmed particle in the rest of the event. The last error includes systematic and charm branching ratio uncertainties.

$\Gamma(\overline{D}^0 X)/\Gamma_{\text{total}}$ — Γ_{28}/Γ

VALUE	DOCUMENT ID		TECN	COMMENT
$0.474 \pm 0.020^{+0.020}_{-0.019}$	[1] AUBERT	07N	BABR	$e^+e^- \to \Upsilon(4S)$
• • • We do not use the following data for averages, fits, limits, etc. • • •				
0.511±0.031±0.028	[1] AUBERT,BE	04B	BABR	Repl. by AUBERT 07N

[1] Events are selected by completely reconstructing one B and searching for a reconstructed charmed particle in the rest of the event. The last error includes systematic and charm branching ratio uncertainties.

$\Gamma(D^0 X)/[\Gamma(D^0 X) + \Gamma(\overline{D}^0 X)]$ — $\Gamma_{27}/(\Gamma_{27}+\Gamma_{28})$

VALUE	DOCUMENT ID		TECN	COMMENT
0.146±0.022±0.006	AUBERT	07N	BABR	$e^+e^- \to \Upsilon(4S)$
• • • We do not use the following data for averages, fits, limits, etc. • • •				
0.110±0.031±0.008	AUBERT,BE	04B	BABR	Repl. by AUBERT 07N

$\Gamma(D^+ X)/\Gamma_{\text{total}}$ — Γ_{29}/Γ

VALUE	CL%	DOCUMENT ID		TECN	COMMENT
<0.039	90	[1] AUBERT	07N	BABR	$e^+e^- \to \Upsilon(4S)$
• • • We do not use the following data for averages, fits, limits, etc. • • •					
<0.051	90	[1] AUBERT,BE	04B	BABR	Repl. by AUBERT 07N

[1] Events are selected by completely reconstructing one B and searching for a reconstructed charmed particle in the rest of the event. The last error includes systematic and charm branching ratio uncertainties.

$\Gamma(D^- X)/\Gamma_{\text{total}}$ — Γ_{30}/Γ

VALUE	DOCUMENT ID		TECN	COMMENT
$0.369 \pm 0.016^{+0.030}_{-0.027}$	[1] AUBERT	07N	BABR	$e^+e^- \to \Upsilon(4S)$
• • • We do not use the following data for averages, fits, limits, etc. • • •				
$0.397 \pm 0.030^{+0.040}_{-0.038}$	[1] AUBERT,BE	04B	BABR	Repl. by AUBERT 07N

[1] Events are selected by completely reconstructing one B and searching for a reconstructed charmed particle in the rest of the event. The last error includes systematic and charm branching ratio uncertainties.

$\Gamma(D^+ X)/[\Gamma(D^+ X) + \Gamma(D^- X)]$ — $\Gamma_{29}/(\Gamma_{29}+\Gamma_{30})$

VALUE	DOCUMENT ID		TECN	COMMENT
0.058±0.028±0.006	AUBERT	07N	BABR	$e^+e^- \to \Upsilon(4S)$
• • • We do not use the following data for averages, fits, limits, etc. • • •				
0.055±0.040±0.006	AUBERT,BE	04B	BABR	Repl. by AUBERT 07N

$\Gamma(D_s^+ X)/\Gamma_{\text{total}}$ — Γ_{31}/Γ

VALUE	DOCUMENT ID		TECN	COMMENT
$0.103 \pm 0.012^{+0.017}_{-0.014}$	[1] AUBERT	07N	BABR	$e^+e^- \to \Upsilon(4S)$
• • • We do not use the following data for averages, fits, limits, etc. • • •				
$0.109 \pm 0.021^{+0.039}_{-0.024}$	[1] AUBERT,BE	04B	BABR	Repl. by AUBERT 07N

[1] Events are selected by completely reconstructing one B and searching for a reconstructed charmed particle in the rest of the event. The last error includes systematic and charm branching ratio uncertainties.

$\Gamma(D_s^- X)/\Gamma_{\text{total}}$ — Γ_{32}/Γ

VALUE	CL%	DOCUMENT ID		TECN	COMMENT
<0.026	90	[1] AUBERT	07N	BABR	$e^+e^- \to \Upsilon(4S)$
• • • We do not use the following data for averages, fits, limits, etc. • • •					
<0.087	90	[1] AUBERT,BE	04B	BABR	Repl. by AUBERT 07N

[1] Events are selected by completely reconstructing one B and searching for a reconstructed charmed particle in the rest of the event. The last error includes systematic and charm branching ratio uncertainties.

$\Gamma(D_s^+ X)/[\Gamma(D_s^+ X) + \Gamma(D_s^- X)]$ — $\Gamma_{31}/(\Gamma_{31}+\Gamma_{32})$

VALUE	DOCUMENT ID		TECN	COMMENT
0.879±0.066±0.005	AUBERT	07N	BABR	$e^+e^- \to \Upsilon(4S)$
• • • We do not use the following data for averages, fits, limits, etc. • • •				
0.733±0.092±0.010	AUBERT,BE	04B	BABR	Repl. by AUBERT 07N

$\Gamma(\Lambda_c^+ X)/\Gamma_{\text{total}}$ — Γ_{33}/Γ

VALUE	CL%	DOCUMENT ID		TECN	COMMENT
<0.031	90	[1] AUBERT	07N	BABR	$e^+e^- \to \Upsilon(4S)$
• • • We do not use the following data for averages, fits, limits, etc. • • •					
<0.038	90	[1] AUBERT,BE	04B	BABR	Repl. by AUBERT 07N

[1] Events are selected by completely reconstructing one B and searching for a reconstructed charmed particle in the rest of the event. The last error includes systematic and charm branching ratio uncertainties.

Int. J. Mod. Phys. A 2026.41. Downloaded from www.worldscientific.com by LIFORNIA @ BERKELEY on 09/16/26. Re-use and distribution is strictly not permitted, except for Open Access articles.

Int. J. Mod. Phys. A 2026.41. Downloaded from www.worldscientific.com by UNIVERSITY OF CALIFORNIA @ BERKELEY on 09/16/26. Re-use and distribution is strictly not permitted, except for Open Access articles.

$\Gamma(\overline{\Lambda}_c^- X)/\Gamma_{total}$ — Γ_{34}/Γ

VALUE	DOCUMENT ID		TECN	COMMENT
$0.05 \pm 0.010^{+0.019}_{-0.011}$	[1] AUBERT	07N	BABR	$e^+e^- \to \Upsilon(4S)$
• • • We do not use the following data for averages, fits, limits, etc. • • •				
$0.049 \pm 0.017^{+0.018}_{-0.011}$	[1] AUBERT,BE	04B	BABR	Repl. by AUBERT 07N

[1] Events are selected by completely reconstructing one B and searching for a reconstructed charmed particle in the rest of the event. The last error includes systematic and charm branching ratio uncertainties.

$\Gamma(\Lambda_c^+ X)/[\Gamma(\Lambda_c^+ X) + \Gamma(\overline{\Lambda}_c^- X)]$ — $\Gamma_{33}/(\Gamma_{33}+\Gamma_{34})$

VALUE	DOCUMENT ID		TECN	COMMENT
$0.243^{+0.119}_{-0.121} \pm 0.003$	AUBERT	07N	BABR	$e^+e^- \to \Upsilon(4S)$
• • • We do not use the following data for averages, fits, limits, etc. • • •				
$0.286 \pm 0.142 \pm 0.007$	AUBERT,BE	04B	BABR	Repl. by AUBERT 07N

$\Gamma(\overline{c}X)/\Gamma_{total}$ — Γ_{35}/Γ

VALUE	DOCUMENT ID		TECN	COMMENT
$0.947 \pm 0.030^{+0.045}_{-0.040}$	[1] AUBERT	07N	BABR	$e^+e^- \to \Upsilon(4S)$
• • • We do not use the following data for averages, fits, limits, etc. • • •				
$1.039 \pm 0.051^{+0.063}_{-0.058}$	[1] AUBERT,BE	04B	BABR	Repl. by AUBERT 07N

[1] Events are selected by completely reconstructing one B and searching for a reconstructed charmed particle in the rest of the event. The last error includes systematic and charm branching ratio uncertainties.

$\Gamma(cX)/\Gamma_{total}$ — Γ_{36}/Γ

VALUE	DOCUMENT ID		TECN	COMMENT
$0.246 \pm 0.024^{+0.021}_{-0.017}$	[1] AUBERT	07N	BABR	$e^+e^- \to \Upsilon(4S)$
• • • We do not use the following data for averages, fits, limits, etc. • • •				
$0.237 \pm 0.036^{+0.041}_{-0.027}$	[1] AUBERT,BE	04B	BABR	Repl. by AUBERT 07N

[1] Events are selected by completely reconstructing one B and searching for a reconstructed charmed particle in the rest of the event. The last error includes systematic and charm branching ratio uncertainties.

$\Gamma(\overline{c}/cX)/\Gamma_{total}$ — Γ_{37}/Γ

VALUE	DOCUMENT ID		TECN	COMMENT
$1.193 \pm 0.030^{+0.053}_{-0.049}$	[1] AUBERT	07N	BABR	$e^+e^- \to \Upsilon(4S)$
• • • We do not use the following data for averages, fits, limits, etc. • • •				
$1.276 \pm 0.062^{+0.088}_{-0.074}$	[1] AUBERT,BE	04B	BABR	Repl. by AUBERT 07N

[1] Events are selected by completely reconstructing one B and searching for a reconstructed charmed particle in the rest of the event. The last error includes systematic and charm branching ratio uncertainties.

$\Gamma(D^-\pi^+)/\Gamma_{total}$ — Γ_{38}/Γ

VALUE (units 10^{-3})	EVTS	DOCUMENT ID		TECN	COMMENT
2.51±0.08 OUR FIT					
2.56±0.08 OUR AVERAGE					
$2.48 \pm 0.01 \pm 0.10$		WAHEED	22	BELL	$e^+e^- \to \Upsilon(4S)$
$2.55 \pm 0.05 \pm 0.16$		[1] AUBERT	07H	BABR	$e^+e^- \to \Upsilon(4S)$
$3.03 \pm 0.23 \pm 0.23$		[2] AUBERT,BE	06J	BABR	$e^+e^- \to \Upsilon(4S)$
$2.68 \pm 0.12 \pm 0.24$		[1,3] AHMED	02B	CLE2	$e^+e^- \to \Upsilon(4S)$
$2.7 \pm 0.6 \pm 0.5$		[4] BORTOLETTO	92	CLEO	$e^+e^- \to \Upsilon(4S)$
$4.8 \pm 1.1 \pm 1.1$	22	[5] ALBRECHT	90J	ARG	$e^+e^- \to \Upsilon(4S)$
$5.1 {}^{+2.8}_{-2.5} {}^{+1.3}_{-1.2}$	4	[6] BEBEK	87	CLEO	$e^+e^- \to \Upsilon(4S)$
• • • We do not use the following data for averages, fits, limits, etc. • • •					
$2.75 \pm 0.20 \pm 0.06$		[1,7] AUBERT,B	04O	BABR	Repl. by AUBERT 07H
$2.85 \pm 0.42 \pm 0.04$	81	[8] ALAM	94	CLE2	Repl. by AHMED 02B
$3.1 \pm 1.3 \pm 1.0$	7	[5] ALBRECHT	88K	ARG	$e^+e^- \to \Upsilon(4S)$

[1] Assumes equal production of B^+ and B^0 at the $\Upsilon(4S)$.

[2] Uses a missing-mass method. Does not depend on D branching fractions or B^+/B^0 production rates.

[3] AHMED 02B reports an additional uncertainty on the branching ratios to account for 4.5% uncertainty on relative production of B^0 and B^+, which is not included here.

[4] BORTOLETTO 92 assumes equal production of B^+ and B^0 at the $\Upsilon(4S)$ and uses Mark III branching fractions for the D.

[5] ALBRECHT 88K assumes $B^0\overline{B}^0$:B^+B^- production ratio is 45:55. Superseded by ALBRECHT 90J which assumes 50:50.

[6] BEBEK 87 value has been updated in BERKELMAN 91 to use same assumptions as noted for BORTOLETTO 92.

[7] AUBERT,B 04O reports $[\Gamma(B^0 \to D^-\pi^+)/\Gamma_{total}] \times [B(D^+ \to K^0_S\pi^+)] = (42.7 \pm 2.1 \pm 2.2)\times 10^{-6}$ which we divide by our best (shown rounded) value $B(D^+ \to K^0_S\pi^+) = (1.554 \pm 0.033) \times 10^{-2}$. Our first error is their experiment's error and our second error is the systematic error from using our best (shown rounded) value.

[8] ALAM 94 reports $[\Gamma(B^0 \to D^-\pi^+)/\Gamma_{total}] \times [B(D^+ \to K^-2\pi^+)] = (0.265 \pm 0.032 \pm 0.023) \times 10^{-3}$ which we divide by our best (shown rounded) value $B(D^+ \to K^-2\pi^+) = (9.31 \pm 0.14) \times 10^{-2}$. Our first error is their experiment's error and our second error is the systematic error from using our best (shown rounded) value. Assumes equal production of B^+ and B^0 at the $\Upsilon(4S)$.

$\Gamma(D^-\ell^+\nu_\ell)/\Gamma(D^-\pi^+)$ — Γ_5/Γ_{38}

VALUE	DOCUMENT ID		TECN	COMMENT
$9.9 \pm 1.0 \pm 0.9$	AALTONEN	09E	CDF	$p\overline{p}$ at 1.96 TeV

$\Gamma(D^-\rho^+)/\Gamma_{total}$ — Γ_{39}/Γ

VALUE	EVTS	DOCUMENT ID		TECN	COMMENT
0.0076±0.0013 OUR AVERAGE					
$0.0076 \pm 0.0013 \pm 0.0001$	79	[1] ALAM	94	CLE2	$e^+e^- \to \Upsilon(4S)$
$0.009 \pm 0.005 \pm 0.003$	9	[2] ALBRECHT	90J	ARG	$e^+e^- \to \Upsilon(4S)$
• • • We do not use the following data for averages, fits, limits, etc. • • •					
$0.022 \pm 0.012 \pm 0.009$	6	[2] ALBRECHT	88K	ARG	$e^+e^- \to \Upsilon(4S)$

[1] ALAM 94 reports $[\Gamma(B^0 \to D^-\rho^+)/\Gamma_{total}] \times [B(D^+ \to K^-2\pi^+)] = 0.000704 \pm 0.000096 \pm 0.000070$ which we divide by our best (shown rounded) value $B(D^+ \to K^-2\pi^+) = (9.31 \pm 0.14) \times 10^{-2}$. Our first error is their experiment's error and our second error is the systematic error from using our best (shown rounded) value. Assumes equal production of B^+ and B^0 at the $\Upsilon(4S)$.

[2] ALBRECHT 88K assumes $B^0\overline{B}^0$:B^+B^- production ratio is 45:55. Superseded by ALBRECHT 90J which assumes 50:50.

$\Gamma(D^-K^0\pi^+)/\Gamma_{total}$ — Γ_{40}/Γ

VALUE (units 10^{-4})	DOCUMENT ID		TECN	COMMENT
$4.9 \pm 0.7 \pm 0.5$	[1] AUBERT,BE	05B	BABR	$e^+e^- \to \Upsilon(4S)$

[1] Assumes equal production of B^+ and B^0 at the $\Upsilon(4S)$.

$\Gamma(D^-K^*(892)^+)/\Gamma_{total}$ — Γ_{41}/Γ

VALUE (units 10^{-4})	DOCUMENT ID		TECN	COMMENT
4.5±0.7 OUR AVERAGE				
$4.6 \pm 0.6 \pm 0.5$	[1] AUBERT,BE	05B	BABR	$e^+e^- \to \Upsilon(4S)$
$3.7 \pm 1.5 \pm 1.0$	[1] MAHAPATRA	02	CLE2	$e^+e^- \to \Upsilon(4S)$

[1] Assumes equal production of B^+ and B^0 at the $\Upsilon(4S)$.

$\Gamma(D^-\omega\pi^+)/\Gamma_{total}$ — Γ_{42}/Γ

VALUE	DOCUMENT ID		TECN	COMMENT
$0.0028 \pm 0.0005 \pm 0.0004$	[1] ALEXANDER	01B	CLE2	$e^+e^- \to \Upsilon(4S)$

[1] Assumes equal production of B^+ and B^0 at the $\Upsilon(4S)$. The signal is consistent with all observed $\omega\pi^+$ having proceeded through the ρ'^+ resonance at mass $1349 \pm 25^{+10}_{-5}$ MeV and width $547 \pm 86^{+46}_{-45}$ MeV.

$\Gamma(D^-K^+)/\Gamma(D^-\pi^+)$ — Γ_{43}/Γ_{38}

VALUE (units 10^{-2})	DOCUMENT ID		TECN	COMMENT
8.19±0.20 OUR AVERAGE				
$8.19 \pm 0.20 \pm 0.23$	WAHEED	22	BELL	$e^+e^- \to \Upsilon(4S)$
$8.22 \pm 0.11 \pm 0.25$	AAIJ	13P	LHCB	pp at 7 TeV
$6.8 \pm 1.5 \pm 0.7$	ABE	01I	BELL	$e^+e^- \to \Upsilon(4S)$

$\Gamma(D^-K^+\pi^+\pi^-)/\Gamma(D^-\pi^+\pi^+\pi^-)$ — Γ_{44}/Γ_{50}

VALUE (units 10^{-2})	DOCUMENT ID		TECN	COMMENT
$5.9 \pm 1.1 \pm 0.5$	AAIJ	12T	LHCB	pp at 7 TeV

$\Gamma(D^-K^+\overline{K}^0)/\Gamma_{total}$ — Γ_{45}/Γ

VALUE (units 10^{-4})	CL%	DOCUMENT ID		TECN	COMMENT
$1.64 \pm 0.24 \pm 0.10$		[1] ADACHI	24L	BEL2	$e^+e^- \to \Upsilon(4S)$
• • • We do not use the following data for averages, fits, limits, etc. • • •					
<3.1	90	[2] DRUTSKOY	02	BELL	$e^+e^- \to \Upsilon(4S)$

[1] Used 362 fb^{-1} Belle II data and $B(\Upsilon(4S) \to B^0\overline{B}^0)$=0.484 ± 0.012.

[2] Assumes equal production of B^+ and B^0 at the $\Upsilon(4S)$.

$\Gamma(D^-K^+\overline{K}^*(892)^0)/\Gamma_{total}$ — Γ_{46}/Γ

VALUE (units 10^{-4})	DOCUMENT ID		TECN	COMMENT
7.7 ±0.6 OUR AVERAGE				
$7.56 \pm 0.45 \pm 0.38$	[1] ADACHI	24L	BEL2	$e^+e^- \to \Upsilon(4S)$
$8.8 \pm 1.1 \pm 1.5$	[2] DRUTSKOY	02	BELL	$e^+e^- \to \Upsilon(4S)$

[1] Used 362 fb^{-1} Belle II data and $B(\Upsilon(4S) \to B^0\overline{B}^0)$=0.484 ± 0.012.

[2] Assumes equal production of B^+ and B^0 at the $\Upsilon(4S)$.

$\Gamma(\overline{D}^0\pi^+\pi^-)/\Gamma_{total}$ — Γ_{47}/Γ

VALUE (units 10^{-4})	CL%	EVTS	DOCUMENT ID		TECN	COMMENT
8.8 ±0.5 OUR AVERAGE						
$8.95 \pm 0.15 \pm 0.52$			[1] AAIJ	15Y	LHCB	pp at 7, 8 TeV
$8.4 \pm 0.4 \pm 0.8$			[2] KUZMIN	07	BELL	$e^+e^- \to \Upsilon(4S)$
• • • We do not use the following data for averages, fits, limits, etc. • • •						
$8.0 \pm 0.6 \pm 1.5$			[2,3] SATPATHY	03	BELL	Repl. by KUZMIN 07
< 16	90		[2] ALAM	94	CLE2	$e^+e^- \to \Upsilon(4S)$
< 70	90		[4] BORTOLETTO	92	CLEO	$e^+e^- \to \Upsilon(4S)$
<340	90		[5] BEBEK	87	CLEO	$e^+e^- \to \Upsilon(4S)$
700 ± 500		5	[6] BEHRENDS	83	CLEO	$e^+e^- \to \Upsilon(4S)$

[1] The second uncertainty combines in quadrature all systematic uncertainties quoted in the paper. AAIJ 15Y reports $B(B^0 \to \overline{D}^0\pi^+\pi^-) = (8.46 \pm 0.14 \pm 0.49) \times 10^{-4}$ in the kinematic region $m(\overline{D}^0\pi^+) > 2.1$ GeV which we corrected to the full phase-space dividing by 0.945 from Belle.

[2] Assumes equal production of B^+ and B^0 at the $\Upsilon(4S)$.

[3] No assumption about the intermediate mechanism is made in the analysis.
[4] BORTOLETTO 92 assumes equal production of B^+ and B^0 at the $\Upsilon(4S)$ and uses Mark III branching fractions for the D. The product branching fraction into $D_0^*(2340)\pi$ followed by $D_0^*(2340) \to D^0\pi$ is < 0.0001 at 90% CL and into $D_2^*(2460)$ followed by $D_2^*(2460) \to D^0\pi$ is < 0.0004 at 90% CL.
[5] BEBEK 87 assume the $\Upsilon(4S)$ decays 43% to $B^0\overline{B}^0$. We rescale to 50%. $B(D^0 \to K^-\pi^+) = (4.2 \pm 0.4 \pm 0.4)\%$ and $B(D^0 \to K^-\pi^+\pi^+\pi^-) = (9.1 \pm 0.8 \pm 0.8)\%$ were used.
[6] Corrected by us using assumptions: $B(D^0 \to K^-\pi^+) = (0.042 \pm 0.006)$ and $B(\Upsilon(4S) \to B^0\overline{B}^0) = 50\%$. The product branching ratio is $B(B^0 \to \overline{D}^0\pi^+\pi^-)B(\overline{D}^0 \to K^+\pi^-) = (0.39 \pm 0.26) \times 10^{-2}$.

$\Gamma(D^*(2010)^-\pi^+)/\Gamma_{total}$ — Γ_{48}/Γ

VALUE (units 10^{-3})	EVTS	DOCUMENT ID		TECN	COMMENT
2.66±0.07 OUR AVERAGE					
2.62±0.08±0.04		[1] KROHN	23	BELL	$e^+e^- \to \Upsilon(4S)$
2.79±0.08±0.17		[2] AUBERT	07H	BABR	$e^+e^- \to \Upsilon(4S)$
2.48±0.34±0.08		[3,4] AUBERT,BE	06J	BABR	$e^+e^- \to \Upsilon(4S)$
2.81±0.24±0.05		[5] BRANDENB...	98	CLE2	$e^+e^- \to \Upsilon(4S)$
2.6 ±0.3 ±0.4	82	[6] ALAM	94	CLE2	$e^+e^- \to \Upsilon(4S)$
3.37±0.96±0.02		[7] BORTOLETTO	92	CLEO	$e^+e^- \to \Upsilon(4S)$
2.36±0.88±0.02	12	[8] ALBRECHT	90J	ARG	$e^+e^- \to \Upsilon(4S)$
$2.36^{+1.50}_{-1.10}$±0.02	5	[9] BEBEK	87	CLEO	$e^+e^- \to \Upsilon(4S)$
• • • We do not use the following data for averages, fits, limits, etc. • • •					
10 ±4 ±1	8	[10] AKERS	94J	OPAL	$e^+e^- \to Z$
2.7 ±1.4 ±1.0	5	[11] ALBRECHT	87C	ARG	$e^+e^- \to \Upsilon(4S)$
3.5 ±2 ±2		[12] ALBRECHT	86F	ARG	$e^+e^- \to \Upsilon(4S)$
17 ±5 ±5	41	[13] GILES	84	CLEO	$e^+e^- \to \Upsilon(4S)$

[1] KROHN 23 reports $(2.623 \pm 0.016 \pm 0.086) \times 10^{-3}$ from a measurement of $[\Gamma(B^0 \to D^*(2010)^-\pi^+)/\Gamma_{total}]$ / $[B(\Upsilon(4S) \to B^0\overline{B}^0)]$ assuming $B(\Upsilon(4S) \to B^0\overline{B}^0) = 0.486 \pm 0.006$, which we rescale to our best (shown rounded) value $B(\Upsilon(4S) \to B^0\overline{B}^0) = (48.6 \pm 0.8) \times 10^{-2}$. Our first error is their experiment's error and our second error is the systematic error from using our best (shown rounded) value.
[2] Assumes equal production of B^+ and B^0 at the $\Upsilon(4S)$.
[3] AUBERT,BE 06J reports $[\Gamma(B^0 \to D^*(2010)^-\pi^+)/\Gamma_{total}]$ / $[B(B^0 \to D^-\pi^+)] = 0.99 \pm 0.11 \pm 0.08$ which we multiply by our best (shown rounded) value $B(B^0 \to D^-\pi^+) = (2.51 \pm 0.08) \times 10^{-3}$. Our first error is their experiment's error and our second error is the systematic error from using our best (shown rounded) value.
[4] Uses a missing-mass method. Does not depend on D branching fractions or B^+/B^0 production rates.
[5] BRANDENBURG 98 assume equal production of B^+ and B^0 at $\Upsilon(4S)$ and use the D^* reconstruction technique. The first error is their experiment's error and the second error is the systematic error from the PDG 96 value of $B(D^* \to D\pi)$.
[6] ALAM 94 assume equal production of B^+ and B^0 at the $\Upsilon(4S)$ and use the CLEO II $B(D^*(2010)^+ \to D^0\pi^+)$ and absolute $B(D^0 \to K^-\pi^+)$ and the PDG 1992 $B(D^0 \to K^-\pi^+\pi^0)/B(D^0 \to K^-\pi^+)$ and $B(D^0 \to K^-2\pi^+\pi^-)/B(D^0 \to K^-\pi^+)$.
[7] BORTOLETTO 92 reports $(4.0 \pm 1.0 \pm 0.7) \times 10^{-3}$ from a measurement of $[\Gamma(B^0 \to D^*(2010)^-\pi^+)/\Gamma_{total}] \times [B(D^*(2010)^+ \to D^0\pi^+)]$ assuming $B(D^*(2010)^+ \to D^0\pi^+) = 0.57 \pm 0.06$, which we rescale to our best (shown rounded) value $B(D^*(2010)^+ \to D^0\pi^+) = (67.7 \pm 0.5) \times 10^{-2}$. Our first error is their experiment's error and our second error is the systematic error from using our best (shown rounded) value. Assumes equal production of B^+ and B^0 at the $\Upsilon(4S)$ and uses Mark III branching fractions for the D.
[8] ALBRECHT 90J reports $(2.8 \pm 0.9 \pm 0.6) \times 10^{-3}$ from a measurement of $[\Gamma(B^0 \to D^*(2010)^-\pi^+)/\Gamma_{total}] \times [B(D^*(2010)^+ \to D^0\pi^+)]$ assuming $B(D^*(2010)^+ \to D^0\pi^+) = 0.57 \pm 0.06$, which we rescale to our best (shown rounded) value $B(D^*(2010)^+ \to D^0\pi^+) = (67.7 \pm 0.5) \times 10^{-2}$. Our first error is their experiment's error and our second error is the systematic error from using our best (shown rounded) value. Assumes equal production of B^+ and B^0 at the $\Upsilon(4S)$ and uses Mark III branching fractions for the D.
[9] BEBEK 87 reports $(2.8^{+1.5}_{-1.2}{}^{+1.0}_{-0.6}) \times 10^{-3}$ from a measurement of $[\Gamma(B^0 \to D^*(2010)^-\pi^+)/\Gamma_{total}] \times [B(D^*(2010)^+ \to D^0\pi^+)]$ assuming $B(D^*(2010)^+ \to D^0\pi^+) = 0.57 \pm 0.06$, which we rescale to our best (shown rounded) value $B(D^*(2010)^+ \to D^0\pi^+) = (67.7 \pm 0.5) \times 10^{-2}$. Our first error is their experiment's error and our second error is the systematic error from using our best (shown rounded) value. Updated in BERKELMAN 91 to use same assumptions as noted for BORTOLETTO 92 and ALBRECHT 90J.
[10] Assumes $B(Z \to b\overline{b}) = 0.217$ and 38% B_d production fraction.
[11] ALBRECHT 87C use PDG 86 branching ratios for D and $D^*(2010)$ and assume $B(\Upsilon(4S) \to B^+B^-) = 55\%$ and $B(\Upsilon(4S) \to B^0\overline{B}^0) = 45\%$. Superseded by ALBRECHT 90J.
[12] ALBRECHT 86F uses pseudomass that is independent of D^0 and D^+ branching ratios.
[13] Assumes $B(D^*(2010)^+ \to D^0\pi^+) = 0.60^{+0.08}_{-0.15}$. Assumes $B(\Upsilon(4S) \to B^0\overline{B}^0) = 0.40 \pm 0.02$ Does not depend on D branching ratios.

$\Gamma(D^*(2010)^-\ell^+\nu_\ell)/\Gamma(D^*(2010)^-\pi^+)$ — Γ_7/Γ_{48}

VALUE	DOCUMENT ID		TECN	COMMENT
16.5±2.3±1.1	AALTONEN	09E	CDF	$p\overline{p}$ at 1.96 TeV

$\Gamma(\overline{D}^0K^+K^-)/\Gamma(\overline{D}^0\pi^+\pi^-)$ — Γ_{49}/Γ_{47}

VALUE	DOCUMENT ID		TECN	COMMENT
0.069±0.004±0.003	AAIJ	18AZ	LHCB	pp at 7, 8 TeV
• • • We do not use the following data for averages, fits, limits, etc. • • •				
0.056±0.011±0.007	[1] AAIJ	12AM	LHCB	pp at 7 TeV

[1] Superseded by AAIJ 21Q.

$\Gamma(D^-\pi^+\pi^+\pi^-)/\Gamma_{total}$ — Γ_{50}/Γ

VALUE	DOCUMENT ID		TECN	COMMENT
0.0060±0.0006 OUR FIT				
0.0080±0.0021±0.0014	[1] BORTOLETTO	92	CLEO	$e^+e^- \to \Upsilon(4S)$

[1] BORTOLETTO 92 assumes equal production of B^+ and B^0 at the $\Upsilon(4S)$ and uses Mark III branching fractions for the D.

$\Gamma(D^-\pi^+\pi^+\pi^-)/\Gamma(D^-\pi^+)$ — Γ_{50}/Γ_{38}

VALUE	DOCUMENT ID		TECN	COMMENT
2.39±0.23 OUR FIT				
2.38±0.11±0.21	AAIJ	11E	LHCB	pp at 7 TeV

$\Gamma((D^-\pi^+\pi^+\pi^-)\text{ nonresonant})/\Gamma_{total}$ — Γ_{51}/Γ

VALUE	DOCUMENT ID		TECN	COMMENT
0.0039±0.0014±0.0013	[1] BORTOLETTO	92	CLEO	$e^+e^- \to \Upsilon(4S)$

[1] BORTOLETTO 92 assumes equal production of B^+ and B^0 at the $\Upsilon(4S)$ and uses Mark III branching fractions for the D.

$\Gamma(D^-\pi^+\rho^0)/\Gamma_{total}$ — Γ_{52}/Γ

VALUE	DOCUMENT ID		TECN	COMMENT
0.0011±0.0009±0.0004	[1] BORTOLETTO	92	CLEO	$e^+e^- \to \Upsilon(4S)$

[1] BORTOLETTO 92 assumes equal production of B^+ and B^0 at the $\Upsilon(4S)$ and uses Mark III branching fractions for the D.

$\Gamma(D^-a_1(1260)^+)/\Gamma_{total}$ — Γ_{53}/Γ

VALUE	DOCUMENT ID		TECN	COMMENT
0.0060±0.0022±0.0024	[1] BORTOLETTO	92	CLEO	$e^+e^- \to \Upsilon(4S)$

[1] BORTOLETTO 92 assumes equal production of B^+ and B^0 at the $\Upsilon(4S)$ and uses Mark III branching fractions for the D.

$\Gamma(D^*(2010)^-\pi^+\pi^0)/\Gamma_{total}$ — Γ_{54}/Γ

VALUE	EVTS	DOCUMENT ID		TECN	COMMENT
0.0152±0.0052±0.0001	51	[1] ALBRECHT	90J	ARG	$e^+e^- \to \Upsilon(4S)$
• • • We do not use the following data for averages, fits, limits, etc. • • •					
0.015 ±0.008 ±0.008	8	[2] ALBRECHT	87C	ARG	$e^+e^- \to \Upsilon(4S)$

[1] ALBRECHT 90J reports $0.018 \pm 0.004 \pm 0.005$ from a measurement of $[\Gamma(B^0 \to D^*(2010)^-\pi^+\pi^0)/\Gamma_{total}] \times [B(D^*(2010)^+ \to D^0\pi^+)]$ assuming $B(D^*(2010)^+ \to D^0\pi^+) = 0.57 \pm 0.06$, which we rescale to our best (shown rounded) value $B(D^*(2010)^+ \to D^0\pi^+) = (67.7 \pm 0.5) \times 10^{-2}$. Our first error is their experiment's error and our second error is the systematic error from using our best (shown rounded) value. Assumes equal production of B^+ and B^0 at the $\Upsilon(4S)$ and uses Mark III branching fractions for the D.
[2] ALBRECHT 87C use PDG 86 branching ratios for D and $D^*(2010)$ and assume $B(\Upsilon(4S) \to B^+B^-) = 55\%$ and $B(\Upsilon(4S) \to B^0\overline{B}^0) = 45\%$. Superseded by ALBRECHT 90J.

$\Gamma(D^*(2010)^-\rho^+)/\Gamma_{total}$ — Γ_{55}/Γ

VALUE (units 10^{-3})	EVTS	DOCUMENT ID		TECN	COMMENT
6.8 ± 0.9 OUR AVERAGE					
6.8 ± 0.3 ± 0.9		[1,2] CSORNA	03	CLE2	$e^+e^- \to \Upsilon(4S)$
16.0 ±11.3 ± 0.1		[3] BORTOLETTO	92	CLEO	$e^+e^- \to \Upsilon(4S)$
5.89± 3.52± 0.04	19	[4] ALBRECHT	90J	ARG	$e^+e^- \to \Upsilon(4S)$
• • • We do not use the following data for averages, fits, limits, etc. • • •					
		[2,5] MATVIENKO	15	BELL	$e^+e^- \to \Upsilon(4S)$
7.4 ± 1.0 ± 1.4	76	[6,7] ALAM	94	CLE2	$e^+e^- \to \Upsilon(4S)$
81 ±29 $^{+59}_{-24}$	19	[8] CHEN	85	CLEO	$e^+e^- \to \Upsilon(4S)$

[1] The second error combines the systematic and theoretical uncertainties in quadrature. CSORNA 03 includes data used in ALAM 94. A full angular fit to three complex helicity amplitudes is performed.
[2] Assumes equal production of B^0 and B^+ at the $\Upsilon(4S)$ resonance.
[3] BORTOLETTO 92 reports $0.019 \pm 0.008 \pm 0.011$ from a measurement of $[\Gamma(B^0 \to D^*(2010)^-\rho^+)/\Gamma_{total}] \times [B(D^*(2010)^+ \to D^0\pi^+)]$ assuming $B(D^*(2010)^+ \to D^0\pi^+) = 0.57 \pm 0.06$, which we rescale to our best (shown rounded) value $B(D^*(2010)^+ \to D^0\pi^+) = (67.7 \pm 0.5) \times 10^{-2}$. Our first error is their experiment's error and our second error is the systematic error from using our best (shown rounded) value. Assumes equal production of B^+ and B^0 at the $\Upsilon(4S)$ and uses Mark III branching fractions for the D.
[4] ALBRECHT 90J reports $0.007 \pm 0.003 \pm 0.003$ from a measurement of $[\Gamma(B^0 \to D^*(2010)^-\rho^+)/\Gamma_{total}] \times [B(D^*(2010)^+ \to D^0\pi^+)]$ assuming $B(D^*(2010)^+ \to D^0\pi^+) = 0.57 \pm 0.06$, which we rescale to our best (shown rounded) value $B(D^*(2010)^+ \to D^0\pi^+) = (67.7 \pm 0.5) \times 10^{-2}$. Our first error is their experiment's error and our second error is the systematic error from using our best (shown rounded) value. Assumes equal production of B^+ and B^0 at the $\Upsilon(4S)$ and uses Mark III branching fractions for the D.
[5] MATVIENKO 15 reports $B(B^0 \to D^*(2010)^-\rho^+,\ \rho^+ \to \omega\pi^+) = (1.48 \pm 0.27^{+0.15}_{-0.09}{}^{+0.21}_{-0.56}) \times 10^{-3}$. The last uncertainty is a model one.
[6] ALAM 94 assume equal production of B^+ and B^0 at the $\Upsilon(4S)$ and use the CLEO II $B(D^*(2010)^+ \to D^0\pi^+)$ and absolute $B(D^0 \to K^-\pi^+)$ and the PDG 1992 $B(D^0 \to K^-\pi^+\pi^0)/B(D^0 \to K^-\pi^+)$ and $B(D^0 \to K^-2\pi^+\pi^-)/B(D^0 \to K^-\pi^+)$.
[7] This decay is nearly completely longitudinally polarized, $\Gamma_L/\Gamma = (93 \pm 5 \pm 5)\%$, as expected from the factorization hypothesis (ROSNER 90). The nonresonant $\pi^+\pi^0$ contribution under the ρ^+ is less than 9% at 90% CL.
[8] Uses $B(D^* \to D^0\pi^+) = 0.6 \pm 0.15$ and $B(\Upsilon(4S) \to B^0\overline{B}^0) = 0.4$. Does not depend on D branching ratios.

Int. J. Mod. Phys. A 2026.41. Downloaded from www.worldscientific.com
by LIFORNIA @ BERKELEY on 09/16/26. Re-use and distribution is strictly not permitted, except for Open Access articles.

Int. J. Mod. Phys. A 2026.41. Downloaded from www.worldscientific.com
by UNIVERSITY OF CALIFORNIA @ BERKELEY on 09/16/26. Re-use and distribution is strictly not permitted, except for Open Access articles.

$\Gamma(D^*(2010)^- K^+)/\Gamma_{total}$ — Γ_{56}/Γ

VALUE (units 10^{-4})	DOCUMENT ID		TECN	COMMENT
2.16±0.08 OUR AVERAGE				
$2.22 \pm 0.10^{+0.03}_{-0.04}$	[1] KROHN	23	BELL	$e^+e^- \to \Upsilon(4S)$
2.07±0.12±0.06	[2] AUBERT	06A	BABR	$e^+e^- \to \Upsilon(4S)$
• • • We do not use the following data for averages, fits, limits, etc. • • •				
2.0 ±0.4 ±0.1	[3] ABE	01I	BELL	Repl. by KROHN 23

[1] KROHN 23 reports (2.221 ± 0.063 ± 0.077) × 10^{-4} from a measurement of $[\Gamma(B^0 \to D^*(2010)^- K^+)/\Gamma_{total}]$ / $[B(\Upsilon(4S) \to B^0\overline{B}^0)]$ assuming $B(\Upsilon(4S) \to B^0\overline{B}^0)$ = 0.486 ± 0.006, which we rescale to our best (shown rounded) value $B(\Upsilon(4S) \to B^0\overline{B}^0)$ = (48.6 ± 0.8) × 10^{-2}. Our first error is their experiment's error and our second error is the systematic error from using our best (shown rounded) value.

[2] AUBERT 06A reports $[\Gamma(B^0 \to D^*(2010)^- K^+)/\Gamma_{total}]$ / $[B(B^0 \to D^*(2010)^- \pi^+)]$ = 0.0776 ± 0.0034 ± 0.0029 which we multiply by our best (shown rounded) value $B(B^0 \to D^*(2010)^- \pi^+)$ = (2.66 ± 0.07) × 10^{-3}. Our first error is their experiment's error and our second error is the systematic error from using our best (shown rounded) value.

[3] ABE 01I reports $[\Gamma(B^0 \to D^*(2010)^- K^+)/\Gamma_{total}]$ / $[B(B^0 \to D^*(2010)^- \pi^+)]$ = 0.074 ± 0.015 ± 0.006 which we multiply by our best (shown rounded) value $B(B^0 \to D^*(2010)^- \pi^+)$ = (2.66 ± 0.07) × 10^{-3}. Our first error is their experiment's error and our second error is the systematic error from using our best (shown rounded) value.

$\Gamma(D^*(2010)^- K^+)/\Gamma(D^*(2010)^- \pi^+)$ — Γ_{56}/Γ_{48}

VALUE (units 10^{-2})	DOCUMENT ID		TECN	COMMENT
8.22±0.29 OUR AVERAGE Error includes scale factor of 1.3.				
8.41±0.24±0.13	KROHN	23	BELL	$e^+e^- \to \Upsilon(4S)$
7.76±0.34±0.26	AAIJ	13AO	LHCB	pp at 7 TeV

$\Gamma(D^*(2010)^- K^0\pi^+)/\Gamma_{total}$ — Γ_{57}/Γ

VALUE (units 10^{-4})	DOCUMENT ID		TECN	COMMENT
3.0±0.7±0.3	[1] AUBERT,BE	05B	BABR	$e^+e^- \to \Upsilon(4S)$

[1] Assumes equal production of B^+ and B^0 at the $\Upsilon(4S)$.

$\Gamma(D^*(2010)^- K^*(892)^+)/\Gamma_{total}$ — Γ_{58}/Γ

VALUE (units 10^{-4})	DOCUMENT ID		TECN	COMMENT
3.3±0.6 OUR AVERAGE				
3.2±0.6±0.3	[1] AUBERT,BE	05B	BABR	$e^+e^- \to \Upsilon(4S)$
3.8±1.3±0.8	[2] MAHAPATRA	02	CLE2	$e^+e^- \to \Upsilon(4S)$

[1] Assumes equal production of B^+ and B^0 at the $\Upsilon(4S)$.

[2] Assumes equal production of B^+ and B^0 at the $\Upsilon(4S)$ and an unpolarized final state.

$\Gamma(D^*(2010)^- K^+\overline{K}^0)/\Gamma_{total}$ — Γ_{59}/Γ

VALUE (units 10^{-4})	CL%	DOCUMENT ID		TECN	COMMENT
1.82±0.38±0.10		[1] ADACHI	24L	BEL2	$e^+e^- \to \Upsilon(4S)$
• • • We do not use the following data for averages, fits, limits, etc. • • •					
<4.7	90	[2] DRUTSKOY	02	BELL	$e^+e^- \to \Upsilon(4S)$

[1] Used 362 fb^{-1} Belle II data and $B(\Upsilon(4S) \to B^0\overline{B}^0)$=0.484 ± 0.012.

[2] Assumes equal production of B^+ and B^0 at the $\Upsilon(4S)$.

$\Gamma(D^*(2010)^- K^+\overline{K}^*(892)^0)/\Gamma_{total}$ — Γ_{60}/Γ

VALUE (units 10^{-4})	DOCUMENT ID		TECN	COMMENT
13.1 ±1.3 OUR AVERAGE				
13.12±1.21±0.71	[1] ADACHI	24L	BEL2	$e^+e^- \to \Upsilon(4S)$
12.9 ±2.2 ±2.5	[2] DRUTSKOY	02	BELL	$e^+e^- \to \Upsilon(4S)$

[1] Used 362 fb^{-1} Belle II data and $B(\Upsilon(4S) \to B^0\overline{B}^0)$=0.484 ± 0.012.

[2] Assumes equal production of B^+ and B^0 at the $\Upsilon(4S)$.

$\Gamma(D^*(2010)^- \pi^+\pi^+\pi^-)/\Gamma_{total}$ — Γ_{61}/Γ

VALUE (units 10^{-3})	CL%	DOCUMENT ID		TECN	COMMENT
7.21±0.29 OUR AVERAGE					
7.26±0.11± 0.31		[1] LEES	16H	BABR	$e^+e^- \to \Upsilon(4S)$
6.81±0.23± 0.72		[2] MAJUMDER	04	BELL	$e^+e^- \to \Upsilon(4S)$
6.3 ±1.0 ± 1.1		[3,4] ALAM	94	CLE2	$e^+e^- \to \Upsilon(4S)$
13.4 ±3.6 ± 0.1		[5] BORTOLETTO	92	CLEO	$e^+e^- \to \Upsilon(4S)$
10.1 ±4.1 ± 0.1		[6] ALBRECHT	90J	ARG	$e^+e^- \to \Upsilon(4S)$
• • • We do not use the following data for averages, fits, limits, etc. • • •					
33 ±9 ±16		[7] ALBRECHT	87C	ARG	$e^+e^- \to \Upsilon(4S)$
<42	90	[8] BEBEK	87	CLEO	$e^+e^- \to \Upsilon(4S)$

[1] Assumes $B(\Upsilon(4S) \to B^0\overline{B}^0)$ = 0.486 ± 0.006.

[2] Assumes equal production of B^+ and B^0 at the $\Upsilon(4S)$.

[3] ALAM 94 assume equal production of B^+ and B^0 at the $\Upsilon(4S)$ and use the CLEO II $B(D^*(2010)^+ \to D^0\pi^+)$ and absolute $B(D^0 \to K^-\pi^+)$ and the PDG 1992 $B(D^0 \to K^-\pi^+\pi^0)/B(D^0 \to K^-\pi^+)$ and $B(D^0 \to K^-2\pi^+\pi^-)/B(D^0 \to K^-\pi^+)$.

[4] The three pion mass is required to be between 1.0 and 1.6 GeV consistent with an a_1 meson. (If this channel is dominated by a_1^+, the branching ratio for $\overline{D}^{*-}a_1^+$ is twice that for $\overline{D}^{*-}\pi^+\pi^+\pi^-$.)

[5] BORTOLETTO 92 reports 0.0159 ± 0.0028 ± 0.0037 from a measurement of $[\Gamma(B^0 \to D^*(2010)^- \pi^+\pi^+\pi^-)/\Gamma_{total}]$ × $[B(D^*(2010)^+ \to D^0\pi^+)]$ assuming $B(D^*(2010)^+ \to D^0\pi^+)$ = 0.57 ± 0.06, which we rescale to our best (shown rounded) value $B(D^*(2010)^+ \to D^0\pi^+)$ = (67.7 ± 0.5) × 10^{-2}. Our first error is their experiment's error and our second error is the systematic error from using our best (shown rounded) value. Assumes equal production of B^+ and B^0 at the $\Upsilon(4S)$ and uses Mark III branching fractions for the D.

[6] ALBRECHT 90J reports 0.012 ± 0.003 ± 0.004 from a measurement of $[\Gamma(B^0 \to D^*(2010)^- \pi^+\pi^+\pi^-)/\Gamma_{total}]$ × $[B(D^*(2010)^+ \to D^0\pi^+)]$ assuming $B(D^*(2010)^+ \to D^0\pi^+)$ = 0.57 ± 0.06, which we rescale to our best (shown rounded) value $B(D^*(2010)^+ \to D^0\pi^+)$ = (67.7 ± 0.5) × 10^{-2}. Our first error is their experiment's error and our second error is the systematic error from using our best (shown rounded) value. Assumes equal production of B^+ and B^0 at the $\Upsilon(4S)$ and uses Mark III branching fractions for the D.

[7] ALBRECHT 87C use PDG 86 branching ratios for D and $D^*(2010)$ and assume $B(\Upsilon(4S) \to B^+B^-)$ = 55% and $B(\Upsilon(4S) \to B^0\overline{B}^0)$ = 45%. Superseded by ALBRECHT 90J.

[8] BEBEK 87 value has been updated in BERKELMAN 91 to use same assumptions as noted for BORTOLETTO 92.

$\Gamma((D^*(2010)^- \pi^+\pi^+\pi^-)$ nonresonant$)/\Gamma_{total}$ — Γ_{62}/Γ

VALUE	DOCUMENT ID		TECN	COMMENT
0.0000±0.0019±0.0016	[1] BORTOLETTO	92	CLEO	$e^+e^- \to \Upsilon(4S)$

[1] BORTOLETTO 92 assumes equal production of B^+ and B^0 at the $\Upsilon(4S)$ and uses Mark III branching fractions for the D and $D^*(2010)$.

$\Gamma(D^*(2010)^- \pi^+\rho^0)/\Gamma_{total}$ — Γ_{63}/Γ

VALUE	DOCUMENT ID		TECN	COMMENT
0.00573±0.00317±0.00004	[1] BORTOLETTO	92	CLEO	$e^+e^- \to \Upsilon(4S)$

[1] BORTOLETTO 92 reports 0.0068 ± 0.0032 ± 0.0021 from a measurement of $[\Gamma(B^0 \to D^*(2010)^- \pi^+\rho^0)/\Gamma_{total}]$ × $[B(D^*(2010)^+ \to D^0\pi^+)]$ assuming $B(D^*(2010)^+ \to D^0\pi^+)$ = 0.57 ± 0.06, which we rescale to our best (shown rounded) value $B(D^*(2010)^+ \to D^0\pi^+)$ = (67.7 ± 0.5) × 10^{-2}. Our first error is their experiment's error and our second error is the systematic error from using our best (shown rounded) value. Assumes equal production of B^+ and B^0 at the $\Upsilon(4S)$ and uses Mark III branching fractions for the D.

$\Gamma(D^*(2010)^- a_1(1260)^+)/\Gamma_{total}$ — Γ_{64}/Γ

VALUE	DOCUMENT ID		TECN	COMMENT
0.0130±0.0027 OUR AVERAGE				
0.0126±0.0020±0.0022	[1,2] ALAM	94	CLE2	$e^+e^- \to \Upsilon(4S)$
0.0152±0.0070±0.0001	[3] BORTOLETTO	92	CLEO	$e^+e^- \to \Upsilon(4S)$

[1] ALAM 94 value is twice their $\Gamma(D^*(2010)^- \pi^+\pi^+\pi^-)/\Gamma_{total}$ value based on their observation that the three pions are dominantly in the $a_1(1260)$ mass range 1.0 to 1.6 GeV.

[2] ALAM 94 assume equal production of B^+ and B^0 at the $\Upsilon(4S)$ and use the CLEO II $B(D^*(2010)^+ \to D^0\pi^+)$ and absolute $B(D^0 \to K^-\pi^+)$ and the PDG 1992 $B(D^0 \to K^-\pi^+\pi^0)/B(D^0 \to K^-\pi^+)$ and $B(D^0 \to K^-2\pi^+\pi^-)/B(D^0 \to K^-\pi^+)$.

[3] BORTOLETTO 92 reports 0.018 ± 0.006 ± 0.006 from a measurement of $[\Gamma(B^0 \to D^*(2010)^- a_1(1260)^+)/\Gamma_{total}]$ × $[B(D^*(2010)^+ \to D^0\pi^+)]$ assuming $B(D^*(2010)^+ \to D^0\pi^+)$ = 0.57 ± 0.06, which we rescale to our best (shown rounded) value $B(D^*(2010)^+ \to D^0\pi^+)$ = (67.7 ± 0.5) × 10^{-2}. Our first error is their experiment's error and our second error is the systematic error from using our best (shown rounded) value. Assumes equal production of B^+ and B^0 at the $\Upsilon(4S)$ and uses Mark III branching fractions for the D.

$\Gamma(\overline{D}_1(2420)^0\pi^-\pi^+, \overline{D}_1^0 \to D^{*-}\pi^+)/\Gamma(D^*(2010)^-\pi^+\pi^+\pi^-)$ — Γ_{65}/Γ_{61}

VALUE	DOCUMENT ID		TECN	COMMENT
(2.04±0.42±0.22) × 10^{-2}	AAIJ	13AO	LHCB	pp at 7 TeV

$\Gamma(D^*(2010)^- K^+\pi^-\pi^+)/\Gamma(D^*(2010)^-\pi^+\pi^+\pi^-)$ — Γ_{66}/Γ_{61}

VALUE	DOCUMENT ID		TECN	COMMENT
(6.47±0.37±0.35) × 10^{-2}	AAIJ	13AO	LHCB	pp at 7 TeV

$\Gamma(D^*(2010)^-\pi^+\pi^+\pi^-\pi^0)/\Gamma_{total}$ — Γ_{67}/Γ

VALUE	EVTS	DOCUMENT ID		TECN	COMMENT
0.0176±0.0027 OUR AVERAGE					
0.0172±0.0014±0.0024		[1] ALEXANDER	01B	CLE2	$e^+e^- \to \Upsilon(4S)$
0.0345±0.0181±0.0003	28	[2] ALBRECHT	90J	ARG	$e^+e^- \to \Upsilon(4S)$

[1] Assumes equal production of B^+ and B^0 at the $\Upsilon(4S)$. The signal is consistent with all observed $\omega\pi^+$ having proceeded through the ρ'^+ resonance at mass 1349 ± 25^{+10}_{-5} MeV and width 547 ± 86^{+46}_{-45} MeV.

[2] ALBRECHT 90J reports 0.041 ± 0.015 ± 0.016 from a measurement of $[\Gamma(B^0 \to D^*(2010)^-\pi^+\pi^+\pi^-\pi^0)/\Gamma_{total}]$ × $[B(D^*(2010)^+ \to D^0\pi^+)]$ assuming $B(D^*(2010)^+ \to D^0\pi^+)$ = 0.57 ± 0.06, which we rescale to our best (shown rounded) value $B(D^*(2010)^+ \to D^0\pi^+)$ = (67.7 ± 0.5) × 10^{-2}. Our first error is their experiment's error and our second error is the systematic error from using our best (shown rounded) value. Assumes equal production of B^+ and B^0 at the $\Upsilon(4S)$ and uses Mark III branching fractions for the D.

$\Gamma(D^{*-}3\pi^+2\pi^-)/\Gamma_{total}$ — Γ_{68}/Γ

VALUE (units 10^{-3})	DOCUMENT ID		TECN	COMMENT
4.72±0.59±0.71	[1] MAJUMDER	04	BELL	$e^+e^- \to \Upsilon(4S)$

[1] Assumes equal production of B^+ and B^0 at the $\Upsilon(4S)$.

$\Gamma(D^*(2010)^-\omega\pi^+)/\Gamma_{total}$ — Γ_{69}/Γ

VALUE (units 10^{-3})	DOCUMENT ID		TECN	COMMENT
2.46±0.18 OUR AVERAGE Error includes scale factor of 1.2.				
2.31±0.11±0.14	[1] MATVIENKO	15	BELL	$e^+e^- \to \Upsilon(4S)$
2.88±0.21±0.31	[1] AUBERT	06L	BABR	$e^+e^- \to \Upsilon(4S)$
2.9 ±0.3 ±0.4	[1,2] ALEXANDER	01B	CLE2	$e^+e^- \to \Upsilon(4S)$

[1] Assumes equal production of B^+ and B^0 at the $\Upsilon(4S)$.
[2] The signal is consistent with all observed $\omega\pi^+$ having proceeded through the ρ'^+ resonance at mass $1349 \pm 25^{+10}_{-5}$ MeV and width $547 \pm 86^{+46}_{-45}$ MeV.

$\Gamma(\overline{D}_1(2430)^0\omega,\ \overline{D}_1^0 \to D^{*-}\pi^+)/\Gamma_{total}$ — Γ_{70}/Γ

VALUE (units 10^{-4})	DOCUMENT ID		TECN	COMMENT
$2.7^{+0.8}_{-0.4}$ OUR AVERAGE				
$2.5 \pm 0.4^{+0.8}_{-0.2}$	[1,2] MATVIENKO	15	BELL	$e^+e^- \to \Upsilon(4S)$
$4.1 \pm 1.2 \pm 1.1$	[3] AUBERT	06L	BABR	$e^+e^- \to \Upsilon(4S)$

[1] Assumes equal production of B^+ and B^0.
[2] The measurement is obtained by amplitude analysis of $B^0 \to D^{*-}\omega\pi^+$. The second uncertainty combines in quadrature experimental systematic and model uncertainties.
[3] Obtained by fitting the events with $\cos\theta_{D^*} < 0.5$ and scaling up the result by a factor of 4/3. No interference effects between $B^0 \to D_1'\omega$ and $D^*\omega\pi$ are assumed.

$\Gamma(D^{*-}\rho(1450)^+,\ \rho^+ \to \omega\pi^+)/\Gamma_{total}$ — Γ_{71}/Γ

VALUE (units 10^{-3})	DOCUMENT ID		TECN	COMMENT
$1.07^{+0.15+0.40}_{-0.31-0.13}$	[1,2] MATVIENKO	15	BELL	$e^+e^- \to \Upsilon(4S)$

[1] Obtained by amplitude analysis of $\overline{B}^0 \to D^{*-}\omega\pi^+$. The second uncertainty combines in qudrature experimental systematic and model uncertainties.
[2] Assumes equal production of B^0 and B^+ at $\Upsilon(4S)$.

$\Gamma(\overline{D}_1(2420)^0\omega,\ \overline{D}_1^0 \to D^{*-}\pi^+)/\Gamma_{total}$ — Γ_{72}/Γ

VALUE (units 10^{-4})	DOCUMENT ID		TECN	COMMENT
$0.7 \pm 0.2 \pm 0.1$	[1,2] MATVIENKO	15	BELL	$e^+e^- \to \Upsilon(4S)$

[1] Obtained by amplitude analysis of $\overline{B}^0 \to D^{*-}\omega\pi^+$. The second uncertainty combines in qudrature experimental systematic and model uncertainties.
[2] Assumes equal production of B^0 and B^+ at $\Upsilon(4S)$.

$\Gamma(\overline{D}_2^*(2460)^0\omega,\ \overline{D}_2^0 \to D^{*-}\pi^+)/\Gamma_{total}$ — Γ_{73}/Γ

VALUE (units 10^{-4})	DOCUMENT ID		TECN	COMMENT
$0.4 \pm 0.1 \pm 0.1$	[1,2] MATVIENKO	15	BELL	$e^+e^- \to \Upsilon(4S)$

[1] Obtained by amplitude analysis of $\overline{B}^0 \to D^{*-}\omega\pi^+$. The second uncertainty combines in qudrature experimental systematic and model uncertainties.
[2] Assumes equal production of B^0 and B^+ at $\Upsilon(4S)$.

$\Gamma(D^{*-}b_1(1235)^+,\ b_1^+ \to \omega\pi^+)/\Gamma_{total}$ — Γ_{74}/Γ

VALUE	CL%	DOCUMENT ID		TECN	COMMENT
$< 0.7 \times 10^{-4}$	90	[1] MATVIENKO	15	BELL	$e^+e^- \to \Upsilon(4S)$

[1] Assumes equal production of B^0 and B^+ at $\Upsilon(4S)$.

$\Gamma(\overline{D}^{**-}\pi^+)/\Gamma_{total}$ — Γ_{75}/Γ

D^{**-} represents an excited state with mass $2.2 < M < 2.8$ GeV/c^2.

VALUE (units 10^{-3})	DOCUMENT ID		TECN	COMMENT
$1.9 \pm 0.9 \pm 0.1$	[1,2] AUBERT,BE	06J	BABR	$e^+e^- \to \Upsilon(4S)$

[1] AUBERT,BE 06J reports $[\Gamma(B^0 \to \overline{D}^{**-}\pi^+)/\Gamma_{total}]$ / $[B(B^0 \to D^-\pi^+)] = 0.77 \pm 0.22 \pm 0.29$ which we multiply by our best (shown rounded) value $B(B^0 \to D^-\pi^+) = (2.51 \pm 0.08) \times 10^{-3}$. Our first error is their experiment's error and our second error is the systematic error from using our best (shown rounded) value.
[2] Uses a missing-mass method. Does not depend on D branching fractions or B^+/B^0 production rates.

$\Gamma(D_1(2420)^-\pi^+,\ D_1^- \to D^-\pi^+\pi^-)/\Gamma_{total}$ — Γ_{76}/Γ

VALUE (units 10^{-4})	DOCUMENT ID		TECN	COMMENT
$0.99^{+0.20}_{-0.25}$ OUR FIT				
$0.89 \pm 0.15^{+0.17}_{-0.32}$	[1] ABE	05A	BELL	$e^+e^- \to \Upsilon(4S)$

[1] Assumes equal production of B^+ and B^0 at the $\Upsilon(4S)$.

$\Gamma(D_1(2420)^-\pi^+,\ D_1^- \to D^-\pi^+\pi^-)/\Gamma(D^-\pi^+\pi^+\pi^-)$ — Γ_{76}/Γ_{50}

VALUE (units 10^{-2})	DOCUMENT ID		TECN	COMMENT
1.7 ± 0.4 OUR FIT				
$2.1 \pm 0.5^{+0.3}_{-0.5}$	AAIJ	11E	LHCB	pp at 7 TeV

$\Gamma(D_1(2420)^-\pi^+,\ D_1^- \to D^{*-}\pi^+\pi^-)/\Gamma_{total}$ — Γ_{77}/Γ

VALUE (units 10^{-4})	CL%	DOCUMENT ID		TECN	COMMENT
< 0.33	90	[1] ABE	05A	BELL	$e^+e^- \to \Upsilon(4S)$

[1] Assumes equal production of B^+ and B^0 at the $\Upsilon(4S)$.

$\Gamma(D^*(2010)^-\pi^+\pi^+\pi^-)/\Gamma(D^*(2010)^-\pi^+)$ — Γ_{61}/Γ_{48}

VALUE	DOCUMENT ID		TECN	COMMENT
$2.64 \pm 0.04 \pm 0.13$	AAIJ	13AO	LHCB	pp at 7 TeV

$\Gamma(\overline{D}_2^*(2460)^-\pi^+,\ D_2^{*-} \to D^0\pi^-)/\Gamma_{total}$ — Γ_{78}/Γ

VALUE (units 10^{-4})	CL%	DOCUMENT ID		TECN	COMMENT
2.38 ± 0.16 OUR AVERAGE					
$2.44 \pm 0.07 \pm 0.16$		[1] AAIJ	15Y	LHCB	pp at 7, 8 TeV
$2.15 \pm 0.17 \pm 0.31$		[2,3] KUZMIN	07	BELL	$e^+e^- \to \Upsilon(4S)$
• • • We do not use the following data for averages, fits, limits, etc. • • •					
< 14.7	90	[2] ALAM	94	CLE2	$e^+e^- \to \Upsilon(4S)$

[1] Result obtained using the isobar formalism. The second uncertainty combines in quadrature all systematic uncertainties quoted in the paper.
[2] Assumes equal production of B^+ and B^0 at the $\Upsilon(4S)$.
[3] Our second uncertainty combines systematics and model errors quoted in the paper.

$\Gamma(\overline{D}_0^*(2400)^-\pi^+,\ D_0^{*-} \to D^0\pi^-)/\Gamma_{total}$ — Γ_{79}/Γ

VALUE (units 10^{-4})	DOCUMENT ID		TECN	COMMENT
0.76 ± 0.08 OUR AVERAGE				
$0.77 \pm 0.05 \pm 0.06$	[1] AAIJ	15Y	LHCB	pp at 7, 8 TeV
$0.60 \pm 0.13 \pm 0.27$	[2,3] KUZMIN	07	BELL	$e^+e^- \to \Upsilon(4S)$

[1] Result obtained using the isobar formalism. The second uncertainty combines in quadrature all systematic uncertainties quoted in the paper.
[2] Assumes equal production of B^+ and B^0 at the $\Upsilon(4S)$.
[3] Our second uncertainty combines systematics and model errors quoted in the paper.

$\Gamma(D_2^*(2460)^-\pi^+,\ D_2^{*-} \to D^{*-}\pi^+\pi^-)/\Gamma_{total}$ — Γ_{80}/Γ

VALUE (units 10^{-4})	CL%	DOCUMENT ID		TECN	COMMENT
< 0.24	90	[1] ABE	05A	BELL	$e^+e^- \to \Upsilon(4S)$

[1] Assumes equal production of B^+ and B^0 at the $\Upsilon(4S)$.

$\Gamma(\overline{D}_2^*(2460)^-\rho^+)/\Gamma_{total}$ — Γ_{81}/Γ

VALUE	CL%	DOCUMENT ID		TECN	COMMENT
< 0.0049	90	[1] ALAM	94	CLE2	$e^+e^- \to \Upsilon(4S)$

[1] ALAM 94 assumes equal production of B^+ and B^0 at the $\Upsilon(4S)$ and use the CLEO II absolute $B(D^0 \to K^-\pi^+)$ and $B(D_2^*(2460)^+ \to D^0\pi^+) = 30\%$.

$\Gamma(D^0\overline{D}^0)/\Gamma_{total}$ — Γ_{82}/Γ

VALUE (units 10^{-4})	CL%	DOCUMENT ID		TECN	COMMENT
$0.14 \pm 0.06 \pm 0.03$		[1] AAIJ	13AP	LHCB	pp at 7 TeV
• • • We do not use the following data for averages, fits, limits, etc. • • •					
< 0.43	90	[2] ADACHI	08	BELL	$e^+e^- \to \Upsilon(4S)$
< 0.6	90	[2] AUBERT,B	06A	BABR	$e^+e^- \to \Upsilon(4S)$

[1] Uses $B(B^0 \to D^-D^+) = (2.11 \pm 0.31) \times 10^{-4}$ and $B(B^+ \to \overline{D}^0 D_s^+) = (10.1 \pm 1.7) \times 10^{-3}$.
[2] Assumes equal production of B^+ and B^0 at the $\Upsilon(4S)$.

$\Gamma(D^{*0}\overline{D}^0)/\Gamma_{total}$ — Γ_{83}/Γ

VALUE (units 10^{-4})	CL%	DOCUMENT ID		TECN	COMMENT
< 2.9	90	[1] AUBERT,B	06A	BABR	$e^+e^- \to \Upsilon(4S)$

[1] Assumes equal production of B^+ and B^0 at the $\Upsilon(4S)$.

$\Gamma(D^-D^+)/\Gamma_{total}$ — Γ_{84}/Γ

VALUE (units 10^{-4})	CL%	DOCUMENT ID		TECN	COMMENT
2.11 ± 0.18 OUR AVERAGE					
$2.12 \pm 0.16 \pm 0.18$		[1] ROHRKEN	12	BELL	$e^+e^- \to \Upsilon(4S)$
$1.97 \pm 0.20 \pm 0.20$		[1] FRATINA	07	BELL	$e^+e^- \to \Upsilon(4S)$
$2.8 \pm 0.4 \pm 0.5$		[1] AUBERT,B	06A	BABR	$e^+e^- \to \Upsilon(4S)$
• • • We do not use the following data for averages, fits, limits, etc. • • •					
$1.91 \pm 0.51 \pm 0.30$		[1] MAJUMDER	05	BELL	Repl. by FRATINA 07
< 9.4	90	[1] LIPELES	00	CLE2	$e^+e^- \to \Upsilon(4S)$
< 59	90	BARATE	98Q	ALEP	$e^+e^- \to Z$
< 12	90	ASNER	97	CLE2	$e^+e^- \to \Upsilon(4S)$

[1] Assumes equal production of B^+ and B^0 at the $\Upsilon(4S)$.

$\Gamma(D^\pm D^{*\mp}(CP\text{-averaged}))/\Gamma_{total}$ — Γ_{85}/Γ

VALUE (units 10^{-4})	DOCUMENT ID		TECN	COMMENT
$6.14 \pm 0.29 \pm 0.50$	[1] ROHRKEN	12	BELL	$e^+e^- \to \Upsilon(4S)$

[1] Assumes equal production of B^+ and B^0 at the $\Upsilon(4S)$.

$\Gamma(D^-D_s^+)/\Gamma_{total}$ — Γ_{86}/Γ

VALUE (units 10^{-3})	EVTS	DOCUMENT ID		TECN	COMMENT
8.1 ± 0.6 OUR AVERAGE	Error includes scale factor of 1.1.				
$8.9 \pm 0.5 \pm 0.5$		[1] ADACHI	24L	BEL2	$e^+e^- \to \Upsilon(4S)$
$7.3 \pm 0.4 \pm 0.7$		[2] ZUPANC	07	BELL	$e^+e^- \to \Upsilon(4S)$
$6.6 \pm 1.4 \pm 0.6$		[3] AUBERT	06N	BABR	$e^+e^- \to \Upsilon(4S)$
$6.8 \pm 2.4 \pm 0.6$		[4] GIBAUT	96	CLE2	$e^+e^- \to \Upsilon(4S)$
$10 \pm 9 \pm 1$		[5] ALBRECHT	92G	ARG	$e^+e^- \to \Upsilon(4S)$
$5.3 \pm 3.0 \pm 0.5$		[6] BORTOLETTO	92	CLEO	$e^+e^- \to \Upsilon(4S)$
• • • We do not use the following data for averages, fits, limits, etc. • • •					
12 ± 7	3	[7] BORTOLETTO	90	CLEO	$e^+e^- \to \Upsilon(4S)$

[1] Used 362 fb^{-1} Belle II data and $B(\Upsilon(4S) \to B^0\overline{B}^0) = 0.484 \pm 0.012$.
[2] ZUPANC 07 reports $(7.5 \pm 0.2 \pm 1.1) \times 10^{-3}$ from a measurement of $[\Gamma(B^0 \to D^-D_s^+)/\Gamma_{total}] \times [B(D_s^+ \to \phi\pi^+)]$ assuming $B(D_s^+ \to \phi\pi^+) = (4.4 \pm 0.6) \times 10^{-2}$, which we rescale to our best (shown rounded) value $B(D_s^+ \to \phi\pi^+) = (4.5 \pm 0.4) \times 10^{-2}$. Our first error is their experiment's error and our second error is the systematic error from using our best (shown rounded) value.

Int. J. Mod. Phys. A 2026.41. Downloaded from www.worldscientific.com
by LIFORNIA @ BERKELEY on 09/16/26. Re-use and distribution is strictly not permitted, except for Open Access articles.

Int. J. Mod. Phys. A 2026.41. Downloaded from www.worldscientific.com
by UNIVERSITY OF CALIFORNIA @ BERKELEY on 09/16/26. Re-use and distribution is strictly not permitted, except for Open Access articles.

[3] AUBERT 06N reports $(0.64 \pm 0.13 \pm 0.10) \times 10^{-2}$ from a measurement of $[\Gamma(B^0 \to D^- D_s^+)/\Gamma_{total}] \times [B(D_s^+ \to \phi\pi^+)]$ assuming $B(D_s^+ \to \phi\pi^+) = 0.0462 \pm 0.0062$, which we rescale to our best (shown rounded) value $B(D_s^+ \to \phi\pi^+) = (4.5 \pm 0.4) \times 10^{-2}$. Our first error is their experiment's error and our second error is the systematic error from using our best (shown rounded) value.

[4] GIBAUT 96 reports $0.0087 \pm 0.0024 \pm 0.0020$ from a measurement of $[\Gamma(B^0 \to D^- D_s^+)/\Gamma_{total}] \times [B(D_s^+ \to \phi\pi^+)]$ assuming $B(D_s^+ \to \phi\pi^+) = 0.035$, which we rescale to our best (shown rounded) value $B(D_s^+ \to \phi\pi^+) = (4.5 \pm 0.4) \times 10^{-2}$. Our first error is their experiment's error and our second error is the systematic error from using our best (shown rounded) value.

[5] ALBRECHT 92G reports $0.017 \pm 0.013 \pm 0.006$ from a measurement of $[\Gamma(B^0 \to D^- D_s^+)/\Gamma_{total}] \times [B(D_s^+ \to \phi\pi^+)]$ assuming $B(D_s^+ \to \phi\pi^+) = 0.027$, which we rescale to our best (shown rounded) value $B(D_s^+ \to \phi\pi^+) = (4.5 \pm 0.4) \times 10^{-2}$. Our first error is their experiment's error and our second error is the systematic error from using our best (shown rounded) value. Assumes PDG 1990 D^+ branching ratios, e.g., $B(D^+ \to K^- 2\pi^+) = 7.7 \pm 1.0\%$.

[6] BORTOLETTO 92 reports $0.0080 \pm 0.0045 \pm 0.0030$ from a measurement of $[\Gamma(B^0 \to D^- D_s^+)/\Gamma_{total}] \times [B(D_s^+ \to \phi\pi^+)]$ assuming $B(D_s^+ \to \phi\pi^+) = 0.030 \pm 0.011$, which we rescale to our best (shown rounded) value $B(D_s^+ \to \phi\pi^+) = (4.5 \pm 0.4) \times 10^{-2}$. Our first error is their experiment's error and our second error is the systematic error from using our best (shown rounded) value. Assumes equal production of B^+ and B^0 at the $\Upsilon(4S)$ and uses Mark III branching fractions for the D.

[7] BORTOLETTO 90 assume $B(D_s \to \phi\pi^+) = 2\%$. Superseded by BORTOLETTO 92.

$\Gamma(D^*(2010)^- D_s^+)/\Gamma_{total}$ — Γ_{88}/Γ

VALUE (units 10^{-3})	EVTS	DOCUMENT ID		TECN	COMMENT
8.2± 0.8 OUR AVERAGE					
8.3± 1.0±0.6		[1] ADACHI	24L	BEL2	$e^+e^- \to \Upsilon(4S)$
7.3± 1.3±0.7		[2] AUBERT	06N	BABR	$e^+e^- \to \Upsilon(4S)$
8.3± 1.5±0.7		[3] AUBERT	03I	BABR	$e^+e^- \to \Upsilon(4S)$
8.8± 1.7±0.8		[4] AHMED	00B	CLE2	$e^+e^- \to \Upsilon(4S)$
8 ± 6 ±1		[5] ALBRECHT	92G	ARG	$e^+e^- \to \Upsilon(4S)$
11 ± 6 ±1		[6] BORTOLETTO	92	CLEO	$e^+e^- \to \Upsilon(4S)$
• • • We do not use the following data for averages, fits, limits, etc. • • •					
7.2± 2.2±0.6		[7] GIBAUT	96	CLE2	Repl. by AHMED 00B
24 ±14	3	[8] BORTOLETTO	90	CLEO	$e^+e^- \to \Upsilon(4S)$

[1] Used 362 fb^{-1} Belle II data and $B(\Upsilon(4S) \to B^0\overline{B}^0)=0.484 \pm 0.012$.

[2] AUBERT 06N reports $(0.71 \pm 0.13 \pm 0.09) \times 10^{-2}$ from a measurement of $[\Gamma(B^0 \to D^*(2010)^- D_s^+)/\Gamma_{total}] \times [B(D_s^+ \to \phi\pi^+)]$ assuming $B(D_s^+ \to \phi\pi^+) = 0.0462 \pm 0.0062$, which we rescale to our best (shown rounded) value $B(D_s^+ \to \phi\pi^+) = (4.5 \pm 0.4) \times 10^{-2}$. Our first error is their experiment's error and our second error is the systematic error from using our best (shown rounded) value.

[3] AUBERT 03I reports $0.0103 \pm 0.0014 \pm 0.0013$ from a measurement of $[\Gamma(B^0 \to D^*(2010)^- D_s^+)/\Gamma_{total}] \times [B(D_s^+ \to \phi\pi^+)]$ assuming $B(D_s^+ \to \phi\pi^+) = 0.036$, which we rescale to our best (shown rounded) value $B(D_s^+ \to \phi\pi^+) = (4.5 \pm 0.4) \times 10^{-2}$. Our first error is their experiment's error and our second error is the systematic error from using our best (shown rounded) value.

[4] AHMED 00B reports $0.0110 \pm 0.0018 \pm 0.0011$ from a measurement of $[\Gamma(B^0 \to D^*(2010)^- D_s^+)/\Gamma_{total}] \times [B(D_s^+ \to \phi\pi^+)]$ assuming $B(D_s^+ \to \phi\pi^+) = 0.036$, which we rescale to our best (shown rounded) value $B(D_s^+ \to \phi\pi^+) = (4.5 \pm 0.4) \times 10^{-2}$. Our first error is their experiment's error and our second error is the systematic error from using our best (shown rounded) value.

[5] ALBRECHT 92G reports $0.014 \pm 0.010 \pm 0.003$ from a measurement of $[\Gamma(B^0 \to D^*(2010)^- D_s^+)/\Gamma_{total}] \times [B(D_s^+ \to \phi\pi^+)]$ assuming $B(D_s^+ \to \phi\pi^+) = 0.027$, which we rescale to our best (shown rounded) value $B(D_s^+ \to \phi\pi^+) = (4.5 \pm 0.4) \times 10^{-2}$. Our first error is their experiment's error and our second error is the systematic error from using our best (shown rounded) value. Assumes PDG 1990 D^+ and $D^*(2010)^+$ branching ratios, e.g., $B(D^0 \to K^-\pi^+) = 3.71 \pm 0.25\%$, $B(D^+ \to K^-2\pi^+) = 7.1 \pm 1.0\%$, and $B(D^*(2010)^+ \to D^0\pi^+) = 55 \pm 4\%$.

[6] BORTOLETTO 92 reports $0.016 \pm 0.009 \pm 0.006$ from a measurement of $[\Gamma(B^0 \to D^*(2010)^- D_s^+)/\Gamma_{total}] \times [B(D_s^+ \to \phi\pi^+)]$ assuming $B(D_s^+ \to \phi\pi^+) = 0.030 \pm 0.011$, which we rescale to our best (shown rounded) value $B(D_s^+ \to \phi\pi^+) = (4.5 \pm 0.4) \times 10^{-2}$. Our first error is their experiment's error and our second error is the systematic error from using our best (shown rounded) value. Assumes equal production of B^+ and B^0 at the $\Upsilon(4S)$ and uses Mark III branching fractions for the D and $D^*(2010)$.

[7] GIBAUT 96 reports $0.0093 \pm 0.0023 \pm 0.0016$ from a measurement of $[\Gamma(B^0 \to D^*(2010)^- D_s^+)/\Gamma_{total}] \times [B(D_s^+ \to \phi\pi^+)]$ assuming $B(D_s^+ \to \phi\pi^+) = 0.035$, which we rescale to our best (shown rounded) value $B(D_s^+ \to \phi\pi^+) = (4.5 \pm 0.4) \times 10^{-2}$. Our first error is their experiment's error and our second error is the systematic error from using our best (shown rounded) value.

[8] BORTOLETTO 90 assume $B(D_s \to \phi\pi^+) = 2\%$. Superseded by BORTOLETTO 92.

$\Gamma(D^*(2010)^- D_s^+,\ D^{*-} \to \overline{D}^0\pi^-, m(\overline{D}^0\pi^-)>2.05\,\text{GeV})/\Gamma(\overline{D}^0 D_s^+\pi^-, m(\overline{D}^0\pi^-)>2.05\,\text{GeV})$ — Γ_{89}/Γ_{87}

VALUE (units 10^{-2})	DOCUMENT ID		TECN	COMMENT
15.8±1.3±2.4	[1] AAIJ	23B	LHCB	pp at 7, 8, 13 TeV

[1] Uses simultaneous fits of $\overline{B}^0 \to \overline{D}^0 D_s^+\pi^-$ and $B^+ \to D^- D_s^+\pi^+$ amplitudes assuming isospin symmetry.

$\Gamma(D_2^*(2460)^- D_s^+,\ D_2^{*-} \to \overline{D}^0\pi^-)/\Gamma(\overline{D}^0 D_s^+\pi^-, m(\overline{D}^0\pi^-)>2.05\,\text{GeV})$ — Γ_{90}/Γ_{87}

VALUE (units 10^{-2})	DOCUMENT ID		TECN	COMMENT
22.38±0.88±0.60	[1] AAIJ	23B	LHCB	pp at 7, 8, 13 TeV

[1] Uses simultaneous fits of $\overline{B}^0 \to \overline{D}^0 D_s^+\pi^-$ and $B^+ \to D^- D_s^+\pi^+$ amplitudes assuming isospin symmetry.

$\Gamma(D_1^*(2600)^- D_s^+,\ D_1^{*-} \to \overline{D}^0\pi^-)/\Gamma(\overline{D}^0 D_s^+\pi^-, m(\overline{D}^0\pi^-)>2.05\,\text{GeV})$ — Γ_{91}/Γ_{87}

VALUE (units 10^{-2})	DOCUMENT ID		TECN	COMMENT
1.35±0.40±0.59	[1] AAIJ	23B	LHCB	pp at 7, 8, 13 TeV

[1] Uses simultaneous fits of $\overline{B}^0 \to \overline{D}^0 D_s^+\pi^-$ and $B^+ \to D^- D_s^+\pi^+$ amplitudes assuming isospin symmetry.

$\Gamma(D_3^*(2750)^- D_s^+,\ D_3^{*-} \to \overline{D}^0\pi^-)/\Gamma(\overline{D}^0 D_s^+\pi^-, m(\overline{D}^0\pi^-)>2.05\,\text{GeV})$ — Γ_{92}/Γ_{87}

VALUE (units 10^{-2})	DOCUMENT ID		TECN	COMMENT
0.31±0.14±0.17	[1] AAIJ	23B	LHCB	pp at 7, 8, 13 TeV

[1] Uses simultaneous fits of $\overline{B}^0 \to \overline{D}^0 D_s^+\pi^-$ and $B^+ \to D^- D_s^+\pi^+$ amplitudes assuming isospin symmetry.

$\Gamma(D_1^*(2760)^- D_s^+,\ D_1^{*-} \to \overline{D}^0\pi^-)/\Gamma(\overline{D}^0 D_s^+\pi^-, m(\overline{D}^0\pi^-)>2.05\,\text{GeV})$ — Γ_{93}/Γ_{87}

VALUE (units 10^{-2})	DOCUMENT ID		TECN	COMMENT
0.28±0.25±1.48	[1] AAIJ	23B	LHCB	pp at 7, 8, 13 TeV

[1] Uses simultaneous fits of $\overline{B}^0 \to \overline{D}^0 D_s^+\pi^-$ and $B^+ \to D^- D_s^+\pi^+$ amplitudes assuming isospin symmetry.

$\Gamma(D_J^*(3000)^- D_s^+,\ D_J^{*-} \to \overline{D}^0\pi^-)/\Gamma(\overline{D}^0 D_s^+\pi^-, m(\overline{D}^0\pi^-)>2.05\,\text{GeV})$ — Γ_{94}/Γ_{87}

VALUE (units 10^{-2})	DOCUMENT ID		TECN	COMMENT
0.45±0.16±0.38	[1] AAIJ	23B	LHCB	pp at 7, 8, 13 TeV

[1] Uses simultaneous fits of $\overline{B}^0 \to \overline{D}^0 D_s^+\pi^-$ and $B^+ \to D^- D_s^+\pi^+$ amplitudes assuming isospin symmetry.

$\Gamma(T_{cs0}^*(2870)^0\overline{D}^0,\ T_{cs0}^{*0} \to D_s^+\pi^-)/\Gamma(\overline{D}^0 D_s^+\pi^-, m(\overline{D}^0\pi^-)>2.05\,\text{GeV})$ — Γ_{95}/Γ_{87}

VALUE (units 10^{-2})	DOCUMENT ID		TECN	COMMENT
2.48±0.67±0.77	[1] AAIJ	23B	LHCB	pp at 7, 8, 13 TeV

[1] Uses simultaneous fits of $\overline{B}^0 \to \overline{D}^0 D_s^+\pi^-$ and $B^+ \to D^- D_s^+\pi^+$ amplitudes assuming isospin symmetry.

$\Gamma(D^- D_s^{*+})/\Gamma_{total}$ — Γ_{96}/Γ

VALUE	DOCUMENT ID		TECN	COMMENT
0.0074±0.0016 OUR AVERAGE				
0.0071±0.0016±0.0006	[1] AUBERT	06N	BABR	$e^+e^- \to \Upsilon(4S)$
0.0078±0.0032±0.0007	[2] GIBAUT	96	CLE2	$e^+e^- \to \Upsilon(4S)$
0.016 ±0.012 ±0.001	[3] ALBRECHT	92G	ARG	$e^+e^- \to \Upsilon(4S)$

[1] AUBERT 06N reports $(0.69 \pm 0.16 \pm 0.09) \times 10^{-2}$ from a measurement of $[\Gamma(B^0 \to D^- D_s^{*+})/\Gamma_{total}] \times [B(D_s^+ \to \phi\pi^+)]$ assuming $B(D_s^+ \to \phi\pi^+) = 0.0462 \pm 0.0062$, which we rescale to our best (shown rounded) value $B(D_s^+ \to \phi\pi^+) = (4.5 \pm 0.4) \times 10^{-2}$. Our first error is their experiment's error and our second error is the systematic error from using our best (shown rounded) value.

[2] GIBAUT 96 reports $0.0100 \pm 0.0035 \pm 0.0022$ from a measurement of $[\Gamma(B^0 \to D^- D_s^{*+})/\Gamma_{total}] \times [B(D_s^+ \to \phi\pi^+)]$ assuming $B(D_s^+ \to \phi\pi^+) = 0.035$, which we rescale to our best (shown rounded) value $B(D_s^+ \to \phi\pi^+) = (4.5 \pm 0.4) \times 10^{-2}$. Our first error is their experiment's error and our second error is the systematic error from using our best (shown rounded) value.

[3] ALBRECHT 92G reports $0.027 \pm 0.017 \pm 0.009$ from a measurement of $[\Gamma(B^0 \to D^- D_s^{*+})/\Gamma_{total}] \times [B(D_s^+ \to \phi\pi^+)]$ assuming $B(D_s^+ \to \phi\pi^+) = 0.027$, which we rescale to our best (shown rounded) value $B(D_s^+ \to \phi\pi^+) = (4.5 \pm 0.4) \times 10^{-2}$. Our first error is their experiment's error and our second error is the systematic error from using our best (shown rounded) value. Assumes PDG 1990 D^+ branching ratios, e.g., $B(D^+ \to K^- 2\pi^+) = 7.7 \pm 1.0\%$.

$\Gamma(D^*(2010)^- D_s^{*+})/\Gamma_{total}$ — Γ_{97}/Γ

VALUE	DOCUMENT ID		TECN	COMMENT
0.0177±0.0014 OUR AVERAGE				
0.0173±0.0018±0.0015	[1] AUBERT	06N	BABR	$e^+e^- \to \Upsilon(4S)$
0.0188±0.0009±0.0017	[2] AUBERT	05V	BABR	$e^+e^- \to \Upsilon(4S)$
0.0158±0.0027±0.0014	[3] AUBERT	03I	BABR	$e^+e^- \to \Upsilon(4S)$
0.015 ±0.004 ±0.001	[4] AHMED	00B	CLE2	$e^+e^- \to \Upsilon(4S)$
0.016 ±0.009 ±0.001	[5] ALBRECHT	92G	ARG	$e^+e^- \to \Upsilon(4S)$
• • • We do not use the following data for averages, fits, limits, etc. • • •				
0.016 ±0.005 ±0.001	[6] GIBAUT	96	CLE2	Repl. by AHMED 00B

[1] AUBERT 06N reports $(1.68 \pm 0.21 \pm 0.19) \times 10^{-2}$ from a measurement of $[\Gamma(B^0 \to D^*(2010)^- D_s^{*+})/\Gamma_{total}] \times [B(D_s^+ \to \phi\pi^+)]$ assuming $B(D_s^+ \to \phi\pi^+) = 0.0462 \pm 0.0062$, which we rescale to our best (shown rounded) value $B(D_s^+ \to \phi\pi^+) = (4.5 \pm$

Int. J. Mod. Phys. A 2026.41. Downloaded from www.worldscientific.com by LIFORNIA @ BERKELEY on 09/16/26. Re-use and distribution is strictly not permitted, except for Open Access articles.

0.4) $\times 10^{-2}$. Our first error is their experiment's error and our second error is the systematic error from using our best (shown rounded) value.

[2] A partial reconstruction technique is used and the result is independent of the particle decay rate of D_S^+ meson. It also provides a model-independent determination of $B(D_S^+ \to \phi\pi^+) = (4.81 \pm 0.52 \pm 0.38)\%$.

[3] AUBERT 03I reports $0.0197 \pm 0.0015 \pm 0.0030$ from a measurement of $[\Gamma(B^0 \to D^*(2010)^- D_s^{*+})/\Gamma_{total}] \times [B(D_s^+ \to \phi\pi^+)]$ assuming $B(D_s^+ \to \phi\pi^+) = 0.036$, which we rescale to our best (shown rounded) value $B(D_s^+ \to \phi\pi^+) = (4.5 \pm 0.4) \times 10^{-2}$. Our first error is their experiment's error and our second error is the systematic error from using our best (shown rounded) value.

[4] AHMED 00B reports $0.0182 \pm 0.0037 \pm 0.0025$ from a measurement of $[\Gamma(B^0 \to D^*(2010)^- D_s^{*+})/\Gamma_{total}] \times [B(D_s^+ \to \phi\pi^+)]$ assuming $B(D_s^+ \to \phi\pi^+) = 0.036$, which we rescale to our best (shown rounded) value $B(D_s^+ \to \phi\pi^+) = (4.5 \pm 0.4) \times 10^{-2}$. Our first error is their experiment's error and our second error is the systematic error from using our best (shown rounded) value.

[5] ALBRECHT 92G reports $0.026 \pm 0.014 \pm 0.006$ from a measurement of $[\Gamma(B^0 \to D^*(2010)^- D_s^{*+})/\Gamma_{total}] \times [B(D_s^+ \to \phi\pi^+)]$ assuming $B(D_s^+ \to \phi\pi^+) = 0.027$, which we rescale to our best (shown rounded) value $B(D_s^+ \to \phi\pi^+) = (4.5 \pm 0.4) \times 10^{-2}$. Our first error is their experiment's error and our second error is the systematic error from using our best (shown rounded) value. Assumes PDG 1990 D^+ and $D^*(2010)^+$ branching ratios, e.g., $B(D^0 \to K^-\pi^+) = 3.71 \pm 0.25\%$, $B(D^+ \to K^-2\pi^+) = 7.1 \pm 1.0\%$, and $B(D^*(2010)^+ \to D^0\pi^+) = 55 \pm 4\%$.

[6] GIBAUT 96 reports $0.0203 \pm 0.0050 \pm 0.0036$ from a measurement of $[\Gamma(B^0 \to D^*(2010)^- D_s^{*+})/\Gamma_{total}] \times [B(D_s^+ \to \phi\pi^+)]$ assuming $B(D_s^+ \to \phi\pi^+) = 0.035$, which we rescale to our best (shown rounded) value $B(D_s^+ \to \phi\pi^+) = (4.5 \pm 0.4) \times 10^{-2}$. Our first error is their experiment's error and our second error is the systematic error from using our best (shown rounded) value.

$\Gamma(D^*(2010)^- D_s^{*+})/\Gamma(D^*(2010)^- D_s^+)$ — Γ_{97}/Γ_{88}

VALUE	DOCUMENT ID		TECN	COMMENT
2.19±0.08±0.01	[1] AAIJ	21S	LHCB	pp at 13 TeV

[1] AAIJ 21S reports $[\Gamma(B^0 \to D^*(2010)^- D_s^{*+})/\Gamma(B^0 \to D^*(2010)^- D_s^+)] \times [B(D_s^{*+} \to D_s^+\gamma)] = 2.045 \pm 0.022 \pm 0.071$ which we divide by our best (shown rounded) value $B(D_s^{*+} \to D_s^+\gamma) = (93.6 \pm 0.4) \times 10^{-2}$. Our first error is their experiment's error and our second error is the systematic error from using our best (shown rounded) value.

$[\Gamma(D^*(2010)^- D_s^+) + \Gamma(D^*(2010)^- D_s^{*+})]/\Gamma_{total}$ — $(\Gamma_{88}+\Gamma_{97})/\Gamma$

VALUE (units 10^{-2})	EVTS	DOCUMENT ID		TECN	COMMENT
2.5 ±0.4 OUR AVERAGE					
2.40±0.35±0.22		[1] AUBERT	03I	BABR	$e^+e^- \to \Upsilon(4S)$
3.3 ±0.9 ±0.3	22	[2] BORTOLETTO	90	CLEO	$e^+e^- \to \Upsilon(4S)$

[1] AUBERT 03I reports $(3.00 \pm 0.19 \pm 0.39) \times 10^{-2}$ from a measurement of $[\left[\Gamma(B^0 \to D^*(2010)^- D_s^+) + \Gamma(B^0 \to D^*(2010)^- D_s^{*+})\right]/\Gamma_{total}] \times [B(D_s^+ \to \phi\pi^+)]$ assuming $B(D_s^+ \to \phi\pi^+) = 0.036$, which we rescale to our best (shown rounded) value $B(D_s^+ \to \phi\pi^+) = (4.5 \pm 0.4) \times 10^{-2}$. Our first error is their experiment's error and our second error is the systematic error from using our best (shown rounded) value.

[2] BORTOLETTO 90 reports $(7.5 \pm 2.0) \times 10^{-2}$ from a measurement of $[\left[\Gamma(B^0 \to D^*(2010)^- D_s^+) + \Gamma(B^0 \to D^*(2010)^- D_s^{*+})\right]/\Gamma_{total}] \times [B(D_s^+ \to \phi\pi^+)]$ assuming $B(D_s^+ \to \phi\pi^+) = 0.02$, which we rescale to our best (shown rounded) value $B(D_s^+ \to \phi\pi^+) = (4.5 \pm 0.4) \times 10^{-2}$. Our first error is their experiment's error and our second error is the systematic error from using our best (shown rounded) value.

$\Gamma(D_{s0}(2317)^- K^+,\ D_{s0}^- \to D_s^-\pi^0)/\Gamma_{total}$ — Γ_{98}/Γ

VALUE (units 10^{-5})	DOCUMENT ID		TECN	COMMENT
$4.2^{+1.4}_{-1.3}\pm0.4$	[1] DRUTSKOY	05	BELL	$e^+e^- \to \Upsilon(4S)$

[1] DRUTSKOY 05 reports $(5.3^{+1.5}_{-1.3} \pm 1.6) \times 10^{-5}$ from a measurement of $[\Gamma(B^0 \to D_{s0}(2317)^- K^+,\ D_{s0}^- \to D_s^-\pi^0)/\Gamma_{total}] \times [B(D_s^+ \to \phi\pi^+)]$ assuming $B(D_s^+ \to \phi\pi^+) = 0.036 \pm 0.009$, which we rescale to our best (shown rounded) value $B(D_s^+ \to \phi\pi^+) = (4.5 \pm 0.4) \times 10^{-2}$. Our first error is their experiment's error and our second error is the systematic error from using our best (shown rounded) value.

$\Gamma(D_{s0}(2317)^- \pi^+,\ D_{s0}^- \to D_s^-\pi^0)/\Gamma_{total}$ — Γ_{99}/Γ

VALUE (units 10^{-5})	CL%	DOCUMENT ID		TECN	COMMENT
<2.5	90	[1] DRUTSKOY	05	BELL	$e^+e^- \to \Upsilon(4S)$

[1] Assumes equal production of B^+ and B^0 at the $\Upsilon(4S)$.

$\Gamma(D_{sJ}(2457)^- K^+,\ D_{sJ}^- \to D_s^-\pi^0)/\Gamma_{total}$ — Γ_{100}/Γ

VALUE (units 10^{-5})	CL%	DOCUMENT ID		TECN	COMMENT
<0.94	90	[1] DRUTSKOY	05	BELL	$e^+e^- \to \Upsilon(4S)$

[1] Assumes equal production of B^+ and B^0 at the $\Upsilon(4S)$.

$\Gamma(D_{sJ}(2457)^- \pi^+,\ D_{sJ}^- \to D_s^-\pi^0)/\Gamma_{total}$ — Γ_{101}/Γ

VALUE (units 10^{-5})	CL%	DOCUMENT ID		TECN	COMMENT
<0.40	90	[1] DRUTSKOY	05	BELL	$e^+e^- \to \Upsilon(4S)$

[1] Assumes equal production of B^+ and B^0 at the $\Upsilon(4S)$.

$\Gamma(D_s^- D_s^+)/\Gamma_{total}$ — Γ_{102}/Γ

VALUE	CL%	DOCUMENT ID		TECN	COMMENT
$< 3.6 \times 10^{-5}$	90	[1] ZUPANC	07	BELL	$e^+e^- \to \Upsilon(4S)$
• • • We do not use the following data for averages, fits, limits, etc. • • •					
$<10 \times 10^{-5}$	90	[1] AUBERT,BE	05F	BABR	$e^+e^- \to \Upsilon(4S)$

[1] Assumes equal production of B^+ and B^0 at the $\Upsilon(4S)$.

$\Gamma(D_s^{*-} D_s^+)/\Gamma_{total}$ — Γ_{103}/Γ

VALUE	CL%	DOCUMENT ID		TECN	COMMENT
$<1.3 \times 10^{-4}$	90	[1] AUBERT,BE	05F	BABR	$e^+e^- \to \Upsilon(4S)$

[1] Assumes equal production of B^+ and B^0 at the $\Upsilon(4S)$.

$\Gamma(D_s^{*-} D_s^{*+})/\Gamma_{total}$ — Γ_{104}/Γ

VALUE	CL%	DOCUMENT ID		TECN	COMMENT
$<2.4 \times 10^{-4}$	90	[1] AUBERT,BE	05F	BABR	$e^+e^- \to \Upsilon(4S)$

[1] Assumes equal production of B^+ and B^0 at the $\Upsilon(4S)$.

$\Gamma(D_{s0}^*(2317)^+ D^-,\ D_{s0}^{*+} \to D_s^+\pi^0)/\Gamma_{total}$ — Γ_{105}/Γ

VALUE (units 10^{-3})	DOCUMENT ID		TECN	COMMENT
1.05±0.16 OUR AVERAGE Error includes scale factor of 1.1.				
$0.99^{+0.16}_{-0.15}\pm0.02$	[1,2] CHOI	15A	BELL	$e^+e^- \to \Upsilon(4S)$
$1.4\ ^{+0.5}_{-0.4}\ \pm0.1$	[2,3] AUBERT,B	04S	BABR	$e^+e^- \to \Upsilon(4S)$
• • • We do not use the following data for averages, fits, limits, etc. • • •				
$0.69^{+0.29}_{-0.24}\pm0.06$	[2,4] KROKOVNY	03B	BELL	Repl. by CHOI 15A

[1] CHOI 15A reports $(10.2^{+1.3}_{-1.2} \pm 1.0 \pm 0.4) \times 10^{-4}$ from a measurement of $[\Gamma(B^0 \to D_{s0}^*(2317)^+ D^-,\ D_{s0}^{*+} \to D_s^+\pi^0)/\Gamma_{total}] \times [B(D_s^+ \to K^+K^-\pi^+)] \times [B(D^+ \to K^-2\pi^+)]$ assuming $B(D_s^+ \to K^+K^-\pi^+) = (5.39 \pm 0.21) \times 10^{-2}$, $B(D^+ \to K^-2\pi^+) = (9.13 \pm 0.19) \times 10^{-2}$, which we rescale to our best (shown rounded) values $B(D_s^+ \to K^+K^-\pi^+) = (5.45 \pm 0.08) \times 10^{-2}$, $B(D^+ \to K^-2\pi^+) = (9.31 \pm 0.14) \times 10^{-2}$. Our first error is their experiment's error and our second error is the systematic error from using our best (shown rounded) values.

[2] Assumes equal production of B^+ and B^0 at the $\Upsilon(4S)$.

[3] AUBERT,B 04S reports $(1.8 \pm 0.4^{+0.7}_{-0.5}) \times 10^{-3}$ from a measurement of $[\Gamma(B^0 \to D_{s0}^*(2317)^+ D^-,\ D_{s0}^{*+} \to D_s^+\pi^0)/\Gamma_{total}] \times [B(D_s^+ \to \phi\pi^+)]$ assuming $B(D_s^+ \to \phi\pi^+) = 0.036 \pm 0.009$, which we rescale to our best (shown rounded) value $B(D_s^+ \to \phi\pi^+) = (4.5 \pm 0.4) \times 10^{-2}$. Our first error is their experiment's error and our second error is the systematic error from using our best (shown rounded) value.

[4] KROKOVNY 03B reports $(0.86^{+0.33}_{-0.26} \pm 0.26) \times 10^{-3}$ from a measurement of $[\Gamma(B^0 \to D_{s0}^*(2317)^+ D^-,\ D_{s0}^{*+} \to D_s^+\pi^0)/\Gamma_{total}] \times [B(D_s^+ \to \phi\pi^+)]$ assuming $B(D_s^+ \to \phi\pi^+) = 0.036 \pm 0.009$, which we rescale to our best (shown rounded) value $B(D_s^+ \to \phi\pi^+) = (4.5 \pm 0.4) \times 10^{-2}$. Our first error is their experiment's error and our second error is the systematic error from using our best (shown rounded) value.

$\Gamma(D_{s0}(2317)^+ D^-,\ D_{s0}^+ \to D_s^{*+}\gamma)/\Gamma_{total}$ — Γ_{106}/Γ

VALUE (units 10^{-3})	CL%	DOCUMENT ID		TECN	COMMENT
<0.95	90	[1] KROKOVNY	03B	BELL	$e^+e^- \to \Upsilon(4S)$

[1] Assumes equal production of B^+ and B^0 at the $\Upsilon(4S)$.

$\Gamma(D_{s0}(2317)^+ D^*(2010)^-,\ D_{s0}^+ \to D_s^+\pi^0)/\Gamma_{total}$ — Γ_{107}/Γ

VALUE (units 10^{-3})	DOCUMENT ID		TECN	COMMENT
$1.5\pm0.4^{+0.5}_{-0.4}$	[1] AUBERT,B	04S	BABR	$e^+e^- \to \Upsilon(4S)$

[1] Assumes equal production of B^+ and B^0 at the $\Upsilon(4S)$.

$\Gamma(D_{sJ}(2457)^+ D^-)/\Gamma_{total}$ — Γ_{108}/Γ

VALUE (units 10^{-3})	DOCUMENT ID		TECN	COMMENT
3.5±1.1 OUR AVERAGE				
2.6±1.5±0.7	[1] AUBERT	06N	BABR	$e^+e^- \to \Upsilon(4S)$
$4.8^{+2.2}_{-1.6}\pm1.1$	[2,3] AUBERT,B	04S	BABR	$e^+e^- \to \Upsilon(4S)$
$3.9^{+1.5}_{-1.3}\pm0.9$	[2,4] KROKOVNY	03B	BELL	$e^+e^- \to \Upsilon(4S)$

[1] Uses a missing-mass method in the events that one of the B mesons is fully reconstructed.

[2] Assumes equal production of B^+ and B^0 at the $\Upsilon(4S)$.

[3] AUBERT,B 04S reports $[\Gamma(B^0 \to D_{sJ}(2457)^+ D^-)/\Gamma_{total}] \times [B(D_{s1}(2460)^+ \to D_s^{*+}\pi^0)] = (2.3^{+1.0}_{-0.7} \pm 0.3) \times 10^{-3}$ which we divide by our best (shown rounded) value $B(D_{s1}(2460)^+ \to D_s^{*+}\pi^0) = (48 \pm 11) \times 10^{-2}$. Our first error is their experiment's error and our second error is the systematic error from using our best (shown rounded) value.

[4] KROKOVNY 03B reports $[\Gamma(B^0 \to D_{sJ}(2457)^+ D^-)/\Gamma_{total}] \times [B(D_{s1}(2460)^+ \to D_s^{*+}\pi^0)] = (1.9^{+0.7}_{-0.6} \pm 0.2) \times 10^{-3}$ which we divide by our best (shown rounded) value $B(D_{s1}(2460)^+ \to D_s^{*+}\pi^0) = (48 \pm 11) \times 10^{-2}$. Our first error is their experiment's error and our second error is the systematic error from using our best (shown rounded) value.

Int. J. Mod. Phys. A 2026.41. Downloaded from www.worldscientific.com
by UNIVERSITY OF CALIFORNIA @ BERKELEY on 09/16/26. Re-use and distribution is strictly not permitted, except for Open Access articles.

$\Gamma(D_{sJ}(2457)^+ D^-,\ D_{sJ}^+ \to D_s^+\gamma)/\Gamma_{total}$ — Γ_{109}/Γ

VALUE (units 10^{-3})	DOCUMENT ID		TECN	COMMENT
$0.65^{+0.17}_{-0.14}$ OUR AVERAGE				
$0.64^{+0.24}_{-0.16}\pm0.06$	[1,2] AUBERT,B	04S	BABR	$e^+e^- \to \Upsilon(4S)$
$0.66^{+0.21}_{-0.19}\pm0.06$	[1,3] KROKOVNY	03B	BELL	$e^+e^- \to \Upsilon(4S)$

[1] Assumes equal production of B^+ and B^0 at the $\Upsilon(4S)$.
[2] AUBERT,B 04S reports $(0.8 \pm 0.2^{+0.3}_{-0.2}) \times 10^{-3}$ from a measurement of $[\Gamma(B^0 \to D_{sJ}(2457)^+ D^-,\ D_{sJ}^+ \to D_s^+\gamma)/\Gamma_{total}] \times [B(D_s^+ \to \phi\pi^+)]$ assuming $B(D_s^+ \to \phi\pi^+) = 0.036 \pm 0.009$, which we rescale to our best (shown rounded) value $B(D_s^+ \to \phi\pi^+) = (4.5 \pm 0.4) \times 10^{-2}$. Our first error is their experiment's error and our second error is the systematic error from using our best (shown rounded) value.
[3] KROKOVNY 03B reports $(0.82^{+0.22}_{-0.19} \pm 0.25) \times 10^{-3}$ from a measurement of $[\Gamma(B^0 \to D_{sJ}(2457)^+ D^-,\ D_{sJ}^+ \to D_s^+\gamma)/\Gamma_{total}] \times [B(D_s^+ \to \phi\pi^+)]$ assuming $B(D_s^+ \to \phi\pi^+) = 0.036 \pm 0.009$, which we rescale to our best (shown rounded) value $B(D_s^+ \to \phi\pi^+) = (4.5 \pm 0.4) \times 10^{-2}$. Our first error is their experiment's error and our second error is the systematic error from using our best (shown rounded) value.

$\Gamma(D_{sJ}(2457)^+ D^-,\ D_{sJ}^+ \to D_s^{*+}\gamma)/\Gamma_{total}$ — Γ_{110}/Γ

VALUE (units 10^{-3})	CL%	DOCUMENT ID		TECN	COMMENT
<0.60	90	[1] KROKOVNY	03B	BELL	$e^+e^- \to \Upsilon(4S)$

[1] Assumes equal production of B^+ and B^0 at the $\Upsilon(4S)$.

$\Gamma(D_{sJ}(2457)^+ D^-,\ D_{sJ}^+ \to D_s^+\pi^+\pi^-)/\Gamma_{total}$ — Γ_{111}/Γ

VALUE (units 10^{-3})	CL%	DOCUMENT ID		TECN	COMMENT
<0.20	90	[1] KROKOVNY	03B	BELL	$e^+e^- \to \Upsilon(4S)$

[1] Assumes equal production of B^+ and B^0 at the $\Upsilon(4S)$.

$\Gamma(D_{sJ}(2457)^+ D^-,\ D_{sJ}^+ \to D_s^+\pi^0)/\Gamma_{total}$ — Γ_{112}/Γ

VALUE (units 10^{-3})	CL%	DOCUMENT ID		TECN	COMMENT
<0.36	90	[1] KROKOVNY	03B	BELL	$e^+e^- \to \Upsilon(4S)$

[1] Assumes equal production of B^+ and B^0 at the $\Upsilon(4S)$.

$\Gamma(D^*(2010)^- D_{sJ}(2457)^+)/\Gamma_{total}$ — Γ_{113}/Γ

VALUE (units 10^{-3})	DOCUMENT ID		TECN	COMMENT
9.3±2.2 OUR AVERAGE				
$8.8\pm2.0\pm1.4$	[1] AUBERT	06N	BABR	$e^+e^- \to \Upsilon(4S)$
$11\ ^{+5}_{-4}\ \pm3$	[2,3] AUBERT,B	04S	BABR	$e^+e^- \to \Upsilon(4S)$

[1] Uses a missing-mass method in the events that one of the B mesons is fully reconstructed.
[2] AUBERT,B 04S reports $[\Gamma(B^0 \to D^*(2010)^- D_{sJ}(2457)^+)/\Gamma_{total}] \times [B(D_{s1}(2460)^+ \to D_s^{*+}\pi^0)] = (5.5 \pm 1.2^{+2.2}_{-1.6}) \times 10^{-3}$ which we divide by our best (shown rounded) value $B(D_{s1}(2460)^+ \to D_s^{*+}\pi^0) = (48 \pm 11) \times 10^{-2}$. Our first error is their experiment's error and our second error is the systematic error from using our best (shown rounded) value.
[3] Assumes equal production of B^+ and B^0 at the $\Upsilon(4S)$.

$\Gamma(D_{sJ}(2457)^+ D^*(2010),\ D_{sJ}^+ \to D_s^+\gamma)/\Gamma_{total}$ — Γ_{114}/Γ

VALUE (units 10^{-3})	DOCUMENT ID		TECN	COMMENT
$2.3\pm0.3^{+0.9}_{-0.6}$	[1] AUBERT,B	04S	BABR	$e^+e^- \to \Upsilon(4S)$

[1] Assumes equal production of B^+ and B^0 at the $\Upsilon(4S)$.

$[\Gamma(D^- D_{s1}(2536)^+,\ D_{s1}^+ \to D^{*0}K^+) + \Gamma(D^{*+}K^0)]/\Gamma_{total}$ — $\Gamma_{115}/\Gamma = (\Gamma_{116}+\Gamma_{117})/\Gamma$

VALUE (units 10^{-4})	DOCUMENT ID		TECN	COMMENT
2.75±0.62±0.36	[1,2] AUSHEV	11	BELL	$e^+e^- \to \Upsilon(4S)$

[1] Uses $\Gamma(D^*(2007)^0 \to D^0\pi^0)\ /\ \Gamma(D^*(2007)^0 \to D^0\gamma) = 1.74 \pm 0.13$ and $\Gamma(D_{s1}(2536)^+ \to D^*(2007)^0 K^+)\ /\ \Gamma(D_{s1}(2536)^+ \to D^*(2010)^+ K^0) = 1.36 \pm 0.2$.
[2] Assumes equal production of B^+ and B^0 at the $\Upsilon(4S)$.

$\Gamma(D^- D_{s1}(2536)^+,\ D_{s1}^+ \to D^{*0}K^+)/\Gamma_{total}$ — Γ_{116}/Γ

VALUE (units 10^{-4})	CL%	DOCUMENT ID		TECN	COMMENT
1.71±0.48±0.32		[1] AUBERT	08B	BABR	$e^+e^- \to \Upsilon(4S)$
• • • We do not use the following data for averages, fits, limits, etc. • • •					
<5	90	AUBERT	03X	BABR	Repl. by AUBERT 08B

[1] Assumes equal production of B^+ and B^0 at the $\Upsilon(4S)$.

$\Gamma(D^- D_{s1}(2536)^+,\ D_{s1}^+ \to D^{*+}K^0)/\Gamma_{total}$ — Γ_{117}/Γ

VALUE (units 10^{-4})	DOCUMENT ID		TECN	COMMENT
2.61±1.03±0.31	[1] AUBERT	08B	BABR	$e^+e^- \to \Upsilon(4S)$

[1] Assumes equal production of B^+ and B^0 at the $\Upsilon(4S)$.

$[\Gamma(D^*(2010)^- D_{s1}(2536)^+,\ D_{s1}^+ \to D^{*0}K^+) + \Gamma(D^{*+}K^0)]/\Gamma_{total}$ — $\Gamma_{118}/\Gamma = (\Gamma_{119}+\Gamma_{120})/\Gamma$

VALUE (units 10^{-4})	DOCUMENT ID		TECN	COMMENT
5.01±1.21±0.70	[1,2] AUSHEV	11	BELL	$e^+e^- \to \Upsilon(4S)$

[1] Uses $\Gamma(D^*(2007)^0 \to D^0\pi^0)\ /\ \Gamma(D^*(2007)^0 \to D^0\gamma) = 1.74 \pm 0.13$ and $\Gamma(D_{s1}(2536)^+ \to D^*(2007)^0 K^+)\ /\ \Gamma(D_{s1}(2536)^+ \to D^*(2010)^+ K^0) = 1.36 \pm 0.2$.
[2] Assumes equal production of B^+ and B^0 at the $\Upsilon(4S)$.

$\Gamma(D^*(2010)^- D_{s1}(2536)^+,\ D_{s1}^+ \to D^{*0}K^+)/\Gamma_{total}$ — Γ_{119}/Γ

VALUE (units 10^{-4})	CL%	DOCUMENT ID		TECN	COMMENT
3.32±0.88±0.66		[1] AUBERT	08B	BABR	$e^+e^- \to \Upsilon(4S)$
• • • We do not use the following data for averages, fits, limits, etc. • • •					
<7	90	AUBERT	03X	BABR	Repl. by AUBERT 08B

[1] Assumes equal production of B^+ and B^0 at the $\Upsilon(4S)$.

$\Gamma(D^{*-} D_{s1}(2536)^+,\ D_{s1}^+ \to D^{*+}K^0)/\Gamma_{total}$ — Γ_{120}/Γ

VALUE (units 10^{-4})	DOCUMENT ID		TECN	COMMENT
5.00±1.51±0.67	[1] AUBERT	08B	BABR	$e^+e^- \to \Upsilon(4S)$

[1] Assumes equal production of B^+ and B^0 at the $\Upsilon(4S)$.

$\Gamma(D^- D_{sJ}(2573)^+,\ D_{sJ}^+ \to D^0K^+)/\Gamma_{total}$ — Γ_{121}/Γ

VALUE (units 10^{-5})	CL%	DOCUMENT ID		TECN	COMMENT
3.4±1.7±0.5		[1] LEES	15C	BABR	$e^+e^- \to \Upsilon(4S)$
• • • We do not use the following data for averages, fits, limits, etc. • • •					
<10	90	AUBERT	03X	BABR	$e^+e^- \to \Upsilon(4S)$

[1] Assumes equal production of B^+ and B^0 at the $\Upsilon(4S)$.

$\Gamma(D^*(2010)^- D_{sJ}(2573)^+,\ D_{sJ}^+ \to D^0K^+)/\Gamma_{total}$ — Γ_{122}/Γ

VALUE (units 10^{-4})	CL%	DOCUMENT ID		TECN	COMMENT
<2	90	AUBERT	03X	BABR	$e^+e^- \to \Upsilon(4S)$

$\Gamma(D^- D_{sJ}(2700)^+,\ D_{sJ}^+ \to D^0K^+)/\Gamma_{total}$ — Γ_{123}/Γ

VALUE (units 10^{-4})	DOCUMENT ID		TECN	COMMENT
7.14±0.96±0.69	[1] LEES	15C	BABR	$e^+e^- \to \Upsilon(4S)$

[1] Assumes equal production of B^+ and B^0 at the $\Upsilon(4S)$.

$\Gamma(D^+\pi^-)/\Gamma_{total}$ — Γ_{124}/Γ

VALUE (units 10^{-7})	DOCUMENT ID		TECN	COMMENT
7.3±1.2±0.2	[1,2] DAS	10	BELL	$e^+e^- \to \Upsilon(4S)$

[1] DAS 10 reports $[\Gamma(B^0 \to D^+\pi^-)/\Gamma_{total}]\ /\ [B(B^0 \to D^-\pi^+)] = (2.92 \pm 0.38 \pm 0.31) \times 10^{-4}$ which we multiply by our best (shown rounded) value $B(B^0 \to D^-\pi^+) = (2.51 \pm 0.08) \times 10^{-3}$. Our first error is their experiment's error and our second error is the systematic error from using our best (shown rounded) value.
[2] Derived using $\tan(\theta_C)\ f_D/f_{D_s} \sqrt{B(B^0 \to D_s^+\pi^-)/B(B^0 \to D^-\pi^+)}$ by assuming the flavor SU(3) symmetry, where θ_C is the Cabibbo angle, f_D (f_{D_s}) is the D (D_s) meson decay constant.

$\Gamma(D_s^+\pi^-)/\Gamma_{total}$ — Γ_{125}/Γ

VALUE (units 10^{-6})	CL%	DOCUMENT ID		TECN	COMMENT
20.3±1.8 OUR FIT					
21.6±2.6 OUR AVERAGE					
$19.9\pm2.6\pm1.8$		[1] DAS	10	BELL	$e^+e^- \to \Upsilon(4S)$
$25\ \pm4\ \pm2$		[1] AUBERT	08AJ	BABR	$e^+e^- \to \Upsilon(4S)$
• • • We do not use the following data for averages, fits, limits, etc. • • •					
$14.0\pm3.5\pm1.3$		[2] AUBERT	07K	BABR	Repl. by AUBERT 08AJ
$25\ \pm9\ \pm2$		[3] AUBERT	03D	BABR	Repl. by AUBERT 07K
$19\ ^{+9}_{-7}\ \pm2$		[4] KROKOVNY	02	BELL	Repl. by DAS 10
< 220	90	[5] ALEXANDER	93B	CLE2	$e^+e^- \to \Upsilon(4S)$
<1300	90	[6] BORTOLETTO	90	CLEO	$e^+e^- \to \Upsilon(4S)$

[1] Assumes equal production of B^+ and B^0 at the $\Upsilon(4S)$.
[2] AUBERT 07K reports $[\Gamma(B^0 \to D_s^+\pi^-)/\Gamma_{total}] \times [B(D_s^+ \to \phi\pi^+)] = (0.63 \pm 0.15 \pm 0.05) \times 10^{-6}$ which we divide by our best (shown rounded) value $B(D_s^+ \to \phi\pi^+) = (4.5 \pm 0.4) \times 10^{-2}$. Our first error is their experiment's error and our second error is the systematic error from using our best (shown rounded) value.
[3] AUBERT 03D reports $[\Gamma(B^0 \to D_s^+\pi^-)/\Gamma_{total}] \times [B(D_s^+ \to \phi\pi^+)] = (1.13 \pm 0.33 \pm 0.21) \times 10^{-6}$ which we divide by our best (shown rounded) value $B(D_s^+ \to \phi\pi^+) = (4.5 \pm 0.4) \times 10^{-2}$. Our first error is their experiment's error and our second error is the systematic error from using our best (shown rounded) value.
[4] KROKOVNY 02 reports $[\Gamma(B^0 \to D_s^+\pi^-)/\Gamma_{total}] \times [B(D_s^+ \to \phi\pi^+)] = (0.86^{+0.37}_{-0.30} \pm 0.11) \times 10^{-6}$ which we divide by our best (shown rounded) value $B(D_s^+ \to \phi\pi^+) = (4.5 \pm 0.4) \times 10^{-2}$. Our first error is their experiment's error and our second error is the systematic error from using our best (shown rounded) value.
[5] ALEXANDER 93B reports $< 270 \times 10^{-6}$ from a measurement of $[\Gamma(B^0 \to D_s^+\pi^-)/\Gamma_{total}] \times [B(D_s^+ \to \phi\pi^+)]$ assuming $B(D_s^+ \to \phi\pi^+) = 0.037$, which we rescale to our best (shown rounded) value $B(D_s^+ \to \phi\pi^+) = 4.5 \times 10^{-2}$.
[6] BORTOLETTO 90 assume $B(D_s \to \phi\pi^+) = 2\%$.

$[\Gamma(D_s^+\pi^-) + \Gamma(D_s^-K^+)]/\Gamma_{total}$ — $(\Gamma_{125}+\Gamma_{135})/\Gamma$

VALUE	CL%	DOCUMENT ID		TECN	COMMENT
$<1.0 \times 10^{-3}$	90	[1] ALBRECHT	93E	ARG	$e^+e^- \to \Upsilon(4S)$

[1] ALBRECHT 93E reports $< 1.7 \times 10^{-3}$ from a measurement of $[\left[\Gamma(B^0 \to D_s^+\pi^-) + \Gamma(B^0 \to D_s^-K^+)\right]/\Gamma_{total}] \times [B(D_s^+ \to \phi\pi^+)]$ assuming $B(D_s^+ \to \phi\pi^+) = 0.027$, which we rescale to our best (shown rounded) value $B(D_s^+ \to \phi\pi^+) = 4.5 \times 10^{-2}$.

Int. J. Mod. Phys. A 2026.41. Downloaded from www.worldscientific.com by CALIFORNIA @ BERKELEY on 09/16/26. Re-use and distribution is strictly not permitted, except for Open Access articles.

$\Gamma(D_s^+\pi^-)/\Gamma(D^-\pi^+)$ — Γ_{125}/Γ_{38}

VALUE (units 10^{-3})	DOCUMENT ID		TECN	COMMENT
8.1±0.7 OUR FIT				
7.7±0.7±0.6	AAIJ	21W	LHCB	pp at 7, 8, 13 TeV

$\Gamma(D_s^{*+}\pi^-)/\Gamma_{total}$ — Γ_{126}/Γ

VALUE (units 10^{-5})	CL%	DOCUMENT ID		TECN	COMMENT
2.1 ±0.4 OUR AVERAGE		Error includes scale factor of 1.4.			
1.75±0.34±0.20		[1] JOSHI	10	BELL	$e^+e^- \to \Upsilon(4S)$
2.6 $^{+0.5}_{-0.4}$ ±0.2		[1] AUBERT	08AJ	BABR	$e^+e^- \to \Upsilon(4S)$
• • • We do not use the following data for averages, fits, limits, etc. • • •					
2.9 ±0.7 ±0.3		[2] AUBERT	07K	BABR	Repl. by AUBERT 08AJ
< 4.1	90	AUBERT	03D	BABR	Repl. by AUBERT 07K
<40	90	[3] ALEXANDER	93B	CLE2	$e^+e^- \to \Upsilon(4S)$

[1] Assumes equal production of B^+ and B^0 at the $\Upsilon(4S)$.
[2] AUBERT 07K reports $[\Gamma(B^0 \to D_s^{*+}\pi^-)/\Gamma_{total}] \times [B(D_s^+ \to \phi\pi^+)] = (1.32 \pm 0.27 \pm 0.15) \times 10^{-6}$ which we divide by our best (shown rounded) value $B(D_s^+ \to \phi\pi^+) = (4.5 \pm 0.4) \times 10^{-2}$. Our first error is their experiment's error and our second error is the systematic error from using our best (shown rounded) value.
[3] ALEXANDER 93B reports $< 44 \times 10^{-5}$ from a measurement of $[\Gamma(B^0 \to D_s^{*+}\pi^-)/\Gamma_{total}] \times [B(D_s^+ \to \phi\pi^+)]$ assuming $B(D_s^+ \to \phi\pi^+) = 0.037$, which we rescale to our best (shown rounded) value $B(D_s^+ \to \phi\pi^+) = 4.5 \times 10^{-2}$.

$[\Gamma(D_s^{*+}\pi^-) + \Gamma(D_s^{*-}K^+)]/\Gamma_{total}$ — $(\Gamma_{126}+\Gamma_{136})/\Gamma$

VALUE	CL%	DOCUMENT ID		TECN	COMMENT
<7 × 10^{-4}	90	[1] ALBRECHT	93E	ARG	$e^+e^- \to \Upsilon(4S)$

[1] ALBRECHT 93E reports $< 1.2 \times 10^{-3}$ from a measurement of $[\left[\Gamma(B^0 \to D_s^{*+}\pi^-) + \Gamma(B^0 \to D_s^{*-}K^+)\right]/\Gamma_{total}] \times [B(D_s^+ \to \phi\pi^+)]$ assuming $B(D_s^+ \to \phi\pi^+) = 0.027$, which we rescale to our best (shown rounded) value $B(D_s^+ \to \phi\pi^+) = 4.5 \times 10^{-2}$.

$\Gamma(D_s^+\rho^-)/\Gamma_{total}$ — Γ_{127}/Γ

VALUE (units 10^{-5})	CL%	DOCUMENT ID		TECN	COMMENT
< 2.4	90	[1] AUBERT	08AJ	BABR	$e^+e^- \to \Upsilon(4S)$
• • • We do not use the following data for averages, fits, limits, etc. • • •					
<130	90	[2] ALBRECHT	93E	ARG	$e^+e^- \to \Upsilon(4S)$
< 50	90	[3] ALEXANDER	93B	CLE2	$e^+e^- \to \Upsilon(4S)$

[1] Assumes equal production of B^+ and B^0 at the $\Upsilon(4S)$.
[2] ALBRECHT 93E reports $< 2.2 \times 10^{-3}$ from a measurement of $[\Gamma(B^0 \to D_s^+\rho^-)/\Gamma_{total}] \times [B(D_s^+ \to \phi\pi^+)]$ assuming $B(D_s^+ \to \phi\pi^+) = 0.027$, which we rescale to our best (shown rounded) value $B(D_s^+ \to \phi\pi^+) = 4.5 \times 10^{-2}$.
[3] ALEXANDER 93B reports $< 6.6 \times 10^{-4}$ from a measurement of $[\Gamma(B^0 \to D_s^+\rho^-)/\Gamma_{total}] \times [B(D_s^+ \to \phi\pi^+)]$ assuming $B(D_s^+ \to \phi\pi^+) = 0.037$, which we rescale to our best (shown rounded) value $B(D_s^+ \to \phi\pi^+) = 4.5 \times 10^{-2}$.

$\Gamma(D_s^{*+}\rho^-)/\Gamma_{total}$ — Γ_{128}/Γ

VALUE (units 10^{-5})	CL%	DOCUMENT ID		TECN	COMMENT
4.1$^{+1.3}_{-1.2}$±0.4		[1] AUBERT	08AJ	BABR	$e^+e^- \to \Upsilon(4S)$
• • • We do not use the following data for averages, fits, limits, etc. • • •					
<150	90	[2] ALBRECHT	93E	ARG	$e^+e^- \to \Upsilon(4S)$
< 60	90	[3] ALEXANDER	93B	CLE2	$e^+e^- \to \Upsilon(4S)$

[1] Assumes equal production of B^+ and B^0 at the $\Upsilon(4S)$.
[2] ALBRECHT 93E reports $< 2.5 \times 10^{-3}$ from a measurement of $[\Gamma(B^0 \to D_s^{*+}\rho^-)/\Gamma_{total}] \times [B(D_s^+ \to \phi\pi^+)]$ assuming $B(D_s^+ \to \phi\pi^+) = 0.027$, which we rescale to our best (shown rounded) value $B(D_s^+ \to \phi\pi^+) = 4.5 \times 10^{-2}$.
[3] ALEXANDER 93B reports $< 7.4 \times 10^{-4}$ from a measurement of $[\Gamma(B^0 \to D_s^{*+}\rho^-)/\Gamma_{total}] \times [B(D_s^+ \to \phi\pi^+)]$ assuming $B(D_s^+ \to \phi\pi^+) = 0.037$, which we rescale to our best (shown rounded) value $B(D_s^+ \to \phi\pi^+) = 4.5 \times 10^{-2}$.

$\Gamma(D_s^+a_0^-)/\Gamma_{total}$ — Γ_{129}/Γ

VALUE (units 10^{-5})	CL%	DOCUMENT ID		TECN	COMMENT
<1.9	90	[1] AUBERT	06X	BABR	$e^+e^- \to \Upsilon(4S)$

[1] Assumes equal production of B^+ and B^0 at the $\Upsilon(4S)$.

$\Gamma(D_s^{*+}a_0^-)/\Gamma_{total}$ — Γ_{130}/Γ

VALUE (units 10^{-5})	CL%	DOCUMENT ID		TECN	COMMENT
<3.6	90	[1] AUBERT	06X	BABR	$e^+e^- \to \Upsilon(4S)$

[1] Assumes equal production of B^+ and B^0 at the $\Upsilon(4S)$.

$\Gamma(D_s^+a_1(1260)^-)/\Gamma_{total}$ — Γ_{131}/Γ

VALUE	CL%	DOCUMENT ID		TECN	COMMENT
<2.1 × 10^{-3}	90	[1] ALBRECHT	93E	ARG	$e^+e^- \to \Upsilon(4S)$

[1] ALBRECHT 93E reports $< 3.5 \times 10^{-3}$ from a measurement of $[\Gamma(B^0 \to D_s^+a_1(1260)^-)/\Gamma_{total}] \times [B(D_s^+ \to \phi\pi^+)]$ assuming $B(D_s^+ \to \phi\pi^+) = 0.027$, which we rescale to our best (shown rounded) value $B(D_s^+ \to \phi\pi^+) = 4.5 \times 10^{-2}$.

$\Gamma(D_s^{*+}a_1(1260)^-)/\Gamma_{total}$ — Γ_{132}/Γ

VALUE	CL%	DOCUMENT ID		TECN	COMMENT
<1.7 × 10^{-3}	90	[1] ALBRECHT	93E	ARG	$e^+e^- \to \Upsilon(4S)$

[1] ALBRECHT 93E reports $< 2.9 \times 10^{-3}$ from a measurement of $[\Gamma(B^0 \to D_s^{*+}a_1(1260)^-)/\Gamma_{total}] \times [B(D_s^+ \to \phi\pi^+)]$ assuming $B(D_s^+ \to \phi\pi^+) = 0.027$, which we rescale to our best (shown rounded) value $B(D_s^+ \to \phi\pi^+) = 4.5 \times 10^{-2}$.

$\Gamma(D_s^+a_2^-)/\Gamma_{total}$ — Γ_{133}/Γ

VALUE (units 10^{-5})	CL%	DOCUMENT ID		TECN	COMMENT
<19	90	[1] AUBERT	06X	BABR	$e^+e^- \to \Upsilon(4S)$

[1] Assumes equal production of B^+ and B^0 at the $\Upsilon(4S)$.

$\Gamma(D_s^{*+}a_2^-)/\Gamma_{total}$ — Γ_{134}/Γ

VALUE (units 10^{-5})	CL%	DOCUMENT ID		TECN	COMMENT
<20	90	[1] AUBERT	06X	BABR	$e^+e^- \to \Upsilon(4S)$

[1] Assumes equal production of B^+ and B^0 at the $\Upsilon(4S)$.

$\Gamma(D_s^-K^+)/\Gamma_{total}$ — Γ_{135}/Γ

VALUE (units 10^{-6})	CL%	DOCUMENT ID		TECN	COMMENT
27 ± 5 OUR FIT		Error includes scale factor of 2.7.			
22 ± 5 OUR AVERAGE		Error includes scale factor of 1.8.			
19.1± 2.4±1.7		[1] DAS	10	BELL	$e^+e^- \to \Upsilon(4S)$
29 ± 4 ±2		[1] AUBERT	08AJ	BABR	$e^+e^- \to \Upsilon(4S)$
• • • We do not use the following data for averages, fits, limits, etc. • • •					
27 ± 5 ±2		[2] AUBERT	07K	BABR	Repl. by AUBERT 08AJ
26 ±10 ±2		[3] AUBERT	03D	BABR	Repl. by AUBERT 07K
36 $^{+11}_{-10}$ ±3		[4] KROKOVNY	02	BELL	Repl. by DAS 10
< 190	90	[5] ALEXANDER	93B	CLE2	$e^+e^- \to \Upsilon(4S)$
<1300	90	[6] BORTOLETTO	90	CLEO	$e^+e^- \to \Upsilon(4S)$

[1] Assumes equal production of B^+ and B^0 at the $\Upsilon(4S)$.
[2] AUBERT 07K reports $[\Gamma(B^0 \to D_s^-K^+)/\Gamma_{total}] \times [B(D_s^+ \to \phi\pi^+)] = (1.21 \pm 0.17 \pm 0.11) \times 10^{-6}$ which we divide by our best (shown rounded) value $B(D_s^+ \to \phi\pi^+) = (4.5 \pm 0.4) \times 10^{-2}$. Our first error is their experiment's error and our second error is the systematic error from using our best (shown rounded) value.
[3] AUBERT 03D reports $[\Gamma(B^0 \to D_s^-K^+)/\Gamma_{total}] \times [B(D_s^+ \to \phi\pi^+)] = (1.16 \pm 0.36 \pm 0.24) \times 10^{-6}$ which we divide by our best (shown rounded) value $B(D_s^+ \to \phi\pi^+) = (4.5 \pm 0.4) \times 10^{-2}$. Our first error is their experiment's error and our second error is the systematic error from using our best (shown rounded) value.
[4] KROKOVNY 02 reports $[\Gamma(B^0 \to D_s^-K^+)/\Gamma_{total}] \times [B(D_s^+ \to \phi\pi^+)] = (1.61^{+0.45}_{-0.38} \pm 0.21) \times 10^{-6}$ which we divide by our best (shown rounded) value $B(D_s^+ \to \phi\pi^+) = (4.5 \pm 0.4) \times 10^{-2}$. Our first error is their experiment's error and our second error is the systematic error from using our best (shown rounded) value.
[5] ALEXANDER 93B reports $< 230 \times 10^{-6}$ from a measurement of $[\Gamma(B^0 \to D_s^-K^+)/\Gamma_{total}] \times [B(D_s^+ \to \phi\pi^+)]$ assuming $B(D_s^+ \to \phi\pi^+) = 0.037$, which we rescale to our best (shown rounded) value $B(D_s^+ \to \phi\pi^+) = 4.5 \times 10^{-2}$.
[6] BORTOLETTO 90 assume $B(D_s \to \phi\pi^+) = 2\%$.

$\Gamma(D_s^-K^+)/\Gamma(D^-\pi^+)$ — Γ_{135}/Γ_{38}

VALUE (units 10^{-2})	DOCUMENT ID		TECN	COMMENT
1.09±0.19 OUR FIT	Error includes scale factor of 2.7.			
1.29±0.05±0.08	AAIJ	15AC	LHCB	pp at 7, 8 TeV

$\Gamma(D_s^{*-}K^+)/\Gamma_{total}$ — Γ_{136}/Γ

VALUE (units 10^{-5})	CL%	DOCUMENT ID		TECN	COMMENT
2.19±0.30 OUR AVERAGE					
2.02±0.33±0.22		[1] JOSHI	10	BELL	$e^+e^- \to \Upsilon(4S)$
2.4 ±0.4 ±0.2		[1] AUBERT	08AJ	BABR	$e^+e^- \to \Upsilon(4S)$
• • • We do not use the following data for averages, fits, limits, etc. • • •					
2.2 ±0.6 ±0.2		[2] AUBERT	07K	BABR	Repl. by AUBERT 08AJ
< 2.5	90	AUBERT	03D	BABR	Repl. by AUBERT 07K
<14	90	[3] ALEXANDER	93B	CLE2	$e^+e^- \to \Upsilon(4S)$

[1] Assumes equal production of B^+ and B^0 at the $\Upsilon(4S)$.
[2] AUBERT 07K reports $[\Gamma(B^0 \to D_s^{*-}K^+)/\Gamma_{total}] \times [B(D_s^+ \to \phi\pi^+)] = (0.97 \pm 0.24 \pm 0.12) \times 10^{-6}$ which we divide by our best (shown rounded) value $B(D_s^+ \to \phi\pi^+) = (4.5 \pm 0.4) \times 10^{-2}$. Our first error is their experiment's error and our second error is the systematic error from using our best (shown rounded) value.
[3] ALEXANDER 93B reports $< 17 \times 10^{-5}$ from a measurement of $[\Gamma(B^0 \to D_s^{*-}K^+)/\Gamma_{total}] \times [B(D_s^+ \to \phi\pi^+)]$ assuming $B(D_s^+ \to \phi\pi^+) = 0.037$, which we rescale to our best (shown rounded) value $B(D_s^+ \to \phi\pi^+) = 4.5 \times 10^{-2}$.

$\Gamma(D_{s1}(2536)^\mp K^\pm,\ D_{s1}^- \to \overline{D}^*(2007)^0K^-)/\Gamma(\overline{D}^0K^+K^-)$ — Γ_{137}/Γ_{49}

VALUE (units 10^{-2})	DOCUMENT ID		TECN	COMMENT
8.4±0.3±0.6	AAIJ	23AY	LHCB	pp at 7, 8, 13 TeV

$\Gamma(D_s^-K^*(892)^+)/\Gamma_{total}$ — Γ_{138}/Γ

VALUE (units 10^{-5})	CL%	DOCUMENT ID		TECN	COMMENT
3.5$^{+1.0}_{-0.9}$±0.4		[1] AUBERT	08AJ	BABR	$e^+e^- \to \Upsilon(4S)$

Int. J. Mod. Phys. A 2026.41. Downloaded from www.worldscientific.com
by UNIVERSITY OF CALIFORNIA @ BERKELEY on 09/16/26. Re-use and distribution is strictly not permitted, except for Open Access articles.

• • • We do not use the following data for averages, fits, limits, etc. • • •

<280	90	[2] ALBRECHT	93E	ARG	$e^+e^- \to \Upsilon(4S)$
< 80	90	[3] ALEXANDER	93B	CLE2	$e^+e^- \to \Upsilon(4S)$

[1] Assumes equal production of B^+ and B^0 at the $\Upsilon(4S)$.

[2] ALBRECHT 93E reports $< 4.6 \times 10^{-3}$ from a measurement of $[\Gamma(B^0 \to D_s^- K^*(892)^+)/\Gamma_{total}] \times [B(D_s^+ \to \phi\pi^+)]$ assuming $B(D_s^+ \to \phi\pi^+) = 0.027$, which we rescale to our best (shown rounded) value $B(D_s^+ \to \phi\pi^+) = 4.5 \times 10^{-2}$.

[3] ALEXANDER 93B reports $< 9.7 \times 10^{-4}$ from a measurement of $[\Gamma(B^0 \to D_s^- K^*(892)^+)/\Gamma_{total}] \times [B(D_s^+ \to \phi\pi^+)]$ assuming $B(D_s^+ \to \phi\pi^+) = 0.037$, which we rescale to our best (shown rounded) value $B(D_s^+ \to \phi\pi^+) = 4.5 \times 10^{-2}$.

$\Gamma(D_s^{*-} K^*(892)^+)/\Gamma_{total}$ — Γ_{139}/Γ

VALUE (units 10^{-5})	CL%	DOCUMENT ID		TECN	COMMENT
$\mathbf{3.2^{+1.4}_{-1.2} \pm 0.4}$		[1] AUBERT	08AJ	BABR	$e^+e^- \to \Upsilon(4S)$

• • • We do not use the following data for averages, fits, limits, etc. • • •

<350	90	[2] ALBRECHT	93E	ARG	$e^+e^- \to \Upsilon(4S)$
< 90	90	[3] ALEXANDER	93B	CLE2	$e^+e^- \to \Upsilon(4S)$

[1] Assumes equal production of B^+ and B^0 at the $\Upsilon(4S)$.

[2] ALBRECHT 93E reports $< 5.8 \times 10^{-3}$ from a measurement of $[\Gamma(B^0 \to D_s^{*-} K^*(892)^+)/\Gamma_{total}] \times [B(D_s^+ \to \phi\pi^+)]$ assuming $B(D_s^+ \to \phi\pi^+) = 0.027$, which we rescale to our best (shown rounded) value $B(D_s^+ \to \phi\pi^+) = 4.5 \times 10^{-2}$.

[3] ALEXANDER 93B reports $< 11.0 \times 10^{-4}$ from a measurement of $[\Gamma(B^0 \to D_s^{*-} K^*(892)^+)/\Gamma_{total}] \times [B(D_s^+ \to \phi\pi^+)]$ assuming $B(D_s^+ \to \phi\pi^+) = 0.037$, which we rescale to our best (shown rounded) value $B(D_s^+ \to \phi\pi^+) = 4.5 \times 10^{-2}$.

$\Gamma(D_s^- \pi^+ K^0)/\Gamma_{total}$ — Γ_{140}/Γ

VALUE (units 10^{-4})	CL%	DOCUMENT ID		TECN	COMMENT
0.97±0.14 OUR AVERAGE					
0.94±0.12±0.10		[1] WIECHCZYN...	15	BELL	$e^+e^- \to \Upsilon(4S)$
1.10±0.26±0.20		[1] AUBERT	08G	BABR	$e^+e^- \to \Upsilon(4S)$

• • • We do not use the following data for averages, fits, limits, etc. • • •

<40	90	[2] ALBRECHT	93E	ARG	$e^+e^- \to \Upsilon(4S)$

[1] Assumes equal production of B^+ and B^0 at the $\Upsilon(4S)$.

[2] ALBRECHT 93E reports $< 7.3 \times 10^{-3}$ from a measurement of $[\Gamma(B^0 \to D_s^- \pi^+ K^0)/\Gamma_{total}] \times [B(D_s^+ \to \phi\pi^+)]$ assuming $B(D_s^+ \to \phi\pi^+) = 0.027$, which we rescale to our best (shown rounded) value $B(D_s^+ \to \phi\pi^+) = 4.5 \times 10^{-2}$.

$\Gamma(D_s^{*-} \pi^+ K^0)/\Gamma_{total}$ — Γ_{141}/Γ

VALUE (units 10^{-4})	CL%	DOCUMENT ID		TECN	COMMENT
< 1.10	90	[1] AUBERT	08G	BABR	$e^+e^- \to \Upsilon(4S)$

• • • We do not use the following data for averages, fits, limits, etc. • • •

<25	90	[2] ALBRECHT	93E	ARG	$e^+e^- \to \Upsilon(4S)$

[1] Assumes equal production of B^+ and B^0 at the $\Upsilon(4S)$.

[2] ALBRECHT 93E reports $< 4.2 \times 10^{-3}$ from a measurement of $[\Gamma(B^0 \to D_s^{*-} \pi^+ K^0)/\Gamma_{total}] \times [B(D_s^+ \to \phi\pi^+)]$ assuming $B(D_s^+ \to \phi\pi^+) = 0.027$, which we rescale to our best (shown rounded) value $B(D_s^+ \to \phi\pi^+) = 4.5 \times 10^{-2}$.

$\Gamma(D_s^- K^+ \pi^+ \pi^-)/\Gamma_{total}$ — Γ_{142}/Γ

VALUE (units 10^{-4})	DOCUMENT ID		TECN	COMMENT
1.71±0.31±0.34	[1] AAIJ	12AX	LHCB	pp at 7 TeV

[1] AAIJ 12AX reports $[\Gamma(B^0 \to D_s^- K^+ \pi^+ \pi^-)/\Gamma_{total}] / [B(B_s^0 \to D_s^- K^+ \pi^+ \pi^-)] = 0.54 \pm 0.07 \pm 0.07$ which we multiply by our best (shown rounded) value $B(B_s^0 \to D_s^- K^+ \pi^+ \pi^-) = (3.2 \pm 0.6) \times 10^{-4}$. Our first error is their experiment's error and our second error is the systematic error from using our best (shown rounded) value.

$\Gamma(D_s^- \pi^+ K^*(892)^0)/\Gamma_{total}$ — Γ_{143}/Γ

VALUE	CL%	DOCUMENT ID		TECN	COMMENT
$\mathbf{<3.0 \times 10^{-3}}$	90	[1] ALBRECHT	93E	ARG	$e^+e^- \to \Upsilon(4S)$

[1] ALBRECHT 93E reports $< 5.0 \times 10^{-3}$ from a measurement of $[\Gamma(B^0 \to D_s^- \pi^+ K^*(892)^0)/\Gamma_{total}] \times [B(D_s^+ \to \phi\pi^+)]$ assuming $B(D_s^+ \to \phi\pi^+) = 0.027$, which we rescale to our best (shown rounded) value $B(D_s^+ \to \phi\pi^+) = 4.5 \times 10^{-2}$.

$\Gamma(D_s^{*-} \pi^+ K^*(892)^0)/\Gamma_{total}$ — Γ_{144}/Γ

VALUE	CL%	DOCUMENT ID		TECN	COMMENT
$\mathbf{<1.6 \times 10^{-3}}$	90	[1] ALBRECHT	93E	ARG	$e^+e^- \to \Upsilon(4S)$

[1] ALBRECHT 93E reports $< 2.7 \times 10^{-3}$ from a measurement of $[\Gamma(B^0 \to D_s^{*-} \pi^+ K^*(892)^0)/\Gamma_{total}] \times [B(D_s^+ \to \phi\pi^+)]$ assuming $B(D_s^+ \to \phi\pi^+) = 0.027$, which we rescale to our best (shown rounded) value $B(D_s^+ \to \phi\pi^+) = 4.5 \times 10^{-2}$.

$\Gamma(\overline{D}^0 K^0)/\Gamma_{total}$ — Γ_{145}/Γ

VALUE (units 10^{-5})	DOCUMENT ID		TECN	COMMENT
5.5±0.4 OUR AVERAGE				
5.6±0.5±0.2	KUMAR	23	BELL	$e^+e^- \to \Upsilon(4S)$
5.3±0.7±0.3	[1] AUBERT,B	06L	BABR	$e^+e^- \to \Upsilon(4S)$

• • • We do not use the following data for averages, fits, limits, etc. • • •

$5.0^{+1.3}_{-1.2} \pm 0.6$	[1] KROKOVNY	03	BELL	Repl. by KUMAR 23

[1] Assumes equal production of B^+ and B^0 at the $\Upsilon(4S)$.

$\Gamma(\overline{D}^0 K^+ \pi^-)/\Gamma_{total}$ — Γ_{146}/Γ

VALUE (units 10^{-6})	DOCUMENT ID		TECN	COMMENT
88±15±9	[1] AUBERT	06A	BABR	$e^+e^- \to \Upsilon(4S)$

[1] Assumes equal production of B^+ and B^0 at the $\Upsilon(4S)$.

$\Gamma(\overline{D}^0 K^+ \pi^-)/\Gamma(\overline{D}^0 \pi^+ \pi^-)$ — Γ_{146}/Γ_{47}

VALUE	DOCUMENT ID		TECN	COMMENT
0.106±0.007±0.008	AAIJ	13AQ	LHCB	pp at 7 TeV

$\Gamma(\overline{D}^0 K^*(892)^0)/\Gamma_{total}$ — Γ_{147}/Γ

VALUE (units 10^{-5})	DOCUMENT ID		TECN	COMMENT
4.5±0.6 OUR AVERAGE				
5.4±0.3±1.1	[1,2] AAIJ	15X	LHCB	pp at 7, 8 TeV
4.0±0.7±0.3	[3] AUBERT,B	06L	BABR	$e^+e^- \to \Upsilon(4S)$
$4.8^{+1.1}_{-1.0} \pm 0.5$	[3] KROKOVNY	03	BELL	$e^+e^- \to \Upsilon(4S)$

• • • We do not use the following data for averages, fits, limits, etc. • • •

5.7±0.9±0.6	[3] AUBERT	06A	BABR	Repl. by AUBERT,B 06L

[1] AAIJ 15X reports $(5.13 \pm 0.20 \pm 0.15 \pm 0.24 \pm 0.60) \times 10^{-5}$ from a measurement of $[\Gamma(B^0 \to \overline{D}^0 K^*(892)^0)/\Gamma_{total}] \times [B(B^0 \to \overline{D}^0 K^+ \pi^-)]$ assuming $B(B^0 \to \overline{D}^0 K^+ \pi^-) = (9.2 \pm 0.6 \pm 0.7 \pm 0.6) \times 10^{-5}$, which we rescale to our best (shown rounded) value $B(B^0 \to \overline{D}^0 K^+ \pi^-) = (8.8 \pm 1.7) \times 10^{-5}$. Our first error is their experiment's error and our second error is the systematic error from using our best (shown rounded) value.

[2] Measured via amplitude analysis of $B^0 \to \overline{D}^0 K^+ \pi^-$, which excludes contribution from decay via $D^*(2010)^-$ resonance.

[3] Assumes equal production of B^+ and B^0 at the $\Upsilon(4S)$.

$\Gamma(\overline{D}^0 K^*(1410)^0)/\Gamma_{total}$ — Γ_{148}/Γ

VALUE	CL%	DOCUMENT ID		TECN	COMMENT
$\mathbf{<6.7 \times 10^{-5}}$	90	[1] AAIJ	15X	LHCB	pp at 7, 8 TeV

[1] Measured via amplitude analysis of $B^0 \to \overline{D}^0 K^+ \pi^-$, which excludes contribution from decay via $D^*(2010)^-$ resonance.

$\Gamma(\overline{D}^0 K_0^*(1430)^0)/\Gamma_{total}$ — Γ_{149}/Γ

VALUE (units 10^{-5})	DOCUMENT ID		TECN	COMMENT
0.7±0.7±0.1	[1,2] AAIJ	15X	LHCB	pp at 7, 8 TeV

[1] AAIJ 15X reports $(0.71 \pm 0.27 \pm 0.33 \pm 0.47 \pm 0.08) \times 10^{-5}$ from a measurement of $[\Gamma(B^0 \to \overline{D}^0 K_0^*(1430)^0)/\Gamma_{total}] \times [B(B^0 \to \overline{D}^0 K^+ \pi^-)]$ assuming $B(B^0 \to \overline{D}^0 K^+ \pi^-) = (9.2 \pm 0.6 \pm 0.7 \pm 0.6) \times 10^{-5}$, which we rescale to our best (shown rounded) value $B(B^0 \to \overline{D}^0 K^+ \pi^-) = (8.8 \pm 1.7) \times 10^{-5}$. Our first error is their experiment's error and our second error is the systematic error from using our best (shown rounded) value.

[2] Measured via amplitude analysis of $B^0 \to \overline{D}^0 K^+ \pi^-$, which excludes contribution from decay via $D^*(2010)^-$ resonance.

$\Gamma(\overline{D}^0 K_2^*(1430)^0)/\Gamma_{total}$ — Γ_{150}/Γ

VALUE (units 10^{-5})	DOCUMENT ID		TECN	COMMENT
2.1±0.8±0.4	[1,2] AAIJ	15X	LHCB	pp at 7, 8 TeV

[1] AAIJ 15X reports $(2.04 \pm 0.45 \pm 0.30 \pm 0.54 \pm 0.25) \times 10^{-5}$ from a measurement of $[\Gamma(B^0 \to \overline{D}^0 K_2^*(1430)^0)/\Gamma_{total}] \times [B(B^0 \to \overline{D}^0 K^+ \pi^-)]$ assuming $B(B^0 \to \overline{D}^0 K^+ \pi^-) = (9.2 \pm 0.6 \pm 0.7 \pm 0.6) \times 10^{-5}$, which we rescale to our best (shown rounded) value $B(B^0 \to \overline{D}^0 K^+ \pi^-) = (8.8 \pm 1.7) \times 10^{-5}$. Our first error is their experiment's error and our second error is the systematic error from using our best (shown rounded) value.

[2] Measured via amplitude analysis of $B^0 \to \overline{D}^0 K^+ \pi^-$, which excludes contribution from decay via $D^*(2010)^-$ resonance.

$\Gamma(D_0^*(2300)^- K^+,\ D_0^{*-} \to \overline{D}^0 \pi^-)/\Gamma_{total}$ — Γ_{151}/Γ

VALUE (units 10^{-5})	DOCUMENT ID		TECN	COMMENT
1.9±0.8±0.4	[1,2] AAIJ	15X	LHCB	pp at 7, 8 TeV

[1] AAIJ 15X reports $(1.77 \pm 0.26 \pm 0.19 \pm 0.67 \pm 0.20) \times 10^{-5}$ from a measurement of $[\Gamma(B^0 \to D_0^*(2300)^- K^+,\ D_0^{*-} \to \overline{D}^0 \pi^-)/\Gamma_{total}] \times [B(B^0 \to \overline{D}^0 K^+ \pi^-)]$ assuming $B(B^0 \to \overline{D}^0 K^+ \pi^-) = (9.2 \pm 0.6 \pm 0.7 \pm 0.6) \times 10^{-5}$, which we rescale to our best (shown rounded) value $B(B^0 \to \overline{D}^0 K^+ \pi^-) = (8.8 \pm 1.7) \times 10^{-5}$. Our first error is their experiment's error and our second error is the systematic error from using our best (shown rounded) value.

[2] Measured via amplitude analysis of $B^0 \to \overline{D}^0 K^+ \pi^-$, which excludes contribution from decay via $D^*(2010)^-$ resonance.

$\Gamma(D_2^*(2460)^- K^+,\ D_2^{*-} \to \overline{D}^0 \pi^-)/\Gamma_{total}$ — Γ_{152}/Γ

VALUE (units 10^{-6})	DOCUMENT ID		TECN	COMMENT
20.3±3.5 OUR AVERAGE				
22 ±2 ±4	[1,2] AAIJ	15X	LHCB	pp at 7, 8 TeV
18.3±4.0±3.1	[3] AUBERT	06A	BABR	$e^+e^- \to \Upsilon(4S)$

[1] AAIJ 15X reports $(2.12 \pm 0.10 \pm 0.11 \pm 0.11 \pm 0.25) \times 10^{-5}$ from a measurement of $[\Gamma(B^0 \to D_2^*(2460)^- K^+,\ D_2^{*-} \to \overline{D}^0 \pi^-)/\Gamma_{total}] \times [B(B^0 \to \overline{D}^0 K^+ \pi^-)]$ assuming $B(B^0 \to \overline{D}^0 K^+ \pi^-) = (9.2 \pm 0.6 \pm 0.7 \pm 0.6) \times 10^{-5}$, which we rescale to our best (shown rounded) value $B(B^0 \to \overline{D}^0 K^+ \pi^-) = (8.8 \pm 1.7) \times 10^{-5}$. Our first error is their experiment's error and our second error is the systematic error from using our best (shown rounded) value.
[2] Measured via amplitude analysis of $B^0 \to \overline{D}^0 K^+ \pi^-$, which excludes contribution from decay via $D^*(2010)^-$ resonance.
[3] Assumes equal production of B^+ and B^0 at the $\Upsilon(4S)$.

$\Gamma(D_3^*(2760)^- K^+,\ D_3^{*-} \to \overline{D}^0 \pi^-)/\Gamma_{total}$ — Γ_{153}/Γ

VALUE	CL%	DOCUMENT ID		TECN	COMMENT
$<0.10 \times 10^{-5}$	90	[1] AAIJ	15X	LHCB	pp at 7, 8 TeV

[1] Measured via amplitude analysis of $B^0 \to \overline{D}^0 K^+ \pi^-$, which excludes contribution from decay via $D^*(2010)^-$ resonance.

$\Gamma(\overline{D}^0 K^+ \pi^-$ nonresonant$)/\Gamma_{total}$ — Γ_{154}/Γ

VALUE (units 10^{-6})	CL%	DOCUMENT ID		TECN	COMMENT
<37	90	[1] AUBERT	06A	BABR	$e^+e^- \to \Upsilon(4S)$

[1] Assumes equal production of B^+ and B^0 at the $\Upsilon(4S)$.

$\Gamma([K^+K^-]_D K^*(892)^0)/\Gamma(\overline{D}^0 K^*(892)^0)$ — $\Gamma_{155}/\Gamma_{147}$

VALUE	DOCUMENT ID		TECN	COMMENT
0.811±0.057±0.017	AAIJ	24M	LHCB	pp at 7, 8, 13 TeV
• • • We do not use the following data for averages, fits, limits, etc. • • •				
0.92 ±0.10 ±0.02	AAIJ	19N	LHCB	Repl. by AAIJ 24M
1.05 $^{+0.17}_{-0.15}$ ±0.04	AAIJ	14BN	LHCB	Repl. by AAIJ 16S
1.36 $^{+0.37}_{-0.32}$ ±0.07	AAIJ	13L	LHCB	Repl. by AAIJ 14BN

$\Gamma([\pi^+\pi^-]_D K^*(892)^0)/\Gamma(\overline{D}^0 K^*(892)^0)$ — $\Gamma_{156}/\Gamma_{147}$

VALUE	DOCUMENT ID		TECN	COMMENT
1.104±0.111±0.026	AAIJ	24M	LHCB	pp at 7, 8, 13 TeV
• • • We do not use the following data for averages, fits, limits, etc. • • •				
1.32 ±0.19 ±0.03	AAIJ	19N	LHCB	Repl. by AAIJ 24M
1.21 $^{+0.28}_{-0.25}$ ±0.05	AAIJ	14BN	LHCB	Repl. by AAIJ 16S

$\Gamma([\pi^+K^-]_D K^*(892)^0)/\Gamma([K^+\pi^-]_D K^*(892)^0)$ — $\Gamma_{157}/\Gamma_{158}$

VALUE	DOCUMENT ID		TECN	COMMENT
0.080±0.015±0.002	AAIJ	19N	LHCB	pp at 7, 8, 13 TeV

$\Gamma([\pi^+\pi^-\pi^+\pi^-]_D K^{*0})/\Gamma(\overline{D}^0 K^*(892)^0)$ — $\Gamma_{159}/\Gamma_{147}$

VALUE	DOCUMENT ID		TECN	COMMENT
0.882±0.086±0.033	AAIJ	24M	LHCB	pp at 7, 8, 13 TeV
• • • We do not use the following data for averages, fits, limits, etc. • • •				
1.01 ±0.16 ±0.04	AAIJ	19N	LHCB	Repl. by AAIJ 24M

$\Gamma([\pi^+K^-\pi^+\pi^-]_D K^{*0})/\Gamma([K^+\pi^-\pi^+\pi^-]_D K^{*0})$ — $\Gamma_{160}/\Gamma_{161}$

VALUE	DOCUMENT ID		TECN	COMMENT
0.073±0.018±0.002	AAIJ	19N	LHCB	pp at 7, 8, 13 TeV

$\Gamma(\overline{D}^0 \pi^0)/\Gamma_{total}$ — Γ_{162}/Γ

VALUE (units 10^{-4})	CL%	DOCUMENT ID		TECN	COMMENT
2.67±0.09 OUR AVERAGE					
2.70±0.06±0.10		BLOOMFIELD	22	BELL	$e^+e^- \to \Upsilon(4S)$
2.69±0.09±0.13		[1] LEES	11M	BABR	$e^+e^- \to \Upsilon(4S)$
2.25±0.14±0.35		[1] BLYTH	06	BELL	$e^+e^- \to \Upsilon(4S)$
2.74 $^{+0.36}_{-0.32}$±0.55		[1] COAN	02	CLE2	$e^+e^- \to \Upsilon(4S)$
• • • We do not use the following data for averages, fits, limits, etc. • • •					
2.9 ±0.2 ±0.3		[1] AUBERT	04B	BABR	Repl. by LEES 11M
3.1 ±0.4 ±0.5		[1] ABE	02J	BELL	Repl. by BLYTH 06
<1.2	90	[2] NEMATI	98	CLE2	Repl. by COAN 02
<4.8	90	[3] ALAM	94	CLE2	Repl. by NEMATI 98

[1] Assumes equal production of B^+ and B^0 at the $\Upsilon(4S)$.
[2] NEMATI 98 assumes equal production of B^+ and B^0 at the $\Upsilon(4S)$ and use the PDG 96 values for D^0, D^{*0}, η, η', and ω branching fractions.
[3] ALAM 94 assume equal production of B^+ and B^0 at the $\Upsilon(4S)$ and use the CLEOII absolute $B(D^0 \to K^-\pi^+)$ and the PDG 1992 $B(D^0 \to K^-\pi^+\pi^0)/B(D^0 \to K^-\pi^+)$ and $B(D^0 \to K^-2\pi^+\pi^-)/B(D^0 \to K^-\pi^+)$.

$\Gamma(\overline{D}^0 \rho^0)/\Gamma_{total}$ — Γ_{163}/Γ

VALUE (units 10^{-4})	CL%	DOCUMENT ID		TECN	COMMENT
3.21±0.21 OUR AVERAGE					
3.21±0.10±0.21		[1] AAIJ	15Y	LHCB	pp at 7, 8 TeV
3.19±0.20±0.45		[2,3] KUZMIN	07	BELL	$e^+e^- \to \Upsilon(4S)$
• • • We do not use the following data for averages, fits, limits, etc. • • •					
2.9 ±1.0 ±0.4		[2] SATPATHY	03	BELL	Repl. by KUZMIN 07
< 3.9	90	[4] NEMATI	98	CLE2	$e^+e^- \to \Upsilon(4S)$
< 5.5	90	[5] ALAM	94	CLE2	Repl. by NEMATI 98
< 6.0	90	[6] BORTOLETTO	92	CLEO	$e^+e^- \to \Upsilon(4S)$
<27.0	90	[7] ALBRECHT	88K	ARG	$e^+e^- \to \Upsilon(4S)$

[1] Measured using isobar formalism in the decay chain $B^0 \to \overline{D}^0 \rho(770)$, $\rho \to \pi^+\pi^-$ assuming $B(\rho(770) \to \pi^+\pi^-) = 1$. The second uncertainty combines in quadrature all systematic uncertainties quoted in the paper.
[2] Assumes equal production of B^+ and B^0 at the $\Upsilon(4S)$.
[3] Our second uncertainty combines systematics and model errors quoted in the paper.
[4] NEMATI 98 assumes equal production of B^+ and B^0 at the $\Upsilon(4S)$ and use the PDG 96 values for D^0, D^{*0}, η, η', and ω branching fractions.
[5] ALAM 94 assume equal production of B^+ and B^0 at the $\Upsilon(4S)$ and use the CLEOII absolute $B(D^0 \to K^-\pi^+)$ and the PDG 1992 $B(D^0 \to K^-\pi^+\pi^0)/B(D^0 \to K^-\pi^+)$ and $B(D^0 \to K^-2\pi^+\pi^-)/B(D^0 \to K^-\pi^+)$.
[6] BORTOLETTO 92 assumes equal production of B^+ and B^0 at the $\Upsilon(4S)$ and uses Mark III branching fractions for the D.
[7] ALBRECHT 88K reports < 0.003 assuming $B^0\overline{B}^0$:B^+B^- production ratio is 45:55. We rescale to 50%.

$\Gamma(\overline{D}^0 f_2)/\Gamma_{total}$ — Γ_{164}/Γ

VALUE (units 10^{-4})	DOCUMENT ID		TECN	COMMENT
1.56±0.21 OUR AVERAGE				
1.68±0.11±0.21	[1] AAIJ	15Y	LHCB	pp at 7, 8 TeV
1.20±0.18±0.38	[2,3] KUZMIN	07	BELL	$e^+e^- \to \Upsilon(4S)$

[1] Result obtained using the isobar formalism. The second uncertainty combines in quadrature all systematic uncertainties quoted in the paper. Measured in the decay chain $B^0 \to \overline{D}^0 f_2(1270)$, $f_2 \to \pi^+\pi^-$.
[2] Assumes equal production of B^+ and B^0 at the $\Upsilon(4S)$.
[3] Our second uncertainty combines systematics and model errors quoted in the paper.

$\Gamma(\overline{D}^0 \eta)/\Gamma_{total}$ — Γ_{165}/Γ

VALUE (units 10^{-4})	CL%	DOCUMENT ID		TECN	COMMENT
2.56±0.12 OUR AVERAGE					
2.66±0.12±0.21		KUMAR	23	BELL	$e^+e^- \to \Upsilon(4S)$
2.53±0.09±0.11		[1] LEES	11M	BABR	$e^+e^- \to \Upsilon(4S)$
• • • We do not use the following data for averages, fits, limits, etc. • • •					
1.77±0.16±0.21		[1] BLYTH	06	BELL	Repl. by KUMAR 23
2.5 ±0.2 ±0.3		[1] AUBERT	04B	BABR	Repl. by LEES 11M
1.4 $^{+0.5}_{-0.4}$ ±0.3		[1] ABE	02J	BELL	Repl. by BLYTH 06
<1.3	90	[2] NEMATI	98	CLE2	$e^+e^- \to \Upsilon(4S)$
<6.8	90	[3] ALAM	94	CLE2	Repl. by NEMATI 98

[1] Assumes equal production of B^+ and B^0 at the $\Upsilon(4S)$.
[2] NEMATI 98 assumes equal production of B^+ and B^0 at the $\Upsilon(4S)$ and use the PDG 96 values for D^0, D^{*0}, η, η', and ω branching fractions.
[3] ALAM 94 assume equal production of B^+ and B^0 at the $\Upsilon(4S)$ and use the CLEOII absolute $B(D^0 \to K^-\pi^+)$ and the PDG 1992 $B(D^0 \to K^-\pi^+\pi^0)/B(D^0 \to K^-\pi^+)$ and $B(D^0 \to K^-2\pi^+\pi^-)/B(D^0 \to K^-\pi^+)$.

$\Gamma(\overline{D}^0 \eta')/\Gamma_{total}$ — Γ_{166}/Γ

VALUE (units 10^{-4})	CL%	DOCUMENT ID		TECN	COMMENT
1.38±0.16 OUR AVERAGE		Error includes scale factor of 1.3.			
1.48±0.13±0.07		[1] LEES	11M	BABR	$e^+e^- \to \Upsilon(4S)$
1.14±0.20 $^{+0.10}_{-0.13}$		[1] SCHUMANN	05	BELL	$e^+e^- \to \Upsilon(4S)$
• • • We do not use the following data for averages, fits, limits, etc. • • •					
1.7 ±0.4 ±0.2		[1] AUBERT	04B	BABR	Repl. by LEES 11M
<9.4	90	[2] NEMATI	98	CLE2	$e^+e^- \to \Upsilon(4S)$
<8.6	90	[3] ALAM	94	CLE2	Repl. by NEMATI 98

[1] Assumes equal production of B^+ and B^0 at the $\Upsilon(4S)$.
[2] NEMATI 98 assumes equal production of B^+ and B^0 at the $\Upsilon(4S)$ and use the PDG 96 values for D^0, D^{*0}, η, η', and ω branching fractions.
[3] ALAM 94 assume equal production of B^+ and B^0 at the $\Upsilon(4S)$ and use the CLEOII absolute $B(D^0 \to K^-\pi^+)$ and the PDG 1992 $B(D^0 \to K^-\pi^+\pi^0)/B(D^0 \to K^-\pi^+)$ and $B(D^0 \to K^-2\pi^+\pi^-)/B(D^0 \to K^-\pi^+)$.

$\Gamma(\overline{D}^0 \eta')/\Gamma(\overline{D}^0 \eta)$ — $\Gamma_{166}/\Gamma_{165}$

VALUE	DOCUMENT ID		TECN	COMMENT
0.54±0.07±0.01	LEES	11M	BABR	$e^+e^- \to \Upsilon(4S)$
• • • We do not use the following data for averages, fits, limits, etc. • • •				
0.7 ±0.2 ±0.1	AUBERT	04B	BABR	Repl. by LEES 11M

$\Gamma(\overline{D}^0 \omega)/\Gamma_{total}$ — Γ_{167}/Γ

VALUE (units 10^{-4})	CL%	DOCUMENT ID		TECN	COMMENT
2.54±0.16 OUR AVERAGE					
2.75±0.72±0.35		[1] AAIJ	15Y	LHCB	pp at 7, 8 TeV
2.57±0.11±0.14		[2] LEES	11M	BABR	$e^+e^- \to \Upsilon(4S)$
2.37±0.23±0.28		[2] BLYTH	06	BELL	$e^+e^- \to \Upsilon(4S)$
• • • We do not use the following data for averages, fits, limits, etc. • • •					
3.0 ±0.3 ±0.4		[2] AUBERT	04B	BABR	Repl. by LEES 11M
1.8 ±0.5 $^{+0.4}_{-0.3}$		[2] ABE	02J	BELL	Repl. by BLYTH 06
<5.1	90	[3] NEMATI	98	CLE2	$e^+e^- \to \Upsilon(4S)$
<6.3	90	[4] ALAM	94	CLE2	Repl. by NEMATI 98

[1] Result obtained using the isobar model. The second uncertainty combines in quadrature all systematic uncertainties quoted in the paper.
[2] Assumes equal production of B^+ and B^0 at the $\Upsilon(4S)$.
[3] NEMATI 98 assumes equal production of B^+ and B^0 at the $\Upsilon(4S)$ and use the PDG 96 values for D^0, D^{*0}, η, η', and ω branching fractions.
[4] ALAM 94 assume equal production of B^+ and B^0 at the $\Upsilon(4S)$ and use the CLEOII absolute $B(D^0 \to K^-\pi^+)$ and the PDG 1992 $B(D^0 \to K^-\pi^+\pi^0)/B(D^0 \to K^-\pi^+)$ and $B(D^0 \to K^-2\pi^+\pi^-)/B(D^0 \to K^-\pi^+)$.

Int. J. Mod. Phys. A 2026.41. Downloaded from www.worldscientific.com
by LIFORNIA @ BERKELEY on 09/16/26. Re-use and distribution is strictly not permitted, except for Open Access articles.

Int. J. Mod. Phys. A 2026.41. Downloaded from www.worldscientific.com
by UNIVERSITY OF CALIFORNIA @ BERKELEY on 09/16/26. Re-use and distribution is strictly not permitted, except for Open Access articles.

$\Gamma(\overline{D}^0\phi)/\Gamma_{total}$ — Γ_{168}/Γ

VALUE (units 10^{-7})	CL%	DOCUMENT ID		TECN	COMMENT
7.7±2.1±1.0		[1] AAIJ	23AZ	LHCB	pp at 7, 8, 13 TeV
• • • We do not use the following data for averages, fits, limits, etc. • • •					
< 23	95	AAIJ	18AY	LHCB	Repl. by AAIJ 23AZ
<116	90	[2] AUBERT	07AO	BABR	$e^+e^- \to \Upsilon(4S)$

[1] The last uncertainty includes the uncertainties of the branching fractions $B(B^0 \to \overline{D}^0 K^+ K^-)$ and $B(\phi \to K^+ K^-)$.
[2] Assumes equal production of B^+ and B^0 at the $\Upsilon(4S)$.

$\Gamma(D^0 K^+\pi^-)/\Gamma_{total}$ — Γ_{169}/Γ

VALUE (units 10^{-6})	CL%	DOCUMENT ID		TECN	COMMENT
• • • We do not use the following data for averages, fits, limits, etc. • • •					
<19	90	[1] AUBERT	06A	BABR	Repl. by AUBERT 09AE

[1] Assumes equal production of B^+ and B^0 at the $\Upsilon(4S)$.

$\Gamma(D^0 K^+\pi^-)/\Gamma(\overline{D}^0 K^+\pi^-)$ — $\Gamma_{169}/\Gamma_{146}$

VALUE	DOCUMENT ID		TECN	COMMENT
0.060±0.034 OUR AVERAGE				
$0.045^{+0.056+0.028}_{-0.050-0.018}$	[1,2] NEGISHI	12	BELL	$e^+e^- \to \Upsilon(4S)$
0.068±0.042	[3] AUBERT	09AE	BABR	$e^+e^- \to \Upsilon(4S)$

[1] Assumes equal production of B^0 and B^+ at $\Upsilon(4S)$.
[2] Uses $D^0 \to K^-\pi^+$mode. Restricts $K^+\pi^-$ mass within ±50 MeV of the nominal K^{*0} mass. Corresponds to the upper limit, < 0.16 at 95% CL.
[3] Reports a signal at the level of 2.5 standard deviations after combining results from $D^0 \to K^+\pi^-$, $K^+\pi^-\pi^0$, and $K^+\pi^-\pi^+\pi^-$.

$\Gamma(D^0 K^*(892)^0)/\Gamma_{total}$ — Γ_{170}/Γ

VALUE (units 10^{-5})	CL%	DOCUMENT ID		TECN	COMMENT
• • • We do not use the following data for averages, fits, limits, etc. • • •					
<1.1	90	[1] AUBERT,B	06L	BABR	$e^+e^- \to \Upsilon(4S)$
<1.8	90	[1] KROKOVNY	03	BELL	$e^+e^- \to \Upsilon(4S)$

[1] Assumes equal production of B^+ and B^0 at the $\Upsilon(4S)$.

$\Gamma(D^0 K^*(892)^0)/\Gamma(\overline{D}^0 K^*(892)^0)$ — $\Gamma_{170}/\Gamma_{147}$

"OUR EVALUATION" is derived from $r_{B^0}(B^0 \to D K^{*0})$ data block listed in "*CP* violation parameters" section.

VALUE (units 10^{-2})	DOCUMENT ID
$6.6^{+1.1}_{-1.2}$ OUR EVALUATION	(Produced by HFLAV)

$\Gamma(\overline{D}^{*0}\gamma)/\Gamma_{total}$ — Γ_{171}/Γ

VALUE	CL%	DOCUMENT ID		TECN	COMMENT
<2.5 × 10^{-5}	90	[1] AUBERT,B	05Q	BABR	$e^+e^- \to \Upsilon(4S)$
• • • We do not use the following data for averages, fits, limits, etc. • • •					
<5.0 × 10^{-5}	90	[1] ARTUSO	00	CLE2	$e^+e^- \to \Upsilon(4S)$

[1] Assumes equal production of B^+ and B^0 at the $\Upsilon(4S)$.

$\Gamma(\overline{D}^*(2007)^0\pi^0)/\Gamma_{total}$ — Γ_{172}/Γ

VALUE (units 10^{-4})	CL%	DOCUMENT ID		TECN	COMMENT
2.2 ±0.6 OUR AVERAGE		Error includes scale factor of 2.6.			See the ideogram below.
3.05±0.14±0.28		[1] LEES	11M	BABR	$e^+e^- \to \Upsilon(4S)$
1.39±0.18±0.26		[1] BLYTH	06	BELL	$e^+e^- \to \Upsilon(4S)$
$2.20^{+0.59}_{-0.52}$±0.79		[1] COAN	02	CLE2	$e^+e^- \to \Upsilon(4S)$
• • • We do not use the following data for averages, fits, limits, etc. • • •					
2.9 ±0.4 ±0.5		[1] AUBERT	04B	BABR	Repl. by LEES 11M
$2.7^{+0.8}_{-0.7}{}^{+0.5}_{-0.6}$		[1] ABE	02J	BELL	Repl. by BLYTH 06
<4.4	90	[2] NEMATI	98	CLE2	Repl. by COAN 02
<9.7	90	[3] ALAM	94	CLE2	Repl. by NEMATI 98

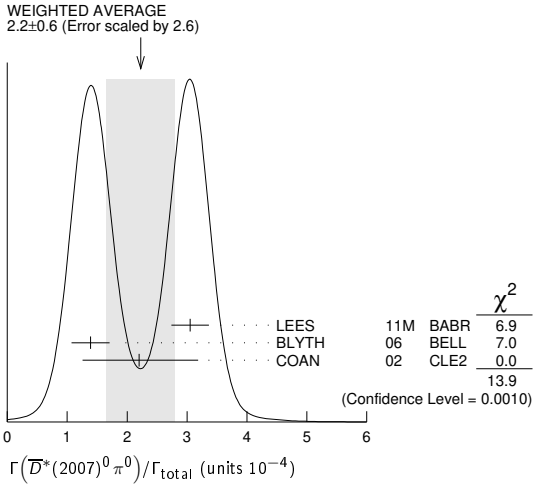

[1] Assumes equal production of B^+ and B^0 at the $\Upsilon(4S)$.
[2] NEMATI 98 assumes equal production of B^+ and B^0 at the $\Upsilon(4S)$ and use the PDG 96 values for D^0, D^{*0}, η, η', and ω branching fractions.
[3] ALAM 94 assume equal production of B^+ and B^0 at the $\Upsilon(4S)$ and use the CLEO II $B(D^*(2007)^0 \to D^0\pi^0)$ and absolute $B(D^0 \to K^-\pi^+)$ and the PDG 1992 $B(D^0 \to K^-\pi^+\pi^0)/B(D^0 \to K^-\pi^+)$ and $B(D^0 \to K^-2\pi^+\pi^-)/B(D^0 \to K^-\pi^+)$.

$\Gamma(\overline{D}^0\pi^0)/\Gamma(\overline{D}^*(2007)^0\pi^0)$ — $\Gamma_{162}/\Gamma_{172}$

VALUE	DOCUMENT ID		TECN	COMMENT
0.90±0.08 OUR AVERAGE				
0.88±0.05±0.06	LEES	11M	BABR	$e^+e^- \to \Upsilon(4S)$
1.62±0.23±0.35	BLYTH	06	BELL	$e^+e^- \to \Upsilon(4S)$
• • • We do not use the following data for averages, fits, limits, etc. • • •				
1.0 ±0.1 ±0.2	AUBERT	04B	BABR	Repl. by LEES 11M

$\Gamma(\overline{D}^*(2007)^0\rho^0)/\Gamma_{total}$ — Γ_{173}/Γ

VALUE	CL%	DOCUMENT ID		TECN	COMMENT
<5.1 × 10^{-4}	90	[1] SATPATHY	03	BELL	$e^+e^- \to \Upsilon(4S)$
• • • We do not use the following data for averages, fits, limits, etc. • • •					
<0.00056	90	[2] NEMATI	98	CLE2	$e^+e^- \to \Upsilon(4S)$
<0.00117	90	[3] ALAM	94	CLE2	Repl. by NEMATI 98

[1] Assumes equal production of B^+ and B^0 at the $\Upsilon(4S)$.
[2] NEMATI 98 assumes equal production of B^+ and B^0 at the $\Upsilon(4S)$ and use the PDG 96 values for D^0, D^{*0}, η, η', and ω branching fractions.
[3] ALAM 94 assume equal production of B^+ and B^0 at the $\Upsilon(4S)$ and use the CLEO II $B(D^*(2007)^0 \to D^0\pi^0)$ and absolute $B(D^0 \to K^-\pi^+)$ and the PDG 1992 $B(D^0 \to K^-\pi^+\pi^0)/B(D^0 \to K^-\pi^+)$ and $B(D^0 \to K^-2\pi^+\pi^-)/B(D^0 \to K^-\pi^+)$.

$\Gamma(\overline{D}^*(2007)^0\eta)/\Gamma_{total}$ — Γ_{174}/Γ

VALUE (units 10^{-4})	CL%	DOCUMENT ID		TECN	COMMENT
2.3 ±0.6 OUR AVERAGE		Error includes scale factor of 2.8.			
2.69±0.14±0.23		[1] LEES	11M	BABR	$e^+e^- \to \Upsilon(4S)$
1.40±0.28±0.26		[1] BLYTH	06	BELL	$e^+e^- \to \Upsilon(4S)$
• • • We do not use the following data for averages, fits, limits, etc. • • •					
2.6 ±0.4 ±0.4		[1] AUBERT	04B	BABR	Repl. by LEES 11M
<4.6	90	[1] ABE	02J	BELL	$e^+e^- \to \Upsilon(4S)$
<2.6	90	[2] NEMATI	98	CLE2	$e^+e^- \to \Upsilon(4S)$
<6.9	90	[3] ALAM	94	CLE2	Repl. by NEMATI 98

[1] Assumes equal production of B^+ and B^0 at the $\Upsilon(4S)$.
[2] NEMATI 98 assumes equal production of B^+ and B^0 at the $\Upsilon(4S)$ and use the PDG 96 values for D^0, D^{*0}, η, η', and ω branching fractions.
[3] ALAM 94 assume equal production of B^+ and B^0 at the $\Upsilon(4S)$ and use the CLEO II $B(D^*(2007)^0 \to D^0\pi^0)$ and absolute $B(D^0 \to K^-\pi^+)$ and the PDG 1992 $B(D^0 \to K^-\pi^+\pi^0)/B(D^0 \to K^-\pi^+)$ and $B(D^0 \to K^-2\pi^+\pi^-)/B(D^0 \to K^-\pi^+)$.

$\Gamma(\overline{D}^0\eta)/\Gamma(\overline{D}^*(2007)^0\eta)$ — $\Gamma_{165}/\Gamma_{174}$

VALUE	DOCUMENT ID		TECN	COMMENT
0.99±0.10 OUR AVERAGE				
0.97±0.07±0.07	LEES	11M	BABR	$e^+e^- \to \Upsilon(4S)$
1.27±0.29±0.25	BLYTH	06	BELL	$e^+e^- \to \Upsilon(4S)$
• • • We do not use the following data for averages, fits, limits, etc. • • •				
0.9 ±0.2 ±0.1	AUBERT	04B	BABR	Repl. by LEES 11M

$\Gamma(\overline{D}^*(2007)^0\eta')/\Gamma(\overline{D}^*(2007)^0\eta)$ — $\Gamma_{175}/\Gamma_{174}$

VALUE	DOCUMENT ID		TECN	COMMENT
0.61±0.14±0.02	LEES	11M	BABR	$e^+e^- \to \Upsilon(4S)$
• • • We do not use the following data for averages, fits, limits, etc. • • •				
0.5 ±0.3 ±0.1	AUBERT	04B	BABR	Repl. by LEES 11M

$\Gamma(\overline{D}^*(2007)^0\eta')/\Gamma_{total}$ — Γ_{175}/Γ

VALUE (units 10^{-4})	CL%	DOCUMENT ID		TECN	COMMENT
1.40±0.22 OUR AVERAGE					
1.48±0.22±0.13		[1] LEES	11M	BABR	$e^+e^- \to \Upsilon(4S)$
1.21±0.34±0.22		[1] SCHUMANN	05	BELL	$e^+e^- \to \Upsilon(4S)$
• • • We do not use the following data for averages, fits, limits, etc. • • •					
1.3 ±0.7 ±0.2		[1,2] AUBERT	04B	BABR	Repl. by LEES 11M
<14	90	BRANDENB...	98	CLE2	$e^+e^- \to \Upsilon(4S)$
<19	90	[3] NEMATI	98	CLE2	$e^+e^- \to \Upsilon(4S)$
<27	90	[4] ALAM	94	CLE2	Repl. by NEMATI 98

[1] Assumes equal production of B^+ and B^0 at the $\Upsilon(4S)$.
[2] Reports an upper limit < 2.6 × 10^{-4} at 90% CL.
[3] NEMATI 98 assumes equal production of B^+ and B^0 at the $\Upsilon(4S)$ and use the PDG 96 values for D^0, D^{*0}, η, η', and ω branching fractions.
[4] ALAM 94 assume equal production of B^+ and B^0 at the $\Upsilon(4S)$ and use the CLEO II $B(D^*(2007)^0 \to D^0\pi^0)$ and absolute $B(D^0 \to K^-\pi^+)$ and the PDG 1992 $B(D^0 \to K^-\pi^+\pi^0)/B(D^0 \to K^-\pi^+)$ and $B(D^0 \to K^-2\pi^+\pi^-)/B(D^0 \to K^-\pi^+)$.

$\Gamma(\overline{D}^0\eta')/\Gamma(\overline{D}^*(2007)^0\eta')$ — $\Gamma_{166}/\Gamma_{175}$

VALUE	DOCUMENT ID		TECN	COMMENT
0.96±0.18±0.06	LEES	11M	BABR	$e^+e^- \to \Upsilon(4S)$
• • • We do not use the following data for averages, fits, limits, etc. • • •				
1.3 ±0.8 ±0.2	AUBERT	04B	BABR	Repl. by LEES 11M

Int. J. Mod. Phys. A 2026.41. Downloaded from www.worldscientific.com by LIFORNIA @ BERKELEY on 09/16/26. Re-use and distribution is strictly not permitted, except for Open Access articles.

$\Gamma(\overline{D}^*(2007)^0\pi^+\pi^-)/\Gamma_{total}$ — Γ_{176}/Γ

VALUE	DOCUMENT ID		TECN	COMMENT
$(6.2\pm1.2\pm1.8)\times10^{-4}$	[1,2] SATPATHY	03	BELL	$e^+e^-\to\Upsilon(4S)$

[1] Assumes equal production of B^+ and B^0 at the $\Upsilon(4S)$.
[2] No assumption about the intermediate mechanism is made in the analysis.

$\Gamma(\overline{D}^*(2007)^0K^+\pi^-)/\Gamma(\overline{D}^*(2007)^0\pi^+\pi^-)$ — $\Gamma_{177}/\Gamma_{176}$

VALUE (units 10^{-2})	DOCUMENT ID		TECN	COMMENT
8.36±0.43±0.61	AAIJ	22N	LHCB	pp at 13 TeV

$\Gamma(\overline{D}^*(2007)^0K^0)/\Gamma_{total}$ — Γ_{178}/Γ

VALUE (units 10^{-5})	CL%	DOCUMENT ID		TECN	COMMENT
3.6±1.2±0.3		[1] AUBERT,B	06L	BABR	$e^+e^-\to\Upsilon(4S)$
• • • We do not use the following data for averages, fits, limits, etc. • • •					
<6.6	90	[1] KROKOVNY	03	BELL	$e^+e^-\to\Upsilon(4S)$

[1] Assumes equal production of B^+ and B^0 at the $\Upsilon(4S)$.

$\Gamma(\overline{D}^*(2007)^0K^*(892)^0)/\Gamma_{total}$ — Γ_{179}/Γ

VALUE	CL%	DOCUMENT ID		TECN	COMMENT
$<6.9\times10^{-5}$	90	[1] KROKOVNY	03	BELL	$e^+e^-\to\Upsilon(4S)$

[1] Assumes equal production of B^+ and B^0 at the $\Upsilon(4S)$.

$\Gamma(\overline{D}^*(2007)^0\phi)/\Gamma_{total}$ — Γ_{180}/Γ

VALUE (units 10^{-6})	DOCUMENT ID		TECN	COMMENT
2.2±0.5±0.3	[1] AAIJ	23AZ	LHCB	pp at 7, 8, 13 TeV

[1] The last uncertainty includes the uncertainties of the branching fraction $B(B^0\to\overline{D}^0K^+K^-)$ and $B(\phi\to K^+K^-)$.

$\Gamma(D^*(2007)^0K^*(892)^0)/\Gamma_{total}$ — Γ_{181}/Γ

VALUE	CL%	DOCUMENT ID		TECN	COMMENT
$<4.0\times10^{-5}$	90	[1] KROKOVNY	03	BELL	$e^+e^-\to\Upsilon(4S)$

[1] Assumes equal production of B^+ and B^0 at the $\Upsilon(4S)$.

$\Gamma(D^*(2007)^0\pi^+\pi^+\pi^-\pi^-)/\Gamma_{total}$ — Γ_{182}/Γ

VALUE (units 10^{-3})	DOCUMENT ID		TECN	COMMENT
2.7 ±0.5 OUR AVERAGE				
2.60±0.47±0.37	[1] MAJUMDER	04	BELL	$e^+e^-\to\Upsilon(4S)$
3.0 ±0.7 ±0.6	[1] EDWARDS	02	CLE2	$e^+e^-\to\Upsilon(4S)$

[1] Assumes equal production of B^+ and B^0 at the $\Upsilon(4S)$.

$\Gamma(D^*(2007)^0\pi^+\pi^+\pi^-\pi^-)/\Gamma(D^*(2010)^-\pi^+\pi^+\pi^-\pi^0)$ — Γ_{182}/Γ_{67}

VALUE	DOCUMENT ID		TECN	COMMENT
0.17±0.04±0.02	[1] EDWARDS	02	CLE2	$e^+e^-\to\Upsilon(4S)$

[1] Assumes equal production of B^+ and B^0 at the $\Upsilon(4S)$.

$\Gamma(D^*(2010)^+D^*(2010)^-)/\Gamma_{total}$ — Γ_{183}/Γ

VALUE (units 10^{-4})	CL%	DOCUMENT ID		TECN	COMMENT
8.0 ±0.6 OUR AVERAGE					
7.82±0.38±0.63		[1] KRONENBIT...	12	BELL	$e^+e^-\to\Upsilon(4S)$
8.1 ±0.6 ±1.0		[1] AUBERT,B	06A	BABR	$e^+e^-\to\Upsilon(4S)$
$9.9\ ^{+4.2}_{-3.3}\pm1.2$		[1] LIPELES	00	CLE2	$e^+e^-\to\Upsilon(4S)$
• • • We do not use the following data for averages, fits, limits, etc. • • •					
8.1 ±0.8 ±1.1		[1] MIYAKE	05	BELL	Repl. by KRONENBITTER 12
8.3 ±1.6 ±1.2		[1,2] AUBERT	02M	BABR	Repl. by AUBERT,B 06B
$6.2\ ^{+4.0}_{-2.9}\pm1.0$		[3] ARTUSO	99	CLE2	Repl. by LIPELES 00
<61	90	[4] BARATE	98Q	ALEP	$e^+e^-\to Z$
<22	90	[5] ASNER	97	CLE2	Repl. by ARTUSO 99

[1] Assumes equal production of B^+ and B^0 at the $\Upsilon(4S)$.
[2] AUBERT 02M also assumes the measured CP-odd fraction of the final states is 0.22 ± 0.18 ± 0.03.
[3] ARTUSO 99 uses $B(\Upsilon(4S)\to B^0\overline{B}^0)=(48\pm4)\%$.
[4] BARATE 98Q (ALEPH) observes 2 events with an expected background of 0.10 ± 0.03 which corresponds to a branching ratio of $(2.3^{+1.9}_{-1.2}\pm0.4)\times10^{-3}$.
[5] ASNER 97 at CLEO observes 1 event with an expected background of 0.022 ± 0.011. This corresponds to a branching ratio of $(5.3^{+7.1}_{-3.7}\pm1.0)\times10^{-4}$.

$\Gamma(\overline{D}^*(2007)^0\omega)/\Gamma_{total}$ — Γ_{184}/Γ

VALUE (units 10^{-4})	CL%	DOCUMENT ID		TECN	COMMENT
3.6 ±1.1 OUR AVERAGE		Error includes scale factor of 3.1.			
4.55±0.24±0.39		[1] LEES	11M	BABR	$e^+e^-\to\Upsilon(4S)$
2.29±0.39±0.40		[1] BLYTH	06	BELL	$e^+e^-\to\Upsilon(4S)$
• • • We do not use the following data for averages, fits, limits, etc. • • •					
4.2 ±0.7 ±0.9	90	[1] AUBERT	04B	BABR	Repl. by LEES 11M
< 7.9	90	[1] ABE	02J	BELL	$e^+e^-\to\Upsilon(4S)$
< 7.4	90	[2] NEMATI	98	CLE2	$e^+e^-\to\Upsilon(4S)$
<21	90	[3] ALAM	94	CLE2	Repl. by NEMATI 98

[1] Assumes equal production of B^+ and B^0 at the $\Upsilon(4S)$.
[2] NEMATI 98 assumes equal production of B^+ and B^0 at the $\Upsilon(4S)$ and use the PDG 96 values for D^0, D^{*0}, η, η', and ω branching fractions.
[3] ALAM 94 assume equal production of B^+ and B^0 at the $\Upsilon(4S)$ and use the CLEO II $B(D^*(2007)^0\to D^0\pi^0)$ and absolute $B(D^0\to K^-\pi^+)$ and the PDG 1992 $B(D^0\to K^-\pi^+\pi^0)/B(D^0\to K^-\pi^+)$ and $B(D^0\to K^-2\pi^+\pi^-)/B(D^0\to K^-\pi^+)$.

$\Gamma(\overline{D}^0\omega)/\Gamma(\overline{D}^*(2007)^0\omega)$ — $\Gamma_{167}/\Gamma_{184}$

VALUE	DOCUMENT ID		TECN	COMMENT
0.58±0.06 OUR AVERAGE				
0.56±0.04±0.04	LEES	11M	BABR	$e^+e^-\to\Upsilon(4S)$
1.04±0.20±0.17	BLYTH	06	BELL	$e^+e^-\to\Upsilon(4S)$
• • • We do not use the following data for averages, fits, limits, etc. • • •				
0.7 ±0.1 ±0.1	AUBERT	04B	BABR	Repl. by LEES 11M

$\Gamma(D^*(2010)^+D^-)/\Gamma_{total}$ — Γ_{185}/Γ

VALUE (units 10^{-4})	CL%	DOCUMENT ID		TECN	COMMENT
6.1±1.5 OUR AVERAGE		Error includes scale factor of 1.6.			
5.7±0.7±0.7		[1] AUBERT,B	06A	BABR	$e^+e^-\to\Upsilon(4S)$
$11.7\pm2.6^{+2.2}_{-2.5}$		[1,2] ABE	02Q	BELL	$e^+e^-\to\Upsilon(4S)$
• • • We do not use the following data for averages, fits, limits, etc. • • •					
8.8±1.0±1.3		[1] AUBERT	03J	BABR	Repl. by AUBERT,B 06B
$14.8\pm3.8^{+2.8}_{-3.1}$		[1,3] ABE	02Q	BELL	$e^+e^-\to\Upsilon(4S)$
< 6.3	90	[1] LIPELES	00	CLE2	$e^+e^-\to\Upsilon(4S)$
<56	90	BARATE	98Q	ALEP	$e^+e^-\to Z$
<18	90	ASNER	97	CLE2	$e^+e^-\to\Upsilon(4S)$

[1] Assumes equal production of B^+ and B^0 at the $\Upsilon(4S)$.
[2] The measurement is performed using fully reconstructed D^* and D^+ decays.
[3] The measurement is performed using a partial reconstruction technique for the D^* and fully reconstructed D^+ decays as a cross check.

$\Gamma(D^*(2007)^0\overline{D}^*(2007)^0)/\Gamma_{total}$ — Γ_{186}/Γ

VALUE (units 10^{-4})	CL%	DOCUMENT ID		TECN	COMMENT
< 0.9	90	[1] AUBERT,B	06A	BABR	$e^+e^-\to\Upsilon(4S)$
• • • We do not use the following data for averages, fits, limits, etc. • • •					
<270	90	BARATE	98Q	ALEP	$e^+e^-\to Z$

[1] Assumes equal production of B^+ and B^0 at the $\Upsilon(4S)$.

$\Gamma(D^-D^0K^+)/\Gamma_{total}$ — Γ_{187}/Γ

VALUE (units 10^{-3})	DOCUMENT ID		TECN	COMMENT
1.07±0.07±0.09	[1] DEL-AMO-SA...	11B	BABR	$e^+e^-\to\Upsilon(4S)$
• • • We do not use the following data for averages, fits, limits, etc. • • •				
1.7 ±0.3 ±0.3	[1] AUBERT	03X	BABR	Repl. by DEL-AMO-SANCHEZ 11B

[1] Assumes equal production of B^+ and B^0 at the $\Upsilon(4S)$.

$\Gamma(D^-D^*(2007)^0K^+)/\Gamma_{total}$ — Γ_{188}/Γ

VALUE (units 10^{-3})	DOCUMENT ID		TECN	COMMENT
3.46±0.18±0.37	[1] DEL-AMO-SA...	11B	BABR	$e^+e^-\to\Upsilon(4S)$
• • • We do not use the following data for averages, fits, limits, etc. • • •				
4.6 ±0.7 ±0.7	[1] AUBERT	03X	BABR	Repl. by DEL-AMO-SANCHEZ 11B

[1] Assumes equal production of B^+ and B^0 at the $\Upsilon(4S)$.

$\Gamma(D^*(2010)^-D^0K^+)/\Gamma_{total}$ — Γ_{189}/Γ

VALUE (units 10^{-3})	DOCUMENT ID		TECN	COMMENT
2.47±0.10±0.18	[1] DEL-AMO-SA...	11B	BABR	$e^+e^-\to\Upsilon(4S)$
• • • We do not use the following data for averages, fits, limits, etc. • • •				
$3.1\ ^{+0.4}_{-0.3}\pm0.4$	[1] AUBERT	03X	BABR	Repl. by DEL-AMO-SANCHEZ 11B

[1] Assumes equal production of B^+ and B^0 at the $\Upsilon(4S)$.

$\Gamma(D^*(2010)^-D^0K^+)/\Gamma(D^-D^0K^+)$ — $\Gamma_{189}/\Gamma_{187}$

VALUE	DOCUMENT ID		TECN	COMMENT
1.754±0.028±0.038	[1] AAIJ	20AN	LHCB	pp at 7, 8, 13 TeV

[1] Uses $D^+\to K^-\pi^+\pi^+$, $D^0\to K^-\pi^+$ and $D^0\to K^-\pi^+\pi^+\pi^-$ decays.

$\Gamma(D^*(2010)^-D^*(2007)^0K^+)/\Gamma_{total}$ — Γ_{190}/Γ

VALUE (units 10^{-3})	DOCUMENT ID		TECN	COMMENT
10.6±0.33±0.86	[1] DEL-AMO-SA...	11B	BABR	$e^+e^-\to\Upsilon(4S)$
• • • We do not use the following data for averages, fits, limits, etc. • • •				
11.8±1.0 ±1.7	[1] AUBERT	03X	BABR	Repl. by DEL-AMO-SANCHEZ 11B

[1] Assumes equal production of B^+ and B^0 at the $\Upsilon(4S)$.

$\Gamma(D^-D^+K^0)/\Gamma_{total}$ — Γ_{191}/Γ

VALUE (units 10^{-3})	CL%	DOCUMENT ID		TECN	COMMENT
0.75±0.12±0.12		[1] DEL-AMO-SA...	11B	BABR	$e^+e^-\to\Upsilon(4S)$
• • • We do not use the following data for averages, fits, limits, etc. • • •					
<1.7	90	[1] AUBERT	03X	BABR	Repl. by DEL-AMO-SANCHEZ 11B

[1] Assumes equal production of B^+ and B^0 at the $\Upsilon(4S)$.

$[\Gamma(D^*(2010)^-D^+K^0)+\Gamma(D^-D^*(2010)^+K^0)]/\Gamma_{total}$ — Γ_{192}/Γ

VALUE (units 10^{-3})	DOCUMENT ID		TECN	COMMENT
6.41±0.36±0.39	[1] DEL-AMO-SA...	11B	BABR	$e^+e^-\to\Upsilon(4S)$
• • • We do not use the following data for averages, fits, limits, etc. • • •				
6.5 ±1.2 ±1.0	[1] AUBERT	03X	BABR	Repl. by DEL-AMO-SANCHEZ 11B

[1] Assumes equal production of B^+ and B^0 at the $\Upsilon(4S)$.

Int. J. Mod. Phys. A 2026.41. Downloaded from www.worldscientific.com
by UNIVERSITY OF CALIFORNIA @ BERKELEY on 09/16/26. Re-use and distribution is strictly not permitted, except for Open Access articles.

$\Gamma(D^*(2010)^- D^*(2010)^+ K^0)/\Gamma_{total}$ — Γ_{193}/Γ

VALUE (units 10^{-3})	DOCUMENT ID		TECN	COMMENT
8.1 ±0.7 OUR AVERAGE				
8.26±0.43±0.67	[1] DEL-AMO-SA...11B		BABR	$e^+e^- \to \Upsilon(4S)$
6.8 ±0.8 ±1.4	[1,2] DALSENO	07	BELL	$e^+e^- \to \Upsilon(4S)$
8.8 ±0.8 ±1.4	[1,2] AUBERT,B	06Q	BABR	$e^+e^- \to \Upsilon(4S)$
• • • We do not use the following data for averages, fits, limits, etc. • • •				
8.8 $^{+1.5}_{-1.4}$ ±1.3	[1] AUBERT	03X	BABR	Repl. by AUBERT,B 06Q

[1] Assumes equal production of B^+ and B^0 at the $\Upsilon(4S)$.
[2] The result is rescaled by a factor of 2 to convert from K^0_S to K^0.

$\Gamma(D^{*-} D_{s1}(2536)^+,\ D^+_{s1} \to D^{*+} K^0)/\Gamma_{total}$ — Γ_{194}/Γ

VALUE (units 10^{-4})	DOCUMENT ID		TECN	COMMENT
8.0±2.4 OUR AVERAGE				
7.6$^{+4.8+1.6}_{-4.2-1.4}$	[1,2] DALSENO	07	BELL	$e^+e^- \to \Upsilon(4S)$
8.2±2.6±1.2	[1,2] AUBERT,B	06Q	BABR	$e^+e^- \to \Upsilon(4S)$

[1] Assumes equal production of B^+ and B^0 at the $\Upsilon(4S)$.
[2] The result is rescaled by a factor of 2 to convert from K^0_S to K^0.

$\Gamma(\overline{D}^0 D^0 K^0)/\Gamma_{total}$ — Γ_{195}/Γ

VALUE (units 10^{-3})	CL%	DOCUMENT ID		TECN	COMMENT
0.27±0.10±0.05		[1] DEL-AMO-SA...11B		BABR	$e^+e^- \to \Upsilon(4S)$
• • • We do not use the following data for averages, fits, limits, etc. • • •					
<1.4	90	[1] AUBERT	03X	BABR	Repl. by DEL-AMO-SANCHEZ 11B

[1] Assumes equal production of B^+ and B^0 at the $\Upsilon(4S)$.

$\Gamma(D^0 \overline{D}^0 K^+\pi^-)/\Gamma(D^*(2010)^- D^0 K^+)$ — $\Gamma_{196}/\Gamma_{189}$

VALUE (%)	DOCUMENT ID		TECN	COMMENT
14.2±1.1±1.0	[1] AAIJ	20AG	LHCB	pp at 7, 8, and 13 TeV

[1] AAIJ 20AG excluded contributions from $B^0 \to D^{*-} D^0 K^+$ transitions with $D^{*-} \to \overline{D}^0 \pi^-$.

$[\Gamma(\overline{D}^0 D^*(2007)^0 K^0) + \Gamma(\overline{D}^*(2007)^0 D^0 K^0)]/\Gamma_{total}$ — Γ_{197}/Γ

VALUE (units 10^{-3})	CL%	DOCUMENT ID		TECN	COMMENT
1.08±0.32±0.36		[1] DEL-AMO-SA...11B		BABR	$e^+e^- \to \Upsilon(4S)$
• • • We do not use the following data for averages, fits, limits, etc. • • •					
<3.7	90	[1] AUBERT	03X	BABR	Repl. by DEL-AMO-SANCHEZ 11B

[1] Assumes equal production of B^+ and B^0 at the $\Upsilon(4S)$.

$\Gamma(\overline{D}^*(2007)^0 D^*(2007)^0 K^0)/\Gamma_{total}$ — Γ_{198}/Γ

VALUE (units 10^{-3})	CL%	DOCUMENT ID		TECN	COMMENT
2.40±0.55±0.67		[1] DEL-AMO-SA...11B		BABR	$e^+e^- \to \Upsilon(4S)$
• • • We do not use the following data for averages, fits, limits, etc. • • •					
<6.6	90	[1] AUBERT	03X	BABR	Repl. by DEL-AMO-SANCHEZ 11B

[1] Assumes equal production of B^+ and B^0 at the $\Upsilon(4S)$.

$\Gamma((\overline{D}+\overline{D}^*)(D+D^*)K)/\Gamma_{total}$ — Γ_{199}/Γ

VALUE (units 10^{-2})	DOCUMENT ID		TECN	COMMENT
3.68±0.10±0.24	[1] DEL-AMO-SA...11B		BABR	$e^+e^- \to \Upsilon(4S)$
• • • We do not use the following data for averages, fits, limits, etc. • • •				
4.3 ±0.3 ±0.6	[1] AUBERT	03X	BABR	Repl. by DEL-AMO-SANCHEZ 11B

[1] Assumes equal production of B^+ and B^0 at the $\Upsilon(4S)$.

$\Gamma(\eta_c K^0)/\Gamma_{total}$ — Γ_{200}/Γ

VALUE (units 10^{-3})	DOCUMENT ID		TECN	COMMENT
1.04±0.13 OUR AVERAGE				
1.13$^{+0.19+0.15}_{-0.16-0.16}$	[1] CHILIKIN	19	BELL	$e^+e^- \to \Upsilon(4S)$
0.75$^{+0.26}_{-0.24}$±0.08	[2,3] AUBERT	07AV	BABR	$e^+e^- \to \Upsilon(4S)$
1.10±0.19±0.09	[2,4] AUBERT,B	04B	BABR	$e^+e^- \to \Upsilon(4S)$
1.23±0.23$^{+0.40}_{-0.41}$	[2] FANG	03	BELL	$e^+e^- \to \Upsilon(4S)$
1.09$^{+0.55}_{-0.42}$±0.33	[5] EDWARDS	01	CLE2	$e^+e^- \to \Upsilon(4S)$

[1] CHILIKIN 19 reports $[\Gamma(B^0 \to \eta_c K^0)/\Gamma_{total}] \times [B(\eta_c(1S) \to p\overline{p}\pi^+\pi^-)] = (38.0^{+6.4+1.3}_{-2.9-4.7}) \times 10^{-7}$ which we divide by our best (shown rounded) value $B(\eta_c(1S) \to p\overline{p}\pi^+\pi^-) = (3.4 \pm 0.5) \times 10^{-3}$. Our first error is their experiment's error and our second error is the systematic error from using our best (shown rounded) value.
[2] Assumes equal production of B^+ and B^0 at the $\Upsilon(4S)$.
[3] AUBERT 07AV reports $[\Gamma(B^0 \to \eta_c K^0)/\Gamma_{total}] \times [B(\eta_c(1S) \to p\overline{p})] = (0.83^{+0.28}_{-0.26} \pm 0.05) \times 10^{-6}$ which we divide by our best (shown rounded) value $B(\eta_c(1S) \to p\overline{p}) = (1.11 \pm 0.12) \times 10^{-3}$. Our first error is their experiment's error and our second error is the systematic error from using our best (shown rounded) value.
[4] AUBERT,B 04B reports $[\Gamma(B^0 \to \eta_c K^0)/\Gamma_{total}] \times [B(\eta_c(1S) \to K\overline{K}\pi)] = (0.0648 \pm 0.0085 \pm 0.0071) \times 10^{-3}$ which we divide by our best (shown rounded) value $B(\eta_c(1S) \to K\overline{K}\pi) = (5.9 \pm 0.5) \times 10^{-2}$. Our first error is their experiment's error and our second error is the systematic error from using our best (shown rounded) value.
[5] EDWARDS 01 assumes equal production of B^0 and B^+ at the $\Upsilon(4S)$. The correlated uncertainties (28.3)% from $B(J/\psi(1S) \to \gamma\eta_c)$ in those modes have been accounted for.

$\Gamma(\eta_c K^0)/\Gamma(J/\psi(1S) K^0)$ — $\Gamma_{200}/\Gamma_{214}$

VALUE	DOCUMENT ID		TECN	COMMENT
1.39±0.20±0.45	[1] AUBERT,B	04B	BABR	$e^+e^- \to \Upsilon(4S)$

[1] Uses BABAR measurement of $B(B^0 \to J/\psi K^0) = (8.5 \pm 0.5 \pm 0.6) \times 10^{-4}$.

$\Gamma(\eta_c(1S) K^+\pi^-)/\Gamma(J/\psi(1S) K^+\pi^-)$ — $\Gamma_{201}/\Gamma_{215}$

VALUE	DOCUMENT ID		TECN	COMMENT
0.68±0.03±0.07	[1] AAIJ	18AN	LHCB	pp at 7, 8, 13 TeV

[1] AAIJ 18AN reports $[\Gamma(B^0 \to \eta_c(1S) K^+\pi^-)/\Gamma(B^0 \to J/\psi(1S) K^+\pi^-)] \times [B(\eta_c(1S) \to p\overline{p})] / [B(J/\psi(1S) \to p\overline{p})] = 0.357 \pm 0.015 \pm 0.008$ which we multiply or divide by our best (shown rounded) values $B(\eta_c(1S) \to p\overline{p}) = (1.11 \pm 0.12) \times 10^{-3}$, $B(J/\psi(1S) \to p\overline{p}) = (2.121 \pm 0.029) \times 10^{-3}$. Our first error is their experiment's error and our second error is the systematic error from using our best (shown rounded) values.

$\Gamma(\eta_c(1S) K^*(1410)^0)/\Gamma(\eta_c(1S) K^+\pi^-)$ — $\Gamma_{204}/\Gamma_{201}$

VALUE (units 10^{-2})	DOCUMENT ID		TECN	COMMENT
32±24±6	[1] AAIJ	18AN	LHCB	pp at 7, 8, 13 TeV

[1] AAIJ 18AN reports $[\Gamma(B^0 \to \eta_c(1S) K^*(1410)^0)/\Gamma(B^0 \to \eta_c(1S) K^+\pi^-)] \times [B(K^*(1410) \to K\pi)] = 0.021 \pm 0.011 \pm 0.011$ which we divide by our best (shown rounded) value $B(K^*(1410) \to K\pi) = (6.6 \pm 1.3) \times 10^{-2}$. Our first error is their experiment's error and our second error is the systematic error from using our best (shown rounded) value.

$\Gamma(\eta_c(1S) K^+\pi^-(NR))/\Gamma(\eta_c(1S) K^+\pi^-)$ — $\Gamma_{202}/\Gamma_{201}$

VALUE (units 10^{-2})	DOCUMENT ID		TECN	COMMENT
10.3±1.4$^{+1.0}_{-1.2}$	AAIJ	18AN	LHCB	pp at 7, 8, 13 TeV

$\Gamma(\eta_c(1S) K^*_0(1430)^0)/\Gamma(\eta_c(1S) K^+\pi^-)$ — $\Gamma_{205}/\Gamma_{201}$

VALUE (units 10^{-2})	DOCUMENT ID		TECN	COMMENT
27±5±3	[1] AAIJ	18AN	LHCB	pp at 7, 8, 13 TeV

[1] AAIJ 18AN reports $[\Gamma(B^0 \to \eta_c(1S) K^*_0(1430)^0)/\Gamma(B^0 \to \eta_c(1S) K^+\pi^-)] \times [B(K^*_0(1430) \to K\pi)] = 0.253 \pm 0.035^{+0.035}_{-0.028}$ which we divide by our best (shown rounded) value $B(K^*_0(1430) \to K\pi) = (93 \pm 10) \times 10^{-2}$. Our first error is their experiment's error and our second error is the systematic error from using our best (shown rounded) value.

$\Gamma(\eta_c(1S) K^*_2(1430)^0)/\Gamma(\eta_c(1S) K^+\pi^-)$ — $\Gamma_{206}/\Gamma_{201}$

VALUE (units 10^{-2})	DOCUMENT ID		TECN	COMMENT
8.2$^{+3.6}_{-4.4}$±0.2	[1] AAIJ	18AN	LHCB	pp at 7, 8, 13 TeV

[1] AAIJ 18AN reports $[\Gamma(B^0 \to \eta_c(1S) K^*_2(1430)^0)/\Gamma(B^0 \to \eta_c(1S) K^+\pi^-)] \times [B(K^*_2(1430) \to K\pi)] = 0.041 \pm 0.015^{+0.010}_{-0.016}$ which we divide by our best (shown rounded) value $B(K^*_2(1430) \to K\pi) = (49.9 \pm 1.2) \times 10^{-2}$. Our first error is their experiment's error and our second error is the systematic error from using our best (shown rounded) value.

$\Gamma(\eta_c(1S) K^*(1680)^0)/\Gamma(\eta_c(1S) K^+\pi^-)$ — $\Gamma_{207}/\Gamma_{201}$

VALUE (units 10^{-2})	DOCUMENT ID		TECN	COMMENT
5.7$^{+6.5}_{-6.8}$±0.4	[1] AAIJ	18AN	LHCB	pp at 7, 8, 13 TeV

[1] AAIJ 18AN reports $[\Gamma(B^0 \to \eta_c(1S) K^*(1680)^0)/\Gamma(B^0 \to \eta_c(1S) K^+\pi^-)] \times [B(K^*(1680) \to K\pi)] = 0.022 \pm 0.020^{+0.015}_{-0.017}$ which we divide by our best (shown rounded) value $B(K^*(1680) \to K\pi) = (38.7 \pm 2.5) \times 10^{-2}$. Our first error is their experiment's error and our second error is the systematic error from using our best (shown rounded) value.

$\Gamma(\eta_c(1S) K^*_0(1950)^0)/\Gamma(\eta_c(1S) K^+\pi^-)$ — $\Gamma_{208}/\Gamma_{201}$

VALUE (units 10^{-2})	DOCUMENT ID		TECN	COMMENT
7$^{+4}_{-6}$±2	[1] AAIJ	18AN	LHCB	pp at 7, 8, 13 TeV

[1] AAIJ 18AN reports $[\Gamma(B^0 \to \eta_c(1S) K^*_0(1950)^0)/\Gamma(B^0 \to \eta_c(1S) K^+\pi^-)] \times [B(K^*_0(1950) \to K^-\pi^+)] = 0.038 \pm 0.018^{+0.014}_{-0.025}$ which we divide by our best (shown rounded) value $B(K^*_0(1950) \to K^-\pi^+) = (52 \pm 14) \times 10^{-2}$. Our first error is their experiment's error and our second error is the systematic error from using our best (shown rounded) value.

$\Gamma(T_{c\overline{c}}(4100)^- K^+,\ T^-_{c\overline{c}} \to \eta_c\pi^-)/\Gamma(\eta_c(1S) K^+\pi^-)$ — $\Gamma_{203}/\Gamma_{201}$

VALUE (units 10^{-2})	DOCUMENT ID		TECN	COMMENT
3.3±1.1$^{+1.2}_{-1.1}$	AAIJ	18AN	LHCB	pp at 7, 8, 13 TeV

$\Gamma(\eta_c K^*(892)^0)/\Gamma_{total}$ — Γ_{209}/Γ

VALUE (units 10^{-4})	DOCUMENT ID		TECN	COMMENT
5.3 $^{+1.0}_{-1.2}$ OUR AVERAGE Error includes scale factor of 2.0. See the ideogram below.				
4.42±0.24$^{+0.54}_{-0.66}$	[1] AAIJ	18AN	LHCB	pp at 7, 8, 13 TeV
7.4 ±0.9 ±0.5	[2,3] AUBERT	08AB	BABR	$e^+e^- \to \Upsilon(4S)$
9.3 $^{+2.9}_{-2.6}$ ±1.0	[4,5] AUBERT	07AV	BABR	$e^+e^- \to \Upsilon(4S)$
16.2 ±3.2 $^{+5.5}_{-6.0}$	[5] FANG	03	BELL	$e^+e^- \to \Upsilon(4S)$

[1] AAIJ 18AN reports $B(B^0 \to \eta_c K^*(892)^0,\ K^*(892)^0 \to K^+\pi^-) = (2.95 \pm 0.16^{+0.36}_{-0.44}) \times 10^{-4}$ using the fitted fraction of $0.514 \pm 0.019^{+0.017}_{-0.048}$ from Dalitz decay of $B(B^0 \to \eta_c K^+\pi^-) = (5.73 \pm 0.24 \pm 0.67) \times 10^{-4}$ and corrected for $B(K^*(892)^0 \to K^+\pi^-) = 2/3$.

[2] AUBERT 08AB reports $[\Gamma(B^0 \to \eta_c K^*(892)^0)/\Gamma_{total}] / [B(B^+ \to \eta_c K^+)] = 0.62 \pm 0.06 \pm 0.05$ which we multiply by our best (shown rounded) value $B(B^+ \to \eta_c K^+) = (1.20 \pm 0.08) \times 10^{-3}$. Our first error is their experiment's error and our second error is the systematic error from using our best (shown rounded) value.

[3] Uses the production ratio of $(B^+B^-)/(B^0\overline{B}^0) = 1.026 \pm 0.032$ at $\Upsilon(4S)$.

[4] AUBERT 07AV reports $[\Gamma(B^0 \to \eta_c K^*(892)^0)/\Gamma_{total}] \times [B(\eta_c(1S) \to p\overline{p})] = (1.03^{+0.27}_{-0.24} \pm 0.17) \times 10^{-6}$ which we divide by our best (shown rounded) value $B(\eta_c(1S) \to p\overline{p}) = (1.11 \pm 0.12) \times 10^{-3}$. Our first error is their experiment's error and our second error is the systematic error from using our best (shown rounded) value.

[5] Assumes equal production of B^+ and B^0 at the $\Upsilon(4S)$.

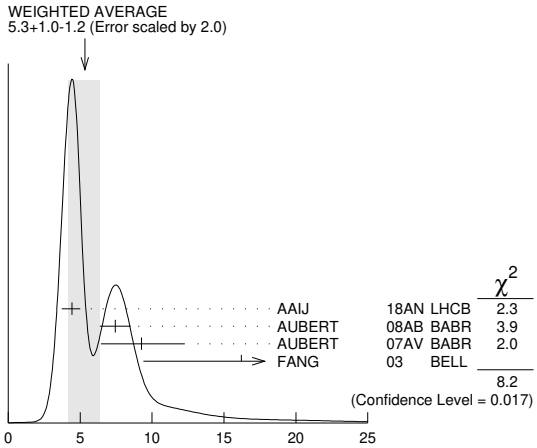

$\Gamma(\eta_c K^*(892)^0)/\Gamma_{total}$ (units 10^{-4})

$\Gamma(\eta_c(2S) K^0_S,\ \eta_c \to p\overline{p}\pi^+\pi^-)/\Gamma_{total}$ — Γ_{210}/Γ

VALUE (units 10^{-7})	DOCUMENT ID		TECN	COMMENT
$4.2^{+1.4}_{-1.2}{}^{+0.3}_{-0.3}$	CHILIKIN	19	BELL	$e^+e^- \to \Upsilon(4S)$

$\Gamma(\eta_c(2S) K^{*0})/\Gamma_{total}$ — Γ_{211}/Γ

VALUE (units 10^{-4})	CL%	DOCUMENT ID		TECN	COMMENT
<3.9	90	[1] AUBERT	08AB	BABR	$e^+e^- \to \Upsilon(4S)$

[1] Uses the production ratio of $(B^+B^-)/(B^0\overline{B}^0) = 1.026 \pm 0.032$ at $\Upsilon(4S)$.

$\Gamma(h_c(1P) K^0_S)/\Gamma_{total}$ — Γ_{212}/Γ

VALUE	DOCUMENT ID		TECN	COMMENT
$<1.4 \times 10^{-5}$	CHILIKIN	19	BELL	$e^+e^- \to \Upsilon(4S)$

$\Gamma(B^0 \to h_c(1P) K^{*0})/\Gamma_{total} \times \Gamma(h_c(1P) \to \gamma\eta_c(1S))/\Gamma_{total}$ — $\Gamma_{213}/\Gamma \times \Gamma^{h_c(1P)}_{30}/\Gamma^{h_c(1P)}$

VALUE (units 10^{-4})	CL%	DOCUMENT ID		TECN	COMMENT
<2.2	90	[1] AUBERT	08AB	BABR	$e^+e^- \to \Upsilon(4S)$

[1] Uses the production ratio of $(B^+B^-)/(B^0\overline{B}^0) = 1.026 \pm 0.032$ at $\Upsilon(4S)$.

$\Gamma(\eta_c K^*(892)^0)/\Gamma(\eta_c K^0)$ — $\Gamma_{209}/\Gamma_{200}$

VALUE	DOCUMENT ID		TECN	COMMENT
$1.33 \pm 0.36^{+0.24}_{-0.33}$	FANG	03	BELL	$e^+e^- \to \Upsilon(4S)$

$\Gamma(J/\psi(1S) K^0)/\Gamma_{total}$ — Γ_{214}/Γ

VALUE (units 10^{-4})	CL%	EVTS	DOCUMENT ID		TECN	COMMENT
8.91±0.21 OUR FIT						
8.91±0.21 OUR AVERAGE						
9.02±0.10±0.26			[1] CHOUDHURY	21	BELL	$e^+e^- \to \Upsilon(4S)$
8.1 ±0.9 ±0.6			[2] CHILIKIN	19	BELL	$e^+e^- \to \Upsilon(4S)$
8.8 $^{+1.4}_{-1.3}$ ±0.1			[3,4] AUBERT	07AV	BABR	$e^+e^- \to \Upsilon(4S)$
8.69±0.22±0.30			[4] AUBERT	05J	BABR	$e^+e^- \to \Upsilon(4S)$
9.5 ±0.8 ±0.6			[4] AVERY	00	CLE2	$e^+e^- \to \Upsilon(4S)$
11.5 ±2.3 ±1.7			[5] ABE	96H	CDF	$p\overline{p}$ at 1.8 TeV
6.93±4.07±0.04			[6] BORTOLETTO	92	CLEO	$e^+e^- \to \Upsilon(4S)$
9.24±7.21±0.05		2	[7] ALBRECHT	90J	ARG	$e^+e^- \to \Upsilon(4S)$
• • • We do not use the following data for averages, fits, limits, etc. • • •						
7.9 ±0.4 ±0.9			[4] ABE	03B	BELL	Repl. by CHOUDHURY 21
8.3 ±0.4 ±0.5			[4] AUBERT	02	BABR	Repl. by AUBERT 05J
8.5 $^{+1.4}_{-1.2}$ ±0.6			[4] JESSOP	97	CLE2	Repl. by AVERY 00
7.5 ±2.4 ±0.8		10	[6] ALAM	94	CLE2	Sup. by JESSOP 97
<50	90		ALAM	86	CLEO	$e^+e^- \to \Upsilon(4S)$

[1] CHOUDHURY 21 uses the relative production fraction of charged (f^{+-}) to neutral (f^{00}) B mesons at $\Upsilon(4S)$ value of $f^{+-}/f^{00} = 1.058 \pm 0.024$.

[2] CHILIKIN 19 reports $[\Gamma(B^0 \to J/\psi(1S) K^0)/\Gamma_{total}] \times [B(J/\psi(1S) \to p\overline{p}\pi^+\pi^-)] = (48.6^{+4.6}_{-4.4}{}^{+2.4}_{-2.6}) \times 10^{-7}$ which we divide by our best (shown rounded) value $B(J/\psi(1S) \to p\overline{p}\pi^+\pi^-) = (6.0 \pm 0.5) \times 10^{-3}$. Our first error is their experiment's error and our second error is the systematic error from using our best (shown rounded) value.

[3] AUBERT 07AV reports $[\Gamma(B^0 \to J/\psi(1S) K^0)/\Gamma_{total}] \times [B(J/\psi(1S) \to p\overline{p})] = (1.87^{+0.28}_{-0.26} \pm 0.07) \times 10^{-6}$ which we divide by our best (shown rounded) value $B(J/\psi(1S) \to p\overline{p}) = (2.121 \pm 0.029) \times 10^{-3}$. Our first error is their experiment's error and our second error is the systematic error from using our best (shown rounded) value.

[4] Assumes equal production of B^+ and B^0 at the $\Upsilon(4S)$.

[5] ABE 96H assumes that $B(B^+ \to J/\psi K^+) = (1.02 \pm 0.14) \times 10^{-3}$.

[6] BORTOLETTO 92 reports $(6 \pm 3 \pm 2) \times 10^{-4}$ from a measurement of $[\Gamma(B^0 \to J/\psi(1S) K^0)/\Gamma_{total}] \times [B(J/\psi(1S) \to e^+e^-)]$ assuming $B(J/\psi(1S) \to e^+e^-) = 0.069 \pm 0.009$, which we rescale to our best (shown rounded) value $B(J/\psi(1S) \to e^+e^-) = (5.971 \pm 0.032) \times 10^{-2}$. Our first error is their experiment's error and our second error is the systematic error from using our best (shown rounded) value. Assumes equal production of B^+ and B^0 at the $\Upsilon(4S)$.

[7] ALBRECHT 90J reports $(8 \pm 6 \pm 2) \times 10^{-4}$ from a measurement of $[\Gamma(B^0 \to J/\psi(1S) K^0)/\Gamma_{total}] \times [B(J/\psi(1S) \to e^+e^-)]$ assuming $B(J/\psi(1S) \to e^+e^-) = 0.069 \pm 0.009$, which we rescale to our best (shown rounded) value $B(J/\psi(1S) \to e^+e^-) = (5.971 \pm 0.032) \times 10^{-2}$. Our first error is their experiment's error and our second error is the systematic error from using our best (shown rounded) value. Assumes equal production of B^+ and B^0 at the $\Upsilon(4S)$.

$\Gamma(J/\psi(1S) K^+\pi^-)/\Gamma_{total}$ — Γ_{215}/Γ

VALUE (units 10^{-3})	CL%	DOCUMENT ID		TECN	COMMENT
1.15 ±0.05 OUR AVERAGE					
1.15 ±0.01 ±0.05		CHILIKIN	14	BELL	$\overline{B}^0 \to J/\psi K^-\pi^+$
1.16 ±0.56 ±0.01		[1] BORTOLETTO	92	CLEO	$e^+e^- \to \Upsilon(4S)$
• • • We do not use the following data for averages, fits, limits, etc. • • •					
1.079±0.011		[2] AUBERT	09AA	BABR	$e^+e^- \to \Upsilon(4S)$
<1.3	90	[3] ALBRECHT	87D	ARG	$e^+e^- \to \Upsilon(4S)$
<6.3	90	GILES	84	CLEO	$e^+e^- \to \Upsilon(4S)$

[1] BORTOLETTO 92 reports $(1.0 \pm 0.4 \pm 0.3) \times 10^{-3}$ from a measurement of $[\Gamma(B^0 \to J/\psi(1S) K^+\pi^-)/\Gamma_{total}] \times [B(J/\psi(1S) \to e^+e^-)]$ assuming $B(J/\psi(1S) \to e^+e^-) = 0.069 \pm 0.009$, which we rescale to our best (shown rounded) value $B(J/\psi(1S) \to e^+e^-) = (5.971 \pm 0.032) \times 10^{-2}$. Our first error is their experiment's error and our second error is the systematic error from using our best (shown rounded) value. Assumes equal production of B^+ and B^0 at the $\Upsilon(4S)$.

[2] Does not report systematic uncertainties.

[3] ALBRECHT 87D assume $B^+B^-/B^0\overline{B}^0$ ratio is 55/45. $K\pi$ system is specifically selected as nonresonant.

$\Gamma(J/\psi(1S) K^*(892)^0)/\Gamma_{total}$ — Γ_{216}/Γ

VALUE (units 10^{-3})	EVTS	DOCUMENT ID		TECN	COMMENT
1.27 ±0.05 OUR FIT					
1.28 ±0.05 OUR AVERAGE					
1.19 ±0.01 ±0.08		CHILIKIN	14	BELL	$\overline{B}^0 \to J/\psi K^-\pi^+$
1.33 $^{+0.22}_{-0.21}$ ±0.02		[1,2] AUBERT	07AV	BABR	$e^+e^- \to \Upsilon(4S)$
1.309±0.026±0.077		[2] AUBERT	05J	BABR	$e^+e^- \to \Upsilon(4S)$
1.29 ±0.05 ±0.13		[2] ABE	02N	BELL	$e^+e^- \to \Upsilon(4S)$
1.74 ±0.20 ±0.18		[3] ABE	98O	CDF	$p\overline{p}$ 1.8 TeV
1.32 ±0.17 ±0.17		[4] JESSOP	97	CLE2	$e^+e^- \to \Upsilon(4S)$
1.27 ±0.65 ±0.01		[5] BORTOLETTO	92	CLEO	$e^+e^- \to \Upsilon(4S)$
1.27 ±0.60 ±0.01	6	[6] ALBRECHT	90J	ARG	$e^+e^- \to \Upsilon(4S)$
4.04 ±1.81 ±0.02	5	[7] BEBEK	87	CLEO	$e^+e^- \to \Upsilon(4S)$
• • • We do not use the following data for averages, fits, limits, etc. • • •					
1.24 ±0.05 ±0.09		[2] AUBERT	02	BABR	Repl. by AUBERT 05J
1.36 ±0.27 ±0.22		[8] ABE	96H	CDF	Sup. by ABE 98O
1.69 ±0.31 ±0.18	29	[9] ALAM	94	CLE2	Sup. by JESSOP 97
		[10] ALBRECHT	94G	ARG	$e^+e^- \to \Upsilon(4S)$
4.0 ±0.30		[11] ALBAJAR	91E	UA1	$E^{p\overline{p}}_{cm} = 630$ GeV
3.3 ±0.18	5	[12] ALBRECHT	87D	ARG	$e^+e^- \to \Upsilon(4S)$
4.1 ±0.18	5	[13] ALAM	86	CLEO	Repl. by BEBEK 87

[1] AUBERT 07AV reports $[\Gamma(B^0 \to J/\psi(1S) K^*(892)^0)/\Gamma_{total}] \times [B(J/\psi(1S) \to p\overline{p})] = (2.82^{+0.30}_{-0.28}{}^{+0.36}_{-0.35}) \times 10^{-6}$ which we divide by our best (shown rounded) value $B(J/\psi(1S) \to p\overline{p}) = (2.121 \pm 0.029) \times 10^{-3}$. Our first error is their experiment's error and our second error is the systematic error from using our best (shown rounded) value.

[2] Assumes equal production of B^+ and B^0 at the $\Upsilon(4S)$.

[3] ABE 98O reports $[B(B^0 \to J/\psi(1S) K^*(892)^0)]/[B(B^+ \to J/\psi(1S) K^+)] = 1.76 \pm 0.14 \pm 0.15$. We multiply by our best value $B(B^+ \to J/\psi(1S) K^+) = (9.9 \pm 1.0) \times 10^{-4}$. Our first error is their experiment's error and our second error is the systematic error from using our best value.

[4] Assumes equal production of B^+ and B^0 at the $\Upsilon(4S)$.

[5] BORTOLETTO 92 reports $(1.1 \pm 0.5 \pm 0.3) \times 10^{-3}$ from a measurement of $[\Gamma(B^0 \to J/\psi(1S) K^*(892)^0)/\Gamma_{total}] \times [B(J/\psi(1S) \to e^+e^-)]$ assuming $B(J/\psi(1S) \to e^+e^-) = 0.069 \pm 0.009$, which we rescale to our best (shown rounded) value $B(J/\psi(1S) \to e^+e^-) = (5.971 \pm 0.032) \times 10^{-2}$. Our first error is their experiment's error and our second error is the systematic error from using our best (shown rounded) value. Assumes equal production of B^+ and B^0 at the $\Upsilon(4S)$.

Int. J. Mod. Phys. A 2026.41. Downloaded from www.worldscientific.com
by LIFORNIA @ BERKELEY on 09/16/26. Re-use and distribution is strictly not permitted, except for Open Access articles.

Int. J. Mod. Phys. A 2026.41. Downloaded from www.worldscientific.com
by UNIVERSITY OF CALIFORNIA @ BERKELEY on 09/16/26. Re-use and distribution is strictly not permitted, except for Open Access articles.

[6] ALBRECHT 90J reports $(1.1 \pm 0.5 \pm 0.2) \times 10^{-3}$ from a measurement of $[\Gamma(B^0 \to J/\psi(1S) K^*(892)^0)/\Gamma_{total}] \times [B(J/\psi(1S) \to e^+e^-)]$ assuming $B(J/\psi(1S) \to e^+e^-) = 0.069 \pm 0.009$, which we rescale to our best (shown rounded) value $B(J/\psi(1S) \to e^+e^-) = (5.971 \pm 0.032) \times 10^{-2}$. Our first error is their experiment's error and our second error is the systematic error from using our best (shown rounded) value. Assumes equal production of B^+ and B^0 at the $\Upsilon(4S)$.

[7] BEBEK 87 reports $(3.5 \pm 1.6 \pm 0.3) \times 10^{-3}$ from a measurement of $[\Gamma(B^0 \to J/\psi(1S) K^*(892)^0)/\Gamma_{total}] \times [B(J/\psi(1S) \to e^+e^-)]$ assuming $B(J/\psi(1S) \to e^+e^-) = 0.069 \pm 0.009$, which we rescale to our best (shown rounded) value $B(J/\psi(1S) \to e^+e^-) = (5.971 \pm 0.032) \times 10^{-2}$. Our first error is their experiment's error and our second error is the systematic error from using our best (shown rounded) value. Updated in BORTOLETTO 92 to use the same assumptions.

[8] ABE 96H assumes that $B(B^+ \to J/\psi K^+) = (1.02 \pm 0.14) \times 10^{-3}$.

[9] The neutral and charged B events together are predominantly longitudinally polarized, $\Gamma_L/\Gamma = 0.080 \pm 0.08 \pm 0.05$. This can be compared with a prediction using HQET, 0.73 (KRAMER 92). This polarization indicates that the $B \to \psi K^*$ decay is dominated by the $CP = -1$ CP eigenstate. Assumes equal production of B^+ and B^0 at the $\Upsilon(4S)$.

[10] ALBRECHT 94G measures the polarization in the vector-vector decay to be predominantly longitudinal, $\Gamma_T/\Gamma = 0.03 \pm 0.16 \pm 0.15$ making the neutral decay a CP eigenstate when the K^{*0} decays through $K^0_S \pi^0$.

[11] ALBAJAR 91E assumes B^0_d production fraction of 36%.

[12] ALBRECHT 87D assume $B^+B^-/B^0\overline{B}^0$ ratio is 55/45. Superseded by ALBRECHT 90J.

[13] ALAM 86 assumes $B^\pm/B^0$ ratio is 60/40. The observation of the decay $B^+ \to J/\psi K^*(892)^+$ (HAAS 85) has been retracted in this paper.

$\Gamma(J/\psi(1S) K^*(892)^0)/\Gamma(J/\psi(1S) K^0)$ — $\Gamma_{216}/\Gamma_{214}$

VALUE	DOCUMENT ID		TECN	COMMENT
1.50±0.09 OUR AVERAGE				
1.51±0.05±0.08	AUBERT	05J	BABR	$e^+e^- \to \Upsilon(4S)$
1.39±0.36±0.10	ABE	96Q	CDF	$p\overline{p}$
• • • We do not use the following data for averages, fits, limits, etc. • • •				
1.49±0.10±0.08	[1] AUBERT	02	BABR	Repl. by AUBERT 05J

[1] Assumes equal production of B^+ and B^0 at the $\Upsilon(4S)$.

$\Gamma(J/\psi(1S)\eta K^0_S)/\Gamma_{total}$ — Γ_{217}/Γ

VALUE (units 10^{-5})	DOCUMENT ID		TECN	COMMENT
5.4 ±0.9 OUR AVERAGE				
5.22±0.78±0.49	[1] IWASHITA	14	BELL	$e^+e^- \to \Upsilon(4S)$
8.4 ±2.6 ±2.7	[1] AUBERT	04Y	BABR	$e^+e^- \to \Upsilon(4S)$

[1] Assumes equal production of B^+ and B^0 at the $\Upsilon(4S)$.

$\Gamma(J/\psi(1S)\eta' K^0_S)/\Gamma_{total}$ — Γ_{218}/Γ

VALUE (units 10^{-5})	CL%	DOCUMENT ID		TECN	COMMENT
<2.5	90	[1] XIE	07	BELL	$e^+e^- \to \Upsilon(4S)$

[1] Assumes equal production of B^+ and B^0 at the $\Upsilon(4S)$.

$\Gamma(J/\psi(1S)\omega K^0)/\Gamma_{total}$ — Γ_{220}/Γ

VALUE (units 10^{-4})	DOCUMENT ID		TECN	COMMENT
2.3±0.3±0.3	[1] DEL-AMO-SA...10B		BABR	$e^+e^- \to \Upsilon(4S)$
• • • We do not use the following data for averages, fits, limits, etc. • • •				
3.1±0.6±0.3	[1] AUBERT	08W	BABR	Repl. by DEL-AMO-SANCHEZ 10B

[1] Assumes equal production of B^+ and B^0 at the $\Upsilon(4S)$.

$\Gamma(\chi_{c0}(3915), \chi_{c0} \to J/\psi\omega)/\Gamma_{total}$ — Γ_{221}/Γ

VALUE (units 10^{-5})	DOCUMENT ID		TECN	COMMENT
2.1±0.9±0.3	[1] DEL-AMO-SA...10B		BABR	$e^+e^- \to \Upsilon(4S)$
• • • We do not use the following data for averages, fits, limits, etc. • • •				
$1.3^{+1.3}_{-1.1}\pm0.2$	[1,2] AUBERT	08W	BABR	Repl. by DEL-AMO-SANCHEZ 10B

[1] Assumes equal production of B^+ and B^0 at the $\Upsilon(4S)$.

[2] Corresponds to upper limit of 3.9×10^{-5} at 90% CL.

$\Gamma(J/\psi(1S)\phi K^0)/\Gamma_{total}$ — Γ_{219}/Γ

VALUE (units 10^{-5})	DOCUMENT ID		TECN	COMMENT
4.9 ±1.0 OUR AVERAGE Error includes scale factor of 1.3.				
4.43±0.76±0.19	LEES	15	BABR	$e^+e^- \to \Upsilon(4S)$
10.2 ±3.8 ±1.0	[1] AUBERT	03O	BABR	$e^+e^- \to \Upsilon(4S)$
$8.8\ ^{+3.5}_{-3.0}\ \pm1.3$	[2] ANASTASSOV	00	CLE2	$e^+e^- \to \Upsilon(4S)$

[1] Assumes equal production of B^+ and B^0 at the $\Upsilon(4S)$.

[2] ANASTASSOV 00 finds 10 events on a background of 0.5 ± 0.2. Assumes equal production of B^0 and B^+ at the $\Upsilon(4S)$, a uniform Dalitz plot distribution, isotropic $J/\psi(1S)$ and ϕ decays, and $B(B^+ \to J/\psi(1S)\phi K^+) = B(B^0 \to J/\psi(1S)\phi K^0)$.

$\Gamma(J/\psi(1S) K(1270)^0)/\Gamma_{total}$ — Γ_{222}/Γ

VALUE (units 10^{-3})	DOCUMENT ID		TECN	COMMENT
1.30±0.34±0.32	[1] ABE	01L	BELL	$e^+e^- \to \Upsilon(4S)$

[1] Assumes equal production of B^+ and B^0 at the $\Upsilon(4S)$ and uses the PDG value of $B(B^+ \to J/\psi(1S) K^+) = (1.00 \pm 0.10) \times 10^{-3}$.

$\Gamma(J/\psi(1S)\pi^0)/\Gamma_{total}$ — Γ_{223}/Γ

VALUE (units 10^{-5})	CL%	DOCUMENT ID		TECN	COMMENT
1.73±0.09 OUR AVERAGE Error includes scale factor of 1.2.					
2.00±0.12±0.09		[1] ADACHI	25C	BELL	$e^+e^- \to \Upsilon(4S)$
1.65±0.10±0.09		[2] AAIJ	24N	LHCB	pp at 7, 8, 13 TeV
1.62±0.11±0.06		[3] PAL	18	BELL	$e^+e^- \to \Upsilon(4S)$
1.69±0.14±0.07		[3] AUBERT	08AU	BABR	$e^+e^- \to \Upsilon(4S)$
$2.5\ ^{+1.1}_{-0.9}\ \pm0.2$		[3] AVERY	00	CLE2	$e^+e^- \to \Upsilon(4S)$
• • • We do not use the following data for averages, fits, limits, etc. • • •					
1.94±0.22±0.17		[3] AUBERT,B	06B	BABR	Repl. by AUBERT 08AU
2.3 ±0.5 ±0.2		[3] ABE	03B	BELL	Repl. by PAL 18
2.0 ±0.6 ±0.2		[3] AUBERT	02	BABR	Repl. by AUBERT,B 06B
< 32	90	[4] ACCIARRI	97C	L3	
< 5.8	90	BISHAI	96	CLE2	Sup. by AVERY 00
<690	90	[3] ALEXANDER	95	CLE2	Sup. by BISHAI 96

[1] ADACHI 25C uses $B(\Upsilon(4S) \to B^+B^-)/B(\Upsilon(4S) \to B^0\overline{B}^0) = 1.052 \pm 0.031$.

[2] AAIJ 24N reports $[\Gamma(B^0 \to J/\psi(1S)\pi^0)/\Gamma_{total}] / [B(B^+ \to J/\psi(1S) K^*(892)^+)] = (1.153 \pm 0.053 \pm 0.048) \times 10^{-2}$ which we multiply by our best (shown rounded) value $B(B^+ \to J/\psi(1S) K^*(892)^+) = (1.43 \pm 0.08) \times 10^{-3}$. Our first error is their experiment's error and our second error is the systematic error from using our best (shown rounded) value.

[3] Assumes equal production of B^+ and B^0 at the $\Upsilon(4S)$.

[4] ACCIARRI 97C assumes B^0 production fraction (39.5 ± 4.0)% and B_s (12.0 ± 3.0)%.

$\Gamma(J/\psi(1S)\eta)/\Gamma_{total}$ — Γ_{224}/Γ

VALUE (units 10^{-6})	CL%	DOCUMENT ID		TECN	COMMENT
$\mathbf{12.3\ ^{+1.8}_{-1.7}\ \pm0.7}$		[1,2] CHANG	12	BELL	$e^+e^- \to \Upsilon(4S)$
• • • We do not use the following data for averages, fits, limits, etc. • • •					
9.92±0.79±0.62		[3] AAIJ	25AN	LHCB	pp at 7, 8 and 13 TeV
8.2 ±2.8 ±0.5		[4] AAIJ	15D	LHCB	Repl. by AAIJ 25AN
9.5 ±1.7 ±0.8		[2] CHANG	07A	BELL	Repl. by CHANG 12
< 27	90	[2] AUBERT	03O	BABR	$e^+e^- \to \Upsilon(4S)$
<1200	90	[5] ACCIARRI	97C	L3	

[1] Reconstructs η in $\gamma\gamma$ and $\pi^+\pi^-\pi^0$ decays.

[2] Assumes equal production of B^+ and B^0 at the $\Upsilon(4S)$.

[3] AAIJ 25AN value obtained by multiplying reported $B(B^0_s \to J/\psi\eta) = (4.58 \pm 0.14 \pm 0.16 \pm 0.26) \times 10^{-4}$ by the ratio $B(B^0 \to J/\psi\eta)/B(B^0_s \to J/\psi\eta) = (2.16 \pm 0.16 \pm 0.05 \pm 0.07) \times 10^{-2}$. The last uncertainty combines the systematic uncertainty with branching fraction uncertainties.

[4] AAIJ 15D reports $[\Gamma(B^0 \to J/\psi(1S)\eta)/\Gamma_{total}] / [B(B^0_s \to J/\psi(1S)\eta)] = (1.85 \pm 0.61 \pm 0.14) \times 10^{-2}$ which we multiply by our best (shown rounded) value $B(B^0_s \to J/\psi(1S)\eta) = (4.45 \pm 0.25) \times 10^{-4}$. Our first error is their experiment's error and our second error is the systematic error from using our best (shown rounded) value.

[5] ACCIARRI 97C assumes B^0 production fraction (39.5 ± 4.0)% and B_s (12.0 ± 3.0)%.

$\Gamma(J/\psi(1S)\pi^+\pi^-)/\Gamma_{total}$ — Γ_{225}/Γ

VALUE (units 10^{-5})	DOCUMENT ID		TECN	COMMENT
3.99±0.15 OUR AVERAGE				
3.97±0.14±0.07	[1,2] AAIJ	13M	LHCB	pp at 7 TeV
4.6 ±0.7 ±0.6	[3] AUBERT	03B	BABR	$e^+e^- \to \Upsilon(4S)$

[1] AAIJ 13M reports $(3.97 \pm 0.09 \pm 0.11 \pm 0.16) \times 10^{-5}$ from a measurement of $[\Gamma(B^0 \to J/\psi(1S)\pi^+\pi^-)/\Gamma_{total}] / [B(B^+ \to J/\psi(1S) K^+)]$ assuming $B(B^+ \to J/\psi(1S) K^+) = (1.018 \pm 0.042) \times 10^{-3}$, which we rescale to our best (shown rounded) value $B(B^+ \to J/\psi(1S) K^+) = (1.019 \pm 0.019) \times 10^{-3}$. Our first error is their experiment's error and our second error is the systematic error from using our best (shown rounded) value.

[2] AAIJ 13M does not report correlations between various measurements of the $J/\psi\pi\pi$ final state.

[3] Assumes equal production of B^+ and B^0 at the $\Upsilon(4S)$.

$\Gamma(J/\psi(1S)\pi^+\pi^-\text{nonresonant})/\Gamma_{total}$ — Γ_{226}/Γ

VALUE (units 10^{-5})	CL%	DOCUMENT ID		TECN	COMMENT
<1.2	90	[1] AUBERT	07AC	BABR	$e^+e^- \to \Upsilon(4S)$

[1] Assumes equal production of B^+ and B^0 at the $\Upsilon(4S)$.

$\Gamma(J/\psi(1S) f_0(500), f_0 \to \pi\pi)/\Gamma_{total}$ — Γ_{227}/Γ

VALUE (units 10^{-6})	DOCUMENT ID		TECN	COMMENT
$\mathbf{8.8\pm0.5\ ^{+1.1}_{-1.5}}$	[1] AAIJ	14X	LHCB	pp at 7, 8 TeV
• • • We do not use the following data for averages, fits, limits, etc. • • •				
$6.4\ ^{+2.5}_{-1.1}\pm0.2$	[2,3] AAIJ	13M	LHCB	Repl. by AAIJ 14X

[1] AAIJ 14X uses Dalitz plot analysis of $B^0 \to J/\psi\pi^+\pi^-$.

[2] AAIJ 13M reports $(6.4 \pm 0.8\ ^{+2.4}_{-0.8}) \times 10^{-6}$ from a measurement of $[\Gamma(B^0 \to J/\psi(1S) f_0(500), f_0 \to \pi\pi)/\Gamma_{total}] / [B(B^0 \to J/\psi(1S)\pi^+\pi^-)]$ assuming $B(B^0 \to J/\psi(1S)\pi^+\pi^-) = (3.97 \pm 0.09 \pm 0.11 \pm 0.16) \times 10^{-5}$, which we rescale to our best (shown rounded) value $B(B^0 \to J/\psi(1S)\pi^+\pi^-) = (3.99 \pm 0.15) \times 10^{-5}$. Our first error is their experiment's error and our second error is the systematic error from using our best (shown rounded) value.

[3] AAIJ 13M does not report correlations between various measurements of the $J/\psi\pi\pi$ final state. Measured in Dalitz plot like analysis of $B^0 \to J/\psi\pi^+\pi^-$.

Int. J. Mod. Phys. A 2026.41. Downloaded from www.worldscientific.com by LIFORNIA @ BERKELEY on 09/16/26. Re-use and distribution is strictly not permitted, except for Open Access articles.

$\Gamma(J/\psi(1S) f_2)/\Gamma_{total}$ — Γ_{228}/Γ

VALUE (units 10^{-5})	CL%	DOCUMENT ID		TECN	COMMENT
$0.33^{+0.05}_{-0.06}$ OUR AVERAGE		Error includes scale factor of 1.5.			
$0.30 \pm 0.03^{+0.02}_{-0.03}$		[1] AAIJ	14X	LHCB	pp at 7, 8 TeV
$0.42 \pm 0.06 \pm 0.02$		[2,3] AAIJ	13M	LHCB	pp at 7 TeV
• • • We do not use the following data for averages, fits, limits, etc. • • •					
<0.5	90	[4,5] AUBERT	07AC	BABR	$e^+e^- \to \Upsilon(4S)$

[1] AAIJ 14X uses Dalitz plot analysis of $B^0 \to J/\psi\pi^+\pi^-$.
[2] AAIJ 13M reports $[\Gamma(B^0 \to J/\psi(1S) f_2)/\Gamma_{total}] \times [B(f_2(1270) \to \pi\pi)] = (3.5 \pm 0.4 \pm 0.4) \times 10^{-6}$ from a measurement of $[\Gamma(B^0 \to J/\psi(1S) f_2)/\Gamma_{total}] \times [B(f_2(1270) \to \pi\pi)] / [B(B^0 \to J/\psi(1S)\pi^+\pi^-)]$ assuming $B(B^0 \to J/\psi(1S)\pi^+\pi^-) = (3.97 \pm 0.09 \pm 0.11 \pm 0.16) \times 10^{-5}$, which we rescale to our best (shown rounded) values $B(f_2(1270) \to \pi\pi) = (84.3^{+2.8}_{-1.0}) \times 10^{-2}$, $B(B^0 \to J/\psi(1S)\pi^+\pi^-) = (3.99 \pm 0.15) \times 10^{-5}$. Our first error is their experiment's error and our second error is the systematic error from using our best (shown rounded) values.
[3] AAIJ 13M does not report correlations between various measurements of the $J/\psi\pi\pi$ final state. Measured in Dalitz plot like analysis of $B^0 \to J/\psi\pi^+\pi^-$.
[4] AUBERT 07AC reports $[\Gamma(B^0 \to J/\psi(1S) f_2)/\Gamma_{total}] \times [B(f_2(1270) \to \pi\pi)] < 0.46 \times 10^{-5}$ which we divide by our best (shown rounded) value $B(f_2(1270) \to \pi\pi) = 84.3 \times 10^{-2}$.
[5] Assumes equal production of B^+ and B^0 at the $\Upsilon(4S)$.

$\Gamma(J/\psi(1S)\rho^0)/\Gamma_{total}$ — Γ_{229}/Γ

VALUE (units 10^{-5})	CL%	DOCUMENT ID		TECN	COMMENT
$2.55^{+0.18}_{-0.16}$ OUR AVERAGE					
$2.50 \pm 0.10^{+0.18}_{-0.15}$		[1] AAIJ	14X	LHCB	pp at 7, 8 TeV
$2.7 \pm 0.3 \pm 0.2$		[2] AUBERT	07AC	BABR	$e^+e^- \to \Upsilon(4S)$
• • • We do not use the following data for averages, fits, limits, etc. • • •					
$2.50^{+0.22}_{-0.23} \pm 0.10$		[3,4] AAIJ	13M	LHCB	Repl. by AAIJ 14X
$1.6 \pm 0.6 \pm 0.4$		[2] AUBERT	03B	BABR	Repl. by AUBERT 07AC
<25	90	BISHAI	96	CLE2	$e^+e^- \to \Upsilon(4S)$

[1] AAIJ 14X uses Dalitz plot analysis of $B^0 \to J/\psi\pi^+\pi^-$. We assume $B(\rho(770)^0 \to \pi^+\pi^-) = 100\%$.
[2] Assumes equal production of B^+ and B^0 at the $\Upsilon(4S)$.
[3] AAIJ 13M reports $(2.49^{+0.20+0.16}_{-0.13-0.23}) \times 10^{-5}$ from a measurement of $[\Gamma(B^0 \to J/\psi(1S)\rho^0)/\Gamma_{total}] / [B(B^0 \to J/\psi(1S)\pi^+\pi^-)]$ assuming $B(B^0 \to J/\psi(1S)\pi^+\pi^-) = (3.97 \pm 0.09 \pm 0.11 \pm 0.16) \times 10^{-5}$, which we rescale to our best (shown rounded) value $B(B^0 \to J/\psi(1S)\pi^+\pi^-) = (3.99 \pm 0.15) \times 10^{-5}$. Our first error is their experiment's error and our second error is the systematic error from using our best (shown rounded) value.
[4] AAIJ 13M does not report correlations between various measurements of the $J/\psi\pi\pi$ final state. Measured in Dalitz plot like analysis of $B^0 \to J/\psi\pi^+\pi^-$. Assumes $B(\rho(770)^0 \to \pi\pi) = 100\%$.

$\Gamma(J/\psi(1S) f_0(980),\ f_0 \to \pi^+\pi^-)/\Gamma_{total}$ — Γ_{230}/Γ

VALUE	CL%	DOCUMENT ID		TECN	COMMENT
$<1.1 \times 10^{-6}$	90	[1] AAIJ	13M	LHCB	pp at 7 TeV

[1] AAIJ 13M does not provide correlations between various measurements of the $J/\psi\pi^+\pi^-$ final state. The measurements were obtained from a Dalitz plot like analysis of $B^0 \to J/\psi\pi^+\pi^-$. Also reports $\Gamma(J/\psi(1S) f_0(980),\ f_0 \to \pi^+\pi^-)/\Gamma_{total} = (6.1^{+3.1+1.7}_{-2.0-1.4}) \times 10^{-6}$.

$\Gamma(J/\psi(1S)\rho(1450)^0,\ \rho^0 \to \pi\pi)/\Gamma_{total}$ — Γ_{231}/Γ

VALUE (units 10^{-6})		DOCUMENT ID		TECN	COMMENT
$2.9^{+1.6}_{-0.7}$ OUR AVERAGE					
$4.6 \pm 1.1 \pm 1.9$		[1] AAIJ	14X	LHCB	pp at 7, 8 TeV
$2.1^{+2.4}_{-0.7} \pm 0.1$		[2,3] AAIJ	13M	LHCB	pp at 7 TeV

[1] AAIJ 14X uses Dalitz plot analysis of $B^0 \to J/\psi\pi^+\pi^-$.
[2] AAIJ 13M reports $(2.1^{+1.0+2.2}_{-0.6-0.4}) \times 10^{-6}$ from a measurement of $[\Gamma(B^0 \to J/\psi(1S)\rho(1450)^0,\ \rho^0 \to \pi\pi)/\Gamma_{total}] / [B(B^0 \to J/\psi(1S)\pi^+\pi^-)]$ assuming $B(B^0 \to J/\psi(1S)\pi^+\pi^-) = (3.97 \pm 0.09 \pm 0.11 \pm 0.16) \times 10^{-5}$, which we rescale to our best (shown rounded) value $B(B^0 \to J/\psi(1S)\pi^+\pi^-) = (3.99 \pm 0.15) \times 10^{-5}$. Our first error is their experiment's error and our second error is the systematic error from using our best (shown rounded) value.
[3] AAIJ 13M does not report correlations between various measurements of the $J/\psi\pi\pi$ final state. Measured in Dalitz plot like analysis of $B^0 \to J/\psi\pi^+\pi^-$.

$\Gamma(J/\psi\rho(1700)^0,\ \rho^0 \to \pi^+\pi^-)/\Gamma_{total}$ — Γ_{232}/Γ

VALUE (units 10^{-6})	DOCUMENT ID		TECN	COMMENT
$2.0 \pm 0.5 \pm 1.2$	[1] AAIJ	14X	LHCB	pp at 7, 8 TeV

[1] AAIJ 14X uses Dalitz plot analysis of $B^0 \to J/\psi\pi^+\pi^-$.

$\Gamma(J/\psi(1S)\omega)/\Gamma_{total}$ — Γ_{233}/Γ

VALUE (units 10^{-5})	CL%	DOCUMENT ID		TECN	COMMENT
2.08 ± 0.29 OUR AVERAGE					
$2.16 \pm 0.30 \pm 0.14$		[1] ADACHI	25E	BELL	$e^+e^- \to \Upsilon(4S)$
$1.8\ ^{+0.7}_{-0.5} \pm 0.1$		[2] AAIJ	14X	LHCB	pp at 7, 8 TeV
• • • We do not use the following data for averages, fits, limits, etc. • • •					
<27	90	BISHAI	96	CLE2	$e^+e^- \to \Upsilon(4S)$

[1] ADACHI 25E uses $B(\Upsilon(4S) \to B^+B^-)/B(\Upsilon(4S) \to B^0\overline{B}^0) = 1.052 \pm 0.031$.
[2] AAIJ 14X reports $[\Gamma(B^0 \to J/\psi(1S)\omega)/\Gamma_{total}] \times [B(\omega(782) \to \pi^+\pi^-)] = (2.7^{+0.8+0.7}_{-0.6-0.5}) \times 10^{-7}$ which we divide by our best (shown rounded) value $B(\omega(782) \to \pi^+\pi^-) = (1.53 \pm 0.12) \times 10^{-2}$. Our first error is their experiment's error and our second error is the systematic error from using our best (shown rounded) value.

$\Gamma(J/\psi(1S)\omega)/\Gamma(J/\psi(1S)\rho^0)$ — $\Gamma_{233}/\Gamma_{229}$

VALUE	DOCUMENT ID		TECN	COMMENT
$0.61^{+0.39}_{-0.21} \pm 0.05$	[1,2] AAIJ	13M	LHCB	pp at 7 TeV

[1] AAIJ 13M reports $0.61^{+0.24+0.31}_{-0.14-0.16}$ from a measurement of $[\Gamma(B^0 \to J/\psi(1S)\omega)/\Gamma(B^0 \to J/\psi(1S)\rho^0)] \times [B(\omega(782) \to \pi^+\pi^-)]$ assuming $B(\omega(782) \to \pi^+\pi^-) = (1.53^{+0.11}_{-0.13}) \times 10^{-2}$, which we rescale to our best (shown rounded) value $B(\omega(782) \to \pi^+\pi^-) = (1.53 \pm 0.12) \times 10^{-2}$. Our first error is their experiment's error and our second error is the systematic error from using our best (shown rounded) value.
[2] AAIJ 13M does not report correlations between various measurements of the $J/\psi\pi\pi$ final state. Measured in Dalitz plot like analysis of $B^0 \to J/\psi\pi^+\pi^-$. Assumes $B(\rho(770)^0 \to \pi\pi) = 100\%$.

$\Gamma(J/\psi(1S)\omega)/\Gamma(J/\psi(1S)\rho^0)$ — $\Gamma_{233}/\Gamma_{229}$

VALUE	DOCUMENT ID		TECN	COMMENT
$0.89 \pm 0.19^{+0.07}_{-0.13}$	AAIJ	13A	LHCB	pp at 7 TeV

$\Gamma(J/\psi(1S) K^+K^-)/\Gamma_{total}$ — Γ_{234}/Γ

VALUE (units 10^{-6})	DOCUMENT ID		TECN	COMMENT
$2.53 \pm 0.35 \pm 0.05$	[1] AAIJ	13BT	LHCB	pp at 7 TeV

[1] AAIJ 13BT reports $(2.53 \pm 0.31 \pm 0.19) \times 10^{-6}$ from a measurement of $[\Gamma(B^0 \to J/\psi(1S) K^+K^-)/\Gamma_{total}] / [B(B^+ \to J/\psi(1S) K^+)]$ assuming $B(B^+ \to J/\psi(1S) K^+) = (1.018 \pm 0.042) \times 10^{-3}$, which we rescale to our best (shown rounded) value $B(B^+ \to J/\psi(1S) K^+) = (1.019 \pm 0.019) \times 10^{-3}$. Our first error is their experiment's error and our second error is the systematic error from using our best (shown rounded) value.

$\Gamma(J/\psi(1S) a_0(980),\ a_0 \to K^+K^-)/\Gamma_{total}$ — Γ_{235}/Γ

VALUE (units 10^{-6})	DOCUMENT ID		TECN	COMMENT
$0.470 \pm 0.331 \pm 0.072$	[1] AAIJ	13BT	LHCB	pp at 7 TeV

[1] AAIJ 13BT uses $B(\overline{B}^0 \to J/\psi K^+K^-) = (2.53 \pm 0.31 \pm 0.19) \times 10^{-6}$ to derive this result. It also reports the equivalent upper limit of $< 9.0 \times 10^{-7}$ at 90% CL.

$\Gamma(J/\psi(1S)\phi)/\Gamma_{total}$ — Γ_{236}/Γ

VALUE	CL%	DOCUMENT ID		TECN	COMMENT
$< 1.1 \times 10^{-7}$	90	AAIJ	21K	LHCB	pp at 7, 8, 13 TeV
• • • We do not use the following data for averages, fits, limits, etc. • • •					
$<10.1 \times 10^{-7}$	90	LEES	15	BABR	$e^+e^- \to \Upsilon(4S)$
$< 1.9 \times 10^{-7}$	90	[1] AAIJ	13BT	LHCB	pp at 7 TeV
$< 9.4 \times 10^{-7}$	90	[2] LIU	08I	BELL	$e^+e^- \to \Upsilon(4S)$
$< 9.2 \times 10^{-6}$	90	[2] AUBERT	03O	BABR	$e^+e^- \to \Upsilon(4S)$

[1] AAIJ 13BT uses $B(B^0 \to J/\psi(1S) K^+K^-) = (2.53 \pm 0.31 \pm 0.19) \times 10^{-6}$ and $B(\phi \to K^+K^-) = (48.9 \pm 0.5)\%$ to obtain this result.
[2] Assumes equal production of B^+ and B^0 at the $\Upsilon(4S)$.

$\Gamma(J/\psi(1S)\eta'(958))/\Gamma_{total}$ — Γ_{237}/Γ

VALUE (units 10^{-6})	CL%	DOCUMENT ID		TECN	COMMENT
• • • We do not use the following data for averages, fits, limits, etc. • • •					
$5.06 \pm 0.48 \pm 0.40$		[1] AAIJ	25AN	LHCB	pp at 7, 8 and 13 TeV
$8.0 \pm 2.4 \pm 0.5$		[2] AAIJ	15D	LHCB	Repl. by AAIJ 25AN
< 7.4	90	[3,4] CHANG	12	BELL	$e^+e^- \to \Upsilon(4S)$
<63	90	[4] AUBERT	03O	BABR	$e^+e^- \to \Upsilon(4S)$

[1] AAIJ 25AN value obtained by multiplying reported $B(B^0_s \to J/\psi\eta') = (3.76 \pm 0.13 \pm 0.19 \pm 0.21) \times 10^{-4}$ by the ratio $B(B^0 \to J/\psi\eta')/B(B^0_s \to J/\psi\eta') = (1.33 \pm 0.12 \pm 0.05) \times 10^{-2}$. The last uncertainty combines the systematic uncertainty with branching fraction uncertainties.
[2] AAIJ 15D reports $[\Gamma(B^0 \to J/\psi(1S)\eta'(958))/\Gamma_{total}] / [B(B^0_s \to J/\psi(1S)\eta')] = (2.28 \pm 0.65 \pm 0.16) \times 10^{-2}$ which we multiply by our best (shown rounded) value $B(B^0_s \to J/\psi(1S)\eta') = (3.53 \pm 0.22) \times 10^{-4}$. Our first error is their experiment's error and our second error is the systematic error from using our best (shown rounded) value.
[3] Reconstructs $\eta'(985)$ in $(etapi + pi)^-$ and $\rho(770)$ decays.
[4] Assumes equal production of B^+ and B^0 at the $\Upsilon(4S)$.

$\Gamma(J/\psi(1S)\eta)/\Gamma(J/\psi(1S)\eta'(958))$ — $\Gamma_{224}/\Gamma_{237}$

VALUE	DOCUMENT ID		TECN	COMMENT
$2.08 \pm 0.26 \pm 0.10$	[1] AAIJ	25AN	LHCB	pp at 7, 8, 13 TeV
• • • We do not use the following data for averages, fits, limits, etc. • • •				
$1.111 \pm 0.475 \pm 0.062$	[2] AAIJ	15D	LHCB	Repl. by AAIJ 25AN

[1] AAIJ 25AN reports $B(B^0 \to J/\psi\eta')/B(B^0 \to J/\psi\eta) = 0.48 \pm 0.06 \pm 0.02 \pm 0.01$ from which the reciprocal of ratio is derived. The last error is total systematic, including the branching ratios of η' uncertainties.
[2] Uses $J/\psi \to \mu^+\mu^-$, $\eta' \to \rho^0\gamma$, and $\eta' \to \eta\pi^+\pi^-$ decays.

Int. J. Mod. Phys. A 2026.41. Downloaded from www.worldscientific.com by UNIVERSITY OF CALIFORNIA @ BERKELEY on 09/16/26. Re-use and distribution is strictly not permitted, except for Open Access articles.

$\Gamma(J/\psi(1S)K^0\pi^+\pi^-)/\Gamma(J/\psi(1S)K^0)$ — $\Gamma_{238}/\Gamma_{214}$

VALUE	DOCUMENT ID		TECN	COMMENT
0.50 ±0.04 OUR AVERAGE				
0.493±0.034±0.027	AAIJ	14L	LHCB	pp at 7 TeV
1.24 ±0.40 ±0.15	AFFOLDER	02B	CDF	$p\overline{p}$ 1.8 TeV

$\Gamma(J/\psi(1S)K^0K^+K^-)/\Gamma_{total}$ — Γ_{240}/Γ

VALUE (units 10^{-6})	DOCUMENT ID		TECN	COMMENT
25 ±7 OUR AVERAGE Error includes scale factor of 1.8.				
34.9±6.7±1.5	LEES	15	BABR	$e^+e^- \to \Upsilon(4S)$
20.2±4.3±1.9	[1] AAIJ	14L	LHCB	pp at 7 TeV

[1] Measured with $B(B^0 \to J/\psi K^0_S K^+K^-)$ / $B(B^0 \to J/\psi K^0_S)$ using PDG 12 for the involved branching fractions.

$\Gamma(J/\psi(1S)K^0K^-\pi^+ + c.c.)/\Gamma_{total}$ — Γ_{239}/Γ

VALUE	CL%	DOCUMENT ID		TECN	COMMENT
<21 × 10^{-6}	90	[1] AAIJ	14L	LHCB	pp at 7 TeV

[1] Measured with $B(B^0 \to J/\psi K^0_S K^\pm\pi^\mp)$ / $B(B^0 \to J/\psi K^0_S \pi^+\pi^-)$ using PDG 12 values for the involved branching fractions.

$\Gamma(J/\psi(1S)K^0\rho^0)/\Gamma_{total}$ — Γ_{242}/Γ

VALUE (units 10^{-4})	DOCUMENT ID		TECN	COMMENT
5.4±2.9±0.9	[1] AFFOLDER	02B	CDF	$p\overline{p}$ 1.8 TeV

[1] Uses $B^0 \to J/\psi(1S)K^0_S$ decay as a reference and $B(B^0 \to J/\psi(1S)K^0) = 8.3\times10^{-4}$.

$\Gamma(J/\psi(1S)K^*(892)^+\pi^-)/\Gamma_{total}$ — Γ_{243}/Γ

VALUE (units 10^{-4})	DOCUMENT ID		TECN	COMMENT
7.7±4.1±1.3	[1] AFFOLDER	02B	CDF	$p\overline{p}$ 1.8 TeV

[1] Uses $B^0 \to J/\psi(1S)K^0_S$ decay as a reference and $B(B^0 \to J/\psi(1S)K^0) = 8.3\times10^{-4}$.

$\Gamma(J/\psi(1S)\pi^+\pi^-\pi^+\pi^-)/\Gamma(J/\psi(1S)\pi^+\pi^-)$ — $\Gamma_{244}/\Gamma_{225}$

VALUE	DOCUMENT ID		TECN	COMMENT
0.361±0.017±0.021	[1] AAIJ	14Y	LHCB	pp at 7, 8 TeV

[1] Excludes contributions from $\psi(2S)$ and $\chi_{c1}(3872)$ decaying to $J/\psi(1S)\pi^+\pi^-$.

$\Gamma(J/\psi(1S)f_1(1285))/\Gamma_{total}$ — Γ_{245}/Γ

VALUE (units 10^{-6})	DOCUMENT ID		TECN	COMMENT
$8.4^{+2.1}_{-2.0}\pm0.5$	[1] AAIJ	14Y	LHCB	pp at 7, 8 TeV

[1] AAIJ 14Y reports $(8.37 \pm 1.95^{+0.71}_{-0.66} \pm 0.35)\times10^{-6}$ from a measurement of $[\Gamma(B^0 \to J/\psi(1S)f_1(1285))/\Gamma_{total}] \times [B(f_1(1285) \to 2\pi^+2\pi^-)]$ assuming $B(f_1(1285) \to 2\pi^+2\pi^-) = 0.11^{+0.007}_{-0.006}$, which we rescale to our best (shown rounded) value $B(f_1(1285) \to 2\pi^+2\pi^-) = (10.9 \pm 0.6)\times10^{-2}$. Our first error is their experiment's error and our second error is the systematic error from using our best (shown rounded) value.

$\Gamma(J/\psi(1S)K^*(892)^0\pi^+\pi^-)/\Gamma_{total}$ — Γ_{246}/Γ

VALUE (units 10^{-4})	DOCUMENT ID		TECN	COMMENT
6.6±1.9±1.1	[1] AFFOLDER	02B	CDF	$p\overline{p}$ 1.8 TeV

[1] Uses $B^0 \to J/\psi(1S)K^*(892)^0$ decay as a reference and $B(B^0 \to J/\psi(1S)K^0) = 12.4\times10^{-4}$.

$\Gamma(\eta_{c2}(1D)K^0_S,\ \eta_{c2} \to h_c\gamma)/\Gamma_{total}$ — Γ_{247}/Γ

VALUE	CL%	DOCUMENT ID		TECN	COMMENT
<3.5 × 10^{-5}	90	CHILIKIN	20	BELL	$e^+e^- \to \Upsilon(4S)$

$\Gamma(\eta_{c2}(1D)\pi^-K^+,\ \eta_{c2} \to h_c\gamma)/\Gamma_{total}$ — Γ_{248}/Γ

VALUE	CL%	DOCUMENT ID		TECN	COMMENT
<1.0 × 10^{-4}	90	CHILIKIN	20	BELL	$e^+e^- \to \Upsilon(4S)$

$\Gamma(\chi_{c1}(3872)K^0)/\Gamma_{total}$ — Γ_{251}/Γ

VALUE (units 10^{-4})	CL%	DOCUMENT ID		TECN	COMMENT
1.1 ±0.4 OUR AVERAGE					
$2.5\ ^{+0.9}_{-0.8}\ \pm0.8$		[1] HIRATA	23	BELL	$e^+e^- \to \Upsilon(4S)$
0.93±0.27±0.29		[2] CHOI	11	BELL	$e^+e^- \to \Upsilon(4S)$
$1.2\ \pm0.6\ ^{+0.4}_{-0.5}$		[3] DEL-AMO-SA...10B		BABR	$e^+e^- \to \Upsilon(4S)$
• • • We do not use the following data for averages, fits, limits, etc. • • •					
<2.5	90	[4,5] BHARDWAJ	11	BELL	$e^+e^- \to \Upsilon(4S)$
2.1 ±1.0 ±0.7		[5,6] AUSHEV	10	BELL	$e^+e^- \to \Upsilon(4S)$
<5	90	[7,8] AUBERT	09B	BABR	$e^+e^- \to \Upsilon(4S)$
4.8 ±2.4 ±1.7		[5,7,9] AUBERT	08B	BABR	$e^+e^- \to \Upsilon(4S)$
<1.4	90	[10] AUBERT	08Y	BABR	$e^+e^- \to \Upsilon(4S)$
<2.4	90	[11] AUBERT	06	BABR	Repl. by AUBERT 08Y
$3.0\ \pm1.4\ ^{+1.6}_{-1.5}$		[12,13] GOKHROO	06	BELL	$e^+e^- \to \Upsilon(4S)$

[1] HIRATA 23 reports $[\Gamma(B^0 \to \chi_{c1}(3872)K^0)/\Gamma_{total}]$ / $[B(B^+ \to \chi_{c1}(3872)K^+)] = 1.34^{+0.47}_{-0.40}{}^{+0.10}_{-0.12}$ which we multiply by our best (shown rounded) value $B(B^+ \to \chi_{c1}(3872)K^+) = (1.9 \pm 0.6)\times10^{-4}$. Our first error is their experiment's error and our second error is the systematic error from using our best (shown rounded) value.

[2] CHOI 11 reports $[\Gamma(B^0 \to \chi_{c1}(3872)K^0)/\Gamma_{total}]$ / $[B(B^+ \to \chi_{c1}(3872)K^+)] = 0.50 \pm 0.14 \pm 0.04$ which we multiply by our best (shown rounded) value $B(B^+ \to \chi_{c1}(3872)K^+) = (1.9 \pm 0.6)\times10^{-4}$. Our first error is their experiment's error and our second error is the systematic error from using our best (shown rounded) value.

[3] DEL-AMO-SANCHEZ 10B reports $[\Gamma(B^0 \to \chi_{c1}(3872)K^0)/\Gamma_{total}] \times [B(\chi_{c1}(3872) \to \omega J/\psi(1S))] = (6 \pm 3 \pm 1)\times10^{-6}$ which we divide by our best (shown rounded) value $B(\chi_{c1}(3872) \to \omega J/\psi(1S)) = (5.0 \pm 1.9)\times10^{-2}$. Our first error is their experiment's error and our second error is the systematic error from using our best (shown rounded) value.

[4] BHARDWAJ 11 reports $[\Gamma(B^0 \to \chi_{c1}(3872)K^0)/\Gamma_{total}] \times [B(\chi_{c1}(3872) \to \gamma J/\psi)] < 2.4\times10^{-6}$ which we divide by our best (shown rounded) value $B(\chi_{c1}(3872) \to \gamma J/\psi) = 10\times10^{-3}$.

[5] Assumes equal production of B^+ and B^0 at the $\Upsilon(4S)$.

[6] AUSHEV 10 reports $[\Gamma(B^0 \to \chi_{c1}(3872)K^0)/\Gamma_{total}] \times [B(\chi_{c1}(3872) \to \overline{D}^{*0}D^0)] = (0.97 \pm 0.46 \pm 0.13)\times10^{-4}$ which we divide by our best (shown rounded) value $B(\chi_{c1}(3872) \to \overline{D}^{*0}D^0) = (46 \pm 16)\times10^{-2}$. Our first error is their experiment's error and our second error is the systematic error from using our best (shown rounded) value.

[7] Uses $B(\Upsilon(4S) \to B^+B^-) = (51.6 \pm 0.6)\%$ and $B(\Upsilon(4S) \to B^0\overline{B}^0) = (48.4 \pm 0.6)\%$.

[8] AUBERT 09B reports $[\Gamma(B^0 \to \chi_{c1}(3872)K^0)/\Gamma_{total}] \times [B(\chi_{c1}(3872) \to \gamma J/\psi)] < 4.9\times10^{-6}$ which we divide by our best (shown rounded) value $B(\chi_{c1}(3872) \to \gamma J/\psi) = 10\times10^{-3}$.

[9] AUBERT 08B reports $[\Gamma(B^0 \to \chi_{c1}(3872)K^0)/\Gamma_{total}] \times [B(\chi_{c1}(3872) \to \overline{D}^{*0}D^0)] = (2.22 \pm 1.05 \pm 0.42)\times10^{-4}$ which we divide by our best (shown rounded) value $B(\chi_{c1}(3872) \to \overline{D}^{*0}D^0) = (46 \pm 16)\times10^{-2}$. Our first error is their experiment's error and our second error is the systematic error from using our best (shown rounded) value.

[10] AUBERT 08Y reports $[\Gamma(B^0 \to \chi_{c1}(3872)K^0)/\Gamma_{total}] \times [B(\chi_{c1}(3872) \to \pi^+\pi^-J/\psi(1S))] < 6.0\times10^{-6}$ which we divide by our best (shown rounded) value $B(\chi_{c1}(3872) \to \pi^+\pi^-J/\psi(1S)) = 4.3\times10^{-2}$.

[11] AUBERT 06 reports $[\Gamma(B^0 \to \chi_{c1}(3872)K^0)/\Gamma_{total}] \times [B(\chi_{c1}(3872) \to \pi^+\pi^-J/\psi(1S))] < 10.3\times10^{-6}$ which we divide by our best (shown rounded) value $B(\chi_{c1}(3872) \to \pi^+\pi^-J/\psi(1S)) = 4.3\times10^{-2}$.

[12] GOKHROO 06 reports $[\Gamma(B^0 \to \chi_{c1}(3872)K^0)/\Gamma_{total}] \times [B(\chi_{c1}(3872) \to D^0\overline{D}^0\pi^0)] = (1.66 \pm 0.70^{+0.32}_{-0.37})\times10^{-4}$ which we divide by our best (shown rounded) value $B(\chi_{c1}(3872) \to D^0\overline{D}^0\pi^0) = (55 \pm 28)\times10^{-2}$. Our first error is their experiment's error and our second error is the systematic error from using our best (shown rounded) value.

[13] Measure the near-threshold enhancements in the $(D^0\overline{D}^0\pi^0)$ system at a mass $3875.2 \pm 0.7^{+0.3}_{-1.6} \pm 0.8$ MeV/c^2.

$\Gamma(\chi_{c1}(3872)^-K^+)/\Gamma_{total}$ — Γ_{249}/Γ

VALUE	CL%	DOCUMENT ID		TECN	COMMENT
<5 × 10^{-4}	90	[1] AUBERT	06E	BABR	$e^+e^- \to \Upsilon(4S)$

[1] Perform measurements of absolute branching fractions using a missing mass technique.

$\Gamma(\chi_{c1}(3872)^-K^+,\ \chi_{c1}(3872)^- \to J/\psi(1S)\pi^-\pi^0)/\Gamma_{total}$ — Γ_{250}/Γ

VALUE (units 10^{-6})	CL%	DOCUMENT ID		TECN	COMMENT
<4.2	90	[1,2] CHOI	11	BELL	$e^+e^- \to \Upsilon(4S)$
• • • We do not use the following data for averages, fits, limits, etc. • • •					
<5.4	90	[2,3] AUBERT	05B	BABR	$e^+e^- \to \Upsilon(4S)$

[1] Assumes $\pi^+\pi^0$ originates from ρ^+.

[2] Assumes equal production of B^+ and B^0 at the $\Upsilon(4S)$.

[3] The isovector-X hypothesis is excluded with a likelihood test at 1×10^{-4} level.

$\Gamma(\chi_{c1}(3872)K^*(892)^0)/\Gamma_{total}$ — Γ_{252}/Γ

VALUE (units 10^{-4})	CL%	DOCUMENT ID		TECN	COMMENT
0.92±0.35±0.29		[1] BALA	15	BELL	$e^+e^- \to \Upsilon(4S)$
• • • We do not use the following data for averages, fits, limits, etc. • • •					
<2.9	90	[2,3] AUBERT	09B	BABR	$e^+e^- \to \Upsilon(4S)$
		[3,4] AUBERT	09B	BABR	$e^+e^- \to \Upsilon(4S)$

[1] BALA 15 reports $[\Gamma(B^0 \to \chi_{c1}(3872)K^*(892)^0)/\Gamma_{total}] \times [B(\chi_{c1}(3872) \to \pi^+\pi^-J/\psi(1S))] = (4.0 \pm 1.5 \pm 0.3)\times10^{-6}$ which we divide by our best (shown rounded) value $B(\chi_{c1}(3872) \to \pi^+\pi^-J/\psi(1S)) = (4.3 \pm 1.4)\times10^{-2}$. Our first error is their experiment's error and our second error is the systematic error from using our best (shown rounded) value.

[2] AUBERT 09B reports $[\Gamma(B^0 \to \chi_{c1}(3872)K^*(892)^0)/\Gamma_{total}] \times [B(\chi_{c1}(3872) \to \gamma J/\psi)] < 2.8\times10^{-6}$ which we divide by our best (shown rounded) value $B(\chi_{c1}(3872) \to \gamma J/\psi) = 10\times10^{-3}$.

[3] Uses $B(\Upsilon(4S) \to B^+B^-) = (51.6 \pm 0.6)\%$ and $B(\Upsilon(4S) \to B^0\overline{B}^0) = (48.4 \pm 0.6)\%$.

[4] AUBERT 09B reports $[\Gamma(B^0 \to \chi_{c1}(3872)K^*(892)^0)/\Gamma_{total}] \times [B(\chi_{c1}(3872) \to \gamma\psi(2S))] < 4.4\times10^{-6}$ at 90% CL.

$\Gamma(\chi_{c1}(3872)K^+\pi^-)/\Gamma_{total}$ — Γ_{253}/Γ

VALUE (units 10^{-4})	DOCUMENT ID		TECN	COMMENT
1.8±0.3±0.6	[1,2] BALA	15	BELL	$e^+e^- \to \Upsilon(4S)$

[1] BALA 15 reports $[\Gamma(B^0 \to \chi_{c1}(3872)K^+\pi^-)/\Gamma_{total}] \times [B(\chi_{c1}(3872) \to \pi^+\pi^-J/\psi(1S))] = (7.9 \pm 1.3 \pm 0.4)\times10^{-6}$ which we divide by our best (shown rounded) value $B(\chi_{c1}(3872) \to \pi^+\pi^-J/\psi(1S)) = (4.3 \pm 1.4)\times10^{-2}$. Our first error is their experiment's error and our second error is the systematic error from using our best (shown rounded) value.

[2] Assumes equal production of B^+ and B^0 at the $\Upsilon(4S)$.

Int. J. Mod. Phys. A 2026.41. Downloaded from www.worldscientific.com by CALIFORNIA @ BERKELEY on 09/16/26. Re-use and distribution is strictly not permitted, except for Open Access articles.

$\Gamma(\chi_{c1}(3872)\gamma)/\Gamma_{total}$ — Γ_{254}/Γ

VALUE	CL%	DOCUMENT ID		TECN	COMMENT
$<1.2\times10^{-5}$	90	[1,2] CHOU	19	BELL	$e^+e^-\to\Upsilon(4S)$

[1] Assumes equal production of B^+ and B^0 at $\Upsilon(4S)$.
[2] CHOU 19 reports $[\Gamma(B^0\to\chi_{c1}(3872)\gamma)/\Gamma_{total}]\times[B(\chi_{c1}(3872)\to\pi^+\pi^-J/\psi(1S))]<5.1\times10^{-7}$ which we divide by our best (shown rounded) value $B(\chi_{c1}(3872)\to\pi^+\pi^-J/\psi(1S))=4.3\times10^{-2}$.

$\Gamma(T_{c\bar{c}1}(4430)^\pm K^\mp,\ T^\pm_{c\bar{c}1}\to\psi(2S)\pi^\pm)/\Gamma_{total}$ — Γ_{255}/Γ

VALUE (units 10^{-5})	CL%	DOCUMENT ID		TECN	COMMENT
$6.0^{+1.7+2.5}_{-2.0-1.4}$		CHILIKIN	13	BELL	$e^+e^-\to\Upsilon(4S)$
• • • We do not use the following data for averages, fits, limits, etc. • • •					
<3.1	95	[1] AUBERT	09AA	BABR	$e^+e^-\to\Upsilon(4S)$
$3.2^{+1.8+5.3}_{-0.9-1.6}$		[1] MIZUK	09	BELL	$e^+e^-\to\Upsilon(4S)$
$4.1\pm1.0\pm1.4$		[1,2] CHOI	08	BELL	Repl. by MIZUK 09

[1] Assumes equal production of B^+ and B^0 at the $\Upsilon(4S)$.
[2] Establishes the $(Z_c4430)^+$ with a significance of 6.5 sigma. Needs confirmation.

$\Gamma(T_{c\bar{c}1}(4430)^\pm K^\mp,\ T^\pm_{c\bar{c}1}\to J/\psi\pi^\pm)/\Gamma_{total}$ — Γ_{256}/Γ

VALUE (units 10^{-6})	CL%	DOCUMENT ID		TECN	COMMENT
$5.4^{+4.0+1.1}_{-1.0-0.6}$		CHILIKIN	14	BELL	$\overline{B}^0\to J/\psi K^-\pi^+$
• • • We do not use the following data for averages, fits, limits, etc. • • •					
<4	95	[1] AUBERT	09AA	BABR	$e^+e^-\to\Upsilon(4S)$

[1] Assumes equal production of B^+ and B^0 at the $\Upsilon(4S)$.

$\Gamma(T_{c\bar{c}1}(3900)^\pm K^\mp,\ T^\pm_{c\bar{c}1}\to J/\psi\pi^\pm)/\Gamma_{total}$ — Γ_{257}/Γ

VALUE	DOCUMENT ID		TECN	COMMENT
$<9\times10^{-7}$	CHILIKIN	14	BELL	$\overline{B}^0\to J/\psi K^-\pi^+$

$\Gamma(T_{c\bar{c}1}(4200)^\pm K^\mp,\ T^\pm_{c\bar{c}1}\to J/\psi\pi^\pm)/\Gamma_{total}$ — Γ_{258}/Γ

VALUE (units 10^{-5})	DOCUMENT ID		TECN	COMMENT
$2.2^{+0.7+1.1}_{-0.5-0.6}$	CHILIKIN	14	BELL	$\overline{B}^0\to J/\psi K^-\pi^+$

$\Gamma(T_{c\bar{c}1}(3900)^\pm K^\mp,\ T^\pm_{c\bar{c}1}\to J/\psi\pi^\pm)/\Gamma(J/\psi(1S)K^*(892)^0)$ — $\Gamma_{257}/\Gamma_{216}$

VALUE	CL%	DOCUMENT ID		TECN	COMMENT
$<1.5\times10^{-2}$	90	ABAZOV	18B	D0	$p\overline{p}$ at 1.96 TeV

$\Gamma(J/\psi(1S)p\overline{p})/\Gamma_{total}$ — Γ_{259}/Γ

VALUE (units 10^{-7})	CL%	DOCUMENT ID		TECN	COMMENT
$4.51\pm0.40\pm0.44$		[1] AAIJ	19U	LHCB	pp at 7, 8, 13 TeV
• • • We do not use the following data for averages, fits, limits, etc. • • •					
<5.2	90	[2] AAIJ	13Z	LHCB	Repl. by AAIJ 19U
<8.3	90	[3] XIE	05	BELL	$e^+e^-\to\Upsilon(4S)$
<19	90	[3] AUBERT	03K	BABR	$e^+e^-\to\Upsilon(4S)$

[1] Measured relative to $B^0_s\to J/\psi\phi$ assuming $B(B^0_s\to J/\psi\phi)=(10.5\pm0.13\pm0.64)\times10^{-4}$ and taking into account small K^+K^- S-wave contribution. Measurement assumes $f_s/f_d=0.259\pm0.015$ for 7, 8 TeV data and f_s/f_d multiplied by 1.068 ± 0.046 for 13 TeV data.
[2] Uses $B(B^0_s\to J/\psi(1S)\pi^+\pi^-)=(1.98\pm0.20)\times10^{-4}$.
[3] Assumes equal production of B^+ and B^0 at the $\Upsilon(4S)$.

$\Gamma(J/\psi(1S)\gamma)/\Gamma_{total}$ — Γ_{260}/Γ

VALUE (units 10^{-6})	CL%	DOCUMENT ID		TECN	COMMENT
<1.5	90	[1] AAIJ	15BB	LHCB	pp at 7, 8 TeV
• • • We do not use the following data for averages, fits, limits, etc. • • •					
<1.6	90	[2] AUBERT,B	04T	BABR	$e^+e^-\to\Upsilon(4S)$

[1] Branching fractions of normalization modes $B^0\to J/\psi\gamma X$ taken from PDG 14. Uses $f_s/f_d=0.259\pm0.015$.
[2] Assumes equal production of B^+ and B^0 at the $\Upsilon(4S)$.

$\Gamma(J/\psi\mu^+\mu^-,\ J/\psi\to\mu^+\mu^-)/\Gamma_{total}$ — Γ_{261}/Γ

VALUE	CL%	DOCUMENT ID		TECN	COMMENT
$<1.0\times10^{-9}$	95	AAIJ	22Q	LHCB	pp at 7, 8, 13 TeV

$\Gamma(J/\psi(1S)\overline{D}^0)/\Gamma_{total}$ — Γ_{262}/Γ

VALUE	CL%	DOCUMENT ID		TECN	COMMENT
$<9.6\times10^{-7}$	90	AAIJ	24F	LHCB	pp at 7, 8, 13 TeV
• • • We do not use the following data for averages, fits, limits, etc. • • •					
$<1.3\times10^{-5}$	90	[1] AUBERT	05U	BABR	$e^+e^-\to\Upsilon(4S)$
$<2.0\times10^{-5}$	90	[1] ZHANG	05B	BELL	$e^+e^-\to\Upsilon(4S)$

[1] Assumes equal production of B^+ and B^0 at the $\Upsilon(4S)$.

$\Gamma(\psi(2S)\pi^0)/\Gamma_{total}$ — Γ_{263}/Γ

VALUE (units 10^{-5})	DOCUMENT ID		TECN	COMMENT
$1.17\pm0.17\pm0.08$	[1] CHOBANOVA	16	BELL	$e^+e^-\to\Upsilon(4S)$

[1] Assumes equal production of B^+ and B^0 at the $\Upsilon(4S)$.

$\Gamma(\psi(2S)K^0)/\Gamma_{total}$ — Γ_{264}/Γ

VALUE (units 10^{-4})	CL%	DOCUMENT ID		TECN	COMMENT
5.8 ± 0.5 OUR FIT					
5.8 ± 0.5 OUR AVERAGE					
$4.7\pm0.7\pm0.7$		[1] AAIJ	14L	LHCB	pp at 7 TeV
$6.46\pm0.65\pm0.51$		[2] AUBERT	05J	BABR	$e^+e^-\to\Upsilon(4S)$
6.7 ± 1.1		[2] ABE	03B	BELL	$e^+e^-\to\Upsilon(4S)$
$5.0\pm1.1\pm0.6$		[2] RICHICHI	01	CLE2	$e^+e^-\to\Upsilon(4S)$
• • • We do not use the following data for averages, fits, limits, etc. • • •					
$6.9\pm1.1\pm1.1$		[2] AUBERT	02	BABR	Repl. by AUBERT 05J
<8	90	[2] ALAM	94	CLE2	$e^+e^-\to\Upsilon(4S)$
<15	90	[2] BORTOLETTO	92	CLEO	$e^+e^-\to\Upsilon(4S)$
<28	90	[2] ALBRECHT	90J	ARG	$e^+e^-\to\Upsilon(4S)$

[1] Measured with $B(B^0\to\psi(2S)K^0_S)\times B(\psi(2S)\to J/\psi\pi^+\pi^-)$ / $B(B^0\to J/\psi K^0_S)$ using PDG 12 values for the involved branching fractions.
[2] Assumes equal production of B^+ and B^0 at the $\Upsilon(4S)$.

$\Gamma(\psi(2S)K^0\pi^+\pi^-)/\Gamma(\psi(2S)K^0)$ — $\Gamma_{265}/\Gamma_{264}$

VALUE	DOCUMENT ID		TECN	COMMENT
$0.480\pm0.013\pm0.032$	TUMASYAN	22AI	CMS	pp at 13 TeV

$\Gamma(\psi(2S)K^0)/\Gamma(J/\psi(1S)K^0)$ — $\Gamma_{264}/\Gamma_{214}$

VALUE	DOCUMENT ID		TECN	COMMENT
$0.82\pm0.13\pm0.12$	[1] AUBERT	02	BABR	$e^+e^-\to\Upsilon(4S)$

[1] Assumes equal production of B^+ and B^0 at the $\Upsilon(4S)$.

$\Gamma(\psi(3770)K^0,\ \psi\to\overline{D}^0D^0)/\Gamma_{total}$ — Γ_{266}/Γ

VALUE (units 10^{-4})	CL%	DOCUMENT ID		TECN	COMMENT
<1.23	90	[1] AUBERT	08B	BABR	$e^+e^-\to\Upsilon(4S)$

[1] Assumes equal production of B^+ and B^0 at the $\Upsilon(4S)$.

$\Gamma(\psi(3770)K^0,\ \psi\to D^-D^+)/\Gamma_{total}$ — Γ_{267}/Γ

VALUE (units 10^{-4})	CL%	DOCUMENT ID		TECN	COMMENT
<1.88	90	[1] AUBERT	08B	BABR	$e^+e^-\to\Upsilon(4S)$

[1] Assumes equal production of B^+ and B^0 at the $\Upsilon(4S)$.

$\Gamma(\psi(2S)\pi^+\pi^-)/\Gamma(J/\psi(1S)\pi^+\pi^-)$ — $\Gamma_{268}/\Gamma_{225}$

VALUE	DOCUMENT ID		TECN	COMMENT
$0.56\pm0.07\pm0.05$	[1] AAIJ	13AA	LHCB	pp at 7 TeV

[1] Assuming lepton universality for dimuon decay modes of J/ψ and $\psi(2S)$ mesons, the ratio $B(J/\psi\to\mu^+\mu^-)/B(\psi(2S)\to\mu^+\mu^-)=B(J/\psi\to e^+e^-)/B(\psi(2S)\to e^+e^-)=7.69\pm0.19$ was used.

$\Gamma(\psi(2S)K^+\pi^-)/\Gamma_{total}$ — Γ_{269}/Γ

VALUE (units 10^{-4})	CL%	DOCUMENT ID		TECN	COMMENT
5.80 ± 0.39		[1,2] CHILIKIN	13	BELL	$e^+e^-\to\Upsilon(4S)$
• • • We do not use the following data for averages, fits, limits, etc. • • •					
5.57 ± 0.16		[3] AUBERT	09AA	BABR	$e^+e^-\to\Upsilon(4S)$
$5.68\pm0.13\pm0.42$		[2] MIZUK	09	BELL	$e^+e^-\to\Upsilon(4S)$
<10	90	[2] ALBRECHT	90J	ARG	$e^+e^-\to\Upsilon(4S)$

[1] Combines measurements with $\psi(2S)\to\ell^+\ell^-$ with measurement from MIZUK 09 which uses $\psi(2S)\to J/\psi\pi^+\pi^-$.
[2] Assumes equal production of B^+ and B^0 at the $\Upsilon(4S)$.
[3] Does not report systematic uncertainties.

$\Gamma(\psi(2S)K^*(892)^0)/\Gamma_{total}$ — Γ_{270}/Γ

VALUE (units 10^{-4})	CL%	DOCUMENT ID		TECN	COMMENT
5.9 ± 0.4 OUR FIT					
$6.0^{+0.5}_{-0.7}$ OUR AVERAGE Error includes scale factor of 1.1.					
$5.55^{+0.22+0.41}_{-0.23-0.84}$		[1] CHILIKIN	13	BELL	$e^+e^-\to\Upsilon(4S)$
$6.49\pm0.59\pm0.97$		[1] AUBERT	05J	BABR	$e^+e^-\to\Upsilon(4S)$
$7.6\pm1.1\pm1.0$		[1] RICHICHI	01	CLE2	$e^+e^-\to\Upsilon(4S)$
$9.0\pm2.2\pm0.9$		[2] ABE	98O	CDF	$p\overline{p}$ 1.8 TeV
• • • We do not use the following data for averages, fits, limits, etc. • • •					
$5.52^{+0.35+0.53}_{-0.32-0.58}$		[1] MIZUK	09	BELL	$e^+e^-\to\Upsilon(4S)$
<19	90	[1] ALAM	94	CLE2	Repl. by RICHICHI 01
$14\pm8\pm4$		[1] BORTOLETTO	92	CLEO	$e^+e^-\to\Upsilon(4S)$
<23	90	[1] ALBRECHT	90J	ARG	$e^+e^-\to\Upsilon(4S)$

[1] Assumes equal production of B^+ and B^0 at the $\Upsilon(4S)$.
[2] ABE 98O reports $[B(B^0\to\psi(2S)K^*(892)^0)]/[B(B^+\to J/\psi(1S)K^+)]=0.908\pm0.194\pm0.10$. We multiply by our best value $B(B^+\to J/\psi(1S)K^+)=(9.9\pm1.0)\times10^{-4}$. Our first error is their experiment's error and our second error is the systematic error from using our best value.

$\Gamma(\psi(2S)K^*(892)^0)/\Gamma(J/\psi(1S)K^*(892)^0)$ — $\Gamma_{270}/\Gamma_{216}$

VALUE	DOCUMENT ID		TECN	COMMENT
$0.488\pm0.018\pm0.014$	[1,2] AAIJ	12L	LHCB	pp at 7 TeV

[1] AAIJ 12L reports $0.476\pm0.014\pm0.010\pm0.012$ from a measurement of $[\Gamma(B^0\to\psi(2S)K^*(892)^0)/\Gamma(B^0\to J/\psi(1S)K^*(892)^0)]\times[B(J/\psi(1S)\to e^+e^-)]$ /

Int. J. Mod. Phys. A 2026.41. Downloaded from www.worldscientific.com by UNIVERSITY OF CALIFORNIA @ BERKELEY on 09/16/26. Re-use and distribution is strictly not permitted, except for Open Access articles.

[B($\psi(2S) \to e^+e^-$)] assuming B($J/\psi(1S) \to e^+e^-$) = (5.94 ± 0.06) × 10^{-2}, B($\psi(2S) \to e^+e^-$) = (7.72 ± 0.17) × 10^{-3}, which we rescale to our best (shown rounded) values B($J/\psi(1S) \to e^+e^-$) = (5.971 ± 0.032) × 10^{-2}, B($\psi(2S) \to e^+e^-$) = (7.95 ± 0.22) × 10^{-3}. Our first error is their experiment's error and our second error is the systematic error from using our best (shown rounded) values.

[2] Assumes B($J/\psi \to \mu^+\mu^-$) / B($\psi(2S) \to \mu^+\mu^-$) = B($J/\psi \to e^+e^-$) / B($\psi(2S) \to e^+e^-$) = 7.69 ± 0.19.

$\Gamma(\psi(2S)K^*(892)^0)/\Gamma(\psi(2S)K^0)$ — $\Gamma_{270}/\Gamma_{264}$

VALUE	DOCUMENT ID		TECN	COMMENT
1.02±0.10 OUR FIT				
1.00±0.14±0.09	AUBERT	05J	BABR	$e^+e^- \to \Upsilon(4S)$

$\Gamma(\chi_{c0}K^0)/\Gamma_{total}$ — Γ_{271}/Γ

VALUE (units 10^{-6})	CL%	DOCUMENT ID		TECN	COMMENT
$\mathbf{195^{+42}_{-36}\pm11}$		[1] AAIJ	18F	LHCB	pp at 7, 8 TeV
• • • We do not use the following data for averages, fits, limits, etc. • • •					
$150^{+106}_{-88}\pm 9$		[2,3] LEES	12I	BABR	$e^+e^- \to \Upsilon(4S)$
148± 30±13		[2,4] LEES	12O	BABR	$e^+e^- \to \Upsilon(4S)$
$142^{+55}_{-44}\pm22$		[2,5] AUBERT	09AU	BABR	$e^+e^- \to \Upsilon(4S)$
< 113	90	[5] GARMASH	07	BELL	$e^+e^- \to \Upsilon(4S)$
<1240	90	[2] AUBERT	05K	BABR	$e^+e^- \to \Upsilon(4S)$
< 500	90	[6] EDWARDS	01	CLE2	$e^+e^- \to \Upsilon(4S)$

[1] AAIJ 18F uses Dalitz plot analysis of the $B^0 \to K^0_S\pi^+\pi^-$ final state decays. For the branching fraction of the reference mode, the PDG 18 average B($B^0 \to K^0_S\pi^+\pi^-$) = (4.96 ± 0.20) × 10^{-5} is used. We compute B($B^0 \to \chi_{c0}K^0$) using the PDG value B($\chi_{c0} \to \pi\pi$) = (8.51 ± 0.33) × 10^{-3} and 2/3 for the $\pi^+\pi^-$ fraction. Our first error is their experiment's error and the second error is systematic error from using our best value.

[2] Assumes equal production of B^+ and B^0 at the $\Upsilon(4S)$.

[3] LEES 12I reports [$\Gamma(B^0 \to \chi_{c0}K^0)/\Gamma_{total}$] × [B($\chi_{c0}(1P) \to K^0_S K^0_S$)] = ($0.46^{+0.25}_{-0.17}$ ± 0.21) × 10^{-6} which we divide by our best (shown rounded) value B($\chi_{c0}(1P) \to K^0_S K^0_S$) = (3.08 ± 0.18) × 10^{-3}. Our first error is their experiment's error and our second error is the systematic error from using our best (shown rounded) value.

[4] Measured in the $B^0 \to K^0_S K^+K^-$ decay.

[5] Uses Dalitz plot analysis of the $B^0 \to K^0\pi^+\pi^-$ final state decays.

[6] EDWARDS 01 assumes equal production of B^0 and B^+ at the $\Upsilon(4S)$. The correlated uncertainties (28.3)% from B($J/\psi(1S) \to \gamma\eta_c$) in those modes have been accounted for.

$\Gamma(\chi_{c0}K^*(892)^0)/\Gamma_{total}$ — Γ_{272}/Γ

VALUE (units 10^{-4})	CL%	DOCUMENT ID		TECN	COMMENT
1.7±0.3±0.2		[1] AUBERT	08BD	BABR	$e^+e^- \to \Upsilon(4S)$
• • • We do not use the following data for averages, fits, limits, etc. • • •					
<7.7	90	[1] AUBERT	05K	BABR	Repl. by AUBERT 08BD

[1] Assumes equal production of B^+ and B^0 at the $\Upsilon(4S)$.

$\Gamma(\chi_{c1}\pi^0)/\Gamma_{total}$ — Γ_{273}/Γ

VALUE (units 10^{-5})	DOCUMENT ID		TECN	COMMENT
1.12±0.25±0.12	[1] KUMAR	08	BELL	$e^+e^- \to \Upsilon(4S)$

[1] Assumes equal production of B^+ and B^0 at the $\Upsilon(4S)$.

$\Gamma(\chi_{c1}K^0)/\Gamma_{total}$ — Γ_{274}/Γ

VALUE (units 10^{-4})	CL%	DOCUMENT ID		TECN	COMMENT
3.95±0.27 OUR AVERAGE					
$15\ ^{+5}_{-4}\pm6$		[1] CHILIKIN	19	BELL	$e^+e^- \to \Upsilon(4S)$
$3.78^{+0.17}_{-0.16}\pm0.33$		[2] BHARDWAJ	11	BELL	$e^+e^- \to \Upsilon(4S)$
4.2 ±0.3 ±0.3		[3] AUBERT	09B	BABR	$e^+e^- \to \Upsilon(4S)$
$3.1\ ^{+1.6}_{-1.1}\pm0.1$		[4] AVERY	00	CLE2	$e^+e^- \to \Upsilon(4S)$
• • • We do not use the following data for averages, fits, limits, etc. • • •					
3.51±0.33±0.45		[2] SONI	06	BELL	Repl. by BHARDWAJ 11
4.53±0.41±0.51		[2] AUBERT	05J	BABR	Repl. by AUBERT 09B
4.4 ±1.4 ±0.2		[5] AUBERT	02	BABR	Repl. by AUBERT 05J
<27	90	[2] ALAM	94	CLE2	$e^+e^- \to \Upsilon(4S)$

[1] CHILIKIN 19 reports [$\Gamma(B^0 \to \chi_{c1}K^0)/\Gamma_{total}$] × [B($\chi_{c1}(1P) \to p\overline{p}\pi^+\pi^-$)] = ($7.4^{+2.4}_{-2.0}{}^{+0.6}_{-0.4}$) × 10^{-7} which we divide by our best (shown rounded) value B($\chi_{c1}(1P) \to p\overline{p}\pi^+\pi^-$) = (5.0 ± 1.9) × 10^{-4}. Our first error is their experiment's error and our second error is the systematic error from using our best (shown rounded) value.

[2] Assumes equal production of B^+ and B^0 at the $\Upsilon(4S)$.

[3] Uses $\chi_{c1,2} \to J/\psi\gamma$. Assumes B($\Upsilon(4S) \to B^+B^-$) = (51.6 ± 0.6)% and B($\Upsilon(4S) \to B^0\overline{B}^0$) = (48.4 ± 0.6)%.

[4] AVERY 00 reports ($3.9^{+1.9}_{-1.3}$ ± 0.4) × 10^{-4} from a measurement of [$\Gamma(B^0 \to \chi_{c1}K^0)/\Gamma_{total}$] × [B($\chi_{c1}(1P) \to \gamma J/\psi(1S)$)] assuming B($\chi_{c1}(1P) \to \gamma J/\psi(1S)$) = 0.273 ± 0.016, which we rescale to our best (shown rounded) value B($\chi_{c1}(1P) \to \gamma J/\psi(1S)$) = (33.9 ± 1.2) × 10^{-2}. Our first error is their experiment's error and our second error is the systematic error from using our best (shown rounded) value. Assumes equal production of B^+ and B^0 at the $\Upsilon(4S)$.

[5] AUBERT 02 reports (5.4 ± 1.4 ± 1.1) × 10^{-4} from a measurement of [$\Gamma(B^0 \to \chi_{c1}K^0)/\Gamma_{total}$] × [B($\chi_{c1}(1P) \to \gamma J/\psi(1S)$)] assuming B($\chi_{c1}(1P) \to \gamma J/\psi(1S)$) = 0.273 ± 0.016, which we rescale to our best (shown rounded) value B($\chi_{c1}(1P) \to \gamma J/\psi(1S)$) = (33.9 ± 1.2) × 10^{-2}. Our first error is their experiment's error and our second error is the systematic error from using our best (shown rounded) value. Assumes equal production of B^+ and B^0 at the $\Upsilon(4S)$.

$\Gamma(\chi_{c1}K^0)/\Gamma(J/\psi(1S)K^0)$ — $\Gamma_{274}/\Gamma_{214}$

VALUE	DOCUMENT ID		TECN	COMMENT
0.53±0.16±0.02	[1] AUBERT	02	BABR	$e^+e^- \to \Upsilon(4S)$

[1] AUBERT 02 reports 0.66 ± 0.11 ± 0.17 from a measurement of [$\Gamma(B^0 \to \chi_{c1}K^0)/\Gamma(B^0 \to J/\psi(1S)K^0)$] × [B($\chi_{c1}(1P) \to \gamma J/\psi(1S)$)] assuming B($\chi_{c1}(1P) \to \gamma J/\psi(1S)$) = 0.273 ± 0.016, which we rescale to our best (shown rounded) value B($\chi_{c1}(1P) \to \gamma J/\psi(1S)$) = (33.9 ± 1.2) × 10^{-2}. Our first error is their experiment's error and our second error is the systematic error from using our best (shown rounded) value. Assumes equal production of B^+ and B^0 at the $\Upsilon(4S)$.

$\Gamma(\chi_{c1}\pi^-K^+)/\Gamma_{total}$ — Γ_{275}/Γ

VALUE (units 10^{-4})	DOCUMENT ID		TECN	COMMENT
4.97±0.12±0.28	[1] BHARDWAJ	16	BELL	$e^+e^- \to \Upsilon(4S)$
• • • We do not use the following data for averages, fits, limits, etc. • • •				
3.83±0.10±0.39	[1] MIZUK	08	BELL	Repl. by BHARDWAJ 16

[1] Assumes equal production of B^+ and B^0 at the $\Upsilon(4S)$.

$\Gamma(\chi_{c1}\pi^-K^+)/\Gamma(J/\psi(1S)K^+\pi^-)$ — $\Gamma_{275}/\Gamma_{215}$

VALUE	DOCUMENT ID		TECN
0.482±0.021±0.017	[1] LEES	12B	BABR

[1] LEES 12B reports 0.474 ± 0.013 ± 0.026 from a measurement of [$\Gamma(B^0 \to \chi_{c1}\pi^-K^+)/\Gamma(B^0 \to J/\psi(1S)K^+\pi^-)$] × [B($\chi_{c1}(1P) \to \gamma J/\psi(1S)$)] assuming B($\chi_{c1}(1P) \to \gamma J/\psi(1S)$) = (34.4 ± 1.5) × 10^{-2}, which we rescale to our best (shown rounded) value B($\chi_{c1}(1P) \to \gamma J/\psi(1S)$) = (33.9 ± 1.2) × 10^{-2}. Our first error is their experiment's error and our second error is the systematic error from using our best (shown rounded) value.

$\Gamma(\chi_{c1}K^*(892)^0)/\Gamma_{total}$ — Γ_{276}/Γ

VALUE (units 10^{-4})	CL%	DOCUMENT ID		TECN	COMMENT
2.38±0.19 OUR FIT Error includes scale factor of 1.2.					
$2.22^{+0.40}_{-0.31}$ OUR AVERAGE Error includes scale factor of 1.6.					
2.5 ±0.2 ±0.2		[1] AUBERT	09B	BABR	$e^+e^- \to \Upsilon(4S)$
$1.73^{+0.15}_{-0.12}{}^{+0.34}_{-0.22}$		[2] MIZUK	08	BELL	$e^+e^- \to \Upsilon(4S)$
• • • We do not use the following data for averages, fits, limits, etc. • • •					
3.14±0.34±0.72		[2] SONI	06	BELL	Repl. by MIZUK 08
3.27±0.42±0.64		[2] AUBERT	05J	BABR	Repl. by AUBERT 09B
3.9 ±1.3 ±0.1		[3] AUBERT	02	BABR	Repl. by AUBERT 05J
<21	90	[4] ALAM	94	CLE2	$e^+e^- \to \Upsilon(4S)$

[1] Uses $\chi_{c1,2} \to J/\psi\gamma$. Assumes B($\Upsilon(4S) \to B^+B^-$) = (51.6 ± 0.6)% and B($\Upsilon(4S) \to B^0\overline{B}^0$) = (48.4 ± 0.6)%.

[2] Assumes equal production of B^+ and B^0 at the $\Upsilon(4S)$.

[3] AUBERT 02 reports (4.8 ± 1.4 ± 0.9) × 10^{-4} from a measurement of [$\Gamma(B^0 \to \chi_{c1}K^*(892)^0)/\Gamma_{total}$] × [B($\chi_{c1}(1P) \to \gamma J/\psi(1S)$)] assuming B($\chi_{c1}(1P) \to \gamma J/\psi(1S)$) = 0.273 ± 0.016, which we rescale to our best (shown rounded) value B($\chi_{c1}(1P) \to \gamma J/\psi(1S)$) = (33.9 ± 1.2) × 10^{-2}. Our first error is their experiment's error and our second error is the systematic error from using our best (shown rounded) value. Assumes equal production of B^+ and B^0 at the $\Upsilon(4S)$.

[4] BORTOLETTO 92 assumes equal production of B^+ and B^0 at the $\Upsilon(4S)$.

$\Gamma(\chi_{c1}K^*(892)^0)/\Gamma(J/\psi(1S)K^*(892)^0)$ — $\Gamma_{276}/\Gamma_{216}$

VALUE (units 10^{-2})	DOCUMENT ID		TECN	COMMENT
18.8±1.5 OUR FIT Error includes scale factor of 1.1.				
19.8±1.1±1.5	[1] AAIJ	13AC	LHCB	pp at 7 TeV

[1] Uses B($\chi_{c1} \to J/\psi\gamma$) = (34.4 ± 1.5)%.

$\Gamma(\chi_{c1}K^*(892)^0)/\Gamma(\chi_{c1}K^0)$ — $\Gamma_{276}/\Gamma_{274}$

VALUE	DOCUMENT ID		TECN	COMMENT
0.72±0.11±0.12	AUBERT	05J	BABR	$e^+e^- \to \Upsilon(4S)$
• • • We do not use the following data for averages, fits, limits, etc. • • •				
0.89±0.34±0.17	[1] AUBERT	02	BABR	Repl. by AUBERT 05J

[1] Assumes equal production of B^+ and B^0 at the $\Upsilon(4S)$.

$\Gamma(T_{c\overline{c}}(4050)^-K^+,\ T^-_{c\overline{c}} \to \chi_{c1}\pi^-)/\Gamma_{total}$ — Γ_{277}/Γ

VALUE (units 10^{-5})	CL%	DOCUMENT ID		TECN	COMMENT
$\mathbf{3.0^{+1.5}_{-0.8}{}^{+3.7}_{-1.6}}$		[1] MIZUK	08	BELL	$e^+e^- \to \Upsilon(4S)$
• • • We do not use the following data for averages, fits, limits, etc. • • •					
<1.8	90	[1,2] LEES	12B	BABR	

[1] Assumes equal production of B^+ and B^0 at the $\Upsilon(4S)$.

[2] Uses $\chi_{c1} \to J/\psi\gamma$ mode. Uses $\chi_{c1} \to J/\psi\gamma$ mode. Finds a good description of the data without this $B^0 \to X(4051)^+K^-$ decay mode in a fit.

Int. J. Mod. Phys. A 2026.41. Downloaded from www.worldscientific.com by LIFORNIA @ BERKELEY on 09/16/26. Re-use and distribution is strictly not permitted, except for Open Access articles.

$\Gamma(T_{c\overline{c}}(4250)^- K^+,\ T_{c\overline{c}}^- \to \chi_{c1}\pi^-)/\Gamma_{total}$ — Γ_{278}/Γ

VALUE (units 10^{-5})	CL%	DOCUMENT ID		TECN	COMMENT
$\mathbf{4.0^{+2.3}_{-0.9}{}^{+19.7}_{-\ 0.5}}$		[1] MIZUK	08	BELL	$e^+e^- \to \Upsilon(4S)$
• • • We do not use the following data for averages, fits, limits, etc. • • •					
<4.0	90	[1,2] LEES	12B	BABR	

[1] Assumes equal production of B^+ and B^0 at the $\Upsilon(4S)$.
[2] Uses $\chi_{c1} \to J/\psi\gamma$ mode. Finds a good description of the data without this $B^0 \to X(4248)^+ K^-$ decay mode in a fit.

$\Gamma(\chi_{c1}\pi^+\pi^- K^0)/\Gamma_{total}$ — Γ_{279}/Γ

VALUE (units 10^{-4})	DOCUMENT ID		TECN	COMMENT
3.16±0.35±0.32	[1] BHARDWAJ	16	BELL	$e^+e^- \to \Upsilon(4S)$

[1] Assumes equal production of B^+ and B^0 at the $\Upsilon(4S)$.

$\Gamma(\chi_{c1}\pi^-\pi^0 K^+)/\Gamma_{total}$ — Γ_{280}/Γ

VALUE (units 10^{-4})	DOCUMENT ID		TECN	COMMENT
3.52±0.52±0.24	[1] BHARDWAJ	16	BELL	$e^+e^- \to \Upsilon(4S)$

[1] Assumes equal production of B^+ and B^0 at the $\Upsilon(4S)$.

$\Gamma(\chi_{c2} K^0)/\Gamma_{total}$ — Γ_{281}/Γ

VALUE	CL%	DOCUMENT ID		TECN	COMMENT
$\mathbf{<1.5\times10^{-5}}$	90	[1] BHARDWAJ	11	BELL	$e^+e^- \to \Upsilon(4S)$
• • • We do not use the following data for averages, fits, limits, etc. • • •					
$<2.8\times10^{-5}$	90	[2] AUBERT	09B	BABR	$e^+e^- \to \Upsilon(4S)$
$<2.6\times10^{-5}$	90	[1] SONI	06	BELL	Repl. by BHARDWAJ 11
$<4.1\times10^{-5}$	90	[1] AUBERT	05K	BABR	$e^+e^- \to \Upsilon(4S)$

[1] Assumes equal production of B^+ and B^0 at the $\Upsilon(4S)$.
[2] Uses $\chi_{c1,2} \to J/\psi\gamma$. Assumes $B(\Upsilon(4S) \to B^+B^-) = (51.6\pm0.6)\%$ and $B(\Upsilon(4S) \to B^0\overline{B}^0) = (48.4\pm0.6)\%$.

$\Gamma(\chi_{c2} K^*(892)^0)/\Gamma_{total}$ — Γ_{282}/Γ

VALUE (units 10^{-5})	CL%	DOCUMENT ID		TECN	COMMENT
4.9±1.2 OUR FIT Error includes scale factor of 1.1.					
6.6±1.8±0.5		[1] AUBERT	09B	BABR	$e^+e^- \to \Upsilon(4S)$
• • • We do not use the following data for averages, fits, limits, etc. • • •					
<7.1	90	[2] SONI	06	BELL	$e^+e^- \to \Upsilon(4S)$
<3.6	90	[2] AUBERT	05K	BABR	Repl. by AUBERT 09B

[1] Uses $\chi_{c1,2} \to J/\psi\gamma$. Assumes $B(\Upsilon(4S) \to B^+B^-) = (51.6\pm0.6)\%$ and $B(\Upsilon(4S) \to B^0\overline{B}^0) = (48.4\pm0.6)\%$.
[2] Assumes equal production of B^+ and B^0 at the $\Upsilon(4S)$.

$\Gamma(\chi_{c2} K^*(892)^0)/\Gamma(\chi_{c1} K^*(892)^0)$ — $\Gamma_{282}/\Gamma_{276}$

VALUE (units 10^{-2})	DOCUMENT ID		TECN	COMMENT
20 ±5 OUR FIT Error includes scale factor of 1.1.				
17.1±5.0±2.0	[1] AAIJ	13AC	LHCB	pp at 7 TeV

[1] Uses $B(\chi_{c1} \to J/\psi\gamma)/B(\chi_{c2} \to J/\psi\gamma) = 1.76 \pm 0.11$.

$\Gamma(\chi_{c2}\pi^- K^+)/\Gamma_{total}$ — Γ_{283}/Γ

VALUE (units 10^{-4})	DOCUMENT ID		TECN	COMMENT
0.72±0.09±0.05	[1] BHARDWAJ	16	BELL	$e^+e^- \to \Upsilon(4S)$

[1] Assumes equal production of B^+ and B^0 at the $\Upsilon(4S)$.

$\Gamma(\chi_{c2}\pi^+\pi^- K^0)/\Gamma_{total}$ — Γ_{284}/Γ

VALUE	CL%	DOCUMENT ID		TECN	COMMENT
$\mathbf{<1.70\times10^{-4}}$	90	[1] BHARDWAJ	16	BELL	$e^+e^- \to \Upsilon(4S)$

[1] Assumes equal production of B^+ and B^0 at the $\Upsilon(4S)$.

$\Gamma(\chi_{c2}\pi^-\pi^0 K^+)/\Gamma_{total}$ — Γ_{285}/Γ

VALUE	CL%	DOCUMENT ID		TECN	COMMENT
$\mathbf{<0.74\times10^{-4}}$	90	[1] BHARDWAJ	16	BELL	$e^+e^- \to \Upsilon(4S)$

[1] Assumes equal production of B^+ and B^0 at the $\Upsilon(4S)$.

$\Gamma(\psi(4660) K^0,\ \psi \to \Lambda_c^+\Lambda_c^-)/\Gamma_{total}$ — Γ_{286}/Γ

VALUE	CL%	DOCUMENT ID		TECN	COMMENT
$\mathbf{<2.3\times10^{-4}}$	90	[1] LI	18D	BELL	$e^+e^- \to \Upsilon(4S)$

[1] Assumes $B(\Upsilon(4S) \to B^0\overline{B}^0) = 48.6\pm0.6\%$ and $B(\Lambda_c^+ \to pK^-\pi^+) = 6.23\pm0.33\%$.

$\Gamma(\psi(4230)^0 K^0,\ \psi^0 \to J/\psi\pi^+\pi^-)/\Gamma_{total}$ — Γ_{287}/Γ

VALUE	CL%	DOCUMENT ID		TECN	COMMENT
$\mathbf{<17\times10^{-6}}$	90	[1] GARG	19	BELL	$e^+e^- \to \Upsilon(4S)$

[1] Assumes equal production of B^0 and B^+ at the $\Upsilon(4S)$.

$\Gamma(K^+\pi^-)/\Gamma_{total}$ — Γ_{288}/Γ

VALUE (units 10^{-6})	CL%	DOCUMENT ID		TECN	COMMENT
20.0 ± 0.4 OUR FIT					
20.0 ± 0.4 OUR AVERAGE					
20.67± 0.37±0.62		ADACHI	24	BELL	$e^+e^- \to \Upsilon(4S)$
20.00± 0.34±0.60		[1] DUH	13	BELL	$e^+e^- \to \Upsilon(4S)$
19.1 ± 0.6 ±0.6		[1] AUBERT	07B	BABR	$e^+e^- \to \Upsilon(4S)$
$18.0\ ^{+2.3}_{-2.1}\ ^{+1.2}_{-0.9}$		[1] BORNHEIM	03	CLE2	$e^+e^- \to \Upsilon(4S)$
• • • We do not use the following data for averages, fits, limits, etc. • • •					
19.9 ± 0.4 ±0.8		[1] LIN	07A	BELL	Repl. by DUH 13
18.5 ± 1.0 ±0.7		[1] CHAO	04	BELL	Repl. by LIN 07A
17.9 ± 0.9 ±0.7		[1] AUBERT	02Q	BABR	Repl. by AUBERT 07B
22.5 ± 1.9 ±1.8		[1] CASEY	02	BELL	Repl. by CHAO 04
$19.3\ ^{+3.4}_{-3.2}\ ^{+1.5}_{-0.6}$		[1] ABE	01H	BELL	Repl. by CASEY 02
16.7 ± 1.6 ±1.3		[1] AUBERT	01E	BABR	Repl. by AUBERT 02Q
< 66	90	[2] ABE	00C	SLD	$e^+e^- \to Z$
$17.2\ ^{+2.5}_{-2.4}$ ±1.2		[1] CRONIN-HEN...	00	CLE2	Repl. by BORNHEIM 03
$15\ ^{+5.}_{-4}$ ±1.4		GODANG	98	CLE2	Repl. by CRONIN-HENNESSY 00
$24\ ^{+17}_{-11}$ ±2		[3] ADAM	96D	DLPH	$e^+e^- \to Z$
< 17	90	ASNER	96	CLE2	Sup. by ADAM 96D
< 30	90	[4] BUSKULIC	96V	ALEP	$e^+e^- \to Z$
< 90	90	[5] ABREU	95N	DLPH	Sup. by ADAM 96D
< 81	90	[6] AKERS	94L	OPAL	$e^+e^- \to Z$
< 26	90	[7] BATTLE	93	CLE2	$e^+e^- \to \Upsilon(4S)$
<180	90	ALBRECHT	91B	ARG	$e^+e^- \to \Upsilon(4S)$
< 90	90	[8] AVERY	89B	CLEO	$e^+e^- \to \Upsilon(4S)$
<320	90	AVERY	87	CLEO	$e^+e^- \to \Upsilon(4S)$

[1] Assumes equal production of B^+ and B^0 at the $\Upsilon(4S)$.
[2] ABE 00C assumes $B(Z \to b\overline{b}) = (21.7 \pm 0.1)\%$ and the B fractions $f_{B^0} = f_{B^+} = (39.7\ ^{+1.8}_{-2.2})\%$ and $f_{B_s} = (10.5\ ^{+1.8}_{-2.2})\%$.
[3] ADAM 96D assumes $f_{B^0} = f_{B^-} = 0.39$ and $f_{B_s} = 0.12$. Contributions from B^0 and B_s decays cannot be separated. Limits are given for the weighted average of the decay rates for the two neutral B mesons.
[4] BUSKULIC 96V assumes PDG 96 production fractions for B^0, B^+, B_s, b baryons.
[5] Assumes a B^0, B^- production fraction of 0.39 and a B_s production fraction of 0.12. Contributions from B^0 and B_s^0 decays cannot be separated. Limits are given for the weighted average of the decay rates for the two neutral B mesons.
[6] Assumes $B(Z \to b\overline{b}) = 0.217$ and B_d^0 (B_s^0) fraction 39.5% (12%).
[7] BATTLE 93 assumes equal production of $B^0\overline{B}^0$ and B^+B^- at $\Upsilon(4S)$.
[8] Assumes the $\Upsilon(4S)$ decays 43% to $B^0\overline{B}^0$.

$\Gamma(K^+\pi^-)/\Gamma(K^0\pi^0)$ — $\Gamma_{288}/\Gamma_{289}$

VALUE	DOCUMENT ID		TECN	COMMENT
2.16±0.16±0.16	LIN	07A	BELL	$e^+e^- \to \Upsilon(4S)$
• • • We do not use the following data for averages, fits, limits, etc. • • •				
$1.20\ ^{+0.50}_{-0.58}\ ^{+0.22}_{-0.32}$	[1] ABE	01H	BELL	Repl. by LIN 07A

[1] Assumes equal production of B^+ and B^0 at the $\Upsilon(4S)$.

$[\Gamma(K^+\pi^-) + \Gamma(\pi^+\pi^-)]/\Gamma_{total}$ — $(\Gamma_{288}+\Gamma_{423})/\Gamma$

VALUE (units 10^{-6})	EVTS	DOCUMENT ID		TECN	COMMENT
19± 6 OUR AVERAGE					
$28\ ^{+15}_{-10}$ ±20		[1] ADAM	96D	DLPH	$e^+e^- \to Z$
$18\ ^{+6}_{-5}\ ^{+3}_{-4}$	17.2	ASNER	96	CLE2	$e^+e^- \to \Upsilon(4S)$
• • • We do not use the following data for averages, fits, limits, etc. • • •					
$24\ ^{+8}_{-7}$ ± 2		[2] BATTLE	93	CLE2	$e^+e^- \to \Upsilon(4S)$

[1] ADAM 96D assumes $f_{B^0} = f_{B^-} = 0.39$ and $f_{B_s} = 0.12$. Contributions from B^0 and B_s decays cannot be separated. Limits are given for the weighted average of the decay rates for the two neutral B mesons.
[2] BATTLE 93 assumes equal production of $B^0\overline{B}^0$ and B^+B^- at $\Upsilon(4S)$.

$\Gamma(K^0\pi^0)/\Gamma_{total}$ — Γ_{289}/Γ

VALUE (units 10^{-6})	CL%	DOCUMENT ID		TECN	COMMENT
10.1 ±0.4 OUR AVERAGE					
10.73±0.63±0.62		[1] ADACHI	24	BELL	$e^+e^- \to \Upsilon(4S)$
9.68±0.46±0.50		[2] DUH	13	BELL	$e^+e^- \to \Upsilon(4S)$
10.1 ±0.6 ±0.4		[2] LEES	13D	BABR	$e^+e^- \to \Upsilon(4S)$
$12.8\ ^{+4.0}_{-3.3}\ ^{+1.7}_{-1.4}$		[2] BORNHEIM	03	CLE2	$e^+e^- \to \Upsilon(4S)$
• • • We do not use the following data for averages, fits, limits, etc. • • •					
8.7 ±0.5 ±0.6		[2] FUJIKAWA	10A	BELL	Repl. by DUH 13
10.3 ±0.7 ±0.6		[2] AUBERT	08E	BABR	Repl. by LEES 13D
9.2 ±0.7 ±0.6		[2] LIN	07A	BELL	Repl. by FUJIKAWA 10A
11.4 ±0.9 ±0.6		[2] AUBERT	05Y	BABR	Repl. by AUBERT 08E
11.4 ±1.7 ±0.8		[2] AUBERT	04M	BABR	Repl. by AUBERT 05Y
$11.7 \pm 2.3\ ^{+1.2}_{-1.3}$		[2] CHAO	04	BELL	Repl. by LIN 07A
$8.0\ ^{+3.3}_{-3.1}$ ±1.6		[2] CASEY	02	BELL	Repl. by CHAO 04
$16.0\ ^{+7.2}_{-5.9}\ ^{+2.5}_{-2.7}$		[2] ABE	01H	BELL	Repl. by CASEY 02
$8.2\ ^{+3.1}_{-2.7}$ ±1.2		[2] AUBERT	01E	BABR	Repl. by AUBERT 04M
$14.6\ ^{+5.9}_{-5.1}\ ^{+2.4}_{-3.3}$		[2] CRONIN-HEN...	00	CLE2	Repl. by BORNHEIM 03
<41	90	GODANG	98	CLE2	Repl. by CRONIN-HENNESSY 00
<40	90	ASNER	96	CLE2	Rep. by GODANG 98

[1] This is the combined result of this analysis (ADACHI 24) and the updated analysis of ADACHI 23E. The individual results are $(10.40 \pm 0.66 \pm 0.60)\times10^{-6}$ and $(11.15 \pm 0.68 \pm 0.62)\times10^{-6}$, respectively.
[2] Assumes equal production of B^+ and B^0 at the $\Upsilon(4S)$.

Int. J. Mod. Phys. A 2026.41. Downloaded from www.worldscientific.com
by UNIVERSITY OF CALIFORNIA @ BERKELEY on 09/16/26. Re-use and distribution is strictly not permitted, except for Open Access articles.

$\Gamma(\eta' K^0)/\Gamma_{total}$ — Γ_{290}/Γ

VALUE (units 10^{-6})	DOCUMENT ID		TECN	COMMENT
66 ± 4 OUR AVERAGE	Error includes scale factor of 1.4.			
$68.5 \pm 2.2 \pm 3.1$	[1] AUBERT	09AV	BABR	$e^+e^- \to \Upsilon(4S)$
$58.9^{+3.6}_{-3.5} \pm 4.3$	[1] SCHUEMANN	06	BELL	$e^+e^- \to \Upsilon(4S)$
$89^{+18}_{-16} \pm 9$	[1] RICHICHI	00	CLE2	$e^+e^- \to \Upsilon(4S)$
• • • We do not use the following data for averages, fits, limits, etc. • • •				
$66.6 \pm 2.6 \pm 2.8$	[1] AUBERT	07AE	BABR	Repl. by AUBERT 09AV
$67.4 \pm 3.3 \pm 3.2$	[1] AUBERT	05M	BABR	AUBERT 07AE
$60.6 \pm 5.6 \pm 4.6$	[1] AUBERT	03W	BABR	Repl. by AUBERT 05M
$55^{+19}_{-16} \pm 8$	[1] ABE	01M	BELL	Repl. by SCHUEMANN 06
$42^{+13}_{-11} \pm 4$	[1] AUBERT	01G	BABR	Repl. by AUBERT 03W
$47^{+27}_{-20} \pm 9$	BEHRENS	98	CLE2	Repl. by RICHICHI 00

[1] Assumes equal production of B^+ and B^0 at the $\Upsilon(4S)$.

$\Gamma(\eta' K^*(892)^0)/\Gamma_{total}$ — Γ_{291}/Γ

VALUE (units 10^{-6})	CL%	DOCUMENT ID		TECN	COMMENT
2.8±0.6 OUR AVERAGE					
$2.6 \pm 0.7 \pm 0.2$		[1] SATO	14	BELL	$e^+e^- \to \Upsilon(4S)$
$3.1^{+0.9}_{-0.8} \pm 0.3$		[1] DEL-AMO-SA...	10A	BABR	$e^+e^- \to \Upsilon(4S)$
• • • We do not use the following data for averages, fits, limits, etc. • • •					
$3.8 \pm 1.1 \pm 0.5$		[1] AUBERT	07E	BABR	Repl. by DEL-AMO-SANCHEZ 10A
< 2.6	90	[1] SCHUEMANN	07	BELL	$e^+e^- \to \Upsilon(4S)$
< 7.6	90	[1] AUBERT,B	04D	BABR	Repl. by AUBERT 07E
<24	90	[1] RICHICHI	00	CLE2	$e^+e^- \to \Upsilon(4S)$
<39	90	BEHRENS	98	CLE2	Repl. by RICHICHI 00

[1] Assumes equal production of B^+ and B^0 at the $\Upsilon(4S)$.

$\Gamma(\eta' K_0^*(1430)^0)/\Gamma_{total}$ — Γ_{292}/Γ

VALUE (units 10^{-6})	DOCUMENT ID		TECN	COMMENT
6.3±1.3±0.9	[1] DEL-AMO-SA...	10A	BABR	$e^+e^- \to \Upsilon(4S)$

[1] Assumes equal production of B^+ and B^0 at the $\Upsilon(4S)$.

$\Gamma(\eta' K_2^*(1430)^0)/\Gamma_{total}$ — Γ_{293}/Γ

VALUE (units 10^{-6})	DOCUMENT ID		TECN	COMMENT
$\mathbf{13.7^{+3.0}_{-2.9} \pm 1.2}$	[1] DEL-AMO-SA...	10A	BABR	$e^+e^- \to \Upsilon(4S)$

[1] Assumes equal production of B^+ and B^0 at the $\Upsilon(4S)$.

$\Gamma(\eta K^0)/\Gamma_{total}$ — Γ_{294}/Γ

VALUE (units 10^{-6})	CL%	DOCUMENT ID		TECN	COMMENT
$\mathbf{1.23^{+0.27}_{-0.24}}$ **OUR AVERAGE**					
$1.27^{+0.33}_{-0.29} \pm 0.08$		[1] HOI	12	BELL	$e^+e^- \to \Upsilon(4S)$
$1.15^{+0.43}_{-0.38} \pm 0.09$		[1] AUBERT	09AV	BABR	$e^+e^- \to \Upsilon(4S)$
• • • We do not use the following data for averages, fits, limits, etc. • • •					
< 1.9	90	[1] CHANG	07B	BELL	Repl. by HOI 12
< 2.9	90	[1] AUBERT,B	06V	BABR	$e^+e^- \to \Upsilon(4S)$
< 2.5	90	[1] AUBERT,B	05K	BABR	$e^+e^- \to \Upsilon(4S)$
< 2.0	90	[1] CHANG	05A	BELL	Repl. by CHANG 07B
< 5.2	90	[1] AUBERT	04H	BABR	Repl. by AUBERT,B 05K
< 9.3	90	[1] RICHICHI	00	CLE2	$e^+e^- \to \Upsilon(4S)$
<33	90	BEHRENS	98	CLE2	Repl. by RICHICHI 00

[1] Assumes equal production of B^+ and B^0 at the $\Upsilon(4S)$.

$\Gamma(\eta K^*(892)^0)/\Gamma_{total}$ — Γ_{295}/Γ

VALUE (units 10^{-6})	CL%	DOCUMENT ID		TECN	COMMENT
15.9±1.0 OUR AVERAGE					
$15.2 \pm 1.2 \pm 1.0$		[1] WANG	07B	BELL	$e^+e^- \to \Upsilon(4S)$
$16.5 \pm 1.1 \pm 0.8$		[1] AUBERT,B	06H	BABR	$e^+e^- \to \Upsilon(4S)$
$13.8^{+5.5}_{-4.6} \pm 1.6$		[1] RICHICHI	00	CLE2	$e^+e^- \to \Upsilon(4S)$
• • • We do not use the following data for averages, fits, limits, etc. • • •					
$18.6 \pm 2.3 \pm 1.2$		[1] AUBERT,B	04D	BABR	Repl. by AUBERT,B 06H
<30	90	BEHRENS	98	CLE2	Repl. by RICHICHI 00

[1] Assumes equal production of B^+ and B^0 at the $\Upsilon(4S)$.

$\Gamma(\eta K_0^*(1430)^0)/\Gamma_{total}$ — Γ_{296}/Γ

VALUE (units 10^{-6})	DOCUMENT ID		TECN	COMMENT
11.0±1.6±1.5	[1] AUBERT,B	06H	BABR	$e^+e^- \to \Upsilon(4S)$

[1] Assumes equal production of B^+ and B^0 at the $\Upsilon(4S)$.

$\Gamma(\eta K_2^*(1430)^0)/\Gamma_{total}$ — Γ_{297}/Γ

VALUE (units 10^{-6})	DOCUMENT ID		TECN	COMMENT
9.6±1.8±1.1	[1] AUBERT,B	06H	BABR	$e^+e^- \to \Upsilon(4S)$

[1] Assumes equal production of B^+ and B^0 at the $\Upsilon(4S)$.

$\Gamma(\omega K^0)/\Gamma_{total}$ — Γ_{298}/Γ

VALUE (units 10^{-6})	CL%	DOCUMENT ID		TECN	COMMENT
4.8±0.4 OUR AVERAGE					
$4.5 \pm 0.4 \pm 0.3$		[1] CHOBANOVA	14	BELL	$e^+e^- \to \Upsilon(4S)$
$5.4 \pm 0.8 \pm 0.3$		[1] AUBERT	07AE	BABR	$e^+e^- \to \Upsilon(4S)$
$10.0^{+5.4}_{-4.2} \pm 1.4$		[1] JESSOP	00	CLE2	$e^+e^- \to \Upsilon(4S)$
• • • We do not use the following data for averages, fits, limits, etc. • • •					
$6.2 \pm 1.0 \pm 0.4$		[1] AUBERT,B	06E	BABR	Repl. by AUBERT 07AE
$4.4^{+0.8}_{-0.7} \pm 0.4$		[1] JEN	06	BELL	Repl. by CHOBANOVA 14
$5.9^{+1.6}_{-1.3} \pm 0.5$		[1] AUBERT	04H	BABR	Repl. by AUBERT,B 06E
$4.0^{+1.9}_{-1.6} \pm 0.5$		[1] WANG	04A	BELL	Repl. by JEN 06
<13	90	[1] AUBERT	01G	BABR	Repl. by AUBERT 04H
<57	90	[1] BERGFELD	98	CLE2	Repl. by JESSOP 00

[1] Assumes equal production of B^+ and B^0 at the $\Upsilon(4S)$.

$\Gamma(a_0(980)^0 K^0,\ a_0^0 \to \eta\pi^0)/\Gamma_{total}$ — Γ_{299}/Γ

VALUE (units 10^{-6})	CL%	DOCUMENT ID		TECN	COMMENT
<7.8	90	[1] AUBERT,BE	04	BABR	$e^+e^- \to \Upsilon(4S)$

[1] Assumes equal production of charged and neutral B mesons at $\Upsilon(4S)$.

$\Gamma(b_1^0 K^0,\ b_1^0 \to \omega\pi^0)/\Gamma_{total}$ — Γ_{300}/Γ

VALUE (units 10^{-6})	CL%	DOCUMENT ID		TECN	COMMENT
<7.8	90	[1] AUBERT	08AG	BABR	$e^+e^- \to \Upsilon(4S)$

[1] Assumes equal production of B^+ and B^0 at the $\Upsilon(4S)$.

$\Gamma(a_0(980)^\pm K^\mp,\ a_0^\pm \to \eta\pi^\pm)/\Gamma_{total}$ — Γ_{301}/Γ

VALUE (units 10^{-6})	CL%	DOCUMENT ID		TECN	COMMENT
<1.9	90	[1] AUBERT	07Y	BABR	$e^+e^- \to \Upsilon(4S)$
• • • We do not use the following data for averages, fits, limits, etc. • • •					
<2.1	90	[1] AUBERT,BE	04	BABR	Repl. by AUBERT 07Y

[1] Assumes equal production of B^+ and B^0 at the $\Upsilon(4S)$.

$\Gamma(b_1^- K^+,\ b_1^- \to \omega\pi^-)/\Gamma_{total}$ — Γ_{302}/Γ

VALUE (units 10^{-6})	DOCUMENT ID		TECN	COMMENT
7.4±1.0±1.0	[1] AUBERT	07BI	BABR	$e^+e^- \to \Upsilon(4S)$

[1] Assumes equal production of B^+ and B^0 at the $\Upsilon(4S)$.

$\Gamma(b_1^0 K^{*0},\ b_1^0 \to \omega\pi^0)/\Gamma_{total}$ — Γ_{303}/Γ

VALUE	CL%	DOCUMENT ID		TECN	COMMENT
$\mathbf{<8.0 \times 10^{-6}}$	90	[1] AUBERT	09AF	BABR	$e^+e^- \to \Upsilon(4S)$

[1] Assumes equal production of B^+ and B^0 at the $\Upsilon(4S)$.

$\Gamma(b_1^- K^{*+},\ b_1^- \to \omega\pi^-)/\Gamma_{total}$ — Γ_{304}/Γ

VALUE	CL%	DOCUMENT ID		TECN	COMMENT
$\mathbf{<5.0 \times 10^{-6}}$	90	[1] AUBERT	09AF	BABR	$e^+e^- \to \Upsilon(4S)$

[1] Assumes equal production of B^+ and B^0 at the $\Upsilon(4S)$.

$\Gamma(a_0(1450)^\pm K^\mp,\ a_0^\pm \to \eta\pi^\pm)/\Gamma_{total}$ — Γ_{305}/Γ

VALUE (units 10^{-6})	CL%	DOCUMENT ID		TECN	COMMENT
<3.1	90	[1] AUBERT	07Y	BABR	$e^+e^- \to \Upsilon(4S)$

[1] Assumes equal production of B^+ and B^0 at the $\Upsilon(4S)$.

$\Gamma(K_S^0 X^0(\text{Familon}))/\Gamma_{total}$ — Γ_{306}/Γ

VALUE (units 10^{-6})	CL%	DOCUMENT ID		TECN	COMMENT
<53	90	[1] AMMAR	01B	CLE2	$e^+e^- \to \Upsilon(4S)$

[1] AMMAR 01B searched for the two-body decay of the B meson to a massless neutral feebly-interacting particle X^0 such as the familon, the Nambu-Goldstone boson associated with a spontaneously broken global family symmetry.

$\Gamma(\omega K^*(892)^0)/\Gamma_{total}$ — Γ_{307}/Γ

VALUE (units 10^{-6})	CL%	DOCUMENT ID		TECN	COMMENT
2.0±0.5 OUR AVERAGE					
$2.2 \pm 0.6 \pm 0.2$		[1] AUBERT	09H	BABR	$e^+e^- \to \Upsilon(4S)$
$1.8 \pm 0.7 \pm 0.3$		[1] GOLDENZWE...	08	BELL	$e^+e^- \to \Upsilon(4S)$
• • • We do not use the following data for averages, fits, limits, etc. • • •					
< 4.2	90	[1] AUBERT,B	06T	BABR	Repl. by AUBERT 09H
< 6.0	90	[1] AUBERT	05O	BABR	Repl. by AUBERT,B 06T
<23	90	[1] BERGFELD	98	CLE2	

[1] Assumes equal production of B^+ and B^0 at the $\Upsilon(4S)$.

$\Gamma(\omega(K\pi)_0^{*0})/\Gamma_{total}$ — Γ_{308}/Γ

$(K\pi)_0^{*0}$ is the total S-wave composed of $K_0^*(1430)$ and nonresonant that are described using LASS shape.

VALUE (units 10^{-6})	DOCUMENT ID		TECN	COMMENT
18.4±1.8±1.7	[1] AUBERT	09H	BABR	$e^+e^- \to \Upsilon(4S)$

[1] Assumes equal production of B^+ and B^0 at the $\Upsilon(4S)$.

Int. J. Mod. Phys. A 2026.41. Downloaded from www.worldscientific.com by LIFORNIA @ BERKELEY on 09/16/26. Re-use and distribution is strictly not permitted, except for Open Access articles.

$\Gamma(\omega K_0^*(1430)^0)/\Gamma_{total}$ — Γ_{309}/Γ

VALUE (units 10^{-6})	DOCUMENT ID		TECN	COMMENT
16.0±1.6±3.0	[1] AUBERT	09H	BABR	$e^+e^- \to \Upsilon(4S)$

[1] Assumes equal production of B^+ and B^0 at the $\Upsilon(4S)$.

$\Gamma(\omega K_2^*(1430)^0)/\Gamma_{total}$ — Γ_{310}/Γ

VALUE (units 10^{-6})	DOCUMENT ID		TECN	COMMENT
10.1±2.0±1.1	[1] AUBERT	09H	BABR	$e^+e^- \to \Upsilon(4S)$

[1] Assumes equal production of B^+ and B^0 at the $\Upsilon(4S)$.

$\Gamma(\omega K^+\pi^-$ nonresonant$)/\Gamma_{total}$ — Γ_{311}/Γ

VALUE (units 10^{-6})	DOCUMENT ID		TECN	COMMENT
5.1±0.7±0.7	[1,2] GOLDENZWE..08		BELL	$e^+e^- \to \Upsilon(4S)$

[1] Assumes equal production of B^+ and B^0 at the $\Upsilon(4S)$.
[2] For the $K\pi$ mass range 0.755–1.250 GeV/c^2, excluding $K^*(892)$.

$\Gamma(K^+\pi^-\pi^0)/\Gamma_{total}$ — Γ_{312}/Γ

VALUE (units 10^{-6})	CL%	DOCUMENT ID		TECN	COMMENT
37.8±3.2 OUR AVERAGE					
38.5±1.0±3.9		[1,2] LEES	11	BABR	$e^+e^- \to \Upsilon(4S)$
$36.6^{+4.2}_{-4.3}\pm3.0$		[1] CHANG	04	BELL	$e^+e^- \to \Upsilon(4S)$
• • • We do not use the following data for averages, fits, limits, etc. • • •					
$35.7^{+2.6}_{-1.5}\pm2.2$		[1] AUBERT	08AQ	BABR	Repl. by LEES 11
<40	90	[1] ECKHART	02	CLE2	$e^+e^- \to \Upsilon(4S)$

[1] Assumes equal production of B^+ and B^0 at the $\Upsilon(4S)$.
[2] Uses Dalitz plot analysis of $B^0 \to K^+\pi^-\pi^0$ decays.

$\Gamma(K^+\rho^-)/\Gamma_{total}$ — Γ_{313}/Γ

VALUE (units 10^{-6})	CL%	DOCUMENT ID		TECN	COMMENT
7.0±0.9 OUR AVERAGE					
6.6±0.5±0.8		[1,2] LEES	11	BABR	$e^+e^- \to \Upsilon(4S)$
$15.1^{+3.4}_{-3.3}{}^{+2.4}_{-2.6}$		[1] CHANG	04	BELL	$e^+e^- \to \Upsilon(4S)$
• • • We do not use the following data for averages, fits, limits, etc. • • •					
$8.0^{+0.8}_{-1.3}\pm0.6$		[1] AUBERT	08AQ	BABR	Repl. by LEES 11
$7.3^{+1.3}_{-1.2}\pm1.3$		[1] AUBERT	03T	BABR	Repl. by AUBERT 08AQ
<32	90	[1] JESSOP	00	CLE2	$e^+e^- \to \Upsilon(4S)$
<35	90	ASNER	96	CLE2	Repl. by JESSOP 00

[1] Assumes equal production of B^+ and B^0 at the $\Upsilon(4S)$.
[2] Uses Dalitz plot analysis of $B^0 \to K^+\pi^-\pi^0$ decays.

$\Gamma(K^+\rho(1450)^-)/\Gamma_{total}$ — Γ_{314}/Γ

VALUE (units 10^{-6})	CL%	DOCUMENT ID		TECN	COMMENT
2.4±1.0±0.6		[1,2] LEES	11	BABR	$e^+e^- \to \Upsilon(4S)$
• • • We do not use the following data for averages, fits, limits, etc. • • •					
<2.1	90	[1] AUBERT	08AQ	BABR	Repl. by LEES 11

[1] Assumes equal production of B^+ and B^0 at the $\Upsilon(4S)$.
[2] Uses Dalitz plot analysis of $B^0 \to K^+\pi^-\pi^0$ decays.

$\Gamma(K^+\rho(1700)^-)/\Gamma_{total}$ — Γ_{315}/Γ

VALUE (units 10^{-6})	CL%	DOCUMENT ID		TECN	COMMENT
0.6±0.6±0.4		[1,2] LEES	11	BABR	$e^+e^- \to \Upsilon(4S)$
• • • We do not use the following data for averages, fits, limits, etc. • • •					
<1.1	90	[1] AUBERT	08AQ	BABR	Repl. by LEES 11

[1] Assumes equal production of B^+ and B^0 at the $\Upsilon(4S)$.
[2] Uses Dalitz plot analysis of $B^0 \to K^+\pi^-\pi^0$ decays.

$\Gamma((K^+\pi^-\pi^0)$ nonresonant$)/\Gamma_{total}$ — Γ_{316}/Γ

VALUE (units 10^{-6})	CL%	DOCUMENT ID		TECN	COMMENT
2.8±0.5±0.4		[1,2] LEES	11	BABR	$e^+e^- \to \Upsilon(4S)$
• • • We do not use the following data for averages, fits, limits, etc. • • •					
4.4±0.9±0.5		[1] AUBERT	08AQ	BABR	Repl. by LEES 11
<9.4	90	[1] CHANG	04	BELL	$e^+e^- \to \Upsilon(4S)$

[1] Assumes equal production of B^+ and B^0 at the $\Upsilon(4S)$.
[2] Uses Dalitz plot analysis of $B^0 \to K^+\pi^-\pi^0$ decays. The quoted value is only for the flat part of the non-resonant component.

$\Gamma((K\pi)_0^{*+}\pi^-,\ (K\pi)_0^{*+} \to K^+\pi^0)/\Gamma_{total}$ — Γ_{317}/Γ

$(K\pi)_0^{*+}$ is the total S-wave composed of $K_0^*(1430)$ and nonresonant that are described using LASS shape.

VALUE (units 10^{-6})	DOCUMENT ID		TECN	COMMENT
34.2±2.4±4.1	[1,2] LEES	11	BABR	$e^+e^- \to \Upsilon(4S)$
• • • We do not use the following data for averages, fits, limits, etc. • • •				
$9.4^{+1.1}_{-1.3}{}^{+2.3}_{-2.1}$	[1] AUBERT	08AQ	BABR	Repl. by LEES 11

[1] Assumes equal production of B^+ and B^0 at the $\Upsilon(4S)$.
[2] Uses Dalitz plot analysis of $B^0 \to K^+\pi^-\pi^0$ decays.

$\Gamma((K\pi)_0^{*0}\pi^0,\ (K\pi)_0^{*0} \to K^+\pi^-)/\Gamma_{total}$ — Γ_{318}/Γ

$(K\pi)_0^{*0}$ is the total S-wave composed of $K_0^*(1430)$ and nonresonant that are described using LASS shape.

VALUE (units 10^{-6})	DOCUMENT ID		TECN	COMMENT
8.6±1.1±1.3	[1,2] LEES	11	BABR	$e^+e^- \to \Upsilon(4S)$
• • • We do not use the following data for averages, fits, limits, etc. • • •				
$8.7^{+1.1}_{-0.9}{}^{+2.8}_{-2.6}$	[1] AUBERT	08AQ	BABR	Repl. by LEES 11

[1] Assumes equal production of B^+ and B^0 at the $\Upsilon(4S)$.
[2] Uses Dalitz plot analysis of $B^0 \to K^+\pi^-\pi^0$ decays.

$\Gamma(K_2^*(1430)^0\pi^0)/\Gamma_{total}$ — Γ_{319}/Γ

VALUE (units 10^{-6})	CL%	DOCUMENT ID		TECN	COMMENT
<4.0	90	[1] AUBERT	08AQ	BABR	$e^+e^- \to \Upsilon(4S)$

[1] Assumes equal production of B^+ and B^0 at the $\Upsilon(4S)$.

$\Gamma(K^*(1680)^0\pi^0)/\Gamma_{total}$ — Γ_{320}/Γ

VALUE (units 10^{-6})	CL%	DOCUMENT ID		TECN	COMMENT
<7.5	90	[1] AUBERT	08AQ	BABR	$e^+e^- \to \Upsilon(4S)$

[1] Assumes equal production of B^+ and B^0 at the $\Upsilon(4S)$.

$\Gamma(K_x^{*0}\pi^0)/\Gamma_{total}$ — Γ_{321}/Γ

K_x^{*0} stands for the possible candidates of $K^*(1410)$, $K_0^*(1430)$ and $K_2^*(1430)$.

VALUE (units 10^{-6})	DOCUMENT ID		TECN	COMMENT
$\mathbf{6.1^{+1.6}_{-1.5}{}^{+0.5}_{-0.6}}$	[1] CHANG	04	BELL	$e^+e^- \to \Upsilon(4S)$

[1] Assumes equal production of B^+ and B^0 at the $\Upsilon(4S)$.

$\Gamma(K^0\pi^+\pi^-)/\Gamma_{total}$ — Γ_{322}/Γ

VALUE (units 10^{-6})	CL%	DOCUMENT ID		TECN	COMMENT
49.7± 1.8 OUR FIT					
49.6± 2.0 OUR AVERAGE					
50.2± 1.5±1.8		[1] AUBERT	09AU	BABR	$e^+e^- \to \Upsilon(4S)$
47.5± 2.4±3.7		[2] GARMASH	07	BELL	$e^+e^- \to \Upsilon(4S)$
$50^{+10}_{-9}\pm7$		[1] ECKHART	02	CLE2	$e^+e^- \to \Upsilon(4S)$
• • • We do not use the following data for averages, fits, limits, etc. • • •					
43.0± 2.3±2.3		[1] AUBERT	06I	BABR	Repl. by AUBERT 09AU
43.7± 3.8±3.4		[1] AUBERT,B	04O	BABR	Repl. by AUBERT 06I
45.4± 5.2±5.9		[1] GARMASH	04	BELL	Repl. by GARMASH 07
<440	90	ALBRECHT	91E	ARG	$e^+e^- \to \Upsilon(4S)$

[1] Assumes equal production of B^+ and B^0 at the $\Upsilon(4S)$.
[2] Uses Dalitz plot analysis of the $B^0 \to K^0\pi^+\pi^-$ final state decays.

$\Gamma(K^0\pi^+\pi^-$ nonresonant$)/\Gamma_{total}$ — Γ_{323}/Γ

VALUE (units 10^{-6})	DOCUMENT ID		TECN	COMMENT
$\mathbf{13.9^{+2.6}_{-1.8}}$ **OUR AVERAGE** Error includes scale factor of 1.6. See the ideogram below.				
12.1±0.6±2.9	[1] AAIJ	18F	LHCB	pp at 7, 8 TeV
$11.1^{+2.5}_{-1.0}\pm0.9$	[2] AUBERT	09AU	BABR	$e^+e^- \to \Upsilon(4S)$
$19.9\pm2.5^{+1.7}_{-2.0}$	[3] GARMASH	07	BELL	$e^+e^- \to \Upsilon(4S)$

[1] Uses Dalitz plot analysis of the $B^0 \to K_S^0\pi^+\pi^-$ final state decays. For the branching fraction of the reference mode, the PDG 18 average $B(B^0 \to K_S^0\pi^+\pi^-) = (4.96 \pm 0.20) \times 10^{-5}$ is used.
[2] Assumes equal production of B^+ and B^0 at the $\Upsilon(4S)$.
[3] Uses Dalitz plot analysis of the $B^0 \to K^0\pi^+\pi^-$ final state decays.

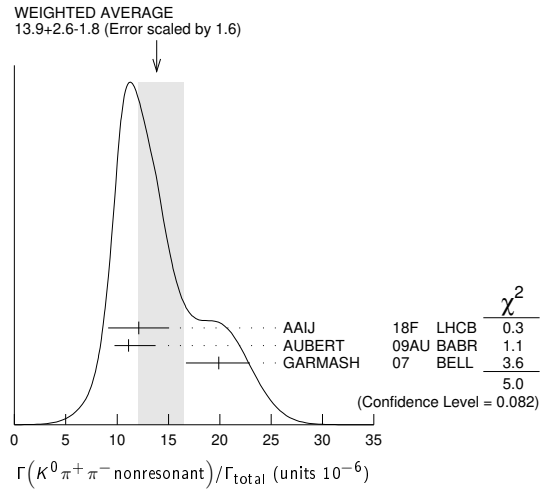

Int. J. Mod. Phys. A 2026.41. Downloaded from www.worldscientific.com
by UNIVERSITY OF CALIFORNIA @ BERKELEY on 09/16/26. Re-use and distribution is strictly not permitted, except for Open Access articles.

$\Gamma(K^0\rho^0)/\Gamma_{total}$ — Γ_{324}/Γ

VALUE (units 10^{-6})	CL%	DOCUMENT ID		TECN	COMMENT
3.4 ±1.1 OUR AVERAGE		Error includes scale factor of 2.3. See the ideogram below.			
$1.89^{+0.55}_{-0.79}\pm0.40$		[1] AAIJ	18F	LHCB	pp at 7, 8 TeV
$4.4\ ^{+0.7}_{-0.6}\ \pm0.3$		[2] AUBERT	09AU	BABR	$e^+e^-\to\Upsilon(4S)$
$6.1\ \pm1.0\ ^{+1.1}_{-1.2}$		[3] GARMASH	07	BELL	$e^+e^-\to\Upsilon(4S)$
• • • We do not use the following data for averages, fits, limits, etc. • • •					
$4.9\ \pm0.8\ \pm0.9$		[2] AUBERT	07F	BABR	Repl. by AUBERT 09AU
<39	90	ASNER	96	CLEO	$e^+e^-\to\Upsilon(4S)$
<320	90	ALBRECHT	91B	ARG	$e^+e^-\to\Upsilon(4S)$
<500	90	[4] AVERY	89B	CLEO	$e^+e^-\to\Upsilon(4S)$

[1] Uses Dalitz plot analysis of the $B^0\to K^0_S\pi^+\pi^-$ final state decays. For the branching fraction of the reference mode, the PDG 18 average $B(B^0\to K^0_S\pi^+\pi^-)=(4.96\pm0.20)\times10^{-5}$ is used.
[2] Assumes equal production of B^+ and B^0 at the $\Upsilon(4S)$.
[3] Uses Dalitz plot analysis of the $B^0\to K^0\pi^+\pi^-$ final state decays.
[4] AVERY 89B reports $<5.8\times10^{-4}$ assuming the $\Upsilon(4S)$ decays 43% to $B^0\overline{B}^0$. We rescale to 50%.

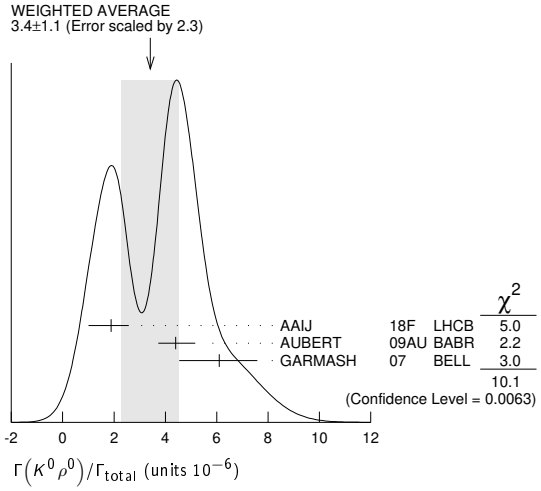

$\Gamma(K^*(892)^+\pi^-)/\Gamma_{total}$ — Γ_{325}/Γ

VALUE (units 10^{-6})	CL%	DOCUMENT ID		TECN	COMMENT
7.5 ±0.4 OUR AVERAGE					
$7.02\pm0.30\pm0.45$		[1] AAIJ	18F	LHCB	pp at 7, 8 TeV
$8.0\ \pm1.1\ \pm0.8$		[2,3] LEES	11	BABR	$e^+e^-\to\Upsilon(4S)$
$8.3\ ^{+0.9}_{-0.8}\ \pm0.8$		[3,4] AUBERT	09AU	BABR	$e^+e^-\to\Upsilon(4S)$
$8.4\ \pm1.1\ ^{+1.0}_{-0.9}$		[4] GARMASH	07	BELL	$e^+e^-\to\Upsilon(4S)$
$16\ ^{+6}_{-5}\ \pm2$		[3] ECKHART	02	CLE2	$e^+e^-\to\Upsilon(4S)$
• • • We do not use the following data for averages, fits, limits, etc. • • •					
$12.6\ ^{+2.7}_{-1.6}\ \pm0.9$		[2,3] AUBERT	08AQ	BABR	Repl. by LEES 11
$11.0\ \pm1.5\ \pm0.71$		[3] AUBERT	06I	BABR	Repl. by AUBERT 09AU
$12.9\ \pm2.4\ \pm1.4$		[3] AUBERT,B	04O	BABR	Repl. by AUBERT 06I
$14.8\ ^{+4.6}_{-4.4}\ ^{+2.8}_{-1.3}$		[3] CHANG	04	BELL	Repl. by GARMASH 07
<72	90	ASNER	96	CLE2	$e^+e^-\to\Upsilon(4S)$
<620	90	ALBRECHT	91B	ARG	$e^+e^-\to\Upsilon(4S)$
<380	90	[5] AVERY	89B	CLEO	$e^+e^-\to\Upsilon(4S)$
<560	90	[6] AVERY	87	CLEO	$e^+e^-\to\Upsilon(4S)$

[1] Uses Dalitz plot analysis of the $B^0\to K^0_S\pi^+\pi^-$ final state decays. For the branching fraction of the reference mode, the PDG 18 average $B(B^0\to K^0_S\pi^+\pi^-)=(4.96\pm0.20)\times10^{-5}$ is used.
[2] Uses Dalitz plot analysis of $B^0\to K^+\pi^-\pi^0$ decays.
[3] Assumes equal production of B^+ and B^0 at the $\Upsilon(4S)$.
[4] Uses Dalitz plot analysis of the $B^0\to K^0\pi^+\pi^-$ final state decays.
[5] AVERY 89B reports $<4.4\times10^{-4}$ assuming the $\Upsilon(4S)$ decays 43% to $B^0\overline{B}^0$. We rescale to 50%.
[6] AVERY 87 reports $<7\times10^{-4}$ assuming the $\Upsilon(4S)$ decays 40% to $B^0\overline{B}^0$. We rescale to 50%.

$\Gamma(K^*_0(1430)^+\pi^-)/\Gamma_{total}$ — Γ_{326}/Γ

VALUE (units 10^{-6})	DOCUMENT ID		TECN	COMMENT
33 ±7 OUR AVERAGE	Error includes scale factor of 2.0.			
$29.9^{+2.3}_{-1.7}\pm3.6$	[1,2] AUBERT	09AU	BABR	$e^+e^-\to\Upsilon(4S)$
$49.7\pm3.8^{+6.8}_{-8.2}$	[2] GARMASH	07	BELL	$e^+e^-\to\Upsilon(4S)$

[1] Assumes equal production of B^+ and B^0 at the $\Upsilon(4S)$.
[2] Uses Dalitz plot analysis of the $B^0\to K^0\pi^+\pi^-$ final state decays.

$\Gamma(K^{*+}_x\pi^-)/\Gamma_{total}$ — Γ_{327}/Γ

K^{*+}_x stands for the possible candidates of $K^*(1410)$, $K^*_0(1430)$ and $K^*_2(1430)$.

VALUE (units 10^{-6})	DOCUMENT ID		TECN	COMMENT
$\mathbf{5.1\pm1.5^{+0.6}_{-0.7}}$	[1] CHANG	04	BELL	$e^+e^-\to\Upsilon(4S)$

[1] Assumes equal production of B^+ and B^0 at the $\Upsilon(4S)$.

$\Gamma(K^*(1410)^+\pi^-,\ K^{*+}\to K^0\pi^+)/\Gamma_{total}$ — Γ_{328}/Γ

VALUE (units 10^{-6})	CL%	DOCUMENT ID		TECN	COMMENT
<3.8	90	[1] GARMASH	07	BELL	$e^+e^-\to\Upsilon(4S)$

[1] Uses Dalitz plot analysis of the $B^0\to K^0\pi^+\pi^-$ final state decays.

$\Gamma((K\pi)^{*+}_0\pi^-,\ (K\pi)^{*+}_0\to K^0\pi^+)/\Gamma_{total}$ — Γ_{329}/Γ

VALUE (units 10^{-6})	DOCUMENT ID		TECN	COMMENT
16.2±0.69±1.15	[1] AAIJ	18F	LHCB	pp at 7, 8 TeV

[1] Uses Dalitz plot analysis of the $B^0\to K^0_S\pi^+\pi^-$ final state decays. $(K\pi)^{*+}_0$ is the S-wave component of $K^0\pi^+$. For the branching fraction of the reference mode, the PDG 18 average $B(B^0\to K^0_S\pi^+\pi^-)=(4.96\pm0.20)\times10^{-5}$ is used.

$\Gamma(f_0(980)K^0,\ f_0\to\pi^+\pi^-)/\Gamma_{total}$ — Γ_{330}/Γ

VALUE (units 10^{-6})	CL%	DOCUMENT ID		TECN	COMMENT
8.1 ±0.8 OUR AVERAGE		Error includes scale factor of 1.3. See the ideogram below.			
$9.23\pm0.40\pm0.79$		[1] AAIJ	18F	LHCB	pp at 7, 8 TeV
$6.9\ \pm0.8\ \pm0.6$		[2] AUBERT	09AU	BABR	$e^+e^-\to\Upsilon(4S)$
$7.6\ \pm1.7\ ^{+0.9}_{-1.3}$		[3] GARMASH	07	BELL	$e^+e^-\to\Upsilon(4S)$
• • • We do not use the following data for averages, fits, limits, etc. • • •					
$5.5\ \pm0.7\ \pm0.6$		[2] AUBERT	06I	BABR	Repl. by AUBERT 09AU
<360	90	[4] AVERY	89B	CLEO	$e^+e^-\to\Upsilon(4S)$

[1] Uses Dalitz plot analysis of the $B^0\to K^0_S\pi^+\pi^-$ final state decays. For the branching fraction of the reference mode, the PDG 18 average $B(B^0\to K^0_S\pi^+\pi^-)=(4.96\pm0.20)\times10^{-5}$ is used.
[2] Assumes equal production of B^+ and B^0 at the $\Upsilon(4S)$.
[3] Uses Dalitz plot analysis of the $B^0\to K^0\pi^+\pi^-$ final state decays.
[4] AVERY 89B reports $<4.2\times10^{-4}$ assuming the $\Upsilon(4S)$ decays 43% to $B^0\overline{B}^0$. We rescale to 50%.

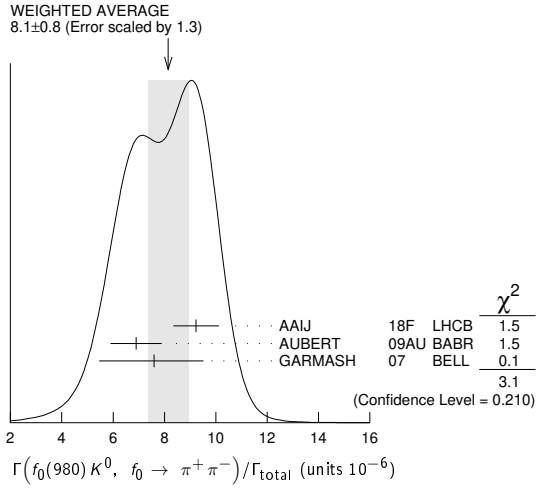

$\Gamma(K^0f_0(500))/\Gamma_{total}$ — Γ_{331}/Γ

VALUE (units 10^{-6})	DOCUMENT ID		TECN	COMMENT
$\mathbf{0.16^{+0.20}_{-0.04}\pm0.15}$	[1] AAIJ	18F	LHCB	pp at 7, 8 TeV

[1] Uses Dalitz plot analysis of the $B^0\to K^0_S\pi^+\pi^-$ final state decays. For the branching fraction of the reference mode, the PDG 18 average $B(B^0\to K^0_S\pi^+\pi^-)=(4.96\pm0.20)\times10^{-5}$ is used.

$\Gamma(K^0f_0(1500))/\Gamma_{total}$ — Γ_{332}/Γ

VALUE (units 10^{-6})	DOCUMENT ID		TECN	COMMENT
1.29±0.27±0.70	[1] AAIJ	18F	LHCB	pp at 7, 8 TeV

[1] Uses Dalitz plot analysis of the $B^0\to K^0_S\pi^+\pi^-$ final state decays. For the branching fraction of the reference mode, the PDG 18 average $B(B^0\to K^0_S\pi^+\pi^-)=(4.96\pm0.20)\times10^{-5}$ is used.

$\Gamma(f_2(1270)K^0)/\Gamma_{total}$ — Γ_{333}/Γ

VALUE (units 10^{-6})	CL%	DOCUMENT ID		TECN	COMMENT
$\mathbf{2.7^{+1.0}_{-0.8}\pm0.9}$		[1] AUBERT	09AU	BABR	$e^+e^-\to\Upsilon(4S)$

Int. J. Mod. Phys. A 2026.41. Downloaded from www.worldscientific.com by LIFORNIA @ BERKELEY on 09/16/26. Re-use and distribution is strictly not permitted, except for Open Access articles.

• • • We do not use the following data for averages, fits, limits, etc. • • •

<2.5	90	[2] GARMASH	07	BELL	$e^+e^- \to \Upsilon(4S)$

[1] Assumes equal production of B^+ and B^0 at the $\Upsilon(4S)$.
[2] GARMASH 07 reports $B(B^0 \to f_2(1270)K^0)\times B(f_2(1270) \to \pi^+\pi^-) < 1.4\times10^{-6}$ using Dalitz plot analysis. We compute $B(B^0 \to f_2(1270)K^0)$ using the PDG value $B(f_2(1270) \to \pi\pi) = 84.3\times10^{-2}$ and 2/3 for the $\pi^+\pi^-$ fraction.

$\Gamma(f_x(1300)K^0, f_x \to \pi^+\pi^-)/\Gamma_{total}$ — Γ_{334}/Γ

VALUE (units 10^{-6})	DOCUMENT ID		TECN	COMMENT
$1.81^{+0.55}_{-0.45}\pm0.48$	[1] AUBERT	09AU	BABR	$e^+e^- \to \Upsilon(4S)$

[1] Assumes equal production of B^+ and B^0 at the $\Upsilon(4S)$.

$\Gamma(K^*(892)^0\pi^0)/\Gamma_{total}$ — Γ_{335}/Γ

VALUE (units 10^{-6})	CL%	DOCUMENT ID		TECN	COMMENT
$3.3\pm0.5\pm0.4$		[1,2] LEES	11	BABR	$e^+e^- \to \Upsilon(4S)$
• • • We do not use the following data for averages, fits, limits, etc. • • •					
$3.6\pm0.7\pm0.4$		[1,2] AUBERT	08AQ	BABR	Repl. by LEES 11
< 3.5	90	[2] CHANG	04	BELL	$e^+e^- \to \Upsilon(4S)$
< 3.6	90	JESSOP	00	CLE2	$e^+e^- \to \Upsilon(4S)$
<28	90	ASNER	96	CLE2	Repl. by JESSOP 00

[1] Uses Dalitz plot analysis of $B^0 \to K^+\pi^-\pi^0$ decays.
[2] Assumes equal production of B^+ and B^0 at the $\Upsilon(4S)$.

$\Gamma(K_2^*(1430)^+\pi^-)/\Gamma_{total}$ — Γ_{336}/Γ

VALUE (units 10^{-6})	CL%	DOCUMENT ID		TECN	COMMENT
$3.65^{+0.15}_{-0.12}\pm0.31$		[1] AAIJ	18F	LHCB	pp at 7, 8 TeV
• • • We do not use the following data for averages, fits, limits, etc. • • •					
< 16.2	90	[2,3] AUBERT	08AQ	BABR	$e^+e^- \to \Upsilon(4S)$
< 6	90	[4] GARMASH	07	BELL	$e^+e^- \to \Upsilon(4S)$
< 18	90	[3] GARMASH	04	BELL	Repl. by GARMASH 07
<2600	90	ALBRECHT	91B	ARG	$e^+e^- \to \Upsilon(4S)$

[1] Uses Dalitz plot analysis of the $B^0 \to K_S^0\pi^+\pi^-$ final state decays. We compute $B(B^0 \to K_2^*(1430)^+\pi^-)$ using the PDG 18 value $B(K_2^*(1430) \to K\pi) = 49.9\times10^{-2}$ and 2/3 for the $K^0\pi^+$ fraction. For the branching fraction of the reference mode, the PDG 18 average $B(B^0 \to K_S^0\pi^+\pi^-) = (4.96\pm0.20)\times10^{-5}$ is used.
[2] Uses Dalitz plot analysis of $B^0 \to K^+\pi^-\pi^0$ decays.
[3] Assumes equal production of B^+ and B^0 at the $\Upsilon(4S)$.
[4] GARMASH 07 reports $B(B^0 \to K_2^*(1430)^+\pi^-)\times B(K_2^{*+} \to K^0\pi^+) < 2.1\times10^{-6}$ using Dalitz plot analysis. We compute $B(B^0 \to K_2^*(1430)^+\pi^-)$ using the PDG value $B(K_2^*(1430) \to K\pi) = 49.9\times10^{-2}$ and 2/3 for the $K^0\pi^+$ fraction.

$\Gamma(K^*(1680)^+\pi^-)/\Gamma_{total}$ — Γ_{337}/Γ

VALUE (units 10^{-6})	CL%	DOCUMENT ID		TECN	COMMENT
$14.1\pm0.58\pm0.84$		[1] AAIJ	18F	LHCB	pp at 7, 8 TeV
• • • We do not use the following data for averages, fits, limits, etc. • • •					
<25	90	[2,3] AUBERT	08AQ	BABR	$e^+e^- \to \Upsilon(4S)$
<10	90	[4] GARMASH	07	BELL	$e^+e^- \to \Upsilon(4S)$

[1] Uses Dalitz plot analysis of the $B^0 \to K_S^0\pi^+\pi^-$ final state decays. We compute $B(B^0 \to K_2^*(1430)^+\pi^-)$ using the PDG 18 value $B(K_2^*(1430) \to K\pi) = (49.9\pm1.2)\times10^{-2}$ and 2/3 for the $K^0\pi^+$ fraction. For the branching fraction of the reference mode, the PDG 18 average $B(B^0 \to K_S^0\pi^+\pi^-) = (4.96\pm0.20)\times10^{-5}$ is used.
[2] Uses Dalitz plot analysis of $B^0 \to K^+\pi^-\pi^0$ decays.
[3] Assumes equal production of B^+ and B^0 at the $\Upsilon(4S)$.
[4] GARMASH 07 reports $B(B^0 \to K^*(1680)^+\pi^-)\times B(K^{*+} \to K^0\pi^+) < 2.6\times10^{-6}$ using Dalitz plot analysis. We compute $B(B^0 \to K^*(1680)^+\pi^-)$ using the PDG value $B(K^*(1680) \to K\pi)=38.7\times10^{-2}$ and 2/3 for the $K^0\pi^+$ fraction.

$\Gamma(K^+\pi^-\pi^+\pi^-)/\Gamma_{total}$ — Γ_{338}/Γ

VALUE	CL%	DOCUMENT ID		TECN	COMMENT
$<2.3\times10^{-4}$	90	[1] ADAM	96D	DLPH	$e^+e^- \to Z$
• • • We do not use the following data for averages, fits, limits, etc. • • •					
$<2.1\times10^{-4}$	90	[2] ABREU	95N	DLPH	Sup. by ADAM 96D

[1] ADAM 96D assumes $f_{B^0} = f_{B^-} = 0.39$ and $f_{B_s} = 0.12$. Contributions from B^0 and B_s decays cannot be separated. Limits are given for the weighted average of the decay rates for the two neutral B mesons.
[2] Assumes a B^0, B^- production fraction of 0.39 and a B_s production fraction of 0.12. Contributions from B^0 and B_s^0 decays cannot be separated. Limits are given for the weighted average of the decay rates for the two neutral B mesons.

$\Gamma(\rho^0K^+\pi^-)/\Gamma_{total}$ — Γ_{339}/Γ

VALUE (units 10^{-6})	DOCUMENT ID		TECN	COMMENT
$2.8\pm0.5\pm0.5$	[1,2] KYEONG	09	BELL	$e^+e^- \to \Upsilon(4S)$

[1] Assumes equal production of B^+ and B^0 at the $\Upsilon(4S)$.
[2] Required $0.75 < m_{K^+\pi^-} < 1.20$ GeV/c^2.

$\Gamma(f_0(980)K^+\pi^-,\ f_0 \to \pi\pi)/\Gamma_{total}$ — Γ_{340}/Γ

VALUE (units 10^{-6})	DOCUMENT ID		TECN	COMMENT
$1.4\pm0.4^{+0.3}_{-0.4}$	[1,2] KYEONG	09	BELL	$e^+e^- \to \Upsilon(4S)$

[1] Assumes equal production of B^+ and B^0 at the $\Upsilon(4S)$.
[2] Required $0.75 < m_{K^+K^-} < 1.2$ GeV/c^2.

$\Gamma(K^+\pi^-\pi^+\pi^-$ nonresonant$)/\Gamma_{total}$ — Γ_{341}/Γ

VALUE	CL%	DOCUMENT ID		TECN	COMMENT
$<2.1\times10^{-6}$	90	[1,2] KYEONG	09	BELL	$e^+e^- \to \Upsilon(4S)$

[1] Assumes equal production of B^+ and B^0 at the $\Upsilon(4S)$.
[2] Required $0.55 < m_{\pi^+\pi^-} < 1.42$ and $0.75 < m_{K^+\pi^-} < 1.20$ GeV/c^2.

$\Gamma(K^*(892)^0\pi^+\pi^-)/\Gamma_{total}$ — Γ_{342}/Γ

VALUE (units 10^{-6})	CL%	DOCUMENT ID		TECN	COMMENT
$54.5\pm2.9\pm4.3$		[1] AUBERT	07AS	BABR	$e^+e^- \to \Upsilon(4S)$
• • • We do not use the following data for averages, fits, limits, etc. • • •					
$4.5^{+1.1}_{-1.0}{}^{+0.9}_{-1.6}$		[1,2] KYEONG	09	BELL	$e^+e^- \to \Upsilon(4S)$
<1400	90	ALBRECHT	91E	ARG	$e^+e^- \to \Upsilon(4S)$

[1] Assumes equal production of B^+ and B^0 at the $\Upsilon(4S)$.
[2] Required $0.55 < m_{\pi^+\pi^-} < 1.42$ GeV/c^2.

$\Gamma(K^*(892)^0\rho^0)/\Gamma_{total}$ — Γ_{343}/Γ

VALUE (units 10^{-6})	CL%	DOCUMENT ID		TECN	COMMENT
3.9±1.3 OUR AVERAGE Error includes scale factor of 1.9.					
$5.1\pm0.6^{+0.6}_{-0.8}$		[1] LEES	12K	BABR	$e^+e^- \to \Upsilon(4S)$
$2.1^{+0.8}_{-0.7}{}^{+0.9}_{-0.5}$		[1] KYEONG	09	BELL	$e^+e^- \to \Upsilon(4S)$
• • • We do not use the following data for averages, fits, limits, etc. • • •					
$5.6\pm0.9\pm1.3$		[1] AUBERT,B	06G	BABR	Repl. by LEES 12K
< 34	90	[2] GODANG	02	CLE2	$e^+e^- \to \Upsilon(4S)$
<286	90	[3] ABE	00C	SLD	$e^+e^- \to Z$
<460	90	ALBRECHT	91B	ARG	$e^+e^- \to \Upsilon(4S)$
<580	90	[4] AVERY	89B	CLEO	$e^+e^- \to \Upsilon(4S)$
<960	90	[5] AVERY	87	CLEO	$e^+e^- \to \Upsilon(4S)$

[1] Assumes equal production of B^+ and B^0 at the $\Upsilon(4S)$.
[2] Assumes a helicity 00 configuration. For a helicity 11 configuration, the limit decreases to 2.4×10^{-5}.
[3] ABE 00C assumes $B(Z \to b\overline{b})=(21.7\pm0.1)\%$ and the B fractions $f_{B^0}=f_{B^+}=(39.7^{+1.8}_{-2.2})\%$ and $f_{B_s}=(10.5^{+1.8}_{-2.2})\%$.
[4] AVERY 89B reports $< 6.7\times10^{-4}$ assuming the $\Upsilon(4S)$ decays 43% to $B^0\overline{B}^0$. We rescale to 50%.
[5] AVERY 87 reports $< 1.2\times10^{-3}$ assuming the $\Upsilon(4S)$ decays 40% to $B^0\overline{B}^0$. We rescale to 50%.

$\Gamma(K^*(892)^0f_0(980),\ f_0 \to \pi\pi)/\Gamma_{total}$ — Γ_{344}/Γ

VALUE (units 10^{-6})	CL%	DOCUMENT ID		TECN	COMMENT
$3.9^{+2.1}_{-1.8}$ **OUR AVERAGE** Error includes scale factor of 3.9.					
$5.7\pm0.6\pm0.4$		[1] LEES	12K	BABR	$e^+e^- \to \Upsilon(4S)$
$1.4^{+0.6}_{-0.5}{}^{+0.6}_{-0.4}$		[1,2] KYEONG	09	BELL	$e^+e^- \to \Upsilon(4S)$
• • • We do not use the following data for averages, fits, limits, etc. • • •					
< 4.3	90	[1] AUBERT,B	06G	BABR	$e^+e^- \to \Upsilon(4S)$
<170	90	[3] AVERY	89B	CLEO	$e^+e^- \to \Upsilon(4S)$

[1] Assumes equal production of B^+ and B^0 at the $\Upsilon(4S)$.
[2] The upper limit is 2.2×10^{-6} at 90% CL.
[3] AVERY 89B reports $< 2.0\times10^{-4}$ assuming the $\Upsilon(4S)$ decays 43% to $B^0\overline{B}^0$. We rescale to 50%.

$\Gamma(K_1(1270)^+\pi^-)/\Gamma_{total}$ — Γ_{345}/Γ

VALUE	CL%	DOCUMENT ID		TECN	COMMENT
$<3.0\times10^{-5}$	90	[1] AUBERT	10D	BABR	$e^+e^- \to \Upsilon(4S)$

[1] Assumes equal production of B^+ and B^0 at the $\Upsilon(4S)$.

$\Gamma(K_1(1400)^+\pi^-)/\Gamma_{total}$ — Γ_{346}/Γ

VALUE	CL%	DOCUMENT ID		TECN	COMMENT
$<2.7\times10^{-5}$	90	[1] AUBERT	10D	BABR	$e^+e^- \to \Upsilon(4S)$
• • • We do not use the following data for averages, fits, limits, etc. • • •					
$<1.1\times10^{-3}$	90	ALBRECHT	91B	ARG	$e^+e^- \to \Upsilon(4S)$

[1] Assumes equal production of B^+ and B^0 at the $\Upsilon(4S)$.

$\Gamma(a_1(1260)^-K^+)/\Gamma_{total}$ — Γ_{347}/Γ

VALUE (units 10^{-6})	CL%	DOCUMENT ID		TECN	COMMENT
$16.3\pm2.9\pm2.3$		[1,2] AUBERT	08F	BABR	$e^+e^- \to \Upsilon(4S)$
• • • We do not use the following data for averages, fits, limits, etc. • • •					
<230	90	[3] ADAM	96D	DLPH	$e^+e^- \to Z$
<390	90	[4] ABREU	95N	DLPH	Sup. by ADAM 96D

[1] Assumes equal production of B^+ and B^0 at the $\Upsilon(4S)$.

[2] Assumes $a_1^\pm$ decays only to 3π and $B(a_1^\pm \to \pi^\pm\pi^\mp\pi^\pm) = 0.5$.

[3] ADAM 96D assumes $f_{B^0} = f_{B^-} = 0.39$ and $f_{B_s} = 0.12$. Contributions from B^0 and B_s decays cannot be separated. Limits are given for the weighted average of the decay rates for the two neutral B mesons.

[4] Assumes a B^0, B^- production fraction of 0.39 and a B_s production fraction of 0.12. Contributions from B^0 and B_s^0 decays cannot be separated. Limits are given for the weighted average of the decay rates for the two neutral B mesons.

$\Gamma(K^*(892)^+\rho^-)/\Gamma_{total}$ — Γ_{348}/Γ

VALUE (units 10^{-6})	CL%	DOCUMENT ID		TECN	COMMENT
10.3±2.3±1.3		[1] LEES	12K	BABR	$e^+e^- \to \Upsilon(4S)$
• • • We do not use the following data for averages, fits, limits, etc. • • •					
<12.0	90	[1] AUBERT,B	06G	BABR	Repl. by LEES 12K

[1] Assumes equal production of B^+ and B^0 at the $\Upsilon(4S)$.

$\Gamma(K_0^*(1430)^+\rho^-)/\Gamma_{total}$ — Γ_{349}/Γ

VALUE (units 10^{-6})	DOCUMENT ID		TECN	COMMENT
28±10±6	[1] LEES	12K	BABR	$e^+e^- \to \Upsilon(4S)$

[1] Assumes equal production of B^+ and B^0 at the $\Upsilon(4S)$.

$\Gamma(K_1(1400)^0\rho^0)/\Gamma_{total}$ — Γ_{350}/Γ

VALUE	CL%	DOCUMENT ID		TECN	COMMENT
$<3.0\times10^{-3}$	90	ALBRECHT	91B	ARG	$e^+e^- \to \Upsilon(4S)$

$\Gamma(K_0^*(1430)^0\rho^0)/\Gamma_{total}$ — Γ_{351}/Γ

VALUE (units 10^{-6})	DOCUMENT ID		TECN	COMMENT
27±4±4	[1] LEES	12K	BABR	$e^+e^- \to \Upsilon(4S)$

[1] Assumes equal production of B^+ and B^0 at the $\Upsilon(4S)$.

$\Gamma(K_0^*(1430)^0 f_0(980),\ f_0 \to \pi\pi)/\Gamma_{total}$ — Γ_{352}/Γ

VALUE (units 10^{-6})	DOCUMENT ID		TECN	COMMENT
2.7±0.7±0.6	[1] LEES	12K	BABR	$e^+e^- \to \Upsilon(4S)$

[1] Assumes equal production of B^+ and B^0 at the $\Upsilon(4S)$.

$\Gamma(K_2^*(1430)^0 f_0(980),\ f_0 \to \pi\pi)/\Gamma_{total}$ — Γ_{353}/Γ

VALUE (units 10^{-6})	DOCUMENT ID		TECN	COMMENT
8.6±1.7±1.0	[1] LEES	12K	BABR	$e^+e^- \to \Upsilon(4S)$

[1] Assumes equal production of B^+ and B^0 at the $\Upsilon(4S)$.

$\Gamma(K^+K^-)/\Gamma_{total}$ — Γ_{354}/Γ

VALUE (units 10^{-8})	CL%	DOCUMENT ID		TECN	COMMENT
7.80± 1.27± 0.84		[1] AAIJ	17G	LHCB	pp at 7 and 8 TeV
• • • We do not use the following data for averages, fits, limits, etc. • • •					
10 ± 8 ± 4		[2,3] DUH	13	BELL	$e^+e^- \to \Upsilon(4S)$
12^{+8}_{-7} ± 1		[4] AAIJ	12AR	LHCB	Repl. by AAIJ 17G
23 ±10 ±10		[5] AALTONEN	12L	CDF	$p\overline{p}$ at 1.96 TeV
< 70	90	[6] AALTONEN	09C	CDF	Repl. by AALTONEN 12L
< 50	90	[3] AUBERT	07B	BABR	$e^+e^- \to \Upsilon(4S)$
< 41	90	[3] LIN	07	BELL	Repl. by DUH 13
< 180	90	[7] ABULENCIA,A	06D	CDF	Repl. by AALTONEN 09C
< 37	90	ABE	05G	BELL	Repl. by LIN 07
< 70	90	CHAO	04	BELL	$e^+e^- \to \Upsilon(4S)$
< 80	90	[3] BORNHEIM	03	CLE2	$e^+e^- \to \Upsilon(4S)$
< 60	90	[3] AUBERT	02Q	BABR	$e^+e^- \to \Upsilon(4S)$
< 90	90	[3] CASEY	02	BELL	$e^+e^- \to \Upsilon(4S)$
< 270	90	[3] ABE	01H	BELL	$e^+e^- \to \Upsilon(4S)$
< 250	90	[3] AUBERT	01E	BABR	$e^+e^- \to \Upsilon(4S)$
< 6600	90	[8] ABE	00C	SLD	$e^+e^- \to Z$
< 190	90	[3] CRONIN-HEN...	00	CLE2	$e^+e^- \to \Upsilon(4S)$
< 430	90	GODANG	98	CLE2	Repl. by CRONIN-HENNESSY 00
< 4600		[9] ADAM	96D	DLPH	$e^+e^- \to Z$
< 400	90	ASNER	96	CLE2	Repl. by GODANG 98
< 1800	90	[10] BUSKULIC	96V	ALEP	$e^+e^- \to Z$
<12000	90	[11] ABREU	95N	DLPH	Sup. by ADAM 96D
< 700	90	[3] BATTLE	93	CLE2	$e^+e^- \to \Upsilon(4S)$

[1] Supercedes results of AAIJ 12AR.

[2] DUH 13 reports also for the same data $B(B^0 \to K^+K^-) < 0.20\times10^{-6}$ at 90% CL.

[3] Assumes equal production of B^+ and B^0 at the $\Upsilon(4S)$.

[4] AAIJ 12AR reports $[\Gamma(B^0 \to K^+K^-)/\Gamma_{total}]$ / $[B(B_s^0 \to K^+K^-)]$ / $[\Gamma(\overline{b} \to B_s^0 \text{at} pp)/\Gamma(\overline{b} \to B^0 \text{at} pp)] = 0.018^{+0.008}_{-0.007} \pm 0.009$ which we multiply by our best (shown rounded) values $B(B_s^0 \to K^+K^-) = (2.61\pm0.16)\times10^{-5}$, $\Gamma(\overline{b} \to B_s^0 \text{at} pp)/\Gamma(\overline{b} \to B^0 \text{at} pp) = 0.251 \pm 0.007$. Our first error is their experiment's error and our second error is the systematic error from using our best (shown rounded) values.

[5] Reported a central value of $(0.23 \pm 0.10 \pm 0.10)\times10^{-6}$ using $B(B^0 \to K^+\pi^-) = (19.4 \pm 0.6)\times10^{-6}$.

[6] Obtains this result from $B(K^+K^-)/B(K^+\pi^-) = 0.020 \pm 0.008 \pm 0.006$, assuming $B(B^0 \to K^+\pi^-) = (19.4 \pm 0.6)\times10^{-6}$.

[7] ABULENCIA,A 06D obtains this from $\Gamma(K^+K^-)/\Gamma(K^+\pi^-) < 0.10$ at 90% CL, assuming $B(B^0 \to K^+\pi^-) = (18.9 \pm 0.7)\times10^{-6}$.

[8] ABE 00C assumes $B(Z \to b\overline{b}) = (21.7 \pm 0.1)\%$ and the B fractions $f_{B^0} = f_{B^+} = (39.7^{+1.8}_{-2.2})\%$ and $f_{B_s} = (10.5^{+1.8}_{-2.2})\%$.

[9] ADAM 96D assumes $f_{B^0} = f_{B^-} = 0.39$ and $f_{B_s} = 0.12$. Contributions from B^0 and B_s decays cannot be separated. Limits are given for the weighted average of the decay rates for the two neutral B mesons.

[10] BUSKULIC 96V assumes PDG 96 production fractions for B^0, B^+, B_s, b baryons.

[11] Assumes a B^0, B^- production fraction of 0.39 and a B_s production fraction of 0.12. Contributions from B^0 and B_s^0 decays cannot be separated. Limits are given for the weighted average of the decay rates for the two neutral B mesons.

$\Gamma(K^0\overline{K}^0)/\Gamma_{total}$ — Γ_{355}/Γ

VALUE (units 10^{-6})	CL%	DOCUMENT ID		TECN	COMMENT
1.21±0.16 OUR AVERAGE					
1.26±0.19±0.05		[1] DUH	13	BELL	$e^+e^- \to \Upsilon(4S)$
1.08±0.28±0.11		[1] AUBERT,BE	06C	BABR	$e^+e^- \to \Upsilon(4S)$
• • • We do not use the following data for averages, fits, limits, etc. • • •					
$0.87^{+0.25}_{-0.20}\pm0.09$		[1] LIN	07	BELL	Repl. by DUH 13
0.8 ±0.3 ±0.9		[1] ABE	05G	BELL	Repl. by LIN 07
$1.19^{+0.40}_{-0.35}\pm0.13$		[1] AUBERT,BE	05E	BABR	Repl. by AUBERT,BE 06C
< 1.8	90	[1] AUBERT	04M	BABR	$e^+e^- \to \Upsilon(4S)$
< 1.5	90	[1] CHAO	04	BELL	Repl. by ABE 05G
< 3.3	90	[1] BORNHEIM	03	CLE2	$e^+e^- \to \Upsilon(4S)$
< 4.1	90	[1] CASEY	02	BELL	$e^+e^- \to \Upsilon(4S)$
<17	90	GODANG	98	CLE2	$e^+e^- \to \Upsilon(4S)$

[1] Assumes equal production of B^+ and B^0 at the $\Upsilon(4S)$.

$\Gamma(K^0\overline{K}^0)/\Gamma(K^0\phi)$ — $\Gamma_{355}/\Gamma_{364}$

VALUE	DOCUMENT ID		TECN	COMMENT
0.17±0.08±0.02	[1] AAIJ	20F	LHCB	pp at 7, 8, 13 TeV

[1] Observed signal with a significance of 3.5 σ.

$\Gamma(K^0K^-\pi^+)/\Gamma_{total}$ — Γ_{356}/Γ

VALUE (units 10^{-6})	CL%	DOCUMENT ID		TECN	COMMENT
6.7±0.5 OUR FIT					
7.0±0.6 OUR AVERAGE					
7.2±0.7±0.3		[1] LAI	19	BELL	$e^+e^- \to \Upsilon(4S)$
6.4±1.0±0.6		[1] DEL-AMO-SA...	10E	BABR	$e^+e^- \to \Upsilon(4S)$
• • • We do not use the following data for averages, fits, limits, etc. • • •					
<18	90	[1] GARMASH	04	BELL	$e^+e^- \to \Upsilon(4S)$
<21	90	[1] ECKHART	02	CLE2	$e^+e^- \to \Upsilon(4S)$

[1] Assumes equal production of B^+ and B^0 at the $\Upsilon(4S)$.

$\Gamma(K^*(892)^\pm K^\mp)/\Gamma_{total}$ — Γ_{357}/Γ

VALUE	CL%	DOCUMENT ID		TECN	COMMENT
$<0.4\times10^{-6}$	90	AAIJ	14BM	LHCB	pp at 7 TeV

$\Gamma(K^0K^-\pi^+)/\Gamma(K^0\pi^+\pi^-)$ — $\Gamma_{356}/\Gamma_{322}$

VALUE	DOCUMENT ID		TECN	COMMENT
0.134±0.011 OUR FIT				
0.123±0.009±0.015	AAIJ	17BP	LHCB	pp at 7, 8 TeV
• • • We do not use the following data for averages, fits, limits, etc. • • •				
0.128±0.017±0.009	AAIJ	13BP	LHCB	Repl. by AAIJ 17BP

$[\Gamma(\overline{K}^{*0}K^0) + \Gamma(K^{*0}\overline{K}^0)]/\Gamma_{total}$ — Γ_{358}/Γ

VALUE (units 10^{-6})	CL%	DOCUMENT ID		TECN	COMMENT
<0.96	90	[1] AAIJ	16	LHCB	pp at 7 TeV
• • • We do not use the following data for averages, fits, limits, etc. • • •					
<1.9	90	[2] AUBERT,BE	06N	BABR	$e^+e^- \to \Upsilon(4S)$

[1] Assumes $B(B^0 \to K^0\pi^+\pi^-) = (4.96 \pm 0.20)\times10^{-5}$.

[2] Assumes equal production of B^+ and B^0 at the $\Upsilon(4S)$.

$\Gamma(K^+K^-\pi^0)/\Gamma_{total}$ — Γ_{359}/Γ

VALUE (units 10^{-6})	CL%	DOCUMENT ID		TECN	COMMENT
2.17±0.60±0.24		[1] GAUR	13	BELL	$e^+e^- \to \Upsilon(4S)$
• • • We do not use the following data for averages, fits, limits, etc. • • •					
<19	90	[1] ECKHART	02	CLE2	$e^+e^- \to \Upsilon(4S)$

[1] Assumes equal production of B^+ and B^0 at the $\Upsilon(4S)$.

$\Gamma(K_S^0K_S^0\pi^0)/\Gamma_{total}$ — Γ_{360}/Γ

VALUE	CL%	DOCUMENT ID		TECN	COMMENT
$<0.9\times10^{-6}$	90	[1] AUBERT	09AD	BABR	$e^+e^- \to \Upsilon(4S)$

[1] Assumes equal production of B^+ and B^0 at the $\Upsilon(4S)$.

$\Gamma(K_S^0K_S^0\eta)/\Gamma_{total}$ — Γ_{361}/Γ

VALUE	CL%	DOCUMENT ID		TECN	COMMENT
$<1.0\times10^{-6}$	90	[1] AUBERT	09AD	BABR	$e^+e^- \to \Upsilon(4S)$

[1] Assumes equal production of B^+ and B^0 at the $\Upsilon(4S)$.

Int. J. Mod. Phys. A 2026.41. Downloaded from www.worldscientific.com
by UNIVERSITY OF CALIFORNIA @ BERKELEY on 09/16/26. Re-use and distribution is strictly not permitted, except for Open Access articles.

Int. J. Mod. Phys. A 2026.41. Downloaded from www.worldscientific.com by LIFORNIA @ BERKELEY on 09/16/26. Re-use and distribution is strictly not permitted, except for Open Access articles.

$\Gamma(K^0_S K^0_S \eta')/\Gamma_{total}$ — Γ_{362}/Γ

VALUE	CL%	DOCUMENT ID		TECN	COMMENT
$<2.0\times10^{-6}$	90	[1] AUBERT	09AD	BABR	$e^+e^-\to\Upsilon(4S)$

[1] Assumes equal production of B^+ and B^0 at the $\Upsilon(4S)$.

$\Gamma(K^0 K^+ K^-)/\Gamma_{total}$ — Γ_{363}/Γ

VALUE (units 10^{-6})	CL%	DOCUMENT ID		TECN	COMMENT
26.8±1.1 OUR FIT					
26.6±1.2 OUR AVERAGE					
26.5±0.9±0.8		[1,2] LEES	12O	BABR	$e^+e^-\to\Upsilon(4S)$
28.3±3.3±4.0		[1] GARMASH	04	BELL	$e^+e^-\to\Upsilon(4S)$
• • • We do not use the following data for averages, fits, limits, etc. • • •					
23.8±2.0±1.6		[1] AUBERT,B	04V	BABR	Repl. by LEES 12O
<1300	90	ALBRECHT	91E	ARG	$e^+e^-\to\Upsilon(4S)$

[1] Assumes equal production of B^+ and B^0 at the $\Upsilon(4S)$.
[2] All intermediate charmonium and charm resonances are removed, except of χ_{c0}.

$\Gamma(K^0 K^+ K^-)/\Gamma(K^0\pi^+\pi^-)$ — $\Gamma_{363}/\Gamma_{322}$

VALUE	DOCUMENT ID		TECN	COMMENT
0.539±0.025 OUR FIT				
0.549±0.018±0.033	AAIJ	17BP	LHCB	pp at 7, 8 TeV
• • • We do not use the following data for averages, fits, limits, etc. • • •				
0.385±0.031±0.023	AAIJ	13BP	LHCB	Repl. by AAIJ 17BP

$\Gamma(K^0\phi)/\Gamma_{total}$ — Γ_{364}/Γ

VALUE (units 10^{-6})	CL%	DOCUMENT ID		TECN	COMMENT
7.3±0.7 OUR AVERAGE					
$7.1\pm0.6^{+0.4}_{-0.3}$		[1] LEES	12O	BABR	$e^+e^-\to\Upsilon(4S)$
$9.0^{+2.2}_{-1.8}\pm0.7$		[1] CHEN	03B	BELL	$e^+e^-\to\Upsilon(4S)$
• • • We do not use the following data for averages, fits, limits, etc. • • •					
$8.4^{+1.5}_{-1.3}\pm0.5$		[1] AUBERT	04A	BABR	Repl. by LEES 12O
$8.1^{+3.1}_{-2.5}\pm0.8$		[1] AUBERT	01D	BABR	$e^+e^-\to\Upsilon(4S)$
< 12.3	90	[1] BRIERE	01	CLE2	$e^+e^-\to\Upsilon(4S)$
< 31	90	[1] BERGFELD	98	CLE2	
< 88	90	ASNER	96	CLE2	$e^+e^-\to\Upsilon(4S)$
< 720	90	ALBRECHT	91B	ARG	$e^+e^-\to\Upsilon(4S)$
< 420	90	[2] AVERY	89B	CLEO	$e^+e^-\to\Upsilon(4S)$
<1000	90	[3] AVERY	87	CLEO	$e^+e^-\to\Upsilon(4S)$

[1] Assumes equal production of B^+ and B^0 at the $\Upsilon(4S)$.
[2] AVERY 89B reports $<4.9\times10^{-4}$ assuming the $\Upsilon(4S)$ decays 43% to $B^0\overline{B}^0$. We rescale to 50%.
[3] AVERY 87 reports $<1.3\times10^{-3}$ assuming the $\Upsilon(4S)$ decays 40% to $B^0\overline{B}^0$. We rescale to 50%.

$\Gamma(f_0(980)K^0,\ f_0\to K^+K^-)/\Gamma_{total}$ — Γ_{365}/Γ

VALUE (units 10^{-6})	DOCUMENT ID		TECN	COMMENT
$7.0^{+2.6}_{-1.8}\pm2.4$	[1] LEES	12O	BABR	$e^+e^-\to\Upsilon(4S)$

[1] Assumes equal production of B^+ and B^0 at the $\Upsilon(4S)$.

$\Gamma(f_0(1500)K^0)/\Gamma_{total}$ — Γ_{366}/Γ

VALUE (units 10^{-6})	DOCUMENT ID		TECN	COMMENT
$13.3^{+5.8}_{-4.4}\pm3.2$	[1] LEES	12O	BABR	$e^+e^-\to\Upsilon(4S)$

[1] Assumes equal production of B^+ and B^0 at the $\Upsilon(4S)$.

$\Gamma(f'_2(1525)^0 K^0)/\Gamma_{total}$ — Γ_{367}/Γ

VALUE (units 10^{-6})	DOCUMENT ID		TECN	COMMENT
$0.29^{+0.27}_{-0.18}\pm0.36$	[1] LEES	12O	BABR	$e^+e^-\to\Upsilon(4S)$

[1] Assumes equal production of B^+ and B^0 at the $\Upsilon(4S)$.

$\Gamma(f_0(1710)K^0,\ f_0\to K^+K^-)/\Gamma_{total}$ — Γ_{368}/Γ

VALUE (units 10^{-6})	DOCUMENT ID		TECN	COMMENT
4.4±0.7±0.5	[1] LEES	12O	BABR	$e^+e^-\to\Upsilon(4S)$

[1] Assumes equal production of B^+ and B^0 at the $\Upsilon(4S)$.

$\Gamma(K^0 K^+ K^-\text{nonresonant})/\Gamma_{total}$ — Γ_{369}/Γ

VALUE (units 10^{-6})	DOCUMENT ID		TECN	COMMENT
33±5±9	[1] LEES	12O	BABR	$e^+e^-\to\Upsilon(4S)$

[1] Assumes equal production of B^+ and B^0 at the $\Upsilon(4S)$.

$\Gamma(K^0_S K^0_S K^0_S)/\Gamma_{total}$ — Γ_{370}/Γ

VALUE (units 10^{-6})	DOCUMENT ID		TECN	COMMENT
6.0 ±0.5 OUR AVERAGE Error includes scale factor of 1.1.				
6.19±0.48±0.19	[1] LEES	12I	BABR	$e^+e^-\to\Upsilon(4S)$
$4.2\ ^{+1.6}_{-1.3}\pm0.8$	[1] GARMASH	04	BELL	$e^+e^-\to\Upsilon(4S)$
• • • We do not use the following data for averages, fits, limits, etc. • • •				
$6.9\ ^{+0.9}_{-0.8}\pm0.6$	[1] AUBERT,B	05	BABR	Repl. by LEES 12I

[1] Assumes equal production of B^+ and B^0 at the $\Upsilon(4S)$.

$\Gamma(f_0(980)K^0,\ f_0\to K^0_S K^0_S)/\Gamma_{total}$ — Γ_{371}/Γ

VALUE (units 10^{-6})	DOCUMENT ID		TECN	COMMENT
$2.7^{+1.3}_{-1.2}\pm1.3$	[1,2] LEES	12I	BABR	$e^+e^-\to\Upsilon(4S)$

[1] Assumes equal production of B^+ and B^0 at the $\Upsilon(4S)$.
[2] Uses Dalitz plot analysis of the $B^0\to K^0_S K^0_S K^0_S$ decay.

$\Gamma(f_0(1710)K^0,\ f_0\to K^0_S K^0_S)/\Gamma_{total}$ — Γ_{372}/Γ

VALUE (units 10^{-6})	DOCUMENT ID		TECN	COMMENT
$0.50^{+0.46}_{-0.24}\pm0.11$	[1,2] LEES	12I	BABR	$e^+e^-\to\Upsilon(4S)$

[1] Assumes equal production of B^+ and B^0 at the $\Upsilon(4S)$.
[2] Uses Dalitz plot analysis of the $B^0\to K^0_S K^0_S K^0_S$ decay.

$\Gamma(f_2(2010)K^0,\ f_2\to K^0_S K^0_S)/\Gamma_{total}$ — Γ_{373}/Γ

VALUE (units 10^{-6})	DOCUMENT ID		TECN	COMMENT
$0.54^{+0.21}_{-0.20}\pm0.52$	[1,2] LEES	12I	BABR	$e^+e^-\to\Upsilon(4S)$

[1] Assumes equal production of B^+ and B^0 at the $\Upsilon(4S)$.
[2] Uses Dalitz plot analysis of the $B^0\to K^0_S K^0_S K^0_S$ decay.

$\Gamma(K^0_S K^0_S K^0_S\text{nonresonant})/\Gamma_{total}$ — Γ_{374}/Γ

VALUE (units 10^{-6})	DOCUMENT ID		TECN	COMMENT
$13.3^{+2.2}_{-2.3}\pm2.2$	[1,2] LEES	12I	BABR	$e^+e^-\to\Upsilon(4S)$

[1] Assumes equal production of B^+ and B^0 at the $\Upsilon(4S)$.
[2] Uses Dalitz plot analysis of the $B^0\to K^0_S K^0_S K^0_S$ decay.

$\Gamma(K^0_S K^0_S K^0_L)/\Gamma_{total}$ — Γ_{375}/Γ

VALUE (units 10^{-6})	CL%	DOCUMENT ID		TECN	COMMENT
<16	90	[1] AUBERT,B	06R	BABR	$e^+e^-\to\Upsilon(4S)$

[1] Assumes equal production of B^+ and B^0 at the $\Upsilon(4S)$.

$\Gamma(K^*(892)^0 K^+ K^-)/\Gamma_{total}$ — Γ_{376}/Γ

VALUE (units 10^{-6})	CL%	DOCUMENT ID		TECN	COMMENT
27.5±1.3±2.2		[1] AUBERT	07AS	BABR	$e^+e^-\to\Upsilon(4S)$
• • • We do not use the following data for averages, fits, limits, etc. • • •					
<610	90	ALBRECHT	91E	ARG	$e^+e^-\to\Upsilon(4S)$

[1] Assumes equal production of B^+ and B^0 at the $\Upsilon(4S)$.

$\Gamma(K^*(892)^0\phi)/\Gamma_{total}$ — Γ_{377}/Γ

VALUE (units 10^{-6})	CL%	DOCUMENT ID		TECN	COMMENT
10.0±0.5 OUR FIT					
10.0±0.5 OUR AVERAGE					
10.4±0.5±0.6		[1] PRIM	13	BELL	$e^+e^-\to\Upsilon(4S)$
9.7±0.5±0.5		[1] AUBERT	08BG	BABR	$e^+e^-\to\Upsilon(4S)$
$11.5^{+4.5}_{-3.7}{}^{+1.8}_{-1.7}$		[1] BRIERE	01	CLE2	$e^+e^-\to\Upsilon(4S)$
• • • We do not use the following data for averages, fits, limits, etc. • • •					
9.2±0.7±0.6		[1] AUBERT	07D	BABR	Repl. by AUBERT 08BG
9.2±0.9±0.5		[1] AUBERT,B	04W	BABR	Repl. by AUBERT 07D
11.2±1.3±0.8		[1] AUBERT	03V	BABR	Repl. by AUBERT,B 04W
$10.0^{+1.6}_{-1.5}{}^{+0.7}_{-0.8}$		[1] CHEN	03B	BELL	Repl. by PRIM 13
$8.7^{+2.5}_{-2.1}\pm1.1$		[1] AUBERT	01D	BABR	Repl. by AUBERT 03V
<384	90	[2] ABE	00C	SLD	$e^+e^-\to Z$
< 21	90	[1] BERGFELD	98	CLE2	
< 43	90	ASNER	96	CLE2	$e^+e^-\to\Upsilon(4S)$
<320	90	ALBRECHT	91B	ARG	$e^+e^-\to\Upsilon(4S)$
<380	90	[3] AVERY	89B	CLEO	$e^+e^-\to\Upsilon(4S)$
<380	90	[4] AVERY	87	CLEO	$e^+e^-\to\Upsilon(4S)$

[1] Assumes equal production of B^+ and B^0 at the $\Upsilon(4S)$.
[2] ABE 00C assumes $B(Z\to b\overline{b})=(21.7\pm0.1)\%$ and the B fractions $f_{B^0}=f_{B^+}=(39.7^{+1.8}_{-2.2})\%$ and $f_{B_s}=(10.5^{+1.8}_{-2.2})\%$.
[3] AVERY 89B reports $<4.4\times10^{-4}$ assuming the $\Upsilon(4S)$ decays 43% to $B^0\overline{B}^0$. We rescale to 50%.
[4] AVERY 87 reports $<4.7\times10^{-4}$ assuming the $\Upsilon(4S)$ decays 40% to $B^0\overline{B}^0$. We rescale to 50%.

$\Gamma(K^+K^-\pi^+\pi^-\text{nonresonant})/\Gamma_{total}$ — Γ_{378}/Γ

VALUE (units 10^{-6})	CL%	DOCUMENT ID		TECN	COMMENT
<71.7	90	[1,2] CHIANG	10	BELL	$e^+e^-\to\Upsilon(4S)$

[1] Measured in the range $0.7<m_{K\pi}<1.7$ and corrected using PS assumption for the full $K\pi$ mass range.
[2] Assumes equal production of B^+ and B^0 at the $\Upsilon(4S)$.

$\Gamma(K^*(892)^0 K^-\pi^+)/\Gamma_{total}$ — Γ_{379}/Γ

VALUE (units 10^{-6})	DOCUMENT ID		TECN	COMMENT
4.5 ±1.3 OUR AVERAGE				
$2.11^{+5.63}_{-5.26}{}^{+4.85}_{-4.75}$	[1,2] CHIANG	10	BELL	$e^+e^-\to\Upsilon(4S)$
4.6 ±1.1 ±0.8	[2] AUBERT	07AS	BABR	$e^+e^-\to\Upsilon(4S)$

Int. J. Mod. Phys. A 2026.41. Downloaded from www.worldscientific.com
by UNIVERSITY OF CALIFORNIA @ BERKELEY on 09/16/26. Re-use and distribution is strictly not permitted, except for Open Access articles.

[1] Measured in the range $0.7 < m_{K\pi} < 1.7$ and corrected using PS assumption for the full $K\pi$ mass range. The quoted result is equivalent to the upper limit of $< 13.9 \times 10^{-6}$ at 90% CL.
[2] Assumes equal production of B^+ and B^0 at the $\Upsilon(4S)$.

$\Gamma(K^*(892)^0 \overline{K}^*(892)^0)/\Gamma_{total}$ — Γ_{380}/Γ

VALUE (units 10^{-6})	CL%	DOCUMENT ID		TECN	COMMENT
0.83±0.24 OUR AVERAGE Error includes scale factor of 1.5. See the ideogram below.					
$0.85 \pm 0.07 \pm 0.20$		[1] AAIJ	19L	LHCB	pp at 7 and 8 TeV
$0.26^{+0.33}_{-0.29}{}^{+0.10}_{-0.08}$		[2,3] CHIANG	10	BELL	$e^+e^- \to \Upsilon(4S)$
$1.28^{+0.35}_{-0.30} \pm 0.11$		[3] AUBERT	08I	BABR	$e^+e^- \to \Upsilon(4S)$
• • • We do not use the following data for averages, fits, limits, etc. • • •					
< 22	90	[4] GODANG	02	CLE2	$e^+e^- \to \Upsilon(4S)$
<469	90	[5] ABE	00C	SLD	$e^+e^- \to Z$

[1] AAIJ 19L reports $[\Gamma(B^0 \to K^*(892)^0 \overline{K}^*(892)^0)/\Gamma_{total}] / [B(B^0_s \to \overline{K}^*(892)^0 K^*(892)^0)] = 0.0758 \pm 0.0057 \pm 0.0030$ which we multiply by our best (shown rounded) value $B(B^0_s \to \overline{K}^*(892)^0 K^*(892)^0) = (1.11 \pm 0.27) \times 10^{-5}$. Our first error is their experiment's error and our second error is the systematic error from using our best (shown rounded) value.
[2] Measured in the range $0.7 < m_{K\pi} < 1.7$ and corrected using PS assumption for the full $K\pi$ mass range. The quoted result is equivalent to the upper limit of $< 0.8 \times 10^{-6}$ at 90% CL.
[3] Assumes equal production of B^+ and B^0 at the $\Upsilon(4S)$.
[4] Assumes a helicity 00 configuration. For a helicity 11 configuration, the limit decreases to 1.9×10^{-5}.
[5] ABE 00C assumes $B(Z \to b\overline{b}) = (21.7 \pm 0.1)\%$ and the B fractions $f_{B^0} = f_{B^+} = (39.7^{+1.8}_{-2.2})\%$ and $f_{B_s} = (10.5^{+1.8}_{-2.2})\%$.

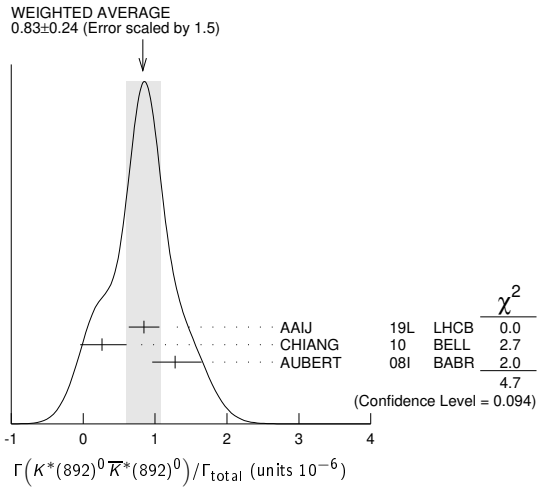

$\Gamma(K^+K^+\pi^-\pi^-$ nonresonant$)/\Gamma_{total}$ — Γ_{381}/Γ

VALUE (units 10^{-6})	CL%	DOCUMENT ID		TECN	COMMENT
<6.0	90	[1] CHIANG	10	BELL	$e^+e^- \to \Upsilon(4S)$

[1] Assumes equal production of B^+ and B^0 at the $\Upsilon(4S)$.

$\Gamma(K^*(892)^0 K^+\pi^-)/\Gamma_{total}$ — Γ_{382}/Γ

VALUE (units 10^{-6})	CL%	DOCUMENT ID		TECN	COMMENT
<2.2	90	[1] AUBERT	07AS	BABR	$e^+e^- \to \Upsilon(4S)$
• • • We do not use the following data for averages, fits, limits, etc. • • •					
<7.6	90	[1] CHIANG	10	BELL	$e^+e^- \to \Upsilon(4S)$

[1] Assumes equal production of B^+ and B^0 at the $\Upsilon(4S)$.

$\Gamma(K^*(892)^0 K^*(892)^0)/\Gamma_{total}$ — Γ_{383}/Γ

VALUE (units 10^{-6})	CL%	DOCUMENT ID		TECN	COMMENT
< 0.2	90	[1] CHIANG	10	BELL	$e^+e^- \to \Upsilon(4S)$
• • • We do not use the following data for averages, fits, limits, etc. • • •					
< 0.41	90	[1] AUBERT	08I	BABR	$e^+e^- \to \Upsilon(4S)$
<37	90	[2] GODANG	02	CLE2	$e^+e^- \to \Upsilon(4S)$

[1] Assumes equal production of B^+ and B^0 at the $\Upsilon(4S)$.
[2] Assumes a helicity 00 configuration. For a helicity 11 configuration, the limit decreases to 2.9×10^{-5}.

$\Gamma(K^*(892)^+ K^*(892)^-)/\Gamma_{total}$ — Γ_{384}/Γ

VALUE (units 10^{-6})	CL%	DOCUMENT ID		TECN	COMMENT
< 2.0	90	[1] AUBERT	08AP	BABR	$e^+e^- \to \Upsilon(4S)$
• • • We do not use the following data for averages, fits, limits, etc. • • •					
<141	90	[2] GODANG	02	CLE2	$e^+e^- \to \Upsilon(4S)$

[1] Assumes equal production of B^+ and B^0 at the $\Upsilon(4S)$.
[2] Assumes a helicity 00 configuration. For a helicity 11 configuration, the limit decreases to 8.9×10^{-5}.

$\Gamma(K_1(1400)^0 \phi)/\Gamma_{total}$ — Γ_{385}/Γ

VALUE	CL%	DOCUMENT ID		TECN	COMMENT
$<5.0 \times 10^{-3}$	90	ALBRECHT	91B	ARG	$e^+e^- \to \Upsilon(4S)$

$\Gamma(\phi(K\pi)^{*0}_0)/\Gamma_{total}$ — Γ_{386}/Γ

This decay refers to the coherent sum of resonant and nonresonant $J^P = 0^+$ $K\pi$ components with $1.13 < m_{K\pi} < 1.53$ GeV/c^2.

VALUE (units 10^{-6})	DOCUMENT ID		TECN	COMMENT
4.3±0.4 OUR AVERAGE				
$4.3 \pm 0.4 \pm 0.4$	[1] PRIM	13	BELL	$e^+e^- \to \Upsilon(4S)$
$4.3 \pm 0.6 \pm 0.4$	[1] AUBERT	08BG	BABR	$e^+e^- \to \Upsilon(4S)$
• • • We do not use the following data for averages, fits, limits, etc. • • •				
$5.0 \pm 0.8 \pm 0.3$	[1] AUBERT	07D	BABR	Repl. by AUBERT 08BG

[1] Assumes equal production of B^+ and B^0 at the $\Upsilon(4S)$.

$\Gamma(\phi(K\pi)^{*0}_0(1.60 < m_{K\pi} < 2.15))/\Gamma_{total}$ — Γ_{387}/Γ

This decay refers to the coherent sum of resonant and nonresonant $J^P = 0^+$ $K\pi$ components with $1.60 < m_{K\pi} < 2.15$ GeV/c^2.

VALUE (units 10^{-6})	CL%	DOCUMENT ID		TECN	COMMENT
<1.7	90	[1] AUBERT	07AO	BABR	$e^+e^- \to \Upsilon(4S)$

[1] Assumes equal production of B^+ and B^0 at the $\Upsilon(4S)$.

$\Gamma(K^*_0(1430)^0 K^-\pi^+)/\Gamma_{total}$ — Γ_{388}/Γ

VALUE (units 10^{-6})	CL%	DOCUMENT ID		TECN	COMMENT
<31.8	90	[1,2] CHIANG	10	BELL	$e^+e^- \to \Upsilon(4S)$

[1] Measured in the range $0.7 < m_{K\pi} < 1.7$ and corrected using PS assumption for the full $K\pi$ mass range.
[2] Assumes equal production of B^+ and B^0 at the $\Upsilon(4S)$.

$\Gamma(K^*_0(1430)^0 \overline{K}^*(892)^0)/\Gamma_{total}$ — Γ_{389}/Γ

VALUE (units 10^{-6})	CL%	DOCUMENT ID		TECN	COMMENT
<3.3	90	[1,2] CHIANG	10	BELL	$e^+e^- \to \Upsilon(4S)$

[1] Measured in the range $0.7 < m_{K\pi} < 1.7$ and corrected using PS assumption for the full $K\pi$ mass range.
[2] Assumes equal production of B^+ and B^0 at the $\Upsilon(4S)$.

$\Gamma(K^*_0(1430)^0 \overline{K}^*_0(1430)^0)/\Gamma_{total}$ — Γ_{390}/Γ

VALUE (units 10^{-6})	CL%	DOCUMENT ID		TECN	COMMENT
<8.4	90	[1,2] CHIANG	10	BELL	$e^+e^- \to \Upsilon(4S)$

[1] Measured in the range $0.7 < m_{K\pi} < 1.7$ and corrected using PS assumption for the full $K\pi$ mass range.
[2] Assumes equal production of B^+ and B^0 at the $\Upsilon(4S)$.

$\Gamma(K^*_0(1430)^0 \phi)/\Gamma_{total}$ — Γ_{391}/Γ

VALUE (units 10^{-6})	DOCUMENT ID		TECN	COMMENT
3.9±0.5±0.6	[1] AUBERT	08BG	BABR	$e^+e^- \to \Upsilon(4S)$
• • • We do not use the following data for averages, fits, limits, etc. • • •				
$4.6 \pm 0.7 \pm 0.6$	[1] AUBERT	07D	BABR	Repl. by AUBERT 08BG
seen	[2] AUBERT,B	04W	BABR	Repl. by AUBERT 07D

[1] Assumes equal production of B^+ and B^0 at the $\Upsilon(4S)$.
[2] Observed 181 ± 17 events with statistical significance greater than 10 σ.

$\Gamma(K^*_0(1430)^0 K^*(892)^0)/\Gamma_{total}$ — Γ_{392}/Γ

VALUE (units 10^{-6})	CL%	DOCUMENT ID		TECN	COMMENT
<1.7	90	[1] CHIANG	10	BELL	$e^+e^- \to \Upsilon(4S)$

[1] Assumes equal production of B^+ and B^0 at the $\Upsilon(4S)$.

$\Gamma(K^*_0(1430)^0 K^*_0(1430)^0)/\Gamma_{total}$ — Γ_{393}/Γ

VALUE (units 10^{-6})	CL%	DOCUMENT ID		TECN	COMMENT
<4.7	90	[1] CHIANG	10	BELL	$e^+e^- \to \Upsilon(4S)$

[1] Assumes equal production of B^+ and B^0 at the $\Upsilon(4S)$.

$\Gamma(K^*(1680)^0 \phi)/\Gamma_{total}$ — Γ_{394}/Γ

VALUE (units 10^{-6})	CL%	DOCUMENT ID		TECN	COMMENT
<3.5	90	[1] AUBERT	07AO	BABR	$e^+e^- \to \Upsilon(4S)$

[1] Assumes equal production of B^+ and B^0 at the $\Upsilon(4S)$.

$\Gamma(K^*(1780)^0 \phi)/\Gamma_{total}$ — Γ_{395}/Γ

VALUE (units 10^{-6})	CL%	DOCUMENT ID		TECN	COMMENT
<2.7	90	[1] AUBERT	07AO	BABR	$e^+e^- \to \Upsilon(4S)$

[1] Assumes equal production of B^+ and B^0 at the $\Upsilon(4S)$.

$\Gamma(K^*(2045)^0 \phi)/\Gamma_{total}$ — Γ_{396}/Γ

VALUE (units 10^{-6})	CL%	DOCUMENT ID		TECN	COMMENT
<15.3	90	[1] AUBERT	07AO	BABR	$e^+e^- \to \Upsilon(4S)$

[1] Assumes equal production of B^+ and B^0 at the $\Upsilon(4S)$.

$\Gamma(K^*_2(1430)^0 \rho^0)/\Gamma_{total}$ — Γ_{397}/Γ

VALUE (units 10^{-6})	CL%	DOCUMENT ID		TECN	COMMENT
$<1.1 \times 10^3$	90	ALBRECHT	91B	ARG	$e^+e^- \to \Upsilon(4S)$

Int. J. Mod. Phys. A 2026.41. Downloaded from www.worldscientific.com by CALIFORNIA @ BERKELEY on 09/16/26. Re-use and distribution is strictly not permitted, except for Open Access articles.

$\Gamma(K_2^*(1430)^0\phi)/\Gamma_{total}$ — Γ_{398}/Γ

VALUE (units 10^{-6})	CL%	DOCUMENT ID		TECN	COMMENT
6.8±0.9 OUR AVERAGE		Error includes scale factor of 1.2.			
$5.5^{+0.9}_{-0.7}\pm1.0$		[1] PRIM	13	BELL	$e^+e^-\to\Upsilon(4S)$
$7.5\pm0.9\pm0.5$		[1] AUBERT	08BG	BABR	$e^+e^-\to\Upsilon(4S)$
• • • We do not use the following data for averages, fits, limits, etc. • • •					
$7.8\pm1.1\pm0.6$		[1] AUBERT	07D	BABR	Repl. by AUBERT 08BG
seen		[2] AUBERT,B	04W	BABR	Repl. by AUBERT 07D
<1400	90	ALBRECHT	91B	ARG	$e^+e^-\to\Upsilon(4S)$

[1] Assumes equal production of B^+ and B^0 at the $\Upsilon(4S)$.
[2] The angular distribution of $B\to\phi K^*(1430)$ provides evidence with statistical significance of 3.2 σ.

$\Gamma(K^0\phi\phi)/\Gamma_{total}$ — Γ_{399}/Γ

VALUE (units 10^{-6})		DOCUMENT ID		TECN	COMMENT
3.7 ±0.7 OUR AVERAGE		Error includes scale factor of 1.3.			
$3.02^{+0.75}_{-0.66}\pm0.20$		[1] MOHANTY	21	BELL	$e^+e^-\to\Upsilon(4S)$
4.5 ±0.8 ±0.3		[1] LEES	11A	BABR	$e^+e^-\to\Upsilon(4S)$
• • • We do not use the following data for averages, fits, limits, etc. • • •					
$4.1\ ^{+1.7}_{-1.4}\ \pm0.4$		[1] AUBERT,BE	06H	BABR	Repl. by LEES 11A

[1] Assumes equal production of B^0 and B^+ at the $\Upsilon(4S)$ and the $\phi\phi$ invariant mass below 2.85 GeV/c^2.

$\Gamma(\eta'\eta'K^0)/\Gamma_{total}$ — Γ_{400}/Γ

VALUE (units 10^{-6})	CL%	DOCUMENT ID		TECN	COMMENT
<31	90	[1] AUBERT,B	06P	BABR	$e^+e^-\to\Upsilon(4S)$

[1] Assumes equal production of B^+ and B^0 at the $\Upsilon(4S)$.

$\Gamma(\eta K^0\gamma)/\Gamma_{total}$ — Γ_{401}/Γ

VALUE (units 10^{-6})		DOCUMENT ID		TECN	COMMENT
7.6±1.8 OUR AVERAGE					
$7.1^{+2.1}_{-2.0}\pm0.4$		[1,2] AUBERT	09	BABR	$e^+e^-\to\Upsilon(4S)$
$8.7^{+3.1}_{-2.7}{}^{+1.9}_{-1.6}$		[2,3] NISHIDA	05	BELL	$e^+e^-\to\Upsilon(4S)$
• • • We do not use the following data for averages, fits, limits, etc. • • •					
$11.3^{+2.8}_{-1.6}\pm0.6$		[1,2] AUBERT,B	06M	BABR	Repl. by AUBERT 09

[1] $m_{\eta K}$ < 3.25 GeV/c^2.
[2] Assumes equal production of B^+ and B^0 at the $\Upsilon(4S)$.
[3] $m_{\eta K}$ < 2.4 GeV/c^2

$\Gamma(\eta' K^0\gamma)/\Gamma_{total}$ — Γ_{402}/Γ

VALUE (units 10^{-6})	CL%	DOCUMENT ID		TECN	COMMENT
<6.4	90	[1,2] WEDD	10	BELL	$e^+e^-\to\Upsilon(4S)$
• • • We do not use the following data for averages, fits, limits, etc. • • •					
<6.6	90	[1,3] AUBERT,B	06M	BABR	$e^+e^-\to\Upsilon(4S)$

[1] Assumes equal production of B^+ and B^0 at the $\Upsilon(4S)$.
[2] $m_{\eta' K}$ < 3.4 GeV/c^2.
[3] $m_{\eta' K}$ < 3.25 GeV/c^2.

$\Gamma(K^0\phi\gamma)/\Gamma_{total}$ — Γ_{403}/Γ

VALUE (units 10^{-6})	CL%	DOCUMENT ID		TECN	COMMENT
2.74±0.60±0.32		[1] SAHOO	11A	BELL	$e^+e^-\to\Upsilon(4S)$
• • • We do not use the following data for averages, fits, limits, etc. • • •					
<2.7	90	[1] AUBERT	07Q	BABR	$e^+e^-\to\Upsilon(4S)$
<8.3	90	[1] DRUTSKOY	04	BELL	$e^+e^-\to\Upsilon(4S)$

[1] Assumes equal production of B^+ and B^0 at $\Upsilon(4S)$.

$\Gamma(K^+\pi^-\gamma)/\Gamma_{total}$ — Γ_{404}/Γ

VALUE	DOCUMENT ID		TECN	COMMENT
$(4.6^{+1.3}_{-1.2}{}^{+0.5}_{-0.7})\times10^{-6}$	[1,2] NISHIDA	02	BELL	$e^+e^-\to\Upsilon(4S)$

[1] Assumes equal production of B^+ and B^0 at the $\Upsilon(4S)$.
[2] 1.25 GeV/c^2 < $M_{K\pi}$ < 1.6 GeV/c^2

$\Gamma(K^*(892)^0\gamma)/\Gamma_{total}$ — Γ_{405}/Γ

VALUE (units 10^{-6})	CL%	DOCUMENT ID		TECN	COMMENT
42.1± 2.4 OUR FIT		Error includes scale factor of 2.0.			
42.0± 2.5 OUR AVERAGE		Error includes scale factor of 2.1.			
$4140\ ^{+132}_{-135}\ ^{+68}_{-63}$		[1] ADACHI	25Z	BELL	$e^+e^-\to\Upsilon(4S)$
39.6± 0.7± 1.4		[2] HORIGUCHI	17	BELL	$e^+e^-\to\Upsilon(4S)$
44.7± 1.0± 1.6		[3] AUBERT	09AO	BABR	$e^+e^-\to\Upsilon(4S)$
$45.5^{+}_{-}\ ^{7.2}_{6.8}\pm3.4$		[4] COAN	00	CLE2	$e^+e^-\to\Upsilon(4S)$
• • • We do not use the following data for averages, fits, limits, etc. • • •					
39.2± 2.0± 2.4		[5] AUBERT,BE	04A	BABR	Repl. by AUBERT 09AO
40.1± 2.1± 1.7		[6] NAKAO	04	BELL	Repl. by HORIGUCHI 17
< 110	90	ACOSTA	02G	CDF	$p\overline{p}$ at 1.8 TeV
42.3± 4.0± 2.2		[6] AUBERT	02C	BABR	Repl. by AUBERT,BE 04A
< 210	90	[7] ADAM	96D	DLPH	$e^+e^-\to Z$
40 ± 17 ± 8		[8] AMMAR	93	CLE2	Repl. by COAN 00
< 420	90	ALBRECHT	89G	ARG	$e^+e^-\to\Upsilon(4S)$
< 240	90	[9] AVERY	89B	CLEO	$e^+e^-\to\Upsilon(4S)$
<2100	90	AVERY	87	CLEO	$e^+e^-\to\Upsilon(4S)$

[1] ADACHI 25Z reports $(4.14\pm0.10\pm0.11)\times10^{-5}$ from a measurement of $[\Gamma(B^0\to K^*(892)^0\gamma)/\Gamma_{total}]\times[B(\Upsilon(4S)\to B^0\overline{B}^0)]$ assuming $B(\Upsilon(4S)\to B^0\overline{B}^0) = 48.61^{+0.74}_{-0.80}$, which we rescale to our best (shown rounded) value $B(\Upsilon(4S)\to B^0\overline{B}^0) = (48.6\pm0.8)\times10^{-2}$. Our first error is their experiment's error and our second error is the systematic error from using our best (shown rounded) value.
[2] Uses $B(\Upsilon(4S)\to B^+B^-) = (51.4\pm0.6)\%$ and $B(\Upsilon(4S)\to B^0\overline{B}^0) = (48.6\pm0.6)\%$.
[3] Uses $B(\Upsilon(4S)\to B^+B^-) = (51.6\pm0.6)\%$ and $B(\Upsilon(4S)\to B^0\overline{B}^0) = (48.4\pm0.6)\%$.
[4] Assumes equal production of B^+ and B^0 at the $\Upsilon(4S)$. No evidence for a nonresonant $K\pi\gamma$ contamination was seen; the central value assumes no contamination.
[5] Uses the production ratio of charged and neutral B from $\Upsilon(4S)$ decays $R^{+/0} = 1.006\pm0.048$.
[6] Assumes equal production of B^+ and B^0 at the $\Upsilon(4S)$.
[7] ADAM 96D assumes $f_{B^0} = f_{B^-} = 0.39$ and $f_{B_s} = 0.12$.
[8] AMMAR 93 observed 6.6 ± 2.8 events above background.
[9] AVERY 89B reports < 2.8×10^{-4} assuming the $\Upsilon(4S)$ decays 43% to $B^0\overline{B}^0$. We rescale to 50%.

$\Gamma(K^*(1410)\gamma)/\Gamma_{total}$ — Γ_{406}/Γ

VALUE	CL%	DOCUMENT ID		TECN	COMMENT
$<1.3\times10^{-4}$	90	[1] NISHIDA	02	BELL	$e^+e^-\to\Upsilon(4S)$

[1] Assumes equal production of B^+ and B^0 at the $\Upsilon(4S)$.

$\Gamma(K^+\pi^-\gamma$ nonresonant$)/\Gamma_{total}$ — Γ_{407}/Γ

VALUE	CL%	DOCUMENT ID		TECN	COMMENT
$<2.6\times10^{-6}$	90	[1,2] NISHIDA	02	BELL	$e^+e^-\to\Upsilon(4S)$

[1] Assumes equal production of B^+ and B^0 at the $\Upsilon(4S)$.
[2] 1.25 GeV/c^2 < $M_{K\pi}$ < 1.6 GeV/c^2

$\Gamma(K^*(892)^0X(214), X\to\mu^+\mu^-)/\Gamma_{total}$ — Γ_{408}/Γ

$X(214)$ is a hypothetical particle of mass 214 MeV/c^2 reported by the HyperCP experiment (PARK 05)

VALUE (units 10^{-8})	CL%	DOCUMENT ID		TECN	COMMENT
<2.26	90	[1,2] HYUN	10	BELL	$e^+e^-\to\Upsilon(4S)$

[1] Assumes equal production of B^+ and B^0 at the $\Upsilon(4S)$.
[2] Based on scalar nature of X particle. With a vector X assumption, the upper limit is 2.27×10^{-8}.

$\Gamma(K^0\pi^+\pi^-\gamma)/\Gamma_{total}$ — Γ_{409}/Γ

VALUE (units 10^{-5})		DOCUMENT ID		TECN	COMMENT
1.99±0.18 OUR AVERAGE					
$2.05\pm0.20^{+0.26}_{-0.22}$		[1,2] DEL-AMO-SA...16		BABR	$e^+e^-\to\Upsilon(4S)$
$1.85\pm0.21\pm0.12$		[1,3] AUBERT	07R	BABR	$e^+e^-\to\Upsilon(4S)$
2.40±0.4 ±0.3		[3,4] YANG	05	BELL	$e^+e^-\to\Upsilon(4S)$

[1] $M_{K\pi\pi}$ < 1.8 GeV/c^2.
[2] Uses $B(\Upsilon(4S)\to B^+B^-) = 0.513\pm0.006$.
[3] Assumes equal production of B^+ and B^0 at the $\Upsilon(4S)$.
[4] $M_{K\pi\pi}$ < 2.0 GeV/c^2.

$\Gamma(K^+\pi^-\pi^0\gamma)/\Gamma_{total}$ — Γ_{410}/Γ

VALUE (units 10^{-5})		DOCUMENT ID		TECN	COMMENT
4.07±0.22±0.31		[1,2] AUBERT	07R	BABR	$e^+e^-\to\Upsilon(4S)$

[1] $M_{K\pi\pi}$ < 1.8 GeV/c^2.
[2] Assumes equal production of B^+ and B^0 at the $\Upsilon(4S)$.

$\Gamma(K_1(1270)^0\gamma)/\Gamma_{total}$ — Γ_{411}/Γ

VALUE (units 10^{-5})	CL%	DOCUMENT ID		TECN	COMMENT
< 5.8	90	[1] YANG	05	BELL	$e^+e^-\to\Upsilon(4S)$
• • • We do not use the following data for averages, fits, limits, etc. • • •					
<700	90	[2] ALBRECHT	89G	ARG	$e^+e^-\to\Upsilon(4S)$

[1] Assumes equal production of B^+ and B^0 at the $\Upsilon(4S)$.
[2] ALBRECHT 89G reports < 0.0078 assuming the $\Upsilon(4S)$ decays 45% to $B^0\overline{B}^0$. We rescale to 50%.

$\Gamma(K_1(1400)^0\gamma)/\Gamma_{total}$ — Γ_{412}/Γ

VALUE (units 10^{-5})	CL%	DOCUMENT ID		TECN	COMMENT
< 1.2	90	[1] YANG	05	BELL	$e^+e^-\to\Upsilon(4S)$
• • • We do not use the following data for averages, fits, limits, etc. • • •					
<430	90	[2] ALBRECHT	89G	ARG	$e^+e^-\to\Upsilon(4S)$

[1] Assumes equal production of B^+ and B^0 at the $\Upsilon(4S)$.
[2] ALBRECHT 89G reports < 0.0048 assuming the $\Upsilon(4S)$ decays 45% to $B^0\overline{B}^0$. We rescale to 50%.

Int. J. Mod. Phys. A 2026.41. Downloaded from www.worldscientific.com
by UNIVERSITY OF CALIFORNIA @ BERKELEY on 09/16/26. Re-use and distribution is strictly not permitted, except for Open Access articles.

$\Gamma(K_2^*(1430)^0\gamma)/\Gamma_{total}$ — Γ_{413}/Γ

VALUE (units 10^{-5})	CL%	DOCUMENT ID		TECN	COMMENT
1.24±0.24 OUR AVERAGE					
1.22±0.25±0.10		[1] AUBERT,B	04U	BABR	$e^+e^- \to \Upsilon(4S)$
1.3 ±0.5 ±0.1		[1] NISHIDA	02	BELL	$e^+e^- \to \Upsilon(4S)$
• • • We do not use the following data for averages, fits, limits, etc. • • •					
<40	90	[2] ALBRECHT	89G	ARG	$e^+e^- \to \Upsilon(4S)$

[1] Assumes equal production of B^+ and B^0 at the $\Upsilon(4S)$.
[2] ALBRECHT 89G reports $< 4.4 \times 10^{-4}$ assuming the $\Upsilon(4S)$ decays 45% to $B^0\overline{B}^0$. We rescale to 50%.

$\Gamma(K^*(1680)^0\gamma)/\Gamma_{total}$ — Γ_{414}/Γ

VALUE	CL%	DOCUMENT ID		TECN	COMMENT
<0.0020	90	[1] ALBRECHT	89G	ARG	$e^+e^- \to \Upsilon(4S)$

[1] ALBRECHT 89G reports < 0.0022 assuming the $\Upsilon(4S)$ decays 45% to $B^0\overline{B}^0$. We rescale to 50%.

$\Gamma(K_3^*(1780)^0\gamma)/\Gamma_{total}$ — Γ_{415}/Γ

VALUE (units 10^{-6})	CL%	DOCUMENT ID		TECN	COMMENT
< 83	90	[1,2] NISHIDA	05	BELL	$e^+e^- \to \Upsilon(4S)$
• • • We do not use the following data for averages, fits, limits, etc. • • •					
<10000	90	[3] ALBRECHT	89G	ARG	$e^+e^- \to \Upsilon(4S)$

[1] Assumes equal production of B^+ and B^0 at the $\Upsilon(4S)$.
[2] Uses $B(K_3^*(1780) \to \eta K) = 0.11^{+0.05}_{-0.04}$.
[3] ALBRECHT 89G reports < 0.011 assuming the $\Upsilon(4S)$ decays 45% to $B^0\overline{B}^0$. We rescale to 50%.

$\Gamma(K_4^*(2045)^0\gamma)/\Gamma_{total}$ — Γ_{416}/Γ

VALUE	CL%	DOCUMENT ID		TECN	COMMENT
<0.0043	90	[1] ALBRECHT	89G	ARG	$e^+e^- \to \Upsilon(4S)$

[1] ALBRECHT 89G reports < 0.0048 assuming the $\Upsilon(4S)$ decays 45% to $B^0\overline{B}^0$. We rescale to 50%.

$\Gamma(\rho^0\gamma)/\Gamma_{total}$ — Γ_{417}/Γ

VALUE (units 10^{-6})	CL%	DOCUMENT ID		TECN	COMMENT
0.80±0.06 OUR FIT Error includes scale factor of 1.4.					
0.83±0.13 OUR AVERAGE					
$0.76 \pm 0.13^{+0.10}_{-0.08}$		ADACHI	25G	BELL	$e^+e^- \to \Upsilon(4S)$
$0.97^{+0.24}_{-0.22} \pm 0.06$		[1] AUBERT	08BH	BABR	$e^+e^- \to \Upsilon(4S)$
• • • We do not use the following data for averages, fits, limits, etc. • • •					
$0.79^{+0.22}_{-0.20} \pm 0.06$		[1] AUBERT	07L	BABR	Repl. by AUBERT 08BH
$1.25^{+0.37}_{-0.33} {}^{+0.07}_{-0.06}$		[1] MOHAPATRA	06	BELL	Repl. by TANIGUCHI 08
0.0 ±0.2 ±0.1	90	[1] AUBERT	05	BABR	Repl. by AUBERT 07L
< 0.8	90	[1] MOHAPATRA	05	BELL	$e^+e^- \to \Upsilon(4S)$
< 1.2	90	[1] AUBERT	04C	BABR	$e^+e^- \to \Upsilon(4S)$
<17	90	[1] COAN	00	CLE2	$e^+e^- \to \Upsilon(4S)$

[1] Assumes equal production of B^+ and B^0 at the $\Upsilon(4S)$.

$\Gamma(\rho^0 X(214), X \to \mu^+\mu^-)/\Gamma_{total}$ — Γ_{418}/Γ

$X(214)$ is a hypothetical particle of mass 214 MeV/c^2 reported by the HyperCP experiment (PARK 05)

VALUE (units 10^{-8})	CL%	DOCUMENT ID		TECN	COMMENT
<1.73	90	[1,2] HYUN	10	BELL	$e^+e^- \to \Upsilon(4S)$

[1] Assumes equal production of B^+ and B^0 at the $\Upsilon(4S)$.
[2] The result is the same for a scalar or vector X particle.

$\Gamma(\rho^0\gamma)/\Gamma(K^*(892)^0\gamma)$ — $\Gamma_{417}/\Gamma_{405}$

VALUE (units 10^{-2})	DOCUMENT ID		TECN	COMMENT
1.90±0.08 OUR FIT				
1.90±0.08 OUR AVERAGE				
1.89±0.07±0.05	AAIJ	25AV	LHCB	pp at 7, 8 and 13 TeV
$2.06^{+0.45}_{-0.43} {}^{+0.14}_{-0.16}$	TANIGUCHI	08	BELL	$e^+e^- \to \Upsilon(4S)$

$\Gamma(\omega\gamma)/\Gamma_{total}$ — Γ_{419}/Γ

VALUE (units 10^{-6})	CL%	DOCUMENT ID		TECN	COMMENT
$0.44^{+0.18}_{-0.16}$ OUR AVERAGE					
$0.50^{+0.27}_{-0.23} \pm 0.09$		[1] AUBERT	08BH	BABR	$e^+e^- \to \Upsilon(4S)$
$0.40^{+0.19}_{-0.17} \pm 0.13$		[1] TANIGUCHI	08	BELL	$e^+e^- \to \Upsilon(4S)$
• • • We do not use the following data for averages, fits, limits, etc. • • •					
$0.40^{+0.24}_{-0.20} \pm 0.05$		[1] AUBERT	07L	BABR	Repl. by AUBERT 08BH
$0.56^{+0.34}_{-0.27} {}^{+0.05}_{-0.10}$		[1] MOHAPATRA	06	BELL	Repl. by TANIGUCHI 08
<1.0	90	[1] AUBERT	05	BABR	Repl. by AUBERT 07L
<0.8	90	[1] MOHAPATRA	05	BELL	Repl. by MOHAPATRA 06
<1.0	90	[1] AUBERT	04C	BABR	$e^+e^- \to \Upsilon(4S)$
<9.2	90	[1] COAN	00	CLE2	$e^+e^- \to \Upsilon(4S)$

[1] Assumes equal production of B^+ and B^0 at the $\Upsilon(4S)$.

$\Gamma(\phi\gamma)/\Gamma_{total}$ — Γ_{420}/Γ

VALUE	CL%	DOCUMENT ID		TECN	COMMENT
$<1.0 \times 10^{-7}$	90	[1] KING	16	BELL	$e^+e^- \to \Upsilon(4S)$
• • • We do not use the following data for averages, fits, limits, etc. • • •					
$<8.5 \times 10^{-7}$	90	[1] AUBERT,BE	05C	BABR	$e^+e^- \to \Upsilon(4S)$
$<3.3 \times 10^{-6}$	90	[1] COAN	00	CLE2	$e^+e^- \to \Upsilon(4S)$

[1] Assumes equal production of B^+ and B^0 at the $\Upsilon(4S)$.

$\Gamma(f_2(1270)\gamma, f_2 \to (KS)^0(KS)^0)/\Gamma_{total}$ — Γ_{421}/Γ

VALUE	DOCUMENT ID		TECN	COMMENT
$<3.1 \times 10^{-7}$	JEON	22	BELL	$e^+e^- \to \Upsilon(4S)$

$\Gamma(f_2'(1525)\gamma, f_2' \to (KS)^0(KS)^0)/\Gamma_{total}$ — Γ_{422}/Γ

VALUE	DOCUMENT ID		TECN	COMMENT
$<2.1 \times 10^{-7}$	JEON	22	BELL	$e^+e^- \to \Upsilon(4S)$

$\Gamma(\pi^+\pi^-)/\Gamma_{total}$ — Γ_{423}/Γ

VALUE (units 10^{-6})	CL%	DOCUMENT ID		TECN	COMMENT
5.37±0.20 OUR FIT Error includes scale factor of 1.3.					
5.43±0.26 OUR AVERAGE Error includes scale factor of 1.4. See the ideogram below.					
5.83±0.22±0.17		ADACHI	24	BELL	$e^+e^- \to \Upsilon(4S)$
5.04±0.21±0.18		[1] DUH	13	BELL	$e^+e^- \to \Upsilon(4S)$
5.5 ±0.4 ±0.3		[1] AUBERT	07B	BABR	$e^+e^- \to \Upsilon(4S)$
$4.5 {}^{+1.4}_{-1.2} {}^{+0.5}_{-0.4}$		[1] BORNHEIM	03	CLE2	$e^+e^- \to \Upsilon(4S)$
• • • We do not use the following data for averages, fits, limits, etc. • • •					
5.1 ±0.2 ±0.2		[1] LIN	07A	BELL	Repl. by DUH 13
4.4 ±0.6 ±0.3		[1] CHAO	04	BELL	Repl. by LIN 07A
4.7 ±0.6 ±0.2		[1] AUBERT	02Q	BABR	Repl. by AUBERT 07B
5.4 ±1.2 ±0.5		[1] CASEY	02	BELL	Repl. by CHAO 04
$5.6 {}^{+2.3}_{-2.0} {}^{+0.4}_{-0.5}$		[1] ABE	01H	BELL	Repl. by CASEY 02
4.1 ±1.0 ±0.7		[1] AUBERT	01E	BABR	Repl. by AUBERT 02Q
< 67	90	[2] ABE	00C	SLD	$e^+e^- \to Z$
$4.3 {}^{+1.6}_{-1.4} \pm 0.5$		[1] CRONIN-HEN...	00	CLE2	Repl. by BORNHEIM 03
< 15	90	GODANG	98	CLE2	Repl. by CRONIN-HENNESSY 00
< 45	90	[3] ADAM	96D	DLPH	$e^+e^- \to Z$
< 20	90	ASNER	96	CLE2	Repl. by GODANG 98
< 41	90	[4] BUSKULIC	96V	ALEP	$e^+e^- \to Z$
< 55	90	[5] ABREU	95N	DLPH	Sup. by ADAM 96D
< 47	90	[6] AKERS	94L	OPAL	$e^+e^- \to Z$
< 29	90	[1] BATTLE	93	CLE2	$e^+e^- \to \Upsilon(4S)$
<130	90	[1] ALBRECHT	90B	ARG	$e^+e^- \to \Upsilon(4S)$
< 77	90	[7] BORTOLETTO	89	CLEO	$e^+e^- \to \Upsilon(4S)$
<260	90	[7] BEBEK	87	CLEO	$e^+e^- \to \Upsilon(4S)$
<500	90	GILES	84	CLEO	$e^+e^- \to \Upsilon(4S)$

[1] Assumes equal production of B^+ and B^0 at the $\Upsilon(4S)$.
[2] ABE 00C assumes $B(Z \to b\overline{b})=(21.7 \pm 0.1)\%$ and the B fractions $f_{B^0}=f_{B^+}=(39.7^{+1.8}_{-2.2})\%$ and $f_{B_s}=(10.5^{+1.8}_{-2.2})\%$.
[3] ADAM 96D assumes $f_{B^0} = f_{B^-} = 0.39$ and $f_{B_s} = 0.12$.
[4] BUSKULIC 96V assumes PDG 96 production fractions for B^0, B^+, B_s, b baryons.
[5] Assumes a B^0, B^- production fraction of 0.39 and a B_s production fraction of 0.12.
[6] Assumes $B(Z \to b\overline{b}) = 0.217$ and B_d^0 (B_s^0) fraction 39.5% (12%).
[7] Paper assumes the $\Upsilon(4S)$ decays 43% to $B^0\overline{B}^0$. We rescale to 50%.

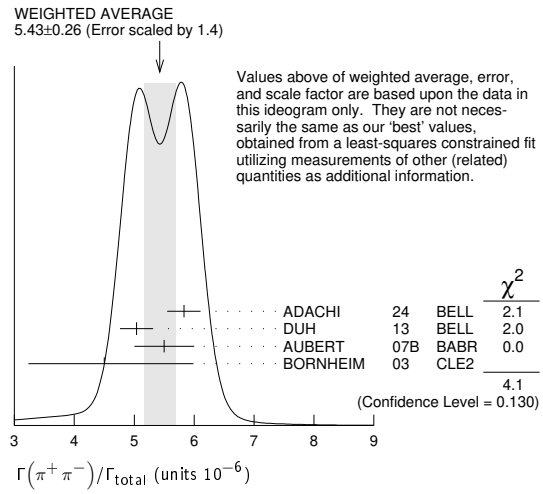

Int. J. Mod. Phys. A 2026.41. Downloaded from www.worldscientific.com
by LIFORNIA @ BERKELEY on 09/16/26. Re-use and distribution is strictly not permitted, except for Open Access articles.

$\Gamma(\pi^+\pi^-)/\Gamma(K^+\pi^-)$ — $\Gamma_{423}/\Gamma_{288}$

VALUE	DOCUMENT ID		TECN	COMMENT
0.268±0.010 OUR FIT	Error includes scale factor of 1.2.			
0.261±0.015 OUR AVERAGE				
0.262±0.009±0.017	AAIJ	12AR	LHCB	pp at 7 TeV
0.259±0.017±0.016	AALTONEN	11N	CDF	$p\overline{p}$ at 1.96 TeV
• • • We do not use the following data for averages, fits, limits, etc. • • •				
0.21 ±0.05 ±0.03	ABULENCIA,A	06D	CDF	Repl. by AALTONEN 11N

$\Gamma(\pi^0\pi^0)/\Gamma_{total}$ — Γ_{424}/Γ

VALUE (units 10^{-6})	CL%	DOCUMENT ID		TECN	COMMENT
1.46±0.19 OUR AVERAGE	Error includes scale factor of 1.3. See the ideogram below.				
1.25±0.20±0.11		ADACHI	25F	BEL2	$e^+e^- \to \Upsilon(4S)$
1.31±0.19±0.19		[1] JULIUS	17	BELL	$e^+e^- \to \Upsilon(4S)$
1.83±0.21±0.13		[1] LEES	13D	BABR	$e^+e^- \to \Upsilon(4S)$
• • • We do not use the following data for averages, fits, limits, etc. • • •					
1.38±0.27±0.22		ABUDINEN	23E	BELL	Repl. by ADACHI 25F
1.47±0.25±0.12		[1] AUBERT	07BC	BABR	Repl. by LEES 13D
1.17±0.32±0.10		[1] AUBERT	05L	BABR	Repl. by AUBERT 07BC
$2.3\ ^{+0.4}_{-0.5}\ ^{+0.2}_{-0.3}$		[1] CHAO	05	BELL	Repl. by JULIUS 17
< 3.6	90	[1] AUBERT	03L	BABR	$e^+e^- \to \Upsilon(4S)$
2.1 ±0.6 ±0.3		[1] AUBERT	03S	BABR	Repl. by AUBERT 05L
< 4.4	90	[1] BORNHEIM	03	CLE2	$e^+e^- \to \Upsilon(4S)$
1.7 ±0.6 ±0.2		[1] LEE	03	BELL	Repl. by CHAO 05
< 5.7	90	[1] ASNER	02	CLE2	$e^+e^- \to \Upsilon(4S)$
< 6.4	90	[1] CASEY	02	BELL	$e^+e^- \to \Upsilon(4S)$
< 9.3	90	GODANG	98	CLE2	Repl. by ASNER 02
< 9.1	90	ASNER	96	CLE2	Repl. by GODANG 98
<60	90	[2] ACCIARRI	95H	L3	$e^+e^- \to Z$

[1] Assumes equal production of B^+ and B^0 at the $\Upsilon(4S)$.
[2] ACCIARRI 95H assumes $f_{B^0} = 39.5 \pm 4.0$ and $f_{B_s} = 12.0 \pm 3.0\%$.

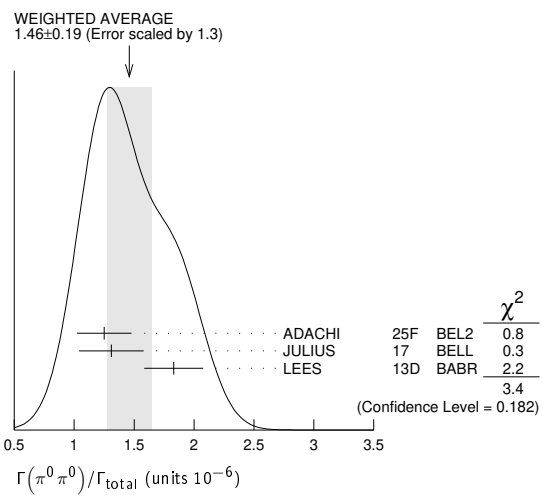

$\Gamma(\eta\pi^0)/\Gamma_{total}$ — Γ_{425}/Γ

VALUE (units 10^{-6})	CL%	DOCUMENT ID		TECN	COMMENT
$\mathbf{0.41\ ^{+0.17}_{-0.15}\ ^{+0.05}_{-0.07}}$		[1,2] PAL	15	BELL	$e^+e^- \to \Upsilon(4S)$
• • • We do not use the following data for averages, fits, limits, etc. • • •					
< 1.5	90	[2] AUBERT	08AH	BABR	$e^+e^- \to \Upsilon(4S)$
< 1.3	90	[2] AUBERT	06W	BABR	Repl. by AUBERT 08AH
< 2.5	90	[2] CHANG	05A	BELL	Repl. by PAL 15
< 2.5	90	[2] AUBERT,B	04D	BABR	Repl. by AUBERT 06W
< 2.9	90	[2] RICHICHI	00	CLE2	$e^+e^- \to \Upsilon(4S)$
< 8	90	BEHRENS	98	CLE2	Repl. by RICHICHI 00
< 250	90	[3] ACCIARRI	95H	L3	$e^+e^- \to Z$
<1800	90	[2] ALBRECHT	90B	ARG	$e^+e^- \to \Upsilon(4S)$

[1] PAL 15 signal significance is 3.0 standard deviations. The measurement corresponds to 90% CL upper limit of $< 6.5 \times 10^{-7}$.
[2] Assumes equal production of B^+ and B^0 at the $\Upsilon(4S)$.
[3] ACCIARRI 95H assumes $f_{B^0} = 39.5 \pm 4.0$ and $f_{B_s} = 12.0 \pm 3.0\%$.

$\Gamma(\eta\eta)/\Gamma_{total}$ — Γ_{426}/Γ

VALUE (units 10^{-6})	CL%	DOCUMENT ID		TECN	COMMENT
< 1.0	90	[1] AUBERT	09AV	BABR	$e^+e^- \to \Upsilon(4S)$
• • • We do not use the following data for averages, fits, limits, etc. • • •					
< 1.8	90	[1] AUBERT,B	06V	BABR	Repl. by AUBERT 09AV
< 2.0	90	[1] CHANG	05A	BELL	$e^+e^- \to \Upsilon(4S)$
< 2.8	90	[1] AUBERT,B	04X	BABR	$e^+e^- \to \Upsilon(4S)$
< 18	90	BEHRENS	98	CLE2	$e^+e^- \to \Upsilon(4S)$
<410	90	[2] ACCIARRI	95H	L3	$e^+e^- \to Z$

[1] Assumes equal production of B^+ and B^0 at the $\Upsilon(4S)$.
[2] ACCIARRI 95H assumes $f_{B^0} = 39.5 \pm 4.0$ and $f_{B_s} = 12.0 \pm 3.0\%$.

$\Gamma(\eta'\pi^0)/\Gamma_{total}$ — Γ_{427}/Γ

VALUE (units 10^{-6})	CL%	DOCUMENT ID		TECN	COMMENT
1.2±0.6 OUR AVERAGE	Error includes scale factor of 1.7.				
0.9±0.4±0.1		[1] AUBERT	08AH	BABR	$e^+e^- \to \Upsilon(4S)$
2.8±1.0±0.3		[1] SCHUEMANN	06	BELL	$e^+e^- \to \Upsilon(4S)$
• • • We do not use the following data for averages, fits, limits, etc. • • •					
$0.8\ ^{+0.8}_{-0.6}$±0.1		[1] AUBERT	06W	BABR	Repl. by AUBERT 08AH
$1.0\ ^{+1.4}_{-1.0}$±0.8	90	[1] AUBERT,B	04D	BABR	Repl. by AUBERT 06W
< 5.7	90	[1] RICHICHI	00	CLE2	$e^+e^- \to \Upsilon(4S)$
<11	90	BEHRENS	98	CLE2	Repl. by RICHICHI 00

[1] Assumes equal production of B^+ and B^0 at the $\Upsilon(4S)$.

$\Gamma(\eta'\eta')/\Gamma_{total}$ — Γ_{428}/Γ

VALUE (units 10^{-6})	CL%	DOCUMENT ID		TECN	COMMENT
< 1.7	90	[1] AUBERT	09AV	BABR	$e^+e^- \to \Upsilon(4S)$
• • • We do not use the following data for averages, fits, limits, etc. • • •					
< 6.5	90	[1] SCHUEMANN	07	BELL	$e^+e^- \to \Upsilon(4S)$
< 2.4	90	[1] AUBERT,B	06V	BABR	Repl. by AUBERT 09AV
<10	90	[1] AUBERT,B	04X	BABR	Repl. by AUBERT,B 06V
<47	90	BEHRENS	98	CLE2	$e^+e^- \to \Upsilon(4S)$

[1] Assumes equal production of B^+ and B^0 at the $\Upsilon(4S)$.

$\Gamma(\eta'\eta)/\Gamma_{total}$ — Γ_{429}/Γ

VALUE (units 10^{-6})	CL%	DOCUMENT ID		TECN	COMMENT
< 1.2	90	[1] AUBERT	08AH	BABR	$e^+e^- \to \Upsilon(4S)$
• • • We do not use the following data for averages, fits, limits, etc. • • •					
< 4.5	90	[1] SCHUEMANN	07	BELL	$e^+e^- \to \Upsilon(4S)$
< 1.7	90	[1] AUBERT	06W	BABR	Repl. by AUBERT 08AH
< 4.6	90	[1] AUBERT,B	04X	BABR	$e^+e^- \to \Upsilon(4S)$
<27	90	BEHRENS	98	CLE2	$e^+e^- \to \Upsilon(4S)$

[1] Assumes equal production of B^+ and B^0 at the $\Upsilon(4S)$.

$\Gamma(\eta'\rho^0)/\Gamma_{total}$ — Γ_{430}/Γ

VALUE (units 10^{-6})	CL%	DOCUMENT ID		TECN	COMMENT
< 1.3	90	[1] SCHUEMANN	07	BELL	$e^+e^- \to \Upsilon(4S)$
• • • We do not use the following data for averages, fits, limits, etc. • • •					
< 2.8	90	[1] DEL-AMO-SA...	10A	BABR	$e^+e^- \to \Upsilon(4S)$
< 3.7	90	AUBERT	07E	BABR	Repl. by DEL-AMO-SANCHEZ 10A
< 4.3	90	[1] AUBERT,B	04D	BABR	Repl. by AUBERT 07E
<12	90	[1] RICHICHI	00	CLE2	$e^+e^- \to \Upsilon(4S)$
<23	90	BEHRENS	98	CLE2	Repl. by RICHICHI 00

[1] Assumes equal production of B^+ and B^0 at the $\Upsilon(4S)$.

$\Gamma(\eta' f_0(980),\ f_0 \to \pi^+\pi^-)/\Gamma_{total}$ — Γ_{431}/Γ

VALUE (units 10^{-6})	CL%	DOCUMENT ID		TECN	COMMENT
<0.9	90	[1] DEL-AMO-SA...	10A	BABR	$e^+e^- \to \Upsilon(4S)$
• • • We do not use the following data for averages, fits, limits, etc. • • •					
<1.5	90	AUBERT	07E	BABR	Repl. by DEL-AMO-SANCHEZ 10A

[1] Assumes equal production of B^+ and B^0 at the $\Upsilon(4S)$.

$\Gamma(\eta\rho^0)/\Gamma_{total}$ — Γ_{432}/Γ

VALUE (units 10^{-6})	CL%	DOCUMENT ID		TECN	COMMENT
< 1.5	90	[1] AUBERT	07Y	BABR	$e^+e^- \to \Upsilon(4S)$
• • • We do not use the following data for averages, fits, limits, etc. • • •					
< 1.9	90	[1] WANG	07B	BELL	$e^+e^- \to \Upsilon(4S)$
< 1.5	90	[1] AUBERT,B	04D	BABR	Repl. by AUBERT 07Y
<10	90	[1] RICHICHI	00	CLE2	$e^+e^- \to \Upsilon(4S)$
<13	90	BEHRENS	98	CLE2	Repl. by RICHICHI 00

[1] Assumes equal production of B^+ and B^0 at the $\Upsilon(4S)$.

$\Gamma(\eta f_0(980),\ f_0 \to \pi^+\pi^-)/\Gamma_{total}$ — Γ_{433}/Γ

VALUE (units 10^{-6})	CL%	DOCUMENT ID		TECN	COMMENT
<0.4	90	[1] AUBERT	07Y	BABR	$e^+e^- \to \Upsilon(4S)$

[1] Assumes equal production of B^+ and B^0 at the $\Upsilon(4S)$.

$\Gamma(\omega\eta)/\Gamma_{total}$ — Γ_{434}/Γ

VALUE (units 10^{-6})	CL%	DOCUMENT ID		TECN	COMMENT
$\mathbf{0.94\ ^{+0.35}_{-0.30}}$±0.09		[1] AUBERT	09AV	BABR	$e^+e^- \to \Upsilon(4S)$
• • • We do not use the following data for averages, fits, limits, etc. • • •					
< 1.9	90	[1] AUBERT,B	05K	BABR	Repl. by AUBERT 09AV
4.0 $^{+1.3}_{-1.2}$ ±0.4		[1] AUBERT,B	04X	BABR	Repl. by AUBERT,B 05K
<12	90	[1] BERGFELD	98	CLE2	

[1] Assumes equal production of B^+ and B^0 at the $\Upsilon(4S)$.

Int. J. Mod. Phys. A 2026.41. Downloaded from www.worldscientific.com
by UNIVERSITY OF CALIFORNIA @ BERKELEY on 09/16/26. Re-use and distribution is strictly not permitted, except for Open Access articles.

$\Gamma(\omega\eta')/\Gamma_{total}$ — Γ_{435}/Γ

VALUE (units 10^{-6})	CL%	DOCUMENT ID		TECN	COMMENT
$1.01^{+0.46}_{-0.38}\pm0.09$		[1] AUBERT	09AV	BABR	$e^+e^-\to\Upsilon(4S)$
• • • We do not use the following data for averages, fits, limits, etc. • • •					
<2.2	90	[1] SCHUEMANN	07	BELL	$e^+e^-\to\Upsilon(4S)$
<2.8	90	[1] AUBERT,B	04X	BABR	$e^+e^-\to\Upsilon(4S)$
<60	90	[1] BERGFELD	98	CLE2	

[1] Assumes equal production of B^+ and B^0 at the $\Upsilon(4S)$.

$\Gamma(\omega\rho^0)/\Gamma_{total}$ — Γ_{436}/Γ

VALUE (units 10^{-6})	CL%	DOCUMENT ID		TECN	COMMENT
<1.6	90	[1] AUBERT	09H	BABR	$e^+e^-\to\Upsilon(4S)$
• • • We do not use the following data for averages, fits, limits, etc. • • •					
<1.5	90	[1] AUBERT,B	06T	BABR	Repl. by AUBERT 09H
<3.3	90	[1] AUBERT	05O	BABR	Repl. by AUBERT,B 06T
<11	90	[1] BERGFELD	98	CLE2	

[1] Assumes equal production of B^+ and B^0 at the $\Upsilon(4S)$.

$\Gamma(\omega f_0(980),\ f_0\to\pi^+\pi^-)/\Gamma_{total}$ — Γ_{437}/Γ

VALUE (units 10^{-6})	CL%	DOCUMENT ID		TECN	COMMENT
<1.5	90	[1] AUBERT	09H	BABR	$e^+e^-\to\Upsilon(4S)$
• • • We do not use the following data for averages, fits, limits, etc. • • •					
<1.5	90	[1] AUBERT,B	06T	BABR	Repl. by AUBERT 09H

[1] Assumes equal production of B^+ and B^0 at the $\Upsilon(4S)$.

$\Gamma(\omega\omega)/\Gamma_{total}$ — Γ_{438}/Γ

VALUE (units 10^{-6})	CL%	DOCUMENT ID		TECN	COMMENT
1.40 ± 0.25 OUR AVERAGE					
$1.54\pm0.34^{+0.02}_{-0.03}$		[1] GUAN	24	BELL	$e^+e^-\to\Upsilon(4S)$
$1.2\ \pm0.3\ ^{+0.3}_{-0.2}$		[2] LEES	14	BABR	$e^+e^-\to\Upsilon(4S)$
• • • We do not use the following data for averages, fits, limits, etc. • • •					
<4.0	90	[2] AUBERT,B	06T	BABR	Repl. by LEES 14
<19	90	[2] BERGFELD	98	CLE2	

[1] GUAN 24 reports $(1.53\pm0.29\pm0.17)\times10^{-6}$ from a measurement of $[\Gamma(B^0\to\omega\omega)/\Gamma_{total}]$ / $[B(\Upsilon(4S)\to B^0\overline{B}^0)]$ assuming $B(\Upsilon(4S)\to B^0\overline{B}^0)=(48.4\pm1.2)\times10^{-2}$, which we rescale to our best (shown rounded) value $B(\Upsilon(4S)\to B^0\overline{B}^0)=(48.6\pm0.8)\times10^{-2}$. Our first error is their experiment's error and our second error is the systematic error from using our best (shown rounded) value.

[2] Assumes equal production of B^+ and B^0 at the $\Upsilon(4S)$.

$\Gamma(\phi\pi^0)/\Gamma_{total}$ — Γ_{439}/Γ

VALUE (units 10^{-6})	CL%	DOCUMENT ID		TECN	COMMENT
<0.15	90	[1] KIM	12A	BELL	$e^+e^-\to\Upsilon(4S)$
• • • We do not use the following data for averages, fits, limits, etc. • • •					
<0.28	90	[1] AUBERT,B	06C	BABR	$e^+e^-\to\Upsilon(4S)$
<1.0	90	[1] AUBERT,B	04D	BABR	Repl. by AUBERT,B 06C
<5	90	[1] BERGFELD	98	CLE2	

[1] Assumes equal production of B^+ and B^0 at the $\Upsilon(4S)$.

$\Gamma(\phi\eta)/\Gamma_{total}$ — Γ_{440}/Γ

VALUE (units 10^{-6})	CL%	DOCUMENT ID		TECN	COMMENT
<0.5	90	[1] AUBERT	09AV	BABR	$e^+e^-\to\Upsilon(4S)$
• • • We do not use the following data for averages, fits, limits, etc. • • •					
<0.6	90	[1] AUBERT,B	06V	BABR	Repl. by AUBERT 09AV
<1.0	90	[1] AUBERT,B	04X	BABR	Repl. by AUBERT,B 06V
<9	90	[1] BERGFELD	98	CLE2	

[1] Assumes equal production of B^+ and B^0 at the $\Upsilon(4S)$.

$\Gamma(\phi\eta')/\Gamma_{total}$ — Γ_{441}/Γ

VALUE (units 10^{-6})	CL%	DOCUMENT ID		TECN	COMMENT
<0.5	90	[1] SCHUEMANN	07	BELL	$e^+e^-\to\Upsilon(4S)$
• • • We do not use the following data for averages, fits, limits, etc. • • •					
<1.1	90	[1] AUBERT	09AV	BABR	$e^+e^-\to\Upsilon(4S)$
<1.0	90	[1] AUBERT,B	06V	BABR	Repl. by AUBERT 09AV
<4.5	90	[1] AUBERT,B	04X	BABR	Repl. by AUBERT,B 06V
<31	90	[1] BERGFELD	98	CLE2	

[1] Assumes equal production of B^+ and B^0 at the $\Upsilon(4S)$.

$\Gamma(\phi\pi^+\pi^-)/\Gamma_{total}$ — Γ_{442}/Γ

VALUE (units 10^{-7})	DOCUMENT ID		TECN	COMMENT
$1.82\pm0.25\pm0.43$	[1] AAIJ	17A	LHCB	pp at 7, 8 TeV

[1] Signal evidence is 4.5 standard deviations.

$\Gamma(\phi\rho^0)/\Gamma_{total}$ — Γ_{443}/Γ

VALUE (units 10^{-6})	CL%	DOCUMENT ID		TECN	COMMENT
<0.33	90	[1] AUBERT	08BK	BABR	$e^+e^-\to\Upsilon(4S)$
• • • We do not use the following data for averages, fits, limits, etc. • • •					
<156	90	[2] ABE	00C	SLD	$e^+e^-\to Z$
<13	90	[1] BERGFELD	98	CLE2	

[1] Assumes equal production of B^+ and B^0 at the $\Upsilon(4S)$.

[2] ABE 00C assumes $B(Z\to b\overline{b})=(21.7\pm0.1)\%$ and the B fractions $f_{B^0}=f_{B^+}=(39.7^{+1.8}_{-2.2})\%$ and $f_{B_s}=(10.5^{+1.8}_{-2.2})\%$.

$\Gamma(\phi f_0(980),\ f_0\to\pi^+\pi^-)/\Gamma_{total}$ — Γ_{444}/Γ

VALUE (units 10^{-6})	CL%	DOCUMENT ID		TECN	COMMENT
<0.38	90	[1] AUBERT	08BK	BABR	$e^+e^-\to\Upsilon(4S)$

[1] Assumes equal production of B^+ and B^0 at the $\Upsilon(4S)$.

$\Gamma(\phi\omega)/\Gamma_{total}$ — Γ_{445}/Γ

VALUE (units 10^{-6})	CL%	DOCUMENT ID		TECN	COMMENT
<0.7	90	[1] LEES	14	BABR	$e^+e^-\to\Upsilon(4S)$
• • • We do not use the following data for averages, fits, limits, etc. • • •					
<1.2	90	[1] AUBERT,B	06T	BABR	Repl. by LEES 14
<21	90	[1] BERGFELD	98	CLE2	

[1] Assumes equal production of B^+ and B^0 at the $\Upsilon(4S)$.

$\Gamma(\phi\phi)/\Gamma_{total}$ — Γ_{446}/Γ

VALUE	CL%	DOCUMENT ID		TECN	COMMENT
$<1.3\times10^{-8}$	90	AAIJ	25AS	LHCB	pp at 7, 8, 13 TeV
• • • We do not use the following data for averages, fits, limits, etc. • • •					
$<2.7\times10^{-8}$	90	AAIJ	19AP	LHCB	Repl. by AAIJ 25AS.
$<2.8\times10^{-8}$	90	AAIJ	15AS	LHCB	Repl. by AAIJ 19AP
$<2\times10^{-7}$	90	[1] AUBERT	08BK	BABR	$e^+e^-\to\Upsilon(4S)$
$<1.5\times10^{-6}$	90	[1] AUBERT,B	04X	BABR	Repl. by AUBERT 08BK
$<3.21\times10^{-4}$	90	[2] ABE	00C	SLD	$e^+e^-\to Z$
$<1.2\times10^{-5}$	90	[1] BERGFELD	98	CLE2	
$<3.9\times10^{-5}$	90	ASNER	96	CLE2	$e^+e^-\to\Upsilon(4S)$

[1] Assumes equal production of B^+ and B^0 at the $\Upsilon(4S)$.

[2] ABE 00C assumes $B(Z\to b\overline{b})=(21.7\pm0.1)\%$ and the B fractions $f_{B^0}=f_{B^+}=(39.7^{+1.8}_{-2.2})\%$ and $f_{B_s}=(10.5^{+1.8}_{-2.2})\%$.

$\Gamma(a_0(980)^\pm\pi^\mp,\ a_0^\pm\to\eta\pi^\pm)/\Gamma_{total}$ — Γ_{447}/Γ

VALUE (units 10^{-6})	CL%	DOCUMENT ID		TECN	COMMENT
<3.1	90	[1] AUBERT	07Y	BABR	$e^+e^-\to\Upsilon(4S)$
• • • We do not use the following data for averages, fits, limits, etc. • • •					
<5.1	90	[1] AUBERT,BE	04	BABR	Repl. by AUBERT 07Y

[1] Assumes equal production of B^+ and B^0 at the $\Upsilon(4S)$.

$\Gamma(a_0(1450)^\pm\pi^\mp,\ a_0^\pm\to\eta\pi^\pm)/\Gamma_{total}$ — Γ_{448}/Γ

VALUE (units 10^{-6})	CL%	DOCUMENT ID		TECN	COMMENT
<2.3	90	[1] AUBERT	07Y	BABR	$e^+e^-\to\Upsilon(4S)$

[1] Assumes equal production of B^+ and B^0 at the $\Upsilon(4S)$.

$\Gamma(\pi^+\pi^-\pi^0)/\Gamma_{total}$ — Γ_{449}/Γ

VALUE	CL%	DOCUMENT ID		TECN	COMMENT
$<7.2\times10^{-4}$	90	[1] ALBRECHT	90B	ARG	$e^+e^-\to\Upsilon(4S)$

[1] ALBRECHT 90B limit assumes equal production of $B^0\overline{B}^0$ and B^+B^- at $\Upsilon(4S)$.

$\Gamma(\rho^0\pi^0)/\Gamma_{total}$ — Γ_{450}/Γ

VALUE (units 10^{-6})	CL%	DOCUMENT ID		TECN	COMMENT
$2.0\ \pm0.5$ OUR AVERAGE					
$3.0\ \pm0.5\ \pm0.7$		[1,2] KUSAKA	08	BELL	$e^+e^-\to\Upsilon(4S)$
$1.4\ \pm0.6\ \pm0.3$		[1] AUBERT	04Z	BABR	$e^+e^-\to\Upsilon(4S)$
$1.6\ ^{+2.0}_{-1.4}\ \pm0.8$		[1] JESSOP	00	CLEO	$e^+e^-\to\Upsilon(4S)$
• • • We do not use the following data for averages, fits, limits, etc. • • •					
$3.12^{+0.88+0.60}_{-0.82-0.76}$		[1] DRAGIC	06	BELL	Repl. by KUSAKA 08
$5.1\ \pm1.6\ \pm0.9$		DRAGIC	04	BELL	Repl. by DRAGIC 06
<5.3	90	[1] GORDON	02	BELL	Repl. by DRAGIC 04
<24	90	ASNER	96	CLEO	Repl. by JESSOP 00
<400	90	[1] ALBRECHT	90B	ARG	$e^+e^-\to\Upsilon(4S)$

[1] Assumes equal production of B^+ and B^0 at the $\Upsilon(4S)$.

[2] This is the first measurement that excludes contributions from $\rho(1450)$ and $\rho(1570)$ resonances.

$\Gamma(\rho^\mp\pi^\pm)/\Gamma_{total}$ — Γ_{451}/Γ

VALUE (units 10^{-6})	CL%	DOCUMENT ID		TECN	COMMENT
23.0 ± 2.3 OUR AVERAGE					
$22.6\pm1.1\pm4.4$		[1,2] KUSAKA	08	BELL	$e^+e^-\to\Upsilon(4S)$
$22.6\pm1.8\pm2.2$		[1] AUBERT	03T	BABR	$e^+e^-\to\Upsilon(4S)$
$27.6^{+8.4}_{-7.4}\pm4.2$		[1] JESSOP	00	CLE2	$e^+e^-\to\Upsilon(4S)$
• • • We do not use the following data for averages, fits, limits, etc. • • •					
$20.8^{+6.0+2.8}_{-6.3-3.1}$		[1] GORDON	02	BELL	Repl. by KUSAKA 08
<88	90	ASNER	96	CLE2	Repl. by JESSOP 00
<520	90	[1] ALBRECHT	90B	ARG	$e^+e^-\to\Upsilon(4S)$
<5200	90	[3] BEBEK	87	CLEO	$e^+e^-\to\Upsilon(4S)$

[1] Assumes equal production of B^+ and B^0 at the $\Upsilon(4S)$.

[2] This is the first measurement that excludes contributions from $\rho(1450)$ and $\rho(1570)$ resonances.

[3] BEBEK 87 reports $<6.1\times10^{-3}$ assuming the $\Upsilon(4S)$ decays 43% to $B^0\overline{B}^0$. We rescale to 50%.

Int. J. Mod. Phys. A 2026.41. Downloaded from www.worldscientific.com
by LIFORNIA @ BERKELEY on 09/16/26. Re-use and distribution is strictly not permitted, except for Open Access articles.

$\Gamma(\pi^+\pi^-\pi^+\pi^-)/\Gamma_{total}$ — Γ_{452}/Γ

VALUE	CL%	DOCUMENT ID		TECN	COMMENT
$<11.2\times10^{-6}$	90	[1] VANHOEFER	14	BELL	$e^+e^-\to\Upsilon(4S)$
• • • We do not use the following data for averages, fits, limits, etc. • • •					
$<23.1\times10^{-6}$	90	[1] AUBERT	08BB	BABR	$e^+e^-\to\Upsilon(4S)$
$<19.3\times10^{-6}$	90	[1] CHIANG	08	BELL	Repl. by VANHOEFER 14
$<2.3\times10^{-4}$	90	[2] ADAM	96D	DLPH	$e^+e^-\to Z$
$<2.8\times10^{-4}$	90	[3] ABREU	95N	DLPH	Sup. by ADAM 96D
$<6.7\times10^{-4}$	90	[1] ALBRECHT	90B	ARG	$e^+e^-\to\Upsilon(4S)$

[1] Assumes equal production of B^+ and B^0 at the $\Upsilon(4S)$.
[2] ADAM 96D assumes $f_{B^0}=f_{B^-}=0.39$ and $f_{B_s}=0.12$.
[3] Assumes a B^0, B^- production fraction of 0.39 and a B_s production fraction of 0.12.

$\Gamma(\rho^0\pi^+\pi^-)/\Gamma_{total}$ — Γ_{453}/Γ

VALUE (units 10^{-6})	CL%	DOCUMENT ID		TECN	COMMENT
< 8.8	90	[1] AUBERT	08BB	BABR	$e^+e^-\to\Upsilon(4S)$
• • • We do not use the following data for averages, fits, limits, etc. • • •					
<12.0	90	[1] VANHOEFER	14	BELL	$e^+e^-\to\Upsilon(4S)$
<12.0	90	[1] CHIANG	08	BELL	Repl. by VANHOEFER 14

[1] Assumes equal production of B^+ and B^0 at the $\Upsilon(4S)$.

$\Gamma(\rho^0\rho^0)/\Gamma_{total}$ — Γ_{454}/Γ

VALUE (units 10^{-6})	CL%	DOCUMENT ID		TECN	COMMENT
0.96±0.15 OUR FIT					
0.97±0.24 OUR AVERAGE					
$1.02\pm0.30\pm0.15$		[1,2] VANHOEFER	14	BELL	$e^+e^-\to\Upsilon(4S)$
$0.92\pm0.32\pm0.14$		[2] AUBERT	08BB	BABR	$e^+e^-\to\Upsilon(4S)$
• • • We do not use the following data for averages, fits, limits, etc. • • •					
$0.4\ \pm0.4\ ^{+0.2}_{-0.3}$		[2] CHIANG	08	BELL	Repl. by VANHOEFER 14
$1.07\pm0.33\pm0.19$		[2] AUBERT	07G	BABR	Repl. by AUBERT 08BB
< 1.1	90	[2] AUBERT	05I	BABR	Repl. by AUBERT 07G
< 2.1	90	[2] AUBERT	03V	BABR	Repl. by AUBERT 05I
< 18	90	[3] GODANG	02	CLE2	$e^+e^-\to\Upsilon(4S)$
<136	90	[4] ABE	00C	SLD	$e^+e^-\to Z$
<280	90	[2] ALBRECHT	90B	ARG	$e^+e^-\to\Upsilon(4S)$
<290	90	[5] BORTOLETTO	89	CLEO	$e^+e^-\to\Upsilon(4S)$
<430	90	[5] BEBEK	87	CLEO	$e^+e^-\to\Upsilon(4S)$

[1] Signal significance 3.4 standard deviations.
[2] Assumes equal production of B^+ and B^0 at the $\Upsilon(4S)$.
[3] Assumes a helicity 00 configuration. For a helicity 11 configuration, the limit decreases to 1.4×10^{-5}.
[4] ABE 00C assumes $B(Z\to b\overline{b})=(21.7\pm0.1)\%$ and the B fractions $f_{B^0}=f_{B^+}=(39.7^{+1.8}_{-2.2})\%$ and $f_{B_s}=(10.5^{+1.8}_{-2.2})\%$.
[5] Paper assumes the $\Upsilon(4S)$ decays 43% to $B^0\overline{B}^0$. We rescale to 50%.

$\Gamma(\rho^0\rho^0)/\Gamma(K^*(892)^0\phi)$ — $\Gamma_{454}/\Gamma_{377}$

VALUE (units 10^{-2})	DOCUMENT ID		TECN	COMMENT
9.5±1.5 OUR FIT				
9.4±1.7±0.9	AAIJ	15T	LHCB	pp at 7, 8 TeV

$\Gamma(f_0(980)\pi^+\pi^-,\ f_0\to\pi^+\pi^-)/\Gamma_{total}$ — Γ_{455}/Γ

VALUE	CL%	DOCUMENT ID		TECN	COMMENT
$<3.0\times10^{-6}$	90	[1] VANHOEFER	14	BELL	$e^+e^-\to\Upsilon(4S)$
• • • We do not use the following data for averages, fits, limits, etc. • • •					
$<3.8\times10^{-6}$	90	[1] CHIANG	08	BELL	$e^+e^-\to\Upsilon(4S)$

[1] Assumes equal production of B^+ and B^0 at the $\Upsilon(4S)$.

$\Gamma(\rho^0 f_0(980),\ f_0\to\pi^+\pi^-)/\Gamma_{total}$ — Γ_{456}/Γ

VALUE (units 10^{-7})	CL%	DOCUMENT ID		TECN	COMMENT
7.8±2.2±1.1		[1,2] VANHOEFER	14	BELL	$e^+e^-\to\Upsilon(4S)$
• • • We do not use the following data for averages, fits, limits, etc. • • •					
<8.1	90	AAIJ	15T	LHCB	pp at 7, 8 TeV
<4.0	90	[2] AUBERT	08BB	BABR	$e^+e^-\to\Upsilon(4S)$
<3	90	[2] CHIANG	08	BELL	Repl. by VANHOEFER 14
<5.3	90	[2] AUBERT	07G	BABR	Repl. by AUBERT 08BB

[1] Signal significance of 3.1 standard deviations.
[2] Assumes equal production of B^+ and B^0 at the $\Upsilon(4S)$.

$\Gamma(f_0(980)f_0(980),\ f_0\to\pi^+\pi^-,\ f_0\to\pi^+\pi^-)/\Gamma_{total}$ — Γ_{457}/Γ

VALUE (units 10^{-6})	CL%	DOCUMENT ID		TECN	COMMENT
<0.19	90	[1] AUBERT	08BB	BABR	$e^+e^-\to\Upsilon(4S)$
• • • We do not use the following data for averages, fits, limits, etc. • • •					
<0.2	90	[1] VANHOEFER	14	BELL	$e^+e^-\to\Upsilon(4S)$
<0.1	90	[1] CHIANG	08	BELL	Repl. by VANHOEFER 14
<0.16	90	[1] AUBERT	07G	BABR	Repl. by AUBERT 08BB

[1] Assumes equal production of B^+ and B^0 at the $\Upsilon(4S)$.

$\Gamma(f_0(980)f_0(980),\ f_0\to\pi^+\pi^-,\ f_0\to K^+K^-)/\Gamma_{total}$ — Γ_{458}/Γ

VALUE (units 10^{-6})	CL%	DOCUMENT ID		TECN	COMMENT
<0.23	90	[1] AUBERT	08BK	BABR	$e^+e^-\to\Upsilon(4S)$

[1] Assumes equal production of B^+ and B^0 at the $\Upsilon(4S)$.

$\Gamma(a_1(1260)^\mp\pi^\pm)/\Gamma_{total}$ — Γ_{459}/Γ

VALUE (units 10^{-6})	CL%	DOCUMENT ID		TECN	COMMENT
26 ±5 OUR AVERAGE		Error includes scale factor of 1.9.			
$22.2\pm2.0\pm2.8$		[1,2] DALSENO	12	BELL	$e^+e^-\to\Upsilon(4S)$
$33.2\pm3.8\pm3.0$		[2,3] AUBERT	06V	BABR	$e^+e^-\to\Upsilon(4S)$
• • • We do not use the following data for averages, fits, limits, etc. • • •					
< 630	90	[2] ALBRECHT	90B	ARG	$e^+e^-\to\Upsilon(4S)$
< 490	90	[4] BORTOLETTO	89	CLEO	$e^+e^-\to\Upsilon(4S)$
<1000	90	[4] BEBEK	87	CLEO	$e^+e^-\to\Upsilon(4S)$

[1] DALSENO 12 reports $B(B^0\to a_1^\pm\pi^\mp)\,B(a_1^\pm\to\pi^\pm\pi^+\pi^-)=(11.1\pm1.0\pm1.4)\times10^{-6}$ which we rescaled assuming $a_1(1260)$ decays only to 3π and $B(a_1^\pm\to\pi^\pm\pi^+\pi^-)=0.5$.
[2] Assumes equal production of B^+ and B^0 at the $\Upsilon(4S)$.
[3] Assumes $a_1(1260)$ decays only to 3π and $B(a_1^\pm\to\pi^\pm\pi^\mp\pi^\pm)=0.5$.
[4] Paper assumes the $\Upsilon(4S)$ decays 43% to $B^0\overline{B}^0$. We rescale to 50%.

$\Gamma(a_2(1320)^\mp\pi^\pm)/\Gamma_{total}$ — Γ_{460}/Γ

VALUE	CL%	DOCUMENT ID		TECN	COMMENT
$<6.3\times10^{-6}$	90	[1] DALSENO	12	BELL	$e^+e^-\to\Upsilon(4S)$
• • • We do not use the following data for averages, fits, limits, etc. • • •					
$<3.0\times10^{-4}$	90	[2] BORTOLETTO	89	CLEO	$e^+e^-\to\Upsilon(4S)$
$<1.4\times10^{-3}$	90	[2] BEBEK	87	CLEO	$e^+e^-\to\Upsilon(4S)$

[1] DALSENO 12 reports $B(B^0\to a_2^\pm\pi^\mp)\,B(a_2^\pm\to\pi^\pm\pi^+\pi^-)<2.2\times10^{-6}$ which we rescaled using $B(a_2^\pm\to\pi^\pm\pi^+\pi^-)=1/2\,B(a_2^\pm\to3\pi)=0.35\pm0.013$.
[2] Paper assumes the $\Upsilon(4S)$ decays 43% to $B^0\overline{B}^0$. We rescale to 50%.

$\Gamma(\pi^+\pi^-\pi^0\pi^0)/\Gamma_{total}$ — Γ_{461}/Γ

VALUE	CL%	DOCUMENT ID		TECN	COMMENT
$<3.1\times10^{-3}$	90	[1] ALBRECHT	90B	ARG	$e^+e^-\to\Upsilon(4S)$

[1] ALBRECHT 90B limit assumes equal production of $B^0\overline{B}^0$ and B^+B^- at $\Upsilon(4S)$.

$\Gamma(\rho^+\rho^-)/\Gamma_{total}$ — Γ_{462}/Γ

VALUE (units 10^{-6})	CL%	DOCUMENT ID		TECN	COMMENT
28.0±1.7 OUR AVERAGE					
$28.9^{+2.3}_{-2.2}\pm2.9^{+}_{-2.7}$		[1] ADACHI	25H	BELL	$e^+e^-\to\Upsilon(4S)$
$28.3\pm1.5\pm1.5$		[2] VANHOEFER	16	BELL	$e^+e^-\to\Upsilon(4S)$
$25.5\pm2.1^{+3.6}_{-3.9}$		[2] AUBERT	07BF	BABR	$e^+e^-\to\Upsilon(4S)$
• • • We do not use the following data for averages, fits, limits, etc. • • •					
$22.8\pm3.8^{+2.3}_{-2.6}$		[2] SOMOV	06	BELL	Repl. by VANHOEFER 16
$25\ ^{+7}_{-6}\ ^{+5}_{-6}$		[2] AUBERT	04G	BABR	Repl. by AUBERT,B 04R
$30\ \pm4\ \pm5$		[2,3] AUBERT,B	04R	BABR	Repl. by AUBERT 07BF
<2200	90	[2] ALBRECHT	90B	ARG	$e^+e^-\to\Upsilon(4S)$

[1] Derived assuming $f_{00}=0.4861^{+0.0074}_{-0.0080}$.
[2] Assumes equal production of B^+ and B^0 at the $\Upsilon(4S)$.
[3] The quoted result is obtained after combining with AUBERT 04G result by AUBERT 04R alone gives $(33\pm4\pm5)\times10^{-6}$.

$\Gamma(a_1(1260)^0\pi^0)/\Gamma_{total}$ — Γ_{463}/Γ

VALUE	CL%	DOCUMENT ID		TECN	COMMENT
$<1.1\times10^{-3}$	90	[1] ALBRECHT	90B	ARG	$e^+e^-\to\Upsilon(4S)$

[1] ALBRECHT 90B limit assumes equal production of $B^0\overline{B}^0$ and B^+B^- at $\Upsilon(4S)$.

$\Gamma(\omega\pi^0)/\Gamma_{total}$ — Γ_{464}/Γ

VALUE (units 10^{-6})	CL%	DOCUMENT ID		TECN	COMMENT
< 0.5	90	[1] AUBERT	08AH	BABR	$e^+e^-\to\Upsilon(4S)$
• • • We do not use the following data for averages, fits, limits, etc. • • •					
< 2.0	90	[1] JEN	06	BELL	$e^+e^-\to\Upsilon(4S)$
< 1.2	90	[1] AUBERT,B	04D	BABR	Repl. by AUBERT 08AH
< 1.9	90	[1] WANG	04A	BELL	$e^+e^-\to\Upsilon(4S)$
< 3	90	[1] AUBERT	01G	BABR	$e^+e^-\to\Upsilon(4S)$
< 5.5	90	[1] JESSOP	00	CLE2	$e^+e^-\to\Upsilon(4S)$
< 14	90	[1] BERGFELD	98	CLE2	Repl. by JESSOP 00
<460	90	[2] ALBRECHT	90B	ARG	$e^+e^-\to\Upsilon(4S)$

[1] Assumes equal production of B^+ and B^0 at the $\Upsilon(4S)$.
[2] ALBRECHT 90B limit assumes equal production of $B^0\overline{B}^0$ and B^+B^- at $\Upsilon(4S)$.

$\Gamma(\pi^+\pi^+\pi^-\pi^-\pi^0)/\Gamma_{total}$ — Γ_{465}/Γ

VALUE	CL%	DOCUMENT ID		TECN	COMMENT
$<9.0\times10^{-3}$	90	[1] ALBRECHT	90B	ARG	$e^+e^-\to\Upsilon(4S)$

[1] ALBRECHT 90B limit assumes equal production of $B^0\overline{B}^0$ and B^+B^- at $\Upsilon(4S)$.

$\Gamma(a_1(1260)^+\rho^-)/\Gamma_{total}$ — Γ_{466}/Γ

VALUE (units 10^{-6})	CL%	DOCUMENT ID		TECN	COMMENT
< 61	90	[1,2] AUBERT,B	06O	BABR	$e^+e^-\to\Upsilon(4S)$
• • • We do not use the following data for averages, fits, limits, etc. • • •					
<3400	90	[1] ALBRECHT	90B	ARG	$e^+e^-\to\Upsilon(4S)$

[1] Assumes equal production of B^+ and B^0 at the $\Upsilon(4S)$.
[2] Assumes $a_1(1260)$ decays only to 3π and $B(a_1^\pm\to\pi^\pm\pi^\mp\pi^\pm)=0.5$.

Int. J. Mod. Phys. A 2026.41. Downloaded from www.worldscientific.com
by UNIVERSITY OF CALIFORNIA @ BERKELEY on 09/16/26. Re-use and distribution is strictly not permitted, except for Open Access articles.

$\Gamma(a_1(1260)^0\rho^0)/\Gamma_{total}$ — Γ_{467}/Γ

VALUE	CL%	DOCUMENT ID		TECN	COMMENT
$<2.4\times10^{-3}$	90	[1] ALBRECHT	90B	ARG	$e^+e^-\to\Upsilon(4S)$

[1] ALBRECHT 90B limit assumes equal production of $B^0\overline{B}^0$ and B^+B^- at $\Upsilon(4S)$.

$\Gamma(b_1^{\mp}\pi^{\pm},\ b_1^{\mp}\to\omega\pi^{\mp})/\Gamma_{total}$ — Γ_{468}/Γ

VALUE (units 10^{-6})	DOCUMENT ID		TECN	COMMENT
10.9±1.2±0.9	[1] AUBERT	07BI	BABR	$e^+e^-\to\Upsilon(4S)$

[1] Assumes equal production of B^+ and B^0 at the $\Upsilon(4S)$.

$\Gamma(b_1^0\pi^0,\ b_1^0\to\omega\pi^0)/\Gamma_{total}$ — Γ_{469}/Γ

VALUE (units 10^{-6})	CL%	DOCUMENT ID		TECN	COMMENT
<1.9	90	[1] AUBERT	08AG	BABR	$e^+e^-\to\Upsilon(4S)$

[1] Assumes equal production of B^+ and B^0 at the $\Upsilon(4S)$.

$\Gamma(b_1^-\rho^+,\ b_1^-\to\omega\pi^-)/\Gamma_{total}$ — Γ_{470}/Γ

VALUE	CL%	DOCUMENT ID		TECN	COMMENT
$<1.4\times10^{-6}$	90	[1] AUBERT	09AF	BABR	$e^+e^-\to\Upsilon(4S)$

[1] Assumes equal production of B^+ and B^0 at the $\Upsilon(4S)$.

$\Gamma(b_1^0\rho^0,\ b_1^0\to\omega\pi^0)/\Gamma_{total}$ — Γ_{471}/Γ

VALUE	CL%	DOCUMENT ID		TECN	COMMENT
$<3.4\times10^{-6}$	90	[1] AUBERT	09AF	BABR	$e^+e^-\to\Upsilon(4S)$

[1] Assumes equal production of B^+ and B^0 at the $\Upsilon(4S)$.

$\Gamma(\pi^+\pi^+\pi^+\pi^-\pi^-\pi^-)/\Gamma_{total}$ — Γ_{472}/Γ

VALUE	CL%	DOCUMENT ID		TECN	COMMENT
$<3.0\times10^{-3}$	90	[1] ALBRECHT	90B	ARG	$e^+e^-\to\Upsilon(4S)$

[1] ALBRECHT 90B limit assumes equal production of $B^0\overline{B}^0$ and B^+B^- at $\Upsilon(4S)$.

$\Gamma(a_1(1260)^+a_1(1260)^-,\ a_1^+\to2\pi^+\pi^-,\ a_1^-\to2\pi^-\pi^+)/\Gamma_{total}$ — Γ_{473}/Γ

VALUE (units 10^{-6})	CL%	DOCUMENT ID		TECN	COMMENT
11.8±2.6±1.6		[1] AUBERT	09AL	BABR	$e^+e^-\to\Upsilon(4S)$
• • • We do not use the following data for averages, fits, limits, etc. • • •					
<6000	90	[1] ALBRECHT	90B	ARG	$e^+e^-\to\Upsilon(4S)$
<2800	90	[2] BORTOLETTO	89	CLEO	$e^+e^-\to\Upsilon(4S)$

[1] Assumes equal production of $B^0\overline{B}^0$ and B^+B^- at $\Upsilon(4S)$.
[2] BORTOLETTO 89 reports $<3.2\times10^{-3}$ assuming the $\Upsilon(4S)$ decays 43% to $B^0\overline{B}^0$. We rescale to 50%.

$\Gamma(\pi^+\pi^+\pi^+\pi^-\pi^-\pi^-\pi^0)/\Gamma_{total}$ — Γ_{474}/Γ

VALUE	CL%	DOCUMENT ID		TECN	COMMENT
$<1.1\times10^{-2}$	90	[1] ALBRECHT	90B	ARG	$e^+e^-\to\Upsilon(4S)$

[1] ALBRECHT 90B limit assumes equal production of $B^0\overline{B}^0$ and B^+B^- at $\Upsilon(4S)$.

$\Gamma(p\overline{p})/\Gamma_{total}$ — Γ_{475}/Γ

VALUE (units 10^{-8})	CL%	DOCUMENT ID		TECN	COMMENT
1.27±0.13±0.06		[1] AAIJ	23T	LHCB	pp at 7, 8 and 13 TeV
• • • We do not use the following data for averages, fits, limits, etc. • • •					
1.25±0.27±0.18		[1] AAIJ	17BJ	LHCB	Repl. by AAIJ 23T
$1.47^{+0.62}_{-0.51}\pm0.14$		[2] AAIJ	13BQ	LHCB	Repl. by AAIJ 17BJ
< 11	90	[3] TSAI	07	BELL	$e^+e^-\to\Upsilon(4S)$
< 41	90	[3] CHANG	05	BELL	$e^+e^-\to\Upsilon(4S)$
< 27	90	[3] AUBERT	04U	BABR	$e^+e^-\to\Upsilon(4S)$
< 140	90	[3] BORNHEIM	03	CLE2	$e^+e^-\to\Upsilon(4S)$
< 120	90	[3] ABE	02O	BELL	$e^+e^-\to\Upsilon(4S)$
< 700	90	[3] COAN	99	CLE2	$e^+e^-\to\Upsilon(4S)$
< 1800	90	[4] BUSKULIC	96V	ALEP	$e^+e^-\to Z$
<35000	90	[5] ABREU	95N	DLPH	Sup. by ADAM 96D
< 3400	90	[6] BORTOLETTO	89	CLEO	$e^+e^-\to\Upsilon(4S)$
<12000	90	[7] ALBRECHT	88F	ARG	$e^+e^-\to\Upsilon(4S)$
<17000	90	[6] BEBEK	87	CLEO	$e^+e^-\to\Upsilon(4S)$

[1] Uses normalization mode $B(B^0\to K^+\pi^-)=(19.6\pm0.5)\times10^{-6}$.
[2] Uses normalization mode $B(B^0\to K^+\pi^-)=(19.55\pm0.54)\times10^{-6}$.
[3] Assumes equal production of B^+ and B^0 at the $\Upsilon(4S)$.
[4] BUSKULIC 96V assumes PDG 96 production fractions for B^0, B^+, B_s, b baryons.
[5] Assumes a B^0, B^- production fraction of 0.39 and a B_s production fraction of 0.12.
[6] Paper assumes the $\Upsilon(4S)$ decays 43% to $B^0\overline{B}^0$. We rescale to 50%.
[7] ALBRECHT 88F reports $<1.3\times10^{-4}$ assuming the $\Upsilon(4S)$ decays 45% to $B^0\overline{B}^0$. We rescale to 50%.

$\Gamma(p\overline{p}\pi^+\pi^-)/\Gamma_{total}$ — Γ_{476}/Γ

VALUE (units 10^{-6})	CL%	DOCUMENT ID		TECN	COMMENT
2.87± 0.15± 0.11		[1,2] AAIJ	17BD	LHCB	pp at 7, 8 TeV
• • • We do not use the following data for averages, fits, limits, etc. • • •					
0.83± 0.17± 0.17		[3] CHU	20	BELL	$e^+e^-\to\Upsilon(4S)$
<950	90	[4] ABREU	95N	DLPH	Sup. by ADAM 96D
<250	90	[5] BEBEK	89	CLEO	$e^+e^-\to\Upsilon(4S)$
540 ±180 ±200		[6] ALBRECHT	88F	ARG	$e^+e^-\to\Upsilon(4S)$

[1] AAIJ 17BD reports $[\Gamma(B^0\to p\overline{p}\pi^+\pi^-)/\Gamma_{total}]$ / $[B(B^0\to J/\psi(1S)K^*(892)^0)]$ / $[B(J/\psi(1S)\to p\overline{p})]$ / $[B(K^*(892)\to(K\pi)^{\pm})]=1.07\pm0.04\pm0.04$ which we multiply by our best (shown rounded) values $B(B^0\to J/\psi(1S)K^*(892)^0)=(1.27\pm0.05)\times10^{-3}$, $B(J/\psi(1S)\to p\overline{p})=(2.121\pm0.029)\times10^{-3}$, $B(K^*(892)\to(K\pi)^{\pm})=(99.896\pm0.010)\times10^{-2}$. Our first error is their experiment's error and our second error is the systematic error from using our best (shown rounded) values.
[2] The branching ratio is given for $m_{p\overline{p}}<2.85$ GeV.
[3] Assumes equal production of B^0 and B^+ from $\Upsilon(4S)$ decays. This measurement is quoted for $M(\pi^+\pi^-)<1.22$ GeV excluding the $0.46<M(\pi^+\pi^-)<0.53$ GeV region.
[4] Assumes a B^0, B^- production fraction of 0.39 and a B_s production fraction of 0.12.
[5] BEBEK 89 reports $<2.9\times10^{-4}$ assuming the $\Upsilon(4S)$ decays 43% to $B^0\overline{B}^0$. We rescale to 50%.
[6] ALBRECHT 88F reports 6.0 ± 2.0 ± 2.2 assuming the $\Upsilon(4S)$ decays 45% to $B^0\overline{B}^0$. We rescale to 50%.

$\Gamma(p\overline{p}\pi^+\pi^-)/\Gamma(p\overline{p}K^+\pi^-)$ — $\Gamma_{476}/\Gamma_{477}$

VALUE	DOCUMENT ID		TECN	COMMENT
• • • We do not use the following data for averages, fits, limits, etc. • • •				
0.46±0.02±0.02	[1] AAIJ	17BD	LHCB	pp at 7, 8 TeV

[1] The ratio is given for $m_{p\overline{p}}<2.85$ GeV.

$\Gamma(p\overline{p}K^0)/\Gamma_{total}$ — Γ_{478}/Γ

VALUE (units 10^{-6})	CL%	DOCUMENT ID		TECN	COMMENT
2.79±0.16 OUR AVERAGE					
2.82±0.08±0.16		[1] AAIJ	25X	LHCB	pp at 7, 8 and 13 TeV
$2.51^{+0.35}_{-0.29}\pm0.21$		[2,3] CHEN	08C	BELL	$e^+e^-\to\Upsilon(4S)$
3.0 ±0.5 ±0.3		[3] AUBERT	07AV	BABR	$e^+e^-\to\Upsilon(4S)$
• • • We do not use the following data for averages, fits, limits, etc. • • •					
$2.40^{+0.64}_{-0.44}\pm0.28$		[3,4,5] WANG	05A	BELL	Repl. by CHEN 08C
$1.88^{+0.77}_{-0.60}\pm0.23$		[3,4,6] WANG	04	BELL	Repl. by WANG 05A
<7.2	90	[3,4] ABE	02K	BELL	Repl. by WANG 04

[1] The last uncertainty includes the systematic uncertainties due to the uncertainty of the branching fraction of the normalisation channel.
[2] Explicitly vetoes resonant production of $p\overline{p}$ from charmonium states.
[3] Assumes equal production of B^+ and B^0 at the $\Upsilon(4S)$.
[4] Explicitly vetoes resonant production of $p\overline{p}$ from charmonium states and pK^0 production from Λ_c.
[5] Provides also results with $M_{p\overline{p}}<2.85$ GeV/c^2 and angular asymmetry of $p\overline{p}$ system.
[6] The branching fraction for $M_{p\overline{p}}<2.85$ is also reported.

$\Gamma(\Theta(1540)^+\overline{p},\ \Theta^+\to pK^0_S)/\Gamma_{total}$ — Γ_{479}/Γ

VALUE (units 10^{-6})	CL%	DOCUMENT ID		TECN	COMMENT
<0.05	90	[1] AUBERT	07AV	BABR	$e^+e^-\to\Upsilon(4S)$
• • • We do not use the following data for averages, fits, limits, etc. • • •					
<0.23	90	[1] WANG	05A	BELL	$e^+e^-\to\Upsilon(4S)$

[1] Assumes equal production of B^+ and B^0 at the $\Upsilon(4S)$.

$\Gamma(f_J(2220)K^0,\ f_J\to p\overline{p})/\Gamma_{total}$ — Γ_{480}/Γ

VALUE (units 10^{-6})	CL%	DOCUMENT ID		TECN	COMMENT
<0.45	90	[1] AUBERT	07AV	BABR	$e^+e^-\to\Upsilon(4S)$

[1] Assumes equal production of B^+ and B^0 at the $\Upsilon(4S)$.

$\Gamma(p\overline{p}K^+\pi^-)/\Gamma_{total}$ — Γ_{477}/Γ

VALUE (units 10^{-6})	DOCUMENT ID		TECN	COMMENT
6.3±0.5±0.2	[1,2] AAIJ	17BD	LHCB	pp at 7, 8 TeV

[1] AAIJ 17BD reports $[\Gamma(B^0\to p\overline{p}K^+\pi^-)/\Gamma_{total}]$ / $[B(B^0\to J/\psi(1S)K^*(892)^0)]$ / $[B(J/\psi(1S)\to p\overline{p})]$ / $[B(K^*(892)\to(K\pi)^{\pm})]=2.34\pm0.12\pm0.12$ which we multiply by our best (shown rounded) values $B(B^0\to J/\psi(1S)K^*(892)^0)=(1.27\pm0.05)\times10^{-3}$, $B(J/\psi(1S)\to p\overline{p})=(2.121\pm0.029)\times10^{-3}$, $B(K^*(892)\to(K\pi)^{\pm})=(99.896\pm0.010)\times10^{-2}$. Our first error is their experiment's error and our second error is the systematic error from using our best (shown rounded) values.
[2] The branching ratio is given for $m_{p\overline{p}}<2.85$ GeV.

$\Gamma(p\overline{p}K^*(892)^0)/\Gamma_{total}$ — Γ_{481}/Γ

VALUE (units 10^{-6})	CL%	DOCUMENT ID		TECN	COMMENT
$1.24^{+0.28}_{-0.25}$ OUR AVERAGE					
$1.18^{+0.29}_{-0.25}\pm0.11$		[1,2] CHEN	08C	BELL	$e^+e^-\to\Upsilon(4S)$
1.47±0.45±0.40		[2] AUBERT	07AV	BABR	$e^+e^-\to\Upsilon(4S)$
• • • We do not use the following data for averages, fits, limits, etc. • • •					
<7.6	90	[2] WANG	04	BELL	$e^+e^-\to\Upsilon(4S)$

[1] Explicitly vetoes resonant production of $p\overline{p}$ from charmonium states.
[2] Assumes equal production of B^+ and B^0 at the $\Upsilon(4S)$.

$\Gamma(p\overline{p}\pi^0)/\Gamma_{total}$ — Γ_{484}/Γ

VALUE (units 10^{-7})	DOCUMENT ID		TECN	COMMENT
5.0±1.8±0.6	PAL	19	BELL	$e^+e^-\to\Upsilon(4S)$

Int. J. Mod. Phys. A 2026.41. Downloaded from www.worldscientific.com by LIFORNIA @ BERKELEY on 09/16/26. Re-use and distribution is strictly not permitted, except for Open Access articles.

$\Gamma(f_J(2220)K_0^*,\ f_J \to p\overline{p})/\Gamma_{total}$ — Γ_{482}/Γ

VALUE (units 10^{-6})	CL%	DOCUMENT ID		TECN	COMMENT
<0.15	90	[1] AUBERT	07AV	BABR	$e^+e^- \to \Upsilon(4S)$

[1] Assumes equal production of B^+ and B^0 at the $\Upsilon(4S)$.

$\Gamma(p\overline{p}K^+K^-)/\Gamma_{total}$ — Γ_{483}/Γ

VALUE (units 10^{-8})	DOCUMENT ID		TECN	COMMENT
12.1±3.1±0.5	[1,2] AAIJ	17BD	LHCB	pp at 7, 8 TeV

[1] AAIJ 17BD reports $[\Gamma(B^0 \to p\overline{p}K^+K^-)/\Gamma_{total}]$ / $[B(B^0 \to J/\psi(1S)K^*(892)^0)]$ / $[B(J/\psi(1S) \to p\overline{p})]$ / $[B(K^*(892) \to (K\pi)^\pm)] = 0.045 \pm 0.011 \pm 0.004$ which we multiply by our best (shown rounded) values $B(B^0 \to J/\psi(1S)K^*(892)^0) = (1.27 \pm 0.05) \times 10^{-3}$, $B(J/\psi(1S) \to p\overline{p}) = (2.121 \pm 0.029) \times 10^{-3}$, $B(K^*(892) \to (K\pi)^\pm) = (99.896 \pm 0.010) \times 10^{-2}$. Our first error is their experiment's error and our second error is the systematic error from using our best (shown rounded) values.

[2] The branching ratio is given for $m_{p\overline{p}} < 2.85$ GeV.

$\Gamma(p\overline{p}K^+K^-)/\Gamma(p\overline{p}K^+\pi^-)$ — $\Gamma_{483}/\Gamma_{477}$

VALUE (%)	DOCUMENT ID		TECN	COMMENT
• • • We do not use the following data for averages, fits, limits, etc. • • •				
$1.9 \pm 0.5 \pm 0.2$	[1] AAIJ	17BD	LHCB	pp at 7, 8 TeV

[1] The ratio is given for $m_{p\overline{p}} < 2.85$ GeV.

$\Gamma(p\overline{p}p\overline{p})/\Gamma_{total}$ — Γ_{485}/Γ

VALUE (units 10^{-8})	CL%	DOCUMENT ID		TECN	COMMENT
2.2±0.4±0.1		[1] AAIJ	23AD	LHCB	pp at 7, 8, 13 TeV
• • • We do not use the following data for averages, fits, limits, etc. • • •					
<20	90	[2] LEES	18C	BABR	$e^+e^- \to \Upsilon(4S)$

[1] AAIJ 23AD reports $(2.2 \pm 0.4 \pm 0.1 \pm 0.1) \times 10^{-8}$ from a measurement of $[\Gamma(B^0 \to p\overline{p}p\overline{p})/\Gamma_{total}]$ / $[B(B^0 \to J/\psi(1S)K^*(892)^0)]$ / $[B(J/\psi(1S) \to p\overline{p})]$ assuming $B(B^0 \to J/\psi(1S)K^*(892)^0) = (1.27 \pm 0.05) \times 10^{-3}$, $B(J/\psi(1S) \to p\overline{p}) = (2.120 \pm 0.029) \times 10^{-3}$, which we rescale to our best (shown rounded) values $B(B^0 \to J/\psi(1S)K^*(892)^0) = (1.27 \pm 0.05) \times 10^{-3}$, $B(J/\psi(1S) \to p\overline{p}) = (2.121 \pm 0.029) \times 10^{-3}$. Our first error is their experiment's error and our second error is the systematic error from using our best (shown rounded) values. It also includes $B(K^*(892)^0 \to K^+\pi^-) = 2/3$.

[2] Assumes equal production of B^+ and B^0 at the $\Upsilon(4S)$.

$\Gamma(p\overline{\Lambda}\pi^-)/\Gamma_{total}$ — Γ_{486}/Γ

VALUE (units 10^{-6})	CL%	DOCUMENT ID		TECN	COMMENT
3.16±0.24 OUR AVERAGE					
$3.21^{+0.28}_{-0.25} \pm 0.16$		[1] CHANG	23	BELL	$e^+e^- \to \Upsilon(4S)$
$3.07 \pm 0.31 \pm 0.23$		[1] AUBERT	09AC	BABR	$e^+e^- \to \Upsilon(4S)$
• • • We do not use the following data for averages, fits, limits, etc. • • •					
$3.23^{+0.33}_{-0.29} \pm 0.29$		[1] WANG	07C	BELL	$e^+e^- \to \Upsilon(4S)$
$2.62^{+0.44}_{-0.40} \pm 0.31$		[1,2] WANG	05A	BELL	Repl. by WANG 07C
$3.97^{+1.00}_{-0.80} \pm 0.56$		[1] WANG	03	BELL	Repl. by WANG 05A
< 13	90	[1] COAN	99	CLE2	$e^+e^- \to \Upsilon(4S)$
<180	90	[3] ALBRECHT	88F	ARG	$e^+e^- \to \Upsilon(4S)$

[1] Assumes equal production of B^+ and B^0 at the $\Upsilon(4S)$.

[2] Provides also results with $M_{p\overline{p}} < 2.85$ GeV/c^2 and angular asymmetry of $p\overline{\Lambda}$ system.

[3] ALBRECHT 88F reports $< 2.0 \times 10^{-4}$ assuming the $\Upsilon(4S)$ decays 45% to $B^0\overline{B}^0$. We rescale to 50%.

$\Gamma(p\overline{\Lambda}\pi^-\gamma)/\Gamma_{total}$ — Γ_{487}/Γ

VALUE	CL%	DOCUMENT ID		TECN	COMMENT
$<6.5 \times 10^{-7}$	90	[1] LAI	14	BELL	$e^+e^- \to \Upsilon(4S)$

[1] Assumes equal production of B^+ and B^0 at the $\Upsilon(4S)$.

$\Gamma(p\overline{\Sigma}(1385)^-)/\Gamma_{total}$ — Γ_{488}/Γ

VALUE (units 10^{-6})	CL%	DOCUMENT ID		TECN	COMMENT
<0.26	90	[1] WANG	07C	BELL	$e^+e^- \to \Upsilon(4S)$

[1] Assumes equal production of B^+ and B^0 at the $\Upsilon(4S)$.

$[\Gamma(\Delta(1232)^+\overline{p}) + \Gamma(\Delta(1232)^-p)]/\Gamma_{total}$ — Γ_{489}/Γ

VALUE	DOCUMENT ID		TECN	COMMENT
$<1.6 \times 10^{-6}$	PAL	19	BELL	$e^+e^- \to \Upsilon(4S)$

$\Gamma(\Delta^0\overline{\Lambda})/\Gamma_{total}$ — Γ_{490}/Γ

VALUE (units 10^{-6})	CL%	DOCUMENT ID		TECN	COMMENT
<0.93	90	[1] WANG	07C	BELL	$e^+e^- \to \Upsilon(4S)$

[1] Assumes equal production of B^+ and B^0 at the $\Upsilon(4S)$.

$\Gamma(p\overline{\Lambda}K^-)/\Gamma_{total}$ — Γ_{491}/Γ

VALUE (units 10^{-6})	CL%	DOCUMENT ID		TECN	COMMENT
<0.82	90	[1] WANG	03	BELL	$e^+e^- \to \Upsilon(4S)$

[1] Assumes equal production of B^+ and B^0 at the $\Upsilon(4S)$.

$\Gamma(p\overline{\Lambda}D^-)/\Gamma_{total}$ — Γ_{492}/Γ

VALUE (units 10^{-6})	DOCUMENT ID		TECN	COMMENT
25.1±2.6±3.5	[1] CHANG	15	BELL	$e^+e^- \to \Upsilon(4S)$

[1] Assumes equal production of B^+ and B^0 at the $\Upsilon(4S)$.

$\Gamma(p\overline{\Lambda}D^{*-})/\Gamma_{total}$ — Γ_{493}/Γ

VALUE (units 10^{-6})	DOCUMENT ID		TECN	COMMENT
33.6±6.3±4.4	[1] CHANG	15	BELL	$e^+e^- \to \Upsilon(4S)$

[1] Assumes equal production of B^+ and B^0 at the $\Upsilon(4S)$.

$\Gamma(p\overline{\Sigma}^0\pi^-)/\Gamma_{total}$ — Γ_{494}/Γ

VALUE (units 10^{-6})	CL%	DOCUMENT ID		TECN	COMMENT
$1.17^{+0.43}_{-0.40} \pm 0.07$		[1] CHANG	23	BELL	$e^+e^- \to \Upsilon(4S)$
• • • We do not use the following data for averages, fits, limits, etc. • • •					
<3.8	90	[1] WANG	03	BELL	$e^+e^- \to \Upsilon(4S)$

[1] Assumes equal production of B^+ and B^0 at the $\Upsilon(4S)$.

$\Gamma(\overline{\Lambda}\Lambda)/\Gamma_{total}$ — Γ_{495}/Γ

VALUE (units 10^{-6})	CL%	DOCUMENT ID		TECN	COMMENT
<0.32	90	[1] TSAI	07	BELL	$e^+e^- \to \Upsilon(4S)$
• • • We do not use the following data for averages, fits, limits, etc. • • •					
<0.69	90	[1] CHANG	05	BELL	Repl. by TSAI 07
<1.2	90	[1] BORNHEIM	03	CLE2	$e^+e^- \to \Upsilon(4S)$
<1.0	90	[1] ABE	02O	BELL	Repl. by CHANG 05
<3.9	90	[1] COAN	99	CLE2	$e^+e^- \to \Upsilon(4S)$

[1] Assumes equal production of B^+ and B^0 at the $\Upsilon(4S)$.

$\Gamma(\overline{\Lambda}\Lambda K^0)/\Gamma_{total}$ — Γ_{496}/Γ

VALUE (units 10^{-6})	DOCUMENT ID		TECN	COMMENT
$4.76^{+0.84}_{-0.68} \pm 0.61$	[1,2] CHANG	09	BELL	$e^+e^- \to \Upsilon(4S)$

[1] Excluding charmonium events in $2.85 < m_{\Lambda\overline{\Lambda}} < 3.128$ GeV/c^2 and $3.315 < m_{\Lambda\overline{\Lambda}} < 3.735$ GeV/c^2. Measurements in various $m_{\Lambda\overline{\Lambda}}$ bins are also reported.

[2] Assumes equal production of B^+ and B^0 at the $\Upsilon(4S)$.

$\Gamma(\overline{\Lambda}\Lambda K^{*0})/\Gamma_{total}$ — Γ_{497}/Γ

VALUE (units 10^{-6})	DOCUMENT ID		TECN	COMMENT
$2.46^{+0.87}_{-0.72} \pm 0.34$	[1,2] CHANG	09	BELL	$e^+e^- \to \Upsilon(4S)$

[1] Excluding charmonium events in $2.85 < m_{\Lambda\overline{\Lambda}} < 3.128$ GeV/c^2 and $3.315 < m_{\Lambda\overline{\Lambda}} < 3.735$ GeV/c^2. Measurements in various $m_{\Lambda\overline{\Lambda}}$ bins are also reported.

[2] Assumes equal production of B^+ and B^0 at the $\Upsilon(4S)$.

$\Gamma(\overline{\Lambda}\Lambda D^0)/\Gamma_{total}$ — Γ_{498}/Γ

VALUE (units 10^{-5})	DOCUMENT ID		TECN	COMMENT
$1.00^{+0.30}_{-0.26}$ OUR AVERAGE				
$0.98^{+0.29}_{-0.26} \pm 0.19$	[1,2] LEES	14B	BABR	$e^+e^- \to \Upsilon(4S)$
$1.05^{+0.57}_{-0.44} \pm 0.14$	[2] CHANG	09	BELL	$e^+e^- \to \Upsilon(4S)$

[1] Evidence for 3.4 st. dev. signal significance.

[2] Assumes equal production of B^+ and B^0 at the $\Upsilon(4S)$.

$\Gamma(D^0\Sigma^0\overline{\Lambda} + c.c.)/\Gamma_{total}$ — Γ_{499}/Γ

VALUE	CL%	DOCUMENT ID		TECN	COMMENT
$<3.1 \times 10^{-5}$	90	[1,2] LEES	14B	BABR	$e^+e^- \to \Upsilon(4S)$

[1] Here $\Sigma^0 \to \Lambda\gamma$.

[2] Assumes equal production of B^+ and B^0 at the $\Upsilon(4S)$.

$\Gamma(\Delta^0\overline{\Delta}^0)/\Gamma_{total}$ — Γ_{500}/Γ

VALUE	CL%	DOCUMENT ID		TECN	COMMENT
<0.0015	90	[1] BORTOLETTO	89	CLEO	$e^+e^- \to \Upsilon(4S)$

[1] BORTOLETTO 89 reports < 0.0018 assuming $\Upsilon(4S)$ decays 43% to $B^0\overline{B}^0$. We rescale to 50%.

$\Gamma(\Delta^{++}\overline{\Delta}^{--})/\Gamma_{total}$ — Γ_{501}/Γ

VALUE	CL%	DOCUMENT ID		TECN	COMMENT
$<1.1 \times 10^{-4}$	90	[1] BORTOLETTO	89	CLEO	$e^+e^- \to \Upsilon(4S)$

[1] BORTOLETTO 89 reports $< 1.3 \times 10^{-4}$ assuming $\Upsilon(4S)$ decays 43% to $B^0\overline{B}^0$. We rescale to 50%.

$\Gamma(\overline{D}^0p\overline{p})/\Gamma_{total}$ — Γ_{502}/Γ

VALUE (units 10^{-4})	DOCUMENT ID		TECN	COMMENT
1.04±0.07 OUR AVERAGE				
$1.02 \pm 0.04 \pm 0.06$	[1,2] DEL-AMO-SA...12		BABR	$e^+e^- \to \Upsilon(4S)$
$1.18 \pm 0.15 \pm 0.16$	[2] ABE	02W	BELL	$e^+e^- \to \Upsilon(4S)$
• • • We do not use the following data for averages, fits, limits, etc. • • •				
$1.13 \pm 0.06 \pm 0.08$	[2] AUBERT,B	06S	BABR	Repl. by DEL-AMO-SANCHEZ 12

[1] Uses the values of D and D^* branching fractions from PDG 08.

[2] Assumes equal production of B^+ and B^0 at the $\Upsilon(4S)$.

Int. J. Mod. Phys. A 2026.41. Downloaded from www.worldscientific.com by UNIVERSITY OF CALIFORNIA @ BERKELEY on 09/16/26. Re-use and distribution is strictly not permitted, except for Open Access articles.

$\Gamma(D_s^- \overline{\Lambda} p)/\Gamma_{total}$ — Γ_{503}/Γ

VALUE (units 10^{-5})	DOCUMENT ID		TECN	COMMENT
2.8±0.8±0.3	[1,2] MEDVEDEVA	07	BELL	$e^+e^- \to \Upsilon(4S)$

[1] Assumes equal production of B^+ and B^0 at the $\Upsilon(4S)$.
[2] MEDVEDEVA 07 reports $(2.9 \pm 0.7 \pm 0.5 \pm 0.4) \times 10^{-5}$ from a measurement of $[\Gamma(B^0 \to D_s^- \overline{\Lambda} p)/\Gamma_{total}] \times [B(D_s^+ \to \phi\pi^+)]$ assuming $B(D_s^+ \to \phi\pi^+) = (4.4 \pm 0.6) \times 10^{-2}$, which we rescale to our best (shown rounded) value $B(D_s^+ \to \phi\pi^+) = (4.5 \pm 0.4) \times 10^{-2}$. Our first error is their experiment's error and our second error is the systematic error from using our best (shown rounded) value.

$\Gamma(\overline{D}^*(2007)^0 p\overline{p})/\Gamma_{total}$ — Γ_{504}/Γ

VALUE (units 10^{-4})	DOCUMENT ID		TECN	COMMENT
0.99±0.11 OUR AVERAGE				
0.97±0.07±0.09	[1,2] DEL-AMO-SA...12		BABR	$e^+e^- \to \Upsilon(4S)$
$1.20^{+0.33}_{-0.29} \pm 0.21$	[2] ABE	02W	BELL	$e^+e^- \to \Upsilon(4S)$
• • • We do not use the following data for averages, fits, limits, etc. • • •				
1.01±0.10±0.09	[2] AUBERT,B	06S	BABR	Repl. by DEL-AMO-SANCHEZ 12

[1] Uses the values of D and D^* branching fractions from PDG 08.
[2] Assumes equal production of B^+ and B^0 at the $\Upsilon(4S)$.

$\Gamma(D^*(2010)^- p\overline{n})/\Gamma_{total}$ — Γ_{505}/Γ

VALUE (units 10^{-4})	DOCUMENT ID		TECN	COMMENT
$\mathbf{14.5^{+3.4}_{-3.0} \pm 2.7}$	[1] ANDERSON	01	CLE2	$e^+e^- \to \Upsilon(4S)$

[1] Assumes equal production of B^+ and B^0 at the $\Upsilon(4S)$.

$\Gamma(D^- p\overline{p}\pi^+)/\Gamma_{total}$ — Γ_{506}/Γ

VALUE (units 10^{-4})	DOCUMENT ID		TECN	COMMENT
3.32±0.10±0.29	[1,2] DEL-AMO-SA...12		BABR	$e^+e^- \to \Upsilon(4S)$
• • • We do not use the following data for averages, fits, limits, etc. • • •				
3.38±0.14±0.29	[2] AUBERT,B	06S	BABR	Repl. by DEL-AMO-SANCHEZ 12

[1] Uses the values of D and D^* branching fractions from PDG 08.
[2] Assumes equal production of B^+ and B^0 at the $\Upsilon(4S)$.

$\Gamma(D^*(2010)^- p\overline{p}\pi^+)/\Gamma_{total}$ — Γ_{507}/Γ

VALUE (units 10^{-4})	DOCUMENT ID		TECN	COMMENT
4.7 ±0.5 OUR AVERAGE Error includes scale factor of 1.2.				
4.55±0.16±0.39	[1,2] DEL-AMO-SA...12		BABR	$e^+e^- \to \Upsilon(4S)$
$6.5\ ^{+1.3}_{-1.2} \pm 1.0$	[2] ANDERSON	01	CLE2	$e^+e^- \to \Upsilon(4S)$
• • • We do not use the following data for averages, fits, limits, etc. • • •				
4.81±0.22±0.44	[2] AUBERT,B	06S	BABR	Repl. by DEL-AMO-SANCHEZ 12

[1] Uses the values of D and D^* branching fractions from PDG 08.
[2] Assumes equal production of B^+ and B^0 at the $\Upsilon(4S)$.

$\Gamma(\overline{D}^0 p\overline{p}\pi^+\pi^-)/\Gamma_{total}$ — Γ_{508}/Γ

VALUE (units 10^{-4})	DOCUMENT ID		TECN	COMMENT
2.99±0.21±0.45	[1,2] DEL-AMO-SA...12		BABR	$e^+e^- \to \Upsilon(4S)$

[1] Uses the values of D and D^* branching fractions from PDG 08.
[2] Assumes equal production of B^+ and B^0 at the $\Upsilon(4S)$.

$\Gamma(\overline{D}^{*0} p\overline{p}\pi^+\pi^-)/\Gamma_{total}$ — Γ_{509}/Γ

VALUE (units 10^{-4})	DOCUMENT ID		TECN	COMMENT
1.91±0.36±0.29	[1,2] DEL-AMO-SA...12		BABR	$e^+e^- \to \Upsilon(4S)$

[1] Uses the values of D and D^* branching fractions from PDG 08.
[2] Assumes equal production of B^+ and B^0 at the $\Upsilon(4S)$.

$\Gamma(\Theta_c \overline{p}\pi^+, \Theta_c \to D^- p)/\Gamma_{total}$ — Γ_{510}/Γ

VALUE (units 10^{-6})	CL%	DOCUMENT ID		TECN	COMMENT
<9	90	[1] AUBERT,B	06S	BABR	$e^+e^- \to \Upsilon(4S)$

[1] Assumes equal production of B^+ and B^0 at the $\Upsilon(4S)$.

$\Gamma(\Theta_c \overline{p}\pi^+, \Theta_c \to D^{*-} p)/\Gamma_{total}$ — Γ_{511}/Γ

VALUE (units 10^{-6})	CL%	DOCUMENT ID		TECN	COMMENT
<14	90	[1] AUBERT,B	06S	BABR	$e^+e^- \to \Upsilon(4S)$

[1] Assumes equal production of B^+ and B^0 at the $\Upsilon(4S)$.

$\Gamma(\overline{\Sigma}_c^{--} \Delta^{++})/\Gamma_{total}$ — Γ_{512}/Γ

VALUE	CL%	DOCUMENT ID		TECN	COMMENT
$\mathbf{<8 \times 10^{-4}}$	90	[1] PROCARIO	94	CLE2	$e^+e^- \to \Upsilon(4S)$

[1] PROCARIO 94 reports < 0.0012 from a measurement of $[\Gamma(B^0 \to \overline{\Sigma}_c^{--} \Delta^{++})/\Gamma_{total}] \times [B(\Lambda_c^+ \to pK^-\pi^+)]$ assuming $B(\Lambda_c^+ \to pK^-\pi^+) = 0.043$, which we rescale to our best (shown rounded) value $B(\Lambda_c^+ \to pK^-\pi^+) = 6.37 \times 10^{-2}$.

$\Gamma(\overline{\Lambda}_c^- p\pi^+\pi^-)/\Gamma_{total}$ — Γ_{513}/Γ

VALUE (units 10^{-3})	DOCUMENT ID		TECN	COMMENT
1.00±0.14 OUR AVERAGE Error includes scale factor of 1.4. See the ideogram below.				
1.23±0.05±0.33	[1,2] LEES	13H	BABR	$e^+e^- \to \Upsilon(4S)$
0.88±0.11±0.03	[1,3] PARK	07	BELL	$e^+e^- \to \Upsilon(4S)$
$1.31^{+0.21}_{-0.20} \pm 0.04$	[4] DYTMAN	02	CLE2	$e^+e^- \to \Upsilon(4S)$
• • • We do not use the following data for averages, fits, limits, etc. • • •				
0.86±0.16±0.03	[5] GABYSHEV	02	BELL	Repl. by PARK 07
$1.33^{+0.46}_{-0.42} \pm 0.37$	[6] FU	97	CLE2	Repl. by DYTMAN 02

[1] Assumes equal production of B^+ and B^0 at the $\Upsilon(4S)$.
[2] Uses $\Lambda_c^+ \to pK^-\pi^+$ mode. The second error includes the uncertainty of the branching fraction of the Λ_c decay, $B(\Lambda_c^+ \to pK^-\pi^+) = (5.0 \pm 1.3)\%$.
[3] PARK 07 reports $(11.2 \pm 0.5 \pm 3.2) \times 10^{-4}$ from a measurement of $[\Gamma(B^0 \to \overline{\Lambda}_c^- p\pi^+\pi^-)/\Gamma_{total}] \times [B(\Lambda_c^+ \to pK^-\pi^+)]$ assuming $B(\Lambda_c^+ \to pK^-\pi^+) = (5.0 \pm 1.3) \times 10^{-2}$, which we rescale to our best (shown rounded) value $B(\Lambda_c^+ \to pK^-\pi^+) = (6.37 \pm 0.21) \times 10^{-2}$. Our first error is their experiment's error and our second error is the systematic error from using our best (shown rounded) value.
[4] DYTMAN 02 reports $(1.67^{+0.27}_{-0.25}) \times 10^{-3}$ from a measurement of $[\Gamma(B^0 \to \overline{\Lambda}_c^- p\pi^+\pi^-)/\Gamma_{total}] \times [B(\Lambda_c^+ \to pK^-\pi^+)]$ assuming $B(\Lambda_c^+ \to pK^-\pi^+) = 0.05$, which we rescale to our best (shown rounded) value $B(\Lambda_c^+ \to pK^-\pi^+) = (6.37 \pm 0.21) \times 10^{-2}$. Our first error is their experiment's error and our second error is the systematic error from using our best (shown rounded) value.
[5] GABYSHEV 02 reports $(1.1 \pm 0.2) \times 10^{-3}$ from a measurement of $[\Gamma(B^0 \to \overline{\Lambda}_c^- p\pi^+\pi^-)/\Gamma_{total}] \times [B(\Lambda_c^+ \to pK^-\pi^+)]$ assuming $B(\Lambda_c^+ \to pK^-\pi^+) = 0.05$, which we rescale to our best (shown rounded) value $B(\Lambda_c^+ \to pK^-\pi^+) = (6.37 \pm 0.21) \times 10^{-2}$. Our first error is their experiment's error and our second error is the systematic error from using our best (shown rounded) value.
[6] FU 97 uses PDG 96 values of Λ_c branching fraction.

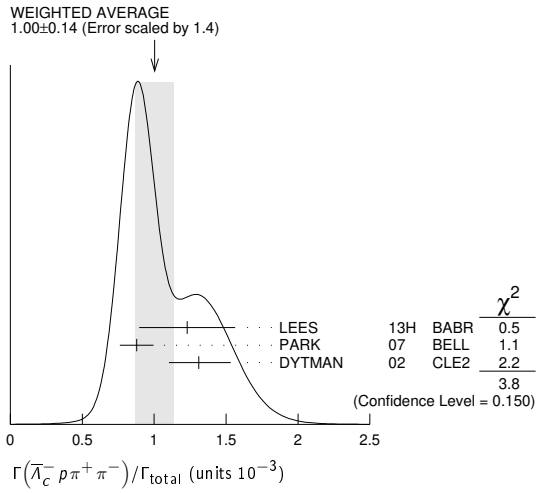

$\Gamma(\overline{\Lambda}_c^- p)/\Gamma_{total}$ — Γ_{514}/Γ

VALUE (units 10^{-5})	CL%	DOCUMENT ID		TECN	COMMENT
1.51±0.17 OUR AVERAGE					
1.48±0.16±0.05		[1,2] AUBERT	08BN	BABR	$e^+e^- \to \Upsilon(4S)$
$2.19^{+0.56}_{-0.49} \pm 0.65$		[1,3] GABYSHEV	03	BELL	$e^+e^- \to \Upsilon(4S)$
• • • We do not use the following data for averages, fits, limits, etc. • • •					
$2.10^{+0.67+0.77}_{-0.55-0.46}$		[1,4] AUBERT	07AV	BABR	Repl. by AUBERT 08BN
< 9	90	[1,5] DYTMAN	02	CLE2	$e^+e^- \to \Upsilon(4S)$
< 3.1	90	[1,4] GABYSHEV	02	BELL	$e^+e^- \to \Upsilon(4S)$
<21	90	[6] FU	97	CLE2	$e^+e^- \to \Upsilon(4S)$

[1] Assumes equal production of B^+ and B^0 at the $\Upsilon(4S)$.
[2] AUBERT 08BN reports $(1.89 \pm 0.21 \pm 0.49) \times 10^{-5}$ from a measurement of $[\Gamma(B^0 \to \overline{\Lambda}_c^- p)/\Gamma_{total}] \times [B(\Lambda_c^+ \to pK^-\pi^+)]$ assuming $B(\Lambda_c^+ \to pK^-\pi^+) = (5.0 \pm 1.3) \times 10^{-2}$, which we rescale to our best (shown rounded) value $B(\Lambda_c^+ \to pK^-\pi^+) = (6.37 \pm 0.21) \times 10^{-2}$. Our first error is their experiment's error and our second error is the systematic error from using our best (shown rounded) value.
[3] The second error for GABYSHEV 03 includes the systematic and the error of $\Lambda_c \to \overline{p}K^+\pi^-$ decay branching fraction.
[4] Uses the value for $\Lambda_c \to pK^-\pi^+$ branching ratio $(5.0 \pm 1.3)\%$.
[5] DYTMAN 02 measurement uses $B(\Lambda_c^- \to \overline{p}K^+\pi^-) = 5.0 \pm 1.3\%$. The second error includes the systematic and the uncertainty of the branching ratio.
[6] FU 97 uses PDG 96 values of Λ_c branching ratio.

$\Gamma(\overline{\Lambda}_c^- p\pi^0)/\Gamma_{total}$ — Γ_{515}/Γ

VALUE (units 10^{-4})	CL%	DOCUMENT ID		TECN	COMMENT
1.52±0.17±0.05		[1,2] AUBERT	10H	BABR	$e^+e^- \to \Upsilon(4S)$
• • • We do not use the following data for averages, fits, limits, etc. • • •					
<5.9	90	[3] FU	97	CLE2	$e^+e^- \to \Upsilon(4S)$

[1] AUBERT 10H reports $(1.94 \pm 0.17 \pm 0.52) \times 10^{-4}$ from a measurement of $[\Gamma(B^0 \to \overline{\Lambda}_c^- p\pi^0)/\Gamma_{total}] \times [B(\Lambda_c^+ \to pK^-\pi^+)]$ assuming $B(\Lambda_c^+ \to pK^-\pi^+) = (5.0 \pm 1.3) \times 10^{-2}$, which we rescale to our best (shown rounded) value $B(\Lambda_c^+ \to pK^-\pi^+) = (6.37 \pm 0.21) \times 10^{-2}$. Our first error is their experiment's error and our second error is the systematic error from using our best (shown rounded) value.
[2] Assumes equal production of B^+ and B^0 at the $\Upsilon(4S)$.
[3] FU 97 uses PDG 96 values of Λ_c branching ratio.

$\Gamma(\Lambda_c^- pK^+K^-)/\Gamma_{total}$ — Γ_{529}/Γ

VALUE (units 10^{-5})		DOCUMENT ID		TECN	COMMENT
$1.96 \pm 0.35^{+0.07}_{-0.06}$	[1,2]	LEES	15B	BABR	$e^+e^- \to \Upsilon(4S)$

[1] LEES 15B reports $[\Gamma(B^0 \to \Lambda_c^- pK^+K^-)/\Gamma_{total}] \times [B(\Lambda_c^+ \to pK^-\pi^+)] = (12.5 \pm 2.0 \pm 1.0) \times 10^{-7}$ which we divide by our best (shown rounded) value $B(\Lambda_c^+ \to pK^-\pi^+) = (6.37 \pm 0.21) \times 10^{-2}$. Our first error is their experiment's error and our second error is the systematic error from using our best (shown rounded) value.
[2] Assumes equal production of B^+ and B^0 at the $\Upsilon(4S)$.

$\Gamma(\Lambda_c^- p\phi)/\Gamma_{total}$ — Γ_{530}/Γ

VALUE	CL%	DOCUMENT ID		TECN	COMMENT
$<9 \times 10^{-6}$	90	[1,2] LEES	15B	BABR	$e^+e^- \to \Upsilon(4S)$

[1] LEES 15B reports $< 1.2 \times 10^{-5}$ from a measurement of $[\Gamma(B^0 \to \Lambda_c^- p\phi)/\Gamma_{total}] \times [B(\Lambda_c^+ \to pK^-\pi^+)]$ assuming $B(\Lambda_c^+ \to pK^-\pi^+) = (5.0 \pm 1.3) \times 10^{-2}$, which we rescale to our best (shown rounded) value $B(\Lambda_c^+ \to pK^-\pi^+) = 6.37 \times 10^{-2}$.
[2] Assumes equal production of B^+ and B^0 at the $\Upsilon(4S)$.

$\Gamma(\Sigma_c(2455)^- p)/\Gamma_{total}$ — Γ_{516}/Γ

VALUE (units 10^{-6})		DOCUMENT ID		TECN	COMMENT
<24	[1,2]	AUBERT	10H	BABR	$e^+e^- \to \Upsilon(4S)$

[1] AUBERT 10H reports $[\Gamma(B^0 \to \Sigma_c(2455)^- p)/\Gamma_{total}] \times [B(\Lambda_c^+ \to pK^-\pi^+)] < 1.5 \times 10^{-6}$ which we divide by our best (shown rounded) value $B(\Lambda_c^+ \to pK^-\pi^+) = 6.37 \times 10^{-2}$.
[2] Assumes equal production of B^+ and B^0 at the $\Upsilon(4S)$.

$\Gamma(\overline{\Lambda}_c^- p\pi^+\pi^-\pi^0)/\Gamma_{total}$ — Γ_{517}/Γ

VALUE	CL%	DOCUMENT ID		TECN	COMMENT
$<5.07 \times 10^{-3}$	90	[1] FU	97	CLE2	$e^+e^- \to \Upsilon(4S)$

[1] FU 97 uses PDG 96 values of Λ_c branching ratio.

$\Gamma(\overline{\Lambda}_c^- p\pi^+\pi^-\pi^+\pi^-)/\Gamma_{total}$ — Γ_{518}/Γ

VALUE	CL%	DOCUMENT ID		TECN	COMMENT
$<2.74 \times 10^{-3}$	90	[1] FU	97	CLE2	$e^+e^- \to \Upsilon(4S)$

[1] FU 97 uses PDG 96 values of Λ_c branching ratio.

$\Gamma(\overline{\Lambda}_c^- p\pi^+\pi^-(\text{nonresonant}))/\Gamma_{total}$ — Γ_{519}/Γ

VALUE (units 10^{-4})		DOCUMENT ID		TECN	COMMENT
5.4 ± 1.0 OUR AVERAGE	Error includes scale factor of 1.3.				
$7.9 \pm 0.4 \pm 2.0$	[1,2]	LEES	13H	BABR	$e^+e^- \to \Upsilon(4S)$
$5.0 \pm 0.8 \pm 0.2$	[1,3]	PARK	07	BELL	$e^+e^- \to \Upsilon(4S)$

[1] Assumes equal production of B^+ and B^0 at the $\Upsilon(4S)$.
[2] Uses $\Lambda_c^+ \to pK^-\pi^+$ mode. The second error includes the uncertainty of the branching fraction of the Λ_c decay, $B(\Lambda_c^+ \to pK^-\pi^+) = (5.0 \pm 1.3)\%$.
[3] PARK 07 reports $(6.4 \pm 0.4 \pm 1.9) \times 10^{-4}$ from a measurement of $[\Gamma(B^0 \to \overline{\Lambda}_c^- p\pi^+\pi^-(\text{nonresonant}))/\Gamma_{total}] \times [B(\Lambda_c^+ \to pK^-\pi^+)]$ assuming $B(\Lambda_c^+ \to pK^-\pi^+) = (5.0 \pm 1.3) \times 10^{-2}$, which we rescale to our best (shown rounded) value $B(\Lambda_c^+ \to pK^-\pi^+) = (6.37 \pm 0.21) \times 10^{-2}$. Our first error is their experiment's error and our second error is the systematic error from using our best (shown rounded) value.

$\Gamma(\overline{\Sigma}_c(2520)^{--} p\pi^+)/\Gamma_{total}$ — Γ_{520}/Γ

VALUE (units 10^{-4})		DOCUMENT ID		TECN	COMMENT
1.01 ± 0.18 OUR AVERAGE					
$1.15 \pm 0.10 \pm 0.30$	[1,2]	LEES	13H	BABR	$e^+e^- \to \Upsilon(4S)$
$0.94 \pm 0.21 \pm 0.03$	[1,3]	PARK	07	BELL	$e^+e^- \to \Upsilon(4S)$
• • • We do not use the following data for averages, fits, limits, etc. • • •					
$1.28^{+0.50}_{-0.45} \pm 0.04$	[4]	GABYSHEV	02	BELL	Repl. by PARK 07

[1] Assumes equal production of B^+ and B^0 at the $\Upsilon(4S)$.
[2] Uses $\Lambda_c^+ \to pK^-\pi^+$ mode. The second error includes the uncertainty of the branching fraction of the Λ_c decay, $B(\Lambda_c^+ \to pK^-\pi^+) = (5.0 \pm 1.3)\%$.
[3] PARK 07 reports $(1.2 \pm 0.1 \pm 0.4) \times 10^{-4}$ from a measurement of $[\Gamma(B^0 \to \overline{\Sigma}_c(2520)^{--} p\pi^+)/\Gamma_{total}] \times [B(\Lambda_c^+ \to pK^-\pi^+)]$ assuming $B(\Lambda_c^+ \to pK^-\pi^+) = (5.0 \pm 1.3) \times 10^{-2}$, which we rescale to our best (shown rounded) value $B(\Lambda_c^+ \to pK^-\pi^+) = (6.37 \pm 0.21) \times 10^{-2}$. Our first error is their experiment's error and our second error is the systematic error from using our best (shown rounded) value.
[4] GABYSHEV 02 reports $(1.63^{+0.64}_{-0.58}) \times 10^{-4}$ from a measurement of $[\Gamma(B^0 \to \overline{\Sigma}_c(2520)^{--} p\pi^+)/\Gamma_{total}] \times [B(\Lambda_c^+ \to pK^-\pi^+)]$ assuming $B(\Lambda_c^+ \to pK^-\pi^+) = 0.05$, which we rescale to our best (shown rounded) value $B(\Lambda_c^+ \to pK^-\pi^+) = (6.37 \pm 0.21) \times 10^{-2}$. Our first error is their experiment's error and our second error is the systematic error from using our best (shown rounded) value.

$\Gamma(\overline{\Sigma}_c(2520)^0 p\pi^-)/\Gamma_{total}$ — Γ_{521}/Γ

VALUE	CL%	DOCUMENT ID		TECN	COMMENT
$<0.31 \times 10^{-4}$	90	[1,2] LEES	13H	BABR	$e^+e^- \to \Upsilon(4S)$
• • • We do not use the following data for averages, fits, limits, etc. • • •					
$<0.38 \times 10^{-4}$	90	[1] PARK	07	BELL	$e^+e^- \to \Upsilon(4S)$
$<1.21 \times 10^{-4}$	90	[1,2] GABYSHEV	02	BELL	Repl. by PARK 07

[1] Assumes equal production of B^+ and B^0 at the $\Upsilon(4S)$.
[2] Uses the value for $\Lambda_c \to pK^-\pi^+$ branching ratio $(5.0 \pm 1.3)\%$.

$\Gamma(\overline{\Sigma}_c(2455)^0 N^0,\ N^0 \to p\pi^-)/\Gamma_{total}$ — Γ_{523}/Γ

N^0 is the $N(1440)\ P_{11}$ or $N(1535)\ S_{11}$ or an admixture of the two baryonic states.

VALUE (units 10^{-4})		DOCUMENT ID		TECN	COMMENT
$0.63 \pm 0.16 \pm 0.02$	[1,2] KIM	08	BELL	$e^+e^- \to \Upsilon(4S)$

[1] Assumes equal production of B^+ and B^0 at the $\Upsilon(4S)$.
[2] KIM 08 reports $(0.80 \pm 0.15 \pm 0.25) \times 10^{-4}$ from a measurement of $[\Gamma(B^0 \to \overline{\Sigma}_c(2455)^0 N^0,\ N^0 \to p\pi^-)/\Gamma_{total}] \times [B(\Lambda_c^+ \to pK^-\pi^+)]$ assuming $B(\Lambda_c^+ \to pK^-\pi^+) = (5.0 \pm 1.3) \times 10^{-2}$, which we rescale to our best (shown rounded) value $B(\Lambda_c^+ \to pK^-\pi^+) = (6.37 \pm 0.21) \times 10^{-2}$. Our first error is their experiment's error and our second error is the systematic error from using our best (shown rounded) value.

$\Gamma(\overline{\Sigma}_c(2455)^0 p\pi^-)/\Gamma_{total}$ — Γ_{522}/Γ

VALUE (units 10^{-4})	CL%	DOCUMENT ID		TECN	COMMENT
1.08 ± 0.09 OUR AVERAGE					
$1.09 \pm 0.06 \pm 0.07$		LI	23E	BELL	$e^+e^- \to \Upsilon(4S)$
$0.91 \pm 0.07 \pm 0.24$		[1,2] LEES	13H	BABR	$e^+e^- \to \Upsilon(4S)$
$1.7 \pm 0.5 \pm 0.1$		[3] DYTMAN	02	CLE2	$e^+e^- \to \Upsilon(4S)$
• • • We do not use the following data for averages, fits, limits, etc. • • •					
$1.10 \pm 0.20 \pm 0.04$		[1,4] PARK	07	BELL	Repl. by LI 23E.
$0.38^{+0.36}_{-0.32} \pm 0.01$	90	[5] GABYSHEV	02	BELL	Repl. by PARK 07

[1] Assumes equal production of B^+ and B^0 at the $\Upsilon(4S)$.
[2] Uses $\Lambda_c^+ \to pK^-\pi^+$ mode. The second error includes the uncertainty of the branching fraction of the Λ_c decay, $B(\Lambda_c^+ \to pK^-\pi^+) = (5.0 \pm 1.3)\%$.
[3] DYTMAN 02 reports $(2.2 \pm 0.7) \times 10^{-4}$ from a measurement of $[\Gamma(B^0 \to \overline{\Sigma}_c(2455)^0 p\pi^-)/\Gamma_{total}] \times [B(\Lambda_c^+ \to pK^-\pi^+)]$ assuming $B(\Lambda_c^+ \to pK^-\pi^+) = 0.05$, which we rescale to our best (shown rounded) value $B(\Lambda_c^+ \to pK^-\pi^+) = (6.37 \pm 0.21) \times 10^{-2}$. Our first error is their experiment's error and our second error is the systematic error from using our best (shown rounded) value.
[4] PARK 07 reports $(1.4 \pm 0.2 \pm 0.4) \times 10^{-4}$ from a measurement of $[\Gamma(B^0 \to \overline{\Sigma}_c(2455)^0 p\pi^-)/\Gamma_{total}] \times [B(\Lambda_c^+ \to pK^-\pi^+)]$ assuming $B(\Lambda_c^+ \to pK^-\pi^+) = (5.0 \pm 1.3) \times 10^{-2}$, which we rescale to our best (shown rounded) value $B(\Lambda_c^+ \to pK^-\pi^+) = (6.37 \pm 0.21) \times 10^{-2}$. Our first error is their experiment's error and our second error is the systematic error from using our best (shown rounded) value.
[5] GABYSHEV 02 reports $(0.48^{+0.46}_{-0.41}) \times 10^{-4}$ from a measurement of $[\Gamma(B^0 \to \overline{\Sigma}_c(2455)^0 p\pi^-)/\Gamma_{total}] \times [B(\Lambda_c^+ \to pK^-\pi^+)]$ assuming $B(\Lambda_c^+ \to pK^-\pi^+) = 0.05$, which we rescale to our best (shown rounded) value $B(\Lambda_c^+ \to pK^-\pi^+) = (6.37 \pm 0.21) \times 10^{-2}$. Our first error is their experiment's error and our second error is the systematic error from using our best (shown rounded) value.

$\Gamma(\overline{\Sigma}_c(2455)^{--} p\pi^+)/\Gamma_{total}$ — Γ_{524}/Γ

VALUE (units 10^{-4})		DOCUMENT ID		TECN	COMMENT
1.89 ± 0.15 OUR AVERAGE					
$1.84 \pm 0.11 \pm 0.12$		LI	23E	BELL	$e^+e^- \to \Upsilon(4S)$
$2.13 \pm 0.10 \pm 0.56$		[1,2] LEES	13H	BABR	$e^+e^- \to \Upsilon(4S)$
$2.9 \pm 0.9 \pm 0.1$		[3] DYTMAN	02	CLE2	$e^+e^- \to \Upsilon(4S)$
• • • We do not use the following data for averages, fits, limits, etc. • • •					
$1.65 \pm 0.25^{+0.06}_{-0.05}$		[1,4] PARK	07	BELL	Repl. by LI 23E.
$1.9^{+0.6}_{-0.5} \pm 0.1$		[5] GABYSHEV	02	BELL	Repl. by PARK 07

[1] Assumes equal production of B^+ and B^0 at the $\Upsilon(4S)$.
[2] Uses $\Lambda_c^+ \to pK^-\pi^+$ mode. The second error includes the uncertainty of the branching fraction of the Λ_c decay, $B(\Lambda_c^+ \to pK^-\pi^+) = (5.0 \pm 1.3)\%$.
[3] DYTMAN 02 reports $(3.7 \pm 1.1) \times 10^{-4}$ from a measurement of $[\Gamma(B^0 \to \overline{\Sigma}_c(2455)^{--} p\pi^+)/\Gamma_{total}] \times [B(\Lambda_c^+ \to pK^-\pi^+)]$ assuming $B(\Lambda_c^+ \to pK^-\pi^+) = 0.05$, which we rescale to our best (shown rounded) value $B(\Lambda_c^+ \to pK^-\pi^+) = (6.37 \pm 0.21) \times 10^{-2}$. Our first error is their experiment's error and our second error is the systematic error from using our best (shown rounded) value.
[4] PARK 07 reports $(2.1 \pm 0.2 \pm 0.6) \times 10^{-4}$ from a measurement of $[\Gamma(B^0 \to \overline{\Sigma}_c(2455)^{--} p\pi^+)/\Gamma_{total}] \times [B(\Lambda_c^+ \to pK^-\pi^+)]$ assuming $B(\Lambda_c^+ \to pK^-\pi^+) = (5.0 \pm 1.3) \times 10^{-2}$, which we rescale to our best (shown rounded) value $B(\Lambda_c^+ \to pK^-\pi^+) = (6.37 \pm 0.21) \times 10^{-2}$. Our first error is their experiment's error and our second error is the systematic error from using our best (shown rounded) value.
[5] GABYSHEV 02 reports $(2.38^{+0.75}_{-0.69}) \times 10^{-4}$ from a measurement of $[\Gamma(B^0 \to \overline{\Sigma}_c(2455)^{--} p\pi^+)/\Gamma_{total}] \times [B(\Lambda_c^+ \to pK^-\pi^+)]$ assuming $B(\Lambda_c^+ \to pK^-\pi^+) = 0.05$, which we rescale to our best (shown rounded) value $B(\Lambda_c^+ \to pK^-\pi^+) = (6.37 \pm 0.21) \times 10^{-2}$. Our first error is their experiment's error and our second error is the systematic error from using our best (shown rounded) value.

Int. J. Mod. Phys. A 2026.41. Downloaded from www.worldscientific.com
by LIFORNIA @ BERKELEY on 09/16/26. Re-use and distribution is strictly not permitted, except for Open Access articles.

Int. J. Mod. Phys. A 2026.41. Downloaded from www.worldscientific.com
by UNIVERSITY OF CALIFORNIA @ BERKELEY on 09/16/26. Re-use and distribution is strictly not permitted, except for Open Access articles.

$\Gamma(\Sigma_c(2455)^0\overline{\Xi}_c^0)/\Gamma_{total}$ — Γ_{527}/Γ

VALUE (units 10^{-4})	DOCUMENT ID	TECN	COMMENT
$4.83\pm1.12^{+0.81}_{-0.70}$	[1] ABUMUSABH 25	BELL	$e^+e^-\to\Upsilon(4S)$

[1] Uses $\Sigma_c(2455)^0\to\Lambda_c^+\pi^-$ and $\overline{\Xi}_c^0\to\overline{\Xi}^+\pi^-$ and $\overline{\Lambda}K^+\pi^-$ decays.

$\Gamma(\Lambda_c^- pK^+\pi^-)/\Gamma_{total}$ — Γ_{525}/Γ

VALUE (units 10^{-5})	DOCUMENT ID	TECN	COMMENT
$3.4\pm0.7\pm0.1$	[1,2] AUBERT 09AG	BABR	$e^+e^-\to\Upsilon(4S)$

[1] AUBERT 09AG reports $(4.33\pm0.82\pm0.33\pm1.13)\times10^{-5}$ from a measurement of $[\Gamma(B^0\to\Lambda_c^- pK^+\pi^-)/\Gamma_{total}]\times[B(\Lambda_c^+\to pK^-\pi^+)]$ assuming $B(\Lambda_c^+\to pK^-\pi^+)=(5.0\pm1.3)\times10^{-2}$, which we rescale to our best (shown rounded) value $B(\Lambda_c^+\to pK^-\pi^+)=(6.37\pm0.21)\times10^{-2}$. Our first error is their experiment's error and our second error is the systematic error from using our best (shown rounded) value.

[2] Assumes equal production of B^+ and B^0 at the $\Upsilon(4S)$.

$\Gamma(\overline{\Sigma}_c(2455)^{--}pK^+,\ \overline{\Sigma}_c^{--}\to\overline{\Lambda}_c^-\pi^-)/\Gamma_{total}$ — Γ_{526}/Γ

VALUE (units 10^{-5})	DOCUMENT ID	TECN	COMMENT
$0.87\pm0.25\pm0.03$	[1,2] AUBERT 09AG	BABR	$e^+e^-\to\Upsilon(4S)$

[1] AUBERT 09AG reports $(1.11\pm0.30\pm0.09\pm0.29)\times10^{-5}$ from a measurement of $[\Gamma(B^0\to\overline{\Sigma}_c(2455)^{--}pK^+,\ \overline{\Sigma}_c^{--}\to\overline{\Lambda}_c^-\pi^-)/\Gamma_{total}]\times[B(\Lambda_c^+\to pK^-\pi^+)]$ assuming $B(\Lambda_c^+\to pK^-\pi^+)=(5.0\pm1.3)\times10^{-2}$, which we rescale to our best (shown rounded) value $B(\Lambda_c^+\to pK^-\pi^+)=(6.37\pm0.21)\times10^{-2}$. Our first error is their experiment's error and our second error is the systematic error from using our best (shown rounded) value.

[2] Assumes equal production of B^+ and B^0 at the $\Upsilon(4S)$.

$\Gamma(\Lambda_c^- pK^*(892)^0)/\Gamma_{total}$ — Γ_{528}/Γ

VALUE (units 10^{-5})	CL%	DOCUMENT ID	TECN	COMMENT
<2.42	90	[1] AUBERT 09AG	BABR	$e^+e^-\to\Upsilon(4S)$

[1] Assumes equal production of B^+ and B^0 at the $\Upsilon(4S)$.

$\Gamma(\Lambda_c^- p\overline{p}p)/\Gamma_{total}$ — Γ_{531}/Γ

VALUE (units 10^{-6})	DOCUMENT ID	TECN	COMMENT
<2.8	[1] LEES 14C	BABR	$e^+e^-\to\Upsilon(4S)$

[1] Assumes equal production of B^+ and B^0 at the $\Upsilon(4S)$ and $B(\Lambda_c^+\to pK^-\pi^+)=0.050\pm0.013$.

$\Gamma(\overline{\Lambda}_c^-\Lambda K^+)/\Gamma_{total}$ — Γ_{532}/Γ

VALUE (units 10^{-5})	DOCUMENT ID	TECN	COMMENT
$4.9\pm1.1\pm0.2$	[1,2] LEES 11F	BABR	$e^+e^-\to\Upsilon(4S)$

[1] Assumes equal production of B^0 and B^+ from Upsilon(4S) decays.

[2] LEES 11F reports $(3.8\pm0.8\pm0.2\pm1.0)\times10^{-5}$ from a measurement of $[\Gamma(B^0\to\overline{\Lambda}_c^-\Lambda K^+)/\Gamma_{total}]\ /\ [B(\Lambda_c^+\to pK^-\pi^+)]\ /\ [B(\Lambda\to p\pi^-)]$ assuming $B(\Lambda_c^+\to pK^-\pi^+)=(5.0\pm1.3)\times10^{-2}$, $B(\Lambda\to p\pi^-)=(63.9\pm0.5)\times10^{-2}$, which we rescale to our best (shown rounded) values $B(\Lambda_c^+\to pK^-\pi^+)=(6.37\pm0.21)\times10^{-2}$, $B(\Lambda\to p\pi^-)=(64.1\pm0.5)\times10^{-2}$. Our first error is their experiment's error and our second error is the systematic error from using our best (shown rounded) values. The reported uncertainties are statistical, systematic, and $\overline{\Lambda}_c^-$ branching fraction uncertainty.

$\Gamma(\overline{\Lambda}_c^-\Lambda_c^+)/\Gamma_{total}$ — Γ_{533}/Γ

VALUE (units 10^{-5})	CL%	DOCUMENT ID	TECN	COMMENT
<1.6	95	[1] AAIJ 14AA	LHCB	pp at 7 TeV
• • • We do not use the following data for averages, fits, limits, etc. • • •				
<6.2	90	[2] UCHIDA 08	BELL	$e^+e^-\to\Upsilon(4S)$

[1] Uses $B(\overline{B}^0\to D^+D_s^-)=(7.2\pm0.8)\times10^{-3}$.

[2] Assumes equal production of B^+ and B^0 at the $\Upsilon(4S)$.

$\Gamma(\overline{\Lambda}_c(2593)^-\ /\ \overline{\Lambda}_c(2625)^-p)/\Gamma_{total}$ — Γ_{534}/Γ

VALUE	CL%	DOCUMENT ID	TECN	COMMENT
$<1.1\times10^{-4}$	90	[1,2] DYTMAN 02	CLE2	$e^+e^-\to\Upsilon(4S)$

[1] Assumes equal production of B^+ and B^0 at the $\Upsilon(4S)$.

[2] DYTMAN 02 measurement uses $B(\Lambda_c^-\to\overline{p}K^+\pi^-)=5.0\pm1.3\%$. The second error includes the systematic and the uncertainty of the branching ratio.

$\Gamma(\overline{\Xi}_c^-\Lambda_c^+)/\Gamma_{total}$ — Γ_{535}/Γ

VALUE (units 10^{-3})	DOCUMENT ID	TECN	COMMENT
$1.14\pm0.80\pm0.04$	[1,2] LI 19C	BELL	$e^+e^-\to\Upsilon(4S)$

[1] Uses fully reconstructed B^0 on tag side with recoil against Λ_c^+.

[2] LI 19C reports $(1.16\pm0.74\pm0.33)\times10^{-3}$ from a measurement of $[\Gamma(B^0\to\overline{\Xi}_c^-\Lambda_c^+)/\Gamma_{total}]\times[B(\Lambda_c^+\to pK^-\pi^+)]$ assuming $B(\Lambda_c^+\to pK^-\pi^+)=(6.28\pm0.32)\times10^{-2}$, which we rescale to our best (shown rounded) value $B(\Lambda_c^+\to pK^-\pi^+)=(6.37\pm0.21)\times10^{-2}$. Our first error is their experiment's error and our second error is the systematic error from using our best (shown rounded) value.

$\Gamma(\overline{\Xi}_c^-\Lambda_c^+,\ \overline{\Xi}_c^-\to\overline{\Xi}^+\pi^-\pi^-)/\Gamma_{total}$ — Γ_{536}/Γ

VALUE (units 10^{-5})	DOCUMENT ID	TECN	COMMENT
$2.3\ \pm1.0$ OUR AVERAGE Error includes scale factor of 1.8.			
$3.3\ \pm0.8\ \pm0.1$	[1] LI 19C	BELL	$e^+e^-\to\Upsilon(4S)$
$1.18\pm0.85\pm0.04$	[2,3] AUBERT 08H	BABR	$e^+e^-\to\Upsilon(4S)$
• • • We do not use the following data for averages, fits, limits, etc. • • •			
$7.3\ ^{+3.3}_{-2.7}\ \pm0.2$	[3,4] CHISTOV 06A	BELL	Repl. by LI 19C

[1] LI 19C reports $(3.32\pm0.74\pm0.33)\times10^{-5}$ from a measurement of $[\Gamma(B^0\to\overline{\Xi}_c^-\Lambda_c^+,\ \overline{\Xi}_c^-\to\overline{\Xi}^+\pi^-\pi^-)/\Gamma_{total}]\times[B(\Lambda_c^+\to pK^-\pi^+)]$ assuming $B(\Lambda_c^+\to pK^-\pi^+)=(6.28\pm0.32)\times10^{-2}$, which we rescale to our best (shown rounded) value $B(\Lambda_c^+\to pK^-\pi^+)=(6.37\pm0.21)\times10^{-2}$. Our first error is their experiment's error and our second error is the systematic error from using our best (shown rounded) value.

[2] AUBERT 08H reports $(1.5\pm1.07\pm0.44)\times10^{-5}$ from a measurement of $[\Gamma(B^0\to\overline{\Xi}_c^-\Lambda_c^+,\ \overline{\Xi}_c^-\to\overline{\Xi}^+\pi^-\pi^-)/\Gamma_{total}]\times[B(\Lambda_c^+\to pK^-\pi^+)]$ assuming $B(\Lambda_c^+\to pK^-\pi^+)=(5.0\pm1.3)\times10^{-2}$, which we rescale to our best (shown rounded) value $B(\Lambda_c^+\to pK^-\pi^+)=(6.37\pm0.21)\times10^{-2}$. Our first error is their experiment's error and our second error is the systematic error from using our best (shown rounded) value.

[3] Assumes equal production of B^+ and B^0 at the $\Upsilon(4S)$.

[4] CHISTOV 06A reports $(9.3^{+3.7}_{-2.8}\pm3.1)\times10^{-5}$ from a measurement of $[\Gamma(B^0\to\overline{\Xi}_c^-\Lambda_c^+,\ \overline{\Xi}_c^-\to\overline{\Xi}^+\pi^-\pi^-)/\Gamma_{total}]\times[B(\Lambda_c^+\to pK^-\pi^+)]$ assuming $B(\Lambda_c^+\to pK^-\pi^+)=(5.0\pm1.3)\times10^{-2}$, which we rescale to our best (shown rounded) value $B(\Lambda_c^+\to pK^-\pi^+)=(6.37\pm0.21)\times10^{-2}$. Our first error is their experiment's error and our second error is the systematic error from using our best (shown rounded) value.

$\Gamma(\overline{\Xi}_c^-\Lambda_c^+,\ \overline{\Xi}_c^-\to\overline{p}K^+\pi^-)/\Gamma_{total}$ — Γ_{537}/Γ

VALUE (units 10^{-6})	DOCUMENT ID	TECN	COMMENT
$5.2\pm1.6\pm0.2$	[1] LI 19C	BELL	$e^+e^-\to\Upsilon(4S)$

[1] LI 19C reports $(5.27\pm1.51\pm0.69)\times10^{-6}$ from a measurement of $[\Gamma(B^0\to\overline{\Xi}_c^-\Lambda_c^+,\ \overline{\Xi}_c^-\to\overline{p}K^+\pi^-)/\Gamma_{total}]\times[B(\Lambda_c^+\to pK^-\pi^+)]$ assuming $B(\Lambda_c^+\to pK^-\pi^+)=(6.28\pm0.32)\times10^{-2}$, which we rescale to our best (shown rounded) value $B(\Lambda_c^+\to pK^-\pi^+)=(6.37\pm0.21)\times10^{-2}$. Our first error is their experiment's error and our second error is the systematic error from using our best (shown rounded) value.

$\Gamma(\Lambda_c^+\Lambda_c^-K^0)/\Gamma_{total}$ — Γ_{538}/Γ

VALUE (units 10^{-4})	DOCUMENT ID	TECN	COMMENT
$4.0\ \pm0.9$ OUR AVERAGE			
$3.99\pm0.76\pm0.51$	[1] LI 18D	BELL	$e^+e^-\to\Upsilon(4S)$
$3.8\ \pm3.1\ \pm2.1$	[2,3] AUBERT 08H	BABR	$e^+e^-\to\Upsilon(4S)$
• • • We do not use the following data for averages, fits, limits, etc. • • •			
$7.9\ ^{+2.9}_{-2.3}\ \pm4.3$	[2,3] GABYSHEV 06	BELL	Repl. by LI 18D

[1] Assumes $B(\Upsilon(4S)\to B^0\overline{B}^0)=48.6\pm0.6\%$ and $B(\Lambda_c^+\to pK^-\pi^+)=6.23\pm0.33\%$.

[2] Assumes $B(\Lambda_c^+\to pK^-\pi^+)=5.0\pm1.3\%$.

[3] Assumes equal production of B^+ and B^0 at the $\Upsilon(4S)$.

$\Gamma(\overline{\Lambda}_c(2910)^-p,\ \overline{\Lambda}_c^-\to\overline{\Sigma}_c(2455)^{--}\pi^+)/\Gamma_{total}$ — Γ_{539}/Γ

VALUE (units 10^{-5})	DOCUMENT ID	TECN	COMMENT
$1.24\pm0.35\pm0.10$	LI 23E	BELL	$e^+e^-\to\Upsilon(4S)$

$\Gamma(\overline{\Lambda}_c(2910)^-p,\ \overline{\Lambda}_c^-\to\overline{\Sigma}_c(2455)^0\pi^-)/\Gamma_{total}$ — Γ_{540}/Γ

VALUE (units 10^{-6})	DOCUMENT ID	TECN	COMMENT
$9.5\pm3.6\pm1.6$	LI 23E	BELL	$e^+e^-\to\Upsilon(4S)$

$\Gamma(\overline{\Xi}_c(2930)^-\Lambda_c^+,\ \overline{\Xi}_c^-\to\Lambda_c^-K^0)/\Gamma_{total}$ — Γ_{541}/Γ

VALUE (units 10^{-4})	DOCUMENT ID	TECN	COMMENT
$2.37\pm0.51\pm0.31$	[1] LI 18D	BELL	$e^+e^-\to\Upsilon(4S)$

[1] Assumes $B(\Upsilon(4S)\to B^0\overline{B}^0)=48.6\pm0.6\%$ and $B(\Lambda_c^+\to pK^-\pi^+)=6.23\pm0.33\%$.

$\Gamma(\Omega_c^0\overline{\Lambda},\ \Omega_c^0\to\Omega^-\pi^+)/\Gamma_{total}$ — Γ_{542}/Γ

VALUE	CL%	DOCUMENT ID	TECN	COMMENT
$<9.7\times10^{-8}$	95	[1] SAVINOV 24	BELL	$e^+e^-\to\Upsilon(4S)$

[1] Uses $B(\Upsilon(4S)\to B^0\overline{B}^0)$ based on the CHOUDHURY 23 to estimate $N(B^0\overline{B}^0)$ pairs.

$\Gamma(\Omega_c(2770)^0\overline{\Lambda},\ \Omega_c^0\to\Omega^-\pi^+)/\Gamma_{total}$ — Γ_{543}/Γ

VALUE	CL%	DOCUMENT ID	TECN	COMMENT
$<3.12\times10^{-7}$	95	[1] SAVINOV 24	BELL	$e^+e^-\to\Upsilon(4S)$

[1] Uses $B(\Upsilon(4S)\to B^0\overline{B}^0)$ based on the CHOUDHURY 23 to estimate $N(B^0\overline{B}^0)$ pairs. $\Omega_c(2770)^0$ is partially reconstructed and assumed to exclusively decay to final states containing Ω_c^0.

$\Gamma(\Omega_c^0\Lambda,\ \Omega_c^0\to\Omega^-\pi^+)/\Gamma_{total}$ — Γ_{544}/Γ

VALUE	CL%	DOCUMENT ID	TECN	COMMENT
$<9.5\times10^{-8}$	95	[1] SAVINOV 24	BELL	$e^+e^-\to\Upsilon(4S)$

[1] Uses $B(\Upsilon(4S)\to B^0\overline{B}^0)$ based on the CHOUDHURY 23 to estimate $N(B^0\overline{B}^0)$ pairs.

Int. J. Mod. Phys. A 2026.41. Downloaded from www.worldscientific.com by LIFORNIA @ BERKELEY on 09/16/26. Re-use and distribution is strictly not permitted, except for Open Access articles.

$\Gamma(\Omega_c(2770)^0 \Lambda,\ \Omega_c^0 \to \Omega^- \pi^+)/\Gamma_{total}$ — Γ_{545}/Γ

VALUE	CL%	DOCUMENT ID		TECN	COMMENT
$<1.00 \times 10^{-7}$	95	[1] SAVINOV	24	BELL	$e^+e^- \to \Upsilon(4S)$

[1] Uses B($\Upsilon(4S) \to B^0\overline{B}^0$) based on the CHOUDHURY 23 to estimate N($B^0\overline{B}^0$) pairs. $\Omega_c(2770)^0$ is partially reconstructed and assumed to exclusively decay to final states containing Ω_c^0.

$\Gamma(\Lambda\psi_{DS})/\Gamma_{total}$ — Γ_{546}/Γ

VALUE	CL%	DOCUMENT ID		TECN	COMMENT
$< 0.13\text{–}5.2 \times 10^{-5}$	90	[1] LEES	23B	BABR	$e^+e^- \to \Upsilon(4S)$
• • • We do not use the following data for averages, fits, limits, etc. • • •					
$<2.1 \times 10^{-5}$	90	[2] HADJIVASILIOU	22	BELL	$e^+e^- \to \Upsilon(4S)$

[1] LEES 23B searched for ψ_{DS} in the recoil mass against Λ and the fully reconstructed accompanying B meson. The cited upper limit is for m(ψ_{DS}) between 1 and 4.1 GeV/c^2.

[2] HADJIVASILIOU 22 searched for ψ_{DS}, in the mass range 1–3.9 GeV/c^2, in the recoil mass against Λ and the accompanying B meson. The cited upper limit is for m(ψ_{DS}) = 2.0 GeV/c^2 and is the most stringent. The least stringent limit is $< 3.8 \times 10^{-5}$ at m(ψ_{DS}) = 3.9 GeV/c^2.

$\Gamma(\gamma\gamma)/\Gamma_{total}$ — Γ_{547}/Γ

Test for ΔB=1 weak neutral current. Allowed by higher-order electroweak interactions.

VALUE	CL%	DOCUMENT ID		TECN	COMMENT
$<6.4 \times 10^{-8}$	90	[1] ADACHI	24J	BEL2	$e^+e^- \to \Upsilon(4S)$
• • • We do not use the following data for averages, fits, limits, etc. • • •					
$<3.2 \times 10^{-7}$	90	[2] DEL-AMO-SA...	11A	BABR	$e^+e^- \to \Upsilon(4S)$
$<6.2 \times 10^{-7}$	90	[2] VILLA	06	BELL	Repl. by ADACHI 24J
$<1.7 \times 10^{-6}$	90	[2] AUBERT	01I	BABR	$e^+e^- \to \Upsilon(4S)$
$<3.9 \times 10^{-5}$	90	[3] ACCIARRI	95I	L3	$e^+e^- \to Z$

[1] Used combined Belle and Belle II data and B(Υ(4S) $\to B^0\overline{B}^0$) = (48.4 ± 1.2)%. A signal with 2.5σ significance, including systematic uncertainties, is observed, corresponding to a branching fraction $(3.7^{+2.2}_{-1.8} \pm 0.5) \times 10^{-8}$.

[2] Assumes equal production of B^+ and B^0 at the $\Upsilon(4S)$.

[3] ACCIARRI 95I assumes $f_{B^0} = 39.5 \pm 4.0$ and $f_{B_s} = 12.0 \pm 3.0$%.

$\Gamma(e^+e^-)/\Gamma_{total}$ — Γ_{548}/Γ

Test for ΔB=1 weak neutral current. Allowed by higher-order electroweak interactions.

VALUE	CL%	DOCUMENT ID		TECN	COMMENT
$< 2.5 \times 10^{-9}$	90	[1] AAIJ	20W	LHCB	pp at 7, 8, 13 TeV
• • • We do not use the following data for averages, fits, limits, etc. • • •					
$< 8.3 \times 10^{-8}$	90	AALTONEN	09P	CDF	$p\overline{p}$ at 1.96 TeV
$<11.3 \times 10^{-8}$	90	[2] AUBERT	08P	BABR	$e^+e^- \to \Upsilon(4S)$
$< 6.1 \times 10^{-8}$	90	[2] AUBERT	05W	BABR	Repl. by AUBERT 08P
$< 1.9 \times 10^{-7}$	90	[2] CHANG	03	BELL	$e^+e^- \to \Upsilon(4S)$
$< 8.3 \times 10^{-7}$	90	[2] BERGFELD	00B	CLE2	$e^+e^- \to \Upsilon(4S)$
$< 1.4 \times 10^{-5}$	90	[3] ACCIARRI	97B	L3	$e^+e^- \to Z$
$< 5.9 \times 10^{-6}$	90	AMMAR	94	CLE2	Repl. by BERGFELD 00B
$< 2.6 \times 10^{-5}$	90	[4] AVERY	89B	CLEO	$e^+e^- \to \Upsilon(4S)$
$< 7.6 \times 10^{-5}$	90	[5] ALBRECHT	87D	ARG	$e^+e^- \to \Upsilon(4S)$
$< 6.4 \times 10^{-5}$	90	[6] AVERY	87	CLEO	$e^+e^- \to \Upsilon(4S)$
$< 3 \times 10^{-4}$	90	GILES	84	CLEO	Repl. by AVERY 87

[1] Assumes no contribution from $B_s^0 \to e^+e^-$ decays.

[2] Assumes equal production of B^+ and B^0 at the $\Upsilon(4S)$.

[3] ACCIARRI 97B assume PDG 96 production fractions for B^+, B^0, B_s, and Λ_b.

[4] AVERY 89B reports $< 3 \times 10^{-5}$ assuming the $\Upsilon(4S)$ decays 43% to $B^0\overline{B}^0$. We rescale to 50%.

[5] ALBRECHT 87D reports $< 8.5 \times 10^{-5}$ assuming the $\Upsilon(4S)$ decays 45% to $B^0\overline{B}^0$. We rescale to 50%.

[6] AVERY 87 reports $< 8 \times 10^{-5}$ assuming the $\Upsilon(4S)$ decays 40% to $B^0\overline{B}^0$. We rescale to 50%.

$\Gamma(e^+e^-\gamma)/\Gamma_{total}$ — Γ_{549}/Γ

Test for ΔB=1 weak neutral current. Allowed by higher-order electroweak interactions.

VALUE	CL%	DOCUMENT ID		TECN	COMMENT
$<1.2 \times 10^{-7}$	90	AUBERT	08C	BABR	$e^+e^- \to \Upsilon(4S)$

$\Gamma(\mu^+\mu^-)/\Gamma_{total}$ — Γ_{550}/Γ

Test for ΔB=1 weak neutral current. Allowed by higher-order electroweak interactions.

VALUE (units 10^{-10})	CL%	DOCUMENT ID		TECN	COMMENT
< 1.5	90	[1,2] TUMASYAN	23A	CMS	pp at 13 TeV
• • • We do not use the following data for averages, fits, limits, etc. • • •					
$1.2^{+0.8}_{-0.7} \pm 0.1$		[3] AAIJ	22	LHCB	pp at 7, 8, 13 TeV
< 3.6	95	[4] SIRUNYAN	20AG		pp at 7, 8, 13 TeV
− 1.9 ± 1.6		[5,6] AABOUD	19L	ATLS	pp at 7, 8, 13 TeV
$1.5^{+1.2}_{-1.0} \pm^{0.2}_{0.1}$		[7] AAIJ	17AI	LHCB	Repl. by AAIJ 22
− 2.5 ± 2.0		[8] AABOUD	16L	ATLS	Repl. by AABOUD 19L
$3.9^{+1.6}_{-1.4}$		[9] KHACHATRY...	15BE	LHC	pp at 7, 8 TeV
< 8.0	90	[10] AAIJ	13B	LHCB	Repl. by AAIJ 13BA
< 6.3	90	[11] AAIJ	13BA	LHCB	Repl. by KHACHATRYAN 15BE
< 38	90	[12] AALTONEN	13F	CDF	$p\overline{p}$ at 1.96 TeV
$3.5^{+2.1}_{-1.8}$		[13] CHATRCHYAN	13AW	CMS	Repl. by SIRUNYAN 20AG
< 26	90	[10] AAIJ	12A	LHCB	Repl. by AAIJ 12W
< 8.1	90	[14] AAIJ	12W	LHCB	Repl. by AAIJ 13B
< 14	90	[14] CHATRCHYAN	12A	CMS	pp at 7 TeV
< 120	90	[15] AAIJ	11B	LHCB	Repl. by AAIJ 12A
< 50	90	[14] AALTONEN	11AG	CDF	$p\overline{p}$ at 1.96 TeV
< 37	90	[14] CHATRCHYAN	11T	CMS	Repl. by CHATRCHYAN 12A

[1] Corresponds to a 95% CL upper limit of $< 1.9 \times 10^{-10}$.

[2] Uses normalization mode B($B^+ \to J/\psi K^+$) = $(1.020 \pm 0.019) \times 10^{-3}$, B($J/\psi \to \mu^+\mu^-$) = $(5.961 \pm 0.033) \times 10^{-2}$.

[3] Corresponds to a 95% CL upper limit of $< 2.6 \times 10^{-10}$.

[4] Uses normalization mode B($B^+ \to J/\psi K^+$) = $(1.01 \pm 0.03) \times 10^{-3}$.

[5] Corresponds to a 95% CL upper limit of $< 2.1 \times 10^{-10}$.

[6] Uses normalization mode B($B^+ \to J/\psi K^+$) = $(1.010 \pm 0.029) \times 10^{-3}$ and B production ratio f($b \to B_s^0$)/f($b \to B^0$) = 0.256 ± 0.013.

[7] Corresponds to a 95% CL upper limit of $< 3.4 \times 10^{-10}$.

[8] This value is obtained from a profile-likelihood fit, see Fig. 9. It corresponds to an uppper limit of $< 0.42 \times 10^{-9}$ at 95% C.L.

[9] Derived from the combined fit to CMS and LHCb data. Uncertainty includes both statistical and systematic component. Also reports B($B^0 \to \mu^+\mu^-$)/B($B_s \to \mu^+\mu^-$) = $0.14^{+0.08}_{-0.06}$.

[10] Uses B($B^+ \to J/\psi K^+ \to \mu^+\mu^- K^+$) = $(6.01 \pm 0.21) \times 10^{-5}$ and B($B^0 \to K^+\pi^-$) = $(1.94 \pm 0.06) \times 10^{-5}$ for normalization.

[11] Reports also a limit of $< 7.4 \times 10^{-10}$ at 95% CL. Uses normalization modes $B^+ \to J/\psi K^+ \to \mu^+\mu^- K^+$ and $B^0 \to K^+\pi^-$.

[12] Uses normalization mode B($B^+ \to J/\psi K^+$) = $(10.22 \pm 0.35) \times 10^{-4}$.

[13] Reports also a limit of $< 9.2 \times 10^{-10}$ at 90% CL. and uses B($B^+ \to J/\psi K^+ \to \mu^+\mu^- K^+$) = $(6.0 \pm 0.2) \times 10^{-5}$ for normalization.

[14] Uses B($B^+ \to J/\psi K^+ \to \mu^+\mu^- K^+$) = $(6.01 \pm 0.21) \times 10^{-5}$.

[15] Uses B production ratio f($\overline{b} \to B^+$)/f($\overline{b} \to B_s^0$) = 3.71 ± 0.47 and three normalization modes.

$\Gamma(\mu^+\mu^-\gamma)/\Gamma_{total}$ — Γ_{551}/Γ

Test for ΔB=1 weak neutral current. Allowed by higher-order electroweak interactions.

VALUE	CL%	DOCUMENT ID		TECN	COMMENT
$<1.6 \times 10^{-7}$	90	AUBERT	08C	BABR	$e^+e^- \to \Upsilon(4S)$

$\Gamma(\tau^+\tau^-)/\Gamma_{total}$ — Γ_{555}/Γ

Test for ΔB=1 weak neutral current. Allowed by higher-order electroweak interactions.

VALUE	CL%	DOCUMENT ID		TECN	COMMENT
$<2.1 \times 10^{-3}$	95	[1] AAIJ	17AJ	LHCB	pp at 7, 8 TeV
• • • We do not use the following data for averages, fits, limits, etc. • • •					
$<4.1 \times 10^{-3}$	90	[2] AUBERT	06S	BABR	$e^+e^- \to \Upsilon(4S)$

[1] Assuming no contribution from $B_s^0 \to \tau^+\tau^-$.

[2] Assumes equal production of B^+ and B^0 at the $\Upsilon(4S)$.

$\Gamma(\mu^+\mu^-\mu^+\mu^-)/\Gamma_{total}$ — Γ_{552}/Γ

VALUE	CL%	DOCUMENT ID		TECN	COMMENT
$<1.8 \times 10^{-10}$	95	AAIJ	22Q	LHCB	pp at 7, 8, 13 TeV
• • • We do not use the following data for averages, fits, limits, etc. • • •					
$<6.9 \times 10^{-10}$	95	AAIJ	17N	LHCB	pp at 7, 8 TeV
$<6.6 \times 10^{-9}$	95	[1] AAIJ	13AW	LHCB	Repl. by AAIJ 17N

[1] Also reports a limit of $< 5.3 \times 10^{-9}$ at 90% CL.

$\Gamma(S P,\ S \to \mu^+\mu^-,\ P \to \mu^+\mu^-)/\Gamma_{total}$ — Γ_{553}/Γ

Here S and P are the hypothetical scalar and pseudoscalar particles with masses of 2.5 GeV/c^2 and 214.3 MeV/c^2, respectively.

VALUE	CL%	DOCUMENT ID		TECN	COMMENT
$<6.0 \times 10^{-10}$	95	AAIJ	17N	LHCB	pp at 7, 8 TeV
• • • We do not use the following data for averages, fits, limits, etc. • • •					
$<5.1 \times 10^{-9}$	90	[1] AAIJ	13AW	LHCB	Repl. by AAIJ 17N

[1] Also reports a limit of $< 6.3 \times 10^{-9}$ at 95% CL.

$\Gamma(a a,\ a \to \mu^+\mu^-)/\Gamma_{total}$ — Γ_{554}/Γ

Here particle a is a scalar with a mass of 1 GeV/c^2.

VALUE	CL%	DOCUMENT ID		TECN	COMMENT
$<2.3 \times 10^{-10}$	95	AAIJ	22Q	LHCB	pp at 7, 8, 13 TeV

$\Gamma(\pi^0\ell^+\ell^-)/\Gamma_{total}$ — Γ_{556}/Γ

VALUE	CL%	DOCUMENT ID		TECN	COMMENT
$<3.8 \times 10^{-8}$	90	[1] ADACHI	24N	BELL	$e^+e^- \to \Upsilon(4S)$
• • • We do not use the following data for averages, fits, limits, etc. • • •					
$<5.3 \times 10^{-8}$	90	[2] LEES	13M	BABR	$e^+e^- \to \Upsilon(4S)$
$<1.5 \times 10^{-7}$	90	[2] WEI	08A	BELL	$e^+e^- \to \Upsilon(4S)$
$<1.2 \times 10^{-7}$	90	[2] AUBERT	07AG	BABR	Repl. by LEES 13M

[1] Where $\ell = e,\ \mu$.

[2] Assumes equal production of B^+ and B^0 at the $\Upsilon(4S)$.

$\Gamma(\pi^0\nu\overline{\nu})/\Gamma_{total}$ — Γ_{566}/Γ

Test for $\Delta B = 1$ weak neutral current. Allowed by higher-order electroweak interaction.

VALUE	CL%	DOCUMENT ID		TECN	COMMENT
$<0.9 \times 10^{-5}$	90	[1] GRYGIER	17	BELL	$e^+e^- \to \Upsilon(4S)$

Int. J. Mod. Phys. A 2026.41. Downloaded from www.worldscientific.com
by UNIVERSITY OF CALIFORNIA @ BERKELEY on 09/16/26. Re-use and distribution is strictly not permitted, except for Open Access articles.

• • • We do not use the following data for averages, fits, limits, etc. • • •

$<6.9\times10^{-5}$	90	[1] LUTZ	13	BELL	$e^+e^-\to\Upsilon(4S)$
$<2.2\times10^{-4}$	90	[1] CHEN	07D	BELL	Repl. by LUTZ 13

[1] Assumes equal production of B^+ and B^0 at the $\Upsilon(4S)$.

$\Gamma(\pi^0 e^+ e^-)/\Gamma_{total}$ — Γ_{557}/Γ

VALUE	CL%	DOCUMENT ID		TECN	COMMENT
$<7.9\times10^{-8}$	90	ADACHI	24N	BELL	$e^+e^-\to\Upsilon(4S)$

• • • We do not use the following data for averages, fits, limits, etc. • • •

$<8.4\times10^{-8}$	90	[1] LEES	13M	BABR	$e^+e^-\to\Upsilon(4S)$
$<2.3\times10^{-7}$	90	[1] WEI	08A	BELL	$e^+e^-\to\Upsilon(4S)$
$<1.4\times10^{-7}$	90	[1] AUBERT	07AG	BABR	Repl. by LEES 13M

[1] Assumes equal production of B^+ and B^0 at the $\Upsilon(4S)$.

$\Gamma(\pi^0\mu^+\mu^-)/\Gamma_{total}$ — Γ_{558}/Γ

VALUE	CL%	DOCUMENT ID		TECN	COMMENT
$<5.9\times10^{-8}$	90	ADACHI	24N	BELL	$e^+e^-\to\Upsilon(4S)$

• • • We do not use the following data for averages, fits, limits, etc. • • •

$<6.9\times10^{-8}$	90	[1] LEES	13M	BABR	$e^+e^-\to\Upsilon(4S)$
$<1.8\times10^{-7}$	90	[1] WEI	08A	BELL	$e^+e^-\to\Upsilon(4S)$
$<5.1\times10^{-7}$	90	[1] AUBERT	07AG	BABR	$e^+e^-\to\Upsilon(4S)$

[1] Assumes equal production of B^+ and B^0 at the $\Upsilon(4S)$.

$\Gamma(\eta\ell^+\ell^-)/\Gamma_{total}$ — Γ_{559}/Γ

VALUE	CL%	DOCUMENT ID		TECN	COMMENT
$<4.8\times10^{-8}$	90	[1] ADACHI	24N	BELL	$e^+e^-\to\Upsilon(4S)$

• • • We do not use the following data for averages, fits, limits, etc. • • •

$<6.4\times10^{-8}$	90	[2] LEES	13M	BABR	$e^+e^-\to\Upsilon(4S)$

[1] Where $\ell = e,\ \mu$.
[2] Assumes equal production of B^+ and B^0 at the $\Upsilon(4S)$.

$\Gamma(\eta e^+ e^-)/\Gamma_{total}$ — Γ_{560}/Γ

VALUE	CL%	DOCUMENT ID		TECN	COMMENT
$<10.5\times10^{-8}$	90	ADACHI	24N	BELL	$e^+e^-\to\Upsilon(4S)$

• • • We do not use the following data for averages, fits, limits, etc. • • •

$<10.8\times10^{-8}$	90	[1] LEES	13M	BABR	$e^+e^-\to\Upsilon(4S)$

[1] Assumes equal production of B^+ and B^0 at the $\Upsilon(4S)$.

$\Gamma(\eta\mu^+\mu^-)/\Gamma_{total}$ — Γ_{561}/Γ

VALUE	CL%	DOCUMENT ID		TECN	COMMENT
$<9.4\times10^{-8}$	90	ADACHI	24N	BELL	$e^+e^-\to\Upsilon(4S)$

• • • We do not use the following data for averages, fits, limits, etc. • • •

$<11.2\times10^{-8}$	90	[1] LEES	13M	BABR	$e^+e^-\to\Upsilon(4S)$

[1] Assumes equal production of B^+ and B^0 at the $\Upsilon(4S)$.

$\Gamma(\rho(770)^0 e^+ e^-)/\Gamma_{total}$ — Γ_{562}/Γ

VALUE	CL%	DOCUMENT ID		TECN	COMMENT
$<45.5\times10^{-8}$	90	ADACHI	24N	BELL	$e^+e^-\to\Upsilon(4S)$

$\Gamma(\omega e^+ e^-)/\Gamma_{total}$ — Γ_{563}/Γ

VALUE	CL%	DOCUMENT ID		TECN	COMMENT
$<30.7\times10^{-8}$	90	ADACHI	24N	BELL	$e^+e^-\to\Upsilon(4S)$

$\Gamma(\omega\mu^+\mu^-)/\Gamma_{total}$ — Γ_{564}/Γ

VALUE	CL%	DOCUMENT ID		TECN	COMMENT
$<24.9\times10^{-8}$	90	ADACHI	24N	BELL	$e^+e^-\to\Upsilon(4S)$

$\Gamma(\omega\ell^+\ell^-)/\Gamma_{total}$ — Γ_{565}/Γ

VALUE	CL%	DOCUMENT ID		TECN	COMMENT
$<22.0\times10^{-8}$	90	[1] ADACHI	24N	BELL	$e^+e^-\to\Upsilon(4S)$

[1] Where $\ell = e,\ \mu$.

$\Gamma(K^0\ell^+\ell^-)/\Gamma_{total}$ — Γ_{567}/Γ

VALUE (units 10^{-7})	CL%	DOCUMENT ID		TECN	COMMENT
3.3 ± 0.6 OUR AVERAGE					
$3.51^{+0.69}_{-0.60}\pm0.10$		CHOUDHURY	21	BELL	$e^+e^-\to\Upsilon(4S)$
$2.1^{+1.5}_{-1.3}\pm0.2$		[1] AUBERT	09T	BABR	$e^+e^-\to\Upsilon(4S)$
• • • We do not use the following data for averages, fits, limits, etc. • • •					
$3.4^{+0.9}_{-0.8}\pm0.2$		[1,2] WEI	09A	BELL	$e^+e^-\to\Upsilon(4S)$
$2.9^{+1.6}_{-1.3}\pm0.3$		[1] AUBERT,B	06J	BABR	Repl. by AUBERT 09T
<6.8	90	[1] ISHIKAWA	03	BELL	$e^+e^-\to\Upsilon(4S)$

[1] Assumes equal production of B^0 and B^+ at $\Upsilon(4S)$.
[2] Superseded by CHOUDHURY 21.

$\Gamma(K^0 e^+ e^-)/\Gamma_{total}$ — Γ_{568}/Γ

Test for ΔB=1 weak neutral current. Allowed by higher-order electroweak interactions.

VALUE (units 10^{-7})	CL%	DOCUMENT ID		TECN	COMMENT
$2.5^{+1.1}_{-0.9}$ OUR AVERAGE Error includes scale factor of 1.3.					
$3.1^{+1.0}_{-0.9}\pm0.08$		CHOUDHURY	21	BELL	$e^+e^-\to\Upsilon(4S)$
$0.8^{+1.5}_{-1.2}\pm0.1$		[1] AUBERT	09T	BABR	$e^+e^-\to\Upsilon(4S)$
• • • We do not use the following data for averages, fits, limits, etc. • • •					
$2.0^{+1.4}_{-1.0}\pm0.1$		[1,2] WEI	09A	BELL	$e^+e^-\to\Upsilon(4S)$
$1.3^{+1.6}_{-1.1}\pm0.2$		[1] AUBERT,B	06J	BABR	Repl. by AUBERT 09T
$-\ 2.1^{+2.3}_{-1.6}\pm0.8$		[1] AUBERT	03U	BABR	$e^+e^-\to\Upsilon(4S)$
$<\ 5.4$	90	[3] ISHIKAWA	03	BELL	$e^+e^-\to\Upsilon(4S)$
$<\ 27$	90	[1] ABE	02	BELL	Repl. by ISHIKAWA 03
$<\ 38$	90	[1] AUBERT	02L	BABR	$e^+e^-\to\Upsilon(4S)$
$<\ 84.5$	90	[4] ANDERSON	01B	CLE2	$e^+e^-\to\Upsilon(4S)$
$<\ 3000$	90	ALBRECHT	91E	ARG	$e^+e^-\to\Upsilon(4S)$
$<\ 5200$	90	[5] AVERY	87	CLEO	$e^+e^-\to\Upsilon(4S)$

[1] Assumes equal production of B^+ and B^0 at the $\Upsilon(4S)$.
[2] Superseded by CHOUDHURY 21.
[3] Assumes equal production of B^0 and B^+ at $\Upsilon(4S)$.
[4] The result is for di-lepton masses above 0.5 GeV.
[5] AVERY 87 reports $<6.5\times10^{-4}$ assuming the $\Upsilon(4S)$ decays 40% to $B^0\overline{B}^0$. We rescale to 50%.

$\Gamma(K^0\nu\overline{\nu})/\Gamma_{total}$ — Γ_{570}/Γ

Test for $\Delta B = 1$ weak neutral current. Allowed by higher-order electroweak interaction.

VALUE	CL%	DOCUMENT ID		TECN	COMMENT
$<2.6\times10^{-5}$	90	[1] GRYGIER	17	BELL	$e^+e^-\to\Upsilon(4S)$

• • • We do not use the following data for averages, fits, limits, etc. • • •

$<4.9\times10^{-5}$	90	[1,2] LEES	13I	BABR	$e^+e^-\to\Upsilon(4S)$
$<19.4\times10^{-5}$	90	[1] LUTZ	13	BELL	$e^+e^-\to\Upsilon(4S)$
$<5.6\times10^{-5}$	90	[1] DEL-AMO-SA...10Q		BABR	Repl. by LEES 13I
$<1.6\times10^{-4}$	90	[1] CHEN	07D	BELL	$e^+e^-\to\Upsilon(4S)$

[1] Assumes equal production of B^+ and B^0 at the $\Upsilon(4S)$.
[2] Also reported a limit $<8.1\times10^{-5}$ at 90% CL obtained using a fully reconstructed hadronic B-tag evnets.

$\Gamma(\rho^0\nu\overline{\nu})/\Gamma_{total}$ — Γ_{571}/Γ

Test for $\Delta B = 1$ weak neutral current. Allowed by higher-order electroweak interaction.

VALUE	CL%	DOCUMENT ID		TECN	COMMENT
$<4.0\ \times10^{-5}$	90	[1] GRYGIER	17	BELL	$e^+e^-\to\Upsilon(4S)$

• • • We do not use the following data for averages, fits, limits, etc. • • •

$<2.08\times10^{-4}$	90	[1] LUTZ	13	BELL	$e^+e^-\to\Upsilon(4S)$
$<4.4\ \times10^{-4}$	90	[1] CHEN	07D	BELL	Repl. by LUTZ 13

[1] Assumes equal production of B^+ and B^0 at the $\Upsilon(4S)$.

$\Gamma(K^0\mu^+\mu^-)/\Gamma_{total}$ — Γ_{569}/Γ

Test for ΔB=1 weak neutral current. Allowed by higher-order electroweak interactions.

VALUE (units 10^{-7})	CL%	DOCUMENT ID		TECN	COMMENT
3.39 ± 0.35 OUR FIT Error includes scale factor of 1.1.					
3.39 ± 0.35 OUR AVERAGE					
$3.9^{+1.0}_{-0.8}\pm0.3$		CHOUDHURY	21	BELL	$e^+e^-\to\Upsilon(4S)$
$3.27\pm0.34\pm0.17$		[1] AAIJ	14M	LHCB	pp at 7, 8 TeV
$4.9^{+2.9}_{-2.5}\pm0.3$		[2] AUBERT	09T	BABR	$e^+e^-\to\Upsilon(4S)$
• • • We do not use the following data for averages, fits, limits, etc. • • •					
$3.1^{+0.7}_{-0.6}$		AAIJ	12AH	LHCB	Repl. by AAIJ 14M
$4.4^{+1.3}_{-1.1}\pm0.3$		[2,3] WEI	09A	BELL	$e^+e^-\to\Upsilon(4S)$
$5.9^{+3.3}_{-2.6}\pm0.7$		[2] AUBERT,B	06J	BABR	Repl. by AUBERT 09T
$1.63^{+0.82}_{-0.63}\pm0.14$		[2] AUBERT	03U	BABR	Repl. by AUBERT,B 06J
$5.6^{+2.9}_{-2.3}\pm0.5$		[4] ISHIKAWA	03	BELL	Repl. by WEI 09A
<33	90	[2] ABE	02	BELL	Repl. by ISHIKAWA 03
<36	90	AUBERT	02L	BABR	$e^+e^-\to\Upsilon(4S)$
<66.4	90	[5] ANDERSON	01B	CLE2	$e^+e^-\to\Upsilon(4S)$
<5200	90	ALBRECHT	91E	ARG	$e^+e^-\to\Upsilon(4S)$
<3600	90	[6] AVERY	87	CLEO	$e^+e^-\to\Upsilon(4S)$

[1] Uses $B(B^0\to J/\psi(1S)K^0) = (0.928\pm0.013\pm0.037)\times10^{-3}$ for normalization.
[2] Assumes equal production of B^+ and B^0 at the $\Upsilon(4S)$.
[3] Superseded by CHOUDHURY 21.
[4] Assumes equal production of B^0 and B^+ at $\Upsilon(4S)$. The second error is a total of systematic uncertainties including model dependence.
[5] The result is for di-lepton masses above 0.5 GeV.
[6] AVERY 87 reports $<4.5\times10^{-4}$ assuming the $\Upsilon(4S)$ decays 40% to $B^0\overline{B}^0$. We rescale to 50%.

$\Gamma(K^0\mu^+\mu^-)/\Gamma(J/\psi(1S)K^0)$ — $\Gamma_{569}/\Gamma_{214}$

VALUE (units 10^{-3})	DOCUMENT ID		TECN	COMMENT
0.38 ± 0.04 OUR FIT Error includes scale factor of 1.1.				
$0.37\pm0.12\pm0.02$	AALTONEN	11AI	CDF	$p\overline{p}$ at 1.96 TeV

$\Gamma(K^*(892)^0\ell^+\ell^-)/\Gamma_{total}$ — Γ_{572}/Γ

Test for ΔB=1 weak neutral current. Allowed by higher-order electroweak interactions.

VALUE (units 10^{-7})	DOCUMENT ID		TECN	COMMENT
$9.9^{+1.2}_{-1.1}$ OUR AVERAGE				
$10.3^{+2.2}_{-2.1}\pm0.7$	[1] AUBERT	09T	BABR	$e^+e^-\to\Upsilon(4S)$

Int. J. Mod. Phys. A 2026.41. Downloaded from www.worldscientific.com by LIFORNIA @ BERKELEY on 09/16/26. Re-use and distribution is strictly not permitted, except for Open Access articles.

$9.7^{+1.3}_{-1.1}\pm0.7$	[1] WEI	09A	BELL	$e^+e^-\to\Upsilon(4S)$
• • • We do not use the following data for averages, fits, limits, etc. • • •				
$8.1^{+2.1}_{-1.9}\pm0.9$	[1] AUBERT,B	06J	BABR	Repl. by AUBERT 09T
$11.7^{+3.0}_{-2.7}\pm0.9$	[1] ISHIKAWA	03	BELL	Repl. by WEI 09A

[1] Assumes equal production of B^0 and B^+ at $\Upsilon(4S)$.

$\Gamma(K^*(892)^0 e^+ e^-)/\Gamma_{total}$ — Γ_{573}/Γ

Test for ΔB=1 weak neutral current. Allowed by higher-order electroweak interactions.

VALUE (units 10^{-7})	CL%	DOCUMENT ID		TECN	COMMENT
$10.3^{+1.9}_{-1.7}$ OUR AVERAGE					
$8.6^{+2.6}_{-2.4}\pm0.5$		[1] AUBERT	09T	BABR	$e^+e^-\to\Upsilon(4S)$
$11.8^{+2.7}_{-2.2}\pm0.9$		[1] WEI	09A	BELL	$e^+e^-\to\Upsilon(4S)$
• • • We do not use the following data for averages, fits, limits, etc. • • •					
$10.4^{+3.3}_{-2.9}\pm1.1$		[1] AUBERT,B	06J	BABR	Repl. by AUBERT 09T
$11.1^{+5.6}_{-4.7}\pm1.1$		[1] AUBERT	03U	BABR	$e^+e^-\to\Upsilon(4S)$
$<$ 24	90	[2] ISHIKAWA	03	BELL	$e^+e^-\to\Upsilon(4S)$
$<$ 64	90	[1] ABE	02	BELL	Repl. by ISHIKAWA 03
$<$ 67	90	[1] AUBERT	02L	BABR	$e^+e^-\to\Upsilon(4S)$
$<$2900	90	ALBRECHT	91E	ARG	$e^+e^-\to\Upsilon(4S)$

[1] Assumes equal production of B^+ and B^0 at the $\Upsilon(4S)$.
[2] Assumes equal production of B^0 and B^+ at $\Upsilon(4S)$.

$\Gamma(K^*(892)^0 \mu^+ \mu^-)/\Gamma_{total}$ — Γ_{574}/Γ

Test for ΔB=1 weak neutral current. Allowed by higher-order electroweak interactions.

VALUE (units 10^{-7})	CL%	DOCUMENT ID		TECN	COMMENT
9.4 ±0.5 OUR FIT					
9.4 ±0.6 OUR AVERAGE					
$9.04^{+0.16}_{-0.15}\pm0.62$		[1] AAIJ	17Q	LHCB	pp at 7, 8 TeV
$13.5\ ^{+4.0}_{-3.7}\ \pm1.0$		[2] AUBERT	09T	BABR	$e^+e^-\to\Upsilon(4S)$
$10.6\ ^{+1.9}_{-1.4}\ \pm0.7$		[2] WEI	09A	BELL	$e^+e^-\to\Upsilon(4S)$
• • • We do not use the following data for averages, fits, limits, etc. • • •					
$10.36^{+0.18}_{-0.17}\pm0.71$		[1] AAIJ	16AO	LHCB	Repl. by AAIJ 17Q
$8.7\ ^{+3.8}_{-3.3}\ \pm1.2$		[2] AUBERT,B	06J	BABR	Repl. by AUBERT 09T
$8.6\ ^{+7.9}_{-5.8}\ \pm1.1$		[2] AUBERT	03U	BABR	Repl. by AUBERT,B 06J
$13.3\ ^{+4.2}_{-3.7}\ \pm1.1$		[3] ISHIKAWA	03	BELL	Repl. by WEI 09A
$<$42	90	[2] ABE	02	BELL	$e^+e^-\to\Upsilon(4S)$
$<$33	90	AUBERT	02L	BABR	$e^+e^-\to\Upsilon(4S)$
$<$40	90	[4] AFFOLDER	99B	CDF	$p\overline{p}$ at 1.8 TeV

[1] Uses $B(B^0\to J/\psi K^*(892)^0)=(1.19\pm0.01\pm0.08)\times10^{-3}$. The second error is the total systematic uncertainty.
[2] Assumes equal production of B^+ and B^0 at the $\Upsilon(4S)$.
[3] Assumes equal production of B^0 and B^+ at $\Upsilon(4S)$. The second error is a total of systematic uncertainties including model dependence.
[4] AFFOLDER 99B measured relative to $B^0\to J/\psi(1S)K^*(892)^0$.

$\Gamma(K^*(892)^0 \mu^+ \mu^-)/\Gamma(J/\psi(1S)K^*(892)^0)$ — $\Gamma_{574}/\Gamma_{216}$

VALUE (units 10^{-3})	DOCUMENT ID		TECN	COMMENT
0.75±0.05 OUR FIT				
0.77±0.08±0.03	AALTONEN	11AI	CDF	$p\overline{p}$ at 1.96 TeV
• • • We do not use the following data for averages, fits, limits, etc. • • •				
0.80±0.10±0.06	AALTONEN	11L	CDF	Repl. by AALTONEN 11AI
0.61±0.23±0.07	AALTONEN	09B	CDF	Repl. by AALTONEN 11L

$\Gamma(K^*(892)^0 \chi,\ \chi\to\mu^+\mu^-)/\Gamma_{total}$ — Γ_{575}/Γ

VALUE	CL%	DOCUMENT ID		TECN	COMMENT
$<\sim10^{-9}$	95	[1] AAIJ	15AZ	LHCB	pp at 7, 8 TeV

[1] The limt is obtained as a function of di-muon mass. A normalizing mode branching fraction value of $B(B^0\to K^{*0}\mu^+\mu^-)=(1.6\pm0.3)\times10^{-7}$ is used.

$\Gamma(K^*(892)^0 \tau^+ \tau^-)/\Gamma_{total}$ — Γ_{576}/Γ

VALUE	CL%	DOCUMENT ID		TECN	COMMENT
$<1.8\times10^{-3}$	90	ADACHI	25V	BEL2	$e^+e^-\to\Upsilon(4S)$
• • • We do not use the following data for averages, fits, limits, etc. • • •					
$<3.1\times10^{-3}$	90	[1] DONG	23	BELL	$e^+e^-\to\Upsilon(4S)$

[1] Uses full reconstruction of companion neutral B.

$\Gamma(\overline{D}^0 \mu^+ \mu^-)/\Gamma_{total}$ — Γ_{577}/Γ

VALUE	CL%	DOCUMENT ID		TECN	COMMENT
$<4.0\times10^{-8}$	90	AAIJ	24F	LHCB	pp at 7, 8, 13 TeV

$\Gamma(\pi^+\pi^-\mu^+\mu^-)/\Gamma_{total}$ — Γ_{578}/Γ

VALUE (units 10^{-8})	DOCUMENT ID		TECN	COMMENT
2.1±0.5±0.1	[1] AAIJ	15S	LHCB	pp at 7, 8 TeV

[1] AAIJ 15S reports (2.11 ± 0.51 ± 0.15 ± 0.16) × 10^{-8} from a measurement of $[\Gamma(B^0\to\pi^+\pi^-\mu^+\mu^-)/\Gamma_{total}]$ / $[B(B^0\to J/\psi(1S)K^*(892)^0)]$ assuming $B(B^0\to J/\psi(1S)K^*(892)^0)=(1.3\pm0.1)\times10^{-3}$, which we rescale to our best (shown rounded) value $B(B^0\to J/\psi(1S)K^*(892)^0)=(1.27\pm0.05)\times10^{-3}$. Our first error is their experiment's error and our second error is the systematic error from using our best (shown rounded) value.

$\Gamma(K^*(892)^0 \nu\overline{\nu})/\Gamma_{total}$ — Γ_{579}/Γ

Test for ΔB=1 weak neutral current. Allowed by higher-order electroweak interactions.

VALUE	CL%	DOCUMENT ID		TECN	COMMENT
$<1.8\times10^{-5}$	90	[1] GRYGIER	17	BELL	$e^+e^-\to\Upsilon(4S)$
• • • We do not use the following data for averages, fits, limits, etc. • • •					
$<1.2\times10^{-4}$	90	[1,2] LEES	13I	BABR	$e^+e^-\to\Upsilon(4S)$
$<5.5\times10^{-5}$	90	[1] LUTZ	13	BELL	$e^+e^-\to\Upsilon(4S)$
$<1.2\times10^{-4}$	90	AUBERT	08BC	BABR	Repl. by LEES 13I
$<3.4\times10^{-4}$	90	[1] CHEN	07D	BELL	$e^+e^-\to\Upsilon(4S)$
$<1.0\times10^{-3}$	90	[3] ADAM	96D	DLPH	$e^+e^-\to Z$

[1] Assumes equal production of B^+ and B^0 at the $\Upsilon(4S)$.
[2] Also reported a limit $<9.3\times10^{-5}$ at 90% CL obtained using a fully reconstructed hadronic B-tag evnets.
[3] ADAM 96D assumes $f_{B^0}=f_{B^-}=0.39$ and $f_{B_s}=0.12$.

$\Gamma(\text{invisible})/\Gamma_{total}$ — Γ_{580}/Γ

VALUE	CL%	DOCUMENT ID		TECN	COMMENT
$<2.4\times10^{-5}$	90	[1] LEES	12T	BABR	$e^+e^-\to\Upsilon(4S)$
• • • We do not use the following data for averages, fits, limits, etc. • • •					
$<1.4\times10^{-4}$	90	[2] ALONSO-ALV...24		THEO	$e^+e^-\to Z$
$<7.8\times10^{-5}$	90	[3] KU	20	BELL	$e^+e^-\to\Upsilon(4S)$
$<13\times10^{-5}$	90	[4] HSU	12	BELL	$e^+e^-\to\Upsilon(4S)$
$<22\times10^{-5}$	90	[1] AUBERT,B	04J	BABR	$e^+e^-\to\Upsilon(4S)$

[1] Uses the fully reconstructed $B^0\to D^{(*)-}\ell^+\nu_\ell$ events as a tag.
[2] A reinterpretation of an old inclusive ALEPH search for b-hadron decays with large missing energy reported in BARATE 01E.
[3] Identified by fully reconstructing a hadronic decay of the accompanying B meson.
[4] Identified by fully reconstructing a hadronic decay of the accompanying B meson and requiring no other particles in the event.

$\Gamma(\nu\overline{\nu}\gamma)/\Gamma_{total}$ — Γ_{581}/Γ

VALUE (units 10^{-5})	CL%	DOCUMENT ID		TECN	COMMENT
<1.6	90	[1] KU	20	BELL	$e^+e^-\to\Upsilon(4S)$
• • • We do not use the following data for averages, fits, limits, etc. • • •					
<1.7	90	[2] LEES	12T	BABR	$e^+e^-\to\Upsilon(4S)$
<4.7	90	[2] AUBERT,B	04J	BABR	Repl. by LEES 12T

[1] Identified by fully reconstructing a hadronic decay of the accompanying B meson.
[2] Uses the fully reconstructed $B^0\to D^{(*)-}\ell^+\nu_\ell$ events as a tag.

$\Gamma(\phi\mu^+\mu^-)/\Gamma_{total}$ — Γ_{582}/Γ

VALUE	CL%	DOCUMENT ID		TECN	COMMENT
$<3.2\times10^{-9}$	90	[1] AAIJ	22S	LHCB	pp at 7, 8, 13 TeV

[1] Using $B(B^0_s\to\phi\mu^+\mu^-)$ as normalization. The limit is set for the full q^2 phase space.

$\Gamma(\phi\nu\overline{\nu})/\Gamma_{total}$ — Γ_{583}/Γ

Test for $\Delta B=1$ weak neutral current. Allowed by higher-order electroweak interaction.

VALUE	CL%	DOCUMENT ID		TECN	COMMENT
$<1.27\times10^{-4}$	90	[1] LUTZ	13	BELL	$e^+e^-\to\Upsilon(4S)$
• • • We do not use the following data for averages, fits, limits, etc. • • •					
$<5.8\times10^{-5}$	90	[1] CHEN	07D	BELL	Repl. by LUTZ 13

[1] Assumes equal production of B^+ and B^0 at the $\Upsilon(4S)$.

$\Gamma(e^\pm\mu^\mp)/\Gamma_{total}$ — Γ_{584}/Γ

Test of lepton family number conservation. Allowed by higher-order electroweak interactions.

VALUE	CL%	DOCUMENT ID		TECN	COMMENT
$<1.0\times10^{-9}$	90	[1] AAIJ	18T	LHCB	pp at 7, 8 TeV
• • • We do not use the following data for averages, fits, limits, etc. • • •					
$<2.8\times10^{-9}$	90	[2] AAIJ	13BM	LHCB	Repl. by AAIJ 18T
$<6.4\times10^{-8}$	90	AALTONEN	09P	CDF	$p\overline{p}$ at 1.96 TeV
$<9.2\times10^{-8}$	90	[3] AUBERT	08P	BABR	$e^+e^-\to\Upsilon(4S)$
$<1.8\times10^{-7}$	90	[3] AUBERT	05W	BABR	$e^+e^-\to\Upsilon(4S)$
$<1.7\times10^{-7}$	90	[3] CHANG	03	BELL	$e^+e^-\to\Upsilon(4S)$
$<15\times10^{-7}$	90	[3] BERGFELD	00B	CLE2	$e^+e^-\to\Upsilon(4S)$
$<3.5\times10^{-6}$	90	ABE	98V	CDF	$p\overline{p}$ at 1.8 TeV
$<1.6\times10^{-5}$	90	[4] ACCIARRI	97B	L3	$e^+e^-\to Z$
$<5.9\times10^{-6}$	90	AMMAR	94	CLE2	$e^+e^-\to\Upsilon(4S)$
$<3.4\times10^{-5}$	90	[5] AVERY	89B	CLEO	$e^+e^-\to\Upsilon(4S)$
$<4.5\times10^{-5}$	90	[6] ALBRECHT	87D	ARG	$e^+e^-\to\Upsilon(4S)$
$<7.7\times10^{-5}$	90	[7] AVERY	87	CLEO	$e^+e^-\to\Upsilon(4S)$
$<3\times10^{-4}$	90	GILES	84	CLEO	Repl. by AVERY 87

[1] AAIJ 18T uses normalization modes $B(B^0\to K^+\pi^-)=(19.6\pm0.5)\times10^{-6}$ and $B(B^+\to J/\psi K^+)=(1.026\pm0.031)\times10^{-3}$.
[2] Uses normalization mode $B(B^0\to K^+\pi^-)=(19.4\pm0.6)\times10^{-6}$.
[3] Assumes equal production of B^+ and B^0 at the $\Upsilon(4S)$.

[4] ACCIARRI 97B assume PDG 96 production fractions for B^+, B^0, B_s, and Λ_b.
[5] Paper assumes the $\Upsilon(4S)$ decays 43% to $B^0\overline{B}^0$. We rescale to 50%.
[6] ALBRECHT 87D reports $< 5 \times 10^{-5}$ assuming the $\Upsilon(4S)$ decays 45% to $B^0\overline{B}^0$. We rescale to 50%.
[7] AVERY 87 reports $< 9 \times 10^{-5}$ assuming the $\Upsilon(4S)$ decays 40% to $B^0\overline{B}^0$. We rescale to 50%.

$\Gamma(\pi^0 e^\pm \mu^\mp)/\Gamma_{total}$ — Γ_{585}/Γ

VALUE	CL%	DOCUMENT ID		TECN	COMMENT
$<1.4 \times 10^{-7}$	90	[1] AUBERT	07AG	BABR	$e^+e^- \to \Upsilon(4S)$

[1] Assumes equal production of B^+ and B^0 at the $\Upsilon(4S)$.

$\Gamma(K^0 e^\pm \mu^\mp)/\Gamma_{total}$ — Γ_{586}/Γ

Test of lepton family number conservation.

VALUE	CL%	DOCUMENT ID		TECN	COMMENT
$< 3.8 \times 10^{-8}$	90	CHOUDHURY	21	BELL	$e^+e^- \to \Upsilon(4S)$
• • • We do not use the following data for averages, fits, limits, etc. • • •					
$< 2.7 \times 10^{-7}$	90	[1] AUBERT,B	06J	BABR	$e^+e^- \to \Upsilon(4S)$
$<40 \times 10^{-7}$	90	[1] AUBERT	02L	BABR	Repl. by AUBERT,B 06J

[1] Assumes equal production of B^+ and B^0 at the $\Upsilon(4S)$.

$\Gamma(K^0_S \tau^+ e^-)/\Gamma_{total}$ — Γ_{587}/Γ

VALUE	CL%	DOCUMENT ID		TECN	COMMENT
$<1.5 \times 10^{-5}$	90	[1] ADACHI	25B	BELL	$e^+e^- \to \Upsilon(4S)$

[1] Uses tagging of the companion B meson in fully hadronic decay modes

$\Gamma(K^0_S \tau^- e^+)/\Gamma_{total}$ — Γ_{588}/Γ

VALUE	CL%	DOCUMENT ID		TECN	COMMENT
$<0.8 \times 10^{-5}$	90	[1] ADACHI	25B	BELL	$e^+e^- \to \Upsilon(4S)$

[1] Uses the tagging of the companion B meson in hadronic decays modes

$\Gamma(K^0_S \tau^+ \mu^-)/\Gamma_{total}$ — Γ_{589}/Γ

VALUE	CL%	DOCUMENT ID		TECN	COMMENT
$<1.1 \times 10^{-5}$	90	[1] ADACHI	25B	BELL	$e^+e^- \to \Upsilon(4S)$

[1] Uses the tagging of the companion B meson in hadronic decays modes

$\Gamma(K^0_S \tau^- \mu^+)/\Gamma_{total}$ — Γ_{590}/Γ

VALUE	CL%	DOCUMENT ID		TECN	COMMENT
$<3.6 \times 10^{-5}$	90	[1] ADACHI	25B	BELL	$e^+e^- \to \Upsilon(4S)$

[1] Uses the tagging of the companion B meson in hadronic decays modes

$\Gamma(K^*(892)^0 e^+ \mu^-)/\Gamma_{total}$ — Γ_{591}/Γ

VALUE	CL%	DOCUMENT ID		TECN	COMMENT
$<6.8 \times 10^{-9}$	90	[1] AAIJ	23G	LHCB	pp at 7, 8, 13 TeV
• • • We do not use the following data for averages, fits, limits, etc. • • •					
$<1.6 \times 10^{-7}$	90	[2] SANDILYA	18	BELL	$e^+e^- \to \Upsilon(4S)$
$<5.3 \times 10^{-7}$	90	[3] AUBERT,B	06J	BABR	$e^+e^- \to \Upsilon(4S)$

[1] Uses the uniform phase space model for the signal decays.
[2] Uses $B(\Upsilon(4S) \to B^0\overline{B}^0) = 0.486 \pm 0.006$.
[3] Assumes equal production of B^0 and B^+ at $\Upsilon(4S)$.

$\Gamma(K^*(892)^0 e^- \mu^+)/\Gamma_{total}$ — Γ_{592}/Γ

VALUE	CL%	DOCUMENT ID		TECN	COMMENT
$<5.7 \times 10^{-9}$	90	[1] AAIJ	23G	LHCB	pp at 7, 8, 13 TeV
• • • We do not use the following data for averages, fits, limits, etc. • • •					
$<1.2 \times 10^{-7}$	90	[2] SANDILYA	18	BELL	$e^+e^- \to \Upsilon(4S)$
$<3.4 \times 10^{-7}$	90	[3] AUBERT,B	06J	BABR	$e^+e^- \to \Upsilon(4S)$

[1] Uses the uniform phase space model for the signal decays.
[2] Uses $B(\Upsilon(4S) \to B^0\overline{B}^0) = 0.486 \pm 0.006$.
[3] Assumes equal production of B^0 and B^+ at $\Upsilon(4S)$.

$\Gamma(K^*(892)^0 e^\pm \mu^\mp)/\Gamma_{total}$ — Γ_{593}/Γ

Test of lepton family number conservation.

VALUE	CL%	DOCUMENT ID		TECN	COMMENT
$< 1.01 \times 10^{-8}$	90	[1] AAIJ	23G	LHCB	pp at 7, 8, 13 TeV
• • • We do not use the following data for averages, fits, limits, etc. • • •					
$< 1.8 \times 10^{-7}$	90	[2] SANDILYA	18	BELL	$e^+e^- \to \Upsilon(4S)$
$< 5.8 \times 10^{-7}$	90	[3] AUBERT,B	06J	BABR	$e^+e^- \to \Upsilon(4S)$
$<34 \times 10^{-7}$	90	[3] AUBERT	02L	BABR	Repl. by AUBERT,B 06J

[1] Uses the uniform phase space model for the signal decays.
[2] Uses $B(\Upsilon(4S) \to B^0\overline{B}^0) = 0.486 \pm 0.006$.
[3] Assumes equal production of B^+ and B^0 at the $\Upsilon(4S)$.

$\Gamma(K^*(892)^0 \tau^+ e^-)/\Gamma_{total}$ — Γ_{594}/Γ

VALUE	CL%	DOCUMENT ID		TECN	COMMENT
$<4.9 \times 10^{-6}$	90	AAIJ	25AR	LHCB	pp at 13 TeV
• • • We do not use the following data for averages, fits, limits, etc. • • •					
$<2.9 \times 10^{-5}$	90	[1] ADACHI	25S	BELL	$e^+e^- \to \Upsilon(4S)$

[1] Uses $B(\Upsilon(4S) \to B^0\overline{B}^0) = 0.4861 \pm 0.0080$.

$\Gamma(K^*(892)^0 \tau^- e^+)/\Gamma_{total}$ — Γ_{595}/Γ

VALUE	CL%	DOCUMENT ID		TECN	COMMENT
$<5.9 \times 10^{-6}$	90	AAIJ	25AR	LHCB	pp at 13 TeV
• • • We do not use the following data for averages, fits, limits, etc. • • •					
$<6.4 \times 10^{-5}$	90	[1] ADACHI	25S	BELL	$e^+e^- \to \Upsilon(4S)$

[1] Uses $B(\Upsilon(4S) \to B^0\overline{B}^0) = 0.4861 \pm 0.0080$.

$\Gamma(K^*(892)^0 \tau^+ \mu^-)/\Gamma_{total}$ — Γ_{596}/Γ

VALUE	CL%	DOCUMENT ID		TECN	COMMENT
$<1.0 \times 10^{-5}$	90	[1] AAIJ	23F	LHCB	pp at 7, 8, 13 TeV
• • • We do not use the following data for averages, fits, limits, etc. • • •					
$<4.2 \times 10^{-5}$	90	[2] ADACHI	25S	BELL	$e^+e^- \to \Upsilon(4S)$

[1] Using $B^0 \to D^- D_s^+$ as normalisation decay.
[2] Uses $B(\Upsilon(4S) \to B^0\overline{B}^0) = 0.4861 \pm 0.0080$.

$\Gamma(K^*(892)^0 \tau^- \mu^+)/\Gamma_{total}$ — Γ_{597}/Γ

VALUE	CL%	DOCUMENT ID		TECN	COMMENT
$<8.2 \times 10^{-6}$	90	[1] AAIJ	23F	LHCB	pp at 7, 8, 13 TeV
• • • We do not use the following data for averages, fits, limits, etc. • • •					
$<5.6 \times 10^{-5}$	90	[2] ADACHI	25S	BELL	$e^+e^- \to \Upsilon(4S)$

[1] Using $B^0 \to D^- D_s^+$ as normalisation decay.
[2] Uses $B(\Upsilon(4S) \to B^0\overline{B}^0) = 0.4861 \pm 0.0080$.

$\Gamma(e^\pm \tau^\mp)/\Gamma_{total}$ — Γ_{598}/Γ

Test of lepton family number conservation. Allowed by higher-order electroweak interactions.

VALUE	CL%	DOCUMENT ID		TECN	COMMENT
$<1.6 \times 10^{-5}$	90	[1] ATMACAN	21	BELL	$e^+e^- \to \Upsilon(4S)$
• • • We do not use the following data for averages, fits, limits, etc. • • •					
$<2.8 \times 10^{-5}$	90	[2] AUBERT	08AD	BABR	$e^+e^- \to \Upsilon(4S)$
$<1.1 \times 10^{-4}$	90	BORNHEIM	04	CLE2	$e^+e^- \to \Upsilon(4S)$
$<5.3 \times 10^{-4}$	90	AMMAR	94	CLE2	Repl. by BORNHEIM 04

[1] Uses events in which one B meson is fully reconstructed in a hadronic decay mode.
[2] Assumes equal production of B^+ and B^0 at the $\Upsilon(4S)$.

$\Gamma(\mu^\pm \tau^\mp)/\Gamma_{total}$ — Γ_{599}/Γ

Test of lepton family number conservation. Allowed by higher-order electroweak interactions.

VALUE	CL%	DOCUMENT ID		TECN	COMMENT
$<1.4 \times 10^{-5}$	95	[1] AAIJ	19AK	LHCB	pp at 7, 8 TeV
• • • We do not use the following data for averages, fits, limits, etc. • • •					
$<1.5 \times 10^{-5}$	90	[2] ATMACAN	21	BELL	$e^+e^- \to \Upsilon(4S)$
$<2.2 \times 10^{-5}$	90	[3] AUBERT	08AD	BABR	$e^+e^- \to \Upsilon(4S)$
$<3.8 \times 10^{-5}$	90	BORNHEIM	04	CLE2	$e^+e^- \to \Upsilon(4S)$
$<8.3 \times 10^{-4}$	90	AMMAR	94	CLE2	Repl. by BORNHEIM 04

[1] Assuming no contribution from $B^0_s \to \mu^\pm \tau^\mp$.
[2] Uses events in which one B meson is fully reconstructed in a hadronic decay mode.
[3] Assumes equal production of B^+ and B^0 at the $\Upsilon(4S)$.

$\Gamma(p\mu^-)/\Gamma_{total}$ — Γ_{600}/Γ

VALUE	CL%	DOCUMENT ID		COMMENT
$<2.6 \times 10^{-9}$	90	[1] AAIJ	23Y	pp at 7, 8, 13 TeV

[1] Assumes that B^0 decay branching fractions to $p\mu^-$ and $\overline{p}\mu^+$ are the same.

$\Gamma(\Lambda_c^+ \mu^-)/\Gamma_{total}$ — Γ_{601}/Γ

VALUE	CL%	DOCUMENT ID		TECN	COMMENT
$<1.4 \times 10^{-6}$	90	[1,2] DEL-AMO-SA...11K		BABR	$e^+e^- \to \Upsilon(4S)$

[1] DEL-AMO-SANCHEZ 11K reports $< 180 \times 10^{-8}$ from a measurement of $[\Gamma(B^0 \to \Lambda_c^+ \mu^-)/\Gamma_{total}] \times [B(\Lambda_c^+ \to pK^-\pi^+)]$ assuming $B(\Lambda_c^+ \to pK^-\pi^+) = (5.0 \pm 1.3) \times 10^{-2}$, which we rescale to our best (shown rounded) value $B(\Lambda_c^+ \to pK^-\pi^+) = 6.37 \times 10^{-2}$.
[2] Uses $B(\Upsilon(4S) \to B^0\overline{B}^0) = (51.6 \pm 0.6)\%$ and $B(\Upsilon(4S) \to B^+B^-) = (48.4 \pm 0.6)\%$.

$\Gamma(\Lambda_c^+ e^-)/\Gamma_{total}$ — Γ_{602}/Γ

VALUE	CL%	DOCUMENT ID		TECN	COMMENT
$<4 \times 10^{-6}$	90	[1,2] DEL-AMO-SA...11K		BABR	$e^+e^- \to \Upsilon(4S)$

[1] DEL-AMO-SANCHEZ 11K reports $< 520 \times 10^{-8}$ from a measurement of $[\Gamma(B^0 \to \Lambda_c^+ e^-)/\Gamma_{total}] \times [B(\Lambda_c^+ \to pK^-\pi^+)]$ assuming $B(\Lambda_c^+ \to pK^-\pi^+) = (5.0 \pm 1.3) \times 10^{-2}$, which we rescale to our best (shown rounded) value $B(\Lambda_c^+ \to pK^-\pi^+) = 6.37 \times 10^{-2}$.
[2] Uses $B(\Upsilon(4S) \to B^0\overline{B}^0) = (51.6 \pm 0.6)\%$ and $B(\Upsilon(4S) \to B^+B^-) = (48.4 \pm 0.6)\%$.

B^0_s CROSS-PARTICLE BRANCHING RATIOS

$\Gamma([K^+K^-]_D K^*(892)^0)/\Gamma_{total} \times B(B^0_s \to [K^+K^-]_D K^*(892)^0)$ — $\Gamma_{155}/\Gamma \times B$

VALUE	DOCUMENT ID		TECN	COMMENT
$0.10 \pm 0.02 \pm 0.01$	AAIJ	14BN	LHCB	pp at 7, 8 TeV

Int. J. Mod. Phys. A 2026.41. Downloaded from www.worldscientific.com
by UNIVERSITY OF CALIFORNIA @ BERKELEY on 09/16/26. Re-use and distribution is strictly not permitted, except for Open Access articles.

Int. J. Mod. Phys. A 2026.41. Downloaded from www.worldscientific.com by UNIVERSITY OF CALIFORNIA @ BERKELEY on 09/16/26. Re-use and distribution is strictly not permitted, except for Open Access articles.

$\Gamma([\pi^+\pi^-]_D K^*(892)^0)/\Gamma_{total} \times B(B^0_s \to [\pi^+\pi^-]_D K^*(892)^0)$ $\Gamma_{156}/\Gamma \times B$

VALUE	DOCUMENT ID		TECN	COMMENT
0.15±0.04±0.01	AAIJ	14BN	LHCB	pp at 7, 8 TeV

See the related review(s):
Polarization in B Decays

POLARIZATION IN B^0 DECAY

In decays involving two vector mesons, one can distinguish among the states in which meson polarizations are both longitudinal (L) or both are transverse and parallel ($\|$) or perpendicular ($\perp$) to each other with the parameters Γ_L/Γ, $\Gamma_\perp/\Gamma$, and the relative phases $\phi_\|$ and $\phi_\perp$. See the definitions in the note on "Polarization in B Decays" review in the B^0 Particle Listings.

Γ_L/Γ in $B^0 \to J/\psi(1S)K^*(892)^0$

VALUE	EVTS	DOCUMENT ID		TECN	COMMENT
0.571±0.007 OUR AVERAGE					
0.572±0.006±0.014		[1] AAIJ	13AT	LHCB	pp at 7 TeV
0.587±0.011±0.013		[2] ABAZOV	09E	D0	$p\overline{p}$ at 1.96 TeV
0.556±0.009±0.010		[3] AUBERT	07AD	BABR	$e^+e^- \to \Upsilon(4S)$
0.562±0.026±0.018		ACOSTA	05	CDF	$p\overline{p}$ at 1.96 TeV
0.574±0.012±0.009		ITOH	05	BELL	$e^+e^- \to \Upsilon(4S)$
0.59 ±0.06 ±0.01		[4] AFFOLDER	00N	CDF	$p\overline{p}$ at 1.8 TeV
0.52 ±0.07 ±0.04		[5] JESSOP	97	CLE2	$e^+e^- \to \Upsilon(4S)$
0.65 ±0.10 ±0.04	65	ABE	95Z	CDF	$p\overline{p}$ at 1.8 TeV
0.97 ±0.16 ±0.15	13	[6] ALBRECHT	94G	ARG	$e^+e^- \to \Upsilon(4S)$
• • • We do not use the following data for averages, fits, limits, etc. • • •					
0.566±0.012±0.005		[3] AUBERT	05P	BABR	Repl. by AUBERT 07AD
0.62 ±0.02 ±0.03		[7] ABE	02N	BELL	Repl. by ITOH 05
0.597±0.028±0.024		[8] AUBERT	01H	BABR	Repl. by AUBERT 07AD
0.80 ±0.08 ±0.05	42	[6] ALAM	94	CLE2	Sup. by JESSOP 97

[1] AAIJ 13AT obtains $\Gamma_\|/\Gamma = 0.227 \pm 0.004 \pm 0.011$. The relation $1 = (\Gamma_L + \Gamma_\perp + \Gamma_\|)/\Gamma$ is used to obtain Γ_L/Γ.
[2] Measured the angular and lifetime parameters for the time-dependent angular untagged decays $B^0_d \to J/\psi K^{*0}$ and $B^0_s \to J/\psi\phi$.
[3] Obtained by combining the B^0 and B^+ modes.
[4] AFFOLDER 00N measurements are based on 190 B^0 candidates obtained from a data sample of 89 pb^{-1}. The P-wave fraction is found to be $0.13^{+0.12}_{-0.09} \pm 0.06$.
[5] JESSOP 97 is the average over a mixture of B^0 and B^+ decays. The P-wave fraction is found to be $0.16 \pm 0.08 \pm 0.04$.
[6] Averaged over an admixture of B^0 and B^+ decays.
[7] Averaged over an admixture of B^0 and B^+ decays and the P wave fraction is $(19 \pm 2 \pm 3)\%$.
[8] Averaged over an admixture of B^0 and B^- decays and the P wave fraction is $(16.0 \pm 3.2 \pm 1.4) \times 10^{-2}$.

$\Gamma_\perp/\Gamma$ in $B^0 \to J/\psi K^{*0}$

VALUE	DOCUMENT ID		TECN	COMMENT
0.211±0.008 OUR AVERAGE	Error includes scale factor of 1.3. See the ideogram below.			
0.201±0.004±0.008	AAIJ	13AT	LHCB	pp at 7 TeV
0.230±0.013±0.025	[1] ABAZOV	09E	D0	$p\overline{p}$ at 1.96 TeV
0.233±0.010±0.005	[2] AUBERT	07AD	BABR	$e^+e^- \to \Upsilon(4S)$
0.215±0.032±0.006	ACOSTA	05	CDF	$p\overline{p}$ at 1.96 TeV
0.195±0.012±0.008	ITOH	05	BELL	$e^+e^- \to \Upsilon(4S)$

[1] Measured the angular and lifetime parameters for the time-dependent angular untagged decays $B^0_d \to J/\psi K^{*0}$ and $B^0_s \to J/\psi\phi$.
[2] Obtained by combining the B^0 and B^+ modes.

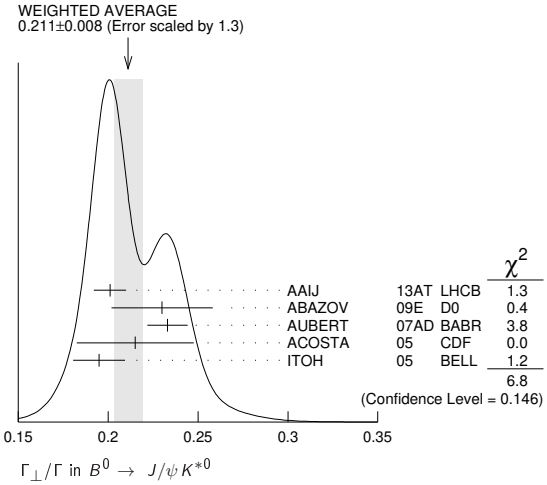

$\phi_\|$ in $B^0 \to J/\psi K^{*0}$

VALUE (rad)	DOCUMENT ID		TECN	COMMENT
−2.92±0.04 OUR AVERAGE	Error includes scale factor of 1.3. See the ideogram below.			
−2.94±0.02±0.03	AAIJ	13AT	LHCB	pp at 7 TeV
−2.69±0.08±0.11	[1] ABAZOV	09E	D0	$p\overline{p}$ at 1.96 TeV
−2.93±0.08±0.04	[2] AUBERT	07AD	BABR	$e^+e^- \to \Upsilon(4S)$

[1] Obtained $\phi_\|$ as $\delta_2 - \delta_1$, assuming they are uncorrelated.
[2] Obtained by combining the B^0 and B^+ modes.

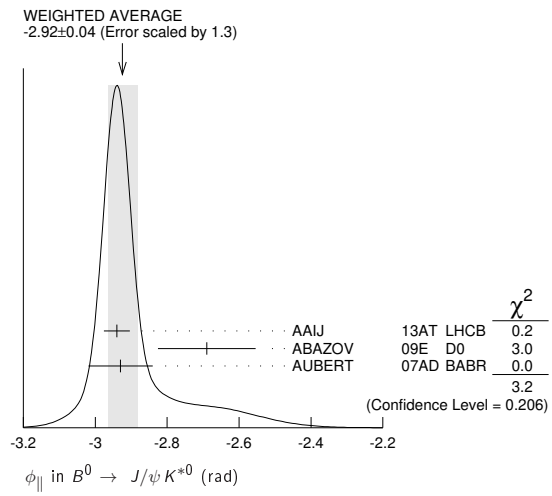

$\phi_\perp$ in $B^0 \to J/\psi K^{*0}$

VALUE (rad)	DOCUMENT ID		TECN	COMMENT
2.96±0.05 OUR AVERAGE	Error includes scale factor of 2.2. See the ideogram below.			
2.94±0.02±0.02	AAIJ	13AT	LHCB	pp at 7 TeV
3.21±0.06±0.06	ABAZOV	09E	D0	$p\overline{p}$ at 1.96 TeV
2.91±0.05±0.03	[1] AUBERT	07AD	BABR	$e^+e^- \to \Upsilon(4S)$

[1] Obtained by combining the B^0 and B^+ modes.

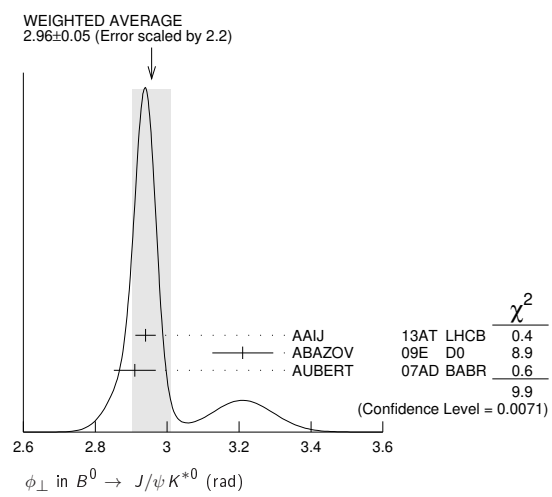

Γ_L/Γ in $B^0 \to \psi(2S)K^*(892)^0$

VALUE	DOCUMENT ID		TECN	COMMENT
$0.463^{+0.028}_{-0.040}$ OUR AVERAGE				
$0.455^{+0.031}_{-0.029}{}^{+0.014}_{-0.049}$	CHILIKIN	13	BELL	$e^+e^- \to \Upsilon(4S)$
0.48 ±0.05 ±0.02	[1] AUBERT	07AD	BABR	$e^+e^- \to \Upsilon(4S)$
0.45 ±0.11 ±0.04	[2] RICHICHI	01	CLE2	$e^+e^- \to \Upsilon(4S)$
• • • We do not use the following data for averages, fits, limits, etc. • • •				
$0.448^{+0.040}_{-0.027}{}^{+0.040}_{-0.053}$	MIZUK	09	BELL	$e^+e^- \to \Upsilon(4S)$

[1] Obtained by combining the B^0 and B^+ modes.
[2] Averages between charged and neutral B mesons.

$\Gamma_\perp/\Gamma$ in $B^0 \to \psi(2S)K^{*0}$

VALUE	DOCUMENT ID		TECN	COMMENT
0.30±0.06±0.02	[1] AUBERT	07AD	BABR	$e^+e^- \to \Upsilon(4S)$

[1] Obtained by combining the B^0 and B^+ modes.

Int. J. Mod. Phys. A 2026.41. Downloaded from www.worldscientific.com
by UNIVERSITY OF CALIFORNIA @ BERKELEY on 09/16/26. Re-use and distribution is strictly not permitted, except for Open Access articles.

$\phi_{\parallel}$ in $B^0 \to \psi(2S) K^{*0}$

VALUE (rad)	DOCUMENT ID		TECN	COMMENT
$-2.8 \pm 0.4 \pm 0.1$	[1] AUBERT	07AD	BABR	$e^+e^- \to \Upsilon(4S)$

[1] Obtained by combining the B^0 and B^+ modes.

$\phi_{\perp}$ in $B^0 \to \psi(2S) K^{*0}$

VALUE (rad)	DOCUMENT ID		TECN	COMMENT
$2.8 \pm 0.3 \pm 0.1$	[1] AUBERT	07AD	BABR	$e^+e^- \to \Upsilon(4S)$

[1] Obtained by combining the B^0 and B^+ modes.

Γ_L/Γ in $B^0 \to \chi_{c1} K^*(892)^0$

VALUE	DOCUMENT ID		TECN	COMMENT
$0.83^{+0.06}_{-0.08}$ OUR AVERAGE Error includes scale factor of 1.3.				
$0.947^{+0.038+0.046}_{-0.048-0.099}$	MIZUK	08	BELL	$e^+e^- \to \Upsilon(4S)$
$0.77 \pm 0.07 \pm 0.04$	[1] AUBERT	07AD	BABR	$e^+e^- \to \Upsilon(4S)$

[1] Obtained by combining the B^0 and B^+ modes.

$\Gamma_{\perp}/\Gamma$ in $B^0 \to \chi_{c1} K^*(892)^0$

VALUE	DOCUMENT ID		TECN	COMMENT
$0.03 \pm 0.04 \pm 0.02$	[1] AUBERT	07AD	BABR	$e^+e^- \to \Upsilon(4S)$

[1] Obtained by combining the B^0 and B^+ modes.

$\phi_{\parallel}$ in $B^0 \to \chi_{c1} K^*(892)^0$

VALUE (rad)	DOCUMENT ID		TECN	COMMENT
$0.0 \pm 0.3 \pm 0.1$	[1] AUBERT	07AD	BABR	$e^+e^- \to \Upsilon(4S)$

[1] Obtained by combining the B^0 and B^+ modes.

Γ_L/Γ in $B^0 \to D^{*-} \ell^+ \nu_\ell$

VALUE	DOCUMENT ID		TECN	COMMENT
$0.487 \pm 0.017 \pm 0.005$	PRIM	23	BELL	$e^+e^- \to \Upsilon(4S)$

Γ_L/Γ in $B^0 \to D^{*-} e^+ \nu_e$

VALUE	DOCUMENT ID		TECN	COMMENT
0.516 ± 0.013 OUR AVERAGE Error includes scale factor of 1.9.				
$0.520 \pm 0.005 \pm 0.005$	ADACHI	23J	BELL	$e^+e^- \to \Upsilon(4S)$
$0.471 \pm 0.024 \pm 0.007$	PRIM	23	BELL	$e^+e^- \to \Upsilon(4S)$

Γ_L/Γ in $B^0 \to D^{*-} \mu^+ \nu_\mu$

VALUE	DOCUMENT ID		TECN	COMMENT
0.525 ± 0.007 OUR AVERAGE				
$0.527 \pm 0.005 \pm 0.005$	ADACHI	23J	BELL	$e^+e^- \to \Upsilon(4S)$
$0.504 \pm 0.023 \pm 0.007$	PRIM	23	BELL	$e^+e^- \to \Upsilon(4S)$

$\Delta(\Gamma_L/\Gamma)$ in $B^0 \to D^{*-} \ell^+ \nu_\ell$

$\Delta(\Gamma_L/\Gamma) = (\Gamma_L/\Gamma)^{\mu} - (\Gamma_L/\Gamma)^{e}$

VALUE	DOCUMENT ID		TECN	COMMENT
0.008 ± 0.008 OUR AVERAGE				
$0.006 \pm 0.007 \pm 0.005$	ADACHI	23J	BELL	$e^+e^- \to \Upsilon(4S)$
$0.033 \pm 0.033 \pm 0.010$	PRIM	23	BELL	$e^+e^- \to \Upsilon(4S)$

Γ_L/Γ in $B^0 \to D^{*-} \tau^+ \nu_\tau$

VALUE	DOCUMENT ID		TECN	COMMENT
$0.41 \pm 0.06 \pm 0.03$	AAIJ	24AN	LHCB	pp at 7, 8, 13 TeV
• • • We do not use the following data for averages, fits, limits, etc. • • •				
$0.52 \pm 0.07 \pm 0.04$	[1] AAIJ	24AN	LHCB	pp at 7, 8, 13 TeV
$0.34 \pm 0.08 \pm 0.02$	[2] AAIJ	24AN	LHCB	pp at 7, 8, 13 TeV

[1] AAIJ 24AN value restricted to $q^2 < 7.0$ GeV$^2/c^4$. Reports correlation of -0.18 with the measurement in the region $q^2 > 7.0$ GeV$^2/c^4$.
[2] AAIJ 24AN value restricted to $q^2 > 7.0$ GeV$^2/c^4$. Reports correlation of -0.18 with the measurement in the region $q^2 < 7.0$ GeV$^2/c^4$.

Γ_L/Γ in $B^0 \to D_s^{*+} D^{*-}$

VALUE	DOCUMENT ID		TECN	COMMENT
0.574 ± 0.014 OUR AVERAGE				
$0.578 \pm 0.010 \pm 0.011$	[1] AAIJ	21S	LHCB	pp at 13 TeV
$0.519 \pm 0.050 \pm 0.028$	[2] AUBERT	03I	BABR	$e^+e^- \to \Upsilon(4S)$
$0.506 \pm 0.139 \pm 0.036$	AHMED	00B	CLE2	$e^+e^- \to \Upsilon(4S)$

[1] AAIJ 21S uses $D_s^{*+} \to D_s^+ \gamma$ decays.
[2] Measurement performed using partial reconstruction of D^{*-} decay.

$|H_+|$ in $B^0 \to D_s^{*+} D^{*-}$

H_+, H_- define parity-even ($\parallel$) and parity-odd ($\perp$) polarization transversity amplitudes $A_{\parallel,\perp} = (H_+ \pm H_-)/\sqrt{2}$.

VALUE	DOCUMENT ID		TECN	COMMENT
$0.195 \pm 0.022 \pm 0.032$	[1] AAIJ	21S	BELL	pp at 13 TeV

[1] AAIJ 21S uses $D_s^{*+} \to D_s^+ \gamma$ decays.

$|H_-|$ in $B^0 \to D_s^{*+} D^{*-}$

H_+, H_- define parity-even ($\parallel$) and parity-odd ($\perp$) polarization transversity amplitudes $A_{\parallel,\perp} = (H_+ \pm H_-)/\sqrt{2}$.

VALUE	DOCUMENT ID		TECN	COMMENT
$0.620 \pm 0.011 \pm 0.013$	[1] AAIJ	21S	LHCB	pp at 13 TeV

[1] AAIJ 21S uses $D_s^{*+} \to D_s^+ \gamma$ decays.

ϕ_+ in $B^0 \to D_s^{*+} D^{*-}$

VALUE	DOCUMENT ID		TECN	COMMENT
$-0.046 \pm 0.102 \pm 0.020$	[1] AAIJ	21S	LHCB	pp at 13 TeV

[1] AAIJ 21S uses $D_s^{*+} \to D_s^+ \gamma$ decays.

ϕ_- in $B^0 \to D_s^{*+} D^{*-}$

VALUE	DOCUMENT ID		TECN	COMMENT
$0.108 \pm 0.170 \pm 0.051$	[1] AAIJ	21S	LHCB	pp at 13 TeV

[1] AAIJ 21S uses $D_s^{*+} \to D_s^+ \gamma$ decays.

Γ_L/Γ in $B^0 \to D^{*-} \rho^+$

VALUE	EVTS	DOCUMENT ID		TECN	COMMENT
$0.885 \pm 0.016 \pm 0.012$		CSORNA	03	CLE2	$e^+e^- \to \Upsilon(4S)$
• • • We do not use the following data for averages, fits, limits, etc. • • •					
$0.93 \pm 0.05 \pm 0.05$	76	ALAM	94	CLE2	$e^+e^- \to \Upsilon(4S)$

Γ_L/Γ in $B^0 \to D_s^{*+} \rho^-$

VALUE	DOCUMENT ID		TECN	COMMENT
$0.84^{+0.26}_{-0.28} \pm 0.13$	[1] AUBERT	08AJ	BABR	$e^+e^- \to \Upsilon(4S)$

[1] Assumes equal production of B^+ and B^0 at the $\Upsilon(4S)$.

Γ_L/Γ in $B^0 \to D_s^{*+} K^{*-}$

VALUE	DOCUMENT ID		TECN	COMMENT
$0.92^{+0.37}_{-0.31} \pm 0.07$	[1] AUBERT	08AJ	BABR	$e^+e^- \to \Upsilon(4S)$

[1] Assumes equal production of B^+ and B^0 at the $\Upsilon(4S)$.

Γ_L/Γ in $B^0 \to D^{*+} D^{*-}$

VALUE	DOCUMENT ID		TECN	COMMENT
$0.624 \pm 0.029 \pm 0.011$	KRONENBIT...	12	BELL	$e^+e^- \to \Upsilon(4S)$
• • • We do not use the following data for averages, fits, limits, etc. • • •				
$0.57 \pm 0.08 \pm 0.02$	MIYAKE	05	BELL	Repl. by KRONENBITTER 12

$\Gamma_{\perp}/\Gamma$ in $B^0 \to D^{*+} D^{*-}$

VALUE	DOCUMENT ID		TECN	COMMENT
0.147 ± 0.019 OUR AVERAGE				
$0.138 \pm 0.024 \pm 0.006$	KRONENBIT...	12	BELL	$e^+e^- \to \Upsilon(4S)$
$0.158 \pm 0.028 \pm 0.006$	AUBERT	09C	BABR	$e^+e^- \to \Upsilon(4S)$
• • • We do not use the following data for averages, fits, limits, etc. • • •				
$0.125 \pm 0.043 \pm 0.023$	VERVINK	09	BELL	Repl. by KRONENBITTER 12
$0.143 \pm 0.034 \pm 0.008$	AUBERT	07BO	BABR	Repl. by AUBERT 09C
$0.125 \pm 0.044 \pm 0.007$	AUBERT,BE	05A	BABR	Repl. by AUBERT 07BO
$0.19 \pm 0.08 \pm 0.01$	MIYAKE	05	BELL	Repl. by VERVINK 09
$0.063 \pm 0.055 \pm 0.009$	AUBERT	03Q	BABR	Repl. by AUBERT,BE 05A

Γ_L/Γ in $B^0 \to \overline{D}^{*0} \omega$

VALUE	DOCUMENT ID		TECN	COMMENT
$0.665 \pm 0.047 \pm 0.015$	LEES	11M	BABR	$e^+e^- \to \Upsilon(4S)$

Γ_L/Γ in $B^0 \to \overline{D}_1(2430)^0 \omega$

VALUE (%)	DOCUMENT ID		TECN	COMMENT
$63.0 \pm 9.1^{+6.5}_{-6.0}$	[1,2] MATVIENKO	15	BELL	$e^+e^- \to \Upsilon(4S)$

[1] Obtained by amplitude analysis of $\overline{B}^0 \to D^{*-} \omega \pi^+$. The second uncertainty combines in qudrature experimental systematic and model uncertainties.
[2] Assumes equal production of B^0 and B^+ at $\Upsilon(4S)$.

Γ_L/Γ in $B^0 \to \overline{D}_1(2420)^0 \omega$

VALUE (%)	DOCUMENT ID		TECN	COMMENT
$67.1 \pm 11.7^{+2.3}_{-5.0}$	[1,2] MATVIENKO	15	BELL	$e^+e^- \to \Upsilon(4S)$

[1] Obtained by amplitude analysis of $\overline{B}^0 \to D^{*-} \omega \pi^+$. The second uncertainty combines in qudrature experimental systematic and model uncertainties.
[2] Assumes equal production of B^0 and B^+ at $\Upsilon(4S)$.

Γ_L/Γ in $B^0 \to \overline{D}_2^*(2460)^0 \omega$

VALUE (%)	DOCUMENT ID		TECN	COMMENT
$76.0^{+18.3+3.5}_{-\ 8.5-2.8}$	[1,2] MATVIENKO	15	BELL	$e^+e^- \to \Upsilon(4S)$

[1] Obtained by amplitude analysis of $\overline{B}^0 \to D^{*-} \omega \pi^+$. The second uncertainty combines in qudrature experimental systematic and model uncertainties.
[2] Assumes equal production of B^0 and B^+ at $\Upsilon(4S)$.

Γ_L/Γ in $B^0 \to D^{*-} \omega \pi^+$

VALUE	DOCUMENT ID		TECN	COMMENT
$0.654 \pm 0.042 \pm 0.016$	[1] AUBERT	06L	BABR	$e^+e^- \to \Upsilon(4S)$

[1] Invariant mass of the $[\omega \pi]$ system is restricted in the region 1.1 and 1.9 GeV.

Γ_L/Γ in $B^0 \to \omega K^{*0}$

VALUE	DOCUMENT ID		TECN	COMMENT
0.69 ± 0.11 OUR AVERAGE				
$0.68 \pm 0.17 \pm 0.16$	AAIJ	19J	LHCB	pp at 7, 8 TeV
$0.72 \pm 0.14 \pm 0.02$	AUBERT	09H	BABR	$e^+e^- \to \Upsilon(4S)$
$0.56 \pm 0.29^{+0.18}_{-0.08}$	GOLDENZWE...	08	BELL	$e^+e^- \to \Upsilon(4S)$

Int. J. Mod. Phys. A 2026.41. Downloaded from www.worldscientific.com
by [redacted]LIFORNIA @ BERKELEY on 09/16/26. Re-use and distribution is strictly not permitted, except for Open Access articles.

$\Gamma_\perp/\Gamma$ in $B^0 \to \omega K^*(892)^0$

VALUE	DOCUMENT ID		TECN	COMMENT
0.10±0.09±0.09	AAIJ	19J	LHCB	pp at 7, 8 TeV

A^0_{CP} in $B^0 \to \omega K^*(892)^0$

VALUE	DOCUMENT ID		TECN	COMMENT
−0.13±0.27±0.13	AAIJ	19J	LHCB	pp at 7, 8 TeV

$A^\perp_{CP}$ in $B^0 \to \omega K^*(892)^0$

VALUE	DOCUMENT ID		TECN	COMMENT
0.3±0.8±0.4	AAIJ	19J	LHCB	pp at 7, 8 TeV

$A^\parallel_{CP}$ in $B^0 \to \omega K^*(892)^0$

VALUE	DOCUMENT ID		TECN	COMMENT
0.26±0.55±0.22	AAIJ	19J	LHCB	pp at 7, 8 TeV

ϕ_0 in $B^0 \to \omega K^*(892)^0$

VALUE	DOCUMENT ID		TECN	COMMENT
−0.86±0.29±0.71	AAIJ	19J	LHCB	pp at 7, 8 TeV

$\phi_\perp$ in $B^0 \to \omega K^*(892)^0$

VALUE	DOCUMENT ID		TECN	COMMENT
1.6±0.4±0.6	AAIJ	19J	LHCB	pp at 7, 8 TeV

$\phi_\parallel$ in $B^0 \to \omega K^*(892)^0$

VALUE	DOCUMENT ID		TECN	COMMENT
−1.83±0.29±0.32	AAIJ	19J	LHCB	pp at 7, 8 TeV

Γ_L/Γ in $B^0 \to \omega K_2^*(1430)^0$

VALUE	DOCUMENT ID		TECN	COMMENT
0.45±0.12±0.02	AUBERT	09H	BABR	$e^+e^- \to \Upsilon(4S)$

Γ_L/Γ in $B^0 \to K^{*0}\overline{K}^{*0}$

VALUE	DOCUMENT ID		TECN	COMMENT
0.74 ±0.05 OUR AVERAGE				
0.724±0.051±0.016	[1] AAIJ	19L	LHCB	pp at 7 and 8 TeV
$0.80\ ^{+0.10}_{-0.12}\ \pm0.06$	AUBERT	08I	BABR	$e^+e^- \to \Upsilon(4S)$

[1] Untagged and time-integrated analysis within 150 MeV of the K^{*0} mass.

Γ_L/Γ in $B^0 \to \phi K^*(892)^0$

VALUE	DOCUMENT ID		TECN	COMMENT
0.497±0.017 OUR AVERAGE				
0.497±0.019±0.015	AAIJ	14AM	LHCB	pp at 7 TeV
0.499±0.030±0.018	PRIM	13	BELL	$e^+e^- \to \Upsilon(4S)$
0.494±0.034±0.013	AUBERT	08BG	BABR	$e^+e^- \to \Upsilon(4S)$
• • • We do not use the following data for averages, fits, limits, etc. • • •				
0.506±0.040±0.015	AUBERT	07D	BABR	Repl. by AUBERT 08BG
0.45 ±0.05 ±0.02	CHEN	05A	BELL	Repl. by PRIM 13
0.52 ±0.05 ±0.02	[1] AUBERT,B	04W	BABR	Repl. by AUBERT 07D
0.65 ±0.07 ±0.02	AUBERT	03V	BABR	Repl. by AUBERT,B 04W
0.41 ±0.10 ±0.04	CHEN	03B	BELL	Repl. by CHEN 05A

[1] AUBERT,B 04W also measures the fraction of parity-odd transverse contribution $f_\perp = 0.22 \pm 0.05 \pm 0.02$ and the phases of the parity-even and parity-odd transverse amplitudes relative to the longitudinal amplitude.

$\Gamma_\perp/\Gamma$ in $B^0 \to \phi K^*(892)^0$

VALUE	DOCUMENT ID		TECN	COMMENT
0.224±0.015 OUR AVERAGE				
0.221±0.016±0.013	AAIJ	14AM	LHCB	pp at 7 TeV
0.238±0.026±0.008	PRIM	13	BELL	$e^+e^- \to \Upsilon(4S)$
0.212±0.032±0.013	AUBERT	08BG	BABR	$e^+e^- \to \Upsilon(4S)$
• • • We do not use the following data for averages, fits, limits, etc. • • •				
0.227±0.038±0.013	AUBERT	07D	BABR	Repl. by AUBERT 08BG
$0.31\ ^{+0.06}_{-0.05}\ \pm0.02$	[1] CHEN	05A	BELL	Repl. by PRIM 13
0.22 ±0.05 ±0.02	AUBERT,B	04W	BABR	Repl. by AUBERT 07D

[1] This quantity was recalculated by the BELLE authors from numbers in the original paper.

$\phi_\parallel$ in $B^0 \to \phi K^*(892)^0$

VALUE (rad)	DOCUMENT ID		TECN	COMMENT
2.43 ±0.11 OUR AVERAGE	Error includes scale factor of 1.8. See the ideogram below.			
2.562±0.069±0.040	AAIJ	14AM	LHCB	pp at 7 TeV
2.23 ±0.10 ±0.02	PRIM	13	BELL	$e^+e^- \to \Upsilon(4S)$
2.40 ±0.13 ±0.08	AUBERT	08BG	BABR	$e^+e^- \to \Upsilon(4S)$
• • • We do not use the following data for averages, fits, limits, etc. • • •				
2.31 ±0.14 ±0.08	AUBERT	07D	BABR	Repl. by AUBERT 08BG
$2.40\ ^{+0.28}_{-0.24}\ \pm0.07$	[1] CHEN	05A	BELL	Repl. by PRIM 13
$2.34\ ^{+0.23}_{-0.20}\ \pm0.05$	AUBERT,B	04W	BABR	Repl. by AUBERT 07D

[1] This quantity was recalculated by the BELLE authors from numbers in the original paper.

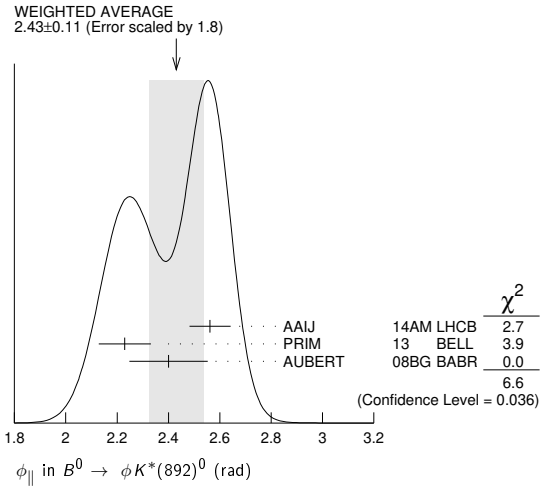

$\phi_\perp$ in $B^0 \to \phi K^*(892)^0$

VALUE (rad)	DOCUMENT ID		TECN	COMMENT
2.53 ±0.09 OUR AVERAGE	Error includes scale factor of 1.7. See the ideogram below.			
2.633±0.062±0.037	AAIJ	14AM	LHCB	pp at 7 TeV
2.37 ±0.10 ±0.04	PRIM	13	BELL	$e^+e^- \to \Upsilon(4S)$
2.35 ±0.13 ±0.09	AUBERT	08BG	BABR	$e^+e^- \to \Upsilon(4S)$
• • • We do not use the following data for averages, fits, limits, etc. • • •				
2.24 ±0.15 ±0.09	AUBERT	07D	BABR	Repl. by AUBERT 08BG
2.51 ±0.25 ±0.06	[1] CHEN	05A	BELL	Repl. by PRIM 13
2.47 ±0.25 ±0.05	AUBERT,B	04W	BABR	Repl. by AUBERT 07D

[1] This quantity was recalculated by the BELLE authors from numbers in the original paper.

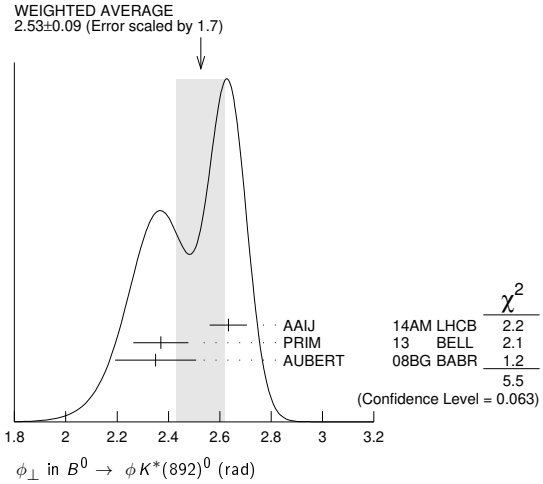

$\delta_0(B^0 \to \phi K^*(892)^0)$

VALUE (rad)	DOCUMENT ID		TECN	COMMENT
2.88±0.10 OUR AVERAGE				
2.91±0.10±0.08	PRIM	13	BELL	$e^+e^- \to \Upsilon(4S)$
2.82±0.15±0.09	AUBERT	08BG	BABR	$e^+e^- \to \Upsilon(4S)$
• • • We do not use the following data for averages, fits, limits, etc. • • •				
2.78±0.17±0.09	AUBERT	07D	BABR	Repl. by AUBERT 08BG

A^0_{CP} in $B^0 \to \phi K^*(892)^0$

VALUE	DOCUMENT ID		TECN	COMMENT
−0.007±0.030 OUR AVERAGE				
−0.003±0.038±0.005	AAIJ	14AM	LHCB	pp at 7 TeV
−0.030±0.061±0.007	PRIM	13	BELL	$e^+e^- \to \Upsilon(4S)$
0.01 ±0.07 ±0.02	AUBERT	08BG	BABR	$e^+e^- \to \Upsilon(4S)$
• • • We do not use the following data for averages, fits, limits, etc. • • •				
−0.03 ±0.08 ±0.02	AUBERT	07D	BABR	Repl. by AUBERT 08BG
0.13 ±0.12 ±0.04	[1] CHEN	05A	BELL	Repl. by PRIM 13
−0.06 ±0.10 ±0.01	AUBERT,B	04W	BABR	Repl. by AUBERT 07D

[1] This quantity was recalculated by the BELLE authors from numbers in the original paper.

$A^\perp_{CP}$ in $B^0 \to \phi K^*(892)^0$

VALUE	DOCUMENT ID		TECN	COMMENT
−0.02 ±0.06 OUR AVERAGE				
0.047±0.074±0.009	AAIJ	14AM	LHCB	pp at 7 TeV
−0.14 ±0.11 ±0.01	PRIM	13	BELL	$e^+e^- \to \Upsilon(4S)$
−0.04 ±0.15 ±0.06	AUBERT	08BG	BABR	$e^+e^- \to \Upsilon(4S)$

Int. J. Mod. Phys. A 2026.41. Downloaded from www.worldscientific.com
by UNIVERSITY OF CALIFORNIA @ BERKELEY on 09/16/26. Re-use and distribution is strictly not permitted, except for Open Access articles.

• • • We do not use the following data for averages, fits, limits, etc. • • •

$-0.03 \pm 0.16 \pm 0.05$	AUBERT	07D	BABR	Repl. by AUBERT 08BG
$-0.20 \pm 0.18 \pm 0.04$	[1] CHEN	05A	BELL	Repl. by PRIM 13
$-0.10 \pm 0.24 \pm 0.05$	AUBERT,B	04W	BABR	Repl. by AUBERT 07D

[1] This quantity was recalculated by the BELLE authors from numbers in the original paper.

$\Delta\phi_\parallel$ in $B^0 \to \phi K^*(892)^0$

VALUE (rad)	DOCUMENT ID		TECN	COMMENT
0.05 ±0.05 OUR AVERAGE				
$0.045 \pm 0.069 \pm 0.015$	AAIJ	14AM	LHCB	pp at 7 TeV
$-0.02 \pm 0.10 \pm 0.01$	PRIM	13	BELL	$e^+e^- \to \Upsilon(4S)$
$0.22 \pm 0.12 \pm 0.08$	AUBERT	08BG	BABR	$e^+e^- \to \Upsilon(4S)$
• • • We do not use the following data for averages, fits, limits, etc. • • •				
$0.24 \pm 0.14 \pm 0.08$	AUBERT	07D	BABR	Repl. by AUBERT 08BG
$-0.32 \pm 0.27 \pm 0.07$	[1] CHEN	05A	BELL	Repl. by PRIM 13
$0.27 {}^{+0.20}_{-0.23} \pm 0.05$	AUBERT,B	04W	BABR	Repl. by AUBERT 07D

[1] This quantity was recalculated by the BELLE authors from numbers in the original paper.

$\Delta\phi_\perp$ in $B^0 \to \phi K^*(892)^0$

VALUE (rad)	DOCUMENT ID		TECN	COMMENT
0.08 ±0.05 OUR AVERAGE				
$0.062 \pm 0.062 \pm 0.005$	AAIJ	14AM	LHCB	pp at 7 TeV
$0.05 \pm 0.10 \pm 0.02$	PRIM	13	BELL	$e^+e^- \to \Upsilon(4S)$
$0.21 \pm 0.13 \pm 0.08$	AUBERT	08BG	BABR	$e^+e^- \to \Upsilon(4S)$
• • • We do not use the following data for averages, fits, limits, etc. • • •				
$0.19 \pm 0.15 \pm 0.08$	AUBERT	07D	BABR	Repl. by AUBERT 08BG
$-0.30 \pm 0.25 \pm 0.06$	[1] CHEN	05A	BELL	Repl. by PRIM 13
$0.36 \pm 0.25 \pm 0.05$	AUBERT,B	04W	BABR	Repl. by AUBERT 07D

[1] This quantity was recalculated by the BELLE authors from numbers in the original paper.

$\Delta\delta_0(B^0 \to \phi K^*(892)^0)$

VALUE (rad)	DOCUMENT ID		TECN	COMMENT
0.13±0.09 OUR AVERAGE				
$0.08 \pm 0.10 \pm 0.01$	PRIM	13	BELL	$e^+e^- \to \Upsilon(4S)$
$0.27 \pm 0.14 \pm 0.08$	AUBERT	08BG	BABR	$e^+e^- \to \Upsilon(4S)$
• • • We do not use the following data for averages, fits, limits, etc. • • •				
$0.21 \pm 0.17 \pm 0.08$	AUBERT	07D	BABR	Repl. by AUBERT 08BG

$\Delta\phi_{00}(B^0 \to \phi K_0^*(1430)^0)$

VALUE (rad)	DOCUMENT ID		TECN	COMMENT
0.28±0.42±0.04	AUBERT	08BG	BABR	$e^+e^- \to \Upsilon(4S)$

Γ_L/Γ in $B^0 \to \phi K_2^*(1430)^0$

VALUE	DOCUMENT ID		TECN	COMMENT
$0.913 {}^{+0.028}_{-0.050}$ OUR AVERAGE				
$0.918 {}^{+0.029}_{-0.060} \pm 0.012$	PRIM	13	BELL	$e^+e^- \to \Upsilon(4S)$
$0.901 {}^{+0.046}_{-0.058} \pm 0.037$	AUBERT	08BG	BABR	$e^+e^- \to \Upsilon(4S)$
• • • We do not use the following data for averages, fits, limits, etc. • • •				
$0.853 {}^{+0.061}_{-0.069} \pm 0.036$	AUBERT	07D	BABR	Repl. by AUBERT 08BG

$\Gamma_\perp/\Gamma$ in $B^0 \to \phi K_2^*(1430)^0$

VALUE	DOCUMENT ID		TECN	COMMENT
$0.027 {}^{+0.031}_{-0.025}$ OUR AVERAGE Error includes scale factor of 1.1.				
$0.056 {}^{+0.050}_{-0.035} \pm 0.009$	PRIM	13	BELL	$e^+e^- \to \Upsilon(4S)$
$0.002 {}^{+0.018}_{-0.002} \pm 0.031$	AUBERT	08BG	BABR	$e^+e^- \to \Upsilon(4S)$
• • • We do not use the following data for averages, fits, limits, etc. • • •				
$0.045 {}^{+0.049}_{-0.040} \pm 0.013$	AUBERT	07D	BABR	Repl. by AUBERT 08BG

$\phi_\parallel$ in $B^0 \to \phi K_2^*(1430)^0$

VALUE (rad)	DOCUMENT ID		TECN	COMMENT
4.0 ±0.4 OUR AVERAGE				
$3.76 \pm 2.88 \pm 1.32$	PRIM	13	BELL	$e^+e^- \to \Upsilon(4S)$
$3.96 \pm 0.38 \pm 0.06$	AUBERT	08BG	BABR	$e^+e^- \to \Upsilon(4S)$
• • • We do not use the following data for averages, fits, limits, etc. • • •				
$2.90 \pm 0.39 \pm 0.06$	AUBERT	07D	BABR	Repl. by AUBERT 08BG

$\phi_\perp$ in $B^0 \to \phi K_2^*(1430)^0$

VALUE (rad)	DOCUMENT ID		TECN	COMMENT
$4.45 {}^{+0.43}_{-0.38} \pm 0.13$	PRIM	13	BELL	$e^+e^- \to \Upsilon(4S)$
• • • We do not use the following data for averages, fits, limits, etc. • • •				
$5.72 {}^{+0.55}_{-0.87} \pm 0.11$	AUBERT	07D	BABR	Repl. by AUBERT 08BG

$\delta_0(B^0 \to \phi K_2^*(1430)^0)$

VALUE (rad)	DOCUMENT ID		TECN	COMMENT
3.46±0.14 OUR AVERAGE				
$3.53 \pm 0.11 \pm 0.19$	PRIM	13	BELL	$e^+e^- \to \Upsilon(4S)$
$3.41 \pm 0.13 \pm 0.13$	AUBERT	08BG	BABR	$e^+e^- \to \Upsilon(4S)$
• • • We do not use the following data for averages, fits, limits, etc. • • •				
$3.54 {}^{+0.12}_{-0.14} \pm 0.06$	AUBERT	07D	BABR	Repl. by AUBERT 08BG

A_{CP}^0 in $B^0 \to \phi K_2^*(1430)^0$

VALUE	DOCUMENT ID		TECN	COMMENT
−0.03 ±0.04 OUR AVERAGE				
$-0.016 {}^{+0.066}_{-0.051} \pm 0.008$	PRIM	13	BELL	$e^+e^- \to \Upsilon(4S)$
$-0.05 \pm 0.06 \pm 0.01$	AUBERT	08BG	BABR	$e^+e^- \to \Upsilon(4S)$

$A_{CP}^\perp$ in $B^0 \to \phi K_2^*(1430)^0$

VALUE	DOCUMENT ID		TECN	COMMENT
$-0.01 {}^{+0.85}_{-0.67} \pm 0.09$	PRIM	13	BELL	$e^+e^- \to \Upsilon(4S)$

$\Delta\phi_\parallel(B^0 \to \phi K_2^*(1430)^0)$

VALUE (rad)	DOCUMENT ID		TECN	COMMENT
−0.9 ±0.4 OUR AVERAGE				
$-0.02 \pm 1.08 \pm 1.01$	PRIM	13	BELL	$e^+e^- \to \Upsilon(4S)$
$-1.00 \pm 0.38 \pm 0.09$	AUBERT	08BG	BABR	$e^+e^- \to \Upsilon(4S)$

$\Delta\phi_\perp(B^0 \to \phi K_2^*(1430)^0)$

VALUE	DOCUMENT ID		TECN	COMMENT
−0.19±0.42±0.11	PRIM	13	BELL	$e^+e^- \to \Upsilon(4S)$

$\Delta\delta_0$ in $B^0 \to \phi K_2^*(1430)^0$

VALUE (rad)	DOCUMENT ID		TECN	COMMENT
0.08±0.09 OUR AVERAGE				
$0.06 \pm 0.11 \pm 0.02$	PRIM	13	BELL	$e^+e^- \to \Upsilon(4S)$
$0.11 \pm 0.13 \pm 0.06$	AUBERT	08BG	BABR	$e^+e^- \to \Upsilon(4S)$

Γ_L/Γ in $B^0 \to K^*(892)^0\rho^0$

VALUE	DOCUMENT ID		TECN	COMMENT
0.173±0.026 OUR AVERAGE				
$0.164 \pm 0.015 \pm 0.022$	AAIJ	19J	LHCB	pp at 7, 8 TeV
$0.40 \pm 0.08 \pm 0.11$	LEES	12K	BABR	$e^+e^- \to \Upsilon(4S)$
• • • We do not use the following data for averages, fits, limits, etc. • • •				
$0.57 \pm 0.09 \pm 0.08$	AUBERT,B	06G	BABR	Repl. by LEES 12K

$\Gamma_\perp/\Gamma$ in $B^0 \to K^*(892)^0\rho^0$

VALUE	DOCUMENT ID		TECN	COMMENT
0.401±0.016±0.037	AAIJ	19J	LHCB	pp at 7, 8 TeV

A_{CP}^0 in $B^0 \to K^*(892)^0\rho^0$

VALUE	DOCUMENT ID		TECN	COMMENT
−0.62±0.09±0.09	AAIJ	19J	LHCB	pp at 7, 8 TeV

$A_{CP}^\perp$ in $B^0 \to K^*(892)^0\rho^0$

VALUE	DOCUMENT ID		TECN	COMMENT
0.050±0.039±0.015	AAIJ	19J	LHCB	pp at 7, 8 TeV

$A_{CP}^\parallel$ in $B^0 \to K^*(892)^0\rho^0$

VALUE	DOCUMENT ID		TECN	COMMENT
0.188±0.037±0.022	AAIJ	19J	LHCB	pp at 7, 8 TeV

ϕ_0 in $B^0 \to K^*(892)^0\rho^0$

VALUE	DOCUMENT ID		TECN	COMMENT
1.57±0.08±0.18	AAIJ	19J	LHCB	pp at 7, 8 TeV

$\phi_\perp$ in $B^0 \to K^*(892)^0\rho^0$

VALUE	DOCUMENT ID		TECN	COMMENT
−2.365±0.032±0.054	AAIJ	19J	LHCB	pp at 7, 8 TeV

$\phi_\parallel$ in $B^0 \to K^*(892)^0\rho^0$

VALUE	DOCUMENT ID		TECN	COMMENT
0.795±0.030±0.068	AAIJ	19J	LHCB	pp at 7, 8 TeV

Γ_L/Γ in $B^0 \to K^{*+}\rho^-$

VALUE	DOCUMENT ID		TECN	COMMENT
0.38±0.13±0.03	LEES	12K	BABR	$e^+e^- \to \Upsilon(4S)$

Γ_L/Γ in $B^0 \to \rho^+\rho^-$

VALUE	DOCUMENT ID		TECN	COMMENT
0.970±0.023 OUR AVERAGE Error includes scale factor of 1.4. See the ideogram below.				
$0.921 {}^{+0.024}_{-0.025} {}^{+0.017}_{-0.015}$	ADACHI	25H	BELL	$e^+e^- \to \Upsilon(4S)$
$0.988 \pm 0.012 \pm 0.023$	VANHOEFER	16	BELL	$e^+e^- \to \Upsilon(4S)$
$0.992 \pm 0.024 {}^{+0.026}_{-0.013}$	AUBERT	07BF	BABR	$e^+e^- \to \Upsilon(4S)$
• • • We do not use the following data for averages, fits, limits, etc. • • •				
$0.941 {}^{+0.034}_{-0.040} \pm 0.030$	SOMOV	06	BELL	Repl. by VANHOEFER 16
$0.978 \pm 0.014 {}^{+0.021}_{-0.029}$	AUBERT,B	05C	BABR	Repl. by AUBERT 07BF

$0.98\ ^{+0.02}_{-0.08}\ \pm0.03$	AUBERT	04G	BABR	Repl. by AUBERT,B 04R	
$0.99\ \pm0.03\ ^{+0.04}_{-0.03}$	AUBERT,B	04R	BABR	Repl. by AUBERT,B 05C	

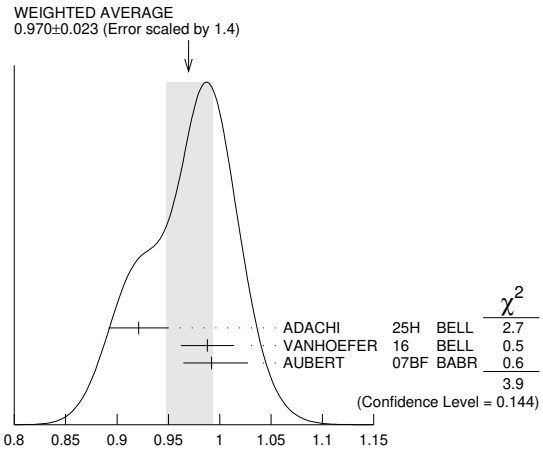

Γ_L/Γ in $B^0 \to \rho^0\rho^0$

VALUE	DOCUMENT ID		TECN	COMMENT
$0.71\ ^{+0.08}_{-0.09}$ OUR AVERAGE Error includes scale factor of 1.6. See the ideogram below.				
$0.745\ ^{+0.048}_{-0.058}\pm0.034$	AAIJ	15T	LHCB	pp at 7, 8 TeV
$0.21\ ^{+0.18}_{-0.22}\ \pm0.15$	VANHOEFER	14	BELL	$e^+e^- \to \Upsilon(4S)$
$0.75\ ^{+0.11}_{-0.14}\ \pm0.05$	AUBERT	08BB	BABR	$e^+e^- \to \Upsilon(4S)$
• • • We do not use the following data for averages, fits, limits, etc. • • •				
$0.87\ \pm0.13\ \pm0.04$	AUBERT	07G	BABR	Repl. by AUBERT 08BB

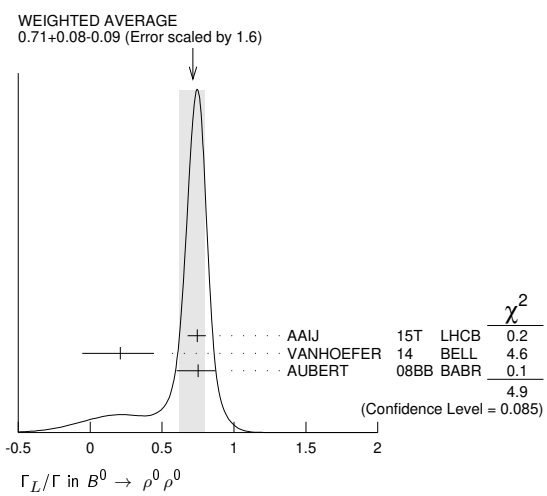

Γ_L/Γ in $B^0 \to \omega\omega$

VALUE	DOCUMENT ID		TECN	COMMENT
$0.87\pm0.13\pm0.13$	GUAN	24	BELL	$e^+e^- \to \Upsilon(4S)$

Γ_L/Γ in $B^0 \to a_1(1260)^+ a_1(1260)^-$

VALUE	DOCUMENT ID		TECN	COMMENT
$0.31\pm0.22\pm0.10$	AUBERT	09AL	BABR	$e^+e^- \to \Upsilon(4S)$

Γ_L/Γ in $B^0 \to p\overline{p}K^*(892)^0$

VALUE	DOCUMENT ID		TECN	COMMENT
$1.01\pm0.13\pm0.03$	CHEN	08C	BELL	$e^+e^- \to \Upsilon(4S)$

Γ_L/Γ in $B^0 \to \Lambda\overline{\Lambda}K^*(892)^0$

VALUE	DOCUMENT ID		TECN	COMMENT
$0.60\pm0.22\pm0.08$	CHANG	09	BELL	$e^+e^- \to \Upsilon(4S)$

Γ_L/Γ in $B^0 \to K^*(892)^0\mu^+\mu^-$ ($0.04 < q^2 < 6.0$ GeV^2/c^4)

VALUE	DOCUMENT ID		TECN	COMMENT
$0.50\pm0.06\pm0.04$	[1] AABOUD	18BY	ATLS	pp at 8 TeV

[1] A set of angular parameters obtained for this decay is also presented.

Γ_L/Γ in $B^0 \to K^*(892)^0\mu^+\mu^-$ ($1.1 < q^2 < 2.0$ GeV^2/c^4)

VALUE	DOCUMENT ID		TECN	COMMENT
$0.709^{+0.073}_{-0.054}\pm0.021$	[1] HAYRAPETY...	25AE	CMS	$p\,p$ at 13 TeV

[1] A set of angular parameters obtained for this decay is also presented.

Γ_L/Γ in $B^0 \to K^*(892)^0\mu^+\mu^-$ ($2.0 < q^2 < 4.3$ GeV^2/c^4)

VALUE	DOCUMENT ID		TECN	COMMENT
$0.810^{+0.036}_{-0.030}\pm0.016$	[1] HAYRAPETY...	25AE	CMS	$p\,p$ at 13 TeV

[1] A set of angular parameters obtained for this decay is also presented.

Γ_L/Γ in $B^0 \to K^*(892)^0\mu^+\mu^-$ ($4.3 < q^2 < 6.0$ GeV^2/c^4)

VALUE	DOCUMENT ID		TECN	COMMENT
$0.714^{+0.032}_{-0.030}\pm0.012$	[1] HAYRAPETY...	25AE	CMS	$p\,p$ at 13 TeV

[1] A set of angular parameters obtained for this decay is also presented.

Γ_L/Γ in $B^0 \to K^*(892)^0 e^+e^-$ (at low q^2)

VALUE	DOCUMENT ID		TECN	COMMENT
$0.044\pm0.026\pm0.014$	[1] AAIJ	20AO	LHCB	pp at 7, 8, 13 TeV
• • • We do not use the following data for averages, fits, limits, etc. • • •				
$0.16\ \pm0.06\ \pm0.03$	[2] AAIJ	15Z	LHCB	Repl. by AAIJ 20AO

[1] Determined in the effective dielectron invariant mass range $0.0008 < q^2 < 0.257$ GeV^2/c^4.
[2] Determined in the effective dielectron invariant mass range $0.002 < q^2 < 1.120$ GeV^2/c^4.

Γ_L/Γ in $B^0 \to K^*(892)^0 e^+e^-$ ($1.1 < q^2 < 6.0$ GeV^2/c^4)

VALUE	DOCUMENT ID		TECN	COMMENT
$0.58\pm0.04\pm0.05$	[1] AAIJ	25W	LHCB	pp at 7, 8, 13 TeV

[1] A set of angular parameters obtained for this decay is also presented.

$A_T^{(2)}$ in $B^0 \to K^*(892)^0 e^+e^-$ (at low q^2)

VALUE	DOCUMENT ID		TECN	COMMENT
$0.11\pm0.10\pm0.02$	[1] AAIJ	20AO	LHCB	pp at 7, 8, 13 TeV
• • • We do not use the following data for averages, fits, limits, etc. • • •				
$-0.23\pm0.23\pm0.05$	[2] AAIJ	15Z	LHCB	Repl. by AAIJ 20AO

[1] Determined in the effective dielectron invariant mass range $0.0008 < q^2 < 0.257$ GeV^2/c^4.
[2] Determined in the effective dielectron invariant mass range $0.002 < q^2 < 1.120$ GeV^2/c^4.

A_T^{Im} in $B^0 \to K^*(892)^0 e^+e^-$ (at low q^2)

VALUE	DOCUMENT ID		TECN	COMMENT
$0.02\pm0.10\pm0.01$	[1] AAIJ	20AO	LHCB	pp at 7, 8, 13 TeV
• • • We do not use the following data for averages, fits, limits, etc. • • •				
$0.14\pm0.22\pm0.05$	[2] AAIJ	15Z	LHCB	Repl. by AAIJ 20AO

[1] Determined in the effective dielectron invariant mass range $0.0008 < q^2 < 0.257$ GeV^2/c^4.
[2] Determined in the effective dielectron invariant mass range $0.002 < q^2 < 1.120$ GeV^2/c^4.

A_T^{Re} in $B^0 \to K^*(892)^0 e^+e^-$ (at low q^2)

Related to A_{FB}, F_L by $A_T^{Re} = (4/3)\ A_{FB}\ /\ (1 - F_L)$.

VALUE	DOCUMENT ID		TECN	COMMENT
$-0.06\pm0.08\pm0.02$	[1] AAIJ	20AO	LHCB	pp at 7, 8, 13 TeV
• • • We do not use the following data for averages, fits, limits, etc. • • •				
$0.10\pm0.18\pm0.05$	[2] AAIJ	15Z	LHCB	Repl. by AAIJ 20AO

[1] Determined in the effective dielectron invariant mass range $0.0008 < q^2 < 0.257$ GeV^2/c^4.
[2] Determined in the effective dielectron invariant mass range $0.002 < q^2 < 1.120$ GeV^2/c^4.

See the related review(s):

$B^0 - \overline{B}^0$ Mixing

B^0-$\overline{B}^0$ MIXING PARAMETERS

For a discussion of B^0-$\overline{B}^0$ mixing see the note on "B^0-$\overline{B}^0$ Mixing" in the B^0 Particle Listings above.

χ_d is a measure of the time-integrated B^0-$\overline{B}^0$ mixing probability that a produced $B^0(\overline{B}^0)$ decays as a $\overline{B}^0(B^0)$. Mixing violates $\Delta B \neq 2$ rule.

$$\chi_d = \frac{x_d^2}{2(1+x_d^2)}$$

$$x_d = \frac{\Delta m_{B^0}}{\Gamma_{B^0}} = (m_{B^0_H} - m_{B^0_L})\ \tau_{B^0}\ ,$$

where H, L stand for heavy and light states of two B^0 CP eigenstates and $\tau_{B^0} = \frac{1}{0.5(\Gamma_{B^0_H} + \Gamma_{B^0_L})}$.

χ_d

This B^0-$\overline{B}^0$ mixing parameter is the probability (integrated over time) that a produced B^0 (or $\overline{B}^0$) decays as a $\overline{B}^0$ (or B^0), e.g. for inclusive lepton decays

$$\chi_d = \Gamma(B^0 \to \ell^- X \text{ (via } \overline{B}^0))/\Gamma(B^0 \to \ell^\pm X)$$
$$= \Gamma(\overline{B}^0 \to \ell^+ X \text{ (via } B^0))/\Gamma(\overline{B}^0 \to \ell^\pm X)$$

Int. J. Mod. Phys. A 2026.41. Downloaded from www.worldscientific.com
by UNIVERSITY OF CALIFORNIA @ BERKELEY on 09/16/26. Re-use and distribution is strictly not permitted, except for Open Access articles.

Int. J. Mod. Phys. A 2026.41. Downloaded from www.worldscientific.com
by UNIVERSITY OF CALIFORNIA @ BERKELEY on 09/16/26. Re-use and distribution is strictly not permitted, except for Open Access articles.

Where experiments have measured the parameter $r = \chi/(1-\chi)$, we have converted to χ. Mixing violates the $\Delta B \neq 2$ rule.

Note that the measurement of χ at energies higher than the $\Upsilon(4S)$ have not separated χ_d from χ_s where the subscripts indicate $B^0(\overline{b}d)$ or $B^0_s(\overline{b}s)$. They are listed in the $B^\pm/B^0/B^0_s/b$-baryon ADMIXTURE section.

The experiments at $\Upsilon(4S)$ make an assumption about the $B^0\overline{B}^0$ fraction and about the ratio of the $B^\pm$ and B^0 semileptonic branching ratios (usually that it equals one).

"OUR EVALUATION" is an average using rescaled values of the data listed below. The averaging/rescaling procedure takes into account correlations between the measurements, includes χ_d calculated from Δm_{B^0} and τ_{B^0}.

VALUE	CL%	DOCUMENT ID		TECN	COMMENT
0.1849±0.0010 OUR EVALUATION		(Produced by HFLAV)			
0.182 ±0.015 OUR AVERAGE					
0.198 ±0.013 ±0.014		[1] BEHRENS	00B	CLE2	$e^+e^- \to \Upsilon(4S)$
0.16 ±0.04 ±0.04		[2] ALBRECHT	94	ARG	$e^+e^- \to \Upsilon(4S)$
0.149 ±0.023 ±0.022		[3] BARTELT	93	CLE2	$e^+e^- \to \Upsilon(4S)$
0.171 ±0.048		[4] ALBRECHT	92L	ARG	$e^+e^- \to \Upsilon(4S)$
• • • We do not use the following data for averages, fits, limits, etc. • • •					
0.20 ±0.13 ±0.12		[5] ALBRECHT	96D	ARG	$e^+e^- \to \Upsilon(4S)$
0.19 ±0.07 ±0.09		[6] ALBRECHT	96D	ARG	$e^+e^- \to \Upsilon(4S)$
0.24 ±0.12		[7] ELSEN	90	JADE	e^+e^- 35–44 GeV
$0.158^{+0.052}_{-0.059}$		ARTUSO	89	CLEO	$e^+e^- \to \Upsilon(4S)$
0.17 ±0.05		[8] ALBRECHT	87I	ARG	$e^+e^- \to \Upsilon(4S)$
<0.19	90	[9] BEAN	87B	CLEO	$e^+e^- \to \Upsilon(4S)$
<0.27	90	[10] AVERY	84	CLEO	$e^+e^- \to \Upsilon(4S)$

[1] BEHRENS 00B uses high-momentum lepton tags and partially reconstructed $\overline{B}^0 \to D^{*+}\pi^-, \rho^-$ decays to determine the flavor of the B meson.

[2] ALBRECHT 94 reports r=0.194 ± 0.062 ± 0.054. We convert to χ for comparison. Uses tagged events (lepton + pion from D^*).

[3] BARTELT 93 analysis performed using tagged events (lepton+pion from D^*). Using dilepton events they obtain $0.157 \pm 0.016^{+0.033}_{-0.028}$.

[4] ALBRECHT 92L is a combined measurement employing several lepton-based techniques. It uses all previous ARGUS data in addition to new data and therefore supersedes ALBRECHT 87I. A value of $r = 20.6 \pm 7.0\%$ is directly measured. The value can be used to measure $x = \Delta M/\Gamma = 0.72 \pm 0.15$ for the B_d meson. Assumes $f_{+-}/f_0 = 1.0 \pm 0.05$ and uses $\tau_{B^\pm}/\tau_{B^0} = (0.95 \pm 0.14)\ (f_{+-}/f_0)$.

[5] Uses $D^{*+}K^\pm$ correlations.

[6] Uses $(D^{*+}\ell^-)\ K^\pm$ correlations.

[7] These experiments see a combination of B_s and B_d mesons.

[8] ALBRECHT 87I is inclusive measurement with like-sign dileptons, with tagged B decays plus leptons, and one fully reconstructed event. Measures r=0.21 ± 0.08. We convert to χ for comparison. Superseded by ALBRECHT 92L.

[9] BEAN 87B measured $r <$ 0.24; we converted to χ.

[10] Same-sign dilepton events. Limit assumes semileptonic BR for B^+ and B^0 equal. If $B^0/B^\pm$ ratio <0.58, no limit exists. The limit was corrected in BEAN 87B from $r <$ 0.30 to $r <$ 0.37. We converted this limit to χ.

$\Delta m_{B^0} = m_{B^0_H} - m_{B^0_L}$

Δm_{B^0} is a measure of 2π times the B^0-$\overline{B}^0$ oscillation frequency in time-dependent mixing experiments.

"OUR EVALUATION" is an average using rescaled values of the data listed below. The averaging/rescaling procedure takes into account correlations between the measurements and includes Δm_d calculated from χ_d measured at $\Upsilon(4S)$.

VALUE ($10^{12}\ \hbar\ s^{-1}$)	DOCUMENT ID		TECN	COMMENT
0.5068±0.0019 OUR EVALUATION	(Produced by HFLAV)			
0.516 ±0.008 ±0.005	[1] ABUDINEN	23D	BELL	$e^+e^- \to \Upsilon(4S)$
0.5050±0.0021±0.0010	[2] AAIJ	16AV	LHCB	pp at 7, 8 TeV
0.503 ±0.011 ±0.013	[3] AAIJ	13CF	LHCB	pp at 7 TeV
0.5156±0.0051±0.0033	[4] AAIJ	13F	LHCB	pp at 7 TeV
0.499 ±0.032 ±0.003	[5] AAIJ	12I	LHCB	pp at 7 TeV
0.506 ±0.020 ±0.016	[6] ABAZOV	06W	D0	$p\overline{p}$ at 1.96 TeV
$0.511 \pm 0.007\ ^{+0.007}_{-0.006}$	[7] AUBERT	06G	BABR	$e^+e^- \to \Upsilon(4S)$
0.511 ±0.005 ±0.006	[8] ABE	05B	BELL	$e^+e^- \to \Upsilon(4S)$
0.531 ±0.025 ±0.007	[9] ABDALLAH	03B	DLPH	$e^+e^- \to Z$
0.492 ±0.018 ±0.013	[10] AUBERT	03C	BABR	$e^+e^- \to \Upsilon(4S)$
0.503 ±0.008 ±0.010	[11] HASTINGS	03	BELL	$e^+e^- \to \Upsilon(4S)$
0.509 ±0.017 ±0.020	[12] ZHENG	03	BELL	$e^+e^- \to \Upsilon(4S)$
0.516 ±0.016 ±0.010	[13] AUBERT	02I	BABR	$e^+e^- \to \Upsilon(4S)$
0.493 ±0.012 ±0.009	[14] AUBERT	02J	BABR	$e^+e^- \to \Upsilon(4S)$
0.497 ±0.024 ±0.025	[15] ABBIENDI,G	00B	OPAL	$e^+e^- \to Z$
0.503 ±0.064 ±0.071	[16] ABE	99K	CDF	$p\overline{p}$ at 1.8 TeV
0.500 ±0.052 ±0.043	[17] ABE	99Q	CDF	$p\overline{p}$ at 1.8 TeV
$0.516 \pm 0.099\ ^{+0.029}_{-0.035}$	[18] AFFOLDER	99C	CDF	$p\overline{p}$ at 1.8 TeV
$0.471\ ^{+0.078}_{-0.068}\ ^{+0.033}_{-0.034}$	[19] ABE	98C	CDF	$p\overline{p}$ at 1.8 TeV
0.458 ±0.046 ±0.032	[20] ACCIARRI	98D	L3	$e^+e^- \to Z$
0.437 ±0.043 ±0.044	[21] ACCIARRI	98D	L3	$e^+e^- \to Z$
0.472 ±0.049 ±0.053	[22] ACCIARRI	98D	L3	$e^+e^- \to Z$
0.523 ±0.072 ±0.043	[23] ABREU	97N	DLPH	$e^+e^- \to Z$
0.493 ±0.042 ±0.027	[21] ABREU	97N	DLPH	$e^+e^- \to Z$
0.499 ±0.053 ±0.015	[24] ABREU	97N	DLPH	$e^+e^- \to Z$
0.480 ±0.040 ±0.051	[20] ABREU	97N	DLPH	$e^+e^- \to Z$
$0.444 \pm 0.029\ ^{+0.020}_{-0.017}$	[21] ACKERSTAFF	97U	OPAL	$e^+e^- \to Z$
$0.430 \pm 0.043\ ^{+0.028}_{-0.030}$	[20] ACKERSTAFF	97V	OPAL	$e^+e^- \to Z$
0.482 ±0.044 ±0.024	[25] BUSKULIC	97D	ALEP	$e^+e^- \to Z$
0.404 ±0.045 ±0.027	[21] BUSKULIC	97D	ALEP	$e^+e^- \to Z$
0.452 ±0.039 ±0.044	[20] BUSKULIC	97D	ALEP	$e^+e^- \to Z$
0.539 ±0.060 ±0.024	[26] ALEXANDER	96V	OPAL	$e^+e^- \to Z$
$0.567 \pm 0.089\ ^{+0.029}_{-0.023}$	[27] ALEXANDER	96V	OPAL	$e^+e^- \to Z$
• • • We do not use the following data for averages, fits, limits, etc. • • •				
0.516 ±0.016 ±0.010	[28] AUBERT	02N	BABR	$e^+e^- \to \Upsilon(4S)$
0.494 ±0.012 ±0.015	[29] HARA	02	BELL	Repl. by ABE 05B
0.528 ±0.017 ±0.011	[30] TOMURA	02	BELL	Repl. by ABE 05B
0.463 ±0.008 ±0.016	[14] ABE	01D	BELL	Repl. by HASTINGS 03
0.444 ±0.028 ±0.028	[31] ACCIARRI	98D	L3	$e^+e^- \to Z$
0.497 ±0.035	[32] ABREU	97N	DLPH	$e^+e^- \to Z$
$0.467 \pm 0.022\ ^{+0.017}_{-0.015}$	[33] ACKERSTAFF	97V	OPAL	$e^+e^- \to Z$
0.446 ±0.032	[34] BUSKULIC	97D	ALEP	$e^+e^- \to Z$
$0.531\ ^{+0.050}_{-0.046} \pm 0.078$	[35] ABREU	96Q	DLPH	Sup. by ABREU 97N
$0.496\ ^{+0.055}_{-0.051} \pm 0.043$	[20] ACCIARRI	96E	L3	Repl. by ACCIARRI 98D
$0.548 \pm 0.050\ ^{+0.023}_{-0.019}$	[36] ALEXANDER	96V	OPAL	$e^+e^- \to Z$
0.496 ±0.046	[37] AKERS	95J	OPAL	Repl. by ACKERSTAFF 97V
$0.462\ ^{+0.040}_{-0.053}\ ^{+0.052}_{-0.035}$	[20] AKERS	95J	OPAL	Repl. by ACKERSTAFF 97V
0.50 ±0.12 ±0.06	[23] ABREU	94M	DLPH	Sup. by ABREU 97N
0.508 ±0.075 ±0.025	[26] AKERS	94C	OPAL	Repl. by ALEXANDER 96V
0.57 ±0.11 ±0.02	[27] AKERS	94H	OPAL	Repl. by ALEXANDER 96V
$0.50\ ^{+0.07}_{-0.06}\ ^{+0.11}_{-0.10}$	[20] BUSKULIC	94B	ALEP	Sup. by BUSKULIC 97D
$0.52\ ^{+0.10}_{-0.11}\ ^{+0.04}_{-0.03}$	[27] BUSKULIC	93K	ALEP	Sup. by BUSKULIC 97D

[1] Measured using $B^0 \to D^{(*)-}\pi^+$ decays.

[2] Uses semileptonic decays of $B^0 \to D^-\mu^+\nu_\mu X$ and $B^0 \to D^{(*)-}\mu^+\nu_\mu X$, where the D mesons are reconstructed in $D^- \to K^+\pi^-\pi^-$ and $D^{(*)-} \to \overline{D}^0\pi^-$ with $\overline{D}^0 \to K^+\pi^-$.

[3] Uses semileptonic decays of $B^0 \to D^-\mu^+\nu_\mu X$ where the D^- mesons are reconstructed in $D^- \to K^+K^-\pi^-$.

[4] Measured using $B^0 \to D^-\pi^+$ and $B^0 \to J/\psi K^*(892)^0$ decays.

[5] Measured using $B^0 \to D^-\pi^+$.

[6] Uses opposite-side flavor-tagging with $B \to D^{(*)}\mu\nu_\mu X$ events.

[7] Measured using a simultaneous fit of the B^0 lifetime and $\overline{B}^0B^0$ oscillation frequency Δm_d in the partially reconstructed $B^0 \to D^{*-}\ell\nu$ decays.

[8] Measurement performed using a combined fit of CP-violation, mixing and lifetimes.

[9] Events with a high transverse momentum lepton were removed and an inclusively reconstructed vertex was required.

[10] AUBERT 03C uses a sample of approximately 14,000 exclusively reconstructed $B^0 \to D^*(2010)^-\ell\nu$ and simultaneously measures the lifetime and oscillation frequency.

[11] HASTINGS 03 measurement based on the time evolution of dilepton events. It also reports $f_+/f_0 = 1.01 \pm 0.03 \pm 0.09$ and CPT violation parameters in B^0-$\overline{B}^0$ mixing.

[12] ZHENG 03 data analyzed using partially reconstructed $\overline{B}^0 \to D^{*-}\pi^+$ decay and a flavor tag based on the charge of the lepton from the accompanying B decay.

[13] Uses a tagged sample of fully-reconstructed neutral B decays at $\Upsilon(4S)$.

[14] Measured based on the time evolution of dilepton events in $\Upsilon(4S)$ decays.

[15] Data analyzed using partially reconstructed $\overline{B}^0 \to D^{*+}\ell^-\overline{\nu}$ decay and a combination of flavor tags from the rest of the event.

[16] Uses di-muon events.

[17] Uses jet-charge and lepton-flavor tagging.

[18] Uses $\ell^-D^{*+}-\ell$ events.

[19] Uses π-B in the same side.

[20] Uses ℓ-ℓ.

[21] Uses ℓ-Q_{hem}.

[22] Uses ℓ-ℓ with impact parameters.

[23] Uses $D^{*\pm}$-Q_{hem}.

[24] Uses $\pi^\pm_s\ell$-Q_{hem}.

[25] Uses $D^{*\pm}$-ℓ/Q_{hem}.

[26] Uses $D^{*\pm}\ell$-Q_{hem}.

[27] Uses $D^{*\pm}$-ℓ.

[28] AUBERT 02N result based on the same analysis and data sample reported in AUBERT 02I.

[29] Uses a tagged sample of B^0 decays reconstructed in the mode $B^0 \to D^*\ell\nu$.

[30] Uses a tagged sample of fully-reconstructed hadronic B^0 decays at $\Upsilon(4S)$.

[31] ACCIARRI 98D combines results from ℓ-ℓ, ℓ-Q_{hem}, and ℓ-ℓ with impact parameters.

[32] ABREU 97N combines results from $D^{*\pm}$-Q_{hem}, ℓ-Q_{hem}, $\pi^\pm_s\ell$-Q_{hem}, and ℓ-ℓ.

[33] ACKERSTAFF 97V combines results from ℓ-ℓ, ℓ-Q_{hem}, D^*-ℓ, and $D^{*\pm}$-Q_{hem}.

[34] BUSKULIC 97D combines results from $D^{*\pm}$-ℓ/Q_{hem}, ℓ-Q_{hem}, and ℓ-ℓ.

[35] ABREU 96Q analysis performed using lepton, kaon, and jet-charge tags.

[36] ALEXANDER 96V combines results from $D^{*\pm}$-ℓ and $D^{*\pm}\ell$-Q_{hem}.

[37] AKERS 95J combines results from charge measurement, $D^{*\pm}\ell$-Q_{hem} and ℓ-ℓ.

Int. J. Mod. Phys. A 2026.41. Downloaded from www.worldscientific.com by CALIFORNIA @ BERKELEY on 09/16/26. Re-use and distribution is strictly not permitted, except for Open Access articles.

$x_d = \Delta m_{B^0}/\Gamma_{B^0}$

"OUR EVALUATION" is an average using rescaled values of the data listed below. The averaging/rescaling procedure takes into account correlations between the measurements and includes Δm_d calculated from χ_d measured at $\Upsilon(4S)$.

VALUE	DOCUMENT ID
0.7659±0.0032 OUR EVALUATION	(Produced by HFLAV)

Re(λ_{CP} / $|\lambda_{CP}|$) Re(z)

The λ_{CP} characterizes B^0 and $\overline{B}^0$ decays to states of charmonium plus K^0_L. Parameter z is used to describe CPT violation in mixing, see the review on "CP Violation" in the reviews section.

VALUE	DOCUMENT ID		TECN	COMMENT
0.047±0.022±0.003	[1] LEES	16E	BABR	$e^+e^- \to \Upsilon(4S)$
• • • We do not use the following data for averages, fits, limits, etc. • • •				
0.014±0.035±0.034	[2] AUBERT,B	04C	BABR	Repl. by LEES 16E

[1] The first uncertainty is the uncertainty from Re(z) and the second uncertainty is from Re($\lambda/|\lambda|$).
[2] Corresponds to 90% confidence range [−0.072, 0.101].

ΔΓ Re(z)

VALUE (ps^{-1})	DOCUMENT ID		TECN	COMMENT
−0.0071±0.0039±0.0020	AUBERT	06T	BABR	$e^+e^- \to \Upsilon(4S)$

Re(z)

VALUE (units 10^{-2})	DOCUMENT ID		TECN	COMMENT
−4 ± 4 OUR AVERAGE Error includes scale factor of 1.4.				
−6.5± 2.8±1.4	[1] LEES	16E	BABR	$e^+e^- \to \Upsilon(4S)$
1.9± 3.7±3.3	[2] HIGUCHI	12	BELL	$e^+e^- \to \Upsilon(4S)$
• • • We do not use the following data for averages, fits, limits, etc. • • •				
0 ±12 ±1	[3] HASTINGS	03	BELL	Repl. by HIGUCHI 12

[1] Measurement uses decays $B^0/\overline{B}^0 \to c\overline{c}K^0_S/K^0_L$.
[2] Measured using $B^0 \to J/\psi K^0_S$, $J/\psi K^0_L$, $D^-\pi^+$, $D^{*-}\pi^+$, $D^{*-}\rho^+$, and $D^{*-}\ell^+\nu$ decays.
[3] Measured using inclusive dilepton events from B^0 decay.

Im(z)

VALUE (units 10^{-2})	DOCUMENT ID		TECN	COMMENT
−0.8 ±0.4 OUR AVERAGE				
1.0 ±3.0 ±1.3	[1] LEES	16E	BABR	$e^+e^- \to \Upsilon(4S)$
−0.57±0.33±0.33	[2] HIGUCHI	12	BELL	$e^+e^- \to \Upsilon(4S)$
−1.39±0.73±0.32	[3] AUBERT	06T	BABR	$e^+e^- \to \Upsilon(4S)$
• • • We do not use the following data for averages, fits, limits, etc. • • •				
3.8 ±2.9 ±2.5	[4] AUBERT,B	04C	BABR	Repl. by AUBERT 06T
−3 ±1 ±3	[5] HASTINGS	03	BELL	Repl. by HIGUCHI 12

[1] Measurement uses decays $B^0/\overline{B}^0 \to c\overline{c}K^0_S/K^0_L$.
[2] Measured using $B^0 \to J/\psi K^0_S$, $J/\psi K^0_L$, $D^-\pi^+$, $D^{*-}\pi^+$, $D^{*-}\rho^+$, and $D^{*-}\ell^+\nu$ decays.
[3] Measurement uses $B^0/\overline{B}^0 \to \ell^+X/\ell^-X$ decays. Assuming $\Delta\Gamma = 0$, the result becomes Im(z) = $(-0.37 \pm 0.54) \times 10^{-2}$.
[4] Corresponds to 90% confidence range [−0.028, 0.104].
[5] Measured using inclusive dilepton events from B^0 decay.

CP VIOLATION PARAMETERS

Re(ϵ_{B^0})/(1+$|\epsilon_{B^0}|^2$)

CP impurity in B^0_d system. It is obtained from either $a_{\ell\ell}$, the charge asymmetry in like-sign dilepton events or a_{cp}, the time-dependent asymmetry of inclusive B^0 and $\overline{B}^0$ decays.

"OUR EVALUATION" is the result of a fit to B_d and B_s CP asymmetries, which includes the B_d measurements listed below and the B_s measurements listed in the B_s section, taking into account correlations between those measurements.

VALUE (units 10^{-3})	DOCUMENT ID		TECN	COMMENT
− 0.5 ± 0.4 OUR EVALUATION (Produced by HFLAV)				
− 0.1 ± 0.4 OUR AVERAGE				
− 0.05 ± 0.48 ±0.75	[1] AAIJ	15F	LHCB	pp at 7, 8 TeV
− 0.975± 0.875±0.475	[2] LEES	15A	BABR	$e^+e^- \to \Upsilon(4S)$
1.55 ± 1.05	[3] ABAZOV	14	D0	$p\overline{p}$ at 1.96 TeV
0.15 ± 0.42 $^{+0.94}_{-0.81}$	[4] LEES	13N	BABR	$e^+e^- \to \Upsilon(4S)$
− 1.7 ± 1.1 ±0.4	[5] ABAZOV	12AC	D0	$p\overline{p}$ at 1.96 TeV
0.4 ± 1.3 ±0.9	[6] AUBERT	06T	BABR	$e^+e^- \to \Upsilon(4S)$
− 0.3 ± 2.0 ±2.1	[7] NAKANO	06	BELL	$e^+e^- \to \Upsilon(4S)$
3.5 ±10.3 ±1.5	[8] JAFFE	01	CLE2	$e^+e^- \to \Upsilon(4S)$
• • • We do not use the following data for averages, fits, limits, etc. • • •				
− 0.3 ± 1.3	[9] ABAZOV	11U	D0	Repl. by ABAZOV 14
− 2.3 ± 1.1 ±0.8	[10] ABAZOV	06S	D0	Repl. by ABAZOV 11U
−14.7 ± 6.7 ±5.7	[11] AUBERT,B	04C	BABR	Repl. by AUBERT 06T
1.2 ± 2.9 ±3.6	[2] AUBERT	02K	BABR	Repl. by LEES 15A
− 3.2 ± 6.5	[12] BARATE	01D	ALEP	$e^+e^- \to Z$
4 ±18 ±3	[13] BEHRENS	00B	CLE2	Repl. by JAFFE 01
1.2 ±13.8 ±3.2	[14] ABBIENDI	99J	OPAL	$e^+e^- \to Z$
2 ± 7 ±3	[15] ACKERSTAFF	97U	OPAL	$e^+e^- \to Z$
< 45	[16] BARTELT	93	CLE2	$e^+e^- \to \Upsilon(4S)$

[1] AAIJ 15F uses semileptonic B^0 decays in the inclusive final states $D^-\mu^+$ and $D^{*-}\mu^+$, where the D^- meson decays into the $K^+\pi^-\pi^-$ final state, and the D^{*-} meson into the $\overline{D}^0(\to K^+\pi^-)\pi^-$ final state. Reports $A^d_{SL} = (-0.02 \pm 0.19 \pm 0.30)\%$, which equals to 4Re($\epsilon_{B^0}$)/(1+$|\epsilon_{B^0}|^2$).
[2] Uses the charge asymmetry in like-sign dilepton events. LEES 15A reports $A^d_{SL} = (-3.9 \pm 3.5 \pm 1.9) \times 10^{-3}$.
[3] ABAZOV 14 uses the dimuon charge asymmetry with different impact parameters from which it reports $A^d_{SL} = (-0.62 \pm 0.42) \times 10^{-2}$.
[4] Uses $B^0 \to D^{*-}X\ell^+\nu_\ell$ and a kaon-tagged sample which yields measurement of $A^d_{SL} = (0.06 \pm 0.17 ^{+0.38}_{-0.32})\%$, corresponding to $\Delta_{CP} = 1-|q/p| = (0.29 \pm 0.84 ^{+1.88}_{-1.61}) \times 10^{-3}$.
[5] ABAZOV 12AC uses $B^0 \to D^-\mu^+X$ and $B^0 \to D^*(2010)^-\mu^+X$ decays without initial state flavor tagging which yields measurement of $A^d_{SL} = (6.8 \pm 4.5 \pm 1.4) \times 10^{-3}$.
[6] AUBERT 06T reports $|q/p|-1=(-0.8\pm2.7\pm1.9)\times10^{-3}$. We convert to $(1-|q/p|^2)/4$.
[7] Uses the charge asymmetry in like-sign dilepton events and reports $|q/p| = 1.0005 \pm 0.0040 \pm 0.0043$.
[8] JAFFE 01 finds $a_{\ell\ell} = 0.013 \pm 0.050 \pm 0.005$ and combines with the previous BEHRENS 00B independent measurement.
[9] ABAZOV 11U uses the dimuon charge asymmetry with different impact parameters from which it reports $A^d_{SL} = (-1.2 \pm 5.2) \times 10^{-3}$.
[10] Uses the dimuon charge asymmetry.
[11] AUBERT 04C reports $|q/p| = 1.029 \pm 0.013 \pm 0.011$ and we converted it to (1- $|q/p|^2$)/4.
[12] BARATE 01D measured by investigating time-dependent asymmetries in semileptonic and fully inclusive B^0_d decays.
[13] BEHRENS 00B uses high-momentum lepton tags and partially reconstructed $\overline{B}^0 \to D^{*+}\pi^-$, ρ^- decays to determine the flavor of the B meson.
[14] Data analyzed using the time-dependent asymmetry of inclusive B^0 decay. The production flavor of B^0 mesons is determined using both the jet charge and the charge of secondary vertex in the opposite hemisphere.
[15] ACKERSTAFF 97U assumes CPT and is based on measuring the charge asymmetry in a sample of B^0 decays defined by lepton and Q_{hem} tags. If CPT is not invoked, Re(ϵ_B) = $-0.006 \pm 0.010 \pm 0.006$ is found. The indirect CPT violation parameter is determined to Im(δB) = $-0.020 \pm 0.016 \pm 0.006$.
[16] BARTELT 93 finds $a_{\ell\ell} = 0.031 \pm 0.096 \pm 0.032$ which corresponds to $|a_{\ell\ell}| < 0.18$, which yields the above |Re(ϵ_{B^0})/(1+$|\epsilon_{B^0}|^2$)|.

$A_{T/CP}$

$A_{T/CP}$ is defined as

$$\frac{P(\overline{B}^0 \to B^0) - P(B^0 \to \overline{B}^0)}{P(\overline{B}^0 \to B^0) + P(B^0 \to \overline{B}^0)},$$

the CPT invariant asymmetry between the oscillation probabilities P($\overline{B}^0 \to B^0$) and P($B^0 \to \overline{B}^0$).

VALUE	DOCUMENT ID		TECN	COMMENT
0.005±0.012±0.014	[1] AUBERT	02K	BABR	$e^+e^- \to \Upsilon(4S)$

[1] AUBERT 02K uses the charge asymmetry in like-sign dilepton events.

$A_{CP}(B^0 \to D^*(2010)^+D^-)$

A_{CP} is defined as

$$\frac{B(\overline{B}^0 \to \overline{f}) - B(B^0 \to f)}{B(\overline{B}^0 \to \overline{f}) + B(B^0 \to f)},$$

the CP-violation charge asymmetry of exclusive B^0 and $\overline{B}^0$ decay.

VALUE	DOCUMENT ID		TECN	COMMENT
0.013±0.014 OUR AVERAGE				
0.008±0.014±0.006	AAIJ	20L	LHCB	pp at 7, 8, 13 TeV
0.06 ±0.05 ±0.02	ROHRKEN	12	BELL	$e^+e^- \to \Upsilon(4S)$
0.008±0.048±0.013	AUBERT	09C	BABR	$e^+e^- \to \Upsilon(4S)$
0.07 ±0.08 ±0.04	[1] AUSHEV	04	BELL	$e^+e^- \to \Upsilon(4S)$
• • • We do not use the following data for averages, fits, limits, etc. • • •				
−0.12 ±0.06 ±0.02	AUBERT	07AI	BABR	Repl. by AUBERT 09C
−0.03 ±0.10 ±0.02	AUBERT,B	06A	BABR	Repl. by AUBERT 07AI
−0.03 ±0.11 ±0.05	AUBERT	03J	BABR	Repl. by AUBERT,B 06B

[1] Combines results from fully and partially reconstructed $B^0 \to D^{*\pm}D^\mp$ decays.

$A_{CP}(B^0 \to \overline{D}^0\pi^0)$

VALUE (units 10^{-2})	DOCUMENT ID		TECN	COMMENT
0.42±2.05±1.22	BLOOMFIELD	22	BELL	$e^+e^- \to \Upsilon(4S)$

$A_{CP}(B^0 \to [K^+K^-]_D K^*(892)^0)$

VALUE	DOCUMENT ID		TECN	COMMENT
−0.047±0.063±0.015	AAIJ	24M	LHCB	pp at 7, 8, 13 TeV
• • • We do not use the following data for averages, fits, limits, etc. • • •				
−0.05 ±0.10 ±0.01	AAIJ	19N	LHCB	Repl. by AAIJ 24M
−0.20 ±0.15 ±0.02	AAIJ	14BN	LHCB	Repl. by AAIJ 16S
−0.45 ±0.23 ±0.02	AAIJ	13L	LHCB	Repl. by AAIJ 14BN

$A_{CP}(B^0 \to [K^+\pi^-]_D K^*(892)^0)$

VALUE	DOCUMENT ID		TECN	COMMENT
0.031±0.017±0.015	AAIJ	24M	LHCB	pp at 7, 8, 13 TeV
• • • We do not use the following data for averages, fits, limits, etc. • • •				
0.047±0.027±0.010	AAIJ	19N	LHCB	Repl. by AAIJ 24M
−0.03 ±0.04 ±0.02	AAIJ	14BN	LHCB	Repl. by AAIJ 19N
−0.08 ±0.08 ±0.01	AAIJ	13L	LHCB	Repl. by AAIJ 14BN

Int. J. Mod. Phys. A 2026.41. Downloaded from www.worldscientific.com
by UNIVERSITY OF CALIFORNIA @ BERKELEY on 09/16/26. Re-use and distribution is strictly not permitted, except for Open Access articles.

$A_{CP}(B^0 \to [K^+\pi^-\pi^+\pi^-]_D K^*(892)^0)$

VALUE	DOCUMENT ID		TECN	COMMENT
−0.012±0.018±0.016	AAIJ	24M	LHCB	pp at 7, 8, 13 TeV
• • • We do not use the following data for averages, fits, limits, etc. • • •				
0.037±0.032±0.010	AAIJ	19N	LHCB	Repl. by AAIJ 24M

$A_{CP}(B^0 \to [K^-\pi^+]_D K^*(892)^0)$

VALUE	DOCUMENT ID		TECN	COMMENT
0.19±0.19±0.01	AAIJ	19N	LHCB	pp at 7, 8, 13 TeV

$A_{CP}(B^0 \to [K^-\pi^+\pi^+\pi^-]_D K^*(892)^0)$

VALUE	DOCUMENT ID		TECN	COMMENT
−0.01±0.24±0.01	AAIJ	19N	LHCB	pp at 7, 8, 13 TeV

$R_d^+ = \Gamma(B^0 \to [\pi^+K^-]_D K^{*0}) / \Gamma(B^0 \to [\pi^-K^+]_D K^{*0})$

VALUE	DOCUMENT ID		TECN	COMMENT
0.069±0.013±0.005	AAIJ	24M	LHCB	pp at 7, 8, 13 TeV
• • • We do not use the following data for averages, fits, limits, etc. • • •				
0.064±0.021±0.002	AAIJ	19N	LHCB	Repl. by AAIJ 24M
0.06 ±0.03 ±0.01	AAIJ	14BN	LHCB	Repl. by AAIJ 19N

$R_d^- = \Gamma(\overline{B}^0 \to [\pi^-K^+]_D K^{*0}) / \Gamma(\overline{B}^0 \to [\pi^+K^-]_D K^{*0})$

VALUE	DOCUMENT ID		TECN	COMMENT
0.093±0.013±0.005	AAIJ	24M	LHCB	pp at 7, 8, 13 TeV
• • • We do not use the following data for averages, fits, limits, etc. • • •				
0.095±0.021±0.003	AAIJ	19N	LHCB	Repl. by AAIJ 24M
0.06 ±0.03 ±0.01	AAIJ	14BN	LHCB	Repl. by AAIJ 19N

$A_{CP}(B^0 \to [\pi^+\pi^-]_D K^*(892)^0)$

VALUE	DOCUMENT ID		TECN	COMMENT
−0.034±0.094±0.016	AAIJ	24M	LHCB	pp at 7, 8, 13 TeV
• • • We do not use the following data for averages, fits, limits, etc. • • •				
−0.18 ±0.14 ±0.01	AAIJ	19N	LHCB	Repl. by AAIJ 24M
−0.09 ±0.22 ±0.02	AAIJ	14BN	LHCB	Repl. by AAIJ 16S

$A_{CP}(B^0 \to [\pi^+\pi^-\pi^+\pi^-]_D K^*(892)^0)$

VALUE	DOCUMENT ID		TECN	COMMENT
0.021±0.087±0.016	AAIJ	24M	LHCB	pp at 7, 8, 13 TeV
• • • We do not use the following data for averages, fits, limits, etc. • • •				
−0.03 ±0.15 ±0.01	AAIJ	19N	LHCB	Repl. by AAIJ 24M

$R_d^+ = \Gamma(B^0 \to [\pi^+K^-\pi^+\pi^-]_D K^{*0}) / \Gamma(B^0 \to [\pi^-K^+\pi^+\pi^-]_D K^{*0})$

VALUE	DOCUMENT ID		TECN	COMMENT
0.060±0.014±0.006	AAIJ	24M	LHCB	pp at 7, 8, 13 TeV
• • • We do not use the following data for averages, fits, limits, etc. • • •				
0.074±0.026±0.002	AAIJ	19N	LHCB	Repl. by AAIJ 24M

$R_d^- = \Gamma(\overline{B}^0 \to [\pi^-K^+\pi^+\pi^-]_D K^{*0}) / \Gamma(\overline{B}^0 \to [\pi^+K^-\pi^+\pi^-]_D K^{*0})$

VALUE	DOCUMENT ID		TECN	COMMENT
0.038±0.014±0.006	AAIJ	24M	LHCB	pp at 7, 8, 13 TeV
• • • We do not use the following data for averages, fits, limits, etc. • • •				
0.072±0.025±0.003	AAIJ	19N	LHCB	Repl. by AAIJ 24M

$A_{CP}(B^0 \to K^+\pi^-)$

VALUE	DOCUMENT ID		TECN	COMMENT
−0.0831±0.0031 OUR AVERAGE				
−0.072 ±0.019 ±0.007	ADACHI	24	BELL	$e^+e^- \to \Upsilon(4S)$
−0.0824±0.0033±0.0033	AAIJ	21O	LHCB	pp at 13 TeV
−0.084 ±0.004 ±0.003	AAIJ	18O	LHCB	pp at 7, 8 TeV
−0.083 ±0.013 ±0.004	AALTONEN	14P	CDF	$p\overline{p}$ at 1.96 TeV
−0.069 ±0.014 ±0.007	DUH	13	BELL	$e^+e^- \to \Upsilon(4S)$
−0.107 ±0.016 $^{+0.006}_{-0.004}$	LEES	13D	BABR	$e^+e^- \to \Upsilon(4S)$
−0.04 ±0.16	[1] CHEN	00	CLE2	$e^+e^- \to \Upsilon(4S)$
• • • We do not use the following data for averages, fits, limits, etc. • • •				
−0.080 ±0.007 ±0.003	AAIJ	13AX	LHCB	Repl. by AAIJ 18O
−0.088 ±0.011 ±0.008	AAIJ	12V	LHCB	Repl. by AAIJ 13AX
−0.086 ±0.023 ±0.009	AALTONEN	11N	CDF	Repl. by AALTONEN 14P
−0.094 ±0.018 ±0.008	LIN	08	BELL	Repl. by DUH 13
−0.107 ±0.018 $^{+0.007}_{-0.004}$	AUBERT	07AF	BABR	Repl. by LEES 13D
−0.013 ±0.078 ±0.012	ABULENCIA,A	06D	CDF	Repl. by AALTONEN 11N
−0.088 ±0.035 ±0.013	[2] CHAO	05A	BELL	Repl. by CHAO 04B
−0.133 ±0.030 ±0.009	[3] AUBERT,B	04K	BABR	Repl. by AUBERT 07AF
−0.101 ±0.025 ±0.005	[4] CHAO	04B	BELL	Repl. by LIN 08
−0.07 ±0.08 ±0.02	[5] AUBERT	02D	BABR	Repl. by AUBERT 02Q
−0.102 ±0.050 ±0.016	[6] AUBERT	02Q	BABR	Repl. by AUBERT,B 04K
−0.06 ±0.09 $^{+0.01}_{-0.02}$	[7] CASEY	02	BELL	Repl. by CHAO 04B
0.044 $^{+0.186}_{-0.167}$ $^{+0.018}_{-0.021}$	[8] ABE	01K	BELL	Repl. by CASEY 02
−0.19 ±0.10 ±0.03	[9] AUBERT	01E	BABR	Repl. by AUBERT 02Q

[1] Corresponds to 90% confidence range $-0.30 < A_{CP} < 0.22$.
[2] Corresponds to a 90% CL interval of $-0.15 < A_{CP} < -0.03$.
[3] Based on a total signal yield of $N(K^-\pi^+) + N(K^+\pi^-) = 1606 \pm 51$ events.
[4] CHAO 04B reports significance of 3.9 standard deviation for deviation of A_{CP} from zero.
[5] Corresponds to 90% confidence range $-0.21 < A_{CP} < 0.07$.
[6] Corresponds to 90% confidence range $-0.188 < A_{CP} < -0.016$.
[7] Corresponds to 90% confidence range $-0.21 < A_{CP} < +0.09$.
[8] Corresponds to 90% confidence range $-0.25 < A_{CP} < 0.37$.
[9] Corresponds to 90% confidence range $-0.35 < A_{CP} < -0.03$.

$A_{CP}(B^0 \to \eta' K^*(892)^0)$

VALUE	DOCUMENT ID		TECN	COMMENT
−0.07±0.18 OUR AVERAGE				
−0.22±0.29±0.07	SATO	14	BELL	$e^+e^- \to \Upsilon(4S)$
0.02±0.23±0.02	DEL-AMO-SA...10A		BABR	$e^+e^- \to \Upsilon(4S)$
• • • We do not use the following data for averages, fits, limits, etc. • • •				
0.08±0.25±0.02	[1] AUBERT	07E	BABR	Repl. by DEL-AMO-SANCHEZ 10A

[1] Reports A_{CP} with the opposite sign convention.

$A_{CP}(B^0 \to \eta' K_0^*(1430)^0)$

VALUE	DOCUMENT ID		TECN	COMMENT
−0.19±0.17±0.02	DEL-AMO-SA...10A		BABR	$e^+e^- \to \Upsilon(4S)$

$A_{CP}(B^0 \to \eta' K_2^*(1430)^0)$

VALUE	DOCUMENT ID		TECN	COMMENT
0.14±0.18±0.02	DEL-AMO-SA...10A		BABR	$e^+e^- \to \Upsilon(4S)$

$A_{CP}(B^0 \to \eta K^*(892)^0)$

VALUE	DOCUMENT ID		TECN	COMMENT
0.19±0.05 OUR AVERAGE				
0.17±0.08±0.01	WANG	07B	BELL	$e^+e^- \to \Upsilon(4S)$
0.21±0.06±0.02	AUBERT,B	06H	BABR	$e^+e^- \to \Upsilon(4S)$
• • • We do not use the following data for averages, fits, limits, etc. • • •				
0.02±0.11±0.02	AUBERT,B	04D	BABR	Repl. by AUBERT,B 06H

$A_{CP}(B^0 \to \eta K_0^*(1430)^0)$

VALUE	DOCUMENT ID		TECN	COMMENT
0.06±0.13±0.02	AUBERT,B	06H	BABR	$e^+e^- \to \Upsilon(4S)$

$A_{CP}(B^0 \to \eta K_2^*(1430)^0)$

VALUE	DOCUMENT ID		TECN	COMMENT
−0.07±0.19±0.02	AUBERT,B	06H	BABR	$e^+e^- \to \Upsilon(4S)$

$A_{CP}(B^0 \to b_1 K^+)$

VALUE	DOCUMENT ID		TECN	COMMENT
−0.07±0.12±0.02	AUBERT	07BI	BABR	$e^+e^- \to \Upsilon(4S)$

$A_{CP}(B^0 \to \omega K^{*0})$

VALUE	DOCUMENT ID		TECN	COMMENT
0.45±0.25±0.02	AUBERT	09H	BABR	$e^+e^- \to \Upsilon(4S)$

$A_{CP}(B^0 \to \omega (K\pi)_0^{*0})$

VALUE	DOCUMENT ID		TECN	COMMENT
−0.07±0.09±0.02	AUBERT	09H	BABR	$e^+e^- \to \Upsilon(4S)$

$A_{CP}(B^0 \to \omega K_2^*(1430)^0)$

VALUE	DOCUMENT ID		TECN	COMMENT
−0.37±0.17±0.02	AUBERT	09H	BABR	$e^+e^- \to \Upsilon(4S)$

$A_{CP}(B^0 \to K^+\pi^-\pi^0)$

VALUE (units 10^{-2})	DOCUMENT ID		TECN	COMMENT
0 ± 6 OUR AVERAGE				
$-3.0^{+4.5}_{-5.1}\pm5.5$	[1] AUBERT	08AQ	BABR	$e^+e^- \to \Upsilon(4S)$
7 ±11 ±1	[2] CHANG	04	BELL	$e^+e^- \to \Upsilon(4S)$

[1] Uses Dalitz plot analysis of $B^0 \to K^+\pi^-\pi^0$ decays.
[2] Corresponds to 90% confidence range $-0.12 < A_{CP} < 0.26$.

$A_{CP}(B^0 \to \rho^- K^+)$

VALUE	DOCUMENT ID		TECN	COMMENT
0.20±0.11 OUR AVERAGE				
0.20±0.09±0.08	[1] LEES	11	BABR	$e^+e^- \to \Upsilon(4S)$
$0.22^{+0.22}_{-0.23}\pm^{0.06}_{0.02}$	[2] CHANG	04	BELL	$e^+e^- \to \Upsilon(4S)$
• • • We do not use the following data for averages, fits, limits, etc. • • •				
$0.11^{+0.14}_{-0.15}\pm0.07$	[1] AUBERT	08AQ	BABR	Repl. by LEES 11
−0.28±0.17±0.08	[3] AUBERT	03T	BABR	Repl. by AUBERT 08AQ

[1] Uses Dalitz plot analysis of $B^0 \to K^+\pi^-\pi^0$ decays.
[2] Corresponds to 90% confidence range $-0.18 < A_{CP} < 0.64$.
[3] The result reported corresponds to $-A_{CP}$.

$A_{CP}(B^0 \to \rho(1450)^- K^+)$

VALUE	DOCUMENT ID		TECN	COMMENT
−0.10±0.32±0.09	[1] LEES	11	BABR	$e^+e^- \to \Upsilon(4S)$

[1] Uses Dalitz plot analysis of $B^0 \to K^+\pi^-\pi^0$ decays.

Int. J. Mod. Phys. A 2026.41. Downloaded from www.worldscientific.com by LIFORNIA @ BERKELEY on 09/16/26. Re-use and distribution is strictly not permitted, except for Open Access articles.

$A_{CP}(B^0 \to \rho(1700)^- K^+)$

VALUE	DOCUMENT ID		TECN	COMMENT
−0.36±0.57±0.23	[1] LEES	11	BABR	$e^+e^- \to \Upsilon(4S)$

[1] Uses Dalitz plot analysis of $B^0 \to K^+\pi^-\pi^0$ decays.

$A_{CP}(B^0 \to K^+\pi^-\pi^0 \text{nonresonant})$

VALUE	DOCUMENT ID		TECN	COMMENT
0.10±0.16±0.08	[1] LEES	11	BABR	$e^+e^- \to \Upsilon(4S)$
• • • We do not use the following data for averages, fits, limits, etc. • • •				
$0.23^{+0.19}_{-0.27}{}^{+0.11}_{-0.10}$	[1] AUBERT	08AQ	BABR	Repl. by LEES 11

[1] Uses Dalitz plot analysis of $B^0 \to K^+\pi^-\pi^0$ decays. The quoted value is only for the flat part of the non-resonant component.

$A_{CP}(B^0 \to K^0\pi^+\pi^-)$

VALUE	DOCUMENT ID		TECN	COMMENT
−0.01±0.05±0.01	[1] AUBERT	09AU	BABR	$e^+e^- \to \Upsilon(4S)$

[1] Uses Dalitz plot analysis of $B^0 \to K^0\pi^+\pi^-$ decays and the first of two equivalent solutions is used.

$A_{CP}(B^0 \to K^*(892)^+\pi^-)$

VALUE	DOCUMENT ID		TECN	COMMENT
−0.27 ±0.04 OUR AVERAGE				
−0.308±0.060±0.016	[1] AAIJ	18F	LHCB	pp at 7, 8 TeV
−0.29 ±0.11 ±0.02	[2] LEES	11	BABR	$e^+e^- \to \Upsilon(4S)$
−0.21 ±0.10 ±0.02	[3,4] AUBERT	09AU	BABR	$e^+e^- \to \Upsilon(4S)$
−0.21 ±0.11 ±0.07	[5] DALSENO	09	BELL	$e^+e^- \to \Upsilon(4S)$
$0.26\ ^{+0.33}_{-0.34}\ ^{+0.10}_{-0.08}$	[6] EISENSTEIN	03	CLE2	$e^+e^- \to \Upsilon(4S)$
• • • We do not use the following data for averages, fits, limits, etc. • • •				
$-0.19\ ^{+0.20}_{-0.15}$ ±0.04	[2] AUBERT	08AQ	BABR	Repl. by LEES 11
−0.11 ±0.14 ±0.05	[3] AUBERT	06I	BABR	Repl. by AUBERT 09AU
0.23 ±0.18 $^{+0.09}_{-0.06}$	AUBERT,B	04O	BABR	Repl. by AUBERT 06I

[1] Uses Dalitz plot analysis of the $B^0 \to K^0_S\pi^+\pi^-$ final state decays.
[2] Uses Dalitz plot analysis of $B^0 \to K^+\pi^-\pi^0$ decays.
[3] Uses Dalitz plot analysis of $B^0 \to K^0\pi^+\pi^-$ decays.
[4] The first of two equivalent solutions is used.
[5] Uses Dalitz plot analysis of $B^0 \to K^0\pi^+\pi^-$ decays and the first of two consistent solutions that may be preferred.
[6] Corresponds to 90% confidence range $-0.31 < A_{CP} < 0.78$.

$A_{CP}(B^0 \to (K\pi)^{*+}_0\pi^-)$

VALUE	DOCUMENT ID		TECN	COMMENT
0.02 ±0.04 OUR AVERAGE				
−0.032±0.047±0.031	[1] AAIJ	18F	LHCB	pp at 7, 8 TeV
0.07 ±0.14 ±0.01	[2] LEES	11	BABR	$e^+e^- \to \Upsilon(4S)$
0.09 ±0.07 ±0.03	[3] AUBERT	09AU	BABR	$e^+e^- \to \Upsilon(4S)$
• • • We do not use the following data for averages, fits, limits, etc. • • •				
$0.17\ ^{+0.11}_{-0.16}$ ±0.22	[2] AUBERT	08AQ	BABR	Repl. by LEES 11

[1] Uses Dalitz plot analysis of the $B^0 \to K^0_S\pi^+\pi^-$ final states decays.
[2] Uses Dalitz plot analysis of $B^0 \to K^+\pi^-\pi^0$ decays.
[3] Uses Dalitz plot analysis of $B^0 \to K^0\pi^+\pi^-$ decays and the first of two equivalent solutions is used.

$A_{CP}(B^0 \to K^*_2(1430)^+\pi^-)$

VALUE	DOCUMENT ID		TECN	COMMENT
−0.29±0.22±0.09	[1] AAIJ	18F	LHCB	pp at 7, 8 TeV

[1] Uses Dalitz plot analysis of the $B^0 \to K^0_S\pi^+\pi^-$ final state decays.

$A_{CP}(B^0 \to K^*(1680)^+\pi^-)$

VALUE	DOCUMENT ID		TECN	COMMENT
−0.07±0.13±0.04	[1] AAIJ	18F	LHCB	pp at 7, 8 TeV

[1] Uses Dalitz plot analysis of the $B^0 \to K^0_S\pi^+\pi^-$ final state decays.

$A_{CP}(B^0 \to f_0(980)K^0_S)$

VALUE	DOCUMENT ID		TECN	COMMENT
0.28±0.27±0.15	[1] AAIJ	18F	LHCB	pp at 7, 8 TeV

[1] Uses Dalitz plot analysis of the $B^0 \to K^0_S\pi^+\pi^-$ final state decays.

$A_{CP}(B^0 \to (K\pi)^{*0}_0\pi^0)$

VALUE	DOCUMENT ID		TECN	COMMENT
−0.15±0.10±0.04	[1] LEES	11	BABR	$e^+e^- \to \Upsilon(4S)$
• • • We do not use the following data for averages, fits, limits, etc. • • •				
$-0.22\pm0.12^{+0.30}_{-0.29}$	[1] AUBERT	08AQ	BABR	Repl. by LEES 11

[1] Uses Dalitz plot analysis of $B^0 \to K^+\pi^-\pi^0$ decays.

$A_{CP}(B^0 \to K^{*0}\pi^0)$

VALUE	DOCUMENT ID		TECN	COMMENT
−0.15±0.12±0.04	[1] LEES	11	BABR	$e^+e^- \to \Upsilon(4S)$
• • • We do not use the following data for averages, fits, limits, etc. • • •				
$-0.09^{+0.21}_{-0.24}$±0.09	[1] AUBERT	08AQ	BABR	Repl. by LEES 11

[1] Uses Dalitz plot analysis of $B^0 \to K^+\pi^-\pi^0$ decays.

$A_{CP}(B^0 \to K^*(892)^0\pi^+\pi^-)$

VALUE	DOCUMENT ID		TECN	COMMENT
0.07±0.04±0.03	AUBERT	07AS	BABR	$e^+e^- \to \Upsilon(4S)$

$A_{CP}(B^0 \to K^*(892)^0\rho^0)$

VALUE	DOCUMENT ID		TECN	COMMENT
−0.06±0.09±0.02	LEES	12K	BABR	$e^+e^- \to \Upsilon(4S)$
• • • We do not use the following data for averages, fits, limits, etc. • • •				
0.09±0.19±0.02	AUBERT,B	06G	BABR	Repl. by LEES 12K

$A_{CP}(B^0 \to K^{*0}f_0(980))$

VALUE	DOCUMENT ID		TECN	COMMENT
0.07±0.10±0.02	LEES	12K	BABR	$e^+e^- \to \Upsilon(4S)$
• • • We do not use the following data for averages, fits, limits, etc. • • •				
−0.17±0.28±0.02	AUBERT,B	06G	BABR	Repl. by LEES 12K

$A_{CP}(B^0 \to K^{*+}\rho^-)$

VALUE	DOCUMENT ID		TECN	COMMENT
0.21±0.15±0.02	LEES	12K	BABR	$e^+e^- \to \Upsilon(4S)$

$A_{CP}(B^0 \to K^*(892)^0K^+K^-)$

VALUE	DOCUMENT ID		TECN	COMMENT
0.01±0.05±0.02	AUBERT	07AS	BABR	$e^+e^- \to \Upsilon(4S)$

$A_{CP}(B^0 \to a_1^- K^+)$

VALUE	DOCUMENT ID		TECN	COMMENT
−0.16±0.12±0.01	AUBERT	08F	BABR	$e^+e^- \to \Upsilon(4S)$

$A_{CP}(B^0 \to K^0K^0)$

VALUE	DOCUMENT ID		TECN	COMMENT
$\mathbf{-0.58^{+0.73}_{-0.66}\pm0.04}$	LIN	07	BELL	$e^+e^- \to \Upsilon(4S)$

$A_{CP}(B^0 \to K^*(892)^0\phi)$

VALUE	DOCUMENT ID		TECN	COMMENT
0.00 ±0.04 OUR AVERAGE				
−0.007±0.048±0.021	PRIM	13	BELL	$e^+e^- \to \Upsilon(4S)$
0.01 ±0.06 ±0.03	AUBERT	08BG	BABR	$e^+e^- \to \Upsilon(4S)$
• • • We do not use the following data for averages, fits, limits, etc. • • •				
−0.03 ±0.07 ±0.03	AUBERT	07D	BABR	Repl. by AUBERT 08BG
0.02 ±0.09 ±0.02	[1] CHEN	05A	BELL	Repl. by PRIM 13
−0.01 ±0.09 ±0.02	AUBERT,B	04W	BABR	Repl. by AUBERT 07D
0.04 ±0.12 ±0.02	AUBERT	03V	BABR	Repl. by AUBERT 04W
0.07 ±0.15 $^{+0.05}_{-0.03}$	[2] CHEN	03B	BELL	Repl. by CHEN 05A
0.00 ±0.27 ±0.03	[3] AUBERT	02E	BABR	Repl. by AUBERT 03V

[1] Corresponds to 90% confidence range $-0.14 < A_{CP} < 0.17$.
[2] Corresponds to 90% confidence range $-0.18 < A_{CP} < 0.33$.
[3] Corresponds to 90% confidence range $-0.44 < A_{CP} < 0.44$.

$A_{CP}(B^0 \to K^*(892)^0K^-\pi^+)$

VALUE	DOCUMENT ID		TECN	COMMENT
0.22±0.33±0.20	AUBERT	07AS	BABR	$e^+e^- \to \Upsilon(4S)$

$A_{CP}(B^0 \to \phi(K\pi)^{*0}_0)$

VALUE	DOCUMENT ID		TECN	COMMENT
0.12 ±0.08 OUR AVERAGE				
0.093±0.094±0.017	PRIM	13	BELL	$e^+e^- \to \Upsilon(4S)$
0.20 ±0.14 ±0.06	AUBERT	08BG	BABR	$e^+e^- \to \Upsilon(4S)$
• • • We do not use the following data for averages, fits, limits, etc. • • •				
0.17 ±0.15 ±0.03	AUBERT	07D	BABR	Repl. by AUBERT 08BG

$A_{CP}(B^0 \to \phi K^*_2(1430)^0)$

VALUE	DOCUMENT ID		TECN	COMMENT
−0.11 ±0.10 OUR AVERAGE				
$-0.155^{+0.152}_{-0.133}$±0.033	PRIM	13	BELL	$e^+e^- \to \Upsilon(4S)$
−0.08 ±0.12 ±0.05	AUBERT	08BG	BABR	$e^+e^- \to \Upsilon(4S)$
• • • We do not use the following data for averages, fits, limits, etc. • • •				
−0.12 ±0.14 ±0.04	AUBERT	07D	BABR	Repl. by AUBERT 08BG

$A_{CP}(B^0 \to K^*(892)^0\gamma)$

VALUE	DOCUMENT ID		TECN	COMMENT
−0.012±0.010 OUR AVERAGE				
−0.033±0.023±0.004	ADACHI	25Z	BELL	$e^+e^- \to \Upsilon(4S)$
−0.013±0.017±0.004	[1] HORIGUCHI	17	BELL	$e^+e^- \to \Upsilon(4S)$
0.008±0.017±0.009	AAIJ	13	LHCB	pp at 7 TeV
−0.016±0.022±0.007	AUBERT	09AO	BABR	$e^+e^- \to \Upsilon(4S)$

[1] Uses $B(\Upsilon(4S) \to B^+B^-) = (51.4 \pm 0.6)\%$ and $B(\Upsilon(4S) \to B^0\overline{B}^0) = (48.6 \pm 0.6)\%$.

Int. J. Mod. Phys. A 2026.41. Downloaded from www.worldscientific.com
by UNIVERSITY OF CALIFORNIA @ BERKELEY on 09/16/26. Re-use and distribution is strictly not permitted, except for Open Access articles.

$A_{CP}(B^0 \to K_2^*(1430)^0\gamma)$

VALUE	DOCUMENT ID		TECN	COMMENT
−0.08±0.15±0.01	AUBERT,B	04U	BABR	$e^+e^- \to \Upsilon(4S)$

$A_{CP}(B^0 \to X_s\gamma)$

VALUE	DOCUMENT ID		TECN	COMMENT
−0.0094±0.0174±0.0047	[1] WATANUKI	19	BELL	$e^+e^- \to \Upsilon(4S)$

[1] Using a sum-of-exclusive technique with $m_{X_s} < 2.8$ GeV/c^2.

$A_{CP}(B^0 \to \rho^+\pi^-)$

VALUE	DOCUMENT ID		TECN	COMMENT
0.13±0.06 OUR AVERAGE	Error includes scale factor of 1.1.			
$0.09^{+0.05}_{-0.06}\pm0.04$	[1] LEES	13J	BABR	$e^+e^- \to \Upsilon(4S)$
0.21±0.08±0.04	[1] KUSAKA	07	BELL	$e^+e^- \to \Upsilon(4S)$
• • • We do not use the following data for averages, fits, limits, etc. • • •				
0.03±0.07±0.04	AUBERT	07AA	BABR	Repl. by LEES 13J
$-0.02\pm0.16^{+0.05}_{-0.02}$	WANG	05	BELL	Repl. by KUSAKA 07
−0.18±0.08±0.03	AUBERT	03T	BABR	Repl. by AUBERT 07AA

[1] Uses time-dependent Dalitz plot analysis of $B^0 \to \pi^+\pi^-\pi^0$ decays.

$A_{CP}(B^0 \to \rho^-\pi^+)$

VALUE	DOCUMENT ID		TECN	COMMENT
−0.08±0.08 OUR AVERAGE				
$-0.12\pm0.08^{+0.04}_{-0.05}$	[1] LEES	13J	BABR	$e^+e^- \to \Upsilon(4S)$
0.08±0.16±0.11	[1] KUSAKA	07	BELL	$e^+e^- \to \Upsilon(4S)$
• • • We do not use the following data for averages, fits, limits, etc. • • •				
$-0.37\pm0.16^{+0.09}_{-0.10}$	AUBERT	07AA	BABR	Repl. by LEES 13J
$-0.53\pm0.29^{+0.09}_{-0.04}$	WANG	05	BELL	Repl. by KUSAKA 07

[1] Uses time-dependent Dalitz plot analysis of $B^0 \to \pi^+\pi^-\pi^0$ decays.

$A_{CP}(B^0 \to \omega\omega)$

VALUE	DOCUMENT ID		TECN	COMMENT
−0.44±0.43±0.11	GUAN	24	BELL	$e^+e^- \to \Upsilon(4S)$

$A_{CP}(B^0 \to a_1(1260)^\pm\pi^\mp)$

VALUE	DOCUMENT ID		TECN	COMMENT
−0.07±0.06 OUR AVERAGE				
−0.06±0.05±0.07	DALSENO	12	BELL	$e^+e^- \to \Upsilon(4S)$
−0.07±0.07±0.02	AUBERT	07O	BABR	$e^+e^- \to \Upsilon(4S)$

$A_{CP}(B^0 \to b_1^-\pi^+)$

VALUE	DOCUMENT ID		TECN	COMMENT
−0.05±0.10±0.02	AUBERT	07BI	BABR	$e^+e^- \to \Upsilon(4S)$

$A_{CP}(B^0 \to p\overline{p}K^*(892)^0)$

VALUE	DOCUMENT ID		TECN	COMMENT
0.05±0.12 OUR AVERAGE				
−0.08±0.20±0.02	CHEN	08C	BELL	$e^+e^- \to \Upsilon(4S)$
0.11±0.13±0.06	AUBERT	07AV	BABR	$e^+e^- \to \Upsilon(4S)$

$A_{CP}(B^0 \to p\overline{\Lambda}\pi^-)$

VALUE	DOCUMENT ID		TECN	COMMENT
0.04±0.07 OUR AVERAGE				
0.10±0.10±0.02	AUBERT	09AC	BABR	$e^+e^- \to \Upsilon(4S)$
−0.02±0.10±0.03	WANG	07C	BELL	$e^+e^- \to \Upsilon(4S)$

$A_{CP}(B^0 \to K^{*0}\ell^+\ell^-)$

VALUE	DOCUMENT ID		TECN	COMMENT
−0.05±0.10 OUR AVERAGE				
0.02±0.20±0.02	AUBERT	09T	BABR	$e^+e^- \to \Upsilon(4S)$
−0.08±0.12±0.02	WEI	09A	BELL	$e^+e^- \to \Upsilon(4S)$

$A_{CP}(B^0 \to K^{*0}e^+e^-)$

VALUE	DOCUMENT ID		TECN	COMMENT
−0.21±0.19±0.02	WEI	09A	BELL	$e^+e^- \to \Upsilon(4S)$

$A_{CP}(B^0 \to K^{*0}\mu^+\mu^-)$

VALUE	DOCUMENT ID		TECN	COMMENT
−0.034±0.024 OUR AVERAGE				
−0.035±0.024±0.003	AAIJ	14AN	LHCB	pp at 7, 8 TeV
0.00 ±0.15 ±0.03	WEI	09A	BELL	$e^+e^- \to \Upsilon(4S)$
• • • We do not use the following data for averages, fits, limits, etc. • • •				
−0.072±0.040±0.005	AAIJ	13E	LHCB	Repl. by AAIJ 14AN

$C_{D^*(2010)^-D^+}$ $(B^0 \to D^*(2010)^-D^+)$

VALUE	DOCUMENT ID		TECN	COMMENT
−0.02 ±0.08 OUR AVERAGE				
−0.028±0.130±0.026	[1] AAIJ	20L	LHCB	pp at 7, 8, 13 TeV
−0.13 ±0.16 ±0.05	[2] ROHRKEN	12	BELL	$e^+e^- \to \Upsilon(4S)$
0.00 ±0.17 ±0.03	AUBERT	09C	BABR	$e^+e^- \to \Upsilon(4S)$
0.23 ±0.25 ±0.06	[3] AUSHEV	04	BELL	$e^+e^- \to \Upsilon(4S)$
• • • We do not use the following data for averages, fits, limits, etc. • • •				
0.23 ±0.15 ±0.04	AUBERT	07AI	BABR	Repl. by AUBERT 09C
0.17 ±0.24 ±0.04	AUBERT,B	05Z	BABR	Repl. by AUBERT 07AI
−0.22 ±0.37 ±0.10	AUBERT	03J	BABR	Repl. by AUBERT,B 05Z

[1] AAIJ 20L reports the measurements of C = −0.059±0.092±0.020 and ΔC = −0.031±0.092 ± 0.016 such that $C_{D^*(2010)^-D^+}$ = C − ΔC.

[2] ROHRKEN 12 reports the measurements of C = −0.01 ± 0.11 ± 0.04 and ΔC = 0.12 ± 0.11 ± 0.03 such that $C_{D^*(2010)^-D^+}$ = C − ΔC .

[3] Combines results from fully and partially reconstructed $B^0 \to D^{*\pm}D^\mp$ decays.

$S_{D^*(2010)^-D^+}$ $(B^0 \to D^*(2010)^-D^+)$

VALUE	DOCUMENT ID		TECN	COMMENT
−0.83 ±0.09 OUR AVERAGE				
−0.880±0.107±0.022	[1] AAIJ	20L	LHCB	pp at 7, 8, 13 TeV
−0.65 ±0.22 ±0.07	[2] ROHRKEN	12	BELL	$e^+e^- \to \Upsilon(4S)$
−0.73 ±0.23 ±0.050	AUBERT	09C	BABR	$e^+e^- \to \Upsilon(4S)$
−0.96 ±0.43 ±0.12	[3] AUSHEV	04	BELL	$e^+e^- \to \Upsilon(4S)$
• • • We do not use the following data for averages, fits, limits, etc. • • •				
−0.44 ±0.22 ±0.06	AUBERT	07AI	BABR	Repl. by AUBERT 09C
−0.29 ±0.33 ±0.07	AUBERT,B	05Z	BABR	Repl. by AUBERT 07AI
−0.24 ±0.69 ±0.12	AUBERT	03J	BABR	Repl. by AUBERT,B 05Z

[1] AAIJ 20L reports the measurements of S = −0.861 ± 0.077 ± 0.019 and ΔS = 0.019 ± 0.075 ± 0.012 such that $S_{D^*(2010)^-D^+}$ = S − ΔS.

[2] ROHRKEN 12 reports the measurements of S = −0.78 ± 0.15 ± 0.05 and ΔS = −0.13 ± 0.15 ± 0.04 such that $S_{D^*(2010)^+D^-}$ = S − ΔS.

[3] Combines results from fully and partially reconstructed $B^0 \to D^{*\pm}D^\mp$ decays.

$C_{D^*(2010)^+D^-}$ $(B^0 \to D^*(2010)^+D^-)$

VALUE	DOCUMENT ID		TECN	COMMENT
−0.03 ±0.09 OUR AVERAGE	Error includes scale factor of 1.1.			
−0.090±0.130±0.026	[1] AAIJ	20L	LHCB	pp at 7, 8, 13 TeV
0.11 ±0.14 ±0.06	[2] ROHRKEN	12	BELL	$e^+e^- \to \Upsilon(4S)$
0.08 ±0.17 ±0.04	AUBERT	09C	BABR	$e^+e^- \to \Upsilon(4S)$
−0.37 ±0.22 ±0.06	[3] AUSHEV	04	BELL	$e^+e^- \to \Upsilon(4S)$
• • • We do not use the following data for averages, fits, limits, etc. • • •				
0.18 ±0.15 ±0.04	AUBERT	07AI	BABR	Repl. by AUBERT 09C
0.09 ±0.25 ±0.06	AUBERT,B	05Z	BABR	Repl. by AUBERT 07AI
−0.47 ±0.40 ±0.12	AUBERT	03J	BABR	Repl. by AUBERT,B 05Z

[1] AAIJ 20L reports the measurements of C = −0.059±0.092±0.020 and ΔC = −0.031±0.092 ± 0.016 such that $C_{D^*(2010)^+D^-}$ = C + ΔC.

[2] ROHRKEN 12 reports the measurements of C = −0.01 ± 0.11 ± 0.04 and ΔC = 0.12 ± 0.11 ± 0.03 such that $C_{D^*(2010)^+D^-}$ = C + ΔC .

[3] Combines results from fully and partially reconstructed $B^0 \to D^{*\pm}D^\mp$ decays.

$S_{D^*(2010)^+D^-}$ $(B^0 \to D^*(2010)^+D^-)$

VALUE	DOCUMENT ID		TECN	COMMENT
−0.80 ±0.09 OUR AVERAGE				
−0.842±0.107±0.022	[1] AAIJ	20L	LHCB	pp at 7, 8, 13 TeV
−0.90 ±0.21 ±0.07	[2] ROHRKEN	12	BELL	$e^+e^- \to \Upsilon(4S)$
−0.62 ±0.21 ±0.03	AUBERT	09C	BABR	$e^+e^- \to \Upsilon(4S)$
−0.55 ±0.39 ±0.12	[3] AUSHEV	04	BELL	$e^+e^- \to \Upsilon(4S)$
• • • We do not use the following data for averages, fits, limits, etc. • • •				
−0.79 ±0.21 ±0.06	AUBERT	07AI	BABR	Repl. by AUBERT 09C
−0.54 ±0.35 ±0.07	AUBERT,B	05Z	BABR	Repl. by AUBERT 07AI
−0.82 ±0.75 ±0.14	AUBERT	03J	BABR	Repl. by AUBERT,B 05Z

[1] AAIJ 20L reports the measurements of S = −0.861 ± 0.077 ± 0.019 and ΔS = 0.019 ± 0.075 ± 0.012 such that $S_{D^*(2010)^+D^-}$ = S + ΔS.

[2] ROHRKEN 12 reports the measurements of S = −0.78 ± 0.15 ± 0.05 and ΔS = −0.13 ± 0.15 ± 0.04 such that $S_{D^*(2010)^+D^-}$ = S + ΔS.

[3] Combines results from fully and partially reconstructed $B^0 \to D^{*\pm}D^\mp$ decays.

$C_{D^{*+}D^{*-}}$ $(B^0 \to D^{*+}D^{*-})$

VALUE	DOCUMENT ID		TECN	COMMENT
0.01±0.09 OUR AVERAGE	Error includes scale factor of 1.6. See the ideogram below.			
−0.15±0.08±0.04	[1,2] KRONENBIT...	12	BELL	$e^+e^- \to \Upsilon(4S)$
+0.15±0.09±0.04	[3] LEES	12AF	BABR	$e^+e^- \to \Upsilon(4S)$
0.05±0.09±0.02	AUBERT	09C	BABR	$e^+e^- \to \Upsilon(4S)$
• • • We do not use the following data for averages, fits, limits, etc. • • •				
−0.15±0.13±0.04	[2] VERVINK	09	BELL	Repl. by KRONENBITTER 12
−0.02±0.11±0.02	[1] AUBERT	07BO	BABR	Repl. by AUBERT 09C
0.26±0.26±0.06	[2] MIYAKE	05	BELL	Repl. by VERVINK 09
0.28±0.23±0.02	[4] AUBERT	03Q	BABR	Repl. by AUBERT 07BO

[1] Assumes both CP-even and CP-odd states having the CP asymmetry.

[2] Belle Collab. quotes $A_{D^{*+}D^{*-}}$ which is equal to $-C_{D^{*+}D^{*-}}$.

[3] Measured partially reconstructed candidates when one D^0 meson is not excplicitely reconstructed. Analysis does not separate CP-even and CP-odd component.

[4] AUBERT 03Q reports $|\lambda|$=0.75 ± 0.19 ± 0.02 and Im(λ)=0.05 ± 0.29 ± 0.10. We convert them to S and C parameters taking into account correlations.

Int. J. Mod. Phys. A 2026.41. Downloaded from www.worldscientific.com
by LIFORNIA @ BERKELEY on 09/16/26. Re-use and distribution is strictly not permitted, except for Open Access articles.

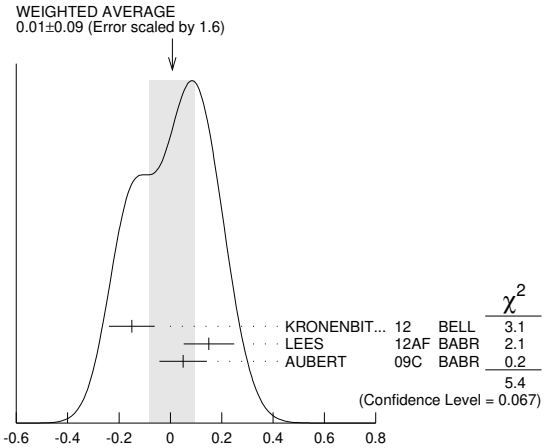

$C_{D^{*+}D^{*-}}$ $(B^0 \to D^{*+}D^{*-})$

$S_{D^{*+}D^{*-}}$ $(B^0 \to D^{*+}D^{*-})$

VALUE	DOCUMENT ID		TECN	COMMENT
−0.59±0.14 OUR AVERAGE	Error includes scale factor of 1.8. See the ideogram below.			
−0.79±0.13±0.03	[1] KRONENBIT...	12	BELL	$e^+e^- \to \Upsilon(4S)$
−0.34±0.12±0.05	[2] LEES	12AF	BABR	$e^+e^- \to \Upsilon(4S)$
−0.70±0.16±0.03	[1] AUBERT	09C	BABR	$e^+e^- \to \Upsilon(4S)$
• • • We do not use the following data for averages, fits, limits, etc. • • •				
$-0.96\pm0.25^{+0.13}_{-0.16}$	VERVINK	09	BELL	Repl. by KRONENBITTER 12
−0.66±0.19±0.04	[1] AUBERT	07BO	BABR	Repl. by AUBERT 09C
−0.75±0.56±0.12	MIYAKE	05	BELL	Repl. by VERVINK 09
0.06±0.37±0.13	[3] AUBERT	03Q	BABR	Repl. by AUBERT 07BO

[1] Assumes both CP-even and CP-odd states having the CP asymmetry.
[2] Measured partially reconstructed candidates when one D^0 meson is not excplicitely reconstructed. Analysis does not separate CP-even and CP-odd component.
[3] AUBERT 03Q reports $|\lambda|$=0.75 ± 0.19 ± 0.02 and Im(λ)=0.05 ± 0.29 ± 0.10. We convert them to S and C parameters taking into account correlations.

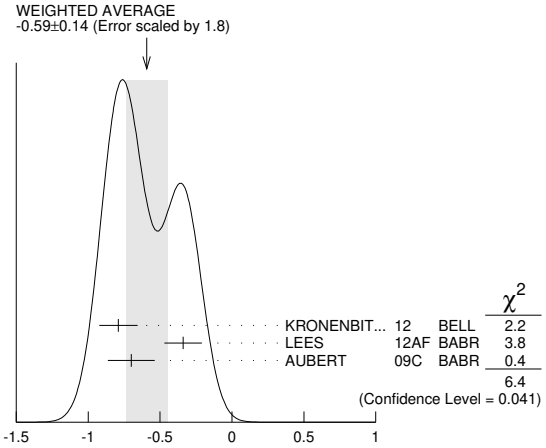

$S_{D^{*+}D^{*-}}$ $(B^0 \to D^{*+}D^{*-})$

C_+ $(B^0 \to D^{*+}D^{*-})$

See the note in the $C_{\pi\pi}$ datablock, but for CP even final state.

VALUE	DOCUMENT ID		TECN	COMMENT
0.00±0.10 OUR AVERAGE	Error includes scale factor of 1.6. See the ideogram below.			
−0.18±0.10±0.05	[1] KRONENBIT...	12	BELL	$e^+e^- \to \Upsilon(4S)$
+0.15±0.09±0.04	[2] LEES	12AF	BABR	$e^+e^- \to \Upsilon(4S)$
0.00±0.12±0.02	AUBERT	09C	BABR	$e^+e^- \to \Upsilon(4S)$
• • • We do not use the following data for averages, fits, limits, etc. • • •				
−0.05±0.14±0.02	AUBERT	07BO	BABR	Repl. by AUBERT 09C
0.06±0.17±0.03	[3] AUBERT,BE	05A	BABR	Repl. by AUBERT 07BO

[1] Belle Collab. quotes $A_{D^{*+}D^{*-}}$ which is equal to $-C_{D^{*+}D^{*-}}$.
[2] Measured partially reconstructed candidates when one D^0 meson is not excplicitely reconstructed. Extracted under assumption of equal C_+ and C_-.
[3] AUBERT,BE 05A reports a CP-odd fraction $R_\perp$ = 0.125 ± 0.044 ± 0.007.

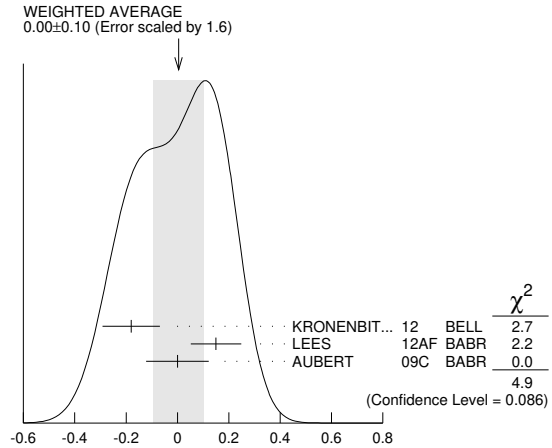

C_+ $(B^0 \to D^{*+}D^{*-})$

S_+ $(B^0 \to D^{*+}D^{*-})$

See the note in the $S_{\pi\pi}$ datablock, but for CP even final state.

VALUE	DOCUMENT ID		TECN	COMMENT
−0.73±0.09 OUR AVERAGE				
−0.81±0.13±0.03	KRONENBIT...	12	BELL	$e^+e^- \to \Upsilon(4S)$
−0.49±0.18±0.08	[1] LEES	12AF	BABR	$e^+e^- \to \Upsilon(4S)$
−0.76±0.16±0.04	AUBERT	09C	BABR	$e^+e^- \to \Upsilon(4S)$
• • • We do not use the following data for averages, fits, limits, etc. • • •				
−0.72±0.19±0.05	AUBERT	07BO	BABR	Repl. by AUBERT 09C
−0.75±0.25±0.03	[2] AUBERT,BE	05A	BABR	Repl. by AUBERT 07BO

[1] Measured partially reconstructed candidates when one D^0 meson is not excplicitely reconstructed. Analysis does not separate CP-even and CP-odd component. Value is obtained from $S = -0.34 \pm 0.12 \pm 0.05$ using $S = S_+ (1 - 2 R_\perp)$ with $R_\perp = 0.158 \pm 0.029$.
[2] AUBERT,BE 05A reports a CP-odd fraction $R_\perp$ = 0.125 ± 0.044 ± 0.007.

C_- $(B^0 \to D^{*+}D^{*-})$

See the note in the $C_{\pi\pi}$ datablock, but for CP odd final state.

VALUE	DOCUMENT ID		TECN	COMMENT
0.19±0.31 OUR AVERAGE				
0.05±0.39±0.08	[1] KRONENBIT...	12	BELL	$e^+e^- \to \Upsilon(4S)$
0.41±0.49±0.08	AUBERT	09C	BABR	$e^+e^- \to \Upsilon(4S)$
• • • We do not use the following data for averages, fits, limits, etc. • • •				
0.23±0.67±0.10	AUBERT	07BO	BABR	Repl. by AUBERT 09C
−0.20±0.96±0.11	[2] AUBERT,BE	05A	BABR	Repl. by AUBERT 07BO

[1] Belle Collab. quotes $A_{D^{*+}D^{*-}}$ which is equal to $-C_{D^{*+}D^{*-}}$.
[2] AUBERT,BE 05A reports a CP-odd fraction $R_\perp$ = 0.125 ± 0.044 ± 0.007.

S_- $(B^0 \to D^{*+}D^{*-})$

See the note in the $S_{\pi\pi}$ datablock, but for CP odd final state.

VALUE	DOCUMENT ID		TECN	COMMENT
−1.6 ±0.5 OUR AVERAGE				
−1.52±0.62±0.12	[1] KRONENBIT...	12	BELL	$e^+e^- \to \Upsilon(4S)$
−1.80±0.70±0.16	AUBERT	09C	BABR	$e^+e^- \to \Upsilon(4S)$
• • • We do not use the following data for averages, fits, limits, etc. • • •				
−1.83±1.04±0.23	AUBERT	07BO	BABR	Repl. by AUBERT 09C
−1.75±1.78±0.22	[2] AUBERT,BE	05A	BABR	Repl. by AUBERT 07BO

[1] KRONENBITTER 12 reported S_- = 1.52 ± 0.62 ± 0.12. A minus sign results from a different convention, see AUBERT 09C.
[2] AUBERT,BE 05A reports a CP-odd fraction $R_\perp$ = 0.125 ± 0.044 ± 0.007.

C $(B^0 \to D^*(2010)^+ D^*(2010)^- K^0_S)$

VALUE	DOCUMENT ID		TECN	COMMENT
0.01±0.28±0.09	[1] DALSENO	07	BELL	$e^+e^- \to \Upsilon(4S)$

[1] Reports value of A which is equal to $-C$.

S $(B^0 \to D^*(2010)^+ D^*(2010)^- K^0_S)$

VALUE	DOCUMENT ID		TECN	COMMENT
$\mathbf{0.06^{+0.45}_{-0.44}\pm0.06}$	[1] DALSENO	07	BELL	$e^+e^- \to \Upsilon(4S)$

[1] This value includes an unknown CP dilution factor D due to possible contributions from intermediate resonances and different partial waves.

$C_{D^+D^-}$ $(B^0 \to D^+D^-)$

VALUE	DOCUMENT ID		TECN	COMMENT
−0.06 ±0.18 OUR AVERAGE	Error includes scale factor of 2.5. See the ideogram below.			
0.128±0.103±0.010	AAIJ	25A	LHCB	pp at 13 TeV
$0.26\ ^{+0.18}_{-0.17}\ \pm0.02$	AAIJ	16AN	LHCB	pp at 7, 8 TeV
−0.43 ±0.16 ±0.05	ROHRKEN	12	BELL	$e^+e^- \to \Upsilon(4S)$
−0.07 ±0.23 ±0.03	AUBERT	09C	BABR	$e^+e^- \to \Upsilon(4S)$
−0.91 ±0.23 ±0.06	[1] FRATINA	07	BELL	$e^+e^- \to \Upsilon(4S)$

Int. J. Mod. Phys. A 2026.41. Downloaded from www.worldscientific.com
by UNIVERSITY OF CALIFORNIA @ BERKELEY on 09/16/26. Re-use and distribution is strictly not permitted, except for Open Access articles.

• • • We do not use the following data for averages, fits, limits, etc. • • •

0.11 ±0.22 ±0.07	AUBERT	07AI	BABR	Repl. by AUBERT 09C
0.11 ±0.35 ±0.06	AUBERT,B	05Z	BABR	Repl. by AUBERT 07AI

[1] The paper reports A, which is equal to $-C$.

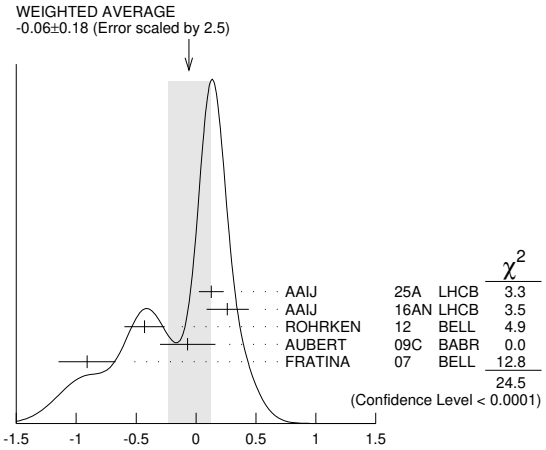

$C_{D^+D^-}$ $(B^0 \to D^+D^-)$

$S_{D^+D^-}$ $(B^0 \to D^+D^-)$

VALUE	DOCUMENT ID		TECN	COMMENT
−0.64 ±0.09 OUR AVERAGE	Error includes scale factor of 1.3. See the ideogram below.			
−0.552±0.100±0.010	AAIJ	25A	LHCB	pp at 13 TeV
$-0.54\ ^{+0.17}_{-0.16}\ \pm0.05$	AAIJ	16AN	LHCB	pp at 7, 8 TeV
$-1.06\ ^{+0.21}_{-0.14}\ \pm0.08$	ROHRKEN	12	BELL	$e^+e^- \to \Upsilon(4S)$
−0.63 ±0.36 ±0.05	AUBERT	09C	BABR	$e^+e^- \to \Upsilon(4S)$
−1.13 ±0.37 ±0.09	FRATINA	07	BELL	$e^+e^- \to \Upsilon(4S)$
• • • We do not use the following data for averages, fits, limits, etc. • • •				
−0.54 ±0.34 ±0.06	AUBERT	07AI	BABR	Repl. by AUBERT 09C
−0.29 ±0.63 ±0.06	AUBERT,B	05Z	BABR	Repl. by AUBERT 07AI

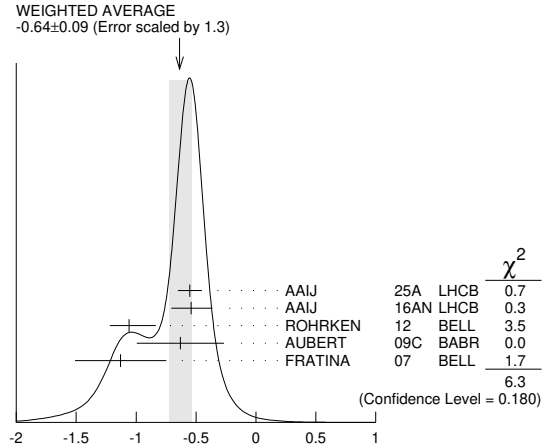

$S_{D^+D^-}$ $(B^0 \to D^+D^-)$

$C_{J/\psi(1S)\pi^0}$ $(B^0 \to J/\psi(1S)\pi^0)$

VALUE	DOCUMENT ID		TECN	COMMENT
0.07±0.09 OUR AVERAGE	Error includes scale factor of 1.1.			
0.13±0.12±0.03	ADACHI	25C	BELL	$e^+e^- \to \Upsilon(4S)$
$0.15\pm0.14\ ^{+0.04}_{-0.03}$	[1] PAL	18	BELL	$e^+e^- \to \Upsilon(4S)$
−0.20±0.19±0.03	AUBERT	08AU	BABR	$e^+e^- \to \Upsilon(4S)$
• • • We do not use the following data for averages, fits, limits, etc. • • •				
−0.08±0.16±0.05	[1] LEE	08A	BELL	Repl. by PAL 18
−0.21±0.26±0.06	AUBERT,B	06B	BABR	Repl. by AUBERT 08AU
0.01±0.29±0.03	[1] KATAOKA	04	BELL	Repl. by LEE 08A
0.38±0.41±0.09	AUBERT	03N	BABR	Repl. by AUBERT,B 06B

[1] BELLE Collab. quotes $A_{J/\psi\pi^0}$ which is equal to $-C_{J/\psi\pi^0}$.

$S_{J/\psi(1S)\pi^0}$ $(B^0 \to J/\psi(1S)\pi^0)$

VALUE	DOCUMENT ID		TECN	COMMENT
−0.88±0.17 OUR AVERAGE	Error includes scale factor of 1.6. See the ideogram below.			
−0.88±0.17±0.03	ADACHI	25C	BELL	$e^+e^- \to \Upsilon(4S)$
−0.59±0.19±0.03	PAL	18	BELL	$e^+e^- \to \Upsilon(4S)$
−1.23±0.21±0.04	AUBERT	08AU	BABR	$e^+e^- \to \Upsilon(4S)$
• • • We do not use the following data for averages, fits, limits, etc. • • •				
−0.65±0.21±0.05	LEE	08A	BELL	Repl. by PAL 18
−0.68±0.30±0.04	AUBERT,B	06B	BABR	Repl. by AUBERT 08AU
−0.72±0.42±0.09	KATAOKA	04	BELL	Repl. by LEE 08A
0.05±0.49±0.16	AUBERT	03N	BABR	Repl. by AUBERT,B 06B

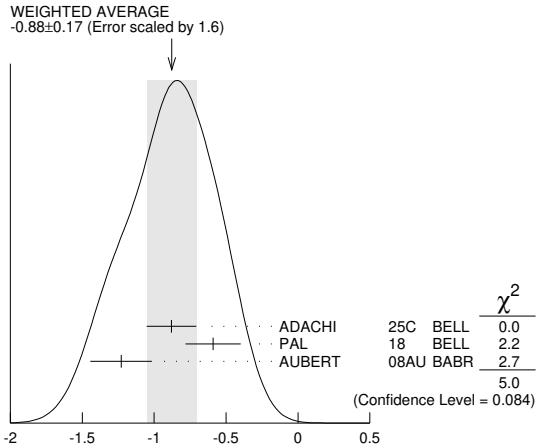

$S_{J/\psi(1S)\pi^0}$ $(B^0 \to J/\psi(1S)\pi^0)$

$C(B^0 \to J/\psi(1S)\rho^0)$

VALUE	DOCUMENT ID		TECN	COMMENT
$\mathbf{-0.063\pm0.056\ ^{+0.019}_{-0.014}}$	[1] AAIJ	15J	LHCB	pp at 7, 8 TeV

[1] Time-dependent CP violation is measured in the $B^0 \to J/\psi\rho^0$ and was used to limit the size of penguin amplitude contributions to ϕ_s in $B^0_s \to J/\psi\phi$ decays to be between $[-1.05°, 1.18°]$ at 95% confidence level.

$S(B^0 \to J/\psi(1S)\rho^0)$

VALUE	DOCUMENT ID		TECN	COMMENT
$\mathbf{-0.66\ ^{+0.13}_{-0.12}\pm0.09_{-0.03}}$	[1] AAIJ	15J	LHCB	pp at 7, 8 TeV

[1] Time-dependent CP violation is measured in the $B^0 \to J/\psi\rho^0$ and was used to limit the size of penguin amplitude contributions to ϕ_s in $B^0_s \to J/\psi\phi$ decays to be between $[-1.05°, 1.18°]$ at 95% confidence level.

$C_{D^{(*)}_{CP}h^0}$ $(B^0 \to D^{(*)}_{CP}h^0)$

VALUE	DOCUMENT ID		TECN	COMMENT
−0.02±0.07±0.03	[1] ABDESSALAM 15			$e^+e^- \to \Upsilon(4S)$
• • • We do not use the following data for averages, fits, limits, etc. • • •				
−0.23±0.16±0.04	AUBERT	07AJ	BABR	Repl. by ABDESSALAM 15

[1] BABAR and BELLE combined analysis uses CP-eigenstate decay modes $D^0 \to K^+K^-$, $K^0_S\pi^0$, $K^0_S\omega$, and $h^0 = \pi^0, \eta, \omega$.

$S_{D^{(*)}_{CP}h^0}$ $(B^0 \to D^{(*)}_{CP}h^0)$

VALUE	DOCUMENT ID		TECN	COMMENT
−0.66±0.10±0.06	[1] ABDESSALAM 15			$e^+e^- \to \Upsilon(4S)$
• • • We do not use the following data for averages, fits, limits, etc. • • •				
−0.56±0.23±0.05	AUBERT	07AJ	BABR	Repl. by ABDESSALAM 15

[1] BABAR and BELLE combined analysis uses CP-eigenstate decay modes $D^0 \to K^+K^-$, $K^0_S\pi^0$, $K^0_S\omega$, and $h^0 = \pi^0, \eta, \omega$.

$C_{K^0\pi^0}$ $(B^0 \to K^0\pi^0)$

VALUE	DOCUMENT ID		TECN	COMMENT
0.00±0.08 OUR AVERAGE				
−0.01±0.12±0.04	[1] ADACHI	24	BELL	$e^+e^- \to \Upsilon(4S)$
−0.14±0.13±0.06	[2] FUJIKAWA	10A	BELL	$e^+e^- \to \Upsilon(4S)$
0.13±0.13±0.03	AUBERT	09I	BABR	$e^+e^- \to \Upsilon(4S)$
• • • We do not use the following data for averages, fits, limits, etc. • • •				
−0.06±0.15±0.04	[3] ADACHI	24	BELL	$e^+e^- \to \Upsilon(4S)$
$-0.04\ ^{+0.14}_{-0.15}\pm0.05$	[4] ADACHI	23E	BELL	$e^+e^- \to \Upsilon(4S)$
0.24±0.15±0.03	AUBERT	08E	BABR	Repl. by AUBERT 09I
0.05±0.14±0.05	[2] CHAO	07	BELL	Repl. by FUJIKAWA 10A
0.06±0.18±0.03	AUBERT	05Y	BABR	Repl. by AUBERT 08E

$-0.16 \pm 0.29 \pm 0.05$	[2,5] CHAO	05A	BELL	Repl. by CHEN 05B
$0.11 \pm 0.20 \pm 0.09$	[2] CHEN	05B	BELL	Repl. by CHAO 07
$-0.03 \pm 0.36 \pm 0.11$	[2] AUBERT	04M	BABR	Repl. by AUBERT,B 04M
$0.40 ^{+0.27}_{-0.28} \pm 0.09$	[6] AUBERT,B	04M	BABR	Repl. by AUBERT 05Y

[1] This is the combined result of this analysis (ADACHI 24) and ADACHI 23E.
[2] Reports A which is equal to $-C$.
[3] The measurement is using BELL II data reported in ADACHI 24. The combination with ADACHI 23E is also reported.
[4] The result has been combined with ADACHI 24.
[5] Corresponds to a 90% CL interval of $-0.33 < A_{CP} < 0.64$.
[6] Based on a total signal yield of 122 ± 16 events.

$S_{K^0\pi^0}$ ($B^0 \to K^0\pi^0$)

VALUE	DOCUMENT ID		TECN	COMMENT
0.64±0.13 OUR AVERAGE				
$0.75 ^{+0.20}_{-0.23} \pm 0.04$	ADACHI	23E	BELL	$e^+e^- \to \Upsilon(4S)$
$0.67 \pm 0.31 \pm 0.08$	FUJIKAWA	10A	BELL	$e^+e^- \to \Upsilon(4S)$
$0.55 \pm 0.20 \pm 0.03$	AUBERT	09I	BABR	$e^+e^- \to \Upsilon(4S)$
• • • We do not use the following data for averages, fits, limits, etc. • • •				
$0.40 \pm 0.23 \pm 0.03$	AUBERT	08E	BABR	Repl. by AUBERT 09I
$0.33 \pm 0.35 \pm 0.08$	CHAO	07	BELL	Repl. by FUJIKAWA 10A
$0.35 ^{+0.30}_{-0.33} \pm 0.04$	AUBERT	05Y	BABR	Repl. by AUBERT 08E
$0.32 \pm 0.61 \pm 0.13$	CHEN	05B	BELL	Repl. by CHAO 07
$0.48 ^{+0.38}_{-0.47} \pm 0.06$	[1] AUBERT,B	04M	BABR	Repl. by AUBERT 05Y

[1] Based on a total signal yield of 122 ± 16 events.

$C_{\eta'(958)K^0_S}$ ($B^0 \to \eta'(958)K^0_S$)

See updated measurements in $C_{\eta' K^0}$

VALUE	DOCUMENT ID		TECN	COMMENT
−0.04±0.20 OUR AVERAGE Error includes scale factor of 2.5.				
$-0.21 \pm 0.10 \pm 0.02$	AUBERT	05M	BABR	$e^+e^- \to \Upsilon(4S)$
$0.19 \pm 0.11 \pm 0.05$	[1] CHEN	05B	BELL	$e^+e^- \to \Upsilon(4S)$
• • • We do not use the following data for averages, fits, limits, etc. • • •				
$-0.26 \pm 0.22 \pm 0.03$	[1] ABE	03C	BELL	Repl. by ABE 03H
$0.01 \pm 0.16 \pm 0.04$	[1] ABE	03H	BELL	Repl. by CHEN 05B
$0.10 \pm 0.22 \pm 0.04$	AUBERT	03W	BABR	Repl. by AUBERT 05M
$-0.13 \pm 0.32 ^{+0.06}_{-0.09}$	[1] CHEN	02B	BELL	Repl. by ABE 03C

[1] BELLE Collab. quotes $A_{\eta'(958)K^0_S}$ which is equal to $-C_{\eta'(958)K^0_S}$.

$S_{\eta'(958)K^0_S}$ ($B^0 \to \eta'(958)K^0_S$)

See updated measurements in $S_{\eta' K^0}$

VALUE	DOCUMENT ID		TECN	COMMENT
0.43±0.17 OUR AVERAGE Error includes scale factor of 1.5.				
$0.30 \pm 0.14 \pm 0.02$	AUBERT	05M	BABR	$e^+e^- \to \Upsilon(4S)$
$0.65 \pm 0.18 \pm 0.04$	CHEN	05B	BELL	$e^+e^- \to \Upsilon(4S)$
• • • We do not use the following data for averages, fits, limits, etc. • • •				
$0.71 \pm 0.37 ^{+0.05}_{-0.06}$	ABE	03C	BELL	Repl. by ABE 03H
$0.43 \pm 0.27 \pm 0.05$	ABE	03H	BELL	Repl. by CHEN 05B
$0.02 \pm 0.34 \pm 0.03$	AUBERT	03W	BABR	Repl. by AUBERT 05M
$0.28 \pm 0.55 ^{+0.07}_{-0.08}$	CHEN	02B	BELL	Repl. by ABE 03C

$C_{\eta' K^0}$ ($B^0 \to \eta' K^0$)

VALUE	DOCUMENT ID		TECN	COMMENT
−0.08±0.04 OUR AVERAGE Error includes scale factor of 1.1.				
$-0.19 \pm 0.08 \pm 0.03$	[1] ADACHI	24P	BEL2	$e^+e^- \to \Upsilon(4S)$
$-0.03 \pm 0.05 \pm 0.04$	[2] SANTELJ	14	BELL	$e^+e^- \to \Upsilon(4S)$
$-0.08 \pm 0.06 \pm 0.02$	AUBERT	09I	BABR	$e^+e^- \to \Upsilon(4S)$
• • • We do not use the following data for averages, fits, limits, etc. • • •				
$-0.16 \pm 0.07 \pm 0.03$	[3] AUBERT	07A	BABR	Repl. by AUBERT 09I
$0.01 \pm 0.07 \pm 0.05$	[2,3] CHEN	07	BELL	Repl. by SANTELJ 14

[1] Asymmetries are measured using $B^0 \to \eta' K^0_S$ decays, with $\eta' \to \eta(\to \gamma\gamma)\pi^+\pi^-$ and $\eta' \to \rho(\to \pi^+\pi^-)\gamma$.
[2] The paper reports A, which is equal to $-C$.
[3] The mixing-induced CP violation is reported with a significance of more than 5 standard deviations in this $b \to s$ penguin dominated mode.

$S_{\eta' K^0}$ ($B^0 \to \eta' K^0$)

VALUE	DOCUMENT ID		TECN	COMMENT
0.64±0.05 OUR AVERAGE				
$0.67 \pm 0.10 \pm 0.03$	[1] ADACHI	24P	BEL2	$e^+e^- \to \Upsilon(4S)$
$0.68 \pm 0.07 \pm 0.03$	SANTELJ	14	BELL	$e^+e^- \to \Upsilon(4S)$
$0.57 \pm 0.08 \pm 0.02$	AUBERT	09I	BABR	$e^+e^- \to \Upsilon(4S)$
• • • We do not use the following data for averages, fits, limits, etc. • • •				
$0.58 \pm 0.10 \pm 0.03$	[2] AUBERT	07A	BABR	Repl. by AUBERT 09I
$0.64 \pm 0.10 \pm 0.04$	[2] CHEN	07	BELL	Repl. by SANTELJ 14

[1] Asymmetries are measured using $B^0 \to \eta' K^0_S$ decays, with $\eta' \to \eta(\to \gamma\gamma)\pi^+\pi^-$ and $\eta' \to \rho(\to \pi^+\pi^-)\gamma$.
[2] The mixing-induced CP violation is reported with a significance of more than 5 standard deviations in this $b \to s$ penguin dominated mode.

$C_{\omega K^0_S}$ ($B^0 \to \omega K^0_S$)

VALUE	DOCUMENT ID		TECN	COMMENT
0.0 ±0.4 OUR AVERAGE Error includes scale factor of 3.0.				
$0.36 \pm 0.19 \pm 0.05$	[1] CHOBANOVA	14	BELL	$e^+e^- \to \Upsilon(4S)$
$-0.52 ^{+0.22}_{-0.20} \pm 0.03$	AUBERT	09I	BABR	$e^+e^- \to \Upsilon(4S)$
• • • We do not use the following data for averages, fits, limits, etc. • • •				
$0.09 \pm 0.29 \pm 0.06$	[1] CHAO	07	BELL	Repl. by CHOBANOVA 14
$-0.55 ^{+0.28}_{-0.26} \pm 0.03$	AUBERT,B	06E	BABR	Repl. by AUBERT 09I
$-0.27 \pm 0.48 \pm 0.15$	[1] CHEN	05B	BELL	Repl. by CHAO 07

[1] Belle Collab. quotes $A_{\omega K^0_S}$ which is equal to $-C_{\omega K^0_S}$.

$S_{\omega K^0_S}$ ($B^0 \to \omega K^0_S$)

VALUE	DOCUMENT ID		TECN	COMMENT
0.70±0.21 OUR AVERAGE				
$0.91 \pm 0.32 \pm 0.05$	CHOBANOVA	14	BELL	$e^+e^- \to \Upsilon(4S)$
$0.55 ^{+0.26}_{-0.29} \pm 0.02$	AUBERT	09I	BABR	$e^+e^- \to \Upsilon(4S)$
• • • We do not use the following data for averages, fits, limits, etc. • • •				
$0.11 \pm 0.46 \pm 0.07$	CHAO	07	BELL	Repl. by CHOBANOVA 14
$0.51 ^{+0.35}_{-0.39} \pm 0.02$	AUBERT,B	06E	BABR	Repl. by AUBERT 09I
$0.76 \pm 0.65 ^{+0.13}_{-0.16}$	CHEN	05B	BELL	Repl. by CHAO 07

C ($B^0 \to K^0_S\pi^0\pi^0$)

VALUE	DOCUMENT ID		TECN	COMMENT
−0.21±0.20 OUR AVERAGE				
$-0.28 \pm 0.21 \pm 0.04$	[1] YUSA	19	BELL	$e^+e^- \to \Upsilon(4S)$
$0.23 \pm 0.52 \pm 0.13$	AUBERT	07AQ	BABR	$e^+e^- \to \Upsilon(4S)$

[1] Reports value of A which is equal to $-C$.

S ($B^0 \to K^0_S\pi^0\pi^0$)

VALUE	DOCUMENT ID		TECN	COMMENT
$0.89 ^{+0.27}_{-0.30}$ OUR AVERAGE				
$0.92 ^{+0.27}_{-0.31} \pm 0.11$	YUSA	19	BELL	$e^+e^- \to \Upsilon(4S)$
$0.72 \pm 0.71 \pm 0.08$	AUBERT	07AQ	BABR	$e^+e^- \to \Upsilon(4S)$

$C_{\rho^0 K^0_S}$ ($B^0 \to \rho^0 K^0_S$)

VALUE	DOCUMENT ID		TECN	COMMENT
−0.04±0.20 OUR AVERAGE				
$-0.05 \pm 0.26 \pm 0.10$	[1] AUBERT	09AU	BABR	$e^+e^- \to \Upsilon(4S)$
$-0.03 ^{+0.24}_{-0.23} \pm 0.15$	[2,3] DALSENO	09	BELL	$e^+e^- \to \Upsilon(4S)$
• • • We do not use the following data for averages, fits, limits, etc. • • •				
$0.64 \pm 0.41 \pm 0.20$	AUBERT	07F	BABR	Repl. by AUBERT 09AU

[1] Uses Dalitz plot analysis of $B^0 \to K^0\pi^+\pi^-$ decays and the first of two equivalent solutions is used.
[2] Quotes $A_{\rho^0 K^0_S}$ which is equal to $-C_{\rho^0 K^0_S}$.
[3] Uses Dalitz plot analysis of $B^0 \to K^0\pi^+\pi^-$ decays and the first of two consistent solutions that may be preferred.

$S_{\rho^0 K^0_S}$ ($B^0 \to \rho^0 K^0_S$)

VALUE	DOCUMENT ID		TECN	COMMENT
$0.50 ^{+0.17}_{-0.21}$ OUR AVERAGE				
$0.35 ^{+0.26}_{-0.31} \pm 0.07$	[1] AUBERT	09AU	BABR	$e^+e^- \to \Upsilon(4S)$
$0.64 ^{+0.19}_{-0.25} \pm 0.13$	[2] DALSENO	09	BELL	$e^+e^- \to \Upsilon(4S)$
• • • We do not use the following data for averages, fits, limits, etc. • • •				
$0.20 \pm 0.52 \pm 0.24$	AUBERT	07F	BABR	Repl. by AUBERT 09AU

[1] Uses Dalitz plot analysis of $B^0 \to K^0\pi^+\pi^-$ decays and the first of two equivalent solutions is used.
[2] Uses Dalitz plot analysis of $B^0 \to K^0\pi^+\pi^-$ decays and the first of two consistent solutions that may be preferred.

$C_{f_0(980)K^0_S}$ ($B^0 \to f_0(980)K^0_S$)

VALUE	DOCUMENT ID		TECN	COMMENT
0.29±0.20 OUR AVERAGE				
$0.28 \pm 0.24 \pm 0.09$	[1] LEES	12O	BABR	$e^+e^- \to \Upsilon(4S)$
$0.30 \pm 0.29 \pm 0.14$	[2,3] NAKAHAMA	10	BELL	$e^+e^- \to \Upsilon(4S)$
• • • We do not use the following data for averages, fits, limits, etc. • • •				
$0.08 \pm 0.19 \pm 0.05$	[4] AUBERT	09AU	BABR	Repl. by LEES 12O
$0.06 \pm 0.17 \pm 0.11$	[2,5] DALSENO	09	BELL	Repl. by NAKAHAMA 10
$-0.41 \pm 0.23 \pm 0.07$	[2] AUBERT	07AX	BABR	Repl. by AUBERT 09AU
$0.15 \pm 0.15 \pm 0.07$	[2] CHAO	07	BELL	Repl. by DALSENO 09
$0.39 \pm 0.27 \pm 0.09$	[2] CHEN	05B	BELL	Repl. by CHAO 07

[1] Uses Dalitz plot analysis of the $B^0 \to K^0_S K^+ K^-$ decay.
[2] Quotes $A_{f_0(980)K^0_S}$ which is equal to $-C_{f_0(980)K^0_S}$.
[3] Uses Dalitz plot analysis of $B^0 \to K^0_S K^+ K^-$ decays and the first of four consistent solutions that may be preferred.
[4] Uses Dalitz plot analysis of $B^0 \to K^0\pi^+\pi^-$ decays and the first of two equivalent solutions is used.
[5] Uses Dalitz plot analysis of $B^0 \to K^0\pi^+\pi^-$ decays and the first of two consistent solutions that may be preferred.

Int. J. Mod. Phys. A 2026.41. Downloaded from www.worldscientific.com
by [redacted]LIFORNIA @ BERKELEY on 09/16/26. Re-use and distribution is strictly not permitted, except for Open Access articles.

Int. J. Mod. Phys. A 2026.41. Downloaded from www.worldscientific.com
by UNIVERSITY OF CALIFORNIA @ BERKELEY on 09/16/26. Re-use and distribution is strictly not permitted, except for Open Access articles.

$S_{f_0(980)K^0_S}$ ($B^0 \to f_0(980)K^0_S$)

VALUE	DOCUMENT ID		TECN	COMMENT
−0.50±0.16 OUR AVERAGE				
−0.55±0.18±0.12	[1] LEES	12O	BABR	$e^+e^- \to \Upsilon(4S)$
$-0.43^{+0.22}_{-0.20}\pm0.14$	[2] DALSENO	09	BELL	$e^+e^- \to \Upsilon(4S)$
• • • We do not use the following data for averages, fits, limits, etc. • • •				
$-0.96^{+0.21}_{-0.04}\pm0.04$	[3] AUBERT	09AU	BABR	Repl. by LEES 12O
−0.25±0.26±0.10	[4] AUBERT	07AX	BABR	Repl. by AUBERT 09AU
0.18±0.23±0.11	CHAO	07	BELL	Repl. by DALSENO 09
0.47±0.41±0.08	CHEN	05B	BELL	Repl. by CHAO 07

[1] Uses Dalitz plot analysis of the $B^0 \to K^0_S K^+ K^-$ decay.
[2] Uses Dalitz plot analysis of $B^0 \to K^0 \pi^+ \pi^-$ decays and the first of two consistent solutions that may be preferred.
[3] Uses Dalitz plot analysis of $B^0 \to K^0 \pi^+ \pi^-$ decays and the first of two equivalent solutions is used.
[4] Reports β_{eff}. We quote S obtained from epaps: E-PRLTAO-99-076741.

$S_{f_2(1270)K^0_S}$ ($B^0 \to f_2(1270)K^0_S$)

VALUE	DOCUMENT ID		TECN	COMMENT
−0.48±0.52±0.12	[1] AUBERT	09AU	BABR	$e^+e^- \to \Upsilon(4S)$

[1] Uses Dalitz plot analysis of $B^0 \to K^0 \pi^+ \pi^-$ decays and the first of two equivalent solutions is used.

$C_{f_2(1270)K^0_S}$ ($B^0 \to f_2(1270)K^0_S$)

VALUE	DOCUMENT ID		TECN	COMMENT
$\mathbf{0.28^{+0.35}_{-0.40}\pm0.11}$	[1] AUBERT	09AU	BABR	$e^+e^- \to \Upsilon(4S)$

[1] Uses Dalitz plot analysis of $B^0 \to K^0 \pi^+ \pi^-$ decays and the first of two equivalent solutions is used.

$S_{f_x(1300)K^0_S}$ ($B^0 \to f_x(1300)K^0_S$)

VALUE	DOCUMENT ID		TECN	COMMENT
−0.20±0.52±0.10	[1] AUBERT	09AU	BABR	$e^+e^- \to \Upsilon(4S)$

[1] Uses Dalitz plot analysis of $B^0 \to K^0 \pi^+ \pi^-$ decays and the first of two equivalent solutions is used.

$C_{f_x(1300)K^0_S}$ ($B^0 \to f_x(1300)K^0_S$)

VALUE	DOCUMENT ID		TECN	COMMENT
$\mathbf{0.13^{+0.33}_{-0.35}\pm0.10}$	[1] AUBERT	09AU	BABR	$e^+e^- \to \Upsilon(4S)$

[1] Uses Dalitz plot analysis of $B^0 \to K^0 \pi^+ \pi^-$ decays and the first of two equivalent solutions is used.

$S_{K^0\pi^+\pi^-}$ ($B^0 \to K^0\pi^+\pi^-$ nonresonant)

VALUE	DOCUMENT ID		TECN	COMMENT
−0.01±0.31±0.10	[1] AUBERT	09AU	BABR	$e^+e^- \to \Upsilon(4S)$

[1] Uses Dalitz plot analysis of $B^0 \to K^0 \pi^+ \pi^-$ decays and the first of two equivalent solutions is used.

$C_{K^0\pi^+\pi^-}$ ($B^0 \to K^0\pi^+\pi^-$ nonresonant)

VALUE	DOCUMENT ID		TECN	COMMENT
0.01±0.25±0.08	[1] AUBERT	09AU	BABR	$e^+e^- \to \Upsilon(4S)$

[1] Uses Dalitz plot analysis of $B^0 \to K^0 \pi^+ \pi^-$ decays and the first of two equivalent solutions is used.

$C_{K^0_S K^0_S}$ ($B^0 \to K^0_S K^0_S$)

VALUE	DOCUMENT ID		TECN	COMMENT
0.0 ±0.4 OUR AVERAGE	Error includes scale factor of 1.4.			
0.38±0.38±0.05	[1] NAKAHAMA	08	BELL	$e^+e^- \to \Upsilon(4S)$
−0.40±0.41±0.06	AUBERT,BE	06C	BABR	$e^+e^- \to \Upsilon(4S)$

[1] Reports $A_{K^0_S K^0_S}$ which equals to $-C_{K^0_S K^0_S}$.

$S_{K^0_S K^0_S}$ ($B^0 \to K^0_S K^0_S$)

VALUE	DOCUMENT ID		TECN	COMMENT
−0.8 ±0.5 OUR AVERAGE				
$-0.38^{+0.69}_{-0.77}\pm0.09$	NAKAHAMA	08	BELL	$e^+e^- \to \Upsilon(4S)$
$-1.28^{+0.80+0.11}_{-0.73-0.16}$	AUBERT,BE	06C	BABR	$e^+e^- \to \Upsilon(4S)$

$C_{K^+K^-K^0_S}$ ($B^0 \to K^+K^-K^0_S$ nonresonant)

VALUE	DOCUMENT ID		TECN	COMMENT
0.06 ±0.08 OUR AVERAGE				
0.02 ±0.09 ±0.03	[1,2] LEES	12O	BABR	$e^+e^- \to \Upsilon(4S)$
0.14 ±0.11 ±0.09	[3,4] NAKAHAMA	10	BELL	$e^+e^- \to \Upsilon(4S)$
• • • We do not use the following data for averages, fits, limits, etc. • • •				
0.054±0.102±0.060	[3,5] AUBERT	07AX	BABR	Repl. by LEES 12O
0.09 ±0.10 ±0.05	[3,5] CHAO	07	BELL	Repl. by NAKAHAMA 10
0.10 ±0.14 ±0.04	[5] AUBERT	05T	BABR	Repl. by AUBERT 07AX
0.09 ±0.12 ±0.07	[3] CHEN	05B	BELL	Repl. by CHAO 07
−0.10 ±0.19 ±0.10	[5] AUBERT,B	04V	BABR	Repl. by AUBERT 05T
$0.40 \pm 0.33 \; ^{+0.28}_{-0.10}$	[3] ABE	03C	BELL	Repl. by ABE 03H
0.17 ±0.16 ±0.04	[3,5] ABE	03H	BELL	Repl. by CHEN 05B

[1] Uses Dalitz plot analysis of the $B^0 \to K^0_S K^+ K^-$ decay.
[2] This measurement is performed on all the isobar components, excluding ϕK^0_S and $f_0(980)K^0_S$.
[3] Quotes $A_{K^+K^-K^0_S}$ which is equal to $-C_{K^+K^-K^0_S}$.
[4] Uses Dalitz plot analysis of $B^0 \to K^0_S K^+ K^-$ decays and the first of four consistent solutions that may be preferred.
[5] Excludes the events from $B^0 \to \phi K^0_S$ decay. The results are derived from a combined sample of $K^+K^-K^0_S$ and $K^+K^-K^0_L$ decays.

$S_{K^+K^-K^0_S}$ ($B^0 \to K^+K^-K^0_S$ nonresonant)

VALUE	DOCUMENT ID		TECN	COMMENT
−0.66 ±0.11 OUR AVERAGE				
−0.65 ±0.12 ±0.03	[1,2] LEES	12O	BABR	$e^+e^- \to \Upsilon(4S)$
$-0.68 \pm 0.15 \; ^{+0.21}_{-0.13}$	[3] CHAO	07	BELL	$e^+e^- \to \Upsilon(4S)$
• • • We do not use the following data for averages, fits, limits, etc. • • •				
$-0.764\pm0.111\,^{+0.071}_{-0.040}$	[3,4] AUBERT	07AX	BABR	Repl. by LEES 12O
−0.42 ±0.17 ±0.03	[3,5] AUBERT	05T	BABR	Repl. by AUBERT 07AX
−0.49 ±0.18 ±0.04	CHEN	05B	BELL	Repl. by CHAO 07
−0.56 ±0.25 ±0.04	[3,6] AUBERT,B	04V	BABR	Repl. by AUBERT 05T
−0.49 ±0.43 ±0.11	ABE	03C	BELL	Repl. by ABE 03H
−0.51 ±0.26 ±0.05	[3,7] ABE	03H	BELL	Repl. by CHEN 05B

[1] Uses Dalitz plot analysis of the $B^0 \to K^0_S K^+ K^-$ decay.
[2] This measurement is performed on all the isobar components, excluding ϕK^0_S and $f_0(980)K^0_S$. Note that the nonresonant component is not a CP eigenstate.
[3] Excludes events from $B^0 \to \phi K^0_S$ decay. The results are derived from a combined sample of $K^+K^-K^0_S$ and $K^+K^-K^0_L$ decays.
[4] Reports β_{eff}. We quote S obtained from epaps: E-PRLTAO-99-076741.
[5] The measured CP-even final states fraction is 0.89 ± 0.08 ± 0.06.
[6] The measured CP-even final states fraction is 0.98 ± 0.15 ± 0.04.
[7] The measured CP-even final states fraction is 1.03 ± 0.15 ± 0.05.

$C_{K^+K^-K^0_S}$ ($B^0 \to K^+K^-K^0_S$ inclusive)

VALUE	DOCUMENT ID		TECN	COMMENT
0.015±0.077±0.053	[1,2] AUBERT	07AX	BABR	$e^+e^- \to \Upsilon(4S)$

[1] Measured using full Dalitz plot fit including ϕ component.
[2] The results are derived from a combined sample of $K^+K^-K^0_S$ and $K^+K^-K^0_L$ decays.

$S_{K^+K^-K^0_S}$ ($B^0 \to K^+K^-K^0_S$ inclusive)

VALUE	DOCUMENT ID		TECN	COMMENT
−0.647±0.116±0.040	[1] AUBERT	07AX	BABR	$e^+e^- \to \Upsilon(4S)$

[1] Measured using full Dalitz plot fit including ϕ component.

$C_{\phi K^0_S}$ ($B^0 \to \phi K^0_S$)

VALUE	DOCUMENT ID		TECN	COMMENT
−0.09±0.12 OUR AVERAGE				
−0.31±0.20±0.05	ADACHI	23I	BELL	$e^+e^- \to \Upsilon(4S)$
0.05±0.18±0.05	[1] LEES	12O	BABR	$e^+e^- \to \Upsilon(4S)$
−0.04±0.20±0.10	[2,3] NAKAHAMA	10	BELL	$e^+e^- \to \Upsilon(4S)$
• • • We do not use the following data for averages, fits, limits, etc. • • •				
0.08±0.18±0.04	[2,4] AUBERT	07AX	BABR	Repl. by LEES 12O
−0.07±0.15±0.05	[2,4] CHEN	07	BELL	Repl. by NAKAHAMA 10
0.00±0.23±0.05	[4] AUBERT	05T	BABR	Repl. by AUBERT 07AX
−0.08±0.22±0.09	[2,4] CHEN	05B	BELL	Repl. by CHEN 07
0.01±0.33±0.10	[4] AUBERT,B	04G	BABR	Repl. by AUBERT 05T
0.56±0.41±0.16	[2] ABE	03C	BELL	Repl. by ABE 03H
0.15±0.29±0.07	[2] ABE	03H	BELL	Repl. by CHEN 05B

[1] Uses Dalitz plot analysis of the $B^0 \to K^0_S K^+ K^-$ decay.
[2] Quotes $A_{\phi K^0_S}$ which is equal to $-C_{\phi K^0_S}$.
[3] Uses Dalitz plot analysis of $B^0 \to K^0_S K^+ K^-$ decays and the first of four consistent solutions that may be preferred.
[4] Result combines B-meson final states ϕK^0_S and ϕK^0_L by assuming $S_{\phi K^0_S} = -S_{\phi K^0_L}$

$S_{\phi K^0_S}$ ($B^0 \to \phi K^0_S$)

VALUE	DOCUMENT ID		TECN	COMMENT
0.58±0.12 OUR AVERAGE				
$0.54\pm0.26\,^{+0.06}_{-0.08}$	ADACHI	23I	BELL	$e^+e^- \to \Upsilon(4S)$
0.66±0.17±0.07	[1] LEES	12O	BABR	$e^+e^- \to \Upsilon(4S)$
0.50±0.21±0.06	[2] CHEN	07	BELL	$e^+e^- \to \Upsilon(4S)$
• • • We do not use the following data for averages, fits, limits, etc. • • •				
0.21±0.26±0.11	[2,3] AUBERT	07AX	BABR	Repl. by LEES 12O
$0.50\pm0.25\,^{+0.07}_{-0.04}$	[2] AUBERT	05T	BABR	Repl. by AUBERT 07AX
0.08±0.33±0.09	[2] CHEN	05B	BELL	Repl. by CHEN 07
$0.47\pm0.34\,^{+0.08}_{-0.06}$	[2] AUBERT,B	04G	BABR	Repl. by AUBERT 05T
−0.73±0.64±0.22	ABE	03C	BELL	Repl. by ABE 03H
$-0.96\pm0.50\,^{+0.09}_{-0.11}$	ABE	03H	BELL	Repl. by CHEN 05B

[1] Uses Dalitz plot analysis of the $B^0 \to K^0_S K^+ K^-$ decay.
[2] Result combines B-meson final states ϕK^0_S and ϕK^0_L by assuming $S_{\phi K^0_S} = -S_{\phi K^0_L}$
[3] Reports β_{eff}. We quote S obtained from epaps: E-PRLTAO-99-076741.

$C_{K_S K_S K_S}(B^0 \to K_S K_S K_S)$

VALUE	CL%	DOCUMENT ID		TECN	COMMENT
-0.14 ± 0.12 OUR AVERAGE					
$-0.12 \pm 0.16 \pm 0.05$		[1] KANG	21	BELL	$e^+e^- \to \Upsilon(4S)$
$-0.17 \pm 0.18 \pm 0.04$		LEES	12I	BABR	$e^+e^- \to \Upsilon(4S)$
• • • We do not use the following data for averages, fits, limits, etc. • • •					
[-0.45, 0.32]	95	[2] ADACHI	24G	BEL2	$e^+e^- \to \Upsilon(4S)$
$0.02 \pm 0.21 \pm 0.05$		AUBERT	07AT	BABR	Repl. by LEES 12I
$-0.31 \pm 0.20 \pm 0.07$		[1] CHEN	07	BELL	Repl. by KANG 21
$-0.34^{+0.28}_{-0.25} \pm 0.05$		AUBERT,B	05	BABR	Repl. by AUBERT 07AT
$-0.54 \pm 0.34 \pm 0.09$		[1] SUMISAWA	05	BELL	Repl. by CHEN 07

[1] KANG 21 quotes $A_{K^0_S K^0_S K^0_S}$ which is equal to $-C_{K^0_S K^0_S K^0_S}$.
[2] The two-dimensional intervals at the 95.5 % CL using 362 fb^{-1} BELL II data.

$S_{K_S K_S K_S}(B^0 \to K_S K_S K_S)$

VALUE	CL%	DOCUMENT ID		TECN	COMMENT
-0.82 ± 0.17 OUR AVERAGE					
$-0.71 \pm 0.23 \pm 0.05$		KANG	21	BELL	$e^+e^- \to \Upsilon(4S)$
$-0.94^{+0.24}_{-0.21} \pm 0.06$		LEES	12I	BABR	$e^+e^- \to \Upsilon(4S)$
• • • We do not use the following data for averages, fits, limits, etc. • • •					
[-1, -0.41]	95	[1] ADACHI	24G	BEL2	$e^+e^- \to \Upsilon(4S)$
$-0.71 \pm 0.24 \pm 0.04$		AUBERT	07AT	BABR	Repl. by LEES 12I
$0.30 \pm 0.32 \pm 0.08$		CHEN	07	BELL	Repl. by KANG 21
$-0.71^{+0.38}_{-0.32} \pm 0.04$		AUBERT,B	05	BABR	Repl. by AUBERT 07AT
$1.26 \pm 0.68 \pm 0.20$		SUMISAWA	05	BELL	Repl. by CHEN 07.

[1] The two-dimensional intervals at the 95.5 % CL using 362 fb^{-1} BELL II data.

$C_{K^0_S \pi^0 \gamma}(B^0 \to K^0_S \pi^0 \gamma)$

VALUE	DOCUMENT ID		TECN	COMMENT
• • • We do not use the following data for averages, fits, limits, etc. • • •				
$-0.06 \pm 0.25 \pm 0.09$	[1] ADACHI	25	BELL	$e^+e^- \to \Upsilon(4S)$
$0.36 \pm 0.33 \pm 0.04$	[2] AUBERT	08BA	BABR	$e^+e^- \to \Upsilon(4S)$
$0.20 \pm 0.20 \pm 0.06$	[3,4] USHIRODA	06	BELL	$e^+e^- \to \Upsilon(4S)$
$-1.0 \pm 0.5 \pm 0.2$	[2] AUBERT,B	05P	BABR	Repl. by AUBERT 08BA
$-0.03 \pm 0.34 \pm 0.11$	[4] USHIRODA	05	BELL	Repl. by USHIRODA 06

[1] Requires $0.6 < M_{K^0_S \pi^0} < 0.8$ GeV/c^2 or $1.0 < M_{K^0_S \pi^0} < 1.8$ GeV/c^2.
[2] Requires $1.1 < M_{K^0_S \pi^0} < 1.8$ GeV/c^2.
[3] Requires $M_{K^0_S \pi^0} < 1.8$ GeV/c^2.
[4] Reports $A_{K^0_S \pi^0 \gamma}$, which is $-C_{K^0_S \pi^0 \gamma}$.

$S_{K^0_S \pi^0 \gamma}(B^0 \to K^0_S \pi^0 \gamma)$

VALUE	DOCUMENT ID		TECN	COMMENT
• • • We do not use the following data for averages, fits, limits, etc. • • •				
$0.04^{+0.45}_{-0.44} \pm 0.10$	[1] ADACHI	25	BELL	$e^+e^- \to \Upsilon(4S)$
$-0.78 \pm 0.59 \pm 0.09$	[2] AUBERT	08BA	BABR	$e^+e^- \to \Upsilon(4S)$
$-0.10 \pm 0.31 \pm 0.07$	[3] USHIRODA	06	BELL	$e^+e^- \to \Upsilon(4S)$
$0.9 \pm 1.0 \pm 0.2$	[2] AUBERT,B	05P	BABR	Repl. by AUBERT 08BA
$-0.58^{+0.46}_{-0.38} \pm 0.11$	USHIRODA	05	BELL	Repl. by USHIRODA 06

[1] Requires $0.6 < M_{K^0_S \pi^0} < 0.8$ GeV/c^2 or $1.0 < M_{K^0_S \pi^0} < 1.8$ GeV/c^2.
[2] Requires $1.1 < M_{K^0_S \pi^0} < 1.8$ GeV/c^2.
[3] Requires $M_{K^0_S \pi^0} < 1.8$ GeV/c^2.

$C_{K^0_S \pi^+ \pi^- \gamma}(B^0 \to K^0_S \pi^+ \pi^- \gamma)$

VALUE	DOCUMENT ID	TECN	COMMENT
$-0.39 \pm 0.20^{+0.03}_{-0.02}$	[1] DEL-AMO-SA...16	BABR	$e^+e^- \to \Upsilon(4S)$

[1] Requires $M_{K\pi\pi} < 1.8$ GeV/c^2, 0.6 GeV/c^2 $< m_{\pi^+\pi^-} < 0.9$ GeV/c^2, $m_{K\pi} < 0.845$ GeV/c^2 or $m_{K\pi} > 0.945$ GeV/c^2.

$S_{K^0_S \pi^+ \pi^- \gamma}(B^0 \to K^0_S \pi^+ \pi^- \gamma)$

VALUE	DOCUMENT ID	TECN	COMMENT
$0.14 \pm 0.25 \pm 0.03$	[1] DEL-AMO-SA...16	BABR	$e^+e^- \to \Upsilon(4S)$

[1] Requires $M_{K\pi\pi} < 1.8$ GeV/c^2, 0.6 GeV/c^2 $< m_{\pi^+\pi^-} < 0.9$ GeV/c^2, $m_{K\pi} < 0.845$ GeV/c^2 or $m_{K\pi} > 0.945$ GeV/c^2.

$C_{K^*(892)^0 \gamma}$ $(B^0 \to K^*(892)^0 \gamma)$

VALUE	DOCUMENT ID		TECN	COMMENT
0.03 ± 0.10 OUR AVERAGE				
$0.10 \pm 0.13 \pm 0.04$	[1] ADACHI	25	BELL	$e^+e^- \to \Upsilon(4S)$
$-0.14 \pm 0.16 \pm 0.03$	[1] AUBERT	08BA	BABR	$e^+e^- \to \Upsilon(4S)$
$0.20 \pm 0.24 \pm 0.05$	[1,2] USHIRODA	06	BELL	$e^+e^- \to \Upsilon(4S)$
• • • We do not use the following data for averages, fits, limits, etc. • • •				
$-0.40 \pm 0.23 \pm 0.03$	AUBERT,B	05P	BABR	Repl. by AUBERT 08BA
$-0.57 \pm 0.32 \pm 0.09$	[3] AUBERT,B	04Z	BABR	Repl. by AUBERT,B 05P

[1] Requires $0.8 < M_{K^0_S \pi^0} < 1.0$ GeV/c^2.
[2] Reports value of A which is equal to $-C$.
[3] Based on a total signal of 105 ± 14 events with $K^*(892)^0 \to K^0_S \pi^0$ only.

$S_{K^*(892)^0 \gamma}$ $(B^0 \to K^*(892)^0 \gamma)$

VALUE	DOCUMENT ID		TECN	COMMENT
-0.08 ± 0.17 OUR AVERAGE				
$0.00^{+0.27}_{-0.26} \pm 0.03$	[1] ADACHI	25	BELL	$e^+e^- \to \Upsilon(4S)$
$-0.03 \pm 0.29 \pm 0.03$	[1] AUBERT	08BA	BABR	$e^+e^- \to \Upsilon(4S)$
$-0.32^{+0.36}_{-0.33} \pm 0.05$	[1] USHIRODA	06	BELL	$e^+e^- \to \Upsilon(4S)$
• • • We do not use the following data for averages, fits, limits, etc. • • •				
$-0.21 \pm 0.40 \pm 0.05$	AUBERT,B	05P	BABR	Repl. by AUBERT 08BA
$-0.79^{+0.63}_{-0.50} \pm 0.10$	[2] USHIRODA	05	BELL	Repl. by USHIRODA 06
$0.25 \pm 0.63 \pm 0.14$	[3] AUBERT,B	04Z	BABR	Repl. by AUBERT,B 05P

[1] Requires $0.8 < M_{K^0_S \pi^0} < 1.0$ GeV/c^2.
[2] Assumes $C(B^0 \to K^*(892)^0 \gamma) = 0$.
[3] Based on a total signal of 105 ± 14 events with $K^*(892)^0 \to K^0_S \pi^0$ only.

$C_{\eta K^0 \gamma}$ $(B^0 \to \eta K^0 \gamma)$

VALUE	DOCUMENT ID		TECN	COMMENT
0.1 ± 0.4 OUR AVERAGE Error includes scale factor of 1.4.				
$0.48 \pm 0.41 \pm 0.07$	[1,2] NAKANO	18	BELL	$e^+e^- \to \Upsilon(4S)$
$-0.32^{+0.40}_{-0.39} \pm 0.07$	[3] AUBERT	09	BABR	$e^+e^- \to \Upsilon(4S)$

[1] Assuming $m_{\eta K^0_S} < 2.1$ GeV.
[2] Reversed the sign for C=-A.
[3] Assuming $m_{\eta K} < 3.25$ GeV.

$S_{\eta K^0 \gamma}$ $(B^0 \to \eta K^0 \gamma)$

VALUE	DOCUMENT ID		TECN	COMMENT
-0.5 ± 0.5 OUR AVERAGE Error includes scale factor of 1.2.				
$-1.32 \pm 0.77 \pm 0.36$	[1] NAKANO	18	BELL	$e^+e^- \to \Upsilon(4S)$
$-0.18^{+0.49}_{-0.46} \pm 0.12$	[2] AUBERT	09	BABR	$e^+e^- \to \Upsilon(4S)$

[1] Assuming $m_{\eta K^0_S} < 2.1$ GeV.
[2] Assuming $m_{\eta K} < 3.25$ GeV.

$C_{K^0 \phi \gamma}$ $(B^0 \to K^0 \phi \gamma)$

VALUE	DOCUMENT ID		TECN	COMMENT
$-0.35 \pm 0.58^{+0.10}_{-0.23}$	[1] SAHOO	11A	BELL	$e^+e^- \to \Upsilon(4S)$

[1] Reports value of A, which is equal to $-C$.

$S_{K^0 \phi \gamma}$ $(B^0 \to K^0 \phi \gamma)$

VALUE	DOCUMENT ID		TECN	COMMENT
$0.74^{+0.72}_{-1.05}{}^{+0.10}_{-0.24}$	SAHOO	11A	BELL	$e^+e^- \to \Upsilon(4S)$

$C(B^0 \to K^0_S \rho^0 \gamma)$

VALUE	DOCUMENT ID		TECN	COMMENT
$-0.05 \pm 0.18 \pm 0.06$	[1,2] LI	08F	BELL	$e^+e^- \to \Upsilon(4S)$

[1] Requires $M_{K^0_S \pi^+ \pi^-} < 1.8$ GeV/c^2 and $0.6 < M_{\pi^+\pi^-} < 0.9$ GeV/c^2 .
[2] Reports value of $A_{\rm eff}$ which is equal to $-C$, and includes the non-resonant $\pi^+\pi^-$ contribution in the ρ^0 region.

$S(B^0 \to K^0_S \rho^0 \gamma)$

VALUE	DOCUMENT ID		TECN	COMMENT
-0.04 ± 0.23 OUR AVERAGE				
$-0.18 \pm 0.32^{+0.06}_{-0.05}$	[1] DEL-AMO-SA...16		BABR	$e^+e^- \to \Upsilon(4S)$
$0.11 \pm 0.33^{+0.05}_{-0.09}$	[2] LI	08F	BELL	$e^+e^- \to \Upsilon(4S)$

[1] Requires $M_{K\pi\pi} < 1.8$ GeV/c^2, 0.6 GeV/c^2 $< m_{\pi^+\pi^-} < 0.9$ GeV/c^2, $m_{K\pi} < 0.845$ GeV/c^2 or $m_{K\pi} > 0.945$ GeV/c^2.
[2] Requires $M_{K\pi\pi} < 1.8$ GeV/c^2.

C $(B^0 \to \rho^0 \gamma)$

VALUE	DOCUMENT ID		TECN	COMMENT
$0.44 \pm 0.49 \pm 0.14$	[1] USHIRODA	08	BELL	$e^+e^- \to \Upsilon(4S)$

[1] Reports value of A which is equal to $-C$.

S $(B^0 \to \rho^0 \gamma)$

VALUE	DOCUMENT ID		TECN	COMMENT
$-0.83 \pm 0.65 \pm 0.18$	USHIRODA	08	BELL	$e^+e^- \to \Upsilon(4S)$

Int. J. Mod. Phys. A 2026.41. Downloaded from www.worldscientific.com
by LIFORNIA @ BERKELEY on 09/16/26. Re-use and distribution is strictly not permitted, except for Open Access articles.

Int. J. Mod. Phys. A 2026.41. Downloaded from www.worldscientific.com
by UNIVERSITY OF CALIFORNIA @ BERKELEY on 09/16/26. Re-use and distribution is strictly not permitted, except for Open Access articles.

$C_{\pi\pi}$ ($B^0 \to \pi^+\pi^-$)

$C_{\pi\pi}$ is defined as $(1-|\lambda|^2)/(1+|\lambda|^2)$, where the quantity $\lambda = q/p\ \overline{A}_f/A_f$ is a phase convention independent observable quantity for the final state f. For details, see the review on "CP Violation" in the Reviews section.

VALUE	DOCUMENT ID		TECN	COMMENT
-0.314 ± 0.030 OUR AVERAGE				
$-0.311 \pm 0.045 \pm 0.015$	AAIJ	21O	LHCB	pp at 13 TeV
$-0.34 \pm 0.06 \pm 0.01$	AAIJ	18O	LHCB	pp at 7, 8 TeV
$-0.33 \pm 0.06 \pm 0.03$	[1] DALSENO	13	BELL	$e^+e^- \to \Upsilon(4S)$
$-0.25 \pm 0.08 \pm 0.02$	LEES	13D	BABR	$e^+e^- \to \Upsilon(4S)$
• • • We do not use the following data for averages, fits, limits, etc. • • •				
$-0.38 \pm 0.15 \pm 0.02$	AAIJ	13BO	LHCB	Repl. by AAIJ 18O
$-0.21 \pm 0.09 \pm 0.02$	AUBERT	07AF	BABR	Repl. by LEES 13D
$-0.55 \pm 0.08 \pm 0.05$	[1] ISHINO	07	BELL	Repl. by DALSENO 13
$-0.56 \pm 0.12 \pm 0.06$	[1] ABE	05D	BELL	Repl. by ISHINO 07
$-0.09 \pm 0.15 \pm 0.04$	AUBERT,BE	05	BABR	Repl. by AUBERT 07AF
$-0.58 \pm 0.15 \pm 0.07$	[1] ABE	04E	BELL	Repl. by ABE 05D
$-0.77 \pm 0.27 \pm 0.08$	[1] ABE	03G	BELL	Repl. by ABE 04E.
$-0.94\ ^{+0.31}_{-0.25} \pm 0.09$	[1] ABE	02M	BELL	Repl. by ABE 03G
$-0.25\ ^{+0.45}_{-0.47} \pm 0.14$	[2] AUBERT	02D	BABR	Repl. by AUBERT 02Q
$-0.30 \pm 0.25 \pm 0.04$	[3] AUBERT	02Q	BABR	Repl. by AUBERT,BE 05

[1] Paper reports $A_{\pi\pi}$ which equals to $-C_{\pi\pi}$.
[2] Corresponds to 90% confidence range $-1.0 < C_{\pi\pi} < 0.47$.
[3] Corresponds to 90% confidence range $-0.72 < C_{\pi\pi} < 0.12$.

$S_{\pi\pi}$ ($B^0 \to \pi^+\pi^-$)

$S_{\pi\pi} = 2\mathrm{Im}\lambda/(1+|\lambda|^2)$, see the note in the $C_{\pi\pi}$ datablock above.

VALUE	DOCUMENT ID		TECN	COMMENT
-0.670 ± 0.030 OUR AVERAGE				
$-0.706 \pm 0.042 \pm 0.013$	AAIJ	21O	LHCB	pp at 13 TeV
$-0.63 \pm 0.05 \pm 0.01$	AAIJ	18O	LHCB	pp at 7, 8 TeV
$-0.64 \pm 0.08 \pm 0.03$	[1] DALSENO	13	BELL	$e^+e^- \to \Upsilon(4S)$
$-0.68 \pm 0.10 \pm 0.03$	LEES	13D	BABR	$e^+e^- \to \Upsilon(4S)$
• • • We do not use the following data for averages, fits, limits, etc. • • •				
$-0.71 \pm 0.13 \pm 0.02$	AAIJ	13BO	LHCB	Repl. by AAIJ 18O
$-0.60 \pm 0.11 \pm 0.03$	AUBERT	07AF	BABR	Repl. by LEES 13D
$-0.61 \pm 0.10 \pm 0.04$	ISHINO	07	BELL	Repl. by DALSENO 13
$-0.67 \pm 0.16 \pm 0.06$	[2] ABE	05D	BELL	Repl. by ISHINO 07
$-0.30 \pm 0.17 \pm 0.03$	AUBERT,BE	05	BABR	Repl. by AUBERT 07AF
$-1.00 \pm 0.21 \pm 0.07$	[3] ABE	04E	BELL	Repl. by ABE 05D
$-1.23 \pm 0.41\ ^{+0.08}_{-0.07}$	ABE	03G	BELL	Repl. by ABE 04E.
$-1.21\ ^{+0.38}_{-0.27}\ ^{+0.16}_{-0.13}$	ABE	02M	BELL	Repl. by ABE 03G
$0.03\ ^{+0.52}_{-0.56} \pm 0.11$	[4] AUBERT	02D	BABR	Repl. by AUBERT 02Q
$0.02 \pm 0.34 \pm 0.05$	[5] AUBERT	02Q	BABR	Repl. by AUBERT,BE 05

[1] An isospin analysis using other BELLE measurements, disfavors the region of $23.8^\circ < \phi_2 < 66.8^\circ$ at 68% CL.
[2] Rule out the CP-conserving case, $C_{\pi\pi} = S_{\pi\pi} = 0$, at the 5.4 sigma level.
[3] Rule out the CP-conserving case, $C_{\pi\pi} = S_{\pi\pi} = 0$, at the 5.2 sigma level.
[4] Corresponds to 90% confidence range $-0.89 < S_{\pi\pi} < 0.85$.
[5] Corresponds to 90% confidence range $-0.54 < S_{\pi\pi} < 0.58$.

$C_{\pi^0\pi^0}$($B^0 \to \pi^0\pi^0$)

VALUE	DOCUMENT ID		TECN	COMMENT
-0.23 ± 0.18 OUR AVERAGE				
$-0.03 \pm 0.30 \pm 0.04$	[1] ADACHI	25F	BEL2	$e^+e^- \to \Upsilon(4S)$
$-0.14 \pm 0.36 \pm 0.10$	[2] JULIUS	17	BELL	$e^+e^- \to \Upsilon(4S)$
$-0.43 \pm 0.26 \pm 0.05$	LEES	13D	BABR	$e^+e^- \to \Upsilon(4S)$
• • • We do not use the following data for averages, fits, limits, etc. • • •				
$0.14 \pm 0.46 \pm 0.07$	[2] ABUDINEN	23E	BELL	Repl. by ADACHI 25F
$-0.49 \pm 0.35 \pm 0.05$	AUBERT	07BC	BABR	Repl. by LEES 13D
$-0.12 \pm 0.56 \pm 0.06$	[3] AUBERT	05L	BABR	Repl. by AUBERT 07BC
$-0.44\ ^{+0.52}_{-0.53} \pm 0.17$	[2] CHAO	05	BELL	Repl. by JULIUS 17

[1] Reports value of A which is equal to $-C$.
[2] Quotes $A_{\pi^0\pi^0} = -0.14 \pm 0.46 \pm 0.07$ (correction published May 22, 2024) which is equal to $-C_{\pi^0\pi^0}$.
[3] Corresponds to a 90% CL interval of $-0.88 < A_{CP} < 0.64$.

$C_{\rho\pi}$ ($B^0 \to \rho^+\pi^-$)

VALUE	DOCUMENT ID		TECN	COMMENT
-0.03 ± 0.07 OUR AVERAGE Error includes scale factor of 1.2.				
$0.016 \pm 0.059 \pm 0.036$	[1] LEES	13J	BABR	$e^+e^- \to \Upsilon(4S)$
$-0.13 \pm 0.09 \pm 0.05$	[1] KUSAKA	07	BELL	$e^+e^- \to \Upsilon(4S)$
• • • We do not use the following data for averages, fits, limits, etc. • • •				
$0.15 \pm 0.09 \pm 0.05$	AUBERT	07AA	BABR	Repl. by LEES 13J
$0.25 \pm 0.17\ ^{+0.02}_{-0.06}$	WANG	05	BELL	Repl. by KUSAKA 07
$0.36 \pm 0.18 \pm 0.04$	AUBERT	03T	BABR	Repl. by AUBERT 07AA

[1] Uses time-dependent Dalitz plot analysis of $B^0 \to \pi^+\pi^-\pi^0$ decays.

$S_{\rho\pi}$ ($B^0 \to \rho^+\pi^-$)

VALUE	DOCUMENT ID		TECN	COMMENT
0.05 ± 0.07 OUR AVERAGE				
$0.053 \pm 0.081 \pm 0.034$	[1] LEES	13J	BABR	$e^+e^- \to \Upsilon(4S)$
$0.06 \pm 0.13 \pm 0.05$	[1] KUSAKA	07	BELL	$e^+e^- \to \Upsilon(4S)$
• • • We do not use the following data for averages, fits, limits, etc. • • •				
$-0.03 \pm 0.11 \pm 0.04$	AUBERT	07AA	BABR	Repl. by LEES 13J
$-0.28 \pm 0.23\ ^{+0.10}_{-0.08}$	WANG	05	BELL	Repl. by KUSAKA 07
$0.19 \pm 0.24 \pm 0.03$	AUBERT	03T	BABR	Repl. by AUBERT 07AA

[1] Uses time-dependent Dalitz plot analysis of $B^0 \to \pi^+\pi^-\pi^0$ decays.

$\Delta C_{\rho\pi}$ ($B^0 \to \rho^+\pi^-$)

$\Delta C_{\rho\pi}$ describes the asymmetry between the rates $\Gamma(B^0 \to \rho^+\pi^-) + \Gamma(\overline{B}^0 \to \rho^-\pi^+)$ and $\Gamma(B^0 \to \rho^-\pi^+) + \Gamma(\overline{B}^0 \to \rho^+\pi^-)$.

VALUE	DOCUMENT ID		TECN	COMMENT
0.27 ± 0.06 OUR AVERAGE				
$0.234 \pm 0.061 \pm 0.048$	[1] LEES	13J	BABR	$e^+e^- \to \Upsilon(4S)$
$0.36 \pm 0.10 \pm 0.05$	[1] KUSAKA	07	BELL	$e^+e^- \to \Upsilon(4S)$
• • • We do not use the following data for averages, fits, limits, etc. • • •				
$0.39 \pm 0.09 \pm 0.09$	AUBERT	07AA	BABR	Repl. by LEES 13J
$0.38 \pm 0.18\ ^{+0.02}_{-0.04}$	WANG	05	BELL	Repl. by KUSAKA 07
$0.28\ ^{+0.18}_{-0.19} \pm 0.04$	AUBERT	03T	BABR	Repl. by AUBERT 07AA

[1] Uses time-dependent Dalitz plot analysis of $B^0 \to \pi^+\pi^-\pi^0$ decays.

$\Delta S_{\rho\pi}$ ($B^0 \to \rho^+\pi^-$)

$\Delta S_{\rho\pi}$ is related to the strong phase difference between the amplitudes contributing to $B^0 \to \rho^+\pi^-$.

VALUE	DOCUMENT ID		TECN	COMMENT
0.01 ± 0.08 OUR AVERAGE				
$0.054 \pm 0.082 \pm 0.039$	[1] LEES	13J	BABR	$e^+e^- \to \Upsilon(4S)$
$-0.08 \pm 0.13 \pm 0.05$	[1] KUSAKA	07	BELL	$e^+e^- \to \Upsilon(4S)$
• • • We do not use the following data for averages, fits, limits, etc. • • •				
$-0.01 \pm 0.14 \pm 0.06$	AUBERT	07AA	BABR	Repl. by LEES 13J
$-0.30 \pm 0.24 \pm 0.09$	WANG	05	BELL	Repl. by KUSAKA 07
$0.15 \pm 0.25 \pm 0.03$	AUBERT	03T	BABR	Repl. by AUBERT 07AA

[1] Uses time-dependent Dalitz plot analysis of $B^0 \to \pi^+\pi^-\pi^0$ decays.

$C_{\rho^0\pi^0}$ ($B^0 \to \rho^0\pi^0$)

VALUE	DOCUMENT ID		TECN	COMMENT
0.27 ± 0.24 OUR AVERAGE				
$0.19 \pm 0.23 \pm 0.15$	[1] LEES	13J	BABR	$e^+e^- \to \Upsilon(4S)$
$0.49 \pm 0.36 \pm 0.28$	[1,2] KUSAKA	07	BELL	$e^+e^- \to \Upsilon(4S)$
• • • We do not use the following data for averages, fits, limits, etc. • • •				
$-0.10 \pm 0.40 \pm 0.53$	AUBERT	07AA	BABR	Repl. by LEES 13J
$0.53\ ^{+0.67}_{-0.84}\ ^{+0.10}_{-0.15}$	[2] DRAGIC	06	BELL	Repl. by KUSAKA 07

[1] Uses time-dependent Dalitz plot analysis of $B^0 \to \pi^+\pi^-\pi^0$ decays.
[2] Quotes $A_{\rho^0\pi^0}$ which is equal to $-C_{\rho^0\pi^0}$.

$S_{\rho^0\pi^0}$ ($B^0 \to \rho^0\pi^0$)

VALUE	DOCUMENT ID		TECN	COMMENT
-0.23 ± 0.34 OUR AVERAGE				
$-0.37 \pm 0.34 \pm 0.20$	[1] LEES	13J	BABR	$e^+e^- \to \Upsilon(4S)$
$0.17 \pm 0.57 \pm 0.35$	[1] KUSAKA	07	BELL	$e^+e^- \to \Upsilon(4S)$
• • • We do not use the following data for averages, fits, limits, etc. • • •				
$0.04 \pm 0.44 \pm 0.18$	AUBERT	07AA	BABR	Repl. by LEES 13J

[1] Uses time-dependent Dalitz plot analysis of $B^0 \to \pi^+\pi^-\pi^0$ decays.

$C_{a_1\pi}$ ($B^0 \to a_1(1260)^+\pi^-$)

VALUE	DOCUMENT ID		TECN	COMMENT
-0.05 ± 0.11 OUR AVERAGE				
$-0.01 \pm 0.11 \pm 0.09$	DALSENO	12	BELL	$e^+e^- \to \Upsilon(4S)$
$-0.10 \pm 0.15 \pm 0.09$	AUBERT	07O	BABR	$e^+e^- \to \Upsilon(4S)$

$S_{a_1\pi}$ ($B^0 \to a_1(1260)^+\pi^-$)

VALUE	DOCUMENT ID		TECN	COMMENT
-0.2 ± 0.4 OUR AVERAGE Error includes scale factor of 3.2.				
$-0.51 \pm 0.14 \pm 0.08$	DALSENO	12	BELL	$e^+e^- \to \Upsilon(4S)$
$0.37 \pm 0.21 \pm 0.07$	AUBERT	07O	BABR	$e^+e^- \to \Upsilon(4S)$

$\Delta C_{a_1\pi}$ ($B^0 \to a_1(1260)^+\pi^-$)

$\Delta C_{a_1\pi}$ describes the asymmetry between the rates $\Gamma(B^0 \to a_1^+\pi^-) + \Gamma(\overline{B}^0 \to a_1^-\pi^+)$ and $\Gamma(B^0 \to a_1^-\pi^+) + \Gamma(\overline{B}^0 \to a_1^+\pi^-)$.

VALUE	DOCUMENT ID		TECN	COMMENT
0.43 ± 0.14 OUR AVERAGE Error includes scale factor of 1.3.				
$0.54 \pm 0.11 \pm 0.07$	DALSENO	12	BELL	$e^+e^- \to \Upsilon(4S)$
$0.26 \pm 0.15 \pm 0.07$	AUBERT	07O	BABR	$e^+e^- \to \Upsilon(4S)$

Int. J. Mod. Phys. A 2026.41. Downloaded from www.worldscientific.com by CALIFORNIA @ BERKELEY on 09/16/26. Re-use and distribution is strictly not permitted, except for Open Access articles.

$\Delta S_{a_1\pi}$ ($B^0 \to a_1(1260)^+\pi^-$)

$\Delta S_{a_1\pi}$ is related to the strong phase difference between the amplitudes contributing to $B^0 \to a_1\pi$ decays.

VALUE	DOCUMENT ID		TECN	COMMENT
−0.11±0.12 OUR AVERAGE				
−0.09±0.14±0.06	DALSENO	12	BELL	$e^+e^- \to \Upsilon(4S)$
−0.14±0.21±0.06	AUBERT	07O	BABR	$e^+e^- \to \Upsilon(4S)$

C ($B^0 \to b_1^- K^+$)

VALUE	DOCUMENT ID		TECN	COMMENT
−0.22±0.23±0.05	AUBERT	07BI	BABR	$e^+e^- \to \Upsilon(4S)$

ΔC ($B^0 \to b_1^- \pi^+$)

VALUE	DOCUMENT ID		TECN	COMMENT
−1.04±0.23±0.08	AUBERT	07BI	BABR	$e^+e^- \to \Upsilon(4S)$

$C_{\rho^0\rho^0}$ ($B^0 \to \rho^0\rho^0$)

VALUE	DOCUMENT ID		TECN	COMMENT
0.2±0.8±0.3	AUBERT	08BB	BABR	$e^+e^- \to \Upsilon(4S)$

$S_{\rho^0\rho^0}$ ($B^0 \to \rho^0\rho^0$)

VALUE	DOCUMENT ID		TECN	COMMENT
0.3±0.7±0.2	AUBERT	08BB	BABR	$e^+e^- \to \Upsilon(4S)$

$C_{\rho\rho}$ ($B^0 \to \rho^+\rho^-$)

VALUE	DOCUMENT ID		TECN	COMMENT
0.00±0.08 OUR AVERAGE				
$-0.02\pm0.12^{+0.06}_{-0.05}$	ADACHI	25H	BELL	$e^+e^- \to \Upsilon(4S)$
0.00±0.10±0.06	[1] VANHOEFER	16	BELL	$e^+e^- \to \Upsilon(4S)$
0.01±0.15±0.06	AUBERT	07BF	BABR	$e^+e^- \to \Upsilon(4S)$
• • • We do not use the following data for averages, fits, limits, etc. • • •				
−0.16±0.21±0.08	[1] SOMOV	07	BELL	Repl. by VANHOEFER 16
−0.00±0.30±0.09	[1] SOMOV	06	BELL	Repl. by SOMOV 07
−0.03±0.18±0.09	AUBERT,B	05C	BABR	Repl. by AUBERT 07BF
−0.17±0.27±0.14	AUBERT,B	04R	BABR	Repl. by AUBERT,B 05C

[1] BELLE Collab. quotes A_{CP} which is equal to $-C$.

$S_{\rho\rho}$ ($B^0 \to \rho^+\rho^-$)

VALUE	DOCUMENT ID		TECN	COMMENT
−0.18±0.11 OUR AVERAGE				
−0.26±0.19±0.08	ADACHI	25H	BELL	$e^+e^- \to \Upsilon(4S)$
−0.13±0.15±0.05	VANHOEFER	16	BELL	$e^+e^- \to \Upsilon(4S)$
$-0.17\pm0.20^{+0.05}_{-0.06}$	AUBERT	07BF	BABR	$e^+e^- \to \Upsilon(4S)$
• • • We do not use the following data for averages, fits, limits, etc. • • •				
0.19±0.30±0.08	SOMOV	07	BELL	Repl. by VANHOEFER 16
0.08±0.41±0.09	SOMOV	06	BELL	Repl. by SOMOV 07
$-0.33\pm0.24^{+0.08}_{-0.14}$	AUBERT,B	05C	BABR	Repl. by AUBERT 07BF
−0.42±0.42±0.14	AUBERT,B	04R	BABR	Repl. by AUBERT,B 05C

$|\lambda|$ ($B^0 \to J/\psi K^*(892)^0$)

VALUE	CL%	DOCUMENT ID		TECN	COMMENT
<0.25	95	[1] AUBERT,B	04H	BABR	$e^+e^- \to \Upsilon(4S)$

[1] Uses the measured cosine coefficients C and $\overline{C}$ and assumes $|q/p| = 1$.

cos 2β ($B^0 \to J/\psi K^*(892)^0$)

β (ϕ_1) is one of the angles of CMK unitarity triangle, see the review on "*CP*" Violation in the Reviews section.

VALUE	DOCUMENT ID		TECN	COMMENT
$1.7\ ^{+0.7}_{-0.9}$ OUR AVERAGE Error includes scale factor of 1.6.				
$2.72^{+0.50}_{-0.79}\pm0.27$	[1] AUBERT	05P	BABR	$e^+e^- \to \Upsilon(4S)$
0.87±0.74±0.12	[2] ITOH	05	BELL	$e^+e^- \to \Upsilon(4S)$

[1] The measurement is obtained when sin 2β is fixed to 0.726 and the sign of cos 2β is positive with 86% confidence level.
[2] The measurement is obtained with sin 2β fixed to 0.731.

cos 2β ($B^0 \to [K^0_S\pi^+\pi^-]_{D(*)}\ h^0$)

VALUE	DOCUMENT ID		TECN	COMMENT
0.91±0.22±0.11	[1] ADACHI	18		$e^+e^- \to \Upsilon(4S)$
• • • We do not use the following data for averages, fits, limits, etc. • • •				
$1.06\pm0.33^{+0.21}_{-0.15}$	[2] VOROBYEV	16	BELL	$e^+e^- \to \Upsilon(4S)$
0.42±0.49±0.16	[3] AUBERT	07BH	BABR	$e^+e^- \to \Upsilon(4S)$
$1.87^{+0.40+0.22}_{-0.53-0.32}$	[4] KROKOVNY	06	BELL	Repl. by VOROBYEV 16

[1] Analyzes joint data sample of Belle and BaBar using Dalitz plot analysis of $D \to K^0_S\pi^+\pi^-$; the second error combines experimental systematic uncertainty and the Dalitz plot model uncertainty.
[2] A model-independent measurement uses the binned Dalitz plot technique.
[3] AUBERT 07BH evaluates the likelihoods for the positive and negative solutions assuming $\sin(2\beta_{eff}) = 0.678$. It quotes $L_+ / (L_+ + L_-) = 0.86$ corresponding to a likelihood ratio of $L_+/L_- = 6.14$ in favor of the positive solution.
[4] KROKOVNY 06 evaluates the likelihoods for the positive and negative solutions assuming $\sin(2\beta_{eff}) = 0.689$. It quotes $L_+ / (L_+ + L_-) = 0.983$ corresponding to a likelihood ratio of $L_+/L_- = 57.8$ in favor of the positive solution.

$(S_+ + S_-)/2$ ($B^0 \to D^{*-}\pi^+$)

$S_\pm = -\frac{2Im(\lambda_\pm)}{1+|\lambda_\pm|^2}$ where λ_+ and λ_- are defined in the $C_{\pi\pi}$ datablock above for $B^0 \to D^{*-}\pi^+$ and $\overline{B}^0 \to D^{*+}\pi^-$.

VALUE	DOCUMENT ID		TECN	COMMENT
−0.039±0.011 OUR AVERAGE				
−0.046±0.013±0.015	[1] BAHINIPATI	11	BELL	$e^+e^- \to \Upsilon(4S)$
−0.040±0.023±0.010	[2] AUBERT	06Y	BABR	$e^+e^- \to \Upsilon(4S)$
−0.034±0.014±0.009	[1] AUBERT	05Z	BABR	$e^+e^- \to \Upsilon(4S)$
• • • We do not use the following data for averages, fits, limits, etc. • • •				
−0.039±0.020±0.013	[3] RONGA	06	BELL	Repl. by BAHINIPATI 11
−0.030±0.028±0.018	[1] GERSHON	05	BELL	Repl. by RONGA 06
−0.068±0.038±0.020	[2] AUBERT	04V	BABR	Repl. by AUBERT 06Y
−0.063±0.024±0.014	[1] AUBERT	04W	BABR	Repl. by AUBERT 05Z
0.060±0.040±0.019	[2] SARANGI	04	BELL	Repl. by RONGA 06

[1] Uses partially reconstructed $B^0 \to D^{*\pm}\pi^\mp$ decays.
[2] Uses fully reconstructed $B^0 \to D^{*\pm}\pi^\mp$ decays.
[3] Combines the results from fully reconstructed and partially reconstructed $D^*\pi$ events by taking weighted averages. Assumes that systematic errors from physics parameters and fit biases in the two measurements are 100% correlated.

$(S_- - S_+)/2$ ($B^0 \to D^{*-}\pi^+$)

VALUE	DOCUMENT ID		TECN	COMMENT
−0.009±0.015 OUR AVERAGE				
−0.015±0.013±0.015	[1] BAHINIPATI	11	BELL	$e^+e^- \to \Upsilon(4S)$
0.049±0.042±0.015	[2] AUBERT	06Y	BABR	$e^+e^- \to \Upsilon(4S)$
−0.019±0.022±0.013	[1] AUBERT	05Z	BABR	$e^+e^- \to \Upsilon(4S)$
• • • We do not use the following data for averages, fits, limits, etc. • • •				
−0.011±0.020±0.013	[3] RONGA	06	BELL	Repl. by BAHINIPATI 11
−0.005±0.028±0.018	[1] GERSHON	05	BELL	Repl. by RONGA 06
0.031±0.070±0.033	[2] AUBERT	04V	BABR	Repl. by AUBERT 06Y
−0.004±0.037±0.014	[1] AUBERT	04W	BABR	Repl. by AUBERT 05Z
0.049±0.040±0.019	[2] SARANGI	04	BELL	Repl. by RONGA 06

[1] Uses partially reconstructed $B^0 \to D^{*\pm}\pi^\mp$ decays.
[2] Uses fully reconstructed $B^0 \to D^{*\pm}\pi^\mp$ decays.
[3] Combines the results from fully reconstructed and partially reconstructed $D^*\pi$ events by taking weighted averages. Assumes that systematic errors from physics parameters and fit biases in the two measurements are 100% correlated.

$(S_+ + S_-)/2$ ($B^0 \to D^-\pi^+$)

VALUE	DOCUMENT ID		TECN	COMMENT
−0.046±0.023 OUR AVERAGE				
−0.010±0.023±0.07	[1] AUBERT	06Y	BABR	$e^+e^- \to \Upsilon(4S)$
−0.050±0.021±0.012	[2] RONGA	06	BELL	$e^+e^- \to \Upsilon(4S)$
• • • We do not use the following data for averages, fits, limits, etc. • • •				
−0.022±0.038±0.020	[1] AUBERT	04V	BABR	Repl. by AUBERT 06Y
−0.062±0.037±0.018	[1] SARANGI	04	BELL	Repl. by RONGA 06

[1] Uses fully reconstructed $B^0 \to D^\pm\pi^\mp$ decays.
[2] Combines the results from fully reconstructed and partially reconstructed $D\pi$ events by taking weighted averages. Assumes that systematic errors from physics parameters and fit biases in the two measurements are 100% correlated.

$(S_- - S_+)/2$ ($B^0 \to D^-\pi^+$)

VALUE	DOCUMENT ID		TECN	COMMENT
−0.022±0.021 OUR AVERAGE				
−0.033±0.042±0.012	[1] AUBERT	06Y	BABR	$e^+e^- \to \Upsilon(4S)$
−0.019±0.021±0.012	[2] RONGA	06	BELL	$e^+e^- \to \Upsilon(4S)$
• • • We do not use the following data for averages, fits, limits, etc. • • •				
0.025±0.068±0.033	[1] AUBERT	04V	BABR	Repl. by AUBERT 06Y
−0.025±0.037±0.018	[1] SARANGI	04	BELL	Repl. by RONGA 06

[1] Uses fully reconstructed $B^0 \to D^\pm\pi^\mp$ decays.
[2] Combines the results from fully reconstructed and partially reconstructed $D\pi$ events by taking weighted averages. Assumes that systematic errors from physics parameters and fit biases in the two measurements are 100% correlated.

S_+ ($B^0 \to D^-\pi^+$)

VALUE	DOCUMENT ID		TECN	COMMENT
0.058±0.020±0.011	[1] AAIJ	18Z	LHCB	pp at 7, 8 TeV

[1] Measured in the simultaneous analysis of $B^0 \to D^\mp\pi^\pm$ decays. AAIJ 18Z reports a statistical (systematic) correlation of 0.6 (−0.41) with the measured value of $S_-(B^0 \to D^+\pi^-)$.

S_- ($B^0 \to D^+\pi^-$)

VALUE	DOCUMENT ID		TECN	COMMENT
0.038±0.020±0.007	[1] AAIJ	18Z	LHCB	pp at 7, 8 TeV

[1] Measured in the simultaneous analysis of $B^0 \to D^\mp\pi^\pm$ decays. AAIJ 18Z reports a statistical (systematic) correlation of 0.6 (−0.41) with the measured value of $S_+(B^0 \to D^-\pi^+)$.

$(S_+ + S_-)/2$ ($B^0 \to D^-\rho^+$)

VALUE	DOCUMENT ID		TECN	COMMENT
−0.024±0.031±0.009	[1] AUBERT	06Y	BABR	$e^+e^- \to \Upsilon(4S)$

[1] Uses fully reconstructed $B^0 \to D^-\rho^+$ decays.

Int. J. Mod. Phys. A 2026.41. Downloaded from www.worldscientific.com
by UNIVERSITY OF CALIFORNIA @ BERKELEY on 09/16/26. Re-use and distribution is strictly not permitted, except for Open Access articles.

$(S_- - S_+)/2$ ($B^0 \to D^- \rho^+$)

VALUE	DOCUMENT ID		TECN	COMMENT
−0.098±0.055±0.018	[1] AUBERT	06Y	BABR	$e^+e^- \to \Upsilon(4S)$

[1] Uses fully reconstructed $B^0 \to D^- \rho^+$ decays.

$C_{\eta_c K^0_S}$ ($B^0 \to \eta_c K^0_S$)

VALUE	DOCUMENT ID		TECN	COMMENT
0.080±0.124±0.029	AUBERT	09K	BABR	$e^+e^- \to \Upsilon(4S)$

$S_{\eta_c K^0_S}$ ($B^0 \to \eta_c K^0_S$)

VALUE	DOCUMENT ID		TECN	COMMENT
0.925±0.160±0.057	AUBERT	09K	BABR	$e^+e^- \to \Upsilon(4S)$

$C_{c\overline{c}K^{(*)0}}$ ($B^0 \to c\overline{c}K^{(*)0}$)

VALUE (units 10^{-2})	DOCUMENT ID		TECN	COMMENT
0.4± 1.0 OUR EVALUATION	(Produced by HFLAV)			
0.4± 1.0 OUR AVERAGE				
0.4± 1.2	[1] AAIJ	24	LHCB	pp at 7, 8 and 13 TeV
− 0.6± 1.6±1.2	[2] ADACHI	12A	BELL	$e^+e^- \to \Upsilon(4S)$
−29 $^{+53}_{-44}$ ±6	[3] AUBERT	09AU	BABR	$e^+e^- \to \Upsilon(4S)$
2.4± 2.0±1.6	[4] AUBERT	09K	BABR	$e^+e^- \to \Upsilon(4S)$
• • • We do not use the following data for averages, fits, limits, etc. • • •				
0.8± 1.2±0.3	[5,6] AAIJ	24	LHCB	pp at 13 TeV
− 1.7± 2.9	[5,7] AAIJ	17BN	LHCB	pp at 7, 8 TeV
− 4 ± 7 ±5	[8] SAHOO	08	BELL	Repl. by ADACHI 12A
4.9± 2.3±1.8	[4] AUBERT	07AY	BABR	Repl. by AUBERT 09K
− 1.8± 2.1±1.4	[9] CHEN	07	BELL	Repl. by ADACHI 12A
− 0.7± 4.1±3.3	[10] ABE	05B	BELL	Repl. by CHEN 07
5.1± 3.2±1.4	[11] AUBERT	05F	BABR	Repl. by AUBERT 07AY
5.1± 5.1±2.6	[12] ABE	02Z	BELL	Repl. by ABE 05B
5.3± 5.4±3.2	[13] AUBERT	02P	BABR	Repl. by AUBERT 05F

[1] A combination of this Run 2 result with the Run 1 result from AAIJ 17BN is reported with a correlation coefficient of 0.40.
[2] Measurement based on $B^0 \to J/\psi K^0_S$, $B^0 \to \psi(2S) K^0_S$, $B^0 \to J/\psi K^0_L$, and $B^0 \to \chi_{c1}(1P) K^0_S$ decays.
[3] Uses Dalitz plot analysis of $B^0 \to K^0\pi^+\pi^-$ decays and the first of two equivalent solutions is used.
[4] Measurement based on $B^0 \to c\overline{c}K(*)0$ decays.
[5] Measurement based on $B^0 \to J/\psi K^0_S$, $B^0 \to \psi(2S) K^0_S$ with $J/\psi \to \mu^+\mu^-$, $J/\psi \to e^+e^-$ and $\psi(2S) \to \mu^+\mu^-$.
[6] AAIJ 24 provides the correlation coefficient ρ=0.441 between the uncertainties of $\sin(2\beta)$ and $C_{c\overline{c}K(*)0}$ ($B^0 \to c\overline{c}K^{(*)0}$) measurements.
[7] AAIJ 17BN provides the correlation coefficient ρ=0.42 between the uncertainties of $S_{B^0 \to c\overline{c}K^{(*)0}}$($B^0 \to c\overline{c}K^{(*)0}$) and $C_{c\overline{c}K^{(*)0}}$ ($B^0 \to c\overline{c}K^{(*)0}$) measurements.
[8] Reports value of A of $B^0 \to \psi(2S) K^0$ which is equal to $-C$.
[9] Reports value of A of $B^0 \to J/\psi K^0$ which is equal to $-C$.
[10] Measurement based on 152×10^6 $B\overline{B}$ pairs.
[11] Measurement based on 227×10^6 $B\overline{B}$ pairs.
[12] Measured with both $\eta_f = \pm 1$ samples.
[13] Measured with the high purity of $\eta_f = -1$ samples.

$\sin(2\beta)$

For a discussion of CP violation, see the review on "CP Violation" in the Reviews section. $\sin(2\beta)$ is a measure of the CP-violating amplitude in the $B^0_d \to J/\psi(1S) K^0_S$.

VALUE	DOCUMENT ID		TECN	COMMENT
0.710±0.011 OUR EVALUATION	(Produced by HFLAV)			
0.710±0.013 OUR AVERAGE	Error includes scale factor of 1.2.			
0.724±0.014	[1] AAIJ	24	LHCB	pp at 7, 8 and 13 TeV
0.724±0.035±0.009	[2] ADACHI	24H	BEL2	$e^+e^- \to \Upsilon(4S)$
0.667±0.023±0.012	[3] ADACHI	12A	BELL	$e^+e^- \to \Upsilon(4S)$
0.57 ±0.58 ±0.06	[4] SATO	12	BELL	$e^+e^- \to \Upsilon(5S)$
0.69 ±0.52 ±0.08	[5] AUBERT	09AU	BABR	$e^+e^- \to \Upsilon(4S)$
0.687±0.028±0.012	[6] AUBERT	09K	BABR	$e^+e^- \to \Upsilon(4S)$
1.56 ±0.42 ±0.21	[7] AUBERT	04R	BABR	$e^+e^- \to \Upsilon(4S)$
0.79 $^{+0.41}_{-0.44}$	[8] AFFOLDER	00C	CDF	$p\overline{p}$ at 1.8 TeV
0.84 $^{+0.82}_{-1.04}$ ±0.16	[9] BARATE	00Q	ALEP	$e^+e^- \to Z$
3.2 $^{+1.8}_{-2.0}$ ±0.5	[10] ACKERSTAFF	98Z	OPAL	$e^+e^- \to Z$
• • • We do not use the following data for averages, fits, limits, etc. • • •				
0.717±0.013±0.008	[11,12] AAIJ	24	LHCB	pp at 13 TeV
0.760±0.034	[11,13] AAIJ	17BN	LHCB	pp at 7, 8 TeV
0.72 ±0.09 ±0.03	[14] SAHOO	08	BELL	Repl. by ADACHI 12A
0.714±0.032±0.018	[6] AUBERT	07AY	BABR	Repl. by AUBERT 09K
0.642±0.031±0.017	CHEN	07	BELL	Repl. by ADACHI 12A
0.728±0.056±0.023	[15] ABE	05B	BELL	Repl. by CHEN 07
0.722±0.040±0.023	[16] AUBERT	05F	BABR	Repl. by AUBERT 07AY
0.99 ±0.14 ±0.06	[17] ABE	02U	BELL	$e^+e^- \to \Upsilon(4S)$
0.719±0.074±0.035	[18] ABE	02Z	BELL	Repl. by ABE 05B
0.59 ±0.14 ±0.05	[19] AUBERT	02N	BABR	$e^+e^- \to \Upsilon(4S)$
0.741±0.067±0.034	[20] AUBERT	02P	BABR	Repl. by AUBERT 05F
0.58 $^{+0.32}_{-0.34}$ $^{+0.09}_{-0.10}$	ABASHIAN	01	BELL	Repl. by ABE 01G
0.99 ±0.14 ±0.06	[21] ABE	01G	BELL	Repl. by ABE 02Z
0.34 ±0.20 ±0.05	AUBERT	01	BABR	Repl. by AUBERT 01B
0.59 ±0.14 ±0.05	[21] AUBERT	01B	BABR	Repl. by AUBERT 02P
1.8 ±1.1 ±0.3	[22] ABE	98U	CDF	Repl. by AFFOLDER 00C

[1] A combination of this Run 2 result with the Run 1 result from AAIJ 17BN is reported with a correlation coefficient of 0.40.
[2] Uses $B^0 \to J/\psi K^0_S$ decays with 362 fb^{-1} BELL II data.
[3] Measurement based on $B^0 \to J/\psi K^0_S$, $B^0 \to \psi(2S) K^0_S$, $B^0 \to J/\psi K^0_L$, and $B^0 \to \chi_{c1}(1P) K^0_S$ decays.
[4] SATO 12 uses 121 fb^{-1} data collected on $\Upsilon(5S)$ resonance. Uses the "$B-\pi$ tagging" where $B\pi^+$ and $B\pi^-$ tagged $J/\psi K^0_S$ events are compared.
[5] Uses Dalitz plot analysis of $B^0 \to K^0\pi^+\pi^-$ decays and the first of two equivalent solutions.
[6] Measurement based on $B^0 \to c\overline{c}K(*)0$ decays.
[7] Measurement in which the J/ψ decays to hadrons or to muons that do not satisfy the standard identification criteria.
[8] AFFOLDER 00C uses about 400 $B^0 \to J/\psi(1S) K^0_S$ events. The production flavor of B^0 was determined using three tagging algorithms: a same-side tag, a jet-charge tag, and a soft-lepton tag.
[9] BARATE 00Q uses 23 candidates for $B^0 \to J/\psi(1S) K^0_S$ decays. A combination of jet-charge, vertex-charge, and same-side tagging techniques were used to determine the B^0 production flavor.
[10] ACKERSTAFF 98Z uses 24 candidates for $B^0_d \to J/\psi(1S) K^0_S$ decay. A combination of jet-charge and vertex-charge techniques were used to tag the B^0_d production flavor.
[11] Measurement based on $B^0 \to J/\psi K^0_S$, $B^0 \to \psi(2S) K^0_S$ with $J/\psi \to \mu^+\mu^-$, $J/\psi \to e^+e^-$ and $\psi(2S) \to \mu^+\mu^-$.
[12] AAIJ 24 provides the correlation coefficient ρ = 0.441 between the uncertainties of $\sin(2\beta)$ and $C_{c\overline{c}K(*)0}$ ($B^0 \to c\overline{c}K^{(*)0}$) measurements.
[13] AAIJ 17BN provides the correlation coefficient ρ = 0.42 between the uncertainties of $\sin(2\beta)$ and $\cos(2\beta)$ measurements.
[14] Based on $B^0 \to \psi(2S) K^0_S$ decays.
[15] Measurement based on 152×10^6 $B\overline{B}$ pairs.
[16] Measurement based on 227×10^6 $B\overline{B}$ pairs.
[17] ABE 02U result is based on the same analysis and data sample reported in ABE 01G.
[18] ABE 02Z result is based on 85×10^6 $B\overline{B}$ pairs.
[19] AUBERT 02N result based on the same analysis and data sample reported in AUBERT 01B.
[20] AUBERT 02P result is based on 88×10^6 $B\overline{B}$ pairs.
[21] First observation of CP violation in B^0 meson system.
[22] ABE 98U uses 198 ± 17 $B^0_d \to J/\psi(1S) K^0$ events. The production flavor of B^0 was determined using the same side tagging technique.

$C_{J/\psi(nS) K^0}$ ($B^0 \to J/\psi(nS) K^0$)

VALUE (units 10^{-2})	DOCUMENT ID		TECN	COMMENT
0.2± 1.0 OUR EVALUATION	(Produced by HFLAV)			
0.1± 1.0 OUR AVERAGE				
0.4± 1.2	[1] AAIJ	24	LHCB	pp at 7, 8 and 13 TeV
− 3.5± 2.6±2.9	[2] ADACHI	24H	BEL2	$e^+e^- \to \Upsilon(4S)$
1.5± 2.1 $^{+2.3}_{-4.5}$	[3,4] ADACHI	12A	BELL	$e^+e^- \to \Upsilon(4S)$
−10.4± 5.5 $^{+2.7}_{-4.7}$	[4,5] ADACHI	12A	BELL	$e^+e^- \to \Upsilon(4S)$
− 1.9± 2.6 $^{+4.1}_{-1.7}$	[4,6] ADACHI	12A	BELL	$e^+e^- \to \Upsilon(4S)$
8.9± 7.6±2.0	[5] AUBERT	09K	BABR	$e^+e^- \to \Upsilon(4S)$
1.6± 2.3±1.8	AUBERT	09K	BABR	$e^+e^- \to \Upsilon(4S)$
• • • We do not use the following data for averages, fits, limits, etc. • • •				
0.8± 1.2±0.3	[7,8] AAIJ	24	LHCB	pp at 13 TeV
− 8.7± 4.8±0.5	[9] AAIJ	24	LHCB	pp at 13 TeV
1.5± 1.3±0.3	[10] AAIJ	24	LHCB	pp at 13 TeV
− 1.7± 2.9	[7,11] AAIJ	17BN	LHCB	pp at 7, 8 TeV
− 1.4± 3.0	[10] AAIJ	17BN	LHCB	pp at 7, 8 TeV
− 5 ±10 ±1	[9] AAIJ	17BN	LHCB	pp at 7, 8 TeV
− 3.8± 3.2±0.5	[12] AAIJ	15N	LHCB	Repl. by AAIJ 17BN
3 ± 9 ±1	[13] AAIJ	13K	LHCB	Repl. by AAIJ 15N
− 4 ± 7 ±5	[4,5] SAHOO	08	BELL	Repl. by ADACHI 12A
− 1.8± 2.1±1.4	[4] CHEN	07	BELL	Repl. by ADACHI 12A

[1] A combination of this Run 2 result with the Run 1 result from AAIJ 17BN is reported with a correlation coefficient of 0.40.
[2] Uses $B^0 \to J/\psi K^0_S$ decays with 362 fb^{-1} BELL II data.
[3] Uses $B^0 \to J/\psi K^0_S$ decays.
[4] The paper reports A, which is equal to $-C$.
[5] Uses $B^0 \to \psi(2S) K^0_S$ decays.
[6] Uses $B^0 \to J/\psi K^0_L$ decays.
[7] Measurement based on $B^0 \to J/\psi K^0_S$, $B^0 \to \psi(2S) K^0_S$ with $J/\psi \to \mu^+\mu^-$, $J/\psi \to e^+e^-$ and $\psi(2S) \to \mu^+\mu^-$.
[8] AAIJ 24 provides the correlation coefficient ρ = 0.441 between the uncertainties of $C_{J/\psi(nS) K^0}$ ($B^0 \to J/\psi(nS) K^0$) and $S_{J/\psi(nS) K^0}$ ($B^0 \to J/\psi(nS) K^0$) measurements.
[9] Measurement based on $B^0 \to \psi(2S) K^0_S$ with $\psi(2S) \to \mu^+\mu^-$.
[10] Measurement based on $B^0 \to J/\psi K^0_S$ with $J/\psi \to \mu^+\mu^-$ and $J/\psi \to e^+e^-$.
[11] AAIJ 17BN provides the correlation coefficient ρ = 0.42 between the uncertainties of $S_{J/\psi(nS) K^0}$ ($B^0 \to J/\psi(nS) K^0$) and $C_{J/\psi(nS) K^0}$ ($B^0 \to J/\psi(nS) K^0$) measurements.

[12] AAIJ 15N uses 41,560 flavor-tagged $B_d \to J/\psi K^0_S$ events from 3 fb^{-1} of integrated luminosity. Provides the correlation coefficient $\rho = 0.483$ between the statistical uncertainties of and measurements.
[13] AAIJ 13K uses 8200 flavor-tagged $B_d \to J/\psi K^0_S$ events from 1 fb^{-1} of integrated luminosity. Provides the correlation coefficient $\rho = 0.42$ between the statistical uncertainties of $S_{J/\psi(nS)K^0}$ ($B^0 \to J/\psi(nS)K^0$) and $C_{J/\psi(nS)K^0}$ ($B^0 \to J/\psi(nS)K^0$) measurements.

$S_{J/\psi(nS)K^0}$ ($B^0 \to J/\psi(nS)K^0$)

VALUE	DOCUMENT ID		TECN	COMMENT
0.711±0.011 OUR EVALUATION	(Produced by HFLAV)			
0.710±0.014 OUR AVERAGE	Error includes scale factor of 1.3.			See the ideogram below.
0.724±0.014	[1] AAIJ	24	LHCB	pp at 7, 8 and 13 TeV
0.724±0.035±0.009	[2] ADACHI	24H	BEL2	$e^+e^- \to \Upsilon(4S)$
0.670±0.029±0.013	[3] ADACHI	12A	BELL	$e^+e^- \to \Upsilon(4S)$
0.738±0.079±0.036	[4] ADACHI	12A	BELL	$e^+e^- \to \Upsilon(4S)$
0.642±0.047±0.021	[5] ADACHI	12A	BELL	$e^+e^- \to \Upsilon(4S)$
0.57 ±0.58 ±0.06	[6] SATO	12	BELL	$e^+e^- \to \Upsilon(5S)$
0.897±0.100±0.036	[4] AUBERT	09K	BABR	$e^+e^- \to \Upsilon(4S)$
0.666±0.031±0.013	AUBERT	09K	BABR	$e^+e^- \to \Upsilon(4S)$
0.79 $^{+0.41}_{-0.44}$	[7] AFFOLDER	00C	CDF	$p\overline{p}$ at 1.8 TeV
0.84 $^{+0.82}_{-1.04}$ ±0.16	[8] BARATE	00Q	ALEP	$e^+e^- \to Z$
3.2 $^{+1.8}_{-2.0}$ ±0.5	[9] ACKERSTAFF	98Z	OPAL	$e^+e^- \to Z$
• • • We do not use the following data for averages, fits, limits, etc. • • •				
0.717±0.013±0.008	[10,11] AAIJ	24	LHCB	pp at 13 TeV
0.649±0.053±0.018	[12] AAIJ	24	LHCB	pp at 13 TeV
0.722±0.014±0.007	[13] AAIJ	24	LHCB	pp at 13 TeV
0.760±0.034	[10,14] AAIJ	17BN	LHCB	pp at 7, 8 TeV
0.75 ±0.04	[13] AAIJ	17BN	LHCB	pp at 7, 8 TeV
0.84 ±0.10 ±0.01	[12] AAIJ	17BN	LHCB	pp at 7, 8 TeV
0.731±0.035±0.020	[15] AAIJ	15N	LHCB	Repl. by AAIJ 17BN
0.73 ±0.07 ±0.04	[16] AAIJ	13K	LHCB	Repl. by AAIJ 15N
0.650±0.029±0.018	[17] SAHOO	08	BELL	Repl. by ADACHI 12A
0.72 ±0.09 ±0.03	[4] SAHOO	08	BELL	Repl. by ADACHI 12A
0.642±0.031±0.017	CHEN	07	BELL	Repl. by ADACHI 12A

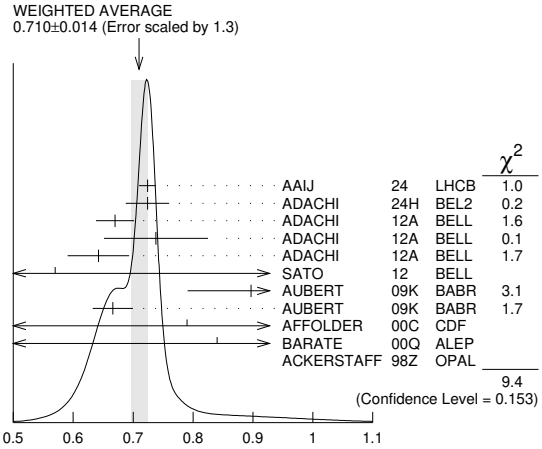

$S_{J/\psi(nS)K^0}$ ($B^0 \to J/\psi(nS)K^0$)

[1] A combination of this Run 2 result with the Run 1 result from AAIJ 17BN is reported with a correlation coefficient of 0.40.
[2] Uses $B^0 \to J/\psi K^0_S$ decays with 362 fb^{-1} BELL II data.
[3] Uses $B^0 \to J/\psi K^0_S$ decays.
[4] Based on $B^0 \to \psi(2S) K^0_S$ decays.
[5] Uses $B^0 \to J/\psi K^0_L$ decays.
[6] SATO 12 uses 121 fb^{-1} data collected at $\Upsilon(5S)$ resonance. Uses the "$B - \pi$ tagging" where $B\pi^+$ and $B\pi^-$ tagged $J/\psi K^0_S$ events are compared.
[7] AFFOLDER 00C uses about 400 $B^0 \to J/\psi(1S) K^0_S$ events. The production flavor of B^0 was determined using three tagging algorithms: a same-side tag, a jet-charge tag, and a soft-lepton tag.
[8] BARATE 00Q uses 23 candidates for $B^0 \to J/\psi(1S) K^0_S$ decays. A combination of jet-charge, vertex-charge, and same-side tagging techniques were used to determine the B^0 production flavor.
[9] ACKERSTAFF 98Z uses 24 candidates for $B^0_d \to J/\psi(1S) K^0_S$ decay. A combination of jet-charge and vertex-charge techniques were used to tag the B^0_d production flavor.
[10] Measurement based on $B^0 \to J/\psi K^0_S$, $B^0 \to \psi(2S) K^0_S$ with $J/\psi \to \mu^+\mu^-$, $J/\psi \to e^+e^-$ and $\psi(2S) \to \mu^+\mu^-$.
[11] AAIJ 24 provides the correlation coefficient $\rho = 0.441$ between the uncertainties of $C_{J/\psi(nS)K^0}$ ($B^0 \to J/\psi(nS)K^0$) and $S_{J/\psi(nS)K^0}$ ($B^0 \to J/\psi(nS)K^0$) measurements.
[12] Measurement based on $B^0 \to \psi(2S) K^0_S$ with $\psi(2S) \to \mu^+\mu^-$.
[13] Measurement based on $B^0 \to J/\psi K^0_S$ with $J/\psi \to \mu^+\mu^-$ and $J/\psi \to e^+e^-$.
[14] AAIJ 17BN provides the correlation coefficient $\rho = 0.42$ between the uncertainties of $S_{J/\psi(nS)K^0}$ ($B^0 \to J/\psi(nS)K^0$) and $C_{J/\psi(nS)K^0}$ ($B^0 \to J/\psi(nS)K^0$) measurements.
[15] AAIJ 15N uses 41,560 flavor-tagged $B_d \to J/\psi K^0_S$ events from 3 fb^{-1} of integrated luminosity. Provides the correlation coefficient $\rho = 0.483$ between the statistical uncertainties of and measurements.
[16] AAIJ 13K uses 8200 flavor-tagged $B_d \to J/\psi K^0_S$ events from 1 fb^{-1} of integrated luminosity. Provides the correlation coefficient $\rho = 0.42$ between the statistical uncertainties of $S_{J/\psi(nS)K^0}$ ($B^0 \to J/\psi(nS)K^0$) and $C_{J/\psi(nS)K^0}$ ($B^0 \to J/\psi(nS)K^0$) measurements.
[17] Combined result of CHEN 07 and SAHOO 08.

$C_{J/\psi K^{*0}}$ ($B^0 \to J/\psi K^{*0}$)

VALUE	DOCUMENT ID		TECN	COMMENT
0.025±0.083±0.054	[1] AUBERT	09K	BABR	$e^+e^- \to \Upsilon(4S)$

[1] Based on $B^0 \to J/\psi K^{*0}$, $K^{*0} \to K^0_S \pi^0$.

$S_{J/\psi K^{*0}}$ ($B^0 \to J/\psi K^{*0}$)

VALUE	DOCUMENT ID		TECN	COMMENT
0.601±0.239±0.087	[1,2] AUBERT	09K	BABR	$e^+e^- \to \Upsilon(4S)$

[1] Based on $B^0 \to J/\psi K^{*0}$, $K^{*0} \to K^0_S \pi^0$.
[2] This $S_{J/\psi K^{*0}}$ value has been corrected for the dilution of the sin(ΔM Δt) coefficient of the CP asymmetry by a factor of $1-R_\perp$, which arises from the mixture of CP-even and CP-odd B decay amplitudes.

$C_{\chi_{c0} K^0_S}$ ($B^0 \to \chi_{c0} K^0_S$)

VALUE	DOCUMENT ID		TECN	COMMENT
$-0.29^{+0.53}_{-0.44}$±0.06	[1] AUBERT	09AU	BABR	$e^+e^- \to \Upsilon(4S)$

[1] Uses Dalitz plot analysis of $B^0 \to K^0\pi^+\pi^-$ decays and the first of two equivalent solutions is used.

$S_{\chi_{c0} K^0_S}$ ($B^0 \to \chi_{c0} K^0_S$)

VALUE	DOCUMENT ID		TECN	COMMENT
−0.69±0.52±0.08	[1] AUBERT	09AU	BABR	$e^+e^- \to \Upsilon(4S)$

[1] Uses Dalitz plot analysis of $B^0 \to K^0\pi^+\pi^-$ decays and the first of two equivalent solutions is used.

$C_{\chi_{c1} K^0_S}$ ($B^0 \to \chi_{c1} K^0_S$)

VALUE	DOCUMENT ID		TECN	COMMENT
0.06 ±0.07 OUR AVERAGE				
0.017±0.083 $^{+0.026}_{-0.046}$	ADACHI	12A	BELL	$e^+e^- \to \Upsilon(4S)$
0.129±0.109±0.025	AUBERT	09K	BABR	$e^+e^- \to \Upsilon(4S)$

$S_{\chi_{c1} K^0_S}$ ($B^0 \to \chi_{c1} K^0_S$)

VALUE	DOCUMENT ID		TECN	COMMENT
0.63 ±0.10 OUR AVERAGE				
0.640±0.117±0.040	ADACHI	12A	BELL	$e^+e^- \to \Upsilon(4S)$
0.614±0.160±0.040	AUBERT	09K	BABR	$e^+e^- \to \Upsilon(4S)$

$\sin(2\beta_{\rm eff})$($B^0 \to \phi K^0$)

VALUE	DOCUMENT ID		TECN	COMMENT
0.22±0.27±0.12	AUBERT	07AX	BABR	$e^+e^- \to \Upsilon(4S)$
• • • We do not use the following data for averages, fits, limits, etc. • • •				
0.50±0.25 $^{+0.07}_{-0.04}$	[1] AUBERT	05T	BABR	Repl. by AUBERT 07AX

[1] Obtained by constraining $C = 0$.

$\sin(2\beta_{\rm eff})$($B^0 \to \phi K^*_0(1430)^0$)

VALUE	DOCUMENT ID		TECN	COMMENT
0.97 $^{+0.03}_{-0.52}$	[1] AUBERT	08BG	BABR	$e^+e^- \to \Upsilon(4S)$

[1] Measured using the CP-violation phase difference $\Delta\phi_{00}$ between the B and $\overline{B}$ decay amplitude.

$\sin(2\beta_{\rm eff})$($B^0 \to K^+K^-K^0_S$)

VALUE	DOCUMENT ID		TECN	COMMENT
0.77±0.11 $^{+0.07}_{-0.04}$	AUBERT	07AX	BABR	$e^+e^- \to \Upsilon(4S)$
• • • We do not use the following data for averages, fits, limits, etc. • • •				
0.55±0.22±0.12	[1] AUBERT	05T	BABR	Repl. by AUBERT 07AX

[1] Obtained by constraining $C = 0$.

$\sin(2\beta_{\rm eff})$($B^0 \to [K^0_S\pi^+\pi^-]_{D(*)} h^0$)

VALUE	DOCUMENT ID		TECN	COMMENT
0.80±0.14±0.07	[1] ADACHI	18		$e^+e^- \to \Upsilon(4S)$
• • • We do not use the following data for averages, fits, limits, etc. • • •				
0.43±0.27±0.08	[2] VOROBYEV	16	BELL	$e^+e^- \to \Upsilon(4S)$
0.29±0.34±0.06	AUBERT	07BH	BABR	$e^+e^- \to \Upsilon(4S)$
0.78±0.44±0.22	KROKOVNY	06	BELL	Repl. by VOROBYEV 16

[1] Analyzes joint data sample of Belle and BaBar using Dalitz plot analysis of $D \to K^0_S\pi^+\pi^-$; the second error combines experimental systematic uncertainty and the Dalitz plot model uncertainty.
[2] A model-independent measurement uses the binned Dalitz plot technique.

Int. J. Mod. Phys. A 2026.41. Downloaded from www.worldscientific.com
by LIFORNIA @ BERKELEY on 09/16/26. Re-use and distribution is strictly not permitted, except for Open Access articles.

Int. J. Mod. Phys. A 2026.41. Downloaded from www.worldscientific.com by UNIVERSITY OF CALIFORNIA @ BERKELEY on 09/16/26. Re-use and distribution is strictly not permitted, except for Open Access articles.

$\beta_{\rm eff}(B^0 \to [K^0_S\pi^+\pi^-]_{D^{(*)}}\, h^0)$

VALUE (°)	DOCUMENT ID		TECN	COMMENT
22.5±4.4±1.3	[1] ADACHI	18		$e^+e^- \to \Upsilon(4S)$
• • • We do not use the following data for averages, fits, limits, etc. • • •				
11.7±7.8±2.1	[2] VOROBYEV	16	BELL	$e^+e^- \to \Upsilon(4S)$

[1] Analyzes joint data sample of Belle and BaBar using Dalitz plot analysis of $D \to K^0_S\pi^+\pi^-$; the second error combines experimental systematic uncertainty and the Dalitz plot model uncertainty.
[2] A model-independent measurement uses the binned Dalitz plot technique.

$2\beta_{\rm eff}(B^0 \to J/\psi\rho^0)$

VALUE (°)	DOCUMENT ID		TECN	COMMENT
$41.7\pm9.6^{+2.8}_{-6.3}$	AAIJ	15J	LHCB	pp at 7, 8 TeV

$|\lambda|\ (B^0 \to [K^0_S\pi^+\pi^-]_{D^{(*)}}\, h^0)$

VALUE	DOCUMENT ID		TECN	COMMENT
1.01±0.08±0.02	AUBERT	07BH	BABR	$e^+e^- \to \Upsilon(4S)$

$|\sin(2\beta+\gamma)|$

β (ϕ_1) and γ (ϕ_3) are angles of CKM unitarity triangle, see the review on "*CP* Violation" in the Reviews section.

VALUE	CL%	DOCUMENT ID		TECN	COMMENT
>0.40	90	[1] AUBERT	06Y	BABR	$e^+e^- \to \Upsilon(4S)$
• • • We do not use the following data for averages, fits, limits, etc. • • •					
>0.77	68	[2] AAIJ	18Z	LHCB	pp at 7, 8 TeV
>0.13	95	[3] RONGA	06	BELL	$e^+e^- \to \Upsilon(4S)$
>0.07	95	[3] RONGA	06	BELL	$e^+e^- \to \Upsilon(4S)$
>0.35	90	[4] AUBERT	05Z	BABR	$e^+e^- \to \Upsilon(4S)$
>0.69	68	[5] AUBERT	04V	BABR	$e^+e^- \to \Upsilon(4S)$
>0.58	95	[6] AUBERT	04W	BABR	Repl. by AUBERT 05Z

[1] Uses fully reconstructed $B^0 \to D^{(*)\pm}\pi^\mp$ and $D^\pm\rho^\mp$ decays and some theoretical assumptions.
[2] Uses a time dependent CP violation measurement in $B^0 \to D^\mp\pi^\pm$ decays with external input and some theoretical assumptions.
[3] Combines the results from fully reconstructed and partially reconstructed $D^{(*)}\pi$ events by taking weighted averages. Assumes that systematic errors from physics parameters and fit biases in the two measurements are 100% correlated.
[4] Uses partially reconstructed $B^0 \to D^{*\pm}\pi^\mp$ decays and some theoretical assumptions.
[5] Uses fully reconstructed $B^0 \to D^{(*)\pm}\pi^\mp$ decays and some theoretical assumptions, such as the SU(3) symmetry relation.
[6] Combining this measurement with the results from AUBERT 04V for fully reconstructed $B^0 \to D^{(*)\pm}\pi^\mp$ and some theoretical assumptions, such as the SU(3) symmetry relation.

$2\beta+\gamma$

VALUE (°)	DOCUMENT ID		TECN	COMMENT
83±53±20	[1] AUBERT	08AC	BABR	$e^+e^- \to \Upsilon(4S)$

[1] Used a time-dependent Dalitz-plot analysis of $B^0 \to D^\mp K^0\pi^\pm$ assuming the ratio of the $b \to u$ and $b \to c$ decay amplitudes to be 0.3.

α

For angle $\alpha(\phi_2)$ of the CKM unitarity triangle, see the review on "*CP* violation" in the reviews section.

VALUE (°)	DOCUMENT ID		TECN	COMMENT
$84.1^{+3.7}_{-3.0}$ OUR EVALUATION	(Produced by HFLAV)			
$91.5^{+4.8}_{-5.2}$	[1] ADACHI	25H	BELL	$e^+e^- \to \Upsilon(4S)$
• • • We do not use the following data for averages, fits, limits, etc. • • •				
93.7±10.6	[1] VANHOEFER	16	BELL	$e^+e^- \to \Upsilon(4S)$
84.9±13.5	[1] VANHOEFER	14	BELL	Repl. by VANHOEFER 16
79 ± 7 ±11	[2] AUBERT	10D	BABR	$e^+e^- \to \Upsilon(4S)$
$92.4^{+6.0}_{-6.5}$	[1] AUBERT	09G	BABR	$e^+e^- \to \Upsilon(4S)$
78.6± 7.3	[3] AUBERT	07O	BABR	$e^+e^- \to \Upsilon(4S)$
88 ±17	[4] SOMOV	06	BELL	Repl. by VANHOEFER 14
100 ±13	[5] AUBERT,B	05C	BABR	Repl. by AUBERT 09G
102^{+16}_{-12} ±14	[6] AUBERT,B	04R	BABR	Repl. by AUBERT,B 05C

[1] Based on an isospin analysis of the $B \to \rho\rho$ system.
[2] Obtained using the time dependent analysis of $B^0 \to a_1(1260)^\pm\pi^\mp$ and branching fraction measurements of $B \to a_1(1260)K$ and $B \to K_1\pi$. Uses SU(3) flavor relations.
[3] The angle $\alpha_{\rm eff}$ is obtained using the measured *CP* parameters of $B^0 \to a_1(1260)^\pm\pi^\mp$ and choosing one of the four solutions that is compatible with the result of SM-based fits.
[4] Obtained using isospin relation and selecting a solution closest to the CKM best fit average; the 90% CL allowed interval is $59^\circ < \phi_2\ (\equiv\alpha) < 115^\circ$.
[5] Obtained using isospin relation and selecting a solution closest to the CKM best fit average; 90% CL allowed interval is $79^\circ < \alpha < 123^\circ$.
[6] Obtained from the measured *CP* parameters of the longitudinal polarization by selecting the solution closest to the CKM best fit central value of $\alpha = 95^\circ - 98^\circ$.

CP VIOLATION PARAMETERS IN $B^0 \to D^0K^{*0}$ DECAY

The parameters r_{B^0} and δ_{B^0} are the magnitude ratio and strong phase difference between the amplitudes of $A(B^0 \to D^0K^{*0})$ and $A(B^0 \to \overline{D}^0K^{*0})$. The measured observables and are defined as $x_\pm = r_{B^0}\cos(\delta_{B^0} \pm \gamma)$ and $y_\pm = r_{B^0}\sin(\delta_{B^0} \pm \gamma)$ where γ is the CKM angle γ.

"OUR EVALUATION" is provided by the Heavy Flavor Averaging Group (HFLAV). The CKM angle γ is listed in the B^+ section for "*CP* VIOLATION PARAMETERS IN $B^+ \to DK^+$ AND SIMILAR DECAYS."

$x_+(B^0 \to DK^{*0})$

VALUE	DOCUMENT ID		TECN	COMMENT
0.07 ±0.08 OUR AVERAGE				
0.074±0.086±0.012	[1] AAIJ	24U	LHCB	pp at 7, 8, 13 TeV
0.04 ±0.16 ±0.11	[2] AAIJ	16S	LHCB	pp at 7, 8 TeV
• • • We do not use the following data for averages, fits, limits, etc. • • •				
0.05 ±0.24 ±0.04	[3] AAIJ	16AA	LHCB	Repl. by AAIJ 16Z
0.05 ±0.35 ±0.02	[4] AAIJ	16Z	LHCB	Repl. by AAIJ 24U

[1] Uses Dalitz plot analysis of $D \to K^0_S\pi^+\pi^-$, $K^0_SK^+K^-$ decays coming from $B^0 \to DK^*(892)^0$ modes. The second error is the systematic contribution from the D decay strong-phase inputs and from the experimental systematic uncertainties.
[2] Uses Dalitz plof of $B^0 \to DK^+\pi^-$ with $D \to K^+K^-$, $\pi^+\pi^-$, or $K^+\pi^-$.
[3] Uses Dalitz plot analysis of $D \to K^0_S\pi^+\pi^-$ decays coming from $B^0 \to DK^*(892)^0$ modes.
[4] Uses Dalitz plot analysis of $D \to K^0_S\pi^+\pi^-$, $K^0_SK^+K^-$ decays coming from $B^0 \to DK^*(892)^0$ modes.

$x_-(B^0 \to DK^{*0})$

VALUE	DOCUMENT ID		TECN	COMMENT
−0.18 ±0.08 OUR AVERAGE				
−0.215±0.086±0.014	[1] AAIJ	24U	LHCB	pp at 7, 8, 13 TeV
−0.02 ±0.13 ±0.14	[2] AAIJ	16S	LHCB	pp at 7, 8 TeV
• • • We do not use the following data for averages, fits, limits, etc. • • •				
−0.15 ±0.14 ±0.03	[3] AAIJ	16AA	LHCB	Repl. by AAIJ 16Z
−0.31 ±0.20 ±0.04	[4] AAIJ	16Z	LHCB	Repl. by AAIJ 24U

[1] Uses Dalitz plot analysis of $D \to K^0_S\pi^+\pi^-$, $K^0_SK^+K^-$ decays coming from $B^0 \to DK^*(892)^0$ modes. The second error is the systematic contribution from the D decay strong-phase inputs and from the experimental systematic uncertainties.
[2] Uses Dalitz plot of $B^0 \to DK^+\pi^-$ with $D \to K^+K^-$, $\pi^+\pi^-$, or $K^+\pi^-$.
[3] Uses Dalitz plot analysis of $D \to K^0_S\pi^+\pi^-$ decays coming from $B^0 \to DK^*(892)^0$ modes.
[4] Uses Dalitz plot analysis of $D \to K^0_S\pi^+\pi^-$, $K^0_SK^+K^-$ decays coming from $B^0 \to DK^*(892)^0$ modes.

$y_+(B^0 \to DK^{*0})$

VALUE	DOCUMENT ID		TECN	COMMENT
−0.35 ±0.10 OUR AVERAGE				
−0.336±0.105±0.019	[1] AAIJ	24U	LHCB	pp at 7, 8, 13 TeV
−0.47 ±0.28 ±0.22	[2] AAIJ	16S	LHCB	pp at 7, 8 TeV
• • • We do not use the following data for averages, fits, limits, etc. • • •				
$-0.65\ ^{+0.24}_{-0.23}$ ±0.08	[3] AAIJ	16AA	LHCB	Repl. by AAIJ 16Z
−0.81 ±0.28 ±0.06	[4] AAIJ	16Z	LHCB	Repl. by AAIJ 24U

[1] Uses Dalitz plot analysis of $D \to K^0_S\pi^+\pi^-$, $K^0_SK^+K^-$ decays coming from $B^0 \to DK^*(892)^0$ modes. The second error is the systematic contribution from the D decay strong-phase inputs and from the experimental systematic uncertainties.
[2] Uses Dalitz plof of $B^0 \to DK^+\pi^-$ with $D \to K^+K^-$, $\pi^+\pi^-$, or $K^+\pi^-$.
[3] Uses Dalitz plot analysis of $D \to K^0_S\pi^+\pi^-$ decays coming from $B^0 \to DK^*(892)^0$ modes.
[4] Uses Dalitz plot analysis of $D \to K^0_S\pi^+\pi^-$, $K^0_SK^+K^-$ decays coming from $B^0 \to DK^*(892)^0$ modes.

$y_-(B^0 \to DK^{*0})$

VALUE	DOCUMENT ID		TECN	COMMENT
−0.03 ±0.13 OUR AVERAGE				
−0.012±0.128±0.026	[1] AAIJ	24U	LHCB	pp at 7, 8, 13 TeV
−0.35 ±0.26 ±0.41	[2] AAIJ	16S	LHCB	pp at 7, 8 TeV
• • • We do not use the following data for averages, fits, limits, etc. • • •				
0.25 ±0.15 ±0.06	[3] AAIJ	16AA	LHCB	Repl. by AAIJ 16Z
0.31 ±0.21 ±0.05	[4] AAIJ	16Z	LHCB	Repl. by AAIJ 24U

[1] Uses Dalitz plot analysis of $D \to K^0_S\pi^+\pi^-$, $K^0_SK^+K^-$ decays coming from $B^0 \to DK^*(892)^0$ modes. The second error is the systematic contribution from the D decay strong-phase inputs and from the experimental systematic uncertainties.
[2] Uses Dalitz plof of $B^0 \to DK^+\pi^-$ with $D \to K^+K^-$, $\pi^+\pi^-$, or $K^+\pi^-$.
[3] Uses Dalitz plot analysis of $D \to K^0_S\pi^+\pi^-$ decays coming from $B^0 \to DK^*(892)^0$ modes.
[4] Uses Dalitz plot analysis of $D \to K^0_S\pi^+\pi^-$, $K^0_SK^+K^-$ decays coming from $B^0 \to DK^*(892)^0$ modes.

$r_{B^0}(B^0 \to DK^{*0})$

VALUE	DOCUMENT ID		TECN	COMMENT
0.250±0.022 OUR EVALUATION	(Produced by HFLAV)			

Int. J. Mod. Phys. A 2026.41. Downloaded from www.worldscientific.com by LIFORNIA @ BERKELEY on 09/16/26. Re-use and distribution is strictly not permitted, except for Open Access articles.

• • • We do not use the following data for averages, fits, limits, etc. • • •

$0.271^{+0.065}_{-0.066}$	[1] AAIJ	24U	LHCB	pp at 7, 8, 13 TeV
0.39 ±0.13	[2] AAIJ	16AA	LHCB	Repl. by AAIJ 16Z
0.56 ±0.17	[3,4] AAIJ	16Z	LHCB	Repl. by AAIJ 24U

[1] Uses Dalitz plot analysis of $D \to K^0_S \pi^+\pi^-$, $K^0_S K^+K^-$ decays coming from $B^0 \to D K^*(892)^0$ modes.
[2] Uses Dalitz plot analysis of $D \to K^0_S \pi^+\pi^-$ decays coming from $B^0 \to D K^*(892)^0$ modes.
[3] Measurement is performed with $K^+\pi^-$ masses within 50 MeV of the K^{*0} mass and an absolute value of the cosine of the K^{*0} helicity angle greater than 0.4. Angle γ is required to satisfy $0 < \gamma < 180$ degrees.
[4] Uses Dalitz plot analysis of $D \to K^0_S \pi^+\pi^-$, $K^0_S K^+K^-$ decays coming from $B^0 \to D K^*(892)^0$ modes.

$\delta_{B^0}(B^0 \to D K^{*0})$

VALUE (°)	DOCUMENT ID	TECN	COMMENT
$202.8^{+10.3}_{-9.0}$ OUR EVALUATION	(Produced by HFLAV)		

• • • We do not use the following data for averages, fits, limits, etc. • • •

236^{+19}_{-21}	[1] AAIJ	24U	LHCB	pp at 7, 8, 13 TeV
197^{+24}_{-20}	[2] AAIJ	16AA	LHCB	Repl. by AAIJ 16Z
204^{+21}_{-20}	[3,4] AAIJ	16Z	LHCB	Repl. by AAIJ 24U

[1] Uses Dalitz plot analysis of $D \to K^0_S \pi^+\pi^-$, $K^0_S K^+K^-$ decays coming from $B^0 \to D K^*(892)^0$ modes.
[2] Uses Dalitz plot analysis of $D \to K^0_S \pi^+\pi^-$ decays coming from $B^0 \to D K^*(892)^0$ modes.
[3] Measurement is performed with $K^+\pi^-$ masses within 50 MeV of the K^{*0} mass and an absolute value of the cosine of the K^{*0} helicity angle greater than 0.4. Angle γ is required to satisfy $0 < \gamma < 180$ degrees.
[4] Uses Dalitz plot analysis of $D \to K^0_S \pi^+\pi^-$, $K^0_S K^+K^-$ decays coming from $B^0 \to D K^*(892)^0$ modes.

$a_{CP}(B^0 \to p\overline{p}K^+\pi^-)$

Observable $a_{CP}(B^0 \to p\overline{p}K^+\pi^-)$ calculated as half of the difference between triple products for B^0 and $\overline{B}^0$, which is sensitive to CP violation.

VALUE (%)	DOCUMENT ID	TECN	COMMENT
0.51±0.85±0.08	[1] AAIJ 23AG	LHCB	pp at 7, 8 and 13 TeV

[1] Phase-space integrated asymmetry.

$a_P(B^0 \to p\overline{p}K^+\pi^-)$

Observable $a_P(B^0 \to p\overline{p}K^+\pi^-)$ calculated as the average of the triple products for B^0 and $\overline{B}^0$, which is sensitive to parity violation.

VALUE (%)	DOCUMENT ID	TECN	COMMENT
1.49±0.85±0.08	[1] AAIJ 23AG	LHCB	pp at 7, 8 and 13 TeV

[1] Phase-space integrated asymmetry.

T and CPT VIOLATION PARAMETERS

Measured values of the T-, CP-, and CPT-asymmetry parameters, defined as the differences in $S^{\pm}_{\alpha,\beta}$ and $C^{\pm}_{\alpha,\beta}$ between symmetry-transformed transitions. The indices $\alpha = \ell^+$, ℓ^- and $\beta = K^0_S$, K^0_L stand for reconstructed the flavor final state and the CP final states from $\Upsilon(4S)$ decay. The sign $\pm$ indicates whether the decay to the flavor final state α occurs before or after the decay to the CP final state.

Alternatively, violations of CPT symmetry and Lorentz invariance are searched for by studying interference effects in B^0 mixing. Results are expressed in terms of the standard model extension parameter Δa, which describes the difference between the couplings of the valence quarks within B^0 meson with the Lorentz-violating fields.

$\Delta S^+_T\ (S^-_{\ell^-,K^0_S} - S^+_{\ell^+,K^0_S})$

VALUE	DOCUMENT ID	TECN	COMMENT
−1.37±0.14±0.06	LEES 12W	BABR	$e^+e^- \to \Upsilon(4S)$

$\Delta S^-_T\ (S^+_{\ell^-,K^0_S} - S^-_{\ell^+,K^0_S})$

VALUE	DOCUMENT ID	TECN	COMMENT
1.17±0.18±0.11	LEES 12W	BABR	$e^+e^- \to \Upsilon(4S)$

$\Delta C^+_T\ (C^-_{\ell^-,K^0_S} - C^+_{\ell^+,K^0_S})$

VALUE	DOCUMENT ID	TECN	COMMENT
0.10±0.14±0.08	LEES 12W	BABR	$e^+e^- \to \Upsilon(4S)$

$\Delta C^-_T\ (C^+_{\ell^-,K^0_S} - C^-_{\ell^+,K^0_S})$

VALUE	DOCUMENT ID	TECN	COMMENT
0.04±0.14±0.08	LEES 12W	BABR	$e^+e^- \to \Upsilon(4S)$

$\Delta S^+_{CP}\ (S^+_{\ell^-,K^0_S} - S^+_{\ell^+,K^0_S})$

VALUE	DOCUMENT ID	TECN	COMMENT
−1.30±0.11±0.07	LEES 12W	BABR	$e^+e^- \to \Upsilon(4S)$

$\Delta S^-_{CP}\ (S^-_{\ell^-,K^0_S} - S^-_{\ell^+,K^0_S})$

VALUE	DOCUMENT ID	TECN	COMMENT
1.33±0.12±0.06	LEES 12W	BABR	$e^+e^- \to \Upsilon(4S)$

$\Delta C^+_{CP}\ (C^+_{\ell^-,K^0_S} - C^+_{\ell^+,K^0_S})$

VALUE	DOCUMENT ID	TECN	COMMENT
0.07±0.09±0.03	LEES 12W	BABR	$e^+e^- \to \Upsilon(4S)$

$\Delta C^-_{CP}\ (C^-_{\ell^-,K^0_S} - C^-_{\ell^+,K^0_S})$

VALUE	DOCUMENT ID	TECN	COMMENT
0.08±0.10±0.04	LEES 12W	BABR	$e^+e^- \to \Upsilon(4S)$

$\Delta S^+_{CPT}\ (S^-_{\ell^+,K^0_S} - S^+_{\ell^+,K^0_S})$

VALUE	DOCUMENT ID	TECN	COMMENT
0.16±0.21±0.09	LEES 12W	BABR	$e^+e^- \to \Upsilon(4S)$

$\Delta S^-_{CPT}\ (S^+_{\ell^+,K^0_S} - S^-_{\ell^+,K^0_S})$

VALUE	DOCUMENT ID	TECN	COMMENT
−0.03±0.13±0.06	LEES 12W	BABR	$e^+e^- \to \Upsilon(4S)$

$\Delta C^+_{CPT}\ (C^-_{\ell^+,K^0_S} - C^+_{\ell^+,K^0_S})$

VALUE	DOCUMENT ID	TECN	COMMENT
0.14±0.15±0.07	LEES 12W	BABR	$e^+e^- \to \Upsilon(4S)$

$\Delta C^-_{CPT}\ (C^+_{\ell^+,K^0_S} - C^-_{\ell^+,K^0_S})$

VALUE	DOCUMENT ID	TECN	COMMENT
0.03±0.12±0.08	LEES 12W	BABR	$e^+e^- \to \Upsilon(4S)$

$\Delta a_{\parallel}$ CPT parameter in B^0 mixing

VALUE (10^{-15} GeV)	DOCUMENT ID	TECN	COMMENT
−0.10±0.82±0.54	[1] AAIJ 16E	LHCB	pp at 7, 8 TeV

[1] Uses $B^0 \to J/\psi K^0_S$ decays.

$\Delta a_{\perp}$ CPT parameter in B^0 mixing

VALUE (10^{-13} GeV)	DOCUMENT ID	TECN	COMMENT
−0.20±0.22±0.04	[1] AAIJ 16E	LHCB	pp at 7, 8 TeV

[1] Uses $B^0 \to J/\psi K^0_S$ decays.

Δa_X CPT parameter in B^0 mixing

VALUE (10^{-15} GeV)	DOCUMENT ID	TECN	COMMENT
+1.97±1.30±0.29	[1] AAIJ 16E	LHCB	pp at 7, 8 TeV

[1] Uses $B^0 \to J/\psi K^0_S$ decays.

Δa_Y CPT parameter in B^0 mixing

VALUE (10^{-15} GeV)	DOCUMENT ID	TECN	COMMENT
+0.44±1.26±0.29	[1] AAIJ 16E	LHCB	pp at 7, 8 TeV

[1] Uses $B^0 \to J/\psi K^0_S$ decays.

$B^0 \to D^{*-}\ell^+\nu_\ell$ FORM FACTORS

R_1 (form factor ratio $\sim V/A_1$)

VALUE	DOCUMENT ID	TECN	COMMENT
1.239±0.029 OUR AVERAGE			
1.229±0.028±0.009	[1] WAHEED 19	BELL	$e^+e^- \to \Upsilon(4S)$
1.56 ±0.07 ±0.15	AUBERT 09A	BABR	$e^+e^- \to \Upsilon(4S)$
1.18 ±0.30 ±0.12	DUBOSCQ 96	CLE2	$e^+e^- \to \Upsilon(4S)$
• • • We do not use the following data for averages, fits, limits, etc. • • •			
1.401±0.034±0.018	[1] DUNGEL 10	BELL	Repl. by WAHEED 19
1.429±0.061±0.044	AUBERT 08R	BABR	Repl. by AUBERT 09A
1.396±0.060±0.044	AUBERT,B 06Z	BABR	Repl. by AUBERT 08R

[1] Uses fully reconstructed $D^{*-}\ell^+\nu$ events ($\ell = e$ or μ).

R_2 (form factor ratio $\sim A_2/A_1$)

VALUE	DOCUMENT ID	TECN	COMMENT
0.84 ±0.04 OUR AVERAGE	Error includes scale factor of 1.8.		
0.852±0.021±0.006	[1] WAHEED 19	BELL	$e^+e^- \to \Upsilon(4S)$
0.66 ±0.05 ±0.09	AUBERT 09A	BABR	$e^+e^- \to \Upsilon(4S)$
0.71 ±0.22 ±0.07	DUBOSCQ 96	CLE2	$e^+e^- \to \Upsilon(4S)$
• • • We do not use the following data for averages, fits, limits, etc. • • •			
0.864±0.024±0.008	[1] DUNGEL 10	BELL	Repl. by WAHEED 19
0.827±0.038±0.022	AUBERT 08R	BABR	Repl. by AUBERT 09A
0.885±0.040±0.026	AUBERT,B 06Z	BABR	Repl. by AUBERT 08R

[1] Uses fully reconstructed $D^{*-}\ell^+\nu$ events ($\ell = e$ or μ).

Int. J. Mod. Phys. A 2026.41. Downloaded from www.worldscientific.com
by UNIVERSITY OF CALIFORNIA @ BERKELEY on 09/16/26. Re-use and distribution is strictly not permitted, except for Open Access articles.

$\rho^2_{A_1}$ (form factor slope)

VALUE	DOCUMENT ID		TECN	COMMENT
1.12 ±0.04 OUR AVERAGE	Error includes scale factor of 1.5.			
1.106±0.031±0.007	[1] WAHEED	19	BELL	$e^+e^- \to \Upsilon(4S)$
1.22 ±0.02 ±0.07	AUBERT	09A	BABR	$e^+e^- \to \Upsilon(4S)$
0.91 ±0.15 ±0.06	DUBOSCQ	96	CLE2	$e^+e^- \to \Upsilon(4S)$
• • • We do not use the following data for averages, fits, limits, etc. • • •				
1.214±0.034±0.009	[1] DUNGEL	10	BELL	Repl. by WAHEED 19
1.191±0.048±0.028	AUBERT	08R	BABR	Repl. by AUBERT 09A
1.145±0.059±0.046	AUBERT,B	06Z	BABR	Repl. by AUBERT 08R

[1] Uses fully reconstructed $D^{*-}\ell^+\nu$ events ($\ell = e$ or μ).

PARTIAL BRANCHING FRACTIONS IN $B^0 \to K^{(*)0}\ell^+\ell^-$

B($B^0 \to K^{*0}e^+e^-$) (0.0009 < q^2 < 1.0 GeV^2/c^4)

VALUE (units 10^{-7})	DOCUMENT ID		TECN	COMMENT
$3.1^{+0.9}_{-0.8}{}^{+0.2}_{-0.3}\pm0.2$	[1] AAIJ	13U	LHCB	pp at 7 TeV

[1] The last uncertainty is due to uncertainties of B($B^0 \to J/\psi K^{*0}$) and B($J/\psi \to e^+e^-$) branching fraction measurements.

B($B^0 \to K^{*0}\ell^+\ell^-$) (0.1 < q^2 < 2.0 GeV^2/c^4)

VALUE (units 10^{-7})	DOCUMENT ID		TECN	COMMENT
$1.24^{+0.23}_{-0.27}$ **OUR AVERAGE**	Error includes scale factor of 1.6.			
$1.14\pm0.11^{+0.11}_{-0.15}$	AAIJ	13Y	LHCB	pp at 7 TeV, $K^{*0}\mu^+\mu^-$
1.80±0.36±0.11	AALTONEN	11AI	CDF	$p\overline{p}$ at 1.96 TeV
• • • We do not use the following data for averages, fits, limits, etc. • • •				
$0.48^{+0.14}_{-0.12}\pm0.04$	[1] CHATRCHYAN	13BL	CMS	pp at 7 TeV
1.16±0.23±0.11	AAIJ	12U	LHCB	Repl. by AAIJ 13Y

[1] CHATRCHYAN 13BL uses, for this bin, 1.0 < q^2 < 2.0 GeV^2/c^4.

B($B^0 \to K^{*0}\ell^+\ell^-$) (2.0 < q^2 < 4.3 GeV^2/c^4)

VALUE (units 10^{-7})	DOCUMENT ID		TECN	COMMENT
0.76 ±0.07 OUR AVERAGE				
0.759±0.115±0.046	KHACHATRY...	16D	CMS	pp at 8 TeV
0.69 ±0.07 ±0.09	AAIJ	13Y	LHCB	pp at 7 TeV, $K^{*0}\mu^+\mu^-$
0.87 ±0.16 ±0.07	CHATRCHYAN	13BL	CMS	pp at 7 TeV
0.84 ±0.28 ±0.06	AALTONEN	11AI	CDF	$p\overline{p}$ at 1.96 TeV
• • • We do not use the following data for averages, fits, limits, etc. • • •				
0.78 ±0.21 ±0.05	AAIJ	12U	LHCB	Repl. by AAIJ 13Y

B($B^0 \to K^{*0}\ell^+\ell^-$) (4.3 < q^2 < 8.68 GeV^2/c^4)

VALUE (units 10^{-7})	DOCUMENT ID		TECN	COMMENT
1.87±0.21 OUR AVERAGE				
$2.15\pm0.18^{+0.22}_{-0.28}$	AAIJ	13Y	LHCB	pp at 7 TeV, $K^{*0}\mu^+\mu^-$
1.62±0.31±0.18	CHATRCHYAN	13BL	CMS	pp at 7 TeV
1.73±0.43±0.15	AALTONEN	11AI	CDF	$p\overline{p}$ at 1.96 TeV
• • • We do not use the following data for averages, fits, limits, etc. • • •				
3.02±0.35±0.22	AAIJ	12U	LHCB	Repl. by AAIJ 13Y

B($B^0 \to K^{*0}\ell^+\ell^-$) (10.09 < q^2 < 12.86 GeV^2/c^4)

VALUE (units 10^{-7})	DOCUMENT ID		TECN	COMMENT
1.49±0.15 OUR AVERAGE	Error includes scale factor of 1.3. See the ideogram below.			
1.72±0.11±0.14	KHACHATRY...	16D	CMS	pp at 8 TeV
$1.19\pm0.11^{+0.14}_{-0.17}$	AAIJ	13Y	LHCB	pp at 7 TeV, $K^{*0}\mu^+\mu^-$
1.50±0.25±0.25	CHATRCHYAN	13BL	CMS	pp at 7 TeV
1.77±0.36±0.12	AALTONEN	11AI	CDF	$p\overline{p}$ at 1.96 TeV
• • • We do not use the following data for averages, fits, limits, etc. • • •				
1.52±0.25±0.19	AAIJ	12U	LHCB	Repl. by AAIJ 13Y

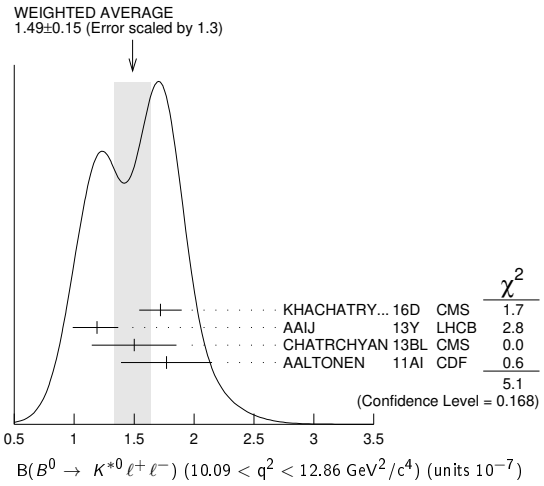

B($B^0 \to K^{*0}\ell^+\ell^-$) (14.18 < q^2 < 16.0 GeV^2/c^4)

VALUE (units 10^{-7})	DOCUMENT ID		TECN	COMMENT
1.09±0.10 OUR AVERAGE	Error includes scale factor of 1.1.			
1.22±0.11±0.09	KHACHATRY...	16D	CMS	pp at 8 TeV
$1.02\pm0.11^{+0.11}_{-0.15}$	AAIJ	13Y	LHCB	pp at 7 TeV, $K^{*0}\mu^+\mu^-$
$0.84^{+0.16}_{-0.15}\pm0.09$	CHATRCHYAN	13BL	CMS	pp at 7 TeV
1.34±0.26±0.08	AALTONEN	11AI	CDF	$p\overline{p}$ at 1.96 TeV
• • • We do not use the following data for averages, fits, limits, etc. • • •				
1.15±0.20±0.09	AAIJ	12U	LHCB	Repl. by AAIJ 13Y

B($B^0 \to K^{*0}\ell^+\ell^-$) (16.0 < q^2 < 19.0 GeV^2/c^4)

VALUE (units 10^{-7})	DOCUMENT ID		TECN	COMMENT
1.27±0.09 OUR AVERAGE				
1.26±0.09±0.09	KHACHATRY...	16D	CMS	pp at 8 TeV
$1.23\pm0.12^{+0.15}_{-0.18}$	AAIJ	13Y	LHCB	pp at 7 TeV, $K^{*0}\mu^+\mu^-$
1.56±0.18±0.15	CHATRCHYAN	13BL	CMS	pp at 7 TeV
0.97±0.26±0.07	AALTONEN	11AI	CDF	$p\overline{p}$ at 1.96 TeV
• • • We do not use the following data for averages, fits, limits, etc. • • •				
1.50±0.24±0.15	AAIJ	12U	LHCB	Repl. by AAIJ 13Y

B($B^0 \to K^*(892)^0\ell^+\ell^-$) (15.0 < q^2 < 19.0 GeV^2/c^4)

VALUE (units 10^{-7})	DOCUMENT ID		TECN	COMMENT
1.80 ±0.13 OUR AVERAGE				
$2.2^{+0.5}_{-0.4}\pm0.2$	[1] WEHLE	21	BELL	$e^+e^- \to \Upsilon(4S)$
$2.0^{+0.6}_{-0.5}\pm0.2$	[2] WEHLE	21	BELL	$e^+e^- \to \Upsilon(4S)$
$1.744^{+0.072}_{-0.076}\pm0.123$	[1] AAIJ	17Q	LHCB	pp at 7, 8 TeV
• • • We do not use the following data for averages, fits, limits, etc. • • •				
$1.95^{+0.08}_{-0.09}\pm0.13$	[1] AAIJ	16AO	LHCB	Repl. by AAIJ 17Q

[1] Measured with $\mu^+\mu^-$ as lepton pair.
[2] Measured with e^+e^- as lepton pair.

B($B^0 \to K^{*0}\ell^+\ell^-$) (1.0 < q^2 < 6.0 GeV^2/c^4)

VALUE (units 10^{-7})	DOCUMENT ID		TECN	COMMENT
1.74±0.11 OUR AVERAGE				
$1.9^{+0.6}_{-0.5}\pm0.3$	[1,2] WEHLE	21	BELL	$e^+e^- \to \Upsilon(4S)$
$1.8^{+0.6}_{-0.6}\pm0.2$	[1,3] WEHLE	21	BELL	$e^+e^- \to \Upsilon(4S)$
1.68±0.083±0.12	[1,2] AAIJ	17Q	LHCB	pp at 7, 8 TeV
1.90±0.20	[2] KHACHATRY...	16D	CMS	pp at 7, 8 TeV
1.42±0.41 ±0.12	[2] AALTONEN	11AI	CDF	$p\overline{p}$ at 1.96 TeV
• • • We do not use the following data for averages, fits, limits, etc. • • •				
$1.92^{+0.10}_{-0.09}\pm0.14$	AAIJ	16AO	LHCB	Repl. by AAIJ 17Q
$1.70\pm0.15^{+0.20}_{-0.25}$	AAIJ	13Y	LHCB	Repl. by AAIJ 16AO
2.20±0.30 ±0.20	CHATRCHYAN	13BL	CMS	Repl. by KHACHATRYAN 16D
2.10±0.30 ±0.15	AAIJ	12U	LHCB	Repl. by AAIJ 13Y

[1] Result is determined for the range 1.1 < q^2 < 6.0 GeV^4/c^2.
[2] Measured with $\mu^+\mu^-$ as lepton pair.
[3] Measured with e^+e^- as lepton pair.

B($B^0 \to K^{*0}\ell^+\ell^-$) (0.0 < q^2 < 4.3 GeV^2/c^4)

VALUE (units 10^{-7})	DOCUMENT ID		TECN	COMMENT
2.60±0.45±0.17	AALTONEN	11AI	CDF	$p\overline{p}$ at 1.96 TeV

B($B^0 \to K^{*0}\mu^+\mu^-$)/B($B^0 \to K^{*0}e^+e^-$) (0.045 < q^2 < 1.1 GeV^2/c^4)

VALUE	DOCUMENT ID		TECN	COMMENT
0.91 ±0.09 OUR AVERAGE				
$0.927^{+0.093}_{-0.087}{}^{+0.036}_{-0.035}$	[1] AAIJ	23AB	LHCB	pp at 7, 8, 13 TeV
$0.46^{+0.55}_{-0.27}\pm0.13$	WEHLE	21	BELL	$e^+e^- \to \Upsilon(4S)$
• • • We do not use the following data for averages, fits, limits, etc. • • •				
$0.66^{+0.11}_{-0.07}\pm0.03$	[2] AAIJ	17W	LHCB	pp at 7, 8 TeV

[1] Measured for the region 0.1 < q^2 < 1.1 GeV^2/c^4.
[2] Superseded by AAIJ 23AB.

B($B^0 \to K^{*0}\mu^+\mu^-$)/B($B^0 \to K^{*0}e^+e^-$) (1.1 < q^2 < 6.0 GeV^2/c^4)

VALUE	DOCUMENT ID		TECN	COMMENT
1.03 ±0.07 OUR AVERAGE				
$1.027^{+0.072}_{-0.068}{}^{+0.027}_{-0.026}$	AAIJ	23AB	LHCB	pp at 7, 8, 13 TeV
$1.06^{+0.63}_{-0.38}\pm0.13$	WEHLE	21	BELL	$e^+e^- \to \Upsilon(4S)$
• • • We do not use the following data for averages, fits, limits, etc. • • •				
$0.69^{+0.11}_{-0.07}\pm0.05$	[1] AAIJ	17W	LHCB	pp at 7, 8 TeV

[1] Superseded by AAIJ 23AB.

Int. J. Mod. Phys. A 2026.41. Downloaded from www.worldscientific.com by LIFORNIA @ BERKELEY on 09/16/26. Re-use and distribution is strictly not permitted, except for Open Access articles.

$B(B^0 \to K^{*0}\mu^+\mu^-)/B(B^0 \to K^{*0}e^+e^-)$ ($15.0 < q^2 < 19.0$ GeV^2/c^4)

VALUE	DOCUMENT ID		TECN	COMMENT
$1.12^{+0.61}_{-0.36}\pm0.10$	WEHLE	21	BELL	$e^+e^- \to \Upsilon(4S)$

$B(B^0 \to K^0\ell^+\ell^-)$ ($q^2 < 2.0$ GeV^2/c^4)

VALUE (units 10^{-7})	DOCUMENT ID		TECN	COMMENT
$0.24^{+0.22}_{-0.20}$ OUR AVERAGE				
$0.21^{+0.27}_{-0.23}$	AAIJ	12AH	LHCB	pp at 7 TeV
$0.31\pm0.37\pm0.02$	AALTONEN	11AI	CDF	$p\overline{p}$ at 1.96 TeV

$B(B^0 \to K^0\ell^+\ell^-)$ ($2.0 < q^2 < 4.3$ GeV^2/c^4)

VALUE (units 10^{-7})	DOCUMENT ID		TECN	COMMENT
$0.24^{+0.35}_{-0.30}$ OUR AVERAGE Error includes scale factor of 1.6.				
$0.07^{+0.25}_{-0.21}$	AAIJ	12AH	LHCB	pp at 7 TeV
$0.93\pm0.49\pm0.07$	AALTONEN	11AI	CDF	$p\overline{p}$ at 1.96 TeV

$B(B^0 \to K^0\ell^+\ell^-)$ ($4.3 < q^2 < 8.68$ GeV^2/c^4)

VALUE (units 10^{-7})	DOCUMENT ID		TECN	COMMENT
1.08 ± 0.27 OUR AVERAGE				
1.23 ± 0.31	AAIJ	12AH	LHCB	pp at 7 TeV
$0.66\pm0.51\pm0.05$	AALTONEN	11AI	CDF	$p\overline{p}$ at 1.96 TeV

$B(B^0 \to K^0\ell^+\ell^-)$ ($10.09 < q^2 < 12.86$ GeV^2/c^4)

VALUE (units 10^{-7})	DOCUMENT ID		TECN	COMMENT
0.27 ± 0.27 OUR AVERAGE Error includes scale factor of 1.8.				
$0.50^{+0.22}_{-0.19}$	AAIJ	12AH	LHCB	pp at 7 TeV
$-0.03\pm0.22\pm0.01$	AALTONEN	11AI	CDF	$p\overline{p}$ at 1.96 TeV

$B(B^0 \to K^0\ell^+\ell^-)$ ($14.18 < q^2 < 16.0$ GeV^2/c^4)

VALUE (units 10^{-7})	DOCUMENT ID		TECN	COMMENT
$0.29^{+0.21}_{-0.15}$ OUR AVERAGE Error includes scale factor of 1.8.				
$0.20^{+0.13}_{-0.09}$	AAIJ	12AH	LHCB	pp at 7 TeV
$0.73\pm0.26\pm0.06$	AALTONEN	11AI	CDF	$p\overline{p}$ at 1.96 TeV

$B(B^0 \to K^0\ell^+\ell^-)$ ($q^2 > 16.0$ GeV^2/c^4)

VALUE (units 10^{-7})	DOCUMENT ID		TECN	COMMENT
$0.31^{+0.16}_{-0.12}$ OUR AVERAGE				
$0.35^{+0.21}_{-0.14}$	AAIJ	12AH	LHCB	pp at 7 TeV
$0.21\pm0.18\pm0.16$	AALTONEN	11AI	CDF	$p\overline{p}$ at 1.96 TeV

$B(B^0 \to K^0\ell^+\ell^-)$ ($1.0 < q^2 < 6.0$ GeV^2/c^4)

VALUE (units 10^{-7})	DOCUMENT ID		TECN	COMMENT
$0.91^{+0.15}_{-0.13}$ OUR AVERAGE				
$0.62^{+0.44}_{-0.32}\pm0.02$	[1] CHOUDHURY	21	BELL	$e^+e^- \to \Upsilon(4S)$
$1.12^{+0.50}_{-0.40}\pm0.04$	[2] CHOUDHURY	21	BELL	$e^+e^- \to \Upsilon(4S)$
$0.916^{+0.172}_{-0.157}\pm0.004$	[3] AAIJ	14M	LHCB	pp at 7, 8 TeV
$0.98\pm0.61\pm0.08$	AALTONEN	11AI	CDF	$p\overline{p}$ at 1.96 TeV
• • • We do not use the following data for averages, fits, limits, etc. • • •				
$0.65^{+0.45}_{-0.35}$	AAIJ	12AH	LHCB	Repl. by AAIJ 14M

[1] Measured for $B^0 \to K^0_S\mu^+\mu^-$ decays. Measurements in other q^2 bins are also reported.
[2] Measured for $B^0 \to K^0_S e^+e^-$ decays. Measurements in other q^2 bins are also reported.
[3] Uses $B(B^0 \to J/\psi(1S)K^0) = (0.928\pm0.013\pm0.037)\times10^{-3}$ for normalisation and $\mu^+\mu^-$ as a lepton pair. Measured in $1.1 < q^2 < 6.0$ GeV^2/c^4.

$B(B^0 \to K^0\mu^+\mu^-)$ / $B(B^0 \to K^0e^+e^-)$ ($1.0 < q^2 < 6.0$ GeV^2/c^4)

VALUE	DOCUMENT ID		TECN	COMMENT
$0.64^{+0.18}_{-0.13}$ OUR AVERAGE				
$0.66^{+0.20}_{-0.14}{}^{+0.02}_{-0.04}$	[1] AAIJ	22J	LHCB	pp at 7, 8, 13 TeV
$0.55^{+0.46}_{-0.34}\pm0.01$	[2] CHOUDHURY	21	BELL	$e^+e^- \to \Upsilon(4S)$

[1] Measured in the range $1.1 < q^2 < 6.0$ GeV^2/c^4.
[2] Measured from the ratio of $K^0_S\mu^+\mu^-$ and $K^0_S e^+e^-$. Measurements in other q^2 bins are also reported.

$B(B^0 \to K^0\ell^+\ell^-)$ ($0.0 < q^2 < 4.3$ GeV^2/c^4)

VALUE (units 10^{-7})	DOCUMENT ID		TECN	COMMENT
$1.27\pm0.62\pm0.10$	AALTONEN	11AI	CDF	$p\overline{p}$ at 1.96 TeV

$B(B^0 \to K^0\ell^+\ell^-)$ ($15.0 < q^2 < 22.0$ GeV^2/c^4)

VALUE (units 10^{-7})	DOCUMENT ID		TECN	COMMENT
$0.67^{+0.11}_{-0.11}\pm0.04$	[1] AAIJ	14M	LHCB	pp at 7, 8 TeV

[1] Uses $B(B^0 \to J/\psi(1S)K^0) = (0.928\pm0.013\pm0.037)\times10^{-3}$ for normalisation and $\mu^+\mu^-$ as a lepton pair.

$B(B^0 \to K^0e^+e^-)$ ($1.1 < q^2 < 6.0$ GeV^2/c^4)

VALUE (units 10^{-8})	DOCUMENT ID		TECN	COMMENT
$13\pm3\pm1$	[1] AAIJ	22J	LHCB	pp at 7, 8, 13 TeV

[1] The reported value is converted from the measured $dB/dq^2 = (2.6\pm0.6\pm0.1)\times10^{-8}$ (GeV^2/c^4)$^{-1}$ by multiplying by the $\Delta q^2 = 4.9$ GeV^2/c^4 range.

$B(B^0 \to K^*_{0,2}(1430)^0\mu^+\mu^-)$ ($1.10 < q^2 < 6.00$ GeV^2/c^4)

VALUE (units 10^{-8})	DOCUMENT ID		TECN	COMMENT
$4.02\pm0.44\pm0.31$	[1,2] AAIJ	16AP	LHCB	pp at 7, 8 TeV

[1] Measured the differential branching fraction and angular moments of the decay $B^0 \to K^+\pi^-\mu^+\mu^-$ in the $K^+\pi^-$ invariant mass range $1330 < m(K^+\pi^-) < 1530$ MeV/c^2.
[2] The reported value is converted from the measured $dB/dq^2 = (0.82\pm0.09\pm0.063)\times10^{-8}$ (GeV^2/c^4)$^{-1}$ by multiplying by the $\Delta q^2 = 4.9$ GeV^2/c^4 range.

$F_H(B^0 \to K^0\mu^+\mu^-)$ ($1.1 < q^2 < 6.0$ GeV^2/c^4)

F_H is a fractional contribution of (pseudo) scalar and tensor amplitudes to the decay width in the massless muon approximation.

VALUE	DOCUMENT ID		TECN	COMMENT
$0.78\pm0.46\pm0.09$	[1] AAIJ	14O	LHCB	pp at 7, 8 TeV

[1] AAIJ 14O reports 68% C.L. interval, which we encode as midpoint with uncertainty as half of the width of interval.

$F_H(B^0 \to K^0\mu^+\mu^-)$ ($15.0 < q^2 < 22.0$ GeV^2/c^4)

VALUE	DOCUMENT ID		TECN	COMMENT
$0.34\pm0.25\pm0.03$	[1] AAIJ	14O	LHCB	pp at 7, 8 TeV

[1] AAIJ 14O reports 68% C.L. interval, which we encode as midpoint with uncertainty as half of the width of interval.

PRODUCTION ASYMMETRIES

$A_P(B^0)$

$A_P(B^0) = [\sigma(\overline{B}^0) - \sigma(B^0)] / [\sigma(\overline{B}^0) + \sigma(B^0)]$

VALUE (units 10^{-2})	DOCUMENT ID		TECN	COMMENT
-0.3 ± 0.6 OUR AVERAGE Error includes scale factor of 1.7. See the ideogram below.				
$0.44\pm0.88\pm0.11$	[1] AAIJ	17BF	LHCB	pp at 7 TeV
$-1.40\pm0.55\pm0.10$	[1] AAIJ	17BF	LHCB	pp at 8 TeV
$0.25\pm0.48\pm0.05$	[2] AABOUD	16G	ATLS	pp at 7, 8 TeV
• • • We do not use the following data for averages, fits, limits, etc. • • •				
$-0.35\pm0.76\pm0.28$	[3] AAIJ	14BP	LHCB	Repl. by AAIJ 17BF, pp at 7 TeV

[1] AAIJ 17BF uses $B^0 \to J/\psi K^{*0}$ decays with B^0 transverse momenta p_T and rapidities y in the region of $0 < p_T < 30$ GeV/c and $2.1 < y < 4.5$.
[2] Based on time-dependent analysis of $B^0 \to J/\psi K^{*0}$ decay in kinematic range $p_T > 10$ GeV/c and $|\eta| < 2.5$.
[3] Based on time-dependent analysis of $B^0 \to J/\psi K^{*0}$ and $B^0 \to D^-\pi^+$ in kinematic range $4 < p_T < 30$ GeV/c and $2.5 < \eta < 4.5$.

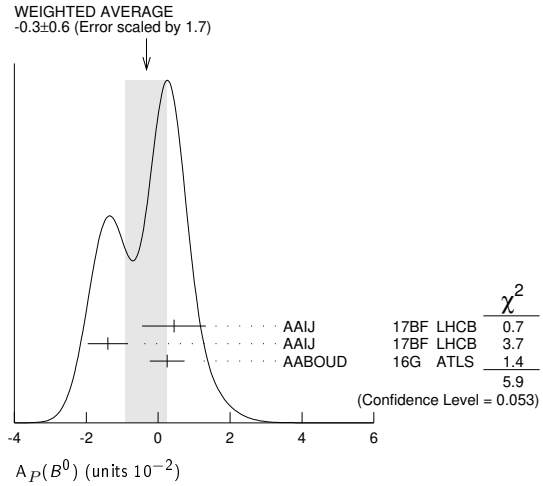

$A(B^0+\overline{B}^0)$ in $K^0_S K^\mp\pi^\pm$

$A(B^0+\overline{B}^0) = [n(K^0_S K^-\pi^+) - n(K^0_S K^+\pi^-)] / [n(K^0_S K^-\pi^+) + n(K^0_S K^+\pi^-)]$

VALUE (units 10^{-2})	DOCUMENT ID		TECN	COMMENT
$-8.5\pm8.9\pm0.2$	LAI	19	BELL	$e^+e^- \to \Upsilon(4S)$

Int. J. Mod. Phys. A 2026.41. Downloaded from www.worldscientific.com
by UNIVERSITY OF CALIFORNIA @ BERKELEY on 09/16/26. Re-use and distribution is strictly not permitted, except for Open Access articles.

FORWARD-BACKWARD ASYMMETRIES

A_{FB} in $B^0 \to D^{*-} e^+ \nu_e$

VALUE	DOCUMENT ID		TECN	COMMENT
0.225±0.018 OUR AVERAGE				
0.228±0.012±0.018	ADACHI	23J	BELL	$e^+e^- \to \Upsilon(4S)$
0.218±0.030±0.009	PRIM	23	BELL	$e^+e^- \to \Upsilon(4S)$

A_{FB} in $B^0 \to D^{*-} \mu^+ \nu_\mu$

VALUE	DOCUMENT ID		TECN	COMMENT
0.235±0.033 OUR AVERAGE Error includes scale factor of 1.7.				
0.211±0.011±0.021	ADACHI	23J	BELL	$e^+e^- \to \Upsilon(4S)$
0.281±0.032±0.007	PRIM	23	BELL	$e^+e^- \to \Upsilon(4S)$

$\Delta(A_{FB}) = (A^{\mu}_{FB} - A^{e}_{FB})$ in $B^0 \to D^{*-} \ell^+ \nu_\ell$

VALUE	DOCUMENT ID		TECN	COMMENT
−0.018±0.020 OUR AVERAGE				
−0.024±0.043±0.016	[1] ADACHI	23H	BELL	$e^+e^- \to \Upsilon(4S)$
−0.017±0.016±0.016	ADACHI	23J	BELL	$e^+e^- \to \Upsilon(4S)$
• • • We do not use the following data for averages, fits, limits, etc. • • •				
0.063±0.044±0.012	PRIM	23	BELL	$e^+e^- \to \Upsilon(4S)$

[1] ADACHI 23H measurement is based on the angular asymmetries of $B^0 \to D^{*-} \ell^+ \nu_\ell$ decays using explicit reconstruction of the B tag. Other asymmetries from $\Delta(S_3)$, $\Delta(S_5)$, $\Delta(S_7)$, and $\Delta(S_9)$ are also reported.

B^0 REFERENCES

AAD	25AM	EPJ C85 736	G. Aad et al.	(ATLAS Collab.)
AAIJ	25A	JHEP 2501 061	R. Aaij et al.	(LHCb Collab.)
AAIJ	25AN	JHEP 2510 113	R. Aaij et al.	(LHCb Collab.)
AAIJ	25AR	JHEP 2511 172	R. Aaij et al.	(LHCb Collab.)
AAIJ	25AS	JHEP 2512 026	R. Aaij et al.	(LHCb Collab.)
AAIJ	25AV	JHEP 2512 151	R. Aaij et al.	(LHCb Collab.)
AAIJ	25G	PRL 134 061801	R. Aaij et al.	(LHCb Collab.)
AAIJ	25W	JHEP 2506 140	R. Aaij et al.	(LHCb Collab.)
AAIJ	25X	JHEP 2507 121	R. Aaij et al.	(LHCb Collab.)
ABUMUSABH	25	PR D112 L051101	M. Abumusabh et al.	(BELLE and BELLE II Collabs.)
ADACHI	25	PRL 134 011802	I. Adachi et al.	(BELLE II Collab.)
ADACHI	25B	PRL 135 041801	I. Adachi et al.	(BELLE and BELLE II Collab.)
ADACHI	25C	PR D111 012011	I. Adachi et al.	(BELLE II Collab.)
ADACHI	25E	PR D111 032012	I. Adachi et al.	(BELLE II Collab.)
ADACHI	25F	PR D111 L071102	I. Adachi et al.	(BELLE II Collab.)
ADACHI	25G	PR D111 L071103	I. Adachi et al.	(BELLE and BELLE II Collab.)
ADACHI	25H	PR D111 092001	I. Adachi et al.	(BELLE II Collab.)
ADACHI	25I	PR D111 112009	I. Adachi et al.	(BELLE II Collab.)
ADACHI	25R	PR D112 032010	I. Adachi et al.	(BELLE II Collab.)
ADACHI	25S	JHEP 2508 184	I. Adachi et al.	(BELLE Collab.)
ADACHI	25V	PRL 135 151801	I. Adachi et al.	(BELLE II Collab.)
ADACHI	25Y	PR D112 112009	I. Adachi et al.	(BELLE II Collab.)
ADACHI	25Z	JHEP 2509 024	I. Adachi et al.	(BELLE II Collab.)
HAYRAPETY...	25AE	PL B864 139406	A. Hayrapetyan et al.	(CMS collaboration)
AAIJ	24	PRL 132 021801	R. Aaij et al.	(LHCb Collab.)
AAIJ	24AN	PR D110 092007	R. Aaij et al.	(LHCb Collab.)
AAIJ	24F	JHEP 2402 032	R. Aaij et al.	(LHCb Collab.)
AAIJ	24M	JHEP 2405 025	R. Aaij et al.	(LHCb Collab.)
AAIJ	24N	JHEP 2405 065	R. Aaij et al.	(LHCb Collab.)
AAIJ	24U	EPJ C84 206	R. Aaij et al.	(LHCb Collab.)
ADACHI	24	PR D109 012001	I. Adachi et al.	(BELLE II Collab.)
ADACHI	24G	PR D109 112020	I. Adachi et al.	(BELLE II Collab.)
ADACHI	24H	PR D110 012001	I. Adachi et al.	(BELLE II Collab.)
ADACHI	24J	PR D110 L031106	I. Adachi et al.	(BELLE and BELLE II Collab.)
ADACHI	24L	JHEP 2408 206	I. Adachi et al.	(BELLE II Collab.)
ADACHI	24N	PRL 133 101804	I. Adachi et al.	(BELLE and BELLE II Collab.)
ADACHI	24P	PR D110 112002	I. Adachi et al.	(BELLE II Collab.)
ALONSO-ALV...	24	EPJ C84 553	G. Alonso-Alvarez, M.E. Abenza	(MCGI, TNTO+)
GUAN	24	PRL 133 081801	Y. Guan et al.	(BELLE Collab.)
SAVINOV	24	PR D110 L031102	V. Savinov et al.	(BELLE Collab.)
AAIJ	23AB	PRL 131 051803	R. Aaij et al.	(LHCb Collab.)
Also		PR D108 032002	R. Aaij et al.	(LHCb Collab.)
AAIJ	23AD	PRL 131 091901	R. Aaij et al.	(LHCb Collab.)
AAIJ	23AG	PR D108 032007	R. Aaij et al.	(LHCb Collab.)
AAIJ	23AR	PRL 131 111802	R. Aaij et al.	(LHCb Collab.)
AAIJ	23AY	JHEP 2310 106	R. Aaij et al.	(LHCb Collab.)
AAIJ	23AZ	JHEP 2310 123	R. Aaij et al.	(LHCb Collab.)
AAIJ	23B	PR D108 012017	R. Aaij et al.	(LHCb Collab.)
AAIJ	23F	JHEP 2306 143	R. Aaij et al.	(LHCb Collab.)
AAIJ	23G	JHEP 2306 073	R. Aaij et al.	(LHCb Collab.)
AAIJ	23T	PR D108 012007	R. Aaij et al.	(LHCb Collab.)
AAIJ	23W	PR D108 012018	R. Aaij et al.	(LHCb Collab.)
Also		PR D109 119902 (errat.)	R. Aaij et al.	(LHCb Collab.)
AAIJ	23Y	PR D108 012021	R. Aaij et al.	(LHCb Collab.)
ABUDINEN	23D	PR D107 L091102	F. Abudinen et al.	(BELLE II Collab.)
ABUDINEN	23E	PR D107 112009	F. Abudinen et al.	(BELLE II Collab.)
ADACHI	23E	PRL 131 111803	I. Adachi et al.	(BELLE II Collab.)
ADACHI	23H	PRL 131 181801	I. Adachi et al.	(BELLE II Collab.)
ADACHI	23I	PR D108 072012	I. Adachi et al.	(BELLE II Collab.)
ADACHI	23J	PR D108 092013	I. Adachi et al.	(BELLE II Collab.)
CAO	23	PRL 131 211801	L. Cao et al.	(BELLE Collab.)
CHANG	23	PR D108 052011	C.-Y. Chang et al.	(BELLE Collab.)
CHOUDHURY	23	PR D107 L031102	S. Choudhury et al.	(BELLE Collab.)
DONG	23	PR D108 L011102	T.V. Dong et al.	(BELLE Collab.)
HIRATA	23	PR D107 112011	H. Hirata et al.	(BELLE Collab.)
KROHN	23	PR D107 012003	J.-F. Krohn et al.	(BELLE Collab.)
KUMAR	23	PR D107 L031101	M. Kumar et al.	(BELLE Collab.)
LEES	23B	PR D107 092001	J.P. Lees et al.	(BABAR Collab.)
LI	23E	PRL 130 031901	Y.B. Li et al.	(BELLE Collab.)
MEIER	23	PR D107 092003	F. Meier et al.	(BELLE Collab.)
PRIM	23	PR D108 012002	M.T. Prim et al.	(BELLE Collab.)
TUMASYAN	23A	PL B842 137955	A. Tumasyan et al.	(CMS Collab.)
AAIJ	22	PRL 128 041801	R. Aaij et al.	(LHCb Collab.)
Also		PR D105 012010	R. Aaij et al.	(LHCb Collab.)
AAIJ	22J	PRL 128 191802	R. Aaij et al.	(LHCb Collab.)
AAIJ	22N	PR D105 072005	R. Aaij et al.	(LHCb Collab.)
AAIJ	22Q	JHEP 2203 109	R. Aaij et al.	(LHCb Collab.)
AAIJ	22S	JHEP 2205 067	R. Aaij et al.	(LHCb Collab.)
BLOOMFIELD	22	PR D105 072007	T. Bloomfield et al.	(BELLE Collab.)
HADJIVASILIOU	22	PR D105 L051101	C. Hadjivasiliou et al.	(BELLE Collab.)
JEON	22	PR D106 012006	H.B. Jeon et al.	(BELLE Collab.)
TUMASYAN	22AI	EPJ C82 499	A. Tumasyan et al.	(CMS Collab.)
WAHEED	22	PR D105 012003	E. Waheed et al.	(BELLE Collab.)
AAIJ	21K	CP C45 043001	R. Aaij et al.	(LHCb Collab.)
AAIJ	21O	JHEP 2103 075	R. Aaij et al.	(LHCb Collab.)
AAIJ	21Q	JHEP 2104 081	R. Aaij et al.	(LHCb Collab.)
AAIJ	21S	JHEP 2106 177	R. Aaij et al.	(LHCb Collab.)
AAIJ	21W	EPJ C81 314	R. Aaij et al.	(LHCb Collab.)
ATMACAN	21	PR D104 L091105	H. Atmacan et al.	(BELLE Collab.)
CAO	21A	PR D104 012008	L. Cao et al.	(BELLE Collab.)
CHOUDHURY	21	JHEP 2103 105	S. Choudhury et al.	(BELLE Collab.)
KANG	21	PR D103 032003	K.H. Kang et al.	(BELLE Collab.)
MOHANTY	21	PR D103 052013	S. Mohanty et al.	(BELLE Collab.)
WAHEED	21	PR D103 079901	E. Waheed et al.	(BELLE Collab.)
WEHLE	21	PRL 126 161801	S. Wehle et al.	(BELLE Collab.)
AAIJ	20AG	PR D102 051102	R. Aaij et al.	(LHCb Collab.)
AAIJ	20AN	JHEP 2012 139	R. Aaij et al.	(LHCb Collab.)
AAIJ	20AO	JHEP 2012 081	R. Aaij et al.	(LHCb Collab.)
AAIJ	20F	PR D102 012011	R. Aaij et al.	(LHCb Collab.)
AAIJ	20L	JHEP 2003 147	R. Aaij et al.	(LHCb Collab.)
AAIJ	20W	PRL 124 211802	R. Aaij et al.	(LHCb Collab.)
CHILIKIN	20	JHEP 2005 034	K. Chilikin et al.	(BELLE Collab.)
CHU	20	PR D101 052012	K. Chu et al.	(BELLE Collab.)
KU	20	PR D102 012003	Y. Ku et al.	(BELLE Collab.)
SIRUNYAN	20AG	JHEP 2004 188	A.M. Sirunyan et al.	(CMS Collab.)
AABOUD	19L	JHEP 1904 098	M. Aaboud et al.	(ATLAS Collab.)
AAIJ	19AK	PRL 123 211801	R. Aaij et al.	(LHCb Collab.)
AAIJ	19AP	JHEP 1912 155	R. Aaij et al.	(LHCb Collab.)
AAIJ	19J	JHEP 1905 026	R. Aaij et al.	(LHCb Collab.)
AAIJ	19L	JHEP 1907 032	R. Aaij et al.	(LHCb Collab.)
AAIJ	19N	JHEP 1908 041	R. Aaij et al.	(LHCb Collab.)
AAIJ	19U	PRL 122 191804	R. Aaij et al.	(LHCb Collab.)
CHILIKIN	19	PR D100 012001	K. Chilikin et al.	(BELLE Collab.)
CHOU	19	PR D100 012002	P.-C. Chou et al.	(BELLE Collab.)
GARG	19	PR D99 071102	R. Garg et al.	(BELLE Collab.)
LAI	19	PR D100 011101	Y.-T. Lai et al.	(BELLE Collab.)
LI	19C	PR D100 031101	Y.B. Li et al.	(BELLE Collab.)
PAL	19	PR D99 091104	B. Pal et al.	(BELLE Collab.)
WAHEED	19	PR D100 052007	E. Waheed et al.	(BELLE Collab.)
WATANUKI	19	PR D99 032012	S. Watanuki et al.	(BELLE Collab.)
YUSA	19	PR D99 011102	Y. Yusa et al.	(BELLE Collab.)
AABOUD	18BY	JHEP 1810 047	M. Aaboud et al.	(ATLAS Collab.)
AAIJ	18AN	EPJ C78 1019	R. Aaij et al.	(LHCb Collab.)
AAIJ	18AY	PR D98 071103	R. Aaij et al.	(LHCb Collab.)
AAIJ	18AZ	PR D98 072006	R. Aaij et al.	(LHCb Collab.)
AAIJ	18D	PRL 120 171802	R. Aaij et al.	(LHCb Collab.)
AAIJ	18F	PRL 120 261801	R. Aaij et al.	(LHCb Collab.)
AAIJ	18O	PR D98 032004	R. Aaij et al.	(LHCb Collab.)
AAIJ	18T	JHEP 1803 078	R. Aaij et al.	(LHCb Collab.)
AAIJ	18Z	JHEP 1806 084	R. Aaij et al.	(LHCb Collab.)
ABAZOV	18B	PR D98 052010	V.M. Abazov et al.	(D0 Collab.)
ADACHI	18	PR D98 112012	I. Adachi et al.	(BELLE and BABAR Collab.)
Also		PRL 121 261801	I. Adachi et al.	(BELLE and BABAR Collab.)
LEES	18C	PR D98 071102	J.P. Lees et al.	(BABAR Collab.)
LI	18D	EPJ C78 928	Y.B. Li et al.	(BELLE Collab.)
NAKANO	18	PR D97 092003	H. Nakano et al.	(BELLE Collab.)
PAL	18	PR D98 112008	B. Pal et al.	(BELLE Collab.)
PDG	18	PR D98 030001	M. Tanabashi et al.	(PDG Collab.)
SANDILYA	18	PR D98 071101	S. Sandilya et al.	(BELLE Collab.)
SIRUNYAN	18BY	EPJ C78 457	A.M. Sirunyan et al.	(CMS Collab.)
SIRUNYAN	18DF	EPJ C78 939	A.M. Sirunyan et al.	(CMS Collab.)
VOSSEN	18	PR D98 012005	A. Vossen et al.	(BELLE Collab.)
AAIJ	17A	PR D95 012006	R. Aaij et al.	(LHCb Collab.)
AAIJ	17AI	PRL 118 191801	R. Aaij et al.	(LHCb Collab.)
AAIJ	17AJ	PRL 118 251802	R. Aaij et al.	(LHCb Collab.)
AAIJ	17BD	PR D96 051103	R. Aaij et al.	(LHCb Collab.)
AAIJ	17BF	PL B774 139	R. Aaij et al.	(LHCb Collab.)
AAIJ	17BJ	PRL 119 232001	R. Aaij et al.	(LHCb Collab.)
AAIJ	17BN	JHEP 1711 170	R. Aaij et al.	(LHCb Collab.)
AAIJ	17BP	JHEP 1711 027	R. Aaij et al.	(LHCb Collab.)
AAIJ	17G	PRL 118 081801	R. Aaij et al.	(LHCb Collab.)
AAIJ	17N	JHEP 1703 001	R. Aaij et al.	(LHCb Collab.)
AAIJ	17Q	JHEP 1704 142	R. Aaij et al.	(LHCb Collab.)
AAIJ	17W	JHEP 1708 055	R. Aaij et al.	(LHCb Collab.)
GRYGIER	17	PR D96 091101	J. Grygier et al.	(BELLE Collab.)
HORIGUCHI	17	PRL 119 191802	T. Horiguchi et al.	(BELLE Collab.)
JULIUS	17	PR D96 032007	T. Julius et al.	(BELLE Collab.)
AABOUD	16G	JHEP 1606 081	M. Aaboud et al.	(ATLAS Collab.)
AABOUD	16L	EPJ C76 513	M. Aaboud et al.	(ATLAS Collab.)
AAIJ	16	JHEP 1601 012	R. Aaij et al.	(LHCb Collab.)
AAIJ	16AA	JHEP 1608 137	R. Aaij et al.	(LHCb Collab.)
AAIJ	16AN	PRL 117 261801	R. Aaij et al.	(LHCb Collab.)
AAIJ	16AO	JHEP 1611 047	R. Aaij et al.	(LHCb Collab.)
AAIJ	16AP	JHEP 1612 065	R. Aaij et al.	(LHCb Collab.)
AAIJ	16AV	EPJ C76 412	R. Aaij et al.	(LHCb Collab.)
AAIJ	16E	PRL 116 241601	R. Aaij et al.	(LHCb Collab.)
AAIJ	16S	PR D93 112018	R. Aaij et al.	(LHCb Collab.)
AAIJ	16Z	JHEP 1606 131	R. Aaij et al.	(LHCb Collab.)
BHARDWAJ	16	PR D93 052016	V. Bhardwaj et al.	(BELLE Collab.)
CHOBANOVA	16	PR D93 031101	V. Chobanova et al.	(BELLE Collab.)
DEL-AMO-SA...	16	PR D93 052013	P. del Amo Sanchez et al.	(BABAR Collab.)
GLATTAUER	16	PR D93 032006	R. Glattauer et al.	(BELLE Collab.)
HAMER	16	PR D93 032007	P. Hamer et al.	(BELLE Collab.)
KHACHATRY...	16D	PL B753 424	V. Khachatryan et al.	(CMS Collab.)
KING	16	PR D93 111101	Z. King et al.	(BELLE Collab.)
LEES	16	PRL 116 041801	J.P. Lees et al.	(BABAR Collab.)
LEES	16E	PR D94 011101	J.P. Lees et al.	(BABAR Collab.)
LEES	16H	PR D94 091101	J.P. Lees et al.	(BABAR Collab.)
SATO	16B	PR D94 072007	Y. Sato et al.	(BELLE Collab.)
VANHOEFER	16	PR D93 032010	P. Vanhoefer et al.	(BELLE Collab.)
Also		PR D94 099903 (errat.)	P. Vanhoefer et al.	(BELLE Collab.)
VOROBYEV	16	PR D94 052004	V. Vorobyev et al.	(BELLE Collab.)
AAIJ	15AC	JHEP 1505 019	R. Aaij et al.	(LHCb Collab.)
AAIJ	15AS	JHEP 1510 053	R. Aaij et al.	(LHCb Collab.)
AAIJ	15AZ	PRL 115 161802	R. Aaij et al.	(LHCb Collab.)
AAIJ	15BB	PR D92 112002	R. Aaij et al.	(LHCb Collab.)
AAIJ	15D	JHEP 1501 024	R. Aaij et al.	(LHCb Collab.)
AAIJ	15F	PRL 114 041601	R. Aaij et al.	(LHCb Collab.)
AAIJ	15J	PL B742 38	R. Aaij et al.	(LHCb Collab.)
AAIJ	15N	PRL 115 031601	R. Aaji et al.	(LHCb Collab.)
AAIJ	15Q	PRL 115 111803	R. Aaij et al.	(LHCb Collab.)
AAIJ	15S	PL B743 46	R. Aaij et al.	(LHCb Collab.)
AAIJ	15T	PL B747 468	R. Aaij et al.	(LHCb Collab.)
AAIJ	15X	PR D92 012012	R. Aaij et al.	(LHCb Collab.)
AAIJ	15Y	PR D92 032002	R. Aaij et al.	(LHCb Collab.)
AAIJ	15Z	JHEP 1504 064	R. Aaij et al.	(LHCb Collab.)
ABAZOV	15A	PRL 114 062001	V.M. Abazov et al.	(D0 Collab.)
ABDESSALAM	15	PRL 115 121604	A. Abdessalam et al.	(BABAR and BELLE Collabs.)
BALA	15	PR D91 051101	A. Bala et al.	(BELLE Collab.)
CHANG	15	PRL 115 221803	Y.-Y. Chang et al.	(BELLE Collab.)
CHOI	15A	PR D91 092011	S.-K. Choi et al.	(BELLE Collab.)
KHACHATRY...	15BE	NAT 522 68	V. Khachatryan et al.	(CMS and LHCb Collab.)
LEES	15	PR D91 012003	J.P. Lees et al.	(BABAR Collab.)
LEES	15A	PRL 114 081801	J.P. Lees et al.	(BABAR Collab.)
LEES	15B	PR D91 031102	J.P. Lees et al.	(BABAR Collab.)

Int. J. Mod. Phys. A 2026.41. Downloaded from www.worldscientific.com
by LIFORNIA @ BERKELEY on 09/16/26. Re-use and distribution is strictly not permitted, except for Open Access articles.

LEES	15C	PR D91 052002	J.P. Lees *et al.*	(BABAR Collab.)
MATVIENKO	15	PR D92 012013	D. Matvienko *et al.*	(BELLE Collab.)
PAL	15	PR D92 011101	B. Pal *et al.*	(BELLE Collab.)
WIECHCZYN...	15	PR D91 032008	J. Wiechczynski *et al.*	(BELLE Collab.)
AAIJ	14AA	PRL 112 202001	R. Aaij *et al.*	(LHCb Collab.)
AAIJ	14AM	JHEP 1405 069	R. Aaij *et al.*	(LHCb Collab.)
AAIJ	14AN	JHEP 1409 177	R. Aaij *et al.*	(LHCb Collab.)
AAIJ	14BM	NJP 16 123001	R. Aaij *et al.*	(LHCb Collab.)
AAIJ	14BN	PR D90 112002	R. Aaij *et al.*	(LHCb Collab.)
AAIJ	14BP	PL B739 218	R. Aaij *et al.*	(LHCb Collab.)
AAIJ	14E	JHEP 1404 114	R. Aaij *et al.*	(LHCb Collab.)
AAIJ	14L	JHEP 1407 140	R. Aaij *et al.*	(LHCb Collab.)
AAIJ	14M	JHEP 1406 133	R. Aaij *et al.*	(LHCb Collab.)
AAIJ	14O	JHEP 1405 082	R. Aaij *et al.*	(LHCb Collab.)
AAIJ	14R	PL B736 446	R. Aaij *et al.*	(LHCb Collab.)
AAIJ	14X	PR D90 012003	R. Aaij *et al.*	(LHCb Collab.)
AAIJ	14Y	PRL 112 091802	R. Aaij *et al.*	(LHCb Collab.)
AALTONEN	14P	PRL 113 242001	T. Aaltonen *et al.*	(CDF Collab.)
ABAZOV	14	PR D89 012002	V.M. Abazov *et al.*	(D0 Collab.)
CHILIKIN	14	PR D90 112009	K. Chilikin *et al.*	(BELLE Collab.)
CHOBANOVA	14	PR D90 012002	V. Chobanova *et al.*	(BELLE Collab.)
IWASHITA	14	PTEP 2014 043C01	T. Iwashita *et al.*	(BELLE Collab.)
LAI	14	PR D89 051103	Y.-T. Lai *et al.*	(BELLE Collab.)
LEES	14	PR D89 051101	J.P. Lees *et al.*	(BABAR Collab.)
LEES	14B	PR D89 112002	J.P. Lees *et al.*	(BABAR Collab.)
LEES	14C	PR D89 071102	J.P. Lees *et al.*	(BABAR Collab.)
PDG	14	CP C38 070001	K. Olive *et al.*	(PDG Collab.)
SANTELJ	14	JHEP 1410 165	L. Santelj *et al.*	(BELLE Collab.)
SATO	14	PR D90 072009	S. Sato *et al.*	(BELLE Collab.)
VANHOEFER	14	PR D89 072008	P. Vanhoefer *et al.*	(BELLE Collab.)
AAD	13U	PR D87 032002	G. Aad *et al.*	(ATLAS Collab.)
AAIJ	13	NP B867 1	R. Aaij *et al.*	(LHCb Collab.)
AAIJ	13A	NP B867 547	R. Aaij *et al.*	(LHCb Collab.)
AAIJ	13AA	NP B871 403	R. Aaij *et al.*	(LHCb Collab.)
AAIJ	13AC	NP B874 663	R. Aaij *et al.*	(LHCb Collab.)
AAIJ	13AO	PR D87 092001	R. Aaij *et al.*	(LHCb Collab.)
AAIJ	13AP	PR D87 092007	R. Aaij *et al.*	(LHCb Collab.)
AAIJ	13AQ	PR D87 112009	R. Aaij *et al.*	(LHCb Collab.)
AAIJ	13AT	PR D88 052002	R. Aaij *et al.*	(LHCb Collab.)
AAIJ	13AW	PRL 110 211801	R. Aaij *et al.*	(LHCb Collab.)
AAIJ	13AX	PRL 110 221601	R. Aaij *et al.*	(LHCb Collab.)
AAIJ	13B	PRL 110 021801	R. Aaij *et al.*	(LHCb Collab.)
AAIJ	13BA	PRL 111 101805	R. Aaij *et al.*	(LHCb Collab.)
AAIJ	13BM	PRL 111 141801	R. Aaij *et al.*	(LHCb Collab.)
AAIJ	13BO	JHEP 1310 183	R. Aaij *et al.*	(LHCb Collab.)
AAIJ	13BP	JHEP 1310 143	R. Aaij *et al.*	(LHCb Collab.)
AAIJ	13BQ	JHEP 1310 005	R. Aaij *et al.*	(LHCb Collab.)
AAIJ	13BT	PR D88 072005	R. Aaij *et al.*	(LHCb Collab.)
AAIJ	13CF	EPJ C73 2655	R. Aaij *et al.*	(LHCb Collab.)
AAIJ	13E	PRL 110 031801	R. Aaij *et al.*	(LHCb Collab.)
AAIJ	13F	PL B719 318	R. Aaij *et al.*	(LHCb Collab.)
AAIJ	13K	PL B721 24	R. Aaij *et al.*	(LHCb Collab.)
AAIJ	13L	JHEP 1303 067	R. Aaij *et al.*	(LHCb Collab.)
AAIJ	13M	PR D87 052001	R. Aaij *et al.*	(LHCb Collab.)
AAIJ	13P	JHEP 1304 001	R. Aaij *et al.*	(LHCb Collab.)
AAIJ	13U	JHEP 1305 159	R. Aaij *et al.*	(LHCb Collab.)
AAIJ	13Y	JHEP 1308 131	R. Aaij *et al.*	(LHCb Collab.)
AAIJ	13Z	JHEP 1309 006	R. Aaij *et al.*	(LHCb Collab.)
AALTONEN	13F	PR D87 072003	T. Aaltonen *et al.*	(CDF Collab.)
CHATRCHYAN	13AW	PRL 111 101804	S. Chatrchyan *et al.*	(CMS Collab.)
CHATRCHYAN	13BL	PL B727 77	S. Chatrchyan *et al.*	(CMS Collab.)
CHILIKIN	13	PR D88 074026	K. Chilikin *et al.*	(BELLE Collab.)
DALSENO	13	PR D88 092003	J. Dalseno *et al.*	(BELLE Collab.)
DUH	13	PR D87 031103	Y. T. Duh *et al.*	(BELLE Collab.)
GAUR	13	PR D87 091101	V. Gaur *et al.*	(BELLE Collab.)
LEES	13D	PR D87 052009	J.P. Lees *et al.*	(BABAR Collab.)
LEES	13H	PR D87 092004	J.P. Lees *et al.*	(BABAR Collab.)
LEES	13I	PR D87 112005	J.P. Lees *et al.*	(BABAR Collab.)
LEES	13J	PR D88 012003	J.P. Lees *et al.*	(BABAR Collab.)
LEES	13M	PR D88 032012	J.P. Lees *et al.*	(BABAR Collab.)
LEES	13N	PRL 111 101802	J.P. Lees *et al.*	(BABAR Collab.)
Also		PRL 111 159901(errat.)	J.P. Lees *et al.*	(BABAR Collab.)
Also		PR D93 032001	J.P. Lees *et al.*	(BABAR Collab.)
LUTZ	13	PR D87 111103	O. Lutz *et al.*	(BELLE Collab.)
PRIM	13	PR D88 072004	M. Prim *et al.*	(BELLE Collab.)
SIBIDANOV	13	PR D88 032005	A. Sibidanov *et al.*	(BELLE Collab.)
AAIJ	12A	PL B708 55	R. Aaij *et al.*	(LHCb Collab.)
AAIJ	12AH	JHEP 1207 133	R. Aaij *et al.*	(LHCb Collab.)
AAIJ	12AM	PRL 109 131801	R. Aaij *et al.*	(LHCb Collab.)
AAIJ	12AR	JHEP 1210 037	R. Aaij *et al.*	(LHCb Collab.)
AAIJ	12AX	PR D86 112005	R. Aaij *et al.*	(LHCb Collab.)
AAIJ	12E	PL B708 241	R. Aaij *et al.*	(LHCb Collab.)
AAIJ	12I	PL B709 177	R. Aaij *et al.*	(LHCb Collab.)
AAIJ	12L	EPJ C72 2118	R. Aaij *et al.*	(LHCb Collab.)
AAIJ	12T	PRL 108 161801	R. Aaij *et al.*	(LHCb Collab.)
AAIJ	12U	PRL 108 181806	R. Aaij *et al.*	(LHCb Collab.)
AAIJ	12V	PRL 108 201601	R. Aaij *et al.*	(LHCb Collab.)
AAIJ	12W	PRL 108 231801	R. Aaij *et al.*	(LHCb Collab.)
AALTONEN	12L	PRL 108 211803	T. Aaltonen *et al.*	(CDF Collab.)
ABAZOV	12AC	PR D86 072009	V.M. Abazov *et al.*	(D0 Collab.)
ABAZOV	12U	PR D85 112003	V.M. Abazov *et al.*	(D0 Collab.)
ADACHI	12A	PRL 108 171802	I. Adachi *et al.*	(BELLE Collab.)
CHANG	12	PR D85 091102	M.-C. Chang *et al.*	(BELLE Collab.)
CHATRCHYAN	12A	JHEP 1204 033	S. Chatrchyan *et al.*	(CMS Collab.)
DALSENO	12	PR D86 092012	J. Dalseno *et al.*	(BELLE Collab.)
DEL-AMO-SA...	12	PR D85 092017	P. del Amo Sanchez *et al.*	(BABAR Collab.)
HIGUCHI	12	PR D85 071105	T. Higuchi *et al.*	(BELLE Collab.)
HOI	12	PRL 108 031801	C.-T. Hoi *et al.*	(BELLE Collab.)
HSU	12	PR D86 032002	C.-L. Hsu *et al.*	(BELLE Collab.)
KIM	12A	PR D86 031101	J.H. Kim *et al.*	(BELLE Collab.)
KRONENBIT...	12	PR D86 071103	B. Kronenbitter *et al.*	(BELLE Collab.)
LEES	12AA	PR D86 092004	J.P. Lees *et al.*	(BABAR Collab.)
LEES	12AF	PR D86 112006	J.P. Lees *et al.*	(BABAR Collab.)
LEES	12B	PR D85 052003	J.P. Lees *et al.*	(BABAR Collab.)
LEES	12D	PRL 109 101802	J.P. Lees *et al.*	(BABAR Collab.)
Also		PR D88 072012	J.P. Lees *et al.*	(BABAR Collab.)
LEES	12I	PR D85 054023	J.P. Lees *et al.*	(BABAR Collab.)
LEES	12K	PR D85 072005	J.P. Lees *et al.*	(BABAR Collab.)
LEES	12O	PR D85 112010	J.P. Lees *et al.*	(BABAR Collab.)
LEES	12T	PR D86 051105	J.P. Lees *et al.*	(BABAR Collab.)
LEES	12W	PRL 109 211801	J.P. Lees *et al.*	(BABAR Collab.)
NEGISHI	12	PR D86 011101	K. Negishi *et al.*	(BELLE Collab.)
PDG	12	PR D86 010001	J. Beringer *et al.*	(PDG Collab.)
ROHRKEN	12	PR D85 091106	M. Rohrken *et al.*	(BELLE Collab.)
SATO	12	PRL 108 171801	Y. Sato *et al.*	(BELLE Collab.)
AAIJ	11B	PL B699 330	R. Aaij *et al.*	(LHCb Collab.)
AAIJ	11E	PR D84 092001	R. Aaij *et al.*	(LHCb Collab.)
Also		PR D85 039904 (errat.)	R. Aaij *et al.*	(LHCb Collab.)
AALTONEN	11	PRL 106 121804	T. Aaltonen *et al.*	(CDF Collab.)
AALTONEN	11AG	PRL 107 191801	T. Aaltonen *et al.*	(CDF Collab.)
Also		PRL 107 239903 (errat.)	T. Aaltonen *et al.*	(CDF Collab.)
AALTONEN	11AI	PRL 107 201802	T. Aaltonen *et al.*	(CDF Collab.)
AALTONEN	11L	PRL 106 161801	T. Aaltonen *et al.*	(CDF Collab.)
AALTONEN	11N	PRL 106 181802	T. Aaltonen *et al.*	(CDF Collab.)
ABAZOV	11U	PR D84 052007	V.M. Abazov *et al.*	(D0 Collab.)
AUSHEV	11	PR D83 051102	T. Aushev *et al.*	(BELLE Collab.)
BAHINIPATI	11	PR D84 021101	S. Bahinipati *et al.*	(BELLE Collab.)
BHARDWAJ	11	PRL 107 091803	V. Bhardwaj *et al.*	(BELLE Collab.)
CHATRCHYAN	11T	PRL 107 191802	S. Chatrchyan *et al.*	(CMS Collab.)
CHOI	11	PR D84 052004	S.-K. Choi *et al.*	(BELLE Collab.)
DEL-AMO-SA...	11A	PR D83 032006	P. del Amo Sanchez *et al.*	(BABAR Collab.)
DEL-AMO-SA...	11B	PR D83 032004	P. del Amo Sanchez *et al.*	(BABAR Collab.)
DEL-AMO-SA...	11C	PR D83 032007	P. del Amo Sanchez *et al.*	(BABAR Collab.)
DEL-AMO-SA...	11F	PR D83 052011	P. del Amo Sanchez *et al.*	(BABAR Collab.)
DEL-AMO-SA...	11K	PR D83 091101	P. del Amo Sanchez *et al.*	(BABAR Collab.)
HA	11	PR D83 071101	H. Ha *et al.*	(BELLE Collab.)
LEES	11	PR D83 112010	J.P. Lees *et al.*	(BABAR Collab.)
LEES	11A	PR D84 012001	J.P. Lees *et al.*	(BABAR Collab.)
LEES	11F	PR D84 071102	J.P. Lees *et al.*	(BABAR Collab.)
LEES	11M	PR D84 112007	J.P. Lees *et al.*	(BABAR Collab.)
Also		PR D87 039901 (errat.)	J.P. Lees *et al.*	(BABAR Collab.)
SAHOO	11A	PR D84 071101	H. Sahoo *et al.*	(BELLE Collab.)
AUBERT	10	PRL 104 011802	B. Aubert *et al.*	(BABAR Collab.)
AUBERT	10D	PR D81 052009	B. Aubert *et al.*	(BABAR Collab.)
AUBERT	10H	PR D82 031102	B. Aubert *et al.*	(BABAR Collab.)
AUSHEV	10	PR D81 031103	T. Aushev *et al.*	(BELLE Collab.)
CHIANG	10	PR D81 071101	C.-C. Chiang *et al.*	(BELLE Collab.)
DAS	10	PR D82 051103	A. Das *et al.*	(BELLE Collab.)
DEL-AMO-SA...	10A	PR D82 011502	P. del Amo Sanchez *et al.*	(BABAR Collab.)
DEL-AMO-SA...	10B	PR D82 011101	P. del Amo Sanchez *et al.*	(BABAR Collab.)
DEL-AMO-SA...	10E	PR D82 031101	P. del Amo Sanchez *et al.*	(BABAR Collab.)
DEL-AMO-SA...	10Q	PR D82 112002	P. del Amo Sanchez *et al.*	(BABAR Collab.)
DUNGEL	10	PR D82 112007	W. Dungel *et al.*	(BELLE Collab.)
FUJIKAWA	10A	PR D81 011101	M. Fujikawa *et al.*	(BELLE Collab.)
HYUN	10	PRL 105 091801	H.J. Hyun *et al.*	(BELLE Collab.)
JOSHI	10	PR D81 031101	N.J. Joshi *et al.*	(BELLE Collab.)
NAKAHAMA	10	PR D82 073011	Y. Nakahama *et al.*	(BELLE Collab.)
WEDD	10	PR D81 111104	R. Wedd *et al.*	(BELLE Collab.)
AALTONEN	09B	PR D79 011104	T. Aaltonen *et al.*	(CDF Collab.)
AALTONEN	09C	PRL 103 031801	T. Aaltonen *et al.*	(CDF Collab.)
AALTONEN	09E	PR D79 032001	T. Aaltonen *et al.*	(CDF Collab.)
AALTONEN	09P	PRL 102 201801	T. Aaltonen *et al.*	(CDF Collab.)
ABAZOV	09E	PRL 102 032001	V.M. Abazov *et al.*	(D0 Collab.)
AUBERT	09	PR D79 011102	B. Aubert *et al.*	(BABAR Collab.)
AUBERT	09A	PR D79 012002	B. Aubert *et al.*	(BABAR Collab.)
AUBERT	09AA	PR D79 112001	B. Aubert *et al.*	(BABAR Collab.)
AUBERT	09AC	PR D79 112009	B. Aubert *et al.*	(BABAR Collab.)
AUBERT	09AD	PR D80 011101	B. Aubert *et al.*	(BABAR Collab.)
AUBERT	09AE	PR D80 031102	B. Aubert *et al.*	(BABAR Collab.)
AUBERT	09AF	PR D80 051101	B. Aubert *et al.*	(BABAR Collab.)
AUBERT	09AG	PR D80 051105	B. Aubert *et al.*	(BABAR Collab.)
AUBERT	09AL	PR D80 092007	B. Aubert *et al.*	(BABAR Collab.)
AUBERT	09AO	PRL 103 211802	B. Aubert *et al.*	(BABAR Collab.)
AUBERT	09AU	PR D80 112001	B. Aubert *et al.*	(BABAR Collab.)
AUBERT	09AV	PR D80 112002	B. Aubert *et al.*	(BABAR Collab.)
AUBERT	09B	PRL 102 132001	B. Aubert *et al.*	(BABAR Collab.)
AUBERT	09C	PR D79 032002	B. Aubert *et al.*	(BABAR Collab.)
AUBERT	09G	PRL 102 141802	B. Aubert *et al.*	(BABAR Collab.)
AUBERT	09H	PR D79 052005	B. Aubert *et al.*	(BABAR Collab.)
AUBERT	09I	PR D79 052003	B. Aubert *et al.*	(BABAR Collab.)
AUBERT	09K	PR D79 072009	B. Aubert *et al.*	(BABAR Collab.)
AUBERT	09S	PR D79 092002	B. Aubert *et al.*	(BABAR Collab.)
AUBERT	09T	PRL 102 091803	B. Aubert *et al.*	(BABAR Collab.)
Also		EPAPS Document No.	E-PRLTAO-102-060910	(BABAR Collab.)
AUBERT	09Y	PRL 103 051803	B. Aubert *et al.*	(BABAR Collab.)
CHANG	09	PR D79 052006	Y.-W. Chang *et al.*	(BELLE Collab.)
DALSENO	09	PR D79 072004	J. Dalseno *et al.*	(BELLE Collab.)
KYEONG	09	PR D80 051103	S.-H. Kyeong *et al.*	(BELLE Collab.)
MIZUK	09	PR D80 031104	R. Mizuk *et al.*	(BELLE Collab.)
VERVINK	09	PR D80 111104	K. Vervink *et al.*	(BELLE Collab.)
WEI	09A	PRL 103 171801	J.-T. Wei *et al.*	(BELLE Collab.)
Also		EPAPS Supplement	J.-T. Wei *et al.*	(BELLE Collab.)
ADACHI	08	PR D77 091101	I. Adachi *et al.*	(BELLE Collab.)
AUBERT	08AB	PR D78 012006	B. Aubert *et al.*	(BABAR Collab.)
AUBERT	08AC	PR D77 071102	B. Aubert *et al.*	(BABAR Collab.)
AUBERT	08AD	PR D77 091104	B. Aubert *et al.*	(BABAR Collab.)
AUBERT	08AF	PR D78 011103	B. Aubert *et al.*	(BABAR Collab.)
AUBERT	08AG	PR D78 011104	B. Aubert *et al.*	(BABAR Collab.)
AUBERT	08AH	PR D78 011107	B. Aubert *et al.*	(BABAR Collab.)
AUBERT	08AJ	PR D78 032005	B. Aubert *et al.*	(BABAR Collab.)
AUBERT	08AP	PR D78 051103	B. Aubert *et al.*	(BABAR Collab.)
AUBERT	08AQ	PR D78 052005	B. Aubert *et al.*	(BABAR Collab.)
AUBERT	08AU	PRL 101 021801	B. Aubert *et al.*	(BABAR Collab.)
AUBERT	08AV	PRL 101 081801	B. Aubert *et al.*	(BABAR Collab.)
AUBERT	08B	PR D77 011102	B. Aubert *et al.*	(BABAR Collab.)
AUBERT	08BA	PR D78 071102	B. Aubert *et al.*	(BABAR Collab.)
AUBERT	08BB	PR D78 071104	B. Aubert *et al.*	(BABAR Collab.)
AUBERT	08BC	PR D78 072007	B. Aubert *et al.*	(BABAR Collab.)
AUBERT	08BD	PR D78 091101	B. Aubert *et al.*	(BABAR Collab.)
AUBERT	08BG	PR D78 092008	B. Aubert *et al.*	(BABAR Collab.)
AUBERT	08BH	PR D78 112001	B. Aubert *et al.*	(BABAR Collab.)
AUBERT	08BK	PRL 101 201801	B. Aubert *et al.*	(BABAR Collab.)
AUBERT	08BL	PRL 101 261802	B. Aubert *et al.*	(BABAR Collab.)
AUBERT	08BN	PR D78 112003	B. Aubert *et al.*	(BABAR Collab.)
AUBERT	08C	PR D77 011104	B. Aubert *et al.*	(BABAR Collab.)
AUBERT	08E	PR D77 012003	B. Aubert *et al.*	(BABAR Collab.)
AUBERT	08F	PRL 100 051803	B. Aubert *et al.*	(BABAR Collab.)
AUBERT	08G	PRL 100 171803	B. Aubert *et al.*	(BABAR Collab.)
AUBERT	08H	PR D77 031101	B. Aubert *et al.*	(BABAR Collab.)
AUBERT	08I	PRL 100 081801	B. Aubert *et al.*	(BABAR Collab.)
AUBERT	08N	PRL 100 021801	B. Aubert *et al.*	(BABAR Collab.)
Also		PR D79 092002	B. Aubert *et al.*	(BABAR Collab.)
AUBERT	08P	PR D77 032007	B. Aubert *et al.*	(BABAR Collab.)
AUBERT	08Q	PRL 100 151802	B. Aubert *et al.*	(BABAR Collab.)
AUBERT	08R	PR D77 032002	B. Aubert *et al.*	(BABAR Collab.)
AUBERT	08W	PRL 101 082001	B. Aubert *et al.*	(BABAR Collab.)
AUBERT	08Y	PR D77 111101	B. Aubert *et al.*	(BABAR Collab.)
CHEN	08C	PRL 100 251801	J.-H. Chen *et al.*	(BELLE Collab.)
CHIANG	08	PR D78 111102	C.C. Chiang *et al.*	(BELLE Collab.)
CHOI	08	PRL 100 142001	S.-K. Choi *et al.*	(BELLE Collab.)
GOLDENZWE...	08	PRL 101 231801	P. Goldenzweig *et al.*	(BELLE Collab.)
KIM	08	PL B669 287	H.O. Kim *et al.*	(BELLE Collab.)
KUMAR	08	PR D78 091104	R. Kumar *et al.*	(BELLE Collab.)
KUSAKA	08	PR D77 072001	A. Kusaka *et al.*	(BELLE Collab.)
LEE	08A	PR D77 071101	S.E. Lee *et al.*	(BELLE Collab.)
LI	08F	PRL 101 251601	J. Li *et al.*	(BELLE Collab.)
LIN	08	NAT 452 332	S.-W. Lin *et al.*	(BELLE Collab.)
LIU	08I	PR D78 011106	Y. Liu *et al.*	(BELLE Collab.)
LIVENTSEV	08	PR D77 091503	D. Liventsev *et al.*	(BELLE Collab.)
MIZUK	08	PR D78 072004	R. Mizuk *et al.*	(BELLE Collab.)
NAKAHAMA	08	PRL 100 121601	Y. Nakahama *et al.*	(BELLE Collab.)
PDG	08	PL B667 1	C. Amsler *et al.*	(PDG Collab.)
SAHOO	08	PR D77 091103	H. Sahoo *et al.*	(BELLE Collab.)
TANIGUCHI	08	PRL 101 111801	N. Taniguchi *et al.*	(BELLE Collab.)

Int. J. Mod. Phys. A 2026.41. Downloaded from www.worldscientific.com
by UNIVERSITY OF CALIFORNIA @ BERKELEY on 09/16/26. Re-use and distribution is strictly not permitted, except for Open Access articles.

UCHIDA	08	PR D77 051101	Y. Uchida *et al.*	(BELLE Collab.)
USHIRODA	08	PRL 100 021602	Y. Ushiroda *et al.*	(BELLE Collab.)
WEI	08A	PR D78 011101	J.-T. Wei *et al.*	(BELLE Collab.)
ABAZOV	07S	PRL 99 142001	V.M. Abazov *et al.*	(D0 Collab.)
ABULENCIA	07A	PRL 98 122001	A. Abulencia *et al.*	(FNAL CDF Collab.)
ADAM	07	PRL 99 041802	N.E. Adam *et al.*	(CLEO Collab.)
Also		PR D76 012007	D.M. Asner *et al.*	(CLEO Collab.)
AUBERT	07A	PRL 98 031801	B. Aubert *et al.*	(BABAR Collab.)
AUBERT	07AA	PR D76 012004	B. Aubert *et al.*	(BABAR Collab.)
AUBERT	07AC	PR D76 031101	B. Aubert *et al.*	(BABAR Collab.)
AUBERT	07AD	PR D76 031102	B. Aubert *et al.*	(BABAR Collab.)
AUBERT	07AE	PR D76 031103	B. Aubert *et al.*	(BABAR Collab.)
AUBERT	07AF	PRL 99 021603	B. Aubert *et al.*	(BABAR Collab.)
AUBERT	07AG	PRL 99 051801	B. Aubert *et al.*	(BABAR Collab.)
AUBERT	07AI	PRL 99 071801	B. Aubert *et al.*	(BABAR Collab.)
AUBERT	07AJ	PRL 99 081801	B. Aubert *et al.*	(BABAR Collab.)
AUBERT	07AN	PR D76 051101	B. Aubert *et al.*	(BABAR Collab.)
AUBERT	07AO	PR D76 051103	B. Aubert *et al.*	(BABAR Collab.)
AUBERT	07AQ	PR D76 071101	B. Aubert *et al.*	(BABAR Collab.)
AUBERT	07AS	PR D76 071104	B. Aubert *et al.*	(BABAR Collab.)
AUBERT	07AT	PR D76 091101	B. Aubert *et al.*	(BABAR Collab.)
AUBERT	07AV	PR D76 092004	B. Aubert *et al.*	(BABAR Collab.)
AUBERT	07AX	PRL 99 161802	B. Aubert *et al.*	(BABAR Collab.)
AUBERT	07AY	PRL 99 171803	B. Aubert *et al.*	(BABAR Collab.)
AUBERT	07B	PR D75 012008	B. Aubert *et al.*	(BABAR Collab.)
AUBERT	07BC	PR D76 091102	B. Aubert *et al.*	(BABAR Collab.)
AUBERT	07BF	PR D76 052007	B. Aubert *et al.*	(BABAR Collab.)
AUBERT	07BH	PRL 99 231802	B. Aubert *et al.*	(BABAR Collab.)
AUBERT	07BI	PRL 99 241803	B. Aubert *et al.*	(BABAR Collab.)
AUBERT	07BO	PR D76 111102	B. Aubert *et al.*	(BABAR Collab.)
AUBERT	07D	PRL 98 051801	B. Aubert *et al.*	(BABAR Collab.)
AUBERT	07E	PRL 98 051802	B. Aubert *et al.*	(BABAR Collab.)
AUBERT	07F	PRL 98 051803	B. Aubert *et al.*	(BABAR Collab.)
AUBERT	07G	PRL 98 111801	B. Aubert *et al.*	(BABAR Collab.)
AUBERT	07H	PR D75 031101	B. Aubert *et al.*	(BABAR Collab.)
AUBERT	07J	PRL 98 091801	B. Aubert *et al.*	(BABAR Collab.)
AUBERT	07K	PRL 98 081801	B. Aubert *et al.*	(BABAR Collab.)
AUBERT	07L	PRL 98 151802	B. Aubert *et al.*	(BABAR Collab.)
AUBERT	07N	PR D75 072002	B. Aubert *et al.*	(BABAR Collab.)
AUBERT	07O	PRL 98 181803	B. Aubert *et al.*	(BABAR Collab.)
AUBERT	07Q	PR D75 051102	B. Aubert *et al.*	(BABAR Collab.)
AUBERT	07R	PRL 98 211804	B. Aubert *et al.*	(BABAR Collab.)
Also		PRL 100 189903E	B. Aubert *et al.*	(BABAR Collab.)
Also		PRL 100 199905E	B. Aubert *et al.*	(BABAR Collab.)
AUBERT	07Y	PR D75 111102	B. Aubert *et al.*	(BABAR Collab.)
CHANG	07A	PRL 98 131803	M.-C. Chang *et al.*	(BELLE Collab.)
CHANG	07B	PR D75 071104	P. Chang *et al.*	(BELLE Collab.)
CHAO	07	PR D76 091103	Y. Chao *et al.*	(BELLE Collab.)
CHEN	07	PRL 98 031802	K.-F. Chen *et al.*	(BELLE Collab.)
CHEN	07D	PRL 99 221802	K.-F. Chen *et al.*	(BELLE Collab.)
DALSENO	07	PR D76 072004	J. Dalseno *et al.*	(BELLE Collab.)
FRATINA	07	PRL 98 221802	S. Fratina *et al.*	(BELLE Collab.)
GARMASH	07	PR D75 012006	A. Garmash *et al.*	(BELLE Collab.)
HOKUUE	07	PL B648 139	T. Hokuue *et al.*	(BELLE Collab.)
ISHINO	07	PRL 98 211801	H. Ishino *et al.*	(BELLE Collab.)
KUSAKA	07	PRL 98 221602	A. Kusaka *et al.*	(BELLE Collab.)
Also		PR D77 072001	A. Kusaka *et al.*	(BELLE Collab.)
KUZMIN	07	PR D76 012006	A. Kuzmin *et al.*	(BELLE Collab.)
LIN	07	PRL 98 181804	S.-W. Lin *et al.*	(BELLE Collab.)
LIN	07A	PRL 99 121601	S.-W. Lin *et al.*	(BELLE Collab.)
MATYJA	07	PRL 99 191807	A. Matyja *et al.*	(BELLE Collab.)
MEDVEDEVA	07	PR D76 051102	T. Medvedeva *et al.*	(BELLE Collab.)
PARK	07	PR D75 011101	K.S. Park *et al.*	(BELLE Collab.)
SCHUEMANN	07	PR D75 092002	J. Schuemann *et al.*	(BELLE Collab.)
SOMOV	07	PR D76 011104	A. Somov *et al.*	(BELLE Collab.)
TSAI	07	PR D75 111101	Y.-T. Tsai *et al.*	(BELLE Collab.)
URQUIJO	07	PR D75 032001	P. Urquijo *et al.*	(BELLE Collab.)
WANG	07B	PR D75 092005	C.H. Wang *et al.*	(BELLE Collab.)
WANG	07C	PR D76 052004	M.-Z. Wang *et al.*	(BELLE Collab.)
XIE	07	PR D75 017101	Q.L. Xie *et al.*	(BELLE Collab.)
ZUPANC	07	PR D75 091102	A. Zupanc *et al.*	(BELLE Collab.)
ABAZOV	06S	PR D74 092001	V.M. Abazov *et al.*	(D0 Collab.)
ABAZOV	06W	PR D74 112002	V.M. Abazov *et al.*	(D0 Collab.)
ABULENCIA,A	06D	PRL 97 211802	A. Abulencia *et al.*	(CDF Collab.)
ACOSTA	06	PRL 96 202001	D. Acosta *et al.*	(CDF Collab.)
AUBERT	06	PR D73 011101	B. Aubert *et al.*	(BABAR Collab.)
AUBERT	06A	PRL 96 011803	B. Aubert *et al.*	(BABAR Collab.)
AUBERT	06E	PRL 96 052002	B. Aubert *et al.*	(BABAR Collab.)
AUBERT	06G	PR D73 012004	B. Aubert *et al.*	(BABAR Collab.)
AUBERT	06I	PR D73 031101	B. Aubert *et al.*	(BABAR Collab.)
AUBERT	06L	PR D74 012001	B. Aubert *et al.*	(BABAR Collab.)
AUBERT	06N	PR D74 031103	B. Aubert *et al.*	(BABAR Collab.)
AUBERT	06S	PRL 96 241802	B. Aubert *et al.*	(BABAR Collab.)
AUBERT	06T	PRL 96 251802	B. Aubert *et al.*	(BABAR Collab.)
AUBERT	06V	PRL 97 051802	B. Aubert *et al.*	(BABAR Collab.)
AUBERT	06W	PR D73 071102	B. Aubert *et al.*	(BABAR Collab.)
AUBERT	06X	PR D73 071103	B. Aubert *et al.*	(BABAR Collab.)
AUBERT	06Y	PR D73 111101	B. Aubert *et al.*	(BABAR Collab.)
AUBERT,B	06A	PR D73 112004	B. Aubert *et al.*	(BABAR Collab.)
AUBERT,B	06B	PR D74 011101	B. Aubert *et al.*	(BABAR Collab.)
AUBERT,B	06C	PR D74 011102	B. Aubert *et al.*	(BABAR Collab.)
AUBERT,B	06E	PR D74 011106	B. Aubert *et al.*	(BABAR Collab.)
AUBERT,B	06G	PRL 97 201801	B. Aubert *et al.*	(BABAR Collab.)
AUBERT,B	06H	PRL 97 201802	B. Aubert *et al.*	(BABAR Collab.)
AUBERT,B	06J	PR D73 092001	B. Aubert *et al.*	(BABAR Collab.)
AUBERT,B	06K	PRL 97 211801	B. Aubert *et al.*	(BABAR Collab.)
AUBERT,B	06L	PR D74 031101	B. Aubert *et al.*	(BABAR Collab.)
AUBERT,B	06M	PR D74 031102	B. Aubert *et al.*	(BABAR Collab.)
AUBERT,B	06O	PR D74 031104	B. Aubert *et al.*	(BABAR Collab.)
AUBERT,B	06P	PR D74 031105	B. Aubert *et al.*	(BABAR Collab.)
AUBERT,B	06Q	PR D74 091101	B. Aubert *et al.*	(BABAR Collab.)
AUBERT,B	06R	PR D74 032005	B. Aubert *et al.*	(BABAR Collab.)
AUBERT,B	06S	PR D74 051101	B. Aubert *et al.*	(BABAR Collab.)
AUBERT,B	06T	PR D74 051102	B. Aubert *et al.*	(BABAR Collab.)
AUBERT,B	06V	PR D74 051106	B. Aubert *et al.*	(BABAR Collab.)
AUBERT,B	06Y	PR D74 091105	B. Aubert *et al.*	(BABAR Collab.)
AUBERT,B	06Z	PR D74 092004	B. Aubert *et al.*	(BABAR Collab.)
AUBERT,BE	06C	PRL 97 171805	B. Aubert *et al.*	(BABAR Collab.)
AUBERT,BE	06H	PRL 97 261803	B. Aubert *et al.*	(BABAR Collab.)
AUBERT,BE	06J	PR D74 111102	B. Aubert *et al.*	(BABAR Collab.)
AUBERT,BE	06N	PR D74 072008	B. Aubert *et al.*	(BABAR Collab.)
BLYTH	06	PR D74 092002	S. Blyth *et al.*	(BELLE Collab.)
CHISTOV	06A	PR D74 111105	R. Chistov *et al.*	(BELLE Collab.)
DRAGIC	06	PR D73 111105	J. Dragic *et al.*	(BELLE Collab.)
GABYSHEV	06	PRL 97 202003	N. Gabyshev *et al.*	(BELLE Collab.)
GOKHROO	06	PRL 97 162002	G. Gokhroo *et al.*	(BELLE Collab.)
JEN	06	PR D74 111101	C.-M. Jen *et al.*	(BELLE Collab.)
KROKOVNY	06	PRL 97 081801	P. Krokovny *et al.*	(BELLE Collab.)
MOHAPATRA	06	PRL 96 221601	D. Mohapatra *et al.*	(BELLE Collab.)
NAKANO	06	PR D73 112002	E. Nakano *et al.*	(BELLE Collab.)
RONGA	06	PR D73 092003	F.J. Ronga *et al.*	(BELLE Collab.)
SCHUEMANN	06	PRL 97 061802	J. Schuemann *et al.*	(BELLE Collab.)
SOMOV	06	PRL 96 171801	A. Somov *et al.*	(BELLE Collab.)
SONI	06	PL B634 155	N. Soni *et al.*	(BELLE Collab.)
USHIRODA	06	PR D74 111104	Y. Ushiroda *et al.*	(BELLE Collab.)
VILLA	06	PR D73 051107	S. Villa *et al.*	(BELLE Collab.)
ABAZOV	05B	PRL 94 042001	V.M. Abazov *et al.*	(D0 Collab.)
ABAZOV	05C	PRL 94 102001	V.M. Abazov *et al.*	(D0 Collab.)
ABAZOV	05D	PRL 94 182001	V.M. Abazov *et al.*	(D0 Collab.)
ABAZOV	05W	PRL 95 171801	V.M. Abazov *et al.*	(D0 Collab.)
ABE	05A	PRL 94 221805	K. Abe *et al.*	(BELLE Collab.)
ABE	05B	PR D71 072003	K. Abe *et al.*	(BELLE Collab.)
Also		PR D71 079903 (errat.)	K. Abe *et al.*	(BELLE Collab.)
ABE	05D	PRL 95 101801	K. Abe *et al.*	(BELLE Collab.)
ABE	05G	PRL 95 231802	K. Abe *et al.*	(BELLE Collab.)
ACOSTA	05	PRL 94 101803	D. Acosta *et al.*	(CDF Collab.)
AUBERT	05	PRL 94 011801	B. Aubert *et al.*	(BABAR Collab.)
AUBERT	05B	PR D71 031501	B. Aubert *et al.*	(BABAR Collab.)
AUBERT	05E	PR D71 051502	B. Aubert *et al.*	(BABAR Collab.)
AUBERT	05F	PRL 94 161803	B. Aubert *et al.*	(BABAR Collab.)
AUBERT	05I	PRL 94 131801	B. Aubert *et al.*	(BABAR Collab.)
AUBERT	05J	PRL 94 141801	B. Aubert *et al.*	(BABAR Collab.)
AUBERT	05K	PRL 94 171801	B. Aubert *et al.*	(BABAR Collab.)
AUBERT	05L	PRL 94 181802	B. Aubert *et al.*	(BABAR Collab.)
AUBERT	05M	PRL 94 191802	B. Aubert *et al.*	(BABAR Collab.)
AUBERT	05O	PR D71 031103	B. Aubert *et al.*	(BABAR Collab.)
AUBERT	05P	PR D71 032005	B. Aubert *et al.*	(BABAR Collab.)
AUBERT	05T	PR D71 091102	B. Aubert *et al.*	(BABAR Collab.)
AUBERT	05U	PR D71 091103	B. Aubert *et al.*	(BABAR Collab.)
AUBERT	05V	PR D71 091104	B. Aubert *et al.*	(BABAR Collab.)
AUBERT	05W	PRL 94 221803	B. Aubert *et al.*	(BABAR Collab.)
AUBERT	05Y	PR D71 111102	B. Aubert *et al.*	(BABAR Collab.)
AUBERT	05Z	PR D71 112003	B. Aubert *et al.*	(BABAR Collab.)
AUBERT,B	05	PRL 95 011801	B. Aubert *et al.*	(BABAR Collab.)
AUBERT,B	05C	PRL 95 041805	B. Aubert *et al.*	(BABAR Collab.)
AUBERT,B	05K	PRL 95 131803	B. Aubert *et al.*	(BABAR Collab.)
AUBERT,B	05O	PR D72 051102	B. Aubert *et al.*	(BABAR Collab.)
AUBERT,B	05P	PR D72 051103	B. Aubert *et al.*	(BABAR Collab.)
AUBERT,B	05Q	PR D72 051106	B. Aubert *et al.*	(BABAR Collab.)
AUBERT,B	05Z	PRL 95 131802	B. Aubert *et al.*	(BABAR Collab.)
AUBERT,BE	05	PRL 95 151803	B. Aubert *et al.*	(BABAR Collab.)
AUBERT,BE	05A	PRL 95 151804	B. Aubert *et al.*	(BABAR Collab.)
AUBERT,BE	05B	PRL 95 171802	B. Aubert *et al.*	(BABAR Collab.)
AUBERT,BE	05C	PR D72 091103	B. Aubert *et al.*	(BABAR Collab.)
AUBERT,BE	05E	PRL 95 221801	B. Aubert *et al.*	(BABAR Collab.)
AUBERT,BE	05F	PR D72 111101	B. Aubert *et al.*	(BABAR Collab.)
CHANG	05	PR D71 072007	M.-C. Chang *et al.*	(BELLE Collab.)
CHANG	05A	PR D71 091106	P. Chang *et al.*	(BELLE Collab.)
CHAO	05	PRL 94 181803	Y. Chao *et al.*	(BELLE Collab.)
CHAO	05A	PR D71 031502	Y. Chao *et al.*	(BELLE Collab.)
CHEN	05A	PRL 94 221804	K.-F. Chen *et al.*	(BELLE Collab.)
CHEN	05B	PR D72 012004	K.-F. Chen *et al.*	(BELLE Collab.)
DRUTSKOY	05	PRL 94 061802	A. Drutskoy *et al.*	(BELLE Collab.)
GERSHON	05	PL B624 11	T. Gershon *et al.*	(BELLE Collab.)
ITOH	05	PRL 95 091601	R. Itoh *et al.*	(BELLE Collab.)
LIVENTSEV	05	PR D72 051109	D. Liventsev *et al.*	(BELLE Collab.)
MAJUMDER	05	PRL 95 041803	G. Majumder *et al.*	(BELLE Collab.)
MIYAKE	05	PL B618 34	H. Miyake *et al.*	(BELLE Collab.)
MOHAPATRA	05	PR D72 011101	D. Mohapatra *et al.*	(BELLE Collab.)
NISHIDA	05	PL B610 23	S. Nishida *et al.*	(BELLE Collab.)
OKABE	05	PL B614 27	T. Okabe *et al.*	(BELLE Collab.)
PARK	05	PRL 94 021801	H.K. Park *et al.*	(FNAL HyperCP Collab.)
SCHUMANN	05	PR D72 011103	J. Schumann *et al.*	(BELLE Collab.)
SUMISAWA	05	PRL 95 061801	K. Sumisawa *et al.*	(BELLE Collab.)
USHIRODA	05	PRL 94 231601	Y. Ushiroda *et al.*	(BELLE Collab.)
WANG	05	PRL 94 121801	C.C. Wang *et al.*	(BELLE Collab.)
WANG	05A	PL B617 141	M.-Z. Wang *et al.*	(BELLE Collab.)
XIE	05	PR D72 051105	Q.L. Xie *et al.*	(BELLE Collab.)
YANG	05	PRL 94 111802	H. Yang *et al.*	(BELLE Collab.)
ZHANG	05B	PR D71 091107	L.M. Zhang *et al.*	(BELLE Collab.)
ABDALLAH	04D	EPJ C33 213	J. Abdallah *et al.*	(DELPHI Collab.)
ABDALLAH	04E	EPJ C33 307	J. Abdallah *et al.*	(DELPHI Collab.)
ABE	04E	PRL 93 021601	K. Abe *et al.*	(BELLE Collab.)
AUBERT	04A	PR D69 011102	B. Aubert *et al.*	(BABAR Collab.)
AUBERT	04B	PR D69 032004	B. Aubert *et al.*	(BABAR Collab.)
AUBERT	04C	PRL 92 111801	B. Aubert *et al.*	(BABAR Collab.)
AUBERT	04G	PR D69 031102	B. Aubert *et al.*	(BABAR Collab.)
AUBERT	04H	PRL 92 061801	B. Aubert *et al.*	(BABAR Collab.)
AUBERT	04M	PRL 92 201802	B. Aubert *et al.*	(BABAR Collab.)
AUBERT	04R	PR D69 052001	B. Aubert *et al.*	(BABAR Collab.)
AUBERT	04U	PR D69 091503	B. Aubert *et al.*	(BABAR Collab.)
AUBERT	04V	PRL 92 251801	B. Aubert *et al.*	(BABAR Collab.)
AUBERT	04W	PRL 92 251802	B. Aubert *et al.*	(BABAR Collab.)
AUBERT	04Y	PRL 93 041801	B. Aubert *et al.*	(BABAR Collab.)
AUBERT	04Z	PRL 93 051802	B. Aubert *et al.*	(BABAR Collab.)
AUBERT,B	04B	PR D70 011101	B. Aubert *et al.*	(BABAR Collab.)
AUBERT,B	04C	PR D70 012007	B. Aubert *et al.*	(BABAR Collab.)
Also		PRL 92 181801	B. Aubert *et al.*	(BABAR Collab.)
AUBERT,B	04D	PR D70 032006	B. Aubert *et al.*	(BABAR Collab.)
AUBERT,B	04G	PRL 93 071801	B. Aubert *et al.*	(BABAR Collab.)
AUBERT,B	04H	PRL 93 081801	B. Aubert *et al.*	(BABAR Collab.)
AUBERT,B	04J	PRL 93 091802	B. Aubert *et al.*	(BABAR Collab.)
AUBERT,B	04K	PRL 93 131801	B. Aubert *et al.*	(BABAR Collab.)
AUBERT,B	04M	PRL 93 131805	B. Aubert	(BABAR Collab.)
AUBERT,B	04O	PR D70 091103	B. Aubert *et al.*	(BABAR Collab.)
AUBERT,B	04R	PRL 93 231801	B. Aubert *et al.*	(BABAR Collab.)
AUBERT,B	04S	PRL 93 181801	B. Aubert *et al.*	(BABAR Collab.)
AUBERT,B	04T	PR D70 091104	B. Aubert *et al.*	(BABAR Collab.)
AUBERT,B	04U	PR D70 091105	B. Aubert *et al.*	(BABAR Collab.)
AUBERT,B	04V	PRL 93 181805	B. Aubert *et al.*	(BABAR Collab.)
AUBERT,B	04W	PRL 93 231804	B. Aubert *et al.*	(BABAR Collab.)
AUBERT,B	04X	PRL 93 181806	B. Aubert *et al.*	(BABAR Collab.)
AUBERT,B	04Z	PRL 93 201801	B. Aubert *et al.*	(BABAR Collab.)
AUBERT,BE	04	PR D70 111102	B. Aubert *et al.*	(BABAR Collab.)
AUBERT,BE	04A	PR D70 112006	B. Aubert *et al.*	(BABAR Collab.)
AUBERT,BE	04B	PR D70 091106	B. Aubert *et al.*	(BABAR Collab.)
AUSHEV	04	PRL 93 201802	T. Aushev *et al.*	(BELLE Collab.)
BORNHEIM	04	PRL 93 241802	A. Bornheim *et al.*	(CLEO Collab.)
CHANG	04	PL B599 148	P. Chang *et al.*	(BELLE Collab.)
CHAO	04	PR D69 111102	Y. Chao *et al.*	(BELLE Collab.)
CHAO	04B	PRL 93 191802	Y. Chao *et al.*	(BELLE Collab.)
DRAGIC	04	PRL 93 131802	J. Dragic	(BELLE Collab.)
DRUTSKOY	04	PRL 92 051801	A. Drutskoy *et al.*	(BELLE Collab.)
GARMASH	04	PR D69 012001	A. Garmash *et al.*	(BELLE Collab.)
KATAOKA	04	PRL 93 261801	S.U. Kataoka *et al.*	(BELLE Collab.)
MAJUMDER	04	PR D70 111103	G. Majumder *et al.*	(BELLE Collab.)
NAKAO	04	PR D69 112001	M. Nakao *et al.*	(BELLE Collab.)
SARANGI	04	PRL 93 031802	T.R. Sarangi *et al.*	(BELLE Collab.)
WANG	04	PRL 92 131801	M.Z. Wang *et al.*	(BELLE Collab.)
WANG	04A	PR D70 012001	C.H. Wang *et al.*	(BELLE Collab.)
ABDALLAH	03B	EPJ C28 155	J. Abdallah *et al.*	(DELPHI Collab.)
ABE	03B	PR D67 032003	K. Abe *et al.*	(BELLE Collab.)
ABE	03C	PR D67 031102	K. Abe *et al.*	(BELLE Collab.)
ABE	03G	PR D68 012001	K. Abe *et al.*	(BELLE Collab.)

Int. J. Mod. Phys. A 2026.41. Downloaded from www.worldscientific.com by [redacted]LIFORNIA @ BERKELEY on 09/16/26. Re-use and distribution is strictly not permitted, except for Open Access articles.

ABE	03H	PRL 91 261602	K. Abe *et al.*	(BELLE Collab.)
ADAM	03	PR D67 032001	N.E. Adam *et al.*	(CLEO Collab.)
ATHAR	03	PR D68 072003	S.B. Athar *et al.*	(CLEO Collab.)
AUBERT	03B	PRL 90 091801	B. Aubert *et al.*	(BABAR Collab.)
AUBERT	03C	PR D67 072002	B. Aubert *et al.*	(BABAR Collab.)
AUBERT	03D	PRL 90 181803	B. Aubert *et al.*	(BABAR Collab.)
AUBERT	03E	PRL 90 181801	B. Aubert *et al.*	(BABAR Collab.)
AUBERT	03H	PR D67 091101	B. Aubert *et al.*	(BABAR Collab.)
AUBERT	03I	PR D67 092003	B. Aubert *et al.*	(BABAR Collab.)
AUBERT	03J	PRL 90 221801	B. Aubert *et al.*	(BABAR Collab.)
AUBERT	03K	PRL 90 231801	B. Aubert *et al.*	(BABAR Collab.)
AUBERT	03L	PRL 91 021801	B. Aubert *et al.*	(BABAR Collab.)
AUBERT	03N	PRL 91 061802	B. Aubert *et al.*	(BABAR Collab.)
AUBERT	03O	PRL 91 071801	B. Aubert *et al.*	(BABAR Collab.)
AUBERT	03Q	PRL 91 131801	B. Aubert *et al.*	(BABAR Collab.)
AUBERT	03S	PRL 91 241801	B. Aubert *et al.*	(BABAR Collab.)
AUBERT	03T	PRL 91 201802	B. Aubert *et al.*	(BABAR Collab.)
AUBERT	03U	PRL 91 221802	B. Aubert *et al.*	(BABAR Collab.)
AUBERT	03V	PRL 91 171802	B. Aubert *et al.*	(BABAR Collab.)
AUBERT	03W	PRL 91 161801	B. Aubert *et al.*	(BABAR Collab.)
AUBERT	03X	PR D68 092001	B. Aubert *et al.*	(BABAR Collab.)
BORNHEIM	03	PR D68 052002	A. Bornheim *et al.*	(CLEO Collab.)
CHANG	03	PR D68 111101	M.-C. Chang *et al.*	(BELLE Collab.)
CHEN	03B	PRL 91 201801	K.-F. Chen *et al.*	(BELLE Collab.)
CSORNA	03	PR D67 112002	S.E. Csorna *et al.*	(CLEO Collab.)
EISENSTEIN	03	PR D68 017101	B.I. Eisenstein *et al.*	(CLEO Collab.)
FANG	03	PRL 90 071801	F. Fang *et al.*	(BELLE Collab.)
GABYSHEV	03	PRL 90 121802	N. Gabyshev *et al.*	(BELLE Collab.)
HASTINGS	03	PR D67 052004	N.C. Hastings *et al.*	(BELLE Collab.)
ISHIKAWA	03	PRL 91 261601	A. Ishikawa *et al.*	(BELLE Collab.)
KROKOVNY	03	PRL 90 141802	P. Krokovny *et al.*	(BELLE Collab.)
KROKOVNY	03B	PRL 91 262002	P. Krokovny *et al.*	(BELLE Collab.)
LEE	03	PRL 91 261801	S.H. Lee *et al.*	(BELLE Collab.)
SATPATHY	03	PL B553 159	A. Satpathy *et al.*	(BELLE Collab.)
WANG	03	PRL 90 201802	M.-Z. Wang *et al.*	(BELLE Collab.)
ZHENG	03	PR D67 092004	Y. Zheng *et al.*	(BELLE Collab.)
ABE	02	PRL 88 021801	K. Abe *et al.*	(BELLE Collab.)
ABE	02E	PL B526 258	K. Abe *et al.*	(BELLE Collab.)
ABE	02F	PL B526 247	K. Abe *et al.*	(BELLE Collab.)
ABE	02H	PRL 88 171801	K. Abe *et al.*	(BELLE Collab.)
ABE	02J	PRL 88 052002	K. Abe *et al.*	(BELLE Collab.)
ABE	02K	PRL 88 181803	K. Abe *et al.*	(BELLE Collab.)
ABE	02M	PRL 89 071801	K. Abe *et al.*	(BELLE Collab.)
ABE	02N	PL B538 11	K. Abe *et al.*	(BELLE Collab.)
ABE	02O	PR D65 091103	K. Abe *et al.*	(BELLE Collab.)
ABE	02Q	PRL 89 122001	K. Abe *et al.*	(BELLE Collab.)
ABE	02U	PR D66 032007	K. Abe *et al.*	(BELLE Collab.)
ABE	02W	PRL 89 151802	K. Abe *et al.*	(BELLE Collab.)
ABE	02Z	PR D66 071102	K. Abe *et al.*	(BELLE Collab.)
ACOSTA	02C	PR D65 092009	D. Acosta *et al.*	(CDF Collab.)
ACOSTA	02G	PR D66 112002	D. Acosta *et al.*	(CDF Collab.)
AFFOLDER	02B	PRL 88 071801	T. Affolder *et al.*	(CDF Collab.)
AHMED	02B	PR D66 031101	S. Ahmed *et al.*	(CLEO Collab.)
ASNER	02	PR D65 031103	D.M. Asner *et al.*	(CLEO Collab.)
AUBERT	02	PR D65 032001	B. Aubert *et al.*	(BABAR Collab.)
AUBERT	02C	PRL 88 101805	B. Aubert *et al.*	(BABAR Collab.)
AUBERT	02D	PR D65 051502	B. Aubert *et al.*	(BABAR Collab.)
AUBERT	02E	PR D65 051101	B. Aubert *et al.*	(BABAR Collab.)
AUBERT	02H	PRL 89 011802	B. Aubert *et al.*	(BABAR Collab.)
Also		PRL 89 169903 (errat.)	B. Aubert *et al.*	(BABAR Collab.)
AUBERT	02I	PRL 88 221802	B. Aubert *et al.*	(BABAR Collab.)
AUBERT	02J	PRL 88 221803	B. Aubert *et al.*	(BABAR Collab.)
AUBERT	02K	PRL 88 231801	B. Aubert *et al.*	(BABAR Collab.)
AUBERT	02L	PRL 88 241801	B. Aubert *et al.*	(BABAR Collab.)
AUBERT	02M	PRL 89 061801	B. Aubert *et al.*	(BABAR Collab.)
AUBERT	02N	PR D66 032003	B. Aubert *et al.*	(BABAR Collab.)
AUBERT	02P	PRL 89 201802	B. Aubert *et al.*	(BABAR Collab.)
AUBERT	02Q	PRL 89 281802	B. Aubert *et al.*	(BABAR Collab.)
BRIERE	02	PRL 89 081803	R. Briere *et al.*	(CLEO Collab.)
CASEY	02	PR D66 092002	B.C.K. Casey *et al.*	(BELLE Collab.)
CHEN	02B	PL B546 196	K.-F. Chen *et al.*	(BELLE Collab.)
COAN	02	PRL 88 062001	T.E. Coan *et al.*	(CLEO Collab.)
Also		PRL 88 069902 (errat.)	T.E. Coan *et al.*	(CLEO Collab.)
DRUTSKOY	02	PL B542 171	A. Drutskoy *et al.*	(BELLE Collab.)
DYTMAN	02	PR D66 091101	S.A. Dytman *et al.*	(CLEO Collab.)
ECKHART	02	PRL 89 251801	E. Eckhart *et al.*	(CLEO Collab.)
EDWARDS	02	PR D65 012002	K.W. Edwards *et al.*	(CLEO Collab.)
GABYSHEV	02	PR D66 091102	N. Gabyshev *et al.*	(BELLE Collab.)
GODANG	02	PRL 88 021802	R. Godang *et al.*	(CLEO Collab.)
GORDON	02	PL B542 183	A. Gordon *et al.*	(BELLE Collab.)
HARA	02	PRL 89 251803	K. Hara *et al.*	(BELLE Collab.)
KROKOVNY	02	PRL 89 231804	P. Korkovny *et al.*	(BELLE Collab.)
MAHAPATRA	02	PRL 88 101803	R. Mahapatra *et al.*	(CLEO Collab.)
NISHIDA	02	PRL 89 231801	S. Nishida *et al.*	(BELLE Collab.)
TOMURA	02	PL B542 207	T. Tomura *et al.*	(BELLE Collab.)
ABASHIAN	01	PRL 86 2509	A. Abashian *et al.*	(BELLE Collab.)
ABE	01D	PRL 86 3228	K. Abe *et al.*	(BELLE Collab.)
ABE	01G	PRL 87 091802	K. Abe *et al.*	(BELLE Collab.)
ABE	01H	PRL 87 101801	K. Abe *et al.*	(BELLE Collab.)
ABE	01I	PRL 87 111801	K. Abe *et al.*	(BELLE Collab.)
ABE	01K	PR D64 071101	K. Abe *et al.*	(BELLE Collab.)
ABE	01L	PRL 87 161601	K. Abe *et al.*	(BELLE Collab.)
ABE	01M	PL B517 309	K. Abe *et al.*	(BELLE Collab.)
ABREU	01H	PL B510 55	P. Abreu *et al.*	(DELPHI Collab.)
ALEXANDER	01B	PR D64 092001	J.P. Alexander *et al.*	(CLEO Collab.)
AMMAR	01B	PRL 87 271801	R. Ammar *et al.*	(CLEO Collab.)
ANDERSON	01	PRL 86 2732	S. Anderson *et al.*	(CLEO Collab.)
ANDERSON	01B	PRL 87 181803	S. Anderson *et al.*	(CLEO Collab.)
AUBERT	01	PRL 86 2515	B. Aubert *et al.*	(BABAR Collab.)
AUBERT	01B	PRL 87 091801	B. Aubert *et al.*	(BABAR Collab.)
AUBERT	01D	PRL 87 151801	B. Aubert *et al.*	(BABAR Collab.)
AUBERT	01E	PRL 87 151802	B. Aubert *et al.*	(BABAR Collab.)
AUBERT	01F	PRL 87 201803	B. Aubert *et al.*	(BABAR Collab.)
AUBERT	01G	PRL 87 221802	B. Aubert *et al.*	(BABAR Collab.)
AUBERT	01H	PRL 87 241801	B. Aubert *et al.*	(BABAR Collab.)
AUBERT	01I	PRL 87 241803	B. Aubert *et al.*	(BABAR Collab.)
BARATE	01D	EPJ C20 431	R. Barate *et al.*	(ALEPH Collab.)
BARATE	01E	EPJ C19 213	R. Barate *et al.*	(ALEPH Collab.)
BRIERE	01	PRL 86 3718	R.A. Biere *et al.*	(CLEO Collab.)
EDWARDS	01	PRL 86 30	K.W. Edwards *et al.*	(CLEO Collab.)
JAFFE	01	PRL 86 5000	D. Jaffe *et al.*	(CLEO Collab.)
RICHICHI	01	PR D63 031103	S.J. Richichi *et al.*	(CLEO Collab.)
ABBIENDI	00Q	PL B482 15	G. Abbiendi *et al.*	(OPAL Collab.)
ABBIENDI,G	00B	PL B493 266	G. Abbiendi *et al.*	(OPAL Collab.)
ABE	00C	PR D62 071101	K. Abe *et al.*	(SLD Collab.)
AFFOLDER	00C	PR D61 072005	T. Affolder *et al.*	(CDF Collab.)
AFFOLDER	00N	PRL 85 4668	T. Affolder *et al.*	(CDF Collab.)
AHMED	00B	PR D62 112003	S. Ahmed *et al.*	(CLEO Collab.)
ANASTASSOV	00	PRL 84 1393	A. Anastassov *et al.*	(CLEO Collab.)
ARTUSO	00	PRL 84 4292	M. Artuso *et al.*	(CLEO Collab.)
AVERY	00	PR D62 051101	P. Avery *et al.*	(CLEO Collab.)
BARATE	00Q	PL B492 259	R. Barate *et al.*	(ALEPH Collab.)
BARATE	00R	PL B492 275	R. Barate *et al.*	(ALEPH Collab.)
BEHRENS	00	PR D61 052001	B.H. Behrens *et al.*	(CLEO Collab.)
BEHRENS	00B	PL B490 36	B.H. Behrens *et al.*	(CLEO Collab.)
BERGFELD	00B	PR D62 091102	T. Bergfeld *et al.*	(CLEO Collab.)
CHEN	00	PRL 85 525	S. Chen *et al.*	(CLEO Collab.)
COAN	00	PRL 84 5283	T.E. Coan *et al.*	(CLEO Collab.)
CRONIN-HEN...	00	PRL 85 515	D. Cronin-Hennessy *et al.*	(CLEO Collab.)
CSORNA	00	PR D61 111101	S.E. Csorna *et al.*	(CLEO Collab.)
JESSOP	00	PRL 85 2881	C.P. Jessop *et al.*	(CLEO Collab.)
LIPELES	00	PR D62 032005	E. Lipeles *et al.*	(CLEO Collab.)
RICHICHI	00	PRL 85 520	S.J. Richichi *et al.*	(CLEO Collab.)
ABBIENDI	99J	EPJ C12 609	G. Abbiendi *et al.*	(OPAL Collab.)
ABE	99K	PR D60 051101	F. Abe *et al.*	(CDF Collab.)
ABE	99Q	PR D60 072003	F. Abe *et al.*	(CDF Collab.)
AFFOLDER	99B	PRL 83 3378	T. Affolder *et al.*	(CDF Collab.)
AFFOLDER	99C	PR D60 112004	T. Affolder *et al.*	(CDF Collab.)
ARTUSO	99	PRL 82 3020	M. Artuso *et al.*	(CLEO Collab.)
BARTELT	99	PRL 82 3746	J. Bartelt *et al.*	(CLEO Collab.)
COAN	99	PR D59 111101	T.E. Coan *et al.*	(CLEO Collab.)
ABE	98B	PR D57 5382	F. Abe *et al.*	(CDF Collab.)
ABE	98C	PRL 80 2057	F. Abe *et al.*	(CDF Collab.)
Also		PR D59 032001	F. Abe *et al.*	(CDF Collab.)
ABE	98O	PR D58 072001	F. Abe *et al.*	(CDF Collab.)
ABE	98Q	PR D58 092002	F. Abe *et al.*	(CDF Collab.)
ABE	98U	PRL 81 5513	F. Abe *et al.*	(CDF Collab.)
ABE	98V	PRL 81 5742	F. Abe *et al.*	(CDF Collab.)
ACCIARRI	98D	EPJ C5 195	M. Acciarri *et al.*	(L3 Collab.)
ACCIARRI	98S	PL B438 417	M. Acciarri *et al.*	(L3 Collab.)
ACKERSTAFF	98Z	EPJ C5 379	K. Ackerstaff *et al.*	(OPAL Collab.)
BARATE	98Q	EPJ C4 387	R. Barate *et al.*	(ALEPH Collab.)
BEHRENS	98	PRL 80 3710	B.H. Behrens *et al.*	(CLEO Collab.)
BERGFELD	98	PRL 81 272	T. Bergfeld *et al.*	(CLEO Collab.)
BRANDENB...	98	PRL 80 2762	G. Brandenbrug *et al.*	(CLEO Collab.)
GODANG	98	PRL 80 3456	R. Godang *et al.*	(CLEO Collab.)
NEMATI	98	PR D57 5363	B. Nemati *et al.*	(CLEO Collab.)
ABE	97J	PRL 79 590	K. Abe *et al.*	(SLD Collab.)
ABREU	97F	ZPHY C74 19	P. Abreu *et al.*	(DELPHI Collab.)
Also		ZPHY C75 579 (errat.)	P. Abreu *et al.*	(DELPHI Collab.)
ABREU	97N	ZPHY C76 579	P. Abreu *et al.*	(DELPHI Collab.)
ACCIARRI	97B	PL B391 474	M. Acciarri *et al.*	(L3 Collab.)
ACCIARRI	97C	PL B391 481	M. Acciarri *et al.*	(L3 Collab.)
ACKERSTAFF	97G	PL B395 128	K. Ackerstaff *et al.*	(OPAL Collab.)
ACKERSTAFF	97U	ZPHY C76 401	K. Ackerstaff *et al.*	(OPAL Collab.)
ACKERSTAFF	97V	ZPHY C76 417	K. Ackerstaff *et al.*	(OPAL Collab.)
ARTUSO	97	PL B399 321	M. Artuso *et al.*	(CLEO Collab.)
ASNER	97	PRL 79 799	D. Asner *et al.*	(CLEO Collab.)
ATHANAS	97	PRL 79 2208	M. Athanas *et al.*	(CLEO Collab.)
BUSKULIC	97	PL B395 373	D. Buskulic *et al.*	(ALEPH Collab.)
BUSKULIC	97D	ZPHY C75 397	D. Buskulic *et al.*	(ALEPH Collab.)
FU	97	PRL 79 3125	X. Fu *et al.*	(CLEO Collab.)
JESSOP	97	PRL 79 4533	C.P. Jessop *et al.*	(CLEO Collab.)
ABE	96B	PR D53 3496	F. Abe *et al.*	(CDF Collab.)
ABE	96C	PRL 76 4462	F. Abe *et al.*	(CDF Collab.)
ABE	96H	PRL 76 2015	F. Abe *et al.*	(CDF Collab.)
ABE	96Q	PR D54 6596	F. Abe *et al.*	(CDF Collab.)
ABREU	96P	ZPHY C71 539	P. Abreu *et al.*	(DELPHI Collab.)
ABREU	96Q	ZPHY C72 17	P. Abreu *et al.*	(DELPHI Collab.)
ACCIARRI	96E	PL B383 487	M. Acciarri *et al.*	(L3 Collab.)
ADAM	96D	ZPHY C72 207	W. Adam *et al.*	(DELPHI Collab.)
ALBRECHT	96D	PL B374 256	H. Albrecht *et al.*	(ARGUS Collab.)
ALEXANDER	96T	PRL 77 5000	J.P. Alexander *et al.*	(CLEO Collab.)
ALEXANDER	96V	ZPHY C72 377	G. Alexander *et al.*	(OPAL Collab.)
ASNER	96	PR D53 1039	D.M. Asner *et al.*	(CLEO Collab.)
BARISH	96B	PRL 76 1570	B.C. Barish *et al.*	(CLEO Collab.)
BISHAI	96	PL B369 186	M. Bishai *et al.*	(CLEO Collab.)
BUSKULIC	96J	ZPHY C71 31	D. Buskulic *et al.*	(ALEPH Collab.)
BUSKULIC	96V	PL B384 471	D. Buskulic *et al.*	(ALEPH Collab.)
DUBOSCQ	96	PRL 76 3898	J.E. Duboscq *et al.*	(CLEO Collab.)
GIBAUT	96	PR D53 4734	D. Gibaut *et al.*	(CLEO Collab.)
PDG	96	PR D54 1	R. M. Barnett *et al.*	(PDG Collab.)
ABE	95Z	PRL 75 3068	F. Abe *et al.*	(CDF Collab.)
ABREU	95N	PL B357 255	P. Abreu *et al.*	(DELPHI Collab.)
ABREU	95Q	ZPHY C68 13	P. Abreu *et al.*	(DELPHI Collab.)
ACCIARRI	95H	PL B363 127	M. Acciarri *et al.*	(L3 Collab.)
ACCIARRI	95I	PL B363 137	M. Acciarri *et al.*	(L3 Collab.)
ADAM	95	ZPHY C68 363	W. Adam *et al.*	(DELPHI Collab.)
AKERS	95J	ZPHY C66 555	R. Akers *et al.*	(OPAL Collab.)
AKERS	95T	ZPHY C67 379	R. Akers *et al.*	(OPAL Collab.)
ALEXANDER	95	PL B341 435	J. Alexander *et al.*	(CLEO Collab.)
Also		PL B347 469 (errat.)	J. Alexander *et al.*	(CLEO Collab.)
BARISH	95	PR D51 1014	B.C. Barish *et al.*	(CLEO Collab.)
BUSKULIC	95N	PL B359 236	D. Buskulic *et al.*	(ALEPH Collab.)
ABE	94D	PRL 72 3456	F. Abe *et al.*	(CDF Collab.)
ABREU	94M	PL B338 409	P. Abreu *et al.*	(DELPHI Collab.)
AKERS	94C	PL B327 411	R. Akers *et al.*	(OPAL Collab.)
AKERS	94H	PL B336 585	R. Akers *et al.*	(OPAL Collab.)
AKERS	94J	PL B337 196	R. Akers *et al.*	(OPAL Collab.)
AKERS	94L	PL B337 393	R. Akers *et al.*	(OPAL Collab.)
ALAM	94	PR D50 43	M.S. Alam *et al.*	(CLEO Collab.)
ALBRECHT	94	PL B324 249	H. Albrecht *et al.*	(ARGUS Collab.)
ALBRECHT	94G	PL B340 217	H. Albrecht *et al.*	(ARGUS Collab.)
AMMAR	94	PR D49 5701	R. Ammar *et al.*	(CLEO Collab.)
ATHANAS	94	PRL 73 3503	M. Athanas *et al.*	(CLEO Collab.)
Also		PRL 74 3090 (errat.)	M. Athanas *et al.*	(CLEO Collab.)
BUSKULIC	94B	PL B322 441	D. Buskulic *et al.*	(ALEPH Collab.)
PDG	94	PR D50 1173	L. Montanet *et al.*	(CERN, LBL, BOST+)
PROCARIO	94	PRL 73 1472	M. Procario *et al.*	(CLEO Collab.)
STONE	94	HEPSY 93-11	S. Stone	
Published in B Decays, 2nd Edition, World Scientific, Singapore				
ABREU	93D	ZPHY C57 181	P. Abreu *et al.*	(DELPHI Collab.)
ABREU	93G	PL B312 253	P. Abreu *et al.*	(DELPHI Collab.)
ACTON	93C	PL B307 247	P.D. Acton *et al.*	(OPAL Collab.)
ALBRECHT	93	ZPHY C57 533	H. Albrecht *et al.*	(ARGUS Collab.)
ALBRECHT	93E	ZPHY C60 11	H. Albrecht *et al.*	(ARGUS Collab.)
ALEXANDER	93B	PL B319 365	J. Alexander *et al.*	(CLEO Collab.)
AMMAR	93	PRL 71 674	R. Ammar *et al.*	(CLEO Collab.)
BARTELT	93	PRL 71 1680	J.E. Bartelt *et al.*	(CLEO Collab.)
BATTLE	93	PRL 71 3922	M. Battle *et al.*	(CLEO Collab.)
BEAN	93B	PRL 70 2681	A. Bean *et al.*	(CLEO Collab.)
BUSKULIC	93D	PL B307 194	D. Buskulic *et al.*	(ALEPH Collab.)
Also		PL B325 537 (errat.)	D. Buskulic *et al.*	(ALEPH Collab.)
BUSKULIC	93K	PL B313 498	D. Buskulic *et al.*	(ALEPH Collab.)
SANGHERA	93	PR D47 791	S. Sanghera *et al.*	(CLEO Collab.)
ALBRECHT	92C	PL B275 195	H. Albrecht *et al.*	(ARGUS Collab.)
ALBRECHT	92G	ZPHY C54 1	H. Albrecht *et al.*	(ARGUS Collab.)
ALBRECHT	92L	ZPHY C55 357	H. Albrecht *et al.*	(ARGUS Collab.)
BORTOLETTO	92	PR D45 21	D. Bortoletto *et al.*	(CLEO Collab.)
HENDERSON	92	PR D45 2212	S. Henderson *et al.*	(CLEO Collab.)
KRAMER	92	PL B279 181	G. Kramer, W.F. Palmer	(HAMB, OSU)
ALBAJAR	91E	PL B273 540	C. Albajar *et al.*	(UA1 Collab.)
ALBRECHT	91B	PL B254 288	H. Albrecht *et al.*	(ARGUS Collab.)
ALBRECHT	91C	PL B255 297	H. Albrecht *et al.*	(ARGUS Collab.)

Int. J. Mod. Phys. A 2026.41. Downloaded from www.worldscientific.com
by UNIVERSITY OF CALIFORNIA @ BERKELEY on 09/16/26. Re-use and distribution is strictly not permitted, except for Open Access articles.

ALBRECHT	91E	PL B262 148	H. Albrecht *et al.*	(ARGUS Collab.)
BERKELMAN	91	ARNPS 41 1	K. Berkelman, S. Stone	(CORN, SYRA)
"Decays of B Mesons"				
FULTON	91	PR D43 651	R. Fulton *et al.*	(CLEO Collab.)
ALBRECHT	90B	PL B241 278	H. Albrecht *et al.*	(ARGUS Collab.)
ALBRECHT	90J	ZPHY C48 543	H. Albrecht *et al.*	(ARGUS Collab.)
ANTREASYAN	90B	ZPHY C48 553	D. Antreasyan *et al.*	(Crystal Ball Collab.)
BORTOLETTO	90	PRL 64 2117	D. Bortoletto *et al.*	(CLEO Collab.)
ELSEN	90	ZPHY C46 349	E. Elsen *et al.*	(JADE Collab.)
ROSNER	90	PR D42 3732	J.L. Rosner	
WAGNER	90	PRL 64 1095	S.R. Wagner *et al.*	(Mark II Collab.)
ALBRECHT	89C	PL B219 121	H. Albrecht *et al.*	(ARGUS Collab.)
ALBRECHT	89G	PL B229 304	H. Albrecht *et al.*	(ARGUS Collab.)
ALBRECHT	89J	PL B229 175	H. Albrecht *et al.*	(ARGUS Collab.)
ALBRECHT	89L	PL B232 554	H. Albrecht *et al.*	(ARGUS Collab.)
ARTUSO	89	PRL 62 2233	M. Artuso *et al.*	(CLEO Collab.)
AVERILL	89	PR D39 123	D.A. Averill *et al.*	(HRS Collab.)
AVERY	89B	PL B223 470	P. Avery *et al.*	(CLEO Collab.)
BEBEK	89	PRL 62 8	C. Bebek *et al.*	(CLEO Collab.)
BORTOLETTO	89	PRL 62 2436	D. Bortoletto *et al.*	(CLEO Collab.)
BORTOLETTO	89B	PRL 63 1667	D. Bortoletto *et al.*	(CLEO Collab.)
ALBRECHT	88F	PL B209 119	H. Albrecht *et al.*	(ARGUS Collab.)
ALBRECHT	88K	PL B215 424	H. Albrecht *et al.*	(ARGUS Collab.)
ALBRECHT	87C	PL B185 218	H. Albrecht *et al.*	(ARGUS Collab.)
ALBRECHT	87D	PL B199 451	H. Albrecht *et al.*	(ARGUS Collab.)
ALBRECHT	87I	PL B192 245	H. Albrecht *et al.*	(ARGUS Collab.)
ALBRECHT	87J	PL B197 452	H. Albrecht *et al.*	(ARGUS Collab.)
AVERY	87	PL B183 429	P. Avery *et al.*	(CLEO Collab.)
BEAN	87B	PRL 58 183	A. Bean *et al.*	(CLEO Collab.)
BEBEK	87	PR D36 1289	C. Bebek *et al.*	(CLEO Collab.)
ALAM	86	PR D34 3279	M.S. Alam *et al.*	(CLEO Collab.)
ALBRECHT	86F	PL B182 95	H. Albrecht *et al.*	(ARGUS Collab.)
PDG	86	PL 170B 1	M. Aguilar-Benitez *et al.*	(CERN, CIT+)
CHEN	85	PR D31 2386	A. Chen *et al.*	(CLEO Collab.)
HAAS	85	PRL 55 1248	J. Haas *et al.*	(CLEO Collab.)
AVERY	84	PRL 53 1309	P. Avery *et al.*	(CLEO Collab.)
GILES	84	PR D30 2279	R. Giles *et al.*	(CLEO Collab.)
BEHRENDS	83	PRL 50 881	S. Behrends *et al.*	(CLEO Collab.)

$B^\pm/B^0$ ADMIXTURE

B DECAY MODES

The branching fraction measurements are for an admixture of B mesons at the $\Upsilon(4S)$. The values quoted assume that $B(\Upsilon(4S) \to B\overline{B}) = 100\%$.

For inclusive branching fractions, *e.g.*, $B \to D^\pm$ *anything*, the treatment of multiple D's in the final state must be defined. One possibility would be to count the number of events with one-or-more D's and divide by the total number of B's. Another possibility would be to count the total number of D's and divide by the total number of B's, which is the definition of average multiplicity. The two definitions are identical if only one D is allowed in the final state. Even though the "one-or-more" definition seems sensible, for practical reasons inclusive branching fractions are almost always measured using the multiplicity definition. For heavy final state particles, authors call their results inclusive branching fractions while for light particles some authors call their results multiplicities. In the B sections, we list all results as inclusive branching fractions, adopting a multiplicity definition. This means that inclusive branching fractions can exceed 100% and that inclusive partial widths can exceed total widths, just as inclusive cross sections can exceed total cross section.

$\overline{B}$ modes are charge conjugates of the modes below. Reactions indicate the weak decay vertex and do not include mixing.

	Mode		Fraction (Γ_i/Γ)	Scale factor/ Confidence level
	Semileptonic and leptonic modes			
Γ_1	$e^+\nu_e$ anything	[a]		
Γ_2	$\mu^+\nu_\mu$ anything	[a]		
Γ_3	$\ell^+\nu_\ell$ anything	[a,b]	(10.82 ± 0.15) %	
Γ_4	$D^-\ell^+\nu_\ell$ anything	[b]	(2.6 ± 0.5) %	
Γ_5	$\overline{D}^0\ell^+\nu_\ell$ anything	[b]	(7.2 ± 1.5) %	
Γ_6	$\overline{D}\ell^+\nu_\ell$		(2.41 ± 0.12) %	
Γ_7	$\overline{D}e^+\nu_e$		seen	
Γ_8	$\overline{D}\mu^+\nu_\mu$		seen	
Γ_9	$D^{*-}\ell^+\nu_\ell$ anything	[c]	$(6.7 \pm 1.3) \times 10^{-3}$	
Γ_{10}	$D^{*0}\ell^+\nu_\ell$ anything			
Γ_{11}	$\overline{D}^*\ell^+\nu_\ell$	[d]	(4.95 ± 0.11) %	
Γ_{12}	$\overline{D}^*e^+\nu_e$			
Γ_{13}	$\overline{D}^*\mu^+\nu_\mu$			
Γ_{14}	$\overline{D}^{**}\ell^+\nu_\ell$	[b,e]	(2.7 ± 0.7) %	
Γ_{15}	$\overline{D}_1(2420)\ell^+\nu_\ell$ anything		$(3.8 \pm 1.3) \times 10^{-3}$	S=2.4
Γ_{16}	$\overline{D}\pi\ell^+\nu_\ell$ anything + $\overline{D}^*\pi\ell^+\nu_\ell$ anything		(2.6 ± 0.5) %	S=1.5
Γ_{17}	$\overline{D}\pi\ell^+\nu_\ell$ anything		(1.5 ± 0.6) %	
Γ_{18}	$\overline{D}^*\pi\ell^+\nu_\ell$ anything		(1.9 ± 0.4) %	
Γ_{19}	$\overline{D}_2^*(2460)\ell^+\nu_\ell$ anything		$(4.4 \pm 1.6) \times 10^{-3}$	
Γ_{20}	$D^{*-}\pi^+\ell^+\nu_\ell$ anything		(1.00 ± 0.34) %	
Γ_{21}	$\overline{D}\pi^+\pi^-\ell^+\nu_\ell$		$(1.62 \pm 0.32) \times 10^{-3}$	
Γ_{22}	$\overline{D}^*\pi^+\pi^-\ell^+\nu_\ell$		$(9.4 \pm 3.2) \times 10^{-4}$	
Γ_{23}	$D_s^-\ell^+\nu_\ell$ anything	[b]	$< 7 \times 10^{-3}$	CL=90%
Γ_{24}	$D_s^-\ell^+\nu_\ell K^+$ anything	[b]	$< 5 \times 10^{-3}$	CL=90%
Γ_{25}	$D_s^-\ell^+\nu_\ell K^0$ anything	[b]	$< 7 \times 10^{-3}$	CL=90%
Γ_{26}	$X_c\ell^+\nu_\ell$		(10.63 ± 0.15) %	
Γ_{27}	$X_u\ell^+\nu_\ell$		$(1.88 \pm 0.27) \times 10^{-3}$	
Γ_{28}	$X_u e^+\nu_e$		$(1.57 \pm 0.19) \times 10^{-3}$	
Γ_{29}	$X_u\mu^+\nu_\mu$		$(1.62 \pm 0.21) \times 10^{-3}$	
Γ_{30}	$K^+\ell^+\nu_\ell$ anything	[b]	(6.3 ± 0.5) %	
Γ_{31}	$K^-\ell^+\nu_\ell$ anything	[b]	$(10 \pm 4) \times 10^{-3}$	
Γ_{32}	$K^0/\overline{K}^0\ell^+\nu_\ell$ anything	[b]	(4.6 ± 0.5) %	
Γ_{33}	$\overline{D}\tau^+\nu_\tau$		$(8.4 \pm 0.7) \times 10^{-3}$	
Γ_{34}	$\overline{D}^*\tau^+\nu_\tau$		(1.43 ± 0.07) %	
	***D*, *D**, or *D*$_s$ modes**			
Γ_{35}	$D^\pm$ anything		(23.3 ± 1.2) %	
Γ_{36}	$D^0/\overline{D}^0$ anything		(64.6 ± 2.0) %	S=1.5
Γ_{37}	$D^*(2010)^\pm$ anything		(22.5 ± 1.5) %	
Γ_{38}	$\overline{D}^*(2007)^0$ anything		(26.0 ± 2.7) %	
Γ_{39}	$D_s^\pm$ anything	[f]	(10.6 ± 0.6) %	S=1.7
Γ_{40}	$D_s^{*\pm}$ anything		(6.3 ± 1.0) %	
Γ_{41}	$D_s^{*\pm}\overline{D}^{(*)}$		(3.4 ± 0.6) %	
Γ_{42}	$\overline{D}D_{s0}(2317)$		seen	
Γ_{43}	$\overline{D}D_{sJ}(2457)$		seen	
Γ_{44}	$D^{(*)}\overline{D}^{(*)}K^0 + D^{(*)}\overline{D}^{(*)}K^\pm$	[f,g]	$(7.1 {}^{+2.7}_{-1.7})$ %	
Γ_{45}	$b \to c\overline{c}s$		(22 ± 4) %	
Γ_{46}	$D_s^{(*)}\overline{D}^{(*)}$	[f,g]	(5.0 ± 0.4) %	
Γ_{47}	$D^*D^*(2010)^\pm$	[f]	$< 5.9 \times 10^{-3}$	CL=90%
Γ_{48}	$DD^*(2010)^\pm + D^*D^\pm$	[f]	$< 5.5 \times 10^{-3}$	CL=90%
Γ_{49}	$DD^\pm$	[f]	$< 3.1 \times 10^{-3}$	CL=90%
Γ_{50}	$D_s^{(*)\pm}\overline{D}^{(*)}X(n\pi^\pm)$	[f,g]	$(9 {}^{+5}_{-4})$ %	
Γ_{51}	$\overline{D}^*(2010)\gamma$		$< 1.1 \times 10^{-3}$	CL=90%
Γ_{52}	$D_s^+\pi^-$, $D_s^{*+}\pi^-$, $D_s^+\rho^-$, $D_s^{*+}\rho^-$, $D_s^+\pi^0$, $D_s^{*+}\pi^0$, $D_s^+\eta$, $D_s^{*+}\eta$, $D_s^+\rho^0$, $D_s^{*+}\rho^0$, $D_s^+\omega$, $D_s^{*+}\omega$	[f]	$< 4 \times 10^{-4}$	CL=90%
Γ_{53}	$D_{s1}(2536)^+$ anything		$< 9.5 \times 10^{-3}$	CL=90%
	Charmonium modes			
Γ_{54}	$J/\psi(1S)$ anything		(1.094 ± 0.032) %	S=1.1
Γ_{55}	$J/\psi(1S)$ (direct) anything		$(7.8 \pm 0.4) \times 10^{-3}$	S=1.1
Γ_{56}	$\psi(2S)$ anything		$(3.07 \pm 0.21) \times 10^{-3}$	
Γ_{57}	$\chi_{c1}(1P)$ anything		$(3.55 \pm 0.27) \times 10^{-3}$	S=1.3
Γ_{58}	$\chi_{c1}(1P)$ (direct) anything		$(3.09 \pm 0.19) \times 10^{-3}$	
Γ_{59}	$\chi_{c2}(1P)$ anything		$(10.0 \pm 1.7) \times 10^{-4}$	S=1.6
Γ_{60}	$\chi_{c2}(1P)$ (direct) anything		$(7.5 \pm 1.1) \times 10^{-4}$	
Γ_{61}	$\eta_c(1S)$ anything		$< 9 \times 10^{-3}$	CL=90%
Γ_{62}	$K\chi_{c1}(3872)$		$(1.9 \pm 0.7) \times 10^{-4}$	
Γ_{63}	$KX(3940)$, $X \to D^{*0}D^0$		$< 6.7 \times 10^{-5}$	CL=90%
Γ_{64}	$K\chi_{c0}(3915)$, $\chi_{c0} \to \omega J/\psi$	[h]	$(7.1 \pm 3.4) \times 10^{-5}$	
	***K* or *K* modes**			
Γ_{65}	$K^\pm$ anything	[f]	(78.9 ± 2.5) %	
Γ_{66}	K^+ anything		(66 ± 5) %	
Γ_{67}	K^- anything		(13 ± 4) %	
Γ_{68}	$K^0/\overline{K}^0$ anything	[f]	(64 ± 4) %	
Γ_{69}	$K^*(892)^\pm$ anything		(18 ± 6) %	
Γ_{70}	$K^*(892)^0/\overline{K}^*(892)^0$ anything	[f]	(14.6 ± 2.6) %	
Γ_{71}	$K^*(892)\gamma$		$(4.10 \pm 0.12) \times 10^{-5}$	
Γ_{72}	$\eta K\gamma$		$(8.5 {}^{+1.8}_{-1.6}) \times 10^{-6}$	
Γ_{73}	$K_1(1400)\gamma$		$< 1.27 \times 10^{-4}$	CL=90%
Γ_{74}	$K_2^*(1430)\gamma$		$(1.7 {}^{+0.6}_{-0.5}) \times 10^{-5}$	
Γ_{75}	$K_2(1770)\gamma$		$< 1.2 \times 10^{-3}$	CL=90%
Γ_{76}	$K_3^*(1780)\gamma$		$< 3.7 \times 10^{-5}$	CL=90%
Γ_{77}	$K_4^*(2045)\gamma$		$< 1.0 \times 10^{-3}$	CL=90%
Γ_{78}	$K\eta'(958)$		$(8.3 \pm 1.1) \times 10^{-5}$	
Γ_{79}	$K^*(892)\eta'(958)$		$(4.1 \pm 1.1) \times 10^{-6}$	
Γ_{80}	$K\eta$		$< 5.2 \times 10^{-6}$	CL=90%
Γ_{81}	$K^*(892)\eta$		$(1.8 \pm 0.5) \times 10^{-5}$	
Γ_{82}	$K\phi\phi$		$(2.3 \pm 0.9) \times 10^{-6}$	
Γ_{83}	$\overline{b} \to \overline{s}\gamma$		$(3.49 \pm 0.19) \times 10^{-4}$	
Γ_{84}	$\overline{b} \to \overline{d}\gamma$		$(9.2 \pm 3.0) \times 10^{-6}$	
Γ_{85}	$\overline{b} \to \overline{s}$gluon		< 6.8 %	CL=90%
Γ_{86}	η anything		$(2.6 {}^{+0.5}_{-0.8}) \times 10^{-4}$	

Γ_{87}	η' anything		(4.2 ± 0.9) × 10^{-4}	
Γ_{88}	K^+ gluon (charmless)		< 1.87 × 10^{-4}	CL=90%
Γ_{89}	K^0 gluon (charmless)		(1.9 ± 0.7) × 10^{-4}	

Light unflavored meson modes

Γ_{90}	$\rho\gamma$		(1.39 ± 0.25) × 10^{-6}	S=1.2
Γ_{91}	$\rho/\omega\gamma$		(1.30 ± 0.23) × 10^{-6}	S=1.2
Γ_{92}	$\pi^{\pm}$ anything	[f,i]	(358 ± 7) %	
Γ_{93}	π^0 anything		(235 ±11) %	
Γ_{94}	η anything		(17.6 ± 1.6) %	
Γ_{95}	ρ^0 anything		(21 ± 5) %	
Γ_{96}	ω anything		< 81 %	CL=90%
Γ_{97}	ϕ anything		(3.43 ± 0.12) %	
Γ_{98}	$\phi K^*(892)$		< 2.2 × 10^{-5}	CL=90%
Γ_{99}	$\overline{b} \to \overline{d}$ gluon			
Γ_{100}	π^+ gluon (charmless)		(3.7 ± 0.8) × 10^{-4}	

Baryon modes

Γ_{101}	$\Lambda_c^+ / \overline{\Lambda}_c^-$ anything		(3.53 ± 0.34) %	
Γ_{102}	Λ_c^+ anything		< 1.3 %	CL=90%
Γ_{103}	$\overline{\Lambda}_c^-$ anything		< 7 %	CL=90%
Γ_{104}	$\overline{\Lambda}_c^- \ell^+$ anything		< 9 × 10^{-4}	CL=90%
Γ_{105}	$\overline{\Lambda}_c^- e^+$ anything		< 1.8 × 10^{-3}	CL=90%
Γ_{106}	$\overline{\Lambda}_c^- \mu^+$ anything		< − 1.4 × 10^{-3}	CL=90%
Γ_{107}	$\overline{\Lambda}_c^- p$ anything		(2.01 ± 0.31) %	
Γ_{108}	$\overline{\Lambda}_c^- p e^+ \nu_e$		< 8 × 10^{-4}	CL=90%
Γ_{109}	$\overline{\Sigma}_c^{--}$ anything		(3.3 ± 1.7) × 10^{-3}	
Γ_{110}	$\overline{\Sigma}_c^-$ anything		< 8 × 10^{-3}	CL=90%
Γ_{111}	$\overline{\Sigma}_c^0$ anything		(3.6 ± 1.7) × 10^{-3}	
Γ_{112}	$\overline{\Sigma}_c^0 N$ ($N = p$ or n)		< 1.1 × 10^{-3}	CL=90%
Γ_{113}	Ξ_c^0 anything, $\Xi_c^0 \to \Xi^- \pi^+$		(1.93 ± 0.30) × 10^{-4}	S=1.1
Γ_{114}	Ξ_c^+, $\Xi_c^+ \to \Xi^- \pi^+ \pi^+$		(4.5 $^{+1.3}_{-1.2}$) × 10^{-4}	
Γ_{115}	$p/\overline{p}$ anything	[f]	(8.0 ± 0.4) %	
Γ_{116}	$p/\overline{p}$ (direct) anything	[f]	(5.5 ± 0.5) %	
Γ_{117}	$\overline{p} e^+ \nu_e$ anything		< 5.9 × 10^{-4}	CL=90%
Γ_{118}	$\Lambda/\overline{\Lambda}$ anything	[f]	(4.0 ± 0.5) %	
Γ_{119}	Λ anything		seen	
Γ_{120}	$\overline{\Lambda}$ anything		seen	
Γ_{121}	$\Xi^-/\overline{\Xi}^+$ anything	[f]	(2.7 ± 0.6) × 10^{-3}	
Γ_{122}	baryons anything		(6.8 ± 0.6) %	
Γ_{123}	$p\overline{p}$ anything		(2.47 ± 0.23) %	
Γ_{124}	$\Lambda\overline{p}/\overline{\Lambda}p$ anything	[f]	(2.5 ± 0.4) %	
Γ_{125}	$\Lambda\overline{\Lambda}$ anything		< 5 × 10^{-3}	CL=90%

Lepton Family number (*LF*) violating modes or $\Delta B = 1$ weak neutral current (*B1*) modes

Γ_{126}	$s e^+ e^-$	B1		(6.7 ± 1.7) × 10^{-6}	S=2.0
Γ_{127}	$s \mu^+ \mu^-$	B1		(4.3 ± 1.0) × 10^{-6}	
Γ_{128}	$s \ell^+ \ell^-$	B1	[b]	(5.8 ± 1.3) × 10^{-6}	S=1.8
Γ_{129}	$\pi \ell^+ \ell^-$	B1		< 5.9 × 10^{-8}	CL=90%
Γ_{130}	$\pi e^+ e^-$	B1		< 1.10 × 10^{-7}	CL=90%
Γ_{131}	$\pi \mu^+ \mu^-$	B1		< 5.0 × 10^{-8}	CL=90%
Γ_{132}	$K e^+ e^-$	B1		(4.4 ± 0.6) × 10^{-7}	
Γ_{133}	$K^*(892) e^+ e^-$	B1		(1.19 ± 0.20) × 10^{-6}	S=1.2
Γ_{134}	$K \mu^+ \mu^-$	B1		(4.4 ± 0.4) × 10^{-7}	
Γ_{135}	$K^*(892) \mu^+ \mu^-$	B1		(1.06 ± 0.09) × 10^{-6}	
Γ_{136}	$K \ell^+ \ell^-$	B1		(4.8 ± 0.4) × 10^{-7}	
Γ_{137}	$K^*(892) \ell^+ \ell^-$	B1		(1.05 ± 0.10) × 10^{-6}	
Γ_{138}	$K \nu \overline{\nu}$	B1		< 1.6 × 10^{-5}	CL=90%
Γ_{139}	$K^* \nu \overline{\nu}$	B1		< 2.7 × 10^{-5}	CL=90%
Γ_{140}	$\pi \nu \overline{\nu}$	B1		< 8 × 10^{-6}	CL=90%
Γ_{141}	$\rho \nu \overline{\nu}$	B1		< 2.8 × 10^{-5}	CL=90%
Γ_{142}	$s e^{\pm} \mu^{\mp}$	LF	[f]	< 2.2 × 10^{-5}	CL=90%
Γ_{143}	$\pi e^{\pm} \mu^{\mp}$	LF		< 9.2 × 10^{-8}	CL=90%
Γ_{144}	$\rho e^{\pm} \mu^{\mp}$	LF		< 3.2 × 10^{-6}	CL=90%
Γ_{145}	$K e^{\pm} \mu^{\mp}$	LF		< 3.8 × 10^{-8}	CL=90%
Γ_{146}	$K^*(892) e^{\pm} \mu^{\mp}$	LF		< 5.1 × 10^{-7}	CL=90%

[a] These values are model dependent.

[b] An ℓ indicates an e or a μ mode, not a sum over these modes.

[c] Here "anything" means at least one particle observed.

[d] This is a $B(B^0 \to D^{*-} \ell^+ \nu_\ell)$ value.

[e] D^{**} stands for the sum of the $D(1\,^1P_1)$, $D(1\,^3P_0)$, $D(1\,^3P_1)$, $D(1\,^3P_2)$, $D(2\,^1S_0)$, and $D(2\,^1S_1)$ resonances.

[f] The value is for the sum of the charge states or particle/antiparticle states indicated.

[g] $D^{(*)}\overline{D}^{(*)}$ stands for the sum of $D^*\overline{D}^*$, $D^*\overline{D}$, $D\overline{D}^*$, and $D\overline{D}$.

[h] $X(3915)$ denotes a near-threshold enhancement in the $\omega J/\psi$ mass spectrum.

[i] Inclusive branching fractions have a multiplicity definition and can be greater than 100%.

$B^{\pm}/B^0$ ADMIXTURE BRANCHING RATIOS

$\Gamma(\ell^+ \nu_\ell \text{anything})/\Gamma_{\text{total}}$ — Γ_3/Γ

These branching fraction values are model dependent.

VALUE (%)	DOCUMENT ID		TECN	COMMENT
10.82±0.15 OUR EVALUATION	(Produced by HFLAV)			
10.49±0.20 OUR AVERAGE	Error includes scale factor of 1.3. See the ideogram below.			
10.34±0.04±0.26	[1] LEES	17B	BABR	$e^+e^- \to \Upsilon(4S)$
10.28±0.18±0.24	[2] URQUIJO	07	BELL	$e^+e^- \to \Upsilon(4S)$
10.91±0.09±0.24	[3] MAHMOOD	04	CLEO	$e^+e^- \to \Upsilon(4S)$
9.7 ±0.5 ±0.4	[4] ALBRECHT	93H	ARG	$e^+e^- \to \Upsilon(4S)$
• • • We do not use the following data for averages, fits, limits, etc. • • •				
9.96±0.19±0.32	[5] AUBERT,B	06Y	BABR	Repl. by LEES 17B
10.85±0.21±0.36	[6] OKABE	05	BELL	Repl. by URQUIJO 07
10.83±0.16±0.06	[7] AUBERT	04X	BABR	Repl. by AUBERT,B 06Y
10.36±0.06±0.23	[8] AUBERT,B	04A	BABR	$e^+e^- \to \Upsilon(4S)$
10.87±0.18±0.30	[9] AUBERT	03	BABR	Repl. by AUBERT 04X
10.90±0.12±0.49	[10] ABE	02Y	BELL	Repl. by OKABE 05
10.49±0.17±0.43	[11] BARISH	96B	CLE2	Repl. by MAHMOOD 04
10.80±0.20±0.56	[12] HENDERSON	92	CLEO	$e^+e^- \to \Upsilon(4S)$
10.0 ±0.4 ±0.3	[13] YANAGISAWA	91	CSB2	$e^+e^- \to \Upsilon(4S)$
10.3 ±0.6 ±0.2	[14] ALBRECHT	90H	ARG	Direct e at $\Upsilon(4S)$
10.0 ±0.6 ±0.2	[15] ALBRECHT	90H	ARG	Direct μ at $\Upsilon(4S)$
11.7 ±0.4 ±1.0	[16] WACHS	89	CBAL	Direct e at $\Upsilon(4S)$
12.0 ±0.7 ±0.5	CHEN	84	CLEO	Direct e at $\Upsilon(4S)$
10.8 ±0.6 ±1.0	CHEN	84	CLEO	Direct μ at $\Upsilon(4S)$
11.2 ±0.9 ±1.0	LEVMAN	84	CUSB	Direct μ at $\Upsilon(4S)$
13.2 ±0.8 ±1.4	[17] KLOPFEN...	83B	CUSB	Direct e at $\Upsilon(4S)$

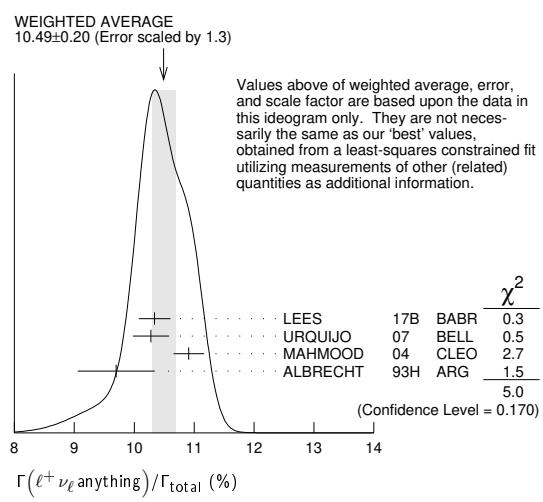

[1] LEES 17B measurement is obtained from semileptonic decays to electrons. The result is averaged over $B^{\pm}$ and B^0 mesons, assuming lepton universality.

[2] URQUIJO 07 report a measurement of (10.07 ± 0.18 ± 0.21)% for the partial branching fraction of $B \to e\nu_e X_c$ decay with electron energy above 0.6 GeV. We converted the result to $B \to e\nu_e X$ branching fraction.

[3] Uses charge and angular correlations in $\Upsilon(4S)$ events with a high-momentum lepton and an additional electron.

[4] ALBRECHT 93H analysis performed using tagged semileptonic decays of the B. This technique is almost model independent for the lepton branching ratio.

[5] The measurements are obtained for charged and neutral B mesons partial rates of semileptonic decay to electrons with momentum above 0.6 GeV/c in the B rest frame. The best precision on the ratio is achieved for a momentum threshold of 1.0 GeV: $B(B^+ \to e^+\nu_e X)$ / $B(B^0 \to e^+\nu_e X) = 1.074 \pm 0.041 \pm 0.026$.

[6] The measurements are obtained for charged and neutral B mesons partial rates of semileptonic decay to electrons with momentum above 0.6 GeV/c in the B rest frame, and their ratio of $B(B^+ \to e^+\nu_e X)/B(B^0 \to e^+\nu_e X) = 1.08 \pm 0.05 \pm 0.02$.

[7] The semileptonic branching ratio, $|V_{cb}|$ and other heavy-quark parameters are determined from a simultaneous fit to moments of the hadronic-mass and lepton-energy distribution.

[8] Uses the high-momentum lepton tag method and requires the electron energy above 0.6 GeV.

[9] Uses the high-momentum lepton tag method. They also report $|V_{cb}| = 0.0423 \pm 0.0007(\text{exp}) \pm 0.0020(\text{theo.})$.

Int. J. Mod. Phys. A 2026.41. Downloaded from www.worldscientific.com
by LIFORNIA @ BERKELEY on 09/16/26. Re-use and distribution is strictly not permitted, except for Open Access articles.

Int. J. Mod. Phys. A 2026.41. Downloaded from www.worldscientific.com
by UNIVERSITY OF CALIFORNIA @ BERKELEY on 09/16/26. Re-use and distribution is strictly not permitted, except for Open Access articles.

[10] Uses the high-momentum lepton tag method. ABE 02Y also reports $|V_{cb}| = 0.0408 \pm 0.0010(\text{exp}) \pm 0.0025(\text{theo.})$. The second error is due to uncertainties of theoretical inputs.
[11] BARISH 96B analysis performed using tagged semileptonic decays of the B. This technique is almost model independent for the lepton branching ratio.
[12] HENDERSON 92 measurement employs e and μ. The systematic error contains 0.004 in quadrature from model dependence. The authors average a variation of the Isgur, Scora, Grinstein, and Wise model with that of the Altarelli-Cabibbo-Corbò-Maiani-Martinelli model for semileptonic decays to correct the acceptance.
[13] YANAGISAWA 91 also measures an average semileptonic branching ratio at the $\Upsilon(5S)$ of 9.6–10.5% depending on assumptions about the relative production of different B meson species.
[14] ALBRECHT 90H uses the model of ALTARELLI 82 to correct over all lepton momenta. 0.099 ± 0.006 is obtained using ISGUR 89B.
[15] ALBRECHT 90H uses the model of ALTARELLI 82 to correct over all lepton momenta. 0.097 ± 0.006 is obtained using ISGUR 89B.
[16] Using data above $p(e) = 2.4$ GeV, WACHS 89 determine $\sigma(B \to e\nu\text{up})/\sigma(B \to e\nu\text{charm}) < 0.065$ at 90% CL.
[17] Ratio $\sigma(b \to e\nu\text{up})/\sigma(b \to e\nu\text{charm}) < 0.055$ at CL = 90%.

$\Gamma(e^+\nu_e\,\text{anything})/\Gamma(\mu^+\nu_\mu\,\text{anything})$ — Γ_1/Γ_2

VALUE	DOCUMENT ID		TECN	COMMENT
1.007±0.005±0.025	[1] HOHMANN	25	BELL	$e^+e^- \to \Upsilon(4S)$
• • • We do not use the following data for averages, fits, limits, etc. • • •				
1.007±0.009±0.019	[2] AGGARWAL	23	BELL	$e^+e^- \to \Upsilon(4S)$

[1] Measured from the partial branching fractions by extrapolating to the full phase-space via a correction factor of 1.0045 ± 0.0001, extracted from a simulation.
[2] The accompanying B meson is fully reconstructed in its hadronic decay modes. Superseded by by HOHMANN 25.

$\Gamma(D^-\ell^+\nu_\ell\,\text{anything})/\Gamma(\ell^+\nu_\ell\,\text{anything})$ — Γ_4/Γ_3

$\ell = e$ or μ.

VALUE	DOCUMENT ID		TECN	COMMENT
0.26±0.07±0.04	[1] FULTON	91	CLEO	$e^+e^- \to \Upsilon(4S)$

[1] FULTON 91 uses $B(D^+ \to K^-\pi^+\pi^+) = (9.1 \pm 1.3 \pm 0.4)\%$ as measured by MARK III.

$\Gamma(\overline{D}^0\ell^+\nu_\ell\,\text{anything})/\Gamma(\ell^+\nu_\ell\,\text{anything})$ — Γ_5/Γ_3

$\ell = e$ or μ.

VALUE	DOCUMENT ID		TECN	COMMENT
0.67±0.09±0.10	[1] FULTON	91	CLEO	$e^+e^- \to \Upsilon(4S)$

[1] FULTON 91 uses $B(D^0 \to K^-\pi^+) = (4.2 \pm 0.4 \pm 0.4)\%$ as measured by MARK III.

$\Gamma(\overline{D}\ell^+\nu_\ell)/\Gamma(\ell^+\nu_\ell\,\text{anything})$ — Γ_6/Γ_3

VALUE	DOCUMENT ID		TECN	COMMENT
0.223±0.006±0.009	[1] AUBERT	10	BABR	$e^+e^- \to \Upsilon(4S)$

[1] Uses a fully reconstructed B meson as a tag on the recoil side.

$\Gamma(\overline{D}e^+\nu_e)/\Gamma(\overline{D}\mu^+\nu_\mu)$ — Γ_7/Γ_8

VALUE	DOCUMENT ID		TECN	COMMENT
1.020±0.020±0.022	[1] ADACHI	25Y	BELL	$e^+e^- \to \Upsilon(4S)$

[1] The second B meson from the $\Upsilon(4S)$ decay is not explicitly reconstructed.

$\Gamma(D^{*-}\ell^+\nu_\ell\,\text{anything})/\Gamma_{\text{total}}$ — Γ_9/Γ

VALUE (units 10^{-2})	DOCUMENT ID		TECN	COMMENT
0.67±0.08±0.10	ABDALLAH	04D	DLPH	$e^+e^- \to Z^0$
• • • We do not use the following data for averages, fits, limits, etc. • • •				
0.6 ±0.3 ±0.1	[1] BARISH	95	CLE2	$e^+e^- \to \Upsilon(4S)$

[1] BARISH 95 use $B(D^0 \to K^-\pi^+) = (3.91 \pm 0.08 \pm 0.17)\%$ and $B(D^{*+} \to D^0\pi^+) = (68.1 \pm 1.0 \pm 1.3)\%$.

$\Gamma(D^{*0}\ell^+\nu_\ell\,\text{anything})/\Gamma_{\text{total}}$ — Γ_{10}/Γ

VALUE (units 10^{-2})	DOCUMENT ID		TECN	COMMENT
• • • We do not use the following data for averages, fits, limits, etc. • • •				
0.6±0.6±0.1	[1] BARISH	95	CLE2	$e^+e^- \to \Upsilon(4S)$

[1] BARISH 95 use $B(D^0 \to K^-\pi^+) = (3.91 \pm 0.08 \pm 0.17)\%$, $B(D^{*+} \to D^0\pi^+) = (68.1 \pm 1.0 \pm 1.3)\%$, $B(D^{*0} \to D^0\pi^0) = (63.6 \pm 2.3 \pm 3.3)\%$.

$\Gamma(\overline{D}^*e^+\nu_e)/\Gamma(\overline{D}^*\mu^+\nu_\mu)$ — Γ_{12}/Γ_{13}

VALUE	DOCUMENT ID		TECN	COMMENT
0.993±0.023±0.023	[1] PRIM	23	BELL	$e^+e^- \to \Upsilon(4S)$

[1] This is the lepton-flavor universality ratio $R_{e\mu}$ for the $B^+ \to \overline{D}^{*0}\ell^+\nu_\ell$ and $B^0 \to D^{*-}\ell^+\nu_\ell$ average.

$\Gamma(\overline{D}^{**}\ell^+\nu_\ell)/\Gamma_{\text{total}}$ — Γ_{14}/Γ

D^{**} stands for the sum of the $D(1\,^1P_1)$, $D(1\,^3P_0)$, $D(1\,^3P_1)$, $D(1\,^3P_2)$, $D(2\,^1S_0)$, and $D(2\,^1S_1)$ resonances. $\ell = e$ or μ, not sum over e and μ modes.

VALUE	CL%	EVTS	DOCUMENT ID		TECN	COMMENT
0.027±0.005±0.005		63	[1] ALBRECHT	93	ARG	$e^+e^- \to \Upsilon(4S)$
• • • We do not use the following data for averages, fits, limits, etc. • • •						
<0.028	95		[2] BARISH	95	CLE2	$e^+e^- \to \Upsilon(4S)$

[1] ALBRECHT 93 assumes the GISW model to correct for unseen modes. Using the BHKT model, the result becomes $0.023 \pm 0.006 \pm 0.004$. Assumes $B(D^{*+} \to D^0\pi^+) = 68.1\%$, $B(D^0 \to K^-\pi^+) = 3.65\%$, $B(D^0 \to K^-\pi^+\pi^-\pi^+) = 7.5\%$. We have taken their average e and μ value.
[2] BARISH 95 use $B(D^0 \to K^-\pi^+) = (3.91 \pm 0.08 \pm 0.17)\%$, assume all nonresonant channels are zero, and use GISW model for relative abundances of D^{**} states.

$\Gamma(\overline{D}_1(2420)\ell^+\nu_\ell\,\text{anything})/\Gamma_{\text{total}}$ — Γ_{15}/Γ

VALUE	DOCUMENT ID		TECN	COMMENT
0.0038±0.0013 OUR AVERAGE	Error includes scale factor of 2.4.			
0.0033±0.0006	[1] ABAZOV	05O	D0	$p\overline{p}$ at 1.96 TeV
0.0074±0.0016	[2] BUSKULIC	97B	ALEP	$e^+e^- \to Z$
• • • We do not use the following data for averages, fits, limits, etc. • • •				
seen	[3] BUSKULIC	95B	ALEP	Repl. by BUSKULIC 97B

[1] Assumes $B(D_1 \to D^*\pi) = 1$, $B(D_1 \to D^*\pi^{\pm}) = 2/3$, and $B(b \to B) = 0.397$.
[2] BUSKULIC 97B assumes $B(D_1(2420) \to D^*\pi) = 1$, $B(D_1(2420) \to D^*\pi^{\pm}) = 2/3$, and $B(b \to B) = 0.378 \pm 0.022$.
[3] BUSKULIC 95B reports $f_B \times B(B \to \overline{D}_1(2420)^0\ell^+\nu_\ell\,\text{anything}) \times B(\overline{D}_1(2420)^0 \to \overline{D}^*(2010)^-\pi^+) = (2.04 \pm 0.58 \pm 0.34)10^{-3}$, where f_B is the production fraction for a single B charge state.

$[\Gamma(\overline{D}\pi\ell^+\nu_\ell\,\text{anything}) + \Gamma(\overline{D}^*\pi\ell^+\nu_\ell\,\text{anything})]/\Gamma_{\text{total}}$ — Γ_{16}/Γ

VALUE	DOCUMENT ID		TECN	COMMENT
0.026 ±0.005 OUR AVERAGE	Error includes scale factor of 1.5.			
0.0340±0.0052±0.0032	[1] ABREU	00R	DLPH	$e^+e^- \to Z$
0.0226±0.0029±0.0033	[2] BUSKULIC	97B	ALEP	$e^+e^- \to Z$

[1] Assumes no contribution from B_s and b baryons. Further assumes contributions from single pion ($D\pi$ and $D^*\pi$) states only, allowing isospin conservation to relate the relative π^0 and π^+ rates.
[2] BUSKULIC 97B assumes $B(b \to B) = 0.378 \pm 0.022$ and uses isospin invariance by assuming that all observed $D^0\pi^+$, $D^{*0}\pi^+$, $D^+\pi^-$, and $D^{*+}\pi^-$ are from D^{**} states. A correction has been applied to account for the production of B_s^0 and Λ_b^0.

$\Gamma(\overline{D}\pi\ell^+\nu_\ell\,\text{anything})/\Gamma_{\text{total}}$ — Γ_{17}/Γ

VALUE	DOCUMENT ID		TECN	COMMENT
0.0154±0.0061	ABREU	00R	DLPH	$e^+e^- \to Z$

$\Gamma(\overline{D}^*\pi\ell^+\nu_\ell\,\text{anything})/\Gamma_{\text{total}}$ — Γ_{18}/Γ

VALUE	DOCUMENT ID		TECN	COMMENT
0.0186±0.0038	ABREU	00R	DLPH	$e^+e^- \to Z$

$\Gamma(\overline{D}_2^*(2460)\ell^+\nu_\ell\,\text{anything})/\Gamma_{\text{total}}$ — Γ_{19}/Γ

VALUE	CL%	DOCUMENT ID		TECN	COMMENT
0.0044±0.0016		[1] ABAZOV	05O	D0	$p\overline{p}$ at 1.96 TeV
• • • We do not use the following data for averages, fits, limits, etc. • • •					
<0.0065	95	[2] BUSKULIC	97B	ALEP	$e^+e^- \to Z$
not seen		[3] BUSKULIC	95B	ALEP	$e^+e^- \to Z$

[1] Assumes $B(D_2^* \to D^*\pi^{\pm}) = 0.30 \pm 0.06$ and $B(b \to B) = 0.397$.
[2] A revised number based on BUSKULIC 97B which assumes $B(D_2^*(2460) \to D^*\pi^{\pm}) = 0.20$ and $B(b \to B) = 0.378 \pm 0.022$.
[3] BUSKULIC 95B reports $f_B \times B(B \to \overline{D}_2^*(2460)^0\ell^+\nu_\ell\,\text{anything}) \times B(\overline{D}_2^*(2460)^0 \to \overline{D}^*(2010)^-\pi^+) \leq 0.81 \times 10^{-3}$ at CL=95%, where f_B is the production fraction for a single B charge state.

$\dfrac{\Gamma(B \to \overline{D}_2^*(2460)\ell^+\nu_\ell\,\text{anything}) \times B(\overline{D}_2^*(2460) \to D^{*-}\pi^+)}{\Gamma(B \to \overline{D}_1(2420)\ell^+\nu_\ell\,\text{anything}) \times B(\overline{D}_1(2420) \to D^{*-}\pi^+)}$

VALUE	DOCUMENT ID		TECN	COMMENT
0.39±0.09±0.12	ABAZOV	05O	D0	$p\overline{p}$ at 1.96 TeV

$\Gamma(D^{*-}\pi^+\ell^+\nu_\ell\,\text{anything})/\Gamma_{\text{total}}$ — Γ_{20}/Γ

Includes resonant and nonresonant contributions.

VALUE (units 10^{-3})	DOCUMENT ID		TECN	COMMENT
10.0±2.7±2.1	[1] BUSKULIC	95B	ALEP	$e^+e^- \to Z$

[1] BUSKULIC 95B reports $f_B \times B(B \to \overline{D}^*(2010)^-\pi^+\ell^+\nu_\ell\,\text{anything}) = (3.7 \pm 1.0 \pm 0.7)10^{-3}$. Above value assumes $f_B = 0.37 \pm 0.03$.

$\Gamma(\overline{D}\pi^+\pi^-\ell^+\nu_\ell)/\Gamma(\overline{D}\ell^+\nu_\ell)$ — Γ_{21}/Γ_6

VALUE (units 10^{-2})	DOCUMENT ID		TECN	COMMENT
6.7±1.0±0.8	[1] LEES	16	BABR	$e^+e^- \to \Upsilon(4S)$

[1] Measurement used electrons and muons as leptons.

$\Gamma(\overline{D}^*\pi^+\pi^-\ell^+\nu_\ell)/\Gamma(\overline{D}^*\ell^+\nu_\ell)$ — Γ_{22}/Γ_{11}

VALUE (units 10^{-2})	DOCUMENT ID		TECN	COMMENT
1.9±0.5±0.4	[1] LEES	16	BABR	$e^+e^- \to \Upsilon(4S)$

[1] Measurement used electrons and muons as leptons.

$\Gamma(D_s^-\ell^+\nu_\ell\,\text{anything})/\Gamma_{\text{total}}$ — Γ_{23}/Γ

VALUE	CL%	DOCUMENT ID		TECN	COMMENT
<7 × 10^{-3}	90	[1] ALBRECHT	93E	ARG	$e^+e^- \to \Upsilon(4S)$

[1] ALBRECHT 93E reports < 0.012 from a measurement of $[\Gamma(B \to D_s^-\ell^+\nu_\ell\,\text{anything})/\Gamma_{\text{total}}] \times [B(D_s^+ \to \phi\pi^+)]$ assuming $B(D_s^+ \to \phi\pi^+) = 0.027$, which we rescale to our best (shown rounded) value $B(D_s^+ \to \phi\pi^+) = 4.5 \times 10^{-2}$.

$\Gamma(D_s^-\ell^+\nu_\ell K^+\,\text{anything})/\Gamma_{\text{total}}$ — Γ_{24}/Γ

VALUE	CL%	DOCUMENT ID		TECN	COMMENT
<5 × 10^{-3}	90	[1] ALBRECHT	93E	ARG	$e^+e^- \to \Upsilon(4S)$

[1] ALBRECHT 93E reports < 0.008 from a measurement of $[\Gamma(B \to D_s^-\ell^+\nu_\ell K^+\,\text{anything})/\Gamma_{\text{total}}] \times [B(D_s^+ \to \phi\pi^+)]$ assuming $B(D_s^+ \to \phi\pi^+) = 0.027$, which we rescale to our best (shown rounded) value $B(D_s^+ \to \phi\pi^+) = 4.5 \times 10^{-2}$.

Int. J. Mod. Phys. A 2026.41. Downloaded from www.worldscientific.com
by CALIFORNIA @ BERKELEY on 09/16/26. Re-use and distribution is strictly not permitted, except for Open Access articles.

$\Gamma(D_s^- \ell^+ \nu_\ell K^0 \text{anything})/\Gamma_{\text{total}}$ — Γ_{25}/Γ

VALUE	CL%	DOCUMENT ID		TECN	COMMENT
$<7\times10^{-3}$	90	[1] ALBRECHT	93E	ARG	$e^+e^- \to \Upsilon(4S)$

[1] ALBRECHT 93E reports <0.012 from a measurement of $[\Gamma(B \to D_s^- \ell^+ \nu_\ell K^0 \text{anything})/\Gamma_{\text{total}}] \times [B(D_s^+ \to \phi\pi^+)]$ assuming $B(D_s^+ \to \phi\pi^+) = 0.027$, which we rescale to our best (shown rounded) value $B(D_s^+ \to \phi\pi^+) = 4.5\times10^{-2}$.

$\Gamma(X_c \ell^+ \nu_\ell)/\Gamma_{\text{total}}$ — Γ_{26}/Γ

VALUE (%)	DOCUMENT ID		TECN	COMMENT
10.63±0.15 OUR EVALUATION	(Produced by HFLAV)			
10.29±0.19 OUR AVERAGE				
10.18±0.03±0.24	[1] LEES	17B	BABR	$e^+e^- \to \Upsilon(4S)$
10.44±0.19±0.22	[2] URQUIJO	07	BELL	$e^+e^- \to \Upsilon(4S)$
• • • We do not use the following data for averages, fits, limits, etc. • • •				
10.64±0.17±0.06	[3] AUBERT	10A	BABR	Repl. by LEES 17B
10.61±0.16±0.06	[4] AUBERT	04X	BABR	Repl. by AUBERT 10A

[1] The measurement is obtained from semileptonic decays to electrons $B \to X e\nu$, and using a theoretical model (GAMBINO 07, GAMBINO 11) to predict the contribution from $B \to X_u e\nu$. The result is averaged over $B^{\pm}$ and B^0 mesons, assuming lepton universality.

[2] Measured the independent B^+ and B^0 partial branching fractions with electron energy above 0.4 GeV.

[3] Obtained from a combined fit to the moments of observed spectra in inclusive $B \to X_c \ell^+ \nu_\ell$ decay.

[4] The semileptonic branching ratio, $|V_{cb}|$ and other heavy-quark parameters are determined from a simultaneous fit to moments of the hadronic-mass and lepton-energy distribution.

$\Gamma(X_u \ell^+ \nu_\ell)/\Gamma_{\text{total}}$ — Γ_{27}/Γ

VALUE (units 10^{-3})	DOCUMENT ID		TECN	COMMENT
1.88 ±0.27 OUR EVALUATION	(Produced by HFLAV)			
1.85 ±0.08 ±0.19	[1] CAO	21A	BELL	$e^+e^- \to \Upsilon(4S)$
$1.665\pm0.087^{+0.103}_{-0.094}$	[2] LEES	17B	BABR	$e^+e^- \to \Upsilon(4S)$
2.01 ±0.15 ±0.25	[3] LEES	12R	BABR	$e^+e^- \to \Upsilon(4S)$
2.53 ±0.24 ±0.24	[4] AUBERT,B	05X	BABR	$e^+e^- \to \Upsilon(4S)$
2.80 ±0.52 ±0.41	[5] LIMOSANI	05	BELL	$e^+e^- \to \Upsilon(4S)$
1.77 ±0.29 ±0.38	[6] BORNHEIM	02	CLE2	$e^+e^- \to \Upsilon(4S)$
• • • We do not use the following data for averages, fits, limits, etc. • • •				
1.39 ±0.14 ±0.22	[7] CAO	23	BELL	$e^+e^- \to \Upsilon(4S)$
1.963±0.173±0.159	[8] URQUIJO	10	BELL	Repl. by CAO 21A
1.18 ±0.09 ±0.07	[9] AUBERT	08AS	BABR	Repl. by LEES 12R
$2.27 \pm0.26 ^{+0.37}_{-0.33}$	[10] AUBERT	06H	BABR	Repl. by LEES 17B
2.24 ±0.27 ±0.47	[11,12] AUBERT	04I	BABR	Repl. by AUBERT,B 05X

[1] Measures several partial branching fractions in different phase space regions. The most inclusive result of the full branching fraction is obtained in the region for lepton energy in B rest frame $E^*_\ell > 1$ GeV, where the measured partial branching fraction is $\Delta B = (1.59 \pm 0.07 \pm 0.16)\times10^{-3}$. The acceptance in that region is reported to be 0.86.

[2] Obtained from the partial rate $\Delta B = (1.554 \pm 0.082^{+0.095}_{-0.086})\times10^{-3}$ for the electron momentum interval of 0.8–2.7 GeV/c based on GGOU1 method ($X_c \ell\nu$, m_c constraint fit of SF parameters).

[3] Measures several partial branching fractions in different phase space regions. The most precise result on the full branching fraction is obtained in the region for lepton momentum in B rest frame $p^*_\ell > 1$ GeV/c, where the measured partial branching fraction is $\Delta B = (1.80 \pm 0.13 \pm 0.15)\times10^{-3}$. The acceptance in that region is reported in a private communication by the Authors to be 0.894. The corresponding $|V_{ub}|$ from the BLNP method is $(4.28 \pm 0.15 \pm 0.18 \pm 0.19)\times10^{-3}$, where the last uncertainty comes from theoretical prediction.

[4] Determined from the partial rate $\Delta B = (4.41\pm0.42\pm0.42)\times10^{-4}$ measured for electron energy > 2 GeV and hadronic mass squared < 3.5 GeV^2, and calculated acceptance 0.174 in that region. The V_{ub} is measured as $(4.41 \pm 0.30^{+0.65}_{-0.47} \pm 0.28)\times10^{-3}$.

[5] Uses electrons in the momentum interval 1.9–2.6 GeV/c in the center-of-mass frame. The V_{ub} is found to be $(5.08 \pm 0.47^{+0.49}_{-0.48})\times10^{-3}$.

[6] BORNHEIM 02 uses the observed yield of leptons from semileptonic B decays in the end-point momentum interval 2.2–2.6 GeV/c with recent CLEO-2 data on $B \to X_s\gamma$. The V_{ub} is found to be $(4.08 \pm 0.34 \pm 0.53)\times10^{-3}$.

[7] Measurement requires lepton energy $E^*_\ell > 1$ GeV in the B rest frame. It is a part of the inclusive and exclusive $|V_{ub}|$ determination.

[8] Uses a multivariate analysis method and requires lepton momentum in the B rest frame, $p^*_\ell > 1.0$ GeV/c.

[9] Measures several partial branching fractions in different phase space regions. The most precise result is obtained in the region for hadronic mass $M_X < 1.55$ GeV/c^2, and is $\Delta B = (1.18 \pm 0.09 \pm 0.07)\times10^{-3}$. The corresponding $|V_{ub}|$ from the BLNP method is $(4.27 \pm 0.16 \pm 0.13 \pm 0.30)\times10^{-3}$, where the last uncertainty comes from the theoretical prediction of the partial rate in the given phase-space region.

[10] Obtained from the partial rate $\Delta B = (0.572 \pm 0.041 \pm 0.065)\times10^{-3}$ for the electron momentum interval of 2.0–2.6 GeV/c based on BLNP method.

[11] Used BaBar measurement of Semileptonic branching fraction $B(B \to X\ell\nu_\ell) = (10.87 \pm 0.18 \pm 0.30)\%$ to convert the ratio of rates to branching fraction.

[12] The third error includes the systematics and theoretical errors summed in quadrature.

$\Gamma(X_u \ell^+ \nu_\ell)/\Gamma(\ell^+ \nu_\ell \text{anything})$ — Γ_{27}/Γ_3

ℓ denotes e or μ, not the sum. These experiments measure this ratio in very limited momentum intervals.

VALUE (units 10^{-2})	CL%	EVTS	DOCUMENT ID		TECN	COMMENT
1.82±0.19 OUR AVERAGE						
1.78±0.15±0.14			[1] HOHMANN	25	BELL	$e^+e^- \to \Upsilon(4S)$
2.06±0.25±0.42			[2] AUBERT	04I	BABR	$e^+e^- \to \Upsilon(4S)$
• • • We do not use the following data for averages, fits, limits, etc. • • •						
			[3] ALBRECHT	94C	ARG	$e^+e^- \to \Upsilon(4S)$
		107	[4] BARTELT	93B	CLE2	$e^+e^- \to \Upsilon(4S)$
		77	[5] ALBRECHT	91C	ARG	$e^+e^- \to \Upsilon(4S)$
		41	[6] ALBRECHT	90	ARG	$e^+e^- \to \Upsilon(4S)$
		76	[7] FULTON	90	CLEO	$e^+e^- \to \Upsilon(4S)$
<4.0	90		[8] BEHRENDS	87	CLEO	$e^+e^- \to \Upsilon(4S)$
<4.0	90		CHEN	84	CLEO	Direct e at $\Upsilon(4S)$
<5.5	90		KLOPFEN...	83B	CUSB	Direct e at $\Upsilon(4S)$

[1] Derived using the ratio of $\Delta B(B^- \to X_u \ell\nu)/\Delta B(B^- \to X_c \ell\nu) = (1.99 \pm 0.17 \pm 0.16)\times10^{-2}$ with the lepton $p_\ell > 1$ GeV, which covers approximately 86% and 78% of the $B(B^- \to X_u \ell\nu)$ and $B(B^- \to X_c \ell\nu)$ phase space.

[2] The third error includes the systematics and theoretical errors summed in quadrature.

[3] ALBRECHT 94C find $\Gamma(b \to c)/\Gamma(b \to \text{all}) = 0.99 \pm 0.02 \pm 0.04$.

[4] BARTELT 93B (CLEO II) measures an excess of $107 \pm 15 \pm 11$ leptons in the lepton momentum interval 2.3–2.6 GeV/c which is attributed to $b \to u\ell\nu_\ell$. This corresponds to a model-dependent partial branching ratio ΔB_{ub} between $(1.15 \pm 0.16 \pm 0.15)\times10^{-4}$, as evaluated using the KS model (KOERNER 88), and $(1.54 \pm 0.22 \pm 0.20)\times10^{-4}$ using the ACCMM model (ARTUSO 93). The corresponding values of $|V_{ub}|/|V_{cb}|$ are 0.056 ± 0.006 and 0.076 ± 0.008, respectively.

[5] ALBRECHT 91C result supersedes ALBRECHT 90. Two events are fully reconstructed providing evidence for the $b \to u$ transition. Using the model of ALTARELLI 82, they obtain $|V_{ub}/V_{cb}| = 0.11 \pm 0.012$ from 77 leptons in the 2.3–2.6 GeV momentum range.

[6] ALBRECHT 90 observes 41 ± 10 excess e and μ (lepton) events in the momentum interval $p = 2.3$–2.6 GeV signaling the presence of the $b \to u$ transition. The events correspond to a model-dependent measurement of $|V_{ub}/V_{cb}| = 0.10 \pm 0.01$.

[7] FULTON 90 observe 76 ± 20 excess e and μ (lepton) events in the momentum interval $p = 2.4$–2.6 GeV signaling the presence of the $b \to u$ transition. The average branching ratio, $(1.8 \pm 0.4 \pm 0.3)\times10^{-4}$, corresponds to a model-dependent measurement of approximately $|V_{ub}/V_{cb}| = 0.1$ using $B(b \to c\ell\nu) = 10.2 \pm 0.2 \pm 0.7\%$.

[8] The quoted possible limits range from 0.018 to 0.04 for the ratio, depending on which model or momentum range is chosen. We select the most conservative limit they have calculated. This corresponds to a limit on $|V_{ub}|/|V_{cb}| < 0.20$. While the endpoint technique employed is more robust than their previous results in CHEN 84, these results do not provide a numerical improvement in the limit.

$\Gamma(X_u e^+ \nu_e)/\Gamma_{\text{total}}$ — Γ_{28}/Γ

Requires $E^*_e > 1$ GeV, where E^*_e is e^+ energy in B rest frame.

VALUE (units 10^{-3})	DOCUMENT ID		TECN	COMMENT
1.57±0.10±0.16	[1] CAO	21A	BELL	$e^+e^- \to \Upsilon(4S)$

[1] The correlation of 53% with $B(B \to X_u \mu^+ \nu_\mu)$(letpon energy in B rest frame $E^*_{\mu^+} > 1$ GeV) is reported.

$\Gamma(X_u \mu^+ \nu_\mu)/\Gamma_{\text{total}}$ — Γ_{29}/Γ

Requires $E^*_\mu > 1$ GeV, where E^*_μ is μ^+ energy in B rest frame.

VALUE (units 10^{-3})	DOCUMENT ID		TECN	COMMENT
1.62±0.10±0.18	[1] CAO	21A	BELL	$e^+e^- \to \Upsilon(4S)$

[1] The correlation of 53% with $B(B \to X_u e^+ \nu_e)$(letpon energy in B rest frame $E^*_{e^+} > 1$ GeV) is reported.

$\Gamma(K^+ \ell^+ \nu_\ell \text{anything})/\Gamma(\ell^+ \nu_\ell \text{anything})$ — Γ_{30}/Γ_3

ℓ denotes e or μ, not the sum.

VALUE	DOCUMENT ID		TECN	COMMENT
0.58 ±0.05 OUR AVERAGE				
0.594±0.021±0.056	ALBRECHT	94C	ARG	$e^+e^- \to \Upsilon(4S)$
0.54 ±0.07 ±0.06	[1] ALAM	87B	CLEO	$e^+e^- \to \Upsilon(4S)$

[1] ALAM 87B measurement relies on lepton-kaon correlations.

$\Gamma(K^- \ell^+ \nu_\ell \text{anything})/\Gamma(\ell^+ \nu_\ell \text{anything})$ — Γ_{31}/Γ_3

ℓ denotes e or μ, not the sum.

VALUE	DOCUMENT ID		TECN	COMMENT
0.092±0.035 OUR AVERAGE				
0.086±0.011±0.044	ALBRECHT	94C	ARG	$e^+e^- \to \Upsilon(4S)$
0.10 ±0.05 ±0.02	[1] ALAM	87B	CLEO	$e^+e^- \to \Upsilon(4S)$

[1] ALAM 87B measurement relies on lepton-kaon correlations.

$\Gamma(K^0/\overline{K}^0 \ell^+ \nu_\ell \text{anything})/\Gamma(\ell^+ \nu_\ell \text{anything})$ — Γ_{32}/Γ_3

ℓ denotes e or μ, not the sum. Sum over K^0 and $\overline{K}^0$ states.

VALUE	DOCUMENT ID		TECN	COMMENT
0.42 ±0.05 OUR AVERAGE				
0.452±0.038±0.056	[1] ALBRECHT	94C	ARG	$e^+e^- \to \Upsilon(4S)$
0.39 ±0.06 ±0.04	[2] ALAM	87B	CLEO	$e^+e^- \to \Upsilon(4S)$

[1] ALBRECHT 94C assume a $K^0/\overline{K}^0$ multiplicity twice that of K^0_S.

[2] ALAM 87B measurement relies on lepton-kaon correlations.

Int. J. Mod. Phys. A 2026.41. Downloaded from www.worldscientific.com by UNIVERSITY OF CALIFORNIA @ BERKELEY on 09/16/26. Re-use and distribution is strictly not permitted, except for Open Access articles.

$\Gamma(\overline{D}\tau^+\nu_\tau)/\Gamma(\overline{D}\ell^+\nu_\ell)$ — Γ_{33}/Γ_6

VALUE (units 10^{-2})	DOCUMENT ID		TECN	COMMENT
34.7 ± 2.5 OUR EVALUATION	(Produced by HFLAV)			
34.3 ± 2.7 OUR AVERAGE				
33.5 ± 5.2	[1] AAIJ	25G	LHCB	pp at 7, 8, 13 TeV
30.7 ± 3.7±1.6	[2] CARIA	20	BELL	$e^+e^- \to \Upsilon(4S)$
37.5 ± 6.4±2.6	[3,4] HUSCHLE	15	BELL	$e^+e^- \to \Upsilon(4S)$
44.0 ± 5.8±4.2	[3,4] LEES	12D	BABR	$e^+e^- \to \Upsilon(4S)$
• • • We do not use the following data for averages, fits, limits, etc. • • •				
4.16±11.7±5.2	[3] AUBERT	08N	BABR	Repl. by LEES 12D

[1] Combines measurement in $B^0 \to D^-\tau^+\nu_\tau$ with $\tau^+ \to \mu^+\nu_\mu\overline{\nu}_\tau$ with results from AAIJ 23AR and AAIJ 23W. Simultaneously extracts also $B(B^0 \to D^*(2010)^-\tau^+\nu_\tau)/B(B^0 \to D^*(2010)^-\mu^+\nu_\mu)$ and reports correlation factor -0.30.

[2] The tag-side B meson is reconstructed in a semileptonic decay mode and the signal-side τ is reconstructed in a purely leptonic decay. The Belle combination of HUSCHLE 15 and CARIA 20 yields $R(D) = (32.6 \pm 3.4) \times 10^{-2}$.

[3] Uses a fully reconstructed B meson as a tag on the recoil side.

[4] Uses $\tau^+ \to e^+\nu_e\overline{\nu}_\tau$ and $\tau^+ \to \mu^+\nu_\mu\overline{\nu}_\tau$ and e^+ or μ^+ as ℓ^+. Obtained from simultaneous fit to B+ and B0 assuming isospin symmetry.

$\Gamma(\overline{D}^*\tau^+\nu_\tau)/\Gamma(\overline{D}^*\ell^+\nu_\ell)$ — Γ_{34}/Γ_{11}

VALUE (units 10^{-2})	DOCUMENT ID		TECN	COMMENT
28.8±1.2 OUR EVALUATION	(Produced by HFLAV)			
28.8±1.2 OUR AVERAGE				
27.9±1.9	[1] AAIJ	25G	LHCB	pp at 7, 8, 13 TeV
$26.2^{+4.1}_{-3.9}{}^{+3.5}_{-3.2}$	[2] ADACHI	24O	BELL	$e^+e^- \to \Upsilon(4S)$
28.3±1.8±1.4	[3] CARIA	20	BELL	$e^+e^- \to \Upsilon(4S)$
$27.0 \pm 3.5^{+2.8}_{-2.5}$	[4] HIROSE	17	BELL	$e^+e^- \to \Upsilon(4S)$
29.3±3.8±1.5	[5] HUSCHLE	15	BELL	$e^+e^- \to \Upsilon(4S)$
33.2±2.4±1.8	[5] LEES	12D	BABR	$e^+e^- \to \Upsilon(4S)$
• • • We do not use the following data for averages, fits, limits, etc. • • •				
28.1±1.8±2.4	[6] AAIJ	23AR	LHCB	Repl. by AAIJ 25G
29.7±5.6±1.8	[7] AUBERT	08N	BABR	Repl. by LEES 12D

[1] Combines measurement in $B^0 \to D^*(2010)^-\tau^+\nu_\tau$ with $\tau^+ \to \mu^+\nu_\mu\overline{\nu}_\tau$ with results from AAIJ 23AR and AAIJ 23W. Simultaneously extracts also $B(B^0 \to D^-\tau^+\nu_\tau)/B(B^0 \to D^-\mu^+\nu_\mu)$ and reports correlation factor -0.30.

[2] Uses leptonic τ decays and a fully reconstructed B meson in hadronic final states as a tag on the recoil side.

[3] The tag-side B meson is reconstructed in a semileptonic decay mode and the signal-side τ is reconstructed in a purely leptonic decay. The Belle combination of HUSCHLE 15, HIROSE 17, and CARIA 20 yields $R(D^*) = 0.238 \pm 0.018$.

[4] Uses a fully reconstructed B meson as a tag on the recoil side.

[5] Uses $\tau^+ \to e^+\nu_e\overline{\nu}_\tau$ and $\tau^+ \to \mu^+\nu_\mu\overline{\nu}_\tau$ and e^+ or μ^+ as ℓ^+. Obtained from simultaneous fit to B+ and B0 assuming isospin symmetry. Uses a fully reconstructed B meson as a tag on the recoil side.

[6] Uses $\tau^+ \to \mu^+\nu_\mu\overline{\nu}_\tau$ and μ^+ as ℓ^+. The measurement combines fully reconstructed D^{*+} sample with sample where only D^0 from D^* decays is reconstructed.

[7] Uses a fully reconstructed B meson as a tag on the recoil side. The results are normalized to the B^+ decay rate.

$\langle n_c \rangle$

VALUE	DOCUMENT ID		TECN	COMMENT
1.10±0.05	[1] GIBBONS	97B	CLE2	$e^+e^- \to \Upsilon(4S)$
• • • We do not use the following data for averages, fits, limits, etc. • • •				
0.98±0.16±0.12	[2] ALAM	87B	CLEO	$e^+e^- \to \Upsilon(4S)$

[1] GIBBONS 97B from charm counting using $B(D_s^+ \to \phi\pi) = 0.036 \pm 0.009$ and $B(\Lambda_c^+ \to pK^-\pi^+) = 0.044 \pm 0.006$.

[2] From the difference between K^- and K^+ widths. ALAM 87B measurement relies on lepton-kaon correlations. It does not consider the possibility of $B\overline{B}$ mixing. We have thus removed it from the average.

$\Gamma(D^{\pm}\text{anything})/\Gamma_{\text{total}}$ — Γ_{35}/Γ

VALUE	EVTS	DOCUMENT ID		TECN	COMMENT
0.233±0.012 OUR AVERAGE					
0.232±0.012±0.004		[1] GIBBONS	97B	CLE2	$e^+e^- \to \Upsilon(4S)$
0.243±0.038±0.004		[2] BORTOLETTO	92	CLEO	$e^+e^- \to \Upsilon(4S)$
0.224±0.052±0.003		[3] ALBRECHT	91H	ARG	$e^+e^- \to \Upsilon(4S)$
• • • We do not use the following data for averages, fits, limits, etc. • • •					
0.204±0.048±0.003	20k	[4] BORTOLETTO	87	CLEO	Sup. by BORTOLETTO 92

[1] GIBBONS 97B reports $[\Gamma(B \to D^{\pm}\text{anything})/\Gamma_{\text{total}}] \times [B(D^+ \to K^-2\pi^+)] = 0.0216 \pm 0.0008 \pm 0.00082$ which we divide by our best (shown rounded) value $B(D^+ \to K^-2\pi^+) = (9.31 \pm 0.14) \times 10^{-2}$. Our first error is their experiment's error and our second error is the systematic error from using our best (shown rounded) value.

[2] BORTOLETTO 92 reports $[\Gamma(B \to D^{\pm}\text{anything})/\Gamma_{\text{total}}] \times [B(D^+ \to K^-2\pi^+)] = 0.0226 \pm 0.0030 \pm 0.0018$ which we divide by our best (shown rounded) value $B(D^+ \to K^-2\pi^+) = (9.31 \pm 0.14) \times 10^{-2}$. Our first error is their experiment's error and our second error is the systematic error from using our best (shown rounded) value.

[3] ALBRECHT 91H reports $[\Gamma(B \to D^{\pm}\text{anything})/\Gamma_{\text{total}}] \times [B(D^+ \to K^-2\pi^+)] = 0.0209 \pm 0.0027 \pm 0.0040$ which we divide by our best (shown rounded) value $B(D^+ \to K^-2\pi^+) = (9.31 \pm 0.14) \times 10^{-2}$. Our first error is their experiment's error and our second error is the systematic error from using our best (shown rounded) value.

[4] BORTOLETTO 87 reports $[\Gamma(B \to D^{\pm}\text{anything})/\Gamma_{\text{total}}] \times [B(D^+ \to K^-2\pi^+)] = 0.019 \pm 0.004 \pm 0.002$ which we divide by our best (shown rounded) value $B(D^+ \to K^-2\pi^+) = (9.31 \pm 0.14) \times 10^{-2}$. Our first error is their experiment's error and our second error is the systematic error from using our best (shown rounded) value.

$\Gamma(D^0/\overline{D}^0\text{anything})/\Gamma_{\text{total}}$ — Γ_{36}/Γ

VALUE	EVTS	DOCUMENT ID		TECN	COMMENT
0.646 ±0.020 OUR AVERAGE		Error includes scale factor of 1.5. See the ideogram below.			
0.6663±0.0004±0.0177		ZHUKOVA	23	BELL	$e^+e^- \to \Upsilon(4S)$
0.638 ±0.024 ±0.005		[1] GIBBONS	97B	CLE2	$e^+e^- \to \Upsilon(4S)$
0.592 ±0.047 ±0.005		[2] BORTOLETTO	92	CLEO	$e^+e^- \to \Upsilon(4S)$
0.493 ±0.074 ±0.004		[3] ALBRECHT	91H	ARG	$e^+e^- \to \Upsilon(4S)$
• • • We do not use the following data for averages, fits, limits, etc. • • •					
0.534 ±0.066 ±0.004	21k	[4] BORTOLETTO	87	CLEO	$e^+e^- \to \Upsilon(4S)$
0.610 ±0.183 ±0.005		[5] GREEN	83	CLEO	Repl. by BORTOLETTO 87

[1] GIBBONS 97B reports $[\Gamma(B \to D^0/\overline{D}^0\text{anything})/\Gamma_{\text{total}}] \times [B(D^0 \to K^-\pi^+)] = 0.0251 \pm 0.0006 \pm 0.00075$ which we divide by our best (shown rounded) value $B(D^0 \to K^-\pi^+) = (3.936 \pm 0.030) \times 10^{-2}$. Our first error is their experiment's error and our second error is the systematic error from using our best (shown rounded) value.

[2] BORTOLETTO 92 reports $[\Gamma(B \to D^0/\overline{D}^0\text{anything})/\Gamma_{\text{total}}] \times [B(D^0 \to K^-\pi^+)] = 0.0233 \pm 0.0012 \pm 0.0014$ which we divide by our best (shown rounded) value $B(D^0 \to K^-\pi^+) = (3.936 \pm 0.030) \times 10^{-2}$. Our first error is their experiment's error and our second error is the systematic error from using our best (shown rounded) value.

[3] ALBRECHT 91H reports $[\Gamma(B \to D^0/\overline{D}^0\text{anything})/\Gamma_{\text{total}}] \times [B(D^0 \to K^-\pi^+)] = 0.0194 \pm 0.0015 \pm 0.0025$ which we divide by our best (shown rounded) value $B(D^0 \to K^-\pi^+) = (3.936 \pm 0.030) \times 10^{-2}$. Our first error is their experiment's error and our second error is the systematic error from using our best (shown rounded) value.

[4] BORTOLETTO 87 reports $[\Gamma(B \to D^0/\overline{D}^0\text{anything})/\Gamma_{\text{total}}] \times [B(D^0 \to K^-\pi^+)] = 0.0210 \pm 0.0015 \pm 0.0021$ which we divide by our best (shown rounded) value $B(D^0 \to K^-\pi^+) = (3.936 \pm 0.030) \times 10^{-2}$. Our first error is their experiment's error and our second error is the systematic error from using our best (shown rounded) value.

[5] GREEN 83 reports $[\Gamma(B \to D^0/\overline{D}^0\text{anything})/\Gamma_{\text{total}}] \times [B(D^0 \to K^-\pi^+)] = 0.024 \pm 0.006 \pm 0.004$ which we divide by our best (shown rounded) value $B(D^0 \to K^-\pi^+) = (3.936 \pm 0.030) \times 10^{-2}$. Our first error is their experiment's error and our second error is the systematic error from using our best (shown rounded) value.

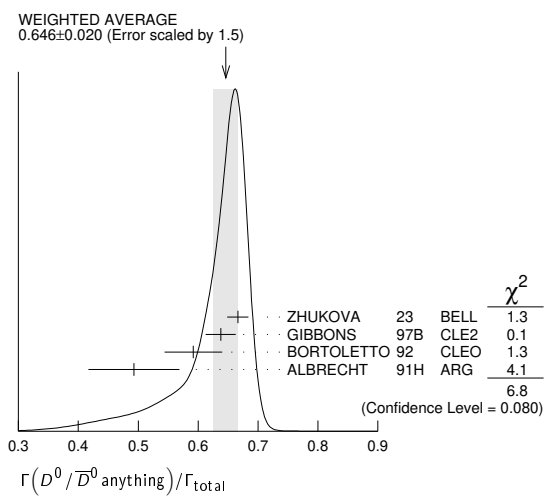

$\Gamma(D^-\ell^+\nu_\ell\text{anything})/\Gamma(\overline{D}^0\ell^+\nu_\ell\text{anything})$ — Γ_4/Γ_5

VALUE	DOCUMENT ID		TECN	COMMENT
0.359±0.006±0.009	[1] AAIJ	19AD	LHCB	pp at 13 TeV

[1] AAIJ 19AD uses $D^0 \to K^-\pi^+$ and $D^+ \to K^-\pi^+\pi^+$ modes.

$\Gamma(D^*(2010)^{\pm}\text{anything})/\Gamma_{\text{total}}$ — Γ_{37}/Γ

VALUE	EVTS	DOCUMENT ID		TECN	COMMENT
0.225±0.015 OUR AVERAGE					
0.247±0.019±0.01		[1] GIBBONS	97B	CLE2	$e^+e^- \to \Upsilon(4S)$
0.205±0.019±0.007		[2] ALBRECHT	96D	ARG	$e^+e^- \to \Upsilon(4S)$
0.230±0.028±0.009		[3] BORTOLETTO	92	CLEO	$e^+e^- \to \Upsilon(4S)$
• • • We do not use the following data for averages, fits, limits, etc. • • •					
0.283±0.053±0.002		[4] ALBRECHT	91H	ARG	Sup. by ALBRECHT 96D
$0.22 \pm 0.04\ ^{+0.07}_{-0.04}$	5200	[5] BORTOLETTO	87	CLEO	$e^+e^- \to \Upsilon(4S)$
$0.27 \pm 0.06\ ^{+0.08}_{-0.06}$	510	[6] CSORNA	85	CLEO	Repl. by BORTOLETTO 87

[1] GIBBONS 97B reports $B(B \to D^*(2010)^+\text{anything}) = 0.239 \pm 0.015 \pm 0.014 \pm 0.009$ using CLEO measured D and D^* branching fractions. We rescale to our PDG 96 values of D and D^* branching ratios. Our first error is their experiment's error and our second error is the systematic error from using our best value.

[2] ALBRECHT 96D reports $B(B \to D^*(2010)^+\text{anything})$ 0.196 ± 0.019 using CLEO measured $B(D^*(2010)^+ \to D^0\pi^+) = 0.681 \pm 0.01 \pm 0.013$, $B(D^0 \to K^-\pi^+) = 0.0401 \pm 0.0014$, $B(D^0 \to K^-\pi^+\pi^+\pi^-) = 0.081 \pm 0.005$., We rescale to our PDG 96 values of D and D^* branching ratios. Our first error is their experiment's error and our second error is the systematic error from using our best value.

[3] BORTOLETTO 92 reports $B(B \to D^*(2010)^+\text{anything}) = 0.25 \pm 0.03 \pm 0.04$ using MARK II $B(D^*(2010)^+ \to D^0\pi^+) = 0.57 \pm 0.06$ and $B(D^0 \to K^-\pi^+) = 0.042 \pm$

Int. J. Mod. Phys. A 2026.41. Downloaded from www.worldscientific.com
by LIFORNIA @ BERKELEY on 09/16/26. Re-use and distribution is strictly not permitted, except for Open Access articles.

0.008. We rescale to our PDG 96 values of D and D^* branching ratios. Our first error is their experiment's error and our second error is the systematic error from using our best value.

[4] ALBRECHT 91H reports 0.348 ± 0.060 ± 0.035 from a measurement of $[\Gamma(B \to D^*(2010)^{\pm}\text{anything})/\Gamma_{\text{total}}] \times [B(D^*(2010)^+ \to D^0\pi^+)]$ assuming $B(D^*(2010)^+ \to D^0\pi^+) = 0.55 \pm 0.04$, which we rescale to our best (shown rounded) value $B(D^*(2010)^+ \to D^0\pi^+) = (67.7 \pm 0.5) \times 10^{-2}$. Our first error is their experiment's error and our second error is the systematic error from using our best (shown rounded) value. Uses the PDG 90 $B(D^0 \to K^-\pi^+) = 0.0371 \pm 0.0025$.

[5] BORTOLETTO 87 uses old MARK III (BALTRUSAITIS 86E) branching ratios $B(D^0 \to K^-\pi^+) = 0.056 \pm 0.004 \pm 0.003$ and also assumes $B(D^*(2010)^+ \to D^0\pi^+) = 0.60^{+0.08}_{-0.15}$. The product branching ratio for $B(B \to D^*(2010)^+)\, B(D^*(2010)^+ \to D^0\pi^+)$ is $0.13 \pm 0.02 \pm 0.012$. Superseded by BORTOLETTO 92.

[6] $V-A$ momentum spectrum used to extrapolate below $p = 1$ GeV. We correct the value assuming $B(D^0 \to K^-\pi^+) = 0.042 \pm 0.006$ and $B(D^{*+} \to D^0\pi^+) = 0.6^{+0.08}_{-0.15}$. The product branching fraction is $B(B \to D^{*+}X) \cdot B(D^{*+} \to \pi^+ D^0) \cdot B(D^0 \to K^-\pi^+) = (68 \pm 15 \pm 9) \times 10^{-4}$.

$\Gamma(\overline{D}^*(2007)^0\,\text{anything})/\Gamma_{\text{total}}$ — Γ_{38}/Γ

VALUE	DOCUMENT ID		TECN	COMMENT
0.260±0.023±0.015	[1] GIBBONS	97B	CLE2	$e^+e^- \to \Upsilon(4S)$

[1] GIBBONS 97B reports $B(B \to D^*(2007)^0\text{anything})$ 0.247 ± 0.012 ± 0.018 ± 0.018 using CLEO measured D and D^* branching fractions. We rescale to our PDG 96 values of D and D^* branching ratios. Our first error is their experiment's error and our second error is the systematic error from using our best value.

$\Gamma(D_s^{\pm}\text{anything})/\Gamma_{\text{total}}$ — Γ_{39}/Γ

VALUE	EVTS	DOCUMENT ID		TECN	COMMENT
0.106 ±0.006 OUR AVERAGE		Error includes scale factor of 1.7. See the ideogram below.			
0.1128±0.0003±0.0043		ZHUKOVA	23	BELL	$e^+e^- \to \Upsilon(4S)$
0.089 ±0.010 ±0.008		[1] ARTUSO	05B	CLE2	$e^+e^- \to \Upsilon(5S)$
0.087 ±0.005 ±0.008		[2] AUBERT	02G	BABR	$e^+e^- \to \Upsilon(4S)$
0.065 ±0.011 ±0.006		[3] ALBRECHT	92G	ARG	$e^+e^- \to \Upsilon(4S)$
0.068 ±0.010 ±0.006	257	[4] BORTOLETTO	90	CLEO	$e^+e^- \to \Upsilon(4S)$
0.085 ±0.022 ±0.008		[5] HAAS	86	CLEO	$e^+e^- \to \Upsilon(4S)$
• • • We do not use the following data for averages, fits, limits, etc. • • •					
0.094 ±0.007 ±0.008		[6] GIBAUT	96	CLE2	Repl. by ARTUSO 05B
0.094 ±0.024 ±0.008		[7] ALBRECHT	87H	ARG	$e^+e^- \to \Upsilon(4S)$

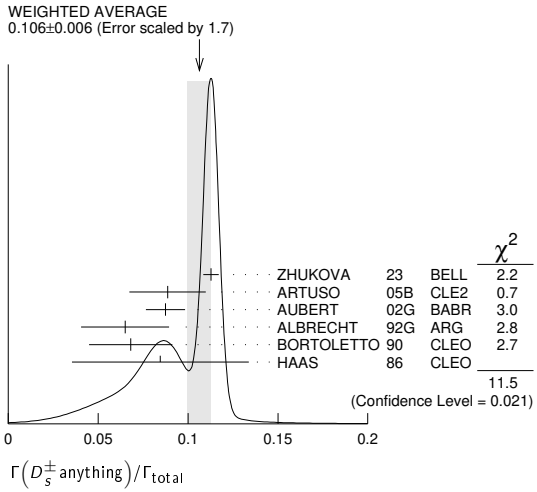

[1] ARTUSO 05B reports 0.0905 ± 0.0025 ± 0.0140 from a measurement of $[\Gamma(B \to D_s^{\pm}\text{anything})/\Gamma_{\text{total}}] \times [B(D_s^+ \to \phi\pi^+)]$ assuming $B(D_s^+ \to \phi\pi^+) = (4.4 \pm 0.5) \times 10^{-2}$, which we rescale to our best (shown rounded) value $B(D_s^+ \to \phi\pi^+) = (4.5 \pm 0.4) \times 10^{-2}$. Our first error is their experiment's error and our second error is the systematic error from using our best (shown rounded) value.

[2] AUBERT 02G reports $[\Gamma(B \to D_s^{\pm}\text{anything})/\Gamma_{\text{total}}] \times [B(D_s^+ \to \phi\pi^+)] = 0.00393 \pm 0.00007 \pm 0.00021$ which we divide by our best (shown rounded) value $B(D_s^+ \to \phi\pi^+) = (4.5 \pm 0.4) \times 10^{-2}$. Our first error is their experiment's error and our second error is the systematic error from using our best (shown rounded) value.

[3] ALBRECHT 92G reports $[\Gamma(B \to D_s^{\pm}\text{anything})/\Gamma_{\text{total}}] \times [B(D_s^+ \to \phi\pi^+)] = 0.00292 \pm 0.00039 \pm 0.00031$ which we divide by our best (shown rounded) value $B(D_s^+ \to \phi\pi^+) = (4.5 \pm 0.4) \times 10^{-2}$. Our first error is their experiment's error and our second error is the systematic error from using our best (shown rounded) value.

[4] BORTOLETTO 90 reports $[\Gamma(B \to D_s^{\pm}\text{anything})/\Gamma_{\text{total}}] \times [B(D_s^+ \to \phi\pi^+)] = 0.00306 \pm 0.00047$ which we divide by our best (shown rounded) value $B(D_s^+ \to \phi\pi^+) = (4.5 \pm 0.4) \times 10^{-2}$. Our first error is their experiment's error and our second error is the systematic error from using our best (shown rounded) value.

[5] HAAS 86 reports $[\Gamma(B \to D_s^{\pm}\text{anything})/\Gamma_{\text{total}}] \times [B(D_s^+ \to \phi\pi^+)] = 0.0038 \pm 0.0010$ which we divide by our best (shown rounded) value $B(D_s^+ \to \phi\pi^+) = (4.5 \pm 0.4) \times 10^{-2}$. Our first error is their experiment's error and our second error is the systematic error from using our best (shown rounded) value. 64 ± 22% decays are 2-body.

[6] GIBAUT 96 reports 0.1211 ± 0.0039 ± 0.0088 from a measurement of $[\Gamma(B \to D_s^{\pm}\text{anything})/\Gamma_{\text{total}}] \times [B(D_s^+ \to \phi\pi^+)]$ assuming $B(D_s^+ \to \phi\pi^+) = 0.035$, which we rescale to our best (shown rounded) value $B(D_s^+ \to \phi\pi^+) = (4.5 \pm 0.4) \times 10^{-2}$. Our first error is their experiment's error and our second error is the systematic error from using our best (shown rounded) value.

[7] ALBRECHT 87H reports $[\Gamma(B \to D_s^{\pm}\text{anything})/\Gamma_{\text{total}}] \times [B(D_s^+ \to \phi\pi^+)] = 0.0042 \pm 0.0009 \pm 0.0006$ which we divide by our best (shown rounded) value $B(D_s^+ \to \phi\pi^+) = (4.5 \pm 0.4) \times 10^{-2}$. Our first error is their experiment's error and our second error is the systematic error from using our best (shown rounded) value. 46 ± 16% of $B \to D_s X$ decays are 2-body. Superseded by ALBRECHT 92G.

$\Gamma(D_s^{*\pm}\text{anything})/\Gamma_{\text{total}}$ — Γ_{40}/Γ

VALUE	DOCUMENT ID		TECN	COMMENT
0.063±0.009±0.006	[1] AUBERT	02G	BABR	$e^+e^- \to \Upsilon(4S)$

[1] AUBERT 02G reports $[\Gamma(B \to D_s^{*\pm}\text{anything})/\Gamma_{\text{total}}] \times [B(D_s^+ \to \phi\pi^+)] = 0.00284 \pm 0.00029 \pm 0.00025$ which we divide by our best (shown rounded) value $B(D_s^+ \to \phi\pi^+) = (4.5 \pm 0.4) \times 10^{-2}$. Our first error is their experiment's error and our second error is the systematic error from using our best (shown rounded) value.

$\Gamma(D_s^{*\pm}\overline{D}^{(*)})/\Gamma(D_s^{*\pm}\text{anything})$ — Γ_{41}/Γ_{40}

Sum over modes

VALUE	DOCUMENT ID		TECN	COMMENT
0.533±0.037±0.037	AUBERT	02G	BABR	$e^+e^- \to \Upsilon(4S)$

$\Gamma(\overline{D}D_{s0}(2317))/\Gamma_{\text{total}}$ — Γ_{42}/Γ

VALUE	DOCUMENT ID		TECN	COMMENT
seen	[1] KROKOVNY	03B	BELL	$e^+e^- \to \Upsilon(4S)$

[1] The product branching ratio for $B(B \to \overline{D}D_{s0}(2317)^+) \times B(D_{s0}(2317)^+ \to D_s\pi^0)$ is measured to be $(8.5^{+2.1}_{-1.9} \pm 2.6) \times 10^{-4}$.

$\Gamma(\overline{D}D_{sJ}(2457))/\Gamma_{\text{total}}$ — Γ_{43}/Γ

VALUE	DOCUMENT ID		TECN	COMMENT
seen	[1] KROKOVNY	03B	BELL	$e^+e^- \to \Upsilon(4S)$

[1] The product branching ratio for $B(B \to \overline{D}D_{s,J}(2457)^+) \times B(D_{s,J}(2457)^+ \to D_s^{*+}\pi^0, D_s^+\gamma)$ are measured to be $(17.8^{+4.5}_{-3.9} \pm 5.3) \times 10^{-4}$ and $(6.7^{+1.3}_{-1.2} \pm 2.0) \times 10^{-4}$, respectively.

$[\Gamma(D^{(*)}\overline{D}^{(*)}K^0) + \Gamma(D^{(*)}\overline{D}^{(*)}K^{\pm})]/\Gamma_{\text{total}}$ — Γ_{44}/Γ

VALUE	DOCUMENT ID		TECN	COMMENT
$0.071^{+0.025}_{-0.015}{}^{+0.010}_{-0.009}$	[1] BARATE	98Q	ALEP	$e^+e^- \to Z$

[1] The systematic error includes the uncertainties due to the charm branching ratios.

$\Gamma(b \to c\overline{c}s)/\Gamma_{\text{total}}$ — Γ_{45}/Γ

VALUE	DOCUMENT ID		TECN	COMMENT
0.219±0.037	[1] COAN	98	CLE2	$e^+e^- \to \Upsilon(4S)$

[1] COAN 98 uses D-ℓ correlation.

$\Gamma(D_s^{(*)}\overline{D}^{(*)})/\Gamma(D_s^{\pm}\text{anything})$ — Γ_{46}/Γ_{39}

Sum over modes.

VALUE	DOCUMENT ID		TECN	COMMENT
0.469±0.017 OUR AVERAGE				
0.464±0.013±0.015	AUBERT	02G	BABR	$e^+e^- \to \Upsilon(4S)$
$0.56\ ^{+0.21}_{-0.15}\ ^{+0.09}_{-0.08}$	[1] BARATE	98Q	ALEP	$e^+e^- \to Z$
0.457±0.019±0.037	GIBAUT	96	CLE2	$e^+e^- \to \Upsilon(4S)$
0.58 ±0.07 ±0.09	ALBRECHT	92G	ARG	$e^+e^- \to \Upsilon(4S)$
0.56 ±0.10	BORTOLETTO	90	CLEO	$e^+e^- \to \Upsilon(4S)$

[1] BARATE 98Q measures $B(B \to D_s^{(*)}\overline{D}^{(*)}) = 0.056^{+0.021}_{-0.015}{}^{+0.009}_{-0.008}{}^{+0.019}_{-0.011}$, where the third error results from the uncertainty on the different D branching ratios and is dominated by the uncertainty on $B(D_s^+ \to \phi\pi^+)$. We divide $B(B \to D_s^{(*)}\overline{D}^{(*)})$ by our best value of $B(B \to D_s\,\text{anything}) = 0.1 \pm 0.025$.

$\Gamma(D^*D^*(2010)^{\pm})/\Gamma_{\text{total}}$ — Γ_{47}/Γ

VALUE	CL%	DOCUMENT ID		TECN	COMMENT
$<5.9 \times 10^{-3}$	90	BARATE	98Q	ALEP	$e^+e^- \to Z$

$[\Gamma(DD^*(2010)^{\pm}) + \Gamma(D^*D^{\pm})]/\Gamma_{\text{total}}$ — Γ_{48}/Γ

VALUE	CL%	DOCUMENT ID		TECN	COMMENT
$<5.5 \times 10^{-3}$	90	BARATE	98Q	ALEP	$e^+e^- \to Z$

$\Gamma(DD^{\pm})/\Gamma_{\text{total}}$ — Γ_{49}/Γ

VALUE	CL%	DOCUMENT ID		TECN	COMMENT
$<3.1 \times 10^{-3}$	90	BARATE	98Q	ALEP	$e^+e^- \to Z$

$\Gamma(D_s^{(*)\pm}\overline{D}^{(*)}X(n\pi^{\pm}))/\Gamma_{\text{total}}$ — Γ_{50}/Γ

VALUE	DOCUMENT ID		TECN	COMMENT
$0.094^{+0.040}_{-0.031}{}^{+0.034}_{-0.024}$	[1] BARATE	98Q	ALEP	$e^+e^- \to Z$

[1] The systematic error includes the uncertainties due to the charm branching ratios.

Int. J. Mod. Phys. A 2026.41. Downloaded from www.worldscientific.com by UNIVERSITY OF CALIFORNIA @ BERKELEY on 09/16/26. Re-use and distribution is strictly not permitted, except for Open Access articles.

$\Gamma(\overline{D}^*(2010)\gamma)/\Gamma_{total}$ — Γ_{51}/Γ

VALUE	CL%	DOCUMENT ID		TECN	COMMENT
$<1.1\times10^{-3}$	90	[1] LESIAK	92	CBAL	$e^+e^-\to\Upsilon(4S)$

[1] LESIAK 92 set a limit on the inclusive process $B(b\to s\gamma)<2.8\times10^{-3}$ at 90% CL for the range of masses of 892–2045 MeV, independent of assumptions about s-quark hadronization.

$\Gamma(D_s^+\pi^-, D_s^{*+}\pi^-, D_s^+\rho^-, D_s^{*+}\rho^-, D_s^+\pi^0, D_s^{*+}\pi^0, D_s^+\eta, D_s^{*+}\eta, D_s^+\rho^0, D_s^{*+}\rho^0, D_s^+\omega, D_s^{*+}\omega)/\Gamma_{total}$ — Γ_{52}/Γ

Sum over modes.

VALUE	CL%	DOCUMENT ID		TECN	COMMENT
$<4\times10^{-4}$	90	[1] ALEXANDER	93B	CLE2	$e^+e^-\to\Upsilon(4S)$

[1] ALEXANDER 93B reports $<4.8\times10^{-4}$ from a measurement of $[\Gamma(B\to D_s^+\pi^-, D_s^{*+}\pi^-, D_s^+\rho^-, D_s^{*+}\rho^-, D_s^+\pi^0, D_s^{*+}\pi^0, D_s^+\eta, D_s^{*+}\eta, D_s^+\rho^0, D_s^{*+}\rho^0, D_s^+\omega, D_s^{*+}\omega)/\Gamma_{total}]\times[B(D_s^+\to\phi\pi^+)]$ assuming $B(D_s^+\to\phi\pi^+)=0.037$, which we rescale to our best (shown rounded) value $B(D_s^+\to\phi\pi^+)=4.5\times10^{-2}$. This branching ratio limit provides a model-dependent upper limit $|V_{ub}|/|V_{cb}|<0.16$ at CL=90%.

$\Gamma(D_{s1}(2536)^+\text{anything})/\Gamma_{total}$ — Γ_{53}/Γ

$D_{s1}(2536)^+$ is the narrow P-wave D_s^+ meson with $J^P=1^+$.

VALUE	CL%	DOCUMENT ID		TECN	COMMENT
<0.0095	90	[1] BISHAI	98	CLE2	$e^+e^-\to\Upsilon(4S)$

[1] Assuming factorization, the decay constant $f_{D_{s1}^+}$ is at least a factor of 2.5 times smaller than $f_{D_s^+}$.

$\Gamma(J/\psi(1S)\text{anything})/\Gamma_{total}$ — Γ_{54}/Γ

VALUE (units 10^{-2})	EVTS	DOCUMENT ID		TECN	COMMENT
1.094±0.032 OUR AVERAGE		Error includes scale factor of 1.1.			
1.057±0.012±0.040		[1] AUBERT	03F	BABR	$e^+e^-\to\Upsilon(4S)$
1.121±0.013±0.042		ANDERSON	02	CLE2	$e^+e^-\to\Upsilon(4S)$
1.29 ±0.45 ±0.01	27	[2] MASCHMANN	90	CBAL	$e^+e^-\to\Upsilon(4S)$
1.24 ±0.27 ±0.01	120	[3] ALBRECHT	87D	ARG	$e^+e^-\to\Upsilon(4S)$
1.35 ±0.24 ±0.01	52	[4] ALAM	86	CLEO	$e^+e^-\to\Upsilon(4S)$
• • • We do not use the following data for averages, fits, limits, etc. • • •					
1.12 ±0.06 ±0.01	1489	[5] BALEST	95B	CLE2	$e^+e^-\to\Upsilon(4S)$
1.4 $^{+0.6}_{-0.5}$	7	[6] ALBRECHT	85H	ARG	$e^+e^-\to\Upsilon(4S)$
1.1 ±0.21 ±0.23	46	[7] HAAS	85	CLEO	Repl. by ALAM 86

[1] AUBERT 03F also reports the momentum distribution and helicity of $J/\psi\to\ell^+\ell^-$ in the $\Upsilon(4S)$ center-of-mass frame.

[2] MASCHMANN 90 reports $(1.12\pm0.33\pm0.25)\times10^{-2}$ from a measurement of $[\Gamma(B\to J/\psi(1S)\text{anything})/\Gamma_{total}]\times[B(J/\psi(1S)\to e^+e^-)]$ assuming $B(J/\psi(1S)\to e^+e^-)=0.069\pm0.009$, which we rescale to our best (shown rounded) value $B(J/\psi(1S)\to e^+e^-)=(5.971\pm0.032)\times10^{-2}$. Our first error is their experiment's error and our second error is the systematic error from using our best (shown rounded) value.

[3] ALBRECHT 87D reports $(1.07\pm0.16\pm0.22)\times10^{-2}$ from a measurement of $[\Gamma(B\to J/\psi(1S)\text{anything})/\Gamma_{total}]\times[B(J/\psi(1S)\to e^+e^-)]$ assuming $B(J/\psi(1S)\to e^+e^-)=0.069\pm0.009$, which we rescale to our best (shown rounded) value $B(J/\psi(1S)\to e^+e^-)=(5.971\pm0.032)\times10^{-2}$. Our first error is their experiment's error and our second error is the systematic error from using our best (shown rounded) value. ALBRECHT 87D find the branching ratio for J/ψ not from $\psi(2S)$ to be 0.0081 ± 0.0023.

[4] ALAM 86 reports $(1.09\pm0.16\pm0.21)\times10^{-2}$ from a measurement of $[\Gamma(B\to J/\psi(1S)\text{anything})/\Gamma_{total}]\times[B(J/\psi(1S)\to\mu^+\mu^-)]$ assuming $B(J/\psi(1S)\to\mu^+\mu^-)=0.074\pm0.012$, which we rescale to our best (shown rounded) value $B(J/\psi(1S)\to\mu^+\mu^-)=(5.961\pm0.033)\times10^{-2}$. Our first error is their experiment's error and our second error is the systematic error from using our best (shown rounded) value.

[5] BALEST 95B reports $(1.12\pm0.04\pm0.06)\times10^{-2}$ from a measurement of $[\Gamma(B\to J/\psi(1S)\text{anything})/\Gamma_{total}]\times[B(J/\psi(1S)\to e^+e^-)]$ assuming $B(J/\psi(1S)\to e^+e^-)=0.0599\pm0.0025$, which we rescale to our best (shown rounded) value $B(J/\psi(1S)\to e^+e^-)=(5.971\pm0.032)\times10^{-2}$. Our first error is their experiment's error and our second error is the systematic error from using our best (shown rounded) value. They measure $J/\psi(1S)\to e^+e^-$ and $\mu^+\mu^-$ and use PDG 1994 values for the branching fractions. The rescaling is the same for either mode so we use e^+e^-.

[6] Statistical and systematic errors were added in quadrature. ALBRECHT 85H also report a CL = 90% limit of 0.007 for $B\to J/\psi(1S)+X$ where $m_X<1$ GeV.

[7] Dimuon and dielectron events used.

$\Gamma(J/\psi(1S)(\text{direct})\text{anything})/\Gamma_{total}$ — Γ_{55}/Γ

VALUE	DOCUMENT ID		TECN	COMMENT
0.0078 ±0.0004 OUR AVERAGE	Error includes scale factor of 1.1.			
0.00740±0.00023±0.00043	[1] AUBERT	03F	BABR	$e^+e^-\to\Upsilon(4S)$
0.00813±0.00017±0.00037	[2] ANDERSON	02	CLE2	$e^+e^-\to\Upsilon(4S)$
• • • We do not use the following data for averages, fits, limits, etc. • • •				
0.0080 ±0.0008	[3] BALEST	95B	CLE2	$e^+e^-\to\Upsilon(4S)$

[1] AUBERT 03F also reports the helicity of $J/\psi\to\ell^+\ell^-$ produced directly in B decay.

[2] Also reports the measurement of $J/\psi\to\ell^+\ell^-$ polarization produced directly from B decay.

[3] BALEST 95B assume PDG 1994 values for sub mode branching ratios. $J/\psi(1S)$ mesons are reconstructed in $J/\psi(1S)\to e^+e^-$ and $J/\psi(1S)\to\mu^+\mu^-$. The $B\to J/\psi(1S)X$ branching ratio contains $J/\psi(1S)$ mesons directly from B decays and also from feeddown through $\psi(2S)\to J/\psi(1S)$, $\chi_{c1}(1P)\to J/\psi(1S)$, or $\chi_{c2}(1P)\to J/\psi(1S)$. Using the measured inclusive rates, BALEST 95B corrects for the feeddown and finds the $B\to J/\psi(1S)(\text{direct})X$ branching ratio.

$\Gamma(\psi(2S)\text{anything})/\Gamma_{total}$ — Γ_{56}/Γ

VALUE	EVTS	DOCUMENT ID		TECN	COMMENT
0.00307±0.00021 OUR AVERAGE					
0.00297±0.00020±0.00020		AUBERT	03F	BABR	$e^+e^-\to\Upsilon(4S)$
0.00316±0.00014±0.00028		[1] ANDERSON	02	CLE2	$e^+e^-\to\Upsilon(4S)$
0.0046 ±0.0017 ±0.0011	8	ALBRECHT	87D	ARG	$e^+e^-\to\Upsilon(4S)$
• • • We do not use the following data for averages, fits, limits, etc. • • •					
0.0034 ±0.0004 ±0.0003	240	[2] BALEST	95B	CLE2	$e^+e^-\to\Upsilon(4S)$

[1] Also reports the measurement of $\psi(2S)\to\ell^+\ell^-$ polarization produced directly from B decay.

[2] BALEST 95B assume PDG 1994 values for sub mode branching ratios. They find $B(B\to\psi(2S)X,\ \psi(2S)\to\ell^+\ell^-)=0.30\pm0.05\pm0.04$ and $B(B\to\psi(2S)X,\ \psi(2S)\to J/\psi(1S)\pi^+\pi^-)=0.37\pm0.05\pm0.05$. Weighted average is quoted for $B(B\to\psi(2S)X)$.

$\Gamma(\chi_{c1}(1P)\text{anything})/\Gamma_{total}$ — Γ_{57}/Γ

VALUE (units 10^{-3})	EVTS	DOCUMENT ID		TECN	COMMENT
3.55±0.27 OUR AVERAGE		Error includes scale factor of 1.3. See the ideogram below.			
3.33±0.05±0.24		[1] BHARDWAJ	16	BELL	$e^+e^-\to\Upsilon(4S)$
3.67±0.35±0.44		AUBERT	03F	BABR	$e^+e^-\to\Upsilon(4S)$
4.35±0.29±0.40		ANDERSON	02	CLE2	$e^+e^-\to\Upsilon(4S)$
• • • We do not use the following data for averages, fits, limits, etc. • • •					
3.63±0.22±0.34		[2] ABE	02L	BELL	Repl. by BHARDWAJ 16
3.3 ±0.4 ±0.1		[3] CHEN	01	CLE2	$e^+e^-\to\Upsilon(4S)$
4.0 ±0.6 ±0.4	112	[4] BALEST	95B	CLE2	Repl. by CHEN 01
10.5 ±3.5 ±2.5		[5] ALBRECHT	92E	ARG	$e^+e^-\to\Upsilon(4S)$

[1] Assumes equal production of B^+ and B^0 at the $\Upsilon(4S)$.

[2] ABE 02L uses PDG 01 values for $B(J/\psi(1S)\to\ell^+\ell^-)$ and $B(\chi_{c1,c2}\to J/\psi(1S)\gamma)$.

[3] CHEN 01 reports $0.00414\pm0.00031\pm0.00040$ from a measurement of $[\Gamma(B\to\chi_{c1}(1P)\text{anything})/\Gamma_{total}]\times[B(\chi_{c1}(1P)\to\gamma J/\psi(1S))]$ assuming $B(\chi_{c1}(1P)\to\gamma J/\psi(1S))=0.273\pm0.016$, which we rescale to our best (shown rounded) value $B(\chi_{c1}(1P)\to\gamma J/\psi(1S))=(33.9\pm1.2)\times10^{-2}$. Our first error is their experiment's error and our second error is the systematic error from using our best (shown rounded) value. Assumes equal production of B^+ and B^0 at the $\Upsilon(4S)$.

[4] BALEST 95B assume $B(\chi_{c1}(1P)\to J/\psi(1S)\gamma)=(27.3\pm1.6)\times10^{-2}$, the PDG 1994 value. Fit to ψ-photon invariant mass distribution allows for a $\chi_{c1}(1P)$ and a $\chi_{c2}(1P)$ component.

[5] ALBRECHT 92E assumes no $\chi_{c2}(1P)$ production.

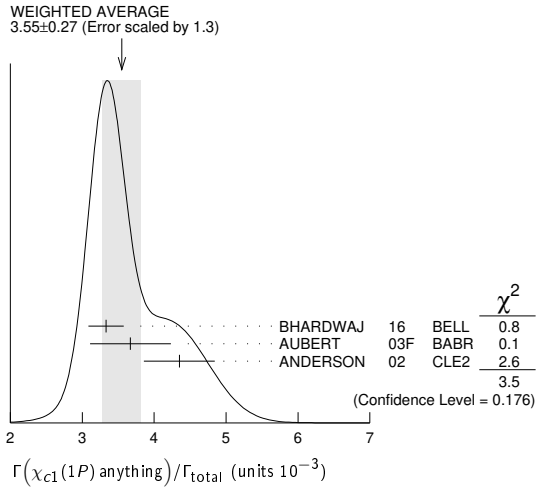

$\Gamma(\chi_{c1}(1P)(\text{direct})\text{anything})/\Gamma_{total}$ — Γ_{58}/Γ

VALUE (units 10^{-3})	DOCUMENT ID		TECN	COMMENT
3.09±0.19 OUR AVERAGE				
3.03±0.05±0.24	[1] BHARDWAJ	16	BELL	$e^+e^-\to\Upsilon(4S)$
3.41±0.35±0.42	AUBERT	03F	BABR	$e^+e^-\to\Upsilon(4S)$
3.1 ±0.4 ±0.1	[2] CHEN	01	CLE2	$e^+e^-\to\Upsilon(4S)$
• • • We do not use the following data for averages, fits, limits, etc. • • •				
3.32±0.22±0.34	[3] ABE	02L	BELL	Repl. by BHARDWAJ 16
3.7 ±0.7	[4] BALEST	95B	CLE2	Repl. by CHEN 01

[1] Assumes equal production of B^+ and B^0 at the $\Upsilon(4S)$.

[2] CHEN 01 reports $0.00383\pm0.00031\pm0.00040$ from a measurement of $[\Gamma(B\to\chi_{c1}(1P)(\text{direct})\text{anything})/\Gamma_{total}]\times[B(\chi_{c1}(1P)\to\gamma J/\psi(1S))]$ assuming $B(\chi_{c1}(1P)\to\gamma J/\psi(1S))=0.273\pm0.016$, which we rescale to our best (shown rounded) value $B(\chi_{c1}(1P)\to\gamma J/\psi(1S))=(33.9\pm1.2)\times10^{-2}$. Our first error is their experiment's error and our second error is the systematic error from using our best (shown rounded) value. Assumes equal production of B^+ and B^0 at the $\Upsilon(4S)$.

[3] ABE 02L uses PDG 01 values for $B(J/\psi(1S)\to\ell^+\ell^-)$ and $B(\chi_{c1,c2}\to J/\psi(1S)\gamma)$.

[4] BALEST 95B assume PDG 1994 values. $J/\psi(1S)$ mesons are reconstructed in the e^+e^- and $\mu^+\mu^-$ modes. The $B\to\chi_{c1}(1P)X$ branching ratio contains $\chi_{c1}(1P)$ mesons directly from B decays and also from feeddown through $\psi(2S)\to\chi_{c1}(1P)\gamma$. Using the measured inclusive rates, BALEST 95B corrects for the feeddown and finds the $B\to\chi_{c1}(1P)(\text{direct})X$ branching ratio.

Int. J. Mod. Phys. A 2026.41. Downloaded from www.worldscientific.com by CALIFORNIA @ BERKELEY on 09/16/26. Re-use and distribution is strictly not permitted, except for Open Access articles.

$\Gamma(\chi_{c2}(1P)\text{anything})/\Gamma_{\text{total}}$ — Γ_{59}/Γ

VALUE (units 10^{-4})	CL%	DOCUMENT ID		TECN	COMMENT
10.0±1.7 OUR AVERAGE		Error includes scale factor of 1.6. See the ideogram below.			
9.8±0.6±1.0		[1] BHARDWAJ	16	BELL	$e^+e^- \to \Upsilon(4S)$
21.0±4.5±3.1		AUBERT	03F	BABR	$e^+e^- \to \Upsilon(4S)$
7.0±3.5±0.3		[2] CHEN	01	CLE2	$e^+e^- \to \Upsilon(4S)$
• • • We do not use the following data for averages, fits, limits, etc. • • •					
$18.0^{+2.3}_{-2.8}\pm2.6$		[3] ABE	02L	BELL	Repl. by BHARDWAJ 16
<38	90	[4] BALEST	95B	CLE2	Repl. by CHEN 01

[1] Assumes equal production of B^+ and B^0 at the $\Upsilon(4S)$.
[2] CHEN 01 reports $(9.8 \pm 4.8 \pm 1.5) \times 10^{-4}$ from a measurement of $[\Gamma(B \to \chi_{c2}(1P)\text{anything})/\Gamma_{\text{total}}] \times [B(\chi_{c2}(1P) \to \gamma J/\psi(1S))]$ assuming $B(\chi_{c2}(1P) \to \gamma J/\psi(1S)) = 0.135 \pm 0.011$, which we rescale to our best (shown rounded) value $B(\chi_{c2}(1P) \to \gamma J/\psi(1S)) = (19.0 \pm 0.8) \times 10^{-2}$. Our first error is their experiment's error and our second error is the systematic error from using our best (shown rounded) value. Assumes equal production of B^+ and B^0 at the $\Upsilon(4S)$.
[3] ABE 02L uses PDG 01 values for $B(J/\psi(1S) \to \ell^+\ell^-)$ and $B(\chi_{c1,c2} \to J/\psi(1S)\gamma)$.
[4] BALEST 95B assume $B(\chi_{c2}(1P) \to J/\psi(1S)\gamma) = (13.5 \pm 1.1) \times 10^{-2}$, the PDG 1994 value. $J/\psi(1S)$ mesons are reconstructed in the e^+e^- and $\mu^+\mu^-$ modes, and PDG 1994 branching fractions are used. If interpreted as signal, the 35 ± 13 events correspond to $B(B \to \chi_{c2}(1P)X) = (0.25 \pm 0.10 \pm 0.03) \times 10^{-2}$.

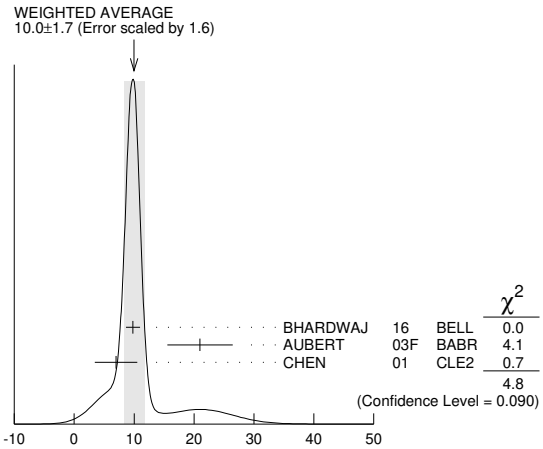

$\Gamma(\chi_{c2}(1P)\text{anything})/\Gamma_{\text{total}}$ — Γ_{59}/Γ

$\Gamma(\chi_{c2}(1P)(\text{direct})\text{anything})/\Gamma_{\text{total}}$ — Γ_{60}/Γ

VALUE (units 10^{-3})	DOCUMENT ID		TECN	COMMENT
0.75±0.11 OUR AVERAGE				
0.70±0.06±0.10	[1] BHARDWAJ	16	BELL	$e^+e^- \to \Upsilon(4S)$
1.90±0.45±0.29	AUBERT	03F	BABR	$e^+e^- \to \Upsilon(4S)$
• • • We do not use the following data for averages, fits, limits, etc. • • •				
$1.53^{+0.23}_{-0.28}\pm0.27$	[2] ABE	02L	BELL	Repl. by BHARDWAJ 16

[1] Assumes equal production of B^+ and B^0 at the $\Upsilon(4S)$.
[2] ABE 02L uses PDG 01 values for $B(J/\psi(1S) \to \ell^+\ell^-)$ and $B(\chi_{c1,c2} \to J/\psi(1S)\gamma)$.

$\Gamma(\eta_c(1S)\text{anything})/\Gamma_{\text{total}}$ — Γ_{61}/Γ

VALUE	CL%	DOCUMENT ID		TECN	COMMENT
<0.009	90	[1] BALEST	95B	CLE2	$e^+e^- \to \Upsilon(4S)$

[1] BALEST 95B assume PDG 1994 values for sub mode branching ratios. $J/\psi(1S)$ mesons are reconstructed in $J/\psi(1S) \to e^+e^-$ and $J/\psi(1S) \to \mu^+\mu^-$. Search region $2960 < m_{\eta_c(1S)} < 3010$ MeV/c^2.

$\Gamma(K\chi_{c1}(3872))/\Gamma_{\text{total}}$ — Γ_{62}/Γ

VALUE (units 10^{-4})	DOCUMENT ID		TECN	COMMENT
1.9±0.7 OUR AVERAGE				
1.7±0.5±0.6	[1] AUSHEV	10	BELL	$e^+e^- \to \Upsilon(4S)$
$2.2^{+0.7}_{-0.8}{}^{+1.2}_{-1.1}$	[2,3] GOKHROO	06	BELL	$e^+e^- \to \Upsilon(4S)$

[1] AUSHEV 10 reports $[\Gamma(B \to K\chi_{c1}(3872))/\Gamma_{\text{total}}] \times [B(\chi_{c1}(3872) \to \overline{D}^{*0}D^0)] = (0.80 \pm 0.20 \pm 0.10) \times 10^{-4}$ which we divide by our best (shown rounded) value $B(\chi_{c1}(3872) \to \overline{D}^{*0}D^0) = (46 \pm 16) \times 10^{-2}$. Our first error is their experiment's error and our second error is the systematic error from using our best (shown rounded) value.
[2] GOKHROO 06 reports $[\Gamma(B \to K\chi_{c1}(3872))/\Gamma_{\text{total}}] \times [B(\chi_{c1}(3872) \to D^0\overline{D}^0\pi^0)] = (1.22 \pm 0.31^{+0.23}_{-0.30}) \times 10^{-4}$ which we divide by our best (shown rounded) value $B(\chi_{c1}(3872) \to D^0\overline{D}^0\pi^0) = (55 \pm 28) \times 10^{-2}$. Our first error is their experiment's error and our second error is the systematic error from using our best (shown rounded) value.
[3] Measure the near-threshold enhancements in the $(D^0\overline{D}^0\pi^0)$ system at a mass $3875.2 \pm 0.7^{+0.3}_{-1.6} \pm 0.8$ MeV/c^2.

$\Gamma(KX(3940),\ X \to D^{*0}D^0)/\Gamma_{\text{total}}$ — Γ_{63}/Γ

VALUE (units 10^{-4})	CL%	DOCUMENT ID		TECN	COMMENT
<0.67	90	AUSHEV	10	BELL	$e^+e^- \to \Upsilon(4S)$

$\Gamma(K\chi_{c0}(3915),\ \chi_{c0} \to \omega J/\psi)/\Gamma_{\text{total}}$ — Γ_{64}/Γ

VALUE (units 10^{-5})	DOCUMENT ID		TECN	COMMENT
7.1±1.3±3.1	[1] CHOI	05	BELL	$e^+e^- \to \Upsilon(4S)$

[1] CHOI 05 reports the observation of a near-threshold enhancement in the $\omega J/\psi$ mass spectrum in exclusive $B \to K\omega J/\psi$. The new state, denoted as $\chi_{c0}(3915)$, is measured to have a mass of $3943 \pm 11 \pm 13$ GeV/c^2 and a width $\Gamma = 87 \pm 22 \pm 26$ MeV.

$\Gamma(K^{\pm}\text{anything})/\Gamma_{\text{total}}$ — Γ_{65}/Γ

VALUE	DOCUMENT ID		TECN	COMMENT
0.789±0.025 OUR AVERAGE				
0.82 ±0.01 ±0.05	ALBRECHT	94C	ARG	$e^+e^- \to \Upsilon(4S)$
0.775±0.015±0.025	[1] ALBRECHT	93I	ARG	$e^+e^- \to \Upsilon(4S)$
0.85 ±0.07 ±0.09	ALAM	87B	CLEO	$e^+e^- \to \Upsilon(4S)$
• • • We do not use the following data for averages, fits, limits, etc. • • •				
seen	[2] BRODY	82	CLEO	$e^+e^- \to \Upsilon(4S)$
seen	[3] GIANNINI	82	CUSB	$e^+e^- \to \Upsilon(4S)$

[1] ALBRECHT 93I value is not independent of the sum of $B \to K^+$ anything and $B \to K^-$ anything ALBRECHT 94C values.
[2] Assuming $\Upsilon(4S) \to B\overline{B}$, a total of $3.38 \pm 0.34 \pm 0.68$ kaons per $\Upsilon(4S)$ decay is found (the second error is systematic). In the context of the standard B-decay model, this leads to a value for (b-quark $\to$ c-quark)/(b-quark $\to$ all) of $1.09 \pm 0.33 \pm 0.13$.
[3] GIANNINI 82 at CESR-CUSB observed 1.58 ± 0.35 K^0 per hadronic event much higher than 0.82 ± 0.10 below threshold. Consistent with predominant $b \to cX$ decay.

$\Gamma(K^+\text{anything})/\Gamma_{\text{total}}$ — Γ_{66}/Γ

VALUE	DOCUMENT ID		TECN	COMMENT
0.66 ±0.05	[1] ALBRECHT	94C	ARG	$e^+e^- \to \Upsilon(4S)$
• • • We do not use the following data for averages, fits, limits, etc. • • •				
0.620±0.013±0.038	[2] ALBRECHT	94C	ARG	$e^+e^- \to \Upsilon(4S)$
0.66 ±0.05 ±0.07	[2] ALAM	87B	CLEO	$e^+e^- \to \Upsilon(4S)$

[1] Measurement relies on lepton-kaon correlations. It is for the weak decay vertex and does not include mixing of the neutral B meson. Mixing effects were corrected for by assuming a mixing parameter r of (18.1 ± 4.3)%.
[2] Measurement relies on lepton-kaon correlations. It includes production through mixing of the neutral B meson.

$\Gamma(K^-\text{anything})/\Gamma_{\text{total}}$ — Γ_{67}/Γ

VALUE	DOCUMENT ID		TECN	COMMENT
0.13 ±0.04	[1] ALBRECHT	94C	ARG	$e^+e^- \to \Upsilon(4S)$
• • • We do not use the following data for averages, fits, limits, etc. • • •				
0.165±0.011±0.036	[2] ALBRECHT	94C	ARG	$e^+e^- \to \Upsilon(4S)$
0.19 ±0.05 ±0.02	[2] ALAM	87B	CLEO	$e^+e^- \to \Upsilon(4S)$

[1] Measurement relies on lepton-kaon correlations. It is for the weak decay vertex and does not include mixing of the neutral B meson. Mixing effects were corrected for by assuming a mixing parameter r of (18.1 ± 4.3)%.
[2] Measurement relies on lepton-kaon correlations. It includes production through mixing of the neutral B meson.

$\Gamma(K^0/\overline{K}^0\text{anything})/\Gamma_{\text{total}}$ — Γ_{68}/Γ

VALUE	DOCUMENT ID		TECN	COMMENT
0.64 ±0.04 OUR AVERAGE				
0.642±0.010±0.042	[1] ALBRECHT	94C	ARG	$e^+e^- \to \Upsilon(4S)$
0.63 ±0.06 ±0.06	ALAM	87B	CLEO	$e^+e^- \to \Upsilon(4S)$

[1] ALBRECHT 94C assume a $K^0/\overline{K}^0$ multiplicity twice that of K^0_S.

$\Gamma(K^*(892)^{\pm}\text{anything})/\Gamma_{\text{total}}$ — Γ_{69}/Γ

VALUE	DOCUMENT ID		TECN	COMMENT
0.182±0.054±0.024	ALBRECHT	94J	ARG	$e^+e^- \to \Upsilon(4S)$

$\Gamma(K^*(892)^0/\overline{K}^*(892)^0\text{anything})/\Gamma_{\text{total}}$ — Γ_{70}/Γ

VALUE	DOCUMENT ID		TECN	COMMENT
0.146±0.016±0.020	ALBRECHT	94J	ARG	$e^+e^- \to \Upsilon(4S)$

$\Gamma(K^*(892)\gamma)/\Gamma_{\text{total}}$ — Γ_{71}/Γ

VALUE (units 10^{-5})	CL%	DOCUMENT ID		TECN	COMMENT
4.10±0.12 OUR AVERAGE					
4.10±0.08±0.09		[1] ADACHI	25Z	BELL	$e^+e^- \to \Upsilon(4S)$
4.24±0.54±0.32		[2] COAN	00	CLE2	$e^+e^- \to \Upsilon(4S)$
• • • We do not use the following data for averages, fits, limits, etc. • • •					
<150	90	[3] LESIAK	92	CBAL	$e^+e^- \to \Upsilon(4S)$
< 24	90	ALBRECHT	88H	ARG	$e^+e^- \to \Upsilon(4S)$

[1] An average of $B(B^+ \to K^*(892)^+\gamma)$ and $B(B^0 \to K^*(892)^0\gamma)$ measurements assuming $B(\Upsilon(4S) \to B^+B^-) = 0.5113^{+0.0073}_{-0.0108}$ and $B(\Upsilon(4S) \to B^0\overline{B}^0) = 0.4861^{+0.0074}_{-0.0080}$.
[2] An average of $B(B^+ \to K^*(892)^+\gamma)$ and $B(B^0 \to K^*(892)^0\gamma)$ measurements reported in COAN 00 by assuming full correlated systematic errors.
[3] LESIAK 92 set a limit on the inclusive process $B(b \to s\gamma) < 2.8 \times 10^{-3}$ at 90% CL for the range of masses of 892–2045 MeV, independent of assumptions about s-quark hadronization.

Int. J. Mod. Phys. A 2026.41. Downloaded from www.worldscientific.com
by UNIVERSITY OF CALIFORNIA @ BERKELEY on 09/16/26. Re-use and distribution is strictly not permitted, except for Open Access articles.

$\Gamma(\eta K\gamma)/\Gamma_{total}$ — Γ_{72}/Γ

VALUE (units 10^{-6})	DOCUMENT ID		TECN	COMMENT
$8.5\pm1.3^{+1.2}_{-0.9}$	[1] NISHIDA	05	BELL	$e^+e^-\to\Upsilon(4S)$

[1] $m_{\eta K}<2.4$ GeV/c^2

$\Gamma(K_1(1400)\gamma)/\Gamma_{total}$ — Γ_{73}/Γ

VALUE	CL%	DOCUMENT ID		TECN	COMMENT
$<12.7\times10^{-5}$	90	[1] COAN	00	CLE2	$e^+e^-\to\Upsilon(4S)$
• • • We do not use the following data for averages, fits, limits, etc. • • •					
$<1.6\times10^{-3}$	90	[2] LESIAK	92	CBAL	$e^+e^-\to\Upsilon(4S)$
$<4.1\times10^{-4}$	90	ALBRECHT	88H	ARG	$e^+e^-\to\Upsilon(4S)$

[1] Assumes equal production of B^+ and B^0 at the $\Upsilon(4S)$.
[2] LESIAK 92 set a limit on the inclusive process $B(b\to s\gamma)<2.8\times10^{-3}$ at 90% CL for the range of masses of 892–2045 MeV, independent of assumptions about s-quark hadronization.

$\Gamma(K_2^*(1430)\gamma)/\Gamma_{total}$ — Γ_{74}/Γ

VALUE (units 10^{-5})	CL%	DOCUMENT ID		TECN	COMMENT
$1.66^{+0.59}_{-0.53}\pm0.13$		[1] COAN	00	CLE2	$e^+e^-\to\Upsilon(4S)$
• • • We do not use the following data for averages, fits, limits, etc. • • •					
<83	90	ALBRECHT	88H	ARG	$e^+e^-\to\Upsilon(4S)$

[1] COAN 00 obtains a fitted signal yield of $15.9^{+5.7}_{-5.2}$ events. A search for contamination by $K^*(1410)$ yielded a rate consistent with 0; the central value assumes no contamination.

$\Gamma(K_2(1770)\gamma)/\Gamma_{total}$ — Γ_{75}/Γ

VALUE	CL%	DOCUMENT ID		TECN	COMMENT
$<1.2\times10^{-3}$	90	[1] LESIAK	92	CBAL	$e^+e^-\to\Upsilon(4S)$

[1] LESIAK 92 set a limit on the inclusive process $B(b\to s\gamma)<2.8\times10^{-3}$ at 90% CL for the range of masses of 892–2045 MeV, independent of assumptions about s-quark hadronization.

$\Gamma(K_3^*(1780)\gamma)/\Gamma_{total}$ — Γ_{76}/Γ

VALUE	CL%	DOCUMENT ID		TECN	COMMENT
$<3.7\times10^{-5}$	90	[1] NISHIDA	05	BELL	$e^+e^-\to\Upsilon(4S)$
• • • We do not use the following data for averages, fits, limits, etc. • • •					
$<3.0\times10^{-3}$	90	ALBRECHT	88H	ARG	$e^+e^-\to\Upsilon(4S)$

[1] Uses $B(K_3^*(1780)\to\eta K)=0.11^{+0.05}_{-0.04}$.

$\Gamma(K_4^*(2045)\gamma)/\Gamma_{total}$ — Γ_{77}/Γ

VALUE	CL%	DOCUMENT ID		TECN	COMMENT
$<1.0\times10^{-3}$	90	[1] LESIAK	92	CBAL	$e^+e^-\to\Upsilon(4S)$

[1] LESIAK 92 set a limit on the inclusive process $B(b\to s\gamma)<2.8\times10^{-3}$ at 90% CL for the range of masses of 892–2045 MeV, independent of assumptions about s-quark hadronization.

$\Gamma(K\eta'(958))/\Gamma_{total}$ — Γ_{78}/Γ

VALUE	DOCUMENT ID		TECN	COMMENT
$(8.3^{+0.9}_{-0.8}\pm0.7)\times10^{-5}$	[1] RICHICHI	00	CLE2	$e^+e^-\to\Upsilon(4S)$

[1] Assumes equal production of B^+ and B^0 at the $\Upsilon(4S)$.

$\Gamma(K^*(892)\eta'(958))/\Gamma_{total}$ — Γ_{79}/Γ

VALUE (units 10^{-6})	CL%	DOCUMENT ID		TECN	COMMENT
$4.1^{+1.0}_{-0.9}\pm0.5$		[1] AUBERT	07E	BABR	$e^+e^-\to\Upsilon(4S)$
• • • We do not use the following data for averages, fits, limits, etc. • • •					
<22	90	[1] RICHICHI	00	CLE2	$e^+e^-\to\Upsilon(4S)$

[1] Assumes equal production of B^+ and B^0 at the $\Upsilon(4S)$.

$\Gamma(K\eta)/\Gamma_{total}$ — Γ_{80}/Γ

VALUE	CL%	DOCUMENT ID		TECN	COMMENT
$<5.2\times10^{-6}$	90	[1] RICHICHI	00	CLE2	$e^+e^-\to\Upsilon(4S)$

[1] Assumes equal production of B^+ and B^0 at the $\Upsilon(4S)$.

$\Gamma(K^*(892)\eta)/\Gamma_{total}$ — Γ_{81}/Γ

VALUE	DOCUMENT ID		TECN	COMMENT
$(1.80^{+0.49}_{-0.43}\pm0.18)\times10^{-5}$	[1] RICHICHI	00	CLE2	$e^+e^-\to\Upsilon(4S)$

[1] Assumes equal production of B^+ and B^0 at the $\Upsilon(4S)$.

$\Gamma(K\phi\phi)/\Gamma_{total}$ — Γ_{82}/Γ

VALUE (units 10^{-6})	DOCUMENT ID		TECN	COMMENT
$2.3^{+0.9}_{-0.8}\pm0.3$	[1] HUANG	03	BELL	$e^+e^-\to\Upsilon(4S)$

[1] Assumes equal production of charged and neutral B meson pairs and isospin symmetry.

$\Gamma(\overline{b}\to\overline{s}\gamma)/\Gamma_{total}$ — Γ_{83}/Γ

VALUE (units 10^{-4})	DOCUMENT ID		TECN	COMMENT
3.49±0.19 OUR AVERAGE				
$3.75\pm0.18\pm0.35$	[1,2] SAITO	15	BELL	$e^+e^-\to\Upsilon(4S)$
$3.52\pm0.20\pm0.51$	[1,3] LEES	12U	BABR	$e^+e^-\to\Upsilon(4S)$
$3.32\pm0.16\pm0.31$	[1,4] LEES	12V	BABR	$e^+e^-\to\Upsilon(4S)$
$3.47\pm0.15\pm0.40$	[1,5] LIMOSANI	09	BELL	$e^+e^-\to\Upsilon(4S)$
$3.90\pm0.91\pm0.64$	[1,6] AUBERT	08O	BABR	$e^+e^-\to\Upsilon(4S)$
$3.29\pm0.44\pm0.29$	[1,7] CHEN	01C	CLE2	$e^+e^-\to\Upsilon(4S)$
• • • We do not use the following data for averages, fits, limits, etc. • • •				
$2.30\pm0.08\pm0.30$	[8] DEL-AMO-SA...	10M	BABR	$e^+e^-\to\Upsilon(4S)$
$4.3\ \pm0.3\ \pm0.7$	[9] AUBERT	09U	BABR	Repl. by DEL-AMO-SANCHEZ 10M
$3.92\pm0.31\pm0.47$	[1,10] AUBERT,BE	06B	BABR	Repl. by LEES 12V
$3.49\pm0.20^{+0.59}_{-0.46}$	[1,11] AUBERT,B	05R	BABR	Repl. by LEES 12U
$3.50\pm0.32\pm0.31$	[1,12] KOPPENBURG	04	BELL	Repl. by LIMOSANI 09
$3.36\pm0.53^{+0.65}_{-0.68}$	[13] ABE	01F	BELL	Repl. by SAITO 15
$2.32\pm0.57\pm0.35$	ALAM	95	CLE2	Repl. by CHEN 01C

[1] We extrapolate the measured value to $E_\gamma>1.6$ GeV using the method of BUCHMUELLER 06 (average of three theoretical models).
[2] SAITO 15 measured $(3.51\pm0.17\pm0.33)\times10^{-4}$ using a sum-of-exclusive approach in which 38 of the hadronic final states with $m_{X_s}<2.8$ GeV/c^2 are reconstructed. The cut of minimum photon energy is $E_\gamma>1.9$ GeV.
[3] Reports $(3.29\pm0.19\pm0.48)\times10^{-4}$ for $E_\gamma>1.9$ GeV.
[4] Reports $(3.21\pm0.15\pm0.29\pm0.08)\times10^{-4}$ for $1.8<E_\gamma<2.8$ GeV, where the last systematic uncertainty is for model dependency. Results with other cutoffs are also reported.
[5] The measurement reported is $(3.45\pm0.15\pm0.40)\times10^{-4}$ for $E_\gamma>1.7$ GeV.
[6] Uses a fully reconstructed B meson as a tag on the recoil side. The measurement reported is $(3.66\pm0.85\pm0.60)\times10^{-4}$ for $E_\gamma>1.9$ GeV.
[7] The measurement reported is $(3.21\pm0.43^{+0.32}_{-0.29})\times10^{-4}$ for $E_\gamma>2.0$ GeV.
[8] Measured using sums of seven exclusive final states $B\to X_{d(s)}\gamma$ where $X_{d(s)}$ is a nonstrange (strange) charmless hadronic system in mass range 0.5–2.0 GeV/c^2.
[9] Measured using sums of seven exclusive final states $B\to X_{d(s)}\gamma$ where $X_{d(s)}$ is a nonstrange (strange) charmless hadronic system in mass range 0.6–1.8 GeV/c^2.
[10] The measurement reported is $(3.67\pm0.29\pm0.45)\times10^{-4}$ for $E_\gamma>1.9$ GeV.
[11] The measurement reported is $(3.27\pm0.18^{+0.55}_{-0.42})\times10^{-4}$ for $E_\gamma>1.9$ GeV.
[12] The measurement reported is $(3.55\pm0.32\pm0.32)\times10^{-4}$ for $E_\gamma>1.8$ GeV.
[13] ABE 01F reports their systematic errors $(\pm0.42^{+0.50}_{-0.54})\times10^{-4}$, where the second error is due to the theoretical uncertainty. We combine them in quadrature.

$\Gamma(\overline{b}\to\overline{d}\gamma)/\Gamma_{total}$ — Γ_{84}/Γ

VALUE (units 10^{-6})	DOCUMENT ID		TECN	COMMENT
9.2±2.0±2.3	[1] DEL-AMO-SA...	10M	BABR	$e^+e^-\to\Upsilon(4S)$
• • • We do not use the following data for averages, fits, limits, etc. • • •				
$14\ \pm5\ \pm4$	[2] AUBERT	09U	BABR	Repl. by DEL-AMO-SANCHEZ 10M

[1] Measured using sums of seven exclusive final states $B\to X_{d(s)}\gamma$ where $X_{d(s)}$ is a nonstrange (strange) charmless hadronic system in mass range 0.5–2.0 GeV/c^2.
[2] Measured using sums of seven exclusive final states $B\to X_{d(s)}\gamma$ where $X_{d(s)}$ is a nonstrange (strange) charmless hadronic system in mass range 0.6–1.8 GeV/c^2.

$\Gamma(\overline{b}\to\overline{d}\gamma)/\Gamma(\overline{b}\to\overline{s}\gamma)$ — Γ_{84}/Γ_{83}

VALUE	DOCUMENT ID		TECN	COMMENT
0.040±0.009±0.010	[1] DEL-AMO-SA...	10M	BABR	$e^+e^-\to\Upsilon(4S)$
• • • We do not use the following data for averages, fits, limits, etc. • • •				
$0.033\pm0.013\pm0.009$	[2] AUBERT	09U	BABR	Repl. by DEL-AMO-SANCHEZ 10M

[1] Measured using sums of seven exclusive final states $B\to X_{d(s)}\gamma$ where $X_{d(s)}$ is a nonstrange (strange) charmless hadronic system in mass range 0.5–2.0 GeV/c^2.
[2] Measured using sums of seven exclusive final states $B\to X_{d(s)}\gamma$ where $X_{d(s)}$ is a nonstrange (strange) charmless hadronic system in mass range 0.6–1.8 GeV/c^2.

$\Gamma(\overline{b}\to\overline{s}\text{gluon})/\Gamma_{total}$ — Γ_{85}/Γ

VALUE	CL%	EVTS	DOCUMENT ID		TECN	COMMENT
<0.068	90		[1] COAN	98	CLE2	$e^+e^-\to\Upsilon(4S)$
• • • We do not use the following data for averages, fits, limits, etc. • • •						
<0.08		2	[2] ALBRECHT	95D	ARG	$e^+e^-\to\Upsilon(4S)$

[1] COAN 98 uses D-ℓ correlation.
[2] ALBRECHT 95D use full reconstruction of one B decay as tag. Two candidate events for charmless B decay can be interpreted as either $b\to s$gluon or $b\to u$ transition. If interpreted as $b\to s$gluon they find a branching ratio of ~0.026 or the upper limit quoted above. Result is highly model dependent.

$\Gamma(\eta\text{ anything})/\Gamma_{total}$ — Γ_{86}/Γ

VALUE (units 10^{-4})	CL%	DOCUMENT ID		TECN	COMMENT
$2.61\pm0.30^{+0.44}_{-0.74}$		[1] NISHIMURA	10	BELL	$e^+e^-\to\Upsilon(4S)$
• • • We do not use the following data for averages, fits, limits, etc. • • •					
$1.69\pm0.29^{+0.36}_{-0.62}$		[2] NISHIMURA	10	BELL	$e^+e^-\to\Upsilon(4S)$
<4.4	90	[3] BROWDER	98	CLE2	$e^+e^-\to\Upsilon(4S)$

[1] Uses $B\to\eta X_s$ with $0.4<m_{X_s}<2.6$ GeV/c^2.
[2] Uses $B\to\eta X_s$ with $1.8<m_{X_s}<2.6$ GeV/c^2.
[3] BROWDER 98 search for high momentum $B\to\eta X_s$ between 2.1 and 2.7 GeV/c.

Int. J. Mod. Phys. A 2026.41. Downloaded from www.worldscientific.com by CALIFORNIA @ BERKELEY on 09/16/26. Re-use and distribution is strictly not permitted, except for Open Access articles.

$\Gamma(\eta' \text{ anything})/\Gamma_{total}$ — Γ_{87}/Γ

VALUE (units 10^{-4})	DOCUMENT ID		TECN	COMMENT
4.2±0.9 OUR AVERAGE				
3.9±0.8±0.9	[1] AUBERT,B	04F	BABR	$e^+e^- \to \Upsilon(4S)$
4.6±1.1±0.6	[2] BONVICINI	03	CLE2	$e^+e^- \to \Upsilon(4S)$
• • • We do not use the following data for averages, fits, limits, etc. • • •				
$6.2\pm1.6^{+1.3}_{-2.0}$	[3] BROWDER	98	CLE2	$e^+e^- \to \Upsilon(4S)$

[1] AUBERT,B 04F reports branching ratio $B \to \eta' X_s$ for high momentum η' between 2.0 and 2.7 GeV/c in the $\Upsilon(4S)$ center-of-mass frame. X_s represents a recoil system consisting of a kaon and zero to four pions.
[2] BONVICINI 03 observed a signal of 61.2 ± 13.9 events in $B \to \eta' X_{nc}$ production for high momentum η' between 2.0 and 2.7 GeV/c in the $\Upsilon(4S)$ center-of-mass frame. The X_{nc} denotes "charmless" hadronic states recoiling against η'. The second error combines systematic and background subtraction uncertainties in quadrature.
[3] BROWDER 98 observed a signal of 39.0 ± 11.6 events in high momentum $B \to \eta' X_s$ production between 2.0 and 2.7 GeV/c. The branching fraction is based on the interpretation of $b \to sg$, where the last error includes additional uncertainties due to the color-suppressed $b \to$ backgrounds.

$\Gamma(K^+ \text{gluon (charmless)})/\Gamma_{total}$ — Γ_{88}/Γ

VALUE (units 10^{-4})	CL%	DOCUMENT ID		TECN	COMMENT
<1.87	90	[1] DEL-AMO-SA...	11	BABR	$e^+e^- \to \Upsilon(4S)$

[1] $B \to K^+ X$ with $m_X < 1.69$ GeV/c^2.

$\Gamma(K^0 \text{gluon (charmless)})/\Gamma_{total}$ — Γ_{89}/Γ

VALUE (units 10^{-4})	DOCUMENT ID		TECN	COMMENT
$\mathbf{1.95^{+0.51}_{-0.45}\pm0.50}$	[1] DEL-AMO-SA...	11	BABR	$e^+e^- \to \Upsilon(4S)$

[1] $B \to K^0 X$ with $m_X < 1.69$ GeV/c^2.

$\Gamma(\rho\gamma)/\Gamma_{total}$ — Γ_{90}/Γ

VALUE (units 10^{-6})	CL%	DOCUMENT ID		TECN	COMMENT
1.39±0.25 OUR AVERAGE		Error includes scale factor of 1.2.			
$1.73^{+0.34}_{-0.32}\pm0.17$		[1,2] AUBERT	08BH	BABR	$e^+e^- \to \Upsilon(4S)$
$1.21^{+0.24}_{-0.22}\pm0.12$		[1,2] TANIGUCHI	08	BELL	$e^+e^- \to \Upsilon(4S)$
• • • We do not use the following data for averages, fits, limits, etc. • • •					
$1.36^{+0.29}_{-0.27}\pm0.10$		[1,3] AUBERT	07L	BABR	Repl. by AUBERT 08BH
< 1.9	90	[1,3] AUBERT	04C	BABR	Repl. by AUBERT 07L
<14	90	[1,4] COAN	00	CLE2	$e^+e^- \to \Upsilon(4S)$

[1] Assumes equal production of B^+ and B^0 at the $\Upsilon(4S)$.
[2] Assumes $\Gamma(B \to \rho\gamma) = \Gamma(B^+ \to \rho^+\gamma) = 2\,\Gamma(B^0 \to \rho^0\gamma)$ and uses lifetime ratio of $\tau_{B^+}/\tau_{B^0} = 1.071 \pm 0.009$.
[3] Assumes $\Gamma(B \to \rho\gamma) = \Gamma(B^+ \to \rho^+\gamma) = 2\,\Gamma(B^0 \to \rho^0\gamma)$ and uses lifetime ratio of $\tau_{B^+}/\tau_{B^0} = 1.083 \pm 0.017$.
[4] COAN 00 reports $B(B \to \rho\gamma)/B(B \to K^*(892)\gamma) < 0.32$ at 90%CL and scaled by the central value of $B(B \to K^*(892)\gamma)=(4.24 \pm 0.54 \pm 0.32) \times 10^{-5}$.

$\Gamma(\rho\gamma)/\Gamma(K^*(892)\gamma)$ — Γ_{90}/Γ_{71}

VALUE (units 10^{-2})	DOCUMENT ID	TECN	COMMENT
$\mathbf{3.02^{+0.60}_{-0.55}+0.26}$ $\mathbf{-0.28}$	TANIGUCHI 08	BELL	$e^+e^- \to \Upsilon(4S)$

$\Gamma(\rho/\omega\gamma)/\Gamma_{total}$ — Γ_{91}/Γ

VALUE (units 10^{-6})	CL%	DOCUMENT ID		TECN	COMMENT
1.30±0.23 OUR AVERAGE		Error includes scale factor of 1.2.			
$1.63^{+0.30}_{-0.28}\pm0.16$		[1,2,3] AUBERT	08BH	BABR	$e^+e^- \to \Upsilon(4S)$
$1.14\pm0.20^{+0.10}_{-0.12}$		[1,3] TANIGUCHI	08	BELL	$e^+e^- \to \Upsilon(4S)$
• • • We do not use the following data for averages, fits, limits, etc. • • •					
$1.25^{+0.25}_{-0.24}\pm0.09$		[4] AUBERT	07L	BABR	Repl. by AUBERT 08BH
$1.32^{+0.34}_{-0.31}+0.10$ -0.09		[4] MOHAPATRA	06	BELL	Repl. by TANIGUCHI 08
0.6 ±0.3 ±0.1		[4] AUBERT	05	BABR	Repl. by AUBERT 07L
<1.4	90	[4] MOHAPATRA	05	BELL	$e^+e^- \to \Upsilon(4S)$

[1] Assumes $\Gamma(B \to \rho\gamma) = \Gamma(B^+ \to \rho^+\gamma) = 2\,\Gamma(B^0 \to \rho^0\gamma)$ and uses lifetime ratio of $\tau_{B^+}/\tau_{B^0} = 1.071 \pm 0.009$.
[2] Also reports $|V_{td}/V_{ts}| = 0.233^{+0.025}_{-0.024}{}^{+0.022}_{-0.021}$.
[3] Assumes equal production of B^+ and B^0 at the $\Upsilon(4S)$.
[4] Assumes $\Gamma(B \to \rho\gamma) = \Gamma(B^+ \to \rho^+\gamma) = 2\,\Gamma(B^0 \to \rho^0\gamma)$ and uses lifetime ratio of $\tau_{B^+}/\tau_{B^0} = 1.083 \pm 0.017$.

$\Gamma(\rho/\omega\gamma)/\Gamma(K^*(892)\gamma)$ — Γ_{91}/Γ_{71}

VALUE (units 10^{-2})	CL%	DOCUMENT ID		TECN	COMMENT
$\mathbf{2.84\pm0.50^{+0.27}_{-0.29}}$		[1] TANIGUCHI	08	BELL	$e^+e^- \to \Upsilon(4S)$
• • • We do not use the following data for averages, fits, limits, etc. • • •					
<3.5	90	MOHAPATRA	05	BELL	Repl. by TANIGUCHI 08

[1] Also reports $|V_{td}/V_{ts}| = 0.195^{+0.020}_{-0.019} \pm 0.015$.

$\Gamma(\pi^{\pm} \text{ anything})/\Gamma_{total}$ — Γ_{92}/Γ

VALUE	DOCUMENT ID		TECN	COMMENT
3.585±0.025±0.070	[1] ALBRECHT	93I	ARG	$e^+e^- \to \Upsilon(4S)$

[1] ALBRECHT 93 excludes $\pi^{\pm}$ from K^0_S and Λ decays. If included, they find 4.105 ± 0.025 ± 0.080.

$\Gamma(\pi^0 \text{ anything})/\Gamma_{total}$ — Γ_{93}/Γ

VALUE	DOCUMENT ID		TECN	COMMENT
2.35±0.02±0.11	[1] ABE	01J	BELL	$e^+e \to \Upsilon(4S)$

[1] From fully inclusive π^0 yield with no corrections from decays of K^0_S or other particles.

$\Gamma(\eta \text{ anything})/\Gamma_{total}$ — Γ_{94}/Γ

VALUE	DOCUMENT ID		TECN	COMMENT
0.176±0.011±0.012	KUBOTA	96	CLE2	$e^+e^- \to \Upsilon(4S)$

$\Gamma(\rho^0 \text{ anything})/\Gamma_{total}$ — Γ_{95}/Γ

VALUE	DOCUMENT ID		TECN	COMMENT
0.208±0.042±0.032	ALBRECHT	94J	ARG	$e^+e^- \to \Upsilon(4S)$

$\Gamma(\omega \text{ anything})/\Gamma_{total}$ — Γ_{96}/Γ

VALUE	CL%	DOCUMENT ID		TECN	COMMENT
<0.81	90	ALBRECHT	94J	ARG	$e^+e^- \to \Upsilon(4S)$

$\Gamma(\phi \text{ anything})/\Gamma_{total}$ — Γ_{97}/Γ

VALUE	DOCUMENT ID		TECN	COMMENT
0.0343±0.0012 OUR AVERAGE				
0.0353±0.0005±0.0030	HUANG	07	CLEO	$e^+e^- \to \Upsilon(4S)$
0.0341±0.0006±0.0012	AUBERT	04S	BABR	$e^+e^- \to \Upsilon(4S)$
0.0390±0.0030±0.0035	ALBRECHT	94J	ARG	$e^+e^- \to \Upsilon(4S)$
0.023 ±0.006 ±0.005	BORTOLETTO	86	CLEO	$e^+e^- \to \Upsilon(4S)$

$\Gamma(\phi K^*(892))/\Gamma_{total}$ — Γ_{98}/Γ

VALUE	CL%	DOCUMENT ID		TECN
$\mathbf{<2.2\times10^{-5}}$	90	[1] BERGFELD	98	CLE2

[1] Assumes equal production of B^+ and B^0 at the $\Upsilon(4S)$.

$\Gamma(\pi^+ \text{ gluon (charmless)})/\Gamma_{total}$ — Γ_{100}/Γ

VALUE (units 10^{-4})	DOCUMENT ID		TECN	COMMENT
$\mathbf{3.72^{+0.50}_{-0.47}\pm0.59}$	[1] DEL-AMO-SA...	11	BABR	$e^+e^- \to \Upsilon(4S)$

[1] $B \to \pi^+ X$ with $m_X < 1.71$ GeV/c^2.

$\Gamma(\Lambda_c^+ / \overline{\Lambda}_c^- \text{ anything})/\Gamma_{total}$ — Γ_{101}/Γ

VALUE (%)	CL%	DOCUMENT ID		TECN	COMMENT
3.53±0.31±0.12		[1] AUBERT	07C	BABR	$e^+e^- \to \Upsilon(4S)$
• • • We do not use the following data for averages, fits, limits, etc. • • •					
6.4 ±0.8 ±0.8		[2] CRAWFORD	92	CLEO	$e^+e^- \to \Upsilon(4S)$
14 ±9		[3] ALBRECHT	88E	ARG	$e^+e^- \to \Upsilon(4S)$
<11.2	90	[4] ALAM	87	CLEO	$e^+e^- \to \Upsilon(4S)$

[1] AUBERT 07C reports 0.045 ± 0.003 ± 0.012 from a measurement of $[\Gamma(B \to \Lambda_c^+ / \overline{\Lambda}_c^- \text{anything})/\Gamma_{total}] \times [B(\Lambda_c^+ \to pK^-\pi^+)]$ assuming $B(\Lambda_c^+ \to pK^-\pi^+) = (5.0 \pm 1.3) \times 10^{-2}$, which we rescale to our best (shown rounded) value $B(\Lambda_c^+ \to pK^-\pi^+) = (6.37 \pm 0.21) \times 10^{-2}$. Our first error is their experiment's error and our second error is the systematic error from using our best (shown rounded) value.
[2] CRAWFORD 92 result derived from lepton baryon correlations. Assumes all charmed baryons in B^0 and $B^{\pm}$ decay are Λ_c.
[3] ALBRECHT 88E measured $B(B \to \Lambda_c^+ X)\cdot B(\Lambda_c^+ \to pK^-\pi^+) = (0.30 \pm 0.12 \pm 0.06)\%$ and used $B(\Lambda_c^+ \to pK^-\pi^+) = (2.2 \pm 1.0)\%$ from ABRAMS 80 to obtain above number.
[4] Assuming all baryons result from charmed baryons, ALAM 86 conclude the branching fraction is 7.4 ± 2.9%. The limit given above is model independent.

$\Gamma(\Lambda_c^+ \text{ anything})/\Gamma(\overline{\Lambda}_c^- \text{ anything})$ — $\Gamma_{102}/\Gamma_{103}$

VALUE	DOCUMENT ID		TECN	COMMENT
0.19±0.13±0.04	[1] AMMAR	97	CLE2	$e^+e^- \to \Upsilon(4S)$

[1] AMMAR 97 uses a high-momentum lepton tag ($P_\ell > 1.4$ GeV/c^2).

$\Gamma(\overline{\Lambda}_c^- \mu^+ \text{ anything})/\Gamma(\overline{\Lambda}_c^- \text{ anything})$ — $\Gamma_{106}/\Gamma_{103}$

VALUE (units 10^{-2})	DOCUMENT ID		TECN	COMMENT
−2.0±2.0±1.9	LEES	12	BABR	$e^+e^- \to \Upsilon(4S)$

$\Gamma(\overline{\Lambda}_c^- \ell^+ \text{ anything})/\Gamma(\Lambda_c^+ / \overline{\Lambda}_c^- \text{ anything})$ — $\Gamma_{104}/\Gamma_{101}$

VALUE	CL%	DOCUMENT ID		TECN	COMMENT
$\mathbf{<2.5\times10^{-2}}$	90	[1] LEES	12	BABR	$e^+e^- \to \Upsilon(4S)$

[1] LEES 12 quotes also the measurement $\Gamma(B \to \overline{\Lambda}_c^- \ell^+ \text{anything})/\Gamma(B \to \Lambda_c^+ / \overline{\Lambda}_c^- \text{anything}) = (1.2 \pm 0.7 \pm 0.4) \times 10^{-2}$.

$\Gamma(\overline{\Lambda}_c^- e^+ \text{ anything})/\Gamma(\Lambda_c^+ / \overline{\Lambda}_c^- \text{ anything})$ — $\Gamma_{105}/\Gamma_{101}$

VALUE	CL%	DOCUMENT ID		TECN	COMMENT
<0.05	90	[1] BONVICINI	98	CLE2	$e^+e^- \to \Upsilon(4S)$

[1] BONVICINI 98 uses the electron with momentum above 0.6 GeV/c.

Int. J. Mod. Phys. A 2026.41. Downloaded from www.worldscientific.com
by UNIVERSITY OF CALIFORNIA @ BERKELEY on 09/16/26. Re-use and distribution is strictly not permitted, except for Open Access articles.

$\Gamma(\overline{\Lambda}_c^- e^+ \text{anything})/\Gamma(\overline{\Lambda}_c^- \text{anything})$ — $\Gamma_{105}/\Gamma_{103}$

VALUE (units 10^{-2})	DOCUMENT ID		TECN	COMMENT
2.5±1.1±0.6	[1] LEES	12	BABR	$e^+e^- \to \Upsilon(4S)$

[1] Uses the full reconstruction of the recoiling B in a hadronic decay as a tag.

$\Gamma(\overline{\Lambda}_c^- \ell^+ \text{anything})/\Gamma(\overline{\Lambda}_c^- \text{anything})$ — $\Gamma_{104}/\Gamma_{103}$

VALUE	CL%	DOCUMENT ID		TECN	COMMENT
$<3.5\times10^{-2}$	90	[1] LEES	12	BABR	$e^+e^- \to \Upsilon(4S)$

[1] LEES 12 quotes also the measurement $\Gamma(B \to \overline{\Lambda}_c^- \ell^+ \text{anything})/\Gamma(B \to \overline{\Lambda}_c^- \text{anything}) = (1.7 \pm 1.0 \pm 0.6)\times10^{-2}$.

$\Gamma(\overline{\Lambda}_c^- p \text{ anything})/\Gamma(\Lambda_c^+ / \overline{\Lambda}_c^- \text{anything})$ — $\Gamma_{107}/\Gamma_{101}$

VALUE	DOCUMENT ID		TECN	COMMENT
0.57±0.05±0.05	BONVICINI	98	CLE2	$e^+e^- \to \Upsilon(4S)$

$\Gamma(\overline{\Lambda}_c^- p e^+ \nu_e)/\Gamma(\overline{\Lambda}_c^- p \text{ anything})$ — $\Gamma_{108}/\Gamma_{107}$

VALUE	CL%	DOCUMENT ID		TECN	COMMENT
<0.04	90	[1] BONVICINI	98	CLE2	$e^+e^- \to \Upsilon(4S)$

[1] BONVICINI 98 uses the electron with momentum above 0.6 GeV/c.

$\Gamma(\overline{\Sigma}_c^{--} \text{anything})/\Gamma_{\text{total}}$ — Γ_{109}/Γ

VALUE	EVTS	DOCUMENT ID		TECN	COMMENT
0.0033±0.0017±0.0001	77	[1] PROCARIO	94	CLE2	$e^+e^- \to \Upsilon(4S)$

[1] PROCARIO 94 reports $[\Gamma(B \to \overline{\Sigma}_c^{--} \text{anything})/\Gamma_{\text{total}}] \times [B(\Lambda_c^+ \to pK^-\pi^+)] = 0.00021\pm0.00008\pm0.00007$ which we divide by our best (shown rounded) value $B(\Lambda_c^+ \to pK^-\pi^+) = (6.37 \pm 0.21)\times10^{-2}$. Our first error is their experiment's error and our second error is the systematic error from using our best (shown rounded) value.

$\Gamma(\overline{\Sigma}_c^- \text{anything})/\Gamma_{\text{total}}$ — Γ_{110}/Γ

VALUE	CL%	DOCUMENT ID		TECN	COMMENT
$<8\times10^{-3}$	90	[1] PROCARIO	94	CLE2	$e^+e^- \to \Upsilon(4S)$

[1] PROCARIO 94 reports $[\Gamma(B \to \overline{\Sigma}_c^- \text{anything})/\Gamma_{\text{total}}] \times [B(\Lambda_c^+ \to pK^-\pi^+)] < 0.00048$ which we divide by our best (shown rounded) value $B(\Lambda_c^+ \to pK^-\pi^+) = 6.37\times10^{-2}$.

$\Gamma(\overline{\Sigma}_c^0 \text{anything})/\Gamma_{\text{total}}$ — Γ_{111}/Γ

VALUE	EVTS	DOCUMENT ID		TECN	COMMENT
0.0036±0.0017±0.0001	76	[1] PROCARIO	94	CLE2	$e^+e^- \to \Upsilon(4S)$

[1] PROCARIO 94 reports $[\Gamma(B \to \overline{\Sigma}_c^0 \text{anything})/\Gamma_{\text{total}}] \times [B(\Lambda_c^+ \to pK^-\pi^+)] = 0.00023\pm0.00008\pm0.00007$ which we divide by our best (shown rounded) value $B(\Lambda_c^+ \to pK^-\pi^+) = (6.37 \pm 0.21)\times10^{-2}$. Our first error is their experiment's error and our second error is the systematic error from using our best (shown rounded) value.

$\Gamma(\overline{\Sigma}_c^0 N\,(N = p \text{ or } n))/\Gamma_{\text{total}}$ — Γ_{112}/Γ

VALUE	CL%	DOCUMENT ID		TECN	COMMENT
$<1.1\times10^{-3}$	90	[1] PROCARIO	94	CLE2	$e^+e^- \to \Upsilon(4S)$

[1] PROCARIO 94 reports <0.0017 from a measurement of $[\Gamma(B \to \overline{\Sigma}_c^0 N(N = p \text{ or } n))/\Gamma_{\text{total}}] \times [B(\Lambda_c^+ \to pK^-\pi^+)]$ assuming $B(\Lambda_c^+ \to pK^-\pi^+) = 0.043$, which we rescale to our best (shown rounded) value $B(\Lambda_c^+ \to pK^-\pi^+) = 6.37\times10^{-2}$.

$\Gamma(\Xi_c^0 \text{anything},\ \Xi_c^0 \to \Xi^-\pi^+)/\Gamma_{\text{total}}$ — Γ_{113}/Γ

VALUE (units 10^{-3})	DOCUMENT ID		TECN	COMMENT
0.193±0.030 OUR AVERAGE	Error includes scale factor of 1.1.			
0.211±0.019±0.025	[1] AUBERT,B	05M	BABR	$e^+e^- \to \Upsilon(4S)$
0.144±0.048±0.021	[2] BARISH	97	CLE2	$e^+e^- \to \Upsilon(4S)$

[1] The yield is obtained by requiring the momentum P < 2.15 GeV/c.
[2] BARISH 97 find 79 ± 27 Ξ_c^0 events.

$\Gamma(\Xi_c^+,\ \Xi_c^+ \to \Xi^-\pi^+\pi^+)/\Gamma_{\text{total}}$ — Γ_{114}/Γ

VALUE (units 10^{-3})	DOCUMENT ID		TECN	COMMENT
$0.453\pm0.096^{+0.085}_{-0.065}$	[1] BARISH	97	CLE2	$e^+e^- \to \Upsilon(4S)$

[1] BARISH 97 find 125 ± 28 Ξ_c^+ events.

$\Gamma(p/\overline{p} \text{ anything})/\Gamma_{\text{total}}$ — Γ_{115}/Γ

Includes p and $\overline{p}$ from Λ and $\overline{\Lambda}$ decay.

VALUE	EVTS	DOCUMENT ID		TECN	COMMENT
0.080±0.004 OUR AVERAGE					
0.080±0.005±0.005		ALBRECHT	93I	ARG	$e^+e^- \to \Upsilon(4S)$
0.080±0.005±0.003		CRAWFORD	92	CLEO	$e^+e^- \to \Upsilon(4S)$
$0.082\pm0.005^{+0.013}_{-0.010}$	2163	[1] ALBRECHT	89K	ARG	$e^+e^- \to \Upsilon(4S)$
• • • We do not use the following data for averages, fits, limits, etc. • • •					
>0.021		[2] ALAM	83B	CLEO	$e^+e^- \to \Upsilon(4S)$

[1] ALBRECHT 89K include direct and nondirect protons.
[2] ALAM 83B reported their result as > 0.036 ± 0.006 ± 0.009. Data are consistent with equal yields of p and $\overline{p}$. Using assumed yields below cut, $B(B \to p+X) = 0.03$ not including protons from Λ decays.

$\Gamma(p/\overline{p}\ (\text{direct}) \text{ anything})/\Gamma_{\text{total}}$ — Γ_{116}/Γ

VALUE	EVTS	DOCUMENT ID		TECN	COMMENT
0.055±0.005 OUR AVERAGE					
0.055±0.005±0.0035		ALBRECHT	93I	ARG	$e^+e^- \to \Upsilon(4S)$
0.056±0.006±0.005		CRAWFORD	92	CLEO	$e^+e^- \to \Upsilon(4S)$
0.055±0.016	1220	[1] ALBRECHT	89K	ARG	$e^+e^- \to \Upsilon(4S)$

[1] ALBRECHT 89K subtract contribution of Λ decay from the inclusive proton yield.

$\Gamma(\overline{p}e^+\nu_e \text{ anything})/\Gamma_{\text{total}}$ — Γ_{117}/Γ

VALUE	CL%	DOCUMENT ID		TECN	COMMENT
$<5.9\times10^{-4}$	90	[1] ADAM	03B	CLE2	$e^+e^- \to \Upsilon(4S)$
• • • We do not use the following data for averages, fits, limits, etc. • • •					
$<16\ \times10^{-4}$	90	ALBRECHT	90H	ARG	$e^+e^- \to \Upsilon(4S)$

[1] Based on $V-A$ model.

$\Gamma(\Lambda/\overline{\Lambda} \text{ anything})/\Gamma_{\text{total}}$ — Γ_{118}/Γ

VALUE	EVTS	DOCUMENT ID		TECN	COMMENT
0.040±0.005 OUR AVERAGE					
0.038±0.004±0.006	2998	CRAWFORD	92	CLEO	$e^+e^- \to \Upsilon(4S)$
0.042±0.005±0.006	943	ALBRECHT	89K	ARG	$e^+e^- \to \Upsilon(4S)$
• • • We do not use the following data for averages, fits, limits, etc. • • •					
0.022±0.003±0.0022		[1] ACKERSTAFF	97N	OPAL	$e^+e^- \to Z$
>0.011		[2] ALAM	83B	CLEO	$e^+e^- \to \Upsilon(4S)$

[1] ACKERSTAFF 97N assumes $B(b \to B) = 0.868 \pm 0.041$, *i.e.*, an admixture of B^0, $B^{\pm}$, and B_s.
[2] ALAM 83B reported their result as > 0.022 ± 0.007 ± 0.004. Values are for $(B(\Lambda X)+B(\overline{\Lambda} X))/2$. Data are consistent with equal yields of p and $\overline{p}$. Using assumed yields below cut, $B(B \to \Lambda X) = 0.03$.

$\Gamma(\Lambda \text{ anything})/\Gamma(\overline{\Lambda} \text{ anything})$ — $\Gamma_{119}/\Gamma_{120}$

VALUE	DOCUMENT ID		TECN	COMMENT
0.43±0.09±0.07	[1] AMMAR	97	CLE2	$e^+e^- \to \Upsilon(4S)$

[1] AMMAR 97 uses a high-momentum lepton tag ($P_\ell > 1.4$ GeV/c^2).

$\Gamma(\Xi^-/\overline{\Xi}^+ \text{anything})/\Gamma_{\text{total}}$ — Γ_{121}/Γ

VALUE	EVTS	DOCUMENT ID		TECN	COMMENT
0.0027±0.0006 OUR AVERAGE					
0.0027±0.0005±0.0004	147	CRAWFORD	92	CLEO	$e^+e^- \to \Upsilon(4S)$
0.0028±0.0014	54	ALBRECHT	89K	ARG	$e^+e^- \to \Upsilon(4S)$

$\Gamma(\text{baryons anything})/\Gamma_{\text{total}}$ — Γ_{122}/Γ

VALUE	DOCUMENT ID		TECN	COMMENT
0.068±0.005±0.003	[1] ALBRECHT	92O	ARG	$e^+e^- \to \Upsilon(4S)$
• • • We do not use the following data for averages, fits, limits, etc. • • •				
0.076±0.014	[2] ALBRECHT	89K	ARG	$e^+e^- \to \Upsilon(4S)$

[1] ALBRECHT 92O result is from simultaneous analysis of p and Λ yields, $p\overline{p}$ and $\Lambda\overline{p}$ correlations, and various lepton-baryon and lepton-baryon-antibaryon correlations. Supersedes ALBRECHT 89K.
[2] ALBRECHT 89K obtain this result by adding their their measurements (5.5 ± 1.6)% for direct protons and (4.2 ± 0.5 ± 0.6)% for inclusive Λ production. They then assume (5.5 ± 1.6)% for neutron production and add it in also. Since each B decay has two baryons, they divide by 2 to obtain (7.6 ± 1.4)%.

$\Gamma(p\overline{p} \text{ anything})/\Gamma_{\text{total}}$ — Γ_{123}/Γ

Includes p and $\overline{p}$ from Λ and $\overline{\Lambda}$ decay.

VALUE	EVTS	DOCUMENT ID		TECN	COMMENT
0.0247±0.0023 OUR AVERAGE					
0.024 ±0.001 ±0.004		CRAWFORD	92	CLEO	$e^+e^- \to \Upsilon(4S)$
0.025 ±0.002 ±0.002	918	ALBRECHT	89K	ARG	$e^+e^- \to \Upsilon(4S)$

$\Gamma(p\overline{p} \text{ anything})/\Gamma(p/\overline{p} \text{ anything})$ — $\Gamma_{123}/\Gamma_{115}$

Includes p and $\overline{p}$ from Λ and $\overline{\Lambda}$ decay.

VALUE	DOCUMENT ID		TECN	COMMENT
• • • We do not use the following data for averages, fits, limits, etc. • • •				
0.30±0.02±0.05	[1] CRAWFORD	92	CLEO	$e^+e^- \to \Upsilon(4S)$

[1] CRAWFORD 92 value is not independent of their $\Gamma(p\overline{p}\text{anything})/\Gamma_{\text{total}}$ value.

$\Gamma(\Lambda\overline{p}/\overline{\Lambda}p \text{ anything})/\Gamma_{\text{total}}$ — Γ_{124}/Γ

Includes p and $\overline{p}$ from Λ and $\overline{\Lambda}$ decay.

VALUE	EVTS	DOCUMENT ID		TECN	COMMENT
0.025±0.004 OUR AVERAGE					
0.029±0.005±0.005		CRAWFORD	92	CLEO	$e^+e^- \to \Upsilon(4S)$
0.023±0.004±0.003	165	ALBRECHT	89K	ARG	$e^+e^- \to \Upsilon(4S)$

$\Gamma(\Lambda\overline{p}/\overline{\Lambda}p \text{ anything})/\Gamma(\Lambda/\overline{\Lambda} \text{ anything})$ — $\Gamma_{124}/\Gamma_{118}$

Includes p and $\overline{p}$ from Λ and $\overline{\Lambda}$ decay.

VALUE	DOCUMENT ID		TECN	COMMENT
• • • We do not use the following data for averages, fits, limits, etc. • • •				
0.76±0.11±0.08	[1] CRAWFORD	92	CLEO	$e^+e^- \to \Upsilon(4S)$

[1] CRAWFORD 92 value is not independent of their $[\Gamma(\Lambda\overline{p}\text{anything})+\Gamma(\overline{\Lambda}p\text{anything})]/\Gamma_{\text{total}}$ value.

Int. J. Mod. Phys. A 2026.41. Downloaded from www.worldscientific.com
by CALIFORNIA @ BERKELEY on 09/16/26. Re-use and distribution is strictly not permitted, except for Open Access articles.

$\Gamma(\Lambda\overline{\Lambda}\text{ anything})/\Gamma_{\text{total}}$ — Γ_{125}/Γ

VALUE	CL%	EVTS	DOCUMENT ID		TECN	COMMENT
<0.005	90		CRAWFORD	92	CLEO	$e^+e^- \to \Upsilon(4S)$
• • • We do not use the following data for averages, fits, limits, etc. • • •						
<0.0088	90	12	ALBRECHT	89K	ARG	$e^+e^- \to \Upsilon(4S)$

$\Gamma(\Lambda\overline{\Lambda}\text{ anything})/\Gamma(\Lambda/\overline{\Lambda}\text{ anything})$ — $\Gamma_{125}/\Gamma_{118}$

VALUE	CL%	DOCUMENT ID		TECN	COMMENT
• • • We do not use the following data for averages, fits, limits, etc. • • •					
<0.13	90	[1] CRAWFORD	92	CLEO	$e^+e^- \to \Upsilon(4S)$

[1] CRAWFORD 92 value is not independent of their $\Gamma(\Lambda\overline{\Lambda}\text{anything})/\Gamma_{\text{total}}$ value.

$\Gamma(s e^+ e^-)/\Gamma_{\text{total}}$ — Γ_{126}/Γ

Test for $\Delta B = 1$ weak neutral current. Allowed by higher-order electroweak interactions.

VALUE (units 10^{-6})	CL%	DOCUMENT ID		TECN	COMMENT
6.7 ±1.7 OUR AVERAGE		Error includes scale factor of 2.0.			
$7.69^{+0.82}_{-0.77}{}^{+0.71}_{-0.60}$		[1] LEES	14D	BABR	$e^+e^- \to \Upsilon(4S)$
$4.04 \pm 1.30^{+0.87}_{-0.83}$		[2] IWASAKI	05	BELL	$e^+e^- \to \Upsilon(4S)$
• • • We do not use the following data for averages, fits, limits, etc. • • •					
6.0 ±1.7 ±1.3		[2] AUBERT,B	04I	BABR	Repl. by LEES 14D
5.0 ±2.3 $^{+1.3}_{-1.1}$		[2] KANEKO	03	BELL	Repl. by IWASAKI 05
< 57	90	GLENN	98	CLEO	$e^+e^- \to \Upsilon(4S)$
<50000	90	BEBEK	81	CLEO	$e^+e^- \to \Upsilon(4S)$

[1] Measured from sum of exclusive modes through K^+, $K^+\pi^0$, $K^+\pi^-$, $K^+\pi^-\pi^0$, $K^+\pi^-\pi^+$, K^0_S, $K^0_S\pi^0$, $K^0_S\pi^+$, $K^0_S\pi^+\pi^0$, and $K^0_S\pi^+\pi^-$ corrected for unobserved modes.
[2] Requires $M_{\ell^+\ell^-} > 0.2$ GeV/c^2.

$\Gamma(s\mu^+\mu^-)/\Gamma_{\text{total}}$ — Γ_{127}/Γ

Test for $\Delta B = 1$ weak neutral current. Allowed by higher-order electroweak interactions.

VALUE (units 10^{-6})	CL%	DOCUMENT ID		TECN	COMMENT
4.3 ±1.0 OUR AVERAGE					
$4.41^{+1.31}_{-1.17}{}^{+0.63}_{-0.50}$		[1] LEES	14D	BABR	$e^+e^- \to \Upsilon(4S)$
$4.13 \pm 1.05^{+0.85}_{-0.81}$		[2] IWASAKI	05	BELL	$e^+e^- \to \Upsilon(4S)$
• • • We do not use the following data for averages, fits, limits, etc. • • •					
5.0 ±2.8 ±1.2		AUBERT,B	04I	BABR	Repl. by LEES 14D
7.9 ±2.1 $^{+2.1}_{-1.5}$		KANEKO	03	BELL	Repl. by IWASAKI 05
< 58	90	GLENN	98	CLEO	$e^+e^- \to \Upsilon(4S)$
<17000	90	CHADWICK	81	CLEO	$e^+e^- \to \Upsilon(4S)$

[1] Measured from sum of exclusive modes through K^+, $K^+\pi^0$, $K^+\pi^-$, $K^+\pi^-\pi^0$, $K^+\pi^-\pi^+$, K^0_S, $K^0_S\pi^0$, $K^0_S\pi^+$, $K^0_S\pi^+\pi^0$, and $K^0_S\pi^+\pi^-$ corrected for unobserved modes.
[2] Requires $M_{\ell^+\ell^-} > 0.2$ GeV/c^2.

$[\Gamma(s e^+ e^-) + \Gamma(s\mu^+\mu^-)]/\Gamma_{\text{total}}$ — $(\Gamma_{126}+\Gamma_{127})/\Gamma$

Test for $\Delta B = 1$ weak neutral current. Allowed by higher-order electroweak interactions.

VALUE	CL%	DOCUMENT ID		TECN	COMMENT
<4.2 $\times 10^{-5}$	90	GLENN	98	CLEO	$e^+e^- \to \Upsilon(4S)$
• • • We do not use the following data for averages, fits, limits, etc. • • •					
<0.0024	90	[1] BEAN	87	CLEO	Repl. by GLENN 98
<0.0062	90	[2] AVERY	84	CLEO	Repl. by BEAN 87

[1] BEAN 87 reports $[(\mu^+\mu^-)+(e^+e^-)]/2$ and we converted it.
[2] Determine ratio of B^+ to B^0 semileptonic decays to be in the range 0.25–2.9.

$\Gamma(s\ell^+\ell^-)/\Gamma_{\text{total}}$ — Γ_{128}/Γ

Test for $\Delta B = 1$ weak neutral current.

VALUE (units 10^{-6})	DOCUMENT ID		TECN	COMMENT
5.8 ±1.3 OUR AVERAGE	Error includes scale factor of 1.8.			
$6.73^{+0.70}_{-0.64}{}^{+0.60}_{-0.56}$	[1] LEES	14D	BABR	$e^+e^- \to \Upsilon(4S)$
$4.11 \pm 0.83^{+0.85}_{-0.81}$	[2] IWASAKI	05	BELL	$e^+e^- \to \Upsilon(4S)$
• • • We do not use the following data for averages, fits, limits, etc. • • •				
5.6 ±1.5 ±1.3	[3] AUBERT,B	04I	BABR	Repl. by LEES 14D
6.1 ±1.4 $^{+1.4}_{-1.1}$	[3] KANEKO	03	BELL	Repl. by IWASAKI 05

[1] Measured from sum of exclusive modes through K^+, $K^+\pi^0$, $K^+\pi^-$, $K^+\pi^-\pi^0$, $K^+\pi^-\pi^+$, K^0_S, $K^0_S\pi^0$, $K^0_S\pi^+$, $K^0_S\pi^+\pi^0$, and $K^0_S\pi^+\pi^-$ corrected for unobserved modes.
[2] Requires $M_{\ell^+\ell^-} > 0.2$ GeV/c^2.
[3] Requires $M_{e^+e^-} > 0.2$ GeV/c^2.

$\Gamma(\pi\ell^+\ell^-)/\Gamma_{\text{total}}$ — Γ_{129}/Γ

VALUE	CL%	DOCUMENT ID		TECN	COMMENT
<5.9 $\times 10^{-8}$	90	[1] LEES	13M	BABR	$e^+e^- \to \Upsilon(4S)$
• • • We do not use the following data for averages, fits, limits, etc. • • •					
<6.2 $\times 10^{-8}$	90	[1] WEI	08A	BELL	$e^+e^- \to \Upsilon(4S)$
<9.1 $\times 10^{-8}$	90	[1] AUBERT	07AG	BABR	$e^+e^- \to \Upsilon(4S)$

[1] Assumes equal production of B^+ and B^0 at the $\Upsilon(4S)$.

$\Gamma(\pi e^+ e^-)/\Gamma_{\text{total}}$ — Γ_{130}/Γ

VALUE	CL%	DOCUMENT ID		TECN	COMMENT
<11.0 $\times 10^{-8}$	90	[1] LEES	13M	BABR	$e^+e^- \to \Upsilon(4S)$

[1] Assumes equal production of B^+ and B^0 at the $\Upsilon(4S)$.

$\Gamma(\pi\mu^+\mu^-)/\Gamma_{\text{total}}$ — Γ_{131}/Γ

VALUE	CL%	DOCUMENT ID		TECN	COMMENT
<5.0 $\times 10^{-8}$	90	[1] LEES	13M	BABR	$e^+e^- \to \Upsilon(4S)$

[1] Assumes equal production of B^+ and B^0 at the $\Upsilon(4S)$.

$\Gamma(K e^+ e^-)/\Gamma_{\text{total}}$ — Γ_{132}/Γ

Test for $\Delta B = 1$ weak neutral current. Allowed by higher-order electroweak interactions.

VALUE (units 10^{-7})	CL%	DOCUMENT ID		TECN	COMMENT
4.4±0.6 OUR AVERAGE					
$3.9^{+0.9}_{-0.8} \pm 0.2$		[1] AUBERT	09T	BABR	$e^+e^- \to \Upsilon(4S)$
$4.8^{+0.8}_{-0.7} \pm 0.3$		[1] WEI	09A	BELL	$e^+e^- \to \Upsilon(4S)$
• • • We do not use the following data for averages, fits, limits, etc. • • •					
$3.3^{+0.9}_{-0.8} \pm 0.2$		[1] AUBERT,B	06J	BABR	Repl. by AUBERT 09T
$7.4^{+1.8}_{-1.6} \pm 0.5$		[1] AUBERT	03U	BABR	Repl. by AUBERT,B 06J
$4.8^{+1.5}_{-1.3} \pm 0.3$		[1,2] ISHIKAWA	03	BELL	Repl. by WEI 09A
<13	90	ABE	02	BELL	Repl. by ISHIKAWA 03

[1] Assumes equal production of B^+ and B^0 at the $\Upsilon(4S)$.
[2] The second error is a total of systematic uncertainties including model dependence.

$\Gamma(K^*(892) e^+ e^-)/\Gamma_{\text{total}}$ — Γ_{133}/Γ

Test for $\Delta B = 1$ weak neutral current. Allowed by higher-order electroweak interactions.

VALUE (units 10^{-7})	CL%	DOCUMENT ID		TECN	COMMENT
11.9±2.0 OUR AVERAGE		Error includes scale factor of 1.2.			
$9.9^{+2.3}_{-2.1} \pm 0.6$		[1] AUBERT	09T	BABR	$e^+e^- \to \Upsilon(4S)$
$13.9^{+2.3}_{-2.0} \pm 1.2$		[1] WEI	09A	BELL	$e^+e^- \to \Upsilon(4S)$
• • • We do not use the following data for averages, fits, limits, etc. • • •					
$9.7^{+3.0}_{-2.7} \pm 1.4$		[1] AUBERT,B	06J	BABR	Repl. by AUBERT 09T
$9.8^{+5.0}_{-4.2} \pm 1.1$		[1] AUBERT	03U	BABR	Repl. by AUBERT,B 06J
$14.9^{+5.2}_{-4.6}{}^{+1.2}_{-1.3}$		[2] ISHIKAWA	03	BELL	Repl. by WEI 09A
<56	90	ABE	02	BELL	Repl. by ISHIKAWA 03

[1] Assumes equal production of B^+ and B^0 at the $\Upsilon(4S)$.
[2] Assumes equal production of B^0 and B^+ at $\Upsilon(4S)$. The second error is a total of systematic uncertainties including model dependence.

$\Gamma(K\mu^+\mu^-)/\Gamma_{\text{total}}$ — Γ_{134}/Γ

Test for $\Delta B = 1$ weak neutral current. Allowed by higher-order electroweak interactions.

VALUE (units 10^{-7})	DOCUMENT ID		TECN	COMMENT
4.4±0.4 OUR AVERAGE				
4.2±0.4±0.2	AALTONEN	11AI	CDF	$p\overline{p}$ at 1.96 TeV
$4.1^{+1.3}_{-1.2} \pm 0.2$	[1] AUBERT	09T	BABR	$e^+e^- \to \Upsilon(4S)$
5.0±0.6±0.3	[1] WEI	09A	BELL	$e^+e^- \to \Upsilon(4S)$
• • • We do not use the following data for averages, fits, limits, etc. • • •				
$3.5^{+1.3}_{-1.1} \pm 0.3$	[1] AUBERT,B	06J	BABR	Repl. by AUBERT 09T
$4.5^{+2.3}_{-1.9} \pm 0.4$	[1] AUBERT	03U	BABR	Repl. by AUBERT,B 06J
$4.8^{+1.2}_{-1.1} \pm 0.4$	[1,2] ISHIKAWA	03	BELL	Repl. by WEI 09A
$9.9^{+4.0}_{-3.2}{}^{+1.3}_{-1.0}$	ABE	02	BELL	Repl. by ISHIKAWA 03

[1] Assumes equal production of B^+ and B^0 at the $\Upsilon(4S)$.
[2] The second error is a total of systematic uncertainties including model dependence.

$\Gamma(K\mu^+\mu^-)/\Gamma(K e^+ e^-)$ — $\Gamma_{134}/\Gamma_{132}$

VALUE	DOCUMENT ID		TECN	COMMENT
$1.01^{+0.19}_{-0.16}$ OUR AVERAGE				
$1.03^{+0.28}_{-0.24} \pm 0.01$	[1] CHOUDHURY	21	BELL	$e^+e^- \to \Upsilon(4S)$
$1.00^{+0.31}_{-0.25} \pm 0.07$	[2] LEES	12S	BABR	$e^+e^- \to \Upsilon(4S)$
$0.96^{+0.44}_{-0.34} \pm 0.05$	AUBERT	09T	BABR	$e^+e^- \to \Upsilon(4S)$
• • • We do not use the following data for averages, fits, limits, etc. • • •				
1.03±0.19±0.06	[3] WEI	09A	BELL	$e^+e^- \to \Upsilon(4S)$
1.06±0.48±0.08	AUBERT,B	06J	BABR	Repl. by AUBERT 09T

[1] For $1.0 < q^2 < 6.0$ GeV^2/c^4. Measurements in other q^2 bins are also reported.
[2] Measured in the union of $0.10 < q^2 < 8.12$ GeV^2/c^4 and $q^2 > 10.11$ GeV^2/c^4. LEES 12s reports also individual measurements $\Gamma(B \to K\mu^+\mu^-)/\Gamma(B \to K e^+e^-) = 0.74^{+0.40}_{-0.31} \pm 0.06$ for $0.10 < q^2 < 8.12$ GeV^2/c^4 and $\Gamma(B \to K\mu^+\mu^-)/\Gamma(B \to K e^+e^-) = 1.43^{+0.65}_{-0.44} \pm 0.12$ for $q^2 > 10.11$ GeV^2/c^4.
[3] Superseded by CHOUDHURY 21.

Int. J. Mod. Phys. A 2026.41. Downloaded from www.worldscientific.com by UNIVERSITY OF CALIFORNIA @ BERKELEY on 09/16/26. Re-use and distribution is strictly not permitted, except for Open Access articles.

$\Gamma(K^*(892)\mu^+\mu^-)/\Gamma_{total}$ — Γ_{135}/Γ

Test for $\Delta B = 1$ weak neutral current. Allowed by higher-order electroweak interactions.

VALUE (units 10^{-7})	CL%	DOCUMENT ID		TECN	COMMENT
10.6±0.9 OUR AVERAGE					
$10.1\pm1.0\pm0.5$		AALTONEN	11AI	CDF	$p\overline{p}$ at 1.96 TeV
$13.5^{+3.5}_{-3.3}\pm1.0$		[1] AUBERT	09T	BABR	$e^+e^-\to\Upsilon(4S)$
$11.0^{+1.6}_{-1.4}\pm0.8$		[1] WEI	09A	BELL	$e^+e^-\to\Upsilon(4S)$
• • • We do not use the following data for averages, fits, limits, etc. • • •					
$8.8^{+3.5}_{-3.0}\pm1.2$		[1] AUBERT,B	06J	BABR	Repl. by AUBERT 09T
$12.7^{+7.6}_{-6.1}\pm1.6$		[1] AUBERT	03U	BABR	Repl. by AUBERT,B 06J
$11.7^{+3.6}_{-3.1}\pm1.0$		[2] ISHIKAWA	03	BELL	Repl. by WEI 09A
<31	90	ABE	02	BELL	Repl. by ISHIKAWA 03

[1] Assumes equal production of B^+ and B^0 at the $\Upsilon(4S)$.
[2] Assumes equal production of B^0 and B^+ at $\Upsilon(4S)$. The second error is a total of systematic uncertainties including model dependence.

$\Gamma(K^*(892)\mu^+\mu^-)/\Gamma(K^*(892)e^+e^-)$ — $\Gamma_{135}/\Gamma_{133}$

VALUE	DOCUMENT ID		TECN	COMMENT
0.98±0.15 OUR AVERAGE				
$1.13^{+0.34}_{-0.26}\pm0.10$	[1] LEES	12S	BABR	$e^+e^-\to\Upsilon(4S)$
$1.37^{+0.53}_{-0.40}\pm0.09$	AUBERT	09T	BABR	$e^+e^-\to\Upsilon(4S)$
$0.83\pm0.17\pm0.08$	WEI	09A	BELL	$e^+e^-\to\Upsilon(4S)$
• • • We do not use the following data for averages, fits, limits, etc. • • •				
$0.91\pm0.45\pm0.06$	AUBERT,B	06J	BABR	Repl. by AUBERT 09T

[1] Measured in the union of $0.10 < q^2 < 8.12$ GeV^2/c^4 and $q^2 > 10.11$ GeV^2/c^4. LEES 12S reports also individual measurements $\Gamma(B\to K^*(892)\mu^+\mu^-)/\Gamma(B\to K^*(892)e^+e^-) = 1.06^{+0.48}_{-0.33}\pm0.08$ for $0.10 < q^2 < 8.12$ GeV^2/c^4 and $\Gamma(B\to K^*(892)\mu^+\mu^-)/\Gamma(B\to K^*(892)e^+e^-) = 1.18^{+0.55}_{-0.37}\pm0.11$ for $q^2 > 10.11$ GeV^2/c^4.

$\Gamma(K\ell^+\ell^-)/\Gamma_{total}$ — Γ_{136}/Γ

Test for $\Delta B = 1$ weak neutral current. Allowed by higher-order electroweak interactions.

VALUE (units 10^{-7})	CL%	DOCUMENT ID		TECN	COMMENT
4.8±0.4 OUR AVERAGE					
$4.7\pm0.6\pm0.2$		LEES	12S	BABR	$e^+e^-\to\Upsilon(4S)$
$4.8^{+0.5}_{-0.4}\pm0.3$		WEI	09A	BELL	$e^+e^-\to\Upsilon(4S)$
• • • We do not use the following data for averages, fits, limits, etc. • • •					
$3.9\pm0.7\pm0.2$		[1] AUBERT	09T	BABR	Repl. by LEES 12S
$3.4\pm0.7\pm0.2$		[1] AUBERT,B	06J	BABR	Repl. by AUBERT 09T
$6.5^{+1.4}_{-1.3}\pm0.4$		[2] AUBERT	03U	BABR	Repl. by AUBERT,B 06J
$4.8^{+1.0}_{-0.9}\pm0.3$		[3] ISHIKAWA	03	BELL	Repl. by WEI 09A
$7.5^{+2.5}_{-2.1}\pm0.6$		[4] ABE	02	BELL	Repl. by ISHIKAWA 03
< 5.1	90	[1] AUBERT	02L	BABR	$e^+e^-\to\Upsilon(4S)$
<17	90	[5] ANDERSON	01B	CLE2	$e^+e^-\to\Upsilon(4S)$

[1] Assumes equal production of B^+ and B^0 at the $\Upsilon(4S)$.
[2] Assumes all four $B\to K\ell^+\ell^-$ modes having equal partial widths in the fit.
[3] Assumes equal production rate for charge and neutral B meson pairs, isospin invariance, lepton universality for $B\to K\ell^+\ell^-$, and $B(B\to K^*(892)\mu^+\mu^-) = 1.33$. The second error is total systematic uncertainties including model dependence.
[4] Assumes lepton universality.
[5] The result is for di-lepton masses above 0.5 GeV.

$\Gamma(K^*(892)\ell^+\ell^-)/\Gamma_{total}$ — Γ_{137}/Γ

Test for $\Delta B = 1$ weak neutral current. Allowed by higher-order electroweak interactions.

VALUE (units 10^{-7})	CL%	DOCUMENT ID		TECN	COMMENT
10.5±1.0 OUR AVERAGE					
$10.2^{+1.4}_{-1.3}\pm0.5$		LEES	12S	BABR	$e^+e^-\to\Upsilon(4S)$
$10.7^{+1.1}_{-1.0}\pm0.9$		WEI	09A	BELL	$e^+e^-\to\Upsilon(4S)$
• • • We do not use the following data for averages, fits, limits, etc. • • •					
$11.1^{+1.9}_{-1.8}\pm0.7$		[1] AUBERT	09T	BABR	Repl. by LEES 12S
$7.8^{+1.9}_{-1.7}\pm1.1$		[1] AUBERT,B	06J	BABR	Repl. by AUBERT 09T
$8.8^{+3.3}_{-2.9}\pm1.0$		[2] AUBERT	03U	BABR	Repl. by AUBERT,B 06J
$11.5^{+2.6}_{-2.4}\pm0.8$		[3] ISHIKAWA	03	BELL	Repl. by WEI 09A
<31	90	[1,4] AUBERT	02L	BABR	Repl. by AUBERT 03U
<33	90	[5] ANDERSON	01B	CLE2	$e^+e^-\to\Upsilon(4S)$

[1] Assumes equal production of B^+ and B^0 at the $\Upsilon(4S)$.
[2] Assumes the partial width ratio of electron and muon modes to be $\Gamma(B\to K^*(892)e^+e^-)/\Gamma(B\to K^*(892)\mu^+\mu^-) = 1.33$.
[3] Assumes equal production rate for charge and neutral B meson pairs, isospin invariance, lepton universality for $B\to K\ell^+\ell^-$, and $B(B\to K^*(892)\mu^+\mu^-) = 1.33$. The second error is total systematic uncertainties including model dependence.
[4] For averaging $K^*(892)\mu^+\mu^-$ and $K^*(892)e^+e^-$ modes, AUBERT 02L assumed $B(B\to K^*(892)e^+e^-)/B(B\to K^*(892)\mu^+\mu^-) = 1.2$.
[5] The result is for di-lepton masses above 0.5 GeV.

$\Gamma(K\nu\overline{\nu})/\Gamma_{total}$ — Γ_{138}/Γ

Test for $\Delta B = 1$ weak neutral current.

VALUE	CL%	DOCUMENT ID		TECN	COMMENT
$<1.6\times10^{-5}$	90	[1] GRYGIER	17	BELL	$e^+e^-\to\Upsilon(4S)$
• • • We do not use the following data for averages, fits, limits, etc. • • •					
$<1.7\times10^{-5}$	90	[1,2] LEES	13I	BABR	$e^+e^-\to\Upsilon(4S)$
$<1.4\times10^{-5}$	90	[1] DEL-AMO-SA...	10Q	BABR	Repl. by LEES 13I

[1] Assumes equal production of B^+ and B^0 at the $\Upsilon(4S)$.
[2] Also reported a limit $< 3.2\times10^{-5}$ at 90% CL obtained using a fully reconstructed hadronic B-tag evnets.

$\Gamma(K^*\nu\overline{\nu})/\Gamma_{total}$ — Γ_{139}/Γ

Test for $\Delta B = 1$ weak neutral current.

VALUE	CL%	DOCUMENT ID		TECN	COMMENT
$<2.7\times10^{-5}$	90	[1] GRYGIER	17	BELL	$e^+e^-\to\Upsilon(4S)$
• • • We do not use the following data for averages, fits, limits, etc. • • •					
$<7.6\times10^{-5}$	90	[1,2] LEES	13I	BABR	$e^+e^-\to\Upsilon(4S)$
$<8\times10^{-5}$	90	AUBERT	08BC	BABR	Repl. by LEES 13I

[1] Assumes equal production of B^+ and B^0 at the $\Upsilon(4S)$.
[2] Also reported a limit $< 7.9\times10^{-5}$ at 90% CL obtained using a fully reconstructed hadronic B-tag evnets.

$\Gamma(\pi\nu\overline{\nu})/\Gamma_{total}$ — Γ_{140}/Γ

VALUE	CL%	DOCUMENT ID		TECN	COMMENT
$<0.8\times10^{-5}$	90	[1] GRYGIER	17	BELL	$e^+e^-\to\Upsilon(4S)$

[1] Assumes equal production of B^+ and B^0 at the $\Upsilon(4S)$.

$\Gamma(\rho\nu\overline{\nu})/\Gamma_{total}$ — Γ_{141}/Γ

VALUE	CL%	DOCUMENT ID		TECN	COMMENT
$<2.8\times10^{-5}$	90	[1] GRYGIER	17	BELL	$e^+e^-\to\Upsilon(4S)$

[1] Assumes equal production of B^+ and B^0 at the $\Upsilon(4S)$.

$\Gamma(s e^{\pm}\mu^{\mp})/\Gamma_{total}$ — Γ_{142}/Γ

Test for lepton family number conservation. Allowed by higher-order electroweak interactions.

VALUE	CL%	DOCUMENT ID		TECN	COMMENT
$<2.2\times10^{-5}$	90	GLENN	98	CLEO	$e^+e^-\to\Upsilon(4S)$

$\Gamma(\pi e^{\pm}\mu^{\mp})/\Gamma_{total}$ — Γ_{143}/Γ

Test of lepton family number conservation.

VALUE	CL%	DOCUMENT ID		TECN	COMMENT
$<9.2\times10^{-8}$	90	[1] AUBERT	07AG	BABR	$e^+e^-\to\Upsilon(4S)$
• • • We do not use the following data for averages, fits, limits, etc. • • •					
$<1.6\times10^{-6}$	90	[1] EDWARDS	02B	CLE2	$e^+e^-\to\Upsilon(4S)$

[1] Assumes equal production of B^+ and B^0 at the $\Upsilon(4S)$.

$\Gamma(\rho e^{\pm}\mu^{\mp})/\Gamma_{total}$ — Γ_{144}/Γ

Test of lepton family number conservation.

VALUE	CL%	DOCUMENT ID		TECN	COMMENT
$<3.2\times10^{-6}$	90	[1] EDWARDS	02B	CLE2	$e^+e^-\to\Upsilon(4S)$

[1] Assumes equal production of B^+ and B^0 at the $\Upsilon(4S)$.

$\Gamma(K e^{\pm}\mu^{\mp})/\Gamma_{total}$ — Γ_{145}/Γ

Test of lepton family number conservation.

VALUE (units 10^{-7})	CL%	DOCUMENT ID		TECN	COMMENT
< 0.38	90	[1] AUBERT,B	06J	BABR	$e^+e^-\to\Upsilon(4S)$
• • • We do not use the following data for averages, fits, limits, etc. • • •					
<16	90	[1] EDWARDS	02B	CLE2	$e^+e^-\to\Upsilon(4S)$

[1] Assumes equal production of B^+ and B^0 at the $\Upsilon(4S)$.

$\Gamma(K^*(892)e^{\pm}\mu^{\mp})/\Gamma_{total}$ — Γ_{146}/Γ

Test of lepton family number conservation.

VALUE (units 10^{-7})	CL%	DOCUMENT ID		TECN	COMMENT
< 5.1	90	[1] AUBERT,B	06J	BABR	$e^+e^-\to\Upsilon(4S)$
• • • We do not use the following data for averages, fits, limits, etc. • • •					
<62	90	[1] EDWARDS	02B	CLE2	$e^+e^-\to\Upsilon(4S)$

[1] Assumes equal production of B^+ and B^0 at the $\Upsilon(4S)$.

CP VIOLATION

A_{CP} is defined as

$$\frac{B(\overline{B}\to\overline{f})-B(B\to f)}{B(\overline{B}\to\overline{f})+B(B\to f)},$$

the *CP*-violation charge asymmetry of inclusive $B^{\pm}$ and B^0 decay.

$A_{CP}(B\to K^*(892)\gamma)$

VALUE	DOCUMENT ID		TECN	COMMENT
−0.003±0.011 OUR AVERAGE				
$-0.004\pm0.014\pm0.003$	[1] HORIGUCHI	17	BELL	$e^+e^-\to\Upsilon(4S)$
$-0.003\pm0.017\pm0.007$	[2] AUBERT	09AO	BABR	$e^+e^-\to\Upsilon(4S)$
$0.08\pm0.13\pm0.03$	[3] COAN	00	CLE2	$e^+e^-\to\Upsilon(4S)$
• • • We do not use the following data for averages, fits, limits, etc. • • •				
$-0.013\pm0.036\pm0.010$	[4] AUBERT,BE	04A	BABR	Repl. by AUBERT 09AO

$-0.015 \pm 0.044 \pm 0.012$	[3] NAKAO	04	BELL	Repl. by HORIGUCHI 17
$-0.044 \pm 0.076 \pm 0.012$	[5] AUBERT	02C	BABR	Repl. by AUBERT,BE 04A

[1] Uses B($\Upsilon(4S) \rightarrow B^+B^-$) = (51.4 ± 0.6)% and B($\Upsilon(4S) \rightarrow B^0\overline{B}^0$) = (48.6 ± 0.6)%.
[2] Corresponds to a 90% CL interval $-0.033 < A_{CP} < 0.028$.
[3] Assumes equal production of B^+ and B^0 at the $\Upsilon(4S)$.
[4] Corresponds to a 90% CL allowed region, $-0.074 < A_{CP} < 0.049$.
[5] A 90% CL range is $-0.170 < A_{CP} < 0.082$.

$A_{CP}(B \rightarrow s\gamma)$

VALUE	DOCUMENT ID		TECN	COMMENT
0.015 ±0.011 OUR AVERAGE				
$0.0144 \pm 0.0128 \pm 0.0011$	[1] WATANUKI	19	BELL	$e^+e^- \rightarrow \Upsilon(4S)$
$0.017 \pm 0.019 \pm 0.010$	[2] LEES	14K	BABR	$e^+e^- \rightarrow \Upsilon(4S)$
• • • We do not use the following data for averages, fits, limits, etc. • • •				
$-0.011 \pm 0.030 \pm 0.014$	[3] AUBERT	08BJ	BABR	Repl. by LEES 14K
$0.025 \pm 0.050 \pm 0.015$	[4] AUBERT,B	04E	BABR	Repl. by AUBERT 08BJ
$0.002 \pm 0.050 \pm 0.030$	[5] NISHIDA	04	BELL	Repl. by WATANUKI 19

[1] Using a sum-of-exclusive technique with $m_{X_s} < 2.8$ GeV/c^2.
[2] Measured with 16 exclusively reconstructed $B \rightarrow X_s\gamma$ decays with $0.6 < m_{X_s} < 2.0$ GeV/c^2 (ten charged and six neutral self-tagging B modes).
[3] Uses a sum of exclusively reconstructed $B \rightarrow X_s$ decay modes, with X_s mass between 0.6 and 2.8 GeV/c^2.
[4] Corresponds to $-0.06 < A_{CP} < 0.11$ at 90% CL.
[5] This measurement is performed inclusively for recoil mass X_s less than 2.1 GeV, which corresponds to $-0.093 < A_{CP} < 0.096$ at 90% CL.

$A_{CP}(B \rightarrow (s+d)\gamma)$

VALUE	DOCUMENT ID		TECN	COMMENT
0.010±0.031 OUR AVERAGE				
$0.022 \pm 0.039 \pm 0.009$	[1] PESANTEZ	15	BELL	$e^+e^- \rightarrow \Upsilon(4S)$
$0.057 \pm 0.060 \pm 0.018$	LEES	12V	BABR	$e^+e^- \rightarrow \Upsilon(4S)$
$-0.10 \pm 0.18 \pm 0.05$	[2] AUBERT	08O	BABR	$e^+e^- \rightarrow \Upsilon(4S)$
$-0.110 \pm 0.115 \pm 0.017$	AUBERT,BE	06B	BABR	$e^+e^- \rightarrow \Upsilon(4S)$
$-0.079 \pm 0.108 \pm 0.022$	[3] COAN	01	CLE2	$e^+e^- \rightarrow \Upsilon(4S)$

[1] Assumes equal production of B^+ and B^0 at the $\Upsilon(4S)$. Uses an opposite side lepton tag. Requires center-of-mass frame $E_\gamma > 2.1$ GeV.
[2] Uses a fully reconstructed B meson as a tag on the recoil side. Requires $E_\gamma > 2.2$ GeV.
[3] Corresponds to $-0.27 < A_{CP} < 0.10$ at 90% CL.

$A_{CP}(B \rightarrow X_s\ell^+\ell^-)$

VALUE	DOCUMENT ID		TECN	COMMENT
0.04±0.11±0.01	[1] LEES	14D	BABR	$e^+e^- \rightarrow \Upsilon(4S)$
• • • We do not use the following data for averages, fits, limits, etc. • • •				
$-0.22 \pm 0.26 \pm 0.02$	[2] AUBERT,B	04I	BABR	Repl. by LEES 14D

[1] Measured from sum of exclusive modes through K^+, $K^+\pi^0$, $K^+\pi^-$, $K^+\pi^-\pi^0$, $K^+\pi^-\pi^+$, $K^0_S\pi^+$, and $K^0_S\pi^+\pi^0$.
[2] The final state flavor is determined by the kaon and pion charges where modes with $X_s = K^0_S$, $K^0_S\pi^0$ or $K^0_S\pi^+\pi^-$ are not used.

$A_{CP}(B \rightarrow X_s\ell^+\ell^-)$ ($1.0 < q^2 < 6.0$ GeV^2/c^4)

VALUE	DOCUMENT ID		TECN	COMMENT
−0.06±0.22±0.01	[1] LEES	14D	BABR	$e^+e^- \rightarrow \Upsilon(4S)$

[1] Measured from sum of exclusive modes through K^+, $K^+\pi^0$, $K^+\pi^-$, $K^+\pi^-\pi^0$, $K^+\pi^-\pi^+$, $K^0_S\pi^+$, and $K^0_S\pi^+\pi^0$.

$A_{CP}(B \rightarrow X_s\ell^+\ell^-)$ ($10.1 < q^2 < 12.9$ or $q^2 > 14.2$ GeV^2/c^4)

VALUE	DOCUMENT ID		TECN	COMMENT
$\mathbf{0.19^{+0.18}_{-0.17} \pm 0.01}$	[1] LEES	14D	BABR	$e^+e^- \rightarrow \Upsilon(4S)$

[1] Measured from sum of exclusive modes through K^+, $K^+\pi^0$, $K^+\pi^-$, $K^+\pi^-\pi^0$, $K^+\pi^-\pi^+$, $K^0_S\pi^+$, and $K^0_S\pi + (pi-)^0$.

$A_{CP}(B \rightarrow K^* e^+e^-)$

VALUE	DOCUMENT ID		TECN	COMMENT
−0.18±0.15±0.01	WEI	09A	BELL	$e^+e^- \rightarrow \Upsilon(4S)$

$A_{CP}(B \rightarrow K^*\mu^+\mu^-)$

VALUE	DOCUMENT ID		TECN	COMMENT
−0.03±0.13±0.02	WEI	09A	BELL	$e^+e^- \rightarrow \Upsilon(4S)$

$A_{CP}(B \rightarrow K^*\ell^+\ell^-)$

VALUE	DOCUMENT ID		TECN	COMMENT
−0.04±0.07 OUR AVERAGE				
$0.03 \pm 0.13 \pm 0.01$	[1] LEES	12S	BABR	$e^+e^- \rightarrow \Upsilon(4S)$
$+0.01^{+0.16}_{-0.15} \pm 0.01$	AUBERT	09T	BABR	$e^+e^- \rightarrow \Upsilon(4S)$
$-0.10 \pm 0.10 \pm 0.01$	WEI	09A	BELL	$e^+e^- \rightarrow \Upsilon(4S)$

[1] Measured in the union of $0.10 < q^2 < 8.12$ GeV^2/c^4 and $q^2 > 10.11$ GeV^2/c^4. LEES 12S reports also individual measurements $A_{CP}(B \rightarrow K^*\ell^+\ell^-) = -0.13^{+0.18}_{-0.19} \pm 0.01$ for $0.10 < q^2 < 8.12$ GeV^2/c^4 and $A_{CP}(B \rightarrow K^*\ell^+\ell^-) = 0.16^{+0.18}_{-0.19} \pm 0.01$ for $q^2 > 10.11$ GeV^2/c^4.

$A_{CP}(B \rightarrow \eta$ anything$)$

VALUE	DOCUMENT ID		TECN	COMMENT
$\mathbf{-0.13 \pm 0.04^{+0.02}_{-0.03}}$	[1] NISHIMURA	10	BELL	$e^+e^- \rightarrow \Upsilon(4S)$

[1] Uses $B \rightarrow \eta X_s$ with $0.4 < m_{X_s} < 2.6$ GeV/c^2.

$\Delta A_{CP}(X_s\gamma) = A_{CP}(B^{\pm} \rightarrow X_s\gamma) - A_{CP}(B^0 \rightarrow X_s\gamma)$

This is the isospin difference of the CP asymmetries.

VALUE	DOCUMENT ID		TECN	COMMENT
0.041 ±0.023 OUR AVERAGE				
$0.0369 \pm 0.0265 \pm 0.0076$	[1] WATANUKI	19	BELL	$e^+e^- \rightarrow \Upsilon(4S)$
$0.050 \pm 0.039 \pm 0.015$	[2] LEES	14K	BABR	$e^+e^- \rightarrow \Upsilon(4S)$

[1] Using a sum-of-exclusive technique with $m_{X_s} < 2.8$ GeV/c^2.
[2] Measured with 16 exclusively reconstructed $B \rightarrow X_s\gamma$ decays with $0.6 < m_{X_s} < 2.0$ GeV/c^2 (ten charged and six neutral self-tagging B modes).

$\overline{A}_{CP}(B \rightarrow X_s\gamma) = (A_{CP}(B^+ \rightarrow X_s\gamma) + A_{CP}(B^0 \rightarrow X_s\gamma))/2$

VALUE	DOCUMENT ID		TECN	COMMENT
0.0091±0.0121±0.0013	[1] WATANUKI	19	BELL	$e^+e^- \rightarrow \Upsilon(4S)$

[1] Using a sum-of-exclusive technique with $m_{X_s} < 2.8$ GeV/c^2.

$\Delta A_{CP}(B \rightarrow K^*\gamma) = A_{CP}(B^+ \rightarrow K^{*+}\gamma) - A_{CP}(B^0 \rightarrow K^{*0}\gamma)$

This is the isospin difference of the CP asymmetries.

VALUE	DOCUMENT ID		TECN	COMMENT
0.025±0.023 OUR AVERAGE				
$0.026 \pm 0.038 \pm 0.006$	ADACHI	25Z	BELL	$e^+e^- \rightarrow \Upsilon(4S)$
$0.024 \pm 0.028 \pm 0.005$	[1] HORIGUCHI	17	BELL	$e^+e^- \rightarrow \Upsilon(4S)$

[1] Uses B($\Upsilon(4S) \rightarrow B^+B^-$) = (51.4 ± 0.6)% and B($\Upsilon(4S) \rightarrow B^0\overline{B}^0$) = (48.6 ± 0.6)%.

$\overline{A}_{CP}(B \rightarrow K^*\gamma) = (A_{CP}(B^+ \rightarrow K^{*+}\gamma) + A_{CP}(B^0 \rightarrow K^{*0}\gamma))/2$

This is the average CP asymmetry.

VALUE	DOCUMENT ID		TECN	COMMENT
−0.009±0.011 OUR AVERAGE				
$-0.024 \pm 0.019 \pm 0.003$	ADACHI	25Z	BELL	$e^+e^- \rightarrow \Upsilon(4S)$
$-0.001 \pm 0.014 \pm 0.003$	[1] HORIGUCHI	17	BELL	$e^+e^- \rightarrow \Upsilon(4S)$

[1] Uses B($\Upsilon(4S) \rightarrow B^+B^-$) = (51.4 ± 0.6)% and B($\Upsilon(4S) \rightarrow B^0\overline{B}^0$) = (48.6 ± 0.6)%.

POLARIZATION IN B DECAY

In decays involving two vector mesons, one can distinguish among the states in which meson polarizations are both longitudinal (L) or both are transverse and parallel ($\|$) or perpendicular ($\perp$) to each other with the parameters Γ_L/Γ, $\Gamma_\perp/\Gamma$, and the relative phases $\phi_\|$ and $\phi_\perp$. See the definitions in the note on "Polarization in B Decays" review in the B^0 Particle Listings.

$F_L(B \rightarrow K^*\ell^+\ell^-)$ ($q^2 > 0.1$ GeV^2/c^4)

VALUE	DOCUMENT ID		TECN	COMMENT
$\mathbf{0.63^{+0.18}_{-0.19} \pm 0.05}$	[1] AUBERT,B	06J	BABR	$e^+e^- \rightarrow \Upsilon(4S)$

[1] Results with different q^2 cuts are also reported.

$F_L(B \rightarrow K^*\ell^+\ell^-)$ ($m_{\ell\ell} < 2.5$ GeV/c^2)

VALUE	DOCUMENT ID		TECN	COMMENT
0.35±0.16±0.04	AUBERT	09N	BABR	$e^+e^- \rightarrow \Upsilon(4S)$

$F_L(B \rightarrow K^*\ell^+\ell^-)$ ($m_{\ell\ell} > 3.2$ GeV/c^2)

VALUE	DOCUMENT ID		TECN	COMMENT
$\mathbf{0.71^{+0.20}_{-0.22} \pm 0.04}$	AUBERT	09N	BABR	$e^+e^- \rightarrow \Upsilon(4S)$

$F_L(B \rightarrow K^*\ell^+\ell^-)$ ($0.10 < q^2 < 0.98$ GeV^2/c^4)

VALUE	DOCUMENT ID		TECN	COMMENT
$\mathbf{0.263^{+0.045}_{-0.044} \pm 0.017}$	AAIJ	16B	LHCB	pp at 7, 8 TeV

$F_L(B \rightarrow K^*\ell^+\ell^-)$ ($1.1 < q^2 < 2.5$ GeV^2/c^4)

VALUE	DOCUMENT ID		TECN	COMMENT
$\mathbf{0.660^{+0.083}_{-0.077} \pm 0.022}$	AAIJ	16B	LHCB	pp at 7, 8 TeV

$F_L(B \rightarrow K^*\ell^+\ell^-)$ ($0.1 < q^2 < 2.0$ GeV^2/c^4)

VALUE	DOCUMENT ID		TECN	COMMENT
$\mathbf{0.34^{+0.08}_{-0.07}}$ **OUR AVERAGE**				
$0.37^{+0.10}_{-0.09} {}^{+0.04}_{-0.03}$	AAIJ	13Y	LHCB	pp at 7 TeV, $K^{*0}\mu^+\mu^-$
$0.30 \pm 0.16 \pm 0.02$	AALTONEN	12I	CDF	$p\overline{p}$ at 1.96 TeV
$0.29^{+0.21}_{-0.18} \pm 0.02$	WEI	09A	BELL	$e^+e^- \rightarrow \Upsilon(4S)$
• • • We do not use the following data for averages, fits, limits, etc. • • •				
$0.60^{+0.00}_{-0.28} \pm 0.19$	[1] CHATRCHYAN	13BL	CMS	pp at 7 TeV
$0.00^{+0.13}_{-0.00} \pm 0.02$	AAIJ	12U	LHCB	Repl. by AAIJ 13Y
$0.53^{+0.32}_{-0.34} \pm 0.07$	AALTONEN	11L	CDF	Repl. by AALTONEN 12I

[1] CHATRCHYAN 13BL uses, for this bin, $1.0 < q^2 < 2.0$ GeV^2/c^4.

Int. J. Mod. Phys. A 2026.41. Downloaded from www.worldscientific.com
by CALIFORNIA @ BERKELEY on 09/16/26. Re-use and distribution is strictly not permitted, except for Open Access articles.

Int. J. Mod. Phys. A 2026.41. Downloaded from www.worldscientific.com
by UNIVERSITY OF CALIFORNIA @ BERKELEY on 09/16/26. Re-use and distribution is strictly not permitted, except for Open Access articles.

$F_L(B \to K^* \ell^+ \ell^-)$ ($2.0 < q^2 < 4.3$ GeV^2/c^4)

VALUE	DOCUMENT ID		TECN	COMMENT
0.77 ±0.05 OUR AVERAGE				
$0.876^{+0.109}_{-0.097}\pm0.017$	[1] AAIJ	16B	LHCB	pp at 7, 8 TeV
$0.80 \pm0.08 \pm0.06$	KHACHATRY...	16D	CMS	pp at 8 TeV
$0.74 ^{+0.10}_{-0.09} ^{+0.02}_{-0.03}$	AAIJ	13Y	LHCB	pp at 7 TeV, $K^{*0}\mu^+\mu^-$
$0.65 \pm0.17 \pm0.03$	CHATRCHYAN	13BL	CMS	pp at 7 TeV
$0.37 ^{+0.25}_{-0.24} \pm0.10$	AALTONEN	12I	CDF	$p\overline{p}$ at 1.96 TeV
$0.71 \pm0.24 \pm0.05$	WEI	09A	BELL	$e^+e^- \to \Upsilon(4S)$
• • • We do not use the following data for averages, fits, limits, etc. • • •				
$0.77 \pm0.15 \pm0.03$	AAIJ	12U	LHCB	Repl. by AAIJ 13Y
$0.40 ^{+0.32}_{-0.33} \pm0.08$	AALTONEN	11L	CDF	Repl. by AALTONEN 12I

[1] Measured in $2.5 < q^2 < 4.0$ GeV^2/c^4.

$F_L(B \to K^* \ell^+ \ell^-)$ ($4.0 < q^2 < 6.0$ GeV^2/c^4)

VALUE	DOCUMENT ID		TECN	COMMENT
$\mathbf{0.611^{+0.052}_{-0.053}\pm0.017}$	AAIJ	16B	LHCB	pp at 7, 8 TeV

$F_L(B \to K^* \ell^+ \ell^-)$ ($6.0 < q^2 < 8.0$ GeV^2/c^4)

VALUE	DOCUMENT ID		TECN	COMMENT
0.579±0.046±0.015	AAIJ	16B	LHCB	pp at 7, 8 TeV

$F_L(B \to K^* \ell^+ \ell^-)$ ($4.3 < q^2 < 8.6$ GeV^2/c^4)

VALUE	DOCUMENT ID		TECN	COMMENT
0.64±0.06 OUR AVERAGE				
$0.57\pm0.07\pm0.03$	AAIJ	13Y	LHCB	pp at 7 TeV, $K^{*0}\mu^+\mu^-$
$0.81^{+0.13}_{-0.12}\pm0.05$	CHATRCHYAN	13BL	CMS	pp at 7 TeV
$0.68^{+0.15}_{-0.17}\pm0.09$	AALTONEN	12I	CDF	$p\overline{p}$ at 1.96 TeV
$0.64^{+0.23}_{-0.24}\pm0.07$	WEI	09A	BELL	$e^+e^- \to \Upsilon(4S)$
• • • We do not use the following data for averages, fits, limits, etc. • • •				
$0.60^{+0.06}_{-0.07}\pm0.01$	AAIJ	12U	LHCB	Repl. by AAIJ 13Y
$0.82^{+0.19}_{-0.23}\pm0.07$	AALTONEN	11L	CDF	Repl. by AALTONEN 12I

$F_L(B \to K^* \ell^+ \ell^-)$ ($10.09 < q^2 < 12.86$ GeV^2/c^4)

VALUE	DOCUMENT ID		TECN	COMMENT
0.448±0.033 OUR AVERAGE				
$0.493^{+0.049}_{-0.047}\pm0.013$	[1] AAIJ	16B	LHCB	pp at 7, 8 TeV
$0.39 \pm0.05 \pm0.04$	KHACHATRY...	16D	CMS	pp at 8 TeV
$0.48 ^{+0.08}_{-0.09} \pm0.03$	AAIJ	13Y	LHCB	pp at 7 TeV, $K^{*0}\mu^+\mu^-$
$0.45 ^{+0.10}_{-0.11} \pm0.04$	CHATRCHYAN	13BL	CMS	pp at 7 TeV
$0.47 \pm0.14 \pm0.03$	AALTONEN	12I	CDF	$p\overline{p}$ at 1.96 TeV
$0.17 ^{+0.17}_{-0.15} \pm0.03$	WEI	09A	BELL	$e^+e^- \to \Upsilon(4S)$
• • • We do not use the following data for averages, fits, limits, etc. • • •				
$0.41 \pm0.11 \pm0.03$	AAIJ	12U	LHCB	Repl. by AAIJ 13Y
$0.31 ^{+0.19}_{-0.18} \pm0.02$	AALTONEN	11L	CDF	Repl. by AALTONEN 12I

[1] Measured in $11.0 < q^2 < 12.5$ GeV^2/c^4.

$F_L(B \to K^* \ell^+ \ell^-)$ ($15.0 < q^2 < 17.0$ GeV^2/c^4)

VALUE	DOCUMENT ID		TECN	COMMENT
0.349±0.039±0.009	AAIJ	16B	LHCB	pp at 7, 8 TeV

$F_L(B \to K^* \ell^+ \ell^-)$ ($17.0 < q^2 < 19.0$ GeV^2/c^4)

VALUE	DOCUMENT ID		TECN	COMMENT
$\mathbf{0.354^{+0.049}_{-0.048}\pm0.025}$	AAIJ	16B	LHCB	pp at 7, 8 TeV

$F_L(B \to K^* \ell^+ \ell^-)$ ($14.18 < q^2 < 16.0$ GeV^2/c^4)

VALUE	DOCUMENT ID		TECN	COMMENT
0.40±0.06 OUR AVERAGE Error includes scale factor of 1.4. See the ideogram below.				
$0.48^{+0.05}_{-0.06}\pm0.04$	KHACHATRY...	16D	CMS	pp at 8 TeV
$0.33^{+0.08}_{-0.07}{}^{+0.02}_{-0.03}$	AAIJ	13Y	LHCB	pp at 7 TeV, $K^{*0}\mu^+\mu^-$
$0.53\pm0.12\pm0.03$	CHATRCHYAN	13BL	CMS	pp at 7 TeV
$0.29^{+0.14}_{-0.13}\pm0.05$	AALTONEN	12I	CDF	$p\overline{p}$ at 1.96 TeV
$-0.15^{+0.27}_{-0.23}\pm0.07$	WEI	09A	BELL	$e^+e^- \to \Upsilon(4S)$
• • • We do not use the following data for averages, fits, limits, etc. • • •				
$0.37\pm0.09\pm0.05$	AAIJ	12U	LHCB	Repl. by AAIJ 13Y
$0.55^{+0.17}_{-0.18}\pm0.02$	AALTONEN	11L	CDF	Repl. by AALTONEN 12I

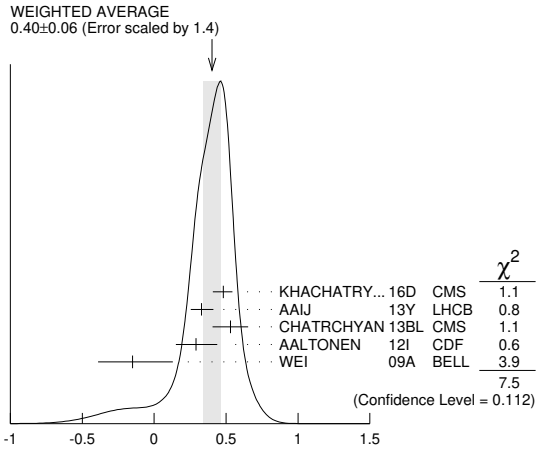

$F_L(B \to K^* \ell^+ \ell^-)$ ($14.18 < q^2 < 16.0$ GeV^2/c^4)

$F_L(B \to K^* \ell^+ \ell^-)$ ($16.0 < q^2 < 19.0$ GeV^2/c^4)

VALUE	DOCUMENT ID		TECN	COMMENT
0.350±0.019 OUR AVERAGE				
$0.345\pm0.020\pm0.007$	[1] AAIJ	20Y	LHCB	pp at 7, 8, 13 TeV
$0.38 ^{+0.05}_{-0.06} \pm0.04$	KHACHATRY...	16D	CMS	pp at 8 TeV
$0.38 ^{+0.09}_{-0.07} \pm0.03$	AAIJ	13Y	LHCB	pp at 7 TeV, $K^{*0}\mu^+\mu^-$
$0.44 \pm0.07 \pm0.03$	CHATRCHYAN	13BL	CMS	pp at 7 TeV
$0.20 ^{+0.19}_{-0.17} \pm0.05$	AALTONEN	12I	CDF	$p\overline{p}$ at 1.96 TeV
$0.12 ^{+0.15}_{-0.13} \pm0.02$	WEI	09A	BELL	$e^+e^- \to \Upsilon(4S)$
• • • We do not use the following data for averages, fits, limits, etc. • • •				
$0.344^{+0.028}_{-0.030}\pm0.008$	[1] AAIJ	16B	LHCB	Repl. by AAIJ 20Y
$0.26 ^{+0.10}_{-0.08} \pm0.03$	AAIJ	12U	LHCB	Repl. by AAIJ 13Y
$0.09 ^{+0.18}_{-0.14} \pm0.03$	AALTONEN	11L	CDF	Repl. by AALTONEN 12I

[1] Measured in $15.0 < q^2 < 19.0$ GeV^2/c^4.

$F_L(B \to K^* \ell^+ \ell^-)$ ($1.0 < q^2 < 6.0$ GeV^2/c^4)

VALUE	DOCUMENT ID		TECN	COMMENT
0.67 ±0.07 OUR AVERAGE Error includes scale factor of 2.8. See the ideogram below.				
$0.700\pm0.025\pm0.013$	[1] AAIJ	20Y	LHCB	pp at 7, 8, 13 TeV
0.72 ± 0.06	KHACHATRY...	16D	CMS	pp at 7, 8 TeV
$0.24 ^{+0.09}_{-0.08} \pm0.02$	[2] LEES	16C	BABR	$e^+e^- \to \Upsilon(4S)$
$0.65 ^{+0.08}_{-0.07} \pm0.03$	AAIJ	13Y	LHCB	pp at 7 TeV, $K^{*0}\mu^+\mu^-$
$0.69 ^{+0.19}_{-0.21} \pm0.08$	AALTONEN	12I	CDF	$p\overline{p}$ at 1.96 TeV
$0.67 \pm0.23 \pm0.05$	WEI	09A	BELL	$e^+e^- \to \Upsilon(4S)$
• • • We do not use the following data for averages, fits, limits, etc. • • •				
$0.690^{+0.035}_{-0.036}\pm0.017$	[1] AAIJ	16B	LHCB	Repl. by AAIJ 20Y
$0.68 \pm0.10 \pm0.02$	CHATRCHYAN	13BL	CMS	Repl. by KHACHATRYAN 16D
$0.55 \pm0.10 \pm0.03$	AAIJ	12U	LHCB	Repl. by AAIJ 13Y
$0.50 ^{+0.27}_{-0.30} \pm0.03$	AALTONEN	11L	CDF	Repl. by AALTONEN 12I

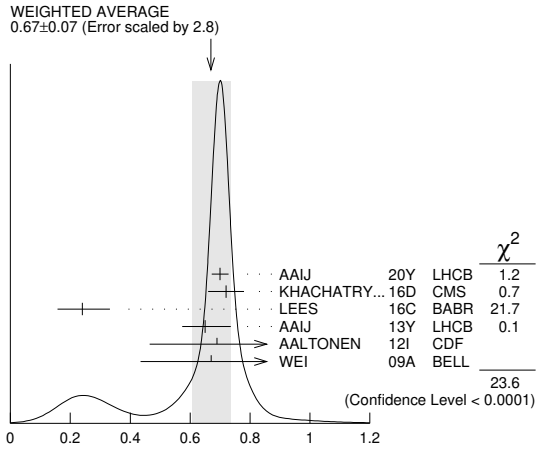

$F_L(B \to K^* \ell^+ \ell^-)$ ($1.0 < q^2 < 6.0$ GeV^2/c^4)

[1] Measured in $1.1 < q^2 < 6.0$ GeV$^2/c^4$.
[2] Measured by combining B^0 and B^+ with e and μ as leptons. Results are also provided separately for B^0 and B^+.

$F_L(B \to K^* \ell^+ \ell^-)$ ($0.0 < q^2 < 4.3$ GeV$^2/c^4$)

VALUE	DOCUMENT ID		TECN	COMMENT
$0.33^{+0.14}_{-0.13} \pm 0.03$	AALTONEN	12I	CDF	$p\overline{p}$ at 1.96 TeV
• • • We do not use the following data for averages, fits, limits, etc. • • •				
$0.47^{+0.23}_{-0.24} \pm 0.03$	AALTONEN	11L	CDF	Repl. by AALTONEN 12I

$A_T^{(2)}$ in $B \to K^* e^+ e^-$ (at low q^2)

VALUE	DOCUMENT ID		TECN	COMMENT
$0.52 \pm 0.53 \pm 0.11$	[1,2] FERLEWICZ	24	BELL	$e^+e^- \to \Upsilon(4S)$

[1] Events are reconstructed in $B^0 \to K^{*0}(\to K^+\pi^-)e^+e^-$ and $B^+ \to K^{*+}(\to K^0_S\pi^+)e^+e^-$ decay modes. The effective dielectron invariant mass is required to be in the range $0.0008 < q^2 < 1.12$ GeV$^2/c^4$.
[2] A_T^{Im} and $A_T^{(2)}$ measure the ratio of the right- and left-handed Wilson coefficients, C_7'/C_7, which constrains non-SM contributions at small q^2.

A_T^{Im} in $B \to K^* e^+ e^-$ (at low q^2)

VALUE	DOCUMENT ID		TECN	COMMENT
$-1.27 \pm 0.52 \pm 0.12$	[1,2] FERLEWICZ	24	BELL	$e^+e^- \to \Upsilon(4S)$

[1] Events are reconstructed in $B^0 \to K^{*0}(\to K^+\pi^-)e^+e^-$ and $B^+ \to K^{*+}(\to K^0_S\pi^+)e^+e^-$ decay modes. The effective dielectron invariant mass is required to be in the range $0.0008 < q^2 < 1.12$ GeV$^2/c^4$.
[2] A_T^{Im} and $A_T^{(2)}$ measure the ratio of the right- and left-handed Wilson coefficients, C_7'/C_7, which constrains non-SM contributions at small q^2.

$P_\tau(B \to D^* \tau^+ \nu_\tau)$

Measures difference in decay widths with positive and negative τ^+ helicities normalized to the sum of those decay widths.

VALUE	DOCUMENT ID		TECN	COMMENT
$-0.38 \pm 0.51^{+0.21}_{-0.16}$	[1] HIROSE	17	BELL	$e^+e^- \to \Upsilon(4S)$

[1] Uses a fully reconstructed B meson as a tag on the recoil side.

Γ_L/Γ in $B \to \overline{D}^* \ell^+ \nu_\ell$

VALUE	DOCUMENT ID		TECN	COMMENT
$0.502 \pm 0.012 \pm 0.004$	[1] PRIM	23	BELL	$e^+e^- \to \Upsilon(4S)$

[1] This is the $B^+ \to \overline{D}^{*0}\ell^+\nu_\ell$ and $B^0 \to D^{*-}\ell^+\nu_\ell$ average.

Γ_L/Γ in $B \to \overline{D}^* e^+ \nu_e$

VALUE	DOCUMENT ID		TECN	COMMENT
$0.485 \pm 0.018 \pm 0.005$	[1] PRIM	23	BELL	$e^+e^- \to \Upsilon(4S)$

[1] This is the $B^+ \to \overline{D}^{*0}e^+\nu_e$ and $B^0 \to D^{*-}e^+\nu_e$ average.

Γ_L/Γ in $B \to \overline{D}^* \mu^+ \nu_\mu$

VALUE	DOCUMENT ID		TECN	COMMENT
$0.515 \pm 0.017 \pm 0.005$	[1] PRIM	23	BELL	$e^+e^- \to \Upsilon(4S)$

[1] This is the $B^+ \to \overline{D}^{*0}\mu^+\nu_\mu$ and $B^0 \to D^{*-}\mu^+\nu_\mu$ average.

$\Delta(\Gamma_L/\Gamma)$ in $B \to \overline{D}^* (leption)^+ \nu_\ell$

$\Delta(\Gamma_L/\Gamma) = (\Gamma_L/\Gamma)^\mu - (\Gamma_L/\Gamma)^e$

VALUE	DOCUMENT ID		TECN	COMMENT
$0.030 \pm 0.025 \pm 0.007$	[1] PRIM	23	BELL	$e^+e^- \to \Upsilon(4S)$

[1] This is the B^+ and B^0 average.

PARTIAL BRANCHING FRACTIONS IN $B \to K^{(*)} \ell^+ \ell^-$

$B(B \to K^* \ell^+ \ell^-)$ ($q^2 < 2.0$ GeV$^2/c^4$)

VALUE (units 10^{-7})	DOCUMENT ID		TECN	COMMENT
1.68±0.23 OUR AVERAGE				
$1.89^{+0.52}_{-0.46} \pm 0.06$	[1] LEES	12S	BABR	$e^+e^- \to \Upsilon(4S)$
$1.73 \pm 0.33 \pm 0.10$	AALTONEN	11AI	CDF	$p\overline{p}$ at 1.96 TeV
$1.46^{+0.40}_{-0.35} \pm 0.11$	WEI	09A	BELL	$e^+e^- \to \Upsilon(4S)$
• • • We do not use the following data for averages, fits, limits, etc. • • •				
$0.98 \pm 0.40 \pm 0.09$	AALTONEN	11L	CDF	Repl. by AALTONEN 11AI

[1] The value reported here from LEES 12S refers to $0.1 < q^2 < 2.0$ GeV$^2/c^2$.

$B(B \to K^* \ell^+ \ell^-)$ ($2.0 < q^2 < 4.3$ GeV$^2/c^4$)

VALUE (units 10^{-7})	DOCUMENT ID		TECN	COMMENT
0.87±0.17 OUR AVERAGE				
$0.95^{+0.35}_{-0.30} \pm 0.04$	LEES	12S	BABR	$e^+e^- \to \Upsilon(4S)$
$0.82 \pm 0.26 \pm 0.06$	AALTONEN	11AI	CDF	$p\overline{p}$ at 1.96 TeV
$0.86^{+0.31}_{-0.27} \pm 0.07$	WEI	09A	BELL	$e^+e^- \to \Upsilon(4S)$
• • • We do not use the following data for averages, fits, limits, etc. • • •				
$1.00 \pm 0.38 \pm 0.09$	AALTONEN	11L	CDF	Repl. by AALTONEN 11AI

$B(B \to K^* \ell^+ \ell^-)$ ($4.3 < q^2 < 8.68$ GeV$^2/c^4$)

VALUE (units 10^{-7})	DOCUMENT ID		TECN	COMMENT
1.67±0.29 OUR AVERAGE				
$1.82^{+0.56}_{-0.52} \pm 0.09$	[1] LEES	12S	BABR	$e^+e^- \to \Upsilon(4S)$
$1.72 \pm 0.41 \pm 0.14$	AALTONEN	11AI	CDF	$p\overline{p}$ at 1.96 TeV
$1.37^{+0.47}_{-0.42} \pm 0.39$	WEI	09A	BELL	$e^+e^- \to \Upsilon(4S)$
• • • We do not use the following data for averages, fits, limits, etc. • • •				
$1.69 \pm 0.57 \pm 0.15$	AALTONEN	11L	CDF	Repl. by AALTONEN 11AI

[1] The value reported here from LEES 12S refers to $4.3 < q^2 < 8.12$ GeV$^2/c^2$.

$B(B \to K^* \ell^+ \ell^-)$ ($10.09 < q^2 < 12.86$ GeV$^2/c^4$)

VALUE (units 10^{-7})	DOCUMENT ID		TECN	COMMENT
1.93±0.25 OUR AVERAGE				
$1.86^{+0.52}_{-0.48} \pm 0.10$	[1] LEES	12S	BABR	$e^+e^- \to \Upsilon(4S)$
$1.77 \pm 0.34 \pm 0.11$	AALTONEN	11AI	CDF	$p\overline{p}$ at 1.96 TeV
$2.24^{+0.44}_{-0.40} \pm 0.19$	WEI	09A	BELL	$e^+e^- \to \Upsilon(4S)$
• • • We do not use the following data for averages, fits, limits, etc. • • •				
$1.97 \pm 0.47 \pm 0.17$	AALTONEN	11L	CDF	Repl. by AALTONEN 11AI

[1] The value reported here from LEES 12S refers to $10.11 < q^2 < 12.89$ GeV$^2/c^2$.

$B(B \to K^* \ell^+ \ell^-)$ ($14.18 < q^2 < 16.0$ GeV$^2/c^4$)

VALUE (units 10^{-7})	DOCUMENT ID		TECN	COMMENT
1.21±0.17 OUR AVERAGE				
$1.46^{+0.41}_{-0.36} \pm 0.06$	[1] LEES	12S	BABR	$e^+e^- \to \Upsilon(4S)$
$1.21 \pm 0.24 \pm 0.07$	AALTONEN	11AI	CDF	$p\overline{p}$ at 1.96 TeV
$1.05^{+0.29}_{-0.26} \pm 0.08$	WEI	09A	BELL	$e^+e^- \to \Upsilon(4S)$
• • • We do not use the following data for averages, fits, limits, etc. • • •				
$1.51 \pm 0.36 \pm 0.13$	AALTONEN	11L	CDF	Repl. by AALTONEN 11AI

[1] The value reported here from LEES 12S refers to $14.21 < q^2 < 16.0$ GeV$^2/c^2$.

$B(B \to K^* \ell^+ \ell^-)$ ($16.0 < q^2$ GeV$^2/c^4$)

VALUE (units 10^{-7})	DOCUMENT ID		TECN	COMMENT
1.3 ±0.4 OUR AVERAGE	Error includes scale factor of 2.3. See the ideogram below.			
$1.02^{+0.47}_{-0.42} \pm 0.06$	LEES	12S	BABR	$e^+e^- \to \Upsilon(4S)$
$0.88 \pm 0.22 \pm 0.05$	AALTONEN	11AI	CDF	$p\overline{p}$ at 1.96 TeV
$2.04^{+0.27}_{-0.24} \pm 0.16$	WEI	09A	BELL	$e^+e^- \to \Upsilon(4S)$
• • • We do not use the following data for averages, fits, limits, etc. • • •				
$1.35 \pm 0.37 \pm 0.12$	AALTONEN	11L	CDF	Repl. by AALTONEN 11AI

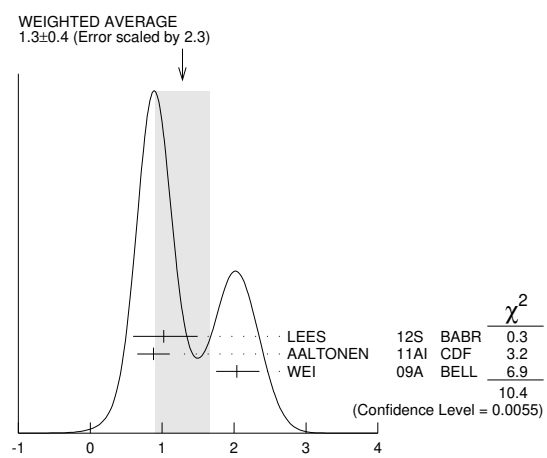

$B(B \to K^* \ell^+ \ell^-)$ ($16.0 < q^2$ GeV$^2/c^4$) (units 10^{-7})

$B(B \to K^* \ell^+ \ell^-)$ ($1.0 < q^2 < 6.0$ GeV$^2/c^4$)

VALUE (units 10^{-7})	DOCUMENT ID		TECN	COMMENT
1.64±0.26 OUR AVERAGE				
$2.05^{+0.53}_{-0.48} \pm 0.07$	LEES	12S	BABR	$e^+e^- \to \Upsilon(4S)$
$1.48 \pm 0.39 \pm 0.12$	AALTONEN	11AI	CDF	$p\overline{p}$ at 1.96 TeV
$1.49^{+0.45}_{-0.40} \pm 0.12$	WEI	09A	BELL	$e^+e^- \to \Upsilon(4S)$
• • • We do not use the following data for averages, fits, limits, etc. • • •				
$1.60 \pm 0.54 \pm 0.14$	AALTONEN	11L	CDF	Repl. by AALTONEN 11AI

$B(B \to K^* \ell^+ \ell^-)$ ($0.0 < q^2 < 4.3$ GeV$^2/c^4$)

VALUE (units 10^{-7})	DOCUMENT ID		TECN	COMMENT
2.53±0.43±0.15	AALTONEN	11AI	CDF	$p\overline{p}$ at 1.96 TeV
• • • We do not use the following data for averages, fits, limits, etc. • • •				
$1.98 \pm 0.55 \pm 0.18$	AALTONEN	11L	CDF	Repl. by AALTONEN 11AI

Int. J. Mod. Phys. A 2026.41. Downloaded from www.worldscientific.com
by [redacted]LIFORNIA @ BERKELEY on 09/16/26. Re-use and distribution is strictly not permitted, except for Open Access articles.

Int. J. Mod. Phys. A 2026.41. Downloaded from www.worldscientific.com
by UNIVERSITY OF CALIFORNIA @ BERKELEY on 09/16/26. Re-use and distribution is strictly not permitted, except for Open Access articles.

$B(B^+ \to K^*\mu^+\mu^-)$ / $B(B^+ \to K^*e^+e^-)$ ($0.045 < q^2 < 1.1$ GeV^2/c^4)

VALUE	DOCUMENT ID		TECN	COMMENT
$0.52^{+0.36}_{-0.26}\pm0.05$	WEHLE	21	BELL	$e^+e^- \to \Upsilon(4S)$

$B(B^+ \to K^*\mu^+\mu^-)$ / $B(B^+ \to K^*e^+e^-)$ ($1.1 < q^2 < 6.0$ GeV^2/c^4)

VALUE	DOCUMENT ID		TECN	COMMENT
$0.96^{+0.45}_{-0.29}\pm0.11$	WEHLE	21	BELL	$e^+e^- \to \Upsilon(4S)$

$B(B^+ \to K^*\mu^+\mu^-)$ / $B(B^+ \to K^*e^+e^-)$ ($15.0 < q^2 < 19.0$ GeV^2/c^4)

VALUE	DOCUMENT ID		TECN	COMMENT
$1.18^{+0.52}_{-0.32}\pm0.10$	WEHLE	21	BELL	$e^+e^- \to \Upsilon(4S)$

$B(B \to K\ell^+\ell^-)$ ($q^2 < 2.0$ GeV^2/c^4)

VALUE (units 10^{-7})	DOCUMENT ID		TECN	COMMENT
0.51 ± 0.16 OUR AVERAGE	Error includes scale factor of 1.9. See the ideogram below.			
$0.71^{+0.20}_{-0.18}\pm0.02$	[1] LEES	12S	BABR	$e^+e^- \to \Upsilon(4S)$
$0.33\pm0.10\pm0.02$	AALTONEN	11AI	CDF	$p\overline{p}$ at 1.96 TeV
$0.81^{+0.18}_{-0.16}\pm0.05$	WEI	09A	BELL	$e^+e^- \to \Upsilon(4S)$
• • • We do not use the following data for averages, fits, limits, etc. • • •				
$0.38\pm0.16\pm0.03$	AALTONEN	11L	CDF	Repl. by AALTONEN 11AI

[1] The value reported here from LEES 12S refers to $0.1 < q^2 < 2.0$ GeV^2/c^2.

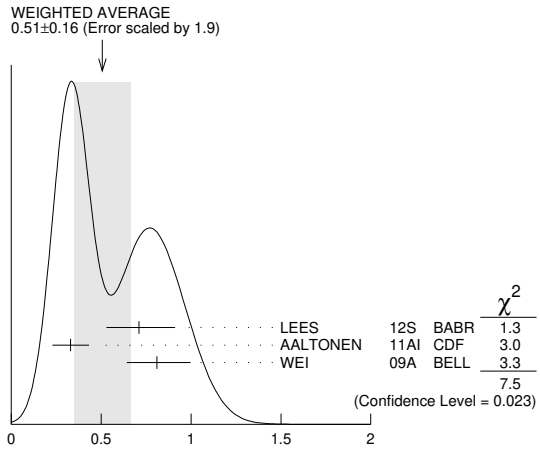

$B(B \to K\ell^+\ell^-)$ ($q^2 < 2.0$ GeV^2/c^4) (units 10^{-7})

$B(B \to K\ell^+\ell^-)$ ($2.0 < q^2 < 4.3$ GeV^2/c^4)

VALUE (units 10^{-7})	DOCUMENT ID		TECN	COMMENT
$0.57^{+0.10}_{-0.09}$ OUR AVERAGE	Error includes scale factor of 1.2.			
$0.49^{+0.15}_{-0.13}\pm0.01$	LEES	12S	BABR	$e^+e^- \to \Upsilon(4S)$
$0.77\pm0.14\pm0.05$	AALTONEN	11AI	CDF	$p\overline{p}$ at 1.96 TeV
$0.46^{+0.14}_{-0.12}\pm0.03$	WEI	09A	BELL	$e^+e^- \to \Upsilon(4S)$
• • • We do not use the following data for averages, fits, limits, etc. • • •				
$0.58\pm0.19\pm0.04$	AALTONEN	11L	CDF	Repl. by AALTONEN 11AI

$B(B \to K\ell^+\ell^-)$ ($4.3 < q^2 < 8.68$ GeV^2/c^4)

VALUE (units 10^{-7})	DOCUMENT ID		TECN	COMMENT
1.00 ± 0.11 OUR AVERAGE				
$0.94^{+0.20}_{-0.19}\pm0.02$	[1] LEES	12S	BABR	$e^+e^- \to \Upsilon(4S)$
$1.05\pm0.17\pm0.07$	AALTONEN	11AI	CDF	$p\overline{p}$ at 1.96 TeV
$1.00^{+0.19}_{-0.18}\pm0.06$	WEI	09A	BELL	$e^+e^- \to \Upsilon(4S)$
• • • We do not use the following data for averages, fits, limits, etc. • • •				
$0.93\pm0.25\pm0.06$	AALTONEN	11L	CDF	Repl. by AALTONEN 11AI

[1] The value reported here from LEES 12S refers to $4.3 < q^2 < 8.12$ GeV^2/c^2.

$B(B \to K\ell^+\ell^-)$ ($10.09 < q^2 < 12.86$ GeV^2/c^4)

VALUE (units 10^{-7})	DOCUMENT ID		TECN	COMMENT
0.57 ± 0.11 OUR AVERAGE	Error includes scale factor of 1.4. See the ideogram below.			
$0.90^{+0.20}_{-0.19}\pm0.04$	[1] LEES	12S	BABR	$e^+e^- \to \Upsilon(4S)$
$0.48\pm0.10\pm0.03$	AALTONEN	11AI	CDF	$p\overline{p}$ at 1.96 TeV
$0.55^{+0.16}_{-0.14}\pm0.03$	WEI	09A	BELL	$e^+e^- \to \Upsilon(4S)$
• • • We do not use the following data for averages, fits, limits, etc. • • •				
$0.72\pm0.17\pm0.05$	AALTONEN	11L	CDF	Repl. by AALTONEN 11AI

[1] The value reported here from LEES 12S refers to $10.11 < q^2 < 12.89$ GeV^2/c^2.

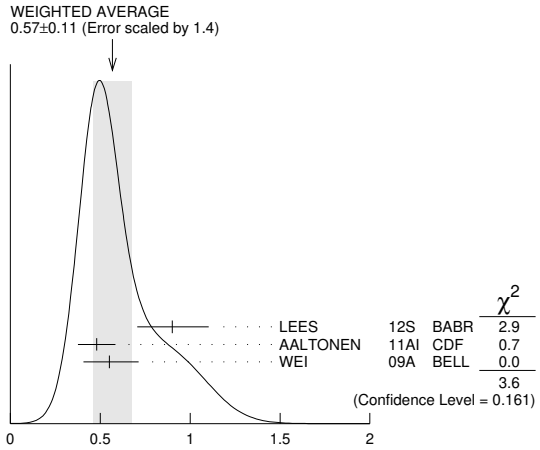

$B(B \to K\ell^+\ell^-)$ ($10.09 < q^2 < 12.86$ GeV^2/c^4) (units 10^{-7})

$B(B \to K\ell^+\ell^-)$ ($14.18 < q^2 < 16.0$ GeV^2/c^4)

VALUE (units 10^{-7})	DOCUMENT ID		TECN	COMMENT
0.49 ± 0.07 OUR AVERAGE				
$0.49^{+0.15}_{-0.14}\pm0.02$	[1] LEES	12S	BABR	$e^+e^- \to \Upsilon(4S)$
$0.52\pm0.09\pm0.03$	AALTONEN	11AI	CDF	$p\overline{p}$ at 1.96 TeV
$0.38^{+0.19}_{-0.12}\pm0.02$	WEI	09A	BELL	$e^+e^- \to \Upsilon(4S)$
• • • We do not use the following data for averages, fits, limits, etc. • • •				
$0.38\pm0.12\pm0.03$	AALTONEN	11L	CDF	Repl. by AALTONEN 11AI

[1] The value reported here from LEES 12S refers to $14.21 < q^2 < 16.0$ GeV^2/c^2.

$B(B \to K\ell^+\ell^-)$ ($16.0 < q^2$ GeV^2/c^4)

VALUE (units 10^{-7})	DOCUMENT ID		TECN	COMMENT
0.52 ± 0.16 OUR AVERAGE	Error includes scale factor of 2.1. See the ideogram below.			
$0.67^{+0.23}_{-0.21}\pm0.05$	LEES	12S	BABR	$e^+e^- \to \Upsilon(4S)$
$0.38\pm0.09\pm0.02$	AALTONEN	11AI	CDF	$p\overline{p}$ at 1.96 TeV
$0.98^{+0.20}_{-0.18}\pm0.06$	WEI	09A	BELL	$e^+e^- \to \Upsilon(4S)$
• • • We do not use the following data for averages, fits, limits, etc. • • •				
$0.35\pm0.13\pm0.02$	AALTONEN	11L	CDF	Repl. by AALTONEN 11AI

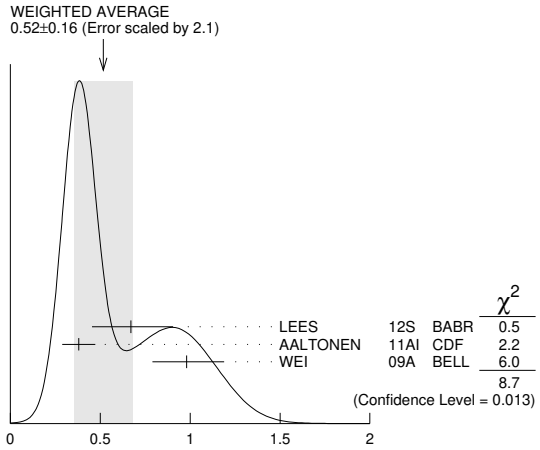

$B(B \to K\ell^+\ell^-)$ ($16.0 < q^2$ GeV^2/c^4) (units 10^{-7})

$B(B \to K\ell^+\ell^-)$ ($1.0 < q^2 < 6.0$ GeV^2/c^4)

VALUE (units 10^{-7})	DOCUMENT ID		TECN	COMMENT
1.33 ± 0.13 OUR AVERAGE				
$1.36^{+0.27}_{-0.24}\pm0.03$	LEES	12S	BABR	$e^+e^- \to \Upsilon(4S)$
$1.29\pm0.18\pm0.08$	AALTONEN	11AI	CDF	$p\overline{p}$ at 1.96 TeV
$1.36^{+0.23}_{-0.21}\pm0.08$	WEI	09A	BELL	$e^+e^- \to \Upsilon(4S)$
• • • We do not use the following data for averages, fits, limits, etc. • • •				
$1.01\pm0.26\pm0.07$	AALTONEN	11L	CDF	Repl. by AALTONEN 11AI

$B(B \to K\ell^+\ell^-)$ ($0.0 < q^2 < 4.3$ GeV^2/c^4)

VALUE (units 10^{-7})	DOCUMENT ID		TECN	COMMENT
$1.07\pm0.17\pm0.07$	AALTONEN	11AI	CDF	$p\overline{p}$ at 1.96 TeV
• • • We do not use the following data for averages, fits, limits, etc. • • •				
$0.96\pm0.25\pm0.06$	AALTONEN	11L	CDF	Repl. by AALTONEN 11AI

Int. J. Mod. Phys. A 2026.41. Downloaded from www.worldscientific.com by CALIFORNIA @ BERKELEY on 09/16/26. Re-use and distribution is strictly not permitted, except for Open Access articles.

$B(B \to X_s \ell^+ \ell^-)$ ($1.0 < q^2 < 6.0$ GeV^2/c^4)

VALUE (units 10^{-6})	DOCUMENT ID		TECN	COMMENT
$1.60^{+0.41}_{-0.39}{}^{+0.25}_{-0.22}$	[1] LEES	14D	BABR	$e^+e^- \to \Upsilon(4S)$

[1] Measured from sum of exclusive modes through K^+, $K^+\pi^0$, $K^+\pi^-$, $K^+\pi^-\pi^0$, $K^+\pi^-\pi^+$, K^0_S, $K^0_S\pi^0$, $K^0_S\pi^+$, $K^0_S\pi^+\pi^0$, and $K^0_S\pi^+\pi^-$ corrected for unobserved modes.

$B(B \to X_s e^+ e^-)$ ($1.0 < q^2 < 6.0$ GeV^2/c^4)

VALUE (units 10^{-6})	DOCUMENT ID		TECN	COMMENT
$1.93^{+0.47}_{-0.45}{}^{+0.28}_{-0.24}$	[1] LEES	14D	BABR	$e^+e^- \to \Upsilon(4S)$

[1] Measured from sum of exclusive modes through K^+, $K^+\pi^0$, $K^+\pi^-$, $K^+\pi^-\pi^0$, $K^+\pi^-\pi^+$, K^0_S, $K^0_S\pi^0$, $K^0_S\pi^+$, $K^0_S\pi^+\pi^0$, and $K^0_S\pi^+\pi^-$ corrected for unobserved modes.

$B(B \to X_s \mu^+ \mu^-)$ ($1.0 < q^2 < 6.0$ GeV^2/c^4)

VALUE (units 10^{-6})	DOCUMENT ID		TECN	COMMENT
$0.66^{+0.82}_{-0.76}{}^{+0.31}_{-0.25}$	[1] LEES	14D	BABR	$e^+e^- \to \Upsilon(4S)$

[1] Measured from sum of exclusive modes through K^+, $K^+\pi^0$, $K^+\pi^-$, $K^+\pi^-\pi^0$, $K^+\pi^-\pi^+$, K^0_S, $K^0_S\pi^0$, $K^0_S\pi^+$, $K^0_S\pi^+\pi^0$, and $K^0_S\pi^+\pi^-$ corrected for unobserved modes.

$B(B \to X_s \ell^+ \ell^-)$ ($14.2 < q^2$ GeV^2/c^4)

VALUE (units 10^{-6})	DOCUMENT ID		TECN	COMMENT
$0.57^{+0.16}_{-0.15}{}^{+0.03}_{-0.02}$	[1] LEES	14D	BABR	$e^+e^- \to \Upsilon(4S)$

[1] Measured from sum of exclusive modes through K^+, $K^+\pi^0$, $K^+\pi^-$, $K^+\pi^-\pi^0$, $K^+\pi^-\pi^+$, K^0_S, $K^0_S\pi^0$, $K^0_S\pi^+$, $K^0_S\pi^+\pi^0$, and $K^0_S\pi^+\pi^-$ corrected for unobserved modes.

$B(B \to X_s e^+ e^-)$ ($14.2 < q^2$ GeV^2/c^4)

VALUE (units 10^{-6})	DOCUMENT ID		TECN	COMMENT
$0.56^{+0.19}_{-0.18}{}^{+0.03}_{-0.03}$	[1] LEES	14D	BABR	$e^+e^- \to \Upsilon(4S)$

[1] Measured from sum of exclusive modes through K^+, $K^+\pi^0$, $K^+\pi^-$, $K^+\pi^-\pi^0$, $K^+\pi^-\pi^+$, K^0_S, $K^0_S\pi^0$, $K^0_S\pi^+$, $K^0_S\pi^+\pi^0$, and $K^0_S\pi^+\pi^-$ corrected for unobserved modes.

$B(B \to X_s \mu^+ \mu^-)$ ($14.2 < q^2$ GeV^2/c^4)

VALUE (units 10^{-6})	DOCUMENT ID		TECN	COMMENT
$0.60^{+0.31}_{-0.29}{}^{+0.05}_{-0.04}$	[1] LEES	14D	BABR	$e^+e^- \to \Upsilon(4S)$

[1] Measured from sum of exclusive modes through K^+, $K^+\pi^0$, $K^+\pi^-$, $K^+\pi^-\pi^0$, $K^+\pi^-\pi^+$, K^0_S, $K^0_S\pi^0$, $K^0_S\pi^+$, $K^0_S\pi^+\pi^0$, and $K^0_S\pi^+\pi^-$ corrected for unobserved modes.

LEPTON (HADRON) FORWARD-BACKWARD ASYMMETRY IN $B \to K^{(*)}\ell^+\ell^-$ ($B \to K/\pi h^+ h^-$) DECAY

The forward-backward angular asymmetry of the lepton pair in $B \to K^{(*)}\ell^+\ell^-$ ($B \to K/\pi h^+ h^-$) decay is defined as

$$A_{FB}(s) = \frac{N(cos\theta>0)-N(cos\theta<0)}{N(cos\theta>0)+N(cos\theta<0)},$$

where $s=q^2/m_B^2$, and θ is the angle of the ℓ^- (h^-) with respect to the flight direction of the B meson, measured in the dilepton (dihadron) rest frame. In addition, the fraction of longitudinal polarization F_L of the K^* and F_S, the relative contribution from scalar and pseudoscalar penguin amplitudes in $B \to K\ell^+\ell^-$, can be measured from the angular distribution of its decay products.

$A_{FB}(B \to K^*\ell^+\ell^-)$ ($q^2 > 0.1$ GeV^2/c^4)

VALUE	CL%	DOCUMENT ID		TECN	COMMENT
$0.50 \pm 0.15 \pm 0.02$		[1] ISHIKAWA	06	BELL	$e^+e^- \to \Upsilon(4S)$
• • • We do not use the following data for averages, fits, limits, etc. • • •					
>0.55	95	[2] AUBERT,B	06J	BABR	$e^+e^- \to \Upsilon(4S)$

[1] Using an unbinned max. likelihood fits to the M_{bc} distribution in five q^2 bins for $\cos\theta > 0$ and $\cos\theta < 0$.
[2] Results with different q^2 cuts are also reported.

$A_{FB}(B \to K^*\ell^+\ell^-)$ ($0.1 < q^2 < 2.0$ GeV^2/c^4)

VALUE	DOCUMENT ID		TECN	COMMENT
-0.01 ± 0.14 OUR AVERAGE	Error includes scale factor of 1.4. See the ideogram below.			
$-0.02 \pm 0.12 \pm 0.01$	AAIJ	13Y	LHCB	pp at 7 TeV, $K^{*0}\mu^+\mu^-$
$-0.35^{+0.26}_{-0.23} \pm 0.10$	AALTONEN	12I	CDF	$p\overline{p}$ at 1.96 TeV
$0.47^{+0.26}_{-0.32} \pm 0.03$	WEI	09A	BELL	$e^+e^- \to \Upsilon(4S)$
• • • We do not use the following data for averages, fits, limits, etc. • • •				
$-0.29^{+0.37}_{-0.00} \pm 0.18$	[1] CHATRCHYAN	13BL	CMS	pp at 7 TeV
$-0.15 \pm 0.20 \pm 0.06$	AAIJ	12U	LHCB	Repl. by AAIJ 13Y
$0.13^{+1.65}_{-0.75} \pm 0.25$	AALTONEN	11L	CDF	Repl. by AALTONEN 12I

[1] CHATRCHYAN 13BL uses, for this bin, $1.0 < q^2 < 2.0$ GeV^2/c^4.

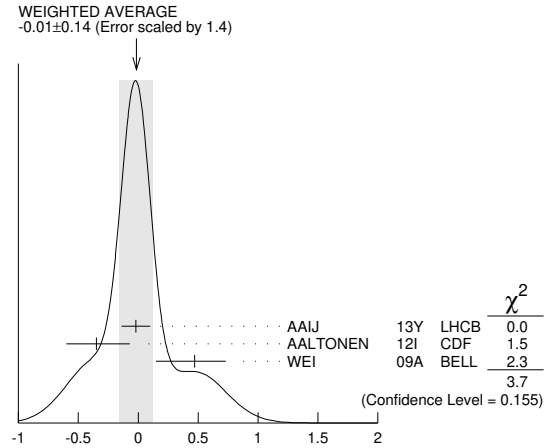

$A_{FB}(B \to K^*\ell^+\ell^-)$ ($0.1 < q^2 < 2.0$ GeV^2/c^4)

$A_{FB}(B \to K^*\ell^+\ell^-)$ ($m_{\ell\ell} < 2.5$ GeV/c^2)

VALUE	DOCUMENT ID		TECN	COMMENT
$0.24^{+0.18}_{-0.23} \pm 0.05$	AUBERT	09N	BABR	$e^+e^- \to \Upsilon(4S)$

$A_{FB}(B \to K^*\ell^+\ell^-)$ ($m_{\ell\ell} > 3.2$ GeV/c^2)

VALUE	DOCUMENT ID		TECN	COMMENT
$0.76^{+0.52}_{-0.32} \pm 0.07$	AUBERT	09N	BABR	$e^+e^- \to \Upsilon(4S)$

$A_{FB}(B \to K^*\ell^+\ell^-)$ ($0.10 < q^2 < 0.98$ GeV^2/c^4)

VALUE	DOCUMENT ID		TECN	COMMENT
$-0.003^{+0.058}_{-0.057} \pm 0.009$	AAIJ	16B	LHCB	pp at 7, 8 TeV

$A_{FB}(B \to K^*\ell^+\ell^-)$ ($1.1 < q^2 < 2.5$ GeV^2/c^4)

VALUE	DOCUMENT ID		TECN	COMMENT
$-0.191^{+0.068}_{-0.080} \pm 0.012$	AAIJ	16B	LHCB	pp at 7, 8 TeV

$A_{FB}(B \to K^*\ell^+\ell^-)$ ($2.0 < q^2 < 4.3$ GeV^2/c^4)

VALUE	DOCUMENT ID		TECN	COMMENT
-0.14 ± 0.05 OUR AVERAGE				
$-0.118^{+0.082}_{-0.090} \pm 0.007$	[1] AAIJ	16B	LHCB	pp at 7, 8 TeV
$-0.12^{+0.15}_{-0.17} \pm 0.05$	KHACHATRY...	16D	CMS	pp at 8 TeV
$-0.20 \pm 0.08 \pm 0.01$	AAIJ	13Y	LHCB	pp at 7 TeV, $K^{*0}\mu^+\mu^-$
$-0.07 \pm 0.20 \pm 0.02$	CHATRCHYAN	13BL	CMS	pp at 7 TeV
$0.29^{+0.32}_{-0.35} \pm 0.15$	AALTONEN	12I	CDF	$p\overline{p}$ at 1.96 TeV
$0.11^{+0.31}_{-0.36} \pm 0.07$	WEI	09A	BELL	$e^+e^- \to \Upsilon(4S)$
• • • We do not use the following data for averages, fits, limits, etc. • • •				
$0.05^{+0.16}_{-0.20} \pm 0.04$	AAIJ	12U	LHCB	Repl. by AAIJ 13Y
$0.19^{+0.40}_{-0.41} \pm 0.14$	AALTONEN	11L	CDF	Repl. by AALTONEN 12I

[1] Measured in $2.5 < q^2 < 4.0$ GeV^2/c^4.

$A_{FB}(B \to K^*\ell^+\ell^-)$ ($0.0 < q^2 < 4.3$ GeV^2/c^4)

VALUE	DOCUMENT ID		TECN	COMMENT
$-0.08^{+0.21}_{-0.20} \pm 0.05$	AALTONEN	12I	CDF	$p\overline{p}$ at 1.96 TeV
• • • We do not use the following data for averages, fits, limits, etc. • • •				
$0.21^{+0.31}_{-0.33} \pm 0.05$	AALTONEN	11L	CDF	Repl. by AALTONEN 12I

$A_{FB}(B \to K^*\ell^+\ell^-)$ ($4.0 < q^2 < 6.0$ GeV^2/c^4)

VALUE	DOCUMENT ID		TECN	COMMENT
$0.025^{+0.051}_{-0.052} \pm 0.004$	AAIJ	16B	LHCB	pp at 7, 8 TeV

$A_{FB}(B \to K^*\ell^+\ell^-)$ ($6.0 < q^2 < 8.0$ GeV^2/c^4)

VALUE	DOCUMENT ID		TECN	COMMENT
$0.152^{+0.041}_{-0.040} \pm 0.008$	AAIJ	16B	LHCB	pp at 7, 8 TeV

$A_{FB}(B \to K^*\ell^+\ell^-)$ ($1.0 < q^2 < 6.0$ GeV^2/c^4)

VALUE	DOCUMENT ID		TECN	COMMENT
-0.078 ± 0.022 OUR AVERAGE	Error includes scale factor of 1.1.			
$-0.073 \pm 0.021 \pm 0.002$	[1] AAIJ	20Y	LHCB	pp at 7, 8, 13 TeV
-0.12 ± 0.08	KHACHATRY...	16D	CMS	pp at 7, 8 TeV
$0.21^{+0.10}_{-0.15}{}^{+0.07}_{-0.09}$	[2] LEES	16C	BABR	$e^+e^- \to \Upsilon(4S)$

Int. J. Mod. Phys. A 2026.41. Downloaded from www.worldscientific.com
by UNIVERSITY OF CALIFORNIA @ BERKELEY on 09/16/26. Re-use and distribution is strictly not permitted, except for Open Access articles.

$-0.17 \pm 0.06 \pm 0.01$	AAIJ	13Y	LHCB	pp at 7 TeV, $K^{*0}\mu^+\mu^-$
$0.29 \pm^{0.20}_{0.23} \pm 0.07$	AALTONEN	12I	CDF	$p\overline{p}$ at 1.96 TeV
$0.26 \pm^{0.27}_{0.30} \pm 0.07$	WEI	09A	BELL	$e^+e^- \to \Upsilon(4S)$
• • • We do not use the following data for averages, fits, limits, etc. • • •				
$-0.075 \pm^{0.032}_{0.034} \pm 0.007$	[1] AAIJ	16B	LHCB	Repl. by AAIJ 20Y
0.55 ± 0.43	[3] SATO	16	BELL	$e^+e^- \to \Upsilon(4S)$
$-0.07 \pm 0.12 \pm 0.01$	CHATRCHYAN	13BL	CMS	Repl. by KHACHATRYAN 16D
$-0.06 \pm^{0.13}_{0.14} \pm 0.07$	AAIJ	12U	LHCB	Repl. by AAIJ 13Y
$0.43 \pm^{0.36}_{0.37} \pm 0.06$	AALTONEN	11L	CDF	Repl. by AALTONEN 12I

[1] Measured in $1.1 < q^2 < 6.0$ GeV^2/c^4.
[2] Measured by combining B^0 and B^+ with e and μ as leptons. Results are also provided separately for B^0 and B^+.
[3] Uses $K^* \to K^-\pi^+$, $K^-\pi^0$, $K^0_S\pi^-$ in the range $M(K\pi) < 1.1$ GeV/c^2. Uncertainty is statistical only.

$A_{FB}(B \to K^*\ell^+\ell^-)$ ($4.3 < q^2 < 8.6$ GeV^2/c^4)

VALUE	DOCUMENT ID		TECN	COMMENT
$0.13 \pm^{0.06}_{0.05}$ OUR AVERAGE	Error includes scale factor of 1.1.			
$0.16 \pm^{0.06}_{0.05} \pm 0.01$	AAIJ	13Y	LHCB	pp at 7 TeV, $K^{*0}\mu^+\mu^-$
$-0.01 \pm 0.11 \pm 0.03$	CHATRCHYAN	13BL	CMS	pp at 7 TeV
$0.01 \pm 0.20 \pm 0.09$	AALTONEN	12I	CDF	$p\overline{p}$ at 1.96 TeV
$0.45 \pm^{0.15}_{0.21} \pm 0.15$	WEI	09A	BELL	$e^+e^- \to \Upsilon(4S)$
• • • We do not use the following data for averages, fits, limits, etc. • • •				
$0.27 \pm^{0.06}_{0.08} \pm 0.02$	AAIJ	12U	LHCB	Repl. by AAIJ 13Y
$-0.06 \pm^{0.30}_{0.28} \pm 0.05$	AALTONEN	11L	CDF	Repl. by AALTONEN 12I

$A_{FB}(B \to K^*\ell^+\ell^-)$ ($10.09 < q^2 < 12.86$ GeV^2/c^4)

VALUE	DOCUMENT ID		TECN	COMMENT
0.288 ± 0.034 OUR AVERAGE	Error includes scale factor of 1.2.			
$0.318 \pm^{0.044}_{0.040} \pm 0.009$	[1] AAIJ	16B	LHCB	pp at 7, 8 TeV
$0.16 \pm 0.06 \pm 0.01$	KHACHATRY...	16D	CMS	pp at 8 TeV
$0.28 \pm^{0.07}_{0.06} \pm 0.02$	AAIJ	13Y	LHCB	pp at 7 TeV, $K^{*0}\mu^+\mu^-$
$0.40 \pm 0.08 \pm 0.05$	CHATRCHYAN	13BL	CMS	pp at 7 TeV
$0.38 \pm^{0.16}_{0.19} \pm 0.09$	AALTONEN	12I	CDF	$p\overline{p}$ at 1.96 TeV
$0.43 \pm^{0.18}_{0.20} \pm 0.03$	WEI	09A	BELL	$e^+e^- \to \Upsilon(4S)$
• • • We do not use the following data for averages, fits, limits, etc. • • •				
$0.27 \pm^{0.11}_{0.13} \pm 0.02$	AAIJ	12U	LHCB	Repl. by AAIJ 13Y
$0.66 \pm^{0.23}_{0.20} \pm 0.07$	AALTONEN	11L	CDF	Repl. by AALTONEN 12I

[1] Measured in $11.0 < q^2 < 12.5$ GeV^2/c^4.

$A_{FB}(B \to K^*\ell^+\ell^-)$ ($14.18 < q^2 < 16.0$ GeV^2/c^4)

VALUE	DOCUMENT ID		TECN	COMMENT
$0.43 \pm^{0.05}_{0.06}$ OUR AVERAGE	Error includes scale factor of 1.6. See the ideogram below.			
$0.39 \pm^{0.04}_{0.06} \pm 0.01$	KHACHATRY...	16D	CMS	pp at 8 TeV
$0.51 \pm^{0.07}_{0.05} \pm 0.02$	AAIJ	13Y	LHCB	pp at 7 TeV, $K^{*0}\mu^+\mu^-$
$0.29 \pm 0.09 \pm 0.05$	CHATRCHYAN	13BL	CMS	pp at 7 TeV
$0.44 \pm^{0.18}_{0.21} \pm 0.10$	AALTONEN	12I	CDF	$p\overline{p}$ at 1.96 TeV
$0.70 \pm^{0.16}_{0.22} \pm 0.10$	WEI	09A	BELL	$e^+e^- \to \Upsilon(4S)$
• • • We do not use the following data for averages, fits, limits, etc. • • •				
$0.47 \pm^{0.06}_{0.08} \pm 0.03$	AAIJ	12U	LHCB	Repl. by AAIJ 13Y
$0.42 \pm 0.16 \pm 0.09$	AALTONEN	11L	CDF	Repl. by AALTONEN 12I

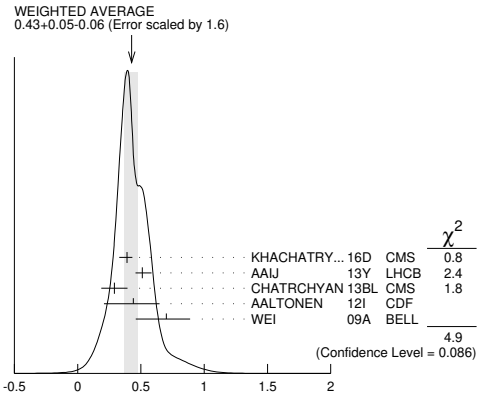

$A_{FB}(B \to K^*\ell^+\ell^-)$ ($14.18 < q^2 < 16.0$ GeV^2/c^4)

$A_{FB}(B \to K^*\ell^+\ell^-)$ ($15.0 < q^2 < 17.0$ GeV^2/c^4)

VALUE	DOCUMENT ID		TECN	COMMENT
$0.411 \pm^{0.41}_{0.037} \pm 0.008$	AAIJ	16B	LHCB	pp at 7, 8 TeV

$A_{FB}(B \to K^*\ell^+\ell^-)$ ($17.0 < q^2 < 19.0$ GeV^2/c^4)

VALUE	DOCUMENT ID		TECN	COMMENT
$0.305 \pm^{0.049}_{0.048} \pm 0.013$	AAIJ	16B	LHCB	pp at 7, 8 TeV

$A_{FB}(B \to K^*\ell^+\ell^-)$ ($16.0 < q^2 < 19.0$ GeV^2/c^4)

VALUE	DOCUMENT ID		TECN	COMMENT
0.362 ± 0.019 OUR AVERAGE				
$0.353 \pm 0.020 \pm 0.010$	[1] AAIJ	20Y	LHCB	pp at 7, 8, 13 TeV
$0.35 \pm 0.07 \pm 0.01$	KHACHATRY...	16D	CMS	pp at 8 TeV
$0.30 \pm 0.08 \pm^{0.01}_{0.02}$	AAIJ	13Y	LHCB	pp at 7 TeV, $K^{*0}\mu^+\mu^-$
$0.41 \pm 0.05 \pm 0.03$	CHATRCHYAN	13BL	CMS	pp at 7 TeV
$0.65 \pm^{0.17}_{0.18} \pm 0.16$	AALTONEN	12I	CDF	$p\overline{p}$ at 1.96 TeV
$0.66 \pm^{0.11}_{0.16} \pm 0.04$	WEI	09A	BELL	$e^+e^- \to \Upsilon(4S)$
• • • We do not use the following data for averages, fits, limits, etc. • • •				
$0.355 \pm 0.027 \pm 0.009$	[1] AAIJ	16B	LHCB	Repl. by AAIJ 20Y
$0.16 \pm^{0.11}_{0.13} \pm 0.06$	AAIJ	12U	LHCB	Repl. by AAIJ 13Y
$0.70 \pm^{0.16}_{0.25} \pm 0.10$	AALTONEN	11L	CDF	Repl. by AALTONEN 12I

[1] Measured in $15.0 < q^2 < 19.0$ GeV^2/c^4.

$A_{FB}(B \to K\ell^+\ell^-)$ ($q^2 > 0.1$ GeV^2/c^4)

VALUE	DOCUMENT ID		TECN	COMMENT
0.11 ± 0.12 OUR AVERAGE				
$0.15 \pm^{0.21}_{0.23} \pm 0.08$	[1] AUBERT,B	06J	BABR	$e^+e^- \to \Upsilon(4S)$
$0.10 \pm 0.14 \pm 0.01$	[2] ISHIKAWA	06	BELL	$e^+e^- \to \Upsilon(4S)$

[1] Results with different q^2 cuts are also reported.
[2] Using an unbinned max. likelihood fits to the M_{bc} distribution in five q^2 bins for $\cos\theta > 0$ and $\cos\theta < 0$.

$A_{FB}(B \to K\ell^+\ell^-)$ ($q^2 < 2.0$ GeV^2/c^4)

VALUE	DOCUMENT ID		TECN	COMMENT
$0.00 \pm^{0.06}_{0.05}$ OUR AVERAGE				
$0.00 \pm^{0.06}_{0.05} \pm^{0.03}_{0.01}$	AAIJ	13H	LHCB	pp at 7 TeV
$0.13 \pm^{0.42}_{0.43} \pm 0.07$	AALTONEN	12I	CDF	$p\overline{p}$ at 1.96 TeV
$0.06 \pm^{0.32}_{0.35} \pm 0.02$	WEI	09A	BELL	$e^+e^- \to \Upsilon(4S)$
• • • We do not use the following data for averages, fits, limits, etc. • • •				
$-0.15 \pm^{0.46}_{0.39} \pm 0.08$	AALTONEN	11L	CDF	Repl. by AALTONEN 12I

$A_{FB}(B \to K\ell^+\ell^-)$ ($2.0 < q^2 < 4.3$ GeV^2/c^4)

VALUE	DOCUMENT ID		TECN	COMMENT
$0.09 \pm^{0.10}_{0.07}$ OUR AVERAGE	Error includes scale factor of 1.4.			
$0.07 \pm^{0.08}_{0.05} \pm^{0.02}_{0.01}$	AAIJ	13H	LHCB	pp at 7 TeV
$0.32 \pm^{0.15}_{0.16} \pm 0.05$	AALTONEN	12I	CDF	$p\overline{p}$ at 1.96 TeV
$-0.43 \pm^{0.38}_{0.40} \pm 0.09$	WEI	09A	BELL	$e^+e^- \to \Upsilon(4S)$
• • • We do not use the following data for averages, fits, limits, etc. • • •				
$0.72 \pm^{0.40}_{0.35} \pm 0.07$	AALTONEN	11L	CDF	Repl. by AALTONEN 12I

$A_{FB}(B \to K\ell^+\ell^-)$ ($0.0 < q^2 < 4.3$ GeV^2/c^4)

VALUE	DOCUMENT ID		TECN	COMMENT
$0.31 \pm 0.16 \pm 0.04$	AALTONEN	12I	CDF	$p\overline{p}$ at 1.96 TeV
• • • We do not use the following data for averages, fits, limits, etc. • • •				
$0.36 \pm^{0.24}_{0.26} \pm 0.06$	AALTONEN	11L	CDF	Repl. by AALTONEN 12I

$A_{FB}(B \to K\ell^+\ell^-)$ ($1.0 < q^2 < 6.0$ GeV^2/c^4)

VALUE	DOCUMENT ID		TECN	COMMENT
$0.034 \pm^{0.040}_{0.029}$ OUR AVERAGE				
$0.02 \pm^{0.05}_{0.03} \pm^{0.02}_{0.01}$	AAIJ	13H	LHCB	pp at 7 TeV
$0.13 \pm 0.09 \pm 0.02$	AALTONEN	12I	CDF	$p\overline{p}$ at 1.96 TeV
$-0.04 \pm^{0.13}_{0.16} \pm 0.05$	WEI	09A	BELL	$e^+e^- \to \Upsilon(4S)$
• • • We do not use the following data for averages, fits, limits, etc. • • •				
0.00 ± 0.13	[1] SATO	16	BELL	$e^+e^- \to \Upsilon(4S)$
$0.08 \pm^{0.27}_{0.22} \pm 0.07$	AALTONEN	11L	CDF	Repl. by AALTONEN 12I

[1] Statistical uncertainty only.

Int. J. Mod. Phys. A 2026.41. Downloaded from www.worldscientific.com
by [redacted]LIFORNIA @ BERKELEY on 09/16/26. Re-use and distribution is strictly not permitted, except for Open Access articles.

$A_{FB}(B \to K\ell^+\ell^-)$ ($4.3 < q^2 < 8.6$ GeV^2/c^4)

VALUE	DOCUMENT ID		TECN	COMMENT
$-0.04^{+0.04}_{-0.05}$ OUR AVERAGE				
$-0.02^{+0.03}_{-0.05}\pm0.03$	AAIJ	13H	LHCB	pp at 7 TeV
$0.01^{+0.13}_{-0.10}\pm0.01$	AALTONEN	12I	CDF	$p\overline{p}$ at 1.96 TeV
$-0.20^{+0.12}_{-0.14}\pm0.03$	WEI	09A	BELL	$e^+e^- \to \Upsilon(4S)$
• • • We do not use the following data for averages, fits, limits, etc. • • •				
$-0.20^{+0.17}_{-0.28}\pm0.03$	AALTONEN	11L	CDF	Repl. by AALTONEN 12I

$A_{FB}(B \to K\ell^+\ell^-)$ ($10.09 < q^2 < 12.86$ GeV^2/c^4)

VALUE	DOCUMENT ID		TECN	COMMENT
-0.05 ± 0.06 OUR AVERAGE				
$-0.03\pm0.07\pm0.01$	AAIJ	13H	LHCB	pp at 7 TeV
$-0.03^{+0.11}_{-0.10}\pm0.04$	AALTONEN	12I	CDF	$p\overline{p}$ at 1.96 TeV
$-0.21^{+0.17}_{-0.15}\pm0.06$	WEI	09A	BELL	$e^+e^- \to \Upsilon(4S)$
• • • We do not use the following data for averages, fits, limits, etc. • • •				
$-0.10^{+0.17}_{-0.15}\pm0.07$	AALTONEN	11L	CDF	Repl. by AALTONEN 12I

$A_{FB}(B \to K\ell^+\ell^-)$ ($14.18 < q^2 < 16.0$ GeV^2/c^4)

VALUE	DOCUMENT ID		TECN	COMMENT
$-0.02^{+0.07}_{-0.05}$ OUR AVERAGE				
$-0.01^{+0.12}_{-0.06}\pm0.01$	AAIJ	13H	LHCB	pp at 7 TeV
$-0.05^{+0.09}_{-0.11}\pm0.03$	AALTONEN	12I	CDF	$p\overline{p}$ at 1.96 TeV
$0.04^{+0.32}_{-0.26}\pm0.05$	WEI	09A	BELL	$e^+e^- \to \Upsilon(4S)$
• • • We do not use the following data for averages, fits, limits, etc. • • •				
$0.03^{+0.49}_{-0.16}\pm0.04$	AALTONEN	11L	CDF	Repl. by AALTONEN 12I

$A_{FB}(B \to K\ell^+\ell^-)$ ($16.0 < q^2 < 18.0$ GeV^2/c^4)

VALUE	DOCUMENT ID		TECN	COMMENT
$-0.09^{+0.07+0.02}_{-0.09-0.01}$	AAIJ	13H	LHCB	pp at 7 TeV

$A_{FB}(B \to K\ell^+\ell^-)$ ($18.0 < q^2 < 22.0$ GeV^2/c^4)

VALUE	DOCUMENT ID		TECN	COMMENT
$0.02\pm0.11\pm0.01$	AAIJ	13H	LHCB	pp at 7 TeV

$A_{FB}(B \to K\ell^+\ell^-)$ ($q^2 > 16.0$ GeV^2/c^4)

VALUE	DOCUMENT ID		TECN	COMMENT
$0.04^{+0.09}_{-0.07}$ OUR AVERAGE				
$0.09^{+0.17}_{-0.13}\pm0.03$	AALTONEN	12I	CDF	$p\overline{p}$ at 1.96 TeV
$0.02^{+0.11}_{-0.08}\pm0.02$	WEI	09A	BELL	$e^+e^- \to \Upsilon(4S)$
• • • We do not use the following data for averages, fits, limits, etc. • • •				
$0.07^{+0.30}_{-0.23}\pm0.02$	AALTONEN	11L	CDF	Repl. by AALTONEN 12I

$A_{FB}(B \to X_s\ell^+\ell^-)$ ($1.0 < q^2 < 6.0$ GeV^2/c^4)

VALUE	DOCUMENT ID		TECN	COMMENT
• • • We do not use the following data for averages, fits, limits, etc. • • •				
0.74 ± 0.54	[1] SATO	16	BELL	$e^+e^- \to \Upsilon(4S)$

[1] Uses the sum of 10 exclusive X_s modes in the range $M(X_s) > 1.1$ GeV/c^2. Uncertainty is statistical only.

$F_S(B \to K\ell^+\ell^-)$ ($q^2 > 0.1$ GeV^2/c^4)

VALUE	DOCUMENT ID		TECN	COMMENT
$0.81^{+0.58}_{-0.61}\pm0.46$	[1] AUBERT,B	06J	BABR	$e^+e^- \to \Upsilon(4S)$

[1] Results with different q^2 cuts are also reported.

$A_{FB}(B \to Kp\overline{p})$ ($m_{p\overline{p}} < 2.85$ GeV/c^2)

VALUE	DOCUMENT ID		TECN	COMMENT
$0.495\pm0.012\pm0.007$	[1] AAIJ	14AF	LHCB	pp at 7, 8 TeV

[1] Measured in $B^+ \to K^+p\overline{p}$ decays.

$A_{FB}(B \to \pi p\overline{p})$ ($m_{p\overline{p}} < 2.85$ GeV/c^2)

VALUE	DOCUMENT ID		TECN	COMMENT
$-0.409\pm0.033\pm0.006$	[1] AAIJ	14AF	LHCB	pp at 7, 8 TeV

[1] Measured in $B^+ \to \pi^+p\overline{p}$ decays.

A_{FB} in $B \to \overline{D}^*e^+\nu_e$

VALUE	DOCUMENT ID		TECN	COMMENT
$0.227\pm0.020\pm0.006$	[1] PRIM	23	BELL	$e^+e^- \to \Upsilon(4S)$

[1] This is the B^+ and B^0 average.

A_{FB} in $B \to \overline{D}^*\mu^+\nu_\mu$

VALUE	DOCUMENT ID		TECN	COMMENT
$0.256\pm0.020\pm0.005$	[1] PRIM	23	BELL	$e^+e^- \to \Upsilon(4S)$

[1] This is the B^+ and B^0 average.

$\Delta(A_{FB}) = (A^{\mu}_{FB} - A^{e}_{FB})$ in $B^0 \to D^{*-}\ell^+\nu_\ell$

VALUE	DOCUMENT ID		TECN	COMMENT
$0.028\pm0.028\pm0.008$	[1] PRIM	23	BELL	$e^+e^- \to \Upsilon(4S)$

[1] This is the B^+ and B^0 average.

ISOSPIN ASYMMETRY

Δ_{0-} is defined as

$$\frac{\Gamma(\overline{B}^0 \to f_d) - \Gamma(B^- \to f_u)}{\Gamma(\overline{B}^0 \to f_d) + \Gamma(B^- \to f_u)},$$

the isospin asymmetry of inclusive neutral and charged B decay.

$\Delta_{0-}(B(B \to X_s\gamma))$

VALUE	DOCUMENT ID		TECN	COMMENT
-0.005 ± 0.020 OUR AVERAGE				
$-0.0048\pm0.0149\pm0.0150$	[1] WATANUKI	19	BELL	$e^+e^- \to \Upsilon(4S)$
$-0.006\pm0.058\pm0.026$	AUBERT,B	05R	BABR	$e^+e^- \to \Upsilon(4S)$

[1] Using a sum-of-exclusive technique with $m_{X_s} < 2.8$ GeV/c^2.

$\Delta_{0-}(B(B \to X_{s+d}\gamma))$

VALUE	DOCUMENT ID		TECN	COMMENT
$-0.06\pm0.15\pm0.07$	[1] AUBERT	08O	BABR	$e^+e^- \to \Upsilon(4S)$

[1] Uses a fully reconstructed B meson as a tag on the recoil side. The result is for $E_\gamma >$ 2.2 GeV.

$\Delta_{0+}(B \to K^*(892)\gamma)$

Δ_{0+} describes the isospin asymmetry between $\Gamma(B^0 \to K^*(892)^0\gamma)$ and $\Gamma(B^+ \to K^*(892)^+\gamma)$.

VALUE	DOCUMENT ID		TECN	COMMENT
0.059 ± 0.014 OUR AVERAGE				
$0.048\pm0.020\pm0.018$	[1] ADACHI	25Z	BELL	$e^+e^- \to \Upsilon(4S)$
$0.062\pm0.015\pm0.013$	[2] HORIGUCHI	17	BELL	$e^+e^- \to \Upsilon(4S)$
$0.066\pm0.021\pm0.022$	[3] AUBERT	09AO	BABR	$e^+e^- \to \Upsilon(4S)$
• • • We do not use the following data for averages, fits, limits, etc. • • •				
$0.050\pm0.045\pm0.037$	[4] AUBERT,BE	04A	BABR	Repl. by AUBERT 09AO
$0.012\pm0.044\pm0.026$	NAKAO	04	BELL	Repl. by HORIGUCHI 17

[1] Uses $B(\Upsilon(4S) \to B^+B^-)=(51.13^{+0.73}_{-1.08})\%$, $B(\Upsilon(4S) \to B^0\overline{B}^0)=(48.61^{+0.74}_{-0.80})\%$.

[2] Uses $B(\Upsilon(4S) \to B^+B^-) = (51.4\pm0.6)\%$ and $B(\Upsilon(4S) \to B^0\overline{B}^0) = (48.6\pm0.6)\%$.

[3] Uses the production ratio of charged and neutral B from $\Upsilon(4S)$ decays and the lifetime ratio $\tau_{B^+}/\tau_{B^0} = 1.071\pm0.009$. The 90% CL interval is $0.017 < \Delta_{0+} < 0.116$

[4] Uses the production ratio of charged and neutral B from $\Upsilon(4S)$ decays $R^{+/0} = 1.006\pm0.048$ and the lifetime ratio of $\tau_{B^+}/\tau_{B^0} = 1.083\pm0.017$. The 90% CL interval is $-0.046 < \Delta_{0+} < 0.146$.

$\Delta_{\rho\gamma} = \Gamma(B^+ \to \rho^+\gamma) / (2\cdot\Gamma(B^0 \to \rho^0\gamma)) - 1$

VALUE	DOCUMENT ID		TECN	COMMENT
-0.36 ± 0.13 OUR AVERAGE				
$-0.197^{+0.190+0.119}_{-0.182-0.127}$	[1] ADACHI	25G	BELL	$e^+e^- \to \Upsilon(4S)$
$-0.43^{+0.25}_{-0.22}\pm0.10$	AUBERT	08BH	BABR	$e^+e^- \to \Upsilon(4S)$
$-0.48^{+0.21}_{-0.19}{}^{+0.08}_{-0.09}$	TANIGUCHI	08	BELL	$e^+e^- \to \Upsilon(4S)$

[1] ADACHI 25G reports the ratio $(2\,\Gamma(B^0 \to \rho^0\gamma) - \Gamma(B^+ \to \rho^+\gamma))\,/\,(2\,\Gamma(B^0 \to \rho^0\gamma) + \Gamma(B^+ \to \rho^+\gamma)) = 0.109^{+0.112+0.068+0.038}_{-0.117-0.062-0.039}$, where the last uncertainty comes from f_{+-}/f_{00} uncertainty combined with the one from τ_{B^+}/τ_{B^0} lifetimes ratio.

$\Delta_{0-}(B(B \to K\ell^+\ell^-))$

VALUE	DOCUMENT ID		TECN	COMMENT
-0.15 ± 0.06 OUR AVERAGE Error includes scale factor of 1.2.				
$-0.31^{+0.13}_{-0.11}\pm0.01$	[1] CHOUDHURY	21	BELL	$e^+e^- \to \Upsilon(4S)$
$-0.10^{+0.08}_{-0.09}\pm0.02$	[2] AAIJ	14M	LHCB	pp at 7, 8 TeV
$-0.09^{+0.08}_{-0.08}\pm0.02$	[3] AAIJ	14M	LHCB	pp at 7, 8 TeV
$-0.58^{+0.29}_{-0.37}\pm0.02$	[4] LEES	12S	BABR	$e^+e^- \to \Upsilon(4S)$
• • • We do not use the following data for averages, fits, limits, etc. • • •				
$-0.35^{+0.23}_{-0.27}$	[5] AAIJ	12AH	LHCB	Repl. by AAIJ 14M
$-1.43^{+0.56}_{-0.85}\pm0.05$	[6,7] AUBERT	09T	BABR	Repl. by LEES 12S
$-0.31^{+0.17}_{-0.14}\pm0.08$	[8,9] WEI	09A	BELL	$e^+e^- \to \Upsilon(4S)$

[1] For $1.0 < q^2 < 6.0$ GeV^2/c^4 using both $\mu^+\mu^-$ and e^+e^- as a lepton pair. Measurements in other q^2 bins are also reported.

[2] For $1.1 < q^2 < 6.0$ GeV^2/c^4 using $\mu^+\mu^-$ as a lepton pair and assuming isospin symmetry for the $B \to J/\psi(1S)K$. Measurements in other q^2 bins are also reported.

Int. J. Mod. Phys. A 2026.41. Downloaded from www.worldscientific.com by UNIVERSITY OF CALIFORNIA @ BERKELEY on 09/16/26. Re-use and distribution is strictly not permitted, except for Open Access articles.

[3] For $15.0 < q^2 < 19.0$ GeV^2/c^4 using $\mu^+\mu^-$ as a lepton pair and assuming isospin symmetry for the $B \to J/\psi(1S)K$. Measurements in other q^2 bins are also reported.
[4] For $0.10 < q^2 < 8.12$ GeV^2/c^4. Measurements in other q^2 bins are also reported.
[5] For $1 < q^2 < 6$ GeV^2/c^4.
[6] For $0.1 < m^2_{\ell^+\ell^-} < 7.02$ GeV^2/c^4.
[7] Assumes equal production of B^+ and B^0 at the $\Upsilon(4S)$.
[8] Superseded by CHOUDHURY 21.
[9] For $q^2 < 8.68$ GeV^2/c^4.

$\Delta_{0-}(B(B \to K^*\ell^+\ell^-))$

VALUE	DOCUMENT ID		TECN	COMMENT
$-0.03^{+0.08}_{-0.07}$ OUR AVERAGE	Error includes scale factor of 1.2.			
$0.00^{+0.12}_{-0.10}\pm0.02$	[1] AAIJ	14M	LHCB	pp at 7, 8 TeV
$0.06^{+0.10}_{-0.09}\pm0.02$	[2] AAIJ	14M	LHCB	pp at 7, 8 TeV
$-0.25^{+0.20}_{-0.17}\pm0.03$	[3] LEES	12S	BABR	$e^+e^- \to \Upsilon(4S)$
$-0.29\pm0.16\pm0.09$	[4] WEI	09A	BELL	$e^+e^- \to \Upsilon(4S)$
• • • We do not use the following data for averages, fits, limits, etc. • • •				
-0.15 ± 0.16	[5] AAIJ	12AH	LHCB	Repl. by AAIJ 14M
$-0.56^{+0.17}_{-0.15}\pm0.03$	[6,7] AUBERT	09T	BABR	Repl. by LEES 12S

[1] For $1.1 < q^2 < 6.0$ GeV^2/c^4 using $\mu^+\mu^-$ as a lepton pair and assuming isospin symmetry for the $B(B \to J/\psi(1S)K^*(892))$. Measurements in other q^2 bins are also reported.
[2] For $15.0 < q^2 < 22.0$ GeV^2/c^4 using $\mu^+\mu^-$ as a lepton pair and assuming isospin symmetry for the $B(B \to J/\psi(1S)K^*(892))$. Measurements in other q^2 bins are also reported.
[3] For $0.10 < q^2 < 8.12$ GeV^2/c^4. Measurements in other q^2 bins are also reported.
[4] For $q^2 < 8.68$ GeV^2/c^4.
[5] For $1 < q^2 < 6$ GeV^2/c^4.
[6] For $0.1 < m^2_{\ell^+\ell^-} < 7.02$ GeV^2/c^4.
[7] Assumes equal production of B^+ and B^0 at the $\Upsilon(4S)$.

$\Delta_{0-}(B(B \to K^{(*)}\ell^+\ell^-))$

VALUE	DOCUMENT ID		TECN	COMMENT
-0.45 ± 0.17 OUR AVERAGE	Error includes scale factor of 1.7.			
$-0.64^{+0.15}_{-0.14}\pm0.03$	[1,2] AUBERT	09T	BABR	$e^+e^- \to \Upsilon(4S)$
$-0.30^{+0.12}_{-0.11}\pm0.08$	[3] WEI	09A	BELL	$e^+e^- \to \Upsilon(4S)$

[1] For $0.1 < m^2_{\ell^+\ell^-} < 7.02$ GeV^2/c^4.
[2] Assumes equal production of B^+ and B^0 at the $\Upsilon(4S)$.
[3] For $q^2 < 8.68$ GeV^2/c^2.

$B \to X_c\ell\nu$ HADRONIC MASS MOMENTS

$\langle M_X^2 - \overline{M}_D^2 \rangle$ (First Moments)

VALUE (GeV^2)	DOCUMENT ID		TECN	COMMENT
0.36 ±0.08 OUR AVERAGE	Error includes scale factor of 1.8.			
$0.467\pm0.038\pm0.068$	[1] ACOSTA	05F	CDF	$p\overline{p}$ at 1.96 TeV
$0.293\pm0.012\pm0.058$	[2] CSORNA	04	CLE2	$e^+e^- \to \Upsilon(4S)$
• • • We do not use the following data for averages, fits, limits, etc. • • •				
$0.251\pm0.023\pm0.062$	[3] CRONIN-HEN...	01B	CLE2	$e^+e^- \to \Upsilon(4S)$

[1] Moments are measured with a minimum lepton momentum of 0.7 GeV/c in the B rest frame;
[2] Uses minimum lepton energy of 1.5 GeV and also reports moments with $E_\ell > 1.0$ GeV.
[3] The leptons are required to have $P_\ell > 1.5$ GeV/c.

$\langle M_X^2 \rangle$ (First Moments)

VALUE (GeV^2)	DOCUMENT ID		TECN	COMMENT
4.156±0.029 OUR AVERAGE				
$4.144\pm0.028\pm0.022$	[1] SCHWANDA	07	BELL	$e^+e^- \to \Upsilon(4S)$
$4.18\ \pm0.04\ \pm0.03$	[1] AUBERT,B	04	BABR	$e^+e^- \to \Upsilon(4S)$

[1] The leptons are required to have $E_\ell > 1.5$ GeV/c.

$\langle (M_X^2 - \overline{M}_X^2)^2 \rangle$ (Second Moments)

VALUE (GeV^4)	DOCUMENT ID		TECN	COMMENT
0.55 ±0.08 OUR AVERAGE				
$0.515\pm0.061\pm0.064$	[1] SCHWANDA	07	BELL	$e^+e^- \to \Upsilon(4S)$
$0.629\pm0.031\pm0.143$	[2] CSORNA	04	CLE2	$e^+e^- \to \Upsilon(4S)$
• • • We do not use the following data for averages, fits, limits, etc. • • •				
$1.05\ \pm0.26\ \pm0.13$	[3] ACOSTA	05F	CDF	$p\overline{p}$ at 1.96 TeV
$0.576\pm0.048\pm0.168$	[1] CRONIN-HEN...	01B	CLE2	$e^+e^- \to \Upsilon(4S)$

[1] The leptons are required to have $E_\ell > 1.5$ GeV/c.
[2] Uses minimum lepton energy of 1.5 GeV and also reports moments with $E_\ell > 1.0$ GeV.
[3] Moments are measured with a minimum lepton momentum of 0.7 GeV/c in the B rest frame;

$\langle (M_X^2 - \overline{M}_D^2)^2 \rangle$ (Second Moments)

VALUE (GeV^4)	DOCUMENT ID		TECN	COMMENT
0.639±0.056±0.178	[1] CRONIN-HEN...	01B	CLE2	$e^+e^- \to \Upsilon(4S)$

[1] The leptons are required to have $E_\ell > 1.5$ GeV/c.

$B \to X_c\ell\nu$ LEPTON MOMENTUM MOMENTS

R_0 ($\Gamma_{E_l>1.7GeV}$ / $\Gamma_{E_l>1.5GeV}$)

VALUE	DOCUMENT ID		TECN	COMMENT
0.6187±0.0014±0.0016	[1] MAHMOOD	03	CLE2	$e^+e^- \to \Upsilon(4S)$

[1] The leptons are required to have $E_l > 1.5$ GeV in the B rest frame.

R_1 ($\langle E_l \rangle_{E_l>1.5GeV}$)

VALUE	DOCUMENT ID		TECN	COMMENT
1.7797±0.0018 OUR AVERAGE	Error includes scale factor of 1.8. See the ideogram below.			
$1.7743\pm0.0019\pm0.0014$	[1] AUBERT,B	04A	BABR	$e^+e^- \to \Upsilon(4S)$
$1.7792\pm0.0021\pm0.0027$	[2] MAHMOOD	04	CLEO	$e^+e^- \to \Upsilon(4S)$
$1.7810\pm0.0007\pm0.0009$	[3] MAHMOOD	03	CLE2	$e^+e^- \to \Upsilon(4S)$

[1] The leptons are required to have $E_l > 1.5$ GeV in the B rest frame. The result with $E_l > 0.6$ GeV is also given.
[2] Uses $E_e > 1.5$ GeV and also reports moments with other minimum minimum E_e conditions, as low as $E_e > 0.6$ GeV.
[3] The leptons are required to have $E_l > 1.5$ GeV in the B rest frame.

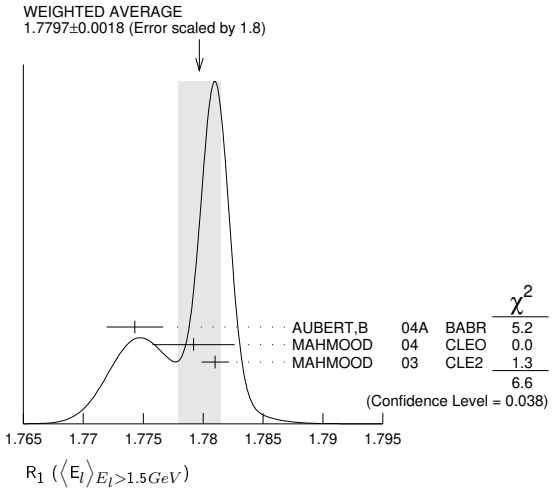

R_2 ($\langle E_l^2 - \overline{E}_l^2 \rangle_{E_l>1.5GeV}$)

VALUE (10^{-3} GeV^2)	DOCUMENT ID		TECN	COMMENT
30.8±0.8 OUR AVERAGE				
$30.3\pm0.9\pm0.5$	[1] AUBERT,B	04A	BABR	$e^+e^- \to \Upsilon(4S)$
$31.6\pm0.8\pm1.0$	[2] MAHMOOD	04	CLEO	$e^+e^- \to \Upsilon(4S)$

[1] The leptons are required to have $E_l > 1.5$ GeV in the B rest frame. The result with $E_l > 0.6$ GeV is also given.
[2] Uses $E_e > 1.5$ GeV and also reports moments with other minimum minimum E_e conditions, as low as $E_e > 0.6$ GeV.

R_3 ($\langle E_l^3 - \overline{E}_l^3 \rangle_{E_l>1.5GeV}$)

VALUE (10^{-3} GeV^3)	DOCUMENT ID		TECN	COMMENT
2.12±0.47±0.20	[1] AUBERT,B	04A	BABR	$e^+e^- \to \Upsilon(4S)$

[1] The leptons are required to have $E_l > 1.5$ GeV in the B rest frame. The result with $E_l > 0.6$ GeV is also given.

$B \to X_s\gamma$ PHOTON ENERGY MOMENTS

$\langle E_\gamma \rangle$

VALUE (GeV)	DOCUMENT ID		TECN	COMMENT
2.314±0.011 OUR AVERAGE				
$2.346\pm0.018^{+0.027}_{-0.022}$	[1,2] LEES	12U	BABR	$e^+e^- \to \Upsilon(4S)$
$2.304\pm0.014\pm0.017$	[2,3] LEES	12V	BABR	$e^+e^- \to \Upsilon(4S)$
$2.311\pm0.009\pm0.015$	[3] LIMOSANI	09	BELL	$e^+e^- \to \Upsilon(4S)$
$2.289\pm0.058\pm0.027$	[3,4] AUBERT	08O	BABR	$e^+e^- \to \Upsilon(4S)$
$2.309\pm0.023\pm0.023$	[2,3] SCHWANDA	08	BELL	$e^+e^- \to \Upsilon(4S)$
• • • We do not use the following data for averages, fits, limits, etc. • • •				
$2.288\pm0.025\pm0.023$	[3] AUBERT,BE	06B	BABR	Repl. by LEES 12V

[1] LEES 12U uses $E_\gamma > 1.897$ GeV to calculate the moments; the moments are used to calculate the HQET parameters $m_b = 4.579^{+0.032}_{-0.029}$ GeV/c^2 and $\mu_\pi^2 = 0.257^{+0.034}_{-0.039}$ GeV^2 in the shape function model. The same HQET parameters are also determined in the kinetic model.
[2] Results for different E_γ threshold values are also measured.
[3] The result is for $E_\gamma > 1.9$ GeV.
[4] Uses a fully reconstructed B meson as a tag on the recoil side.

Int. J. Mod. Phys. A 2026.41. Downloaded from www.worldscientific.com
by CALIFORNIA @ BERKELEY on 09/16/26. Re-use and distribution is strictly not permitted, except for Open Access articles.

$\langle E_\gamma^2 \rangle - \langle E_\gamma \rangle^2$

VALUE (10^{-2} GeV^2)	DOCUMENT ID		TECN	COMMENT
3.03±0.25 OUR AVERAGE				
$2.11 \pm 0.57^{+0.55}_{-0.69}$	[1,2] LEES	12U	BABR	$e^+e^- \to \Upsilon(4S)$
$3.62 \pm 0.33 \pm 0.33$	[2,3] LEES	12V	BABR	$e^+e^- \to \Upsilon(4S)$
$3.02 \pm 0.19 \pm 0.30$	[3] LIMOSANI	09	BELL	$e^+e^- \to \Upsilon(4S)$
$3.34 \pm 1.24 \pm 0.62$	[3,4] AUBERT	08O	BABR	$e^+e^- \to \Upsilon(4S)$
$2.17 \pm 0.60 \pm 0.55$	[2,3] SCHWANDA	08	BELL	$e^+e^- \to \Upsilon(4S)$
• • • We do not use the following data for averages, fits, limits, etc. • • •				
$3.28 \pm 0.40 \pm 0.43$	[3] AUBERT,BE	06B	BABR	Repl. by LEES 12V

[1] LEES 12U uses $E_\gamma > 1.897$ GeV to calculate the moments; the moments are used to calculate the HQET parameters $m_b = 4.579^{+0.032}_{-0.029}$ GeV/c^2 and $\mu_\pi^2 = 0.257^{+0.034}_{-0.039}$ GeV^2 in the shape function model. The same HQET parameters are also determined in the kinetic model.

[2] Results for different E_γ threshold values are also measured.

[3] The result is for $E_\gamma > 1.9$ GeV.

[4] Uses a fully reconstructed B meson as a tag on the recoil side.

$B^{\pm}/B^{0}$ ADMIXTURE REFERENCES

AAIJ	25G	PRL 134 061801	R. Aaij et al.	(LHCb Collab.)
ADACHI	25G	PR D111 L071103	I. Adachi et al.	(BELLE and BELLE II Collab.)
ADACHI	25Y	PR D112 112009	I. Adachi et al.	(BELLE II Collab.)
ADACHI	25Z	JHEP 2509 024	I. Adachi et al.	(BELLE II Collab.)
HOHMANN	25	PR D111 092016	M. Hohmann et al.	(BELLE Collab.)
ADACHI	24O	PR D110 072020	I. Adachi et al.	(BELLE II Collab.)
FERLEWICZ	24	PR D110 072005	D. Ferlewicz et al.	(BELLE Collab.)
AAIJ	23AR	PRL 131 111802	R. Aaij et al.	(LHCb Collab.)
AAIJ	23W	PR D108 012018	R. Aaij et al.	(LHCb Collab.)
Also		PR D109 119902 (errat.)	R. Aaij et al.	(LHCb Collab.)
AGGARWAL	23	PRL 131 051804	L. Aggarwal et al.	(BELLE II Collab.)
CAO	23	PRL 131 211801	L. Cao et al.	(BELLE Collab.)
PRIM	23	PR D108 012002	M.T. Prim et al.	(BELLE Collab.)
ZHUKOVA	23	JHEP 2308 131	V. Zhukova et al.	(BELLE Collab.)
CAO	21A	PR D104 012008	L. Cao et al.	(BELLE Collab.)
CHOUDHURY	21	JHEP 2103 105	S. Choudhury et al.	(BELLE Collab.)
WEHLE	21	PRL 126 161801	S. Wehle et al.	(BELLE Collab.)
AAIJ	20Y	PRL 125 011802	R. Aaij et al.	(LHCb Collab.)
CARIA	20	PRL 124 161803	G. Caria et al.	(BELLE Collab.)
AAIJ	19AD	PR D100 031102	R. Aaij et al.	(LHCb Collab.)
WATANUKI	19	PR D99 032012	S. Watanuki et al.	(BELLE Collab.)
GRYGIER	17	PR D96 091101	J. Grygier et al.	(BELLE Collab.)
HIROSE	17	PRL 118 211801	S. Hirose et al.	(BELLE Collab.)
Also		PR D97 012004	S. Hirose et al.	(BELLE Collab.)
HORIGUCHI	17	PRL 119 191802	T. Horiguchi et al.	(BELLE Collab.)
LEES	17B	PR D95 072001	J.P. Lees et al.	(BABAR Collab.)
AAIJ	16B	JHEP 1602 104	R. Aaij et al.	(LHCb Collab.)
BHARDWAJ	16	PR D93 052016	V. Bhardwaj et al.	(BELLE Collab.)
KHACHATRY...	16D	PL B753 424	V. Khachatryan et al.	(CMS Collab.)
LEES	16	PRL 116 041801	J.P. Lees et al.	(BABAR Collab.)
LEES	16C	PR D93 052015	J.P. Lees et al.	(BABAR Collab.)
SATO	16	PR D93 032008	Y. Sato et al.	(BELLE Collab.)
Also		PR D93 059901 (errat.)	Y. Sato et al.	(BELLE Collab.)
HUSCHLE	15	PR D92 072014	M. Huschle et al.	(BELLE Collab.)
PESANTEZ	15	PRL 114 151601	L. Pesantez et al.	(BELLE Collab.)
SAITO	15	PR D91 052004	T. Saito et al.	(BELLE Collab.)
AAIJ	14AF	PRL 113 141801	R. Aaij et al.	(LHCb Collab.)
Also		PRL 134 179901 (errat.)	R. Aaij et al.	(LHCb Collab.)
AAIJ	14M	JHEP 1406 133	R. Aaij et al.	(LHCb Collab.)
LEES	14D	PRL 112 211802	J.P. Lees et al.	(BABAR Collab.)
LEES	14K	PR D90 092001	J.P. Lees et al.	(BABAR Collab.)
AAIJ	13H	JHEP 1302 105	R. Aaij et al.	(LHCb Collab.)
AAIJ	13Y	JHEP 1308 131	R. Aaij et al.	(LHCb Collab.)
CHATRCHYAN	13BL	PL B727 77	S. Chatrchyan et al.	(CMS Collab.)
LEES	13I	PR D87 112005	J.P. Lees et al.	(BABAR Collab.)
LEES	13M	PR D88 032012	J.P. Lees et al.	(BABAR Collab.)
AAIJ	12AH	JHEP 1207 133	R. Aaij et al.	(LHCb Collab.)
AAIJ	12U	PRL 108 181806	R. Aaij et al.	(LHCb Collab.)
AALTONEN	12I	PRL 108 081807	T. Aaltonen et al.	(CDF Collab.)
LEES	12	PR D85 011102	J.P. Lees et al.	(BABAR Collab.)
LEES	12D	PRL 109 101802	J.P. Lees et al.	(BABAR Collab.)
Also		PR D88 072012	J.P. Lees et al.	(BABAR Collab.)
LEES	12R	PR D86 032004	J.P. Lees et al.	(BABAR Collab.)
LEES	12S	PR D86 032012	J.P. Lees et al.	(BABAR Collab.)
LEES	12U	PR D86 052012	J.P. Lees et al.	(BABAR Collab.)
LEES	12V	PRL 109 191801	J.P. Lees	(BABAR Collab.)
Also		PR D86 112008	J.P. Lees et al.	(BABAR Collab.)
AALTONEN	11AI	PRL 107 201802	T. Aaltonen et al.	(CDF Collab.)
AALTONEN	11L	PRL 106 161801	T. Aaltonen et al.	(CDF Collab.)
DEL-AMO-SA...	11	PR D83 031103	P. del Amo Sanchez et al.	(BABAR Collab.)
GAMBINO	11	JHEP 1109 055	P. Gambino	(LCGT)
AUBERT	10	PRL 104 011802	B. Aubert et al.	(BABAR Collab.)
AUBERT	10A	PR D81 032003	B. Aubert et al.	(BABAR Collab.)
AUSHEV	10	PR D81 031103	T. Aushev et al.	(BELLE Collab.)
DEL-AMO-SA...	10M	PR D82 051101	P. del Amo Sanchez et al.	(BABAR Collab.)
DEL-AMO-SA...	10Q	PR D82 112002	P. del Amo Sanchez et al.	(BABAR Collab.)
NISHIMURA	10	PRL 105 191803	K. Nishimura et al.	(BELLE Collab.)
URQUIJO	10	PRL 104 021801	P. Urquijo et al.	(BELLE Collab.)
AUBERT	09AO	PRL 103 211802	B. Aubert et al.	(BABAR Collab.)
AUBERT	09N	PR D79 031102	B. Aubert et al.	(BABAR Collab.)
AUBERT	09T	PRL 102 091803	B. Aubert et al.	(BABAR Collab.)
Also		EPAPS Document No. E-PRLTAO-102-060910		(BABAR Collab.)
AUBERT	09U	PRL 102 161803	B. Aubert et al.	(BABAR Collab.)
LIMOSANI	09	PRL 103 241801	A. Limosani et al.	(BELLE Collab.)
WEI	09A	PRL 103 171801	J.-T. Wei et al.	(BELLE Collab.)
Also		EPAPS Supplement	J.-T. Wei et al.	(BELLE Collab.)
AUBERT	08AS	PRL 100 171802	B. Aubert et al.	(BABAR Collab.)
AUBERT	08BC	PR D78 072007	B. Aubert et al.	(BABAR Collab.)
AUBERT	08BH	PR D78 112001	B. Aubert et al.	(BABAR Collab.)
AUBERT	08BJ	PRL 101 171804	B. Aubert et al.	(BABAR Collab.)
AUBERT	08N	PRL 100 021801	B. Aubert et al.	(BABAR Collab.)
Also		PR D79 092002	B. Aubert et al.	(BABAR Collab.)
AUBERT	08O	PR D77 051103	B. Aubert et al.	(BABAR Collab.)
SCHWANDA	08	PR D78 032016	C. Schwanda et al.	(BELLE Collab.)
TANIGUCHI	08	PRL 101 111801	N. Taniguchi et al.	(BELLE Collab.)
WEI	08A	PR D78 011101	J.-T. Wei et al.	(BELLE Collab.)
AUBERT	07AG	PRL 99 051801	B. Aubert et al.	(BABAR Collab.)
AUBERT	07C	PR D75 012003	B. Aubert et al.	(BABAR Collab.)
AUBERT	07E	PRL 98 051802	B. Aubert et al.	(BABAR Collab.)
AUBERT	07L	PRL 98 151802	B. Aubert et al.	(BABAR Collab.)
GAMBINO	07	JHEP 0710 058	P. Gambino et al.	
HUANG	07	PR D75 012002	G.S. Huang et al.	(CLEO Collab.)
SCHWANDA	07	PR D75 032005	C. Schwanda et al.	(BELLE Collab.)
URQUIJO	07	PR D75 032001	P. Urquijo et al.	(BELLE Collab.)
AUBERT	06H	PR D73 012006	B. Aubert et al.	(BABAR Collab.)
AUBERT,B	06J	PR D73 092001	B. Aubert et al.	(BABAR Collab.)
AUBERT,B	06Y	PR D74 091105	B. Aubert et al.	(BABAR Collab.)
AUBERT,BE	06B	PRL 97 171803	B. Aubert et al.	(BABAR Collab.)
BUCHMUEL...	06	PR D73 073008	O.L. Buchmueller, H.U. Flacher	(RHBL)
GOKHROO	06	PRL 97 162002	G. Gokhroo et al.	(BELLE Collab.)
ISHIKAWA	06	PRL 96 251801	A. Ishikawa et al.	(BELLE Collab.)
MOHAPATRA	06	PRL 96 221601	D. Mohapatra et al.	(BELLE Collab.)
ABAZOV	05O	PRL 95 171803	V.M. Abazov et al.	(D0 Collab.)
ACOSTA	05F	PR D71 051103	D. Acosta et al.	(CDF Collab.)
ARTUSO	05B	PRL 95 261801	M. Artuso et al.	(CLEO Collab.)
AUBERT	05	PRL 94 011801	B. Aubert et al.	(BABAR Collab.)
AUBERT,B	05M	PRL 95 142003	B. Aubert et al.	(BABAR Collab.)
AUBERT,B	05R	PR D72 052004	B. Aubert et al.	(BABAR Collab.)
AUBERT,B	05X	PRL 95 111801	B. Aubert et al.	(BABAR Collab.)
Also		PRL 97 019903 (errat.)	B. Aubert et al.	(BABAR Collab.)
CHOI	05	PRL 94 182002	S.-K. Choi et al.	(BELLE Collab.)
IWASAKI	05	PR D72 092005	M. Iwasaki et al.	(BELLE Collab.)
LIMOSANI	05	PL B621 28	A. Limosani et al.	(BELLE Collab.)
MOHAPATRA	05	PR D72 011101	D. Mohapatra et al.	(BELLE Collab.)
NISHIDA	05	PL B610 23	S. Nishida et al.	(BELLE Collab.)
OKABE	05	PL B614 27	T. Okabe et al.	(BELLE Collab.)
ABDALLAH	04D	EPJ C33 213	J. Abdallah et al.	(DELPHI Collab.)
AUBERT	04C	PRL 92 111801	B. Aubert et al.	(BABAR Collab.)
AUBERT	04I	PRL 92 071802	B. Aubert et al.	(BABAR Collab.)
AUBERT	04S	PR D69 052005	B. Aubert et al.	(BABAR Collab.)
AUBERT	04X	PRL 93 011803	B. Aubert et al.	(BABAR Collab.)
AUBERT,B	04	PR D69 111103	B. Aubert et al.	(BABAR Collab.)
AUBERT,B	04A	PR D69 111104	B. Aubert et al.	(BABAR Collab.)
AUBERT,B	04E	PRL 93 021804	B. Aubert et al.	(BABAR Collab.)
AUBERT,B	04F	PRL 93 061801	B. Aubert et al.	(BABAR Collab.)
AUBERT,B	04I	PRL 93 081802	B. Aubert et al.	(BABAR Collab.)
AUBERT,BE	04A	PR D70 112006	B. Aubert et al.	(BABAR Collab.)
CSORNA	04	PR D70 032002	S.E. Csorna et al.	(CLEO Collab.)
KOPPENBURG	04	PRL 93 061803	P. Koppenburg et al.	(BELLE Collab.)
MAHMOOD	04	PR D70 032003	A.H. Mahmodd et al.	(CLEO Collab.)
NAKAO	04	PR D69 112001	M. Nakao et al.	(BELLE Collab.)
NISHIDA	04	PRL 93 031803	S. Nishida et al.	(BELLE Collab.)
ADAM	03B	PR D68 012004	N.E. Adam et al.	(CLEO Collab.)
AUBERT	03	PR D67 031101	B. Aubert et al.	(BABAR Collab.)
AUBERT	03F	PR D67 032002	B. Aubert et al.	(BABAR Collab.)
AUBERT	03U	PRL 91 221802	B. Aubert et al.	(BABAR Collab.)
BONVICINI	03	PR D68 011101	G. Bonvicini et al.	(CLEO Collab.)
HUANG	03	PRL 91 241802	H.-C. Huang et al.	(BELLE Collab.)
ISHIKAWA	03	PRL 91 261601	A. Ishikawa et al.	(BELLE Collab.)
KANEKO	03	PRL 90 021801	J. Kaneko et al.	(BELLE Collab.)
KROKOVNY	03B	PRL 91 262002	P. Krokovny et al.	(BELLE Collab.)
MAHMOOD	03	PR D67 072001	A.H. Mahmood et al.	(CLEO Collab.)
ABE	02	PRL 88 021801	K. Abe et al.	(BELLE Collab.)
ABE	02L	PRL 89 011803	K. Abe et al.	(BELLE Collab.)
ABE	02Y	PL B547 181	K. Abe et al.	(BELLE Collab.)
ANDERSON	02	PRL 89 282001	S. Anderson et al.	(CLEO Collab.)
AUBERT	02C	PRL 88 101805	B. Aubert et al.	(BABAR Collab.)
AUBERT	02G	PR D65 091104	B. Aubert et al.	(BABAR Collab.)
AUBERT	02L	PRL 88 241801	B. Aubert et al.	(BABAR Collab.)
BORNHEIM	02	PRL 88 231803	A. Bornheim et al.	(CLEO Collab.)
EDWARDS	02B	PR D65 111102	K.W. Edwards et al.	(CLEO Collab.)
ABE	01F	PL B511 151	K. Abe et al.	(BELLE Collab.)
ABE	01J	PR D64 072001	K. Abe et al.	(BELLE Collab.)
ANDERSON	01B	PRL 87 181803	S. Anderson et al.	(CLEO Collab.)
CHEN	01	PR D63 031102	S. Chen et al.	(CLEO Collab.)
CHEN	01C	PRL 87 251807	S. Chen et al.	(CLEO Collab.)
COAN	01	PRL 86 5661	T.E. Coan et al.	(CLEO Collab.)
CRONIN-HEN...	01B	PRL 87 251808	D. Cronin-Hennessy et al.	(CLEO Collab.)
PDG	01	Unofficial 2001 WWW edition		
ABREU	00R	PL B475 407	P. Abreu et al.	(DELPHI Collab.)
COAN	00	PRL 84 5283	T.E. Coan et al.	(CLEO Collab.)
RICHICHI	00	PRL 85 520	S.J. Richichi et al.	(CLEO Collab.)
BARATE	98Q	EPJ C4 387	R. Barate et al.	(ALEPH Collab.)
BERGFELD	98	PRL 81 272	T. Bergfeld et al.	(CLEO Collab.)
BISHAI	98	PR D57 3847	M. Bishai et al.	(CLEO Collab.)
BONVICINI	98	PR D57 6604	G. Bonvicini et al.	(CLEO Collab.)
BROWDER	98	PRL 81 1786	T.E. Browder et al.	(CLEO Collab.)
COAN	98	PRL 80 1150	T.E. Coan et al.	(CLEO Collab.)
GLENN	98	PRL 80 2289	S. Glenn et al.	(CLEO Collab.)
ACKERSTAFF	97N	ZPHY C74 423	K. Ackerstaff et al.	(OPAL Collab.)
AMMAR	97	PR D55 13	R. Ammar et al.	(CLEO Collab.)
BARISH	97	PRL 79 3599	B. Barish et al.	(CLEO Collab.)
BUSKULIC	97B	ZPHY C73 601	D. Buskulic et al.	(ALEPH Collab.)
GIBBONS	97B	PR D56 3783	L. Gibbons et al.	(CLEO Collab.)
ALBRECHT	96D	PL B374 256	H. Albrecht et al.	(ARGUS Collab.)
BARISH	96B	PRL 76 1570	B.C. Barish et al.	(CLEO Collab.)
GIBAUT	96	PR D53 4734	D. Gibaut et al.	(CLEO Collab.)
KUBOTA	96	PR D53 6033	Y. Kubota et al.	(CLEO Collab.)
PDG	96	PR D54 1	R. M. Barnett et al.	(PDG Collab.)
ALAM	95	PRL 74 2885	M.S. Alam et al.	(CLEO Collab.)
ALBRECHT	95D	PL B353 554	H. Albrecht et al.	(ARGUS Collab.)
BALEST	95B	PR D52 2661	R. Balest et al.	(CLEO Collab.)
BARISH	95	PR D51 1014	B.C. Barish et al.	(CLEO Collab.)
BUSKULIC	95B	PL B345 103	D. Buskulic et al.	(ALEPH Collab.)
ALBRECHT	94C	ZPHY C62 371	H. Albrecht et al.	(ARGUS Collab.)
ALBRECHT	94J	ZPHY C61 1	H. Albrecht et al.	(ARGUS Collab.)
PROCARIO	94	PRL 73 1472	M. Procario et al.	(CLEO Collab.)
ALBRECHT	93	ZPHY C57 533	H. Albrecht et al.	(ARGUS Collab.)
ALBRECHT	93E	ZPHY C60 11	H. Albrecht et al.	(ARGUS Collab.)
ALBRECHT	93H	PL B318 397	H. Albrecht et al.	(ARGUS Collab.)
ALBRECHT	93I	ZPHY C58 191	H. Albrecht et al.	(ARGUS Collab.)
ALEXANDER	93B	PL B319 365	J. Alexander et al.	(CLEO Collab.)
ARTUSO	93	PL B311 307	M. Artuso	(SYRA)
BARTELT	93B	PRL 71 4111	J.E. Bartelt et al.	(CLEO Collab.)
ALBRECHT	92E	PL B277 209	H. Albrecht et al.	(ARGUS Collab.)
ALBRECHT	92G	ZPHY C54 1	H. Albrecht et al.	(ARGUS Collab.)
ALBRECHT	92O	ZPHY C56 1	H. Albrecht et al.	(ARGUS Collab.)
BORTOLETTO	92	PR D45 21	D. Bortoletto et al.	(CLEO Collab.)
CRAWFORD	92	PR D45 752	G. Crawford et al.	(CLEO Collab.)
HENDERSON	92	PR D45 2212	S. Henderson et al.	(CLEO Collab.)
LESIAK	92	ZPHY C55 33	T. Lesiak et al.	(Crystal Ball Collab.)
ALBRECHT	91C	PL B255 297	H. Albrecht et al.	(ARGUS Collab.)
ALBRECHT	91H	ZPHY C52 353	H. Albrecht et al.	(ARGUS Collab.)
FULTON	91	PR D43 651	R. Fulton et al.	(CLEO Collab.)
YANAGISAWA	91	PRL 66 2436	C. Yanagisawa et al.	(CUSB II Collab.)
ALBRECHT	90	PL B234 409	H. Albrecht et al.	(ARGUS Collab.)
ALBRECHT	90H	PL B249 359	H. Albrecht et al.	(ARGUS Collab.)
BORTOLETTO	90	PRL 64 2117	D. Bortoletto et al.	(CLEO Collab.)
Also		PR D45 21	D. Bortoletto et al.	(CLEO Collab.)
FULTON	90	PRL 64 16	R. Fulton et al.	(CLEO Collab.)
MASCHMANN	90	ZPHY C46 555	W.S. Maschmann et al.	(Crystal Ball Collab.)
PDG	90	PL B239 1	J.J. Hernandez et al.	(IFIC, BOST, CIT+)

ALBRECHT	89K	ZPHY C42 519	H. Albrecht *et al.*	(ARGUS Collab.)
ISGUR	89B	PR D39 799	N. Isgur *et al.*	(TNTO, CIT)
WACHS	89	ZPHY C42 33	K. Wachs *et al.*	(Crystal Ball Collab.)
ALBRECHT	88E	PL B210 263	H. Albrecht *et al.*	(ARGUS Collab.)
ALBRECHT	88H	PL B210 258	H. Albrecht *et al.*	(ARGUS Collab.)
KOERNER	88	ZPHY C38 511	J.G. Korner, G.A. Schuler	(MAINZ, DESY)
ALAM	87	PRL 59 22	M.S. Alam *et al.*	(CLEO Collab.)
ALAM	87B	PRL 58 1814	M.S. Alam *et al.*	(CLEO Collab.)
ALBRECHT	87D	PL B199 451	H. Albrecht *et al.*	(ARGUS Collab.)
ALBRECHT	87H	PL B187 425	H. Albrecht *et al.*	(ARGUS Collab.)
BEAN	87	PR D35 3533	A. Bean *et al.*	(CLEO Collab.)
BEHRENDS	87	PRL 59 407	S. Behrends *et al.*	(CLEO Collab.)
BORTOLETTO	87	PR D35 19	D. Bortoletto *et al.*	(CLEO Collab.)
ALAM	86	PR D34 3279	M.S. Alam *et al.*	(CLEO Collab.)
BALTRUSAIT...	86E	PRL 56 2140	R.M. Baltrusaitis *et al.*	(Mark III Collab.)
BORTOLETTO	86	PRL 56 800	D. Bortoletto *et al.*	(CLEO Collab.)
HAAS	86	PRL 56 2781	J. Haas *et al.*	(CLEO Collab.)
ALBRECHT	85H	PL 162B 395	H. Albrecht *et al.*	(ARGUS Collab.)
CSORNA	85	PRL 54 1894	S.E. Csorna *et al.*	(CLEO Collab.)
HAAS	85	PRL 55 1248	J. Haas *et al.*	(CLEO Collab.)
AVERY	84	PRL 53 1309	P. Avery *et al.*	(CLEO Collab.)
CHEN	84	PRL 52 1084	A. Chen *et al.*	(CLEO Collab.)
LEVMAN	84	PL 141B 271	G.M. Levman *et al.*	(CUSB Collab.)
ALAM	83B	PRL 51 1143	M.S. Alam *et al.*	(CLEO Collab.)
GREEN	83	PRL 51 347	J. Green *et al.*	(CLEO Collab.)
KLOPFEN...	83B	PL 130B 444	C. Klopfenstein *et al.*	(CUSB Collab.)
ALTARELLI	82	NP B208 365	G. Altarelli *et al.*	(ROMA, INFN, FRAS)
BRODY	82	PRL 48 1070	A.D. Brody *et al.*	(CLEO Collab.)
GIANNINI	82	NP B206 1	G. Giannini *et al.*	(CUSB Collab.)
BEBEK	81	PRL 46 84	C. Bebek *et al.*	(CLEO Collab.)
CHADWICK	81	PRL 46 88	K. Chadwick *et al.*	(CLEO Collab.)
ABRAMS	80	PRL 44 10	G.S. Abrams *et al.*	(SLAC, LBL)

$B^{\pm}/B^0/B^0_s/b$-baryon ADMIXTURE

$B^{\pm}/B^0/B^0_s/b$-baryon ADMIXTURE MEAN LIFE

Each measurement of the B mean life is an average over an admixture of various bottom mesons and baryons which decay weakly. Different techniques emphasize different admixtures of produced particles, which could result in a different B mean life.

"OUR EVALUATION" is an average using rescaled values of the data listed below. This is a weighted average of the lifetimes of the five main b-hadron species (B^+, B^0, B^0_{sH}, B^0_{sL}, and Λ_b) that assumes the production fractions in Z decays (given at the end of this section) and equal production fractions of B^0_{sH} and B^0_{sL} mesons.

VALUE (10^{-12} s)	EVTS	DOCUMENT ID		TECN	COMMENT
1.5673±0.0029 OUR EVALUATION		(Produced by HFLAV)			
• • • We do not use the following data for averages, fits, limits, etc. • • •					
1.570 ±0.005 ±0.008		[1] ABDALLAH	04E	DLPH	$e^+e^- \to Z$
1.533 ±0.015 $^{+0.035}_{-0.031}$		[2] ABE	98B	CDF	$p\overline{p}$ at 1.8 TeV
1.549 ±0.009 ±0.015		[3] ACCIARRI	98	L3	$e^+e^- \to Z$
1.611 ±0.010 ±0.027		[4] ACKERSTAFF	97F	OPAL	$e^+e^- \to Z$
1.582 ±0.011 ±0.027		[4] ABREU	96E	DLPH	$e^+e^- \to Z$
1.575 ±0.010 ±0.026		[5] ABREU	96E	DLPH	$e^+e^- \to Z$
1.533 ±0.013 ±0.022	29.8k	[6] BUSKULIC	96F	ALEP	$e^+e^- \to Z$
1.564 ±0.030 ±0.036		[7] ABE,K	95B	SLD	$e^+e^- \to Z$
1.542 ±0.021 ±0.045		[8] ABREU	94L	DLPH	$e^+e^- \to Z$
1.50 $^{+0.24}_{-0.21}$ ±0.03		[9] ABREU	94P	DLPH	$e^+e^- \to Z$
1.46 ±0.06 ±0.06	5344	[10] ABE	93J	CDF	Repl. by ABE 98B
1.23 $^{+0.14}_{-0.13}$ ±0.15	188	[11] ABREU	93D	DLPH	Sup. by ABREU 94L
1.49 ±0.11 ±0.12	253	[12] ABREU	93G	DLPH	Sup. by ABREU 94L
1.51 $^{+0.16}_{-0.14}$ ±0.11	130	[13] ACTON	93C	OPAL	$e^+e^- \to Z$
1.523 ±0.034 ±0.038	5372	[14] ACTON	93L	OPAL	$e^+e^- \to Z$
1.535 ±0.035 ±0.028	7357	[14] ADRIANI	93K	L3	Repl. by ACCIARRI 98
1.511 ±0.022 ±0.078		[15] BUSKULIC	93O	ALEP	$e^+e^- \to Z$
1.28 ±0.10		[16] ABREU	92	DLPH	Sup. by ABREU 94L
1.37 ±0.07 ±0.06	1354	[17] ACTON	92	OPAL	Sup. by ACTON 93L
1.49 ±0.03 ±0.06		[18] BUSKULIC	92F	ALEP	Sup. by BUSKULIC 96F
1.35 $^{+0.19}_{-0.17}$ ±0.05		[19] BUSKULIC	92G	ALEP	$e^+e^- \to Z$
1.32 ±0.08 ±0.09	1386	[20] ADEVA	91H	L3	Sup. by ADRIANI 93K
1.32 $^{+0.31}_{-0.25}$ ±0.15	37	[21] ALEXANDER	91G	OPAL	$e^+e^- \to Z$
1.29 ±0.06 ±0.10	2973	[22] DECAMP	91C	ALEP	Sup. by BUSKULIC 92F
1.36 $^{+0.25}_{-0.23}$		[23] HAGEMANN	90	JADE	E^{ee}_{cm}= 35 GeV
1.13 ±0.15		[24] LYONS	90	RVUE	
1.35 ±0.10 ±0.24		BRAUNSCH...	89B	TASS	E^{ee}_{cm}= 35 GeV
0.98 ±0.12 ±0.13		ONG	89	MRK2	E^{ee}_{cm}= 29 GeV
1.17 $^{+0.27}_{-0.22}$ $^{+0.17}_{-0.16}$		KLEM	88	DLCO	E^{ee}_{cm}= 29 GeV
1.29 ±0.20 ±0.21		[25] ASH	87	MAC	E^{ee}_{cm}= 29 GeV
1.02 $^{+0.42}_{-0.39}$	301	[26] BROM	87	HRS	E^{ee}_{cm}= 29 GeV

[1] Measurement performed using an inclusive reconstruction and B flavor identification technique.
[2] Measured using inclusive $J/\psi(1S) \to \mu^+\mu^-$ vertex.
[3] ACCIARRI 98 uses inclusively reconstructed secondary vertex and lepton impact parameter.
[4] ACKERSTAFF 97F uses inclusively reconstructed secondary vertices.
[5] Combines ABREU 96E secondary vertex result with ABREU 94L impact parameter result.
[6] BUSKULIC 96F analyzed using 3D impact parameter.
[7] ABE,K 95B uses an inclusive topological technique.
[8] ABREU 94L uses charged particle impact parameters. Their result from inclusively reconstructed secondary vertices is superseded by ABREU 96E.
[9] From proper time distribution of $b \to J/\psi(1S)$ anything.
[10] ABE 93J analyzed using $J/\psi(1S) \to \mu\mu$ vertices.
[11] ABREU 93D data analyzed using $D/D^*\ell$ anything event vertices.
[12] ABREU 93G data analyzed using charged and neutral vertices.
[13] ACTON 93C analysed using $D/D^*\ell$ anything event vertices.
[14] ACTON 93L and ADRIANI 93K analyzed using lepton (e and μ) impact parameter at Z.
[15] BUSKULIC 93O analyzed using dipole method.
[16] ABREU 92 is combined result of muon and hadron impact parameter analyses. Hadron tracks gave $(12.7 \pm 0.4 \pm 1.2) \times 10^{-13}$ s for an admixture of B species weighted by production fraction and mean charge multiplicity, while muon tracks gave $(13.0 \pm 1.0 \pm 0.8) \times 10^{-13}$ s for an admixture weighted by production fraction and semileptonic branching fraction.
[17] ACTON 92 is combined result of muon and electron impact parameter analyses.
[18] BUSKULIC 92F uses the lepton impact parameter distribution for data from the 1991 run.
[19] BUSKULIC 92G use $J/\psi(1S)$ tags to measure the average b lifetime. This is comparable to other methods only if the $J/\psi(1S)$ branching fractions of the different b-flavored hadrons are in the same ratio.
[20] Using $Z \to e^+X$ or μ^+X, ADEVA 91H determined the average lifetime for an admixture of B hadrons from the impact parameter distribution of the lepton.
[21] Using $Z \to J/\psi(1S)X$, $J/\psi(1S) \to \ell^+\ell^-$, ALEXANDER 91G determined the average lifetime for an admixture of B hadrons from the decay point of the $J/\psi(1S)$.
[22] Using $Z \to eX$ or μX, DECAMP 91C determines the average lifetime for an admixture of B hadrons from the signed impact parameter distribution of the lepton.
[23] HAGEMANN 90 uses electrons and muons in an impact parameter analysis.
[24] LYONS 90 combine the results of the B lifetime measurements of ONG 89, BRAUNSCHWEIG 89B, KLEM 88, and ASH 87, and JADE data by private communication. They use statistical techniques which include variation of the error with the mean life, and possible correlations between the systematic errors. This result is not independent of the measured results used in our average.
[25] We have combined an overall scale error of 15% in quadrature with the systematic error of ±0.7 to obtain ±2.1 systematic error.
[26] Statistical and systematic errors were combined by BROM 87.

CHARGED b-HADRON ADMIXTURE MEAN LIFE

VALUE (10^{-12} s)	DOCUMENT ID		TECN	COMMENT
1.72±0.08±0.06	[1] ADAM	95	DLPH	$e^+e^- \to Z$

[1] ADAM 95 data analyzed using vertex-charge technique to tag b-hadron charge.

NEUTRAL b-HADRON ADMIXTURE MEAN LIFE

VALUE (10^{-12} s)	DOCUMENT ID		TECN	COMMENT
1.58±0.11±0.09	[1] ADAM	95	DLPH	$e^+e^- \to Z$

[1] ADAM 95 data analyzed using vertex-charge technique to tag b-hadron charge.

MEAN LIFE RATIO $\tau_{\text{charged } b\text{-hadron}}/\tau_{\text{neutral } b\text{-hadron}}$

VALUE	DOCUMENT ID		TECN	COMMENT
$1.09^{+0.11}_{-0.10}$±0.08	[1] ADAM	95	DLPH	$e^+e^- \to Z$

[1] ADAM 95 data analyzed using vertex-charge technique to tag b-hadron charge.

$|\Delta\tau_b|/\tau_{b,\overline{b}}$

$\tau_{b,\overline{b}}$ and $|\Delta\tau_b|$ are the mean life average and difference between b and $\overline{b}$ hadrons.

VALUE	DOCUMENT ID		TECN	COMMENT
−0.001±0.012±0.008	[1] ABBIENDI	99J	OPAL	$e^+e^- \to Z$

[1] Data analyzed using both the jet charge and the charge of secondary vertex in the opposite hemisphere.

$\overline{b}$ PRODUCTION FRACTIONS AND DECAY MODES

The branching fraction measurements are for an admixture of B mesons and baryons at energies above the $\Upsilon(4S)$. Only the highest energy results (LHC, LEP, Tevatron, Sp$\overline{p}$S) are used in the branching fraction averages. In the following, the production fractions are provided separately at three different colliders (LEP, $p\overline{p}$ Tevatron, and pp LHC) and are used for the subsequent measurements accordingly.

For inclusive branching fractions, *e.g.*, $B \to D^{\pm}$ anything, the values usually are multiplicities, not branching fractions. They can be greater than one.

The modes below are listed for a $\overline{b}$ initial state. b modes are their charge conjugates. Reactions indicate the weak decay vertex and do not include mixing.

Int. J. Mod. Phys. A 2026.41. Downloaded from www.worldscientific.com
by UNIVERSITY OF CALIFORNIA @ BERKELEY on 09/16/26. Re-use and distribution is strictly not permitted, except for Open Access articles.

Meson Particle Listings

$B^{\pm}/B^0/B^0_s/b$-baryon ADMIXTURE

	Mode		Fraction (Γ_i/Γ)	Scale factor/ Confidence level

PRODUCTION FRACTIONS

The production fractions for weakly decaying b-hadrons at high energy have been calculated from the best values of mean lives, mixing parameters, and branching fractions in this edition by the Heavy Flavor Averaging Group (HFLAV) as described in the note "B^0-$\overline{B}^0$ Mixing" in the B^0 Particle Listings. We no longer provide world averages of the b-hadron production fractions, where results from LEP, Tevatron and LHC are averaged together; indeed the available data (from CDF and LHCb) shows that the fractions depend on the kinematics (in particular the p_T) of the produced b hadron. Hence, we would like to list the fractions at LEP Z decays, at $p\overline{p}$ collision at the Tevatron, and at pp collision at LHC, separately, when they are available.

Values assume:

$B(\overline{b} \to B^+) = B(\overline{b} \to B^0)$

$B(\overline{b} \to B^+) + B(\overline{b} \to B^0) + B(\overline{b} \to B^0_s) + B(b \to b\text{-baryon}) = 100\%$.

The notation for production fractions varies in the literature (f_d, d_{B^0}, $f(b \to \overline{B}^0)$, $Br(b \to \overline{B}^0)$). We use our own branching fraction notation here, $B(\overline{b} \to B^0 \text{ at } Z)$ at LEP, $B(\overline{b} \to B^0 \text{ at } p\overline{p})$ at Tevatron, $B(\overline{b} \to B^0 \text{ at } pp)$ at LHC. The $B(\overline{b} \to B^+_c)$ is a placeholder for the future measurements, and is negligible in the $\overline{b}$-production fractions.

Note these production fractions are b-hadronization fractions, not the conventional branching fractions of b-quark to a B-hadron, which may have considerable dependence on the initial and final state kinematic and production environment.

Production fractions at Z

The correlation coefficients between the reported production fractions are:

$cor(B^0_s \text{ at } Z, b\text{-baryon at } Z) = 0.064$

$cor(B^0_s \text{ at } Z, B^{\pm}{=}B^0 \text{ at } Z) = -0.633$

$cor(b\text{-baryon at } Z, B^{\pm}{=}B^0 \text{ at } Z) = -0.813$.

Γ_1	B^+ at Z		(40.8 ± 0.7) %
Γ_2	B^0 at Z		(40.8 ± 0.7) %
Γ_3	B^0_s at Z		(10.0 ± 0.8) %
Γ_4	b-baryon at Z		(8.4 ± 1.1) %
Γ_5	B^+_c at Z		

Production fractions at $p\overline{p}$

The correlation coefficients between the reported production fractions are:

$cor(B^0_s \text{ at } p\overline{p}, b\text{-baryon at } p\overline{p}) = -0.429$

$cor(B^0_s \text{ at } p\overline{p}, B^{\pm}{=}B^0 \text{ at } p\overline{p}) = +0.159$

$cor(b\text{-baryon at } p\overline{p}, B^{\pm}{=}B^0 \text{ at } p\overline{p}) = -0.960$.

as obtained with the Tevatron average of time-integrated mixing parameter $\overline{\chi} = 0.147 \pm 0.011$.

Γ_6	B^+ at $p\overline{p}$		(34.4 ± 2.1) %
Γ_7	B^0 at $p\overline{p}$		(34.4 ± 2.1) %
Γ_8	B^0_s at $p\overline{p}$		(11.5 ± 1.3) %
Γ_9	b-baryon at $p\overline{p}$		(19.8 ± 4.6) %
Γ_{10}	B^+_c at $p\overline{p}$		

Production fractions at pp

Γ_{11}	B^+ at pp		(36.0 ± 0.5) %
Γ_{12}	B^0 at pp		(36.0 ± 0.5) %
Γ_{13}	B^0_s at pp		(9.04 ± 0.25) %
Γ_{14}	b-baryon at pp		(18.7 ± 1.1) %
Γ_{15}	B^+_c at pp		(2.7 ± 0.5) $\times 10^{-3}$

DECAY MODES

Semileptonic and leptonic modes

Γ_{16}	ν anything		(23.1 ± 1.5) %	
Γ_{17}	$\ell^+ \nu_\ell$ anything	[a]	(10.69 ± 0.22) %	
Γ_{18}	$e^+ \nu_e$ anything		(10.86 ± 0.35) %	
Γ_{19}	$\mu^+ \nu_\mu$ anything		($10.95^{+0.29}_{-0.25}$) %	
Γ_{20}	$D^- \ell^+ \nu_\ell$ anything	[a]	(2.2 ± 0.4) %	S=1.8
Γ_{21}	$D^- \pi^+ \ell^+ \nu_\ell$ anything		(4.9 ± 1.9) $\times 10^{-3}$	
Γ_{22}	$D^- \pi^- \ell^+ \nu_\ell$ anything		(2.6 ± 1.6) $\times 10^{-3}$	
Γ_{23}	$\overline{D}^0 \ell^+ \nu_\ell$ anything	[a]	(6.80 ± 0.34) %	
Γ_{24}	$\overline{D}^0 \pi^- \ell^+ \nu_\ell$ anything		(1.07 ± 0.27) %	
Γ_{25}	$\overline{D}^0 \pi^+ \ell^+ \nu_\ell$ anything		(2.3 ± 1.6) $\times 10^{-3}$	
Γ_{26}	$D^{*-} \ell^+ \nu_\ell$ anything	[a]	(2.75 ± 0.19) %	
Γ_{27}	$D^{*-} \pi^- \ell^+ \nu_\ell$ anything		(6 ± 7) $\times 10^{-4}$	
Γ_{28}	$D^{*-} \pi^+ \ell^+ \nu_\ell$ anything		(4.8 ± 1.0) $\times 10^{-3}$	
Γ_{29}	$\overline{D}^0_j \ell^+ \nu_\ell$ anything $\times$ $B(\overline{D}^0_j \to D^{*+} \pi^-)$	[a,b]	(2.6 ± 0.9) $\times 10^{-3}$	
Γ_{30}	$D^-_j \ell^+ \nu_\ell$ anything $\times$ $B(D^-_j \to D^0 \pi^-)$	[a,b]	(7.0 ± 2.3) $\times 10^{-3}$	
Γ_{31}	$\overline{D}^*_2(2460)^0 \ell^+ \nu_\ell$ anything $\times$ $B(\overline{D}^*_2(2460)^0 \to D^{*-} \pi^+)$		< 1.4 $\times 10^{-3}$	CL=90%
Γ_{32}	$D^*_2(2460)^- \ell^+ \nu_\ell$ anything $\times$ $B(D^*_2(2460)^- \to D^0 \pi^-)$		($4.2^{+1.5}_{-1.8}$) $\times 10^{-3}$	
Γ_{33}	$\overline{D}^*_2(2460)^0 \ell^+ \nu_\ell$ anything $\times$ $B(\overline{D}^*_2(2460)^0 \to D^- \pi^+)$		(1.6 ± 0.8) $\times 10^{-3}$	
Γ_{34}	charmless $\ell \overline{\nu}_\ell$	[a]	(1.7 ± 0.5) $\times 10^{-3}$	
Γ_{35}	$\tau^+ \nu_\tau$ anything		(2.41 ± 0.23) %	
Γ_{36}	$D^{*-} \tau \nu_\tau$ anything		(9 ± 4) $\times 10^{-3}$	
Γ_{37}	$\overline{c} \to \ell^- \overline{\nu}_\ell$ anything	[a]	(8.02 ± 0.19) %	
Γ_{38}	$c \to \ell^+ \nu$ anything		($1.6^{+0.4}_{-0.5}$) %	

Charmed meson and baryon modes

Γ_{39}	$\overline{D}^0$ anything		(58.9 ± 2.8) %	
Γ_{40}	$D^0 D^{\pm}_s$ anything	[c]	($9.1^{+4.0}_{-2.8}$) %	
Γ_{41}	$D^{\mp} D^{\pm}_s$ anything	[c]	($4.0^{+2.3}_{-1.8}$) %	
Γ_{42}	$\overline{D}^0 D^0$ anything	[c]	($5.1^{+2.0}_{-1.8}$) %	
Γ_{43}	$D^0 D^{\pm}$ anything	[c]	($2.7^{+1.8}_{-1.6}$) %	
Γ_{44}	$D^{\pm} D^{\mp}$ anything	[c]	< 9 $\times 10^{-3}$	CL=90%
Γ_{45}	D^0 anything			
Γ_{46}	D^+ anything			
Γ_{47}	D^- anything		(22.9 ± 1.6) %	
Γ_{48}	$D^*(2010)^+$ anything		(17.3 ± 2.0) %	
Γ_{49}	$D_1(2420)^0$ anything		(5.0 ± 1.5) %	
Γ_{50}	$D^*(2010)^{\mp} D^{\pm}_s$ anything	[c]	($3.3^{+1.6}_{-1.3}$) %	
Γ_{51}	$D^0 D^*(2010)^{\pm}$ anything	[c]	($3.0^{+1.1}_{-0.9}$) %	
Γ_{52}	$D^*(2010)^{\pm} D^{\mp}$ anything	[c]	($2.5^{+1.2}_{-1.0}$) %	
Γ_{53}	$D^*(2010)^{\pm} D^*(2010)^{\mp}$ anything	[c]	(1.2 ± 0.4) %	
Γ_{54}	$\overline{D} D$ anything		(10^{+11}_{-10}) %	
Γ_{55}	$D^*_2(2460)^0$ anything		(4.7 ± 2.7) %	
Γ_{56}	D^-_s anything		(14.7 ± 2.1) %	
Γ_{57}	D^+_s anything		(10.1 ± 3.1) %	
Γ_{58}	Λ^+_c anything		(7.6 ± 1.1) %	
Γ_{59}	$\overline{c}/c$ anything	[d]	(116.2 ± 3.2) %	

Charmonium modes

Γ_{60}	$J/\psi(1S)$ anything		(1.16 ± 0.10) %	
Γ_{61}	$\psi(2S)$ anything		(3.06 ± 0.30) $\times 10^{-3}$	
Γ_{62}	$\chi_{c0}(1P)$ anything		(2.9 ± 0.6) $\times 10^{-3}$	
Γ_{63}	$\chi_{c1}(1P)$ anything		(5.6 ± 1.5) $\times 10^{-3}$	S=1.3
Γ_{64}	$\chi_{c2}(1P)$ anything		(1.4 ± 1.0) $\times 10^{-3}$	
Γ_{65}	$\chi_c(2P)$ anything, $\chi_c \to \phi\phi$		< 2.8 $\times 10^{-7}$	CL=95%
Γ_{66}	$\eta_c(1S)$ anything		(5.7 ± 0.7) $\times 10^{-3}$	
Γ_{67}	$\eta_c(2S)$ anything, $\eta_c \to \phi\phi$		(3.3 ± 1.4) $\times 10^{-7}$	
Γ_{68}	$\chi_{c1}(3872)$ anything, $\chi_{c1} \to \phi\phi$		< 4.5 $\times 10^{-7}$	CL=95%
Γ_{69}	$\chi_{c0}(3915)$ anything, $\chi_{c0} \to \phi\phi$		< 3.1 $\times 10^{-7}$	CL=95%

K or K^* modes

Γ_{70}	$\overline{s}\gamma$		(3.1 ± 1.1) $\times 10^{-4}$	
Γ_{71}	$\overline{s}\nu\nu$	B1	< 6.4 $\times 10^{-4}$	CL=90%
Γ_{72}	$K^{\pm}$ anything		(74 ± 6) %	
Γ_{73}	K^0_S anything		(29.0 ± 2.9) %	

Pion modes

Γ_{74}	$\pi^{\pm}$ anything		(397 ± 21) %	
Γ_{75}	π^0 anything	[d]	(280 ± 60) %	
Γ_{76}	ϕ anything		(2.82 ± 0.23) %	

Baryon modes

Γ_{77}	$p/\overline{p}$ anything		(13.1 ± 1.1) %	
Γ_{78}	$\Lambda/\overline{\Lambda}$ anything		(5.9 ± 0.6) %	
Γ_{79}	b-baryon anything		(10.2 ± 2.8) %	

Int. J. Mod. Phys. A 2026.41. Downloaded from www.worldscientific.com
by [redacted]LIFORNIA @ BERKELEY on 09/16/26. Re-use and distribution is strictly not permitted, except for Open Access articles.

Int. J. Mod. Phys. A 2026.41. Downloaded from www.worldscientific.com by UNIVERSITY OF CALIFORNIA @ BERKELEY on 09/16/26. Re-use and distribution is strictly not permitted, except for Open Access articles.

Γ_{80}	$\overline{\Lambda}^0_b$ anything		
Γ_{81}	Ξ^+_b anything		

Other modes

Γ_{82}	charged anything	[d]	(497 ± 7) %
Γ_{83}	hadron$^+$ hadron$^-$		$(1.7 {}^{+1.0}_{-0.7}) \times 10^{-5}$
Γ_{84}	charmless		$(7 \pm 21) \times 10^{-3}$

$\Delta B = 1$ weak neutral current ($B1$) modes

Γ_{85}	e^+e^- anything				
Γ_{86}	$\mu^+\mu^-$ anything	$B1$	$<$	3.2×10^{-4}	CL=90%
Γ_{87}	$\nu\overline{\nu}$ anything				

[a] An ℓ indicates an e or a μ mode, not a sum over these modes.

[b] D_j represents an unresolved mixture of pseudoscalar and tensor D^{**} (P-wave) states.

[c] The value is for the sum of the charge states or particle/antiparticle states indicated.

[d] Inclusive branching fractions have a multiplicity definition and can be greater than 100%.

$B^{\pm}/B^0/B^0_s/b$-baryon ADMIXTURE BRANCHING RATIOS

$\Gamma(B^+ \text{at} Z)/\Gamma_{\text{total}}$ — Γ_1/Γ

"OUR EVALUATION" is an average from Z decay.

VALUE	DOCUMENT ID		TECN	COMMENT
0.408 ±0.007 OUR EVALUATION	(Produced by HFLAV)			
0.4099±0.0082±0.0111	[1] ABDALLAH	03K	DLPH	$e^+e^- \to Z$

[1] The analysis is based on a neural network, to estimate the charge of the weakly-decaying b hadron by distinguishing its decay products from particles produced at the primary vertex.

$\Gamma(B^0_s \text{at} Z)/[\Gamma(B^+ \text{at} Z) + \Gamma(B^0 \text{at} Z)]$ — $\Gamma_3/(\Gamma_1+\Gamma_2)$

"OUR EVALUATION" is an average from Z decay.

VALUE	DOCUMENT ID
0.1230±0.0115 OUR EVALUATION	(Produced by HFLAV)

$\Gamma(b\text{-baryon at} Z)/[\Gamma(B^+ \text{at} Z) + \Gamma(B^0 \text{at} Z)]$ — $\Gamma_4/(\Gamma_1+\Gamma_2)$

VALUE	DOCUMENT ID
0.103±0.015 OUR EVALUATION	

$\Gamma(B^+ \text{at} p\overline{p})/\Gamma(B^0 \text{at} p\overline{p})$ — Γ_6/Γ_7

VALUE	DOCUMENT ID		TECN	COMMENT
$1.054 \pm 0.018 {}^{+0.062}_{-0.074}$	AALTONEN	08N	CDF	$p\overline{p}$ at 1.96 TeV

$\Gamma(B^0_s \text{at} p\overline{p})/[\Gamma(B^+ \text{at} p\overline{p}) + \Gamma(B^0 \text{at} p\overline{p})]$ — $\Gamma_8/(\Gamma_6+\Gamma_7)$

VALUE	DOCUMENT ID		TECN	COMMENT
0.17 ±0.02 OUR EVALUATION				
• • • We do not use the following data for averages, fits, limits, etc. • • •				
$0.128 {}^{+0.011}_{-0.010} \pm 0.011$	[1] AALTONEN	08N	CDF	$p\overline{p}$ at 1.96 TeV
0.213 ± 0.068	[2] AFFOLDER	00E	CDF	$p\overline{p}$ at 1.8 TeV
$0.21 \pm 0.036 {}^{+0.038}_{-0.030}$	[3] ABE	99P	CDF	$\overline{p}p$ at 1.8 TeV

[1] AALTONEN 08N reports $[\Gamma(\overline{b} \to B^0_s \text{at} Z)/[\Gamma(\overline{b} \to B^+ \text{at} Z) + \Gamma(\overline{b} \to B^0 \text{at} Z)]] \times [B(D^+_s \to \phi\pi^+)] = (5.76 \pm 0.18 {}^{+0.45}_{-0.42}) \times 10^{-3}$ which we divide by our best (shown rounded) value $B(D^+_s \to \phi\pi^+) = (4.5 \pm 0.4) \times 10^{-2}$. Our first error is their experiment's error and our second error is the systematic error from using our best (shown rounded) value.

[2] AFFOLDER 00E uses several electron-charm final states in $b \to ce^-X$.

[3] ABE 99P uses the numbers of $K^*(892)^0$, $K^*(892)^+$, and $\phi(1020)$ events produced in association with the double semileptonic decays $b \to c\mu^-X$ with $c \to s\mu^+X$.

$\Gamma(b\text{-baryon at} p\overline{p})/[\Gamma(B^+ \text{at} p\overline{p}) + \Gamma(B^0 \text{at} p\overline{p})]$ — $\Gamma_9/(\Gamma_6+\Gamma_7)$

VALUE	DOCUMENT ID		TECN	COMMENT
0.29 ±0.08 OUR EVALUATION				
• • • We do not use the following data for averages, fits, limits, etc. • • •				
$0.31 \pm 0.11 {}^{+0.12}_{-0.08}$	[1] AALTONEN	09E	CDF	$p\overline{p}$ at 1.8 TeV
$0.22 {}^{+0.08}_{-0.07} \pm 0.01$	[2] AALTONEN	08N	CDF	$p\overline{p}$ at 1.96 TeV
0.118 ± 0.042	[1,3] AFFOLDER	00E	CDF	$p\overline{p}$ at 1.8 TeV

[1] AALTONEN 09E errata to the measurement reported in AFFOLDER 00E using the p_T spectra from fully reconstructed B^0 and Λ_b decays.

[2] AALTONEN 08N reports $[\Gamma(\overline{b} \to b\text{-baryon at} p\overline{p})/[\Gamma(\overline{b} \to B^+ \text{at} p\overline{p}) + \Gamma(\overline{b} \to B^0 \text{at} p\overline{p})]] \times [B(\Lambda^+_c \to pK^-\pi^+)] = (14.1 \pm 0.6 {}^{+5.3}_{-4.4}) \times 10^{-3}$ which we divide by our best (shown rounded) value $B(\Lambda^+_c \to pK^-\pi^+) = (6.37 \pm 0.21) \times 10^{-2}$. Our first error is their experiment's error and our second error is the systematic error from using our best (shown rounded) value.

[3] AFFOLDER 00E uses several electron-charm final states in $b \to ce^-X$.

$\Gamma(B^0_s \text{at} pp)/[\Gamma(B^+ \text{at} pp) + \Gamma(B^0 \text{at} pp)]$ — $\Gamma_{13}/(\Gamma_{11}+\Gamma_{12})$

VALUE	DOCUMENT ID		TECN	COMMENT
0.1254±0.0033 OUR FIT				
0.127 ±0.004 OUR AVERAGE				
$0.124 \pm 0.002 \pm 0.005$	[1,2] AAIJ	20V	LHCB	pp at 7 TeV
$0.128 \pm 0.002 \pm 0.005$	[1,3] AAIJ	20V	LHCB	pp at 8 TeV
$0.133 \pm 0.002 \pm 0.005$	[1,4,5] AAIJ	20V	LHCB	pp at 13 TeV
0.122 ± 0.006	[6] AAIJ	19AD	LHCB	pp at 13 TeV
$0.134 \pm 0.004 {}^{+0.011}_{-0.010}$	[7] AAIJ	12J	LHCB	pp at 7 TeV
$0.1265 \pm 0.0085 \pm 0.0131$	[8] AAIJ	11F	LHCB	pp at 7 TeV

[1] AAIJ 20V measures the average value using the observed $B^0_s \to J/\psi\phi$ and $B^+ \to J/\psi K^+$ yields, over the ranges b-hadron p_T of 0.5 and 40 GeV and η of 2.0 and 6.5. The value is not used in averages as BR-related systematic uncertainties are not evaluated.

[2] AAIJ 20V reports $[\Gamma(\overline{b} \to B^0_s \text{at} pp)/\Gamma(\overline{b} \to B^+ \text{at} pp)] \times [B(B^0_s \to J/\psi(1S)\phi)] / [B(B^+ \to J/\psi(1S)K^+)] = 0.1238 \pm 0.0010 \pm 0.0022$ which we multiply or divide by our best (shown rounded) values $B(B^0_s \to J/\psi(1S)\phi) = (1.01 \pm 0.04) \times 10^{-3}$, $B(B^+ \to J/\psi(1S)K^+) = (1.019 \pm 0.019) \times 10^{-3}$. Our first error is their experiment's error and our second error is the systematic error from using our best (shown rounded) values.

[3] AAIJ 20V reports $[\Gamma(\overline{b} \to B^0_s \text{at} pp)/\Gamma(\overline{b} \to B^+ \text{at} pp)] \times [B(B^0_s \to J/\psi(1S)\phi)] / [B(B^+ \to J/\psi(1S)K^+)] = 0.1270 \pm 0.0007 \pm 0.0022$ which we multiply or divide by our best (shown rounded) values $B(B^0_s \to J/\psi(1S)\phi) = (1.01 \pm 0.04) \times 10^{-3}$, $B(B^+ \to J/\psi(1S)K^+) = (1.019 \pm 0.019) \times 10^{-3}$. Our first error is their experiment's error and our second error is the systematic error from using our best (shown rounded) values.

[4] AAIJ 20V reports the results in two different data sets, and we quote here the weighted average.

[5] AAIJ 20V reports $[\Gamma(\overline{b} \to B^0_s \text{at} pp)/\Gamma(\overline{b} \to B^+ \text{at} pp)] \times [B(B^0_s \to J/\psi(1S)\phi)] / [B(B^+ \to J/\psi(1S)K^+)] = 0.1326 \pm 0.0007 \pm 0.0023$ which we multiply or divide by our best (shown rounded) values $B(B^0_s \to J/\psi(1S)\phi) = (1.01 \pm 0.04) \times 10^{-3}$, $B(B^+ \to J/\psi(1S)K^+) = (1.019 \pm 0.019) \times 10^{-3}$. Our first error is their experiment's error and our second error is the systematic error from using our best (shown rounded) values.

[6] AAIJ 19AD measured the average value using b-hadron semileptonic decays and assuming isospin symmetry for b-hadron p_T of 4 and 25 GeV and η of 2 and 5.

[7] AAIJ 12J measured this value using b-hadron semileptonic decays and assuming isospin symmetry.

[8] AAIJ 11F measured $f_s/f_d = 0.253 \pm 0.017 \pm 0.017 \pm 0.020$, where the errors are statistical, systematic, and theoretical. We divide their value by 2. Our second error combines systematic and theoretical uncertainties.

$\Gamma(B^0_s \text{at} pp)/\Gamma(B^0 \text{at} pp)$ — Γ_{13}/Γ_{12}

VALUE	DOCUMENT ID		TECN	COMMENT
0.251 ±0.007 OUR FIT				
0.239 ±0.016 OUR AVERAGE				
$0.240 \pm 0.004 \pm 0.020$	[1] AAD	15CM	ATLS	pp at 7 TeV
$0.238 \pm 0.004 \pm 0.026$	[2] AAIJ	13P	LHCB	pp at 7 TeV
• • • We do not use the following data for averages, fits, limits, etc. • • •				
0.2385 ± 0.0075	[3] AAIJ	21Y	LHCB	pp at 8 TeV
0.2539 ± 0.0079	[3] AAIJ	21Y	LHCB	pp at 13 TeV
0.2390 ± 0.0076	[3] AAIJ	21Y	LHCB	pp at 7 TeV

[1] AAD 15CM measurement is derived from the observed $B^0_s \to J/\psi\phi$ and $B^0_d \to J/\psi K^{*0}$ yields and a recent theory prediction of $B(B^0_s \to J/\psi\phi)/B(B^0_d \to J/\psi K^{*0})$. The second uncertainty combines in quadrature systematic and theoretical uncertainties.

[2] AAIJ 13P studies also separately the $p_T(B)$ and $\eta(B)$ dependency of $\Gamma(\overline{b} \to B^0_s \text{at} pp)/\Gamma(\overline{b} \to B^0 \text{at} pp)$, finding $f_s/f_d(p_T) = (0.256 \pm 0.020) + (-2.0 \pm 0.6)\ 10^{-3}$ /GeV/c $(p_T - \langle p_T \rangle)$ and $f_s/f_d(\eta) = (0.256 \pm 0.020) + (0.005 \pm 0.006)\ (\eta - \langle \eta \rangle)$, where $\langle p_T \rangle = 10.4$ GeV/c and $\langle \eta \rangle = 3.28$. AAIJ 13P reports the measurement as $0.238 \pm 0.004 \pm 0.015 \pm 0.021$ where the last uncertainly is theoretical.

[3] AAIJ 21Y uses hadronic decays $B^0 \to D^-\pi^+$, $B^0 \to D^-K^+$, $B^0_s \to D^-_s\pi^+$ and $B^0_s \to J/\psi\phi$ as well as semileptonic B^0 and B^0_s decays. Measured within the p_T range [0.5,40] GeV/c, η range [2, 6.4].

$\Gamma(B^+_c \text{at} pp)/[\Gamma(B^+ \text{at} pp) + \Gamma(B^0 \text{at} pp)]$ — $\Gamma_{15}/(\Gamma_{11}+\Gamma_{12})$

VALUE (units 10^{-3})	DOCUMENT ID		TECN	COMMENT
3.7 ±0.6 OUR FIT				
3.7 ±0.6 OUR AVERAGE				
$3.63 \pm 0.08 \pm 0.87$	[1] AAIJ	19AI	LHCB	pp at 7 TeV
$3.78 \pm 0.04 \pm 0.90$	[1] AAIJ	19AI	LHCB	pp at 13 TeV

[1] Measured using B^+_c semileptonic decays.

$\Gamma(b\text{-baryon at} pp)/[\Gamma(B^+ \text{at} pp) + \Gamma(B^0 \text{at} pp)]$ — $\Gamma_{14}/(\Gamma_{11}+\Gamma_{12})$

VALUE	DOCUMENT ID		TECN	COMMENT
0.259±0.018 OUR FIT				
0.259±0.018	[1] AAIJ	19AD	LHCB	pp at 13 TeV
• • • We do not use the following data for averages, fits, limits, etc. • • •				
$0.305 \pm 0.010 \pm 0.081$	[2] AAIJ	12J	LHCB	pp at 7 TeV

[1] AAIJ 19AD measured the average value for Λ^0_b using semileptonic decays and assuming isospin symmetry for b-hadron p_T of 4 and 25 GeV and η of 2 and 5.

[2] AAIJ 12J measured the ratio to be $(0.404 \pm 0.017 \pm 0.027 \pm 0.105) \times [1 - (0.031 \pm 0.004 \pm 0.003) \times P_T]$ using b-hadron semileptonic decays where the P_T is the momentum of charmed hadron-muon pair in GeV/c. We quote their weighted average value where the second error combines systematic and the error on $B(\Lambda^+_c \to pK^-\pi^+)$.

Int. J. Mod. Phys. A 2026.41. Downloaded from www.worldscientific.com
by LIFORNIA @ BERKELEY on 09/16/26. Re-use and distribution is strictly not permitted, except for Open Access articles.

$\Gamma(\nu\,\text{anything})/\Gamma_{\text{total}}$ — Γ_{16}/Γ

VALUE	DOCUMENT ID		TECN	COMMENT
0.2308 ± 0.0077 ± 0.0124	[1,2] ACCIARRI	96C	L3	$e^+e^- \to Z$

[1] ACCIARRI 96C assumes relative b semileptonic decay rates e:μ:τ of 1:1:0.25. Based on missing-energy spectrum.
[2] Assumes Standard Model value for R_B.

$\Gamma(\ell^+\nu_\ell\,\text{anything})/\Gamma_{\text{total}}$ — Γ_{17}/Γ

"OUR EVALUATION" is an average of the data listed below, excluding all asymmetry measurements, performed by the LEP Electroweak Working Group as described in the "Note on the Z boson" in the Z Particle Listings.

VALUE	DOCUMENT ID		TECN	COMMENT
0.1069 ± 0.0022 OUR EVALUATION				
0.1064 ± 0.0016 OUR AVERAGE				
0.1070 ± 0.0010 ± 0.0035	[1] HEISTER	02G	ALEP	$e^+e^- \to Z$
0.1070 ± 0.0008 $^{+0.0037}_{-0.0049}$	[2] ABREU	01L	DLPH	$e^+e^- \to Z$
0.1083 ± 0.0010 $^{+0.0028}_{-0.0024}$	[3] ABBIENDI	00E	OPAL	$e^+e^- \to Z$
0.1016 ± 0.0013 ± 0.0030	[4] ACCIARRI	00	L3	$e^+e^- \to Z$
0.1085 ± 0.0012 ± 0.0047	[5,6] ACCIARRI	96C	L3	$e^+e^- \to Z$
• • • We do not use the following data for averages, fits, limits, etc. • • •				
0.1106 ± 0.0039 ± 0.0022	[7] ABREU	95D	DLPH	$e^+e^- \to Z$
0.114 ± 0.003 ± 0.004	[8] BUSKULIC	94G	ALEP	$e^+e^- \to Z$
0.100 ± 0.007 ± 0.007	[9] ABREU	93C	DLPH	$e^+e^- \to Z$
0.105 ± 0.006 ± 0.005	[10] AKERS	93B	OPAL	Repl. by ABBIENDI 00E

[1] Uses the combination of lepton transverse momentum spectrum and the correlation between the charge of the lepton and opposite jet charge. The first error is statistic and the second error is the total systematic error including the modeling.
[2] The experimental systematic and model uncertainties are combined in quadrature.
[3] ABBIENDI 00E result is determined by comparing the distribution of several kinematic variables of leptonic events in a lifetime tagged $Z \to b\overline{b}$ sample using artificial neural network techniques. The first error is statistic; the second error is the total systematic error.
[4] ACCIARRI 00 result obtained from a combined fit of $R_b = \Gamma(Z \to b\overline{b})/\Gamma(Z \to \text{hadrons})$ and $B(b \to \ell\nu X)$, using double-tagging method.
[5] ACCIARRI 96C result obtained by a fit to the single lepton spectrum.
[6] Assumes Standard Model value for R_B.
[7] ABREU 95D give systematic errors ±0.0019 (model) and 0.0012 (R_c). We combine these in quadrature.
[8] BUSKULIC 94G uses e and μ events. This value is from a global fit to the lepton p and p_T (relative to jet) spectra which also determines the b and c production fractions, the fragmentation functions, and the forward-backward asymmetries. This branching ratio depends primarily on the ratio of dileptons to single leptons at high p_T, but the lower p_T portion of the lepton spectrum is included in the global fit to reduce the model dependence. The model dependence is ±0.0026 and is included in the systematic error.
[9] ABREU 93C event count includes ee events. Combining ee, $\mu\mu$, and $e\mu$ events, they obtain 0.100 ± 0.007 ± 0.007.
[10] AKERS 93B analysis performed using single and dilepton events.

$\Gamma(e^+\nu_e\,\text{anything})/\Gamma_{\text{total}}$ — Γ_{18}/Γ

VALUE	EVTS	DOCUMENT ID		TECN	COMMENT
0.1086 ± 0.0035 OUR AVERAGE					
0.1078 ± 0.0008 $^{+0.0050}_{-0.0046}$		[1] ABBIENDI	00E	OPAL	$e^+e^- \to Z$
0.1089 ± 0.0020 ± 0.0051		[2,3] ACCIARRI	96C	L3	$e^+e^- \to Z$
0.107 ± 0.015 ± 0.007	260	[4] ABREU	93C	DLPH	$e^+e^- \to Z$
0.138 ± 0.032 ± 0.008		[5] ADEVA	91C	L3	$e^+e^- \to Z$
• • • We do not use the following data for averages, fits, limits, etc. • • •					
0.086 ± 0.027 ± 0.008		[6] ABE	93E	VNS	E^{ee}_{cm} = 58 GeV
0.109 $^{+0.014}_{-0.013}$ ± 0.0055	2719	[7] AKERS	93B	OPAL	Repl. by ABBIENDI 00E
0.111 ± 0.028 ± 0.026		BEHREND	90D	CELL	E^{ee}_{cm} = 43 GeV
0.150 ± 0.011 ± 0.022		BEHREND	90D	CELL	E^{ee}_{cm} = 35 GeV
0.112 ± 0.009 ± 0.011		ONG	88	MRK2	E^{ee}_{cm} = 29 GeV
0.149 $^{+0.022}_{-0.019}$		PAL	86	DLCO	E^{ee}_{cm} = 29 GeV
0.110 ± 0.018 ± 0.010		AIHARA	85	TPC	E^{ee}_{cm} = 29 GeV
0.111 ± 0.034 ± 0.040		ALTHOFF	84J	TASS	E^{ee}_{cm} = 34.6 GeV
0.146 ± 0.028		KOOP	84	DLCO	Repl. by PAL 86
0.116 ± 0.021 ± 0.017		NELSON	83	MRK2	E^{ee}_{cm} = 29 GeV

[1] ABBIENDI 00E result is determined by comparing the distribution of several kinematic variables of leptonic events in a lifetime tagged $Z \to b\overline{b}$ sample using artificial neural network techniques. The first error is statistic; the second error is the total systematic error.
[2] ACCIARRI 96C result obtained by a fit to the single lepton spectrum.
[3] Assumes Standard Model value for R_B.
[4] ABREU 93C event count includes ee events. Combining ee, $\mu\mu$, and $e\mu$ events, they obtain 0.100 ± 0.007 ± 0.007.
[5] ADEVA 91C measure the average $B(b \to eX)$ branching ratio using single and double tagged b enhanced Z events. Combining e and μ results, they obtain 0.113 ± 0.010 ± 0.006. Constraining the initial number of b quarks by the Standard Model prediction (378 ± 3 MeV) for the decay of the Z into $b\overline{b}$, the electron result gives 0.112 ± 0.004 ± 0.008. They obtain 0.119 ± 0.003 ± 0.006 when e and μ results are combined. Used to measure the $b\overline{b}$ width itself, this electron result gives 370 ± 12 ± 24 MeV and combined with the muon result gives 385 ± 7 ± 22 MeV.
[6] ABE 93E experiment also measures forward-backward asymmetries and fragmentation functions for b and c.
[7] AKERS 93B analysis performed using single and dilepton events.

$\Gamma(\mu^+\nu_\mu\,\text{anything})/\Gamma_{\text{total}}$ — Γ_{19}/Γ

VALUE	EVTS	DOCUMENT ID		TECN	COMMENT
0.1095 $^{+0.0029}_{-0.0025}$ OUR AVERAGE					
0.1096 ± 0.0008 $^{+0.0034}_{-0.0027}$		[1] ABBIENDI	00E	OPAL	$e^+e^- \to Z$
0.1082 ± 0.0015 ± 0.0059		[2,3] ACCIARRI	96C	L3	$e^+e^- \to Z$
0.110 ± 0.012 ± 0.007	656	[4] ABREU	93C	DLPH	$e^+e^- \to Z$
0.113 ± 0.012 ± 0.006		[5] ADEVA	91C	L3	$e^+e^- \to Z$
• • • We do not use the following data for averages, fits, limits, etc. • • •					
0.122 ± 0.006 ± 0.007		[3] UENO	96	AMY	e^+e^- at 57.9 GeV
0.101 $^{+0.010}_{-0.009}$ ± 0.0055	4248	[6] AKERS	93B	OPAL	Repl. by ABBIENDI 00E
0.104 ± 0.023 ± 0.016		BEHREND	90D	CELL	E^{ee}_{cm} = 43 GeV
0.148 ± 0.010 ± 0.016		BEHREND	90D	CELL	E^{ee}_{cm} = 35 GeV
0.118 ± 0.012 ± 0.010		ONG	88	MRK2	E^{ee}_{cm} = 29 GeV
0.117 ± 0.016 ± 0.015		BARTEL	87	JADE	E^{ee}_{cm} = 34.6 GeV
0.114 ± 0.018 ± 0.025		BARTEL	85J	JADE	Repl. by BARTEL 87
0.117 ± 0.028 ± 0.010		ALTHOFF	84G	TASS	E^{ee}_{cm} = 34.5 GeV
0.105 ± 0.015 ± 0.013		ADEVA	83B	MRKJ	E^{ee}_{cm} = 33–38.5 GeV
0.155 $^{+0.054}_{-0.029}$		FERNANDEZ	83D	MAC	E^{ee}_{cm} = 29 GeV

[1] ABBIENDI 00E result is determined by comparing the distribution of several kinematic variables of leptonic events in a lifetime tagged $Z \to b\overline{b}$ sample using artificial neural network techniques. The first error is statistic; the second error is the total systematic error.
[2] ACCIARRI 96C result obtained by a fit to the single lepton spectrum.
[3] Assumes Standard Model value for R_B.
[4] ABREU 93C event count includes $\mu\mu$ events. Combining ee, $\mu\mu$, and $e\mu$ events, they obtain 0.100 ± 0.007 ± 0.007.
[5] ADEVA 91C measure the average $B(b \to eX)$ branching ratio using single and double tagged b enhanced Z events. Combining e and μ results, they obtain 0.113 ± 0.010 ± 0.006. Constraining the initial number of b quarks by the Standard Model prediction (378 ± 3 MeV) for the decay of the Z into $b\overline{b}$, the muon result gives 0.123 ± 0.003 ± 0.006. They obtain 0.119 ± 0.003 ± 0.006 when e and μ results are combined. Used to measure the $b\overline{b}$ width itself, this muon result gives 394 ± 9 ± 22 MeV and combined with the electron result gives 385 ± 7 ± 22 MeV.
[6] AKERS 93B analysis performed using single and dilepton events.

$\Gamma(D^-\ell^+\nu_\ell\,\text{anything})/\Gamma_{\text{total}}$ — Γ_{20}/Γ

VALUE	DOCUMENT ID		TECN	COMMENT
0.022 ± 0.004 OUR AVERAGE Error includes scale factor of 1.8.				
0.0272 ± 0.0028 ± 0.0018	[1] ABREU	00R	DLPH	$e^+e^- \to Z$
0.0195 ± 0.0025 ± 0.0003	[2] AKERS	95Q	OPAL	$e^+e^- \to Z$

[1] ABREU 00R reports their experiment's uncertainties ±0.0019 ± 0.0016 ± 0.0018, where the first error is statistical, the second is systematic, and the third is the uncertainty due to the D branching fraction. We combine first two in quadrature.
[2] AKERS 95Q reports $[\Gamma(\overline{b} \to D^-\ell^+\nu_\ell\,\text{anything})/\Gamma_{\text{total}}] \times [B(D^+ \to K^-2\pi^+)] = (1.82 \pm 0.20 \pm 0.12) \times 10^{-3}$ which we divide by our best (shown rounded) value $B(D^+ \to K^-2\pi^+) = (9.31 \pm 0.14) \times 10^{-2}$. Our first error is their experiment's error and our second error is the systematic error from using our best (shown rounded) value.

$\Gamma(D^-\pi^+\ell^+\nu_\ell\,\text{anything})/\Gamma_{\text{total}}$ — Γ_{21}/Γ

VALUE	DOCUMENT ID		TECN	COMMENT
0.0049 ± 0.0018 ± 0.0007	ABREU	00R	DLPH	$e^+e^- \to Z$

$\Gamma(D^-\pi^-\ell^+\nu_\ell\,\text{anything})/\Gamma_{\text{total}}$ — Γ_{22}/Γ

VALUE	DOCUMENT ID		TECN	COMMENT
0.0026 ± 0.0015 ± 0.0004	ABREU	00R	DLPH	$e^+e^- \to Z$

$\Gamma(\overline{D}^0\ell^+\nu_\ell\,\text{anything})/\Gamma_{\text{total}}$ — Γ_{23}/Γ

VALUE	DOCUMENT ID		TECN	COMMENT
0.0680 ± 0.0034 OUR AVERAGE				
0.0704 ± 0.0040 ± 0.0017	[1] ABREU	00R	DLPH	$e^+e^- \to Z$
0.0640 ± 0.0056 ± 0.0005	[2] AKERS	95Q	OPAL	$e^+e^- \to Z$

[1] ABREU 00R reports their experiment's uncertainties ±0.0034 ± 0.0036 ± 0.0017, where the first error is statistical, the second is systematic, and the third is the uncertainty due to the D branching fraction. We combine first two in quadrature.
[2] AKERS 95Q reports $[\Gamma(\overline{b} \to \overline{D}^0\ell^+\nu_\ell\,\text{anything})/\Gamma_{\text{total}}] \times [B(D^0 \to K^-\pi^+)] = (2.52 \pm 0.14 \pm 0.17) \times 10^{-3}$ which we divide by our best (shown rounded) value $B(D^0 \to K^-\pi^+) = (3.936 \pm 0.030) \times 10^{-2}$. Our first error is their experiment's error and our second error is the systematic error from using our best (shown rounded) value.

$\Gamma(\overline{D}^0\pi^-\ell^+\nu_\ell\,\text{anything})/\Gamma_{\text{total}}$ — Γ_{24}/Γ

VALUE	DOCUMENT ID		TECN	COMMENT
0.0107 ± 0.0025 ± 0.0011	ABREU	00R	DLPH	$e^+e^- \to Z$

$\Gamma(\overline{D}^0\pi^+\ell^+\nu_\ell\,\text{anything})/\Gamma_{\text{total}}$ — Γ_{25}/Γ

VALUE	DOCUMENT ID		TECN	COMMENT
0.0023 ± 0.0015 ± 0.0004	ABREU	00R	DLPH	$e^+e^- \to Z$

$\Gamma(D^{*-}\ell^+\nu_\ell\,\text{anything})/\Gamma_{\text{total}}$ — Γ_{26}/Γ

VALUE	DOCUMENT ID		TECN	COMMENT
0.0275 ± 0.0019 OUR AVERAGE				
0.0275 ± 0.0021 ± 0.0009	[1] ABREU	00R	DLPH	$e^+e^- \to Z$
0.0276 ± 0.0027 ± 0.0011	[2] AKERS	95Q	OPAL	$e^+e^- \to Z$

Int. J. Mod. Phys. A 2026.41. Downloaded from www.worldscientific.com by UNIVERSITY OF CALIFORNIA @ BERKELEY on 09/16/26. Re-use and distribution is strictly not permitted, except for Open Access articles.

[1] ABREU 00R reports their experiment's uncertainties $\pm 0.0017 \pm 0.0013 \pm 0.0009$, where the first error is statistical, the second is systematic, and the third is the uncertainty due to the D branching fraction. We combine first two in quadrature.

[2] AKERS 95Q reports $[B(\overline{b} \to D^* \ell^+ \nu_\ell X) \times B(D^{*+} \to D^0 \pi^+) \times B(D^0 \to K^- \pi^+)] = ((7.53 \pm 0.47 \pm 0.56) \times 10^{-4})$ and uses $B(D^{*+} \to D^0 \pi^+) = 0.681 \pm 0.013$ and $B(D^0 \to K^- \pi^+) = 0.0401 \pm 0.0014$ to obtain the above result. The first error is the experiments error and the second error is the systematic error from the D^{*+} and D^0 branching ratios.

$\Gamma(D^{*-}\pi^-\ell^+\nu_\ell \text{anything})/\Gamma_{total}$ — Γ_{27}/Γ

VALUE	DOCUMENT ID		TECN	COMMENT
0.0006±0.0007±0.0002	ABREU	00R	DLPH	$e^+e^- \to Z$

$\Gamma(D^{*-}\pi^+\ell^+\nu_\ell \text{anything})/\Gamma_{total}$ — Γ_{28}/Γ

VALUE	DOCUMENT ID		TECN	COMMENT
0.0048±0.0009±0.0005	ABREU	00R	DLPH	$e^+e^- \to Z$

$\Gamma(\overline{D}^0_j \ell^+\nu_\ell \text{anything} \times B(\overline{D}^0_j \to D^{*+}\pi^-))/\Gamma_{total}$ — Γ_{29}/Γ

D_j represents an unresolved mixture of pseudoscalar and tensor D^{**} (P-wave) states.

VALUE (units 10^{-3})	DOCUMENT ID		TECN	COMMENT
2.64±0.79±0.39	ABBIENDI	03M	OPAL	$e^+e^- \to Z$
• • • We do not use the following data for averages, fits, limits, etc. • • •				
6.1 ±1.3 ±1.3	AKERS	95Q	OPAL	Repl. by ABBIENDI 03M

$\Gamma(D^-_j \ell^+\nu_\ell \text{anything} \times B(D^-_j \to D^0\pi^-))/\Gamma_{total}$ — Γ_{30}/Γ

D_j represents an unresolved mixture of pseudoscalar and tensor D^{**} (P-wave) states.

VALUE (units 10^{-3})	DOCUMENT ID		TECN	COMMENT
$7.0 \pm 1.9^{+1.2}_{-1.3}$	AKERS	95Q	OPAL	$e^+e^- \to Z$

$\Gamma(\overline{D}^*_2(2460)^0 \ell^+\nu_\ell \text{anything} \times B(\overline{D}^*_2(2460)^0 \to D^{*-}\pi^+))/\Gamma_{total}$ — Γ_{31}/Γ

VALUE (units 10^{-3})	CL%	DOCUMENT ID		TECN	COMMENT
<1.4	90	ABBIENDI	03M	OPAL	$e^+e^- \to Z$

$\Gamma(D^*_2(2460)^- \ell^+\nu_\ell \text{anything} \times B(D^*_2(2460)^- \to D^0\pi^-))/\Gamma_{total}$ — Γ_{32}/Γ

VALUE (units 10^{-3})	DOCUMENT ID		TECN	COMMENT
$4.2 \pm 1.3^{+0.7}_{-1.2}$	AKERS	95Q	OPAL	$e^+e^- \to Z$

$\Gamma(\overline{D}^*_2(2460)^0 \ell^+\nu_\ell \text{anything} \times B(\overline{D}^*_2(2460)^0 \to D^-\pi^+))/\Gamma_{total}$ — Γ_{33}/Γ

VALUE (units 10^{-3})	DOCUMENT ID		TECN	COMMENT
1.6±0.7±0.3	AKERS	95Q	OPAL	$e^+e^- \to Z$

$\Gamma(\text{charmless } \ell\overline{\nu}_\ell)/\Gamma_{total}$ — Γ_{34}/Γ

"OUR EVALUATION" is an average of the data listed below performed by the LEP Heavy Flavour Steering Group. The averaging procedure takes into account correlations between the measurements.

VALUE	DOCUMENT ID		TECN	COMMENT
0.00171±0.00052 OUR EVALUATION				
0.0017 ±0.0004 OUR AVERAGE				
$0.00163 \pm 0.00053^{+0.00055}_{-0.00062}$	[1] ABBIENDI	01R	OPAL	$e^+e^- \to Z$
0.00157±0.00035±0.00055	[2] ABREU	00D	DLPH	$e^+e^- \to Z$
0.00173±0.00055±0.00055	[3] BARATE	99G	ALEP	$e^+e^- \to Z$
0.0033 ±0.0010 ±0.0017	[4] ACCIARRI	98K	L3	$e^+e^- \to Z$

[1] Obtained from the best fit of the MC simulated events to the data based on the $b \to X_u \ell \nu$ neutral network output distributions.

[2] ABREU 00D result obtained from a fit to the numbers of decays in $b \to u$ enriched and depleted samples and their lepton spectra, and assuming $|V_{cb}| = 0.0384 \pm 0.0033$ and $\tau_b = 1.564 \pm 0.014$ ps.

[3] Uses lifetime tagged $b\overline{b}$ sample.

[4] ACCIARRI 98K assumes $R_b = 0.2174 \pm 0.0009$ at Z decay.

$\Gamma(\tau^+\nu_\tau \text{anything})/\Gamma_{total}$ — Γ_{35}/Γ

VALUE (units 10^{-2})	EVTS	DOCUMENT ID		TECN	COMMENT
2.41±0.23 OUR AVERAGE					
2.78±0.18±0.51		[1] ABBIENDI	01Q	OPAL	$e^+e^- \to Z$
2.43±0.20±0.25		[2] BARATE	01E	ALEP	$e^+e^- \to Z$
2.19±0.24±0.39		[3] ABREU	00C	DLPH	$e^+e^- \to Z$
1.7 ±0.5 ±1.1		[4,5] ACCIARRI	96C	L3	$e^+e^- \to Z$
2.4 ±0.7 ±0.8	1032	[6] ACCIARRI	94C	L3	$e^+e^- \to Z$
• • • We do not use the following data for averages, fits, limits, etc. • • •					
2.75±0.30±0.37	405	[7] BUSKULIC	95	ALEP	Repl. by BARATE 01E
4.08±0.76±0.62		BUSKULIC	93B	ALEP	Repl. by BUSKULIC 95

[1] ABBIENDI 01Q uses a missing energy technique.

[2] The energy-flow and b-tagging algorithms were used.

[3] Uses the missing energy in $Z \to b\overline{b}$ decays without identifying leptons.

[4] ACCIARRI 96C result obtained from missing energy spectrum.

[5] Assumes Standard Model value for R_B.

[6] This is a direct result using tagged $b\overline{b}$ events at the Z, but species are not separated.

[7] BUSKULIC 95 uses missing-energy technique.

$\Gamma(D^{*-}\tau\nu_\tau \text{anything})/\Gamma_{total}$ — Γ_{36}/Γ

VALUE	DOCUMENT ID		TECN	COMMENT
$(0.88 \pm 0.31 \pm 0.28) \times 10^{-2}$	[1] BARATE	01E	ALEP	$e^+e^- \to Z$

[1] The energy-flow and b-tagging algorithms were used.

$\Gamma(\overline{b} \to \overline{c} \to \ell^-\overline{\nu}_\ell \text{anything})/\Gamma_{total}$ — Γ_{37}/Γ

"OUR EVALUATION" is an average of the data listed below, excluding all asymmetry measurements, performed by the LEP Electroweak Working Group as described in the "Note on the Z boson" in the Z Particle Listings.

VALUE	DOCUMENT ID		TECN	COMMENT
0.0802±0.0019 OUR EVALUATION				
0.0817±0.0020 OUR AVERAGE				
$0.0818 \pm 0.0015^{+0.0024}_{-0.0026}$	[1] HEISTER	02G	ALEP	$e^+e^- \to Z$
$0.0798 \pm 0.0022^{+0.0025}_{-0.0029}$	[2] ABREU	01L	DLPH	$e^+e^- \to Z$
$0.0840 \pm 0.0016^{+0.0039}_{-0.0036}$	[3] ABBIENDI	00E	OPAL	$e^+e^- \to Z$
• • • We do not use the following data for averages, fits, limits, etc. • • •				
0.0770±0.0097±0.0046	[4] ABREU	95D	DLPH	$e^+e^- \to Z$
0.082 ±0.003 ±0.012	[5] BUSKULIC	94G	ALEP	$e^+e^- \to Z$
0.077 ±0.004 ±0.007	[6] AKERS	93B	OPAL	Repl. by ABBIENDI 00E

[1] Uses the combination of lepton transverse momentum spectrum and the correlation between the charge of the lepton and opposite jet charge. The first error is statistic and the second error is the total systematic error including the modeling.

[2] The experimental systematic and model uncertainties are combined in quadrature.

[3] ABBIENDI 00E result is determined by comparing the distribution of several kinematic variables of leptonic events in a lifetime tagged $Z \to b\overline{b}$ sample using artificial neural network techniques. The first error is statistic; the second error is the total systematic error.

[4] ABREU 95D give systematic errors ± 0.0033 (model) and 0.0032 (R_C). We combine these in quadrature. This result is from the same global fit as their $\Gamma(\overline{b} \to \ell^+\nu_\ell X)$ data.

[5] BUSKULIC 94G uses e and μ events. This value is from the same global fit as their $\Gamma(\overline{b} \to \ell^+\nu_\ell \text{anything})/\Gamma_{total}$ data.

[6] AKERS 93B analysis performed using single and dilepton events.

$\Gamma(c \to \ell^+\nu \text{anything})/\Gamma_{total}$ — Γ_{38}/Γ

VALUE	DOCUMENT ID		TECN	COMMENT
$0.0161 \pm 0.0020^{+0.0034}_{-0.0047}$	[1] ABREU	01L	DLPH	$e^+e^- \to Z$

[1] The experimental systematic and model uncertainties are combined in quadrature.

$\Gamma(\overline{D}^0 \text{anything})/\Gamma_{total}$ — Γ_{39}/Γ

VALUE	DOCUMENT ID		TECN	COMMENT
0.589±0.028±0.004	[1] BUSKULIC	96Y	ALEP	$e^+e^- \to Z$

[1] BUSKULIC 96Y reports $0.605 \pm 0.024 \pm 0.016$ from a measurement of $[\Gamma(\overline{b} \to \overline{D}^0 \text{anything})/\Gamma_{total}] \times [B(D^0 \to K^-\pi^+)]$ assuming $B(D^0 \to K^-\pi^+) = 0.0383$, which we rescale to our best (shown rounded) value $B(D^0 \to K^-\pi^+) = (3.936 \pm 0.030) \times 10^{-2}$. Our first error is their experiment's error and our second error is the systematic error from using our best (shown rounded) value.

$\Gamma(D^0 D^{\pm}_s \text{anything})/\Gamma_{total}$ — Γ_{40}/Γ

VALUE	DOCUMENT ID		TECN	COMMENT
$0.091^{+0.020}_{-0.018}{}^{+0.034}_{-0.022}$	[1] BARATE	98Q	ALEP	$e^+e^- \to Z$

[1] The systematic error includes the uncertainties due to the charm branching ratios.

$\Gamma(D^{\mp} D^{\pm}_s \text{anything})/\Gamma_{total}$ — Γ_{41}/Γ

VALUE	DOCUMENT ID		TECN	COMMENT
$0.040^{+0.017}_{-0.014}{}^{+0.016}_{-0.011}$	[1] BARATE	98Q	ALEP	$e^+e^- \to Z$

[1] The systematic error includes the uncertainties due to the charm branching ratios.

$[\Gamma(D^0 D^{\pm}_s \text{anything}) + \Gamma(D^{\mp} D^{\pm}_s \text{anything})]/\Gamma_{total}$ — $(\Gamma_{40}+\Gamma_{41})/\Gamma$

VALUE	DOCUMENT ID		TECN	COMMENT
$0.131^{+0.026}_{-0.022}{}^{+0.048}_{-0.031}$	[1] BARATE	98Q	ALEP	$e^+e^- \to Z$

[1] The systematic error includes the uncertainties due to the charm branching ratios.

$\Gamma(\overline{D}^0 D^0 \text{anything})/\Gamma_{total}$ — Γ_{42}/Γ

VALUE	DOCUMENT ID		TECN	COMMENT
$0.051^{+0.016}_{-0.014}{}^{+0.012}_{-0.011}$	[1] BARATE	98Q	ALEP	$e^+e^- \to Z$

[1] The systematic error includes the uncertainties due to the charm branching ratios.

$\Gamma(D^0 D^{\pm} \text{anything})/\Gamma_{total}$ — Γ_{43}/Γ

VALUE	DOCUMENT ID		TECN	COMMENT
$0.027^{+0.015}_{-0.013}{}^{+0.010}_{-0.009}$	[1] BARATE	98Q	ALEP	$e^+e^- \to Z$

[1] The systematic error includes the uncertainties due to the charm branching ratios.

$[\Gamma(\overline{D}^0 D^0 \text{anything}) + \Gamma(D^0 D^{\pm} \text{anything})]/\Gamma_{total}$ — $(\Gamma_{42}+\Gamma_{43})/\Gamma$

VALUE	DOCUMENT ID		TECN	COMMENT
$0.078^{+0.020}_{-0.018}{}^{+0.018}_{-0.016}$	[1] BARATE	98Q	ALEP	$e^+e^- \to Z$

[1] The systematic error includes the uncertainties due to the charm branching ratios.

Int. J. Mod. Phys. A 2026.41. Downloaded from www.worldscientific.com
by CALIFORNIA @ BERKELEY on 09/16/26. Re-use and distribution is strictly not permitted, except for Open Access articles.

$\Gamma(D^{\pm}D^{\mp}\text{anything})/\Gamma_{\text{total}}$ — Γ_{44}/Γ

VALUE	CL%	DOCUMENT ID		TECN	COMMENT
<0.009	90	BARATE	98Q	ALEP	$e^+e^- \to Z$

$[\Gamma(D^0\text{anything}) + \Gamma(D^+\text{anything})]/\Gamma_{\text{total}}$ — $(\Gamma_{45}+\Gamma_{46})/\Gamma$

VALUE	DOCUMENT ID		TECN	COMMENT
0.093±0.017±0.014	[1] ABDALLAH	03E	DLPH	$e^+e^- \to Z$

[1] The second error is the total of systematic uncertainties including the branching fractions used in the measurement.

$\Gamma(D^-\text{anything})/\Gamma_{\text{total}}$ — Γ_{47}/Γ

VALUE	DOCUMENT ID		TECN	COMMENT
0.229±0.016±0.003	[1] BUSKULIC	96Y	ALEP	$e^+e^- \to Z$

[1] BUSKULIC 96Y reports 0.234 ± 0.013 ± 0.010 from a measurement of $[\Gamma(\overline{b} \to D^-\text{anything})/\Gamma_{\text{total}}] \times [B(D^+ \to K^-2\pi^+)]$ assuming $B(D^+ \to K^-2\pi^+) = 0.091$, which we rescale to our best (shown rounded) value $B(D^+ \to K^-2\pi^+) = (9.31 \pm 0.14) \times 10^{-2}$. Our first error is their experiment's error and our second error is the systematic error from using our best (shown rounded) value.

$\Gamma(D^*(2010)^+\text{anything})/\Gamma_{\text{total}}$ — Γ_{48}/Γ

VALUE	DOCUMENT ID		TECN	COMMENT
0.173±0.016±0.012	[1] ACKERSTAFF	98E	OPAL	$e^+e^- \to Z$

[1] Uses lepton tags to select $Z \to b\overline{b}$ events.

$\Gamma(D_1(2420)^0\text{anything})/\Gamma_{\text{total}}$ — Γ_{49}/Γ

VALUE	DOCUMENT ID		TECN	COMMENT
0.050±0.014±0.006	[1] ACKERSTAFF	97W	OPAL	$e^+e^- \to Z$

[1] ACKERSTAFF 97W assumes $B(D_2^*(2460)^0 \to D^{*+}\pi^-) = 0.21 \pm 0.04$ and $\Gamma_{b\overline{b}}/\Gamma_{\text{hadrons}} = 0.216$ at Z decay.

$\Gamma(D^*(2010)^{\mp}D_s^{\pm}\text{anything})/\Gamma_{\text{total}}$ — Γ_{50}/Γ

VALUE	DOCUMENT ID		TECN	COMMENT
$\mathbf{0.033^{+0.010}_{-0.009}{}^{+0.012}_{-0.009}}$	[1] BARATE	98Q	ALEP	$e^+e^- \to Z$

[1] The systematic error includes the uncertainties due to the charm branching ratios.

$\Gamma(D^0D^*(2010)^{\pm}\text{anything})/\Gamma_{\text{total}}$ — Γ_{51}/Γ

VALUE	DOCUMENT ID		TECN	COMMENT
$\mathbf{0.030^{+0.009}_{-0.008}{}^{+0.007}_{-0.005}}$	[1] BARATE	98Q	ALEP	$e^+e^- \to Z$

[1] The systematic error includes the uncertainties due to the charm branching ratios.

$\Gamma(D^*(2010)^{\pm}D^{\mp}\text{anything})/\Gamma_{\text{total}}$ — Γ_{52}/Γ

VALUE	DOCUMENT ID		TECN	COMMENT
$\mathbf{0.025^{+0.010}_{-0.009}{}^{+0.006}_{-0.005}}$	[1] BARATE	98Q	ALEP	$e^+e^- \to Z$

[1] The systematic error includes the uncertainties due to the charm branching ratios.

$\Gamma(D^*(2010)^{\pm}D^*(2010)^{\mp}\text{anything})/\Gamma_{\text{total}}$ — Γ_{53}/Γ

VALUE	DOCUMENT ID		TECN	COMMENT
$\mathbf{0.012^{+0.004}_{-0.003}\pm0.002}$	[1] BARATE	98Q	ALEP	$e^+e^- \to Z$

[1] The systematic error includes the uncertainties due to the charm branching ratios.

$\Gamma(\overline{D}D\text{anything})/\Gamma_{\text{total}}$ — Γ_{54}/Γ

VALUE	DOCUMENT ID		TECN	COMMENT
$\mathbf{0.10\pm0.032^{+0.107}_{-0.095}}$	[1] ABBIENDI	04I	OPAL	$e^+e^- \to Z$

[1] Measurement performed using an inclusive identification of B mesons and the D candidates.

$\Gamma(D_2^*(2460)^0\text{anything})/\Gamma_{\text{total}}$ — Γ_{55}/Γ

VALUE	DOCUMENT ID		TECN	COMMENT
0.047±0.024±0.013	[1] ACKERSTAFF	97W	OPAL	$e^+e^- \to Z$

[1] ACKERSTAFF 97W assumes $B(D_2^*(2460)^0 \to D^{*+}\pi^-) = 0.21 \pm 0.04$ and $\Gamma_{b\overline{b}}/\Gamma_{\text{hadrons}} = 0.216$ at Z decay.

$\Gamma(D_s^-\text{anything})/\Gamma_{\text{total}}$ — Γ_{56}/Γ

VALUE	DOCUMENT ID		TECN	COMMENT
0.147±0.017±0.013	[1] BUSKULIC	96Y	ALEP	$e^+e^- \to Z$

[1] BUSKULIC 96Y reports 0.183 ± 0.019 ± 0.009 from a measurement of $[\Gamma(\overline{b} \to D_s^-\text{anything})/\Gamma_{\text{total}}] \times [B(D_s^+ \to \phi\pi^+)]$ assuming $B(D_s^+ \to \phi\pi^+) = 0.036$, which we rescale to our best (shown rounded) value $B(D_s^+ \to \phi\pi^+) = (4.5 \pm 0.4) \times 10^{-2}$. Our first error is their experiment's error and our second error is the systematic error from using our best (shown rounded) value.

$\Gamma(D_s^+\text{anything})/\Gamma_{\text{total}}$ — Γ_{57}/Γ

VALUE	DOCUMENT ID		TECN	COMMENT
0.101±0.010±0.029	[1] ABDALLAH	03E	DLPH	$e^+e^- \to Z$

[1] The second error is the total of systematic uncertainties including the branching fractions used in the measurement.

$\Gamma(b \to \Lambda_c^+\text{anything})/\Gamma_{\text{total}}$ — Γ_{58}/Γ

VALUE	DOCUMENT ID		TECN	COMMENT
$\mathbf{0.076\pm0.011^{+0.003}_{-0.002}}$	[1] BUSKULIC	96Y	ALEP	$e^+e^- \to Z$

[1] BUSKULIC 96Y reports 0.110 ± 0.014 ± 0.006 from a measurement of $[\Gamma(b \to \Lambda_c^+\text{anything})/\Gamma_{\text{total}}] \times [B(\Lambda_c^+ \to pK^-\pi^+)]$ assuming $B(\Lambda_c^+ \to pK^-\pi^+) = 0.044$, which we rescale to our best (shown rounded) value $B(\Lambda_c^+ \to pK^-\pi^+) = (6.37 \pm 0.21) \times 10^{-2}$. Our first error is their experiment's error and our second error is the systematic error from using our best (shown rounded) value.

$\Gamma(\overline{c}/c\text{ anything})/\Gamma_{\text{total}}$ — Γ_{59}/Γ

VALUE	DOCUMENT ID		TECN	COMMENT
1.162±0.032 OUR AVERAGE				
$1.12\ ^{+0.11}_{-0.10}$	[1] ABBIENDI	04I	OPAL	$e^+e^- \to Z$
1.166±0.031±0.080	[2] ABREU	00	DLPH	$e^+e^- \to Z$
1.147±0.041	[3] ABREU	98D	DLPH	$e^+e^- \to Z$
1.230±0.036±0.065	[4] BUSKULIC	96Y	ALEP	$e^+e^- \to Z$

[1] Measurement performed using an inclusive identification of B mesons and the D candidates.
[2] Evaluated via summation of exclusive and inclusive channels.
[3] ABREU 98D results are extracted from a fit to the b-tagging probability distribution based on the impact parameter.
[4] BUSKULIC 96Y assumes PDG 96 production fractions for B^0, B^+, B_s, b baryons, and PDG 96 branching ratios for charm decays. This is sum of their inclusive $\overline{D}^0$, D^-, $\overline{D}_s$, and Λ_c branching ratios, corrected to include inclusive Ξ_c and charmonium.

$\Gamma(J/\psi(1S)\text{anything})/\Gamma_{\text{total}}$ — Γ_{60}/Γ

VALUE (units 10^{-2})	CL%	EVTS	DOCUMENT ID		TECN	COMMENT
1.16±0.10 OUR AVERAGE						
1.12±0.12±0.10			[1] ABREU	94P	DLPH	$e^+e^- \to Z$
1.16±0.16±0.14		121	[2] ADRIANI	93J	L3	$e^+e^- \to Z$
1.21±0.13±0.08			BUSKULIC	92G	ALEP	$e^+e^- \to Z$
• • • We do not use the following data for averages, fits, limits, etc. • • •						
1.3 ±0.2 ±0.2			[3] ADRIANI	92	L3	$e^+e^- \to Z$
<4.9	90		MATTEUZZI	83	MRK2	E^{ee}_{cm}= 29 GeV

[1] ABREU 94P is an inclusive measurement from b decays at the Z. Uses $J/\psi(1S) \to e^+e^-$ and $\mu^+\mu^-$ channels. Assumes $\Gamma(Z \to b\overline{b})/\Gamma_{\text{hadron}}$=0.22.
[2] ADRIANI 93J is an inclusive measurement from b decays at the Z. Uses $J/\psi(1S) \to \mu^+\mu^-$ and $J/\psi(1S) \to e^+e^-$ channels.
[3] ADRIANI 92 measurement is an inclusive result for $B(Z \to J/\psi(1S)X) = (4.1 \pm 0.7 \pm 0.3) \times 10^{-3}$ which is used to extract the b-hadron contribution to $J/\psi(1S)$ production.

$\Gamma(\psi(2S)\text{anything})/\Gamma_{\text{total}}$ — Γ_{61}/Γ

VALUE	DOCUMENT ID		TECN	COMMENT
• • • We do not use the following data for averages, fits, limits, etc. • • •				
0.0048±0.0022±0.0010	[1] ABREU	94P	DLPH	$e^+e^- \to Z$

[1] ABREU 94P is an inclusive measurement from b decays at the Z. Uses $\psi(2S) \to J/\psi(1S)\pi^+\pi^-$, $J/\psi(1S) \to \mu^+\mu^-$ channels. Assumes $\Gamma(Z \to b\overline{b})/\Gamma_{\text{hadron}}$=0.22.

$\Gamma(\psi(2S)\text{anything})/\Gamma(J/\psi(1S)\text{anything})$ — Γ_{61}/Γ_{60}

VALUE	DOCUMENT ID		TECN	COMMENT
0.263±0.013 OUR AVERAGE				
0.265±0.002±0.016	[1] AAIJ	20G	LHCB	pp at 13 TeV
0.266±0.06 ±0.03	[2,3] AAIJ	12BD	LHCB	pp at 7 TeV
0.257±0.015±0.019	[4,5] CHATRCHYAN	12AK	CMS	pp at 7 TeV

[1] The first error is statistic; the second error is the total systematic error.
[2] AAIJ 12BD reports $B(b \to \psi(2S)X) = (3.08 \pm 0.07 \pm 0.36 \pm 0.27) \times 10^{-3}$ and we divided our best value of $B(b \to \psi(1S)X) = (1.16 \pm 0.10) \times 10^{-2}$ as the ratio listed here.
[3] Assumes lepton universality imposing $B(\psi(2s) \to \mu^+\mu^-) = B(\psi(2s) \to e^+e^-)$.
[4] CHATRCHYAN 12AK really reports $\Gamma_{61}/\Gamma = (3.08\pm0.12\pm0.13\pm0.42)\times10^{-3}$ assuming PDG 10 value of $\Gamma_{60}/\Gamma = (1.16 \pm 0.10) \times 10^{-2}$ which we present as a ratio of $\Gamma_{61}/\Gamma_{60} = (26.5 \pm 1.0 \pm 1.1 \pm 2.8) \times 10^{-2}$.
[5] CHATRCHYAN 12AK reports $(26.5 \pm 1.0 \pm 1.1 \pm 2.8) \times 10^{-2}$ from a measurement of $[\Gamma(\overline{b} \to \psi(2S)\text{anything})/\Gamma(\overline{b} \to J/\psi(1S)\text{anything})] \times [B(\psi(2S) \to \mu^+\mu^-)] / [B(J/\psi(1S) \to \mu^+\mu^-)]$ assuming $B(\psi(2S) \to \mu^+\mu^-) = (7.7 \pm 0.8) \times 10^{-3}$, $B(J/\psi(1S) \to \mu^+\mu^-) = (5.93 \pm 0.06) \times 10^{-2}$, which we rescale to our best (shown rounded) values $B(\psi(2S) \to \mu^+\mu^-) = (8.0 \pm 0.6) \times 10^{-3}$, $B(J/\psi(1S) \to \mu^+\mu^-) = (5.961 \pm 0.033) \times 10^{-2}$. Our first error is their experiment's error and our second error is the systematic error from using our best (shown rounded) values.

$\Gamma(\chi_{c0}(1P)\text{anything})/\Gamma_{\text{total}}$ — Γ_{62}/Γ

VALUE (units 10^{-3})	DOCUMENT ID		TECN	COMMENT
2.9±0.6±0.1	[1] AAIJ	24AP	LHCB	pp at 13 TeV

[1] AAIJ 24AP reports $[\Gamma(\overline{b} \to \chi_{c0}(1P)\text{anything})/\Gamma_{\text{total}}] \times [B(\chi_{c0}(1P) \to p\overline{p})] = (6.74 \pm 1.18 \pm 0.62) \times 10^{-7}$ which we divide by our best (shown rounded) value $B(\chi_{c0}(1P) \to p\overline{p}) = (2.35 \pm 0.12) \times 10^{-4}$. Our first error is their experiment's error and our second error is the systematic error from using our best (shown rounded) value.

$\Gamma(\chi_{c0}(1P)\text{anything})/\Gamma(\eta_c(1S)\text{anything})$ — Γ_{62}/Γ_{66}

VALUE	DOCUMENT ID		TECN	COMMENT
0.26±0.04±0.07	[1] AAIJ	17BB	LHCB	pp at 7, 8 TeV

[1] AAIJ 17BB reports $[\Gamma(\overline{b} \to \chi_{c0}(1P)\,\text{anything})/\Gamma(\overline{b} \to \eta_c(1S)\,\text{anything})]$ / $[B(\eta_c(1S) \to \phi\phi)] \times [B(\chi_{c0}(1P) \to \phi\phi)] = 0.147 \pm 0.023 \pm 0.011$ which we multiply or divide by our best (shown rounded) values $B(\eta_c(1S) \to \phi\phi) = (1.4 \pm 0.4) \times 10^{-3}$, $B(\chi_{c0}(1P) \to \phi\phi) = (8.3 \pm 0.4) \times 10^{-4}$. Our first error is their experiment's error and our second error is the systematic error from using our best (shown rounded) values.

$\Gamma(\chi_{c1}(1P)\,\text{anything})/\Gamma_{\text{total}}$ — Γ_{63}/Γ

VALUE (units 10^{-3})	EVTS	DOCUMENT ID		TECN	COMMENT
5.6±1.5 OUR AVERAGE		Error includes scale factor of 1.3.			
4.9±1.2±0.2		[1] AAIJ	24AP	LHCB	pp at 13 TeV
$11.3^{+5.8}_{-5.1}\pm0.4$		[2] ABREU	94P	DLPH	$e^+e^- \to Z$
19 ±7 ±1	19	[3] ADRIANI	93J	L3	$e^+e^- \to Z$

[1] AAIJ 24AP reports $[\Gamma(\overline{b} \to \chi_{c1}(1P)\,\text{anything})/\Gamma_{\text{total}}] \times [B(\chi_{c1}(1P) \to p\overline{p})] = (3.88 \pm 0.91 \pm 0.36) \times 10^{-7}$ which we divide by our best (shown rounded) value $B(\chi_{c1}(1P) \to p\overline{p}) = (7.97 \pm 0.29) \times 10^{-5}$. Our first error is their experiment's error and our second error is the systematic error from using our best (shown rounded) value.

[2] ABREU 94P reports $(1.4 \pm 0.6^{+0.4}_{-0.2}) \times 10^{-2}$ from a measurement of $[\Gamma(\overline{b} \to \chi_{c1}(1P)\,\text{anything})/\Gamma_{\text{total}}] \times [B(\chi_{c1}(1P) \to \gamma J/\psi(1S))]$ assuming $B(\chi_{c1}(1P) \to \gamma J/\psi(1S)) = (27.3 \pm 1.6) \times 10^{-2}$, which we rescale to our best (shown rounded) value $B(\chi_{c1}(1P) \to \gamma J/\psi(1S)) = (33.9 \pm 1.2) \times 10^{-2}$. Our first error is their experiment's error and our second error is the systematic error from using our best (shown rounded) value. Assumes no $\chi_{c2}(1P)$ and $\Gamma(Z \to b\overline{b})/\Gamma_{\text{hadron}} = 0.22$.

[3] ADRIANI 93J reports $(2.4 \pm 0.9 \pm 0.2) \times 10^{-2}$ from a measurement of $[\Gamma(\overline{b} \to \chi_{c1}(1P)\,\text{anything})/\Gamma_{\text{total}}] \times [B(\chi_{c1}(1P) \to \gamma J/\psi(1S))]$ assuming $B(\chi_{c1}(1P) \to \gamma J/\psi(1S)) = (27.3 \pm 1.6) \times 10^{-2}$, which we rescale to our best (shown rounded) value $B(\chi_{c1}(1P) \to \gamma J/\psi(1S)) = (33.9 \pm 1.2) \times 10^{-2}$. Our first error is their experiment's error and our second error is the systematic error from using our best (shown rounded) value.

$\Gamma(\chi_{c1}(1P)\,\text{anything})/\Gamma(J/\psi(1S)\,\text{anything})$ — Γ_{63}/Γ_{60}

VALUE	EVTS	DOCUMENT ID		TECN	COMMENT
• • • We do not use the following data for averages, fits, limits, etc. • • •					
1.92±0.82	121	[1] ADRIANI	93J	L3	$e^+e^- \to Z$

[1] ADRIANI 93J is a ratio of inclusive measurements from b decays at the Z using only the $J/\psi(1S) \to \mu^+\mu^-$ channel since some systematics cancel.

$\Gamma(\chi_{c1}(1P)\,\text{anything})/\Gamma(\chi_{c0}(1P)\,\text{anything})$ — Γ_{63}/Γ_{62}

VALUE	DOCUMENT ID		TECN	COMMENT
1.06±0.22 OUR AVERAGE				
1.7 ±0.7 ±0.1	[1] AAIJ	24AP	LHCB	pp at 13 TeV
0.99±0.22±0.06	[2] AAIJ	17BB	LHCB	pp at 7, 8 TeV

[1] AAIJ 24AP reports $[\Gamma(\overline{b} \to \chi_{c1}(1P)\,\text{anything})/\Gamma(\overline{b} \to \chi_{c0}(1P)\,\text{anything})]$ / $[B(\chi_{c0}(1P) \to p\overline{p})] \times [B(\chi_{c1}(1P) \to p\overline{p})] = 0.58 \pm 0.23 \pm 0.02$ which we multiply or divide by our best (shown rounded) values $B(\chi_{c0}(1P) \to p\overline{p}) = (2.35 \pm 0.12) \times 10^{-4}$, $B(\chi_{c1}(1P) \to p\overline{p}) = (7.97 \pm 0.29) \times 10^{-5}$. Our first error is their experiment's error and our second error is the systematic error from using our best (shown rounded) values.

[2] AAIJ 17BB reports $[\Gamma(\overline{b} \to \chi_{c1}(1P)\,\text{anything})/\Gamma(\overline{b} \to \chi_{c0}(1P)\,\text{anything})]$ / $[B(\chi_{c0}(1P) \to \phi\phi)] \times [B(\chi_{c1}(1P) \to \phi\phi)] = 0.50 \pm 0.11 \pm 0.01$ which we multiply or divide by our best (shown rounded) values $B(\chi_{c0}(1P) \to \phi\phi) = (8.3 \pm 0.4) \times 10^{-4}$, $B(\chi_{c1}(1P) \to \phi\phi) = (4.22 \pm 0.20) \times 10^{-4}$. Our first error is their experiment's error and our second error is the systematic error from using our best (shown rounded) values.

$\Gamma(\chi_{c1}(1P)\,\text{anything})/\Gamma(\eta_c(1S)\,\text{anything})$ — Γ_{63}/Γ_{66}

VALUE	DOCUMENT ID		TECN	COMMENT
0.25±0.06±0.07	[1] AAIJ	17BB	LHCB	pp at 7, 8 TeV

[1] AAIJ 17BB reports $[\Gamma(\overline{b} \to \chi_{c1}(1P)\,\text{anything})/\Gamma(\overline{b} \to \eta_c(1S)\,\text{anything})]$ / $[B(\eta_c(1S) \to \phi\phi)] \times [B(\chi_{c1}(1P) \to \phi\phi)] = 0.073 \pm 0.016 \pm 0.006$ which we multiply or divide by our best (shown rounded) values $B(\eta_c(1S) \to \phi\phi) = (1.4 \pm 0.4) \times 10^{-3}$, $B(\chi_{c1}(1P) \to \phi\phi) = (4.22 \pm 0.20) \times 10^{-4}$. Our first error is their experiment's error and our second error is the systematic error from using our best (shown rounded) values.

$\Gamma(\chi_{c2}(1P)\,\text{anything})/\Gamma_{\text{total}}$ — Γ_{64}/Γ

VALUE (units 10^{-3})	DOCUMENT ID		TECN	COMMENT
1.4±1.0±0.1	[1] AAIJ	24AP	LHCB	pp at 13 TeV

[1] AAIJ 24AP reports $[\Gamma(\overline{b} \to \chi_{c2}(1P)\,\text{anything})/\Gamma_{\text{total}}] \times [B(\chi_{c2}(1P) \to p\overline{p})] = (1.13 \pm 0.83 \pm 0.10) \times 10^{-7}$ which we divide by our best (shown rounded) value $B(\chi_{c2}(1P) \to p\overline{p}) = (8.06 \pm 0.33) \times 10^{-5}$. Our first error is their experiment's error and our second error is the systematic error from using our best (shown rounded) value.

$\Gamma(\chi_{c2}(1P)\,\text{anything})/\Gamma(\chi_{c0}(1P)\,\text{anything})$ — Γ_{64}/Γ_{62}

VALUE	DOCUMENT ID		TECN	COMMENT
0.39±0.07 OUR AVERAGE				
0.50±0.35±0.03	[1] AAIJ	24AP	LHCB	pp at 13 TeV
0.38±0.07±0.03	[2] AAIJ	17BB	LHCB	pp at 7, 8 TeV

[1] AAIJ 24AP reports $[\Gamma(\overline{b} \to \chi_{c2}(1P)\,\text{anything})/\Gamma(\overline{b} \to \chi_{c0}(1P)\,\text{anything})]$ / $[B(\chi_{c0}(1P) \to p\overline{p})] \times [B(\chi_{c2}(1P) \to p\overline{p})] = 0.17 \pm 0.12 \pm 0.01$ which we multiply or divide by our best (shown rounded) values $B(\chi_{c0}(1P) \to p\overline{p}) = (2.35 \pm 0.12) \times 10^{-4}$, $B(\chi_{c2}(1P) \to p\overline{p}) = (8.06 \pm 0.33) \times 10^{-5}$. Our first error is their experiment's error and our second error is the systematic error from using our best (shown rounded) values.

[2] AAIJ 17BB reports $[\Gamma(\overline{b} \to \chi_{c2}(1P)\,\text{anything})/\Gamma(\overline{b} \to \chi_{c0}(1P)\,\text{anything})]$ / $[B(\chi_{c0}(1P) \to \phi\phi)] \times [B(\chi_{c2}(1P) \to \phi\phi)] = 0.56 \pm 0.10 \pm 0.01$ which we multiply or divide by our best (shown rounded) values $B(\chi_{c0}(1P) \to \phi\phi) = (8.3 \pm 0.4) \times 10^{-4}$, $B(\chi_{c2}(1P) \to \phi\phi) = (1.22 \pm 0.07) \times 10^{-3}$. Our first error is their experiment's error and our second error is the systematic error from using our best (shown rounded) values.

$\Gamma(\chi_{c2}(1P)\,\text{anything})/\Gamma(\eta_c(1S)\,\text{anything})$ — Γ_{64}/Γ_{66}

VALUE	DOCUMENT ID		TECN	COMMENT
0.096±0.016±0.027	[1] AAIJ	17BB	LHCB	pp at 7, 8 TeV

[1] AAIJ 17BB reports $[\Gamma(\overline{b} \to \chi_{c2}(1P)\,\text{anything})/\Gamma(\overline{b} \to \eta_c(1S)\,\text{anything})]$ / $[B(\eta_c(1S) \to \phi\phi)] \times [B(\chi_{c2}(1P) \to \phi\phi)] = 0.081 \pm 0.013 \pm 0.005$ which we multiply or divide by our best (shown rounded) values $B(\eta_c(1S) \to \phi\phi) = (1.4 \pm 0.4) \times 10^{-3}$, $B(\chi_{c2}(1P) \to \phi\phi) = (1.22 \pm 0.07) \times 10^{-3}$. Our first error is their experiment's error and our second error is the systematic error from using our best (shown rounded) values.

$\Gamma(\chi_c(2P)\,\text{anything},\ \chi_c \to \phi\phi)/\Gamma_{\text{total}}$ — Γ_{65}/Γ

VALUE	CL%	DOCUMENT ID		TECN	COMMENT
$<2.8 \times 10^{-7}$	95	AAIJ	17BB	LHCB	pp at 7, 8 TeV

$\Gamma(\eta_c(1S)\,\text{anything})/\Gamma(J/\psi(1S)\,\text{anything})$ — Γ_{66}/Γ_{60}

VALUE	DOCUMENT ID		TECN	COMMENT
0.49±0.04 OUR AVERAGE				
0.49±0.03±0.05	[1] AAIJ	24AP	LHCB	pp at 13 TeV
0.48±0.03±0.06	AAIJ	20H	LHCB	pp at 13 TeV

[1] Using $\eta_c(1S)$ and $J/\psi(1S)$ decays to $p\overline{p}$.

$\Gamma(\eta_c(2S)\,\text{anything},\ \eta_c \to \phi\phi)/\Gamma(\eta_c(1S)\,\text{anything})$ — Γ_{67}/Γ_{66}

VALUE (units 10^{-5})	DOCUMENT ID		TECN	COMMENT
5.8±1.7±1.6	[1] AAIJ	17BB	LHCB	pp at 7, 8 TeV

[1] AAIJ 17BB reports $[\Gamma(\overline{b} \to \eta_c(2S)\,\text{anything},\ \eta_c \to \phi\phi)/\Gamma(\overline{b} \to \eta_c(1S)\,\text{anything})]$ / $[B(\eta_c(1S) \to \phi\phi)] = 0.040 \pm 0.011 \pm 0.004$ which we multiply by our best (shown rounded) value $B(\eta_c(1S) \to \phi\phi) = (1.4 \pm 0.4) \times 10^{-3}$. Our first error is their experiment's error and our second error is the systematic error from using our best (shown rounded) value.

$\Gamma(\chi_{c1}(3872)\,\text{anything},\ \chi_{c1} \to \phi\phi)/\Gamma_{\text{total}}$ — Γ_{68}/Γ

VALUE	CL%	DOCUMENT ID		TECN	COMMENT
$<4.5 \times 10^{-7}$	95	AAIJ	17BB	LHCB	pp at 7, 8 TeV

$\Gamma(\chi_{c0}(3915)\,\text{anything},\ \chi_{c0} \to \phi\phi)/\Gamma_{\text{total}}$ — Γ_{69}/Γ

VALUE	CL%	DOCUMENT ID		TECN	COMMENT
$<3.1 \times 10^{-7}$	95	AAIJ	17BB	LHCB	pp at 7, 8 TeV

$\Gamma(\overline{s}\gamma)/\Gamma_{\text{total}}$ — Γ_{70}/Γ

VALUE (units 10^{-4})	CL%	DOCUMENT ID		TECN	COMMENT
3.11±0.80±0.72		[1] BARATE	98I	ALEP	$e^+e^- \to Z$
• • • We do not use the following data for averages, fits, limits, etc. • • •					
< 5.4	90	[2] ADAM	96D	DLPH	$e^+e^- \to Z$
<12	90	[3] ADRIANI	93L	L3	$e^+e^- \to Z$

[1] BARATE 98I uses lifetime tagged $Z \to b\overline{b}$ sample.

[2] ADAM 96D assumes $f_{B^0} = f_{B^-} = 0.39$ and $f_{B_s} = 0.12$.

[3] ADRIANI 93L result is for $\overline{b} \to \overline{s}\gamma$ is performed inclusively.

$\Gamma(\overline{s}\overline{\nu}\nu)/\Gamma_{\text{total}}$ — Γ_{71}/Γ

VALUE	CL%	DOCUMENT ID		TECN	COMMENT
$<6.4 \times 10^{-4}$	90	[1] BARATE	01E	ALEP	$e^+e^- \to Z$

[1] The energy-flow and b-tagging algorithms were used.

$\Gamma(K^{\pm}\,\text{anything})/\Gamma_{\text{total}}$ — Γ_{72}/Γ

VALUE	DOCUMENT ID		TECN	COMMENT
0.74±0.06 OUR AVERAGE				
0.72±0.02±0.06	BARATE	98V	ALEP	$e^+e^- \to Z$
0.88±0.05±0.18	ABREU	95C	DLPH	$e^+e^- \to Z$

$\Gamma(K^0_S\,\text{anything})/\Gamma_{\text{total}}$ — Γ_{73}/Γ

VALUE	DOCUMENT ID		TECN	COMMENT
0.290±0.011±0.027	ABREU	95C	DLPH	$e^+e^- \to Z$

$\Gamma(\pi^{\pm}\,\text{anything})/\Gamma_{\text{total}}$ — Γ_{74}/Γ

VALUE	DOCUMENT ID		TECN	COMMENT
3.97±0.02±0.21	BARATE	98V	ALEP	$e^+e^- \to Z$

$\Gamma(\pi^0\,\text{anything})/\Gamma_{\text{total}}$ — Γ_{75}/Γ

VALUE	DOCUMENT ID		TECN	COMMENT
2.78±0.15±0.60	[1] ADAM	96	DLPH	$e^+e^- \to Z$

[1] ADAM 96 measurement obtained from a fit to the rapidity distribution of $\pi^{0's}$ in $Z \to b\,b$ events.

$\Gamma(\phi\,\text{anything})/\Gamma_{\text{total}}$ — Γ_{76}/Γ

VALUE	DOCUMENT ID		TECN	COMMENT
0.0282±0.0013±0.0019	ABBIENDI	00Z	OPAL	$e^+e^- \to Z$

$\Gamma(p/\overline{p}\,\text{anything})/\Gamma_{\text{total}}$ — Γ_{77}/Γ

VALUE	DOCUMENT ID		TECN	COMMENT
0.131±0.011 OUR AVERAGE				
0.131±0.004±0.011	BARATE	98V	ALEP	$e^+e^- \to Z$
0.141±0.018±0.056	ABREU	95C	DLPH	$e^+e^- \to Z$

Int. J. Mod. Phys. A 2026.41. Downloaded from www.worldscientific.com
by UNIVERSITY OF CALIFORNIA @ BERKELEY on 09/16/26. Re-use and distribution is strictly not permitted, except for Open Access articles.

Int. J. Mod. Phys. A 2026.41. Downloaded from www.worldscientific.com by CALIFORNIA @ BERKELEY on 09/16/26. Re-use and distribution is strictly not permitted, except for Open Access articles.

$\Gamma(\Lambda/\overline{\Lambda}\text{anything})/\Gamma_{\text{total}}$ — Γ_{78}/Γ

VALUE	DOCUMENT ID		TECN	COMMENT
0.059 ±0.006 OUR AVERAGE				
0.0587±0.0046±0.0048	ACKERSTAFF	97N	OPAL	$e^+e^- \to Z$
0.059 ±0.007 ±0.009	ABREU	95C	DLPH	$e^+e^- \to Z$

$\Gamma(b\text{-baryon anything})/\Gamma_{\text{total}}$ — Γ_{79}/Γ

VALUE	DOCUMENT ID		TECN	COMMENT
0.102±0.007±0.027	[1] BARATE	98V	ALEP	$e^+e^- \to Z$

[1] BARATE 98V assumes $B(B_s \to pX) = 8 \pm 4\%$ and $B(b\text{-baryon} \to pX) = 58 \pm 6\%$.

$\Gamma(\Xi_b^+\text{anything})/\Gamma(\Lambda_b^0\text{anything})$ — Γ_{81}/Γ_{80}

VALUE (units 10^{-2})	DOCUMENT ID		TECN	COMMENT
7.3±1.7 OUR AVERAGE				
6.7±0.5±2.1	[1] AAIJ	19AB	LHCB	pp at 7 and 8 TeV
8.2±0.7±2.6	[1] AAIJ	19AB	LHCB	pp at 13 TeV

[1] Measured from $R = [B(\overline{b} \to \Xi_b^+)\times B(\Xi_b \to J/\psi\Xi^+)]/[B(\overline{b} \to \overline{\Lambda}_b^0)\times B(\overline{\Lambda}_b^0 \to J/\psi\overline{\Lambda}^0)]$ and assumes $\Gamma_{\Xi_b^+ \to J/\psi\Xi^+}/\Gamma_{\overline{\Lambda}_b^0 \to J/\psi\overline{\Lambda}^0} = 3/2$ related through SU(3) flavor symmetry.

$\Gamma(\text{charged anything})/\Gamma_{\text{total}}$ — Γ_{82}/Γ

VALUE	DOCUMENT ID		TECN	COMMENT
4.97±0.03±0.06	[1] ABREU	98H	DLPH	$e^+e^- \to Z$
• • • We do not use the following data for averages, fits, limits, etc. • • •				
5.84±0.04±0.38	ABREU	95C	DLPH	Repl. by ABREU 98H

[1] ABREU 98H measurement excludes the contribution from K^0 and Λ decay.

$\Gamma(\text{hadron}^+\text{hadron}^-)/\Gamma_{\text{total}}$ — Γ_{83}/Γ

VALUE (units 10^{-5})	DOCUMENT ID		TECN	COMMENT
$1.7^{+1.0}_{-0.7}\pm0.2$	[1,2] BUSKULIC	96V	ALEP	$e^+e^- \to Z$

[1] BUSKULIC 96V assumes PDG 96 production fractions for B^0, B^+, B_s, b baryons.
[2] Average branching fraction of weakly decaying B hadrons into two long-lived charged hadrons, weighted by their production cross section and lifetimes.

$\Gamma(\text{charmless})/\Gamma_{\text{total}}$ — Γ_{84}/Γ

VALUE	DOCUMENT ID		TECN	COMMENT
0.007±0.021	[1] ABREU	98D	DLPH	$e^+e^- \to Z$

[1] ABREU 98D results are extracted from a fit to the b-tagging probability distribution based on the impact parameter. The expected hidden charm contribution of 0.026 ± 0.004 has been subtracted.

$\Gamma(\mu^+\mu^-\text{anything})/\Gamma_{\text{total}}$ — Γ_{86}/Γ

Test for $\Delta B = 1$ weak neutral current.

VALUE	CL%	DOCUMENT ID		TECN	COMMENT
$<3.2 \times 10^{-4}$	90	ABBOTT	98B	D0	$p\overline{p}$ 1.8 TeV
• • • We do not use the following data for averages, fits, limits, etc. • • •					
$<5.0 \times 10^{-5}$	90	[1] ALBAJAR	91C	UA1	$E^{p\overline{p}}_{\text{cm}}$= 630 GeV
<0.02	95	ALTHOFF	84G	TASS	E^{ee}_{cm}= 34.5 GeV
<0.007	95	ADEVA	83	MRKJ	E^{ee}_{cm}= 30–38 GeV
<0.007	95	BARTEL	83B	JADE	E^{ee}_{cm}= 33–37 GeV

[1] Both ABBOTT 98B and GLENN 98 claim that the efficiency quoted in ALBAJAR 91C was overestimated by a large factor.

$[\Gamma(e^+e^-\text{anything}) + \Gamma(\mu^+\mu^-\text{anything})]/\Gamma_{\text{total}}$ — $(\Gamma_{85}+\Gamma_{86})/\Gamma$

Test for $\Delta B = 1$ weak neutral current.

VALUE	CL%	DOCUMENT ID		TECN	COMMENT
• • • We do not use the following data for averages, fits, limits, etc. • • •					
<0.008	90	MATTEUZZI	83	MRK2	E^{ee}_{cm}= 29 GeV

$\Gamma(\nu\overline{\nu}\text{anything})/\Gamma_{\text{total}}$ — Γ_{87}/Γ

VALUE	DOCUMENT ID		TECN	COMMENT
• • • We do not use the following data for averages, fits, limits, etc. • • •				
$<3.9 \times 10^{-4}$	[1] GROSSMAN	96	RVUE	$e^+e^- \to Z$

[1] GROSSMAN 96 limit is derived from the ALEPH BUSKULIC 95 limit $B(B^+ \to \tau^+\nu_\tau) < 1.8 \times 10^{-3}$ at CL=90% using conservative simplifying assumptions.

χ_b AT HIGH ENERGY

χ_b is the average B-$\overline{B}$ mixing parameter at high-energy $\chi_b = f'_d\chi_d + f'_s\chi_s$ where f'_d and f'_s are the fractions of B^0 and B^0_s hadrons in an unbiased sample of semileptonic b-hadron decays. We consider here $\overline{\chi}$ for hadrons produced in Z decays.

VALUE (units 10^{-2})	EVTS	DOCUMENT ID		TECN	COMMENT
12.59± 0.42 OUR EVALUATION		(from LEP-SLC 06, eq. 5.39)			
12.6 ± 0.4 OUR AVERAGE					
13.12± 0.49±0.42		[1] ABBIENDI	03P	OPAL	$e^+e^- \to Z$
12.7 ± 1.3 ±0.6		[2] ABREU	01L	DLPH	$e^+e^- \to Z$
11.92± 0.68±0.51		[3] ACCIARRI	99D	L3	$e^+e^- \to Z$
12.1 ± 1.6 ±0.6		[4] ABREU	94J	DLPH	$e^+e^- \to Z$
11.4 ± 1.4 ±0.8		[5] BUSKULIC	94G	ALEP	$e^+e^- \to Z$
12.9 ± 2.2		[6] BUSKULIC	92B	ALEP	$e^+e^- \to Z$
• • • We do not use the following data for averages, fits, limits, etc. • • •					
13.2 ± 0.1 ±2.4		[7] ABAZOV	06S	D0	$p\overline{p}$ at 1.96 TeV
15.2 ± 0.7 ±1.1		[8] ACOSTA	04A	CDF	$p\overline{p}$ at 1.8 TeV
13.1 ± 2.0 ±1.6		[9] ABE	97I	CDF	Repl. by ACOSTA 04A
11.07± 0.62±0.55		[10] ALEXANDER	96	OPAL	Rep. by ABBIENDI 03P
13.6 ± 3.7 ±4.0		[11] UENO	96	AMY	e^+e^- at 57.9 GeV
14.4 ± 1.4 $^{+1.7}_{-1.1}$		[12] ABREU	94F	DLPH	Sup. by ABREU 94J
13.1 ± 1.4		[13] ABREU	94J	DLPH	$e^+e^- \to Z$
12.3 ± 1.2 ±0.8		ACCIARRI	94D	L3	Repl. by ACCIARRI 99D
15.7 ± 2.0 ±3.2		[14] ALBAJAR	94	UA1	$\sqrt{s}$ = 630 GeV
12.1 $^{+4.4}_{-4.0}$ ±1.7	1665	[15] ABREU	93C	DLPH	Sup. by ABREU 94J
14.3 $^{+2.2}_{-2.1}$ ±0.7		[16] AKERS	93B	OPAL	Sup. by ALEXANDER 96
14.5 $^{+4.1}_{-3.5}$ ±1.8		[17] ACTON	92C	OPAL	$e^+e^- \to Z$
12.1 ± 1.7 ±0.6		[18] ADEVA	92C	L3	Sup. by ACCIARRI 94D
17.6 ± 3.1 ±3.2	1112	[19] ABE	91G	CDF	$p\overline{p}$ 1.8 TeV
14.8 ± 2.9 ±1.7		[20] ALBAJAR	91D	UA1	$p\overline{p}$ 630 GeV
13.2 ±22.0 $^{+1.5}_{-1.2}$	823	[21] DECAMP	91	ALEP	$e^+e^- \to Z$
17.8 $^{+4.9}_{-4.0}$ ±2.0		[22] ADEVA	90P	L3	$e^+e^- \to Z$
17 $^{+15}_{-8}$		[23,24] WEIR	90	MRK2	e^+e^- 29 GeV
21 $^{+29}_{-15}$		[23] BAND	88	MAC	E^{ee}_{cm}= 29 GeV
>2 at 90%CL		[23] BAND	88	MAC	E^{ee}_{cm}= 29 GeV
12.1 ± 4.7		[23,25] ALBAJAR	87C	UA1	Repl. by ALBAJAR 91D
<12 at 90%CL		[23,26] SCHAAD	85	MRK2	E^{ee}_{cm}= 29 GeV

[1] The average B mixing parameter is determined simultaneously with b and c forward-backward asymmetries in the fit.
[2] The experimental systematic and model uncertainties are combined in quadrature.
[3] ACCIARRI 99D uses maximum-likelihood fits to extract χ_b as well as the A^b_{FB} in $Z \to b\overline{b}$ events containing prompt leptons.
[4] This ABREU 94J result is from 5182 $\ell\ell$ and 279 $\Lambda\ell$ events. The systematic error includes 0.004 for model dependence.
[5] BUSKULIC 94G data analyzed using ee, $e\mu$, and $\mu\mu$ events.
[6] BUSKULIC 92B uses a jet charge technique combined with electrons and muons.
[7] Uses the dimuon charge asymmetry. Averaged over the mix of b-flavored hadrons.
[8] Measurement performed using events containing a dimuon or an e/μ pair.
[9] Uses di-muon events.
[10] ALEXANDER 96 uses a maximum likelihood fit to simultaneously extract χ as well as the forward-backward asymmetries in $e^+e^- \to Z \to b\overline{b}$ and $c\overline{c}$.
[11] UENO 96 extracted χ from the energy dependence of the forward-backward asymmetry.
[12] ABREU 94F uses the average electric charge sum of the jets recoiling against a b-quark jet tagged by a high p_T muon. The result is for $\overline{\chi} = f_d\chi_d + 0.9 f_s\chi_s$.
[13] This ABREU 94J result combines $\ell\ell$, $\Lambda\ell$, and jet-charge ℓ (ABREU 94F) analyses. It is for $\overline{\chi} = f_d\chi_d + 0.96 f_s\chi_s$.
[14] ALBAJAR 94 uses dimuon events. Not independent of ALBAJAR 91D.
[15] ABREU 93C data analyzed using ee, $e\mu$, and $\mu\mu$ events.
[16] AKERS 93B analysis performed using dilepton events.
[17] ACTON 92C uses electrons and muons. Superseded by AKERS 93B.
[18] ADEVA 92C uses electrons and muons.
[19] ABE 91G measurement of χ is done with $e\mu$ and ee events.
[20] ALBAJAR 91D measurement of χ is done with dimuons.
[21] DECAMP 91 done with opposite and like-sign dileptons. Superseded by BUSKULIC 92B.
[22] ADEVA 90P measurement uses ee, $\mu\mu$, and $e\mu$ events from 118k events at the Z. Superseded by ADEVA 92C.
[23] These experiments are not in the average because the combination of B_s and B_d mesons which they see could differ from those at higher energy.
[24] The WEIR 90 measurement supersedes the limit obtained in SCHAAD 85. The 90% CL are 0.06 and 0.38.
[25] ALBAJAR 87C measured $\chi = (\overline{B}^0 \to B^0 \to \mu^+X)$ divided by the average production weighted semileptonic branching fraction for B hadrons at 546 and 630 GeV.
[26] Limit is average probability for hadron containing B quark to produce a positive lepton.

CP VIOLATION PARAMETERS in semileptonic b-hadron decays.

$\text{Re}(\epsilon_b) / (1 + |\epsilon_b|^2)$

CP impurity in semileptonic b-hadron decays.

VALUE (units 10^{-3})	DOCUMENT ID		TECN	COMMENT
• • • We do not use the following data for averages, fits, limits, etc. • • •				
−6.2 ±5.2 ±4.7	[1] AABOUD	17E	ATLS	pp at 8 TeV
−1.24±0.38±0.18	[2] ABAZOV	14	D0	$p\overline{p}$ at 1.96 TeV
−1.97±0.43±0.23	[3] ABAZOV	11U	D0	Repl. by ABAZOV 14
−2.39±0.63±0.37	[4] ABAZOV	10H	D0	Repl. by ABAZOV 11U

[1] AABOUD 17E reports a measurement of charge asymmetry of $A^b_{SL} = (-25 \pm 21 \pm 19) \times 10^{-3}$ in lepton + jets $t\overline{t}$ events in which a b-hadron decays semileptonically to a soft muon.
[2] ABAZOV 14 reports a measurement of like-sign dimuon charge asymmetry of $A^b_{SL} = (-4.96 \pm 1.53 \pm 0.72) \times 10^{-3}$ in semileptonic b-hadron decays.
[3] ABAZOV 11U reports a measurement of like-sign dimuon charge asymmetry of $A^b_{SL} = (-7.87 \pm 1.72 \pm 0.93) \times 10^{-3}$ in semileptonic b-hadron decays.
[4] ABAZOV 10H reports a measurement of like-sign dimuon charge asymmetry of $A^b_{SL}=(-9.57 \pm 2.51 \pm 1.46) \times 10^{-3}$ in semileptonic b-hadron decays. Using the measured production ratio of B^0_d and B^0_s, and the asymmetry of B^0_d $A^d_{SL}=(-4.7 \pm 4.6) \times 10^{-3}$ measured from B-factories, they obtain the asymmetry for B^0_s as $A^s_{SL}=(-14.6 \pm 7.5) \times 10^{-3}$.

Int. J. Mod. Phys. A 2026.41. Downloaded from www.worldscientific.com
by UNIVERSITY OF CALIFORNIA @ BERKELEY on 09/16/26. Re-use and distribution is strictly not permitted, except for Open Access articles.

PRODUCTION ASYMMETRIES

$A_C^{b\overline{b}}$

$A_C^{b\overline{b}} = [N(\Delta y > 0) - N(\Delta y < 0)] / [N(\Delta y > 0) + N(\Delta y < 0)]$ with $\Delta y = |y_b| - |y_{\overline{b}}|$ where $y_{b/\overline{b}}$ is rapidity of b or $\overline{b}$ quarks.

VALUE (units 10^{-2})	DOCUMENT ID		TECN	COMMENT
Average is meaningless.				
$0.4 \pm 0.4 \pm 0.3$	[1] AAIJ	14AS	LHCB	pp at 7 TeV
$2.0 \pm 0.9 \pm 0.6$	[2] AAIJ	14AS	LHCB	pp at 7 TeV
$1.6 \pm 1.7 \pm 0.6$	[3] AAIJ	14AS	LHCB	pp at 7 TeV

[1] Measured for $40 < M(b\overline{b}) < 75$ GeV/c^2.
[2] Measured for $75 < M(b\overline{b}) < 105$ GeV/c^2.
[3] Measured for $M(b\overline{b}) > 105$ GeV/c^2.

$B^{\pm}/B^0/B^0_s/b$-baryon ADMIXTURE REFERENCES

AAIJ	24AP	EPJ C84 1274	R. Aaij et al.	(LHCb Collab.)
AAIJ	21Y	PR D104 032005	R. Aaij et al.	(LHCb Collab.)
AAIJ	20G	EPJ C80 185	R. Aaij et al.	(LHCb Collab.)
AAIJ	20H	EPJ C80 191	R. Aaij et al.	(LHCb Collab.)
AAIJ	20V	PRL 124 122002	R. Aaij et al.	(LHCb Collab.)
AAIJ	19AB	PR D99 052006	R. Aaij et al.	(LHCb Collab.)
AAIJ	19AD	PR D100 031102	R. Aaij et al.	(LHCb Collab.)
AAIJ	19AI	PR D100 112006	R. Aaij et al.	(LHCb Collab.)
AABOUD	17E	JHEP 1702 071	M. Aaboud et al.	(ATLAS Collab.)
AAIJ	17BB	EPJ C77 609	R. Aaij et al.	(LHCb Collab.)
AAD	15CM	PRL 115 262001	G. Aad et al.	(ATLAS Collab.)
AAIJ	14AS	PRL 113 082003	R. Aaij et al.	(LHCb Collab.)
ABAZOV	14	PR D89 012002	V.M. Abazov et al.	(D0 Collab.)
AAIJ	13P	JHEP 1304 001	R. Aaij et al.	(LHCb Collab.)
AAIJ	12BD	EPJ C72 2100	R. Aaij et al.	(LHCb Collab.)
Also		EPJ C80 49 (errat.)	R. Aaij et al.	(LHCb Collab.)
AAIJ	12J	PR D85 032008	R. Aaji et al.	(LHCb Collab.)
CHATRCHYAN	12AK	JHEP 1202 011	S. Chatrchyan et al.	(CMS Collab.)
AAIJ	11F	PRL 107 211801	R. Aaij et al.	(LHCb Collab.)
ABAZOV	11U	PR D84 052007	V.M. Abazov et al.	(D0 Collab.)
ABAZOV	10H	PRL 105 081801	V.M. Abazov et al.	(D0 Collab.)
Also		PR D82 032001	V.M. Abazov et al.	(D0 Collab.)
PDG	10	JP G37 075021	K. Nakamura et al.	(PDG Collab.)
AALTONEN	09E	PR D79 032001	T. Aaltonen et al.	(CDF Collab.)
AALTONEN	08N	PR D77 072003	T. Aaltonen et al.	(CDF Collab.)
ABAZOV	06S	PR D74 092001	V.M. Abazov et al.	(D0 Collab.)
LEP-SLC	06	PRPL 427 257	ALEPH, DELPHI, L3, OPAL, SLD and working groups	
ABBIENDI	04I	EPJ C35 149	G. Abbiendi et al.	(OPAL Collab.)
ABDALLAH	04E	EPJ C33 307	J. Abdallah et al.	(DELPHI Collab.)
ACOSTA	04A	PR D69 012002	D. Acosta et al.	(CDF Collab.)
ABBIENDI	03M	EPJ C30 467	G. Abbiendi et al.	(OPAL Collab.)
ABBIENDI	03P	PL B577 18	G. Abbiendi et al.	(OPAL Collab.)
ABDALLAH	03E	PL B561 26	J. Abdallah et al.	(DELPHI Collab.)
ABDALLAH	03K	PL B576 29	J. Abdallah et al.	(DELPHI Collab.)
HEISTER	02G	EPJ C22 613	A. Heister et al.	(ALEPH Collab.)
ABBIENDI	01Q	PL B520 1	G. Abbiendi et al.	(OPAL Collab.)
ABBIENDI	01R	EPJ C21 399	G. Abbiendi et al.	(OPAL Collab.)
ABREU	01L	EPJ C20 455	P. Abreu et al.	(DELPHI Collab.)
BARATE	01E	EPJ C19 213	R. Barate et al.	(ALEPH Collab.)
ABBIENDI	00E	EPJ C13 225	G. Abbiendi et al.	(OPAL Collab.)
ABBIENDI	00Z	PL B492 13	G. Abbiendi et al.	(OPAL Collab.)
ABREU	00	EPJ C12 225	P. Abreu et al.	(DELPHI Collab.)
ABREU	00C	PL B496 43	P. Abreu et al.	(DELPHI Collab.)
ABREU	00D	PL B478 14	P. Abreu et al.	(DELPHI Collab.)
ABREU	00R	PL B475 407	P. Abreu et al.	(DELPHI Collab.)
ACCIARRI	00	EPJ C13 47	M. Acciarri et al.	(L3 Collab.)
AFFOLDER	00E	PRL 84 1663	T. Affolder et al.	(CDF Collab.)
ABBIENDI	99J	EPJ C12 609	G. Abbiendi et al.	(OPAL Collab.)
ABE	99P	PR D60 092005	F. Abe et al.	(CDF Collab.)
ACCIARRI	99D	PL B448 152	M. Acciarri et al.	(L3 Collab.)
BARATE	99G	EPJ C6 555	R. Barate et al.	(ALEPH Collab.)
ABBOTT	98B	PL B423 419	B. Abbott et al.	(D0 Collab.)
ABE	98B	PR D57 5382	F. Abe et al.	(CDF Collab.)
ABREU	98D	PL B426 193	P. Abreu et al.	(DELPHI Collab.)
ABREU	98H	PL B425 399	P. Abreu et al.	(DELPHI Collab.)
ACCIARRI	98	PL B416 220	M. Acciarri et al.	(L3 Collab.)
ACCIARRI	98K	PL B436 174	M. Acciarri et al.	(L3 Collab.)
ACKERSTAFF	98E	EPJ C1 439	K. Ackerstaff et al.	(OPAL Collab.)
BARATE	98I	PL B429 169	R. Barate et al.	(ALEPH Collab.)
BARATE	98Q	EPJ C4 387	R. Barate et al.	(ALEPH Collab.)
BARATE	98V	EPJ C5 205	R. Barate et al.	(ALEPH Collab.)
GLENN	98	PRL 80 2289	S. Glenn et al.	(CLEO Collab.)
ABE	97I	PR D55 2546	F. Abe et al.	(CDF Collab.)
ACKERSTAFF	97F	ZPHY C73 397	K. Ackerstaff et al.	(OPAL Collab.)
ACKERSTAFF	97N	ZPHY C74 423	K. Ackerstaff et al.	(OPAL Collab.)
ACKERSTAFF	97W	ZPHY C76 425	K. Ackerstaff et al.	(OPAL Collab.)
ABREU	96E	PL B377 195	P. Abreu et al.	(DELPHI Collab.)
ACCIARRI	96C	ZPHY C71 379	M. Acciarri et al.	(L3 Collab.)
ADAM	96	ZPHY C69 561	W. Adam et al.	(DELPHI Collab.)
ADAM	96D	ZPHY C72 207	W. Adam et al.	(DELPHI Collab.)
ALEXANDER	96	ZPHY C70 357	G. Alexander et al.	(OPAL Collab.)
BUSKULIC	96F	PL B369 151	D. Buskulic et al.	(ALEPH Collab.)
BUSKULIC	96V	PL B384 471	D. Buskulic et al.	(ALEPH Collab.)
BUSKULIC	96Y	PL B388 648	D. Buskulic et al.	(ALEPH Collab.)
GROSSMAN	96	NP B465 369	Y. Grossman, Z. Ligeti, E. Nardi	(REHO, CIT)
Also		NP B480 753 (errat.)	Y. Grossman, Z. Ligeti, E. Nardi	
PDG	96	PR D54 1	R. M. Barnett et al.	(PDG Collab.)
UENO	96	PL B381 365	K. Ueno et al.	(AMY Collab.)
ABE,K	95B	PRL 75 3624	K. Abe et al.	(SLD Collab.)
ABREU	95C	PL B347 447	P. Abreu et al.	(DELPHI Collab.)
ABREU	95D	ZPHY C66 323	P. Abreu et al.	(DELPHI Collab.)
ADAM	95	ZPHY C68 363	W. Adam et al.	(DELPHI Collab.)
AKERS	95Q	ZPHY C67 57	R. Akers et al.	(OPAL Collab.)
BUSKULIC	95	PL B343 444	D. Buskulic et al.	(ALEPH Collab.)
ABREU	94F	PL B322 459	P. Abreu et al.	(DELPHI Collab.)
ABREU	94J	PL B332 488	P. Abreu et al.	(DELPHI Collab.)
ABREU	94L	ZPHY C63 3	P. Abreu et al.	(DELPHI Collab.)
ABREU	94P	PL B341 109	P. Abreu et al.	(DELPHI Collab.)
ACCIARRI	94C	PL B332 201	M. Acciarri et al.	(L3 Collab.)
ACCIARRI	94D	PL B335 542	M. Acciarri et al.	(L3 Collab.)
ALBAJAR	94	ZPHY C61 41	C. Albajar et al.	(UA1 Collab.)
BUSKULIC	94G	ZPHY C62 179	D. Buskulic et al.	(ALEPH Collab.)
ABE	93E	PL B313 288	K. Abe et al.	(VENUS Collab.)
ABE	93J	PRL 71 3421	F. Abe et al.	(CDF Collab.)
ABREU	93C	PL B301 145	P. Abreu et al.	(DELPHI Collab.)
ABREU	93D	ZPHY C57 181	P. Abreu et al.	(DELPHI Collab.)
ABREU	93G	PL B312 253	P. Abreu et al.	(DELPHI Collab.)
ACTON	93C	PL B307 247	P.D. Acton et al.	(OPAL Collab.)
ACTON	93L	ZPHY C60 217	P.D. Acton et al.	(OPAL Collab.)
ADRIANI	93J	PL B317 467	O. Adriani et al.	(L3 Collab.)
ADRIANI	93K	PL B317 474	O. Adriani et al.	(L3 Collab.)
ADRIANI	93L	PL B317 637	O. Adriani et al.	(L3 Collab.)
AKERS	93B	ZPHY C60 199	R. Akers et al.	(OPAL Collab.)
BUSKULIC	93B	PL B298 479	D. Buskulic et al.	(ALEPH Collab.)
BUSKULIC	93O	PL B314 459	D. Buskulic et al.	(ALEPH Collab.)
ABREU	92	ZPHY C53 567	P. Abreu et al.	(DELPHI Collab.)
ACTON	92	PL B274 513	D.P. Acton et al.	(OPAL Collab.)
ACTON	92C	PL B276 379	D.P. Acton et al.	(OPAL Collab.)
ADEVA	92C	PL B288 395	B. Adeva et al.	(L3 Collab.)
ADRIANI	92	PL B288 412	O. Adriani et al.	(L3 Collab.)
BUSKULIC	92B	PL B284 177	D. Buskulic et al.	(ALEPH Collab.)
BUSKULIC	92F	PL B295 174	D. Buskulic et al.	(ALEPH Collab.)
BUSKULIC	92G	PL B295 396	D. Buskulic et al.	(ALEPH Collab.)
ABE	91G	PRL 67 3351	F. Abe et al.	(CDF Collab.)
ADEVA	91C	PL B261 177	B. Adeva et al.	(L3 Collab.)
ADEVA	91H	PL B270 111	B. Adeva et al.	(L3 Collab.)
ALBAJAR	91C	PL B262 163	C. Albajar et al.	(UA1 Collab.)
ALBAJAR	91D	PL B262 171	C. Albajar et al.	(UA1 Collab.)
ALEXANDER	91G	PL B266 485	G. Alexander et al.	(OPAL Collab.)
DECAMP	91	PL B258 236	D. Decamp et al.	(ALEPH Collab.)
DECAMP	91C	PL B257 492	D. Decamp et al.	(ALEPH Collab.)
ADEVA	90P	PL B252 703	B. Adeva et al.	(L3 Collab.)
BEHREND	90D	ZPHY C47 333	H.J. Behrend et al.	(CELLO Collab.)
HAGEMANN	90	ZPHY C48 401	J. Hagemann et al.	(JADE Collab.)
LYONS	90	PR D41 982	L. Lyons, A.J. Martin, D.H. Saxon	(OXF, BRIS+)
WEIR	90	PL B240 289	A.J. Weir et al.	(Mark II Collab.)
BRAUNSCH...	89B	ZPHY C44 1	R. Braunschweig et al.	(TASSO Collab.)
ONG	89	PRL 62 1236	R.A. Ong et al.	(Mark II Collab.)
BAND	88	PL B200 221	H.R. Band et al.	(MAC Collab.)
KLEM	88	PR D37 41	D.E. Klem et al.	(DELCO Collab.)
ONG	88	PRL 60 2587	R.A. Ong et al.	(Mark II Collab.)
ALBAJAR	87C	PL B186 247	C. Albajar et al.	(UA1 Collab.)
ASH	87	PRL 58 640	W.W. Ash et al.	(MAC Collab.)
BARTEL	87	ZPHY C33 339	W. Bartel et al.	(JADE Collab.)
BROM	87	PL B195 301	J.M. Brom et al.	(HRS Collab.)
PAL	86	PR D33 2708	T. Pal et al.	(DELCO Collab.)
AIHARA	85	ZPHY C27 39	H. Aihara et al.	(TPC Collab.)
BARTEL	85J	PL 163B 277	W. Bartel et al.	(JADE Collab.)
SCHAAD	85	PL 160B 188	T. Schaad et al.	(Mark II Collab.)
ALTHOFF	84G	ZPHY C22 219	M. Althoff et al.	(TASSO Collab.)
ALTHOFF	84J	PL 146B 443	M. Althoff et al.	(TASSO Collab.)
KOOP	84	PRL 52 970	D.E. Koop et al.	(DELCO Collab.)
ADEVA	83	PRL 50 799	B. Adeva et al.	(Mark-J Collab.)
ADEVA	83B	PRL 51 443	B. Adeva et al.	(Mark-J Collab.)
BARTEL	83B	PL 132B 241	W. Bartel et al.	(JADE Collab.)
FERNANDEZ	83D	PRL 50 2054	E. Fernandez et al.	(MAC Collab.)
MATTEUZZI	83	PL 129B 141	C. Matteuzzi et al.	(Mark II Collab.)
NELSON	83	PRL 50 1542	M.E. Nelson et al.	(Mark II Collab.)

V_{cb} and V_{ub} CKM Matrix Elements

OMITTED FROM SUMMARY TABLE

See the related review(s):

Semileptonic B Hadron Decays, Determination of V_{cb} and V_{ub}

V_{cb} MEASUREMENTS

For the discussion of V_{cb} measurements, which is not repeated here, see the review on "Determination of $|V_{cb}|$ and $|V_{ub}|$."

The CKM matrix element $|V_{cb}|$ can be determined by studying the rate of the semileptonic decay $B \to D^{(*)} \ell \nu$ as a function of the recoil kinematics of $D^{(*)}$ mesons. Taking advantage of theoretical constraints on the normalization and a linear ω dependence of the form factors ($F(\omega)$, $G(\omega)$) provided by Heavy Quark Effective Theory (HQET), the $|V_{cb}| \times F(\omega)$ and ρ^2 can be simultaneously extracted from data, where ω is the scalar product of the two-meson four velocities, $F(1)$ is the form factor at zero recoil (ω=1) and ρ^2 is the slope. Using the theoretical input of $F(1)$, a value of $|V_{cb}|$ can be obtained.

$|V_{cb}| \times F(1)$ (from $B^0 \to D^{*-} \ell^+ \nu$)

VALUE (units 10^{-2})	DOCUMENT ID		TECN	COMMENT
3.522±0.037 OUR EVALUATION (Produced by HFLAV) with ρ^2=1.139 ± 0.020 and a correlation 0.268. The fitted χ^2 is 63.2 for 27 degrees of freedom.				
3.62 ±0.05 OUR AVERAGE Error includes scale factor of 1.6. See the ideogram below.				
3.66 ±0.05	[1] PRIM	24	BELL	$e^+e^- \to \Upsilon(4S)$
3.676±0.028±0.086	[2] ADACHI	23J	BELL2	$e^+e^- \to \Upsilon(4S)$
3.506±0.015±0.056	[3] WAHEED	21	BELL	$e^+e^- \to \Upsilon(4S)$
3.59 ±0.02 ±0.12	[4] AUBERT	09A	BABR	$e^+e^- \to \Upsilon(4S)$
3.92 ±0.18 ±0.23	[5] ABDALLAH	04D	DLPH	$e^+e^- \to Z^0$
4.31 ±0.13 ±0.18	[6] ADAM	03	CLE2	$e^+e^- \to \Upsilon(4S)$
3.55 ±0.14 $^{+0.23}_{-0.24}$	[7] ABREU	01H	DLPH	$e^+e^- \to Z$
3.71 ±0.10 ±0.20	[8] ABBIENDI	00Q	OPAL	$e^+e^- \to Z$
3.19 ±0.18 ±0.19	[9] BUSKULIC	97	ALEP	$e^+e^- \to Z$
• • • We do not use the following data for averages, fits, limits, etc. • • •				
3.64 ±0.09	[10] PRIM	23	BELL	$e^+e^- \to \Upsilon(4S)$, Repl. by PRIM 24
3.483±0.015±0.056	[3] WAHEED	19	BELL	Repl. by WAHEED 21
3.46 ±0.02 ±0.10	[11] DUNGEL	10	BELL	Rep. by WAHEED 19
3.59 ±0.06 ±0.14	[12] AUBERT	08AT	BABR	Repl. by AUBERT 09A
3.44 ±0.03 ±0.11	[13] AUBERT	08R	BABR	Repl. by AUBERT 09A
3.55 ±0.03 ±0.16	[14] AUBERT	05E	BABR	Repl. by AUBERT 08R

3.77 ±0.11 ±0.19	[15] ABDALLAH	04D	DLPH	$e^+e^- \to Z^0$
3.54 ±0.19 ±0.18	[16] ABE	02F	BELL	Repl. by DUNGEL 10
4.31 ±0.13 ±0.18	[17] BRIERE	02	CLE2	$e^+e^- \to \Upsilon(4S)$
3.28 ±0.19 ±0.22	ACKERSTAFF	97G	OPAL	Repl. by ABBIENDI 00Q
3.50 ±0.19 ±0.23	[18] ABREU	96P	DLPH	Repl. by ABREU 01H
3.51 ±0.19 ±0.20	[19] BARISH	95	CLE2	Repl. by ADAM 03
3.14 ±0.23 ±0.25	BUSKULIC	95N	ALEP	Repl. by BUSKULIC 97

[1] PRIM 24 value established from a complete set of angular coefficients for exclusive $B \to \overline{D}^* \ell^+ \nu_\ell$ decays with hadronic tag-side reconstruction. The $|V_{cb}| \times F(1)$ is derived from the extracted the BGL and CNL form factor parameters: $|V_{cb}|_{\rm BGL} = (40.7 \pm 0.7) \times 10^{-3}$ with the zero-recoil lattice QCD point $F(1) = 0.900 \pm 0.009$ and $|V_{cb}|_{\rm CNL} = (40.3 \pm 0.6) \times 10^{-3}$.

[2] ADACHI 23J result comes from differential shapes of exclusive $B \to D^* \ell^- \nu_\ell$ ($\ell = e$ or μ) decays. Using CNL form factor parametrization and the zero-recoil lattice QCD point $F(1) = 0.906 \pm 0.013$ ADACHI 23J finds $|V_{cb}|_{\rm CNL} = (40.57 \pm 0.31 \pm 0.95 \pm 0.58) \times 10^{-3}$ where the last uncertainty is due to the prediction of $F(1)$. Also reports a measurement of $|V_{cb}|_{\rm BGL} = (40.13 \pm 0.27 \pm 0.93 \pm 0.58) \times 10^{-3}$ using BGL form factors parametrization.

[3] WAHEED 21 uses fully reconstructed $D^{*-} \ell^+ \nu$ events ($\ell = e$ or μ) and $\eta_{EW} = 1.0066$.

[4] Obtained from a global fit to $B \to D^{(*)} \ell \nu_\ell$ events, with reconstructed $D^0 \ell$ and $D^+ \ell$ final states and $\rho^2 = 1.22 \pm 0.02 \pm 0.07$.

[5] Measurement using fully reconstructed D^* sample with a $\rho^2 = 1.32 \pm 0.15 \pm 0.33$.

[6] Average of the $B^0 \to D^*(2010)^- \ell^+ \nu$ and $B^+ \to \overline{D}^*(2007)) \ell^+ \nu$ modes with $\rho^2 = 1.61 \pm 0.09 \pm 0.21$ and $f_{+-} = 0.521 \pm 0.012$.

[7] ABREU 01H measured using about 5000 partial reconstructed D^* sample with a $\rho^2 = 1.34 \pm 0.14^{+0.24}_{-0.22}$.

[8] ABBIENDI 00Q: measured using both inclusively and exclusively reconstructed $D^{*\pm}$ samples with a $\rho^2 = 1.21 \pm 0.12 \pm 0.20$. The statistical and systematic correlations between $|V_{cb}| \times F(1)$ and ρ^2 are 0.90 and 0.54 respectively.

[9] BUSKULIC 97: measured using exclusively reconstructed $D^{*\pm}$ with a $a^2 = 0.31 \pm 0.17 \pm 0.08$. The statistical correlation is 0.92.

[10] Measured from differential shapes of exclusive $B \to D^* \ell^- \nu_\ell$ decays with hadronic tag-side reconstruction and extracting the CNL and BGL form factor parameters. PRIM 23 finds $|V_{cb}|_{\rm CNL} = (40.2 \pm 0.9) \times 10^{-3}$ with the zero-recoil lattice QCD point $F(1) = 0.906 \pm 0.013$. PRIM 23 provides also a measurement of $|V_{cb}|_{\rm BGL} = (40.7 \pm 1.0) \times 10^{-3}$.

[11] Uses fully reconstructed $D^{*-} \ell^+ \nu$ events ($\ell = e$ or μ).

[12] Measured using the dependence of $B^- \to D^{*0} e^- \overline{\nu}_e$ decay differential rate and the form factor description by CAPRINI 98 with $\rho^2 = 1.16 \pm 0.06 \pm 0.08$.

[13] Measured using fully reconstructed D^* sample and a simultaneous fit to the Caprini-Lellouch-Neubert form factor parameters: $\rho^2 = 1.191 \pm 0.048 \pm 0.028$, $R_1(1) = 1.429 \pm 0.061 \pm 0.044$, and $R_2(1) = 0.827 \pm 0.038 \pm 0.022$.

[14] Measurement using fully reconstructed D^* sample with a $\rho^2 = 1.29 \pm 0.03 \pm 0.27$.

[15] Combines with previous partial reconstructed D^* measurement with a $\rho^2 = 1.39 \pm 0.10 \pm 0.33$.

[16] Measured using exclusive $B^0 \to D^*(892)^- e^+ \nu$ decays with $\rho^2 = 1.35 \pm 0.17 \pm 0.19$ and a correlation of 0.91.

[17] BRIERE 02 result is based on the same analysis and data sample reported in ADAM 03.

[18] ABREU 96P: measured using both inclusively and exclusively reconstructed $D^{*\pm}$ samples.

[19] BARISH 95: measured using both exclusive reconstructed $B^0 \to D^{*-} \ell^+ \nu$ and $B^+ \to D^{*0} \ell^+ \nu$ samples. They report their experiment's uncertainties $\pm 0.0019 \pm 0.0018 \pm 0.0008$, where the first error is statistical, the second is systematic, and the third is the uncertainty in the lifetimes. We combine the last two in quadrature.

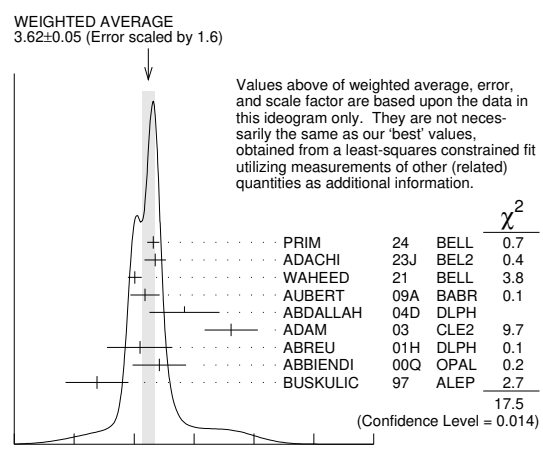

$|V_{cb}| \times F(1)$ (from $B^0 \to D^{*-} \ell^+ \nu$)

$|V_{cb}| \times G(1)$ (from $B \to D^- \ell^+ \nu$)

VALUE (units 10^{-2})	DOCUMENT ID		TECN	COMMENT
4.121±0.100 OUR EVALUATION (Produced by HFLAV) with $\rho^2 = 1.128 \pm 0.033$ and a correlation 0.747. The fitted χ^2 is 4.8 for 8 degrees of freedom.				
4.15 ±0.07 OUR AVERAGE				
4.06 ±0.14	[1] ADACHI	25Y	BELL	$e^+e^- \to \Upsilon(4S)$
4.109±0.116	[2] LEES	24	BABR	$e^+e^- \to \Upsilon(4S)$
4.229±0.137	[3] GLATTAUER	16	BELL	$e^+e^- \to \Upsilon(4S)$
4.23 ±0.19 ±0.14	[4] AUBERT	10	BABR	$e^+e^- \to \Upsilon(4S)$
4.31 ±0.08 ±0.23	[5] AUBERT	09A	BABR	$e^+e^- \to \Upsilon(4S)$
4.16 ±0.47 ±0.37	[6] BARTELT	99	CLE2	$e^+e^- \to \Upsilon(4S)$
2.78 ±0.68 ±0.65	[7] BUSKULIC	97	ALEP	$e^+e^- \to Z$
• • • We do not use the following data for averages, fits, limits, etc. • • •				
4.11 ±0.44 ±0.52	[8] ABE	02E	BELL	Repl. by GLATTAUER 16
3.37 ±0.44 $^{+0.72}_{-0.49}$	[9] ATHANAS	97	CLE2	Repl. by BARTELT 99

[1] The listed value, obtained by averaging B^0 and B^+ results, is based on CLN form factor model. ADACHI 25Y also lists $|V_{cb}| = (39.2 \pm 0.9) \times 10^{-3}$ based on BCL form factor model, which results in more precise than the value based on CLN.

[2] Obtained from a 2D fit to the combined $B \to \overline{D} \ell^+ \nu_\ell$ sample with a model-independent parametrization according to Boyd-Grinstein-Lebed (BGL), in which a hadronic decay of the second B meson is fully reconstructed.

[3] Obtained from a fit to the combined partially reconstructed $B \to \overline{D} \ell \nu_\ell$ sample while tagged by the other fully reconstructed B meson in the event. Also reports fitted $\rho^2 = 1.09 \pm 0.05$.

[4] Obtained from a fit to the combined $B \to \overline{D} \ell^+ \nu_\ell$ sample in which a hadronic decay of the second B meson is fully reconstructed and $\rho^2 = 1.20 \pm 0.09 \pm 0.04$.

[5] Obtained from a global fit to $B \to D^{(*)} \ell \nu_\ell$ events, with reconstructed $D^0 \ell$ and $D^+ \ell$ final states and $\rho^2 = 1.20 \pm 0.04 \pm 0.07$.

[6] BARTELT 99: measured using both exclusive reconstructed $B^0 \to D^- \ell^+ \nu$ and $B^+ \to D^0 \ell^+ \nu$ samples.

[7] BUSKULIC 97: measured using exclusively reconstructed $D^\pm$ with a $a^2 = -0.05 \pm 0.53 \pm 0.38$. The statistical correlation is 0.99.

[8] Using the missing energy and momentum to extract kinematic information about the undetected neutrino in the $B^0 \to D^- \ell^+ \nu$ decay.

[9] ATHANAS 97: measured using both exclusive reconstructed $B^0 \to D^- \ell^+ \nu$ and $B^+ \to D^0 \ell^+ \nu$ samples with a $\rho^2 = 0.59 \pm 0.22 \pm 0.12^{+0.59}_{-0}$. They report their experiment's uncertainties $\pm 0.0044 \pm 0.0048^{+0.0053}_{-0.0012}$, where the first error is statistical, the second is systematic, and the third is the uncertainty due to the form factor model variations. We combine the last two in quadrature.

$|V_{cb}|$ (from $D_s^{*-} \mu^+ \nu_\mu$)

VALUE (units 10^{-3})	DOCUMENT ID		TECN	COMMENT
41.4±0.6±0.9±1.2	[1] AAIJ	20E	LHCB	pp at 7, 8 TeV

[1] Measured from an inclusive sample of $D_s^- \mu^+$ candidates using CNL parameterization of the form factor. AAIJ 20E provides also measurement of $|V_{cb}| = (42.3 \pm 0.8 \pm 0.9 \pm 1.2) \times 10^{-3}$ using BGL parameterization of the form factor. The third uncertainty is due to the external inputs used in the measurement.

V_{ub} MEASUREMENTS

For the discussion of V_{ub} measurements, which is not repeated here, see the review on "Determination of $|V_{cb}|$ and $|V_{ub}|$."

The CKM matrix element $|V_{ub}|$ can be determined by studying the rate of the charmless semileptonic decay $b \to u \ell \nu$. The relevant branching ratio measurements based on exclusive and inclusive decays can be found in the B Listings, and are not repeated here.

V_{cb} and V_{ub} CKM Matrix Elements REFERENCES

ADACHI	25Y	PR D112 112009	I. Adachi et al.	(BELLE II Collab.)
LEES	24	PR D110 032018	J.P. Lees et al.	(BABAR Collab.)
PRIM	24	PRL 133 131801	M.T. Prim et al.	(BELLE Collab.)
ADACHI	23J	PR D108 092013	I. Adachi et al.	(BELLE II Collab.)
PRIM	23	PR D108 012002	M.T. Prim et al.	(BELLE Collab.)
WAHEED	21	PR D103 079901	E. Waheed et al.	(BELLE Collab.)
AAIJ	20E	PR D101 072004	R. Aaij et al.	(LHCb Collab.)
WAHEED	19	PR D100 052007	E. Waheed et al.	(BELLE Collab.)
GLATTAUER	16	PR D93 032006	R. Glattauer et al.	(BELLE Collab.)
AUBERT	10	PRL 104 011802	B. Aubert et al.	(BABAR Collab.)
DUNGEL	10	PR D82 112007	W. Dungel et al.	(BELLE Collab.)
AUBERT	09A	PR D79 012002	B. Aubert et al.	(BABAR Collab.)
AUBERT	08AT	PRL 100 231803	B. Aubert et al.	(BABAR Collab.)
AUBERT	08R	PR D77 032002	B. Aubert et al.	(BABAR Collab.)
AUBERT	05E	PR D71 051502	B. Aubert et al.	(BABAR Collab.)
ABDALLAH	04D	EPJ C33 213	J. Abdallah et al.	(DELPHI Collab.)
ADAM	03	PR D67 032001	N.E. Adam et al.	(CLEO Collab.)
ABE	02E	PL B526 258	K. Abe et al.	(BELLE Collab.)
ABE	02F	PL B526 247	K. Abe et al.	(BELLE Collab.)
BRIERE	02	PRL 89 081803	R. Briere et al.	(CLEO Collab.)
ABREU	01H	PL B510 55	P. Abreu et al.	(DELPHI Collab.)
ABBIENDI	00Q	PL B482 15	G. Abbiendi et al.	(OPAL Collab.)
BARTELT	99	PRL 82 3746	J. Bartelt et al.	(CLEO Collab.)
CAPRINI	98	NP B530 153	I. Caprini, L. Lellouch, M. Neubert	(BCIP, CERN)
ACKERSTAFF	97G	PL B395 128	K. Ackerstaff et al.	(OPAL Collab.)
ATHANAS	97	PRL 79 2208	M. Athanas et al.	(CLEO Collab.)
BUSKULIC	97	PL B395 373	D. Buskulic et al.	(ALEPH Collab.)
ABREU	96P	ZPHY C71 539	P. Abreu et al.	(DELPHI Collab.)
BARISH	95	PR D51 1014	B.C. Barish et al.	(CLEO Collab.)
BUSKULIC	95N	PL B359 236	D. Buskulic et al.	(ALEPH Collab.)

Int. J. Mod. Phys. A 2026.41. Downloaded from www.worldscientific.com
by LIFORNIA @ BERKELEY on 09/16/26. Re-use and distribution is strictly not permitted, except for Open Access articles.

Int. J. Mod. Phys. A 2026.41. Downloaded from www.worldscientific.com
by UNIVERSITY OF CALIFORNIA @ BERKELEY on 09/16/26. Re-use and distribution is strictly not permitted, except for Open Access articles.

B^*

$I(J^P) = \frac{1}{2}(1^-)$
I, J, P need confirmation.

Quantum numbers shown are quark-model predictions.

B^* MASS

From mass difference below and the average of our B masses $(m_{B^\pm} + m_{B^0})/2$.

VALUE (MeV)	DOCUMENT ID
5324.75 ± 0.20 OUR FIT	

$m_{B^*} - m_B$

VALUE (MeV)	EVTS	DOCUMENT ID		TECN	COMMENT
45.18 ± 0.20 OUR FIT					
45.42 ± 0.26 OUR AVERAGE		Includes data from the datablock that follows this one.			
46.2 ± 0.3 ± 0.8		[1] ACKERSTAFF	97M	OPAL	$e^+e^- \to Z$
45.3 ± 0.35 ± 0.87	4227	[1] BUSKULIC	96D	ALEP	E^{ee}_{cm} = 88–94 GeV
45.5 ± 0.3 ± 0.8		[1] ABREU	95R	DLPH	E^{ee}_{cm} = 88–94 GeV
46.3 ± 1.9	1378	[1] ACCIARRI	95B	L3	E^{ee}_{cm} = 88–94 GeV
46.4 ± 0.3 ± 0.8		[2] AKERIB	91	CLE2	$e^+e^- \to \gamma X$
45.6 ± 0.8		[2] WU	91	CSB2	$e^+e^- \to \gamma X, \gamma \ell X$
45.4 ± 1.0		[3] LEE-FRANZINI	90	CSB2	$e^+e^- \to \Upsilon(5S)$
• • • We do not use the following data for averages, fits, limits, etc. • • •					
52 ± 2 ± 4	1400	[4] HAN	85	CUSB	$e^+e^- \to \gamma e X$

[1] u, d, s flavor averaged.
[2] These papers report E_γ in the B^* center of mass. The $m_{B^*} - m_B$ is 0.2 MeV higher. E_{cm} = 10.61–10.7 GeV. Admixture of B^0 and B^+ mesons, but not B_s.
[3] LEE-FRANZINI 90 value is for an admixture of B^0 and B^+. They measure 46.7 ± 0.4 ± 0.2 MeV for an admixture of B^0, B^+, and B_s, and use the shape of the photon line to separate the above value.
[4] HAN 85 is for E_{cm} = 10.6–11.2 GeV, giving an admixture of B^0, B^+, and B_s.

$m_{B^{*+}} - m_{B^+}$

VALUE (MeV)	DOCUMENT ID		TECN	COMMENT
The data in this block is included in the average printed for a previous datablock.				
45.34 ± 0.20 OUR FIT				
45.01 ± 0.30 ± 0.23	[5] AAIJ	13O	LHCB	pp at 7 TeV

[5] Obtained the mass difference between $B^{*+}K^-$ and B^+K^- from $B^*_{s2}(5840)^0$ decay.

$|(m_{B^{*+}} - m_{B^+}) - (m_{B^{*0}} - m_{B^0})|$

VALUE (MeV)	CL%	DOCUMENT ID		TECN	COMMENT
<6	95	ABREU	95R	DLPH	E^{ee}_{cm} = 88–94 GeV

$m_{B^{*0}} - m_{B^{*+}}$

VALUE (MeV)	DOCUMENT ID		TECN	COMMENT
0.91 ± 0.24 ± 0.09	[6] SIRUNYAN	18DF	CMS	pp at 8 TeV

[6] Uses exclusively reconstructed final states containing a $J/\psi \to \mu^+\mu^-$ decay.

B^* DECAY MODES

	Mode	Fraction (Γ_i/Γ)
Γ_1	$B\gamma$	seen

B^* REFERENCES

SIRUNYAN	18DF	EPJ C78 939	A.M. Sirunyan et al.	(CMS Collab.)
AAIJ	13O	PRL 110 151803	R. Aaij et al.	(LHCb Collab.)
ACKERSTAFF	97M	ZPHY C74 413	K. Ackerstaff et al.	(OPAL Collab.)
BUSKULIC	96D	ZPHY C69 393	D. Buskulic et al.	(ALEPH Collab.)
ABREU	95R	ZPHY C68 353	P. Abreu et al.	(DELPHI Collab.)
ACCIARRI	95B	PL B345 589	M. Acciarri et al.	(L3 Collab.)
AKERIB	91	PRL 67 1692	D.S. Akerib et al.	(CLEO Collab.)
WU	91	PL B273 177	Q.W. Wu et al.	(CUSB II Collab.)
LEE-FRANZINI	90	PRL 65 2947	J. Lee-Franzini et al.	(CUSB II Collab.)
HAN	85	PRL 55 36	K. Han et al.	(COLU, LSU, MPIM, STON)

$B_1(5721)$

$I(J^P) = \frac{1}{2}(1^+)$
I, J, P need confirmation.

Quantum numbers shown are quark-model predictions.

$B_1(5721)$ MASS

$B_1(5721)^+$ mass

OUR FIT uses $m_{B^{*0}}$ and $m_{B_1^+} - m_{B^{*0}}$ to determine $m_{B_1(5721)^+}$.

VALUE (MeV)	DOCUMENT ID
$5726.0^{+2.5}_{-2.7}$ OUR FIT	

$m_{B_1^+} - m_{B^{*0}}$

VALUE (MeV)	EVTS	DOCUMENT ID		TECN	COMMENT
$401.2^{+2.4}_{-2.7}$ OUR FIT					
$401.2^{+2.4}_{-2.7}$ OUR AVERAGE					
400.5 ± 1.8 ± 3.1	8k	[1] AAIJ	15AB	LHCB	pp at 7, 8 TeV
402 ± 3 $^{+1}_{-3}$		[2] AALTONEN	14I	CDF	$p\overline{p}$ at 1.96 TeV

[1] AAIJ 15AB reports $[m_{B_1^+} - m_{B^0}] - (m_{B^{*0}} - m_{B^0}) - m_{\pi^+}$ = 260.9 ± 1.8 ± 3.1 MeV which we adjust by the π^+ mass and assume $(m_{B^{*0}} - m_{B^0}) = (m_{B^{*+}} - m_{B^+})$ = 45.01 ± 0.30 ± 0.23 MeV. The masses inside the square brackets were measured for each candidate event.
[2] AALTONEN 14I reports $m_{B_1(5721)^+} - m_{B^{*0}} - m_{\pi^+}$ = 262 ± 3 $^{+1}_{-3}$ MeV which we adjusted by the π^+ mass.

$B_1(5721)^0$ mass

OUR FIT uses mass differences measurements listed below to determine the mass $m_{B_1(5721)^0}$.

VALUE (MeV)	DOCUMENT ID
5726.1 ± 1.2 OUR FIT Error includes scale factor of 1.2.	

$m_{B_1^0} - m_{B^+}$

VALUE (MeV)	DOCUMENT ID		TECN	COMMENT
446.7 ± 1.2 OUR FIT Error includes scale factor of 1.2.				
441.5 ± 2.4 ± 1.3	[1] ABAZOV	07T	D0	$p\overline{p}$ at 1.96 TeV
• • • We do not use the following data for averages, fits, limits, etc. • • •				
$446.2^{+1.9}_{-2.1}{}^{+1.0}_{-1.2}$	[1] AALTONEN	09D	CDF	Repl. by AALTONEN 14I

[1] Observed in $B_1^0 \to B^{*+}\pi^-$.

$m_{B_1^0} - m_{B^{*+}}$

VALUE (MeV)	EVTS	DOCUMENT ID		TECN	COMMENT
401.4 ± 1.2 OUR FIT Error includes scale factor of 1.2.					
402.8 ± 1.1 OUR AVERAGE					
403.4 ± 0.7 ± 1.5	35k	[1] AAIJ	15AB	LHCB	pp at 7, 8 TeV
$402.3 \pm 0.9^{+1.1}_{-1.2}$		[2] AALTONEN	14I	CDF	$p\overline{p}$ at 1.96 TeV

[1] AAIJ 15AB reports $[m_{B_1^0} - m_{B^+}] - (m_{B^{*+}} - m_{B^+}) - m_{\pi^-}$ = 263.9 ± 0.7 ± 1.4 MeV which we adjust by the π^- mass and $(m_{B^{*+}} - m_{B^+})$ = 45.01 ± 0.30 ± 0.23 MeV. The masses inside the square brackets were measured for each candidate event.
[2] AALTONEN 14I reports $m_{B_1(5721)^0} - m_{B^{*+}} - m_{\pi^-}$ = 262.7 ± 0.9 $^{+1.1}_{-1.2}$ MeV which we adjusted by the π^- mass.

$B_1(5721)$ WIDTH

$B_1(5721)^+$ width

VALUE (MeV)	EVTS	DOCUMENT ID		TECN	COMMENT
31 ± 6 OUR AVERAGE Error includes scale factor of 1.1.					
29.1 ± 3.6 ± 4.3	8k	AAIJ	15AB	LHCB	pp at 7, 8 TeV
49 $^{+12}_{-10}$ $^{+2}_{-13}$		AALTONEN	14I	CDF	$p\overline{p}$ at 1.96 TeV

$B_1(5721)^0$ width

VALUE (MeV)	EVTS	DOCUMENT ID		TECN	COMMENT
27.5 ± 3.4 OUR AVERAGE Error includes scale factor of 1.1.					
30.1 ± 1.5 ± 3.5	35k	AAIJ	15AB	LHCB	pp at 7, 8 TeV
23 ± 3 ± 4		AALTONEN	14I	CDF	$p\overline{p}$ at 1.96 TeV

$B_1(5721)$ DECAY MODES

	Mode	Fraction (Γ_i/Γ)
Γ_1	$B^*\pi$	seen

$B_1(5721)$ BRANCHING RATIOS

$\Gamma(B^*\pi)/\Gamma_{total}$ — Γ_1/Γ

VALUE	DOCUMENT ID		TECN	CHG	COMMENT
seen	AAIJ	15AB	LHCB	±0	pp at 7, 8 TeV
seen	AALTONEN	14I	CDF	±	$p\overline{p}$ at 1.96 TeV
seen	AALTONEN	09D	CDF	0	$p\overline{p}$ at 1.96 TeV
seen	[1] ABAZOV	07T	D0	0	$p\overline{p}$ at 1.96 TeV

[1] Observed in $B_1^0 \to B^{*+}\pi^-$ with $B^{*+} \to B^+\gamma$ and $B^+ \to J/\psi\pi^+$.

$B_1(5721)$ REFERENCES

AAIJ	15AB	JHEP 1504 024	R. Aaij et al.	(LHCb Collab.)
AALTONEN	14I	PR D90 012013	T. Aaltonen et al.	(CDF Collab.)
AALTONEN	09D	PRL 102 102003	T. Aaltonen et al.	(CDF Collab.)
ABAZOV	07T	PRL 99 172001	V.M. Abazov et al.	(D0 Collab.)

Int. J. Mod. Phys. A 2026.41. Downloaded from www.worldscientific.com by CALIFORNIA @ BERKELEY on 09/16/26. Re-use and distribution is strictly not permitted, except for Open Access articles.

$B_J^*(5732)$

$I(J^P) = ?(?^?)$

OMITTED FROM SUMMARY TABLE

Signal can be interpreted as stemming from several narrow and broad resonances.

$B_J^*(5732)$ MASS

VALUE (MeV)	EVTS	DOCUMENT ID		TECN	COMMENT
5698± 8 OUR AVERAGE		Error includes scale factor of 1.2.			
5710 ± 20		[1] AFFOLDER	01F	CDF	$p\overline{p}$ at 1.8 TeV
5695^{+17}_{-19}		[2] BARATE	98L	ALEP	$e^+e^- \to Z$
$5704 \pm 4 \pm 10$	1944	[3] BUSKULIC	96D	ALEP	E^{ee}_{cm}= 88–94 GeV
$5732 \pm 5 \pm 20$	2157	ABREU	95B	DLPH	E^{ee}_{cm}= 88–94 GeV
5681 ± 11	1738	AKERS	95E	OPAL	E^{ee}_{cm}= 88–94 GeV
• • • We do not use the following data for averages, fits, limits, etc. • • •					
5713 ± 2		[4] ACCIARRI	99N	L3	$e^+e^- \to Z$

[1] AFFOLDER 01F uses the reconstructed B meson through semileptonic decay channels. The fraction of light B mesons that are produced at L=1 B^{**} states is measured to be $0.28 \pm 0.06 \pm 0.03$.

[2] BARATE 98L uses fully reconstructed B mesons to search for B^{**} production in the $B\pi^{\pm}$ system. In the framework of heavy quark symmetry (HQS), they also measured the mass of B_2^* to be $5739^{+8}_{-11}{}^{+6}_{-4}$ MeV/c^2 and the relative production rate of $B(b \to B_2^* \to B^{(*)}\pi)/B(b \to B_{u,d}) = (31 \pm 9^{+6}_{-5})\%$.

[3] Using $m_{B\pi} - m_B = 424 \pm 4 \pm 10$ MeV.

[4] ACCIARRI 99N uses inclusive reconstructed B mesons to search for B^{**} production in the $B^{(*)}\pi^{\pm}$ system. In the framework of HQET, they measured the mass of B_1^* and B_2^* to be $5670 \pm 10 \pm 13$ MeV and $5768 \pm 5 \pm 6$ with the $B(b \to B^{**}) = (32 \pm 3 \pm 6) \times 10^{-2}$. They also reported the evidence for the existence of an excited B-meson state or mixture of states in the region 5.9–6.0 GeV.

$B_J^*(5732)$ WIDTH

VALUE (MeV)	EVTS	DOCUMENT ID		TECN	COMMENT
128±18 OUR AVERAGE					
145 ± 28	2157	ABREU	95B	DLPH	E^{ee}_{cm}= 88–94 GeV
116 ± 24	1738	AKERS	95E	OPAL	E^{ee}_{cm}= 88–94 GeV

$B_J^*(5732)$ DECAY MODES

	Mode	Fraction (Γ_i/Γ)
Γ_1	$B^*\pi + B\pi$	seen
Γ_2	$B^*\pi(X)$	[a] (85 ± 29) %

[a] X refers to decay modes with or without additional accompanying decay particles.

$B_J^*(5732)$ BRANCHING RATIOS

X refers to decay modes with or without additional accompanying decay particles.

$\Gamma(B^*\pi(X))/\Gamma_{total}$ — Γ_2/Γ

VALUE	DOCUMENT ID		TECN	COMMENT
$0.85^{+0.26}_{-0.27} \pm 0.12$	ABBIENDI	02E	OPAL	$e^+e^- \to Z$

$B_J^*(5732)$ REFERENCES

ABBIENDI	02E	EPJ C23 437	G. Abbiendi *et al.*	(OPAL Collab.)
AFFOLDER	01F	PR D64 072002	T. Affolder *et al.*	(CDF Collab.)
ACCIARRI	99N	PL B465 323	M. Acciarri *et al.*	(L3 Collab.)
BARATE	98L	PL B425 215	R. Barate *et al.*	(ALEPH Collab.)
BUSKULIC	96D	ZPHY C69 393	D. Buskulic *et al.*	(ALEPH Collab.)
ABREU	95B	PL B345 598	P. Abreu *et al.*	(DELPHI Collab.)
AKERS	95E	ZPHY C66 19	R. Akers *et al.*	(OPAL Collab.)

$B_2^*(5747)$

$I(J^P) = \frac{1}{2}(2^+)$

I, J, P need confirmation.

Quantum numbers shown are quark-model predictions.

$B_2^*(5747)$ MASS

$B_2^*(5747)^+$ mass

OUR FIT uses m_{B^0} and $m_{B_2^{*+}} - m_{B^0}$ to determine $m_{B_2^*(5747)^+}$.

VALUE (MeV)	DOCUMENT ID
5737.3±0.7 OUR FIT	

$m_{B_2^{*+}} - m_{B^0}$

VALUE (MeV)	EVTS	DOCUMENT ID		TECN	COMMENT
457.5 ±0.7 OUR FIT					
457.5 ±0.7 OUR AVERAGE					
$457.62 \pm 0.72 \pm 0.40$	4k	[1] AAIJ	15AB	LHCB	pp at 7, 8 TeV
$457.3 \pm 1.3\ ^{+0.3}_{-0.9}$		[2] AALTONEN	14I	CDF	$p\overline{p}$ at 1.96 TeV

[1] AAIJ 15AB reports $[m_{B_2^{*+}} - m_{B^0}] - m_{\pi^+} = 318.1 \pm 0.7 \pm 0.4$ MeV which we adjust by the π^+ mass. The masses inside the square brackets were measured for each candidate event.

[2] AALTONEN 14I reports $m_{B_2^*(5747)^+} - m_{B^0} - m_{\pi^+} = 317.7 \pm 1.2^{+0.3}_{-0.9}$ MeV which we adjusted by the π^+ mass.

$B_2^*(5747)^0$ mass

OUR FIT uses m_{B^+}, $m_{B_1^0} - m_{B^+}$, and mass differences below to determine $m_{B_2^*(5747)^0}$. The -0.659 correlation between statistical uncertainties of $m_{B_1^0} - m_{B^+}$ and $m_{B_2^{*0}} - m_{B_1^0}$ measurements reported by ABAZOV 07T is taken into account.

VALUE (MeV)	DOCUMENT ID
5739.6±0.7 OUR FIT Error includes scale factor of 1.4.	

$m_{B_2^{*0}} - m_{B_1^0}$

VALUE (MeV)	DOCUMENT ID		TECN	COMMENT
13.5±1.4 OUR FIT Error includes scale factor of 1.3.				
26.2±3.1±0.9	[1] ABAZOV	07T	D0	$p\overline{p}$ at 1.96 TeV
• • • We do not use the following data for averages, fits, limits, etc. • • •				
$14.9^{+2.2}_{-2.5}{}^{+1.2}_{-1.4}$	[1] AALTONEN	09D	CDF	Repl. by AALTONEN 14I

[1] Observed in $B_2^{*0} \to B^{*+}\pi^-$ and $B_2^{*0} \to B^+\pi^-$.

$m_{B_2^{*0}} - m_{B^+}$

VALUE (MeV)	EVTS	DOCUMENT ID		TECN	COMMENT
460.2 ±0.6 OUR FIT Error includes scale factor of 1.4.					
459.9 ±0.8 OUR AVERAGE Error includes scale factor of 1.8.					
$460.18 \pm 0.37 \pm 0.33$	17k	[1] AAIJ	15AB	LHCB	pp at 7, 8 TeV
$457.5 \pm 1.2\ ^{+0.8}_{-0.9}$		[2] AALTONEN	14I	CDF	$p\overline{p}$ at 1.96 TeV

[1] AAIJ 15AB reports $[m_{B_2^{*0}} - m_{B^+}] - m_{\pi^-} = 320.6 \pm 0.4 \pm 0.3$ MeV which we adjust by the π^- mass. The masses inside the square brackets were measured for each candidate event.

[2] AALTONEN 14I reports $m_{B_2^*(5747)^0} - m_{B^+} - m_{\pi^-} = 317.9 \pm 1.2^{+0.8}_{-0.9}$ MeV which we adjusted by the π^- mass.

$B_2^*(5747)$ WIDTH

$B_2^*(5747)^+$ width

VALUE (MeV)	EVTS	DOCUMENT ID		TECN	COMMENT
20 ±5 OUR AVERAGE Error includes scale factor of 2.2.					
$23.6 \pm 2.0 \pm 2.1$	4k	AAIJ	15AB	LHCB	pp at 7, 8 TeV
$11\ ^{+4}_{-3}\ ^{+3}_{-4}$		AALTONEN	14I	CDF	$p\overline{p}$ at 1.96 TeV

$B_2^*(5747)^0$ width

VALUE (MeV)	EVTS	DOCUMENT ID		TECN	COMMENT
24.2±1.7 OUR AVERAGE					
$24.5 \pm 1.0 \pm 1.5$	17k	AAIJ	15AB	LHCB	pp at 7, 8 TeV
$22\ ^{+3}_{-2}\ ^{+4}_{-5}$		AALTONEN	14I	CDF	$p\overline{p}$ at 1.96 TeV
• • • We do not use the following data for averages, fits, limits, etc. • • •					
$22.7^{+3.8}_{-3.2}{}^{+3.2}_{-10.2}$		AALTONEN	09D	CDF	Repl. by AALTONEN 14I

$B_2^*(5747)$ DECAY MODES

	Mode	Fraction (Γ_i/Γ)
Γ_1	$B\pi$	seen
Γ_2	$B^*\pi$	seen

$B_2^*(5747)$ BRANCHING RATIOS

$\Gamma(B\pi)/\Gamma_{total}$ — Γ_1/Γ

VALUE	EVTS	DOCUMENT ID		TECN	CHG	COMMENT
seen	4k,17k	AAIJ	15AB	LHCB	±0	pp at 7, 8 TeV
seen		AALTONEN	14I	CDF	±	$p\overline{p}$ at 1.96 TeV
seen		AALTONEN	09D	CDF	0	$p\overline{p}$ at 1.96 TeV
seen		ABAZOV	07T	D0	0	$p\overline{p}$ at 1.96 TeV

$\Gamma(B^*\pi)/\Gamma_{total}$ — Γ_2/Γ

VALUE	EVTS	DOCUMENT ID		TECN	CHG	COMMENT
seen	4k,17k	AAIJ	15AB	LHCB	±0	pp at 7, 8 TeV
seen		AALTONEN	09D	CDF	0	$p\overline{p}$ at 1.96 TeV
seen		ABAZOV	07T	D0	0	$p\overline{p}$ at 1.96 TeV

Int. J. Mod. Phys. A 2026.41. Downloaded from www.worldscientific.com
by UNIVERSITY OF CALIFORNIA @ BERKELEY on 09/16/26. Re-use and distribution is strictly not permitted, except for Open Access articles.

$\Gamma(B^*\pi)/\Gamma(B\pi)$ — Γ_2/Γ_1

VALUE	EVTS	DOCUMENT ID		TECN	CHG	COMMENT
0.84±0.27 OUR AVERAGE						
0.71±0.14±0.30	17k	AAIJ	15AB	LHCB	0	pp at 7, 8 TeV
1.0 ±0.5 ±0.8	4k	AAIJ	15AB	LHCB	±	pp at 7, 8 TeV
1.10±0.42±0.31		[1] ABAZOV	07T	D0	0	$p\overline{p}$ at 1.96 TeV

[1] Converted from measured ratio of R = B($B_2^{*0} \to B^{*+}\pi^-$) / B($B_2^{*0} \to B^{(*)+}\pi^-$) = 0.475 ± 0.095 ± 0.069.

$B_2^*(5747)$ REFERENCES

AAIJ	15AB	JHEP 1504 024	R. Aaij *et al.*	(LHCb Collab.)
AALTONEN	14I	PR D90 012013	T. Aaltonen *et al.*	(CDF Collab.)
AALTONEN	09D	PRL 102 102003	T. Aaltonen *et al.*	(CDF Collab.)
ABAZOV	07T	PRL 99 172001	V.M. Abazov *et al.*	(D0 Collab.)

$B_J(5840)$

$I(J^P) = \frac{1}{2}(?^?)$
I, J, P need confirmation.

OMITTED FROM SUMMARY TABLE

Quantum numbers shown are quark-model predictions.

$B_J(5840)$ MASS

$B_J(5840)^+$ MASS

OUR FIT uses m_{B^0} and $m_{B_J(5840)^+} - m_{B^0}$ to determine $m_{B_J(5840)^+}$.

VALUE (MeV)	DOCUMENT ID
5851±19 OUR FIT	

$m_{B_J(5840)^+} - m_{B^0}$

VALUE (MeV)	EVTS	DOCUMENT ID		TECN	COMMENT
571±19 OUR FIT					
571±13±14	7k	[1] AAIJ	15AB	LHCB	pp at 7, 8 TeV
• • • We do not use the following data for averages, fits, limits, etc. • • •					
595±26±14	7k	[2] AAIJ	15AB	LHCB	pp at 7, 8 TeV

[1] AAIJ 15AB reports $[m_{B_J^+} - m_{B^0}] - m_{\pi^+} = 431 \pm 13 \pm 14$ MeV which we adjust by the π^+ mass. The masses inside the square brackets were measured for each candidate event. The result assumes $P = (-1)^J$ and uses two relativistic Breit-Wigner functions in the fit for mass difference.

[2] AAIJ 15AB reports $[m_{B_J^+} - m_{B^0}] - m_{\pi^+} = 455 \pm 26 \pm 14$ MeV which we adjust by the π^+ mass. The masses inside the square brackets were measured for each candidate event. The result assumes $P = (-1)^J$ and uses three relativistic Breit-Wigner functions in the fit for mass difference.

$m_{B_J(5840)^+} - m_{B^{*0}}$

VALUE (MeV)	EVTS	DOCUMENT ID		TECN	COMMENT
• • • We do not use the following data for averages, fits, limits, etc. • • •					
565±15±14	7k	[1] AAIJ	15AB	LHCB	pp at 7, 8 TeV

[1] AAIJ 15AB reports $[m_{B_J^+} - m_{B^0}] - (m_{B^{*+}} - m_{B^+}) - m_{\pi^+} = 425 \pm 15 \pm 14$ MeV which we adjust by the π^+ mass. The masses inside the square brackets were measured for each candidate event. The result assumes $P = -(-1)^J$, $(m_{B^{*0}} - m_{B^0}) = (m_{B^{*+}} - m_{B^+}) = 45.01 \pm 0.30 \pm 0.23$ MeV, and uses three relativistic Breit-Wigner functions in the fit for mass difference.

$B_J(5840)^0$ MASS

OUR FIT uses m_{B^+} and $m_{B_J(5840)^0} - m_{B^+}$ to determine $m_{B_J(5840)^0}$.

VALUE (MeV)	DOCUMENT ID
5863±9 OUR FIT	

$m_{B_J(5840)^0} - m_{B^+}$

VALUE (MeV)	EVTS	DOCUMENT ID		TECN	COMMENT
584± 9 OUR FIT					
584± 5±7	12k	[1] AAIJ	15AB	LHCB	pp at 7, 8 TeV
• • • We do not use the following data for averages, fits, limits, etc. • • •					
610±22±7	12k	[2] AAIJ	15AB	LHCB	pp at 7, 8 TeV

[1] AAIJ 15AB reports $[m_{B_J^0} - m_{B^+}] - m_{\pi^-} = 444 \pm 5 \pm 7$ MeV which we adjust by the π^- mass. The masses inside the square brackets were measured for each candidate event. The result assumes $P = (-1)^J$ and uses two relativistic Breit-Wigner functions in the fit for mass difference.

[2] AAIJ 15AB reports $[m_{B_J^0} - m_{B^+}] - m_{\pi^-} = 471 \pm 22 \pm 7$ MeV which we adjust by the π^- mass. The masses inside the square brackets were measured for each candidate event. The result assumes $P = (-1)^J$ and uses three relativistic Breit-Wigner functions in the fit for mass difference.

$m_{B_J(5840)^0} - m_{B^{*+}}$

VALUE (MeV)	EVTS	DOCUMENT ID		TECN	COMMENT
• • • We do not use the following data for averages, fits, limits, etc. • • •					
584±5±7	12k	[1] AAIJ	15AB	LHCB	pp at 7, 8 TeV

[1] AAIJ 15AB reports $[m_{B_J^0} - m_{B^+}] - (m_{B^{*+}} - m_{B^+}) - m_{\pi^-} = 444 \pm 5 \pm 7$ MeV which we adjust by the π^- mass. The masses inside the square brackets were measured for each candidate event. The result assumes $P = -(-1)^J$, $(m_{B^{*+}} - m_{B^+}) = 45.01 \pm 0.30 \pm 0.23$ MeV, and uses three relativistic Breit-Wigner functions in the fit for mass difference.

$B_J(5840)$ WIDTH

$B_J(5840)^+$ WIDTH

VALUE (MeV)	EVTS	DOCUMENT ID		TECN	COMMENT
224±24±80	7k	[1] AAIJ	15AB	LHCB	pp at 7, 8 TeV
• • • We do not use the following data for averages, fits, limits, etc. • • •					
215±27±80	7k	[2] AAIJ	15AB	LHCB	pp at 7, 8 TeV
229±27±80	7k	[3] AAIJ	15AB	LHCB	pp at 7, 8 TeV

[1] Assuming $P = (-1)^J$ and using two relativistic Breit-Wigner functions in the fit for mass difference.
[2] Assuming $P = (-1)^J$ and using three relativistic Breit-Wigner functions in the fit for mass difference.
[3] Assuming $P = -(-1)^J$ and using three relativistic Breit-Wigner functions in the fit for mass difference.

$B_J(5840)^0$ WIDTH

VALUE (MeV)	EVTS	DOCUMENT ID		TECN	COMMENT
127±17±34	12k	[1] AAIJ	15AB	LHCB	pp at 7, 8 TeV
• • • We do not use the following data for averages, fits, limits, etc. • • •					
107±20±34	12k	[2] AAIJ	15AB	LHCB	pp at 7, 8 TeV
119±17±34	12k	[3] AAIJ	15AB	LHCB	pp at 7, 8 TeV

[1] Assuming $P = (-1)^J$ and using two relativistic Breit-Wigner functions in the fit for mass difference.
[2] Assuming $P = (-1)^J$ and using three relativistic Breit-Wigner functions in the fit for mass difference.
[3] Assuming $P = -(-1)^J$ and using three relativistic Breit-Wigner functions in the fit for mass difference.

$B_J(5840)$ DECAY MODES

	Mode	Fraction (Γ_i/Γ)
Γ_1	$B^*\pi$	seen
Γ_2	$B\pi$	possibly seen

$B_J(5840)$ BRANCHING RATIOS

$\Gamma(B^*\pi)/\Gamma_{total}$ — Γ_1/Γ

VALUE	EVTS	DOCUMENT ID		TECN	CHG	COMMENT
seen	7k	AAIJ	15AB	LHCB	±	pp at 7, 8 TeV
seen	12k	AAIJ	15AB	LHCB	0	pp at 7, 8 TeV

$\Gamma(B\pi)/\Gamma_{total}$ — Γ_2/Γ

VALUE	EVTS	DOCUMENT ID		TECN	CHG	COMMENT
possibly seen	7k	[1] AAIJ	15AB	LHCB	±	pp at 7, 8 TeV
possibly seen		[1] AAIJ	15AB	LHCB	0	pp at 7, 8 TeV

[1] A $B\pi$ decay is forbidden from a $P = -(-1)^J$ parent, whereas $B^*\pi$ is allowed.

$B_J(5840)$ REFERENCES

AAIJ	15AB	JHEP 1504 024	R. Aaij *et al.*	(LHCb Collab.)

$B_J(5970)$

$I(J^P) = \frac{1}{2}(?^?)$
I, J, P need confirmation.

Quantum numbers shown are quark-model predictions.

$B_J(5970)$ MASS

$B_J(5970)^+$ MASS

OUR FIT uses m_{B^0} and $m_{B_J(5970)^+} - m_{B^0}$ to determine $m_{B_J(5970)^+}$.

VALUE (MeV)	DOCUMENT ID
5965±5 OUR FIT	

$m_{B_J(5970)^+} - m_{B^0}$

VALUE (MeV)	EVTS	DOCUMENT ID		TECN	COMMENT
685 ±5 OUR FIT					
685 ±5 OUR AVERAGE					
685.3±4.1± 2.5	2k	[1] AAIJ	15AB	LHCB	pp at 7, 8 TeV
681 ±5 ±12	1.4k	[2] AALTONEN	14I	CDF	$p\overline{p}$ at 1.96 TeV
• • • We do not use the following data for averages, fits, limits, etc. • • •					
686.8±4.5± 2.5	2k	[3] AAIJ	15AB	LHCB	pp at 7, 8 TeV

[1] AAIJ 15AB reports $[m_{B_J^+} - m_{B^0}] - m_{\pi^+} = 545.8 \pm 4.1 \pm 2.5$ MeV which we adjust by the π^+ mass. The masses inside the square brackets were measured for each candidate event. The result assumes $P = (-1)^J$ and uses two relativistic Breit-Wigner functions in the fit for mass difference.

[2] AALTONEN 14I reports $m_{B_J(5970)^+} - m_{B^0} - m_{\pi^+} = 541 \pm 5 \pm 12$ MeV which we adjusted by the π^+ mass.
[3] AAIJ 15AB reports $[m_{B_J^+} - m_{B^0}] - m_{\pi^+} = 547 \pm 5 \pm 3$ MeV which we adjust by the π^+ mass. The masses inside the square brackets were measured for each candidate event. The result assumes $P = (-1)^J$ and uses three relativistic Breit-Wigner functions in the fit for mass difference.

$m_{B_J(5970)^+} - m_{B^{*0}}$

VALUE (MeV)	EVTS	DOCUMENT ID		TECN	COMMENT
• • • We do not use the following data for averages, fits, limits, etc. • • •					
$686.0 \pm 4.0 \pm 2.5$	2k	[1] AAIJ	15AB	LHCB	pp at 7, 8 TeV

[1] AAIJ 15AB reports $[m_{B_J^+} - m_{B^0}] - (m_{B^{*+}} - m_{B^+}) - m_{\pi^+} = 547 \pm 4 \pm 3$ MeV which we adjust by the π^+ mass. The masses inside the square brackets were measured for each candidate event. The result assumes $P = -(-1)^J$, $(m_{B^{*0}} - m_{B^0}) = (m_{B^{*+}} - m_{B^+}) = 45.01 \pm 0.30 \pm 0.23$ MeV, and uses three relativistic Breit-Wigner functions in the fit for mass difference.

$B_J(5970)^0$ MASS

OUR FIT uses m_{B^+} and $m_{B_J(5970)^0} - m_{B^+}$ to determine $m_{B_J(5970)^0}$.

VALUE (MeV)	DOCUMENT ID
5971 ± 5 OUR FIT	

$m_{B_J(5970)^0} - m_{B^+}$

VALUE (MeV)	EVTS	DOCUMENT ID		TECN	COMMENT
691 ± 5 OUR FIT					
691 ± 5 OUR AVERAGE					
$689.9 \pm 2.9 \pm 5.1$	10k	[1] AAIJ	15AB	LHCB	pp at 7, 8 TeV
$698 \pm 5 \pm 12$	2.6k	[2] AALTONEN	14I	CDF	$p\overline{p}$ at 1.96 TeV
• • • We do not use the following data for averages, fits, limits, etc. • • •					
$714.3 \pm 6.4 \pm 5.1$	10k	[3] AAIJ	15AB	LHCB	pp at 7, 8 TeV

[1] AAIJ 15AB reports $[m_{B_J^0} - m_{B^+}] - m_{\pi^-} = 550.4 \pm 2.9 \pm 5.1$ MeV which we adjust by the π^- mass. The masses inside the square brackets were measured for each candidate event. The result assumes $P = (-1)^J$ and uses two relativistic Breit-Wigner functions in the fit for mass difference.
[2] AALTONEN 14I reports $m_{B_J(5970)^0} - m_{B^+} - m_{\pi^-} = 558 \pm 5 \pm 12$ MeV which we adjusted by the π^- mass.
[3] AAIJ 15AB reports $[m_{B_J^0} - m_{B^+}] - m_{\pi^-} = 575 \pm 6 \pm 5$ MeV which we adjust by the π^- mass. The masses inside the square brackets were measured for each candidate event. The result assumes $P = (-1)^J$ and uses three relativistic Breit-Wigner functions in the fit for mass difference.

$m_{B_J(5970)^0} - m_{B^{*+}}$

VALUE (MeV)	EVTS	DOCUMENT ID		TECN	COMMENT
• • • We do not use the following data for averages, fits, limits, etc. • • •					
$691.6 \pm 3.7 \pm 5.1$	10k	[1] AAIJ	15AB	LHCB	pp at 7, 8 TeV

[1] AAIJ 15AB reports $[m_{B_J^0} - m_{B^+}] - (m_{B^{*+}} - m_{B^+}) - m_{\pi^-} = 552 \pm 4 \pm 5$ MeV which we adjust by the π^- mass. The masses inside the square brackets were measured for each candidate event. The result assumes $P = -(-1)^J$, $(m_{B^{*+}} - m_{B^+}) = 45.01 \pm 0.30 \pm 0.23$ MeV, and uses three relativistic Breit-Wigner functions in the fit for mass difference.

$B_J(5970)$ WIDTH

$B_J(5970)^+$ WIDTH

VALUE (MeV)	EVTS	DOCUMENT ID		TECN	COMMENT
62 ± 20 OUR AVERAGE					
$63 \pm 15 \pm 17$	2k	[1] AAIJ	15AB	LHCB	pp at 7, 8 TeV
$60^{+30}_{-20} \pm 40$	1.4k	AALTONEN	14I	CDF	$p\overline{p}$ at 1.96 TeV
• • • We do not use the following data for averages, fits, limits, etc. • • •					
$61 \pm 14 \pm 17$	2k	[2] AAIJ	15AB	LHCB	pp at 7, 8 TeV
$61 \pm 15 \pm 17$	2k	[3] AAIJ	15AB	LHCB	pp at 7, 8 TeV

[1] Assuming $P = (-1)^J$ and using two relativistic Breit-Wigner functions in the fit for mass difference.
[2] Assuming $P = (-1)^J$ and using three relativistic Breit-Wigner functions in the fit for mass difference.
[3] Assuming $P = -(-1)^J$ and using three relativistic Breit-Wigner functions in the fit for mass difference.

$B_J(5970)^0$ WIDTH

VALUE (MeV)	EVTS	DOCUMENT ID		TECN	COMMENT
81 ± 12 OUR AVERAGE					
$82 \pm 8 \pm 9$	10k	[1] AAIJ	15AB	LHCB	pp at 7, 8 TeV
$70^{+30}_{-20} \pm 30$	2.6k	AALTONEN	14I	CDF	$p\overline{p}$ at 1.96 TeV
• • • We do not use the following data for averages, fits, limits, etc. • • •					
$56 \pm 7 \pm 9$	10k	[2] AAIJ	15AB	LHCB	pp at 7, 8 TeV
$82 \pm 10 \pm 9$	10k	[3] AAIJ	15AB	LHCB	pp at 7, 8 TeV

[1] Assuming $P = (-1)^J$ and using two relativistic Breit-Wigner functions in the fit for mass difference.
[2] Assuming $P = (-1)^J$ and using three relativistic Breit-Wigner functions in the fit for mass difference.
[3] Assuming $P = -(-1)^J$ and using three relativistic Breit-Wigner functions in the fit for mass difference.

$B_J(5970)$ DECAY MODES

	Mode	Fraction (Γ_i/Γ)
Γ_1	$B\pi$	possibly seen
Γ_2	$B^*\pi$	seen

$B_J(5970)$ BRANCHING RATIOS

$\Gamma(B\pi)/\Gamma_{total}$ — Γ_1/Γ

VALUE	EVTS	DOCUMENT ID		TECN	CHG	COMMENT
possibly seen	2k	[1] AAIJ	15AB	LHCB	±	pp at 7, 8 TeV
possibly seen	10k	[1] AAIJ	15AB	LHCB	0	pp at 7, 8 TeV
possibly seen	2.6k	AALTONEN	14I	CDF	0	$p\overline{p}$ at 1.96 TeV
possibly seen	1.4k	AALTONEN	14I	CDF	±	$p\overline{p}$ at 1.96 TeV

[1] A $B\pi$ decay is forbidden from a $P = -(-1)^J$ parent, whereas $B^*\pi$ is allowed.

$\Gamma(B^*\pi)/\Gamma_{total}$ — Γ_2/Γ

VALUE	EVTS	DOCUMENT ID		TECN	CHG	COMMENT
seen	10k	AAIJ	15AB	LHCB	0	pp at 7, 8 TeV
seen	2k	AAIJ	15AB	LHCB	±	pp at 7, 8 TeV
seen	2.6k	AALTONEN	14I	CDF	0	$p\overline{p}$ at 1.96 TeV
seen	1.4k	AALTONEN	14I	CDF	±	$p\overline{p}$ at 1.96 TeV

$B_J(5970)$ REFERENCES

AAIJ 15AB JHEP 1504 024 R. Aaij et al. (LHCb Collab.)
AALTONEN 14I PR D90 012013 T. Aaltonen et al. (CDF Collab.)

Int. J. Mod. Phys. A 2026.41. Downloaded from www.worldscientific.com
by [redacted]LIFORNIA @ BERKELEY on 09/16/26. Re-use and distribution is strictly not permitted, except for Open Access articles.

Int. J. Mod. Phys. A 2026.41. Downloaded from www.worldscientific.com by UNIVERSITY OF CALIFORNIA @ BERKELEY on 09/16/26. Re-use and distribution is strictly not permitted, except for Open Access articles.

BOTTOM, STRANGE MESONS ($B = \pm1$, $S = \mp1$)

$B_s^0 = s\overline{b}$, $\overline{B}_s^0 = \overline{s}b$, similarly for B_s^*'s

B_s^0

$I(J^P) = 0(0^-)$

I, J, P need confirmation. Quantum numbers shown are quark-model predictions.

B_s^0 MASS

VALUE (MeV)	EVTS	DOCUMENT ID		TECN	COMMENT
5366.93± 0.10 OUR FIT					
5366.91± 0.11 OUR AVERAGE					
5366.98± 0.07±0.13		[1] AAIJ	21C	LHCB	pp at 7, 8, 13 TeV
5366.85± 0.19±0.13		[2] AAIJ	19U	LHCB	pp at 7, 8, 13 TeV
5366.83± 0.25±0.27		[3] AAIJ	18AC	LHCB	pp at 7, 8, 13 TeV
5367.08± 0.38±0.15	128	[4] AAIJ	16U	LHCB	pp at 7, 8 TeV
5366.90± 0.28±0.23		[5] AAIJ	12E	LHCB	pp at 7 TeV
5364.4 ± 1.3 ±0.7		LOUVOT	09	BELL	$e^+e^- \to \Upsilon(5S)$
5366.01± 0.73±0.33		[6] ACOSTA	06	CDF	$p\overline{p}$ at 1.96 TeV
5369.9 ± 2.3 ±1.3	32	[7] ABE	96B	CDF	$p\overline{p}$ at 1.8 TeV
5374 ±16 ±2	3	ABREU	94D	DLPH	$e^+e^- \to Z$
5359 ±19 ±7	1	[7] AKERS	94J	OPAL	$e^+e^- \to Z$
5368.6 ± 5.6 ±1.5	2	BUSKULIC	93G	ALEP	$e^+e^- \to Z$
• • • We do not use the following data for averages, fits, limits, etc. • • •					
5370 ± 1 ±3		DRUTSKOY	07A	BELL	Repl. by LOUVOT 09
5370 ±40	6	[8] AKERS	94J	OPAL	$e^+e^- \to Z$
5383.3 ± 4.5 ±5.0	14	ABE	93F	CDF	Repl. by ABE 96B

[1] Uses $B_s^0 \to J/\psi\pi^+\pi^-K^+K^-$ decays.
[2] Uses $B_s^0 \to J/\psi p\overline{p}$ decays.
[3] Uses $B_s \to \chi_{c1}K^+K^-$ mode.
[4] Uses $J/\psi \to \mu^+\mu^-$, $\phi \to K^+K^-$ decays, and observes 128 ± 13 events of $B_s^0 \to J/\psi\phi\phi$.
[5] Uses $B_s^0 \to J/\psi\phi$ fully reconstructed decays.
[6] Uses exclusively reconstructed final states containing a $J/\psi \to \mu^+\mu^-$ decays.
[7] From the decay $B_s \to J/\psi(1S)\phi$.
[8] From the decay $B_s \to D_s^-\pi^+$.

$m_{B_s^0} - m_B$

m_B is the average of our B masses $(m_{B^\pm}+m_{B^0})/2$.

VALUE (MeV)	CL%	DOCUMENT ID		TECN	COMMENT
87.37±0.12 OUR FIT					
87.42±0.24 OUR AVERAGE					
87.60±0.44±0.09		[1] AAIJ	15U	LHCB	pp at 7, 8 TeV
87.42±0.30±0.09		[2] AAIJ	12E	LHCB	pp at 7 TeV
86.64±0.80±0.08		[3] ACOSTA	06	CDF	$p\overline{p}$ at 1.96 TeV
• • • We use the following data for averages but not for fits. • • •					
89.7 ±2.7 ±1.2		ABE	96B	CDF	$p\overline{p}$ at 1.8 TeV
• • • We do not use the following data for averages, fits, limits, etc. • • •					
80 to 130	68	LEE-FRANZINI	90	CSB2	$e^+e^- \to \Upsilon(5S)$

[1] The reported result is $m_{B_s^0} - m_{B^0} = 87.45 \pm 0.44 \pm 0.09$ MeV. We convert it to the mass difference with respect to the average of $(m_{B^\pm} + m_{B^0})/2$. Uses the mode $B_s^0 \to \psi(2S)K^-\pi^+$.
[2] The reported result is $m_{B_s^0} - m_{B^+} = 87.52 \pm 0.30 \pm 0.12$ MeV. We convert it to the mass difference with respect to the average of $(m_{B^\pm} + m_{B^0})/2$.
[3] The reported result is $m_{B_s^0} - m_{B^0} = 86.38 \pm 0.90 \pm 0.06$ MeV. We convert it to the mass difference with respect to the average of $(m_{B^\pm} + m_{B^0})/2$.

$m_{B^0_{sH}} - m_{B^0_{sL}}$

See the B_s^0-$\overline{B}_s^0$ MIXING section near the end of these B_s^0 Listings.

B_s^0 MEAN LIFE

The mean B_s^0 lifetime is defined and computed as $1/\Gamma_{B_s^0}$, where $\Gamma_{B_s^0}$ is the average decay width of the B_s^0 mass eigenstates.

VALUE (10^{-12} s)	EVTS	DOCUMENT ID		TECN	COMMENT
1.515±0.006 OUR EVALUATION (Produced by HFLAV)					
• • • We do not use the following data for averages, fits, limits, etc. • • •					
1.518±0.041±0.027		[1] AALTONEN	11AP	CDF	$p\overline{p}$ at 1.96 TeV
1.398±0.044$^{+0.028}_{-0.025}$		[2] ABAZOV	06V	D0	$p\overline{p}$ at 1.96 TeV
1.42 $^{+0.14}_{-0.13}$ ±0.03		[3] ABREU	00Y	DLPH	$e^+e^- \to Z$
1.53 $^{+0.16}_{-0.15}$ ±0.07		[4] ABREU,P	00G	DLPH	$e^+e^- \to Z$
1.36 ±0.09 $^{+0.06}_{-0.05}$		[5] ABE	99D	CDF	$p\overline{p}$ at 1.8 TeV
1.72 $^{+0.20}_{-0.19}$ $^{+0.18}_{-0.17}$		[6] ACKERSTAFF	98F	OPAL	$e^+e^- \to Z$
1.50 $^{+0.16}_{-0.15}$ ±0.04		[5] ACKERSTAFF	98G	OPAL	$e^+e^- \to Z$
1.47 ±0.14 ±0.08		[4] BARATE	98C	ALEP	$e^+e^- \to Z$
1.51 ±0.11		[7] BARATE	98C	ALEP	$e^+e^- \to Z$
1.56 $^{+0.29}_{-0.26}$ $^{+0.08}_{-0.07}$		[5] ABREU	96F	DLPH	Repl. by ABREU 00Y
1.65 $^{+0.34}_{-0.31}$ ±0.12		[4] ABREU	96F	DLPH	Repl. by ABREU 00Y
1.76 ±0.20 $^{+0.15}_{-0.10}$		[8] ABREU	96F	DLPH	Repl. by ABREU 00Y
1.60 ±0.26 $^{+0.13}_{-0.15}$		[9] ABREU	96F	DLPH	Repl. by ABREU,P 00G
1.67 ±0.14		[10] ABREU	96F	DLPH	$e^+e^- \to Z$
1.61 $^{+0.30}_{-0.29}$ $^{+0.18}_{-0.16}$	90	[4] BUSKULIC	96E	ALEP	Repl. by BARATE 98C
1.54 $^{+0.14}_{-0.13}$ ±0.04		[5] BUSKULIC	96M	ALEP	$e^+e^- \to Z$
1.42 $^{+0.27}_{-0.23}$ ±0.11	76	[5] ABE	95R	CDF	Repl. by ABE 99D
1.74 $^{+1.08}_{-0.69}$ ±0.07	8	[11] ABE	95R	CDF	Sup. by ABE 96N
1.54 $^{+0.25}_{-0.21}$ ±0.06	79	[5] AKERS	95G	OPAL	Repl. by ACKERSTAFF 98G
1.59 $^{+0.17}_{-0.15}$ ±0.03	134	[5] BUSKULIC	95O	ALEP	Sup. by BUSKULIC 96M
0.96 ±0.37	41	[12] ABREU	94E	DLPH	Sup. by ABREU 96F
1.92 $^{+0.45}_{-0.35}$ ±0.04	31	[5] BUSKULIC	94C	ALEP	Sup. by BUSKULIC 95O
1.13 $^{+0.35}_{-0.26}$ ±0.09	22	[5] ACTON	93H	OPAL	Sup. by AKERS 95G

[1] AALTONEN 11AP combines the fully reconstrcuted $B_s^0 \to D_s^-\pi^+$ decays and partially reconstructed $B_s^0 \to D_sX$ decays.
[2] Measured using $D_s\mu^+$ vertices.
[3] Uses $D_s^-\ell^+$, and $\phi\ell^+$ vertices.
[4] Measured using D_s hadron vertices.
[5] Measured using $D_s^-\ell^+$ vertices.
[6] ACKERSTAFF 98F use fully reconstructed $D_s^- \to \phi\pi^-$ and $D_s^- \to K^{*0}K^-$ in the inclusive B_s^0 decay.
[7] Combined results from $D_s^-\ell^+$ and D_s hadron.
[8] Measured using $\phi\ell$ vertices.
[9] Measured using inclusive D_s vertices.
[10] Combined result for the four ABREU 96F methods.
[11] Exclusive reconstruction of $B_s \to \psi\phi$.
[12] ABREU 94E uses the flight-distance distribution of D_s vertices, ϕ-lepton vertices, and $D_s\mu$ vertices.

$\Gamma_{B_s^0}$

"OUR EVALUATION" includes the measurements of $\Gamma_{B_s^0}$ and $\Delta\Gamma_{B_s^0}$ listed in this section, as well as constraints from effective lifetimes with pure CP modes and flavor-specific modes.

VALUE (10^{12} s^{-1})	DOCUMENT ID		TECN	COMMENT
0.6600±0.0024 OUR EVALUATION (Produced by HFLAV)				
0.6617±0.0026 OUR AVERAGE Error includes scale factor of 2.0. See the ideogram below.				
0.6613±0.0015±0.0034	[1] HAYRAPETY...	26A	CMS	pp at 13 TeV
0.6527$^{+0.0013}_{-0.0015}$±0.0022	[2] AAIJ	24A	LHCB	pp at 13 TeV
0.6687±0.0015±0.0022	[3,4] AAD	21AE	ATLS	pp at 13 TeV
0.608 ±0.018 ±0.012	[5] AAIJ	21AN	LHCB	pp at 7, 8 TeV
0.650 ±0.006 ±0.004	[6] AAIJ	17V	LHCB	pp at 7, 8 TeV
0.676 ±0.004 ±0.004	[4,7] AAD	16AP	ATLS	pp at 8 TeV
0.668 ±0.011 ±0.006	[8] AAIJ	16AK	LHCB	pp at 7, 8 TeV
0.6704±0.0043±0.0055	[4] KHACHATRY...	16S	CMS	pp at 8 TeV
0.6603±0.0027±0.0015	[9] AAIJ	15I	LHCB	pp at 7, 8 TeV
0.677 ±0.007 ±0.004	[4] AAD	14U	ATLS	pp at 7 TeV
0.654 ±0.008 ±0.004	[4] AALTONEN	12AJ	CDF	$p\overline{p}$ at 1.96 TeV
0.693 $^{+0.018}_{-0.017}$	[4] ABAZOV	12D	D0	$p\overline{p}$ at 1.96 TeV
• • • We do not use the following data for averages, fits, limits, etc. • • •				
0.6531±0.0042±0.0026	[4,10] SIRUNYAN	21E	CMS	Repl. by HAYRAPETYAN 26A
0.6563±0.0021	[4,11] AAIJ	19Q	LHCB	Repl. by AAIJ 24A
0.661 ±0.004 ±0.006	[12] AAIJ	13AR	LHCB	Repl. by AAIJ 15I
0.677 ±0.007 ±0.004	[4] AAD	12CV	ATLS	Repl. by AAD 14U
0.657 ±0.009 ±0.008	[4] AAIJ	12D	LHCB	Repl. by AAIJ 13AR
0.654 ±0.011 ±0.005	[4,13] AALTONEN	12D	CDF	Repl. by AALTONEN 12AJ
0.672 ±0.027 ±0.013	[4] ABAZOV	09E	D0	Repl. by ABAZOV 08AM
0.658 ±0.017 ±0.009	[4,14] AALTONEN	08J	CDF	Repl. by AALTONEN 12D

0.658 ±0.022 ±0.004	[4] ABAZOV	08AM	D0	Repl. by ABAZOV 12D
0.658 ±0.035 $^{+0.0130}_{-0.004}$	[4,14] ABAZOV	07	D0	Repl. by ABAZOV 09E
0.714 $^{+0.007}_{-0.008}$ ±0.010	[4,14] ACOSTA	05	CDF	Repl. by AALTONEN 08J

[1] Measured using a time-dependent angular analysis of $B^0_s \to J/\psi\phi$ decays with the ML-improved flavor-tagging algorithm.
[2] Reports $\Gamma_s - \Gamma_d = -0.0056^{+0.0013}_{-0.0015} \pm 0.0014$ ps^{-1} using a time-dependent angular analysis of $B^0_s \to J/\psi K^+K^-$ decays and the current B^0 lifetime of 1.517 ± 0.004 ps^{-1}.
[3] Reports a combination of 0.6703 ± 0.0014 ± 0.0018 ps^{-1} with AAD 16AP.
[4] Measured using a time-dependent angular analysis of $B^0_s \to J/\psi\phi$ decays.
[5] Measured using a time-dependent angular analysis of $B^0_s \to J/\psi\phi$ decays with $J/\psi \to e^+e^-$.
[6] Measured using time-dependent angular analysis of $B^0_s \to J/\psi K^+K^-$ in the region m(KK) > 1.05 GeV.
[7] Reports a combination of 0.675 ± 0.003 ± 0.003 ps^{-1} with AAD 14U.
[8] Measured using a time-dependent angular analysis of $B^0_s \to \psi(2S)\phi$ decays.
[9] Measured using a time-dependent angular analysis of $B^0_s \to J/\psi K^+K^-$ decays.
[10] Reports a combination of 0.6590 ± 0.0032 ± 0.0023 ps^{-1} with KHACHATRYAN 16S.
[11] Reports $\Gamma_s - \Gamma_d = -0.0041 \pm 0.0024 \pm 0.0015$ ps^{-1} using a time-dependent angular analysis of $B^0_s \to J/\psi K^+K^-$ decays and the B^0 lifetime of 1.520 ± 0.004 ps^{-1}. The results are further combined with those coming from $B^0_s \to J/\psi\pi^+\pi^-$, $B^0_s \to \psi(2S)\phi$, and $B^0_s \to D^+_s D^-_s$.
[12] Measured using a combined time-dependent angular analysis of $B^0_s \to J/\psi K^+K^-$ and $B^0_s \to J/\psi\pi^+\pi^-$ decays.
[13] Assuming CPV phase $\phi_s = -0.04$.
[14] Assuming CPV phase $\phi_s = 0$.

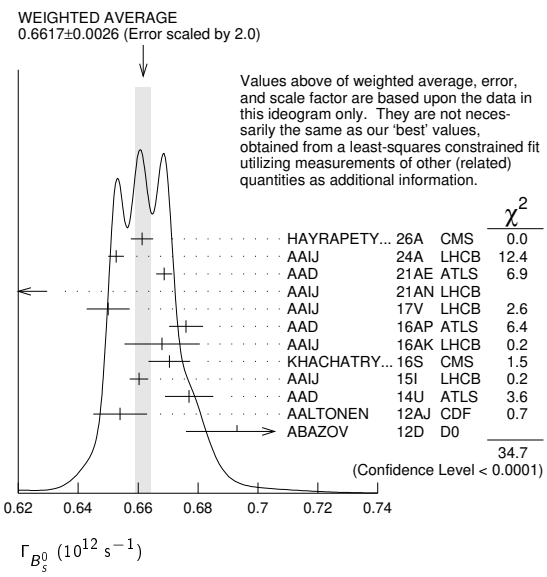

$\Delta\Gamma_{B^0_s}$

"OUR EVALUATION" includes the measurements of $\Gamma_{B^0_s}$ and $\Delta\Gamma_{B^0_s}$ listed in this section, as well as constraints from effective lifetimes with pure *CP* modes and flavor-specific modes.

VALUE (10^{12} s^{-1})	*DOCUMENT ID*		*TECN*	*COMMENT*
0.0783±0.0035 OUR EVALUATION	(Produced by HFLAV)			
0.0776±0.0034 OUR AVERAGE	Error includes scale factor of 1.3. See the ideogram below.			
0.0761±0.0040±0.0024	[1,2] HAYRAPETY...	26A	CMS	pp at 13 TeV
0.0845±0.0044±0.0024	[3] AAIJ	24A	LHCB	pp at 13 TeV
0.087 ±0.012 ±0.009	[4] AAIJ	24O	LHCB	pp at 7, 8, 13 TeV
0.0607±0.0047±0.0043	[5,6] AAD	21AE	ATLS	pp at 13 TeV
0.115 ±0.045 ±0.011	[7] AAIJ	21AN	LHCB	pp at 7, 8 TeV
0.066 ±0.018 ±0.010	[8] AAIJ	17V	LHCB	pp at 7, 8 TeV
0.101 ±0.013 ±0.007	[5,9] AAD	16AP	ATLS	pp at 8 TeV
0.066 $^{+0.041}_{-0.044}$ ±0.007	[10] AAIJ	16AK	LHCB	pp at 7, 8 TeV
0.095 ±0.013 ±0.007	[5] KHACHATRY...	16S	CMS	pp at 8 TeV
0.0805±0.0091±0.0032	[3] AAIJ	15I	LHCB	pp at 7, 8 TeV
0.053 ±0.021 ±0.010	[5] AAD	14U	ATLS	pp at 7 TeV
0.068 ±0.026 ±0.009	[5] AALTONEN	12AJ	CDF	$p\overline{p}$ at 1.96 TeV
0.163 $^{+0.065}_{-0.064}$	[5,11] ABAZOV	12D	D0	$p\overline{p}$ at 1.96 TeV

• • • We do not use the following data for averages, fits, limits, etc. • • •

0.114 ±0.014 ±0.007	[5,12] SIRUNYAN	21E	CMS	Repl. by HAYRAPETYAN 26A
0.077 ±0.008 ±0.003	[3] AAIJ	19Q	LHCB	Repl. by AAIJ 24A
0.106 ±0.011 ±0.007	[13] AAIJ	13AR	LHCB	Repl. by AAIJ 15I
0.053 ±0.021 ±0.010	[5] AAD	12CV	ATLS	Repl. by AAD 14U
0.123 ±0.029 ±0.011	[5] AAIJ	12D	LHCB	Repl. by AAIJ 13AR
0.075 ±0.035 ±0.006	[14] AALTONEN	12D	CDF	Repl. by AALTONEN 12AJ
0.085 $^{+0.072}_{-0.078}$ ±0.001	[15] ABAZOV	09E	D0	Repl. by ABAZOV 08AM
0.076 $^{+0.059}_{-0.063}$ ±0.006	[16] AALTONEN	08J	CDF	Repl. by AALTONEN 12D
0.19 ±0.07 $^{+0.02}_{-0.01}$	[5,17] ABAZOV	08AM	D0	Repl. by ABAZOV 12D
0.12 $^{+0.08}_{-0.10}$ ±0.02	[16,18] ABAZOV	07	D0	Repl. by ABAZOV 07N
0.13 ±0.09	[19] ABAZOV	07N	D0	Repl. by ABAZOV 09E
0.47 $^{+0.19}_{-0.24}$ ±0.01	[16] ACOSTA	05	CDF	Repl. by AALTONEN 08J

[1] Measured using a time-dependent angular analysis of $B^0_s \to J/\psi\phi$ decays with the ML-improved flavor-tagging algorithm.
[2] Reports a combination of 0.0780 ± 0.0045 ps^{-1} with KHACHATRYAN 16S.
[3] Measured using time-dependent angular analysis of $B^0_s \to J/\psi K^+K^-$ decays.
[4] Measured using *CP* eigenstates $B^0_s \to J/\psi\eta'$ and $B^0_s \to J/\psi\pi^+\pi^-$ (selected to be predominantly *CP*-odd). Negligible *CP* violation and $\Gamma_{B^0_s} = 0.6628 \pm 0.0035$ ps^{-1} are assumed.
[5] Measured using the time-dependent angular analysis of $B^0_s \to J/\psi\phi$ decays.
[6] Reports a combination of 0.0657 ± 0.0043 ± 0.0037 ps^{-1} with AAD 16AP
[7] Measured using a time-dependent angular analysis of $B^0_s \to J/\psi\phi$ decays with $J/\psi \to e^+e^-$.
[8] Measured using time-dependent angular analysis of $B^0_s \to J/\psi K^+K^-$ in the region m(KK) > 1.05 GeV.
[9] Reports a combination pf $0.066^{+0.041}_{-0.044}$ ± 0.007 ps^{-1} with AAD 14U.
[10] Measured using time-dependent angular analysis of $B^0_s \to \psi(2S)\phi$ decays.
[11] The error includes both statistical and systematic uncertainties.
[12] Reports a combination of 0.1032 ± 0.0095 ± 0.0048 ps^{-1} with KHACHATRYAN 16S.
[13] AAIJ 13AR result comes from a combined fit to $B^0_s \to J/\psi K^+K^-$ and $B^0_s \to J/\psi\pi^+\pi^-$ data sets. Also reports $\Delta\Gamma_s = 0.100 \pm 0.016 \pm 0.003$ ps^{-1} from a fit to $B^0_s \to J/\psi K^+K^-$ decays.
[14] Uses the time-dependent angular analysis of $B^0_s \to J/\psi\phi$ decays and assuming *CP*-violating angle $\beta_s(B^0 \to J/\psi\phi) = 0.02$.
[15] Measured the angular and lifetime parameters for the time-dependent angular untagged decays $B^0_d \to J/\psi K^{*0}$ and $B^0_s \to J/\psi\phi$.
[16] Measured using the time-dependent angular analysis of $B^0_s \to J/\psi\phi$ decays and assuming *CP*-violating phase $\phi_s = 0$.
[17] Obtaines 90% CL interval $-0.06 < \Delta\Gamma_s < 0.30$.
[18] ABAZOV 07 reports 0.17 ± 0.09 ± 0.02 with *CP*-violating phase ϕ_s as a free parameter.
[19] Combines D^0 measurements of time-dependent angular distributions in $B^0_s \to J/\psi\phi$ and charge asymmetry in semileptonic decays. There is a 4-fold ambiguity in the solution.

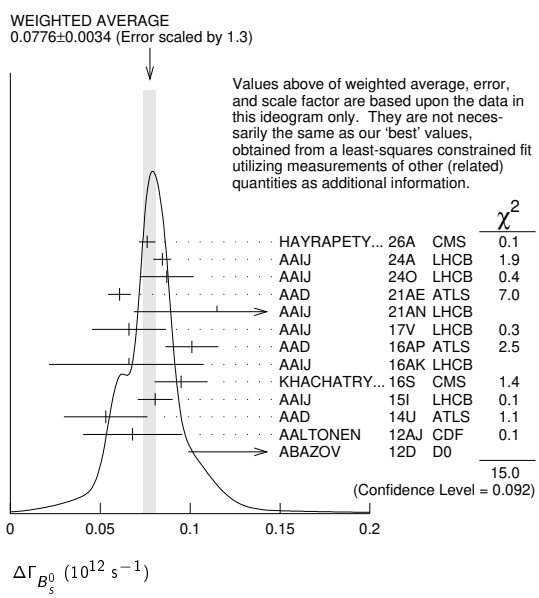

Int. J. Mod. Phys. A 2026.41. Downloaded from www.worldscientific.com
by CALIFORNIA @ BERKELEY on 09/16/26. Re-use and distribution is strictly not permitted, except for Open Access articles.

Int. J. Mod. Phys. A 2026.41. Downloaded from www.worldscientific.com
by UNIVERSITY OF CALIFORNIA @ BERKELEY on 09/16/26. Re-use and distribution is strictly not permitted, except for Open Access articles.

$\Delta\Gamma_{B^0_s}/\Gamma_{B^0_s}$

$\Gamma_{B^0_s}$ and $\Delta\Gamma_{B^0_s}$ are the decay rate average and difference between two B^0_s CP eigenstates (light − heavy). "OUR EVALUATION" is derived from the averages of $\Gamma_{B^0_s}$ and $\Delta\Gamma_{B^0_s}$ (and their correlation).

VALUE	CL%	DOCUMENT ID		TECN	COMMENT
0.118±0.006 OUR EVALUATION		(Produced by HFLAV)			
• • • We do not use the following data for averages, fits, limits, etc. • • •					
$0.090\pm0.009\pm0.023$		[1] ESEN	13	BELL	$e^+e^-\to\Upsilon(5S)$
		[2] AAIJ	12D	LHCB	pp at 7 TeV
		[3] AALTONEN	12D	CDF	$p\overline{p}$ at 1.96 TeV
		[4] ABAZOV	12D	D0	$p\overline{p}$ at 1.96 TeV
$0.147^{+0.036}_{-0.030}{}^{+0.042}_{-0.041}$		[1] ESEN	10	BELL	$e^+e^-\to\Upsilon(5S)$
$0.072\pm0.021\pm0.022$		[5] ABAZOV	09I	D0	$p\overline{p}$ at 1.96 TeV
>0.012	95	[5] AALTONEN	08F	CDF	$p\overline{p}$ at 1.96 TeV
$0.116^{+0.09}_{-0.10}\pm0.010$		[6] AALTONEN	08J	CDF	Repl. by AALTONEN 12D
$0.079^{+0.038}_{-0.035}{}^{+0.031}_{-0.030}$		[5] ABAZOV	07Y	D0	Repl. by ABAZOV 09I
$0.24\ ^{+0.28}_{-0.38}\ ^{+0.03}_{-0.04}$		[6,7] ABAZOV	05W	D0	Repl. by ABAZOV 08AM
$0.65\ ^{+0.25}_{-0.33}\pm0.01$		[6] ACOSTA	05	CDF	Repl. by AALTONEN 08J
<0.46	95	[8] ABREU	00Y	DLPH	$e^+e^-\to Z$
<0.69	95	[9] ABREU,P	00G	DLPH	$e^+e^-\to Z$
$0.25\ ^{+0.21}_{-0.14}$		[10] BARATE	00K	ALEP	$e^+e^-\to Z$
<0.83	95	[11] ABE	99D	CDF	$p\overline{p}$ at 1.8 TeV
<0.67	95	[12] ACCIARRI	98S	L3	$e^+e^-\to Z$

[1] Assumes CP violation is negligible.
[2] Measured using the time-dependent angular analysis of $B^0_s\to J/\psi\phi$ decays.
[3] Uses the time-dependent angular analysis of $B^0_s\to J/\psi\phi$ decays and assuming CP-violating angle $\beta_s(B^0\to J/\psi\phi)=0.02$.
[4] Measured using fully reconstructed $B_s\to J/\psi\phi$ decays.
[5] Assumes $2\,B(B^0_s\to D^{(*)}_s D^{(*)}_s)\simeq\Delta\Gamma^{CP}_s/\Gamma_s$.
[6] Measured using the time-dependent angular analysis of $B^0_s\to J/\psi\phi$ decays.
[7] Uses $|A_0|^2-|A_\parallel|^2=0.355\pm0.066$ from ACOSTA 05.
[8] Uses $D^-_s\ell^+$, and $\phi\ell^+$ vertices.
[9] Measured using D_s hadron vertices.
[10] Uses $\phi\phi$ correlations from $B^0_s\to D^{(*)+}_s D^{(*)-}_s$.
[11] ABE 99D assumes $\tau_{B^0_s}=1.55\pm0.05$ ps.
[12] ACCIARRI 98S assumes $\tau_{B^0_s}=1.49\pm0.06$ ps and PDG 98 values of b production fraction.

B^0_{sH} MEAN LIFE

B^0_{sH} is the heavy mass state of two B^0_s CP eigenstates.

VALUE (10^{-12} s)	DOCUMENT ID		TECN	COMMENT
1.611±0.008 OUR EVALUATION	(Produced by HFLAV)			
• • • We do not use the following data for averages, fits, limits, etc. • • •				
$1.59\pm0.07\pm0.03$	[1] HAYRAPETY...24AX		CMS	pp at 13 TeV
$0.99\ ^{+0.42}_{-0.07}\pm0.17$	[2] AAD	23BY	ATLS	pp at 13 TeV
$1.83\ ^{+0.23}_{-0.20}\pm0.04$	[2] TUMASYAN	23A	CMS	pp at 13 TeV
$2.07\pm0.29\pm0.03$	[2] AAIJ	22	LHCB	pp at 7, 8, 13 TeV
$1.70\ ^{+0.60}_{-0.43}\pm0.09$	[2] SIRUNYAN	20AG	CMS	pp at 7, 8, 13 TeV
$1.677\pm0.034\pm0.011$	[3] SIRUNYAN	18BY	CMS	pp at 8 TeV
$2.04\pm0.44\pm0.05$	[2] AAIJ	17AI	LHCB	pp at 7, 8, 13 TeV
$1.70\pm0.14\pm0.05$	[4] ABAZOV	16C	D0	$p\overline{p}$ at 1.96 TeV
$1.75\pm0.12\pm0.07$	[1] AAIJ	13AB	LHCB	pp at 7 TeV
$1.652\pm0.024\pm0.024$	[5] AAIJ	13AR	LHCB	pp at 7 TeV
$1.700\pm0.040\pm0.026$	[6] AAIJ	12AN	LHCB	pp at 7 TeV
	[7] AALTONEN	12D	CDF	$p\overline{p}$ at 1.96 TeV
$1.70\ ^{+0.12}_{-0.11}\pm0.03$	[6] AALTONEN	11AB	CDF	$p\overline{p}$ at 1.96 TeV
$1.613^{+0.123}_{-0.113}$	[8,9] AALTONEN	08J	CDF	Repl. by AALTONEN 12D
$1.58\ ^{+0.39}_{-0.42}\ ^{+0.01}_{-0.02}$	[9] ABAZOV	05W	D0	Repl. by ABAZOV 08AM
$2.07\ ^{+0.58}_{-0.46}\pm0.03$	[9] ACOSTA	05	CDF	Repl. by AALTONEN 08J

[1] Measured using a pure CP-odd final state $J/\psi K^0_S$ with the assumption that contributions from penguin diagrams are small.
[2] Measured using $B_s\to\mu^+\mu^-$ decays which, in the Standard Model, correspond to B^0_{sH} decays. Assumes $-2\,\mathrm{Re}(\lambda)/(1+|\lambda|^2)=1$.
[3] Measured using $B^0_s\to J/\psi\pi^+\pi^-$ decays with $0.9240<m(\pi\pi)<1.0204$ GeV, which is dominated by the $f_0(980)$ resonance, making it a CP-odd state.
[4] Measured using $J/\psi\pi^+\pi^-$ mode with $0.880<m(\pi\pi)<1.080$ GeV/c^2, which is mostly $J/\psi f(0)(980)$ mode, a pure CP-odd final state.
[5] Measured using $B_s\to J/\psi\pi^+\pi^-$ decays which, in the limit of $\phi_s=0$ and $|\lambda|=1$, correspond to B^0_{sH} decays.
[6] Measured using a pure CP-odd final state $J/\psi f_0(980)$.
[7] Uses the time-dependent angular analysis of $B^0_s\to J/\psi\phi$ decays assuming CP-violating angle $\beta_s(B^0\to J/\psi\phi)=0.02$.
[8] Obtained from $\Delta\Gamma_s$ and Γ_s fit with a correlation of 0.6.
[9] Measured using the time-dependent angular analysis of $B^0_s\to J/\psi\phi$ decays.

B^0_{sL} MEAN LIFE

B^0_{sL} is the light mass state of two B^0_s CP eigenstates.

VALUE (10^{-12} s)	DOCUMENT ID		TECN	COMMENT
1.430±0.006 OUR EVALUATION	(Produced by HFLAV)			
1.452±0.016 OUR AVERAGE				
$1.445\pm0.016\pm0.008$	[1,2] AAIJ	23P	LHCB	pp at 7, 8, 13 TeV
$1.479\pm0.034\pm0.011$	[1] AAIJ	16AL	LHCB	pp at 7, 8 TeV
• • • We do not use the following data for averages, fits, limits, etc. • • •				
1.40 ± 0.02	[3] SIRUNYAN	18BY	CMS	pp at 8 TeV
$1.379\pm0.026\pm0.017$	[4] AAIJ	14F	LHCB	pp at 7, 8 TeV
$1.407\pm0.016\pm0.007$	[5] AAIJ	14R	LHCB	pp at 7 TeV
$1.440\pm0.096\pm0.009$	[5] AAIJ	12	LHCB	pp at 7 TeV
$1.455\pm0.046\pm0.006$	[5] AAIJ	12R	LHCB	Repl. by AAIJ 14R
	[6] AALTONEN	12D	CDF	$p\overline{p}$ at 1.96 TeV
$1.437^{+0.054}_{-0.047}$	[7,8] AALTONEN	08J	CDF	Repl. by AALTONEN 12D
$1.24\ ^{+0.14}_{-0.11}\ ^{+0.01}_{-0.02}$	[8] ABAZOV	05W	D0	Repl. by ABAZOV 08AM
$1.05\ ^{+0.16}_{-0.13}\pm0.02$	[8] ACOSTA	05	CDF	Repl. by AALTONEN 08J
$1.27\pm0.33\pm0.08$	[9] BARATE	00K	ALEP	$e^+e^-\to Z$

[1] Uses $B^0_s\to J/\psi\eta$ decays.
[2] AAIJ 23P reports a τ_L value combined with AAIJ 16AL result as $\tau_L=1.452\pm0.014\pm0.007$ ps.
[3] Measured using results in SIRUNYAN 18BY for the heavy B^0_s lifetime obtained from $B^0_s\to J/\psi\pi^+\pi^-$ decays and the average effective $B^0_s\to J/\psi\phi$ lifetime, and magnitude squared of the CP-odd amplitude $|A_\perp|^2=0.250\pm0.006$. The uncertainty includes all statistical and systematic contributions.
[4] Measured using $B^0_s\to D^-_s D^+_s$. The effective lifetime is translated into a decay width of $\Gamma_L=0.725\pm0.014\pm0.009$ ps^{-1}.
[5] Measured using $B^0_s\to K^+K^-$ decays. There may still be CPV in the decay.
[6] Uses the time-dependent angular analysis of $B^0_s\to J/\psi\phi$ decays and assuming CP-violating angle $\beta_s(B^0\to J/\psi\phi)=0.02$.
[7] Obtained from $\Delta\Gamma_s$ and Γ_s fit with a correlation of 0.6.
[8] Measured using the time-dependent angular analysis of $B^0_s\to J/\psi\phi$ decays.
[9] Uses $\phi\phi$ correlations from $B^0_s\to D^{(*)+}_s D^{(*)-}_s$.

B^0_s MEAN LIFE (Flavor specific)

VALUE (10^{-12} s)	DOCUMENT ID		TECN	COMMENT
1.527±0.011 OUR EVALUATION				
1.526±0.015 OUR AVERAGE	Error includes scale factor of 1.3. See the ideogram below.			
$1.547\pm0.013\pm0.011$	[1] AAIJ	17AN	LHCB	pp at 7, 8 TeV
$1.479\pm0.010\pm0.021$	[2] ABAZOV	15A	D0	$p\overline{p}$ at 1.96 TeV
$1.535\pm0.015\pm0.014$	[3] AAIJ	14AX	LHCB	pp at 7 TeV
$1.52\pm0.15\pm0.01$	[4] AAIJ	14F	LHCB	pp at 7, 8 TeV
$1.60\pm0.06\pm0.01$	[5] AAIJ	14R	LHCB	pp at 7 TeV
$1.518\pm0.041\pm0.027$	[6] AALTONEN	11AP	CDF	$p\overline{p}$ at 1.96 TeV
$1.42\ ^{+0.14}_{-0.13}\pm0.03$	[7] ABREU	00Y	DLPH	$e^+e^-\to Z$
$1.36\pm0.09\ ^{+0.06}_{-0.05}$	[8] ABE	99D	CDF	$p\overline{p}$ at 1.8 TeV
$1.50\ ^{+0.16}_{-0.15}\pm0.04$	[8] ACKERSTAFF	98G	OPAL	$e^+e^-\to Z$
$1.54\ ^{+0.14}_{-0.13}\pm0.04$	[8] BUSKULIC	96M	ALEP	$e^+e^-\to Z$
• • • We do not use the following data for averages, fits, limits, etc. • • •				
$1.398\pm0.044^{+0.028}_{-0.025}$	[9] ABAZOV	06V	D0	Repl. by ABAZOV 15A

[1] AAIJ 17AN value was measured using $B^0_s\to D^{(*)-}_s\mu^+\nu_\mu$ decays relative to $B^0\to D^{(*)-}\mu^+\nu_\mu$ decays.
[2] Measured using $B^0_s\to D^-_s\mu^+\nu_\mu X$ decays.
[3] Measured using the $B^0_s\to D^-_s\pi^+$ decays.
[4] Measured using $B^0_s\to D^+D^-_s$.
[5] Measured using $B^0_s\to\pi^+K^-$ decays.
[6] AALTONEN 11AP combines the fully reconstrcuted $B^0_s\to D^-_s\pi^+$ decays and partially reconstructed $B^0_s\to D_s X$ decays.
[7] Uses $D^-_s\ell^+$, and $\phi\ell^+$ vertices.
[8] Measured using $D^-_s\ell^+$ vertices.
[9] Measured using $D^-_s\mu^+$ vertices.

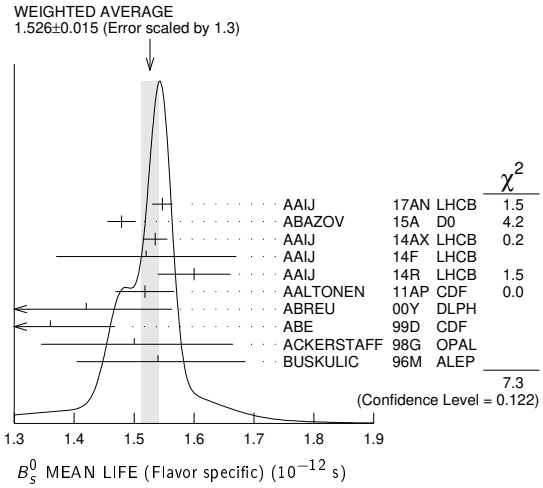

B^0_s MEAN LIFE (partial)

B^0_s mean life ($B_s \to D^+_s D^-_s$)

VALUE (10^{-12} s)	DOCUMENT ID		TECN	COMMENT
1.379±0.031 OUR EVALUATION	(Produced by HFLAV)			
1.379±0.026±0.017	[1] AAIJ	14F	LHCB	pp at 7, 8 TeV

[1] Measured using $B^0_s \to D^-_s D^+_s$. The effective lifetime is translated into a decay width of $\Gamma_L = 0.725 \pm 0.014 \pm 0.009$ ps^{-1}.

B^0_s mean life ($B_s \to J/\psi\phi$)

VALUE (10^{-12} s)	DOCUMENT ID		TECN	COMMENT
1.480±0.007 OUR EVALUATION				
1.480±0.007 OUR AVERAGE				
1.481±0.007±0.005	[1] SIRUNYAN	18BY	CMS	pp at 8 TeV
1.480±0.011±0.005	[1] AAIJ	14E	LHCB	pp at 7 TeV
$1.444^{+0.098}_{-0.090}\pm0.020$	[1] ABAZOV	05B	D0	$p\overline{p}$ at 1.96 TeV
$1.34\ ^{+0.23}_{-0.19}\ \pm0.05$	[2] ABE	98B	CDF	$p\overline{p}$ at 1.8 TeV
• • • We do not use the following data for averages, fits, limits, etc. • • •				
$1.39\ ^{+0.13}_{-0.16}\ ^{+0.01}_{-0.02}$	[2] ABAZOV	05W	D0	$p\overline{p}$ at 1.96 TeV
$1.34\ ^{+0.23}_{-0.19}\ \pm0.05$	[3] ABE	96N	CDF	Repl. by ABE 98B

[1] Measured using fully reconstructed $B_s \to J/\psi\phi$ decays.
[2] Measured using the time-dependent angular analysis of $B^0_s \to J/\psi\phi$ decays.
[3] ABE 96N uses 58 ± 12 exclusive $B_s \to J/\psi\phi$ events.

B^0_s mean life ($B_s \to J/\psi\eta$)

VALUE (10^{-12} s)	DOCUMENT ID		TECN	COMMENT
1.452±0.016 OUR EVALUATION	(Produced by HFLAV)			
1.452±0.016 OUR AVERAGE				
1.445±0.016±0.008	[1,2] AAIJ	23P	LHCB	pp at 7, 8, 13 TeV
1.479±0.034±0.011	[1] AAIJ	16L	LHCB	pp at 7, 8 TeV

[1] Uses $B^0_s \to J/\psi\eta$ decays.
[2] AAIJ 23P reports a τ_L value combined with AAIJ 16AL result as $\tau_L = 1.452 \pm 0.014 \pm 0.007$ ps.

B^0_s mean life ($B_s \to J/\psi K^0_S$)

VALUE (10^{-12} s)	DOCUMENT ID		TECN	COMMENT
1.63±0.07 OUR EVALUATION	(Produced by HFLAV)			
1.63±0.07 OUR AVERAGE				
1.59±0.07±0.03	[1] HAYRAPETY...	24AX	CMS	pp at 13 TeV
1.75±0.12±0.07	[1] AAIJ	13AB	LHCB	pp at 7 TeV

[1] Measured using a pure CP-odd final state $J/\psi K^0_S$ with the assumption that contributions from penguin diagrams are small.

B^0_s mean life ($B_s \to J/\psi\pi^+\pi^-$)

VALUE (10^{-12} s)	DOCUMENT ID		TECN	COMMENT
1.641±0.013 OUR EVALUATION	(Produced by HFLAV)			
1.660±0.022 OUR AVERAGE				
1.632±0.013±0.05	[1] AAIJ	19AF	LHCB	pp at 13 TeV
1.677±0.034±0.011	[2] SIRUNYAN	18BY	CMS	pp at 8 TeV
1.70 ±0.14 ±0.05	[3] ABAZOV	16C	D0	$p\overline{p}$ at 1.96 TeV
1.652±0.024±0.024	[4] AAIJ	13AR	LHCB	pp at 7 TeV
$1.70\ ^{+0.12}_{-0.11}\ \pm0.03$	[5] AALTONEN	11AB	CDF	$p\overline{p}$ at 1.96 TeV
• • • We do not use the following data for averages, fits, limits, etc. • • •				
1.700±0.040±0.026	[5] AAIJ	12AN	LHCB	Repl. by AAIJ 13AR

[1] Based on $\Delta\Gamma = \Gamma_H - \Gamma_{B^0} = -0.05 \pm 0.004 \pm 0.004$ ps^{-1} and $\tau_{B^0} = 1.517 \pm 0.004$ ps. The first error is due to the combined $\Delta\Gamma$ uncertainty and the second is from τ_{B^0} uncertainty.
[2] Measured using $B^0_s \to J/\psi\pi^+\pi^-$ decays with $0.9240 < m(\pi\pi) < 1.0204$ GeV, which is dominated by the $f_0(980)$ resonance, making it a CP-odd state.
[3] Measured using $J/\psi\pi^+\pi^-$ mode with $0.880 < m(\pi\pi) < 1.080$ GeV/c^2, which is mostly $J/\psi f(0)(980)$ mode, a pure CP-odd final state.
[4] Measured using $B_s \to J/\psi\pi^+\pi^-$ decays which, in the limit of $\phi_s = 0$ and $|\lambda| = 1$, correspond to B^0_{sH} decays.
[5] Measured using a pure CP-odd final state $J/\psi f_0(980)$.

B^0_s mean life ($B_s \to K^+K^-$)

VALUE (10^{-12} s)	DOCUMENT ID		TECN	COMMENT
1.408±0.017 OUR EVALUATION	(Produced by HFLAV)			
1.408±0.017 OUR AVERAGE				
1.407±0.016±0.007	[1] AAIJ	14R	LHCB	pp at 7 TeV
1.440±0.096±0.009	[1] AAIJ	12	LHCB	pp at 7 TeV

[1] Measured using $B^0_s \to K^+K^-$ decays. There may still be CPV in the decay.

B^0_s mean life ($B_s \to \mu\mu$)

VALUE (10^{-12} s)	DOCUMENT ID		TECN	COMMENT
1.79±0.17 OUR EVALUATION	(Produced by HFLAV)			
$\mathbf{1.80^{+0.24}_{-0.18}}$ **OUR AVERAGE**	Error includes scale factor of 1.4. See the ideogram below.			
$0.99^{+0.42}_{-0.07}\pm0.17$	[1] AAD	23BY	ATLS	pp at 13 TeV
$1.83^{+0.23}_{-0.20}\pm0.04$	[1] TUMASYAN	23A	CMS	pp at 13 TeV
2.07±0.29±0.03	[1] AAIJ	22	LHCB	pp at 7, 8, 13 TeV
• • • We do not use the following data for averages, fits, limits, etc. • • •				
$1.70^{+0.60}_{-0.43}\pm0.09$	[1] SIRUNYAN	20AG	CMS	Repl. by TUMASYAN 23A
2.04±0.44±0.05	[1] AAIJ	17AI	LHCB	Repl. by AAIJ 22

[1] Measured using $B_s \to \mu^+\mu^-$ decays which, in the Standard Model, correspond to B^0_{sH} decays. Assumes $-2\,\mathrm{Re}(\lambda)/(1+|\lambda|^2) = 1$.

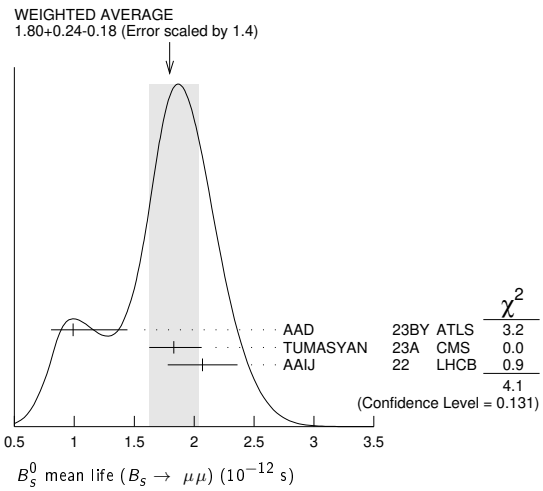

B^0_{sL} mean life ($B_s \to J/\psi\eta$, $B_s \to D^+_s D^-_s$)

VALUE (10^{-12} s)	DOCUMENT ID
1.437±0.014 OUR EVALUATION	(Produced by HFLAV)

B^0_{sH} mean life ($B_s \to J/\psi f_0$, $B_s \to J/\psi\pi\pi$)

VALUE (10^{-12} s)	DOCUMENT ID
1.641±0.013 OUR EVALUATION	(Produced by HFLAV)

$\tau_{B^0_s}/\tau_{B^0}$ mean life ratio

$\tau_{B^0_s}/\tau_{B^0}$ (direct measurements)

VALUE	DOCUMENT ID		TECN	COMMENT
0.980±0.006±0.003	[1] SIRUNYAN	18BY	CMS	pp at 8 TeV

[1] Measured using $B^0_s \to J/\psi\phi(1020)$ and $B^0 \to J/\psi K^*(892)^0$ decays.

$\Gamma_{B^0_s} - \Gamma_{B^0}$

VALUE (10^{12} s^{-1})	DOCUMENT ID		TECN	COMMENT
−0.0041±0.0024±0.0015	[1] AAIJ	19Q	LHCB	pp at 13 TeV

[1] Measured using time-dependent angular analysis of $B^0_s \to J/\psi K^+K^-$ decays.

Int. J. Mod. Phys. A 2026.41. Downloaded from www.worldscientific.com
by CALIFORNIA @ BERKELEY on 09/16/26. Re-use and distribution is strictly not permitted, except for Open Access articles.

Int. J. Mod. Phys. A 2026.41. Downloaded from www.worldscientific.com
by UNIVERSITY OF CALIFORNIA @ BERKELEY on 09/16/26. Re-use and distribution is strictly not permitted, except for Open Access articles.

$\Gamma_{B^0_{sH}} - \Gamma_{B^0}$

VALUE (10^{12} s^{-1})	DOCUMENT ID		TECN	COMMENT
$-0.050 \pm 0.004 \pm 0.004$	[1] AAIJ	19AF	LHCB	pp at 7, 8, 13 TeV

[1] Measured in $B^0_s \to J/\psi \pi^+ \pi^-$ decays.

B^0_s DECAY MODES

These branching fractions all scale with $B(\overline{b} \to B^0_s)$.

The branching fraction $B(B^0_s \to D^-_s \ell^+ \nu_\ell \text{anything})$ is not a pure measurement since the measured product branching fraction $B(\overline{b} \to B^0_s) \times B(B^0_s \to D^-_s \ell^+ \nu_\ell \text{anything})$ was used to determine $B(\overline{b} \to B^0_s)$, as described in the note on "B^0-$\overline{B}^0$ Mixing"

For inclusive branching fractions, *e.g.*, $B \to D^\pm$ anything, the values usually are multiplicities, not branching fractions. They can be greater than one.

	Mode		Fraction (Γ_i/Γ)	Scale factor/ Confidence level
Γ_1	D^-_s anything			
Γ_2	$D^\pm_s$ anything		(65 ± 5) %	
Γ_3	$D^0/\overline{D}^0$ anything		(24 ± 4) %	
Γ_4	$D^\pm$ anything		(13 ± 5) %	
Γ_5	$\ell \nu_\ell X$		(9.6 ± 0.8) %	
Γ_6	$e^+ \nu X^-$		(9.1 ± 0.8) %	
Γ_7	$\mu^+ \nu X^-$		(10.2 ± 1.0) %	
Γ_8	$D^-_s \ell^+ \nu_\ell$ anything	[a]	(8.1 ± 1.3) %	
Γ_9	$D^{*-}_s \ell^+ \nu_\ell$ anything		(5.4 ± 1.1) %	
Γ_{10}	$D^-_s \mu^+ \nu_\mu$		(2.31 ± 0.21) %	
Γ_{11}	$D^{*-}_s \mu^+ \nu_\mu$		(5.2 ± 0.5) %	
Γ_{12}	$D_{s1}(2536)^- \mu^+ \nu_\mu$, $D^-_{s1} \to D^{*-} K^0_S$		$(2.7 \pm 0.7) \times 10^{-3}$	
Γ_{13}	$D_{s1}(2536)^- X \mu^+ \nu$, $D^-_{s1} \to \overline{D}^0 K^+$		$(4.4 \pm 1.3) \times 10^{-3}$	
Γ_{14}	$D_{s2}(2573)^- X \mu^+ \nu$, $D^-_{s2} \to \overline{D}^0 K^+$		$(2.7 \pm 1.0) \times 10^{-3}$	
Γ_{15}	$K^- \mu^+ \nu_\mu$		$(1.06 \pm 0.09) \times 10^{-4}$	
Γ_{16}	$D^-_s \pi^+$		$(2.98 \pm 0.13) \times 10^{-3}$	
Γ_{17}	$D^-_s \rho^+$		$(6.9 \pm 1.4) \times 10^{-3}$	
Γ_{18}	$D^-_s \pi^+ \pi^+ \pi^-$		$(6.1 \pm 1.0) \times 10^{-3}$	
Γ_{19}	$D_{s1}(2536)^- \pi^+$, $D^-_{s1} \to D^-_s \pi^+ \pi^-$		$(2.4 \pm 0.8) \times 10^{-5}$	
Γ_{20}	$D^\mp_s K^\pm$		$(2.25 \pm 0.12) \times 10^{-4}$	
Γ_{21}	$D_{s1}(2536)^\mp K^\pm$, $D^-_{s1} \to \overline{D}^*(2007)^0 K^-$		$(2.48 \pm 0.28) \times 10^{-5}$	
Γ_{22}	$D^-_s K^+ \pi^+ \pi^-$		$(3.2 \pm 0.6) \times 10^{-4}$	
Γ_{23}	$D^+_s D^-_s$		$(4.5 \pm 0.6) \times 10^{-3}$	S=1.3
Γ_{24}	$D^-_s D^+$		$(3.1 \pm 0.5) \times 10^{-4}$	
Γ_{25}	$D^+ D^-$		$(2.2 \pm 0.6) \times 10^{-4}$	
Γ_{26}	$D^{*+} D^-$			
Γ_{27}	$D^{*-} D^+$			
Γ_{28}	$D^{*+} D^{*-}$		$(2.14 \pm 0.32) \times 10^{-4}$	
Γ_{29}	$D^0 \overline{D}^0$		$(1.9 \pm 0.5) \times 10^{-4}$	
Γ_{30}	$D^{*-}_s \pi^+$		$(1.9 {}^{+0.5}_{-0.4}) \times 10^{-3}$	
Γ_{31}	$D^{*\mp}_s K^\pm$		$(1.32 {}^{+0.40}_{-0.32}) \times 10^{-4}$	
Γ_{32}	$D^{*-}_s \rho^+$		$(9.5 \pm 2.0) \times 10^{-3}$	
Γ_{33}	$D^{*+}_s D^-_s + D^{*-}_s D^+_s$		(1.51 ± 0.13) %	
Γ_{34}	$D^{*+}_s D^{*-}_s$		(1.58 ± 0.20) %	S=1.3
Γ_{35}	$D^{(*)+}_s D^{(*)-}_s$		(4.5 ± 1.4) %	
Γ_{36}	$D^{*-} D^+_s$		$(4.0 \pm 0.7) \times 10^{-4}$	
Γ_{37}	$\overline{D}^{*0} \overline{K}^0$		$(2.8 \pm 1.1) \times 10^{-4}$	
Γ_{38}	$\overline{D}^0 \overline{K}^0$		$(4.3 \pm 0.9) \times 10^{-4}$	
Γ_{39}	$\overline{D}^0 K^- \pi^+$		$(1.04 \pm 0.13) \times 10^{-3}$	
Γ_{40}	$\overline{D}^*(2007)^0 K^- \pi^+$		$(7.3 \pm 2.6) \times 10^{-4}$	
Γ_{41}	$\overline{D}^0 \overline{K}^*(892)^0$		$(4.4 \pm 0.6) \times 10^{-4}$	
Γ_{42}	$\overline{D}^0 \overline{K}^*(1410)$		$(3.9 \pm 3.5) \times 10^{-4}$	
Γ_{43}	$\overline{D}^0 \overline{K}^*_0(1430)$		$(3.0 \pm 0.7) \times 10^{-4}$	
Γ_{44}	$\overline{D}^0 \overline{K}^*_2(1430)$		$(1.1 \pm 0.4) \times 10^{-4}$	
Γ_{45}	$\overline{D}^0 \overline{K}^*(1680)$		$< 7.8 \times 10^{-5}$	CL=90%
Γ_{46}	$\overline{D}^0 \overline{K}^*_0(1950)$		$< 1.1 \times 10^{-4}$	CL=90%
Γ_{47}	$\overline{D}^0 \overline{K}^*_3(1780)$		$< 2.6 \times 10^{-5}$	CL=90%
Γ_{48}	$\overline{D}^0 \overline{K}^*_4(2045)$		$< 3.1 \times 10^{-5}$	CL=90%
Γ_{49}	$\overline{D}^0 K^- \pi^+$ (non-resonant)		$(2.1 \pm 0.8) \times 10^{-4}$	
Γ_{50}	$[K^+ K^-]_D \overline{K}^*(892)^0$		$(4.4 \pm 0.6) \times 10^{-4}$	
Γ_{51}	$[\pi^+ \pi^-]_D \overline{K}^*(892)^0$		$(4.4 \pm 0.6) \times 10^{-4}$	
Γ_{52}	$[\pi^+ K^-]_D \overline{K}^*(892)^0$			
Γ_{53}	$[K^+ \pi^-]_D \overline{K}^*(892)^0$			
Γ_{54}	$[\pi^+ \pi^- \pi^+ \pi^-]_D \overline{K}^*(892)^0$		$(4.4 \pm 0.6) \times 10^{-4}$	
Γ_{55}	$[\pi^+ K^- \pi^+ \pi^-]_D \overline{K}^*(892)^0$			
Γ_{56}	$[K^+ \pi^- \pi^+ \pi^-]_D \overline{K}^*(892)^0$			
Γ_{57}	$D^*_{s2}(2573)^- \pi^+$, $D^*_{s2} \to \overline{D}^0 K^-$		$(2.6 \pm 0.4) \times 10^{-4}$	
Γ_{58}	$D^*_{s1}(2700)^- \pi^+$, $D^*_{s1} \to \overline{D}^0 K^-$		$(1.6 \pm 0.8) \times 10^{-5}$	
Γ_{59}	$D^*_{s1}(2860)^- \pi^+$, $D^*_{s1} \to \overline{D}^0 K^-$		$(5 \pm 4) \times 10^{-5}$	
Γ_{60}	$D^*_{s3}(2860)^- \pi^+$, $D^*_{s3} \to \overline{D}^0 K^-$		$(2.2 \pm 0.6) \times 10^{-5}$	
Γ_{61}	$\overline{D}^0 K^+ K^-$		$(5.6 \pm 0.9) \times 10^{-5}$	
Γ_{62}	$\overline{D}^0 f_0(980)$		$< 3.1 \times 10^{-6}$	CL=90%
Γ_{63}	$\overline{D}^0 \phi$		$(2.30 \pm 0.25) \times 10^{-5}$	
Γ_{64}	$\overline{D}^{*0} \phi$		$(3.2 \pm 0.4) \times 10^{-5}$	
Γ_{65}	$D^{*\mp} \pi^\pm$		$< 6.1 \times 10^{-6}$	CL=90%
Γ_{66}	$\eta_c \phi$		$(5.0 \pm 0.9) \times 10^{-4}$	
Γ_{67}	$\eta' X_{s\overline{s}}$			
Γ_{68}	$\eta_c \pi^+ \pi^-$		$(1.8 \pm 0.7) \times 10^{-4}$	
Γ_{69}	$J/\psi(1S) \phi$		$(1.01 \pm 0.04) \times 10^{-3}$	
Γ_{70}	$J/\psi(1S) \phi \phi$		$(1.17 {}^{+0.14}_{-0.16}) \times 10^{-5}$	
Γ_{71}	$J/\psi(1S) \pi^0$		$< 1.21 \times 10^{-5}$	CL=90%
Γ_{72}	$J/\psi(1S) \eta$		$(4.45 \pm 0.25) \times 10^{-4}$	S=1.1
Γ_{73}	$J/\psi(1S) K^0_S$		$(1.92 \pm 0.14) \times 10^{-5}$	
Γ_{74}	$J/\psi(1S) \overline{K}^*(892)^0$		$(3.95 \pm 0.24) \times 10^{-5}$	
Γ_{75}	$J/\psi(1S) \eta'$		$(3.53 \pm 0.22) \times 10^{-4}$	S=1.1
Γ_{76}	$J/\psi(1S) \pi^+ \pi^-$		$(2.00 \pm 0.17) \times 10^{-4}$	S=1.7
Γ_{77}	$J/\psi(1S) f_0(500)$, $f_0 \to \pi^+ \pi^-$		$< 4 \times 10^{-6}$	CL=90%
Γ_{78}	$J/\psi(1S) \rho$, $\rho \to \pi^+ \pi^-$		$< 3.4 \times 10^{-6}$	CL=90%
Γ_{79}	$J/\psi(1S) f_0(980)$, $f_0 \to \pi^+ \pi^-$		$(1.23 \pm 0.15) \times 10^{-4}$	S=2.1
Γ_{80}	$J/\psi(1S) f_2(1270)$, $f_2 \to \pi^+ \pi^-$		$(1.0 \pm 0.4) \times 10^{-6}$	
Γ_{81}	$J/\psi(1S) f_2(1270)_0$, $f_2 \to \pi^+ \pi^-$		$(7.2 \pm 1.6) \times 10^{-7}$	
Γ_{82}	$J/\psi(1S) f_2(1270)_\parallel$, $f_2 \to \pi^+ \pi^-$		$(1.04 \pm 0.32) \times 10^{-6}$	
Γ_{83}	$J/\psi(1S) f_2(1270)_\perp$, $f_2 \to \pi^+ \pi^-$		$(1.3 \pm 0.7) \times 10^{-6}$	
Γ_{84}	$J/\psi(1S) f_0(1370)$, $f_0 \to \pi^+ \pi^-$		$(4.4 {}^{+0.6}_{-4.0}) \times 10^{-5}$	
Γ_{85}	$J/\psi(1S) f_0(1500)$, $f_0 \to \pi^+ \pi^-$		$(2.02 {}^{+0.32}_{-0.24}) \times 10^{-5}$	
Γ_{86}	$J/\psi(1S) f'_2(1525)_0$, $f'_2 \to \pi^+ \pi^-$		$(1.02 \pm 0.22) \times 10^{-6}$	
Γ_{87}	$J/\psi(1S) f'_2(1525)_\parallel$, $f'_2 \to \pi^+ \pi^-$		$(1.2 {}^{+2.6}_{-0.8}) \times 10^{-7}$	
Γ_{88}	$J/\psi(1S) f'_2(1525)_\perp$, $f'_2 \to \pi^+ \pi^-$		$(5 \pm 4) \times 10^{-7}$	
Γ_{89}	$J/\psi(1S) f_0(1790)$, $f_0 \to \pi^+ \pi^-$		$(4.8 {}^{+10.0}_{-1.0}) \times 10^{-6}$	
Γ_{90}	$J/\psi(1S) \pi^+ \pi^-$ (nonresonant)		$(1.72 {}^{+1.00}_{-0.34}) \times 10^{-5}$	
Γ_{91}	$J/\psi(1S) \overline{K}^0 \pi^+ \pi^-$		$< 4.4 \times 10^{-5}$	CL=90%
Γ_{92}	$J/\psi(1S) K^+ K^-$		$(7.9 \pm 0.7) \times 10^{-4}$	
Γ_{93}	$J/\psi(1S) K^0 K^- \pi^+ +$ c.c.		$(9.5 \pm 1.3) \times 10^{-4}$	
Γ_{94}	$J/\psi(1S) \overline{K}^0 K^+ K^-$		$< 1.2 \times 10^{-5}$	CL=90%
Γ_{95}	$J/\psi K^*(892)^0 \overline{K}^*(892)^0$		$(1.07 \pm 0.09) \times 10^{-4}$	
Γ_{96}	$J/\psi(1S) f'_2(1525)$		$(2.6 \pm 0.6) \times 10^{-4}$	
Γ_{97}	$J/\psi(1S) p \overline{p}$		$(3.6 \pm 0.4) \times 10^{-6}$	
Γ_{98}	$J/\psi(1S) \gamma$		$< 7.3 \times 10^{-6}$	CL=90%
Γ_{99}	$J/\psi \mu^+ \mu^-$, $J/\psi \to \mu^+ \mu^-$		$< 2.6 \times 10^{-9}$	CL=95%
Γ_{100}	$J/\psi(1S) \pi^+ \pi^- \pi^+ \pi^-$		$(7.4 \pm 0.8) \times 10^{-5}$	
Γ_{101}	$J/\psi(1S) f_1(1285)$		$(7.2 \pm 1.4) \times 10^{-5}$	
Γ_{102}	$J/\psi(1S) \overline{D}^0$		$< 1.0 \times 10^{-6}$	CL=90%
Γ_{103}	$\psi(2S) \eta$		$(3.7 \pm 0.8) \times 10^{-4}$	
Γ_{104}	$\psi(2S) \eta'$		$(1.37 \pm 0.33) \times 10^{-4}$	
Γ_{105}	$\psi(2S) \pi^+ \pi^-$		$(6.8 \pm 1.2) \times 10^{-5}$	
Γ_{106}	$\psi(2S) \phi$		$(5.1 \pm 0.4) \times 10^{-4}$	

Int. J. Mod. Phys. A 2026.41. Downloaded from www.worldscientific.com
by CALIFORNIA @ BERKELEY on 09/16/26. Re-use and distribution is strictly not permitted, except for Open Access articles.

Γ_{107}	$\psi(2S)K^0$		$(1.9 \pm 0.5) \times 10^{-5}$	
Γ_{108}	$\psi(2S)K^-\pi^+$		$(3.1 \pm 0.4) \times 10^{-5}$	
Γ_{109}	$\psi(2S)\overline{K}^*(892)^0$		$(3.3 \pm 0.5) \times 10^{-5}$	
Γ_{110}	$\chi_{c1}\phi$		$(1.92 \pm 0.25) \times 10^{-4}$	
Γ_{111}	$\chi_{c1}K^+K^-$			
Γ_{112}	$\chi_{c2}K^+K^-$			
Γ_{113}	$\chi_{c1}(3872)\phi$		$(9.6 \pm 3.2) \times 10^{-5}$	
Γ_{114}	$\chi_{c1}(3872)(K^+K^-)_{non-\phi}$		$(7.6 \pm 3.0) \times 10^{-5}$	
Γ_{115}	$\chi_{c1}(3872)\pi^+\pi^-$		$(3.7 \pm 1.5) \times 10^{-5}$	
Γ_{116}	$\pi^+\pi^-$		$(7.1 \pm 0.8) \times 10^{-7}$	
Γ_{117}	$\pi^0\pi^0$		$< 7.7 \times 10^{-6}$	CL=90%
Γ_{118}	$\eta\pi^0$		$< 1.0 \times 10^{-3}$	CL=90%
Γ_{119}	$\eta\eta$		$< 1.43 \times 10^{-4}$	CL=90%
Γ_{120}	$\rho^0\rho^0$		$< 3.20 \times 10^{-4}$	CL=90%
Γ_{121}	$\eta' K_S^0$		$< 8.16 \times 10^{-6}$	CL=90%
Γ_{122}	$\eta'\eta$		$< 6.5 \times 10^{-5}$	CL=90%
Γ_{123}	$\eta'\eta'$		$(3.3 \pm 0.7) \times 10^{-5}$	
Γ_{124}	$\eta'\phi$		$< 8.2 \times 10^{-7}$	CL=90%
Γ_{125}	$\phi f_0(980)$, $f_0(980) \to \pi^+\pi^-$		$(1.12 \pm 0.21) \times 10^{-6}$	
Γ_{126}	$\phi f_2(1270)$, $f_2(1270) \to \pi^+\pi^-$		$(6.1 {}^{+1.8}_{-1.5}) \times 10^{-7}$	
Γ_{127}	$\phi\rho^0$		$(2.7 \pm 0.8) \times 10^{-7}$	
Γ_{128}	$\phi\pi^+\pi^-$		$(3.5 \pm 0.5) \times 10^{-6}$	
Γ_{129}	$\phi\phi$		$(1.83 \pm 0.14) \times 10^{-5}$	
Γ_{130}	$\phi\phi\phi$		$(2.1 \pm 0.6) \times 10^{-6}$	
Γ_{131}	π^+K^-		$(5.9 \pm 0.6) \times 10^{-6}$	
Γ_{132}	K^+K^-		$(2.61 \pm 0.16) \times 10^{-5}$	
Γ_{133}	$K^0\overline{K}^0$		$(1.76 \pm 0.31) \times 10^{-5}$	
Γ_{134}	$K^0\pi^+\pi^-$		$(9.5 \pm 2.1) \times 10^{-6}$	
Γ_{135}	$K^0K^\pm\pi^\mp$		$(8.4 \pm 0.9) \times 10^{-5}$	
Γ_{136}	$K^*(892)^-\pi^+$		$(2.9 \pm 1.1) \times 10^{-6}$	
Γ_{137}	$K^*(892)^\pm K^\mp$		$(1.9 \pm 0.5) \times 10^{-5}$	
Γ_{138}	$K_0^*(1430)^\pm K^\mp$		$(3.1 \pm 2.5) \times 10^{-5}$	
Γ_{139}	$K_2^*(1430)^\pm K^\mp$		$(1.0 \pm 1.7) \times 10^{-5}$	
Γ_{140}	$K^*(892)^0\overline{K}^0 +$ c.c.		$(2.0 \pm 0.6) \times 10^{-5}$	
Γ_{141}	$K_0^*(1430)\overline{K}^0 +$ c.c.		$(3.3 \pm 1.0) \times 10^{-5}$	
Γ_{142}	$K_2^*(1430)^0\overline{K}^0 +$ c.c.		$(1.7 \pm 2.2) \times 10^{-5}$	
Γ_{143}	$K_S^0\overline{K}^*(892)^0 +$ c.c.		$(1.6 \pm 0.4) \times 10^{-5}$	
Γ_{144}	$K^0K^+K^-$		$(1.3 \pm 0.6) \times 10^{-6}$	
Γ_{145}	$\overline{K}^*(892)^0\rho^0$		$< 7.67 \times 10^{-4}$	CL=90%
Γ_{146}	$\overline{K}^*(892)^0K^*(892)^0$		$(1.11 \pm 0.27) \times 10^{-5}$	
Γ_{147}	$K^*(892)^0\overline{K}_2^*(1430)^0$			
Γ_{148}	$K_2^*(1430)^0\overline{K}^*(892)^0$			
Γ_{149}	$K_2^*(1430)^0\overline{K}_2^*(1430)^0$			
Γ_{150}	$\phi K^*(892)^0$		$(1.14 \pm 0.30) \times 10^{-6}$	
Γ_{151}	$p\overline{p}$		$< 4.4 \times 10^{-9}$	CL=90%
Γ_{152}	$p\overline{p}K^0$		$(9.1 \pm 2.0) \times 10^{-7}$	
Γ_{153}	$p\overline{p}K^+K^-$		$(4.5 \pm 0.5) \times 10^{-6}$	
Γ_{154}	$p\overline{p}K^+\pi^-$		$(1.39 \pm 0.26) \times 10^{-6}$	
Γ_{155}	$p\overline{p}\pi^+\pi^-$		$(4.3 \pm 2.0) \times 10^{-7}$	
Γ_{156}	$p\overline{p}p\overline{p}$		$(2.3 \pm 1.0) \times 10^{-8}$	
Γ_{157}	$p\overline{\Lambda}K^- +$ c.c.		$(5.5 \pm 1.0) \times 10^{-6}$	
Γ_{158}	$\Lambda_c^-\Lambda\pi^+$		$(3.6 \pm 1.6) \times 10^{-4}$	
Γ_{159}	$\Lambda_c^-\Lambda_c^+$		$< 8.0 \times 10^{-5}$	CL=95%

Lepton family (LF), lepton (L), baryon (B) number violating modes or $\Delta B = 1$ weak neutral current ($B1$) modes

Γ_{160}	$\gamma\gamma$	$B1$		$< 3.1 \times 10^{-6}$	CL=90%
Γ_{161}	$\phi\gamma$	$B1$		$(3.4 \pm 0.4) \times 10^{-5}$	
Γ_{162}	$f_2(1270)\gamma$	$B1$		$(9 {}^{+4}_{-5}) \times 10^{-6}$	
Γ_{163}	$f_2'(1525)\gamma$	$B1$		$(6.7 {}^{+0.9}_{-0.8}) \times 10^{-6}$	
Γ_{164}	$\phi(1680)\gamma$, $\phi \to K^+K^-$	$B1$		$(9.3 \pm 2.4) \times 10^{-7}$	
Γ_{165}	$\phi_3(1850)\gamma$, $\phi_3 \to K^+K^-$	$B1$		$(7 {}^{+6}_{-5}) \times 10^{-8}$	
Γ_{166}	$f_2(2010)\gamma$, $f_2 \to K^+K^-$	$B1$		$(1.0 {}^{+0.7}_{-0.5}) \times 10^{-7}$	
Γ_{167}	$\mu^+\mu^-$	$B1$		$(3.34 \pm 0.27) \times 10^{-9}$	
Γ_{168}	e^+e^-	$B1$		$< 9.4 \times 10^{-9}$	CL=90%
Γ_{169}	$\tau^+\tau^-$	$B1$		$< 6.8 \times 10^{-3}$	CL=95%
Γ_{170}	$\mu^+\mu^-\gamma$	$B1$		$< 4.2 \times 10^{-8}$	CL=95%
Γ_{171}	$\mu^+\mu^-\mu^+\mu^-$	$B1$		$< 8.6 \times 10^{-10}$	CL=95%
Γ_{172}	SP, $S \to \mu^+\mu^-$, $P \to \mu^+\mu^-$	$B1$	[b]	$< 2.2 \times 10^{-9}$	CL=95%
Γ_{173}	aa, $a \to \mu^+\mu^-$	$B1$		$< 5.8 \times 10^{-10}$	CL=95%
Γ_{174}	$\phi(1020)\mu^+\mu^-$	$B1$		$(8.2 \pm 0.4) \times 10^{-7}$	
Γ_{175}	$f_2'(1525)\mu^+\mu^-$	$B1$		$(1.57 \pm 0.22) \times 10^{-7}$	
Γ_{176}	$\overline{K}^*(892)^0\mu^+\mu^-$	$B1$		$(2.9 \pm 1.1) \times 10^{-8}$	
Γ_{177}	$\pi^+\pi^-\mu^+\mu^-$	$B1$		$(8.4 \pm 1.7) \times 10^{-8}$	
Γ_{178}	$\overline{D}^0\mu^+\mu^-$	$B1$		$< 1.2 \times 10^{-7}$	CL=90%
Γ_{179}	$\phi\nu\overline{\nu}$	$B1$		$< 5.4 \times 10^{-3}$	CL=90%
Γ_{180}	invisible	$B1$			
Γ_{181}	$e^\pm\mu^\mp$	LF	[c]	$< 5.4 \times 10^{-9}$	CL=90%
Γ_{182}	$e^\pm\tau^\mp$	LF		$< 1.4 \times 10^{-3}$	CL=90%
Γ_{183}	$\mu^\pm\tau^\mp$	LF		$< 4.2 \times 10^{-5}$	CL=95%
Γ_{184}	$\phi\mu^\pm e^\mp$	LF		$< 1.6 \times 10^{-8}$	CL=90%
Γ_{185}	$\phi\mu^\pm\tau^\mp$	LF		$< 1.0 \times 10^{-5}$	CL=90%
Γ_{186}	$p\mu^-$	L,B		$< 1.21 \times 10^{-8}$	CL=90%

[a] Not a pure measurement. See note at head of B_s^0 Decay Modes.

[b] Here S and P are the hypothetical scalar and pseudoscalar particles with masses of 2.5 GeV/c^2 and 214.3 MeV/c^2, respectively.

[c] The value is for the sum of the charge states or particle/antiparticle states indicated.

FIT INFORMATION

An overall fit to 16 branching ratios uses 28 measurements to determine 9 parameters. The overall fit has a $\chi^2 = 32.6$ for 19 degrees of freedom.

The following *off-diagonal* array elements are the correlation coefficients $\langle \delta x_i \delta x_j \rangle / (\delta x_i \cdot \delta x_j)$, in percent, from the fit to the branching fractions, $x_i \equiv \Gamma_i/\Gamma_{total}$.

x_{18}	17							
x_{20}	81	13						
x_{69}	0	0	0					
x_{72}	0	0	0	46				
x_{75}	0	0	0	39	83			
x_{76}	0	0	0	41	19	16		
x_{79}	0	0	0	29	14	11	52	
x_{129}	0	0	0	15	7	6	6	4
	x_{16}	x_{18}	x_{20}	x_{69}	x_{72}	x_{75}	x_{76}	x_{79}

B_s^0 BRANCHING RATIOS

$\Gamma(D_s^\pm \text{anything})/\Gamma_{total}$ — Γ_2/Γ

VALUE	EVTS	DOCUMENT ID		TECN	CHG	COMMENT
0.65 ±0.05 OUR AVERAGE						
0.634±0.045±0.022		[1,2] ADACHI	25O	BEL2	±	$e^+e^- \to \Upsilon(5S)$
0.91 ±0.18 ±0.41		[3] DRUTSKOY	07	BELL	−	$e^+e^- \to \Upsilon(5S)$
0.81 ±0.24 ±0.22	90	[4] BUSKULIC	96E	ALEP	−	$e^+e^- \to Z$
1.56 ±0.58 ±0.44	147	[5] ACTON	92N	OPAL	−	$e^+e^- \to Z$
• • • We do not use the following data for averages, fits, limits, etc. • • •						
0.92 ±0.11		[6] ZHUKOVA	23	BELL	±	$e^+e^- \to \Upsilon(5S)$
0.605±0.058±0.022		[7,8] WANG	22	BELL	−	$e^+e^- \to \Upsilon(5S)$

[1] ADACHI 25O branching fraction is measured to be $0.0686 \pm 0.072 \pm 0.040$. They improve the measurement by averaging this result with the previous BELLE measurement with semileptonic tagging in WANG 22 after rescaling the previous measurement with the most recent values of D_s^+ branching fractions and taking into account correlated uncertainties.

[2] Supersedes ZHUKOVA 23 and partially WANG 22.

[3] The extraction of this result takes into account the correlation between the measurements of $B(\Upsilon(5S) \to D_s X)$ and $B(\Upsilon(5S) \to D^0 X)$.

[4] BUSKULIC 96E separate $c\overline{c}$ and $b\overline{b}$ sources of D_s^+ mesons using a lifetime tag, subtract generic $\overline{b} \to W^+ \to D_s^+$ events, and obtain $B(\overline{b} \to B_s^0) \times B(B_s^0 \to D_s^- \text{anything}) = 0.088 \pm 0.020 \pm 0.020$ assuming $B(D_s \to \phi\pi) = (3.5 \pm 0.4) \times 10^{-2}$ and PDG 1994 values for the relative partial widths to other D_s channels. We evaluate using our current values $B(\overline{b} \to B_s^0) = 0.107 \pm 0.014$ and $B(D_s \to \phi\pi) = 0.036 \pm 0.009$. Our first error is their experiment's and our second error is that due to $B(\overline{b} \to B_s^0)$ and $B(D_s \to \phi\pi)$.

[5] ACTON 92N assume that excess of 147 ± 48 D_s^0 events over that expected from B^0, B^+, and $c\overline{c}$ is all from B_s^0 decay. The product branching fraction is measured to be $B(\overline{b} \to B_s^0)B(B_s^0 \to D_s^- \text{anything}) \times B(D_s^- \to \phi\pi^-) = (5.9 \pm 1.9 \pm 1.1) \times 10^{-3}$. We evaluate using our current values $B(\overline{b} \to B_s^0) = 0.107 \pm 0.014$ and $B(D_s \to \phi\pi) = 0.036 \pm 0.009$. Our first error is their experiment's and our second error is that due to $B(\overline{b} \to B_s^0)$ and $B(D_s \to \phi\pi)$.

[6] Repl. by ADACHI 25O.

[7] WANG 22 selects the B_s events by tagging the accompanying B_s via partial reconstruction of the semileptonic decays $B_s \to D_s X \ell^+ \nu$. Partially superseded by ADACHI 25O.

[8] This measurement, originally $0.602 \pm 0.058 \pm 0.023$, has been rescaled by ADACHI 25O with the most recent values of D_s^+ branching fractions.

Int. J. Mod. Phys. A 2026.41. Downloaded from www.worldscientific.com
by UNIVERSITY OF CALIFORNIA @ BERKELEY on 09/16/26. Re-use and distribution is strictly not permitted, except for Open Access articles.

$\Gamma(D^0/\overline{D}^0 \text{anything})/\Gamma(D_s^\pm \text{anything})$ — Γ_3/Γ_2

VALUE	DOCUMENT ID		TECN	COMMENT
0.416±0.018±0.092	ZHUKOVA	23	BELL	$e^+e^- \to \Upsilon(5S)$

$\Gamma(D^0/\overline{D}^0 \text{anything})/\Gamma_{\text{total}}$ — Γ_3/Γ

VALUE	DOCUMENT ID		TECN	COMMENT
0.239±0.041±0.018	[1] ADACHI	25O	BEL2	$e^+e^- \to \Upsilon(5S)$

[1] ADACHI 25O direct measurement of the branching fraction is 0.215±0.061±0.018. They improve the measurement by averaging this result with the previous BELLE measurement of $B(B_s^0 \to D^0/\overline{D}^0 X)/B(B_s^0 \to D_s^\pm X) = 0.416 \pm 0.018 \pm 0.092$ of ZHUKOVA 23, multiplied by best value of $B(B_s^0 \to D_s^\pm X)$ obtained by ADACHI 25O, and taking into account correlated uncertainties.

$\Gamma(D^\pm \text{anything})/\Gamma_{\text{total}}$ — Γ_4/Γ

VALUE	DOCUMENT ID		TECN	COMMENT
0.126±0.046±0.013	ADACHI	25O	BEL2	$e^+e^- \to \Upsilon(5S)$

$\Gamma(\ell\nu_\ell X)/\Gamma_{\text{total}}$ — Γ_5/Γ

VALUE (units 10^{-2})	DOCUMENT ID		TECN	COMMENT
9.6±0.8 OUR AVERAGE				
9.6±0.4±0.7	[1] OSWALD	13	BELL	$e^+e^- \to \Upsilon(5S)$
$9.5^{+2.5}_{-2.0}{}^{+1.1}_{-1.9}$	[2] LEES	12A	BABR	e^+e^-

[1] The measurement corresponds to the average of the electron and muon branching fractions.

[2] The measurement corresponds to a branching fraction where the lepton originates from bottom decay and is the average between the electron and muon branching fractions. LEES 12A uses the correlation of the production of ϕ mesons in association with a lepton in e^+e^- data taken at center-of-mass energies between 10.54 and 11.2 GeV.

$\Gamma(e^+\nu X^-)/\Gamma_{\text{total}}$ — Γ_6/Γ

VALUE (units 10^{-2})	DOCUMENT ID		TECN	COMMENT
9.1±0.5±0.6	OSWALD	13	BELL	$e^+e^- \to \Upsilon(5S)$

$\Gamma(\mu^+\nu X^-)/\Gamma_{\text{total}}$ — Γ_7/Γ

VALUE (units 10^{-2})	DOCUMENT ID		TECN	COMMENT
10.2±0.6±0.8	OSWALD	13	BELL	$e^+e^- \to \Upsilon(5S)$

$\Gamma(D_s^-\ell^+\nu_\ell \text{anything})/\Gamma_{\text{total}}$ — Γ_8/Γ

The values and averages in this section serve only to show what values result if one assumes our $B(\overline{b} \to B_s^0)$. They cannot be thought of as measurements since the underlying product branching fractions were also used to determine $B(\overline{b} \to B_s^0)$ as described in the note on "Production and Decay of b-Flavored Hadrons."

VALUE (units 10^{-2})	EVTS	DOCUMENT ID		TECN	COMMENT
8.1±1.3 OUR AVERAGE					
8.2±0.2±1.5		[1] OSWALD	15	BELL	$e^+e^- \to \Upsilon(5S)$
7.6±1.2±2.1	134	[2] BUSKULIC	95O	ALEP	$e^+e^- \to Z$
10.7±4.3±2.9		[3] ABREU	92M	DLPH	$e^+e^- \to Z$
10.3±3.6±2.8	18	[4] ACTON	92N	OPAL	$e^+e^- \to Z$
• • • We do not use the following data for averages, fits, limits, etc. • • •					
13 ±4 ±4	27	[5] BUSKULIC	92E	ALEP	$e^+e^- \to Z$

[1] Obtains $B_s \to D_s X e\nu$, and $D_s X \mu\nu$ separately, then combines them by assuming systematic uncertainties are fully correlated, except for the one on lepton identification. The third uncertainty adds in quadrature systematic uncertainties from external sources (number of B_s events, and $D_s^{(*)}$ branching fractions). OSWALD 15 also measures the cross-section $\sigma(e^+e^- \to B_s^{(*)}\overline{B}_s^{(*)}) = 53.8 \pm 1.4 \pm 5.3$ pb at $\sqrt{s} = 10.86$ GeV.

[2] BUSKULIC 95O use $D_s\ell$ correlations. The measured product branching ratio is $B(\overline{b} \to B_s) \times B(B_s \to D_s^-\ell^+\nu_\ell \text{anything}) = (0.82 \pm 0.09^{+0.13}_{-0.14})\%$ assuming $B(D_s \to \phi\pi) = (3.5 \pm 0.4) \times 10^{-2}$ and PDG 1994 values for the relative partial widths to the six other D_s channels used in this analysis. Combined with results from $\Upsilon(4S)$ experiments this can be used to extract $B(\overline{b} \to B_s) = (11.0 \pm 1.2^{+2.5}_{-2.6})\%$. We evaluate using our current values $B(\overline{b} \to B_s^0) = 0.107 \pm 0.014$ and $B(D_s \to \phi\pi) = 0.036 \pm 0.009$. Our first error is their experiment's and our second error is that due to $B(\overline{b} \to B_s^0)$ and $B(D_s \to \phi\pi)$.

[3] ABREU 92M measured muons only and obtained product branching ratio $B(Z \to b \text{ or } \overline{b}) \times B(\overline{b} \to B_s) \times B(B_s \to D_s\mu^+\nu_\mu \text{anything}) \times B(D_s \to \phi\pi) = (18 \pm 8) \times 10^{-5}$. We evaluate using our current values $B(\overline{b} \to B_s^0) = 0.107 \pm 0.014$ and $B(D_s \to \phi\pi) = 0.036 \pm 0.009$. Our first error is their experiment's and our second error is that due to $B(\overline{b} \to B_s^0)$ and $B(D_s \to \phi\pi)$. We use $B(Z \to b \text{ or } \overline{b}) = 2B(Z \to b\overline{b}) = 2\times(0.2212 \pm 0.0019)$.

[4] ACTON 92N is measured using $D_s \to \phi\pi^+$ and $K^*(892)^0 K^+$ events. The product branching fraction measured is measured to be $B(\overline{b} \to B_s^0)B(B_s^0 \to D_s^-\ell^+\nu_\ell \text{anything}) \times B(D_s^- \to \phi\pi^-) = (3.9 \pm 1.1 \pm 0.8) \times 10^{-4}$. We evaluate using our current values $B(\overline{b} \to B_s^0) = 0.107 \pm 0.014$ and $B(D_s \to \phi\pi) = 0.036 \pm 0.009$. Our first error is their experiment's and our second error is that due to $B(\overline{b} \to B_s^0)$ and $B(D_s \to \phi\pi)$.

[5] BUSKULIC 92E is measured using $D_s \to \phi\pi^+$ and $K^*(892)^0 K^+$ events. They use 2.7 ± 0.7% for the $\phi\pi^+$ branching fraction. The average product branching fraction is measured to be $B(\overline{b} \to B_s^0)B(B_s^0 \to D_s^-\ell^+\nu_\ell \text{anything}) = 0.020 \pm 0.0055^{+0.005}_{-0.006}$. We evaluate using our current values $B(\overline{b} \to B_s^0) = 0.107 \pm 0.014$ and $B(D_s \to \phi\pi) = 0.036 \pm 0.009$. Our first error is their experiment's and our second error is that due to $B(\overline{b} \to B_s^0)$ and $B(D_s \to \phi\pi)$. Superseded by BUSKULIC 95O.

$\Gamma(D_s^{*-}\ell^+\nu_\ell \text{anything})/\Gamma_{\text{total}}$ — Γ_9/Γ

VALUE (units 10^{-2})	DOCUMENT ID		TECN	COMMENT
5.4±0.4±1.0	[1] OSWALD	15	BELL	$e^+e^- \to \Upsilon(5S)$

[1] Obtains $B_s \to D_s^* X e\nu$, and $D_s^* X \mu\nu$ separately, then combines them by assuming systematic uncertainties are fully correlated, except for the one on lepton identification. The third uncertainty adds in quadrature systematic uncertainties from external sources (number of B_s events, and $D_s^{(*)}$ branching fractions). OSWALD 15 also measures the cross-section $\sigma(e^+e^- \to B_s^{(*)}\overline{B}_s^{(*)}) = 53.8 \pm 1.4 \pm 5.3$ pb at $\sqrt{s} = 10.86$ GeV.

$\Gamma(D_s^-\mu^+\nu_\mu)/\Gamma_{\text{total}}$ — Γ_{10}/Γ

VALUE (units 10^{-2})	DOCUMENT ID		TECN	COMMENT
2.31±0.20±0.07	[1] AAIJ	20E	LHCB	pp at 7, 8 TeV

[1] AAIJ 20E reports $[\Gamma(B_s^0 \to D_s^-\mu^+\nu_\mu)/\Gamma_{\text{total}}] / [B(B^0 \to D^-\ell^+\nu_\ell)] = 1.09 \pm 0.05 \pm 0.06 \pm 0.05$ which we multiply by our best (shown rounded) value $B(B^0 \to D^-\ell^+\nu_\ell) = (2.12 \pm 0.06) \times 10^{-2}$. Our first error is their experiment's error and our second error is the systematic error from using our best (shown rounded) value.

$\Gamma(D_s^{*-}\mu^+\nu_\mu)/\Gamma_{\text{total}}$ — Γ_{11}/Γ

VALUE (units 10^{-2})	DOCUMENT ID		TECN	COMMENT
5.2±0.5±0.1	[1] AAIJ	20E	LHCB	pp at 7, 8 TeV

[1] AAIJ 20E reports $[\Gamma(B_s^0 \to D_s^{*-}\mu^+\nu_\mu)/\Gamma_{\text{total}}] / [B(B^0 \to D^*(2010)^-\ell^+\nu_\ell)] = 1.06 \pm 0.05 \pm 0.07 \pm 0.05$ which we multiply by our best (shown rounded) value $B(B^0 \to D^*(2010)^-\ell^+\nu_\ell) = (4.90 \pm 0.12) \times 10^{-2}$. Our first error is their experiment's error and our second error is the systematic error from using our best (shown rounded) value.

$\Gamma(D_s^-\mu^+\nu_\mu)/\Gamma(D_s^{*-}\mu^+\nu_\mu)$ — Γ_{10}/Γ_{11}

VALUE	DOCUMENT ID		TECN	COMMENT
• • • We do not use the following data for averages, fits, limits, etc. • • •				
0.464±0.013±0.043	[1] AAIJ	20E	LHCB	pp at 7, 8 TeV

[1] AAIJ 20E value is not independent of other reported measurements.

$\Gamma(D_{s1}(2536)^-\mu^+\nu_\mu,\ D_{s1}^- \to D^{*-}K_S^0)/\Gamma_{\text{total}}$ — Γ_{12}/Γ

VALUE (units 10^{-3})	DOCUMENT ID		TECN	COMMENT
2.7±0.7±0.2	[1] ABAZOV	09G	D0	$p\overline{p}$ at 1.96 TeV

[1] ABAZOV 09G reports $[\Gamma(B_s^0 \to D_{s1}(2536)^-\mu^+\nu_\mu,\ D_{s1}^- \to D^{*-}K_S^0)/\Gamma_{\text{total}}] \times [B(\overline{b} \to B_s^0 \text{ at } Z)] = (2.66 \pm 0.52 \pm 0.45) \times 10^{-4}$ which we divide by our best (shown rounded) value $B(\overline{b} \to B_s^0 \text{ at } Z) = (10.0 \pm 0.8) \times 10^{-2}$. Our first error is their experiment's error and our second error is the systematic error from using our best (shown rounded) value.

$\Gamma(D_{s1}(2536)^-X\mu^+\nu,\ D_{s1}^- \to \overline{D}^0K^+)/\Gamma(D_s^-\ell^+\nu_\ell \text{anything})$ — Γ_{13}/Γ_8

VALUE (units 10^{-2})	DOCUMENT ID		TECN	COMMENT
5.4±1.2±0.5	AAIJ	11A	LHCB	pp at 7 TeV

$\Gamma(D_{s2}(2573)^-X\mu^+\nu,\ D_{s2}^- \to \overline{D}^0K^+)/\Gamma(D_s^-\ell^+\nu_\ell \text{anything})$ — Γ_{14}/Γ_8

VALUE (units 10^{-2})	DOCUMENT ID		TECN	COMMENT
3.3±1.0±0.4	AAIJ	11A	LHCB	pp at 7 TeV

$\Gamma(D_{s1}(2536)^-X\mu^+\nu,\ D_{s1}^- \to \overline{D}^0K^+)/\Gamma(D_{s2}(2573)^-X\mu^+\nu,\ D_{s2}^- \to \overline{D}^0K^+)$ — Γ_{13}/Γ_{14}

VALUE	DOCUMENT ID		TECN	COMMENT
• • • We do not use the following data for averages, fits, limits, etc. • • •				
0.61±0.14±0.05	[1] AAIJ	11A	LHCB	pp at 7 TeV

[1] Not independent of other AAIJ 11A measurements.

$\Gamma(K^-\mu^+\nu_\mu)/\Gamma(D_s^-\mu^+\nu_\mu)$ — Γ_{15}/Γ_{10}

VALUE (units 10^{-3})	DOCUMENT ID		TECN	COMMENT
4.89±0.21±0.25	[1,2] AAIJ	21G	LHCB	pp at 8 TeV

[1] AAIJ 21G measures $B(B_s^0 \to K^-\mu^+\nu_\mu)/B(B_s^0 \to D_s^-\mu^+\nu_\mu) = (4.89 \pm 0.21^{+0.20}_{-0.21} \pm 0.14) \times 10^{-3}$ over the whole q^2 range, where the last uncertainty is due to the $D_s^- \to K^+K^-\pi^-$ branching fraction.

[2] AAIJ 21G reports this branching ratio for $q^2 < 7$ GeV^2 as $(1.66 \pm 0.08 \pm 0.07 \pm 0.05) \times 10^{-3}$ and for $q^2 > 7$ GeV^2 as $(3.25 \pm 0.21^{+0.16}_{-0.17} \pm 0.09) \times 10^{-3}$.

$\Gamma(K^-\mu^+\nu_\mu)/\Gamma_{\text{total}}$ — Γ_{15}/Γ

VALUE (units 10^{-4})	DOCUMENT ID		TECN	COMMENT
1.06±0.05±0.08	[1] AAIJ	21G	LHCB	pp at 8 TeV

[1] The total systematic error includes D_s^- branching fractions, B_s^0 lifetime, $|V_{cb}|$, and $B_s^0 \to D_s^-$ form factor integral uncertainties.

$\Gamma(D_s^-\pi^+)/\Gamma_{\text{total}}$ — Γ_{16}/Γ

VALUE (units 10^{-3})	EVTS	DOCUMENT ID		TECN	COMMENT
2.98±0.13 OUR FIT					
2.98±0.13 OUR AVERAGE					
2.96±0.10±0.09		[1] AAIJ	21Y	LHCB	pp at 7, 8, 13 TeV
3.4 ±0.5 ±0.2		[2] LOUVOT	09	BELL	$e^+e^- \to \Upsilon(5S)$
2.8 ±0.6 ±0.1		[3] ABULENCIA	07C	CDF	$p\overline{p}$ at 1.96 TeV

Int. J. Mod. Phys. A 2026.41. Downloaded from www.worldscientific.com
by CALIFORNIA @ BERKELEY on 09/16/26. Re-use and distribution is strictly not permitted, except for Open Access articles.

• • • We do not use the following data for averages, fits, limits, etc. • • •

$2.95 \pm 0.05^{+0.25}_{-0.28}$	[4] AAIJ	12AG	LHCB	Repl. by AAIJ 21Y
$6.8 \pm 2.2 \pm 1.6$	DRUTSKOY	07A	BELL	Repl. by LOUVOT 09
$3.3 \pm 1.1 \pm 0.1$	[5] ABULENCIA	06J	CDF	Repl. by ABULENCIA 07C
<130	[6] AKERS	94J	OPAL	$e^+e^- \to Z$
seen	[1] BUSKULIC	93G	ALEP	$e^+e^- \to Z$

[1] AAIJ 21Y reports $[\Gamma(B^0_s \to D^-_s \pi^+)/\Gamma_{total}] / [B(B^0 \to D^- \pi^+)] = 1.18 \pm 0.04$ which we multiply by our best (shown rounded) value $B(B^0 \to D^- \pi^+) = (2.51 \pm 0.08) \times 10^{-3}$. Our first error is their experiment's error and our second error is the systematic error from using our best (shown rounded) value.

[2] LOUVOT 09 reports $(3.67^{+0.35}_{-0.33}{}^{+0.65}_{-0.645}) \times 10^{-3}$ from a measurement of $[\Gamma(B^0_s \to D^-_s \pi^+)/\Gamma_{total}] \times [B(\Upsilon(10860) \to B^{(*)}_s \overline{B}^{(*)}_s)]$ assuming $B(\Upsilon(10860) \to B^{(*)}_s \overline{B}^{(*)}_s) = (19.5 \pm 2.6) \times 10^{-2}$, which we rescale to our best (shown rounded) value $B(\Upsilon(10860) \to B^{(*)}_s \overline{B}^{(*)}_s) = (21.3 \pm 1.5) \times 10^{-2}$. Our first error is their experiment's error and our second error is the systematic error from using our best (shown rounded) value.

[3] ABULENCIA 07C reports $[\Gamma(B^0_s \to D^-_s \pi^+)/\Gamma_{total}] / [B(B^0 \to D^- \pi^+)] = 1.13 \pm 0.08 \pm 0.23$ which we multiply by our best (shown rounded) value $B(B^0 \to D^- \pi^+) = (2.51 \pm 0.08) \times 10^{-3}$. Our first error is their experiment's error and our second error is the systematic error from using our best (shown rounded) value.

[4] AAIJ 12AG reports $(2.95 \pm 0.05 \pm 0.17^{+0.18}_{-0.22}) \times 10^{-3}$ where the last uncertainty comes from the semileptonic f_s/f_d measurement. We combined the systematics in quadrature.

[5] ABULENCIA 06J reports $[\Gamma(B^0_s \to D^-_s \pi^+)/\Gamma_{total}] / [B(B^0 \to D^- \pi^+)] = 1.32 \pm 0.18 \pm 0.38$ which we multiply by our best (shown rounded) value $B(B^0 \to D^- \pi^+) = (2.51 \pm 0.08) \times 10^{-3}$. Our first error is their experiment's error and our second error is the systematic error from using our best (shown rounded) value.

[6] AKERS 94J sees ≤ 6 events and measures the limit on the product branching fraction $f(\overline{b} \to B^0_s) \cdot B(B^0_s \to D^-_s \pi^+) < 1.3\%$ at CL = 90%. We divide by our current value $B(\overline{b} \to B^0_s) = 0.105$.

$\Gamma(D^-_s \rho^+)/\Gamma(D^-_s \pi^+)$ — Γ_{17}/Γ_{16}

VALUE	DOCUMENT ID		TECN	COMMENT
2.3±0.4±0.2	LOUVOT	10	BELL	$e^+e^- \to \Upsilon(5S)$

$\Gamma(D^-_s \pi^+ \pi^+ \pi^-)/\Gamma_{total}$ — Γ_{18}/Γ

VALUE (units 10^{-3})	DOCUMENT ID		TECN	COMMENT
6.1±1.0 OUR FIT				
6.3±1.4±0.6	[1] ABULENCIA	07C	CDF	$p\overline{p}$ at 1.96 TeV

[1] ABULENCIA 07C reports $[\Gamma(B^0_s \to D^-_s \pi^+ \pi^+ \pi^-)/\Gamma_{total}] / [B(B^0 \to D^- \pi^+ \pi^+ \pi^-)] = 1.05 \pm 0.10 \pm 0.22$ which we multiply by our best (shown rounded) value $B(B^0 \to D^- \pi^+ \pi^+ \pi^-) = (6.0 \pm 0.6) \times 10^{-3}$. Our first error is their experiment's error and our second error is the systematic error from using our best (shown rounded) value.

$\Gamma(D^-_s \pi^+ \pi^+ \pi^-)/\Gamma(D^-_s \pi^+)$ — Γ_{18}/Γ_{16}

VALUE	DOCUMENT ID		TECN	COMMENT
2.05±0.33 OUR FIT				
2.01±0.37±0.20	AAIJ	11E	LHCB	pp at 7 TeV

$\Gamma(D_{s1}(2536)^- \pi^+, D^-_{s1} \to D^-_s \pi^+ \pi^-)/\Gamma(D^-_s \pi^+ \pi^+ \pi^-)$ — Γ_{19}/Γ_{18}

VALUE (units 10^{-3})	DOCUMENT ID		TECN	COMMENT
4.0±1.0±0.4	AAIJ	12AX	LHCB	pp at 7 TeV

$\Gamma(D^{\mp}_s K^{\pm})/\Gamma_{total}$ — Γ_{20}/Γ

VALUE (units 10^{-4})	DOCUMENT ID		TECN	COMMENT
2.25±0.12 OUR FIT				
$\mathbf{2.2^{+1.1}_{-0.9}{}^{+0.2}_{-0.1}}$	[1] LOUVOT	09	BELL	$e^+e^- \to \Upsilon(5S)$

[1] LOUVOT 09 reports $(2.4^{+1.2}_{-1.0} \pm 0.42) \times 10^{-4}$ from a measurement of $[\Gamma(B^0_s \to D^{\mp}_s K^{\pm})/\Gamma_{total}] \times [B(\Upsilon(10860) \to B^{(*)}_s \overline{B}^{(*)}_s)]$ assuming $B(\Upsilon(10860) \to B^{(*)}_s \overline{B}^{(*)}_s) = (19.5 \pm 2.6) \times 10^{-2}$, which we rescale to our best (shown rounded) value $B(\Upsilon(10860) \to B^{(*)}_s \overline{B}^{(*)}_s) = (21.3 \pm 1.5) \times 10^{-2}$. Our first error is their experiment's error and our second error is the systematic error from using our best (shown rounded) value.

$\Gamma(D_{s1}(2536)^{\mp} K^{\pm}, D^-_{s1} \to \overline{D}^*(2007)^0 K^-)/\Gamma_{total}$ — Γ_{21}/Γ

VALUE (units 10^{-5})	DOCUMENT ID		TECN	COMMENT
2.48±0.18±0.22	[1] AAIJ	23AY	LHCB	pp at 7, 8, 13 TeV

[1] AAIJ 23AY reports $[\Gamma(B^0_s \to D_{s1}(2536)^{\mp} K^{\pm}, D^-_{s1} \to \overline{D}^*(2007)^0 K^-)/\Gamma_{total}] / [B(B^0 \to \overline{D}^0 K^+ K^-)] = 0.409 \pm 0.019 \pm 0.022$ which we multiply by our best (shown rounded) value $B(B^0 \to \overline{D}^0 K^+ K^-) = (6.1 \pm 0.5) \times 10^{-5}$. Our first error is their experiment's error and our second error is the systematic error from using our best (shown rounded) value.

$\Gamma(D^{\mp}_s K^{\pm})/\Gamma(D^-_s \pi^+)$ — Γ_{20}/Γ_{16}

VALUE (units 10^{-2})	DOCUMENT ID		TECN	COMMENT
7.55±0.24 OUR FIT				
7.55±0.24 OUR AVERAGE				
$7.52 \pm 0.15 \pm 0.19$	AAIJ	15AC	LHCB	pp at 7, 8 TeV
$9.7 \pm 1.8 \pm 0.9$	AALTONEN	09AQ	CDF	$p\overline{p}$ at 1.96 TeV

• • • We do not use the following data for averages, fits, limits, etc. • • •

$6.46 \pm 0.43 \pm 0.25$	AAIJ	12AG	LHCB	Repl. by AAIJ 15AC

$\Gamma(D^-_s K^+ \pi^+ \pi^-)/\Gamma(D^-_s \pi^+ \pi^+ \pi^-)$ — Γ_{22}/Γ_{18}

VALUE (units 10^{-2})	DOCUMENT ID		TECN	COMMENT
5.2±0.5±0.3	AAIJ	12AX	LHCB	pp at 7 TeV

$\Gamma(D^+_s D^-_s)/\Gamma_{total}$ — Γ_{23}/Γ

VALUE (units 10^{-3})	CL%	DOCUMENT ID		TECN	COMMENT
4.5±0.6 OUR AVERAGE		Error includes scale factor of 1.3. See the ideogram below.			
$4.0 \pm 0.2 \pm 0.5$		[1] AAIJ	13AP	LHCB	pp at 7 TeV
$5.8^{+1.1}_{-0.9} \pm 1.3$		[2] ESEN	13	BELL	$e^+e^- \to \Upsilon(5S)$
$6.1 \pm 0.9 \pm 0.7$		[3] AALTONEN	12C	CDF	$p\overline{p}$ at 1.96 TeV

• • • We do not use the following data for averages, fits, limits, etc. • • •

$10.3^{+3.9}_{-3.2}{}^{+2.6}_{-2.5}$	[4] ESEN	10	BELL	Repl. by ESEN 13
$12 \pm 4 \pm 1$	[5] AALTONEN	08F	CDF	Repl. by AALTONEN 12C
<67 90	DRUTSKOY	07A	BELL	Repl. by ESEN 10

[1] Uses $B(B^0 \to D^- D^+_s) = (7.2 \pm 0.8) \times 10^{-3}$.

[2] Use $\Upsilon(5S) \to B^*_s \overline{B}^*_s$ decays assuming $B(\Upsilon(5S) \to B^*_s \overline{B}^*_s) = (17.1 \pm 3.0)\%$ and $\Gamma(\Upsilon(5S) \to B^*_s \overline{B}^*_s) / \Gamma(\Upsilon(5S) \to B^{(*)}_s \overline{B}^{(*)}_s) = (87.0 \pm 1.7)\%$.

[3] AALTONEN 12C reports $(f_s/f_d)\,(B(B^0_s \to D^+_s D^-_s) / B(B^0 \to D^- D^+_s)) = 0.183 \pm 0.021 \pm 0.017$. We multiply this result by our best value of $B(B^0 \to D^- D^+_s) = (8.1 \pm 0.6) \times 10^{-3}$ and divide by our best value of f_s/f_d, where $1/2\ f_s/f_d = 0.1230 \pm 0.0115$. Our first quoted uncertainty is the combined experiment's uncertainty and our second is the systematic uncertainty from using out best values.

[4] Uses $\Upsilon(10860) \to B^*_s \overline{B}^*_s$ assuming $B(\Upsilon(10860) \to B^{(*)}_s \overline{B}^{(*)}_s) = (19.3 \pm 2.9)\%$ and $\Gamma(\Upsilon(10860) \to B^*_s \overline{B}^*_s) / \Gamma(\Upsilon(10860) \to B^{(*)}_s \overline{B}^{(*)}_s) = (90.1^{+3.8}_{-4.0})\%$.

[5] AALTONEN 08F reports $[\Gamma(B^0_s \to D^+_s D^-_s)/\Gamma_{total}] / [B(B^0 \to D^- D^+_s)] = 1.44^{+0.48}_{-0.44}$ which we multiply by our best (shown rounded) value $B(B^0 \to D^- D^+_s) = (8.1 \pm 0.6) \times 10^{-3}$. Our first error is their experiment's error and our second error is the systematic error from using our best (shown rounded) value.

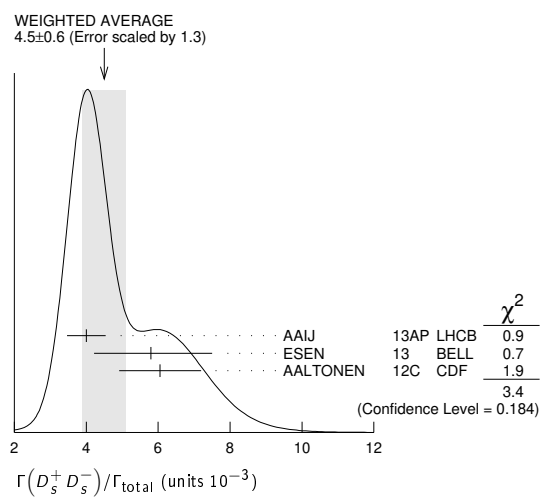

$\Gamma(D^-_s D^+)/\Gamma_{total}$ — Γ_{24}/Γ

VALUE (units 10^{-4})	DOCUMENT ID		TECN	COMMENT
3.1±0.4±0.2	[1] AAIJ	14AA	LHCB	pp at 7 TeV

• • • We do not use the following data for averages, fits, limits, etc. • • •

$3.6 \pm 0.6 \pm 0.5$	[2] AAIJ	13AP	LHCB	Repl. by AAIJ 14AA

[1] AAIJ 14AA reports $[\Gamma(B^0_s \to D^-_s D^+)/\Gamma_{total}] / [B(B^0 \to D^- D^+_s)] = 0.038 \pm 0.004 \pm 0.003$ which we multiply by our best (shown rounded) value $B(B^0 \to D^- D^+_s) = (8.1 \pm 0.6) \times 10^{-3}$. Our first error is their experiment's error and our second error is the systematic error from using our best (shown rounded) value..

[2] Uses $B(B^0 \to D^- D^+_s) = (7.2 \pm 0.8) \times 10^{-3}$.

$\Gamma(D^+ D^-)/\Gamma_{total}$ — Γ_{25}/Γ

VALUE (units 10^{-4})	DOCUMENT ID		TECN	COMMENT
2.2±0.4±0.4	[1] AAIJ	13AP	LHCB	pp at 7 TeV

[1] Uses $B(B^0 \to D^- D^+) = (2.11 \pm 0.31) \times 10^{-4}$ and $B(B^+ \to \overline{D}^0 D^+_s) = (10.1 \pm 1.7) \times 10^{-3}$.

$\Gamma(D^0 \overline{D}^0)/\Gamma_{total}$ — Γ_{29}/Γ

VALUE (units 10^{-4})	DOCUMENT ID		TECN	COMMENT
1.9±0.3±0.4	[1] AAIJ	13AP	LHCB	pp at 7 TeV

[1] Uses $B(B^0 \to D^- D^+) = (2.11 \pm 0.31) \times 10^{-4}$ and $B(B^+ \to \overline{D}^0 D^+_s) = (10.1 \pm 1.7) \times 10^{-3}$.

Int. J. Mod. Phys. A 2026.41. Downloaded from www.worldscientific.com
by UNIVERSITY OF CALIFORNIA @ BERKELEY on 09/16/26. Re-use and distribution is strictly not permitted, except for Open Access articles.

$\Gamma(D^{*+}D^{*-})/\Gamma_{total}$ — Γ_{28}/Γ

VALUE (units 10^{-4})	DOCUMENT ID		TECN	COMMENT
$2.14\pm0.28^{+0.17}_{-0.16}$	[1,2] AAIJ	23J	LHCB	pp at 7, 8, 13 TeV

[1] AAIJ 23J reports $[\Gamma(B_s^0 \to D^{*+}D^{*-})/\Gamma_{total}]$ / $[B(B^0 \to D^*(2010)^+D^*(2010)^-)]$ $= 0.269 \pm 0.032 \pm 0.011 \pm 0.008$ which we multiply by our best (shown rounded) value $B(B^0 \to D^*(2010)^+D^*(2010)^-) = (8.0 \pm 0.6)\times10^{-4}$. Our first error is their experiment's error and our second error is the systematic error from using our best (shown rounded) value.

[2] Uses average B_s^0 lifetime of 1.5215 ps.

$\Gamma(D_s^{*-}\pi^+)/\Gamma(D_s^-\pi^+)$ — Γ_{30}/Γ_{16}

VALUE	DOCUMENT ID		TECN	COMMENT
$0.65^{+0.15}_{-0.13}\pm0.07$	LOUVOT	10	BELL	$e^+e^- \to \Upsilon(5S)$

$\Gamma(D_s^{*\mp}K^\pm)/\Gamma(D_s^{*-}\pi^+)$ — Γ_{31}/Γ_{30}

VALUE	DOCUMENT ID		TECN	COMMENT
$0.068\pm0.005^{+0.003}_{-0.002}$	AAIJ	15AD	LHCB	pp at 7, 8 TeV

$\Gamma(D_s^{*-}\rho^+)/\Gamma(D_s^-\pi^+)$ — Γ_{32}/Γ_{16}

VALUE	DOCUMENT ID		TECN	COMMENT
$3.2\pm0.6\pm0.3$	LOUVOT	10	BELL	$e^+e^- \to \Upsilon(5S)$

$\Gamma(D_s^{*-}\rho^+)/\Gamma(D_s^-\rho^+)$ — Γ_{32}/Γ_{17}

VALUE	DOCUMENT ID		TECN	COMMENT
• • • We do not use the following data for averages, fits, limits, etc. • • •				
$1.4\pm0.3\pm0.1$	[1] LOUVOT	10	BELL	$e^+e^- \to \Upsilon(5S)$

[1] Not independent of other LOUVOT 10 measurements.

$[\Gamma(D_s^{*+}D_s^-)+\Gamma(D_s^{*-}D_s^+)]/\Gamma_{total}$ — Γ_{33}/Γ

VALUE (units 10^{-3})	CL%	DOCUMENT ID		TECN	COMMENT
15.1±1.3 OUR AVERAGE					
$15.3\pm1.2\pm1.1$		[1] AAIJ	16P	LHCB	pp at 7 TeV
$17.6^{+2.3}_{-2.2}\pm4.0$		[2] ESEN	13	BELL	$e^+e^- \to \Upsilon(5S)$
$14.0\pm1.9\pm1.6$		[3] AALTONEN	12C	CDF	$p\overline{p}$ at 1.96 TeV
• • • We do not use the following data for averages, fits, limits, etc. • • •					
$27.5^{+8.3}_{-7.1}\pm6.9$		[4] ESEN	10	BELL	Repl. by ESEN 13
<121	90	DRUTSKOY	07A	BELL	Repl. by ESEN 10

[1] AAIJ 16P reports $[\left[\Gamma(B_s^0 \to D_s^{*+}D_s^-)+\Gamma(D_s^{*-}D_s^+)\right]/\Gamma_{total}]$ / $[B(B^0 \to D^-D_s^+)]$ $= 1.88 \pm 0.08 \pm 0.12$ which we multiply by our best (shown rounded) value $B(B^0 \to D^-D_s^+) = (8.1\pm0.6)\times10^{-3}$. Our first error is their experiment's error and our second error is the systematic error from using our best (shown rounded) value.

[2] Use $\Upsilon(5S) \to B_s^*\overline{B}_s^*$ decays assuming $B(\Upsilon(5S) \to B_s^*\overline{B}_s^*) = (17.1 \pm 3.0)\%$ and $\Gamma(\Upsilon(5S) \to B_s^*\overline{B}_s^*)$ / $\Gamma(\Upsilon(5S) \to B_s^{(*)}\overline{B}_s^{(*)}) = (87.0 \pm 1.7)\%$.

[3] AALTONEN 12C reports (f_s/f_d) $(B(B_s^0 \to D_s^{*+}D_s^- + D_s^{*-}D_s^+)$ / $B(B^0 \to D^-D_s^+))$ $= 0.424 \pm 0.046 \pm 0.035$. We multiply this result by our best value of $B(B^0 \to D^-D_s^+) = (8.1\pm0.6)\times10^{-3}$ and divide by our best value of f_s/f_d, where $1/2\ f_s/f_d = 0.1230\pm0.0115$. Our first quoted uncertainty is the combined experiment's uncertainty and our second is the systematic uncertainty from using out best values.

[4] Uses $\Upsilon(10860) \to B_s^*\overline{B}_s^*$ assuming $B(\Upsilon(10860) \to B_s^{(*)}\overline{B}_s^{(*)}) = (19.3\pm2.9)\%$ and $\Gamma(\Upsilon(10860) \to B_s^*\overline{B}_s^*)$ / $\Gamma(\Upsilon(10860) \to B_s^{(*)}\overline{B}_s^{(*)}) = (90.1^{+3.8}_{-4.0})\%$.

$\Gamma(D_s^{*+}D_s^{*-})/\Gamma_{total}$ — Γ_{34}/Γ

VALUE (units 10^{-3})	CL%	DOCUMENT ID		TECN	COMMENT
15.8± 2.0 OUR AVERAGE Error includes scale factor of 1.3. See the ideogram below.					
$14.3\pm1.4\pm1.0$		[1] AAIJ	16P	LHCB	pp at 7 TeV
$19.8^{+3.3+5.2}_{-3.1-5.0}$		[2] ESEN	13	BELL	$e^+e^- \to \Upsilon(5S)$
$21.6\pm3.2\pm2.5$		[3] AALTONEN	12C	CDF	$p\overline{p}$ at 1.96 TeV
• • • We do not use the following data for averages, fits, limits, etc. • • •					
$30.8^{+12.2+8.5}_{-10.4-8.6}$		[4] ESEN	10	BELL	Repl. by ESEN 13
<257	90	DRUTSKOY	07A	BELL	Repl. by ESEN 10

[1] AAIJ 16P reports $[\Gamma(B_s^0 \to D_s^{*+}D_s^{*-})/\Gamma_{total}]$ / $[B(B^0 \to D^-D_s^+)] = 1.76 \pm 0.11 \pm 0.14$ which we multiply by our best (shown rounded) value $B(B^0 \to D^-D_s^+) = (8.1\pm0.6)\times10^{-3}$. Our first error is their experiment's error and our second error is the systematic error from using our best (shown rounded) value.

[2] Use $\Upsilon(5S) \to B_s^*\overline{B}_s^*$ decays assuming $B(\Upsilon(5S) \to B_s^*\overline{B}_s^*) = (17.1 \pm 3.0)\%$ and $\Gamma(\Upsilon(5S) \to B_s^*\overline{B}_s^*)$ / $\Gamma(\Upsilon(5S) \to B_s^{(*)}\overline{B}_s^{(*)}) = (87.0 \pm 1.7)\%$.

[3] AALTONEN 12C reports (f_s/f_d) $(B(B_s^0 \to D_s^{*+}D_s^{*-})$ / $B(B^0 \to D^-D_s^+))$ $= 0.654 \pm 0.072 \pm 0.065$. We multiply this result by our best value of $B(B^0 \to D^-D_s^+) = (8.1 \pm 0.6)\times10^{-3}$ and divide by our best value of f_s/f_d, where $1/2\ f_s/f_d = 0.1230\pm0.0115$. Our first quoted uncertainty is the combined experiment's uncertainty and our second is the systematic uncertainty from using out best values.

[4] Uses $\Upsilon(10860) \to B_s^*\overline{B}_s^*$ assuming $B(\Upsilon(10860) \to B_s^{(*)}\overline{B}_s^{(*)}) = (19.3 \pm 2.9)\%$ and $\Gamma(\Upsilon(10860) \to B_s^*\overline{B}_s^*)$ / $\Gamma(\Upsilon(10860) \to B_s^{(*)}\overline{B}_s^{(*)}) = (90.1^{+3.8}_{-4.0})\%$.

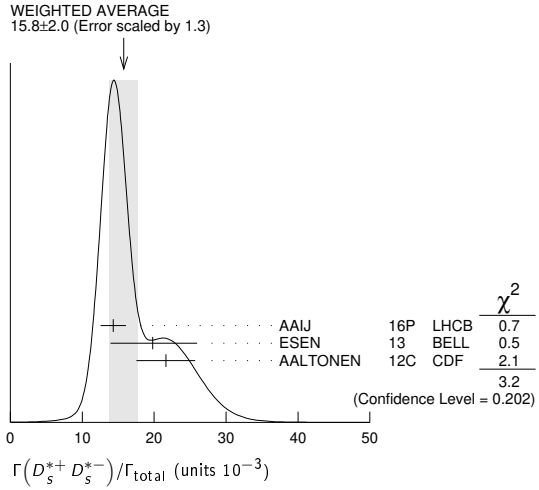

$\Gamma(D_s^{(*)+}D_s^{(*)-})/\Gamma_{total}$ — Γ_{35}/Γ

VALUE (%)	CL%	DOCUMENT ID		TECN	COMMENT
4.5 ±1.4 OUR EVALUATION (Produced by HFLAV)					
3.66±0.29 OUR AVERAGE					
$3.45\pm0.25\pm0.24$		[1] AAIJ	16P	LHCB	pp at 7 TeV
$4.32^{+0.42+1.04}_{-0.39-1.03}$		[2] ESEN	13	BELL	$e^+e^- \to \Upsilon(5S)$
$4.2\ \pm0.5\ \pm0.5$		[3] AALTONEN	12C	CDF	$p\overline{p}$ at 1.96 TeV
$3.5\ \pm1.0\ \pm1.1$		[4] ABAZOV	09I	D0	$p\overline{p}$ at 1.96 TeV
$14\ \pm6\ \pm3$		[5,6] BARATE	00K	ALEP	$e^+e^- \to Z$
• • • We do not use the following data for averages, fits, limits, etc. • • •					
$6.85^{+1.53+1.79}_{-1.30-1.80}$		[7,8] ESEN	10	BELL	Repl. by ESEN 13
$3.9\ ^{+1.9\ +1.6}_{-1.7\ -1.5}$		[4] ABAZOV	07Y	D0	Repl. by ABAZOV 09I
<0.218	90	BARATE	98Q	ALEP	$e^+e^- \to Z$

[1] AAIJ 16P reports $[\Gamma(B_s^0 \to D_s^{(*)+}D_s^{(*)-})/\Gamma_{total}]$ / $[B(B^0 \to D^-D_s^+)] = 4.24 \pm 0.14 \pm 0.27$ which we multiply by our best (shown rounded) value $B(B^0 \to D^-D_s^+) = (8.1\pm0.6)\times10^{-3}$. Our first error is their experiment's error and our second error is the systematic error from using our best (shown rounded) value.

[2] Use $\Upsilon(5S) \to B_s^*\overline{B}_s^*$ decays assuming $B(\Upsilon(5S) \to B_s^*\overline{B}_s^*) = (17.1 \pm 3.0)\%$ and $\Gamma(\Upsilon(5S) \to B_s^*\overline{B}_s^*)$ / $\Gamma(\Upsilon(5S) \to B_s^{(*)}\overline{B}_s^{(*)}) = (87.0 \pm 1.7)\%$.

[3] AALTONEN 12C reports (f_s/f_d) $(B(B_s^0 \to D_s^{(*)+}D_s^{(*)-})$ / $B(B^0 \to D^-D_s^+))$ $= 1.261 \pm 0.095 \pm 0.112$. We multiply this result by our best value of $B(B^0 \to D^-D_s^+) = (8.1\pm0.6)\times10^{-3}$ and divide by our best value of f_s/f_d, where $1/2\ f_s/f_d = 0.1230\pm0.0115$. Our first quoted uncertainty is the combined experiment's uncertainty and our second is the systematic uncertainty from using out best values.

[4] Uses the final states where $D_s^+ \to \phi\pi^+$ and $D_s^- \to \phi\mu^-\overline{\nu}_\mu$.

[5] Reports $B(B_s^0(\text{short}) \to D_s^{(*)}D_s^{(*)}) = (0.23 \pm 0.10 \pm 0.05) \cdot [0.17/B(D_s \to \phi\chi)]^2$ assuming $B(B_s^0 \to B_s^0(\text{short})) = 50\%$. We use our best value of $B(D_s \to \phi\chi) = 15.7 \pm 1.0\%$ to obtain the quoted result.

[6] Uses $\phi\phi$ correlations from $B_s^0(\text{short}) \to D_s^{(*)+}D_s^{(*)-}$.

[7] Sum of exclusive $B_s \to D_s^+D_s^-$, $B_s \to D_s^{*\pm}D_s^\mp$ and $B_s \to D_s^{*+}D_s^{*-}$.

[8] Uses $\Upsilon(10860) \to B_s^*\overline{B}_s^*$ assuming $B(\Upsilon(10860) \to B_s^{(*)}\overline{B}_s^{(*)}) = (19.3 \pm 2.9)\%$ and $\Gamma(\Upsilon(10860) \to B_s^*\overline{B}_s^*)$ / $\Gamma(\Upsilon(10860) \to B_s^{(*)}\overline{B}_s^{(*)}) = (90.1^{+3.8}_{-4.0})\%$.

$\Gamma(D^{*-}D_s^+)/\Gamma_{total}$ — Γ_{36}/Γ

VALUE (units 10^{-4})	DOCUMENT ID		TECN	COMMENT
4.0±0.6±0.4	[1] AAIJ	21S	LHCB	pp at 13 TeV

[1] AAIJ 21S reports $[\Gamma(B_s^0 \to D^{*-}D_s^+)/\Gamma_{total}]$ / $[B(B^0 \to D^*(2010)^-D_s^+)] = 0.049 \pm 0.006 \pm 0.0036$ which we multiply by our best (shown rounded) value $B(B^0 \to D^*(2010)^-D_s^+) = (8.2 \pm 0.8)\times10^{-3}$. Our first error is their experiment's error and our second error is the systematic error from using our best (shown rounded) value.

$[\Gamma(D^{*+}D^-)+\Gamma(D^{*-}D^+)]/\Gamma_{total}$ — $(\Gamma_{26}+\Gamma_{27})/\Gamma$

VALUE (units 10^{-5})	DOCUMENT ID		TECN	COMMENT
8.4±1.1±0.8	[1] AAIJ	21N	LHCB	pp at 7, 8, 13 TeV

[1] AAIJ 21N reports $[\left[\Gamma(B_s^0 \to D^{*+}D^-)+\Gamma(B_s^0 \to D^{*-}D^+)\right]/\Gamma_{total}]$ / $[B(B^0 \to D^\pm D^{*\mp}(CP\text{-averaged}))] = 0.137\pm0.017\pm0.006$ which we multiply by our best (shown rounded) value $B(B^0 \to D^\pm D^{*\mp}(CP\text{-averaged})) = (6.1\pm0.6)\times10^{-4}$. Our first error is their experiment's error and our second error is the systematic error from using our best (shown rounded) value.

Int. J. Mod. Phys. A 2026.41. Downloaded from www.worldscientific.com by CALIFORNIA @ BERKELEY on 09/16/26. Re-use and distribution is strictly not permitted, except for Open Access articles.

$\Gamma(\overline{D}^{*0}\overline{K}^0)/\Gamma_{total}$ — Γ_{37}/Γ

VALUE (units 10^{-4})	DOCUMENT ID		TECN	COMMENT
2.8±1.0±0.5	[1] AAIJ	16C	LHCB	pp at 7, 8 TeV

[1] Measured and normalized to the $B_s^0 \to \overline{D}^{*0} K_S^0$ decay with $f_s/f_d = 0.259 \pm 0.015$. Signal significance is 4.4 standard deviations.

$\Gamma(\overline{D}^0\overline{K}^0)/\Gamma_{total}$ — Γ_{38}/Γ

VALUE (units 10^{-4})	DOCUMENT ID		TECN	COMMENT
4.3±0.5±0.7	[1] AAIJ	16C	LHCB	pp at 7, 8 TeV

[1] Measured and normalized to the $B^0 \to \overline{D}^0 K_S^0$ decay with $f_s/f_d = 0.259 \pm 0.015$.

$\Gamma(\overline{D}^0 K^-\pi^+)/\Gamma_{total}$ — Γ_{39}/Γ

VALUE (units 10^{-4})	DOCUMENT ID		TECN	COMMENT
10.4±1.1±0.5	[1] AAIJ	13AQ	LHCB	pp at 7 TeV

[1] AAIJ 13AQ reports $[\Gamma(B_s^0 \to \overline{D}^0 K^-\pi^+)/\Gamma_{total}]$ / $[B(B^0 \to \overline{D}^0\pi^+\pi^-)] = 1.18 \pm 0.05 \pm 0.12$ which we multiply by our best (shown rounded) value $B(B^0 \to \overline{D}^0\pi^+\pi^-) = (8.8 \pm 0.5) \times 10^{-4}$. Our first error is their experiment's error and our second error is the systematic error from using our best (shown rounded) value.

$\Gamma(\overline{D}^*(2007)^0 K^-\pi^+)/\Gamma_{total}$ — Γ_{40}/Γ

VALUE (units 10^{-4})	DOCUMENT ID		TECN	COMMENT
7.3±0.6±2.5	[1] AAIJ	22N	LHCB	pp at 13 TeV

[1] AAIJ 22N reports $[\Gamma(B_s^0 \to \overline{D}^*(2007)^0 K^-\pi^+)/\Gamma_{total}]$ / $[B(B^0 \to \overline{D}^*(2007)^0\pi^+\pi^-)] = 1.178 \pm 0.029 \pm 0.091 \pm 0.037$ which we multiply by our best (shown rounded) value $B(B^0 \to \overline{D}^*(2007)^0\pi^+\pi^-) = (6.2 \pm 2.2) \times 10^{-4}$. Our first error is their experiment's error and our second error is the systematic error from using our best (shown rounded) value.

$\Gamma(\overline{D}^0\overline{K}^*(892)^0)/\Gamma_{total}$ — Γ_{41}/Γ

VALUE (units 10^{-4})	DOCUMENT ID		TECN	COMMENT
4.4 ±0.6 OUR AVERAGE				
4.29±0.09±0.65	[1] AAIJ	14BH	LHCB	pp at 7, 8 TeV
4.7 ±1.2 ±0.3	[2] AAIJ	11D	LHCB	pp at 7 TeV
• • • We do not use the following data for averages, fits, limits, etc. • • •				
3.5 ±0.4 ±0.4	[3] AAIJ	13BX	LHCB	Repl. by AAIJ 14BH

[1] Uses Dalitz plot analysis of $B_s^0 \to \overline{D}^0 K^-\pi^+$ decays.

[2] AAIJ 11D reports $[\Gamma(B_s^0 \to \overline{D}^0\overline{K}^*(892)^0)/\Gamma_{total}]$ / $[B(B^0 \to \overline{D}^0\rho^0)] = 1.48 \pm 0.34 \pm 0.19$ which we multiply by our best (shown rounded) value $B(B^0 \to \overline{D}^0\rho^0) = (3.21 \pm 0.21) \times 10^{-4}$. Our first error is their experiment's error and our second error is the systematic error from using our best (shown rounded) value.

[3] AAIJ 13BX reports $[\Gamma(B_s^0 \to \overline{D}^0\overline{K}^*(892)^0)/\Gamma_{total}]$ / $[B(B^0 \to \overline{D}^0 K^*(892)^0)] = 7.8 \pm 0.7 \pm 0.3 \pm 0.6$ which we multiply by our best (shown rounded) value $B(B^0 \to \overline{D}^0 K^*(892)^0) = (4.5 \pm 0.6) \times 10^{-5}$. Our first error is their experiment's error and our second error is the systematic error from using our best (shown rounded) value.

$\Gamma(\overline{D}^0\overline{K}^*(1410))/\Gamma_{total}$ — Γ_{42}/Γ

VALUE (units 10^{-5})	DOCUMENT ID		TECN	COMMENT
38.6±11.4±33.3	[1] AAIJ	14BH	LHCB	pp at 7, 8 TeV

[1] Uses Dalitz plot analysis of $B_s^0 \to \overline{D}^0 K^-\pi^+$ decays.

$\Gamma(\overline{D}^0\overline{K}_0^*(1430))/\Gamma_{total}$ — Γ_{43}/Γ

VALUE (units 10^{-5})	DOCUMENT ID		TECN	COMMENT
30.0±2.4±6.8	[1] AAIJ	14BH	LHCB	pp at 7, 8 TeV

[1] Uses Dalitz plot analysis of $B_s^0 \to \overline{D}^0 K^-\pi^+$ decays. Corresponds to the resonant $K_0^*(1430)$ part of LASS parametrization.

$\Gamma(\overline{D}^0\overline{K}_2^*(1430))/\Gamma_{total}$ — Γ_{44}/Γ

VALUE (units 10^{-5})	DOCUMENT ID		TECN	COMMENT
11.1±1.8±3.8	[1] AAIJ	14BH	LHCB	pp at 7, 8 TeV

[1] Uses Dalitz plot analysis of $B_s^0 \to \overline{D}^0 K^-\pi^+$ decays.

$\Gamma(\overline{D}^0\overline{K}^*(1680))/\Gamma_{total}$ — Γ_{45}/Γ

VALUE (units 10^{-5})	CL%	DOCUMENT ID		TECN	COMMENT
<7.8	90	[1] AAIJ	14BH	LHCB	pp at 7, 8 TeV

[1] Uses Dalitz plot analysis of $B_s^0 \to \overline{D}^0 K^-\pi^+$ decays.

$\Gamma(\overline{D}^0\overline{K}_0^*(1950))/\Gamma_{total}$ — Γ_{46}/Γ

VALUE (units 10^{-5})	CL%	DOCUMENT ID		TECN	COMMENT
<11	90	[1] AAIJ	14BH	LHCB	pp at 7, 8 TeV

[1] Uses Dalitz plot analysis of $B_s^0 \to \overline{D}^0 K^-\pi^+$ decays.

$\Gamma(\overline{D}^0\overline{K}_3^*(1780))/\Gamma_{total}$ — Γ_{47}/Γ

VALUE (units 10^{-5})	CL%	DOCUMENT ID		TECN	COMMENT
<2.6	90	[1] AAIJ	14BH	LHCB	pp at 7, 8 TeV

[1] Uses Dalitz plot analysis of $B_s^0 \to \overline{D}^0 K^-\pi^+$ decays.

$\Gamma(\overline{D}^0\overline{K}_4^*(2045))/\Gamma_{total}$ — Γ_{48}/Γ

VALUE (units 10^{-5})	CL%	DOCUMENT ID		TECN	COMMENT
<3.1	90	[1] AAIJ	14BH	LHCB	pp at 7, 8 TeV

[1] Uses Dalitz plot analysis of $B_s^0 \to \overline{D}^0 K^-\pi^+$ decays.

$\Gamma(\overline{D}^0 K^-\pi^+(\text{non-resonant}))/\Gamma_{total}$ — Γ_{49}/Γ

VALUE (units 10^{-5})	DOCUMENT ID		TECN	COMMENT
20.6±3.8±7.3	[1] AAIJ	14BH	LHCB	pp at 7, 8 TeV

[1] Uses Dalitz plot analysis of $B_s^0 \to \overline{D}^0 K^-\pi^+$ decays. Corresponds to the non-resonant part of the LASS parametrization.

$\Gamma([K^+K^-]_D\overline{K}^*(892)^0)/\Gamma(\overline{D}^0\overline{K}^*(892)^0)$ — Γ_{50}/Γ_{41}

VALUE	DOCUMENT ID		TECN	COMMENT
1.000±0.034±0.016	AAIJ	24M	LHCB	pp at 7, 8, 13 TeV

$\Gamma([\pi^+\pi^-]_D\overline{K}^*(892)^0)/\Gamma(\overline{D}^0\overline{K}^*(892)^0)$ — Γ_{51}/Γ_{41}

VALUE	DOCUMENT ID		TECN	COMMENT
0.996±0.057±0.023	AAIJ	24M	LHCB	pp at 7, 8, 13 TeV

$\Gamma([\pi^+\pi^-\pi^+\pi^-]_D\overline{K}^*(892)^0)/\Gamma(\overline{D}^0\overline{K}^*(892)^0)$ — Γ_{54}/Γ_{41}

VALUE	DOCUMENT ID		TECN	COMMENT
1.010±0.048±0.033	AAIJ	24M	LHCB	pp at 7, 8, 13 TeV

$\Gamma(D_{s2}^*(2573)^-\pi^+,\ D_{s2}^* \to \overline{D}^0 K^-)/\Gamma_{total}$ — Γ_{57}/Γ

VALUE (units 10^{-5})	DOCUMENT ID		TECN	COMMENT
25.7±0.7±4.0	[1] AAIJ	14BH	LHCB	pp at 7, 8 TeV

[1] Uses Dalitz plot analysis of $B_s^0 \to \overline{D}^0 K^-\pi^+$ decays.

$\Gamma(D_{s1}^*(2700)^-\pi^+,\ D_{s1}^* \to \overline{D}^0 K^-)/\Gamma_{total}$ — Γ_{58}/Γ

VALUE (units 10^{-5})	DOCUMENT ID		TECN	COMMENT
1.6±0.4±0.7	[1] AAIJ	14BH	LHCB	pp at 7, 8 TeV

[1] Uses Dalitz plot analysis of $B_s^0 \to \overline{D}^0 K^-\pi^+$ decays.

$\Gamma(D_{s1}^*(2860)^-\pi^+,\ D_{s1}^* \to \overline{D}^0 K^-)/\Gamma_{total}$ — Γ_{59}/Γ

VALUE (units 10^{-5})	DOCUMENT ID		TECN	COMMENT
5.0±1.2±3.4	[1] AAIJ	14BH	LHCB	pp at 7, 8 TeV

[1] Uses Dalitz plot analysis of $B_s^0 \to \overline{D}^0 K^-\pi^+$ decays.

$\Gamma(D_{s3}^*(2860)^-\pi^+,\ D_{s3}^* \to \overline{D}^0 K^-)/\Gamma_{total}$ — Γ_{60}/Γ

VALUE (units 10^{-5})	DOCUMENT ID		TECN	COMMENT
2.2±0.1±0.6	[1] AAIJ	14BH	LHCB	pp at 7, 8 TeV

[1] Uses Dalitz plot analysis of $B_s^0 \to \overline{D}^0 K^-\pi^+$ decays.

$\Gamma(\overline{D}^0 K^+K^-)/\Gamma_{total}$ — Γ_{61}/Γ

VALUE (units 10^{-5})	DOCUMENT ID		TECN	COMMENT
5.6±0.7±0.5	[1] AAIJ	18AZ	LHCB	pp at 7, 8 TeV
• • • We do not use the following data for averages, fits, limits, etc. • • •				
5.5±2.0±0.5	[2,3] AAIJ	12AM	LHCB	Repl. by AAIJ 18AZ

[1] AAIJ 18AZ reports $[\Gamma(B_s^0 \to \overline{D}^0 K^+K^-)/\Gamma_{total}]$ / $[B(B^0 \to \overline{D}^0 K^+K^-)] = 0.930 \pm 0.089 \pm 0.069$ which we multiply by our best (shown rounded) value $B(B^0 \to \overline{D}^0 K^+K^-) = (6.1 \pm 0.5) \times 10^{-5}$. Our first error is their experiment's error and our second error is the systematic error from using our best (shown rounded) value.

[2] AAIJ 12AM reports $[\Gamma(B_s^0 \to \overline{D}^0 K^+K^-)/\Gamma_{total}]$ / $[B(B^0 \to \overline{D}^0 K^+K^-)] = 0.90 \pm 0.27 \pm 0.20$ which we multiply by our best (shown rounded) value $B(B^0 \to \overline{D}^0 K^+K^-) = (6.1 \pm 0.5) \times 10^{-5}$. Our first error is their experiment's error and our second error is the systematic error from using our best (shown rounded) value.

[3] Uses $B(b \to B_s^0)/B(b \to B^0) = 0.267^{+0.023}_{-0.020}$ measured by the same authors.

$\Gamma(\overline{D}^0 f_0(980))/\Gamma_{total}$ — Γ_{62}/Γ

VALUE	CL%	DOCUMENT ID		TECN	COMMENT
<3.1 × 10^{-6}	90	AAIJ	15AG	LHCB	pp at 7, 8 TeV

$\Gamma(\overline{D}^0\phi)/\Gamma_{total}$ — Γ_{63}/Γ

VALUE (units 10^{-5})	DOCUMENT ID		TECN	COMMENT
2.30±0.10±0.23	[1] AAIJ	23AZ	LHCB	pp at 7, 8, 13 TeV
• • • We do not use the following data for averages, fits, limits, etc. • • •				
3.0 ±0.4 ±0.2	[2] AAIJ	18AY	LHCB	Repl. by AAIJ 23AZ

[1] AAIJ 23AZ result's last uncertainty includes the uncertainty of the branching fraction of $B(B^0 \to \overline{D}^0 K^+K^-)$ and of f_s/f_d ratio.

[2] AAIJ 18AY reports $[\Gamma(B_s^0 \to \overline{D}^0\phi)/\Gamma_{total}]$ / $[B(B^0 \to \overline{D}^0\pi^+\pi^-)] = (3.4 \pm 0.4 \pm 0.3) \times 10^{-2}$ which we multiply by our best (shown rounded) value $B(B^0 \to \overline{D}^0\pi^+\pi^-) = (8.8 \pm 0.5) \times 10^{-4}$. Our first error is their experiment's error and our second error is the systematic error from using our best (shown rounded) value.

$\Gamma(\overline{D}^0\phi)/\Gamma(\overline{D}^0\overline{K}^*(892)^0)$ — Γ_{63}/Γ_{41}

VALUE	DOCUMENT ID		TECN	COMMENT
• • • We do not use the following data for averages, fits, limits, etc. • • •				
0.069±0.013±0.007	AAIJ	13BX	LHCB	Repl. by AAIJ 18AY

Int. J. Mod. Phys. A 2026.41. Downloaded from www.worldscientific.com
by UNIVERSITY OF CALIFORNIA @ BERKELEY on 09/16/26. Re-use and distribution is strictly not permitted, except for Open Access articles.

$\Gamma(\overline{D}^{*0}\phi)/\Gamma_{total}$ — Γ_{64}/Γ

VALUE (units 10^{-5})	DOCUMENT ID		TECN	COMMENT
3.17±0.16±0.32	[1] AAIJ	23AZ	LHCB	pp at 7, 8, 13 TeV
• • • We do not use the following data for averages, fits, limits, etc. • • •				
3.7 ±0.6 ±0.2	[2] AAIJ	18AY	LHCB	Repl. by AAIJ 23AZ

[1] AAIJ 23AZ result's last uncertainty includes the uncertainties of the branching fraction of $B(B^0 \to \overline{D}^0 K^+ K^-)$ and of f_s/f_d ratio.

[2] AAIJ 18AY reports $[\Gamma(B_s^0 \to \overline{D}^{*0}\phi)/\Gamma_{total}] / [B(B^0 \to \overline{D}^0\pi^+\pi^-)] = (4.2 \pm 0.5 \pm 0.4) \times 10^{-2}$ which we multiply by our best (shown rounded) value $B(B^0 \to \overline{D}^0\pi^+\pi^-) = (8.8 \pm 0.5) \times 10^{-4}$. Our first error is their experiment's error and our second error is the systematic error from using our best (shown rounded) value.

$\Gamma(D^{*\mp}\pi^{\pm})/\Gamma_{total}$ — Γ_{65}/Γ

VALUE	CL%	DOCUMENT ID		TECN	COMMENT
$<6.1 \times 10^{-6}$	90	[1] AAIJ	13AL	LHCB	pp at 7 TeV

[1] Uses $f_s/f_d = 0.256 \pm 0.020$ and $B(B^0 \to D^{*-}\pi^+) = (2.76 \pm 0.13) \times 10^{-3}$.

$\Gamma(\eta_c\phi)/\Gamma_{total}$ — Γ_{66}/Γ

VALUE (units 10^{-4})	DOCUMENT ID		TECN	COMMENT
5.01±0.53±0.68	[1] AAIJ	17U	LHCB	pp at 7, 8 TeV

[1] The last uncertainty includes the limited knowledge of the external branching fractions where the η_c is reconstructed in the $p\overline{p}, K^+K^-\pi^+\pi^-$, $\pi^+\pi^-\pi^+\pi^-$, and $K^+K^-K^+K^-$ decays and $\phi(1020) \to K^+K^-$.

$\Gamma(\eta_c\pi^+\pi^-)/\Gamma_{total}$ — Γ_{68}/Γ

VALUE (units 10^{-4})	DOCUMENT ID		TECN	COMMENT
1.76±0.59±0.31	[1] AAIJ	17U	LHCB	pp at 7, 8 TeV

[1] The last uncertainty includes the limited knowledge of the external branching fractions where the η_c is reconstructed in the $p\overline{p}, K^+K^-\pi^+\pi^-$, $\pi^+\pi^-\pi^+\pi^-$, and $K^+K^-K^+K^-$ decays. The significance of the signal, including systematic uncertainties, is 4.6 standard deviations.

$\Gamma(J/\psi(1S)\phi)/\Gamma_{total}$ — Γ_{69}/Γ

VALUE (units 10^{-3})	EVTS	DOCUMENT ID		TECN	COMMENT
1.01 ±0.04 OUR FIT					
1.02 ±0.04 OUR AVERAGE					
1.016±0.031±0.022		[1] AAIJ	21Y	LHCB	pp at 7, 8, 13 TeV
1.25 ±0.07 ±0.23		[2] THORNE	13	BELL	$e^+e^- \to \Upsilon(5S)$
1.5 ±0.5 ±0.1		[3] ABE	96Q	CDF	$p\overline{p}$
• • • We do not use the following data for averages, fits, limits, etc. • • •					
1.050±0.013±0.104		[4] AAIJ	13AN	LHCB	Repl. by AAIJ 21Y
<6	1	[5] AKERS	94J	OPAL	$e^+e^- \to Z$
seen	14	[6] ABE	93F	CDF	$p\overline{p}$ at 1.8 TeV
seen	1	[7] ACTON	92N	OPAL	Sup. by AKERS 94J

[1] AAIJ 21Y reports $[\Gamma(B_s^0 \to J/\psi(1S)\phi)/\Gamma_{total}] \times [B(\phi(1020) \to K^+K^-)] = (5.01 \pm 0.16 \pm 0.17) \times 10^{-4}$ from a measurement of $[\Gamma(B_s^0 \to J/\psi(1S)\phi)/\Gamma_{total}] \times [B(\phi(1020) \to K^+K^-)] / [B(B^+ \to J/\psi(1S)K^+)]$ assuming $B(B^+ \to J/\psi(1S)K^+) = (1.003 \pm 0.035) \times 10^{-3}$, which we rescale to our best (shown rounded) values $B(\phi(1020) \to K^+K^-) = (50.1 \pm 0.6) \times 10^{-2}$, $B(B^+ \to J/\psi(1S)K^+) = (1.019 \pm 0.019) \times 10^{-3}$. Our first error is their experiment's error and our second error is the systematic error from using our best (shown rounded) values.

[2] THORNE 13 uses $f_s = (17.2 \pm 3.0)\%$ as the fraction of $\Upsilon(5S)$ decaying to $B_s^{(*)}\overline{B}_s^{(*)}$.

[3] ABE 96Q reports $[\Gamma(B_s^0 \to J/\psi(1S)\phi)/\Gamma_{total}] \times [\Gamma(\overline{b} \to B_s^0 \text{ at } Z)/\left[\Gamma(\overline{b} \to B^+ \text{ at } Z) + \Gamma(\overline{b} \to B^0 \text{ at } Z)\right]] = (0.185 \pm 0.055 \pm 0.020) \times 10^{-3}$ which we divide by our best (shown rounded) value $\Gamma(\overline{b} \to B_s^0 \text{ at } Z)/\left[\Gamma(\overline{b} \to B^+ \text{ at } Z) + \Gamma(\overline{b} \to B^0 \text{ at } Z)\right] = 0.1230 \pm 0.0115$. Our first error is their experiment's error and our second error is the systematic error from using our best (shown rounded) value.

[4] AAIJ 13AN uses $f_s/f_d = 0.256 \pm 0.020$ and $B(B^+ \to J/\psi K^+) = (10.18 \pm 0.42) \times 10^{-4}$.

[5] AKERS 94J sees one event and measures the limit on the product branching fraction $f(\overline{b} \to B_s^0) \cdot B(B_s^0 \to J/\psi(1S)\phi) < 7 \times 10^{-4}$ at CL = 90%. We divide by $B(\overline{b} \to B_s^0) = 0.112$.

[6] ABE 93F measured using $J/\psi(1S) \to \mu^+\mu^-$ and $\phi \to K^+K^-$.

[7] In ACTON 92N a limit on the product branching fraction is measured to be $f(\overline{b} \to B_s^0) \cdot B(B_s^0 \to J/\psi(1S)\phi) \leq 0.22 \times 10^{-2}$.

$\Gamma(J/\psi(1S)\phi\phi)/\Gamma(J/\psi(1S)\phi)$ — Γ_{70}/Γ_{69}

VALUE (units 10^{-2})	EVTS	DOCUMENT ID		TECN	COMMENT
$1.15 \pm 0.12^{+0.05}_{-0.09}$	128	[1] AAIJ	16U	LHCB	pp at 7, 8 TeV

[1] Uses $J/\psi \to \mu^+\mu^-$, $\phi \to K^+K^-$ decays, and observes 128 ± 13 events of $B_s^0 \to J/\psi\phi\phi$.

$\Gamma(J/\psi(1S)\pi^0)/\Gamma_{total}$ — Γ_{71}/Γ

VALUE	CL%	DOCUMENT ID		TECN	COMMENT
$<1.21 \times 10^{-5}$	90	[1] KUMAR	24	BELL	$e^+e^- \to \Upsilon(5S)$
• • • We do not use the following data for averages, fits, limits, etc. • • •					
$<1.2 \times 10^{-3}$	90	[2] ACCIARRI	97C	L3	

[1] KUMAR 24 uses $f_s = (22.0^{+2.0}_{-2.1})\%$ as the fraction of $\Upsilon(5S)$ decaying to $B_s^{(*)}\overline{B}_s^{(*)}$.

[2] ACCIARRI 97C assumes B^0 production fraction (39.5 ± 4.0%) and B_s (12.0 ± 3.0%).

$\Gamma(J/\psi(1S)\eta)/\Gamma_{total}$ — Γ_{72}/Γ

VALUE (units 10^{-4})	CL%	DOCUMENT ID		TECN	COMMENT
4.45±0.25 OUR FIT Error includes scale factor of 1.1.					
4.3 ±0.7 OUR AVERAGE Error includes scale factor of 1.5. See the ideogram below.					
5.7 ±0.5 ±0.9		[1,2] AAIJ	25AN	LHCB	pp at 7, 8, 13 TeV
$3.6^{+0.5}_{-0.6}{}^{+0.3}_{-0.2}$		[3] AAIJ	13A	LHCB	pp at 7 TeV
$5.10 \pm 0.50^{+1.17}_{-0.83}$		[4] LI	12	BELL	$e^+e^- \to \Upsilon(4S)$
• • • We do not use the following data for averages, fits, limits, etc. • • •					
<38	90	[5] ACCIARRI	97C	L3	

[1] AAIJ 25AN reports $B(B^0 \to J/\psi\eta)/B(B_s^0 \to J/\psi\eta) = (2.16 \pm 0.16 \pm 0.05 \pm 0.07) \times 10^{-2}$ where the last uncertainty is due to f_s/f_d ratio. We use the inverse of this branching ratio to obtain the listed value.

[2] AAIJ 25AN reports $[\Gamma(B_s^0 \to J/\psi(1S)\eta)/\Gamma_{total}] / [B(B^0 \to J/\psi(1S)\eta)] = 46.3 \pm 3.4 \pm 1.8$ which we multiply by our best (shown rounded) value $B(B^0 \to J/\psi(1S)\eta) = (1.23 \pm 0.19) \times 10^{-5}$. Our first error is their experiment's error and our second error is the systematic error from using our best (shown rounded) value.

[3] AAIJ 13A reports $[\Gamma(B_s^0 \to J/\psi(1S)\eta)/\Gamma_{total}] / [B(B^0 \to J/\psi(1S)\rho^0)] = 14.0 \pm 1.2^{+1.1}_{-1.5}{}^{+1.1}_{-1.0}$ which we multiply by our best (shown rounded) value $B(B^0 \to J/\psi(1S)\rho^0) = (2.55^{+0.18}_{-0.16}) \times 10^{-5}$. Our first error is their experiment's error and our second error is the systematic error from using our best (shown rounded) value.

[4] Observed for the first time with significances over 10 σ. The second error are total systematic uncertainties including the error on $N(B_s^{(*)}\overline{B}_s^{(*)})$.

[5] ACCIARRI 97C assumes B^0 production fraction (39.5 ± 4.0%) and B_s (12.0 ± 3.0%).

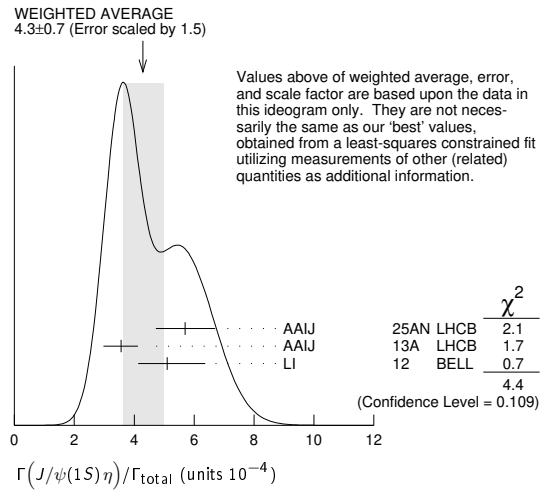

$\Gamma(J/\psi(1S)\eta)/\Gamma(J/\psi(1S)\phi)$ — Γ_{72}/Γ_{69}

VALUE (units 10^{-1})	DOCUMENT ID		TECN	COMMENT
4.39±0.22 OUR FIT Error includes scale factor of 1.1.				
4.50±0.14±0.21	[1] AAIJ	25AN	LHCB	pp at 7, 8 and 13 TeV

[1] The last uncertainty combines the systematic uncertainty with branching fraction uncertainties.

$\Gamma(J/\psi(1S)K_S^0)/\Gamma_{total}$ — Γ_{73}/Γ

VALUE (units 10^{-5})	DOCUMENT ID		TECN	COMMENT
1.92±0.14 OUR AVERAGE				
1.92±0.14±0.05	[1] AAIJ	15AL	LHCB	pp at 7, 8 TeV
2.0 ±0.4 ±0.2	[2] AALTONEN	11A	CDF	$p\overline{p}$ at 1.96 TeV
• • • We do not use the following data for averages, fits, limits, etc. • • •				
1.99±0.16±0.07	[3] AAIJ	13AB	LHCB	Repl. by AAIJ 15AL
$1.99^{+0.26}_{-0.25} \pm 0.07$	[4] AAIJ	12O	LHCB	Repl. by AAIJ 13AB

[1] AAIJ 15AL reports $[\Gamma(B_s^0 \to J/\psi(1S)K_S^0)/\Gamma_{total}] / [B(B^0 \to J/\psi(1S)K_S^0)] = (4.31 \pm 0.17 \pm 0.12 \pm 0.25) \times 10^{-2}$ which we multiply by our best (shown rounded) value $B(B^0 \to J/\psi(1S)K_S^0) = (4.45 \pm 0.11) \times 10^{-4}$. Our first error is their experiment's error and our second error is the systematic error from using our best (shown rounded) value.

[2] AALTONEN 11A reports $[\Gamma(B_s^0 \to J/\psi(1S)K_S^0)/\Gamma_{total}] \times [B(\overline{b} \to B_s^0 \text{ at } Z)] / [B(\overline{b} \to B^0 \text{ at } Z)] / [B(B^0 \to J/\psi(1S)K_S^0)] = (1.09 \pm 0.19 \pm 0.11) \times 10^{-2}$ which we multiply or divide by our best values $B(\overline{b} \to B_s^0 \text{ at } Z) = (10.0 \pm 0.8) \times 10^{-2}$, $B(\overline{b} \to B^0 \text{ at } Z) = (40.8 \pm 0.7) \times 10^{-2}$, $B(B^0 \to J/\psi(1S)K_S^0) = 1/2 \times B(B^0 \to J/\psi(1S)K^0) = 1/2 \times (8.91 \pm 0.21) \times 10^{-4}$. Our first error is their experiment's error and our second error is the systematic error from using our best values.

[3] AAIJ 13AB reports $(1.97 \pm 0.14 \pm 0.07 \pm 0.15 \pm 0.08) \times 10^{-5}$ from a measurement of $[\Gamma(B_s^0 \to J/\psi(1S)K_S^0)/\Gamma_{total}] / [B(B^0 \to J/\psi(1S)K^0)] \times [\Gamma(\overline{b} \to B_s^0 \text{ at } pp)/\Gamma(\overline{b} \to B^0 \text{ at } pp)]$ assuming $B(B^0 \to J/\psi(1S)K^0) = (8.98 \pm 0.35) \times 10^{-4}$, $\Gamma(\overline{b} \to B_s^0 \text{ at } pp)/\Gamma(\overline{b} \to B^0 \text{ at } pp) = 0.256 \pm 0.020$, which we rescale to our best (shown rounded) values $B(B^0 \to J/\psi(1S)K^0) = (8.91 \pm 0.21) \times 10^{-4}$, $\Gamma(\overline{b} \to B_s^0 \text{ at } pp)/$

Int. J. Mod. Phys. A 2026.41. Downloaded from www.worldscientific.com by CALIFORNIA @ BERKELEY on 09/16/26. Re-use and distribution is strictly not permitted, except for Open Access articles.

$\Gamma(\overline{b} \to B^0 \text{ at } pp) = 0.251 \pm 0.007$. Our first error is their experiment's error and our second error is the systematic error from using our best (shown rounded) values.

[4] AAIJ 12O reports $(1.83 \pm 0.21 \pm 0.10 \pm 0.14 \pm 0.07) \times 10^{-5}$ from a measurement of $[\Gamma(B_s^0 \to J/\psi(1S) K_S^0)/\Gamma_{total}] / [B(B^0 \to J/\psi(1S) K^0)] \times [\Gamma(\overline{b} \to B_s^0 \text{ at } pp)/\Gamma(\overline{b} \to B^0 \text{ at } pp)]$ assuming $B(B^0 \to J/\psi(1S) K^0) = (8.71 \pm 0.32) \times 10^{-4}$, $\Gamma(\overline{b} \to B_s^0 \text{ at } pp)/\Gamma(\overline{b} \to B^0 \text{ at } pp) = 0.267^{+0.021}_{-0.02}$, which we rescale to our best (shown rounded) values $B(B^0 \to J/\psi(1S) K^0) = (8.91 \pm 0.21) \times 10^{-4}$, $\Gamma(\overline{b} \to B_s^0 \text{ at } pp)/\Gamma(\overline{b} \to B^0 \text{ at } pp) = 0.251 \pm 0.007$. Our first error is their experiment's error and our second error is the systematic error from using our best (shown rounded) values.

$\Gamma(J/\psi(1S)\overline{K}^*(892)^0)/\Gamma_{total}$ — Γ_{74}/Γ

VALUE (units 10^{-5})	DOCUMENT ID		TECN	COMMENT
3.95±0.19±0.14	[1] AAIJ	25AQ	LHCB	pp at 7, 8, 13 TeV
• • • We do not use the following data for averages, fits, limits, etc. • • •				
3.90±0.20±0.14	[2] AAIJ	25AQ	LHCB	pp at 13 TeV
4.14±0.18±0.35	[3] AAIJ	15AV	LHCB	Repl. by AAIJ 25AQ
$4.4\ ^{+0.5}_{-0.4} \pm 0.8$	[4] AAIJ	12AP	LHCB	Repl. by AAIJ 15AV
9 ±4 ±1	[5] AALTONEN	11A	CDF	$p\overline{p}$ at 1.96 TeV

[1] AAIJ 25AQ reports $[\Gamma(B_s^0 \to J/\psi(1S)\overline{K}^*(892)^0)/\Gamma_{total}] / [B(B^0 \to J/\psi(1S) K^*(892)^0)] = (3.12 \pm 0.09 \pm 0.06 \pm 0.10) \times 10^{-2}$ which we multiply by our best (shown rounded) value $B(B^0 \to J/\psi(1S) K^*(892)^0) = (1.27 \pm 0.05) \times 10^{-3}$. Our first error is their experiment's error and our second error is the systematic error from using our best (shown rounded) value.

[2] AAIJ 25AQ reports $[\Gamma(B_s^0 \to J/\psi(1S)\overline{K}^*(892)^0)/\Gamma_{total}] / [B(B^0 \to J/\psi(1S) K^*(892)^0)] = (3.08 \pm 0.11 \pm 0.06 \pm 0.10) \times 10^{-2}$ which we multiply by our best (shown rounded) value $B(B^0 \to J/\psi(1S) K^*(892)^0) = (1.27 \pm 0.05) \times 10^{-3}$. Our first error is their experiment's error and our second error is the systematic error from using our best (shown rounded) value.

[3] AAIJ 15AV result combines two measurements with different normalizing modes of $B^0 \to J/\psi K^*(892)^0$ and $B_s^0 \to J/\psi\phi$.

[4] AAIJ 12AP reports $B(B_s^0 \to J/\psi(1S)\overline{K}^*(892)^0)/B(B^0 \to J/\psi(1S) K^*(892)^0) = (3.43^{+0.34}_{-0.36} \pm 0.50) \times 10^{-2}$ and $B(B^0 \to J/\psi(1S) K^*(892)^0) = (1.29 \pm 0.05 \pm 0.13) \times 10^{-3}$ after correcting for the contribution from $K\pi$ S-wave beneath the K^* peak.

[5] AALTONEN 11A reports $[\Gamma(B_s^0 \to J/\psi(1S)\overline{K}^*(892)^0)/\Gamma_{total}] \times [B(\overline{b} \to B_s^0 \text{ at } Z)] / [B(\overline{b} \to B^0 \text{ at } Z)] / [B(B^0 \to J/\psi(1S) K^*(892)^0)] = 0.0168 \pm 0.0024 \pm 0.0068$ which we multiply or divide by our best (shown rounded) values $B(\overline{b} \to B_s^0 \text{ at } Z) = (10.0 \pm 0.8) \times 10^{-2}$, $B(\overline{b} \to B^0 \text{ at } Z) = (40.8 \pm 0.7) \times 10^{-2}$, $B(B^0 \to J/\psi(1S) K^*(892)^0) = (1.27 \pm 0.05) \times 10^{-3}$. Our first error is their experiment's error and our second error is the systematic error from using our best (shown rounded) values.

$\Gamma(J/\psi(1S)\eta')/\Gamma_{total}$ — Γ_{75}/Γ

VALUE (units 10^{-4})	DOCUMENT ID		TECN	COMMENT
3.53±0.22 OUR FIT Error includes scale factor of 1.1.				
3.3 ±0.4 OUR AVERAGE				
$3.2\ ^{+0.4}_{-0.5} \pm 0.2$	[1] AAIJ	13A	LHCB	pp at 7 TeV
$3.71 \pm 0.61^{+0.85}_{-0.60}$	[2] LI	12	BELL	$e^+e^- \to \Upsilon(4S)$

[1] AAIJ 13A reports $[\Gamma(B_s^0 \to J/\psi(1S)\eta')/\Gamma_{total}] / [B(B^0 \to J/\psi(1S)\rho^0)] = 12.7 \pm 1.1^{+0.5+1.0}_{-1.3-0.9}$ which we multiply by our best (shown rounded) value $B(B^0 \to J/\psi(1S)\rho^0) = (2.55^{+0.18}_{-0.16}) \times 10^{-5}$. Our first error is their experiment's error and our second error is the systematic error from using our best (shown rounded) value.

[2] Observed for the first time with significances over 10 σ. The second error are total systematic uncertainties including the error on $N(B_s^{(*)}\overline{B}_s^{(*)})$.

$\Gamma(J/\psi(1S)\eta')/\Gamma(J/\psi(1S)\eta)$ — Γ_{75}/Γ_{72}

VALUE	DOCUMENT ID		TECN	COMMENT
0.793±0.028 OUR FIT				
0.797±0.028 OUR AVERAGE				
0.80 ±0.02 ±0.02	[1] AAIJ	25AN	LHCB	pp at 7, 8 and 13 TeV
0.73 ±0.14 ±0.02	[2] LI	12	BELL	$e^+e^- \to \Upsilon(4S)$
• • • We do not use the following data for averages, fits, limits, etc. • • •				
0.902±0.072±0.045	[3] AAIJ	15D	LHCB	Repl. by AAIJ 25AN
$0.90\ \pm 0.09\ ^{+0.06}_{-0.02}$	[2] AAIJ	13A	LHCB	Repl. by AAIJ 15D

[1] The last uncertainty combines the systematic uncertainty with branching fraction uncertainties.

[2] Strongly correlated with measurements of $\Gamma(J/\psi(1S)\eta)/\Gamma$ and $\Gamma(J/\psi(1S)\eta')/\Gamma$ reported in the same reference.

[3] Uses $J/\psi \to \mu^+\mu^-$, $\eta' \to \rho^0\gamma$, and $\eta' \to \eta\pi^+\pi^-$ decays.

$\Gamma(J/\psi(1S)\pi^+\pi^-)/\Gamma(J/\psi(1S)\phi)$ — Γ_{76}/Γ_{69}

VALUE (units 10^{-2})	DOCUMENT ID		TECN	COMMENT
19.8±1.5 OUR FIT Error includes scale factor of 2.2.				
20.3±0.7±0.2	[1] AAIJ	12AO	LHCB	pp at 7 TeV

[1] AAIJ 12AO reports $(19.79 \pm 0.47 \pm 0.52) \times 10^{-2}$ from a measurement of $[\Gamma(B_s^0 \to J/\psi(1S)\pi^+\pi^-)/\Gamma(B_s^0 \to J/\psi(1S)\phi)] / [B(\phi(1020) \to K^+K^-)]$ assuming $B(\phi(1020) \to K^+K^-) = (48.9 \pm 0.5) \times 10^{-2}$, which we rescale to our best (shown rounded) value $B(\phi(1020) \to K^+K^-) = (50.1 \pm 0.6) \times 10^{-2}$. Our first error is their experiment's error and our second error is the systematic error from using our best (shown rounded) value.

$\Gamma(J/\psi(1S) f_0(500),\ f_0 \to \pi^+\pi^-)/\Gamma(J/\psi(1S) f_0(980),\ f_0 \to \pi^+\pi^-)$ — Γ_{77}/Γ_{79}

VALUE	CL%	DOCUMENT ID		TECN	COMMENT
<0.034	90	[1] AAIJ	14BR	LHCB	pp at 7, 8 TeV

[1] Reported first of two solutions using the full Dalitz analysis.

$\Gamma(J/\psi(1S)\rho,\ \rho \to \pi^+\pi^-)/\Gamma(J/\psi(1S)\pi^+\pi^-)$ — Γ_{78}/Γ_{76}

VALUE	CL%	DOCUMENT ID		TECN	COMMENT
<0.017	90	[1] AAIJ	14BR	LHCB	pp at 7, 8 TeV

[1] Reported first of two solutions using the full Dalitz analysis.

$\Gamma(J/\psi(1S) f_0(980),\ f_0 \to \pi^+\pi^-)/\Gamma_{total}$ — Γ_{79}/Γ

VALUE (units 10^{-4})	DOCUMENT ID		TECN	COMMENT
1.23±0.15 OUR FIT Error includes scale factor of 2.1.				
$1.16^{+0.31+0.30}_{-0.19-0.25}$	[1] LI	11	BELL	$e^+e^- \to \Upsilon(5S)$

[1] The second error includes both the detector systematic and the uncertainty in the number of produced $\Upsilon(5S) \to B_s^{(*)}\overline{B}_s^{(*)}$ pairs.

$\Gamma(J/\psi(1S) f_0(980),\ f_0 \to \pi^+\pi^-)/\Gamma(J/\psi(1S)\phi)$ — Γ_{79}/Γ_{69}

VALUE	DOCUMENT ID		TECN	COMMENT
$0.121^{+0.013}_{-0.015}$ **OUR FIT** Error includes scale factor of 2.4.				
$0.113^{+0.020}_{-0.018}$ **OUR AVERAGE** Error includes scale factor of 2.5. See the ideogram below.				
0.070±0.012±0.001	[1] KHACHATRY...	16Q	CMS	pp at 7 TeV
$0.142^{+0.026}_{-0.014} \pm 0.002$	[2,3] AAIJ	12AO	LHCB	pp at 7 TeV
0.138±0.037±0.002	[4] ABAZOV	12C	D0	$p\overline{p}$ at 1.96 TeV
0.129±0.012±0.001	[5] AALTONEN	11AB	CDF	$p\overline{p}$ at 1.96 TeV
• • • We do not use the following data for averages, fits, limits, etc. • • •				
$0.126^{+0.027}_{-0.023} \pm 0.001$	[6] AAIJ	11	LHCB	Repl. by AAIJ 12AO

[1] KHACHATRYAN 16Q reports $[\Gamma(B_s^0 \to J/\psi(1S) f_0(980),\ f_0 \to \pi^+\pi^-)/\Gamma(B_s^0 \to J/\psi(1S)\phi)] / [B(\phi(1020) \to K^+K^-)] = 0.140 \pm 0.008 \pm 0.023$ which we multiply by our best (shown rounded) value $B(\phi(1020) \to K^+K^-) = (50.1 \pm 0.6) \times 10^{-2}$. Our first error is their experiment's error and our second error is the systematic error from using our best (shown rounded) value.

[2] AAIJ 12AO reports $(13.9 \pm 0.6^{+2.5}_{-1.2}) \times 10^{-2}$ from a measurement of $[\Gamma(B_s^0 \to J/\psi(1S) f_0(980),\ f_0 \to \pi^+\pi^-)/\Gamma(B_s^0 \to J/\psi(1S)\phi)] / [B(\phi(1020) \to K^+K^-)]$ assuming $B(\phi(1020) \to K^+K^-) = (48.9 \pm 0.5) \times 10^{-2}$, which we rescale to our best (shown rounded) value $B(\phi(1020) \to K^+K^-) = (50.1 \pm 0.6) \times 10^{-2}$. Our first error is their experiment's error and our second error is the systematic error from using our best (shown rounded) value.

[3] Measured in Dalitz plot like analysis of $B_s \to J/\psi\pi^+\pi^-$ decays.

[4] ABAZOV 12C reports $[\Gamma(B_s^0 \to J/\psi(1S) f_0(980),\ f_0 \to \pi^+\pi^-)/\Gamma(B_s^0 \to J/\psi(1S)\phi)] / [B(\phi(1020) \to K^+K^-)] = 0.275 \pm 0.041 \pm 0.061$ which we multiply by our best (shown rounded) value $B(\phi(1020) \to K^+K^-) = (50.1 \pm 0.6) \times 10^{-2}$. Our first error is their experiment's error and our second error is the systematic error from using our best (shown rounded) value.

[5] AALTONEN 11AB reports $[\Gamma(B_s^0 \to J/\psi(1S) f_0(980),\ f_0 \to \pi^+\pi^-)/\Gamma(B_s^0 \to J/\psi(1S)\phi)] / [B(\phi(1020) \to K^+K^-)] = 0.257 \pm 0.020 \pm 0.014$ which we multiply by our best (shown rounded) value $B(\phi(1020) \to K^+K^-) = (50.1 \pm 0.6) \times 10^{-2}$. Our first error is their experiment's error and our second error is the systematic error from using our best (shown rounded) value.

[6] AAIJ 11 reports $[\Gamma(B_s^0 \to J/\psi(1S) f_0(980),\ f_0 \to \pi^+\pi^-)/\Gamma(B_s^0 \to J/\psi(1S)\phi)] / [B(\phi(1020) \to K^+K^-)] = 0.252^{+0.046+0.027}_{-0.032-0.033}$ which we multiply by our best (shown rounded) value $B(\phi(1020) \to K^+K^-) = (50.1 \pm 0.6) \times 10^{-2}$. Our first error is their experiment's error and our second error is the systematic error from using our best (shown rounded) value.

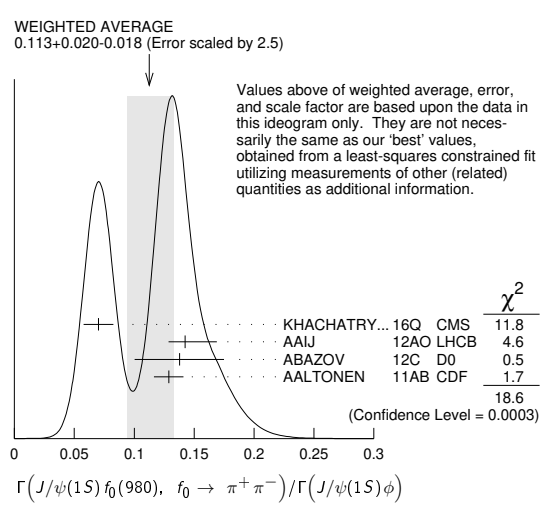

Int. J. Mod. Phys. A 2026.41. Downloaded from www.worldscientific.com
by UNIVERSITY OF CALIFORNIA @ BERKELEY on 09/16/26. Re-use and distribution is strictly not permitted, except for Open Access articles.

$\Gamma(J/\psi(1S) f_0(980),\ f_0 \to \pi^+\pi^-)/\Gamma(J/\psi(1S)\pi^+\pi^-)$ — Γ_{79}/Γ_{76}

VALUE	DOCUMENT ID		TECN	COMMENT
0.61 $^{+0.05}_{-0.07}$ OUR FIT	Error includes scale factor of 2.1.			
0.703±0.015$^{+0.004}_{-0.051}$	[1] AAIJ	14BR	LHCB	pp at 7, 8 TeV

[1] Reported first of two solutions using the full Dalitz analysis.

$\Gamma(J/\psi(1S) f_2(1270),\ f_2 \to \pi^+\pi^-)/\Gamma(J/\psi(1S)\phi)$ — Γ_{80}/Γ_{69}

VALUE (units 10^{-4})	DOCUMENT ID		TECN	COMMENT
10.0$^{+3.4}_{-3.7}$±0.1	[1,2] AAIJ	12AO	LHCB	pp at 7 TeV

[1] AAIJ 12AO reports $(0.098 \pm 0.033^{+0.006}_{-0.015}) \times 10^{-2}$ from a measurement of $[\Gamma(B_s^0 \to J/\psi(1S) f_2(1270),\ f_2 \to \pi^+\pi^-)/\Gamma(B_s^0 \to J/\psi(1S)\phi)]$ / $[B(\phi(1020) \to K^+K^-)]$ assuming $B(\phi(1020) \to K^+K^-) = (48.9 \pm 0.5) \times 10^{-2}$, which we rescale to our best (shown rounded) value $B(\phi(1020) \to K^+K^-) = (50.1 \pm 0.6) \times 10^{-2}$. Our first error is their experiment's error and our second error is the systematic error from using our best (shown rounded) value.

[2] Measured in Dalitz plot like analysis of $B_s \to J/\psi\pi^+\pi^-$ decays for the f_2 helicity state $\lambda = 0$.

$\Gamma(J/\psi(1S) f_2(1270)_0,\ f_2 \to \pi^+\pi^-)/\Gamma(J/\psi(1S)\pi^+\pi^-)$ — Γ_{81}/Γ_{76}

VALUE (%)	DOCUMENT ID		TECN	COMMENT
0.36±0.07±0.03	[1] AAIJ	14BR	LHCB	pp at 7, 8 TeV

[1] Reported first of two solutions using the full Dalitz analysis.

$\Gamma(J/\psi(1S) f_2(1270)_\parallel,\ f_2 \to \pi^+\pi^-)/\Gamma(J/\psi(1S)\pi^+\pi^-)$ — Γ_{82}/Γ_{76}

VALUE (%)	DOCUMENT ID		TECN	COMMENT
0.52±0.15$^{+0.05}_{-0.02}$	[1] AAIJ	14BR	LHCB	pp at 7, 8 TeV

[1] Reported first of two solutions using the full Dalitz analysis.

$\Gamma(J/\psi(1S) f_2(1270)_\perp,\ f_2 \to \pi^+\pi^-)/\Gamma(J/\psi(1S)\pi^+\pi^-)$ — Γ_{83}/Γ_{76}

VALUE (%)	DOCUMENT ID		TECN	COMMENT
0.63±0.34$^{+0.16}_{-0.08}$	[1] AAIJ	14BR	LHCB	pp at 7, 8 TeV

[1] Reported first of two solutions using the full Dalitz analysis.

$\Gamma(J/\psi(1S) f_0(1370),\ f_0 \to \pi^+\pi^-)/\Gamma_{total}$ — Γ_{84}/Γ

VALUE (units 10^{-4})	DOCUMENT ID		TECN	COMMENT
• • • We do not use the following data for averages, fits, limits, etc. • • •				
$0.34^{+0.11}_{-0.14}{}^{+0.085}_{-0.054}$	[1] LI	11	BELL	$e^+e^- \to \Upsilon(5S)$

[1] The second error includes both the detector systematic and the uncertainty in the number of produced $Y(5S) \to B_s^{(*)}\overline{B}_s^{(*)}$ pairs.

$\Gamma(J/\psi(1S) f_0(1370),\ f_0 \to \pi^+\pi^-)/\Gamma(J/\psi(1S)\phi)$ — Γ_{84}/Γ_{69}

VALUE (units 10^{-2})	DOCUMENT ID		TECN	COMMENT
4.29$^{+0.56}_{-3.83}$±0.05	[1,2] AAIJ	12AO	LHCB	pp at 7 TeV

[1] AAIJ 12AO reports $(4.19 \pm 0.53^{+0.12}_{-3.7}) \times 10^{-2}$ from a measurement of $[\Gamma(B_s^0 \to J/\psi(1S) f_0(1370),\ f_0 \to \pi^+\pi^-)/\Gamma(B_s^0 \to J/\psi(1S)\phi)]$ / $[B(\phi(1020) \to K^+K^-)]$ assuming $B(\phi(1020) \to K^+K^-) = (48.9 \pm 0.5) \times 10^{-2}$, which we rescale to our best (shown rounded) value $B(\phi(1020) \to K^+K^-) = (50.1 \pm 0.6) \times 10^{-2}$. Our first error is their experiment's error and our second error is the systematic error from using our best (shown rounded) value.

[2] Measured in Dalitz plot like analysis of $B_s \to J/\psi\pi^+\pi^-$ decays.

$\Gamma(J/\psi(1S) f_0(1500),\ f_0 \to \pi^+\pi^-)/\Gamma(J/\psi(1S)\pi^+\pi^-)$ — Γ_{85}/Γ_{76}

VALUE	DOCUMENT ID		TECN	COMMENT
0.101±0.008$^{+0.011}_{-0.003}$	[1] AAIJ	14BR	LHCB	pp at 7, 8 TeV

[1] Reported first of two solutions using the full Dalitz analysis.

$\Gamma(J/\psi(1S) f_2'(1525)_0,\ f_2' \to \pi^+\pi^-)/\Gamma(J/\psi(1S)\pi^+\pi^-)$ — Γ_{86}/Γ_{76}

VALUE (%)	DOCUMENT ID		TECN	COMMENT
0.51±0.09$^{+0.05}_{-0.04}$	[1] AAIJ	14BR	LHCB	pp at 7, 8 TeV

[1] Reported first of two solutions using the full Dalitz analysis.

$\Gamma(J/\psi(1S) f_2'(1525)_\parallel,\ f_2' \to \pi^+\pi^-)/\Gamma(J/\psi(1S)\pi^+\pi^-)$ — Γ_{87}/Γ_{76}

VALUE (%)	DOCUMENT ID		TECN	COMMENT
0.06$^{+0.13}_{-0.04}$±0.01	[1] AAIJ	14BR	LHCB	pp at 7, 8 TeV

[1] Reported first of two solutions using the full Dalitz analysis.

$\Gamma(J/\psi(1S) f_2'(1525)_\perp,\ f_2' \to \pi^+\pi^-)/\Gamma(J/\psi(1S)\pi^+\pi^-)$ — Γ_{88}/Γ_{76}

VALUE (%)	DOCUMENT ID		TECN	COMMENT
0.26±0.18$^{+0.06}_{-0.04}$	[1] AAIJ	14BR	LHCB	pp at 7, 8 TeV

[1] Reported first of two solutions using the full Dalitz analysis.

$\Gamma(J/\psi(1S) f_0(1790),\ f_0 \to \pi^+\pi^-)/\Gamma(J/\psi(1S)\pi^+\pi^-)$ — Γ_{89}/Γ_{76}

VALUE	DOCUMENT ID		TECN	COMMENT
0.024±0.004$^{+0.050}_{-0.002}$	[1] AAIJ	14BR	LHCB	pp at 7, 8 TeV

[1] Reported first of two solutions using the full Dalitz analysis.

$\Gamma(J/\psi(1S)\pi^+\pi^-(\text{nonresonant}))/\Gamma(J/\psi(1S)\phi)$ — Γ_{90}/Γ_{69}

VALUE (units 10^{-2})	DOCUMENT ID		TECN	COMMENT
1.70$^{+1.03}_{-0.33}$±0.02	[1,2] AAIJ	12AO	LHCB	pp at 7 TeV

[1] AAIJ 12AO reports $(1.66 \pm 0.31^{+0.96}_{-0.08}) \times 10^{-2}$ from a measurement of $[\Gamma(B_s^0 \to J/\psi(1S)\pi^+\pi^-(\text{nonresonant}))/\Gamma(B_s^0 \to J/\psi(1S)\phi)]$ / $[B(\phi(1020) \to K^+K^-)]$ assuming $B(\phi(1020) \to K^+K^-) = (48.9 \pm 0.5) \times 10^{-2}$, which we rescale to our best (shown rounded) value $B(\phi(1020) \to K^+K^-) = (50.1 \pm 0.6) \times 10^{-2}$. Our first error is their experiment's error and our second error is the systematic error from using our best (shown rounded) value.

[2] Measured in Dalitz plot like analysis of $B_s \to J/\psi\pi^+\pi^-$ decays.

$\Gamma(J/\psi(1S)\overline{K}^0\pi^+\pi^-)/\Gamma_{total}$ — Γ_{91}/Γ

VALUE	CL%	DOCUMENT ID		TECN	COMMENT
<4.4 × 10^{-5}	90	[1] AAIJ	14L	LHCB	pp at 7 TeV

[1] Measured with $B(B_s^0 \to J/\psi K_S^0\pi^+\pi^-)$ / $B(B^0 \to J/\psi K_S^0\pi^+\pi^-)$ using PDG 12 values for the involved branching fractions.

$\Gamma(J/\psi(1S) K^+K^-)/\Gamma_{total}$ — Γ_{92}/Γ

VALUE (units 10^{-4})	DOCUMENT ID		TECN	COMMENT
7.9 ±0.7 OUR AVERAGE				
7.70±0.08±0.72	[1] AAIJ	13AN	LHCB	pp at 7 TeV
10.1 ±0.9 ±2.1	[2] THORNE	13	BELL	$e^+e^- \to \Upsilon(5S)$

[1] Uses $f_s/f_d = 0.256 \pm 0.020$ and $B(B^+ \to J/\psi K^+) = (10.18 \pm 0.42) \times 10^{-4}$.

[2] Uses $f_s = (17.2 \pm 3.0)\%$ as the fraction of $\Upsilon(5S)$ decaying to $B_s^{(*)}\overline{B}_s^{(*)}$.

$\Gamma(J/\psi(1S) K^0K^-\pi^+ + \text{c.c.})/\Gamma_{total}$ — Γ_{93}/Γ

VALUE (units 10^{-4})	DOCUMENT ID		TECN	COMMENT
9.5±1.0±0.8	[1] AAIJ	14L	LHCB	pp at 7 TeV

[1] AAIJ 14L reports $[\Gamma(B_s^0 \to J/\psi(1S) K^0K^-\pi^+ + \text{c.c.})/\Gamma_{total}]$ / $[B(B^0 \to J/\psi(1S) K^0\pi^+\pi^-)] = 2.12 \pm 0.15 \pm 0.18$ which we multiply by our best (shown rounded) value $B(B^0 \to J/\psi(1S) K^0\pi^+\pi^-) = (4.5 \pm 0.4) \times 10^{-4}$. Our first error is their experiment's error and our second error is the systematic error from using our best (shown rounded) value. This is an observation of $B_s^0 \to J/\psi K_S^0 K^\pm\pi^\mp$ with more than 10 standard deviations.

$\Gamma(J/\psi(1S)\overline{K}^0 K^+K^-)/\Gamma_{total}$ — Γ_{94}/Γ

VALUE	CL%	DOCUMENT ID		TECN	COMMENT
<12 × 10^{-6}	90	[1] AAIJ	14L	LHCB	pp at 7 TeV

[1] Measured with $B(B_s^0 \to J/\psi K_S^0 K^+K^-)/B(B^0 \to J/\psi K_S^0\pi^+\pi^-)$ using PDG 12 values for the involved branching fractions.

$\Gamma(J/\psi(1S) f_2'(1525))/\Gamma_{total}$ — Γ_{96}/Γ

VALUE (units 10^{-4})	DOCUMENT ID		TECN	COMMENT
2.61±0.20$^{+0.56}_{-0.50}$	[1] AAIJ	13AN	LHCB	pp at 7 TeV

[1] Uses $f_s/f_d = 0.256 \pm 0.020$ and $B(B^+ \to J/\psi K^+) = (10.18 \pm 0.42) \times 10^{-4}$.

$\Gamma(J/\psi(1S) f_2'(1525))/\Gamma(J/\psi(1S)\phi)$ — Γ_{96}/Γ_{69}

VALUE (units 10^{-2})	DOCUMENT ID		TECN	COMMENT
21 ±4 OUR AVERAGE				
21.5±4.9±2.6	[1] THORNE	13	BELL	$e^+e^- \to \Upsilon(5S)$
21 ±7 ±1	[2,3] ABAZOV	12AF	D0	$p\overline{p}$ at 1.96 TeV
• • • We do not use the following data for averages, fits, limits, etc. • • •				
27 ±4 ±1	[4] AAIJ	12S	LHCB	Repl. by AAIJ 13AN

[1] Uses $B(f_2'(1525) \to K^+K^-) = (44.4 \pm 1.1)\%$.

[2] ABAZOV 12AF reports $[\Gamma(B_s^0 \to J/\psi(1S) f_2'(1525))/\Gamma(B_s^0 \to J/\psi(1S)\phi)] \times B(f_2'(1525) \to K^+K^-)$ / $B(\phi(1020) \to K^+K^-) = 0.19 \pm 0.05 \pm 0.04$ which we divide and multiply by our best values $B(f_2'(1525) \to K^+K^-) = \frac{1}{2}(88.8 \pm 2.2) \times 10^{-2}$, $B(\phi(1020) \to K^+K^-) = (50.1 \pm 0.6) \times 10^{-2}$. Our first error is their experiment's error and our second error is the systematic error from using our best values.

[3] ABAZOV 12AF fits the invariant masses of the K^+K^- pair in the range $1.35 < M(K^+K^-) < 2$ GeV.

[4] AAIJ 12S reports $[(26.4 \pm 2.7 \pm 2.4) \times 10^{-2}$ from a measurement of $\Gamma(B_s^0 \to J/\psi(1S) f_2'(1525))/\Gamma(B_s^0 \to J/\psi(1S)\phi)] \times B(f_2'(1525) \to K^+K^-)$ / $B(\phi(1020) \to K^+K^-)$ assuming $B(f_2'(1525) \to K^+K^-) = (44.4 \pm 1.1) \times 10^{-2}$, $B(\phi(1020) \to K^+K^-) = (48.9 \pm 0.5) \times 10^{-2}$, which we rescale to our best values $B(f_2'(1525) \to K^+K^-) = \frac{1}{2}(88.8 \pm 2.2) \times 10^{-2}$, $B(\phi(1020) \to K^+K^-) = (50.1 \pm 0.6) \times 10^{-2}$. Our first error is their experiment's error and our second error is the systematic error from using our best values.

Int. J. Mod. Phys. A 2026.41. Downloaded from www.worldscientific.com by CALIFORNIA @ BERKELEY on 09/16/26. Re-use and distribution is strictly not permitted, except for Open Access articles.

$\Gamma(J/\psi(1S)p\overline{p})/\Gamma_{total}$ — Γ_{97}/Γ

VALUE (units 10^{-6})	CL%	DOCUMENT ID		TECN	COMMENT
3.58±0.19±0.39		[1] AAIJ	19U	LHCB	pp at 7, 8, 13 TeV
• • • We do not use the following data for averages, fits, limits, etc. • • •					
<4.8	90	[2] AAIJ	13Z	LHCB	Repl. by AAIJ 19U

[1] Measured relative to $B_s^0 \to J/\psi\phi$ assuming $B(B_s^0 \to J/\psi\phi) = (10.5 \pm 0.13 \pm 0.64) \times 10^{-4}$ and taking into account small K^+K^- S-wave contribution.
[2] Uses $B(B_s^0 \to J/\psi(1S)\pi^+\pi^-) = (1.98 \pm 0.20) \times 10^{-4}$.

$\Gamma(J/\psi(1S)\gamma)/\Gamma_{total}$ — Γ_{98}/Γ

VALUE	CL%	DOCUMENT ID		TECN	COMMENT
<7.3 × 10^{-6}	90	[1] AAIJ	15BB	LHCB	pp at 7, 8 TeV

[1] Branching fractions of normalization modes $B_s^0 \to J/\psi\gamma X$ taken from PDG 14. Uses $f_s/f_d = 0.259 \pm 0.015$.

$\Gamma(J/\psi\mu^+\mu^-, J/\psi \to \mu^+\mu^-)/\Gamma_{total}$ — Γ_{99}/Γ

VALUE	CL%	DOCUMENT ID		TECN	COMMENT
<2.6 × 10^{-9}	95	AAIJ	22Q	LHCB	pp at 7, 8, 13 TeV

$\Gamma(J/\psi(1S)\pi^+\pi^-\pi^+\pi^-)/\Gamma(J/\psi(1S)\pi^+\pi^-)$ — Γ_{100}/Γ_{76}

VALUE	DOCUMENT ID		TECN	COMMENT
0.371±0.015±0.022	[1] AAIJ	14Y	LHCB	pp at 7,8 TeV

[1] Excludes contributions from $\psi(2S)$ and $\chi_{c1}(3872)$ decaying to $J/\psi(1S)\pi^+\pi^-$.

$\Gamma(J/\psi(1S)f_1(1285))/\Gamma_{total}$ — Γ_{101}/Γ

VALUE (units 10^{-5})	DOCUMENT ID		TECN	COMMENT
7.2±1.3±0.4	[1] AAIJ	14Y	LHCB	pp at 7, 8 TeV

[1] AAIJ 14Y reports $(7.14 \pm 0.99^{+0.83}_{-0.91} \pm 0.41) \times 10^{-5}$ from a measurement of $[\Gamma(B_s^0 \to J/\psi(1S)f_1(1285))/\Gamma_{total}] \times [B(f_1(1285) \to 2\pi^+2\pi^-)]$ assuming $B(f_1(1285) \to 2\pi^+2\pi^-) = 0.11^{+0.007}_{-0.006}$, which we rescale to our best (shown rounded) value $B(f_1(1285) \to 2\pi^+2\pi^-) = (10.9 \pm 0.6) \times 10^{-2}$. Our first error is their experiment's error and our second error is the systematic error from using our best (shown rounded) value.

$\Gamma(J/\psi(1S)\overline{D}^0)/\Gamma_{total}$ — Γ_{102}/Γ

VALUE	CL%	DOCUMENT ID		TECN	COMMENT
<1.0 × 10^{-6}	90	AAIJ	24F	LHCB	pp at 7, 8, 13 TeV

$\Gamma(\psi(2S)\eta)/\Gamma(J/\psi(1S)\eta)$ — Γ_{103}/Γ_{72}

VALUE	DOCUMENT ID		TECN	COMMENT
0.83±0.14±0.12	[1] AAIJ	13AA	LHCB	pp at 7 TeV

[1] Assuming lepton universality for dimuon decay modes of J/ψ and $\psi(2S)$ mesons, the ratio $B(J/\psi \to \mu^+\mu^-)/B(\psi(2S) \to \mu^+\mu^-) = B(J/\psi \to e^+e^-)/B(\psi(2S) \to e^+e^-) = 7.69 \pm 0.19$ was used.

$\Gamma(\psi(2S)\eta')/\Gamma(J/\psi(1S)\eta')$ — Γ_{104}/Γ_{75}

VALUE (units 10^{-2})	DOCUMENT ID		TECN	COMMENT
38.7±9.0±1.6	[1] AAIJ	15D	LHCB	pp at 7, 8 TeV

[1] Uses $J/\psi \to \mu^+\mu^-$, $\eta' \to \rho^0\gamma$, and $\eta' \to \eta\pi^+\pi^-$ decays.

$\Gamma(\psi(2S)\pi^+\pi^-)/\Gamma(J/\psi(1S)\pi^+\pi^-)$ — Γ_{105}/Γ_{76}

VALUE	DOCUMENT ID		TECN	COMMENT
0.34±0.04±0.03	[1] AAIJ	13AA	LHCB	pp at 7 TeV

[1] Assuming lepton universality for dimuon decay modes of J/ψ and $\psi(2S)$ mesons, the ratio $B(J/\psi \to \mu^+\mu^-)/B(\psi(2S) \to \mu^+\mu^-) = B(J/\psi \to e^+e^-)/B(\psi(2S) \to e^+e^-) = 7.69 \pm 0.19$ was used.

$\Gamma(\psi(2S)\phi)/\Gamma_{total}$ — Γ_{106}/Γ

VALUE (units 10^{-4})	EVTS	DOCUMENT ID		TECN	COMMENT
• • • We do not use the following data for averages, fits, limits, etc. • • •					
seen	1	BUSKULIC	93G	ALEP	$e^+e^- \to Z$

$\Gamma(\psi(2S)\phi)/\Gamma(J/\psi(1S)\phi)$ — Γ_{106}/Γ_{69}

VALUE	DOCUMENT ID		TECN	COMMENT
0.504±0.035 OUR AVERAGE				
0.501±0.034±0.014	[1,2] AAIJ	12L	LHCB	pp at 7 TeV
0.53 ±0.10 ±0.09	ABAZOV	09Y	D0	$p\overline{p}$ at 1.96 TeV
0.52 ±0.13 ±0.07	ABULENCIA	06N	CDF	$p\overline{p}$ at 1.96 TeV

[1] AAIJ 12L reports $0.489 \pm 0.026 \pm 0.021 \pm 0.012$ from a measurement of $[\Gamma(B_s^0 \to \psi(2S)\phi)/\Gamma(B_s^0 \to J/\psi(1S)\phi)] \times [B(J/\psi(1S) \to e^+e^-)] / [B(\psi(2S) \to e^+e^-)]$ assuming $B(J/\psi(1S) \to e^+e^-) = (5.94 \pm 0.06) \times 10^{-2}$, $B(\psi(2S) \to e^+e^-) = (7.72 \pm 0.17) \times 10^{-3}$, which we rescale to our best (shown rounded) values $B(J/\psi(1S) \to e^+e^-) = (5.971 \pm 0.032) \times 10^{-2}$, $B(\psi(2S) \to e^+e^-) = (7.95 \pm 0.22) \times 10^{-3}$. Our first error is their experiment's error and our second error is the systematic error from using our best (shown rounded) values.
[2] Assumes $B(J/\psi \to \mu^+\mu^-) / B(\psi(2S) \to \mu^+\mu^-) = B(J/\psi \to e^+e^-) / B(\psi(2S) \to e^+e^-) = 7.69 \pm 0.19$.

$\Gamma(\psi(2S)K^0)/\Gamma_{total}$ — Γ_{107}/Γ

VALUE (units 10^{-5})	DOCUMENT ID		TECN	COMMENT
1.9±0.5±0.2	[1] TUMASYAN	22AI	CMS	pp at 13 TeV

[1] TUMASYAN 22AI reports $[\Gamma(B_s^0 \to \psi(2S)K^0)/\Gamma_{total}] / [B(B^0 \to \psi(2S)K^0)] = (3.33 \pm 0.69 \pm 0.11 \pm 0.34) \times 10^{-2}$ which we multiply by our best (shown rounded) value $B(B^0 \to \psi(2S)K^0) = (5.8 \pm 0.5) \times 10^{-4}$. Our first error is their experiment's error and our second error is the systematic error from using our best (shown rounded) value.

$\Gamma(\psi(2S)K^-\pi^+)/\Gamma_{total}$ — Γ_{108}/Γ

VALUE (units 10^{-5})	DOCUMENT ID		TECN	COMMENT
3.12±0.30±0.21	[1] AAIJ	15U	LHCB	pp at 7, 8 TeV

[1] AAIJ 15U reports $[\Gamma(B_s^0 \to \psi(2S)K^-\pi^+)/\Gamma_{total}] / [B(B^0 \to \psi(2S)K^+\pi^-)] = (5.38 \pm 0.36 \pm 0.22 \pm 0.31) \times 10^{-2}$ which we multiply by our best (shown rounded) value $B(B^0 \to \psi(2S)K^+\pi^-) = (5.8 \pm 0.4) \times 10^{-4}$. Our first error is their experiment's error and our second error is the systematic error from using our best (shown rounded) value.

$\Gamma(\psi(2S)\overline{K}^*(892)^0)/\Gamma_{total}$ — Γ_{109}/Γ

VALUE (units 10^{-5})	DOCUMENT ID		TECN	COMMENT
3.3±0.5$^{+0.2}_{-0.3}$	[1] AAIJ	15U	LHCB	pp at 7, 8 TeV

[1] AAIJ 15U reports $[\Gamma(B_s^0 \to \psi(2S)\overline{K}^*(892)^0)/\Gamma_{total}] / [B(B^0 \to \psi(2S)K^*(892)^0)] = (5.58 \pm 0.57 \pm 0.40 \pm 0.32) \times 10^{-2}$ which we multiply by our best (shown rounded) value $B(B^0 \to \psi(2S)K^*(892)^0) = (5.9 \pm 0.4) \times 10^{-4}$. Our first error is their experiment's error and our second error is the systematic error from using our best (shown rounded) value.

$\Gamma(\chi_{c1}\phi)/\Gamma(J/\psi(1S)\phi)$ — Γ_{110}/Γ_{69}

VALUE (units 10^{-2})	DOCUMENT ID		TECN	COMMENT
18.9±1.8±1.5	[1] AAIJ	13AC	LHCB	pp at 7 TeV

[1] Uses $B(\chi_{c1} \to J/\psi\gamma) = (34.4 \pm 1.5)\%$.

$\Gamma(\chi_{c2}K^+K^-)/\Gamma(\chi_{c1}K^+K^-)$ — $\Gamma_{112}/\Gamma_{111}$

VALUE (units 10^{-2})	DOCUMENT ID		TECN	COMMENT
17.1±3.1±1.0	[1] AAIJ	18AC	LHCB	pp at 7, 8, 13 TeV

[1] Measures the ratio for ±15 MeV window around ϕ mass.

$\Gamma(\chi_{c1}(3872)\phi)/\Gamma(\psi(2S)\phi)$ — $\Gamma_{113}/\Gamma_{106}$

VALUE	DOCUMENT ID		TECN	COMMENT
0.19±0.06 OUR AVERAGE				
0.19±0.02±0.06	[1] AAIJ	21C	LHCB	pp at 7, 8, 13 TeV
0.18±0.03±0.06	[2] SIRUNYAN	20BB	CMS	pp at 13 TeV

[1] AAIJ 21C reports $[\Gamma(B_s^0 \to \chi_{c1}(3872)\phi)/\Gamma(B_s^0 \to \psi(2S)\phi)] \times [B(\chi_{c1}(3872) \to \pi^+\pi^-J/\psi(1S))] / [B(\psi(2S) \to J/\psi(1S)\pi^+\pi^-)] = (2.42 \pm 0.23 \pm 0.07) \times 10^{-2}$ which we multiply or divide by our best (shown rounded) values $B(\chi_{c1}(3872) \to \pi^+\pi^-J/\psi(1S)) = (4.3 \pm 1.4) \times 10^{-2}$, $B(\psi(2S) \to J/\psi(1S)\pi^+\pi^-) = (34.78 \pm 0.33) \times 10^{-2}$. Our first error is their experiment's error and our second error is the systematic error from using our best (shown rounded) values.
[2] SIRUNYAN 20BB reports $[\Gamma(B_s^0 \to \chi_{c1}(3872)\phi)/\Gamma(B_s^0 \to \psi(2S)\phi)] \times [B(\chi_{c1}(3872) \to \pi^+\pi^-J/\psi(1S))] / [B(\psi(2S) \to J/\psi(1S)\pi^+\pi^-)] = (2.21 \pm 0.29 \pm 0.17) \times 10^{-2}$ which we multiply or divide by our best (shown rounded) values $B(\chi_{c1}(3872) \to \pi^+\pi^-J/\psi(1S)) = (4.3 \pm 1.4) \times 10^{-2}$, $B(\psi(2S) \to J/\psi(1S)\pi^+\pi^-) = (34.78 \pm 0.33) \times 10^{-2}$. Our first error is their experiment's error and our second error is the systematic error from using our best (shown rounded) values.

$\Gamma(\chi_{c1}(3872)\pi^+\pi^-)/\Gamma(\psi(2S)\pi^+\pi^-)$ — $\Gamma_{115}/\Gamma_{105}$

VALUE	DOCUMENT ID		TECN	COMMENT
0.54±0.09±0.17	[1] AAIJ	23AP	LHCB	pp at 7, 8, 13 TeV

[1] AAIJ 23AP reports $[\Gamma(B_s^0 \to \chi_{c1}(3872)\pi^+\pi^-)/\Gamma(B_s^0 \to \psi(2S)\pi^+\pi^-)] \times [B(\chi_{c1}(3872) \to \pi^+\pi^-J/\psi(1S))] / [B(\psi(2S) \to J/\psi(1S)\pi^+\pi^-)] = (6.8 \pm 1.1 \pm 0.2) \times 10^{-2}$ which we multiply or divide by our best (shown rounded) values $B(\chi_{c1}(3872) \to \pi^+\pi^-J/\psi(1S)) = (4.3 \pm 1.4) \times 10^{-2}$, $B(\psi(2S) \to J/\psi(1S)\pi^+\pi^-) = (34.78 \pm 0.33) \times 10^{-2}$. Our first error is their experiment's error and our second error is the systematic error from using our best (shown rounded) values.

$\Gamma(J/\psi K^*(892)^0\overline{K}^*(892)^0)/\Gamma(\psi(2S)\phi)$ — Γ_{95}/Γ_{106}

VALUE	DOCUMENT ID		TECN	COMMENT
0.209±0.006±0.003	[1] AAIJ	21C	LHCB	pp at 7, 8, 13 TeV

[1] AAIJ 21C reports $\Gamma(B_s^0 \to J/\psi K^*(892)^0\overline{K}^*(892)^0)/\Gamma(B_s^0 \to \psi(2S)\phi)\ B^2(K^{*0} \to K^+\pi^-)/B(\psi(2S) \to J/\psi\pi^+\pi^-)/B(\phi \to K^+K^-) = 1.22 \pm 0.03 \pm 0.04$ which we adjust with PDG 20 values of $B(K^{*0} \to K^+\pi^-) = (99.902 \pm 0.009) \times 10^{-2}$, $B(\psi(2S) \to J/\psi\pi^+\pi^-) = (34.68 \pm 0.30) \times 10^{-2}$, and $B(\phi \to K^+K^-) = (49.2 \pm 0.5) \times 10^{-2}$. The first uncertainty is the total experiment's one and the second is due to the adjustment branching fractions.

$\Gamma(\chi_{c1}(3872)(K^+K^-)_{non-\phi})/\Gamma(\chi_{c1}(3872)\phi)$ — $\Gamma_{114}/\Gamma_{113}$

VALUE	DOCUMENT ID		TECN	COMMENT
0.79±0.17±0.01	[1] AAIJ	21C	LHCB	pp at 7, 8, 13 TeV

[1] AAIJ 21C reports $[\Gamma(B_s^0 \to \chi_{c1}(3872)(K^+K^-)_{non-\phi})/\Gamma(B_s^0 \to \chi_{c1}(3872)\phi)] / [B(\phi(1020) \to K^+K^-)] = 1.57 \pm 0.32 \pm 0.12$ which we multiply by our best (shown rounded) value $B(\phi(1020) \to K^+K^-) = (50.1 \pm 0.6) \times 10^{-2}$. Our first error is their experiment's error and our second error is the systematic error from using our best (shown rounded) value.

Int. J. Mod. Phys. A 2026.41. Downloaded from www.worldscientific.com by UNIVERSITY OF CALIFORNIA @ BERKELEY on 09/16/26. Re-use and distribution is strictly not permitted, except for Open Access articles.

$\Gamma(\pi^+\pi^-)/\Gamma_{total}$ — Γ_{116}/Γ

VALUE (units 10^{-7})	CL%	DOCUMENT ID		TECN	COMMENT
7.1±0.8 OUR AVERAGE					
7.3±0.9±0.2		[1] AAIJ	17G	LHCB	pp at 7 and 8 TeV
6.4±1.8±0.2		[2] AALTONEN	12L	CDF	$p\overline{p}$ at 1.96 TeV
• • • We do not use the following data for averages, fits, limits, etc. • • •					
$10.7^{+2.5}_{-2.1}\pm0.5$		[3] AAIJ	12AR	LHCB	Repl. by AAIJ 17G
< 120	90	[4] PENG	10	BELL	$e^+e^-\to\Upsilon(5S)$
< 12	90	[5] AALTONEN	09C	CDF	Repl. by AALTONEN 12L
< 17	90	[6] ABULENCIA,A	06D	CDF	Repl. by AALTONEN 09C
<2320	90	[7] ABE	00C	SLD	$e^+e^-\to Z$
<1700	90	[8] BUSKULIC	96V	ALEP	$e^+e^-\to Z$

[1] AAIJ 17G reports $[\Gamma(B^0_s\to\pi^+\pi^-)/\Gamma_{total}]$ / $[B(B^0\to K^+\pi^-)]\times[\Gamma(\overline{b}\to B^0_s\,at\,pp)/\Gamma(\overline{b}\to B^0\,at\,pp)]=(9.15\pm0.71\pm0.83)\times10^{-3}$ which we multiply or divide by our best (shown rounded) values $B(B^0\to K^+\pi^-)=(2.00\pm0.04)\times10^{-5}$, $\Gamma(\overline{b}\to B^0_s\,at\,pp)/\Gamma(\overline{b}\to B^0\,at\,pp)=0.251\pm0.007$. Our first error is their experiment's error and our second error is the systematic error from using our best (shown rounded) values.

[2] AALTONEN 12L reports $[\Gamma(B^0_s\to\pi^+\pi^-)/\Gamma_{total}]$ / $[B(B^0\to K^+\pi^-)]\times[\Gamma(\overline{b}\to B^0_s\,at\,pp)/\Gamma(\overline{b}\to B^0\,at\,pp)]=0.008\pm0.002\pm0.001$ which we multiply or divide by our best (shown rounded) values $B(B^0\to K^+\pi^-)=(2.00\pm0.04)\times10^{-5}$, $\Gamma(\overline{b}\to B^0_s\,at\,pp)/\Gamma(\overline{b}\to B^0\,at\,pp)=0.251\pm0.007$. Our first error is their experiment's error and our second error is the systematic error from using our best (shown rounded) values.

[3] AAIJ 12AR reports $[\Gamma(B^0_s\to\pi^+\pi^-)/\Gamma_{total}]$ / $[B(B^0\to\pi^+\pi^-)]\times[\Gamma(\overline{b}\to B^0_s\,at\,pp)/\Gamma(\overline{b}\to B^0\,at\,pp)]=0.050^{+0.011}_{-0.009}\pm0.004$ which we multiply or divide by our best (shown rounded) values $B(B^0\to\pi^+\pi^-)=(5.37\pm0.20)\times10^{-6}$, $\Gamma(\overline{b}\to B^0_s\,at\,pp)/\Gamma(\overline{b}\to B^0\,at\,pp)=0.251\pm0.007$. Our first error is their experiment's error and our second error is the systematic error from using our best (shown rounded) values.

[4] Uses $\Upsilon(10860)\to B^*_s\overline{B}^*_s$ and assumes $B(\Upsilon(10860)\to B^{(*)}_s\overline{B}^{(*)}_s)=(19.3\pm2.9)\%$ and $\Gamma(\Upsilon(10860)\to B^*_s\overline{B}^*_s)$ / $\Gamma(\Upsilon(10860)\to B^{(*)}_s\overline{B}^{(*)}_s)=(90.1^{+3.8}_{-4.0})\%$.

[5] Obtains this result from $(f_s/f_d)\cdot B(B_s\to\pi^+\pi^-)/B(B^0\to K^+\pi^-)=0.007\pm0.004\pm0.005$, assuming $f_s/f_d=0.276\pm0.034$ and $B(B^0\to K^+\pi^-)=(19.4\pm0.6)\times10^{-6}$.

[6] ABULENCIA,A 06D obtains this from $B(B_s\to\pi^+\pi^-)$ / $B(B_s\to K^+K^-)<0.05$ at 90% CL, assuming $B(B_s\to K^+K^-)=(33\pm6\pm7)\times10^{-6}$.

[7] ABE 00C assumes $B(Z\to b\overline{b})=(21.7\pm0.1)\%$ and the B fractions $f_{B^0}=f_{B^+}=(39.7^{+1.8}_{-2.2})\%$ and $f_{B_s}=(10.5^{+1.8}_{-2.2})\%$.

[8] BUSKULIC 96V assumes PDG 96 production fractions for B^0, B^+, B_s, b baryons.

$\Gamma(\pi^0\pi^0)/\Gamma_{total}$ — Γ_{117}/Γ

VALUE	CL%	DOCUMENT ID		TECN	COMMENT
<7.7 × 10^{-6}	90	[1] BORAH	23	BELL	$e^+e^-\to\Upsilon(5S)$
• • • We do not use the following data for averages, fits, limits, etc. • • •					
<2.1 × 10^{-4}	90	[2] ACCIARRI	95H	L3	$e^+e^-\to Z$

[1] BORAH 23 assumes $f_{B_s}=20.1\pm3.1\%$.

[2] ACCIARRI 95H assumes $f_{B^0}=39.5\pm4.0$ and $f_{B_s}=12.0\pm3.0\%$.

$\Gamma(\eta\pi^0)/\Gamma_{total}$ — Γ_{118}/Γ

VALUE	CL%	DOCUMENT ID		TECN	COMMENT
<1.0 × 10^{-3}	90	[1] ACCIARRI	95H	L3	$e^+e^-\to Z$

[1] ACCIARRI 95H assumes $f_{B^0}=39.5\pm4.0$ and $f_{B_s}=12.0\pm3.0\%$.

$\Gamma(\eta\eta)/\Gamma_{total}$ — Γ_{119}/Γ

VALUE	CL%	DOCUMENT ID		TECN	COMMENT
<1.43 × 10^{-4}	90	BHUYAN	22	BELL	$e^+e^-\to\Upsilon(5S)$
• • • We do not use the following data for averages, fits, limits, etc. • • •					
<1.5 × 10^{-3}	90	[1] ACCIARRI	95H	L3	$e^+e^-\to Z$

[1] ACCIARRI 95H assumes $f_{B^0}=39.5\pm4.0$ and $f_{B_s}=12.0\pm3.0\%$.

$\Gamma(\rho^0\rho^0)/\Gamma_{total}$ — Γ_{120}/Γ

VALUE	CL%	DOCUMENT ID		TECN	COMMENT
<3.20 × 10^{-4}	90	[1] ABE	00C	SLD	$e^+e^-\to Z$

[1] ABE 00C assumes $B(Z\to b\overline{b})=(21.7\pm0.1)\%$ and the B fractions $f_{B^0}=f_{B^+}=(39.7^{+1.8}_{-2.2})\%$ and $f_{B_s}=(10.5^{+1.8}_{-2.2})\%$.

$\Gamma(\eta' K^0_S)/\Gamma_{total}$ — Γ_{121}/Γ

VALUE	CL%	DOCUMENT ID		TECN	COMMENT
<8.16 × 10^{-6}	90	[1] PANG	22	BELL	$e^+e^-\to\Upsilon(5S)$

[1] Uses $\Upsilon(10860)\to B^{(*)}_s\overline{B}^{(*)}_s$ decays and assumes $B(\Upsilon(10860)\to B^{(*)}_s\overline{B}^{(*)}_s)=(20.1\pm3.1)\%$.

$\Gamma(\eta'\eta)/\Gamma_{total}$ — Γ_{122}/Γ

VALUE	CL%	DOCUMENT ID		TECN	COMMENT
<6.5 × 10^{-5}	90	[1] NISAR	21	BELL	$e^+e^-\to\Upsilon(5S)$

[1] Uses $\Upsilon(10860)\to B^*_s\overline{B}^*_s$ decays and assumes $B(\Upsilon(10860)\to B^{(*)}_s\overline{B}^{(*)}_s)=(20.1\pm3.1)\%$.

$\Gamma(\eta'\eta')/\Gamma_{total}$ — Γ_{123}/Γ

VALUE (units 10^{-5})	DOCUMENT ID		TECN	COMMENT
3.3±0.7±0.1	[1] AAIJ	15O	LHCB	pp at 7, 8 TeV

[1] AAIJ 15O reports $[\Gamma(B^0_s\to\eta'\eta')/\Gamma_{total}]$ / $[B(B^+\to\eta' K^+)]=0.47\pm0.09\pm0.04$ which we multiply by our best (shown rounded) value $B(B^+\to\eta' K^+)=(7.04\pm0.25)\times10^{-5}$. Our first error is their experiment's error and our second error is the systematic error from using our best (shown rounded) value.

$\Gamma(\eta'\phi)/\Gamma_{total}$ — Γ_{124}/Γ

VALUE	CL%	DOCUMENT ID		TECN	COMMENT
<0.82 × 10^{-6}	90	[1] AAIJ	17BA	LHCB	pp at 7, 8 TeV

[1] Corresponds to the 95% CL upper limit 1.01×10^{-6}. Uses the normalization mode $B^+\to\eta' K^+$ with branching fraction $(70.6\pm2.5)\times10^{-6}$ and the ratio of hadronisation fractions $f_s/f_d=0.259\pm0.015$, which is assumed equal to f_s/f_u.

$\Gamma(\eta' X_{s\overline{s}})/\Gamma_{total}$ — Γ_{67}/Γ

VALUE (units 10^{-3})	CL%	DOCUMENT ID		TECN	COMMENT
<1.4	90	[1] DUBEY	21	BELL	$e^+e^-\to\Upsilon(4S)$

[1] DUBEY 21 result is for $m(X_{s\overline{s}})<2.85$ GeV/c^2.

$\Gamma(\phi f_0(980),\ f_0(980)\to\pi^+\pi^-)/\Gamma_{total}$ — Γ_{125}/Γ

VALUE (units 10^{-6})	DOCUMENT ID		TECN	COMMENT
1.12±0.16±0.14	[1] AAIJ	17A	LHCB	pp at 7, 8 TeV

[1] Signal is observed with 8 standard deviations significance.

$\Gamma(\phi f_2(1270),\ f_2(1270)\to\pi^+\pi^-)/\Gamma_{total}$ — Γ_{126}/Γ

VALUE (units 10^{-6})	DOCUMENT ID		TECN	COMMENT
$0.61\pm0.13^{+0.13}_{-0.08}$	[1] AAIJ	17A	LHCB	pp at 7, 8 TeV

[1] Signal is observed with 5 standard deviations significance.

$\Gamma(\phi\rho^0)/\Gamma_{total}$ — Γ_{127}/Γ

VALUE (units 10^{-7})	CL%	DOCUMENT ID		TECN	COMMENT
2.7±0.7±0.3		[1] AAIJ	17A	LHCB	pp at 7, 8 TeV
• • • We do not use the following data for averages, fits, limits, etc. • • •					
<6170	90	[2] ABE	00C	SLD	$e^+e^-\to Z$

[1] Signal evidence is 4 standard deviations.

[2] ABE 00C assumes $B(Z\to b\overline{b})=(21.7\pm0.1)\%$ and the B fractions $f_{B^0}=f_{B^+}=(39.7^{+1.8}_{-2.2})\%$ and $f_{B_s}=(10.5^{+1.8}_{-2.2})\%$.

$\Gamma(\phi\pi^+\pi^-)/\Gamma_{total}$ — Γ_{128}/Γ

VALUE (units 10^{-6})	DOCUMENT ID		TECN	COMMENT
3.48±0.23±0.39	[1] AAIJ	17A	LHCB	pp at 7, 8 TeV

[1] Inclusive decays in mass range $400<m(\pi^+\pi^-)<1600$ MeV/c^2.

$\Gamma(\phi\phi)/\Gamma_{total}$ — Γ_{129}/Γ

VALUE (units 10^{-6})	CL%	DOCUMENT ID		TECN	COMMENT
18.3±1.4 OUR FIT					
18.5±1.4±1.0		[1] AAIJ	15AS	LHCB	pp at 7, 8 TeV
• • • We do not use the following data for averages, fits, limits, etc. • • •					
$14^{+6}_{-5}\pm6$		[2] ACOSTA	05J	CDF	Repl. by AALTONEN 11AN
<1183	90	[3] ABE	00C	SLD	$e^+e^-\to Z$

[1] AAIJ 15AS reports $[\Gamma(B^0_s\to\phi\phi)/\Gamma_{total}]$ / $[B(B^0\to K^*(892)^0\phi)]=1.84\pm0.05\pm0.13$ which we multiply by our best (shown rounded) value $B(B^0\to K^*(892)^0\phi)=(1.00\pm0.05)\times10^{-5}$. Our first error is their experiment's error and our second error is the systematic error from using our best (shown rounded) value.

[2] Uses $B(B^0\to J/\psi\phi)=(1.38\pm0.49)\times10^{-3}$ and production cross-section ratio of $\sigma(B_s)/\sigma(B^0)=0.26\pm0.04$.

[3] ABE 00C assumes $B(Z\to b\overline{b})=(21.7\pm0.1)\%$ and the B fractions $f_{B^0}=f_{B^+}=(39.7^{+1.8}_{-2.2})\%$ and $f_{B_s}=(10.5^{+1.8}_{-2.2})\%$.

$\Gamma(\phi\phi)/\Gamma(J/\psi(1S)\phi)$ — Γ_{129}/Γ_{69}

VALUE (units 10^{-2})	DOCUMENT ID		TECN	COMMENT
1.81±0.15 OUR FIT				
1.78±0.14±0.20	AALTONEN	11AN	CDF	$p\overline{p}$ at 1.96 TeV

$\Gamma(\phi\phi\phi)/\Gamma(\phi\phi)$ — $\Gamma_{130}/\Gamma_{129}$

VALUE	DOCUMENT ID		TECN	COMMENT
0.117±0.030±0.015	AAIJ	17BB	LHCB	pp at 7, 8 TeV

$\Gamma(\pi^+K^-)/\Gamma_{total}$ — Γ_{131}/Γ

VALUE (units 10^{-6})	CL%	DOCUMENT ID		TECN	COMMENT
5.9±0.6 OUR AVERAGE					
5.9±0.7±0.2		[1] AAIJ	12AR	LHCB	pp at 7 TeV
5.8±1.0±0.5		[2] AALTONEN	09C	CDF	$p\overline{p}$ at 1.96 TeV
• • • We do not use the following data for averages, fits, limits, etc. • • •					
< 26	90	[3] PENG	10	BELL	$e^+e^-\to\Upsilon(5S)$
< 5.6	90	[4] ABULENCIA,A	06D	CDF	Repl. by AALTONEN 09C
<261	90	[5] ABE	00C	SLD	$e^+e^-\to Z$
<210	90	[6] BUSKULIC	96V	ALEP	$e^+e^-\to Z$
<260	90	[7] AKERS	94L	OPAL	$e^+e^-\to Z$

[1] AAIJ 12AR reports $[\Gamma(B^0_s \to \pi^+ K^-)/\Gamma_{total}]$ / $[B(B^0 \to K^+\pi^-)] \times [\Gamma(\overline{b} \to B^0_s \text{ at } pp)/\Gamma(\overline{b} \to B^0 \text{ at } pp)] = 0.074 \pm 0.006 \pm 0.006$ which we multiply or divide by our best (shown rounded) values $B(B^0 \to K^+\pi^-) = (2.00 \pm 0.04) \times 10^{-5}$, $\Gamma(\overline{b} \to B^0_s \text{ at } pp)/\Gamma(\overline{b} \to B^0 \text{ at } pp) = 0.251 \pm 0.007$. Our first error is their experiment's error and our second error is the systematic error from using our best (shown rounded) values.

[2] AALTONEN 09C reports $[\Gamma(B^0_s \to \pi^+ K^-)/\Gamma_{total}]$ / $[B(B^0 \to K^+\pi^-)] \times [B(\overline{b} \to B^0_s \text{ at } Z)]$ / $[B(\overline{b} \to B^0 \text{ at } Z)] = 0.071 \pm 0.010 \pm 0.007$ which we multiply or divide by our best (shown rounded) values $B(B^0 \to K^+\pi^-) = (2.00 \pm 0.04) \times 10^{-5}$, $B(\overline{b} \to B^0_s \text{ at } Z) = (10.0 \pm 0.8) \times 10^{-2}$, $B(\overline{b} \to B^0 \text{ at } Z) = (40.8 \pm 0.7) \times 10^{-2}$. Our first error is their experiment's error and our second error is the systematic error from using our best (shown rounded) values.

[3] Uses $\Upsilon(10860) \to B^*_s \overline{B}^*_s$ and assumes $B(\Upsilon(10860) \to B^{(*)}_s \overline{B}^{(*)}_s) = (19.3 \pm 2.9)\%$ and $\Gamma(\Upsilon(10860) \to B^*_s \overline{B}^*_s)$ / $\Gamma(\Upsilon(10860) \to B^{(*)}_s \overline{B}^{(*)}_s) = (90.1^{+3.8}_{-4.0})\%$.

[4] ABULENCIA,A 06D obtains this from (f_s/f_d) $(B(B_s \to \pi^+K^-)$ / $B(B^0 \to K^+\pi^-))$ < 0.08 at 90% CL, assuming $f_s/f_d = 0.260 \pm 0.039$ and $B(B^0 \to K^+\pi^-) = (18.9 \pm 0.7) \times 10^{-6}$.

[5] ABE 00C assumes $B(Z \to b\overline{b}) = (21.7 \pm 0.1)\%$ and the B fractions $f_{B^0} = f_{B^+} = (39.7^{+1.8}_{-2.2})\%$ and $f_{B_s} = (10.5^{+1.8}_{-2.2})\%$.

[6] BUSKULIC 96V assumes PDG 96 production fractions for B^0, B^+, B_s, b baryons.

[7] Assumes $B(Z \to b\overline{b}) = 0.217$ and B^0_d (B^0_s) fraction 39.5% (12%).

$\Gamma(K^+K^-)/\Gamma_{total}$ — Γ_{132}/Γ

VALUE (units 10^{-6})	CL%	DOCUMENT ID		TECN	COMMENT
26.1 ± 1.6 OUR AVERAGE					
25.2 ± 1.7 ± 0.8		[1] AAIJ	12AR	LHCB	pp at 7 TeV
28.3 ± 2.4 ± 2.7		[2] AALTONEN	11N	CDF	$p\overline{p}$ at 1.96 TeV
38 $^{+10}_{-9}$ ± 7		[3] PENG	10	BELL	$e^+e^- \to \Upsilon(5S)$
• • • We do not use the following data for averages, fits, limits, etc. • • •					
<310	90	DRUTSKOY	07A	BELL	$e^+e^- \to \Upsilon(5S)$
33 ± 6 ± 7		[4] ABULENCIA,A	06D	CDF	Repl. by AALTONEN 11N
<283	90	[5] ABE	00C	SLD	$e^+e^- \to Z$
< 59	90	[6] BUSKULIC	96V	ALEP	$e^+e^- \to Z$
<140	90	[7] AKERS	94L	OPAL	$e^+e^- \to Z$

[1] AAIJ 12AR reports $[\Gamma(B^0_s \to K^+K^-)/\Gamma_{total}]$ / $[B(B^0 \to K^+\pi^-)] \times [\Gamma(\overline{b} \to B^0_s \text{ at } pp)/\Gamma(\overline{b} \to B^0 \text{ at } pp)] = 0.316 \pm 0.009 \pm 0.019$ which we multiply or divide by our best (shown rounded) values $B(B^0 \to K^+\pi^-) = (2.00 \pm 0.04) \times 10^{-5}$, $\Gamma(\overline{b} \to B^0_s \text{ at } pp)/\Gamma(\overline{b} \to B^0 \text{ at } pp) = 0.251 \pm 0.007$. Our first error is their experiment's error and our second error is the systematic error from using our best (shown rounded) values.

[2] AALTONEN 11N reports (f_s/f_d) $(B(B^0_s \to K^+K^-)$ / $B(B^0 \to K^+\pi^-)) = 0.347 \pm 0.020 \pm 0.021$. We multiply this result by our best value of $B(B^0 \to K^+\pi^-) = (2.00 \pm 0.04) \times 10^{-5}$ and divide by our best value of f_s/f_d, where $1/2\ f_s/f_d = 0.1230 \pm 0.0115$. Our first quoted uncertainty is the combined experiment's uncertainty and our second is the systematic uncertainty from using our best values.

[3] Uses $\Upsilon(10860) \to B^*_s \overline{B}^*_s$ and assumes $B(\Upsilon(10860) \to B^{(*)}_s \overline{B}^{(*)}_s) = (19.3 \pm 2.9)\%$ and $\Gamma(\Upsilon(10860) \to B^*_s \overline{B}^*_s)$ / $\Gamma(\Upsilon(10860) \to B^{(*)}_s \overline{B}^{(*)}_s) = (90.1^{+3.8}_{-4.0})\%$.

[4] ABULENCIA,A 06D obtains this from (f_s/f_d) $(B(B_s \to K^+K^-)$ / $B(B^0 \to K^+\pi^-))$ $= 0.46 \pm 0.08 \pm 0.07$, assuming $f_s/f_d = 0.260 \pm 0.039$ and $B(B^0 \to K^+\pi^-) = (18.9 \pm 0.7) \times 10^{-6}$.

[5] ABE 00C assumes $B(Z \to b\overline{b}) = (21.7 \pm 0.1)\%$ and the B fractions $f_{B^0} = f_{B^+} = (39.7^{+1.8}_{-2.2})\%$ and $f_{B_s} = (10.5^{+1.8}_{-2.2})\%$.

[6] BUSKULIC 96V assumes PDG 96 production fractions for B^0, B^+, B_s, b baryons.

[7] Assumes $B(Z \to b\overline{b}) = 0.217$ and B^0_d (B^0_s) fraction 39.5% (12%).

$\Gamma(K^0\overline{K}^0)/\Gamma_{total}$ — Γ_{133}/Γ

VALUE (units 10^{-5})	CL%	DOCUMENT ID		TECN	COMMENT
1.76 ± 0.31 OUR AVERAGE					
$1.68 \pm 0.34^{+0.16}_{-0.15}$		[1] AAIJ	20F	LHCB	pp at 7, 8, 13 TeV
$1.96^{+0.58}_{-0.51} \pm 0.10 \pm 0.20$		[2] PAL	16	BELL	$e^+e^- \to \Upsilon(5S)$
• • • We do not use the following data for averages, fits, limits, etc. • • •					
<6.6	90	[3] PENG	10	BELL	Repl. by PAL 16

[1] AAIJ 20F reports $[\Gamma(B^0_s \to K^0\overline{K}^0)/\Gamma_{total}]$ / $[B(B^0 \to K^0\phi)] = 2.3 \pm 0.4 \pm 0.2 \pm 0.1$ which we multiply by our best (shown rounded) value $B(B^0 \to K^0\phi) = (7.3 \pm 0.7) \times 10^{-6}$. Our first error is their experiment's error and our second error is the systematic error from using our best (shown rounded) value.

[2] Observed in $B^0_s \to K^0_S K^0_S$ with significance of 5.1 σ. The last uncertainty is due to the uncertainty of the total number of $B^0_s\overline{B}^0_s$ pairs.

[3] Uses $\Upsilon(10860) \to B^*_s \overline{B}^*_s$ and assumes $B(\Upsilon(10860) \to B^{(*)}_s \overline{B}^{(*)}_s) = (19.3 \pm 2.9)\%$ and $\Gamma(\Upsilon(10860) \to B^*_s \overline{B}^*_s)$ / $\Gamma(\Upsilon(10860) \to B^{(*)}_s \overline{B}^{(*)}_s) = (90.1^{+3.8}_{-4.0})\%$.

$\Gamma(K^0\pi^+\pi^-)/\Gamma_{total}$ — Γ_{134}/Γ

VALUE (units 10^{-6})	DOCUMENT ID		TECN	COMMENT
9.5 ± 2.1 ± 0.3	[1,2] AAIJ	17BP	LHCB	pp at 7, 8 TeV
• • • We do not use the following data for averages, fits, limits, etc. • • •				
14 ± 4 ± 1	[3] AAIJ	13BP	LHCB	Repl. by AAIJ 17BP

[1] AAIJ 17BP reports $[\Gamma(B^0_s \to K^0\pi^+\pi^-)/\Gamma_{total}]$ / $[B(B^0 \to K^0\pi^+\pi^-)] = 0.191 \pm 0.027 \pm 0.033$ which we multiply by our best (shown rounded) value $B(B^0 \to K^0\pi^+\pi^-) = (4.97 \pm 0.18) \times 10^{-5}$. Our first error is their experiment's error and our second error is the systematic error from using our best (shown rounded) value.

[2] Used $f_s/f_d = 0.259 \pm 0.015$.

[3] AAIJ 13BP reports $[\Gamma(B^0_s \to K^0\pi^+\pi^-)/\Gamma_{total}]$ / $[B(B^0 \to K^0\pi^+\pi^-)] = 0.29 \pm 0.06 \pm 0.04$ which we multiply by our best (shown rounded) value $B(B^0 \to K^0\pi^+\pi^-) = (4.97 \pm 0.18) \times 10^{-5}$. Our first error is their experiment's error and our second error is the systematic error from using our best (shown rounded) value.

$\Gamma(K^0K^\pm\pi^\mp)/\Gamma_{total}$ — Γ_{135}/Γ

VALUE (units 10^{-5})	DOCUMENT ID		TECN	COMMENT
8.4 ± 0.8 ± 0.3	[1,2] AAIJ	17BP	LHCB	pp at 7, 8 TeV
• • • We do not use the following data for averages, fits, limits, etc. • • •				
7.4 ± 0.9 ± 0.3	[3] AAIJ	13BP	LHCB	Repl. by AAIJ 17BP

[1] AAIJ 17BP reports $[\Gamma(B^0_s \to K^0K^\pm\pi^\mp)/\Gamma_{total}]$ / $[B(B^0 \to K^0\pi^+\pi^-)] = 1.70 \pm 0.07 \pm 0.15$ which we multiply by our best (shown rounded) value $B(B^0 \to K^0\pi^+\pi^-) = (4.97 \pm 0.18) \times 10^{-5}$. Our first error is their experiment's error and our second error is the systematic error from using our best (shown rounded) value.

[2] Used $f_s/f_d = 0.259 \pm 0.015$.

[3] AAIJ 13BP reports $[\Gamma(B^0_s \to K^0K^\pm\pi^\mp)/\Gamma_{total}]$ / $[B(B^0 \to K^0\pi^+\pi^-)] = 1.48 \pm 0.12 \pm 0.14$ which we multiply by our best (shown rounded) value $B(B^0 \to K^0\pi^+\pi^-) = (4.97 \pm 0.18) \times 10^{-5}$. Our first error is their experiment's error and our second error is the systematic error from using our best (shown rounded) value.

$\Gamma(K^*(892)^-\pi^+)/\Gamma_{total}$ — Γ_{136}/Γ

VALUE (units 10^{-6})	DOCUMENT ID		TECN	COMMENT
2.9 ± 1.0 ± 0.2	[1,2] AAIJ	14BM	LHCB	pp at 7 TeV

[1] AAIJ 14BM reports $[\Gamma(B^0_s \to K^*(892)^-\pi^+)/\Gamma_{total}]$ / $[B(B^0 \to K^*(892)^+\pi^-)] = 0.39 \pm 0.13 \pm 0.05$ which we multiply by our best (shown rounded) value $B(B^0 \to K^*(892)^+\pi^-) = (7.5 \pm 0.4) \times 10^{-6}$. Our first error is their experiment's error and our second error is the systematic error from using our best (shown rounded) value.

[2] Uses $f_s/f_d = 0.259 \pm 0.015$.

$\Gamma(K^*(892)^\pm K^\mp)/\Gamma_{total}$ — Γ_{137}/Γ

VALUE (units 10^{-5})	DOCUMENT ID		TECN	COMMENT
1.86 ± 0.12 ± 0.45	[1,2] AAIJ	19K	LHCB	pp at 7, 8 TeV
• • • We do not use the following data for averages, fits, limits, etc. • • •				
$1.12 \pm 0.21^{+0.07}_{-0.06}$	[3,4] AAIJ	14BM	LHCB	Repl. by AAIJ 19K

[1] AAIJ 19K reports $(18.6 \pm 1.2 \pm 0.8 \pm 4.0 \pm 2.0) \times 10^{-6}$ as the measured value. We have combined in quadrature all systematic uncertainties into a single one.

[2] Measured in Dalitz plot analysis of $B^0_s \to K^0_S K^\pm\pi^\mp$ decays.

[3] AAIJ 14BM reports $[\Gamma(B^0_s \to K^*(892)^\pm K^\mp)/\Gamma_{total}]$ / $[B(B^0 \to K^*(892)^+\pi^-)]$ $= 1.49 \pm 0.22 \pm 0.18$ which we multiply by our best (shown rounded) value $B(B^0 \to K^*(892)^+\pi^-) = (7.5 \pm 0.4) \times 10^{-6}$. Our first error is their experiment's error and our second error is the systematic error from using our best (shown rounded) value.

[4] Uses $f_s/f_d = 0.259 \pm 0.015$.

$\Gamma(K^*_0(1430)^\pm K^\mp)/\Gamma_{total}$ — Γ_{138}/Γ

VALUE (units 10^{-5})	DOCUMENT ID		TECN	COMMENT
3.13 ± 0.23 ± 2.53	[1,2] AAIJ	19K	LHCB	pp at 7, 8 TeV

[1] AAIJ 19K reports $(31.3 \pm 2.3 \pm 0.7 \pm 25.1 \pm 3.3) \times 10^{-6}$ as the measured value. We have combined in quadrature all systematic uncertainties into a single one.

[2] Measured in Dalitz plot analysis of $B^0_s \to K^0_S K^\pm\pi^\mp$ decays.

$\Gamma(K^*_2(1430)^\pm K^\mp)/\Gamma_{total}$ — Γ_{139}/Γ

VALUE (units 10^{-5})	DOCUMENT ID		TECN	COMMENT
1.03 ± 0.25 ± 1.64	[1,2] AAIJ	19K	LHCB	pp at 7, 8 TeV

[1] AAIJ 19K reports $(10.3 \pm 2.5 \pm 1.1 \pm 16.3 \pm 1.1) \times 10^{-6}$ as the measured value. We have combined in quadrature all systematic uncertainties into a single one.

[2] Measured in Dalitz plot analysis of $B^0_s \to K^0_S K^\pm\pi^\mp$ decays.

$\Gamma(K^*(892)^0\overline{K}^0 + c.c.)/\Gamma_{total}$ — Γ_{140}/Γ

VALUE (units 10^{-5})	DOCUMENT ID		TECN	COMMENT
1.98 ± 0.28 ± 0.50	[1,2] AAIJ	19K	LHCB	pp at 7, 8 TeV

[1] AAIJ 19K reports $(19.8 \pm 2.8 \pm 1.2 \pm 4.4 \pm 2.1) \times 10^{-6}$ as the measured value. We have combined in quadrature all systematic uncertainties into a single one.

[2] Measured in Dalitz plot analysis of $B^0_s \to K^0_S K^\pm\pi^\mp$ decays.

$\Gamma(K^*_0(1430)\overline{K}^0 + c.c.)/\Gamma_{total}$ — Γ_{141}/Γ

VALUE (units 10^{-5})	DOCUMENT ID		TECN	COMMENT
3.30 ± 0.25 ± 0.98	[1,2] AAIJ	19K	LHCB	pp at 7, 8 TeV

[1] AAIJ 19K reports $(33.0 \pm 2.5 \pm 0.9 \pm 9.1 \pm 3.5) \times 10^{-6}$ as the measured value. We have combined in quadrature all systematic uncertainties into a single one.

[2] Measured in Dalitz plot analysis of $B^0_s \to K^0_S K^\pm\pi^\mp$ decays.

$\Gamma(K^*_2(1430)^0\overline{K}^0 + c.c.)/\Gamma_{total}$ — Γ_{142}/Γ

VALUE (units 10^{-5})	DOCUMENT ID		TECN	COMMENT
1.68 ± 0.45 ± 2.13	[1,2] AAIJ	19K	LHCB	pp at 7, 8 TeV

[1] AAIJ 19K reports $(16.8 \pm 4.5 \pm 1.7 \pm 21.2 \pm 1.8) \times 10^{-6}$ as the measured value. We have combined in quadrature all systematic uncertainties into a single one.

[2] Measured in Dalitz plot analysis of $B^0_s \to K^0_S K^\pm\pi^\mp$ decays.

Int. J. Mod. Phys. A 2026.41. Downloaded from www.worldscientific.com
by LIFORNIA @ BERKELEY on 09/16/26. Re-use and distribution is strictly not permitted, except for Open Access articles.

Int. J. Mod. Phys. A 2026.41. Downloaded from www.worldscientific.com
by UNIVERSITY OF CALIFORNIA @ BERKELEY on 09/16/26. Re-use and distribution is strictly not permitted, except for Open Access articles.

$\Gamma(K_S^0 \overline{K}^*(892)^0 + \text{c.c.})/\Gamma_{\text{total}}$ — Γ_{143}/Γ

VALUE (units 10^{-6})	DOCUMENT ID		TECN	COMMENT
16.4±3.4±2.3	[1] AAIJ	16	LHCB	pp at 7 TeV

[1] Measured relative to $B^0 \to K_S^0 \pi^+ \pi^-$ using the value of $B(B^0 \to K^0 \pi^+ \pi^-) = (4.96 \pm 0.2) \times 10^{-5}$.

$\Gamma(K^0 K^+ K^-)/\Gamma_{\text{total}}$ — Γ_{144}/Γ

VALUE (units 10^{-7})	CL%	DOCUMENT ID		TECN	COMMENT
12.9±6.5±0.5		[1,2,3] AAIJ	17BP	LHCB	pp at 7, 8 TeV
• • • We do not use the following data for averages, fits, limits, etc. • • •					
<34	90	[4] AAIJ	13BP	LHCB	Repl. by AAIJ 17BP

[1] AAIJ 17BP reports $[\Gamma(B_s^0 \to K^0 K^+ K^-)/\Gamma_{\text{total}}] / [B(B^0 \to K^0 \pi^+ \pi^-)] = 0.026 \pm 0.011 \pm 0.007$ which we multiply by our best (shown rounded) value $B(B^0 \to K^0 \pi^+ \pi^-) = (4.97 \pm 0.18) \times 10^{-5}$. Our first error is their experiment's error and our second error is the systematic error from using our best (shown rounded) value.

[2] AAIJ 17BP also set the limit range 4–25 $\times 10^{-7}$ at 90% CL using the world average value $B(B^0 \to K^0 \pi^+ \pi^-) = (4.96 \pm 0.20) \times 10^{-5}$.

[3] Used $f_s/f_d = 0.259 \pm 0.015$.

[4] AAIJ 13BP reports $[\Gamma(B_s^0 \to K^0 K^+ K^-)/\Gamma_{\text{total}}] / [B(B^0 \to K^0 \pi^+ \pi^-)] < 0.068$ which we multiply by our best (shown rounded) value $B(B^0 \to K^0 \pi^+ \pi^-) = 4.97 \times 10^{-5}$.

$\Gamma(\overline{K}^*(892)^0 \rho^0)/\Gamma_{\text{total}}$ — Γ_{145}/Γ

VALUE	CL%	DOCUMENT ID		TECN	COMMENT
<7.67 × 10^{-4}	90	[1] ABE	00C	SLD	$e^+ e^- \to Z$

[1] ABE 00C assumes $B(Z \to b\overline{b})$=(21.7 ± 0.1)% and the B fractions $f_{B^0}=f_{B^+}=(39.7^{+1.8}_{-2.2})$% and $f_{B_s}=(10.5^{+1.8}_{-2.2})$%.

$\Gamma(\overline{K}^*(892)^0 K^*(892)^0)/\Gamma_{\text{total}}$ — Γ_{146}/Γ

VALUE (units 10^{-5})	CL%	DOCUMENT ID		TECN	COMMENT
1.11±0.26±0.06		[1] AAIJ	15AF	LHCB	pp at 7 TeV
• • • We do not use the following data for averages, fits, limits, etc. • • •					
2.81±0.46±0.56		[2] AAIJ	12F	LHCB	Repl. by AAIJ 15AF
<168.1	90	[3] ABE	00C	SLD	$e^+ e^- \to Z$

[1] AAIJ 15AF reports $[\Gamma(B_s^0 \to \overline{K}^*(892)^0 K^*(892)^0)/\Gamma_{\text{total}}] / [B(B^0 \to K^*(892)^0 \phi)] = 1.11 \pm 0.22 \pm 0.12 \pm 0.06$ which we multiply by our best (shown rounded) value $B(B^0 \to K^*(892)^0 \phi) = (1.00 \pm 0.05) \times 10^{-5}$. Our first error is their experiment's error and our second error is the systematic error from using our best (shown rounded) value.

[2] Uses $B^0 \to J/\psi K^{*0}$ for normalization and assumes $B(B^0 \to J/\psi K^{*0})\, B(J/\psi \to \mu^+ \mu^-)\, B(K^{*0} \to K^+ \pi^-) = (1.33 \pm 0.06) \times 10^{-3}$ and $f_s/f_d = 0.253 \pm 0.031$. The second quoted error is total uncertainty including the error of 0.34 on f_s/f_d.

[3] ABE 00C assumes $B(Z \to b\overline{b})$=(21.7 ± 0.1)% and the B fractions $f_{B^0}=f_{B^+}=(39.7^{+1.8}_{-2.2})$% and $f_{B_s}=(10.5^{+1.8}_{-2.2})$%.

$\Gamma(\phi K^*(892)^0)/\Gamma_{\text{total}}$ — Γ_{150}/Γ

VALUE (units 10^{-6})	CL%	DOCUMENT ID		TECN	COMMENT
1.14±0.29±0.06		[1] AAIJ	13BW	LHCB	pp at 7 TeV
• • • We do not use the following data for averages, fits, limits, etc. • • •					
<1013	90	[2] ABE	00C	SLD	$e^+ e^- \to Z$

[1] AAIJ 13BW reports $[\Gamma(B_s^0 \to \phi K^*(892)^0)/\Gamma_{\text{total}}] / [B(B^0 \to K^*(892)^0 \phi)] = 0.113 \pm 0.024 \pm 0.016$ which we multiply by our best (shown rounded) value $B(B^0 \to K^*(892)^0 \phi) = (1.00 \pm 0.05) \times 10^{-5}$. Our first error is their experiment's error and our second error is the systematic error from using our best (shown rounded) value.

[2] ABE 00C assumes $B(Z \to b\overline{b})$=(21.7 ± 0.1)% and the B fractions $f_{B^0}=f_{B^+}=(39.7^{+1.8}_{-2.2})$% and $f_{B_s}=(10.5^{+1.8}_{-2.2})$%.

$\Gamma(p\overline{p})/\Gamma_{\text{total}}$ — Γ_{151}/Γ

Test for ΔB=1 weak neutral current. Allowed by higher-order electroweak interactions.

VALUE (units 10^{-8})	CL%	DOCUMENT ID		TECN	COMMENT
< 0.44	90	[1] AAIJ	23T	LHCB	pp at 13 TeV
• • • We do not use the following data for averages, fits, limits, etc. • • •					
< 1.5	90	[2] AAIJ	17BJ	LHCB	Repl. by AAIJ 23T
$2.84^{+2.03+0.85}_{-1.68-0.18}$		[3] AAIJ	13BQ	LHCB	Repl. by AAIJ 17BJ
<5900	90	[4] BUSKULIC	96V	ALEP	$e^+ e^- \to Z$

[1] Uses normalization mode $B(B^0 \to K^+ \pi^-) = (19.6 \pm 0.5) \times 10^{-6}$ and B production ratio $f(\overline{b} \to B_s^0)/f(\overline{b} \to B_d^0) = 0.2539 \pm 0.0079$.

[2] Uses normalization mode $B(B^0 \to K^+ \pi^-) = (19.6 \pm 0.5) \times 10^{-6}$ and B production ratio $f(\overline{b} \to B_s^0)/f(\overline{b} \to B_d^0) = 0.259 \pm 0.015$.

[3] Uses normalization mode $B(B^0 \to K^+ \pi^-) = (19.55 \pm 0.54) \times 10^{-6}$ and B production ratio $f(\overline{b} \to B_s^0)/f(\overline{b} \to B_d^0) = 0.256 \pm 0.020$.

[4] BUSKULIC 96V assumes PDG 96 production fractions for B^0, B^+, B_s, b baryons.

$\Gamma(p\overline{p}K^0)/\Gamma_{\text{total}}$ — Γ_{152}/Γ

VALUE (units 10^{-7})	DOCUMENT ID		TECN	COMMENT
9.14±1.69±0.98	[1] AAIJ	25X	LHCB	pp at 7, 8 and 13 TeV

[1] The last error includes the systematic uncertainties due to the uncertainties of the branching fraction of the normalisation channel, and f_s/f_d.

$\Gamma(p\overline{p}K^+ K^-)/\Gamma_{\text{total}}$ — Γ_{153}/Γ

VALUE (units 10^{-6})	DOCUMENT ID		TECN	COMMENT
4.5±0.4±0.2	[1,2] AAIJ	17BD	LHCB	pp at 7, 8 TeV

[1] AAIJ 17BD reports $[\Gamma(B_s^0 \to p\overline{p}K^+ K^-)/\Gamma_{\text{total}}] / [B(B^0 \to J/\psi(1S) K^*(892)^0)] / [B(J/\psi(1S) \to p\overline{p})] / [B(K^*(892) \to (K\pi)^{\pm})] = 1.67 \pm 0.12 \pm 0.11$ which we multiply by our best (shown rounded) values $B(B^0 \to J/\psi(1S) K^*(892)^0) = (1.27 \pm 0.05) \times 10^{-3}$, $B(J/\psi(1S) \to p\overline{p}) = (2.121 \pm 0.029) \times 10^{-3}$, $B(K^*(892) \to (K\pi)^{\pm}) = (99.896 \pm 0.010) \times 10^{-2}$. Our first error is their experiment's error and our second error is the systematic error from using our best (shown rounded) values. Reported value assumes $f_s/f_d = 0.259 \pm 0.015$.

[2] The branching ratio is given for $m_{p\overline{p}}$ <2.85 GeV.

$\Gamma(p\overline{p}K^+ \pi^-)/\Gamma_{\text{total}}$ — Γ_{154}/Γ

VALUE (units 10^{-7})	DOCUMENT ID		TECN	COMMENT
13.9±2.5±0.5	[1,2] AAIJ	17BD	LHCB	pp at 7, 8 TeV

[1] AAIJ 17BD reports $[\Gamma(B_s^0 \to p\overline{p}K^+ \pi^-)/\Gamma_{\text{total}}] / [B(B^0 \to J/\psi(1S) K^*(892)^0)] / [B(J/\psi(1S) \to p\overline{p})] / [B(K^*(892) \to (K\pi)^{\pm})] = 0.52 \pm 0.08 \pm 0.05$ which we multiply by our best (shown rounded) values $B(B^0 \to J/\psi(1S) K^*(892)^0) = (1.27 \pm 0.05) \times 10^{-3}$, $B(J/\psi(1S) \to p\overline{p}) = (2.121 \pm 0.029) \times 10^{-3}$, $B(K^*(892) \to (K\pi)^{\pm}) = (99.896 \pm 0.010) \times 10^{-2}$. Our first error is their experiment's error and our second error is the systematic error from using our best (shown rounded) values. Reported value assumes $f_s/f_d = 0.259 \pm 0.015$.

[2] The branching ratio is given for $m_{p\overline{p}}$ <2.85 GeV.

$\Gamma(p\overline{p}K^+ \pi^-)/\Gamma(p\overline{p}K^+ K^-)$ — $\Gamma_{154}/\Gamma_{153}$

VALUE	DOCUMENT ID		TECN	COMMENT
0.31±0.05±0.02	[1,2] AAIJ	17BD	LHCB	pp at 7, 8 TeV

[1] Reports $B(B_s^0 \to p\overline{p}K^+ \pi^-) / B(B^0 \to p\overline{p}K^+ \pi^-) = 0.22 \pm 0.04 \pm 0.02 \pm 0.01$, where the third error is due to f_s/f_d.

[2] The ratio is given for $m_{p\overline{p}}$ <2.85 GeV and assuming $f_s/f_d = 0.259 \pm 0.015$.

$\Gamma(p\overline{p}\pi^+ \pi^-)/\Gamma_{\text{total}}$ — Γ_{155}/Γ

VALUE (units 10^{-7})	DOCUMENT ID		TECN	COMMENT
4.3±2.0±0.2	[1,2] AAIJ	17BD	LHCB	pp at 7, 8 TeV

[1] AAIJ 17BD reports $[\Gamma(B_s^0 \to p\overline{p}\pi^+ \pi^-)/\Gamma_{\text{total}}] / [B(B^0 \to J/\psi(1S) K^*(892)^0)] / [B(J/\psi(1S) \to p\overline{p})] / [B(K^*(892) \to (K\pi)^{\pm})] = 0.16 \pm 0.07 \pm 0.02$ which we multiply by our best (shown rounded) values $B(B^0 \to J/\psi(1S) K^*(892)^0) = (1.27 \pm 0.05) \times 10^{-3}$, $B(J/\psi(1S) \to p\overline{p}) = (2.121 \pm 0.029) \times 10^{-3}$, $B(K^*(892) \to (K\pi)^{\pm}) = (99.896 \pm 0.010) \times 10^{-2}$. Our first error is their experiment's error and our second error is the systematic error from using our best (shown rounded) values. Reported value assumes $f_s/f_d = 0.259 \pm 0.015$.

[2] The branching ratio is given for $m_{p\overline{p}}$ <2.85 GeV.

$\Gamma(p\overline{p}p\overline{p})/\Gamma_{\text{total}}$ — Γ_{156}/Γ

VALUE (units 10^{-8})	DOCUMENT ID		TECN	COMMENT
2.3±1.0±0.1	[1] AAIJ	23AD	LHCB	pp at 7, 8, 13 TeV

[1] AAIJ 23AD reports $(2.3 \pm 1.0 \pm 0.2 \pm 0.1) \times 10^{-8}$ from a measurement of $[\Gamma(B_s^0 \to p\overline{p}p\overline{p})/\Gamma_{\text{total}}] / [B(B_s^0 \to J/\psi(1S)\phi)] / [B(\phi(1020) \to K^+ K^-)] / [B(J/\psi(1S) \to p\overline{p})]$ assuming $B(B_s^0 \to J/\psi(1S)\phi) = (1.04 \pm 0.04) \times 10^{-3}$, $B(\phi(1020) \to K^+ K^-) = 0.491 \pm 0.005$, $B(J/\psi(1S) \to p\overline{p}) = (2.120 \pm 0.029) \times 10^{-3}$, which we rescale to our best (shown rounded) values $B(B_s^0 \to J/\psi(1S)\phi) = (1.01 \pm 0.04) \times 10^{-3}$, $B(\phi(1020) \to K^+ K^-) = (50.1 \pm 0.6) \times 10^{-2}$, $B(J/\psi(1S) \to p\overline{p}) = (2.121 \pm 0.029) \times 10^{-3}$. Our first error is their experiment's error and our second error is the systematic error from using our best (shown rounded) values.

$\Gamma(p\overline{\Lambda}K^- + \text{c.c.})/\Gamma_{\text{total}}$ — Γ_{157}/Γ

VALUE (units 10^{-6})	DOCUMENT ID		TECN	COMMENT
5.5±0.9±0.4	[1,2] AAIJ	17AL	LHCB	pp at 7, 8 TeV

[1] AAIJ 17AL reports $(5.46 \pm 0.61 \pm 0.82) \times 10^{-6}$ from a measurement of $[\Gamma(B_s^0 \to p\overline{\Lambda}K^- + \text{c.c.})/\Gamma_{\text{total}}] / [B(B^0 \to p\overline{\Lambda}\pi^-)]$ assuming $B(B^0 \to p\overline{\Lambda}\pi^-) = (3.14 \pm 0.29) \times 10^{-6}$, which we rescale to our best (shown rounded) value $B(B^0 \to p\overline{\Lambda}\pi^-) = (3.16 \pm 0.24) \times 10^{-6}$. Our first error is their experiment's error and our second error is the systematic error from using our best (shown rounded) value.

[2] AAIJ 17AL value represents the sum of $B_s^0 \to p\overline{\Lambda}K^-$ and $B_s^0 \to \overline{p}\Lambda K^+$ and assumes the fraction $f_s/f_d = 0.259 \pm 0.015$.

$\Gamma(\Lambda_c^- \Lambda\pi^+)/\Gamma_{\text{total}}$ — Γ_{158}/Γ

VALUE (units 10^{-4})	DOCUMENT ID		TECN	COMMENT
3.6±1.1±1.2	[1] SOLOVIEVA	13	BELL	$e^+ e^- \to \Upsilon(4S)$

[1] The second error is the total systematic uncertainty including the Λ_c absolute branching fractions and the normalizion number of B_s events.

$\Gamma(\Lambda_c^- \Lambda_c^+)/\Gamma_{\text{total}}$ — Γ_{159}/Γ

VALUE	CL%	DOCUMENT ID		TECN	COMMENT
<8.0 × 10^{-5}	95	[1] AAIJ	14AA	LHCB	pp at 7 TeV

[1] Uses $B(\overline{B}^0 \to D^+ D_s^-) = (7.2 \pm 0.8) \times 10^{-3}$.

Int. J. Mod. Phys. A 2026.41. Downloaded from www.worldscientific.com
by CALIFORNIA @ BERKELEY on 09/16/26. Re-use and distribution is strictly not permitted, except for Open Access articles.

$\Gamma(\gamma\gamma)/\Gamma_{total}$ — Γ_{160}/Γ

Test for ΔB=1 weak neutral current.

VALUE (units 10^{-6})	CL%	DOCUMENT ID		TECN	COMMENT
< 3.1	90	[1] DUTTA	15	BELL	$e^+e^- \to \Upsilon(5S)$
• • • We do not use the following data for averages, fits, limits, etc. • • •					
< 8.7	90	[2] WICHT	08A	BELL	Repl. by DUTTA 15
< 53	90	DRUTSKOY	07A	BELL	Repl. by WICHT 08A
<148	90	[3] ACCIARRI	95I	L3	$e^+e^- \to Z$

[1] Assumes the fraction of $B_s^{(*)}\overline{B}_s^{(*)}$ in $b\overline{b}$ events is $f_s = (17.2 \pm 3.0)\%$.
[2] Assumes $\Upsilon(5S) \to B_s^*\overline{B}_s^* = (19.5^{+3.0}_{-2.3})\%$.
[3] ACCIARRI 95I assumes $f_{B^0} = 39.5 \pm 4.0$ and $f_{B_s} = (12.0 \pm 3.0)\%$.

$\Gamma(\phi\gamma)/\Gamma_{total}$ — Γ_{161}/Γ

VALUE (units 10^{-6})	CL%	DOCUMENT ID		TECN	COMMENT
34 ± 4 OUR AVERAGE					
36 ± 5 ± 7		[1] DUTTA	15	BELL	$e^+e^- \to \Upsilon(5S)$
34.1± 3.4± 1.9		[2] AAIJ	13	LHCB	pp at 7 TeV
• • • We do not use the following data for averages, fits, limits, etc. • • •					
39 ± 5		[3] AAIJ	12AE	LHCB	Repl. by AAIJ 13
$57^{+18}_{-15}{}^{+12}_{-11}$		[4] WICHT	08A	BELL	Repl. by DUTTA 15
<390	90	DRUTSKOY	07A	BELL	$e^+e^- \to \Upsilon(5S)$
<120	90	ACOSTA	02G	CDF	$p\overline{p}$ at 1.8 TeV
<700	90	[5] ADAM	96D	DLPH	$e^+e^- \to Z$

[1] Assumes the fraction of $B_s^{(*)}\overline{B}_s^{(*)}$ in $b\overline{b}$ events is $f_s = (17.2 \pm 3.0)\%$. The systematic uncertainty from f_s is 0.6×10^{-5}.
[2] AAIJ 13 reports $[\Gamma(B_s^0 \to \phi\gamma)/\Gamma_{total}]$ / $[B(B^0 \to K^*(892)^0\gamma)] = 0.81 \pm 0.04 \pm 0.07$ which we multiply by our best (shown rounded) value $B(B^0 \to K^*(892)^0\gamma) = (4.21 \pm 0.24) \times 10^{-5}$. Our first error is their experiment's error and our second error is the systematic error from using our best (shown rounded) value.
[3] Measures $B(B^0 \to K^{*0}\gamma)/B(B_s \to \phi\gamma) = 1.12 \pm 0.08(\text{stat})^{+0.06}_{-0.04}(\text{sys})^{+0.09}_{-0.08}(f_s/f_d)$ and uses current world-average value of $B(B^0 \to K^{*0}\gamma) = (4.33 \pm 0.15) \times 10^{-5}$.
[4] Assumes $\Upsilon(5S) \to B_s^*\overline{B}_s^* = (19.5^{+3.0}_{-2.3})\%$.
[5] ADAM 96D assumes $f_{B^0} = f_{B^-} = 0.39$ and $f_{B_s} = 0.12$.

$\Gamma(f_2(1270)\gamma)/\Gamma(\phi\gamma)$ — $\Gamma_{162}/\Gamma_{161}$

VALUE (%)	DOCUMENT ID		TECN	COMMENT
$\mathbf{26^{+11}_{-13}{}^{+2}_{-3}}$	[1] AAIJ	24S	LHCB	pp at 7, 8, 13 TeV

[1] AAIJ 24S reports $[\Gamma(B_s^0 \to f_2(1270)\gamma)/\Gamma(B_s^0 \to \phi\gamma)] \times B(f_2(1270) \to K^+K^-)$ / $B(\phi(1020) \to K^+K^-) = 1.2^{+0.4}_{-0.3}{}^{+0.3}_{-0.5}$% which we divide and multiply by our best values $B(f_2(1270) \to K^+K^-) = \frac{1}{2}(4.6 \pm 0.4) \times 10^{-2}$, $B(\phi(1020) \to K^+K^-) = (50.1 \pm 0.6) \times 10^{-2}$. Our first error is their experiment's error and our second error is the systematic error from using our best values.

$\Gamma(f_2'(1525)\gamma)/\Gamma(\phi\gamma)$ — $\Gamma_{163}/\Gamma_{161}$

VALUE (%)	DOCUMENT ID		TECN	COMMENT
$\mathbf{19.5^{+1.7}_{-1.0} \pm 0.5}$	[1] AAIJ	24S	LHCB	pp at 7, 8, 13 TeV

[1] AAIJ 24S reports $[\Gamma(B_s^0 \to f_2'(1525)\gamma)/\Gamma(B_s^0 \to \phi\gamma)] \times B(f_2'(1525) \to K^+K^-)$ / $B(\phi(1020) \to K^+K^-) = 17.3^{+0.8}_{-0.7}{}^{+1.3}_{-0.5}$% which we divide and multiply by our best values $B(f_2'(1525) \to K^+K^-) = \frac{1}{2}(88.8 \pm 2.2) \times 10^{-2}$, $B(\phi(1020) \to K^+K^-) = (50.1 \pm 0.6) \times 10^{-2}$. Our first error is their experiment's error and our second error is the systematic error from using our best values.

$\Gamma(\phi(1680)\gamma,\ \phi \to K^+K^-)/\Gamma(\phi\gamma)$ — $\Gamma_{164}/\Gamma_{161}$

VALUE (%)	DOCUMENT ID		TECN	COMMENT
$\mathbf{2.71^{+0.67}_{-0.63} \pm 0.03}$	[1] AAIJ	24S	LHCB	pp at 7, 8, 13 TeV

[1] AAIJ 24S reports $[\Gamma(B_s^0 \to \phi(1680)\gamma,\ \phi \to K^+K^-)/\Gamma(B_s^0 \to \phi\gamma)]$ / $[B(\phi(1020) \to K^+K^-)] = 5.4^{+0.9}_{-0.6}{}^{+1.0}_{-1.1}$ % which we multiply by our best (shown rounded) value $B(\phi(1020) \to K^+K^-) = (50.1 \pm 0.6) \times 10^{-2}$. Our first error is their experiment's error and our second error is the systematic error from using our best (shown rounded) value.

$\Gamma(\phi_3(1850)\gamma,\ \phi_3 \to K^+K^-)/\Gamma(\phi\gamma)$ — $\Gamma_{165}/\Gamma_{161}$

VALUE (%)	DOCUMENT ID		TECN	COMMENT
$\mathbf{0.200^{+0.181}_{-0.142} \pm 0.002}$	[1] AAIJ	24S	LHCB	pp at 7, 8, 13 TeV

[1] AAIJ 24S reports $[\Gamma(B_s^0 \to \phi_3(1850)\gamma,\ \phi_3 \to K^+K^-)/\Gamma(B_s^0 \to \phi\gamma)]$ / $[B(\phi(1020) \to K^+K^-)] = 0.4^{+0.3}_{-0.2}{}^{+0.2}_{-0.2}$ % which we multiply by our best (shown rounded) value $B(\phi(1020) \to K^+K^-) = (50.1 \pm 0.6) \times 10^{-2}$. Our first error is their experiment's error and our second error is the systematic error from using our best (shown rounded) value.

$\Gamma(f_2(2010)\gamma,\ f_2 \to K^+K^-)/\Gamma(\phi\gamma)$ — $\Gamma_{166}/\Gamma_{161}$

VALUE (%)	DOCUMENT ID		TECN	COMMENT
$\mathbf{0.301^{+0.213}_{-0.142} \pm 0.003}$	[1] AAIJ	24S	LHCB	pp at 7, 8, 13 TeV

[1] AAIJ 24S reports $[\Gamma(B_s^0 \to f_2(2010)\gamma,\ f_2 \to K^+K^-)/\Gamma(B_s^0 \to \phi\gamma)]$ / $[B(\phi(1020) \to K^+K^-)] = 0.6^{+0.3}_{-0.2}{}^{+0.3}_{-0.2}$ % which we multiply by our best (shown rounded) value $B(\phi(1020) \to K^+K^-) = (50.1 \pm 0.6) \times 10^{-2}$. Our first error is their experiment's error and our second error is the systematic error from using our best (shown rounded) value.

$\Gamma(\mu^+\mu^-)/\Gamma_{total}$ — Γ_{167}/Γ

Test for $\Delta B = 1$ weak neutral current.

VALUE (units 10^{-9})	CL%	DOCUMENT ID		TECN	COMMENT
3.34±0.27 OUR AVERAGE					
$3.83^{+0.24}_{-0.36}{}^{+0.24}_{-0.21}$		[1] TUMASYAN	23A	CMS	pp at 13 TeV
$3.09^{+0.46}_{-0.43}{}^{+0.15}_{-0.11}$		AAIJ	22	LHCB	pp at 7, 8, 13 TeV
2.9 ±0.6 ±0.4		[2] SIRUNYAN	20AG	CMS	pp at 7, 8, 13 TeV
$2.8\ ^{+0.8}_{-0.7}$		[3] AABOUD	19L	ATLS	pp at 7, 8, 13 TeV
• • • We do not use the following data for averages, fits, limits, etc. • • •					
$3.0 \pm 0.6\ ^{+0.3}_{-0.2}$		AAIJ	17AI	LHCB	Repl. by AAIJ 22
$0.9\ ^{+1.1}_{-0.8}$		[4] AABOUD	16L	ATLS	Repl. by AABOUD 19L
$2.8\ ^{+0.7}_{-0.6}$		[5] KHACHATRY...	15BE	LHC	pp at 7, 8 TeV
$3.2\ ^{+1.4}_{-1.2}{}^{+0.5}_{-0.3}$		[6] AAIJ	13B	LHCB	Repl. by AAIJ 13BA
$2.9\ ^{+1.1}_{-1.0}{}^{+0.3}_{-0.1}$		[7] AAIJ	13BA	LHCB	Repl. by KHACHATRYAN 15BE
$13\ ^{+9}_{-7}$		[8] AALTONEN	13F	CDF	$p\overline{p}$ at 1.96 TeV
<12	90	[9] ABAZOV	13C	D0	$p\overline{p}$ at 1.96 TeV
$3.0\ ^{+1.0}_{-0.9}$		[10] CHATRCHYAN	13AW	CMS	Repl. by SIRUNYAN 20AG
<19	90	[11] AAD	12AE	ATLS	pp at 7 TeV
<12	90	[12] AAIJ	12A	LHCB	Repl. by AAIJ 12W
< 3.8	90	[13] AAIJ	12W	LHCB	Repl. by AAIJ 13B
< 6.4	90	[14] CHATRCHYAN	12A	CMS	pp at 7 TeV
<43	90	[15] AAIJ	11B	LHCB	Repl. by AAIJ 12A
<35	90	[16] AALTONEN	11AG	CDF	$p\overline{p}$ at 1.96 TeV
<16	90	[17] CHATRCHYAN	11T	CMS	Repl. by CHATRCHYAN 12A
<42	90	[18] ABAZOV	10S	D0	$p\overline{p}$ at 1.96 TeV

[1] Uses normalization mode $B(B^+ \to J/\psi K^+) = (1.020 \pm 0.019) \times 10^{-3}$, $B(J/\psi \to \mu^+\mu^-) = (5.961 \pm 0.033) \times 10^{-2}$ and B production ratio $f(b \to B_s^0)/f(b \to B^+) = 0.231 \pm 0.008$.
[2] Uses normalization mode $B(B^+ \to J/\psi K^+) = (1.01 \pm 0.03) \times 10^{-3}$ and B production ratio $f(b \to B_s^0)/f(b \to B^+) = 0.252 \pm 0.012 \pm 0.015$.
[3] Uses normalization mode $B(B^+ \to J/\psi K^+) = (1.010 \pm 0.029) \times 10^{-3}$ and B production ratio $f(b \to B_s^0)/f(b \to B^0) = 0.256 \pm 0.013$.
[4] This value corresponds to an upper limit of $< 3.0 \times 10^{-9}$ at 95% C.L. It uses $f_s/f_d = 0.24 \pm 0.02$.
[5] Determined from the joint fit to CMS and LHCb data. Uncertainty includes both statistical and systematic component.
[6] Uses B production ratio $f(\overline{b} \to B_s^0)/f(\overline{b} \to B_d^0) = 0.256 \pm 0.020$ and two normalization modes: $B(B^+ \to J/\psi K^+ \to \mu^+\mu^-K^+) = (6.01 \pm 0.21) \times 10^{-5}$ and $B(B^0 \to K^+\pi^-) = (1.94 \pm 0.06) \times 10^{-5}$.
[7] Uses B production ratio $f(\overline{b} \to B_s^0)/f(\overline{b} \to B_d^0) = 0.259 \pm 0.015$ and normalization modes $B^+ \to J/\psi K^+ \to \mu^+\mu^-K^+$ and $B^0 \to K^+\pi^-$.
[8] Uses normalization mode $B(B^+ \to J/\psi K^+) = (10.22 \pm 0.35) \times 10^{-4}$ and B production ratio $f(\overline{b} \to B_s^0)/f(\overline{b} \to B_d^0) = 0.28 \pm 0.04$.
[9] Uses normalization mode $B(B^+ \to J/\psi K^+ \to \mu^+\mu^-K^+) = (6.01 \pm 0.21) \times 10^{-5}$ and B production ratio $f(\overline{b} \to B_s^0)/f(\overline{b} \to B_d^0) = 0.263 \pm 0.017$.
[10] Uses B production ratio $f(\overline{b} \to B_s^0)/f(\overline{b} \to B_d^0) = 0.256 \pm 0.020$ and $B(B^+ \to J/\psi K^+ \to \mu^+\mu^-K^+) = (6.0 \pm 0.2) \times 10^{-5}$ for normalization.
[11] Uses B production ratio $f(\overline{b} \to B^+)/f(\overline{b} \to B_s^0) = 3.75 \pm 0.29$ and $B(B^+ \to J/\psi K^+ \to \mu^+\mu^-K^+) = (6.0 \pm 0.2) \times 10^{-5}$.
[12] Uses B production ratio $f(\overline{b} \to B_s^0)/f(\overline{b} \to B_d^0) = 0.267^{+0.021}_{-0.020}$ and three normalization modes $B(B^+ \to J/\psi K^+ \to \mu^+\mu^-K^+) = (6.01 \pm 0.21) \times 10^{-5}$, $B(B^0 \to K^+\pi^-) = (1.94 \pm 0.06) \times 10^{-5}$, and $B(B_s^0 \to J/\psi\phi \to \mu^+\mu^-K^+K^-) = (3.4 \pm 0.9) \times 10^{-5}$.
[13] Uses B production ratio $f(\overline{b} \to B_s^0)/f(\overline{b} \to B_d^0) = 0.267^{+0.021}_{-0.020}$ and three normalization modes of $B^+ \to J/\psi K^+$, $B^0 \to K^+\pi^-$, and $B_s^0 \to J/\psi\phi$.
[14] Uses $f_s/f_u = 0.267 \pm 0.021$ and $B(B^+ \to J/\psi K^+ \to \mu^+\mu^-K^+) = (6.0 \pm 0.2) \times 10^{-5}$.
[15] Uses B production ratio $f(\overline{b} \to B^+)/f(\overline{b} \to B_s^0) = 3.71 \pm 0.47$ and three normalization modes.
[16] Uses B production ratio $f(\overline{b} \to B^+)/f(\overline{b} \to B_s^0) = 3.55 \pm 0.47$ and $B(B^+ \to J/\psi K^+ \to \mu^+\mu^-K^+) = (6.01 \pm 0.21) \times 10^{-5}$.
[17] Uses B production ratio $f(\overline{b} \to B^+)/f(\overline{b} \to B_s^0) = 3.55 \pm 0.42$ and $B(B^+ \to J/\psi K^+ \to \mu^+\mu^-K^+) = (6.0 \pm 0.2) \times 10^{-5}$.
[18] Uses B production ratio $f(\overline{b} \to B^+)/f(\overline{b} \to B_s^0) = 3.86 \pm 0.59$, and the number of $B^+ \to J/\psi K^+$ decays.

$\Gamma(e^+e^-)/\Gamma_{total}$ — Γ_{168}/Γ

Test for $\Delta B = 1$ weak neutral current.

VALUE	CL%	DOCUMENT ID		TECN	COMMENT
$\mathbf{<9.4 \times 10^{-9}}$	90	[1] AAIJ	20W	LHCB	pp at 7, 8, 13 TeV
• • • We do not use the following data for averages, fits, limits, etc. • • •					
$<2.8 \times 10^{-7}$	90	AALTONEN	09P	CDF	$p\overline{p}$ at 1.96 TeV
$<5.4 \times 10^{-5}$	90	[2] ACCIARRI	97B	L3	$e^+e^- \to Z$

Int. J. Mod. Phys. A 2026.41. Downloaded from www.worldscientific.com
by UNIVERSITY OF CALIFORNIA @ BERKELEY on 09/16/26. Re-use and distribution is strictly not permitted, except for Open Access articles.

[1] Assumes no contribution from $B^0 \to e^+e^-$ decays.
[2] ACCIARRI 97B assume PDG 96 production fractions for B^+, B^0, B_s, and Λ_b.

$\Gamma(\tau^+\tau^-)/\Gamma_{total}$ — Γ_{169}/Γ

VALUE	CL%	DOCUMENT ID		TECN	COMMENT
$<6.8 \times 10^{-3}$	95	[1] AAIJ	17AJ	LHCB	pp at 7, 8 TeV

[1] Assuming no contribution from $B^0 \to \tau^+\tau^-$.

$\Gamma(\mu^+\mu^-\gamma)/\Gamma_{total}$ — Γ_{170}/Γ

VALUE	CL%	DOCUMENT ID		TECN	COMMENT
$<4.2 \times 10^{-8}$	95	[1] AAIJ	24Q	LHCB	pp at 13 TeV
• • • We do not use the following data for averages, fits, limits, etc. • • •					
$<2.0 \times 10^{-9}$	95	[2,3] AAIJ	22	LHCB	pp at 7, 8, 13 TeV

[1] The exclusion limit is quoted at 95% CL for the dimuon mass region $[3.92 - m_{B_s^0}]$ GeV/c^2. The limits are also reported for other dimuon mass regions: $< 4.2 \times 10^{-8}$ in $[2m_\mu - 1.7]$ GeV/c^2; $< 7.7 \times 10^{-8}$ in [1.70–2.88] GeV/c^2; $< 2.8 \times 10^{-8}$ in $[2m_\mu - 1.7]$ GeV/c^2 and excluding ϕ mass.
[2] The exclusion is limited to the range $m_{\mu\mu} > 4.9$ GeV/c^2.
[3] For the mass region $4.9 - m_{B_s^0}$ GeV/c^2.

$\Gamma(\mu^+\mu^-\mu^+\mu^-)/\Gamma_{total}$ — Γ_{171}/Γ

VALUE	CL%	DOCUMENT ID		TECN	COMMENT
$<8.6 \times 10^{-10}$	95	AAIJ	22Q	LHCB	pp at 7, 8, 13 TeV
• • • We do not use the following data for averages, fits, limits, etc. • • •					
$<2.5 \times 10^{-9}$	95	AAIJ	17N	LHCB	pp at 7, 8 TeV
$<1.6 \times 10^{-8}$	95	[1] AAIJ	13AW	LHCB	Repl. by AAIJ 17N

[1] Also reports a limit of $< 1.2 \times 10^{-8}$ at 90% CL.

$\Gamma(\overline{D}^0\mu^+\mu^-)/\Gamma_{total}$ — Γ_{178}/Γ

VALUE	CL%	DOCUMENT ID		TECN	COMMENT
$<1.2 \times 10^{-7}$	90	AAIJ	24F	LHCB	pp at 7, 8, 13 TeV

$\Gamma(SP,\ S \to \mu^+\mu^-,\ P \to \mu^+\mu^-)/\Gamma_{total}$ — Γ_{172}/Γ

Here S and P are the hypothetical scalar and pseudoscalar particles with masses of 2.5 GeV/c^2 and 214.3 MeV/c^2, respectively.

VALUE	CL%	DOCUMENT ID		TECN	COMMENT
$<2.2 \times 10^{-9}$	95	AAIJ	17N	LHCB	pp at 7, 8 TeV
• • • We do not use the following data for averages, fits, limits, etc. • • •					
$<1.2 \times 10^{-8}$	90	[1] AAIJ	13AW	LHCB	Repl. by AAIJ 17N

[1] Also reports a limit of $< 1.6 \times 10^{-8}$ at 95% CL.

$\Gamma(aa,\ a \to \mu^+\mu^-)/\Gamma_{total}$ — Γ_{173}/Γ

Here particle a is a scalar with a mass of 1 GeV/c^2.

VALUE	CL%	DOCUMENT ID		TECN	COMMENT
$<5.8 \times 10^{-10}$	95	AAIJ	22Q	LHCB	pp at 7, 8, 13 TeV

$\Gamma(\phi(1020)\mu^+\mu^-)/\Gamma_{total}$ — Γ_{174}/Γ

Test for $\Delta B = 1$ weak neutral current.

VALUE (units 10^{-7})	CL%	DOCUMENT ID		TECN	COMMENT
• • • We do not use the following data for averages, fits, limits, etc. • • •					
<32	90	[1] ABAZOV	06G	D0	$p\overline{p}$ at 1.96 TeV
$< 4.7 \times 10^2$	90	ACOSTA	02D	CDF	$p\overline{p}$ at 1.8 TeV

[1] Uses $B(B_s^0 \to J/\psi\phi) = 9.3 \times 10^{-4}$.

$\Gamma(\phi(1020)\mu^+\mu^-)/\Gamma(J/\psi(1S)\phi)$ — Γ_{174}/Γ_{69}

VALUE (units 10^{-3})	CL%	DOCUMENT ID		TECN	COMMENT
0.806±0.026 OUR AVERAGE					
0.800±0.021±0.016		AAIJ	21AG	LHCB	pp at 7, 8, 13 TeV
1.13 ±0.19 ±0.07		AALTONEN	11AI	CDF	$p\overline{p}$ at 1.96 TeV
• • • We do not use the following data for averages, fits, limits, etc. • • •					
$0.741^{+0.042}_{-0.040} \pm 0.029$		AAIJ	15AQ	LHCB	Repl. by AAIJ 21AG
$0.674^{+0.061}_{-0.056} \pm 0.016$		AAIJ	13X	LHCB	Repl. by AAIJ 15AQ
1.11 ±0.25 ±0.09		AALTONEN	11L	CDF	Repl. by AALTONEN 11AI
< 2.3	90	AALTONEN	09B	CDF	Repl. by AALTONEN 11L

$\Gamma(\overline{K}^*(892)^0\mu^+\mu^-)/\Gamma_{total}$ — Γ_{176}/Γ

VALUE (units 10^{-8})	DOCUMENT ID		TECN	COMMENT
2.9±1.0±0.4	[1] AAIJ	18AB	LHCB	pp at 7, 8, 13 TeV

[1] Normalizes to $B(B^0 \to J/\psi K^{*0}) = 1.19 \pm 0.01 \pm 0.08\%$ and $B(J/\psi \to \mu^+\mu^-) = 5.96 \pm 0.03\%$, and uses $f_s/f_d = 0.259 \pm 0.015$.

$\Gamma(f_2'(1525)\mu^+\mu^-)/\Gamma(J/\psi(1S)\phi)$ — Γ_{175}/Γ_{69}

VALUE (units 10^{-4})	DOCUMENT ID		TECN	COMMENT
1.55±0.19±0.08	[1] AAIJ	21AG	LHCB	pp at 7, 8, 13 TeV

[1] Measured by combining the q^2 regions [0.1, 0.98], [1.1, 8.0], and [11.0, 12.5] GeV^2/c^4.

$\Gamma(\pi^+\pi^-\mu^+\mu^-)/\Gamma_{total}$ — Γ_{177}/Γ

VALUE (units 10^{-8})	DOCUMENT ID		TECN	COMMENT
8.4±1.6±0.3	[1] AAIJ	15S	LHCB	pp at 7, 8 TeV

[1] AAIJ 15S reports $(8.6 \pm 1.5 \pm 0.7 \pm 0.7) \times 10^{-8}$ from a measurement of $[\Gamma(B_s^0 \to \pi^+\pi^-\mu^+\mu^-)/\Gamma_{total}]$ / $[B(B^0 \to J/\psi(1S)K^*(892)^0)]$ assuming $B(B^0 \to J/\psi(1S)K^*(892)^0) = (1.3 \pm 0.1) \times 10^{-3}$, which we rescale to our best (shown rounded) value $B(B^0 \to J/\psi(1S)K^*(892)^0) = (1.27 \pm 0.05) \times 10^{-3}$. Our first error is their experiment's error and our second error is the systematic error from using our best (shown rounded) value.

$\Gamma(\phi\nu\overline{\nu})/\Gamma_{total}$ — Γ_{179}/Γ

Test for $\Delta B = 1$ weak neutral current.

VALUE	CL%	DOCUMENT ID		TECN	COMMENT
$<5.4 \times 10^{-3}$	90	[1] ADAM	96D	DLPH	$e^+e^- \to Z$

[1] ADAM 96D assumes $f_{B^0} = f_{B^-} = 0.39$ and $f_{B_s} = 0.12$.

$\Gamma(\text{invisible})/\Gamma_{total}$ — Γ_{180}/Γ

VALUE	CL%	DOCUMENT ID		TECN	COMMENT
• • • We do not use the following data for averages, fits, limits, etc. • • •					
$<5.6 \times 10^{-4}$	90	[1] ALONSO-ALV...24		THEO	$e^+e^- \to Z$

[1] A reinterpretation of an old inclusive ALEPH search for b-hadron decays with large missing energy reported in BARATE 01E.

$\Gamma(e^\pm\mu^\mp)/\Gamma_{total}$ — Γ_{181}/Γ

Test of lepton family number conservation.

VALUE	CL%	DOCUMENT ID		TECN	COMMENT
$<5.4 \times 10^{-9}$	90	[1] AAIJ	18T	LHCB	pp at 7, 8 TeV
• • • We do not use the following data for averages, fits, limits, etc. • • •					
$<1.1 \times 10^{-8}$	90	[2] AAIJ	13BM	LHCB	Repl. by AAIJ 18T
$<2.0 \times 10^{-7}$	90	AALTONEN	09P	CDF	$p\overline{p}$ at 1.96 TeV
$<6.1 \times 10^{-6}$	90	ABE	98V	CDF	Repl. by AALTONEN 09P
$<4.1 \times 10^{-5}$	90	[3] ACCIARRI	97B	L3	$e^+e^- \to Z$

[1] AAIJ 18T uses normalization modes $B(B^0 \to K^+\pi^-) = (19.6 \pm 0.5) \times 10^{-6}$ and $B(B^+ \to J/\psi K^+) = (1.026 \pm 0.031) \times 10^{-3}$ with B production ratio $f(\overline{b} \to B_s^0)/f(\overline{b} \to B_d^0) = 0.259 \pm 0.015$. The upper limit increases to 6×10^{-9} with the assumption of B_L-dominated decay amplitude.
[2] Uses normalization mode $B(B^0 \to K^+\pi^-) = (19.4 \pm 0.6) \times 10^{-6}$ and B production ratio $f(\overline{b} \to B_s^0)/f(\overline{b} \to B_d^0) = 0.256 \pm 0.020$.
[3] ACCIARRI 97B assume PDG 96 production fractions for B^+, B^0, B_s, and Λ_b.

$\Gamma(e^\pm\tau^\mp)/\Gamma_{total}$ — Γ_{182}/Γ

VALUE	CL%	DOCUMENT ID		COMMENT
$<1.4 \times 10^{-3}$	90	[1] NAYAK	23	$e^+e^- \to \Upsilon(4S)$

[1] Reconstructs the accompanying B_s^0 meson in the semileptonic decay modes.

$\Gamma(\mu^\pm\tau^\mp)/\Gamma_{total}$ — Γ_{183}/Γ

VALUE	CL%	DOCUMENT ID		TECN	COMMENT
$<4.2 \times 10^{-5}$	95	[1] AAIJ	19AK	LHCB	pp at 7, 8 TeV
• • • We do not use the following data for averages, fits, limits, etc. • • •					
$<7.3 \times 10^{-4}$	90	[2] NAYAK	23	BELL	$e^+e^- \to \Upsilon(4S)$

[1] Assuming no contribution from $B^0 \to \mu^\pm\tau^\mp$.
[2] Reconstructs the accompanying B_s^0 meson in the semileptonic decay modes.

$\Gamma(\phi\mu^\pm e^\mp)/\Gamma_{total}$ — Γ_{184}/Γ

VALUE	CL%	DOCUMENT ID		TECN	COMMENT
$<1.6 \times 10^{-8}$	90	[1] AAIJ	23G	LHCB	pp at 7, 8, 13 TeV

[1] Uses the uniform phase space model for the signal decays.

$\Gamma(\phi\mu^\pm\tau^\mp)/\Gamma_{total}$ — Γ_{185}/Γ

VALUE	CL%	DOCUMENT ID		TECN	COMMENT
$<1.0 \times 10^{-5}$	90	AAIJ	24AK	LHCB	pp at 7, 8 and 13 TeV

$\Gamma(p\mu^-)/\Gamma_{total}$ — Γ_{186}/Γ

VALUE	CL%	DOCUMENT ID		COMMENT
$<1.21 \times 10^{-8}$	90	[1] AAIJ	23Y	pp at 7, 8, 13 TeV

[1] Assumes that B_s^0 decay branching fractions to $p\mu^-$ and $\overline{p}\mu^+$ are the same.

POLARIZATION IN B_s^0 DECAY

In decays involving two vector mesons, one can distinguish among the states in which meson polarizations are both longitudinal (L), or both are transverse and parallel ($\|$), or perpendicular ($\perp$) to each other with the parameters Γ_L/Γ, $\Gamma_\perp/\Gamma$, and the relative phases $\phi_\|$ and $\phi_\perp$. In decays involving two tensor mesons, the transverse polarization states are described by parameters $\Gamma_{\|1}$, $\Gamma_{\|2}$, $\Gamma_{\perp 1}$, $\Gamma_{\perp 2}$ and their relative phases $\phi_{\|1}$, $\phi_{\|2}$, $\phi_{\perp 1}$, $\phi_{\perp 2}$. See also the review on "Polarization in B Decays."

Γ_L/Γ in $B_s^0 \to D_s^*\rho^+$

VALUE	DOCUMENT ID		TECN	COMMENT
$1.05^{+0.08+0.03}_{-0.10-0.04}$	LOUVOT	10	BELL	$e^+e^- \to \Upsilon(5S)$

Int. J. Mod. Phys. A 2026.41. Downloaded from www.worldscientific.com
by CALIFORNIA @ BERKELEY on 09/16/26. Re-use and distribution is strictly not permitted, except for Open Access articles.

Γ_L/Γ in $B_s^0 \to J/\psi(1S)\phi$

VALUE	DOCUMENT ID		TECN	COMMENT
0.518 ±0.004 OUR AVERAGE	Error includes scale factor of 1.5. See the ideogram below.			
$0.5300 \pm 0.0015 \pm 0.0086$	[1] HAYRAPETY...	26A	CMS	pp at 13 TeV
$0.5179 \pm 0.0017 \pm 0.0032$	[2] AAIJ	24A	LHCB	pp at 13 TeV
$0.5152 \pm 0.0012 \pm 0.0034$	[3] AAD	21AE	ATLS	pp at 7, 8, 13 TeV
$0.524 \pm 0.013 \pm 0.015$	[4] AALTONEN	12D	CDF	$p\overline{p}$ at 1.96 TeV
$0.558 {}^{+0.017}_{-0.019}$	[4,5] ABAZOV	12D	D0	$p\overline{p}$ at 1.96 TeV
$0.61 \pm 0.14 \pm 0.02$	[6] AFFOLDER	00N	CDF	$p\overline{p}$ at 1.8 TeV
$0.56 \pm 0.21 {}^{+0.02}_{-0.04}$	ABE	95Z	CDF	$p\overline{p}$ at 1.8 TeV
• • • We do not use the following data for averages, fits, limits, etc. • • •				
$0.5350 \pm 0.0047 \pm 0.0049$	[4] SIRUNYAN	21E	CMS	pp at 13 TeV
$0.5289 \pm 0.0038 \pm 0.0041$	[4] SIRUNYAN	21E	CMS	Repl. by HAYRAPETYAN 26A
$0.5186 \pm 0.0029 \pm 0.0023$	AAIJ	19Q	LHCB	Repl. by AAIJ 24A
$0.522 \pm 0.003 \pm 0.007$	[3] AAD	16AP	ATLS	Repl. by AAD 21AE
$0.510 \pm 0.005 \pm 0.011$	[4] KHACHATRY...	16S	CMS	pp at 8 TeV
$0.5241 \pm 0.0034 \pm 0.0067$	AAIJ	15I	LHCB	Repl. by AAIJ 19Q
$0.529 \pm 0.006 \pm 0.012$	[3] AAD	14U	ATLS	Repl. by AAD 16AP
$0.539 \pm 0.014 \pm 0.016$	[4] AAD	12CV	ATLS	Repl. by AAD 14U
$0.555 \pm 0.027 \pm 0.006$	[7] ABAZOV	09E	D0	Repl. by ABAZOV 12D
$0.531 \pm 0.020 \pm 0.007$	[4] AALTONEN	08J	CDF	Repl. by AALTONEN 12D
$0.62 \pm 0.06 \pm 0.01$	ACOSTA	05	CDF	Repl. by AALTONEN 08J

[1] Measured using a time-dependent angular analysis of $B_s^0 \to J/\psi\phi$ decays with the ML-improved flavor-tagging algorithm.
[2] Measured using a time-dependent angular analysis of $B_s^0 \to J/\psi K^+ K^-$ decays.
[3] Measured using the flavor tagged, time-dependent angular analysis of $B_s^0 \to J/\psi\phi$ decays.
[4] Measured using the time-dependent angular analysis of $B_s^0 \to J/\psi\phi$ decays.
[5] The error includes both statistical and systematic uncertainties.
[6] AFFOLDER 00N measurements are based on 40 B_s^0 candidates obtained from a data sample of 89 pb^{-1}. The P-wave fraction is found to be $0.23 \pm 0.19 \pm 0.04$.
[7] Measured the angular and lifetime parameters for the time-dependent angular untagged decays $B_d^0 \to J/\psi K^{*0}$ and $B_s^0 \to J/\psi\phi$.

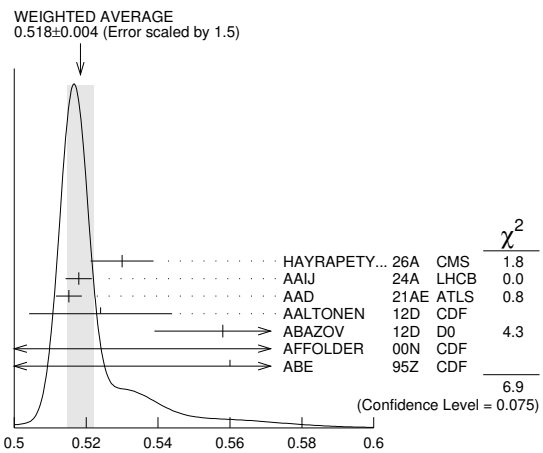

Γ_L/Γ in $B_s^0 \to J/\psi(1S)\phi$

Γ_L/Γ in $B_s^0 \to D_s^{*+} D_s^{*-}$

VALUE	DOCUMENT ID		TECN	COMMENT
$\mathbf{0.06 {}^{+0.18}_{-0.17} \pm 0.03}$	ESEN	13	BELL	$e^+e^- \to \Upsilon(5S)$

$\Gamma_\parallel/\Gamma$ in $B_s^0 \to J/\psi(1S)\phi$

VALUE	DOCUMENT ID		TECN	COMMENT
0.2222±0.0027 OUR AVERAGE				
$0.2220 \pm 0.0017 \pm 0.0021$	[1] AAD	21AE	ATLS	pp at 7, 8, 13 TeV
$0.231 \pm 0.014 \pm 0.015$	[2] AALTONEN	12D	CDF	$p\overline{p}$ at 1.96 TeV
$0.231 {}^{+0.024}_{-0.030}$	[2,3] ABAZOV	12D	D0	$p\overline{p}$ at 1.96 TeV
• • • We do not use the following data for averages, fits, limits, etc. • • •				
$0.227 \pm 0.004 \pm 0.006$	[1] AAD	16AP	ATLS	Repl. by AAD 21AE
$0.220 \pm 0.008 \pm 0.009$	[1] AAD	14U	ATLS	Repl. by AAD 16AP
$0.224 \pm 0.010 \pm 0.009$	[2] AAD	12CV	ATLS	Repl. by AAD 14U
$0.244 \pm 0.032 \pm 0.014$	[4] ABAZOV	09E	D0	Repl. by ABAZOV 12D
$0.230 \pm 0.029 \pm 0.011$	[2] AALTONEN	08J	CDF	Repl. by AALTONEN 12D
$0.260 \pm 0.084 \pm 0.013$	ACOSTA	05	CDF	Repl. by AALTONEN 08J

[1] Measured using a tagged, time-dependent angular analysis of $B_s^0 \to J/\psi\phi$ decays.
[2] Measured using the time-dependent angular analysis of $B_s^0 \to J/\psi\phi$ decays.
[3] The error includes both statistical and systematic uncertainties.
[4] Measured the angular and lifetime parameters for the time-dependent angular untagged decays $B_d^0 \to J/\psi K^{*0}$ and $B_s^0 \to J/\psi\phi$.

$\Gamma_\perp/\Gamma$ in $B_s^0 \to J/\psi(1S)\phi$

VALUE	DOCUMENT ID		TECN	COMMENT
0.2447±0.0028 OUR AVERAGE				
$0.2409 \pm 0.0020 \pm 0.0047$	[1] HAYRAPETY...	26A	CMS	pp at 13 TeV
$0.2463 \pm 0.0023 \pm 0.0024$	[2] AAIJ	24A	LHCB	pp at 13 TeV
• • • We do not use the following data for averages, fits, limits, etc. • • •				
$0.2337 \pm 0.0063 \pm 0.0045$	[3] SIRUNYAN	21E	CMS	pp at 13 TeV
$0.2393 \pm 0.0050 \pm 0.0037$	SIRUNYAN	21E	CMS	Repl. by HAYRAPETYAN 26A
$0.2456 \pm 0.0040 \pm 0.0019$	AAIJ	19Q	LHCB	Repl. by AAIJ 24A
$0.243 \pm 0.008 \pm 0.012$	KHACHATRY...	16S	CMS	pp at 8 TeV
$0.2504 \pm 0.0049 \pm 0.0036$	AAIJ	15I	LHCB	Repl. by AAIJ 19Q

[1] Measured using a time-dependent angular analysis of $B_s^0 \to J/\psi\phi$ decays with the ML-improved flavor-tagging algorithm.
[2] Measured using a time-dependent angular analysis of $B_s^0 \to J/\psi K^+ K^-$ decays.
[3] Measured with a combination of result from KHACHATRYAN 16S.

Γ_S/Γ in $B_s^0 \to J/\psi(1S)\phi$

$B_s^0 \to J/\psi(1S)\phi$ in S-wave.

VALUE (units 10^{-3})	DOCUMENT ID		TECN	COMMENT
$\mathbf{6.7 {}^{+3.4}_{-2.7} \pm 1.3}$	[1] HAYRAPETY...	26A	CMS	pp at 13 TeV

[1] Measured using a time-dependent angular analysis of $B_s^0 \to J/\psi\phi$ decays with the ML-improved flavor-tagging algorithm.

$\phi_\parallel$ in $B_s^0 \to J/\psi(1S)\phi$

VALUE (rad)	DOCUMENT ID		TECN	COMMENT
3.19 ±0.05 OUR AVERAGE	Error includes scale factor of 1.1.			
$3.145 \pm 0.077 \pm 0.033$	[1] HAYRAPETY...	26A	CMS	pp at 13 TeV
$3.146 \pm 0.061 \pm 0.052$	[2] AAIJ	24A	LHCB	pp at 13 TeV
$3.36 \pm 0.05 \pm 0.09$	[3] AAD	21AE	ATLS	pp at 7, 8, 13 TeV
3.15 ± 0.22	[4] ABAZOV	12D	D0	$p\overline{p}$ at 1.96 TeV
• • • We do not use the following data for averages, fits, limits, etc. • • •				
$3.18 \pm 0.12 \pm 0.003$	SIRUNYAN	21E	CMS	pp at 13 TeV
$3.19 \pm 0.12 \pm 0.04$	SIRUNYAN	21E	CMS	Repl. by HAYRAPETYAN 26A
$3.06 {}^{+0.08}_{-0.07} \pm 0.04$	AAIJ	19Q	LHCB	Repl. by AAIJ 24A
$3.15 \pm 0.10 \pm 0.05$	AAD	16AP	ATLS	Repl. by AAD 21AE
$3.48 {}^{+0.07}_{-0.09} \pm 0.68$	KHACHATRY...	16S	CMS	pp at 8 TeV
$3.26 {}^{+0.10}_{-0.17} {}^{+0.06}_{-0.07}$	AAIJ	15I	LHCB	Repl. by AAIJ 19Q
$2.72 {}^{+1.12}_{-0.27} \pm 0.26$	ABAZOV	09E	D0	Repl. by ABAZOV 12D

[1] Measured using a time-dependent angular analysis of $B_s^0 \to J/\psi\phi$ decays with the ML-improved flavor-tagging algorithm.
[2] Measured using a time-dependent angular analysis of $B_s^0 \to J/\psi K^+ K^-$ decays.
[3] The fit found another solution with $\phi_\parallel = 2.95 \pm 0.05 \pm 0.09$ rad.
[4] The error includes both statistical and systematic uncertainties.

$\phi_\perp$ in $B_s^0 \to J/\psi(1S)\phi$

VALUE (rad)	DOCUMENT ID		TECN	COMMENT
3.00 ±0.10 OUR AVERAGE	Error includes scale factor of 1.6. See the ideogram below.			
$2.931 \pm 0.096 \pm 0.063$	[1,2] HAYRAPETY...	26A	CMS	pp at 13 TeV
$2.903 {}^{+0.075}_{-0.074} \pm 0.048$	[3] AAIJ	24A	LHCB	pp at 13 TeV
$3.22 \pm 0.10 \pm 0.05$	[4] AAD	21AE	ATLS	pp at 7, 8, 13 TeV
• • • We do not use the following data for averages, fits, limits, etc. • • •				
$2.77 \pm 0.16 \pm 0.05$	[5] SIRUNYAN	21E	CMS	pp at 13 TeV
$2.78 \pm 0.15 \pm 0.06$	[5] SIRUNYAN	21E	CMS	Repl. by HAYRAPETYAN 26A
$2.64 \pm 0.13 \pm 0.10$	AAIJ	19Q	LHCB	Repl. by AAIJ 24A
$4.15 \pm 0.32 \pm 0.16$	[5] AAD	16AP	ATLS	Repl. by AAD 21AE
$2.98 \pm 0.36 \pm 0.66$	[5] KHACHATRY...	16S	CMS	pp at 8 TeV
$3.08 {}^{+0.14}_{-0.15} \pm 0.06$	AAIJ	15I	LHCB	Repl. by AAIJ 19Q
$3.89 \pm 0.47 \pm 0.11$	[5] AAD	14U	ATLS	Repl. by AAD 16AP

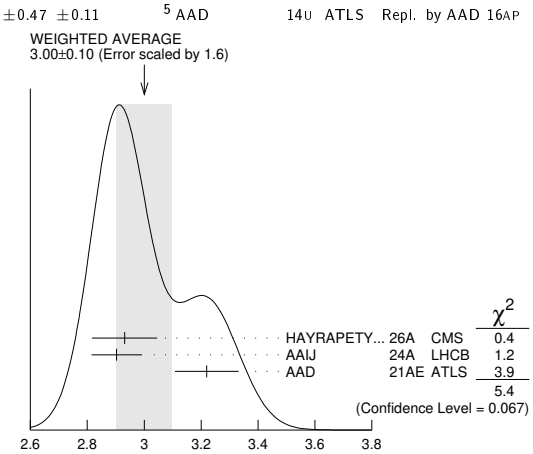

$\phi_\perp$ in $B_s^0 \to J/\psi(1S)\phi$ (rad)

[1] Measured using a time-dependent angular analysis of $B_s^0 \to J/\psi\phi$ decays with the ML-improved flavor-tagging algorithm.
[2] The difference between the P- and S-wave phases is also reported $\phi_{S_\perp} = \phi_S - \phi_\perp = 0.48^{+0.11}_{-0.16} \pm 0.07$ rad.
[3] Measured using a time-dependent angular analysis of $B_s^0 \to J/\psi K^+ K^-$ decays.
[4] The fit found another solution with $\phi_\perp = 3.03 \pm 0.05 \pm 0.09$ rad.
[5] Measured using a tagged, time-dependent angular analysis of $B_s^0 \to J/\psi\phi$ decays.

$\Gamma_\perp/\Gamma$ in $B_s^0 \to \psi(2S)\phi$

VALUE	DOCUMENT ID		TECN	COMMENT
$0.264^{+0.024}_{-0.023} \pm 0.002$	[1] AAIJ	16AK	LHCB	pp at 7, 8 TeV

[1] Measured using time-dependent angular analysis of $B_s^0 \to \psi(2S)\phi$ decays.

$\phi_\parallel$ in $B_s^0 \to \psi(2S)\phi$

VALUE (rad)	DOCUMENT ID		TECN	COMMENT
$3.67^{+0.13}_{-0.18} \pm 0.03$	[1] AAIJ	16AK	LHCB	pp at 7, 8 TeV

[1] Measured using time-dependent angular analysis of $B_s^0 \to \psi(2S)\phi$ decays.

$\phi_\perp$ in $B_s^0 \to \psi(2S)\phi$

VALUE (rad)	DOCUMENT ID		TECN	COMMENT
$3.29^{+0.43}_{-0.39} \pm 0.04$	[1] AAIJ	16AK	LHCB	pp at 7, 8 TeV

[1] Measured using time-dependent angular analysis of $B_s^0 \to \psi(2S)\phi$ decays.

Γ_L/Γ for $B_s^0 \to J/\psi(1S)\overline{K}^*(892)^0$

Longitudinal polarization fraction, equals to f_L using notation of "Polarization in B decays" review.

VALUE	DOCUMENT ID		TECN	COMMENT
$0.528 \pm 0.011 \pm 0.009$	[1] AAIJ	25AQ	LHCB	pp at 7, 8, 13 TeV
• • • We do not use the following data for averages, fits, limits, etc. • • •				
$0.534 \pm 0.012 \pm 0.009$	AAIJ	25AQ	LHCB	pp at 13 TeV
$0.497 \pm 0.025 \pm 0.025$	AAIJ	15AV	LHCB	Repl. by AAIJ 25AQ
$0.50 \pm 0.08 \pm 0.02$	[2] AAIJ	12AP	LHCB	Repl. by AAIJ 15AV

[1] Combination with measurement from AAIJ 15AV.
[2] The non-resonant $K\pi$ background contributions are subtracted. Also reports an S-wave amplitude $|A_S|^2 = 0.07^{+0.15}_{-0.07}$.

$\Gamma_\parallel/\Gamma$ for $B_s^0 \to J/\psi(1S)\overline{K}^*(892)^0$

Parallel polarization fraction, equals to $1 - f_L - f_\perp$ using notation of "Polarization in B decays" review.

VALUE	DOCUMENT ID		TECN	COMMENT
$0.205 \pm 0.012 \pm 0.005$	[1] AAIJ	25AQ	LHCB	pp at 7, 8, 13 TeV
• • • We do not use the following data for averages, fits, limits, etc. • • •				
$0.211 \pm 0.014 \pm 0.005$	AAIJ	25AQ	LHCB	pp at 13 TeV
$0.179 \pm 0.027 \pm 0.013$	AAIJ	15AV	LHCB	Repl. by AAIJ 25AQ
$0.19 \; ^{+0.10}_{-0.08} \pm 0.02$	[2] AAIJ	12AP	LHCB	Repl. by AAIJ 15AV

[1] Combination with measurement from AAIJ 15AV.
[2] The non-resonant $K\pi$ background contributions are subtracted. Also reports an S-wave amplitude $|A_S|^2 = 0.07^{+0.15}_{-0.07}$.

$\phi_\parallel$ in $B_s^0 \to J/\psi(1S)\overline{K}^*(892)^0$

VALUE	DOCUMENT ID		TECN	COMMENT
$2.879 \pm 0.085 \pm 0.018$	AAIJ	25AQ	LHCB	pp at 13 TeV

$\phi_\perp$ in $B_s^0 \to J/\psi(1S)\overline{K}^*(892)^0$

VALUE	DOCUMENT ID		TECN	COMMENT
$0.057 \pm 0.065 \pm 0.018$	AAIJ	25AQ	LHCB	pp at 13 TeV

$\Gamma_\parallel/\Gamma$ of $K^*(892)^0$ in $B_s^0 \to \psi(2S)\overline{K}^*(892)^0$

VALUE	DOCUMENT ID		TECN	COMMENT
$0.524 \pm 0.056 \pm 0.029$	AAIJ	15U	LHCB	pp at 7, 8 TeV

Γ_L/Γ in $B_s^0 \to \phi\phi$

VALUE	DOCUMENT ID		TECN	COMMENT
0.379 ± 0.008 OUR AVERAGE	Error includes scale factor of 1.2.			
$0.384 \pm 0.007 \pm 0.003$	AAIJ	23AT	LHCB	pp at 13 TeV
$0.364 \pm 0.012 \pm 0.009$	AAIJ	14AE	LHCB	pp at 7, 8 TeV
$0.348 \pm 0.041 \pm 0.021$	AALTONEN	11AN	CDF	$p\overline{p}$ at 1.96 TeV
• • • We do not use the following data for averages, fits, limits, etc. • • •				
$0.381 \pm 0.007 \pm 0.012$	AAIJ	19AP	LHCB	pp at 7, 8, partial 13 TeV
$0.365 \pm 0.022 \pm 0.012$	AAIJ	12P	LHCB	Repl. by AAIJ 14AE

$\Gamma_\perp/\Gamma$ in $B_s^0 \to \phi\phi$

VALUE	DOCUMENT ID		TECN	COMMENT
0.310 ± 0.006 OUR AVERAGE				
$0.310 \pm 0.006 \pm 0.003$	AAIJ	23AT	LHCB	pp at 13 TeV
$0.305 \pm 0.013 \pm 0.005$	AAIJ	14AE	LHCB	pp at 7, 8 TeV
$0.365 \pm 0.044 \pm 0.027$	AALTONEN	11AN	CDF	$p\overline{p}$ at 1.96 TeV
• • • We do not use the following data for averages, fits, limits, etc. • • •				
$0.290 \pm 0.008 \pm 0.005$	[1] AAIJ	19AP	LHCB	pp at 7, 8, partial 13 TeV
$0.291 \pm 0.024 \pm 0.010$	AAIJ	12P	LHCB	Repl. by AAIJ 14AE

[1] Note: in the summary of AAIJ 19AP the systematic uncertainty is 0.007. We take the systematic uncertainty as given in Table 5 in the paper.

$\phi_\parallel$ in $B_s^0 \to \phi\phi$

VALUE (rad)	DOCUMENT ID		TECN	COMMENT
2.469 ± 0.029 OUR AVERAGE				
$2.463 \pm 0.029 \pm 0.009$	AAIJ	23AT	LHCB	pp at 13 TeV
$2.54 \pm 0.07 \pm 0.09$	[1] AAIJ	14AE	LHCB	pp at 7, 8 TeV
$2.71 \; ^{+0.31}_{-0.36} \pm 0.22$	[2] AALTONEN	11AN	CDF	$p\overline{p}$ at 1.96 TeV
• • • We do not use the following data for averages, fits, limits, etc. • • •				
$2.559 \pm 0.045 \pm 0.033$	AAIJ	19AP	LHCB	pp at 7, 8, partial 13 TeV
$2.57 \pm 0.15 \pm 0.06$	[3] AAIJ	12P	LHCB	Repl. by AAIJ 14AE

[1] AAIJ 14AE reports measurement of $\phi_\perp$ and $\phi_\perp - \phi_\parallel$, which we convert into $\phi_\parallel$. Statistical uncertainty includes correlation between measured parameters, while systematic uncertainties are assumed uncorrelated.
[2] AALTONEN 11AN quotes $\cos\phi_\parallel = -0.91^{+0.15}_{-0.13} \pm 0.09$ which we convert to $\phi_\parallel$ taking the smaller solution.
[3] AAIJ 12P quotes $\cos\phi_\parallel = -0.844 \pm 0.068 \pm 0.029$ which we convert to $\phi_\parallel$, taking the smaller solution.

$\phi_\perp$ in $B_s^0 \to \phi\phi$

VALUE (rad)	DOCUMENT ID		TECN	COMMENT
2.75 ± 0.10 OUR AVERAGE				
$2.769 \pm 0.105 \pm 0.011$	AAIJ	23AT	LHCB	pp at 13 TeV
$2.67 \pm 0.23 \pm 0.07$	AAIJ	14AE	LHCB	pp at 7, 8 TeV
• • • We do not use the following data for averages, fits, limits, etc. • • •				
$2.818 \pm 0.178 \pm 0.073$	AAIJ	19AP	LHCB	pp at 7, 8, partial 13 TeV

Γ_L/Γ in $B_s^0 \to K^{*0}\overline{K}^{*0}$

VALUE	DOCUMENT ID		TECN	COMMENT
$0.240 \pm 0.031 \pm 0.025$	[1] AAIJ	19L	LHCB	pp at 7 and 8 TeV
• • • We do not use the following data for averages, fits, limits, etc. • • •				
$0.208 \pm 0.032 \pm 0.046$	[2] AAIJ	18S	LHCB	Repl. by AAIJ 19L
$0.201 \pm 0.057 \pm 0.040$	[3] AAIJ	15AF	LHCB	Repl. by AAIJ 18S
$0.31 \pm 0.12 \pm 0.04$	AAIJ	12F	LHCB	Repl. by AAIJ 15AF

[1] Untagged and time-integrated analysis within 150 MeV of the K^{*0} mass.
[2] Measured in angular analysis, which takes into account S-, P- and D-wave. contributions.
[3] Measured in angular analysis, which takes into account S-wave contributions.

$\Gamma_\perp/\Gamma$ in $B_s^0 \to K^{*0}\overline{K}^{*0}$

VALUE	DOCUMENT ID		TECN	COMMENT
$0.38 \pm 0.11 \pm 0.04$	AAIJ	12F	LHCB	pp at 7 TeV

$\Gamma_\parallel/\Gamma$ in $B_s^0 \to K^*(892)^0\overline{K}^*(892)^0$

VALUE	DOCUMENT ID		TECN	COMMENT
$0.297 \pm 0.029 \pm 0.042$	[1] AAIJ	18S	LHCB	pp at 7, 8 TeV
• • • We do not use the following data for averages, fits, limits, etc. • • •				
$0.215 \pm 0.046 \pm 0.015$	AAIJ	15AF	LHCB	Repl. by AAIJ 18S

[1] Measured in angular analysis, which takes into account S-, P- and D-wave. contributions.

$\Phi_\parallel$ in $B_s^0 \to K^*(892)^0\overline{K}^*(892)^0$

VALUE	DOCUMENT ID		TECN	COMMENT
$2.40 \pm 0.11 \pm 0.33$	[1] AAIJ	18S	LHCB	pp at 7, 8 TeV
• • • We do not use the following data for averages, fits, limits, etc. • • •				
$5.31 \pm 0.24 \pm 0.14$	AAIJ	15AF	LHCB	Repl. by AAIJ 18S

[1] Measured in angular analysis, which takes into account S-, P- and D-wave. contributions.

$\Phi_\perp$ in $B_s^0 \to K^*(892)^0\overline{K}^*(892)^0$

VALUE (rad)	DOCUMENT ID		TECN	COMMENT
$2.62 \pm 0.26 \pm 0.64$	[1] AAIJ	18S	LHCB	pp at 7, 8 TeV

[1] Measured in angular analysis, which takes into account S-, P- and D-wave. contributions.

Γ_L/Γ in $B_s^0 \to \phi\overline{K}^{*0}$

VALUE	DOCUMENT ID		TECN	COMMENT
$0.51 \pm 0.15 \pm 0.07$	AAIJ	13BW	LHCB	pp at 7 TeV

$\Gamma_\parallel/\Gamma$ in $B_s^0 \to \phi\overline{K}^{*0}$

VALUE	DOCUMENT ID		TECN	COMMENT
$0.21 \pm 0.11 \pm 0.02$	AAIJ	13BW	LHCB	pp at 7 TeV

$\phi_\parallel$ in $B_s^0 \to \phi\overline{K}^{*0}$

VALUE (rad)	DOCUMENT ID		TECN	COMMENT
$1.75 \pm 0.53 \pm 0.29$	[1] AAIJ	13BW	LHCB	pp at 7 TeV

[1] Measures $\cos(\phi_\parallel) = -0.18 \pm 0.52 \pm 0.29$, which we convert to $\phi_\parallel$ by taking the smaller solution.

Γ_L/Γ in $B_s^0 \to \overline{D}^{*0}\phi$

VALUE	DOCUMENT ID		TECN	COMMENT
$0.531 \pm 0.060 \pm 0.019$	AAIJ	23AZ	LHCB	pp at 7, 8, 13 TeV
• • • We do not use the following data for averages, fits, limits, etc. • • •				
$0.73 \pm 0.15 \pm 0.04$	AAIJ	18AY	LHCB	Repl. by AAIJ 23AZ

Γ_L/Γ in $B_s^0 \to K^*(892)^0\overline{K}_2^*(1430)^0$

VALUE	DOCUMENT ID		TECN	COMMENT
$0.911 \pm 0.020 \pm 0.165$	[1] AAIJ	18S	LHCB	pp at 7, 8 TeV

[1] Measured in angular analysis, which takes into account S-, P- and D-wave. contributions.

Int. J. Mod. Phys. A 2026.41. Downloaded from www.worldscientific.com
by UNIVERSITY OF CALIFORNIA @ BERKELEY on 09/16/26. Re-use and distribution is strictly not permitted, except for Open Access articles.

Int. J. Mod. Phys. A 2026.41. Downloaded from www.worldscientific.com
by CALIFORNIA @ BERKELEY on 09/16/26. Re-use and distribution is strictly not permitted, except for Open Access articles.

$\Gamma_{\parallel}/\Gamma$ in $B_s^0 \to K^*(892)^0 \overline{K}_2^*(1430)^0$

VALUE	DOCUMENT ID		TECN	COMMENT
0.012±0.008±0.053	[1] AAIJ	18S	LHCB	pp at 7, 8 TeV

[1] Measured in angular analysis, which takes into account S-, P- and D-wave. contributions.

Γ_L/Γ in $B_s^0 \to K_2^*(1430)^0 \overline{K}^*(892)^0$

VALUE	DOCUMENT ID		TECN	COMMENT
0.62±0.16±0.25	[1] AAIJ	18S	LHCB	pp at 7, 8 TeV

[1] Measured in angular analysis, which takes into account S-, P- and D-wave. contributions.

$\Gamma_{\parallel}/\Gamma$ in $B_s^0 \to K_2^*(1430)^0 \overline{K}^*(892)^0$

VALUE	DOCUMENT ID		TECN	COMMENT
0.24±0.10±0.14	[1] AAIJ	18S	LHCB	pp at 7, 8 TeV

[1] Measured in angular analysis, which takes into account S-, P- and D-wave. contributions.

Γ_L/Γ in $B_s^0 \to K_2^*(1430)^0 \overline{K}_2^*(1430)^0$

VALUE	DOCUMENT ID		TECN	COMMENT
0.25±0.14±0.18	[1] AAIJ	18S	LHCB	pp at 7, 8 TeV

[1] Measured in angular analysis, which takes into account S-, P- and D-wave. contributions.

$\Gamma_{\parallel 1}/\Gamma$ in $B_s^0 \to K_2^*(1430)^0 \overline{K}_2^*(1430)^0$

VALUE	DOCUMENT ID		TECN	COMMENT
0.17±0.11±0.14	[1] AAIJ	18S	LHCB	pp at 7, 8 TeV

[1] Measured in angular analysis, which takes into account S-, P- and D-wave. contributions.

$\Gamma_{\perp 1}/\Gamma$ in $B_s^0 \to K_2^*(1430)^0 \overline{K}_2^*(1430)^0$

VALUE	DOCUMENT ID		TECN	COMMENT
0.30±0.18±0.21	[1] AAIJ	18S	LHCB	pp at 7, 8 TeV

[1] Measured in angular analysis, which takes into account S-, P- and D-wave. contributions.

$\Gamma_{\parallel 2}/\Gamma$ in $B_s^0 \to K_2^*(1430)^0 \overline{K}_2^*(1430)^0$

VALUE	DOCUMENT ID		TECN	COMMENT
0.015±0.033±0.107	[1] AAIJ	18S	LHCB	pp at 7, 8 TeV

[1] Measured in angular analysis, which takes into account S-, P- and D-wave . contributions.

$F_L(B_s^0 \to \phi e^+ e^-)$ $(0.0009 < q^2 < 0.2615$ GeV$^2/c^4)$

VALUE	CL%	DOCUMENT ID		TECN	COMMENT
<0.115	90	AAIJ	25S	LHCB	pp at 7, 8 and 13 TeV

$A_T^{(2)}(B_s^0 \to \phi e^+ e^-)$ $(0.0009 < q^2 < 0.2615$ GeV$^2/c^4)$

VALUE	DOCUMENT ID		TECN	COMMENT
−0.045±0.235±0.014	AAIJ	25S	LHCB	pp at 7, 8 and 13 TeV

$A_T^{ImCP}(B_s^0 \to \phi e^+ e^-)$ $(0.0009 < q^2 < 0.2615$ GeV$^2/c^4)$

VALUE	DOCUMENT ID		TECN	COMMENT
0.002±0.247±0.016	AAIJ	25S	LHCB	pp at 7, 8 and 13 TeV

$A_T^{ReCP}(B_s^0 \to \phi e^+ e^-)$ $(0.0009 < q^2 < 0.2615$ GeV$^2/c^4)$

VALUE	DOCUMENT ID		TECN	COMMENT
0.116±0.155±0.006	AAIJ	25S	LHCB	pp at 7, 8 and 13 TeV

$F_L(B_s^0 \to \phi e^+ e^-)$ $(0.1 < q^2 < 1.1$ GeV$^2/c^4)$

VALUE	DOCUMENT ID		TECN	COMMENT
0.25±0.12±0.06	AAIJ	25AC	LHCB	pp at 7, 8, 13 TeV

$F_L(B_s^0 \to \phi e^+ e^-)$ $(1.1 < q^2 < 6.0$ GeV$^2/c^4)$

VALUE	DOCUMENT ID		TECN	COMMENT
$0.67^{+0.12}_{-0.13}$±0.06	AAIJ	25AC	LHCB	pp at 7, 8, 13 TeV

$F_L(B_s^0 \to \phi e^+ e^-)$ $(15.0 < q^2 < 19.0$ GeV$^2/c^4)$

VALUE	DOCUMENT ID		TECN	COMMENT
$0.43^{+0.11}_{-0.10}$±0.05	AAIJ	25AC	LHCB	pp at 7, 8, 13 TeV

$F_L(B_s^0 \to \phi \mu^+ \mu^-)$ $(0.10 < q^2 < 2.00$ GeV$^2/c^4)$

VALUE	DOCUMENT ID		TECN	COMMENT
$0.20^{+0.08}_{-0.09}$±0.02	AAIJ	15AQ	LHCB	pp at 7, 8 TeV
• • • We do not use the following data for averages, fits, limits, etc. • • •				
$0.37^{+0.19}_{-0.17}$±0.07	AAIJ	13X	LHCB	Repl. by AAIJ 15AQ

$F_L(B_s^0 \to \phi \mu^+ \mu^-)$ $(2.00 < q^2 < 5.0$ GeV$^2/c^4)$

VALUE	DOCUMENT ID		TECN	COMMENT
$0.68^{+0.16}_{-0.13}$±0.03	AAIJ	15AQ	LHCB	pp at 7, 8 TeV
• • • We do not use the following data for averages, fits, limits, etc. • • •				
$0.53^{+0.25}_{-0.23}$±0.10	[1] AAIJ	13X	LHCB	Repl. by AAIJ 15AQ

[1] Measured in $2.0 < q^2 < 4.3$ GeV$^2/c^4$.

$F_L(B_s^0 \to \phi \mu^+ \mu^-)$ $(5.0 < q^2 < 8.0$ GeV$^2/c^4)$

VALUE	DOCUMENT ID		TECN	COMMENT
$0.54^{+0.10}_{-0.09}$±0.02	AAIJ	15AQ	LHCB	pp at 7, 8 TeV
• • • We do not use the following data for averages, fits, limits, etc. • • •				
$0.81^{+0.11}_{-0.13}$±0.05	[1] AAIJ	13X	LHCB	Repl. by AAIJ 15AQ

[1] Measured in $4.3 < q^2 < 8.68$ GeV$^2/c^4$.

$F_L(B_s^0 \to \phi \mu^+ \mu^-)$ $(11.0 < q^2 < 12.5$ GeV$^2/c^4)$

VALUE	DOCUMENT ID		TECN	COMMENT
0.29±0.11±0.04	AAIJ	15AQ	LHCB	pp at 7, 8 TeV
• • • We do not use the following data for averages, fits, limits, etc. • • •				
$0.33^{+0.14}_{-0.12}$±0.06	[1] AAIJ	13X	LHCB	Repl. by AAIJ 15AQ

[1] Measured in $10.09 < q^2 < 12.90$ GeV$^2/c^4$.

$F_L(B_s^0 \to \phi \mu^+ \mu^-)$ $(15.0< q^2 < 17.0$ GeV$^2/c^4)$

VALUE	DOCUMENT ID		TECN	COMMENT
$0.23^{+0.09}_{-0.08}$±0.02	AAIJ	15AQ	LHCB	pp at 7, 8 TeV
• • • We do not use the following data for averages, fits, limits, etc. • • •				
$0.34^{+0.18}_{-0.17}$±0.07	[1] AAIJ	13X	LHCB	Repl. by AAIJ 15AQ

[1] Measured in $14.18 < q^2 < 16$ GeV$^2/c^4$.

$F_L(B_s^0 \to \phi \mu^+ \mu^-)$ $(17.0 < q^2 < 19.0$ GeV$^2/c^4)$

VALUE	DOCUMENT ID		TECN	COMMENT
$0.40^{+0.13}_{-0.15}$±0.02	AAIJ	15AQ	LHCB	pp at 7, 8 TeV
• • • We do not use the following data for averages, fits, limits, etc. • • •				
$0.16^{+0.17}_{-0.10}$±0.07	[1] AAIJ	13X	LHCB	Repl. by AAIJ 15AQ

[1] Measured in $16.0 < q^2 < 19.0$ GeV$^2/c^4$.

$F_L(B_s^0 \to \phi \mu^+ \mu^-)$ $(15.0 < q^2 < 18.9$ GeV$^2/c^4)$

VALUE	DOCUMENT ID		TECN	COMMENT
0.359±0.031±0.019	AAIJ	21AK	LHCB	pp at 7, 8, 13 TeV

$F_L(B_s^0 \to \phi \mu^+ \mu^-)$ $(1.00 < q^2 < 6.00$ GeV$^2/c^4)$

VALUE	DOCUMENT ID		TECN	COMMENT
0.715±0.036±0.013	AAIJ	21AK	LHCB	pp at 7, 8, 13 TeV
• • • We do not use the following data for averages, fits, limits, etc. • • •				
$0.63\ ^{+0.09}_{-0.09}$ ±0.03	AAIJ	15AQ	LHCB	Repl. by AAIJ 21AK
$0.56\ ^{+0.17}_{-0.16}$ ±0.09	AAIJ	13X	LHCB	Repl. by AAIJ 15AQ

B_s^0-$\overline{B}_s^0$ MIXING

For a discussion of B_s^0-$\overline{B}_s^0$ mixing see the note on "B^0-$\overline{B}^0$ Mixing" in the B^0 Particle Listings above.

χ_s is a measure of the time-integrated B_s^0-$\overline{B}_s^0$ mixing probability that produced $B_s^0(\overline{B}_s^0)$ decays as a $\overline{B}_s^0(B_s^0)$. Mixing violates $\Delta B \neq 2$ rule.

$$\chi_s = \frac{x_s^2}{2(1+x_s^2)}$$

$$x_s = \frac{\Delta m_{B_s^0}}{\Gamma_{B_s^0}} = (m_{B_{sH}^0} - m_{B_{sL}^0})\,\tau_{B_s^0}\ ,$$

where H, L stand for heavy and light states of two B_s^0 CP eigenstates and $\tau_{B_s^0} = \frac{1}{0.5(\Gamma_{B_{sH}^0}+\Gamma_{B_{sL}^0})}$.

$\Delta m_{B_s^0} = m_{B_{sH}^0} - m_{B_{sL}^0}$

$\Delta m_{B_s^0}$ is a measure of 2π times the B_s^0-$\overline{B}_s^0$ oscillation frequency in time-dependent mixing experiments.

VALUE ($10^{12}\ \hbar\ s^{-1}$)	CL%	DOCUMENT ID		TECN	COMMENT
17.766 ±0.006 OUR EVALUATION (Produced by HFLAV)					
17.765 ±0.005 OUR AVERAGE					
17.757 ±0.040 ±0.023		[1] HAYRAPETY...	26A	CMS	pp at 13 TeV
17.743 ±0.033 ±0.009		[2] AAIJ	24A	LHCB	pp at 13 TeV
17.7683±0.0051±0.0032		[3] AAIJ	22B	LHCB	pp at 13 TeV
17.757 ±0.007 ±0.008		[4] AAIJ	21M	LHCB	pp at 7, 8, 13 TeV
17.768 ±0.023 ±0.006		[3] AAIJ	13BI	LHCB	pp at 7 TeV
17.93 ±0.22 ±0.15		[5] AAIJ	13CF	LHCB	pp at 7 TeV
17.77 ±0.10 ±0.07		[6] ABULENCIA,A	06G	CDF	$p\overline{p}$ at 1.96 TeV
• • • We do not use the following data for averages, fits, limits, etc. • • •					
17.51 $^{+0.10}_{-0.09}$ ±0.03		[7] SIRUNYAN	21E	CMS	Repl. by HAYRAPETYAN 26A
17.703 ±0.059 ±0.018		[2] AAIJ	19Q	LHCB	Repl. by AAIJ 24A

$17.711\ ^{+0.055}_{-0.057}\ \pm0.011$	[2] AAIJ	15I	LHCB	Repl. by AAIJ 19Q
$17.63\ \pm0.11\ \pm0.02$	[8] AAIJ	12I	LHCB	Repl. by AAIJ 21M
17–21 90	[9] ABAZOV	06B	D0	$p\overline{p}$ at 1.96 TeV
$17.31\ ^{+0.33}_{-0.18}\ \pm0.07$	[10] ABULENCIA	06Q	CDF	Repl. by ABULENCIA,A 06G
> 8.0 95	[11] ABDALLAH	04J	DLPH	$e^+e^- \to Z^0$
> 4.9 95	[12] ABDALLAH	04J	DLPH	$e^+e^- \to Z^0$
> 8.5 95	[13] ABDALLAH	04J	DLPH	$e^+e^- \to Z^0$
> 5.0 95	[14] ABDALLAH	03B	DLPH	$e^+e^- \to Z$
>10.3 95	[15] ABE	03	SLD	$e^+e^- \to Z$
>10.9 95	[16] HEISTER	03E	ALEP	$e^+e^- \to Z$
> 5.3 95	[17] ABE	02V	SLD	$e^+e^- \to Z$
> 1.0 95	[18] ABBIENDI	01D	OPAL	$e^+e^- \to Z$
> 7.4 95	[19] ABREU	00Y	DLPH	Repl. by ABDALLAH 04J
> 4.0 95	[20] ABREU,P	00G	DLPH	$e^+e^- \to Z$
> 5.2 95	[21] ABBIENDI	99S	OPAL	$e^+e^- \to Z$
<96 95	[22] ABE	99D	CDF	$p\overline{p}$ at 1.8 TeV
> 5.8 95	[23] ABE	99J	CDF	$p\overline{p}$ at 1.8 TeV
> 9.6 95	[24] BARATE	99J	ALEP	$e^+e^- \to Z$
> 7.9 95	[25] BARATE	98C	ALEP	Repl. by BARATE 99J
> 3.1 95	[26] ACKERSTAFF	97U	OPAL	Repl. by ABBIENDI 99S
> 2.2 95	[27] ACKERSTAFF	97V	OPAL	Repl. by ABBIENDI 99S
> 6.5 95	[28] ADAM	97	DLPH	Repl. by ABREU 00Y
> 6.6 95	[29] BUSKULIC	96M	ALEP	Repl. by BARATE 98C
> 2.2 95	[27] AKERS	95J	OPAL	Sup. by ACKERSTAFF 97V
> 5.7 95	[30] BUSKULIC	95J	ALEP	$e^+e^- \to Z$
> 1.8 95	[27] BUSKULIC	94B	ALEP	$e^+e^- \to Z$

[1] Measured using a time-dependent angular analysis of $B_s^0 \to J/\psi\phi$ decays with the ML-improved flavor-tagging algorithm.

[2] Measured using time-dependent angular analysis of $B_s^0 \to J/\psi K^+K^-$ decays.

[3] Measured using $B_s^0 \to D_s^-\pi^+$ decays.

[4] Measured using $B_s^0 \to D_s^-\pi^+\pi^-\pi^+$ decays.

[5] Measured using $B_s^0 \to D_s^-\mu^+\nu_\mu X$ decays.

[6] Significance of oscillation signal is 5.4 σ. Also reports $|V_{td}\ /\ V_{ts}| = 0.2060 \pm 0.0007\ ^{+0.0081}_{-0.0060}$.

[7] Measured using time-dependent angular analysis of $B_s^0 \to J/\psi\phi$ decays.

[8] Measured using $B_s^0 \to D_s^-\pi^+$ and $D_s^-\pi^+\pi^-\pi^+$ decays.

[9] A likelihood scan over the oscillation frequency, Δm_s, gives a most probable value of 19 ps^{-1} and a range of 17< Δm_s <21 (ps^{-1}) at 90% C.L. assuming Gaussian uncertainties. Also excludes Δm_s <14.8 ps^{-1} at 95% C.L

[10] Significance of oscillation signal is 0.2%. Also reported the value $|V_{td}\ /\ V_{ts}| = 0.208\ ^{+0.001}_{-0.002}\ ^{+0.008}_{-0.006}$.

[11] Uses leptons emitted with large momentum transverse to a jet and improved techniques for vertexing and flavor-tagging.

[12] Updates of D_s-lepton analysis.

[13] Combined results from all Delphi analyses.

[14] Events with a high transverse momentum lepton were removed and an inclusively reconstructed vertex was required.

[15] ABE 03 uses the novel "charge dipole" technique to reconstruct separate secondary and tertiary vertices originating from the $B \to D$ decay chain. The analysis excludes Δm_s <4.9 ps^{-1} and 7.9< Δm_s <10.3 ps^{-1}.

[16] Three analyses based on complementary event selections: (1) fully-reconstructed hadronic decays; (2) semileptonic decays with D_s exclusively reconstructed; (3) inclusive semileptonic decays.

[17] ABE 02V uses exclusively reconstructed D_s^- mesons and excludes Δm_s <1.4 ps^{-1} and 2.4< Δm_s <5.3 ps^{-1} at 95%CL.

[18] Uses fully or partially reconstructed $D_s\ell$ vertices and a mixing tag as a flavor tagging.

[19] Replaced by ABDALLAH 04A. Uses $D_s^-\ell^+$, and $\phi\ell^+$ vertices, and a multi-variable discriminant as a flavor tagging.

[20] Uses inclusive D_s vertices and fully reconstructed B_s decays and a multi-variable discriminant as a flavor tagging.

[21] Uses ℓ-$Q_{\rm hem}$ and ℓ-ℓ.

[22] ABE 99D assumes $\tau_{B_s^0}$= 1.55 ± 0.05 ps and $\Delta\Gamma/\Delta m$= (5.6 ± 2.6) × 10^{-3}.

[23] ABE 99J uses ϕ ℓ-ℓ correlation.

[24] BARATE 99J uses combination of an inclusive lepton and D_s^--based analyses.

[25] BARATE 98C combines results from $D_s h$-$\ell/Q_{\rm hem}$, $D_s h$-K in the same side, $D_s\ell$-$\ell/Q_{\rm hem}$ and $D_s\ell$-K in the same side.

[26] Uses ℓ-$Q_{\rm hem}$.

[27] Uses ℓ-ℓ.

[28] ADAM 97 combines results from $D_s\ell$-$Q_{\rm hem}$, ℓ-$Q_{\rm hem}$, and ℓ-ℓ.

[29] BUSKULIC 96M uses D_s lepton correlations and lepton, kaon, and jet charge tags.

[30] BUSKULIC 95J uses ℓ-$Q_{\rm hem}$. They find Δm_s > 5.6 [> 6.1] for f_s=10% [12%]. We interpolate to our central value f_s=10.5%.

$x_s = \Delta m_{B_s^0}/\Gamma_{B_s^0}$

Derived from the results on $\Delta m_{B_s^0}$ and "OUR EVALUATION" of the B_s^0 mean lifetime.

VALUE	DOCUMENT ID
26.91±0.11 OUR EVALUATION	(Produced by HFLAV)

χ_s

This is a B_s^0-$\overline{B}_s^0$ integrated mixing parameter derived from x_s above and OUR EVALUATION of $\Delta\Gamma_{B_s^0}/\Gamma_{B_s^0}$.

VALUE	DOCUMENT ID
0.499313±0.000006 OUR EVALUATION	(Produced by HFLAV)

CP VIOLATION PARAMETERS in B_s^0

$\mathrm{Re}(\epsilon_{B_s^0})\ /\ (1 + |\epsilon_{B_s^0}|^2)$

CP impurity in B_s^0 system.

"OUR EVALUATION" is the result of a fit to B_d and B_s *CP* asymmetries, which includes the B_s measurements listed below and the B_d measurements listed in the B_d section, and takes into account correlations between those measurements.

VALUE (units 10^{-3})	DOCUMENT ID		TECN	COMMENT
−0.15±0.70 OUR EVALUATION	(Produced by HFLAV)			
0.0 ±1.1 OUR AVERAGE	Error includes scale factor of 1.6. See the ideogram below.			
0.98±0.65±0.5	[1] AAIJ	16G	LHCB	pp at 7, 8 TeV
−2.15±1.85	[2] ABAZOV	14	D0	$p\overline{p}$ at 1.96 TeV
−2.8 ±1.9 ±0.4	[3] ABAZOV	13	D0	$p\overline{p}$ at 1.96 TeV
• • • We do not use the following data for averages, fits, limits, etc. • • •				
−0.15±1.25±0.90	[4] AAIJ	14D	LHCB	Repl. by AAIJ 16G
−4.5 ±2.7	[5] ABAZOV	11U	D0	Repl. by ABAZOV 14
−0.4 ±2.3 ±0.4	[6] ABAZOV	10E	D0	Repl. by ABAZOV 13
−3.6 ±1.9	[7] ABAZOV	10H	D0	Repl. by ABAZOV 11U
6.1 ±4.8 ±0.9	[8] ABAZOV	07A	D0	Repl. by ABAZOV 10E

[1] AAIJ 16G reports a measurement of time-integrated flavor-specific asymmetry in $B_s^0 \to \mu^+D_s^-X$ decays, A^s_{SL} = (0.39 ± 0.26 ± 0.20)%, which is approximately equal to 4 × $\mathrm{Re}(\epsilon_{B_s^0})\ /\ (1 + |\epsilon_{B_s^0}|^2)$.

[2] ABAZOV 14 uses the dimuon charge asymmetry with different impact parameters from which it reports A^s_{SL} = (−0.86 ± 0.74) × 10^{-2}.

[3] ABAZOV 13 reports a measurement of time-integrated flavor-specific asymmetry in mixed semileptonic $B_s^0 \to \mu^+D_s^-X$ decays A^s_{SL} = (−1.12 ± 0.74 ± 0.17)% which is approximately equal to 4 × $\mathrm{Re}(\epsilon_{B_s^0})\ /\ (1 + |\epsilon_{B_s^0}|^2)$.

[4] AAIJ 14D reports a measurement of time-integrated flavor-specific asymmetry in $B_s^0 \to \mu^+D_s^-X$ decays, A^s_{SL} = (−0.06 ± 0.50 ± 0.36)%, which is approximately equal to4 × $\mathrm{Re}(\epsilon_{B_s^0})\ /\ (1 + |\epsilon_{B_s^0}|^2)$.

[5] ABAZOV 11U uses the dimuon charge asymmetry with different impact parameters from which it reports A^s_{SL} = (−18.1 ± 10.6) × 10^{-3}.

[6] ABAZOV 10E reports a measurement of flavor-specific asymmetry in $B^0_{(s)} \to \mu^+D^{*-}_{(s)}X$ decays with a decay-time analysis including initial-state flavor tagging, A^s_{SL} = (−1.7 ± 9.1 $^{+1.4}_{-1.5}$) × 10^{-3} which is approximately equal to 4 × $\mathrm{Re}(\epsilon_{B_s^0})\ /\ (1 + |\epsilon_{B_s^0}|^2)$.

[7] ABAZOV 10H reports a measurement of like-sign dimuon charge asymmetry of A^s_{SL} = (−9.57 ± 2.51 ± 1.46) × 10^{-3} in semileptonic b-hadron decays. Using the measured production ratio of B_d^0 and B_0^0, and the asymmetry of B_d^0 A^s_{SL} = (−4.7 ± 4.6) × 10^{-3} measured from B-factories, they obtain the asymmetry for B_s^0.

[8] The first direct measurement of the time integrated flavor untagged charge asymmetry in semileptonic B_s^0 decays is reported as 2 × A^s_{SL}(untagged) = A^s_{SL} = (2.45 ± 1.93 ± 0.35) × 10^{-2}.

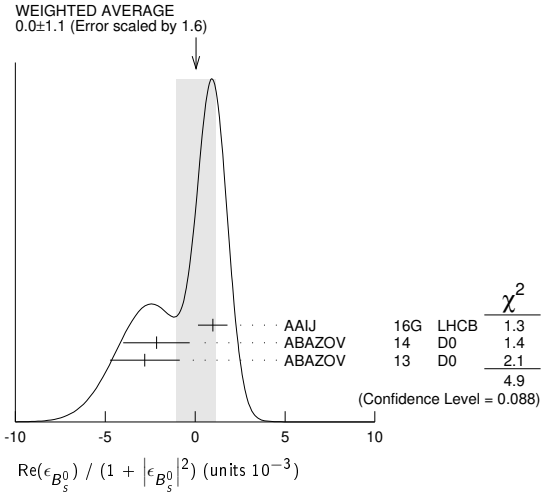

Int. J. Mod. Phys. A 2026.41. Downloaded from www.worldscientific.com
by UNIVERSITY OF CALIFORNIA @ BERKELEY on 09/16/26. Re-use and distribution is strictly not permitted, except for Open Access articles.

Int. J. Mod. Phys. A 2026.41. Downloaded from www.worldscientific.com by CALIFORNIA @ BERKELEY on 09/16/26. Re-use and distribution is strictly not permitted, except for Open Access articles.

$C_{KK}(B_s^0 \to K^+K^-)$

VALUE	DOCUMENT ID		TECN	COMMENT
0.162±0.035 OUR AVERAGE				
0.164±0.034±0.014	AAIJ	21O	LHCB	pp at 13 TeV
0.14 ±0.11 ±0.03	AAIJ	13BO	LHCB	pp at 7 TeV

$S_{KK}(B_s^0 \to K^+K^-)$

VALUE	DOCUMENT ID		TECN	COMMENT
0.14 ±0.05 OUR AVERAGE	Error includes scale factor of 1.3.			
0.123±0.034±0.015	AAIJ	21O	LHCB	pp at 13 TeV
0.30 ±0.12 ±0.04	AAIJ	13BO	LHCB	pp at 7 TeV

$r_B(B_s^0 \to D_s^\mp K^\pm)$

r_B and δ_B are the amplitude ratio and relative strong phase between the amplitudes of $A(B_s^0 \to D_s^+ K^-)$ and $A(B_s^0 \to D_s^- K^+)$,

VALUE	DOCUMENT ID		TECN	COMMENT
$\mathbf{0.318^{+0.034}_{-0.033}}$	[1,2] AAIJ	25T	LHCB	pp at 7, 8, 13 TeV
• • • We do not use the following data for averages, fits, limits, etc. • • •				
$0.327^{+0.039}_{-0.037}$	[1] AAIJ	25T	LHCB	$p\,p$ at 13 TeV
$0.37\ ^{+0.10}_{-0.09}$	[3] AAIJ	18U	LHCB	pp at 7, 8 TeV
$0.53\ ^{+0.17}_{-0.16}$	[4] AAIJ	14BF	LHCB	Repl. by AAIJ 18U

[1] Measured in $B_s^0 \to D_s^\mp K^\pm$ decays, constraining $-2\beta_s$ by the measurement of $\phi_s = -0.031 \pm 0.018$ rad. The value is modulo 180°.
[2] Combines the result with that of AAIJ 18U, for which the values of the nuisance parameters Δm_s, Γ_s and $\Delta\Gamma_s$ have been re-evaluated and the related systematic uncertainties updated.
[3] Measured in $B_s^0 \to D_s^\mp K^\pm$ decays, constraining $-2\beta_s$ by the measurement of $\phi_s = -0.030 \pm 0.033$ from HFLAV.
[4] Measured in $B_s^0 \to D_s^\mp K^\pm$ decays, constraining $-2\beta_s$ by the measurement of $\phi_s = 0.01 \pm 0.07 \pm 0.0$ from AAIJ 13AR. At 68% CL.

$r_B(B_s^0 \to D_s^\mp K^\pm \pi^\pm \pi^\mp)$

VALUE	DOCUMENT ID		TECN	COMMENT
$\mathbf{0.47\pm0.08^{+0.02}_{-0.03}}$	[1,2] AAIJ	21M	LHCB	pp at 7, 8, 13 TeV

[1] Measured in restricted phase space with $m(K^+\pi^+\pi^-) < 1950$ MeV, $m(K^+\pi^-) < 1200$ MeV and $m(\pi^+\pi^-) < 1200$ MeV.
[2] A model-independent coherence factor for the decay $B_s \to D_s K\pi\pi$ (in the restricted phase space region) is also reported.

$\delta_B(B_s^0 \to D_s^\pm K^\mp)$

VALUE (°)	DOCUMENT ID		TECN	COMMENT
347.6± 6.3	[1,2] AAIJ	25T	LHCB	pp at 7, 8, 13 TeV
• • • We do not use the following data for averages, fits, limits, etc. • • •				
$346.9^{+\ 6.8}_{-\ 6.6}$	[1] AAIJ	25T	LHCB	$p\,p$ at 13 TeV
$358\ ^{+13}_{-14}$	[3] AAIJ	18U	LHCB	pp at 7, 8 TeV
$3\ ^{+19}_{-20}$	[4] AAIJ	14BF	LHCB	Repl. by AAIJ 18U

[1] Measured in $B_s^0 \to D_s^\mp K^\pm$ decays, constraining $-2\beta_s$ by the measurement of $\phi_s = -0.031 \pm 0.018$ rad. The value is modulo 180°.
[2] Combines the result with that of AAIJ 18U, for which the values of the nuisance parameters Δm_s, Γ_s and $\Delta\Gamma_s$ have been re-evaluated and the related systematic uncertainties updated.
[3] Measured in $B_s^0 \to D_s^\mp K^\pm$ decays, constraining $-2\beta_s$ by the measurement of $\phi_s = 0.030 \pm 0.033$ from HFLAV. The value is modulo 180°.
[4] Measured in $B_s^0 \to D_s^\mp K^\pm$ decays, constraining $-2\beta_s$ by the measurement of $\phi_s = 0.01 \pm 0.07 \pm 0.0$ from AAIJ 13AR. The value is modulo 180° at 68% CL.

$\delta_B(B_s^0 \to D_s^\pm K^\mp \pi^\pm \pi^\mp)$

VALUE (°)	DOCUMENT ID		TECN	COMMENT
$\mathbf{-6^{+10+2}_{-12-4}}$	[1,2] AAIJ	21M	LHCB	pp at 7, 8, 13 TeV

[1] Measured in restricted phase space with $m(K^+\pi^+\pi^-) < 1950$ MeV, $m(K^+\pi^-) < 1200$ MeV and $m(\pi^+\pi^-) < 1200$ MeV. The value is modulo 180°.
[2] A model-independent coherence factor for the decay $B_s \to D_s K\pi\pi$ (in the restricted phase space region) is also reported.

CP Violation phase β_s ($b \to c\bar{c}s$)

$-2\beta_s$ is the weak phase difference between B_s^0 mixing amplitude and the $B_s^0 \to J/\psi\phi$ decay amplitude driven by the $b \to c\bar{c}s$ transition (such as $B_s \to J/\psi\phi$, $J/\psi K^+K^-$, $J/\psi\pi^+\pi^-$, and $D_s^+D_s^-$). The Standard Model value of β_s is $\arg(-\frac{V_{ts}V_{tb}^*}{V_{cs}V_{cb}^*})$ if penguin contributions are neglected.

VALUE (10^{-2} rad)	DOCUMENT ID		TECN	COMMENT
2.7 ± 0.7 OUR EVALUATION	(Produced by HFLAV)			
2.5 ± 0.7 OUR AVERAGE				
3.65± 1.10±0.50	[1,2] HAYRAPETY...	26A	CMS	pp at 13 TeV
4.3 ± 5.3 ±1.4	[3] AAIJ	25A	LHCB	pp at 13 TeV
1.9 ± 1.1 ±0.3	[4] AAIJ	24A	LHCB	pp at 13 TeV
4.05± 2.05±1.10	[5,6] AAD	21AE	ATLS	pp at 13 TeV
0 ±14 ±4	[7] AAIJ	21AN	LHCB	pp at 7, 8 TeV
2.85± 3.00±0.55	[8,9] AAIJ	19AF	LHCB	pp at 13 TeV
− 5.95± 5.35±1.70	[10] AAIJ	17V	LHCB	pp at 7, 8 TeV
5.05± 4.10±2.10	[11,12] AAD	16AP	ATLS	pp at 8 TeV
$-11.5\ ^{+14}_{-14.5}$ ±1	[13] AAIJ	16AK	LHCB	pp at 7, 8 TeV
3.75± 4.85±1.55	[14] KHACHATRY...	16S	CMS	pp at 8 TeV
2.9 ± 2.5 ±0.3	[15] AAIJ	15I	LHCB	pp at 7, 8 TeV
− 6 ±13 ±3	[16] AAD	14U	ATLS	pp at 7 TeV
− 1 ± 9 ±1	[17] AAIJ	14AY	LHCB	pp at 7, 8 TeV
− 3.5 ± 3.4 ±0.4	[18] AAIJ	14S	LHCB	pp at 7, 8 TeV
	[19] AALTONEN	12AJ	CDF	$p\overline{p}$ at 1.96 TeV
$28\ ^{+18}_{-19}$	[20] ABAZOV	12D	D0	$p\overline{p}$ at 1.96 TeV
• • • We do not use the following data for averages, fits, limits, etc. • • •				
0.5 ± 2.5 ±0.5	[21,22] SIRUNYAN	21E	CMS	Repl. by HAYRAPETYAN 26A
4.15± 2.05±0.30	[23] AAIJ	19Q	LHCB	Repl. by AAIJ 24A
5.0 ± 6.5 ±7.0	[24] AAIJ	18S	LHCB	pp at 7, 8 TeV
$6\ ^{+\ 8}_{-\ 7}$	[25,26] AAIJ	15K	LHCB	pp at 7, 8 TeV
− 0.5 ± 3.5 ±0.5	[27] AAIJ	13AR	LHCB	Repl. by AAIJ 15I
−11.0 ±20.5 ±5.0	[28] AAD	12CV	ATLS	Repl. by AAD 14U
22 ±22 ±1	[29] AAIJ	12B	LHCB	Repl. by AAIJ 12Q
− 8 ± 9 ±3	[30] AAIJ	12D	LHCB	Repl. by AAIJ 13AR
$0.95^{+\ 8.70+0.15}_{-\ 8.65-0.20}$	[31] AAIJ	12Q	LHCB	Repl. by AAIJ 13AR
	[32] AALTONEN	12D	CDF	Repl. by AALTONEN 12AJ
	[33] AALTONEN	08G	CDF	Repl. by AALTONEN 12D
$28\ ^{+12}_{-15}\ ^{+4}_{-1}$	[20,34] ABAZOV	08AM	D0	Repl. by ABAZOV 12D
$39.5\ \pm28.0\ ^{+0.5}_{-7.0}$	[35,36] ABAZOV	07	D0	Repl. by ABAZOV 07N
$35\ ^{+20}_{-24}$	[36,37] ABAZOV	07N	D0	Repl. by ABAZOV 08AM

[1] HAYRAPETYAN 26A measured $\phi_s = -2\,\beta_s = (-7.3 \pm 2.2 \pm 1.0) \times 10^{-2}$ rad. using a time-dependent angular analysis of $B_s^0 \to J/\psi\phi$ decays with the ML-improved flavor-tagging algorithm.
[2] Reports a combination of $\beta_s = (3.70 \pm 1.15) \times 10^{-2}$ rad with KHACHATRYAN 16S.
[3] AAIJ 25A reports $\phi_s = -2\,\beta_s = -0.086 \pm 0.106 \pm 0.028$ rad. in a time-dependent fit to $B_s^0 \to D_s^+D_s^-$, while allowing *CP* violation in decay.
[4] AAIJ 19Q reports $\phi_s = -2\,\beta_s = -0.039 \pm 0.022 \pm 0.006$ rad. measured using a time-dependent angular analysis of $B_s^0 \to J/\psi K^+K^-$ decays.
[5] Reports a combination of $0.0435 \pm 0.0180 \pm 0.0105$ with AAD 16AP.
[6] AAD 21AE measured $\phi_s = -2\,\beta_s = -0.087 \pm 0.036 \pm 0.021$ rad. using a time-dependent angular analysis of $B_s^0 \to J/\psi\phi$ decays.
[7] AAIJ 21AN measured $\phi_s = -2\beta_s = 0.00 \pm 0.28 \pm 0.07$ rad, using a time-dependent angular analysis of $B_s^0 \to J/\psi\phi$ decays with $J/\psi \to e^+e^-$.
[8] Reports a combination of $-0.001 \pm 0.022 \pm 0.006$ with AAIJ 14S.
[9] AAIJ 19AF reports $\phi_s = -2\,\beta_s = 0.002 \pm 0.044 \pm 0.012$ rad. and $|\lambda| = 0.949 \pm 0.036 \pm 0.019$, when direct *CP* violation is allowed. Measured using a time-dependent fit to $B_s^0 \to J/\psi\pi^+\pi^-$ decays.
[10] Measured $\phi_s = -2\,\beta_s = 0.119 \pm 0.107 \pm 0.034$ rad using time-dependent angular analysis of $B_s^0 \to J/\psi K^+K^-$ in the region $m(KK) > 1.05$ GeV.
[11] Reports a combination of $0.0435 \pm 0.0180 \pm 0.0105$ with AAD 14U.
[12] AAD 16AP reports $\phi_s = -2\,\beta_s = -0.090 \pm 0.078 \pm 0.041$ rad. that was measured using a time-dependent angular analysis of $B_s^0 \to J/\psi\phi$ decays.
[13] AAIJ 16AK reports $\phi_s = -2\,\beta_s = 0.23^{+0.29}_{-0.28} \pm 0.02$ rad. that was measured using a time-dependent angular analysis of $B_s^0 \to \psi(2S)\phi$ decays.
[14] KHACHATRYAN 16S reports $\phi_s = -2\,\beta_s = -0.075 \pm 0.097 \pm 0.031$ rad. that was measured using a time-dependent angular analysis of $B_s^0 \to J/\psi\phi$ decays.
[15] AAIJ 15I reports $\phi_s = -2\,\beta_s = -0.058 \pm 0.049 \pm 0.006$ rad. that was measured using a time-dependent angular analysis of $B_s^0 \to J/\psi K^+K^-$ decays. It also combines this result with that of AAIJ 14S and quotes $\phi_s = -2\,\beta_s = -0.010 \pm 0.039$ rad.
[16] AAD 14U reports $\phi_s = -2\,\beta_s = 0.12 \pm 0.25 \pm 0.05$ rad. that was measured using a time-dependent angular analysis of $B_s^0 \to J/\psi\phi$ decays.
[17] AAIJ 14AY reports $\phi_s = -2\,\beta_s = 0.02 \pm 0.17 \pm 0.02$ rad. in a time-dependent fit to $B_s^0 \to D_s^+D_s^-$, while allowing *CP* violation in decay.
[18] AAIJ 14S reports $\phi_s = -2\,\beta_s = 0.070 \pm 0.068 \pm 0.008$ rad. and $|\lambda| = 0.89 \pm 0.05 \pm 0.01$, when direct *CP* violation is allowed. Measured using a time-dependent fit to $B_s^0 \to J/\psi\pi^+\pi^-$ decays.
[19] AALTONEN 12AJ reports $-\pi/2 < \beta_s < -1.51$ or $-0.06 < \beta_s < 0.30$, or $1.26 < \beta_s < \pi/2$ rad. at 68% CL. Measured using the time-dependent angular analysis of $B_s^0 \to J/\psi\phi$ decays.
[20] ABAZOV 12D reports $\phi_s = -2\,\beta_s = -0.55^{+0.38}_{-0.36}$ rad. that was measured using a time-dependent angular analysis of $B_s^0 \to J/\psi\phi$ decays. A single error includes both statistical and systematic uncertainties.
[21] Reports a combination of $0.0105 \pm 0.0220 \pm 0.0050$ with KHACHATRYAN 16S.
[22] SIRUNYAN 21E measured $\phi_s = -2\,\beta_s = -0.021 \pm 0.044 \pm 0.010$ rad. using a time-dependent angular analysis of $B_s^0 \to J/\psi\phi$ decays.
[23] AAIJ 19Q reports $\phi_s = -2\,\beta_s = -0.083 \pm 0.041 \pm 0.006$ rad. that was measured using a time-dependent angular analysis of $B_s^0 \to J/\psi K^+K^-$ decays.

[24] AAIJ 18S reports $\phi_s = -2\,\beta_s = -0.10 \pm 0.13 \pm 0.14$ rad measured in $B^0_s \to (K^+\pi^-)(K^-\pi^+)$ in the region $0.75 < m(K^\pm\pi^\mp) < 1.6$ GeV. This is a $b \to d\overline{d}s$ transition with a decay amplitude phase different from that of $b \to c\overline{c}s$ transition.

[25] AAIJ 15K reports $-2\beta_s = -0.12^{+0.14}_{-0.16}$ rad. The value was obtained by measuring time-dependent *CP* asymmetry in $B^0_s \to K^+K^-$ and using a U-spin relation between $B^0_s \to K^+K^-$ and $B^0 \to \pi^+\pi^-$.

[26] Results are also presented using additional inputs on $B^0 \to \pi^0\pi^0$ and $B^+ \to \pi^+\pi^0$ decays from other experiments and isospin symmetry assumptions. The dependence of the results on the maximum allowed amount of U-spin breaking up to 50% is also included.

[27] AAIJ 13AR reports $\phi_s = -2\beta_s = 0.01 \pm 0.07 \pm 0.01$ rad. obtained from combined fit to $B^0_s \to J/\psi K^+K^-$ and $B^0_s \to J/\psi\pi^+\pi^-$ data sets. Also reports separate results of $\phi_s = 0.07 \pm 0.09 \pm 0.01$ rad. from $B^0_s \to J/\psi K^+K^-$ decays and $\phi_s = -0.14^{+0.17}_{-0.16} \pm 0.01$ rad. from $B^0_s \to J/\psi\pi^+\pi^-$ decays.

[28] AAD 12CV reports $\phi_s = -2\,\beta_s = 0.22 \pm 0.41 \pm 0.10$ rad. that was measured using a time-dependent angular analysis of $B^0_s \to J/\psi\phi$ decays.

[29] Reports $\phi_s = -2\,\beta_s = -0.44 \pm 0.44 \pm 0.02$ rad. that was measured using a time-dependent fit to $B^0_s \to J/\psi f_0(980)$ decays.

[30] Reports $\phi_s = -2\,\beta_s = 0.15 \pm 0.18 \pm 0.06$ rad. that was measured using a time-dependent angular analysis of $B^0_s \to J/\psi\phi$ decays.

[31] Reports $\phi_s = -2\,\beta_s = -0.019^{+0.173+0.004}_{-0.174-0.003}$ rad. which was measured using a time-dependent fit to $B^0_s \to J/\psi\pi^+\pi^-$ decays, with the $\pi^+\pi^-$ mass within 775–1550 MeV. Searches for, but finds no evidence, for direct *CP* violation in $B^0_s \to J/\psi\pi\pi$ decays.

[32] Reports $0.02 < \phi_s < 0.52$ or $1.08 < \phi_s < 1.55$ rad. at 68% C.L. confidence regions in the two-dimensional space of ϕ_s and $\Delta\Gamma_{B^0_s}$ from $B^0_s \to J/\psi\phi$ decays.

[33] Reports $0.32 < 2\beta_s < 2.82$ rad. at 68% C.L. and confidence regions in the two-dimensional space of $2\beta_s$ and $\Delta\Gamma$ from the first measurement of $B^0_s \to J/\psi\phi$ decays using flavor tagging. The probability of a deviation from SM prediction as large as the level of observed data is 15%.

[34] Reports $\phi_s = -2\,\beta_s$ and obtains 90% CL interval $-0.03 < \beta_s < 0.60$ rad.

[35] The first direct measurement of the *CP*-violating mixing phase is reported from the time-dependent analysis of flavor untagged $B^0_s \to J/\psi\phi$ decays.

[36] Reports ϕ_s which equals to $-2\beta_s$.

[37] Combines D0 collaboration measurements of time-dependent angular distributions in $B^0_s \to J/\psi\phi$ and charge asymmetry in semileptonic decays. There is a 4-fold ambiguity in the solution.

CP Violation phase β_s ($b \to s\overline{s}s$)

VALUE (10^{-2} rad)		DOCUMENT ID		TECN	COMMENT
3.7 ±3.5	1,2	AAIJ	23AT	LHCB	pp at 7, 8, 13 TeV
• • • We do not use the following data for averages, fits, limits, etc. • • •					
2.1 ±3.8±0.5	3	AAIJ	23AT	LHCB	pp at 13 TeV
3.7 ±5.8±1.4	4,5	AAIJ	19AP	LHCB	Repl. by AAIJ 23AT
8.5 ±7.5±1.5	6	AAIJ	14AE	LHCB	Repl. by AAIJ 19AP
0.38 to 1.23	7	AAIJ	13AY	LHCB	Repl. by AAIJ 14AE

[1] AAIJ 23AT reports $\phi_s^{s\overline{s}s} = -0.074 \pm 0.069$ rad and $|\lambda| = 1.009 \pm 0.030$. Measured using a time-dependent fit to $B^0_s \to \phi\phi$ decays, assuming independence of the helicity of the $\phi\phi$ decay.

[2] AAIJ 23AT also reports polarisation-dependent results assuming that the longitudinal weak phase is *CP*-conserving and that there is no direct *CP* violation.

[3] Measured using a time-dependent fit to $B^0_s \to \phi\phi$ decays, assuming independence of the helicity of the $\phi\phi$ decay.

[4] AAIJ 19AP reports $\phi_s^{s\overline{s}s} = -0.073 \pm 0.115 \pm 0.027$ rad and $|\lambda| = 0.99 \pm 0.05 \pm 0.01$. Measured using a time-dependent fit to $B^0_s \to \phi\phi$ decays, assuming independence of the helicity of the $\phi\phi$ decay.

[5] AAIJ 19AP reports also polarisation-dependent results assuming that the longitudinal weak phase is *CP*-conserving and that there is no direct *CP* violation, giving $\phi_{s,\parallel}^{s\overline{s}s} = 0.014 \pm 0.055 \pm 0.011$ rad and $\phi_{s,\perp}^{s\overline{s}s} = 0.044 \pm 0.059 \pm 0.019$ rad.

[6] AAIJ 14AE value measured in $B^0_s \to \phi\phi$ decays. Also reports $\phi_s^{s\overline{s}s} = -0.17 \pm 0.15 \pm 0.03$ rad.

[7] AAIJ 13AY uses $B^0_s \to \phi\phi$ mode, and reports the 68% CL interval of $\phi_s^{s\overline{s}s} = -2\,\beta_s^{s\overline{s}s}$ as $[-2.46, -0.76]$ rad.

CP Violation phase β_s ($B^0_s \to J/\psi(1S)\phi$)

VALUE (10^{-2} rad)		DOCUMENT ID		TECN	COMMENT
3.0 ± 0.7 OUR EVALUATION (Produced by HFLAV)					
3.0 ± 0.7 OUR AVERAGE					
3.65 ± 1.10 ± 0.50	1,2	HAYRAPETY...	26A	CMS	pp at 13 TeV
1.9 ± 1.1 ± 0.3	3	AAIJ	24A	LHCB	pp at 13 TeV
4.05 ± 2.05 ± 1.10	4,5	AAD	21AE	ATLS	pp at 13 TeV
0 ± 14 ± 4	6	AAIJ	21AN	LHCB	pp at 7, 8 TeV
5.05 ± 4.10 ± 2.10	7,8	AAD	16AP	ATLS	pp at 8 TeV
3.75 ± 4.85 ± 1.55	9	KHACHATRY...	16S	CMS	pp at 8 TeV
2.9 ± 2.5 ± 0.3	10	AAIJ	15I	LHCB	pp at 7, 8 TeV
− 6 ± 13 ± 3	11	AAD	14U	ATLS	pp at 7 TeV
	12	AALTONEN	12AJ	CDF	$p\overline{p}$ at 1.96 TeV
$28\ ^{+18}_{-19}$	13	ABAZOV	12D	D0	$p\overline{p}$ at 1.96 TeV
• • • We do not use the following data for averages, fits, limits, etc. • • •					
0.5 ± 2.5 ± 0.5	14,15	SIRUNYAN	21E	CMS	Repl. by HAYRAPETYAN 26A
4.15 ± 2.05 ± 0.30	16	AAIJ	19Q	LHCB	Repl. by AAIJ 24A
− 0.5 ± 3.5 ± 0.5	17	AAIJ	13AR	LHCB	Repl. by AAIJ 15I
−11.0 ± 20.5 ± 5.0	18	AAD	12CV	ATLS	Repl. by AAD 14U
22 ± 22 ± 1	19	AAIJ	12B	LHCB	Repl. by AAIJ 12Q
− 8 ± 9 ± 3	20	AAIJ	12D	LHCB	Repl. by AAIJ 13AR
$0.95^{+8.70+0.15}_{-8.65-0.20}$	21	AAIJ	12Q	LHCB	Repl. by AAIJ 13AR
	22	AALTONEN	12D	CDF	Repl. by AALTONEN 12AJ
	23	AALTONEN	08G	CDF	Repl. by AALTONEN 12D
$28\ ^{+12}_{-15}\ ^{+4}_{-1}$	13,24	ABAZOV	08AM	D0	Repl. by ABAZOV 12D
$39.5 \pm 28.0\ ^{+0.5}_{-7.0}$	25,26	ABAZOV	07	D0	Repl. by ABAZOV 07N
$35\ ^{+20}_{-24}$	26,27	ABAZOV	07N	D0	Repl. by ABAZOV 08AM

[1] HAYRAPETYAN 26A measured $\phi_s = -2\,\beta_s = (-7.3 \pm 2.2 \pm 1.0) \times 10^{-2}$ rad. using a time-dependent angular analysis of $B^0_s \to J/\psi\phi$ decays with the ML-improved flavor-tagging algorithm.

[2] Reports a combination of $\beta_s = (3.70 \pm 1.15) \times 10^{-2}$ rad with KHACHATRYAN 16S.

[3] AAIJ 19Q reports $\phi_s = -2\,\beta_s = -0.039 \pm 0.022 \pm 0.006$ rad. measured using a time-dependent angular analysis of $B^0_s \to J/\psi K^+K^-$ decays.

[4] Reports a combination of $0.0435 \pm 0.0180 \pm 0.0105$ with AAD 16AP.

[5] AAD 21AE measured $\phi_s = -2\,\beta_s = -0.087 \pm 0.036 \pm 0.021$ rad. using a time-dependent angular analysis of $B^0_s \to J/\psi\phi$ decays.

[6] AAIJ 21AN measured $\phi_s = -2\beta_s = 0.00 \pm 0.28 \pm 0.07$ rad, using a time-dependent angular analysis of $B^0_s \to J/\psi\phi$ decays with $J/\psi \to e^+e^-$.

[7] Reports a combination of $0.0435 \pm 0.0180 \pm 0.0105$ with AAD 14U.

[8] AAD 16AP reports $\phi_s = -2\,\beta_s = -0.090 \pm 0.078 \pm 0.041$ rad. that was measured using a time-dependent angular analysis of $B^0_s \to J/\psi\phi$ decays.

[9] KHACHATRYAN 16S reports $\phi_s = -2\,\beta_s = -0.075 \pm 0.097 \pm 0.031$ rad. that was measured using a time-dependent angular analysis of $B^0_s \to J/\psi\phi$ decays.

[10] AAIJ 15I reports $\phi_s = -2\,\beta_s = -0.058 \pm 0.049 \pm 0.006$ rad. that was measured using a time-dependent angular analysis of $B^0_s \to J/\psi K^+K^-$ decays. It also combines this result with that of AAIJ 14S and quotes $\phi_s = -2\,\beta_s = -0.010 \pm 0.039$ rad.

[11] AAD 14U reports $\phi_s = -2\,\beta_s = 0.12 \pm 0.25 \pm 0.05$ rad. that was measured using a time-dependent angular analysis of $B^0_s \to J/\psi\phi$ decays.

[12] AALTONEN 12AJ reports $-\pi/2 < \beta_s < -1.51$ or $-0.06 < \beta_s < 0.30$, or $1.26 < \beta_s < \pi/2$ rad. at 68% CL. Measured using the time-dependent angular analysis of $B^0_s \to J/\psi\phi$ decays.

[13] ABAZOV 12D reports $\phi_s = -2\,\beta_s = -0.55^{+0.38}_{-0.36}$ rad. that was measured using a time-dependent angular analysis of $B^0_s \to J/\psi\phi$ decays. A single error includes both statistical and systematic uncertainties.

[14] Reports a combination of $0.0105 \pm 0.0220 \pm 0.0050$ with KHACHATRYAN 16S.

[15] SIRUNYAN 21E measured $\phi_s = -2\,\beta_s = -0.021 \pm 0.044 \pm 0.010$ rad. using a time-dependent angular analysis of $B^0_s \to J/\psi\phi$ decays.

[16] AAIJ 19Q reports $\phi_s = -2\,\beta_s = -0.083 \pm 0.041 \pm 0.006$ rad. that was measured using a time-dependent angular analysis of $B^0_s \to J/\psi K^+K^-$ decays.

[17] AAIJ 13AR reports $\phi_s = -2\beta_s = 0.01 \pm 0.07 \pm 0.01$ rad. obtained from combined fit to $B^0_s \to J/\psi K^+K^-$ and $B^0_s \to J/\psi\pi^+\pi^-$ data sets. Also reports separate results of $\phi_s = 0.07 \pm 0.09 \pm 0.01$ rad. from $B^0_s \to J/\psi K^+K^-$ decays and $\phi_s = -0.14^{+0.17}_{-0.16} \pm 0.01$ rad. from $B^0_s \to J/\psi\pi^+\pi^-$ decays.

[18] AAD 12CV reports $\phi_s = -2\,\beta_s = 0.22 \pm 0.41 \pm 0.10$ rad. that was measured using a time-dependent angular analysis of $B^0_s \to J/\psi\phi$ decays.

[19] Reports $\phi_s = -2\,\beta_s = -0.44 \pm 0.44 \pm 0.02$ rad. that was measured using a time-dependent fit to $B^0_s \to J/\psi f_0(980)$ decays.

[20] Reports $\phi_s = -2\,\beta_s = 0.15 \pm 0.18 \pm 0.06$ rad. that was measured using a time-dependent angular analysis of $B^0_s \to J/\psi\phi$ decays.

[21] Reports $\phi_s = -2\,\beta_s = -0.019^{+0.173+0.004}_{-0.174-0.003}$ rad. which was measured using a time-dependent fit to $B^0_s \to J/\psi\pi^+\pi^-$ decays, with the $\pi^+\pi^-$ mass within 775–1550 MeV. Searches for, but finds no evidence, for direct *CP* violation in $B^0_s \to J/\psi\pi\pi$ decays.

[22] Reports $0.02 < \phi_s < 0.52$ or $1.08 < \phi_s < 1.55$ rad. at 68% C.L. confidence regions in the two-dimensional space of ϕ_s and $\Delta\Gamma_{B^0_s}$ from $B^0_s \to J/\psi\phi$ decays.

[23] Reports $0.32 < 2\beta_s < 2.82$ rad. at 68% C.L. and confidence regions in the two-dimensional space of $2\beta_s$ and $\Delta\Gamma$ from the first measurement of $B^0_s \to J/\psi\phi$ decays using flavor tagging. The probability of a deviation from SM prediction as large as the level of observed data is 15%.

[24] Reports $\phi_s = -2\,\beta_s$ and obtains 90% CL interval $-0.03 < \beta_s < 0.60$ rad.

[25] The first direct measurement of the *CP*-violating mixing phase is reported from the time-dependent analysis of flavor untagged $B^0_s \to J/\psi\phi$ decays.

[26] Reports ϕ_s which equals to $-2\beta_s$.

[27] Combines D0 collaboration measurements of time-dependent angular distributions in $B^0_s \to J/\psi\phi$ and charge asymmetry in semileptonic decays. There is a 4-fold ambiguity in the solution.

$|\lambda|$ ($B^0_s \to J/\psi(1S)\phi$)

$\lambda = q/p \cdot A_f/\overline{A}_f$ is a phase-convention-independent observable quantity for the final state f. See the review on "*CP* Violation in the Quark Sector" for details.

VALUE	DOCUMENT ID		TECN	COMMENT
0.995±0.009 OUR EVALUATION (Produced by HFLAV)				
0.994±0.009 OUR AVERAGE				
1.011±0.014±0.015	1 HAYRAPETY...	26A	CMS	pp at 13 TeV
0.990±0.010	AAIJ	24A	LHCB	pp at 7, 8, 13 TeV

Int. J. Mod. Phys. A 2026.41. Downloaded from www.worldscientific.com
by UNIVERSITY OF CALIFORNIA @ BERKELEY on 09/16/26. Re-use and distribution is strictly not permitted, except for Open Access articles.

Int. J. Mod. Phys. A 2026.41. Downloaded from www.worldscientific.com by CALIFORNIA @ BERKELEY on 09/16/26. Re-use and distribution is strictly not permitted, except for Open Access articles.

• • • We do not use the following data for averages, fits, limits, etc. • • •

$0.877^{+0.112}_{-0.116}\pm0.031$	AAIJ	21AN	LHCB	Repl. by AAIJ 24A
$0.972\pm0.026\pm0.008$	[2] SIRUNYAN	21E	CMS	Repl. by HAYRAPETYAN 26A
$1.012\pm0.016\pm0.006$	AAIJ	19Q	LHCB	Repl. by AAIJ 24A
$0.964\pm0.019\pm0.007$	AAIJ	15I	LHCB	Repl. by AAIJ 24A
$0.93\ \pm0.03\ \pm0.02$	AAIJ	13AR	LHCB	Repl. by AAIJ 15I

[1] Measured using a time-dependent angular analysis of $B_s^0 \to J/\psi\phi$ decays with the ML-improved flavor-tagging algorithm.
[2] Measured using time-dependent angular analysis of $B_s^0 \to J/\psi\phi$ decays.

$|\lambda|$ ($b \to c\overline{c}s$)

$\lambda = q/p \cdot A_f/\overline{A}_f$ is a phase-convention-independent observable quantity for the final state f. See the review on "*CP* Violation in the Quark Sector" for details.

VALUE	DOCUMENT ID		TECN	COMMENT
0.989±0.008 OUR AVERAGE				
$1.145\pm0.126\pm0.031$	[1] AAIJ	25A	LHCB	pp at 13 TeV
0.990 ± 0.010	[2] AAIJ	24A	LHCB	pp at 7, 8, 13 TeV
$0.972\pm0.026\pm0.008$	[3] SIRUNYAN	21E	CMS	pp at 13 TeV
$0.949\pm0.036\pm0.019$	[4] AAIJ	19AF	LHCB	pp at 7, 8, 13 TeV
$0.994\pm0.018\pm0.006$	[5] AAIJ	17V	LHCB	pp at 7, 8 TeV
$1.045^{+0.069}_{-0.050}\pm0.007$	[6] AAIJ	16AK	LHCB	pp at 7, 8 TeV
$0.91\ ^{+0.18}_{-0.15}\ \pm0.02$	[1] AAIJ	14AY	LHCB	pp at 7, 8 TeV
• • • We do not use the following data for averages, fits, limits, etc. • • •				
$1.004\pm0.030\pm0.009$	[7] AAIJ	23AT	LHCB	pp at 13 TeV
1.009 ± 0.030	[7] AAIJ	23AT	LHCB	pp at 7, 8 and 13 TeV
$0.877^{+0.112}_{-0.116}\pm0.031$	AAIJ	21AN	LHCB	Repl. by AAIJ 24A
$0.99\ \pm0.05\ \pm0.01$	[7] AAIJ	19AP	LHCB	Repl. by AAIJ 23AT
$1.012\pm0.016\pm0.006$	AAIJ	19Q	LHCB	Repl. by AAIJ 24A
$1.035\pm0.034\pm0.089$	[8] AAIJ	18S	LHCB	pp at 7, 8 TeV
$0.964\pm0.019\pm0.007$	AAIJ	15I	LHCB	Repl. by AAIJ 24A
$1.04\ \pm0.07\ \pm0.03$	[7] AAIJ	14AE	LHCB	Repl. by AAIJ 19AP
$0.93\ \pm0.03\ \pm0.02$	AAIJ	13AR	LHCB	Repl. by AAIJ 15I

[1] Measured in $B_s^0 \to D_s^+ D_s^-$ decays.
[2] Measured using time-dependent angular analysis of $B_s^0 \to J/\psi K^+ K^-$ in the region $m(K\,K)$ in the vicinity of the $\phi(1020)$ resonance.
[3] Measured using time-dependent angular analysis of $B_s^0 \to J/\psi\phi$ decays.
[4] Measured using time-dependent analysis of $B_s^0 \to J/\psi\pi^+\pi^-$ decays.
[5] Measured using time-dependent angular analysis of $B_s^0 \to J/\psi K^+ K^-$ in the region $m(K\,K) > 1.05$ GeV.
[6] Measured using time-dependent angular analysis of $B_s^0 \to \psi(2S)\,\phi$ decays.
[7] Measured in $B_s^0 \to \phi\phi$ decays.
[8] Measured in $B_s^0 \to (K^+\pi^-)(K^-\pi^+)$ in the region $0.75 < m(K^\pm\pi^\mp) < 1.6$ GeV.

A, *CP* violation parameter

$A = -2\,\mathrm{Re}(\lambda)\ /\ (1 + |\lambda|^2)$

VALUE	DOCUMENT ID		TECN	COMMENT
−0.79±0.08 OUR AVERAGE				
$-0.83\pm0.05\pm0.09$	[1] AAIJ	21O	LHCB	pp at 13 TeV
$-0.79\pm0.07\pm0.10$	[1] AAIJ	18O	LHCB	pp at 7, 8 TeV
$0.49^{+0.77}_{-0.65}\pm0.06$	[2] AAIJ	15AL	LHCB	pp at 7, 8 TeV

[1] Measured in $B_s^0 \to K^+ K^-$ decays.
[2] Measured in $B_s^0 \to J/\psi K_S^0$ decays.

C, *CP* violation parameter

$C = (1 - |\lambda|^2)\ /\ (1 + |\lambda|^2)$

VALUE	DOCUMENT ID		TECN	COMMENT
0.19±0.06 OUR AVERAGE				
$0.20\pm0.06\pm0.02$	[1] AAIJ	18O	LHCB	pp at 7, 8 TeV
$-0.28\pm0.41\pm0.08$	[2] AAIJ	15AL	LHCB	pp at 7, 8 TeV

[1] Measured in $B_s^0 \to K^+ K^-$ decays.
[2] Measured in $B_s^0 \to J/\psi K_S^0$ decays.

S, *CP* violation parameter

$S = -2\,\mathrm{Im}(\lambda)\ /\ (1 + |\lambda|^2)$

VALUE	DOCUMENT ID		TECN	COMMENT
0.17±0.06 OUR AVERAGE				
$0.18\pm0.06\pm0.02$	[1] AAIJ	18O	LHCB	pp at 7, 8 TeV
$-0.08\pm0.40\pm0.08$	[2] AAIJ	15AL	LHCB	pp at 7, 8 TeV

[1] Measured in $B_s^0 \to K^+ K^-$ decays.
[2] Measured in $B_s^0 \to J/\psi K_S^0$ decays.

$A_{CP}^{L}(B_s \to J/\psi\overline{K}^*(892)^0)$

VALUE	DOCUMENT ID		TECN	COMMENT
0.021±0.026±0.007	[1] AAIJ	25AQ	LHCB	pp at 7, 8, 13 TeV
• • • We do not use the following data for averages, fits, limits, etc. • • •				
$0.014\pm0.029\pm0.007$	AAIJ	25AQ	LHCB	pp at 13 TeV
$-0.048\pm0.057\pm0.020$	AAIJ	15AV	LHCB	Repl. by AAIJ 25AQ

[1] Combination with measurement from refAAIJ 2025AQ.

$A_{CP}^{\parallel}(B_s \to J/\psi\overline{K}^*(892)^0)$

VALUE	DOCUMENT ID		TECN	COMMENT
−0.073±0.060±0.007	[1] AAIJ	25AQ	LHCB	pp at 7, 8, 13 TeV
• • • We do not use the following data for averages, fits, limits, etc. • • •				
$-0.055\pm0.065\pm0.007$	AAIJ	25AQ	LHCB	pp at 13 TeV
$0.171\pm0.152\pm0.028$	AAIJ	15AV	LHCB	Repl. by AAIJ 25AQ

[1] Combination with measurement from AAIJ 15AV.

$A_{CP}^{\perp}(B_s \to J/\psi\overline{K}^*(892)^0)$

VALUE	DOCUMENT ID		TECN	COMMENT
0.057±0.049±0.014	[1] AAIJ	25AQ	LHCB	pp at 7, 8, 13 TeV
• • • We do not use the following data for averages, fits, limits, etc. • • •				
$0.060\pm0.057\pm0.016$	AAIJ	25AQ	LHCB	pp at 13 TeV
$-0.049\pm0.096\pm0.025$	AAIJ	15AV	LHCB	Repl. by AAIJ 25AQ

[1] Combination with measurement from AAIJ 15AV.

$A_{CP}(B_s \to \pi^+ K^-)$

A_{CP} is defined as

$$\frac{B(\overline{B}_s^0 \to f) - B(B_s^0 \to \overline{f})}{B(\overline{B}_s^0 \to f) + B(B_s^0 \to \overline{f})},$$

the *CP*-violation asymmetry of exclusive B_s^0 and $\overline{B}_s^0$ decay.

VALUE	DOCUMENT ID		TECN	COMMENT
0.224±0.012 OUR AVERAGE				
$0.236\pm0.013\pm0.011$	AAIJ	21O	LHCB	pp at 13 TeV
$0.213\pm0.015\pm0.007$	AAIJ	18O	LHCB	pp at 7, 8 TeV
$0.22\ \pm0.07\ \pm0.02$	AALTONEN	14P	CDF	$p\overline{p}$ at 1.96 TeV
• • • We do not use the following data for averages, fits, limits, etc. • • •				
$0.27\ \pm0.04\ \pm0.01$	AAIJ	13AX	LHCB	Repl. by AAIJ 18O
$0.27\ \pm0.08\ \pm0.02$	AAIJ	12V	LHCB	Repl. by AAIJ 13AX
$0.39\ \pm0.15\ \pm0.08$	AALTONEN	11N	CDF	Repl. by AALTONEN 14P

$A_{CP}(B_s^0 \to [K^+K^-]_D\overline{K}^*(892)^0)$

VALUE	DOCUMENT ID		TECN	COMMENT
0.062±0.032±0.021	AAIJ	24M	LHCB	pp at 7, 8, 13 TeV
• • • We do not use the following data for averages, fits, limits, etc. • • •				
$-0.04\ \pm0.07\ \pm0.02$	AAIJ	14BN	LHCB	Repl. by AAIJ 24M
$0.04\ \pm0.16\ \pm0.01$	AAIJ	13L	LHCB	Repl. by AAIJ 14BN

$A_{CP}(B_s^0 \to [\pi^+K^-]_D K^*(892)^0)$

VALUE	DOCUMENT ID		TECN	COMMENT
−0.009±0.011±0.020	AAIJ	24M	LHCB	pp at 7, 8, 13 TeV
• • • We do not use the following data for averages, fits, limits, etc. • • •				
$-0.01\ \pm0.03\ \pm0.02$	AAIJ	14BN	LHCB	Repl. by AAIJ 24M

$A_{CP}(B_s^0 \to [K^+\pi^-]_D\overline{K}^*(892)^0)$

$A_{CP}(B_s^0 \to [\pi^+\pi^-]_D K^*(892)^0)$

VALUE	DOCUMENT ID		TECN	COMMENT
−0.001±0.056±0.021	AAIJ	24M	LHCB	pp at 7, 8, 13 TeV
• • • We do not use the following data for averages, fits, limits, etc. • • •				
$0.06\ \pm0.13\ \pm0.02$	AAIJ	14BN	LHCB	Repl. by AAIJ 24M

$A_{CP}(B_s^0 \to [K^+\pi^-\pi^+\pi^-]_D\overline{K}^*(892)^0)$

VALUE	DOCUMENT ID		TECN	COMMENT
−0.029±0.012±0.021	AAIJ	24M	LHCB	pp at 7, 8, 13 TeV

$A_{CP}(B_s^0 \to [K^-\pi^+\pi^+\pi^-]_D\overline{K}^*(892)^0)$

$A_{CP}(B_s^0 \to [\pi^+\pi^-\pi^+\pi^-]_D\overline{K}^*(892)^0)$

VALUE	DOCUMENT ID		TECN	COMMENT
0.017±0.044±0.022	AAIJ	24M	LHCB	pp at 7, 8, 13 TeV

$R_s^+ = \Gamma(B_s^0 \to [\pi^-K^+]_D\overline{K}^{*0})\ /\ \Gamma(B_s^0 \to [\pi^+K^-]_D\overline{K}^{*0})$

VALUE	DOCUMENT ID		TECN	COMMENT
0.004±0.002±0.006	AAIJ	24M	LHCB	pp at 7, 8, 13 TeV

$R_s^- = \Gamma(\overline{B}_s^0 \to [\pi^+K^-]_D K^{*0})\ /\ \Gamma(\overline{B}_s^0 \to [\pi^-K^+]_D K^{*0})$

VALUE	DOCUMENT ID		TECN	COMMENT
0.004±0.002±0.006	AAIJ	24M	LHCB	pp at 7, 8, 13 TeV

$R_s^+ = \Gamma(B_s^0 \to [\pi^-K^+\pi^+\pi^-]_D\overline{K}^{*0})\ /\ \Gamma(B_s^0 \to [\pi^+K^-\pi^+\pi^-]_D\overline{K}^{*0})$

VALUE	DOCUMENT ID		TECN	COMMENT
0.019±0.004±0.007	AAIJ	24M	LHCB	pp at 7, 8, 13 TeV

$R_s^- = \Gamma(\overline{B}_s^0 \to [\pi^+K^-\pi^+\pi^-]_D K^{*0})\ /\ \Gamma(\overline{B}_s^0 \to [\pi^-K^+\pi^+\pi^-]_D K^{*0})$

VALUE	DOCUMENT ID		TECN	COMMENT
0.015±0.004±0.007	AAIJ	24M	LHCB	pp at 7, 8, 13 TeV

$S(B_s^0 \to \phi\gamma)$

VALUE	DOCUMENT ID		TECN	COMMENT
0.43±0.30±0.11	[1] AAIJ	19AE	LHCB	pp at 7, 8 TeV

[1] Measured in flavor tagged time dependent analysis.

Int. J. Mod. Phys. A 2026.41. Downloaded from www.worldscientific.com
by UNIVERSITY OF CALIFORNIA @ BERKELEY on 09/16/26. Re-use and distribution is strictly not permitted, except for Open Access articles.

$C(B_s^0 \to \phi\gamma)$

VALUE	DOCUMENT ID		TECN	COMMENT
0.11±0.29±0.11	[1] AAIJ	19AE	LHCB	pp at 7, 8 TeV

[1] Measured in flavor tagged time dependent analysis.

$A^{\Delta}(B_s^0 \to \phi\gamma)$

$A^{\Delta}(B_s \to \phi\gamma)$ is the multiplicative coefficient of the sinh($\Delta\Gamma t/2$) term in the $B_s \to \phi\gamma$ decay rate time dependence.

VALUE	DOCUMENT ID		TECN	COMMENT
$-0.67^{+0.37}_{-0.41}\pm0.17$	[1] AAIJ	19AE	LHCB	pp at 7, 8 TeV
• • • We do not use the following data for averages, fits, limits, etc. • • •				
$-0.98^{+0.46}_{-0.52}\pm0.23$	[2] AAIJ	17B	LHCB	Repl. by AAIJ 19AE

[1] Measured in flavor tagged time dependent analysis, using tagged and un-tagged events. This result updates AAIJ 17B with better selection efficiency and other analysis improvements.
[2] Measured in time dependent analysis without initial flavor tagging.

CPT VIOLATION PARAMETERS

In the B_s^0 mixing, propagating mass eigenstates can be written as

$$|B_{sL}\rangle \propto p\sqrt{1-\xi}\,|B_s^0\rangle + q\sqrt{1+\xi}\,|\overline{B}_s^0\rangle$$
$$|B_{sH}\rangle \propto p\sqrt{1+\xi}\,|B_s^0\rangle - q\sqrt{1-\xi}\,|\overline{B}_s^0\rangle$$

where parameter ξ controls CPT violation. If ξ is zero, then CPT is conserved. The parameter ξ can be written as

$$\xi = \frac{2(M_{11}-M_{22})-i(\Gamma_{11}-\Gamma_{22})}{-2\Delta m_s - i\Delta\Gamma_s} \approx \frac{-2\beta^{\mu}\Delta a_{\mu}}{2\Delta m_s - i\Delta\Gamma_s},$$

where M_{ii}, Γ_{ii}, Δm_s, and $\Delta\Gamma_s$ are parameters of Hamiltonian governing B_s oscillations, β^{μ} is the B_s^0 meson velocity and Δa_{μ} characterizes Lorentz-invariance violation.

$\Delta a_{\perp}$

VALUE (10^{-12} GeV)	CL%	DOCUMENT ID		TECN	COMMENT
$-0.47\pm0.39\pm0.08$		[1] AAIJ	16E	LHCB	pp at 7, 8 TeV
< 1.2	95	[2] ABAZOV	15L	D0	$p\overline{p}$ at 1.96 TeV

[1] Uses $B_s^0 \to J/\psi K^+ K^-$ decays.
[2] Measured in semileptonic $B_s^0 \to D_s^- \mu^+ X$ decays. Also extracts limit on time and longitudinal components ($-0.8 < \Delta a_T - 0.396\,\Delta a_Z < 3.9$) 10^{-13} GeV.

$\Delta a_{\parallel}$

VALUE (10^{-14} GeV)	DOCUMENT ID		TECN	COMMENT
$-0.89\pm1.41\pm0.36$	[1] AAIJ	16E	LHCB	pp at 7, 8 TeV

[1] Uses $B_s^0 \to J/\psi K^+ K^-$ decays.

Δa_X

VALUE (10^{-14} GeV)	DOCUMENT ID		TECN	COMMENT
$+1.01\pm2.08\pm0.71$	[1] AAIJ	16E	LHCB	pp at 7, 8 TeV

[1] Uses $B_s^0 \to J/\psi K^+ K^-$ decays.

Δa_Y

VALUE (10^{-14} GeV)	DOCUMENT ID		TECN	COMMENT
$-3.83\pm2.09\pm0.71$	[1] AAIJ	16E	LHCB	pp at 7, 8 TeV

[1] Uses $B_s^0 \to J/\psi K^+ K^-$ decays.

Re(ξ)

VALUE	DOCUMENT ID		TECN	COMMENT
$-0.022\pm0.033\pm0.003$	[1] AAIJ	16E	LHCB	pp at 7, 8 TeV

[1] Uses $B_s^0 \to J/\psi K^+ K^-$ decays.

Im(ξ)

VALUE	DOCUMENT ID		TECN	COMMENT
0.004±0.011±0.002	[1] AAIJ	16E	LHCB	pp at 7, 8 TeV

[1] Uses $B_s^0 \to J/\psi K^+ K^-$ decays.

PARTIAL BRANCHING FRACTIONS IN $B_s \to \phi\ell^+\ell^-$

B($B_s \to \phi\ell^+\ell^-$) (0.1 < q^2 < 2.0 GeV^2/c^4)

VALUE (units 10^{-7})	DOCUMENT ID		TECN	COMMENT
1.14 ±0.16 OUR AVERAGE				
$1.11\ ^{+0.14}_{-0.13}\pm0.09$	[1] AAIJ	15AQ	LHCB	pp at 7, 8 TeV
2.78 ±0.95 ±0.89	AALTONEN	11AI	CDF	$p\overline{p}$ at 1.96 TeV
• • • We do not use the following data for averages, fits, limits, etc. • • •				
$0.897^{+0.207}_{-0.186}\pm0.097$	[1] AAIJ	13X	LHCB	Repl. by AAIJ 15AQ

[1] Measured in $B_s^0 \to \phi\mu^+\mu^-$ decays.

B($B_s^0 \to \phi\ell^+\ell^-$) (0.1 < q^2 < 0.98 GeV^2/c^4)

VALUE (units 10^{-8})	DOCUMENT ID		TECN	COMMENT
6.81±0.47±0.34	[1] AAIJ	21AG	LHCB	pp at 7, 8, 13 TeV

[1] Measured in $B_s^0 \to \phi\mu^+\mu^-$ decays

B($B_s^0 \to \phi\ell^+\ell^-$) (1.1 < q^2 < 2.5 GeV^2/c^4)

VALUE (units 10^{-8})	DOCUMENT ID		TECN	COMMENT
4.41±0.41±0.24	[1] AAIJ	21AG	LHCB	pp at 7, 8, 13 TeV

[1] Measured in $B_s^0 \to \phi\mu^+\mu^-$ decays

B($B_s \to \phi\ell^+\ell^-$) (2.0 < q^2 < 5.0 GeV^2/c^4)

VALUE (units 10^{-7})	DOCUMENT ID		TECN	COMMENT
0.77 ±0.12 ±0.06	[1] AAIJ	15AQ	LHCB	pp at 7, 8 TeV
• • • We do not use the following data for averages, fits, limits, etc. • • •				
$0.529^{+0.182}_{-0.159}\pm0.057$	[1,2] AAIJ	13X	LHCB	Repl. by AAIJ 15AQ
0.58 ±0.55 ±0.19	[2] AALTONEN	11AI	CDF	$p\overline{p}$ at 1.96 TeV

[1] Measured in $B_s^0 \to \phi\mu^+\mu^-$ decays.
[2] Measured in 2<q^2 <4.3 GeV^2/c^4.

B($B_s^0 \to \phi\ell^+\ell^-$) (2.5 < q^2 < 4.0 GeV^2/c^4)

VALUE (units 10^{-8})	DOCUMENT ID		TECN	COMMENT
3.51±0.39±0.18	[1] AAIJ	21AG	LHCB	pp at 7, 8, 13 TeV

[1] Measured in $B_s^0 \to \phi\mu^+\mu^-$ decays

B($B_s^0 \to \phi\ell^+\ell^-$) (4.0 < q^2 < 6.0 GeV^2/c^4)

VALUE (units 10^{-8})	DOCUMENT ID		TECN	COMMENT
6.22±0.48±0.32	[1] AAIJ	21AG	LHCB	pp at 7, 8, 13 TeV

[1] Measured in $B_s^0 \to \phi\mu^+\mu^-$ decays

B($B_s \to \phi\ell^+\ell^-$) (5.0 < q^2 < 8.0 GeV^2/c^4)

VALUE (units 10^{-7})	DOCUMENT ID		TECN	COMMENT
0.96±0.13±0.08	[1] AAIJ	15AQ	LHCB	pp at 7, 8 TeV
• • • We do not use the following data for averages, fits, limits, etc. • • •				
$1.38^{+0.25}_{-0.23}\pm0.14$	[1,2] AAIJ	13X	LHCB	Repl. by AAIJ 15AQ
1.34±0.83±0.43	[2] AALTONEN	11AI	CDF	$p\overline{p}$ at 1.96 TeV

[1] Measured in $B_s^0 \to \phi\mu^+\mu^-$ decays.
[2] Measured in 4.3<q^2 <8.68 GeV^2/c^4.

B($B_s^0 \to \phi\ell^+\ell^-$) (6.0 < q^2 < 8.0 GeV^2/c^4)

VALUE (units 10^{-8})	DOCUMENT ID		TECN	COMMENT
6.30±0.48±0.32	[1] AAIJ	21AG	LHCB	pp at 7, 8, 13 TeV

[1] Measured in $B_s^0 \to \phi\mu^+\mu^-$ decays

B($B_s \to \phi\ell^+\ell^-$) (11.0 < q^2 < 12.5 GeV^2/c^4)

VALUE (units 10^{-7})	DOCUMENT ID		TECN	COMMENT
0.717±0.045±0.036	[1] AAIJ	21AG	LHCB	pp at 7, 8, 13 TeV
• • • We do not use the following data for averages, fits, limits, etc. • • •				
0.71 ±0.10 ±0.06	[1] AAIJ	15AQ	LHCB	Repl. by AAIJ 21AG
$1.18\ ^{+0.22}_{-0.21}\pm0.14$	[1,2] AAIJ	13X	LHCB	Repl. by AAIJ 15AQ
2.98 ±0.95 ±0.95	[2] AALTONEN	11AI	CDF	$p\overline{p}$ at 1.96 TeV

[1] Measured in $B_s^0 \to \phi\mu^+\mu^-$ decays.
[2] Measured in 10.9<q^2 <12.86 GeV^2/c^4.

B($B_s^0 \to \phi\ell^+\ell^-$) (15.0 < q^2 < 19.0 GeV^2/c^4)

VALUE (units 10^{-8})	DOCUMENT ID		TECN	COMMENT
18.52±0.80±1.00	[1] AAIJ	21AG	LHCB	pp at 7, 8, 13 TeV

[1] Measured in $B_s^0 \to \phi\mu^+\mu^-$ decays

B($B_s \to \phi\ell^+\ell^-$) (15.0 < q^2 < 17.0 GeV^2/c^4)

VALUE (units 10^{-7})	DOCUMENT ID		TECN	COMMENT
1.050±0.058±0.054	[1] AAIJ	21AG	LHCB	pp at 7, 8, 13 TeV
• • • We do not use the following data for averages, fits, limits, etc. • • •				
0.90 ±0.11 ±0.07	[1] AAIJ	15AQ	LHCB	Repl. by AAIJ 21AG
$0.760^{+0.189}_{-0.169}\pm0.087$	[1,2] AAIJ	13X	LHCB	Repl. by AAIJ 15AQ
1.86 ±0.66 ±0.59	[2] AALTONEN	11AI	CDF	$p\overline{p}$ at 1.96 TeV

[1] Measured in $B_s^0 \to \phi\mu^+\mu^-$ decays.
[2] Measured in 14.18<q^2 <16 GeV^2/c^4.

B($B_s \to \phi\ell^+\ell^-$) (17.0 < q^2 < 19.0 GeV^2/c^4)

VALUE (units 10^{-7})	DOCUMENT ID		TECN	COMMENT
0.838±0.058±0.046	[1] AAIJ	21AG	LHCB	pp at 7, 8, 13 TeV
• • • We do not use the following data for averages, fits, limits, etc. • • •				
0.79 ±0.11 ±0.07	[1] AAIJ	15AQ	LHCB	Repl. by AAIJ 21AG
$1.06\ ^{+0.23}_{-0.21}\pm0.12$	[1,2] AAIJ	13X	LHCB	Repl. by AAIJ 15AQ
2.32 ±0.76 ±0.74	[2] AALTONEN	11AI	CDF	$p\overline{p}$ at 1.96 TeV

[1] Measured in $B_s^0 \to \phi\mu^+\mu^-$ decays.
[2] Measured in 16<q^2 <19 GeV^2/c^4.

Int. J. Mod. Phys. A 2026.41. Downloaded from www.worldscientific.com by CALIFORNIA @ BERKELEY on 09/16/26. Re-use and distribution is strictly not permitted, except for Open Access articles.

$B(B_s \to \phi \ell^+ \ell^-)$ $(1.0 < q^2 < 6.0\ \mathrm{GeV}^2/c^4)$

VALUE (units 10^{-7})	DOCUMENT ID		TECN	COMMENT
1.44 ±0.11 OUR AVERAGE				
1.440±0.075±0.075	[1] AAIJ	21AG	LHCB	pp at 7, 8, 13 TeV
1.14 ±0.79 ±0.36	AALTONEN	11AI	CDF	$p\overline{p}$ at 1.96 TeV
• • • We do not use the following data for averages, fits, limits, etc. • • •				
1.29 ±0.16 ±0.10	[1] AAIJ	15AQ	LHCB	Repl. by AAIJ 21AG
1.14 $^{+0.25}_{-0.23}$ ±0.13	[1] AAIJ	13X	LHCB	Repl. by AAIJ 15AQ

[1] Measured in $B_s^0 \to \phi\mu^+\mu^-$ decays.

$B(B_s \to \phi \ell^+ \ell^-)$ $(0.0 < q^2 < 4.3\ \mathrm{GeV}^2/c^4)$

VALUE (units 10^{-7})	DOCUMENT ID		TECN	COMMENT
3.30±1.09±1.05	AALTONEN	11AI	CDF	$p\overline{p}$ at 1.96 TeV

$B(B_s \to \phi e^+ e^-)$ $(0.1 < q^2 < 1.1\ \mathrm{GeV}^2/c^4)$

VALUE (units 10^{-7})	DOCUMENT ID		TECN	COMMENT
$1.38^{+0.25}_{-0.22}$±0.20	[1] AAIJ	25K	LHCB	pp at 7, 8 and 13 TeV

[1] The second uncertainty includes the systematic, the uncertainties on the ratio of $dB(B_s^0 \to \phi\mu^+\mu^-)/dq^2/B(B_s^0 \to J/\psi\phi)$, and $B(B_s^0 \to J/\psi\phi)$.

$B(B_s \to \phi e^+ e^-)$ $(1.1 < q^2 < 6.0\ \mathrm{GeV}^2/c^4)$

VALUE (units 10^{-7})	DOCUMENT ID		TECN	COMMENT
1.27±0.29±0.085	[1] AAIJ	25K	LHCB	pp at 7, 8 and 13 TeV

[1] The second uncertainty includes the systematic, the uncertainties on the ratio of $dB(B_s^0 \to \phi\mu^+\mu^-)/dq^2/B(B_s^0 \to J/\psi\phi)$, and $B(B_s^0 \to J/\psi\phi)$.

$B(B_s \to \phi e^+ e^-)$ $(15.0 < q^2 < 19.0\ \mathrm{GeV}^2/c^4)$

VALUE (units 10^{-7})	DOCUMENT ID		TECN	COMMENT
1.56±0.44±0.20	[1] AAIJ	25K	LHCB	pp at 7, 8 and 13 TeV

[1] The second uncertainty includes the systematic, the uncertainties on the ratio of $dB(B_s^0 \to \phi\mu^+\mu^-)/dq^2/B(B_s^0 \to J/\psi\phi)$, and $B(B_s^0 \to J/\psi\phi)$.

$[B(B_s \to \phi e^+ e^-)/B(B_s \to J/\psi(J/\psi \to e^+e^-)\phi)]/[B(B_s \to \phi\mu^+\mu^-)/B(B_s \to J/\psi(J/\psi \to \mu^+\mu^-)\phi)]$ $(0.1 < q^2 < 1.1\ \mathrm{GeV}^2/c^4)$

VALUE	DOCUMENT ID		TECN	COMMENT
$1.57^{+0.28}_{-0.25}$±0.05	AAIJ	25K	LHCB	pp at 7, 8 and 13 TeV

$[B(B_s \to \phi e^+ e^-)/B(B_s \to J/\psi(J/\psi \to e^+e^-)\phi)]/[B(B_s \to \phi\mu^+\mu^-)/B(B_s \to J/\psi(J/\psi \to \mu^+\mu^-)\phi)]$ $(1.1 < q^2 < 6.0\ \mathrm{GeV}^2/c^4)$

VALUE	DOCUMENT ID		TECN	COMMENT
$0.91^{+0.20}_{-0.19}$±0.05	AAIJ	25K	LHCB	pp at 7, 8 and 13 TeV

$[B(B_s \to \phi e^+ e^-)/B(B_s \to J/\psi(J/\psi \to e^+e^-)\phi)]/[B(B_s \to \phi\mu^+\mu^-)/B(B_s \to J/\psi(J/\psi \to \mu^+\mu^-)\phi)]$ $(15.0 < q^2 < 19.0\ \mathrm{GeV}^2/c^4)$

VALUE	DOCUMENT ID		TECN	COMMENT
$0.85^{+0.24}_{-0.23}$±0.10	AAIJ	25K	LHCB	pp at 7, 8 and 13 TeV

PRODUCTION ASYMMETRIES

$A_P(B_s^0)$

$A_P(B_s^0) = [\sigma(\overline{B}_s^0) - \sigma(B_s^0)] / [\sigma(\overline{B}_s^0) + \sigma(B_s^0)]$

VALUE (units 10^{-2})	DOCUMENT ID		TECN	COMMENT
1.2 ±1.6 OUR AVERAGE				
−0.65±2.88±0.59	[1] AAIJ	17BF	LHCB	pp at 7 TeV
1.98±1.90±0.59	[1] AAIJ	17BF	LHCB	pp at 8 TeV
• • • We do not use the following data for averages, fits, limits, etc. • • •				
1.09±2.61±0.66	[2] AAIJ	14BP	LHCB	Repl. by AAIJ 17BF, pp at 7 TeV

[1] Based on time-dependent analysis of $B_s^0 \to D_s^- \pi^+$ in kinematic range $2 < p_T < 30$ GeV/c and $2.1 < \eta < 4.5$.

[2] Based on time-dependent analysis of $B_s^0 \to D_s^- \pi^+$ in kinematic range $4 < p_T < 30$ GeV/c and $2.5 < \eta < 4.5$.

$B_s^0 \to D_s^{*-} \ell^+ \nu_\ell$ FORM FACTORS

ρ^2 (form factor slope)

VALUE	DOCUMENT ID		TECN	COMMENT
1.17±0.08 OUR AVERAGE				
1.16±0.05±0.07	[1] AAIJ	20AW	LHCB	pp at 13 TeV
1.23±0.17±0.05	[2] AAIJ	20E	LHCB	pp at 7,8 TeV

[1] The $B_s^0 \to D_s^{*-} \mu^+ \nu_\mu$ decay is reconstructed through the decays of $D_s^{*-} \to D_s^- \gamma$, $D_s^- \to K^- K^+ \pi^-$.

[2] The $B_s^0 \to D_s^{*-} \mu^+ \nu_\mu$ decay is reconstructed inclusively without γ from the decays of $D_s^{*-} \to D_s^- \gamma$, $D_s^- \to K^- K^+ \pi^-$.

B_s^0 REFERENCES

HAYRAPETY...	26A	arXiv:2412.19952	A. Hayrapetyan et al.	(CMS Collab.)
AAIJ	25A	JHEP 2501 061	R. Aaij et al.	(LHCb Collab.)
AAIJ	25AC	JHEP 2507 069	R. Aaij et al.	(LHCb Collab.)
AAIJ	25AN	JHEP 2510 113	R. Aaij et al.	(LHCb Collab.)
AAIJ	25AQ	JHEP 2510 173	R. Aaij et al.	(LHCb Collab.)
AAIJ	25K	PRL 134 121803	R. Aaij et al.	(LHCb Collab.)
AAIJ	25S	JHEP 2503 047	R. Aaij et al.	(LHCb Collab.)
AAIJ	25T	JHEP 2503 139	R. Aaij et al.	(LHCb Collab.)
AAIJ	25X	JHEP 2507 121	R. Aaij et al.	(LHCb Collab.)
ADACHI	25O	JHEP 2504 114	I. Adachi et al.	(BELLE and BELLEII Collab.)
AAIJ	24A	PRL 132 051802	R. Aaij et al.	(LHCb Collab.)
AAIJ	24AK	PR D110 072014	R. Aaij et al.	(LHCb Collab.)
AAIJ	24F	JHEP 2402 032	R. Aaij et al.	(LHCb Collab.)
AAIJ	24M	JHEP 2405 025	R. Aaij et al.	(LHCb Collab.)
AAIJ	24O	JHEP 2405 253	R. Aaij et al.	(LHCb Collab.)
AAIJ	24Q	JHEP 2407 101	R. Aaij et al.	(LHCb Collab.)
AAIJ	24S	JHEP 2408 093	R. Aaij et al.	(LHCb Collab.)
ALONSO-ALV...	24	EPJ C84 553	G. Alonso-Alvarez, M.E. Abenza	(MCGI, TNTO+)
HAYRAPETY...	24AX	JHEP 2410 247	A. Hayrapetyan et al.	(CMS Collab.)
KUMAR	24	PR D109 032007	D. Kumar et al.	(BELLE Collab.)
AAD	23BY	JHEP 2309 199	G. Aad et al.	(ATLAS Collab.)
AAIJ	23AD	PRL 131 091901	R. Aaij et al.	(LHCb Collab.)
AAIJ	23AP	JHEP 2307 084	R. Aaij et al.	(LHCb Collab.)
AAIJ	23AT	PRL 131 171802	R. Aaij et al.	(LHCb Collab.)
AAIJ	23AY	JHEP 2310 106	R. Aaij et al.	(LHCb Collab.)
AAIJ	23AZ	JHEP 2310 123	R. Aaij et al.	(LHCb Collab.)
AAIJ	23G	JHEP 2306 073	R. Aaij et al.	(LHCb Collab.)
AAIJ	23J	JHEP 2307 119	R. Aaij et al.	(LHCb Collab.)
AAIJ	23P	EPJ C83 629	R. Aaij et al.	(LHCb Collab.)
AAIJ	23T	PR D108 012007	R. Aaij et al.	(LHCb Collab.)
AAIJ	23Y	PR D108 012021	R. Aaij et al.	(LHCb Collab.)
BORAH	23	PR D107 L051101	J. Borah et al.	(BELLE Collab.)
NAYAK	23	JHEP 2308 178	M. Nayak et al.	(BELLE Collab.)
TUMASYAN	23A	PL B842 137955	A. Tumasyan et al.	(CMS Collab.)
ZHUKOVA	23	JHEP 2308 131	V. Zhukova et al.	(BELLE Collab.)
AAIJ	22	PRL 128 041801	R. Aaij et al.	(LHCb Collab.)
Also		PR D105 012010	R. Aaij et al.	(LHCb Collab.)
AAIJ	22B	NATP 18 1	R. Aaij et al.	(LHCb Collab.)
AAIJ	22N	PR D105 072005	R. Aaij et al.	(LHCb Collab.)
AAIJ	22Q	JHEP 2203 109	R. Aaij et al.	(LHCb Collab.)
BHUYAN	22	PR D105 012007	B. Bhuyan et al.	(BELLE Collab.)
PANG	22	PR D106 L051103	T. Pang et al.	(BELLE Collab.)
TUMASYAN	22AI	EPJ C82 499	A. Tumasyan et al.	(CMS Collab.)
WANG	22	PR D105 012004	B. Wang et al.	(BELLE Collab.)
AAD	21AE	EPJ C81 342	G. Aad et al.	(ATLAS Collab.)
AAIJ	21AG	PRL 127 151801	R. Aaij et al.	(LHCb Collab.)
AAIJ	21AK	JHEP 2111 043	R. Aaij et al.	(LHCb Collab.)
AAIJ	21AN	EPJ C81 1026	R. Aaij et al.	(LHCb Collab.)
AAIJ	21C	JHEP 2102 024	R. Aaij et al.	(LHCb Collab.)
AAIJ	21G	PRL 126 081804	R. Aaij et al.	(LHCb Collab.)
AAIJ	21M	JHEP 2103 137	R. Aaij et al.	(LHCb Collab.)
AAIJ	21N	JHEP 2103 099	R. Aaij et al.	(LHCb Collab.)
AAIJ	21O	JHEP 2103 075	R. Aaij et al.	(LHCb Collab.)
AAIJ	21S	JHEP 2106 177	R. Aaij et al.	(LHCb Collab.)
AAIJ	21Y	PR D104 032005	R. Aaij et al.	(LHCb Collab.)
DUBEY	21	PR D104 012007	S. Dubey et al.	(BELLE Collab.)
NISAR	21	PR D104 L031101	N.K. Nisar et al.	(BELLE Collab.)
SIRUNYAN	21E	PL B816 136188	A.M. Sirunyan et al.	(CMS Collab.)
AAIJ	20AW	JHEP 2012 144	R. Aaij et al.	(LHCb Collab.)
AAIJ	20E	PR D101 072004	R. Aaij et al.	(LHCb Collab.)
AAIJ	20F	PR D102 012011	R. Aaij et al.	(LHCb Collab.)
AAIJ	20W	PRL 124 211802	R. Aaij et al.	(LHCb Collab.)
PDG	20	PTEP 2020 083C01	P.A. Zyla et al.	(PDG Collab.)
SIRUNYAN	20AG	JHEP 2004 188	A.M. Sirunyan et al.	(CMS Collab.)
SIRUNYAN	20BB	PRL 125 152001	A.M. Sirunyan et al.	(CMS Collab.)
AABOUD	19L	JHEP 1904 098	M. Aaboud et al.	(ATLAS Collab.)
AAIJ	19AE	PRL 123 081802	R. Aaij et al.	(LHCb Collab.)
AAIJ	19AF	PL B797 134789	R. Aaij et al.	(LHCb Collab.)
AAIJ	19AK	PRL 123 211801	R. Aaij et al.	(LHCb Collab.)
AAIJ	19AP	JHEP 1912 155	R. Aaij et al.	(LHCb Collab.)
AAIJ	19K	JHEP 1906 114	R. Aaij et al.	(LHCb Collab.)
AAIJ	19L	JHEP 1907 032	R. Aaij et al.	(LHCb Collab.)
AAIJ	19Q	EPJ C79 706	R. Aaij et al.	(LHCb Collab.)
Also		EPJ C80 601 (errat.)	R. Aaij et al.	(LHCb Collab.)
AAIJ	19U	PRL 122 191804	R. Aaij et al.	(LHCb Collab.)
AAIJ	18AB	JHEP 1807 020	R. Aaij et al.	(LHCb Collab.)
AAIJ	18AC	JHEP 1808 191	R. Aaij et al.	(LHCb Collab.)
AAIJ	18AY	PR D98 071103	R. Aaij et al.	(LHCb Collab.)
AAIJ	18AZ	PR D98 072006	R. Aaij et al.	(LHCb Collab.)
AAIJ	18O	PR D98 032004	R. Aaij et al.	(LHCb Collab.)
AAIJ	18S	JHEP 1803 140	R. Aaij et al.	(LHCb Collab.)
AAIJ	18T	JHEP 1803 078	R. Aaij et al.	(LHCb Collab.)
AAIJ	18U	JHEP 1803 059	R. Aaij et al.	(LHCb Collab.)
SIRUNYAN	18BY	EPJ C78 457	A.M. Sirunyan et al.	(CMS Collab.)
AAIJ	17A	PR D95 012006	R. Aaij et al.	(LHCb Collab.)
AAIJ	17AI	PRL 118 191801	R. Aaij et al.	(LHCb Collab.)
AAIJ	17AJ	PRL 118 251802	R. Aaij et al.	(LHCb Collab.)
AAIJ	17AL	PRL 119 041802	R. Aaij et al.	(LHCb Collab.)
AAIJ	17AN	PRL 119 101801	R. Aaij et al.	(LHCb Collab.)
AAIJ	17B	PRL 118 021801	R. Aaij et al.	(LHCb Collab.)
AAIJ	17BA	JHEP 1705 158	R. Aaij et al.	(LHCb Collab.)
AAIJ	17BB	EPJ C77 609	R. Aaij et al.	(LHCb Collab.)
AAIJ	17BD	PR D96 051103	R. Aaij et al.	(LHCb Collab.)
AAIJ	17BF	PL B774 139	R. Aaij et al.	(LHCb Collab.)
AAIJ	17BJ	PRL 119 232001	R. Aaij et al.	(LHCb Collab.)
AAIJ	17BP	JHEP 1711 027	R. Aaij et al.	(LHCb Collab.)
AAIJ	17G	PRL 118 081801	R. Aaij et al.	(LHCb Collab.)
AAIJ	17N	JHEP 1703 001	R. Aaij et al.	(LHCb Collab.)
AAIJ	17U	JHEP 1707 021	R. Aaij et al.	(LHCb Collab.)
AAIJ	17V	JHEP 1708 037	R. Aaij et al.	(LHCb Collab.)
AABOUD	16L	EPJ C76 513	M. Aaboud et al.	(ATLAS Collab.)
AAD	16AP	JHEP 1608 147	G. Aad et al.	(ATLAS Collab.)
AAIJ	16	JHEP 1601 012	R. Aaij et al.	(LHCb Collab.)
AAIJ	16AK	PL B762 253	R. Aaij et al.	(LHCb Collab.)
AAIJ	16AL	PL B762 484	R. Aaij et al.	(LHCb Collab.)
AAIJ	16C	PRL 116 161802	R. Aaij et al.	(LHCb Collab.)
AAIJ	16E	PRL 116 241601	R. Aaij et al.	(LHCb Collab.)
AAIJ	16G	PRL 117 061803	R. Aaij et al.	(LHCb Collab.)
AAIJ	16L	PL B760 117	R. Aaij et al.	(LHCb Collab.)
AAIJ	16P	PR D93 092008	R. Aaij et al.	(LHCb Collab.)
AAIJ	16U	JHEP 1603 040	R. Aaij et al.	(LHCb Collab.)
ABAZOV	16C	PR D94 012001	V.M. Abazov et al.	(D0 Collab.)
KHACHATRY...	16Q	PL B756 84	V. Khachatryan et al.	(CMS Collab.)
KHACHATRY...	16S	PL B757 97	V. Khachatryan et al.	(CMS Collab.)
PAL	16	PRL 116 161801	B. Pal et al.	(BELLE Collab.)
AAIJ	15AC	JHEP 1505 019	R. Aaij et al.	(LHCb Collab.)
AAIJ	15AD	JHEP 1506 130	R. Aaij et al.	(LHCb Collab.)
AAIJ	15AF	JHEP 1507 166	R. Aaij et al.	(LHCb Collab.)
AAIJ	15AG	JHEP 1508 005	R. Aaij et al.	(LHCb Collab.)

Int. J. Mod. Phys. A 2026.41. Downloaded from www.worldscientific.com
by UNIVERSITY OF CALIFORNIA @ BERKELEY on 09/16/26. Re-use and distribution is strictly not permitted, except for Open Access articles.

AAIJ	15AL	JHEP 1506 131	R. Aaji *et al.*	(LHCb Collab.)
AAIJ	15AQ	JHEP 1509 179	R. Aaij *et al.*	(LHCb Collab.)
AAIJ	15AS	JHEP 1510 053	R. Aaij *et al.*	(LHCb Collab.)
AAIJ	15AV	JHEP 1511 082	R. Aaij *et al.*	(LHCb Collab.)
AAIJ	15BB	PR D92 112002	R. Aaij *et al.*	(LHCb Collab.)
AAIJ	15D	JHEP 1501 024	R. Aaij *et al.*	(LHCb Collab.)
AAIJ	15I	PRL 114 041801	R. Aaij *et al.*	(LHCb Collab.)
AAIJ	15K	PL B741 1	R. Aaij *et al.*	(LHCb Collab.)
AAIJ	15O	PRL 115 051801	R. Aaij *et al.*	(LHCb Collab.)
AAIJ	15S	PL B743 46	R. Aaij *et al.*	(LHCb Collab.)
AAIJ	15U	PL B747 484	R. Aaij *et al.*	(LHCb Collab.)
ABAZOV	15A	PRL 114 062001	V.M. Abazov *et al.*	(D0 Collab.)
ABAZOV	15L	PRL 115 161601	V.M. Abazov *et al.*	(D0 Collab.)
DUTTA	15	PR D91 011101	D. Dutta *et al.*	(BELLE Collab.)
KHACHATRY...	15BE	NAT 522 68	V. Khachatryan *et al.*	(CMS and LHCb Collab.)
OSWALD	15	PR D92 072013	C. Oswald *et al.*	(BELLE Collab.)
AAD	14U	PR D90 052007	G. Aad *et al.*	(ATLAS Collab.)
AAIJ	14AA	PRL 112 202001	R. Aaij *et al.*	(LHCb Collab.)
AAIJ	14AE	PR D90 052011	R. Aaij *et al.*	(LHCb Collab.)
AAIJ	14AX	PRL 113 172001	R. Aaij *et al.*	(LHCb Collab.)
AAIJ	14AY	PRL 113 211801	R. Aaij *et al.*	(LHCb Collab.)
AAIJ	14BF	JHEP 1411 060	R. Aaij *et al.*	(LHCb Collab.)
AAIJ	14BH	PR D90 072003	R. Aaij *et al.*	(LHCb Collab.)
AAIJ	14BM	NJP 16 123001	R. Aaij *et al.*	(LHCb Collab.)
AAIJ	14BN	PR D90 112002	R. Aaij *et al.*	(LHCb Collab.)
AAIJ	14BP	PL B739 218	R. Aaij *et al.*	(LHCb Collab.)
AAIJ	14BR	PR D89 092006	R. Aaij *et al.*	(LHCb Collab.)
AAIJ	14D	PL B728 607	R. Aaij *et al.*	(LHCb Collab.)
AAIJ	14E	JHEP 1404 114	R. Aaij *et al.*	(LHCb Collab.)
AAIJ	14F	PRL 112 111802	R. Aaij *et al.*	(LHCb Collab.)
AAIJ	14L	JHEP 1407 140	R. Aaij *et al.*	(LHCb Collab.)
AAIJ	14R	PL B736 446	R. Aaij *et al.*	(LHCb Collab.)
AAIJ	14S	PL B736 186	R. Aaij *et al.*	(LHCb Collab.)
AAIJ	14Y	PRL 112 091802	R. Aaij *et al.*	(LHCb Collab.)
AALTONEN	14P	PRL 113 242001	T. Aaltonen *et al.*	(CDF Collab.)
ABAZOV	14	PR D89 012002	V.M. Abazov *et al.*	(D0 Collab.)
PDG	14	CP C38 070001	K. Olive *et al.*	(PDG Collab.)
AAIJ	13	NP B867 1	R. Aaij *et al.*	(LHCb Collab.)
AAIJ	13A	NP B867 547	R. Aaij *et al.*	(LHCb Collab.)
AAIJ	13AA	NP B871 403	R. Aaij *et al.*	(LHCb Collab.)
AAIJ	13AB	NP B873 275	R. Aaij *et al.*	(LHCb Collab.)
AAIJ	13AC	NP B874 663	R. Aaij *et al.*	(LHCb Collab.)
AAIJ	13AL	PR D87 071101	R. Aaij *et al.*	(LHCb Collab.)
AAIJ	13AN	PR D87 072004	R. Aaij *et al.*	(LHCb Collab.)
AAIJ	13AP	PR D87 092007	R. Aaij *et al.*	(LHCb Collab.)
AAIJ	13AQ	PR D87 112009	R. Aaij *et al.*	(LHCb Collab.)
AAIJ	13AR	PR D87 112010	R. Aaij *et al.*	(LHCb Collab.)
AAIJ	13AW	PRL 110 211801	R. Aaij *et al.*	(LHCb Collab.)
AAIJ	13AX	PRL 110 221601	R. Aaij *et al.*	(LHCb Collab.)
AAIJ	13AY	PRL 110 241802	R. Aaij *et al.*	(LHCb Collab.)
AAIJ	13B	PRL 110 021801	R. Aaij *et al.*	(LHCb Collab.)
AAIJ	13BA	PRL 111 101805	R. Aaij *et al.*	(LHCb Collab.)
AAIJ	13BI	NJP 15 053021	R. Aaij *et al.*	(LHCb Collab.)
AAIJ	13BM	PRL 111 141801	R. Aaij *et al.*	(LHCb Collab.)
AAIJ	13BO	JHEP 1310 183	R. Aaij *et al.*	(LHCb Collab.)
AAIJ	13BP	JHEP 1310 143	R. Aaij *et al.*	(LHCb Collab.)
AAIJ	13BQ	JHEP 1310 005	R. Aaij *et al.*	(LHCb Collab.)
AAIJ	13BW	JHEP 1311 092	R. Aaij *et al.*	(LHCb Collab.)
AAIJ	13BX	PL B727 403	R. Aaij *et al.*	(LHCb Collab.)
AAIJ	13CF	EPJ C73 2655	R. Aaij *et al.*	(LHCb Collab.)
AAIJ	13L	JHEP 1303 067	R. Aaij *et al.*	(LHCb Collab.)
AAIJ	13X	JHEP 1307 084	R. Aaij *et al.*	(LHCb Collab.)
AAIJ	13Z	JHEP 1309 006	R. Aaij *et al.*	(LHCb Collab.)
AALTONEN	13F	PR D87 072003	T. Aaltonen *et al.*	(CDF Collab.)
ABAZOV	13	PRL 110 011801	V.M. Abazov *et al.*	(D0 Collab.)
ABAZOV	13C	PR D87 072006	V.M. Abazov *et al.*	(D0 Collab.)
CHATRCHYAN	13AW	PRL 111 101804	S. Chatrchyan *et al.*	(CMS Collab.)
ESEN	13	PR D87 031101	S. Esen *et al.*	(BELLE Collab.)
OSWALD	13	PR D87 072008	C. Oswald *et al.*	(BELLE Collab.)
Also		PR D90 119901 (errat.)	C. Oswald *et al.*	(BELLE Collab.)
SOLOVIEVA	13	PL B726 206	E. Solovieva *et al.*	(BELLE Collab.)
THORNE	13	PR D88 114006	F. Thorne *et al.*	(BELLE Collab.)
AAD	12AE	PL B713 387	G. Aad *et al.*	(ATLAS Collab.)
AAD	12CV	JHEP 1212 072	G. Aad *et al.*	(ATLAS Collab.)
AAIJ	12	PL B707 349	R. Aaij *et al.*	(LHCb Collab.)
AAIJ	12A	PL B708 55	R. Aaij *et al.*	(LHCb Collab.)
AAIJ	12AE	PR D85 112013	R. Aaij *et al.*	(LHCb Collab.)
AAIJ	12AG	JHEP 1206 115	R. Aaij *et al.*	(LHCb Collab.)
AAIJ	12AM	PRL 109 131801	R. Aaij *et al.*	(LHCb Collab.)
AAIJ	12AN	PRL 109 152002	R. Aaij *et al.*	(LHCb Collab.)
AAIJ	12AO	PR D86 052006	R. Aaij *et al.*	(LHCb Collab.)
AAIJ	12AP	PR D86 071102	R. Aaij *et al.*	(LHCb Collab.)
AAIJ	12AR	JHEP 1210 037	R. Aaij *et al.*	(LHCb Collab.)
AAIJ	12AX	PR D86 112005	R. Aaij *et al.*	(LHCb Collab.)
AAIJ	12B	PL B707 497	R. Aaij *et al.*	(LHCb Collab.)
AAIJ	12D	PRL 108 101803	R. Aaij *et al.*	(LHCb Collab.)
AAIJ	12E	PL B708 241	R. Aaij *et al.*	(LHCb Collab.)
AAIJ	12F	PL B709 50	R. Aaij *et al.*	(LHCb Collab.)
AAIJ	12I	PL B709 177	R. Aaij *et al.*	(LHCb Collab.)
AAIJ	12L	EPJ C72 2118	R. Aaij *et al.*	(LHCb Collab.)
AAIJ	12O	PL B713 172	R. Aaij *et al.*	(LHCb Collab.)
AAIJ	12P	PL B713 369	R. Aaij *et al.*	(LHCb Collab.)
AAIJ	12Q	PL B713 378	R. Aaij *et al.*	(LHCb Collab.)
AAIJ	12R	PL B716 393	R. Aaij *et al.*	(LHCb Collab.)
AAIJ	12S	PRL 108 151801	R. Aaij *et al.*	(LHCb Collab.)
AAIJ	12V	PRL 108 201601	R. Aaij *et al.*	(LHCb Collab.)
AAIJ	12W	PRL 108 231801	R. Aaij *et al.*	(LHCb Collab.)
AALTONEN	12AJ	PRL 109 171802	T. Aaltonen *et al.*	(CDF Collab.)
AALTONEN	12C	PRL 108 201801	T. Aaltonen *et al.*	(CDF Collab.)
AALTONEN	12D	PR D85 072002	T. Aaltonen *et al.*	(CDF Collab.)
AALTONEN	12L	PRL 108 211803	T. Aaltonen *et al.*	(CDF Collab.)
ABAZOV	12AF	PR D86 092011	V.M. Abazov *et al.*	(D0 Collab.)
ABAZOV	12C	PR D85 011103	V.M. Abazov *et al.*	(D0 Collab.)
ABAZOV	12D	PR D85 032006	V.M. Abazov *et al.*	(D0 Collab.)
CHATRCHYAN	12A	JHEP 1204 033	S. Chatrchyan *et al.*	(CMS Collab.)
LEES	12A	PR D85 011101	J.P. Lees *et al.*	(BABAR Collab.)
LI	12	PRL 108 181808	J. Li *et al.*	(BELLE Collab.)
PDG	12	PR D86 010001	J. Beringer *et al.*	(PDG Collab.)
AAIJ	11	PL B698 115	R. Aaij *et al.*	(LHCb Collab.)
AAIJ	11A	PL B698 14	R. Aaij *et al.*	(LHCb Collab.)
AAIJ	11B	PL B699 330	R. Aaij *et al.*	(LHCb Collab.)
AAIJ	11D	PL B706 32	R. Aaij	(LHCb Collab.)
AAIJ	11E	PR D84 092001	R. Aaij *et al.*	(LHCb Collab.)
Also		PR D85 039904 (errat.)	R. Aaij *et al.*	(LHCb Collab.)
AALTONEN	11A	PR D83 052012	T. Aaltonen *et al.*	(CDF Collab.)
AALTONEN	11AB	PR D84 052012	T. Aaltonen *et al.*	(CDF Collab.)
AALTONEN	11AG	PRL 107 191801	T. Aaltonen *et al.*	(CDF Collab.)
Also		PRL 107 239903 (errat.)	T. Aaltonen *et al.*	(CDF Collab.)
AALTONEN	11AI	PRL 107 201802	T. Aaltonen *et al.*	(CDF Collab.)
AALTONEN	11AN	PRL 107 261802	T. Aaltonen *et al.*	(CDF Collab.)
AALTONEN	11AP	PRL 107 272001	T. Aaltonen *et al.*	(CDF Collab.)
AALTONEN	11L	PRL 106 161801	T. Aaltonen *et al.*	(CDF Collab.)
AALTONEN	11N	PRL 106 181802	T. Aaltonen *et al.*	(CDF Collab.)
ABAZOV	11U	PR D84 052007	V.M. Abazov *et al.*	(D0 Collab.)
CHATRCHYAN	11T	PRL 107 191802	S. Chatrchyan *et al.*	(CMS Collab.)
LI	11	PRL 106 121802	J. Li *et al.*	(BELLE Collab.)
ABAZOV	10E	PR D82 012003	V.M. Abazov *et al.*	(D0 Collab.)
ABAZOV	10H	PRL 105 081801	V.M. Abazov *et al.*	(D0 Collab.)
Also		PR D82 032001	V.M. Abazov *et al.*	(D0 Collab.)
ABAZOV	10S	PL B693 539	V.M. Abazov *et al.*	(D0 Collab.)
ESEN	10	PRL 105 201802	S. Esen *et al.*	(BELLE Collab.)
LOUVOT	10	PRL 104 231801	R. LOUVOT *et al.*	(BELLE Collab.)
PENG	10	PR D82 072007	C.-C. Peng *et al.*	(BELLE Collab.)
AALTONEN	09AQ	PRL 103 191802	T. Aaltonen *et al.*	(CDF Collab.)
AALTONEN	09B	PR D79 011104	T. Aaltonen *et al.*	(CDF Collab.)
AALTONEN	09C	PRL 103 031801	T. Aaltonen *et al.*	(CDF Collab.)
AALTONEN	09P	PRL 102 201801	T. Aaltonen *et al.*	(CDF Collab.)
ABAZOV	09E	PRL 102 032001	V.M. Abazov *et al.*	(D0 Collab.)
ABAZOV	09G	PRL 102 051801	V.M. Abazov *et al.*	(D0 Collab.)
ABAZOV	09I	PRL 102 091801	V.M. Abazov *et al.*	(D0 Collab.)
ABAZOV	09Y	PR D79 111102	V.M. Abazov *et al.*	(D0 Collab.)
LOUVOT	09	PRL 102 021801	R. Louvot *et al.*	(BELLE Collab.)
AALTONEN	08F	PRL 100 021803	T. Aaltonen *et al.*	(CDF Collab.)
AALTONEN	08G	PRL 100 161802	T. Aaltonen *et al.*	(CDF Collab.)
AALTONEN	08J	PRL 100 121803	T. Aaltonen *et al.*	(CDF Collab.)
ABAZOV	08AM	PRL 101 241801	V.M. Abazov *et al.*	(D0 Collab.)
WICHT	08A	PRL 100 121801	J. Wicht *et al.*	(BELLE Collab.)
ABAZOV	07	PRL 98 121801	V.M. Abazov *et al.*	(D0 Collab.)
ABAZOV	07A	PRL 98 151801	V.M. Abazov *et al.*	(D0 Collab.)
ABAZOV	07N	PR D76 057101	V.M. Abazov *et al.*	(D0 Collab.)
ABAZOV	07Y	PRL 99 241801	V.M. Abazov *et al.*	(D0 Collab.)
ABULENCIA	07C	PRL 98 061802	A. Abulencia *et al.*	(CDF Collab.)
DRUTSKOY	07	PRL 98 052001	A. Drutskoy *et al.*	(BELLE Collab.)
DRUTSKOY	07A	PR D76 012002	A. Drutskoy *et al.*	(BELLE Collab.)
ABAZOV	06B	PRL 97 021802	V.M. Abazov *et al.*	(D0 Collab.)
ABAZOV	06G	PR D74 031107	V.M. Abazov *et al.*	(D0 Collab.)
ABAZOV	06V	PRL 97 241801	V.M. Abazov *et al.*	(D0 Collab.)
ABULENCIA	06J	PRL 96 191801	A. Abulencia *et al.*	(CDF Collab.)
ABULENCIA	06N	PRL 96 231801	A. Abulencia *et al.*	(CDF Collab.)
ABULENCIA	06Q	PRL 97 062003	A. Abulencia *et al.*	(CDF Collab.)
ABULENCIA,A	06D	PRL 97 211802	A. Abulencia *et al.*	(CDF Collab.)
ABULENCIA,A	06G	PRL 97 242003	A. Abulencia *et al.*	(CDF Collab.)
ACOSTA	06	PRL 96 202001	D. Acosta *et al.*	(CDF Collab.)
ABAZOV	05B	PRL 94 042001	V.M. Abazov *et al.*	(D0 Collab.)
ABAZOV	05W	PRL 95 171801	V.M. Abazov *et al.*	(D0 Collab.)
ACOSTA	05	PRL 94 101803	D. Acosta *et al.*	(CDF Collab.)
ACOSTA	05J	PRL 95 031801	D. Acosta *et al.*	(CDF Collab.)
ABDALLAH	04A	PL B585 63	J. Abdallah *et al.*	(DELPHI Collab.)
ABDALLAH	04J	EPJ C35 35	J. Abdallah *et al.*	(DELPHI Collab.)
ABDALLAH	03B	EPJ C28 155	J. Abdallah *et al.*	(DELPHI Collab.)
ABE	03	PR D67 012006	K. Abe *et al.*	(SLD Collab.)
HEISTER	03E	EPJ C29 143	A. Heister *et al.*	(ALEPH Collab.)
ABE	02V	PR D66 032009	K. Abe *et al.*	(SLD Collab.)
ACOSTA	02D	PR D65 111101	D. Acosta *et al.*	(CDF Collab.)
ACOSTA	02G	PR D66 112002	D. Acosta *et al.*	(CDF Collab.)
ABBIENDI	01D	EPJ C19 241	G. Abbiendi *et al.*	(OPAL Collab.)
BARATE	01E	EPJ C19 213	R. Barate *et al.*	(ALEPH Collab.)
ABE	00C	PR D62 071101	K. Abe *et al.*	(SLD Collab.)
ABREU	00Y	EPJ C16 555	P. Abreu *et al.*	(DELPHI Collab.)
ABREU,P	00G	EPJ C18 229	P. Abreu *et al.*	(DELPHI Collab.)
AFFOLDER	00N	PRL 85 4668	T. Affolder *et al.*	(CDF Collab.)
BARATE	00K	PL B486 286	R. Barate *et al.*	(ALEPH Collab.)
ABBIENDI	99S	EPJ C11 587	G. Abbiendi *et al.*	(OPAL Collab.)
ABE	99D	PR D59 032004	F. Abe *et al.*	(CDF Collab.)
ABE	99J	PRL 82 3576	F. Abe *et al.*	(CDF Collab.)
BARATE	99J	EPJ C7 553	R. Barate *et al.*	(ALEPH Collab.)
Also		EPJ C12 181 (errat.)	R. Barate *et al.*	(ALEPH Collab.)
ABE	98B	PR D57 5382	F. Abe *et al.*	(CDF Collab.)
ABE	98V	PRL 81 5742	F. Abe *et al.*	(CDF Collab.)
ACCIARRI	98S	PL B438 417	M. Acciarri *et al.*	(L3 Collab.)
ACKERSTAFF	98F	EPJ C2 407	K. Ackerstaff *et al.*	(OPAL Collab.)
ACKERSTAFF	98G	PL B426 161	K. Ackerstaff *et al.*	(OPAL Collab.)
BARATE	98C	EPJ C4 367	R. Barate *et al.*	(ALEPH Collab.)
BARATE	98Q	EPJ C4 387	R. Barate *et al.*	(ALEPH Collab.)
PDG	98	EPJ C3 1	C. Caso *et al.*	(PDG Collab.)
ACCIARRI	97B	PL B391 474	M. Acciarri *et al.*	(L3 Collab.)
ACCIARRI	97C	PL B391 481	M. Acciarri *et al.*	(L3 Collab.)
ACKERSTAFF	97U	ZPHY C76 401	K. Ackerstaff *et al.*	(OPAL Collab.)
ACKERSTAFF	97V	ZPHY C76 417	K. Ackerstaff *et al.*	(OPAL Collab.)
ADAM	97	PL B414 382	W. Adam *et al.*	(DELPHI Collab.)
ABE	96B	PR D53 3496	F. Abe *et al.*	(CDF Collab.)
ABE	96N	PRL 77 1945	F. Abe *et al.*	(CDF Collab.)
ABE	96Q	PR D54 6596	F. Abe *et al.*	(CDF Collab.)
ABREU	96F	ZPHY C71 11	P. Abreu *et al.*	(DELPHI Collab.)
ADAM	96D	ZPHY C72 207	W. Adam *et al.*	(DELPHI Collab.)
BUSKULIC	96E	ZPHY C69 585	D. Buskulic *et al.*	(ALEPH Collab.)
BUSKULIC	96M	PL B377 205	D. Buskulic *et al.*	(ALEPH Collab.)
BUSKULIC	96V	PL B384 471	D. Buskulic *et al.*	(ALEPH Collab.)
PDG	96	PR D54 1	R. M. Barnett *et al.*	(PDG Collab.)
ABE	95R	PRL 74 4988	F. Abe *et al.*	(CDF Collab.)
ABE	95Z	PRL 75 3068	F. Abe *et al.*	(CDF Collab.)
ACCIARRI	95H	PL B363 127	M. Acciarri *et al.*	(L3 Collab.)
ACCIARRI	95I	PL B363 137	M. Acciarri *et al.*	(L3 Collab.)
AKERS	95G	PL B350 273	R. Akers *et al.*	(OPAL Collab.)
AKERS	95J	ZPHY C66 555	R. Akers *et al.*	(OPAL Collab.)
BUSKULIC	95J	PL B356 409	D. Buskulic *et al.*	(ALEPH Collab.)
BUSKULIC	95O	PL B361 221	D. Buskulic *et al.*	(ALEPH Collab.)
ABREU	94D	PL B324 500	P. Abreu *et al.*	(DELPHI Collab.)
ABREU	94E	ZPHY C61 407	P. Abreu *et al.*	(DELPHI Collab.)
Also		PL B289 199	P. Abreu *et al.*	(DELPHI Collab.)
AKERS	94J	PL B337 196	R. Akers *et al.*	(OPAL Collab.)
AKERS	94L	PL B337 393	R. Akers *et al.*	(OPAL Collab.)
BUSKULIC	94B	PL B322 441	D. Buskulic *et al.*	(ALEPH Collab.)
BUSKULIC	94C	PL B322 275	D. Buskulic *et al.*	(ALEPH Collab.)
ABE	93F	PRL 71 1685	F. Abe *et al.*	(CDF Collab.)
ACTON	93H	PL B312 501	P.D. Acton *et al.*	(OPAL Collab.)
BUSKULIC	93G	PL B311 425	D. Buskulic *et al.*	(ALEPH Collab.)
ABREU	92M	PL B289 199	P. Abreu *et al.*	(DELPHI Collab.)
ACTON	92N	PL B295 357	P.D. Acton *et al.*	(OPAL Collab.)
BUSKULIC	92E	PL B294 145	D. Buskulic *et al.*	(ALEPH Collab.)
LEE-FRANZINI	90	PRL 65 2947	J. Lee-Franzini *et al.*	(CUSB II Collab.)

Int. J. Mod. Phys. A 2026.41. Downloaded from www.worldscientific.com by CALIFORNIA @ BERKELEY on 09/16/26. Re-use and distribution is strictly not permitted, except for Open Access articles.

B_s^*

$I(J^P) = 0(1^-)$

I, J, P need confirmation. Quantum numbers shown are quark-model predictions.

B_s^* MASS

From mass difference below and the B_s^0 mass.

VALUE (MeV)	DOCUMENT ID		TECN	COMMENT
5415.4±1.4 OUR FIT Error includes scale factor of 2.6.				
5415.8±1.5 OUR AVERAGE Error includes scale factor of 2.6.				
5416.4±0.4±0.5	LOUVOT	09	BELL	$e^+e^- \to \Upsilon(5S)$
5411.7±1.6±0.6	[1] AQUINES	06	CLEO	$e^+e^- \to \Upsilon(5S)$
• • • We do not use the following data for averages, fits, limits, etc. • • •				
5418 ±1 ±3	DRUTSKOY	07A	BELL	Repl. by LOUVOT 09
5414 ±1 ±3	[2] BONVICINI	06	CLEO	$e^+e^- \to \Upsilon(5S)$

[1] Utilized the beam constrained invariant mass peak positions for B^* and B_s^* to extract the measurement.
[2] Uses 14 candidates consistent with B_s decays into final states with a J/ψ and a $D_s^{(*)-}$.

$m_{B_s^*} - m_{B_s}$

VALUE (MeV)	DOCUMENT ID		TECN	COMMENT
48.5±1.4 OUR FIT Error includes scale factor of 2.6.				
46.1±1.5 OUR AVERAGE				
45.7±1.7±0.7	[3] AQUINES	06	CLEO	$e^+e^- \to \Upsilon(5S)$
47.0±2.6	[4] LEE-FRANZINI	90	CSB2	$e^+e^- \to \Upsilon(5S)$
• • • We do not use the following data for averages, fits, limits, etc. • • •				
48 ±1 ±3	[5] BONVICINI	06	CLEO	Repl. by AQUINES 06

[3] Utilized the beam constrained invariant mass peak positions for B^* and B_s^* to extract the measurement.
[4] LEE-FRANZINI 90 measure 46.7 ± 0.4 ± 0.2 MeV for an admixture of B^0, B^+, and B_s. They use the shape of the photon line to separate the above value for B_s.
[5] Uses 14 candidates consistent with B_s decays into final states with a J/ψ and a $D_s^{(*)-}$.

$|(m_{B_s^*} - m_{B_s}) - (m_{B^*} - m_B)|$

VALUE (MeV)	CL%	DOCUMENT ID		TECN	COMMENT
<6	95	ABREU	95R	DLPH	E_{cm}^{ee}= 88–94 GeV

B_s^* DECAY MODES

	Mode	Fraction (Γ_i/Γ)
Γ_1	$B_s\gamma$	seen

B_s^* REFERENCES

LOUVOT	09	PRL 102 021801	R. Louvot *et al.*	(BELLE Collab.)
DRUTSKOY	07A	PR D76 012002	A. Drutskoy *et al.*	(BELLE Collab.)
AQUINES	06	PRL 96 152001	O. Aquines *et al.*	(CLEO Collab.)
BONVICINI	06	PRL 96 022002	G. Bonvicini *et al.*	(CLEO Collab.)
ABREU	95R	ZPHY C68 353	P. Abreu *et al.*	(DELPHI Collab.)
LEE-FRANZINI	90	PRL 65 2947	J. Lee-Franzini *et al.*	(CUSB II Collab.)

$B_{s1}(5830)^0$

$I(J^P) = 0(1^+)$

I, J, P need confirmation.

Quantum numbers shown are quark-model predictions.

$B_{s1}(5830)^0$ MASS

VALUE (MeV)	DOCUMENT ID		TECN	COMMENT
5828.73±0.20 OUR FIT				
5828.65±0.24 OUR AVERAGE				
5828.78±0.09±0.29	SIRUNYAN	18DF	CMS	pp at 8 TeV
5828.40±0.04±0.41	[1] AAIJ	13O	LHCB	pp at 7 TeV
• • • We do not use the following data for averages, fits, limits, etc. • • •				
5829.4 ±0.7	[2] AALTONEN	08K	CDF	Repl. by AALTONEN 14I

[1] Uses $B_{s1}(5830)^0 \to B^{*+}K^-$ decay.
[2] Uses two-body decays into K^- and B^+ mesons reconstructed as $B^+ \to J/\psi K^+$, $J/\psi \to \mu^+\mu^-$ or $B^+ \to \overline{D}^0\pi^+$, $\overline{D}^0 \to K^+\pi^-$.

$m_{B_{s1}^0} - m_{B^{*+}}$

VALUE (MeV)	DOCUMENT ID		TECN	COMMENT
503.98±0.17 OUR FIT				
504.03±0.12±0.15	[1] AALTONEN	14I	CDF	$p\overline{p}$ at 1.96 TeV
• • • We do not use the following data for averages, fits, limits, etc. • • •				
504.41±0.21±0.14	[2] AALTONEN	08K	CDF	Repl. by AALTONEN 14I

[1] AALTONEN 14I reports $m_{B_{s1}(5830)^0} - m_{B^{*+}} - m_{K^-} = 10.35 \pm 0.12 \pm 0.15$ MeV which we adjusted by the K^- mass.
[2] Uses two-body decays into K^- and B^+ mesons reconstructed as $B^+ \to J/\psi K^+$, $J/\psi \to \mu^+\mu^-$ or $B^+ \to \overline{D}^0\pi^+$, $\overline{D}^0 \to K^+\pi^-$.

$B_{s1}(5830)^0$ WIDTH

VALUE (MeV)	DOCUMENT ID		TECN	COMMENT
0.5±0.3±0.3	AALTONEN	14I	CDF	$p\overline{p}$ at 1.96 TeV

$B_{s1}(5830)^0$ DECAY MODES

	Mode	Fraction (Γ_i/Γ)
Γ_1	$B^{*+}K^-$	seen
Γ_2	$B^{*0}K_S^0$	

$B_{s1}(5830)^0$ BRANCHING RATIOS

$\Gamma(B^{*+}K^-)/\Gamma_{total}$ — **Γ_1/Γ**

VALUE	DOCUMENT ID		TECN	COMMENT
seen	AALTONEN	08K	CDF	$p\overline{p}$ at 1.96 TeV

$\Gamma(B^{*0}K_S^0)/\Gamma(B^{*+}K^-)$ — **Γ_2/Γ_1**

VALUE	DOCUMENT ID		TECN	COMMENT
0.49±0.12±0.07	[1] SIRUNYAN	18DF	CMS	pp at 8 TeV

[1] With the branching fractions $B(B^+ \to J/\psi K^+) = (1.026 \pm 0.031) \times 10^{-3}$ and $B(B^0 \to J/\psi K^{*0}) = (1.28 \pm 0.05) \times 10^{-3}$.

$B_{s1}(5830)^0$ REFERENCES

SIRUNYAN	18DF	EPJ C78 939	A.M. Sirunyan *et al.*	(CMS Collab.)
AALTONEN	14I	PR D90 012013	T. Aaltonen *et al.*	(CDF Collab.)
AAIJ	13O	PRL 110 151803	R. Aaij *et al.*	(LHCb Collab.)
AALTONEN	08K	PRL 100 082001	T. Aaltonen *et al.*	(CDF Collab.)

$B_{s2}^*(5840)^0$

$I(J^P) = 0(2^+)$

I, J, P need confirmation.

Quantum numbers shown are quark-model predictions.

$B_{s2}^*(5840)^0$ MASS

VALUE (MeV)	DOCUMENT ID		TECN	COMMENT
5839.88±0.12 OUR FIT				
5839.92±0.14 OUR AVERAGE				
5839.86±0.09±0.17	SIRUNYAN	18DF	CMS	pp at 8 TeV
5839.99±0.05±0.20	AAIJ	13O	LHCB	pp at 7 TeV
5839.6 ±1.1 ±0.7	[1] ABAZOV	08E	D0	$p\overline{p}$ at 1.96 TeV
• • • We do not use the following data for averages, fits, limits, etc. • • •				
5839.7 ±0.7	[2] AALTONEN	08K	CDF	Repl. by AALTONEN 14I

[1] Observed in $B_{s2}^{*0} \to B^+K^-$. Measured production rate of B_{s2}^{*0} relative to B^+ to be (1.15 ± 0.23 ± 0.13)%.
[2] Uses two-body decays into K^- and B^+ mesons reconstructed as $B^+ \to J/\psi K^+$, $J/\psi \to \mu^+\mu^-$ or $B^+ \to \overline{D}^0\pi^+$, $\overline{D}^0 \to K^+\pi^-$.

$m_{B_{s2}^{*0}} - m_{B_{s1}^0}$

VALUE (MeV)	DOCUMENT ID		TECN	COMMENT
• • • We do not use the following data for averages, fits, limits, etc. • • •				
10.5±0.6	[1] AALTONEN	08K	CDF	Repl. by AALTONEN 14I

[1] Uses two-body decays into K^- and B^+ mesons reconstructed as $B^+ \to J/\psi K^+$, $J/\psi \to \mu^+\mu^-$ or $B^+ \to \overline{D}^0\pi^+$, $\overline{D}^0 \to K^+\pi^-$.

$m_{B_{s2}^{*0}} - m_{B^+}$

VALUE (MeV)	DOCUMENT ID		TECN	COMMENT
560.48±0.12 OUR FIT				
560.41±0.13±0.14	[1] AALTONEN	14I	CDF	$p\overline{p}$ at 1.96 TeV

[1] AALTONEN 14I reports $m_{B_{s2}(5840)^0} - m_{B^+} - m_{K^-} = 66.73 \pm 0.13 \pm 0.14$ MeV which we adjusted by the K^- mass.

$B_{s2}^*(5840)^0$ WIDTH

VALUE (MeV)	DOCUMENT ID		TECN	COMMENT
1.49±0.27 OUR AVERAGE				
1.52±0.34±0.30	SIRUNYAN	18DF	CMS	pp at 8 TeV
1.4 ±0.4 ±0.2	AALTONEN	14I	CDF	$p\overline{p}$ at 1.96 TeV
1.56±0.13±0.47	[1] AAIJ	13O	LHCB	pp at 7 TeV

[1] Uses $B_{s2}^*(5840)^0 \to B^{*+}K^-$ decays.

Int. J. Mod. Phys. A 2026.41. Downloaded from www.worldscientific.com by UNIVERSITY OF CALIFORNIA @ BERKELEY on 09/16/26. Re-use and distribution is strictly not permitted, except for Open Access articles.

$B^*_{s2}(5840)^0$ DECAY MODES

Branching fractions are given relative to the one **DEFINED AS 1**.

	Mode	Fraction (Γ_i/Γ)
Γ_1	$B^+ K^-$	**DEFINED AS 1**
Γ_2	$B^{*+} K^-$	0.093±0.018
Γ_3	$B^0 K^0_S$	0.43 ±0.11
Γ_4	$B^{*0} K^0_S$	0.04 ±0.04

$B^*_{s2}(5840)^0$ BRANCHING RATIOS

$\Gamma(B^+ K^-)/\Gamma_{total}$ — **Γ_1/Γ**

VALUE	DOCUMENT ID		TECN	COMMENT
seen	AALTONEN	08K	CDF	$p\overline{p}$ at 1.96 TeV
seen	[1] ABAZOV	08E	D0	$p\overline{p}$ at 1.96 TeV

[1] Measured production rate of B^{*0}_{s2} relative to B^+ to be (1.15 ± 0.23 ± 0.13)%.

$\Gamma(B^{*+} K^-)/\Gamma(B^+ K^-)$ — **Γ_2/Γ_1**

VALUE	DOCUMENT ID		TECN	COMMENT
0.093±0.013±0.012	AAIJ	13O	LHCB	pp at 7 TeV

$\Gamma(B^{*0} K^0_S)/\Gamma(B^0 K^0_S)$ — **Γ_4/Γ_3**

VALUE	DOCUMENT ID		TECN	COMMENT
0.093±0.086±0.014	[1] SIRUNYAN	18DF	CMS	pp at 8 TeV

[1] With the branching fraction B($B^0 \to J/\psi K^{*0}$) = (1.28 ± 0.05) × 10^{-3}.

$\Gamma(B^0 K^0_S)/\Gamma(B^+ K^-)$ — **Γ_3/Γ_1**

VALUE	DOCUMENT ID		TECN	COMMENT
0.432±0.077±0.078	[1] SIRUNYAN	18DF	CMS	pp at 8 TeV

[1] With the branching fractions B($B^+ \to J/\psi K^+$) = (1.026 ± 0.031) × 10^{-3} and B($B^0 \to J/\psi K^{*0}$) = (1.28 ± 0.05) × 10^{-3}.

$\Gamma(B^{*+} K^-)/\Gamma(B^+ K^-)$ — **Γ_2/Γ_1**

VALUE	DOCUMENT ID		TECN	COMMENT
0.081±0.021±0.015	[1] SIRUNYAN	18DF	CMS	pp at 8 TeV

[1] With the branching fraction B($B^+ \to J/\psi K^+$) = (1.026 ± 0.031) × 10^{-3}.

$B^*_{s2}(5840)^0$ REFERENCES

SIRUNYAN	18DF	EPJ C78 939	A.M. Sirunyan *et al.*	(CMS Collab.)
AALTONEN	14I	PR D90 012013	T. Aaltonen *et al.*	(CDF Collab.)
AAIJ	13O	PRL 110 151803	R. Aaij *et al.*	(LHCb Collab.)
AALTONEN	08K	PRL 100 082001	T. Aaltonen *et al.*	(CDF Collab.)
ABAZOV	08E	PRL 100 082002	V.M. Abazov *et al.*	(D0 Collab.)

$B^*_{sJ}(5850)$

$I(J^P) = ?(?^?)$

OMITTED FROM SUMMARY TABLE

Signal can be interpreted as coming from $\overline{b}s$ states. Needs confirmation.

$B^*_{sJ}(5850)$ MASS

VALUE (MeV)	EVTS	DOCUMENT ID		TECN	COMMENT
5853±15	141	AKERS	95E	OPAL	E^{ee}_{cm}= 88–94 GeV

$B^*_{sJ}(5850)$ WIDTH

VALUE (MeV)	EVTS	DOCUMENT ID		TECN	COMMENT
47±22	141	AKERS	95E	OPAL	E^{ee}_{cm}= 88–94 GeV

$B^*_{sJ}(5850)$ REFERENCES

AKERS	95E	ZPHY C66 19	R. Akers *et al.*	(OPAL Collab.)

$B_{sJ}(6063)^0$

$I(J^P) = 0(?^?)$

OMITTED FROM SUMMARY TABLE

$B_{sJ}(6063)^0$ MASS

VALUE (MeV)	DOCUMENT ID		TECN	COMMENT
6063.5±1.2±0.8	[1] AAIJ	21D	LHCB	pp at 7, 8, 13 TeV

[1] Seen in the decay channel $B^\pm K^\mp$. Integrated luminosity = 9 fb^{-1}.

$B_{sJ}(6063)^0$ WIDTH

VALUE (MeV)	DOCUMENT ID		TECN	COMMENT
26±4±4	[1] AAIJ	21D	LHCB	pp at 7, 8, 13 TeV

[1] Seen in the decay channel $B^\pm K^\mp$. Integrated luminosity = 9 fb^{-1}.

$B_{sJ}(6063)^0$ DECAY MODES

	Mode	Fraction (Γ_i/Γ)
Γ_1	$B^+ K^-$	seen

$B_{sJ}(6063)^0$ BRANCHING RATIOS

$\Gamma(B^+ K^-)/\Gamma_{total}$ — **Γ_1/Γ**

VALUE	DOCUMENT ID		TECN	COMMENT
seen	AAIJ	21D	LHCB	$B^\pm K^\mp$ mass spectrum

$B_{sJ}(6063)^0$ REFERENCES

AAIJ	21D	EPJ C81 601	R. Aaij *et al.*	(LHCb Collab.)

$B_{sJ}(6114)^0$

$I(J^P) = 0(?^?)$

OMITTED FROM SUMMARY TABLE

$B_{sJ}(6114)^0$ MASS

VALUE (MeV)	DOCUMENT ID		TECN	COMMENT
6114±3±5	[1] AAIJ	21D	LHCB	pp at 7, 8, 13 TeV

[1] Seen in the decay channel $B^\pm K^\mp$. Integrated luminosity = 9 fb^{-1}.

$B_{sJ}(6114)^0$ WIDTH

VALUE (MeV)	DOCUMENT ID		TECN	COMMENT
66±18±21	[1] AAIJ	21D	LHCB	pp at 7, 8, 13 TeV

[1] Seen in the decay channel $B^\pm K^\mp$. Integrated luminosity = 9 fb^{-1}.

$B_{sJ}(6114)^0$ DECAY MODES

	Mode	Fraction (Γ_i/Γ)
Γ_1	$B^+ K^-$	seen

$B_{sJ}(6114)^0$ BRANCHING RATIOS

$\Gamma(B^+ K^-)/\Gamma_{total}$ — **Γ_1/Γ**

VALUE	DOCUMENT ID		TECN	COMMENT
seen	AAIJ	21D	LHCB	$B^\pm K^\mp$ mass spectrum

$B_{sJ}(6114)^0$ REFERENCES

AAIJ	21D	EPJ C81 601	R. Aaij *et al.*	(LHCb Collab.)

BOTTOM, CHARMED MESONS
($B = C = \pm 1$)

$B_c^+ = c\overline{b}$, $B_c^- = \overline{c}b$, similarly for B_c^*'s

B_c^+

$I(J^P) = 0(0^-)$
I, J, P need confirmation.

Quantum numbers shown are quark-model predictions.

B_c^+ MASS

VALUE (MeV)	DOCUMENT ID		TECN	COMMENT
6274.47± 0.27± 0.17	[1] AAIJ	20R	LHCB	pp at 7, 8, 13 TeV
• • • We do not use the following data for averages, fits, limits, etc. • • •				
6274.28± 1.40± 0.32	[2] AAIJ	17L	LHCB	Repl. by AAIJ 20R
6274.0 ± 1.8 ± 0.4	[3] AAIJ	14AQ	LHCB	Repl. by AAIJ 20R
6276.28± 1.44± 0.36	[4] AAIJ	13AS	LHCB	Repl. by AAIJ 20R
6273.7 ± 1.3 ± 1.6	[5] AAIJ	12AV	LHCB	Repl. by AAIJ 20R
6275.6 ± 2.9 ± 2.5	[6] AALTONEN	08M	CDF	$p\overline{p}$ at 1.96 TeV
6300 ± 14 ± 5	[6] ABAZOV	08T	D0	$p\overline{p}$ at 1.96 TeV
6285.7 ± 5.3 ± 1.2	[6] ABULENCIA	06C	CDF	Repl. by AALTONEN 08M
6400 ±390 ±130	[7] ABE	98M	CDF	$p\overline{p}$ at 1.8 TeV
6320 ± 60	[8] ACKERSTAFF	98O	OPAL	$e^+e^- \to Z$

[1] AAIJ 20R uses the $B_c^+ \to J/\psi\pi^+$, $J/\psi\pi^+\pi^-\pi^+$, $J/\psi p\overline{p}\pi^+$, $J/\psi D_s^+$, $J/\psi D^0 K^+$ and $B_s^0\pi^+$ modes.

[2] Measured using $B_c^+ \to J/\psi D^0 K^+$ decays.

[3] Uses $B_c^+ \to J/\psi p\overline{p}\pi^+$ decays.

[4] AAIJ 13AS uses the $B_c^+ \to J/\psi D_s^+$.

[5] AAIJ 12AV uses the $B_c^+ \to J/\psi\pi^+$ mode and also measures the mass difference $M(B_c^+) - M(B^+) = 994.6 \pm 1.3 \pm 0.6$ MeV/c^2.

[6] Measured using a fully reconstructed decay mode of $B_c \to J/\psi\pi$.

[7] ABE 98M observed $20.4^{+6.2}_{-5.5}$ events in the $B_c^+ \to J/\psi(1s)\ell\nu_\ell$ with a significance of > 4.8 standard deviations. The mass value is estimated from $m(J/\psi(1S)\ell)$.

[8] ACKERSTAFF 98O observed 2 candidate events in the $B_c^+ \to J/\psi(1S)\pi^+$ channel with an estimated background of 0.63 ± 0.20 events.

$m_{B_c^+} - m_{B_s^0}$

VALUE (MeV)	DOCUMENT ID		TECN	COMMENT
907.75±0.37±0.27	[1] AAIJ	20R	LHCB	pp at 7, 8, 13 TeV

[1] AAIJ 20R uses the $B_c^+ \to J/\psi\pi^+$, $J/\psi\pi^+\pi^-\pi^+$, $J/\psi p\overline{p}\pi^+$, $J/\psi D_s^+$, $J/\psi D^0 K^+$ and $B_s^0\pi^+$ modes.

B_c^+ MEAN LIFE

VALUE (10^{-12} s)	DOCUMENT ID		TECN	COMMENT
0.510 ±0.009 OUR EVALUATION	(Produced by HFLAV)			
0.510 ±0.009 OUR AVERAGE				
0.541 ±0.026 ±0.014	[1] SIRUNYAN	18BY	CMS	pp at 8 TeV
0.5134±0.0110±0.0057	[2,3] AAIJ	15G	LHCB	pp at 7, 8 TeV
0.509 ±0.008 ±0.012	[4] AAIJ	14G	LHCB	pp at 8 TeV
0.452 ±0.048 ±0.027	[3] AALTONEN	13	CDF	$p\overline{p}$ at 1.96 TeV
0.448 $^{+0.038}_{-0.036}$ ±0.032	[5] ABAZOV	09H	D0	$p\overline{p}$ at 1.96 TeV
0.463 $^{+0.073}_{-0.065}$ ±0.036	[5] ABULENCIA	06O	CDF	$p\overline{p}$ at 1.96 TeV
0.46 $^{+0.18}_{-0.16}$ ±0.03	[5] ABE	98M	CDF	$p\overline{p}$ 1.8 TeV

[1] The lifetime is measured using the decays $B_c^+ \to J/\psi\pi^+$ and $B^+ \to J/\psi K^+$.

[2] Also measures the width difference $\Delta\Gamma = \Gamma_{B_c^+} - \Gamma_{B^+} = 4.46 \pm 0.14 \pm 0.07$ mm^{-1} c.

[3] Uses fully reconstructed $B_c^+ \to J/\psi\pi^+$ decays.

[4] Measured using $B_c^+ \to J/\psi\mu^+\nu_\mu X$ decays.

[5] The lifetime is measured from the $J/\psi e$ decay vertices.

B_c^+ DECAY MODES × B($\overline{b} \to B_c$)

The following quantities are not pure branching ratios; rather the fractions $\Gamma_i/\Gamma \times B(\overline{b} \to B_c)$. B_c^- modes are charge conjugates of the modes below.

	Mode	Fraction (Γ_i/Γ)	Confidence level
Γ_1	$J/\psi(1S)\ell^+\nu_\ell$ anything	seen	
Γ_2	$J/\psi(1S)\mu^+\nu_\mu$	seen	
Γ_3	$J/\psi(1S)\tau^+\nu_\tau$	seen	
Γ_4	$J/\psi(1S)\pi^+$	seen	
Γ_5	$J/\psi(1S)K^+$	seen	
Γ_6	$J/\psi(1S)\pi^+\pi^0$		
Γ_7	$J/\psi(1S)\pi^+\pi^+\pi^-$	seen	
Γ_8	$J/\psi(1S)K^+\pi^-\pi^+$		
Γ_9	$J/\psi(1S)K^+K^-K^+$		
Γ_{10}	$J/\psi(1S)a_1(1260)$	not seen	
Γ_{11}	$J/\psi(1S)K^+K^-\pi^+$	seen	
Γ_{12}	$J/\psi(1S)\pi^+\pi^+\pi^+\pi^-\pi^-$	seen	
Γ_{13}	$\psi(2S)\pi^+$	seen	
Γ_{14}	$\psi(2S)\pi^+$, $\psi(2S) \to J/\psi\pi^+\pi^-$		
Γ_{15}	$\psi(2S)\pi^+\pi^-\pi^+$		
Γ_{16}	$\psi(2S)K^+K^-\pi^+$		
Γ_{17}	$J/\psi(1S)D^0K^+$	seen	
Γ_{18}	$J/\psi(1S)D^*(2007)^0K^+$	seen	
Γ_{19}	$J/\psi(1S)D^*(2010)^+K^{*0}$	seen	
Γ_{20}	$J/\psi(1S)D^+K^{*0}$	seen	
Γ_{21}	$J/\psi(1S)D_s^+$	seen	
Γ_{22}	$J/\psi(1S)D_s^{*+}$	seen	
Γ_{23}	$J/\psi(1S)p\overline{p}\pi^+$	seen	
Γ_{24}	$\chi_{c0}\pi^+$		
Γ_{25}	$\chi_{c1}\pi^+$		
Γ_{26}	$\chi_{c2}\pi^+$		
Γ_{27}	$\chi_{c1}(3872)\pi^+$, $\chi_{c1}(3872) \to J/\psi\pi^+\pi^-$		
Γ_{28}	$p\overline{p}\pi^+$	not seen	
Γ_{29}	D^0K^+	seen	
Γ_{30}	$D^0\pi^+$	not seen	
Γ_{31}	$D^{*0}\pi^+$	not seen	
Γ_{32}	$D^{*0}K^+$	not seen	
Γ_{33}	$D_s^+\overline{D}^0$	$<7.2 \times 10^{-4}$	90%
Γ_{34}	$D_s^+D^0$	$<3.0 \times 10^{-4}$	90%
Γ_{35}	$D^+\overline{D}^0$	$<1.9 \times 10^{-4}$	90%
Γ_{36}	D^+D^0	$<1.4 \times 10^{-4}$	90%
Γ_{37}	$D_s^{*+}\overline{D}^0$	$<5.3 \times 10^{-4}$	90%
Γ_{38}	$D_s^+\overline{D}^*(2007)^0$	$<4.6 \times 10^{-4}$	90%
Γ_{39}	$D_s^{*+}D^0$	$<9 \times 10^{-4}$	90%
Γ_{40}	$D_s^+D^*(2007)^0$	$<6.6 \times 10^{-4}$	90%
Γ_{41}	$D^*(2010)^+\overline{D}^0$	$<3.8 \times 10^{-4}$	90%
Γ_{42}	$D^*(2010)^+\overline{D}^0$, $D^{*+} \to D^+\pi^0/\gamma$	not seen	
Γ_{43}	$D^+\overline{D}^*(2007)^0$	$<6.5 \times 10^{-4}$	90%
Γ_{44}	$D^*(2007)^+D^0$	$<2.0 \times 10^{-4}$	90%
Γ_{45}	$D^*(2010)^+D^0$, $D^{*+} \to D^+\pi^0/\gamma$	not seen	
Γ_{46}	$D^+D^*(2007)^0$	$<3.7 \times 10^{-4}$	90%
Γ_{47}	$D_s^{*+}\overline{D}^*(2007)^0$	$<1.3 \times 10^{-3}$	90%
Γ_{48}	$D_s^{*+}D^*(2007)^0$	$<1.3 \times 10^{-3}$	90%
Γ_{49}	$D^*(2010)^+\overline{D}^*(2007)^0$	$<1.0 \times 10^{-3}$	90%
Γ_{50}	$D^*(2010)^+D^*(2007)^0$	$<7.7 \times 10^{-4}$	90%
Γ_{51}	D^+K^{*0}	not seen	
Γ_{52}	$D^+\overline{K}^{*0}$	not seen	
Γ_{53}	$D_s^+K^{*0}$	not seen	
Γ_{54}	$D_s^+\overline{K}^{*0}$	not seen	
Γ_{55}	$D_s^+\phi$	not seen	
Γ_{56}	K^+K^0	not seen	
Γ_{57}	π^+B^{*0}, $B^{*0} \to \mu^+\mu^-$		
Γ_{58}	$\pi^+B_s^{*0}$, $B_s^{*0} \to \mu^+\mu^-$		
Γ_{59}	$B_s^0\pi^+$ / B($\overline{b} \to B_s$)	seen	
Γ_{60}	$B_s^0\pi^+$		
Γ_{61}	$\pi^+\mu^+\mu^-$		
Γ_{62}	$D_s^+\mu^+\mu^-$		

B_c^+ BRANCHING RATIOS

$\Gamma(J/\psi(1S)\ell^+\nu_\ell \text{anything})/\Gamma_{\text{total}} \times B(\overline{b} \to B_c \text{ at } Z)$ — $\Gamma_1/\Gamma \times B$

VALUE (units 10^{-5})	CL%	DOCUMENT ID		TECN	COMMENT
8.2±1.3 OUR AVERAGE	Error includes scale factor of 1.4.				
8.8±1.0±0.2		[1,2] AALTONEN	16A	CDF	$p\overline{p}$ at 1.96 TeV
$5.2^{+2.4}_{-2.1}$		[3] ABE	98M	CDF	$p\overline{p}$ 1.8 TeV
• • • We do not use the following data for averages, fits, limits, etc. • • •					
<16	90	[4] ACKERSTAFF	98O	OPAL	$e^+e^- \to Z$
<19	90	[5] ABREU	97E	DLPH	$e^+e^- \to Z$
<12	90	[6] BARATE	97H	ALEP	$e^+e^- \to Z$

[1] AALTONEN 16A reports $[\Gamma(B_c^+ \to J/\psi(1S)\ell^+\nu_\ell \text{anything})/\Gamma_{\text{total}} \times B(\overline{b} \to B_c \text{ at } Z)]$ / $[B(\overline{b} \to B^+ \text{ at } Z)]$ / $[B(B^+ \to J/\psi(1S)K^+)] = 0.211 \pm 0.012^{+0.021}_{-0.020}$ which we

Int. J. Mod. Phys. A 2026.41. Downloaded from www.worldscientific.com
by CALIFORNIA @ BERKELEY on 09/16/26. Re-use and distribution is strictly not permitted, except for Open Access articles.

multiply by our best (shown rounded) values $B(\overline{b} \to B^+ \text{ at } Z) = (40.8 \pm 0.7) \times 10^{-2}$, $B(B^+ \to J/\psi(1S) K^+) = (1.019 \pm 0.019) \times 10^{-3}$. Our first error is their experiment's error and our second error is the systematic error from using our best (shown rounded) values.

[2] AALTONEN 16A also measures the cross-section $\sigma(B_c) \times B(B_c \to J/\psi \mu \nu_\mu) = 0.60 \pm 0.09$ nb and estimates the total cross-section $\sigma(B_c)$ to be in the range 25 ± 4 to 52 ± 8 nb for $p_T(B_c) > 6$ GeV/c and $|y(B_c)| < 1$.

[3] ABE 98M result is derived from the measurement of $[\sigma(B_c) \times B(B_c \to J/\psi(1S) \ell \nu_\ell)] / [\sigma(B^+) \times B(B^+ \to J/\psi(1S) K^+)] = 0.132 ^{+0.041}_{-0.037}(\text{stat}) \pm 0.031(\text{sys}) ^{+0.032}_{-0.020}(\text{lifetime})$ by using PDG 98 values of $B(b \to B^+)$ and $B(B^+ \to J/\psi(1S) K^+)$.

[4] ACKERSTAFF 98O reports $B(Z \to B_c X)/B(Z \to q q) \times B(B_c \to J/\psi(1S) \ell \nu_\ell) < 6.95 \times 10^{-5}$ at 90%CL. We rescale to our PDG 98 values of $B(Z \to b \overline{b})$.

[5] ABREU 97E value listed is for an assumed $\tau_{B_c} = 0.4$ ps and improves to 1.6×10^{-4} for $\tau_{B_c} = 1.4$ ps.

[6] BARATE 97H reports $B(Z \to B_c X)/B(Z \to q q) \cdot B(B_c \to J/\psi(1S) \ell \nu_\ell) < 5.2 \times 10^{-5}$ at 90%CL. We rescale to our PDG 96 values of $B(Z \to b \overline{b})$. A $B_c^+ \to J/\psi(1S) \mu^+ \nu_\mu$ candidate event is found, compared to all the known background sources 2×10^{-3}, which gives $m_{B_c} = 5.96 ^{+0.25}_{-0.19}$ GeV and $\tau_{B_c} = 1.77 \pm 0.17$ ps.

$\Gamma(J/\psi(1S) \tau^+ \nu_\tau)/\Gamma(J/\psi(1S) \mu^+ \nu_\mu)$ — Γ_3/Γ_2

VALUE	DOCUMENT ID		TECN	COMMENT
0.52±0.26 OUR AVERAGE	Error includes scale factor of 1.3.			
$0.17 ^{+0.18}_{-0.17} \pm 0.28$	[1] HAYRAPETY...25K		CMS	pp at 13 TeV
$0.71 \pm 0.17 \pm 0.18$	[1] AAIJ	18C	LHCB	pp at 7, 8 TeV

[1] Uses $\tau^+ \to \mu^+ \nu_\mu \overline{\nu}_\tau$ mode to obtain the ratio value.

$\Gamma(J/\psi(1S) \pi^+)/\Gamma_{total} \times B(\overline{b} \to B_c \text{ at } Z)$ — $\Gamma_4/\Gamma \times B$

VALUE	CL%	DOCUMENT ID		TECN	COMMENT
seen		[1] AABOUD	21	ATLS	pp at 8 TeV
seen		[2] AAIJ	15M	LHCB	pp at 8 TeV
seen		[3] KHACHATRY...15AA		CMS	pp at 7 TeV
seen		AALTONEN	13	CDF	$p\overline{p}$ at 1.96 TeV
seen		[4] AAIJ	12AV	LHCB	pp at 7 TeV
seen		AALTONEN	08M	CDF	$p\overline{p}$ at 1.96 TeV
seen		ABAZOV	08T	D0	$p\overline{p}$ at 1.96 TeV
• • • We do not use the following data for averages, fits, limits, etc. • • •					
$<2.4 \times 10^{-4}$	90	[5] ACKERSTAFF	98O	OPAL	$e^+e^- \to Z$
$<3.4 \times 10^{-4}$	90	[6] ABREU	97E	DLPH	$e^+e^- \to Z$
$<8.2 \times 10^{-5}$	90	[7] BARATE	97H	ALEP	$e^+e^- \to Z$
$<2.0 \times 10^{-5}$	95	[8] ABE	96R	CDF	$p\overline{p}$ 1.8 TeV

[1] AABOUD 21 reports a measurement of $B(B_c^+ \to J/\psi \pi^+) / B(B^+ \to J/\psi K^+) \cdot f_c/f_u = (0.34 \pm 0.04 ^{+0.06}_{-0.02} \pm 0.01)$ %, at $p_T > 13$ GeV and $|y| < 2.3$.

[2] AAIJ 15M reports a measurement of $B(B_c^+ \to J/\psi \pi^+) / B(B^+ \to J/\psi K^+) \cdot f_c/f_u = (0.683 \pm 0.018 \pm 0.009)$% at $p_T(B) < 20$ GeV and $2.0 < y(B) < 4.5$.

[3] KHACHATRYAN 15AA reports a measurement of $B(B_c^+ \to J/\psi \pi^+) / B(B^+ \to J/\psi K^+) \cdot f_c/f_u = (0.48 \pm 0.05 \pm 0.03 \pm 0.05)$%, at $p_T > 15$ GeV and $|\eta(B)| < 1.6$.

[4] AAIJ 12AV reports a measurement of $B(B_c^+ \to J/\psi \pi^+)/B(B^+ \to J/\psi K^+)\ f_c/f_u = (0.68 \pm 0.10 \pm 0.03 \pm 0.05)$% at $p_T(B) > 4$ GeV and $2.5 < \eta(B) < 4.5$.

[5] ACKERSTAFF 98O reports $B(Z \to B_c X)/B(Z \to q q) \times B(B_c \to J/\psi(1S) \pi^+) < 1.06 \times 10^{-4}$ at 90%CL. We rescale to our PDG 98 values of $B(Z \to b \overline{b})$.

[6] ABREU 97E value listed is for an assumed $\tau_{B_c} = 0.4$ ps and improves to 2.7×10^{-4} for $\tau_{B_c} = 1.4$ ps.

[7] BARATE 97H reports $B(Z \to B_c X)/B(Z \to q q) \cdot B(B_c \to J/\psi(1S) \pi) < 3.6 \times 10^{-5}$ at 90%CL. We rescale to our PDG 96 values of $B(Z \to b \overline{b})$.

[8] ABE 96R reports $B(b \to B_c X)/B(b \to B^+ X) \cdot B(B_c^+ \to J/\psi(1S) \pi^+)/B(B^+ \to J/\psi(1S) K^+) < 0.053$ at 95%CL for $\tau_{B_c} = 0.8$ ps. It changes from 0.15 to 0.04 for 0.17 ps$< \tau_{B_c} < 1.6$ ps. We rescale to our PDG 96 values of $B(b \to B^+) = 0.378 \pm 0.022$ and $B(B^+ \to J/\psi(1S) K^+) = 0.00101 \pm 0.00014$.

$\Gamma(J/\psi(1S) \pi^+)/\Gamma(J/\psi(1S) \mu^+ \nu_\mu)$ — Γ_4/Γ_2

VALUE (units 10^{-2})	DOCUMENT ID		TECN	COMMENT
4.69±0.28±0.46	[1] AAIJ	14W	LHCB	pp at 7 TeV

[1] AAIJ 14W reports also a measurement $B(B_c^+ \to J/\psi \pi^+) / B(B_c^+ \to J/\psi \mu^+ \nu_\mu) = 0.271 \pm 0.016 \pm 0.016$ in the region $m_{J/\psi \mu^+} > 5.3$ GeV.

$\Gamma(J/\psi(1S) K^+)/\Gamma(J/\psi(1S) \pi^+)$ — Γ_5/Γ_4

VALUE	EVTS	DOCUMENT ID		TECN	COMMENT
0.079±0.007±0.003		AAIJ	16AF	LHCB	pp at 7, 8 TeV
• • • We do not use the following data for averages, fits, limits, etc. • • •					
$0.069 \pm 0.019 \pm 0.005$	50	AAIJ	13BY	LHCB	Repl. by AAIJ 16AF

$\Gamma(J/\psi(1S) \pi^+ \pi^0)/\Gamma(J/\psi(1S) \pi^+)$ — Γ_6/Γ_4

VALUE	DOCUMENT ID		TECN	COMMENT
2.80±0.15±0.19	AAIJ	24L	LHCB	pp at 7, 8, 13 TeV

$\Gamma(J/\psi(1S) \pi^+ \pi^+ \pi^-)/\Gamma_{total} \times B(\overline{b} \to B_c \text{ at } Z)$ — $\Gamma_7/\Gamma \times B$

VALUE	CL%	DOCUMENT ID		TECN	COMMENT
seen		AAIJ	12Y	LHCB	pp at 7 TeV
• • • We do not use the following data for averages, fits, limits, etc. • • •					
$<5.7 \times 10^{-4}$	90	[1] ABREU	97E	DLPH	$e^+e^- \to Z$

[1] ABREU 97E value listed is independent of 0.4 ps$< \tau_{B_c} < 1.4$ ps.

$\Gamma(J/\psi(1S) \pi^+ \pi^+ \pi^-)/\Gamma(J/\psi(1S) \pi^+)$ — Γ_7/Γ_4

VALUE	DOCUMENT ID		TECN	COMMENT
2.4 ±0.4 OUR AVERAGE				
$2.55 \pm 0.80 \pm 0.33 ^{+0.04}_{-0.01}$	KHACHATRY...15AA		CMS	pp at 7 TeV
$2.41 \pm 0.30 \pm 0.33$	AAIJ	12Y	LHCB	pp at 7 TeV

$\Gamma(J/\psi(1S) K^+ \pi^- \pi^+)/\Gamma(J/\psi(1S) K^+ K^- \pi^+)$ — Γ_8/Γ_{11}

VALUE	DOCUMENT ID		TECN	COMMENT
0.35±0.06±0.01	AAIJ	22P	LHCB	pp at 7, 8, 13 TeV

$\Gamma(J/\psi(1S) K^+ K^- K^+)/\Gamma(J/\psi(1S) K^+ K^- \pi^+)$ — Γ_9/Γ_{11}

VALUE	DOCUMENT ID		TECN	COMMENT
$(7.0 \pm 1.8 \pm 0.2) \times 10^{-2}$	AAIJ	22P	LHCB	pp at 7, 8, 13 TeV

$\Gamma(J/\psi(1S) a_1(1260))/\Gamma_{total} \times B(\overline{b} \to B_c \text{ at } Z)$ — $\Gamma_{10}/\Gamma \times B$

VALUE	CL%	DOCUMENT ID		TECN	COMMENT
$<1.2 \times 10^{-3}$	90	[1] ACKERSTAFF	98O	OPAL	$e^+e^- \to Z$

[1] ACKERSTAFF 98O reports $B(Z \to B_c X)/B(Z \to q q) \times B(B_c \to J/\psi(1S) a_1(1260)) < 5.29 \times 10^{-4}$ at 90%CL. We rescale to our PDG 98 values of $B(Z \to b \overline{b})$.

$\Gamma(J/\psi(1S) K^+ K^- \pi^+)/\Gamma_{total} \times B(\overline{b} \to B_c \text{ at } Z)$ — $\Gamma_{11}/\Gamma \times B$

VALUE	DOCUMENT ID		TECN	COMMENT
seen	[1] AAIJ	13CA	LHCB	pp at 7, 8 TeV

[1] A signal yield of 78 ± 14 decays is reported with a significance of 6.2 standard deviations using an integrated luminosity of 3 fb^{-1} data.

$\Gamma(J/\psi(1S) K^+ K^- \pi^+)/\Gamma(J/\psi(1S) \pi^+)$ — Γ_{11}/Γ_4

VALUE	DOCUMENT ID		TECN	COMMENT
0.53±0.10±0.05	[1] AAIJ	13CA	LHCB	pp at 7, 8 TeV

[1] A signal yield of 78 ± 14 decays is reported with a significance of 6.2 standard deviations using an integrated luminosity of 3 fb^{-1} data.

$\Gamma(J/\psi(1S) K^+ K^- \pi^+)/\Gamma(J/\psi(1S) \pi^+ \pi^+ \pi^-)$ — Γ_{11}/Γ_7

VALUE	DOCUMENT ID		TECN	COMMENT
0.185±0.013±0.006	AAIJ	22P	LHCB	pp at 7, 8, 13 TeV

$\Gamma(J/\psi(1S) \pi^+ \pi^+ \pi^+ \pi^- \pi^-)/\Gamma(J/\psi(1S) \pi^+)$ — Γ_{12}/Γ_4

VALUE	DOCUMENT ID		TECN	COMMENT
1.74±0.44±0.24	[1] AAIJ	14P	LHCB	pp at 7, 8 TeV

[1] A signal yield of 32 ± 8 decays is reported with a significance of 4.5 standard deviations.

$\Gamma(\psi(2S) \pi^+)/\Gamma(J/\psi(1S) \pi^+)$ — Γ_{13}/Γ_4

VALUE	DOCUMENT ID		TECN	COMMENT
0.254±0.018±0.006	[1,2] AAIJ	24W	LHCB	pp at 7, 8 and 13 TeV
• • • We do not use the following data for averages, fits, limits, etc. • • •				
$0.268 \pm 0.032 \pm 0.007 \pm 0.006$	[3,4] AAIJ	15AY	LHCB	pp at 7, 8 TeV
$0.250 \pm 0.068 \pm 0.014 \pm 0.006$	[3] AAIJ	13AM	LHCB	Repl. by AAIJ 15AY

[1] The last uncertainty includes the uncertainties on the branching fractions of the leptonic J/ψ and $\psi(2S)$ decays (± 0.005).

[2] Supersedes AAIJ 15AY.

[3] The last uncertainty is due to the uncertainty of the $B(\psi(2S) \to \mu^+ \mu^-)/B(J/\psi \to \mu^+ \mu^-)$ ratio measurement.

[4] Replaced by AAIJ 24W.

$\Gamma(\psi(2S) \pi^+)/\Gamma(J/\psi(1S) \pi^+ \pi^+ \pi^-)$ — Γ_{13}/Γ_7

VALUE	DOCUMENT ID		TECN	COMMENT
$(3.5 \pm 0.6 \pm 0.2) \times 10^{-2}$	AAIJ	22P	LHCB	pp at 7, 8, 13 TeV

$\Gamma(\psi(2S) \pi^+ \pi^- \pi^+)/\Gamma(J/\psi(1S) \pi^+ \pi^+ \pi^-)$ — Γ_{15}/Γ_7

VALUE	DOCUMENT ID		TECN	COMMENT
$(1.9 \pm 0.4 \pm 0.1) \times 10^{-2}$	AAIJ	22P	LHCB	pp at 7, 8, 13 TeV

$\Gamma(\psi(2S) K^+ K^- \pi^+)/\Gamma(J/\psi(1S) K^+ K^- \pi^+)$ — Γ_{16}/Γ_{11}

VALUE	DOCUMENT ID		TECN	COMMENT
$(3.7 \pm 1.2 \pm 0.1) \times 10^{-2}$	AAIJ	22P	LHCB	pp at 7, 8, 13 TeV

$\Gamma(J/\psi(1S) D^0 K^+)/\Gamma(J/\psi(1S) \pi^+)$ — Γ_{17}/Γ_4

VALUE	DOCUMENT ID		TECN	COMMENT
0.432±0.136±0.028	AAIJ	17L	LHCB	pp at 7, 8 TeV

$\Gamma(J/\psi(1S) D^*(2007)^0 K^+)/\Gamma(J/\psi(1S) D^0 K^+)$ — Γ_{18}/Γ_{17}

VALUE	DOCUMENT ID		TECN	COMMENT
5.1±1.8±0.4	AAIJ	17L	LHCB	pp at 7, 8 TeV

Int. J. Mod. Phys. A 2026.41. Downloaded from www.worldscientific.com
by UNIVERSITY OF CALIFORNIA @ BERKELEY on 09/16/26. Re-use and distribution is strictly not permitted, except for Open Access articles.

Int. J. Mod. Phys. A 2026.41. Downloaded from www.worldscientific.com by CALIFORNIA @ BERKELEY on 09/16/26. Re-use and distribution is strictly not permitted, except for Open Access articles.

$\Gamma(J/\psi(1S)D^*(2010)^+K^{*0})/\Gamma(J/\psi(1S)D^0K^+)$ — Γ_{19}/Γ_{17}

VALUE	DOCUMENT ID		TECN	COMMENT
2.10±1.08±0.34	AAIJ	17L	LHCB	pp at 7, 8 TeV

$\Gamma(J/\psi(1S)D^+K^{*0})/\Gamma(J/\psi(1S)D^0K^+)$ — Γ_{20}/Γ_{17}

VALUE	DOCUMENT ID		TECN	COMMENT
0.63±0.39±0.08	AAIJ	17L	LHCB	pp at 7, 8 TeV

$\Gamma(J/\psi(1S)D_s^+)/\Gamma_{total}\times B(\overline{b}\to B_c \text{ at } Z)$ — $\Gamma_{21}/\Gamma\times B$

VALUE (units 10^{-6})	DOCUMENT ID		TECN	COMMENT
6.7±0.8±0.1	[1] AAIJ	24F	LHCB	pp at 7, 8, 13 TeV

[1] AAIJ 24F reports $[\Gamma(B_c^+\to J/\psi(1S)D_s^+)/\Gamma_{total}\times B(\overline{b}\to B_c \text{ at } Z)]$ / $[B(\overline{b}\to B^+ \text{ at } Z)] = (1.63\pm0.15\pm0.13)\times10^{-5}$ which we multiply by our best (shown rounded) value $B(\overline{b}\to B^+ \text{ at } Z) = (40.8\pm0.7)\times10^{-2}$. Our first error is their experiment's error and our second error is the systematic error from using our best (shown rounded) value.

$\Gamma(J/\psi(1S)D_s^+)/\Gamma(J/\psi(1S)\pi^+)$ — Γ_{21}/Γ_4

VALUE	DOCUMENT ID		TECN	COMMENT
2.8 ±0.4 OUR AVERAGE				
2.76±0.33±0.33	[1] AAD	22O	ATLS	pp at 13 TeV
2.90±0.57±0.24	AAIJ	13AS	LHCB	pp at 7, 8 TeV
• • • We do not use the following data for averages, fits, limits, etc. • • •				
3.8 ±1.1 ±0.4	AAD	16H	ATLS	pp at 7, 8 TeV

[1] Supersedes the measurement of AAD 16H.

$\Gamma(J/\psi(1S)D_s^{*+})/\Gamma(J/\psi(1S)\pi^+)$ — Γ_{22}/Γ_4

VALUE	DOCUMENT ID		TECN	COMMENT
5.33±0.61±0.74	AAD	22O	ATLS	pp at 13 TeV
• • • We do not use the following data for averages, fits, limits, etc. • • •				
10.4 ±3.1 ±1.6	AAD	16H	ATLS	Repl. by AAD 22O

$\Gamma(J/\psi(1S)D_s^{*+})/\Gamma(J/\psi(1S)D_s^+)$ — Γ_{22}/Γ_{21}

VALUE	DOCUMENT ID		TECN	COMMENT
1.95±0.16 OUR AVERAGE				
1.91±0.20±0.07	AAIJ	24F	LHCB	pp at 7, 8, 13 TeV
1.93±0.24±0.09	[1] AAD	22O	ATLS	pp at 13 TeV
2.37±0.56±0.10	AAIJ	13AS	LHCB	pp at 7, 8 TeV
• • • We do not use the following data for averages, fits, limits, etc. • • •				
2.8 $^{+1.2}_{-0.8}$ ±0.3	AAD	16H	ATLS	pp at 7, 8 TeV

[1] Supersedes the measurement of AAD 16H.

$\Gamma(J/\psi(1S)p\overline{p}\pi^+)/\Gamma(J/\psi(1S)\pi^+)$ — Γ_{23}/Γ_4

VALUE	DOCUMENT ID		TECN	COMMENT
0.143$^{+0.041}_{-0.036}$	AAIJ	14AQ	LHCB	pp at 7, 8 TeV

$\Gamma(\chi_{c0}\pi^+)/\Gamma_{total}\times B(\overline{b}\to B_c \text{ at } Z)$ — $\Gamma_{24}/\Gamma\times B$

VALUE (units 10^{-6})	DOCUMENT ID		TECN	COMMENT
24.0$^{+8.6}_{-7.6}$±4.4	[1,2] AAIJ	16AT	LHCB	pp at 7 and 8 TeV

[1] AAIJ 16AT reports $[\Gamma(B_c^+\to\chi_{c0}\pi^+)/\Gamma_{total}\times B(\overline{b}\to B_c \text{ at } Z)]\times[\Gamma(\overline{b}\to B^+ \text{ at } Z)/\Gamma_{total}] = (9.8^{+3.4}_{-3.0}\pm0.8)\times10^{-6}$ which we divide by our best (shown rounded) value $\Gamma(\overline{b}\to B^+ \text{ at } Z)/\Gamma_{total} = 0.408\pm0.007$. Our first error is their experiment's error and our second error is the systematic error from using our best (shown rounded) value.

[2] The significance of the observed signal is 4.0 standard deviations.

$\Gamma(\chi_{c1}\pi^+)/\Gamma(\chi_{c2}\pi^+)$ — Γ_{25}/Γ_{26}

VALUE	CL%	DOCUMENT ID		TECN	COMMENT
<0.49	90	AAIJ	24I	LHCB	pp at 7, 8 and 13 TeV

$\Gamma(\chi_{c2}\pi^+)/\Gamma(J/\psi(1S)\pi^+)$ — Γ_{26}/Γ_4

VALUE	DOCUMENT ID		TECN	COMMENT
0.37±0.06±0.022	[1] AAIJ	24I	LHCB	pp at 7, 8 and 13 TeV

[1] The last uncertainty includes the knowledge of the $\chi_{c2}\to J/\psi\gamma$ branching fraction (±0.01).

$\Gamma(\chi_{c1}(3872)\pi^+,\ \chi_{c1}(3872)\to J/\psi\pi^+\pi^-)/\Gamma(\psi(2S)\pi^+,\ \psi(2S)\to J/\psi\pi^+\pi^-)$ — Γ_{27}/Γ_{14}

VALUE	CL%	DOCUMENT ID		TECN	COMMENT
<5 × 10^{-2}	90	AAIJ	25V	LHCB	pp at 7, 8, 13 TeV

$\Gamma(p\overline{p}\pi^+)/\Gamma_{total}$ — Γ_{28}/Γ

VALUE	DOCUMENT ID		TECN	COMMENT
not seen	[1] AAIJ	16K	LHCB	pp at 7, 8 TeV

[1] Measures the ratio $(f_c/f_u)\times B(B_c^+\to p\overline{p}\pi^+) < 3.6\times10^{-8}$ at 95% CL, in the region $m(p\overline{p}) < 2.85$ GeV/c^2, where f_c (f_u) represents the fragmentation fraction of the b-quark into the B_c^+ (B_u^+) meson.

$\Gamma(D^0K^+)/\Gamma_{total}\times B(\overline{b}\to B_c \text{ at } Z)$ — $\Gamma_{29}/\Gamma\times B$

VALUE (units 10^{-7})	DOCUMENT ID		TECN	COMMENT
3.8$^{+1.2}_{-1.0}$±0.1	[1] AAIJ	17AG	LHCB	pp at 7, 8 TeV

[1] AAIJ 17AG reports $[\Gamma(B_c^+\to D^0K^+)/\Gamma_{total}\times B(\overline{b}\to B_c \text{ at } Z)]$ / $[B(\overline{b}\to B^+ \text{ at } Z)] = (9.3^{+2.8}_{-2.5}\pm0.6)\times10^{-7}$ which we multiply by our best (shown rounded) value $B(\overline{b}\to B^+ \text{ at } Z) = (40.8\pm0.7)\times10^{-2}$. Our first error is their experiment's error and our second error is the systematic error from using our best (shown rounded) value.

$\Gamma(D^0\pi^+)/\Gamma_{total}\times B(\overline{b}\to B_c \text{ at } Z)$ — $\Gamma_{30}/\Gamma\times B$

VALUE	CL%	DOCUMENT ID		TECN	COMMENT
<1.6 × 10^{-7}	95	[1] AAIJ	17AG	LHCB	pp at 7, 8 TeV

[1] AAIJ 17AG reports $[\Gamma(B_c^+\to D^0\pi^+)/\Gamma_{total}\times B(\overline{b}\to B_c \text{ at } Z)]$ / $[B(\overline{b}\to B^+ \text{ at } Z)] < 3.9\times10^{-7}$ which we multiply by our best (shown rounded) value $B(\overline{b}\to B^+ \text{ at } Z) = 40.8\times10^{-2}$.

$\Gamma(D^{*0}\pi^+)/\Gamma_{total}\times B(\overline{b}\to B_c \text{ at } Z)$ — $\Gamma_{31}/\Gamma\times B$

VALUE	CL%	DOCUMENT ID		TECN	COMMENT
<4 × 10^{-7}	95	[1] AAIJ	17AG	LHCB	pp at 7, 8 TeV

[1] AAIJ 17AG reports $[\Gamma(B_c^+\to D^{*0}\pi^+)/\Gamma_{total}\times B(\overline{b}\to B_c \text{ at } Z)]$ / $[B(\overline{b}\to B^+ \text{ at } Z)] < 1.1\times10^{-6}$ which we multiply by our best (shown rounded) value $B(\overline{b}\to B^+ \text{ at } Z) = 40.8\times10^{-2}$.

$\Gamma(D^{*0}K^+)/\Gamma_{total}\times B(\overline{b}\to B_c \text{ at } Z)$ — $\Gamma_{32}/\Gamma\times B$

VALUE	CL%	DOCUMENT ID		TECN	COMMENT
<4 × 10^{-7}	95	[1] AAIJ	17AG	LHCB	pp at 7, 8 TeV

[1] AAIJ 17AG reports $[\Gamma(B_c^+\to D^{*0}K^+)/\Gamma_{total}\times B(\overline{b}\to B_c \text{ at } Z)]$ / $[B(\overline{b}\to B^+ \text{ at } Z)] < 1.1\times10^{-6}$ which we multiply by our best (shown rounded) value $B(\overline{b}\to B^+ \text{ at } Z) = 40.8\times10^{-2}$.

$\Gamma(D_s^+\overline{D}^0)/\Gamma_{total}\times B(\overline{b}\to B_c \text{ at } Z)$ — $\Gamma_{33}/\Gamma\times B$

VALUE	CL%	DOCUMENT ID		TECN	COMMENT
<1.4 × 10^{-7}	90	[1] AAIJ	18P	LHCB	pp at 7, 8 TeV

[1] AAIJ 18P reports $[\Gamma(B_c^+\to D_s^+\overline{D}^0)/\Gamma_{total}\times B(\overline{b}\to B_c \text{ at } Z)]$ / $[B(\overline{b}\to B^+ \text{ at } Z)]$ / $[B(B^+\to\overline{D}^0D^+)] < 0.9\times10^{-3}$ which we multiply by our best (shown rounded) values $B(\overline{b}\to B^+ \text{ at } Z) = 40.8\times10^{-2}$, $B(B^+\to\overline{D}^0D^+) = 3.8\times10^{-4}$.

$\Gamma(D_s^+D^0)/\Gamma_{total}\times B(\overline{b}\to B_c \text{ at } Z)$ — $\Gamma_{34}/\Gamma\times B$

VALUE	CL%	DOCUMENT ID		TECN	COMMENT
<6 × 10^{-8}	90	[1] AAIJ	18P	LHCB	pp at 7, 8 TeV

[1] AAIJ 18P reports $[\Gamma(B_c^+\to D_s^+D^0)/\Gamma_{total}\times B(\overline{b}\to B_c \text{ at } Z)]$ / $[B(\overline{b}\to B^+ \text{ at } Z)]$ / $[B(B^+\to\overline{D}^0D^+)] < 3.7\times10^{-4}$ which we multiply by our best (shown rounded) values $B(\overline{b}\to B^+ \text{ at } Z) = 40.8\times10^{-2}$, $B(B^+\to\overline{D}^0D^+) = 3.8\times10^{-4}$.

$\Gamma(D^+\overline{D}^0)/\Gamma_{total}\times B(\overline{b}\to B_c \text{ at } Z)$ — $\Gamma_{35}/\Gamma\times B$

VALUE	CL%	DOCUMENT ID		TECN	COMMENT
<3.0 × 10^{-6}	90	[1] AAIJ	18P	LHCB	pp at 7, 8 TeV

[1] AAIJ 18P reports $[\Gamma(B_c^+\to D^+\overline{D}^0)/\Gamma_{total}\times B(\overline{b}\to B_c \text{ at } Z)]$ / $[B(\overline{b}\to B^+ \text{ at } Z)]$ / $[B(B^+\to\overline{D}^0D^+)] < 1.9\times10^{-2}$ which we multiply by our best (shown rounded) values $B(\overline{b}\to B^+ \text{ at } Z) = 40.8\times10^{-2}$, $B(B^+\to\overline{D}^0D^+) = 3.8\times10^{-4}$.

$\Gamma(D^+D^0)/\Gamma_{total}\times B(\overline{b}\to B_c \text{ at } Z)$ — $\Gamma_{36}/\Gamma\times B$

VALUE	CL%	DOCUMENT ID		TECN	COMMENT
• • • We do not use the following data for averages, fits, limits, etc. • • •					
<1.9 × 10^{-6}	90	[1] AAIJ	18P	LHCB	Repl. by AAIJ 21AF

[1] AAIJ 18P reports $[\Gamma(B_c^+\to D^+D^0)/\Gamma_{total}\times B(\overline{b}\to B_c \text{ at } Z)]$ / $[B(\overline{b}\to B^+ \text{ at } Z)]$ / $[B(B^+\to\overline{D}^0D^+)] < 1.2\times10^{-2}$ which we multiply by our best (shown rounded) values $B(\overline{b}\to B^+ \text{ at } Z) = 40.8\times10^{-2}$, $B(B^+\to\overline{D}^0D^+) = 3.8\times10^{-4}$.

$[\Gamma(D_s^{*+}\overline{D}^0)+\Gamma(D_s^+\overline{D}^*(2007)^0)]/\Gamma_{total}\times B(\overline{b}\to B_c \text{ at } Z)$ — $(\Gamma_{37}+\Gamma_{38})/\Gamma\times B$

VALUE	CL%	DOCUMENT ID		TECN	COMMENT
• • • We do not use the following data for averages, fits, limits, etc. • • •					
<4 × 10^{-7}	90	[1] AAIJ	18P	LHCB	Repl. by AAIJ 21AF

[1] AAIJ 18P reports $[\left[\Gamma(B_c^+\to D_s^{*+}\overline{D}^0)+\Gamma(B_c^+\to D_s^+\overline{D}^*(2007)^0)\right]/\Gamma_{total}\times B(\overline{b}\to B_c \text{ at } Z)]$ / $[B(\overline{b}\to B^+ \text{ at } Z)]$ / $[B(B^+\to\overline{D}^0D^+)] < 2.8\times10^{-3}$ which we multiply by our best (shown rounded) values $B(\overline{b}\to B^+ \text{ at } Z) = 40.8\times10^{-2}$, $B(B^+\to\overline{D}^0D^+) = 3.8\times10^{-4}$.

$[\Gamma(D_s^{*+}D^0)+\Gamma(D_s^+D^*(2007)^0)]/\Gamma_{total}\times B(\overline{b}\to B_c \text{ at } Z)$ — $(\Gamma_{39}+\Gamma_{40})/\Gamma\times B$

VALUE	CL%	DOCUMENT ID		TECN	COMMENT
• • • We do not use the following data for averages, fits, limits, etc. • • •					
<5 × 10^{-7}	90	[1] AAIJ	18P	LHCB	Repl. by AAIJ 21AF

[1] AAIJ 18P reports $[\left[\Gamma(B_c^+\to D_s^{*+}D^0)+\Gamma(B_c^+\to D_s^+D^*(2007)^0)\right]/\Gamma_{total}\times B(\overline{b}\to B_c \text{ at } Z)]$ / $[B(\overline{b}\to B^+ \text{ at } Z)]$ / $[B(B^+\to\overline{D}^0D^+)] < 3.0\times10^{-3}$ which we multiply by our best (shown rounded) values $B(\overline{b}\to B^+ \text{ at } Z) = 40.8\times10^{-2}$, $B(B^+\to\overline{D}^0D^+) = 3.8\times10^{-4}$.

See key on page 1227

Int. J. Mod. Phys. A 2026.41. Downloaded from www.worldscientific.com
by UNIVERSITY OF CALIFORNIA @ BERKELEY on 09/16/26. Re-use and distribution is strictly not permitted, except for Open Access articles.

$\Gamma(D^*(2010)^+\overline{D}^0)/\Gamma_{total} \times B(\overline{b} \to B_c \text{ at } Z)$ — $\Gamma_{41}/\Gamma \times B$

VALUE	CL%	DOCUMENT ID		TECN	COMMENT
$<6.2 \times 10^{-3}$	90	[1] BARATE	98Q	ALEP	$e^+e^- \to Z$

[1] BARATE 98Q reports $B(Z \to B_c X) \times B(B_c \to D^*(2010)^+\overline{D}^0) < 1.9 \times 10^{-3}$ at 90%CL. We rescale to our PDG 98 values of $B(Z \to b\overline{b})$.

$[\Gamma(D^*(2010)^+\overline{D}^0,\ D^{*+} \to D^+\pi^0/\gamma) + \Gamma(D^+\overline{D}^*(2007)^0)]/\Gamma_{total} \times B(\overline{b} \to B_c \text{ at } Z)$ — $(\Gamma_{42}+\Gamma_{43})/\Gamma \times B$

VALUE	CL%	DOCUMENT ID		TECN	COMMENT
• • • We do not use the following data for averages, fits, limits, etc. • • •					
$<9 \times 10^{-6}$	90	[1] AAIJ	18P	LHCB	Repl. by AAIJ 21AF

[1] AAIJ 18P reports $[[\Gamma(B_c^+ \to D^*(2010)^+\overline{D}^0,\ D^{*+} \to D^+\pi^0/\gamma) + \Gamma(B_c^+ \to D^+\overline{D}^*(2007)^0)]/\Gamma_{total} \times B(\overline{b} \to B_c \text{ at } Z)] / [B(\overline{b} \to B^+ \text{ at } Z)] / [B(B^+ \to \overline{D}^0 D^+)] < 5.5 \times 10^{-2}$ which we multiply by our best (shown rounded) values $B(\overline{b} \to B^+ \text{ at } Z) = 40.8 \times 10^{-2}$, $B(B^+ \to \overline{D}^0 D^+) = 3.8 \times 10^{-4}$.

$[\Gamma(D^*(2010)^+ D^0,\ D^{*+} \to D^+\pi^0/\gamma) + \Gamma(D^+ D^*(2007)^0)]/\Gamma_{total} \times B(\overline{b} \to B_c \text{ at } Z)$ — $(\Gamma_{45}+\Gamma_{46})/\Gamma \times B$

VALUE	CL%	DOCUMENT ID		TECN	COMMENT
• • • We do not use the following data for averages, fits, limits, etc. • • •					
$<3.4 \times 10^{-6}$	90	[1] AAIJ	18P	LHCB	Repl. by AAIJ 21AF

[1] AAIJ 18P reports $[[\Gamma(B_c^+ \to D^*(2010)^+ D^0,\ D^{*+} \to D^+\pi^0/\gamma) + \Gamma(B_c^+ \to D^+ D^*(2007)^0)]/\Gamma_{total} \times B(\overline{b} \to B_c \text{ at } Z)] / [B(\overline{b} \to B^+ \text{ at } Z)] / [B(B^+ \to \overline{D}^0 D^+)] < 2.2 \times 10^{-2}$ which we multiply by our best (shown rounded) values $B(\overline{b} \to B^+ \text{ at } Z) = 40.8 \times 10^{-2}$, $B(B^+ \to \overline{D}^0 D^+) = 3.8 \times 10^{-4}$.

$\Gamma(D_s^{*+}\overline{D}^*(2007)^0)/\Gamma_{total} \times B(\overline{b} \to B_c \text{ at } Z)$ — $\Gamma_{47}/\Gamma \times B$

VALUE	CL%	DOCUMENT ID		TECN	COMMENT
• • • We do not use the following data for averages, fits, limits, etc. • • •					
$<1.7 \times 10^{-6}$	90	[1] AAIJ	18P	LHCB	Repl. by AAIJ 21AF

[1] AAIJ 18P reports $[\Gamma(B_c^+ \to D_s^{*+}\overline{D}^*(2007)^0)/\Gamma_{total} \times B(\overline{b} \to B_c \text{ at } Z)] / [B(\overline{b} \to B^+ \text{ at } Z)] / [B(B^+ \to \overline{D}^0 D^+)] < 1.1 \times 10^{-2}$ which we multiply by our best (shown rounded) values $B(\overline{b} \to B^+ \text{ at } Z) = 40.8 \times 10^{-2}$, $B(B^+ \to \overline{D}^0 D^+) = 3.8 \times 10^{-4}$.

$\Gamma(D_s^{*+} D^*(2007)^0)/\Gamma_{total} \times B(\overline{b} \to B_c \text{ at } Z)$ — $\Gamma_{48}/\Gamma \times B$

VALUE	CL%	DOCUMENT ID		TECN	COMMENT
• • • We do not use the following data for averages, fits, limits, etc. • • •					
$<3.1 \times 10^{-6}$	90	[1] AAIJ	18P	LHCB	Repl. by AAIJ 21AF

[1] AAIJ 18P reports $[\Gamma(B_c^+ \to D_s^{*+} D^*(2007)^0)/\Gamma_{total} \times B(\overline{b} \to B_c \text{ at } Z)] / [B(\overline{b} \to B^+ \text{ at } Z)] / [B(B^+ \to \overline{D}^0 D^+)] < 2.0 \times 10^{-2}$ which we multiply by our best (shown rounded) values $B(\overline{b} \to B^+ \text{ at } Z) = 40.8 \times 10^{-2}$, $B(B^+ \to \overline{D}^0 D^+) = 3.8 \times 10^{-4}$.

$\Gamma(D^*(2010)^+\overline{D}^*(2007)^0)/\Gamma_{total} \times B(\overline{b} \to B_c \text{ at } Z)$ — $\Gamma_{49}/\Gamma \times B$

VALUE	CL%	DOCUMENT ID		TECN	COMMENT
• • • We do not use the following data for averages, fits, limits, etc. • • •					
$<1.0 \times 10^{-4}$	90	[1] AAIJ	18P	LHCB	Repl. by AAIJ 21AF

[1] AAIJ 18P reports $[\Gamma(B_c^+ \to D^*(2010)^+\overline{D}^*(2007)^0)/\Gamma_{total} \times B(\overline{b} \to B_c \text{ at } Z)] / [B(\overline{b} \to B^+ \text{ at } Z)] / [B(B^+ \to \overline{D}^0 D^+)] < 6.5 \times 10^{-1}$ which we multiply by our best (shown rounded) values $B(\overline{b} \to B^+ \text{ at } Z) = 40.8 \times 10^{-2}$, $B(B^+ \to \overline{D}^0 D^+) = 3.8 \times 10^{-4}$.

$\Gamma(D^*(2010)^+ D^*(2007)^0)/\Gamma_{total} \times B(\overline{b} \to B_c \text{ at } Z)$ — $\Gamma_{50}/\Gamma \times B$

VALUE	CL%	DOCUMENT ID		TECN	COMMENT
• • • We do not use the following data for averages, fits, limits, etc. • • •					
$<2.0 \times 10^{-5}$	90	[1] AAIJ	18P	LHCB	Repl. by AAIJ 21AF

[1] AAIJ 18P reports $[\Gamma(B_c^+ \to D^*(2010)^+ D^*(2007)^0)/\Gamma_{total} \times B(\overline{b} \to B_c \text{ at } Z)] / [B(\overline{b} \to B^+ \text{ at } Z)] / [B(B^+ \to \overline{D}^0 D^+)] < 1.3 \times 10^{-1}$ which we multiply by our best (shown rounded) values $B(\overline{b} \to B^+ \text{ at } Z) = 40.8 \times 10^{-2}$, $B(B^+ \to \overline{D}^0 D^+) = 3.8 \times 10^{-4}$.

$\Gamma(D^+ K^{*0})/\Gamma_{total} \times B(\overline{b} \to B_c \text{ at } Z)$ — $\Gamma_{51}/\Gamma \times B$

VALUE	CL%	DOCUMENT ID		TECN	COMMENT
$<2.0 \times 10^{-7}$	90	[1] AAIJ	13R	LHCB	pp at 7 TeV

[1] AAIJ 13R reports $[\Gamma(B_c^+ \to D^+ K^{*0})/\Gamma_{total} \times B(\overline{b} \to B_c \text{ at } Z)] / [B(\overline{b} \to B^+ \text{ at } Z)] < 0.5 \times 10^{-6}$ which we multiply by our best (shown rounded) value $B(\overline{b} \to B^+ \text{ at } Z) = 40.8 \times 10^{-2}$.

$\Gamma(D^+\overline{K}^{*0})/\Gamma_{total} \times B(\overline{b} \to B_c \text{ at } Z)$ — $\Gamma_{52}/\Gamma \times B$

VALUE	CL%	DOCUMENT ID		TECN	COMMENT
$<1.6 \times 10^{-7}$	90	[1] AAIJ	13R	LHCB	pp at 7 TeV

[1] AAIJ 13R reports $[\Gamma(B_c^+ \to D^+\overline{K}^{*0})/\Gamma_{total} \times B(\overline{b} \to B_c \text{ at } Z)] / [B(\overline{b} \to B^+ \text{ at } Z)] < 0.4 \times 10^{-6}$ which we multiply by our best (shown rounded) value $B(\overline{b} \to B^+ \text{ at } Z) = 40.8 \times 10^{-2}$.

$\Gamma(D_s^+ K^{*0})/\Gamma_{total} \times B(\overline{b} \to B_c \text{ at } Z)$ — $\Gamma_{53}/\Gamma \times B$

VALUE	CL%	DOCUMENT ID		TECN	COMMENT
$<2.9 \times 10^{-7}$	90	[1] AAIJ	13R	LHCB	pp at 7 TeV

[1] AAIJ 13R reports $[\Gamma(B_c^+ \to D_s^+ K^{*0})/\Gamma_{total} \times B(\overline{b} \to B_c \text{ at } Z)] / [B(\overline{b} \to B^+ \text{ at } Z)] < 0.7 \times 10^{-6}$ which we multiply by our best (shown rounded) value $B(\overline{b} \to B^+ \text{ at } Z) = 40.8 \times 10^{-2}$.

$\Gamma(D_s^+\overline{K}^{*0})/\Gamma_{total} \times B(\overline{b} \to B_c \text{ at } Z)$ — $\Gamma_{54}/\Gamma \times B$

VALUE	CL%	DOCUMENT ID		TECN	COMMENT
$<4 \times 10^{-7}$	90	[1] AAIJ	13R	LHCB	pp at 7 TeV

[1] AAIJ 13R reports $[\Gamma(B_c^+ \to D_s^+\overline{K}^{*0})/\Gamma_{total} \times B(\overline{b} \to B_c \text{ at } Z)] / [B(\overline{b} \to B^+ \text{ at } Z)] < 1.1 \times 10^{-6}$ which we multiply by our best (shown rounded) value $B(\overline{b} \to B^+ \text{ at } Z) = 40.8 \times 10^{-2}$.

$\Gamma(D_s^+\phi)/\Gamma_{total} \times B(\overline{b} \to B_c \text{ at } Z)$ — $\Gamma_{55}/\Gamma \times B$

VALUE	CL%	DOCUMENT ID		TECN	COMMENT
$<3.3 \times 10^{-7}$	90	[1] AAIJ	13R	LHCB	pp at 7 TeV

[1] AAIJ 13R reports $[\Gamma(B_c^+ \to D_s^+\phi)/\Gamma_{total} \times B(\overline{b} \to B_c \text{ at } Z)] / [B(\overline{b} \to B^+ \text{ at } Z)] < 0.8 \times 10^{-6}$ which we multiply by our best (shown rounded) value $B(\overline{b} \to B^+ \text{ at } Z) = 40.8 \times 10^{-2}$.

$\Gamma(K^+ K^0)/\Gamma_{total} \times B(\overline{b} \to B_c \text{ at } Z)$ — $\Gamma_{56}/\Gamma \times B$

VALUE	CL%	DOCUMENT ID		TECN	COMMENT
$<4.6 \times 10^{-7}$	90	[1] AAIJ	13BS	LHCB	pp at 7 TeV

[1] Derived from $\Gamma(K^+ K^0)/\Gamma \times B(\overline{b} \to B_c) / (B(B^+ \to K^0\pi^+)\, B(\overline{b} \to B^+)) < 5.8\%$ at 90% CL using normalization mode $B(B^+ \to K^0\pi^+) = (23.97 \pm 0.53 \pm 0.71) \times 10^{-6}$ and assuming a B production ratio $f(\overline{b} \to B_u^+) = 0.33$.

$\Gamma(B_s^0\pi^+ / B(\overline{b} \to B_s))/\Gamma_{total} \times B(\overline{b} \to B_c \text{ at } Z)$ — $\Gamma_{59}/\Gamma \times B$

VALUE (units 10^{-3})	DOCUMENT ID		TECN	COMMENT
$2.37 \pm 0.31 \pm 0.11 {}^{+0.17}_{-0.13}$	[1] AAIJ	13BU	LHCB	pp at 7, 8 TeV

[1] The last uncertinty is due to the uncertainty of the B_c^+ lifetime measurument.

$\Gamma(D_s^+\overline{D}^0)/\Gamma_{total}$ — Γ_{33}/Γ

VALUE	CL%	DOCUMENT ID		TECN	COMMENT
$<7.2 \times 10^{-4}$	90	[1] AAIJ	21AF	LHCB	pp at 13 TeV

[1] Uses $B(\overline{b} \to B_c)/B(\overline{b} \to B^+) = 0.76\%$ determined by AAIJ 19AI.

$\Gamma(D_s^+ D^0)/\Gamma_{total}$ — Γ_{34}/Γ

VALUE	CL%	DOCUMENT ID		TECN	COMMENT
$<3.0 \times 10^{-4}$	90	[1] AAIJ	21AF	LHCB	pp at 13 TeV

[1] Uses $B(\overline{b} \to B_c)/B(\overline{b} \to B^+) = 0.76\%$ determined by AAIJ 19AI.

$\Gamma(D^+\overline{D}^0)/\Gamma_{total}$ — Γ_{35}/Γ

VALUE	CL%	DOCUMENT ID		TECN	COMMENT
$<1.9 \times 10^{-4}$	90	[1] AAIJ	21AF	LHCB	pp at 13 TeV

[1] Uses $B(\overline{b} \to B_c)/B(\overline{b} \to B^+) = 0.76\%$ determined by AAIJ 19AI.

$\Gamma(D^+ D^0)/\Gamma_{total}$ — Γ_{36}/Γ

VALUE	CL%	DOCUMENT ID		TECN	COMMENT
$<1.4 \times 10^{-4}$	90	[1] AAIJ	21AF	LHCB	pp at 13 TeV

[1] Uses $B(\overline{b} \to B_c)/B(\overline{b} \to B^+) = 0.76\%$ determined by AAIJ 19AI.

$\Gamma(D_s^{*+}\overline{D}^0)/\Gamma_{total}$ — Γ_{37}/Γ

VALUE	CL%	DOCUMENT ID		TECN	COMMENT
$<5.3 \times 10^{-4}$	90	[1] AAIJ	21AF	LHCB	pp at 13 TeV

[1] Uses $B(\overline{b} \to B_c)/B(\overline{b} \to B^+) = 0.76\%$ determined by AAIJ 19AI.

$\Gamma(D_s^+\overline{D}^*(2007)^0)/\Gamma_{total}$ — Γ_{38}/Γ

VALUE	CL%	DOCUMENT ID		TECN	COMMENT
$<4.6 \times 10^{-4}$	90	[1] AAIJ	21AF	LHCB	pp at 13 TeV

[1] Uses $B(\overline{b} \to B_c)/B(\overline{b} \to B^+) = 0.76\%$ determined by AAIJ 19AI.

$\Gamma(D_s^{*+} D^0)/\Gamma_{total}$ — Γ_{39}/Γ

VALUE	CL%	DOCUMENT ID		TECN	COMMENT
$<0.9 \times 10^{-3}$	90	[1] AAIJ	21AF	LHCB	pp at 13 TeV

[1] Uses $B(\overline{b} \to B_c)/B(\overline{b} \to B^+) = 0.76\%$ determined by AAIJ 19AI.

$\Gamma(D_s^+ D^*(2007)^0)/\Gamma_{total}$ — Γ_{40}/Γ

VALUE	CL%	DOCUMENT ID		TECN	COMMENT
$<6.6 \times 10^{-4}$	90	[1] AAIJ	21AF	LHCB	pp at 13 TeV

[1] Uses $B(\overline{b} \to B_c)/B(\overline{b} \to B^+) = 0.76\%$ determined by AAIJ 19AI.

$\Gamma(D^*(2010)^+\overline{D}^0)/\Gamma_{total}$ — Γ_{41}/Γ

VALUE	CL%	DOCUMENT ID		TECN	COMMENT
$<3.8 \times 10^{-4}$	90	[1] AAIJ	21AF	LHCB	pp at 13 TeV

[1] Uses $B(\overline{b} \to B_c)/B(\overline{b} \to B^+) = 0.76\%$ determined by AAIJ 19AI.

Int. J. Mod. Phys. A 2026.41. Downloaded from www.worldscientific.com
by CALIFORNIA @ BERKELEY on 09/16/26. Re-use and distribution is strictly not permitted, except for Open Access articles.

$\Gamma(D^*(2007)^+ D^0)/\Gamma_{total}$ — Γ_{44}/Γ

VALUE	CL%	DOCUMENT ID		TECN	COMMENT
$<2.0 \times 10^{-4}$	90	[1] AAIJ	21AF	LHCB	pp at 13 TeV

[1] Uses $B(\overline{b} \to B_c)/B(\overline{b} \to B^+) = 0.76\%$ determined by AAIJ 19AI.

$\Gamma(D^+ \overline{D}^*(2007)^0)/\Gamma_{total}$ — Γ_{43}/Γ

VALUE	CL%	DOCUMENT ID		TECN	COMMENT
$<6.5 \times 10^{-4}$	90	[1] AAIJ	21AF	LHCB	pp at 13 TeV

[1] Uses $B(\overline{b} \to B_c)/B(\overline{b} \to B^+) = 0.76\%$ determined by AAIJ 19AI.

$\Gamma(D^+ D^*(2007)^0)/\Gamma_{total}$ — Γ_{46}/Γ

VALUE	CL%	DOCUMENT ID		TECN	COMMENT
$<3.7 \times 10^{-4}$	90	[1] AAIJ	21AF	LHCB	pp at 13 TeV

[1] Uses $B(\overline{b} \to B_c)/B(\overline{b} \to B^+) = 0.76\%$ determined by AAIJ 19AI.

$\Gamma(D_s^{*+} \overline{D}^*(2007)^0)/\Gamma_{total}$ — Γ_{47}/Γ

VALUE	CL%	DOCUMENT ID		TECN	COMMENT
$<1.3 \times 10^{-3}$	90	[1] AAIJ	21AF	LHCB	pp at 13 TeV

[1] Uses $B(\overline{b} \to B_c)/B(\overline{b} \to B^+) = 0.76\%$ determined by AAIJ 19AI.

$\Gamma(D_s^{*+} D^*(2007)^0)/\Gamma_{total}$ — Γ_{48}/Γ

VALUE	CL%	DOCUMENT ID		TECN	COMMENT
$<1.3 \times 10^{-3}$	90	[1] AAIJ	21AF	LHCB	pp at 13 TeV

[1] Uses $B(\overline{b} \to B_c)/B(\overline{b} \to B^+) = 0.76\%$ determined by AAIJ 19AI.

$\Gamma(D^*(2010)^+ \overline{D}^*(2007)^0)/\Gamma_{total}$ — Γ_{49}/Γ

VALUE	CL%	DOCUMENT ID		TECN	COMMENT
$<1.0 \times 10^{-3}$	90	[1] AAIJ	21AF	LHCB	pp at 13 TeV

[1] Uses $B(\overline{b} \to B_c)/B(\overline{b} \to B^+) = 0.76\%$ determined by AAIJ 19AI.

$\Gamma(D^*(2010)^+ D^*(2007)^0)/\Gamma_{total}$ — Γ_{50}/Γ

VALUE	CL%	DOCUMENT ID		TECN	COMMENT
$<7.7 \times 10^{-4}$	90	[1] AAIJ	21AF	LHCB	pp at 13 TeV

[1] Uses $B(\overline{b} \to B_c)/B(\overline{b} \to B^+) = 0.76\%$ determined by AAIJ 19AI.

$\Gamma(\pi^+ B^{*0},\ B^{*0} \to \mu^+\mu^-)/\Gamma(J/\psi(1S)\pi^+)$ — Γ_{57}/Γ_4

VALUE	CL%	DOCUMENT ID		TECN	COMMENT
$<3.8 \times 10^{-5}$	90	AAIJ	25Z	LHCB	pp at 7, 8, 13 TeV

$\Gamma(\pi^+ B_s^{*0},\ B_s^{*0} \to \mu^+\mu^-)/\Gamma(J/\psi(1S)\pi^+)$ — Γ_{58}/Γ_4

VALUE	CL%	DOCUMENT ID		TECN	COMMENT
$<5.0 \times 10^{-5}$	90	AAIJ	25Z	LHCB	pp at 7, 8, 13 TeV

$\Gamma(B_s^0 \pi^+)/\Gamma(J/\psi(1S)\pi^+)$ — Γ_{60}/Γ_4

VALUE	DOCUMENT ID		TECN	COMMENT
$91 \pm 10 \pm 8.5$	[1] AAIJ	23M	LHCB	pp at 13 TeV

[1] The B_s^0 mesons are reconstructed via the decays $B_s^0 \to J/\psi\phi$ and $B_s^0 \to D_s^- \pi^+$. The third uncertainty includes systematic (± 8) and imprecise knowledge of the branching fractions (± 3).

$\Gamma(\pi^+ \mu^+ \mu^-)/\Gamma(J/\psi(1S)\pi^+)$ — Γ_{61}/Γ_4

VALUE	CL%	DOCUMENT ID		TECN	COMMENT
$<2.1 \times 10^{-4}$	90	AAIJ	24W	LHCB	pp at 7, 8 and 13 TeV

$\Gamma(D_s^+ \mu^+ \mu^-)/\Gamma_{total} \times B(\overline{b} \to B_c \text{ at } Z)$ — $\Gamma_{62}/\Gamma \times B$

VALUE	CL%	DOCUMENT ID		TECN	COMMENT
$<3.1 \times 10^{-8}$	90	[1] AAIJ	24F	LHCB	pp at 7, 8, 13 TeV

[1] AAIJ 24F reports $[\Gamma(B_c^+ \to D_s^+ \mu^+ \mu^-)/\Gamma_{total} \times B(\overline{b} \to B_c \text{ at } Z)] / [B(\overline{b} \to B^+ \text{ at } Z)] < 7.5 \times 10^{-8}$ which we multiply by our best (shown rounded) value $B(\overline{b} \to B^+ \text{ at } Z) = 40.8 \times 10^{-2}$.

POLARIZATION IN B_c^+ DECAY

In decays involving two vector mesons, one can distinguish among the states in which meson polarizations are both longitudinal (L) or both are transverse and parallel ($\|$) or perpendicular ($\perp$) to each other with the parameters Γ_L/Γ, $\Gamma_\perp/\Gamma$, and the relative phases $\phi_\|$ and $\phi_\perp$. See the definitions in the note on "Polarization in B Decays" review in the B^0 Particle Listings.

Γ_L/Γ in $B_c^+ \to J/\psi D_s^{*+}$

VALUE	DOCUMENT ID		TECN	COMMENT
0.34±0.09 OUR AVERAGE				
$0.30 \pm 0.10 \pm 0.04$	[1,2] AAD	22O	ATLS	pp at 13 TeV
0.48 ± 0.20	[3] AAIJ	13AS	LHCB	pp at 7, 8 TeV
• • • We do not use the following data for averages, fits, limits, etc. • • •				
0.62 ± 0.24	[4] AAD	16H	ATLS	pp at 7, 8 TeV

[1] Supersedes the measurement of AAD 16H.
[2] AAD 22O measures $1 - \Gamma_L/\Gamma = 0.70 \pm 0.10 \pm 0.04$.
[3] AAIJ 13AS measures $1 - \Gamma_L/\Gamma = 0.52 \pm 0.20$.
[4] AAD 16H measures $1 - \Gamma_L/\Gamma = 0.38 \pm 0.24$.

$A_P(B_c^+)$

$$A_P(B_c^+) = [\sigma(B_c^-) - \sigma(B_c^+)] \ / \ [\sigma(B_c^-) + \sigma(B_c^+)]$$

VALUE (units 10^{-2})	DOCUMENT ID		TECN	COMMENT
−1.0±1.0 OUR AVERAGE				
$-2.5 \pm 2.1 \pm 0.5$	[1] AAIJ	19AI	LHCB	pp at 7 TeV
$-0.5 \pm 1.1 \pm 0.4$	[1] AAIJ	19AI	LHCB	pp at 13 TeV

[1] Measured using B_c^+ semileptonic decays.

B_c^+ REFERENCES

AAIJ	25V	JHEP 2506 013	R. Aaij *et al.*	(LHCb Collab.)
AAIJ	25Z	EPJ C85 20	R. Aaij *et al.*	(LHCb Collab.)
HAYRAPETY...	25K	PR D111 L051102	A. Hayrapetyan *et al.*	(CMS collaboration)
AAIJ	24F	JHEP 2402 032	R. Aaij *et al.*	(LHCb Collab.)
AAIJ	24I	JHEP 2402 173	R. Aaij *et al.*	(LHCb Collab.)
AAIJ	24L	JHEP 2404 151	R. Aaij *et al.*	(LHCb Collab.)
AAIJ	24W	EPJ C84 468	R. Aaij *et al.*	(LHCb Collab.)
AAIJ	23M	JHEP 2307 066	R. Aaij *et al.*	(LHCb Collab.)
AAD	22O	JHEP 2208 087	G. Aad *et al.*	(ATLAS Collab.)
AAIJ	22P	JHEP 2201 065	R. Aaij *et al.*	(LHCb Collab.)
AABOUD	21	PR D104 012010	M. Aaboud *et al.*	(ATLAS Collab.)
AAIJ	21AF	JHEP 2112 117	R. Aaij *et al.*	(LHCb Collab.)
AAIJ	20R	JHEP 2007 123	R. Aaij *et al.*	(LHCb Collab.)
AAIJ	19AI	PR D100 112006	R. Aaij *et al.*	(LHCb Collab.)
AAIJ	18C	PRL 120 121801	R. Aaij *et al.*	(LHCb Collab.)
AAIJ	18P	NP B930 563	R. Aaij *et al.*	(LHCb Collab.)
SIRUNYAN	18BY	EPJ C78 457	A.M. Sirunyan *et al.*	(CMS Collab.)
AAIJ	17AG	PRL 118 111803	R. Aaij *et al.*	(LHCb Collab.)
AAIJ	17L	PR D95 032005	R. Aaij *et al.*	(LHCb Collab.)
AAD	16H	EPJ C76 4	G. Aad *et al.*	(ATLAS Collab.)
AAIJ	16AF	JHEP 1609 153	R. Aaij *et al.*	(LHCb Collab.)
AAIJ	16AT	PR D94 091102	R. Aaij *et al.*	(LHCb Collab.)
AAIJ	16K	PL B759 313	R. Aaij *et al.*	(LHCb Collab.)
AALTONEN	16A	PR D93 052001	T. Aaltonen *et al.*	(CDF Collab.)
AAIJ	15AY	PR D92 072007	R. Aaij *et al.*	(LHCb Collab.)
AAIJ	15G	PL B742 29	R. Aaij *et al.*	(LHCb Collab.)
AAIJ	15M	PRL 114 132001	R. Aaij *et al.*	(LHCb Collab.)
KHACHATRY...	15AA	JHEP 1501 063	V. Khachatryan *et al.*	(CMS Collab.)
AAIJ	14AQ	PRL 113 152003	R. Aaij *et al.*	(LHCb Collab.)
AAIJ	14G	EPJ C74 2839	R. Aaij *et al.*	(LHCb Collab.)
AAIJ	14P	JHEP 1405 148	R. Aaij *et al.*	(LHCb Collab.)
AAIJ	14W	PR D90 032009	R. Aaij *et al.*	(LHCb Collab.)
AAIJ	13AM	PR D87 071103	R. Aaij *et al.*	(LHCb Collab.)
AAIJ	13AS	PR D87 112012	R. Aaij *et al.*	(LHCb Collab.)
Also		PR D89 019901 (errat.)	R. Aaij *et al.*	(LHCb Collab.)
AAIJ	13BS	PL B726 646	R. Aaij *et al.*	(LHCb Collab.)
AAIJ	13BU	PRL 111 181801	R. Aaij *et al.*	(LHCb Collab.)
AAIJ	13BY	JHEP 1309 075	R. Aaij *et al.*	(LHCb Collab.)
AAIJ	13CA	JHEP 1311 094	R. Aaij *et al.*	(LHCb Collab.)
AAIJ	13R	JHEP 1302 043	R. Aaij *et al.*	(LHCb Collab.)
AALTONEN	13	PR D87 011101	T. Aaltonen *et al.*	(CDF Collab.)
AAIJ	12AV	PRL 109 232001	R. Aaij *et al.*	(LHCb Collab.)
AAIJ	12Y	PRL 108 251802	R. Aaij *et al.*	(LHCb Collab.)
ABAZOV	09H	PRL 102 092001	V.M. Abazov *et al.*	(D0 Collab.)
AALTONEN	08M	PRL 100 182002	T. Aaltonen *et al.*	(CDF Collab.)
ABAZOV	08T	PRL 101 012001	V.M. Abazov *et al.*	(D0 Collab.)
ABULENCIA	06C	PRL 96 082002	A. Abulencia *et al.*	(CDF Collab.)
ABULENCIA	06O	PRL 97 012002	A. Abulencia *et al.*	(CDF Collab.)
ABE	98M	PRL 81 2432	F. Abe *et al.*	(CDF Collab.)
Also		PR D58 112004	F. Abe *et al.*	(CDF Collab.)
ACKERSTAFF	98O	PL B420 157	K. Ackerstaff *et al.*	(OPAL Collab.)
BARATE	98Q	EPJ C4 387	R. Barate *et al.*	(ALEPH Collab.)
PDG	98	EPJ C3 1	C. Caso *et al.*	(PDG Collab.)
ABREU	97E	PL B398 207	P. Abreu *et al.*	(DELPHI Collab.)
BARATE	97H	PL B402 213	R. Barate *et al.*	(ALEPH Collab.)
ABE	96R	PRL 77 5176	F. Abe *et al.*	(CDF Collab.)
PDG	96	PR D54 1	R. M. Barnett *et al.*	(PDG Collab.)

$B_c(1P)^\pm$

$I(J^P) = 0(?^?)$

OMITTED FROM SUMMARY TABLE

$B_c(1P)^\pm$ MASS

VALUE (MeV)	DOCUMENT ID		TECN	COMMENT
• • • We do not use the following data for averages, fits, limits, etc. • • •				
$6704.8 \pm 5.5 \pm 2.8$	[1,2] AAIJ	25AE	LHCB	pp at 7, 8, 13 TeV
$6752.4 \pm 9.5 \pm 3.1$	[2,3] AAIJ	25AE	LHCB	pp at 7, 8, 13 TeV

[1] The observed structure in $B_c^\pm \gamma$ is described by two Gaussian functions with power-law tails, the other one is at 6752.4 MeV.
[2] Consistent with unresolved contributions from $^3P_0$, $^3P_2$, mixed $^3P_1$ and $^1P_1$ (both decaying radiatively to $B_c^\pm$ and $B_c^{*\pm}$) (see AAIJ 25AF).
[3] The observed structure in $B_c^\pm \gamma$ is described by two Gaussian functions with power-law tails, the other one is at 6704.8 MeV.

$B_c(1P)^\pm$ DECAY MODES

	Mode	Fraction (Γ_i/Γ)
Γ_1	$B_c^\pm \gamma$	seen

$B_c(1P)^\pm$ BRANCHING RATIOS

$\Gamma(B_c^\pm \gamma)/\Gamma_{total}$ — Γ_1/Γ

VALUE	DOCUMENT ID		TECN	COMMENT
seen	AAIJ	25AE	LHCB	pp at 7, 8, 13 TeV

$B_c(1P)^\pm$ REFERENCES

AAIJ	25AE	PRL 135 231902	R. Aaij *et al.*	(LHCb Collab.)
AAIJ	25AF	PR D112 112003	R. Aaij *et al.*	(LHCb Collab.)

$B_c(2S)^\pm$

$I(J^P) = 0(0^-)$

Quantum numbers neither measured nor confirmed.

$B_c(2S)^\pm$ MASS

VALUE (MeV)	EVTS	DOCUMENT ID		TECN	COMMENT
6871.2±1.0 OUR AVERAGE					
6871.7±1.3±0.3	24	[1,2] AAIJ	19Y	LHCB	pp at 7, 8, 13 TeV
6870.6±1.4±0.3	51	[3,4] SIRUNYAN	19M	CMS	pp at 13 TeV
• • • We do not use the following data for averages, fits, limits, etc. • • •					
not seen		[5] AAIJ	18AL	LHCB	pp at 8 TeV
6842 ±4 ±5	57	[6,7] AAD	14AQ	ATLS	pp at 7, 8 TeV

[1] AAIJ 19Y observed $B_c(2S)^+$ in the decay mode $B_c(2S)^+ \to B_c^+\pi^+\pi^-$ ($B_c^+ \to J/\psi\pi^+$) with 2.2 (3.2) global (local) standard deviations significance.

[2] AAIJ 19Y reports mass difference measurement of $M(B_c(2S)^+) - M(B_c^+) = 597.2 \pm 1.3 \pm 0.1$ MeV. We have adjusted this measurement with our best value of $M(B_c^+) = 6274.47 \pm 0.32$ MeV. The first uncertainty of the $M(B_c(2S)^+)$ value is a total of uncertainties reported by the experiment and the second one comes from our best value of $M(B_c^+)$.

[3] SIRUNYAN 19M observed $B_c(2S)^+$ in the decay mode $B_c(2S)^+ \to B_c^+\pi^+\pi^-$ ($B_c^+ \to J/\psi\pi^+$) with 6.5 standard deviations significance.

[4] SIRUNYAN 19M reports mass difference measurement of $M(B_c(2S)^+) - M(B_c^+) = 596.1 \pm 1.2 \pm 0.8$ MeV. We have adjusted this measurement with our best value of $M(B_c^+) = 6274.47 \pm 0.32$ MeV. The first uncertainty of the $M(B_c(2S)^+)$ value is a total of uncertainties reported by the experiment and the second one comes from our best value of $M(B_c^+)$.

[5] AAIJ 18AL reports an upper limit on the ratio of production cross sections for $[\sigma(B_c(2S)^+)/\sigma(B_c^+)]\cdot B(B_c(2S)^+ \to B_c^+\pi^+\pi^-) < 0.04$–$0.09$ at 95% CL for the mass value reported by AAD 14AQ.

[6] Observed in the decay mode $B_c(2S)^+ \to B_c^+\pi^+\pi^-$ ($B_c^+ \to J/\psi\pi^+$) with 5.2 standard deviations significance.

[7] Might be the $B_c^*(2S)$.

$B_c(2S)^\pm$ DECAY MODES × $B(\overline{b} \to B_c(2S))$

The following quantities are not pure branching ratios; rather the fractions $\Gamma_i/\Gamma \times B(\overline{b} \to B_c(2S))$.

	Mode	Fraction (Γ_i/Γ)
Γ_1	$B_c^+\pi^+\pi^-$	seen

$B_c(2S)^\pm$ BRANCHING RATIOS

$\Gamma(B_c^+\pi^+\pi^-)/\Gamma_{total}$ — Γ_1/Γ

VALUE	EVTS	DOCUMENT ID		TECN	COMMENT
seen		SIRUNYAN	19M	CMS	pp at 13 TeV
seen	57	[1] AAD	14AQ	ATLS	pp at 7, 8 TeV
• • • We do not use the following data for averages, fits, limits, etc. • • •					
not seen		[2] AAIJ	18AL	LHCB	pp at 8 TeV

[1] Observed with 5.2 standard deviations significance.

[2] AAIJ 18AL reports an upper limit on the ratio of production cross sections for $[\sigma(B_c(2S)^+)/\sigma(B_c^+)]\cdot B(B_c(2S)^+ \to B_c^+\pi^+\pi^-) < 0.04$–$0.09$ at 95% CL for the mass value reported by AAD 14AQ.

$B_c(2S)^\pm$ REFERENCES

AAIJ	19Y	PRL 122 232001	R. Aaij *et al.*	(LHCb Collab.)
SIRUNYAN	19M	PRL 122 132001	A.M. Sirunyan *et al.*	(CMS Collab.)
AAIJ	18AL	JHEP 1801 138	R. Aaij *et al.*	(LHCb Collab.)
AAD	14AQ	PRL 113 212004	G. Aad *et al.*	(ATLAS Collab.)

See the related review(s):

Spectroscopy of Mesons Containing Two Heavy Quarks

Int. J. Mod. Phys. A 2026.41. Downloaded from www.worldscientific.com
by UNIVERSITY OF CALIFORNIA @ BERKELEY on 09/16/26. Re-use and distribution is strictly not permitted, except for Open Access articles.

$c\overline{c}$ MESONS (including possibly non-$q\overline{q}$ states)

Updated March 2024.

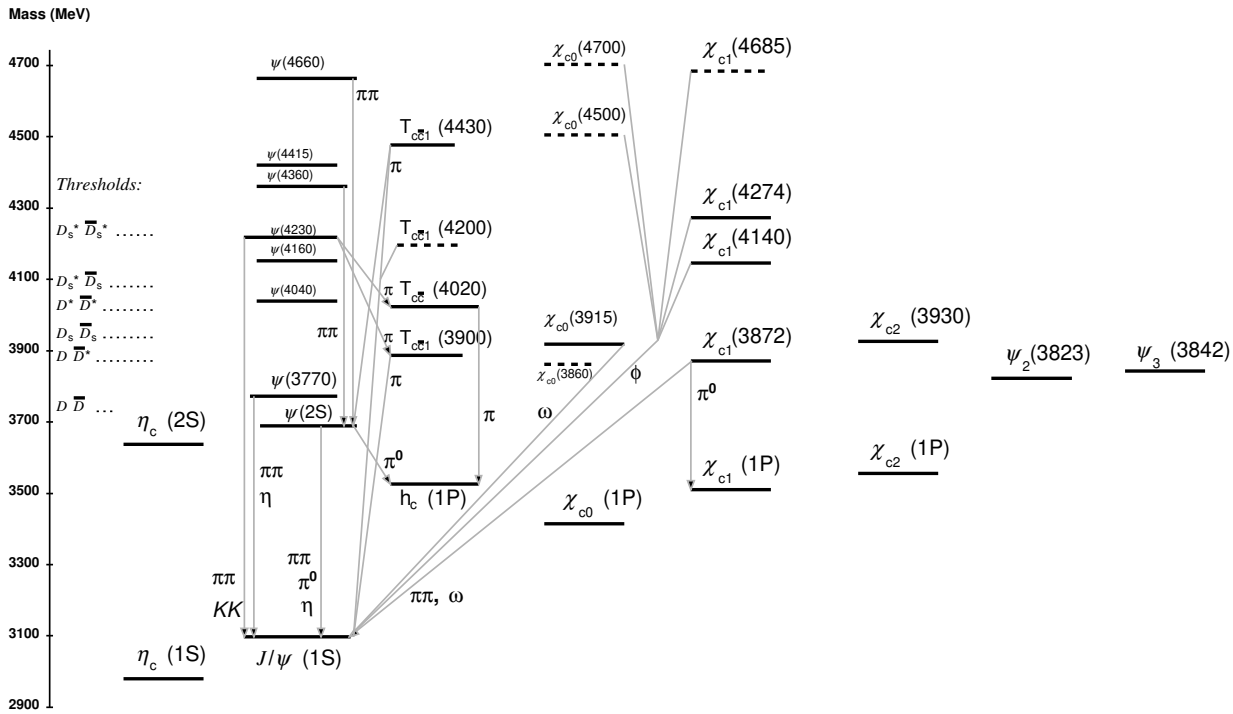

The level scheme of meson states containing a minimal quark content of $c\overline{c}$ and having $S = C = B = 0$. The name of a state is determined by its quantum numbers $I^G J^{PC}$ (see the review "Naming Scheme for Hadrons"). States included in the Summary Tables are shown with solid lines; selected states not in the Summary Tables, but with assigned quantum numbers, are shown with dotted lines. The arrows indicate the most dominant hadronic transitions. Single photon transitions, including $\psi(nS) \to \gamma\eta_c(mS)$, $\psi(nS) \to \gamma\chi_{cJ}(1P)$, and $\chi_{cJ}(1P) \to \gamma J/\psi$, are omitted for clarity. For orientation, the location of the thresholds related to a pair of ground state open charm mesons is indicated in the figure. The J^P of $T_{c\overline{c}}(4020)$ is not established. Decays to open flavour final states are not shown in the figure.

$\eta_c(1S)$

$I^G(J^{PC}) = 0^+(0^{-+})$

$\eta_c(1S)$ MASS

VALUE (MeV)	EVTS	DOCUMENT ID		TECN	COMMENT
2984.09 ± 0.30 OUR AVERAGE		Error includes scale factor of 1.2.			
2984.14 ± 0.13 ± 0.38		[1] ABLIKIM	25R	BES3	$\psi(2S) \to \gamma\eta_c \to \gamma 2(\pi^+\pi^-)\eta$
2985.01 ± 0.17 ± 0.89	35k	AAIJ	23AH	LHCB	$B^+ \to K^+(K^0_S K\pi)$
2983.9 ± 0.7 ± 0.1		[2] AAIJ	20H	LHCB	$pp \to bX \to p\overline{p}X$
2985.9 ± 0.7 ± 2.1	1705	ABLIKIM	19AV	BES3	$J/\psi \to \gamma\omega\omega$
2984.6 ± 0.7 ± 2.2	2673	XU	18	BELL	$e^+e^- \to e^+e^-\eta'\pi^+\pi^-$
2986.7 ± 0.5 ± 0.9	11k	[3] AAIJ	17AD	LHCB	$pp \to B^+X \to p\overline{p}K^+X$
2982.8 ± 1.0 ± 0.5	6.4k	[4] AAIJ	17BB	LHCB	$pp \to b\overline{b}X \to 2(K^+K^-)X$
2982.2 ± 1.5 ± 0.1	2.0k	[5] AAIJ	15BI	LHCB	$pp \to \eta_c(1S)X$
2983.5 ± 1.4 $^{+1.6}_{-3.6}$		[6] ANASHIN	14	KEDR	$J/\psi \to \gamma\eta_c$
2979.8 ± 0.8 ± 3.5	4.5k	[7,8] LEES	14E	BABR	$\gamma\gamma \to K^+K^-\pi^0$
2984.1 ± 1.1 ± 2.1	900	[7,8,9] LEES	14E	BABR	$\gamma\gamma \to K^+K^-\eta$
2984.3 ± 0.6 ± 0.6		[10,11] ABLIKIM	12F	BES3	$\psi(2S) \to \gamma\eta_c$
2984.49 ± 1.16 ± 0.52	832	[7] ABLIKIM	12N	BES3	$\psi(2S) \to \pi^0\gamma$ hadrons
2982.7 ± 1.8 ± 2.2	486	ZHANG	12A	BELL	$e^+e^- \to e^+e^-\eta'\pi^+\pi^-$
2984.5 ± 0.8 ± 3.1	11k	DEL-AMO-SA..	11M	BABR	$\gamma\gamma \to K^+K^-\pi^+\pi^-\pi^0$
2985.4 ± 1.5 $^{+0.5}_{-2.0}$	920	[11] VINOKUROVA	11	BELL	$B^\pm \to K^\pm(K^0_S K^\pm\pi^\mp)$
2982.2 ± 0.4 ± 1.6	14k	[12] LEES	10	BABR	10.6 $e^+e^- \to e^+e^-K^0_S K^\pm\pi^\mp$
2985.8 ± 1.5 ± 3.1	0.9k	AUBERT	08AB	BABR	$B \to \eta_c(1S)K^{(*)} \to K\overline{K}\pi K^{(*)}$
2986.1 ± 1.0 ± 2.5	7.5k	UEHARA	08	BELL	$\gamma\gamma \to \eta_c \to$ hadrons
2970 ± 5 ± 6	501	[13] ABE	07	BELL	$e^+e^- \to J/\psi(c\overline{c})$
2971 ± 3 $^{+2}_{-1}$	195	WU	06	BELL	$B^+ \to p\overline{p}K^+$
2974 ± 7 $^{+2}_{-1}$	20	WU	06	BELL	$B^+ \to \Lambda\overline{\Lambda}K^+$
2981.8 ± 1.3 ± 1.5	592	ASNER	04	CLEO	$\gamma\gamma \to \eta'_c \to K^0_S K^\pm\pi^\mp$
2984.1 ± 2.1 ± 1.0	190	[14] AMBROGIANI	03	E835	$\overline{p}p \to \eta_c \to \gamma\gamma$
• • • We do not use the following data for averages, fits, limits, etc. • • •					
2982.5 ± 0.4 ± 1.4	12k	[15] DEL-AMO-SA..	11M	BABR	$\gamma\gamma \to K^0_S K^\pm\pi^\mp$
2982.2 ± 0.6		[16] MITCHELL	09	CLEO	$e^+e^- \to \gamma X$
2982 ± 5	270	[17] AUBERT	06E	BABR	$B^\pm \to K^\pm X_{c\overline{c}}$
2982.5 ± 1.1 ± 0.9	2.5k	[18] AUBERT	04D	BABR	$\gamma\gamma \to \eta_c(1S) \to K\overline{K}\pi$
2977.5 ± 1.0 ± 1.2		[16,19] BAI	03	BES	$J/\psi \to \gamma\eta_c$

Int. J. Mod. Phys. A 2026.41. Downloaded from www.worldscientific.com
by LIFORNIA @ BERKELEY on 09/16/26. Re-use and distribution is strictly not permitted, except for Open Access articles.

$2979.6 \pm 2.3 \pm 1.6$	180	[20] FANG	03	BELL	$B \to \eta_c K$
$2976.3 \pm 2.3 \pm 1.2$		[16,21] BAI	00F	BES	$J/\psi,\ \psi(2S) \to \gamma\eta_c$
$2976.6 \pm 2.9 \pm 1.3$	140	[16,22] BAI	00F	BES	$J/\psi \to \gamma\eta_c$
$2980.4 \pm 2.3 \pm 0.6$		[23] BRANDENB...	00B	CLE2	$\gamma\gamma \to \eta_c \to K^\pm K^0_S \pi^\mp$
$2975.8 \pm 3.9 \pm 1.2$		[22] BAI	99B	BES	Sup. by BAI 00F
2999 ± 8	25	ABREU	98O	DLPH	$e^+e^- \to e^+e^-$ +hadrons
$2988.3^{+3.3}_{-3.1}$		ARMSTRONG	95F	E760	$\overline{p}p \to \gamma\gamma$
2974.4 ± 1.9		[16,24] BISELLO	91	DM2	$J/\psi \to \eta_c\gamma$
$2969 \pm 4 \pm 4$	80	[16] BAI	90B	MRK3	$J/\psi \to \gamma K^+K^-K^+K^-$
$2956 \pm 12 \pm 12$		[16] BAI	90B	MRK3	$J/\psi \to \gamma K^+K^-K^0_S K^0_L$
$2982.6^{+2.7}_{-2.3}$	12	BAGLIN	87B	SPEC	$\overline{p}p \to \gamma\gamma$
2980.2 ± 1.6		[16,24] BALTRUSAIT...	86	MRK3	$J/\psi \to \eta_c\gamma$
$2984 \pm 2.3 \pm 4.0$		[16] GAISER	86	CBAL	$J/\psi \to \gamma X,\ \psi(2S) \to \gamma X$
2976 ± 8		[16,25] BALTRUSAIT...	84	MRK3	$J/\psi \to 2\phi\gamma$
2982 ± 8	18	[26] HIMEL	80B	MRK2	e^+e^-
2980 ± 9		[26] PARTRIDGE	80B	CBAL	e^+e^-

[1] Average between constructive and destructive interference with background.
[2] AAIJ 20H report $m_{J/\psi} - m_{\eta_c(1S)} = 113.0 \pm 0.7 \pm 0.1$ MeV. We use the current value $m_{J/\psi} = 3096.900 \pm 0.006$ MeV to obtain the quoted mass.
[3] AAIJ 17AD report $m_{J/\psi} - m_{\eta_c(1S)} = 110.2 \pm 0.5 \pm 0.9$ MeV. We use the current value $m_{J/\psi} = 3096.900 \pm 0.006$ MeV to obtain the quoted mass.
[4] From a fit of the $\phi\phi$ invariant mass with the mass and width of $\eta_c(1S)$ as free parameters.
[5] AAIJ 15BI reports $m_{J/\psi} - m_{\eta_c(1S)} = 114.7 \pm 1.5 \pm 0.1$ MeV from a sample of $\eta_c(1S)$ and J/ψ produced in b-hadron decays. We have used current value of $m_{J/\psi} = 3096.900 \pm 0.006$ MeV to arrive at the quoted $m_{\eta_c(1S)}$ result.
[6] Taking into account an asymmetric photon lineshape.
[7] With floating width.
[8] Ignoring possible interference with the non-resonant 0^- amplitude.
[9] Using both, $\eta \to \gamma\gamma$ and $\eta \to \pi^+\pi^-\pi^0$ decays.
[10] From a simultaneous fit to six decay modes of the η_c.
[11] Accounts for interference with non-resonant continuum.
[12] Taking into account interference with the non-resonant $J^P = 0^-$ amplitude.
[13] From a fit of the J/ψ recoil mass spectrum. Supersedes ABE,K 02 and ABE 04G.
[14] Using mass of $\psi(2S) = 3686.00$ MeV.
[15] Not independent from the measurements reported by LEES 10.
[16] MITCHELL 09 observes a significant asymmetry in the lineshapes of $\psi(2S) \to \gamma\eta_c$ and $J/\psi \to \gamma\eta_c$ transitions. If ignored, this asymmetry could lead to significant bias whenever the mass and width are measured in $\psi(2S)$ or J/ψ radiative decays.
[17] From the fit of the kaon momentum spectrum. Systematic errors not evaluated.
[18] Superseded by LEES 10.
[19] From a simultaneous fit of five decay modes of the η_c.
[20] Superseded by VINOKUROVA 11.
[21] Weighted average of the $\psi(2S)$ and $J/\psi(1S)$ samples. Using an η_c width of 13.2 MeV.
[22] Average of several decay modes. Using an η_c width of 13.2 MeV.
[23] Superseded by ASNER 04.
[24] Average of several decay modes.
[25] $\eta_c \to \phi\phi$.
[26] Mass adjusted by us to correspond to $J/\psi(1S)$ mass = 3097 MeV.

$\eta_c(1S)$ WIDTH

VALUE (MeV)	EVTS	DOCUMENT ID		TECN	COMMENT
30.0 ± 0.5 OUR FIT Error includes scale factor of 1.2.					
30.2 ± 0.5 OUR AVERAGE Error includes scale factor of 1.2.					
$28.82 \pm 0.11 \pm 0.82$		[1] ABLIKIM	25R	BES3	$\psi(2S) \to \gamma\eta_c \to \gamma 2(\pi^+\pi^-)\eta$
$29.7 \pm 0.5 \pm 0.2$	35k	AAIJ	23AH	LHCB	$B^+ \to K^+(K^0_S K\pi)$
$33.8 \pm 1.6 \pm 4.1$	1705	ABLIKIM	19AV	BES3	$J/\psi \to \gamma\omega\omega$
$30.8^{+2.3}_{-2.2} \pm 2.9$	2673	XU	18	BELL	$e^+e^- \to e^+e^-\eta'\pi^+\pi^-$
$34.0 \pm 1.9 \pm 1.3$	11k	AAIJ	17AD	LHCB	$pp \to B^+X \to p\overline{p}K^+X$
$31.4 \pm 3.5 \pm 2.0$	6.4k	[2] AAIJ	17BB	LHCB	$pp \to b\overline{b}X \to 2(K^+K^-)X$
$27.2 \pm 3.1\ ^{+5.4}_{-2.6}$		[3] ANASHIN	14	KEDR	$J/\psi \to \gamma\eta_c$
$25.2 \pm 2.6 \pm 2.4$	4.5k	[4,5] LEES	14E	BABR	$\gamma\gamma \to K^+K^-\pi^0$
$34.8 \pm 3.1 \pm 4.0$	900	[4,5,6] LEES	14E	BABR	$\gamma\gamma \to K^+K^-\eta$
$32.0 \pm 1.2 \pm 1.0$		[7,8] ABLIKIM	12F	BES3	$\psi(2S) \to \gamma\eta_c$
$36.4 \pm 3.2 \pm 1.7$	832	[4] ABLIKIM	12N	BES3	$\psi(2S) \to \pi^0\gamma$ hadrons
$37.8^{+5.8}_{-5.3} \pm 3.1$	486	ZHANG	12A	BELL	$e^+e^- \to e^+e^-\eta'\pi^+\pi^-$
$36.2 \pm 2.8 \pm 3.0$	11k	DEL-AMO-SA...	11M	BABR	$\gamma\gamma \to K^+K^-\pi^+\pi^-\pi^0$
$35.1 \pm 3.1\ ^{+1.0}_{-1.6}$	920	[8] VINOKUROVA	11	BELL	$B^\pm \to K^\pm(K^0_S K^\pm\pi^\mp)$
$31.7 \pm 1.2 \pm 0.8$	14k	[9] LEES	10	BABR	$10.6\ e^+e^- \to e^+e^-K^0_S K^\pm\pi^\mp$
$36.3^{+3.7}_{-3.6} \pm 4.4$	0.9k	AUBERT	08AB	BABR	$B \to \eta_c(1S)K^{(*)} \to K\overline{K}\pi K^{(*)}$
$28.1 \pm 3.2 \pm 2.2$	7.5k	UEHARA	08	BELL	$\gamma\gamma \to \eta_c \to$ hadrons
$48^{+8}_{-7} \pm 5$	195	WU	06	BELL	$B^+ \to p\overline{p}K^+$
$40 \pm 19 \pm 5$	20	WU	06	BELL	$B^+ \to \Lambda\overline{\Lambda}K^+$
$24.8 \pm 3.4 \pm 3.5$	592	ASNER	04	CLEO	$\gamma\gamma \to \eta'_c \to K^0_S K^\pm\pi^\mp$
$20.4^{+7.7}_{-6.7} \pm 2.0$	190	AMBROGIANI	03	E835	$\overline{p}p \to \eta_c \to \gamma\gamma$
$23.9^{+12.6}_{-7.1}$		ARMSTRONG	95F	E760	$\overline{p}p \to \gamma\gamma$
• • • We do not use the following data for averages, fits, limits, etc. • • •					
$32.1 \pm 1.1 \pm 1.3$	12k	[10] DEL-AMO-SA...	11M	BABR	$\gamma\gamma \to K^0_S K^\pm\pi^\mp$
$34.3 \pm 2.3 \pm 0.9$	2.5k	[11] AUBERT	04D	BABR	$\gamma\gamma \to \eta_c(1S) \to K\overline{K}\pi$
$17.0 \pm 3.7 \pm 7.4$		[12] BAI	03	BES	$J/\psi \to \gamma\eta_c$
$29 \pm 8 \pm 6$	180	[13] FANG	03	BELL	$B \to \eta_c K$
$11.0 \pm 8.1 \pm 4.1$		[14] BAI	00F	BES	$J/\psi \to \gamma\eta_c$ and $\psi(2S) \to \gamma\eta_c$
$27.0 \pm 5.8 \pm 1.4$		[15] BRANDENB...	00B	CLE2	$\gamma\gamma \to \eta_c \to K^\pm K^0_S\pi^\mp$
$7.0^{+7.5}_{-7.0}$	12	BAGLIN	87B	SPEC	$\overline{p}p \to \gamma\gamma$
$10.1^{+33.0}_{-8.2}$	23	[16] BALTRUSAIT...	86	MRK3	$J/\psi \to \gamma p\overline{p}$
11.5 ± 4.5		GAISER	86	CBAL	$J/\psi \to \gamma X,\ \psi(2S) \to \gamma X$
< 40 90% CL	18	HIMEL	80B	MRK2	e^+e^-
< 20 90% CL		PARTRIDGE	80B	CBAL	e^+e^-

[1] Average between constructive and destructive interference with background.
[2] From a fit of the $\phi\phi$ invariant mass with the mass and width of $\eta_c(1S)$ as free parameters.
[3] Taking into account an asymmetric photon lineshape.
[4] With floating mass.
[5] Ignoring possible interference with the non-resonant 0^- amplitude.
[6] Using both, $\eta \to \gamma\gamma$ and $\eta \to \pi^+\pi^-\pi^0$ decays.
[7] From a simultaneous fit to six decay modes of the η_c.
[8] Accounts for interference with non-resonant continuum.
[9] Taking into account interference with the non-resonant $J^P = 0^-$ amplitude.
[10] Not independent from the measurements reported by LEES 10.
[11] Superseded by LEES 10.
[12] From a simultaneous fit of five decay modes of the η_c.
[13] Superseded by VINOKUROVA 11.
[14] From a fit to the 4-prong invariant mass in $\psi(2S) \to \gamma\eta_c$ and $J/\psi(1S) \to \gamma\eta_c$ decays.
[15] Superseded by ASNER 04.
[16] Positive and negative errors correspond to 90% confidence level.

$\eta_c(1S)$ DECAY MODES

	Mode	Fraction (Γ_i/Γ)	Scale factor/ Confidence level
	Decays involving hadronic resonances		
Γ_1	$\eta'(958)\pi\pi$	(1.59 ± 0.34) %	S=1.7
Γ_2	$\eta'(958)K\overline{K}$	(1.37 ± 0.31) %	
Γ_3	$\eta'(958)\eta\eta$	$(2.7 \pm 0.5) \times 10^{-3}$	
Γ_4	$\rho\rho$	(1.41 ± 0.34) %	
Γ_5	$K^*(892)^0K^-\pi^+ +$ c.c.	(1.43 ± 0.35) %	
Γ_6	$K^*(892)\overline{K}^*(892)$	$(5.5 \pm 1.1) \times 10^{-3}$	S=1.2
Γ_7	$K^*(892)^0\overline{K}^*(892)^0\pi^+\pi^-$	(1.1 ± 0.4) %	
Γ_8	ϕK^+K^-	$(3.0\ ^{+1.2}_{-1.0}) \times 10^{-3}$	
Γ_9	$\phi\phi$	$(1.4 \pm 0.4) \times 10^{-3}$	S=2.9
Γ_{10}	$\phi 2(\pi^+\pi^-)$	$< 3.3 \times 10^{-3}$	CL=90%
Γ_{11}	$a_0(980)\pi$	seen	
Γ_{12}	$a_2(1320)\pi$	seen	
Γ_{13}	$K^*(892)\overline{K} +$ c.c.	< 1.28 %	CL=90%
Γ_{14}	$f_2(1270)\eta$	seen	
Γ_{15}	$f_2(1270)\eta'$	seen	
Γ_{16}	$\omega\omega$	$(2.1 \pm 0.8) \times 10^{-3}$	S=2.4
Γ_{17}	$\omega\phi$	$(3.0 \pm 0.8) \times 10^{-5}$	
Γ_{18}	$f_2(1270)f_2(1270)$	$(8.4 \pm 2.4) \times 10^{-3}$	S=1.2
Γ_{19}	$f_2(1270)f'_2(1525)$	$(7.7 \pm 2.5) \times 10^{-3}$	
Γ_{20}	$f_0(500)\eta$	seen	
Γ_{21}	$f_0(500)\eta'$	seen	
Γ_{22}	$f_0(980)\eta$	seen	
Γ_{23}	$f_0(980)\eta'$	seen	
Γ_{24}	$f_0(1500)\eta$	seen	
Γ_{25}	$f_0(1710)\eta'$	seen	
Γ_{26}	$f_0(2100)\eta'$	seen	
Γ_{27}	$f_0(2200)\eta$	seen	
Γ_{28}	$a_0(1320)\pi$	seen	
Γ_{29}	$a_0(1450)\pi$	seen	
Γ_{30}	$a_2(1700)\pi$	seen	
Γ_{31}	$a_0(1710)\pi$	seen	
Γ_{32}	$a_0(1950)\pi$	seen	
Γ_{33}	$K^*_0(1430)\overline{K} +$ c.c.	seen	
Γ_{34}	$K^*_2(1430)\overline{K} +$ c.c.	seen	
Γ_{35}	$K^*_0(1950)\overline{K} +$ c.c.	seen	
Γ_{36}	$K^*_0(2600)\overline{K} +$ c.c.	seen	

Int. J. Mod. Phys. A 2026.41. Downloaded from www.worldscientific.com
by UNIVERSITY OF CALIFORNIA @ BERKELEY on 09/16/26. Re-use and distribution is strictly not permitted, except for Open Access articles.

Int. J. Mod. Phys. A 2026.41. Downloaded from www.worldscientific.com by [redacted]LIFORNIA @ BERKELEY on 09/16/26. Re-use and distribution is strictly not permitted, except for Open Access articles.

Decays into stable hadrons

Γ_{37}	$K\overline{K}\pi$	(5.9 ±0.5) %	S=1.8
Γ_{38}	$K\overline{K}\eta$	(1.11±0.15) %	S=1.3
Γ_{39}	$\eta\pi^+\pi^-$	(1.5 ±0.4) %	
Γ_{40}	$\eta 2(\pi^+\pi^-)$	(4.0 ±1.2) %	
Γ_{41}	$K^+K^-\pi^+\pi^-$	(6.7 ±1.8) $\times 10^{-3}$	S=2.4
Γ_{42}	$K^+K^-\pi^+\pi^-\pi^0$	(2.8 ±0.5) %	
Γ_{43}	$K^0K^-\pi^+\pi^-\pi^+$ + c.c.	(5.1 ±1.4) %	
Γ_{44}	$K^+K^-2(\pi^+\pi^-)$	(6.9 ±2.0) $\times 10^{-3}$	
Γ_{45}	$2(K^+K^-)$	(1.2 ±0.4) $\times 10^{-3}$	S=1.6
Γ_{46}	$\pi^+\pi^-\pi^0$	< 4 $\times 10^{-4}$	CL=90%
Γ_{47}	$\pi^+\pi^-\pi^0\pi^0$	(4.3 ±1.0) %	
Γ_{48}	$2(\pi^+\pi^-)$	(7.5 ±1.3) $\times 10^{-3}$	S=1.6
Γ_{49}	$2\pi^+2\pi^-\eta$		
Γ_{50}	$2(\pi^+\pi^-\pi^0)$	(15.5 ±2.0) %	
Γ_{51}	$3(\pi^+\pi^-)$	(1.55±0.28) %	
Γ_{52}	$p\overline{p}$	(1.11±0.12) $\times 10^{-3}$	S=1.4
Γ_{53}	$p\overline{p}\pi^0$	(3.2 ±1.2) $\times 10^{-3}$	
Γ_{54}	$p\overline{p}\pi^+\pi^-$	(3.4 ±0.5) $\times 10^{-3}$	S=1.2
Γ_{55}	$\Lambda\overline{\Lambda}$	(9.4 ±1.8) $\times 10^{-4}$	S=1.2
Γ_{56}	$K^+\overline{p}\Lambda$ + c.c.	(2.26±0.34) $\times 10^{-3}$	
Γ_{57}	$\overline{\Lambda}(1520)\Lambda$ + c.c.	(2.8 ±1.2) $\times 10^{-3}$	
Γ_{58}	$\Sigma^+\overline{\Sigma}^-$	(1.98±0.35) $\times 10^{-3}$	
Γ_{59}	$\Xi^-\overline{\Xi}^+$	(8.3 ±1.8) $\times 10^{-4}$	

Radiative decays

Γ_{60}	$\gamma\gamma$	(2.13±0.15) $\times 10^{-4}$	S=1.5
Γ_{61}	$\gamma\phi$	($1.15^{+0.33}_{-0.40}$) $\times 10^{-5}$	

Charge conjugation (C), Parity (P), Lepton Family number (LF) violating modes

Γ_{62}	$\pi^+\pi^-$	P,CP < 1.0 $\times 10^{-4}$	CL=90%
Γ_{63}	$\pi^0\pi^0$	P,CP < 3.3 $\times 10^{-5}$	CL=90%
Γ_{64}	K^+K^-	P,CP < 5 $\times 10^{-4}$	CL=90%
Γ_{65}	$K^0_SK^0_S$	P,CP < 2.9 $\times 10^{-4}$	CL=90%

FIT INFORMATION

A multiparticle fit to $\eta_c(1S)$, $J/\psi(1S)$, $\psi(2S)$, $h_c(1P)$, and $B^\pm$ with the total width, 10 combinations of partial widths obtained from integrated cross section, and 38 branching ratios uses 115 measurements to determine 19 parameters. The overall fit has a $\chi^2 = 215.4$ for 96 degrees of freedom.

The following *off-diagonal* array elements are the correlation coefficients $\langle \delta p_i \delta p_j \rangle / (\delta p_i \cdot \delta p_j)$, in percent, from the fit to parameters p_i, including the branching fractions, $x_i \equiv \Gamma_i/\Gamma_{total}$.

	x_1	x_6	x_9	x_{16}	x_{18}	x_{37}	x_{38}	x_{41}	x_{45}	x_{48}
x_6	16									
x_9	13	14								
x_{16}	8	9	8							
x_{18}	10	12	12	7						
x_{37}	32	30	26	15	20					
x_{38}	19	18	15	9	12	59				
x_{41}	9	9	8	5	6	19	12			
x_{45}	7	6	6	3	4	17	10	5		
x_{48}	14	18	18	10	15	29	17	10	6	
x_{52}	22	23	21	12	17	45	27	13	12	25
x_{54}	10	10	10	5	7	28	17	7	13	11
x_{55}	9	11	13	7	10	22	13	7	7	16
x_{60}	−41	−37	−29	−17	−22	−76	−45	−20	−16	−33
Γ	−2	−1	−1	−1	−1	−3	−2	−1	−1	−1

	x_{52}	x_{54}	x_{55}	x_{60}
x_{54}	22			
x_{55}	20	16		
x_{60}	−51	−23	−20	
Γ	1	−1	−1	−15

$\eta_c(1S)$ PARTIAL WIDTHS

$\Gamma(\gamma\gamma)$ — Γ_{60}

VALUE (keV)	EVTS	DOCUMENT ID		TECN	COMMENT
6.4± 0.5 OUR FIT Error includes scale factor of 1.5.					
• • • We do not use the following data for averages, fits, limits, etc. • • •					
5.8± 1.1	486	[1] ZHANG	12A	BELL	$e^+e^- \to e^+e^-\eta'\pi^+\pi^-$
5.2± 1.2	273 ± 43	[2,3] AUBERT	06E	BABR	$B^\pm \to K^\pm X_{c\overline{c}}$
5.5± 1.2± 1.8	157 ± 33	[4] KUO	05	BELL	$\gamma\gamma \to p\overline{p}$
7.4± 0.4± 2.3		[5] ASNER	04	CLEO	$\gamma\gamma \to \eta'_c \to K^0_SK^\pm\pi^\mp$
13.9± 2.0± 3.0	41	[6] ABDALLAH	03J	DLPH	$\gamma\gamma \to \eta_c$
$3.8^{+1.1}_{-1.0}{}^{+1.9}_{-1.0}$	190	[7] AMBROGIANI	03	E835	$\overline{p}p \to \eta_c \to \gamma\gamma$
7.6± 0.8± 2.3		[5,8] BRANDENB...	00B	CLE2	$\gamma\gamma \to \eta_c \to K^\pm K^0_S\pi^\mp$
6.9± 1.7± 2.1	76	[9] ACCIARRI	99T	L3	$e^+e^- \to e^+e^-\eta_c$
27 ±16 ±10	5	[5] SHIRAI	98	AMY	58 e^+e^-
$6.7^{+2.4}_{-1.7}$ ± 2.3		[4] ARMSTRONG	95F	E760	$\overline{p}p \to \gamma\gamma$
11.3± 4.2		[10] ALBRECHT	94H	ARG	$e^+e^- \to e^+e^-\eta_c$
8.0± 2.3± 2.4	17	[11] ADRIANI	93N	L3	$e^+e^- \to e^+e^-\eta_c$
$5.9^{+2.1}_{-1.8}$ ± 1.9		[7] CHEN	90B	CLEO	$e^+e^- \to e^+e^-\eta_c$
$6.4^{+5.0}_{-3.4}$		[12] AIHARA	88D	TPC	$e^+e^- \to e^+e^-X$
$4.3^{+3.4}_{-3.7}$ ± 2.4		[4] BAGLIN	87B	SPEC	$\overline{p}p \to \gamma\gamma$
28 ±15		[5,13] BERGER	86	PLUT	$\gamma\gamma \to K\overline{K}\pi$

[1] Assuming there is no interference with the non-resonant background.
[2] Calculated by us using $\Gamma(\eta_c \to K\overline{K}\pi) \times \Gamma(\eta_c \to \gamma\gamma) / \Gamma = 0.44 \pm 0.05$ keV from PDG 06 and $B(\eta_c \to K\overline{K}\pi) = (8.5 \pm 1.8)\%$ from AUBERT 06E.
[3] Systematic errors not evaluated.
[4] Normalized to $B(\eta_c \to p\overline{p}) = (1.3 \pm 0.4) \times 10^{-3}$.
[5] Normalized to $B(\eta_c \to K^\pm K^0_S\pi^\mp)$.
[6] Average of $K^0_SK^\pm\pi^\mp$, $\pi^+\pi^-K^+K^-$, and $2(K^+K^-)$ decay modes.
[7] Normalized to the sum of $B(\eta_c \to K^\pm K^0_S\pi^\mp)$, $B(\eta_c \to K^+K^-\pi^+\pi^-)$, and $B(\eta_c \to 2\pi^+2\pi^-)$.
[8] Superseded by ASNER 04.
[9] Normalized to the sum of 9 branching ratios.
[10] Normalized to the sum of $B(\eta_c \to K^\pm K^0_S\pi^\mp)$, $B(\eta_c \to \phi\phi)$, $B(\eta_c \to K^+K^-\pi^+\pi^-)$, and $B(\eta_c \to 2\pi^+2\pi^-)$.
[11] Superseded by ACCIARRI 99T.
[12] Normalized to the sum of $B(\eta_c \to K^\pm K^0_S\pi^\mp)$, $B(\eta_c \to 2K^+2K^-)$, $B(\eta_c \to K^+K^-\pi^+\pi^-)$, and $B(\eta_c \to 2\pi^+2\pi^-)$.
[13] Re-evaluated by AIHARA 88D.

$\eta_c(1S)$ $\Gamma(i)\Gamma(\gamma\gamma)/\Gamma(\text{total})$

$\Gamma(\eta'(958)\pi\pi) \times \Gamma(\gamma\gamma)/\Gamma_{total}$ — $\Gamma_1\Gamma_{60}/\Gamma$

VALUE (eV)	EVTS	DOCUMENT ID		TECN	COMMENT
102 ±18 OUR FIT Error includes scale factor of 1.5.					
98.1± 3.9±11.7	2673	XU	18	BELL	$e^+e^- \to e^+e^-\eta'\pi^+\pi^-$
• • • We do not use the following data for averages, fits, limits, etc. • • •					
$75.8^{+6.3}_{-6.2}$ ± 8.4	486	[1] ZHANG	12A	BELL	$e^+e^- \to e^+e^-\eta'\pi^+\pi^-$

[1] Superseded by XU 18.

$\Gamma(\rho\rho) \times \Gamma(\gamma\gamma)/\Gamma_{total}$ — $\Gamma_4\Gamma_{60}/\Gamma$

VALUE (eV)	CL%	EVTS	DOCUMENT ID		TECN	COMMENT
• • • We do not use the following data for averages, fits, limits, etc. • • •						
<39	90	< 1556	UEHARA	08	BELL	$\gamma\gamma \to 2(\pi^+\pi^-)$

$\Gamma(K^*(892)\overline{K}^*(892)) \times \Gamma(\gamma\gamma)/\Gamma_{total}$ — $\Gamma_6\Gamma_{60}/\Gamma$

VALUE (eV)	EVTS	DOCUMENT ID		TECN	COMMENT
35 ±6 OUR FIT					
32.4±4.2±5.8	882 ± 115	UEHARA	08	BELL	$\gamma\gamma \to \pi^+\pi^-K^+K^-$

$\Gamma(\phi\phi) \times \Gamma(\gamma\gamma)/\Gamma_{total}$ — $\Gamma_9\Gamma_{60}/\Gamma$

VALUE (eV)	EVTS	DOCUMENT ID		TECN	COMMENT
9.2 ±2.2 OUR FIT Error includes scale factor of 2.7.					
7.75±0.66±0.62	386 ± 31	[1] LIU	12B	BELL	$\gamma\gamma \to 2(K^+K^-)$
• • • We do not use the following data for averages, fits, limits, etc. • • •					
6.8 ±1.2 ±1.3	132 ± 23	UEHARA	08	BELL	$\gamma\gamma \to 2(K^+K^-)$

[1] Supersedes UEHARA 08. Using $B(\phi \to K^+K^-) = (48.9 \pm 0.5)\%$.

$\Gamma(\omega\omega) \times \Gamma(\gamma\gamma)/\Gamma_{total}$ — $\Gamma_{16}\Gamma_{60}/\Gamma$

VALUE (eV)	EVTS	DOCUMENT ID		TECN	COMMENT
13 ±4 OUR FIT Error includes scale factor of 2.1.					
8.67±2.86±0.96	85 ± 29	[1] LIU	12B	BELL	$\gamma\gamma \to 2(\pi^+\pi^-\pi^0)$

[1] Using $B(\omega \to \pi^+\pi^-\pi^0) = (89.2 \pm 0.7)\%$.

Int. J. Mod. Phys. A 2026.41. Downloaded from www.worldscientific.com
by UNIVERSITY OF CALIFORNIA @ BERKELEY on 09/16/26. Re-use and distribution is strictly not permitted, except for Open Access articles.

$\Gamma(\omega\phi) \times \Gamma(\gamma\gamma)/\Gamma_{total}$ — $\Gamma_{17}\Gamma_{60}/\Gamma$

VALUE (eV)	CL%	DOCUMENT ID		TECN	COMMENT
• • • We do not use the following data for averages, fits, limits, etc. • • •					
<0.49	90	[1] LIU	12B	BELL	$\gamma\gamma \to K^+K^-\pi^+\pi^-\pi^0$

[1] Using $B(\phi \to K^+K^-) = (48.9 \pm 0.5)\%$ and $B(\omega \to \pi^+\pi^-\pi^0) = (89.2 \pm 0.7)\%$.

$\Gamma(f_2(1270)f_2(1270)) \times \Gamma(\gamma\gamma)/\Gamma_{total}$ — $\Gamma_{18}\Gamma_{60}/\Gamma$

VALUE (eV)	EVTS	DOCUMENT ID		TECN	COMMENT
54±13 OUR FIT					
69±17±12	3182±766	UEHARA	08	BELL	$\gamma\gamma \to 2(\pi^+\pi^-)$

$\Gamma(f_2(1270)f'_2(1525)) \times \Gamma(\gamma\gamma)/\Gamma_{total}$ — $\Gamma_{19}\Gamma_{60}/\Gamma$

VALUE (eV)	EVTS	DOCUMENT ID		TECN	COMMENT
49±9±13	1128±206	UEHARA	08	BELL	$\gamma\gamma \to \pi^+\pi^-K^+K^-$

$\Gamma(K\overline{K}\pi) \times \Gamma(\gamma\gamma)/\Gamma_{total}$ — $\Gamma_{37}\Gamma_{60}/\Gamma$

VALUE (keV)	CL%	EVTS	DOCUMENT ID		TECN	COMMENT
0.377±0.020 OUR FIT Error includes scale factor of 1.4.						
0.396±0.016 OUR AVERAGE						
0.386±0.008±0.021		12k	DEL-AMO-SA...	11M	BABR	$\gamma\gamma \to K^0_S K^\pm\pi^\mp$
0.374±0.009±0.031		14k	[1] LEES	10	BABR	10.6 $e^+e^- \to e^+e^-K^0_S K^\pm\pi^\mp$
0.407±0.022±0.028			[2,3] ASNER	04	CLEO	$\gamma\gamma \to \eta'_c \to K^0_S K^\pm\pi^\mp$
0.60 ±0.12 ±0.09		41	[3,4] ABDALLAH	03J	DLPH	$\gamma\gamma \to K^0_S K^\pm\pi^\mp$
1.47 ±0.87 ±0.27			[3] SHIRAI	98	AMY	$\gamma\gamma \to \eta_c \to K^\pm K^0_S\pi^\mp$
0.84 ±0.21			[3] ALBRECHT	94H	ARG	$\gamma\gamma \to K^\pm K^0_S\pi^\mp$
0.60 $^{+0.23}_{-0.20}$			[3] CHEN	90B	CLEO	$\gamma\gamma \to \eta_c K^\pm K^0_S\pi^\mp$
1.06 ±0.41 ±0.27		11	[3] BRAUNSCH...	89	TASS	$\gamma\gamma \to K\overline{K}\pi$
1.5 $^{+0.60}_{-0.45}$ ±0.3		7	[3] BERGER	86	PLUT	$\gamma\gamma \to K\overline{K}\pi$
• • • We do not use the following data for averages, fits, limits, etc. • • •						
0.418±0.044±0.022			[3,5] BRANDENB...	00B	CLE2	$\gamma\gamma \to \eta_c \to K^\pm K^0_S\pi^\mp$
<0.63	95		[3] BEHREND	89	CELL	$\gamma\gamma \to K^0_S K^\pm\pi^\mp$
<4.4	95		ALTHOFF	85B	TASS	$\gamma\gamma \to K\overline{K}\pi$

[1] From the corrected and unfolded mass spectrum.
[2] Calculated by us from the value reported in ASNER 04 that assumes $B(\eta_c \to K\overline{K}\pi) = 5.5 \pm 1.7\%$
[3] We have multiplied $K^\pm K^0_S\pi^\mp$ measurement by 3 to obtain $K\overline{K}\pi$.
[4] Calculated by us from the value reported in ABDALLAH 03J, which uses $B(\eta_c \to K^0_S K^\pm\pi^\mp) = (1.5 \pm 0.4)\%$.
[5] Superseded by ASNER 04.

$\Gamma(K^+K^-\pi^+\pi^-) \times \Gamma(\gamma\gamma)/\Gamma_{total}$ — $\Gamma_{41}\Gamma_{60}/\Gamma$

VALUE (eV)	EVTS	DOCUMENT ID		TECN	COMMENT
42 ± 10 OUR FIT Error includes scale factor of 2.2.					
27 ± 6 OUR AVERAGE					
25.7± 3.2± 4.9	2019±248	UEHARA	08	BELL	$\gamma\gamma \to \pi^+\pi^-K^+K^-$
280 ±100 ±60	42	[1] ABDALLAH	03J	DLPH	$\gamma\gamma \to \pi^+\pi^-K^+K^-$
170 ± 80 ±20	13.9 ± 6.6	ALBRECHT	94H	ARG	$\gamma\gamma \to \pi^+\pi^-K^+K^-$

[1] Calculated by us from the value reported in ABDALLAH 03J, which uses $B(\eta_c \to \pi^+\pi^-K^+K^-) = (2.0 \pm 0.7)\%$.

$\Gamma(K^+K^-\pi^+\pi^-\pi^0) \times \Gamma(\gamma\gamma)/\Gamma_{total}$ — $\Gamma_{42}\Gamma_{60}/\Gamma$

VALUE (keV)	EVTS	DOCUMENT ID		TECN	COMMENT
0.190±0.006±0.028	11k	DEL-AMO-SA...	11M	BABR	$\gamma\gamma \to K^+K^-\pi^+\pi^-\pi^0$

$\Gamma(2(K^+K^-)) \times \Gamma(\gamma\gamma)/\Gamma_{total}$ — $\Gamma_{45}\Gamma_{60}/\Gamma$

VALUE (eV)	EVTS	DOCUMENT ID		TECN	COMMENT
7.5± 2.3 OUR FIT Error includes scale factor of 1.5.					
5.8± 1.9 OUR AVERAGE					
5.6± 1.1± 1.6	216 ± 42	UEHARA	08	BELL	$\gamma\gamma \to 2(K^+K^-)$
350 ±90 ±60	46	[1] ABDALLAH	03J	DLPH	$\gamma\gamma \to 2(K^+K^-)$
231 ±90 ±23	9.1 ± 3.3	[2] ALBRECHT	94H	ARG	$\gamma\gamma \to 2(K^+K^-)$

[1] Calculated by us from the value reported in ABDALLAH 03J, which uses $B(\eta_c \to) 2(K^+K^-) = (2.1 \pm 1.2)\%$.
[2] Includes all topological modes except $\eta_c \to \phi\phi$.

$\Gamma(2(\pi^+\pi^-)) \times \Gamma(\gamma\gamma)/\Gamma_{total}$ — $\Gamma_{48}\Gamma_{60}/\Gamma$

VALUE (eV)	EVTS	DOCUMENT ID		TECN	COMMENT
48 ± 7 OUR FIT Error includes scale factor of 1.4.					
42 ± 6 OUR AVERAGE					
40.7± 3.7± 5.3	5381±492	UEHARA	08	BELL	$\gamma\gamma \to 2(\pi^+\pi^-)$
180 ±70 ±20	21.4 ± 8.6	ALBRECHT	94H	ARG	$\gamma\gamma \to 2(\pi^+\pi^-)$

$\Gamma(p\overline{p}) \times \Gamma(\gamma\gamma)/\Gamma_{total}$ — $\Gamma_{52}\Gamma_{60}/\Gamma$

VALUE (eV)	EVTS	DOCUMENT ID		TECN	COMMENT
7.1 ±0.6 OUR FIT Error includes scale factor of 1.2.					
6.2 $^{+1.1}_{-1.0}$ OUR AVERAGE Error includes scale factor of 1.1.					
7.20±1.53$^{+0.67}_{-0.75}$	157 ± 33	[1] KUO	05	BELL	$\gamma\gamma \to p\overline{p}$
4.6 $^{+1.3}_{-1.1}$ ±0.4	190	AMBROGIANI	03	E835	$\overline{p}p \to \gamma\gamma$
8.1 $^{+2.9}_{-2.0}$		ARMSTRONG	95F	E760	$\overline{p}p \to \gamma\gamma$

[1] Not independent from the $\Gamma_{\gamma\gamma}$ reported by the same experiment.

$\eta_c(1S)$ BRANCHING RATIOS

HADRONIC DECAYS

$\Gamma(\eta'(958)K\overline{K})/\Gamma(\eta'(958)\pi\pi)$ — Γ_2/Γ_1

VALUE	DOCUMENT ID		TECN	COMMENT
0.859±0.052±0.043	[1] LEES	21A	BABR	$\gamma\gamma \to \eta' K^+K^-$, $\eta'\pi^+\pi^-$

[1] Based on Dalitz-plot analysis of the $\eta_c \to \eta' K^+K^-$, $\eta'\pi^+\pi^-$ final states where the fit fractions and relative phases are determined for numerous two-body intermediate states.

$\Gamma(\eta'(958)\eta\eta)/\Gamma_{total}$ — Γ_3/Γ

VALUE (units 10^{-3})	DOCUMENT ID		TECN	COMMENT
2.7±0.4±0.2	[1] ABLIKIM	21C	BES3	$J/\psi(1S) \to \gamma\eta\eta\eta'$

[1] ABLIKIM 21C reports $[\Gamma(\eta_c(1S) \to \eta'(958)\eta\eta)/\Gamma_{total}] \times [B(J/\psi(1S) \to \gamma\eta_c(1S))] = (4.86 \pm 0.62 \pm 0.45) \times 10^{-5}$ which we divide by our best (shown rounded) value $B(J/\psi(1S) \to \gamma\eta_c(1S)) = (1.82 \pm 0.15) \times 10^{-2}$. Our first error is their experiment's error and our second error is the systematic error from using our best (shown rounded) value.

$\Gamma(\rho\rho)/\Gamma_{total}$ — Γ_4/Γ

VALUE (units 10^{-2})	CL%	EVTS	DOCUMENT ID		TECN	COMMENT
• • • We do not use the following data for averages, fits, limits, etc. • • •						
0.9±0.4±0.1		72	[1] ABLIKIM	05L	BES2	$J/\psi \to \pi^+\pi^-\pi^+\pi^-\gamma$
1.8±0.4±0.1		113	[2,3] BISELLO	91	DM2	$J/\psi \to \gamma\rho^0\rho^0$
1.6±0.8±0.1		32	[4,5] BISELLO	91	DM2	$J/\psi \to \gamma\rho^+\rho^-$
<14	90		[6] BALTRUSAIT...	86	MRK3	$J/\psi \to \eta_c\gamma$

[1] ABLIKIM 05L reports $[\Gamma(\eta_c(1S) \to \rho\rho)/\Gamma_{total}] \times [B(J/\psi(1S) \to \gamma\eta_c(1S))] = (1.6 \pm 0.6 \pm 0.4) \times 10^{-4}$ which we divide by our best (shown rounded) value $B(J/\psi(1S) \to \gamma\eta_c(1S)) = (1.82 \pm 0.15) \times 10^{-2}$. Our first error is their experiment's error and our second error is the systematic error from using our best (shown rounded) value.
[2] BISELLO 91 reports $[\Gamma(\eta_c(1S) \to \rho\rho)/\Gamma_{total}] \times [B(J/\psi(1S) \to \gamma\eta_c(1S))] = (3.30 \pm 0.30 \pm 0.60) \times 10^{-4}$ which we divide by our best (shown rounded) value $B(J/\psi(1S) \to \gamma\eta_c(1S)) = (1.82 \pm 0.15) \times 10^{-2}$. Our first error is their experiment's error and our second error is the systematic error from using our best (shown rounded) value.
[3] The value reported by BISELLO 91 has been multiplied by 3 to account for isospin symmetry.
[4] BISELLO 91 reports $[\Gamma(\eta_c(1S) \to \rho\rho)/\Gamma_{total}] \times [B(J/\psi(1S) \to \gamma\eta_c(1S))] = (3.0 \pm 1.3 \pm 0.6) \times 10^{-4}$ which we divide by our best (shown rounded) value $B(J/\psi(1S) \to \gamma\eta_c(1S)) = (1.82 \pm 0.15) \times 10^{-2}$. Our first error is their experiment's error and our second error is the systematic error from using our best (shown rounded) value.
[5] The value reported by BISELLO 91 has been multiplied by 3/2 to account for isospin symmetry.
[6] Using $B(J/\psi(1S) \to \gamma\eta_c(1S)) = 0.0127 \pm 0.0036$.

$\Gamma(K^*(892)^0K^-\pi^+ + \text{c.c.})/\Gamma_{total}$ — Γ_5/Γ

VALUE (units 10^{-2})	EVTS	DOCUMENT ID		TECN	COMMENT
• • • We do not use the following data for averages, fits, limits, etc. • • •					
1.43±0.33±0.12	63	[1] BALTRUSAIT...86		MRK3	$J/\psi \to \eta_c\gamma$

[1] BALTRUSAITIS 86 reports $[\Gamma(\eta_c(1S) \to K^*(892)^0K^-\pi^+ + \text{c.c.})/\Gamma_{total}] \times [B(J/\psi(1S) \to \gamma\eta_c(1S))] = (2.6 \pm 0.6) \times 10^{-4}$ which we divide by our best (shown rounded) value $B(J/\psi(1S) \to \gamma\eta_c(1S)) = (1.82 \pm 0.15) \times 10^{-2}$. Our first error is their experiment's error and our second error is the systematic error from using our best (shown rounded) value.

$\Gamma(K^*(892)^0\overline{K}^*(892)^0\pi^+\pi^-)/\Gamma_{total}$ — Γ_7/Γ

VALUE (units 10^{-4})	EVTS	DOCUMENT ID		TECN	COMMENT
• • • We do not use the following data for averages, fits, limits, etc. • • •					
105±44±9	45	[1] ABLIKIM	06A	BES2	$J/\psi \to K^{*0}\overline{K}^{*0}\pi^+\pi^-\gamma$

[1] ABLIKIM 06A reports $[\Gamma(\eta_c(1S) \to K^*(892)^0\overline{K}^*(892)^0\pi^+\pi^-)/\Gamma_{total}] \times [B(J/\psi(1S) \to \gamma\eta_c(1S))] = (1.91 \pm 0.64 \pm 0.48) \times 10^{-4}$ which we divide by our best (shown rounded) value $B(J/\psi(1S) \to \gamma\eta_c(1S)) = (1.82 \pm 0.15) \times 10^{-2}$. Our first error is their experiment's error and our second error is the systematic error from using our best (shown rounded) value.

$\Gamma(\phi K^+K^-)/\Gamma_{total}$ — Γ_8/Γ

VALUE (units 10^{-3})	EVTS	DOCUMENT ID		TECN	COMMENT
• • • We do not use the following data for averages, fits, limits, etc. • • •					
2.9$^{+0.9}_{-0.8}$±1.1	14.1$^{+4.4}_{-3.7}$	[1,2] HUANG	03	BELL	$B^+ \to (\phi K^+K^-)K^+$

[1] Using $B(B^+ \to \eta_c K^+) = (1.25 \pm 0.12^{+0.10}_{-0.12}) \times 10^{-3}$ from FANG 03 and $B(\eta_c \to K\overline{K}\pi) = (5.5 \pm 1.7) \times 10^{-2}$.
[2] Not used since the same experimental measurement has been used in another related quantity included elsewhere in the fit.

$\Gamma(\phi 2(\pi^+\pi^-))/\Gamma_{total}$ — Γ_{10}/Γ

VALUE (units 10^{-4})	CL%	DOCUMENT ID		TECN	COMMENT
<33	90	[1] ABLIKIM	06A	BES2	$J/\psi \to \phi 2(\pi^+\pi^-)\gamma$

[1] ABLIKIM 06A reports $[\Gamma(\eta_c(1S) \to \phi 2(\pi^+\pi^-))/\Gamma_{total}] \times [B(J/\psi(1S) \to \gamma\eta_c(1S))] < 0.603 \times 10^{-4}$ which we divide by our best (shown rounded) value $B(J/\psi(1S) \to \gamma\eta_c(1S)) = 1.82 \times 10^{-2}$.

$\Gamma(a_0(980)\pi)/\Gamma_{total}$ — Γ_{11}/Γ

VALUE	CL%	DOCUMENT ID		TECN	COMMENT
seen		AAIJ	23AH	LHCB	$B^+ \to K^+(K^0_S K\pi)$
seen		LEES	21A	BABR	Dalitz anal. of $\eta_c \to \pi^+\pi^-\eta$
seen		LEES	14E	BABR	Dalitz anal. of $\eta_c \to K^+K^-\pi^0$
• • • We do not use the following data for averages, fits, limits, etc. • • •					
<0.02	90	[1,2] BALTRUSAIT...86		MRK3	$J/\psi \to \eta_c\gamma$

[1] The quoted branching ratio uses $B(J/\psi(1S) \to \gamma\eta_c(1S)) = 0.0127 \pm 0.0036$.
[2] We are assuming $B(a_0(980) \to \eta\pi) > 0.5$.

$\Gamma(a_2(1320)\pi)/\Gamma_{total}$ — Γ_{12}/Γ

VALUE	CL%	DOCUMENT ID		TECN	COMMENT
seen		LEES	21A	BABR	Dalitz anal. of $\eta_c \to \pi^+\pi^-\eta$
• • • We do not use the following data for averages, fits, limits, etc. • • •					
<0.02	90	[1] BALTRUSAIT...86		MRK3	$J/\psi \to \eta_c\gamma$

[1] The quoted branching ratio uses $B(J/\psi(1S) \to \gamma\eta_c(1S)) = 0.0127 \pm 0.0036$.

$\Gamma(K^*(892)\overline{K} + c.c.)/\Gamma_{total}$ — Γ_{13}/Γ

VALUE	CL%	DOCUMENT ID		TECN	COMMENT
<0.0128	90	BISELLO	91	DM2	$J/\psi \to \gamma K^0_S K^\pm\pi^\mp$
<0.0132	90	[1] BISELLO	91	DM2	$J/\psi \to \gamma K^+K^-\pi^0$

[1] The quoted branching ratios use $B(J/\psi(1S) \to \gamma\eta_c(1S)) = 0.0127 \pm 0.0036$.

$\Gamma(f_2(1270)\eta)/\Gamma_{total}$ — Γ_{14}/Γ

VALUE	CL%	DOCUMENT ID		TECN	COMMENT
seen		LEES	21A	BABR	Dalitz anal. of $\eta_c \to \pi^+\pi^-\eta$
• • • We do not use the following data for averages, fits, limits, etc. • • •					
<0.011	90	[1] BALTRUSAIT...86		MRK3	$J/\psi \to \eta_c\gamma$

[1] The quoted branching ratio uses $B(J/\psi(1S) \to \gamma\eta_c(1S)) = 0.0127 \pm 0.0036$.

$\Gamma(f_2(1270)\eta')/\Gamma_{total}$ — Γ_{15}/Γ

VALUE	DOCUMENT ID		TECN	COMMENT
seen	LEES	21A	BABR	Dalitz anal. of $\eta_c \to \pi^+\pi^-\eta'$; $K^+K^-\eta'$

$\Gamma(\omega\phi)/\Gamma_{total}$ — Γ_{17}/Γ

VALUE (units 10^{-5})	CL%	EVTS	DOCUMENT ID		TECN	COMMENT
3.0±0.8±0.2		118	[1] ABLIKIM	25AC	BES3	$J/\psi(1S) \to \gamma\eta_c$
• • • We do not use the following data for averages, fits, limits, etc. • • •						
< 25	90		[2] ABLIKIM	17P	BES3	$J/\psi \to \pi^+\pi^-\pi^0K^+K^-\gamma$
<170	90		[3] ABLIKIM	05L	BES2	$J/\psi \to \pi^+\pi^-\pi^0K^+K^-\gamma$

[1] ABLIKIM 25AC reports $(3.86 \pm 0.92 \pm 0.62) \times 10^{-5}$ from a measurement of $[\Gamma(\eta_c(1S) \to \omega\phi)/\Gamma_{total}] \times [B(J/\psi(1S) \to \gamma\eta_c(1S))]$ assuming $B(J/\psi(1S) \to \gamma\eta_c(1S)) = (1.41 \pm 0.14) \times 10^{-2}$, which we rescale to our best (shown rounded) value $B(J/\psi(1S) \to \gamma\eta_c(1S)) = (1.82 \pm 0.15) \times 10^{-2}$. Our first error is their experiment's error and our second error is the systematic error from using our best (shown rounded) value.
[2] Using $B(J/\psi \to \gamma\eta_c) = 0.017 \pm 0.004$.
[3] The quoted branching ratio uses $B(J/\psi(1S) \to \gamma\eta_c(1S)) = 0.0127 \pm 0.0036$.

$\Gamma(f_0(500)\eta)/\Gamma_{total}$ — Γ_{20}/Γ

VALUE	DOCUMENT ID		TECN	COMMENT
seen	LEES	21A	BABR	Dalitz anal. of $\eta_c \to \pi^+\pi^-\eta$

$\Gamma(f_0(500)\eta')/\Gamma_{total}$ — Γ_{21}/Γ

VALUE	DOCUMENT ID		TECN	COMMENT
seen	LEES	21A	BABR	Dalitz anal. of $\eta_c(1S) \to \pi^+\pi^-\eta'$

$\Gamma(f_0(980)\eta)/\Gamma_{total}$ — Γ_{22}/Γ

VALUE	DOCUMENT ID		TECN	COMMENT
seen	LEES	21A	BABR	Dalitz anal. of $\eta_c \to \pi^+\pi^-\eta$
seen	LEES	14E	BABR	Dalitz anal. of $\eta_c \to K^+K^-\eta$

$\Gamma(f_0(980)\eta')/\Gamma_{total}$ — Γ_{23}/Γ

VALUE	DOCUMENT ID		TECN	COMMENT
seen	LEES	21A	BABR	Dalitz anal. of $\eta_c \to \pi^+\pi^-\eta'$, $K^+K^-\eta'$

$\Gamma(f_0(1500)\eta)/\Gamma_{total}$ — Γ_{24}/Γ

VALUE	DOCUMENT ID		TECN	COMMENT
seen	LEES	21A	BABR	Dalitz anal. of $\eta_c \to \pi^+\pi^-\eta$
seen	LEES	14E	BABR	Dalitz anal. of $\eta_c \to K^+K^-\eta$

$\Gamma(f_0(1710)\eta')/\Gamma_{total}$ — Γ_{25}/Γ

VALUE	DOCUMENT ID		TECN	COMMENT
seen	LEES	21A	BABR	Dalitz anal. of $\eta_c \to K^+K^-\eta'$

$\Gamma(f_0(2100)\eta')/\Gamma_{total}$ — Γ_{26}/Γ

VALUE	DOCUMENT ID		TECN	COMMENT
seen	LEES	21A	BABR	Dalitz anal. of $\eta_c \to \pi^+\pi^-\eta$

$\Gamma(f_0(2200)\eta)/\Gamma_{total}$ — Γ_{27}/Γ

VALUE	DOCUMENT ID		TECN	COMMENT
seen	LEES	14E	BABR	Dalitz anal. of $\eta_c \to K^+K^-\eta$

$\Gamma(a_0(1320)\pi)/\Gamma_{total}$ — Γ_{28}/Γ

VALUE	DOCUMENT ID		TECN	COMMENT
seen	AAIJ	23AH	LHCB	$B^+ \to K^+(K^0_S K\pi)$
seen	LEES	14E	BABR	Dalitz anal. of $\eta_c \to K^+K^-\pi^0$

$\Gamma(a_0(1450)\pi)/\Gamma_{total}$ — Γ_{29}/Γ

VALUE	DOCUMENT ID		TECN	COMMENT
seen	AAIJ	23AH	LHCB	$B^+ \to K^+(K^0_S K\pi)$
seen	LEES	21A	BABR	Dalitz anal. of $\eta_c \to \pi^+\pi^-\eta$
seen	LEES	14E	BABR	Dalitz anal. of $\eta_c \to K^+K^-\pi^0$

$\Gamma(a_2(1700)\pi)/\Gamma_{total}$ — Γ_{30}/Γ

VALUE	DOCUMENT ID		TECN	COMMENT
seen	AAIJ	23AH	LHCB	$B^+ \to K^+(K^0_S K\pi)$

$\Gamma(a_0(1710)\pi)/\Gamma_{total}$ — Γ_{31}/Γ

VALUE	DOCUMENT ID		TECN	COMMENT
seen	AAIJ	23AH	LHCB	$B^+ \to K^+(K^0_S K\pi)$
seen	LEES	21A	BABR	Dalitz anal. of $\eta_c \to \pi^+\pi^-\eta'$

$\Gamma(a_0(1950)\pi)/\Gamma_{total}$ — Γ_{32}/Γ

VALUE	EVTS	DOCUMENT ID		TECN	COMMENT
seen		LEES	21A	BABR	Dalitz anal. of $\eta_c(1S) \to \pi^+\pi^-\eta'$
seen	12k	[1] LEES	16A	BABR	$\gamma\gamma \to \eta_c(1S) \to K\overline{K}\pi$

[1] From a model-independant partial wave analysis.

$\Gamma(K^*_0(1430)\overline{K} + c.c.)/\Gamma_{total}$ — Γ_{33}/Γ

VALUE	EVTS	DOCUMENT ID		TECN	COMMENT
seen	12k	[1] LEES	16A	BABR	$\gamma\gamma \to \eta_c(1S) \to K\overline{K}\pi$
seen		LEES	14E	BABR	Dalitz anal. of $\eta_c \to K^+K^-\eta/\pi^0$

[1] From a model-independant partial wave analysis.

$\Gamma(K^*_2(1430)\overline{K} + c.c.)/\Gamma_{total}$ — Γ_{34}/Γ

VALUE	DOCUMENT ID		TECN	COMMENT
seen	AAIJ	23AH	LHCB	$B^+ \to K^+(K^0_S K\pi)$
seen	LEES	21A	BABR	Dalitz anal. of $\eta_c \to K^+K^-\eta'$
seen	LEES	14E	BABR	Dalitz anal. of $\eta_c \to K^+K^-\pi^0$

$\Gamma(K^*_0(1950)\overline{K} + c.c.)/\Gamma_{total}$ — Γ_{35}/Γ

VALUE	EVTS	DOCUMENT ID		TECN	COMMENT
seen		AAIJ	23AH	LHCB	$B^+ \to K^+(K^0_S K\pi)$
seen		LEES	21A	BABR	Dalitz anal. of $\eta_c \to K^+K^-\eta'$
seen	12k	[1] LEES	16A	BABR	$\gamma\gamma \to \eta_c(1S) \to K\overline{K}\pi$
seen		LEES	14E	BABR	Dalitz anal. of $\eta_c \to K^+K^-\eta/\pi^0$

[1] From a Dalitz plot analysis using an isobar model.

$\Gamma(K^*_0(2600)\overline{K} + c.c.)/\Gamma_{total}$ — Γ_{36}/Γ

VALUE	DOCUMENT ID		TECN	COMMENT
seen	AAIJ	23AH	LHCB	$B^+ \to K^+(K^0_S K\pi)$

$\Gamma(K\overline{K}\pi)/\Gamma_{total}$ — Γ_{37}/Γ

VALUE (units 10^{-2})	EVTS	DOCUMENT ID		TECN	COMMENT
5.9±0.5 OUR FIT Error includes scale factor of 1.8.					
7.4±0.6 OUR AVERAGE					
6.9±0.7±0.6	146	[1] ABLIKIM	19AP	BES3	$h_c \to \gamma\eta_c$
7.8±0.6±0.6	267	[2] ABLIKIM	19AP	BES3	$h_c \to \gamma\eta_c$
• • • We do not use the following data for averages, fits, limits, etc. • • •					
5.7±1.1±0.6	55	[3,4,5] ABLIKIM	12N	BES3	$\psi(2S) \to \pi^0\gamma K^+K^-\pi^0$
7.2±1.2±0.8	107	[5,6,7] ABLIKIM	12N	BES3	$\psi(2S) \to \pi^0\gamma K^0_S K^\mp\pi^\pm$
8.5±1.8		[5,8] AUBERT	06E	BABR	$B^\pm \to K^\pm X_{c\overline{c}}$
3.6±1.0±0.3	0.6k	[5,9,10] BAI	04	BES	$J/\psi \to \gamma K^\pm\pi^\mp K^0_S$
4.8±1.4±0.4	33	[5,11,12] BISELLO	91	DM2	$J/\psi \to \gamma K^+K^-\pi^0$
3.8±0.9±0.3	68	[5,13,14] BISELLO	91	DM2	$J/\psi \to \gamma K^\pm\pi^\mp K^0_S$
4.8±1.7	95	[5,15,16] BALTRUSAIT...86		MRK3	$J/\psi \to \eta_c\gamma$
4.3±1.6±0.3	32	[5,17,18] BALTRUSAIT...86		MRK3	$J/\psi \to \gamma K^+K^-\pi^0$
3.1±0.8±0.3	63	[5,19,20] BALTRUSAIT...86		MRK3	$J/\psi \to \gamma K^\pm\pi^\mp K^0_S$
$12\ ^{+7}_{-5} \pm 2$		[5,21] HIMEL	80B	MRK2	$\psi(2S) \to \eta_c\gamma$
< 10.7 90% CL		[16] PARTRIDGE	80B	CBAL	$J/\psi \to \eta_c\gamma$

Int. J. Mod. Phys. A 2026.41. Downloaded from www.worldscientific.com
by [redacted]LIFORNIA @ BERKELEY on 09/16/26. Re-use and distribution is strictly not permitted, except for Open Access articles.

See key on page 1227

[1] ABLIKIM 19AP quotes $B(\eta_c \to K^+K^-\pi^0) = (1.15 \pm 0.12 \pm 0.10) \times 10^{-2}$ which we multiply by 6 to account for isospin symmetry.
[2] ABLIKIM 19AP quotes $B(\eta_c \to K^0_S K^\pm \pi^\mp) = (2.60 \pm 0.21 \pm 0.20) \times 10^{-2}$ which we multiply by 3 to account for isospin symmetry.
[3] ABLIKIM 12N quotes $B(\psi(2S) \to \pi^0 h_c) \cdot B(h_c \to \gamma\eta_c) \cdot B(\eta_c \to K^+K^-\pi^0) = (4.54 \pm 0.76 \pm 0.48) \times 10^{-6}$ which we multiply by 6 to account for isospin symmetry.
[4] ABLIKIM 12N reports $[\Gamma(\eta_c(1S) \to K\overline{K}\pi)/\Gamma_{total}] \times [B(\psi(2S) \to h_c(1P)\pi^0)] \times [B(h_c(1P) \to \gamma\eta_c(1S))] = (27.24 \pm 4.56 \pm 2.88) \times 10^{-6}$ which we divide by our best (shown rounded) values $B(\psi(2S) \to h_c(1P)\pi^0) = (7.4 \pm 0.5) \times 10^{-4}$, $B(h_c(1P) \to \gamma\eta_c(1S)) = (64 \pm 5) \times 10^{-2}$. Our first error is their experiment's error and our second error is the systematic error from using our best (shown rounded) values.
[5] Not used since the same experimental measurement has been used in another related quantity included elsewhere in the fit.
[6] ABLIKIM 12N quotes $B(\psi(2S) \to \pi^0 h_c) \cdot B(h_c \to \gamma\eta_c) \cdot B(\eta_c \to K^0_S K^\pm\pi^\mp) = (11.35 \pm 1.25 \pm 1.50) \times 10^{-6}$ which we multiply by 3 to account for isospin symmetry.
[7] ABLIKIM 12N reports $[\Gamma(\eta_c(1S) \to K\overline{K}\pi)/\Gamma_{total}] \times [B(\psi(2S) \to h_c(1P)\pi^0)] \times [B(h_c(1P) \to \gamma\eta_c(1S))] = (34.05 \pm 3.75 \pm 4.50) \times 10^{-6}$ which we divide by our best (shown rounded) values $B(\psi(2S) \to h_c(1P)\pi^0) = (7.4 \pm 0.5) \times 10^{-4}$, $B(h_c(1P) \to \gamma\eta_c(1S)) = (64 \pm 5) \times 10^{-2}$. Our first error is their experiment's error and our second error is the systematic error from using our best (shown rounded) values.
[8] Determined from the ratio of $B(B^\pm \to K^\pm\eta_c)\, B(\eta_c \to K\overline{K}\pi) = (7.4 \pm 0.5 \pm 0.7) \times 10^{-5}$ reported in AUBERT,B 04B and $B(B^\pm \to K^\pm\eta_c) = (8.7 \pm 1.5) \times 10^{-3}$ reported in AUBERT 06E.
[9] BAI 04 reports $B(J/\psi \to \gamma\eta_c) \cdot B(\eta_c \to K^\pm K^0_S \pi^\mp) = (2.2 \pm 0.3 \pm 0.5) \times 10^{-4}$ which we multiply by 3 to account for isospin symmetry.
[10] BAI 04 reports $[\Gamma(\eta_c(1S) \to K\overline{K}\pi)/\Gamma_{total}] \times [B(J/\psi(1S) \to \gamma\eta_c(1S))] = (6.6 \pm 0.9 \pm 1.5) \times 10^{-4}$ which we divide by our best (shown rounded) value $B(J/\psi(1S) \to \gamma\eta_c(1S)) = (1.82 \pm 0.15) \times 10^{-2}$. Our first error is their experiment's error and our second error is the systematic error from using our best (shown rounded) value.
[11] BISELLO 91 reports $[\Gamma(\eta_c(1S) \to K\overline{K}\pi)/\Gamma_{total}] \times [B(J/\psi(1S) \to \gamma\eta_c(1S))] = (8.76 \pm 1.80 \pm 1.68) \times 10^{-4}$ which we divide by our best (shown rounded) value $B(J/\psi(1S) \to \gamma\eta_c(1S)) = (1.82 \pm 0.15) \times 10^{-2}$. Our first error is their experiment's error and our second error is the systematic error from using our best (shown rounded) value.
[12] BISELLO 91 reports $B(J/\psi \to \gamma\eta_c) \cdot B(\eta_c \to K^+K^-\pi^0) = (1.46 \pm 0.30 \pm 0.28) \times 10^{-4}$ which we multiply by 6 to account for isospin symmetry.
[13] BISELLO 91 reports $[\Gamma(\eta_c(1S) \to K\overline{K}\pi)/\Gamma_{total}] \times [B(J/\psi(1S) \to \gamma\eta_c(1S))] = (6.9 \pm 1.2 \pm 1.2) \times 10^{-4}$ which we divide by our best (shown rounded) value $B(J/\psi(1S) \to \gamma\eta_c(1S)) = (1.82 \pm 0.15) \times 10^{-2}$. Our first error is their experiment's error and our second error is the systematic error from using our best (shown rounded) value.
[14] BISELLO 91 reports $B(J/\psi \to \gamma\eta_c) \cdot B(\eta_c \to K^\pm K^0_S \pi^\mp) = (2.3 \pm 0.4 \pm 0.4) \times 10^{-4}$ which we multiply by 3 to account for isospin symmetry.
[15] Average from $K^+K^-\pi^0$ and $K^\pm K^0_S \pi^\mp$ decay channels.
[16] The quoted branching ratios use $B(J/\psi(1S) \to \gamma\eta_c(1S)) = 0.0127 \pm 0.0036$. Where relevant, the error in this branching ratio is treated as a common systematic in computing averages.
[17] BALTRUSAITIS 86 reports $[\Gamma(\eta_c(1S) \to K\overline{K}\pi)/\Gamma_{total}] \times [B(J/\psi(1S) \to \gamma\eta_c(1S))] = (7.8 \pm 3.0) \times 10^{-4}$ which we divide by our best (shown rounded) value $B(J/\psi(1S) \to \gamma\eta_c(1S)) = (1.82 \pm 0.15) \times 10^{-2}$. Our first error is their experiment's error and our second error is the systematic error from using our best (shown rounded) value.
[18] BALTRUSAITIS 86 reports $B(J/\psi \to \gamma\eta_c) \cdot B(\eta_c \to K^+K^-\pi^0) = (1.3 \pm 0.5) \times 10^{-4}$ which we multiply by 6 to account for isospin symmetry.
[19] BALTRUSAITIS 86 reports $[\Gamma(\eta_c(1S) \to K\overline{K}\pi)/\Gamma_{total}] \times [B(J/\psi(1S) \to \gamma\eta_c(1S))] = (5.7 \pm 1.5) \times 10^{-4}$ which we divide by our best (shown rounded) value $B(J/\psi(1S) \to \gamma\eta_c(1S)) = (1.82 \pm 0.15) \times 10^{-2}$. Our first error is their experiment's error and our second error is the systematic error from using our best (shown rounded) value.
[20] BALTRUSAITIS 86 reports $B(J/\psi \to \gamma\eta_c) \cdot B(\eta_c \to K^\pm K^0_S \pi^\mp) = (1.9 \pm 0.5) \times 10^{-4}$ which we multiply by 3 to account for isospin symmetry.
[21] HIMEL 80B reports $[\Gamma(\eta_c(1S) \to K\overline{K}\pi)/\Gamma_{total}] \times [B(\psi(2S) \to \gamma\eta_c(1S))] = (4.5^{+2.4}_{-1.8}) \times 10^{-4}$ which we divide by our best (shown rounded) value $B(\psi(2S) \to \gamma\eta_c(1S)) = (3.6 \pm 0.5) \times 10^{-3}$. Our first error is their experiment's error and our second error is the systematic error from using our best (shown rounded) value.

$\Gamma(\phi K^+K^-)/\Gamma(K\overline{K}\pi)$ — Γ_8/Γ_{37}

VALUE	EVTS	DOCUMENT ID		TECN	COMMENT
$\mathbf{0.052^{+0.016}_{-0.014} \pm 0.014}$	7	[1] HUANG	03	BELL	$B^\pm \to K^\pm\phi\phi$

[1] Using $B(B^+ \to \eta_c K^+) = (1.25 \pm 0.12^{+0.10}_{-0.12}) \times 10^{-3}$ from FANG 03 and $B(\eta_c \to K\overline{K}\pi) = (5.5 \pm 1.7) \times 10^{-2}$.

$\Gamma(K\overline{K}\eta)/\Gamma_{total}$ — Γ_{38}/Γ

VALUE (units 10^{-2})	CL%	EVTS	DOCUMENT ID		TECN	COMMENT
• • • We do not use the following data for averages, fits, limits, etc. • • •						
$0.9 \pm 0.4 \pm 0.1$		7	[1,2,3] ABLIKIM	12N	BES3	$\psi(2S) \to \pi^0\gamma\eta K^+K^-$
<3.1	90		[4] BALTRUSAIT...86		MRK3	$J/\psi \to \eta_c\gamma$

[1] Not used since the same experimental measurement has been used in another related quantity included elsewhere in the fit.
[2] ABLIKIM 12N quotes $B(\psi(2S) \to \pi^0 h_c) \cdot B(h_c \to \gamma\eta_c) \cdot B(\eta_c \to K^+K^-\eta) = (2.11 \pm 1.01 \pm 0.32) \times 10^{-6}$ which we multiply by 2 to account for isospin symmetry.
[3] ABLIKIM 12N reports $[\Gamma(\eta_c(1S) \to K\overline{K}\eta)/\Gamma_{total}] \times [B(\psi(2S) \to h_c(1P)\pi^0)] \times [B(h_c(1P) \to \gamma\eta_c(1S))] = (4.22 \pm 2.02 \pm 0.64) \times 10^{-6}$ which we divide by our best (shown rounded) values $B(\psi(2S) \to h_c(1P)\pi^0) = (7.4 \pm 0.5) \times 10^{-4}$, $B(h_c(1P) \to \gamma\eta_c(1S)) = (64 \pm 5) \times 10^{-2}$. Our first error is their experiment's error and our second error is the systematic error from using our best (shown rounded) values.
[4] The quoted branching ratios use $B(J/\psi(1S) \to \gamma\eta_c(1S)) = 0.0127 \pm 0.0036$.

$\Gamma(K\overline{K}\eta)/\Gamma(K\overline{K}\pi)$ — Γ_{38}/Γ_{37}

VALUE	EVTS	DOCUMENT ID		TECN	COMMENT
0.188±0.018 OUR FIT					
0.190±0.008±0.017	5.4k	[1] LEES	14E	BABR	$\gamma\gamma \to K^+K^-\eta/\pi^0$

[1] LEES 14E reports $B(\eta_c(1S) \to K^+K^-\eta)/B(\eta_c(1S) \to K^+K^-\pi^0) = 0.571 \pm 0.025 \pm 0.051$, which we divide by 3 to account for isospin symmetry. It uses both $\eta \to \gamma\gamma$ and $\eta \to \pi^+\pi^-\pi^0$ decays.

$\Gamma(\eta\pi^+\pi^-)/\Gamma_{total}$ — Γ_{39}/Γ

VALUE (units 10^{-2})	EVTS	DOCUMENT ID		TECN	COMMENT
1.5±0.4±0.2	33	[1] ABLIKIM	12N	BES3	$\psi(2S) \to \pi^0\gamma\eta\pi^+\pi^-$
• • • We do not use the following data for averages, fits, limits, etc. • • •					
5.4 ± 2.0	75	[2,3] BALTRUSAIT...86		MRK3	$J/\psi \to \eta_c\gamma$
$3.7 \pm 1.3 \pm 2.0$	18	[2,3] PARTRIDGE	80B	CBAL	$J/\psi \to \eta\pi^+\pi^-\gamma$

[1] ABLIKIM 12N reports $[\Gamma(\eta_c(1S) \to \eta\pi^+\pi^-)/\Gamma_{total}] \times [B(\psi(2S) \to h_c(1P)\pi^0)] \times [B(h_c(1P) \to \gamma\eta_c(1S))] = (7.22 \pm 1.47 \pm 1.11) \times 10^{-6}$ which we divide by our best (shown rounded) values $B(\psi(2S) \to h_c(1P)\pi^0) = (7.4 \pm 0.5) \times 10^{-4}$, $B(h_c(1P) \to \gamma\eta_c(1S)) = (64 \pm 5) \times 10^{-2}$. Our first error is their experiment's error and our second error is the systematic error from using our best (shown rounded) values.
[2] Not used since the same experimental measurement has been used in another related quantity.
[3] The quoted branching ratios use $B(J/\psi(1S) \to \gamma\eta_c(1S)) = 0.0127 \pm 0.0036$. Where relevant, the error in this branching ratio is treated as a common systematic in computing averages.

$\Gamma(\eta 2(\pi^+\pi^-))/\Gamma_{total}$ — Γ_{40}/Γ

VALUE (units 10^{-2})	EVTS	DOCUMENT ID		TECN	COMMENT
4.0±1.1±0.4	39	[1] ABLIKIM	12N	BES3	$\psi(2S) \to \pi^0\gamma\eta 2(\pi^+\pi^-)$

[1] ABLIKIM 12N reports $[\Gamma(\eta_c(1S) \to \eta 2(\pi^+\pi^-))/\Gamma_{total}] \times [B(\psi(2S) \to h_c(1P)\pi^0)] \times [B(h_c(1P) \to \gamma\eta_c(1S))] = (19.17 \pm 3.77 \pm 3.72) \times 10^{-6}$ which we divide by our best (shown rounded) values $B(\psi(2S) \to h_c(1P)\pi^0) = (7.4 \pm 0.5) \times 10^{-4}$, $B(h_c(1P) \to \gamma\eta_c(1S)) = (64 \pm 5) \times 10^{-2}$. Our first error is their experiment's error and our second error is the systematic error from using our best (shown rounded) values.

$\Gamma(K^+K^-\pi^+\pi^-\pi^0)/\Gamma(K\overline{K}\pi)$ — Γ_{42}/Γ_{37}

VALUE	EVTS	DOCUMENT ID		TECN	COMMENT
0.477±0.017±0.070	11k	[1] DEL-AMO-SA...11M		BABR	$\gamma\gamma \to K^+K^-\pi^+\pi^-\pi^0$

[1] We have multiplied the value of $\Gamma(K^+K^-\pi^+\pi^-\pi^0)/\Gamma(K^0_S K^\pm\pi^\mp)$ reported in DEL-AMO-SANCHEZ 11M by a factor 1/3 to obtain $\Gamma(K^+K^-\pi^+\pi^-\pi^0)/\Gamma(K\overline{K}\pi)$. Not independent from other measurements reported in DEL-AMO-SANCHEZ 11M.

$\Gamma(K^0K^-\pi^+\pi^-\pi^+ + \text{c.c.})/\Gamma_{total}$ — Γ_{43}/Γ

VALUE (units 10^{-2})	EVTS	DOCUMENT ID		TECN	COMMENT
5.1±1.3±0.5	43	[1,2] ABLIKIM	12N	BES3	$\psi(2S) \to \pi^0\gamma K^0_S K^\mp\pi^\mp 2\pi^\pm$

[1] ABLIKIM 12N quotes $B(\psi(2S) \to \pi^0 h_c) \cdot B(h_c \to \gamma\eta_c) \cdot B(\eta_c \to K^0_S K^-\pi^-2\pi^+) = (12.01 \pm 2.22 \pm 2.04) \times 10^{-6}$ which we multiply by 2 to take c.c. into account.
[2] ABLIKIM 12N reports $[\Gamma(\eta_c(1S) \to K^0K^-\pi^+\pi^-\pi^+ + \text{c.c.})/\Gamma_{total}] \times [B(\psi(2S) \to h_c(1P)\pi^0)] \times [B(h_c(1P) \to \gamma\eta_c(1S))] = (24.02 \pm 4.44 \pm 4.08) \times 10^{-6}$ which we divide by our best (shown rounded) values $B(\psi(2S) \to h_c(1P)\pi^0) = (7.4 \pm 0.5) \times 10^{-4}$, $B(h_c(1P) \to \gamma\eta_c(1S)) = (64 \pm 5) \times 10^{-2}$. Our first error is their experiment's error and our second error is the systematic error from using our best (shown rounded) values.

$\Gamma(K^+K^-2(\pi^+\pi^-))/\Gamma_{total}$ — Γ_{44}/Γ

VALUE (units 10^{-3})	EVTS	DOCUMENT ID		TECN	COMMENT
6.9±2.0 OUR AVERAGE					
$8 \pm 4 \pm 1$	10	[1] ABLIKIM	12N	BES3	$\psi(2S) \to \pi^0\gamma K^+K^-2(\pi^+\pi^-)$
$6.7 \pm 2.2 \pm 0.5$	100	[2] ABLIKIM	06A	BES2	$J/\psi \to K^+K^-2(\pi^+\pi^-)\gamma$

[1] ABLIKIM 12N reports $[\Gamma(\eta_c(1S) \to K^+K^-2(\pi^+\pi^-))/\Gamma_{total}] \times [B(\psi(2S) \to h_c(1P)\pi^0)] \times [B(h_c(1P) \to \gamma\eta_c(1S))] = (3.60 \pm 1.71 \pm 0.64) \times 10^{-6}$ which we divide by our best (shown rounded) values $B(\psi(2S) \to h_c(1P)\pi^0) = (7.4 \pm 0.5) \times 10^{-4}$, $B(h_c(1P) \to \gamma\eta_c(1S)) = (64 \pm 5) \times 10^{-2}$. Our first error is their experiment's error and our second error is the systematic error from using our best (shown rounded) values.
[2] ABLIKIM 06A reports $[\Gamma(\eta_c(1S) \to K^+K^-2(\pi^+\pi^-))/\Gamma_{total}] \times [B(J/\psi(1S) \to \gamma\eta_c(1S))] = (1.21 \pm 0.32 \pm 0.24) \times 10^{-4}$ which we divide by our best (shown rounded) value $B(J/\psi(1S) \to \gamma\eta_c(1S)) = (1.82 \pm 0.15) \times 10^{-2}$. Our first error is their experiment's error and our second error is the systematic error from using our best (shown rounded) value.

$\Gamma(\pi^+\pi^-\pi^0)/\Gamma_{total}$ — Γ_{46}/Γ

VALUE	CL%	DOCUMENT ID		TECN	COMMENT
$<4 \times 10^{-4}$	90	[1] ABLIKIM	17AJ	BES3	$\psi(2S) \to \gamma\pi^+\pi^-\pi^0$

[1] ABLIKIM 17AJ reports $[\Gamma(\eta_c(1S) \to \pi^+\pi^-\pi^0)/\Gamma_{total}] \times [B(\psi(2S) \to \gamma\eta_c(1S))] < 1.6 \times 10^{-6}$ which we divide by our best (shown rounded) value $B(\psi(2S) \to \gamma\eta_c(1S)) = 3.6 \times 10^{-3}$.

$\Gamma(\pi^+\pi^-\pi^0\pi^0)/\Gamma_{total}$ — Γ_{47}/Γ

VALUE (units 10^{-2})	EVTS	DOCUMENT ID		TECN	COMMENT
4.3±0.8±0.5	118	[1] ABLIKIM	12N	BES3	$\psi(2S) \to \pi^0\gamma\pi^+\pi^-2\pi^0$

[1] ABLIKIM 12N reports $[\Gamma(\eta_c(1S) \to \pi^+\pi^-\pi^0\pi^0)/\Gamma_{total}] \times [B(\psi(2S) \to h_c(1P)\pi^0)] \times [B(h_c(1P) \to \gamma\eta_c(1S))] = (20.31 \pm 2.20 \pm 3.33) \times 10^{-6}$ which we divide by our best (shown rounded) values $B(\psi(2S) \to h_c(1P)\pi^0) = (7.4 \pm 0.5) \times 10^{-4}$, $B(h_c(1P) \to \gamma\eta_c(1S)) = (64 \pm 5) \times 10^{-2}$. Our first error is their experiment's error and our second error is the systematic error from using our best (shown rounded) values.

Int. J. Mod. Phys. A 2026.41. Downloaded from www.worldscientific.com
by UNIVERSITY OF CALIFORNIA @ BERKELEY on 09/16/26. Re-use and distribution is strictly not permitted, except for Open Access articles.

Int. J. Mod. Phys. A 2026.41. Downloaded from www.worldscientific.com by CALIFORNIA @ BERKELEY on 09/16/26. Re-use and distribution is strictly not permitted, except for Open Access articles.

$\Gamma(2(\pi^+\pi^-\pi^0))/\Gamma_{total}$ — Γ_{50}/Γ

VALUE (units 10^{-2})	EVTS	DOCUMENT ID		TECN	COMMENT
15.5±2.0 OUR AVERAGE					
15.3±1.8±1.8	333	ABLIKIM	19AP	BES3	$h_c \to \gamma\eta_c$
15.8±2.6±1.7	175	[1] ABLIKIM	12N	BES3	$\psi(2S) \to \pi^0\gamma 2(\pi^+\pi^-\pi^0)$

[1] ABLIKIM 12N reports $[\Gamma(\eta_c(1S) \to 2(\pi^+\pi^-\pi^0))/\Gamma_{total}] \times [B(\psi(2S) \to h_c(1P)\pi^0)] \times [B(h_c(1P) \to \gamma\eta_c(1S))] = (75.13 \pm 7.42 \pm 9.99) \times 10^{-6}$ which we divide by our best (shown rounded) values $B(\psi(2S) \to h_c(1P)\pi^0) = (7.4 \pm 0.5) \times 10^{-4}$, $B(h_c(1P) \to \gamma\eta_c(1S)) = (64 \pm 5) \times 10^{-2}$. Our first error is their experiment's error and our second error is the systematic error from using our best (shown rounded) values.

$\Gamma(3(\pi^+\pi^-))/\Gamma_{total}$ — Γ_{51}/Γ

VALUE (units 10^{-3})	EVTS	DOCUMENT ID		TECN	COMMENT
15.5±2.8 OUR AVERAGE					
19 ±5 ±2	51	[1] ABLIKIM	12N	BES3	$\psi(2S) \to \pi^0\gamma 3(\pi^+\pi^-)$
14.2±3.1±1.2	479	[2] ABLIKIM	06A	BES2	$J/\psi \to 3(\pi^+\pi^-)\gamma$

[1] ABLIKIM 12N reports $[\Gamma(\eta_c(1S) \to 3(\pi^+\pi^-))/\Gamma_{total}] \times [B(\psi(2S) \to h_c(1P)\pi^0)] \times [B(h_c(1P) \to \gamma\eta_c(1S))] = (8.82 \pm 1.57 \pm 1.59) \times 10^{-6}$ which we divide by our best (shown rounded) values $B(\psi(2S) \to h_c(1P)\pi^0) = (7.4 \pm 0.5) \times 10^{-4}$, $B(h_c(1P) \to \gamma\eta_c(1S)) = (64 \pm 5) \times 10^{-2}$. Our first error is their experiment's error and our second error is the systematic error from using our best (shown rounded) values.

[2] ABLIKIM 06A reports $[\Gamma(\eta_c(1S) \to 3(\pi^+\pi^-))/\Gamma_{total}] \times [B(J/\psi(1S) \to \gamma\eta_c(1S))] = (2.59 \pm 0.32 \pm 0.47) \times 10^{-4}$ which we divide by our best (shown rounded) value $B(J/\psi(1S) \to \gamma\eta_c(1S)) = (1.82 \pm 0.15) \times 10^{-2}$. Our first error is their experiment's error and our second error is the systematic error from using our best (shown rounded) value.

$\Gamma(p\overline{p})/\Gamma_{total}$ — Γ_{52}/Γ

VALUE (units 10^{-4})	EVTS	DOCUMENT ID		TECN	COMMENT
11.1± 1.2 OUR FIT Error includes scale factor of 1.4.					
12.0± 2.6±1.5	34	ABLIKIM	19AP	BES3	$h_c \to \gamma\eta_c$
• • • We do not use the following data for averages, fits, limits, etc. • • •					
14 ± 5 ±1	15	[1,2] ABLIKIM	12N	BES3	$\psi(2S) \to \pi^0\gamma p\overline{p}$
$11.8^{+1.6}_{-1.9} \pm 0.8$	195	[2,3] WU	06	BELL	$B^+ \to p\overline{p}K^+$
10.4± 2.3±0.8	213	[2,4] BAI	04	BES	$J/\psi \to \gamma p\overline{p}$
7.1± 2.7±0.6	18	[2,5] BISELLO	91	DM2	$J/\psi \to \gamma p\overline{p}$
8 ± 4 ±1	23	[2,6] BALTRUSAIT...86		MRK3	$J/\psi \to \eta_c\gamma$
$22^{+22}_{-11} \pm 3$		[2,7] HIMEL	80B	MRK2	$\psi(2S) \to \eta_c\gamma$

[1] ABLIKIM 12N reports $[\Gamma(\eta_c(1S) \to p\overline{p})/\Gamma_{total}] \times [B(\psi(2S) \to h_c(1P)\pi^0)] \times [B(h_c(1P) \to \gamma\eta_c(1S))] = (0.65 \pm 0.19 \pm 0.10) \times 10^{-6}$ which we divide by our best (shown rounded) values $B(\psi(2S) \to h_c(1P)\pi^0) = (7.4 \pm 0.5) \times 10^{-4}$, $B(h_c(1P) \to \gamma\eta_c(1S)) = (64 \pm 5) \times 10^{-2}$. Our first error is their experiment's error and our second error is the systematic error from using our best (shown rounded) values.

[2] Not used since the same experimental measurement has been used in another related quantity included elsewhere in the fit.

[3] WU 06 reports $[\Gamma(\eta_c(1S) \to p\overline{p})/\Gamma_{total}] \times [B(B^+ \to \eta_c K^+)] = (1.42 \pm 0.11^{+0.16}_{-0.20}) \times 10^{-6}$ which we divide by our best (shown rounded) value $B(B^+ \to \eta_c K^+) = (1.20 \pm 0.08) \times 10^{-3}$. Our first error is their experiment's error and our second error is the systematic error from using our best (shown rounded) value.

[4] BAI 04 reports $[\Gamma(\eta_c(1S) \to p\overline{p})/\Gamma_{total}] \times [B(J/\psi(1S) \to \gamma\eta_c(1S))] = (1.9 \pm 0.3 \pm 0.3) \times 10^{-5}$ which we divide by our best (shown rounded) value $B(J/\psi(1S) \to \gamma\eta_c(1S)) = (1.82 \pm 0.15) \times 10^{-2}$. Our first error is their experiment's error and our second error is the systematic error from using our best (shown rounded) value.

[5] BISELLO 91 reports $[\Gamma(\eta_c(1S) \to p\overline{p})/\Gamma_{total}] \times [B(J/\psi(1S) \to \gamma\eta_c(1S))] = (0.13 \pm 0.04 \pm 0.03) \times 10^{-4}$ which we divide by our best (shown rounded) value $B(J/\psi(1S) \to \gamma\eta_c(1S)) = (1.82 \pm 0.15) \times 10^{-2}$. Our first error is their experiment's error and our second error is the systematic error from using our best (shown rounded) value.

[6] BALTRUSAITIS 86 reports $[\Gamma(\eta_c(1S) \to p\overline{p})/\Gamma_{total}] \times [B(J/\psi(1S) \to \gamma\eta_c(1S))] = (1.4 \pm 0.7) \times 10^{-5}$ which we divide by our best (shown rounded) value $B(J/\psi(1S) \to \gamma\eta_c(1S)) = (1.82 \pm 0.15) \times 10^{-2}$. Our first error is their experiment's error and our second error is the systematic error from using our best (shown rounded) value.

[7] HIMEL 80B reports $[\Gamma(\eta_c(1S) \to p\overline{p})/\Gamma_{total}] \times [B(\psi(2S) \to \gamma\eta_c(1S))] = (8^{+8}_{-4}) \times 10^{-6}$ which we divide by our best (shown rounded) value $B(\psi(2S) \to \gamma\eta_c(1S)) = (3.6 \pm 0.5) \times 10^{-3}$. Our first error is their experiment's error and our second error is the systematic error from using our best (shown rounded) value.

$\Gamma(p\overline{p})/\Gamma_{total} \times \Gamma(\phi\phi)/\Gamma_{total}$ — $\Gamma_{52}/\Gamma \times \Gamma_9/\Gamma$

VALUE (units 10^{-5})	DOCUMENT ID		TECN	COMMENT
0.16±0.06 OUR FIT Error includes scale factor of 2.8.				
$4.0^{+3.5}_{-3.2}$	BAGLIN	89	SPEC	$\overline{p}p \to K^+K^-K^+K^-$

$\Gamma(p\overline{p}\pi^0)/\Gamma_{total}$ — Γ_{53}/Γ

VALUE (units 10^{-2})	EVTS	DOCUMENT ID		TECN	COMMENT
• • • We do not use the following data for averages, fits, limits, etc. • • •					
0.32±0.11±0.03	14	[1] ABLIKIM	12N	BES3	$\psi(2S) \to \pi^0\gamma p\overline{p}\pi^0$

[1] ABLIKIM 12N reports $[\Gamma(\eta_c(1S) \to p\overline{p}\pi^0)/\Gamma_{total}] \times [B(\psi(2S) \to h_c(1P)\pi^0)] \times [B(h_c(1P) \to \gamma\eta_c(1S))] = (1.53 \pm 0.49 \pm 0.23) \times 10^{-6}$ which we divide by our best (shown rounded) values $B(\psi(2S) \to h_c(1P)\pi^0) = (7.4 \pm 0.5) \times 10^{-4}$, $B(h_c(1P) \to \gamma\eta_c(1S)) = (64 \pm 5) \times 10^{-2}$. Our first error is their experiment's error and our second error is the systematic error from using our best (shown rounded) values.

$\Gamma(K^+\overline{p}\Lambda + c.c.)/\Gamma_{total}$ — Γ_{56}/Γ

VALUE (units 10^{-3})	EVTS	DOCUMENT ID		TECN	COMMENT
$2.26^{+0.31}_{-0.29} \pm 0.16$	157	[1] LU	19	BELL	$B^+ \to \overline{p}\Lambda K^+K^+$

[1] LU 19 reports $(2.83^{+0.36}_{-0.34} \pm 0.35) \times 10^{-3}$ from a measurement of $[\Gamma(\eta_c(1S) \to K^+\overline{p}\Lambda + c.c.)/\Gamma_{total}] \times [B(B^+ \to \eta_c K^+)]$ assuming $B(B^+ \to \eta_c K^+) = (9.6 \pm 1.1) \times 10^{-4}$, which we rescale to our best (shown rounded) value $B(B^+ \to \eta_c K^+) = (1.20 \pm 0.08) \times 10^{-3}$. Our first error is their experiment's error and our second error is the systematic error from using our best (shown rounded) value.

$\Gamma(\overline{\Lambda}(1520)\Lambda + c.c.)/\Gamma_{total}$ — Γ_{57}/Γ

VALUE (units 10^{-3})	EVTS	DOCUMENT ID		TECN	COMMENT
2.8±1.2±0.2	43	[1] LU	19	BELL	$B^+ \to \overline{p}\Lambda K^+K^+$

[1] LU 19 reports $(3.48 \pm 1.48 \pm 0.46) \times 10^{-3}$ from a measurement of $[\Gamma(\eta_c(1S) \to \overline{\Lambda}(1520)\Lambda + c.c.)/\Gamma_{total}] \times [B(B^+ \to \eta_c K^+)]$ assuming $B(B^+ \to \eta_c K^+) = (9.6 \pm 1.1) \times 10^{-4}$, which we rescale to our best (shown rounded) value $B(B^+ \to \eta_c K^+) = (1.20 \pm 0.08) \times 10^{-3}$. Our first error is their experiment's error and our second error is the systematic error from using our best (shown rounded) value.

$\Gamma(\Sigma^+\overline{\Sigma}^-)/\Gamma_{total}$ — Γ_{58}/Γ

VALUE (units 10^{-3})	EVTS	DOCUMENT ID		TECN	COMMENT
• • • We do not use the following data for averages, fits, limits, etc. • • •					
1.98±0.31±0.16	112	[1] ABLIKIM	13C	BES3	$J/\psi \to \gamma p\overline{p}\pi^0\pi^0$

[1] ABLIKIM 13C reports $[\Gamma(\eta_c(1S) \to \Sigma^+\overline{\Sigma}^-)/\Gamma_{total}] \times [B(J/\psi(1S) \to \gamma\eta_c(1S))] = (3.60 \pm 0.48 \pm 0.31) \times 10^{-5}$ which we divide by our best (shown rounded) value $B(J/\psi(1S) \to \gamma\eta_c(1S)) = (1.82 \pm 0.15) \times 10^{-2}$. Our first error is their experiment's error and our second error is the systematic error from using our best (shown rounded) value.

$\Gamma(\Xi^-\overline{\Xi}^+)/\Gamma_{total}$ — Γ_{59}/Γ

VALUE (units 10^{-3})	EVTS	DOCUMENT ID		TECN	COMMENT
• • • We do not use the following data for averages, fits, limits, etc. • • •					
0.83±0.17±0.07	78	[1] ABLIKIM	13C	BES3	$J/\psi \to \gamma\Lambda\overline{\Lambda}\pi^+\pi^-$

[1] ABLIKIM 13C reports $[\Gamma(\eta_c(1S) \to \Xi^-\overline{\Xi}^+)/\Gamma_{total}] \times [B(J/\psi(1S) \to \gamma\eta_c(1S))] = (1.51 \pm 0.27 \pm 0.14) \times 10^{-5}$ which we divide by our best (shown rounded) value $B(J/\psi(1S) \to \gamma\eta_c(1S)) = (1.82 \pm 0.15) \times 10^{-2}$. Our first error is their experiment's error and our second error is the systematic error from using our best (shown rounded) value.

RADIATIVE DECAYS

$\Gamma(\gamma\gamma)/\Gamma_{total}$ — Γ_{60}/Γ

VALUE (units 10^{-4})	CL%	EVTS	DOCUMENT ID		TECN	COMMENT
2.13±0.15 OUR FIT Error includes scale factor of 1.5.						
• • • We do not use the following data for averages, fits, limits, etc. • • •						
2.5 ±0.7 ±0.2		73	[1,2] ABLIKIM	13I	BES3	$\psi(2S) \to \pi^+\pi^- J/\psi$
$0.7^{+1.5}_{-0.6} \pm 0.1$		$1.2^{+2.8}_{-1.1}$	[1,3] ADAMS	08	CLEO	$\psi(2S) \to \pi^+\pi^- J/\psi$
$1.8^{+0.8}_{-0.6} \pm 0.1$		13	[1,4] WICHT	08	BELL	$B^\pm \to K^\pm\gamma\gamma$
$1.87 \pm 0.32^{+0.95}_{-0.50}$			[1] AMBROGIANI	03	E835	$\overline{p}p \to \gamma\gamma$
$2.80^{+0.67}_{-0.58} \pm 1.0$			[1] ARMSTRONG	95F	E760	$\overline{p}p \to \gamma\gamma$
< 9	90		[1,5] BISELLO	91	DM2	$J/\psi \to \gamma\gamma\gamma$
$6^{+4}_{-3} \pm 4$			[1] BAGLIN	87B	SPEC	$\overline{p}p \to \gamma\gamma$
< 18	90		[6] BLOOM	83	CBAL	$J/\psi \to \eta_c\gamma$

[1] Not used since the same experimental measurement has been used in another related quantity included elsewhere in the fit.

[2] ABLIKIM 13I reports $[\Gamma(\eta_c(1S) \to \gamma\gamma)/\Gamma_{total}] \times [B(J/\psi(1S) \to \gamma\eta_c(1S))] = (4.5 \pm 1.2 \pm 0.6) \times 10^{-6}$ which we divide by our best (shown rounded) value $B(J/\psi(1S) \to \gamma\eta_c(1S)) = (1.82 \pm 0.15) \times 10^{-2}$. Our first error is their experiment's error and our second error is the systematic error from using our best (shown rounded) value.

[3] ADAMS 08 reports $[\Gamma(\eta_c(1S) \to \gamma\gamma)/\Gamma_{total}] \times [B(J/\psi(1S) \to \gamma\eta_c(1S))] = (1.2^{+2.7}_{-1.1} \pm 0.3) \times 10^{-6}$ which we divide by our best (shown rounded) value $B(J/\psi(1S) \to \gamma\eta_c(1S)) = (1.82 \pm 0.15) \times 10^{-2}$. Our first error is their experiment's error and our second error is the systematic error from using our best (shown rounded) value.

[4] WICHT 08 reports $[\Gamma(\eta_c(1S) \to \gamma\gamma)/\Gamma_{total}] \times [B(B^+ \to \eta_c K^+)] = (2.2^{+0.9}_{-0.7}{}^{+0.4}_{-0.2}) \times 10^{-7}$ which we divide by our best (shown rounded) value $B(B^+ \to \eta_c K^+) = (1.20 \pm 0.08) \times 10^{-3}$. Our first error is their experiment's error and our second error is the systematic error from using our best (shown rounded) value.

[5] The quoted branching ratios use $B(J/\psi(1S) \to \gamma\eta_c(1S)) = 0.0127 \pm 0.0036$.

[6] Using $B(J/\psi(1S) \to \gamma\eta_c(1S)) = 0.0127 \pm 0.0036$.

$\Gamma(p\overline{p})/\Gamma_{total} \times \Gamma(\gamma\gamma)/\Gamma_{total}$ — $\Gamma_{52}/\Gamma \times \Gamma_{60}/\Gamma$

VALUE (units 10^{-6})	EVTS	DOCUMENT ID		TECN	COMMENT
0.237±0.020 OUR FIT Error includes scale factor of 1.2.					
0.26 ±0.05 OUR AVERAGE Error includes scale factor of 1.4.					
$0.224^{+0.038}_{-0.037} \pm 0.020$	190	AMBROGIANI	03	E835	$\overline{p}p \to \eta_c \to \gamma\gamma$
$0.336^{+0.080}_{-0.070}$		ARMSTRONG	95F	E760	$\overline{p}p \to \gamma\gamma$
$0.68^{+0.42}_{-0.31}$	12	BAGLIN	87B	SPEC	$\overline{p}p \to \gamma\gamma$

Int. J. Mod. Phys. A 2026.41. Downloaded from www.worldscientific.com
by UNIVERSITY OF CALIFORNIA @ BERKELEY on 09/16/26. Re-use and distribution is strictly not permitted, except for Open Access articles.

$\Gamma(\gamma\phi)/\Gamma_{total}$ — Γ_{61}/Γ

VALUE (units 10^{-6})	DOCUMENT ID		TECN	COMMENT
$11.5^{+3.2}_{-4.2}\pm0.9$	[1] ABLIKIM	25P	BES3	$J/\psi \to \phi\gamma\gamma$

[1] ABLIKIM 25P reports $[\Gamma(\eta_c(1S) \to \gamma\phi)/\Gamma_{total}] \times [B(J/\psi(1S) \to \gamma\eta_c(1S))] = (2.1 \pm 0.3^{+0.5}_{-0.7}) \times 10^{-7}$ which we divide by our best (shown rounded) value $B(J/\psi(1S) \to \gamma\eta_c(1S)) = (1.82 \pm 0.15) \times 10^{-2}$. Our first error is their experiment's error and our second error is the systematic error from using our best (shown rounded) value.

Charge conjugation (C), Parity (P), Lepton family number (LF) violating modes

$\Gamma(\pi^+\pi^-)/\Gamma_{total}$ — Γ_{62}/Γ

VALUE (units 10^{-5})	CL%	DOCUMENT ID		TECN	COMMENT
<10	90	[1] ABLIKIM	11G	BES3	$J/\psi \to \gamma\pi^+\pi^-$
• • • We do not use the following data for averages, fits, limits, etc. • • •					
<60	90	[2] ABLIKIM	06B	BES2	$J/\psi \to \pi^+\pi^-\gamma$

[1] ABLIKIM 11G reports $[\Gamma(\eta_c(1S) \to \pi^+\pi^-)/\Gamma_{total}] \times [B(J/\psi(1S) \to \gamma\eta_c(1S))] < 1.82 \times 10^{-6}$ which we divide by our best (shown rounded) value $B(J/\psi(1S) \to \gamma\eta_c(1S)) = 1.82 \times 10^{-2}$.

[2] ABLIKIM 06B reports $[\Gamma(\eta_c(1S) \to \pi^+\pi^-)/\Gamma_{total}] \times [B(J/\psi(1S) \to \gamma\eta_c(1S))] < 1.1 \times 10^{-5}$ which we divide by our best (shown rounded) value $B(J/\psi(1S) \to \gamma\eta_c(1S)) = 1.82 \times 10^{-2}$.

$\Gamma(\pi^0\pi^0)/\Gamma_{total}$ — Γ_{63}/Γ

VALUE (units 10^{-5})	CL%	DOCUMENT ID		TECN	COMMENT
< 3.3	90	[1] ABLIKIM	11G	BES3	$J/\psi \to \gamma\pi^0\pi^0$
• • • We do not use the following data for averages, fits, limits, etc. • • •					
<40	90	[2] ABLIKIM	06B	BES2	$J/\psi \to \pi^0\pi^0\gamma$

[1] ABLIKIM 11G reports $[\Gamma(\eta_c(1S) \to \pi^0\pi^0)/\Gamma_{total}] \times [B(J/\psi(1S) \to \gamma\eta_c(1S))] < 6.0 \times 10^{-7}$ which we divide by our best (shown rounded) value $B(J/\psi(1S) \to \gamma\eta_c(1S)) = 1.82 \times 10^{-2}$.

[2] ABLIKIM 06B reports $[\Gamma(\eta_c(1S) \to \pi^0\pi^0)/\Gamma_{total}] \times [B(J/\psi(1S) \to \gamma\eta_c(1S))] < 0.71 \times 10^{-5}$ which we divide by our best (shown rounded) value $B(J/\psi(1S) \to \gamma\eta_c(1S)) = 1.82 \times 10^{-2}$.

$\Gamma(K^+K^-)/\Gamma_{total}$ — Γ_{64}/Γ

VALUE (units 10^{-5})	CL%	DOCUMENT ID		TECN	COMMENT
<50	90	[1] ABLIKIM	06B	BES2	$J/\psi \to K^+K^-\gamma$

[1] ABLIKIM 06B reports $[\Gamma(\eta_c(1S) \to K^+K^-)/\Gamma_{total}] \times [B(J/\psi(1S) \to \gamma\eta_c(1S))] < 0.96 \times 10^{-5}$ which we divide by our best (shown rounded) value $B(J/\psi(1S) \to \gamma\eta_c(1S)) = 1.82 \times 10^{-2}$.

$\Gamma(K^0_S K^0_S)/\Gamma_{total}$ — Γ_{65}/Γ

VALUE (units 10^{-5})	CL%	DOCUMENT ID		TECN	COMMENT
<29	90	[1] ABLIKIM	06B	BES2	$J/\psi \to K^0_S K^0_S \gamma$
• • • We do not use the following data for averages, fits, limits, etc. • • •					
<32	90	[2,3] UEHARA	13	BELL	$\gamma\gamma \to K^0_S K^0_S$
< 5.6	90	[4,5] UEHARA	13	BELL	$\gamma\gamma \to K^0_S K^0_S$

[1] ABLIKIM 06B reports $[\Gamma(\eta_c(1S) \to K^0_S K^0_S)/\Gamma_{total}] \times [B(J/\psi(1S) \to \gamma\eta_c(1S))] < 0.53 \times 10^{-5}$ which we divide by our best (shown rounded) value $B(J/\psi(1S) \to \gamma\eta_c(1S)) = 1.82 \times 10^{-2}$.

[2] Using $\Gamma(\gamma\gamma)(\eta_c) = 5.3 \pm 0.5$ keV. UEHARA 13 reports $\Gamma(\gamma\gamma) \times B(K^0_S K^0_S) < 1.6$ eV.

[3] Taking into account interference with the non-resonant continuum.

[4] Using $\Gamma(\gamma\gamma)(\eta_c) = 5.3 \pm 0.5$ keV. UEHARA 13 reports $\Gamma(\gamma\gamma) \times B(K^0_S K^0_S) < 0.29$ eV.

[5] Neglecting interference with the non-resonant continuum.

$\eta_c(1S)$ CROSS-PARTICLE BRANCHING RATIOS

$\Gamma(\eta_c(1S) \to \eta'(958)\pi\pi)/\Gamma_{total} \times \Gamma(J/\psi(1S) \to \gamma\eta_c(1S))/\Gamma_{total}$ — $\Gamma_1/\Gamma \times \Gamma^{J/\psi(1S)}_{248}/\Gamma^{J/\psi(1S)}$

VALUE (units 10^{-4})	EVTS	DOCUMENT ID		TECN	COMMENT
2.9 ±0.6 OUR FIT Error includes scale factor of 1.5.					
5.25±1.65	14	[1] BALTRUSAITIS...86		MRK3	$J/\psi \to \eta_c\gamma$

[1] The value reported by BALTRUSAITIS 86 has been multiplied by 3/2 to account for isospin symmetry.

$\Gamma(\eta_c(1S) \to \rho\rho)/\Gamma_{total} \times \Gamma(J/\psi(1S) \to \gamma\eta_c(1S))/\Gamma_{total}$ — $\Gamma_4/\Gamma \times \Gamma^{J/\psi(1S)}_{248}/\Gamma^{J/\psi(1S)}$

VALUE (units 10^{-4})	EVTS	DOCUMENT ID		TECN	COMMENT
2.6 ±0.6 OUR AVERAGE Error includes scale factor of 1.2.					
1.6 ±0.6 ±0.4	72	ABLIKIM	05L	BES2	$J/\psi \to \pi^+\pi^-\pi^+\pi^-\gamma$
3.30±0.30±0.60	113	[1] BISELLO	91	DM2	$J/\psi \to \gamma\rho^0\rho^0$
3.0 ±1.3 ±0.6	32	[2] BISELLO	91	DM2	$J/\psi \to \gamma\rho^+\rho^-$

[1] The value reported by BISELLO 91 has been multiplied by 3 to account for isospin symmetry.

[2] The value reported by BISELLO 91 has been multiplied by 3/2 to account for isospin symmetry.

$\Gamma(\eta_c(1S) \to K^*(892)^0 K^-\pi^+ + \text{c.c.})/\Gamma_{total} \times \Gamma(J/\psi(1S) \to \gamma\eta_c(1S))/\Gamma_{total}$ — $\Gamma_5/\Gamma \times \Gamma^{J/\psi(1S)}_{248}/\Gamma^{J/\psi(1S)}$

VALUE (units 10^{-4})	EVTS	DOCUMENT ID		TECN	COMMENT
2.6±0.6	63	BALTRUSAIT...86		MRK3	$J/\psi \to \eta_c\gamma$

$\Gamma(\eta_c(1S) \to K^*(892)\overline{K}^*(892))/\Gamma_{total} \times \Gamma(J/\psi(1S) \to \gamma\eta_c(1S))/\Gamma_{total}$ — $\Gamma_6/\Gamma \times \Gamma^{J/\psi(1S)}_{248}/\Gamma^{J/\psi(1S)}$

VALUE (units 10^{-4})	EVTS	DOCUMENT ID		TECN	COMMENT
1.00±0.18 OUR FIT					
1.17±0.29 OUR AVERAGE					
1.4 ±0.3 ±0.5	60	ABLIKIM	05L	BES2	$J/\psi \to K^+K^-\pi^+\pi^-\gamma$
1.04±0.36±0.18	14	[1] BISELLO	91	DM2	$e^+e^- \to \gamma K^+K^-\pi^+\pi^-$
1.2 ±0.6	9	[1] BALTRUSAIT...86		MRK3	$J/\psi \to \eta_c\gamma$

[1] The reported value has been multiplied by 2 to account for isospin symmetry.

$\Gamma(\eta_c(1S) \to K^*(892)^0\overline{K}^*(892)^0\pi^+\pi^-)/\Gamma_{total} \times \Gamma(J/\psi(1S) \to \gamma\eta_c(1S))/\Gamma_{total}$ — $\Gamma_7/\Gamma \times \Gamma^{J/\psi(1S)}_{248}/\Gamma^{J/\psi(1S)}$

VALUE (units 10^{-4})	EVTS	DOCUMENT ID		TECN	COMMENT
1.91±0.64±0.48	45	ABLIKIM	06A	BES2	$J/\psi \to K^{*0}\overline{K}^{*0}\pi^+\pi^-\gamma$

$\Gamma(\eta_c(1S) \to \phi K^+K^-)/\Gamma_{total} \times \Gamma(B^+ \to \eta_c K^+)/\Gamma_{total}$ — $\Gamma_8/\Gamma \times \Gamma^{B^\pm}_{274}/\Gamma^{B^\pm}$

VALUE (units 10^{-6})	EVTS	DOCUMENT ID		TECN	COMMENT
$3.6^{+1.1}_{-0.9}\pm0.8$	$14.1^{+4.4}_{-3.7}$	HUANG	03	BELL	$B^+ \to (\phi K^+K^-)\ K^+$

$\Gamma(\eta_c(1S) \to \phi\phi)/\Gamma_{total} \times \Gamma(J/\psi(1S) \to \gamma\eta_c(1S))/\Gamma_{total}$ — $\Gamma_9/\Gamma \times \Gamma^{J/\psi(1S)}_{248}/\Gamma^{J/\psi(1S)}$

VALUE (units 10^{-5})	EVTS	DOCUMENT ID		TECN	COMMENT
2.6±0.6 OUR FIT Error includes scale factor of 2.3.					
4.1±0.6 OUR AVERAGE Error includes scale factor of 1.2.					
$4.3\pm0.5^{+0.5}_{-1.2}$	1.2k	ABLIKIM	17P	BES3	$J/\psi \to \gamma K^+K^-K^+K^-$
3.3±0.6±0.6	72	ABLIKIM	05L	BES2	$J/\psi \to \gamma K^+K^-K^+K^-$
3.9±0.9±0.7	19	BISELLO	91	DM2	$J/\psi \to \gamma K^+K^-K^+K^-$
$3.8^{+2.3}_{-1.5}\pm0.7$	5	BISELLO	91	DM2	$J/\psi \to \gamma K^+K^-K^0_S K^0_L$
9.3±2.0±1.6	80	BAI	90B	MRK3	$J/\psi \to \gamma K^+K^-K^+K^-$
8.5±2.7±1.8		BAI	90B	MRK3	$J/\psi \to \gamma K^+K^-K^0_S K^0_L$
• • • We do not use the following data for averages, fits, limits, etc. • • •					
3.3±0.6±0.6	357	[1] BAI	04	BES	$J/\psi \to \gamma K^+K^-K^+K^-$

[1] Superseded by ABLIKIM 05L.

$\Gamma(\eta_c(1S) \to \phi\phi)/\Gamma_{total} \times \Gamma(B^+ \to \eta_c K^+)/\Gamma_{total}$ — $\Gamma_9/\Gamma \times \Gamma^{B^\pm}_{274}/\Gamma^{B^\pm}$

VALUE (units 10^{-6})	EVTS	DOCUMENT ID		TECN	COMMENT
1.7±0.4 OUR FIT Error includes scale factor of 2.5.					
$3.3^{+1.2}_{-1.0}$ OUR AVERAGE Error includes scale factor of 1.5.					
4.7±1.2±0.5		AUBERT,B	04B	BABR	$B^\pm \to K^\pm\eta_c$
$2.2^{+1.0}_{-0.7}\pm0.5$	7	HUANG	03	BELL	$B^\pm \to K^\pm\phi\phi$

$\Gamma(\eta_c(1S) \to \omega\omega)/\Gamma_{total} \times \Gamma(J/\psi(1S) \to \gamma\eta_c(1S))/\Gamma_{total}$ — $\Gamma_{16}/\Gamma \times \Gamma^{J/\psi(1S)}_{248}/\Gamma^{J/\psi(1S)}$

VALUE (units 10^{-5})	EVTS	DOCUMENT ID		TECN	COMMENT
3.8 ±1.2 OUR FIT Error includes scale factor of 2.1.					
4.90±0.17±0.77	1705	ABLIKIM	19AV	BES3	$J/\psi \to \gamma\omega\omega$

$\Gamma(\eta_c(1S) \to f_2(1270)f_2(1270))/\Gamma_{total} \times \Gamma(J/\psi(1S) \to \gamma\eta_c(1S))/\Gamma_{total}$ — $\Gamma_{18}/\Gamma \times \Gamma^{J/\psi(1S)}_{248}/\Gamma^{J/\psi(1S)}$

VALUE (units 10^{-4})	EVTS	DOCUMENT ID		TECN	COMMENT
1.5±0.4 OUR FIT					
$1.3\pm0.3^{+0.3}_{-0.4}$	91.2 ± 19.8	ABLIKIM	04M	BES	$J/\psi \to \gamma 2\pi^+ 2\pi^-$

$\Gamma(\eta_c(1S) \to K\overline{K}\pi)/\Gamma_{total} \times \Gamma(J/\psi(1S) \to \gamma\eta_c(1S))/\Gamma_{total}$ — $\Gamma_{37}/\Gamma \times \Gamma^{J/\psi(1S)}_{248}/\Gamma^{J/\psi(1S)}$

VALUE (units 10^{-4})	EVTS	DOCUMENT ID		TECN	COMMENT
10.7 ±1.0 OUR FIT Error includes scale factor of 1.7.					
6.7 ±0.8 OUR AVERAGE					
6.6 ±0.9 ±1.5	0.6k	[1] BAI	04	BES	$J/\psi \to \gamma K^\pm\pi^\mp K^0_S$
8.76±1.80±1.68	33	[2] BISELLO	91	DM2	$J/\psi \to \gamma K^+K^-\pi^0$
6.9 ±1.2 ±1.2	68	[3] BISELLO	91	DM2	$J/\psi \to \gamma K^\pm\pi^\mp K^0_S$
7.8 ±3.0	32	[4] BALTRUSAIT...86		MRK3	$J/\psi \to \gamma K^+K^-\pi^0$
5.7 ±1.5	63	[5] BALTRUSAIT...86		MRK3	$J/\psi \to \gamma K^\pm\pi^\mp K^0_S$

[1] BAI 04 reports $B(J/\psi \to \gamma\eta_c) \cdot B(\eta_c \to K^\pm K^0_S\pi^\mp) = (2.2 \pm 0.3 \pm 0.5) \times 10^{-4}$ which we multiply by 3 to account for isospin symmetry.

[2] BISELLO 91 reports $B(J/\psi \to \gamma\eta_c) \cdot B(\eta_c \to K^+K^-\pi^0) = (1.46 \pm 0.30 \pm 0.28) \times 10^{-4}$ which we multiply by 6 to account for isospin symmetry.

[3] BISELLO 91 reports $B(J/\psi \to \gamma\eta_c) \cdot B(\eta_c \to K^\pm K^0_S\pi^\mp) = (2.3 \pm 0.4 \pm 0.4) \times 10^{-4}$ which we multiply by 3 to account for isospin symmetry.

[4] BALTRUSAITIS 86 reports $B(J/\psi \to \gamma\eta_c) \cdot B(\eta_c \to K^+K^-\pi^0) = (1.3 \pm 0.5) \times 10^{-4}$ which we multiply by 6 to account for isospin symmetry.

[5] BALTRUSAITIS 86 reports $B(J/\psi \to \gamma\eta_c) \cdot B(\eta_c \to K^\pm K^0_S\pi^\mp) = (1.9 \pm 0.5) \times 10^{-4}$ which we multiply by 3 to account for isospin symmetry.

Int. J. Mod. Phys. A 2026.41. Downloaded from www.worldscientific.com by CALIFORNIA @ BERKELEY on 09/16/26. Re-use and distribution is strictly not permitted, except for Open Access articles.

$\Gamma(\eta_c(1S) \to K\overline{K}\pi)/\Gamma_{total} \times \Gamma(B^+ \to \eta_c K^+)/\Gamma_{total}$ $\quad \Gamma_{37}/\Gamma \times \Gamma^{B^\pm}_{274}/\Gamma^{B^\pm}$

VALUE (units 10^{-5})	DOCUMENT ID		TECN	COMMENT
7.1 ±0.6 OUR FIT	Error includes scale factor of 1.3.			
7.5 ±0.8 OUR AVERAGE				
$8.01 \pm 0.42^{+1.71}_{-1.65}$	[1] VINOKUROVA 11		BELL	$e^+e^- \to \Upsilon(4S)$
7.4 ±0.5 ±0.7	AUBERT,B	04B	BABR	$B^\pm \to K^\pm \eta_c$

[1] VINOKUROVA 11 reports $B(B^+ \to \eta_c K^+,\ \eta_c \to K^0_S K^\pm \pi^\mp) = (26.7 \pm 1.4^{+2.9}_{-2.6} \pm 4.9) \times 10^{-6}$, where the first uncertainty is statistical, the second is due to systematics, and the third comes from interference of $\eta_c(1S) \to K^0_S K^\pm \pi^\mp$ with nonresonant $K^0_S K^\pm \pi^\mp$. We combined both systematic uncertainties to single values. We multiply the reported result by 3 to account for isospin symmetry.

$\Gamma(\eta_c(1S) \to K\overline{K}\pi)/\Gamma_{total} \times \Gamma(\psi(2S) \to \gamma\eta_c(1S))/\Gamma_{total}$ $\quad \Gamma_{37}/\Gamma \times \Gamma^{\psi(2S)}_{199}/\Gamma^{\psi(2S)}$

VALUE (units 10^{-4})	DOCUMENT ID		TECN	COMMENT
2.1±0.4 OUR FIT	Error includes scale factor of 1.6.			
$\mathbf{4.5^{+2.4}_{-1.8}}$	HIMEL	80B	MRK2	$\psi(2S) \to \eta_c \gamma$

$\Gamma(\eta_c(1S) \to K\overline{K}\pi)/\Gamma_{total} \times \Gamma(h_c(1P) \to \gamma\eta_c(1S))/\Gamma_{total}$ $\quad \Gamma_{37}/\Gamma \times \Gamma^{h_c(1P)}_{30}/\Gamma^{h_c(1P)}$

VALUE (units 10^{-2})	EVTS	DOCUMENT ID		TECN	COMMENT
3.8±0.4 OUR FIT	Error includes scale factor of 1.3.				
4.1±0.6 OUR AVERAGE					
3.7±0.7±0.3	55	[1,2] ABLIKIM	12N	BES3	$\psi(2S) \to \pi^0\gamma K^+K^-\pi^0$
4.6±0.8±0.3	107	[3,4] ABLIKIM	12N	BES3	$\psi(2S) \to \pi^0\gamma K^0_S K^\mp\pi^\pm$

[1] ABLIKIM 12N quotes $B(\psi(2S) \to \pi^0 h_c) \cdot B(h_c \to \gamma\eta_c) \cdot B(\eta_c \to K^+K^-\pi^0) = (4.54 \pm 0.76 \pm 0.48) \times 10^{-6}$ which we multiply by 6 to account for isospin symmetry.

[2] ABLIKIM 12N reports $[\Gamma(\eta_c(1S) \to K\overline{K}\pi)/\Gamma_{total} \times \Gamma(h_c(1P) \to \gamma\eta_c(1S))/\Gamma_{total}] \times [B(\psi(2S) \to h_c(1P)\pi^0)] = (27.24 \pm 4.56 \pm 2.88) \times 10^{-6}$ which we divide by our best (shown rounded) value $B(\psi(2S) \to h_c(1P)\pi^0) = (7.4 \pm 0.5) \times 10^{-4}$. Our first error is their experiment's error and our second error is the systematic error from using our best (shown rounded) value.

[3] ABLIKIM 12N quotes $B(\psi(2S) \to \pi^0 h_c) \cdot B(h_c \to \gamma\eta_c) \cdot B(\eta_c \to K^0_S K^\pm\pi^\mp) = (11.35 \pm 1.25 \pm 1.50) \times 10^{-6}$ which we multiply by 3 to account for isospin symmetry.

[4] ABLIKIM 12N reports $[\Gamma(\eta_c(1S) \to K\overline{K}\pi)/\Gamma_{total} \times \Gamma(h_c(1P) \to \gamma\eta_c(1S))/\Gamma_{total}] \times [B(\psi(2S) \to h_c(1P)\pi^0)] = (34.05 \pm 3.75 \pm 4.50) \times 10^{-6}$ which we divide by our best (shown rounded) value $B(\psi(2S) \to h_c(1P)\pi^0) = (7.4 \pm 0.5) \times 10^{-4}$. Our first error is their experiment's error and our second error is the systematic error from using our best (shown rounded) value.

$\Gamma(\eta_c(1S) \to K\overline{K}\eta)/\Gamma_{total} \times \Gamma(h_c(1P) \to \gamma\eta_c(1S))/\Gamma_{total}$ $\quad \Gamma_{38}/\Gamma \times \Gamma^{h_c(1P)}_{30}/\Gamma^{h_c(1P)}$

VALUE (units 10^{-3})	EVTS	DOCUMENT ID		TECN	COMMENT
7.1±1.0 OUR FIT	Error includes scale factor of 1.2.				
5.7±2.9±0.4	7	[1,2] ABLIKIM	12N	BES3	$\psi(2S) \to \pi^0\gamma\eta K^+K^-$

[1] ABLIKIM 12N quotes $B(\psi(2S) \to \pi^0 h_c) \cdot B(h_c \to \gamma\eta_c) \cdot B(\eta_c \to K^+K^-\eta) = (2.11 \pm 1.01 \pm 0.32) \times 10^{-6}$ which we multiply by 2 to account for isospin symmetry.

[2] ABLIKIM 12N reports $[\Gamma(\eta_c(1S) \to K\overline{K}\eta)/\Gamma_{total} \times \Gamma(h_c(1P) \to \gamma\eta_c(1S))/\Gamma_{total}] \times [B(\psi(2S) \to h_c(1P)\pi^0)] = (4.22 \pm 2.02 \pm 0.64) \times 10^{-6}$ which we divide by our best (shown rounded) value $B(\psi(2S) \to h_c(1P)\pi^0) = (7.4 \pm 0.5) \times 10^{-4}$. Our first error is their experiment's error and our second error is the systematic error from using our best (shown rounded) value.

$\Gamma(\eta_c(1S) \to \eta\pi^+\pi^-)/\Gamma_{total} \times \Gamma(h_c(1P) \to \gamma\eta_c(1S))/\Gamma_{total}$ $\quad \Gamma_{39}/\Gamma \times \Gamma^{h_c(1P)}_{30}/\Gamma^{h_c(1P)}$

VALUE (units 10^{-3})	EVTS	DOCUMENT ID		TECN	COMMENT
9.7±2.5±0.7	33	[1] ABLIKIM	12N	BES3	$\psi(2S) \to \pi^0\gamma\eta\pi^+\pi^-$

[1] ABLIKIM 12N reports $[\Gamma(\eta_c(1S) \to \eta\pi^+\pi^-)/\Gamma_{total} \times \Gamma(h_c(1P) \to \gamma\eta_c(1S))/\Gamma_{total}] \times [B(\psi(2S) \to h_c(1P)\pi^0)] = (7.22 \pm 1.47 \pm 1.11) \times 10^{-6}$ which we divide by our best (shown rounded) value $B(\psi(2S) \to h_c(1P)\pi^0) = (7.4 \pm 0.5) \times 10^{-4}$. Our first error is their experiment's error and our second error is the systematic error from using our best (shown rounded) value.

$\Gamma(\eta_c(1S) \to \eta\pi^+\pi^-)/\Gamma_{total} \times \Gamma(J/\psi(1S) \to \gamma\eta_c(1S))/\Gamma_{total}$ $\quad \Gamma_{39}/\Gamma \times \Gamma^{J/\psi(1S)}_{248}/\Gamma^{J/\psi(1S)}$

VALUE (units 10^{-4})	EVTS	DOCUMENT ID		TECN	COMMENT
4.2±0.9 OUR AVERAGE					
4.6±1.1	75	BALTRUSAIT...86		MRK3	$J/\psi \to \eta_c\gamma$
3.1±1.1±1.5	18	PARTRIDGE	80B	CBAL	$J/\psi \to \eta\pi^+\pi^-\gamma$

$\Gamma(\eta_c(1S) \to \eta 2(\pi^+\pi^-))/\Gamma_{total} \times \Gamma(h_c(1P) \to \gamma\eta_c(1S))/\Gamma_{total}$ $\quad \Gamma_{40}/\Gamma \times \Gamma^{h_c(1P)}_{30}/\Gamma^{h_c(1P)}$

VALUE (units 10^{-2})	EVTS	DOCUMENT ID		TECN	COMMENT
2.6±0.7±0.2	39	[1] ABLIKIM	12N	BES3	$\psi(2S) \to \pi^0\gamma\eta 2(\pi^+\pi^-)$

[1] ABLIKIM 12N reports $[\Gamma(\eta_c(1S) \to \eta 2(\pi^+\pi^-))/\Gamma_{total} \times \Gamma(h_c(1P) \to \gamma\eta_c(1S))/\Gamma_{total}] \times [B(\psi(2S) \to h_c(1P)\pi^0)] = (19.17 \pm 3.77 \pm 3.72) \times 10^{-6}$ which we divide by our best (shown rounded) value $B(\psi(2S) \to h_c(1P)\pi^0) = (7.4 \pm 0.5) \times 10^{-4}$. Our first error is their experiment's error and our second error is the systematic error from using our best (shown rounded) value.

$\Gamma(\eta_c(1S) \to K^+K^-\pi^+\pi^-)/\Gamma_{total} \times \Gamma(J/\psi(1S) \to \gamma\eta_c(1S))/\Gamma_{total}$ $\quad \Gamma_{41}/\Gamma \times \Gamma^{J/\psi(1S)}_{248}/\Gamma^{J/\psi(1S)}$

VALUE (units 10^{-4})	EVTS	DOCUMENT ID		TECN	COMMENT
1.21±0.29 OUR FIT	Error includes scale factor of 2.2.				
1.9 ±0.6 OUR AVERAGE	Error includes scale factor of 2.4.				
1.5 ±0.2 ±0.2	0.4k	BAI	04	BES	$J/\psi \to \gamma K^+K^-\pi^+\pi^-$
2.7 ±0.4	110	BALTRUSAIT...86		MRK3	$J/\psi \to \eta_c\gamma$

$\Gamma(\eta_c(1S) \to K^+K^-\pi^+\pi^-)/\Gamma_{total} \times \Gamma(\psi(2S) \to \gamma\eta_c(1S))/\Gamma_{total}$ $\quad \Gamma_{41}/\Gamma \times \Gamma^{\psi(2S)}_{199}/\Gamma^{\psi(2S)}$

VALUE (units 10^{-5})	DOCUMENT ID		TECN	COMMENT
2.4±0.8 OUR FIT	Error includes scale factor of 2.1.			
$\mathbf{4.0^{+6.0}_{-2.5}}$	HIMEL	80B	MRK2	$\psi(2S) \to \eta_c\gamma$

$\Gamma(\eta_c(1S) \to K^+K^-\pi^+\pi^-)/\Gamma_{total} \times \Gamma(h_c(1P) \to \gamma\eta_c(1S))/\Gamma_{total}$ $\quad \Gamma_{41}/\Gamma \times \Gamma^{h_c(1P)}_{30}/\Gamma^{h_c(1P)}$

VALUE (units 10^{-3})	EVTS	DOCUMENT ID		TECN	COMMENT
4.2±1.1 OUR FIT	Error includes scale factor of 2.0.				
5.6±1.3±0.4	38	[1] ABLIKIM	12N	BES3	$\psi(2S) \to \pi^0\gamma K^+K^-\pi^+\pi^-$

[1] ABLIKIM 12N reports $[\Gamma(\eta_c(1S) \to K^+K^-\pi^+\pi^-)/\Gamma_{total} \times \Gamma(h_c(1P) \to \gamma\eta_c(1S))/\Gamma_{total}] \times [B(\psi(2S) \to h_c(1P)\pi^0)] = (4.16 \pm 0.76 \pm 0.59) \times 10^{-6}$ which we divide by our best (shown rounded) value $B(\psi(2S) \to h_c(1P)\pi^0) = (7.4 \pm 0.5) \times 10^{-4}$. Our first error is their experiment's error and our second error is the systematic error from using our best (shown rounded) value.

$\Gamma(\eta_c(1S) \to K^0K^-\pi^+\pi^-\pi^+ + c.c.)/\Gamma_{total} \times \Gamma(h_c(1P) \to \gamma\eta_c(1S))/\Gamma_{total}$ $\quad \Gamma_{43}/\Gamma \times \Gamma^{h_c(1P)}_{30}/\Gamma^{h_c(1P)}$

VALUE (units 10^{-2})	DOCUMENT ID		TECN	COMMENT
3.2±0.8±0.2	[1,2] ABLIKIM	12N	BES3	$\psi(2S) \to \pi^0\gamma K^0_S K^\mp\pi^\mp 2\pi^\pm$

[1] ABLIKIM 12N quotes $B(\psi(2S) \to \pi^0 h_c) \cdot B(h_c \to \gamma\eta_c) \cdot B(\eta_c \to K^0_S K^-\pi^-2\pi^+) = (12.01 \pm 2.22 \pm 2.04) \times 10^{-6}$ which we multiply by 2 to take c.c. into account.

[2] ABLIKIM 12N reports $[\Gamma(\eta_c(1S) \to K^0K^-\pi^+\pi^-\pi^+ + c.c.)/\Gamma_{total} \times \Gamma(h_c(1P) \to \gamma\eta_c(1S))/\Gamma_{total}] \times [B(\psi(2S) \to h_c(1P)\pi^0)] = (24.02 \pm 4.44 \pm 4.08) \times 10^{-6}$ which we divide by our best (shown rounded) value $B(\psi(2S) \to h_c(1P)\pi^0) = (7.4 \pm 0.5) \times 10^{-4}$. Our first error is their experiment's error and our second error is the systematic error from using our best (shown rounded) value.

$\Gamma(\eta_c(1S) \to K^+K^-2(\pi^+\pi^-))/\Gamma_{total} \times \Gamma(J/\psi(1S) \to \gamma\eta_c(1S))/\Gamma_{total}$ $\quad \Gamma_{44}/\Gamma \times \Gamma^{J/\psi(1S)}_{248}/\Gamma^{J/\psi(1S)}$

VALUE (units 10^{-4})	EVTS	DOCUMENT ID		TECN	COMMENT
1.21±0.32±0.24	100	ABLIKIM	06A	BES2	$J/\psi \to K^+K^-2(\pi^+\pi^-)\gamma$

$\Gamma(\eta_c(1S) \to K^+K^-2(\pi^+\pi^-))/\Gamma_{total} \times \Gamma(h_c(1P) \to \gamma\eta_c(1S))/\Gamma_{total}$ $\quad \Gamma_{44}/\Gamma \times \Gamma^{h_c(1P)}_{30}/\Gamma^{h_c(1P)}$

VALUE (units 10^{-3})	EVTS	DOCUMENT ID		TECN	COMMENT
4.8±2.5±0.3	10	[1] ABLIKIM	12N	BES3	$\psi(2S) \to \pi^0\gamma K^+K^-2(\pi^+\pi^-)$

[1] ABLIKIM 12N reports $[\Gamma(\eta_c(1S) \to K^+K^-2(\pi^+\pi^-))/\Gamma_{total} \times \Gamma(h_c(1P) \to \gamma\eta_c(1S))/\Gamma_{total}] \times [B(\psi(2S) \to h_c(1P)\pi^0)] = (3.60 \pm 1.71 \pm 0.64) \times 10^{-6}$ which we divide by our best (shown rounded) value $B(\psi(2S) \to h_c(1P)\pi^0) = (7.4 \pm 0.5) \times 10^{-4}$. Our first error is their experiment's error and our second error is the systematic error from using our best (shown rounded) value.

$\Gamma(\eta_c(1S) \to 2(K^+K^-))/\Gamma_{total} \times \Gamma(B^+ \to \eta_c K^+)/\Gamma_{total}$ $\quad \Gamma_{45}/\Gamma \times \Gamma^{B^\pm}_{274}/\Gamma^{B^\pm}$

VALUE (units 10^{-6})	EVTS	DOCUMENT ID		TECN	COMMENT
1.4±0.4 OUR FIT	Error includes scale factor of 1.5.				
$\mathbf{1.8^{+0.6}_{-0.5}}$	$14.5^{+4.6}_{-3.0}$	HUANG	03	BELL	$B^+ \to 2(K^+K^-)K^+$

$\Gamma(\eta_c(1S) \to 2(K^+K^-))/\Gamma_{total} \times \Gamma(h_c(1P) \to \gamma\eta_c(1S))/\Gamma_{total}$ $\quad \Gamma_{45}/\Gamma \times \Gamma^{h_c(1P)}_{30}/\Gamma^{h_c(1P)}$

VALUE (units 10^{-3})	EVTS	DOCUMENT ID		TECN	COMMENT
0.75±0.24 OUR FIT	Error includes scale factor of 1.5.				
1.3 ±0.5 ±0.1	7	[1] ABLIKIM	12N	BES3	$\psi(2S) \to \pi^0\gamma 2(K^+K^-)$

[1] ABLIKIM 12N reports $[\Gamma(\eta_c(1S) \to 2(K^+K^-))/\Gamma_{total} \times \Gamma(h_c(1P) \to \gamma\eta_c(1S))/\Gamma_{total}] \times [B(\psi(2S) \to h_c(1P)\pi^0)] = (0.94 \pm 0.37 \pm 0.14) \times 10^{-6}$ which we divide by our best (shown rounded) value $B(\psi(2S) \to h_c(1P)\pi^0) = (7.4 \pm 0.5) \times 10^{-4}$. Our first error is their experiment's error and our second error is the systematic error from using our best (shown rounded) value.

$\Gamma(\eta_c(1S) \to \pi^+\pi^-\pi^0\pi^0)/\Gamma_{total} \times \Gamma(h_c(1P) \to \gamma\eta_c(1S))/\Gamma_{total}$ $\quad \Gamma_{47}/\Gamma \times \Gamma^{h_c(1P)}_{30}/\Gamma^{h_c(1P)}$

VALUE (units 10^{-2})	EVTS	DOCUMENT ID		TECN	COMMENT
2.7±0.5±0.2	118	[1] ABLIKIM	12N	BES3	$\psi(2S) \to \pi^0\gamma\pi^+\pi^-2\pi^0$

[1] ABLIKIM 12N reports $[\Gamma(\eta_c(1S) \to \pi^+\pi^-\pi^0\pi^0)/\Gamma_{total} \times \Gamma(h_c(1P) \to \gamma\eta_c(1S))/\Gamma_{total}] \times [B(\psi(2S) \to h_c(1P)\pi^0)] = (20.31 \pm 2.20 \pm 3.33) \times 10^{-6}$ which we divide by our best (shown rounded) value $B(\psi(2S) \to h_c(1P)\pi^0) = (7.4 \pm 0.5) \times 10^{-4}$. Our first error is their experiment's error and our second error is the systematic error from using our best (shown rounded) value.

Int. J. Mod. Phys. A 2026.41. Downloaded from www.worldscientific.com
by UNIVERSITY OF CALIFORNIA @ BERKELEY on 09/16/26. Re-use and distribution is strictly not permitted, except for Open Access articles.

$\Gamma(\eta_c(1S) \to 2(\pi^+\pi^-))/\Gamma_{total} \times \Gamma(J/\psi(1S) \to \gamma\eta_c(1S))/\Gamma_{total}$ $\Gamma_{48}/\Gamma \times \Gamma_{248}^{J/\psi(1S)}/\Gamma^{J/\psi(1S)}$

VALUE (units 10^{-4})	EVTS	DOCUMENT ID		TECN	COMMENT
1.37±0.19 OUR FIT	Error includes scale factor of 1.3.				
1.36±0.23 OUR AVERAGE					
1.3 ±0.2 ±0.4	0.5k	BAI	04	BES	$J/\psi \to \gamma 2(\pi^+\pi^-)$
1.33±0.22±0.20	137	BISELLO	91	DM2	$J/\psi \to \gamma 2(\pi^+\pi^-)$
1.6 ±0.6	25	BALTRUSAIT...86		MRK3	$J/\psi \to \gamma\eta_c$

$\Gamma(\eta_c(1S) \to 2(\pi^+\pi^-))/\Gamma_{total} \times \Gamma(\psi(2S) \to \gamma\eta_c(1S))/\Gamma_{total}$ $\Gamma_{48}/\Gamma \times \Gamma_{199}^{\psi(2S)}/\Gamma^{\psi(2S)}$

VALUE (units 10^{-5})	DOCUMENT ID			TECN	COMMENT
2.7±0.6 OUR FIT	Error includes scale factor of 1.6.				
$5.7^{+3.9}_{-2.4}$	HIMEL		80B	MRK2	$\psi(2S) \to \eta_c\gamma$

$\Gamma(\eta_c(1S) \to 2\pi^+2\pi^-\eta)/\Gamma_{total} \times \Gamma(\psi(2S) \to \gamma\eta_c(1S))/\Gamma_{total}$ $\Gamma_{49}/\Gamma \times \Gamma_{199}^{\psi(2S)}/\Gamma^{\psi(2S)}$

VALUE (units 10^{-5})	DOCUMENT ID			TECN	COMMENT
• • • We do not use the following data for averages, fits, limits, etc. • • •					
2.01±0.17±0.64	[1] ABLIKIM		25R	BES3	$e^+e^- \to \psi(2S)$

[1] Destructive interference with background. The constructive interference solution is $(0.95 \pm 0.17 \pm 0.44) \times 10^{-5}$.

$\Gamma(\eta_c(1S) \to 2(\pi^+\pi^-))/\Gamma_{total} \times \Gamma(h_c(1P) \to \gamma\eta_c(1S))/\Gamma_{total}$ $\Gamma_{48}/\Gamma \times \Gamma_{30}^{h_c(1P)}/\Gamma^{h_c(1P)}$

VALUE (units 10^{-2})	EVTS	DOCUMENT ID		TECN	COMMENT
0.48±0.09 OUR FIT	Error includes scale factor of 1.4.				
1.01±0.19±0.07	100	[1] ABLIKIM	12N	BES3	$\psi(2S) \to \pi^0\gamma 2(\pi^+\pi^-)$

[1] ABLIKIM 12N reports $[\Gamma(\eta_c(1S) \to 2(\pi^+\pi^-))/\Gamma_{total} \times \Gamma(h_c(1P) \to \gamma\eta_c(1S))/\Gamma_{total}] \times [B(\psi(2S) \to h_c(1P)\pi^0)] = (7.51 \pm 0.85 \pm 1.11) \times 10^{-6}$ which we divide by our best (shown rounded) value $B(\psi(2S) \to h_c(1P)\pi^0) = (7.4 \pm 0.5) \times 10^{-4}$. Our first error is their experiment's error and our second error is the systematic error from using our best (shown rounded) value.

$\Gamma(\eta_c(1S) \to 2(\pi^+\pi^-\pi^0))/\Gamma_{total} \times \Gamma(h_c(1P) \to \gamma\eta_c(1S))/\Gamma_{total}$ $\Gamma_{50}/\Gamma \times \Gamma_{30}^{h_c(1P)}/\Gamma^{h_c(1P)}$

VALUE (units 10^{-2})	EVTS	DOCUMENT ID		TECN	COMMENT
10.1±1.7±0.7	175	[1] ABLIKIM	12N	BES3	$\psi(2S) \to \pi^0\gamma 2(\pi^+\pi^-\pi^0)$

[1] ABLIKIM 12N reports $[\Gamma(\eta_c(1S) \to 2(\pi^+\pi^-\pi^0))/\Gamma_{total} \times \Gamma(h_c(1P) \to \gamma\eta_c(1S))/\Gamma_{total}] \times [B(\psi(2S) \to h_c(1P)\pi^0)] = (75.13 \pm 7.42 \pm 9.99) \times 10^{-6}$ which we divide by our best (shown rounded) value $B(\psi(2S) \to h_c(1P)\pi^0) = (7.4 \pm 0.5) \times 10^{-4}$. Our first error is their experiment's error and our second error is the systematic error from using our best (shown rounded) value.

$\Gamma(\eta_c(1S) \to 3(\pi^+\pi^-))/\Gamma_{total} \times \Gamma(J/\psi(1S) \to \gamma\eta_c(1S))/\Gamma_{total}$ $\Gamma_{51}/\Gamma \times \Gamma_{248}^{J/\psi(1S)}/\Gamma^{J/\psi(1S)}$

VALUE (units 10^{-4})	EVTS	DOCUMENT ID		TECN	COMMENT
2.59±0.32±0.47	471	ABLIKIM	06A	BES2	$J/\psi \to 3(\pi^+\pi^-)\gamma$

$\Gamma(\eta_c(1S) \to 3(\pi^+\pi^-))/\Gamma_{total} \times \Gamma(h_c(1P) \to \gamma\eta_c(1S))/\Gamma_{total}$ $\Gamma_{51}/\Gamma \times \Gamma_{30}^{h_c(1P)}/\Gamma^{h_c(1P)}$

VALUE (units 10^{-2})	EVTS	DOCUMENT ID		TECN	COMMENT
1.19±0.30±0.08	51	[1] ABLIKIM	12N	BES3	$\psi(2S) \to \pi^0\gamma 3(\pi^+\pi^-)$

[1] ABLIKIM 12N reports $[\Gamma(\eta_c(1S) \to 3(\pi^+\pi^-))/\Gamma_{total} \times \Gamma(h_c(1P) \to \gamma\eta_c(1S))/\Gamma_{total}] \times [B(\psi(2S) \to h_c(1P)\pi^0)] = (8.82 \pm 1.57 \pm 1.59) \times 10^{-6}$ which we divide by our best (shown rounded) value $B(\psi(2S) \to h_c(1P)\pi^0) = (7.4 \pm 0.5) \times 10^{-4}$. Our first error is their experiment's error and our second error is the systematic error from using our best (shown rounded) value.

$\Gamma(\eta_c(1S) \to p\overline{p})/\Gamma_{total} \times \Gamma(J/\psi(1S) \to \gamma\eta_c(1S))/\Gamma_{total}$ $\Gamma_{52}/\Gamma \times \Gamma_{248}^{J/\psi(1S)}/\Gamma^{J/\psi(1S)}$

VALUE (units 10^{-5})	EVTS	DOCUMENT ID		TECN	COMMENT
2.02±0.19 OUR FIT	Error includes scale factor of 1.2.				
1.61±0.29 OUR AVERAGE					
1.9 ±0.3 ±0.3	213	BAI	04	BES	$J/\psi \to \gamma p\overline{p}$
1.3 ±0.4 ±0.3	18	BISELLO	91	DM2	$J/\psi \to \gamma p\overline{p}$
1.4 ±0.7	23	BALTRUSAIT...86		MRK3	$J/\psi \to \eta_c\gamma$

$\Gamma(\eta_c(1S) \to p\overline{p})/\Gamma_{total} \times \Gamma(h_c(1P) \to \gamma\eta_c(1S))/\Gamma_{total}$ $\Gamma_{52}/\Gamma \times \Gamma_{30}^{h_c(1P)}/\Gamma^{h_c(1P)}$

VALUE (units 10^{-4})	EVTS	DOCUMENT ID		TECN	COMMENT
7.1±0.8 OUR FIT	Error includes scale factor of 1.2.				
8.7±2.9±0.6	15	[1] ABLIKIM	12N	BES3	$\psi(2S) \to \pi^0\gamma p\overline{p}$

[1] ABLIKIM 12N reports $[\Gamma(\eta_c(1S) \to p\overline{p})/\Gamma_{total} \times \Gamma(h_c(1P) \to \gamma\eta_c(1S))/\Gamma_{total}] \times [B(\psi(2S) \to h_c(1P)\pi^0)] = (0.65 \pm 0.19 \pm 0.10) \times 10^{-6}$ which we divide by our best (shown rounded) value $B(\psi(2S) \to h_c(1P)\pi^0) = (7.4 \pm 0.5) \times 10^{-4}$. Our first error is their experiment's error and our second error is the systematic error from using our best (shown rounded) value.

$\Gamma(\eta_c(1S) \to p\overline{p})/\Gamma_{total} \times \Gamma(\psi(2S) \to \gamma\eta_c(1S))/\Gamma_{total}$ $\Gamma_{52}/\Gamma \times \Gamma_{199}^{\psi(2S)}/\Gamma^{\psi(2S)}$

VALUE (units 10^{-6})	DOCUMENT ID			TECN	COMMENT
4.0±0.7 OUR FIT	Error includes scale factor of 1.4.				
8^{+8}_{-4}	HIMEL		80B	MRK2	$\psi(2S) \to \eta_c\gamma$

$\Gamma(\eta_c(1S) \to p\overline{p})/\Gamma_{total} \times \Gamma(B^+ \to \eta_c K^+)/\Gamma_{total}$ $\Gamma_{52}/\Gamma \times \Gamma_{274}^{B^\pm}/\Gamma^{B^\pm}$

VALUE (units 10^{-6})	EVTS	DOCUMENT ID		TECN	COMMENT
1.34±0.13 OUR FIT	Error includes scale factor of 1.2.				
1.54±0.19 OUR AVERAGE	Error includes scale factor of 1.1.				
$1.42 \pm 0.11^{+0.16}_{-0.20}$	195	WU	06	BELL	$B^+ \to p\overline{p}K^+$
$1.8^{+0.3}_{-0.2} \pm 0.2$		AUBERT,B	05L	BABR	$e^+e^- \to \Upsilon(4S)$

$\Gamma(\eta_c(1S) \to p\overline{p}\pi^0)/\Gamma_{total} \times \Gamma(h_c(1P) \to \gamma\eta_c(1S))/\Gamma_{total}$ $\Gamma_{53}/\Gamma \times \Gamma_{30}^{h_c(1P)}/\Gamma^{h_c(1P)}$

VALUE (units 10^{-3})	DOCUMENT ID			TECN	COMMENT
2.1±0.7±0.1	[1] ABLIKIM		12N	BES3	$\psi(2S) \to \pi^0\gamma p\overline{p}\pi^0$

[1] ABLIKIM 12N reports $[\Gamma(\eta_c(1S) \to p\overline{p}\pi^0)/\Gamma_{total} \times \Gamma(h_c(1P) \to \gamma\eta_c(1S))/\Gamma_{total}] \times [B(\psi(2S) \to h_c(1P)\pi^0)] = (1.53 \pm 0.49 \pm 0.23) \times 10^{-6}$ which we divide by our best (shown rounded) value $B(\psi(2S) \to h_c(1P)\pi^0) = (7.4 \pm 0.5) \times 10^{-4}$. Our first error is their experiment's error and our second error is the systematic error from using our best (shown rounded) value.

$\Gamma(\eta_c(1S) \to p\overline{p}\pi^+\pi^-)/\Gamma_{total} \times \Gamma(h_c(1P) \to \gamma\eta_c(1S))/\Gamma_{total}$ $\Gamma_{54}/\Gamma \times \Gamma_{30}^{h_c(1P)}/\Gamma^{h_c(1P)}$

VALUE (units 10^{-3})	EVTS	DOCUMENT ID		TECN	COMMENT
2.15±0.31 OUR FIT	Error includes scale factor of 1.1.				
3.1 ±1.0 ±0.2	19	[1] ABLIKIM	12N	BES3	$\psi(2S) \to \pi^0\gamma p\overline{p}\pi^+\pi^-$

[1] ABLIKIM 12N reports $[\Gamma(\eta_c(1S) \to p\overline{p}\pi^+\pi^-)/\Gamma_{total} \times \Gamma(h_c(1P) \to \gamma\eta_c(1S))/\Gamma_{total}] \times [B(\psi(2S) \to h_c(1P)\pi^0)] = (2.30 \pm 0.65 \pm 0.36) \times 10^{-6}$ which we divide by our best (shown rounded) value $B(\psi(2S) \to h_c(1P)\pi^0) = (7.4 \pm 0.5) \times 10^{-4}$. Our first error is their experiment's error and our second error is the systematic error from using our best (shown rounded) value.

$\Gamma(\eta_c(1S) \to p\overline{p}\pi^+\pi^-)/\Gamma_{total} \times \Gamma(B^+ \to \eta_c K^+)/\Gamma_{total}$ $\Gamma_{54}/\Gamma \times \Gamma_{274}^{B^\pm}/\Gamma^{B^\pm}$

VALUE (units 10^{-6})	DOCUMENT ID			TECN	COMMENT
4.0 ±0.4 OUR FIT					
$3.94^{+0.41}_{-0.39}{}^{+0.22}_{-0.18}$	CHILIKIN		19	BELL	$e^+e^- \to \Upsilon(4S)$

$\Gamma(\eta_c(1S) \to \Lambda\overline{\Lambda})/\Gamma_{total} \times \Gamma(J/\psi(1S) \to \gamma\eta_c(1S))/\Gamma_{total}$ $\Gamma_{55}/\Gamma \times \Gamma_{248}^{J/\psi(1S)}/\Gamma^{J/\psi(1S)}$

VALUE (units 10^{-5})	DOCUMENT ID			TECN	COMMENT
1.72±0.28 OUR FIT					
1.98±0.21±0.32	ABLIKIM		12B	BES3	$J/\psi \to \Lambda\overline{\Lambda}\gamma$

$\Gamma(\eta_c(1S) \to \Lambda\overline{\Lambda})/\Gamma_{total} \times \Gamma(B^+ \to \eta_c K^+)/\Gamma_{total}$ $\Gamma_{55}/\Gamma \times \Gamma_{274}^{B^\pm}/\Gamma^{B^\pm}$

VALUE (units 10^{-6})	EVTS	DOCUMENT ID		TECN	COMMENT
1.13±0.19 OUR FIT	Error includes scale factor of 1.1.				
$0.95^{+0.25}_{-0.22}{}^{+0.08}_{-0.11}$	20	WU	06	BELL	$B^+ \to \Lambda\overline{\Lambda}K^+$

$\Gamma(\eta_c(1S) \to \Sigma^+\overline{\Sigma}^-)/\Gamma_{total} \times \Gamma(J/\psi(1S) \to \gamma\eta_c(1S))/\Gamma_{total}$ $\Gamma_{58}/\Gamma \times \Gamma_{248}^{J/\psi(1S)}/\Gamma^{J/\psi(1S)}$

VALUE (units 10^{-5})	EVTS	DOCUMENT ID		TECN	COMMENT
3.60±0.48±0.31	112	ABLIKIM	13C	BES3	$J/\psi \to \gamma p\overline{p}\pi^0\pi^0$

$\Gamma(\eta_c(1S) \to \Xi^-\overline{\Xi}^+)/\Gamma_{total} \times \Gamma(J/\psi(1S) \to \gamma\eta_c(1S))/\Gamma_{total}$ $\Gamma_{59}/\Gamma \times \Gamma_{248}^{J/\psi(1S)}/\Gamma^{J/\psi(1S)}$

VALUE (units 10^{-5})	EVTS	DOCUMENT ID		TECN	COMMENT
1.51±0.27±0.14	78	ABLIKIM	13C	BES3	$J/\psi \to \gamma\Lambda\overline{\Lambda}\pi^+\pi^-$

$\Gamma(\eta_c(1S) \to \gamma\gamma)/\Gamma_{total} \times \Gamma(J/\psi(1S) \to \gamma\eta_c(1S))/\Gamma_{total}$ $\Gamma_{60}/\Gamma \times \Gamma_{248}^{J/\psi(1S)}/\Gamma^{J/\psi(1S)}$

VALUE (units 10^{-6})	EVTS	DOCUMENT ID		TECN	COMMENT
3.9 ±0.4 OUR FIT	Error includes scale factor of 1.5.				
5.1 ±0.4 OUR AVERAGE					
5.23±0.26±0.30	678	ABLIKIM	25D	BES3	$\psi(2S) \to \pi^+\pi^-J/\psi$
4.5 ±1.2 ±0.6	73	ABLIKIM	13I	BES3	$\psi(2S) \to \pi^+\pi^-J/\psi$
$1.2^{+2.7}_{-1.1} \pm 0.3$	$1.2^{+2.8}_{-1.1}$	ADAMS	08	CLEO	$\psi(2S) \to \pi^+\pi^-J/\psi$

$\Gamma(\eta_c(1S) \to \gamma\gamma)/\Gamma_{total} \times \Gamma(B^+ \to \eta_c K^+)/\Gamma_{total}$ $\Gamma_{60}/\Gamma \times \Gamma_{274}^{B^\pm}/\Gamma^{B^\pm}$

VALUE (units 10^{-6})	EVTS	DOCUMENT ID		TECN	COMMENT
0.256±0.028 OUR FIT	Error includes scale factor of 1.4.				
$0.22^{+0.09}_{-0.07}{}^{+0.04}_{-0.02}$	13	WICHT	08	BELL	$B^\pm \to K^\pm\gamma\gamma$

Int. J. Mod. Phys. A 2026.41. Downloaded from www.worldscientific.com by CALIFORNIA @ BERKELEY on 09/16/26. Re-use and distribution is strictly not permitted, except for Open Access articles.

$\eta_c(1S)$ REFERENCES

ABLIKIM	25AC	PR D112 012012	M. Ablikim *et al.*	(BESIII Collab.)
ABLIKIM	25D	PRL 134 181901	M. Ablikim *et al.*	(BESIII Collab.)
ABLIKIM	25P	PR D111 052011	M. Ablikim *et al.*	(BESIII Collab.)
ABLIKIM	25R	PR D111 052013	M. Ablikim *et al.*	(BESIII Collab.)
AAIJ	23AH	PR D108 032010	R. Aaij *et al.*	(LHCb Collab.)
ABLIKIM	21C	PR D103 012009	M. Ablikim *et al.*	(BESIII Collab.)
LEES	21A	PR D104 072002	J.P. Lees *et al.*	(BABAR Collab.)
AAIJ	20H	EPJ C80 191	R. Aaij *et al.*	(LHCb Collab.)
ABLIKIM	19AP	PR D100 012003	M. Ablikim *et al.*	(BESIII Collab.)
ABLIKIM	19AV	PR D100 052012	M. Ablikim *et al.*	(BESIII Collab.)
CHILIKIN	19	PR D100 012001	K. Chilikin *et al.*	(BELLE Collab.)
LU	19	PR D99 032003	P.-C. Lu *et al.*	(BELLE Collab.)
XU	18	PR D98 072001	Q.N. Xu *et al.*	(BELLE Collab.)
AAIJ	17AD	PL B769 305	R. Aaij *et al.*	(LHCb Collab.)
AAIJ	17BB	EPJ C77 609	R. Aaij *et al.*	(LHCb Collab.)
ABLIKIM	17AJ	PR D96 112008	M. Ablikim *et al.*	(BESIII Collab.)
ABLIKIM	17P	PR D95 092004	M. Ablikim *et al.*	(BESIII Collab.)
LEES	16A	PR D93 012005	J.P. Lees *et al.*	(BABAR Collab.)
AAIJ	15BI	EPJ C75 311	R. Aaij *et al.*	(LHCb Collab.)
ANASHIN	14	PL B738 391	V.V. Anashin *et al.*	(KEDR Collab.)
LEES	14E	PR D89 112004	J.P. Lees *et al.*	(BABAR Collab.)
ABLIKIM	13C	PR D87 012003	M. Ablikim *et al.*	(BESIII Collab.)
ABLIKIM	13I	PR D87 032003	M. Ablikim *et al.*	(BESIII Collab.)
UEHARA	13	PTEP 2013 123C01	S. Uehara *et al.*	(BELLE Collab.)
ABLIKIM	12B	PR D86 032008	M. Ablikim *et al.*	(BESIII Collab.)
ABLIKIM	12F	PRL 108 222002	M. Ablikim *et al.*	(BESIII Collab.)
ABLIKIM	12N	PR D86 092009	M. Ablikim *et al.*	(BESIII Collab.)
LIU	12B	PRL 108 232001	Z.Q. Liu *et al.*	(BELLE Collab.)
ZHANG	12A	PR D86 052002	C.C. Zhang *et al.*	(BELLE Collab.)
ABLIKIM	11G	PR D84 032006	M. Ablikim *et al.*	(BESIII Collab.)
DEL-AMO-SA...	11M	PR D84 012004	P. del Amo Sanchez *et al.*	(BABAR Collab.)
VINOKUROVA	11	PL B706 139	A. Vinokurova *et al.*	(BELLE Collab.)
LEES	10	PR D81 052010	J.P. Lees *et al.*	(BABAR Collab.)
MITCHELL	09	PRL 102 011801	R.E. Mitchell *et al.*	(CLEO Collab.)
ADAMS	08	PRL 101 101801	G.S. Adams *et al.*	(CLEO Collab.)
AUBERT	08AB	PR D78 012006	B. Aubert *et al.*	(BABAR Collab.)
UEHARA	08	EPJ C53 1	S. Uehara *et al.*	(BELLE Collab.)
WICHT	08	PL B662 323	J. Wicht *et al.*	(BELLE Collab.)
ABE	07	PRL 98 082001	K. Abe *et al.*	(BELLE Collab.)
ABLIKIM	06A	PL B633 19	M. Ablikim *et al.*	(BES Collab.)
ABLIKIM	06B	EPJ C45 337	M. Ablikim *et al.*	(BES Collab.)
AUBERT	06E	PRL 96 052002	B. Aubert *et al.*	(BABAR Collab.)
PDG	06	JP G33 1	W.-M. Yao *et al.*	(PDG Collab.)
WU	06	PRL 97 162003	C.-H. Wu *et al.*	(BELLE Collab.)
ABLIKIM	05L	PR D72 072005	M. Ablikim *et al.*	(BES Collab.)
AUBERT,B	05L	PR D72 051101	B. Aubert *et al.*	(BABAR Collab.)
KUO	05	PL B621 41	C.C. Kuo *et al.*	(BELLE Collab.)
ABE	04G	PR D70 071102	K. Abe *et al.*	(BELLE Collab.)
ABLIKIM	04M	PR D70 112008	M. Ablikim *et al.*	(BES Collab.)
ASNER	04	PRL 92 142001	D.M. Asner *et al.*	(CLEO Collab.)
AUBERT	04D	PRL 92 142002	B. Aubert *et al.*	(BABAR Collab.)
AUBERT,B	04B	PR D70 011101	B. Aubert *et al.*	(BABAR Collab.)
BAI	04	PL B578 16	J.Z. Bai *et al.*	(BES Collab.)
ABDALLAH	03J	EPJ C31 481	J. Abdallah *et al.*	(DELPHI Collab.)
AMBROGIANI	03	PL B566 45	M. Ambrogiani *et al.*	(FNAL E835 Collab.)
BAI	03	PL B555 174	J.Z. Bai *et al.*	(BES Collab.)
FANG	03	PRL 90 071801	F. Fang *et al.*	(BELLE Collab.)
HUANG	03	PRL 91 241802	H.-C. Huang *et al.*	(BELLE Collab.)
ABE,K	02	PRL 89 142001	K. Abe *et al.*	(BELLE Collab.)
BAI	00F	PR D62 072001	J.Z. Bai *et al.*	(BES Collab.)
BRANDENB...	00B	PRL 85 3095	G. Brandenburg *et al.*	(CLEO Collab.)
ACCIARRI	99T	PL B461 155	M. Acciarri *et al.*	(L3 Collab.)
BAI	99B	PR D60 072001	J.Z. Bai *et al.*	(BES Collab.)
ABREU	98O	PL B441 479	P. Abreu *et al.*	(DELPHI Collab.)
SHIRAI	98	PL B424 405	M. Shirai *et al.*	(AMY Collab.)
ARMSTRONG	95F	PR D52 4839	T.A. Armstrong *et al.*	(FNAL, FERR, GENO+)
ALBRECHT	94H	PL B338 390	H. Albrecht *et al.*	(ARGUS Collab.)
ADRIANI	93N	PL B318 575	O. Adriani *et al.*	(L3 Collab.)
BISELLO	91	NP B350 1	D. Bisello *et al.*	(DM2 Collab.)
BAI	90B	PRL 65 1309	Z. Bai *et al.*	(Mark III Collab.)
CHEN	90B	PL B243 169	W.Y. Chen *et al.*	(CLEO Collab.)
BAGLIN	89	PL B231 557	C. Baglin, S. Baird, G. Bassompierre	(R704 Collab.)
BEHREND	89	ZPHY C42 367	H.J. Behrend *et al.*	(CELLO Collab.)
BRAUNSCH...	89	ZPHY C41 533	W. Braunschweig *et al.*	(TASSO Collab.)
AIHARA	88D	PRL 60 2355	H. Aihara *et al.*	(TPC Collab.)
BAGLIN	87B	PL B187 191	C. Baglin *et al.*	(R704 Collab.)
BALTRUSAIT...	86	PR D33 629	R.M. Baltrusaitis *et al.*	(Mark III Collab.)
BERGER	86	PL 167B 120	C. Berger *et al.*	(PLUTO Collab.)
GAISER	86	PR D34 711	J. Gaiser *et al.*	(Crystal Ball Collab.)
ALTHOFF	85B	ZPHY C29 189	M. Althoff *et al.*	(TASSO Collab.)
BALTRUSAIT...	84	PRL 52 2126	R.M. Baltrusaitis *et al.*	(CIT, UCSC+) JP
BLOOM	83	ARNS 33 143	E.D. Bloom, C. Peck	(SLAC, CIT)
HIMEL	80B	PRL 45 1146	T.M. Himel *et al.*	(SLAC, LBL, UCB)
PARTRIDGE	80B	PRL 45 1150	R. Partridge *et al.*	(CIT, HARV, PRIN+)

$J/\psi(1S)$

$I^G(J^{PC}) = 0^-(1^{--})$

$J/\psi(1S)$ MASS

VALUE (MeV)	EVTS	DOCUMENT ID		TECN	COMMENT
3096.900±0.006 OUR AVERAGE					
3096.900±0.002±0.006		[1] ANASHIN	15	KEDR	$e^+e^- \to$ hadrons
3096.89 ±0.09	502	[2] ARTAMONOV	00	OLYA	$e^+e^- \to$ hadrons
3096.91 ±0.03 ±0.01		[3] ARMSTRONG	93B	E760	$\overline{p}p \to e^+e^-$
3096.95 ±0.1 ±0.3	193	BAGLIN	87	SPEC	$\overline{p}p \to e^+e^-X$
• • • We do not use the following data for averages, fits, limits, etc. • • •					
3096.66 ±0.19 ±0.02	6.1k	[4] AAIJ	15BI	LHCB	$pp \to J/\psi X$
3096.917±0.010±0.007		AULCHENKO	03	KEDR	$e^+e^- \to$ hadrons
3097.5 ±0.3		GRIBUSHIN	96	FMPS	515 π^-Be $\to 2\mu X$
3098.4 ±2.0	38k	LEMOIGNE	82	GOLI	185 π^-Be $\to \gamma\mu^+\mu^-$A
3096.93 ±0.09	502	[5] ZHOLENTZ	80	REDE	e^+e^-
3097.0 ±1		[6] BRANDELIK	79C	DASP	e^+e^-

[1] Supersedes AULCHENKO 03.
[2] Reanalysis of ZHOLENTZ 80 using new electron mass (COHEN 87) and radiative corrections (KURAEV 85).
[3] Mass central value and systematic error recalculated by us according to Eq. (16) in ARMSTRONG 93B, using the value for the $\psi(2S)$ mass from AULCHENKO 03.
[4] From a sample of $\eta_c(1S)$ and J/ψ produced in b-hadron decays. Systematic uncertainties not estimated.
[5] Superseded by ARTAMONOV 00.
[6] From a simultaneous fit to e^+e^-, $\mu^+\mu^-$ and hadronic channels assuming $\Gamma(e^+e^-) = \Gamma(\mu^+\mu^-)$.

$J/\psi(1S)$ WIDTH

VALUE (keV)	EVTS	DOCUMENT ID		TECN	COMMENT
92.6 ± 1.7 OUR AVERAGE		Error includes scale factor of 1.1.			
92.45 ± 1.40±1.48		[1] ANASHIN	20	KEDR	e^+e^-
96.1 ± 3.2	13k	[2] ADAMS	06A	CLEO	$e^+e^- \to \mu^+\mu^-\gamma$
84.4 ± 8.9		BAI	95B	BES	e^+e^-
91 ±11 ±6		[3] ARMSTRONG	93B	E760	$\overline{p}p \to e^+e^-$
85.5 $^{+6.1}_{-5.8}$		[4] HSUEH	92	RVUE	See Υ mini-review
• • • We do not use the following data for averages, fits, limits, etc. • • •					
92.94 ± 1.83		[5,6] ANASHIN	18A	KEDR	e^+e^-
94.1 ± 2.7		[7] ANASHIN	10	KEDR	3.097 $e^+e^- \to e^+e^-, \mu^+\mu^-$
93.7 ± 3.5	7.8k	[2] AUBERT	04	BABR	$e^+e^- \to \mu^+\mu^-\gamma$

[1] Based on the same dataset as ANASHIN 18A and correlated to the values reported there.
[2] Calculated by us from the reported values of $\Gamma(e^+e^-)\times B(\mu^+\mu^-)$ using $B(e^+e^-) = (5.94 \pm 0.06)\%$ and $B(\mu^+\mu^-) = (5.93 \pm 0.06)\%$.
[3] The initial-state radiation correction reevaluated by ANDREOTTI 07 in its Ref. [4].
[4] Using data from COFFMAN 92, BALDINI-CELIO 75, BOYARSKI 75, ESPOSITO 75B, BRANDELIK 79C.
[5] Using $\Gamma(e^+e^-)$ from ANASHIN 18A and $B(J/\psi(1S) \to e^+e^-) = (5.971 \pm 0.032)\%$ from PDG 16.
[6] Superseded by ANASHIN 20 that is based on the same dataset.
[7] Assuming $\Gamma(e^+e^-) = \Gamma(\mu^+\mu^-)$ and using $\Gamma(e^+e^-)/\Gamma_{total} = (5.94 \pm 0.06)\%$.

$J/\psi(1S)$ DECAY MODES

	Mode		Fraction (Γ_i/Γ)	Scale factor/ Confidence level
Γ_1	hadrons		(87.7 ± 0.5) %	
Γ_2	virtual$\gamma \to$ hadrons		(13.46 ± 0.07) %	
Γ_3	ggg		(64.1 ± 1.0) %	
Γ_4	γgg		(8.8 ± 1.1) %	
Γ_5	e^+e^-		(5.971± 0.032) %	
Γ_6	$e^+e^-\gamma$	[a]	(8.8 ± 1.4) $\times 10^{-3}$	
Γ_7	$\mu^+\mu^-$		(5.961± 0.033) %	
Γ_8	$e^+e^-e^+e^-$		(5.5 ± 0.5) $\times 10^{-5}$	
Γ_9	$e^+e^-\mu^+\mu^-$		(3.53 ± 0.26) $\times 10^{-5}$	
Γ_{10}	$\mu^+\mu^-\mu^+\mu^-$		(1.11 ± 0.11) $\times 10^{-6}$	
	Decays involving hadronic resonances			
Γ_{11}	$\rho\pi$		(1.88 ± 0.12) %	S=2.6
Γ_{12}	$\rho^0\pi^0$		(6.2 ± 0.6) $\times 10^{-3}$	
Γ_{13}	$a_2(1320)^0\pi^+\pi^- \to 2(\pi^+\pi^-)\pi^0$		(2.8 ± 0.6) $\times 10^{-3}$	
Γ_{14}	$a_2(1320)^+\pi^-\pi^0$ + c.c $\to 2(\pi^+\pi^-)\pi^0$		(3.7 ± 0.7) $\times 10^{-3}$	
Γ_{15}	$a_2(1320)\rho$		(1.09 ± 0.22) %	
Γ_{16}	$\eta\pi^+\pi^-$		(3.8 ± 0.7) $\times 10^{-4}$	
Γ_{17}	$\eta\rho$		(1.93 ± 0.23) $\times 10^{-4}$	
Γ_{18}	$\eta\pi^+\pi^-\pi^0$		(1.17 ± 0.20) %	
Γ_{19}	$\eta\pi^+\pi^-3\pi^0$		(4.9 ± 1.0) $\times 10^{-3}$	
Γ_{20}	$\eta\phi(2170) \to \eta\phi f_0(980) \to \eta\phi\pi^+\pi^-$		(1.2 ± 0.4) $\times 10^{-4}$	
Γ_{21}	$\eta\phi(2170) \to \eta K^*(892)^0\overline{K}^*(892)^0$		< 2.52 $\times 10^{-4}$	CL=90%
Γ_{22}	ηK^+K^-		(8.6 ± 3.0) $\times 10^{-4}$	
Γ_{23}	$\eta K^\pm K^0_S\pi^\mp$	[b]	(2.2 ± 0.4) $\times 10^{-3}$	
Γ_{24}	$\eta K^*(892)^0\overline{K}^*(892)^0$		(1.15 ± 0.26) $\times 10^{-3}$	
Γ_{25}	$\rho\eta'(958)$		(8.1 ± 0.8) $\times 10^{-5}$	S=1.6
Γ_{26}	$\rho^\pm\pi^\mp\pi^+\pi^-2\pi^0$		(2.8 ± 0.8) %	
Γ_{27}	$\rho^+\rho^-\pi^+\pi^-\pi^0$		(6 ± 4) $\times 10^{-3}$	
Γ_{28}	$\rho^+K^+K^-\pi^-$ + c.c $\to K^+K^-\pi^+\pi^-\pi^0$		(3.5 ± 0.8) $\times 10^{-3}$	
Γ_{29}	$\rho^\mp K^\pm K^0_S$		(1.9 ± 0.4) $\times 10^{-3}$	
Γ_{30}	$h_1(1415)\eta' \to \gamma\eta\eta'$			
Γ_{31}	$h_1(1595)\eta' \to \gamma\eta\eta'$			
Γ_{32}	$\rho(1450)\pi$		seen	
Γ_{33}	$\rho(1450)\pi \to \pi^+\pi^-\pi^0$		(2.2 ± 1.1) $\times 10^{-4}$	
Γ_{34}	$\rho(1450)^\pm\pi^\mp \to K^0_S K^\pm\pi^\mp$		(3.3 ± 0.6) $\times 10^{-4}$	
Γ_{35}	$\rho(1450)^0\pi^0 \to K^+K^-\pi^0$		(2.7 ± 0.6) $\times 10^{-4}$	

Int. J. Mod. Phys. A 2026.41. Downloaded from www.worldscientific.com
by UNIVERSITY OF CALIFORNIA @ BERKELEY on 09/16/26. Re-use and distribution is strictly not permitted, except for Open Access articles.

Γ_{36}	$\rho(1450)\eta'(958) \to \pi^+\pi^-\eta'(958)$		$(3.3 \pm 0.7) \times 10^{-6}$	
Γ_{37}	$\rho(1700)\pi$		seen	
Γ_{38}	$\rho(1700)\pi \to \pi^+\pi^-\pi^0$		$(1.6 \pm 1.1) \times 10^{-4}$	
Γ_{39}	$\rho(2150)\pi$		seen	
Γ_{40}	$\rho(2150)\pi \to \pi^+\pi^-\pi^0$		$(10 \pm 40) \times 10^{-6}$	
Γ_{41}	$\rho_3(1690)\pi \to \pi^+\pi^-\pi^0$			
Γ_{42}	$\omega\pi^0$		$(4.5 \pm 0.5) \times 10^{-4}$	S=1.4
Γ_{43}	$\omega\pi^0 \to \pi^+\pi^-\pi^0$		$(1.6 \pm 0.7) \times 10^{-5}$	
Γ_{44}	$\omega\pi^+\pi^-$		$(8.5 \pm 1.0) \times 10^{-3}$	S=1.3
Γ_{45}	$\omega\pi^0\pi^0$		$(3.4 \pm 0.8) \times 10^{-3}$	
Γ_{46}	$\omega 3\pi^0$		$(1.9 \pm 0.6) \times 10^{-3}$	
Γ_{47}	$\omega f_2(1270)$		$(4.3 \pm 0.6) \times 10^{-3}$	
Γ_{48}	$\omega\eta$		$(1.74 \pm 0.20) \times 10^{-3}$	S=1.6
Γ_{49}	$\omega\pi^+\pi^-\pi^0$		$(4.0 \pm 0.7) \times 10^{-3}$	
Γ_{50}	$\omega\pi^0\eta$		$(3.4 \pm 1.7) \times 10^{-4}$	
Γ_{51}	$\omega\pi^+\pi^+\pi^-\pi^-$		$(8.5 \pm 3.4) \times 10^{-3}$	
Γ_{52}	$\omega\pi^+\pi^-2\pi^0$		(3.3 ± 0.5) %	
Γ_{53}	$\omega\eta'\pi^+\pi^-$		$(1.12 \pm 0.13) \times 10^{-3}$	
Γ_{54}	$\omega\eta'(958)$		$(1.89 \pm 0.18) \times 10^{-4}$	
Γ_{55}	$\omega f_0(980)$		$(1.4 \pm 0.5) \times 10^{-4}$	
Γ_{56}	$\omega f_0(1710) \to \omega K\overline{K}$		$(4.8 \pm 1.1) \times 10^{-4}$	
Γ_{57}	$\omega f_1(1420)$		$(6.8 \pm 2.4) \times 10^{-4}$	
Γ_{58}	$\omega f'_2(1525)$		$< 2.2 \times 10^{-4}$	CL=90%
Γ_{59}	$\omega X(1835) \to \omega p\overline{p}$		$< 3.9 \times 10^{-6}$	CL=95%
Γ_{60}	$\omega K^+K^-\eta$		$(3.33 \pm 0.12) \times 10^{-4}$	
Γ_{61}	$\omega X(1835),\ X \to \eta'\pi^+\pi^-$		$< 6.2 \times 10^{-5}$	
Γ_{62}	ωK^+K^-		$(1.52 \pm 0.31) \times 10^{-3}$	
Γ_{63}	$\omega K^\pm K^0_S\pi^\mp$	[b]	$(3.4 \pm 0.5) \times 10^{-3}$	
Γ_{64}	$\omega K\overline{K}$		$(1.9 \pm 0.4) \times 10^{-3}$	
Γ_{65}	$\omega K^*(892)\overline{K}+$ c.c.		$(6.1 \pm 0.9) \times 10^{-3}$	
Γ_{66}	$\eta' K^{*\pm}K^\mp$		$(1.48 \pm 0.13) \times 10^{-3}$	
Γ_{67}	$\eta' K^{*0}\overline{K}^0+$ c.c.		$(1.66 \pm 0.21) \times 10^{-3}$	
Γ_{68}	$\eta' h_1(1415) \to \eta' K^*\overline{K}+$ c.c.		$(2.16 \pm 0.31) \times 10^{-4}$	
Γ_{69}	$\eta' h_1(1415) \to \eta' K^{*\pm}K^\mp$		$(1.51 \pm 0.23) \times 10^{-4}$	
Γ_{70}	$\eta' h_1(1415) \to \gamma\eta'\eta'$		$(4.7 {}^{+1.1}_{-2.0}) \times 10^{-7}$	
Γ_{71}	$\overline{K}K^*(892)+$c.c.		seen	
Γ_{72}	$\overline{K}K^*(892)+$c.c. $\to K^0_S K^\pm\pi^\mp$		$(4.8 \pm 0.5) \times 10^{-3}$	
Γ_{73}	$K^+K^*(892)^-+$ c.c.		$(6.0 {}^{+0.8}_{-1.0}) \times 10^{-3}$	S=2.9
Γ_{74}	$K^+K^*(892)^-+$ c.c. $\to K^+K^-\pi^0$		$(2.69 {}^{+0.13}_{-0.20}) \times 10^{-3}$	
Γ_{75}	$K^+K^*(892)^-+$ c.c. $\to K^0K^\pm\pi^\mp+$ c.c.		$(3.0 \pm 0.4) \times 10^{-3}$	
Γ_{76}	$K^0\overline{K}^*(892)^0+$ c.c.		$(4.2 \pm 0.4) \times 10^{-3}$	
Γ_{77}	$K^0\overline{K}^*(892)^0+$ c.c. $\to K^0K^\pm\pi^\mp+$ c.c.		$(3.2 \pm 0.4) \times 10^{-3}$	
Γ_{78}	$\overline{K}^*(892)^0K^+\pi^-+$ c.c.		$(5.7 \pm 0.8) \times 10^{-3}$	
Γ_{79}	$K^*(892)^\pm K^\mp\pi^0$		$(4.1 \pm 1.3) \times 10^{-3}$	
Γ_{80}	$K^*(892)^+K^0_S\pi^-+$ c.c.		$(2.0 \pm 0.5) \times 10^{-3}$	
Γ_{81}	$K^*(892)^+K^0_S\pi^-+$ c.c. $\to K^0_S K^0_S\pi^+\pi^-$		$(6.7 \pm 2.2) \times 10^{-4}$	
Γ_{82}	$K^*(892)^0K^-\pi^++$ c.c. $\to K^+K^-\pi^+\pi^-$		$(3.8 \pm 0.5) \times 10^{-3}$	
Γ_{83}	$K^*(892)^0K^0_S \to \gamma K^0_S K^0_S$		$(6.3 {}^{+0.6}_{-0.5}) \times 10^{-6}$	
Γ_{84}	$K^*(892)^0K^0_S\pi^0$		$(7 \pm 4) \times 10^{-4}$	
Γ_{85}	$K^*(892)^\pm K^*(700)^\mp$		$(1.1 {}^{+1.0}_{-0.6}) \times 10^{-3}$	
Γ_{86}	$K^*(892)^0\overline{K}^*(892)^0$		$(2.3 \pm 0.6) \times 10^{-4}$	
Γ_{87}	$K^*(892)^\pm K^*(892)^\mp$		$(1.00 {}^{+0.22}_{-0.40}) \times 10^{-3}$	
Γ_{88}	$K_1(1400)^\pm K^\mp$		$(3.8 \pm 1.4) \times 10^{-3}$	
Γ_{89}	$K^*(1410)\overline{K}+$c.c.		seen	
Γ_{90}	$K^*(1410)\overline{K}+$c.c $\to K^\pm K^\mp\pi^0$		$(7 \pm 4) \times 10^{-5}$	
Γ_{91}	$K^*(1410)\overline{K}+$ c.c. $\to K^0_S K^\pm\pi^\mp$		$(8 \pm 5) \times 10^{-5}$	
Γ_{92}	$K^*_2(1430)\overline{K}+$c.c.		seen	
Γ_{93}	$K^*_2(1430)\overline{K}+$c.c. $\to K^\pm K^\mp\pi^0$		$(1.0 \pm 0.5) \times 10^{-4}$	
Γ_{94}	$K^*_2(1430)\overline{K}+$ c.c. $\to K^0_S K^\pm\pi^\mp$		$(3.8 \pm 1.0) \times 10^{-4}$	
Γ_{95}	$\overline{K}^*_2(1430)K+$ c.c.		$< 4.0 \times 10^{-3}$	CL=90%
Γ_{96}	$K^*_2(1430)^+K^-+$ c.c. $\to K^+K^-\pi^0$		$(2.69 {}^{+0.25}_{-0.19}) \times 10^{-4}$	
Γ_{97}	$K^*_2(1430)^0K^-\pi^++$ c.c. $\to K^+K^-\pi^+\pi^-$		$(2.6 \pm 0.9) \times 10^{-3}$	
Γ_{98}	$K^*_2(1430)^+K^0_S\pi^-+$ c.c.		$(3.6 \pm 1.8) \times 10^{-3}$	
Γ_{99}	$\overline{K}^*_2(1430)^0K^*(892)^0+$ c.c.		$(4.67 \pm 0.29) \times 10^{-3}$	
Γ_{100}	$K^*_2(1430)^-K^*(892)^++$ c.c.		$(3.4 \pm 2.9) \times 10^{-3}$	
Γ_{101}	$K^*_2(1430)^-K^*(892)^++$ c.c. $\to K^*(892)^+K^0_S\pi^-+$ c.c.		$(4 \pm 4) \times 10^{-4}$	
Γ_{102}	$K^*_2(1430)^0\overline{K}^*_2(1430)^0$		$< 2.9 \times 10^{-3}$	CL=90%
Γ_{103}	$\overline{K}_2(1770)^0K^*(892)^0+$ c.c. $\to K^*(892)^0K^-\pi^++$ c.c.		$(6.9 \pm 0.9) \times 10^{-4}$	
Γ_{104}	$K^*_2(1980)^+K^-+$ c.c. $\to K^+K^-\pi^0$		$(1.10 {}^{+0.60}_{-0.14}) \times 10^{-5}$	
Γ_{105}	$K^*_4(2045)^+K^-+$ c.c. $\to K^+K^-\pi^0$		$(6.2 {}^{+2.9}_{-1.6}) \times 10^{-6}$	
Γ_{106}	$K_1(1270)^\pm K^\mp$		$< 3.0 \times 10^{-3}$	CL=90%
Γ_{107}	$K_1(1270)K^0_S \to \gamma K^0_S K^0_S$		$(8.5 \pm 2.5) \times 10^{-7}$	
Γ_{108}	$a_2(1320)^\pm\pi^\mp$	[b]	$< 4.3 \times 10^{-3}$	CL=90%
Γ_{109}	$\phi\pi^0$		3×10^{-6} or 1×10^{-7}	
Γ_{110}	$\phi\pi^+\pi^-$		$(9.4 \pm 1.5) \times 10^{-4}$	S=1.7
Γ_{111}	$\phi\pi^0\pi^0$		$(4.9 \pm 1.0) \times 10^{-4}$	
Γ_{112}	$\phi 2(\pi^+\pi^-)$		$(1.60 \pm 0.32) \times 10^{-3}$	
Γ_{113}	$\phi\eta$		$(7.4 \pm 0.6) \times 10^{-4}$	S=1.2
Γ_{114}	$\phi\eta'(958)$		$(4.6 \pm 0.5) \times 10^{-4}$	S=2.2
Γ_{115}	$\phi\eta\eta'$		$(2.32 \pm 0.17) \times 10^{-4}$	
Γ_{116}	$\phi f_0(980)$		$(3.2 \pm 0.9) \times 10^{-4}$	S=1.9
Γ_{117}	$\phi f_0(980) \to \phi\pi^+\pi^-$		$(2.57 \pm 0.34) \times 10^{-4}$	
Γ_{118}	$\phi f_0(980) \to \phi\pi^0\pi^0$		$(1.7 \pm 0.5) \times 10^{-4}$	
Γ_{119}	$\phi\pi^0 f_0(980) \to \phi\pi^0\pi^+\pi^-$		$(4.5 \pm 1.0) \times 10^{-6}$	
Γ_{120}	$\phi\pi^0 f_0(980) \to \phi\pi^0 p^0\pi^0$		$(1.7 \pm 0.6) \times 10^{-6}$	
Γ_{121}	$\phi f_0(980)\eta \to \eta\phi\pi^+\pi^-$		$(3.2 \pm 1.0) \times 10^{-4}$	
Γ_{122}	$\phi a_0(980)^0 \to \phi\eta\pi^0$			
Γ_{123}	$\phi(1680)^0\pi^0 \to \phi\eta\pi^0$		$(6.7 \pm 1.1) \times 10^{-6}$	
Γ_{124}	$X(2000)^0\pi^0 \to \phi\eta\pi^0$		$(1.70 {}^{+0.50}_{-0.23}) \times 10^{-6}$	
Γ_{125}	$h_1(1900)^0\pi^0 \to \phi\eta\pi^0$		$(8.4 {}^{+1.4}_{-1.3}) \times 10^{-6}$	
Γ_{126}	$\phi f_2(1270)$		$(3.2 \pm 0.6) \times 10^{-4}$	
Γ_{127}	$\phi f_1(1285)$		$(2.6 \pm 0.5) \times 10^{-4}$	
Γ_{128}	$\phi f_1(1285) \to \phi\pi^0 f_0(980) \to \phi\pi^0\pi^+\pi^-$		$(9.4 \pm 2.8) \times 10^{-7}$	
Γ_{129}	$\phi f_1(1285) \to \phi\pi^0 f_0(980) \to \phi 3\pi^0$		$(2.1 \pm 2.2) \times 10^{-7}$	
Γ_{130}	$\phi\eta(1405) \to \phi\eta\pi^+\pi^-$		$(2.0 \pm 1.0) \times 10^{-5}$	
Γ_{131}	$\phi f'_2(1525)$		$(8 \pm 4) \times 10^{-4}$	S=2.7
Γ_{132}	$\phi X(1835) \to \phi p\overline{p}$		$< 2.1 \times 10^{-7}$	CL=90%
Γ_{133}	$\phi X(1835) \to \phi\eta\pi^+\pi^-$		$< 2.8 \times 10^{-4}$	CL=90%
Γ_{134}	$\phi X(1870) \to \phi\eta\pi^+\pi^-$		$< 6.13 \times 10^{-5}$	CL=90%
Γ_{135}	$\phi K\overline{K}$		$(1.77 \pm 0.16) \times 10^{-3}$	S=1.3
Γ_{136}	$\phi f_0(1710) \to \phi K\overline{K}$		$(3.6 \pm 0.6) \times 10^{-4}$	
Γ_{137}	ϕK^+K^-		$(8.2 \pm 1.1) \times 10^{-4}$	
Γ_{138}	$\phi K^0_S K^0_S$		$(5.8 \pm 1.5) \times 10^{-4}$	
Γ_{139}	$\phi K^\pm K^0_S\pi^\mp$	[b]	$(7.2 \pm 0.8) \times 10^{-4}$	
Γ_{140}	$\phi K^*(892)\overline{K}+$ c.c.		$(2.18 \pm 0.23) \times 10^{-3}$	
Γ_{141}	$b_1(1235)^\pm\pi^\mp$	[b]	$(3.0 \pm 0.5) \times 10^{-3}$	
Γ_{142}	$b_1(1235)^0\pi^0$		$(2.3 \pm 0.6) \times 10^{-3}$	
Γ_{143}	$f'_2(1525)K^+K^-$		$(1.04 \pm 0.35) \times 10^{-3}$	
Γ_{144}	$\Delta(1232)^+\overline{p}$		$< 1 \times 10^{-4}$	CL=90%
Γ_{145}	$\Delta(1232)^{++}\overline{p}\pi^-$		$(1.6 \pm 0.5) \times 10^{-3}$	
Γ_{146}	$\Delta(1232)^{++}\overline{\Delta}(1232)^{--}$		$(1.10 \pm 0.29) \times 10^{-3}$	
Γ_{147}	$\overline{\Sigma}(1385)^0pK^-$		$(5.1 \pm 3.2) \times 10^{-4}$	
Γ_{148}	$\Sigma(1385)^0\overline{\Lambda}+$ c.c.		$< 8.2 \times 10^{-6}$	CL=90%
Γ_{149}	$\Sigma(1385)^-\overline{\Sigma}^++$ c.c.	[b]	$(3.0 \pm 0.7) \times 10^{-4}$	
Γ_{150}	$\Sigma(1385)^+\overline{\Sigma}^-+$ c.c.		$(3.3 \pm 0.8) \times 10^{-4}$	
Γ_{151}	$\Sigma(1385)^-\overline{\Sigma}(1385)^++$ c.c.	[b]	$(1.08 \pm 0.06) \times 10^{-3}$	
Γ_{152}	$\Sigma(1385)^+\overline{\Sigma}(1385)^-+$ c.c.		$(1.25 \pm 0.07) \times 10^{-3}$	
Γ_{153}	$\Sigma(1385)^0\overline{\Sigma}(1385)^0$		$(1.07 \pm 0.08) \times 10^{-3}$	
Γ_{154}	$\Lambda(1520)\overline{\Lambda}+$ c.c. $\to \gamma\Lambda\overline{\Lambda}$		$< 4.1 \times 10^{-6}$	CL=90%
Γ_{155}	$\overline{\Lambda}(1520)\Lambda+$ c.c.		$< 1.80 \times 10^{-3}$	CL=90%
Γ_{156}	$\Xi^0\overline{\Xi}^0$		$(1.17 \pm 0.04) \times 10^{-3}$	
Γ_{157}	$\Xi(1530)^-\overline{\Xi}^++$ c.c.		$(3.18 \pm 0.08) \times 10^{-4}$	
Γ_{158}	$\Xi(1530)^0\overline{\Xi}^0$		$(3.2 \pm 1.4) \times 10^{-4}$	

Int. J. Mod. Phys. A 2026.41. Downloaded from www.worldscientific.com
by [redacted] LIFORNIA @ BERKELEY on 09/16/26. Re-use and distribution is strictly not permitted, except for Open Access articles.

Γ_{159}	$\Theta(1540)\overline{\Theta}(1540) \to K^0_S p K^- \overline{n} +$ c.c.	[c]	$< 1.1 \times 10^{-5}$	CL=90%
Γ_{160}	$\Theta(1540) K^- \overline{n} \to K^0_S p K^- \overline{n}$	[c]	$< 2.1 \times 10^{-5}$	CL=90%
Γ_{161}	$\Theta(1540) K^0_S \overline{p} \to K^0_S \overline{p} K^+ n$	[c]	$< 1.6 \times 10^{-5}$	CL=90%
Γ_{162}	$\overline{\Theta}(1540) K^+ n \to K^0_S \overline{p} K^+ n$	[c]	$< 5.6 \times 10^{-5}$	CL=90%
Γ_{163}	$\overline{\Theta}(1540) K^0_S p \to K^0_S p K^- \overline{n}$	[c]	$< 1.1 \times 10^{-5}$	CL=90%

Decays into stable hadrons

Γ_{164}	$2(\pi^+\pi^-)\pi^0$		(4.2 ± 0.4) %	S=2.1
Γ_{165}	$3(\pi^+\pi^-)\pi^0$		(2.9 ± 0.6) %	
Γ_{166}	$\pi^+\pi^- 3\pi^0$		(1.9 ± 0.9) %	
Γ_{167}	$\rho^\pm\pi^\mp\pi^0\pi^0$		(1.41 ± 0.22) %	
Γ_{168}	$\rho^+\rho^-\pi^0$		$(6.0 \pm 1.1) \times 10^{-3}$	
Γ_{169}	$\pi^+\pi^- 4\pi^0$		$(6.5 \pm 1.3) \times 10^{-3}$	
Γ_{170}	$\pi^+\pi^-\pi^0$		(2.00 ± 0.07) %	S=2.0
Γ_{171}	$2(\pi^+\pi^-\pi^0)$		(1.61 ± 0.20) %	
Γ_{172}	$\pi^+\pi^-\pi^0 K^+ K^-$		(1.52 ± 0.27) %	S=1.4
Γ_{173}	$\pi^+\pi^-$		$(1.47 \pm 0.14) \times 10^{-4}$	
Γ_{174}	$2(\pi^+\pi^-)$		$(3.20 \pm 0.25) \times 10^{-3}$	S=1.2
Γ_{175}	$3(\pi^+\pi^-)$		$(4.3 \pm 0.4) \times 10^{-3}$	
Γ_{176}	$2(\pi^+\pi^-)3\pi^0$		(6.2 ± 0.9) %	
Γ_{177}	$4(\pi^+\pi^-)\pi^0$		$(9.0 \pm 3.0) \times 10^{-3}$	
Γ_{178}	$2(\pi^+\pi^-)\eta$		$(2.29 \pm 0.28) \times 10^{-3}$	
Γ_{179}	$3(\pi^+\pi^-)\eta$		$(7.2 \pm 1.5) \times 10^{-4}$	
Γ_{180}	$2(\pi^+\pi^-\pi^0)\eta$		$(1.6 \pm 0.5) \times 10^{-3}$	
Γ_{181}	$\pi^+\pi^-\pi^0\pi^0\eta$		$(2.4 \pm 0.5) \times 10^{-3}$	
Γ_{182}	$\rho^\pm\pi^\mp\pi^0\eta$		$(1.9 \pm 0.8) \times 10^{-3}$	
Γ_{183}	K^+K^-		$(3.06 \pm 0.05) \times 10^{-4}$	
Γ_{184}	$K^0_S K^0_L$		$(1.95 \pm 0.11) \times 10^{-4}$	S=2.4
Γ_{185}	$K^0_S K^0_S$		$< 4.7 \times 10^{-9}$	CL=90%
Γ_{186}	$K\overline{K}\pi$		$(6.1 \pm 1.0) \times 10^{-3}$	
Γ_{187}	$K^+K^-\pi^0$		$(2.88 \pm 0.12) \times 10^{-3}$	
Γ_{188}	$K^0_S K^\pm\pi^\mp$		$(5.3 \pm 0.5) \times 10^{-3}$	
Γ_{189}	$K^0_S K^0_L \pi^0$		$(2.06 \pm 0.26) \times 10^{-3}$	
Γ_{190}	$K^*(892)^0\overline{K}^0 +$ c.c. $\to K^0_S K^0_L \pi^0$		$(1.21 \pm 0.18) \times 10^{-3}$	
Γ_{191}	$K^*_2(1430)^0\overline{K}^0 +$ c.c. $\to K^0_S K^0_L \pi^0$		$(4.3 \pm 1.3) \times 10^{-4}$	
Γ_{192}	$K^+K^-\pi^+\pi^-$		$(7.0 \pm 1.0) \times 10^{-3}$	
Γ_{193}	$K^+K^-\pi^0\pi^0$		$(2.13 \pm 0.22) \times 10^{-3}$	
Γ_{194}	$K^+K^-\pi^0\pi^0\pi^0$		$(1.61 \pm 0.29) \times 10^{-3}$	
Γ_{195}	$K^0_S K^\pm\pi^\mp\pi^0\pi^0$		$(5.3 \pm 0.7) \times 10^{-3}$	
Γ_{196}	$K^0_S K^\pm\pi^\mp\pi^+\pi^-$		$(6.3 \pm 0.4) \times 10^{-3}$	
Γ_{197}	$K^0_S K^\pm\rho(770)^\pm\pi^0$		$(2.9 \pm 0.8) \times 10^{-3}$	
Γ_{198}	$K^0_S K^0_L \pi^+\pi^-$		$(3.8 \pm 0.6) \times 10^{-3}$	
Γ_{199}	$K^0_S K^0_L \pi^0\pi^0$		$(1.9 \pm 0.4) \times 10^{-3}$	
Γ_{200}	$K^0_S K^0_L \eta$		$(1.45 \pm 0.33) \times 10^{-3}$	
Γ_{201}	$K^0_S K^0_S \pi^+\pi^-$		$(1.68 \pm 0.19) \times 10^{-3}$	
Γ_{202}	$K^\mp K^0_S \pi^\pm\pi^0$		$(5.7 \pm 0.5) \times 10^{-3}$	
Γ_{203}	$K^0_S K^\pm\pi^\mp\rho(770)^0$		$(3.1 \pm 0.5) \times 10^{-3}$	
Γ_{204}	$K^+K^- 2(\pi^+\pi^-)$		$(3.1 \pm 1.3) \times 10^{-3}$	
Γ_{205}	$K^+K^-\pi^+\pi^-\eta$		$(4.7 \pm 0.7) \times 10^{-3}$	
Γ_{206}	$2(K^+K^-)$		$(7.2 \pm 0.8) \times 10^{-4}$	
Γ_{207}	$K^+K^- K^0_S K^0_S$		$(4.2 \pm 0.7) \times 10^{-4}$	
Γ_{208}	$K^0_S K^*(892)^0\pi^+\pi^-$		$(1.7 \pm 0.6) \times 10^{-3}$	
Γ_{209}	$K^0_S K^*(892)^0\pi^0\pi^0$		$(1.01 \pm 0.18) \times 10^{-3}$	
Γ_{210}	$K^\mp K^*(892)^\pm\pi^+\pi^-$		$(3.4 \pm 1.2) \times 10^{-3}$	
Γ_{211}	$K^*(892)^\pm K^*(892)^0\pi^\mp$		$(4.8 \pm 1.0) \times 10^{-3}$	
Γ_{212}	$K^\mp K^*(892)^\pm\pi^0\pi^0$		$(1.57 \pm 0.32) \times 10^{-3}$	
Γ_{213}	$K^*(892)^+ K^*(892)^-\pi^0$		(1.12 ± 0.23) %	
Γ_{214}	$p\overline{p}$		$(2.121 \pm 0.029) \times 10^{-3}$	
Γ_{215}	$p\overline{p}\pi^0$		$(1.19 \pm 0.08) \times 10^{-3}$	S=1.1
Γ_{216}	$p\overline{p}\pi^+\pi^-$		$(6.0 \pm 0.5) \times 10^{-3}$	S=1.3
Γ_{217}	$p\overline{p}\pi^+\pi^-\pi^0$	[d]	$(2.3 \pm 0.9) \times 10^{-3}$	S=1.9
Γ_{218}	$p\overline{p}\eta$		$(1.513 \pm 0.023) \times 10^{-3}$	
Γ_{219}	$p\overline{p}\rho$		$< 3.1 \times 10^{-4}$	CL=90%
Γ_{220}	$p\overline{p}\omega$		$(9.8 \pm 1.0) \times 10^{-4}$	S=1.3
Γ_{221}	$p\overline{p}\eta'(958)$		$(1.29 \pm 0.14) \times 10^{-4}$	S=2.0
Γ_{222}	$p\overline{p}a_0(980) \to p\overline{p}\pi^0\eta$		$(6.8 \pm 1.8) \times 10^{-5}$	
Γ_{223}	$p\overline{p}\phi$		$(5.19 \pm 0.33) \times 10^{-5}$	
Γ_{224}	$p\overline{n}\pi^-$		$(2.12 \pm 0.09) \times 10^{-3}$	
Γ_{225}	$n\overline{n}$		$(2.09 \pm 0.16) \times 10^{-3}$	
Γ_{226}	$n\overline{n}\pi^+\pi^-$		$(4 \pm 4) \times 10^{-3}$	
Γ_{227}	$nN(1440)$		seen	
Γ_{228}	$nN(1520)$		seen	
Γ_{229}	$nN(1535)$		seen	
Γ_{230}	$\Lambda\overline{\Lambda}$		$(1.88 \pm 0.08) \times 10^{-3}$	S=2.6
Γ_{231}	$\Lambda\overline{\Lambda}\pi^0$		$(3.8 \pm 0.4) \times 10^{-5}$	
Γ_{232}	$\Lambda\overline{\Lambda}\pi^+\pi^-$		$(4.3 \pm 1.0) \times 10^{-3}$	
Γ_{233}	$\Lambda\overline{\Lambda}\eta$		$(1.62 \pm 0.17) \times 10^{-4}$	
Γ_{234}	$\Lambda\overline{\Sigma}^+\pi^+ +$ c.c.	[b]	$(1.26 \pm 0.05) \times 10^{-3}$	S=1.2
Γ_{235}	$\Lambda\overline{\Sigma}^+\pi^- +$ c.c.		$(1.21 \pm 0.07) \times 10^{-3}$	S=1.8
Γ_{236}	$pK^-\overline{\Lambda} +$c.c.		$(8.6 \pm 1.1) \times 10^{-4}$	
Γ_{237}	$pK^-\overline{\Sigma}^0$		$(2.9 \pm 0.8) \times 10^{-4}$	
Γ_{238}	$pK^0_S\overline{\Sigma}^- +$c.c.		$(2.73 \pm 0.05) \times 10^{-4}$	
Γ_{239}	$\overline{\Lambda}nK^0_S +$ c.c.		$(6.5 \pm 1.1) \times 10^{-4}$	
Γ_{240}	$\Lambda\overline{\Sigma} +$ c.c.		$(2.83 \pm 0.23) \times 10^{-5}$	
Γ_{241}	$\Sigma^+\overline{\Sigma}^-$		$(1.07 \pm 0.04) \times 10^{-3}$	
Γ_{242}	$\Sigma^0\overline{\Sigma}^0$		$(1.172 \pm 0.032) \times 10^{-3}$	S=1.4
Γ_{243}	$\Sigma^+\overline{\Sigma}^-\eta$		$(6.3 \pm 0.4) \times 10^{-5}$	
Γ_{244}	$\Xi^-\overline{\Xi}^+$		$(9.7 \pm 0.8) \times 10^{-4}$	S=1.4
Γ_{245}	$\Xi^0\overline{\Sigma}^- K^+ +$ c.c		$(5.64 \pm 0.33) \times 10^{-5}$	
Γ_{246}	$\Xi^0\overline{\Sigma}^0 K^0_S +$ c.c		$(2.2 \pm 0.4) \times 10^{-5}$	
Γ_{247}	$\Xi^0\overline{\Lambda}K^0_S +$ c.c		$(3.76 \pm 0.27) \times 10^{-5}$	

Radiative decays

Γ_{248}	$\gamma\eta_c(1S)$		(1.82 ± 0.15) %	S=1.6
Γ_{249}	$\gamma\eta_c(1S) \to 3\gamma$		seen	
Γ_{250}	$\gamma\eta_c(1S) \to \gamma\eta\eta\eta'$		seen	
Γ_{251}	3γ		$(1.16 \pm 0.22) \times 10^{-5}$	
Γ_{252}	4γ		$< 9 \times 10^{-6}$	CL=90%
Γ_{253}	5γ		$< 1.5 \times 10^{-5}$	CL=90%
Γ_{254}	$\gamma\pi^0$		$(3.39 \pm 0.08) \times 10^{-5}$	
Γ_{255}	$\gamma\pi^0\pi^0$		$(1.15 \pm 0.05) \times 10^{-3}$	
Γ_{256}	$\gamma 2\pi^+ 2\pi^-$		$(2.8 \pm 0.5) \times 10^{-3}$	S=1.9
Γ_{257}	$\gamma f_2(1270) f_2(1270)$		$(9.5 \pm 1.7) \times 10^{-4}$	
Γ_{258}	$\gamma f_2(1270) f_2(1270)$ (non resonant)		$(8.2 \pm 1.9) \times 10^{-4}$	
Γ_{259}	$\gamma\pi^+\pi^- 2\pi^0$		$(8.3 \pm 3.1) \times 10^{-3}$	
Γ_{260}	$\gamma K^0_S K^0_S$		$(8.1 \pm 0.4) \times 10^{-4}$	
Γ_{261}	$\gamma(K\overline{K}\pi)$ $[J^{PC} = 0^{-+}]$		$(7 \pm 4) \times 10^{-4}$	S=2.1
Γ_{262}	$\gamma K^+K^-\pi^+\pi^-$		$(2.1 \pm 0.6) \times 10^{-3}$	
Γ_{263}	$\gamma K^*(892)\overline{K}^*(892)$		$(4.0 \pm 1.3) \times 10^{-3}$	
Γ_{264}	$\gamma\eta$		$(1.090 \pm 0.013) \times 10^{-3}$	
Γ_{265}	$\gamma\eta\pi^0$		$(2.14 \pm 0.31) \times 10^{-5}$	
Γ_{266}	$\gamma f_0(500) \to \gamma\pi\pi$			
Γ_{267}	$\gamma f_0(500) \to \gamma K\overline{K}$			
Γ_{268}	$\gamma f_0(500) \to \gamma\eta\eta$			
Γ_{269}	$\gamma a_0(980)^0 \to \gamma\eta\pi^0$		$< 2.5 \times 10^{-6}$	CL=95%
Γ_{270}	$\gamma a_2(1320)^0 \to \gamma\eta\pi^0$		$< 6.6 \times 10^{-6}$	CL=95%
Γ_{271}	$\gamma\eta\pi\pi$		$(6.1 \pm 1.0) \times 10^{-3}$	
Γ_{272}	$\gamma\eta_2(1870) \to \gamma\eta\pi^+\pi^-$		$(6.2 \pm 2.4) \times 10^{-4}$	
Γ_{273}	$\gamma\eta'(958)$		$(5.28 \pm 0.06) \times 10^{-3}$	S=1.3
Γ_{274}	$\gamma f_0(980) \to \gamma\pi\pi$			
Γ_{275}	$\gamma f_0(980) \to \gamma K\overline{K}$			
Γ_{276}	$\gamma\rho\rho$		$(4.5 \pm 0.8) \times 10^{-3}$	
Γ_{277}	$\gamma\rho\omega$		$< 5.4 \times 10^{-4}$	CL=90%
Γ_{278}	$\gamma\rho\phi$		$< 8.8 \times 10^{-5}$	CL=90%
Γ_{279}	$\gamma\omega\omega$		$(1.61 \pm 0.33) \times 10^{-3}$	
Γ_{280}	$\gamma\phi\phi$		$(4.0 \pm 1.2) \times 10^{-4}$	S=2.1
Γ_{281}	$\gamma\eta(1405/1475) \to \gamma K\overline{K}\pi$		$(2.8 \pm 0.6) \times 10^{-3}$	S=1.6
Γ_{282}	$\gamma\eta(1405/1475) \to \gamma\gamma\rho^0$		$(7.8 \pm 2.0) \times 10^{-5}$	S=1.8
Γ_{283}	$\gamma\eta(1405/1475) \to \gamma\eta\pi^+\pi^-$		$(3.0 \pm 0.5) \times 10^{-4}$	
Γ_{284}	$\gamma\eta(1405/1475) \to \gamma\rho^0\rho^0$		$(1.7 \pm 0.4) \times 10^{-3}$	S=1.3
Γ_{285}	$\gamma\eta(1405/1475) \to \gamma\gamma\phi$		$(3.6 \pm 0.6) \times 10^{-6}$	
Γ_{286}	$\gamma\eta(1405) \to \gamma f_0(980)\pi^0 \to \gamma\pi^+\pi^-\pi^0$		$(1.50 \pm 0.16) \times 10^{-5}$	
Γ_{287}	$\gamma\eta(1405) \to \gamma f_0(980)\pi^0 \to \gamma\pi^0\pi^0\pi^0$		$(6.64 {}^{+1.10}_{-0.23}) \times 10^{-6}$	
Γ_{288}	$\gamma\eta(1405) \to \gamma\gamma\gamma$		$< 2.63 \times 10^{-6}$	CL=90%
Γ_{289}	$\gamma\eta(1475) \to \gamma\gamma\gamma$		$< 1.86 \times 10^{-6}$	CL=90%
Γ_{290}	$\gamma\eta(1760) \to \gamma\rho^0\rho^0$		$(1.3 \pm 0.9) \times 10^{-4}$	
Γ_{291}	$\gamma\eta(1760) \to \gamma\omega\omega$		$(1.98 \pm 0.33) \times 10^{-3}$	
Γ_{292}	$\gamma\eta(1760) \to \gamma\gamma\gamma$		$< 4.80 \times 10^{-6}$	CL=90%
Γ_{293}	$\gamma\eta(2225)$		$(3.14 {}^{+0.50}_{-0.19}) \times 10^{-4}$	
Γ_{294}	$\gamma f_2(1270)$		$(1.63 \pm 0.12) \times 10^{-3}$	S=1.3
Γ_{295}	$\gamma f_2(1270) \to \gamma K^0_S K^0_S$		$(2.58 {}^{+0.60}_{-0.22}) \times 10^{-5}$	
Γ_{296}	$\gamma f_1(1285)$		$(6.1 \pm 0.8) \times 10^{-4}$	

Int. J. Mod. Phys. A 2026.41. Downloaded from www.worldscientific.com
by UNIVERSITY OF CALIFORNIA @ BERKELEY on 09/16/26. Re-use and distribution is strictly not permitted, except for Open Access articles.

Γ_{297}	$\gamma f_1(1285) \to \gamma\gamma\phi$	$(2.9 \pm^{1.1}_{0.9}) \times 10^{-7}$	
Γ_{298}	$\gamma f_1(1285) \to \gamma\pi^0 f_0(980) \to \gamma\pi^0\pi^0\pi^0$	$(5.6 \pm^{0.9}_{3.1}) \times 10^{-7}$	
Γ_{299}	$\gamma f_1(1285) \to \gamma a_0(980)^0\pi^0 \to \gamma K^0_S K^0_S \pi^0$	$(8.6 \pm^{3.4}_{1.1}) \times 10^{-6}$	
Γ_{300}	$\gamma f_0(1370) \to \gamma\pi\pi$		
Γ_{301}	$\gamma f_0(1370) \to \gamma K\overline{K}$	$(4.2 \pm 1.5) \times 10^{-4}$	
Γ_{302}	$\gamma f_0(1370) \to \gamma K^0_S K^0_S$	$(1.1 \pm 0.4) \times 10^{-5}$	
Γ_{303}	$\gamma f_0(1370) \to \gamma\eta\eta$		
Γ_{304}	$\gamma f_0(1370) \to \gamma\eta\eta'$		
Γ_{305}	$\gamma f_1(1420) \to \gamma K\overline{K}\pi$	$(7.9 \pm 1.3) \times 10^{-4}$	
Γ_{306}	$\gamma f_1(1420) \to \gamma K^*(892)^0 K^0_S \to \gamma K^0_S K^0_S \pi^0$	$(7.2 \pm^{0.7}_{1.3}) \times 10^{-5}$	
Γ_{307}	$\gamma f_1(1420) \to \gamma a_0(980)^0\pi^0 \to \gamma K^0_S K^0_S \pi^0$	$(4.6 \pm^{2.4}_{2.0}) \times 10^{-6}$	
Γ_{308}	$\gamma f_1(1420) \to \gamma\gamma\phi$	$(5.5 \pm 1.9) \times 10^{-7}$	
Γ_{309}	$\gamma f_1(1420) \to \gamma\pi^0 f_0(980) \to \gamma\pi^0\pi^0\pi^0$	$(2.23 \pm^{0.26}_{1.20}) \times 10^{-6}$	
Γ_{310}	$\gamma f_0(1500) \to \gamma\pi\pi$	$(1.09 \pm 0.24) \times 10^{-4}$	
Γ_{311}	$\gamma f_0(1500) \to \gamma\eta\eta$	$(1.7 \pm^{0.6}_{1.4}) \times 10^{-5}$	
Γ_{312}	$\gamma f_0(1500) \to \gamma K^0_S K^0_S$	$(1.59 \pm^{0.24}_{0.60}) \times 10^{-5}$	
Γ_{313}	$\gamma f_0(1500) \to \gamma\eta\eta'$		
Γ_{314}	$\gamma f_1(1510) \to \gamma\eta\pi^+\pi^-$	$(4.5 \pm 1.2) \times 10^{-4}$	
Γ_{315}	$\gamma f_1(1510) \to \gamma\gamma\phi$	$(7.8 \pm^{3.5}_{3.1}) \times 10^{-7}$	
Γ_{316}	$\gamma f_1(1510) \to \gamma\pi^0 f_0(980) \to \gamma\pi^0\pi^0\pi^0$		
Γ_{317}	$\gamma f'_2(1525)$	$(5.7 \pm^{0.8}_{0.5}) \times 10^{-4}$	S=1.5
Γ_{318}	$\gamma f'_2(1525) \to \gamma K^0_S K^0_S$	$(8.0 \pm^{0.7}_{0.5}) \times 10^{-5}$	
Γ_{319}	$\gamma f'_2(1525) \to \gamma K^*(892)^0 K^0_S \to \gamma K^0_S K^0_S \pi^0$	$(9.5 \pm^{1.6}_{0.8}) \times 10^{-6}$	
Γ_{320}	$\gamma f'_2(1525) \to \gamma\eta\eta$	$(3.4 \pm 1.4) \times 10^{-5}$	
Γ_{321}	$\gamma f_2(1565) \to \gamma\eta\eta'$		
Γ_{322}	$\gamma f'_2(1525) \to \gamma\gamma\phi$	$(2.8 \pm^{0.9}_{0.6}) \times 10^{-6}$	
Γ_{323}	$\gamma f_2(1640) \to \gamma\omega\omega$	$(2.8 \pm 1.8) \times 10^{-4}$	
Γ_{324}	$\gamma f_0(1710) \to \gamma\pi\pi$	$(3.8 \pm 0.5) \times 10^{-4}$	
Γ_{325}	$\gamma f_0(1710) \to \gamma K\overline{K}$	$(9.5 \pm^{0.9}_{0.5}) \times 10^{-4}$	S=1.4
Γ_{326}	$\gamma f_0(1710) \to \gamma\omega\omega$	$(3.1 \pm 1.0) \times 10^{-4}$	
Γ_{327}	$\gamma f_0(1710) \to \gamma\eta\eta$	$(2.4 \pm^{1.2}_{0.7}) \times 10^{-4}$	
Γ_{328}	$\gamma f_0(1710) \to \gamma\eta\eta'$		
Γ_{329}	$\gamma f_0(1710) \to \gamma\omega\phi$	$(2.5 \pm 0.6) \times 10^{-4}$	
Γ_{330}	$\gamma f_0(1810) \to \gamma\pi\pi$		
Γ_{331}	$\gamma f_0(1810) \to \gamma K^0_S K^0_S$	$(1.11 \pm^{0.20}_{0.33}) \times 10^{-5}$	
Γ_{332}	$\gamma f_0(1810) \to \gamma K\overline{K}$		
Γ_{333}	$\gamma f_0(1810) \to \gamma\eta\eta$		
Γ_{334}	$\gamma f_0(1810) \to \gamma\eta\eta'$		
Γ_{335}	$\gamma f_0(1810) \to \gamma\omega\phi$		
Γ_{336}	$\gamma f_2(1810) \to \gamma\eta\eta$	$(5.4 \pm^{3.5}_{2.4}) \times 10^{-5}$	
Γ_{337}	$\gamma\eta_1(1855) \to \gamma\eta\eta'$	$(2.7 \pm^{0.4}_{0.5}) \times 10^{-6}$	
Γ_{338}	$\gamma f_2(1910) \to \gamma\omega\omega$	$(2.0 \pm 1.4) \times 10^{-4}$	
Γ_{339}	$\gamma f_2(1950) \to \gamma K^*(892)\overline{K}^*(892)$	$(7.0 \pm 2.2) \times 10^{-4}$	
Γ_{340}	$\gamma f_2(1950) \to \gamma\gamma\phi$	$(10.0 \pm^{3.5}_{2.2}) \times 10^{-6}$	
Γ_{341}	$\gamma f_2(2010) \to \gamma\eta\eta'$		
Γ_{342}	$\gamma f_2(2010) \to \gamma\gamma\phi$	$(4.6 \pm 1.5) \times 10^{-6}$	
Γ_{343}	$\gamma f_0(2020) \to \gamma\pi\pi$		
Γ_{344}	$\gamma f_0(2020) \to \gamma K\overline{K}$		
Γ_{345}	$\gamma f_0(2020) \to \gamma\eta\eta$		
Γ_{346}	$\gamma f_0(2020) \to \gamma\eta'\eta'$	$(2.63 \pm^{0.32}_{0.50}) \times 10^{-4}$	
Γ_{347}	$\gamma f_0(2020) \to \gamma\eta\eta'$		
Γ_{348}	$\gamma f_4(2050)$	$(2.7 \pm 0.7) \times 10^{-3}$	
Γ_{349}	$\gamma f_4(2050) \to \gamma\eta\eta'$		
Γ_{350}	$\gamma f_0(2100) \to \gamma\eta\eta$	$(1.13 \pm^{0.60}_{0.30}) \times 10^{-4}$	
Γ_{351}	$\gamma f_0(2100) \to \gamma K\overline{K}$		
Γ_{352}	$\gamma f_0(2100) \to \gamma\pi\pi$	$(6.2 \pm 1.0) \times 10^{-4}$	
Γ_{353}	$\gamma f_0(2200)$	seen	
Γ_{354}	$\gamma f_0(2200) \to \gamma K\overline{K}$	$(5.9 \pm 1.3) \times 10^{-4}$	
Γ_{355}	$\gamma f_0(2200) \to \gamma K^0_S K^0_S$	$(2.72 \pm^{0.19}_{0.50}) \times 10^{-4}$	
Γ_{356}	$\gamma f_0(2200) \to \gamma\pi\pi$		
Γ_{357}	$\gamma f_0(2200) \to \gamma\eta\eta$		
Γ_{358}	$\gamma f_0(2200) \to \gamma\gamma\phi$	$(2.0 \pm^{0.6}_{0.8}) \times 10^{-7}$	
Γ_{359}	$\gamma f_J(2220)$	seen	
Γ_{360}	$\gamma f_J(2220) \to \gamma\pi\pi$	$< 3.9 \times 10^{-5}$	CL=90%
Γ_{361}	$\gamma f_J(2220) \to \gamma K\overline{K}$	$< 4.1 \times 10^{-5}$	CL=90%
Γ_{362}	$\gamma f_J(2220) \to \gamma p\overline{p}$	$(1.5 \pm 0.8) \times 10^{-5}$	
Γ_{363}	$\gamma f_0(2330) \to \gamma K^0_S K^0_S$	$(4.9 \pm 0.7) \times 10^{-5}$	
Γ_{364}	$\gamma f_0(2330) \to \gamma\pi\pi$		
Γ_{365}	$\gamma f_0(2330) \to \gamma\eta\eta$		
Γ_{366}	$\gamma f_0(2330) \to \gamma\eta'\eta'$	$(6.1 \pm^{4.0}_{1.8}) \times 10^{-6}$	
Γ_{367}	$\gamma f_0(2330) \to \gamma\eta\eta'$		
Γ_{368}	$\gamma f_2(2340) \to \gamma\eta\eta$	$(5.6 \pm^{2.4}_{2.2}) \times 10^{-5}$	
Γ_{369}	$\gamma f_2(2340) \to \gamma K^0_S K^0_S$	$(5.5 \pm^{4.0}_{1.5}) \times 10^{-5}$	
Γ_{370}	$\gamma f_2(2340) \to \gamma\eta'\eta'$	$(8.7 \pm^{0.9}_{1.8}) \times 10^{-6}$	
Γ_{371}	$\gamma f_0(2470) \to \gamma\eta'\eta'$	$(8.2 \pm^{4.0}_{2.8}) \times 10^{-7}$	
Γ_{372}	$\gamma X(1835) \to \gamma\pi^+\pi^-\eta'$	$(2.7 \pm^{0.6}_{0.8}) \times 10^{-4}$	S=1.6
Γ_{373}	$\gamma X(1835) \to \gamma p\overline{p}$	$(7.7 \pm^{1.5}_{0.9}) \times 10^{-5}$	
Γ_{374}	$\gamma X(1835) \to \gamma K^0_S K^0_S \eta$	$(3.3 \pm^{2.0}_{1.3}) \times 10^{-5}$	
Γ_{375}	$\gamma X(1835) \to \gamma\gamma\phi(1020)$	$(3.4 \pm^{0.8}_{1.1}) \times 10^{-6}$	
Γ_{376}	$\gamma X(1835) \to \gamma\gamma\gamma$	$< 3.56 \times 10^{-6}$	CL=90%
Γ_{377}	$\gamma X(1835) \to \gamma 3(\pi^+\pi^-)$	$(2.4 \pm^{0.7}_{0.8}) \times 10^{-5}$	
Γ_{378}	$\gamma\eta(2370) \to \gamma K^+K^-\eta'$	$(1.8 \pm 0.7) \times 10^{-5}$	
Γ_{379}	$\gamma\eta(2370) \to \gamma K^0_S K^0_S \eta'$	$(1.2 \pm 0.5) \times 10^{-5}$	
Γ_{380}	$\gamma\eta(2370) \to \gamma\eta\eta\eta'$	$< 9.2 \times 10^{-6}$	CL=90%
Γ_{381}	$\gamma D^0 +$ c.c.	$< 9.1 \times 10^{-8}$	CL=90%
Γ_{382}	$\gamma p\overline{p}$	$(3.8 \pm 1.0) \times 10^{-4}$	
Γ_{383}	$\gamma p\overline{p}\pi^+\pi^-$	$< 7.9 \times 10^{-4}$	CL=90%
Γ_{384}	$\gamma\Lambda\overline{\Lambda}$	$< 1.3 \times 10^{-4}$	CL=90%
Γ_{385}	$\gamma A^0 \to \gamma$ invisible	[e] $< 1.7 \times 10^{-6}$	CL=90%
Γ_{386}	$\gamma A^0 \to \gamma\gamma\gamma$	$< 4.9 \times 10^{-7}$	CL=95%
Γ_{387}	$\gamma A^0 \to \gamma\mu^+\mu^-$	[f] $< 7.8 \times 10^{-7}$	CL=90%

Dalitz decays

Γ_{388}	$\pi^0 e^+ e^-$	$(8.1 \pm 0.5) \times 10^{-7}$	
Γ_{389}	$\eta e^+ e^-$	$(1.42 \pm 0.08) \times 10^{-5}$	
Γ_{390}	$\eta'(958) e^+ e^-$	$(6.59 \pm 0.18) \times 10^{-5}$	
Γ_{391}	$\eta(1405) e^+ e^- \to f_0(980)\pi^0 e^+ e^- \to \pi^+\pi^-\pi^0 e^+ e^-$	$(2.04 \pm 0.22) \times 10^{-7}$	
Γ_{392}	$X(1835) e^+ e^-,\ X \to \pi^+\pi^-\eta'$	$(3.58 \pm 0.25) \times 10^{-6}$	
Γ_{393}	$X(2120) e^+ e^-,\ X \to \pi^+\pi^-\eta'$	$(8.2 \pm 1.3) \times 10^{-7}$	
Γ_{394}	$\eta(2370) e^+ e^-,\ \eta \to \pi^+\pi^-\eta'$	$(1.08 \pm 0.17) \times 10^{-6}$	
Γ_{395}	$\eta U \to \eta e^+ e^-$	[g] $< 9.11 \times 10^{-7}$	CL=90%
Γ_{396}	$\eta'(958) U \to \eta'(958) e^+ e^-$	[g] $< 2.0 \times 10^{-7}$	CL=90%
Γ_{397}	$\phi e^+ e^-$	$< 1.2 \times 10^{-7}$	CL=90%

Weak decays

Γ_{398}	$D^- e^+ \nu_e +$ c.c.	$< 7.1 \times 10^{-8}$	CL=90%
Γ_{399}	$D^- \mu^+ \nu_\mu +$ c.c.	$< 5.6 \times 10^{-7}$	CL=90%
Γ_{400}	$\overline{D}^0 e^+ e^- +$ c.c.	$< 8.5 \times 10^{-8}$	CL=90%
Γ_{401}	$D^0 \mu^+ \mu^- +$ c.c.	$< 1.1 \times 10^{-7}$	CL=90%
Γ_{402}	$D^-_s e^+ \nu_e +$ c.c.	$< 1.3 \times 10^{-6}$	CL=90%
Γ_{403}	$D^{*-}_s e^+ \nu_e +$ c.c.	$< 1.8 \times 10^{-6}$	CL=90%
Γ_{404}	$D^- \pi^+ +$ c.c.	$< 7.0 \times 10^{-8}$	CL=90%
Γ_{405}	$D^- \rho^+ +$ c.c	$< 6.0 \times 10^{-7}$	CL=90%
Γ_{406}	$\overline{D}^0 \pi^0 +$ c.c	$< 4.7 \times 10^{-7}$	CL=90%
Γ_{407}	$\overline{D}^0 \overline{K}^0 +$ c.c.	$< 1.7 \times 10^{-4}$	CL=90%
Γ_{408}	$\overline{D}^0 \overline{K}^{*0} +$ c.c.	$< 2.5 \times 10^{-6}$	CL=90%
Γ_{409}	$\overline{D}^0 \eta +$ c.c	$< 6.8 \times 10^{-7}$	CL=90%
Γ_{410}	$\overline{D}^0 \rho^0 +$ c.c	$< 5.2 \times 10^{-7}$	CL=90%
Γ_{411}	$D^-_s \pi^+ +$ c.c.	$< 4.1 \times 10^{-7}$	CL=90%
Γ_{412}	$D^-_s \rho^+ +$ c.c.	$< 8.0 \times 10^{-7}$	CL=90%

Int. J. Mod. Phys. A 2026.41. Downloaded from www.worldscientific.com
by CALIFORNIA @ BERKELEY on 09/16/26. Re-use and distribution is strictly not permitted, except for Open Access articles.

Charge conjugation (C), Parity (P), Lepton Family number (LF) violating modes

Γ_{413}	$\gamma\gamma$	C	$<$ 2.7	$\times 10^{-7}$	CL=90%
Γ_{414}	$\gamma\phi$	C	$<$ 1.4	$\times 10^{-6}$	CL=90%
Γ_{415}	$e^{\pm}\mu^{\mp}$	LF	$<$ 1.6	$\times 10^{-7}$	CL=90%
Γ_{416}	$e^{\pm}\tau^{\mp}$	LF	$<$ 7.5	$\times 10^{-8}$	CL=90%
Γ_{417}	$\mu^{\pm}\tau^{\mp}$	LF	$<$ 2.0	$\times 10^{-6}$	CL=90%
Γ_{418}	$K^+K^+e^-e^-$ + c.c.	L	$<$ 2.1	$\times 10^{-9}$	CL=90%
Γ_{419}	pe^- + c.c.	L,B	$<$ 3.1	$\times 10^{-8}$	CL=90%
Γ_{420}	$\Lambda_c^+ e^-$+c.c.		$<$ 6.9	$\times 10^{-8}$	CL=90%

Other decays

Γ_{421}	invisible		$<$ 7	$\times 10^{-4}$	CL=90%
Γ_{422}	$\mu^+\mu^-X^0 \rightarrow \mu^+\mu^-$ + invisible				
Γ_{423}	ϕ + invisible$X$				

[a] For $E_\gamma > 100$ MeV.
[b] The value is for the sum of the charge states or particle/antiparticle states indicated.
[c] $\Theta(1540)$ is a hypothetical pentaquark state of 1.54 GeV/c^2 mass and a width of less than 25 MeV/c^2.
[d] Includes $p\overline{p}\pi^+\pi^-\gamma$ and excludes $p\overline{p}\eta$, $p\overline{p}\omega$, $p\overline{p}\eta'$.
[e] For a narrow state A with mass less than 960 MeV.
[f] For a narrow scalar or pseudoscalar A^0 with mass 0.21–3.0 GeV.
[g] For a dark photon U with mass between 100 and 2100 MeV.

FIT INFORMATION

A multiparticle fit to $\eta_c(1S)$, $J/\psi(1S)$, $\psi(2S)$, $h_c(1P)$, and $B^{\pm}$ with the total width, 10 combinations of partial widths obtained from integrated cross section, and 38 branching ratios uses 115 measurements to determine 19 parameters. The overall fit has a $\chi^2 = 215.4$ for 96 degrees of freedom.

$J/\psi(1S)$ PARTIAL WIDTHS

Γ(hadrons) — Γ_1

VALUE (keV)	DOCUMENT ID		TECN	COMMENT
81.37± 1.36±1.30	[1] ANASHIN	20	KEDR	e^+e^-
• • • We do not use the following data for averages, fits, limits, etc. • • •				
74.1 ± 8.1	BAI	95B	BES	e^+e^-
59 ±24	BALDINI-...	75	FRAG	e^+e^-
59 ±14	BOYARSKI	75	MRK1	e^+e^-
50 ±25	ESPOSITO	75B	FRAM	e^+e^-

[1] Based on the same dataset as ANASHIN 18A and correlated to the values reported there.

$\Gamma(e^+e^-)$ — Γ_5

VALUE (keV)	EVTS	DOCUMENT ID		TECN	COMMENT
5.53 ±0.10 OUR AVERAGE					
5.550±0.056±0.089		[1,2] ANASHIN	18A	KEDR	e^+e^-
5.36 $^{+0.29}_{-0.28}$		[3] HSUEH	92	RVUE	See Υ mini-review
• • • We do not use the following data for averages, fits, limits, etc. • • •					
5.58 ±0.05 ±0.08		[4] ABLIKIM	16Q	BES3	3.773 $e^+e^- \rightarrow \mu^+\mu^-\gamma$
5.71 ±0.16	13k	[5] ADAMS	06A	CLEO	$e^+e^- \rightarrow \mu^+\mu^-\gamma$
5.57 ±0.19	7.8k	[5] AUBERT	04	BABR	$e^+e^- \rightarrow \mu^+\mu^-\gamma$
5.14 ±0.39		BAI	95B	BES	e^+e^-
4.72 ±0.35		ALEXANDER	89	RVUE	See Υ mini-review
4.4 ±0.6		[3] BRANDELIK	79C	DASP	e^+e^-
4.6 ±0.8		[6] BALDINI-...	75	FRAG	e^+e^-
4.8 ±0.6		BOYARSKI	75	MRK1	e^+e^-
4.6 ±1.0		ESPOSITO	75B	FRAM	e^+e^-

[1] From the cross sections of $e^+e^- \rightarrow e^+e^-$ and $e^+e^- \rightarrow$ hadrons near the $J/\psi(1S)$ peak.
[2] Based on the same dataset as ANASHIN 20 and correlated to the values reported there.
[3] From a simultaneous fit to e^+e^-, $\mu^+\mu^-$, and hadronic channels assuming $\Gamma(e^+e^-) = \Gamma(\mu^+\mu^-)$.
[4] Using $B(J/\psi \rightarrow \mu^+\mu^-) = (5.973 \pm 0.007 \pm 0.037)\%$ from ABLIKIM 13R.
[5] Calculated by us from the reported values of $\Gamma(e^+e^-)\times B(\mu^+\mu^-)$ using $B(\mu^+\mu^-) = (5.93 \pm 0.06)\%$.
[6] Assuming equal partial widths for e^+e^- and $\mu^+\mu^-$.

$\Gamma(\mu^+\mu^-)$ — Γ_7

VALUE (keV)	DOCUMENT ID		TECN	COMMENT
• • • We do not use the following data for averages, fits, limits, etc. • • •				
5.13±0.52	BAI	95B	BES	e^+e^-
4.8 ±0.6	BOYARSKI	75	MRK1	e^+e^-
5 ±1	ESPOSITO	75B	FRAM	e^+e^-

$\Gamma(\gamma\gamma)$ — Γ_{413}

VALUE (eV)	CL%	DOCUMENT ID		TECN	COMMENT
<5.4	90	BRANDELIK	79C	DASP	e^+e^-

$J/\psi(1S)$ $\Gamma(i)\Gamma(e^+e^-)/\Gamma$(total)

This combination of a partial width with the partial width into e^+e^- and with the total width is obtained from the integrated cross section into channel(i) in the e^+e^- annihilation.

Γ(hadrons) $\times$ $\Gamma(e^+e^-)/\Gamma_{total}$ — $\Gamma_1\Gamma_5/\Gamma$

VALUE (keV)	DOCUMENT ID		TECN	COMMENT
• • • We do not use the following data for averages, fits, limits, etc. • • •				
4.884±0.048±0.078	[1,2] ANASHIN	18A	KEDR	e^+e^-
4 ±0.8	[3] BALDINI-...	75	FRAG	e^+e^-
3.9 ±0.8	[3] ESPOSITO	75B	FRAM	e^+e^-

[1] From the cross sections of $e^+e^- \rightarrow e^+e^-$ and $e^+e^- \rightarrow$ hadrons near the $J/\psi(1S)$ peak.
[2] Based on the same dataset as ANASHIN 20 and correlated to the values reported there.
[3] Data redundant with branching ratios or partial widths above.

$\Gamma(e^+e^-)$ $\times$ $\Gamma(e^+e^-)/\Gamma_{total}$ — $\Gamma_5\Gamma_5/\Gamma$

VALUE (eV)	DOCUMENT ID		TECN	COMMENT
• • • We do not use the following data for averages, fits, limits, etc. • • •				
333.1± 6.6±4.0	[1,2] ANASHIN	18A	KEDR	e^+e^-
332.3± 6.4±4.8	ANASHIN	10	KEDR	3.097 $e^+e^- \rightarrow e^+e^-$
350 ± 20	BRANDELIK	79C	DASP	e^+e^-
320 ± 70	[3] BALDINI-...	75	FRAG	e^+e^-
340 ± 90	[3] ESPOSITO	75B	FRAM	e^+e^-
360 ±100	[3] FORD	75	SPEC	e^+e^-

[1] From the cross sections of $e^+e^- \rightarrow e^+e^-$ and $e^+e^- \rightarrow$ hadrons near the $J/\psi(1S)$ peak.
[2] Based on the same dataset as ANASHIN 20 and correlated to the values reported there.
[3] Data redundant with branching ratios or partial widths above.

$\Gamma(\mu^+\mu^-)$ $\times$ $\Gamma(e^+e^-)/\Gamma_{total}$ — $\Gamma_7\Gamma_5/\Gamma$

VALUE (eV)	EVTS	DOCUMENT ID		TECN	COMMENT
333 ± 4 OUR AVERAGE					
333.4± 2.5±4.4		ABLIKIM	16Q	BES3	3.773 $e^+e^- \rightarrow \mu^+\mu^-\gamma$
331.8± 5.2±6.3		ANASHIN	10	KEDR	3.097 $e^+e^- \rightarrow \mu^+\mu^-$
338.4± 5.8±7.1	13k	ADAMS	06A	CLEO	$e^+e^- \rightarrow \mu^+\mu^-\gamma$
330.1± 7.7±7.3	7.8k	AUBERT	04	BABR	$e^+e^- \rightarrow \mu^+\mu^-\gamma$
• • • We do not use the following data for averages, fits, limits, etc. • • •					
510 ±90		DASP	75	DASP	e^+e^-
380 ±50		[1] ESPOSITO	75B	FRAM	e^+e^-

[1] Data redundant with branching ratios or partial widths above.

$\Gamma(\eta\pi^+\pi^-)$ $\times$ $\Gamma(e^+e^-)/\Gamma_{total}$ — $\Gamma_{16}\Gamma_5/\Gamma$

VALUE (eV)	EVTS	DOCUMENT ID		TECN	COMMENT
2.3 ±0.4 OUR AVERAGE					
2.34±0.43±0.16	49	LEES	18	BABR	$e^+e^- \rightarrow \eta\pi^+\pi^-\gamma$
2.22±0.96±0.02	9	[1] AUBERT	07AU	BABR	10.6 $e^+e^- \rightarrow \eta\pi^+\pi^-\gamma$

[1] AUBERT 07AU reports $[\Gamma(J/\psi(1S) \rightarrow \eta\pi^+\pi^-) \times \Gamma(J/\psi(1S) \rightarrow e^+e^-)/\Gamma_{total}] \times [B(\eta \rightarrow \pi^+\pi^-\pi^0)] = 0.51 \pm 0.22 \pm 0.03$ eV which we divide by our best (shown rounded) value $B(\eta \rightarrow \pi^+\pi^-\pi^0) = (23.02 \pm 0.25) \times 10^{-2}$. Our first error is their experiment's error and our second error is the systematic error from using our best (shown rounded) value.

$\Gamma(\eta\pi^+\pi^-\pi^0)$ $\times$ $\Gamma(e^+e^-)/\Gamma_{total}$ — $\Gamma_{18}\Gamma_5/\Gamma$

VALUE (eV)	EVTS	DOCUMENT ID		TECN	COMMENT
64.8±11.1±0.4	200	[1] LEES	21C	BABR	$e^+e^- \rightarrow \gamma_{ISR}(\pi^+\pi^-4\pi^0)$

[1] LEES 21C reports $[\Gamma(J/\psi(1S) \rightarrow \eta\pi^+\pi^-\pi^0) \times \Gamma(J/\psi(1S) \rightarrow e^+e^-)/\Gamma_{total}] \times [B(\eta \rightarrow 3\pi^0)] = 21.1 \pm 1.7 \pm 3.2$ eV which we divide by our best (shown rounded) value $B(\eta \rightarrow 3\pi^0) = (32.56 \pm 0.21) \times 10^{-2}$. Our first error is their experiment's error and our second error is the systematic error from using our best (shown rounded) value.

$\Gamma(\eta\pi^+\pi^-3\pi^0)$ $\times$ $\Gamma(e^+e^-)/\Gamma_{total}$ — $\Gamma_{19}\Gamma_5/\Gamma$

VALUE (eV)	EVTS	DOCUMENT ID		TECN	COMMENT
26.9±5.7±0.1	101	[1] LEES	21C	BABR	$e^+e^- \rightarrow \gamma_{ISR}(\pi^+\pi^-3\pi^0\gamma\gamma)$

[1] LEES 21C reports $[\Gamma(J/\psi(1S) \rightarrow \eta\pi^+\pi^-3\pi^0) \times \Gamma(J/\psi(1S) \rightarrow e^+e^-)/\Gamma_{total}] \times [B(\eta \rightarrow 2\gamma)] = 10.6 \pm 1.6 \pm 1.6$ eV which we divide by our best (shown rounded) value $B(\eta \rightarrow 2\gamma) = (39.36 \pm 0.18) \times 10^{-2}$. Our first error is their experiment's error and our second error is the systematic error from using our best (shown rounded) value.

$\Gamma(\eta K^+K^-)$ $\times$ $\Gamma(e^+e^-)/\Gamma_{total}$ — $\Gamma_{22}\Gamma_5/\Gamma$

VALUE (eV)	DOCUMENT ID		TECN	COMMENT
4.76±1.64±0.03	[1] LEES	23	BABR	$e^+e^- \rightarrow \gamma_{ISR}$hadrons

[1] LEES 23 reports $[\Gamma(J/\psi(1S) \rightarrow \eta K^+K^-) \times \Gamma(J/\psi(1S) \rightarrow e^+e^-)/\Gamma_{total}] \times [B(\eta \rightarrow 3\pi^0)] = 1.55 \pm 0.51 \pm 0.16$ eV which we divide by our best (shown rounded) value $B(\eta \rightarrow 3\pi^0) = (32.56 \pm 0.21) \times 10^{-2}$. Our first error is their experiment's error and our second error is the systematic error from using our best (shown rounded) value.

$\Gamma(\eta K^{\pm}K^0_S\pi^{\mp})$ $\times$ $\Gamma(e^+e^-)/\Gamma_{total}$ — $\Gamma_{23}\Gamma_5/\Gamma$

VALUE (eV)	EVTS	DOCUMENT ID		TECN	COMMENT
7.3±1.4±0.4	44	LEES	17D	BABR	$e^+e^- \rightarrow K^0_S K^{\pm}\pi^{\mp}\pi^0\gamma$

Int. J. Mod. Phys. A 2026.41. Downloaded from www.worldscientific.com
by UNIVERSITY OF CALIFORNIA @ BERKELEY on 09/16/26. Re-use and distribution is strictly not permitted, except for Open Access articles.

$\Gamma(\rho^\pm\pi^\mp\pi^+\pi^-2\pi^0) \times \Gamma(e^+e^-)/\Gamma_{total}$ — $\Gamma_{26}\Gamma_5/\Gamma$

VALUE (eV)	EVTS	DOCUMENT ID		TECN	COMMENT
155±26±36	14k	LEES	21	BABR	$10.6\ e^+e^- \to 2(\pi^+\pi^-)3\pi^0\gamma$

$\Gamma(\rho^+\rho^-\pi^+\pi^-\pi^0) \times \Gamma(e^+e^-)/\Gamma_{total}$ — $\Gamma_{27}\Gamma_5/\Gamma$

VALUE (eV)	EVTS	DOCUMENT ID		TECN	COMMENT
32±13±15	14k	LEES	21	BABR	$10.6\ e^+e^- \to 2(\pi^+\pi^-)3\pi^0\gamma$

$\Gamma(\rho^\mp K^\pm K^0_S) \times \Gamma(e^+e^-)/\Gamma_{total}$ — $\Gamma_{29}\Gamma_5/\Gamma$

VALUE (eV)	EVTS	DOCUMENT ID		TECN	COMMENT
10.4±1.0±1.9	130	LEES	17D	BABR	$e^+e^- \to K^0_S K^\pm\pi^\mp\pi^0\gamma$

$\Gamma(\omega\pi^+\pi^-) \times \Gamma(e^+e^-)/\Gamma_{total}$ — $\Gamma_{44}\Gamma_5/\Gamma$

VALUE (eV)	EVTS	DOCUMENT ID		TECN	COMMENT
53.6±5.0±0.4	788	[1] AUBERT	07AU	BABR	$10.6\ e^+e^- \to \omega\pi^+\pi^-\gamma$

[1] AUBERT 07AU reports $[\Gamma(J/\psi(1S) \to \omega\pi^+\pi^-) \times \Gamma(J/\psi(1S) \to e^+e^-)/\Gamma_{total}] \times [B(\omega(782) \to \pi^+\pi^-\pi^0)] = 47.8 \pm 3.1 \pm 3.2$ eV which we divide by our best (shown rounded) value $B(\omega(782) \to \pi^+\pi^-\pi^0) = (89.2 \pm 0.7) \times 10^{-2}$. Our first error is their experiment's error and our second error is the systematic error from using our best (shown rounded) value.

$\Gamma(\omega\pi^0\pi^0) \times \Gamma(e^+e^-)/\Gamma_{total}$ — $\Gamma_{45}\Gamma_5/\Gamma$

VALUE (eV)	EVTS	DOCUMENT ID		TECN	COMMENT
27.8±3.5±0.2	398	[1] LEES	18E	BABR	$10.6\ e^+e^- \to \pi^+\pi^-3\pi^0\gamma$

[1] LEES 18E reports $[\Gamma(J/\psi(1S) \to \omega\pi^0\pi^0) \times \Gamma(J/\psi(1S) \to e^+e^-)/\Gamma_{total}] \times [B(\omega(782) \to \pi^+\pi^-\pi^0)] = 24.8 \pm 1.8 \pm 2.5$ eV which we divide by our best (shown rounded) value $B(\omega(782) \to \pi^+\pi^-\pi^0) = (89.2 \pm 0.7) \times 10^{-2}$. Our first error is their experiment's error and our second error is the systematic error from using our best (shown rounded) value.

$\Gamma(\omega 3\pi^0) \times \Gamma(e^+e^-)/\Gamma_{total}$ — $\Gamma_{46}\Gamma_5/\Gamma$

VALUE (eV)	EVTS	DOCUMENT ID		TECN	COMMENT
10.5±3.1±0.1	89	[1] LEES	21C	BABR	$e^+e^- \to \gamma_{ISR}(\pi^+\pi^-4\pi^0)$

[1] LEES 21C reports $[\Gamma(J/\psi(1S) \to \omega 3\pi^0) \times \Gamma(J/\psi(1S) \to e^+e^-)/\Gamma_{total}] \times [B(\omega(782) \to \pi^+\pi^-\pi^0)] = 9.4 \pm 2.3 \pm 1.5$ eV which we divide by our best (shown rounded) value $B(\omega(782) \to \pi^+\pi^-\pi^0) = (89.2 \pm 0.7) \times 10^{-2}$. Our first error is their experiment's error and our second error is the systematic error from using our best (shown rounded) value.

$\Gamma(\omega\eta) \times \Gamma(e^+e^-)/\Gamma_{total}$ — $\Gamma_{48}\Gamma_5/\Gamma$

VALUE (eV)	DOCUMENT ID		TECN	COMMENT
16.9±7.6±0.2	[1] LEES	21C	BABR	$e^+e^- \to \gamma_{ISR}(\pi^+\pi^-4\pi^0)$

[1] Different final state as in AUBERT 06. LEES 21C reports $[\Gamma(J/\psi(1S) \to \omega\eta) \times \Gamma(J/\psi(1S) \to e^+e^-)/\Gamma_{total}] \times [B(\eta \to 3\pi^0)] \times [B(\omega(782) \to \pi^+\pi^-\pi^0)] = 4.9 \pm 2.1 \pm 0.7$ eV which we divide by our best (shown rounded) values $B(\eta \to 3\pi^0) = (32.56 \pm 0.21) \times 10^{-2}$, $B(\omega(782) \to \pi^+\pi^-\pi^0) = (89.2 \pm 0.7) \times 10^{-2}$. Our first error is their experiment's error and our second error is the systematic error from using our best (shown rounded) values.

$\Gamma(\omega\pi^+\pi^-\pi^0) \times \Gamma(e^+e^-)/\Gamma_{total}$ — $\Gamma_{49}\Gamma_5/\Gamma$

VALUE (10^{-2} keV)	EVTS	DOCUMENT ID		TECN	COMMENT
2.2±0.3±0.2	170	AUBERT	06D	BABR	$10.6\ e^+e^- \to \omega\pi^+\pi^-\pi^0\gamma$

$\Gamma(\omega\pi^0\eta) \times \Gamma(e^+e^-)/\Gamma_{total}$ — $\Gamma_{50}\Gamma_5/\Gamma$

VALUE (eV)	EVTS	DOCUMENT ID		TECN	COMMENT
1.90±0.96±0.01	27	[1] LEES	18E	BABR	$10.6\ e^+e^- \to \pi^+\pi^-\pi^0\pi^0\eta\gamma$

[1] LEES 18E reports $[\Gamma(J/\psi(1S) \to \omega\pi^0\eta) \times \Gamma(J/\psi(1S) \to e^+e^-)/\Gamma_{total}] \times [B(\omega(782) \to \pi^+\pi^-\pi^0)] = 1.7 \pm 0.8 \pm 0.3$ eV which we divide by our best (shown rounded) value $B(\omega(782) \to \pi^+\pi^-\pi^0) = (89.2 \pm 0.7) \times 10^{-2}$. Our first error is their experiment's error and our second error is the systematic error from using our best (shown rounded) value.

$\Gamma(\omega\pi^+\pi^-2\pi^0) \times \Gamma(e^+e^-)/\Gamma_{total}$ — $\Gamma_{52}\Gamma_5/\Gamma$

VALUE (eV)	EVTS	DOCUMENT ID		TECN	COMMENT
185±30±1	14k	[1] LEES	21	BABR	$10.6\ e^+e^- \to 2(\pi^+\pi^-)3\pi^0\gamma$

[1] LEES 21 reports $[\Gamma(J/\psi(1S) \to \omega\pi^+\pi^-2\pi^0) \times \Gamma(J/\psi(1S) \to e^+e^-)/\Gamma_{total}] \times [B(\omega(782) \to \pi^+\pi^-\pi^0)] = 165 \pm 9 \pm 25$ eV which we divide by our best (shown rounded) value $B(\omega(782) \to \pi^+\pi^-\pi^0) = (89.2 \pm 0.7) \times 10^{-2}$. Our first error is their experiment's error and our second error is the systematic error from using our best (shown rounded) value.

$\Gamma(\omega K\overline{K}) \times \Gamma(e^+e^-)/\Gamma_{total}$ — $\Gamma_{64}\Gamma_5/\Gamma$

VALUE (eV)	EVTS	DOCUMENT ID		TECN	COMMENT
3.70±1.98±0.03	24	[1] AUBERT	07AU	BABR	$10.6\ e^+e^- \to \omega K^+K^-\gamma$

[1] AUBERT 07AU reports $[\Gamma(J/\psi(1S) \to \omega K\overline{K}) \times \Gamma(J/\psi(1S) \to e^+e^-)/\Gamma_{total}] \times [B(\omega(782) \to \pi^+\pi^-\pi^0)] = 3.3 \pm 1.3 \pm 1.2$ eV which we divide by our best (shown rounded) value $B(\omega(782) \to \pi^+\pi^-\pi^0) = (89.2 \pm 0.7) \times 10^{-2}$. Our first error is their experiment's error and our second error is the systematic error from using our best (shown rounded) value.

$\Gamma(K^+K^*(892)^- + c.c.) \times \Gamma(e^+e^-)/\Gamma_{total}$ — $\Gamma_{73}\Gamma_5/\Gamma$

VALUE (eV)	DOCUMENT ID		TECN	COMMENT
29.0±1.7±1.3	AUBERT	08S	BABR	$10.6\ e^+e^- \to K^+K^*(892)^-\gamma$

$\Gamma(K^+K^*(892)^- + c.c. \to K^+K^-\pi^0) \times \Gamma(e^+e^-)/\Gamma_{total}$ — $\Gamma_{74}\Gamma_5/\Gamma$

VALUE (eV)	EVTS	DOCUMENT ID		TECN	COMMENT
10.96±0.85±0.70	155	AUBERT	08S	BABR	$10.6\ e^+e^- \to K^+K^-\pi^0\gamma$

$\Gamma(K^+K^*(892)^- + c.c. \to K^0K^\pm\pi^\mp + c.c.) \times \Gamma(e^+e^-)/\Gamma_{total}$ — $\Gamma_{75}\Gamma_5/\Gamma$

VALUE (eV)	EVTS	DOCUMENT ID		TECN	COMMENT
16.76±1.70±1.00	89	AUBERT	08S	BABR	$10.6\ e^+e^- \to K^0_S K^\pm\pi^\mp\gamma$

$\Gamma(K^0\overline{K}^*(892)^0 + c.c.) \times \Gamma(e^+e^-)/\Gamma_{total}$ — $\Gamma_{76}\Gamma_5/\Gamma$

VALUE (eV)	DOCUMENT ID		TECN	COMMENT
26.6±2.5±1.5	AUBERT	08S	BABR	$10.6\ e^+e^- \to K^0\overline{K}^*(892)^0\gamma$

$\Gamma(K^0\overline{K}^*(892)^0 + c.c. \to K^0K^\pm\pi^\mp + c.c.) \times \Gamma(e^+e^-)/\Gamma_{total}$ — $\Gamma_{77}\Gamma_5/\Gamma$

VALUE (eV)	EVTS	DOCUMENT ID		TECN	COMMENT
17.70±1.70±1.00	94	AUBERT	08S	BABR	$10.6\ e^+e^- \to K^0_S K^\pm\pi^\mp\gamma$

$\Gamma(\overline{K}^*(892)^0K^+\pi^- + c.c.) \times \Gamma(e^+e^-)/\Gamma_{total}$ — $\Gamma_{78}\Gamma_5/\Gamma$

VALUE (eV)	EVTS	DOCUMENT ID		TECN	COMMENT
42.6±4.8±7.2	99	[1] LEES	17D	BABR	$e^+e^- \to K^0_S K^\pm\pi^\mp\pi^0\gamma$

[1] Dividing by 1/6 to account for $B(K^*(892)^0 \to K^0_S\pi^0)$=1/6.

$\Gamma(K^*(892)^\pm K^\mp\pi^0) \times \Gamma(e^+e^-)/\Gamma_{total}$ — $\Gamma_{79}\Gamma_5/\Gamma$

VALUE (eV)	EVTS	DOCUMENT ID		TECN	COMMENT
22.8±2.8±6.8	80	[1] LEES	17D	BABR	$e^+e^- \to K^0_S K^\pm\pi^\mp\pi^0\gamma$

[1] Dividing by 1/4 to account for $B(K^*(892)^\pm \to K^0_S\pi^\pm) = 1/4$.

$\Gamma(K^*(892)^+K^0_S\pi^- + c.c.) \times \Gamma(e^+e^-)/\Gamma_{total}$ — $\Gamma_{80}\Gamma_5/\Gamma$

VALUE (eV)	EVTS	DOCUMENT ID		TECN	COMMENT
11.0±2.8 OUR AVERAGE					
9.2±1.2±3.2	64	[1] LEES	17D	BABR	$e^+e^- \to K^0_S K^\pm\pi^\mp\pi^0\gamma$
14.8±4.8±1.2	53	[2] LEES	14H	BABR	$e^+e^- \to \pi^+\pi^-K^0_S K^0_S\gamma$

[1] Dividing by 1/2 to take into account $B(K^*(892)^\pm \to K^\pm\pi^\mp) = 1/2$.
[2] Dividing by 1/4 to take into account $B(K^*(892) \to K^0_S\pi) = 1/4$.

$\Gamma(K^*(892)^+K^0_S\pi^- + c.c. \to K^0_S K^0_S\pi^+\pi^-) \times \Gamma(e^+e^-)/\Gamma_{total}$ — $\Gamma_{81}\Gamma_5/\Gamma$

VALUE (eV)	EVTS	DOCUMENT ID		TECN	COMMENT
3.7±1.2±0.3	53	LEES	14H	BABR	$e^+e^- \to \pi^+\pi^-K^0_S K^0_S\gamma$

$\Gamma(K^*(892)^0K^0_S\pi^0) \times \Gamma(e^+e^-)/\Gamma_{total}$ — $\Gamma_{84}\Gamma_5/\Gamma$

VALUE (eV)	EVTS	DOCUMENT ID		TECN	COMMENT
3.60±0.75±2.25	34	[1] LEES	17D	BABR	$e^+e^- \to K^0_S K^\pm\pi^\mp\pi^0\gamma$

[1] Dividing by 2/3 to account for $B(K^*(892)^0 \to K^+\pi^-) = 2/3$.

$\Gamma(K^*(892)^0\overline{K}^*(892)^0) \times \Gamma(e^+e^-)/\Gamma_{total}$ — $\Gamma_{86}\Gamma_5/\Gamma$

VALUE (eV)	EVTS	DOCUMENT ID		TECN	COMMENT
1.28±0.34±0.07	47±12	[1] LEES	12F	BABR	$10.6\ e^+e^- \to \pi^+\pi^-K^+K^-\gamma$
• • • We do not use the following data for averages, fits, limits, etc. • • •					
1.28±0.40±0.11	25 ± 8	[1,2] AUBERT	07AK	BABR	$10.6\ e^+e^- \to \pi^+\pi^-K^+K^-\gamma$

[1] Dividing by $(2/3)^2$ to take twice into account that $B(K^{*0} \to K^+\pi^-) = 2/3\ B(K^{*0} \to K\pi)$.
[2] Superseded by LEES 12F.

$\Gamma(K^*(892)^\pm K^*(892)^\mp) \times \Gamma(e^+e^-)/\Gamma_{total}$ — $\Gamma_{87}\Gamma_5/\Gamma$

VALUE (eV)	EVTS	DOCUMENT ID		TECN	COMMENT
0.80±0.48±0.32	1 ± 5	[1] LEES	14H	BABR	$e^+e^- \to \pi^+\pi^-K^0_S K^0_S\gamma$

[1] Dividing by $(1/4)^2$ to take twice into account $B(K^*(892) \to K^0_S\pi) = 1/4$.

$\Gamma(K^*_2(1430)^+K^0_S\pi^- + c.c.) \times \Gamma(e^+e^-)/\Gamma_{total}$ — $\Gamma_{98}\Gamma_5/\Gamma$

VALUE (eV)	EVTS	DOCUMENT ID		TECN	COMMENT
20.1±9.8±0.5	35	[1,2] LEES	14H	BABR	$e^+e^- \to \pi^+\pi^-K^0_S K^0_S\gamma$

[1] Dividing by 1/4 to take into account $B(K^*(1430) \to K^0_S\pi) = 1/4\ B(K^*(1430) \to K\pi)$.
[2] LEES 14H reports $[\Gamma(J/\psi(1S) \to K^*_2(1430)^+K^0_S\pi^- + c.c.) \times \Gamma(J/\psi(1S) \to e^+e^-)/\Gamma_{total}] \times [B(K^*_2(1430) \to K\pi)] = 10.0 \pm 4.8 \pm 0.8$ eV which we divide by our best (shown rounded) value $B(K^*_2(1430) \to K\pi) = (49.9 \pm 1.2) \times 10^{-2}$. Our first error is their experiment's error and our second error is the systematic error from using our best (shown rounded) value.

$\Gamma(\overline{K}^*_2(1430)^0K^*(892)^0 + c.c.) \times \Gamma(e^+e^-)/\Gamma_{total}$ — $\Gamma_{99}\Gamma_5/\Gamma$

VALUE (eV)	EVTS	DOCUMENT ID		TECN	COMMENT
25.8±1.4±0.6	710	[1,2,3] LEES	12F	BABR	$10.6\ e^+e^- \to \pi^+\pi^-K^+K^-\gamma$
• • • We do not use the following data for averages, fits, limits, etc. • • •					
33 ±4 ±1	317	[2,4] AUBERT	07AK	BABR	$10.6\ e^+e^- \to \pi^+\pi^-K^+K^-\gamma$

[1] LEES 12F reports $[\Gamma(J/\psi(1S) \to \overline{K}^*_2(1430)^0K^*(892)^0 + c.c.) \times \Gamma(J/\psi(1S) \to e^+e^-)/\Gamma_{total}] \times [B(K^*_2(1430) \to K\pi)] = 12.89 \pm 0.54 \pm 0.41$ eV which we divide by our best (shown rounded) value $B(K^*_2(1430) \to K\pi) = (49.9 \pm 1.2) \times 10^{-2}$.

Int. J. Mod. Phys. A 2026.41. Downloaded from www.worldscientific.com
by LIFORNIA @ BERKELEY on 09/16/26. Re-use and distribution is strictly not permitted, except for Open Access articles.

Our first error is their experiment's error and our second error is the systematic error from using our best (shown rounded) value.

[2] Dividing by 2/3 to take into account that $B(K^{*0} \to K^+\pi^-) = 2/3\ B(K^{*0} \to K\pi)$.

[3] The $K_2^*(1430)$ cannot be distinguished from the $K_0^*(1430)$.

[4] Superseded by LEES 12F. AUBERT 07AK reports $[\Gamma(J/\psi(1S) \to \overline{K}_2^*(1430)^0 K^*(892)^0 + \text{c.c.}) \times \Gamma(J/\psi(1S) \to e^+e^-)/\Gamma_{total}] \times [B(K_2^*(1430) \to K\pi)] = 16.4 \pm 1.1 \pm 1.4$ eV which we divide by our best (shown rounded) value $B(K_2^*(1430) \to K\pi) = (49.9 \pm 1.2) \times 10^{-2}$. Our first error is their experiment's error and our second error is the systematic error from using our best (shown rounded) value.

$\Gamma(K_2^*(1430)^- K^*(892)^+ + \text{c.c.}) \times \Gamma(e^+e^-)/\Gamma_{total}$ — $\Gamma_{100}\Gamma_5/\Gamma$

VALUE (eV)	EVTS	DOCUMENT ID		TECN	COMMENT
18.6±16.1±0.4	8 ± 8	[1,2] LEES	14H	BABR	$e^+e^- \to \pi^+\pi^- K_S^0 K_S^0 \gamma$

[1] Dividing by $(1/4)^2$ to take into account $B(K^*(892) \to K_S^0\pi) = 1/4$ and $B(K^*(1430) \to K_S^0\pi) = 1/4\ B(K^*(1430) \to K\pi)$.

[2] LEES 14H reports $[\Gamma(J/\psi(1S) \to K_2^*(1430)^- K^*(892)^+ + \text{c.c.}) \times \Gamma(J/\psi(1S) \to e^+e^-)/\Gamma_{total}] \times [B(K_2^*(1430) \to K\pi)] = 9.28 \pm 8.0 \pm 0.32$ eV which we divide by our best (shown rounded) value $B(K_2^*(1430) \to K\pi) = (49.9 \pm 1.2) \times 10^{-2}$. Our first error is their experiment's error and our second error is the systematic error from using our best (shown rounded) value.

$\Gamma(K_2^*(1430)^- K^*(892)^+ + \text{c.c.} \to K^*(892)^+ K_S^0\pi^- + \text{c.c.}) \times \Gamma(e^+e^-)/\Gamma_{total}$ — $\Gamma_{101}\Gamma_5/\Gamma$

VALUE (eV)	EVTS	DOCUMENT ID		TECN	COMMENT
2.32±2.00±0.08	8 ± 8	[1] LEES	14H	BABR	$e^+e^- \to \pi^+\pi^- K_S^0 K_S^0 \gamma$

[1] Dividing by 1/4 to take into account $B(K^*(892) \to K_S^0\pi) = 1/4$.

$\Gamma(\overline{K}_2(1770)^0 K^*(892)^0 + \text{c.c.} \to K^*(892)^0 K^-\pi^+ + \text{c.c.}) \times \Gamma(e^+e^-)/\Gamma_{total}$ — $\Gamma_{103}\Gamma_5/\Gamma$

VALUE (eV)	EVTS	DOCUMENT ID		TECN	COMMENT
3.8±0.4±0.3	110 ± 14	[1] AUBERT	07AK	BABR	$10.6\ e^+e^- \to \pi^+\pi^- K^+K^-\gamma$

[1] Dividing by 2/3 to take into account that $B(K^{*0} \to K^+\pi^-) = 2/3$.

$\Gamma(\phi\pi^+\pi^-) \times \Gamma(e^+e^-)/\Gamma_{total}$ — $\Gamma_{110}\Gamma_5/\Gamma$

VALUE (eV)	EVTS	DOCUMENT ID		TECN	COMMENT
4.39±0.34 OUR AVERAGE					
4.37±0.48±0.05	181	[1] LEES	12F	BABR	$10.6\ e^+e^- \to K^+K^-\pi^+\pi^-\gamma$
4.42±0.47±0.05	254 ± 23	[2] SHEN	09	BELL	$10.6\ e^+e^- \to K^+K^-\pi^+\pi^-\gamma$
• • • We do not use the following data for averages, fits, limits, etc. • • •					
5.2 ±0.7 ±0.1	103	[3] AUBERT,BE	06D	BABR	$10.6\ e^+e^- \to K^+K^-\pi^+\pi^-\gamma$

[1] LEES 12F reports $[\Gamma(J/\psi(1S) \to \phi\pi^+\pi^-) \times \Gamma(J/\psi(1S) \to e^+e^-)/\Gamma_{total}] \times [B(\phi(1020) \to K^+K^-)] = 2.19 \pm 0.23 \pm 0.07$ eV which we divide by our best (shown rounded) value $B(\phi(1020) \to K^+K^-) = (50.1 \pm 0.6) \times 10^{-2}$. Our first error is their experiment's error and our second error is the systematic error from using our best (shown rounded) value.

[2] SHEN 09 reports $4.50 \pm 0.41 \pm 0.26$ eV from a measurement of $[\Gamma(J/\psi(1S) \to \phi\pi^+\pi^-) \times \Gamma(J/\psi(1S) \to e^+e^-)/\Gamma_{total}] \times [B(\phi(1020) \to K^+K^-)]$ assuming $B(\phi(1020) \to K^+K^-) = (49.2 \pm 0.6) \times 10^{-2}$, which we rescale to our best (shown rounded) value $B(\phi(1020) \to K^+K^-) = (50.1 \pm 0.6) \times 10^{-2}$. Our first error is their experiment's error and our second error is the systematic error from using our best (shown rounded) value.

[3] Superseded by LEES 12F. AUBERT,BE 06D reports $[\Gamma(J/\psi(1S) \to \phi\pi^+\pi^-) \times \Gamma(J/\psi(1S) \to e^+e^-)/\Gamma_{total}] \times [B(\phi(1020) \to K^+K^-)] = 2.61 \pm 0.30 \pm 0.18$ eV which we divide by our best (shown rounded) value $B(\phi(1020) \to K^+K^-) = (50.1 \pm 0.6) \times 10^{-2}$. Our first error is their experiment's error and our second error is the systematic error from using our best (shown rounded) value.

$\Gamma(\phi\pi^0\pi^0) \times \Gamma(e^+e^-)/\Gamma_{total}$ — $\Gamma_{111}\Gamma_5/\Gamma$

VALUE (eV)	EVTS	DOCUMENT ID		TECN	COMMENT
2.71±0.56±0.03	45	[1] LEES	12F	BABR	$10.6\ e^+e^- \to K^+K^-\pi^0\pi^0\gamma$
• • • We do not use the following data for averages, fits, limits, etc. • • •					
3.07±0.86±0.03	23	[2] AUBERT,BE	06D	BABR	$10.6\ e^+e^- \to K^+K^-\pi^0\pi^0\gamma$

[1] LEES 12F reports $[\Gamma(J/\psi(1S) \to \phi\pi^0\pi^0) \times \Gamma(J/\psi(1S) \to e^+e^-)/\Gamma_{total}] \times [B(\phi(1020) \to K^+K^-)] = 1.36 \pm 0.27 \pm 0.07$ eV which we divide by our best (shown rounded) value $B(\phi(1020) \to K^+K^-) = (50.1 \pm 0.6) \times 10^{-2}$. Our first error is their experiment's error and our second error is the systematic error from using our best (shown rounded) value.

[2] Superseded by LEES 12F. AUBERT,BE 06D reports $[\Gamma(J/\psi(1S) \to \phi\pi^0\pi^0) \times \Gamma(J/\psi(1S) \to e^+e^-)/\Gamma_{total}] \times [B(\phi(1020) \to K^+K^-)] = 1.54 \pm 0.40 \pm 0.16$ eV which we divide by our best (shown rounded) value $B(\phi(1020) \to K^+K^-) = (50.1 \pm 0.6) \times 10^{-2}$. Our first error is their experiment's error and our second error is the systematic error from using our best (shown rounded) value.

$\Gamma(\phi 2(\pi^+\pi^-)) \times \Gamma(e^+e^-)/\Gamma_{total}$ — $\Gamma_{112}\Gamma_5/\Gamma$

VALUE (10^{-2} keV)	EVTS	DOCUMENT ID		TECN	COMMENT
0.94±0.19±0.01	35	[1] AUBERT	06D	BABR	$10.6\ e^+e^- \to \phi 2(\pi^+\pi^-)\gamma$

[1] AUBERT 06D reports $[\Gamma(J/\psi(1S) \to \phi 2(\pi^+\pi^-)) \times \Gamma(J/\psi(1S) \to e^+e^-)/\Gamma_{total}] \times [B(\phi(1020) \to K^+K^-)] = (0.47 \pm 0.09 \pm 0.03) \times 10^{-2}$ keV which we divide by our best (shown rounded) value $B(\phi(1020) \to K^+K^-) = (50.1 \pm 0.6) \times 10^{-2}$. Our first error is their experiment's error and our second error is the systematic error from using our best (shown rounded) value.

$\Gamma(\phi\eta) \times \Gamma(e^+e^-)/\Gamma_{total}$ — $\Gamma_{113}\Gamma_5/\Gamma$

VALUE (eV)	EVTS	DOCUMENT ID		TECN	COMMENT
4.6±1.4 OUR AVERAGE					
4.1±1.6±0.4		[1] LEES	23	BABR	$e^+e^- \to \gamma_{ISR}$hadrons
6.1±2.7±0.4	6	[2] AUBERT	07AU	BABR	$10.6\ e^+e^- \to \phi\eta\gamma$

[1] LEES 23 quotes $\Gamma_{ee}^{J/\psi} \cdot B(J/\psi \to \phi\eta) \cdot B(\phi \to K^+K^-) \cdot B(\eta \to 3\pi^0) = 0.64 \pm 0.26 \pm 0.06$ eV.

[2] AUBERT 07AU quotes $\Gamma_{ee}^{J/\psi} \cdot B(J/\psi \to \phi\eta) \cdot B(\phi \to K^+K^-) \cdot B(\eta \to 3\pi) = 0.84 \pm 0.37 \pm 0.05$ eV.

$\Gamma(\phi f_0(980) \to \phi\pi^+\pi^-) \times \Gamma(e^+e^-)/\Gamma_{total}$ — $\Gamma_{117}\Gamma_5/\Gamma$

VALUE (eV)	EVTS	DOCUMENT ID		TECN	COMMENT
1.42±0.18 OUR AVERAGE					
1.38±0.24±0.02	57 ± 9	[1] LEES	12F	BABR	$10.6\ e^+e^- \to \pi^+\pi^- K^+K^-\gamma$
1.48±0.27±0.09	60±11	[2] SHEN	09	BELL	$10.6\ e^+e^- \to K^+K^-\pi^+\pi^-\gamma$
• • • We do not use the following data for averages, fits, limits, etc. • • •					
1.00±0.23±0.01	20 ± 5	[3] AUBERT	07AK	BABR	$10.6\ e^+e^- \to \pi^+\pi^- K^+K^-\gamma$

[1] LEES 12F reports $[\Gamma(J/\psi(1S) \to \phi f_0(980) \to \phi\pi^+\pi^-) \times \Gamma(J/\psi(1S) \to e^+e^-)/\Gamma_{total}] \times [B(\phi(1020) \to K^+K^-)] = 0.69 \pm 0.11 \pm 0.05$ eV which we divide by our best (shown rounded) value $B(\phi(1020) \to K^+K^-) = (50.1 \pm 0.6) \times 10^{-2}$. Our first error is their experiment's error and our second error is the systematic error from using our best (shown rounded) value.

[2] Multiplied by 2/3 to take into account the $\phi\pi^+\pi^-$ mode only. Using $B(\phi \to K^+K^-) = (49.2 \pm 0.6)\%$.

[3] Superseded by LEES 12F. AUBERT 07AK reports $[\Gamma(J/\psi(1S) \to \phi f_0(980) \to \phi\pi^+\pi^-) \times \Gamma(J/\psi(1S) \to e^+e^-)/\Gamma_{total}] \times [B(\phi(1020) \to K^+K^-)] = 0.50 \pm 0.11 \pm 0.04$ eV which we divide by our best (shown rounded) value $B(\phi(1020) \to K^+K^-) = (50.1 \pm 0.6) \times 10^{-2}$. Our first error is their experiment's error and our second error is the systematic error from using our best (shown rounded) value.

$\Gamma(\phi f_0(980) \to \phi\pi^0\pi^0) \times \Gamma(e^+e^-)/\Gamma_{total}$ — $\Gamma_{118}\Gamma_5/\Gamma$

VALUE (eV)	EVTS	DOCUMENT ID		TECN	COMMENT
0.96±0.26±0.01	16 ± 4	[1] LEES	12F	BABR	$10.6\ e^+e^- \to \pi^0\pi^0 K^+K^-\gamma$
• • • We do not use the following data for averages, fits, limits, etc. • • •					
0.94±0.39±0.01	7.0 ± 2.8	[2] AUBERT	07AK	BABR	$10.6\ e^+e^- \to \pi^0\pi^0 K^+K^-\gamma$

[1] LEES 12F reports $[\Gamma(J/\psi(1S) \to \phi f_0(980) \to \phi\pi^0\pi^0) \times \Gamma(J/\psi(1S) \to e^+e^-)/\Gamma_{total}] \times [B(\phi(1020) \to K^+K^-)] = 0.48 \pm 0.12 \pm 0.05$ eV which we divide by our best (shown rounded) value $B(\phi(1020) \to K^+K^-) = (50.1 \pm 0.6) \times 10^{-2}$. Our first error is their experiment's error and our second error is the systematic error from using our best (shown rounded) value.

[2] Superseded by LEES 12F. AUBERT 07AK reports $[\Gamma(J/\psi(1S) \to \phi f_0(980) \to \phi\pi^0\pi^0) \times \Gamma(J/\psi(1S) \to e^+e^-)/\Gamma_{total}] \times [B(\phi(1020) \to K^+K^-)] = 0.47 \pm 0.19 \pm 0.05$ eV which we divide by our best (shown rounded) value $B(\phi(1020) \to K^+K^-) = (50.1 \pm 0.6) \times 10^{-2}$. Our first error is their experiment's error and our second error is the systematic error from using our best (shown rounded) value.

$\Gamma(\phi f_2(1270)) \times \Gamma(e^+e^-)/\Gamma_{total}$ — $\Gamma_{126}\Gamma_5/\Gamma$

VALUE (eV)	EVTS	DOCUMENT ID		TECN	COMMENT
$1.79 \pm 0.32^{+0.02}_{-0.06}$	61	[1,2,3] LEES	12F	BABR	$10.6\ e^+e^- \to \pi^+\pi^- K^+K^-\gamma$
• • • We do not use the following data for averages, fits, limits, etc. • • •					
$4.08 \pm 0.73^{+0.05}_{-0.14}$	44	[2,4] AUBERT	07AK	BABR	$10.6\ e^+e^- \to \pi^+\pi^- K^+K^-\gamma$

[1] LEES 12F reports $[\Gamma(J/\psi(1S) \to \phi f_2(1270)) \times \Gamma(J/\psi(1S) \to e^+e^-)/\Gamma_{total}] \times [B(f_2(1270) \to \pi\pi)] = 1.51 \pm 0.25 \pm 0.10$ eV which we divide by our best (shown rounded) value $B(f_2(1270) \to \pi\pi) = (84.3^{+2.8}_{-1.0}) \times 10^{-2}$. Our first error is their experiment's error and our second error is the systematic error from using our best (shown rounded) value.

[2] Using $B(\phi \to K^+K^-) = (48.9 \pm 0.5)\%$.

[3] Using $\pi^+\pi^-$ invariant mass between 1.1 and 1.5 GeV. May include other sources such as $f_0(1370)$.

[4] Superseded by LEES 12F. AUBERT 07AK reports $[\Gamma(J/\psi(1S) \to \phi f_2(1270)) \times \Gamma(J/\psi(1S) \to e^+e^-)/\Gamma_{total}] \times [B(f_2(1270) \to \pi\pi)] = 3.44 \pm 0.55 \pm 0.28$ eV which we divide by our best (shown rounded) value $B(f_2(1270) \to \pi\pi) = (84.3^{+2.8}_{-1.0}) \times 10^{-2}$. Our first error is their experiment's error and our second error is the systematic error from using our best (shown rounded) value.

$\Gamma(\phi f_2'(1525)) \times \Gamma(e^+e^-)/\Gamma_{total}$ — $\Gamma_{131}\Gamma_5/\Gamma$

VALUE (eV)	EVTS	DOCUMENT ID		TECN	COMMENT
8.1±3.2±0.2	11	[1,2] LEES	14H	BABR	$e^+e^- \to K_S^0 K_S^0 K^+K^-\gamma$

[1] Dividing by 1/4 to take into account $B(f_2'(1525) \to K_S^0 K_S^0) = 1/4\ B(f_2'(1525) \to K\overline{K})$ and using $B(\phi \to K^+K^-) = (48.9 \pm 0.5)\%$.

[2] LEES 14H reports $[\Gamma(J/\psi(1S) \to \phi f_2'(1525)) \times \Gamma(J/\psi(1S) \to e^+e^-)/\Gamma_{total}] \times [B(f_2'(1525) \to K\overline{K})] = 7.2 \pm 2.8 \pm 0.3$ eV which we divide by our best (shown rounded) value $B(f_2'(1525) \to K\overline{K}) = (88.8 \pm 2.2) \times 10^{-2}$. Our first error is their experiment's error and our second error is the systematic error from using our best (shown rounded) value.

Int. J. Mod. Phys. A 2026.41. Downloaded from www.worldscientific.com
by UNIVERSITY OF CALIFORNIA @ BERKELEY on 09/16/26. Re-use and distribution is strictly not permitted, except for Open Access articles.

$\Gamma(\phi K^+ K^-) \times \Gamma(e^+ e^-)/\Gamma_{total}$ — $\Gamma_{137}\Gamma_5/\Gamma$

VALUE (eV)	EVTS	DOCUMENT ID		TECN	COMMENT
4.51±0.61±0.05	163	[1] LEES	12F	BABR	10.6 $e^+e^- \to K^+K^-K^+K^-\gamma$

[1] LEES 12F reports $[\Gamma(J/\psi(1S) \to \phi K^+K^-) \times \Gamma(J/\psi(1S) \to e^+e^-)/\Gamma_{total}] \times [B(\phi(1020) \to K^+K^-)] = 2.26 \pm 0.26 \pm 0.16$ eV which we divide by our best (shown rounded) value $B(\phi(1020) \to K^+K^-) = (50.1 \pm 0.6) \times 10^{-2}$. Our first error is their experiment's error and our second error is the systematic error from using our best (shown rounded) value.

$\Gamma(\phi K^0_S K^0_S) \times \Gamma(e^+ e^-)/\Gamma_{total}$ — $\Gamma_{138}\Gamma_5/\Gamma$

VALUE (eV)	EVTS	DOCUMENT ID		TECN	COMMENT
3.19±0.82±0.04	29	[1] LEES	14H	BABR	$e^+e^- \to K^0_S K^0_S K^+K^-\gamma$

[1] LEES 14H reports $[\Gamma(J/\psi(1S) \to \phi K^0_S K^0_S) \times \Gamma(J/\psi(1S) \to e^+e^-)/\Gamma_{total}] \times [B(\phi(1020) \to K^+K^-)] = 1.6 \pm 0.4 \pm 0.1$ eV which we divide by our best (shown rounded) value $B(\phi(1020) \to K^+K^-) = (50.1 \pm 0.6) \times 10^{-2}$. Our first error is their experiment's error and our second error is the systematic error from using our best (shown rounded) value.

$\Gamma(f'_2(1525) K^+K^-) \times \Gamma(e^+ e^-)/\Gamma_{total}$ — $\Gamma_{143}\Gamma_5/\Gamma$

VALUE (eV)	EVTS	DOCUMENT ID		TECN	COMMENT
5.8±1.9±0.1	16	[1,2] LEES	14H	BABR	$e^+e^- \to K^0_S K^0_S K^+K^-\gamma$

[1] Dividing by 1/4 to take into account $B(f'_2(1525) \to K^0_S K^0_S) = 1/4\ B(f'_2(1525) \to K\overline{K})$.

[2] LEES 14H reports $[\Gamma(J/\psi(1S) \to f'_2(1525) K^+K^-) \times \Gamma(J/\psi(1S) \to e^+e^-)/\Gamma_{total}] \times [B(f'_2(1525) \to K\overline{K})] = 5.12 \pm 1.68 \pm 0.20$ eV which we divide by our best (shown rounded) value $B(f'_2(1525) \to K\overline{K}) = (88.8 \pm 2.2) \times 10^{-2}$. Our first error is their experiment's error and our second error is the systematic error from using our best (shown rounded) value.

$\Gamma(2(\pi^+\pi^-)\pi^0) \times \Gamma(e^+ e^-)/\Gamma_{total}$ — $\Gamma_{164}\Gamma_5/\Gamma$

VALUE (eV)	EVTS	DOCUMENT ID		TECN	COMMENT
303±5±18	4990	AUBERT	07AU	BABR	10.6 $e^+e^- \to 2(\pi^+\pi^-)\pi^0\gamma$

$\Gamma(\pi^+\pi^-3\pi^0) \times \Gamma(e^+ e^-)/\Gamma_{total}$ — $\Gamma_{166}\Gamma_5/\Gamma$

VALUE (eV)	EVTS	DOCUMENT ID		TECN	COMMENT
100 ±50 OUR AVERAGE					Error includes scale factor of 4.3.
55 ±16 ± 1	14k	[1] LEES	21	BABR	10.6 $e^+e^- \to 2(\pi^+\pi^-)3\pi^0\gamma$
150.0± 4.0±15.0	2.3k	LEES	18E	BABR	10.6 $e^+e^- \to \pi^+\pi^-3\pi^0\gamma$

[1] LEES 21 reports $[\Gamma(J/\psi(1S) \to \pi^+\pi^-3\pi^0) \times \Gamma(J/\psi(1S) \to e^+e^-)/\Gamma_{total}] \times [\Gamma(\psi(2S) \to J/\psi(1S)\pi^+\pi^-)/\Gamma_{total}] = 19.2 \pm 4.5 \pm 3.2$ eV which we divide by our best (shown rounded) value $\Gamma(\psi(2S) \to J/\psi(1S)\pi^+\pi^-)/\Gamma_{total} = 0.3478 \pm 0.0033$. Our first error is their experiment's error and our second error is the systematic error from using our best (shown rounded) value.

$\Gamma(\pi^+\pi^-4\pi^0) \times \Gamma(e^+ e^-)/\Gamma_{total}$ — $\Gamma_{169}\Gamma_5/\Gamma$

VALUE (eV)	EVTS	DOCUMENT ID		TECN	COMMENT
35.8±4.4±5.4	340	LEES	21C	BABR	$e^+e^- \to \gamma_{ISR}(\pi^+\pi^-4\pi^0)$

$\Gamma(\rho^\pm\pi^\mp\pi^0\pi^0) \times \Gamma(e^+ e^-)/\Gamma_{total}$ — $\Gamma_{167}\Gamma_5/\Gamma$

VALUE (eV)	EVTS	DOCUMENT ID		TECN	COMMENT
78.0±9.0±8.0	1.2k	LEES	18E	BABR	10.6 $e^+e^- \to \pi^+\pi^-3\pi^0\gamma$

$\Gamma(\rho^+\rho^-\pi^0) \times \Gamma(e^+ e^-)/\Gamma_{total}$ — $\Gamma_{168}\Gamma_5/\Gamma$

VALUE (eV)	EVTS	DOCUMENT ID		TECN	COMMENT
33.0±5.0±3.3	529	LEES	18E	BABR	10.6 $e^+e^- \to \pi^+\pi^-3\pi^0\gamma$

$\Gamma(\pi^+\pi^-\pi^0) \times \Gamma(e^+ e^-)/\Gamma_{total}$ — $\Gamma_{170}\Gamma_5/\Gamma$

VALUE (keV)	DOCUMENT ID		TECN	COMMENT
0.1248±0.0019±0.0026	LEES	21B	BABR	10.5 $e^+e^- \to \pi^+\pi^-\pi^0\gamma$
• • • We do not use the following data for averages, fits, limits, etc. • • •				
0.122 ±0.005 ±0.008	AUBERT,B	04N	BABR	10.6 $e^+e^- \to \pi^+\pi^-\pi^0\gamma$

$\Gamma(2(\pi^+\pi^-\pi^0)) \times \Gamma(e^+ e^-)/\Gamma_{total}$ — $\Gamma_{171}\Gamma_5/\Gamma$

VALUE (10^{-2} keV)	EVTS	DOCUMENT ID		TECN	COMMENT
8.9±0.5±1.0	761	AUBERT	06D	BABR	10.6 $e^+e^- \to 2(\pi^+\pi^-\pi^0)\gamma$

$\Gamma(\pi^+\pi^-\pi^0 K^+K^-) \times \Gamma(e^+ e^-)/\Gamma_{total}$ — $\Gamma_{172}\Gamma_5/\Gamma$

VALUE (eV)	EVTS	DOCUMENT ID		TECN	COMMENT
107.0±4.3±6.4	768	AUBERT	07AU	BABR	10.6 $e^+e^- \to K^+K^-\pi^+\pi^-\pi^0\gamma$

$\Gamma(2(\pi^+\pi^-)) \times \Gamma(e^+ e^-)/\Gamma_{total}$ — $\Gamma_{174}\Gamma_5/\Gamma$

VALUE (eV)	EVTS	DOCUMENT ID		TECN	COMMENT
20.4±0.9±0.4		LEES	12E	BABR	10.6 $e^+e^- \to 2\pi^+2\pi^-\gamma$
• • • We do not use the following data for averages, fits, limits, etc. • • •					
19.5±1.4±1.3	270	[1] AUBERT	05D	BABR	10.6 $e^+e^- \to 2(\pi^+\pi^-)\gamma$

[1] Superseded by LEES 12E.

$\Gamma(3(\pi^+\pi^-)) \times \Gamma(e^+ e^-)/\Gamma_{total}$ — $\Gamma_{175}\Gamma_5/\Gamma$

VALUE (10^{-2} keV)	EVTS	DOCUMENT ID		TECN	COMMENT
2.37±0.16±0.14	496	AUBERT	06D	BABR	10.6 $e^+e^- \to 3(\pi^+\pi^-)\gamma$

$\Gamma(2(\pi^+\pi^-)3\pi^0) \times \Gamma(e^+ e^-)/\Gamma_{total}$ — $\Gamma_{176}\Gamma_5/\Gamma$

VALUE (eV)	EVTS	DOCUMENT ID		TECN	COMMENT
345±10±50	14k	LEES	21	BABR	10.6 $e^+e^- \to 2(\pi^+\pi^-)3\pi^0\gamma$

$\Gamma(2(\pi^+\pi^-)\eta) \times \Gamma(e^+ e^-)/\Gamma_{total}$ — $\Gamma_{178}\Gamma_5/\Gamma$

VALUE (eV)	EVTS	DOCUMENT ID		TECN	COMMENT
13.1±2.4±0.1	85	[1] AUBERT	07AU	BABR	10.6 $e^+e^- \to 2(\pi^+\pi^-)\eta\gamma$

[1] AUBERT 07AU reports $[\Gamma(J/\psi(1S) \to 2(\pi^+\pi^-)\eta) \times \Gamma(J/\psi(1S) \to e^+e^-)/\Gamma_{total}] \times [B(\eta \to 2\gamma)] = 5.16 \pm 0.85 \pm 0.39$ eV which we divide by our best (shown rounded) value $B(\eta \to 2\gamma) = (39.36 \pm 0.18) \times 10^{-2}$. Our first error is their experiment's error and our second error is the systematic error from using our best (shown rounded) value.

$\Gamma(2(\pi^+\pi^-\pi^0)\eta) \times \Gamma(e^+ e^-)/\Gamma_{total}$ — $\Gamma_{180}\Gamma_5/\Gamma$

VALUE (eV)	EVTS	DOCUMENT ID		TECN	COMMENT
9.1±2.6±1.4	14k	LEES	21	BABR	10.6 $e^+e^- \to 2(\pi^+\pi^-)3\pi^0\gamma$

$\Gamma(\pi^+\pi^-\pi^0\pi^0\eta) \times \Gamma(e^+ e^-)/\Gamma_{total}$ — $\Gamma_{181}\Gamma_5/\Gamma$

VALUE (eV)	EVTS	DOCUMENT ID		TECN	COMMENT
13.1± 2.7 OUR AVERAGE					
26.1±17.9±0.3	14k	[1] LEES	21	BABR	10.6 $e^+e^- \to 2(\pi^+\pi^-)3\pi^0\gamma$
12.8± 1.8±2.0	203	LEES	18E	BABR	10.6 $e^+e^- \to \pi^+\pi^-\pi^0\pi^0\eta\gamma$

[1] LEES 21 reports $[\Gamma(J/\psi(1S) \to \pi^+\pi^-\pi^0\pi^0\eta) \times \Gamma(J/\psi(1S) \to e^+e^-)/\Gamma_{total}] \times [B(\eta \to \pi^+\pi^-\pi^0)] = 6 \pm 4 \pm 1$ eV which we divide by our best (shown rounded) value $B(\eta \to \pi^+\pi^-\pi^0) = (23.02 \pm 0.25) \times 10^{-2}$. Our first error is their experiment's error and our second error is the systematic error from using our best (shown rounded) value.

$\Gamma(\rho^\pm\pi^\mp\pi^0\eta) \times \Gamma(e^+ e^-)/\Gamma_{total}$ — $\Gamma_{182}\Gamma_5/\Gamma$

VALUE (eV)	EVTS	DOCUMENT ID		TECN	COMMENT
10.5±4.1±1.6	168	LEES	18E	BABR	10.6 $e^+e^- \to \pi^+\pi^-\pi^0\pi^0\eta\gamma$

$\Gamma(K^+K^-) \times \Gamma(e^+ e^-)/\Gamma_{total}$ — $\Gamma_{183}\Gamma_5/\Gamma$

VALUE (eV)	EVTS	DOCUMENT ID		TECN	COMMENT
• • • We do not use the following data for averages, fits, limits, etc. • • •					
1.78±0.11±0.05	462	[1] LEES	15J	BABR	$e^+e^- \to K^+K^-\gamma$
1.94±0.11±0.05	462	[2] LEES	15J	BABR	$e^+e^- \to K^+K^-\gamma$
1.42±0.23±0.08	51	[3] LEES	13Q	BABR	$e^+e^- \to K^+K^-\gamma$

[1] $\sin\phi > 0$.
[2] $\sin\phi < 0$.
[3] Interference with non-resonant K^+K^- production not taken into account.

$\Gamma(K^0_S K^0_L \pi^0) \times \Gamma(e^+ e^-)/\Gamma_{total}$ — $\Gamma_{189}\Gamma_5/\Gamma$

VALUE (eV)	EVTS	DOCUMENT ID		TECN	COMMENT
11.4±1.3±0.6	182	LEES	17A	BABR	$e^+e^- \to K^0_S K^0_L \pi^0\gamma$

$\Gamma(K^*(892)^0\overline{K}^0 + \text{c.c.} \to K^0_S K^0_L \pi^0) \times \Gamma(e^+ e^-)/\Gamma_{total}$ — $\Gamma_{190}\Gamma_5/\Gamma$

VALUE (eV)	EVTS	DOCUMENT ID		TECN	COMMENT
6.7±0.9±0.4	106	LEES	17A	BABR	$e^+e^- \to K^0_S K^0_L \pi^0\gamma$

$\Gamma(K^*_2(1430)^0\overline{K}^0 + \text{c.c.} \to K^0_S K^0_L \pi^0) \times \Gamma(e^+ e^-)/\Gamma_{total}$ — $\Gamma_{191}\Gamma_5/\Gamma$

VALUE (eV)	EVTS	DOCUMENT ID		TECN	COMMENT
2.4±0.7±0.1	37	LEES	17A	BABR	$e^+e^- \to K^0_S K^0_L \pi^0\gamma$

$\Gamma(K^+K^-\pi^+\pi^-) \times \Gamma(e^+ e^-)/\Gamma_{total}$ — $\Gamma_{192}\Gamma_5/\Gamma$

VALUE (eV)	EVTS	DOCUMENT ID		TECN	COMMENT
37.94±0.81±1.10	3.1k	LEES	12F	BABR	10.6 $e^+e^- \to \pi^+\pi^-K^+K^-\gamma$
• • • We do not use the following data for averages, fits, limits, etc. • • •					
36.3 ±1.3 ±2.1	1.5k	[1] AUBERT	07AK	BABR	10.6 $e^+e^- \to \pi^+\pi^-K^+K^-\gamma$
33.6 ±2.7 ±2.7	233	[2] AUBERT	05D	BABR	10.6 $e^+e^- \to K^+K^-\pi^+\pi^-\gamma$

[1] Superseded by LEES 12F.
[2] Superseded by AUBERT 07AK.

$\Gamma(K^+K^-\pi^0\pi^0) \times \Gamma(e^+ e^-)/\Gamma_{total}$ — $\Gamma_{193}\Gamma_5/\Gamma$

VALUE (eV)	EVTS	DOCUMENT ID		TECN	COMMENT
11.75±0.81±0.90	388	LEES	12F	BABR	10.6 $e^+e^- \to \pi^0\pi^0K^+K^-\gamma$
• • • We do not use the following data for averages, fits, limits, etc. • • •					
13.6 ±1.1 ±1.3	203	[1] AUBERT	07AK	BABR	10.6 $e^+e^- \to \pi^0\pi^0K^+K^-\gamma$

[1] Superseded by LEES 12F.

$\Gamma(K^+K^-\pi^0\pi^0\pi^0) \times \Gamma(e^+ e^-)/\Gamma_{total}$ — $\Gamma_{194}\Gamma_5/\Gamma$

VALUE (eV)	DOCUMENT ID		TECN	COMMENT
8.9±1.3±0.9	LEES	23	BABR	$e^+e^- \to \gamma_{ISR}$hadrons

$\Gamma(K^0_S K^\pm\pi^\mp\pi^0\pi^0) \times \Gamma(e^+ e^-)/\Gamma_{total}$ — $\Gamma_{195}\Gamma_5/\Gamma$

VALUE (eV)	DOCUMENT ID		TECN	COMMENT
29.3±2.6±2.9	LEES	23	BABR	$e^+e^- \to \gamma_{ISR}$hadrons

$\Gamma(K^0_S K^\pm\pi^\mp\pi^+\pi^-) \times \Gamma(e^+ e^-)/\Gamma_{total}$ — $\Gamma_{196}\Gamma_5/\Gamma$

VALUE (eV)	DOCUMENT ID		TECN	COMMENT
34.6±1.4±1.8	LEES	23	BABR	$e^+e^- \to \gamma_{ISR}$hadrons

Int. J. Mod. Phys. A 2026.41. Downloaded from www.worldscientific.com by CALIFORNIA @ BERKELEY on 09/16/26. Re-use and distribution is strictly not permitted, except for Open Access articles.

$\Gamma(K^0_S K^\pm \rho(770)^\pm \pi^0) \times \Gamma(e^+e^-)/\Gamma_{total}$ — $\Gamma_{197}\Gamma_5/\Gamma$

VALUE (eV)	DOCUMENT ID		TECN	COMMENT
16.0±4.1±1.6	LEES	23	BABR	$e^+e^- \to \gamma_{ISR}$hadrons

$\Gamma(K^0_S K^0_L \pi^+\pi^-) \times \Gamma(e^+e^-)/\Gamma_{total}$ — $\Gamma_{198}\Gamma_5/\Gamma$

VALUE (eV)	EVTS	DOCUMENT ID		TECN	COMMENT
20.8±2.3±2.1	248	LEES	14H	BABR	$e^+e^- \to \pi^+\pi^- K^0_S K^0_L \gamma$

$\Gamma(K^0_S K^0_L \pi^0\pi^0) \times \Gamma(e^+e^-)/\Gamma_{total}$ — $\Gamma_{199}\Gamma_5/\Gamma$

VALUE (eV)	EVTS	DOCUMENT ID		TECN	COMMENT
10.3±2.3±0.5	47	LEES	17A	BABR	$e^+e^- \to K^0_S K^0_L \pi^0\pi^0\gamma$

$\Gamma(K^0_S K^0_L \eta) \times \Gamma(e^+e^-)/\Gamma_{total}$ — $\Gamma_{200}\Gamma_5/\Gamma$

VALUE (eV)	EVTS	DOCUMENT ID		TECN	COMMENT
8.0±1.8±0.4	45	LEES	17A	BABR	$e^+e^- \to K^0_S K^0_L \eta\gamma$

$\Gamma(K^0_S K^0_S \pi^+\pi^-) \times \Gamma(e^+e^-)/\Gamma_{total}$ — $\Gamma_{201}\Gamma_5/\Gamma$

VALUE (eV)	EVTS	DOCUMENT ID		TECN	COMMENT
9.3±0.9±0.5	133	LEES	14H	BABR	$e^+e^- \to \pi^+\pi^- K^0_S K^0_S \gamma$

$\Gamma(K^\mp K^0_S \pi^\pm \pi^0) \times \Gamma(e^+e^-)/\Gamma_{total}$ — $\Gamma_{202}\Gamma_5/\Gamma$

VALUE (eV)	EVTS	DOCUMENT ID		TECN	COMMENT
31.7±1.9±1.8	393	LEES	17D	BABR	$e^+e^- \to K^0_S K^\pm \pi^\mp \pi^0 \gamma$

$\Gamma(K^0_S K^\pm \pi^\mp \rho(770)^0) \times \Gamma(e^+e^-)/\Gamma_{total}$ — $\Gamma_{203}\Gamma_5/\Gamma$

VALUE (eV)	DOCUMENT ID		TECN	COMMENT
17.3±2.1±1.7	LEES	23	BABR	$e^+e^- \to \gamma_{ISR}$hadrons

$\Gamma(K^+K^- 2(\pi^+\pi^-)) \times \Gamma(e^+e^-)/\Gamma_{total}$ — $\Gamma_{204}\Gamma_5/\Gamma$

VALUE (10^{-2} keV)	EVTS	DOCUMENT ID		TECN	COMMENT
2.75±0.23±0.17	205	AUBERT	06D	BABR	10.6 $e^+e^- \to K^+K^- 2(\pi^+\pi^-)\gamma$

$\Gamma(K^+K^-\pi^+\pi^-\eta) \times \Gamma(e^+e^-)/\Gamma_{total}$ — $\Gamma_{205}\Gamma_5/\Gamma$

VALUE (eV)	EVTS	DOCUMENT ID		TECN	COMMENT
25.9±3.9±0.1	73	[1] AUBERT	07AU	BABR	10.6 $e^+e^- \to K^+K^-\pi^+\pi^-\eta\gamma$

[1] AUBERT 07AU reports $[\Gamma(J/\psi(1S) \to K^+K^-\pi^+\pi^-\eta) \times \Gamma(J/\psi(1S) \to e^+e^-)/\Gamma_{total}] \times [B(\eta \to 2\gamma)] = 10.2 \pm 1.3 \pm 0.8$ eV which we divide by our best (shown rounded) value $B(\eta \to 2\gamma) = (39.36 \pm 0.18) \times 10^{-2}$. Our first error is their experiment's error and our second error is the systematic error from using our best (shown rounded) value.

$\Gamma(2(K^+K^-)) \times \Gamma(e^+e^-)/\Gamma_{total}$ — $\Gamma_{206}\Gamma_5/\Gamma$

VALUE (eV)	EVTS	DOCUMENT ID		TECN	COMMENT
4.00±0.33±0.29	287 ± 24	LEES	12F	BABR	10.6 $e^+e^- \to 2(K^+K^-)\gamma$
• • • We do not use the following data for averages, fits, limits, etc. • • •					
4.11±0.39±0.30	156 ± 15	[1] AUBERT	07AK	BABR	10.6 $e^+e^- \to 2(K^+K^-)\gamma$
4.0 ±0.7 ±0.6	38	[2] AUBERT	05D	BABR	10.6 $e^+e^- \to 2(K^+K^-)\gamma$

[1] Superseded by LEES 12F.
[2] Superseded by AUBERT 07AK.

$\Gamma(K^+K^-K^0_S K^0_S) \times \Gamma(e^+e^-)/\Gamma_{total}$ — $\Gamma_{207}\Gamma_5/\Gamma$

VALUE (eV)	EVTS	DOCUMENT ID		TECN	COMMENT
2.3±0.4±0.1	29	LEES	14H	BABR	$e^+e^- \to K^0_S K^0_S K^+K^-\gamma$

$\Gamma(K^0_S K^*(892)^0 \pi^+\pi^-) \times \Gamma(e^+e^-)/\Gamma_{total}$ — $\Gamma_{208}\Gamma_5/\Gamma$

VALUE (eV)	DOCUMENT ID		TECN	COMMENT
9.45±3.15±0.90	LEES	23	BABR	$e^+e^- \to \gamma_{ISR}$hadrons

$\Gamma(K^0_S K^*(892)^0 \pi^0\pi^0) \times \Gamma(e^+e^-)/\Gamma_{total}$ — $\Gamma_{209}\Gamma_5/\Gamma$

VALUE (eV)	DOCUMENT ID		TECN	COMMENT
5.59±0.79±0.55	LEES	23	BABR	$e^+e^- \to \gamma_{ISR}$hadrons

$\Gamma(K^\mp K^*(892)^\pm \pi^+\pi^-) \times \Gamma(e^+e^-)/\Gamma_{total}$ — $\Gamma_{210}\Gamma_5/\Gamma$

VALUE (eV)	DOCUMENT ID		TECN	COMMENT
18.6±6.3±1.8	LEES	23	BABR	$e^+e^- \to \gamma_{ISR}$hadrons

$\Gamma(K^*(892)^\pm K^*(892)^0 \pi^\mp) \times \Gamma(e^+e^-)/\Gamma_{total}$ — $\Gamma_{211}\Gamma_5/\Gamma$

VALUE (eV)	DOCUMENT ID		TECN	COMMENT
26.6±4.5±2.7	LEES	23	BABR	$e^+e^- \to \gamma_{ISR}$hadrons

$\Gamma(K^\mp K^*(892)^\pm \pi^0\pi^0) \times \Gamma(e^+e^-)/\Gamma_{total}$ — $\Gamma_{212}\Gamma_5/\Gamma$

VALUE (eV)	DOCUMENT ID		TECN	COMMENT
8.67±1.56±0.84	LEES	23	BABR	$e^+e^- \to \gamma_{ISR}$hadrons

$\Gamma(K^*(892)^+ K^*(892)^- \pi^0) \times \Gamma(e^+e^-)/\Gamma_{total}$ — $\Gamma_{213}\Gamma_5/\Gamma$

VALUE (eV)	DOCUMENT ID		TECN	COMMENT
62.1±10.8±6.30	LEES	23	BABR	$e^+e^- \to \gamma_{ISR}$hadrons

$\Gamma(p\overline{p}) \times \Gamma(e^+e^-)/\Gamma_{total}$ — $\Gamma_{214}\Gamma_5/\Gamma$

VALUE (eV)	EVTS	DOCUMENT ID		TECN	COMMENT
11.9±0.6 OUR AVERAGE Error includes scale factor of 1.8. See the ideogram below.					
11.3±0.4±0.3	821	[1] LEES	13O	BABR	$e^+e^- \to p\overline{p}\gamma$
12.9±0.4±0.4	918	[2] LEES	13Y	BABR	$e^+e^- \to p\overline{p}\gamma$
9.7±1.7		[3] ARMSTRONG	93B	E760	$\overline{p}p \to e^+e^-$
• • • We do not use the following data for averages, fits, limits, etc. • • •					
12.0±0.6±0.5	438	[4] AUBERT	06B	BABR	$e^+e^- \to p\overline{p}\gamma$

[1] ISR photon reconstructed in the detector
[2] ISR photon undetected
[3] Using $\Gamma_{total} = 85.5^{+6.1}_{-5.8}$ MeV.
[4] Superseded by LEES 13O

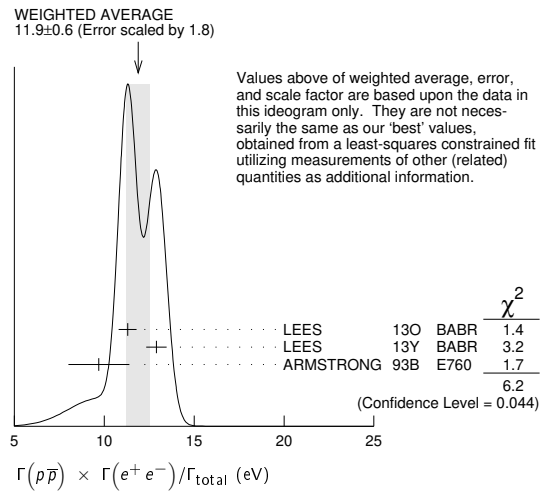

$\Gamma(\Lambda\overline{\Lambda}) \times \Gamma(e^+e^-)/\Gamma_{total}$ — $\Gamma_{230}\Gamma_5/\Gamma$

VALUE (eV)	DOCUMENT ID		TECN	COMMENT
10.7±0.9±0.7	AUBERT	07BD	BABR	10.6 $e^+e^- \to \Lambda\overline{\Lambda}\gamma$

$\Gamma(\Sigma^+\overline{\Sigma}^-) \times \Gamma(e^+e^-)/\Gamma_{total}$ — $\Gamma_{241}\Gamma_5/\Gamma$

VALUE (eV)	DOCUMENT ID		TECN	COMMENT
• • • We do not use the following data for averages, fits, limits, etc. • • •				
6.8±1.5±0.8	GONG	23	BELL	$e^+e^- \to \Sigma^+\overline{\Sigma}^-$

$\Gamma(\Sigma^0\overline{\Sigma}^0) \times \Gamma(e^+e^-)/\Gamma_{total}$ — $\Gamma_{242}\Gamma_5/\Gamma$

VALUE (eV)	DOCUMENT ID		TECN	COMMENT
• • • We do not use the following data for averages, fits, limits, etc. • • •				
5.2±1.5±0.6	GONG	23	BELL	$e^+e^- \to \Sigma^0\overline{\Sigma}^0$
6.4±1.2±0.6	AUBERT	07BD	BABR	10.6 $e^+e^- \to \Sigma^0\overline{\Sigma}^0\gamma$

$J/\psi(1S)$ BRANCHING RATIOS

For the first four branching ratios, see also the partial widths, and (partial widths) $\times \Gamma(e^+e^-)/\Gamma_{total}$ above.

$\Gamma(\text{hadrons})/\Gamma_{total}$ — Γ_1/Γ

VALUE	DOCUMENT ID		TECN	COMMENT
0.877±0.005 OUR AVERAGE				
0.878±0.005	BAI	95B	BES	e^+e^-
0.86 ±0.02	BOYARSKI	75	MRK1	e^+e^-

$\Gamma(\text{virtual}\,\gamma \to \text{hadrons})/\Gamma_{total}$ — Γ_2/Γ

VALUE	DOCUMENT ID		TECN	COMMENT
0.1346±0.0007	[1] LIAO	23	RVUE	e^+e^-
• • • We do not use the following data for averages, fits, limits, etc. • • •				
0.135 ±0.003	[2,3] SETH	04	RVUE	e^+e^-
0.17 ±0.02	[2] BOYARSKI	75	MRK1	e^+e^-

[1] Using $B(J/\psi(1S) \to \ell^+\ell^-) = (5.967 \pm 0.023)\%$ and $R = 2.26 \pm 0.01$ determined by a fit to data from Mark-I, DM2, BESII, KEDR, and BESIII.
[2] Included in $\Gamma(\text{hadrons})/\Gamma_{total}$.
[3] Using $B(J/\psi \to \ell^+\ell^-) = (5.90 \pm 0.09)\%$ from RPP-2002 and $R = 2.28 \pm 0.04$ determined by a fit to data from BAI 00 and BAI 02C. Superseded by LIAO 23.

$\Gamma(ggg)/\Gamma_{total}$ — Γ_3/Γ

VALUE (units 10^{-2})	EVTS	DOCUMENT ID		TECN	COMMENT
64.1±1.0	6 M	[1] BESSON	08	CLEO	$\psi(2S) \to \pi^+\pi^-+$ hadrons

[1] Calculated using the value $\Gamma(\gamma gg)/\Gamma(ggg) = 0.137 \pm 0.001 \pm 0.016 \pm 0.004$ from BESSON 08 and the PDG 08 values of $B(\ell^+\ell^-)$, B(virtual $\gamma \to$ hadrons), and $B(\gamma\eta_c)$. The statistical error is negligible and the systematic error is partially correlated with that of $\Gamma(\gamma gg)/\Gamma_{total}$ measurement of BESSON 08.

Int. J. Mod. Phys. A 2026.41. Downloaded from www.worldscientific.com
by UNIVERSITY OF CALIFORNIA @ BERKELEY on 09/16/26. Re-use and distribution is strictly not permitted, except for Open Access articles.

$\Gamma(\gamma gg)/\Gamma_{total}$ — Γ_4/Γ

VALUE (units 10^{-2})	EVTS	DOCUMENT ID		TECN	COMMENT
8.79±1.05	200 k	[1] BESSON	08	CLEO	$\psi(2S) \to \pi^+\pi^-\gamma$ + hadrons

[1] Calculated using the value $\Gamma(\gamma gg)/\Gamma(ggg) = 0.137 \pm 0.001 \pm 0.016 \pm 0.004$ from BESSON 08 and the value of $\Gamma(ggg)/\Gamma_{total}$. The statistical error is negligible and the systematic error is partially correlated with that of $\Gamma(ggg)/\Gamma_{total}$ measurement of BESSON 08.

$\Gamma(\gamma gg)/\Gamma(ggg)$ — Γ_4/Γ_3

VALUE (units 10^{-2})	EVTS	DOCUMENT ID		TECN	COMMENT
13.7±0.1±0.7	6 M	BESSON	08	CLEO	$\psi(2S) \to \pi^+\pi^- J/\psi$

$\Gamma(e^+e^-)/\Gamma_{total}$ — Γ_5/Γ

VALUE (units 10^{-2})	EVTS	DOCUMENT ID		TECN	COMMENT
5.971±0.032 OUR AVERAGE					
5.983±0.007±0.037	720k	ABLIKIM	13R	BES3	$\psi(2S) \to J/\psi\pi^+\pi^-$
5.945±0.067±0.042	15k	LI	05C	CLEO	$\psi(2S) \to J/\psi\pi^+\pi^-$
5.90 ±0.05 ±0.10		BAI	98D	BES	$\psi(2S) \to J/\psi\pi^+\pi^-$
6.09 ±0.33		BAI	95B	BES	e^+e^-
5.92 ±0.15 ±0.20		COFFMAN	92	MRK3	$\psi(2S) \to J/\psi\pi^+\pi^-$
6.9 ±0.9		BOYARSKI	75	MRK1	e^+e^-

$\Gamma(e^+e^-\gamma)/\Gamma_{total}$ — Γ_6/Γ

VALUE (units 10^{-3})	DOCUMENT ID		TECN	COMMENT
8.8±1.3±0.4	[1] ARMSTRONG	96	E760	$\overline{p}p \to e^+e^-\gamma$

[1] For $E_\gamma > 100$ MeV.

$\Gamma(\mu^+\mu^-)/\Gamma_{total}$ — Γ_7/Γ

VALUE (units 10^{-2})	EVTS	DOCUMENT ID		TECN	COMMENT
5.961±0.033 OUR AVERAGE					
5.973±0.007±0.038	770k	ABLIKIM	13R	BES3	$\psi(2S) \to J/\psi\pi^+\pi^-$
5.960±0.065±0.050	17k	LI	05C	CLEO	$\psi(2S) \to J/\psi\pi^+\pi^-$
5.84 ±0.06 ±0.10		BAI	98D	BES	$\psi(2S) \to J/\psi\pi^+\pi^-$
6.08 ±0.33		BAI	95B	BES	e^+e^-
5.90 ±0.15 ±0.19		COFFMAN	92	MRK3	$\psi(2S) \to J/\psi\pi^+\pi^-$
6.9 ±0.9		BOYARSKI	75	MRK1	e^+e^-

$\Gamma(e^+e^-)/\Gamma(\mu^+\mu^-)$ — Γ_5/Γ_7

VALUE	DOCUMENT ID		TECN	COMMENT
1.0016±0.0031 OUR AVERAGE				
1.0022±0.0044±0.0048	[1] AULCHENKO	14	KEDR	3.097 $e^+e^- \to e^+e^-,\mu^+\mu^-$
1.0017±0.0017±0.0033	[2] ABLIKIM	13R	BES3	$\psi(2S) \to J/\psi\pi^+\pi^-$
1.002 ±0.021 ±0.013	[3] ANASHIN	10	KEDR	3.097 $e^+e^- \to e^+e^-,\mu^+\mu^-$
0.997 ±0.012 ±0.006	LI	05C	CLEO	$\psi(2S) \to J/\psi\pi^+\pi^-$
• • • We do not use the following data for averages, fits, limits, etc. • • •				
1.011 ±0.013 ±0.016	BAI	98D	BES	$\psi(2S) \to J/\psi\pi^+\pi^-$
1.00 ±0.07	BAI	95B	BES	e^+e^-
1.00 ±0.05	BOYARSKI	75	MRK1	e^+e^-
0.91 ±0.15	ESPOSITO	75B	FRAM	e^+e^-
0.93 ±0.10	FORD	75	SPEC	e^+e^-

[1] From 235.3k $J/\psi \to e^+e^-$ and 156.6k $J/\psi \to \mu^+\mu^-$ observed events.
[2] Not independent of the corresponding measurements of $\Gamma(e+ e-)/\Gamma_{total}$ and $\Gamma(mu+ mu-)/\Gamma_{total}$.
[3] Not independent of the corresponding measurements of $\Gamma(e^+e^-) \times \Gamma(e^+e^-)/\Gamma_{total}$ and $\Gamma(\mu^+\mu^-) \times \Gamma(e^+e^-)/\Gamma_{total}$.

$\Gamma(e^+e^-e^+e^-)/\Gamma_{total}$ — Γ_8/Γ

VALUE (units 10^{-5})	EVTS	DOCUMENT ID		TECN	COMMENT
5.48±0.31±0.45	700	[1] ABLIKIM	24L	BES3	$\psi(2S) \to \pi^+\pi^- J/\psi$

[1] $B(\psi(2S) \to \pi^+\pi^- J/\psi) = (34.68 \pm 0.30)\%$ from PDG 20 was used.

$\Gamma(e^+e^-\mu^+\mu^-)/\Gamma_{total}$ — Γ_9/Γ

VALUE (units 10^{-5})	EVTS	DOCUMENT ID		TECN	COMMENT
3.53±0.22±0.13	354	[1] ABLIKIM	24L	BES3	$\psi(2S) \to \pi^+\pi^- J/\psi$

[1] $B(\psi(2S) \to \pi^+\pi^- J/\psi) = (34.68 \pm 0.30)\%$ from PDG 20 was used.

$\Gamma(\mu^+\mu^-\mu^+\mu^-)/\Gamma_{total}$ — Γ_{10}/Γ

VALUE (units 10^{-7})	CL%	EVTS	DOCUMENT ID		TECN	COMMENT
• • • We do not use the following data for averages, fits, limits, etc. • • •						
11.3±1.1±0.1		452	[1] AAIJ	24AE	LHCB	$J/\psi \to \mu^+\mu^-\mu^+\mu^-$
<16	90	3.4	[2] ABLIKIM	24L	BES3	$\psi(2S) \to \pi^+\pi^- J/\psi$
$10.1^{+3.3}_{-2.8}\pm0.1$		12	[3] HAYRAPETY...	24A	CMS	$J/\psi \to \mu^+\mu^-\mu^+\mu^-$

[1] AAIJ 24AE reports $[\Gamma(J/\psi(1S) \to \mu^+\mu^-\mu^+\mu^-)/\Gamma_{total}] / [B(J/\psi(1S) \to \mu^+\mu^-)] = (1.89 \pm 0.17 \pm 0.09) \times 10^{-5}$ which we multiply by our best (shown rounded) value $B(J/\psi(1S) \to \mu^+\mu^-) = (5.961 \pm 0.033) \times 10^{-2}$. Our first error is their experiment's error and our second error is the systematic error from using our best (shown rounded) value.
[2] Measured with $\psi(2S) \to \pi^+\pi^- J/\psi$, $J/\psi \to \mu^+\mu^-\mu^+\mu^-$. $B(\psi(2S) \to \pi^+\pi^- J/\psi) = (34.68 \pm 0.30)\%$ from PDG 20 was used.
[3] HAYRAPETYAN 24A reports $[\Gamma(J/\psi(1S) \to \mu^+\mu^-\mu^+\mu^-)/\Gamma_{total}] / [B(J/\psi(1S) \to \mu^+\mu^-)] = (16.9^{+5.5}_{-4.6} \pm 0.6) \times 10^{-6}$ which we multiply by our best (shown rounded) value $B(J/\psi(1S) \to \mu^+\mu^-) = (5.961 \pm 0.033) \times 10^{-2}$. Our first error is their experiment's error and our second error is the systematic error from using our best (shown rounded) value.

$\Gamma(\mu^+\mu^-\mu^+\mu^-)/\Gamma(\mu^+\mu^-)$ — Γ_{10}/Γ_7

VALUE (units 10^{-6})	EVTS	DOCUMENT ID		TECN	COMMENT
18.7±1.8 OUR AVERAGE					
18.9±1.7±0.9	452	[1] AAIJ	24AE	LHCB	$J/\psi \to \mu^+\mu^-\mu^+\mu^-$
$16.9^{+5.5}_{-4.6}\pm0.6$	12	HAYRAPETY...	24A	CMS	$J/\psi \to \mu^+\mu^-\mu^+\mu^-$

[1] Includes prompt production and inclusive decays of b-hadrons.

HADRONIC DECAYS

$\Gamma(\rho\pi)/\Gamma_{total}$ — Γ_{11}/Γ

VALUE (units 10^{-2})	EVTS	DOCUMENT ID		TECN	COMMENT
1.88 ±0.12 OUR AVERAGE		Error includes scale factor of 2.6.			See the ideogram below.
2.072±0.017±0.062	19.8k	[1] ANASHIN	23	KEDR	$e^+e^- \to J/\psi \to \pi^+\pi^-\pi^0$
2.18 ±0.19		[2,3] AUBERT,B	04N	BABR	10.6 $e^+e^- \to \pi^+\pi^-\pi^0\gamma$
2.184±0.005±0.201	220k	[3,4] BAI	04H	BES	$e^+e^- \to J/\psi \to \pi^+\pi^-\pi^0$
2.091±0.021±0.116		[3,5] BAI	04H	BES	$\psi(2S) \to \pi^+\pi^- J/\psi$
1.21 ±0.20		BAI	96D	BES	$e^+e^- \to \rho\pi$
1.42 ±0.01 ±0.19		COFFMAN	88	MRK3	e^+e^-
1.3 ±0.3	150	FRANKLIN	83	MRK2	e^+e^-
1.6 ±0.4	183	ALEXANDER	78	PLUT	e^+e^-
1.33 ±0.21		BRANDELIK	78B	DASP	e^+e^-
1.0 ±0.2	543	BARTEL	76	CNTR	e^+e^-
1.3 ±0.3	153	JEAN-MARIE	76	MRK1	e^+e^-

[1] By a simultaneous fit of the $\pi\pi$ invariant mass distribution over the decay modes $J/\psi \to \rho^0\pi^0$, $J/\psi \to \rho^+\pi^-$, $J/\psi \to \rho^-\pi^+$. In the fit only the intermediate states $\rho(770)\pi$ and $\rho(1450)\pi$ are considered.
[2] From the ratio of $\Gamma(e^+e^-)\ B(\pi^+\pi^-\pi^0)$ and $\Gamma(e^+e^-)\ B(\mu^+\mu^-)$ (AUBERT 04).
[3] Not independent of their $B(\pi^+\pi^-\pi^0)$.
[4] From $J/\psi \to \pi^+\pi^-\pi^0$ events directly.
[5] Obtained comparing the rates for $\pi^+\pi^-\pi^0$ and $\mu^+\mu^-$, using J/ψ events produced via $\psi(2S) \to \pi^+\pi^- J/\psi$ and with $B(J/\psi \to \mu^+\mu^-) = 5.88 \pm 0.10\%$.

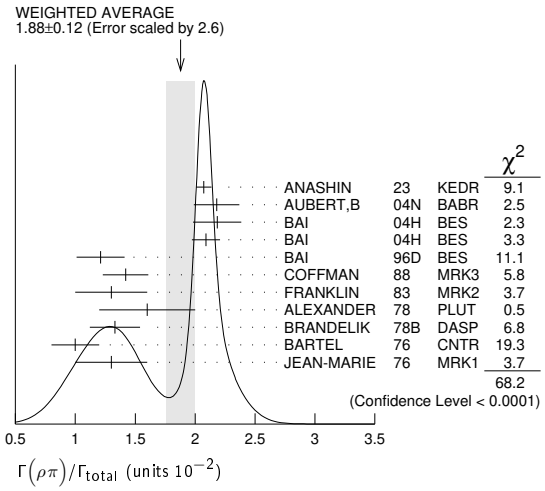

$\Gamma(\rho\pi)/\Gamma(\pi^+\pi^-\pi^0)$ — Γ_{11}/Γ_{170}

VALUE	EVTS	DOCUMENT ID		TECN	COMMENT
1.142±0.011±0.026	20k	[1] LEES	17C	BABR	$J/\psi \to \pi^+\pi^-\pi^0$
• • • We do not use the following data for averages, fits, limits, etc. • • •					
1.331±0.033	20k	[2] LEES	17C	BABR	$J/\psi \to \pi^+\pi^-\pi^0$

[1] From a Dalitz plot analysis in an isobar model.
[2] From a Dalitz plot analysis in a Veneziano model.

$\Gamma(\rho^0\pi^0)/\Gamma(\rho\pi)$ — Γ_{12}/Γ_{11}

VALUE	DOCUMENT ID		TECN	COMMENT
0.328±0.005±0.027	COFFMAN	88	MRK3	e^+e^-
• • • We do not use the following data for averages, fits, limits, etc. • • •				
0.35 ±0.08	ALEXANDER	78	PLUT	e^+e^-
0.32 ±0.08	BRANDELIK	78B	DASP	e^+e^-
0.39 ±0.11	BARTEL	76	CNTR	e^+e^-
0.37 ±0.09	JEAN-MARIE	76	MRK1	e^+e^-

$\Gamma(a_2(1320)^0\pi^+\pi^- \to 2(\pi^+\pi^-)\pi^0)/\Gamma_{total}$ — Γ_{13}/Γ

VALUE (units 10^{-3})	EVTS	DOCUMENT ID		TECN	COMMENT
2.84±0.08±0.60	1317	ANASHIN	22	KEDR	$J/\psi \to 2(\pi^+\pi^-)\pi^0$

Int. J. Mod. Phys. A 2026.41. Downloaded from www.worldscientific.com by CALIFORNIA @ BERKELEY on 09/16/26. Re-use and distribution is strictly not permitted, except for Open Access articles.

$\Gamma(a_2(1320)^+\pi^-\pi^0 + \text{c.c} \to 2(\pi^+\pi^-)\pi^0)/\Gamma_{total}$ — Γ_{14}/Γ

VALUE (units 10^{-3})	EVTS	DOCUMENT ID		TECN	COMMENT
3.67±0.09±0.73	1628	ANASHIN	22	KEDR	$J/\psi \to 2(\pi^+\pi^-)\pi^0$

$\Gamma(a_2(1320)\rho)/\Gamma_{total}$ — Γ_{15}/Γ

VALUE (units 10^{-3})	EVTS	DOCUMENT ID		TECN	COMMENT
10.9±2.2 OUR AVERAGE					
11.7±0.7±2.5	7584	AUGUSTIN	89	DM2	$J/\psi \to \rho^0\rho^\pm\pi^\mp$
8.4±4.5	36	VANNUCCI	77	MRK1	$e^+e^- \to 2(\pi^+\pi^-)\pi^0$

$\Gamma(\eta\pi^+\pi^-)/\Gamma_{total}$ — Γ_{16}/Γ

VALUE (units 10^{-4})	EVTS	DOCUMENT ID		TECN	COMMENT
3.78±0.68	471	[1] ABLIKIM	19Q	BES3	$e^+e^- \to J/\psi \to \eta\pi^+\pi^-$

[1] From an energy scan of $e^+e^- \to J/\psi \to \eta\pi^+\pi^-$ assuming PDG 16 values for $\Gamma(e^+e^-)$, $\Gamma(\mu^+\mu^-)$, and Γ(total).

$\Gamma(\eta\rho)/\Gamma_{total}$ — Γ_{17}/Γ

VALUE (units 10^{-3})	EVTS	DOCUMENT ID		TECN	COMMENT
0.193±0.023 OUR AVERAGE					
0.194±0.017±0.029	299	JOUSSET	90	DM2	$J/\psi \to$ hadrons
0.193±0.013±0.029		COFFMAN	88	MRK3	$e^+e^- \to \pi^+\pi^-\eta$

$\Gamma(\eta\phi(2170) \to \eta\phi f_0(980) \to \eta\phi\pi^+\pi^-)/\Gamma_{total}$ — Γ_{20}/Γ

VALUE (units 10^{-4})	EVTS	DOCUMENT ID		TECN	COMMENT
1.20±0.14±0.37	471	ABLIKIM	15H	BES3	$e^+e^- \to J/\psi \to \phi\eta\pi^+\pi^-$

$\Gamma(\eta\phi(2170) \to \eta K^*(892)^0\overline{K}^*(892)^0)/\Gamma_{total}$ — Γ_{21}/Γ

VALUE	CL%	DOCUMENT ID		TECN	COMMENT
<2.52 × 10^{-4}	90	ABLIKIM	10C	BES2	$J/\psi \to \eta K^+\pi^- K^-\pi^+$

$\Gamma(\eta K^\pm K^0_S\pi^\mp)/\Gamma_{total}$ — Γ_{23}/Γ

VALUE (units 10^{-4})	EVTS	DOCUMENT ID		TECN	COMMENT
21.8±2.2±3.4	232 ± 23	ABLIKIM	08E	BES2	$e^+e^- \to J/\psi$

$\Gamma(\eta K^*(892)^0\overline{K}^*(892)^0)/\Gamma_{total}$ — Γ_{24}/Γ

VALUE (units 10^{-3})	EVTS	DOCUMENT ID		TECN	COMMENT
1.15±0.13±0.22	209	ABLIKIM	10C	BES2	$J/\psi \to \eta K^+\pi^- K^-\pi^+$

$\Gamma(\rho\eta'(958))/\Gamma_{total}$ — Γ_{25}/Γ

VALUE (units 10^{-5})	EVTS	DOCUMENT ID		TECN	COMMENT
8.1 ±0.8 OUR AVERAGE	Error includes scale factor of 1.6.				
7.90±0.19±0.49	3476	[1] ABLIKIM	17AK	BES3	$J/\psi \to \pi^+\pi^-\eta'$
8.3 ±3.0 ±1.2	19	JOUSSET	90	DM2	$J/\psi \to$ hadrons
11.4 ±1.4 ±1.6		COFFMAN	88	MRK3	$J/\psi \to \pi^+\pi^-\eta'$

[1] From a partial wave analysis of the decay $J/\psi \to \pi^+\pi^-\eta'$.

$\Gamma(\rho^+K^+K^-\pi^- + \text{c.c} \to K^+K^-\pi^+\pi^-\pi^0)/\Gamma_{total}$ — Γ_{28}/Γ

VALUE (units 10^{-3})	EVTS	DOCUMENT ID		TECN	COMMENT
3.53±0.16±0.81	485	ANASHIN	22	KEDR	$J/\psi \to K^+K^-\pi^+\pi^-\pi^0$

$\Gamma(h_1(1415)\eta' \to \gamma\eta\eta')/\Gamma_{total}$ — Γ_{30}/Γ

VALUE (units 10^{-5})	DOCUMENT ID		TECN	COMMENT
• • • We do not use the following data for averages, fits, limits, etc. • • •				
$0.08\pm0.01^{+0.01}_{-0.02}$	[1] ABLIKIM	22AS	BES3	$J/\psi(1S) \to \gamma\eta\eta'$

[1] From a Breit-Wigner fit involving 9 resonances and a resonating exotic $\eta_1(1855) \to \eta\eta'$ P-wave.

$\Gamma(h_1(1595)\eta' \to \gamma\eta\eta')/\Gamma_{total}$ — Γ_{31}/Γ

VALUE (units 10^{-5})	DOCUMENT ID		TECN	COMMENT
• • • We do not use the following data for averages, fits, limits, etc. • • •				
$0.16\pm0.02^{+0.03}_{-0.01}$	[1] ABLIKIM	22AS	BES3	$J/\psi(1S) \to \gamma\eta\eta'$

[1] From a Breit-Wigner fit involving 9 resonances and a resonating exotic $\eta_1(1855) \to \eta\eta'$ P-wave.

$\Gamma(\rho(1450)\pi \to \pi^+\pi^-\pi^0)/\Gamma_{total}$ — Γ_{33}/Γ

VALUE (units 10^{-4})	EVTS	DOCUMENT ID		TECN	COMMENT
2.2±0.2±1.1	19.8k	[1] ANASHIN	23	KEDR	$e^+e^- \to J/\psi \to \pi^+\pi^-\pi^0$

[1] By a simultaneous fit of the $\pi\pi$ invariant mass distribution over the decay modes $J/\psi \to \rho^0\pi^0$, $J/\psi \to \rho^+\pi^-$, $J/\psi \to \rho^-\pi^+$. In the fit only the intermediate states $\rho(770)\pi$ and $\rho(1450)\pi$ are considered.

$\Gamma(\rho(1450)\pi \to \pi^+\pi^-\pi^0)/\Gamma(\pi^+\pi^-\pi^0)$ — Γ_{33}/Γ_{170}

VALUE (%)	EVTS	DOCUMENT ID		TECN	COMMENT
• • • We do not use the following data for averages, fits, limits, etc. • • •					
10.9 ±1.7 ±2.7	20k	[1] LEES	17C	BABR	$J/\psi \to \pi^+\pi^-\pi^0$
0.80±0.27	20k	[2] LEES	17C	BABR	$J/\psi \to \pi^+\pi^-\pi^0$

[1] From a Dalitz plot analysis in an isobar model.
[2] From a Dalitz plot analysis in a Veneziano model.

$\Gamma(\rho(1450)^\pm\pi^\mp \to K^0_S K^\pm\pi^\mp)/\Gamma(K^0_S K^\pm\pi^\mp)$ — Γ_{34}/Γ_{188}

VALUE (%)	EVTS	DOCUMENT ID		TECN	COMMENT
6.3±0.8±0.6	4k	[1] LEES	17C	BABR	$J/\psi \to K^0_S K^\pm\pi^\mp$

[1] From a Dalitz plot analysis in an isobar model.

$\Gamma(\rho(1450)^0\pi^0 \to K^+K^-\pi^0)/\Gamma(K^+K^-\pi^0)$ — Γ_{35}/Γ_{187}

VALUE (%)	EVTS	DOCUMENT ID		TECN	COMMENT
9.3±2.0±0.6	2k	[1] LEES	17C	BABR	$J/\psi \to K^+K^-\pi^0$

[1] From a Dalitz plot analysis in an isobar model.

$\Gamma(\rho(1450)\eta'(958) \to \pi^+\pi^-\eta'(958))/\Gamma_{total}$ — Γ_{36}/Γ

VALUE (units 10^{-6})	EVTS	DOCUMENT ID		TECN	COMMENT
3.28±0.55±0.44	119	[1] ABLIKIM	17AK	BES3	$J/\psi \to \pi^+\pi^-\eta'$

[1] From a partial wave analysis of the decay $J/\psi \to \pi^+\pi^-\eta'$.

$\Gamma(\rho(1700)\pi \to \pi^+\pi^-\pi^0)/\Gamma(\pi^+\pi^-\pi^0)$ — Γ_{38}/Γ_{170}

VALUE (units 10^{-3})	EVTS	DOCUMENT ID		TECN	COMMENT
8±2±5	20k	[1] LEES	17C	BABR	$J/\psi \to \pi^+\pi^-\pi^0$
• • • We do not use the following data for averages, fits, limits, etc. • • •					
22±6	20k	[2] LEES	17C	BABR	$J/\psi \to \pi^+\pi^-\pi^0$

[1] From a Dalitz plot analysis in an isobar model.
[2] From a Dalitz plot analysis in a Veneziano model.

$\Gamma(\rho(2150)\pi \to \pi^+\pi^-\pi^0)/\Gamma(\pi^+\pi^-\pi^0)$ — Γ_{40}/Γ_{170}

VALUE (units 10^{-4})	EVTS	DOCUMENT ID		TECN	COMMENT
4± 1±20	20k	[1] LEES	17C	BABR	$J/\psi \to \pi^+\pi^-\pi^0$
• • • We do not use the following data for averages, fits, limits, etc. • • •					
600±250	20k	[2] LEES	17C	BABR	$J/\psi \to \pi^+\pi^-\pi^0$

[1] From a Dalitz plot analysis in an isobar model.
[2] From a Dalitz plot analysis in a Veneziano model.

$\Gamma(\rho_3(1690)\pi \to \pi^+\pi^-\pi^0)/\Gamma(\pi^+\pi^-\pi^0)$ — Γ_{41}/Γ_{170}

VALUE (units 10^{-3})	EVTS	DOCUMENT ID		TECN	COMMENT
• • • We do not use the following data for averages, fits, limits, etc. • • •					
4.0±0.8	20k	[1] LEES	17C	BABR	$J/\psi \to \pi^+\pi^-\pi^0$

[1] From a Dalitz plot analysis in a Veneziano model.

$\Gamma(\omega\pi^0)/\Gamma_{total}$ — Γ_{42}/Γ

VALUE (units 10^{-3})	EVTS	DOCUMENT ID		TECN	COMMENT
0.45 ±0.05 OUR AVERAGE	Error includes scale factor of 1.4. See the ideogram below.				
0.538±0.012±0.065	2090	[1] ABLIKIM	06F	BES2	$J/\psi \to \omega\pi^0$
0.360±0.028±0.054	222	JOUSSET	90	DM2	$J/\psi \to$ hadrons
0.482±0.019±0.064		COFFMAN	88	MRK3	$e^+e^- \to \pi^0\pi^+\pi^-\pi^0$

[1] Using $B(\omega \to \pi^+\pi^-\pi^0) = (89.1 \pm 0.7)\%$.

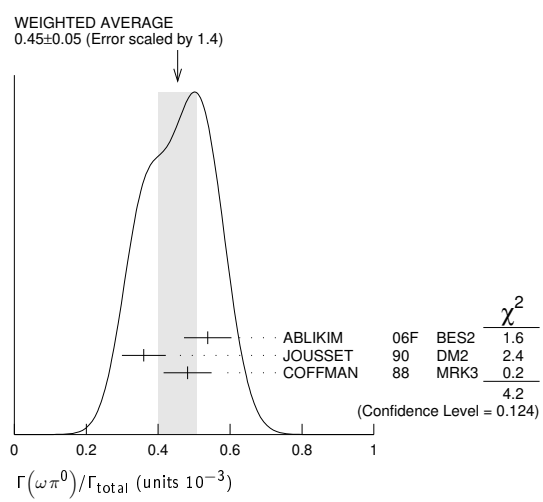

$\Gamma(\omega\pi^0 \to \pi^+\pi^-\pi^0)/\Gamma(\pi^+\pi^-\pi^0)$ — Γ_{43}/Γ_{170}

VALUE (units 10^{-4})	EVTS	DOCUMENT ID		TECN	COMMENT
8±3±2	20k	[1] LEES	17C	BABR	$J/\psi \to \pi^+\pi^-\pi^0$

[1] From a Dalitz plot analysis in an isobar model and significance 4.9 σ.

$\Gamma(\omega\pi^+\pi^-)/\Gamma_{total}$ — Γ_{44}/Γ

VALUE (units 10^{-3})	EVTS	DOCUMENT ID		TECN	COMMENT
8.5±1.0 OUR AVERAGE	Error includes scale factor of 1.3. See the ideogram below.				
10.6±1.2±0.1	3531	[1] ANASHIN	22	KEDR	$J/\psi \to 2(\pi^+\pi^-)\pi^0$
7.0±1.6	18058	AUGUSTIN	89	DM2	$J/\psi \to 2(\pi^+\pi^-)\pi^0$
7.8±1.6	215	BURMESTER	77D	PLUT	e^+e^-
6.8±1.9	348	VANNUCCI	77	MRK1	$e^+e^- \to 2(\pi^+\pi^-)\pi^0$

Int. J. Mod. Phys. A 2026.41. Downloaded from www.worldscientific.com
by UNIVERSITY OF CALIFORNIA @ BERKELEY on 09/16/26. Re-use and distribution is strictly not permitted, except for Open Access articles.

[1] ANASHIN 22 reports $[\Gamma(J/\psi(1S) \to \omega\pi^+\pi^-)/\Gamma_{total}] \times [B(\omega(782) \to \pi^+\pi^-\pi^0)] = (0.946 \pm 0.016 \pm 0.108) \times 10^{-2}$ which we divide by our best (shown rounded) value $B(\omega(782) \to \pi^+\pi^-\pi^0) = (89.2 \pm 0.7) \times 10^{-2}$. Our first error is their experiment's error and our second error is the systematic error from using our best (shown rounded) value.

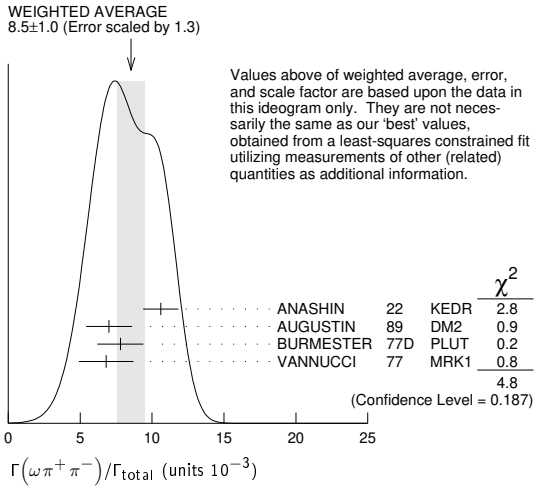

$\Gamma(\omega\pi^0\pi^0)/\Gamma_{total}$ — Γ_{45}/Γ

VALUE (units 10^{-3})	EVTS	DOCUMENT ID		TECN	COMMENT
3.4±0.3±0.7	509	AUGUSTIN	89	DM2	$J/\psi \to \pi^+\pi^-3\pi^0$

$\Gamma(\omega f_2(1270))/\Gamma_{total}$ — Γ_{47}/Γ

VALUE (units 10^{-3})	EVTS	DOCUMENT ID		TECN	COMMENT
4.3±0.6 OUR AVERAGE					
4.3±0.2±0.6	5860	AUGUSTIN	89	DM2	e^+e^-
4.0±1.6	70	BURMESTER	77D	PLUT	e^+e^-
• • • We do not use the following data for averages, fits, limits, etc. • • •					
1.9±0.8	81	VANNUCCI	77	MRK1	$e^+e^- \to 2(\pi^+\pi^-)\pi^0$

$\Gamma(\omega\eta)/\Gamma_{total}$ — Γ_{48}/Γ

VALUE (units 10^{-3})	EVTS	DOCUMENT ID		TECN	COMMENT
1.74 ±0.20 OUR AVERAGE	Error includes scale factor of 1.6. See the ideogram below.				
2.352±0.273	5k	[1] ABLIKIM	06F	BES2	$J/\psi \to \omega\eta$
1.44 ±0.40 ±0.14	13	[2] AUBERT	06D	BABR	10.6 $e^+e^- \to \omega\eta\gamma$
1.43 ±0.10 ±0.21	378	JOUSSET	90	DM2	$J/\psi \to$ hadrons
1.71 ±0.08 ±0.20		COFFMAN	88	MRK3	$e^+e^- \to 3\pi\eta$

[1] Using $B(\eta \to 2\gamma) = (39.43 \pm 0.26)\%$, $B(\eta \to \pi^+\pi^-\pi^0) = 22.6 \pm 0.4\%$, $B(\eta \to \pi^+\pi^-\gamma) = 4.68 \pm 0.11\%$, and $B(\omega \to \pi^+\pi^-\pi^0) = (89.1 \pm 0.7)\%$.
[2] Using $\Gamma(J/\psi \to e^+e^-) = 5.52 \pm 0.14 \pm 0.04$ keV.

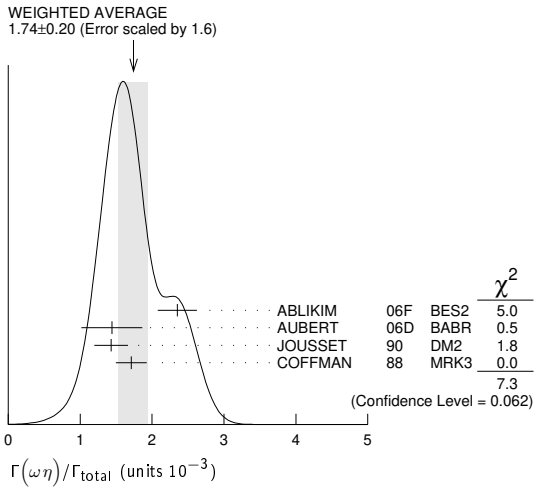

$\Gamma(\omega\pi^+\pi^+\pi^-\pi^-)/\Gamma_{total}$ — Γ_{51}/Γ

VALUE (units 10^{-4})	EVTS	DOCUMENT ID		TECN	COMMENT
85±34	140	VANNUCCI	77	MRK1	$e^+e^- \to 3(\pi^+\pi^-)\pi^0$

$\Gamma(\omega\eta'\pi^+\pi^-)/\Gamma_{total}$ — Γ_{53}/Γ

VALUE (units 10^{-3})	EVTS	DOCUMENT ID		TECN	COMMENT
1.12±0.02±0.13	14k	[1] ABLIKIM	19AC	BES3	$J/\psi \to \omega\eta'\pi^+\pi^-$

[1] Using the decays $\omega \to \pi^+\pi^-\pi^0$ and $\eta' \to \eta\pi^+\pi^-$.

$\Gamma(\omega\eta'(958))/\Gamma_{total}$ — Γ_{54}/Γ

VALUE (units 10^{-4})	EVTS	DOCUMENT ID		TECN	COMMENT
1.89±0.18 OUR AVERAGE					
2.08±0.30±0.14	137	[1] ABLIKIM	17AK	BES3	$J/\psi \to \pi^+\pi^-\eta'$
2.26±0.43	218	[2] ABLIKIM	06F	BES2	$J/\psi \to \omega\eta'$
$1.8\ ^{+1.0}_{-0.8}\ \pm0.3$	6	JOUSSET	90	DM2	$J/\psi \to$ hadrons
1.66±0.17±0.19		COFFMAN	88	MRK3	$e^+e^- \to 3\pi\eta'$

[1] From a partial wave analysis of the decay $J/\psi \to \pi^+\pi^-\eta'$.
[2] Using $B(\eta' \to \pi^+\pi^-\eta) = (44.3 \pm 1.5)\%$, $B(\eta' \to \pi^+\pi^-\gamma) = 29.5 \pm 1.0\%$, $B(\eta \to 2\gamma) = 39.43 \pm 0.26\%$, and $B(\omega \to \pi^+\pi^-\pi^0) = (89.1 \pm 0.7)\%$.

$\Gamma(\omega f_0(980))/\Gamma_{total}$ — Γ_{55}/Γ

VALUE (units 10^{-4})	DOCUMENT ID		TECN	COMMENT
1.41±0.27±0.47	[1] AUGUSTIN	89	DM2	$J/\psi \to 2(\pi^+\pi^-)\pi^0$

[1] Assuming $B(f_0(980) \to \pi\pi) = 0.78$.

$\Gamma(\omega f_0(1710) \to \omega K\overline{K})/\Gamma_{total}$ — Γ_{56}/Γ

VALUE (units 10^{-4})	DOCUMENT ID		TECN	COMMENT
4.8±1.1±0.3	[1,2] FALVARD	88	DM2	$J/\psi \to$ hadrons

[1] Includes unknown branching fraction $f_0(1710) \to K\overline{K}$.
[2] Addition of $f_0(1710) \to K^+K^-$ and $f_0(1710) \to K^0\overline{K}^0$ branching ratios.

$\Gamma(\omega f_1(1420))/\Gamma_{total}$ — Γ_{57}/Γ

VALUE (units 10^{-4})	EVTS	DOCUMENT ID		TECN	COMMENT
$\mathbf{6.8^{+1.9}_{-1.6}\pm1.7}$	111^{+31}_{-26}	BECKER	87	MRK3	$e^+e^- \to$ hadrons

$\Gamma(\omega f_2'(1525))/\Gamma_{total}$ — Γ_{58}/Γ

VALUE	CL%	DOCUMENT ID		TECN	COMMENT
$<2.2 \times 10^{-4}$	90	[1] VANNUCCI	77	MRK1	$e^+e^- \to \pi^+\pi^-\pi^0K^+K^-$
• • • We do not use the following data for averages, fits, limits, etc. • • •					
$<2.8 \times 10^{-4}$	90	[1] FALVARD	88	DM2	$J/\psi \to$ hadrons

[1] Re-evaluated assuming $B(f_2'(1525) \to K\overline{K}) = 0.713$.

$\Gamma(\omega X(1835) \to \omega p\overline{p})/\Gamma_{total}$ — Γ_{59}/Γ

VALUE	CL%	DOCUMENT ID		TECN	COMMENT
$<3.9 \times 10^{-6}$	95	ABLIKIM	13P	BES3	$J/\psi \to \gamma\pi^0p\overline{p}$

$\Gamma(\omega X(1835),\ X \to \eta'\pi^+\pi^-)/\Gamma_{total}$ — Γ_{61}/Γ

VALUE	DOCUMENT ID		TECN	COMMENT
$<6.2 \times 10^{-5}$	[1] ABLIKIM	19AC	BES3	$J/\psi \to \omega\eta'\pi^+\pi^-$

[1] Using the decays $\omega \to \pi^+\pi^-\pi^0$ and $\eta' \to \eta\pi^+\pi^-$.

$\Gamma(\omega K^+K^-)/\Gamma_{total}$ — Γ_{62}/Γ

VALUE (units 10^{-3})	EVTS	DOCUMENT ID		TECN	COMMENT
1.52±0.30±0.01	276	[1] ANASHIN	22	KEDR	$J/\psi \to K^+K^-\pi^+\pi^-\pi^0$

[1] ANASHIN 22 reports $[\Gamma(J/\psi(1S) \to \omega K^+K^-)/\Gamma_{total}] \times [B(\omega(782) \to \pi^+\pi^-\pi^0)] = (0.136 \pm 0.008 \pm 0.026) \times 10^{-2}$ which we divide by our best (shown rounded) value $B(\omega(782) \to \pi^+\pi^-\pi^0) = (89.2 \pm 0.7) \times 10^{-2}$. Our first error is their experiment's error and our second error is the systematic error from using our best (shown rounded) value.

$\Gamma(\omega K^+K^-\eta)/\Gamma_{total}$ — Γ_{60}/Γ

VALUE (units 10^{-4})	DOCUMENT ID		TECN	COMMENT
3.33±0.02±0.12	ABLIKIM	24BQ	BES3	$e^+e^- \to J/\psi(1S)$

$\Gamma(\omega K^\pm K^0_S\pi^\mp)/\Gamma_{total}$ — Γ_{63}/Γ

VALUE (units 10^{-4})	EVTS	DOCUMENT ID		TECN	COMMENT
34 ±5 OUR AVERAGE					
37.7±0.8±5.8	1972 ± 41	ABLIKIM	08E	BES2	$e^+e^- \to J/\psi$
29.5±1.4±7.0	879 ± 41	BECKER	87	MRK3	$e^+e^- \to$ hadrons

$\Gamma(\omega K\overline{K})/\Gamma_{total}$ — Γ_{64}/Γ

VALUE (units 10^{-4})	EVTS	DOCUMENT ID		TECN	COMMENT
19 ± 4 OUR AVERAGE					
19.8± 2.1±3.9		[1] FALVARD	88	DM2	$J/\psi \to$ hadrons
16 ±10	22	FELDMAN	77	MRK1	e^+e^-

[1] Addition of ωK^+K^- and $\omega K^0\overline{K}^0$ branching ratios.

$\Gamma(\omega K^*(892)\overline{K} + c.c.)/\Gamma_{total}$ — Γ_{65}/Γ

VALUE (units 10^{-4})	EVTS	DOCUMENT ID		TECN	COMMENT
61 ± 9 OUR AVERAGE					
62.0± 6.8±10.6	899 ± 98	ABLIKIM	08E	BES2	$J/\psi \to \omega K^0_S K^\pm\pi^\mp$
65.3±10.2±13.5	176 ± 28	ABLIKIM	08E	BES2	$J/\psi \to \omega K^+K^-\pi^0$
53 ±14 ±14	530 ± 140	BECKER	87	MRK3	$e^+e^- \to$ hadrons

$\Gamma(\eta' K^{*\pm}K^\mp)/\Gamma_{total}$ — Γ_{66}/Γ

VALUE (units 10^{-3})	DOCUMENT ID		TECN	COMMENT
1.48±0.13 OUR AVERAGE				
1.50±0.02±0.19	[1] ABLIKIM	18AB	BES3	$J/\psi \to \eta' K^*\overline{K}$
1.47±0.03±0.17	[2] ABLIKIM	18AB	BES3	$J/\psi \to \eta' K^*\overline{K}$

[1] From $\eta' K^+K^-\pi^0$.
[2] From $\eta' K^0_S K^\pm\pi^\mp$.

Int. J. Mod. Phys. A 2026.41. Downloaded from www.worldscientific.com
by [redacted]LIFORNIA @ BERKELEY on 09/16/26. Re-use and distribution is strictly not permitted, except for Open Access articles.

$\Gamma(\eta' K^{*0}\overline{K}^0 + \text{c.c.})/\Gamma_{\text{total}}$ — Γ_{67}/Γ

VALUE (units 10^{-3})	DOCUMENT ID		TECN	COMMENT
1.66±0.03±0.21	[1] ABLIKIM	18AB	BES3	$J/\psi \to \eta' K^* \overline{K}$

[1] From $\eta' K^0_S K^\pm \pi^\mp$.

$\Gamma(\eta' h_1(1415) \to \eta' K^* \overline{K} + \text{c.c.})/\Gamma_{\text{total}}$ — Γ_{68}/Γ

VALUE (units 10^{-4})	EVTS	DOCUMENT ID		TECN	COMMENT
2.16±0.12±0.29	1.1k	[1] ABLIKIM	18AB	BES3	$J/\psi \to \eta' h_1 \to \eta' K^* \overline{K}$

[1] From $\eta' K^0_S K^\pm \pi^\mp$.

$\Gamma(\eta' h_1(1415) \to \eta' K^{*\pm} K^\mp)/\Gamma_{\text{total}}$ — Γ_{69}/Γ

VALUE (units 10^{-4})	EVTS	DOCUMENT ID		TECN	COMMENT
1.51±0.09±0.21	1.0k	[1] ABLIKIM	18AB	BES3	$J/\psi \to \eta' h_1 \to \eta' K^* \overline{K}$

[1] From $\eta' K^+ K^- \pi^0$.

$\Gamma(\eta' h_1(1415) \to \gamma \eta' \eta')/\Gamma_{\text{total}}$ — Γ_{70}/Γ

VALUE (units 10^{-7})	DOCUMENT ID		TECN	COMMENT
$4.69 \pm 0.80 {}^{+0.74}_{-1.82}$	[1] ABLIKIM	22C	BES3	$J/\psi \to \gamma \eta' \eta' \to 4/5 \gamma 2(\pi^+\pi^-)$

[1] From a partial wave analysis of the systems (γX), with $X \to \eta' \eta'$, and $(\eta' X)$, with $X \to \gamma \eta'$ in the decay $J/\psi \to \gamma \eta' \eta'$. The intermediate resonance X is parametrized by a constant-width, relativistic Breit-Wigner.

$\Gamma(\overline{K} K^*(892) + \text{c.c.} \to K^0_S K^\pm \pi^\mp)/\Gamma(K^0_S K^\pm \pi^\mp)$ — Γ_{72}/Γ_{188}

VALUE (%)	EVTS	DOCUMENT ID		TECN	COMMENT
90.5±0.9±3.8	4k	[1] LEES	17C	BABR	$J/\psi \to K^0_S K^\pm \pi^\mp$

[1] From a Dalitz plot analysis in an isobar model.

$\Gamma(K^+ K^*(892)^- + \text{c.c.})/\Gamma_{\text{total}}$ — Γ_{73}/Γ

VALUE (units 10^{-3})	EVTS	DOCUMENT ID		TECN	COMMENT
$6.0 {}^{+0.8}_{-1.0}$ OUR AVERAGE Error includes scale factor of 2.9. See the ideogram below.					
$8.07 \pm 0.04 {}^{+0.38}_{-0.61}$	183k	ABLIKIM	19AQ	BES	$J/\psi \to K^+ K^- \pi^0$
$4.57 \pm 0.17 \pm 0.70$	2285	JOUSSET	90	DM2	$J/\psi \to$ hadrons
$5.26 \pm 0.13 \pm 0.53$		COFFMAN	88	MRK3	$J/\psi \to K^\pm K^0_S \pi^\mp$, $K^+ K^- \pi^0$
• • • We do not use the following data for averages, fits, limits, etc. • • •					
2.6 ± 0.6	24	FRANKLIN	83	MRK2	$J/\psi \to K^+ K^- \pi^0$
3.2 ± 0.6	48	VANNUCCI	77	MRK1	$J/\psi \to K^\pm K^0_S \pi^\mp$
4.1 ± 1.2	39	BRAUNSCH...	76	DASP	$J/\psi \to K^\pm X$

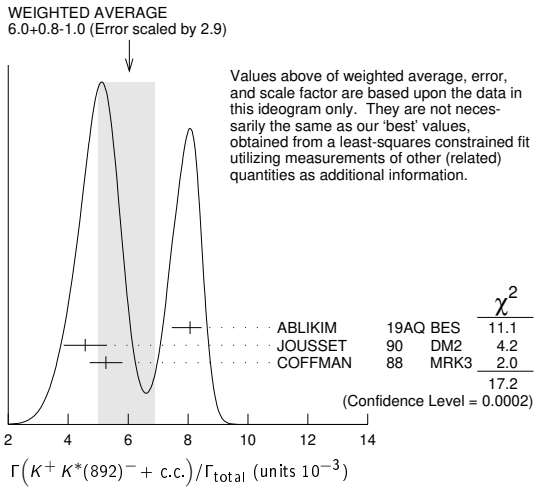

$\Gamma(K^+ K^*(892)^- + \text{c.c.} \to K^+ K^- \pi^0)/\Gamma_{\text{total}}$ — Γ_{74}/Γ

VALUE (units 10^{-3})	EVTS	DOCUMENT ID		TECN	COMMENT
$2.69 \pm 0.01 {}^{+0.13}_{-0.20}$	183k	ABLIKIM	19AQ	BES	$J/\psi \to K^+ K^- \pi^0$

$\Gamma(K^+ K^*(892)^- + \text{c.c.} \to K^+ K^- \pi^0)/\Gamma(K^+ K^- \pi^0)$ — Γ_{74}/Γ_{187}

VALUE (%)	EVTS	DOCUMENT ID		TECN	COMMENT
92.4±1.5±3.4	2k	[1] LEES	17C	BABR	$J/\psi \to K^+ K^- \pi^0$

[1] From a Dalitz plot analysis in an isobar model.

$\Gamma(K^0 \overline{K}^*(892)^0 + \text{c.c.})/\Gamma_{\text{total}}$ — Γ_{76}/Γ

VALUE (units 10^{-3})	EVTS	DOCUMENT ID		TECN	COMMENT
4.2 ±0.4 OUR AVERAGE					
$3.96 \pm 0.15 \pm 0.60$	1192	JOUSSET	90	DM2	$J/\psi \to$ hadrons
$4.33 \pm 0.12 \pm 0.45$		COFFMAN	88	MRK3	$J/\psi \to K^\pm K^0_S \pi^\mp$
• • • We do not use the following data for averages, fits, limits, etc. • • •					
2.7 ± 0.6	45	VANNUCCI	77	MRK1	$J/\psi \to K^\pm K^0_S \pi^\mp$

$\Gamma(\overline{K}^*(892)^0 K^+ \pi^- + \text{c.c.})/\Gamma_{\text{total}}$ — Γ_{78}/Γ

VALUE (units 10^{-3})	DOCUMENT ID		TECN	COMMENT
5.73±0.14±0.82	[1] ANASHIN	22	KEDR	$J/\psi \to K^+ K^- \pi^+ \pi^-$
• • • We do not use the following data for averages, fits, limits, etc. • • •				
seen	[2] ABLIKIM	06C	BES2	$J/\psi \to \overline{K}^*(892)^0 K^+ \pi^-$

[1] Obtained from $J/\psi \to K^*(892) K^- \pi^+ +$ c.c. $\to K^+ K^- \pi^+ \pi^-$ taking the value 2/3 for the probability of the $K^*(892)^0 \to K^+ \pi^-$ decay.

[2] A $K^*_0(700)$ is observed by ABLIKIM 06C in the $K^+ \pi^-$ mass spectrum of the $\overline{K}^*(892)^0 K^+ \pi^-$ final state against the $\overline{K}^*(892)$. A corresponding branching fraction of the $J/\psi(1S)$ is not presented.

$\Gamma(K^*(892)^0 K^- \pi^+ + \text{c.c.} \to K^+ K^- \pi^+ \pi^-)/\Gamma_{\text{total}}$ — Γ_{82}/Γ

VALUE (units 10^{-3})	EVTS	DOCUMENT ID		TECN	COMMENT
3.81±0.10±0.54	1559	ANASHIN	22	KEDR	$J/\psi \to K^+ K^- \pi^+ \pi^-$

$\Gamma(K^*(892)^0 K^0_S \to \gamma K^0_S K^0_S)/\Gamma_{\text{total}}$ — Γ_{83}/Γ

VALUE (units 10^{-6})	DOCUMENT ID		TECN	COMMENT
$6.28 {}^{+0.16}_{-0.17} {}^{+0.59}_{-0.52}$	ABLIKIM	18AA	BES3	$J/\psi \to \gamma K^0_S K^0_S$

$\Gamma(K^*(892)^\pm K^*(700)^\mp)/\Gamma_{\text{total}}$ — Γ_{85}/Γ

VALUE (units 10^{-3})	EVTS	DOCUMENT ID		TECN	COMMENT
$1.09 \pm 0.18 {}^{+0.94}_{-0.54}$	655	ABLIKIM	10E	BES2	$J/\psi \to K^\pm K^0_S \pi^\mp \pi^0$

$\Gamma(K^*(892)^0 \overline{K}^*(892)^0)/\Gamma_{\text{total}}$ — Γ_{86}/Γ

VALUE (units 10^{-4})	CL%	DOCUMENT ID		TECN	COMMENT
• • • We do not use the following data for averages, fits, limits, etc. • • •					
<5	90	VANNUCCI	77	MRK1	$e^+ e^- \to \pi^+ \pi^- K^+ K^-$

$\Gamma(K^*(892)^\pm K^*(892)^\mp)/\Gamma_{\text{total}}$ — Γ_{87}/Γ

VALUE (units 10^{-3})	EVTS	DOCUMENT ID		TECN	COMMENT
$1.00 \pm 0.19 {}^{+0.11}_{-0.32}$	323	ABLIKIM	10E	BES2	$J/\psi \to K^\pm K^0_S \pi^\mp \pi^0$

$\Gamma(K_1(1400)^\pm K^\mp)/\Gamma_{\text{total}}$ — Γ_{88}/Γ

VALUE (units 10^{-3})	DOCUMENT ID		TECN	COMMENT
3.8±0.8±1.2	[1] BAI	99C	BES	$e^+ e^-$

[1] Assuming $B(K_1(1400) \to K^* \pi) = 0.94 \pm 0.06$

$\Gamma(K^*(1410) \overline{K} + \text{c.c} \to K^\pm K^\mp \pi^0)/\Gamma(K^+ K^- \pi^0)$ — Γ_{90}/Γ_{187}

VALUE (%)	EVTS	DOCUMENT ID		TECN	COMMENT
2.3±1.1±0.7	2k	[1] LEES	17C	BABR	$J/\psi \to K^+ K^- \pi^0$

[1] From a Dalitz plot analysis in an isobar model.

$\Gamma(K^*(1410) \overline{K} + \text{c.c.} \to K^0_S K^\pm \pi^\mp)/\Gamma(K^0_S K^\pm \pi^\mp)$ — Γ_{91}/Γ_{188}

VALUE (%)	EVTS	DOCUMENT ID		TECN	COMMENT
1.5±0.5±0.9	4k	[1] LEES	17C	BABR	$J/\psi \to K^0_S K^\pm \pi^\mp$

[1] From a Dalitz plot analysis in an isobar model.

$\Gamma(K^*_2(1430) \overline{K} + \text{c.c.} \to K^\pm K^\mp \pi^0)/\Gamma(K^+ K^- \pi^0)$ — Γ_{93}/Γ_{187}

VALUE (%)	EVTS	DOCUMENT ID		TECN	COMMENT
3.5±1.3±0.9	2k	[1] LEES	17C	BABR	$J/\psi \to K^+ K^- \pi^0$

[1] From a Dalitz plot analysis in an isobar model.

$\Gamma(K^*_2(1430) \overline{K} + \text{c.c.} \to K^0_S K^\pm \pi^\mp)/\Gamma(K^0_S K^\pm \pi^\mp)$ — Γ_{94}/Γ_{188}

VALUE (%)	EVTS	DOCUMENT ID		TECN	COMMENT
7.1±1.3±1.2	4k	[1] LEES	17C	BABR	$J/\psi \to K^0_S K^\pm \pi^\mp$

[1] From a Dalitz plot analysis in an isobar model.

$\Gamma(\overline{K}^*_2(1430) K + \text{c.c.})/\Gamma_{\text{total}}$ — Γ_{95}/Γ

VALUE	CL%	DOCUMENT ID		TECN	COMMENT
$<40 \times 10^{-4}$	90	VANNUCCI	77	MRK1	$e^+ e^- \to K^0 \overline{K}^{*0}_2$
• • • We do not use the following data for averages, fits, limits, etc. • • •					
$<66 \times 10^{-4}$	90	BRAUNSCH...	76	DASP	$e^+ e^- \to K^\pm \overline{K}^{*\mp}_2$

$\Gamma(K^*_2(1430)^+ K^- + \text{c.c.} \to K^+ K^- \pi^0)/\Gamma_{\text{total}}$ — Γ_{96}/Γ

VALUE (units 10^{-4})	EVTS	DOCUMENT ID		TECN	COMMENT
$2.69 \pm 0.04 {}^{+0.25}_{-0.19}$	183k	ABLIKIM	19AQ	BES	$J/\psi \to K^+ K^- \pi^0$

$\Gamma(K^*_2(1430)^0 K^- \pi^+ + \text{c.c.} \to K^+ K^- \pi^+ \pi^-)/\Gamma_{\text{total}}$ — Γ_{97}/Γ

VALUE (units 10^{-3})	EVTS	DOCUMENT ID		TECN	COMMENT
2.65±0.80±0.44	1094	ANASHIN	22	KEDR	$J/\psi \to K^+ K^- \pi^+ \pi^-$

$\Gamma(\overline{K}^*_2(1430)^0 K^*(892)^0 + \text{c.c.})/\Gamma_{\text{total}}$ — Γ_{99}/Γ

VALUE (units 10^{-3})	EVTS	DOCUMENT ID		TECN	COMMENT
• • • We do not use the following data for averages, fits, limits, etc. • • •					
6.7 ± 2.6	40	VANNUCCI	77	MRK1	$e^+ e^- \to \pi^+ \pi^- K^+ K^-$

Int. J. Mod. Phys. A 2026.41. Downloaded from www.worldscientific.com
by UNIVERSITY OF CALIFORNIA @ BERKELEY on 09/16/26. Re-use and distribution is strictly not permitted, except for Open Access articles.

$\Gamma(K_2^*(1430)^0 \overline{K}_2^*(1430)^0)/\Gamma_{total}$ — Γ_{102}/Γ

VALUE	CL%	DOCUMENT ID		TECN	COMMENT
$<29 \times 10^{-4}$	90	VANNUCCI	77	MRK1	$e^+e^- \to \pi^+\pi^- K^+K^-$

$\Gamma(K_2^*(1980)^+ K^- + \text{c.c.} \to K^+K^-\pi^0)/\Gamma_{total}$ — Γ_{104}/Γ

VALUE (units 10^{-5})	EVTS	DOCUMENT ID		TECN	COMMENT
$1.1 \pm 0.1^{+0.6}_{-0.1}$	183k	ABLIKIM	19AQ	BES	$J/\psi \to K^+K^-\pi^0$

$\Gamma(K_4^*(2045)^+ K^- + \text{c.c.} \to K^+K^-\pi^0)/\Gamma_{total}$ — Γ_{105}/Γ

VALUE (units 10^{-6})	EVTS	DOCUMENT ID		TECN	COMMENT
$6.2 \pm 0.7^{+2.8}_{-1.4}$	183k	ABLIKIM	19AQ	BES	$J/\psi \to K^+K^-\pi^0$

$\Gamma(K_1(1270)^\pm K^\mp)/\Gamma_{total}$ — Γ_{106}/Γ

VALUE	CL%	DOCUMENT ID		TECN	COMMENT
$<3.0 \times 10^{-3}$	90	[1] BAI	99C	BES	e^+e^-

[1] Assuming $B(K_1(1270) \to K\rho) = 0.42 \pm 0.06$

$\Gamma(K_1(1270) K_S^0 \to \gamma K_S^0 K_S^0)/\Gamma_{total}$ — Γ_{107}/Γ

VALUE (units 10^{-7})	DOCUMENT ID		TECN	COMMENT
$8.54^{+1.07}_{-1.20}{}^{+2.35}_{-2.13}$	ABLIKIM	18AA	BES3	$J/\psi \to \gamma K_S^0 K_S^0$

$\Gamma(a_2(1320)^\pm \pi^\mp)/\Gamma_{total}$ — Γ_{108}/Γ

VALUE	CL%	DOCUMENT ID		TECN	COMMENT
$<43 \times 10^{-4}$	90	BRAUNSCH...	76	DASP	e^+e^-

$\Gamma(\phi\pi^0)/\Gamma_{total}$ — Γ_{109}/Γ

The two different fit values of ABLIKIM 15K below have the same statistical significance of 6.4 σ and cannot be distinguished at this moment.

VALUE (units 10^{-6})	CL%	EVTS	DOCUMENT ID		TECN	COMMENT
$2.94 \pm 0.16 \pm 0.16$		0.8k	[1] ABLIKIM	15K	BES3	$e^+e^- \to J/\psi \to K^+K^-\gamma\gamma$
$0.124 \pm 0.033 \pm 0.030$		35 ± 9	[2] ABLIKIM	15K	BES3	$e^+e^- \to J/\psi \to K^+K^-\gamma\gamma$
• • • We do not use the following data for averages, fits, limits, etc. • • •						
<6.4	90		[3] ABLIKIM	05B	BES2	$e^+e^- \to J/\psi \to \phi\gamma\gamma$
<6.8	90		COFFMAN	88	MRK3	$e^+e^- \to K^+K^-\pi^0$

[1] Corresponding to one of the two fit solutions with $\delta = (-95.9 \pm 1.5)^\circ$ for the phase angle between the resonant $J/\psi \to \phi\pi^0$ and non-phi $J/\psi \to K^+K^-\pi^0$ contributions.
[2] Corresponding to one of the two fit solutions with $\delta = (-152.1 \pm 7.7)^\circ$ for the phase angle between the resonant $J/\psi \to \phi\pi^0$ and non-phi $J/\psi \to K^+K^-\pi^0$ contributions.
[3] Superseded by ABLIKIM 15K.

$\Gamma(\phi\pi^+\pi^-)/\Gamma_{total}$ — Γ_{110}/Γ

VALUE (units 10^{-3})	EVTS	DOCUMENT ID		TECN	COMMENT
0.94 ± 0.15 OUR AVERAGE	Error includes scale factor of 1.7.				
$1.09 \pm 0.02 \pm 0.13$		ABLIKIM	05	BES2	$J/\psi \to \phi\pi^+\pi^-$
$0.78 \pm 0.03 \pm 0.12$		FALVARD	88	DM2	$J/\psi \to$ hadrons
2.1 ± 0.9	23	FELDMAN	77	MRK1	e^+e^-

$\Gamma(\phi 2(\pi^+\pi^-))/\Gamma_{total}$ — Γ_{112}/Γ

VALUE (units 10^{-4})	DOCUMENT ID		TECN	COMMENT
$16.0 \pm 1.0 \pm 3.0$	FALVARD	88	DM2	$J/\psi \to$ hadrons

$\Gamma(\phi\eta)/\Gamma_{total}$ — Γ_{113}/Γ

VALUE (units 10^{-3})	EVTS	DOCUMENT ID		TECN	COMMENT
0.74 ± 0.06 OUR AVERAGE	Error includes scale factor of 1.2.				
$0.71 \pm 0.10 \pm 0.05$	99 ± 14	[1] ZHU	23	BELL	$e^+e^- \to \Upsilon(nS) \to \phi\eta\gamma$
$0.898 \pm 0.024 \pm 0.089$		ABLIKIM	05B	BES2	$e^+e^- \to J/\psi \to$ hadr
$0.64 \pm 0.04 \pm 0.11$	346	JOUSSET	90	DM2	$J/\psi \to$ hadrons
$0.661 \pm 0.045 \pm 0.078$		COFFMAN	88	MRK3	$e^+e^- \to K^+K^-\eta$

[1] From a fit to the combined $\phi\eta$ invariant mass spectrum with a Gaussian function for the J/ψ signals and a second-order polynomial function for the backgrounds.

$\Gamma(\phi\eta'(958))/\Gamma_{total}$ — Γ_{114}/Γ

VALUE (units 10^{-4})	CL%	EVTS	DOCUMENT ID		TECN	COMMENT
4.6 ± 0.5 OUR AVERAGE	Error includes scale factor of 2.2. See the ideogram below.					
$5.10 \pm 0.03 \pm 0.32$		31k	ABLIKIM	16M	BES3	$e^+e^- \to J/\psi \to$ hadrons
$5.46 \pm 0.31 \pm 0.56$			ABLIKIM	05B	BES2	$e^+e^- \to J/\psi \to$ hadrons
$4.1 \pm 0.3 \pm 0.8$		167	JOUSSET	90	DM2	$J/\psi \to$ hadrons
$3.08 \pm 0.34 \pm 0.36$			COFFMAN	88	MRK3	$e^+e^- \to K^+K^-\eta'$
• • • We do not use the following data for averages, fits, limits, etc. • • •						
< 13	90		VANNUCCI	77	MRK1	e^+e^-

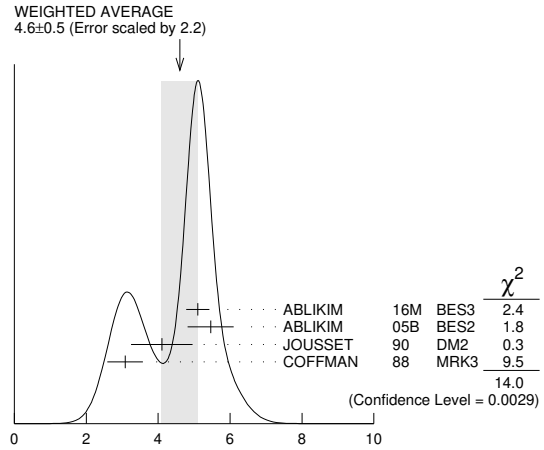

$\Gamma(\phi\eta\eta')/\Gamma_{total}$ — Γ_{115}/Γ

VALUE (units 10^{-4})	EVTS	DOCUMENT ID		TECN	COMMENT
$2.32 \pm 0.06 \pm 0.16$	2.2k	[1] ABLIKIM	19AN	BES3	$e^+e^- \to J/\psi \to$ hadrons

[1] Including contributions from intermediate resonances. Evidence for an intermediate resonance at M $\approx$ 2 GeV and $\Gamma \approx 150$ MeV decaying to $\phi\eta'$ with $J^P = 1^+$ or $J^P = 1^-$, and $B(J/\psi \to \eta X) \times B(X \to \phi\eta') \approx 10^{-4}$.

$\Gamma(\phi f_0(980))/\Gamma_{total}$ — Γ_{116}/Γ

VALUE (units 10^{-4})	EVTS	DOCUMENT ID		TECN	COMMENT
3.2 ± 0.9 OUR AVERAGE	Error includes scale factor of 1.9.				
$4.6 \pm 0.4 \pm 0.8$		[1] FALVARD	88	DM2	$J/\psi \to$ hadrons
2.6 ± 0.6	50	[1] GIDAL	81	MRK2	$J/\psi \to K^+K^-K^+K^-$

[1] Assuming $B(f_0(980) \to \pi\pi) = 0.78$.

$\Gamma(\phi\pi^0 f_0(980) \to \phi\pi^0\pi^+\pi^-)/\Gamma_{total}$ — Γ_{119}/Γ

VALUE (units 10^{-6})	EVTS	DOCUMENT ID		TECN	COMMENT
$4.50 \pm 0.80 \pm 0.61$	355	ABLIKIM	15P	BES3	$J/\psi \to K^+K^-3\pi$

$\Gamma(\phi\pi^0 f_0(980) \to \phi\pi^0 p^0\pi^0)/\Gamma_{total}$ — Γ_{120}/Γ

VALUE (units 10^{-6})	EVTS	DOCUMENT ID		TECN	COMMENT
$1.67 \pm 0.50 \pm 0.24$	70	ABLIKIM	15P	BES3	$J/\psi \to K^+K^-3\pi$

$\Gamma(\phi f_0(980)\eta \to \eta\phi\pi^+\pi^-)/\Gamma_{total}$ — Γ_{121}/Γ

VALUE (units 10^{-4})	EVTS	DOCUMENT ID		TECN	COMMENT
$3.23 \pm 0.75 \pm 0.73$	52	ABLIKIM	08F	BES	$J/\psi \to \eta\phi f_0(980)$

$\Gamma(\phi a_0(980)^0 \to \phi\eta\pi^0)/\Gamma_{total}$ — Γ_{122}/Γ

VALUE (units 10^{-6})	DOCUMENT ID		TECN	COMMENT
• • • We do not use the following data for averages, fits, limits, etc. • • •				
$3.24 \pm 0.20^{+0.52}_{-0.22}$	[1] ABLIKIM	24CB	BES3	$J/\psi \to \phi\eta\pi^0$
$2.74 \pm 0.13^{+0.15}_{-0.16}$	[2] ABLIKIM	24CB	BES3	$J/\psi \to \phi\eta\pi^0$
4.37 ± 1.35	[3,4] ABLIKIM	18D	BES3	$J/\psi \to \phi\eta\pi^0$
$5.0 \pm 2.7 \pm 2.5$	[5] ABLIKIM	11D	BES3	$J/\psi \to \phi\eta\pi^0$

[1] $J/\psi \to \phi a_0(980)$ electromagnetic decay.
[2] $J/\psi \to \phi f_0(980)$, $\phi a_0(980)$ mixing.
[3] Assuming constructive interference between $a_0(980) - f_0(980)$ mixing and electromagnetic decay. Destructive interference gives a value of $(4.93 \pm 1.77) \times 10^{-6}$ for this branching fraction.
[4] Superseded by ABLIKIM 24CB.
[5] Assuming $a_0(980) - f_0(980)$ mixing and isospin breaking via γ^* and K^*K loops.

$\Gamma(\phi(1680)^0\pi^0 \to \phi\eta\pi^0)/\Gamma_{total}$ — Γ_{123}/Γ

VALUE (units 10^{-6})	DOCUMENT ID		TECN	COMMENT
$6.66 \pm 0.26^{+1.1}_{-1.0}$	ABLIKIM	24CB	BES3	$J/\psi \to \phi\eta\pi^0$

$\Gamma(X(2000)^0\pi^0 \to \phi\eta\pi^0)/\Gamma_{total}$ — Γ_{124}/Γ

VALUE (units 10^{-6})	DOCUMENT ID		TECN	COMMENT
$1.70 \pm 0.19^{+0.48}_{-0.13}$	ABLIKIM	24CB	BES3	$J/\psi \to \phi\eta\pi^0$

$\Gamma(h_1(1900)^0\pi^0 \to \phi\eta\pi^0)/\Gamma_{total}$ — Γ_{125}/Γ

VALUE (units 10^{-6})	DOCUMENT ID		TECN	COMMENT
$8.44 \pm 0.35^{+1.4}_{-1.2}$	ABLIKIM	24CB	BES3	$J/\psi \to \phi\eta\pi^0$

Int. J. Mod. Phys. A 2026.41. Downloaded from www.worldscientific.com
by CALIFORNIA @ BERKELEY on 09/16/26. Re-use and distribution is strictly not permitted, except for Open Access articles.

$\Gamma(\phi f_2(1270))/\Gamma_{total}$ — Γ_{126}/Γ

VALUE (units 10^{-3})	CL%	DOCUMENT ID		TECN	COMMENT
• • • We do not use the following data for averages, fits, limits, etc. • • •					
< 0.45	90	FALVARD	88	DM2	$J/\psi \to$ hadrons
< 0.37	90	VANNUCCI	77	MRK1	$e^+e^- \to \pi^+\pi^- K^+K^-$

$\Gamma(\phi f_1(1285))/\Gamma_{total}$ — Γ_{127}/Γ

VALUE (units 10^{-4})	EVTS	DOCUMENT ID		TECN	COMMENT
2.6±0.5 OUR AVERAGE					
$3.4\pm1.8\pm1.5$	1.1k	[1] ABLIKIM	15H	BES3	$e^+e^- \to J/\psi \to \phi\eta\pi^+\pi^-$
$3.2\pm0.6\pm0.4$		JOUSSET	90	DM2	$J/\psi \to \phi(\pi^+\pi^-)$
$2.1\pm0.5\pm0.4$	25	[2] JOUSSET	90	DM2	$J/\psi \to \phi\eta\pi^+\pi^-$
• • • We do not use the following data for averages, fits, limits, etc. • • •					
$0.6\pm0.2\pm0.1$	16	BECKER	87	MRK3	$J/\psi \to \phi K\overline{K}\pi$

[1] ABLIKIM 15H reports $[\Gamma(J/\psi(1S) \to \phi f_1(1285))/\Gamma_{total}] \times [B(f_1(1285) \to \eta\pi^+\pi^-)] = (1.20 \pm 0.6 \pm 0.14) \times 10^{-4}$ which we divide by our best (shown rounded) value $B(f_1(1285) \to \eta\pi^+\pi^-) = (35 \pm 15) \times 10^{-2}$. Our first error is their experiment's error and our second error is the systematic error from using our best (shown rounded) value.

[2] We attribute to the $f_1(1285)$ the signal observed in the $\pi^+\pi^-\eta$ invariant mass distribution at 1297 MeV.

$\Gamma(\phi f_1(1285) \to \phi\pi^0 f_0(980) \to \phi\pi^0\pi^+\pi^-)/\Gamma_{total}$ — Γ_{128}/Γ

VALUE (units 10^{-7})	EVTS	DOCUMENT ID		TECN	COMMENT
9.36±2.31±1.54	78	ABLIKIM	15P	BES3	$J/\psi \to K^+K^-3\pi$

$\Gamma(\phi f_1(1285) \to \phi\pi^0 f_0(980) \to \phi 3\pi^0)/\Gamma_{total}$ — Γ_{129}/Γ

VALUE (units 10^{-7})	EVTS	DOCUMENT ID		TECN	COMMENT
2.08±1.63±1.47	9	ABLIKIM	15P	BES3	$J/\psi \to K^+K^-3\pi$

$\Gamma(\phi\eta(1405) \to \phi\eta\pi^+\pi^-)/\Gamma_{total}$ — Γ_{130}/Γ

VALUE (units 10^{-5})	CL%	EVTS	DOCUMENT ID		TECN	COMMENT
2.01±0.58±0.82		172	[1] ABLIKIM	15H	BES3	$e^+e^- \to J/\psi \to \phi\eta\pi^+\pi^-$
• • • We do not use the following data for averages, fits, limits, etc. • • •						
< 17	90		[2] FALVARD	88	DM2	$J/\psi \to$ hadrons

[1] With 3.6 σ significance.

[2] Includes unknown branching fraction $\eta(1405) \to \eta\pi\pi$.

$\Gamma(\phi f'_2(1525))/\Gamma_{total}$ — Γ_{131}/Γ

VALUE (units 10^{-4})	EVTS	DOCUMENT ID		TECN	COMMENT
8 ±4 OUR AVERAGE Error includes scale factor of 2.7.					
$12.3\pm0.6\pm2.0$		[1,2] FALVARD	88	DM2	$J/\psi \to$ hadrons
4.8 ± 1.8	46	[1] GIDAL	81	MRK2	$J/\psi \to K^+K^-K^+K^-$

[1] Re-evaluated using $B(f'_2(1525) \to K\overline{K}) = 0.713$.

[2] Including interference with $f_0(1710)$.

$\Gamma(\phi X(1835) \to \phi p\overline{p})/\Gamma_{total}$ — Γ_{132}/Γ

VALUE	CL%	DOCUMENT ID		TECN	COMMENT
$<2.1 \times 10^{-7}$	90	[1] ABLIKIM	16K	BES3	$J/\psi \to p\overline{p}K^0_S K^0_L$, $p\overline{p}K^+K^-$

[1] Upper limit applies to any $p\overline{p}$ mass enhancement near threshold.

$\Gamma(\phi X(1835) \to \phi\eta\pi^+\pi^-)/\Gamma_{total}$ — Γ_{133}/Γ

VALUE	CL%	DOCUMENT ID		TECN	COMMENT
$<2.8 \times 10^{-4}$	90	ABLIKIM	15H	BES3	$e^+e^- \to J/\psi \to \phi\eta\pi^+\pi^-$

$\Gamma(\phi X(1870) \to \phi\eta\pi^+\pi^-)/\Gamma_{total}$ — Γ_{134}/Γ

VALUE	CL%	DOCUMENT ID		TECN	COMMENT
$<6.13 \times 10^{-5}$	90	ABLIKIM	15H	BES3	$e^+e^- \to J/\psi \to \phi\eta\pi^+\pi^-$

$\Gamma(\phi K\overline{K})/\Gamma_{total}$ — Γ_{135}/Γ

VALUE (units 10^{-4})	EVTS	DOCUMENT ID		TECN	COMMENT
17.7± 1.6 OUR AVERAGE Error includes scale factor of 1.3. See the ideogram below.					
$16.6\pm 1.9\pm1.2$	163 ± 19	LEES	12F	BABR	$10.6\ e^+e^- \to 2(K^+K^-)\gamma$
$21.4\pm 0.4\pm2.2$		ABLIKIM	05	BES2	$J/\psi \to \phi\pi^+\pi^-$
$48\ ^{+20}_{-16}\ \pm6$	$9.0^{+3.7}_{-3.0}$	[1,2] HUANG	03	BELL	$B^+ \to (\phi K^+K^-)\ K^+$
$14.6\pm 0.8\pm2.1$		[3] FALVARD	88	DM2	$J/\psi \to$ hadrons
$18\ \pm 8$	14	FELDMAN	77	MRK1	e^+e^-

[1] We have multiplied K^+K^- measurement by 2 to obtain $K\overline{K}$.

[2] Using $B(B^+ \to J/\psi K^+) = (1.01 \pm 0.05) \times 10^{-3}$.

[3] Addition of ϕK^+K^- and $\phi K^0\overline{K}^0$ branching ratios.

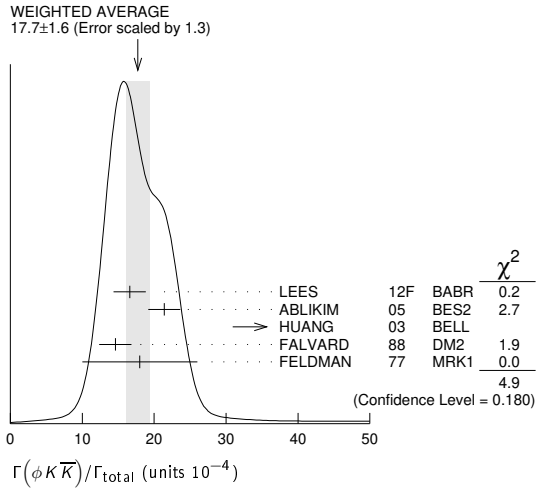

$\Gamma(\phi f_0(1710) \to \phi K\overline{K})/\Gamma_{total}$ — Γ_{136}/Γ

VALUE (units 10^{-4})	DOCUMENT ID		TECN	COMMENT
3.6±0.2±0.6	[1,2] FALVARD	88	DM2	$J/\psi \to$ hadrons

[1] Including interference with $f'_2(1525)$.

[2] Includes unknown branching fraction $f_0(1710) \to K\overline{K}$.

$\Gamma(\phi K^\pm K^0_S \pi^\mp)/\Gamma_{total}$ — Γ_{139}/Γ

VALUE (units 10^{-4})	EVTS	DOCUMENT ID		TECN	COMMENT
7.2±0.8 OUR AVERAGE					
$7.4\pm0.6\pm1.4$	227 ± 19	ABLIKIM	08E	BES2	$e^+e^- \to J/\psi$
$7.4\pm0.9\pm1.1$		FALVARD	88	DM2	$J/\psi \to$ hadrons
$7\ \pm0.6\pm1.0$	163 ± 15	BECKER	87	MRK3	$e^+e^- \to$ hadrons

$\Gamma(\phi K^*(892)\overline{K} + c.c.)/\Gamma_{total}$ — Γ_{140}/Γ

VALUE (units 10^{-4})	EVTS	DOCUMENT ID		TECN	COMMENT
21.8±2.3 OUR AVERAGE					
$20.8\pm2.7\pm3.9$	195 ± 25	ABLIKIM	08E	BES2	$J/\psi \to \phi K^0_S K^\pm\pi^\mp$
$29.6\pm3.7\pm4.7$	238 ± 30	ABLIKIM	08E	BES2	$J/\psi \to \phi K^+K^-\pi^0$
$20.7\pm2.4\pm3.0$		FALVARD	88	DM2	$J/\psi \to$ hadrons
$20\ \pm3\ \pm3$	155 ± 20	BECKER	87	MRK3	$e^+e^- \to$ hadrons

$\Gamma(b_1(1235)^\pm\pi^\mp)/\Gamma_{total}$ — Γ_{141}/Γ

VALUE (units 10^{-4})	EVTS	DOCUMENT ID		TECN	COMMENT
30±5 OUR AVERAGE					
31 ± 6	4600	AUGUSTIN	89	DM2	$J/\psi \to 2(\pi^+\pi^-)\pi^0$
29 ± 7	87	BURMESTER	77D	PLUT	e^+e^-

$\Gamma(b_1(1235)^0\pi^0)/\Gamma_{total}$ — Γ_{142}/Γ

VALUE (units 10^{-4})	EVTS	DOCUMENT ID		TECN	COMMENT
23±3±5	229	AUGUSTIN	89	DM2	e^+e^-

$\Gamma(\Delta(1232)^+\overline{p})/\Gamma_{total}$ — Γ_{144}/Γ

VALUE	CL%	DOCUMENT ID		TECN	COMMENT
$<0.1 \times 10^{-3}$	90	HENRARD	87	DM2	e^+e^-

$\Gamma(\Delta(1232)^{++}\overline{p}\pi^-)/\Gamma_{total}$ — Γ_{145}/Γ

VALUE (units 10^{-3})	EVTS	DOCUMENT ID		TECN	COMMENT
1.58±0.23±0.40	332	EATON	84	MRK2	e^+e^-

$\Gamma(\Delta(1232)^{++}\overline{\Delta}(1232)^{--})/\Gamma_{total}$ — Γ_{146}/Γ

VALUE (units 10^{-3})	EVTS	DOCUMENT ID		TECN	COMMENT
1.10±0.09±0.28	233	EATON	84	MRK2	e^+e^-

$\Gamma(\overline{\Sigma}(1385)^0 pK^-)/\Gamma_{total}$ — Γ_{147}/Γ

VALUE (units 10^{-3})	EVTS	DOCUMENT ID		TECN	COMMENT
0.51±0.26±0.18	89	EATON	84	MRK2	e^+e^-

$\Gamma(\Sigma(1385)^0\overline{\Lambda} + c.c.)/\Gamma_{total}$ — Γ_{148}/Γ

VALUE	CL%	DOCUMENT ID		TECN	COMMENT
$<0.82 \times 10^{-5}$	90	ABLIKIM	13F	BES3	$J/\psi \to p\overline{p}\pi^+\pi^-\gamma\gamma$
• • • We do not use the following data for averages, fits, limits, etc. • • •					
$<0.2\ \times 10^{-3}$	90	HENRARD	87	DM2	e^+e^-

$\Gamma(\Sigma(1385)^-\overline{\Sigma}^+ + c.c.)/\Gamma_{total}$ — Γ_{149}/Γ

VALUE (units 10^{-3})	EVTS	DOCUMENT ID		TECN	COMMENT
0.30±0.07 OUR AVERAGE					
$0.30\pm0.03\pm0.08$	74 ± 8	HENRARD	87	DM2	e^+e^-
$0.29\pm0.11\pm0.10$	26	EATON	84	MRK2	e^+e^-

Int. J. Mod. Phys. A 2026.41. Downloaded from www.worldscientific.com by UNIVERSITY OF CALIFORNIA @ BERKELEY on 09/16/26. Re-use and distribution is strictly not permitted, except for Open Access articles.

$\Gamma(\Sigma(1385)^+\overline{\Sigma}^- + \text{c.c.})/\Gamma_{\text{total}}$ — Γ_{150}/Γ

VALUE (units 10^{-3})	EVTS	DOCUMENT ID		TECN	COMMENT
0.33±0.08 OUR AVERAGE					
0.34±0.04±0.08	77	HENRARD	87	DM2	e^+e^-
0.31±0.11±0.11	28	EATON	84	MRK2	e^+e^-

$\Gamma(\Sigma(1385)^-\overline{\Sigma}(1385)^+ + \text{c.c.})/\Gamma_{\text{total}}$ — Γ_{151}/Γ

VALUE (units 10^{-3})	EVTS	DOCUMENT ID		TECN	COMMENT
1.08 ±0.06 OUR AVERAGE					
1.096±0.012±0.071	43k	ABLIKIM	16L	BES3	e^+e^-
1.23 ±0.07 ±0.30	0.8k	ABLIKIM	12P	BES2	e^+e^-
1.00 ±0.04 ±0.21	0.6k	HENRARD	87	DM2	e^+e^-
0.86 ±0.18 ±0.22	56	EATON	84	MRK2	e^+e^-

$\Gamma(\Sigma(1385)^+\overline{\Sigma}(1385)^- + \text{c.c.})/\Gamma_{\text{total}}$ — Γ_{152}/Γ

VALUE (units 10^{-3})	EVTS	DOCUMENT ID		TECN	COMMENT
1.25 ±0.07 OUR AVERAGE					
1.258±0.014±0.078	53k	ABLIKIM	16L	BES3	e^+e^-
1.50 ±0.08 ±0.38	1k	ABLIKIM	12P	BES2	e^+e^-
1.19 ±0.04 ±0.25	0.7k	HENRARD	87	DM2	e^+e^-
1.03 ±0.24 ±0.25	68	EATON	84	MRK2	e^+e^-

$\Gamma(\Sigma(1385)^0\overline{\Sigma}(1385)^0)/\Gamma_{\text{total}}$ — Γ_{153}/Γ

VALUE (units 10^{-3})	EVTS	DOCUMENT ID		TECN	COMMENT
1.071±0.009±0.082	103k	ABLIKIM	17E	BES3	$e^+e^- \to J/\psi \to$ hadrons

$\Gamma(\Lambda(1520)\overline{\Lambda} + \text{c.c.} \to \gamma\Lambda\overline{\Lambda})/\Gamma_{\text{total}}$ — Γ_{154}/Γ

VALUE	CL%	DOCUMENT ID		TECN	COMMENT
$<4.1\times10^{-6}$	90	ABLIKIM	12B	BES3	$J/\psi \to \Lambda\overline{\Lambda}\gamma$

$\Gamma(\overline{\Lambda}(1520)\Lambda + \text{c.c.})/\Gamma_{\text{total}}$ — Γ_{155}/Γ

VALUE	CL%	DOCUMENT ID		TECN	COMMENT
$<1.80\times10^{-3}$	90	LU	19	BELL	$B^+ \to \overline{p}\Lambda K^+K^+$

$\Gamma(\Xi^0\overline{\Xi}^0)/\Gamma_{\text{total}}$ — Γ_{156}/Γ

VALUE (units 10^{-3})	EVTS	DOCUMENT ID		TECN	COMMENT
1.17 ±0.04 OUR AVERAGE					
1.165±0.004±0.043	135k	ABLIKIM	17E	BES3	$e^+e^- \to J/\psi \to$ hadrons
1.20 ±0.12 ±0.21	206	ABLIKIM	08O	BES2	$e^+e^- \to J/\psi$

$\Gamma(\Xi(1530)^-\overline{\Xi}^+ + \text{c.c.})/\Gamma_{\text{total}}$ — Γ_{157}/Γ

VALUE (units 10^{-3})	EVTS	DOCUMENT ID		TECN	COMMENT
0.318±0.008 OUR AVERAGE					
0.317±0.002±0.008	70k	ABLIKIM	20	BES3	$e^+e^- \to J/\psi$
0.59 ±0.09 ±0.12	75	HENRARD	87	DM2	e^+e^-

$\Gamma(\Xi(1530)^0\overline{\Xi}^0)/\Gamma_{\text{total}}$ — Γ_{158}/Γ

VALUE (units 10^{-3})	EVTS	DOCUMENT ID		TECN	COMMENT
0.32±0.12±0.07	24 ± 9	HENRARD	87	DM2	e^+e^-

$\Gamma(\Theta(1540)\overline{\Theta}(1540) \to K^0_S pK^-\overline{n} + \text{c.c.})/\Gamma_{\text{total}}$ — Γ_{159}/Γ

VALUE	CL%	DOCUMENT ID		TECN	COMMENT
$<1.1\times10^{-5}$	90	BAI	04G	BES2	e^+e^-

$\Gamma(\Theta(1540)K^-\overline{n} \to K^0_S pK^-\overline{n})/\Gamma_{\text{total}}$ — Γ_{160}/Γ

VALUE	CL%	DOCUMENT ID		TECN	COMMENT
$<2.1\times10^{-5}$	90	BAI	04G	BES2	e^+e^-

$\Gamma(\Theta(1540)K^0_S\overline{p} \to K^0_S\overline{p}K^+n)/\Gamma_{\text{total}}$ — Γ_{161}/Γ

VALUE	CL%	DOCUMENT ID		TECN	COMMENT
$<1.6\times10^{-5}$	90	BAI	04G	BES2	e^+e^-

$\Gamma(\overline{\Theta}(1540)K^+n \to K^0_S\overline{p}K^+n)/\Gamma_{\text{total}}$ — Γ_{162}/Γ

VALUE	CL%	DOCUMENT ID		TECN	COMMENT
$<5.6\times10^{-5}$	90	BAI	04G	BES2	e^+e^-

$\Gamma(\overline{\Theta}(1540)K^0_S p \to K^0_S pK^-\overline{n})/\Gamma_{\text{total}}$ — Γ_{163}/Γ

VALUE	CL%	DOCUMENT ID		TECN	COMMENT
$<1.1\times10^{-5}$	90	BAI	04G	BES2	e^+e^-

STABLE HADRONS

$\Gamma(2(\pi^+\pi^-)\pi^0)/\Gamma_{\text{total}}$ — Γ_{164}/Γ

VALUE (units 10^{-2})	EVTS	DOCUMENT ID		TECN	COMMENT
4.2 ±0.4 OUR AVERAGE Error includes scale factor of 2.1. See the ideogram below.					
5.44±0.07±0.33	23k	ANASHIN	22	KEDR	$J/\psi \to 2(\pi^+\pi^-)\pi^0$
3.5 ±0.8 ±0.1	14k	[1] LEES	21	BABR	10.6 $e^+e^- \to 2(\pi^+\pi^-)3\pi^0\gamma$
4.73±0.44	228k	[2] ABLIKIM	19Q	BES3	$J/\psi \to 2(\pi^+\pi^-)\pi^0$
3.25±0.49	46055	AUGUSTIN	89	DM2	$J/\psi \to 2(\pi^+\pi^-)\pi^0$
3.17±0.42	147	FRANKLIN	83	MRK2	$e^+e^- \to$ hadrons
3.64±0.52	1500	BURMESTER	77D	PLUT	e^+e^-
4 ±1	675	JEAN-MARIE	76	MRK1	e^+e^-

[1] LEES 21 reports $[\Gamma(J/\psi(1S) \to 2(\pi^+\pi^-)\pi^0)/\Gamma_{\text{total}}] \times [\Gamma(\psi(2S) \to e^+e^-)] \times [B(\psi(2S) \to J/\psi(1S)\pi^0\pi^0)] = (14.8 \pm 2.6 \pm 2.2) \times 10^{-3}$ keV which we divide by our best (shown rounded) values $\Gamma(\psi(2S) \to e^+e^-) = 2.33 \pm 0.04$ keV, $B(\psi(2S) \to J/\psi(1S)\pi^0\pi^0) = (18.3 \pm 0.5) \times 10^{-2}$. Our first error is their experiment's error and our second error is the systematic error from using our best (shown rounded) values.

[2] From an energy scan of $e^+e^- \to J/\psi \to 2(\pi^+\pi^-)\pi^0$, assuming PDG 16 values for $\Gamma(e^+e^-)$, $\Gamma(\mu^+\mu^-)$, and $\Gamma(\text{total})$, and for a phase difference between strong and electromagnetic amplitudes of $(84.9 \pm 3.6)^\circ$. An alternative solution is $(4.85 \pm 0.45)\%$ with a phase of $(-84.7 \pm 3.1)^\circ$.

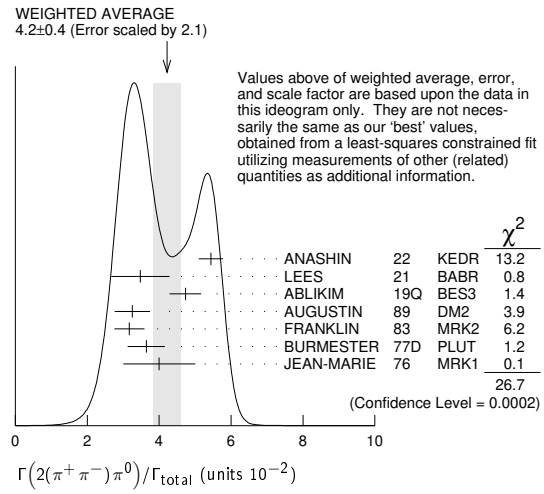

$\Gamma(3(\pi^+\pi^-)\pi^0)/\Gamma_{\text{total}}$ — Γ_{165}/Γ

VALUE	EVTS	DOCUMENT ID		TECN	COMMENT
0.029±0.006 OUR AVERAGE					
0.028±0.009	11	FRANKLIN	83	MRK2	$e^+e^- \to$ hadrons
0.029±0.007	181	JEAN-MARIE	76	MRK1	e^+e^-

$\Gamma(\pi^+\pi^-\pi^0)/\Gamma_{\text{total}}$ — Γ_{170}/Γ

VALUE (units 10^{-3})	EVTS	DOCUMENT ID		TECN	COMMENT
20.0 ±0.7 OUR AVERAGE Error includes scale factor of 2.0. See the ideogram below.					
18.78±0.13±0.51	19.8k	[1] ANASHIN	23	KEDR	$e^+e^- \to J/\psi \to \pi^+\pi^-\pi^0$
$21.37\pm0.04^{+0.64}_{-0.62}$	1.8M	[2] ABLIKIM	12H	BES3	$e^+e^- \to J/\psi \to \pi^+\pi^-\pi^0$
23.0 ±2.0 ±0.4	256	[3] AUBERT	07AU	BABR	10.6 $e^+e^- \to J/\psi\pi^+\pi^-\gamma$
21.84±0.05±2.01	220k	[4,5] BAI	04H	BES	e^+e^-
20.91±0.21±1.16		[5,6] BAI	04H	BES	e^+e^-
15 ±2	168	FRANKLIN	83	MRK2	e^+e^-

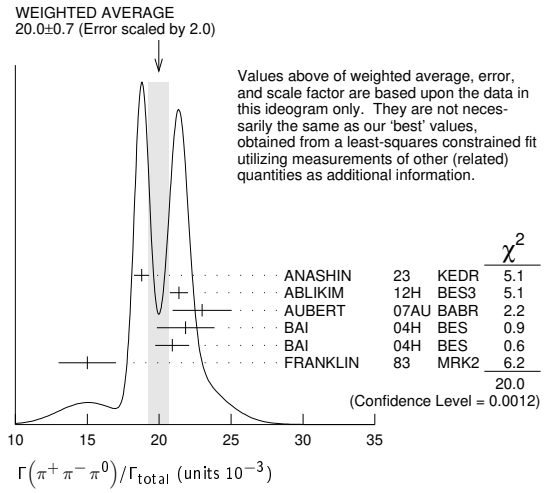

[1] By a simultaneous fit of the $\pi\pi$ invariant mass distribution over the decay modes $J/\psi \to \rho^0\pi^0$, $J/\psi \to \rho^+\pi^-$, $J/\psi \to \rho^-\pi^+$. In the fit only the intermediate states $\rho(770)\pi$ and $\rho(1450)\pi$ are considered.

[2] The quoted systematic error includes a contribution of 1.23% (added in quadrature) from the uncertainty on the number of J/ψ events.

[3] AUBERT 07AU reports $[\Gamma(J/\psi(1S) \to \pi^+\pi^-\pi^0)/\Gamma_{\text{total}}] \times [\Gamma(\psi(2S) \to J/\psi(1S)\pi^+\pi^-) \times \Gamma(\psi(2S) \to e^+e^-)/\Gamma_{\text{total}}] = (18.6 \pm 1.2 \pm 1.1) \times 10^{-3}$ keV which we divide by our best (shown rounded) value $\Gamma(\psi(2S) \to J/\psi(1S)\pi^+\pi^-) \times \Gamma(\psi(2S) \to e^+e^-)/\Gamma_{\text{total}} = 0.809 \pm 0.014$ keV. Our first error is their experiment's error and our second error is the systematic error from using our best (shown rounded) value.

Int. J. Mod. Phys. A 2026.41. Downloaded from www.worldscientific.com by LIFORNIA @ BERKELEY on 09/16/26. Re-use and distribution is strictly not permitted, except for Open Access articles.

[4] From $J/\psi \to \pi^+\pi^-\pi^0$ events directly.
[5] Mostly $\rho\pi$, see also $\rho\pi$ subsection.
[6] Obtained comparing the rates for $\pi^+\pi^-\pi^0$ and $\mu^+\mu^-$, using J/ψ events produced via $\psi(2S) \to \pi^+\pi^- J/\psi$ and with $B(J/\psi \to \mu^+\mu^-) = 5.88 \pm 0.10\%$.

$\Gamma(\pi^+\pi^-\pi^0 K^+ K^-)/\Gamma_{total}$ — Γ_{172}/Γ

VALUE (units 10^{-2})	EVTS	DOCUMENT ID		TECN	COMMENT
1.52±0.27 OUR AVERAGE		Error includes scale factor of 1.4.			
1.74±0.08±0.24	2616	ANASHIN	22	KEDR	$J/\psi \to K^+K^-\pi^+\pi^-\pi^0$
1.2 ±0.3	309	VANNUCCI	77	MRK1	e^+e^-

$\Gamma(\pi^+\pi^-)/\Gamma_{total}$ — Γ_{173}/Γ

VALUE (units 10^{-4})	EVTS	DOCUMENT ID		TECN	COMMENT
1.47±0.14 OUR AVERAGE					
1.47±0.13±0.13	140	[1] METREVELI	12		$\psi(2S) \to 2(\pi^+\pi^-)$
1.58±0.20±0.15	84	BALTRUSAIT...85D		MRK3	e^+e^-
1.0 ±0.5	5	BRANDELIK	78B	DASP	e^+e^-
1.6 ±1.6	1	VANNUCCI	77	MRK1	e^+e^-

[1] Obtained by analyzing CLEO-c data but not authored by the CLEO Collaboration.

$\Gamma(2(\pi^+\pi^-))/\Gamma_{total}$ — Γ_{174}/Γ

VALUE (units 10^{-3})	EVTS	DOCUMENT ID		TECN	COMMENT
3.20±0.25 OUR AVERAGE		Error includes scale factor of 1.2.			
2.88±0.14±0.24	2654	ANASHIN	22	KEDR	$J/\psi \to 2(\pi^+\pi^-)$
3.53±0.12±0.29	1107	[1] ABLIKIM	05H	BES2	$e^+e^- \to \psi(2S) \to J/\psi\pi^+\pi^-$, $J/\psi \to 2(\pi^+\pi^-)$
4.0 ±1.0	76	JEAN-MARIE	76	MRK1	e^+e^-

[1] Computed using $B(J/\psi \to \mu^+\mu^-) = 0.0588 \pm 0.0010$.

$\Gamma(3(\pi^+\pi^-))/\Gamma_{total}$ — Γ_{175}/Γ

VALUE (units 10^{-4})	EVTS	DOCUMENT ID		TECN	COMMENT
• • • We do not use the following data for averages, fits, limits, etc. • • •					
40±20	32	JEAN-MARIE	76	MRK1	e^+e^-

$\Gamma(4(\pi^+\pi^-)\pi^0)/\Gamma_{total}$ — Γ_{177}/Γ

VALUE (units 10^{-4})	EVTS	DOCUMENT ID		TECN	COMMENT
90±30	13	JEAN-MARIE	76	MRK1	e^+e^-

$\Gamma(2(\pi^+\pi^-)\eta)/\Gamma_{total}$ — Γ_{178}/Γ

VALUE (units 10^{-3})	EVTS	DOCUMENT ID		TECN	COMMENT
2.29±0.28 OUR AVERAGE					
3.1 ±1.5 ±0.1	14k	[1] LEES	21	BABR	10.6 $e^+e^- \to 2(\pi^+\pi^-)3\pi^0\gamma$
2.26±0.08±0.27	4.8k	ABLIKIM	05C	BES2	$e^+e^- \to 2(\pi^+\pi^-)\eta$

[1] LEES 21 reports $[\Gamma(J/\psi(1S) \to 2(\pi^+\pi^-)\eta)/\Gamma_{total}] \times [\Gamma(J/\psi(1S) \to e^+e^-)] \times [B(\eta \to 3\pi^0)] = (5.6 \pm 2.6 \pm 0.8) \times 10^{-3}$ keV which we divide by our best (shown rounded) values $\Gamma(J/\psi(1S) \to e^+e^-) = 5.53 \pm 0.10$ keV, $B(\eta \to 3\pi^0) = (32.56 \pm 0.21) \times 10^{-2}$. Our first error is their experiment's error and our second error is the systematic error from using our best (shown rounded) values.

$\Gamma(3(\pi^+\pi^-)\eta)/\Gamma_{total}$ — Γ_{179}/Γ

VALUE (units 10^{-4})	EVTS	DOCUMENT ID		TECN	COMMENT
7.24±0.96±1.11	616	ABLIKIM	05C	BES2	$e^+e^- \to 3(\pi^+\pi^-)\eta$

$\Gamma(K^+K^-)/\Gamma_{total}$ — Γ_{183}/Γ

VALUE (units 10^{-4})	EVTS	DOCUMENT ID		TECN	COMMENT
3.06 ±0.05 OUR AVERAGE					
3.072±0.023±0.050	1.8 k	[1] ABLIKIM	24AB	BES3	$\psi(2S) \to \pi^+\pi^-K^+K^-$
2.86 ±0.09 ±0.19	1k	[2] METREVELI	12		$\psi(2S) \to \pi^+\pi^-K^+K^-$
• • • We do not use the following data for averages, fits, limits, etc. • • •					
2.39 ±0.24 ±0.22	107	[3] BALTRUSAIT...85D		MRK3	e^+e^-
2.2 ±0.9	6	[3] BRANDELIK	79C	DASP	e^+e^-

[1] Using $B(J/\psi \to \mu^+\mu^-) = (5.916 \pm 0.033)\%$.
[2] Obtained by analyzing CLEO-c data but not authored by the CLEO Collaboration.
[3] Interference with non-resonant K^+K^- production not taken into account.

$\Gamma(K^0_S K^0_L)/\Gamma_{total}$ — Γ_{184}/Γ

VALUE (units 10^{-4})	EVTS	DOCUMENT ID		TECN	COMMENT
1.95±0.11 OUR AVERAGE		Error includes scale factor of 2.4. See the ideogram below.			
1.93±0.01±0.05	110k	ABLIKIM	17AH	BES3	$J/\psi \to K^0_S K^0_L \to \pi^+\pi^- X$
2.62±0.15±0.14	0.3k	[1] METREVELI	12		$\psi(2S) \to \pi^+\pi^- K^0_S K^0_L$
1.82±0.04±0.13	2.1k	[2] BAI	04A	BES2	$J/\psi \to K^0_S K^0_L \to \pi^+\pi^- X$
• • • We do not use the following data for averages, fits, limits, etc. • • •					
1.18±0.12±0.18		JOUSSET	90	DM2	$J/\psi \to$ hadrons
1.01±0.16±0.09	74	BALTRUSAIT...85D		MRK3	e^+e^-

[1] Obtained by analyzing CLEO-c data but not authored by the CLEO Collaboration.
[2] Using $B(K^0_S \to \pi^+\pi^-) = 0.6868 \pm 0.0027$.

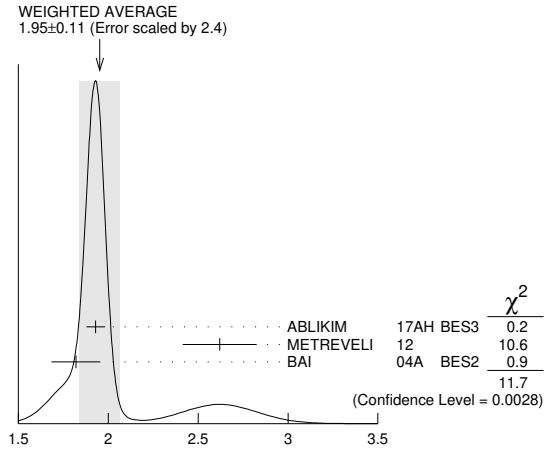

$\Gamma(K^0_S K^0_L)/\Gamma_{total}$ — Γ_{184}/Γ

$\Gamma(K^0_S K^0_S)/\Gamma_{total}$ — Γ_{185}/Γ

VALUE	CL%	DOCUMENT ID		TECN	COMMENT
<4.7 × 10^{-9}	90	ABLIKIM	25CC	BES3	$J/\psi \to K^0_S K^0_S \to \pi^+\pi^-\pi^+\pi^-$
• • • We do not use the following data for averages, fits, limits, etc. • • •					
<1.4 × 10^{-8}	95	[1] ABLIKIM	17AH	BES3	$J/\psi \to K^0_S K^0_S \to \pi^+\pi^-\pi^+\pi^-$
<1 × 10^{-6}	95	[1] BAI	04D	BES	$e^+e^- \to J/\psi \to K^0_S K^0_S$
<5.2 × 10^{-6}	90	[1] BALTRUSAIT...85C		MRK3	e^+e^-

[1] Forbidden by *CP*.

$\Gamma(K\overline{K}\pi)/\Gamma_{total}$ — Γ_{186}/Γ

VALUE (units 10^{-4})	EVTS	DOCUMENT ID		TECN	COMMENT
61 ±10 OUR AVERAGE					
55.2±12.0	25	FRANKLIN	83	MRK2	$e^+e^- \to K^+K^-\pi^0$
78.0±21.0	126	VANNUCCI	77	MRK1	$e^+e^- \to K^0_S K^\pm\pi^\mp$

$\Gamma(K^+K^-\pi^0)/\Gamma_{total}$ — Γ_{187}/Γ

VALUE (units 10^{-3})	EVTS	DOCUMENT ID		TECN	COMMENT
2.88±0.01±0.12	183k	ABLIKIM	19AQ	BES	$J/\psi \to K^+K^-\pi^0$

$\Gamma(K^+K^-\pi^0)/\Gamma(\pi^+\pi^-\pi^0)$ — $\Gamma_{187}/\Gamma_{170}$

VALUE (%)	EVTS	DOCUMENT ID		TECN	COMMENT
12.0±0.3±0.9	23k	LEES	17C	BABR	$J/\psi \to h^+h^-\pi^0$

$\Gamma(K^0_S K^\pm\pi^\mp)/\Gamma(\pi^+\pi^-\pi^0)$ — $\Gamma_{188}/\Gamma_{170}$

VALUE (%)	EVTS	DOCUMENT ID		TECN	COMMENT
26.5±0.5±2.1	24k	LEES	17C	BABR	$J/\psi \to h^0h^+h^-$

$\Gamma(K^+K^-\pi^+\pi^-)/\Gamma_{total}$ — Γ_{192}/Γ

VALUE (units 10^{-3})	EVTS	DOCUMENT ID		TECN	COMMENT
7.04±0.26±0.92	2671	ANASHIN	22	KEDR	$J/\psi \to K^+K^-\pi^+\pi^-$
• • • We do not use the following data for averages, fits, limits, etc. • • •					
7.2 ±2.3	205	VANNUCCI	77	MRK1	e^+e^-

$\Gamma(K^+K^-2(\pi^+\pi^-))/\Gamma_{total}$ — Γ_{204}/Γ

VALUE (units 10^{-4})	EVTS	DOCUMENT ID		TECN	COMMENT
31±13	30	VANNUCCI	77	MRK1	e^+e^-

$\Gamma(2(K^+K^-))/\Gamma_{total}$ — Γ_{206}/Γ

VALUE (units 10^{-3})	EVTS	DOCUMENT ID		TECN	COMMENT
• • • We do not use the following data for averages, fits, limits, etc. • • •					
$1.4^{+0.5}_{-0.4}\pm0.2$	$11.0^{+4.3}_{-3.5}$	[1] HUANG	03	BELL	$B^+ \to 2(K^+K^-)K^+$
0.7±0.3		VANNUCCI	77	MRK1	e^+e^-

[1] Using $B(B^+ \to J/\psi K^+) = (1.01 \pm 0.05) \times 10^{-3}$.

$\Gamma(p\overline{p})/\Gamma_{total}$ — Γ_{214}/Γ

VALUE (units 10^{-3})	EVTS	DOCUMENT ID		TECN	COMMENT
2.121±0.029 OUR AVERAGE					
2.112±0.004±0.031	314k	ABLIKIM	12C	BES3	e^+e^-
2.17 ±0.16 ±0.04	317	[1] WU	06	BELL	$B^+ \to p\overline{p}K^+$
2.26 ±0.01 ±0.14	63316	BAI	04E	BES2	$e^+e^- \to J/\psi$
1.97 ±0.22	99	BALDINI	98	FENI	e^+e^-
1.91 ±0.04 ±0.30		PALLIN	87	DM2	e^+e^-
2.16 ±0.07 ±0.15	1420	EATON	84	MRK2	e^+e^-
2.5 ±0.4	133	BRANDELIK	79C	DASP	e^+e^-
2.0 ±0.5		BESCH	78	BONA	e^+e^-

Int. J. Mod. Phys. A 2026.41. Downloaded from www.worldscientific.com
by UNIVERSITY OF CALIFORNIA @ BERKELEY on 09/16/26. Re-use and distribution is strictly not permitted, except for Open Access articles.

2.2 ±0.2	331	[2] PERUZZI	78	MRK1	e^+e^-

• • • We do not use the following data for averages, fits, limits, etc. • • •

2.0 ±0.3	48	ANTONELLI	93	SPEC	e^+e^-

[1] WU 06 reports $[\Gamma(J/\psi(1S) \to p\overline{p})/\Gamma_{total}] \times [B(B^+ \to J/\psi(1S)K^+)] = (2.21 \pm 0.13 \pm 0.10) \times 10^{-6}$ which we divide by our best (shown rounded) value $B(B^+ \to J/\psi(1S)K^+) = (1.019 \pm 0.019) \times 10^{-3}$. Our first error is their experiment's error and our second error is the systematic error from using our best (shown rounded) value.

[2] Assuming angular distribution $(1+\cos^2\theta)$.

$\Gamma(p\overline{p}\pi^0)/\Gamma_{total}$ — Γ_{215}/Γ

VALUE (units 10^{-3})	EVTS	DOCUMENT ID		TECN	COMMENT
1.19±0.08 OUR AVERAGE	Error includes scale factor of 1.1.				
1.33±0.02±0.11	11k	ABLIKIM	09B	BES2	e^+e^-
1.13±0.09±0.09	685	EATON	84	MRK2	e^+e^-
1.4 ±0.4		BRANDELIK	79C	DASP	e^+e^-
1.00±0.15	109	PERUZZI	78	MRK1	e^+e^-

$\Gamma(p\overline{p}\pi^+\pi^-)/\Gamma_{total}$ — Γ_{216}/Γ

VALUE (units 10^{-3})	EVTS	DOCUMENT ID		TECN	COMMENT
6.0 ±0.5 OUR AVERAGE	Error includes scale factor of 1.3. See the ideogram below.				
6.46±0.17±0.43	1435	EATON	84	MRK2	e^+e^-
3.8 ±1.6	48	BESCH	81	BONA	e^+e^-
5.5 ±0.6	533	PERUZZI	78	MRK1	e^+e^-

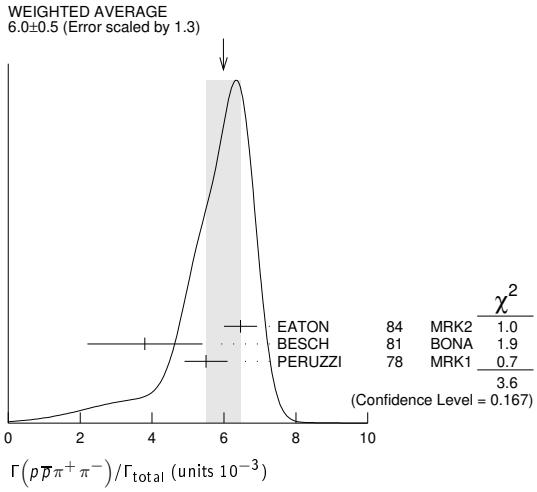

$\Gamma(p\overline{p}\pi^+\pi^-\pi^0)/\Gamma_{total}$ — Γ_{217}/Γ

Including $p\overline{p}\pi^+\pi^-\gamma$ and excluding ω, η, η'

VALUE (units 10^{-3})	EVTS	DOCUMENT ID		TECN	COMMENT
2.3 ±0.9 OUR AVERAGE	Error includes scale factor of 1.9.				
3.36±0.65±0.28	364	EATON	84	MRK2	e^+e^-
1.6 ±0.6	39	PERUZZI	78	MRK1	e^+e^-

$\Gamma(p\overline{p}\eta)/\Gamma_{total}$ — Γ_{218}/Γ

VALUE (units 10^{-3})	EVTS	DOCUMENT ID		TECN	COMMENT
1.513±0.023 OUR AVERAGE					
1.496±0.001±0.023	3.2M	[1] ABLIKIM	24BV	BES3	e^+e^-
1.91 ±0.02 ±0.17	13k	[1] ABLIKIM	09	BES2	e^+e^-
2.03 ±0.13 ±0.15	826	EATON	84	MRK2	e^+e^-
2.5 ±1.2		BRANDELIK	79C	DASP	e^+e^-
2.3 ±0.4	197	PERUZZI	78	MRK1	e^+e^-

[1] Combining the $p\overline{p}\eta \to p\overline{p}\gamma\gamma$ and $p\overline{p}\eta \to p\overline{p}\pi^+\pi^-\pi^0$ channels.

$\Gamma(p\overline{p}\rho)/\Gamma_{total}$ — Γ_{219}/Γ

VALUE	CL%	DOCUMENT ID		TECN	COMMENT
$<0.31 \times 10^{-3}$	90	EATON	84	MRK2	$e^+e^- \to$ hadronsγ

$\Gamma(p\overline{p}\omega)/\Gamma_{total}$ — Γ_{220}/Γ

VALUE (units 10^{-3})	EVTS	DOCUMENT ID		TECN	COMMENT
0.98±0.10 OUR AVERAGE	Error includes scale factor of 1.3. See the ideogram below.				
0.90±0.02±0.09	2670	ABLIKIM	13P	BES3	e^+e^-
0.98±0.03±0.14	2449	ABLIKIM	08	BES2	e^+e^-
1.10±0.17±0.18	486	EATON	84	MRK2	e^+e^-
1.6 ±0.3	77	PERUZZI	78	MRK1	e^+e^-

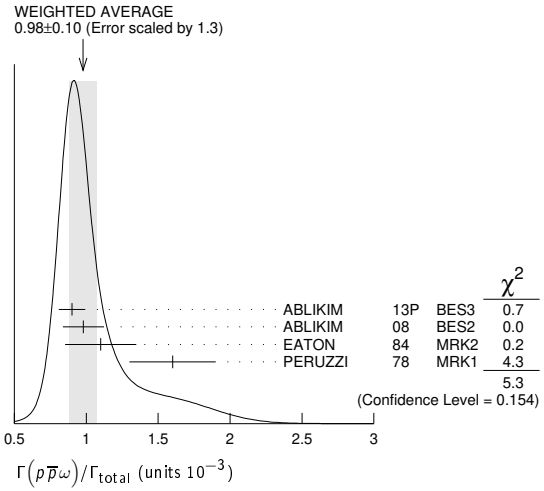

$\Gamma(p\overline{p}\eta'(958))/\Gamma_{total}$ — Γ_{221}/Γ

VALUE (units 10^{-3})	EVTS	DOCUMENT ID		TECN	COMMENT
0.129±0.014 OUR AVERAGE	Error includes scale factor of 2.0.				
0.126±0.002±0.007	16k	[1] ABLIKIM	19N	BES3	e^+e^-
0.200±0.023±0.028	265 ± 31	[2] ABLIKIM	09	BES2	e^+e^-
0.68 ±0.23 ±0.17	19	EATON	84	MRK2	e^+e^-
1.8 ±0.6	19	PERUZZI	78	MRK1	e^+e^-

[1] From the combination of $p\overline{p}\eta' \to p\overline{p}\pi^+\pi^-\eta$ and $p\overline{p}\eta' \to p\overline{p}\pi^+\pi^-\gamma$ channels.

[2] From the combination of $p\overline{p}\eta' \to p\overline{p}\pi^+\pi^-\eta$ and $p\overline{p}\eta' \to p\overline{p}\gamma\rho^0$ channels.

$\Gamma(p\overline{p}a_0(980) \to p\overline{p}\pi^0\eta)/\Gamma_{total}$ — Γ_{222}/Γ

VALUE (units 10^{-5})	DOCUMENT ID		TECN	COMMENT
6.8±1.2±1.3	ABLIKIM	14N	BES3	$e^+e^- \to J/\psi$

$\Gamma(p\overline{p}\phi)/\Gamma_{total}$ — Γ_{223}/Γ

VALUE (units 10^{-4})	EVTS	DOCUMENT ID		TECN	COMMENT
0.519±0.033 OUR AVERAGE					
0.523±0.006±0.033	14k	ABLIKIM	16K	BES3	$J/\psi \to p\overline{p}K^0_S K^0_L$, $p\overline{p}K^+K^-$
0.45 ±0.13 ±0.07		FALVARD	88	DM2	$J/\psi \to$ hadrons

$\Gamma(p\overline{n}\pi^-)/\Gamma_{total}$ — Γ_{224}/Γ

VALUE (units 10^{-3})	EVTS	DOCUMENT ID		TECN	COMMENT
2.12±0.09 OUR AVERAGE					
2.36±0.02±0.21	59k	ABLIKIM	06K	BES2	$J/\psi \to p\pi^-\overline{n}$
2.47±0.02±0.24	55k	ABLIKIM	06K	BES2	$J/\psi \to \overline{p}\pi^+n$
2.02±0.07±0.16	1288	EATON	84	MRK2	$e^+e^- \to p\pi^-$
1.93±0.07±0.16	1191	EATON	84	MRK2	$e^+e^- \to \overline{p}\pi^+$
1.7 ±0.7	32	BESCH	81	BONA	$e^+e^- \to p\pi^-$
1.6 ±1.2	5	BESCH	81	BONA	$e^+e^- \to \overline{p}\pi^+$
2.16±0.29	194	PERUZZI	78	MRK1	$e^+e^- \to p\pi^-$
2.04±0.27	204	PERUZZI	78	MRK1	$e^+e^- \to \overline{p}\pi^+$

$\Gamma(n\overline{n})/\Gamma_{total}$ — Γ_{225}/Γ

VALUE (units 10^{-3})	EVTS	DOCUMENT ID		TECN	COMMENT
2.09±0.16 OUR AVERAGE					
2.07±0.01±0.17	36k	ABLIKIM	12C	BES3	e^+e^-
2.31±0.49	79	BALDINI	98	FENI	e^+e^-
1.8 ±0.9		BESCH	78	BONA	e^+e^-

• • • We do not use the following data for averages, fits, limits, etc. • • •

1.90±0.55	40	ANTONELLI	93	SPEC	e^+e^-

$\Gamma(n\overline{n}\pi^+\pi^-)/\Gamma_{total}$ — Γ_{226}/Γ

VALUE (units 10^{-3})	EVTS	DOCUMENT ID		TECN	COMMENT
3.8±3.6	5	BESCH	81	BONA	e^+e^-

$\Gamma(\Lambda\overline{\Lambda})/\Gamma_{total}$ — Γ_{230}/Γ

VALUE (units 10^{-3})	EVTS	DOCUMENT ID		TECN	COMMENT
1.88 ±0.08 OUR AVERAGE	Error includes scale factor of 2.6. See the ideogram below.				
1.64 ±0.12 ±0.09		ABLIKIM	23S	BES3	$e^+e^- \to \gamma\Lambda\overline{\Lambda}$
1.943±0.003±0.033	441k	ABLIKIM	17L	BES3	e^+e^-
2.03 ±0.03 ±0.15	8887	ABLIKIM	06	BES2	$J/\psi \to \Lambda\overline{\Lambda}$
1.96 $^{+0.47}_{-0.44}$ ±0.04	46	[1] WU	06	BELL	$B^+ \to \Lambda\overline{\Lambda}K^+$
1.08 ±0.06 ±0.24	631	BAI	98G	BES	e^+e^-
1.38 ±0.05 ±0.20	1847	PALLIN	87	DM2	e^+e^-
1.58 ±0.08 ±0.19	365	EATON	84	MRK2	e^+e^-
2.6 ±1.6	5	BESCH	81	BONA	e^+e^-
1.1 ±0.2	196	PERUZZI	78	MRK1	e^+e^-

[1] WU 06 reports $[\Gamma(J/\psi(1S) \to \Lambda\overline{\Lambda})/\Gamma_{total}] \times [B(B^+ \to J/\psi(1S)K^+)] = (2.00^{+0.34}_{-0.29} \pm 0.34) \times 10^{-6}$ which we divide by our best (shown rounded) value $B(B^+ \to J/\psi(1S)K^+) = (1.019 \pm 0.019) \times 10^{-3}$. Our first error is their experiment's error and our second error is the systematic error from using our best (shown rounded) value.

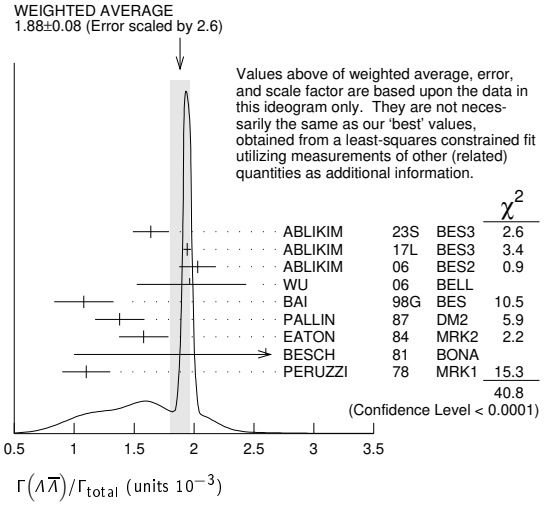

$\Gamma(\Lambda\overline{\Lambda}\pi^0)/\Gamma_{total}$ — Γ_{231}/Γ

VALUE (units 10^{-5})	CL%	EVTS	DOCUMENT ID		TECN	COMMENT
3.78±0.27±0.30		323	[1] ABLIKIM	13F	BES3	$J/\psi \to p\overline{p}\pi^+\pi^-\gamma\gamma$
• • • We do not use the following data for averages, fits, limits, etc. • • •						
< 6.4	90		[2] ABLIKIM	07H	BES2	$e^+e^- \to \psi(2S)$
23 ±7 ±8		11	BAI	98G	BES	e^+e^-
22 ±5 ±5		19	HENRARD	87	DM2	e^+e^-

[1] Using $B(\Lambda \to \pi^- p) = 63.9\%$ and $B(\pi^0 \to \gamma\gamma) = 98.8\%$.
[2] Using $B(\Lambda \to \pi^- p) = 63.9\%$.

$\Gamma(\Lambda\overline{\Lambda}\pi^+\pi^-)/\Gamma_{total}$ — Γ_{232}/Γ

VALUE (units 10^{-3})	EVTS	DOCUMENT ID		TECN	COMMENT
4.30±0.13±0.99	2.4k	ABLIKIM	12P	BES2	J/ψ

$\Gamma(\Lambda\overline{\Lambda}\eta)/\Gamma_{total}$ — Γ_{233}/Γ

VALUE (units 10^{-5})	EVTS	DOCUMENT ID		TECN	COMMENT
16.2±1.7 OUR AVERAGE					
15.7±0.80±1.54	454	[1] ABLIKIM	13F	BES3	$J/\psi \to p\overline{p}\pi^+\pi^-\gamma\gamma$
26.2±6.0 ±4.4	44	[2] ABLIKIM	07H	BES2	$e^+e^- \to \psi(2S)$

[1] Using $B(\Lambda \to \pi^- p) = 63.9\%$ and $B(\eta \to \gamma\gamma) = 39.31\%$.
[2] Using $B(\Lambda \to \pi^- p) = 63.9\%$ and $B(\eta \to \gamma\gamma) = 39.4\%$.

$\Gamma(\Lambda\overline{\Sigma}^-\pi^+ + c.c.)/\Gamma_{total}$ — Γ_{234}/Γ

VALUE (units 10^{-3})	EVTS	DOCUMENT ID		TECN	COMMENT
1.26 ±0.05 OUR AVERAGE Error includes scale factor of 1.2.					
1.244±0.002±0.045	2.6M	ABLIKIM	23BU	BES3	e^+e^-
1.52 ±0.08 ±0.16	589	[1] ABLIKIM	07H	BES2	e^+e^-
1.11 ±0.06 ±0.20	342 ± 18	HENRARD	87	DM2	e^+e^-
1.38 ±0.21 ±0.35	118	EATON	84	MRK2	e^+e^-

[1] Using $B(\Lambda \to \pi^- p) = 63.9\%$ and $B(\Sigma^+ \to \pi^0 p) = 51.6\%$.

$\Gamma(\Lambda\overline{\Sigma}^+\pi^- + c.c.)/\Gamma_{total}$ — Γ_{235}/Γ

VALUE (units 10^{-3})	EVTS	DOCUMENT ID		TECN	COMMENT
1.21 ±0.07 OUR AVERAGE Error includes scale factor of 1.8.					
1.221±0.002±0.038	2.7M	ABLIKIM	23BU	BES3	e^+e^-
0.90 ±0.06 ±0.16	225	HENRARD	87	DM2	e^+e^-
1.53 ±0.17 ±0.38	135	EATON	84	MRK2	e^+e^-

$\Gamma(pK^-\overline{\Lambda}+c.c.)/\Gamma_{total}$ — Γ_{236}/Γ

VALUE (units 10^{-3})	EVTS	DOCUMENT ID		TECN	COMMENT
0.86±0.11 OUR AVERAGE					
$0.84^{+0.17}_{-0.15} \pm 0.02$	45	[1] LU	19	BELL	$B^+ \to \overline{p}\Lambda K^+K^+$
0.89±0.07±0.14	307	EATON	84	MRK2	e^+e^-

[1] LU 19 reports $(8.32^{+1.63}_{-1.45} \pm 0.49) \times 10^{-4}$ from a measurement of $[\Gamma(J/\psi(1S) \to pK^-\overline{\Lambda}+c.c.)/\Gamma_{total}] \times [B(B^+ \to J/\psi(1S)K^+)]$ assuming $B(B^+ \to J/\psi(1S)K^+) = (1.026 \pm 0.031) \times 10^{-3}$, which we rescale to our best (shown rounded) value $B(B^+ \to J/\psi(1S)K^+) = (1.019 \pm 0.019) \times 10^{-3}$. Our first error is their experiment's error and our second error is the systematic error from using our best (shown rounded) value.

$\Gamma(pK^-\overline{\Sigma}^0)/\Gamma_{total}$ — Γ_{237}/Γ

VALUE (units 10^{-3})	EVTS	DOCUMENT ID		TECN	COMMENT
0.29±0.06±0.05	90	EATON	84	MRK2	e^+e^-

$\Gamma(pK^0_S\overline{\Sigma}^- + c.c.)/\Gamma_{total}$ — Γ_{238}/Γ

VALUE (units 10^{-4})	EVTS	DOCUMENT ID		TECN	COMMENT
2.725±0.009±0.050	120k	[1] ABLIKIM	24H	BES3	$e^+e^- \to J/\psi$

[1] The branching fractions for the charge-conjugate channels are measured separately as $(1.361 \pm 0.006 \pm 0.025) \times 10^{-4}$ for $\overline{p}K^0_S\Sigma^+$ and $(1.352 \pm 0.006 \pm 0.025) \times 10^{-4}$ for $pK^0_S\overline{\Sigma}^-$.

$\Gamma(\overline{\Lambda}nK^0_S + c.c.)/\Gamma_{total}$ — Γ_{239}/Γ

VALUE (units 10^{-4})	EVTS	DOCUMENT ID		TECN	COMMENT
6.46±0.20±1.07	1058	[1] ABLIKIM	08C	BES2	$e^+e^- \to J/\psi$

[1] Using $B(\overline{\Lambda} \to \overline{p}\pi^+) = 63.9\%$ and $B(K^0_S \to \pi^+\pi^-) = 69.2\%$.

$\Gamma(\Lambda\overline{\Sigma} + c.c.)/\Gamma_{total}$ — Γ_{240}/Γ

VALUE (units 10^{-5})	CL%	EVTS	DOCUMENT ID		TECN	COMMENT
2.83±0.23 OUR AVERAGE						
2.74±0.24±0.22		234 ± 21	[1] ABLIKIM	12B	BES3	$J/\psi \to \Lambda\overline{\Sigma}^0$
2.92±0.22±0.24		308 ± 24	[2] ABLIKIM	12B	BES3	$J/\psi \to \overline{\Lambda}\Sigma^0$
• • • We do not use the following data for averages, fits, limits, etc. • • •						
<18			[2] HENRARD	87	DM2	$J/\psi \to \overline{\Lambda}\Sigma^0$
<15		90	PERUZZI	78	MRK1	$e^+e^- \to \Lambda X$

[1] ABLIKIM 12B quotes $B(J/\psi \to \Lambda\overline{\Sigma}^0)$ which we multiply by 2.
[2] ABLIKIM 12B and HENRARD 87 quote results for $B(J/\psi \to \overline{\Lambda}\Sigma^0)$ which we multiply by 2.

$\Gamma(\Sigma^+\overline{\Sigma}^-)/\Gamma_{total}$ — Γ_{241}/Γ

VALUE (units 10^{-3})	EVTS	DOCUMENT ID		TECN	COMMENT
1.07 ±0.04 OUR AVERAGE					
1.061±0.004±0.036	87k	ABLIKIM	21AT	BES3	$J/\psi \to p\pi^0\overline{p}\pi^0$
1.50 ±0.10 ±0.22	399	ABLIKIM	08O	BES2	$e^+e^- \to J/\psi$

$\Gamma(\Sigma^0\overline{\Sigma}^0)/\Gamma_{total}$ — Γ_{242}/Γ

VALUE (units 10^{-3})	EVTS	DOCUMENT ID		TECN	COMMENT
1.172±0.032 OUR AVERAGE Error includes scale factor of 1.4.					
1.164±0.004±0.023	111k	ABLIKIM	17L	BES3	$J/\psi \to \Sigma^0\overline{\Sigma}^0$
1.33 ±0.04 ±0.11	1.7k	ABLIKIM	06	BES2	$J/\psi \to \Sigma^0\overline{\Sigma}^0$
1.06 ±0.04 ±0.23	884	PALLIN	87	DM2	$e^+e^- \to \Sigma^0\overline{\Sigma}^0$
1.58 ±0.16 ±0.25	90	EATON	84	MRK2	$e^+e^- \to \Sigma^0\overline{\Sigma}^0$
1.3 ±0.4	52	PERUZZI	78	MRK1	$e^+e^- \to \Sigma^0\overline{\Sigma}^0$
• • • We do not use the following data for averages, fits, limits, etc. • • •					
2.4 ±2.6	3	BESCH	81	BONA	$e^+e^- \to \Sigma^+\overline{\Sigma}^-$

$\Gamma(\Sigma^+\overline{\Sigma}^-\eta)/\Gamma_{total}$ — Γ_{243}/Γ

VALUE (units 10^{-5})	EVTS	DOCUMENT ID		TECN	COMMENT
6.34±0.21±0.37	1821	ABLIKIM	22AY	BES3	$J/\psi \to \Sigma^+\overline{\Sigma}^-\eta$

$\Gamma(\Xi^-\overline{\Xi}^+)/\Gamma_{total}$ — Γ_{244}/Γ

VALUE (units 10^{-3})	EVTS	DOCUMENT ID		TECN	COMMENT
0.97 ±0.08 OUR AVERAGE Error includes scale factor of 1.4. See the ideogram below.					
1.040±0.006±0.074	43k	ABLIKIM	16L	BES3	$J/\psi \to \Xi^-\overline{\Xi}^+$
0.90 ±0.03 ±0.18	961	ABLIKIM	12P	BES2	$J/\psi \to \Xi^-\overline{\Xi}^+$
0.70 ±0.06 ±0.12	132	HENRARD	87	DM2	$e^+e^- \to \Xi^-\overline{\Xi}^+$
1.14 ±0.08 ±0.20	194	EATON	84	MRK2	$e^+e^- \to \Xi^-\overline{\Xi}^+$
1.4 ±0.5	51	PERUZZI	78	MRK1	$e^+e^- \to \Xi^-\overline{\Xi}^+$

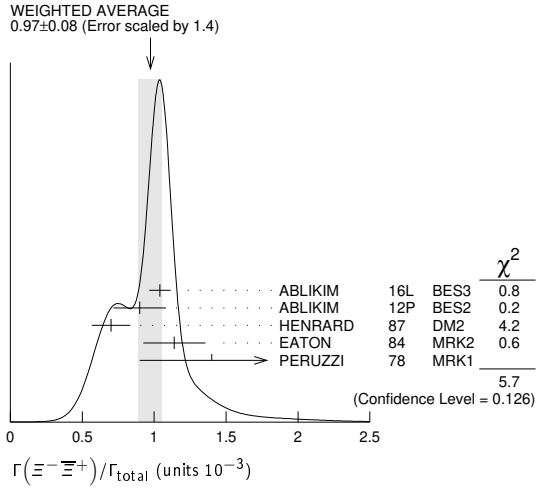

$\Gamma(\Xi^0\overline{\Sigma}^-K^+ + c.c)/\Gamma_{total}$ — Γ_{245}/Γ

VALUE (units 10^{-5})	EVTS	DOCUMENT ID		TECN	COMMENT
5.64±0.17±0.28	1284	ABLIKIM	25BW	BES3	$J/\psi \to \Xi^0\overline{\Sigma}^-K^+$

Int. J. Mod. Phys. A 2026.41. Downloaded from www.worldscientific.com
by [redacted]LIFORNIA @ BERKELEY on 09/16/26. Re-use and distribution is strictly not permitted, except for Open Access articles.

Int. J. Mod. Phys. A 2026.41. Downloaded from www.worldscientific.com
by UNIVERSITY OF CALIFORNIA @ BERKELEY on 09/16/26. Re-use and distribution is strictly not permitted, except for Open Access articles.

$\Gamma(\Xi^0\overline{\Sigma}^0 K^0_S + c.c)/\Gamma_{total}$ — Γ_{246}/Γ

VALUE (units 10^{-5})	EVTS	DOCUMENT ID		TECN	COMMENT
2.24±0.32±0.31	91	ABLIKIM	25BW	BES3	$J/\psi \to \Xi^0\overline{\Sigma}^0 K^0_S$

$\Gamma(\Xi^0\overline{\Lambda} K^0_S + c.c)/\Gamma_{total}$ — Γ_{247}/Γ

VALUE (units 10^{-5})	EVTS	DOCUMENT ID		TECN	COMMENT
3.76±0.14±0.23	982	ABLIKIM	25BW	BES3	$J/\psi \to \Xi^0\overline{\Lambda} K^0_S$

RADIATIVE DECAYS

$\Gamma(\gamma\eta_c(1S))/\Gamma_{total}$ — Γ_{248}/Γ

VALUE (units 10^{-2})	DOCUMENT ID		TECN	COMMENT
1.82±0.15 OUR FIT Error includes scale factor of 1.6.				
1.7 ±0.4 OUR AVERAGE Error includes scale factor of 1.5.				
1.99±0.31±0.02	[1] MITCHELL	09	CLEO	$e^+e^- \to \gamma X$
1.27±0.36	GAISER	86	CBAL	$J/\psi \to \gamma X$
• • • We do not use the following data for averages, fits, limits, etc. • • •				
3.40±0.33	[2] ANASHIN	14	KEDR	$J/\psi \to \gamma\eta_c$

[1] MITCHELL 09 reports (1.98 ± 0.09 ± 0.30) × 10^{-2} from a measurement of $[\Gamma(J/\psi(1S) \to \gamma\eta_c(1S))/\Gamma_{total}] \times [B(\psi(2S) \to J/\psi(1S)\pi^+\pi^-)]$ assuming $B(\psi(2S) \to J/\psi(1S)\pi^+\pi^-) = (35.04 \pm 0.07 \pm 0.77) \times 10^{-2}$, which we rescale to our best (shown rounded) value $B(\psi(2S) \to J/\psi(1S)\pi^+\pi^-) = (34.78 \pm 0.33) \times 10^{-2}$. Our first error is their experiment's error and our second error is the systematic error from using our best (shown rounded) value.

[2] Statistical uncertainty only.

$\Gamma(3\gamma)/\Gamma_{total}$ — Γ_{251}/Γ

VALUE (units 10^{-6})	CL%	EVTS	DOCUMENT ID		TECN	COMMENT
11.6±2.2 OUR AVERAGE						
11.3±1.8±2.0		113 ± 18	ABLIKIM	13I	BES3	$\psi(2S) \to \pi^+\pi^- J/\psi$
12 ±3 ±2		$24.2^{+7.2}_{-6.0}$	ADAMS	08	CLEO	$\psi(2S) \to \pi^+\pi^- J/\psi$
• • • We do not use the following data for averages, fits, limits, etc. • • •						
<55	90		PARTRIDGE	80	CBAL	e^+e^-

$\Gamma(4\gamma)/\Gamma_{total}$ — Γ_{252}/Γ

VALUE	CL%	DOCUMENT ID		TECN	COMMENT
<9 × 10^{-6}	90	ADAMS	08	CLEO	$\psi(2S) \to \pi^+\pi^- J/\psi$

$\Gamma(5\gamma)/\Gamma_{total}$ — Γ_{253}/Γ

VALUE	CL%	DOCUMENT ID		TECN	COMMENT
<15 × 10^{-6}	90	ADAMS	08	CLEO	$\psi(2S) \to \pi^+\pi^- J/\psi$

$\Gamma(\gamma\pi^0)/\Gamma_{total}$ — Γ_{254}/Γ

VALUE (units 10^{-5})	EVTS	DOCUMENT ID		TECN	COMMENT
3.39±0.08 OUR AVERAGE					
3.34±0.02±0.09	176k	ABLIKIM	23BD	BES3	$J/\psi \to \pi^0\gamma$
3.58±0.20±0.03	1.6k	[1] ABLIKIM	18O	BES3	$\psi(2S) \to \pi^+\pi^-\gamma\gamma\gamma$
3.63±0.36±0.13		PEDLAR	09	CLE3	$J/\psi \to \pi^0\gamma$
$3.13^{+0.65}_{-0.47}$	586	ABLIKIM	06E	BES2	$J/\psi \to \pi^0\gamma$
• • • We do not use the following data for averages, fits, limits, etc. • • •					
3.6 ±1.1 ±0.7		BLOOM	83	CBAL	e^+e^-
7.3 ±4.7	10	BRANDELIK	79C	DASP	e^+e^-

[1] ABLIKIM 18O reports $[\Gamma(J/\psi(1S) \to \gamma\pi^0)/\Gamma_{total}] \times [B(\pi^0 \to 2\gamma)] = (3.57 \pm 0.12 \pm 0.16) \times 10^{-5}$ from a measurement of $[\Gamma(J/\psi(1S) \to \gamma\pi^0)/\Gamma_{total}] \times [B(\pi^0 \to 2\gamma)] \times [B(\psi(2S) \to J/\psi(1S)\pi^+\pi^-)]$ assuming $B(\psi(2S) \to J/\psi(1S)\pi^+\pi^-) = (34.49 \pm 0.30) \times 10^{-2}$, which we rescale to our best (shown rounded) values $B(\pi^0 \to 2\gamma) = (98.823 \pm 0.034) \times 10^{-2}$, $B(\psi(2S) \to J/\psi(1S)\pi^+\pi^-) = (34.78 \pm 0.33) \times 10^{-2}$. Our first error is their experiment's error and our second error is the systematic error from using our best (shown rounded) values.

$\Gamma(\gamma\pi^0\pi^0)/\Gamma_{total}$ — Γ_{255}/Γ

VALUE (units 10^{-3})	DOCUMENT ID		TECN	COMMENT
1.15±0.05	[1] ABLIKIM	15AE	BES3	$J/\psi \to \gamma\pi^0\pi^0$

[1] The uncertainty is systematic as statistical is netligible.

$\Gamma(\gamma 2\pi^+ 2\pi^-)/\Gamma_{total}$ — Γ_{256}/Γ

VALUE (units 10^{-3})	DOCUMENT ID		TECN	COMMENT
2.8 ±0.5 OUR AVERAGE Error includes scale factor of 1.9. See the ideogram below.				
4.32±0.14±0.73	[1] BISELLO	89B	DM2	$J/\psi \to 4\pi\gamma$
2.08±0.13±0.35	[2] BISELLO	89B	DM2	$J/\psi \to 4\pi\gamma$
3.05±0.08±0.45	[2] BALTRUSAIT...	86B	MRK3	$J/\psi \to 4\pi\gamma$
4.85±0.45±1.20	[3] BURKE	82	MRK2	e^+e^-

[1] 4π mass less than 3.0 GeV.
[2] 4π mass less than 2.0 GeV.
[3] 4π mass less than 2.5 GeV.

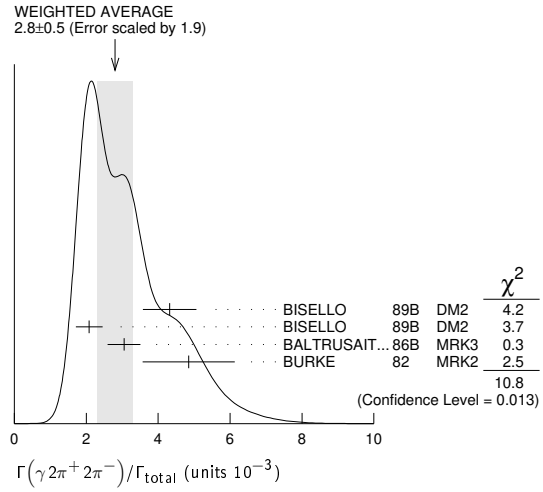

$\Gamma(\gamma f_2(1270) f_2(1270))/\Gamma_{total}$ — Γ_{257}/Γ

VALUE (units 10^{-4})	EVTS	DOCUMENT ID		TECN	COMMENT
9.5±0.7±1.6	646 ± 45	ABLIKIM	04M	BES	$J/\psi \to \gamma 2\pi^+ 2\pi^-$

$\Gamma(\gamma f_2(1270) f_2(1270)(\text{non resonant}))/\Gamma_{total}$ — Γ_{258}/Γ

VALUE (units 10^{-4})	DOCUMENT ID		TECN	COMMENT
8.2±0.8±1.7	[1] ABLIKIM	04M	BES	$J/\psi \to \gamma 2\pi^+ 2\pi^-$

[1] Subtracting contribution from intermediate $\eta_c(1S)$ decays.

$\Gamma(\gamma\pi^+\pi^- 2\pi^0)/\Gamma_{total}$ — Γ_{259}/Γ

VALUE (units 10^{-3})	DOCUMENT ID		TECN	COMMENT
8.3±0.2±3.1	[1] BALTRUSAIT...	86B	MRK3	$J/\psi \to 4\pi\gamma$

[1] 4π mass less than 2.0 GeV.

$\Gamma(\gamma K^0_S K^0_S)/\Gamma_{total}$ — Γ_{260}/Γ

VALUE (units 10^{-4})	DOCUMENT ID		TECN	COMMENT
8.1±0.4	ABLIKIM	18AA	BES3	$J/\psi \to \gamma K^0_S K^0_S$

$\Gamma(\gamma(K\overline{K}\pi)[J^{PC} = 0^{-+}])/\Gamma_{total}$ — Γ_{261}/Γ

VALUE (units 10^{-3})	DOCUMENT ID		TECN	COMMENT
0.7 ±0.4 OUR AVERAGE Error includes scale factor of 2.1.				
0.58±0.03±0.20	[1] BAI	00D	BES	$J/\psi \to \gamma K^\pm K^0_S \pi^\mp$
2.1 ±0.1 ±0.7	[2] BAI	00D	BES	$J/\psi \to \gamma K^\pm K^0_S \pi^\mp$

[1] For a broad structure around 1800 MeV.
[2] For a broad structure around 2040 MeV.

$\Gamma(\gamma K^+ K^- \pi^+\pi^-)/\Gamma_{total}$ — Γ_{262}/Γ

VALUE (units 10^{-3})	EVTS	DOCUMENT ID		TECN	COMMENT
2.1±0.1±0.6	1516	BAI	00B	BES	$J/\psi \to \gamma K^+ K^0 \pi^+\pi^-$

$\Gamma(\gamma K^*(892)\overline{K}^*(892))/\Gamma_{total}$ — Γ_{263}/Γ

VALUE (units 10^{-3})	EVTS	DOCUMENT ID		TECN	COMMENT
4.0±0.3±1.3	320	[1] BAI	00B	BES	$J/\psi \to \gamma K^+ K^0 \pi^+\pi^-$

[1] Summed over all charges.

$\Gamma(\gamma f_1(1420) \to \gamma K^*(892)^0 K^0_S \to \gamma K^0_S K^0_S \pi^0)/\Gamma_{total}$ — Γ_{306}/Γ

VALUE (units 10^{-5})	EVTS	DOCUMENT ID		TECN	COMMENT
$7.25 \pm 0.12^{+0.73}_{-1.25}$	126k	ABLIKIM	23M	BES3	$J/\psi \to \gamma K^0_S K^0_S \pi^0$

$\Gamma(\gamma f_1(1420) \to \gamma a_0(980)^0\pi^0 \to \gamma K^0_S K^0_S \pi^0)/\Gamma_{total}$ — Γ_{307}/Γ

VALUE (units 10^{-6})	EVTS	DOCUMENT ID		TECN	COMMENT
$4.62 \pm 0.36^{+2.36}_{-1.94}$	126k	ABLIKIM	23M	BES3	$J/\psi \to \gamma K^0_S K^0_S \pi^0$

$\Gamma(\gamma\eta)/\Gamma_{total}$ — Γ_{264}/Γ

VALUE (units 10^{-3})	EVTS	DOCUMENT ID		TECN	COMMENT
1.090±0.013 OUR AVERAGE					
1.096±0.001±0.019	2.2M	ABLIKIM	23BD	BES3	$J/\psi \to \eta\gamma$
1.067±0.005±0.023	87.9k	ABLIKIM	21AM	BES3	$e^+e^- \to J/\psi$
1.11 ±0.05 ±0.01	18.6k	[1] ABLIKIM	18O	BES3	$\psi(2S) \to \pi^+\pi^-\gamma\gamma\gamma$
1.101±0.029±0.022		PEDLAR	09	CLE3	$J/\psi \to \eta\gamma$
1.123±0.089	11k	ABLIKIM	06E	BES2	$J/\psi \to \eta\gamma$
• • • We do not use the following data for averages, fits, limits, etc. • • •					
0.88 ±0.08 ±0.11		BLOOM	83	CBAL	e^+e^-
0.82 ±0.10		BRANDELIK	79C	DASP	e^+e^-
1.3 ±0.4	21	BARTEL	77	CNTR	e^+e^-

[1] ABLIKIM 18O reports $[\Gamma(J/\psi(1S) \to \gamma\eta)/\Gamma_{total}] \times [B(\eta \to 2\gamma)] = (4.42 \pm 0.04 \pm 0.18) \times 10^{-4}$ from a measurement of $[\Gamma(J/\psi(1S) \to \gamma\eta)/\Gamma_{total}] \times [B(\eta \to 2\gamma)] \times [B(\psi(2S) \to J/\psi(1S)\pi^+\pi^-)]$ assuming $B(\psi(2S) \to J/\psi(1S)\pi^+\pi^-) = (34.49 \pm 0.30) \times 10^{-2}$, which we rescale to our best (shown rounded) values $B(\eta \to 2\gamma) = (39.36 \pm 0.18) \times 10^{-2}$, $B(\psi(2S) \to J/\psi(1S)\pi^+\pi^-) = (34.78 \pm 0.33) \times 10^{-2}$. Our first error is their experiment's error and our second error is the systematic error from using our best (shown rounded) values.

$\Gamma(\gamma\eta\pi^0)/\Gamma_{total}$ — Γ_{265}/Γ

VALUE (units 10^{-6})	EVTS	DOCUMENT ID		TECN	COMMENT
21.4±1.8±2.5	596	ABLIKIM	16P	BES3	$J/\psi \to 5\gamma$

$\Gamma(\gamma f_0(500) \to \gamma\pi\pi)/\Gamma_{total}$ — Γ_{266}/Γ

VALUE (units 10^{-4})	DOCUMENT ID		TECN	COMMENT
• • • We do not use the following data for averages, fits, limits, etc. • • •				
10.5±2.0	SARANTSEV	21	RVUE	$J/\psi(1S) \to \gamma(\pi\pi,\ K\overline{K},\ \eta\eta,\ \omega\phi)$

$\Gamma(\gamma f_0(500) \to \gamma K\overline{K})/\Gamma_{total}$ — Γ_{267}/Γ

VALUE (units 10^{-5})	DOCUMENT ID		TECN	COMMENT
• • • We do not use the following data for averages, fits, limits, etc. • • •				
5±5	SARANTSEV	21	RVUE	$J/\psi(1S) \to \gamma(\pi\pi,\ K\overline{K},\ \eta\eta,\ \omega\phi)$

$\Gamma(\gamma f_0(500) \to \gamma\eta\eta)/\Gamma_{total}$ — Γ_{268}/Γ

VALUE (units 10^{-5})	DOCUMENT ID		TECN	COMMENT
• • • We do not use the following data for averages, fits, limits, etc. • • •				
4±3	SARANTSEV	21	RVUE	$J/\psi(1S) \to \gamma(\pi\pi,\ K\overline{K},\ \eta\eta,\ \omega\phi)$

$\Gamma(\gamma a_0(980)^0 \to \gamma\eta\pi^0)/\Gamma_{total}$ — Γ_{269}/Γ

VALUE	CL%	DOCUMENT ID		TECN	COMMENT
$<2.5 \times 10^{-6}$	95	ABLIKIM	16P	BES3	$J/\psi \to 5\gamma$

$\Gamma(\gamma a_2(1320)^0 \to \gamma\eta\pi^0)/\Gamma_{total}$ — Γ_{270}/Γ

VALUE	CL%	DOCUMENT ID		TECN	COMMENT
$<6.6 \times 10^{-6}$	95	ABLIKIM	16P	BES3	$J/\psi \to 5\gamma$

$\Gamma(\gamma\eta\pi\pi)/\Gamma_{total}$ — Γ_{271}/Γ

VALUE (units 10^{-3})	DOCUMENT ID		TECN	COMMENT
6.1 ±1.0 OUR AVERAGE				
5.85±0.3±1.05	[1] EDWARDS	83B	CBAL	$J/\psi \to \eta\pi^+\pi^-$
7.8 ±1.2±2.4	[1] EDWARDS	83B	CBAL	$J/\psi \to \eta 2\pi^0$

[1] Broad enhancement at 1700 MeV.

$\Gamma(\gamma\eta_2(1870) \to \gamma\eta\pi^+\pi^-)/\Gamma_{total}$ — Γ_{272}/Γ

VALUE (units 10^{-4})	DOCUMENT ID		TECN	COMMENT
6.2±2.2±0.9	BAI	99	BES	$J/\psi \to \gamma\eta\pi^+\pi^-$

$\Gamma(\gamma\eta'(958))/\Gamma_{total}$ — Γ_{273}/Γ

VALUE (units 10^{-3})	EVTS	DOCUMENT ID		TECN	COMMENT
5.28±0.06 OUR AVERAGE Error includes scale factor of 1.3. See the ideogram below.					
5.40±0.01±0.11	638k	ABLIKIM	23BD	BES3	$J/\psi \to \gamma\eta'$
5.27±0.03±0.05	36k	ABLIKIM	19T	BES	$J/\psi \to \gamma\eta'$
5.42±0.23±0.09	5.0k	[1] ABLIKIM	18O	BES3	$\psi(2S) \to \pi^+\pi^-\gamma\gamma\gamma$
4.76±0.22±0.06		[2] ABLIKIM	11	BES3	$J/\psi \to \eta'\gamma$
5.24±0.12±0.11		PEDLAR	09	CLE3	$J/\psi \to \eta'\gamma$
5.55±0.44	35k	ABLIKIM	06E	BES2	$J/\psi \to \eta'\gamma$
• • • We do not use the following data for averages, fits, limits, etc. • • •					
4.50±0.14±0.53		BOLTON	92B	MRK3	$J/\psi \to \gamma\pi^+\pi^-\eta,\ \eta \to \gamma\gamma$
4.30±0.31±0.71		BOLTON	92B	MRK3	$J/\psi \to \gamma\pi^+\pi^-\eta,\ \eta \to \pi^+\pi^-\pi^0$
4.04±0.16±0.85	622	AUGUSTIN	90	DM2	$J/\psi \to \gamma\eta\pi^+\pi^-$
4.39±0.09±0.66	2420	AUGUSTIN	90	DM2	$J/\psi \to \gamma\gamma\pi^+\pi^-$
4.1 ±0.3 ±0.6		BLOOM	83	CBAL	$e^+e^- \to 3\gamma +$ hadrons
2.9 ±1.1	6	BRANDELIK	79C	DASP	$e^+e^- \to 3\gamma$
2.4 ±0.7	57	BARTEL	76	CNTR	$e^+e^- \to 2\gamma\rho$

[1] ABLIKIM 18O reports $[\Gamma(J/\psi(1S) \to \gamma\eta'(958))/\Gamma_{total}] \times [B(\eta'(958) \to \gamma\gamma)] = (1.26 \pm 0.02 \pm 0.05) \times 10^{-4}$ from a measurement of $[\Gamma(J/\psi(1S) \to \gamma\eta'(958))/\Gamma_{total}] \times [B(\eta'(958) \to \gamma\gamma)] \times [B(\psi(2S) \to J/\psi(1S)\pi^+\pi^-)]$ assuming $B(\psi(2S) \to J/\psi(1S)\pi^+\pi^-) = (34.49 \pm 0.30) \times 10^{-2}$, which we rescale to our best (shown rounded) values $B(\eta'(958) \to \gamma\gamma) = (2.307 \pm 0.033) \times 10^{-2}$, $B(\psi(2S) \to J/\psi(1S)\pi^+\pi^-) = (34.78 \pm 0.33) \times 10^{-2}$. Our first error is their experiment's error and our second error is the systematic error from using our best (shown rounded) values.

[2] ABLIKIM 11 reports $(4.84 \pm 0.03 \pm 0.24) \times 10^{-3}$ from a measurement of $[\Gamma(J/\psi(1S) \to \gamma\eta'(958))/\Gamma_{total}]$ / $[B(\eta'(958) \to \pi^+\pi^-\eta)]$ / $[B(\eta \to 2\gamma)]$ assuming $B(\eta'(958) \to \pi^+\pi^-\eta) = (43.2 \pm 0.7) \times 10^{-2}$, $B(\eta \to 2\gamma) = (39.31 \pm 0.20) \times 10^{-2}$, which we rescale to our best (shown rounded) values $B(\eta'(958) \to \pi^+\pi^-\eta) = (42.5 \pm 0.5) \times 10^{-2}$, $B(\eta \to 2\gamma) = (39.36 \pm 0.18) \times 10^{-2}$. Our first error is their experiment's error and our second error is the systematic error from using our best (shown rounded) values.

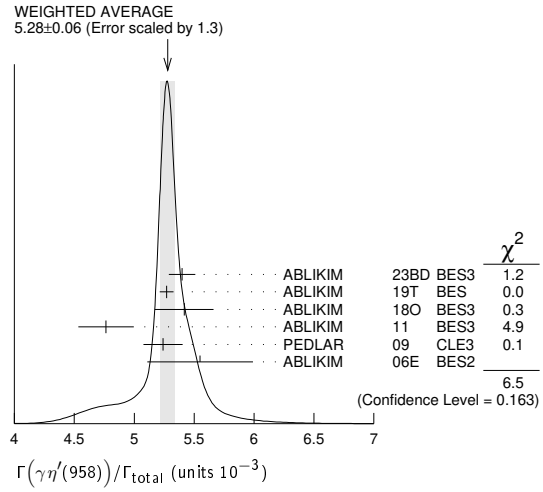

$\Gamma(\gamma f_0(980) \to \gamma\pi\pi)/\Gamma_{total}$ — Γ_{274}/Γ

VALUE (units 10^{-5})	DOCUMENT ID		TECN	COMMENT
• • • We do not use the following data for averages, fits, limits, etc. • • •				
1.3±0.2	SARANTSEV	21	RVUE	$J/\psi(1S) \to \gamma(\pi\pi,\ K\overline{K},\ \eta\eta,\ \omega\phi)$

$\Gamma(\gamma f_0(980) \to \gamma K\overline{K})/\Gamma_{total}$ — Γ_{275}/Γ

VALUE (units 10^{-5})	DOCUMENT ID		TECN	COMMENT
• • • We do not use the following data for averages, fits, limits, etc. • • •				
0.8±0.3	SARANTSEV	21	RVUE	$J/\psi(1S) \to \gamma(\pi\pi,\ K\overline{K},\ \eta\eta,\ \omega\phi)$

$\Gamma(\gamma\rho\rho)/\Gamma_{total}$ — Γ_{276}/Γ

VALUE (units 10^{-3})	CL%	DOCUMENT ID		TECN	COMMENT
4.5 ±0.8 OUR AVERAGE					
4.7 ±0.3 ±0.9		[1] BALTRUSAIT...	86B	MRK3	$J/\psi \to 4\pi\gamma$
3.75±1.05±1.20		[2] BURKE	82	MRK2	$J/\psi \to 4\pi\gamma$
• • • We do not use the following data for averages, fits, limits, etc. • • •					
<0.09	90	[3] BISELLO	89B		$J/\psi \to 4\pi\gamma$

[1] 4π mass less than 2.0 GeV.
[2] 4π mass less than 2.0 GeV. We have multiplied $2\rho^0$ measurement by 3 to obtain 2ρ.
[3] 4π mass in the range 2.0–25 GeV.

$\Gamma(\gamma\rho\omega)/\Gamma_{total}$ — Γ_{277}/Γ

VALUE	CL%	DOCUMENT ID		TECN	COMMENT
$<5.4 \times 10^{-4}$	90	ABLIKIM	08A	BES2	$e^+e^- \to J/\psi$

$\Gamma(\gamma\rho\phi)/\Gamma_{total}$ — Γ_{278}/Γ

VALUE	CL%	DOCUMENT ID		TECN	COMMENT
$<8.8 \times 10^{-5}$	90	ABLIKIM	08A	BES2	$e^+e^- \to J/\psi$

$\Gamma(\gamma\omega\omega)/\Gamma_{total}$ — Γ_{279}/Γ

VALUE (units 10^{-3})	EVTS	DOCUMENT ID		TECN	COMMENT
1.61±0.33 OUR AVERAGE					
6.0 ±4.8 ±1.8		ABLIKIM	08A	BES2	$J/\psi \to \gamma\omega\pi^+\pi^-$
1.41±0.2 ±0.42	120 ± 17	BISELLO	87	SPEC	e^+e^-, hadronsγ
1.76±0.09±0.45		BALTRUSAIT...	85C	MRK3	$e^+e^- \to$ hadronsγ

$\Gamma(\gamma\phi\phi)/\Gamma_{total}$ — Γ_{280}/Γ

VALUE (units 10^{-4})	EVTS	DOCUMENT ID		TECN	COMMENT
4.0±1.2 OUR AVERAGE Error includes scale factor of 2.1. See the ideogram below.					
7.5±0.6±1.2	168	BAI	90B	MRK3	$J/\psi \to \gamma 4K$
3.4±0.8±0.6	33 ± 7	[1] BISELLO	90	DM2	$J/\psi \to \gamma K^+K^-K^0_SK^0_L$
3.1±0.7±0.4		[1] BISELLO	86B	DM2	$J/\psi \to \gamma K^+K^-K^+K^-$

[1] $\phi\phi$ mass less than 2.9 GeV, η_c excluded.

Int. J. Mod. Phys. A 2026.41. Downloaded from www.worldscientific.com
by CALIFORNIA @ BERKELEY on 09/16/26. Re-use and distribution is strictly not permitted, except for Open Access articles.

Int. J. Mod. Phys. A 2026.41. Downloaded from www.worldscientific.com
by UNIVERSITY OF CALIFORNIA @ BERKELEY on 09/16/26. Re-use and distribution is strictly not permitted, except for Open Access articles.

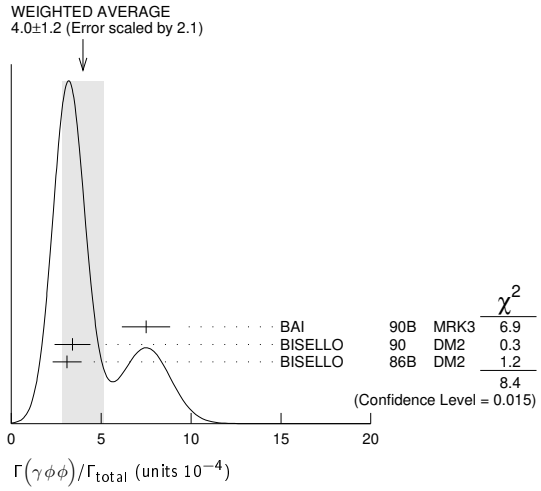

$\Gamma(\gamma\eta(1405/1475)\to\gamma K\overline{K}\pi)/\Gamma_{total}$ — Γ_{281}/Γ

VALUE (units 10^{-3})		DOCUMENT ID		TECN	COMMENT
2.8 ±0.6 OUR AVERAGE	Error includes scale factor of 1.6. See the ideogram below.				
1.66±0.1 ±0.58		[1,2] BAI	00D	BES	$J/\psi\to\gamma K^\pm K^0_S\pi^\mp$
3.8 ±0.3 ±0.6		[3] AUGUSTIN	90	DM2	$J/\psi\to\gamma K\overline{K}\pi$
4.0 ±0.7 ±1.0		[3] EDWARDS	82E	CBAL	$J/\psi\to K^+K^-\pi^0\gamma$
4.3 ±1.7		[3,4] SCHARRE	80	MRK2	e^+e^-
• • • We do not use the following data for averages, fits, limits, etc. • • •					
1.78±0.21±0.33		[3,5,6] AUGUSTIN	92	DM2	$J/\psi\to\gamma K\overline{K}\pi$
0.83±0.13±0.18		[3,7,8] AUGUSTIN	92	DM2	$J/\psi\to\gamma K\overline{K}\pi$
$0.66^{+0.17}_{-0.16}{}^{+0.24}_{-0.15}$		[3,6,9] BAI	90C	MRK3	$J/\psi\to\gamma K^0_S K^\pm\pi^\mp$
$1.03^{+0.21}_{-0.18}{}^{+0.26}_{-0.19}$		[3,8,10] BAI	90C	MRK3	$J/\psi\to\gamma K^0_S K^\pm\pi^\mp$

[1] Interference with the $J/\psi(1S)$ radiative transition to the broad $K\overline{K}\pi$ pseudoscalar state around 1800 is $(0.15\pm0.01\pm0.05)\times10^{-3}$.
[2] Interference with $J/\psi\to\gamma f_1(1420)$ is $(-0.03\pm0.01\pm0.01)\times10^{-3}$.
[3] Includes unknown branching fraction $\eta(1405)\to K\overline{K}\pi$.
[4] Corrected for spin-zero hypothesis for $\eta(1405)$.
[5] From fit to the $a_0(980)\pi$ 0^{-+} partial wave.
[6] $a_0(980)\pi$ mode.
[7] From fit to the $K^*(892)K$ 0^{-+} partial wave.
[8] K^*K mode.
[9] From $a_0(980)\pi$ final state.
[10] From $K^*(890)K$ final state.

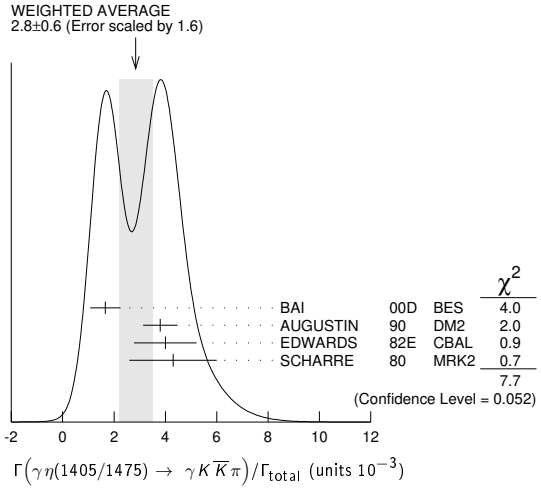

$\Gamma(\gamma\eta(1405/1475)\to\gamma\gamma\rho^0)/\Gamma_{total}$ — Γ_{282}/Γ

VALUE (units 10^{-4})		DOCUMENT ID		TECN	COMMENT
0.78±0.20 OUR AVERAGE	Error includes scale factor of 1.8.				
1.07±0.17±0.11		[1] BAI	04J	BES2	$J/\psi\to\gamma\gamma\pi^+\pi^-$
0.64±0.12±0.07		[1] COFFMAN	90	MRK3	$J/\psi\to\gamma\gamma\pi^+\pi^-$

[1] Includes unknown branching fraction $\eta(1405)\to\gamma\rho^0$.

$\Gamma(\gamma\eta(1405/1475)\to\gamma\eta\pi^+\pi^-)/\Gamma_{total}$ — Γ_{283}/Γ

VALUE (units 10^{-4})	EVTS	DOCUMENT ID		TECN	COMMENT
3.0 ±0.5 OUR AVERAGE					
2.6 ±0.7 ±0.4		BAI	99	BES	$J/\psi\to\gamma\eta\pi^+\pi^-$
3.38±0.33±0.64		[1] BOLTON	92B	MRK3	$J/\psi\to\gamma\eta\pi^+\pi^-$
• • • We do not use the following data for averages, fits, limits, etc. • • •					
7.0 ±0.6 ±1.1	261	[2] AUGUSTIN	90	DM2	$J/\psi\to\gamma\eta\pi^+\pi^-$

[1] Via $a_0(980)\pi$.
[2] Includes unknown branching fraction to $\eta\pi^+\pi^-$.

$\Gamma(\gamma\eta(1405/1475)\to\gamma\rho^0\rho^0)/\Gamma_{total}$ — Γ_{284}/Γ

VALUE (units 10^{-3})		DOCUMENT ID		TECN	COMMENT
1.7 ±0.4 OUR AVERAGE	Error includes scale factor of 1.3.				
2.1 ±0.4		BUGG	95	MRK3	$J/\psi\to\gamma\pi^+\pi^-\pi^+\pi^-$
1.36±0.38		[1,2] BISELLO	89B	DM2	$J/\psi\to4\pi\gamma$

[1] Estimated by us from various fits.
[2] Includes unknown branching fraction to $\rho^0\rho^0$.

$\Gamma(\gamma\eta(1405/1475)\to\gamma\gamma\phi)/\Gamma_{total}$ — Γ_{285}/Γ

VALUE (units 10^{-6})	CL%	EVTS	DOCUMENT ID		TECN	COMMENT
$\mathbf{3.57\pm0.18^{+0.59}_{-0.61}}$			[1] ABLIKIM	25P	BES3	$J/\psi\to\gamma\gamma\phi$
• • • We do not use the following data for averages, fits, limits, etc. • • •						
7.03±0.92±0.91		1.3k	[2] ABLIKIM	18I	BES3	$J/\psi\to\gamma\gamma\phi(1020)$
10.36±1.51±1.54		1.9k	[3] ABLIKIM	18I	BES3	$J/\psi\to\gamma\gamma\phi(1020)$
<82	95		BAI	04J	BES2	$J/\psi\to\gamma\gamma K^+K^-$

[1] From a partial wave analysis of $J/\psi\to\gamma\gamma\phi$ with significance 18.9σ.
[2] Constructive interference between the $X(1835)$ and $\eta(1405)/\eta(1475)$ is assumed in a fit to the $\gamma\phi$ invariant mass.
[3] Destructive interference between the $X(1835)$ and $\eta(1405)/\eta(1475)$ is assumed in a fit to the $\gamma\phi$ invariant mass.

$\Gamma(\gamma\eta(1405)\to\gamma f_0(980)\pi^0\to\gamma\pi^+\pi^-\pi^0)/\Gamma_{total}$ — Γ_{286}/Γ

VALUE (units 10^{-5})	EVTS	DOCUMENT ID		TECN	COMMENT
1.5±0.11±0.11	743	ABLIKIM	12E	BES3	$J/\psi\to\gamma\eta(1405)$

$\Gamma(\gamma\eta(1405)\to\gamma f_0(980)\pi^0\to\gamma\pi^0\pi^0\pi^0)/\Gamma_{total}$ — Γ_{287}/Γ

VALUE (units 10^{-6})	EVTS	DOCUMENT ID		TECN	COMMENT
$\mathbf{6.64^{+1.10}_{-0.23}}$ **OUR AVERAGE**					
$4.62\pm0.15^{+5.08}_{-0.18}$		[1] ABLIKIM	25AB	BES3	$J/\psi\to\gamma\pi^0 f_0(980)\to\gamma\pi^0\pi^0\pi^0$
7.10±0.82±0.72	198	ABLIKIM	12E	BES3	$J/\psi\to\gamma\eta(1405)$

[1] ABLIKIM 25AB measured $J/\psi\to\gamma\eta(1405)\to\gamma\pi^0 f_0(980)$ / 0^{++} *PHSP* $\to\gamma\pi^0\pi^0\pi^0$. Here $\gamma\pi^0 f_0(980)$ / 0^{++} *PHSP* indicates an intermediate state which could be either $\gamma\pi^0 f_0(980)$ or $\gamma\pi^0$ 0^{++} phase space.

$\Gamma(\gamma\eta(1405)\to\gamma\gamma\gamma)/\Gamma_{total}$ — Γ_{288}/Γ

VALUE	CL%	DOCUMENT ID		TECN	COMMENT
$\mathbf{<2.63\times10^{-6}}$	90	ABLIKIM	18O	BES3	$\psi(2S)\to\pi^+\pi^-\gamma\gamma\gamma$

$\Gamma(\gamma\eta(1475)\to\gamma\gamma\gamma)/\Gamma_{total}$ — Γ_{289}/Γ

VALUE	CL%	DOCUMENT ID		TECN	COMMENT
$\mathbf{<1.86\times10^{-6}}$	90	ABLIKIM	18O	BES3	$\psi(2S)\to\pi^+\pi^-\gamma\gamma\gamma$

$\Gamma(\gamma\eta(1760)\to\gamma\rho^0\rho^0)/\Gamma_{total}$ — Γ_{290}/Γ

VALUE (units 10^{-3})		DOCUMENT ID		TECN	COMMENT
0.13±0.09		[1,2] BISELLO	89B	DM2	$J/\psi\to4\pi\gamma$

[1] Estimated by us from various fits.
[2] Includes unknown branching fraction to $\rho^0\rho^0$.

$\Gamma(\gamma\eta(1760)\to\gamma\omega\omega)/\Gamma_{total}$ — Γ_{291}/Γ

VALUE (units 10^{-3})	EVTS	DOCUMENT ID		TECN	COMMENT
1.98±0.08±0.32	1045	ABLIKIM	06H	BES	$J/\psi\to\gamma\omega\omega$

$\Gamma(\gamma\eta(1760)\to\gamma\gamma\gamma)/\Gamma_{total}$ — Γ_{292}/Γ

VALUE	CL%	DOCUMENT ID		TECN	COMMENT
$\mathbf{<4.80\times10^{-6}}$	90	ABLIKIM	18O	BES3	$\psi(2S)\to\pi^+\pi^-\gamma\gamma\gamma$

$\Gamma(\gamma\eta(2225))/\Gamma_{total}$ — Γ_{293}/Γ

VALUE (units 10^{-4})	EVTS	DOCUMENT ID		TECN	COMMENT
$\mathbf{3.14^{+0.50}_{-0.19}}$ **OUR AVERAGE**					
$2.40\pm0.10^{+2.47}_{-0.18}$		[1,2] ABLIKIM	16N	BES3	$J/\psi\to\gamma K^+K^-K^+K^-$
4.4 ±0.4 ±0.8	196	[2] ABLIKIM	08I	BES	$J/\psi\to\gamma K^+K^-K^0_S K^0_L$
3.3 ±0.8 ±0.5		[2] BAI	90B	MRK3	$J/\psi\to\gamma K^+K^-K^+K^-$
2.7 ±0.6 ±0.6		[2] BAI	90B	MRK3	$J/\psi\to\gamma K^+K^-K^0_S K^0_L$
$2.4^{+1.5}_{-1.0}$		[3,4] BISELLO	89B	DM2	$J/\psi\to4\pi\gamma$

[1] From a partial wave analysis of $J/\psi\to\gamma\phi\phi$ that also finds significant signals for for $\eta(2100)$, 0^{-+} phase space, $f_0(2100)$, $f_2(2010)$, $f_2(2300)$, $f_2(2340)$, and a previously unseen 0^{-+} state $X(2500)$ ($M=2470^{+15}_{-19}{}^{+101}_{-23}$ MeV, $\Gamma=230^{+64}_{-35}{}^{+56}_{-33}$ MeV).
[2] Includes unknown branching fraction to $\phi\phi$.
[3] Estimated by us from various fits.
[4] Includes unknown branching fraction to $\rho^0\rho^0$.

Int. J. Mod. Phys. A 2026.41. Downloaded from www.worldscientific.com by CALIFORNIA @ BERKELEY on 09/16/26. Re-use and distribution is strictly not permitted, except for Open Access articles.

$\Gamma(\gamma f_2(1270))/\Gamma_{total}$ — Γ_{294}/Γ

VALUE (units 10^{-3})	EVTS	DOCUMENT ID		TECN	COMMENT
1.63±0.12 OUR AVERAGE		Error includes scale factor of 1.3. See the ideogram below.			
$2.07\pm0.16^{+0.02}_{-0.07}$	2.4k	[1,2] DOBBS	15		$J/\psi \to \gamma\pi\pi$
$1.63\pm0.26^{+0.02}_{-0.05}$		[3] ABLIKIM	06V	BES2	$e^+e^- \to J/\psi \to \gamma\pi^+\pi^-$
$1.42\pm0.21^{+0.02}_{-0.05}$		[4] ABLIKIM	06V	BES2	$e^+e^- \to J/\psi \to \gamma\pi^0\pi^0$
$1.33\pm0.05\pm0.20$		[5] AUGUSTIN	87	DM2	$J/\psi \to \gamma\pi^+\pi^-$
$1.36\pm0.09\pm0.23$		[5] BALTRUSAIT...	87	MRK3	$J/\psi \to \gamma\pi^+\pi^-$
$1.48\pm0.25\pm0.30$	178	EDWARDS	82B	CBAL	$e^+e^- \to 2\pi^0\gamma$
$2.0\ \pm0.7$	35	ALEXANDER	78	PLUT	e^+e^-
$1.2\ \pm0.6$	30	[6] BRANDELIK	78B	DASP	$e^+e^- \to \pi^+\pi^-\gamma$

[1] Using CLEO-c data but not authored by the CLEO Collaboration.
[2] DOBBS 15 reports $[\Gamma(J/\psi(1S) \to \gamma f_2(1270))/\Gamma_{total}] \times [B(f_2(1270) \to \pi\pi)] = (1.744 \pm 0.052 \pm 0.122) \times 10^{-3}$ which we divide by our best (shown rounded) value $B(f_2(1270) \to \pi\pi) = (84.3^{+2.8}_{-1.0}) \times 10^{-2}$. Our first error is their experiment's error and our second error is the systematic error from using our best (shown rounded) value.
[3] ABLIKIM 06V reports $[\Gamma(J/\psi(1S) \to \gamma f_2(1270))/\Gamma_{total}] \times [B(f_2(1270) \to \pi\pi)] = (1.371 \pm 0.010 \pm 0.222) \times 10^{-3}$ which we divide by our best (shown rounded) value $B(f_2(1270) \to \pi\pi) = (84.3^{+2.8}_{-1.0}) \times 10^{-2}$. Our first error is their experiment's error and our second error is the systematic error from using our best (shown rounded) value.
[4] ABLIKIM 06V reports $[\Gamma(J/\psi(1S) \to \gamma f_2(1270))/\Gamma_{total}] \times [B(f_2(1270) \to \pi\pi)] = (1.200 \pm 0.027 \pm 0.174) \times 10^{-3}$ which we divide by our best (shown rounded) value $B(f_2(1270) \to \pi\pi) = (84.3^{+2.8}_{-1.0}) \times 10^{-2}$. Our first error is their experiment's error and our second error is the systematic error from using our best (shown rounded) value.
[5] Estimated using $B(f_2(1270) \to \pi\pi)=0.843 \pm 0.012$. The errors do not contain the uncertainty in the $f_2(1270)$ decay.
[6] Restated by us to take account of spread of E1, M2, E3 transitions.

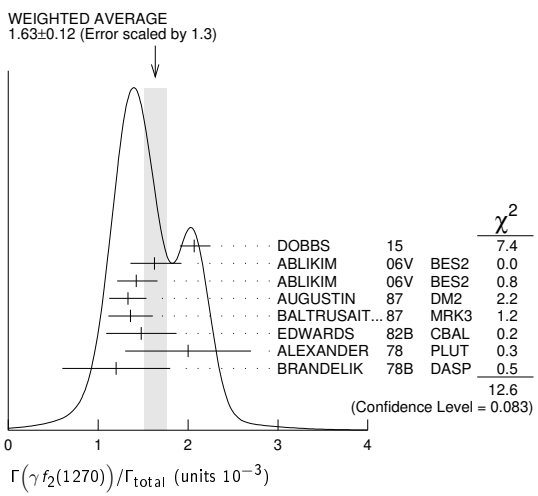

$\Gamma(\gamma f_2(1270) \to \gamma K^0_S K^0_S)/\Gamma_{total}$ — Γ_{295}/Γ

VALUE (units 10^{-5})	DOCUMENT ID		TECN	COMMENT
$\mathbf{2.58^{+0.08}_{-0.09}{}^{+0.59}_{-0.20}}$	ABLIKIM	18AA	BES3	$J/\psi \to \gamma K^0_S K^0_S$

$\Gamma(\gamma f_1(1285))/\Gamma_{total}$ — Γ_{296}/Γ

VALUE (units 10^{-3})	DOCUMENT ID		TECN	COMMENT
0.61 ±0.08 OUR AVERAGE				
$0.69\ \pm0.16\ \pm0.20$	[1] BAI	04J	BES2	$J/\psi \to \gamma\gamma\rho^0$
$0.61\ \pm0.04\ \pm0.21$	[2] BAI	00D	BES	$J/\psi \to \gamma K^\pm K^0_S \pi^\mp$
$0.45\ \pm0.09\ \pm0.17$	[3] BAI	99	BES	$J/\psi \to \gamma\eta\pi^+\pi^-$
$0.625\pm0.063\pm0.103$	[4] BOLTON	92	MRK3	$J/\psi \to \gamma f_1(1285)$
$0.70\ \pm0.08\ \pm0.16$	[5] BOLTON	92B	MRK3	$J/\psi \to \gamma\eta\pi^+\pi^-$

[1] Assuming $B(f_1(1285) \to \rho^0\gamma) = 0.055 \pm 0.013$.
[2] Assuming $\Gamma(f_1(1285) \to K\overline{K}\pi)/\Gamma_{total} = 0.090 \pm 0.004$.
[3] Assuming $\Gamma(f_1(1285) \to \eta\pi\pi)/\Gamma_{total} = 0.5 \pm 0.18$.
[4] Obtained summing the sequential decay channels
$B(J/\psi \to \gamma f_1(1285), f_1(1285) \to \pi\pi\pi\pi) = (1.44 \pm 0.39 \pm 0.27) \times 10^{-4}$;
$B(J/\psi \to \gamma f_1(1285), f_1(1285) \to a_0(980)\pi, a_0(980) \to \eta\pi) = (3.90 \pm 0.42 \pm 0.87) \times 10^{-4}$;
$B(J/\psi \to \gamma f_1(1285), f_1(1285) \to a_0(980)\pi, a_0(980) \to K\overline{K}) = (0.66 \pm 0.26 \pm 0.29) \times 10^{-4}$;
$B(J/\psi \to \gamma f_1(1285), f_1(1285) \to \gamma\rho^0) = (0.25 \pm 0.07 \pm 0.03) \times 10^{-4}$.
[5] Using $B(f_1(1285) \to a_0(980)\pi) = 0.37$, and including unknown branching ratio for $a_0(980) \to \eta\pi$.

$\Gamma(\gamma f_1(1285) \to \gamma\gamma\phi)/\Gamma_{total}$ — Γ_{297}/Γ

VALUE (units 10^{-6})	DOCUMENT ID		TECN	COMMENT
$\mathbf{0.29\pm0.03^{+0.11}_{-0.09}}$	[1] ABLIKIM	25P	BES3	$J/\psi \to \gamma\gamma\phi$

[1] From a partial wave analysis of $J/\psi \to \gamma\gamma\phi$ with significance 17.3σ.

$\Gamma(\gamma f_1(1285) \to \gamma\pi^0 f_0(980) \to \gamma\pi^0\pi^0\pi^0)/\Gamma_{total}$ — Γ_{298}/Γ

VALUE (units 10^{-7})	DOCUMENT ID		TECN
$\mathbf{5.64\pm0.45^{+0.74}_{-3.05}}$	[1] ABLIKIM	25AB	BES3

[1] ABLIKIM 25AB measured $J/\psi \to \gamma f_1(1285) \to \gamma\pi^0 f_0(980)$ / 0^{++} *PHSP* $\to \gamma\pi^0\pi^0\pi^0$. Here $\gamma\pi^0 f_0(980)$ / 0^{++} *PHSP* indicates an intermediate state which could be either $\gamma\pi^0 f_0(980)$ or $\gamma\pi^0\ 0^{++}$ phase space.

$\Gamma(\gamma f_1(1285) \to \gamma a_0(980)^0\pi^0 \to \gamma K^0_S K^0_S \pi^0)/\Gamma_{total}$ — Γ_{299}/Γ

VALUE (units 10^{-6})	EVTS	DOCUMENT ID		TECN	COMMENT
$\mathbf{8.55\pm0.41^{+3.42}_{-1.04}}$	126k	ABLIKIM	23M	BES3	$J/\psi \to \gamma K^0_S K^0_S \pi^0$

$\Gamma(\gamma f_0(1370) \to \gamma\pi\pi)/\Gamma_{total}$ — Γ_{300}/Γ

VALUE (units 10^{-5})	DOCUMENT ID		TECN	COMMENT
• • • We do not use the following data for averages, fits, limits, etc. • • •				
38 ± 10	SARANTSEV	21	RVUE	$J/\psi(1S) \to \gamma(\pi\pi,\ K\overline{K},\ \eta\eta,\ \omega\phi)$

$\Gamma(\gamma f_0(1370) \to \gamma K\overline{K})/\Gamma_{total}$ — Γ_{301}/Γ

VALUE (units 10^{-4})	EVTS	DOCUMENT ID		TECN	COMMENT
$\mathbf{4.19\pm0.73\pm1.34}$	478	[1] DOBBS	15		$J/\psi \to \gamma K\overline{K}$
• • • We do not use the following data for averages, fits, limits, etc. • • •					
$1.3\ \pm0.4$		SARANTSEV	21	RVUE	$J/\psi(1S) \to \gamma(\pi\pi,\ K\overline{K},\ \eta\eta,\ \omega\phi)$

[1] Using CLEO-c data but not authored by the CLEO Collaboration.

$\Gamma(\gamma f_0(1370) \to \gamma K^0_S K^0_S)/\Gamma_{total}$ — Γ_{302}/Γ

VALUE (units 10^{-5})	DOCUMENT ID		TECN	COMMENT
$\mathbf{1.07^{+0.08}_{-0.07}{}^{+0.36}_{-0.34}}$	ABLIKIM	18AA	BES3	$J/\psi \to \gamma K^0_S K^0_S$

$\Gamma(\gamma f_0(1370) \to \gamma\eta\eta)/\Gamma_{total}$ — Γ_{303}/Γ

VALUE (units 10^{-5})	DOCUMENT ID		TECN	COMMENT
• • • We do not use the following data for averages, fits, limits, etc. • • •				
3.5 ± 1.0	SARANTSEV	21	RVUE	$J/\psi(1S) \to \gamma(\pi\pi,\ K\overline{K},\ \eta\eta,\ \omega\phi)$

$\Gamma(\gamma f_0(1370) \to \gamma\eta\eta')/\Gamma_{total}$ — Γ_{304}/Γ

VALUE (units 10^{-5})	DOCUMENT ID		TECN	COMMENT
• • • We do not use the following data for averages, fits, limits, etc. • • •				
0.9 ± 0.3	SARANTSEV	21	RVUE	$J/\psi(1S) \to \gamma(\pi\pi,\ K\overline{K},\ \eta\eta,\ \omega\phi)$

$\Gamma(\gamma f_1(1420) \to \gamma K\overline{K}\pi)/\Gamma_{total}$ — Γ_{305}/Γ

VALUE (units 10^{-3})	DOCUMENT ID		TECN	COMMENT
0.79±0.13 OUR AVERAGE				
$0.68\pm0.04\pm0.24$	BAI	00D	BES	$J/\psi \to \gamma K^\pm K^0_S \pi^\mp$
$0.76\pm0.15\pm0.21$	[1,2] AUGUSTIN	92	DM2	$J/\psi \to \gamma K\overline{K}\pi$
$0.87\pm0.14^{+0.14}_{-0.11}$	[1] BAI	90C	MRK3	$J/\psi \to \gamma K^0_S K^\pm \pi^\mp$

[1] Included unknown branching fraction $f_1(1420) \to K\overline{K}\pi$.
[2] From fit to the $K^*(892)K$ 1^{++} partial wave.

$\Gamma(\gamma f_1(1420) \to \gamma\gamma\phi)/\Gamma_{total}$ — Γ_{308}/Γ

VALUE (units 10^{-6})	DOCUMENT ID		TECN	COMMENT
$\mathbf{0.55\pm0.07^{+0.18}_{-0.17}}$	[1] ABLIKIM	25P	BES3	$J/\psi \to \gamma\gamma\phi$

[1] From a partial wave analysis of $J/\psi \to \gamma\gamma\phi$ with significance 9.0σ.

$\Gamma(\gamma f_1(1420) \to \gamma\pi^0 f_0(980) \to \gamma\pi^0\pi^0\pi^0)/\Gamma_{total}$ — Γ_{309}/Γ

VALUE (units 10^{-6})	DOCUMENT ID		TECN
$\mathbf{2.23\pm0.16^{+0.20}_{-1.20}}$	[1] ABLIKIM	25AB	BES3

[1] ABLIKIM 25AB measured $J/\psi \to \gamma f_1(1420) \to \gamma\pi^0 f_0(980)$ / 0^{++} *PHSP* $\to \gamma\pi^0\pi^0\pi^0$. Here $\gamma\pi^0 f_0(980)$ / 0^{++} *PHSP* indicates an intermediate state which could be either $\gamma\pi^0 f_0(980)$ or $\gamma\pi^0\ 0^{++}$ phase space.

$\Gamma(\gamma f_0(1500) \to \gamma\pi\pi)/\Gamma_{total}$ — Γ_{310}/Γ

VALUE (units 10^{-4})	EVTS	DOCUMENT ID		TECN	COMMENT
1.09±0.24 OUR AVERAGE					
$1.21\pm0.29\pm0.24$	174	[1] DOBBS	15		$J/\psi \to \gamma\pi\pi$
$1.00\pm0.03\pm0.45$		[2] ABLIKIM	06V	BES2	$e^+e^- \to J/\psi \to \gamma\pi^+\pi^-$
$1.02\pm0.09\pm0.45$		[2] ABLIKIM	06V	BES2	$e^+e^- \to J/\psi \to \gamma\pi^0\pi^0$
• • • We do not use the following data for averages, fits, limits, etc. • • •					
0.90 ± 0.17		SARANTSEV	21	RVUE	$J/\psi(1S) \to \gamma(\pi\pi,\ K\overline{K},\ \eta\eta,\ \omega\phi)$
$5.7\ \pm0.8$		[3,4] BUGG	95	MRK3	$J/\psi \to \gamma\pi^+\pi^-\pi^+\pi^-$

[1] Using CLEO-c data but not authored by the CLEO Collaboration.
[2] Including unknown branching fraction to $\pi\pi$.
[3] Including unknown branching ratio for $f_0(1500) \to \pi^+\pi^-\pi^+\pi^-$.
[4] Assuming that $f_0(1500)$ decays only to two S-wave dipions.

Int. J. Mod. Phys. A 2026.41. Downloaded from www.worldscientific.com by UNIVERSITY OF CALIFORNIA @ BERKELEY on 09/16/26. Re-use and distribution is strictly not permitted, except for Open Access articles.

$\Gamma(\gamma f_0(1500) \to \gamma\eta\eta)/\Gamma_{total}$ — Γ_{311}/Γ

VALUE (units 10^{-5})	EVTS	DOCUMENT ID		TECN	COMMENT
$1.65^{+0.26+0.51}_{-0.31-1.40}$	5.5k	[1] ABLIKIM	13N	BES3	$J/\psi \to \gamma\eta\eta$
• • • We do not use the following data for averages, fits, limits, etc. • • •					
1.1 ±0.4		SARANTSEV	21	RVUE	$J/\psi(1S) \to \gamma(\pi\pi, K\overline{K}, \eta\eta, \omega\phi)$

[1] From partial wave analysis including all possible combinations of 0^{++}, 2^{++}, and 4^{++} resonances.

$\Gamma(\gamma f_0(1500) \to \gamma K^0_S K^0_S)/\Gamma_{total}$ — Γ_{312}/Γ

VALUE (units 10^{-5})	DOCUMENT ID		TECN	COMMENT
$1.59 \pm 0.16^{+0.18}_{-0.56}$	ABLIKIM	18AA	BES3	$J/\psi \to \gamma K^0_S K^0_S$
• • • We do not use the following data for averages, fits, limits, etc. • • •				
0.7 ±0.3	SARANTSEV	21	RVUE	$J/\psi(1S) \to \gamma(\pi\pi, K\overline{K}, \eta\eta, \omega\phi)$

$\Gamma(\gamma f_0(1500) \to \gamma\eta\eta')/\Gamma_{total}$ — Γ_{313}/Γ

VALUE (units 10^{-6})	DOCUMENT ID		TECN	COMMENT
• • • We do not use the following data for averages, fits, limits, etc. • • •				
$18.1 \pm 1.1^{+1.9}_{-1.3}$	[1] ABLIKIM	22AS	BES3	$J/\psi(1S) \to \gamma\eta\eta'$
12 ±5	SARANTSEV	21	RVUE	$J/\psi(1S) \to \gamma(\pi\pi, K\overline{K}, \eta\eta, \omega\phi)$

[1] From a Breit-Wigner fit involving 9 resonances and a resonating exotic $\eta_1(1855) \to \eta\eta'$ P-wave.

$\Gamma(\gamma f_1(1510) \to \gamma\eta\pi^+\pi^-)/\Gamma_{total}$ — Γ_{314}/Γ

VALUE (units 10^{-4})	DOCUMENT ID		TECN	COMMENT
$4.5 \pm 1.0 \pm 0.7$	BAI	99	BES	$J/\psi \to \gamma\eta\pi^+\pi^-$

$\Gamma(\gamma f_1(1510) \to \gamma\gamma\phi)/\Gamma_{total}$ — Γ_{315}/Γ

VALUE (units 10^{-6})	DOCUMENT ID		TECN	COMMENT
$0.78 \pm 0.09^{+0.34}_{-0.30}$	[1] ABLIKIM	25P	BES3	$J/\psi \to \gamma\gamma\phi$

[1] From a partial wave analysis of $J/\psi \to \gamma\gamma\phi$ with significance 5.3σ.

$\Gamma(\gamma f_1(1510) \to \gamma\pi^0 f_0(980) \to \gamma\pi^0\pi^0\pi^0)/\Gamma_{total}$ — Γ_{316}/Γ

VALUE (units 10^{-7})	DOCUMENT ID		TECN
• • • We do not use the following data for averages, fits, limits, etc. • • •			
$7.91 \pm 1.20^{+0.74}_{-3.83}$	[1] ABLIKIM	25AB	BES3

[1] ABLIKIM 25AB measured $J/\psi \to \gamma f_1(1510) \to \gamma\pi^0 f_0(980)$ / 0^{++} *PHSP* $\to \gamma\pi^0\pi^0\pi^0$. Here $\gamma\pi^0 f_0(980)$ / 0^{++} *PHSP* indicates an intermediate state which could be either $\gamma\pi^0 f_0(980)$ or $\gamma\pi^0$ 0^{++} phase space. Evidence for the $f_1(1510)$ is seen with a 5σ significance in the partial wave analysis.

$\Gamma(\gamma f'_2(1525))/\Gamma_{total}$ — Γ_{317}/Γ

VALUE (units 10^{-4})	CL%	EVTS	DOCUMENT ID		TECN	COMMENT
$5.7^{+0.8}_{-0.5}$ OUR AVERAGE Error includes scale factor of 1.5. See the ideogram below.						
8.0 ±0.9 ±0.2		750	[1,2] DOBBS	15		$J/\psi \to \gamma K\overline{K}$
$3.85 \pm 0.17^{+1.91}_{-0.73}$			[3] BAI	03G	BES	$J/\psi \to \gamma K\overline{K}$
$3.6 \pm 0.4^{+1.4}_{-0.4}$			[3] BAI	96C	BES	$J/\psi \to \gamma K^+K^-$
5.6 ±1.4 ±0.9			[3] AUGUSTIN	88	DM2	$J/\psi \to \gamma K^+K^-$
4.5 ±0.4 ±0.9			[3] AUGUSTIN	88	DM2	$J/\psi \to \gamma K^0_S K^0_S$
6.8 ±1.6 ±1.4			[3] BALTRUSAIT...87		MRK3	$J/\psi \to \gamma K^+K^-$
• • • We do not use the following data for averages, fits, limits, etc. • • •						
<3.4	90	4	[4] BRANDELIK	79C	DASP	$e^+e^- \to \pi^+\pi^-\gamma$
<2.3	90	3	ALEXANDER	78	PLUT	$e^+e^- \to K^+K^-\gamma$

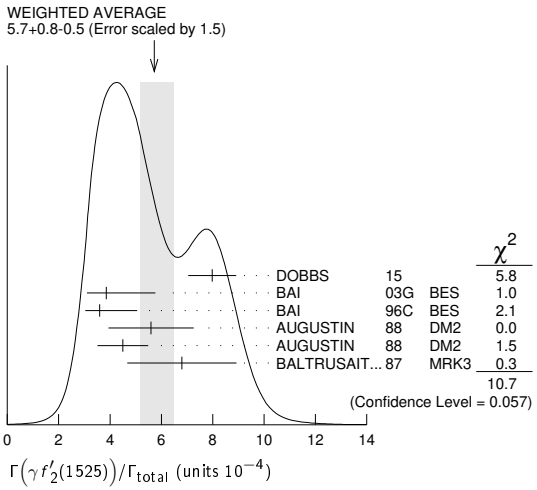

[1] Using CLEO-c data but not authored by the CLEO Collaboration.

[2] DOBBS 15 reports $[\Gamma(J/\psi(1S) \to \gamma f'_2(1525))/\Gamma_{total}] \times [B(f'_2(1525) \to K\overline{K})] = (7.09 \pm 0.46 \pm 0.67) \times 10^{-4}$ which we divide by our best (shown rounded) value $B(f'_2(1525) \to K\overline{K}) = (88.8 \pm 2.2) \times 10^{-2}$. Our first error is their experiment's error and our second error is the systematic error from using our best (shown rounded) value.

[3] Using $B(f'_2(1525) \to K\overline{K}) = 0.888$.

[4] Assuming isotropic production and decay of the $f'_2(1525)$ and isospin.

$\Gamma(\gamma f'_2(1525) \to \gamma K^0_S K^0_S)/\Gamma_{total}$ — Γ_{318}/Γ

VALUE (units 10^{-5})	DOCUMENT ID		TECN	COMMENT
$7.99^{+0.03+0.69}_{-0.04-0.50}$	ABLIKIM	18AA	BES3	$J/\psi \to \gamma K^0_S K^0_S$

$\Gamma(\gamma f'_2(1525) \to \gamma K^*(892)^0 K^0_S \to \gamma K^0_S K^0_S \pi^0)/\Gamma_{total}$ — Γ_{319}/Γ

VALUE (units 10^{-6})	EVTS	DOCUMENT ID		TECN	COMMENT
$9.47 \pm 0.43^{+1.51}_{-0.66}$	126k	ABLIKIM	23M	BES3	$J/\psi \to \gamma K^0_S K^0_S \pi^0$

$\Gamma(\gamma f'_2(1525) \to \gamma\eta\eta)/\Gamma_{total}$ — Γ_{320}/Γ

VALUE (units 10^{-5})	EVTS	DOCUMENT ID		TECN	COMMENT
$3.42^{+0.43+1.37}_{-0.51-1.30}$	5.5k	[1] ABLIKIM	13N	BES3	$J/\psi \to \gamma\eta\eta$

[1] From partial wave analysis including all possible combinations of 0^{++}, 2^{++}, and 4^{++} resonances.

$\Gamma(\gamma f'_2(1525) \to \gamma\gamma\phi)/\Gamma_{total}$ — Γ_{322}/Γ

VALUE (units 10^{-6})	DOCUMENT ID		TECN	COMMENT
$2.76 \pm 0.18^{+0.90}_{-0.61}$	[1] ABLIKIM	25P	BES3	$J/\psi \to \gamma\gamma\phi$

[1] From a partial wave analysis of $J/\psi \to \gamma\gamma\phi$ with significance 16.4σ.

$\Gamma(\gamma f_2(1565) \to \gamma\eta\eta')/\Gamma_{total}$ — Γ_{321}/Γ

VALUE (units 10^{-5})	DOCUMENT ID		TECN	COMMENT
• • • We do not use the following data for averages, fits, limits, etc. • • •				
$0.32 \pm 0.05^{+0.12}_{-0.02}$	[1] ABLIKIM	22AS	BES3	$J/\psi(1S) \to \gamma\eta\eta'$

[1] From a Breit-Wigner fit involving 9 resonances and a resonating exotic $\eta_1(1855) \to \eta\eta'$ P-wave.

$\Gamma(\gamma f_2(1640) \to \gamma\omega\omega)/\Gamma_{total}$ — Γ_{323}/Γ

VALUE (units 10^{-3})	EVTS	DOCUMENT ID		TECN	COMMENT
$0.28 \pm 0.05 \pm 0.17$	141	ABLIKIM	06H	BES	$J/\psi \to \gamma\omega\omega$

$\Gamma(\gamma f_0(1710) \to \gamma\pi\pi)/\Gamma_{total}$ — Γ_{324}/Γ

VALUE (units 10^{-4})	EVTS	DOCUMENT ID		TECN	COMMENT
3.8 ±0.5 OUR AVERAGE					
3.72±0.30±0.43	483	[1] DOBBS	15		$J/\psi \to \gamma\pi\pi$
3.96±0.06±1.12		[2] ABLIKIM	06V	BES2	$e^+e^- \to J/\psi \to \gamma\pi^+\pi^-$
3.99±0.15±2.64		[2] ABLIKIM	06V	BES2	$e^+e^- \to J/\psi \to \gamma\pi^0\pi^0$
• • • We do not use the following data for averages, fits, limits, etc. • • •					
0.6 ±0.2		[3] SARANTSEV	21	RVUE	$J/\psi(1S) \to \gamma(\pi\pi, K\overline{K}, \eta\eta, \omega\phi)$
2.5 ±1.6 ±0.8		BAI	98H	BES	$J/\psi \to \gamma\pi^0\pi^0$

[1] Using CLEO-c data but not authored by the CLEO Collaboration.

[2] Including unknown branching fraction to $\pi\pi$.

[3] There is a further $(2.4 \pm 0.8) \times 10^{-4}$ scalar contribution at 1765 MeV.

$\Gamma(\gamma f_0(1710) \to \gamma K\overline{K})/\Gamma_{total}$ — Γ_{325}/Γ

VALUE (units 10^{-4})	CL%	EVTS	DOCUMENT ID		TECN	COMMENT
$9.5^{+0.9}_{-0.5}$ OUR AVERAGE Error includes scale factor of 1.4. See the ideogram below.						
$8.00^{+0.12+1.24}_{-0.08-0.40}$			[1] ABLIKIM	18AA	BES3	$J/\psi \to \gamma K^0_S K^0_S$
11.76±0.54±0.94		1.2k	[2] DOBBS	15		$J/\psi \to \gamma K\overline{K}$
$9.62 \pm 0.29^{+3.51}_{-1.86}$			[3] BAI	03G	BES	$J/\psi \to \gamma K\overline{K}$
$5.0 \pm 0.8^{+1.8}_{-0.4}$			[1,4] BAI	96C	BES	$J/\psi \to \gamma K^+K^-$
9.2 ±1.4 ±1.4			[1] AUGUSTIN	88	DM2	$J/\psi \to \gamma K^+K^-$
10.4 ±1.2 ±1.6			[1] AUGUSTIN	88	DM2	$J/\psi \to \gamma K^0_S K^0_S$
9.6 ±1.2 ±1.8			[1] BALTRUSAIT...87		MRK3	$J/\psi \to \gamma K^+K^-$
• • • We do not use the following data for averages, fits, limits, etc. • • •						
2.3 ±0.8			[5] SARANTSEV	21	RVUE	$J/\psi(1S) \to \gamma(\pi\pi, K\overline{K}, \eta\eta, \omega\phi)$
$1.6 \pm 0.2^{+0.6}_{-0.2}$			[1,6] BAI	96C	BES	$J/\psi \to \gamma K^+K^-$
< 0.8	90		[7] BISELLO	89B		$J/\psi \to 4\pi\gamma$
1.6 ±0.4 ±0.3			[8] BALTRUSAIT...87		MRK3	$J/\psi \to \gamma\pi^+\pi^-$
3.8 ±1.6			[9] EDWARDS	82D	CBAL	$e^+e^- \to \eta\eta\gamma$

[1] Includes unknown branching fraction to K^+K^- or $K^0_S K^0_S$. We have multiplied K^+K^- measurement by 2, and $K^0_S K^0_S$ by 4 to obtain $K\overline{K}$ result.

[2] Using CLEO-c data but not authored by the CLEO Collaboration.

[3] Includes unknown branching ratio to K^+K^- or $K^0_S K^0_S$.
[4] Assuming $J^P = 2^+$ for $f_0(1710)$.
[5] There is a further $(6 \pm 2) \times 10^{-4}$ scalar contribution at 1765 MeV.
[6] Assuming $J^P = 0^+$ for $f_0(1710)$.
[7] Includes unknown branching fraction to $\rho^0\rho^0$.
[8] Includes unknown branching fraction to $\pi^+\pi^-$.
[9] Includes unknown branching fraction to $\eta\eta$.

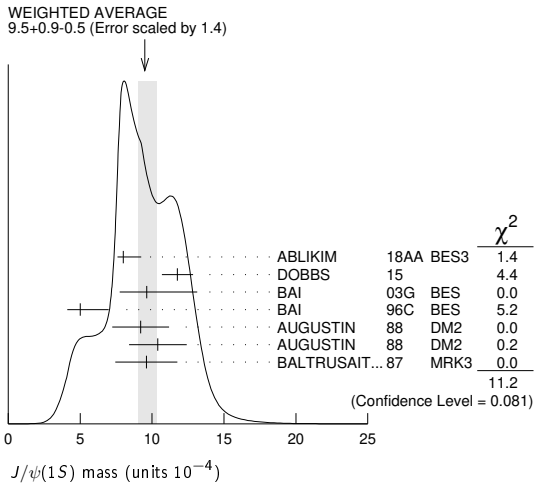

$\Gamma(\gamma f_0(1710) \to \gamma\omega\omega)/\Gamma_{total}$ — Γ_{326}/Γ

VALUE (units 10^{-3})	EVTS	DOCUMENT ID		TECN	COMMENT
$0.31 \pm 0.06 \pm 0.08$	180	ABLIKIM	06H	BES	$J/\psi \to \gamma\omega\omega$

$\Gamma(\gamma f_0(1710) \to \gamma\eta\eta)/\Gamma_{total}$ — Γ_{327}/Γ

VALUE (units 10^{-4})	EVTS	DOCUMENT ID		TECN	COMMENT
$2.35^{+0.13+1.24}_{-0.11-0.74}$	5.5k	[1] ABLIKIM	13N	BES3	$J/\psi \to \gamma\eta\eta$
• • • We do not use the following data for averages, fits, limits, etc. • • •					
1.2 ± 0.4		[2] SARANTSEV	21	RVUE	$J/\psi(1S) \to \gamma(\pi\pi, K\overline{K}, \eta\eta, \omega\phi)$

[1] From partial wave analysis including all possible combinations of 0^{++}, 2^{++}, and 4^{++} resonances.
[2] There is a further $(0.7 \pm 0.1) \times 10^{-4}$ scalar contribution at 1765 MeV.

$\Gamma(\gamma f_0(1710) \to \gamma\eta\eta')/\Gamma_{total}$ — Γ_{328}/Γ

VALUE (units 10^{-5})	DOCUMENT ID		TECN	COMMENT
• • • We do not use the following data for averages, fits, limits, etc. • • •				
6.5 ± 2.5	[1] SARANTSEV	21	RVUE	$J/\psi(1S) \to \gamma(\pi\pi, K\overline{K}, \eta\eta, \omega\phi)$

[1] There is a further $(2.5 \pm 1.1) \times 10^{-5}$ scalar contribution at 1765 MeV.

$\Gamma(\gamma f_0(1710) \to \gamma\omega\phi)/\Gamma_{total}$ — Γ_{329}/Γ

VALUE (units 10^{-4})	EVTS	DOCUMENT ID		TECN	COMMENT
2.5 ± 0.6 OUR AVERAGE					
$2.00 \pm 0.08^{+1.38}_{-1.64}$	1.3k	ABLIKIM	13J	BES3	$J/\psi \to \gamma\omega\phi$
$2.61 \pm 0.27 \pm 0.65$	95	ABLIKIM	06J	BES2	$J/\psi \to \gamma\omega\phi$
• • • We do not use the following data for averages, fits, limits, etc. • • •					
0.1 ± 0.1		[1] SARANTSEV	21	RVUE	$J/\psi(1S) \to \gamma(\pi\pi, K\overline{K}, \eta\eta, \omega\phi)$

[1] There is a further $(2.2 \pm 0.4) \times 10^{-4}$ scalar contribution at 1765 MeV.

$\Gamma(\gamma f_0(1810) \to \gamma\pi\pi)/\Gamma_{total}$ — Γ_{330}/Γ

VALUE (units 10^{-4})	DOCUMENT ID		TECN	COMMENT
• • • We do not use the following data for averages, fits, limits, etc. • • •				
2.4 ± 0.8	SARANTSEV	21	RVUE	$J/\psi(1S) \to \gamma(\pi\pi)$

$\Gamma(\gamma f_0(1810) \to \gamma K^0_S K^0_S)/\Gamma_{total}$ — Γ_{331}/Γ

VALUE (units 10^{-5})	DOCUMENT ID		TECN	COMMENT
$1.11 \pm 0.06^{+0.19}_{-0.32}$	ABLIKIM	18AA	BES3	$J/\psi \to \gamma K^0_S K^0_S$

$\Gamma(\gamma f_0(1810) \to \gamma K\overline{K})/\Gamma_{total}$ — Γ_{332}/Γ

VALUE (units 10^{-4})	DOCUMENT ID		TECN	COMMENT
• • • We do not use the following data for averages, fits, limits, etc. • • •				
6 ± 2	SARANTSEV	21	RVUE	$J/\psi \to \gamma(K\overline{K})$

$\Gamma(\gamma f_0(1810) \to \gamma\eta\eta)/\Gamma_{total}$ — Γ_{333}/Γ

VALUE (units 10^{-4})	DOCUMENT ID		TECN	COMMENT
• • • We do not use the following data for averages, fits, limits, etc. • • •				
0.7 ± 0.1	SARANTSEV	21	RVUE	$J/\psi \to \gamma(\eta\eta)$

$\Gamma(\gamma f_0(1810) \to \gamma\eta\eta')/\Gamma_{total}$ — Γ_{334}/Γ

VALUE (units 10^{-5})	DOCUMENT ID		TECN	COMMENT
• • • We do not use the following data for averages, fits, limits, etc. • • •				
$0.11 \pm 0.01^{+0.04}_{-0.03}$	[1] ABLIKIM	22AS	BES3	$J/\psi(1S) \to \gamma\eta\eta'$
2.5 ± 1.1	SARANTSEV	21	RVUE	$J/\psi \to \gamma(\eta\eta')$

[1] From a Breit-Wigner fit involving 9 resonances and a resonating exotic $\eta_1(1855) \to \eta\eta'$ P-wave.

$\Gamma(\gamma f_0(1810) \to \gamma\omega\phi)/\Gamma_{total}$ — Γ_{335}/Γ

VALUE (units 10^{-4})	DOCUMENT ID		TECN	COMMENT
• • • We do not use the following data for averages, fits, limits, etc. • • •				
2.2 ± 0.4	SARANTSEV	21	RVUE	$J/\psi \to \gamma(\omega\phi)$

$\Gamma(\gamma f_2(1810) \to \gamma\eta\eta)/\Gamma_{total}$ — Γ_{336}/Γ

VALUE (units 10^{-5})	EVTS	DOCUMENT ID		COMMENT
$5.40^{+0.60+3.42}_{-0.67-2.35}$	5.5k	[1] ABLIKIM	13N	$J/\psi \to \gamma\eta\eta$

[1] From partial wave analysis including all possible combinations of 0^{++}, 2^{++}, and 4^{++} resonances.

$\Gamma(\gamma\eta_1(1855) \to \gamma\eta\eta')/\Gamma_{total}$ — Γ_{337}/Γ

VALUE (units 10^{-6})	DOCUMENT ID		TECN	COMMENT
$2.70 \pm 0.41^{+0.16}_{-0.35}$	[1] ABLIKIM	22AI	BES3	$J/\psi(1S) \to \gamma\eta\eta'$

[1] From a Breit-Wigner fit involving 9 resonances and the resonating exotic $\eta_1(1855) \to \eta\eta'$ P-wave. For analysis details see ABLIKIM 22AS.

$\Gamma(\gamma f_2(1910) \to \gamma\omega\omega)/\Gamma_{total}$ — Γ_{338}/Γ

VALUE (units 10^{-3})	EVTS	DOCUMENT ID		TECN	COMMENT
$0.20 \pm 0.04 \pm 0.13$	151	ABLIKIM	06H	BES	$J/\psi \to \gamma\omega\omega$

$\Gamma(\gamma f_2(1950) \to \gamma K^*(892)\overline{K}^*(892))/\Gamma_{total}$ — Γ_{339}/Γ

VALUE (units 10^{-3})	DOCUMENT ID		TECN	COMMENT
$0.7 \pm 0.1 \pm 0.2$	BAI	00B	BES	$J/\psi \to \gamma K^+ K^0 \pi^+\pi^-$

$\Gamma(\gamma f_2(1950) \to \gamma\gamma\phi)/\Gamma_{total}$ — Γ_{340}/Γ

VALUE (units 10^{-6})	DOCUMENT ID		TECN	COMMENT
$9.96 \pm 0.60^{+3.44}_{-2.13}$	[1] ABLIKIM	25P	BES3	$J/\psi \to \gamma\gamma\phi$

[1] From a partial wave analysis of $J/\psi \to \gamma\gamma\phi$ with significance 13.1σ.

$\Gamma(\gamma f_2(2010) \to \gamma\eta\eta')/\Gamma_{total}$ — Γ_{341}/Γ

VALUE (units 10^{-5})	DOCUMENT ID		TECN	COMMENT
• • • We do not use the following data for averages, fits, limits, etc. • • •				
$0.71 \pm 0.06^{+0.10}_{-0.06}$	[1] ABLIKIM	22AS	BES3	$J/\psi(1S) \to \gamma\eta\eta'$

[1] From a Breit-Wigner fit involving 9 resonances and a resonating exotic $\eta_1(1855) \to \eta\eta'$ P-wave.

$\Gamma(\gamma f_2(2010) \to \gamma\gamma\phi)/\Gamma_{total}$ — Γ_{342}/Γ

VALUE (units 10^{-6})	DOCUMENT ID		TECN	COMMENT
$4.63 \pm 0.43^{+1.42}_{-1.46}$	[1] ABLIKIM	25P	BES3	$J/\psi \to \gamma\gamma\phi$

[1] From a partial wave analysis of $J/\psi \to \gamma\gamma\phi$ with significance 11.3σ.

$\Gamma(\gamma f_0(2020) \to \gamma\pi\pi)/\Gamma_{total}$ — Γ_{343}/Γ

VALUE (units 10^{-5})	DOCUMENT ID		TECN	COMMENT
• • • We do not use the following data for averages, fits, limits, etc. • • •				
42 ± 10	SARANTSEV	21	RVUE	$J/\psi(1S) \to \gamma(\pi\pi, K\overline{K}, \eta\eta, \omega\phi)$

$\Gamma(\gamma f_0(2020) \to \gamma K\overline{K})/\Gamma_{total}$ — Γ_{344}/Γ

VALUE (units 10^{-5})	DOCUMENT ID		TECN	COMMENT
• • • We do not use the following data for averages, fits, limits, etc. • • •				
55 ± 25	SARANTSEV	21	RVUE	$J/\psi(1S) \to \gamma(\pi\pi, K\overline{K}, \eta\eta, \omega\phi)$

$\Gamma(\gamma f_0(2020) \to \gamma\eta\eta)/\Gamma_{total}$ — Γ_{345}/Γ

VALUE (units 10^{-5})	DOCUMENT ID		TECN	COMMENT
• • • We do not use the following data for averages, fits, limits, etc. • • •				
10 ± 10	SARANTSEV	21	RVUE	$J/\psi(1S) \to \gamma(\pi\pi, K\overline{K}, \eta\eta, \omega\phi)$

$\Gamma(\gamma f_0(2020) \to \gamma\eta'\eta')/\Gamma_{total}$ — Γ_{346}/Γ

VALUE (units 10^{-4})	DOCUMENT ID		TECN	COMMENT
$2.63 \pm 0.06^{+0.31}_{-0.46}$	[1] ABLIKIM	22C	BES3	$J/\psi \to \gamma\eta'\eta' \to 4/5\gamma 2(\pi^+\pi^-)$

[1] From a partial wave analysis of the systems (γX), with $X \to \eta'\eta'$, and $(\eta' X)$, with $X \to \gamma\eta'$ in the decay $J/\psi \to \gamma\eta'\eta'$. The intermediate resonance X is parametrized by a constant-width, relativistic Breit-Wigner.

Int. J. Mod. Phys. A 2026.41. Downloaded from www.worldscientific.com
by LIFORNIA @ BERKELEY on 09/16/26. Re-use and distribution is strictly not permitted, except for Open Access articles.

Int. J. Mod. Phys. A 2026.41. Downloaded from www.worldscientific.com
by UNIVERSITY OF CALIFORNIA @ BERKELEY on 09/16/26. Re-use and distribution is strictly not permitted, except for Open Access articles.

$\Gamma(\gamma f_0(2020) \to \gamma\eta\eta')/\Gamma_{total}$ — Γ_{347}/Γ

VALUE (units 10^{-5})	DOCUMENT ID	TECN	COMMENT
• • • We do not use the following data for averages, fits, limits, etc. • • •			
$2.28 \pm 0.12^{+0.29}_{-0.20}$	[1] ABLIKIM 22AS	BES3	$J/\psi(1S) \to \gamma\eta\eta'$

[1] From a Breit-Wigner fit involving 9 resonances and a resonating exotic $\eta_1(1855) \to \eta\eta'$ P-wave.

$\Gamma(\gamma f_4(2050))/\Gamma_{total}$ — Γ_{348}/Γ

VALUE (units 10^{-3})	DOCUMENT ID	TECN	COMMENT
$2.7 \pm 0.5 \pm 0.5$	[1] BALTRUSAIT...87	MRK3	$J/\psi \to \gamma\pi^+\pi^-$

[1] Assuming branching fraction $f_4(2050) \to \pi\pi/$ total $= 0.167$.

$\Gamma(\gamma f_4(2050) \to \gamma\eta\eta')/\Gamma_{total}$ — Γ_{349}/Γ

VALUE (units 10^{-5})	DOCUMENT ID	TECN	COMMENT
• • • We do not use the following data for averages, fits, limits, etc. • • •			
$0.06 \pm 0.01^{+0.03}_{-0.01}$	[1] ABLIKIM 22AS	BES3	$J/\psi(1S) \to \gamma\eta\eta'$

[1] From a Breit-Wigner fit involving 9 resonances and a resonating exotic $\eta_1(1855) \to \eta\eta'$ P-wave.

$\Gamma(\gamma f_0(2100) \to \gamma\eta\eta)/\Gamma_{total}$ — Γ_{350}/Γ

VALUE (units 10^{-4})	EVTS	DOCUMENT ID	TECN	COMMENT
$1.13^{+0.09+0.64}_{-0.10-0.28}$	5.5k	[1] ABLIKIM 13N	BES3	$J/\psi \to \gamma\eta\eta$
• • • We do not use the following data for averages, fits, limits, etc. • • •				
1.8 ± 1.5		SARANTSEV 21	RVUE	$J/\psi(1S) \to \gamma(\pi\pi, K\overline{K}, \eta\eta, \omega\phi)$

[1] From partial wave analysis including all possible combinations of 0^{++}, 2^{++}, and 4^{++} resonances.

$\Gamma(\gamma f_0(2100) \to \gamma K\overline{K})/\Gamma_{total}$ — Γ_{351}/Γ

VALUE (units 10^{-5})	DOCUMENT ID	TECN	COMMENT
• • • We do not use the following data for averages, fits, limits, etc. • • •			
32 ± 20	SARANTSEV 21	RVUE	$J/\psi(1S) \to \gamma(\pi\pi, K\overline{K}, \eta\eta, \omega\phi)$

$\Gamma(\gamma f_0(2100) \to \gamma\pi\pi)/\Gamma_{total}$ — Γ_{352}/Γ

VALUE (units 10^{-4})	EVTS	DOCUMENT ID	TECN	COMMENT
$6.24 \pm 0.48 \pm 0.87$	744	[1] DOBBS 15		$J/\psi \to \gamma\pi\pi$
• • • We do not use the following data for averages, fits, limits, etc. • • •				
2.0 ± 0.8		SARANTSEV 21	RVUE	$J/\psi(1S) \to \gamma(\pi\pi, K\overline{K}, \eta\eta, \omega\phi)$

[1] Using CLEO-c data but not authored by the CLEO Collaboration.

$\Gamma(\gamma f_0(2200))/\Gamma_{total}$ — Γ_{353}/Γ

VALUE (units 10^{-4})	DOCUMENT ID	TECN	COMMENT
• • • We do not use the following data for averages, fits, limits, etc. • • •			
1.5	[1] AUGUSTIN 88	DM2	$J/\psi \to \gamma K^0_S K^0_S$

[1] Includes unknown branching fraction to $K^0_S K^0_S$.

$\Gamma(\gamma f_0(2200) \to \gamma K\overline{K})/\Gamma_{total}$ — Γ_{354}/Γ

VALUE (units 10^{-4})	EVTS	DOCUMENT ID	TECN	COMMENT
$5.86 \pm 0.49 \pm 1.20$	490	[1] DOBBS 15		$J/\psi \to \gamma K\overline{K}$
• • • We do not use the following data for averages, fits, limits, etc. • • •				
0.5 ± 0.5		SARANTSEV 21	RVUE	$J/\psi(1S) \to \gamma(\pi\pi, K\overline{K}, \eta\eta, \omega\phi)$

[1] Using CLEO-c data but not authored by the CLEO Collaboration.

$\Gamma(\gamma f_0(2200) \to \gamma K^0_S K^0_S)/\Gamma_{total}$ — Γ_{355}/Γ

VALUE (units 10^{-4})	DOCUMENT ID	TECN	COMMENT
$2.72^{+0.08+0.17}_{-0.06-0.47}$	ABLIKIM 18AA	BES3	$J/\psi \to \gamma K^0_S K^0_S$

$\Gamma(\gamma f_0(2200) \to \gamma\pi\pi)/\Gamma_{total}$ — Γ_{356}/Γ

VALUE (units 10^{-5})	DOCUMENT ID	TECN	COMMENT
• • • We do not use the following data for averages, fits, limits, etc. • • •			
5 ± 2	SARANTSEV 21	RVUE	$J/\psi(1S) \to \gamma(\pi\pi, K\overline{K}, \eta\eta, \omega\phi)$

$\Gamma(\gamma f_0(2200) \to \gamma\eta\eta)/\Gamma_{total}$ — Γ_{357}/Γ

VALUE (units 10^{-5})	DOCUMENT ID	TECN	COMMENT
• • • We do not use the following data for averages, fits, limits, etc. • • •			
0.7 ± 0.4	SARANTSEV 21	RVUE	$J/\psi(1S) \to \gamma(\pi\pi, K\overline{K}, \eta\eta, \omega\phi)$

$\Gamma(\gamma f_0(2200) \to \gamma\gamma\phi)/\Gamma_{total}$ — Γ_{358}/Γ

VALUE (units 10^{-6})	DOCUMENT ID	TECN	COMMENT
$0.20 \pm 0.04^{+0.05}_{-0.07}$	[1] ABLIKIM 25P	BES3	$J/\psi \to \gamma\gamma\phi$

[1] From a partial wave analysis of $J/\psi \to \gamma\gamma\phi$ with significance 6.3σ.

$\Gamma(\gamma f_J(2220))/\Gamma_{total}$ — Γ_{359}/Γ

VALUE (units 10^{-5})	CL%	EVTS	DOCUMENT ID	TECN	COMMENT
• • • We do not use the following data for averages, fits, limits, etc. • • •					
>300			[1] BAI 96B	BES	$e^+e^- \to \gamma\overline{p}p$, $K\overline{K}$
>250	99.9		[2] HASAN 96	SPEC	$\overline{p}p \to \pi^+\pi^-$
< 2.3	95		[3] AUGUSTIN 88	DM2	$J/\psi \to \gamma K^+K^-$
< 1.6	95		[3] AUGUSTIN 88	DM2	$J/\psi \to \gamma K^0_S K^0_S$
$12.4^{+6.4}_{-5.2} \pm 2.8$		23	[3] BALTRUSAIT...86D	MRK3	$J/\psi \to \gamma K^0_S K^0_S$
$8.4^{+3.4}_{-2.8} \pm 1.6$		93	[3] BALTRUSAIT...86D	MRK3	$J/\psi \to \gamma K^+K^-$

[1] Using BARNES 93.
[2] Using BAI 96B.
[3] Includes unknown branching fraction to K^+K^- or $K^0_S K^0_S$.

$\Gamma(\gamma f_J(2220) \to \gamma\pi\pi)/\Gamma_{total}$ — Γ_{360}/Γ

VALUE (units 10^{-5})	CL%	DOCUMENT ID	TECN	COMMENT
< 3.9	90	[1,2] DOBBS 15		$J/\psi \to \gamma\pi\pi$
• • • We do not use the following data for averages, fits, limits, etc. • • •				
$14 \pm 8 \pm 4$		BAI 98H	BES	$J/\psi \to \gamma\pi^0\pi^0$
$8.4 \pm 2.6 \pm 3.0$		BAI 96B	BES	$e^+e^- \to J/\psi \to \gamma\pi^+\pi^-$

[1] Using CLEO-c data but not authored by the CLEO Collaboration.
[2] For $\Gamma = 20/50$ MeV, the 90% CL upper limits for $\pi^+\pi^-$ and $\pi^0\pi^0$ are $2.6/5.2 \times 10^{-5}$ and $1.3/1.9 \times 10^{-5}$, respectively.

$\Gamma(\gamma f_J(2220) \to \gamma K\overline{K})/\Gamma_{total}$ — Γ_{361}/Γ

VALUE (units 10^{-5})	CL%	DOCUMENT ID	TECN	COMMENT
< 4.1	90	[1,2] DOBBS 15		$J/\psi \to \gamma K\overline{K}$
• • • We do not use the following data for averages, fits, limits, etc. • • •				
< 3.6		[3] DEL-AMO-SA...10O	BABR	$e^+e^- \to J/\psi \to \gamma K^+K^-$
< 2.9		[3] DEL-AMO-SA...10O	BABR	$e^+e^- \to J/\psi \to \gamma K^0_S K^0_S$
$6.6 \pm 2.9 \pm 2.4$		BAI 96B	BES	$e^+e^- \to J/\psi \to \gamma K^+K^-$
$10.8 \pm 4.0 \pm 3.2$		BAI 96B	BES	$e^+e^- \to J/\psi \to \gamma K^0_S K^0_S$

[1] Using CLEO-c data but not authored by the CLEO Collaboration.
[2] For $\Gamma = 20/50$ MeV, the 90% CL upper limits for K^+K^- and $K^0_S K^0_S$ are $1.7/3.1 \times 10^{-5}$ and $1.2/2.0 \times 10^{-5}$, respectively.
[3] For spin 2 and helicity 0; other combinations lead to more stringent upper limits.

$\Gamma(\gamma f_J(2220) \to \gamma p\overline{p})/\Gamma_{total}$ — Γ_{362}/Γ

VALUE (units 10^{-5})	DOCUMENT ID	TECN	COMMENT
$1.5 \pm 0.6 \pm 0.5$	BAI 96B	BES	$e^+e^- \to J/\psi \to \gamma p\overline{p}$

$\Gamma(\gamma f_0(2330) \to \gamma K^0_S K^0_S)/\Gamma_{total}$ — Γ_{363}/Γ

VALUE (units 10^{-5})	DOCUMENT ID	TECN	COMMENT
$4.95 \pm 0.21^{+0.66}_{-0.72}$	ABLIKIM 18AA	BES3	$J/\psi \to \gamma K^0_S K^0_S$
• • • We do not use the following data for averages, fits, limits, etc. • • •			
0.6 ± 0.1	SARANTSEV 21	RVUE	$J/\psi(1S) \to \gamma(\pi\pi, K\overline{K}, \eta\eta, \omega\phi)$

$\Gamma(\gamma f_0(2330) \to \gamma\pi\pi)/\Gamma_{total}$ — Γ_{364}/Γ

VALUE (units 10^{-5})	DOCUMENT ID	TECN	COMMENT
• • • We do not use the following data for averages, fits, limits, etc. • • •			
4 ± 2	SARANTSEV 21	RVUE	$J/\psi(1S) \to \gamma(\pi\pi, K\overline{K}, \eta\eta, \omega\phi)$

$\Gamma(\gamma f_0(2330) \to \gamma\eta\eta)/\Gamma_{total}$ — Γ_{365}/Γ

VALUE (units 10^{-5})	DOCUMENT ID	TECN	COMMENT
• • • We do not use the following data for averages, fits, limits, etc. • • •			
1.5 ± 0.4	SARANTSEV 21	RVUE	$J/\psi(1S) \to \gamma(\pi\pi, K\overline{K}, \eta\eta, \omega\phi)$

$\Gamma(\gamma f_0(2330) \to \gamma\eta'\eta')/\Gamma_{total}$ — Γ_{366}/Γ

VALUE (units 10^{-6})	DOCUMENT ID	TECN	COMMENT
$6.09 \pm 0.64^{+4.00}_{-1.68}$	[1] ABLIKIM 22C	BES3	$J/\psi \to \gamma\eta'\eta' \to 4/5\gamma 2(\pi^+\pi^-)$

[1] From a partial wave analysis of the systems (γX), with $X \to \eta'\eta'$, and $(\eta' X)$, with $X \to \gamma\eta'$ in the decay $J/\psi \to \gamma\eta'\eta'$. The intermediate resonance X is parametrized by a constant-width, relativistic Breit-Wigner.

$\Gamma(\gamma f_0(2330) \to \gamma\eta\eta')/\Gamma_{total}$ — Γ_{367}/Γ

VALUE (units 10^{-5})	DOCUMENT ID	TECN	COMMENT
• • • We do not use the following data for averages, fits, limits, etc. • • •			
$0.10 \pm 0.02^{+0.01}_{-0.02}$	[1] ABLIKIM 22AS	BES3	$J/\psi(1S) \to \gamma\eta\eta'$

[1] From a Breit-Wigner fit involving 9 resonances and a resonating exotic $\eta_1(1855) \to \eta\eta'$ P-wave.

$\Gamma(\gamma f_2(2340) \to \gamma\eta\eta)/\Gamma_{total}$ — Γ_{368}/Γ

VALUE (units 10^{-5})	EVTS	DOCUMENT ID	TECN	COMMENT
$5.60^{+0.62+2.37}_{-0.65-2.07}$	5.5k	[1] ABLIKIM 13N	BES3	$J/\psi \to \gamma\eta\eta$

[1] From partial wave analysis including all possible combinations of 0^{++}, 2^{++}, and 4^{++} resonances.

Int. J. Mod. Phys. A 2026.41. Downloaded from www.worldscientific.com by CALIFORNIA @ BERKELEY on 09/16/26. Re-use and distribution is strictly not permitted, except for Open Access articles.

$\Gamma(\gamma f_2(2340) \to \gamma K^0_S K^0_S)/\Gamma_{total}$ — Γ_{369}/Γ

VALUE (units 10^{-5})	DOCUMENT ID		TECN	COMMENT
$5.54^{+0.34+3.82}_{-0.40-1.49}$	ABLIKIM	18AA	BES3	$J/\psi \to \gamma K^0_S K^0_S$

$\Gamma(\gamma f_2(2340) \to \gamma\eta'\eta')/\Gamma_{total}$ — Γ_{370}/Γ

VALUE (units 10^{-6})	DOCUMENT ID		TECN	COMMENT
$8.67\pm0.70^{+0.61}_{-1.67}$	[1] ABLIKIM	22C	BES3	$J/\psi \to \gamma\eta'\eta' \to 4/5\gamma 2(\pi^+\pi^-)$

[1] From a partial wave analysis of the systems (γX), with $X \to \eta'\eta'$, and $(\eta' X)$, with $X \to \gamma\eta'$ in the decay $J/\psi \to \gamma\eta'\eta'$. The intermediate resonance X is parametrized by a constant-width, relativistic Breit-Wigner.

$\Gamma(\gamma f_0(2470) \to \gamma\eta'\eta')/\Gamma_{total}$ — Γ_{371}/Γ

VALUE (units 10^{-7})	DOCUMENT ID		TECN	COMMENT
$8.18\pm1.77^{+3.73}_{-2.23}$	[1] ABLIKIM	22C	BES3	$J/\psi \to \gamma\eta'\eta' \to 4/5\gamma 2(\pi^+\pi^-)$

[1] From a partial wave analysis of the systems (γX), with $X \to \eta'\eta'$, and $(\eta' X)$, with $X \to \gamma\eta'$ in the decay $J/\psi \to \gamma\eta'\eta'$. The intermediate resonance X is parametrized by a constant-width, relativistic Breit-Wigner.

$\Gamma(\gamma X(1835) \to \gamma\pi^+\pi^-\eta')/\Gamma_{total}$ — Γ_{372}/Γ

VALUE (units 10^{-4})	EVTS	DOCUMENT ID		TECN	COMMENT
$2.7\ ^{+0.6}_{-0.8}$ **OUR AVERAGE** Error includes scale factor of 1.6.					
$3.93\pm0.38^{+0.31}_{-0.84}$		[1] ABLIKIM	16J	BES3	$J/\psi \to \gamma\pi^+\pi^-\eta'$
$2.2\ \pm0.4\ \pm0.4$	264	ABLIKIM	05R	BES2	$J/\psi \to \gamma\pi^+\pi^-\eta'$
• • • We do not use the following data for averages, fits, limits, etc. • • •					
$2.87\pm0.09^{+0.49}_{-0.52}$	4265	[2] ABLIKIM	11C	BES3	$J/\psi \to \gamma\pi^+\pi^-\eta'$

[1] From a fit of the measured $\pi^+\pi^-\eta'$ lineshape that accounts for the abrupt distortion observed at the $p\overline{p}$ threshold with a Flatte formula in addition to known backgrounds and contributors, as well as an *ad hoc* Breit-Wigner (M $\approx$ 1919 MeV; $\Gamma \approx$ 51 MeV) that is required for a good fit. Another explanation for the distortion provided by ABLIKIM 16J is that a second resonance near 1870 MeV interferes with the $X(1835)$; fits to this possibility yield product branching fraction values compatible with that shown within the respective systematic uncertainties.

[2] From a fit of the $\pi^+\pi^-\eta'$ mass distribution to a combination of $\gamma f_1(1510)$, $\gamma X(1835)$, and two states $\gamma X(2120)$ and $\gamma\eta(2370)$, for $M(\pi^+\pi^-\eta') < 2.8$ GeV,and accounting for backgrounds from non-η' events and $J/\psi \to \pi^0\pi^+\pi^-\eta'$.

$\Gamma(\gamma X(1835) \to \gamma p\overline{p})/\Gamma_{total}$ — Γ_{373}/Γ

VALUE (units 10^{-4})	EVTS	DOCUMENT ID		TECN	COMMENT
$0.77^{+0.15}_{-0.09}$ **OUR AVERAGE**					
$0.90^{+0.04+0.27}_{-0.11-0.55}$		[1] ABLIKIM	12D	BES3	$J/\psi \to \gamma p\overline{p}$
$1.14^{+0.43+0.42}_{-0.30-0.26}$	231	[2] ALEXANDER	10	CLEO	$J/\psi \to \gamma p\overline{p}$
$0.70\pm0.04^{+0.19}_{-0.08}$		BAI	03F	BES2	$J/\psi \to \gamma p\overline{p}$

[1] From the fit including final state interaction effects in isospin 0 S-wave according to SIBIRTSEV 05A.

[2] From a fit of the $p\overline{p}$ mass distribution to a combination of $\gamma X(1835)$, γR with $M(R) = 2100$ MeV and $\Gamma(R) = 160$ MeV, and $\gamma p\overline{p}$ phase space, for $M(p\overline{p}) < 2.85$ GeV.

$\Gamma(\gamma X(1835) \to \gamma K^0_S K^0_S \eta)/\Gamma_{total}$ — Γ_{374}/Γ

VALUE (units 10^{-5})	DOCUMENT ID		TECN	COMMENT
$3.31^{+0.33+1.96}_{-0.30-1.29}$	ABLIKIM	15T	BES3	$J/\psi \to \gamma K^0_S K^0_S \eta$

$\Gamma(\gamma X(1835) \to \gamma\gamma\phi(1020))/\Gamma_{total}$ — Γ_{375}/Γ

VALUE (units 10^{-6})	EVTS	DOCUMENT ID		TECN	COMMENT
$3.37\pm0.19^{+0.78}_{-1.10}$		[1] ABLIKIM	25P	BES3	$J/\psi \to \gamma\gamma\phi$
• • • We do not use the following data for averages, fits, limits, etc. • • •					
$1.77\pm0.35\pm0.25$	305	[2] ABLIKIM	18I	BES3	$J/\psi \to \gamma\gamma\phi(1020)$
$8.09\pm1.99\pm1.36$	1.3k	[3] ABLIKIM	18I	BES3	$J/\psi \to \gamma\gamma\phi(1020)$

[1] From a partial wave analysis of $J/\psi \to \gamma\gamma\phi$ with significance 15.3σ.

[2] Constructive interference between the $X(1835)$ and $\eta(1405)/\eta(1475)$ is assumed in a fit to the $\gamma\phi$ invariant mass.

[3] Destructive interference between the $X(1835)$ and $\eta(1405)/\eta(1475)$ is assumed in a fit to the $\gamma\phi$ invariant mass.

$\Gamma(\gamma X(1835) \to \gamma\gamma\gamma)/\Gamma_{total}$ — Γ_{376}/Γ

VALUE	CL%	DOCUMENT ID		TECN	COMMENT
$<3.56\times10^{-6}$	90	ABLIKIM	18O	BES3	$\psi(2S) \to \pi^+\pi^-\gamma\gamma\gamma$

$\Gamma(\gamma X(1835) \to \gamma 3(\pi^+\pi^-))/\Gamma_{total}$ — Γ_{377}/Γ

VALUE (units 10^{-5})	EVTS	DOCUMENT ID		TECN	COMMENT
$2.44\pm0.36^{+0.60}_{-0.74}$	0.6k	ABLIKIM	13U	BES3	$J/\psi \to \gamma 3(\pi^+\pi^-)$

$\Gamma(\gamma\eta(2370) \to \gamma K^+K^-\eta')/\Gamma_{total}$ — Γ_{378}/Γ

VALUE (units 10^{-5})	DOCUMENT ID		TECN	COMMENT
$1.79\pm0.23\pm0.65$	ABLIKIM	20Q	BES3	$J/\psi \to \gamma K^+K^-\eta'$

$\Gamma(\gamma\eta(2370) \to \gamma K^0_S K^0_S \eta')/\Gamma_{total}$ — Γ_{379}/Γ

VALUE (units 10^{-5})	DOCUMENT ID		TECN	COMMENT
$1.18\pm0.32\pm0.39$	ABLIKIM	20Q	BES3	$J/\psi \to \gamma K^0_S K^0_S \eta'$
• • • We do not use the following data for averages, fits, limits, etc. • • •				
$1.31\pm0.22^{+2.85}_{-0.84}$	[1] ABLIKIM	24	BES3	$J/\psi \to \gamma K^0_S K^0_S \eta'$

[1] Decaying via the intermediate $f_0(980)\eta'$, fitted together with $X(1835)$, a 600 MeV broad structure around 2.8 GeV, and the tail of the $\eta_c(1S)$.

$\Gamma(\gamma\eta(2370) \to \gamma\eta\eta\eta')/\Gamma_{total}$ — Γ_{380}/Γ

VALUE	CL%	DOCUMENT ID		TECN	COMMENT
$<9.2\times10^{-6}$	90	ABLIKIM	21C	BES3	$J/\psi(1S) \to \gamma\eta\eta\eta'$

$\Gamma(\gamma D^0 + \text{c.c.})/\Gamma_{total}$ — Γ_{381}/Γ

VALUE	CL%	DOCUMENT ID		TECN	COMMENT
$<9.1\times10^{-8}$	90	ABLIKIM	24BZ	BES3	$e^+e^- \to J/\psi(1S)$

$\Gamma(\gamma p\overline{p})/\Gamma_{total}$ — Γ_{382}/Γ

VALUE (units 10^{-3})	CL%	EVTS	DOCUMENT ID		TECN	COMMENT
$0.38\pm0.07\pm0.07$		49	EATON	84	MRK2	e^+e^-
• • • We do not use the following data for averages, fits, limits, etc. • • •						
<0.11	90		PERUZZI	78	MRK1	e^+e^-

$\Gamma(\gamma p\overline{p}\pi^+\pi^-)/\Gamma_{total}$ — Γ_{383}/Γ

VALUE	CL%	DOCUMENT ID		TECN	COMMENT
$<0.79\times10^{-3}$	90	EATON	84	MRK2	e^+e^-

$\Gamma(\gamma\Lambda\overline{\Lambda})/\Gamma_{total}$ — Γ_{384}/Γ

VALUE	CL%	DOCUMENT ID		TECN	COMMENT
$<0.13\times10^{-3}$	90	HENRARD	87	DM2	e^+e^-
• • • We do not use the following data for averages, fits, limits, etc. • • •					
$<0.16\times10^{-3}$	90	BAI	98G	BES	e^+e^-

$\Gamma(\gamma A^0 \to \gamma\text{invisible})/\Gamma_{total}$ — Γ_{385}/Γ

VALUE	CL%	EVTS	DOCUMENT ID		TECN	COMMENT
$<1.7\times10^{-6}$	90	88M	[1] ABLIKIM	20K	BES3	$\psi(2S) \to J/\psi\pi^+\pi^-$
• • • We do not use the following data for averages, fits, limits, etc. • • •						
$<6.3\times10^{-6}$	90	3.7M	[2] INSLER	10	CLEO	$\psi(2S) \to J/\psi\pi^+\pi^-$

[1] For a narrow state, A^0, with mass $m_{A^0} < 1.2$ GeV. The limit varies with m_{A^0}, reaching its largest value of 1.7×10^{-6} at 1.2 GeV and being 7.0×10^{-7} for $m_{A^0} = 0$.

[2] The limit varies with mass m_{A^0} of a narrow state A^0 and is 4.3×10^{-6} for $m_{A^0} = 0$, reaches its largest value of 6.3×10^{-6} at $m_{A^0} = 500$ MeV, and is 3.6×10^{-6} at $m_{A^0} = 960$ MeV.

$\Gamma(\gamma A^0 \to \gamma\gamma\gamma)/\Gamma_{total}$ — Γ_{386}/Γ

VALUE	CL%	DOCUMENT ID		TECN	COMMENT
$<4.9\times10^{-7}$	95	[1] ABLIKIM	24AD	BES3	$J/\psi \to \gamma\gamma\gamma$
• • • We do not use the following data for averages, fits, limits, etc. • • •					
$<1.8\times10^{-6}$	95	[2] ABLIKIM	23E	BES3	$J/\psi \to \gamma\gamma\gamma$

[1] For a light pseudoscalar axion-like particle, A^0, with a mass in the range 0.18–2.85 GeV. The measured 95% CL limit as a function of m_{A^0} ranges from 3.7×10^{-8} to 4.85×10^{-7}.

[2] For a light pseudoscalar axion-like particle, A^0, with a mass in the range 0.165–2.84 GeV. The measured 95% CL limit as a function of m_{A^0} ranges from 8.3×10^{-8} to 1.8×10^{-6}.

$\Gamma(\gamma A^0 \to \gamma\mu^+\mu^-)/\Gamma_{total}$ (narrow state A^0 with 0.2 GeV $< m_{A^0} <$ 3 GeV) — Γ_{387}/Γ

VALUE	CL%	DOCUMENT ID		TECN	COMMENT
$<7.8\times10^{-7}$	90	[1] ABLIKIM	22H	BES3	$J/\psi \to \gamma\mu^+\mu^-$
• • • We do not use the following data for averages, fits, limits, etc. • • •					
$<0.5\times10^{-5}$	90	[2] ABLIKIM	16E	BES3	$J/\psi \to \gamma\mu^+\mu^-$
$<2.1\times10^{-5}$	90	[3] ABLIKIM	12	BES3	$J/\psi \to \gamma\mu^+\mu^-$

[1] For a narrow scalar or pseudoscalar, A^0, with a mass in the range 0.212–3.0 GeV. The measured 90% CL limit as a function of m_{A^0} is in the range $(1.2–778.0)\times10^{-9}$.

[2] For a narrow scalar or pseudoscalar, A^0, with a mass in the range 0.212–3 GeV. The measured 90% CL limit as a function of m_{A^0} is in the range $(2.8–495.3)\times10^{-8}$.

[3] For a narrow scalar or pseudoscalar, A^0, with a mass in the range 0.21–3.00 GeV. The measured 90% CL limit as a function of m_{A^0} ranges from 4×10^{-7} to 2.1×10^{-5}.

DALITZ DECAYS

$\Gamma(\pi^0 e^+e^-)/\Gamma_{total}$ — Γ_{388}/Γ

VALUE (units 10^{-7})	EVTS	DOCUMENT ID		TECN	COMMENT
$8.06\pm0.31\pm0.38$		[1] ABLIKIM	25AD	BES3	$J/\psi \to \pi^0 e^+e^-$
• • • We do not use the following data for averages, fits, limits, etc. • • •					
$7.56\pm1.32\pm0.50$	39	ABLIKIM	14I	BES3	$J/\psi \to \pi^0 e^+e^-$

[1] Includes the $\rho-\omega$ resonant contribution.

Int. J. Mod. Phys. A 2026.41. Downloaded from www.worldscientific.com
by UNIVERSITY OF CALIFORNIA @ BERKELEY on 09/16/26. Re-use and distribution is strictly not permitted, except for Open Access articles.

$\Gamma(\eta e^+ e^-)/\Gamma_{total}$ — Γ_{389}/Γ

VALUE (units 10^{-5})	EVTS	DOCUMENT ID		TECN	COMMENT
1.42±0.04±0.07	2.47k	[1,2] ABLIKIM	19A	BES3	$J/\psi \to \eta e^+ e^-$
• • • We do not use the following data for averages, fits, limits, etc. • • •					
1.16±0.07±0.06	320	[1] ABLIKIM	14I	BES3	$J/\psi \to \eta e^+ e^-$

[1] Using both $\eta \to \gamma\gamma$ and $\eta \to \pi^+\pi^-\pi^0$ decays.
[2] Approximation of the transition form factor squared as an incoherent sum of the ρ-meson and one-pole non-resonant amplitudes gives the pole mass $m(A) = 2.56 \pm 0.04 \pm 0.03$ GeV. Supersedes ABLIKIM 14I.

$\Gamma(\eta'(958) e^+ e^-)/\Gamma_{total}$ — Γ_{390}/Γ

VALUE (units 10^{-5})	EVTS	DOCUMENT ID		TECN	COMMENT
6.59±0.07±0.17	8.9k	[1] ABLIKIM	19H	BES3	$J/\psi \to \eta'(958) e^+ e^-$
• • • We do not use the following data for averages, fits, limits, etc. • • •					
5.81±0.16±0.31	1.4k	[1,2] ABLIKIM	14I	BES3	$J/\psi \to \eta'(958) e^+ e^-$

[1] Using both $\eta' \to \gamma\pi^+\pi^-$ and $\eta' \to \pi^+\pi^-\eta$ decays.
[2] Superseded by ABLIKIM 19H.

$\Gamma(\eta(1405) e^+ e^- \to f_0(980)\pi^0 e^+ e^- \to \pi^+\pi^-\pi^0 e^+ e^-)/\Gamma_{total}$ — Γ_{391}/Γ

VALUE (units 10^{-7})	EVTS	DOCUMENT ID		TECN	COMMENT
2.04±0.20±0.08	203	[1] ABLIKIM	24I	BES3	$J/\psi \to e^+ e^- \eta(1405)$

[1] With a significance of 9.8 σ.

$\Gamma(X(1835) e^+ e^-, X \to \pi^+\pi^-\eta')/\Gamma_{total}$ — Γ_{392}/Γ

VALUE (units 10^{-6})	EVTS	DOCUMENT ID		TECN	COMMENT
3.58±0.19±0.16	1364	[1] ABLIKIM	22B	BES3	$J/\psi \to \pi^+\pi^-\eta' e^+ e^-$

[1] Assuming constructive interference. Destructive interference gives a value of $(4.43 \pm 0.23 \pm 0.19) \times 10^{-6}$ for this branching fraction.

$\Gamma(X(2120) e^+ e^-, X \to \pi^+\pi^-\eta')/\Gamma_{total}$ — Γ_{393}/Γ

VALUE (units 10^{-6})	EVTS	DOCUMENT ID		TECN	COMMENT
0.82±0.12±0.06	310	ABLIKIM	22B	BES3	$J/\psi \to \pi^+\pi^-\eta' e^+ e^-$

$\Gamma(\eta(2370) e^+ e^-, \eta \to \pi^+\pi^-\eta')/\Gamma_{total}$ — Γ_{394}/Γ

VALUE (units 10^{-6})	EVTS	DOCUMENT ID		TECN	COMMENT
1.08±0.14±0.10	397	ABLIKIM	22B	BES3	$J/\psi \to \pi^+\pi^-\eta' e^+ e^-$

$\Gamma(\eta U \to \eta e^+ e^-)/\Gamma_{total}$ — Γ_{395}/Γ

VALUE	CL%	DOCUMENT ID		TECN	COMMENT
<9.11 × 10^{-7}	90	[1] ABLIKIM	19A	BES3	$J/\psi \to \eta e^+ e^-$

[1] For a dark photon U with mass between 10 and 2400 MeV. Obtained 90% C.L. limits as a function of m_U range from 1.9×10^{-8} to 91.1×10^{-8}.

$\Gamma(\eta'(958) U \to \eta'(958) e^+ e^-)/\Gamma_{total}$ — Γ_{396}/Γ

VALUE	CL%	DOCUMENT ID		TECN	COMMENT
<2.0 × 10^{-7}	90	[1] ABLIKIM	19H	BES3	$J/\psi \to \eta'(958) e^+ e^-$

[1] For a dark photon U with mass between 100 and 2100 MeV. Obtained 90% C.L. limits as a function of m_U range from 1.8×10^{-8} to 2.0×10^{-7}. The corresponding limits on the branching fraction $J/\psi \to \eta' U$ range from 5.7×10^{-8} to 7.4×10^{-7}.

$\Gamma(\phi e^+ e^-)/\Gamma_{total}$ — Γ_{397}/Γ

VALUE (units 10^{-7})	CL%	DOCUMENT ID		TECN	COMMENT
<1.2	90	[1] ABLIKIM	19AB	BES3	$J/\psi \to \phi e^+ e^-$

[1] Using $B(\phi \to K^+K^-) = (48.9 \pm 0.5)\%$ and $B(\psi(2S) \to \pi^+\pi^- J/\psi) = (34.49 \pm 0.30)\%$.

WEAK DECAYS

$\Gamma(D^- e^+ \nu_e + c.c.)/\Gamma_{total}$ — Γ_{398}/Γ

VALUE	CL%	DOCUMENT ID		TECN	COMMENT
<7.1 × 10^{-8}	90	ABLIKIM	21Q	BES3	$e^+ e^- \to J/\psi$
• • • We do not use the following data for averages, fits, limits, etc. • • •					
<1.2 × 10^{-5}	90	ABLIKIM	06M	BES2	$e^+ e^- \to J/\psi$

$\Gamma(D^- \mu^+ \nu_\mu + c.c.)/\Gamma_{total}$ — Γ_{399}/Γ

VALUE	CL%	DOCUMENT ID		TECN	COMMENT
<5.6 × 10^{-7}	90	[1] ABLIKIM	24AM	BES3	$e^+ e^- \to J/\psi$

[1] Using $B(D^- \to K^+\pi^-\pi^-) = 9.38 \pm 0.16$ %.

$\Gamma(\overline{D}^0 e^+ e^- + c.c.)/\Gamma_{total}$ — Γ_{400}/Γ

VALUE	CL%	DOCUMENT ID		TECN	COMMENT
<8.5 × 10^{-8}	90	[1] ABLIKIM	17AF	BES3	$e^+ e^- \to J/\psi$
• • • We do not use the following data for averages, fits, limits, etc. • • •					
<1.1 × 10^{-5}	90	ABLIKIM	06M	BES2	$e^+ e^- \to J/\psi$

[1] Using D^0 decays to $K^-\pi^+$, $K^-\pi^+\pi^0$, and $K^-\pi^+\pi^+\pi^-$.

$\Gamma(D^0 \mu^+ \mu^- + c.c.)/\Gamma_{total}$ — Γ_{401}/Γ

VALUE	CL%	DOCUMENT ID		TECN	COMMENT
<1.1 × 10^{-7}	90	[1] ABLIKIM	25AH	BES3	$e^+ e^- \to J/\psi$

[1] Using D^0 decays to $K^-\pi^+$, $K^-\pi^+\pi^0$, and $K^-\pi^+\pi^+\pi^-$.

$\Gamma(D_s^- e^+ \nu_e + c.c.)/\Gamma_{total}$ — Γ_{402}/Γ

VALUE	CL%	DOCUMENT ID		TECN	COMMENT
<1.3 × 10^{-6}	90	ABLIKIM	14R	BES3	$e^+ e^- \to J/\psi$
• • • We do not use the following data for averages, fits, limits, etc. • • •					
<3.6 × 10^{-5}	90	[1] ABLIKIM	06M	BES2	$e^+ e^- \to J/\psi$

[1] Using $B(D_s^- \to \phi\pi^-) = 4.4 \pm 0.5$ %.

$\Gamma(D_s^{*-} e^+ \nu_e + c.c.)/\Gamma_{total}$ — Γ_{403}/Γ

VALUE	CL%	DOCUMENT ID		TECN	COMMENT
<1.8 × 10^{-6}	90	ABLIKIM	14R	BES3	$e^+ e^- \to J/\psi$

$\Gamma(D^- \pi^+ + c.c.)/\Gamma_{total}$ — Γ_{404}/Γ

VALUE	CL%	DOCUMENT ID		TECN	COMMENT
<7.0 × 10^{-8}	90	ABLIKIM	24BI	BES3	$e^+ e^- \to J/\psi$
• • • We do not use the following data for averages, fits, limits, etc. • • •					
<7.5 × 10^{-5}	90	ABLIKIM	08J	BES2	$e^+ e^- \to J/\psi$

$\Gamma(D^- \rho^+ + c.c)/\Gamma_{total}$ — Γ_{405}/Γ

VALUE	CL%	DOCUMENT ID		TECN	COMMENT
<6.0 × 10^{-7}	90	ABLIKIM	24BI	BES3	$e^+ e^- \to J/\psi$

$\Gamma(\overline{D}^0 \pi^0 + c.c)/\Gamma_{total}$ — Γ_{406}/Γ

VALUE	CL%	DOCUMENT ID		TECN	COMMENT
<4.7 × 10^{-7}	90	ABLIKIM	24BI	BES3	$e^+ e^- \to J/\psi$

$\Gamma(\overline{D}^0 K^0 + c.c.)/\Gamma_{total}$ — Γ_{407}/Γ

VALUE	CL%	DOCUMENT ID		TECN	COMMENT
<1.7 × 10^{-4}	90	ABLIKIM	08J	BES2	$e^+ e^- \to J/\psi$

$\Gamma(\overline{D}^0 K^{*0} + c.c.)/\Gamma_{total}$ — Γ_{408}/Γ

VALUE	CL%	DOCUMENT ID		TECN	COMMENT
<2.5 × 10^{-6}	90	ABLIKIM	14K	BES3	$e^+ e^- \to J/\psi$

$\Gamma(\overline{D}^0 \eta + c.c)/\Gamma_{total}$ — Γ_{409}/Γ

VALUE	CL%	DOCUMENT ID		TECN	COMMENT
<6.8 × 10^{-7}	90	ABLIKIM	24BI	BES3	$e^+ e^- \to J/\psi$

$\Gamma(\overline{D}^0 \rho^0 + c.c)/\Gamma_{total}$ — Γ_{410}/Γ

VALUE	CL%	DOCUMENT ID		TECN	COMMENT
<5.2 × 10^{-7}	90	ABLIKIM	24BI	BES3	$e^+ e^- \to J/\psi$

$\Gamma(D_s^- \pi^+ + c.c.)/\Gamma_{total}$ — Γ_{411}/Γ

VALUE	CL%	DOCUMENT ID		TECN	COMMENT
<4.1 × 10^{-7}	90	ABLIKIM	25CG	BES3	$e^+ e^- \to J/\psi$
• • • We do not use the following data for averages, fits, limits, etc. • • •					
<1.3 × 10^{-4}	90	[1] ABLIKIM	08J	BES2	$e^+ e^- \to J/\psi$

[1] Superseeded by ABLIKIM 25CG.

$\Gamma(D_s^- \rho^+ + c.c.)/\Gamma_{total}$ — Γ_{412}/Γ

VALUE	CL%	DOCUMENT ID		TECN	COMMENT
<8.0 × 10^{-7}	90	ABLIKIM	25CG	BES3	$e^+ e^- \to J/\psi$
• • • We do not use the following data for averages, fits, limits, etc. • • •					
<1.3 × 10^{-5}	90	ABLIKIM	14K	BES3	$e^+ e^- \to J/\psi$

CHARGE CONJUGATION (C), PARITY (P), LEPTON FAMILY NUMBER (LF) VIOLATING MODES

$\Gamma(\gamma\gamma)/\Gamma_{total}$ — Γ_{413}/Γ

VALUE	CL%	DOCUMENT ID		TECN	COMMENT
< 2.7 × 10^{-7}	90	ABLIKIM	14Q	BES3	$\psi(2S) \to \pi^+\pi^- J/\psi$
• • • We do not use the following data for averages, fits, limits, etc. • • •					
< 0.5 × 10^{-5}	90	ADAMS	08	CLEO	$\psi(2S) \to \pi^+\pi^- J/\psi$
< 1.6 × 10^{-4}	90	[1] WICHT	08	BELL	$B^\pm \to K^\pm\gamma\gamma$
< 2.2 × 10^{-5}	90	ABLIKIM	07J	BES2	$\psi(2S) \to J/\psi\pi^+\pi^-$
<50 × 10^{-5}	90	BARTEL	77	CNTR	$e^+ e^-$

[1] WICHT 08 reports $[\Gamma(J/\psi(1S) \to \gamma\gamma)/\Gamma_{total}] \times [B(B^+ \to J/\psi(1S) K^+)] < 0.16 \times 10^{-6}$ which we divide by our best (shown rounded) value $B(B^+ \to J/\psi(1S) K^+) = 1.019 \times 10^{-3}$.

$\Gamma(\gamma\phi)/\Gamma_{total}$ — Γ_{414}/Γ

VALUE	CL%	DOCUMENT ID		TECN	COMMENT
<1.4 × 10^{-6}	90	ABLIKIM	14Q	BES3	$\psi(2S) \to \pi^+\pi^- J/\psi$

$\Gamma(e^\pm \mu^\mp)/\Gamma_{total}$ — Γ_{415}/Γ

VALUE	CL%	DOCUMENT ID		TECN	COMMENT
<1.6 × 10^{-7}	90	ABLIKIM	13L	BES3	$e^+ e^- \to J/\psi$
• • • We do not use the following data for averages, fits, limits, etc. • • •					
<1.1 × 10^{-6}	90	BAI	03D	BES	$e^+ e^- \to J/\psi$

$\Gamma(e^\pm \tau^\mp)/\Gamma_{total}$ — Γ_{416}/Γ

VALUE	CL%	DOCUMENT ID		TECN	COMMENT
<7.5 × 10^{-8}	90	ABLIKIM	21M	BES3	$e^+ e^- \to J/\psi$

Int. J. Mod. Phys. A 2026.41. Downloaded from www.worldscientific.com
by CALIFORNIA @ BERKELEY on 09/16/26. Re-use and distribution is strictly not permitted, except for Open Access articles.

• • • We do not use the following data for averages, fits, limits, etc. • • •

$<8.3\times10^{-6}$	90	[1] ABLIKIM	04	BES	$e^+e^-\to J/\psi$

[1] Superseded by ABLIKIM 21M.

$\Gamma(\mu^\pm\tau^\mp)/\Gamma_{total}$ — Γ_{417}/Γ

VALUE	CL%	DOCUMENT ID		TECN	COMMENT
$<2.0\times10^{-6}$	90	ABLIKIM	04	BES	$e^+e^-\to J/\psi$

$\Gamma(K^+K^+e^-e^-+\text{c.c.})/\Gamma_{total}$ — Γ_{418}/Γ

VALUE	CL%	DOCUMENT ID		TECN	COMMENT
$<2.1\times10^{-9}$	90	ABLIKIM	26	BES3	$e^+e^-\to J/\psi$

$\Gamma(pe^-+\text{c.c.})/\Gamma_{total}$ — Γ_{419}/Γ

VALUE	CL%	DOCUMENT ID		TECN	COMMENT
$<3.1\times10^{-8}$	90	[1] ABLIKIM	25AA	BES3	$\psi(2S)\to\pi^+\pi^-J/\psi(1S)$

[1] Using $\psi(2S)\to\pi^+\pi^-J/\psi(1S)$ branching fraction from PDG 24.

$\Gamma(\Lambda_c^+e^-+\text{c.c.})/\Gamma_{total}$ — Γ_{420}/Γ

VALUE	CL%	DOCUMENT ID		TECN	COMMENT
$<6.9\times10^{-8}$	90	ABLIKIM	19AF	BES3	$e^+e^-\to J/\psi\to pK^-\pi^+e^-$ (+ c.c.)

OTHER DECAYS

$\Gamma(\text{invisible})/\Gamma(e^+e^-)$ — Γ_{421}/Γ_5

VALUE	CL%	DOCUMENT ID		TECN	COMMENT
$<6.6\times10^{-2}$	90	LEES	13I	BABR	$B\to K^{(*)}J/\psi$

$\Gamma(\text{invisible})/\Gamma(\mu^+\mu^-)$ — Γ_{421}/Γ_7

VALUE	CL%	DOCUMENT ID		TECN	COMMENT
$<1.2\times10^{-2}$	90	ABLIKIM	08G	BES2	$\psi(2S)\to\pi^+\pi^-J/\psi$

$\Gamma(\mu^+\mu^-X^0\to\mu^+\mu^-+\text{invisible})/\Gamma_{total}$ — Γ_{422}/Γ

VALUE	CL%	DOCUMENT ID		TECN	COMMENT
$<5.5\times10^{-7}$	90	[1] ABLIKIM	24G	BES3	$J/\psi\to\mu^+\mu^-X^0$(scalar) $\to\mu^+\mu^-+$ invisible
$<9.6\times10^{-7}$	90	[2] ABLIKIM	24G	BES3	$J/\psi\to\mu^+\mu^-X^0$(vector) $\to\mu^+\mu^-+$ invisible

[1] For a light scalar, X^0, with a mass in the range 1–1000 MeV. The measured limit at the 90% credibility level as a function of m_{X^0} ranges from 6.2×10^{-9} to 5.5×10^{-7}.

[2] For a light vector, X^0, with a mass in the range 1–1000 MeV. The measured limit at the 90% credibility level as a function of m_{X^0} ranges from 4.5×10^{-9} to 9.6×10^{-7}.

$\Gamma(\phi+\text{invisible}X)/\Gamma_{total}$ — Γ_{423}/Γ

VALUE	CL%	DOCUMENT ID		TECN	COMMENT
• • • We do not use the following data for averages, fits, limits, etc. • • •					
$<7.0\times10^{-8}$	90	[1] ABLIKIM	25BS	BES3	m_X range: 0–0.96 GeV

[1] For an invisible particle X with a mass in the interval 0–0.96 GeV, the measured 90% CL limit as a function of the mass ranges from 4×10^{-9} to 4×10^{-8}.

$J/\psi(1S)$ REFERENCES

ABLIKIM	26	CP C50 013107	M. Ablikim et al.	(BESIII Collab.)
ABLIKIM	25AA	PR D111 112010	M. Ablikim et al.	(BESIII Collab.)
ABLIKIM	25AB	PR D112 032007	M. Ablikim et al.	(BESIII Collab.)
ABLIKIM	25AD	PR D112 L011101	M. Ablikim et al.	(BESIII Collab.)
ABLIKIM	25AH	JHEP 2504 061	M. Ablikim et al.	(BESIII Collab.)
ABLIKIM	25BS	PRL 135 151804	M. Ablikim et al.	(BESIII Collab.)
ABLIKIM	25BW	PR D112 112012	M. Ablikim et al.	(BESIII Collab.)
ABLIKIM	25CC	PR D112 052010	M. Ablikim et al.	(BESIII Collab.)
ABLIKIM	25CG	JHEP 2512 077	M. Ablikim et al.	(BESIII Collab.)
ABLIKIM	25P	PR D111 052011	M. Ablikim et al.	(BESIII Collab.)
AAIJ	24AE	JHEP 2412 062	R. Aaij et al.	(LHCb Collab.)
ABLIKIM	24	PRL 132 181901	M. Ablikim et al.	(BESIII Collab.)
ABLIKIM	24AB	PR D110 032006	M. Ablikim et al.	(BESIII Collab.)
ABLIKIM	24AD	PR D110 L031101	M. Ablikim et al.	(BESIII Collab.)
ABLIKIM	24AM	JHEP 2401 126	M. Ablikim et al.	(BESIII Collab.)
ABLIKIM	24BI	PR D110 032020	M. Ablikim et al.	(BESIII Collab.)
ABLIKIM	24BQ	PR D110 052005	M. Ablikim et al.	(BESIII Collab.)
ABLIKIM	24BV	PR D110 072021	M. Ablikim et al.	(BESIII Collab.)
Also		PR D111 099902 (errat.)	M. Ablikim et al.	(BESIII Collab.)
ABLIKIM	24BZ	PR D110 112012	M. Ablikim et al.	(BESIII Collab.)
ABLIKIM	24CB	PR D110 112014	M. Ablikim et al.	(BESIII Collab.)
ABLIKIM	24G	PR D109 L031102	M. Ablikim et al.	(BESIII Collab.)
ABLIKIM	24H	PR D109 012006	M. Ablikim et al.	(BESIII Collab.)
ABLIKIM	24I	PR D109 012007	M. Ablikim et al.	(BESIII Collab.)
ABLIKIM	24L	PR D109 052006	M. Ablikim et al.	(BESIII Collab.)
HAYRAPETY...	24A	PR D109 L111101	A. Hayrapetyan et al.	(CMS Collab.)
PDG	24	PR D110 030001	S. Navas et al.	(PDG Collab.)
ABLIKIM	23BD	PR D108 092002	M. Ablikim et al.	(BESIII Collab.)
ABLIKIM	23BU	PR D108 112012	M. Ablikim et al.	(BESIII Collab.)
ABLIKIM	23E	PL B838 137698	M. Ablikim et al.	(BESIII Collab.)
ABLIKIM	23M	JHEP 2303 121	M. Ablikim et al.	(BESIII Collab.)
ABLIKIM	23S	PR D107 072005	M. Ablikim et al.	(BESIII Collab.)
ANASHIN	23	JHEP 2306 196	V.V. Anashin et al.	(KEDR Collab.)
GONG	23	PR D107 072008	G. Gong et al.	(BELLE Collab.)
LEES	23	PR D107 072001	J.P. Lees et al.	(BABAR Collab.)
LIAO	23	PR D107 112007	L. Liao et al.	
ZHU	23	PR D107 012006	W. Zhu et al.	(BELLE Collab.)
ABLIKIM	22AI	PRL 129 192002	M. Ablikim et al.	(BESIII Collab.)
Also		PR D106 072012	M. Ablikim et al.	(BESIII Collab.)
ABLIKIM	22AS	PR D106 072012	M. Ablikim et al.	(BESIII Collab.)
Also		PR D107 079901 (errat.)	M. Ablikim et al.	(BESIII Collab.)
ABLIKIM	22AY	PR D106 112007	M. Ablikim et al.	(BESIII Collab.)
ABLIKIM	22B	PRL 129 022002	M. Ablikim et al.	(BESIII Collab.)
ABLIKIM	22C	PR D105 072002	M. Ablikim et al.	(BESIII Collab.)
ABLIKIM	22H	PR D105 012008	M. Ablikim et al.	(BESIII Collab.)
ANASHIN	22	EPJ C82 938	V.V. Anashin et al.	(KEDR Collab.)
ABLIKIM	21AM	PR D104 092004	M. Ablikim et al.	(BESIII Collab.)
ABLIKIM	21AT	JHEP 2111 226	M. Ablikim et al.	(BESIII Collab.)
ABLIKIM	21C	PR D103 012009	M. Ablikim et al.	(BESIII Collab.)
ABLIKIM	21M	PR D103 112007	M. Ablikim et al.	(BESIII Collab.)
ABLIKIM	21Q	JHEP 2106 157	M. Ablikim et al.	(BESIII Collab.)
LEES	21	PR D103 092001	J.P. Lees et al.	(BABAR Collab.)
LEES	21B	PR D104 112003	J.P. Lees et al.	(BABAR Collab.)
LEES	21C	PR D104 112004	J.P. Lees et al.	(BABAR Collab.)
SARANTSEV	21	PL B816 136227	A.V. Sarantsev et al.	(BONN, PNPI)
ABLIKIM	20	PR D101 012004	M. Ablikim et al.	(BESIII Collab.)
ABLIKIM	20K	PR D101 112005	M. Ablikim et al.	(BESIII Collab.)
ABLIKIM	20Q	EPJ C80 746	M. Ablikim et al.	(BESIII Collab.)
ANASHIN	20	JHEP 2007 112	V.V. Anashin et al.	(KEDR Collab.)
PDG	20	PTEP 2020 083C01	P.A. Zyla et al.	(PDG Collab.)
ABLIKIM	19A	PR D99 012006	M. Ablikim et al.	(BESIII Collab.)
Also		PR D104 099901 (errat.)	M. Ablikim et al.	(BESIII Collab.)
ABLIKIM	19AB	PR D99 052010	M. Ablikim et al.	(BESIII Collab.)
ABLIKIM	19AC	PR D99 071101	M. Ablikim et al.	(BESIII Collab.)
ABLIKIM	19AF	PR D99 072006	M. Ablikim et al.	(BESIII Collab.)
ABLIKIM	19AN	PR D99 112008	M. Ablikim et al.	(BESIII Collab.)
ABLIKIM	19AQ	PR D100 032004	M. Ablikim et al.	(BESIII Collab.)
ABLIKIM	19H	PR D99 012013	M. Ablikim et al.	(BESIII Collab.)
ABLIKIM	19N	PR D99 032006	M. Ablikim et al.	(BESIII Collab.)
ABLIKIM	19Q	PL B791 375	M. Ablikim et al.	(BESIII Collab.)
ABLIKIM	19T	PRL 122 142002	M. Ablikim et al.	(BESIII Collab.)
LU	19	PR D99 032003	P.-C. Lu et al.	(BELLE Collab.)
ABLIKIM	18AA	PR D98 072003	M. Ablikim et al.	(BESIII Collab.)
ABLIKIM	18AB	PR D98 072005	M. Ablikim et al.	(BESIII Collab.)
ABLIKIM	18D	PRL 121 022001	M. Ablikim et al.	(BESIII Collab.)
ABLIKIM	18I	PR D97 051101	M. Ablikim et al.	(BESIII Collab.)
ABLIKIM	18O	PR D97 072014	M. Ablikim et al.	(BESIII Collab.)
ANASHIN	18A	JHEP 1805 119	V.V. Anashin et al.	(KEDR Collab.)
LEES	18	PR D97 052007	J.P. Lees et al.	(BABAR Collab.)
LEES	18E	PR D98 112015	J.P. Lees et al.	(BABAR Collab.)
ABLIKIM	17AF	PR D96 111101	M. Ablikim et al.	(BESIII Collab.)
ABLIKIM	17AH	PR D96 112001	M. Ablikim et al.	(BESIII Collab.)
ABLIKIM	17AK	PR D96 112012	M. Ablikim et al.	(BESIII Collab.)
ABLIKIM	17E	PL B770 217	M. Ablikim et al.	(BESIII Collab.)
ABLIKIM	17L	PR D95 052003	M. Ablikim et al.	(BESIII Collab.)
LEES	17A	PR D95 052001	J.P. Lees et al.	(BABAR Collab.)
LEES	17C	PR D95 072007	J.P. Lees et al.	(BABAR Collab.)
LEES	17D	PR D95 092005	J.P. Lees et al.	(BABAR Collab.)
ABLIKIM	16E	PR D93 052005	M. Ablikim et al.	(BESIII Collab.)
ABLIKIM	16J	PRL 117 042002	M. Ablikim et al.	(BESIII Collab.)
ABLIKIM	16K	PR D93 052010	M. Ablikim et al.	(BESIII Collab.)
ABLIKIM	16L	PR D93 072003	M. Ablikim et al.	(BESIII Collab.)
ABLIKIM	16M	PR D93 072008	M. Ablikim et al.	(BESIII Collab.)
ABLIKIM	16N	PR D93 112011	M. Ablikim	(BESIII Collab.)
ABLIKIM	16P	PR D94 072005	M. Ablikim et al.	(BESIII Collab.)
ABLIKIM	16Q	PL B761 98	M. Ablikim et al.	(BESIII Collab.)
PDG	16	CP C40 100001	C. Patrignani et al.	(PDG Collab.)
AAIJ	15BI	EPJ C75 311	R. Aaij et al.	(LHCb Collab.)
ABLIKIM	15AE	PR D92 052003	M. Ablikim et al.	(BESIII Collab.)
ABLIKIM	15H	PR D91 052017	M. Ablikim et al.	(BESIII Collab.)
ABLIKIM	15K	PR D91 112001	M. Ablikim et al.	(BESIII Collab.)
ABLIKIM	15P	PR D92 012007	M. Ablikim et al.	(BESIII Collab.)
ABLIKIM	15T	PRL 115 091803	M. Ablikim et al.	(BESIII Collab.)
ANASHIN	15	PL B749 50	V.V. Anashin et al.	(KEDR Collab.)
DOBBS	15	PR D91 052006	S. Dobbs et al.	(NWES)
LEES	15J	PR D92 072008	J.P. Lees et al.	(BABAR Collab.)
ABLIKIM	14I	PR D89 092008	M. Ablikim et al.	(BESIII Collab.)
ABLIKIM	14K	PR D89 071101	M. Ablikim et al.	(BESIII Collab.)
ABLIKIM	14N	PR D90 052009	M. Ablikim et al.	(BESIII Collab.)
ABLIKIM	14Q	PR D90 092002	M. Ablikim et al.	(BESIII Collab.)
ABLIKIM	14R	PR D90 112014	M. Ablikim et al.	(BESIII Collab.)
ANASHIN	14	PL B738 391	V.V. Anashin et al.	(KEDR Collab.)
AULCHENKO	14	PL B731 227	V.M. Aulchenko et al.	(KEDR Collab.)
LEES	14H	PR D89 092002	J.P. Lees et al.	(BABAR Collab.)
ABLIKIM	13F	PR D87 052007	M. Ablikim et al.	(BESIII Collab.)
ABLIKIM	13I	PR D87 032003	M. Ablikim et al.	(BESIII Collab.)
ABLIKIM	13J	PR D87 032008	M. Ablikim et al.	(BESIII Collab.)
ABLIKIM	13L	PR D87 112007	M. Ablikim et al.	(BESIII Collab.)
ABLIKIM	13N	PR D87 092009	M. Ablikim et al.	(BESIII Collab.)
ABLIKIM	13P	PR D87 112004	M. Ablikim et al.	(BESIII Collab.)
ABLIKIM	13R	PR D88 032007	M. Ablikim et al.	(BESIII Collab.)
ABLIKIM	13U	PR D88 091502	M. Ablikim et al.	(BESIII Collab.)
LEES	13I	PR D87 112005	J.P. Lees et al.	(BABAR Collab.)
LEES	13O	PR D87 092005	J.P. Lees et al.	(BABAR Collab.)
LEES	13Q	PR D88 032013	J.P. Lees et al.	(BABAR Collab.)
LEES	13Y	PR D88 072009	J.P. Lees et al.	(BABAR Collab.)
ABLIKIM	12	PR D85 092012	M. Ablikim et al.	(BESIII Collab.)
ABLIKIM	12B	PR D86 032008	M. Ablikim et al.	(BESIII Collab.)
ABLIKIM	12C	PR D86 032014	M. Ablikim et al.	(BESIII Collab.)
ABLIKIM	12D	PRL 108 112003	M. Ablikim et al.	(BESIII Collab.)
ABLIKIM	12E	PRL 108 182001	M. Ablikim et al.	(BESIII Collab.)
ABLIKIM	12H	PL B710 594	M. Ablikim et al.	(BESIII Collab.)
ABLIKIM	12P	CP C36 1031	M. Ablikim et al.	(BES II Collab.)
LEES	12E	PR D85 112009	J.P. Lees et al.	(BABAR Collab.)
LEES	12F	PR D86 012008	J.P. Lees et al.	(BABAR Collab.)
METREVELI	12	PR D85 092007	Z. Metreveli et al.	(NWES, FLOR, WAYN+)
ABLIKIM	11	PR D83 012003	M. Ablikim et al.	(BESIII Collab.)
ABLIKIM	11C	PRL 106 072002	M. Ablikim et al.	(BESIII Collab.)
ABLIKIM	11D	PR D83 032003	M. Ablikim et al.	(BESIII Collab.)
ABLIKIM	10C	PL B685 27	M. Ablikim et al.	(BES II Collab.)
ABLIKIM	10E	PL B693 88	M. Ablikim et al.	(BES II Collab.)
ALEXANDER	10	PR D82 092002	J.P. Alexander et al.	(CLEO Collab.)
ANASHIN	10	PL B685 134	V.V. Anashin et al.	(KEDR Collab.)
DEL-AMO-SA...	10O	PRL 105 172001	P. del Amo Sanchez et al.	(BABAR Collab.)
INSLER	10	PR D81 091101	J. Insler et al.	(CLEO Collab.)
ABLIKIM	09	PL B676 25	M. Ablikim et al.	(BES Collab.)
ABLIKIM	09B	PR D80 052004	M. Ablikim et al.	(BES II Collab.)
MITCHELL	09	PRL 102 011801	R.E. Mitchell et al.	(CLEO Collab.)
PEDLAR	09	PR D79 111101	T.K. Pedlar et al.	(CLEO Collab.)
SHEN	09	PR D80 031101	C.P. Shen et al.	(BELLE Collab.)
ABLIKIM	08	EPJ C53 15	M. Ablikim et al.	(BES Collab.)
ABLIKIM	08A	PR D77 012001	M. Ablikim et al.	(BES Collab.)
ABLIKIM	08C	PL B659 789	M. Ablikim et al.	(BES Collab.)
ABLIKIM	08E	PR D77 032005	M. Ablikim et al.	(BES Collab.)
ABLIKIM	08F	PRL 100 102003	M. Ablikim et al.	(BES Collab.)
ABLIKIM	08G	PRL 100 192001	M. Ablikim et al.	(BES Collab.)
ABLIKIM	08I	PL B662 330	M. Ablikim et al.	(BES Collab.)
ABLIKIM	08J	PL B663 297	M. Ablikim et al.	(BES Collab.)
ABLIKIM	08O	PR D78 092005	M. Ablikim et al.	(BES Collab.)
ADAMS	08	PRL 101 101801	G.S. Adams et al.	(CLEO Collab.)
AUBERT	08S	PR D77 092002	B. Aubert et al.	(BABAR Collab.)
BESSON	08	PR D78 032012	D. Besson et al.	(CLEO Collab.)
PDG	08	PL B667 1	C. Amsler et al.	(PDG Collab.)
WICHT	08	PL B662 323	J. Wicht et al.	(BELLE Collab.)
ABLIKIM	07H	PR D76 092003	M. Ablikim et al.	(BES Collab.)
ABLIKIM	07J	PR D76 117101	M. Ablikim et al.	(BES Collab.)

Int. J. Mod. Phys. A 2026.41. Downloaded from www.worldscientific.com
by UNIVERSITY OF CALIFORNIA @ BERKELEY on 09/16/26. Re-use and distribution is strictly not permitted, except for Open Access articles.

ANDREOTTI	07	PL B654 74	M. Andreotti *et al.*	(Femilab E835 Collab.)
AUBERT	07AK	PR D76 012008	B. Aubert *et al.*	(BABAR Collab.)
AUBERT	07AU	PR D76 092005	B. Aubert *et al.*	(BABAR Collab.)
Also		PR D77 119902E (errat.)	B. Aubert *et al.*	(BABAR Collab.)
AUBERT	07BD	PR D76 092006	B. Aubert *et al.*	(BABAR Collab.)
ABLIKIM	06	PL B632 181	M. Ablikim *et al.*	(BES Collab.)
ABLIKIM	06C	PL B633 681	M. Ablikim *et al.*	(BES Collab.)
ABLIKIM	06E	PR D73 052008	M. Ablikim *et al.*	(BES Collab.)
ABLIKIM	06F	PR D73 052007	M. Ablikim *et al.*	(BES Collab.)
ABLIKIM	06H	PR D73 112007	M. Ablikim *et al.*	(BES Collab.)
ABLIKIM	06J	PRL 96 162002	M. Ablikim *et al.*	(BES Collab.)
ABLIKIM	06K	PRL 97 062001	M. Ablikim *et al.*	(BES II Collab.)
ABLIKIM	06M	PL B639 418	M. Ablikim *et al.*	(BES Collab.)
ABLIKIM	06V	PL B642 441	M. Ablikim *et al.*	(BES Collab.)
ADAMS	06A	PR D73 051103	G.S. Adams *et al.*	(CLEO Collab.)
AUBERT	06	PR D73 011101	B. Aubert *et al.*	(BABAR Collab.)
AUBERT	06B	PR D73 012005	B. Aubert *et al.*	(BABAR Collab.)
AUBERT	06D	PR D73 052003	B. Aubert *et al.*	(BABAR Collab.)
AUBERT,BE	06D	PR D74 091103	B. Aubert *et al.*	(BABAR Collab.)
WU	06	PRL 97 162003	C.-H. Wu *et al.*	(BELLE Collab.)
ABLIKIM	05	PL B607 243	M. Ablikim *et al.*	(BES Collab.)
ABLIKIM	05B	PR D71 032003	M. Ablikim *et al.*	(BES Collab.)
ABLIKIM	05C	PL B610 192	M. Ablikim *et al.*	(BES Collab.)
ABLIKIM	05H	PR D72 012002	M. Ablikim *et al.*	(BES Collab.)
ABLIKIM	05R	PRL 95 262001	M. Ablikim *et al.*	(BES Collab.)
AUBERT	05D	PR D71 052001	B. Aubert *et al.*	(BABAR Collab.)
LI	05C	PR D71 111103	Z. Li *et al.*	(CLEO Collab.)
SIBIRTSEV	05A	PR D71 054010	A. Sibirtsev, J. Haidenbauer	
ABLIKIM	04	PL B598 172	M. Ablikim *et al.*	(BES Collab.)
ABLIKIM	04M	PR D70 112008	M. Ablikim *et al.*	(BES Collab.)
AUBERT	04	PR D69 011103	B. Aubert *et al.*	(BABAR Collab.)
AUBERT,B	04N	PR D70 072004	B. Aubert *et al.*	(BABAR Collab.)
BAI	04A	PR D69 012003	J.Z. Bai *et al.*	(BES Collab.)
BAI	04D	PL B589 7	J.Z. Bai *et al.*	(BES Collab.)
BAI	04E	PL B591 42	J.Z. Bai *et al.*	(BES Collab.)
BAI	04G	PR D70 012004	J.Z. Bai *et al.*	(BES Collab.)
BAI	04H	PR D70 012005	J.Z. Bai *et al.*	(BES Collab.)
BAI	04J	PL B594 47	J.Z. Bai *et al.*	(BES Collab.)
SETH	04	PR D69 097503	K.K. Seth	
AULCHENKO	03	PL B573 63	V.M. Aulchenko *et al.*	(KEDR Collab.)
BAI	03D	PL B561 49	J.Z. Bai *et al.*	(BES Collab.)
BAI	03F	PRL 91 022001	J.Z. Bai *et al.*	(BES II Collab.)
BAI	03G	PR D68 052003	J.Z. Bai *et al.*	(BES Collab.)
HUANG	03	PRL 91 241802	H.-C. Huang *et al.*	(BELLE Collab.)
BAI	02C	PRL 88 101802	J.Z. Bai *et al.*	(BES Collab.)
ARTAMONOV	00	PL B474 427	A.S. Artamonov *et al.*	
BAI	00	PRL 84 594	J.Z. Bai *et al.*	(BES Collab.)
BAI	00B	PL B472 200	J.Z. Bai *et al.*	(BES Collab.)
BAI	00D	PL B476 25	J.Z. Bai *et al.*	(BES Collab.)
BAI	99	PL B446 356	J.Z. Bai *et al.*	(BES Collab.)
BAI	99C	PRL 83 1918	J.Z. Bai *et al.*	(BES Collab.)
BAI	98D	PR D58 092006	J.Z. Bai *et al.*	(BES Collab.)
BAI	98G	PL B424 213	J.Z. Bai *et al.*	(BES Collab.)
BAI	98H	PRL 81 1179	J.Z. Bai *et al.*	(BES Collab.)
BALDINI	98	PL B444 111	R. Baldini *et al.*	(FENICE Collab.)
ARMSTRONG	96	PR D54 7067	T.A. Armstrong *et al.*	(E760 Collab.)
BAI	96B	PRL 76 3502	J.Z. Bai *et al.*	(BES Collab.)
BAI	96C	PRL 77 3959	J.Z. Bai *et al.*	(BES Collab.)
BAI	96D	PR D54 1221	J.Z. Bai *et al.*	(BES Collab.)
GRIBUSHIN	96	PR D53 4723	A. Gribushin *et al.*	(E672 and E706 Collab.)
HASAN	96	PL B388 376	A. Hasan, D.V. Bugg	(BRUN, LOQM)
BAI	95B	PL B355 374	J.Z. Bai *et al.*	(BES Collab.)
BUGG	95	PL B353 378	D.V. Bugg *et al.*	(LOQM, PNPI, WASH)
ANTONELLI	93	PL B301 317	A. Antonelli *et al.*	(FENICE Collab.)
ARMSTRONG	93B	PR D47 772	T.A. Armstrong *et al.*	(FNAL E760 Collab.)
BARNES	93	PL B309 469	P.D. Barnes *et al.*	(PS185 Collab.)
AUGUSTIN	92	PR D46 1951	J.E. Augustin, G. Cosme	(DM2 Collab.)
BOLTON	92	PL B278 495	T. Bolton *et al.*	(Mark III Collab.)
BOLTON	92B	PRL 69 1328	T. Bolton *et al.*	(Mark III Collab.)
COFFMAN	92	PRL 68 282	D.M. Coffman *et al.*	(Mark III Collab.)
HSUEH	92	PR D45 2181	S. Hsueh, S. Palestini	(FNAL, TORI)
AUGUSTIN	90	PR D42 10	J.E. Augustin *et al.*	(DM2 Collab.)
BAI	90B	PRL 65 1309	Z. Bai *et al.*	(Mark III Collab.)
BAI	90C	PRL 65 2507	Z. Bai *et al.*	(Mark III Collab.)
BISELLO	90	PL B241 617	D. Bisello *et al.*	(DM2 Collab.)
COFFMAN	90	PR D41 1410	D.M. Coffman *et al.*	(Mark III Collab.)
JOUSSET	90	PR D41 1389	J. Jousset *et al.*	(DM2 Collab.)
ALEXANDER	89	NP B320 45	J.P. Alexander *et al.*	(LBL, MICH, SLAC)
AUGUSTIN	89	NP B320 1	J.E. Augustin, G. Cosme	(DM2 Collab.)
BISELLO	89B	PR D39 701	G. Busetto *et al.*	(DM2 Collab.)
AUGUSTIN	88	PRL 60 2238	J.E. Augustin *et al.*	(DM2 Collab.)
COFFMAN	88	PR D38 2695	D.M. Coffman *et al.*	(Mark III Collab.)
FALVARD	88	PR D38 2706	A. Falvard *et al.*	(CLER, FRAS, LALO+)
AUGUSTIN	87	ZPHY C36 369	J.E. Augustin *et al.*	(LALO, CLER, FRAS+)
BAGLIN	87	NP B286 592	C. Baglin *et al.*	(LAPP, CERN, GENO, LYON+)
BALTRUSAIT...	87	PR D35 2077	R.M. Baltrusaitis *et al.*	(Mark III Collab.)
BECKER	87	PRL 59 186	J.J. Becker *et al.*	(Mark III Collab.)
BISELLO	87	PL B192 239	D. Bisello *et al.*	(PADO, CLER, FRAS+)
COHEN	87	RMP 59 1121	E.R. Cohen, B.N. Taylor	(RISC, NBS)
HENRARD	87	NP B292 670	P. Henrard *et al.*	(CLER, FRAS, LALO+)
PALLIN	87	NP B292 653	D. Pallin *et al.*	(CLER, FRAS, LALO, PADO)
BALTRUSAIT...	86B	PR D33 1222	R.M. Baltrusaitis *et al.*	(Mark III Collab.)
BALTRUSAIT...	86D	PRL 56 107	R.M. Baltrusaitis	(CIT, UCSC, ILL, SLAC+)
BISELLO	86B	PL B179 294	D. Bisello *et al.*	(DM2 Collab.)
GAISER	86	PR D34 711	J. Gaiser *et al.*	(Crystal Ball Collab.)
BALTRUSAIT...	85C	PRL 55 1723	R.M. Baltrusaitis *et al.*	(CIT, UCSC+)
BALTRUSAIT...	85D	PR D32 566	R.M. Baltrusaitis *et al.*	(CIT, UCSC+)
KURAEV	85	SJNP 41 466	E.A. Kuraev, V.S. Fadin	(NOVO)
		Translated from YAF 41 733.		
EATON	84	PR D29 804	M.W. Eaton *et al.*	(LBL, SLAC)
BLOOM	83	ARNS 33 143	E.D. Bloom, C. Peck	(SLAC, CIT)
EDWARDS	83B	PRL 51 859	C. Edwards *et al.*	(CIT, HARV, PRIN+)
FRANKLIN	83	PRL 51 963	M.E.B. Franklin *et al.*	(LBL, SLAC)
BURKE	82	PRL 49 632	D.L. Burke *et al.*	(LBL, SLAC)
EDWARDS	82B	PR D25 3065	C. Edwards *et al.*	(CIT, HARV, PRIN+)
EDWARDS	82D	PRL 48 458	C. Edwards *et al.*	(CIT, HARV, PRIN+)
Also		ARNS 33 143	E.D. Bloom, C. Peck	(SLAC, CIT)
EDWARDS	82E	PRL 49 259	C. Edwards *et al.*	(CIT, HARV, PRIN+)
LEMOIGNE	82	PL 113B 509	Y. Lemoigne *et al.*	(SACL, LOIC, SHMP+)
BESCH	81	ZPHY C8 1	H.J. Besch *et al.*	(BONN, DESY, MAINZ)
GIDAL	81	PL 107B 153	G. Gidal *et al.*	(SLAC, LBL)
PARTRIDGE	80	PRL 44 712	R. Partridge *et al.*	(CIT, HARV, PRIN+)
SCHARRE	80	PL 97B 329	D.L. Scharre *et al.*	(SLAC, LBL)
ZHOLENTZ	80	PL 96B 214	A.A. Zholents *et al.*	(NOVO)
Also		SJNP 34 814	A.A. Zholents *et al.*	(NOVO)
		Translated from YAF 34 1471.		
BRANDELIK	79C	ZPHY C1 233	R. Brandelik *et al.*	(DASP Collab.)
ALEXANDER	78	PL 72B 493	G. Alexander *et al.*	(DESY, HAMB, SIEG+)
BESCH	78	PL 78B 347	H.J. Besch *et al.*	(BONN, DESY, MAINZ)
BRANDELIK	78B	PL 74B 292	R. Brandelik *et al.*	(DASP Collab.)
PERUZZI	78	PR D17 2901	I. Peruzzi *et al.*	(SLAC, LBL)
BARTEL	77	PL 66B 489	W. Bartel *et al.*	(DESY, HEIDP)
BURMESTER	77D	PL 72B 135	J. Burmester *et al.*	(DESY, HAMB, SIEG+)
FELDMAN	77	PRPL 33C 285	G.J. Feldman, M.L. Perl	(LBL, SLAC)
VANNUCCI	77	PR D15 1814	F. Vannucci *et al.*	(SLAC, LBL)
BARTEL	76	PL 64B 483	W. Bartel *et al.*	(DESY, HEIDP)
BRAUNSCH...	76	PL 63B 487	W. Braunschweig *et al.*	(DASP Collab.)
JEAN-MARIE	76	PRL 36 291	B. Jean-Marie *et al.*	(SLAC, LBL) IG
BALDINI-...	75	PL 58B 471	R. Baldini-Celio *et al.*	(FRAS, ROMA)
BOYARSKI	75	PRL 34 1357	A.M. Boyarski *et al.*	(SLAC, LBL) JPC
DASP	75	PL 56B 491	W. Braunschweig *et al.*	(DASP Collab.)
ESPOSITO	75B	LNC 14 73	B. Esposito *et al.*	(FRAS, NAPL, PADO+)
FORD	75	PRL 34 604	R.L. Ford *et al.*	(SLAC, PENN)

BRANCHING RATIOS OF $\psi(2S)$, $\chi_{c0,1,2}$ AND η_c

Updated March 2026 by J.J. Hernández-Rey (IFIC, CSIC-UV, Valencia), R. Mitchell (Indiana U.), S. Navas (U. of Granada), C. Patrignani (Bologna Univ., INFN), and C.-Z. Yuan (IHEP, Beijing)

Since 2002, the treatment of the branching ratios of the $\psi(2S)$ and $\chi_{c0,1,2}$ has undergone an important restructuring [1]. Since the 2023 online edition, the η_c(1S) is now treated in a similar way.

When measuring a branching fraction experimentally, it is not always possible to normalize the number of events observed in the corresponding decay mode to the total number of particles produced. Therefore, the experimenters sometimes report the number of observed decays with respect to another decay mode of the same or another particle in the relevant decay chain. This is actually equivalent to measuring combinations of branching ratios of several decay modes.

To extract the branching fraction of a given decay mode, the collaborations use some previously reported measurements of the required branching ratios. However, the values are frequently taken from the *Review of Particle Physics* (RPP), which in turn uses the branching fraction reported by the experiment in the following edition, giving rise either to correlations or to plain vicious circles, as has been pointed out in several publications [2,3,4].

The way to avoid these dependencies and correlations is to extract the branching fractions through a fit that uses the truly measured combinations of branching ratios and partial widths.

In the case of the $\psi(2S)$, χ_{c0}, χ_{c1}, and χ_{c2}, such a fit involves decays from the four particles and, occasionally, some combinations of branching ratios of more than one of them. We tried to identify those branching ratios which can be correlated in a non-trivial way, and although we cannot preclude the existence of other cases, we are confident that the most relevant correlations have already been removed.

The η_c(1S) can be produced in $\gamma\gamma$ collisions, in the radiative decays of vector and axial-vector charmonia (J/ψ, ψ(2S) and h_c(1P)) or in B meson decays. As in the previous case, we now obtain the corresponding branching fractions using the products of branching ratios originally measured by the experiments, which sometimes involve several particles (cross-particle branching ratios) and performing an overall fit.

The PDG policy is to quote the results of the collaborations in a manner as close as possible to what appears in their original publications. However, in order to avoid the problems mentioned above, we had in some cases to work out the values originally measured, using the number of events and detection efficiencies given by the collaborations, or rescaling back the published

Int. J. Mod. Phys. A 2026.41. Downloaded from www.worldscientific.com
by [redacted]LIFORNIA @ BERKELEY on 09/16/26. Re-use and distribution is strictly not permitted, except for Open Access articles.

results. The information was sometimes spread over several articles, and some articles referred to papers still unpublished, which in turn contained the relevant numbers in footnotes.

Even though the experimental collaborations are entitled to extract whatever branching ratios they consider appropriate by using other published results, we would like to encourage them to also quote explicitly in their articles the actual quantities measured, so that they can be used directly in averages and fits of different experimental determinations. For recent experiments our policy is not to use anymore extracted branching fractions, so that if the original measured quantity is missing in the relevant publication, the value will not be used by us in our averages and fits.

To inform the reader how we computed some of the values, we use footnotes to indicate the branching fractions actually given by the experiments and the quantities they use to derive them from the true combination of branching ratios actually measured. Likewise, we show the values of derived quantities even if they are not used in the fit, but to avoid confusion, we include in these measurements the footnote 'Not used since the same experimental measurement has been used in another related quantity included elsewhere in the fit.

1. Fit Information for the $\psi(2S)$ and $\chi_{c0,1,2}$

This is an overall fit to 4 total widths, 1 partial width, 27 combinations of partial widths, 8 branching fractions, and 80 branching ratios or combinations thereof. Of the latter, 57 involve decays of more than one particle.

The overall fit uses 263 measurements to determine 50 parameters and gives a χ^2 of 435.4 for 213 degrees of freedom.

We have applied scaling factors in the final errors of the fitted values following the procedure described in section 5.2.3 of our Introduction. After rescaling, the total χ^2 is 156.1.

In the listing we provide the inter-particle correlation coefficients $\langle \delta x_i \delta x_j \rangle / (\delta x_i \cdot \delta x_j)$, in percent, from the fit to the corresponding parameter x_i.

2. Fit Information for the η_c(1S)

This is an overall fit to 1 total width, 10 combinations of partial widths, 6 branching fractions and 32 branching ratios or combinations thereof. Of the latter, 29 involve decays of more than one particle.

The overall fit uses 115 measurements to determine 19 parameters and has a χ^2 of 215.4 for 96 degrees of freedom.

We have applied scaling factors in the final errors of the fitted values following the procedure described in section 5.2.3 of our Introduction. After rescaling, the total χ^2 is 78.4.

In the listing we provide the inter-particle correlation coefficients $\langle \delta x_i \delta x_j \rangle / (\delta x_i \cdot \delta x_j)$, in percent, from the fit to the corresponding parameter x_i.

References

1. K. Hagiwara *et al.* (Particle Data Group), Phys. Rev. **D68**, 010001 (2002).
2. Y.F. Gu and X.H. Li, Phys. Lett. **B449**, 361 (1999).
3. C. Patrignani, Phys. Rev. **D64**, 034017 (2001).
4. H. Wang and C.-Z. Yuan, Chin. Phys. **C46**, 071001 (2022).

$\chi_{c0}(1P)$

$I^G(J^{PC}) = 0^+(0^{++})$

$\chi_{c0}(1P)$ MASS

VALUE (MeV)	EVTS	DOCUMENT ID		TECN	COMMENT
3415.50± 0.19 OUR AVERAGE		Error includes scale factor of 1.7. See the ideogram below.			
3415.63± 0.07±0.10		[1] ABLIKIM	25CH	BES3	$\psi(2S) \to \gamma\chi_{c0}$
3413.0 ± 1.9 ±0.6	933	[2] AAIJ	17BB	LHCB	$pp \to b\overline{b}X \to 2(K^+K^-)X$
3414.2 ± 0.5 ±2.3	5.4k	UEHARA	08	BELL	$\gamma\gamma \to \chi_{c0} \to$ hadrons
3406 ± 7 ±6	230	[3] ABE	07	BELL	$e^+e^- \to J/\psi(c\overline{c})$
3414.21± 0.39±0.27		ABLIKIM	05G	BES2	$\psi(2S) \to \gamma\chi_{c0}$
3414.7 $^{+0.7}_{-0.6}$ ±0.2		[4] ANDREOTTI	03	E835	$\overline{p}p \to \chi_{c0} \to \pi^0\pi^0$
3415.5 ± 0.4 ±0.4	392	[5] BAGNASCO	02	E835	$\overline{p}p \to \chi_{c0} \to J/\psi\gamma$
3417.4 $^{+1.8}_{-1.9}$ ±0.2		[4] AMBROGIANI	99B	E835	$\overline{p}p \to e^+e^-\gamma$
3414.1 ± 0.6 ±0.8		BAI	99B	BES	$\psi(2S) \to \gamma X$
3417.8 ± 0.4 ±4		[4] GAISER	86	CBAL	$\psi(2S) \to \gamma X$
3416 ± 3 ±4		[6] TANENBAUM	78	MRK1	e^+e^-
• • • We do not use the following data for averages, fits, limits, etc. • • •					
3414.6 ± 1.1	266	UEHARA	13	BELL	$\gamma\gamma \to K^0_S K^0_S$
3416.5 ± 3.0		EISENSTEIN	01	CLE2	$e^+e^- \to e^+e^-\chi_{c0}$
3422 ±10		[6] BARTEL	78B	CNTR	$e^+e^- \to J/\psi 2\gamma$
3415 ± 9		[6] BIDDICK	77	CNTR	$e^+e^- \to \gamma X$

[1] From a measurement of $M(\chi_{c2}(1P)) - M(\chi_{c0}(1P)) = 140.54 \pm 0.07 \pm 0.07$ MeV and using $M(\chi_{c2}(1P)) = 3556.17 \pm 0.07$ MeV from PDG 24.
[2] From a fit of the $\phi\phi$ invariant mass with the width of $\chi_{c0}(1P)$ fixed to the PDG 16 value.
[3] From a fit of the J/ψ recoil mass spectrum. Supersedes ABE,K 02 and ABE 04G.
[4] Using mass of $\psi(2S) = 3686.0$ MeV.
[5] Recalculated by ANDREOTTI 05A, using the value of $\psi(2S)$ mass from AULCHENKO 03.
[6] Mass value shifted by us by amount appropriate for $\psi(2S)$ mass = 3686 MeV and $J/\psi(1S)$ mass = 3097 MeV.

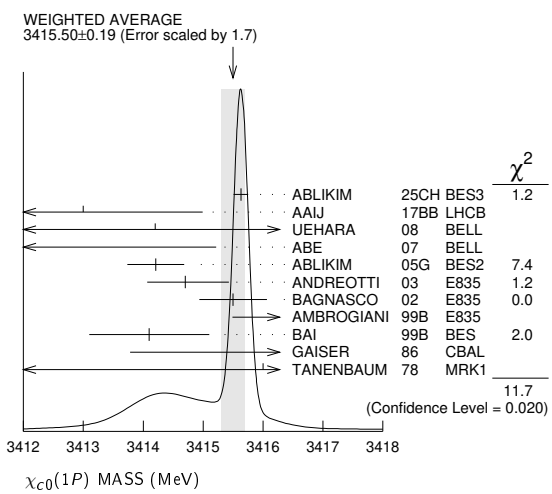

$\chi_{c0}(1P)$ WIDTH

VALUE (MeV)	EVTS	DOCUMENT ID		TECN	COMMENT
12.40±0.27 OUR FIT		Error includes scale factor of 1.6.			
12.4 ±0.5 OUR AVERAGE		Error includes scale factor of 2.8.			
12.52±0.12±0.13		ABLIKIM	25CH	BES3	$\psi(2S) \to \gamma\chi_{c0}$
10.6 ±1.9 ±2.6	5.4k	UEHARA	08	BELL	$\gamma\gamma \to \chi_{c0} \to$ hadrons
12.6 $^{+1.5}_{-1.6}$ $^{+0.9}_{-1.1}$		ABLIKIM	05G	BES2	$\psi(2S) \to \gamma\chi_{c0}$
8.6 $^{+1.7}_{-1.3}$ ±0.1		ANDREOTTI	03	E835	$\overline{p}p \to \chi_{c0} \to \pi^0\pi^0$
9.7 ±1.0	392	[1] BAGNASCO	02	E835	$\overline{p}p \to \chi_{c0} \to J/\psi\gamma$
16.6 $^{+5.2}_{-3.7}$ ±0.1		AMBROGIANI	99B	E835	$\overline{p}p \to e^+e^-\gamma$
14.3 ±2.0 ±3.0		BAI	98I	BES	$\psi(2S) \to \gamma\pi^+\pi^-$
13.5 ±3.3 ±4.2		GAISER	86	CBAL	$\psi(2S) \to \gamma X, \gamma\pi^0\pi^0$
• • • We do not use the following data for averages, fits, limits, etc. • • •					
13.2 ±2.1	266	UEHARA	13	BELL	$\gamma\gamma \to K^0_S K^0_S$

[1] Recalculated by ANDREOTTI 05A.

Int. J. Mod. Phys. A 2026.41. Downloaded from www.worldscientific.com
by UNIVERSITY OF CALIFORNIA @ BERKELEY on 09/16/26. Re-use and distribution is strictly not permitted, except for Open Access articles.

$\chi_{c0}(1P)$ DECAY MODES

	Mode	Fraction (Γ_i/Γ)	Scale factor/ Confidence level
	Hadronic decays		
Γ_1	$2(\pi^+\pi^-)$	(2.10 ± 0.10) %	S=1.2
Γ_2	$\rho^0\pi^+\pi^-$	$(8.2\ \pm2.6\ )\times10^{-3}$	
Γ_3	$\rho^0\rho^0$		
Γ_4	$f_0(980)\,f_0(980)$	$(6.5\ \pm2.1\ )\times10^{-4}$	
Γ_5	$\pi^+\pi^-\pi^0\pi^0$	$(3.2\ \pm0.4\ )$ %	
Γ_6	$\rho^+\pi^-\pi^0+$ c.c.	$(2.8\ \pm0.4\ )$ %	
Γ_7	$4\pi^0$	$(3.2\ \pm0.4\ )\times10^{-3}$	
Γ_8	$\pi^+\pi^-K^+K^-$	(1.73 ± 0.15) %	S=1.1
Γ_9	$K_0^*(1430)^0\overline{K}_0^*(1430)^0\to\pi^+\pi^-K^+K^-$	$(9.6\ ^{+3.5}_{-2.8}\ )\times10^{-4}$	
Γ_{10}	$K_0^*(1430)^0\overline{K}_2^*(1430)^0+$ c.c. $\to\pi^+\pi^-K^+K^-$	$(7.8\ ^{+1.9}_{-2.4}\ )\times10^{-4}$	
Γ_{11}	$K_1(1270)^+K^-+$ c.c. $\to\pi^+\pi^-K^+K^-$	$(6.1\ \pm1.8\ )\times10^{-3}$	
Γ_{12}	$K_1(1400)^+K^-+$ c.c. $\to\pi^+\pi^-K^+K^-$	$<2.6\ \times10^{-3}$	CL=90%
Γ_{13}	$f_0(980)\,f_0(980)$	$(1.6\ ^{+1.0}_{-0.9}\ )\times10^{-4}$	
Γ_{14}	$f_0(980)\,f_0(2200)$	$(7.7\ ^{+2.0}_{-2.4}\ )\times10^{-4}$	
Γ_{15}	$f_0(1370)\,f_0(1370)$	$<2.7\ \times10^{-4}$	CL=90%
Γ_{16}	$f_0(1370)\,f_0(1500)$	$<1.7\ \times10^{-4}$	CL=90%
Γ_{17}	$f_0(1370)\,f_0(1710)$	$(6.5\ ^{+3.4}_{-2.3}\ )\times10^{-4}$	
Γ_{18}	$f_0(1500)\,f_0(1370)$	$<1.3\ \times10^{-4}$	CL=90%
Γ_{19}	$f_0(1500)\,f_0(1500)$	$<5\ \times10^{-5}$	CL=90%
Γ_{20}	$f_0(1500)\,f_0(1710)$	$<7\ \times10^{-5}$	CL=90%
Γ_{21}	$K^+K^-\pi^+\pi^-\pi^0$	$(8.6\ \pm0.9\ )\times10^{-3}$	
Γ_{22}	$K_S^0K^\pm\pi^\mp\pi^+\pi^-$	$(4.1\ \pm0.4\ )\times10^{-3}$	
Γ_{23}	$K^+K^-\pi^0\pi^0$	$(5.4\ \pm0.9\ )\times10^{-3}$	
Γ_{24}	$K^+\pi^-\overline{K}^0\pi^0+$ c.c.	(2.42 ± 0.32) %	
Γ_{25}	$\rho^+K^-K^0+$ c.c.	(1.17 ± 0.20) %	
Γ_{26}	$K^*(892)^-K^+\pi^0\to K^+\pi^-\overline{K}^0\pi^0+$ c.c.	$(4.5\ \pm1.1\ )\times10^{-3}$	
Γ_{27}	$K_S^0K_S^0\pi^+\pi^-$	$(5.5\ \pm1.0\ )\times10^{-3}$	
Γ_{28}	$K^+K^-\eta\pi^0$	$(2.9\ \pm0.7\ )\times10^{-3}$	
Γ_{29}	$3(\pi^+\pi^-)$	(1.97 ± 0.22) %	S=3.0
Γ_{30}	$K^+\overline{K}^*(892)^0\pi^-+$ c.c.	$(7.0\ \pm1.5\ )\times10^{-3}$	
Γ_{31}	$K^*(892)^0\overline{K}^*(892)^0$	$(1.7\ \pm0.6\ )\times10^{-3}$	
Γ_{32}	$\pi\pi$	$(8.76\pm0.26)\times10^{-3}$	S=1.4
Γ_{33}	$\pi^0\eta$	$<1.7\ \times10^{-4}$	
Γ_{34}	$\pi^0\eta'$	$<1.1\ \times10^{-3}$	
Γ_{35}	$\pi^0\eta_c$	$<1.6\ \times10^{-3}$	CL=90%
Γ_{36}	$\eta\eta$	$(2.94\pm0.22)\times10^{-3}$	S=1.2
Γ_{37}	$\eta\eta'$	$(8.9\ \pm1.1\ )\times10^{-5}$	
Γ_{38}	$\eta'\eta'$	$(2.11\pm0.12)\times10^{-3}$	
Γ_{39}	$\omega\omega$	$(1.02\pm0.05)\times10^{-3}$	
Γ_{40}	$\omega\phi$	$(1.21\pm0.10)\times10^{-4}$	S=1.4
Γ_{41}	ωK^+K^-	$(1.87\pm0.20)\times10^{-3}$	
Γ_{42}	K^+K^-	$(6.15\pm0.19)\times10^{-3}$	S=1.4
Γ_{43}	$K_S^0K_S^0$	$(3.08\pm0.18)\times10^{-3}$	S=1.1
Γ_{44}	$\pi^+\pi^-\eta$	$<1.9\ \times10^{-4}$	CL=90%
Γ_{45}	$2\pi^+2\pi^-\eta$	$(4.4\ \pm0.4\ )\times10^{-3}$	
Γ_{46}	$\pi^+\pi^-\eta'$	$<3.5\ \times10^{-4}$	CL=90%
Γ_{47}	$\eta\eta\eta'$	$<2.5\ \times10^{-5}$	CL=90%
Γ_{48}	$\overline{K}^0K^+\pi^-+$ c.c.	$<9\ \times10^{-5}$	CL=90%
Γ_{49}	$K^+K^-\pi^0$	$<6\ \times10^{-5}$	CL=90%
Γ_{50}	$K^+K^-\eta$	$<2.2\ \times10^{-4}$	CL=90%
Γ_{51}	$K^+K^-K_S^0K_S^0$	$(1.4\ \pm0.5\ )\times10^{-3}$	
Γ_{52}	$K_S^0K_S^0K_S^0K_S^0$	$(5.6\ \pm0.5\ )\times10^{-4}$	
Γ_{53}	$K^+K^-K^+K^-$	$(2.7\ \pm0.4\ )\times10^{-3}$	S=1.5
Γ_{54}	$K^+K^-\phi$	$(9.4\ \pm2.4\ )\times10^{-4}$	
Γ_{55}	$\overline{K}^0K^+\pi^-\phi+$ c.c.	$(3.7\ \pm0.6\ )\times10^{-3}$	
Γ_{56}	$K^+K^-\pi^0\phi$	$(1.90\pm0.35)\times10^{-3}$	
Γ_{57}	$K_S^0K_S^0K_S^0K^\pm\pi^\mp$	$(7.7\ \pm0.8\ )\times10^{-5}$	
Γ_{58}	$3(K^+K^-)$	$(1.04\pm0.21)\times10^{-5}$	
Γ_{59}	$\phi\pi^+\pi^-\pi^0$	$(1.14\pm0.14)\times10^{-3}$	
Γ_{60}	$\phi\phi$	$(8.3\ \pm0.4\ )\times10^{-4}$	S=1.1
Γ_{61}	$\phi\phi\eta$	$(8.2\ \pm0.9\ )\times10^{-4}$	
Γ_{62}	$p\overline{p}$	$(2.35\pm0.12)\times10^{-4}$	S=1.9
Γ_{63}	$p\overline{p}\pi^0$	$(6.8\ \pm0.7\ )\times10^{-4}$	S=1.3
Γ_{64}	$p\overline{p}\eta$	$(3.4\ \pm0.4\ )\times10^{-4}$	
Γ_{65}	$p\overline{p}\omega$	$(5.1\ \pm0.6\ )\times10^{-4}$	
Γ_{66}	$p\overline{p}\pi^+\pi^-$	$(1.9\ \pm1.1\ )\times10^{-3}$	S=2.3
Γ_{67}	$p\overline{p}\pi^0\pi^0$	$(1.01\pm0.27)\times10^{-3}$	
Γ_{68}	$p\overline{p}\eta\pi^0$	$(2.35\pm0.20)\times10^{-4}$	
Γ_{69}	$p\overline{p}\eta\eta$	$(5.6\ \pm0.7\ )\times10^{-5}$	
Γ_{70}	$p\overline{p}K^+K^-$	$(2.48\pm0.17)\times10^{-4}$	
Γ_{71}	$p\overline{p}K^+K^-$ (non-resonant)	$(1.19\pm0.26)\times10^{-4}$	
Γ_{72}	$K^+\overline{p}\Lambda(1520)+$ c.c.	$(2.9\ \pm0.7\ )\times10^{-4}$	
Γ_{73}	$\Lambda(1520)\overline{\Lambda}(1520)$	$(3.0\ \pm1.2\ )\times10^{-4}$	
Γ_{74}	$p\overline{p}\phi$	$(5.9\ \pm1.4\ )\times10^{-5}$	
Γ_{75}	$p\overline{p}K_S^0K_S^0$	$<8\ \times10^{-4}$	CL=90%
Γ_{76}	$p\overline{p}K_S^0K^-\pi^++$ c.c.	$(2.5\ \pm0.4\ )\times10^{-5}$	
Γ_{77}	$p\overline{n}\pi^-$	$(1.23\pm0.11)\times10^{-3}$	
Γ_{78}	$\overline{p}n\pi^+$	$(1.33\pm0.12)\times10^{-3}$	
Γ_{79}	$p\overline{n}\pi^-\pi^0$	$(2.28\pm0.20)\times10^{-3}$	
Γ_{80}	$\overline{p}n\pi^+\pi^0$	$(2.15\pm0.18)\times10^{-3}$	
Γ_{81}	$\Lambda\overline{\Lambda}$	$(3.50\pm0.17)\times10^{-4}$	S=1.1
Γ_{82}	$\Lambda\overline{\Lambda}\pi^+\pi^-$	$(1.15\pm0.12)\times10^{-3}$	
Γ_{83}	$\Lambda\overline{\Lambda}\pi^+\pi^-$ (non-resonant)	$<5\ \times10^{-4}$	CL=90%
Γ_{84}	$\Sigma(1385)^+\overline{\Lambda}\pi^-+$ c.c.	$<5\ \times10^{-4}$	CL=90%
Γ_{85}	$\Sigma(1385)^-\overline{\Lambda}\pi^++$ c.c.	$<5\ \times10^{-4}$	CL=90%
Γ_{86}	$\Lambda\overline{\Lambda}\eta$	$(2.2\ \pm0.4\ )\times10^{-4}$	
Γ_{87}	$\Lambda\overline{\Lambda}\eta'$	$(7.3\ \pm1.6\ )\times10^{-5}$	
Γ_{88}	$\Lambda\overline{\Lambda}\omega$	$(2.31\pm0.33)\times10^{-4}$	
Γ_{89}	$\Lambda\overline{\Lambda}\phi$	$(2.9\ \pm1.2\ )\times10^{-5}$	
Γ_{90}	$K^+\overline{p}\Lambda+$ c.c.	$(1.21\pm0.12)\times10^{-3}$	S=1.3
Γ_{91}	$nK_S^0\overline{\Lambda}+$ c.c.	$(6.5\ \pm0.5\ )\times10^{-4}$	
Γ_{92}	$K^*(892)^+\overline{p}\Lambda+$ c.c.	$(4.7\ \pm0.9\ )\times10^{-4}$	
Γ_{93}	$\overline{p}\Lambda(1520)K_S^0\pi^++$ c.c.	$(1.6\ \pm0.7\ )\times10^{-5}$	
Γ_{94}	$\Sigma^0\overline{\Sigma}^0$	$(4.56\pm0.32)\times10^{-4}$	
Γ_{95}	$\Sigma^+\overline{p}K_S^0+$ c.c.	$(3.43\pm0.27)\times10^{-4}$	
Γ_{96}	$\Sigma^0\overline{p}K^++$ c.c.	$(2.95\pm0.20)\times10^{-4}$	
Γ_{97}	$\Sigma^+\overline{\Sigma}^-$	$(4.5\ \pm0.8\ )\times10^{-4}$	S=2.6
Γ_{98}	$\Sigma^+\overline{\Sigma}^-\eta$	$(1.23\pm0.23)\times10^{-4}$	
Γ_{99}	$\Sigma^-\overline{\Sigma}^+$	$(5.0\ \pm0.5\ )\times10^{-4}$	
Γ_{100}	$\Sigma(1385)^+\overline{\Sigma}(1385)^-$	$(1.6\ \pm0.6\ )\times10^{-4}$	
Γ_{101}	$\Sigma(1385)^-\overline{\Sigma}(1385)^+$	$(2.3\ \pm0.6\ )\times10^{-4}$	
Γ_{102}	$K^-\Lambda\overline{\Xi}^++$ c.c.	$(1.89\pm0.34)\times10^{-4}$	
Γ_{103}	$\Xi^0\overline{\Xi}^0$	$(4.3\ \pm0.5\ )\times10^{-4}$	S=1.7
Γ_{104}	$\Xi^-\overline{\Xi}^+$	$(4.34\pm0.20)\times10^{-4}$	
Γ_{105}	$\Omega^-\overline{\Omega}^+$	$(3.4\ \pm0.6\ )\times10^{-5}$	
Γ_{106}	$\eta_c\pi^+\pi^-$	$<7\ \times10^{-4}$	CL=90%
	Radiative decays		
Γ_{107}	$\gamma J/\psi(1S)$	(1.35 ± 0.09) %	S=1.8
Γ_{108}	$\gamma\rho^0$	$<9\ \times10^{-6}$	CL=90%
Γ_{109}	$\gamma\omega$	$<8\ \times10^{-6}$	CL=90%
Γ_{110}	$\gamma\phi$	$<6\ \times10^{-6}$	CL=90%
Γ_{111}	$\gamma\gamma$	$(1.96\pm0.08)\times10^{-4}$	S=1.1
Γ_{112}	$e^+e^-J/\psi(1S)$	$(1.29\pm0.29)\times10^{-4}$	
Γ_{113}	$\mu^+\mu^-J/\psi(1S)$	$<1.8\ \times10^{-5}$	CL=90%

CONSTRAINED FIT INFORMATION

A multiparticle fit to $\chi_{c1}(1P)$, $\chi_{c0}(1P)$, $\chi_{c2}(1P)$, and $\psi(2S)$ with 4 total widths, a partial width, 27 combinations of partial widths obtained from integrated cross section, and 87 branching ratios uses 263 measurements to determine 50 parameters. The overall fit has a $\chi^2 = 435.4$ for 213 degrees of freedom.

The following *off-diagonal* array elements are the correlation coefficients $\langle\delta p_i\delta p_j\rangle/(\delta p_i\cdot\delta p_j)$, in percent, from the fit to parameters p_i, including the branching fractions, $x_i \equiv \Gamma_i/\Gamma_{\rm total}$.

	x_1	x_2	x_8	x_{21}	x_{30}	x_{32}	x_{36}	x_{42}	x_{43}	x_{53}
x_2	15									
x_8	8	1								
x_{21}	12	2	4							
x_{30}	2	0	31	1						
x_{32}	47	7	13	21	3					
x_{36}	18	3	5	8	1	31				
x_{42}	46	7	13	21	3	83	31			
x_{43}	23	4	7	10	2	41	15	41		
x_{53}	6	1	3	3	1	10	4	10	5	
x_{60}	30	5	9	14	2	53	20	53	26	7
x_{62}	19	3	5	9	1	34	11	34	17	4
x_{81}	30	5	8	13	2	53	20	52	26	7
x_{107}	6	1	1	3	0	11	5	11	5	1
x_{111}	9	1	−11	2	−8	25	8	25	10	−5
Γ	−10	−2	−9	−6	−4	−15	−6	−15	−8	−5

x_{62}	22				
x_{81}	34	22			
x_{107}	7	−19	7		
x_{111}	13	10	16	6	
Γ	−11	−6	−9	−2	−20
	x_{60}	x_{62}	x_{81}	x_{107}	x_{111}

$\chi_{c0}(1P)$ PARTIAL WIDTHS

$\chi_{c0}(1P)$ $\Gamma(i)\Gamma(\gamma\gamma)/\Gamma(\text{total})$

$\Gamma(2(\pi^+\pi^-)) \times \Gamma(\gamma\gamma)/\Gamma_{\text{total}}$ — $\Gamma_1\Gamma_{111}/\Gamma$

VALUE (eV)	EVTS	DOCUMENT ID		TECN	COMMENT
51.1± 3.3 OUR FIT Error includes scale factor of 1.2.					
49 ±10 OUR AVERAGE Error includes scale factor of 1.8.					
44.7± 3.6±4.9	3.6k	UEHARA	08	BELL	$\gamma\gamma \to \chi_{c0} \to 2(\pi^+\pi^-)$
75 ±13 ±8		EISENSTEIN	01	CLE2	$e^+e^- \to e^+e^-\chi_{c0}$

$\Gamma(\rho^0\rho^0) \times \Gamma(\gamma\gamma)/\Gamma_{\text{total}}$ — $\Gamma_3\Gamma_{111}/\Gamma$

VALUE (eV)	CL%	EVTS	DOCUMENT ID		TECN	COMMENT
• • • We do not use the following data for averages, fits, limits, etc. • • •						
<12	90	<252	UEHARA	08	BELL	$\gamma\gamma \to \chi_{c0} \to 2(\pi^+\pi^-)$

$\Gamma(\pi^+\pi^-K^+K^-) \times \Gamma(\gamma\gamma)/\Gamma_{\text{total}}$ — $\Gamma_8\Gamma_{111}/\Gamma$

VALUE (eV)	EVTS	DOCUMENT ID		TECN	COMMENT
42 ±4 OUR FIT Error includes scale factor of 1.1.					
38.8±3.7±4.7	1.7k	UEHARA	08	BELL	$\gamma\gamma \to \chi_{c0} \to K^+K^-\pi^+\pi^-$

$\Gamma(K^+K^-\pi^+\pi^-\pi^0) \times \Gamma(\gamma\gamma)/\Gamma_{\text{total}}$ — $\Gamma_{21}\Gamma_{111}/\Gamma$

VALUE (eV)	EVTS	DOCUMENT ID		TECN	COMMENT
20.9±2.3 OUR FIT Error includes scale factor of 1.1.					
26 ±4 ±4	1094	DEL-AMO-SA...	11M	BABR	$\gamma\gamma \to K^+K^-\pi^+\pi^-\pi^0$

$\Gamma(K^+\overline{K}^*(892)^0\pi^- + \text{c.c.}) \times \Gamma(\gamma\gamma)/\Gamma_{\text{total}}$ — $\Gamma_{30}\Gamma_{111}/\Gamma$

VALUE (eV)	EVTS	DOCUMENT ID		TECN	COMMENT
17 ±4 OUR FIT					
16.7±6.1±3.0	495 ± 182	UEHARA	08	BELL	$\gamma\gamma \to \chi_{c0} \to K^+K^-\pi^+\pi^-$

$\Gamma(K^*(892)^0\overline{K}^*(892)^0) \times \Gamma(\gamma\gamma)/\Gamma_{\text{total}}$ — $\Gamma_{31}\Gamma_{111}/\Gamma$

VALUE (eV)	CL%	EVTS	DOCUMENT ID		TECN	COMMENT
• • • We do not use the following data for averages, fits, limits, etc. • • •						
<6	90	<148	UEHARA	08	BELL	$\gamma\gamma \to \chi_{c0} \to K^+K^-\pi^+\pi^-$

$\Gamma(\pi\pi) \times \Gamma(\gamma\gamma)/\Gamma_{\text{total}}$ — $\Gamma_{32}\Gamma_{111}/\Gamma$

VALUE (eV)	EVTS	DOCUMENT ID		TECN	COMMENT
21.3± 1.2 OUR FIT Error includes scale factor of 1.2.					
23 ± 5 OUR AVERAGE					
$29.7^{+17.4}_{-12.0}\pm4.8$	103^{+60}_{-42}	[1] UEHARA	09	BELL	10.6 $e^+e^- \to e^+e^-\pi^0\pi^0$
22.7± 3.2±3.5	129 ± 18	[2] NAKAZAWA	05	BELL	10.6 $e^+e^- \to e^+e^-\pi^+\pi^-$

[1] We multiplied the measurement by 3 to convert from $\pi^0\pi^0$ to $\pi\pi$. Interference with the continuum included.
[2] We have multiplied $\pi^+\pi^-$ measurement by 3/2 to obtain $\pi\pi$.

$\Gamma(\eta\eta) \times \Gamma(\gamma\gamma)/\Gamma_{\text{total}}$ — $\Gamma_{36}\Gamma_{111}/\Gamma$

VALUE (eV)	EVTS	DOCUMENT ID		TECN	COMMENT
7.2±0.6 OUR FIT Error includes scale factor of 1.2.					
9.4±2.3±1.2	22	[1] UEHARA	10A	BELL	10.6 $e^+e^- \to e^+e^-\eta\eta$

[1] Interference with the continuum not included.

$\Gamma(\omega\omega) \times \Gamma(\gamma\gamma)/\Gamma_{\text{total}}$ — $\Gamma_{39}\Gamma_{111}/\Gamma$

VALUE (eV)	CL%	DOCUMENT ID		TECN	COMMENT
• • • We do not use the following data for averages, fits, limits, etc. • • •					
<3.9	90	[1] LIU	12B	BELL	$\gamma\gamma \to 2(\pi^+\pi^-\pi^0)$

[1] Using $B(\omega \to \pi^+\pi^-\pi^0) = (89.2 \pm 0.7)\%$.

$\Gamma(\omega\phi) \times \Gamma(\gamma\gamma)/\Gamma_{\text{total}}$ — $\Gamma_{40}\Gamma_{111}/\Gamma$

VALUE (eV)	CL%	DOCUMENT ID		TECN	COMMENT
• • • We do not use the following data for averages, fits, limits, etc. • • •					
<0.34	90	[1] LIU	12B	BELL	$\gamma\gamma \to K^+K^-\pi^+\pi^-\pi^0$

[1] Using $B(\phi \to K^+K^-) = (48.9 \pm 0.5)\%$ and $B(\omega \to \pi^+\pi^-\pi^0) = (89.2 \pm 0.7)\%$.

$\Gamma(K^+K^-) \times \Gamma(\gamma\gamma)/\Gamma_{\text{total}}$ — $\Gamma_{42}\Gamma_{111}/\Gamma$

VALUE (eV)	EVTS	DOCUMENT ID		TECN	COMMENT
15.0±0.8 OUR FIT Error includes scale factor of 1.2.					
14.3±1.6±2.3	153 ± 17	NAKAZAWA	05	BELL	10.6 $e^+e^- \to e^+e^-K^+K^-$

$\Gamma(K^0_SK^0_S) \times \Gamma(\gamma\gamma)/\Gamma_{\text{total}}$ — $\Gamma_{43}\Gamma_{111}/\Gamma$

VALUE (eV)	EVTS	DOCUMENT ID		TECN	COMMENT
7.5 ±0.6 OUR FIT Error includes scale factor of 1.2.					
8.7 ±1.7 ±0.9	266	[1] UEHARA	13	BELL	$\gamma\gamma \to K^0_SK^0_S$
• • • We do not use the following data for averages, fits, limits, etc. • • •					
7.00±0.65±0.71	134 ± 12	CHEN	07B	BELL	$e^+e^- \to e^+e^-\chi_{c0}$

[1] Supersedes CHEN 07B.

$\Gamma(K^+K^-K^+K^-) \times \Gamma(\gamma\gamma)/\Gamma_{\text{total}}$ — $\Gamma_{53}\Gamma_{111}/\Gamma$

VALUE (eV)	EVTS	DOCUMENT ID		TECN	COMMENT
6.6±1.0 OUR FIT Error includes scale factor of 1.4.					
7.9±1.3±1.1	215 ± 36	UEHARA	08	BELL	$\gamma\gamma \to \chi_{c0} \to 2(K^+K^-)$

$\Gamma(\phi\phi) \times \Gamma(\gamma\gamma)/\Gamma_{\text{total}}$ — $\Gamma_{60}\Gamma_{111}/\Gamma$

VALUE (eV)	EVTS	DOCUMENT ID		TECN	COMMENT
2.03±0.13 OUR FIT Error includes scale factor of 1.2.					
1.72±0.33±0.14	56 ± 11	[1] LIU	12B	BELL	$\gamma\gamma \to 2(K^+K^-)$
• • • We do not use the following data for averages, fits, limits, etc. • • •					
2.3 ±0.9 ±0.4	23.6 ± 9.6	UEHARA	08	BELL	$\gamma\gamma \to \chi_{c0} \to 2(K^+K^-)$

[1] Supersedes UEHARA 08. Using $B(\phi \to K^+K^-) = (48.9 \pm 0.5)\%$.

$\chi_{c0}(1P)$ BRANCHING RATIOS

HADRONIC DECAYS

$\Gamma(2(\pi^+\pi^-))/\Gamma_{\text{total}}$ — Γ_1/Γ

VALUE (%)	EVTS	DOCUMENT ID		TECN	COMMENT
• • • We do not use the following data for averages, fits, limits, etc. • • •					
2.07±0.09±0.05	1946k	[1,2] ABLIKIM	24BT	BES3	$\psi(2S) \to \gamma 2\pi^+2\pi^-$

[1] ABLIKIM 24BT reports 2.127 ± 0.002 ± 0.101 % from a measurement of $[\Gamma(\chi_{c0}(1P) \to 2(\pi^+\pi^-))/\Gamma_{\text{total}}] \times [B(\psi(2S) \to \gamma\chi_{c0}(1P))]$ assuming $B(\psi(2S) \to \gamma\chi_{c0}(1P)) = (9.79 \pm 0.20) \times 10^{-2}$, which we rescale to our best (shown rounded) value $B(\psi(2S) \to \gamma\chi_{c0}(1P)) = (10.06 \pm 0.27) \times 10^{-2}$. Our first error is their experiment's error and our second error is the systematic error from using our best (shown rounded) value.
[2] Not used since the same experimental measurement has been used in another related quantity included elsewhere in the fit.

$\Gamma(\rho^0\pi^+\pi^-)/\Gamma(2(\pi^+\pi^-))$ — Γ_2/Γ_1

VALUE	DOCUMENT ID		TECN	COMMENT
0.39±0.12 OUR FIT				
0.39±0.12	TANENBAUM	78	MRK1	$\psi(2S) \to \gamma\chi_{c0}$

$\Gamma(f_0(980)f_0(980))/\Gamma_{\text{total}}$ — Γ_4/Γ

VALUE (units 10^{-4})	EVTS	DOCUMENT ID		TECN	COMMENT
6.5±2.1±0.2	36 ± 9	[1] ABLIKIM	04G	BES	$\psi(2S) \to \gamma 2\pi^+2\pi^-$

[1] ABLIKIM 04G reports $[\Gamma(\chi_{c0}(1P) \to f_0(980)f_0(980))/\Gamma_{\text{total}}] \times [B(\psi(2S) \to \gamma\chi_{c0}(1P))] = (6.5 \pm 1.6 \pm 1.3) \times 10^{-5}$ which we divide by our best (shown rounded) value $B(\psi(2S) \to \gamma\chi_{c0}(1P)) = (10.06 \pm 0.27) \times 10^{-2}$. Our first error is their experiment's error and our second error is the systematic error from using our best (shown rounded) value.

$\Gamma(\pi^+\pi^-\pi^0\pi^0)/\Gamma_{\text{total}}$ — Γ_5/Γ

VALUE (%)	EVTS	DOCUMENT ID		TECN	COMMENT
3.2±0.4±0.1	1751.4	[1] HE	08B	CLEO	$e^+e^- \to \gamma h^+h^-h^0h^0$

[1] HE 08B reports 3.54 ± 0.10 ± 0.43 ± 0.18 % from a measurement of $[\Gamma(\chi_{c0}(1P) \to \pi^+\pi^-\pi^0\pi^0)/\Gamma_{\text{total}}] \times [B(\psi(2S) \to \gamma\chi_{c0}(1P))]$ assuming $B(\psi(2S) \to \gamma\chi_{c0}(1P)) = (9.22 \pm 0.11 \pm 0.46) \times 10^{-2}$, which we rescale to our best (shown rounded) value $B(\psi(2S) \to \gamma\chi_{c0}(1P)) = (10.06 \pm 0.27) \times 10^{-2}$. Our first error is their experiment's error and our second error is the systematic error from using our best (shown rounded) value.

$\Gamma(\rho^+\pi^-\pi^0 + \text{c.c.})/\Gamma_{\text{total}}$ — Γ_6/Γ

VALUE (%)	EVTS	DOCUMENT ID		TECN	COMMENT
2.8±0.4±0.1	1358.5	[1,2] HE	08B	CLEO	$e^+e^- \to \gamma h^+h^-h^0h^0$

[1] HE 08B reports 3.04 ± 0.18 ± 0.42 ± 0.16 % from a measurement of $[\Gamma(\chi_{c0}(1P) \to \rho^+\pi^-\pi^0 + \text{c.c.})/\Gamma_{\text{total}}] \times [B(\psi(2S) \to \gamma\chi_{c0}(1P))]$ assuming $B(\psi(2S) \to \gamma\chi_{c0}(1P)) = (9.22 \pm 0.11 \pm 0.46) \times 10^{-2}$, which we rescale to our best (shown rounded) value $B(\psi(2S) \to \gamma\chi_{c0}(1P)) = (10.06 \pm 0.27) \times 10^{-2}$. Our first error is their experiment's error and our second error is the systematic error from using our best (shown rounded) value.
[2] Calculated by us. We have added the values from HE 08B for $\rho^+\pi^-\pi^0$ and $\rho^-\pi^+\pi^0$ decays assuming uncorrelated statistical and fully correlated systematic uncertainties.

$\Gamma(4\pi^0)/\Gamma_{\text{total}}$ — Γ_7/Γ

VALUE (units 10^{-3})	EVTS	DOCUMENT ID		TECN	COMMENT
3.2±0.4±0.1	3296	[1] ABLIKIM	11A	BES3	$e^+e^- \to \psi(2S) \to \gamma\chi_{c0}$

[1] ABLIKIM 11A reports $(3.34 \pm 0.06 \pm 0.44) \times 10^{-3}$ from a measurement of $[\Gamma(\chi_{c0}(1P) \to 4\pi^0)/\Gamma_{\text{total}}] \times [B(\psi(2S) \to \gamma\chi_{c0}(1P))]$ assuming $B(\psi(2S) \to \gamma\chi_{c0}(1P)) = (9.62 \pm 0.31) \times 10^{-2}$, which we rescale to our best (shown rounded) value $B(\psi(2S) \to \gamma\chi_{c0}(1P)) = (10.06 \pm 0.27) \times 10^{-2}$. Our first error is their experiment's error and our second error is the systematic error from using our best (shown rounded) value.

$\Gamma(K^*_0(1430)^0\overline{K}^*_0(1430)^0 \to \pi^+\pi^-K^+K^-)/\Gamma_{\text{total}}$ — Γ_9/Γ

VALUE (units 10^{-4})	EVTS	DOCUMENT ID		TECN	COMMENT
$\mathbf{9.6^{+3.5}_{-2.7}\pm0.3}$	83	[1] ABLIKIM	05Q	BES2	$\psi(2S) \to \gamma\pi^+\pi^-K^+K^-$

[1] ABLIKIM 05Q reports $(10.44 \pm 2.37^{+3.05}_{-1.90}) \times 10^{-4}$ from a measurement of $[\Gamma(\chi_{c0}(1P) \to K^*_0(1430)^0\overline{K}^*_0(1430)^0 \to \pi^+\pi^-K^+K^-)/\Gamma_{\text{total}}] \times [B(\psi(2S) \to \gamma\chi_{c0}(1P))]$ assuming $B(\psi(2S) \to \gamma\chi_{c0}(1P)) = (9.22 \pm 0.11 \pm 0.46) \times 10^{-2}$, which we rescale to our best (shown rounded) value $B(\psi(2S) \to \gamma\chi_{c0}(1P)) = (10.06 \pm 0.27) \times 10^{-2}$. Our first error is their experiment's error and our second error is the systematic error from using our best (shown rounded) value.

Int. J. Mod. Phys. A 2026.41. Downloaded from www.worldscientific.com
by CALIFORNIA @ BERKELEY on 09/16/26. Re-use and distribution is strictly not permitted, except for Open Access articles.

Int. J. Mod. Phys. A 2026.41. Downloaded from www.worldscientific.com
by UNIVERSITY OF CALIFORNIA @ BERKELEY on 09/16/26. Re-use and distribution is strictly not permitted, except for Open Access articles.

$\Gamma(K_0^*(1430)^0\overline{K}_2^*(1430)^0 + \text{c.c.} \to \pi^+\pi^-K^+K^-)/\Gamma_{total}$ — Γ_{10}/Γ

VALUE (units 10^{-4})	EVTS	DOCUMENT ID		TECN	COMMENT
$7.8^{+1.9}_{-2.3}\pm0.2$	62	[1] ABLIKIM	05Q	BES2	$\psi(2S) \to \gamma\pi^+\pi^-K^+K^-$

[1] ABLIKIM 05Q reports $(8.49\pm1.66^{+1.32}_{-1.99})\times10^{-4}$ from a measurement of $[\Gamma(\chi_{c0}(1P) \to K_0^*(1430)^0\overline{K}_2^*(1430)^0 + \text{c.c.} \to \pi^+\pi^-K^+K^-)/\Gamma_{total}] \times [B(\psi(2S) \to \gamma\chi_{c0}(1P))]$ assuming $B(\psi(2S) \to \gamma\chi_{c0}(1P)) = (9.22 \pm 0.11 \pm 0.46)\times10^{-2}$, which we rescale to our best (shown rounded) value $B(\psi(2S) \to \gamma\chi_{c0}(1P)) = (10.06 \pm 0.27)\times10^{-2}$. Our first error is their experiment's error and our second error is the systematic error from using our best (shown rounded) value.

$\Gamma(K_1(1270)^+K^- + \text{c.c.} \to \pi^+\pi^-K^+K^-)/\Gamma_{total}$ — Γ_{11}/Γ

VALUE (units 10^{-3})	EVTS	DOCUMENT ID		TECN	COMMENT
$6.1^{+1.9}_{-1.8}\pm0.2$	68	[1] ABLIKIM	05Q	BES2	$\psi(2S) \to \gamma\pi^+\pi^-K^+K^-$

[1] ABLIKIM 05Q reports $(6.66\pm1.31^{+1.60}_{-1.51})\times10^{-3}$ from a measurement of $[\Gamma(\chi_{c0}(1P) \to K_1(1270)^+K^- + \text{c.c.} \to \pi^+\pi^-K^+K^-)/\Gamma_{total}] \times [B(\psi(2S) \to \gamma\chi_{c0}(1P))]$ assuming $B(\psi(2S) \to \gamma\chi_{c0}(1P)) = (9.22 \pm 0.11 \pm 0.46)\times10^{-2}$, which we rescale to our best (shown rounded) value $B(\psi(2S) \to \gamma\chi_{c0}(1P)) = (10.06 \pm 0.27)\times10^{-2}$. Our first error is their experiment's error and our second error is the systematic error from using our best (shown rounded) value. The measurement assumes $B(K_1(1270) \to K\rho(770)) = 42 \pm 6\%$.

$\Gamma(K_1(1400)^+K^- + \text{c.c.} \to \pi^+\pi^-K^+K^-)/\Gamma_{total}$ — Γ_{12}/Γ

VALUE (units 10^{-3})	CL%	DOCUMENT ID		TECN	COMMENT
<2.6	90	[1] ABLIKIM	05Q	BES2	$\psi(2S) \to \gamma\pi^+\pi^-K^+K^-$

[1] ABLIKIM 05Q reports $< 2.85 \times 10^{-3}$ from a measurement of $[\Gamma(\chi_{c0}(1P) \to K_1(1400)^+K^- + \text{c.c.} \to \pi^+\pi^-K^+K^-)/\Gamma_{total}] \times [B(\psi(2S) \to \gamma\chi_{c0}(1P))]$ assuming $B(\psi(2S) \to \gamma\chi_{c0}(1P)) = (9.22 \pm 0.11 \pm 0.46)\times10^{-2}$, which we rescale to our best (shown rounded) value $B(\psi(2S) \to \gamma\chi_{c0}(1P)) = 10.06\times10^{-2}$. The measurement assumes $B(K_1(1400) \to K^*(892)\pi) = 94 \pm 6\%$.

$\Gamma(f_0(980)f_0(980))/\Gamma_{total}$ — Γ_{13}/Γ

VALUE (units 10^{-5})	EVTS	DOCUMENT ID		TECN	COMMENT
$15.8^{+10.2}_{-8.7}\pm0.4$	28	[1] ABLIKIM	05Q	BES2	$\psi(2S) \to \gamma\pi^+\pi^-K^+K^-$

[1] ABLIKIM 05Q reports $[\Gamma(\chi_{c0}(1P) \to f_0(980)f_0(980))/\Gamma_{total}] \times [B(\psi(2S) \to \gamma\chi_{c0}(1P))] = (1.59\pm0.50^{+0.89}_{-0.72})\times10^{-5}$ which we divide by our best (shown rounded) value $B(\psi(2S) \to \gamma\chi_{c0}(1P)) = (10.06 \pm 0.27)\times10^{-2}$. Our first error is their experiment's error and our second error is the systematic error from using our best (shown rounded) value. One of the $f_0(980)$ mesons is identified via decay to $\pi^+\pi^-$ while the other via K^+K^- decay.

$\Gamma(f_0(980)f_0(2200))/\Gamma_{total}$ — Γ_{14}/Γ

VALUE (units 10^{-4})	EVTS	DOCUMENT ID		TECN	COMMENT
$7.7^{+2.0}_{-2.4}\pm0.2$	77	[1] ABLIKIM	05Q	BES2	$\psi(2S) \to \gamma\pi^+\pi^-K^+K^-$

[1] ABLIKIM 05Q reports $(8.42\pm1.42^{+1.65}_{-2.29})\times10^{-4}$ from a measurement of $[\Gamma(\chi_{c0}(1P) \to f_0(980)f_0(2200))/\Gamma_{total}] \times [B(\psi(2S) \to \gamma\chi_{c0}(1P))]$ assuming $B(\psi(2S) \to \gamma\chi_{c0}(1P)) = (9.22 \pm 0.11 \pm 0.46)\times10^{-2}$, which we rescale to our best (shown rounded) value $B(\psi(2S) \to \gamma\chi_{c0}(1P)) = (10.06 \pm 0.27)\times10^{-2}$. Our first error is their experiment's error and our second error is the systematic error from using our best (shown rounded) value. The f_0 mesons are identified via $f_0(980) \to \pi^+\pi^-$ and $f_0(2200) \to K^+K^-$ decays.

$\Gamma(f_0(1370)f_0(1370))/\Gamma_{total}$ — Γ_{15}/Γ

VALUE (units 10^{-4})	CL%	DOCUMENT ID		TECN	COMMENT
<2.7	90	[1] ABLIKIM	05Q	BES2	$\psi(2S) \to \gamma\pi^+\pi^-K^+K^-$

[1] ABLIKIM 05Q reports $< 2.9 \times 10^{-4}$ from a measurement of $[\Gamma(\chi_{c0}(1P) \to f_0(1370)f_0(1370))/\Gamma_{total}] \times [B(\psi(2S) \to \gamma\chi_{c0}(1P))]$ assuming $B(\psi(2S) \to \gamma\chi_{c0}(1P)) = (9.22 \pm 0.11 \pm 0.46)\times10^{-2}$, which we rescale to our best (shown rounded) value $B(\psi(2S) \to \gamma\chi_{c0}(1P)) = 10.06\times10^{-2}$. One of the $f_0(1370)$ mesons is identified via decay to $\pi^+\pi^-$ while the other via K^+K^- decay. Both branching fractions for these f_0 decays are implicitly included in the quoted result.

$\Gamma(f_0(1370)f_0(1500))/\Gamma_{total}$ — Γ_{16}/Γ

VALUE (units 10^{-4})	CL%	DOCUMENT ID		TECN	COMMENT
<1.7	90	[1] ABLIKIM	05Q	BES2	$\psi(2S) \to \gamma\pi^+\pi^-K^+K^-$

[1] ABLIKIM 05Q reports $< 1.8 \times 10^{-4}$ from a measurement of $[\Gamma(\chi_{c0}(1P) \to f_0(1370)f_0(1500))/\Gamma_{total}] \times [B(\psi(2S) \to \gamma\chi_{c0}(1P))]$ assuming $B(\psi(2S) \to \gamma\chi_{c0}(1P)) = (9.22 \pm 0.11 \pm 0.46)\times10^{-2}$, which we rescale to our best (shown rounded) value $B(\psi(2S) \to \gamma\chi_{c0}(1P)) = 10.06\times10^{-2}$. The f_0 mesons are identified via $f_0(1370) \to \pi^+\pi^-$ and $f_0(1500) \to K^+K^-$ decays. Both branching fractions for these f_0 decays are implicitly included in the quoted result.

$\Gamma(f_0(1370)f_0(1710))/\Gamma_{total}$ — Γ_{17}/Γ

VALUE (units 10^{-4})	EVTS	DOCUMENT ID		TECN	COMMENT
$6.5^{+3.4}_{-2.3}\pm0.2$	61	[1] ABLIKIM	05Q	BES2	$\psi(2S) \to \gamma\pi^+\pi^-K^+K^-$

[1] ABLIKIM 05Q reports $(7.12\pm1.85^{+3.28}_{-1.68})\times10^{-4}$ from a measurement of $[\Gamma(\chi_{c0}(1P) \to f_0(1370)f_0(1710))/\Gamma_{total}] \times [B(\psi(2S) \to \gamma\chi_{c0}(1P))]$ assuming $B(\psi(2S) \to \gamma\chi_{c0}(1P)) = (9.22 \pm 0.11 \pm 0.46)\times10^{-2}$, which we rescale to our best (shown rounded) value $B(\psi(2S) \to \gamma\chi_{c0}(1P)) = (10.06 \pm 0.27)\times10^{-2}$. Our first error is their experiment's error and our second error is the systematic error from using our best (shown rounded) value. The f_0 mesons are identified via $f_0(1370) \to \pi^+\pi^-$ and $f_0(1710) \to K^+K^-$ decays. Both branching fractions for these f_0 decays are implicitly included in the quoted result.

$\Gamma(f_0(1500)f_0(1370))/\Gamma_{total}$ — Γ_{18}/Γ

VALUE (units 10^{-4})	CL%	DOCUMENT ID		TECN	COMMENT
<1.3	90	[1] ABLIKIM	05Q	BES2	$\psi(2S) \to \gamma\pi^+\pi^-K^+K^-$

[1] ABLIKIM 05Q reports $< 1.4 \times 10^{-4}$ from a measurement of $[\Gamma(\chi_{c0}(1P) \to f_0(1500)f_0(1370))/\Gamma_{total}] \times [B(\psi(2S) \to \gamma\chi_{c0}(1P))]$ assuming $B(\psi(2S) \to \gamma\chi_{c0}(1P)) = (9.22 \pm 0.11 \pm 0.46)\times10^{-2}$, which we rescale to our best (shown rounded) value $B(\psi(2S) \to \gamma\chi_{c0}(1P)) = 10.06\times10^{-2}$. The f_0 mesons are identified via $f_0(1500) \to \pi^+\pi^-$ and $f_0(1370) \to K^+K^-$ decays. Both branching fractions for these f_0 decays are implicitly included in the quoted result.

$\Gamma(f_0(1500)f_0(1500))/\Gamma_{total}$ — Γ_{19}/Γ

VALUE (units 10^{-4})	CL%	DOCUMENT ID		TECN	COMMENT
<0.5	90	[1] ABLIKIM	05Q	BES2	$\psi(2S) \to \gamma\pi^+\pi^-K^+K^-$

[1] ABLIKIM 05Q reports $< 0.55 \times 10^{-4}$ from a measurement of $[\Gamma(\chi_{c0}(1P) \to f_0(1500)f_0(1500))/\Gamma_{total}] \times [B(\psi(2S) \to \gamma\chi_{c0}(1P))]$ assuming $B(\psi(2S) \to \gamma\chi_{c0}(1P)) = (9.22 \pm 0.11 \pm 0.46)\times10^{-2}$, which we rescale to our best (shown rounded) value $B(\psi(2S) \to \gamma\chi_{c0}(1P)) = 10.06\times10^{-2}$. One of the $f_0(1500)$ is identified via decay to $\pi^+\pi^-$ while the other via K^+K^- decay. Both branching fractions for these f_0 decays are implicitly included in the quoted result.

$\Gamma(f_0(1500)f_0(1710))/\Gamma_{total}$ — Γ_{20}/Γ

VALUE (units 10^{-4})	CL%	DOCUMENT ID		TECN	COMMENT
<0.7	90	[1] ABLIKIM	05Q	BES2	$\psi(2S) \to \gamma\pi^+\pi^-K^+K^-$

[1] ABLIKIM 05Q reports $< 0.73 \times 10^{-4}$ from a measurement of $[\Gamma(\chi_{c0}(1P) \to f_0(1500)f_0(1710))/\Gamma_{total}] \times [B(\psi(2S) \to \gamma\chi_{c0}(1P))]$ assuming $B(\psi(2S) \to \gamma\chi_{c0}(1P)) = (9.22 \pm 0.11 \pm 0.46)\times10^{-2}$, which we rescale to our best (shown rounded) value $B(\psi(2S) \to \gamma\chi_{c0}(1P)) = 10.06\times10^{-2}$. The f_0 mesons are identified via $f_0(1500) \to \pi^+\pi^-$ and $f_0(1710) \to K^+K^-$ decays. Both branching fractions for these f_0 decays are implicitly included in the quoted result.

$\Gamma(K^+K^-\pi^+\pi^-\pi^0)/\Gamma_{total}$ — Γ_{21}/Γ

VALUE (units 10^{-3})	EVTS	DOCUMENT ID		TECN	COMMENT
8.6 ± 0.9 OUR FIT					
• • • We do not use the following data for averages, fits, limits, etc. • • •					
$8.3\pm0.9\pm0.2$	9.0k	[1,2] ABLIKIM	13B	BES3	$e^+e^- \to \psi(2S) \to \gamma\chi_{c0}$

[1] ABLIKIM 13B reports $(8.61\pm0.13\pm0.94)\times10^{-3}$ from a measurement of $[\Gamma(\chi_{c0}(1P) \to K^+K^-\pi^+\pi^-\pi^0)/\Gamma_{total}] \times [B(\psi(2S) \to \gamma\chi_{c0}(1P))]$ assuming $B(\psi(2S) \to \gamma\chi_{c0}(1P)) = (9.68 \pm 0.31)\times10^{-2}$, which we rescale to our best (shown rounded) value $B(\psi(2S) \to \gamma\chi_{c0}(1P)) = (10.06 \pm 0.27)\times10^{-2}$. Our first error is their experiment's error and our second error is the systematic error from using our best (shown rounded) value.

[2] Not used since the same experimental measurement has been used in another related quantity included elsewhere in the fit.

$\Gamma(K_S^0K^\pm\pi^\mp\pi^+\pi^-)/\Gamma_{total}$ — Γ_{22}/Γ

VALUE (units 10^{-3})	EVTS	DOCUMENT ID		TECN	COMMENT
$4.1\pm0.4\pm0.1$	2.7k	[1] ABLIKIM	13B	BES3	$e^+e^- \to \psi(2S) \to \gamma\chi_{c0}$

[1] ABLIKIM 13B reports $(4.22\pm0.10\pm0.43)\times10^{-3}$ from a measurement of $[\Gamma(\chi_{c0}(1P) \to K_S^0K^\pm\pi^\mp\pi^+\pi^-)/\Gamma_{total}] \times [B(\psi(2S) \to \gamma\chi_{c0}(1P))]$ assuming $B(\psi(2S) \to \gamma\chi_{c0}(1P)) = (9.68 \pm 0.31)\times10^{-2}$, which we rescale to our best (shown rounded) value $B(\psi(2S) \to \gamma\chi_{c0}(1P)) = (10.06 \pm 0.27)\times10^{-2}$. Our first error is their experiment's error and our second error is the systematic error from using our best (shown rounded) value.

$\Gamma(K^+K^-\pi^0\pi^0)/\Gamma_{total}$ — Γ_{23}/Γ

VALUE (%)	EVTS	DOCUMENT ID		TECN	COMMENT
$0.54\pm0.09\pm0.01$	213.5	[1] HE	08B	CLEO	$e^+e^- \to \gamma h^+h^-h^0h^0$

[1] HE 08B reports $0.59 \pm 0.05 \pm 0.08 \pm 0.03$ % from a measurement of $[\Gamma(\chi_{c0}(1P) \to K^+K^-\pi^0\pi^0)/\Gamma_{total}] \times [B(\psi(2S) \to \gamma\chi_{c0}(1P))]$ assuming $B(\psi(2S) \to \gamma\chi_{c0}(1P)) = (9.22 \pm 0.11 \pm 0.46)\times10^{-2}$, which we rescale to our best (shown rounded) value $B(\psi(2S) \to \gamma\chi_{c0}(1P)) = (10.06 \pm 0.27)\times10^{-2}$. Our first error is their experiment's error and our second error is the systematic error from using our best (shown rounded) value.

$\Gamma(K^+\pi^-\overline{K}^0\pi^0 + \text{c.c.})/\Gamma_{total}$ — Γ_{24}/Γ

VALUE (%)	EVTS	DOCUMENT ID		TECN	COMMENT
$2.42\pm0.32\pm0.06$	401.7	[1] HE	08B	CLEO	$e^+e^- \to \gamma h^+h^-h^0h^0$

[1] HE 08B reports $2.64 \pm 0.15 \pm 0.31 \pm 0.14$ % from a measurement of $[\Gamma(\chi_{c0}(1P) \to K^+\pi^-\overline{K}^0\pi^0 + \text{c.c.})/\Gamma_{total}] \times [B(\psi(2S) \to \gamma\chi_{c0}(1P))]$ assuming $B(\psi(2S) \to \gamma\chi_{c0}(1P)) = (9.22 \pm 0.11 \pm 0.46)\times10^{-2}$, which we rescale to our best (shown rounded) value $B(\psi(2S) \to \gamma\chi_{c0}(1P)) = (10.06 \pm 0.27)\times10^{-2}$. Our first error is their experiment's error and our second error is the systematic error from using our best (shown rounded) value.

Int. J. Mod. Phys. A 2026.41. Downloaded from www.worldscientific.com by LIFORNIA @ BERKELEY on 09/16/26. Re-use and distribution is strictly not permitted, except for Open Access articles.

$\Gamma(\rho^+ K^- K^0 + \text{c.c.})/\Gamma_{total}$ — Γ_{25}/Γ

VALUE (%)	EVTS	DOCUMENT ID		TECN	COMMENT
1.17±0.20±0.03	179.7	[1] HE	08B	CLEO	$e^+e^- \to \gamma h^+ h^- h^0 h^0$

[1] HE 08B reports 1.28 ± 0.16 ± 0.15 ± 0.07 % from a measurement of $[\Gamma(\chi_{c0}(1P) \to \rho^+ K^- K^0 + \text{c.c.})/\Gamma_{total}] \times [B(\psi(2S) \to \gamma\chi_{c0}(1P))]$ assuming $B(\psi(2S) \to \gamma\chi_{c0}(1P)) = (9.22 \pm 0.11 \pm 0.46) \times 10^{-2}$, which we rescale to our best (shown rounded) value $B(\psi(2S) \to \gamma\chi_{c0}(1P)) = (10.06 \pm 0.27) \times 10^{-2}$. Our first error is their experiment's error and our second error is the systematic error from using our best (shown rounded) value.

$\Gamma(K^*(892)^- K^+ \pi^0 \to K^+ \pi^- \overline{K}^0 \pi^0 + \text{c.c.})/\Gamma_{total}$ — Γ_{26}/Γ

VALUE (%)	EVTS	DOCUMENT ID		TECN	COMMENT
0.45±0.11±0.01	64.1	[1] HE	08B	CLEO	$e^+e^- \to \gamma h^+ h^- h^0 h^0$

[1] HE 08B reports 0.49 ± 0.10 ± 0.07 ± 0.03 % from a measurement of $[\Gamma(\chi_{c0}(1P) \to K^*(892)^- K^+ \pi^0 \to K^+ \pi^- \overline{K}^0 \pi^0 + \text{c.c.})/\Gamma_{total}] \times [B(\psi(2S) \to \gamma\chi_{c0}(1P))]$ assuming $B(\psi(2S) \to \gamma\chi_{c0}(1P)) = (9.22 \pm 0.11 \pm 0.46) \times 10^{-2}$, which we rescale to our best (shown rounded) value $B(\psi(2S) \to \gamma\chi_{c0}(1P)) = (10.06 \pm 0.27) \times 10^{-2}$. Our first error is their experiment's error and our second error is the systematic error from using our best (shown rounded) value.

$\Gamma(K^0_S K^0_S \pi^+ \pi^-)/\Gamma_{total}$ — Γ_{27}/Γ

VALUE (units 10^{-3})	EVTS	DOCUMENT ID		TECN	COMMENT
5.5±1.0±0.1	152 ± 14	[1] ABLIKIM	05O	BES2	$\psi(2S) \to \gamma\chi_{c0}$

[1] ABLIKIM 05O reports $[\Gamma(\chi_{c0}(1P) \to K^0_S K^0_S \pi^+ \pi^-)/\Gamma_{total}] \times [B(\psi(2S) \to \gamma\chi_{c0}(1P))] = (0.558 \pm 0.051 \pm 0.089) \times 10^{-3}$ which we divide by our best (shown rounded) value $B(\psi(2S) \to \gamma\chi_{c0}(1P)) = (10.06 \pm 0.27) \times 10^{-2}$. Our first error is their experiment's error and our second error is the systematic error from using our best (shown rounded) value.

$\Gamma(K^+ K^- \eta\pi^0)/\Gamma_{total}$ — Γ_{28}/Γ

VALUE (%)	EVTS	DOCUMENT ID		TECN	COMMENT
0.29±0.07±0.01	56.4	[1] HE	08B	CLEO	$e^+e^- \to \gamma h^+ h^- h^0 h^0$

[1] HE 08B reports 0.32 ± 0.05 ± 0.05 ± 0.02 % from a measurement of $[\Gamma(\chi_{c0}(1P) \to K^+ K^- \eta\pi^0)/\Gamma_{total}] \times [B(\psi(2S) \to \gamma\chi_{c0}(1P))]$ assuming $B(\psi(2S) \to \gamma\chi_{c0}(1P)) = (9.22 \pm 0.11 \pm 0.46) \times 10^{-2}$, which we rescale to our best (shown rounded) value $B(\psi(2S) \to \gamma\chi_{c0}(1P)) = (10.06 \pm 0.27) \times 10^{-2}$. Our first error is their experiment's error and our second error is the systematic error from using our best (shown rounded) value.

$\Gamma(3(\pi^+\pi^-))/\Gamma_{total}$ — Γ_{29}/Γ

VALUE (units 10^{-3})	EVTS	DOCUMENT ID		TECN	COMMENT
19.7±2.2 OUR AVERAGE	Error includes scale factor of 3.0.				
20.2±0.5±0.5	145k	[1] ABLIKIM	22Q	BES3	$\psi(2S) \to \gamma 3(\pi^+\pi^-)$
10.8±2.1±0.3	191	[2] BAI	99B	BES	$\psi(2S) \to \gamma\chi_{c0}$
13.9±5.0±0.4	37	[3] TANENBAUM	78	MRK1	$\psi(2S) \to \gamma\chi_{c0}$

[1] ABLIKIM 22Q reports (2.080 ± 0.006 ± 0.068) × 10^{-2} from a measurement of $[\Gamma(\chi_{c0}(1P) \to 3(\pi^+\pi^-))/\Gamma_{total}] \times [B(\psi(2S) \to \gamma\chi_{c0}(1P))]$ assuming $B(\psi(2S) \to \gamma\chi_{c0}(1P)) = (9.79 \pm 0.2) \times 10^{-2}$, which we rescale to our best (shown rounded) value $B(\psi(2S) \to \gamma\chi_{c0}(1P)) = (10.06 \pm 0.27) \times 10^{-2}$. Our first error is their experiment's error and our second error is the systematic error from using our best (shown rounded) value.

[2] BAI 99B reports (11.7 ± 1.0 ± 2.3) × 10^{-3} from a measurement of $[\Gamma(\chi_{c0}(1P) \to 3(\pi^+\pi^-))/\Gamma_{total}] \times [B(\psi(2S) \to \gamma\chi_{c0}(1P))]$ assuming $B(\psi(2S) \to \gamma\chi_{c0}(1P)) = (9.3 \pm 0.8) \times 10^{-2}$, which we rescale to our best (shown rounded) value $B(\psi(2S) \to \gamma\chi_{c0}(1P)) = (10.06 \pm 0.27) \times 10^{-2}$. Our first error is their experiment's error and our second error is the systematic error from using our best (shown rounded) value.

[3] TANENBAUM 78 reports $[\Gamma(\chi_{c0}(1P) \to 3(\pi^+\pi^-))/\Gamma_{total}] \times [B(\psi(2S) \to \gamma\chi_{c0}(1P))] = (1.4 \pm 0.5) \times 10^{-3}$ which we divide by our best (shown rounded) value $B(\psi(2S) \to \gamma\chi_{c0}(1P)) = (10.06 \pm 0.27) \times 10^{-2}$. Our first error is their experiment's error and our second error is the systematic error from using our best (shown rounded) value.

$\Gamma(K^+ \overline{K}^*(892)^0 \pi^- + \text{c.c.})/\Gamma(\pi^+\pi^- K^+ K^-)$ — Γ_{30}/Γ_8

VALUE	DOCUMENT ID		TECN	COMMENT
0.41±0.09 OUR FIT				
0.41±0.10	TANENBAUM	78	MRK1	$\psi(2S) \to \gamma\chi_{c0}$

$\Gamma(K^*(892)^0 \overline{K}^*(892)^0)/\Gamma_{total}$ — Γ_{31}/Γ

VALUE (units 10^{-3})	EVTS	DOCUMENT ID		TECN	COMMENT
$1.67^{+0.58}_{-0.53}$±0.04	64	[1] ABLIKIM	05Q	BES2	$\psi(2S) \to \gamma\pi^+\pi^- K^+ K^-$
• • • We do not use the following data for averages, fits, limits, etc. • • •					
1.52±0.39±0.04	30 ± 6	[2,3] ABLIKIM	04H	BES	Repl. by ABLIKIM 05Q

[1] ABLIKIM 05Q reports $[\Gamma(\chi_{c0}(1P) \to K^*(892)^0 \overline{K}^*(892)^0)/\Gamma_{total}] \times [B(\psi(2S) \to \gamma\chi_{c0}(1P))] = (0.168 \pm 0.035^{+0.047}_{-0.040}) \times 10^{-3}$ which we divide by our best (shown rounded) value $B(\psi(2S) \to \gamma\chi_{c0}(1P)) = (10.06 \pm 0.27) \times 10^{-2}$. Our first error is their experiment's error and our second error is the systematic error from using our best (shown rounded) value.

[2] Assumes $B(K^*(892)^0 \to K^-\pi^+) = 2/3$.

[3] ABLIKIM 04H reports $[\Gamma(\chi_{c0}(1P) \to K^*(892)^0 \overline{K}^*(892)^0)/\Gamma_{total}] \times [B(2S) \to \gamma\chi_{c0}(1P))] = (1.53 \pm 0.29 \pm 0.26) \times 10^{-4}$ which we divide by our best (shown rounded) value $B(\psi(2S) \to \gamma\chi_{c0}(1P)) = (10.06 \pm 0.27) \times 10^{-2}$. Our first error is their experiment's error and our second error is the systematic error from using our best (shown rounded) value.

$\Gamma(\pi^0 \eta_c)/\Gamma_{total}$ — Γ_{35}/Γ

VALUE	CL%	DOCUMENT ID		TECN	COMMENT
<1.6 × 10^{-3}	90	[1] ABLIKIM	15N	BES3	$\psi(2s) e^+e^- \to \gamma\pi^0 \eta_c$

[1] Using $B(\eta_c \to K^0_S K^\pm \pi^\mp) \times B(K^0_S \to \pi^+\pi^-) \times B(\pi^0 \to \gamma\gamma) = (1.66 \pm 0.11) \times 10^{-2}$.

$\Gamma(\eta\eta')/\Gamma_{total}$ — Γ_{37}/Γ

VALUE (units 10^{-5})	CL%	EVTS	DOCUMENT ID		TECN	COMMENT
8.9±1.0±0.2		85	[1] ABLIKIM	17AI	BES3	$\psi(2S) \to \gamma\eta'\eta$
• • • We do not use the following data for averages, fits, limits, etc. • • •						
<23	90	35 ± 13	[2] ASNER	09	CLEO	$\psi(2S) \to \gamma\eta'\eta$
<50	90		[3] ADAMS	07	CLEO	$\psi(2S) \to \gamma\chi_{c0}$

[1] ABLIKIM 17AI reports (8.92±0.84±0.65)×10^{-5} from a measurement of $[\Gamma(\chi_{c0}(1P) \to \eta\eta')/\Gamma_{total}] \times [B(\psi(2S) \to \gamma\chi_{c0}(1P))]$ assuming $B(\psi(2S) \to \gamma\chi_{c0}(1P)) = (9.99 \pm 0.27) \times 10^{-2}$, which we rescale to our best (shown rounded) value $B(\psi(2S) \to \gamma\chi_{c0}(1P)) = (10.06 \pm 0.27) \times 10^{-2}$. Our first error is their experiment's error and our second error is the systematic error from using our best (shown rounded) value.

[2] ASNER 09 reports < 0.25 × 10^{-3} from a measurement of $[\Gamma(\chi_{c0}(1P) \to \eta\eta')/\Gamma_{total}] \times [B(\psi(2S) \to \gamma\chi_{c0}(1P))]$ assuming $B(\psi(2S) \to \gamma\chi_{c0}(1P)) = (9.22 \pm 0.11 \pm 0.46) \times 10^{-2}$, which we rescale to our best (shown rounded) value $B(\psi(2S) \to \gamma\chi_{c0}(1P)) = 10.06 \times 10^{-2}$.

[3] Superseded by ASNER 09. ADAMS 07 reports < 0.5 × 10^{-3} from a measurement of $[\Gamma(\chi_{c0}(1P) \to \eta\eta')/\Gamma_{total}] \times [B(\psi(2S) \to \gamma\chi_{c0}(1P))]$ assuming $B(\psi(2S) \to \gamma\chi_{c0}(1P)) = (9.22 \pm 0.11 \pm 0.46) \times 10^{-2}$, which we rescale to our best (shown rounded) value $B(\psi(2S) \to \gamma\chi_{c0}(1P)) = 10.06 \times 10^{-2}$.

$\Gamma(\eta'\eta')/\Gamma_{total}$ — Γ_{38}/Γ

VALUE (units 10^{-3})	EVTS	DOCUMENT ID		TECN	COMMENT
2.11±0.12 OUR AVERAGE					
2.18±0.13±0.06	2.5k	[1] ABLIKIM	17AI	BES3	$\psi(2S) \to \gamma\eta'\eta'$
1.94±0.20±0.05	0.4k	[2] ASNER	09	CLEO	$\psi(2S) \to \gamma\eta'\eta'$
• • • We do not use the following data for averages, fits, limits, etc. • • •					
1.56±0.40±0.04	23	[3] ADAMS	07	CLEO	$\psi(2S) \to \gamma\chi_{c0}$

[1] ABLIKIM 17AI reports (2.19±0.03±0.14)×10^{-3} from a measurement of $[\Gamma(\chi_{c0}(1P) \to \eta'\eta')/\Gamma_{total}] \times [B(\psi(2S) \to \gamma\chi_{c0}(1P))]$ assuming $B(\psi(2S) \to \gamma\chi_{c0}(1P)) = (9.99 \pm 0.27) \times 10^{-2}$, which we rescale to our best (shown rounded) value $B(\psi(2S) \to \gamma\chi_{c0}(1P)) = (10.06 \pm 0.27) \times 10^{-2}$. Our first error is their experiment's error and our second error is the systematic error from using our best (shown rounded) value.

[2] ASNER 09 reports (2.12 ± 0.13 ± 0.21) × 10^{-3} from a measurement of $[\Gamma(\chi_{c0}(1P) \to \eta'\eta')/\Gamma_{total}] \times [B(\psi(2S) \to \gamma\chi_{c0}(1P))]$ assuming $B(\psi(2S) \to \gamma\chi_{c0}(1P)) = (9.22 \pm 0.11 \pm 0.46) \times 10^{-2}$, which we rescale to our best (shown rounded) value $B(\psi(2S) \to \gamma\chi_{c0}(1P)) = (10.06 \pm 0.27) \times 10^{-2}$. Our first error is their experiment's error and our second error is the systematic error from using our best (shown rounded) value.

[3] Superseded by ASNER 09. ADAMS 07 reports (1.7 ± 0.4 ± 0.2) × 10^{-3} from a measurement of $[\Gamma(\chi_{c0}(1P) \to \eta'\eta')/\Gamma_{total}] \times [B(\psi(2S) \to \gamma\chi_{c0}(1P))]$ assuming $B(\psi(2S) \to \gamma\chi_{c0}(1P)) = 0.0922 \pm 0.0011 \pm 0.0046$, which we rescale to our best (shown rounded) value $B(\psi(2S) \to \gamma\chi_{c0}(1P)) = (10.06 \pm 0.27) \times 10^{-2}$. Our first error is their experiment's error and our second error is the systematic error from using our best (shown rounded) value.

$\Gamma(\omega\omega)/\Gamma_{total}$ — Γ_{39}/Γ

VALUE (units 10^{-3})	EVTS	DOCUMENT ID		TECN	COMMENT
1.02±0.05 OUR AVERAGE					
1.04±0.05±0.03	17.5k	[1] ABLIKIM	25K	BES3	$\psi(2S) \to \gamma 2(\pi^+\pi^-\pi^0)$
0.91±0.11±0.02	991	[2] ABLIKIM	11K	BES3	$\psi(2S) \to \gamma$ hadrons
2.1 ±0.6 ±0.1	38.1±9.6	[3] ABLIKIM	05N	BES2	$\psi(2S) \to \gamma\chi_{c0} \to \gamma 6\pi$

[1] ABLIKIM 25K reports (10.66 ± 0.11 ± 0.57) × 10^{-4} from a measurement of $[\Gamma(\chi_{c0}(1P) \to \omega\omega)/\Gamma_{total}] \times [B(\psi(2S) \to \gamma\chi_{c0}(1P))]$ assuming $B(\psi(2S) \to \gamma\chi_{c0}(1P)) = (9.79 \pm 0.20) \times 10^{-2}$, which we rescale to our best (shown rounded) value $B(\psi(2S) \to \gamma\chi_{c0}(1P)) = (10.06 \pm 0.27) \times 10^{-2}$. Our first error is their experiment's error and our second error is the systematic error from using our best (shown rounded) value.

[2] ABLIKIM 11K reports (0.95±0.03±0.11)×10^{-3} from a measurement of $[\Gamma(\chi_{c0}(1P) \to \omega\omega)/\Gamma_{total}] \times [B(\psi(2S) \to \gamma\chi_{c0}(1P))]$ assuming $B(\psi(2S) \to \gamma\chi_{c0}(1P)) = (9.62 \pm 0.31) \times 10^{-2}$, which we rescale to our best (shown rounded) value $B(\psi(2S) \to \gamma\chi_{c0}(1P)) = (10.06 \pm 0.27) \times 10^{-2}$. Our first error is their experiment's error and our second error is the systematic error from using our best (shown rounded) value.

[3] ABLIKIM 05N reports $[\Gamma(\chi_{c0}(1P) \to \omega\omega)/\Gamma_{total}] \times [B(\psi(2S) \to \gamma\chi_{c0}(1P))] = (0.212 \pm 0.053 \pm 0.037) \times 10^{-3}$ which we divide by our best (shown rounded) value $B(\psi(2S) \to \gamma\chi_{c0}(1P)) = (10.06 \pm 0.27) \times 10^{-2}$. Our first error is their experiment's error and our second error is the systematic error from using our best (shown rounded) value.

$\Gamma(\omega\phi)/\Gamma_{total}$ — Γ_{40}/Γ

VALUE (units 10^{-4})	EVTS	DOCUMENT ID		TECN	COMMENT
1.21±0.10 OUR AVERAGE	Error includes scale factor of 1.4.				
1.15±0.07±0.03	1.9k	[1] ABLIKIM	25K	BES3	$\psi(2S) \to \gamma\pi^+\pi^-\pi^0 K^+ K^-$
1.38±0.12±0.04	486	[2] ABLIKIM	19J	BES3	$\psi(2S) \to \gamma$ hadrons
• • • We do not use the following data for averages, fits, limits, etc. • • •					
1.15±0.21±0.03	76	[3,4] ABLIKIM	11K	BES3	$\psi(2S) \to \gamma$ hadrons

[1] ABLIKIM 25K reports (1.18±0.03±0.07)×10^{-4} from a measurement of $[\Gamma(\chi_{c0}(1P) \to \omega\phi)/\Gamma_{total}] \times [B(\psi(2S) \to \gamma\chi_{c0}(1P))]$ assuming $B(\psi(2S) \to \gamma\chi_{c0}(1P)) = (9.79 \pm 0.20) \times 10^{-2}$, which we rescale to our best (shown rounded) value $B(\psi(2S) \to \gamma\chi_{c0}(1P)) = (10.06 \pm 0.27) \times 10^{-2}$. Our first error is their experiment's error and our second error is the systematic error from using our best (shown rounded) value.

Int. J. Mod. Phys. A 2026.41. Downloaded from www.worldscientific.com
by UNIVERSITY OF CALIFORNIA @ BERKELEY on 09/16/26. Re-use and distribution is strictly not permitted, except for Open Access articles.

[2] ABLIKIM 19J reports $[\Gamma(\chi_{c0}(1P) \to \omega\phi)/\Gamma_{total}] \times [B(\psi(2S) \to \gamma\chi_{c0}(1P))] = (13.83 \pm 0.70 \pm 1.01) \times 10^{-6}$ which we divide by our best (shown rounded) value $B(\psi(2S) \to \gamma\chi_{c0}(1P)) = (10.06 \pm 0.27) \times 10^{-2}$. Our first error is their experiment's error and our second error is the systematic error from using our best (shown rounded) value.

[3] ABLIKIM 11K reports $(1.2 \pm 0.1 \pm 0.2) \times 10^{-4}$ from a measurement of $[\Gamma(\chi_{c0}(1P) \to \omega\phi)/\Gamma_{total}] \times [B(\psi(2S) \to \gamma\chi_{c0}(1P))]$ assuming $B(\psi(2S) \to \gamma\chi_{c0}(1P)) = (9.62 \pm 0.31) \times 10^{-2}$, which we rescale to our best (shown rounded) value $B(\psi(2S) \to \gamma\chi_{c0}(1P)) = (10.06 \pm 0.27) \times 10^{-2}$. Our first error is their experiment's error and our second error is the systematic error from using our best (shown rounded) value.

[4] Superseded by ABLIKIM 19J.

$\Gamma(\omega K^+ K^-)/\Gamma_{total}$ — Γ_{41}/Γ

VALUE (units 10^{-3})	EVTS	DOCUMENT ID		TECN	COMMENT
1.87±0.19±0.05	1.4k	[1] ABLIKIM	13B	BES3	$e^+e^- \to \psi(2S) \to \gamma\chi_{c0}$

[1] ABLIKIM 13B reports $(1.94 \pm 0.06 \pm 0.20) \times 10^{-3}$ from a measurement of $[\Gamma(\chi_{c0}(1P) \to \omega K^+ K^-)/\Gamma_{total}] \times [B(\psi(2S) \to \gamma\chi_{c0}(1P))]$ assuming $B(\psi(2S) \to \gamma\chi_{c0}(1P)) = (9.68 \pm 0.31) \times 10^{-2}$, which we rescale to our best (shown rounded) value $B(\psi(2S) \to \gamma\chi_{c0}(1P)) = (10.06 \pm 0.27) \times 10^{-2}$. Our first error is their experiment's error and our second error is the systematic error from using our best (shown rounded) value.

$\Gamma(\pi^+\pi^-\eta)/\Gamma_{total}$ — Γ_{44}/Γ

VALUE (units 10^{-3})	CL%	DOCUMENT ID		TECN	COMMENT
<0.19	90	[1] ATHAR	07	CLEO	$\psi(2S) \to \gamma h^+ h^- h^0$
• • • We do not use the following data for averages, fits, limits, etc. • • •					
<1.0	90	[2] ABLIKIM	06R	BES2	$\psi(2S) \to \gamma\chi_{c0}$

[1] ATHAR 07 reports $< 0.21 \times 10^{-3}$ from a measurement of $[\Gamma(\chi_{c0}(1P) \to \pi^+\pi^-\eta)/\Gamma_{total}] \times [B(\psi(2S) \to \gamma\chi_{c0}(1P))]$ assuming $B(\psi(2S) \to \gamma\chi_{c0}(1P)) = (9.22 \pm 0.11 \pm 0.46) \times 10^{-2}$, which we rescale to our best (shown rounded) value $B(\psi(2S) \to \gamma\chi_{c0}(1P)) = 10.06 \times 10^{-2}$.

[2] ABLIKIM 06R reports $< 1.1 \times 10^{-3}$ from a measurement of $[\Gamma(\chi_{c0}(1P) \to \pi^+\pi^-\eta)/\Gamma_{total}] \times [B(\psi(2S) \to \gamma\chi_{c0}(1P))]$ assuming $B(\psi(2S) \to \gamma\chi_{c0}(1P)) = (9.2 \pm 0.4) \times 10^{-2}$, which we rescale to our best (shown rounded) value $B(\psi(2S) \to \gamma\chi_{c0}(1P)) = 10.06 \times 10^{-2}$.

$\Gamma(\pi^+\pi^-\eta')/\Gamma_{total}$ — Γ_{46}/Γ

VALUE (units 10^{-3})	CL%	DOCUMENT ID		TECN	COMMENT
<0.35	90	[1] ATHAR	07	CLEO	$\psi(2S) \to \gamma h^+ h^- h^0$

[1] ATHAR 07 reports $< 0.38 \times 10^{-3}$ from a measurement of $[\Gamma(\chi_{c0}(1P) \to \pi^+\pi^-\eta')/\Gamma_{total}] \times [B(\psi(2S) \to \gamma\chi_{c0}(1P))]$ assuming $B(\psi(2S) \to \gamma\chi_{c0}(1P)) = (9.22 \pm 0.11 \pm 0.46) \times 10^{-2}$, which we rescale to our best (shown rounded) value $B(\psi(2S) \to \gamma\chi_{c0}(1P)) = 10.06 \times 10^{-2}$.

$\Gamma(\eta\eta\eta')/\Gamma_{total}$ — Γ_{47}/Γ

VALUE	CL%	DOCUMENT ID		TECN	COMMENT
<2.5 × 10⁻⁵	90	[1] ABLIKIM	25CJ	BES3	$\psi(2S) \to \gamma\chi_c^0 \to \gamma\eta\eta\eta'$

[1] ABLIKIM 25CJ reports $< 2.59 \times 10^{-5}$ from a measurement of $[\Gamma(\chi_{c0}(1P) \to \eta\eta\eta')/\Gamma_{total}] \times [B(\psi(2S) \to \gamma\chi_{c0}(1P))]$ assuming $B(\psi(2S) \to \gamma\chi_{c0}(1P)) = (9.77 \pm 0.23) \times 10^{-2}$, which we rescale to our best (shown rounded) value $B(\psi(2S) \to \gamma\chi_{c0}(1P)) = 10.06 \times 10^{-2}$.

$\Gamma(\overline{K}^0 K^+\pi^- + c.c.)/\Gamma_{total}$ — Γ_{48}/Γ

VALUE (units 10^{-3})	CL%	DOCUMENT ID		TECN	COMMENT
<0.09	90	[1] ATHAR	07	CLEO	$\psi(2S) \to \gamma h^+ h^- h^0$
• • • We do not use the following data for averages, fits, limits, etc. • • •					
<0.6	90	[2,3] ABLIKIM	06R	BES2	$\psi(2S) \to \gamma\chi_{c0}$
<0.7	90	[3,4] BAI	99B	BES	$\psi(2S) \to \gamma\chi_{c0}$

[1] ATHAR 07 reports $< 0.10 \times 10^{-3}$ from a measurement of $[\Gamma(\chi_{c0}(1P) \to \overline{K}^0 K^+\pi^- + c.c.)/\Gamma_{total}] \times [B(\psi(2S) \to \gamma\chi_{c0}(1P))]$ assuming $B(\psi(2S) \to \gamma\chi_{c0}(1P)) = (9.22 \pm 0.11 \pm 0.46) \times 10^{-2}$, which we rescale to our best (shown rounded) value $B(\psi(2S) \to \gamma\chi_{c0}(1P)) = 10.06 \times 10^{-2}$.

[2] ABLIKIM 06R reports $< 0.70 \times 10^{-3}$ from a measurement of $[\Gamma(\chi_{c0}(1P) \to \overline{K}^0 K^+\pi^- + c.c.)/\Gamma_{total}] \times [B(\psi(2S) \to \gamma\chi_{c0}(1P))]$ assuming $B(\psi(2S) \to \gamma\chi_{c0}(1P)) = (9.2 \pm 0.4) \times 10^{-2}$, which we rescale to our best (shown rounded) value $B(\psi(2S) \to \gamma\chi_{c0}(1P)) = 10.06 \times 10^{-2}$.

[3] We have multiplied the $K^0_S K^+\pi^-$ measurement by a factor of 2 to convert to $K^0 K^+\pi^-$.

[4] Rescaled by us using $B(\psi(2S) \to \gamma\chi_{c0}) = (9.4 \pm 0.4)\%$ and $B(\psi(2S) \to J/\psi(1S)\pi^+\pi^-) = (32.6 \pm 0.5)\%$.

$\Gamma(K^+K^-\pi^0)/\Gamma_{total}$ — Γ_{49}/Γ

VALUE (units 10^{-3})	CL%	DOCUMENT ID		TECN	COMMENT
<0.06	90	[1] ATHAR	07	CLEO	$\psi(2S) \to \gamma h^+ h^- h^0$

[1] ATHAR 07 reports $< 0.06 \times 10^{-3}$ from a measurement of $[\Gamma(\chi_{c0}(1P) \to K^+K^-\pi^0)/\Gamma_{total}] \times [B(\psi(2S) \to \gamma\chi_{c0}(1P))]$ assuming $B(\psi(2S) \to \gamma\chi_{c0}(1P)) = (9.22 \pm 0.11 \pm 0.46) \times 10^{-2}$, which we rescale to our best (shown rounded) value $B(\psi(2S) \to \gamma\chi_{c0}(1P)) = 10.06 \times 10^{-2}$.

$\Gamma(K^+K^-\eta)/\Gamma_{total}$ — Γ_{50}/Γ

VALUE (units 10^{-3})	CL%	DOCUMENT ID		TECN	COMMENT
<0.22	90	[1] ATHAR	07	CLEO	$\psi(2S) \to \gamma h^+ h^- h^0$

[1] ATHAR 07 reports $< 0.24 \times 10^{-3}$ from a measurement of $[\Gamma(\chi_{c0}(1P) \to K^+K^-\eta)/\Gamma_{total}] \times [B(\psi(2S) \to \gamma\chi_{c0}(1P))]$ assuming $B(\psi(2S) \to \gamma\chi_{c0}(1P)) = (9.22 \pm 0.11 \pm 0.46) \times 10^{-2}$, which we rescale to our best (shown rounded) value $B(\psi(2S) \to \gamma\chi_{c0}(1P)) = 10.06 \times 10^{-2}$.

$\Gamma(K^+K^-K^0_S K^0_S)/\Gamma_{total}$ — Γ_{51}/Γ

VALUE (units 10^{-3})	EVTS	DOCUMENT ID		TECN	COMMENT
1.37±0.46±0.04	16.8±4.8	[1] ABLIKIM	05O	BES2	$\psi(2S) \to \gamma\chi_{c0}$

[1] ABLIKIM 05O reports $[\Gamma(\chi_{c0}(1P) \to K^+K^-K^0_S K^0_S)/\Gamma_{total}] \times [B(\psi(2S) \to \gamma\chi_{c0}(1P))] = (0.138 \pm 0.039 \pm 0.025) \times 10^{-3}$ which we divide by our best (shown rounded) value $B(\psi(2S) \to \gamma\chi_{c0}(1P)) = (10.06 \pm 0.27) \times 10^{-2}$. Our first error is their experiment's error and our second error is the systematic error from using our best (shown rounded) value.

$\Gamma(K^0_S K^0_S K^0_S K^0_S)/\Gamma_{total}$ — Γ_{52}/Γ

VALUE (units 10^{-4})	EVTS	DOCUMENT ID		TECN	COMMENT
5.6±0.5±0.1	319	[1] ABLIKIM	19AA	BES3	$\psi(2S) \to \gamma 4K^0_S$

[1] Using $B(K^0_S \to \pi^+\pi^-) = (69.20 \pm 0.05)\%$. ABLIKIM 19AA reports $[\Gamma(\chi_{c0}(1P) \to K^0_S K^0_S K^0_S K^0_S)/\Gamma_{total}] \times [B(\psi(2S) \to \gamma\chi_{c0}(1P))] = (5.64 \pm 0.33 \pm 0.37) \times 10^{-5}$ which we divide by our best (shown rounded) value $B(\psi(2S) \to \gamma\chi_{c0}(1P)) = (10.06 \pm 0.27) \times 10^{-2}$. Our first error is their experiment's error and our second error is the systematic error from using our best (shown rounded) value..

$\Gamma(K^+K^-\phi)/\Gamma_{total}$ — Γ_{54}/Γ

VALUE (units 10^{-3})	EVTS	DOCUMENT ID		TECN	COMMENT
0.94±0.24±0.02	38	[1] ABLIKIM	06T	BES2	$\psi(2S) \to \gamma 2K^+ 2K^-$

[1] ABLIKIM 06T reports $(1.03 \pm 0.22 \pm 0.15) \times 10^{-3}$ from a measurement of $[\Gamma(\chi_{c0}(1P) \to K^+K^-\phi)/\Gamma_{total}] \times [B(\psi(2S) \to \gamma\chi_{c0}(1P))]$ assuming $B(\psi(2S) \to \gamma\chi_{c0}(1P)) = (9.2 \pm 0.4) \times 10^{-2}$, which we rescale to our best (shown rounded) value $B(\psi(2S) \to \gamma\chi_{c0}(1P)) = (10.06 \pm 0.27) \times 10^{-2}$. Our first error is their experiment's error and our second error is the systematic error from using our best (shown rounded) value.

$\Gamma(\overline{K}^0 K^+\pi^-\phi + c.c.)/\Gamma_{total}$ — Γ_{55}/Γ

VALUE (units 10^{-3})	DOCUMENT ID		TECN	COMMENT
3.68±0.30±0.50	ABLIKIM	15M	BES3	$\psi(2S) \to \gamma\chi_{c0}$

$\Gamma(K^+K^-\pi^0\phi)/\Gamma_{total}$ — Γ_{56}/Γ

VALUE (units 10^{-3})	DOCUMENT ID		TECN	COMMENT
1.90±0.14±0.32	ABLIKIM	15M	BES3	$\psi(2S) \to \gamma\chi_{c0}$

$\Gamma(\phi\pi^+\pi^-\pi^0)/\Gamma_{total}$ — Γ_{59}/Γ

VALUE (units 10^{-3})	EVTS	DOCUMENT ID		TECN	COMMENT
1.14±0.14±0.03	538	[1] ABLIKIM	13B	BES3	$e^+e^- \to \psi(2S) \to \gamma\chi_{c0}$

[1] ABLIKIM 13B reports $(1.18 \pm 0.07 \pm 0.13) \times 10^{-3}$ from a measurement of $[\Gamma(\chi_{c0}(1P) \to \phi\pi^+\pi^-\pi^0)/\Gamma_{total}] \times [B(\psi(2S) \to \gamma\chi_{c0}(1P))]$ assuming $B(\psi(2S) \to \gamma\chi_{c0}(1P)) = (9.68 \pm 0.31) \times 10^{-2}$, which we rescale to our best (shown rounded) value $B(\psi(2S) \to \gamma\chi_{c0}(1P)) = (10.06 \pm 0.27) \times 10^{-2}$. Our first error is their experiment's error and our second error is the systematic error from using our best (shown rounded) value.

$\Gamma(\phi\phi)/\Gamma_{total}$ — Γ_{60}/Γ

VALUE (units 10^{-3})	EVTS	DOCUMENT ID		TECN	COMMENT
0.83 ±0.04 OUR FIT	Error includes scale factor of 1.1.				
• • • We do not use the following data for averages, fits, limits, etc. • • •					
0.836±0.028±0.022	2701	[1,2,3] ABLIKIM	23N	BES3	$\psi(2S) \to \gamma$hadrons

[1] Using $B(\phi \to K^+K^-) = (49.2 \pm 0.5) \times 10^{-2}$ from PDG 22.

[2] ABLIKIM 23N reports $(8.59 \pm 0.27 \pm 0.20) \times 10^{-4}$ from a measurement of $[\Gamma(\chi_{c0}(1P) \to \phi\phi)/\Gamma_{total}] \times [B(\psi(2S) \to \gamma\chi_{c0}(1P))]$ assuming $B(\psi(2S) \to \gamma\chi_{c0}(1P)) = (9.79 \pm 0.20) \times 10^{-2}$, which we rescale to our best (shown rounded) value $B(\psi(2S) \to \gamma\chi_{c0}(1P)) = (10.06 \pm 0.27) \times 10^{-2}$. Our first error is their experiment's error and our second error is the systematic error from using our best (shown rounded) value.

[3] Not used since the same experimental measurement has been used in another related quantity included elsewhere in the fit.

$\Gamma(\phi\phi\eta)/\Gamma_{total}$ — Γ_{61}/Γ

VALUE (units 10^{-4})	EVTS	DOCUMENT ID		TECN	COMMENT
8.2±0.9±0.2	186.6	[1] ABLIKIM	20B	BES3	$\psi(2S) \to \gamma\phi\phi\eta$

[1] ABLIKIM 20B reports $(8.41 \pm 0.74 \pm 0.62) \times 10^{-4}$ from a measurement of $[\Gamma(\chi_{c0}(1P) \to \phi\phi\eta)/\Gamma_{total}] \times [B(\psi(2S) \to \gamma\chi_{c0}(1P))]$ assuming $B(\psi(2S) \to \gamma\chi_{c0}(1P)) = (9.79 \pm 0.20) \times 10^{-2}$, which we rescale to our best (shown rounded) value $B(\psi(2S) \to \gamma\chi_{c0}(1P)) = (10.06 \pm 0.27) \times 10^{-2}$. Our first error is their experiment's error and our second error is the systematic error from using our best (shown rounded) value.

$\Gamma(p\overline{p})/\Gamma_{total} \times \Gamma(\pi\pi)/\Gamma_{total}$ — $\Gamma_{62}/\Gamma \times \Gamma_{32}/\Gamma$

VALUE (units 10^{-7})	DOCUMENT ID		TECN	COMMENT
20.6±1.4 OUR FIT	Error includes scale factor of 1.7.			
15.3±2.4±0.8	[1] ANDREOTTI	03	E835	$\overline{p}p \to \chi_{c0} \to \pi^0\pi^0$

[1] We have multiplied $B(p\overline{p}) \cdot B(\pi^0\pi^0)$ measurement by 3 to obtain $B(p\overline{p}) \cdot B(\pi\pi)$.

$\Gamma(p\overline{p})/\Gamma_{total} \times \Gamma(\pi^0\eta)/\Gamma_{total}$ — $\Gamma_{62}/\Gamma \times \Gamma_{33}/\Gamma$

VALUE (units 10^{-7})	DOCUMENT ID		TECN	COMMENT
<0.4	ANDREOTTI	05C	E835	$\overline{p}p \to \pi^0\eta$

Int. J. Mod. Phys. A 2026.41. Downloaded from www.worldscientific.com by [redacted]LIFORNIA @ BERKELEY on 09/16/26. Re-use and distribution is strictly not permitted, except for Open Access articles.

$\Gamma(p\overline{p})/\Gamma_{total} \times \Gamma(\pi^0\eta')/\Gamma_{total}$ — $\Gamma_{62}/\Gamma \times \Gamma_{34}/\Gamma$

VALUE (units 10^{-7})	DOCUMENT ID		TECN	COMMENT
<2.5	ANDREOTTI	05C	E835	$\overline{p}p \to \pi^0\eta$

$\Gamma(p\overline{p})/\Gamma_{total} \times \Gamma(\eta\eta)/\Gamma_{total}$ — $\Gamma_{62}/\Gamma \times \Gamma_{36}/\Gamma$

VALUE (units 10^{-7})	DOCUMENT ID		TECN	COMMENT
6.9±0.7 OUR FIT Error includes scale factor of 1.4.				
$4.0\pm1.2^{+0.5}_{-0.3}$	ANDREOTTI	05C	E835	$\overline{p}p \to \eta\eta$

$\Gamma(p\overline{p})/\Gamma_{total} \times \Gamma(\eta\eta')/\Gamma_{total}$ — $\Gamma_{62}/\Gamma \times \Gamma_{37}/\Gamma$

VALUE (units 10^{-6})	DOCUMENT ID		TECN	COMMENT
• • • We do not use the following data for averages, fits, limits, etc. • • •				
$2.1^{+2.3}_{-1.5}$	ANDREOTTI	05C	E835	$\overline{p}p \to \pi^0\eta$

$\Gamma(p\overline{p}\pi^0)/\Gamma_{total}$ — Γ_{63}/Γ

VALUE (units 10^{-3})	DOCUMENT ID		TECN	COMMENT
0.68±0.07 OUR AVERAGE Error includes scale factor of 1.3.				
0.71±0.06±0.02	[1] ONYISI	10	CLE3	$\psi(2S) \to \gamma p\overline{p}X$
0.54±0.11±0.01	[2] ATHAR	07	CLEO	$\psi(2S) \to \gamma h^+h^-h^0$

[1] ONYISI 10 reports $(7.76 \pm 0.37 \pm 0.51 \pm 0.39) \times 10^{-4}$ from a measurement of $[\Gamma(\chi_{c0}(1P) \to p\overline{p}\pi^0)/\Gamma_{total}] \times [B(\psi(2S) \to \gamma\chi_{c0}(1P))]$ assuming $B(\psi(2S) \to \gamma\chi_{c0}(1P)) = (9.22 \pm 0.11 \pm 0.46) \times 10^{-2}$, which we rescale to our best (shown rounded) value $B(\psi(2S) \to \gamma\chi_{c0}(1P)) = (10.06 \pm 0.27) \times 10^{-2}$. Our first error is their experiment's error and our second error is the systematic error from using our best (shown rounded) value.

[2] ATHAR 07 reports $(0.59 \pm 0.10 \pm 0.08) \times 10^{-3}$ from a measurement of $[\Gamma(\chi_{c0}(1P) \to p\overline{p}\pi^0)/\Gamma_{total}] \times [B(\psi(2S) \to \gamma\chi_{c0}(1P))]$ assuming $B(\psi(2S) \to \gamma\chi_{c0}(1P)) = (9.22 \pm 0.11 \pm 0.46) \times 10^{-2}$, which we rescale to our best (shown rounded) value $B(\psi(2S) \to \gamma\chi_{c0}(1P)) = (10.06 \pm 0.27) \times 10^{-2}$. Our first error is their experiment's error and our second error is the systematic error from using our best (shown rounded) value.

$\Gamma(p\overline{p}\eta)/\Gamma_{total}$ — Γ_{64}/Γ

VALUE (units 10^{-3})	DOCUMENT ID		TECN	COMMENT
0.34±0.04 OUR AVERAGE				
0.34±0.04±0.01	[1] ONYISI	10	CLE3	$\psi(2S) \to \gamma p\overline{p}X$
0.36±0.11±0.01	[2] ATHAR	07	CLEO	$\psi(2S) \to \gamma h^+h^-h^0$

[1] ONYISI 10 reports $(3.73 \pm 0.38 \pm 0.28 \pm 0.19) \times 10^{-4}$ from a measurement of $[\Gamma(\chi_{c0}(1P) \to p\overline{p}\eta)/\Gamma_{total}] \times [B(\psi(2S) \to \gamma\chi_{c0}(1P))]$ assuming $B(\psi(2S) \to \gamma\chi_{c0}(1P)) = (9.22 \pm 0.11 \pm 0.46) \times 10^{-2}$, which we rescale to our best (shown rounded) value $B(\psi(2S) \to \gamma\chi_{c0}(1P)) = (10.06 \pm 0.27) \times 10^{-2}$. Our first error is their experiment's error and our second error is the systematic error from using our best (shown rounded) value.

[2] ATHAR 07 reports $(0.39 \pm 0.11 \pm 0.04) \times 10^{-3}$ from a measurement of $[\Gamma(\chi_{c0}(1P) \to p\overline{p}\eta)/\Gamma_{total}] \times [B(\psi(2S) \to \gamma\chi_{c0}(1P))]$ assuming $B(\psi(2S) \to \gamma\chi_{c0}(1P)) = (9.22 \pm 0.11 \pm 0.46) \times 10^{-2}$, which we rescale to our best (shown rounded) value $B(\psi(2S) \to \gamma\chi_{c0}(1P)) = (10.06 \pm 0.27) \times 10^{-2}$. Our first error is their experiment's error and our second error is the systematic error from using our best (shown rounded) value.

$\Gamma(p\overline{p}\omega)/\Gamma_{total}$ — Γ_{65}/Γ

VALUE (units 10^{-3})	DOCUMENT ID		TECN	COMMENT
0.51±0.05±0.01	[1] ONYISI	10	CLE3	$\psi(2S) \to \gamma p\overline{p}X$

[1] ONYISI 10 reports $(5.57 \pm 0.48 \pm 0.42 \pm 0.14) \times 10^{-4}$ from a measurement of $[\Gamma(\chi_{c0}(1P) \to p\overline{p}\omega)/\Gamma_{total}] \times [B(\psi(2S) \to \gamma\chi_{c0}(1P))]$ assuming $B(\psi(2S) \to \gamma\chi_{c0}(1P)) = (9.22 \pm 0.11 \pm 0.46) \times 10^{-2}$, which we rescale to our best (shown rounded) value $B(\psi(2S) \to \gamma\chi_{c0}(1P)) = (10.06 \pm 0.27) \times 10^{-2}$. Our first error is their experiment's error and our second error is the systematic error from using our best (shown rounded) value.

$\Gamma(p\overline{p}\pi^+\pi^-)/\Gamma_{total}$ — Γ_{66}/Γ

VALUE (units 10^{-3})	EVTS	DOCUMENT ID		TECN	COMMENT
1.9 ±1.1 OUR AVERAGE Error includes scale factor of 2.3.					
1.45±0.52±0.04	81	[1] BAI	99B	BES	$\psi(2S) \to \gamma\chi_{c0}$
4.7 ±1.3 ±0.1	23	[2] TANENBAUM	78	MRK1	$\psi(2S) \to \gamma\chi_{c0}$

[1] BAI 99B reports $(1.57 \pm 0.21 \pm 0.54) \times 10^{-3}$ from a measurement of $[\Gamma(\chi_{c0}(1P) \to p\overline{p}\pi^+\pi^-)/\Gamma_{total}] \times [B(\psi(2S) \to \gamma\chi_{c0}(1P))]$ assuming $B(\psi(2S) \to \gamma\chi_{c0}(1P)) = (9.3 \pm 0.8) \times 10^{-2}$, which we rescale to our best (shown rounded) value $B(\psi(2S) \to \gamma\chi_{c0}(1P)) = (10.06 \pm 0.27) \times 10^{-2}$. Our first error is their experiment's error and our second error is the systematic error from using our best (shown rounded) value.

[2] TANENBAUM 78 reports $[\Gamma(\chi_{c0}(1P) \to p\overline{p}\pi^+\pi^-)/\Gamma_{total}] \times [B(\psi(2S) \to \gamma\chi_{c0}(1P))] = (4.7 \pm 1.3) \times 10^{-4}$ which we divide by our best (shown rounded) value $B(\psi(2S) \to \gamma\chi_{c0}(1P)) = (10.06 \pm 0.27) \times 10^{-2}$. Our first error is their experiment's error and our second error is the systematic error from using our best (shown rounded) value.

$\Gamma(p\overline{p}\pi^0\pi^0)/\Gamma_{total}$ — Γ_{67}/Γ

VALUE (%)	EVTS	DOCUMENT ID		TECN	COMMENT
0.101±0.027±0.003	39.5	[1] HE	08B	CLEO	$e^+e^- \to \gamma h^+h^-h^0h^0$

[1] HE 08B reports $0.11 \pm 0.02 \pm 0.02 \pm 0.01$ % from a measurement of $[\Gamma(\chi_{c0}(1P) \to p\overline{p}\pi^0\pi^0)/\Gamma_{total}] \times [B(\psi(2S) \to \gamma\chi_{c0}(1P))]$ assuming $B(\psi(2S) \to \gamma\chi_{c0}(1P)) = (9.22 \pm 0.11 \pm 0.46) \times 10^{-2}$, which we rescale to our best (shown rounded) value $B(\psi(2S) \to \gamma\chi_{c0}(1P)) = (10.06 \pm 0.27) \times 10^{-2}$. Our first error is their experiment's error and our second error is the systematic error from using our best (shown rounded) value.

$\Gamma(p\overline{p}\eta\pi^0)/\Gamma_{total}$ — Γ_{68}/Γ

VALUE (units 10^{-4})	EVTS	DOCUMENT ID		TECN	COMMENT
2.35±0.19±0.06	1898	[1] ABLIKIM	25L	BES3	$\psi(3686) \to \gamma p\overline{p}\eta\pi^0$

[1] ABLIKIM 25L reports $(2.42 \pm 0.07 \pm 0.19) \times 10^{-4}$ from a measurement of $[\Gamma(\chi_{c0}(1P) \to p\overline{p}\eta\pi^0)/\Gamma_{total}] \times [B(\psi(2S) \to \gamma\chi_{c0}(1P))]$ assuming $B(\psi(2S) \to \gamma\chi_{c0}(1P)) = (9.77 \pm 0.23) \times 10^{-2}$, which we rescale to our best (shown rounded) value $B(\psi(2S) \to \gamma\chi_{c0}(1P)) = (10.06 \pm 0.27) \times 10^{-2}$. Our first error is their experiment's error and our second error is the systematic error from using our best (shown rounded) value.

$\Gamma(p\overline{p}\eta\eta)/\Gamma_{total}$ — Γ_{69}/Γ

VALUE (units 10^{-5})	EVTS	DOCUMENT ID		TECN	COMMENT
5.6±0.7±0.1	180	[1] ABLIKIM	25CE	BES3	$\psi(2S) \to \gamma\chi_{c0}$

[1] ABLIKIM 25CE reports $(5.75 \pm 0.59 \pm 0.42) \times 10^{-5}$ from a measurement of $[\Gamma(\chi_{c0}(1P) \to p\overline{p}\eta\eta)/\Gamma_{total}] \times [B(\psi(2S) \to \gamma\chi_{c0}(1P))]$ assuming $B(\psi(2S) \to \gamma\chi_{c0}(1P)) = (9.77 \pm 0.23) \times 10^{-2}$, which we rescale to our best (shown rounded) value $B(\psi(2S) \to \gamma\chi_{c0}(1P)) = (10.06 \pm 0.27) \times 10^{-2}$. Our first error is their experiment's error and our second error is the systematic error from using our best (shown rounded) value.

$\Gamma(p\overline{p}K^+K^-)/\Gamma_{total}$ — Γ_{70}/Γ

VALUE (units 10^{-4})	EVTS	DOCUMENT ID		TECN	COMMENT
2.48±0.15±0.07	9952	[1] ABLIKIM	25V	BES3	$\psi(2S) \to \gamma p\overline{p}K^+K^-$

[1] ABLIKIM 25V reports $[\Gamma(\chi_{c0}(1P) \to p\overline{p}K^+K^-)/\Gamma_{total}] \times [B(\psi(2S) \to \gamma\chi_{c0}(1P))] = (2.49 \pm 0.03 \pm 0.15) \times 10^{-5}$ which we divide by our best (shown rounded) value $B(\psi(2S) \to \gamma\chi_{c0}(1P)) = (10.06 \pm 0.27) \times 10^{-2}$. Our first error is their experiment's error and our second error is the systematic error from using our best (shown rounded) value.

$\Gamma(p\overline{p}K^+K^-(\text{non-resonant}))/\Gamma_{total}$ — Γ_{71}/Γ

VALUE (units 10^{-4})	EVTS	DOCUMENT ID		TECN	COMMENT
1.19±0.25±0.03	48 ± 8	[1] ABLIKIM	11F	BES3	$\psi(2S) \to \gamma p\overline{p}K^+K^-$

[1] ABLIKIM 11F reports $(1.24 \pm 0.20 \pm 0.18) \times 10^{-4}$ from a measurement of $[\Gamma(\chi_{c0}(1P) \to p\overline{p}K^+K^-(\text{non-resonant}))/\Gamma_{total}] \times [B(\psi(2S) \to \gamma\chi_{c0}(1P))]$ assuming $B(\psi(2S) \to \gamma\chi_{c0}(1P)) = (9.62 \pm 0.31) \times 10^{-2}$, which we rescale to our best (shown rounded) value $B(\psi(2S) \to \gamma\chi_{c0}(1P)) = (10.06 \pm 0.27) \times 10^{-2}$. Our first error is their experiment's error and our second error is the systematic error from using our best (shown rounded) value.

$\Gamma(K^+\overline{p}\Lambda(1520)+\text{c.c.})/\Gamma_{total}$ — Γ_{72}/Γ

VALUE (units 10^{-4})	EVTS	DOCUMENT ID		TECN	COMMENT
2.9±0.7±0.1	62 ± 12	[1] ABLIKIM	11F	BES3	$\psi(2S) \to \gamma p\overline{p}K^+K^-$

[1] ABLIKIM 11F reports $(3.00 \pm 0.58 \pm 0.50) \times 10^{-4}$ from a measurement of $[\Gamma(\chi_{c0}(1P) \to K^+\overline{p}\Lambda(1520)+\text{c.c.})/\Gamma_{total}] \times [B(\psi(2S) \to \gamma\chi_{c0}(1P))]$ assuming $B(\psi(2S) \to \gamma\chi_{c0}(1P)) = (9.62 \pm 0.31) \times 10^{-2}$, which we rescale to our best (shown rounded) value $B(\psi(2S) \to \gamma\chi_{c0}(1P)) = (10.06 \pm 0.27) \times 10^{-2}$. Our first error is their experiment's error and our second error is the systematic error from using our best (shown rounded) value.

$\Gamma(\Lambda(1520)\overline{\Lambda}(1520))/\Gamma_{total}$ — Γ_{73}/Γ

VALUE (units 10^{-4})	EVTS	DOCUMENT ID		TECN	COMMENT
3.0±1.2±0.1	28 ± 10	[1] ABLIKIM	11F	BES3	$\psi(2S) \to \gamma p\overline{p}K^+K^-$

[1] ABLIKIM 11F reports $(3.18 \pm 1.11 \pm 0.53) \times 10^{-4}$ from a measurement of $[\Gamma(\chi_{c0}(1P) \to \Lambda(1520)\overline{\Lambda}(1520))/\Gamma_{total}] \times [B(\psi(2S) \to \gamma\chi_{c0}(1P))]$ assuming $B(\psi(2S) \to \gamma\chi_{c0}(1P)) = (9.62 \pm 0.31) \times 10^{-2}$, which we rescale to our best (shown rounded) value $B(\psi(2S) \to \gamma\chi_{c0}(1P)) = (10.06 \pm 0.27) \times 10^{-2}$. Our first error is their experiment's error and our second error is the systematic error from using our best (shown rounded) value.

$\Gamma(p\overline{p}\phi)/\Gamma_{total}$ — Γ_{74}/Γ

VALUE (units 10^{-5})	EVTS	DOCUMENT ID		TECN	COMMENT
5.9±1.4±0.2	42 ± 8	[1] ABLIKIM	11F	BES3	$\psi(2S) \to \gamma p\overline{p}K^+K^-$

[1] ABLIKIM 11F reports $(6.12 \pm 1.18 \pm 0.86) \times 10^{-5}$ from a measurement of $[\Gamma(\chi_{c0}(1P) \to p\overline{p}\phi)/\Gamma_{total}] \times [B(\psi(2S) \to \gamma\chi_{c0}(1P))]$ assuming $B(\psi(2S) \to \gamma\chi_{c0}(1P)) = (9.62 \pm 0.31) \times 10^{-2}$, which we rescale to our best (shown rounded) value $B(\psi(2S) \to \gamma\chi_{c0}(1P)) = (10.06 \pm 0.27) \times 10^{-2}$. Our first error is their experiment's error and our second error is the systematic error from using our best (shown rounded) value.

$\Gamma(p\overline{p}K^0_SK^0_S)/\Gamma_{total}$ — Γ_{75}/Γ

VALUE	CL%	DOCUMENT ID		TECN	COMMENT
$<8 \times 10^{-4}$	90	[1] ABLIKIM	06D	BES2	$\psi(2S) \to \chi_{c0}\gamma$

[1] ABLIKIM 06D reports $< 8.8 \times 10^{-4}$ from a measurement of $[\Gamma(\chi_{c0}(1P) \to p\overline{p}K^0_SK^0_S)/\Gamma_{total}] \times [B(\psi(2S) \to \gamma\chi_{c0}(1P))]$ assuming $B(\psi(2S) \to \gamma\chi_{c0}(1P)) = (9.2 \pm 0.5) \times 10^{-2}$, which we rescale to our best (shown rounded) value $B(\psi(2S) \to \gamma\chi_{c0}(1P)) = 10.06 \times 10^{-2}$.

$\Gamma(p\overline{n}\pi^-)/\Gamma_{total}$ — Γ_{77}/Γ

VALUE (units 10^{-4})	EVTS	DOCUMENT ID		TECN	COMMENT
12.3±1.1 OUR AVERAGE					
12.5±1.1±0.3	5150	[1] ABLIKIM	12J	BES3	$\psi(2S) \to \gamma p\overline{n}\pi^-$
10.9±3.0±0.3		[2] ABLIKIM	06I	BES2	$\psi(2S) \to \gamma p\pi^-X$

Int. J. Mod. Phys. A 2026.41. Downloaded from www.worldscientific.com
by UNIVERSITY OF CALIFORNIA @ BERKELEY on 09/16/26. Re-use and distribution is strictly not permitted, except for Open Access articles.

[1] ABLIKIM 12J reports $[\Gamma(\chi_{c0}(1P) \to p\overline{n}\pi^-)/\Gamma_{total}] \times [B(\psi(2S) \to \gamma\chi_{c0}(1P))] = (1.26 \pm 0.02 \pm 0.11) \times 10^{-4}$ which we divide by our best (shown rounded) value $B(\psi(2S) \to \gamma\chi_{c0}(1P)) = (10.06 \pm 0.27) \times 10^{-2}$. Our first error is their experiment's error and our second error is the systematic error from using our best (shown rounded) value.

[2] ABLIKIM 06I reports $[\Gamma(\chi_{c0}(1P) \to p\overline{n}\pi^-)/\Gamma_{total}] \times [B(\psi(2S) \to \gamma\chi_{c0}(1P))] = (1.10 \pm 0.24 \pm 0.18) \times 10^{-4}$ which we divide by our best (shown rounded) value $B(\psi(2S) \to \gamma\chi_{c0}(1P)) = (10.06 \pm 0.27) \times 10^{-2}$. Our first error is their experiment's error and our second error is the systematic error from using our best (shown rounded) value.

$\Gamma(\overline{p}n\pi^+)/\Gamma_{total}$ — Γ_{78}/Γ

VALUE (units 10^{-4})	EVTS	DOCUMENT ID		TECN	COMMENT
13.3±1.1±0.4	5808	[1] ABLIKIM	12J	BES3	$\psi(2S) \to \gamma\overline{p}n\pi^+$

[1] ABLIKIM 12J reports $[\Gamma(\chi_{c0}(1P) \to \overline{p}n\pi^+)/\Gamma_{total}] \times [B(\psi(2S) \to \gamma\chi_{c0}(1P))] = (1.34 \pm 0.03 \pm 0.11) \times 10^{-4}$ which we divide by our best (shown rounded) value $B(\psi(2S) \to \gamma\chi_{c0}(1P)) = (10.06 \pm 0.27) \times 10^{-2}$. Our first error is their experiment's error and our second error is the systematic error from using our best (shown rounded) value.

$\Gamma(p\overline{n}\pi^-\pi^0)/\Gamma_{total}$ — Γ_{79}/Γ

VALUE (units 10^{-4})	EVTS	DOCUMENT ID		TECN	COMMENT
22.8±2.0±0.6	2480	[1] ABLIKIM	12J	BES3	$\psi(2S) \to \gamma p\overline{n}\pi^-\pi^0$

[1] ABLIKIM 12J reports $[\Gamma(\chi_{c0}(1P) \to p\overline{n}\pi^-\pi^0)/\Gamma_{total}] \times [B(\psi(2S) \to \gamma\chi_{c0}(1P))] = (2.29 \pm 0.08 \pm 0.18) \times 10^{-4}$ which we divide by our best (shown rounded) value $B(\psi(2S) \to \gamma\chi_{c0}(1P)) = (10.06 \pm 0.27) \times 10^{-2}$. Our first error is their experiment's error and our second error is the systematic error from using our best (shown rounded) value.

$\Gamma(\overline{p}n\pi^+\pi^0)/\Gamma_{total}$ — Γ_{80}/Γ

VALUE (units 10^{-4})	EVTS	DOCUMENT ID		TECN	COMMENT
21.5±1.7±0.6	2757	[1] ABLIKIM	12J	BES3	$\psi(2S) \to \gamma\overline{p}n\pi^+\pi^0$

[1] ABLIKIM 12J reports $[\Gamma(\chi_{c0}(1P) \to \overline{p}n\pi^+\pi^0)/\Gamma_{total}] \times [B(\psi(2S) \to \gamma\chi_{c0}(1P))] = (2.16 \pm 0.07 \pm 0.16) \times 10^{-4}$ which we divide by our best (shown rounded) value $B(\psi(2S) \to \gamma\chi_{c0}(1P)) = (10.06 \pm 0.27) \times 10^{-2}$. Our first error is their experiment's error and our second error is the systematic error from using our best (shown rounded) value.

$\Gamma(\Lambda\overline{\Lambda}\pi^+\pi^-)/\Gamma_{total}$ — Γ_{82}/Γ

VALUE (units 10^{-5})	CL%	EVTS	DOCUMENT ID		TECN	COMMENT
115±12±3		426	[1] ABLIKIM	12I	BES3	$\psi(2S) \to \gamma\Lambda\overline{\Lambda}\pi^+\pi^-$
• • • We do not use the following data for averages, fits, limits, etc. • • •						
<400	90		[2] ABLIKIM	06D	BES2	$\psi(2S) \to \chi_{c0}\gamma$

[1] ABLIKIM 12I reports $(119.0 \pm 6.4 \pm 11.4) \times 10^{-5}$ from a measurement of $[\Gamma(\chi_{c0}(1P) \to \Lambda\overline{\Lambda}\pi^+\pi^-)/\Gamma_{total}] \times [B(\psi(2S) \to \gamma\chi_{c0}(1P))]$ assuming $B(\psi(2S) \to \gamma\chi_{c0}(1P)) = (9.68 \pm 0.31) \times 10^{-2}$, which we rescale to our best (shown rounded) value $B(\psi(2S) \to \gamma\chi_{c0}(1P)) = (10.06 \pm 0.27) \times 10^{-2}$. Our first error is their experiment's error and our second error is the systematic error from using our best (shown rounded) value.

[2] Using $B(\psi(2S) \to \chi_{c0}\gamma) = (9.2 \pm 0.5)\%$

$\Gamma(\Lambda\overline{\Lambda}\pi^+\pi^-(\text{non-resonant}))/\Gamma_{total}$ — Γ_{83}/Γ

VALUE (units 10^{-5})	CL%	DOCUMENT ID		TECN	COMMENT
<50	90	[1] ABLIKIM	12I	BES3	$\psi(2S) \to \gamma\Lambda\overline{\Lambda}\pi^+\pi^-$

[1] ABLIKIM 12I reports $< 54 \times 10^{-5}$ from a measurement of $[\Gamma(\chi_{c0}(1P) \to \Lambda\overline{\Lambda}\pi^+\pi^-(\text{non-resonant}))/\Gamma_{total}] \times [B(\psi(2S) \to \gamma\chi_{c0}(1P))]$ assuming $B(\psi(2S) \to \gamma\chi_{c0}(1P)) = (9.68 \pm 0.31) \times 10^{-2}$, which we rescale to our best (shown rounded) value $B(\psi(2S) \to \gamma\chi_{c0}(1P)) = 10.06 \times 10^{-2}$.

$\Gamma(\Sigma(1385)^+\overline{\Lambda}\pi^- + c.c.)/\Gamma_{total}$ — Γ_{84}/Γ

VALUE (units 10^{-5})	CL%	DOCUMENT ID		TECN	COMMENT
<50	90	[1] ABLIKIM	12I	BES3	$\psi(2S) \to \gamma\Sigma(1385)^+\overline{\Lambda}\pi^-$

[1] ABLIKIM 12I reports $< 55 \times 10^{-5}$ from a measurement of $[\Gamma(\chi_{c0}(1P) \to \Sigma(1385)^+\overline{\Lambda}\pi^- + c.c.)/\Gamma_{total}] \times [B(\psi(2S) \to \gamma\chi_{c0}(1P))]$ assuming $B(\psi(2S) \to \gamma\chi_{c0}(1P)) = (9.68 \pm 0.31) \times 10^{-2}$, which we rescale to our best (shown rounded) value $B(\psi(2S) \to \gamma\chi_{c0}(1P)) = 10.06 \times 10^{-2}$.

$\Gamma(\Sigma(1385)^-\overline{\Lambda}\pi^+ + c.c.)/\Gamma_{total}$ — Γ_{85}/Γ

VALUE (units 10^{-5})	CL%	DOCUMENT ID		TECN	COMMENT
<50	90	[1] ABLIKIM	12I	BES3	$\psi(2S) \to \gamma\Sigma(1385)^-\overline{\Lambda}\pi^+$

[1] ABLIKIM 12I reports $< 50 \times 10^{-5}$ from a measurement of $[\Gamma(\chi_{c0}(1P) \to \Sigma(1385)^-\overline{\Lambda}\pi^+ + c.c.)/\Gamma_{total}] \times [B(\psi(2S) \to \gamma\chi_{c0}(1P))]$ assuming $B(\psi(2S) \to \gamma\chi_{c0}(1P)) = (9.68 \pm 0.31) \times 10^{-2}$, which we rescale to our best (shown rounded) value $B(\psi(2S) \to \gamma\chi_{c0}(1P)) = 10.06 \times 10^{-2}$.

$\Gamma(K^+\overline{p}\Lambda + c.c.)/\Gamma_{total}$ — Γ_{90}/Γ

VALUE (units 10^{-3})	EVTS	DOCUMENT ID		TECN	COMMENT
1.21±0.12 OUR AVERAGE Error includes scale factor of 1.3.					
1.27±0.09±0.03	9k	[1,2] ABLIKIM	13D	BES3	$\psi(2S) \to \gamma\Lambda\overline{p}K^+$
0.98±0.18±0.03		[3] ATHAR	07	CLEO	$\psi(2S) \to \gamma h^+h^-h^0$

[1] ABLIKIM 13D reports $(1.32 \pm 0.03 \pm 0.10) \times 10^{-3}$ from a measurement of $[\Gamma(\chi_{c0}(1P) \to K^+\overline{p}\Lambda + c.c.)/\Gamma_{total}] \times [B(\psi(2S) \to \gamma\chi_{c0}(1P))]$ assuming $B(\psi(2S) \to \gamma\chi_{c0}(1P)) = (9.68 \pm 0.31) \times 10^{-2}$, which we rescale to our best (shown rounded) value $B(\psi(2S) \to \gamma\chi_{c0}(1P)) = (10.06 \pm 0.27) \times 10^{-2}$. Our first error is their experiment's error and our second error is the systematic error from using our best (shown rounded) value.

[2] Using $B(\Lambda \to p\pi^-) = 63.9\%$.

[3] ATHAR 07 reports $(1.07 \pm 0.17 \pm 0.12) \times 10^{-3}$ from a measurement of $[\Gamma(\chi_{c0}(1P) \to K^+\overline{p}\Lambda + c.c.)/\Gamma_{total}] \times [B(\psi(2S) \to \gamma\chi_{c0}(1P))]$ assuming $B(\psi(2S) \to \gamma\chi_{c0}(1P)) = (9.22 \pm 0.11 \pm 0.46) \times 10^{-2}$, which we rescale to our best (shown rounded) value $B(\psi(2S) \to \gamma\chi_{c0}(1P)) = (10.06 \pm 0.27) \times 10^{-2}$. Our first error is their experiment's error and our second error is the systematic error from using our best (shown rounded) value.

$\Gamma(K^*(892)^+\overline{p}\Lambda + c.c.)/\Gamma_{total}$ — Γ_{92}/Γ

VALUE (units 10^{-4})	EVTS	DOCUMENT ID		TECN	COMMENT
4.7±0.9±0.1	254	[1] ABLIKIM	19AU	BES3	$\psi(2S) \to \gamma K^{*+}\overline{p}\Lambda$

[1] ABLIKIM 19AU reports $[\Gamma(\chi_{c0}(1P) \to K^*(892)^+\overline{p}\Lambda + c.c.)/\Gamma_{total}] \times [B(\psi(2S) \to \gamma\chi_{c0}(1P))] = (4.7 \pm 0.7 \pm 0.5) \times 10^{-5}$ which we divide by our best (shown rounded) value $B(\psi(2S) \to \gamma\chi_{c0}(1P)) = (10.06 \pm 0.27) \times 10^{-2}$. Our first error is their experiment's error and our second error is the systematic error from using our best (shown rounded) value.

$\Gamma(nK^0_S\overline{\Lambda} + c.c.)/\Gamma_{total}$ — Γ_{91}/Γ

VALUE (units 10^{-4})	EVTS	DOCUMENT ID		TECN	COMMENT
6.5±0.5±0.2	1284	[1] ABLIKIM	21AV	BES3	$\psi(2S) \to \gamma nK^0_S\overline{\Lambda}$ + c.c.

[1] ABLIKIM 21AV reports $(6.65 \pm 0.26 \pm 0.41) \times 10^{-4}$ from a measurement of $[\Gamma(\chi_{c0}(1P) \to nK^0_S\overline{\Lambda} + c.c.)/\Gamma_{total}] \times [B(\psi(2S) \to \gamma\chi_{c0}(1P))]$ assuming $B(\psi(2S) \to \gamma\chi_{c0}(1P)) = 0.0979 \pm 0.0020$, which we rescale to our best (shown rounded) value $B(\psi(2S) \to \gamma\chi_{c0}(1P)) = (10.06 \pm 0.27) \times 10^{-2}$. Our first error is their experiment's error and our second error is the systematic error from using our best (shown rounded) value. Also uses $B(\overline{\Lambda} \to \overline{p}\pi^+) = (63.9 \pm 0.5)\%$ and $B(K^0_S \to \pi^+\pi^-) = (69.20 \pm 0.05)\%$.

$\Gamma(\Sigma^0\overline{\Sigma}^0)/\Gamma_{total}$ — Γ_{94}/Γ

VALUE (units 10^{-4})	EVTS	DOCUMENT ID		TECN	COMMENT
4.56±0.32 OUR AVERAGE					
4.69±0.33±0.12	1046	[1] ABLIKIM	18V	BES3	$\psi(2S) \to \gamma\Sigma^0\overline{\Sigma}^0$
4.0 ±0.6 ±0.1	78 ± 10	[2] NAIK	08	CLEO	$\psi(2S) \to \gamma\Sigma^0\overline{\Sigma}^0$
• • • We do not use the following data for averages, fits, limits, etc. • • •					
4.6 ±0.5 ±0.1	243	[3,4] ABLIKIM	13H	BES3	$\psi(2S) \to \gamma\Sigma^0\overline{\Sigma}^0$

[1] ABLIKIM 18V reports $[\Gamma(\chi_{c0}(1P) \to \Sigma^0\overline{\Sigma}^0)/\Gamma_{total}] \times [B(\psi(2S) \to \gamma\chi_{c0}(1P))] = (4.72 \pm 0.18 \pm 0.28) \times 10^{-5}$ which we divide by our best (shown rounded) value $B(\psi(2S) \to \gamma\chi_{c0}(1P)) = (10.06 \pm 0.27) \times 10^{-2}$. Our first error is their experiment's error and our second error is the systematic error from using our best (shown rounded) value.

[2] NAIK 08 reports $(4.41 \pm 0.56 \pm 0.47) \times 10^{-4}$ from a measurement of $[\Gamma(\chi_{c0}(1P) \to \Sigma^0\overline{\Sigma}^0)/\Gamma_{total}] \times [B(\psi(2S) \to \gamma\chi_{c0}(1P))]$ assuming $B(\psi(2S) \to \gamma\chi_{c0}(1P)) = (9.22 \pm 0.11 \pm 0.46) \times 10^{-2}$, which we rescale to our best (shown rounded) value $B(\psi(2S) \to \gamma\chi_{c0}(1P)) = (10.06 \pm 0.27) \times 10^{-2}$. Our first error is their experiment's error and our second error is the systematic error from using our best (shown rounded) value.

[3] ABLIKIM 13H reports $(4.78 \pm 0.34 \pm 0.39) \times 10^{-4}$ from a measurement of $[\Gamma(\chi_{c0}(1P) \to \Sigma^0\overline{\Sigma}^0)/\Gamma_{total}] \times [B(\psi(2S) \to \gamma\chi_{c0}(1P))]$ assuming $B(\psi(2S) \to \gamma\chi_{c0}(1P)) = (9.62 \pm 0.31) \times 10^{-2}$, which we rescale to our best (shown rounded) value $B(\psi(2S) \to \gamma\chi_{c0}(1P)) = (10.06 \pm 0.27) \times 10^{-2}$. Our first error is their experiment's error and our second error is the systematic error from using our best (shown rounded) value.

[4] Superseded by ABLIKIM 18V

$\Gamma(\Sigma^+\overline{\Sigma}^-)/\Gamma_{total}$ — Γ_{97}/Γ

VALUE (units 10^{-4})	EVTS	DOCUMENT ID		TECN	COMMENT
4.5 ±0.8 OUR AVERAGE Error includes scale factor of 2.6.					
4.96±0.34±0.13	747	[1] ABLIKIM	18V	BES3	$\psi(2S) \to \gamma\Sigma^+\overline{\Sigma}^-$
3.0 ±0.6 ±0.1	39 ± 7	[2] NAIK	08	CLEO	$\psi(2S) \to \gamma\Sigma^+\overline{\Sigma}^-$
• • • We do not use the following data for averages, fits, limits, etc. • • •					
4.3 ±0.5 ±0.1	148	[3,4] ABLIKIM	13H	BES3	$\psi(2S) \to \gamma\Sigma^+\overline{\Sigma}^-$

[1] ABLIKIM 18V reports $[\Gamma(\chi_{c0}(1P) \to \Sigma^+\overline{\Sigma}^-)/\Gamma_{total}] \times [B(\psi(2S) \to \gamma\chi_{c0}(1P))] = (4.99 \pm 0.24 \pm 0.24) \times 10^{-5}$ which we divide by our best (shown rounded) value $B(\psi(2S) \to \gamma\chi_{c0}(1P)) = (10.06 \pm 0.27) \times 10^{-2}$. Our first error is their experiment's error and our second error is the systematic error from using our best (shown rounded) value.

[2] NAIK 08 reports $(3.25 \pm 0.57 \pm 0.43) \times 10^{-4}$ from a measurement of $[\Gamma(\chi_{c0}(1P) \to \Sigma^+\overline{\Sigma}^-)/\Gamma_{total}] \times [B(\psi(2S) \to \gamma\chi_{c0}(1P))]$ assuming $B(\psi(2S) \to \gamma\chi_{c0}(1P)) = (9.22 \pm 0.11 \pm 0.46) \times 10^{-2}$, which we rescale to our best (shown rounded) value $B(\psi(2S) \to \gamma\chi_{c0}(1P)) = (10.06 \pm 0.27) \times 10^{-2}$. Our first error is their experiment's error and our second error is the systematic error from using our best (shown rounded) value.

[3] ABLIKIM 13H reports $(4.54 \pm 0.42 \pm 0.30) \times 10^{-4}$ from a measurement of $[\Gamma(\chi_{c0}(1P) \to \Sigma^+\overline{\Sigma}^-)/\Gamma_{total}] \times [B(\psi(2S) \to \gamma\chi_{c0}(1P))]$ assuming $B(\psi(2S) \to \gamma\chi_{c0}(1P)) = (9.62 \pm 0.31) \times 10^{-2}$, which we rescale to our best (shown rounded) value $B(\psi(2S) \to \gamma\chi_{c0}(1P)) = (10.06 \pm 0.27) \times 10^{-2}$. Our first error is their experiment's error and our second error is the systematic error from using our best (shown rounded) value.

[4] Superseded by ABLIKIM 18V

Int. J. Mod. Phys. A 2026.41. Downloaded from www.worldscientific.com by CALIFORNIA @ BERKELEY on 09/16/26. Re-use and distribution is strictly not permitted, except for Open Access articles.

$\Gamma(\Sigma^+\overline{\Sigma}^-\eta)/\Gamma_{total}$ — Γ_{98}/Γ

VALUE (units 10^{-5})	EVTS	DOCUMENT ID		TECN	COMMENT
12.3±2.3±0.3	74	[1] ABLIKIM	24CA	BES3	$\psi(2S) \to \gamma\chi_{c0}(1P)$

[1] ABLIKIM 24CA reports $(12.6 \pm 2.0 \pm 1.3) \times 10^{-5}$ from a measurement of $[\Gamma(\chi_{c0}(1P) \to \Sigma^+\overline{\Sigma}^-\eta)/\Gamma_{total}] \times [B(\psi(2S) \to \gamma\chi_{c0}(1P))]$ assuming $B(\psi(2S) \to \gamma\chi_{c0}(1P)) = (9.79 \pm 0.20) \times 10^{-2}$, which we rescale to our best (shown rounded) value $B(\psi(2S) \to \gamma\chi_{c0}(1P)) = (10.06 \pm 0.27) \times 10^{-2}$. Our first error is their experiment's error and our second error is the systematic error from using our best (shown rounded) value.

$\Gamma(\Sigma^-\overline{\Sigma}^+)/\Gamma_{total}$ — Γ_{99}/Γ

VALUE (units 10^{-4})	EVTS	DOCUMENT ID		TECN	COMMENT
5.0±0.5±0.1	2143	[1] ABLIKIM	20I	BES3	$\psi(2S) \to \gamma\Sigma^-\overline{\Sigma}^+$

[1] ABLIKIM 20I reports $(5.13 \pm 0.24 \pm 0.41) \times 10^{-4}$ from a measurement of $[\Gamma(\chi_{c0}(1P) \to \Sigma^-\overline{\Sigma}^+)/\Gamma_{total}] \times [B(\psi(2S) \to \gamma\chi_{c0}(1P))]$ assuming $B(\psi(2S) \to \gamma\chi_{c0}(1P)) = (9.79 \pm 0.20) \times 10^{-2}$, which we rescale to our best (shown rounded) value $B(\psi(2S) \to \gamma\chi_{c0}(1P)) = (10.06 \pm 0.27) \times 10^{-2}$. Our first error is their experiment's error and our second error is the systematic error from using our best (shown rounded) value.

$\Gamma(\Sigma(1385)^+\overline{\Sigma}(1385)^-)/\Gamma_{total}$ — Γ_{100}/Γ

VALUE (units 10^{-5})	EVTS	DOCUMENT ID		TECN	COMMENT
15.8±5.7±0.4	27	[1] ABLIKIM	12I	BES3	$\psi(2S) \to \gamma\Lambda\overline{\Lambda}\pi^+\pi^-$

[1] ABLIKIM 12I reports $(16.4 \pm 5.7 \pm 1.6) \times 10^{-5}$ from a measurement of $[\Gamma(\chi_{c0}(1P) \to \Sigma(1385)^+\overline{\Sigma}(1385)^-)/\Gamma_{total}] \times [B(\psi(2S) \to \gamma\chi_{c0}(1P))]$ assuming $B(\psi(2S) \to \gamma\chi_{c0}(1P)) = (9.68 \pm 0.31) \times 10^{-2}$, which we rescale to our best (shown rounded) value $B(\psi(2S) \to \gamma\chi_{c0}(1P)) = (10.06 \pm 0.27) \times 10^{-2}$. Our first error is their experiment's error and our second error is the systematic error from using our best (shown rounded) value.

$\Gamma(\Sigma(1385)^-\overline{\Sigma}(1385)^+)/\Gamma_{total}$ — Γ_{101}/Γ

VALUE (units 10^{-5})	EVTS	DOCUMENT ID		TECN	COMMENT
23±6±1	33	[1] ABLIKIM	12I	BES3	$\psi(2S) \to \gamma\Lambda\overline{\Lambda}\pi^+\pi^-$

[1] ABLIKIM 12I reports $(23.5 \pm 6.2 \pm 2.3) \times 10^{-5}$ from a measurement of $[\Gamma(\chi_{c0}(1P) \to \Sigma(1385)^-\overline{\Sigma}(1385)^+)/\Gamma_{total}] \times [B(\psi(2S) \to \gamma\chi_{c0}(1P))]$ assuming $B(\psi(2S) \to \gamma\chi_{c0}(1P)) = (9.68 \pm 0.31) \times 10^{-2}$, which we rescale to our best (shown rounded) value $B(\psi(2S) \to \gamma\chi_{c0}(1P)) = (10.06 \pm 0.27) \times 10^{-2}$. Our first error is their experiment's error and our second error is the systematic error from using our best (shown rounded) value.

$\Gamma(K^-\Lambda\overline{\Xi}^+ + \text{c.c.})/\Gamma_{total}$ — Γ_{102}/Γ

VALUE (units 10^{-4})	EVTS	DOCUMENT ID		TECN	COMMENT
1.89±0.34±0.05	57	[1] ABLIKIM	15I	BES3	$\psi(2S) \to \gamma K^-\Lambda\overline{\Xi}^+ + \text{c.c.}$

[1] ABLIKIM 15I reports $[\Gamma(\chi_{c0}(1P) \to K^-\Lambda\overline{\Xi}^+ + \text{c.c.})/\Gamma_{total}] \times [B(\psi(2S) \to \gamma\chi_{c0}(1P))] = (1.90 \pm 0.30 \pm 0.16) \times 10^{-5}$ which we divide by our best (shown rounded) value $B(\psi(2S) \to \gamma\chi_{c0}(1P)) = (10.06 \pm 0.27) \times 10^{-2}$. Our first error is their experiment's error and our second error is the systematic error from using our best (shown rounded) value.

$\Gamma(\Xi^0\overline{\Xi}^0)/\Gamma_{total}$ — Γ_{103}/Γ

VALUE (units 10^{-4})	EVTS	DOCUMENT ID		TECN	COMMENT
4.3 ±0.5 OUR AVERAGE	Error includes scale factor of 1.7.				
4.55±0.30±0.12	1741	[1] ABLIKIM	22O	BES3	$\psi(2S) \to \gamma\Xi^0\overline{\Xi}^0$
3.1 ±0.8 ±0.1	23.3±4.9	[2] NAIK	08	CLEO	$\psi(2S) \to \gamma\Xi^0\overline{\Xi}^0$

[1] ABLIKIM 22O reports $(4.67 \pm 0.19 \pm 0.26) \times 10^{-4}$ from a measurement of $[\Gamma(\chi_{c0}(1P) \to \Xi^0\overline{\Xi}^0)/\Gamma_{total}] \times [B(\psi(2S) \to \gamma\chi_{c0}(1P))]$ assuming $B(\psi(2S) \to \gamma\chi_{c0}(1P)) = (9.79 \pm 0.2) \times 10^{-2}$, which we rescale to our best (shown rounded) value $B(\psi(2S) \to \gamma\chi_{c0}(1P)) = (10.06 \pm 0.27) \times 10^{-2}$. Our first error is their experiment's error and our second error is the systematic error from using our best (shown rounded) value.

[2] NAIK 08 reports $(3.34 \pm 0.70 \pm 0.48) \times 10^{-4}$ from a measurement of $[\Gamma(\chi_{c0}(1P) \to \Xi^0\overline{\Xi}^0)/\Gamma_{total}] \times [B(\psi(2S) \to \gamma\chi_{c0}(1P))]$ assuming $B(\psi(2S) \to \gamma\chi_{c0}(1P)) = (9.22 \pm 0.11 \pm 0.46) \times 10^{-2}$, which we rescale to our best (shown rounded) value $B(\psi(2S) \to \gamma\chi_{c0}(1P)) = (10.06 \pm 0.27) \times 10^{-2}$. Our first error is their experiment's error and our second error is the systematic error from using our best (shown rounded) value.

$\Gamma(\Xi^-\overline{\Xi}^+)/\Gamma_{total}$ — Γ_{104}/Γ

VALUE (units 10^{-4})	CL%	EVTS	DOCUMENT ID		TECN	COMMENT
4.34±0.20 OUR AVERAGE						
4.31±0.17±0.11		4932	[1] ABLIKIM	22O	BES3	$\psi(2S) \to \gamma\Xi^-\overline{\Xi}^+$
4.7 ±0.7 ±0.1		95	[2] NAIK	08	CLEO	$\psi(2S) \to \gamma\Xi^+\overline{\Xi}^-$
• • • We do not use the following data for averages, fits, limits, etc. • • •						
<10.3	90		[3] ABLIKIM	06D	BES2	$\psi(2S) \to \chi_{c0}\gamma$

[1] ABLIKIM 22O reports $(4.43 \pm 0.08 \pm 0.18) \times 10^{-4}$ from a measurement of $[\Gamma(\chi_{c0}(1P) \to \Xi^-\overline{\Xi}^+)/\Gamma_{total}] \times [B(\psi(2S) \to \gamma\chi_{c0}(1P))]$ assuming $B(\psi(2S) \to \gamma\chi_{c0}(1P)) = (9.79 \pm 0.2) \times 10^{-2}$, which we rescale to our best (shown rounded) value $B(\psi(2S) \to \gamma\chi_{c0}(1P)) = (10.06 \pm 0.27) \times 10^{-2}$. Our first error is their experiment's error and our second error is the systematic error from using our best (shown rounded) value.

[2] NAIK 08 reports $(5.14 \pm 0.60 \pm 0.47) \times 10^{-4}$ from a measurement of $[\Gamma(\chi_{c0}(1P) \to \Xi^-\overline{\Xi}^+)/\Gamma_{total}] \times [B(\psi(2S) \to \gamma\chi_{c0}(1P))]$ assuming $B(\psi(2S) \to \gamma\chi_{c0}(1P)) = (9.22 \pm 0.11 \pm 0.46) \times 10^{-2}$, which we rescale to our best (shown rounded) value $B(\psi(2S) \to \gamma\chi_{c0}(1P)) = (10.06 \pm 0.27) \times 10^{-2}$. Our first error is their experiment's error and our second error is the systematic error from using our best (shown rounded) value.

[3] Using $B(\psi(2S) \to \chi_{c0}\gamma) = (9.2 \pm 0.5)\%$

$\Gamma(\Omega^-\overline{\Omega}^+)/\Gamma_{total}$ — Γ_{105}/Γ

VALUE (units 10^{-5})	EVTS	DOCUMENT ID		TECN	COMMENT
3.4±0.6±0.1	284	[1] ABLIKIM	23T	BES3	$\chi_c^0 \to \Omega^-\overline{\Omega}^+$

[1] ABLIKIM 23T reports $(3.51 \pm 0.54 \pm 0.29) \times 10^{-5}$ from a measurement of $[\Gamma(\chi_{c0}(1P) \to \Omega^-\overline{\Omega}^+)/\Gamma_{total}] \times [B(\psi(2S) \to \gamma\chi_{c0}(1P))]$ assuming $B(\psi(2S) \to \gamma\chi_{c0}(1P)) = (9.79 \pm 0.20) \times 10^{-2}$, which we rescale to our best (shown rounded) value $B(\psi(2S) \to \gamma\chi_{c0}(1P)) = (10.06 \pm 0.27) \times 10^{-2}$. Our first error is their experiment's error and our second error is the systematic error from using our best (shown rounded) value.

$\Gamma(\eta_c\pi^+\pi^-)/\Gamma_{total}$ — Γ_{106}/Γ

VALUE	CL%	DOCUMENT ID		TECN	COMMENT
< 7 × 10⁻⁴	90	[1,2] ABLIKIM	13B	BES3	$e^+e^- \to \psi(2S) \to \gamma\chi_{c0}$
• • • We do not use the following data for averages, fits, limits, etc. • • •					
$<41 \times 10^{-4}$	90	[3,4] ABLIKIM	13B	BES3	$e^+e^- \to \psi(2S) \to \gamma\chi_{c0}$

[1] From the $\eta_c \to K^0_S K^\pm\pi^\mp$ decays.

[2] ABLIKIM 13B reports $< 7 \times 10^{-4}$ from a measurement of $[\Gamma(\chi_{c0}(1P) \to \eta_c\pi^+\pi^-)/\Gamma_{total}] \times [B(\psi(2S) \to \gamma\chi_{c0}(1P))]$ assuming $B(\psi(2S) \to \gamma\chi_{c0}(1P)) = (9.68 \pm 0.31) \times 10^{-2}$, which we rescale to our best (shown rounded) value $B(\psi(2S) \to \gamma\chi_{c0}(1P)) = 10.06 \times 10^{-2}$.

[3] Using 1.06×10^8 $\psi(2S)$ mesons and $B(\psi(2S) \to \chi_{c0}\gamma) = (9.68 \pm 0.31)\%$.

[4] From the $\eta_c \to K^+K^-\pi^0$ decays.

RADIATIVE DECAYS

$\Gamma(\gamma\rho^0)/\Gamma_{total}$ — Γ_{108}/Γ

VALUE (units 10^{-6})	CL%	EVTS	DOCUMENT ID		TECN	COMMENT
< 9	90	1.2 ± 4.5	[1] BENNETT	08A	CLEO	$\psi(2S) \to \gamma\gamma\rho^0$
• • • We do not use the following data for averages, fits, limits, etc. • • •						
<10	90	6 ± 12	[2] ABLIKIM	11E	BES3	$\psi(2S) \to \gamma\gamma\rho^0$

[1] BENNETT 08A reports $< 9.6 \times 10^{-6}$ from a measurement of $[\Gamma(\chi_{c0}(1P) \to \gamma\rho^0)/\Gamma_{total}] \times [B(\psi(2S) \to \gamma\chi_{c0}(1P))]$ assuming $B(\psi(2S) \to \gamma\chi_{c0}(1P)) = (9.2 \pm 0.4) \times 10^{-2}$, which we rescale to our best (shown rounded) value $B(\psi(2S) \to \gamma\chi_{c0}(1P)) = 10.06 \times 10^{-2}$.

[2] ABLIKIM 11E reports $< 10.5 \times 10^{-6}$ from a measurement of $[\Gamma(\chi_{c0}(1P) \to \gamma\rho^0)/\Gamma_{total}] \times [B(\psi(2S) \to \gamma\chi_{c0}(1P))]$ assuming $B(\psi(2S) \to \gamma\chi_{c0}(1P)) = (9.62 \pm 0.31) \times 10^{-2}$, which we rescale to our best (shown rounded) value $B(\psi(2S) \to \gamma\chi_{c0}(1P)) = 10.06 \times 10^{-2}$.

$\Gamma(\gamma\omega)/\Gamma_{total}$ — Γ_{109}/Γ

VALUE (units 10^{-6})	CL%	EVTS	DOCUMENT ID		TECN	COMMENT
< 8	90	0.0 ± 2.8	[1] BENNETT	08A	CLEO	$\psi(2S) \to \gamma\gamma\omega$
• • • We do not use the following data for averages, fits, limits, etc. • • •						
<12	90	5 ± 11	[2] ABLIKIM	11E	BES3	$\psi(2S) \to \gamma\gamma\omega$

[1] BENNETT 08A reports $< 8.8 \times 10^{-6}$ from a measurement of $[\Gamma(\chi_{c0}(1P) \to \gamma\omega)/\Gamma_{total}] \times [B(\psi(2S) \to \gamma\chi_{c0}(1P))]$ assuming $B(\psi(2S) \to \gamma\chi_{c0}(1P)) = (9.2 \pm 0.4) \times 10^{-2}$, which we rescale to our best (shown rounded) value $B(\psi(2S) \to \gamma\chi_{c0}(1P)) = 10.06 \times 10^{-2}$.

[2] ABLIKIM 11E reports $< 12.9 \times 10^{-6}$ from a measurement of $[\Gamma(\chi_{c0}(1P) \to \gamma\omega)/\Gamma_{total}] \times [B(\psi(2S) \to \gamma\chi_{c0}(1P))]$ assuming $B(\psi(2S) \to \gamma\chi_{c0}(1P)) = (9.62 \pm 0.31) \times 10^{-2}$, which we rescale to our best (shown rounded) value $B(\psi(2S) \to \gamma\chi_{c0}(1P)) = 10.06 \times 10^{-2}$.

$\Gamma(\gamma\phi)/\Gamma_{total}$ — Γ_{110}/Γ

VALUE (units 10^{-6})	CL%	EVTS	DOCUMENT ID		TECN	COMMENT
< 6	90	0.1 ± 1.6	[1] BENNETT	08A	CLEO	$\psi(2S) \to \gamma\gamma\phi$
• • • We do not use the following data for averages, fits, limits, etc. • • •						
<15	90	15 ± 7	[2] ABLIKIM	11E	BES3	$\psi(2S) \to \gamma\gamma\phi$

[1] BENNETT 08A reports $< 6.4 \times 10^{-6}$ from a measurement of $[\Gamma(\chi_{c0}(1P) \to \gamma\phi)/\Gamma_{total}] \times [B(\psi(2S) \to \gamma\chi_{c0}(1P))]$ assuming $B(\psi(2S) \to \gamma\chi_{c0}(1P)) = (9.2 \pm 0.4) \times 10^{-2}$, which we rescale to our best (shown rounded) value $B(\psi(2S) \to \gamma\chi_{c0}(1P)) = 10.06 \times 10^{-2}$.

[2] ABLIKIM 11E reports $< 16.2 \times 10^{-6}$ from a measurement of $[\Gamma(\chi_{c0}(1P) \to \gamma\phi)/\Gamma_{total}] \times [B(\psi(2S) \to \gamma\chi_{c0}(1P))]$ assuming $B(\psi(2S) \to \gamma\chi_{c0}(1P)) = (9.62 \pm 0.31) \times 10^{-2}$, which we rescale to our best (shown rounded) value $B(\psi(2S) \to \gamma\chi_{c0}(1P)) = 10.06 \times 10^{-2}$.

$\Gamma(e^+e^-J/\psi(1S))/\Gamma_{total}$ — Γ_{112}/Γ

VALUE (units 10^{-4})	EVTS	DOCUMENT ID		TECN	COMMENT
• • • We do not use the following data for averages, fits, limits, etc. • • •					
1.50±0.32±0.04	56	[1,2] ABLIKIM	17I	BES3	$\psi(2S) \to \gamma e^+e^- J/\psi$

[1] ABLIKIM 17I reports $(1.51 \pm 0.30 \pm 0.13) \times 10^{-4}$ from a measurement of $[\Gamma(\chi_{c0}(1P) \to e^+e^-J/\psi(1S))/\Gamma_{total}] \times [B(\psi(2S) \to \gamma\chi_{c0}(1P))]$ assuming $B(\psi(2S) \to \gamma\chi_{c0}(1P)) = (9.99 \pm 0.27) \times 10^{-2}$, which we rescale to our best (shown rounded) value $B(\psi(2S) \to \gamma\chi_{c0}(1P)) = (10.06 \pm 0.27) \times 10^{-2}$. Our first error is their experiment's error and our second error is the systematic error from using our best (shown rounded) value.

[2] Not independent from other measurements reported by ABLIKIM 17I

$\Gamma(e^+e^-J/\psi(1S))/\Gamma(\gamma J/\psi(1S))$ — $\Gamma_{112}/\Gamma_{107}$

VALUE (units 10^{-3})	EVTS	DOCUMENT ID		TECN	COMMENT
9.5±1.9±0.7	56	[1] ABLIKIM	17I	BES3	$\psi(2S) \to e^+e^-\gamma J/\psi$

[1] Uses $B(\psi(2S) \to \gamma\chi_{c0}(1P)) \times B(\chi_{c0}(1P) \to \gamma J/\psi(1S)) = (15.8 \pm 0.3 \pm 0.6) \times 10^{-4}$ from ABLIKIM 17N and accounts for common systematic errors.

Int. J. Mod. Phys. A 2026.41. Downloaded from www.worldscientific.com
by UNIVERSITY OF CALIFORNIA @ BERKELEY on 09/16/26. Re-use and distribution is strictly not permitted, except for Open Access articles.

$\Gamma(\mu^+\mu^- J/\psi(1S))/\Gamma(e^+e^- J/\psi(1S))$ — $\Gamma_{113}/\Gamma_{112}$

VALUE	CL%	EVTS	DOCUMENT ID		TECN	COMMENT
<0.14	90	<9.5	ABLIKIM	19Z	BES3	$\psi(2S) \to \gamma\chi_c \to \gamma(\mu^+\mu^- J/\psi)$

$\Gamma(\gamma\gamma)/\Gamma(\gamma J/\psi(1S))$ — $\Gamma_{111}/\Gamma_{107}$

VALUE (units 10^{-2})	DOCUMENT ID		TECN	COMMENT
1.45±0.12 OUR FIT Error includes scale factor of 1.6.				
2.0 ±0.4 OUR AVERAGE				
2.2 $\pm0.4\ ^{+0.1}_{-0.2}$	[1] ANDREOTTI	04	E835	$p\overline{p} \to \chi_{c0} \to \gamma\gamma$
1.45±0.74	[2] AMBROGIANI	00B	E835	$\overline{p}p \to \chi_{c2} \to \gamma\gamma, \gamma J/\psi$

[1] The values of $B(p\overline{p})B(\gamma\gamma)$ and $B(\gamma\gamma)B(\gamma J/\psi)$ measured by ANDREOTTI 04 are not independent. The latter is used in the fit because of smaller systematics.
[2] Calculated by us using $B(J/\psi(1S) \to e^+e^-) = 0.0593 \pm 0.0010$.

$\Gamma(p\overline{p})/\Gamma_{total} \times \Gamma(\gamma J/\psi(1S))/\Gamma_{total}$ — $\Gamma_{62}/\Gamma \times \Gamma_{107}/\Gamma$

VALUE (units 10^{-7})	EVTS	DOCUMENT ID		TECN	COMMENT
31.8±2.3 OUR FIT Error includes scale factor of 1.6.					
28.2±2.1 OUR AVERAGE					
28.0±1.9±1.3	392	[1,2,3] BAGNASCO	02	E835	$\overline{p}p \to \chi_{c0} \to J/\psi\gamma$
$29.3\ ^{+5.7}_{-4.7}\pm1.5$	89	[1,2] AMBROGIANI	99B		$\overline{p}p \to \chi_{c0} \to J/\psi\gamma$

[1] Values in $(\Gamma(p\overline{p}) \times \Gamma(\gamma J/\psi(1S))/\Gamma_{total})$ and $(\Gamma(p\overline{p})/\Gamma_{total} \times \Gamma(\gamma J/\psi(1S))/\Gamma_{total})$ are not independent. The latter is used in the fit since it is less correlated to the total width.
[2] Calculated by us using $B(J/\psi(1S) \to e^+e^-) = 0.0593 \pm 0.0010$.
[3] Recalculated by ANDREOTTI 05A.

$\chi_{c0}(1P)$ CROSS-PARTICLE BRANCHING RATIOS

$\Gamma(\chi_{c0}(1P) \to 2(\pi^+\pi^-))/\Gamma_{total} \times \Gamma(\psi(2S) \to \gamma\chi_{c0}(1P))/\Gamma(\psi(2S) \to J/\psi(1S)\pi^+\pi^-)$ — $\Gamma_1/\Gamma \times \Gamma_{196}^{\psi(2S)}/\Gamma_{12}^{\psi(2S)}$

VALUE (units 10^{-3})	DOCUMENT ID		TECN	COMMENT
6.07±0.25 OUR FIT Error includes scale factor of 1.1.				
6.9 ±2.4 OUR AVERAGE Error includes scale factor of 3.8.				
4.4 ±0.1 ±0.9	[1] BAI	99B	BES	$\psi(2S) \to \gamma\chi_{c0}$
9.3 ±0.9	[2] TANENBAUM	78	MRK1	$\psi(2S) \to \gamma\chi_{c0}$

[1] Calculated by us. The value for $B(\chi_{c0} \to 2\pi^+2\pi^-)$ reported in BAI 99B is derived using $B(\psi(2S) \to \gamma\chi_{c0}) = (9.3 \pm 0.8)\%$ and $B(\psi(2S) \to J/\psi(1S)\pi^+\pi^-) = (32.4 \pm 2.6)\%$ [BAI 98D].
[2] The value $B(\psi(1S) \to \gamma\chi_{c0}) \times B(\chi_{c0} \to 2\pi^+2\pi^-)$ reported in TANENBAUM 78 is derived using $B(\psi(2S) \to J/\psi(1S)\pi^+\pi^-) \times B(J/\psi(1S) \to \ell^+\ell^-) = (4.6 \pm 0.7)\%$. Calculated by us using $B(J/\psi(1S) \to \ell^+\ell^-) = 0.1181 \pm 0.0020$.

$\Gamma(\chi_{c0}(1P) \to 2(\pi^+\pi^-))/\Gamma_{total} \times \Gamma(\psi(2S) \to \gamma\chi_{c0}(1P))/\Gamma_{total}$ — $\Gamma_1/\Gamma \times \Gamma_{196}^{\psi(2S)}/\Gamma^{\psi(2S)}$

VALUE (units 10^{-3})	EVTS	DOCUMENT ID		TECN	COMMENT
2.11 ±0.09 OUR FIT Error includes scale factor of 1.1.					
2.082±0.002±0.089	1946k	[1] ABLIKIM	24BT	BES3	$\psi(2S) \to \gamma\chi_{c0}$

[1] Calculated by us. The value given here is derived from the value of $B(\chi_{c0} \to 2(\pi^+\pi^-))$ reported in ABLIKIM 24BT using $B(\psi(2S) \to \gamma\chi_{c0}) = (9.79 \pm 0.20)\%$ [PDG 22].

$\Gamma(\chi_{c0}(1P) \to \pi^+\pi^- K^+K^-)/\Gamma_{total} \times \Gamma(\psi(2S) \to \gamma\chi_{c0}(1P))/\Gamma_{total}$ — $\Gamma_8/\Gamma \times \Gamma_{196}^{\psi(2S)}/\Gamma^{\psi(2S)}$

VALUE (units 10^{-3})	DOCUMENT ID		TECN	COMMENT
1.74±0.15 OUR FIT Error includes scale factor of 1.1.				
1.64±0.05±0.2	ABLIKIM	05Q	BES2	$\psi(2S) \to \gamma\chi_{c0}$

$\Gamma(\chi_{c0}(1P) \to \pi^+\pi^- K^+K^-)/\Gamma_{total} \times \Gamma(\psi(2S) \to \gamma\chi_{c0}(1P))/\Gamma(\psi(2S) \to J/\psi(1S)\pi^+\pi^-)$ — $\Gamma_8/\Gamma \times \Gamma_{196}^{\psi(2S)}/\Gamma_{12}^{\psi(2S)}$

VALUE (units 10^{-3})	DOCUMENT ID		TECN	COMMENT
5.0 ±0.4 OUR FIT Error includes scale factor of 1.1.				
5.8 ±1.6 OUR AVERAGE Error includes scale factor of 2.3.				
4.22±0.20±0.97	BAI	99B	BES	$\psi(2S) \to \gamma\chi_{c0}$
7.4 ±1.0	[1] TANENBAUM	78	MRK1	$\psi(2S) \to \gamma\chi_{c0}$

[1] The reported value is derived using $B(\psi(2S) \to \pi^+\pi^- J/\psi) \times B(J/\psi \to \ell^+\ell^-) = (4.6 \pm 0.7)\%$. Calculated by us using $B(J/\psi \to \ell^+\ell^-) = 0.1181 \pm 0.0020$.

$\Gamma(\chi_{c0}(1P) \to K^+K^-\pi^+\pi^-\pi^0)/\Gamma_{total} \times \Gamma(\psi(2S) \to \gamma\chi_{c0}(1P))/\Gamma_{total}$ — $\Gamma_{21}/\Gamma \times \Gamma_{196}^{\psi(2S)}/\Gamma^{\psi(2S)}$

VALUE (units 10^{-4})	EVTS	DOCUMENT ID		TECN	COMMENT
8.6 ±0.8 OUR FIT					
8.33±0.13±0.87	9.0k	[1] ABLIKIM	13B	BES3	$e^+e^- \to \psi(2S) \to \gamma\chi_{c0}$

[1] Calculated by us using $B(\psi(2S) \to \chi_{c0}\gamma) = (9.68 \pm 0.10)\%$.

$\Gamma(\chi_{c0}(1P) \to \pi\pi)/\Gamma_{total} \times \Gamma(\psi(2S) \to \gamma\chi_{c0}(1P))/\Gamma_{total}$ — $\Gamma_{32}/\Gamma \times \Gamma_{196}^{\psi(2S)}/\Gamma^{\psi(2S)}$

VALUE (units 10^{-4})	EVTS	DOCUMENT ID		TECN	COMMENT
8.81±0.10 OUR FIT Error includes scale factor of 1.1.					
8.87±0.10 OUR AVERAGE					
8.88±0.03±0.10		[1] ABLIKIM	25CH	BES3	$\psi(2S) \to \gamma\chi_{c0}$
9.11±0.08±0.65	17k	[2] ABLIKIM	10A	BES3	$e^+e^- \to \psi(2S) \to \gamma\chi_{c0}$
8.81±0.11±0.43	8.9k	[3] ASNER	09	CLEO	$\psi(2S) \to \gamma\pi^+\pi^-$
8.13±0.19±0.89	2.8k	[4] ASNER	09	CLEO	$\psi(2S) \to \gamma\pi^0\pi^0$

[1] Calculated by us. ABLIKIM 25CH reports $B(\chi_{c0} \to \pi^+\pi^-) = (6.06 \pm 0.02 \pm 0.07) \times 10^{-3}$ using $B(\psi(2S) \to \gamma\chi_{c0}) = (9.77 \pm 0.23)\%$. We have multiplied the $\pi^+\pi^-$ measurement by 3/2 to obtain $\pi\pi$.
[2] Calculated by us. ABLIKIM 10A reports $B(\chi_{c0} \to \pi^0\pi^0) = (3.23 \pm 0.03 \pm 0.23 \pm 0.14) \times 10^{-3}$ using $B(\psi(2S) \to \gamma\chi_{c0}) = (9.4 \pm 0.4)\%$. We have multiplied the $\pi^0\pi^0$ measurement by 3 to obtain $\pi\pi$.
[3] Calculated by us. ASNER 09 reports $B(\chi_{c0} \to \pi^+\pi^-) = (6.37 \pm 0.08 \pm 0.31 \pm 0.32) \times 10^{-3}$ using $B(\psi(2S) \to \gamma\chi_{c0}) = (9.22 \pm 0.11 \pm 0.46)\%$. We have multiplied the $\pi^+\pi^-$ measurement by 3/2 to obtain $\pi\pi$.
[4] Calculated by us. ASNER 09 reports $B(\chi_{c0} \to \pi^0\pi^0) = (2.94 \pm 0.07 \pm 0.32 \pm 0.15) \times 10^{-3}$ using $B(\psi(2S) \to \gamma\chi_{c0}) = (9.22 \pm 0.11 \pm 0.46)\%$. We have multiplied the $\pi^0\pi^0$ measurement by 3 to obtain $\pi\pi$.

$\Gamma(\chi_{c0}(1P) \to \pi\pi)/\Gamma_{total} \times \Gamma(\psi(2S) \to \gamma\chi_{c0}(1P))/\Gamma(\psi(2S) \to J/\psi(1S)\pi^+\pi^-)$ — $\Gamma_{32}/\Gamma \times \Gamma_{196}^{\psi(2S)}/\Gamma_{12}^{\psi(2S)}$

VALUE (units 10^{-4})	EVTS	DOCUMENT ID		TECN	COMMENT
25.3±0.4 OUR FIT Error includes scale factor of 1.1.					
20.7±1.7 OUR AVERAGE					
23.9±2.7±4.1	97 ± 11	[1] BAI	03C	BES	$\psi(2S) \to \gamma\chi_{c0} \to \gamma\pi^0\pi^0$
20.2±1.1±1.5	720 ± 32	[2] BAI	98I	BES	$\psi(2S) \to \gamma\chi_{c0} \to \gamma\pi^+\pi^-$

[1] We have multiplied $\pi^0\pi^0$ measurement by 3 to obtain $\pi\pi$.
[2] Calculated by us. The value for $B(\chi_{c0} \to \pi^+\pi^-)$ reported in BAI 98I is derived using $B(\psi' \to \gamma\chi_{c0}) = (9.3 \pm 0.8)\%$ and $B(\psi' \to J/\psi\pi^+\pi^-) = (32.4 \pm 2.6)\%$ [BAI 98D]. We have multiplied $\pi^+\pi^-$ measurement by 3/2 to obtain $\pi\pi$.

$\Gamma(\chi_{c0}(1P) \to \eta\eta)/\Gamma_{total} \times \Gamma(\psi(2S) \to \gamma\chi_{c0}(1P))/\Gamma_{total}$ — $\Gamma_{36}/\Gamma \times \Gamma_{196}^{\psi(2S)}/\Gamma^{\psi(2S)}$

VALUE (units 10^{-4})	EVTS	DOCUMENT ID		TECN	COMMENT
2.96±0.21 OUR FIT Error includes scale factor of 1.2.					
3.12±0.19 OUR AVERAGE					
3.23±0.09±0.23	2132	[1] ABLIKIM	10A	BES3	$e^+e^- \to \psi(2S) \to \gamma\chi_{c0}$
2.93±0.12±0.29	0.9k	[2] ASNER	09	CLEO	$\psi(2S) \to \gamma\eta\eta$
• • • We do not use the following data for averages, fits, limits, etc. • • •					
2.86±0.46±0.37	48	[3] ADAMS	07	CLEO	$\psi(2S) \to \gamma\chi_{c0}$

[1] Calculated by us. ABLIKIM 10A reports $B(\chi_{c0} \to \eta\eta) = (3.44 \pm 0.10 \pm 0.24 \pm 0.13) \times 10^{-3}$ using $B(\psi(2S) \to \gamma\chi_{c0}) = (9.4 \pm 0.4)\%$.
[2] Calculated by us. ASNER 09 reports $B(\chi_{c0} \to \eta\eta) = (3.18 \pm 0.13 \pm 0.31 \pm 0.16) \times 10^{-3}$ using $B(\psi(2S) \to \gamma\chi_{c0}) = (9.22 \pm 0.11 \pm 0.46)\%$.
[3] Superseded by ASNER 09. Calculated by us. The value of $B(\chi_{c0}(1P) \to \eta\eta)$ reported by ADAMS 07 was derived using $B(\psi(2S) \to \gamma\chi_{c0}(1P)) = (9.22 \pm 0.11 \pm 0.46)\%$ (ATHAR 04).

$\Gamma(\chi_{c0}(1P) \to \eta\eta)/\Gamma_{total} \times \Gamma(\psi(2S) \to \gamma\chi_{c0}(1P))/\Gamma(\psi(2S) \to J/\psi(1S)\pi^+\pi^-)$ — $\Gamma_{36}/\Gamma \times \Gamma_{196}^{\psi(2S)}/\Gamma_{12}^{\psi(2S)}$

VALUE (units 10^{-3})	DOCUMENT ID		TECN	COMMENT
0.85 ±0.06 OUR FIT Error includes scale factor of 1.2.				
0.578±0.241±0.158	BAI	03C	BES	$\psi(2S) \to \gamma\eta\eta$

$\Gamma(\chi_{c0}(1P) \to K^+K^-)/\Gamma_{total} \times \Gamma(\psi(2S) \to \gamma\chi_{c0}(1P))/\Gamma_{total}$ — $\Gamma_{42}/\Gamma \times \Gamma_{196}^{\psi(2S)}/\Gamma^{\psi(2S)}$

VALUE (units 10^{-4})	EVTS	DOCUMENT ID		TECN	COMMENT
6.19±0.08 OUR FIT					
6.20±0.08 OUR AVERAGE					
6.21±0.02±0.08		[1] ABLIKIM	25CH	BES3	$\psi(2S) \to \gamma\chi_{c0}$
5.97±0.07±0.32	8.1k	[2] ASNER	09	CLEO	$\psi(2S) \to \gamma K^+K^-$

[1] Calculated by us. ABLIKIM 25CH reports $B(\chi_{c0} \to K^+K^-) = (6.36 \pm 0.02 \pm 0.08) \times 10^{-3}$ using $B(\psi(2S) \to \gamma\chi_{c0}) = (9.77 \pm 0.23)\%$.
[2] Calculated by us. ASNER 09 reports $B(\chi_{c0} \to K^+K^-) = (6.47 \pm 0.08 \pm 0.35 \pm 0.32) \times 10^{-3}$ using $B(\psi(2S) \to \gamma\chi_{c0}) = (9.22 \pm 0.11 \pm 0.46)\%$.

$\Gamma(\chi_{c0}(1P) \to K^+K^-)/\Gamma_{total} \times \Gamma(\psi(2S) \to \gamma\chi_{c0}(1P))/\Gamma(\psi(2S) \to J/\psi(1S)\pi^+\pi^-)$ — $\Gamma_{42}/\Gamma \times \Gamma_{196}^{\psi(2S)}/\Gamma_{12}^{\psi(2S)}$

VALUE (units 10^{-3})	EVTS	DOCUMENT ID		TECN	COMMENT
1.779±0.028 OUR FIT					
1.63 ±0.10 ±0.15	774 ± 38	[1] BAI	98I	BES	$\psi(2S) \to \gamma K^+K^-$

[1] Calculated by us. The value for $B(\chi_{c0} \to K^+K^-)$ reported by BAI 98I is derived using $B(\psi(2S) \to \gamma\chi_{c0}) = (9.3 \pm 0.8)\%$ and $B(\psi(2S) \to J/\psi\pi^+\pi^-) = (32.4 \pm 2.6)\%$ [BAI 98D].

$\Gamma(\chi_{c0}(1P) \to K^0_S K^0_S)/\Gamma_{total} \times \Gamma(\psi(2S) \to \gamma\chi_{c0}(1P))/\Gamma_{total}$ — $\Gamma_{43}/\Gamma \times \Gamma_{196}^{\psi(2S)}/\Gamma^{\psi(2S)}$

VALUE (units 10^{-4})	EVTS	DOCUMENT ID		TECN	COMMENT
3.09±0.16 OUR FIT					
3.18±0.17 OUR AVERAGE					
3.22±0.07±0.17	2.1k	[1] ASNER	09	CLEO	$\psi(2S) \to \gamma K^0_S K^0_S$
3.02±0.19±0.33	322	ABLIKIM	05O	BES2	$\psi(2S) \to \gamma K^0_S K^0_S$

[1] Calculated by us. ASNER 09 reports $B(\chi_{c0} \to K^0_S K^0_S) = (3.49 \pm 0.08 \pm 0.18 \pm 0.17) \times 10^{-3}$ using $B(\psi(2S) \to \gamma\chi_{c0}) = (9.22 \pm 0.11 \pm 0.46)\%$.

Int. J. Mod. Phys. A 2026.41. Downloaded from www.worldscientific.com by [redacted]LIFORNIA @ BERKELEY on 09/16/26. Re-use and distribution is strictly not permitted, except for Open Access articles.

$\Gamma(\chi_{c0}(1P) \to K^0_S K^0_S)/\Gamma_{total} \times \Gamma(\psi(2S) \to \gamma\chi_{c0}(1P))/\Gamma(\psi(2S) \to J/\psi(1S)\pi^+\pi^-)$ — $\Gamma_{43}/\Gamma \times \Gamma^{\psi(2S)}_{196}/\Gamma^{\psi(2S)}_{12}$

VALUE (units 10^{-4})		DOCUMENT ID		TECN	COMMENT
8.9±0.5 OUR FIT					
5.6±0.8±1.3		[1] BAI	99B	BES	$\psi(2S) \to \gamma K^0_S K^0_S$

[1] Calculated by us. The value of $B(\chi_{c0} \to K^0_S K^0_S)$ reported by BAI 99B was derived using $B(\psi(2S) \to \gamma\chi_{c0}(1P)) = (9.3 \pm 0.8)\%$ and $B(\psi(2S) \to J/\psi\pi^+\pi^-) = (32.4 \pm 2.6)\%$ [BAI 98D].

$\Gamma(\chi_{c0}(1P) \to 2\pi^+2\pi^-\eta)/\Gamma_{total} \times \Gamma(\psi(2S) \to \gamma\chi_{c0}(1P))/\Gamma_{total}$ — $\Gamma_{45}/\Gamma \times \Gamma^{\psi(2S)}_{196}/\Gamma^{\psi(2S)}$

VALUE (units 10^{-5})	EVTS	DOCUMENT ID		TECN	COMMENT
44.4±0.3±3.7	43k	ABLIKIM	25R	BES3	$e^+e^- \to \psi(2S)$

$\Gamma(\chi_{c0}(1P) \to K^+K^-K^+K^-)/\Gamma_{total} \times \Gamma(\psi(2S) \to \gamma\chi_{c0}(1P))/\Gamma_{total}$ — $\Gamma_{53}/\Gamma \times \Gamma^{\psi(2S)}_{196}/\Gamma^{\psi(2S)}$

VALUE (units 10^{-4})	EVTS	DOCUMENT ID		TECN	COMMENT
2.7 ±0.4 OUR FIT Error includes scale factor of 1.4.					
3.20±0.11±0.41	278	[1] ABLIKIM	06T	BES2	$\psi(2S) \to \gamma 2K^+2K^-$

[1] Calculated by us. The value of $B(\chi_{c0} \to 2K^+2K^-)$ reported by ABLIKIM 06T was derived using $B(\psi(2S) \to \gamma\chi_{c0}(1P)) = (9.2 \pm 0.4)\%$.

$\Gamma(\chi_{c0}(1P) \to K^+K^-K^+K^-)/\Gamma_{total} \times \Gamma(\psi(2S) \to \gamma\chi_{c0}(1P))/\Gamma(\psi(2S) \to J/\psi(1S)\pi^+\pi^-)$ — $\Gamma_{53}/\Gamma \times \Gamma^{\psi(2S)}_{196}/\Gamma^{\psi(2S)}_{12}$

VALUE (units 10^{-4})		DOCUMENT ID		TECN	COMMENT
7.9±1.1 OUR FIT Error includes scale factor of 1.4.					
6.1±0.8±0.9		[1] BAI	99B	BES	$\psi(2S) \to \gamma 2K^+2K^-$

[1] Calculated by us. The value of $B(\chi_{c0} \to 2K^+2K^-)$ reported by BAI 99B was derived using $B(\psi(2S) \to \gamma\chi_{c0}(1P)) = (9.3 \pm 0.8)\%$ and $B(\psi(2S) \to J/\psi\pi^+\pi^-) = (32.4 \pm 2.6)\%$ [BAI 98D].

$\Gamma(\chi_{c0}(1P) \to K^0_S K^0_S K^0_S K^\pm\pi^\mp)/\Gamma_{total} \times \Gamma(\psi(2S) \to \gamma\chi_{c0}(1P))/\Gamma_{total}$ — $\Gamma_{57}/\Gamma \times \Gamma^{\psi(2S)}_{196}/\Gamma^{\psi(2S)}$

VALUE (units 10^{-6})	EVTS	DOCUMENT ID		TECN	COMMENT
7.78±0.49±0.64	343	[1] ABLIKIM	25AY	BES3	$\psi(3686) \to \gamma\chi_{c0}$

[1] ABLIKIM 24AY reports also a measurement $B(\chi_{c0}(1P) \to K^0_S K^0_S K^0_S K^\pm\pi^\mp) = (7.95 \pm 0.50 \pm 0.65) \times 10^{-5}$ from this product branching fraction using PDG 24 $B(\psi(2S) \to \gamma\chi_{c0})$ value.

$\Gamma(\chi_{c0}(1P) \to 3(K^+K^-))/\Gamma_{total} \times \Gamma(\psi(2S) \to \gamma\chi_{c0}(1P))/\Gamma_{total}$ — $\Gamma_{58}/\Gamma \times \Gamma^{\psi(2S)}_{196}/\Gamma^{\psi(2S)}$

VALUE (units 10^{-7})	EVTS	DOCUMENT ID		TECN	COMMENT
10.5±1.8±1.1	37.7 ± 6.2	[1] ABLIKIM	24P	BES3	$e^+e^- \to \psi(2S)$

[1] Systematic error derived by us, based on the text.

$\Gamma(\chi_{c0}(1P) \to \phi\phi)/\Gamma_{total} \times \Gamma(\psi(2S) \to \gamma\chi_{c0}(1P))/\Gamma_{total}$ — $\Gamma_{60}/\Gamma \times \Gamma^{\psi(2S)}_{196}/\Gamma^{\psi(2S)}$

VALUE (units 10^{-4})	EVTS	DOCUMENT ID		TECN	COMMENT
0.838±0.030 OUR FIT					
0.843±0.030 OUR AVERAGE					
0.84 ±0.03 ±0.01	2701	[1] ABLIKIM	23N	BES3	$\psi(2S) \to \gamma 2K^+2K^-$
0.88 ±0.07 ±0.1	179	[2,3] ABLIKIM	11K	BES3	$\psi(2S) \to \gamma K^+K^-\pi^+\pi^-\pi^0$
0.86 ±0.19 ±0.12	26	[4] ABLIKIM	06T	BES2	$\psi(2S) \to \gamma 2K^+2K^-$
• • • We do not use the following data for averages, fits, limits, etc. • • •					
0.75 ±0.04 ±0.07	433	[2,5,6] ABLIKIM	11K	BES3	$\psi(2S) \to \gamma 2(K^+K^-)$

[1] Calculated by us. The value of $B(\chi_{c0} \to \phi\phi)$ reported by ABLIKIM 23N was derived using $B(\psi(2S) \to \gamma\chi_{c0}(1P)) = (9.79 \pm 0.20)\%$.
[2] Calculated by us. The value of $B(\chi_{c0} \to \phi\phi)$ reported by ABLIKIM 11K was derived using $B(\psi(2S) \to \gamma\chi_{c0}(1P)) = (9.62 \pm 0.31)\%$.
[3] Using $\phi\phi \to K^+K^-\pi^+\pi^-\pi^0$.
[4] Calculated by us. The value of $B(\chi_{c0} \to \phi\phi)$ reported by ABLIKIM 06T was derived using $B(\psi(2S) \to \gamma\chi_{c0}(1P)) = (9.2 \pm 0.4)\%$.
[5] Using $\phi\phi \to 2(K^+K^-)$.
[6] Superseded by ABLIKIM 23N.

$\Gamma(\chi_{c0}(1P) \to \phi\phi)/\Gamma_{total} \times \Gamma(\psi(2S) \to \gamma\chi_{c0}(1P))/\Gamma(\psi(2S) \to J/\psi(1S)\pi^+\pi^-)$ — $\Gamma_{60}/\Gamma \times \Gamma^{\psi(2S)}_{196}/\Gamma^{\psi(2S)}_{12}$

VALUE (units 10^{-4})		DOCUMENT ID		TECN	COMMENT
2.41±0.09 OUR FIT					
2.6 ±1.0 ±1.1		[1] BAI	99B	BES	$\psi(2S) \to \gamma 2K^+2K^-$

[1] Calculated by us. The value of $B(\chi_{c0} \to \phi\phi)$ reported by BAI 99B was derived using $B(\psi(2S) \to \gamma\chi_{c0}(1P)) = (9.3 \pm 0.8)\%$ and $B(\psi(2S) \to J/\psi\pi^+\pi^-) = (32.4 \pm 2.6)\%$ [BAI 98D].

$\Gamma(\chi_{c0}(1P) \to p\overline{p})/\Gamma_{total} \times \Gamma(\psi(2S) \to \gamma\chi_{c0}(1P))/\Gamma_{total}$ — $\Gamma_{62}/\Gamma \times \Gamma^{\psi(2S)}_{196}/\Gamma^{\psi(2S)}$

VALUE (units 10^{-6})	EVTS	DOCUMENT ID		TECN	COMMENT
23.6±1.1 OUR FIT Error includes scale factor of 1.9.					
24.5±0.6 OUR AVERAGE					
24.6±0.2±0.6	31268	[1] ABLIKIM	25H	BES3	$\psi(2S) \to \gamma p\overline{p}$
23.7±1.4±1.4	383 ± 22	[2] NAIK	08	CLEO	$\psi(2S) \to \gamma p\overline{p}$
$23.6^{+3.7}_{-3.4} \pm 3.4$	89.5^{+14}_{-13}	BAI	04F	BES	$\psi(2S) \to \gamma\chi_{c0}(1P) \to \gamma\overline{p}p$
• • • We do not use the following data for averages, fits, limits, etc. • • •					
23.7±0.8±0.9	1222	[3] ABLIKIM	13V	BES3	$\psi(2S) \to \gamma p\overline{p}$

[1] Calculated by us. ABLIKIM 25H reports $B(\chi_{c0} \to p\overline{p}) = (2.51 \pm 0.02 \pm 0.08) \times 10^{-4}$ using $B(\psi(2S) \to \gamma\chi_{c0}) = (9.79 \pm 0.20)\%$.
[2] Calculated by us. NAIK 08 reports $B(\chi_{c0} \to p\overline{p}) = (25.7 \pm 1.5 \pm 1.5 \pm 1.3) \times 10^{-5}$ using $B(\psi(2S) \to \gamma\chi_{c0}) = (9.22 \pm 0.11 \pm 0.46)\%$.
[3] Superseded by ABLIKIM 25H

$\Gamma(\chi_{c0}(1P) \to p\overline{p})/\Gamma_{total} \times \Gamma(\psi(2S) \to \gamma\chi_{c0}(1P))/\Gamma(\psi(2S) \to J/\psi(1S)\pi^+\pi^-)$ — $\Gamma_{62}/\Gamma \times \Gamma^{\psi(2S)}_{196}/\Gamma^{\psi(2S)}_{12}$

VALUE (units 10^{-5})		DOCUMENT ID		TECN	COMMENT
6.79±0.32 OUR FIT Error includes scale factor of 1.9.					
4.6 ±1.9		[1] BAI	98I	BES	$\psi(2S) \to \gamma\chi_{c0} \to \gamma\overline{p}p$

[1] Calculated by us. The value for $B(\chi_{c0} \to p\overline{p})$ reported in BAI 98I is derived using $B(\psi(2S) \to \gamma\chi_{c0}) = (9.3 \pm 0.8)\%$ and $B(\psi(2S) \to J/\psi(1S)\pi^+\pi^-) = (32.4 \pm 2.6)\%$ [BAI 98D].

$\Gamma(\chi_{c0}(1P) \to p\overline{p}K^0_S K^-\pi^+ + c.c.)/\Gamma_{total} \times \Gamma(\psi(2S) \to \gamma\chi_{c0}(1P))/\Gamma_{total}$ — $\Gamma_{76}/\Gamma \times \Gamma^{\psi(2S)}_{196}/\Gamma^{\psi(2S)}$

VALUE (units 10^{-6})	EVTS	DOCUMENT ID		TECN	COMMENT
2.55±0.26±0.31	173	ABLIKIM	24BX	BES3	$\psi(2S) \to \gamma\chi_{c0}$

$\Gamma(\chi_{c0}(1P) \to \Lambda\overline{\Lambda})/\Gamma_{total} \times \Gamma(\psi(2S) \to \gamma\chi_{c0}(1P))/\Gamma_{total}$ — $\Gamma_{81}/\Gamma \times \Gamma^{\psi(2S)}_{196}/\Gamma^{\psi(2S)}$

VALUE (units 10^{-6})	EVTS	DOCUMENT ID		TECN	COMMENT
35.2±1.3 OUR FIT					
35.1±1.4 OUR AVERAGE Error includes scale factor of 1.1.					
35.6±1.0±1.0	1486	ABLIKIM	21L	BES3	$\psi(2S) \to \gamma p\pi^-\overline{p}\pi^+$
31.2±3.3±2.0	131	[1] NAIK	08	CLEO	$\psi(2S) \to \gamma\Lambda\overline{\Lambda}$
• • • We do not use the following data for averages, fits, limits, etc. • • •					
32.0±1.9±2.2	369	[2,3] ABLIKIM	13H	BES3	$\psi(2S) \to \gamma\Lambda\overline{\Lambda}$

[1] Calculated by us. NAIK 08 reports $B(\chi_{c0} \to \Lambda\overline{\Lambda}) = (33.8 \pm 3.6 \pm 2.2 \pm 1.7) \times 10^{-5}$ using $B(\psi(2S) \to \gamma\chi_{c0}) = (9.22 \pm 0.11 \pm 0.46)\%$.
[2] Superseded by ABLIKIM 21L
[3] Calculated by us. ABLIKIM 13H reports $B(\chi_{c0} \to \Lambda\overline{\Lambda}) = (33.3 \pm 2.0 \pm 2.6) \times 10^{-5}$ from a measurement of $B(\chi_{c0} \to \Lambda\overline{\Lambda}) \times B(\psi(2S) \to \gamma\chi_{c0})$ assuming $B(\psi(2S) \to \gamma\chi_{c0}) = (9.62 \pm 0.31)\%$.

$\Gamma(\chi_{c0}(1P) \to \Lambda\overline{\Lambda})/\Gamma_{total} \times \Gamma(\psi(2S) \to \gamma\chi_{c0}(1P))/\Gamma(\psi(2S) \to J/\psi(1S)\pi^+\pi^-)$ — $\Gamma_{81}/\Gamma \times \Gamma^{\psi(2S)}_{196}/\Gamma^{\psi(2S)}_{12}$

VALUE (units 10^{-5})	EVTS	DOCUMENT ID		TECN	COMMENT
10.1±0.4 OUR FIT					
$\mathbf{13.0^{+3.6}_{-3.5} \pm 2.5}$	$15.2^{+4.2}_{-4.0}$	[1] BAI	03E	BES	$\psi(2S) \to \gamma\Lambda\overline{\Lambda}$

[1] BAI 03E reports $[B(\chi_{c0} \to \Lambda\overline{\Lambda})\, B(\psi(2S) \to \gamma\chi_{c0}) / B(\psi(2S) \to J/\psi\pi^+\pi^-)] \times [B^2(\Lambda \to \pi^-p) / B(J/\psi \to p\overline{p})] = (2.45^{+0.68}_{-0.65} \pm 0.46)\%$. We calculate from this measurement the presented value using $B(\Lambda \to \pi^-p) = (63.9 \pm 0.5)\%$ and $B(J/\psi \to p\overline{p}) = (2.17 \pm 0.07) \times 10^{-3}$.

$\Gamma(\chi_{c0}(1P) \to \Lambda\overline{\Lambda}\eta)/\Gamma_{total} \times \Gamma(\psi(2S) \to \gamma\chi_{c0}(1P))/\Gamma_{total}$ — $\Gamma_{86}/\Gamma \times \Gamma^{\psi(2S)}_{196}/\Gamma^{\psi(2S)}$

VALUE (units 10^{-5})	EVTS	DOCUMENT ID		TECN	COMMENT
2.26±0.30±0.20	67	ABLIKIM	22AO	BES3	$\psi(2S) \to \gamma p\pi^-\overline{p}\pi^+\gamma\gamma$

$\Gamma(\chi_{c0}(1P) \to \Lambda\overline{\Lambda}\eta')/\Gamma_{total} \times \Gamma(\psi(2S) \to \gamma\chi_{c0}(1P))/\Gamma_{total}$ — $\Gamma_{87}/\Gamma \times \Gamma^{\psi(2S)}_{196}/\Gamma^{\psi(2S)}$

VALUE (units 10^{-6})	DOCUMENT ID		TECN	COMMENT
7.39±1.39±0.86	[1] ABLIKIM	25BX	BES3	$\psi(2S) \to \gamma\chi_{c0}$

[1] Calculated by us. ABLIKIM 25BX reports $B(\chi_{c0} \to \Lambda\overline{\Lambda}\eta') = (7.56 \pm 1.42 \pm 0.90) \times 10^{-5}$ from a measurement of $B(\chi_{c0} \to \Lambda\overline{\Lambda}\eta') \times B(\psi(2S) \to \gamma\chi_{c0})$ assuming $B(\psi(2S) \to \gamma\chi_{c0}) = (9.77 \pm 0.23)\%$.

$\Gamma(\chi_{c0}(1P) \to \Lambda\overline{\Lambda}\omega)/\Gamma_{total} \times \Gamma(\psi(2S) \to \gamma\chi_{c0}(1P))/\Gamma_{total}$ — $\Gamma_{88}/\Gamma \times \Gamma^{\psi(2S)}_{196}/\Gamma^{\psi(2S)}$

VALUE (units 10^{-6})	EVTS	DOCUMENT ID		TECN	COMMENT
23.2±2.2±2.4	316 ± 30	[1] ABLIKIM	24BE	BES3	$e^+e^- \to \psi(2S) \to \gamma\chi_{c0}$

[1] Calculated by us. The authors report $B(\chi_{c0} \to \Lambda\overline{\Lambda}\omega)$ obtained from a product using PDG 22 value of $B(\psi(2S) \to \gamma\chi_{c0})$.

Int. J. Mod. Phys. A 2026.41. Downloaded from www.worldscientific.com
by UNIVERSITY OF CALIFORNIA @ BERKELEY on 09/16/26. Re-use and distribution is strictly not permitted, except for Open Access articles.

$\Gamma(\chi_{c0}(1P) \to \Lambda\overline{\Lambda}\phi)/\Gamma_{total} \times \Gamma(\psi(2S) \to \gamma\chi_{c0}(1P))/\Gamma_{total}$ $\Gamma_{89}/\Gamma \times \Gamma_{196}^{\psi(2S)}/\Gamma^{\psi(2S)}$

VALUE (units 10^{-6})	EVTS	DOCUMENT ID		TECN	COMMENT
2.92±1.22±0.19	7.2	ABLIKIM	24AC	BES3	$\psi(2S) \to \gamma\chi_{c0}$

$\Gamma(\chi_{c0}(1P) \to \overline{p}\Lambda(1520)K^0_S\pi^+ + \text{c.c.})/\Gamma_{total} \times \Gamma(\psi(2S) \to \gamma\chi_{c0}(1P))/\Gamma_{total}$ $\Gamma_{93}/\Gamma \times \Gamma_{196}^{\psi(2S)}/\Gamma^{\psi(2S)}$

VALUE (units 10^{-6})	EVTS	DOCUMENT ID		TECN	COMMENT
$1.57^{+0.66}_{-0.62}\pm0.22$	27	ABLIKIM	24BX	BES3	$\psi(2S) \to \gamma\chi_{c0}$

$\Gamma(\chi_{c0}(1P) \to \Sigma^+\overline{p}K^0_S + \text{c.c.})/\Gamma_{total} \times \Gamma(\psi(2S) \to \gamma\chi_{c0}(1P))/\Gamma_{total}$ $\Gamma_{95}/\Gamma \times \Gamma_{196}^{\psi(2S)}/\Gamma^{\psi(2S)}$

VALUE (units 10^{-5})	EVTS	DOCUMENT ID		TECN	COMMENT
3.45±0.17±0.19	493	[1] ABLIKIM	19BB	BES3	$\psi(2S) \to \gamma\Sigma^+\overline{p}K^0_S$ + c.c.

[1] Calculated by us. ABLIKIM 19BB reports $B(\chi_c^0 \to \Sigma^+\overline{p}K^0_S + \text{c.c.}) = (3.52 \pm 0.19 \pm 0.21) \times 10^{-4}$ using $B(\psi(2S) \to \gamma\chi_c^0) = (9.79 \pm 0.20)\%$ and other branching fractions from PDG 18.

$\Gamma(\chi_{c0}(1P) \to \Sigma^0\overline{p}K^+ + \text{c.c.})/\Gamma_{total} \times \Gamma(\psi(2S) \to \gamma\chi_{c0}(1P))/\Gamma_{total}$ $\Gamma_{96}/\Gamma \times \Gamma_{196}^{\psi(2S)}/\Gamma^{\psi(2S)}$

VALUE (units 10^{-5})	EVTS	DOCUMENT ID		TECN	COMMENT
2.97±0.12±0.14	871	[1] ABLIKIM	20AE	BES3	$\psi(2S) \to \gamma\Sigma^0\overline{p}K^+$ + c.c.

[1] Calculated by us. ABLIKIM 20AE reports $B(\chi_c^0 \to \Sigma^0\overline{p}K^+ + \text{c.c.}) = (3.03 \pm 0.12 \pm 0.15) \times 10^{-4}$ using $B(\psi(2S) \to \gamma\chi_c^0) = (9.79 \pm 0.20)\%$ and other branching fractions from PDG 20.

$\Gamma(\chi_{c0}(1P) \to \gamma J/\psi(1S))/\Gamma_{total} \times \Gamma(\psi(2S) \to \gamma\chi_{c0}(1P))/\Gamma_{total}$ $\Gamma_{107}/\Gamma \times \Gamma_{196}^{\psi(2S)}/\Gamma^{\psi(2S)}$

VALUE (units 10^{-2})	EVTS	DOCUMENT ID		TECN	COMMENT
0.136±0.009 OUR FIT	Error includes scale factor of 1.8.				
0.147±0.029 OUR AVERAGE	Error includes scale factor of 4.6.				
0.158±0.003±0.006	4.8k	[1] ABLIKIM	17N	BES3	$\psi(2S) \to \gamma\gamma J/\psi$
0.024±0.015±0.205	12k	ABLIKIM	17U	BES3	$e^+e^- \to \gamma X$
0.069±0.018		[2] OREGLIA	82	CBAL	$\psi(2S) \to \gamma\chi_{c0}$
0.4 ±0.3		[3] BRANDELIK	79B	DASP	$\psi(2S) \to \gamma\chi_{c0}$
0.16 ±0.11		[3] BARTEL	78B	CNTR	$\psi(2S) \to \gamma\chi_{c0}$
3.3 ±1.7		[4] BIDDICK	77	CNTR	$e^+e^- \to \gamma X$
• • • We do not use the following data for averages, fits, limits, etc. • • •					
0.151±0.003±0.010	4.3k	[5] ABLIKIM	12O	BES3	$\psi(2S) \to \gamma\chi_{c0}$
0.125±0.007±0.013	560	[6] MENDEZ	08	CLEO	$\psi(2S) \to \gamma\chi_{c0}$
0.18 ±0.01 ±0.02	172	[7] ADAM	05A	CLEO	$\psi(2S) \to \gamma\chi_{c0}$

[1] Uses $B(J/\psi \to e^+e^-) = (5.971 \pm 0.032)\%$ and $B(J/\psi \to \mu^+\mu^-) = (5.961 \pm 0.033)\%$.
[2] Recalculated by us using $B(J/\psi(1S) \to \ell^+\ell^-) = 0.1181 \pm 0.0020$.
[3] Recalculated by us using $B(J/\psi(1S) \to \mu^+\mu^-) = 0.0588 \pm 0.0010$.
[4] Assumes isotropic gamma distribution.
[5] Superseded by ABLIKIM 17N.
[6] Not used since the same experimental measurement has been used in another related quantity included elsewhere in the fit.
[7] Superseded by MENDEZ 08.

$\Gamma(\chi_{c0}(1P) \to \gamma J/\psi(1S))/\Gamma_{total} \times \Gamma(\psi(2S) \to \gamma\chi_{c0}(1P))/\Gamma(\psi(2S) \to J/\psi(1S)\pi^+\pi^-)$ $\Gamma_{107}/\Gamma \times \Gamma_{196}^{\psi(2S)}/\Gamma_{12}^{\psi(2S)}$

VALUE (units 10^{-2})	EVTS	DOCUMENT ID		TECN	COMMENT
0.392±0.026 OUR FIT	Error includes scale factor of 1.7.				
0.358±0.020±0.037	560	MENDEZ	08	CLEO	$\psi(2S) \to \gamma\chi_{c0}$
• • • We do not use the following data for averages, fits, limits, etc. • • •					
0.55 ±0.04 ±0.06	172	[1] ADAM	05A	CLEO	$\psi(2S) \to \gamma\chi_{c0}$

[1] Superseded by MENDEZ 08.

$\Gamma(\chi_{c0}(1P) \to \gamma\gamma)/\Gamma_{total} \times \Gamma(\psi(2S) \to \gamma\chi_{c0}(1P))/\Gamma_{total}$ $\Gamma_{111}/\Gamma \times \Gamma_{196}^{\psi(2S)}/\Gamma^{\psi(2S)}$

VALUE (units 10^{-5})	EVTS	DOCUMENT ID		TECN	COMMENT
1.97±0.08 OUR FIT	Error includes scale factor of 1.1.				
1.95±0.09 OUR AVERAGE					
1.93±0.08±0.05	3.5k	ABLIKIM	17AE	BES3	$\psi(2S) \to \gamma\chi_{c0} \to 3\gamma$
2.17±0.32±0.10	0.2k	ECKLUND	08A	CLEO	$\psi(2S) \to \gamma\chi_{c0} \to 3\gamma$
3.7 ±1.8 ±1.0		LEE	85	CBAL	$\psi(2S) \to \gamma\chi_{c0}$
• • • We do not use the following data for averages, fits, limits, etc. • • •					
2.17±0.17±0.12	0.8k	[1] ABLIKIM	12A	BES3	$\psi(2S) \to \gamma\chi_{c0} \to 3\gamma$

[1] Superseded by ABLIKIM 17AE.

$\chi_{c0}(1P)$ REFERENCES

ABLIKIM	25AY	PR D112 012007	M. Ablikim et al.	(BESIII Collab.)
ABLIKIM	25BX	PR D112 112015	M. Ablikim et al.	(BESIII Collab.)
ABLIKIM	25CE	JHEP 2510 090	M. Ablikim et al.	(BESIII Collab.)
ABLIKIM	25CH	CP C49 091001	M. Ablikim et al.	(BESIII Collab.)
ABLIKIM	25CJ	CP C49 123001	M. Ablikim et al.	(BESIII Collab.)
ABLIKIM	25H	PR D111 012003	M. Ablikim et al.	(BESIII Collab.)
ABLIKIM	25K	PR D111 032001	M. Ablikim et al.	(BESIII Collab.)
ABLIKIM	25L	PR D111 032008	M. Ablikim et al.	(BESIII Collab.)
ABLIKIM	25R	PR D111 052013	M. Ablikim et al.	(BESIII Collab.)
ABLIKIM	25V	PR D111 072001	M. Ablikim et al.	(BESIII Collab.)
ABLIKIM	24AC	PR D110 032016	M. Ablikim et al.	(BESIII Collab.)
ABLIKIM	24AY	PR D109 L071103	M. Ablikim et al.	(BESIII Collab.)
ABLIKIM	24BE	PR D110 032022	M. Ablikim et al.	(BESIII Collab.)
ABLIKIM	24BT	PR D110 072009	M. Ablikim et al.	(BESIII Collab.)
ABLIKIM	24BX	PR D110 112009	M. Ablikim et al.	(BESIII Collab.)
ABLIKIM	24CA	PR D110 112013	M. Ablikim et al.	(BESIII Collab.)
ABLIKIM	24P	PR D109 072016	M. Ablikim et al.	(BESIII Collab.)
PDG	24	PR D110 030001	S. Navas et al.	(PDG Collab.)
ABLIKIM	23N	JHEP 2305 069	M. Ablikim et al.	(BESIII Collab.)
ABLIKIM	23T	PR D107 092004	M. Ablikim et al.	(BESIII Collab.)
ABLIKIM	22AO	PR D106 072004	M. Ablikim et al.	(BESIII Collab.)
ABLIKIM	22O	JHEP 2206 074	M. Ablikim et al.	(BESIII Collab.)
ABLIKIM	22Q	PR D106 032014	M. Ablikim et al.	(BESIII Collab.)
PDG	22	PTEP 2022 083C01	R.L. Workman et al.	(PDG Collab.)
ABLIKIM	21AV	JHEP 2111 217	M. Ablikim et al.	(BESIII Collab.)
ABLIKIM	21L	PR D103 112004	M. Ablikim et al.	(BESIII Collab.)
ABLIKIM	20AE	PR D102 092006	M. Ablikim et al.	(BESIII Collab.)
ABLIKIM	20B	PR D101 012012	M. Ablikim et al.	(BESIII Collab.)
ABLIKIM	20I	PR D101 092002	M. Ablikim et al.	(BESIII Collab.)
PDG	20	PTEP 2020 083C01	P.A. Zyla et al.	(PDG Collab.)
ABLIKIM	19AA	PR D99 052008	M. Ablikim et al.	(BESIII Collab.)
ABLIKIM	19AU	PR D100 052010	M. Ablikim et al.	(BESIII Collab.)
ABLIKIM	19BB	PR D100 092006	M. Ablikim et al.	(BESIII Collab.)
ABLIKIM	19J	PR D99 012015	M. Ablikim et al.	(BESIII Collab.)
ABLIKIM	19Z	PR D99 051101	M. Ablikim et al.	(BESIII Collab.)
ABLIKIM	18V	PR D97 052011	M. Ablikim et al.	(BESIII Collab.)
PDG	18	PR D98 030001	M. Tanabashi et al.	(PDG Collab.)
AAIJ	17BB	EPJ C77 609	R. Aaij et al.	(LHCb Collab.)
ABLIKIM	17AE	PR D96 092007	M. Ablikim et al.	(BESIII Collab.)
ABLIKIM	17AI	PR D96 112006	M. Ablikim et al.	(BESIII Collab.)
ABLIKIM	17I	PRL 118 221802	M. Ablikim et al.	(BESIII Collab.)
ABLIKIM	17N	PR D95 072004	M. Ablikim et al.	(BESIII Collab.)
ABLIKIM	17U	PR D96 032001	M. Ablikim et al.	(BESIII Collab.)
PDG	16	CP C40 100001	C. Patrignani et al.	(PDG Collab.)
ABLIKIM	15I	PR D91 092006	M. Ablikim et al.	(BESIII Collab.)
ABLIKIM	15M	PR D91 112008	M. Ablikim et al.	(BESIII Collab.)
ABLIKIM	15N	PR D91 112018	M. Ablikim et al.	(BESIII Collab.)
ABLIKIM	13B	PR D87 012002	M. Ablikim et al.	(BESIII Collab.)
ABLIKIM	13D	PR D87 012007	M. Ablikim et al.	(BESIII Collab.)
ABLIKIM	13H	PR D87 032007	M. Ablikim et al.	(BESIII Collab.)
ABLIKIM	13V	PR D88 112001	M. Ablikim et al.	(BESIII Collab.)
UEHARA	13	PTEP 2013 123C01	S. Uehara et al.	(BELLE Collab.)
ABLIKIM	12A	PR D85 112008	M. Ablikim et al.	(BESIII Collab.)
ABLIKIM	12I	PR D86 052004	M. Ablikim et al.	(BESIII Collab.)
ABLIKIM	12J	PR D86 052011	M. Ablikim et al.	(BESIII Collab.)
ABLIKIM	12O	PRL 109 172002	M. Ablikim et al.	(BESIII Collab.)
LIU	12B	PRL 108 232001	Z.Q. Liu et al.	(BELLE Collab.)
ABLIKIM	11A	PR D83 012006	M. Ablikim et al.	(BESIII Collab.)
ABLIKIM	11E	PR D83 112005	M. Ablikim et al.	(BESIII Collab.)
ABLIKIM	11F	PR D83 112009	M. Ablikim et al.	(BESIII Collab.)
ABLIKIM	11K	PRL 107 092001	M. Ablikim et al.	(BESIII Collab.)
DEL-AMO-SA...	11M	PR D84 012004	P. del Amo Sanchez et al.	(BABAR Collab.)
ABLIKIM	10A	PR D81 052005	M. Ablikim et al.	(BESIII Collab.)
ONYISI	10	PR D82 011103	P.U.E. Onyisi et al.	(CLEO Collab.)
UEHARA	10A	PR D82 114031	S. Uehara et al.	(BELLE Collab.)
ASNER	09	PR D79 072007	D.M. Asner et al.	(CLEO Collab.)
UEHARA	09	PR D79 052009	S. Uehara et al.	(BELLE Collab.)
BENNETT	08A	PRL 101 151801	J.V. Bennett et al.	(CLEO Collab.)
ECKLUND	08A	PR D78 091501	K.M. Ecklund et al.	(CLEO Collab.)
HE	08B	PR D78 092004	Q. He et al.	(CLEO Collab.)
MENDEZ	08	PR D78 011102	H. Mendez et al.	(CLEO Collab.)
NAIK	08	PR D78 031101	P. Naik et al.	(CLEO Collab.)
UEHARA	08	EPJ C53 1	S. Uehara et al.	(BELLE Collab.)
ABE	07	PRL 98 082001	K. Abe et al.	(BELLE Collab.)
ADAMS	07	PR D75 071101	G.S. Adams et al.	(CLEO Collab.)
ATHAR	07	PR D75 032002	S.B. Athar et al.	(CLEO Collab.)
CHEN	07B	PL B651 15	W.T. Chen et al.	(BELLE Collab.)
ABLIKIM	06D	PR D73 052006	M. Ablikim et al.	(BES Collab.)
ABLIKIM	06I	PR D74 012004	M. Ablikim et al.	(BES Collab.)
ABLIKIM	06R	PR D74 072001	M. Ablikim et al.	(BES Collab.)
ABLIKIM	06T	PL B642 197	M. Ablikim et al.	(BES Collab.)
ABLIKIM	05G	PR D71 092002	M. Ablikim et al.	(BES Collab.)
ABLIKIM	05N	PL B630 7	M. Ablikim et al.	(BES Collab.)
ABLIKIM	05O	PL B630 21	M. Ablikim et al.	(BES Collab.)
ABLIKIM	05Q	PR D72 092002	M. Ablikim et al.	(BES Collab.)
ADAM	05A	PRL 94 232002	N.E. Adam et al.	(CLEO Collab.)
ANDREOTTI	05A	NP B717 34	M. Andreotti et al.	(FNAL E835 Collab.)
ANDREOTTI	05C	PR D72 112002	M. Andreotti et al.	(FNAL E835 Collab.)
NAKAZAWA	05	PL B615 39	H. Nakazawa et al.	(BELLE Collab.)
ABE	04G	PR D70 071102	K. Abe et al.	(BELLE Collab.)
ABLIKIM	04G	PR D70 092002	M. Ablikim et al.	(BES Collab.)
ABLIKIM	04H	PR D70 092003	M. Ablikim et al.	(BES Collab.)
ANDREOTTI	04	PL B584 16	M. Andreotti et al.	(E835 Collab.)
ATHAR	04	PR D70 112002	S.B. Athar et al.	(CLEO Collab.)
BAI	04F	PR D69 092001	J.Z. Bai et al.	(BES Collab.)
ANDREOTTI	03	PRL 91 091801	M. Andreotti et al.	(FNAL E835 Collab.)
AULCHENKO	03	PL B573 63	V.M. Aulchenko et al.	(KEDR Collab.)
BAI	03C	PR D67 032004	J.Z. Bai et al.	(BES Collab.)
BAI	03E	PR D67 112001	J.Z. Bai et al.	(BES Collab.)
ABE,K	02	PRL 89 142001	K. Abe et al.	(BELLE Collab.)
BAGNASCO	02	PL B533 237	S. Bagnasco et al.	(FNAL E835 Collab.)
EISENSTEIN	01	PRL 87 061801	B.I. Eisenstein et al.	(CLEO Collab.)
AMBROGIANI	00B	PR D62 052002	M. Ambrogiani et al.	(FNAL E835 Collab.)
AMBROGIANI	99B	PRL 83 2902	M. Ambrogiani et al.	(FNAL E835 Collab.)
BAI	99B	PR D60 072001	J.Z. Bai et al.	(BES Collab.)
BAI	98D	PR D58 092006	J.Z. Bai et al.	(BES Collab.)
BAI	98I	PRL 81 3091	J.Z. Bai et al.	(BES Collab.)
GAISER	86	PR D34 711	J. Gaiser et al.	(Crystal Ball Collab.)
LEE	85	SLAC 282	R.A. Lee	(SLAC)
OREGLIA	82	PR D25 2259	M.J. Oreglia et al.	(SLAC, CIT, HARV+)
BRANDELIK	79B	NP B160 426	R. Brandelik et al.	(DASP Collab.)
BARTEL	78B	PL 79B 492	W. Bartel et al.	(DESY, HEIDP)
TANENBAUM	78	PR D17 1731	W.M. Tanenbaum et al.	(SLAC, LBL)
Also		Private Comm.	G. Trilling	(LBL, UCB)
BIDDICK	77	PRL 38 1324	C.J. Biddick et al.	(UCSD, UMD, PAVI+)

Int. J. Mod. Phys. A 2026.41. Downloaded from www.worldscientific.com
by [redacted]LIFORNIA @ BERKELEY on 09/16/26. Re-use and distribution is strictly not permitted, except for Open Access articles.

$\chi_{c1}(1P)$

$I^G(J^{PC}) = 0^+(1^{++})$

See the Review on "Branching Ratios of $\psi(2S)$, $\chi_{c0,1,2}$ and $\eta_c(1S)$" before the $\chi_{c0}(1P)$ Listings.

$\chi_{c1}(1P)$ MASS

VALUE (MeV)	EVTS	DOCUMENT ID		TECN	COMMENT
3510.67 ± 0.05 OUR AVERAGE		Error includes scale factor of 1.2.			
3509.84 ± 0.69 ± 0.64	2.8k	AAIJ	23AH	LHCB	$B^+ \to K^+(K^0_S K\pi)$
3508.4 ± 1.9 ± 0.7	460	[1] AAIJ	17BB	LHCB	$pp \to b\overline{b}X \to 2(K^+K^-)X$
3510.71 ± 0.04 ± 0.09	4.8k	[2] AAIJ	17BI	LHCB	$\chi_{c1} \to J/\psi\mu^+\mu^-$
3510.30 ± 0.14 ± 0.16		ABLIKIM	05G	BES2	$\psi(2S) \to \gamma\chi_{c1}$
3510.719 ± 0.051 ± 0.019		ANDREOTTI	05A	E835	$p\overline{p} \to e^+e^-\gamma$
3509.4 ± 0.9		BAI	99B	BES	$\psi(2S) \to \gamma X$
3510.60 ± 0.087 ± 0.019	513	[3] ARMSTRONG	92	E760	$\overline{p}p \to e^+e^-\gamma$
3511.3 ± 0.4 ± 0.4	30	BAGLIN	86B	SPEC	$\overline{p}p \to e^+e^-X$
3512.3 ± 0.3 ± 4.0		[4] GAISER	86	CBAL	$\psi(2S) \to \gamma X$
3507.4 ± 1.7	91	[5] LEMOIGNE	82	GOLI	185 π^-Be $\to \gamma\mu^+\mu^-$A
3510.4 ± 0.6		OREGLIA	82	CBAL	$e^+e^- \to J/\psi 2\gamma$
3510.1 ± 1.1	254	[6] HIMEL	80	MRK2	$e^+e^- \to J/\psi 2\gamma$
3509 ± 11	21	BRANDELIK	79B	DASP	$e^+e^- \to J/\psi 2\gamma$
3507 ± 3		[6] BARTEL	78B	CNTR	$e^+e^- \to J/\psi 2\gamma$
3505.0 ± 4 ± 4		[6,7] TANENBAUM	78	MRK1	e^+e^-
3513 ± 7	367	[6] BIDDICK	77	CNTR	$\psi(2S) \to \gamma X$
• • • We do not use the following data for averages, fits, limits, etc. • • •					
3500 ± 10	40	TANENBAUM	75	MRK1	Hadrons γ

[1] From a fit of the $\phi\phi$ invariant mass with the width of $\chi_{c1}(1P)$ fixed to the PDG 16 value.
[2] AAIJ 17BI reports also $m(\chi_{c2}) - m(\chi_{c1}) = 45.39 \pm 0.07 \pm 0.03$ MeV.
[3] Recalculated by ANDREOTTI 05A, using the value of $\psi(2S)$ mass from AULCHENKO 03.
[4] Using mass of $\psi(2S) = 3686.0$ MeV.
[5] $J/\psi(1S)$ mass constrained to 3097 MeV.
[6] Mass value shifted by us by amount appropriate for $\psi(2S)$ mass = 3686 MeV and $J/\psi(1S)$ mass = 3097 MeV.
[7] From a simultaneous fit to radiative and hadronic decay channels.

$\chi_{c1}(1P)$ WIDTH

VALUE (MeV)	CL%	EVTS	DOCUMENT ID		TECN	COMMENT
0.82 ± 0.04 OUR FIT			Error includes scale factor of 1.1.			
0.88 ± 0.05 OUR AVERAGE						
$1.39^{+0.40}_{-0.38} \pm^{0.26}_{-0.77}$			ABLIKIM	05G	BES2	$\psi(2S) \to \gamma\chi_{c1}$
0.876 ± 0.045 ± 0.026			ANDREOTTI	05A	E835	$p\overline{p} \to e^+e^-\gamma$
0.87 ± 0.11 ± 0.08		513	[1] ARMSTRONG	92	E760	$\overline{p}p \to e^+e^-\gamma$
• • • We do not use the following data for averages, fits, limits, etc. • • •						
<1.3		95	BAGLIN	86B	SPEC	$\overline{p}p \to e^+e^-X$
<3.8		90	GAISER	86	CBAL	$\psi(2S) \to \gamma X$

[1] Recalculated by ANDREOTTI 05A.

$\chi_{c1}(1P)$ DECAY MODES

	Mode	Fraction (Γ_i/Γ)	Scale factor/ Confidence level
Γ_1	hadrons		
Γ_2	e^+e^-	$(1.5^{+1.6}_{-1.0}) \times 10^{-7}$	
	Hadronic decays		
Γ_3	$3(\pi^+\pi^-)$	(1.06 ± 0.11) %	S=3.0
Γ_4	$2(\pi^+\pi^-)$	$(6.6 \pm 0.7) \times 10^{-3}$	S=2.4
Γ_5	$\rho^0\pi^+\pi^-$	$(1.6 \pm 1.3) \times 10^{-3}$	
Γ_6	$\pi^+\pi^-\pi^0\pi^0$	(1.18 ± 0.15) %	
Γ_7	$\rho^+\pi^-\pi^0$ + c.c.	(1.44 ± 0.24) %	
Γ_8	$4\pi^0$	$(5.3 \pm 0.8) \times 10^{-4}$	
Γ_9	$\pi^+\pi^-K^+K^-$	$(4.5 \pm 1.0) \times 10^{-3}$	
Γ_{10}	$K^+K^-\pi^0\pi^0$	$(1.10 \pm 0.27) \times 10^{-3}$	
Γ_{11}	$K^+K^-\pi^+\pi^-\pi^0$	(1.07 ± 0.12) %	
Γ_{12}	$K^0_S K^\pm\pi^\mp\pi^+\pi^-$	$(7.0 \pm 0.7) \times 10^{-3}$	
Γ_{13}	$K^+\pi^-\overline{K}^0\pi^0$ + c.c.	$(8.5 \pm 1.3) \times 10^{-3}$	
Γ_{14}	$\rho^-K^+\overline{K}^0$ + c.c.	$(5.0 \pm 1.2) \times 10^{-3}$	
Γ_{15}	$K^*(892)^0\overline{K}^0\pi^0 \to K^+\pi^-\overline{K}^0\pi^0$ + c.c.	$(2.3 \pm 0.6) \times 10^{-3}$	
Γ_{16}	$K^+K^-\eta\pi^0$	$(1.10 \pm 0.34) \times 10^{-3}$	
Γ_{17}	$\pi^+\pi^-K^0_S K^0_S$	$(6.8 \pm 2.9) \times 10^{-4}$	
Γ_{18}	$K^+K^-\eta$	$(3.1 \pm 1.0) \times 10^{-4}$	
Γ_{19}	$\overline{K}^0K^+\pi^-$ + c.c.	$(6.9 \pm 0.6) \times 10^{-3}$	S=1.1
Γ_{20}	$K^*(892)^0\overline{K}^0$ + c.c.	$(1.04 \pm 0.15) \times 10^{-3}$	
Γ_{21}	$K^*(892)^+K^-$ + c.c.	$(1.22 \pm 0.23) \times 10^{-3}$	
Γ_{22}	$K^*_J(1430)^0\overline{K}^0$ + c.c. $\to K^0_S K^+\pi^-$ + c.c.	$< 8 \times 10^{-4}$	CL=90%
Γ_{23}	$K^*_J(1430)^+K^-$ + c.c. $\to K^0_S K^+\pi^-$ + c.c.	$< 2.1 \times 10^{-3}$	CL=90%
Γ_{24}	$K^+K^-\pi^0$	$(1.80 \pm 0.24) \times 10^{-3}$	
Γ_{25}	$\eta\pi^+\pi^-$	$(4.57 \pm 0.23) \times 10^{-3}$	
Γ_{26}	$a_0(980)^+\pi^-$ + c.c. $\to \eta\pi^+\pi^-$	$(3.2 \pm 0.4) \times 10^{-3}$	S=2.1
Γ_{27}	$a_2(1320)^+\pi^-$ + c.c. $\to \eta\pi^+\pi^-$	$(1.74 \pm 0.24) \times 10^{-4}$	
Γ_{28}	$a_2(1700)^+\pi^-$ + c.c. $\to \eta\pi^+\pi^-$	$(4.6 \pm 0.7) \times 10^{-5}$	
Γ_{29}	$f_2(1270)\eta \to \eta\pi^+\pi^-$	$(3.5 \pm 0.6) \times 10^{-4}$	
Γ_{30}	$f_4(2050)\eta \to \eta\pi^+\pi^-$	$(2.5 \pm 0.9) \times 10^{-5}$	
Γ_{31}	$\pi_1(1400)^+\pi^-$ + c.c. $\to \eta\pi^+\pi^-$	$< 4 \times 10^{-5}$	CL=90%
Γ_{32}	$\pi_1(1600)^+\pi^-$ + c.c. $\to \eta\pi^+\pi^-$	$< 1.5 \times 10^{-5}$	CL=90%
Γ_{33}	$\pi_1(2015)^+\pi^-$ + c.c. $\to \eta\pi^+\pi^-$	$< 8 \times 10^{-6}$	CL=90%
Γ_{34}	$2\pi^+2\pi^-\eta$	$(8.0 \pm 0.8) \times 10^{-3}$	
Γ_{35}	$f_2(1270)\eta$	$(6.6 \pm 1.1) \times 10^{-4}$	
Γ_{36}	$\pi^+\pi^-\eta'$	$(2.2 \pm 0.4) \times 10^{-3}$	
Γ_{37}	$K^+K^-\eta'(958)$	$(8.4 \pm 0.5) \times 10^{-4}$	
Γ_{38}	$K^*_0(1430)^+K^-$ + c.c. $\to K^+K^-\eta'(958)$	$(6.4^{+2.2}_{-2.8}) \times 10^{-4}$	
Γ_{39}	$f_0(980)\eta'(958) \to K^+K^-\eta'(958)$	$(1.6^{+1.4}_{-0.7}) \times 10^{-4}$	
Γ_{40}	$f_0(1710)\eta'(958) \to K^+K^-\eta'(958)$	$(7^{+7}_{-5}) \times 10^{-5}$	
Γ_{41}	$f'_2(1525)\eta'(958) \to K^+K^-\eta'(958)$	$(9 \pm 6) \times 10^{-5}$	
Γ_{42}	$\eta\eta\eta'$	$(1.39 \pm 0.16) \times 10^{-4}$	
Γ_{43}	$K^*_2(1430)^+K^-$ + c.c.	$(1.63 \pm 0.31) \times 10^{-3}$	
Γ_{44}	$K^*_2(1430)\overline{K}^0$ + c.c.	$(1.18 \pm 0.20) \times 10^{-3}$	
Γ_{45}	$\pi^0 f_0(980) \to \pi^0\pi^+\pi^-$	$(3.5 \pm 0.9) \times 10^{-7}$	
Γ_{46}	$K^+\overline{K}^*(892)^0\pi^-$ + c.c.	$(1.6 \pm 0.9) \times 10^{-3}$	
Γ_{47}	$K^*(892)^0\overline{K}^*(892)^0$	$(1.4 \pm 0.4) \times 10^{-3}$	
Γ_{48}	$K^+K^-K^0_S K^0_S$	$< 4 \times 10^{-4}$	CL=90%
Γ_{49}	$K^0_S K^0_S K^0_S K^0_S$	$(3.5 \pm 1.0) \times 10^{-5}$	
Γ_{50}	$K^+K^-K^+K^-$	$(5.3 \pm 1.1) \times 10^{-4}$	
Γ_{51}	$K^+K^-\phi$	$(4.1 \pm 1.5) \times 10^{-4}$	
Γ_{52}	$\overline{K}^0K^+\pi^-\phi$ + c.c.	$(3.3 \pm 0.5) \times 10^{-3}$	
Γ_{53}	$K^+K^-\pi^0\phi$	$(1.62 \pm 0.30) \times 10^{-3}$	
Γ_{54}	$K^0_S K^0_S K^0_S K^\pm\pi^\mp$	$(2.60 \pm 0.22) \times 10^{-4}$	
Γ_{55}	$3(K^+K^-)$	$(4.2 \pm 1.1) \times 10^{-6}$	
Γ_{56}	$\phi\pi^+\pi^-\pi^0$	$(7.0 \pm 0.9) \times 10^{-4}$	
Γ_{57}	$\omega\omega$	$(6.25 \pm 0.30) \times 10^{-4}$	
Γ_{58}	ωK^+K^-	$(7.3 \pm 0.8) \times 10^{-4}$	
Γ_{59}	$\omega\phi$	$(2.13 \pm 0.30) \times 10^{-5}$	S=1.5
Γ_{60}	$\phi\phi$	$(4.22 \pm 0.20) \times 10^{-4}$	
Γ_{61}	$\phi\phi\eta$	$(2.9 \pm 0.5) \times 10^{-4}$	
Γ_{62}	$p\overline{p}$	$(7.97 \pm 0.29) \times 10^{-5}$	S=1.3
Γ_{63}	$p\overline{p}\pi^0$	$(1.54 \pm 0.18) \times 10^{-4}$	
Γ_{64}	$p\overline{p}\eta$	$(1.44 \pm 0.24) \times 10^{-4}$	
Γ_{65}	$p\overline{p}\omega$	$(2.10 \pm 0.30) \times 10^{-4}$	
Γ_{66}	$p\overline{p}\pi^+\pi^-$	$(5.0 \pm 1.9) \times 10^{-4}$	
Γ_{67}	$p\overline{p}\pi^0\pi^0$	$< 5 \times 10^{-4}$	CL=90%
Γ_{68}	$p\overline{p}\eta\pi^0$	$(1.93 \pm 0.13) \times 10^{-4}$	
Γ_{69}	$p\overline{p}\eta\eta$	$(1.4 \pm 0.4) \times 10^{-5}$	
Γ_{70}	$p\overline{p}K^+K^-$	$(1.86 \pm 0.12) \times 10^{-4}$	
Γ_{71}	$p\overline{p}K^+K^-$ (non-resonant)	$(1.26 \pm 0.22) \times 10^{-4}$	
Γ_{72}	$K^+\overline{p}\Lambda(1520)$ + c.c.	$(1.7 \pm 0.4) \times 10^{-4}$	
Γ_{73}	$\Lambda(1520)\overline{\Lambda}(1520)$	$< 9 \times 10^{-5}$	CL=90%
Γ_{74}	$p\overline{p}\phi$	$< 1.7 \times 10^{-5}$	CL=90%
Γ_{75}	$p\overline{p}K^0_S K^0_S$	$< 4 \times 10^{-4}$	CL=90%
Γ_{76}	$p\overline{p}K^0_S K^-\pi^+$ + c.c.	$(4.1 \pm 0.5) \times 10^{-5}$	
Γ_{77}	$p\overline{n}\pi^-$	$(3.8 \pm 0.5) \times 10^{-4}$	
Γ_{78}	$\overline{p}n\pi^+$	$(3.9 \pm 0.5) \times 10^{-4}$	
Γ_{79}	$p\overline{n}\pi^-\pi^0$	$(1.02 \pm 0.12) \times 10^{-3}$	
Γ_{80}	$\overline{p}n\pi^+\pi^0$	$(9.9 \pm 1.2) \times 10^{-4}$	
Γ_{81}	$\Lambda\overline{\Lambda}$	$(1.26 \pm 0.09) \times 10^{-4}$	S=1.1
Γ_{82}	$\Lambda\overline{\Lambda}\pi^+\pi^-$	$(2.9 \pm 0.5) \times 10^{-4}$	
Γ_{83}	$\Lambda\overline{\Lambda}\pi^+\pi^-$ (non-resonant)	$(2.4 \pm 0.6) \times 10^{-4}$	
Γ_{84}	$\Sigma(1385)^+\overline{\Lambda}\pi^-$ + c.c.	$< 1.3 \times 10^{-4}$	CL=90%
Γ_{85}	$\Sigma(1385)^-\overline{\Lambda}\pi^+$ + c.c.	$< 1.3 \times 10^{-4}$	CL=90%
Γ_{86}	$\Lambda\overline{\Lambda}\eta$	$(5.8 \pm 1.5) \times 10^{-5}$	
Γ_{87}	$\Lambda\overline{\Lambda}\eta'$	$(1.5 \pm 0.5) \times 10^{-5}$	

Int. J. Mod. Phys. A 2026.41. Downloaded from www.worldscientific.com by UNIVERSITY OF CALIFORNIA @ BERKELEY on 09/16/26. Re-use and distribution is strictly not permitted, except for Open Access articles.

Γ_{88}	$\Lambda\overline{\Lambda}\omega$	$(9.9 \pm 1.5) \times 10^{-5}$	
Γ_{89}	$\Lambda\overline{\Lambda}\phi$	$(5.9 \pm 1.0) \times 10^{-5}$	
Γ_{90}	$K^+\overline{p}\Lambda$+c.c.	$(4.1 \pm 0.4) \times 10^{-4}$	S=1.2
Γ_{91}	$nK^0_S\overline{\Lambda}$ + c.c.	$(1.64 \pm 0.17) \times 10^{-4}$	
Γ_{92}	$\overline{p}\Lambda(1520)K^0_S\pi^+$ + c.c.	$(4.0 \pm 0.9) \times 10^{-5}$	
Γ_{93}	$K^*(892)^+\overline{p}\Lambda$+ c.c.	$(4.9 \pm 0.7) \times 10^{-4}$	
Γ_{94}	$\Sigma^0\overline{\Sigma}^0$	$(4.2 \pm 0.6) \times 10^{-5}$	
Γ_{95}	$\Sigma^+\overline{p}K^0_S$ + c.c.	$(1.51 \pm 0.12) \times 10^{-4}$	
Γ_{96}	$\Sigma^0\overline{p}K^+$+ c.c.	$(1.44 \pm 0.10) \times 10^{-4}$	
Γ_{97}	$\Sigma^+\overline{\Sigma}^-$	$(3.6 \pm 0.6) \times 10^{-5}$	
Γ_{98}	$\Sigma^+\overline{\Sigma}^-\eta$	$(5.0 \pm 1.4) \times 10^{-5}$	
Γ_{99}	$\Sigma^-\overline{\Sigma}^+$	$(5.6 \pm 1.5) \times 10^{-5}$	
Γ_{100}	$\Sigma(1385)^+\overline{\Sigma}(1385)^-$	$< 9 \times 10^{-5}$	CL=90%
Γ_{101}	$\Sigma(1385)^-\overline{\Sigma}(1385)^+$	$< 5 \times 10^{-5}$	CL=90%
Γ_{102}	$K^-\Lambda\overline{\Xi}^+$ + c.c.	$(1.34 \pm 0.24) \times 10^{-4}$	
Γ_{103}	$\Xi^0\overline{\Xi}^0$	$(7.4 \pm 1.2) \times 10^{-5}$	
Γ_{104}	$\Xi^-\overline{\Xi}^+$	$(5.9 \pm 0.6) \times 10^{-5}$	
Γ_{105}	$\Omega^-\overline{\Omega}^+$	$(1.47 \pm 0.25) \times 10^{-5}$	
Γ_{106}	$\pi^+\pi^-$ + K^+K^-	$< 1.5 \times 10^{-3}$	CL=90%
Γ_{107}	$K^0_S K^0_S$	$< 6 \times 10^{-5}$	CL=90%
Γ_{108}	$\eta_c\pi^+\pi^-$	$< 3.1 \times 10^{-4}$	CL=90%
	Radiative decays		
Γ_{109}	$\gamma J/\psi(1S)$	(33.9 ± 1.2) %	S=1.3
Γ_{110}	$\gamma\rho^0$	$(2.14 \pm 0.17) \times 10^{-4}$	
Γ_{111}	$\gamma\omega$	$(6.7 \pm 0.8) \times 10^{-5}$	
Γ_{112}	$\gamma\phi$	$(2.4 \pm 0.5) \times 10^{-5}$	
Γ_{113}	$\gamma\gamma$	$< 6 \times 10^{-6}$	CL=90%
Γ_{114}	$e^+e^-J/\psi(1S)$	$(3.42 \pm 0.23) \times 10^{-3}$	
Γ_{115}	$\mu^+\mu^-J/\psi(1S)$	$(2.30 \pm 0.29) \times 10^{-4}$	

CONSTRAINED FIT INFORMATION

A multiparticle fit to $\chi_{c1}(1P)$, $\chi_{c0}(1P)$, $\chi_{c2}(1P)$, and $\psi(2S)$ with 4 total widths, a partial width, 27 combinations of partial widths obtained from integrated cross section, and 87 branching ratios uses 263 measurements to determine 50 parameters. The overall fit has a $\chi^2 = 435.4$ for 213 degrees of freedom.

The following *off-diagonal* array elements are the correlation coefficients $\langle \delta p_i \delta p_j \rangle / (\delta p_i \cdot \delta p_j)$, in percent, from the fit to parameters p_i, including the branching fractions, $x_i \equiv \Gamma_i/\Gamma_{total}$.

x_{50}	4				
x_{62}	15	6			
x_{81}	11	5	17		
x_{109}	17	7	13	20	
Γ	−16	−7	−58	−18	−55
	x_{19}	x_{50}	x_{62}	x_{81}	x_{109}

$\chi_{c1}(1P)$ PARTIAL WIDTHS

$\Gamma(e^+e^-)$ — Γ_2

VALUE (eV)	EVTS	DOCUMENT ID		TECN	COMMENT
$\mathbf{0.12^{+0.13}_{-0.08}}$	250	[1] ABLIKIM	22AF	BES3	$e^+e^- \to \chi_{c1} \to \gamma J/\psi$

[1] Assuming $\Gamma(\chi_{c1} \to \gamma J/\psi) = 0.28$ MeV.

$\chi_{c1}(1P)$ $\Gamma(i)\Gamma(\gamma J/\psi(1S))/\Gamma(total)$

$\Gamma(p\overline{p}) \times \Gamma(\gamma J/\psi(1S))/\Gamma_{total}$ — $\Gamma_{62}\Gamma_{109}/\Gamma$

VALUE (eV)	DOCUMENT ID		TECN	COMMENT
22.1±0.8 OUR FIT				
21.4±0.9 OUR AVERAGE				
21.5±0.5±0.8	[1] ANDREOTTI	05A	E835	$p\overline{p} \to e^+e^-\gamma$
21.4±1.5±2.2	[1,2] ARMSTRONG	92	E760	$\overline{p}p \to e^+e^-\gamma$
$19.9^{+4.4}_{-4.0}$	[1] BAGLIN	86B	SPEC	$\overline{p}p \to e^+e^-X$

[1] Calculated by us using $B(J/\psi(1S) \to e^+e^-) = 0.0593 \pm 0.0010$.
[2] Recalculated by ANDREOTTI 05A.

$\chi_{c1}(1P)$ BRANCHING RATIOS

HADRONIC DECAYS

$\Gamma(3(\pi^+\pi^-))/\Gamma_{total}$ — Γ_3/Γ

VALUE (units 10^{-3})	EVTS	DOCUMENT ID		TECN	COMMENT
10.6 ±1.1 OUR AVERAGE Error includes scale factor of 3.0.					
10.81±0.23±0.29	84k	[1] ABLIKIM	22Q	BES3	$\psi(2S) \to \gamma 3(\pi^+\pi^-)$
5.1 ±1.1 ±0.1	98	[2] BAI	99B	BES	$\psi(2S) \to \gamma\chi_{c1}$
19 ±7 ±1	48	[3] TANENBAUM	78	MRK1	$\psi(2S) \to \gamma\chi_{c1}$

[1] ABLIKIM 22Q reports $(1.092 \pm 0.004 \pm 0.035) \times 10^{-2}$ from a measurement of $[\Gamma(\chi_{c1}(1P) \to 3(\pi^+\pi^-))/\Gamma_{total}] \times [B(\psi(2S) \to \gamma\chi_{c1}(1P))]$ assuming $B(\psi(2S) \to \gamma\chi_{c1}(1P)) = (9.75 \pm 0.24) \times 10^{-2}$, which we rescale to our best (shown rounded) value $B(\psi(2S) \to \gamma\chi_{c1}(1P)) = (9.85 \pm 0.26) \times 10^{-2}$. Our first error is their experiment's error and our second error is the systematic error from using our best (shown rounded) value.
[2] BAI 99B reports $(5.8 \pm 0.7 \pm 1.2) \times 10^{-3}$ from a measurement of $[\Gamma(\chi_{c1}(1P) \to 3(\pi^+\pi^-))/\Gamma_{total}] \times [B(\psi(2S) \to \gamma\chi_{c1}(1P))]$ assuming $B(\psi(2S) \to \gamma\chi_{c1}(1P)) = (8.7 \pm 0.8) \times 10^{-2}$, which we rescale to our best (shown rounded) value $B(\psi(2S) \to \gamma\chi_{c1}(1P)) = (9.85 \pm 0.26) \times 10^{-2}$. Our first error is their experiment's error and our second error is the systematic error from using our best (shown rounded) value.
[3] TANENBAUM 78 reports $[\Gamma(\chi_{c1}(1P) \to 3(\pi^+\pi^-))/\Gamma_{total}] \times [B(\psi(2S) \to \gamma\chi_{c1}(1P))] = (1.9 \pm 0.7) \times 10^{-3}$ which we divide by our best (shown rounded) value $B(\psi(2S) \to \gamma\chi_{c1}(1P)) = (9.85 \pm 0.26) \times 10^{-2}$. Our first error is their experiment's error and our second error is the systematic error from using our best (shown rounded) value.

$\Gamma(2(\pi^+\pi^-))/\Gamma_{total}$ — Γ_4/Γ

VALUE (units 10^{-3})	EVTS	DOCUMENT ID		TECN	COMMENT
6.6 ±0.7 OUR AVERAGE Error includes scale factor of 2.4.					
6.78±0.26±0.18	670k	[1] ABLIKIM	24BT	BES3	$\psi(2S) \to \gamma\chi_{c1}$
4.0 ±0.9 ±0.1	277	[2] BAI	99B	BES	$\psi(2S) \to \gamma\chi_{c1}$
14.2 ±4.1 ±0.4	74	[3] TANENBAUM	78	MRK1	$\psi(2S) \to \gamma\chi_{c1}$

[1] ABLIKIM 24BT reports $(0.685 \pm 0.001 \pm 0.031) \times 10^{-2}$ from a measurement of $[\Gamma(\chi_{c1}(1P) \to 2(\pi^+\pi^-))/\Gamma_{total}] \times [B(\psi(2S) \to \gamma\chi_{c1}(1P))]$ assuming $B(\psi(2S) \to \gamma\chi_{c1}(1P)) = (9.75 \pm 0.24) \times 10^{-2}$, which we rescale to our best (shown rounded) value $B(\psi(2S) \to \gamma\chi_{c1}(1P)) = (9.85 \pm 0.26) \times 10^{-2}$. Our first error is their experiment's error and our second error is the systematic error from using our best (shown rounded) value.
[2] BAI 99B reports $(0.49 \pm 0.04 \pm 0.12) \times 10^{-2}$ from a measurement of $[\Gamma(\chi_{c1}(1P) \to 2(\pi^+\pi^-))/\Gamma_{total}] \times [B(\psi(2S) \to \gamma\chi_{c1}(1P))] \times [B(\psi(2S) \to J/\psi(1S)\pi^+\pi^-)]$ assuming $B(\psi(2S) \to \gamma\chi_{c1}(1P)) = (8.7 \pm 0.8) \times 10^{-2}$, $B(\psi(2S) \to J/\psi(1S)\pi^+\pi^-) = (32.4 \pm 2.6) \times 10^{-2}$, which we rescale to our best (shown rounded) values $B(\psi(2S) \to \gamma\chi_{c1}(1P)) = (9.85 \pm 0.26) \times 10^{-2}$, $B(\psi(2S) \to J/\psi(1S)\pi^+\pi^-) = (34.78 \pm 0.33) \times 10^{-2}$. Our first error is their experiment's error and our second error is the systematic error from using our best (shown rounded) values.
[3] TANENBAUM 78 reports $[\Gamma(\chi_{c1}(1P) \to 2(\pi^+\pi^-))/\Gamma_{total}] \times [B(\psi(2S) \to \gamma\chi_{c1}(1P))] = (1.4 \pm 0.4) \times 10^{-3}$ which we divide by our best (shown rounded) value $B(\psi(2S) \to \gamma\chi_{c1}(1P)) = (9.85 \pm 0.26) \times 10^{-2}$. Our first error is their experiment's error and our second error is the systematic error from using our best (shown rounded) value.

$\Gamma(\rho^0\pi^+\pi^-)/\Gamma_{total}$ — Γ_5/Γ

VALUE (units 10^{-3})	DOCUMENT ID		TECN	COMMENT
• • • We do not use the following data for averages, fits, limits, etc. • • •				
3.9±3.5	[1] TANENBAUM	78	MRK1	$\psi(2S) \to \gamma\chi_{c1}$

[1] Estimated using $B(\psi(2S) \to \gamma\chi_{c1}(1P)) = 0.087$. The errors do not contain the uncertainty in the $\psi(2S)$ decay.

$\Gamma(\rho^0\pi^+\pi^-)/\Gamma(2(\pi^+\pi^-))$ — Γ_5/Γ_4

VALUE	DOCUMENT ID		TECN	COMMENT
0.24±0.20	TANENBAUM	78	MRK1	$\psi(2S) \to \gamma\chi_{c1}$

$\Gamma(\pi^+\pi^-\pi^0\pi^0)/\Gamma_{total}$ — Γ_6/Γ

VALUE (%)	EVTS	DOCUMENT ID		TECN	COMMENT
1.18±0.15±0.03	604.7	[1] HE	08B	CLEO	$e^+e^- \to \gamma h^+h^-h^0h^0$

[1] HE 08B reports $1.28 \pm 0.06 \pm 0.15 \pm 0.08$ % from a measurement of $[\Gamma(\chi_{c1}(1P) \to \pi^+\pi^-\pi^0\pi^0)/\Gamma_{total}] \times [B(\psi(2S) \to \gamma\chi_{c1}(1P))]$ assuming $B(\psi(2S) \to \gamma\chi_{c1}(1P)) = (9.07 \pm 0.11 \pm 0.54) \times 10^{-2}$, which we rescale to our best (shown rounded) value $B(\psi(2S) \to \gamma\chi_{c1}(1P)) = (9.85 \pm 0.26) \times 10^{-2}$. Our first error is their experiment's error and our second error is the systematic error from using our best (shown rounded) value.

$\Gamma(\rho^+\pi^-\pi^0 + c.c.)/\Gamma_{total}$ — Γ_7/Γ

VALUE (%)	EVTS	DOCUMENT ID		TECN	COMMENT
1.44±0.24±0.04	712.3	[1,2] HE	08B	CLEO	$e^+e^- \to \gamma h^+h^-h^0h^0$

[1] HE 08B reports $1.56 \pm 0.13 \pm 0.22 \pm 0.10$ % from a measurement of $[\Gamma(\chi_{c1}(1P) \to \rho^+\pi^-\pi^0 + c.c.)/\Gamma_{total}] \times [B(\psi(2S) \to \gamma\chi_{c1}(1P))]$ assuming $B(\psi(2S) \to \gamma\chi_{c1}(1P)) = (9.07 \pm 0.11 \pm 0.54) \times 10^{-2}$, which we rescale to our best (shown rounded) value $B(\psi(2S) \to \gamma\chi_{c1}(1P)) = (9.85 \pm 0.26) \times 10^{-2}$. Our first error is their experiment's error and our second error is the systematic error from using our best (shown rounded) value.
[2] Calculated by us. We have added the values from HE 08B for $\rho^+\pi^-\pi^0$ and $\rho^-\pi^+\pi^0$ decays assuming uncorrelated statistical and fully correlated systematic uncertainties.

$\Gamma(4\pi^0)/\Gamma_{total}$ — Γ_8/Γ

VALUE (units 10^{-4})	EVTS	DOCUMENT ID		TECN	COMMENT
5.3±0.8±0.1	608	[1] ABLIKIM	11A	BES3	$e^+e^- \to \psi(2S) \to \gamma\chi_{c1}$

[1] ABLIKIM 11A reports $(0.57 \pm 0.03 \pm 0.08) \times 10^{-3}$ from a measurement of $[\Gamma(\chi_{c1}(1P) \to 4\pi^0)/\Gamma_{total}] \times [B(\psi(2S) \to \gamma\chi_{c1}(1P))]$ assuming $B(\psi(2S) \to \gamma\chi_{c1}(1P)) = (9.2 \pm 0.4) \times 10^{-2}$, which we rescale to our best (shown rounded) value $B(\psi(2S) \to \gamma\chi_{c1}(1P)) = (9.85 \pm 0.26) \times 10^{-2}$. Our first error is their experiment's error and our second error is the systematic error from using our best (shown rounded) value.

Int. J. Mod. Phys. A 2026.41. Downloaded from www.worldscientific.com by CALIFORNIA @ BERKELEY on 09/16/26. Re-use and distribution is strictly not permitted, except for Open Access articles.

$\Gamma(\pi^+\pi^-K^+K^-)/\Gamma_{total}$ — Γ_9/Γ

VALUE (units 10^{-3})	DOCUMENT ID		TECN	COMMENT
4.5±1.0 OUR EVALUATION	Treating systematic error as correlated.			
4.5±0.9 OUR AVERAGE				
4.2±0.4±0.9	[1] BAI	99B	BES	$\psi(2S)\to\gamma\chi_{c1}$
7.3±3.0±0.4	[1] TANENBAUM	78	MRK1	$\psi(2S)\to\gamma\chi_{c1}$

[1] Rescaled by us using $B(\psi(2S)\to\gamma\chi_{c1})=(8.8\pm0.4)\%$ and $B(\psi(2S)\to J/\psi(1S)\pi^+\pi^-)=(32.6\pm0.5)\%$.

$\Gamma(K^+K^-\pi^0\pi^0)/\Gamma_{total}$ — Γ_{10}/Γ

VALUE (units 10^{-3})	EVTS	DOCUMENT ID		TECN	COMMENT
1.10±0.27±0.03	45.1	[1] HE	08B	CLEO	$e^+e^-\to\gamma h^+h^-h^0h^0$

[1] HE 08B reports $(0.12\pm0.02\pm0.02\pm0.01)\times10^{-2}$ from a measurement of $[\Gamma(\chi_{c1}(1P)\to K^+K^-\pi^0\pi^0)/\Gamma_{total}]\times[B(\psi(2S)\to\gamma\chi_{c1}(1P))]$ assuming $B(\psi(2S)\to\gamma\chi_{c1}(1P))=(9.07\pm0.11\pm0.54)\times10^{-2}$, which we rescale to our best (shown rounded) value $B(\psi(2S)\to\gamma\chi_{c1}(1P))=(9.85\pm0.26)\times10^{-2}$. Our first error is their experiment's error and our second error is the systematic error from using our best (shown rounded) value.

$\Gamma(K^+K^-\pi^+\pi^-\pi^0)/\Gamma_{total}$ — Γ_{11}/Γ

VALUE (units 10^{-3})	EVTS	DOCUMENT ID		TECN	COMMENT
10.7±1.1±0.3	12k	[1] ABLIKIM	13B	BES3	$e^+e^-\to\psi(2S)\to\gamma\chi_{c1}$

[1] ABLIKIM 13B reports $(11.46\pm0.12\pm1.29)\times10^{-3}$ from a measurement of $[\Gamma(\chi_{c1}(1P)\to K^+K^-\pi^+\pi^-\pi^0)/\Gamma_{total}]\times[B(\psi(2S)\to\gamma\chi_{c1}(1P))]$ assuming $B(\psi(2S)\to\gamma\chi_{c1}(1P))=(9.2\pm0.4)\times10^{-2}$, which we rescale to our best (shown rounded) value $B(\psi(2S)\to\gamma\chi_{c1}(1P))=(9.85\pm0.26)\times10^{-2}$. Our first error is their experiment's error and our second error is the systematic error from using our best (shown rounded) value.

$\Gamma(K^0_SK^\pm\pi^\mp\pi^+\pi^-)/\Gamma_{total}$ — Γ_{12}/Γ

VALUE (units 10^{-3})	EVTS	DOCUMENT ID		TECN	COMMENT
7.0±0.7±0.2	5.1k	[1] ABLIKIM	13B	BES3	$e^+e^-\to\psi(2S)\to\gamma\chi_{c1}$

[1] ABLIKIM 13B reports $(7.52\pm0.11\pm0.79)\times10^{-3}$ from a measurement of $[\Gamma(\chi_{c1}(1P)\to K^0_SK^\pm\pi^\mp\pi^+\pi^-)/\Gamma_{total}]\times[B(\psi(2S)\to\gamma\chi_{c1}(1P))]$ assuming $B(\psi(2S)\to\gamma\chi_{c1}(1P))=(9.2\pm0.4)\times10^{-2}$, which we rescale to our best (shown rounded) value $B(\psi(2S)\to\gamma\chi_{c1}(1P))=(9.85\pm0.26)\times10^{-2}$. Our first error is their experiment's error and our second error is the systematic error from using our best (shown rounded) value.

$\Gamma(K^+\pi^-\overline{K}^0\pi^0+c.c.)/\Gamma_{total}$ — Γ_{13}/Γ

VALUE (%)	EVTS	DOCUMENT ID		TECN	COMMENT
0.85±0.13±0.02	141.3	[1] HE	08B	CLEO	$e^+e^-\to\gamma h^+h^-h^0h^0$

[1] HE 08B reports $0.92\pm0.09\pm0.11\pm0.06$ % from a measurement of $[\Gamma(\chi_{c1}(1P)\to K^+\pi^-\overline{K}^0\pi^0+c.c.)/\Gamma_{total}]\times[B(\psi(2S)\to\gamma\chi_{c1}(1P))]$ assuming $B(\psi(2S)\to\gamma\chi_{c1}(1P))=(9.07\pm0.11\pm0.54)\times10^{-2}$, which we rescale to our best (shown rounded) value $B(\psi(2S)\to\gamma\chi_{c1}(1P))=(9.85\pm0.26)\times10^{-2}$. Our first error is their experiment's error and our second error is the systematic error from using our best (shown rounded) value.

$\Gamma(\rho^-K^+\overline{K}^0+c.c.)/\Gamma_{total}$ — Γ_{14}/Γ

VALUE (%)	EVTS	DOCUMENT ID		TECN	COMMENT
0.50±0.12±0.01	141.3	[1] HE	08B	CLEO	$e^+e^-\to\gamma h^+h^-h^0h^0$

[1] HE 08B reports $0.54\pm0.11\pm0.07\pm0.03$ % from a measurement of $[\Gamma(\chi_{c1}(1P)\to\rho^-K^+\overline{K}^0+c.c.)/\Gamma_{total}]\times[B(\psi(2S)\to\gamma\chi_{c1}(1P))]$ assuming $B(\psi(2S)\to\gamma\chi_{c1}(1P))=(9.07\pm0.11\pm0.54)\times10^{-2}$, which we rescale to our best (shown rounded) value $B(\psi(2S)\to\gamma\chi_{c1}(1P))=(9.85\pm0.26)\times10^{-2}$. Our first error is their experiment's error and our second error is the systematic error from using our best (shown rounded) value.

$\Gamma(K^*(892)^0\overline{K}^0\pi^0\to K^+\pi^-\overline{K}^0\pi^0+c.c.)/\Gamma_{total}$ — Γ_{15}/Γ

VALUE (%)	EVTS	DOCUMENT ID		TECN	COMMENT
0.23±0.06±0.01	141.3	[1] HE	08B	CLEO	$e^+e^-\to\gamma h^+h^-h^0h^0$

[1] HE 08B reports $0.25\pm0.06\pm0.03\pm0.02$ % from a measurement of $[\Gamma(\chi_{c1}(1P)\to K^*(892)^0\overline{K}^0\pi^0\to K^+\pi^-\overline{K}^0\pi^0+c.c.)/\Gamma_{total}]\times[B(\psi(2S)\to\gamma\chi_{c1}(1P))]$ assuming $B(\psi(2S)\to\gamma\chi_{c1}(1P))=(9.07\pm0.11\pm0.54)\times10^{-2}$, which we rescale to our best (shown rounded) value $B(\psi(2S)\to\gamma\chi_{c1}(1P))=(9.85\pm0.26)\times10^{-2}$. Our first error is their experiment's error and our second error is the systematic error from using our best (shown rounded) value.

$\Gamma(K^+K^-\eta\pi^0)/\Gamma_{total}$ — Γ_{16}/Γ

VALUE (%)	EVTS	DOCUMENT ID		TECN	COMMENT
0.110±0.034±0.003	141.3	[1] HE	08B	CLEO	$e^+e^-\to\gamma h^+h^-h^0h^0$

[1] HE 08B reports $0.12\pm0.03\pm0.02\pm0.01$ % from a measurement of $[\Gamma(\chi_{c1}(1P)\to K^+K^-\eta\pi^0)/\Gamma_{total}]\times[B(\psi(2S)\to\gamma\chi_{c1}(1P))]$ assuming $B(\psi(2S)\to\gamma\chi_{c1}(1P))=(9.07\pm0.11\pm0.54)\times10^{-2}$, which we rescale to our best (shown rounded) value $B(\psi(2S)\to\gamma\chi_{c1}(1P))=(9.85\pm0.26)\times10^{-2}$. Our first error is their experiment's error and our second error is the systematic error from using our best (shown rounded) value.

$\Gamma(\pi^+\pi^-K^0_SK^0_S)/\Gamma_{total}$ — Γ_{17}/Γ

VALUE (units 10^{-4})	EVTS	DOCUMENT ID		TECN	COMMENT
6.8±2.9±0.2	19.8±7.7	[1] ABLIKIM	05O	BES2	$\psi(2S)\to\chi_{c1}\gamma$

[1] ABLIKIM 05O reports $[\Gamma(\chi_{c1}(1P)\to\pi^+\pi^-K^0_SK^0_S)/\Gamma_{total}]\times[B(\psi(2S)\to\gamma\chi_{c1}(1P))]=(0.67\pm0.26\pm0.11)\times10^{-4}$ which we divide by our best (shown rounded) value $B(\psi(2S)\to\gamma\chi_{c1}(1P))=(9.85\pm0.26)\times10^{-2}$. Our first error is their experiment's error and our second error is the systematic error from using our best (shown rounded) value.

$\Gamma(K^+K^-\eta)/\Gamma_{total}$ — Γ_{18}/Γ

VALUE (units 10^{-4})	EVTS	DOCUMENT ID		TECN	COMMENT
3.1 ±1.0 ±0.1		[1] ATHAR	07	CLEO	$\psi(2S)\to\gamma h^+h^-h^0$
• • • We do not use the following data for averages, fits, limits, etc. • • •					
4.30±0.05	8690	[2] ABLIKIM	24BW	BES3	$\psi(2S)\to\gamma\chi_{c1}$

[1] ATHAR 07 reports $(0.34\pm0.10\pm0.04)\times10^{-3}$ from a measurement of $[\Gamma(\chi_{c1}(1P)\to K^+K^-\eta)/\Gamma_{total}]\times[B(\psi(2S)\to\gamma\chi_{c1}(1P))]$ assuming $B(\psi(2S)\to\gamma\chi_{c1}(1P))=0.0907\pm0.0011\pm0.0054$, which we rescale to our best (shown rounded) value $B(\psi(2S)\to\gamma\chi_{c1}(1P))=(9.85\pm0.26)\times10^{-2}$. Our first error is their experiment's error and our second error is the systematic error from using our best (shown rounded) value.

[2] No systematic error reported.

$\Gamma(K^*(892)^0\overline{K}^0+c.c.)/\Gamma_{total}$ — Γ_{20}/Γ

VALUE (units 10^{-3})	EVTS	DOCUMENT ID		TECN	COMMENT
1.04±0.15 OUR AVERAGE					
1.05±0.14±0.09	262	[1] AAIJ	23AH	LHCB	$B^+\to K^+(K^0_SK\pi)$
0.97±0.36±0.03	22	[2] ABLIKIM	06R	BES2	$\psi(2S)\to\gamma\chi_{c1}$

[1] AAIJ 23AH reports $(1.04\pm0.13\pm0.04\pm0.09)\times10^{-3}$ from a measurement of $[\Gamma(\chi_{c1}(1P)\to K^*(892)^0\overline{K}^0+c.c.)/\Gamma_{total}]\times[B(\chi_{c1}(1P)\to\overline{K}^0K^+\pi^-+c.c.)]$ assuming $B(\chi_{c1}(1P)\to\overline{K}^0K^+\pi^-+c.c.)=(7.0\pm0.6)\times10^{-3}$, which we rescale to our best (shown rounded) value $B(\chi_{c1}(1P)\to\overline{K}^0K^+\pi^-+c.c.)=(6.9\pm0.6)\times10^{-3}$. Our first error is their experiment's error and our second error is the systematic error from using our best (shown rounded) value.

[2] ABLIKIM 06R reports $(1.1\pm0.4\pm0.1)\times10^{-3}$ from a measurement of $[\Gamma(\chi_{c1}(1P)\to K^*(892)^0\overline{K}^0+c.c.)/\Gamma_{total}]\times[B(\psi(2S)\to\gamma\chi_{c1}(1P))]$ assuming $B(\psi(2S)\to\gamma\chi_{c1}(1P))=(8.7\pm0.4)\times10^{-2}$, which we rescale to our best (shown rounded) value $B(\psi(2S)\to\gamma\chi_{c1}(1P))=(9.85\pm0.26)\times10^{-2}$. Our first error is their experiment's error and our second error is the systematic error from using our best (shown rounded) value.

$\Gamma(K^*(892)^+K^-+c.c.)/\Gamma_{total}$ — Γ_{21}/Γ

VALUE (units 10^{-3})	EVTS	DOCUMENT ID		TECN	COMMENT
1.22±0.23 OUR AVERAGE					
1.19±0.22±0.10	288	[1] AAIJ	23AH	LHCB	$B^+\to K^+(K^0_SK\pi)$
1.41±0.64±0.04	27	[2] ABLIKIM	06R	BES2	$\psi(2S)\to\gamma\chi_{c1}$

[1] AAIJ 23AH reports $(1.18\pm0.17\pm0.14\pm0.10)\times10^{-3}$ from a measurement of $[\Gamma(\chi_{c1}(1P)\to K^*(892)^+K^-+c.c.)/\Gamma_{total}]\times[B(\chi_{c1}(1P)\to\overline{K}^0K^+\pi^-+c.c.)]$ assuming $B(\chi_{c1}(1P)\to\overline{K}^0K^+\pi^-+c.c.)=(7.0\pm0.6)\times10^{-3}$, which we rescale to our best (shown rounded) value $B(\chi_{c1}(1P)\to\overline{K}^0K^+\pi^-+c.c.)=(6.9\pm0.6)\times10^{-3}$. Our first error is their experiment's error and our second error is the systematic error from using our best (shown rounded) value.

[2] ABLIKIM 06R reports $(1.6\pm0.7\pm0.2)\times10^{-3}$ from a measurement of $[\Gamma(\chi_{c1}(1P)\to K^*(892)^+K^-+c.c.)/\Gamma_{total}]\times[B(\psi(2S)\to\gamma\chi_{c1}(1P))]$ assuming $B(\psi(2S)\to\gamma\chi_{c1}(1P))=(8.7\pm0.4)\times10^{-2}$, which we rescale to our best (shown rounded) value $B(\psi(2S)\to\gamma\chi_{c1}(1P))=(9.85\pm0.26)\times10^{-2}$. Our first error is their experiment's error and our second error is the systematic error from using our best (shown rounded) value.

$\Gamma(K^*_J(1430)^0\overline{K}^0+c.c.\to K^0_SK^+\pi^-+c.c.)/\Gamma_{total}$ — Γ_{22}/Γ

VALUE	CL%	DOCUMENT ID		TECN	COMMENT
<8 × 10^{-4}	90	[1] ABLIKIM	06R	BES2	$\psi(2S)\to\gamma\chi_{c1}$

[1] ABLIKIM 06R reports $<0.9\times10^{-3}$ from a measurement of $[\Gamma(\chi_{c1}(1P)\to K^*_J(1430)^0\overline{K}^0+c.c.\to K^0_SK^+\pi^-+c.c.)/\Gamma_{total}]\times[B(\psi(2S)\to\gamma\chi_{c1}(1P))]$ assuming $B(\psi(2S)\to\gamma\chi_{c1}(1P))=(8.7\pm0.4)\times10^{-2}$, which we rescale to our best (shown rounded) value $B(\psi(2S)\to\gamma\chi_{c1}(1P))=9.85\times10^{-2}$.

$\Gamma(K^*_J(1430)^+K^-+c.c.\to K^0_SK^+\pi^-+c.c.)/\Gamma_{total}$ — Γ_{23}/Γ

VALUE	CL%	DOCUMENT ID		TECN	COMMENT
<2.1 × 10^{-3}	90	[1] ABLIKIM	06R	BES2	$\psi(2S)\to\gamma\chi_{c1}$

[1] ABLIKIM 06R reports $<2.4\times10^{-3}$ from a measurement of $[\Gamma(\chi_{c1}(1P)\to K^*_J(1430)^+K^-+c.c.\to K^0_SK^+\pi^-+c.c.)/\Gamma_{total}]\times[B(\psi(2S)\to\gamma\chi_{c1}(1P))]$ assuming $B(\psi(2S)\to\gamma\chi_{c1}(1P))=(8.7\pm0.4)\times10^{-2}$, which we rescale to our best (shown rounded) value $B(\psi(2S)\to\gamma\chi_{c1}(1P))=9.85\times10^{-2}$.

$\Gamma(K^+K^-\pi^0)/\Gamma_{total}$ — Γ_{24}/Γ

VALUE (units 10^{-3})	DOCUMENT ID		TECN	COMMENT
1.80±0.23±0.05	[1] ATHAR	07	CLEO	$\psi(2S)\to\gamma h^+h^-h^0$

[1] ATHAR 07 reports $(1.95\pm0.16\pm0.23)\times10^{-3}$ from a measurement of $[\Gamma(\chi_{c1}(1P)\to K^+K^-\pi^0)/\Gamma_{total}]\times[B(\psi(2S)\to\gamma\chi_{c1}(1P))]$ assuming $B(\psi(2S)\to\gamma\chi_{c1}(1P))=0.0907\pm0.0011\pm0.0054$, which we rescale to our best (shown rounded) value $B(\psi(2S)\to\gamma\chi_{c1}(1P))=(9.85\pm0.26)\times10^{-2}$. Our first error is their experiment's error and our second error is the systematic error from using our best (shown rounded) value.

Int. J. Mod. Phys. A 2026.41. Downloaded from www.worldscientific.com
by UNIVERSITY OF CALIFORNIA @ BERKELEY on 09/16/26. Re-use and distribution is strictly not permitted, except for Open Access articles.

$\Gamma(\eta\pi^+\pi^-)/\Gamma_{total}$ — Γ_{25}/Γ

VALUE (units 10^{-3})	EVTS	DOCUMENT ID		TECN	COMMENT
4.57±0.23 OUR AVERAGE					
4.53±0.23±0.12		[1,2] ABLIKIM	17K	BES3	$\psi(2S) \to \gamma\eta\pi^+\pi^-$
4.6 ±0.5 ±0.1		[3] ATHAR	07	CLEO	$\psi(2S) \to \gamma h^+ h^- h^0$
5.2 ±0.9 ±0.1	222	[4] ABLIKIM	06R	BES2	$\psi(2S) \to \gamma\chi_{c1}$

[1] From an amplitude analysis using an isobar model.
[2] ABLIKIM 17K reports $(4.67 \pm 0.03 \pm 0.23 \pm 0.16) \times 10^{-3}$ from a measurement of $[\Gamma(\chi_{c1}(1P) \to \eta\pi^+\pi^-)/\Gamma_{total}] \times [B(\psi(2S) \to \gamma\chi_{c1}(1P))]$ assuming $B(\psi(2S) \to \gamma\chi_{c1}(1P)) = (9.55 \pm 0.31) \times 10^{-2}$, which we rescale to our best (shown rounded) value $B(\psi(2S) \to \gamma\chi_{c1}(1P)) = (9.85 \pm 0.26) \times 10^{-2}$. Our first error is their experiment's error and our second error is the systematic error from using our best (shown rounded) value.
[3] ATHAR 07 reports $(5.0 \pm 0.3 \pm 0.5) \times 10^{-3}$ from a measurement of $[\Gamma(\chi_{c1}(1P) \to \eta\pi^+\pi^-)/\Gamma_{total}] \times [B(\psi(2S) \to \gamma\chi_{c1}(1P))]$ assuming $B(\psi(2S) \to \gamma\chi_{c1}(1P)) = 0.0907 \pm 0.0011 \pm 0.0054$, which we rescale to our best (shown rounded) value $B(\psi(2S) \to \gamma\chi_{c1}(1P)) = (9.85 \pm 0.26) \times 10^{-2}$. Our first error is their experiment's error and our second error is the systematic error from using our best (shown rounded) value.
[4] ABLIKIM 06R reports $(5.9 \pm 0.7 \pm 0.8) \times 10^{-3}$ from a measurement of $[\Gamma(\chi_{c1}(1P) \to \eta\pi^+\pi^-)/\Gamma_{total}] \times [B(\psi(2S) \to \gamma\chi_{c1}(1P))]$ assuming $B(\psi(2S) \to \gamma\chi_{c1}(1P)) = (8.7 \pm 0.4) \times 10^{-2}$, which we rescale to our best (shown rounded) value $B(\psi(2S) \to \gamma\chi_{c1}(1P)) = (9.85 \pm 0.26) \times 10^{-2}$. Our first error is their experiment's error and our second error is the systematic error from using our best (shown rounded) value.

$\Gamma(a_0(980)^+\pi^- + c.c. \to \eta\pi^+\pi^-)/\Gamma_{total}$ — Γ_{26}/Γ

VALUE (units 10^{-3})	EVTS	DOCUMENT ID		TECN	COMMENT
3.2 ±0.4 OUR AVERAGE	Error includes scale factor of 2.1.				
3.30±0.19±0.09		[1,2] ABLIKIM	17K	BES3	$\psi(2S) \to \gamma\eta\pi^+\pi^-$
1.77±0.62±0.05	58	[3] ABLIKIM	06R	BES2	$\psi(2S) \to \gamma\chi_{c1}$

[1] From an amplitude analysis using an isobar model.
[2] ABLIKIM 17K reports $(3.40 \pm 0.03 \pm 0.19 \pm 0.11) \times 10^{-3}$ from a measurement of $[\Gamma(\chi_{c1}(1P) \to a_0(980)^+\pi^- + c.c. \to \eta\pi^+\pi^-)/\Gamma_{total}] \times [B(\psi(2S) \to \gamma\chi_{c1}(1P))]$ assuming $B(\psi(2S) \to \gamma\chi_{c1}(1P)) = (9.55 \pm 0.31) \times 10^{-2}$, which we rescale to our best (shown rounded) value $B(\psi(2S) \to \gamma\chi_{c1}(1P)) = (9.85 \pm 0.26) \times 10^{-2}$. Our first error is their experiment's error and our second error is the systematic error from using our best (shown rounded) value.
[3] ABLIKIM 06R reports $(2.0 \pm 0.5 \pm 0.5) \times 10^{-3}$ from a measurement of $[\Gamma(\chi_{c1}(1P) \to a_0(980)^+\pi^- + c.c. \to \eta\pi^+\pi^-)/\Gamma_{total}] \times [B(\psi(2S) \to \gamma\chi_{c1}(1P))]$ assuming $B(\psi(2S) \to \gamma\chi_{c1}(1P)) = (8.7 \pm 0.4) \times 10^{-2}$, which we rescale to our best (shown rounded) value $B(\psi(2S) \to \gamma\chi_{c1}(1P)) = (9.85 \pm 0.26) \times 10^{-2}$. Our first error is their experiment's error and our second error is the systematic error from using our best (shown rounded) value.

$\Gamma(a_2(1320)^+\pi^- + c.c. \to \eta\pi^+\pi^-)/\Gamma_{total}$ — Γ_{27}/Γ

VALUE (units 10^{-3})	DOCUMENT ID		TECN	COMMENT
0.174±0.023±0.005	[1,2] ABLIKIM	17K	BES3	$\psi(2S) \to \gamma\eta\pi^+\pi^-$

[1] From an amplitude analysis using an isobar model.
[2] ABLIKIM 17K reports $(0.18 \pm 0.01 \pm 0.02 \pm 0.01) \times 10^{-3}$ from a measurement of $[\Gamma(\chi_{c1}(1P) \to a_2(1320)^+\pi^- + c.c. \to \eta\pi^+\pi^-)/\Gamma_{total}] \times [B(\psi(2S) \to \gamma\chi_{c1}(1P))]$ assuming $B(\psi(2S) \to \gamma\chi_{c1}(1P)) = (9.55 \pm 0.31) \times 10^{-2}$, which we rescale to our best (shown rounded) value $B(\psi(2S) \to \gamma\chi_{c1}(1P)) = (9.85 \pm 0.26) \times 10^{-2}$. Our first error is their experiment's error and our second error is the systematic error from using our best (shown rounded) value.

$\Gamma(a_2(1700)^+\pi^- + c.c. \to \eta\pi^+\pi^-)/\Gamma_{total}$ — Γ_{28}/Γ

VALUE (units 10^{-5})	DOCUMENT ID		TECN	COMMENT
4.6±0.7±0.1	[1,2] ABLIKIM	17K	BES3	$\psi(2S) \to \gamma\eta\pi^+\pi^-$

[1] From an amplitude analysis using an isobar model.
[2] ABLIKIM 17K reports $(4.7 \pm 0.4 \pm 0.6 \pm 0.2) \times 10^{-5}$ from a measurement of $[\Gamma(\chi_{c1}(1P) \to a_2(1700)^+\pi^- + c.c. \to \eta\pi^+\pi^-)/\Gamma_{total}] \times [B(\psi(2S) \to \gamma\chi_{c1}(1P))]$ assuming $B(\psi(2S) \to \gamma\chi_{c1}(1P)) = (9.55 \pm 0.31) \times 10^{-2}$, which we rescale to our best (shown rounded) value $B(\psi(2S) \to \gamma\chi_{c1}(1P)) = (9.85 \pm 0.26) \times 10^{-2}$. Our first error is their experiment's error and our second error is the systematic error from using our best (shown rounded) value.

$\Gamma(f_2(1270)\eta \to \eta\pi^+\pi^-)/\Gamma_{total}$ — Γ_{29}/Γ

VALUE (units 10^{-4})	DOCUMENT ID		TECN	COMMENT
3.5±0.6±0.1	[1,2] ABLIKIM	17K	BES3	$\psi(2S) \to \gamma\eta\pi^+\pi^-$

[1] From an amplitude analysis using an isobar model.
[2] ABLIKIM 17K reports $(0.36 \pm 0.01 \pm 0.06 \pm 0.01) \times 10^{-3}$ from a measurement of $[\Gamma(\chi_{c1}(1P) \to f_2(1270)\eta \to \eta\pi^+\pi^-)/\Gamma_{total}] \times [B(\psi(2S) \to \gamma\chi_{c1}(1P))]$ assuming $B(\psi(2S) \to \gamma\chi_{c1}(1P)) = (9.55 \pm 0.31) \times 10^{-2}$, which we rescale to our best (shown rounded) value $B(\psi(2S) \to \gamma\chi_{c1}(1P)) = (9.85 \pm 0.26) \times 10^{-2}$. Our first error is their experiment's error and our second error is the systematic error from using our best (shown rounded) value.

$\Gamma(f_4(2050)\eta \to \eta\pi^+\pi^-)/\Gamma_{total}$ — Γ_{30}/Γ

VALUE (units 10^{-5})	DOCUMENT ID		TECN	COMMENT
2.5±0.9±0.1	[1,2] ABLIKIM	17K	BES3	$\psi(2S) \to \gamma\eta\pi^+\pi^-$

[1] From an amplitude analysis using an isobar model.
[2] ABLIKIM 17K reports $(2.6 \pm 0.4 \pm 0.8 \pm 0.1) \times 10^{-5}$ from a measurement of $[\Gamma(\chi_{c1}(1P) \to f_4(2050)\eta \to \eta\pi^+\pi^-)/\Gamma_{total}] \times [B(\psi(2S) \to \gamma\chi_{c1}(1P))]$ assuming $B(\psi(2S) \to \gamma\chi_{c1}(1P)) = (9.55 \pm 0.31) \times 10^{-2}$, which we rescale to our best (shown rounded) value $B(\psi(2S) \to \gamma\chi_{c1}(1P)) = (9.85 \pm 0.26) \times 10^{-2}$. Our first error is their experiment's error and our second error is the systematic error from using our best (shown rounded) value.

$\Gamma(\pi_1(1400)^+\pi^- + c.c. \to \eta\pi^+\pi^-)/\Gamma_{total}$ — Γ_{31}/Γ

VALUE	CL%	DOCUMENT ID		TECN	COMMENT
<4 × 10^{-5}	90	[1,2] ABLIKIM	17K	BES3	$\psi(2S) \to \gamma\eta\pi^+\pi^-$

[1] From an amplitude analysis using an isobar model.
[2] ABLIKIM 17K reports $< 4.6 \times 10^{-5}$ from a measurement of $[\Gamma(\chi_{c1}(1P) \to \pi_1(1400)^+\pi^- + c.c. \to \eta\pi^+\pi^-)/\Gamma_{total}] \times [B(\psi(2S) \to \gamma\chi_{c1}(1P))]$ assuming $B(\psi(2S) \to \gamma\chi_{c1}(1P)) = (9.55 \pm 0.31) \times 10^{-2}$, which we rescale to our best (shown rounded) value $B(\psi(2S) \to \gamma\chi_{c1}(1P)) = 9.85 \times 10^{-2}$.

$\Gamma(\pi_1(1600)^+\pi^- + c.c. \to \eta\pi^+\pi^-)/\Gamma_{total}$ — Γ_{32}/Γ

VALUE	CL%	DOCUMENT ID		TECN	COMMENT
<1.5 × 10^{-5}	90	[1,2] ABLIKIM	17K	BES3	$\psi(2S) \to \gamma\eta\pi^+\pi^-$

[1] From an amplitude analysis using an isobar model.
[2] ABLIKIM 17K reports $< 1.5 \times 10^{-5}$ from a measurement of $[\Gamma(\chi_{c1}(1P) \to \pi_1(1600)^+\pi^- + c.c. \to \eta\pi^+\pi^-)/\Gamma_{total}] \times [B(\psi(2S) \to \gamma\chi_{c1}(1P))]$ assuming $B(\psi(2S) \to \gamma\chi_{c1}(1P)) = (9.55 \pm 0.31) \times 10^{-2}$, which we rescale to our best (shown rounded) value $B(\psi(2S) \to \gamma\chi_{c1}(1P)) = 9.85 \times 10^{-2}$.

$\Gamma(\pi_1(2015)^+\pi^- + c.c. \to \eta\pi^+\pi^-)/\Gamma_{total}$ — Γ_{33}/Γ

VALUE	CL%	DOCUMENT ID		TECN	COMMENT
<8 × 10^{-6}	90	[1,2] ABLIKIM	17K	BES3	$\psi(2S) \to \gamma\eta\pi^+\pi^-$

[1] From an amplitude analysis using an isobar model.
[2] ABLIKIM 17K reports $< 8 \times 10^{-6}$ from a measurement of $[\Gamma(\chi_{c1}(1P) \to \pi_1(2015)^+\pi^- + c.c. \to \eta\pi^+\pi^-)/\Gamma_{total}] \times [B(\psi(2S) \to \gamma\chi_{c1}(1P))]$ assuming $B(\psi(2S) \to \gamma\chi_{c1}(1P)) = (9.55 \pm 0.31) \times 10^{-2}$, which we rescale to our best (shown rounded) value $B(\psi(2S) \to \gamma\chi_{c1}(1P)) = 9.85 \times 10^{-2}$.

$\Gamma(f_2(1270)\eta)/\Gamma_{total}$ — Γ_{35}/Γ

VALUE (units 10^{-3})	EVTS	DOCUMENT ID		TECN	COMMENT
0.66±0.11 OUR AVERAGE					
0.62±0.10±0.02		[1,2] ABLIKIM	17K	BES3	$\psi(2S) \to \gamma\eta\pi^+\pi^-$
2.6 ±0.7 ±0.1	53	[3] ABLIKIM	06R	BES2	$\psi(2S) \to \gamma\chi_{c1}$

[1] ABLIKIM 17K reports $(6.4 \pm 1.1) \times 10^{-4}$ from a measurement of $[\Gamma(\chi_{c1}(1P) \to f_2(1270)\eta)/\Gamma_{total}] \times [B(\psi(2S) \to \gamma\chi_{c1}(1P))]$ assuming $B(\psi(2S) \to \gamma\chi_{c1}(1P)) = (9.55 \pm 0.31) \times 10^{-2}$, which we rescale to our best (shown rounded) value $B(\psi(2S) \to \gamma\chi_{c1}(1P)) = (9.85 \pm 0.26) \times 10^{-2}$. Our first error is their experiment's error and our second error is the systematic error from using our best (shown rounded) value.
[2] From an amplitude analysis using an isobar model.
[3] ABLIKIM 06R reports $(3.0 \pm 0.7 \pm 0.5) \times 10^{-3}$ from a measurement of $[\Gamma(\chi_{c1}(1P) \to f_2(1270)\eta)/\Gamma_{total}] \times [B(\psi(2S) \to \gamma\chi_{c1}(1P))]$ assuming $B(\psi(2S) \to \gamma\chi_{c1}(1P)) = (8.7 \pm 0.4) \times 10^{-2}$, which we rescale to our best (shown rounded) value $B(\psi(2S) \to \gamma\chi_{c1}(1P)) = (9.85 \pm 0.26) \times 10^{-2}$. Our first error is their experiment's error and our second error is the systematic error from using our best (shown rounded) value.

$\Gamma(\pi^+\pi^-\eta')/\Gamma_{total}$ — Γ_{36}/Γ

VALUE (units 10^{-3})	DOCUMENT ID		TECN	COMMENT
2.2±0.4±0.1	[1] ATHAR	07	CLEO	$\psi(2S) \to \gamma h^+ h^- h^0$

[1] ATHAR 07 reports $(2.4 \pm 0.4 \pm 0.3) \times 10^{-3}$ from a measurement of $[\Gamma(\chi_{c1}(1P) \to \pi^+\pi^-\eta')/\Gamma_{total}] \times [B(\psi(2S) \to \gamma\chi_{c1}(1P))]$ assuming $B(\psi(2S) \to \gamma\chi_{c1}(1P)) = 0.0907 \pm 0.0011 \pm 0.0054$, which we rescale to our best (shown rounded) value $B(\psi(2S) \to \gamma\chi_{c1}(1P)) = (9.85 \pm 0.26) \times 10^{-2}$. Our first error is their experiment's error and our second error is the systematic error from using our best (shown rounded) value.

$\Gamma(K^+K^-\eta'(958))/\Gamma_{total}$ — Γ_{37}/Γ

VALUE (units 10^{-4})	EVTS	DOCUMENT ID		TECN	COMMENT
8.4±0.4±0.2		[1] ABLIKIM	25I	BES3	$\psi(2S) \to \gamma K^+K^-\eta'(958)$
• • • We do not use the following data for averages, fits, limits, etc. • • •					
8.2±0.7±0.2	529	[2,3] ABLIKIM	14J	BES3	$\psi(2S) \to \gamma K^+K^-\eta'(958)$

[1] ABLIKIM 25I reports $(8.48 \pm 0.10 \pm 0.47) \times 10^{-4}$ from a measurement of $[\Gamma(\chi_{c1}(1P) \to K^+K^-\eta'(958))/\Gamma_{total}] \times [B(\psi(2S) \to \gamma\chi_{c1}(1P))]$ assuming $B(\psi(2S) \to \gamma\chi_{c1}(1P)) = (9.75 \pm 0.24) \times 10^{-2}$, which we rescale to our best (shown rounded) value $B(\psi(2S) \to \gamma\chi_{c1}(1P)) = (9.85 \pm 0.26) \times 10^{-2}$. Our first error is their experiment's error and our second error is the systematic error from using our best (shown rounded) value.
[2] ABLIKIM 14J reports $(8.75 \pm 0.87) \times 10^{-4}$ from a measurement of $[\Gamma(\chi_{c1}(1P) \to K^+K^-\eta'(958))/\Gamma_{total}] \times [B(\psi(2S) \to \gamma\chi_{c1}(1P))]$ assuming $B(\psi(2S) \to \gamma\chi_{c1}(1P)) = (9.2 \pm 0.4) \times 10^{-2}$, which we rescale to our best (shown rounded) value $B(\psi(2S) \to \gamma\chi_{c1}(1P)) = (9.85 \pm 0.26) \times 10^{-2}$. Our first error is their experiment's error and our second error is the systematic error from using our best (shown rounded) value.
[3] Superseded by ABLIKIM 25I.

$\Gamma(K_0^*(1430)^+K^- + c.c. \to K^+K^-\eta'(958))/\Gamma_{total}$ — Γ_{38}/Γ

VALUE (units 10^{-4})	DOCUMENT ID		TECN	COMMENT
$6.41 \pm 0.57^{+2.09}_{-2.71}$	[1] ABLIKIM	14J	BES3	$\psi(2S) \to \gamma K^+K^-\eta'(958)$

[1] From an overall fit to all the intermediate states of $K^+K^-\eta'(958)$ which yields $B(\chi_{c1} \to K^+K^-\eta'(958)) = (8.75 \pm 0.87) \times 10^{-4}$.

$\Gamma(f_0(980)\eta'(958) \to K^+K^-\eta'(958))/\Gamma_{total}$ — Γ_{39}/Γ

VALUE (units 10^{-4})	DOCUMENT ID		TECN	COMMENT
$1.65 \pm 0.47^{+1.32}_{-0.56}$	[1] ABLIKIM	14J	BES3	$\psi(2S) \to \gamma K^+K^-\eta'(958)$

[1] From an overall fit to all the intermediate states of $K^+K^-\eta'(958)$ which yields $B(\chi_{c1} \to K^+K^-\eta'(958)) = (8.75 \pm 0.87) \times 10^{-4}$.

$\Gamma(f_0(1710)\eta'(958) \to K^+K^-\eta'(958))/\Gamma_{total}$ — Γ_{40}/Γ

VALUE (units 10^{-4})	DOCUMENT ID		TECN	COMMENT
$0.71 \pm 0.22^{+0.68}_{-0.48}$	[1] ABLIKIM	14J	BES3	$\psi(2S) \to \gamma K^+K^-\eta'(958)$

[1] From an overall fit to all the intermediate states of $K^+K^-\eta'(958)$ which yields $B(\chi_{c1} \to K^+K^-\eta'(958)) = (8.75 \pm 0.87) \times 10^{-4}$.

$\Gamma(f_2'(1525)\eta'(958) \to K^+K^-\eta'(958))/\Gamma_{total}$ — Γ_{41}/Γ

VALUE (units 10^{-4})	DOCUMENT ID		TECN	COMMENT
$0.92 \pm 0.23^{+0.55}_{-0.51}$	[1] ABLIKIM	14J	BES3	$\psi(2S) \to \gamma K^+K^-\eta'(958)$

[1] From an overall fit to all the intermediate states of $K^+K^-\eta'(958)$ which yields $B(\chi_{c1} \to K^+K^-\eta'(958)) = (8.75 \pm 0.87) \times 10^{-4}$.

$\Gamma(\eta\eta\eta')/\Gamma_{total}$ — Γ_{42}/Γ

VALUE (units 10^{-4})	EVTS	DOCUMENT ID		TECN	COMMENT
$1.39 \pm 0.15 \pm 0.04$	37K	[1] ABLIKIM	25CJ	BES3	$\psi(2S) \to \gamma\chi_{c1} \to \gamma\eta\eta\eta'$

[1] ABLIKIM 25CJ reports $(1.40 \pm 0.13 \pm 0.09) \times 10^{-4}$ from a measurement of $[\Gamma(\chi_{c1}(1P) \to \eta\eta\eta')/\Gamma_{total}] \times [B(\psi(2S) \to \gamma\chi_{c1}(1P))]$ assuming $B(\psi(2S) \to \gamma\chi_{c1}(1P)) = (9.75 \pm 0.27) \times 10^{-2}$, which we rescale to our best (shown rounded) value $B(\psi(2S) \to \gamma\chi_{c1}(1P)) = (9.85 \pm 0.26) \times 10^{-2}$. Our first error is their experiment's error and our second error is the systematic error from using our best (shown rounded) value.

$\Gamma(K_2^*(1430)^+K^- + c.c.)/\Gamma_{total}$ — Γ_{43}/Γ

VALUE (units 10^{-3})	EVTS	DOCUMENT ID		TECN	COMMENT
$1.63 \pm 0.27 \pm 0.14$	351	[1] AAIJ	23AH	LHCB	$B^+ \to K^+(K_S^0 K\pi)$

[1] AAIJ 23AH reports $(1.61 \pm 0.19 \pm 0.19 \pm 0.14) \times 10^{-3}$ from a measurement of $[\Gamma(\chi_{c1}(1P) \to K_2^*(1430)^+K^- + c.c.)/\Gamma_{total}] \times [B(\chi_{c1}(1P) \to \overline{K}^0K^+\pi^- + c.c.)]$ assuming $B(\chi_{c1}(1P) \to \overline{K}^0K^+\pi^- + c.c.) = (7.0 \pm 0.6) \times 10^{-3}$, which we rescale to our best (shown rounded) value $B(\chi_{c1}(1P) \to \overline{K}^0K^+\pi^- + c.c.) = (6.9 \pm 0.6) \times 10^{-3}$. Our first error is their experiment's error and our second error is the systematic error from using our best (shown rounded) value.

$\Gamma(K_2^*(1430)\overline{K}^0 + c.c.)/\Gamma_{total}$ — Γ_{44}/Γ

VALUE (units 10^{-3})	EVTS	DOCUMENT ID		TECN	COMMENT
$1.18 \pm 0.17 \pm 0.10$	278	[1] AAIJ	23AH	LHCB	$B^+ \to K^+(K_S^0 K\pi)$

[1] AAIJ 23AH reports $(1.17 \pm 0.16 \pm 0.05 \pm 0.10) \times 10^{-3}$ from a measurement of $[\Gamma(\chi_{c1}(1P) \to K_2^*(1430)\overline{K}^0 + c.c.)/\Gamma_{total}] \times [B(\chi_{c1}(1P) \to \overline{K}^0K^+\pi^- + c.c.)]$ assuming $B(\chi_{c1}(1P) \to \overline{K}^0K^+\pi^- + c.c.) = (7.0 \pm 0.6) \times 10^{-3}$, which we rescale to our best (shown rounded) value $B(\chi_{c1}(1P) \to \overline{K}^0K^+\pi^- + c.c.) = (6.9 \pm 0.6) \times 10^{-3}$. Our first error is their experiment's error and our second error is the systematic error from using our best (shown rounded) value.

$\Gamma(\pi^0 f_0(980) \to \pi^0\pi^+\pi^-)/\Gamma_{total}$ — Γ_{45}/Γ

VALUE (units 10^{-6})	CL%	DOCUMENT ID		TECN	COMMENT
0.35 ± 0.09		ABLIKIM	18D	BES3	$\psi(2S) \to \gamma\pi^0\pi^+\pi^-$
• • • We do not use the following data for averages, fits, limits, etc. • • •					
<6	90	[1] ABLIKIM	11D	BES3	$\psi(2S) \to \gamma\pi^0\pi^+\pi^-$

[1] ABLIKIM 11D reports $[\Gamma(\chi_{c1}(1P) \to \pi^0 f_0(980) \to \pi^0\pi^+\pi^-)/\Gamma_{total}] \times [B(\psi(2S) \to \gamma\chi_{c1}(1P))] < 6.0 \times 10^{-7}$ which we divide by our best (shown rounded) value $B(\psi(2S) \to \gamma\chi_{c1}(1P)) = 9.85 \times 10^{-2}$.

$\Gamma(K^+\overline{K}^*(892)^0\pi^- + c.c.)/\Gamma_{total}$ — Γ_{46}/Γ

VALUE (units 10^{-4})	DOCUMENT ID		TECN	COMMENT
• • • We do not use the following data for averages, fits, limits, etc. • • •				
32 ± 21	[1] TANENBAUM	78	MRK1	$\psi(2S) \to \gamma\chi_{c1}$

[1] Estimated using $B(\psi(2S) \to \gamma\chi_{c1}(1P)) = 0.087$. The errors do not contain the uncertainty in the $\psi(2S)$ decay.

$\Gamma(K^+\overline{K}^*(892)^0\pi^- + c.c.)/\Gamma(\pi^+\pi^-K^+K^-)$ — Γ_{46}/Γ_9

VALUE	DOCUMENT ID		TECN	COMMENT
0.35 ± 0.18	TANENBAUM	78	MRK1	$\psi(2S) \to \gamma\chi_{c1}$

$\Gamma(K^*(892)^0\overline{K}^*(892)^0)/\Gamma_{total}$ — Γ_{47}/Γ

VALUE (units 10^{-3})	EVTS	DOCUMENT ID		TECN	COMMENT
$1.42 \pm 0.35 \pm 0.04$	28.4 ± 5.5	[1,2] ABLIKIM	04H	BES	$\psi(2S) \to \gamma K^+K^-\pi^+\pi^-$

[1] ABLIKIM 04H reports $[\Gamma(\chi_{c1}(1P) \to K^*(892)^0\overline{K}^*(892)^0)/\Gamma_{total}] \times [B(\psi(2S) \to \gamma\chi_{c1}(1P))] = (1.40 \pm 0.27 \pm 0.22) \times 10^{-4}$ which we divide by our best (shown rounded) value $B(\psi(2S) \to \gamma\chi_{c1}(1P)) = (9.85 \pm 0.26) \times 10^{-2}$. Our first error is their experiment's error and our second error is the systematic error from using our best (shown rounded) value.

[2] Assumes $B(K^*(892)^0 \to K^-\pi^+) = 2/3$.

$\Gamma(K^+K^-K_S^0K_S^0)/\Gamma_{total}$ — Γ_{48}/Γ

VALUE	CL%	EVTS	DOCUMENT ID		TECN	COMMENT
$<4 \times 10^{-4}$	90	3.2 ± 2.4	[1] ABLIKIM	05O	BES2	$\psi(2S) \to \chi_{c1}\gamma$

[1] ABLIKIM 05O reports $[\Gamma(\chi_{c1}(1P) \to K^+K^-K_S^0K_S^0)/\Gamma_{total}] \times [B(\psi(2S) \to \gamma\chi_{c1}(1P))] < 4.2 \times 10^{-5}$ which we divide by our best (shown rounded) value $B(\psi(2S) \to \gamma\chi_{c1}(1P)) = 9.85 \times 10^{-2}$.

$\Gamma(K_S^0K_S^0K_S^0K_S^0)/\Gamma_{total}$ — Γ_{49}/Γ

VALUE (units 10^{-4})	EVTS	DOCUMENT ID		TECN	COMMENT
$0.35 \pm 0.10 \pm 0.01$	22	[1] ABLIKIM	19AA	BES3	$\psi(2S) \to \gamma 4K_S^0$

[1] Using $B(K_S^0 \to \pi^+\pi^-) = (69.20 \pm 0.05)\%$. ABLIKIM 19AA reports $[\Gamma(\chi_{c1}(1P) \to K_S^0K_S^0K_S^0K_S^0)/\Gamma_{total}] \times [B(\psi(2S) \to \gamma\chi_{c1}(1P))] = (3.4 \pm 0.9 \pm 0.3) \times 10^{-6}$ which we divide by our best (shown rounded) value $B(\psi(2S) \to \gamma\chi_{c1}(1P)) = (9.85 \pm 0.26) \times 10^{-2}$. Our first error is their experiment's error and our second error is the systematic error from using our best (shown rounded) value..

$\Gamma(K^+K^-\phi)/\Gamma_{total}$ — Γ_{51}/Γ

VALUE (units 10^{-3})	EVTS	DOCUMENT ID		TECN	COMMENT
$0.41 \pm 0.15 \pm 0.01$	17	[1] ABLIKIM	06T	BES2	$\psi(2S) \to \gamma 2K^+2K^-$

[1] ABLIKIM 06T reports $(0.46 \pm 0.16 \pm 0.06) \times 10^{-3}$ from a measurement of $[\Gamma(\chi_{c1}(1P) \to K^+K^-\phi)/\Gamma_{total}] \times [B(\psi(2S) \to \gamma\chi_{c1}(1P))]$ assuming $B(\psi(2S) \to \gamma\chi_{c1}(1P)) = (8.7 \pm 0.4) \times 10^{-2}$, which we rescale to our best (shown rounded) value $B(\psi(2S) \to \gamma\chi_{c1}(1P)) = (9.85 \pm 0.26) \times 10^{-2}$. Our first error is their experiment's error and our second error is the systematic error from using our best (shown rounded) value.

$\Gamma(\overline{K}^0K^+\pi^-\phi + c.c.)/\Gamma_{total}$ — Γ_{52}/Γ

VALUE (units 10^{-3})	DOCUMENT ID		TECN	COMMENT
$3.27 \pm 0.28 \pm 0.46$	ABLIKIM	15M	BES3	$\psi(2S) \to \gamma\chi_{c1}$

$\Gamma(K^+K^-\pi^0\phi)/\Gamma_{total}$ — Γ_{53}/Γ

VALUE (units 10^{-3})	DOCUMENT ID		TECN	COMMENT
$1.62 \pm 0.12 \pm 0.28$	ABLIKIM	15M	BES3	$\psi(2S) \to \gamma\chi_{c1}$

$\Gamma(\phi\pi^+\pi^-\pi^0)/\Gamma_{total}$ — Γ_{56}/Γ

VALUE (units 10^{-3})	EVTS	DOCUMENT ID		TECN	COMMENT
$0.70 \pm 0.09 \pm 0.02$	373	[1] ABLIKIM	13B	BES3	$e^+e^- \to \psi(2S) \to \gamma\chi_{c1}$

[1] ABLIKIM 13B reports $(0.75 \pm 0.06 \pm 0.08) \times 10^{-3}$ from a measurement of $[\Gamma(\chi_{c1}(1P) \to \phi\pi^+\pi^-\pi^0)/\Gamma_{total}] \times [B(\psi(2S) \to \gamma\chi_{c1}(1P))]$ assuming $B(\psi(2S) \to \gamma\chi_{c1}(1P)) = (9.2 \pm 0.4) \times 10^{-2}$, which we rescale to our best (shown rounded) value $B(\psi(2S) \to \gamma\chi_{c1}(1P)) = (9.85 \pm 0.26) \times 10^{-2}$. Our first error is their experiment's error and our second error is the systematic error from using our best (shown rounded) value.

$\Gamma(\omega\omega)/\Gamma_{total}$ — Γ_{57}/Γ

VALUE (units 10^{-4})	EVTS	DOCUMENT ID		TECN	COMMENT
6.25 ± 0.30 OUR AVERAGE					
$6.36 \pm 0.27 \pm 0.17$	11.7k	[1] ABLIKIM	25K	BES3	$\psi(2S) \to \gamma 2(\pi^+\pi^-\pi^0)$
$5.6 \pm 0.7 \pm 0.1$	597	[2] ABLIKIM	11K	BES3	$\psi(2S) \to \gamma$ hadrons

[1] ABLIKIM 25K reports $(6.43 \pm 0.07 \pm 0.31) \times 10^{-4}$ from a measurement of $[\Gamma(\chi_{c1}(1P) \to \omega\omega)/\Gamma_{total}] \times [B(\psi(2S) \to \gamma\chi_{c1}(1P))]$ assuming $B(\psi(2S) \to \gamma\chi_{c1}(1P)) = (9.75 \pm 0.24) \times 10^{-2}$, which we rescale to our best (shown rounded) value $B(\psi(2S) \to \gamma\chi_{c1}(1P)) = (9.85 \pm 0.26) \times 10^{-2}$. Our first error is their experiment's error and our second error is the systematic error from using our best (shown rounded) value.

[2] ABLIKIM 11K reports $(6.0 \pm 0.3 \pm 0.7) \times 10^{-4}$ from a measurement of $[\Gamma(\chi_{c1}(1P) \to \omega\omega)/\Gamma_{total}] \times [B(\psi(2S) \to \gamma\chi_{c1}(1P))]$ assuming $B(\psi(2S) \to \gamma\chi_{c1}(1P)) = (9.2 \pm 0.4) \times 10^{-2}$, which we rescale to our best (shown rounded) value $B(\psi(2S) \to \gamma\chi_{c1}(1P)) = (9.85 \pm 0.26) \times 10^{-2}$. Our first error is their experiment's error and our second error is the systematic error from using our best (shown rounded) value.

$\Gamma(\omega K^+K^-)/\Gamma_{total}$ — Γ_{58}/Γ

VALUE (units 10^{-3})	EVTS	DOCUMENT ID		TECN	COMMENT
$0.73 \pm 0.08 \pm 0.02$	628	[1] ABLIKIM	13B	BES3	$e^+e^- \to \psi(2S) \to \gamma\chi_{c1}$

[1] ABLIKIM 13B reports $(0.78 \pm 0.04 \pm 0.08) \times 10^{-3}$ from a measurement of $[\Gamma(\chi_{c1}(1P) \to \omega K^+K^-)/\Gamma_{total}] \times [B(\psi(2S) \to \gamma\chi_{c1}(1P))]$ assuming $B(\psi(2S) \to \gamma\chi_{c1}(1P)) = (9.2 \pm 0.4) \times 10^{-2}$, which we rescale to our best (shown rounded) value $B(\psi(2S) \to \gamma\chi_{c1}(1P)) = (9.85 \pm 0.26) \times 10^{-2}$. Our first error is their experiment's error and our second error is the systematic error from using our best (shown rounded) value.

$\Gamma(\omega\phi)/\Gamma_{total}$ — Γ_{59}/Γ

VALUE (units 10^{-5})	EVTS	DOCUMENT ID		TECN	COMMENT
2.13 ± 0.30 OUR AVERAGE	Error includes scale factor of 1.5.				
$1.98 \pm 0.22 \pm 0.05$	356	[1] ABLIKIM	25K	BES3	$\psi(2S) \to \gamma\pi^+\pi^-\pi^0K^+K^-$
$2.7 \pm 0.4 \pm 0.1$	105	[2] ABLIKIM	19J	BES3	$\psi(2S) \to \gamma$ hadrons
• • • We do not use the following data for averages, fits, limits, etc. • • •					
$2.1 \pm 0.6 \pm 0.1$	15	[3,4] ABLIKIM	11K	BES3	$\psi(2S) \to \gamma$ hadrons

[1] ABLIKIM 25K reports $(0.20 \pm 0.02 \pm 0.01) \times 10^{-4}$ from a measurement of $[\Gamma(\chi_{c1}(1P) \to \omega\phi)/\Gamma_{total}] \times [B(\psi(2S) \to \gamma\chi_{c1}(1P))]$ assuming $B(\psi(2S) \to \gamma\chi_{c1}(1P)) = (9.75 \pm 0.24) \times 10^{-2}$, which we rescale to our best (shown rounded) value $B(\psi(2S) \to \gamma\chi_{c1}(1P)) = (9.85 \pm 0.26) \times 10^{-2}$. Our first error is their experiment's error and our second error is the systematic error from using our best (shown rounded) value.

[2] ABLIKIM 19J reports $[\Gamma(\chi_{c1}(1P) \to \omega\phi)/\Gamma_{total}] \times [B(\psi(2S) \to \gamma\chi_{c1}(1P))] = (2.67 \pm 0.31 \pm 0.27) \times 10^{-6}$ which we divide by our best (shown rounded) value $B(\psi(2S) \to \gamma\chi_{c1}(1P)) = (9.85 \pm 0.26) \times 10^{-2}$. Our first error is their experiment's error and our second error is the systematic error from using our best (shown rounded) value.

Int. J. Mod. Phys. A 2026.41. Downloaded from www.worldscientific.com
by LIFORNIA @ BERKELEY on 09/16/26. Re-use and distribution is strictly not permitted, except for Open Access articles.

Int. J. Mod. Phys. A 2026.41. Downloaded from www.worldscientific.com
by UNIVERSITY OF CALIFORNIA @ BERKELEY on 09/16/26. Re-use and distribution is strictly not permitted, except for Open Access articles.

[3] ABLIKIM 11K reports $(0.22 \pm 0.06 \pm 0.02) \times 10^{-4}$ from a measurement of $[\Gamma(\chi_{c1}(1P) \to \omega\phi)/\Gamma_{total}] \times [B(\psi(2S) \to \gamma\chi_{c1}(1P))]$ assuming $B(\psi(2S) \to \gamma\chi_{c1}(1P)) = (9.2 \pm 0.4) \times 10^{-2}$, which we rescale to our best (shown rounded) value $B(\psi(2S) \to \gamma\chi_{c1}(1P)) = (9.85 \pm 0.26) \times 10^{-2}$. Our first error is their experiment's error and our second error is the systematic error from using our best (shown rounded) value.

[4] Superseded by ABLIKIM 19J.

$\Gamma(\phi\phi)/\Gamma_{total}$ — Γ_{60}/Γ

VALUE (units 10^{-4})	EVTS	DOCUMENT ID		TECN	COMMENT
4.22±0.17±0.11	1529	[1,2] ABLIKIM	23N	BES3	$\psi(2S) \to \gamma$hadrons
• • • We do not use the following data for averages, fits, limits, etc. • • •					
4.1 ±0.5 ±0.1	366	[3] ABLIKIM	11K	BES3	$\psi(2S) \to \gamma$hadrons

[1] Using $B(\phi \to K^+K^-) = (49.2 \pm 0.5) \times 10^{-2}$ from PDG 22.

[2] ABLIKIM 23N reports $(4.26 \pm 0.13 \pm 0.15) \times 10^{-4}$ from a measurement of $[\Gamma(\chi_{c1}(1P) \to \phi\phi)/\Gamma_{total}] \times [B(\psi(2S) \to \gamma\chi_{c1}(1P))]$ assuming $B(\psi(2S) \to \gamma\chi_{c1}(1P)) = (9.75 \pm 0.24) \times 10^{-2}$, which we rescale to our best (shown rounded) value $B(\psi(2S) \to \gamma\chi_{c1}(1P)) = (9.85 \pm 0.26) \times 10^{-2}$. Our first error is their experiment's error and our second error is the systematic error from using our best (shown rounded) value.

[3] ABLIKIM 11K reports $(4.4 \pm 0.3 \pm 0.5) \times 10^{-4}$ from a measurement of $[\Gamma(\chi_{c1}(1P) \to \phi\phi)/\Gamma_{total}] \times [B(\psi(2S) \to \gamma\chi_{c1}(1P))]$ assuming $B(\psi(2S) \to \gamma\chi_{c1}(1P)) = (9.2 \pm 0.4) \times 10^{-2}$, which we rescale to our best (shown rounded) value $B(\psi(2S) \to \gamma\chi_{c1}(1P)) = (9.85 \pm 0.26) \times 10^{-2}$. Our first error is their experiment's error and our second error is the systematic error from using our best (shown rounded) value.

$\Gamma(\phi\phi\eta)/\Gamma_{total}$ — Γ_{61}/Γ

VALUE (units 10^{-4})	EVTS	DOCUMENT ID		TECN	COMMENT
2.9±0.5±0.1	83.6	[1] ABLIKIM	20B	BES3	$\psi(2S) \to \gamma\phi\phi\eta$

[1] ABLIKIM 20B reports $(2.96 \pm 0.43 \pm 0.22) \times 10^{-4}$ from a measurement of $[\Gamma(\chi_{c1}(1P) \to \phi\phi\eta)/\Gamma_{total}] \times [B(\psi(2S) \to \gamma\chi_{c1}(1P))]$ assuming $B(\psi(2S) \to \gamma\chi_{c1}(1P)) = (9.75 \pm 0.24) \times 10^{-2}$, which we rescale to our best (shown rounded) value $B(\psi(2S) \to \gamma\chi_{c1}(1P)) = (9.85 \pm 0.26) \times 10^{-2}$. Our first error is their experiment's error and our second error is the systematic error from using our best (shown rounded) value.

$\Gamma(p\overline{p}\pi^0)/\Gamma_{total}$ — Γ_{63}/Γ

VALUE (units 10^{-3})	DOCUMENT ID		TECN	COMMENT
0.154±0.018 OUR AVERAGE				
0.161±0.019±0.004	[1] ONYISI	10	CLE3	$\psi(2S) \to \gamma p\overline{p}X$
0.110±0.046±0.003	[2] ATHAR	07	CLEO	$\psi(2S) \to \gamma h^+h^-h^0$

[1] ONYISI 10 reports $(1.75 \pm 0.16 \pm 0.13 \pm 0.11) \times 10^{-4}$ from a measurement of $[\Gamma(\chi_{c1}(1P) \to p\overline{p}\pi^0)/\Gamma_{total}] \times [B(\psi(2S) \to \gamma\chi_{c1}(1P))]$ assuming $B(\psi(2S) \to \gamma\chi_{c1}(1P)) = (9.07 \pm 0.11 \pm 0.54) \times 10^{-2}$, which we rescale to our best (shown rounded) value $B(\psi(2S) \to \gamma\chi_{c1}(1P)) = (9.85 \pm 0.26) \times 10^{-2}$. Our first error is their experiment's error and our second error is the systematic error from using our best (shown rounded) value.

[2] ATHAR 07 reports $(1.2 \pm 0.5 \pm 0.1) \times 10^{-4}$ from a measurement of $[\Gamma(\chi_{c1}(1P) \to p\overline{p}\pi^0)/\Gamma_{total}] \times [B(\psi(2S) \to \gamma\chi_{c1}(1P))]$ assuming $B(\psi(2S) \to \gamma\chi_{c1}(1P)) = (9.07 \pm 0.11 \pm 0.54) \times 10^{-2}$, which we rescale to our best (shown rounded) value $B(\psi(2S) \to \gamma\chi_{c1}(1P)) = (9.85 \pm 0.26) \times 10^{-2}$. Our first error is their experiment's error and our second error is the systematic error from using our best (shown rounded) value.

$\Gamma(p\overline{p}\eta)/\Gamma_{total}$ — Γ_{64}/Γ

VALUE (units 10^{-3})	CL%	DOCUMENT ID		TECN	COMMENT
0.144±0.024±0.004		[1] ONYISI	10	CLE3	$\psi(2S) \to \gamma p\overline{p}X$
• • • We do not use the following data for averages, fits, limits, etc. • • •					
<0.15	90	[2] ATHAR	07	CLEO	$\psi(2S) \to \gamma h^+h^-h^0$

[1] ONYISI 10 reports $(1.56 \pm 0.22 \pm 0.14 \pm 0.10) \times 10^{-4}$ from a measurement of $[\Gamma(\chi_{c1}(1P) \to p\overline{p}\eta)/\Gamma_{total}] \times [B(\psi(2S) \to \gamma\chi_{c1}(1P))]$ assuming $B(\psi(2S) \to \gamma\chi_{c1}(1P)) = (9.07 \pm 0.11 \pm 0.54) \times 10^{-2}$, which we rescale to our best (shown rounded) value $B(\psi(2S) \to \gamma\chi_{c1}(1P)) = (9.85 \pm 0.26) \times 10^{-2}$. Our first error is their experiment's error and our second error is the systematic error from using our best (shown rounded) value.

[2] ATHAR 07 reports $< 0.16 \times 10^{-3}$ from a measurement of $[\Gamma(\chi_{c1}(1P) \to p\overline{p}\eta)/\Gamma_{total}] \times [B(\psi(2S) \to \gamma\chi_{c1}(1P))]$ assuming $B(\psi(2S) \to \gamma\chi_{c1}(1P)) = (9.07 \pm 0.11 \pm 0.54) \times 10^{-2}$, which we rescale to our best (shown rounded) value $B(\psi(2S) \to \gamma\chi_{c1}(1P)) = 9.85 \times 10^{-2}$.

$\Gamma(p\overline{p}\omega)/\Gamma_{total}$ — Γ_{65}/Γ

VALUE (units 10^{-3})	DOCUMENT ID		TECN	COMMENT
0.210±0.030±0.006	[1] ONYISI	10	CLE3	$\psi(2S) \to \gamma p\overline{p}X$

[1] ONYISI 10 reports $(2.28 \pm 0.28 \pm 0.16 \pm 0.14) \times 10^{-4}$ from a measurement of $[\Gamma(\chi_{c1}(1P) \to p\overline{p}\omega)/\Gamma_{total}] \times [B(\psi(2S) \to \gamma\chi_{c1}(1P))]$ assuming $B(\psi(2S) \to \gamma\chi_{c1}(1P)) = (9.07 \pm 0.11 \pm 0.54) \times 10^{-2}$, which we rescale to our best (shown rounded) value $B(\psi(2S) \to \gamma\chi_{c1}(1P)) = (9.85 \pm 0.26) \times 10^{-2}$. Our first error is their experiment's error and our second error is the systematic error from using our best (shown rounded) value.

$\Gamma(p\overline{p}\pi^+\pi^-)/\Gamma_{total}$ — Γ_{66}/Γ

VALUE (units 10^{-3})	EVTS	DOCUMENT ID		TECN	COMMENT
0.50±0.19 OUR EVALUATION		Treating systematic error as correlated.			
0.47±0.18 OUR AVERAGE					
0.43±0.18±0.01	27	[1] BAI	99B	BES	$\psi(2S) \to \gamma\chi_{c1}$
1.22±0.81±0.03	6	[2] TANENBAUM	78	MRK1	$\psi(2S) \to \gamma\chi_{c1}$

[1] BAI 99B reports $(0.49 \pm 0.13 \pm 0.17) \times 10^{-3}$ from a measurement of $[\Gamma(\chi_{c1}(1P) \to p\overline{p}\pi^+\pi^-)/\Gamma_{total}] \times [B(\psi(2S) \to \gamma\chi_{c1}(1P))]$ assuming $B(\psi(2S) \to \gamma\chi_{c1}(1P)) = (8.7 \pm 0.8) \times 10^{-2}$, which we rescale to our best (shown rounded) value $B(\psi(2S) \to \gamma\chi_{c1}(1P)) = (9.85 \pm 0.26) \times 10^{-2}$. Our first error is their experiment's error and our second error is the systematic error from using our best (shown rounded) value.

[2] TANENBAUM 78 reports $[\Gamma(\chi_{c1}(1P) \to p\overline{p}\pi^+\pi^-)/\Gamma_{total}] \times [B(\psi(2S) \to \gamma\chi_{c1}(1P))] = (1.2 \pm 0.8) \times 10^{-4}$ which we divide by our best (shown rounded) value $B(\psi(2S) \to \gamma\chi_{c1}(1P)) = (9.85 \pm 0.26) \times 10^{-2}$. Our first error is their experiment's error and our second error is the systematic error from using our best (shown rounded) value.

$\Gamma(p\overline{p}\pi^0\pi^0)/\Gamma_{total}$ — Γ_{67}/Γ

VALUE	CL%	DOCUMENT ID		TECN	COMMENT
<5 × 10⁻⁴	90	[1] HE	08B	CLEO	$e^+e^- \to \gamma h^+h^-h^0h^0$

[1] HE 08B reports $< 0.05 \times 10^{-2}$ from a measurement of $[\Gamma(\chi_{c1}(1P) \to p\overline{p}\pi^0\pi^0)/\Gamma_{total}] \times [B(\psi(2S) \to \gamma\chi_{c1}(1P))]$ assuming $B(\psi(2S) \to \gamma\chi_{c1}(1P)) = (9.07 \pm 0.11 \pm 0.54) \times 10^{-2}$, which we rescale to our best (shown rounded) value $B(\psi(2S) \to \gamma\chi_{c1}(1P)) = 9.85 \times 10^{-2}$.

$\Gamma(p\overline{p}\eta\pi^0)/\Gamma_{total}$ — Γ_{68}/Γ

VALUE (units 10^{-4})	EVTS	DOCUMENT ID		TECN	COMMENT
1.93±0.12±0.05	1695	[1] ABLIKIM	25L	BES3	$\psi(3686) \to \gamma p\overline{p}\eta\pi^0$

[1] ABLIKIM 25L reports $(1.95 \pm 0.05 \pm 0.12) \times 10^{-4}$ from a measurement of $[\Gamma(\chi_{c1}(1P) \to p\overline{p}\eta\pi^0)/\Gamma_{total}] \times [B(\psi(2S) \to \gamma\chi_{c1}(1P))]$ assuming $B(\psi(2S) \to \gamma\chi_{c1}(1P)) = (9.75 \pm 0.27) \times 10^{-2}$, which we rescale to our best (shown rounded) value $B(\psi(2S) \to \gamma\chi_{c1}(1P)) = (9.85 \pm 0.26) \times 10^{-2}$. Our first error is their experiment's error and our second error is the systematic error from using our best (shown rounded) value.

$\Gamma(p\overline{p}\eta\eta)/\Gamma_{total}$ — Γ_{69}/Γ

VALUE (units 10^{-5})	EVTS	DOCUMENT ID		TECN	COMMENT
1.39±0.37±0.04	51	[1] ABLIKIM	25CE	BES3	$\psi(2S) \to \gamma\chi_{c1}$

[1] ABLIKIM 25CE reports $(1.40 \pm 0.33 \pm 0.17) \times 10^{-5}$ from a measurement of $[\Gamma(\chi_{c1}(1P) \to p\overline{p}\eta\eta)/\Gamma_{total}] \times [B(\psi(2S) \to \gamma\chi_{c1}(1P))]$ assuming $B(\psi(2S) \to \gamma\chi_{c1}(1P)) = (9.75 \pm 0.27) \times 10^{-2}$, which we rescale to our best (shown rounded) value $B(\psi(2S) \to \gamma\chi_{c1}(1P)) = (9.85 \pm 0.26) \times 10^{-2}$. Our first error is their experiment's error and our second error is the systematic error from using our best (shown rounded) value.

$\Gamma(p\overline{p}K^+K^-)/\Gamma_{total}$ — Γ_{70}/Γ

VALUE (units 10^{-4})	EVTS	DOCUMENT ID		TECN	COMMENT
1.86±0.11±0.05	8721	[1] ABLIKIM	25V	BES3	$\psi(2S) \to \gamma p\overline{p}K^+K^-$

[1] ABLIKIM 25V reports $[\Gamma(\chi_{c1}(1P) \to p\overline{p}K^+K^-)/\Gamma_{total}] \times [B(\psi(2S) \to \gamma\chi_{c1}(1P))] = (1.83 \pm 0.02 \pm 0.11) \times 10^{-5}$ which we divide by our best (shown rounded) value $B(\psi(2S) \to \gamma\chi_{c1}(1P)) = (9.85 \pm 0.26) \times 10^{-2}$. Our first error is their experiment's error and our second error is the systematic error from using our best (shown rounded) value.

$\Gamma(p\overline{p}K^+K^-(\text{non-resonant}))/\Gamma_{total}$ — Γ_{71}/Γ

VALUE (units 10^{-4})	EVTS	DOCUMENT ID		TECN	COMMENT
1.26±0.22±0.03	82 ± 9	[1] ABLIKIM	11F	BES3	$\psi(2S) \to \gamma p\overline{p}K^+K^-$

[1] ABLIKIM 11F reports $(1.35 \pm 0.15 \pm 0.19) \times 10^{-4}$ from a measurement of $[\Gamma(\chi_{c1}(1P) \to p\overline{p}K^+K^-(\text{non-resonant}))/\Gamma_{total}] \times [B(\psi(2S) \to \gamma\chi_{c1}(1P))]$ assuming $B(\psi(2S) \to \gamma\chi_{c1}(1P)) = (9.2 \pm 0.4) \times 10^{-2}$, which we rescale to our best (shown rounded) value $B(\psi(2S) \to \gamma\chi_{c1}(1P)) = (9.85 \pm 0.26) \times 10^{-2}$. Our first error is their experiment's error and our second error is the systematic error from using our best (shown rounded) value.

$\Gamma(K^+\overline{p}\Lambda(1520) + \text{c.c.})/\Gamma_{total}$ — Γ_{72}/Γ

VALUE (units 10^{-4})	EVTS	DOCUMENT ID		TECN	COMMENT
1.69±0.43±0.04	48 ± 10	[1] ABLIKIM	11F	BES3	$\psi(2S) \to \gamma p\overline{p}K^+K^-$

[1] ABLIKIM 11F reports $(1.81 \pm 0.38 \pm 0.28) \times 10^{-4}$ from a measurement of $[\Gamma(\chi_{c1}(1P) \to K^+\overline{p}\Lambda(1520) + \text{c.c.})/\Gamma_{total}] \times [B(\psi(2S) \to \gamma\chi_{c1}(1P))]$ assuming $B(\psi(2S) \to \gamma\chi_{c1}(1P)) = (9.2 \pm 0.4) \times 10^{-2}$, which we rescale to our best (shown rounded) value $B(\psi(2S) \to \gamma\chi_{c1}(1P)) = (9.85 \pm 0.26) \times 10^{-2}$. Our first error is their experiment's error and our second error is the systematic error from using our best (shown rounded) value.

$\Gamma(\Lambda(1520)\overline{\Lambda}(1520))/\Gamma_{total}$ — Γ_{73}/Γ

VALUE	CL%	DOCUMENT ID		TECN	COMMENT
<9 × 10⁻⁵	90	[1] ABLIKIM	11F	BES3	$\psi(2S) \to \gamma p\overline{p}K^+K^-$

[1] ABLIKIM 11F reports $< 1.00 \times 10^{-4}$ from a measurement of $[\Gamma(\chi_{c1}(1P) \to \Lambda(1520)\overline{\Lambda}(1520))/\Gamma_{total}] \times [B(\psi(2S) \to \gamma\chi_{c1}(1P))]$ assuming $B(\psi(2S) \to \gamma\chi_{c1}(1P)) = (9.2 \pm 0.4) \times 10^{-2}$, which we rescale to our best (shown rounded) value $B(\psi(2S) \to \gamma\chi_{c1}(1P)) = 9.85 \times 10^{-2}$.

$\Gamma(p\overline{p}\phi)/\Gamma_{total}$ — Γ_{74}/Γ

VALUE	CL%	DOCUMENT ID		TECN	COMMENT
<1.7 × 10⁻⁵	90	[1] ABLIKIM	11F	BES3	$\psi(2S) \to \gamma p\overline{p}K^+K^-$

[1] ABLIKIM 11F reports $< 1.82 \times 10^{-5}$ from a measurement of $[\Gamma(\chi_{c1}(1P) \to p\overline{p}\phi)/\Gamma_{total}] \times [B(\psi(2S) \to \gamma\chi_{c1}(1P))]$ assuming $B(\psi(2S) \to \gamma\chi_{c1}(1P)) = (9.2 \pm 0.4) \times 10^{-2}$, which we rescale to our best (shown rounded) value $B(\psi(2S) \to \gamma\chi_{c1}(1P)) = 9.85 \times 10^{-2}$.

Int. J. Mod. Phys. A 2026.41. Downloaded from www.worldscientific.com by CALIFORNIA @ BERKELEY on 09/16/26. Re-use and distribution is strictly not permitted, except for Open Access articles.

$\Gamma(p\overline{p}K^0_S K^0_S)/\Gamma_{total}$ — Γ_{75}/Γ

VALUE	CL%	DOCUMENT ID		TECN	COMMENT
$<4\times10^{-4}$	90	[1] ABLIKIM	06D	BES2	$\psi(2S)\to\gamma\chi_{c1}$

[1] ABLIKIM 06D reports $<4.5\times10^{-4}$ from a measurement of $[\Gamma(\chi_{c1}(1P)\to p\overline{p}K^0_S K^0_S)/\Gamma_{total}]\times[B(\psi(2S)\to\gamma\chi_{c2}(1P))]$ assuming $B(\psi(2S)\to\gamma\chi_{c2}(1P))=(9.1\pm0.6)\times10^{-2}$, which we rescale to our best (shown rounded) value $B(\psi(2S)\to\gamma\chi_{c2}(1P))=9.63\times10^{-2}$.

$\Gamma(p\overline{n}\pi^-)/\Gamma_{total}$ — Γ_{77}/Γ

VALUE (units 10^{-4})	EVTS	DOCUMENT ID		TECN	COMMENT
3.8±0.5±0.1	1412	[1] ABLIKIM	12J	BES3	$\psi(2S)\to\gamma p\overline{n}\pi^-$

[1] ABLIKIM 12J reports $[\Gamma(\chi_{c1}(1P)\to p\overline{n}\pi^-)/\Gamma_{total}]\times[B(\psi(2S)\to\gamma\chi_{c1}(1P))]=(0.37\pm0.02\pm0.04)\times10^{-4}$ which we divide by our best (shown rounded) value $B(\psi(2S)\to\gamma\chi_{c1}(1P))=(9.85\pm0.26)\times10^{-2}$. Our first error is their experiment's error and our second error is the systematic error from using our best (shown rounded) value.

$\Gamma(\overline{p}n\pi^+)/\Gamma_{total}$ — Γ_{78}/Γ

VALUE (units 10^{-4})	EVTS	DOCUMENT ID		TECN	COMMENT
3.9±0.5±0.1	1625	[1] ABLIKIM	12J	BES3	$\psi(2S)\to\gamma\overline{p}n\pi^+$

[1] ABLIKIM 12J reports $[\Gamma(\chi_{c1}(1P)\to\overline{p}n\pi^+)/\Gamma_{total}]\times[B(\psi(2S)\to\gamma\chi_{c1}(1P))]=(0.38\pm0.02\pm0.04)\times10^{-4}$ which we divide by our best (shown rounded) value $B(\psi(2S)\to\gamma\chi_{c1}(1P))=(9.85\pm0.26)\times10^{-2}$. Our first error is their experiment's error and our second error is the systematic error from using our best (shown rounded) value.

$\Gamma(p\overline{n}\pi^-\pi^0)/\Gamma_{total}$ — Γ_{79}/Γ

VALUE (units 10^{-4})	EVTS	DOCUMENT ID		TECN	COMMENT
10.2±1.1±0.3	1082	[1] ABLIKIM	12J	BES3	$\psi(2S)\to\gamma p\overline{n}\pi^-\pi^0$

[1] ABLIKIM 12J reports $[\Gamma(\chi_{c1}(1P)\to p\overline{n}\pi^-\pi^0)/\Gamma_{total}]\times[B(\psi(2S)\to\gamma\chi_{c1}(1P))]=(1.00\pm0.05\pm0.10)\times10^{-4}$ which we divide by our best (shown rounded) value $B(\psi(2S)\to\gamma\chi_{c1}(1P))=(9.85\pm0.26)\times10^{-2}$. Our first error is their experiment's error and our second error is the systematic error from using our best (shown rounded) value.

$\Gamma(\overline{p}n\pi^+\pi^0)/\Gamma_{total}$ — Γ_{80}/Γ

VALUE (units 10^{-4})	EVTS	DOCUMENT ID		TECN	COMMENT
9.9±1.1±0.3	1261	[1] ABLIKIM	12J	BES3	$\psi(2S)\to\gamma\overline{p}n\pi^+\pi^0$

[1] ABLIKIM 12J reports $[\Gamma(\chi_{c1}(1P)\to\overline{p}n\pi^+\pi^0)/\Gamma_{total}]\times[B(\psi(2S)\to\gamma\chi_{c1}(1P))]=(0.98\pm0.05\pm0.10)\times10^{-4}$ which we divide by our best (shown rounded) value $B(\psi(2S)\to\gamma\chi_{c1}(1P))=(9.85\pm0.26)\times10^{-2}$. Our first error is their experiment's error and our second error is the systematic error from using our best (shown rounded) value.

$\Gamma(\Lambda\overline{\Lambda}\pi^+\pi^-)/\Gamma_{total}$ — Γ_{82}/Γ

VALUE (units 10^{-5})	CL%	EVTS	DOCUMENT ID		TECN	COMMENT
29±5±1		105	[1] ABLIKIM	12I	BES3	$\psi(2S)\to\gamma\Lambda\overline{\Lambda}\pi^+\pi^-$
• • • We do not use the following data for averages, fits, limits, etc. • • •						
<150	90		[2] ABLIKIM	06D	BES2	$\psi(2S)\to\gamma\chi_{c1}$

[1] ABLIKIM 12I reports $(31.1\pm3.4\pm3.9)\times10^{-5}$ from a measurement of $[\Gamma(\chi_{c1}(1P)\to\Lambda\overline{\Lambda}\pi^+\pi^-)/\Gamma_{total}]\times[B(\psi(2S)\to\gamma\chi_{c1}(1P))]$ assuming $B(\psi(2S)\to\gamma\chi_{c1}(1P))=(9.2\pm0.4)\times10^{-2}$, which we rescale to our best (shown rounded) value $B(\psi(2S)\to\gamma\chi_{c1}(1P))=(9.85\pm0.26)\times10^{-2}$. Our first error is their experiment's error and our second error is the systematic error from using our best (shown rounded) value.

[2] Using $B(\psi(2S)\to\chi_{c1}\gamma)$ (9.1 ± 0.6)%.

$\Gamma(\Lambda\overline{\Lambda}\pi^+\pi^-(\text{non-resonant}))/\Gamma_{total}$ — Γ_{83}/Γ

VALUE (units 10^{-5})	EVTS	DOCUMENT ID		TECN	COMMENT
24±6±1	13	[1] ABLIKIM	12I	BES3	$\psi(2S)\to\gamma\Lambda\overline{\Lambda}\pi^+\pi^-$

[1] ABLIKIM 12I reports $(26.2\pm5.5\pm3.3)\times10^{-5}$ from a measurement of $[\Gamma(\chi_{c1}(1P)\to\Lambda\overline{\Lambda}\pi^+\pi^-(\text{non-resonant}))/\Gamma_{total}]\times[B(\psi(2S)\to\gamma\chi_{c1}(1P))]$ assuming $B(\psi(2S)\to\gamma\chi_{c1}(1P))=(9.2\pm0.4)\times10^{-2}$, which we rescale to our best (shown rounded) value $B(\psi(2S)\to\gamma\chi_{c1}(1P))=(9.85\pm0.26)\times10^{-2}$. Our first error is their experiment's error and our second error is the systematic error from using our best (shown rounded) value.

$\Gamma(\Sigma(1385)^+\overline{\Lambda}\pi^-+\text{c.c.})/\Gamma_{total}$ — Γ_{84}/Γ

VALUE	CL%	DOCUMENT ID		TECN	COMMENT
$<1.3\times10^{-4}$	90	[1] ABLIKIM	12I	BES3	$\psi(2S)\to\gamma\Sigma(1385)^+\overline{\Lambda}\pi^-$

[1] ABLIKIM 12I reports $<14\times10^{-5}$ from a measurement of $[\Gamma(\chi_{c1}(1P)\to\Sigma(1385)^+\overline{\Lambda}\pi^-+\text{c.c.})/\Gamma_{total}]\times[B(\psi(2S)\to\gamma\chi_{c1}(1P))]$ assuming $B(\psi(2S)\to\gamma\chi_{c1}(1P))=(9.2\pm0.4)\times10^{-2}$, which we rescale to our best (shown rounded) value $B(\psi(2S)\to\gamma\chi_{c1}(1P))=9.85\times10^{-2}$.

$\Gamma(\Sigma(1385)^-\overline{\Lambda}\pi^++\text{c.c.})/\Gamma_{total}$ — Γ_{85}/Γ

VALUE (units 10^{-5})	CL%	DOCUMENT ID		TECN	COMMENT
<13	90	[1] ABLIKIM	12I	BES3	$\psi(2S)\to\gamma\Sigma(1385)^-\overline{\Lambda}\pi^+$

[1] ABLIKIM 12I reports $<14\times10^{-5}$ from a measurement of $[\Gamma(\chi_{c1}(1P)\to\Sigma(1385)^-\overline{\Lambda}\pi^++\text{c.c.})/\Gamma_{total}]\times[B(\psi(2S)\to\gamma\chi_{c1}(1P))]$ assuming $B(\psi(2S)\to\gamma\chi_{c1}(1P))=(9.2\pm0.4)\times10^{-2}$, which we rescale to our best (shown rounded) value $B(\psi(2S)\to\gamma\chi_{c1}(1P))=9.85\times10^{-2}$.

$\Gamma(K^+\overline{p}\Lambda+\text{c.c.})/\Gamma_{total}$ — Γ_{90}/Γ

VALUE (units 10^{-4})	EVTS	DOCUMENT ID		TECN	COMMENT
4.1±0.4 OUR AVERAGE	Error includes scale factor of 1.2.				
$9.2^{+2.8}_{-2.4}\pm0.4$	24	[1] LU	19	BELL	$B^+\to\overline{p}\Lambda K^+K^+$
$4.2\pm0.4\pm0.1$	3k	[2,3] ABLIKIM	13D	BES3	$\psi(2S)\to\gamma\Lambda\overline{p}K^+$
$3.0\pm0.9\pm0.1$		[4] ATHAR	07	CLEO	$\psi(2S)\to\gamma h^+h^-h^0$

[1] LU 19 reports $(9.15^{+2.63}_{-2.25}\pm0.86)\times10^{-4}$ from a measurement of $[\Gamma(\chi_{c1}(1P)\to K^+\overline{p}\Lambda+\text{c.c.})/\Gamma_{total}]\times[B(B^+\to\chi_{c1}(1P)K^+)]$ assuming $B(B^+\to\chi_{c1}(1P)K^+)=(4.79\pm0.23)\times10^{-4}$, which we rescale to our best (shown rounded) value $B(B^+\to\chi_{c1}(1P)K^+)=(4.74\pm0.22)\times10^{-4}$. Our first error is their experiment's error and our second error is the systematic error from using our best (shown rounded) value.

[2] ABLIKIM 13D reports $(4.5\pm0.2\pm0.4)\times10^{-4}$ from a measurement of $[\Gamma(\chi_{c1}(1P)\to K^+\overline{p}\Lambda+\text{c.c.})/\Gamma_{total}]\times[B(\psi(2S)\to\gamma\chi_{c1}(1P))]$ assuming $B(\psi(2S)\to\gamma\chi_{c1}(1P))=(9.2\pm0.4)\times10^{-2}$, which we rescale to our best (shown rounded) value $B(\psi(2S)\to\gamma\chi_{c1}(1P))=(9.85\pm0.26)\times10^{-2}$. Our first error is their experiment's error and our second error is the systematic error from using our best (shown rounded) value.

[3] Using $B(\Lambda\to p\pi^-)=63.9$%.

[4] ATHAR 07 reports $(3.3\pm0.9\pm0.4)\times10^{-4}$ from a measurement of $[\Gamma(\chi_{c1}(1P)\to K^+\overline{p}\Lambda+\text{c.c.})/\Gamma_{total}]\times[B(\psi(2S)\to\gamma\chi_{c1}(1P))]$ assuming $B(\psi(2S)\to\gamma\chi_{c1}(1P))=(9.07\pm0.11\pm0.54)\times10^{-2}$, which we rescale to our best (shown rounded) value $B(\psi(2S)\to\gamma\chi_{c1}(1P))=(9.85\pm0.26)\times10^{-2}$. Our first error is their experiment's error and our second error is the systematic error from using our best (shown rounded) value.

$\Gamma(nK^0_S\overline{\Lambda}+\text{c.c.})/\Gamma_{total}$ — Γ_{91}/Γ

VALUE (units 10^{-4})	EVTS	DOCUMENT ID		TECN	COMMENT
1.64±0.16±0.04	399	[1] ABLIKIM	21AV	BES3	$\psi(2S)\to\gamma nK^0_S\overline{\Lambda}+\text{c.c.}$

[1] ABLIKIM 21AV reports $(1.66\pm0.12\pm0.12)\times10^{-4}$ from a measurement of $[\Gamma(\chi_{c1}(1P)\to nK^0_S\overline{\Lambda}+\text{c.c.})/\Gamma_{total}]\times[B(\psi(2S)\to\gamma\chi_{c1}(1P))]$ assuming $B(\psi(2S)\to\gamma\chi_{c1}(1P))=0.0975\pm0.0024$, which we rescale to our best (shown rounded) value $B(\psi(2S)\to\gamma\chi_{c1}(1P))=(9.85\pm0.26)\times10^{-2}$. Our first error is their experiment's error and our second error is the systematic error from using our best (shown rounded) value. Also uses $B(\overline{\Lambda}\to\overline{p}\pi^+)=(63.9\pm0.5)$% and $B(K^0_S\to\pi^+\pi^-)=(69.20\pm0.05)$%.

$\Gamma(K^*(892)^+\overline{p}\Lambda+\text{c.c.})/\Gamma_{total}$ — Γ_{93}/Γ

VALUE (units 10^{-4})	EVTS	DOCUMENT ID		TECN	COMMENT
4.9±0.6±0.1	328	[1] ABLIKIM	19AU	BES3	$\psi(2S)\to\gamma K^{*+}\overline{p}\Lambda$

[1] ABLIKIM 19AU reports $[\Gamma(\chi_{c1}(1P)\to K^*(892)^+\overline{p}\Lambda+\text{c.c.})/\Gamma_{total}]\times[B(\psi(2S)\to\gamma\chi_{c1}(1P))]=(4.8\pm0.5\pm0.4)\times10^{-5}$ which we divide by our best (shown rounded) value $B(\psi(2S)\to\gamma\chi_{c1}(1P))=(9.85\pm0.26)\times10^{-2}$. Our first error is their experiment's error and our second error is the systematic error from using our best (shown rounded) value.

$\Gamma(\Sigma^0\overline{\Sigma}^0)/\Gamma_{total}$ — Γ_{94}/Γ

VALUE (units 10^{-5})	CL%	EVTS	DOCUMENT ID		TECN	COMMENT
4.2±0.6±0.1		103	[1] ABLIKIM	18V	BES3	$\psi(2S)\to\gamma\Sigma^0\overline{\Sigma}^0$
• • • We do not use the following data for averages, fits, limits, etc. • • •						
<6	90		[2] ABLIKIM	13H	BES3	$\psi(2S)\to\gamma\Sigma^0\overline{\Sigma}^0$
<4	90	3.8 ± 2.5	[3] NAIK	08	CLEO	$\psi(2S)\to\gamma\Sigma^0\overline{\Sigma}^0$

[1] ABLIKIM 18V reports $[\Gamma(\chi_{c1}(1P)\to\Sigma^0\overline{\Sigma}^0)/\Gamma_{total}]\times[B(\psi(2S)\to\gamma\chi_{c1}(1P))]=(0.41\pm0.05\pm0.03)\times10^{-5}$ which we divide by our best (shown rounded) value $B(\psi(2S)\to\gamma\chi_{c1}(1P))=(9.85\pm0.26)\times10^{-2}$. Our first error is their experiment's error and our second error is the systematic error from using our best (shown rounded) value.

[2] ABLIKIM 13H reports $<0.62\times10^{-4}$ from a measurement of $[\Gamma(\chi_{c1}(1P)\to\Sigma^0\overline{\Sigma}^0)/\Gamma_{total}]\times[B(\psi(2S)\to\gamma\chi_{c1}(1P))]$ assuming $B(\psi(2S)\to\gamma\chi_{c1}(1P))=(9.2\pm0.4)\times10^{-2}$, which we rescale to our best (shown rounded) value $B(\psi(2S)\to\gamma\chi_{c1}(1P))=9.85\times10^{-2}$.

[3] NAIK 08 reports $<0.44\times10^{-4}$ from a measurement of $[\Gamma(\chi_{c1}(1P)\to\Sigma^0\overline{\Sigma}^0)/\Gamma_{total}]\times[B(\psi(2S)\to\gamma\chi_{c1}(1P))]$ assuming $B(\psi(2S)\to\gamma\chi_{c1}(1P))=(9.07\pm0.11\pm0.54)\times10^{-2}$, which we rescale to our best (shown rounded) value $B(\psi(2S)\to\gamma\chi_{c1}(1P))=9.85\times10^{-2}$.

$\Gamma(\Sigma^+\overline{\Sigma}^-)/\Gamma_{total}$ — Γ_{97}/Γ

VALUE (units 10^{-5})	CL%	EVTS	DOCUMENT ID		TECN	COMMENT
3.6±0.6±0.1		59	[1] ABLIKIM	18V	BES3	$\psi(2S)\to\gamma\Sigma^+\overline{\Sigma}^-$
• • • We do not use the following data for averages, fits, limits, etc. • • •						
<8	90		[2] ABLIKIM	13H	BES3	$\psi(2S)\to\gamma\Sigma^+\overline{\Sigma}^-$
<6	90	4.3 ± 2.3	[3] NAIK	08	CLEO	$\psi(2S)\to\gamma\Sigma^+\overline{\Sigma}^-$

[1] ABLIKIM 18V reports $[\Gamma(\chi_{c1}(1P)\to\Sigma^+\overline{\Sigma}^-)/\Gamma_{total}]\times[B(\psi(2S)\to\gamma\chi_{c1}(1P))]=(0.35\pm0.06\pm0.02)\times10^{-5}$ which we divide by our best (shown rounded) value $B(\psi(2S)\to\gamma\chi_{c1}(1P))=(9.85\pm0.26)\times10^{-2}$. Our first error is their experiment's error and our second error is the systematic error from using our best (shown rounded) value.

[2] ABLIKIM 13H reports $<0.87\times10^{-4}$ from a measurement of $[\Gamma(\chi_{c1}(1P)\to\Sigma^+\overline{\Sigma}^-)/\Gamma_{total}]\times[B(\psi(2S)\to\gamma\chi_{c1}(1P))]$ assuming $B(\psi(2S)\to\gamma\chi_{c1}(1P))=(9.2\pm0.4)\times10^{-2}$, which we rescale to our best (shown rounded) value $B(\psi(2S)\to\gamma\chi_{c1}(1P))=9.85\times10^{-2}$.

[3] NAIK 08 reports $<0.65\times10^{-4}$ from a measurement of $[\Gamma(\chi_{c1}(1P)\to\Sigma^+\overline{\Sigma}^-)/\Gamma_{total}]\times[B(\psi(2S)\to\gamma\chi_{c1}(1P))]$ assuming $B(\psi(2S)\to\gamma\chi_{c1}(1P))=(9.07\pm0.11\pm0.54)\times10^{-2}$, which we rescale to our best (shown rounded) value $B(\psi(2S)\to\gamma\chi_{c1}(1P))=9.85\times10^{-2}$.

Int. J. Mod. Phys. A 2026.41. Downloaded from www.worldscientific.com
by UNIVERSITY OF CALIFORNIA @ BERKELEY on 09/16/26. Re-use and distribution is strictly not permitted, except for Open Access articles.

$\Gamma(\Sigma^+\overline{\Sigma}^-\eta)/\Gamma_{total}$ — Γ_{98}/Γ

VALUE (units 10^{-5})	EVTS	DOCUMENT ID		TECN	COMMENT
5.0±1.4±0.1	36	[1] ABLIKIM	24CA	BES3	$\psi(2S) \to \gamma\chi_{c1}(1P)$

[1] ABLIKIM 24CA reports $(5.10 \pm 1.21 \pm 0.67) \times 10^{-5}$ from a measurement of $[\Gamma(\chi_{c1}(1P) \to \Sigma^+\overline{\Sigma}^-\eta)/\Gamma_{total}] \times [B(\psi(2S) \to \gamma\chi_{c1}(1P))]$ assuming $B(\psi(2S) \to \gamma\chi_{c1}(1P)) = (9.75 \pm 0.24) \times 10^{-2}$, which we rescale to our best (shown rounded) value $B(\psi(2S) \to \gamma\chi_{c1}(1P)) = (9.85 \pm 0.26) \times 10^{-2}$. Our first error is their experiment's error and our second error is the systematic error from using our best (shown rounded) value.

$\Gamma(\Sigma^-\overline{\Sigma}^+)/\Gamma_{total}$ — Γ_{99}/Γ

VALUE (units 10^{-5})	EVTS	DOCUMENT ID		TECN	COMMENT
5.6±1.5±0.1	214	[1] ABLIKIM	20I	BES3	$\psi(2S) \to \gamma\Sigma^-\overline{\Sigma}^+$

[1] ABLIKIM 20I reports $(5.7 \pm 1.4 \pm 0.6) \times 10^{-5}$ from a measurement of $[\Gamma(\chi_{c1}(1P) \to \Sigma^-\overline{\Sigma}^+)/\Gamma_{total}] \times [B(\psi(2S) \to \gamma\chi_{c1}(1P))]$ assuming $B(\psi(2S) \to \gamma\chi_{c1}(1P)) = (9.75 \pm 0.24) \times 10^{-2}$, which we rescale to our best (shown rounded) value $B(\psi(2S) \to \gamma\chi_{c1}(1P)) = (9.85 \pm 0.26) \times 10^{-2}$. Our first error is their experiment's error and our second error is the systematic error from using our best (shown rounded) value.

$\Gamma(\Sigma(1385)^+\overline{\Sigma}(1385)^-)/\Gamma_{total}$ — Γ_{100}/Γ

VALUE	CL%	DOCUMENT ID		TECN	COMMENT
<9 × 10^{-5}	90	[1] ABLIKIM	12I	BES3	$\psi(2S) \to \gamma\Lambda\overline{\Lambda}\pi^+\pi^-$

[1] ABLIKIM 12I reports $< 10 \times 10^{-5}$ from a measurement of $[\Gamma(\chi_{c1}(1P) \to \Sigma(1385)^+\overline{\Sigma}(1385)^-)/\Gamma_{total}] \times [B(\psi(2S) \to \gamma\chi_{c1}(1P))]$ assuming $B(\psi(2S) \to \gamma\chi_{c1}(1P)) = (9.2 \pm 0.4) \times 10^{-2}$, which we rescale to our best (shown rounded) value $B(\psi(2S) \to \gamma\chi_{c1}(1P)) = 9.85 \times 10^{-2}$.

$\Gamma(\Sigma(1385)^-\overline{\Sigma}(1385)^+)/\Gamma_{total}$ — Γ_{101}/Γ

VALUE	CL%	DOCUMENT ID		TECN	COMMENT
<5 × 10^{-5}	90	[1] ABLIKIM	12I	BES3	$\psi(2S) \to \gamma\Lambda\overline{\Lambda}\pi^+\pi^-$

[1] ABLIKIM 12I reports $< 5.7 \times 10^{-5}$ from a measurement of $[\Gamma(\chi_{c1}(1P) \to \Sigma(1385)^-\overline{\Sigma}(1385)^+)/\Gamma_{total}] \times [B(\psi(2S) \to \gamma\chi_{c1}(1P))]$ assuming $B(\psi(2S) \to \gamma\chi_{c1}(1P)) = (9.2 \pm 0.4) \times 10^{-2}$, which we rescale to our best (shown rounded) value $B(\psi(2S) \to \gamma\chi_{c1}(1P)) = 9.85 \times 10^{-2}$.

$\Gamma(K^-\Lambda\overline{\Xi}^+ + \text{c.c.})/\Gamma_{total}$ — Γ_{102}/Γ

VALUE (units 10^{-4})	EVTS	DOCUMENT ID		TECN	COMMENT
1.34±0.24±0.04	49	[1] ABLIKIM	15I	BES3	$\psi(2S) \to \gamma K^-\Lambda\overline{\Xi}^+ + \text{c.c.}$

[1] ABLIKIM 15I reports $[\Gamma(\chi_{c1}(1P) \to K^-\Lambda\overline{\Xi}^+ + \text{c.c.})/\Gamma_{total}] \times [B(\psi(2S) \to \gamma\chi_{c1}(1P))] = (1.32 \pm 0.20 \pm 0.12) \times 10^{-5}$ which we divide by our best (shown rounded) value $B(\psi(2S) \to \gamma\chi_{c1}(1P)) = (9.85 \pm 0.26) \times 10^{-2}$. Our first error is their experiment's error and our second error is the systematic error from using our best (shown rounded) value.

$\Gamma(\Xi^0\overline{\Xi}^0)/\Gamma_{total}$ — Γ_{103}/Γ

VALUE (units 10^{-5})	CL%	EVTS	DOCUMENT ID		TECN	COMMENT
7.4±1.2±0.2		325	[1] ABLIKIM	22O	BES3	$\psi(2S) \to \gamma\Xi^0\overline{\Xi}^0$
• • • We do not use the following data for averages, fits, limits, etc. • • •						
<6	90	1.7 ± 2.4	[2] NAIK	08	CLEO	$\psi(2S) \to \gamma\Xi^0\overline{\Xi}^0$

[1] ABLIKIM 22O reports $(0.75 \pm 0.11 \pm 0.06) \times 10^{-4}$ from a measurement of $[\Gamma(\chi_{c1}(1P) \to \Xi^0\overline{\Xi}^0)/\Gamma_{total}] \times [B(\psi(2S) \to \gamma\chi_{c1}(1P))]$ assuming $B(\psi(2S) \to \gamma\chi_{c1}(1P)) = (9.75 \pm 0.24) \times 10^{-2}$, which we rescale to our best (shown rounded) value $B(\psi(2S) \to \gamma\chi_{c1}(1P)) = (9.85 \pm 0.26) \times 10^{-2}$. Our first error is their experiment's error and our second error is the systematic error from using our best (shown rounded) value.

[2] NAIK 08 reports $< 0.60 \times 10^{-4}$ from a measurement of $[\Gamma(\chi_{c1}(1P) \to \Xi^0\overline{\Xi}^0)/\Gamma_{total}] \times [B(\psi(2S) \to \gamma\chi_{c1}(1P))]$ assuming $B(\psi(2S) \to \gamma\chi_{c1}(1P)) = (9.07 \pm 0.11 \pm 0.54) \times 10^{-2}$, which we rescale to our best (shown rounded) value $B(\psi(2S) \to \gamma\chi_{c1}(1P)) = 9.85 \times 10^{-2}$.

$\Gamma(\Xi^-\overline{\Xi}^+)/\Gamma_{total}$ — Γ_{104}/Γ

VALUE (units 10^{-4})	CL%	EVTS	DOCUMENT ID		TECN	COMMENT
0.59±0.06 OUR AVERAGE						
0.57±0.06±0.02		692	[1] ABLIKIM	22O	BES3	$\psi(2S) \to \gamma\Xi^-\overline{\Xi}^+$
0.79±0.21±0.02		16.4±4.3	[2] NAIK	08	CLEO	$\psi(2S) \to \gamma\Xi^+\overline{\Xi}^-$
• • • We do not use the following data for averages, fits, limits, etc. • • •						
< 3.4		90	[3] ABLIKIM	06D	BES2	$\psi(2S) \to \gamma\chi_{c1}$

[1] ABLIKIM 22O reports $(0.58 \pm 0.04 \pm 0.05) \times 10^{-4}$ from a measurement of $[\Gamma(\chi_{c1}(1P) \to \Xi^-\overline{\Xi}^+)/\Gamma_{total}] \times [B(\psi(2S) \to \gamma\chi_{c1}(1P))]$ assuming $B(\psi(2S) \to \gamma\chi_{c1}(1P)) = (9.75 \pm 0.24) \times 10^{-2}$, which we rescale to our best (shown rounded) value $B(\psi(2S) \to \gamma\chi_{c1}(1P)) = (9.85 \pm 0.26) \times 10^{-2}$. Our first error is their experiment's error and our second error is the systematic error from using our best (shown rounded) value.

[2] NAIK 08 reports $(0.86 \pm 0.22 \pm 0.08) \times 10^{-4}$ from a measurement of $[\Gamma(\chi_{c1}(1P) \to \Xi^-\overline{\Xi}^+)/\Gamma_{total}] \times [B(\psi(2S) \to \gamma\chi_{c1}(1P))]$ assuming $B(\psi(2S) \to \gamma\chi_{c1}(1P)) = (9.07 \pm 0.11 \pm 0.54) \times 10^{-2}$, which we rescale to our best (shown rounded) value $B(\psi(2S) \to \gamma\chi_{c1}(1P)) = (9.85 \pm 0.26) \times 10^{-2}$. Our first error is their experiment's error and our second error is the systematic error from using our best (shown rounded) value.

[3] Using $B(\psi(2S) \to \chi_{c1}\gamma)$ $(9.1 \pm 0.6)\%$.

$\Gamma(\Omega^-\overline{\Omega}^+)/\Gamma_{total}$ — Γ_{105}/Γ

VALUE (units 10^{-5})	EVTS	DOCUMENT ID		TECN	COMMENT
1.47±0.25±0.04	277	[1] ABLIKIM	23T	BES3	$\chi_{c1} \to \Omega^-\overline{\Omega}^+$

[1] ABLIKIM 23T reports $(1.49 \pm 0.23 \pm 0.10) \times 10^{-5}$ from a measurement of $[\Gamma(\chi_{c1}(1P) \to \Omega^-\overline{\Omega}^+)/\Gamma_{total}] \times [B(\psi(2S) \to \gamma\chi_{c1}(1P))]$ assuming $B(\psi(2S) \to \gamma\chi_{c1}(1P)) = (9.75 \pm 0.24) \times 10^{-2}$, which we rescale to our best (shown rounded) value $B(\psi(2S) \to \gamma\chi_{c1}(1P)) = (9.85 \pm 0.26) \times 10^{-2}$. Our first error is their experiment's error and our second error is the systematic error from using our best (shown rounded) value.

$[\Gamma(\pi^+\pi^-) + \Gamma(K^+K^-)]/\Gamma_{total}$ — Γ_{106}/Γ

VALUE	CL%	DOCUMENT ID		TECN	COMMENT
<1.5 × 10^{-3}	90	[1] FELDMAN	77	MRK1	$\psi(2S) \to \gamma\chi_{c1}$
• • • We do not use the following data for averages, fits, limits, etc. • • •					
<3.8 × 10^{-3}	90	[2] BRANDELIK	79B	DASP	$\psi(2S) \to \gamma\chi_{c1}$

[1] FELDMAN 77 reports $[[\Gamma(\chi_{c1}(1P) \to \pi^+\pi^-) + \Gamma(K^+K^-)]/\Gamma_{total}] \times [B(\psi(2S) \to \gamma\chi_{c1}(1P))] < 1.5 \times 10^{-4}$ which we divide by our best (shown rounded) value $B(\psi(2S) \to \gamma\chi_{c1}(1P)) = 9.85 \times 10^{-2}$.

[2] Estimated using $B(\psi(2S) \to \gamma\chi_{c1}(1P)) = 0.087$. The errors do not contain the uncertainty in the $\psi(2S)$ decay.

$\Gamma(K^0_S K^0_S)/\Gamma_{total}$ — Γ_{107}/Γ

VALUE	CL%	DOCUMENT ID		TECN	COMMENT
<6 × 10^{-5}	90	[1] ABLIKIM	05O	BES2	$\psi(2S) \to \chi_{c1}\gamma$

[1] ABLIKIM 05O reports $[\Gamma(\chi_{c1}(1P) \to K^0_S K^0_S)/\Gamma_{total}] \times [B(\psi(2S) \to \gamma\chi_{c1}(1P))] < 0.6 \times 10^{-5}$ which we divide by our best (shown rounded) value $B(\psi(2S) \to \gamma\chi_{c1}(1P)) = 9.85 \times 10^{-2}$.

$\Gamma(\eta_c\pi^+\pi^-)/\Gamma_{total}$ — Γ_{108}/Γ

VALUE	CL%	DOCUMENT ID		TECN	COMMENT
<3.1 × 10^{-4}	90	[1,2] ABLIKIM	25BZ	BES3	$e^+e^- \to \psi(2S) \to \gamma\chi_{c1}$
• • • We do not use the following data for averages, fits, limits, etc. • • •					
<3.2 × 10^{-3}	90	[3,4] ABLIKIM	13B	BES3	$e^+e^- \to \psi(2S) \to \gamma\chi_{c1}$
<4.4 × 10^{-3}	90	[3,5] ABLIKIM	13B	BES3	$e^+e^- \to \psi(2S) \to \gamma\chi_{c1}$

[1] ABLIKIM 25BZ reports $< 3.1 \times 10^{-4}$ from a measurement of $[\Gamma(\chi_{c1}(1P) \to \eta_c\pi^+\pi^-)/\Gamma_{total}] \times [B(\psi(2S) \to \gamma\chi_{c1}(1P))]$ assuming $B(\psi(2S) \to \gamma\chi_{c1}(1P)) = (9.75 \pm 0.27) \times 10^{-2}$, which we rescale to our best (shown rounded) value $B(\psi(2S) \to \gamma\chi_{c1}(1P)) = 9.85 \times 10^{-2}$.

[2] Using 16 η_c decay channels.

[3] Using 1.06×10^8 $\psi(2S)$ mesons and $B(\psi(2S) \to \chi_{c1}\gamma) = (9.2 \pm 0.4)\%$.

[4] Using the $\eta_c \to K^0_S K^\pm\pi^\mp$ decays.

[5] Using the $\eta_c \to K^+K^-\pi^0$ decays.

RADIATIVE DECAYS

$\Gamma(\gamma\rho^0)/\Gamma_{total}$ — Γ_{110}/Γ

VALUE (units 10^{-6})	EVTS	DOCUMENT ID		TECN	COMMENT
214±17 OUR AVERAGE					
213±22±6	432 ± 25	[1] ABLIKIM	11E	BES3	$\psi(2S) \to \gamma\gamma\rho^0$
215±24±6	186 ± 15	[2] BENNETT	08A	CLEO	$\psi(2S) \to \gamma\gamma\rho^0$

[1] ABLIKIM 11E reports $(228 \pm 13 \pm 22) \times 10^{-6}$ from a measurement of $[\Gamma(\chi_{c1}(1P) \to \gamma\rho^0)/\Gamma_{total}] \times [B(\psi(2S) \to \gamma\chi_{c1}(1P))]$ assuming $B(\psi(2S) \to \gamma\chi_{c1}(1P)) = (9.2 \pm 0.4) \times 10^{-2}$, which we rescale to our best (shown rounded) value $B(\psi(2S) \to \gamma\chi_{c1}(1P)) = (9.85 \pm 0.26) \times 10^{-2}$. Our first error is their experiment's error and our second error is the systematic error from using our best (shown rounded) value.

[2] BENNETT 08A reports $(243 \pm 19 \pm 22) \times 10^{-6}$ from a measurement of $[\Gamma(\chi_{c1}(1P) \to \gamma\rho^0)/\Gamma_{total}] \times [B(\psi(2S) \to \gamma\chi_{c1}(1P))]$ assuming $B(\psi(2S) \to \gamma\chi_{c1}(1P)) = (8.7 \pm 0.4) \times 10^{-2}$, which we rescale to our best (shown rounded) value $B(\psi(2S) \to \gamma\chi_{c1}(1P)) = (9.85 \pm 0.26) \times 10^{-2}$. Our first error is their experiment's error and our second error is the systematic error from using our best (shown rounded) value.

$\Gamma(\gamma\omega)/\Gamma_{total}$ — Γ_{111}/Γ

VALUE (units 10^{-6})	EVTS	DOCUMENT ID		TECN	COMMENT
67± 8 OUR AVERAGE					
65± 9±2	136 ± 14	[1] ABLIKIM	11E	BES3	$\psi(2S) \to \gamma\gamma\omega$
73±17±2	39 ± 7	[2] BENNETT	08A	CLEO	$\psi(2S) \to \gamma\gamma\omega$

[1] ABLIKIM 11E reports $(69.7 \pm 7.2 \pm 6.6) \times 10^{-6}$ from a measurement of $[\Gamma(\chi_{c1}(1P) \to \gamma\omega)/\Gamma_{total}] \times [B(\psi(2S) \to \gamma\chi_{c1}(1P))]$ assuming $B(\psi(2S) \to \gamma\chi_{c1}(1P)) = (9.2 \pm 0.4) \times 10^{-2}$, which we rescale to our best (shown rounded) value $B(\psi(2S) \to \gamma\chi_{c1}(1P)) = (9.85 \pm 0.26) \times 10^{-2}$. Our first error is their experiment's error and our second error is the systematic error from using our best (shown rounded) value.

[2] BENNETT 08A reports $(83 \pm 15 \pm 12) \times 10^{-6}$ from a measurement of $[\Gamma(\chi_{c1}(1P) \to \gamma\omega)/\Gamma_{total}] \times [B(\psi(2S) \to \gamma\chi_{c1}(1P))]$ assuming $B(\psi(2S) \to \gamma\chi_{c1}(1P)) = (8.7 \pm 0.4) \times 10^{-2}$, which we rescale to our best (shown rounded) value $B(\psi(2S) \to \gamma\chi_{c1}(1P)) = (9.85 \pm 0.26) \times 10^{-2}$. Our first error is their experiment's error and our second error is the systematic error from using our best (shown rounded) value.

$\Gamma(\gamma\phi)/\Gamma_{total}$ — Γ_{112}/Γ

VALUE (units 10^{-6})	CL%	EVTS	DOCUMENT ID		TECN	COMMENT
24±5±1		43 ± 9	[1] ABLIKIM	11E	BES3	$\psi(2S) \to \gamma\gamma\phi$
• • • We do not use the following data for averages, fits, limits, etc. • • •						
<23	90	5.2 ± 3.1	[2] BENNETT	08A	CLEO	$\psi(2S) \to \gamma\gamma\phi$

[1] ABLIKIM 11E reports $(25.8 \pm 5.2 \pm 2.3) \times 10^{-6}$ from a measurement of $[\Gamma(\chi_{c1}(1P) \to \gamma\phi)/\Gamma_{total}] \times [B(\psi(2S) \to \gamma\chi_{c1}(1P))]$ assuming $B(\psi(2S) \to \gamma\chi_{c1}(1P)) = (9.2 \pm 0.4) \times 10^{-2}$, which we rescale to our best (shown rounded) value $B(\psi(2S) \to \gamma\chi_{c1}(1P))$

$= (9.85 \pm 0.26) \times 10^{-2}$. Our first error is their experiment's error and our second error is the systematic error from using our best (shown rounded) value.

[2] BENNETT 08A reports $< 26 \times 10^{-6}$ from a measurement of $[\Gamma(\chi_{c1}(1P) \to \gamma\phi)/\Gamma_{total}] \times [B(\psi(2S) \to \gamma\chi_{c1}(1P))]$ assuming $B(\psi(2S) \to \gamma\chi_{c1}(1P)) = (8.7 \pm 0.4) \times 10^{-2}$, which we rescale to our best (shown rounded) value $B(\psi(2S) \to \gamma\chi_{c1}(1P)) = 9.85 \times 10^{-2}$.

$\Gamma(\gamma\gamma)/\Gamma_{total}$ — Γ_{113}/Γ

VALUE	CL%	DOCUMENT ID		TECN	COMMENT
$< 6 \times 10^{-6}$	90	[1,2] ABLIKIM	17AE	BES3	$\psi(2S) \to \gamma\chi_{c1} \to 3\gamma$
• • • We do not use the following data for averages, fits, limits, etc. • • •					
$< 3.5 \times 10^{-5}$	90	ECKLUND	08A	CLEO	$\psi(2S) \to \gamma\chi_{c1} \to 3\gamma$
$< 150 \times 10^{-5}$	90	[3] YAMADA	77	DASP	$e^+e^- \to 3\gamma$

[1] ABLIKIM 17AE reports $< 6.3 \times 10^{-6}$ from a measurement of $[\Gamma(\chi_{c1}(1P) \to \gamma\gamma)/\Gamma_{total}] \times [B(\psi(2S) \to \gamma\chi_{c1}(1P))]$ assuming $B(\psi(2S) \to \gamma\chi_{c1}(1P)) = (9.55 \pm 0.31) \times 10^{-2}$, which we rescale to our best (shown rounded) value $B(\psi(2S) \to \gamma\chi_{c1}(1P)) = 9.85 \times 10^{-2}$.

[2] Decay forbidden by the Landau-Yang theorem.

[3] Estimated using $B(\psi(2S) \to \gamma\chi_{c1}(1P)) = 0.087$. The errors do not contain the uncertainty in the $\psi(2S)$ decay.

$\Gamma(e^+e^- J/\psi(1S))/\Gamma_{total}$ — Γ_{114}/Γ

VALUE (units 10^{-3})	EVTS	DOCUMENT ID		TECN	COMMENT
• • • We do not use the following data for averages, fits, limits, etc. • • •					
$3.62 \pm 0.23 \pm 0.10$	1.9k	[1,2] ABLIKIM	17I	BES3	$\psi(2S) \to \gamma e^+e^- J/\psi$

[1] ABLIKIM 17I reports $(3.73 \pm 0.09 \pm 0.25) \times 10^{-3}$ from a measurement of $[\Gamma(\chi_{c1}(1P) \to e^+e^- J/\psi(1S))/\Gamma_{total}] \times [B(\psi(2S) \to \gamma\chi_{c1}(1P))]$ assuming $B(\psi(2S) \to \gamma\chi_{c1}(1P)) = (9.55 \pm 0.31) \times 10^{-2}$, which we rescale to our best (shown rounded) value $B(\psi(2S) \to \gamma\chi_{c1}(1P)) = (9.85 \pm 0.26) \times 10^{-2}$. Our first error is their experiment's error and our second error is the systematic error from using our best (shown rounded) value.

[2] Not independent from other measurements reported by ABLIKIM 17I

$\Gamma(e^+e^- J/\psi(1S))/\Gamma(\gamma J/\psi(1S))$ — $\Gamma_{114}/\Gamma_{109}$

VALUE (units 10^{-3})	EVTS	DOCUMENT ID		TECN	COMMENT
$10.1 \pm 0.3 \pm 0.5$	1.9k	[1] ABLIKIM	17I	BES3	$\psi(2S) \to e^+e^-\gamma J/\psi$

[1] Uses $B(\psi(2S) \to \gamma\chi_{c1}(1P)) \times B(\chi_{c1}(1P) \to \gamma J/\psi(1S)) = (351.8 \pm 1.0 \pm 12.0) \times 10^{-4}$ from ABLIKIM 17N and accounts for common systematic errors.

$\Gamma(\mu^+\mu^- J/\psi(1S))/\Gamma(e^+e^- J/\psi(1S))$ — $\Gamma_{115}/\Gamma_{114}$

VALUE (units 10^{-2})	EVTS	DOCUMENT ID		TECN	COMMENT
$6.73 \pm 0.51 \pm 0.50$	222	ABLIKIM	19Z	BES3	$\psi(2S) \to \gamma\chi_c \to \gamma(\mu^+\mu^- J/\psi)$

$\chi_{c1}(1P)$ CROSS-PARTICLE BRANCHING RATIOS

$\Gamma(\chi_{c1}(1P) \to 2(\pi^+\pi^-))/\Gamma_{total} \times \Gamma(\psi(2S) \to \gamma\chi_{c1}(1P))/\Gamma_{total}$ — $\Gamma_4/\Gamma \times \Gamma_{197}^{\psi(2S)}/\Gamma^{\psi(2S)}$

VALUE (units 10^{-4})	EVTS	DOCUMENT ID		TECN	COMMENT
• • • We do not use the following data for averages, fits, limits, etc. • • •					
$6.68 \pm 0.01 \pm 0.25$	670k	[1,2] ABLIKIM	24BT	BES3	$\psi(2S) \to \gamma\chi_{c1}$

[1] Calculated by us. The value given here is derived from the value of $B(\chi_{c1} \to 2(\pi^+\pi^-))$ reported in ABLIKIM 24BT using $B(\psi(2S) \to \gamma\chi_{c1}) = (9.75 \pm 0.24)\%$ [PDG 22].

[2] Not used since the same experimental measurement has been used in another related quantity elsewhere.

$\Gamma(\chi_{c1}(1P) \to \overline{K}^0 K^+\pi^- + c.c.)/\Gamma_{total} \times \Gamma(\psi(2S) \to \gamma\chi_{c1}(1P))/\Gamma_{total}$ — $\Gamma_{19}/\Gamma \times \Gamma_{197}^{\psi(2S)}/\Gamma^{\psi(2S)}$

VALUE (units 10^{-4})	DOCUMENT ID		TECN	COMMENT
6.8 ± 0.6 OUR FIT Error includes scale factor of 1.1.				
7.2 ± 0.6 OUR AVERAGE				
$7.3 \pm 0.5 \pm 0.5$	[1] ATHAR	07	CLEO	$\psi(2S) \to \gamma K^0_S K^+\pi^-$
$7.0 \pm 0.5 \pm 0.9$	[2] ABLIKIM	06R	BES2	$\psi(2S) \to \gamma\chi_{c1}$

[1] Calculated by us. The value of $B(\chi_{c1} \to K^0 K^+\pi^- + c.c.)$ reported by ATHAR 07 was derived using $B(\psi(2S) \to \gamma\chi_{c1}(1P)) = (9.07 \pm 0.11 \pm 0.54)\%$.

[2] Calculated by us. ABLIKIM 06R reports $B(\chi_{c1} \to K^0_S K^+\pi^-) = (4.0 \pm 0.3 \pm 0.5) \times 10^{-3}$. We use $B(\psi(2S) \to \gamma\chi_{c1}) = (8.7 \pm 0.4) \times 10^{-2}$.

$\Gamma(\chi_{c1}(1P) \to \overline{K}^0 K^+\pi^- + c.c.)/\Gamma_{total} \times \Gamma(\psi(2S) \to \gamma\chi_{c1}(1P))/\Gamma(\psi(2S) \to J/\psi(1S)\pi^+\pi^-)$ — $\Gamma_{19}/\Gamma \times \Gamma_{197}^{\psi(2S)}/\Gamma_{12}^{\psi(2S)}$

VALUE (units 10^{-4})	DOCUMENT ID		TECN	COMMENT
19.6 ± 1.6 OUR FIT Error includes scale factor of 1.1.				
$13.2 \pm 2.4 \pm 3.2$	[1] BAI	99B	BES	$\psi(2S) \to \gamma K^0_S K^+\pi^-$

[1] Calculated by us. The value of $B(\chi_{c1} \to K^0_S K^+\pi^-)$ reported by BAI 99B was derived using $B(\psi(2S) \to \gamma\chi_{c1}(1P)) = (8.7 \pm 0.8)\%$ and $B(\psi(2S) \to J/\psi\pi^+\pi^-) = (32.4 \pm 2.6)\%$ [BAI 98D].

$\Gamma(\chi_{c1}(1P) \to 2\pi^+2\pi^-\eta)/\Gamma_{total} \times \Gamma(\psi(2S) \to \gamma\chi_{c1}(1P))/\Gamma_{total}$ — $\Gamma_{34}/\Gamma \times \Gamma_{197}^{\psi(2S)}/\Gamma^{\psi(2S)}$

VALUE (units 10^{-5})	EVTS	DOCUMENT ID		TECN	COMMENT
$78.7 \pm 0.3 \pm 7.4$	78k	ABLIKIM	25R	BES3	$e^+e^- \to \psi(2S)$

$\Gamma(\chi_{c1}(1P) \to K^+K^-K^+K^-)/\Gamma_{total} \times \Gamma(\psi(2S) \to \gamma\chi_{c1}(1P))/\Gamma_{total}$ — $\Gamma_{50}/\Gamma \times \Gamma_{197}^{\psi(2S)}/\Gamma^{\psi(2S)}$

VALUE (units 10^{-4})	EVTS	DOCUMENT ID		TECN	COMMENT
0.53 ± 0.11 OUR FIT					
$0.61 \pm 0.11 \pm 0.08$	54	[1] ABLIKIM	06T	BES2	$\psi(2S) \to \gamma K^+K^+K^-K^-$

[1] Calculated by us. The value of $B(\chi_{c1} \to 2K^+2K^-)$ reported by ABLIKIM 06T was derived using $B(\psi(2S) \to \gamma\chi_{c1}(1P)) = (8.7 \pm 0.8)\%$.

$\Gamma(\chi_{c1}(1P) \to K^+K^-K^+K^-)/\Gamma_{total} \times \Gamma(\psi(2S) \to \gamma\chi_{c1}(1P))/\Gamma(\psi(2S) \to J/\psi(1S)\pi^+\pi^-)$ — $\Gamma_{50}/\Gamma \times \Gamma_{197}^{\psi(2S)}/\Gamma_{12}^{\psi(2S)}$

VALUE (units 10^{-4})	DOCUMENT ID		TECN	COMMENT
1.51 ± 0.31 OUR FIT				
$1.13 \pm 0.40 \pm 0.29$	[1] BAI	99B	BES	$\psi(2S) \to \gamma K^+K^+K^-K^-$

[1] Calculated by us. The value of $B(\chi_{c1} \to 2K^+2K^-)$ reported by BAI 99B was derived using $B(\psi(2S) \to \gamma\chi_{c1}(1P)) = (8.7 \pm 0.8)\%$ and $B(\psi(2S) \to J/\psi\pi^+\pi^-) = (32.4 \pm 2.6)\%$ [BAI 98D].

$\Gamma(\chi_{c1}(1P) \to K^0_S K^0_S K^0_S K^\pm\pi^\mp)/\Gamma_{total} \times \Gamma(\psi(2S) \to \gamma\chi_{c1}(1P))/\Gamma_{total}$ — $\Gamma_{54}/\Gamma \times \Gamma_{197}^{\psi(2S)}/\Gamma^{\psi(2S)}$

VALUE (units 10^{-6})	EVTS	DOCUMENT ID		TECN	COMMENT
$25.6 \pm 0.8 \pm 1.9$	1190	[1] ABLIKIM	25AY	BES3	$\psi(3686) \to \gamma\chi_{c1}$

[1] ABLIKIM 24AY reports also a measurement $B(\chi_{c1}(1P) \to K^0_S K^0_S K^0_S K^\pm\pi^\mp) = (26.2 \pm 0.8 \pm 1.9) \times 10^{-5}$ from this product branching fraction using PDG 24 $B(\psi(2S) \to \gamma\chi_{c1})$ value.

$\Gamma(\chi_{c1}(1P) \to 3(K^+K^-))/\Gamma_{total} \times \Gamma(\psi(2S) \to \gamma\chi_{c1}(1P))/\Gamma_{total}$ — $\Gamma_{55}/\Gamma \times \Gamma_{197}^{\psi(2S)}/\Gamma^{\psi(2S)}$

VALUE (units 10^{-7})	EVTS	DOCUMENT ID		TECN	COMMENT
$4.1 \pm 0.9 \pm 0.5$	24.9 ± 5.1	[1] ABLIKIM	24P	BES3	$e^+e^- \to \psi(2S)$

[1] Systematic error derived by us, based on the text.

$\Gamma(\chi_{c1}(1P) \to p\overline{p})/\Gamma_{total} \times \Gamma(\psi(2S) \to \gamma\chi_{c1}(1P))/\Gamma_{total}$ — $\Gamma_{62}/\Gamma \times \Gamma_{197}^{\psi(2S)}/\Gamma^{\psi(2S)}$

VALUE (units 10^{-6})	EVTS	DOCUMENT ID		TECN	COMMENT
7.85 ± 0.26 OUR FIT Error includes scale factor of 1.6.					
7.93 ± 0.17 OUR AVERAGE					
$7.96 \pm 0.09 \pm 0.15$	11279	[1] ABLIKIM	25H	BES3	$\psi(2S) \to \gamma p\overline{p}$
$8.2 \pm 0.7 \pm 0.4$	141 ± 13	[2] NAIK	08	CLEO	$\psi(2S) \to \gamma p\overline{p}$
$4.8 {}^{+1.4}_{-1.3} \pm 0.6$	$18.2 {}^{+5.5}_{-4.9}$	BAI	04F	BES	$\psi(2S) \to \gamma\chi_{c1}(1P) \to \gamma\overline{p}p$
• • • We do not use the following data for averages, fits, limits, etc. • • •					
$7.9 \pm 0.4 \pm 0.3$	453	[3] ABLIKIM	13V	BES3	$\psi(2S) \to \gamma p\overline{p}$

[1] Calculated by us. ABLIKIM 25H reports $B(\chi_{c1} \to p\overline{p}) = (8.16 \pm 0.09 \pm 0.25) \times 10^{-5}$ using $B(\psi(2S) \to \gamma\chi_{c1}) = (9.75 \pm 0.24)\%$.

[2] Calculated by us. NAIK 08 reports $B(\chi_{c1} \to p\overline{p}) = (9.0 \pm 0.8 \pm 0.4 \pm 0.5) \times 10^{-5}$ using $B(\psi(2S) \to \gamma\chi_{c1}) = (9.07 \pm 0.11 \pm 0.54)\%$.

[3] Superseded by ABLIKIM 25H

$\Gamma(\chi_{c1}(1P) \to p\overline{p})/\Gamma_{total} \times \Gamma(\psi(2S) \to \gamma\chi_{c1}(1P))/\Gamma(\psi(2S) \to J/\psi(1S)\pi^+\pi^-)$ — $\Gamma_{62}/\Gamma \times \Gamma_{197}^{\psi(2S)}/\Gamma_{12}^{\psi(2S)}$

VALUE (units 10^{-5})	DOCUMENT ID		TECN	COMMENT
2.26 ± 0.08 OUR FIT Error includes scale factor of 1.5.				
1.1 ± 1.0	[1] BAI	98I	BES	$\psi(2S) \to \gamma\chi_{c1} \to \gamma\overline{p}p$

[1] Calculated by us. The value for $B(\chi_{c1} \to p\overline{p})$ reported in BAI 98I is derived using $B(\psi(2S) \to \gamma\chi_{c1}) = (8.7 \pm 0.8)\%$ and $B(\psi(2S) \to J/\psi(1S)\pi^+\pi^-) = (32.4 \pm 2.6)\%$ [BAI 98D].

$\Gamma(\chi_{c1}(1P) \to p\overline{p}K^0_S K^-\pi^+ + c.c.)/\Gamma_{total} \times \Gamma(\psi(2S) \to \gamma\chi_{c1}(1P))/\Gamma_{total}$ — $\Gamma_{76}/\Gamma \times \Gamma_{197}^{\psi(2S)}/\Gamma^{\psi(2S)}$

VALUE (units 10^{-6})	EVTS	DOCUMENT ID		TECN	COMMENT
$4.05 \pm 0.24 \pm 0.39$	396	ABLIKIM	24BX	BES3	$\psi(2S) \to \gamma\chi_{c1}$

$\Gamma(\chi_{c1}(1P) \to \Lambda\overline{\Lambda})/\Gamma_{total} \times \Gamma(\psi(2S) \to \gamma\chi_{c1}(1P))/\Gamma_{total}$ — $\Gamma_{81}/\Gamma \times \Gamma_{197}^{\psi(2S)}/\Gamma^{\psi(2S)}$

VALUE (units 10^{-6})	EVTS	DOCUMENT ID		TECN	COMMENT
12.4 ± 0.9 OUR FIT Error includes scale factor of 1.1.					
12.3 ± 0.9 OUR AVERAGE Error includes scale factor of 1.2.					
$12.8 \pm 0.6 \pm 0.6$	528	ABLIKIM	21L	BES3	$\psi(2S) \to \gamma p\pi^-\overline{p}\pi^+$
$10.5 \pm 1.6 \pm 0.6$	46	[1] NAIK	08	CLEO	$\psi(2S) \to \gamma\Lambda\overline{\Lambda}$
• • • We do not use the following data for averages, fits, limits, etc. • • •					
$11.2 \pm 1.0 \pm 0.9$	136	[2,3] ABLIKIM	13H	BES3	$\psi(2S) \to \gamma\Lambda\overline{\Lambda}$

[1] Calculated by us. NAIK 08 reports $B(\chi_{c1} \to \Lambda\overline{\Lambda}) = (11.6 \pm 1.8 \pm 0.7 \pm 0.7) \times 10^{-5}$ using $B(\psi(2S) \to \gamma\chi_{c1}) = (9.07 \pm 0.11 \pm 0.54)\%$.

[2] Superseded by ABLIKIM 21L

[3] Calculated by us. ABLIKIM 13H reports $B(\chi_{c1} \to \Lambda\overline{\Lambda}) = (12.2 \pm 1.1 \pm 1.1) \times 10^{-5}$ from a measurement of $B(\chi_{c1} \to \Lambda\overline{\Lambda}) \times B(\psi(2S) \to \gamma\chi_{c1})$ assuming $B(\psi(2S) \to \gamma\chi_{c1}) = (9.2 \pm 0.4)\%$.

Int. J. Mod. Phys. A 2026.41. Downloaded from www.worldscientific.com
by LIFORNIA @ BERKELEY on 09/16/26. Re-use and distribution is strictly not permitted, except for Open Access articles.

Int. J. Mod. Phys. A 2026.41. Downloaded from www.worldscientific.com
by UNIVERSITY OF CALIFORNIA @ BERKELEY on 09/16/26. Re-use and distribution is strictly not permitted, except for Open Access articles.

$\Gamma(\chi_{c1}(1P) \to \Lambda\overline{\Lambda})/\Gamma_{total} \times \Gamma(\psi(2S) \to \gamma\chi_{c1}(1P))/\Gamma(\psi(2S) \to J/\psi(1S)\pi^+\pi^-)$ — $\Gamma_{81}/\Gamma \times \Gamma^{\psi(2S)}_{197}/\Gamma^{\psi(2S)}_{12}$

VALUE (units 10^{-5})	EVTS	DOCUMENT ID		TECN	COMMENT
3.57±0.25 OUR FIT	Error includes scale factor of 1.1.				
7.1 $^{+2.8}_{-2.4}$ ±1.3	$9.0^{+3.5}_{-3.1}$	[1] BAI	03E	BES	$\psi(2S) \to \gamma\Lambda\overline{\Lambda}$

[1] BAI 03E reports [$B(\chi_{c1} \to \Lambda\overline{\Lambda})\, B(\psi(2S) \to \gamma\chi_{c1})$ / $B(\psi(2S) \to J/\psi\pi^+\pi^-)$] × [$B^2(\Lambda \to \pi^- p)$ / $B(J/\psi \to p\overline{p})$] = $(1.33^{+0.52}_{-0.46} \pm 0.25)$%. We calculate from this measurement the presented value using $B(\Lambda \to \pi^- p) = (63.9 \pm 0.5)$% and $B(J/\psi \to p\overline{p}) = (2.17 \pm 0.07) \times 10^{-3}$.

$\Gamma(\chi_{c1}(1P) \to \Lambda\overline{\Lambda}\eta)/\Gamma_{total} \times \Gamma(\psi(2S) \to \gamma\chi_{c1}(1P))/\Gamma_{total}$ — $\Gamma_{86}/\Gamma \times \Gamma^{\psi(2S)}_{197}/\Gamma^{\psi(2S)}$

VALUE (units 10^{-6})	EVTS	DOCUMENT ID		TECN	COMMENT
5.72±1.34±0.65	21	ABLIKIM	22AO	BES3	$\psi(2S) \to \gamma p\pi^-\overline{p}\pi^+\gamma\gamma$

$\Gamma(\chi_{c1}(1P) \to \Lambda\overline{\Lambda}\eta')/\Gamma_{total} \times \Gamma(\psi(2S) \to \gamma\chi_{c1}(1P))/\Gamma_{total}$ — $\Gamma_{87}/\Gamma \times \Gamma^{\psi(2S)}_{197}/\Gamma^{\psi(2S)}$

VALUE (units 10^{-6})	DOCUMENT ID		TECN	COMMENT
1.50±0.50±0.15	[1] ABLIKIM	25BX	BES3	$\psi(2S) \to \gamma\chi_{c1}$

[1] Calculated by us. ABLIKIM 25BX reports $B(\chi_{c1} \to \Lambda\overline{\Lambda}\eta') = (1.54 \pm 0.51 \pm 0.16) \times 10^{-5}$ from a measurement of $B(\chi_{c1} \to \Lambda\overline{\Lambda}\eta') \times B(\psi(2S) \to \gamma\chi_{c1})$ assuming $B(\psi(2S) \to \gamma\chi_{c1}) = (9.75 \pm 0.27)$%.

$\Gamma(\chi_{c1}(1P) \to \Lambda\overline{\Lambda}\omega)/\Gamma_{total} \times \Gamma(\psi(2S) \to \gamma\chi_{c1}(1P))/\Gamma_{total}$ — $\Gamma_{88}/\Gamma \times \Gamma^{\psi(2S)}_{197}/\Gamma^{\psi(2S)}$

VALUE (units 10^{-6})	EVTS	DOCUMENT ID		TECN	COMMENT
9.8±1.0±1.1	202 ± 20	[1] ABLIKIM	24BE	BES3	$e^+e^- \to \psi(2S) \to \gamma\chi_{c1}$

[1] Calculated by us. The authors report $B(\chi_{c1} \to \Lambda\overline{\Lambda}\omega)$ obtained from a product using PDG 22 value of $B(\psi(2S) \to \gamma\chi_{c1})$.

$\Gamma(\chi_{c1}(1P) \to \Lambda\overline{\Lambda}\phi)/\Gamma_{total} \times \Gamma(\psi(2S) \to \gamma\chi_{c1}(1P))/\Gamma_{total}$ — $\Gamma_{89}/\Gamma \times \Gamma^{\psi(2S)}_{197}/\Gamma^{\psi(2S)}$

VALUE (units 10^{-6})	EVTS	DOCUMENT ID		TECN	COMMENT
5.86±0.87±0.39	51.6	ABLIKIM	24AC	BES3	$\psi(2S) \to \gamma\chi_{c1}$

$\Gamma(\chi_{c1}(1P) \to \overline{p}\Lambda(1520)K^0_S\pi^+ + c.c.)/\Gamma_{total} \times \Gamma(\psi(2S) \to \gamma\chi_{c1}(1P))/\Gamma_{total}$ — $\Gamma_{92}/\Gamma \times \Gamma^{\psi(2S)}_{197}/\Gamma^{\psi(2S)}$

VALUE (units 10^{-6})	EVTS	DOCUMENT ID		TECN	COMMENT
$3.96^{+0.77}_{-0.74}$±0.50	88	ABLIKIM	24BX	BES3	$\psi(2S) \to \gamma\chi_{c1}$

$\Gamma(\chi_{c1}(1P) \to \Sigma^+\overline{p}K^0_S + c.c.)/\Gamma_{total} \times \Gamma(\psi(2S) \to \gamma\chi_{c1}(1P))/\Gamma_{total}$ — $\Gamma_{95}/\Gamma \times \Gamma^{\psi(2S)}_{197}/\Gamma^{\psi(2S)}$

VALUE (units 10^{-5})	EVTS	DOCUMENT ID		TECN	COMMENT
1.49±0.09±0.07	258	[1] ABLIKIM	19BB	BES3	$\psi(2S) \to \gamma\Sigma^+\overline{p}K^0_S$ + c.c.

[1] Calculated by us. ABLIKIM 19BB reports $B(\chi_{c1} \to \Sigma^+\overline{p}K^0_S + c.c.) = (1.53 \pm 0.10 \pm 0.08) \times 10^{-4}$ using $B(\psi(2S) \to \gamma\chi_{c1}) = (9.75 \pm 0.24)$% and other branching fractions from PDG 18.

$\Gamma(\chi_{c1}(1P) \to \Sigma^0\overline{p}K^+ + c.c.)/\Gamma_{total} \times \Gamma(\psi(2S) \to \gamma\chi_{c1}(1P))/\Gamma_{total}$ — $\Gamma_{96}/\Gamma \times \Gamma^{\psi(2S)}_{197}/\Gamma^{\psi(2S)}$

VALUE (units 10^{-5})	EVTS	DOCUMENT ID		TECN	COMMENT
1.42±0.07±0.06	493	[1] ABLIKIM	20AE	BES3	$\psi(2S) \to \gamma\Sigma^0\overline{p}K^+$ + c.c.

[1] Calculated by us. ABLIKIM 20AE reports $B(\chi_{c1} \to \Sigma^0\overline{p}K^+ + c.c.) = (1.46 \pm 0.07 \pm 0.07) \times 10^{-4}$ using $B(\psi(2S) \to \gamma\chi^0_c) = (9.75 \pm 0.24)$% and other branching fractions from PDG 20.

$\Gamma(\chi_{c1}(1P) \to \gamma J/\psi(1S))/\Gamma_{total} \times \Gamma(\psi(2S) \to \gamma\chi_{c1}(1P))/\Gamma_{total}$ — $\Gamma_{109}/\Gamma \times \Gamma^{\psi(2S)}_{197}/\Gamma^{\psi(2S)}$

VALUE (units 10^{-2})	EVTS	DOCUMENT ID		TECN	COMMENT
3.34 ±0.10 OUR FIT	Error includes scale factor of 1.7.				
3.24 ±0.16 OUR AVERAGE	Error includes scale factor of 2.1. See the ideogram below.				
3.518±0.010±0.120	143k	[1] ABLIKIM	17N	BES3	$\psi(2S) \to \gamma\gamma J/\psi$
3.442±0.010±0.132	1.9M	ABLIKIM	17U	BES3	$e^+e^- \to \gamma X$
2.81 ±0.05 ±0.23	13k	BAI	04I	BES2	$\psi(2S) \to J/\psi\gamma\gamma$
2.56 ±0.12 ±0.20		GAISER	86	CBAL	$\psi(2S) \to \gamma X$
2.78 ±0.30		[2] OREGLIA	82	CBAL	$\psi(2S) \to \gamma\chi_{c1}$
2.2 ±0.5		[3] BRANDELIK	79B	DASP	$\psi(2S) \to \gamma\chi_{c1}$
2.9 ±0.5		[3] BARTEL	78B	CNTR	$\psi(2S) \to \gamma\chi_{c1}$
5.0 ±1.5		[4] BIDDICK	77	CNTR	$e^+e^- \to \gamma X$
2.8 ±0.9		[2] WHITAKER	76	MRK1	e^+e^-
• • • We do not use the following data for averages, fits, limits, etc. • • •					
3.377±0.009±0.183	142k	[5] ABLIKIM	12O	BES3	$\psi(2S) \to \gamma\chi_{c1}$
3.56 ±0.03 ±0.12	24.9k	[6] MENDEZ	08	CLEO	$\psi(2S) \to \gamma\chi_{c1}$
3.44 ±0.06 ±0.13	3.7k	[7] ADAM	05A	CLEO	Repl. by MENDEZ 08

[1] Uses $B(J/\psi \to e^+e^-) = (5.971 \pm 0.032)$% and $B(J/\psi \to \mu^+\mu^-) = (5.961 \pm 0.033)$%.
[2] Recalculated by us using $B(J/\psi(1S) \to \ell^+\ell^-) = 0.1181 \pm 0.0020$.
[3] Recalculated by us using $B(J/\psi(1S) \to \mu^+\mu^-) = 0.0588 \pm 0.0010$.
[4] Assumes isotropic gamma distribution.
[5] Superseded by ABLIKIM 17N.
[6] Not independent from other measurements of MENDEZ 08.
[7] Not independent from other values reported by ADAM 05A.

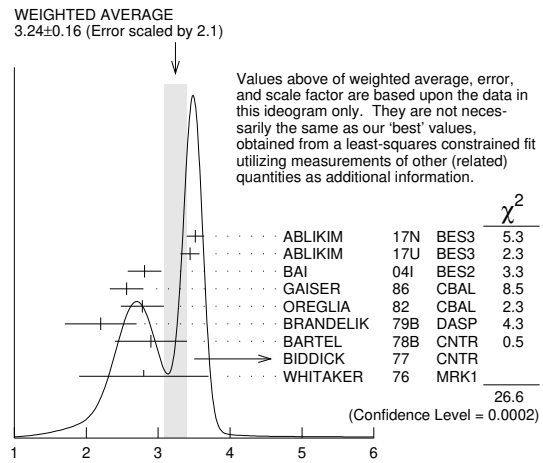

$\Gamma(\chi_{c1}(1P) \to \gamma J/\psi(1S))/\Gamma_{total} \times \Gamma(\psi(2S) \to \gamma\chi_{c1}(1P))/\Gamma_{total}$ (units 10^{-2})

$\Gamma(\chi_{c1}(1P) \to \gamma J/\psi(1S))/\Gamma_{total} \times \Gamma(\psi(2S) \to \gamma\chi_{c1}(1P))/\Gamma(\psi(2S) \to J/\psi(1S)\pi^+\pi^-)$ — $\Gamma_{109}/\Gamma \times \Gamma^{\psi(2S)}_{197}/\Gamma^{\psi(2S)}_{12}$

VALUE (units 10^{-2})	EVTS	DOCUMENT ID		TECN	COMMENT
9.59±0.29 OUR FIT	Error includes scale factor of 1.7.				
10.15±0.28 OUR AVERAGE					
10.17±0.07±0.27	24.9k	MENDEZ	08	CLEO	$\psi(2S) \to \gamma\chi_{c1}$
12.6 ±0.3 ±3.8	3k	[1] ABLIKIM	04B	BES	$\psi(2S) \to J/\psi X$
8.5 ±2.1		[2] HIMEL	80	MRK2	$\psi(2S) \to \gamma\chi_{c1}$
• • • We do not use the following data for averages, fits, limits, etc. • • •					
10.24±0.17±0.23	3.7k	[3] ADAM	05A	CLEO	Repl. by MENDEZ 08

[1] From a fit to the J/ψ recoil mass spectra.
[2] The value for $B(\psi(2S) \to \gamma\chi_{c1}) \times B(\chi_{c1} \to \gamma J/\psi(1S))$ quoted in HIMEL 80 is derived using $B(\psi(2S) \to J/\psi(1S)\pi^+\pi^-) = (33 \pm 3)$% and $B(J/\psi(1S) \to \ell^+\ell^-) = 0.138 \pm 0.018$. Calculated by us using $B(J/\psi(1S) \to \ell^+\ell^-) = 0.1181 \pm 0.0020$.
[3] Not independent from other values reported by ADAM 05A.

MULTIPOLE AMPLITUDES IN $\chi_{c1}(1P) \to \gamma J/\psi(1S)$

$a_2 = M2/\sqrt{E1^2 + M2^2}$ Magnetic quadrupole fractional transition amplitude

VALUE (units 10^{-2})	EVTS	DOCUMENT ID		TECN	COMMENT
−6.7 ±0.9 OUR AVERAGE	Error includes scale factor of 2.6. See the ideogram below.				
−7.40±0.33±0.34	164k	[1] ABLIKIM	17N	BES3	$\psi(2S) \to \gamma\gamma\ell^+\ell^-$
−6.26±0.63±0.24	39k	ARTUSO	09	CLEO	$\psi(2S) \to \gamma\gamma\ell^+\ell^-$
0.2 ±3.2 ±0.4	2090	AMBROGIANI	02	E835	$p\overline{p} \to \chi_{c1} \to J/\psi\gamma$
−0.2 $^{+0.8}_{-2.0}$	921	OREGLIA	82	CBAL	$\psi(2S) \to \chi_{c1}\gamma \to J/\psi\gamma\gamma$

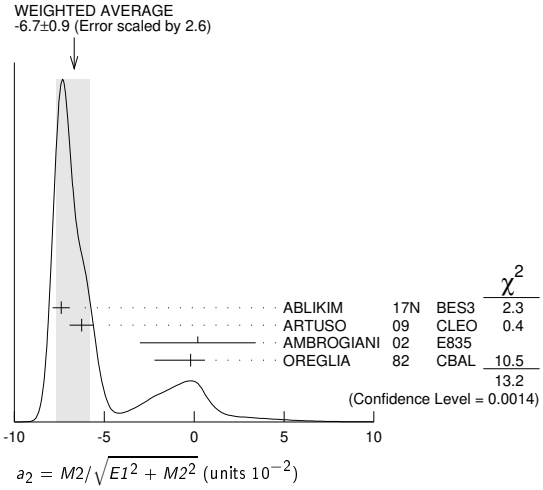

$a_2 = M2/\sqrt{E1^2 + M2^2}$ (units 10^{-2})

Int. J. Mod. Phys. A 2026.41. Downloaded from www.worldscientific.com by UNIVERSITY OF CALIFORNIA @ BERKELEY on 09/16/26. Re-use and distribution is strictly not permitted, except for Open Access articles.

[1] Correlated with b_2 with correlation coefficient $\rho_{a_2 b_2} = 0.133$.

MULTIPOLE AMPLITUDES IN $\psi(2S) \to \gamma\chi_{c1}(1S)$ RADIATIVE DECAY

$b_2 = M2/\sqrt{E1^2 + M2^2}$ Magnetic quadrupole fractional transition amplitude

VALUE (units 10^{-2})	EVTS	DOCUMENT ID		TECN	COMMENT
2.5 ±0.4 OUR AVERAGE					
2.29±0.39±0.27	164k	[1] ABLIKIM	17N	BES3	$\psi(2S) \to \gamma\gamma\ell^+\ell^-$
2.76±0.73±0.23	39k	ARTUSO	09	CLEO	$\psi(2S) \to \gamma\gamma\ell^+\ell^-$
$7.7\ ^{+5.0}_{-4.5}$	921	OREGLIA	82	CBAL	$\psi(2S) \to \gamma\gamma\ell^+\ell^-$

[1] Correlated with a_2 with correlation coefficient $\rho_{a_2 b_2} = 0.133$.

MULTIPOLE AMPLITUDE RATIOS IN RADIATIVE DECAYS $\psi(2S) \to \gamma\chi_{c1}(1S)$ and $\chi_{c1} \to \gamma J/\psi(1S)$

a_2/b_2 Magnetic quadrupole transition amplitude ratio

VALUE	EVTS	DOCUMENT ID		TECN	COMMENT
$\mathbf{-2.27^{+0.57}_{-0.99}}$	39k	[1] ARTUSO	09	CLEO	$\psi(2S) \to \gamma\gamma\ell^+\ell^-$

[1] Statistical and systematic errors combined. Not independent of $a_2(\chi_{c1})$ and $b_2(\chi_{c1})$ values from ARTUSO 09.

$\chi_{c1}(1P)$ REFERENCES

ABLIKIM	25AY	PR D112 012007	M. Ablikim et al.	(BESIII Collab.)
ABLIKIM	25BX	PR D112 112015	M. Ablikim et al.	(BESIII Collab.)
ABLIKIM	25BZ	PR D112 112018	M. Ablikim et al.	(BESIII Collab.)
ABLIKIM	25CE	JHEP 2510 090	M. Ablikim et al.	(BESIII Collab.)
ABLIKIM	25CJ	CP C49 123001	M. Ablikim et al.	(BESIII Collab.)
ABLIKIM	25H	PR D111 012003	M. Ablikim et al.	(BESIII Collab.)
ABLIKIM	25I	PR D111 012004	M. Ablikim et al.	(BESIII Collab.)
ABLIKIM	25K	PR D111 032001	M. Ablikim et al.	(BESIII Collab.)
ABLIKIM	25L	PR D111 032008	M. Ablikim et al.	(BESIII Collab.)
ABLIKIM	25R	PR D111 052013	M. Ablikim et al.	(BESIII Collab.)
ABLIKIM	25V	PR D111 072001	M. Ablikim et al.	(BESIII Collab.)
ABLIKIM	24AC	PR D110 032016	M. Ablikim et al.	(BESIII Collab.)
ABLIKIM	24AY	PR D109 L071103	M. Ablikim et al.	(BESIII Collab.)
ABLIKIM	24BE	PR D110 032022	M. Ablikim et al.	(BESIII Collab.)
ABLIKIM	24BT	PR D110 072009	M. Ablikim et al.	(BESIII Collab.)
ABLIKIM	24BW	PR D110 092003	M. Ablikim et al.	(BESIII Collab.)
ABLIKIM	24BX	PR D110 112009	M. Ablikim et al.	(BESIII Collab.)
ABLIKIM	24CA	PR D110 112013	M. Ablikim et al.	(BESIII Collab.)
ABLIKIM	24P	PR D109 072016	M. Ablikim et al.	(BESIII Collab.)
PDG	24	PR D110 030001	S. Navas et al.	(PDG Collab.)
AAIJ	23AH	PR D108 032010	R. Aaij et al.	(LHCb Collab.)
ABLIKIM	23N	JHEP 2305 069	M. Ablikim et al.	(BESIII Collab.)
ABLIKIM	23T	PR D107 092004	M. Ablikim et al.	(BESIII Collab.)
ABLIKIM	22AF	PRL 129 122001	M. Ablikim et al.	(BESIII Collab.)
ABLIKIM	22AO	PR D106 072004	M. Ablikim et al.	(BESIII Collab.)
ABLIKIM	22O	JHEP 2206 074	M. Ablikim et al.	(BESIII Collab.)
ABLIKIM	22Q	PR D106 032014	M. Ablikim et al.	(BESIII Collab.)
PDG	22	PTEP 2022 083C01	R.L. Workman et al.	(PDG Collab.)
ABLIKIM	21AV	JHEP 2111 217	M. Ablikim et al.	(BESIII Collab.)
ABLIKIM	21L	PR D103 112004	M. Ablikim et al.	(BESIII Collab.)
ABLIKIM	20AE	PR D102 092006	M. Ablikim et al.	(BESIII Collab.)
ABLIKIM	20B	PR D101 012012	M. Ablikim et al.	(BESIII Collab.)
ABLIKIM	20I	PR D101 092002	M. Ablikim et al.	(BESIII Collab.)
PDG	20	PTEP 2020 083C01	P.A. Zyla et al.	(PDG Collab.)
ABLIKIM	19AA	PR D99 052008	M. Ablikim et al.	(BESIII Collab.)
ABLIKIM	19AU	PR D100 052010	M. Ablikim et al.	(BESIII Collab.)
ABLIKIM	19BB	PR D100 092006	M. Ablikim et al.	(BESIII Collab.)
ABLIKIM	19J	PR D99 012015	M. Ablikim et al.	(BESIII Collab.)
ABLIKIM	19Z	PR D99 051101	M. Ablikim et al.	(BESIII Collab.)
LU	19	PR D99 032003	P.-C. Lu et al.	(BELLE Collab.)
ABLIKIM	18D	PRL 121 022001	M. Ablikim et al.	(BESIII Collab.)
ABLIKIM	18V	PR D97 052011	M. Ablikim et al.	(BESIII Collab.)
PDG	18	PR D98 030001	M. Tanabashi et al.	(PDG Collab.)
AAIJ	17BB	EPJ C77 609	R. Aaij et al.	(LHCb Collab.)
AAIJ	17BI	PRL 119 221801	R. Aaij et al.	(LHCb Collab.)
ABLIKIM	17AE	PR D96 092007	M. Ablikim et al.	(BESIII Collab.)
ABLIKIM	17I	PRL 118 221802	M. Ablikim et al.	(BESIII Collab.)
ABLIKIM	17K	PR D95 032002	M. Ablikim et al.	(BESIII Collab.)
ABLIKIM	17N	PR D95 072004	M. Ablikim et al.	(BESIII Collab.)
ABLIKIM	17U	PR D96 032001	M. Ablikim et al.	(BESIII Collab.)
PDG	16	CP C40 100001	C. Patrignani et al.	(PDG Collab.)
ABLIKIM	15I	PR D91 092006	M. Ablikim et al.	(BESIII Collab.)
ABLIKIM	15M	PR D91 112008	M. Ablikim et al.	(BESIII Collab.)
ABLIKIM	14J	PR D89 074030	M. Ablikim et al.	(BESIII Collab.)
ABLIKIM	13B	PR D87 012002	M. Ablikim et al.	(BESIII Collab.)
ABLIKIM	13D	PR D87 012007	M. Ablikim et al.	(BESIII Collab.)
ABLIKIM	13H	PR D87 032007	M. Ablikim et al.	(BESIII Collab.)
ABLIKIM	13V	PR D88 112001	M. Ablikim et al.	(BESIII Collab.)
ABLIKIM	12I	PR D86 052004	M. Ablikim et al.	(BESIII Collab.)
ABLIKIM	12J	PR D86 052011	M. Ablikim et al.	(BESIII Collab.)
ABLIKIM	12O	PRL 109 172002	M. Ablikim et al.	(BESIII Collab.)
ABLIKIM	11A	PR D83 012006	M. Ablikim et al.	(BESIII Collab.)
ABLIKIM	11D	PR D83 032003	M. Ablikim et al.	(BESIII Collab.)
ABLIKIM	11E	PR D83 112005	M. Ablikim et al.	(BESIII Collab.)
ABLIKIM	11F	PR D83 112009	M. Ablikim et al.	(BESIII Collab.)
ABLIKIM	11K	PRL 107 092001	M. Ablikim et al.	(BESIII Collab.)
ONYISI	10	PR D82 011103	P.U.E. Onyisi et al.	(CLEO Collab.)
ARTUSO	09	PR D80 112003	M. Artuso et al.	(CLEO Collab.)
BENNETT	08A	PRL 101 151801	J.V. Bennett et al.	(CLEO Collab.)
ECKLUND	08A	PR D78 091501	K.M. Ecklund et al.	(CLEO Collab.)
HE	08B	PR D78 092004	Q. He et al.	(CLEO Collab.)
MENDEZ	08	PR D78 011102	H. Mendez et al.	(CLEO Collab.)
NAIK	08	PR D78 031101	P. Naik et al.	(CLEO Collab.)
ATHAR	07	PR D75 032002	S.B. Athar et al.	(CLEO Collab.)
ABLIKIM	06D	PR D73 052006	M. Ablikim et al.	(BES Collab.)
ABLIKIM	06R	PR D74 072001	M. Ablikim et al.	(BES Collab.)
ABLIKIM	06T	PL B642 197	M. Ablikim et al.	(BES Collab.)
ABLIKIM	05G	PR D71 092002	M. Ablikim et al.	(BES Collab.)
ABLIKIM	05O	PL B630 21	M. Ablikim et al.	(BES Collab.)
ADAM	05A	PRL 94 232002	N.E. Adam et al.	(CLEO Collab.)
ANDREOTTI	05A	NP B717 34	M. Andreotti et al.	(FNAL E835 Collab.)
ABLIKIM	04B	PR D70 012003	M. Ablikim et al.	(BES Collab.)
ABLIKIM	04H	PR D70 092003	M. Ablikim et al.	(BES Collab.)
BAI	04F	PR D69 092001	J.Z. Bai et al.	(BES Collab.)
BAI	04I	PR D70 012006	J.Z. Bai et al.	(BES Collab.)
AULCHENKO	03	PL B573 63	V.M. Aulchenko et al.	(KEDR Collab.)
BAI	03E	PR D67 112001	J.Z. Bai et al.	(BES Collab.)
AMBROGIANI	02	PR D65 052002	M. Ambrogiani et al.	(FNAL E835 Collab.)
BAI	99B	PR D60 072001	J.Z. Bai et al.	(BES Collab.)
BAI	98D	PR D58 092006	J.Z. Bai et al.	(BES Collab.)
BAI	98I	PRL 81 3091	J.Z. Bai et al.	(BES Collab.)
ARMSTRONG	92	NP B373 35	T.A. Armstrong et al.	(FNAL, FERR, GENO+)
Also		PRL 68 1468	T.A. Armstrong et al.	(FNAL, FERR, GENO+)
BAGLIN	86B	PL B172 455	C. Baglin	(LAPP, CERN, GENO, LYON, OSLO+)
GAISER	86	PR D34 711	J. Gaiser et al.	(Crystal Ball Collab.)
LEMOIGNE	82	PL 113B 509	Y. Lemoigne et al.	(SACL, LOIC, SHMP+)
OREGLIA	82	PR D25 2259	M.J. Oreglia et al.	(SLAC, CIT, HARV+)
Also		Private Comm.	M.J. Oreglia	(EFI)
HIMEL	80	PRL 44 920	T. Himel et al.	(LBL, SLAC)
Also		Private Comm.	G. Trilling	(LBL, UCB)
BRANDELIK	79B	NP B160 426	R. Brandelik et al.	(DASP Collab.)
BARTEL	78B	PL 79B 492	W. Bartel et al.	(DESY, HEIDP)
TANENBAUM	78	PR D17 1731	W.M. Tanenbaum et al.	(SLAC, LBL)
Also		Private Comm.	G. Trilling	(LBL, UCB)
BIDDICK	77	PRL 38 1324	C.J. Biddick et al.	(UCSD, UMD, PAVI+)
FELDMAN	77	PRPL 33C 285	G.J. Feldman, M.L. Perl	(LBL, SLAC)
YAMADA	77	Hamburg Conf. 69	S. Yamada	(DASP Collab.)
WHITAKER	76	PRL 37 1596	J.S. Whitaker et al.	(SLAC, LBL)
TANENBAUM	75	PRL 35 1323	W.M. Tanenbaum et al.	(LBL, SLAC)

$h_c(1P)$

$I^G(J^{PC}) = 0^-(1^{+-})$

Quantum numbers are quark model prediction, $C = -$ established by $\eta_c\gamma$ decay.

$h_c(1P)$ MASS

VALUE (MeV)	EVTS	DOCUMENT ID		TECN	COMMENT
3525.37±0.14 OUR AVERAGE	Error includes scale factor of 1.2.				
3525.32±0.06±0.15	23k	ABLIKIM	22AQ	BES3	$\psi(2S) \to \pi^0$ hadrons; $\pi^0\gamma(\eta_c)$
3525.20±0.18±0.12	1282	[1] DOBBS	08A	CLEO	$\psi(2S) \to \pi^0\eta_c\gamma$
3525.8 ±0.2 ±0.2	13	ANDREOTTI	05B	E835	$\overline{p}p \to \eta_c\gamma$
• • • We do not use the following data for averages, fits, limits, etc. • • •					
3525.31±0.11±0.14	832	[2,3] ABLIKIM	12N	BES3	$\psi(2S) \to \pi^0\gamma$ hadrons
3525.40±0.13±0.18	3679	[2] ABLIKIM	10B	BES3	$\psi(2S) \to \pi^0\gamma\eta_c$
3525.6 ±0.5	92	ADAMS	09	CLEO	$\psi(2S) \to 2(\pi^+\pi^-\pi^0)$
3524.4 ±0.6 ±0.4	168	[4] ROSNER	05	CLEO	$\psi(2S) \to \pi^0\eta_c\gamma$
3527 ±8	42	ANTONIAZZI	94	E705	300 $\pi^\pm$, pLi $\to J/\psi\pi^0$X
3526.28±0.18±0.19	59	[5] ARMSTRONG	92D	E760	$\overline{p}p \to J/\psi\pi^0$
3525.4 ±0.8 ±0.4	5	BAGLIN	86	SPEC	$\overline{p}p \to J/\psi$X

[1] Combination of exclusive and inclusive analyses for the reaction $\psi(2S) \to \pi^0 h_c \to \pi^0\eta_c\gamma$. This result is the average of DOBBS 08A and ROSNER 05.
[2] Superseded by ABLIKIM 22AQ
[3] With floating width.
[4] Superseded by DOBBS 08A.
[5] Mass central value and systematic error recalculated by us according to Eq. (16) in ARMSTRONG 93B, using the value for the $\psi(2S)$ mass from AULCHENKO 03.

$h_c(1P)$ WIDTH

VALUE (MeV)	CL%	EVTS	DOCUMENT ID		TECN	COMMENT
$\mathbf{0.78^{+0.27}_{-0.24}\pm0.12}$		23k	ABLIKIM	22AQ	BES3	$\psi(2S) \to \pi^0$ hadrons; $\pi^0\gamma(\eta_c)$
• • • We do not use the following data for averages, fits, limits, etc. • • •						
0.70±0.28±0.22		832	[1,2] ABLIKIM	12N	BES3	$\psi(2S) \to \pi^0\gamma$ hadrons
< 1.44	90	3679	[3] ABLIKIM	10B	BES3	$\psi(2S) \to \pi^0\gamma\eta_c$
< 1		13	ANDREOTTI	05B	E835	$\overline{p}p \to \eta_c\gamma$
< 1.1	90	59	ARMSTRONG	92D	E760	$\overline{p}p \to J/\psi\pi^0$

[1] Superseded by ABLIKIM 22AQ
[2] With floating mass.
[3] The central value is $\Gamma = 0.73 \pm 0.45 \pm 0.28$ MeV.

$h_c(1P)$ DECAY MODES

	Mode	Fraction (Γ_i/Γ)	Scale factor/ Confidence level
Γ_1	$J/\psi(1S)\pi^0$	$< 5 \times 10^{-4}$	CL=90%
Γ_2	$J/\psi(1S)\pi\pi$	$< 9 \times 10^{-5}$	CL=90%
Γ_3	$J/\psi(1S)\pi^+\pi^-$	$< 9 \times 10^{-4}$	CL=90%
Γ_4	$p\overline{p}$	$< 4 \times 10^{-5}$	CL=90%
Γ_5	$p\overline{p}\pi^0$	$< 8 \times 10^{-4}$	CL=90%
Γ_6	$p\overline{p}\pi^+\pi^-$	$(3.3 \pm 0.6) \times 10^{-3}$	
Γ_7	$p\overline{p}\pi^0\pi^0$	$< 6 \times 10^{-4}$	CL=90%
Γ_8	$p\overline{p}\pi^+\pi^-\pi^0$	$(4.4 \pm 1.3) \times 10^{-3}$	
Γ_9	$p\overline{p}\eta$	$(7.4 \pm 2.2) \times 10^{-4}$	
Γ_{10}	$\pi^+\pi^-\pi^0$	$(1.57 \pm 0.13) \times 10^{-3}$	
Γ_{11}	$\pi^+\pi^-\eta$	$< 5 \times 10^{-4}$	CL=90%
Γ_{12}	$\pi^+\pi^-\pi^0\eta$	$(8.3 \pm 2.4) \times 10^{-3}$	
Γ_{13}	$2\pi^+2\pi^-\pi^0\eta$	$(7.2 \pm 1.7) \times 10^{-3}$	

Int. J. Mod. Phys. A 2026.41. Downloaded from www.worldscientific.com
by UNIVERSITY OF CALIFORNIA @ BERKELEY on 09/16/26. Re-use and distribution is strictly not permitted, except for Open Access articles.

Γ_{14}	$2\pi^+2\pi^-\pi^0$	$(9.4 \pm 1.7) \times 10^{-3}$	
Γ_{15}	$2\pi^+2\pi^-\eta$	$< 6 \times 10^{-4}$	CL=90%
Γ_{16}	$3\pi^+3\pi^-\pi^0$	$(9.1 \pm 1.5) \times 10^{-3}$	
Γ_{17}	$2\pi^+2\pi^-\omega$	$(3.9 \pm 1.0) \times 10^{-3}$	
Γ_{18}	$K^+K^-\pi^+\pi^-$	$< 7 \times 10^{-4}$	CL=90%
Γ_{19}	$K^+K^-\pi^+\pi^-\pi^0$	$(3.8 \pm 0.8) \times 10^{-3}$	
Γ_{20}	$K^+K^-\pi^+\pi^-\eta$	$< 2.7 \times 10^{-3}$	CL=90%
Γ_{21}	$K^+K^-\pi^0$	$(3.8 \pm 0.9) \times 10^{-4}$	
Γ_{22}	$K^+K^-\pi^0\eta$	$< 2.4 \times 10^{-3}$	CL=90%
Γ_{23}	$K^+K^-\eta$	$(3.6 \pm 1.2) \times 10^{-4}$	
Γ_{24}	$2K^+2K^-\pi^0$	$< 2.8 \times 10^{-4}$	CL=90%
Γ_{25}	$K^0_S K^\pm\pi^\mp$	$(7.1 \pm 1.9) \times 10^{-4}$	
Γ_{26}	$K^0_S K^\pm\pi^\mp\pi^+\pi^-$	$(3.2 \pm 1.0) \times 10^{-3}$	

Radiative decays

Γ_{27}	$\gamma\eta$	$(3.8 \pm 0.6) \times 10^{-4}$	
Γ_{28}	$\gamma\eta'(958)$	$(1.41 \pm 0.15) \times 10^{-3}$	
Γ_{29}	$\gamma\pi^0$	$< 5 \times 10^{-5}$	
Γ_{30}	$\gamma\eta_c(1S)$	(64 ± 5) %	S=1.2
Γ_{31}	$\gamma\pi^+\pi^-$	$(3.0 \pm 0.7) \times 10^{-4}$	
Γ_{32}	$\gamma\pi^+\pi^-\eta$	$(3.5 \pm 0.6) \times 10^{-3}$	
Γ_{33}	$\gamma 2\pi^+2\pi^-$	$(2.18 \pm 0.30) \times 10^{-3}$	
Γ_{34}	$\gamma p\overline{p}$	$(3.3 \pm 0.7) \times 10^{-4}$	
Γ_{35}	$e^+e^-\eta_c(1S)$	$(3.8 \pm 0.8) \times 10^{-3}$	
Γ_{36}	$\gamma f_2(1270) \to \gamma\pi^+\pi^-$	$(1.8 \pm 0.4) \times 10^{-4}$	

FIT INFORMATION

A multiparticle fit to $\eta_c(1S)$, $J/\psi(1S)$, $\psi(2S)$, $h_c(1P)$, and $B^\pm$ with the total width, 10 combinations of partial widths obtained from integrated cross section, and 38 branching ratios uses 115 measurements to determine 19 parameters. The overall fit has a $\chi^2 = 215.4$ for 96 degrees of freedom.

$h_c(1P)$ PARTIAL WIDTHS

$h_c(1P)$ $\Gamma(i)\Gamma(\overline{p}p)/\Gamma(\text{total})$

$\Gamma(\gamma\eta_c(1S)) \times \Gamma(p\overline{p})/\Gamma_{\text{total}}$ — $\Gamma_{30}\Gamma_4/\Gamma$

VALUE (eV)	EVTS	DOCUMENT ID		TECN	COMMENT
• • • We do not use the following data for averages, fits, limits, etc. • • •					
12.0 ± 4.5	13	[1] ANDREOTTI	05B	E835	$\overline{p}p \to \eta_c\gamma$

[1] Assuming $\Gamma = 1$ MeV.

$h_c(1P)$ BRANCHING RATIOS

$\Gamma(J/\psi(1S)\pi^0)/\Gamma(\gamma\eta_c(1S))$ — Γ_1/Γ_{30}

VALUE	CL%	DOCUMENT ID		TECN	COMMENT
$<7 \times 10^{-4}$	90	[1] ABLIKIM	22N	BES3	$e^+e^- \to \pi^+\pi^- h_c$

[1] ABLIKIM 22N reports $[\Gamma(h_c(1P) \to J/\psi(1S)\pi^0)/\Gamma(h_c(1P) \to \gamma\eta_c(1S))] / [B(\eta_c \to K^+K^-\pi^0)] < 7.5 \times 10^{-2}$ which we multiply by our best value $B(\eta_c \to K^+K^-\pi^0) = 1/6\ B(\eta_c(1S) \to K\overline{K}\pi) = 1/6\ (5.9 \times 10^{-2})$.

$\Gamma(J/\psi(1S)\pi\pi)/\Gamma(J/\psi(1S)\pi^0)$ — Γ_2/Γ_1

VALUE	CL%	DOCUMENT ID		TECN	COMMENT
<0.18	90	ARMSTRONG	92D	E760	$\overline{p}p \to J/\psi\pi^0$

$\Gamma(J/\psi(1S)\pi^+\pi^-)/\Gamma_{\text{total}}$ — Γ_3/Γ

VALUE	CL%	DOCUMENT ID		TECN	COMMENT
$<9 \times 10^{-4}$	90	[1] ABLIKIM	24BY	BES3	$\psi(2S) \to \pi^0\pi^+\pi^- J/\psi$
• • • We do not use the following data for averages, fits, limits, etc. • • •					
$<2.7 \times 10^{-3}$	90	[2] ABLIKIM	18M	BES3	$\psi(2S) \to \pi^0\pi^+\pi^- J/\psi$

[1] ABLIKIM 24BY reports $[\Gamma(h_c(1P) \to J/\psi(1S)\pi^+\pi^-)/\Gamma_{\text{total}}] \times [B(\psi(2S) \to h_c(1P)\pi^0)] < 6.7 \times 10^{-7}$ which we divide by our best (shown rounded) value $B(\psi(2S) \to h_c(1P)\pi^0) = 7.4 \times 10^{-4}$.

[2] ABLIKIM 18M reports $[\Gamma(h_c(1P) \to J/\psi(1S)\pi^+\pi^-)/\Gamma_{\text{total}}] \times [B(\psi(2S) \to h_c(1P)\pi^0)] < 2.0 \times 10^{-6}$ which we divide by our best (shown rounded) value $B(\psi(2S) \to h_c(1P)\pi^0) = 7.4 \times 10^{-4}$.

$\Gamma(p\overline{p})/\Gamma_{\text{total}}$ — Γ_4/Γ

VALUE	CL%	DOCUMENT ID		TECN	COMMENT
$<4 \times 10^{-5}$	90	[1] ABLIKIM	24R	BES3	$\psi(2S) \to \pi^0 h_c(1P)$

[1] ABLIKIM 24R reports $[\Gamma(h_c(1P) \to p\overline{p})/\Gamma_{\text{total}}] \times [B(\psi(2S) \to h_c(1P)\pi^0)] < 3.22 \times 10^{-8}$ which we divide by our best (shown rounded) value $B(\psi(2S) \to h_c(1P)\pi^0) = 7.4 \times 10^{-4}$.

$\Gamma(p\overline{p}\pi^0)/\Gamma_{\text{total}}$ — Γ_5/Γ

VALUE	CL%	DOCUMENT ID		TECN	COMMENT
$<8 \times 10^{-4}$	90	[1] ABLIKIM	22M	BES3	$\psi(2S) \to \pi^0 h_c(1P)$

[1] ABLIKIM 22M reports $[\Gamma(h_c(1P) \to p\overline{p}\pi^0)/\Gamma_{\text{total}}] \times [B(\psi(2S) \to h_c(1P)\pi^0)] < 5.67 \times 10^{-7}$ which we divide by our best (shown rounded) value $B(\psi(2S) \to h_c(1P)\pi^0) = 7.4 \times 10^{-4}$.

$\Gamma(p\overline{p}\pi^+\pi^-)/\Gamma_{\text{total}}$ — Γ_6/Γ

VALUE (units 10^{-3})	EVTS	DOCUMENT ID		TECN	COMMENT
$3.3 \pm 0.5 \pm 0.2$	230	[1] ABLIKIM	19AG	BES3	$\psi(2S) \to \pi^0 h_c(1P)$

[1] ABLIKIM 19AG reports $[\Gamma(h_c(1P) \to p\overline{p}\pi^+\pi^-)/\Gamma_{\text{total}}] \times [B(\psi(2S) \to h_c(1P)\pi^0)] = (2.49 \pm 0.27 \pm 0.28) \times 10^{-6}$ which we divide by our best (shown rounded) value $B(\psi(2S) \to h_c(1P)\pi^0) = (7.4 \pm 0.5) \times 10^{-4}$. Our first error is their experiment's error and our second error is the systematic error from using our best (shown rounded) value.

$\Gamma(p\overline{p}\pi^0\pi^0)/\Gamma_{\text{total}}$ — Γ_7/Γ

VALUE	CL%	EVTS	DOCUMENT ID		TECN	COMMENT
$<6 \times 10^{-4}$	90	12	[1] ABLIKIM	20AH	BES3	$\psi(2S) \to \pi^0 h_c(1P)$

[1] ABLIKIM 20AH reports $[\Gamma(h_c(1P) \to p\overline{p}\pi^0\pi^0)/\Gamma_{\text{total}}] \times [B(\psi(2S) \to h_c(1P)\pi^0)] < 4.4 \times 10^{-7}$ which we divide by our best (shown rounded) value $B(\psi(2S) \to h_c(1P)\pi^0) = 7.4 \times 10^{-4}$.

$\Gamma(p\overline{p}\pi^+\pi^-\pi^0)/\Gamma_{\text{total}}$ — Γ_8/Γ

VALUE (units 10^{-3})	EVTS	DOCUMENT ID		TECN	COMMENT
$4.4 \pm 1.2 \pm 0.3$	86	[1] ABLIKIM	22M	BES3	$\psi(2S) \to \pi^0 h_c(1P)$

[1] ABLIKIM 22M reports $[\Gamma(h_c(1P) \to p\overline{p}\pi^+\pi^-\pi^0)/\Gamma_{\text{total}}] \times [B(\psi(2S) \to h_c(1P)\pi^0)] = (3.30 \pm 0.71 \pm 0.59) \times 10^{-6}$ which we divide by our best (shown rounded) value $B(\psi(2S) \to h_c(1P)\pi^0) = (7.4 \pm 0.5) \times 10^{-4}$. Our first error is their experiment's error and our second error is the systematic error from using our best (shown rounded) value.

$\Gamma(p\overline{p}\eta)/\Gamma_{\text{total}}$ — Γ_9/Γ

VALUE (units 10^{-4})	EVTS	DOCUMENT ID		TECN	COMMENT
$7.4 \pm 2.1 \pm 0.5$	20	[1] ABLIKIM	22M	BES3	$\psi(2S) \to \pi^0 h_c(1P)$

[1] ABLIKIM 22M reports $[\Gamma(h_c(1P) \to p\overline{p}\eta)/\Gamma_{\text{total}}] \times [B(\psi(2S) \to h_c(1P)\pi^0)] = (5.51 \pm 1.50 \pm 0.46) \times 10^{-7}$ which we divide by our best (shown rounded) value $B(\psi(2S) \to h_c(1P)\pi^0) = (7.4 \pm 0.5) \times 10^{-4}$. Our first error is their experiment's error and our second error is the systematic error from using our best (shown rounded) value.

$\Gamma(\pi^+\pi^-\pi^0)/\Gamma_{\text{total}}$ — Γ_{10}/Γ

VALUE (units 10^{-3})	CL%	EVTS	DOCUMENT ID		TECN	COMMENT
$1.57 \pm 0.06 \pm 0.11$		472	[1] ABLIKIM	24BF	BES3	$\psi(2S) \to \pi^0 h_c(1P)$
• • • We do not use the following data for averages, fits, limits, etc. • • •						
$1.9 \pm 0.5 \pm 0.1$		101	[2,3] ABLIKIM	19AG	BES3	$\psi(2S) \to \pi^0 h_c(1P)$
<2.6	90		[4] ADAMS	09	CLEO	$\psi(2S) \to \pi^0\gamma\eta_c$

[1] ABLIKIM 24BF reports $(1.36 \pm 0.16 \pm 0.14) \times 10^{-3}$ from a measurement of $[\Gamma(h_c(1P) \to \pi^+\pi^-\pi^0)/\Gamma_{\text{total}}] \times [B(\psi(2S) \to h_c(1P)\pi^0)]$ assuming $B(\psi(2S) \to h_c(1P)\pi^0) = (8.6 \pm 1.3) \times 10^{-4}$, which we rescale to our best (shown rounded) value $B(\psi(2S) \to h_c(1P)\pi^0) = (7.4 \pm 0.5) \times 10^{-4}$. Our first error is their experiment's error and our second error is the systematic error from using our best (shown rounded) value.

[2] ABLIKIM 19AG reports $[\Gamma(h_c(1P) \to \pi^+\pi^-\pi^0)/\Gamma_{\text{total}}] \times [B(\psi(2S) \to h_c(1P)\pi^0)] = (1.38 \pm 0.35 \pm 0.17) \times 10^{-6}$ which we divide by our best (shown rounded) value $B(\psi(2S) \to h_c(1P)\pi^0) = (7.4 \pm 0.5) \times 10^{-4}$. Our first error is their experiment's error and our second error is the systematic error from using our best (shown rounded) value.

[3] Superseded by ABLIKIM 24BF.

[4] ADAMS 09 reports $[\Gamma(h_c(1P) \to \pi^+\pi^-\pi^0)/\Gamma_{\text{total}}] \times [B(\psi(2S) \to h_c(1P)\pi^0)] < 0.19 \times 10^{-5}$ which we divide by our best (shown rounded) value $B(\psi(2S) \to h_c(1P)\pi^0) = 7.4 \times 10^{-4}$.

$\Gamma(\pi^+\pi^-\eta)/\Gamma_{\text{total}}$ — Γ_{11}/Γ

VALUE	CL%	EVTS	DOCUMENT ID		TECN	COMMENT
$<5 \times 10^{-4}$	90	44.5	[1] ABLIKIM	24BF	BES3	$\psi(2S) \to \pi^0 h_c(1P)$

[1] ABLIKIM 24BF reports $< 4.0 \times 10^{-4}$ from a measurement of $[\Gamma(h_c(1P) \to \pi^+\pi^-\eta)/\Gamma_{\text{total}}] \times [B(\psi(2S) \to h_c(1P)\pi^0)]$ assuming $B(\psi(2S) \to h_c(1P)\pi^0) = (8.6 \pm 1.3) \times 10^{-4}$, which we rescale to our best (shown rounded) value $B(\psi(2S) \to h_c(1P)\pi^0) = 7.4 \times 10^{-4}$.

$\Gamma(\pi^+\pi^-\pi^0\eta)/\Gamma_{\text{total}}$ — Γ_{12}/Γ

VALUE (units 10^{-3})	EVTS	DOCUMENT ID		TECN	COMMENT
$8.3 \pm 2.3 \pm 0.6$	35	[1] ABLIKIM	20AH	BES3	$\psi(2S) \to \pi^0 h_c(1P)$

[1] ABLIKIM 20AH reports $[\Gamma(h_c(1P) \to \pi^+\pi^-\pi^0\eta)/\Gamma_{\text{total}}] \times [B(\psi(2S) \to h_c(1P)\pi^0)] = (6.2 \pm 1.6 \pm 0.7) \times 10^{-6}$ which we divide by our best (shown rounded) value $B(\psi(2S) \to h_c(1P)\pi^0) = (7.4 \pm 0.5) \times 10^{-4}$. Our first error is their experiment's error and our second error is the systematic error from using our best (shown rounded) value.

$\Gamma(2\pi^+2\pi^-\pi^0\eta)/\Gamma_{\text{total}}$ — Γ_{13}/Γ

VALUE (units 10^{-3})	DOCUMENT ID		TECN	COMMENT
$7.2 \pm 1.7 \pm 0.5$	[1] ABLIKIM	24R	BES3	$\psi(2S) \to \pi^0 h_c(1P)$

[1] ABLIKIM 24R reports $[\Gamma(h_c(1P) \to 2\pi^+2\pi^-\pi^0\eta)/\Gamma_{\text{total}}] \times [B(\psi(2S) \to h_c(1P)\pi^0)] = (5.33 \pm 1.10 \pm 0.56) \times 10^{-6}$ which we divide by our best (shown rounded) value $B(\psi(2S) \to h_c(1P)\pi^0) = (7.4 \pm 0.5) \times 10^{-4}$. Our first error is their experiment's error and our second error is the systematic error from using our best (shown rounded) value.

Int. J. Mod. Phys. A 2026.41. Downloaded from www.worldscientific.com by CALIFORNIA @ BERKELEY on 09/16/26. Re-use and distribution is strictly not permitted, except for Open Access articles.

$\Gamma(2\pi^+2\pi^-\pi^0)/\Gamma_{total}$ — Γ_{14}/Γ

VALUE (units 10^{-2})	EVTS	DOCUMENT ID		TECN	COMMENT
0.94±0.17 OUR AVERAGE					
0.86±0.16±0.06	254	[1] ABLIKIM	19AG	BES3	$\psi(2S) \to \pi^0 h_c(1P)$
$2.5^{+0.9}_{-0.7}$ ±0.2	92	[2] ADAMS	09	CLEO	$\psi(2S) \to \pi^0 \gamma \eta_c$

[1] ABLIKIM 19AG reports $[\Gamma(h_c(1P) \to 2\pi^+2\pi^-\pi^0)/\Gamma_{total}] \times [B(\psi(2S) \to h_c(1P)\pi^0)] = (6.40 \pm 0.81 \pm 0.87) \times 10^{-6}$ which we divide by our best (shown rounded) value $B(\psi(2S) \to h_c(1P)\pi^0) = (7.4 \pm 0.5) \times 10^{-4}$. Our first error is their experiment's error and our second error is the systematic error from using our best (shown rounded) value.

[2] ADAMS 09 reports $[\Gamma(h_c(1P) \to 2\pi^+2\pi^-\pi^0)/\Gamma_{total}] \times [B(\psi(2S) \to h_c(1P)\pi^0)] = (1.88^{+0.48}_{-0.45}{}^{+0.47}_{-0.30}) \times 10^{-5}$ which we divide by our best (shown rounded) value $B(\psi(2S) \to h_c(1P)\pi^0) = (7.4 \pm 0.5) \times 10^{-4}$. Our first error is their experiment's error and our second error is the systematic error from using our best (shown rounded) value.

$\Gamma(2\pi^+2\pi^-\eta)/\Gamma_{total}$ — Γ_{15}/Γ

VALUE	CL%	DOCUMENT ID		TECN	COMMENT
$<6 \times 10^{-4}$	90	[1] ABLIKIM	24R	BES3	$\psi(2S) \to \pi^0 h_c(1P)$

[1] ABLIKIM 24R reports $[\Gamma(h_c(1P) \to 2\pi^+2\pi^-\eta)/\Gamma_{total}] \times [B(\psi(2S) \to h_c(1P)\pi^0)] < 4.53 \times 10^{-7}$ which we divide by our best (shown rounded) value $B(\psi(2S) \to h_c(1P)\pi^0) = 7.4 \times 10^{-4}$.

$\Gamma(3\pi^+3\pi^-\pi^0)/\Gamma_{total}$ — Γ_{16}/Γ

VALUE (units 10^{-3})	CL%	DOCUMENT ID		TECN	COMMENT
9.1±1.3±0.6		[1] ABLIKIM	24R	BES3	$\psi(2S) \to \pi^0 h_c(1P)$
• • • We do not use the following data for averages, fits, limits, etc. • • •					
<10	90	[2] ABLIKIM	19AG	BES3	$\psi(2S) \to \pi^0 h_c(1P)$
<34	90	[3] ADAMS	09	CLEO	$\psi(2S) \to \pi^0 \gamma \eta_c$

[1] ABLIKIM 24R reports $[\Gamma(h_c(1P) \to 3\pi^+3\pi^-\pi^0)/\Gamma_{total}] \times [B(\psi(2S) \to h_c(1P)\pi^0)] = (6.79 \pm 0.83 \pm 0.56) \times 10^{-6}$ which we divide by our best (shown rounded) value $B(\psi(2S) \to h_c(1P)\pi^0) = (7.4 \pm 0.5) \times 10^{-4}$. Our first error is their experiment's error and our second error is the systematic error from using our best (shown rounded) value.

[2] ABLIKIM 19AG reports $[\Gamma(h_c(1P) \to 3\pi^+3\pi^-\pi^0)/\Gamma_{total}] \times [B(\psi(2S) \to h_c(1P)\pi^0)] < 7.5 \times 10^{-6}$ which we divide by our best (shown rounded) value $B(\psi(2S) \to h_c(1P)\pi^0) = 7.4 \times 10^{-4}$. Superseded by ABLIKIM 24R.

[3] ADAMS 09 reports $[\Gamma(h_c(1P) \to 3\pi^+3\pi^-\pi^0)/\Gamma_{total}] \times [B(\psi(2S) \to h_c(1P)\pi^0)] < 2.5 \times 10^{-5}$ which we divide by our best (shown rounded) value $B(\psi(2S) \to h_c(1P)\pi^0) = 7.4 \times 10^{-4}$.

$\Gamma(2\pi^+2\pi^-\omega)/\Gamma_{total}$ — Γ_{17}/Γ

VALUE (units 10^{-3})	DOCUMENT ID		TECN	COMMENT
3.9±0.9±0.3	[1] ABLIKIM	24R	BES3	$\psi(2S) \to \pi^0 h_c(1P)$

[1] ABLIKIM 24R reports $[\Gamma(h_c(1P) \to 2\pi^+2\pi^-\omega)/\Gamma_{total}] \times [B(\psi(2S) \to h_c(1P)\pi^0)] = (2.93 \pm 0.63 \pm 0.26) \times 10^{-6}$ which we divide by our best (shown rounded) value $B(\psi(2S) \to h_c(1P)\pi^0) = (7.4 \pm 0.5) \times 10^{-4}$. Our first error is their experiment's error and our second error is the systematic error from using our best (shown rounded) value.

$\Gamma(K^+K^-\pi^+\pi^-)/\Gamma_{total}$ — Γ_{18}/Γ

VALUE	CL%	DOCUMENT ID		TECN	COMMENT
$<7 \times 10^{-4}$	90	[1] ABLIKIM	19AG	BES3	$\psi(2S) \to \pi^0 h_c(1P)$

[1] ABLIKIM 19AG reports $[\Gamma(h_c(1P) \to K^+K^-\pi^+\pi^-)/\Gamma_{total}] \times [B(\psi(2S) \to h_c(1P)\pi^0)] < 0.5 \times 10^{-6}$ which we divide by our best (shown rounded) value $B(\psi(2S) \to h_c(1P)\pi^0) = 7.4 \times 10^{-4}$.

$\Gamma(K^+K^-\pi^+\pi^-\pi^0)/\Gamma_{total}$ — Γ_{19}/Γ

VALUE (units 10^{-3})	EVTS	DOCUMENT ID		TECN	COMMENT
3.8±0.8±0.3	80	[1] ABLIKIM	20AH	BES3	$\psi(2S) \to \pi^0 h_c(1P)$

[1] ABLIKIM 20AH reports $[\Gamma(h_c(1P) \to K^+K^-\pi^+\pi^-\pi^0)/\Gamma_{total}] \times [B(\psi(2S) \to h_c(1P)\pi^0)] = (2.8 \pm 0.5 \pm 0.3) \times 10^{-6}$ which we divide by our best (shown rounded) value $B(\psi(2S) \to h_c(1P)\pi^0) = (7.4 \pm 0.5) \times 10^{-4}$. Our first error is their experiment's error and our second error is the systematic error from using our best (shown rounded) value.

$\Gamma(K^+K^-\pi^+\pi^-\eta)/\Gamma_{total}$ — Γ_{20}/Γ

VALUE	CL%	EVTS	DOCUMENT ID		TECN	COMMENT
$<2.7 \times 10^{-3}$	90	24	[1] ABLIKIM	20AH	BES3	$\psi(2S) \to \pi^0 h_c(1P)$

[1] ABLIKIM 20AH reports $[\Gamma(h_c(1P) \to K^+K^-\pi^+\pi^-\eta)/\Gamma_{total}] \times [B(\psi(2S) \to h_c(1P)\pi^0)] < 2.0 \times 10^{-6}$ which we divide by our best (shown rounded) value $B(\psi(2S) \to h_c(1P)\pi^0) = 7.4 \times 10^{-4}$.

$\Gamma(K^+K^-\pi^0)/\Gamma_{total}$ — Γ_{21}/Γ

VALUE (units 10^{-4})	CL%	EVTS	DOCUMENT ID		TECN	COMMENT
3.8±0.9±0.3		62	[1] ABLIKIM	24BF	BES3	$\psi(2S) \to \pi^0 h_c(1P)$
• • • We do not use the following data for averages, fits, limits, etc. • • •						
<6	90	20	[2,3] ABLIKIM	20AH	BES3	$\psi(2S) \to \pi^0 h_c(1P)$

[1] ABLIKIM 24BF reports $(3.26 \pm 0.84 \pm 0.36) \times 10^{-4}$ from a measurement of $[\Gamma(h_c(1P) \to K^+K^-\pi^0)/\Gamma_{total}] \times [B(\psi(2S) \to h_c(1P)\pi^0)]$ assuming $B(\psi(2S) \to h_c(1P)\pi^0) = (8.6 \pm 1.3) \times 10^{-4}$, which we rescale to our best (shown rounded) value $B(\psi(2S) \to h_c(1P)\pi^0) = (7.4 \pm 0.5) \times 10^{-4}$. Our first error is their experiment's error and our second error is the systematic error from using our best (shown rounded) value. Significance 3.5σ.

[2] ABLIKIM 20AH reports $[\Gamma(h_c(1P) \to K^+K^-\pi^0)/\Gamma_{total}] \times [B(\psi(2S) \to h_c(1P)\pi^0)] < 4.8 \times 10^{-7}$ which we divide by our best (shown rounded) value $B(\psi(2S) \to h_c(1P)\pi^0) = 7.4 \times 10^{-4}$.

[3] Superseded by ABLIKIM 24BF.

$\Gamma(K^+K^-\pi^0\eta)/\Gamma_{total}$ — Γ_{22}/Γ

VALUE	CL%	EVTS	DOCUMENT ID		TECN	COMMENT
$<2.4 \times 10^{-3}$	90	20	[1] ABLIKIM	20AH	BES3	$\psi(2S) \to \pi^0 h_c(1P)$

[1] ABLIKIM 20AH reports $[\Gamma(h_c(1P) \to K^+K^-\pi^0\eta)/\Gamma_{total}] \times [B(\psi(2S) \to h_c(1P)\pi^0)] < 1.8 \times 10^{-6}$ which we divide by our best (shown rounded) value $B(\psi(2S) \to h_c(1P)\pi^0) = 7.4 \times 10^{-4}$.

$\Gamma(K^+K^-\eta)/\Gamma_{total}$ — Γ_{23}/Γ

VALUE (units 10^{-4})	CL%	EVTS	DOCUMENT ID		TECN	COMMENT
3.6±1.2±0.3		32	[1] ABLIKIM	24BF	BES3	$\psi(2S) \to \pi^0 h_c(1P)$
• • • We do not use the following data for averages, fits, limits, etc. • • •						
<10	90	18	[2,3] ABLIKIM	20AH	BES3	$\psi(2S) \to \pi^0 h_c(1P)$

[1] ABLIKIM 24BF reports $(3.13 \pm 1.08 \pm 0.38) \times 10^{-4}$ from a measurement of $[\Gamma(h_c(1P) \to K^+K^-\eta)/\Gamma_{total}] \times [B(\psi(2S) \to h_c(1P)\pi^0)]$ assuming $B(\psi(2S) \to h_c(1P)\pi^0) = (8.6 \pm 1.3) \times 10^{-4}$, which we rescale to our best (shown rounded) value $B(\psi(2S) \to h_c(1P)\pi^0) = (7.4 \pm 0.5) \times 10^{-4}$. Our first error is their experiment's error and our second error is the systematic error from using our best (shown rounded) value. Significance 3.3σ.

[2] ABLIKIM 20AH reports $[\Gamma(h_c(1P) \to K^+K^-\eta)/\Gamma_{total}] \times [B(\psi(2S) \to h_c(1P)\pi^0)] < 7.5 \times 10^{-7}$ which we divide by our best (shown rounded) value $B(\psi(2S) \to h_c(1P)\pi^0) = 7.4 \times 10^{-4}$.

[3] Superseded by ABLIKIM 24BF.

$\Gamma(2K^+2K^-\pi^0)/\Gamma_{total}$ — Γ_{24}/Γ

VALUE	CL%	EVTS	DOCUMENT ID		TECN	COMMENT
$<2.8 \times 10^{-4}$	90	11	[1] ABLIKIM	20AH	BES3	$\psi(2S) \to \pi^0 h_c(1P)$

[1] ABLIKIM 20AH reports $[\Gamma(h_c(1P) \to 2K^+2K^-\pi^0)/\Gamma_{total}] \times [B(\psi(2S) \to h_c(1P)\pi^0)] < 2.1 \times 10^{-7}$ which we divide by our best (shown rounded) value $B(\psi(2S) \to h_c(1P)\pi^0) = 7.4 \times 10^{-4}$.

$\Gamma(K^0_S K^\pm\pi^\mp)/\Gamma_{total}$ — Γ_{25}/Γ

VALUE (units 10^{-4})	CL%	DOCUMENT ID		TECN	COMMENT
7.1±1.8±0.5		[1] ABLIKIM	24Y	BES3	$\psi(2S) \to \pi^0 h_c(1P)$
• • • We do not use the following data for averages, fits, limits, etc. • • •					
<6	90	[2,3] ABLIKIM	20AH	BES3	$\psi(2S) \to \pi^0 h_c(1P)$

[1] ABLIKIM 24Y reports $[\Gamma(h_c(1P) \to K^0_S K^\pm\pi^\mp)/\Gamma_{total}] \times [B(\psi(2S) \to h_c(1P)\pi^0)] = (5.3 \pm 1.3 \pm 0.4) \times 10^{-7}$ which we divide by our best (shown rounded) value $B(\psi(2S) \to h_c(1P)\pi^0) = (7.4 \pm 0.5) \times 10^{-4}$. Our first error is their experiment's error and our second error is the systematic error from using our best (shown rounded) value.

[2] ABLIKIM 20AH reports $[\Gamma(h_c(1P) \to K^0_S K^\pm\pi^\mp)/\Gamma_{total}] \times [B(\psi(2S) \to h_c(1P)\pi^0)] < 4.8 \times 10^{-7}$ which we divide by our best (shown rounded) value $B(\psi(2S) \to h_c(1P)\pi^0) = 7.4 \times 10^{-4}$.

[3] Superseded by ABLIKIM 24Y.

$\Gamma(K^0_S K^\pm\pi^\mp\pi^+\pi^-)/\Gamma_{total}$ — Γ_{26}/Γ

VALUE (units 10^{-3})	EVTS	DOCUMENT ID		TECN	COMMENT
3.2±1.0±0.2	41	[1] ABLIKIM	20AH	BES3	$\psi(2S) \to \pi^0 h_c(1P)$

[1] ABLIKIM 20AH reports $[\Gamma(h_c(1P) \to K^0_S K^\pm\pi^\mp\pi^+\pi^-)/\Gamma_{total}] \times [B(\psi(2S) \to h_c(1P)\pi^0)] = (2.4 \pm 0.7 \pm 0.3) \times 10^{-6}$ which we divide by our best (shown rounded) value $B(\psi(2S) \to h_c(1P)\pi^0) = (7.4 \pm 0.5) \times 10^{-4}$. Our first error is their experiment's error and our second error is the systematic error from using our best (shown rounded) value.

RADIATIVE DECAYS

$\Gamma(\gamma\eta)/\Gamma_{total}$ — Γ_{27}/Γ

VALUE (units 10^{-4})	EVTS	DOCUMENT ID		TECN	COMMENT
3.8±0.6 OUR AVERAGE					
3.8±0.6±0.3		[1] ABLIKIM	24BJ	BES3	$\psi(2S) \to \pi^0 h_c(1P)$
4.7±1.5±1.4	18	ABLIKIM	16I	BES3	$\psi(2S) \to \pi^0 \gamma\eta$

[1] ABLIKIM 24BJ reports $(3.77 \pm 0.55 \pm 0.29) \times 10^{-4}$ from a measurement of $[\Gamma(h_c(1P) \to \gamma\eta)/\Gamma_{total}] \times [B(\psi(2S) \to h_c(1P)\pi^0)]$ assuming $B(\psi(2S) \to h_c(1P)\pi^0) = (7.4 \pm 0.5) \times 10^{-4}$.

$\Gamma(\gamma\eta'(958))/\Gamma_{total}$ — Γ_{28}/Γ

VALUE (units 10^{-3})	EVTS	DOCUMENT ID		TECN	COMMENT
1.41±0.15 OUR AVERAGE					
1.40±0.11±0.11		[1] ABLIKIM	24BJ	BES3	$\psi(2S) \to \pi^0 \gamma\eta'$
1.52±0.27±0.29	44	ABLIKIM	16I	BES3	$\psi(2S) \to \pi^0 \gamma\eta'(958)$

Int. J. Mod. Phys. A 2026.41. Downloaded from www.worldscientific.com
by UNIVERSITY OF CALIFORNIA @ BERKELEY on 09/16/26. Re-use and distribution is strictly not permitted, except for Open Access articles.

[1] ABLIKIM 24BJ reports $(1.40 \pm 0.11 \pm 0.11) \times 10^{-3}$ from a measurement of $[\Gamma(h_c(1P) \to \gamma\eta'(958))/\Gamma_{total}] \times [B(\psi(2S) \to h_c(1P)\pi^0)]$ assuming $B(\psi(2S) \to h_c(1P)\pi^0) = (7.4 \pm 0.5) \times 10^{-4}$.

$\Gamma(\gamma\pi^0)/\Gamma_{total}$ — Γ_{29}/Γ

VALUE	DOCUMENT ID		TECN	COMMENT
$<5 \times 10^{-5}$	[1] ABLIKIM	24BJ	BES3	$\psi(2S) \to \pi^0 h_c(1P)$

[1] ABLIKIM 24BJ reports $< 5.0 \times 10^{-5}$ from a measurement of $[\Gamma(h_c(1P) \to \gamma\pi^0)/\Gamma_{total}] \times [B(\psi(2S) \to h_c(1P)\pi^0)]$ assuming $B(\psi(2S) \to h_c(1P)\pi^0) = (7.4 \pm 0.5) \times 10^{-4}$.

$\Gamma(\gamma\eta_c(1S))/\Gamma_{total}$ — Γ_{30}/Γ

VALUE (units 10^{-2})	EVTS	DOCUMENT ID		TECN	COMMENT
64± 5 OUR FIT Error includes scale factor of 1.2.					
57± 5 OUR AVERAGE					
57± 4±4	23k	[1] ABLIKIM	22AQ	BES3	$\psi(2S) \to \pi^0$ hadrons; $\pi^0\gamma(\eta_c)$
56± 6±4		[2] DOBBS	08A	CLEO	$\psi(2S) \to \pi^0\eta_c\gamma$
• • • We do not use the following data for averages, fits, limits, etc. • • •					
62± 9±4	3679	[3,4] ABLIKIM	10B	BES3	$\psi(2S) \to \pi^0\eta_c\gamma$
56± 7±4	1282	[5] DOBBS	08A	CLEO	$\psi(2S) \to \pi^0\eta_c\gamma$
54±14±4	168	[6] ROSNER	05	CLEO	$\psi(2S) \to \pi^0\eta_c\gamma$

[1] ABLIKIM 22AQ reports $[\Gamma(h_c(1P) \to \gamma\eta_c(1S))/\Gamma_{total}] \times [B(\psi(2S) \to h_c(1P)\pi^0)] = (4.22^{+0.27}_{-0.26} \pm 0.19) \times 10^{-4}$ which we divide by our best (shown rounded) value $B(\psi(2S) \to h_c(1P)\pi^0) = (7.4 \pm 0.5) \times 10^{-4}$. Our first error is their experiment's error and our second error is the systematic error from using our best (shown rounded) value.

[2] Average of DOBBS 08A and ROSNER 05. DOBBS 08A reports $[\Gamma(h_c(1P) \to \gamma\eta_c(1S))/\Gamma_{total}] \times [B(\psi(2S) \to h_c(1P)\pi^0)] = (4.16 \pm 0.30 \pm 0.37) \times 10^{-4}$ which we divide by our best (shown rounded) value $B(\psi(2S) \to h_c(1P)\pi^0) = (7.4 \pm 0.5) \times 10^{-4}$. Our first error is their experiment's error and our second error is the systematic error from using our best (shown rounded) value.

[3] ABLIKIM 10B reports $[\Gamma(h_c(1P) \to \gamma\eta_c(1S))/\Gamma_{total}] \times [B(\psi(2S) \to h_c(1P)\pi^0)] = (4.58 \pm 0.40 \pm 0.50) \times 10^{-4}$ which we divide by our best (shown rounded) value $B(\psi(2S) \to h_c(1P)\pi^0) = (7.4 \pm 0.5) \times 10^{-4}$. Our first error is their experiment's error and our second error is the systematic error from using our best (shown rounded) value.

[4] Superseded by ABLIKIM 22AQ

[5] DOBBS 08A reports $[\Gamma(h_c(1P) \to \gamma\eta_c(1S))/\Gamma_{total}] \times [B(\psi(2S) \to h_c(1P)\pi^0)] = (4.19 \pm 0.32 \pm 0.45) \times 10^{-4}$ which we divide by our best (shown rounded) value $B(\psi(2S) \to h_c(1P)\pi^0) = (7.4 \pm 0.5) \times 10^{-4}$. Our first error is their experiment's error and our second error is the systematic error from using our best (shown rounded) value.

[6] ROSNER 05 reports $[\Gamma(h_c(1P) \to \gamma\eta_c(1S))/\Gamma_{total}] \times [B(\psi(2S) \to h_c(1P)\pi^0)] = (4.0 \pm 0.8 \pm 0.7) \times 10^{-4}$ which we divide by our best (shown rounded) value $B(\psi(2S) \to h_c(1P)\pi^0) = (7.4 \pm 0.5) \times 10^{-4}$. Our first error is their experiment's error and our second error is the systematic error from using our best (shown rounded) value.

$\Gamma(\gamma\pi^+\pi^-)/\Gamma_{total}$ — Γ_{31}/Γ

VALUE (units 10^{-4})	EVTS	DOCUMENT ID		TECN	COMMENT
3.1±0.5±0.4	127 ± 22	[1] ABLIKIM	25G	BES3	$\psi(2S) \to \pi^0 h_c(1P)$

[1] ABLIKIM 25G reports $(3.06 \pm 0.54 \pm 0.43) \times 10^{-4}$ from a measurement of $[\Gamma(h_c(1P) \to \gamma\pi^+\pi^-)/\Gamma_{total}] \times [B(\psi(2S) \to h_c(1P)\pi^0)]$ assuming $B(\psi(2S) \to h_c(1P)\pi^0) = (7.4 \pm 0.5) \times 10^{-4}$.

$\Gamma(\gamma\pi^+\pi^-\eta)/\Gamma_{total}$ — Γ_{32}/Γ

VALUE (units 10^{-3})	EVTS	DOCUMENT ID		TECN	COMMENT
3.5±0.5±0.4	192 ± 27	[1] ABLIKIM	25G	BES3	$\psi(2S) \to \pi^0 h_c(1P)$

[1] ABLIKIM 25G reports $(3.52 \pm 0.50 \pm 0.38) \times 10^{-3}$ from a measurement of $[\Gamma(h_c(1P) \to \gamma\pi^+\pi^-\eta)/\Gamma_{total}] \times [B(\psi(2S) \to h_c(1P)\pi^0)]$ assuming $B(\psi(2S) \to h_c(1P)\pi^0) = (7.4 \pm 0.5) \times 10^{-4}$.

$\Gamma(\gamma 2\pi^+ 2\pi^-)/\Gamma_{total}$ — Γ_{33}/Γ

VALUE (units 10^{-3})	EVTS	DOCUMENT ID		TECN	COMMENT
2.19±0.20±0.22	495 ± 45	[1] ABLIKIM	25G	BES3	$\psi(2S) \to \pi^0 h_c(1P)$

[1] ABLIKIM 25G reports $(2.19 \pm 0.20 \pm 0.22) \times 10^{-3}$ from a measurement of $[\Gamma(h_c(1P) \to \gamma 2\pi^+ 2\pi^-)/\Gamma_{total}] \times [B(\psi(2S) \to h_c(1P)\pi^0)]$ assuming $B(\psi(2S) \to h_c(1P)\pi^0) = (7.4 \pm 0.5) \times 10^{-4}$.

$\Gamma(\gamma p\overline{p})/\Gamma_{total}$ — Γ_{34}/Γ

VALUE (units 10^{-4})	EVTS	DOCUMENT ID		TECN	COMMENT
3.3±0.5±0.4	127 ± 20	[1] ABLIKIM	25G	BES3	$\psi(2S) \to \pi^0 h_c(1P)$

[1] ABLIKIM 25G reports $(3.34 \pm 0.53 \pm 0.40) \times 10^{-4}$ from a measurement of $[\Gamma(h_c(1P) \to \gamma p\overline{p})/\Gamma_{total}] \times [B(\psi(2S) \to h_c(1P)\pi^0)]$ assuming $B(\psi(2S) \to h_c(1P)\pi^0) = (7.4 \pm 0.5) \times 10^{-4}$.

$\Gamma(e^+e^-\eta_c(1S))/\Gamma(\gamma\eta_c(1S))$ — Γ_{35}/Γ_{30}

VALUE (units 10^{-3})	EVTS	DOCUMENT ID		TECN	COMMENT
5.9±1.0±0.4	961	[1] ABLIKIM	24CC	BES3	$\psi(3686) \to \pi^0 h_c$, $e^+e^- \to \pi^+\pi^- h_c$

[1] Average between $\pi^0 h_c$ $(4.6 \pm 1.2 \pm 0.5) \times 10^{-3}$ and $\pi^+\pi^- h_c$ $(8.9 \pm 1.8 \pm 0.9) \times 10^{-3}$.

$\Gamma(\gamma f_2(1270) \to \gamma\pi^+\pi^-)/\Gamma_{total}$ — Γ_{36}/Γ

VALUE (units 10^{-4})	EVTS	DOCUMENT ID		TECN	COMMENT
1.81±0.35±0.22	72 ± 14	[1] ABLIKIM	25G	BES3	$\psi(2S) \to \pi^0 h_c(1P)$

[1] ABLIKIM 25G reports $(1.81 \pm 0.35 \pm 0.22) \times 10^{-4}$ from a measurement of $[\Gamma(h_c(1P) \to \gamma f_2(1270) \to \gamma\pi^+\pi^-)/\Gamma_{total}] \times [B(\psi(2S) \to h_c(1P)\pi^0)]$ assuming $B(\psi(2S) \to h_c(1P)\pi^0) = (7.4 \pm 0.5) \times 10^{-4}$.

$h_c(1P)$ REFERENCES

ABLIKIM	25G	PRL 134 241902	M. Ablikim et al.	(BESIII Collab.)
ABLIKIM	24BF	PR D110 032023	M. Ablikim et al.	(BESIII Collab.)
ABLIKIM	24BJ	JHEP 2408 180	M. Ablikim et al.	(BESIII Collab.)
ABLIKIM	24BY	PR D110 112010	M. Ablikim et al.	(BESIII Collab.)
ABLIKIM	24CC	PR D110 L111101	M. Ablikim et al.	(BESIII Collab.)
ABLIKIM	24R	PR D109 072018	M. Ablikim et al.	(BESIII Collab.)
ABLIKIM	24Y	PR D110 012007	M. Ablikim et al.	(BESIII Collab.)
ABLIKIM	22AQ	PR D106 072007	M. Ablikim et al.	(BESIII Collab.)
ABLIKIM	22M	JHEP 2205 108	M. Ablikim et al.	(BESIII Collab.)
Also		JHEP 2303 022 (errat.)	M. Ablikim et al.	(BESIII Collab.)
ABLIKIM	22N	JHEP 2205 003	M. Ablikim	(BESIII Collab.)
ABLIKIM	20AH	PR D102 112007	M. Ablikim et al.	(BESIII Collab.)
ABLIKIM	19AG	PR D99 072008	M. Ablikim et al.	(BESIII Collab.)
ABLIKIM	18M	PR D97 052008	M. Ablikim et al.	(BESIII Collab.)
ABLIKIM	16I	PRL 116 251802	M. Ablikim et al.	(BESIII Collab.)
ABLIKIM	12N	PR D86 092009	M. Ablikim et al.	(BESIII Collab.)
ABLIKIM	10B	PRL 104 132002	M. Ablikim et al.	(BESIII Collab.)
ADAMS	09	PR D80 051106	G.S. Adams et al.	(CLEO Collab.)
DOBBS	08A	PRL 101 182003	S. Dobbs et al.	(CLEO Collab.)
ANDREOTTI	05B	PR D72 032001	M. Andreotti et al.	(FNAL E835 Collab.)
ROSNER	05	PRL 95 102003	J.L. Rosner et al.	(CLEO Collab.)
AULCHENKO	03	PL B573 63	V.M. Aulchenko et al.	(KEDR Collab.)
ANTONIAZZI	94	PR D50 4258	L. Antoniazzi et al.	(E705 Collab.)
ARMSTRONG	93B	PR D47 772	T.A. Armstrong et al.	(FNAL E760 Collab.)
ARMSTRONG	92D	PRL 69 2337	T.A. Armstrong et al.	(FNAL, FERR, GENO+)
BAGLIN	86	PL B171 135	C. Baglin et al.	(LAPP, CERN, TORI, STRB+)

$\chi_{c2}(1P)$

$I^G(J^{PC}) = 0^+(2^{++})$

See the Review on "Branching Ratios of $\psi(2S)$, $\chi_{c0,1,2}$ and $\eta_c(1S)$" before the $\chi_{c0}(1P)$ Listings.

$\chi_{c2}(1P)$ MASS

VALUE (MeV)	EVTS	DOCUMENT ID		TECN	COMMENT
3556.17 ± 0.07 OUR AVERAGE					
3557.3 ± 1.7 ±0.7	611	[1] AAIJ	17BB	LHCB	$pp \to b\overline{b}X \to 2(K^+K^-)X$
3556.10 ± 0.06 ±0.11	4.0k	[2] AAIJ	17BI	LHCB	$\chi_{c2} \to J/\psi\mu^+\mu^-$
3555.3 ± 0.6 ±2.2	2.5k	UEHARA	08	BELL	$\gamma\gamma \to$ hadrons
3555.70 ± 0.59 ±0.39		ABLIKIM	05G	BES2	$\psi(2S) \to \gamma\chi_{c2}$
3556.173± 0.123±0.020		ANDREOTTI	05A	E835	$p\overline{p} \to e^+e^-\gamma$
3559.9 ± 2.9		EISENSTEIN	01	CLE2	$e^+e^- \to e^+e^-\chi_{c2}$
3556.4 ± 0.7		BAI	99B	BES	$\psi(2S) \to \gamma X$
3556.22 ± 0.131±0.020	585	[3] ARMSTRONG	92	E760	$\overline{p}p \to e^+e^-\gamma$
3556.9 ± 0.4 ±0.5	50	BAGLIN	86B	SPEC	$\overline{p}p \to e^+e^-X$
3557.8 ± 0.2 ±4		[4] GAISER	86	CBAL	$\psi(2S) \to \gamma X$
3553.4 ± 2.2	66	[5] LEMOIGNE	82	GOLI	185 π^-Be $\to \gamma\mu^+\mu^-$A
3555.9 ± 0.7		[6] OREGLIA	82	CBAL	$e^+e^- \to J/\psi 2\gamma$
3557 ± 1.5	69	[7] HIMEL	80	MRK2	$e^+e^- \to J/\psi 2\gamma$
3551 ±11	15	BRANDELIK	79B	DASP	$e^+e^- \to J/\psi 2\gamma$
3553 ± 4		[7] BARTEL	78B	CNTR	$e^+e^- \to J/\psi 2\gamma$
3553 ± 4 ±4		[7,8] TANENBAUM	78	MRK1	e^+e^-
3563 ± 7	360	[7] BIDDICK	77	CNTR	$e^+e^- \to \gamma X$
• • • We do not use the following data for averages, fits, limits, etc. • • •					
3555.4 ± 1.3	53	UEHARA	13	BELL	$\gamma\gamma \to K^0_S K^0_S$
3543 ±10	4	WHITAKER	76	MRK1	$e^+e^- \to J/\psi 2\gamma$

[1] From a fit of the $\phi\phi$ invariant mass with the width of $\chi_{c2}(1P)$ fixed to the PDG 16 value.

[2] AAIJ 17BI reports also $m(\chi_{c2}) - m(\chi_{c1}) = 45.39 \pm 0.07 \pm 0.03$ MeV.

[3] Recalculated by ANDREOTTI 05A, using the value of $\psi(2S)$ mass from AULCHENKO 03.

[4] Using mass of $\psi(2S) = 3686.0$ MeV.

[5] $J/\psi(1S)$ mass constrained to 3097 MeV.

[6] Assuming $\psi(2S)$ mass = 3686 MeV and $J/\psi(1S)$ mass = 3097 MeV.

[7] Mass value shifted by us by amount appropriate for $\psi(2S)$ mass = 3686 MeV and $J/\psi(1S)$ mass = 3097 MeV.

[8] From a simultaneous fit to radiative and hadronic decay channels.

$\chi_{c2}(1P)$ WIDTH

VALUE (MeV)	EVTS	DOCUMENT ID		TECN	COMMENT
1.94 ±0.09 OUR FIT Error includes scale factor of 1.1.					
2.00 ±0.11 OUR AVERAGE					
2.10 ±0.20 ±0.02	4.0k	AAIJ	17BI	LHCB	$\chi_{c2} \to J/\psi\mu^+\mu^-$
1.915±0.188±0.013		ANDREOTTI	05A	E835	$p\overline{p} \to e^+e^-\gamma$
1.96 ±0.17 ±0.07	585	[1] ARMSTRONG	92	E760	$\overline{p}p \to e^+e^-\gamma$
2.6 $^{+1.4}_{-1.0}$	50	BAGLIN	86B	SPEC	$\overline{p}p \to e^+e^-X$
2.8 $^{+2.1}_{-2.0}$		[2] GAISER	86	CBAL	$\psi(2S) \to \gamma X$

[1] Recalculated by ANDREOTTI 05A.
[2] Errors correspond to 90% confidence level; authors give only width range.

$\chi_{c2}(1P)$ DECAY MODES

	Mode	Fraction (Γ_i/Γ)	Scale factor/ Confidence level
	Hadronic decays		
Γ_1	$2(\pi^+\pi^-)$	(1.11 ± 0.07) %	S=1.2
Γ_2	$\rho\rho$		
Γ_3	$\pi^+\pi^-\pi^0\pi^0$	(1.81 ± 0.23) %	
Γ_4	$\rho^+\pi^-\pi^0$ + c.c.	(2.16 ± 0.34) %	
Γ_5	$4\pi^0$	$(1.10\pm0.15)\times10^{-3}$	
Γ_6	$K^+K^-\pi^0\pi^0$	$(2.0\pm0.4)\times10^{-3}$	
Γ_7	$K^+\pi^-\overline{K}^0\pi^0$ + c.c.	(1.37 ± 0.19) %	
Γ_8	$\rho^-K^+\overline{K}^0$ + c.c.	$(4.1\pm1.2)\times10^{-3}$	
Γ_9	$K^*(892)^0K^-\pi^+\to K^-\pi^+K^0\pi^0$ + c.c.	$(2.9\pm0.8)\times10^{-3}$	
Γ_{10}	$K^*(892)^0\overline{K}^0\pi^0\to K^+\pi^-\overline{K}^0\pi^0$ + c.c.	$(3.8\pm0.9)\times10^{-3}$	
Γ_{11}	$K^*(892)^-K^+\pi^0\to K^+\pi^-\overline{K}^0\pi^0$ + c.c.	$(3.7\pm0.8)\times10^{-3}$	
Γ_{12}	$K^*(892)^+\overline{K}^0\pi^-\to K^+\pi^-\overline{K}^0\pi^0$ + c.c.	$(2.9\pm0.8)\times10^{-3}$	
Γ_{13}	$K^+K^-\eta\pi^0$	$(1.3\pm0.4)\times10^{-3}$	
Γ_{14}	$K^+K^-\pi^+\pi^-$	$(8.4\pm1.1)\times10^{-3}$	S=1.2
Γ_{15}	$K^+K^-\pi^+\pi^-\pi^0$	(1.06 ± 0.11) %	
Γ_{16}	$K^0_SK^\pm\pi^\mp\pi^+\pi^-$	$(6.6\pm0.7)\times10^{-3}$	
Γ_{17}	$K^+\overline{K}^*(892)^0\pi^-$ + c.c.	$(2.1\pm1.1)\times10^{-3}$	
Γ_{18}	$K^*(892)^0\overline{K}^*(892)^0$	$(2.3\pm0.9)\times10^{-3}$	S=2.1
Γ_{19}	$3(\pi^+\pi^-)$	(1.51 ± 0.17) %	S=3.3
Γ_{20}	$\phi\phi$	$(1.22\pm0.07)\times10^{-3}$	S=1.6
Γ_{21}	$\phi\phi\eta$	$(5.3\pm0.6)\times10^{-4}$	
Γ_{22}	$\omega\omega$	$(8.6\pm0.4)\times10^{-4}$	
Γ_{23}	ωK^+K^-	$(6.6\pm0.8)\times10^{-4}$	
Γ_{24}	$\omega\phi$	$(9.8\pm1.3)\times10^{-6}$	
Γ_{25}	$\pi\pi$	$(2.33\pm0.06)\times10^{-3}$	S=1.2
Γ_{26}	$\rho^0\pi^+\pi^-$	$(3.9\pm1.6)\times10^{-3}$	
Γ_{27}	$\pi^+\pi^-\pi^0$ (non-resonant)	$(2.0\pm0.4)\times10^{-5}$	
Γ_{28}	$\rho(770)^\pm\pi^\mp$	$(6\pm4)\times10^{-6}$	
Γ_{29}	$\pi^+\pi^-\eta$	$(4.7\pm1.3)\times10^{-4}$	
Γ_{30}	$2\pi^+2\pi^-\eta$	$(5.7\pm0.6)\times10^{-3}$	
Γ_{31}	$\pi^+\pi^-\eta'$	$(4.9\pm1.8)\times10^{-4}$	
Γ_{32}	$\eta\eta$	$(5.4\pm0.4)\times10^{-4}$	
Γ_{33}	K^+K^-	$(1.16\pm0.05)\times10^{-3}$	S=1.7
Γ_{34}	$K^0_SK^0_S$	$(5.2\pm0.4)\times10^{-4}$	
Γ_{35}	$K^*(892)^\pm K^\mp$	$(1.42\pm0.21)\times10^{-4}$	
Γ_{36}	$K^*(892)^0\overline{K}^0$ + c.c.	$(1.23\pm0.27)\times10^{-4}$	
Γ_{37}	$K^*_2(1430)^\pm K^\mp$	$(1.47\pm0.12)\times10^{-3}$	
Γ_{38}	$K^*_2(1430)^0\overline{K}^0$ + c.c.	$(1.23\pm0.17)\times10^{-3}$	
Γ_{39}	$K^*_3(1780)^\pm K^\mp$	$(5.1\pm0.8)\times10^{-4}$	
Γ_{40}	$K^*_3(1780)^0\overline{K}^0$ + c.c.	$(5.6\pm2.1)\times10^{-4}$	
Γ_{41}	$a_2(1320)^0\pi^0$	$(1.28\pm0.34)\times10^{-3}$	
Γ_{42}	$a_2(1320)^\pm\pi^\mp$	$(1.7\pm0.6)\times10^{-3}$	
Γ_{43}	$\overline{K}^0K^+\pi^-$ + c.c.	$(1.27\pm0.18)\times10^{-3}$	
Γ_{44}	$K^+K^-\pi^0$	$(3.0\pm0.8)\times10^{-4}$	
Γ_{45}	$K^+K^-\eta$	$<3.2\times10^{-4}$	CL=90%
Γ_{46}	$K^+K^-\eta'(958)$	$(1.51\pm0.09)\times10^{-4}$	
Γ_{47}	$\eta\eta'$	$(2.1\pm0.5)\times10^{-5}$	
Γ_{48}	$\eta'\eta'$	$(4.5\pm0.6)\times10^{-5}$	
Γ_{49}	$\eta\eta\eta'$	$(4.1\pm0.9)\times10^{-5}$	
Γ_{50}	$\pi^+\pi^-K^0_SK^0_S$	$(2.2\pm0.5)\times10^{-3}$	
Γ_{51}	$K^+K^-K^0_SK^0_S$	$<4\times10^{-4}$	CL=90%
Γ_{52}	$K^0_SK^0_SK^0_SK^0_S$	$(1.12\pm0.18)\times10^{-4}$	
Γ_{53}	$K^+K^-K^+K^-$	$(1.64\pm0.22)\times10^{-3}$	S=1.1
Γ_{54}	$K^+K^-\phi$	$(1.41\pm0.29)\times10^{-3}$	
Γ_{55}	$\overline{K}^0K^+\pi^-\phi$ + c.c.	$(4.8\pm0.7)\times10^{-3}$	
Γ_{56}	$K^+K^-\pi^0\phi$	$(2.7\pm0.5)\times10^{-3}$	
Γ_{57}	$K^0_SK^0_SK^0_SK^\pm\pi^\mp$	$(1.70\pm0.16)\times10^{-4}$	
Γ_{58}	$3(K^+K^-)$	$(7.1\pm1.4)\times10^{-6}$	
Γ_{59}	$\phi\pi^+\pi^-\pi^0$	$(8.4\pm1.0)\times10^{-4}$	
Γ_{60}	$p\overline{p}$	$(8.06\pm0.33)\times10^{-5}$	S=1.6
Γ_{61}	$p\overline{p}\pi^0$	$(4.6\pm0.4)\times10^{-4}$	
Γ_{62}	$p\overline{p}\eta$	$(1.72\pm0.25)\times10^{-4}$	
Γ_{63}	$p\overline{p}\omega$	$(3.6\pm0.4)\times10^{-4}$	
Γ_{64}	$p\overline{p}\pi^+\pi^-$	$(1.32\pm0.34)\times10^{-3}$	
Γ_{65}	$p\overline{p}\pi^0\pi^0$	$(7.8\pm2.3)\times10^{-4}$	
Γ_{66}	$p\overline{p}\eta\pi^0$	$(1.29\pm0.09)\times10^{-4}$	
Γ_{67}	$p\overline{p}\eta\eta$	$(2.6\pm0.5)\times10^{-5}$	
Γ_{68}	$p\overline{p}K^+K^-$	$(2.52\pm0.17)\times10^{-4}$	
Γ_{69}	$p\overline{p}K^+K^-$ (non-resonant)	$(1.89\pm0.32)\times10^{-4}$	
Γ_{70}	$K^+\overline{p}\Lambda(1520)$ + c.c.	$(2.8\pm0.7)\times10^{-4}$	
Γ_{71}	$\Lambda(1520)\overline{\Lambda}(1520)$	$(4.6\pm1.4)\times10^{-4}$	
Γ_{72}	$p\overline{p}\phi$	$(2.8\pm0.9)\times10^{-5}$	
Γ_{73}	$p\overline{p}K^0_SK^0_S$	$<8\times10^{-4}$	CL=90%
Γ_{74}	$p\overline{p}K^0_SK^-\pi^+$ + c.c.	$(5.6\pm0.5)\times10^{-5}$	
Γ_{75}	$p\overline{n}\pi^-$	$(8.4\pm0.9)\times10^{-4}$	
Γ_{76}	$\overline{p}n\pi^+$	$(8.8\pm0.8)\times10^{-4}$	
Γ_{77}	$p\overline{n}\pi^-\pi^0$	$(2.15\pm0.18)\times10^{-3}$	
Γ_{78}	$\overline{p}n\pi^+\pi^0$	$(2.09\pm0.18)\times10^{-3}$	
Γ_{79}	$\Lambda\overline{\Lambda}$	$(1.81\pm0.16)\times10^{-4}$	
Γ_{80}	$\Lambda\overline{\Lambda}\pi^+\pi^-$	$(1.24\pm0.15)\times10^{-3}$	
Γ_{81}	$\Lambda\overline{\Lambda}\pi^+\pi^-$ (non-resonant)	$(6.5\pm1.5)\times10^{-4}$	
Γ_{82}	$\Sigma(1385)^+\overline{\Lambda}\pi^-$ + c.c.	$<4\times10^{-4}$	CL=90%
Γ_{83}	$\Sigma(1385)^-\overline{\Lambda}\pi^+$ + c.c.	$<6\times10^{-4}$	CL=90%
Γ_{84}	$\Lambda\overline{\Lambda}\eta$	$(1.04\pm0.25)\times10^{-4}$	
Γ_{85}	$\Lambda\overline{\Lambda}\eta'$	$(3.0\pm0.7)\times10^{-5}$	
Γ_{86}	$\Lambda\overline{\Lambda}\omega$	$(1.38\pm0.21)\times10^{-4}$	
Γ_{87}	$\Lambda\overline{\Lambda}\phi$	$(7.1\pm0.9)\times10^{-5}$	
Γ_{88}	$K^+\overline{p}\Lambda$ + c.c.	$(7.7\pm0.5)\times10^{-4}$	
Γ_{89}	$nK^0_S\overline{\Lambda}$ + c.c.	$(3.54\pm0.28)\times10^{-4}$	
Γ_{90}	$K^*(892)^+\overline{p}\Lambda$ + c.c.	$(8.1\pm1.1)\times10^{-4}$	
Γ_{91}	$\overline{p}\Lambda(1520)K^0_S\pi^+$ + c.c.	$(4.0\pm0.9)\times10^{-5}$	
Γ_{92}	$\Sigma^0\overline{\Sigma}^0$	$(3.6\pm0.6)\times10^{-5}$	
Γ_{93}	$\Sigma^+\overline{p}K^0_S$ + c.c.	$(8.2\pm0.9)\times10^{-5}$	
Γ_{94}	$\Sigma^0\overline{p}K^+$ + c.c.	$(9.0\pm0.8)\times10^{-5}$	
Γ_{95}	$\Sigma^+\overline{\Sigma}^-$	$(3.3\pm0.7)\times10^{-5}$	
Γ_{96}	$\Sigma^+\overline{\Sigma}^-\eta$	$(5.4\pm1.3)\times10^{-5}$	
Γ_{97}	$\Sigma^-\overline{\Sigma}^+$	$(4.4\pm1.8)\times10^{-5}$	
Γ_{98}	$\Sigma(1385)^+\overline{\Sigma}(1385)^-$	$<1.5\times10^{-4}$	CL=90%
Γ_{99}	$\Sigma(1385)^-\overline{\Sigma}(1385)^+$	$<8\times10^{-5}$	CL=90%
Γ_{100}	$K^-\Lambda\overline{\Xi}^+$ + c.c.	$(1.75\pm0.31)\times10^{-4}$	
Γ_{101}	$\Xi^0\overline{\Xi}^0$	$(1.81\pm0.22)\times10^{-4}$	
Γ_{102}	$\Xi^-\overline{\Xi}^+$	$(1.42\pm0.12)\times10^{-4}$	
Γ_{103}	$\Omega^-\overline{\Omega}^+$	$(4.47\pm0.30)\times10^{-5}$	
Γ_{104}	$J/\psi(1S)\pi^+\pi^-\pi^0$	<1.5 %	CL=90%
Γ_{105}	$\pi^0\eta_c$	$<3.2\times10^{-3}$	CL=90%
Γ_{106}	$\eta_c(1S)\pi^+\pi^-$	$<5\times10^{-3}$	CL=90%
	Radiative decays		
Γ_{107}	$\gamma J/\psi(1S)$	(19.0 ± 0.8) %	S=1.5
Γ_{108}	$\gamma\rho^0$	$<1.9\times10^{-5}$	CL=90%
Γ_{109}	$\gamma\omega$	$<6\times10^{-6}$	CL=90%
Γ_{110}	$\gamma\phi$	$<7\times10^{-6}$	CL=90%
Γ_{111}	$\gamma\gamma$	$(2.88\pm0.10)\times10^{-4}$	S=1.1
Γ_{112}	$e^+e^-J/\psi(1S)$	$(2.14\pm0.15)\times10^{-3}$	
Γ_{113}	$\mu^+\mu^-J/\psi(1S)$	$(2.01\pm0.33)\times10^{-4}$	

CONSTRAINED FIT INFORMATION

A multiparticle fit to $\chi_{c1}(1P)$, $\chi_{c0}(1P)$, $\chi_{c2}(1P)$, and $\psi(2S)$ with 4 total widths, a partial width, 27 combinations of partial widths obtained from integrated cross section, and 87 branching ratios uses 263 measurements to determine 50 parameters. The overall fit has a $\chi^2 = 435.4$ for 213 degrees of freedom.

The following *off-diagonal* array elements are the correlation coefficients $\langle\delta p_i\delta p_j\rangle/(\delta p_i\cdot\delta p_j)$, in percent, from the fit to parameters p_i, including the branching fractions, $x_i \equiv \Gamma_i/\Gamma_{\rm total}$.

	x_1	x_{14}	x_{17}	x_{18}	x_{20}	x_{25}	x_{26}	x_{32}	x_{33}	x_{34}
x_{14}		5								
x_{17}		1	26							
x_{18}		2	2	0						
x_{20}		14	5	1	2					
x_{25}		30	6	1	3	31				
x_{26}		11	1	0	0	2	4			
x_{32}		10	2	0	1	10	24	1		
x_{33}		18	4	1	2	18	42	2	14	
x_{34}		11	3	1	1	11	24	1	8	14
x_{43}		6	1	0	1	6	13	1	4	8	4
x_{53}		6	3	1	1	7	13	1	4	8	5
x_{60}		17	6	2	2	17	36	2	12	21	13
x_{79}		10	2	0	1	10	23	1	8	14	8
x_{107}		19	10	3	3	19	37	3	12	22	14
x_{111}		14	−7	−2	−1	14	43	1	15	25	13
Γ		−25	−19	−5	−5	−26	−43	−4	−15	−26	−18

Int. J. Mod. Phys. A 2026.41. Downloaded from www.worldscientific.com
by [redacted] LIFORNIA @ BERKELEY on 09/16/26. Re-use and distribution is strictly not permitted, except for Open Access articles.

x_{53}	2					
x_{60}	7	8				
x_{79}	4	4	11			
x_{107}	7	9	3	12		
x_{111}	7	5	28	14	22	
Γ	−8	−12	−41	−14	−49	−46
	x_{43}	x_{53}	x_{60}	x_{79}	x_{107}	x_{111}

$\chi_{c2}(1P)$ PARTIAL WIDTHS

$\chi_{c2}(1P)$ $\Gamma(i)\Gamma(\gamma J/\psi(1S))/\Gamma(\text{total})$

$\Gamma(p\overline{p}) \times \Gamma(\gamma J/\psi(1S))/\Gamma_{\text{total}}$ — $\Gamma_{60}\Gamma_{107}/\Gamma$

VALUE (eV)	DOCUMENT ID		TECN	COMMENT
29.6±1.3 OUR FIT Error includes scale factor of 1.3.				
27.5±1.5 OUR AVERAGE				
27.0±1.5±1.1	[1] ANDREOTTI	05A	E835	$p\overline{p} \to e^+e^-\gamma$
27.7±1.5±2.0	[1,2] ARMSTRONG	92	E760	$\overline{p}p \to e^+e^-\gamma$
36 ±8	[1] BAGLIN	86B	SPEC	$\overline{p}p \to e^+e^-X$

[1] Calculated by us using $B(J/\psi(1S) \to e^+e^-) = 0.0593 \pm 0.0010$.
[2] Recalculated by ANDREOTTI 05A.

$\Gamma(\gamma\gamma) \times \Gamma(\gamma J/\psi(1S))/\Gamma_{\text{total}}$ — $\Gamma_{111}\Gamma_{107}/\Gamma$

VALUE (eV)	EVTS	DOCUMENT ID		TECN	COMMENT
106 ± 5 OUR FIT Error includes scale factor of 1.4.					
123 ± 6 OUR AVERAGE					
124.1± 2.5± 5.9	4960	[1] SEINO	23	BELL	$e^+e^- \to e^+e^-\chi_{c2}$
111 ± 12 ± 9	147	[2] DOBBS	06	CLE3	$e^+e^- \to e^+e^-\chi_{c2}$
139 ± 55 ± 21		[2,3] ACCIARRI	99E	L3	$e^+e^- \to e^+e^-\chi_{c2}$
242 ± 65 ± 51		[2,4] ACKER..,K...	98	OPAL	$e^+e^- \to e^+e^-\chi_{c2}$
150 ± 42 ± 36		[2,5] DOMINICK	94	CLE2	$e^+e^- \to e^+e^-\chi_{c2}$
470 ±240 ±120		[2,6] BAUER	93	TPC	$e^+e^- \to e^+e^-\chi_{c2}$
• • • We do not use the following data for averages, fits, limits, etc. • • •					
114 ± 11 ± 9	136	[2,7] ABE	02T	BELL	$e^+e^- \to e^+e^-\chi_{c2}$

[1] Calculated from the measured $\Gamma_{\gamma\gamma} \times B(\chi_{c2}(1S) \to \gamma J/\psi(1S)) \times B(J/\psi(1S) \to \ell^+\ell^-) = 14.8 \pm 0.3 \pm 0.7$ eV, using $B(J/\psi(1S) \to \ell^+\ell^-) = 11.93 \pm 0.05\%$.
[2] Calculated by us using $B(J/\psi \to \ell^+\ell^-) = 0.1187 \pm 0.0008$.
[3] The value for $\Gamma(\chi_{c2} \to \gamma\gamma)$ reported in ACCIARRI 99E is derived using $B(\chi_{c2} \to \gamma J/\psi(1S)) \times B(J/\psi(1S) \to \ell^+\ell^-) = 0.0162 \pm 0.0014$.
[4] The value for $\Gamma(\chi_{c2} \to \gamma\gamma)$ reported in ACKERSTAFF,K 98 is derived using $B(\chi_{c2} \to \gamma J/\psi(1S)) = 0.135 \pm 0.011$ and $B(J/\psi(1S) \to \ell^+\ell^-) = 0.1203 \pm 0.0038$.
[5] The value for $\Gamma(\chi_{c2} \to \gamma\gamma)$ reported in DOMINICK 94 is derived using $B(\chi_{c2} \to \gamma J/\psi(1S)) = 0.135 \pm 0.011$, $B(J/\psi(1S) \to e^+e^-) = 0.0627 \pm 0.0020$, and $B(J/\psi(1S) \to \mu^+\mu^-) = 0.0597 \pm 0.0025$.
[6] The value for $\Gamma(\chi_{c2} \to \gamma\gamma)$ reported in BAUER 93 is derived using $B(\chi_{c2} \to \gamma J/\psi(1S)) = 0.135 \pm 0.011$, $B(J/\psi(1S) \to e^+e^-) = 0.0627 \pm 0.0020$, and $B(J/\psi(1S) \to \mu^+\mu^-) = 0.0597 \pm 0.0025$.
[7] All systematic errors added in quadrature. Superseded by SEINO 23.

$\chi_{c2}(1P)$ $\Gamma(i)\Gamma(\gamma\gamma)/\Gamma(\text{total})$

$\Gamma(2(\pi^+\pi^-)) \times \Gamma(\gamma\gamma)/\Gamma_{\text{total}}$ — $\Gamma_1\Gamma_{111}/\Gamma$

VALUE (eV)	EVTS	DOCUMENT ID		TECN	COMMENT
6.2 ±0.4 OUR FIT Error includes scale factor of 1.3.					
5.2 ±0.7 OUR AVERAGE					
5.01±0.44±0.55	1597±138	UEHARA	08	BELL	$\gamma\gamma \to \chi_{c2} \to 2(\pi^+\pi^-)$
6.4 ±1.8 ±0.8		EISENSTEIN	01	CLE2	$e^+e^- \to e^+e^-\chi_{c2}$

$\Gamma(\rho\rho) \times \Gamma(\gamma\gamma)/\Gamma_{\text{total}}$ — $\Gamma_2\Gamma_{111}/\Gamma$

VALUE (eV)	CL%	EVTS	DOCUMENT ID		TECN	COMMENT
• • • We do not use the following data for averages, fits, limits, etc. • • •						
<7.8	90	<598	UEHARA	08	BELL	$\gamma\gamma \to \chi_{c2} \to 2(\pi^+\pi^-)$

$\Gamma(K^+K^-\pi^+\pi^-) \times \Gamma(\gamma\gamma)/\Gamma_{\text{total}}$ — $\Gamma_{14}\Gamma_{111}/\Gamma$

VALUE (eV)	EVTS	DOCUMENT ID		TECN	COMMENT
4.7 ±0.6 OUR FIT Error includes scale factor of 1.2.					
4.42±0.42±0.53	780 ± 74	UEHARA	08	BELL	$\gamma\gamma \to \chi_{c2} \to K^+K^-\pi^+\pi^-$

$\Gamma(K^+K^-\pi^+\pi^-\pi^0) \times \Gamma(\gamma\gamma)/\Gamma_{\text{total}}$ — $\Gamma_{15}\Gamma_{111}/\Gamma$

VALUE (eV)	EVTS	DOCUMENT ID		TECN	COMMENT
6.5±0.9±1.5	1250	DEL-AMO-SA...11M		BABR	$\gamma\gamma \to K^+K^-\pi^+\pi^-\pi^0$

$\Gamma(K^*(892)^0\overline{K}^*(892)^0) \times \Gamma(\gamma\gamma)/\Gamma_{\text{total}}$ — $\Gamma_{18}\Gamma_{111}/\Gamma$

VALUE (eV)	EVTS	DOCUMENT ID		TECN	COMMENT
1.3±0.5 OUR FIT Error includes scale factor of 2.1.					
0.8±0.17±0.27	151 ± 30	UEHARA	08	BELL	$\gamma\gamma \to \chi_{c2} \to K^+K^-\pi^+\pi^-$

$\Gamma(\phi\phi) \times \Gamma(\gamma\gamma)/\Gamma_{\text{total}}$ — $\Gamma_{20}\Gamma_{111}/\Gamma$

VALUE (eV)	EVTS	DOCUMENT ID		TECN	COMMENT
0.68±0.04 OUR FIT Error includes scale factor of 1.5.					
0.62±0.07±0.05	89 ± 11	[1] LIU	12B	BELL	$\gamma\gamma \to 2(K^+K^-)$
• • • We do not use the following data for averages, fits, limits, etc. • • •					
0.58±0.18±0.16	26.5±8.1	UEHARA	08	BELL	$\gamma\gamma \to \chi_{c2} \to 2(K^+K^-)$

[1] Supersedes UEHARA 08. Using $B(\phi \to K^+K^-) = (48.9 \pm 0.5)\%$.

$\Gamma(\omega\omega) \times \Gamma(\gamma\gamma)/\Gamma_{\text{total}}$ — $\Gamma_{22}\Gamma_{111}/\Gamma$

VALUE (eV)	CL%	DOCUMENT ID		TECN	COMMENT
• • • We do not use the following data for averages, fits, limits, etc. • • •					
<0.64	90	[1] LIU	12B	BELL	$\gamma\gamma \to 2(\pi^+\pi^-\pi^0)$

[1] Using $B(\omega \to \pi^+\pi^-\pi^0) = (89.2 \pm 0.7)\%$.

$\Gamma(\omega\phi) \times \Gamma(\gamma\gamma)/\Gamma_{\text{total}}$ — $\Gamma_{24}\Gamma_{111}/\Gamma$

VALUE (eV)	CL%	DOCUMENT ID		TECN	COMMENT
• • • We do not use the following data for averages, fits, limits, etc. • • •					
<0.04	90	[1] LIU	12B	BELL	$\gamma\gamma \to K^+K^-\pi^+\pi^-\pi^0$

[1] Using $B(\phi \to K^+K^-) = (48.9 \pm 0.5)\%$ and $B(\omega \to \pi^+\pi^-\pi^0) = (89.2 \pm 0.7)\%$.

$\Gamma(\pi\pi) \times \Gamma(\gamma\gamma)/\Gamma_{\text{total}}$ — $\Gamma_{25}\Gamma_{111}/\Gamma$

VALUE (eV)	EVTS	DOCUMENT ID		TECN	COMMENT
1.30±0.06 OUR FIT Error includes scale factor of 1.3.					
1.18±0.25 OUR AVERAGE					
1.44±0.54±0.47	34 ± 13	[1] UEHARA	09	BELL	10.6 $e^+e^- \to e^+e^-\pi^0\pi^0$
1.14±0.21±0.17	54 ± 10	[2] NAKAZAWA	05	BELL	10.6 $e^+e^- \to e^+e^-\pi^+\pi^-$

[1] We multiplied the measurement by 3 to convert from $\pi^0\pi^0$ to $\pi\pi$. Interference with the continuum included.
[2] We have multiplied $\pi^+\pi^-$ measurement by 3/2 to obtain $\pi\pi$.

$\Gamma(\rho^0\pi^+\pi^-) \times \Gamma(\gamma\gamma)/\Gamma_{\text{total}}$ — $\Gamma_{26}\Gamma_{111}/\Gamma$

VALUE (eV)	EVTS	DOCUMENT ID		TECN	COMMENT
2.2±0.9 OUR FIT					
3.2±1.9±0.5	986 ± 578	UEHARA	08	BELL	$\gamma\gamma \to \chi_{c2} \to 2(\pi^+\pi^-)$

$\Gamma(\eta\eta) \times \Gamma(\gamma\gamma)/\Gamma_{\text{total}}$ — $\Gamma_{32}\Gamma_{111}/\Gamma$

VALUE (eV)	EVTS	DOCUMENT ID		TECN	COMMENT
0.53±0.22±0.09	8	[1] UEHARA	10A	BELL	10.6 $e^+e^- \to e^+e^-\eta\eta$

[1] Interference with the continuum not included.

$\Gamma(K^+K^-) \times \Gamma(\gamma\gamma)/\Gamma_{\text{total}}$ — $\Gamma_{33}\Gamma_{111}/\Gamma$

VALUE (eV)	EVTS	DOCUMENT ID		TECN	COMMENT
0.65±0.04 OUR FIT Error includes scale factor of 1.6.					
0.44±0.11±0.07	33 ± 8	NAKAZAWA	05	BELL	10.6 $e^+e^- \to e^+e^-K^+K^-$

$\Gamma(K^0_SK^0_S) \times \Gamma(\gamma\gamma)/\Gamma_{\text{total}}$ — $\Gamma_{34}\Gamma_{111}/\Gamma$

VALUE (eV)	EVTS	DOCUMENT ID		TECN	COMMENT
0.290±0.024 OUR FIT					
0.27 $^{+0.07}_{-0.06}$ ±0.03	53	[1] UEHARA	13	BELL	$\gamma\gamma \to K^0_SK^0_S$
• • • We do not use the following data for averages, fits, limits, etc. • • •					
0.31 ±0.05 ±0.03	38 ± 7	CHEN	07B	BELL	$e^+e^- \to e^+e^-\chi_{c2}$

[1] Supersedes CHEN 07B.

$\Gamma(\overline{K}^0K^+\pi^- + \text{c.c.}) \times \Gamma(\gamma\gamma)/\Gamma_{\text{total}}$ — $\Gamma_{43}\Gamma_{111}/\Gamma$

VALUE (eV)	EVTS	DOCUMENT ID		TECN	COMMENT
0.71±0.11 OUR FIT					
1.20±0.33±0.13	126	[1] DEL-AMO-SA...11M		BABR	$\gamma\gamma \to K^0_SK^\pm\pi^\mp$

[1] We have multiplied $\overline{K}K\pi$ by 2/3 to obtain $\overline{K}^0K^+\pi^- + \text{c.c.}$

$\Gamma(K^+K^-K^+K^-) \times \Gamma(\gamma\gamma)/\Gamma_{\text{total}}$ — $\Gamma_{53}\Gamma_{111}/\Gamma$

VALUE (eV)	EVTS	DOCUMENT ID		TECN	COMMENT
0.92±0.13 OUR FIT Error includes scale factor of 1.1.					
1.10±0.21±0.15	126 ± 24	UEHARA	08	BELL	$\gamma\gamma \to \chi_{c2} \to 2(K^+K^-)$

$\Gamma(\eta_c(1S)\pi^+\pi^-) \times \Gamma(\gamma\gamma)/\Gamma_{\text{total}}$ — $\Gamma_{106}\Gamma_{111}/\Gamma$

VALUE (eV)	CL%	DOCUMENT ID		TECN	COMMENT
<15.7	90	LEES	12AE	BABR	$e^+e^- \to e^+e^-\pi^+\pi^-\eta_c$

$\chi_{c2}(1P)$ BRANCHING RATIOS

HADRONIC DECAYS

$\Gamma(2(\pi^+\pi^-))/\Gamma_{\text{total}}$ — Γ_1/Γ

VALUE (%)	EVTS	DOCUMENT ID		TECN	COMMENT
1.11±0.07 OUR FIT Error includes scale factor of 1.2.					
• • • We do not use the following data for averages, fits, limits, etc. • • •					
1.14±0.06±0.03	1042k	[1,2] ABLIKIM	24BT	BES3	$\psi(2S) \to \gamma\chi_{c2}$

[1] ABLIKIM 24BT reports $1.153 \pm 0.001 \pm 0.063$ % from a measurement of $[\Gamma(\chi_{c2}(1P) \to 2(\pi^+\pi^-))/\Gamma_{\text{total}}] \times [B(\psi(2S) \to \gamma\chi_{c2}(1P))]$ assuming $B(\psi(2S) \to \gamma\chi_{c2}(1P)) = (9.52 \pm 0.20) \times 10^{-2}$, which we rescale to our best (shown rounded) value $B(\psi(2S) \to \gamma\chi_{c2}(1P)) = (9.63 \pm 0.23) \times 10^{-2}$. Our first error is their experiment's error and our second error is the systematic error from using our best (shown rounded) value.
[2] Not used since the same experimental measurement has been used in another related quantity included elsewhere in the fit.

$\Gamma(\pi^+\pi^-\pi^0\pi^0)/\Gamma_{\text{total}}$ — Γ_3/Γ

VALUE (%)	EVTS	DOCUMENT ID		TECN	COMMENT
1.81±0.23±0.04	903.5	[1] HE	08B	CLEO	$e^+e^- \to \gamma h^+h^-h^0h^0$

Int. J. Mod. Phys. A 2026.41. Downloaded from www.worldscientific.com
by UNIVERSITY OF CALIFORNIA @ BERKELEY on 09/16/26. Re-use and distribution is strictly not permitted, except for Open Access articles.

[1] HE 08B reports 1.87 ± 0.07 ± 0.22 ± 0.13 % from a measurement of $[\Gamma(\chi_{c2}(1P) \to \pi^+\pi^-\pi^0\pi^0)/\Gamma_{total}] \times [B(\psi(2S) \to \gamma\chi_{c2}(1P))]$ assuming $B(\psi(2S) \to \gamma\chi_{c2}(1P)) = (9.33 \pm 0.14 \pm 0.61) \times 10^{-2}$, which we rescale to our best (shown rounded) value $B(\psi(2S) \to \gamma\chi_{c2}(1P)) = (9.63 \pm 0.23) \times 10^{-2}$. Our first error is their experiment's error and our second error is the systematic error from using our best (shown rounded) value.

$\Gamma(\rho^+\pi^-\pi^0 + \text{c.c.})/\Gamma_{total}$ — Γ_4/Γ

VALUE (%)	EVTS	DOCUMENT ID		TECN	COMMENT
2.16±0.33±0.05	1031.9	[1,2] HE	08B	CLEO	$e^+e^- \to \gamma h^+ h^- h^0 h^0$

[1] HE 08B reports 2.23 ± 0.11 ± 0.32 ± 0.16 % from a measurement of $[\Gamma(\chi_{c2}(1P) \to \rho^+\pi^-\pi^0 + \text{c.c.})/\Gamma_{total}] \times [B(\psi(2S) \to \gamma\chi_{c2}(1P))]$ assuming $B(\psi(2S) \to \gamma\chi_{c2}(1P)) = (9.33 \pm 0.14 \pm 0.61) \times 10^{-2}$, which we rescale to our best (shown rounded) value $B(\psi(2S) \to \gamma\chi_{c2}(1P)) = (9.63 \pm 0.23) \times 10^{-2}$. Our first error is their experiment's error and our second error is the systematic error from using our best (shown rounded) value.

[2] Calculated by us. We have added the values from HE 08B for $\rho^+\pi^-\pi^0$ and $\rho^-\pi^+\pi^0$ decays assuming uncorrelated statistical and fully correlated systematic uncertainties.

$\Gamma(4\pi^0)/\Gamma_{total}$ — Γ_5/Γ

VALUE (units 10^{-3})	EVTS	DOCUMENT ID		TECN	COMMENT
1.10±0.15±0.03	1164	[1] ABLIKIM	11A	BES3	$e^+e^- \to \psi(2S) \to \gamma\chi_{c2}$

[1] ABLIKIM 11A reports $(1.21 \pm 0.05 \pm 0.16) \times 10^{-3}$ from a measurement of $[\Gamma(\chi_{c2}(1P) \to 4\pi^0)/\Gamma_{total}] \times [B(\psi(2S) \to \gamma\chi_{c2}(1P))]$ assuming $B(\psi(2S) \to \gamma\chi_{c2}(1P)) = (8.74 \pm 0.35) \times 10^{-2}$, which we rescale to our best (shown rounded) value $B(\psi(2S) \to \gamma\chi_{c2}(1P)) = (9.63 \pm 0.23) \times 10^{-2}$. Our first error is their experiment's error and our second error is the systematic error from using our best (shown rounded) value.

$\Gamma(K^+K^-\pi^0\pi^0)/\Gamma_{total}$ — Γ_6/Γ

VALUE (%)	EVTS	DOCUMENT ID		TECN	COMMENT
0.204±0.040±0.005	76.9	[1] HE	08B	CLEO	$e^+e^- \to \gamma h^+ h^- h^0 h^0$

[1] HE 08B reports 0.21 ± 0.03 ± 0.03 ± 0.01 % from a measurement of $[\Gamma(\chi_{c2}(1P) \to K^+K^-\pi^0\pi^0)/\Gamma_{total}] \times [B(\psi(2S) \to \gamma\chi_{c2}(1P))]$ assuming $B(\psi(2S) \to \gamma\chi_{c2}(1P)) = (9.33 \pm 0.14 \pm 0.61) \times 10^{-2}$, which we rescale to our best (shown rounded) value $B(\psi(2S) \to \gamma\chi_{c2}(1P)) = (9.63 \pm 0.23) \times 10^{-2}$. Our first error is their experiment's error and our second error is the systematic error from using our best (shown rounded) value.

$\Gamma(K^+\pi^-\overline{K}^0\pi^0 + \text{c.c.})/\Gamma_{total}$ — Γ_7/Γ

VALUE (%)	EVTS	DOCUMENT ID		TECN	COMMENT
1.37±0.19±0.03	211.6	[1] HE	08B	CLEO	$e^+e^- \to \gamma h^+ h^- h^0 h^0$

[1] HE 08B reports 1.41 ± 0.11 ± 0.16 ± 0.10 % from a measurement of $[\Gamma(\chi_{c2}(1P) \to K^+\pi^-\overline{K}^0\pi^0 + \text{c.c.})/\Gamma_{total}] \times [B(\psi(2S) \to \gamma\chi_{c2}(1P))]$ assuming $B(\psi(2S) \to \gamma\chi_{c2}(1P)) = (9.33 \pm 0.14 \pm 0.61) \times 10^{-2}$, which we rescale to our best (shown rounded) value $B(\psi(2S) \to \gamma\chi_{c2}(1P)) = (9.63 \pm 0.23) \times 10^{-2}$. Our first error is their experiment's error and our second error is the systematic error from using our best (shown rounded) value.

$\Gamma(\rho^-K^+\overline{K}^0 + \text{c.c.})/\Gamma_{total}$ — Γ_8/Γ

VALUE (%)	EVTS	DOCUMENT ID		TECN	COMMENT
0.41±0.12±0.01	62.9	[1] HE	08B	CLEO	$e^+e^- \to \gamma h^+ h^- h^0 h^0$

[1] HE 08B reports 0.42 ± 0.11 ± 0.06 ± 0.03 % from a measurement of $[\Gamma(\chi_{c2}(1P) \to \rho^-K^+\overline{K}^0 + \text{c.c.})/\Gamma_{total}] \times [B(\psi(2S) \to \gamma\chi_{c2}(1P))]$ assuming $B(\psi(2S) \to \gamma\chi_{c2}(1P)) = (9.33 \pm 0.14 \pm 0.61) \times 10^{-2}$, which we rescale to our best (shown rounded) value $B(\psi(2S) \to \gamma\chi_{c2}(1P)) = (9.63 \pm 0.23) \times 10^{-2}$. Our first error is their experiment's error and our second error is the systematic error from using our best (shown rounded) value.

$\Gamma(K^*(892)^0K^-\pi^+ \to K^-\pi^+K^0\pi^0 + \text{c.c.})/\Gamma_{total}$ — Γ_9/Γ

VALUE (%)	EVTS	DOCUMENT ID		TECN	COMMENT
0.29±0.08±0.01	38.7	[1] HE	08B	CLEO	$e^+e^- \to \gamma h^+ h^- h^0 h^0$

[1] HE 08B reports 0.30 ± 0.07 ± 0.04 ± 0.02 % from a measurement of $[\Gamma(\chi_{c2}(1P) \to K^*(892)^0K^-\pi^+ \to K^-\pi^+K^0\pi^0 + \text{c.c.})/\Gamma_{total}] \times [B(\psi(2S) \to \gamma\chi_{c2}(1P))]$ assuming $B(\psi(2S) \to \gamma\chi_{c2}(1P)) = (9.33 \pm 0.14 \pm 0.61) \times 10^{-2}$, which we rescale to our best (shown rounded) value $B(\psi(2S) \to \gamma\chi_{c2}(1P)) = (9.63 \pm 0.23) \times 10^{-2}$. Our first error is their experiment's error and our second error is the systematic error from using our best (shown rounded) value.

$\Gamma(K^*(892)^0\overline{K}^0\pi^0 \to K^+\pi^-\overline{K}^0\pi^0 + \text{c.c.})/\Gamma_{total}$ — Γ_{10}/Γ

VALUE (%)	EVTS	DOCUMENT ID		TECN	COMMENT
0.38±0.08±0.01	63.0	[1] HE	08B	CLEO	$e^+e^- \to \gamma h^+ h^- h^0 h^0$

[1] HE 08B reports 0.39 ± 0.07 ± 0.05 ± 0.03 % from a measurement of $[\Gamma(\chi_{c2}(1P) \to K^*(892)^0\overline{K}^0\pi^0 \to K^+\pi^-\overline{K}^0\pi^0 + \text{c.c.})/\Gamma_{total}] \times [B(\psi(2S) \to \gamma\chi_{c2}(1P))]$ assuming $B(\psi(2S) \to \gamma\chi_{c2}(1P)) = (9.33 \pm 0.14 \pm 0.61) \times 10^{-2}$, which we rescale to our best (shown rounded) value $B(\psi(2S) \to \gamma\chi_{c2}(1P)) = (9.63 \pm 0.23) \times 10^{-2}$. Our first error is their experiment's error and our second error is the systematic error from using our best (shown rounded) value.

$\Gamma(K^*(892)^-K^+\pi^0 \to K^+\pi^-\overline{K}^0\pi^0 + \text{c.c.})/\Gamma_{total}$ — Γ_{11}/Γ

VALUE (%)	EVTS	DOCUMENT ID		TECN	COMMENT
0.37±0.08±0.01	51.1	[1] HE	08B	CLEO	$e^+e^- \to \gamma h^+ h^- h^0 h^0$

[1] HE 08B reports 0.38 ± 0.07 ± 0.04 ± 0.03 % from a measurement of $[\Gamma(\chi_{c2}(1P) \to K^*(892)^-K^+\pi^0 \to K^+\pi^-\overline{K}^0\pi^0 + \text{c.c.})/\Gamma_{total}] \times [B(\psi(2S) \to \gamma\chi_{c2}(1P))]$ assuming $B(\psi(2S) \to \gamma\chi_{c2}(1P)) = (9.33 \pm 0.14 \pm 0.61) \times 10^{-2}$, which we rescale to our best (shown rounded) value $B(\psi(2S) \to \gamma\chi_{c2}(1P)) = (9.63 \pm 0.23) \times 10^{-2}$. Our first error is their experiment's error and our second error is the systematic error from using our best (shown rounded) value.

$\Gamma(K^*(892)^+\overline{K}^0\pi^- \to K^+\pi^-\overline{K}^0\pi^0 + \text{c.c.})/\Gamma_{total}$ — Γ_{12}/Γ

VALUE (%)	EVTS	DOCUMENT ID		TECN	COMMENT
0.29±0.08±0.01	39.3	[1] HE	08B	CLEO	$e^+e^- \to \gamma h^+ h^- h^0 h^0$

[1] HE 08B reports 0.30 ± 0.07 ± 0.04 ± 0.02 % from a measurement of $[\Gamma(\chi_{c2}(1P) \to K^*(892)^+\overline{K}^0\pi^- \to K^+\pi^-\overline{K}^0\pi^0 + \text{c.c.})/\Gamma_{total}] \times [B(\psi(2S) \to \gamma\chi_{c2}(1P))]$ assuming $B(\psi(2S) \to \gamma\chi_{c2}(1P)) = (9.33 \pm 0.14 \pm 0.61) \times 10^{-2}$, which we rescale to our best (shown rounded) value $B(\psi(2S) \to \gamma\chi_{c2}(1P)) = (9.63 \pm 0.23) \times 10^{-2}$. Our first error is their experiment's error and our second error is the systematic error from using our best (shown rounded) value.

$\Gamma(K^+K^-\eta\pi^0)/\Gamma_{total}$ — Γ_{13}/Γ

VALUE (%)	EVTS	DOCUMENT ID		TECN	COMMENT
0.126±0.044±0.003	22.9	[1] HE	08B	CLEO	$e^+e^- \to \gamma h^+ h^- h^0 h^0$

[1] HE 08B reports 0.13 ± 0.04 ± 0.02 ± 0.01 % from a measurement of $[\Gamma(\chi_{c2}(1P) \to K^+K^-\eta\pi^0)/\Gamma_{total}] \times [B(\psi(2S) \to \gamma\chi_{c2}(1P))]$ assuming $B(\psi(2S) \to \gamma\chi_{c2}(1P)) = (9.33 \pm 0.14 \pm 0.61) \times 10^{-2}$, which we rescale to our best (shown rounded) value $B(\psi(2S) \to \gamma\chi_{c2}(1P)) = (9.63 \pm 0.23) \times 10^{-2}$. Our first error is their experiment's error and our second error is the systematic error from using our best (shown rounded) value.

$\Gamma(K^+K^-\pi^+\pi^-\pi^0)/\Gamma_{total}$ — Γ_{15}/Γ

VALUE (units 10^{-3})	EVTS	DOCUMENT ID		TECN	COMMENT
10.6±1.1±0.3	11k	[1] ABLIKIM	13B	BES3	$e^+e^- \to \psi(2S) \to \gamma\chi_{c2}$

[1] ABLIKIM 13B reports $(11.69 \pm 0.13 \pm 1.31) \times 10^{-3}$ from a measurement of $[\Gamma(\chi_{c2}(1P) \to K^+K^-\pi^+\pi^-\pi^0)/\Gamma_{total}] \times [B(\psi(2S) \to \gamma\chi_{c2}(1P))]$ assuming $B(\psi(2S) \to \gamma\chi_{c2}(1P)) = (8.72 \pm 0.34) \times 10^{-2}$, which we rescale to our best (shown rounded) value $B(\psi(2S) \to \gamma\chi_{c2}(1P)) = (9.63 \pm 0.23) \times 10^{-2}$. Our first error is their experiment's error and our second error is the systematic error from using our best (shown rounded) value.

$\Gamma(K^0_S K^\pm\pi^\mp\pi^+\pi^-)/\Gamma_{total}$ — Γ_{16}/Γ

VALUE (units 10^{-3})	EVTS	DOCUMENT ID		TECN	COMMENT
6.6±0.6±0.2	4.5k	[1] ABLIKIM	13B	BES3	$e^+e^- \to \psi(2S) \to \gamma\chi_{c2}$

[1] ABLIKIM 13B reports $(7.30 \pm 0.11 \pm 0.75) \times 10^{-3}$ from a measurement of $[\Gamma(\chi_{c2}(1P) \to K^0_S K^\pm\pi^\mp\pi^+\pi^-)/\Gamma_{total}] \times [B(\psi(2S) \to \gamma\chi_{c2}(1P))]$ assuming $B(\psi(2S) \to \gamma\chi_{c2}(1P)) = (8.72 \pm 0.34) \times 10^{-2}$, which we rescale to our best (shown rounded) value $B(\psi(2S) \to \gamma\chi_{c2}(1P)) = (9.63 \pm 0.23) \times 10^{-2}$. Our first error is their experiment's error and our second error is the systematic error from using our best (shown rounded) value.

$\Gamma(K^+\overline{K}^*(892)^0\pi^- + \text{c.c.})/\Gamma(K^+K^-\pi^+\pi^-)$ — Γ_{17}/Γ_{14}

VALUE	DOCUMENT ID		TECN	COMMENT
0.25±0.13 OUR FIT				
0.25±0.13	TANENBAUM	78	MRK1	$\psi(2S) \to \gamma\chi_{c2}$

$\Gamma(3(\pi^+\pi^-))/\Gamma_{total}$ — Γ_{19}/Γ

VALUE (units 10^{-3})	EVTS	DOCUMENT ID		TECN	COMMENT
15.1±1.7 OUR AVERAGE	Error includes scale factor of 3.3.				
15.5±0.3±0.4	112k	[1] ABLIKIM	22Q	BES3	$\psi(2S) \to \gamma 3(\pi^+\pi^-)$
7.3±1.7±0.2	112	[2] BAI	99B	BES	$\psi(2S) \to \gamma\chi_{c2}$
9.3±6.2±0.2	23	[3] TANENBAUM	78	MRK1	$\psi(2S) \to \gamma\chi_{c2}$

[1] ABLIKIM 22Q reports $(1.565 \pm 0.005 \pm 0.048) \times 10^{-2}$ from a measurement of $[\Gamma(\chi_{c2}(1P) \to 3(\pi^+\pi^-))/\Gamma_{total}] \times [B(\psi(2S) \to \gamma\chi_{c2}(1P))]$ assuming $B(\psi(2S) \to \gamma\chi_{c2}(1P)) = (9.52 \pm 0.20) \times 10^{-2}$, which we rescale to our best (shown rounded) value $B(\psi(2S) \to \gamma\chi_{c2}(1P)) = (9.63 \pm 0.23) \times 10^{-2}$. Our first error is their experiment's error and our second error is the systematic error from using our best (shown rounded) value.

[2] BAI 99B reports $(9.0 \pm 1.0 \pm 2.0) \times 10^{-3}$ from a measurement of $[\Gamma(\chi_{c2}(1P) \to 3(\pi^+\pi^-))/\Gamma_{total}] \times [B(\psi(2S) \to \gamma\chi_{c2}(1P))]$ assuming $B(\psi(2S) \to \gamma\chi_{c2}(1P)) = (7.8 \pm 0.8) \times 10^{-2}$, which we rescale to our best (shown rounded) value $B(\psi(2S) \to \gamma\chi_{c2}(1P)) = (9.63 \pm 0.23) \times 10^{-2}$. Our first error is their experiment's error and our second error is the systematic error from using our best (shown rounded) value.

[3] TANENBAUM 78 reports $[\Gamma(\chi_{c2}(1P) \to 3(\pi^+\pi^-))/\Gamma_{total}] \times [B(\psi(2S) \to \gamma\chi_{c2}(1P))] = (0.9 \pm 0.6) \times 10^{-3}$ which we divide by our best (shown rounded) value $B(\psi(2S) \to \gamma\chi_{c2}(1P)) = (9.63 \pm 0.23) \times 10^{-2}$. Our first error is their experiment's error and our second error is the systematic error from using our best (shown rounded) value.

$\Gamma(\phi\phi)/\Gamma_{total}$ — Γ_{20}/Γ

VALUE (units 10^{-3})	EVTS	DOCUMENT ID		TECN	COMMENT
1.22 ±0.07 OUR FIT	Error includes scale factor of 1.6.				
• • • We do not use the following data for averages, fits, limits, etc. • • •					
1.253±0.034±0.030	4247	[1,2] ABLIKIM	23N	BES3	$\psi(2S) \to \gamma$hadrons

Int. J. Mod. Phys. A 2026.41. Downloaded from www.worldscientific.com
by CALIFORNIA @ BERKELEY on 09/16/26. Re-use and distribution is strictly not permitted, except for Open Access articles.

[1] ABLIKIM 23N reports $(12.67 \pm 0.28 \pm 0.33) \times 10^{-4}$ from a measurement of $[\Gamma(\chi_{c2}(1P) \to \phi\phi)/\Gamma_{total}] \times [B(\psi(2S) \to \gamma\chi_{c2}(1P))]$ assuming $B(\psi(2S) \to \gamma\chi_{c2}(1P)) = (9.52 \pm 0.20) \times 10^{-2}$, which we rescale to our best (shown rounded) value $B(\psi(2S) \to \gamma\chi_{c2}(1P)) = (9.63 \pm 0.23) \times 10^{-2}$. Our first error is their experiment's error and our second error is the systematic error from using our best (shown rounded) value.

[2] Not used since the same experimental measurement has been used in another related quantity included elsewhere in the fit.

$\Gamma(\phi\phi\eta)/\Gamma_{total}$ — Γ_{21}/Γ

VALUE (units 10^{-4})	EVTS	DOCUMENT ID		TECN	COMMENT
5.3±0.6±0.1	143.6	[1] ABLIKIM	20B	BES3	$\psi(2S) \to \gamma\phi\phi\eta$

[1] ABLIKIM 20B reports $(5.33 \pm 0.52 \pm 0.39) \times 10^{-4}$ from a measurement of $[\Gamma(\chi_{c2}(1P) \to \phi\phi\eta)/\Gamma_{total}] \times [B(\psi(2S) \to \gamma\chi_{c2}(1P))]$ assuming $B(\psi(2S) \to \gamma\chi_{c2}(1P)) = (9.52 \pm 0.20) \times 10^{-2}$, which we rescale to our best (shown rounded) value $B(\psi(2S) \to \gamma\chi_{c2}(1P)) = (9.63 \pm 0.23) \times 10^{-2}$. Our first error is their experiment's error and our second error is the systematic error from using our best (shown rounded) value.

$\Gamma(\omega\omega)/\Gamma_{total}$ — Γ_{22}/Γ

VALUE (units 10^{-3})	EVTS	DOCUMENT ID		TECN	COMMENT
0.86±0.04 OUR AVERAGE					
$0.87 \pm 0.04 \pm 0.02$	14.3k	[1] ABLIKIM	25K	BES3	$\psi(2S) \to \gamma 2(\pi^+\pi^-\pi^0)$
$0.81 \pm 0.10 \pm 0.02$	762	[2] ABLIKIM	11K	BES3	$\psi(2S) \to \gamma$ hadrons
$1.71 \pm 0.57 \pm 0.04$	27.7 ± 7.4	[3] ABLIKIM	05N	BES2	$\psi(2S) \to \gamma\chi_{c2} \to \gamma 6\pi$

[1] ABLIKIM 25K reports $(8.75 \pm 0.08 \pm 0.42) \times 10^{-4}$ from a measurement of $[\Gamma(\chi_{c2}(1P) \to \omega\omega)/\Gamma_{total}] \times [B(\psi(2S) \to \gamma\chi_{c2}(1P))]$ assuming $B(\psi(2S) \to \gamma\chi_{c2}(1P)) = (9.52 \pm 0.20) \times 10^{-2}$, which we rescale to our best (shown rounded) value $B(\psi(2S) \to \gamma\chi_{c2}(1P)) = (9.63 \pm 0.23) \times 10^{-2}$. Our first error is their experiment's error and our second error is the systematic error from using our best (shown rounded) value.

[2] ABLIKIM 11K reports $(8.9 \pm 0.3 \pm 1.1) \times 10^{-4}$ from a measurement of $[\Gamma(\chi_{c2}(1P) \to \omega\omega)/\Gamma_{total}] \times [B(\psi(2S) \to \gamma\chi_{c2}(1P))]$ assuming $B(\psi(2S) \to \gamma\chi_{c2}(1P)) = (8.74 \pm 0.35) \times 10^{-2}$, which we rescale to our best (shown rounded) value $B(\psi(2S) \to \gamma\chi_{c2}(1P)) = (9.63 \pm 0.23) \times 10^{-2}$. Our first error is their experiment's error and our second error is the systematic error from using our best (shown rounded) value.

[3] ABLIKIM 05N reports $[\Gamma(\chi_{c2}(1P) \to \omega\omega)/\Gamma_{total}] \times [B(\psi(2S) \to \gamma\chi_{c2}(1P))] = (0.165 \pm 0.044 \pm 0.032) \times 10^{-3}$ which we divide by our best (shown rounded) value $B(\psi(2S) \to \gamma\chi_{c2}(1P)) = (9.63 \pm 0.23) \times 10^{-2}$. Our first error is their experiment's error and our second error is the systematic error from using our best (shown rounded) value.

$\Gamma(\omega K^+K^-)/\Gamma_{total}$ — Γ_{23}/Γ

VALUE (units 10^{-3})	EVTS	DOCUMENT ID		TECN	COMMENT
0.66±0.08±0.02	512	[1] ABLIKIM	13B	BES3	$e^+e^- \to \psi(2S) \to \gamma\chi_{c2}$

[1] ABLIKIM 13B reports $(0.73 \pm 0.04 \pm 0.08) \times 10^{-3}$ from a measurement of $[\Gamma(\chi_{c2}(1P) \to \omega K^+K^-)/\Gamma_{total}] \times [B(\psi(2S) \to \gamma\chi_{c2}(1P))]$ assuming $B(\psi(2S) \to \gamma\chi_{c2}(1P)) = (8.72 \pm 0.34) \times 10^{-2}$, which we rescale to our best (shown rounded) value $B(\psi(2S) \to \gamma\chi_{c2}(1P)) = (9.63 \pm 0.23) \times 10^{-2}$. Our first error is their experiment's error and our second error is the systematic error from using our best (shown rounded) value.

$\Gamma(\omega\phi)/\Gamma_{total}$ — Γ_{24}/Γ

VALUE (units 10^{-6})	CL%	EVTS	DOCUMENT ID		TECN	COMMENT
9.8±1.3 OUR AVERAGE						
$9.9 \pm 1.4 \pm 0.2$		151	[1] ABLIKIM	25K	BES3	$\psi(2S) \to \gamma\pi^+\pi^-\pi^0K^+K^-$
$9.5 \pm 2.7 \pm 0.2$		33	[2] ABLIKIM	19J	BES3	$\psi(2S) \to \gamma$ hadrons
• • • We do not use the following data for averages, fits, limits, etc. • • •						
<18	90		[3,4] ABLIKIM	11K	BES3	$\psi(2S) \to \gamma$ hadrons

[1] ABLIKIM 25K reports $(0.10 \pm 0.01 \pm 0.01) \times 10^{-4}$ from a measurement of $[\Gamma(\chi_{c2}(1P) \to \omega\phi)/\Gamma_{total}] \times [B(\psi(2S) \to \gamma\chi_{c2}(1P))]$ assuming $B(\psi(2S) \to \gamma\chi_{c2}(1P)) = (9.52 \pm 0.20) \times 10^{-2}$, which we rescale to our best (shown rounded) value $B(\psi(2S) \to \gamma\chi_{c2}(1P)) = (9.63 \pm 0.23) \times 10^{-2}$. Our first error is their experiment's error and our second error is the systematic error from using our best (shown rounded) value.

[2] ABLIKIM 19J reports $[\Gamma(\chi_{c2}(1P) \to \omega\phi)/\Gamma_{total}] \times [B(\psi(2S) \to \gamma\chi_{c2}(1P))] = (0.91 \pm 0.23 \pm 0.12) \times 10^{-6}$ which we divide by our best (shown rounded) value $B(\psi(2S) \to \gamma\chi_{c2}(1P)) = (9.63 \pm 0.23) \times 10^{-2}$. Our first error is their experiment's error and our second error is the systematic error from using our best (shown rounded) value.

[3] ABLIKIM 11K reports $< 2 \times 10^{-5}$ from a measurement of $[\Gamma(\chi_{c2}(1P) \to \omega\phi)/\Gamma_{total}] \times [B(\psi(2S) \to \gamma\chi_{c2}(1P))]$ assuming $B(\psi(2S) \to \gamma\chi_{c2}(1P)) = (8.74 \pm 0.35) \times 10^{-2}$, which we rescale to our best (shown rounded) value $B(\psi(2S) \to \gamma\chi_{c2}(1P)) = 9.63 \times 10^{-2}$.

[4] Superseded by ABLIKIM 19J.

$\Gamma(\rho^0\pi^+\pi^-)/\Gamma(2(\pi^+\pi^-))$ — Γ_{26}/Γ_1

VALUE	DOCUMENT ID	TECN	COMMENT
0.36±0.15 OUR FIT			
0.31±0.17	TANENBAUM 78	MRK1	$\psi(2S) \to \gamma\chi_{c2}$

$\Gamma(\pi^+\pi^-\pi^0(\text{non-resonant}))/\Gamma_{total}$ — Γ_{27}/Γ

VALUE (units 10^{-5})	EVTS	DOCUMENT ID		TECN	COMMENT
1.99±0.42±0.05	64	[1] ABLIKIM	17AG	BES3	$\psi(2S) \to \gamma\pi^+\pi^-\pi^0$

[1] ABLIKIM 17AG reports $(2.1 \pm 0.4 \pm 0.2) \times 10^{-5}$ from a measurement of $[\Gamma(\chi_{c2}(1P) \to \pi^+\pi^-\pi^0(\text{non-resonant}))/\Gamma_{total}] \times [B(\psi(2S) \to \gamma\chi_{c2}(1P))]$ assuming $B(\psi(2S) \to \gamma\chi_{c2}(1P)) = (9.11 \pm 0.31) \times 10^{-2}$, which we rescale to our best (shown rounded) value $B(\psi(2S) \to \gamma\chi_{c2}(1P)) = (9.63 \pm 0.23) \times 10^{-2}$. Our first error is their experiment's error and our second error is the systematic error from using our best (shown rounded) value.

$\Gamma(\rho(770)^\pm\pi^\mp)/\Gamma_{total}$ — Γ_{28}/Γ

VALUE (units 10^{-5})	EVTS	DOCUMENT ID		TECN	COMMENT
0.61±0.37±0.01	15	[1] ABLIKIM	17AG	BES3	$\psi(2S) \to \gamma\pi^+\pi^-\pi^0$

[1] ABLIKIM 17AG reports $(0.64 \pm 0.39 \pm 0.07) \times 10^{-5}$ from a measurement of $[\Gamma(\chi_{c2}(1P) \to \rho(770)^\pm\pi^\mp)/\Gamma_{total}] \times [B(\psi(2S) \to \gamma\chi_{c2}(1P))]$ assuming $B(\psi(2S) \to \gamma\chi_{c2}(1P)) = (9.11 \pm 0.31) \times 10^{-2}$, which we rescale to our best (shown rounded) value $B(\psi(2S) \to \gamma\chi_{c2}(1P)) = (9.63 \pm 0.23) \times 10^{-2}$. Our first error is their experiment's error and our second error is the systematic error from using our best (shown rounded) value.

$\Gamma(\pi^+\pi^-\eta)/\Gamma_{total}$ — Γ_{29}/Γ

VALUE (units 10^{-3})	CL%	DOCUMENT ID		TECN	COMMENT
0.47±0.13±0.01		[1] ATHAR	07	CLEO	$\psi(2S) \to \gamma h^+h^-h^0$
• • • We do not use the following data for averages, fits, limits, etc. • • •					
<1.4	90	[2] ABLIKIM	06R	BES2	$\psi(2S) \to \gamma\chi_{c2}$

[1] ATHAR 07 reports $(0.49 \pm 0.12 \pm 0.06) \times 10^{-3}$ from a measurement of $[\Gamma(\chi_{c2}(1P) \to \pi^+\pi^-\eta)/\Gamma_{total}] \times [B(\psi(2S) \to \gamma\chi_{c2}(1P))]$ assuming $B(\psi(2S) \to \gamma\chi_{c2}(1P)) = (9.33 \pm 0.14 \pm 0.61) \times 10^{-2}$, which we rescale to our best (shown rounded) value $B(\psi(2S) \to \gamma\chi_{c2}(1P)) = (9.63 \pm 0.23) \times 10^{-2}$. Our first error is their experiment's error and our second error is the systematic error from using our best (shown rounded) value.

[2] ABLIKIM 06R reports $< 1.7 \times 10^{-3}$ from a measurement of $[\Gamma(\chi_{c2}(1P) \to \pi^+\pi^-\eta)/\Gamma_{total}] \times [B(\psi(2S) \to \gamma\chi_{c2}(1P))]$ assuming $B(\psi(2S) \to \gamma\chi_{c2}(1P)) = (8.1 \pm 0.4) \times 10^{-2}$, which we rescale to our best (shown rounded) value $B(\psi(2S) \to \gamma\chi_{c2}(1P)) = 9.63 \times 10^{-2}$.

$\Gamma(\pi^+\pi^-\eta')/\Gamma_{total}$ — Γ_{31}/Γ

VALUE (units 10^{-3})	DOCUMENT ID		TECN	COMMENT
0.49±0.18±0.01	[1] ATHAR	07	CLEO	$\psi(2S) \to \gamma h^+h^-h^0$

[1] ATHAR 07 reports $(0.51 \pm 0.18 \pm 0.06) \times 10^{-3}$ from a measurement of $[\Gamma(\chi_{c2}(1P) \to \pi^+\pi^-\eta')/\Gamma_{total}] \times [B(\psi(2S) \to \gamma\chi_{c2}(1P))]$ assuming $B(\psi(2S) \to \gamma\chi_{c2}(1P)) = (9.33 \pm 0.14 \pm 0.61) \times 10^{-2}$, which we rescale to our best (shown rounded) value $B(\psi(2S) \to \gamma\chi_{c2}(1P)) = (9.63 \pm 0.23) \times 10^{-2}$. Our first error is their experiment's error and our second error is the systematic error from using our best (shown rounded) value.

$\Gamma(K^*(892)^\pm K^\mp)/\Gamma_{total}$ — Γ_{35}/Γ

VALUE (units 10^{-4})	DOCUMENT ID		TECN	COMMENT
1.42±0.21±0.03	[1] ABLIKIM	17AG	BES3	$\psi(2S) \to \gamma K\overline{K}\pi$
• • • We do not use the following data for averages, fits, limits, etc. • • •				
$1.70 \pm 0.26 \pm 0.04$	[2] ABLIKIM	17AG	BES3	$\psi(2S) \to \gamma K^+K^-\pi^0$
$1.32 \pm 0.26 \pm 0.03$	[3] ABLIKIM	17AG	BES3	$\psi(2S) \to \gamma K^0_S K^\pm\pi^\mp$

[1] ABLIKIM 17AG reports $(1.5 \pm 0.1 \pm 0.2) \times 10^{-4}$ from a measurement of $[\Gamma(\chi_{c2}(1P) \to K^*(892)^\pm K^\mp)/\Gamma_{total}] \times [B(\psi(2S) \to \gamma\chi_{c2}(1P))]$ assuming $B(\psi(2S) \to \gamma\chi_{c2}(1P)) = (9.11 \pm 0.31) \times 10^{-2}$, which we rescale to our best (shown rounded) value $B(\psi(2S) \to \gamma\chi_{c2}(1P)) = (9.63 \pm 0.23) \times 10^{-2}$. Our first error is their experiment's error and our second error is the systematic error from using our best (shown rounded) value.

[2] ABLIKIM 17AG reports $(1.8 \pm 0.2 \pm 0.2) \times 10^{-4}$ from a measurement of $[\Gamma(\chi_{c2}(1P) \to K^*(892)^\pm K^\mp)/\Gamma_{total}] \times [B(\psi(2S) \to \gamma\chi_{c2}(1P))]$ assuming $B(\psi(2S) \to \gamma\chi_{c2}(1P)) = (9.11 \pm 0.31) \times 10^{-2}$, which we rescale to our best (shown rounded) value $B(\psi(2S) \to \gamma\chi_{c2}(1P)) = (9.63 \pm 0.23) \times 10^{-2}$. Our first error is their experiment's error and our second error is the systematic error from using our best (shown rounded) value.

[3] ABLIKIM 17AG reports $(1.4 \pm 0.2 \pm 0.2) \times 10^{-4}$ from a measurement of $[\Gamma(\chi_{c2}(1P) \to K^*(892)^\pm K^\mp)/\Gamma_{total}] \times [B(\psi(2S) \to \gamma\chi_{c2}(1P))]$ assuming $B(\psi(2S) \to \gamma\chi_{c2}(1P)) = (9.11 \pm 0.31) \times 10^{-2}$, which we rescale to our best (shown rounded) value $B(\psi(2S) \to \gamma\chi_{c2}(1P)) = (9.63 \pm 0.23) \times 10^{-2}$. Our first error is their experiment's error and our second error is the systematic error from using our best (shown rounded) value.

$\Gamma(K^*(892)^0\overline{K}^0 + \text{c.c.})/\Gamma_{total}$ — Γ_{36}/Γ

VALUE (units 10^{-4})	DOCUMENT ID		TECN	COMMENT
1.23±0.26±0.03	[1] ABLIKIM	17AG	BES3	$\psi(2S) \to \gamma K^0_S K^\pm\pi^\mp$

[1] ABLIKIM 17AG reports $(1.3 \pm 0.2 \pm 0.2) \times 10^{-4}$ from a measurement of $[\Gamma(\chi_{c2}(1P) \to K^*(892)^0\overline{K}^0 + \text{c.c.})/\Gamma_{total}] \times [B(\psi(2S) \to \gamma\chi_{c2}(1P))]$ assuming $B(\psi(2S) \to \gamma\chi_{c2}(1P)) = (9.11 \pm 0.31) \times 10^{-2}$, which we rescale to our best (shown rounded) value $B(\psi(2S) \to \gamma\chi_{c2}(1P)) = (9.63 \pm 0.23) \times 10^{-2}$. Our first error is their experiment's error and our second error is the systematic error from using our best (shown rounded) value.

$\Gamma(K^*_2(1430)^\pm K^\mp)/\Gamma_{total}$ — Γ_{37}/Γ

VALUE (units 10^{-4})	DOCUMENT ID		TECN	COMMENT
14.7±1.2±0.3	[1] ABLIKIM	17AG	BES3	$\psi(2S) \to \gamma K\overline{K}\pi$
• • • We do not use the following data for averages, fits, limits, etc. • • •				
$17.2 \pm 1.6 \pm 0.4$	[2] ABLIKIM	17AG	BES3	$\psi(2S) \to \gamma K^+K^-\pi^0$
$12.9 \pm 1.5 \pm 0.3$	[3] ABLIKIM	17AG	BES3	$\psi(2S) \to \gamma K^0_S K^\pm\pi^\mp$

[1] ABLIKIM 17AG reports $(15.5 \pm 0.6 \pm 1.2) \times 10^{-4}$ from a measurement of $[\Gamma(\chi_{c2}(1P) \to K^*_2(1430)^\pm K^\mp)/\Gamma_{total}] \times [B(\psi(2S) \to \gamma\chi_{c2}(1P))]$ assuming $B(\psi(2S) \to \gamma\chi_{c2}(1P)) = (9.11 \pm 0.31) \times 10^{-2}$, which we rescale to our best (shown rounded) value $B(\psi(2S) \to \gamma\chi_{c2}(1P)) = (9.63 \pm 0.23) \times 10^{-2}$. Our first error is their experiment's error and our second error is the systematic error from using our best (shown rounded) value.

Int. J. Mod. Phys. A 2026.41. Downloaded from www.worldscientific.com
by UNIVERSITY OF CALIFORNIA @ BERKELEY on 09/16/26. Re-use and distribution is strictly not permitted, except for Open Access articles.

Int. J. Mod. Phys. A 2026.41. Downloaded from www.worldscientific.com by CALIFORNIA @ BERKELEY on 09/16/26. Re-use and distribution is strictly not permitted, except for Open Access articles.

[2] ABLIKIM 17AG reports $(18.2 \pm 0.8 \pm 1.6) \times 10^{-4}$ from a measurement of $[\Gamma(\chi_{c2}(1P) \to K_2^*(1430)^{\pm} K^{\mp})/\Gamma_{total}] \times [B(\psi(2S) \to \gamma\chi_{c2}(1P))]$ assuming $B(\psi(2S) \to \gamma\chi_{c2}(1P)) = (9.11 \pm 0.31) \times 10^{-2}$, which we rescale to our best (shown rounded) value $B(\psi(2S) \to \gamma\chi_{c2}(1P)) = (9.63 \pm 0.23) \times 10^{-2}$. Our first error is their experiment's error and our second error is the systematic error from using our best (shown rounded) value.

[3] ABLIKIM 17AG reports $(13.6 \pm 0.8 \pm 1.4) \times 10^{-4}$ from a measurement of $[\Gamma(\chi_{c2}(1P) \to K_2^*(1430)^{\pm} K^{\mp})/\Gamma_{total}] \times [B(\psi(2S) \to \gamma\chi_{c2}(1P))]$ assuming $B(\psi(2S) \to \gamma\chi_{c2}(1P)) = (9.11 \pm 0.31) \times 10^{-2}$, which we rescale to our best (shown rounded) value $B(\psi(2S) \to \gamma\chi_{c2}(1P)) = (9.63 \pm 0.23) \times 10^{-2}$. Our first error is their experiment's error and our second error is the systematic error from using our best (shown rounded) value.

$\Gamma(K_2^*(1430)^0 \overline{K}^0 + c.c.)/\Gamma_{total}$ — Γ_{38}/Γ

VALUE (units 10^{-4})	DOCUMENT ID		TECN	COMMENT
12.3±1.7±0.3	[1] ABLIKIM	17AG	BES3	$\psi(2S) \to \gamma K_S^0 K^{\pm}\pi^{\mp}$

[1] ABLIKIM 17AG reports $(13.0 \pm 1.0 \pm 1.5) \times 10^{-4}$ from a measurement of $[\Gamma(\chi_{c2}(1P) \to K_2^*(1430)^0 \overline{K}^0 + c.c.)/\Gamma_{total}] \times [B(\psi(2S) \to \gamma\chi_{c2}(1P))]$ assuming $B(\psi(2S) \to \gamma\chi_{c2}(1P)) = (9.11 \pm 0.31) \times 10^{-2}$, which we rescale to our best (shown rounded) value $B(\psi(2S) \to \gamma\chi_{c2}(1P)) = (9.63 \pm 0.23) \times 10^{-2}$. Our first error is their experiment's error and our second error is the systematic error from using our best (shown rounded) value.

$\Gamma(K_3^*(1780)^{\pm} K^{\mp})/\Gamma_{total}$ — Γ_{39}/Γ

VALUE (units 10^{-4})	DOCUMENT ID		TECN	COMMENT
5.1±0.8±0.1	[1] ABLIKIM	17AG	BES3	$\psi(2S) \to \gamma K \overline{K} \pi$
• • • We do not use the following data for averages, fits, limits, etc. • • •				
5.0±1.0±0.1	[2] ABLIKIM	17AG	BES3	$\psi(2S) \to \gamma K^+ K^- \pi^0$
5.6±1.8±0.1	[3] ABLIKIM	17AG	BES3	$\psi(2S) \to \gamma K_S^0 K^{\pm}\pi^{\mp}$

[1] ABLIKIM 17AG reports $(5.4 \pm 0.5 \pm 0.7) \times 10^{-4}$ from a measurement of $[\Gamma(\chi_{c2}(1P) \to K_3^*(1780)^{\pm} K^{\mp})/\Gamma_{total}] \times [B(\psi(2S) \to \gamma\chi_{c2}(1P))]$ assuming $B(\psi(2S) \to \gamma\chi_{c2}(1P)) = (9.11 \pm 0.31) \times 10^{-2}$, which we rescale to our best (shown rounded) value $B(\psi(2S) \to \gamma\chi_{c2}(1P)) = (9.63 \pm 0.23) \times 10^{-2}$. Our first error is their experiment's error and our second error is the systematic error from using our best (shown rounded) value.

[2] ABLIKIM 17AG reports $(5.3 \pm 0.5 \pm 0.9) \times 10^{-4}$ from a measurement of $[\Gamma(\chi_{c2}(1P) \to K_3^*(1780)^{\pm} K^{\mp})/\Gamma_{total}] \times [B(\psi(2S) \to \gamma\chi_{c2}(1P))]$ assuming $B(\psi(2S) \to \gamma\chi_{c2}(1P)) = (9.11 \pm 0.31) \times 10^{-2}$, which we rescale to our best (shown rounded) value $B(\psi(2S) \to \gamma\chi_{c2}(1P)) = (9.63 \pm 0.23) \times 10^{-2}$. Our first error is their experiment's error and our second error is the systematic error from using our best (shown rounded) value.

[3] ABLIKIM 17AG reports $(5.9 \pm 1.1 \pm 1.5) \times 10^{-4}$ from a measurement of $[\Gamma(\chi_{c2}(1P) \to K_3^*(1780)^{\pm} K^{\mp})/\Gamma_{total}] \times [B(\psi(2S) \to \gamma\chi_{c2}(1P))]$ assuming $B(\psi(2S) \to \gamma\chi_{c2}(1P)) = (9.11 \pm 0.31) \times 10^{-2}$, which we rescale to our best (shown rounded) value $B(\psi(2S) \to \gamma\chi_{c2}(1P)) = (9.63 \pm 0.23) \times 10^{-2}$. Our first error is their experiment's error and our second error is the systematic error from using our best (shown rounded) value.

$\Gamma(K_3^*(1780)^0 \overline{K}^0 + c.c.)/\Gamma_{total}$ — Γ_{40}/Γ

VALUE (units 10^{-4})	DOCUMENT ID		TECN	COMMENT
5.6±2.1±0.1	[1] ABLIKIM	17AG	BES3	$\psi(2S) \to \gamma K_S^0 K^{\pm}\pi^{\mp}$

[1] ABLIKIM 17AG reports $(5.9 \pm 1.6 \pm 1.5) \times 10^{-4}$ from a measurement of $[\Gamma(\chi_{c2}(1P) \to K_3^*(1780)^0 \overline{K}^0 + c.c.)/\Gamma_{total}] \times [B(\psi(2S) \to \gamma\chi_{c2}(1P))]$ assuming $B(\psi(2S) \to \gamma\chi_{c2}(1P)) = (9.11 \pm 0.31) \times 10^{-2}$, which we rescale to our best (shown rounded) value $B(\psi(2S) \to \gamma\chi_{c2}(1P)) = (9.63 \pm 0.23) \times 10^{-2}$. Our first error is their experiment's error and our second error is the systematic error from using our best (shown rounded) value.

$\Gamma(a_2(1320)^0 \pi^0)/\Gamma_{total}$ — Γ_{41}/Γ

VALUE (units 10^{-4})	DOCUMENT ID		TECN	COMMENT
12.8±3.4±0.3	[1] ABLIKIM	17AG	BES3	$\psi(2S) \to \gamma K^+ K^- \pi^0$

[1] ABLIKIM 17AG reports $(13.5 \pm 1.6 \pm 3.2) \times 10^{-4}$ from a measurement of $[\Gamma(\chi_{c2}(1P) \to a_2(1320)^0 \pi^0)/\Gamma_{total}] \times [B(\psi(2S) \to \gamma\chi_{c2}(1P))]$ assuming $B(\psi(2S) \to \gamma\chi_{c2}(1P)) = (9.11 \pm 0.31) \times 10^{-2}$, which we rescale to our best (shown rounded) value $B(\psi(2S) \to \gamma\chi_{c2}(1P)) = (9.63 \pm 0.23) \times 10^{-2}$. Our first error is their experiment's error and our second error is the systematic error from using our best (shown rounded) value.

$\Gamma(a_2(1320)^{\pm} \pi^{\mp})/\Gamma_{total}$ — Γ_{42}/Γ

VALUE (units 10^{-4})	DOCUMENT ID		TECN	COMMENT
17.4±6.0±0.4	[1] ABLIKIM	17AG	BES3	$\psi(2S) \to \gamma K_S^0 K^{\pm}\pi^{\mp}$

[1] ABLIKIM 17AG reports $(18.4 \pm 3.3 \pm 5.5) \times 10^{-4}$ from a measurement of $[\Gamma(\chi_{c2}(1P) \to a_2(1320)^{\pm} \pi^{\mp})/\Gamma_{total}] \times [B(\psi(2S) \to \gamma\chi_{c2}(1P))]$ assuming $B(\psi(2S) \to \gamma\chi_{c2}(1P)) = (9.11 \pm 0.31) \times 10^{-2}$, which we rescale to our best (shown rounded) value $B(\psi(2S) \to \gamma\chi_{c2}(1P)) = (9.63 \pm 0.23) \times 10^{-2}$. Our first error is their experiment's error and our second error is the systematic error from using our best (shown rounded) value.

$\Gamma(K^+ K^- \pi^0)/\Gamma_{total}$ — Γ_{44}/Γ

VALUE (units 10^{-3})	DOCUMENT ID		TECN	COMMENT
0.30±0.08±0.01	[1] ATHAR	07	CLEO	$\psi(2S) \to \gamma h^+ h^- h^0$

[1] ATHAR 07 reports $(0.31 \pm 0.07 \pm 0.04) \times 10^{-3}$ from a measurement of $[\Gamma(\chi_{c2}(1P) \to K^+ K^- \pi^0)/\Gamma_{total}] \times [B(\psi(2S) \to \gamma\chi_{c2}(1P))]$ assuming $B(\psi(2S) \to \gamma\chi_{c2}(1P)) = (9.33 \pm 0.14 \pm 0.61) \times 10^{-2}$, which we rescale to our best (shown rounded) value $B(\psi(2S) \to \gamma\chi_{c2}(1P)) = (9.63 \pm 0.23) \times 10^{-2}$. Our first error is their experiment's error and our second error is the systematic error from using our best (shown rounded) value.

$\Gamma(K^+ K^- \eta)/\Gamma_{total}$ — Γ_{45}/Γ

VALUE (units 10^{-3})	CL%	EVTS	DOCUMENT ID		TECN	COMMENT
<0.32	90		[1] ATHAR	07	CLEO	$\psi(2S) \to \gamma h^+ h^- h^0$
• • • We do not use the following data for averages, fits, limits, etc. • • •						
0.181±0.004		3693	[2] ABLIKIM	24BW	BES3	$\psi(2S) \to \gamma\chi_{c2}$

[1] ATHAR 07 reports $< 0.33 \times 10^{-3}$ from a measurement of $[\Gamma(\chi_{c2}(1P) \to K^+ K^- \eta)/\Gamma_{total}] \times [B(\psi(2S) \to \gamma\chi_{c2}(1P))]$ assuming $B(\psi(2S) \to \gamma\chi_{c2}(1P)) = (9.33 \pm 0.14 \pm 0.61) \times 10^{-2}$, which we rescale to our best (shown rounded) value $B(\psi(2S) \to \gamma\chi_{c2}(1P)) = 9.63 \times 10^{-2}$.

[2] No systematic error reported.

$\Gamma(K^+ K^- \eta'(958))/\Gamma_{total}$ — Γ_{46}/Γ

VALUE (units 10^{-4})	EVTS	DOCUMENT ID		TECN	COMMENT
1.51±0.08±0.04		[1] ABLIKIM	25I	BES3	$\psi(2S) \to \gamma K^+ K^- \eta'(958)$
• • • We do not use the following data for averages, fits, limits, etc. • • •					
1.76±0.30±0.04	107	[2,3] ABLIKIM	14J	BES3	$\psi(2S) \to \gamma K^+ K^- \eta'(958)$

[1] ABLIKIM 25I reports $(1.53 \pm 0.04 \pm 0.08) \times 10^{-4}$ from a measurement of $[\Gamma(\chi_{c2}(1P) \to K^+ K^- \eta'(958))/\Gamma_{total}] \times [B(\psi(2S) \to \gamma\chi_{c2}(1P))]$ assuming $B(\psi(2S) \to \gamma\chi_{c2}(1P)) = (9.52 \pm 0.20) \times 10^{-2}$, which we rescale to our best (shown rounded) value $B(\psi(2S) \to \gamma\chi_{c2}(1P)) = (9.63 \pm 0.23) \times 10^{-2}$. Our first error is their experiment's error and our second error is the systematic error from using our best (shown rounded) value.

[2] ABLIKIM 14J reports $(1.94 \pm 0.34) \times 10^{-4}$ from a measurement of $[\Gamma(\chi_{c2}(1P) \to K^+ K^- \eta'(958))/\Gamma_{total}] \times [B(\psi(2S) \to \gamma\chi_{c2}(1P))]$ assuming $B(\psi(2S) \to \gamma\chi_{c2}(1P)) = (8.72 \pm 0.34) \times 10^{-2}$, which we rescale to our best (shown rounded) value $B(\psi(2S) \to \gamma\chi_{c2}(1P)) = (9.63 \pm 0.23) \times 10^{-2}$. Our first error is their experiment's error and our second error is the systematic error from using our best (shown rounded) value.

[3] Superseded by ABLIKIM 25I.

$\Gamma(\eta\eta')/\Gamma_{total}$ — Γ_{47}/Γ

VALUE (units 10^{-5})	CL%	EVTS	DOCUMENT ID		TECN	COMMENT
2.1±0.5±0.1		20	[1] ABLIKIM	17AI	BES3	$\psi(2S) \to \gamma\eta'\eta$
• • • We do not use the following data for averages, fits, limits, etc. • • •						
< 6	90	3.3 ± 8.0	[2] ASNER	09	CLEO	$\psi(2S) \to \gamma\eta\eta'$
<22	90		[3] ADAMS	07	CLEO	$\psi(2S) \to \gamma\chi_{c2}$

[1] ABLIKIM 17AI reports $(2.27 \pm 0.43 \pm 0.25) \times 10^{-5}$ from a measurement of $[\Gamma(\chi_{c2}(1P) \to \eta\eta')/\Gamma_{total}] \times [B(\psi(2S) \to \gamma\chi_{c2}(1P))]$ assuming $B(\psi(2S) \to \gamma\chi_{c2}(1P)) = (9.11 \pm 0.31) \times 10^{-2}$, which we rescale to our best (shown rounded) value $B(\psi(2S) \to \gamma\chi_{c2}(1P)) = (9.63 \pm 0.23) \times 10^{-2}$. Our first error is their experiment's error and our second error is the systematic error from using our best (shown rounded) value.

[2] ASNER 09 reports $< 0.6 \times 10^{-4}$ from a measurement of $[\Gamma(\chi_{c2}(1P) \to \eta\eta')/\Gamma_{total}] \times [B(\psi(2S) \to \gamma\chi_{c2}(1P))]$ assuming $B(\psi(2S) \to \gamma\chi_{c2}(1P)) = (9.33 \pm 0.14 \pm 0.61) \times 10^{-2}$, which we rescale to our best (shown rounded) value $B(\psi(2S) \to \gamma\chi_{c2}(1P)) = 9.63 \times 10^{-2}$.

[3] Superseded by ASNER 09. ADAMS 07 reports $< 2.3 \times 10^{-4}$ from a measurement of $[\Gamma(\chi_{c2}(1P) \to \eta\eta')/\Gamma_{total}] \times [B(\psi(2S) \to \gamma\chi_{c2}(1P))]$ assuming $B(\psi(2S) \to \gamma\chi_{c2}(1P)) = 0.0933 \pm 0.0014 \pm 0.0061$, which we rescale to our best (shown rounded) value $B(\psi(2S) \to \gamma\chi_{c2}(1P)) = 9.63 \times 10^{-2}$.

$\Gamma(\eta'\eta')/\Gamma_{total}$ — Γ_{48}/Γ

VALUE (units 10^{-5})	CL%	EVTS	DOCUMENT ID		TECN	COMMENT
4.5±0.6±0.1		60	[1] ABLIKIM	17AI	BES3	$\psi(2S) \to \gamma\eta'\eta'$
• • • We do not use the following data for averages, fits, limits, etc. • • •						
<10	90	12 ± 7	[2] ASNER	09	CLEO	$\psi(2S) \to \gamma\eta'\eta'$
<30	90		[3] ADAMS	07	CLEO	$\psi(2S) \to \gamma\chi_{c2}$

[1] ABLIKIM 17AI reports $(4.76 \pm 0.56 \pm 0.38) \times 10^{-5}$ from a measurement of $[\Gamma(\chi_{c2}(1P) \to \eta'\eta')/\Gamma_{total}] \times [B(\psi(2S) \to \gamma\chi_{c2}(1P))]$ assuming $B(\psi(2S) \to \gamma\chi_{c2}(1P)) = (9.11 \pm 0.31) \times 10^{-2}$, which we rescale to our best (shown rounded) value $B(\psi(2S) \to \gamma\chi_{c2}(1P)) = (9.63 \pm 0.23) \times 10^{-2}$. Our first error is their experiment's error and our second error is the systematic error from using our best (shown rounded) value.

[2] ASNER 09 reports $< 1.0 \times 10^{-4}$ from a measurement of $[\Gamma(\chi_{c2}(1P) \to \eta'\eta')/\Gamma_{total}] \times [B(\psi(2S) \to \gamma\chi_{c2}(1P))]$ assuming $B(\psi(2S) \to \gamma\chi_{c2}(1P)) = (9.33 \pm 0.14 \pm 0.61) \times 10^{-2}$, which we rescale to our best (shown rounded) value $B(\psi(2S) \to \gamma\chi_{c2}(1P)) = 9.63 \times 10^{-2}$.

[3] Superseded by ASNER 09. ADAMS 07 reports $< 3.1 \times 10^{-4}$ from a measurement of $[\Gamma(\chi_{c2}(1P) \to \eta'\eta')/\Gamma_{total}] \times [B(\psi(2S) \to \gamma\chi_{c2}(1P))]$ assuming $B(\psi(2S) \to \gamma\chi_{c2}(1P)) = 0.0933 \pm 0.0014 \pm 0.0061$, which we rescale to our best (shown rounded) value $B(\psi(2S) \to \gamma\chi_{c2}(1P)) = 9.63 \times 10^{-2}$.

$\Gamma(\eta\eta\eta')/\Gamma_{total}$ — Γ_{49}/Γ

VALUE (units 10^{-5})	EVTS	DOCUMENT ID		TECN	COMMENT
4.1±0.9±0.1	11k	[1] ABLIKIM	25CJ	BES3	$\psi(2S) \to \gamma\chi_{c2} \to \gamma\eta\eta\eta'$

[1] ABLIKIM 25CJ reports $(4.18 \pm 0.84 \pm 0.48) \times 10^{-5}$ from a measurement of $[\Gamma(\chi_{c2}(1P) \to \eta\eta\eta')/\Gamma_{total}] \times [B(\psi(2S) \to \gamma\chi_{c2}(1P))]$ assuming $B(\psi(2S) \to \gamma\chi_{c2}(1P)) = (9.36 \pm 0.23) \times 10^{-2}$, which we rescale to our best (shown rounded) value $B(\psi(2S) \to \gamma\chi_{c2}(1P)) = (9.63 \pm 0.23) \times 10^{-2}$. Our first error is their experiment's error and our second error is the systematic error from using our best (shown rounded) value.

Int. J. Mod. Phys. A 2026.41. Downloaded from www.worldscientific.com by UNIVERSITY OF CALIFORNIA @ BERKELEY on 09/16/26. Re-use and distribution is strictly not permitted, except for Open Access articles.

$\Gamma(\pi^+\pi^-K^0_S K^0_S)/\Gamma_{total}$ — Γ_{50}/Γ

VALUE (units 10^{-3})	EVTS	DOCUMENT ID		TECN	COMMENT
2.2±0.5±0.1	57 ± 11	[1] ABLIKIM	05O	BES2	$\psi(2S) \to \gamma\chi_{c2}$

[1] ABLIKIM 05O reports $[\Gamma(\chi_{c2}(1P) \to \pi^+\pi^-K^0_S K^0_S)/\Gamma_{total}] \times [B(\psi(2S) \to \gamma\chi_{c2}(1P))] = (0.207 \pm 0.039 \pm 0.033) \times 10^{-3}$ which we divide by our best (shown rounded) value $B(\psi(2S) \to \gamma\chi_{c2}(1P)) = (9.63 \pm 0.23) \times 10^{-2}$. Our first error is their experiment's error and our second error is the systematic error from using our best (shown rounded) value.

$\Gamma(K^+K^-K^0_S K^0_S)/\Gamma_{total}$ — Γ_{51}/Γ

VALUE (units 10^{-4})	CL%	EVTS	DOCUMENT ID		TECN	COMMENT
<4	90	2.3 ± 2.2	[1] ABLIKIM	05O	BES2	$e^+e^- \to \chi_{c2}\gamma$

[1] ABLIKIM 05O reports $[\Gamma(\chi_{c2}(1P) \to K^+K^-K^0_S K^0_S)/\Gamma_{total}] \times [B(\psi(2S) \to \gamma\chi_{c2}(1P))] < 3.5 \times 10^{-5}$ which we divide by our best (shown rounded) value $B(\psi(2S) \to \gamma\chi_{c2}(1P)) = 9.63 \times 10^{-2}$.

$\Gamma(K^0_S K^0_S K^0_S K^0_S)/\Gamma_{total}$ — Γ_{52}/Γ

VALUE (units 10^{-4})	EVTS	DOCUMENT ID		TECN	COMMENT
1.12±0.18±0.03	68	[1] ABLIKIM	19AA	BES3	$\psi(2S) \to \gamma 4K^0_S$

[1] Using $B(K^0_S \to \pi^+\pi^-) = (69.20 \pm 0.05)\%$. ABLIKIM 19AA reports $[\Gamma(\chi_{c2}(1P) \to K^0_S K^0_S K^0_S K^0_S)/\Gamma_{total}] \times [B(\psi(2S) \to \gamma\chi_{c2}(1P))] = (10.8 \pm 1.5 \pm 0.8) \times 10^{-6}$ which we divide by our best (shown rounded) value $B(\psi(2S) \to \gamma\chi_{c2}(1P)) = (9.63 \pm 0.23) \times 10^{-2}$. Our first error is their experiment's error and our second error is the systematic error from using our best (shown rounded) value..

$\Gamma(K^+K^-\phi)/\Gamma_{total}$ — Γ_{54}/Γ

VALUE (units 10^{-3})	EVTS	DOCUMENT ID		TECN	COMMENT
1.41±0.29±0.03	52	[1] ABLIKIM	06T	BES2	$\psi(2S) \to \gamma 2K^+2K^-$

[1] ABLIKIM 06T reports $(1.67 \pm 0.26 \pm 0.24) \times 10^{-3}$ from a measurement of $[\Gamma(\chi_{c2}(1P) \to K^+K^-\phi)/\Gamma_{total}] \times [B(\psi(2S) \to \gamma\chi_{c2}(1P))]$ assuming $B(\psi(2S) \to \gamma\chi_{c2}(1P)) = (8.1 \pm 0.4) \times 10^{-2}$, which we rescale to our best (shown rounded) value $B(\psi(2S) \to \gamma\chi_{c2}(1P)) = (9.63 \pm 0.23) \times 10^{-2}$. Our first error is their experiment's error and our second error is the systematic error from using our best (shown rounded) value.

$\Gamma(\overline{K}^0K^+\pi^-\phi + \text{c.c.})/\Gamma_{total}$ — Γ_{55}/Γ

VALUE (units 10^{-3})	DOCUMENT ID		TECN	COMMENT
4.83±0.32±0.66	ABLIKIM	15M	BES3	$\psi(2S) \to \gamma\chi_{c2}$

$\Gamma(K^+K^-\pi^0\phi)/\Gamma_{total}$ — Γ_{56}/Γ

VALUE (units 10^{-3})	DOCUMENT ID		TECN	COMMENT
2.74±0.16±0.44	ABLIKIM	15M	BES3	$\psi(2S) \to \gamma\chi_{c2}$

$\Gamma(\phi\pi^+\pi^-\pi^0)/\Gamma_{total}$ — Γ_{59}/Γ

VALUE (units 10^{-3})	EVTS	DOCUMENT ID		TECN	COMMENT
0.84±0.10±0.02	408	[1] ABLIKIM	13B	BES3	$e^+e^- \to \psi(2S) \to \gamma\chi_{c2}$

[1] ABLIKIM 13B reports $(0.93 \pm 0.06 \pm 0.10) \times 10^{-3}$ from a measurement of $[\Gamma(\chi_{c2}(1P) \to \phi\pi^+\pi^-\pi^0)/\Gamma_{total}] \times [B(\psi(2S) \to \gamma\chi_{c2}(1P))]$ assuming $B(\psi(2S) \to \gamma\chi_{c2}(1P)) = (8.72 \pm 0.34) \times 10^{-2}$, which we rescale to our best (shown rounded) value $B(\psi(2S) \to \gamma\chi_{c2}(1P)) = (9.63 \pm 0.23) \times 10^{-2}$. Our first error is their experiment's error and our second error is the systematic error from using our best (shown rounded) value.

$\Gamma(p\overline{p}\pi^0)/\Gamma_{total}$ — Γ_{61}/Γ

VALUE (units 10^{-3})	DOCUMENT ID		TECN	COMMENT
0.46±0.04 OUR AVERAGE				
0.47±0.04±0.01	[1] ONYISI	10	CLE3	$\psi(2S) \to \gamma p\overline{p}X$
0.43±0.09±0.01	[2] ATHAR	07	CLEO	$\psi(2S) \to \gamma h^+h^-h^0$

[1] ONYISI 10 reports $(4.83 \pm 0.25 \pm 0.35 \pm 0.31) \times 10^{-4}$ from a measurement of $[\Gamma(\chi_{c2}(1P) \to p\overline{p}\pi^0)/\Gamma_{total}] \times [B(\psi(2S) \to \gamma\chi_{c2}(1P))]$ assuming $B(\psi(2S) \to \gamma\chi_{c2}(1P)) = (9.33 \pm 0.14 \pm 0.61) \times 10^{-2}$, which we rescale to our best (shown rounded) value $B(\psi(2S) \to \gamma\chi_{c2}(1P)) = (9.63 \pm 0.23) \times 10^{-2}$. Our first error is their experiment's error and our second error is the systematic error from using our best (shown rounded) value.

[2] ATHAR 07 reports $(0.44 \pm 0.08 \pm 0.05) \times 10^{-3}$ from a measurement of $[\Gamma(\chi_{c2}(1P) \to p\overline{p}\pi^0)/\Gamma_{total}] \times [B(\psi(2S) \to \gamma\chi_{c2}(1P))]$ assuming $B(\psi(2S) \to \gamma\chi_{c2}(1P)) = (9.33 \pm 0.14 \pm 0.61) \times 10^{-2}$, which we rescale to our best (shown rounded) value $B(\psi(2S) \to \gamma\chi_{c2}(1P)) = (9.63 \pm 0.23) \times 10^{-2}$. Our first error is their experiment's error and our second error is the systematic error from using our best (shown rounded) value.

$\Gamma(p\overline{p}\eta)/\Gamma_{total}$ — Γ_{62}/Γ

VALUE (units 10^{-3})	DOCUMENT ID		TECN	COMMENT
0.172±0.025 OUR AVERAGE				
0.171±0.026±0.004	[1] ONYISI	10	CLE3	$\psi(2S) \to \gamma p\overline{p}X$
0.184±0.069±0.004	[2] ATHAR	07	CLEO	$\psi(2S) \to \gamma h^+h^-h^0$

[1] ONYISI 10 reports $(1.76 \pm 0.23 \pm 0.14 \pm 0.11) \times 10^{-4}$ from a measurement of $[\Gamma(\chi_{c2}(1P) \to p\overline{p}\eta)/\Gamma_{total}] \times [B(\psi(2S) \to \gamma\chi_{c2}(1P))]$ assuming $B(\psi(2S) \to \gamma\chi_{c2}(1P)) = (9.33 \pm 0.14 \pm 0.61) \times 10^{-2}$, which we rescale to our best (shown rounded) value $B(\psi(2S) \to \gamma\chi_{c2}(1P)) = (9.63 \pm 0.23) \times 10^{-2}$. Our first error is their experiment's error and our second error is the systematic error from using our best (shown rounded) value.

[2] ATHAR 07 reports $(0.19 \pm 0.07 \pm 0.02) \times 10^{-3}$ from a measurement of $[\Gamma(\chi_{c2}(1P) \to p\overline{p}\eta)/\Gamma_{total}] \times [B(\psi(2S) \to \gamma\chi_{c2}(1P))]$ assuming $B(\psi(2S) \to \gamma\chi_{c2}(1P)) = (9.33 \pm 0.14 \pm 0.61) \times 10^{-2}$, which we rescale to our best (shown rounded) value $B(\psi(2S) \to \gamma\chi_{c2}(1P)) = (9.63 \pm 0.23) \times 10^{-2}$. Our first error is their experiment's error and our second error is the systematic error from using our best (shown rounded) value.

$\Gamma(p\overline{p}\omega)/\Gamma_{total}$ — Γ_{63}/Γ

VALUE (units 10^{-3})	DOCUMENT ID		TECN	COMMENT
0.36±0.04±0.01	[1] ONYISI	10	CLE3	$\psi(2S) \to \gamma p\overline{p}X$

[1] ONYISI 10 reports $(3.68 \pm 0.35 \pm 0.26 \pm 0.24) \times 10^{-4}$ from a measurement of $[\Gamma(\chi_{c2}(1P) \to p\overline{p}\omega)/\Gamma_{total}] \times [B(\psi(2S) \to \gamma\chi_{c2}(1P))]$ assuming $B(\psi(2S) \to \gamma\chi_{c2}(1P)) = (9.33 \pm 0.14 \pm 0.61) \times 10^{-2}$, which we rescale to our best (shown rounded) value $B(\psi(2S) \to \gamma\chi_{c2}(1P)) = (9.63 \pm 0.23) \times 10^{-2}$. Our first error is their experiment's error and our second error is the systematic error from using our best (shown rounded) value.

$\Gamma(p\overline{p}\pi^+\pi^-)/\Gamma_{total}$ — Γ_{64}/Γ

VALUE (units 10^{-3})	EVTS	DOCUMENT ID		TECN	COMMENT
1.32±0.34 OUR EVALUATION Treating systematic error as correlated.					
1.1 ±0.5 OUR AVERAGE Error includes scale factor of 1.6.					
1.00±0.31±0.02	51	[1] BAI	99B	BES	$\psi(2S) \to \gamma\chi_{c2}$
2.7 ±1.0 ±0.1	13	[2] TANENBAUM	78	MRK1	$\psi(2S) \to \gamma\chi_{c2}$

[1] BAI 99B reports $(1.23 \pm 0.20 \pm 0.35) \times 10^{-3}$ from a measurement of $[\Gamma(\chi_{c2}(1P) \to p\overline{p}\pi^+\pi^-)/\Gamma_{total}] \times [B(\psi(2S) \to \gamma\chi_{c2}(1P))]$ assuming $B(\psi(2S) \to \gamma\chi_{c2}(1P)) = (7.8 \pm 0.8) \times 10^{-2}$, which we rescale to our best (shown rounded) value $B(\psi(2S) \to \gamma\chi_{c2}(1P)) = (9.63 \pm 0.23) \times 10^{-2}$. Our first error is their experiment's error and our second error is the systematic error from using our best (shown rounded) value.

[2] TANENBAUM 78 reports $[\Gamma(\chi_{c2}(1P) \to p\overline{p}\pi^+\pi^-)/\Gamma_{total}] \times [B(\psi(2S) \to \gamma\chi_{c2}(1P))] = (0.26 \pm 0.10) \times 10^{-3}$ which we divide by our best (shown rounded) value $B(\psi(2S) \to \gamma\chi_{c2}(1P)) = (9.63 \pm 0.23) \times 10^{-2}$. Our first error is their experiment's error and our second error is the systematic error from using our best (shown rounded) value.

$\Gamma(p\overline{p}\pi^0\pi^0)/\Gamma_{total}$ — Γ_{65}/Γ

VALUE (%)	EVTS	DOCUMENT ID		TECN	COMMENT
0.078±0.023±0.002	29.2	[1] HE	08B	CLEO	$e^+e^- \to \gamma h^+h^-h^0h^0$

[1] HE 08B reports $0.08 \pm 0.02 \pm 0.01 \pm 0.01$ % from a measurement of $[\Gamma(\chi_{c2}(1P) \to p\overline{p}\pi^0\pi^0)/\Gamma_{total}] \times [B(\psi(2S) \to \gamma\chi_{c2}(1P))]$ assuming $B(\psi(2S) \to \gamma\chi_{c2}(1P)) = (9.33 \pm 0.14 \pm 0.61) \times 10^{-2}$, which we rescale to our best (shown rounded) value $B(\psi(2S) \to \gamma\chi_{c2}(1P)) = (9.63 \pm 0.23) \times 10^{-2}$. Our first error is their experiment's error and our second error is the systematic error from using our best (shown rounded) value.

$\Gamma(p\overline{p}\eta\pi^0)/\Gamma_{total}$ — Γ_{66}/Γ

VALUE (units 10^{-4})	EVTS	DOCUMENT ID		TECN	COMMENT
1.29±0.09±0.03	1059	[1] ABLIKIM	25L	BES3	$\psi(3686) \to \gamma p\overline{p}\eta\pi^0$

[1] ABLIKIM 25L reports $(1.33 \pm 0.05 \pm 0.08) \times 10^{-4}$ from a measurement of $[\Gamma(\chi_{c2}(1P) \to p\overline{p}\eta\pi^0)/\Gamma_{total}] \times [B(\psi(2S) \to \gamma\chi_{c2}(1P))]$ assuming $B(\psi(2S) \to \gamma\chi_{c2}(1P)) = (9.36 \pm 0.23) \times 10^{-2}$, which we rescale to our best (shown rounded) value $B(\psi(2S) \to \gamma\chi_{c2}(1P)) = (9.63 \pm 0.23) \times 10^{-2}$. Our first error is their experiment's error and our second error is the systematic error from using our best (shown rounded) value.

$\Gamma(p\overline{p}\eta\eta)/\Gamma_{total}$ — Γ_{67}/Γ

VALUE (units 10^{-5})	EVTS	DOCUMENT ID		TECN	COMMENT
2.6±0.5±0.1	87	[1] ABLIKIM	25CE	BES3	$\psi(2S) \to \gamma\chi_{c2}$

[1] ABLIKIM 25CE reports $(2.64 \pm 0.40 \pm 0.27) \times 10^{-5}$ from a measurement of $[\Gamma(\chi_{c2}(1P) \to p\overline{p}\eta\eta)/\Gamma_{total}] \times [B(\psi(2S) \to \gamma\chi_{c2}(1P))]$ assuming $B(\psi(2S) \to \gamma\chi_{c2}(1P)) = (9.36 \pm 0.23) \times 10^{-2}$, which we rescale to our best (shown rounded) value $B(\psi(2S) \to \gamma\chi_{c2}(1P)) = (9.63 \pm 0.23) \times 10^{-2}$. Our first error is their experiment's error and our second error is the systematic error from using our best (shown rounded) value.

$\Gamma(p\overline{p}K^+K^-)/\Gamma_{total}$ — Γ_{68}/Γ

VALUE (units 10^{-4})	EVTS	DOCUMENT ID		TECN	COMMENT
2.52±0.16±0.06	11463	[1] ABLIKIM	25V	BES3	$\psi(2S) \to \gamma p\overline{p}K^+K^-$

[1] ABLIKIM 25V reports $[\Gamma(\chi_{c2}(1P) \to p\overline{p}K^+K^-)/\Gamma_{total}] \times [B(\psi(2S) \to \gamma\chi_{c2}(1P))] = (2.43 \pm 0.02 \pm 0.15) \times 10^{-5}$ which we divide by our best (shown rounded) value $B(\psi(2S) \to \gamma\chi_{c2}(1P)) = (9.63 \pm 0.23) \times 10^{-2}$. Our first error is their experiment's error and our second error is the systematic error from using our best (shown rounded) value.

$\Gamma(p\overline{p}K^+K^-(\text{non-resonant}))/\Gamma_{total}$ — Γ_{69}/Γ

VALUE (units 10^{-4})	EVTS	DOCUMENT ID		TECN	COMMENT
1.89±0.31±0.04	131 ± 12	[1] ABLIKIM	11F	BES3	$\psi(2S) \to \gamma p\overline{p}K^+K^-$

[1] ABLIKIM 11F reports $(2.08 \pm 0.19 \pm 0.30) \times 10^{-4}$ from a measurement of $[\Gamma(\chi_{c2}(1P) \to p\overline{p}K^+K^-(\text{non-resonant}))/\Gamma_{total}] \times [B(\psi(2S) \to \gamma\chi_{c2}(1P))]$ assuming $B(\psi(2S) \to \gamma\chi_{c2}(1P)) = (8.74 \pm 0.35) \times 10^{-2}$, which we rescale to our best (shown rounded) value $B(\psi(2S) \to \gamma\chi_{c2}(1P)) = (9.63 \pm 0.23) \times 10^{-2}$. Our first error is their experiment's error and our second error is the systematic error from using our best (shown rounded) value.

$\Gamma(K^+\overline{p}\Lambda(1520) + \text{c.c.})/\Gamma_{total}$ — Γ_{70}/Γ

VALUE (units 10^{-4})	EVTS	DOCUMENT ID		TECN	COMMENT
2.8±0.7±0.1	79 ± 13	[1] ABLIKIM	11F	BES3	$\psi(2S) \to \gamma p\overline{p}K^+K^-$

[1] ABLIKIM 11F reports $(3.06 \pm 0.50 \pm 0.54) \times 10^{-4}$ from a measurement of $[\Gamma(\chi_{c2}(1P) \to K^+ \overline{p} \Lambda(1520) + \text{c.c.})/\Gamma_{total}] \times [B(\psi(2S) \to \gamma\chi_{c2}(1P))]$ assuming $B(\psi(2S) \to \gamma\chi_{c2}(1P)) = (8.74 \pm 0.35) \times 10^{-2}$, which we rescale to our best (shown rounded) value $B(\psi(2S) \to \gamma\chi_{c2}(1P)) = (9.63 \pm 0.23) \times 10^{-2}$. Our first error is their experiment's error and our second error is the systematic error from using our best (shown rounded) value.

$\Gamma(\Lambda(1520)\overline{\Lambda}(1520))/\Gamma_{total}$ — Γ_{71}/Γ

VALUE (units 10^{-4})	EVTS	DOCUMENT ID		TECN	COMMENT
4.6±1.4±0.1	29 ± 7	[1] ABLIKIM	11F	BES3	$\psi(2S) \to \gamma p \overline{p} K^+ K^-$

[1] ABLIKIM 11F reports $(5.05 \pm 1.29 \pm 0.93) \times 10^{-4}$ from a measurement of $[\Gamma(\chi_{c2}(1P) \to \Lambda(1520)\overline{\Lambda}(1520))/\Gamma_{total}] \times [B(\psi(2S) \to \gamma\chi_{c2}(1P))]$ assuming $B(\psi(2S) \to \gamma\chi_{c2}(1P)) = (8.74 \pm 0.35) \times 10^{-2}$, which we rescale to our best (shown rounded) value $B(\psi(2S) \to \gamma\chi_{c2}(1P)) = (9.63 \pm 0.23) \times 10^{-2}$. Our first error is their experiment's error and our second error is the systematic error from using our best (shown rounded) value.

$\Gamma(p\overline{p}\phi)/\Gamma_{total}$ — Γ_{72}/Γ

VALUE (units 10^{-5})	EVTS	DOCUMENT ID		TECN	COMMENT
2.8±0.9±0.1	24 ± 7	[1] ABLIKIM	11F	BES3	$\psi(2S) \to \gamma p \overline{p} K^+ K^-$

[1] ABLIKIM 11F reports $(3.04 \pm 0.85 \pm 0.43) \times 10^{-5}$ from a measurement of $[\Gamma(\chi_{c2}(1P) \to p\overline{p}\phi)/\Gamma_{total}] \times [B(\psi(2S) \to \gamma\chi_{c2}(1P))]$ assuming $B(\psi(2S) \to \gamma\chi_{c2}(1P)) = (8.74 \pm 0.35) \times 10^{-2}$, which we rescale to our best (shown rounded) value $B(\psi(2S) \to \gamma\chi_{c2}(1P)) = (9.63 \pm 0.23) \times 10^{-2}$. Our first error is their experiment's error and our second error is the systematic error from using our best (shown rounded) value.

$\Gamma(p\overline{p}K^0_S K^0_S)/\Gamma_{total}$ — Γ_{73}/Γ

VALUE	CL%	DOCUMENT ID		TECN	COMMENT
$<8 \times 10^{-4}$	90	[1] ABLIKIM	06D	BES2	$\psi(2S) \to \gamma\chi_{c2}$

[1] ABLIKIM 06D reports $< 7.9 \times 10^{-4}$ from a measurement of $[\Gamma(\chi_{c2}(1P) \to p\overline{p}K^0_S K^0_S)/\Gamma_{total}] \times [B(\psi(2S) \to \gamma\chi_{c2}(1P))]$ assuming $B(\psi(2S) \to \gamma\chi_{c2}(1P)) = (9.3 \pm 0.6) \times 10^{-2}$, which we rescale to our best (shown rounded) value $B(\psi(2S) \to \gamma\chi_{c2}(1P)) = 9.63 \times 10^{-2}$.

$\Gamma(p\overline{n}\pi^-)/\Gamma_{total}$ — Γ_{75}/Γ

VALUE (units 10^{-4})	EVTS	DOCUMENT ID		TECN	COMMENT
8.4±0.9 OUR AVERAGE					
8.3±1.0±0.2	3309	[1] ABLIKIM	12J	BES3	$\psi(2S) \to \gamma p \overline{n} \pi^-$
10.1±3.4±0.2		[2] ABLIKIM	06I	BES2	$\psi(2S) \to \gamma p \pi^- X$

[1] ABLIKIM 12J reports $[\Gamma(\chi_{c2}(1P) \to p\overline{n}\pi^-)/\Gamma_{total}] \times [B(\psi(2S) \to \gamma\chi_{c2}(1P))] = (0.80 \pm 0.02 \pm 0.09) \times 10^{-4}$ which we divide by our best (shown rounded) value $B(\psi(2S) \to \gamma\chi_{c2}(1P)) = (9.63 \pm 0.23) \times 10^{-2}$. Our first error is their experiment's error and our second error is the systematic error from using our best (shown rounded) value.

[2] ABLIKIM 06I reports $[\Gamma(\chi_{c2}(1P) \to p\overline{n}\pi^-)/\Gamma_{total}] \times [B(\psi(2S) \to \gamma\chi_{c2}(1P))] = (0.97 \pm 0.20 \pm 0.26) \times 10^{-4}$ which we divide by our best (shown rounded) value $B(\psi(2S) \to \gamma\chi_{c2}(1P)) = (9.63 \pm 0.23) \times 10^{-2}$. Our first error is their experiment's error and our second error is the systematic error from using our best (shown rounded) value.

$\Gamma(\overline{p}n\pi^+)/\Gamma_{total}$ — Γ_{76}/Γ

VALUE (units 10^{-4})	EVTS	DOCUMENT ID		TECN	COMMENT
8.8±0.8±0.2	3732	[1] ABLIKIM	12J	BES3	$\psi(2S) \to \gamma \overline{p} n \pi^+$

[1] ABLIKIM 12J reports $[\Gamma(\chi_{c2}(1P) \to \overline{p}n\pi^+)/\Gamma_{total}] \times [B(\psi(2S) \to \gamma\chi_{c2}(1P))] = (0.85 \pm 0.02 \pm 0.07) \times 10^{-4}$ which we divide by our best (shown rounded) value $B(\psi(2S) \to \gamma\chi_{c2}(1P)) = (9.63 \pm 0.23) \times 10^{-2}$. Our first error is their experiment's error and our second error is the systematic error from using our best (shown rounded) value.

$\Gamma(p\overline{n}\pi^-\pi^0)/\Gamma_{total}$ — Γ_{77}/Γ

VALUE (units 10^{-4})	EVTS	DOCUMENT ID		TECN	COMMENT
21.5±1.7±0.5	2128	[1] ABLIKIM	12J	BES3	$\psi(2S) \to \gamma p \overline{n} \pi^- \pi^0$

[1] ABLIKIM 12J reports $[\Gamma(\chi_{c2}(1P) \to p\overline{n}\pi^-\pi^0)/\Gamma_{total}] \times [B(\psi(2S) \to \gamma\chi_{c2}(1P))] = (2.07 \pm 0.06 \pm 0.15) \times 10^{-4}$ which we divide by our best (shown rounded) value $B(\psi(2S) \to \gamma\chi_{c2}(1P)) = (9.63 \pm 0.23) \times 10^{-2}$. Our first error is their experiment's error and our second error is the systematic error from using our best (shown rounded) value.

$\Gamma(\overline{p}n\pi^+\pi^0)/\Gamma_{total}$ — Γ_{78}/Γ

VALUE (units 10^{-4})	EVTS	DOCUMENT ID		TECN	COMMENT
20.9±1.8±0.5	2352	[1] ABLIKIM	12J	BES3	$\psi(2S) \to \gamma \overline{p} n \pi^+ \pi^0$

[1] ABLIKIM 12J reports $[\Gamma(\chi_{c2}(1P) \to \overline{p}n\pi^+\pi^0)/\Gamma_{total}] \times [B(\psi(2S) \to \gamma\chi_{c2}(1P))] = (2.01 \pm 0.06 \pm 0.16) \times 10^{-4}$ which we divide by our best (shown rounded) value $B(\psi(2S) \to \gamma\chi_{c2}(1P)) = (9.63 \pm 0.23) \times 10^{-2}$. Our first error is their experiment's error and our second error is the systematic error from using our best (shown rounded) value.

$\Gamma(\Lambda\overline{\Lambda}\pi^+\pi^-)/\Gamma_{total}$ — Γ_{80}/Γ

VALUE (units 10^{-5})	CL%	EVTS	DOCUMENT ID		TECN	COMMENT
124±15±3		371	[1] ABLIKIM	12I	BES3	$\psi(2S) \to \gamma \Lambda \overline{\Lambda} \pi^+ \pi^-$
• • • We do not use the following data for averages, fits, limits, etc. • • •						
<350	90		[2] ABLIKIM	06D	BES2	$\psi(2S) \to \chi_{c2}\gamma$

[1] ABLIKIM 12I reports $(137.0 \pm 7.6 \pm 15.7) \times 10^{-5}$ from a measurement of $[\Gamma(\chi_{c2}(1P) \to \Lambda\overline{\Lambda}\pi^+\pi^-)/\Gamma_{total}] \times [B(\psi(2S) \to \gamma\chi_{c2}(1P))]$ assuming $B(\psi(2S) \to \gamma\chi_{c2}(1P)) = (8.72 \pm 0.34) \times 10^{-2}$, which we rescale to our best (shown rounded) value $B(\psi(2S) \to \gamma\chi_{c2}(1P)) = (9.63 \pm 0.23) \times 10^{-2}$. Our first error is their experiment's error and our second error is the systematic error from using our best (shown rounded) value.

[2] Using $B(\psi(2S) \to \chi_{c2}\gamma) = (9.3 \pm 0.6)\%$.

$\Gamma(\Lambda\overline{\Lambda}\pi^+\pi^-(\text{non-resonant}))/\Gamma_{total}$ — Γ_{81}/Γ

VALUE (units 10^{-5})	EVTS	DOCUMENT ID		TECN	COMMENT
65±15±2	36	[1] ABLIKIM	12I	BES3	$\psi(2S) \to \gamma \Lambda \overline{\Lambda} \pi^+ \pi^-$

[1] ABLIKIM 12I reports $(71.8 \pm 14.5 \pm 8.2) \times 10^{-5}$ from a measurement of $[\Gamma(\chi_{c2}(1P) \to \Lambda\overline{\Lambda}\pi^+\pi^-(\text{non-resonant}))/\Gamma_{total}] \times [B(\psi(2S) \to \gamma\chi_{c2}(1P))]$ assuming $B(\psi(2S) \to \gamma\chi_{c2}(1P)) = (8.72 \pm 0.34) \times 10^{-2}$, which we rescale to our best (shown rounded) value $B(\psi(2S) \to \gamma\chi_{c2}(1P)) = (9.63 \pm 0.23) \times 10^{-2}$. Our first error is their experiment's error and our second error is the systematic error from using our best (shown rounded) value.

$\Gamma(\Sigma(1385)^+\overline{\Lambda}\pi^- + \text{c.c.})/\Gamma_{total}$ — Γ_{82}/Γ

VALUE (units 10^{-5})	CL%	DOCUMENT ID		TECN	COMMENT
<40	90	[1] ABLIKIM	12I	BES3	$\psi(2S) \to \gamma \Sigma(1385)^+ \overline{\Lambda} \pi^-$

[1] ABLIKIM 12I reports $< 42 \times 10^{-5}$ from a measurement of $[\Gamma(\chi_{c2}(1P) \to \Sigma(1385)^+\overline{\Lambda}\pi^- + \text{c.c.})/\Gamma_{total}] \times [B(\psi(2S) \to \gamma\chi_{c2}(1P))]$ assuming $B(\psi(2S) \to \gamma\chi_{c2}(1P)) = (8.72 \pm 0.34) \times 10^{-2}$, which we rescale to our best (shown rounded) value $B(\psi(2S) \to \gamma\chi_{c2}(1P)) = 9.63 \times 10^{-2}$.

$\Gamma(\Sigma(1385)^-\overline{\Lambda}\pi^+ + \text{c.c.})/\Gamma_{total}$ — Γ_{83}/Γ

VALUE (units 10^{-5})	CL%	DOCUMENT ID		TECN	COMMENT
<60	90	[1] ABLIKIM	12I	BES3	$\psi(2S) \to \gamma \Sigma(1385)^- \overline{\Lambda} \pi^+$

[1] ABLIKIM 12I reports $< 61 \times 10^{-5}$ from a measurement of $[\Gamma(\chi_{c2}(1P) \to \Sigma(1385)^-\overline{\Lambda}\pi^+ + \text{c.c.})/\Gamma_{total}] \times [B(\psi(2S) \to \gamma\chi_{c2}(1P))]$ assuming $B(\psi(2S) \to \gamma\chi_{c2}(1P)) = (8.72 \pm 0.34) \times 10^{-2}$, which we rescale to our best (shown rounded) value $B(\psi(2S) \to \gamma\chi_{c2}(1P)) = 9.63 \times 10^{-2}$.

$\Gamma(K^+\overline{p}\Lambda + \text{c.c.})/\Gamma_{total}$ — Γ_{88}/Γ

VALUE (units 10^{-4})	EVTS	DOCUMENT ID		TECN	COMMENT
7.7±0.5 OUR AVERAGE					
7.6±0.5±0.2	5k	[1,2] ABLIKIM	13D	BES3	$\psi(2S) \to \gamma \Lambda \overline{p} K^+$
8.2±1.6±0.2		[3] ATHAR	07	CLEO	$\psi(2S) \to \gamma h^+ h^- h^0$

[1] ABLIKIM 13D reports $(8.4 \pm 0.3 \pm 0.6) \times 10^{-4}$ from a measurement of $[\Gamma(\chi_{c2}(1P) \to K^+\overline{p}\Lambda + \text{c.c.})/\Gamma_{total}] \times [B(\psi(2S) \to \gamma\chi_{c2}(1P))]$ assuming $B(\psi(2S) \to \gamma\chi_{c2}(1P)) = (8.72 \pm 0.34) \times 10^{-2}$, which we rescale to our best (shown rounded) value $B(\psi(2S) \to \gamma\chi_{c2}(1P)) = (9.63 \pm 0.23) \times 10^{-2}$. Our first error is their experiment's error and our second error is the systematic error from using our best (shown rounded) value.

[2] Using $B(\Lambda \to p\pi^-) = 63.9\%$.

[3] ATHAR 07 reports $(8.5 \pm 1.4 \pm 1.0) \times 10^{-4}$ from a measurement of $[\Gamma(\chi_{c2}(1P) \to K^+\overline{p}\Lambda + \text{c.c.})/\Gamma_{total}] \times [B(\psi(2S) \to \gamma\chi_{c2}(1P))]$ assuming $B(\psi(2S) \to \gamma\chi_{c2}(1P)) = (9.33 \pm 0.14 \pm 0.61) \times 10^{-2}$, which we rescale to our best (shown rounded) value $B(\psi(2S) \to \gamma\chi_{c2}(1P)) = (9.63 \pm 0.23) \times 10^{-2}$. Our first error is their experiment's error and our second error is the systematic error from using our best (shown rounded) value.

$\Gamma(nK^0_S\overline{\Lambda} + \text{c.c.})/\Gamma_{total}$ — Γ_{89}/Γ

VALUE (units 10^{-4})	EVTS	DOCUMENT ID		TECN	COMMENT
3.54±0.27±0.08	879	[1] ABLIKIM	21AV	BES3	$\psi(2S) \to \gamma n K^0_S \overline{\Lambda}$ + c.c.

[1] ABLIKIM 21AV reports $(3.58 \pm 0.16 \pm 0.23) \times 10^{-4}$ from a measurement of $[\Gamma(\chi_{c2}(1P) \to nK^0_S\overline{\Lambda} + \text{c.c.})/\Gamma_{total}] \times [B(\psi(2S) \to \gamma\chi_{c2}(1P))]$ assuming $B(\psi(2S) \to \gamma\chi_{c2}(1P)) = 0.0952 \pm 0.0020$, which we rescale to our best (shown rounded) value $B(\psi(2S) \to \gamma\chi_{c2}(1P)) = (9.63 \pm 0.23) \times 10^{-2}$. Our first error is their experiment's error and our second error is the systematic error from using our best (shown rounded) value. Also uses $B(\overline{\Lambda} \to \overline{p}\pi^+) = (63.9 \pm 0.5)\%$ and $B(K^0_S \to \pi^+\pi^-) = (69.20 \pm 0.05)\%$.

$\Gamma(K^*(892)^+\overline{p}\Lambda + \text{c.c.})/\Gamma_{total}$ — Γ_{90}/Γ

VALUE (units 10^{-4})	EVTS	DOCUMENT ID		TECN	COMMENT
8.1±1.1±0.2	476	[1] ABLIKIM	19AU	BES3	$\psi(2S) \to \gamma K^{*+} \overline{p} \Lambda$

[1] ABLIKIM 19AU reports $[\Gamma(\chi_{c2}(1P) \to K^*(892)^+\overline{p}\Lambda + \text{c.c.})/\Gamma_{total}] \times [B(\psi(2S) \to \gamma\chi_{c2}(1P))] = (7.8 \pm 0.9 \pm 0.6) \times 10^{-5}$ which we divide by our best (shown rounded) value $B(\psi(2S) \to \gamma\chi_{c2}(1P)) = (9.63 \pm 0.23) \times 10^{-2}$. Our first error is their experiment's error and our second error is the systematic error from using our best (shown rounded) value.

$\Gamma(\Sigma^0\overline{\Sigma}^0)/\Gamma_{total}$ — Γ_{92}/Γ

VALUE (units 10^{-5})	CL%	EVTS	DOCUMENT ID		TECN	COMMENT
3.6±0.6±0.1		91	[1] ABLIKIM	18V	BES3	$\psi(2S) \to \gamma \Sigma^0 \overline{\Sigma}^0$
• • • We do not use the following data for averages, fits, limits, etc. • • •						
<6	90		[2] ABLIKIM	13H	BES3	$\psi(2S) \to \gamma \Sigma^0 \overline{\Sigma}^0$
<7	90	7.5 ± 3.4	[3] NAIK	08	CLEO	$\psi(2S) \to \gamma \Sigma^0 \overline{\Sigma}^0$

[1] ABLIKIM 18V reports $[\Gamma(\chi_{c2}(1P) \to \Sigma^0\overline{\Sigma}^0)/\Gamma_{total}] \times [B(\psi(2S) \to \gamma\chi_{c2}(1P))] = (0.35 \pm 0.05 \pm 0.02) \times 10^{-5}$ which we divide by our best (shown rounded) value $B(\psi(2S) \to \gamma\chi_{c2}(1P)) = (9.63 \pm 0.23) \times 10^{-2}$. Our first error is their experiment's

Int. J. Mod. Phys. A 2026.41. Downloaded from www.worldscientific.com
by CALIFORNIA @ BERKELEY on 09/16/26. Re-use and distribution is strictly not permitted, except for Open Access articles.

Int. J. Mod. Phys. A 2026.41. Downloaded from www.worldscientific.com by UNIVERSITY OF CALIFORNIA @ BERKELEY on 09/16/26. Re-use and distribution is strictly not permitted, except for Open Access articles.

error and our second error is the systematic error from using our best (shown rounded) value.

[2] ABLIKIM 13H reports $< 0.65 \times 10^{-4}$ from a measurement of $[\Gamma(\chi_{c2}(1P) \to \Sigma^0\overline{\Sigma}^0)/\Gamma_{total}] \times [B(\psi(2S) \to \gamma\chi_{c2}(1P))]$ assuming $B(\psi(2S) \to \gamma\chi_{c2}(1P)) = (8.74 \pm 0.35) \times 10^{-2}$, which we rescale to our best (shown rounded) value $B(\psi(2S) \to \gamma\chi_{c2}(1P)) = 9.63 \times 10^{-2}$.

[3] NAIK 08 reports $< 0.75 \times 10^{-4}$ from a measurement of $[\Gamma(\chi_{c2}(1P) \to \Sigma^0\overline{\Sigma}^0)/\Gamma_{total}] \times [B(\psi(2S) \to \gamma\chi_{c2}(1P))]$ assuming $B(\psi(2S) \to \gamma\chi_{c2}(1P)) = (9.33 \pm 0.14 \pm 0.61) \times 10^{-2}$, which we rescale to our best (shown rounded) value $B(\psi(2S) \to \gamma\chi_{c2}(1P)) = 9.63 \times 10^{-2}$.

$\Gamma(\Sigma^+\overline{\Sigma}^-)/\Gamma_{total}$ — Γ_{95}/Γ

VALUE (units 10^{-5})	CL%	EVTS	DOCUMENT ID		TECN	COMMENT
3.3±0.7±0.1		55	[1] ABLIKIM	18V	BES3	$\psi(2S) \to \gamma\Sigma^+\overline{\Sigma}^-$
• • • We do not use the following data for averages, fits, limits, etc. • • •						
<8	90		[2] ABLIKIM	13H	BES3	$\psi(2S) \to \gamma\Sigma^+\overline{\Sigma}^-$
<6	90	4.0 ± 3.5	[3] NAIK	08	CLEO	$\psi(2S) \to \gamma\Sigma^+\overline{\Sigma}^-$

[1] ABLIKIM 18V reports $[\Gamma(\chi_{c2}(1P) \to \Sigma^+\overline{\Sigma}^-)/\Gamma_{total}] \times [B(\psi(2S) \to \gamma\chi_{c2}(1P))] = (0.32 \pm 0.06 \pm 0.03) \times 10^{-5}$ which we divide by our best (shown rounded) value $B(\psi(2S) \to \gamma\chi_{c2}(1P)) = (9.63 \pm 0.23) \times 10^{-2}$. Our first error is their experiment's error and our second error is the systematic error from using our best (shown rounded) value.

[2] ABLIKIM 13H reports $< 0.88 \times 10^{-4}$ from a measurement of $[\Gamma(\chi_{c2}(1P) \to \Sigma^+\overline{\Sigma}^-)/\Gamma_{total}] \times [B(\psi(2S) \to \gamma\chi_{c2}(1P))]$ assuming $B(\psi(2S) \to \gamma\chi_{c2}(1P)) = (8.74 \pm 0.35) \times 10^{-2}$, which we rescale to our best (shown rounded) value $B(\psi(2S) \to \gamma\chi_{c2}(1P)) = 9.63 \times 10^{-2}$.

[3] NAIK 08 reports $< 0.67 \times 10^{-4}$ from a measurement of $[\Gamma(\chi_{c2}(1P) \to \Sigma^+\overline{\Sigma}^-)/\Gamma_{total}] \times [B(\psi(2S) \to \gamma\chi_{c2}(1P))]$ assuming $B(\psi(2S) \to \gamma\chi_{c2}(1P)) = (9.33 \pm 0.14 \pm 0.61) \times 10^{-2}$, which we rescale to our best (shown rounded) value $B(\psi(2S) \to \gamma\chi_{c2}(1P)) = 9.63 \times 10^{-2}$.

$\Gamma(\Sigma^+\overline{\Sigma}^-\eta)/\Gamma_{total}$ — Γ_{96}/Γ

VALUE (units 10^{-5})	EVTS	DOCUMENT ID		TECN	COMMENT
5.4±1.3±0.1	35	[1] ABLIKIM	24CA	BES3	$\psi(2S) \to \gamma\chi_{c2}(1P)$

[1] ABLIKIM 24CA reports $(5.46 \pm 1.18 \pm 0.50) \times 10^{-5}$ from a measurement of $[\Gamma(\chi_{c2}(1P) \to \Sigma^+\overline{\Sigma}^-\eta)/\Gamma_{total}] \times [B(\psi(2S) \to \gamma\chi_{c2}(1P))]$ assuming $B(\psi(2S) \to \gamma\chi_{c2}(1P)) = (9.52 \pm 0.20) \times 10^{-2}$, which we rescale to our best (shown rounded) value $B(\psi(2S) \to \gamma\chi_{c2}(1P)) = (9.63 \pm 0.23) \times 10^{-2}$. Our first error is their experiment's error and our second error is the systematic error from using our best (shown rounded) value.

$\Gamma(\Sigma^-\overline{\Sigma}^+)/\Gamma_{total}$ — Γ_{97}/Γ

VALUE (units 10^{-5})	EVTS	DOCUMENT ID		TECN	COMMENT
4.4±1.8±0.1	131	[1] ABLIKIM	20I	BES3	$\psi(2S) \to \gamma\Sigma^-\overline{\Sigma}^+$

[1] ABLIKIM 20I reports $(4.4 \pm 1.7 \pm 0.5) \times 10^{-5}$ from a measurement of $[\Gamma(\chi_{c2}(1P) \to \Sigma^-\overline{\Sigma}^+)/\Gamma_{total}] \times [B(\psi(2S) \to \gamma\chi_{c2}(1P))]$ assuming $B(\psi(2S) \to \gamma\chi_{c2}(1P)) = (9.52 \pm 0.20) \times 10^{-2}$, which we rescale to our best (shown rounded) value $B(\psi(2S) \to \gamma\chi_{c2}(1P)) = (9.63 \pm 0.23) \times 10^{-2}$. Our first error is their experiment's error and our second error is the systematic error from using our best (shown rounded) value.

$\Gamma(\Sigma(1385)^+\overline{\Sigma}(1385)^-)/\Gamma_{total}$ — Γ_{98}/Γ

VALUE (units 10^{-5})	CL%	DOCUMENT ID		TECN	COMMENT
<15	90	[1] ABLIKIM	12I	BES3	$\psi(2S) \to \gamma\Sigma(1385)^+\overline{\Sigma}(1385)^-$

[1] ABLIKIM 12I reports $< 17 \times 10^{-5}$ from a measurement of $[\Gamma(\chi_{c2}(1P) \to \Sigma(1385)^+\overline{\Sigma}(1385)^-)/\Gamma_{total}] \times [B(\psi(2S) \to \gamma\chi_{c2}(1P))]$ assuming $B(\psi(2S) \to \gamma\chi_{c2}(1P)) = (8.72 \pm 0.34) \times 10^{-2}$, which we rescale to our best (shown rounded) value $B(\psi(2S) \to \gamma\chi_{c2}(1P)) = 9.63 \times 10^{-2}$.

$\Gamma(\Sigma(1385)^-\overline{\Sigma}(1385)^+)/\Gamma_{total}$ — Γ_{99}/Γ

VALUE (units 10^{-5})	CL%	DOCUMENT ID		TECN	COMMENT
<8	90	[1] ABLIKIM	12I	BES3	$\psi(2S) \to \gamma\Sigma(1385)^-\overline{\Sigma}(1385)^+$

[1] ABLIKIM 12I reports $< 8.5 \times 10^{-5}$ from a measurement of $[\Gamma(\chi_{c2}(1P) \to \Sigma(1385)^-\overline{\Sigma}(1385)^+)/\Gamma_{total}] \times [B(\psi(2S) \to \gamma\chi_{c2}(1P))]$ assuming $B(\psi(2S) \to \gamma\chi_{c2}(1P)) = (8.72 \pm 0.34) \times 10^{-2}$, which we rescale to our best (shown rounded) value $B(\psi(2S) \to \gamma\chi_{c2}(1P)) = 9.63 \times 10^{-2}$.

$\Gamma(K^-\Lambda\overline{\Xi}^+ + \text{c.c.})/\Gamma_{total}$ — Γ_{100}/Γ

VALUE (units 10^{-4})	EVTS	DOCUMENT ID		TECN	COMMENT
1.75±0.31±0.04	51	[1] ABLIKIM	15I	BES3	$\psi(2S) \to \gamma K^-\Lambda\overline{\Xi}^+ + \text{c.c.}$

[1] ABLIKIM 15I reports $[\Gamma(\chi_{c2}(1P) \to K^-\Lambda\overline{\Xi}^+ + \text{c.c.})/\Gamma_{total}] \times [B(\psi(2S) \to \gamma\chi_{c2}(1P))] = (1.68 \pm 0.26 \pm 0.15) \times 10^{-5}$ which we divide by our best (shown rounded) value $B(\psi(2S) \to \gamma\chi_{c2}(1P)) = (9.63 \pm 0.23) \times 10^{-2}$. Our first error is their experiment's error and our second error is the systematic error from using our best (shown rounded) value.

$\Gamma(\Xi^0\overline{\Xi}^0)/\Gamma_{total}$ — Γ_{101}/Γ

VALUE (units 10^{-4})	CL%	EVTS	DOCUMENT ID		TECN	COMMENT
1.81±0.21±0.04		804	[1] ABLIKIM	22O	BES3	$\psi(2S) \to \gamma\Xi^0\overline{\Xi}^0$
• • • We do not use the following data for averages, fits, limits, etc. • • •						
<1.0	90	3	[2] NAIK	08	CLEO	$\psi(2S) \to \gamma\Xi^0\overline{\Xi}^0$

[1] ABLIKIM 22O reports $(1.83 \pm 0.15 \pm 0.16) \times 10^{-4}$ from a measurement of $[\Gamma(\chi_{c2}(1P) \to \Xi^0\overline{\Xi}^0)/\Gamma_{total}] \times [B(\psi(2S) \to \gamma\chi_{c2}(1P))]$ assuming $B(\psi(2S) \to \gamma\chi_{c2}(1P)) = (9.52 \pm 0.20) \times 10^{-2}$, which we rescale to our best (shown rounded) value $B(\psi(2S) \to \gamma\chi_{c2}(1P)) = (9.63 \pm 0.23) \times 10^{-2}$. Our first error is their experiment's error and our second error is the systematic error from using our best (shown rounded) value.

[2] NAIK 08 reports $< 1.06 \times 10^{-4}$ from a measurement of $[\Gamma(\chi_{c2}(1P) \to \Xi^0\overline{\Xi}^0)/\Gamma_{total}] \times [B(\psi(2S) \to \gamma\chi_{c2}(1P))]$ assuming $B(\psi(2S) \to \gamma\chi_{c2}(1P)) = (9.33 \pm 0.14 \pm 0.61) \times 10^{-2}$, which we rescale to our best (shown rounded) value $B(\psi(2S) \to \gamma\chi_{c2}(1P)) = 9.63 \times 10^{-2}$.

$\Gamma(\Xi^-\overline{\Xi}^+)/\Gamma_{total}$ — Γ_{102}/Γ

VALUE (units 10^{-4})	CL%	EVTS	DOCUMENT ID		TECN	COMMENT
1.42±0.12 OUR AVERAGE						
1.42±0.12±0.03		1691	[1] ABLIKIM	22O	BES3	$\psi(2S) \to \gamma\Xi^-\overline{\Xi}^+$
1.41±0.31±0.03		29 ± 5	[2] NAIK	08	CLEO	$\psi(2S) \to \gamma\Xi^+\overline{\Xi}^-$
• • • We do not use the following data for averages, fits, limits, etc. • • •						
< 3.7	90		[3] ABLIKIM	06D	BES2	$\psi(2S) \to \chi_{c2}\gamma$

[1] ABLIKIM 22O reports $(1.44 \pm 0.06 \pm 0.11) \times 10^{-4}$ from a measurement of $[\Gamma(\chi_{c2}(1P) \to \Xi^-\overline{\Xi}^+)/\Gamma_{total}] \times [B(\psi(2S) \to \gamma\chi_{c2}(1P))]$ assuming $B(\psi(2S) \to \gamma\chi_{c2}(1P)) = (9.52 \pm 0.20) \times 10^{-2}$, which we rescale to our best (shown rounded) value $B(\psi(2S) \to \gamma\chi_{c2}(1P)) = (9.63 \pm 0.23) \times 10^{-2}$. Our first error is their experiment's error and our second error is the systematic error from using our best (shown rounded) value.

[2] NAIK 08 reports $(1.45 \pm 0.30 \pm 0.15) \times 10^{-4}$ from a measurement of $[\Gamma(\chi_{c2}(1P) \to \Xi^-\overline{\Xi}^+)/\Gamma_{total}] \times [B(\psi(2S) \to \gamma\chi_{c2}(1P))]$ assuming $B(\psi(2S) \to \gamma\chi_{c2}(1P)) = (9.33 \pm 0.14 \pm 0.61) \times 10^{-2}$, which we rescale to our best (shown rounded) value $B(\psi(2S) \to \gamma\chi_{c2}(1P)) = (9.63 \pm 0.23) \times 10^{-2}$. Our first error is their experiment's error and our second error is the systematic error from using our best (shown rounded) value.

[3] Using $B(\psi(2S) \to \chi_{c2}\gamma) = (9.3 \pm 0.6)\%$.

$\Gamma(\Omega^-\overline{\Omega}^+)/\Gamma_{total}$ — Γ_{103}/Γ

VALUE (units 10^{-5})	EVTS	DOCUMENT ID		TECN	COMMENT
4.47±0.28±0.11	1038	[1] ABLIKIM	23T	BES3	$\chi_{c2} \to \Omega^-\overline{\Omega}^+$

[1] ABLIKIM 23T reports $(4.52 \pm 0.24 \pm 0.18) \times 10^{-5}$ from a measurement of $[\Gamma(\chi_{c2}(1P) \to \Omega^-\overline{\Omega}^+)/\Gamma_{total}] \times [B(\psi(2S) \to \gamma\chi_{c2}(1P))]$ assuming $B(\psi(2S) \to \gamma\chi_{c2}(1P)) = (9.52 \pm 0.20) \times 10^{-2}$, which we rescale to our best (shown rounded) value $B(\psi(2S) \to \gamma\chi_{c2}(1P)) = (9.63 \pm 0.23) \times 10^{-2}$. Our first error is their experiment's error and our second error is the systematic error from using our best (shown rounded) value.

$\Gamma(J/\psi(1S)\pi^+\pi^-\pi^0)/\Gamma_{total}$ — Γ_{104}/Γ

VALUE	CL%	DOCUMENT ID		TECN	COMMENT
<0.015	90	BARATE	81	SPEC	190 GeV π^-Be $\to 2\pi 2\mu$

$\Gamma(\pi^0\eta_c)/\Gamma_{total}$ — Γ_{105}/Γ

VALUE	CL%	DOCUMENT ID		TECN	COMMENT
<3.2 × 10⁻³	90	[1] ABLIKIM	15N	BES3	$\psi(2S)e^+e^- \to \pi^0\eta_c$

[1] Using $B(\eta_c \to K^0_S K^\pm\pi^\mp) \times B(K^0_S \to \pi^+\pi^-) \times B(\pi^0 \to \gamma\gamma) = (1.66 \pm 0.11) \times 10^{-2}$.

$\Gamma(\eta_c(1S)\pi^+\pi^-)/\Gamma_{total}$ — Γ_{106}/Γ

VALUE	CL%	DOCUMENT ID		TECN	COMMENT
<5 × 10⁻³	90	[1,2] ABLIKIM	13B	BES3	$e^+e^- \to \psi(2S) \to \gamma\chi_{c2}$
• • • We do not use the following data for averages, fits, limits, etc. • • •					
<0.011	90	[3,4] ABLIKIM	13B	BES3	$e^+e^- \to \psi(2S) \to \gamma\chi_{c2}$

[1] From the $\eta_c \to K^0_S K^\pm\pi^\mp$ decays.

[2] ABLIKIM 13B reports $< 5.4 \times 10^{-3}$ from a measurement of $[\Gamma(\chi_{c2}(1P) \to \eta_c(1S)\pi^+\pi^-)/\Gamma_{total}] \times [B(\psi(2S) \to \gamma\chi_{c2}(1P))]$ assuming $B(\psi(2S) \to \gamma\chi_{c2}(1P)) = (8.72 \pm 0.34) \times 10^{-2}$, which we rescale to our best (shown rounded) value $B(\psi(2S) \to \gamma\chi_{c2}(1P)) = 9.63 \times 10^{-2}$.

[3] From the $\eta_c \to K^+K^-\pi^0$ decays.

[4] ABLIKIM 13B reports $< 1.2 \times 10^{-2}$ from a measurement of $[\Gamma(\chi_{c2}(1P) \to \eta_c(1S)\pi^+\pi^-)/\Gamma_{total}] \times [B(\psi(2S) \to \gamma\chi_{c2}(1P))]$ assuming $B(\psi(2S) \to \gamma\chi_{c2}(1P)) = (8.72 \pm 0.34) \times 10^{-2}$, which we rescale to our best (shown rounded) value $B(\psi(2S) \to \gamma\chi_{c2}(1P)) = 9.63 \times 10^{-2}$.

$\Gamma(\eta_c(1S)\pi^+\pi^-)/\Gamma(\overline{K}^0K^+\pi^- + \text{c.c.})$ — Γ_{106}/Γ_{43}

VALUE	CL%	DOCUMENT ID		TECN	COMMENT
<16.4	90	[1] LEES	12AE	BABR	$e^+e^- \to e^+e^-\pi^+\pi^-\eta_c$

[1] We divided the reported limit by 2 to take into account the $K^0_L K^+\pi^-$ mode.

RADIATIVE DECAYS

$\Gamma(\gamma\rho^0)/\Gamma_{total}$ — Γ_{108}/Γ

VALUE (units 10^{-6})	CL%	EVTS	DOCUMENT ID		TECN	COMMENT
<19	90	13 ± 11	[1] ABLIKIM	11E	BES3	$\psi(2S) \to \gamma\gamma\rho^0$
• • • We do not use the following data for averages, fits, limits, etc. • • •						
<40	90	17.2 ± 6.8	[2] BENNETT	08A	CLEO	$\psi(2S) \to \gamma\gamma\rho^0$

[1] ABLIKIM 11E reports $< 20.8 \times 10^{-6}$ from a measurement of $[\Gamma(\chi_{c2}(1P) \to \gamma\rho^0)/\Gamma_{total}] \times [B(\psi(2S) \to \gamma\chi_{c2}(1P))]$ assuming $B(\psi(2S) \to \gamma\chi_{c2}(1P)) = (8.74 \pm 0.35) \times 10^{-2}$, which we rescale to our best (shown rounded) value $B(\psi(2S) \to \gamma\chi_{c2}(1P)) = 9.63 \times 10^{-2}$.

[2] BENNETT 08A reports $< 50 \times 10^{-6}$ from a measurement of $[\Gamma(\chi_{c2}(1P) \to \gamma\rho^0)/\Gamma_{total}] \times [B(\psi(2S) \to \gamma\chi_{c2}(1P))]$ assuming $B(\psi(2S) \to \gamma\chi_{c2}(1P)) = (8.1 \pm 0.4) \times 10^{-2}$, which we rescale to our best (shown rounded) value $B(\psi(2S) \to \gamma\chi_{c2}(1P)) = 9.63 \times 10^{-2}$.

$\Gamma(\gamma\omega)/\Gamma_{total}$ — Γ_{109}/Γ

VALUE (units 10^{-6})	CL%	EVTS	DOCUMENT ID		TECN	COMMENT
<6	90	1 ± 6	[1] ABLIKIM	11E	BES3	$\psi(2S) \to \gamma\gamma\omega$
• • • We do not use the following data for averages, fits, limits, etc. • • •						
<6	90	0.0 ± 1.8	[2] BENNETT	08A	CLEO	$\psi(2S) \to \gamma\gamma\omega$

[1] ABLIKIM 11E reports $< 6.1 \times 10^{-6}$ from a measurement of $[\Gamma(\chi_{c2}(1P) \to \gamma\omega)/\Gamma_{total}] \times [B(\psi(2S) \to \gamma\chi_{c2}(1P))]$ assuming $B(\psi(2S) \to \gamma\chi_{c2}(1P)) = (8.74 \pm 0.35) \times 10^{-2}$, which we rescale to our best (shown rounded) value $B(\psi(2S) \to \gamma\chi_{c2}(1P)) = 9.63 \times 10^{-2}$.

[2] BENNETT 08A reports $< 7.0 \times 10^{-6}$ from a measurement of $[\Gamma(\chi_{c2}(1P) \to \gamma\omega)/\Gamma_{total}] \times [B(\psi(2S) \to \gamma\chi_{c2}(1P))]$ assuming $B(\psi(2S) \to \gamma\chi_{c2}(1P)) = (8.1 \pm 0.4) \times 10^{-2}$, which we rescale to our best (shown rounded) value $B(\psi(2S) \to \gamma\chi_{c2}(1P)) = 9.63 \times 10^{-2}$.

$\Gamma(\gamma\phi)/\Gamma_{total}$ — Γ_{110}/Γ

VALUE (units 10^{-6})	CL%	EVTS	DOCUMENT ID		TECN	COMMENT
< 7	90	5 ± 5	[1] ABLIKIM	11E	BES3	$\psi(2S) \to \gamma\gamma\phi$
• • • We do not use the following data for averages, fits, limits, etc. • • •						
<11	90	1.3 ± 2.5	[2] BENNETT	08A	CLEO	$\psi(2S) \to \gamma\gamma\phi$

[1] ABLIKIM 11E reports $< 8.1 \times 10^{-6}$ from a measurement of $[\Gamma(\chi_{c2}(1P) \to \gamma\phi)/\Gamma_{total}] \times [B(\psi(2S) \to \gamma\chi_{c2}(1P))]$ assuming $B(\psi(2S) \to \gamma\chi_{c2}(1P)) = (8.74 \pm 0.35) \times 10^{-2}$, which we rescale to our best (shown rounded) value $B(\psi(2S) \to \gamma\chi_{c2}(1P)) = 9.63 \times 10^{-2}$.

[2] BENNETT 08A reports $< 13 \times 10^{-6}$ from a measurement of $[\Gamma(\chi_{c2}(1P) \to \gamma\phi)/\Gamma_{total}] \times [B(\psi(2S) \to \gamma\chi_{c2}(1P))]$ assuming $B(\psi(2S) \to \gamma\chi_{c2}(1P)) = (8.1 \pm 0.4) \times 10^{-2}$, which we rescale to our best (shown rounded) value $B(\psi(2S) \to \gamma\chi_{c2}(1P)) = 9.63 \times 10^{-2}$.

$\Gamma(\gamma\gamma)/\Gamma(\gamma J/\psi(1S))$ — $\Gamma_{111}/\Gamma_{107}$

VALUE (units 10^{-3})	DOCUMENT ID		TECN	COMMENT
1.52±0.07 OUR FIT Error includes scale factor of 1.4.				
0.99±0.18	[1] AMBROGIANI	00B	E835	$\overline{p}p \to \chi_{c2} \to \gamma\gamma, \gamma J/\psi$

[1] Calculated by us using $B(J/\psi(1S) \to e^+e^-) = 0.0593 \pm 0.0010$.

$\Gamma(\gamma\gamma)/\Gamma_{total} \times \Gamma(p\overline{p})/\Gamma_{total}$ — $\Gamma_{111}/\Gamma \times \Gamma_{60}/\Gamma$

VALUE (units 10^{-8})	DOCUMENT ID		TECN	COMMENT
2.32±0.14 OUR FIT Error includes scale factor of 1.3.				
1.7 ±0.4 OUR AVERAGE				
1.60±0.42	ARMSTRONG	93	E760	$\overline{p}p \to \gamma\gamma X$
9.9 ±4.5	BAGLIN	87B	SPEC	$\overline{p}p \to \gamma\gamma X$

$\Gamma(e^+e^- J/\psi(1S))/\Gamma_{total}$ — Γ_{112}/Γ

VALUE (units 10^{-3})	EVTS	DOCUMENT ID		TECN	COMMENT
• • • We do not use the following data for averages, fits, limits, etc. • • •					
2.35±0.15±0.06	1.3k	[1,2] ABLIKIM	17I	BES3	$\psi(2S) \to \gamma e^+e^- J/\psi$

[1] ABLIKIM 17I reports $(2.48 \pm 0.08 \pm 0.16) \times 10^{-3}$ from a measurement of $[\Gamma(\chi_{c2}(1P) \to e^+e^- J/\psi(1S))/\Gamma_{total}] \times [B(\psi(2S) \to \gamma\chi_{c2}(1P))]$ assuming $B(\psi(2S) \to \gamma\chi_{c2}(1P)) = (9.11 \pm 0.31) \times 10^{-2}$, which we rescale to our best (shown rounded) value $B(\psi(2S) \to \gamma\chi_{c2}(1P)) = (9.63 \pm 0.23) \times 10^{-2}$. Our first error is their experiment's error and our second error is the systematic error from using our best (shown rounded) value.

[2] Not independent from other measurements reported by ABLIKIM 17I

$\Gamma(e^+e^- J/\psi(1S))/\Gamma(\gamma J/\psi(1S))$ — $\Gamma_{112}/\Gamma_{107}$

VALUE (units 10^{-3})	EVTS	DOCUMENT ID		TECN	COMMENT
11.3±0.4±0.5	1.3k	[1] ABLIKIM	17I	BES3	$\psi(2S) \to e^+e^-\gamma J/\psi$

[1] Uses $B(\psi(2S) \to \gamma\chi_{c2}(1P)) \times B(\chi_{c2}(1P) \to \gamma J/\psi(1S)) = (199.6 \pm 0.8 \pm 7.0) \times 10^{-4}$ from ABLIKIM 17N and accounts for common systematic errors.

$\Gamma(\mu^+\mu^- J/\psi(1S))/\Gamma(e^+e^- J/\psi(1S))$ — $\Gamma_{113}/\Gamma_{112}$

VALUE (units 10^{-2})	EVTS	DOCUMENT ID		TECN	COMMENT
9.40±0.79±1.15	219	ABLIKIM	19Z	BES3	$\psi(2S) \to \gamma\chi_c \to \gamma(\mu^+\mu^- J/\psi)$

$\chi_{c2}(1P)$ CROSS-PARTICLE BRANCHING RATIOS

$\Gamma(\chi_{c2}(1P) \to 2(\pi^+\pi^-))/\Gamma_{total} \times \Gamma(\psi(2S) \to \gamma\chi_{c2}(1P))/\Gamma_{total}$ — $\Gamma_1/\Gamma \times \Gamma_{198}^{\psi(2S)}/\Gamma^{\psi(2S)}$

VALUE (units 10^{-3})	EVTS	DOCUMENT ID		TECN	COMMENT
1.06 ±0.06 OUR FIT Error includes scale factor of 1.3.					
1.098±0.001±0.055	1042k	[1] ABLIKIM	24BT	BES3	$\psi(2S) \to \gamma\chi_{c2}$

[1] Calculated by us. The value given here is derived from the value of $B(\chi_{c2} \to 2(\pi^+\pi^-))$ reported in ABLIKIM 24BT using $B(\psi(2S) \to \gamma\chi_{c2}) = (9.52 \pm 0.20)\%$ [PDG 22].

$\Gamma(\chi_{c2}(1P) \to 2(\pi^+\pi^-))/\Gamma_{total} \times \Gamma(\psi(2S) \to \gamma\chi_{c2}(1P))/\Gamma(\psi(2S) \to J/\psi(1S)\pi^+\pi^-)$ — $\Gamma_1/\Gamma \times \Gamma_{198}^{\psi(2S)}/\Gamma_{12}^{\psi(2S)}$

VALUE (units 10^{-3})	DOCUMENT ID		TECN	COMMENT
3.06±0.17 OUR FIT Error includes scale factor of 1.3.				
3.1 ±1.0 OUR AVERAGE Error includes scale factor of 2.5.				
2.3 ±0.1 ±0.5	[1] BAI	99B	BES	$\psi(2S) \to \gamma\chi_{c2}$
4.3 ±0.6	[2] TANENBAUM	78	MRK1	$\psi(2S) \to \gamma\chi_{c2}$

[1] Calculated by us. The value for $B(\chi_{c2} \to 2\pi^+2\pi^-)$ reported in BAI 99B is derived using $B(\psi(2S) \to \gamma\chi_{c2}) = (7.8 \pm 0.8)\%$ and $B(\psi(2S) \to J/\psi(1S)\pi^+\pi^-) = (32.4 \pm 2.6)\%$ [BAI 98D].

[2] The value for $B(\psi(2S) \to \gamma\chi_{c2}) \times B(\chi_{c2} \to 2\pi^+2\pi^-)$ reported in TANENBAUM 78 is derived using $B(\psi(2S) \to J/\psi(1S)\pi^+\pi^-) \times B(J/\psi(1S)\ell^+\ell^-) = (4.6 \pm 0.7)\%$. Calculated by us using $B(J/\psi(1S) \to \ell^+\ell^-) = 0.1181 \pm 0.0020$.

$\Gamma(\chi_{c2}(1P) \to K^+K^-\pi^+\pi^-)/\Gamma_{total} \times \Gamma(\psi(2S) \to \gamma\chi_{c2}(1P))/\Gamma(\psi(2S) \to J/\psi(1S)\pi^+\pi^-)$ — $\Gamma_{14}/\Gamma \times \Gamma_{198}^{\psi(2S)}/\Gamma_{12}^{\psi(2S)}$

VALUE (units 10^{-3})	DOCUMENT ID		TECN	COMMENT
2.33±0.32 OUR FIT Error includes scale factor of 1.2.				
2.5 ±0.9 OUR AVERAGE Error includes scale factor of 2.3.				
1.90±0.14±0.44	BAI	99B	BES	$\psi(2S) \to \gamma\chi_{c2}$
3.8 ±0.67	[1] TANENBAUM	78	MRK1	$\psi(2S) \to \gamma\chi_{c2}$

[1] The reported value is derived using $B(\psi(2S) \to \pi^+\pi^- J/\psi) \times B(J/\psi \to \ell^+\ell^-) = (4.6 \pm 0.7)\%$. Calculated by us using $B(J/\psi \to \ell^+\ell^-) = 0.1181 \pm 0.0020$.

$\Gamma(\chi_{c2}(1P) \to K^*(892)^0\overline{K}^*(892)^0)/\Gamma_{total} \times \Gamma(\psi(2S) \to \gamma\chi_{c2}(1P))/\Gamma_{total}$ — $\Gamma_{18}/\Gamma \times \Gamma_{198}^{\psi(2S)}/\Gamma^{\psi(2S)}$

VALUE (units 10^{-4})	DOCUMENT ID		TECN	COMMENT
2.2 ±0.9 OUR FIT Error includes scale factor of 2.2.				
3.11±0.36±0.48	ABLIKIM	04H	BES2	$\psi(2S) \to \gamma\chi_{c2}$

$\Gamma(\chi_{c2}(1P) \to \phi\phi)/\Gamma_{total} \times \Gamma(\psi(2S) \to \gamma\chi_{c2}(1P))/\Gamma_{total}$ — $\Gamma_{20}/\Gamma \times \Gamma_{198}^{\psi(2S)}/\Gamma^{\psi(2S)}$

VALUE (units 10^{-4})	EVTS	DOCUMENT ID		TECN	COMMENT
1.18±0.06 OUR FIT Error includes scale factor of 1.9.					
1.18±0.09 OUR AVERAGE Error includes scale factor of 2.5.					
1.21±0.03±0.02	4.2k	[1] ABLIKIM	23N	BES3	$\psi(2S) \to \gamma 2K^+2K^-$
0.94±0.06±0.08	219	[2,3] ABLIKIM	11K	BES3	$\psi(2S) \to \gamma K^+K^-\pi^+\pi^-\pi^0$
1.38±0.24±0.23	41	[4] ABLIKIM	06T	BES2	$\psi(2S) \to \gamma 2K^+2K^-$
• • • We do not use the following data for averages, fits, limits, etc. • • •					
0.94±0.03±0.09	630	[2,5,6] ABLIKIM	11K	BES3	$\psi(2S) \to \gamma 2K^+2K^-$

[1] Calculated by us. The value of $B(\chi_{c2} \to \phi\phi)$ reported by ABLIKIM 23N was derived using $B(\psi(2S) \to \gamma\chi_{c2}(1P)) = (9.52 \pm 0.20)\%$.

[2] Calculated by us. The value of $B(\chi_{c2} \to \phi\phi)$ reported by ABLIKIM 11K was derived using $B(\psi(2S) \to \gamma\chi_{c2}(1P)) = (8.74 \pm 0.35)\%$.

[3] Using $\phi\phi \to K^+K^-\pi^+\pi^-\pi^0$.

[4] Calculated by us. The value of $B(\chi_{c2} \to \phi\phi)$ reported by ABLIKIM 06T was derived using $B(\psi(2S) \to \gamma\chi_{c2}(1P)) = (8.1 \pm 0.4)\%$.

[5] Using $\phi\phi \to 2(K^+K^-)$.

[6] Superseded by ABLIKIM 23N.

$\Gamma(\chi_{c2}(1P) \to \phi\phi)/\Gamma_{total} \times \Gamma(\psi(2S) \to \gamma\chi_{c2}(1P))/\Gamma(\psi(2S) \to J/\psi(1S)\pi^+\pi^-)$ — $\Gamma_{20}/\Gamma \times \Gamma_{198}^{\psi(2S)}/\Gamma_{12}^{\psi(2S)}$

VALUE (units 10^{-4})	DOCUMENT ID		TECN	COMMENT
3.38±0.18 OUR FIT Error includes scale factor of 1.8.				
4.8 ±1.3 ±1.3	[1] BAI	99B	BES	$\psi(2S) \to \gamma 2K^+2K^-$

[1] Calculated by us. The value of $B(\chi_{c2} \to \phi\phi)$ reported by BAI 99B was derived using $B(\psi(2S) \to \gamma\chi_{c2}(1P)) = (7.8 \pm 0.8)\%$ and $B(\psi(2S) \to J/\psi\pi^+\pi^-) = (32.4 \pm 2.6)\%$ [BAI 98D].

$\Gamma(\chi_{c2}(1P) \to \pi\pi)/\Gamma_{total} \times \Gamma(\psi(2S) \to \gamma\chi_{c2}(1P))/\Gamma_{total}$ — $\Gamma_{25}/\Gamma \times \Gamma_{198}^{\psi(2S)}/\Gamma^{\psi(2S)}$

VALUE (units 10^{-5})	EVTS	DOCUMENT ID		TECN	COMMENT
22.41±0.33 OUR FIT Error includes scale factor of 1.1.					
22.49±0.30 OUR AVERAGE					
22.6 ±0.1 ±0.3		[1] ABLIKIM	25CH	BES3	$\psi(2S) \to \gamma\chi_{c2}$
21.9 ±0.5 ±1.5	4.5k	[2] ABLIKIM	10A	BES3	$e^+e^- \to \psi(2S) \to \gamma\chi_{c2}$
22.3 ±0.6 ±1.0	2.5k	[3] ASNER	09	CLEO	$\psi(2S) \to \gamma\pi^+\pi^-$
19.0 ±0.8 ±2.0	0.8k	[4] ASNER	09	CLEO	$\psi(2S) \to \gamma\pi^0\pi^0$

[1] Calculated by us. ABLIKIM 25CH reports $B(\chi_{c2} \to \pi^+\pi^-) = (1.61 \pm 0.01 \pm 0.02) \times 10^{-3}$ using $B(\psi(2S) \to \gamma\chi_{c2}) = (9.36 \pm 0.23)\%$. We have multiplied the $\pi^+\pi^-$ measurement by 3/2 to obtain $\pi\pi$.

[2] Calculated by us. ABLIKIM 10A reports $B(\chi_{c2} \to \pi^0\pi^0) = (0.88 \pm 0.02 \pm 0.06 \pm 0.04) \times 10^{-3}$ using $B(\psi(2S) \to \gamma\chi_{c2}) = (8.3 \pm 0.4)\%$. We have multiplied the $\pi^0\pi^0$ measurement by 3 to obtain $\pi\pi$.

[3] Calculated by us. ASNER 09 reports $B(\chi_{c2} \to \pi^+\pi^-) = (1.59 \pm 0.04 \pm 0.07 \pm 0.10) \times 10^{-3}$ using $B(\psi(2S) \to \gamma\chi_{c2}) = (9.33 \pm 0.14 \pm 0.61)\%$. We have multiplied the $\pi^+\pi^-$ measurement by 3/2 to obtain $\pi\pi$.

[4] Calculated by us. ASNER 09 reports $B(\chi_{c2} \to \pi^0\pi^0) = (0.68 \pm 0.03 \pm 0.07 \pm 0.04) \times 10^{-3}$ using $B(\psi(2S) \to \gamma\chi_{c2}) = (9.33 \pm 0.14 \pm 0.61)\%$. We have multiplied the $\pi^0\pi^0$ measurement by 3 to obtain $\pi\pi$.

Int. J. Mod. Phys. A 2026.41. Downloaded from www.worldscientific.com
by LIFORNIA @ BERKELEY on 09/16/26. Re-use and distribution is strictly not permitted, except for Open Access articles.

Int. J. Mod. Phys. A 2026.41. Downloaded from www.worldscientific.com by UNIVERSITY OF CALIFORNIA @ BERKELEY on 09/16/26. Re-use and distribution is strictly not permitted, except for Open Access articles.

$\Gamma(\chi_{c2}(1P)\to\pi\pi)/\Gamma_{total}\times\Gamma(\psi(2S)\to\gamma\chi_{c2}(1P))/\Gamma(\psi(2S)\to J/\psi(1S)\pi^+\pi^-)$ — $\Gamma_{25}/\Gamma\times\Gamma^{\psi(2S)}_{198}/\Gamma^{\psi(2S)}_{12}$

VALUE (units 10^{-3})	EVTS	DOCUMENT ID		TECN	COMMENT
0.644±0.011 OUR FIT Error includes scale factor of 1.1.					
0.54 ±0.06 OUR AVERAGE					
0.66 ±0.18 ±0.37	21 ± 6	[1] BAI	03C	BES	$\psi(2S)\to\gamma\pi^0\pi^0$
0.54 ±0.05 ±0.04	185 ± 16	[2] BAI	98I	BES	$\psi(2S)\to\gamma\pi^+\pi^-$

[1] We have multiplied $\pi^0\pi^0$ measurement by 3 to obtain $\pi\pi$.
[2] Calculated by us. The value for $B(\chi_{c2}\to\pi^+\pi^-)$ reported by BAI 98I is derived using $B(\psi(2S)\to\gamma\chi_{c2}) = (7.8\pm0.8)\%$ and $B(\psi(2S)\to J/\psi\pi^+\pi^-) = (32.4\pm2.6)\%$ [BAI 98D]. We have multiplied $\pi^+\pi^-$ measurement by 3/2 to obtain $\pi\pi$.

$\Gamma(\chi_{c2}(1P)\to 2\pi^+2\pi^-\eta)/\Gamma_{total}\times\Gamma(\psi(2S)\to\gamma\chi_{c2}(1P))/\Gamma_{total}$ — $\Gamma_{30}/\Gamma\times\Gamma^{\psi(2S)}_{198}/\Gamma^{\psi(2S)}$

VALUE (units 10^{-5})	EVTS	DOCUMENT ID		TECN	COMMENT
55.3±0.3±5.3	51k	ABLIKIM	25R	BES3	$e^+e^-\to\psi(2S)$

$\Gamma(\chi_{c2}(1P)\to\eta\eta)/\Gamma_{total}\times\Gamma(\psi(2S)\to\gamma\chi_{c2}(1P))/\Gamma_{total}$ — $\Gamma_{32}/\Gamma\times\Gamma^{\psi(2S)}_{198}/\Gamma^{\psi(2S)}$

VALUE (units 10^{-4})	CL%	EVTS	DOCUMENT ID		TECN	COMMENT
0.52±0.04 OUR FIT						
0.52±0.04 OUR AVERAGE						
0.54±0.03±0.04		386	[1] ABLIKIM	10A	BES3	$e^+e^-\to\psi(2S)\to\gamma\chi_{c2}$
0.47±0.05±0.05		156	ASNER	09	CLEO	$\psi(2S)\to\gamma\eta\eta$
• • • We do not use the following data for averages, fits, limits, etc. • • •						
< 0.44	90		[2] ADAMS	07	CLEO	$\psi(2S)\to\gamma\chi_{c2}$
< 3	90		BAI	03C	BES	$\psi(2S)\to\gamma\eta\eta\to5\gamma$
0.62±0.31±0.19			LEE	85	CBAL	$\psi(2S)\to$ photons

[1] Calculated by us. ABLIKIM 10A reports $B(\chi_{c2}\to\eta\eta) = (0.65\pm0.04\pm0.05\pm0.03)\times10^{-3}$ using $B(\psi(2S)\to\gamma\chi_{c2}) = (8.3\pm0.4)\%$.
[2] Superseded by ASNER 09.

$\Gamma(\chi_{c2}(1P)\to K^+K^-)/\Gamma_{total}\times\Gamma(\psi(2S)\to\gamma\chi_{c2}(1P))/\Gamma_{total}$ — $\Gamma_{33}/\Gamma\times\Gamma^{\psi(2S)}_{198}/\Gamma^{\psi(2S)}$

VALUE (units 10^{-5})	EVTS	DOCUMENT ID		TECN	COMMENT
11.2 ±0.5 OUR FIT Error includes scale factor of 2.2.					
11.31±0.27 OUR AVERAGE Error includes scale factor of 1.3.					
11.4 ±0.1 ±0.2		[1] ABLIKIM	25CH	BES3	$\psi(2S)\to\gamma\chi_{c2}$
10.5 ±0.3 ±0.6	1.6k	[2] ASNER	09	CLEO	$\psi(2S)\to\gamma K^+K^-$

[1] Calculated by us. ABLIKIM 25CH reports $B(\chi_{c2}\to K^+K^-) = (1.22\pm0.01\pm0.02)\times10^{-3}$ using $B(\psi(2S)\to\gamma\chi_{c2}) = (9.36\pm0.23)\%$.
[2] Calculated by us. ASNER 09 reports $B(\chi_{c2}\to K^+K^-) = (1.13\pm0.03\pm0.06\pm0.07)\times10^{-3}$ using $B(\psi(2S)\to\gamma\chi_{c2}) = (9.33\pm0.14\pm0.61)\%$.

$\Gamma(\chi_{c2}(1P)\to K^+K^-)/\Gamma_{total}\times\Gamma(\psi(2S)\to\gamma\chi_{c2}(1P))/\Gamma(\psi(2S)\to J/\psi(1S)\pi^+\pi^-)$ — $\Gamma_{33}/\Gamma\times\Gamma^{\psi(2S)}_{198}/\Gamma^{\psi(2S)}_{12}$

VALUE (units 10^{-3})	EVTS	DOCUMENT ID		TECN	COMMENT
0.321±0.014 OUR FIT Error includes scale factor of 2.1.					
0.190±0.034±0.019	115 ± 13	[1] BAI	98I	BES	$\psi(2S)\to\gamma K^+K^-$

[1] Calculated by us. The value for $B(\chi_{c2}\to K^+K^-)$ reported by BAI 98I is derived using $B(\psi(2S)\to\gamma\chi_{c2}) = (7.8\pm0.8)\%$ and $B(\psi(2S)\to J/\psi\pi^+\pi^-) = (32.4\pm2.6)\%$ [BAI 98D].

$\Gamma(\chi_{c2}(1P)\to K^0_SK^0_S)/\Gamma_{total}\times\Gamma(\psi(2S)\to\gamma\chi_{c2}(1P))/\Gamma_{total}$ — $\Gamma_{34}/\Gamma\times\Gamma^{\psi(2S)}_{198}/\Gamma^{\psi(2S)}$

VALUE (units 10^{-5})	EVTS	DOCUMENT ID		TECN	COMMENT
5.0 ±0.4 OUR FIT					
5.0 ±0.4 OUR AVERAGE					
4.9 ±0.3 ±0.3	373 ± 20	[1] ASNER	09	CLEO	$\psi(2S)\to\gamma K^0_SK^0_S$
5.72±0.76±0.63	65	ABLIKIM	05O	BES2	$\psi(2S)\to\gamma K^0_SK^0_S$

[1] Calculated by us. ASNER 09 reports $B(\chi_{c2}\to K^0_SK^0_S) = (0.53\pm0.03\pm0.03\pm0.03)\times10^{-3}$ using $B(\psi(2S)\to\gamma\chi_{c2}) = (9.33\pm0.14\pm0.61)\%$.

$\Gamma(\chi_{c2}(1P)\to K^0_SK^0_S)/\Gamma_{total}\times\Gamma(\psi(2S)\to\gamma\chi_{c2}(1P))/\Gamma(\psi(2S)\to J/\psi(1S)\pi^+\pi^-)$ — $\Gamma_{34}/\Gamma\times\Gamma^{\psi(2S)}_{198}/\Gamma^{\psi(2S)}_{12}$

VALUE (units 10^{-5})	DOCUMENT ID		TECN	COMMENT
14.4±1.1 OUR FIT				
14.7±4.1±3.3	[1] BAI	99B	BES	$\psi(2S)\to\gamma K^0_SK^0_S$

[1] Calculated by us. The value of $B(\chi_{c2}\to K^0_SK^0_S)$ reported by BAI 99B was derived using $B(\psi(2S)\to\gamma\chi_{c2}(1P)) = (7.8\pm0.8)\%$ and $B(\psi(2S)\to J/\psi\pi^+\pi^-) = (32.4\pm2.6)\%$ [BAI 98D].

$\Gamma(\chi_{c2}(1P)\to\overline{K}^0K^+\pi^-+\text{c.c.})/\Gamma_{total}\times\Gamma(\psi(2S)\to\gamma\chi_{c2}(1P))/\Gamma_{total}$ — $\Gamma_{43}/\Gamma\times\Gamma^{\psi(2S)}_{198}/\Gamma^{\psi(2S)}$

VALUE (units 10^{-4})	EVTS	DOCUMENT ID		TECN	COMMENT
1.22±0.18 OUR FIT					
1.15±0.18 OUR AVERAGE					
1.21±0.19±0.09	37	[1] ATHAR	07	CLEO	$\psi(2S)\to\gamma K^0_SK^\pm\pi^\mp$
0.97±0.32±0.13	28	[2] ABLIKIM	06R	BES2	$\psi(2S)\to\gamma K^0_SK^\pm\pi^\mp$

[1] Calculated by us. ATHAR 07 reports $B(\chi_{c2}\to\overline{K}^0K^+\pi^-+\text{c.c.}) = (1.3\pm0.2\pm0.1\pm0.1)\times10^{-3}$ using $B(\psi(2S)\to\gamma\chi_{c2}) = (9.33\pm0.14\pm0.61)\%$.
[2] Calculated by us. ABLIKIM 06R reports $B(\chi_{c2}\to K^0_SK^\pm\pi^\mp) = (0.6\pm0.2\pm0.1)\times10^{-3}$ using $B(\psi(2S)\to\gamma\chi_{c2}) = (8.1\pm0.6)\%$. We have multiplied by 2 to obtain $\overline{K}^0K^+\pi^-+$ c.c. from $K^0_SK^\pm\pi^\mp$.

$\Gamma(\chi_{c2}(1P)\to K^+K^-K^+K^-)/\Gamma_{total}\times\Gamma(\psi(2S)\to\gamma\chi_{c2}(1P))/\Gamma_{total}$ — $\Gamma_{53}/\Gamma\times\Gamma^{\psi(2S)}_{198}/\Gamma^{\psi(2S)}$

VALUE (units 10^{-4})	EVTS	DOCUMENT ID		TECN	COMMENT
1.58±0.21 OUR FIT Error includes scale factor of 1.1.					
1.76±0.16±0.24	160	[1] ABLIKIM	06T	BES2	$\psi(2S)\to\gamma2K^+2K^-$

[1] Calculated by us. The value of $B(\chi_{c2}\to2K^+2K^-)$ reported by ABLIKIM 06T was derived using $B(\psi(2S)\to\gamma\chi_{c2}(1P)) = (8.1\pm0.4)\%$.

$\Gamma(\chi_{c2}(1P)\to K^+K^-K^+K^-)/\Gamma_{total}\times\Gamma(\psi(2S)\to\gamma\chi_{c2}(1P))/\Gamma(\psi(2S)\to J/\psi(1S)\pi^+\pi^-)$ — $\Gamma_{53}/\Gamma\times\Gamma^{\psi(2S)}_{198}/\Gamma^{\psi(2S)}_{12}$

VALUE (units 10^{-4})	DOCUMENT ID		TECN	COMMENT
4.5±0.6 OUR FIT Error includes scale factor of 1.1.				
3.6±0.6±0.6	[1] BAI	99B	BES	$\psi(2S)\to\gamma2K^+2K^-$

[1] Calculated by us. The value of $B(\chi_{c2}\to2K^+2K^-)$ reported by BAI 99B was derived using $B(\psi(2S)\to\gamma\chi_{c2}(1P)) = (7.8\pm0.8)\%$ and $B(\psi(2S)\to J/\psi\pi^+\pi^-) = (32.4\pm2.6)\%$ [BAI 98D].

$\Gamma(\chi_{c2}(1P)\to K^0_SK^0_SK^0_SK^\pm\pi^\mp)/\Gamma_{total}\times\Gamma(\psi(2S)\to\gamma\chi_{c2}(1P))/\Gamma_{total}$ — $\Gamma_{57}/\Gamma\times\Gamma^{\psi(2S)}_{198}/\Gamma^{\psi(2S)}$

VALUE (units 10^{-6})	EVTS	DOCUMENT ID		TECN	COMMENT
16.4±0.6±1.4	767	[1] ABLIKIM	25AY	BES3	$\psi(3686)\to\gamma\chi_{c2}$

[1] ABLIKIM 24AY reports also a measurement $B(\chi_{c2}(1P)\to K^0_SK^0_SK^0_SK^\pm\pi^\mp) = (17.2\pm0.7\pm1.5)\times10^{-5}$ from this product branching fraction using PDG 24 $B(\psi(2S)\to\gamma\chi_{c2})$ value.

$\Gamma(\chi_{c2}(1P)\to3(K^+K^-))/\Gamma_{total}\times\Gamma(\psi(2S)\to\gamma\chi_{c2}(1P))/\Gamma_{total}$ — $\Gamma_{58}/\Gamma\times\Gamma^{\psi(2S)}_{198}/\Gamma^{\psi(2S)}$

VALUE (units 10^{-7})	EVTS	DOCUMENT ID		TECN	COMMENT
6.8±1.1±0.8	46.4 ± 7.0	[1] ABLIKIM	24P	BES3	$e^+e^-\to\psi(2S)$

[1] Systematic error derived by us, based on the text.

$\Gamma(\chi_{c2}(1P)\to p\overline{p})/\Gamma_{total}\times\Gamma(\psi(2S)\to\gamma\chi_{c2}(1P))/\Gamma(\psi(2S)\to J/\psi(1S)\pi^+\pi^-)$ — $\Gamma_{60}/\Gamma\times\Gamma^{\psi(2S)}_{198}/\Gamma^{\psi(2S)}_{12}$

VALUE (units 10^{-5})	DOCUMENT ID		TECN	COMMENT
2.23±0.09 OUR FIT Error includes scale factor of 1.9.				
1.4 ±1.1	[1] BAI	98I	BES	$\psi(2S)\to\gamma\chi_{c2}\to\gamma\overline{p}p$

[1] Calculated by us. The value for $B(\chi_{c2}\to p\overline{p})$ reported in BAI 98I is derived using $B(\psi(2S)\to\gamma\chi_{c2}) = (7.8\pm0.8)\%$ and $B(\psi(2S)\to J/\psi(1S)\pi^+\pi^-) = (32.4\pm2.6)\%$ [BAI 98D].

$\Gamma(\chi_{c2}(1P)\to p\overline{p})/\Gamma_{total}\times\Gamma(\psi(2S)\to\gamma\chi_{c2}(1P))/\Gamma_{total}$ — $\Gamma_{60}/\Gamma\times\Gamma^{\psi(2S)}_{198}/\Gamma^{\psi(2S)}$

VALUE (units 10^{-6})	EVTS	DOCUMENT ID		TECN	COMMENT
7.75±0.29 OUR FIT Error includes scale factor of 2.0.					
7.87±0.15 OUR AVERAGE					
7.93±0.09±0.13	10672	[1] ABLIKIM	25H	BES3	$\psi(2S)\to\gamma p\overline{p}$
7.2 ±0.7 ±0.4	121 ± 12	[2] NAIK	08	CLEO	$\psi(2S)\to\gamma p\overline{p}$
4.4 $^{+1.6}_{-1.4}$ ±0.6	$14.3^{+5.2}_{-4.7}$	BAI	04F	BES	$\psi(2S)\to\gamma\chi_{c2}(1P)\to\gamma\overline{p}p$
• • • We do not use the following data for averages, fits, limits, etc. • • •					
7.3 ±0.4 ±0.3	405	[3] ABLIKIM	13V	BES3	$\psi(2S)\to\gamma p\overline{p}$

[1] Calculated by us. ABLIKIM 25H reports $B(\chi_{c2}\to p\overline{p}) = (8.33\pm0.09\pm0.22)\times10^{-5}$ using $B(\psi(2S)\to\gamma\chi_{c2}) = (9.52\pm0.20)\%$.
[2] Calculated by us. NAIK 08 reports $B(\chi_{c2}\to p\overline{p}) = (7.7\pm0.8\pm0.4\pm0.5)\times10^{-5}$ using $B(\psi(2S)\to\gamma\chi_{c2}) = (9.33\pm0.14\pm0.61)\%$.
[3] Superseded by ABLIKIM 25H

$\Gamma(\chi_{c2}(1P)\to p\overline{p}K^0_SK^-\pi^++\text{c.c.})/\Gamma_{total}\times\Gamma(\psi(2S)\to\gamma\chi_{c2}(1P))/\Gamma_{total}$ — $\Gamma_{74}/\Gamma\times\Gamma^{\psi(2S)}_{198}/\Gamma^{\psi(2S)}$

VALUE (units 10^{-6})	EVTS	DOCUMENT ID		TECN	COMMENT
5.36±0.26±0.43	574	ABLIKIM	24BX	BES3	$\psi(2S)\to\gamma\chi_{c2}$

$\Gamma(\chi_{c2}(1P)\to\Lambda\overline{\Lambda})/\Gamma_{total}\times\Gamma(\psi(2S)\to\gamma\chi_{c2}(1P))/\Gamma_{total}$ — $\Gamma_{79}/\Gamma\times\Gamma^{\psi(2S)}_{198}/\Gamma^{\psi(2S)}$

VALUE (units 10^{-6})	EVTS	DOCUMENT ID		TECN	COMMENT
17.4±1.4 OUR FIT					
17.3±1.5 OUR AVERAGE					
18.2±0.8±1.7	670	ABLIKIM	21L	BES3	$\psi(2S)\to\gamma p\pi^-\overline{p}\pi^+$
15.9±2.1±1.0	71	[1] NAIK	08	CLEO	$\psi(2S)\to\gamma\Lambda\overline{\Lambda}$
• • • We do not use the following data for averages, fits, limits, etc. • • •					
18.2±1.4±0.9	207	[2,3] ABLIKIM	13H	BES3	$\psi(2S)\to\gamma\Lambda\overline{\Lambda}$

[1] Calculated by us. NAIK 08 reports $B(\chi_{c2} \to \Lambda\overline{\Lambda}) = (17.0 \pm 2.2 \pm 1.1 \pm 1.1) \times 10^{-5}$ using $B(\psi(2S) \to \gamma\chi_{c2}) = (9.33 \pm 0.14 \pm 0.61)\%$.
[2] Superseded by ABLIKIM 21L
[3] Calculated by us. ABLIKIM 13H reports $B(\chi_{c2} \to \Lambda\overline{\Lambda}) = (20.8 \pm 1.6 \pm 2.3) \times 10^{-5}$ from a measurement of $B(\chi_{c2} \to \Lambda\overline{\Lambda}) \times B(\psi(2S) \to \gamma\chi_{c2})$ assuming $B(\psi(2S) \to \gamma\chi_{c2}) = (8.74 \pm 0.35)\%$.

$\Gamma(\chi_{c2}(1P) \to \Lambda\overline{\Lambda})/\Gamma_{total} \times \Gamma(\psi(2S) \to \gamma\chi_{c2}(1P))/\Gamma(\psi(2S) \to J/\psi(1S)\pi^+\pi^-)$ — $\Gamma_{79}/\Gamma \times \Gamma_{198}^{\psi(2S)}/\Gamma_{12}^{\psi(2S)}$

VALUE (units 10^{-5})	EVTS	DOCUMENT ID		TECN	COMMENT
5.0±0.4 OUR FIT					
$7.1^{+3.1}_{-2.9}\pm1.3$	$8.3^{+3.7}_{-3.4}$	[1] BAI	03E	BES	$\psi(2S) \to \gamma\Lambda\overline{\Lambda}$

[1] BAI 03E reports $[B(\chi_{c2} \to \Lambda\overline{\Lambda})\, B(\psi(2S) \to \gamma\chi_{c2}) / B(\psi(2S) \to J/\psi\pi^+\pi^-)] \times [B^2(\Lambda \to \pi^- p) / B(J/\psi \to p\overline{p})] = (1.33^{+0.59}_{-0.55} \pm 0.25)\%$. We calculate from this measurement the presented value using $B(\Lambda \to \pi^- p) = (63.9 \pm 0.5)\%$ and $B(J/\psi \to p\overline{p}) = (2.17 \pm 0.07) \times 10^{-3}$.

$\Gamma(\chi_{c2}(1P) \to \Lambda\overline{\Lambda}\eta)/\Gamma_{total} \times \Gamma(\psi(2S) \to \gamma\chi_{c2}(1P))/\Gamma_{total}$ — $\Gamma_{84}/\Gamma \times \Gamma_{198}^{\psi(2S)}/\Gamma^{\psi(2S)}$

VALUE (units 10^{-5})	EVTS	DOCUMENT ID		TECN	COMMENT
1.00±0.20±0.14	32	ABLIKIM	22AO	BES3	$\psi(2S) \to \gamma p\pi^-\overline{p}\pi^+\gamma\gamma$

$\Gamma(\chi_{c2}(1P) \to \Lambda\overline{\Lambda}\eta')/\Gamma_{total} \times \Gamma(\psi(2S) \to \gamma\chi_{c2}(1P))/\Gamma_{total}$ — $\Gamma_{85}/\Gamma \times \Gamma_{198}^{\psi(2S)}/\Gamma^{\psi(2S)}$

VALUE (units 10^{-6})	DOCUMENT ID		TECN	COMMENT
2.84±0.57±0.26	[1] ABLIKIM	25BX	BES3	$\psi(2S) \to \gamma\chi_{c2}$

[1] Calculated by us. ABLIKIM 25BX reports $B(\chi_{c2} \to \Lambda\overline{\Lambda}\eta') = (3.03 \pm 0.61 \pm 0.29) \times 10^{-5}$ from a measurement of $B(\chi_{c2} \to \Lambda\overline{\Lambda}\eta') \times B(\psi(2S) \to \gamma\chi_{c2})$ assuming $B(\psi(2S) \to \gamma\chi_{c2}) = (9.36 \pm 0.23)\%$.

$\Gamma(\chi_{c2}(1P) \to \Lambda\overline{\Lambda}\omega)/\Gamma_{total} \times \Gamma(\psi(2S) \to \gamma\chi_{c2}(1P))/\Gamma_{total}$ — $\Gamma_{86}/\Gamma \times \Gamma_{198}^{\psi(2S)}/\Gamma^{\psi(2S)}$

VALUE (units 10^{-6})	EVTS	DOCUMENT ID		TECN	COMMENT
13.3±1.2±1.6	251 ± 23	[1] ABLIKIM	24BE	BES3	$e^+e^- \to \psi(2S) \to \gamma\chi_{c2}$

[1] Calculated by us. The authors report $B(\chi_{c2} \to \Lambda\overline{\Lambda}\omega)$ obtained from a product using PDG 22 value of $B(\psi(2S) \to \gamma\chi_{c2})$.

$\Gamma(\chi_{c2}(1P) \to \Lambda\overline{\Lambda}\phi)/\Gamma_{total} \times \Gamma(\psi(2S) \to \gamma\chi_{c2}(1P))/\Gamma_{total}$ — $\Gamma_{87}/\Gamma \times \Gamma_{198}^{\psi(2S)}/\Gamma^{\psi(2S)}$

VALUE (units 10^{-6})	EVTS	DOCUMENT ID		TECN	COMMENT
6.79±0.77±0.35	94.4	ABLIKIM	24AC	BES3	$\psi(2S) \to \gamma\chi_{c2}$

$\Gamma(\chi_{c2}(1P) \to \overline{p}\Lambda(1520)K_S^0\pi^+ + c.c.)/\Gamma_{total} \times \Gamma(\psi(2S) \to \gamma\chi_{c2}(1P))/\Gamma_{total}$ — $\Gamma_{91}/\Gamma \times \Gamma_{198}^{\psi(2S)}/\Gamma^{\psi(2S)}$

VALUE (units 10^{-6})	EVTS	DOCUMENT ID		TECN	COMMENT
$3.89^{+0.83}_{-0.80}\pm0.39$	94	ABLIKIM	24BX	BES3	$\psi(2S) \to \gamma\chi_{c2}$

$\Gamma(\chi_{c2}(1P) \to \Sigma^+\overline{p}K_S^0 + c.c.)/\Gamma_{total} \times \Gamma(\psi(2S) \to \gamma\chi_{c2}(1P))/\Gamma_{total}$ — $\Gamma_{93}/\Gamma \times \Gamma_{198}^{\psi(2S)}/\Gamma^{\psi(2S)}$

VALUE (units 10^{-6})	EVTS	DOCUMENT ID		TECN	COMMENT
7.85±0.77±0.44	129	[1] ABLIKIM	19BB	BES3	$\psi(2S) \to \gamma\Sigma^+\overline{p}K_S^0$ + c.c.

[1] Calculated by us. ABLIKIM 19BB reports $B(\chi_{c2} \to \Sigma^+\overline{p}K_S^0 + c.c.) = (8.25 \pm 0.83 \pm 0.49) \times 10^{-5}$ using $B(\psi(2S) \to \gamma\chi_{c2}) = (9.52 \pm 0.20)\%$ and other branching fractions from PDG 18.

$\Gamma(\chi_{c2}(1P) \to \Sigma^0\overline{p}K^+ + c.c.)/\Gamma_{total} \times \Gamma(\psi(2S) \to \gamma\chi_{c2}(1P))/\Gamma_{total}$ — $\Gamma_{94}/\Gamma \times \Gamma_{198}^{\psi(2S)}/\Gamma^{\psi(2S)}$

VALUE (units 10^{-5})	EVTS	DOCUMENT ID		TECN	COMMENT
0.87±0.06±0.04	271	[1] ABLIKIM	20AE	BES3	$\psi(2S) \to \gamma\Sigma^0\overline{p}K^+$ + c.c.

[1] Calculated by us. ABLIKIM 20AE reports $B(\chi_{c2} \to \Sigma^0\overline{p}K^+ + c.c.) = (0.91 \pm 0.06 \pm 0.05) \times 10^{-4}$ using $B(\psi(2S) \to \gamma\chi_{c2}) = (9.52 \pm 0.20)\%$ and other branching fractions from PDG 20.

$\Gamma(\chi_{c2}(1P) \to \gamma J/\psi(1S))/\Gamma_{total} \times \Gamma(\psi(2S) \to \gamma\chi_{c2}(1P))/\Gamma_{total}$ — $\Gamma_{107}/\Gamma \times \Gamma_{198}^{\psi(2S)}/\Gamma^{\psi(2S)}$

VALUE (units 10^{-2})	EVTS	DOCUMENT ID		TECN	COMMENT
1.82 ±0.07 OUR FIT Error includes scale factor of 1.9.					
1.69 ±0.16 OUR AVERAGE Error includes scale factor of 3.4. See the ideogram below.					
1.996±0.008±0.070	81k	[1] ABLIKIM	17N	BES3	$\psi(2S) \to \gamma\gamma J/\psi$
1.793±0.008±0.163	1.0M	ABLIKIM	17U	BES3	$e^+e^- \to \gamma X$
1.62 ±0.04 ±0.12	5.8k	BAI	04I	BES2	$\psi(2S) \to J/\psi\gamma\gamma$
0.99 ±0.10 ±0.08		GAISER	86	CBAL	$\psi(2S) \to \gamma X$
1.47 ±0.17		[2] OREGLIA	82	CBAL	$\psi(2S) \to \gamma\chi_{c2}$
1.8 ±0.5		[3] BRANDELIK	79B	DASP	$\psi(2S) \to \gamma\chi_{c2}$
1.2 ±0.2		[3] BARTEL	78B	CNTR	$\psi(2S) \to \gamma\chi_{c2}$
2.2 ±1.2		[4] BIDDICK	77	CNTR	$e^+e^- \to \gamma X$
1.2 ±0.7		[2] WHITAKER	76	MRK1	e^+e^-
• • • We do not use the following data for averages, fits, limits, etc. • • •					
1.874±0.007±0.102	76k	[5] ABLIKIM	12O	BES3	$\psi(2S) \to \gamma\chi_{c2}$
1.95 ±0.02 ±0.07	12.4k	[6] MENDEZ	08	CLEO	$\psi(2S) \to \gamma\chi_{c2}$
1.85 ±0.04 ±0.07	1.9k	[7] ADAM	05A	CLEO	Repl. by MENDEZ 08

[1] Uses $B(J/\psi \to e^+e^-) = (5.971 \pm 0.032)\%$ and $B(J/\psi \to \mu^+\mu^-) = (5.961 \pm 0.033)\%$.
[2] Recalculated by us using $B(J/\psi(1S) \to \ell^+\ell^-) = 0.1181 \pm 0.0020$.
[3] Recalculated by us using $B(J/\psi(1S) \to \mu^+\mu^-) = 0.0588 \pm 0.0010$.
[4] Assumes isotropic gamma distribution.
[5] Superseded by ABLIKIM 17N.
[6] Not independent from other measurements of MENDEZ 08.
[7] Not independent from other values reported by ADAM 05A.

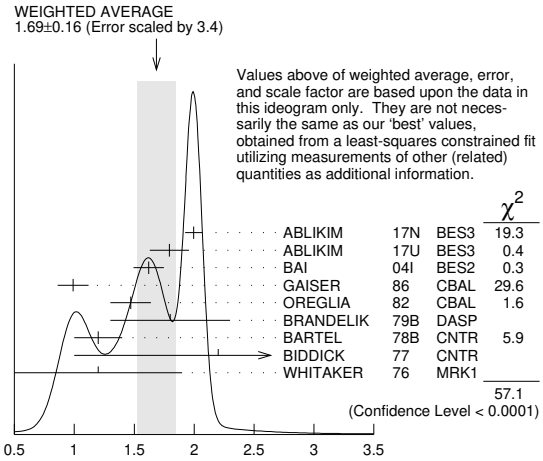

$\Gamma(\chi_{c2}(1P) \to \gamma J/\psi(1S))/\Gamma_{total} \times \Gamma(\psi(2S) \to \gamma\chi_{c2}(1P))/\Gamma_{total}$ (units 10^{-2})

$\Gamma(\chi_{c2}(1P) \to \gamma J/\psi(1S))/\Gamma_{total} \times \Gamma(\psi(2S) \to \gamma\chi_{c2}(1P))/\Gamma(\psi(2S) \to J/\psi(1S)\pi^+\pi^-)$ — $\Gamma_{107}/\Gamma \times \Gamma_{198}^{\psi(2S)}/\Gamma_{12}^{\psi(2S)}$

VALUE (units 10^{-2})	EVTS	DOCUMENT ID		TECN	COMMENT
5.25±0.19 OUR FIT Error includes scale factor of 1.8.					
5.53±0.17 OUR AVERAGE					
5.56±0.05±0.16	12.4k	MENDEZ	08	CLEO	$\psi(2S) \to \gamma\chi_{c2}$
6.0 ±2.8	1.3k	[1] ABLIKIM	04B	BES	$\psi(2S) \to J/\psi X$
3.9 ±1.2		[2] HIMEL	80	MRK2	$\psi(2S) \to \gamma\chi_{c2}$
• • • We do not use the following data for averages, fits, limits, etc. • • •					
5.52±0.13±0.13	1.9k	[3] ADAM	05A	CLEO	Repl. by MENDEZ 08

[1] From a fit to the J/ψ recoil mass spectra.
[2] The value for $B(\psi(2S) \to \gamma\chi_{c2}) \times B(\chi_{c2} \to \gamma J/\psi(1S))$ reported in HIMEL 80 is derived using $B(\psi(2S) \to J/\psi(1S)\pi^+\pi^-) = (33 \pm 3)\%$ and $B(J/\psi(1S) \to \ell^+\ell^-) = 0.138 \pm 0.018$. Calculated by us using $B(J/\psi(1S) \to \ell^+\ell^-) = (0.1181 \pm 0.0020)$.
[3] Not independent from other values reported by ADAM 05A.

$\Gamma(\chi_{c2}(1P) \to \gamma\gamma)/\Gamma_{total} \times \Gamma(\psi(2S) \to \gamma\chi_{c2}(1P))/\Gamma_{total}$ — $\Gamma_{111}/\Gamma \times \Gamma_{198}^{\psi(2S)}/\Gamma^{\psi(2S)}$

VALUE (units 10^{-5})	EVTS	DOCUMENT ID		TECN	COMMENT
2.78±0.09 OUR FIT Error includes scale factor of 1.1.					
2.82±0.10 OUR AVERAGE					
2.83±0.08±0.06	5k	[1] ABLIKIM	17AE	BES3	$\psi(2S) \to \gamma\chi_{c2} \to 3\gamma$
2.68±0.28±0.15	0.3k	ECKLUND	08A	CLEO	$\psi(2S) \to \gamma\chi_{c2} \to 3\gamma$
7.0 ±2.1 ±2.0		LEE	85	CBAL	$\psi(2S) \to \gamma\chi_{c2}$
• • • We do not use the following data for averages, fits, limits, etc. • • •					
2.81±0.17±0.15	1.1k	[2] ABLIKIM	12A	BES3	$\psi(2S) \to \gamma\chi_{c2} \to 3\gamma$

[1] ABLIKIM 17AE measures the ratio of two-photon partial widths for the helicity $\lambda = 0$ and helicity $\lambda = 2$ components to be $f_{0/2} = \Gamma_{\gamma\gamma}^{\lambda=0} / \Gamma_{\gamma\gamma}^{\lambda=2} = 0.000 \pm 0.006 \pm 0.012$.
[2] ABLIKIM 12A measures the ratio of two-photon partial widths for the helicity $\lambda = 0$ and helicity $\lambda = 2$ components to be $f_{0/2} = \Gamma_{\gamma\gamma}^{\lambda=0}/\Gamma_{\gamma\gamma}^{\lambda=2} = 0.00 \pm 0.02 \pm 0.02$. Superseded by ABLIKIM 17AE.

$\Gamma(\chi_{c2}(1P) \to \gamma\gamma)/\Gamma(\chi_{c0}(1P) \to \gamma\gamma)$ — $\Gamma_{111}/\Gamma_{111}^{\chi_{c0}(1P)}$

VALUE	EVTS	DOCUMENT ID		TECN	COMMENT
0.292±0.028 OUR AVERAGE					
0.295±0.014±0.028	8k	[1] ABLIKIM	17AE	BES3	$\psi(2S) \to \gamma\chi_{cJ} \to 3\gamma$
0.278±0.050±0.036	0.5k	[1] ECKLUND	08A	CLEO	$\psi(2S) \to \gamma\chi_{cJ} \to 3\gamma$
• • • We do not use the following data for averages, fits, limits, etc. • • •					
0.271±0.029±0.030	1.9k	[1,2] ABLIKIM	12A	BES3	$\psi(2S) \to \gamma\chi_{cJ} \to 3\gamma$

[1] Not independent from the values of $\Gamma(\chi_{c0}, \chi_{c2})$ and $B(\psi(2S) \to \chi_{c0}, \chi_{c2})$.
[2] Superseded by ABLIKIM 17AE.

Int. J. Mod. Phys. A 2026.41. Downloaded from www.worldscientific.com
by LIFORNIA @ BERKELEY on 09/16/26. Re-use and distribution is strictly not permitted, except for Open Access articles.

Int. J. Mod. Phys. A 2026.41. Downloaded from www.worldscientific.com by UNIVERSITY OF CALIFORNIA @ BERKELEY on 09/16/26. Re-use and distribution is strictly not permitted, except for Open Access articles.

MULTIPOLE AMPLITUDES IN $\chi_{c2}(1P) \to \gamma J/\psi(1S)$ RADIATIVE DECAY

$a_2 = M2/\sqrt{E1^2 + M2^2 + E3^2}$ Magnetic quadrupole fractional transition amplitude

VALUE (units 10^{-2})	EVTS	DOCUMENT ID		TECN	COMMENT
−11.0± 1.0 OUR AVERAGE					
−12.0± 1.3±0.4	89k	[1] ABLIKIM	17N	BES3	$\psi(2S) \to \gamma\gamma\ell^+\ell^-$
− 9.3± 1.6±0.3	19.8k	[2] ARTUSO	09	CLEO	$\psi(2S) \to \gamma\gamma\ell^+\ell^-$
$-9.3^{+3.9}_{-4.1}\pm0.6$	5.9k	[3] AMBROGIANI	02	E835	$p\overline{p} \to \chi_{c2} \to J/\psi\gamma$
−14 ± 6	1.9k	[3] ARMSTRONG	93E	E760	$p\overline{p} \to \chi_{c2} \to J/\psi\gamma$
$-33.3^{+11.6}_{-29.2}$	441	[3] OREGLIA	82	CBAL	$\psi(2S) \to \chi_{c1}\gamma \to J/\psi\gamma\gamma$
• • • We do not use the following data for averages, fits, limits, etc. • • •					
− 7.9± 1.9±0.3	19.8k	[4] ARTUSO	09	CLEO	$\psi(2S) \to \gamma\gamma\ell^+\ell^-$

[1] Correlated with a_3, b_2, and b_3 with correlation coefficients $\rho_{a_2 a_3} = 0.733$, $\rho_{a_2 b_2} = -0.605$, and $\rho_{a_2 b_3} = -0.095$.

[2] From a fit with floating $M2$ amplitudes a_2 and b_2, and fixed $E3$ amplitudes $a_3{=}b_3{=}0$.

[3] Assuming $a_3{=}0$.

[4] From a fit with floating $M2$ and $E3$ amplitudes a_2, b_2, and a_3, and b_3.

$a_3 = E3/\sqrt{E1^2 + M2^2 + E3^2}$ Electric octupole fractional transition amplitude

VALUE (units 10^{-2})	EVTS	DOCUMENT ID		TECN	COMMENT
−0.3±1.0 OUR AVERAGE Error includes scale factor of 1.3. See the ideogram below.					
−1.3±0.9±0.4	89k	[1] ABLIKIM	17N	BES3	$\psi(2S) \to \gamma\gamma\ell^+\ell^-$
1.7±1.4±0.3	19.8k	[2] ARTUSO	09	CLEO	$\psi(2S) \to \gamma\gamma\ell^+\ell^-$
$2.0^{+5.5}_{-4.4}\pm0.9$	5908	AMBROGIANI	02	E835	$p\overline{p} \to \chi_{c2} \to J/\psi\gamma$
0^{+6}_{-5}	1904	ARMSTRONG	93E	E760	$p\overline{p} \to \chi_{c2} \to J/\psi\gamma$

[1] Correlated with a_2, b_2, and b_3 with correlation coefficients $\rho_{a_2 a_3} = 0.733$, $\rho_{a_3 b_2} = -0.422$, and $\rho_{a_3 b_3} = -0.024$.

[2] From a fit with floating $M2$ and $E3$ amplitudes a_2, b_2, and a_3, and b_3.

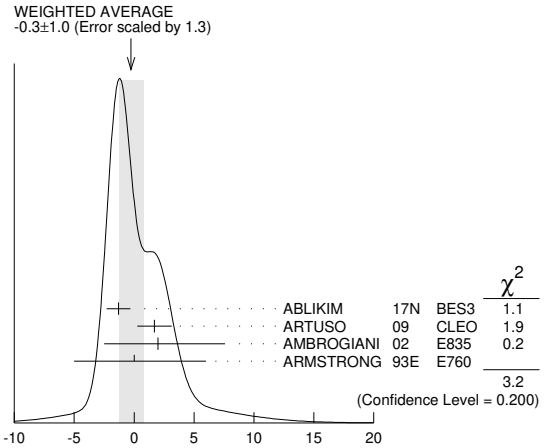

$a_3 = E3/\sqrt{E1^2 + M2^2 + E3^2}$ Electric octupole fractional transition amplitude (units 10^{-2})

MULTIPOLE AMPLITUDES IN $\psi(2S) \to \gamma\chi_{c2}(1P)$ RADIATIVE DECAY

$b_2 = M2/\sqrt{E1^2 + M2^2 + E3^2}$ Magnetic quadrupole fractional transition amplitude

VALUE (units 10^{-2})	EVTS	DOCUMENT ID		TECN	COMMENT
1.9±0.9 OUR AVERAGE Error includes scale factor of 1.4. See the ideogram below.					
1.7±0.8±0.2	89k	[1] ABLIKIM	17N	BES3	$\psi(2S) \to \gamma\gamma\ell^+\ell^-$
4.6±1.0±1.3	13.8k	[2] ABLIKIM	11I	BES3	$\psi(2S) \to \gamma\pi^+\pi^-, \gamma K^+K^-$
0.2±1.5±0.4	19.8k	[3] ARTUSO	09	CLEO	$\psi(2S) \to \gamma\gamma\ell^+\ell^-$
$-5.1^{+5.4}_{-3.6}$	721	[2] ABLIKIM	04I	BES2	$\psi(2S) \to \gamma\pi^+\pi^-, \gamma K^+K^-$
$13.2^{+9.8}_{-7.5}$	441	[4] OREGLIA	82	CBAL	$\psi(2S) \to \gamma\gamma\ell^+\ell^-$
• • • We do not use the following data for averages, fits, limits, etc. • • •					
1.0±1.3±0.3	19.8k	[4] ARTUSO	09	CLEO	$\psi(2S) \to \gamma\gamma\ell^+\ell^-$

[1] Correlated with a_2, a_3, and b_3 with correlation coefficients $\rho_{a_2 b_2} = -0.605$, $\rho_{a_3 b_2} = -0.422$, and $\rho_{b_2 b_3} = 0.384$.

[2] From a fit with floating $M2$ and $E3$ amplitudes b_2 and b_3.

[3] From a fit with floating $M2$ and $E3$ amplitudes a_2, b_2, and a_3, and b_3.

[4] From a fit with floating $M2$ amplitudes a_2 and b_2, and fixed $E3$ amplitudes $a_3{=}b_3{=}0$.

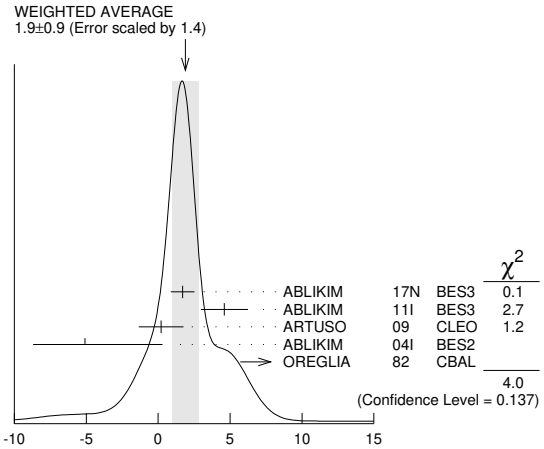

$b_2 = M2/\sqrt{E1^2 + M2^2 + E3^2}$ Magnetic quadrupole fractional transition amplitude (units 10^{-2})

$b_3 = E3/\sqrt{E1^2 + M2^2 + E3^2}$ Electric octupole fractional transition amplitude

VALUE (units 10^{-2})	EVTS	DOCUMENT ID		TECN	COMMENT
−1.0±0.6 OUR AVERAGE					
−1.4±0.7±0.4	89k	[1] ABLIKIM	17N	BES3	$\psi(2S) \to \gamma\gamma\ell^+\ell^-$
1.5±0.8±1.8	13.8k	[2] ABLIKIM	11I	BES3	$\psi(2S) \to \gamma\pi^+\pi^-, \gamma K^+K^-$
−0.8±1.2±0.2	19.8k	ARTUSO	09	CLEO	$\psi(2S) \to \gamma\gamma\ell^+\ell^-$
$-2.7^{+4.3}_{-2.9}$	721	[2] ABLIKIM	04I	BES2	$\psi(2S) \to \gamma\pi^+\pi^-, \gamma K^+K^-$

[1] Correlated with a_2, a_3, and b_2 with correlation coefficients $\rho_{a_2 b_3} = -0.095$, $\rho_{a_3 b_3} = -0.024$, and $\rho_{b_2 b_3} = 0.384$.

[2] From a fit with floating $M2$ and $E3$ amplitudes b_2 and b_3.

MULTIPOLE AMPLITUDE RATIOS IN RADIATIVE DECAYS $\psi(2S) \to \gamma\chi_{c2}(1P)$ and $\chi_{c2} \to \gamma J/\psi(1S)$

b_2/a_2 Magnetic quadrupole transition amplitude ratio

VALUE (units 10^{-2})	EVTS	DOCUMENT ID		TECN	COMMENT
$\mathbf{-11^{+14}_{-15}}$	19.8k	[1] ARTUSO	09	CLEO	$\psi(2S) \to \gamma\gamma\ell^+\ell^-$

[1] Statistical and systematic errors combined. From a fit with floating $M2$ amplitudes a_2 and b_2, and fixed $E3$ amplitudes $a_3{=}b_3{=}0$. Not independent of values for $a_2(\chi_{c2}(1P))$ and $b_2(\chi_{c2}(1P))$ from ARTUSO 09.

$\chi_{c2}(1P)$ REFERENCES

ABLIKIM	25AY	PR D112 012007	M. Ablikim *et al.*	(BESIII Collab.)
ABLIKIM	25BX	PR D112 112015	M. Ablikim *et al.*	(BESIII Collab.)
ABLIKIM	25CE	JHEP 2510 090	M. Ablikim *et al.*	(BESIII Collab.)
ABLIKIM	25CH	CP C49 091001	M. Ablikim *et al.*	(BESIII Collab.)
ABLIKIM	25CJ	CP C49 123001	M. Ablikim *et al.*	(BESIII Collab.)
ABLIKIM	25H	PR D111 012003	M. Ablikim *et al.*	(BESIII Collab.)
ABLIKIM	25I	PR D111 012004	M. Ablikim *et al.*	(BESIII Collab.)
ABLIKIM	25K	PR D111 032001	M. Ablikim *et al.*	(BESIII Collab.)
ABLIKIM	25L	PR D111 032008	M. Ablikim *et al.*	(BESIII Collab.)
ABLIKIM	25R	PR D111 052013	M. Ablikim *et al.*	(BESIII Collab.)
ABLIKIM	25V	PR D111 072001	M. Ablikim *et al.*	(BESIII Collab.)
ABLIKIM	24AC	PR D110 032016	M. Ablikim *et al.*	(BESIII Collab.)
ABLIKIM	24AY	PR D109 L071103	M. Ablikim *et al.*	(BESIII Collab.)
ABLIKIM	24BE	PR D110 032022	M. Ablikim *et al.*	(BESIII Collab.)
ABLIKIM	24BT	PR D110 072009	M. Ablikim *et al.*	(BESIII Collab.)
ABLIKIM	24BW	PR D110 092003	M. Ablikim *et al.*	(BESIII Collab.)
ABLIKIM	24BX	PR D110 112009	M. Ablikim *et al.*	(BESIII Collab.)
ABLIKIM	24CA	PR D110 112013	M. Ablikim *et al.*	(BESIII Collab.)
ABLIKIM	24P	PR D109 072016	M. Ablikim *et al.*	(BESIII Collab.)
PDG	24	PR D110 030001	S. Navas *et al.*	(PDG Collab.)
ABLIKIM	23N	JHEP 2305 069	M. Ablikim *et al.*	(BESIII Collab.)
ABLIKIM	23T	PR D107 092004	M. Ablikim *et al.*	(BESIII Collab.)
SEINO	23	JHEP 2301 160	Y. Seino *et al.*	(BELLE Collab.)
ABLIKIM	22AO	PR D106 072004	M. Ablikim *et al.*	(BESIII Collab.)
ABLIKIM	22O	JHEP 2206 074	M. Ablikim *et al.*	(BESIII Collab.)
ABLIKIM	22Q	PR D106 032014	M. Ablikim *et al.*	(BESIII Collab.)
PDG	22	PTEP 2022 083C01	R.L. Workman *et al.*	(PDG Collab.)
ABLIKIM	21AV	JHEP 2111 217	M. Ablikim *et al.*	(BESIII Collab.)
ABLIKIM	21L	PR D103 112004	M. Ablikim *et al.*	(BESIII Collab.)
ABLIKIM	20AE	PR D102 092006	M. Ablikim *et al.*	(BESIII Collab.)
ABLIKIM	20B	PR D101 012012	M. Ablikim *et al.*	(BESIII Collab.)
ABLIKIM	20I	PR D101 092002	M. Ablikim *et al.*	(BESIII Collab.)
PDG	20	PTEP 2020 083C01	P.A. Zyla *et al.*	(PDG Collab.)
ABLIKIM	19AA	PR D99 052008	M. Ablikim *et al.*	(BESIII Collab.)
ABLIKIM	19AU	PR D100 052010	M. Ablikim *et al.*	(BESIII Collab.)
ABLIKIM	19BB	PR D100 092006	M. Ablikim *et al.*	(BESIII Collab.)
ABLIKIM	19J	PR D99 012015	M. Ablikim *et al.*	(BESIII Collab.)
ABLIKIM	19Z	PR D99 051101	M. Ablikim *et al.*	(BESIII Collab.)
ABLIKIM	18V	PR D97 052011	M. Ablikim *et al.*	(BESIII Collab.)
PDG	18	PR D98 030001	M. Tanabashi *et al.*	(PDG Collab.)
AAIJ	17BB	EPJ C77 609	R. Aaij *et al.*	(LHCb Collab.)
AAIJ	17BI	PRL 119 221801	R. Aaij *et al.*	(LHCb Collab.)
ABLIKIM	17AE	PR D96 092007	M. Ablikim *et al.*	(BESIII Collab.)
ABLIKIM	17AG	PR D96 111102	M. Ablikim *et al.*	(BESIII Collab.)
ABLIKIM	17AI	PR D96 112006	M. Ablikim *et al.*	(BESIII Collab.)
ABLIKIM	17I	PRL 118 221802	M. Ablikim *et al.*	(BESIII Collab.)
ABLIKIM	17N	PR D95 072004	M. Ablikim *et al.*	(BESIII Collab.)
ABLIKIM	17U	PR D96 032001	M. Ablikim *et al.*	(BESIII Collab.)

Int. J. Mod. Phys. A 2026.41. Downloaded from www.worldscientific.com
by CALIFORNIA @ BERKELEY on 09/16/26. Re-use and distribution is strictly not permitted, except for Open Access articles.

PDG	16	CP C40 100001	C. Patrignani *et al.*	(PDG Collab.)
ABLIKIM	15I	PR D91 092006	M. Ablikim *et al.*	(BESIII Collab.)
ABLIKIM	15M	PR D91 112008	M. Ablikim *et al.*	(BESIII Collab.)
ABLIKIM	15N	PR D91 112018	M. Ablikim *et al.*	(BESIII Collab.)
ABLIKIM	14J	PR D89 074030	M. Ablikim *et al.*	(BESIII Collab.)
ABLIKIM	13B	PR D87 012002	M. Ablikim *et al.*	(BESIII Collab.)
ABLIKIM	13D	PR D87 012007	M. Ablikim *et al.*	(BESIII Collab.)
ABLIKIM	13H	PR D87 032007	M. Ablikim *et al.*	(BESIII Collab.)
ABLIKIM	13V	PR D88 112001	M. Ablikim *et al.*	(BESIII Collab.)
UEHARA	13	PTEP 2013 123C01	S. Uehara *et al.*	(BELLE Collab.)
ABLIKIM	12A	PR D85 112008	M. Ablikim *et al.*	(BESIII Collab.)
ABLIKIM	12I	PR D86 052004	M. Ablikim *et al.*	(BESIII Collab.)
ABLIKIM	12J	PR D86 052011	M. Ablikim *et al.*	(BESIII Collab.)
ABLIKIM	12O	PRL 109 172002	M. Ablikim *et al.*	(BESIII Collab.)
LEES	12AE	PR D86 092005	J.P. Lees *et al.*	(BABAR Collab.)
LIU	12B	PRL 108 232001	Z.Q. Liu *et al.*	(BELLE Collab.)
ABLIKIM	11A	PR D83 012006	M. Ablikim *et al.*	(BESIII Collab.)
ABLIKIM	11E	PR D83 112005	M. Ablikim *et al.*	(BESIII Collab.)
ABLIKIM	11F	PR D83 112009	M. Ablikim *et al.*	(BESIII Collab.)
ABLIKIM	11I	PR D84 092006	M. Ablikim *et al.*	(BESIII Collab.)
ABLIKIM	11K	PRL 107 092001	M. Ablikim *et al.*	(BESIII Collab.)
DEL-AMO-SA...	11M	PR D84 012004	P. del Amo Sanchez *et al.*	(BABAR Collab.)
ABLIKIM	10A	PR D81 052005	M. Ablikim *et al.*	(BESIII Collab.)
ONYISI	10	PR D82 011103	P.U.E. Onyisi *et al.*	(CLEO Collab.)
UEHARA	10A	PR D82 114031	S. Uehara *et al.*	(BELLE Collab.)
ARTUSO	09	PR D80 112003	M. Artuso *et al.*	(CLEO Collab.)
ASNER	09	PR D79 072007	D.M. Asner *et al.*	(CLEO Collab.)
UEHARA	09	PR D79 052009	S. Uehara *et al.*	(BELLE Collab.)
BENNETT	08A	PRL 101 151801	J.V. Bennett *et al.*	(CLEO Collab.)
ECKLUND	08A	PR D78 091501	K.M. Ecklund *et al.*	(CLEO Collab.)
HE	08B	PR D78 092004	Q. He *et al.*	(CLEO Collab.)
MENDEZ	08	PR D78 011102	H. Mendez *et al.*	(CLEO Collab.)
NAIK	08	PR D78 031101	P. Naik *et al.*	(CLEO Collab.)
UEHARA	08	EPJ C53 1	S. Uehara *et al.*	(BELLE Collab.)
ADAMS	07	PR D75 071101	G.S. Adams *et al.*	(CLEO Collab.)
ATHAR	07	PR D75 032002	S.B. Athar *et al.*	(CLEO Collab.)
CHEN	07B	PL B651 15	W.T. Chen *et al.*	(BELLE Collab.)
ABLIKIM	06D	PR D73 052006	M. Ablikim *et al.*	(BES Collab.)
ABLIKIM	06I	PR D74 012004	M. Ablikim *et al.*	(BES Collab.)
ABLIKIM	06R	PR D74 072001	M. Ablikim *et al.*	(BES Collab.)
ABLIKIM	06T	PL B642 197	M. Ablikim *et al.*	(BES Collab.)
DOBBS	06	PR D73 071101	S. Dobbs *et al.*	(CLEO Collab.)
ABLIKIM	05G	PR D71 092002	M. Ablikim *et al.*	(BES Collab.)
ABLIKIM	05N	PL B630 7	M. Ablikim *et al.*	(BES Collab.)
ABLIKIM	05O	PL B630 21	M. Ablikim *et al.*	(BES Collab.)
ADAM	05A	PRL 94 232002	N.E. Adam *et al.*	(CLEO Collab.)
ANDREOTTI	05A	NP B717 34	M. Andreotti *et al.*	(FNAL E835 Collab.)
NAKAZAWA	05	PL B615 39	H. Nakazawa *et al.*	(BELLE Collab.)
ABLIKIM	04B	PR D70 012003	M. Ablikim *et al.*	(BES Collab.)
ABLIKIM	04H	PR D70 092003	M. Ablikim *et al.*	(BES Collab.)
ABLIKIM	04I	PR D70 092004	M. Ablikim *et al.*	(BES Collab.)
BAI	04F	PR D69 092001	J.Z. Bai *et al.*	(BES Collab.)
BAI	04I	PR D70 012006	J.Z. Bai *et al.*	(BES Collab.)
AULCHENKO	03	PL B573 63	V.M. Aulchenko *et al.*	(KEDR Collab.)
BAI	03C	PR D67 032004	J.Z. Bai *et al.*	(BES Collab.)
BAI	03E	PR D67 112001	J.Z. Bai *et al.*	(BES Collab.)
ABE	02T	PL B540 33	K. Abe *et al.*	(BELLE Collab.)
AMBROGIANI	02	PR D65 052002	M. Ambrogiani *et al.*	(FNAL E835 Collab.)
EISENSTEIN	01	PRL 87 061801	B.I. Eisenstein *et al.*	(CLEO Collab.)
AMBROGIANI	00B	PR D62 052002	M. Ambrogiani *et al.*	(FNAL E835 Collab.)
ACCIARRI	99E	PL B453 73	M. Acciarri *et al.*	(L3 Collab.)
BAI	99B	PR D60 072001	J.Z. Bai *et al.*	(BES Collab.)
ACKER..,K...	98	PL B439 197	K. Ackerstaff *et al.*	(OPAL Collab.)
BAI	98D	PR D58 092006	J.Z. Bai *et al.*	(BES Collab.)
BAI	98I	PRL 81 3091	J.Z. Bai *et al.*	(BES Collab.)
DOMINICK	94	PR D50 4265	J. Dominick *et al.*	(CLEO Collab.)
ARMSTRONG	93	PRL 70 2988	T.A. Armstrong *et al.*	(FNAL E760 Collab.)
ARMSTRONG	93E	PR D48 3037	T.A. Armstrong *et al.*	(FNAL-E760 Collab.)
BAUER	93	PL B302 345	D.A. Bauer *et al.*	(TPC Collab.)
ARMSTRONG	92	NP B373 35	T.A. Armstrong *et al.*	(FNAL, FERR, GENO+)
Also		PRL 68 1468	T.A. Armstrong *et al.*	(FNAL, FERR, GENO+)
BAGLIN	87B	PL B187 191	C. Baglin *et al.*	(R704 Collab.)
BAGLIN	86B	PL B172 455	C. Baglin	(LAPP, CERN, GENO, LYON, OSLO+)
GAISER	86	PR D34 711	J. Gaiser *et al.*	(Crystal Ball Collab.)
LEE	85	SLAC 282	R.A. Lee	(SLAC)
LEMOIGNE	82	PL 113B 509	Y. Lemoigne *et al.*	(SACL, LOIC, SHMP+)
OREGLIA	82	PR D25 2259	M.J. Oreglia *et al.*	(SLAC, CIT, HARV+)
Also		Private Comm.	M.J. Oreglia	(EFI)
BARATE	81	PR D24 2994	R. Barate *et al.*	(SACL, LOIC, SHMP, CERN+)
HIMEL	80	PRL 44 920	T. Himel *et al.*	(LBL, SLAC)
Also		Private Comm.	G. Trilling	(LBL, UCB)
BRANDELIK	79B	NP B160 426	R. Brandelik *et al.*	(DASP Collab.)
BARTEL	78B	PL 79B 492	W. Bartel *et al.*	(DESY, HEIDP)
TANENBAUM	78	PR D17 1731	W.M. Tanenbaum *et al.*	(SLAC, LBL)
Also		Private Comm.	G. Trilling	(LBL, UCB)
BIDDICK	77	PRL 38 1324	C.J. Biddick *et al.*	(UCSD, UMD, PAVI+)
WHITAKER	76	PRL 37 1596	J.S. Whitaker *et al.*	(SLAC, LBL)

$\eta_c(2S)$

$I^G(J^{PC}) = 0^+(0^{-+})$

Quantum numbers are quark model predictions.

$\eta_c(2S)$ MASS

VALUE (MeV)	EVTS	DOCUMENT ID		TECN	COMMENT
3637.8 ±0.6 OUR AVERAGE		Error includes scale factor of 1.1.			
3637.8 ±0.8 ±0.2	1.6k	ABLIKIM	24J	BES3	$\psi(2S) \to \gamma\eta_c \to \gamma K\overline{K}\pi$
3637.90±0.54±1.40	3.7k	AAIJ	23AH	LHCB	$B^+ \to K^+(K^0_S K\pi)$
3643.4 ±2.3 ±4.4	569	ABLIKIM	22Q	BES3	$\psi(2S) \to \gamma 3(\pi^+\pi^-)$
3635.1 ±3.7 ±2.9	106	XU	18	BELL	$e^+e^- \to e^+e^-\eta'\pi^+\pi^-$
3633.6 ±1.7 ±0.6	106	[1] AAIJ	17AD	LHCB	$pp \to B^+X \to p\overline{p}K^+X$
3636.4 ±4.1 ±0.7	365	[2] AAIJ	17BB	LHCB	$pp \to b\overline{b}X \to 2(K^+K^-)X$
3637.0 ±5.7 ±3.4	178	[3,4] LEES	14E	BABR	$\gamma\gamma \to K^+K^-\pi^0$
3635.1 ±5.8 ±2.1	47	[3,5] LEES	14E	BABR	$\gamma\gamma \to K^+K^-\eta$
3646.9 ±1.6 ±3.6	57	ABLIKIM	13K	BES3	$\psi(2S) \to \gamma K^0_S K^\pm\pi^\mp\pi^+\pi^-$
3637.6 ±2.9 ±1.6	127	[6] ABLIKIM	12G	BES3	$\psi(2S) \to \gamma K^0 K\pi$, $KK\pi^0$
3638.5 ±1.5 ±0.8	624	[3] DEL-AMO-SA...11M		BABR	$\gamma\gamma \to K^0_S K^\pm\pi^\mp$
3640.5 ±3.2 ±2.5	1201	[3] DEL-AMO-SA...11M		BABR	$\gamma\gamma \to K^+K^-\pi^+\pi^-\pi^0$
3636.1 $^{+3.9}_{-4.2}$ $^{+0.7}_{-2.0}$	128	[7] VINOKUROVA	11	BELL	$B^\pm \to K^\pm(K^0_S K^\pm\pi^\mp)$
3626 ±5 ±6	311	[8] ABE	07	BELL	$e^+e^- \to J/\psi(c\overline{c})$
3645.0 ±5.5 $^{+4.9}_{-7.8}$	121	AUBERT	05C	BABR	$e^+e^- \to J/\psi c\overline{c}$
3642.9 ±3.1 ±1.5	61	ASNER	04	CLEO	$\gamma\gamma \to \eta'_c \to K^0_S K^\pm\pi^\mp$
• • • We do not use the following data for averages, fits, limits, etc. • • •					
3639 ±7	98	[9] AUBERT	06E	BABR	$B^\pm \to K^\pm X_{c\overline{c}}$
3630.8 ±3.4 ±1.0	112	[10] AUBERT	04D	BABR	$\gamma\gamma \to \eta_c(2S) \to K\overline{K}\pi$
3654 ±6 ±8	39	[11] CHOI	02	BELL	$B \to KK_SK^-\pi^+$
3594 ±5		[12] EDWARDS	82C	CBAL	$e^+e^- \to \gamma X$

[1] AAIJ 17AD report $m_{\psi(2S)} - m_{\eta_c(2S)} = 52.5 \pm 1.7 \pm 0.6$ MeV. We use the current value $m_{\psi(2S)} = 3686.097 \pm 0.025$ MeV to obtain the quoted mass.
[2] From a fit of the $\phi\phi$ invariant mass with the width of $\eta_c(2S)$ fixed to the PDG 16 value.
[3] Ignoring possible interference with continuum.
[4] With a width fixed to 11.3 MeV.
[5] With a width fixed to 11.3 MeV. Using both $\eta \to \gamma\gamma$ and $\eta \to \pi^+\pi^-\pi^0$ decays.
[6] From a simultaneous fit to $K^0_S K^\pm\pi^\mp$ and $K^+K^-\pi^0$ decay modes.
[7] Accounts for interference with non-resonant continuum.
[8] From a fit of the J/ψ recoil mass spectrum. Supersedes ABE,K 02 and ABE 04G.
[9] From the fit of the kaon momentum spectrum. Systematic errors not evaluated.
[10] Superseded by DEL-AMO-SANCHEZ 11M.
[11] Superseded by VINOKUROVA 11.
[12] Assuming mass of $\psi(2S) = 3686$ MeV.

$\eta_c(2S)$ WIDTH

VALUE (MeV)	CL%	EVTS	DOCUMENT ID		TECN	COMMENT
11.6 ± 1.4 OUR AVERAGE						
10.5 ± 1.7 ±3.5		1.6k	ABLIKIM	24J	BES3	$\psi(2S) \to \gamma\eta_c \to \gamma K\overline{K}\pi$
10.77± 1.62±1.08		3.7k	AAIJ	23AH	LHCB	$B^+ \to K^+(K^0_S K\pi)$
19.8 ± 3.9 ±3.1		569	ABLIKIM	22Q	BES3	$\psi(2S) \to \gamma 3(\pi^+\pi^-)$
9.9 ± 4.8 ±2.9		57	ABLIKIM	13K	BES3	$\psi(2S) \to \gamma K^0_S K^\pm\pi^\mp\pi^+\pi^-$
16.9 ± 6.4 ±4.8		127	[1] ABLIKIM	12G	BES3	$\psi(2S) \to \gamma K^0 K\pi$, $KK\pi^0$
13.4 ± 4.6 ±3.2		624	[2] DEL-AMO-SA...11M		BABR	$\gamma\gamma \to K^0_S K^\pm\pi^\mp$
6.6 $^{+8.4}_{-5.1}$ $^{+2.6}_{-0.9}$		128	[3] VINOKUROVA	11	BELL	$B^\pm \to K^\pm(K^0_S K^\pm\pi^\mp)$
6.3 ±12.4 ±4.0		61	ASNER	04	CLEO	$\gamma\gamma \to \eta'_c \to K^0_S K^\pm\pi^\mp$
• • • We do not use the following data for averages, fits, limits, etc. • • •						
< 23	90	98	[4] AUBERT	06E	BABR	$B^\pm \to K^\pm X_{c\overline{c}}$
22 ±14		121	AUBERT	05C	BABR	$e^+e^- \to J/\psi c\overline{c}$
17.0 ± 8.3 ±2.5		112	[5] AUBERT	04D	BABR	$\gamma\gamma \to \eta_c(2S) \to K\overline{K}\pi$
<55	90	39	[6] CHOI	02	BELL	$B \to KK_SK^-\pi^+$
<8.0	95		[7] EDWARDS	82C	CBAL	$e^+e^- \to \gamma X$

[1] From a simultaneous fit to $K^0_S K^\pm\pi^\mp$ and $K^+K^-\pi^0$ decay modes.
[2] Ignoring possible interference with continuum.
[3] Accounts for interference with non-resonant continuum.
[4] From the fit of the kaon momentum spectrum. Systematic errors not evaluated.
[5] Superseded by DEL-AMO-SANCHEZ 11M.
[6] For a mass value of 3654 ± 6 MeV. Superseded by VINOKUROVA 11.
[7] For a mass value of 3594 ± 5 MeV

$\eta_c(2S)$ DECAY MODES

	Mode	Fraction (Γ_i/Γ)	Confidence level
Γ_1	hadrons	seen	
Γ_2	$K\overline{K}\pi$	$(1.9^{+1.2}_{-1.0})$ %	
Γ_3	$K\overline{K}\eta$	$(7\ ^{+5}_{-4}) \times 10^{-3}$	
Γ_4	$K\overline{K}\eta'$	$(2.1\pm1.6) \times 10^{-3}$	
Γ_5	$2\pi^+2\pi^-$	$< 2.6 \times 10^{-3}$	90%
Γ_6	$a_0(1450)\pi$	seen	
Γ_7	$a_2(1700)\pi$	seen	
Γ_8	$a_0(1710)\pi$	seen	
Γ_9	$\rho^0\rho^0$	$< 2.3 \times 10^{-3}$	90%
Γ_{10}	$3\pi^+3\pi^-$	$(1.7^{+0.9}_{-1.1})$ %	
Γ_{11}	$K^+K^-\pi^+\pi^-$	$< 2.5 \times 10^{-3}$	90%
Γ_{12}	$K^{*0}\overline{K}^{*0}$	$< 4 \times 10^{-3}$	90%

Int. J. Mod. Phys. A 2026.41. Downloaded from www.worldscientific.com
by UNIVERSITY OF CALIFORNIA @ BERKELEY on 09/16/26. Re-use and distribution is strictly not permitted, except for Open Access articles.

Γ_{13}	$K^+K^-\pi^+\pi^-\pi^0$	$(1.5^{+1.0}_{-0.9})$ %		
Γ_{14}	$K^+K^-2\pi^+2\pi^-$	< 1.8	%	90%
Γ_{15}	$K^0_S K^-2\pi^+\pi^- +$ c.c.	$(1.4^{+0.8}_{-1.0})$ %		
Γ_{16}	$2K^+2K^-$	< 1.4	$\times 10^{-3}$	90%
Γ_{17}	$K^*_2(1430)\overline{K}+$ c.c.	seen		
Γ_{18}	$K^*_0(1950)\overline{K}+$ c.c.	seen		
Γ_{19}	$K^*_0(2600)\overline{K}+$ c.c.	seen		
Γ_{20}	$\phi\phi$	< 1.4	$\times 10^{-3}$	90%
Γ_{21}	$\omega\omega$	< 1.9	$\times 10^{-3}$	90%
Γ_{22}	$\omega\phi$	< 3.4	$\times 10^{-4}$	90%
Γ_{23}	$p\overline{p}$	< 3.2	$\times 10^{-4}$	90%
Γ_{24}	$p\overline{p}\pi^+\pi^-$	seen		
Γ_{25}	$p\overline{p}K^+K^-$	$(3.6\pm2.9)\times10^{-4}$		
Γ_{26}	$\gamma\gamma$	$(1.8^{+1.0}_{-1.1})\times10^{-4}$		
Γ_{27}	$\gamma J/\psi(1S)$	< 1.8	%	90%
Γ_{28}	$\pi^+\pi^-\eta$	$(5.5^{+3.3}_{-4.0})\times10^{-3}$		
Γ_{29}	$2\pi^+2\pi^-\eta$	$(1.6^{+0.9}_{-1.0})$ %		
Γ_{30}	$\pi^+\pi^-\eta'$	$(2.7^{+2.0}_{-1.8})\times10^{-3}$		
Γ_{31}	$\pi^+\pi^-\eta_c(1S)$	< 4	%	90%

FIT INFORMATION

A multiparticle fit to $\eta_c(2S)$ and $\psi(2S)$ with 4 branching ratios uses 5 measurements to determine 3 parameters. The overall fit has a $\chi^2 = 2.6$ for 2 degrees of freedom.

The following *off-diagonal* array elements are the correlation coefficients $\langle \delta x_i \delta x_j \rangle / (\delta x_i \cdot \delta x_j)$, in percent, from the fit to the branching fractions, $x_i \equiv \Gamma_i/\Gamma_{total}$.

x_3 92
x_2

$\eta_c(2S)$ PARTIAL WIDTHS

$\Gamma(\gamma\gamma)$ — Γ_{26}

VALUE (keV)	EVTS	DOCUMENT ID		TECN	COMMENT
• • • We do not use the following data for averages, fits, limits, etc. • • •					
0.44 ± 0.14	106	[1] XU	18	BELL	$e^+e^- \to e^+e^-\eta'\pi^+\pi^-$
$1.3\ \pm0.6$		[2] ASNER	04	CLEO	$\gamma\gamma \to \eta'_c \to K^0_S K^\pm\pi^\mp$

[1] Assuming that the branching fraction into $\eta'\pi^+\pi^-$ is the same as for $\eta_c(1S)$.
[2] They measure $\Gamma(\eta_c(2S)\gamma\gamma)\ B(\eta_c(2S) \to K\overline{K}\pi) = (0.18 \pm 0.05 \pm 0.02)\ \Gamma(\eta_c(1S)\gamma\gamma)\ B(\eta_c(1S) \to K\overline{K}\pi)$. The value for $\Gamma(\eta_c(2S) \to \gamma\gamma)$ is derived assuming that the branching fractions for $\eta_c(2S)$ and $\eta_c(1S)$ decays to $K_S K\pi$ are equal and using $\Gamma(\eta_c(1S) \to \gamma\gamma) = 7.4 \pm 0.4 \pm 2.3$ keV.

$\eta_c(2S)\ \Gamma(i)\Gamma(\gamma\gamma)/\Gamma(\text{total})$

$\Gamma(K\overline{K}\pi) \times \Gamma(\gamma\gamma)/\Gamma_{total}$ — $\Gamma_2\Gamma_{26}/\Gamma$

VALUE (eV)	EVTS	DOCUMENT ID		TECN	COMMENT
39 ±6 OUR AVERAGE					
$41\ \pm4\ \pm6$	624	DEL-AMO-SA...	11M	BABR	$\gamma\gamma \to K^0_S K^\pm\pi^\mp$
$33.6\pm7.2\pm8.1$		[1] NAKAZAWA	08	BELL	$\gamma\gamma \to K^0_S K^\pm\pi^\mp$

[1] NAKAZAWA 08 reports $B(\eta_c(2S) \to K^0_S K^\pm\pi^\mp) \times \Gamma(\gamma\gamma) = 11.2 \pm 2.4 \pm 2.7$ eV which we multiplied by 3 to account for isospin symmetry.

$\Gamma(2\pi^+2\pi^-) \times \Gamma(\gamma\gamma)/\Gamma_{total}$ — $\Gamma_5\Gamma_{26}/\Gamma$

VALUE (eV)	CL%	DOCUMENT ID		TECN	COMMENT
• • • We do not use the following data for averages, fits, limits, etc. • • •					
<6.5	90	UEHARA	08	BELL	$\gamma\gamma \to \eta_c(2S) \to 2(\pi^+\pi^-)$

$\Gamma(K^+K^-\pi^+\pi^-) \times \Gamma(\gamma\gamma)/\Gamma_{total}$ — $\Gamma_{11}\Gamma_{26}/\Gamma$

VALUE (eV)	CL%	DOCUMENT ID		TECN	COMMENT
<5.0	90	UEHARA	08	BELL	$\gamma\gamma \to \eta_c(2S) \to K^+K^-\pi^+\pi^-$

$\Gamma(K^+K^-\pi^+\pi^-\pi^0) \times \Gamma(\gamma\gamma)/\Gamma_{total}$ — $\Gamma_{13}\Gamma_{26}/\Gamma$

VALUE (eV)	EVTS	DOCUMENT ID		TECN	COMMENT
30±6±5	1201	DEL-AMO-SA...	11M	BABR	$\gamma\gamma \to K^+K^-\pi^+\pi^-\pi^0$

$\Gamma(2K^+2K^-) \times \Gamma(\gamma\gamma)/\Gamma_{total}$ — $\Gamma_{16}\Gamma_{26}/\Gamma$

VALUE (eV)	CL%	DOCUMENT ID		TECN	COMMENT
<2.9	90	UEHARA	08	BELL	$\gamma\gamma \to \eta_c(2S) \to 2(K^+K^-)$

$\Gamma(\pi^+\pi^-\eta') \times \Gamma(\gamma\gamma)/\Gamma_{total}$ — $\Gamma_{30}\Gamma_{26}/\Gamma$

VALUE (eV)	EVTS	DOCUMENT ID		TECN	COMMENT
$5.6^{+1.2}_{-1.1}\pm1.1$	106	XU	18	BELL	$e^+e^- \to e^+e^-\eta'\pi^+\pi^-$

$\Gamma(\pi^+\pi^-\eta_c(1S)) \times \Gamma(\gamma\gamma)/\Gamma_{total}$ — $\Gamma_{31}\Gamma_{26}/\Gamma$

VALUE (eV)	CL%	DOCUMENT ID		TECN	COMMENT
<133	90	LEES	12AE	BABR	$e^+e^- \to e^+e^-\pi^+\pi^-\eta_c$

$\eta_c(2S)\ \Gamma(i)\Gamma(\gamma\gamma)/\Gamma^2(\text{total})$

$\Gamma(p\overline{p})/\Gamma_{total} \times \Gamma(\gamma\gamma)/\Gamma_{total}$ — $\Gamma_{23}/\Gamma \times \Gamma_{26}/\Gamma$

VALUE (units 10^{-8})	CL%	DOCUMENT ID		TECN	COMMENT
< 5.6	90	[1,2,3] AMBROGIANI	01	E835	$\overline{p}p \to \gamma\gamma$
• • • We do not use the following data for averages, fits, limits, etc. • • •					
< 8.0	90	[1,2,4] AMBROGIANI	01	E835	$\overline{p}p \to \gamma\gamma$
<12.0	90	[2,4] AMBROGIANI	01	E835	$\overline{p}p \to \gamma\gamma$

[1] Including the measurements of of ARMSTRONG 95F in the AMBROGIANI 01 analysis.
[2] For a total width Γ=5 MeV.
[3] For the resonance mass region 3589–3599 MeV/c^2.
[4] For the resonance mass region 3575–3660 MeV/c^2.

$\eta_c(2S)$ BRANCHING RATIOS

$\Gamma(\text{hadrons})/\Gamma_{total}$ — Γ_1/Γ

VALUE	DOCUMENT ID		TECN	COMMENT
• • • We do not use the following data for averages, fits, limits, etc. • • •				
not seen	ABREU	98O	DLPH	$e^+e^- \to e^+e^-$ + hadrons
seen	[1] EDWARDS	82C	CBAL	$e^+e^- \to \gamma X$

[1] For a mass value of 3594 ± 5 MeV

$\Gamma(K\overline{K}\pi)/\Gamma_{total}$ — Γ_2/Γ

VALUE (units 10^{-2})	EVTS	DOCUMENT ID		TECN	COMMENT
$1.9^{+1.2}_{-1.0}$ OUR FIT					
1.9±0.4±1.1	59 ± 12	[1] AUBERT	08AB	BABR	$B \to \eta_c(2S)K \to K\overline{K}\pi K$
• • • We do not use the following data for averages, fits, limits, etc. • • •					
seen	127 ± 18	ABLIKIM	12G	BES3	$\psi(2S) \to \gamma K\overline{K}\pi$
seen	39 ± 11	[2] CHOI	02	BELL	$B \to K K_S K^-\pi^+$

[1] Derived from a measurement of $[B(B^+ \to \eta_c(2S)K^+) \times B(\eta_c(2S) \to K\overline{K}\pi)] / [B(B^+ \to \eta_c K^+) \times B(\eta_c \to K\overline{K}\pi)] = (9.6^{+2.0}_{-1.9} \pm 2.5)\%$ and using $B(B^+ \to \eta_c(2S)K^+) = (3.4 \pm 1.8) \times 10^{-4}$, and $[B(B^+ \to \eta_c K^+) \times B(\eta_c \to K\overline{K}\pi)] = (6.88 \pm 0.77^{+0.55}_{-0.66}) \times 10^{-5}$.
[2] For a mass value of 3654 ± 6 MeV

$\Gamma(K\overline{K}\eta)/\Gamma(K\overline{K}\pi)$ — Γ_3/Γ_2

VALUE (units 10^{-2})	EVTS	DOCUMENT ID		TECN	COMMENT
39 ±10 OUR FIT Error includes scale factor of 1.3.					
27.3± 7.0±9.0	225	[1] LEES	14E	BABR	$\gamma\gamma \to K^+K^-\gamma\gamma$

[1] LEES 14E reports $B(\eta_c(2S) \to K^+K^-\eta)/B(\eta_c(2S) \to K^+K^-\pi^0) = 0.82 \pm 0.21 \pm 0.27$, which we divide by 3 to account for isospin symmetry.

$\Gamma(2\pi^+2\pi^-)/\Gamma_{total}$ — Γ_5/Γ

VALUE	DOCUMENT ID		TECN	COMMENT
• • • We do not use the following data for averages, fits, limits, etc. • • •				
not seen	UEHARA	08	BELL	$\gamma\gamma \to \eta_c(2S)$

$\Gamma(a_0(1450)\pi)/\Gamma_{total}$ — Γ_6/Γ

VALUE	DOCUMENT ID		TECN	COMMENT
seen	[1] AAIJ	23AH	LHCB	$B^+ \to K^+(K^0_S K\pi)$

[1] From a Dalitz plot analysis of $\eta_c(2S) \to K^0_S K^+\pi^-$ + c.c..

$\Gamma(a_2(1700)\pi)/\Gamma_{total}$ — Γ_7/Γ

VALUE	DOCUMENT ID		TECN	COMMENT
seen	[1] AAIJ	23AH	LHCB	$B^+ \to K^+(K^0_S K\pi)$

[1] From a Dalitz plot analysis of $\eta_c(2S) \to K^0_S K^+\pi^-$ + c.c..

$\Gamma(a_0(1710)\pi)/\Gamma_{total}$ — Γ_8/Γ

VALUE	DOCUMENT ID		TECN	COMMENT
seen	[1] AAIJ	23AH	LHCB	$B^+ \to K^+(K^0_S K\pi)$

[1] From a Dalitz plot analysis of $\eta_c(2S) \to K^0_S K^+\pi^-$ + c.c..

$\Gamma(\rho^0\rho^0)/\Gamma_{total}$ — Γ_9/Γ

VALUE	DOCUMENT ID		TECN	COMMENT
• • • We do not use the following data for averages, fits, limits, etc. • • •				
not seen	ABLIKIM	11H	BES3	$\psi(2S) \to \gamma 2\pi^+2\pi^-$

Int. J. Mod. Phys. A 2026.41. Downloaded from www.worldscientific.com by LIFORNIA @ BERKELEY on 09/16/26. Re-use and distribution is strictly not permitted, except for Open Access articles.

$\Gamma(K^+K^-\pi^+\pi^-)/\Gamma_{total}$ — Γ_{11}/Γ

VALUE	DOCUMENT ID	TECN	COMMENT
• • • We do not use the following data for averages, fits, limits, etc. • • •			
not seen	UEHARA 08	BELL	$\gamma\gamma \to \eta_c(2S)$

$\Gamma(K^{*0}\overline{K}^{*0})/\Gamma_{total}$ — Γ_{12}/Γ

VALUE	DOCUMENT ID	TECN	COMMENT
• • • We do not use the following data for averages, fits, limits, etc. • • •			
not seen	ABLIKIM 11H	BES3	$\psi(2S) \to \gamma K^+K^-\pi^+\pi^-$

$\Gamma(K^+K^-\pi^+\pi^-\pi^0)/\Gamma(K\overline{K}\pi)$ — Γ_{13}/Γ_2

VALUE	EVTS	DOCUMENT ID	TECN	COMMENT
• • • We do not use the following data for averages, fits, limits, etc. • • •				
$0.73\pm0.17\pm0.17$	1201	[1] DEL-AMO-SA...11M	BABR	$\gamma\gamma \to K^+K^-\pi^+\pi^-\pi^0$

[1] Not independent from other measurements reported in DEL-AMO-SANCHEZ 11M. We have multiplied the value of $\Gamma(K^+K^-\pi^+\pi^-\pi^0)/\Gamma(K^0_S K^\pm\pi^\mp)$ reported in DEL-AMO-SANCHEZ 11M by a factor 1/3 to obtain $\Gamma(K^+K^-\pi^+\pi^-\pi^0)/\Gamma(K\overline{K}\pi)$.

$\Gamma(K^0_S K^-2\pi^+\pi^- + c.c.)/\Gamma_{total}$ — Γ_{15}/Γ

VALUE	EVTS	DOCUMENT ID	TECN	COMMENT
• • • We do not use the following data for averages, fits, limits, etc. • • •				
seen	57 ± 17	ABLIKIM 13K	BES3	$\psi(2S) \to \gamma K^0_S K^\pm\pi^\mp\pi^+\pi^-$

$\Gamma(2K^+2K^-)/\Gamma_{total}$ — Γ_{16}/Γ

VALUE	DOCUMENT ID	TECN	COMMENT
• • • We do not use the following data for averages, fits, limits, etc. • • •			
not seen	UEHARA 08	BELL	$\gamma\gamma \to \eta_c(2S)$

$\Gamma(K^*_2(1430)\overline{K} + c.c.)/\Gamma_{total}$ — Γ_{17}/Γ

VALUE	DOCUMENT ID	TECN	COMMENT
seen	[1] AAIJ 23AH	LHCB	$B^+ \to K^+(K^0_S K\pi)$

[1] From a Dalitz plot analysis of $\eta_c(2S) \to K^0_S K^+\pi^- +$ c.c..

$\Gamma(K^*_0(1950)\overline{K} + c.c.)/\Gamma_{total}$ — Γ_{18}/Γ

VALUE	DOCUMENT ID	TECN	COMMENT
seen	[1] AAIJ 23AH	LHCB	$B^+ \to K^+(K^0_S K\pi)$

[1] From a Dalitz plot analysis of $\eta_c(2S) \to K^0_S K^+\pi^- +$ c.c..

$\Gamma(K^*_0(2600)\overline{K} + c.c.)/\Gamma_{total}$ — Γ_{19}/Γ

VALUE	DOCUMENT ID	TECN	COMMENT
seen	[1] AAIJ 23AH	LHCB	$B^+ \to K^+(K^0_S K\pi)$

[1] From a Dalitz plot analysis of $\eta_c(2S) \to K^0_S K^+\pi^- +$ c.c..

$\Gamma(\phi\phi)/\Gamma_{total}$ — Γ_{20}/Γ

VALUE	DOCUMENT ID	TECN	COMMENT
• • • We do not use the following data for averages, fits, limits, etc. • • •			
not seen	ABLIKIM 11H	BES3	$\psi(2S) \to \gamma K^+K^-K^+K^-$

$\Gamma(p\overline{p})/\Gamma_{total}$ — Γ_{23}/Γ

VALUE	EVTS	DOCUMENT ID	TECN	COMMENT
• • • We do not use the following data for averages, fits, limits, etc. • • •				
seen	106	[1] AAIJ 17AD	LHCB	$pp \to B^+X \to p\overline{p}K^+X$

[1] AAIJ 17AD report a 6.4 standard deviation signal, with $B(B^+ \to \eta_c(2S)K^+ \to p\overline{p}K^+)/B(B^+ \to J/\psi K^+ \to p\overline{p}K^+) = (1.58 \pm 0.33 \pm 0.09)\times10^{-2}$.

$\Gamma(p\overline{p}\pi^+\pi^-)/\Gamma_{total}$ — Γ_{24}/Γ

VALUE	EVTS	DOCUMENT ID	TECN	COMMENT
seen	110	[1] CHILIKIN 19	BELL	$e^+e^- \to \Upsilon(4S)$

[1] CHILIKIN 19 reports signals in $B^+ \to \eta_c(2S)K^+$ and $B^0 \to \eta_c(2S)K^0_S$ with 12.3 and 5.9 standard deviations, respectively.

$\Gamma(\gamma\gamma)/\Gamma_{total}$ — Γ_{26}/Γ

VALUE	CL%	DOCUMENT ID	TECN	COMMENT
• • • We do not use the following data for averages, fits, limits, etc. • • •				
$<4 \times 10^{-4}$	90	[1] WICHT 08	BELL	$B^\pm \to K^\pm\gamma\gamma$
not seen		AMBROGIANI 01	E835	$\overline{p}p \to \gamma\gamma$
<0.01	90	LEE 85	CBAL	$\psi' \to$ photons

[1] WICHT 08 reports $[\Gamma(\eta_c(2S) \to \gamma\gamma)/\Gamma_{total}] \times [B(B^+ \to \eta_c(2S)K^+)] < 0.18\times10^{-6}$ which we divide by our best (shown rounded) value $B(B^+ \to \eta_c(2S)K^+) = 4.4\times10^{-4}$.

$\Gamma(\pi^+\pi^-\eta_c(1S))/\Gamma(K\overline{K}\pi)$ — Γ_{31}/Γ_2

VALUE	CL%	DOCUMENT ID	TECN	COMMENT
• • • We do not use the following data for averages, fits, limits, etc. • • •				
<3.33	90	[1] LEES 12AE	BABR	$e^+e^- \to e^+e^-\pi^+\pi^-\eta_c$

[1] We divided the reported limit by 3 to take into account isospin relations.

$\eta_c(2S)$ CROSS-PARTICLE BRANCHING RATIOS

$\Gamma(\eta_c(2S) \to K\overline{K}\pi)/\Gamma_{total} \times \Gamma(\psi(2S) \to \gamma\eta_c(2S))/\Gamma_{total}$ — $\Gamma_2/\Gamma \times \Gamma^{\psi(2S)}_{200}/\Gamma^{\psi(2S)}$

VALUE (units 10^{-5})	EVTS	DOCUMENT ID	TECN	COMMENT
1.03 ± 0.12 OUR FIT Error includes scale factor of 1.2.				
1.00 ± 0.10 OUR AVERAGE				
$0.97\pm0.06\pm0.09$	1.6k	ABLIKIM 24J	BES3	$\psi(2S) \to \gamma\eta_c \to \gamma K\overline{K}\pi$
$1.30\pm0.20\pm0.30$	127	ABLIKIM 12G	BES3	$\psi(2S) \to \gamma\eta_c \to \gamma K\overline{K}\pi$

$\Gamma(\eta_c(2S) \to K\overline{K}\eta)/\Gamma_{total} \times \Gamma(\psi(2S) \to \gamma\eta_c(2S))/\Gamma_{total}$ — $\Gamma_3/\Gamma \times \Gamma^{\psi(2S)}_{200}/\Gamma^{\psi(2S)}$

VALUE (units 10^{-6})	CL%	EVTS	DOCUMENT ID	TECN	COMMENT
4.0 ± 1.0 OUR FIT Error includes scale factor of 1.3.					
$4.78\pm0.64\pm0.68$		362	[1] ABLIKIM 24BW	BES3	$\psi(2S) \to \gamma K^+K^-\eta$
• • • We do not use the following data for averages, fits, limits, etc. • • •					
<11.8	90		[2] CRONIN-HEN..10	CLEO	$\psi(2S) \to \gamma K^+K^-\eta$

[1] ABLIKIM 24BW reports a value of $(2.39 \pm 0.32 \pm 0.34)\times10^{-6}$ for the decay $\eta_c(2S) \to K^+K^-\eta$ which we multiply by 2 to account for isospin symmetry.

[2] CRONIN-HENNESSY 10 reports a limit of $< 5.9 \times 10^{-6}$ for the decay $\eta_c(2S) \to K^+K^-\eta$ which we multiply by 2 account for isospin symmetry. It assumes $\Gamma(\eta_c(2S)) = 14$ MeV. It also gives the analytic dependence of limits on width.

$\Gamma(\eta_c(2S) \to K\overline{K}\eta')/\Gamma_{total} \times \Gamma(\psi(2S) \to \gamma\eta_c(2S))/\Gamma_{total}$ — $\Gamma_4/\Gamma \times \Gamma^{\psi(2S)}_{200}/\Gamma^{\psi(2S)}$

VALUE (units 10^{-7})	DOCUMENT ID	TECN	COMMENT
$11.56\pm4.86\pm1.9$	[1] ABLIKIM 25I	BES3	$\psi(2S) \to \gamma K^+K^-\eta'$

[1] ABLIKIM 25I reports a value of $(5.78 \pm 2.43 \pm 0.95)\times10^{-7}$ for $K^+K^-\eta'$ which we multiply by 2 to account for isospin symmetry.

$\Gamma(\eta_c(2S) \to 2\pi^+2\pi^-)/\Gamma_{total} \times \Gamma(\psi(2S) \to \gamma\eta_c(2S))/\Gamma_{total}$ — $\Gamma_5/\Gamma \times \Gamma^{\psi(2S)}_{200}/\Gamma^{\psi(2S)}$

VALUE	CL%	DOCUMENT ID	TECN	COMMENT
$< 1.43 \times 10^{-6}$	90	ABLIKIM 24BT	BES3	$\psi(2S) \to \gamma 2\pi^+2\pi^-$
• • • We do not use the following data for averages, fits, limits, etc. • • •				
$<14.6 \times 10^{-6}$	90	[1] CRONIN-HEN..10	CLEO	$\psi(2S) \to \gamma 2\pi^+2\pi^-$

[1] Assuming $\Gamma(\eta_c(2S)) = 14$ MeV. CRONIN-HENNESSY 10 gives the analytic dependence of limits on width.

$\Gamma(\eta_c(2S) \to \rho^0\rho^0)/\Gamma_{total} \times \Gamma(\psi(2S) \to \gamma\eta_c(2S))/\Gamma_{total}$ — $\Gamma_9/\Gamma \times \Gamma^{\psi(2S)}_{200}/\Gamma^{\psi(2S)}$

VALUE	CL%	DOCUMENT ID	TECN	COMMENT
$<12.7 \times 10^{-7}$	90	ABLIKIM 11H	BES3	$\psi(2S) \to \gamma 2\pi^+2\pi^-$

$\Gamma(\eta_c(2S) \to 3\pi^+3\pi^-)/\Gamma_{total} \times \Gamma(\psi(2S) \to \gamma\eta_c(2S))/\Gamma_{total}$ — $\Gamma_{10}/\Gamma \times \Gamma^{\psi(2S)}_{200}/\Gamma^{\psi(2S)}$

VALUE (units 10^{-6})	CL%	EVTS	DOCUMENT ID	TECN	COMMENT
$9.2\pm1.0\pm1.2$		569	ABLIKIM 22Q	BES3	$\psi(2S) \to \gamma 3(\pi^+\pi^-)$
• • • We do not use the following data for averages, fits, limits, etc. • • •					
<13.2	90		[1] CRONIN-HEN..10	CLEO	$\psi(2S) \to \gamma 3\pi^+3\pi^-$

[1] Assuming $\Gamma(\eta_c(2S)) = 14$ MeV. CRONIN-HENNESSY 10 gives the analytic dependence of limits on width.

$\Gamma(\eta_c(2S) \to K^+K^-\pi^+\pi^-)/\Gamma_{total} \times \Gamma(\psi(2S) \to \gamma\eta_c(2S))/\Gamma_{total}$ — $\Gamma_{11}/\Gamma \times \Gamma^{\psi(2S)}_{200}/\Gamma^{\psi(2S)}$

VALUE	CL%	DOCUMENT ID	TECN	COMMENT
• • • We do not use the following data for averages, fits, limits, etc. • • •				
$<9.6 \times 10^{-6}$	90	[1] CRONIN-HEN..10	CLEO	$\psi(2S) \to \gamma K^+K^-\pi^+\pi^-$

[1] Assuming $\Gamma(\eta_c(2S)) = 14$ MeV. CRONIN-HENNESSY 10 gives the analytic dependence of limits on width.

$\Gamma(\eta_c(2S) \to K^{*0}\overline{K}^{*0})/\Gamma_{total} \times \Gamma(\psi(2S) \to \gamma\eta_c(2S))/\Gamma_{total}$ — $\Gamma_{12}/\Gamma \times \Gamma^{\psi(2S)}_{200}/\Gamma^{\psi(2S)}$

VALUE	CL%	DOCUMENT ID	TECN	COMMENT
$<19.6 \times 10^{-7}$	90	ABLIKIM 11H	BES3	$\psi(2S) \to \gamma K^+K^-\pi^+\pi^-$

$\Gamma(\eta_c(2S) \to K^+K^-\pi^+\pi^-\pi^0)/\Gamma_{total} \times \Gamma(\psi(2S) \to \gamma\eta_c(2S))/\Gamma_{total}$ — $\Gamma_{13}/\Gamma \times \Gamma^{\psi(2S)}_{200}/\Gamma^{\psi(2S)}$

VALUE	CL%	DOCUMENT ID	TECN	COMMENT
• • • We do not use the following data for averages, fits, limits, etc. • • •				
$<43.0 \times 10^{-6}$	90	[1] CRONIN-HEN..10	CLEO	$\psi(2S) \to \gamma K^+K^-\pi^+\pi^-\pi^0$

[1] Assuming $\Gamma(\eta_c(2S)) = 14$ MeV. CRONIN-HENNESSY 10 gives the analytic dependence of limits on width.

$\Gamma(\eta_c(2S) \to K^+K^-2\pi^+2\pi^-)/\Gamma_{total} \times \Gamma(\psi(2S) \to \gamma\eta_c(2S))/\Gamma_{total}$ — $\Gamma_{14}/\Gamma \times \Gamma^{\psi(2S)}_{200}/\Gamma^{\psi(2S)}$

VALUE	CL%	DOCUMENT ID	TECN	COMMENT
$<9.7 \times 10^{-6}$	90	[1] CRONIN-HEN..10	CLEO	$\psi(2S) \to \gamma K^+K^-2\pi^+2\pi^-$

[1] Assuming $\Gamma(\eta_c(2S)) = 14$ MeV. CRONIN-HENNESSY 10 gives the analytic dependence of limits on width.

Int. J. Mod. Phys. A 2026.41. Downloaded from www.worldscientific.com
by UNIVERSITY OF CALIFORNIA @ BERKELEY on 09/16/26. Re-use and distribution is strictly not permitted, except for Open Access articles.

$\Gamma(\eta_c(2S) \to K^0_S K^- 2\pi^+\pi^- + \text{c.c.})/\Gamma_{total} \times \Gamma(\psi(2S) \to \gamma\eta_c(2S))/\Gamma_{total}$ — $\Gamma_{15}/\Gamma \times \Gamma^{\psi(2S)}_{200}/\Gamma^{\psi(2S)}$

VALUE (units 10^{-6})	CL%	EVTS	DOCUMENT ID		TECN	COMMENT
7.9 ±1.8 OUR AVERAGE						
9.31±0.72±2.77		3140	ABLIKIM	24Q	BES3	$\psi(2S) \to \gamma K^0_S K^- 2\pi^+\pi^- +$c.c.
7.03±2.10±0.7		60	ABLIKIM	13K	BES3	$\psi(2S) \to \gamma K^0_S K^- 2\pi^+\pi^- +$c.c.
• • • We do not use the following data for averages, fits, limits, etc. • • •						
< 15.2	90		[1] CRONIN-HEN..	10	CLEO	$\psi(2S) \to \gamma K^0_S K^- 2\pi^+\pi^- +$c.c.

[1] Assuming $\Gamma(\eta_c(2S)) = 14$ MeV. CRONIN-HENNESSY 10 gives the analytic dependence of limits on width.

$\Gamma(\eta_c(2S) \to \phi\phi)/\Gamma_{total} \times \Gamma(\psi(2S) \to \gamma\eta_c(2S))/\Gamma_{total}$ — $\Gamma_{20}/\Gamma \times \Gamma^{\psi(2S)}_{200}/\Gamma^{\psi(2S)}$

VALUE	CL%	DOCUMENT ID		TECN	COMMENT
<7.8 × 10^{-7}	90	ABLIKIM	11H	BES3	$\psi(2S) \to \gamma K^+K^-K^+K^-$

$\Gamma(\eta_c(2S) \to p\overline{p})/\Gamma_{total} \times \Gamma(\psi(2S) \to \gamma\eta_c(2S))/\Gamma_{total}$ — $\Gamma_{23}/\Gamma \times \Gamma^{\psi(2S)}_{200}/\Gamma^{\psi(2S)}$

VALUE	CL%	DOCUMENT ID		TECN	COMMENT
<2.4 × 10^{-7}	90	ABLIKIM	25H	BES3	$\psi(2S) \to \gamma p\overline{p}$
• • • We do not use the following data for averages, fits, limits, etc. • • •					
<1.4 × 10^{-6}	90	[1] ABLIKIM	13V	BES3	$\psi(2S) \to \gamma p\overline{p}$

[1] Superseded by ABLIKIM 25H.

$\Gamma(\eta_c(2S) \to p\overline{p}K^+K^-)/\Gamma_{total} \times \Gamma(\psi(2S) \to \gamma\eta_c(2S))/\Gamma_{total}$ — $\Gamma_{25}/\Gamma \times \Gamma^{\psi(2S)}_{200}/\Gamma^{\psi(2S)}$

VALUE (units 10^{-7})	EVTS	DOCUMENT ID		TECN	COMMENT
1.98±0.41±0.99	84	ABLIKIM	25V	BES3	$e^+e^- \to \psi(2S)$

$\Gamma(\eta_c(2S) \to \gamma J/\psi(1S))/\Gamma_{total} \times \Gamma(\psi(2S) \to \gamma\eta_c(2S))/\Gamma_{total}$ — $\Gamma_{27}/\Gamma \times \Gamma^{\psi(2S)}_{200}/\Gamma^{\psi(2S)}$

VALUE	CL%	EVTS	DOCUMENT ID		TECN	COMMENT
<9.7 × 10^{-6}	90	33	[1] ABLIKIM	17N	BES3	$\psi(2S) \to \gamma\gamma J/\psi$

[1] Uses B($J/\psi \to e^+e^-$) = (5.971 ± 0.032)% and B($J/\psi \to \mu^+\mu^-$) = (5.961 ± 0.033)%.

$\Gamma(\eta_c(2S) \to \pi^+\pi^-\eta)/\Gamma_{total} \times \Gamma(\psi(2S) \to \gamma\eta_c(2S))/\Gamma_{total}$ — $\Gamma_{28}/\Gamma \times \Gamma^{\psi(2S)}_{200}/\Gamma^{\psi(2S)}$

VALUE (units 10^{-6})	CL%	EVTS	DOCUMENT ID		TECN	COMMENT
2.97±0.81±0.26		106	ABLIKIM	23Q	BES3	$\psi(2S) \to \gamma\pi^+\pi^-\eta$
• • • We do not use the following data for averages, fits, limits, etc. • • •						
<4.3	90		[1] CRONIN-HEN..	10	CLEO	$\psi(2S) \to \gamma\pi^+\pi^-\eta$

[1] Assuming $\Gamma(\eta_c(2S)) = 14$ MeV. CRONIN-HENNESSY 10 gives the analytic dependence of limits on width.

$\Gamma(\eta_c(2S) \to 2\pi^+2\pi^-\eta)/\Gamma_{total} \times \Gamma(\psi(2S) \to \gamma\eta_c(2S))/\Gamma_{total}$ — $\Gamma_{29}/\Gamma \times \Gamma^{\psi(2S)}_{200}/\Gamma^{\psi(2S)}$

VALUE (units 10^{-5})	EVTS	DOCUMENT ID		TECN	COMMENT
0.85±0.04±0.13	565	ABLIKIM	25R	BES3	$e^+e^- \to \psi(2S)$

$\Gamma(\eta_c(2S) \to \pi^+\pi^-\eta')/\Gamma_{total} \times \Gamma(\psi(2S) \to \gamma\eta_c(2S))/\Gamma_{total}$ — $\Gamma_{30}/\Gamma \times \Gamma^{\psi(2S)}_{200}/\Gamma^{\psi(2S)}$

VALUE	CL%	DOCUMENT ID		TECN	COMMENT
• • • We do not use the following data for averages, fits, limits, etc. • • •					
<14.2 × 10^{-6}	90	[1] CRONIN-HEN..	10	CLEO	$\psi(2S) \to \gamma\pi^+\pi^-\eta'$

[1] Assuming $\Gamma(\eta_c(2S)) = 14$ MeV. CRONIN-HENNESSY 10 gives the analytic dependence of limits on width.

$\Gamma(\eta_c(2S) \to \pi^+\pi^-\eta_c(1S))/\Gamma_{total} \times \Gamma(\psi(2S) \to \gamma\eta_c(2S))/\Gamma_{total}$ — $\Gamma_{31}/\Gamma \times \Gamma^{\psi(2S)}_{200}/\Gamma^{\psi(2S)}$

VALUE	CL%	DOCUMENT ID		TECN	COMMENT
<2.21 × 10^{-5}	90	[1] ABLIKIM	24Q	BES3	$\psi(2S) \to \gamma\pi^+\pi^-\eta_c(1S)$
• • • We do not use the following data for averages, fits, limits, etc. • • •					
<1.7 × 10^{-4}	90	[2] CRONIN-HEN..	10	CLEO	$\psi(2S) \to \gamma\pi^+\pi^-\eta_c(1S)$

[1] $\eta_c(1S)$ reconstructed in the final states $K^+K^-\pi^0$ and $K^0_S K^\pm\pi^\mp$.

[2] Assuming $\Gamma(\eta_c(2S)) = 14$ MeV. CRONIN-HENNESSY 10 gives the analytic dependence of limits on width.

$\Gamma(\eta_c(2S) \to \omega\omega)/\Gamma_{total} \times \Gamma(\psi(2S) \to \gamma\eta_c(2S))/\Gamma_{total}$ — $\Gamma_{21}/\Gamma \times \Gamma^{\psi(2S)}_{200}/\Gamma^{\psi(2S)}$

VALUE	CL%	DOCUMENT ID		TECN	COMMENT
<1.04 × 10^{-6}	90	ABLIKIM	25K	BES3	$\psi(2S) \to \gamma 2(\pi^+\pi^-\pi^0)$

$\Gamma(\eta_c(2S) \to \omega\phi)/\Gamma_{total} \times \Gamma(\psi(2S) \to \gamma\eta_c(2S))/\Gamma_{total}$ — $\Gamma_{22}/\Gamma \times \Gamma^{\psi(2S)}_{200}/\Gamma^{\psi(2S)}$

VALUE	CL%	DOCUMENT ID		TECN	COMMENT
<1.85 × 10^{-7}	90	ABLIKIM	25K	BES3	$\psi(2S) \to \gamma\pi^+\pi^-\pi^0K^+K^-$

$\eta_c(2S)$ REFERENCES

ABLIKIM	25H	PR D111 012003	M. Ablikim et al.	(BESIII Collab.)
ABLIKIM	25I	PR D111 012004	M. Ablikim et al.	(BESIII Collab.)
ABLIKIM	25K	PR D111 032001	M. Ablikim et al.	(BESIII Collab.)
ABLIKIM	25R	PR D111 052013	M. Ablikim et al.	(BESIII Collab.)
ABLIKIM	25V	PR D111 072001	M. Ablikim et al.	(BESIII Collab.)
ABLIKIM	24BT	PR D110 072009	M. Ablikim et al.	(BESIII Collab.)
ABLIKIM	24BW	PR D110 092003	M. Ablikim et al.	(BESIII Collab.)
ABLIKIM	24J	PR D109 032004	M. Ablikim et al.	(BESIII Collab.)
ABLIKIM	24Q	PR D109 072017	M. Ablikim et al.	(BESIII Collab.)
AAIJ	23AH	PR D108 032010	R. Aaij et al.	(LHCb Collab.)
ABLIKIM	23Q	PR D107 052007	M. Ablikim et al.	(BESIII Collab.)
ABLIKIM	22Q	PR D106 032014	M. Ablikim et al.	(BESIII Collab.)
CHILIKIN	19	PR D100 012001	K. Chilikin et al.	(BELLE Collab.)
XU	18	PR D98 072001	Q.N. Xu et al.	(BELLE Collab.)
AAIJ	17AD	PL B769 305	R. Aaij et al.	(LHCb Collab.)
AAIJ	17BB	EPJ C77 609	R. Aaij et al.	(LHCb Collab.)
ABLIKIM	17N	PR D95 072004	M. Ablikim et al.	(BESIII Collab.)
PDG	16	CP C40 100001	C. Patrignani et al.	(PDG Collab.)
LEES	14E	PR D89 112004	J.P. Lees et al.	(BABAR Collab.)
ABLIKIM	13K	PR D87 052005	M. Ablikim et al.	(BESIII Collab.)
ABLIKIM	13V	PR D88 112001	M. Ablikim et al.	(BESIII Collab.)
ABLIKIM	12G	PRL 109 042003	M. Ablikim et al.	(BESIII Collab.)
LEES	12AE	PR D86 092005	J.P. Lees et al.	(BABAR Collab.)
ABLIKIM	11H	PR D84 091102	M. Ablikim et al.	(BESIII Collab.)
DEL-AMO-SA...	11M	PR D84 012004	P. del Amo Sanchez et al.	(BABAR Collab.)
VINOKUROVA	11	PL B706 139	A. Vinokurova et al.	(BELLE Collab.)
CRONIN-HEN...	10	PR D81 052002	D. Cronin-Hennessey et al.	(CLEO Collab.)
AUBERT	08AB	PR D78 012006	B. Aubert et al.	(BABAR Collab.)
NAKAZAWA	08	NPBPS 184 220	H. Nakazawa	(BELLE Collab.)
UEHARA	08	EPJ C53 1	S. Uehara et al.	(BELLE Collab.)
WICHT	08	PL B662 323	J. Wicht et al.	(BELLE Collab.)
ABE	07	PRL 98 082001	K. Abe et al.	(BELLE Collab.)
AUBERT	06E	PRL 96 052002	B. Aubert et al.	(BABAR Collab.)
AUBERT	05C	PR D72 031101	B. Aubert et al.	(BABAR Collab.)
ABE	04G	PR D70 071102	K. Abe et al.	(BELLE Collab.)
ASNER	04	PRL 92 142001	D.M. Asner et al.	(CLEO Collab.)
AUBERT	04D	PRL 92 142002	B. Aubert et al.	(BABAR Collab.)
ABE,K	02	PRL 89 142001	K. Abe et al.	(BELLE Collab.)
CHOI	02	PRL 89 102001	S.-K. Choi et al.	(BELLE Collab.)
AMBROGIANI	01	PR D64 052003	M. Ambrogiani et al.	(FNAL E835 Collab.)
ABREU	98O	PL B441 479	P. Abreu et al.	(DELPHI Collab.)
ARMSTRONG	95F	PR D52 4839	T.A. Armstrong et al.	(FNAL, FERR, GENO+)
LEE	85	SLAC 282	R.A. Lee	(SLAC)
EDWARDS	82C	PRL 48 70	C. Edwards et al.	(CIT, HARV, PRIN+)

$\psi(2S)$

$I^G(J^{PC}) = 0^-(1^{--})$

See the Review on "Branching Ratios of $\psi(2S)$, $\chi_{c0,1,2}$ and $\eta_c(1S)$" before the $\chi_{c0}(1P)$ Listings.

$\psi(2S)$ MASS

OUR FIT includes measurements of $m_{\psi(2S)}$, $m_{\psi(3770)}$, and $m_{\psi(3770)} - m_{\psi(2S)}$.

VALUE (MeV)	EVTS	DOCUMENT ID		TECN	COMMENT
3686.097±0.011 OUR FIT Error includes scale factor of 1.1.					
3686.097±0.010 OUR AVERAGE					
3686.099±0.004±0.009		[1] ANASHIN	15	KEDR	$e^+e^- \to$ hadrons
3686.12 ±0.06 ±0.10	4k	AAIJ	12H	LHCB	$pp \to J/\psi\pi^+\pi^-X$
3685.95 ±0.10	413	[2] ARTAMONOV	00	OLYA	$e^+e^- \to$ hadrons
3685.98 ±0.09 ±0.04		[3] ARMSTRONG	93B	E760	$\overline{p}p \to e^+e^-$
• • • We do not use the following data for averages, fits, limits, etc. • • •					
3686.08 ±0.07	1301	[4] AAIJ	23AP	LHCB	$B^0_s \to J/\psi 2(\pi^+\pi^-)$
3686.114±0.007 $^{+0.011}_{-0.016}$		[5] ANASHIN	12	KEDR	$e^+e^- \to$ hadrons
3686.111±0.025±0.009		AULCHENKO	03	KEDR	$e^+e^- \to$ hadrons
3686.00 ±0.10	413	[6] ZHOLENTZ	80	OLYA	e^+e^-

[1] Supersedes AULCHENKO 03 and ANASHIN 12.

[2] Reanalysis of ZHOLENTZ 80 using new electron mass (COHEN 87) and radiative corrections (KURAEV 85).

[3] Mass central value and systematic error recalculated by us according to Eq. (16) in ARMSTRONG 93B, using the value for the $J/\psi(1S)$ mass from AULCHENKO 03.

[4] From a fit of a relativistic S-wave Breit-Wigner convolved with the detector resolution. The width of $\psi(2S)$ is constrained to the PDG 22 value. Systematic errors not evaluated.

[5] From the scans in 2004 and 2006. ANASHIN 12 reports the value 3686.114 ± 0.007 ± 0.011 $^{+0.002}_{-0.012}$ MeV, where the third uncertainty is due to assumptions on the interference between the resonance and hadronic continuum. We combined the two systematic uncertainties.

[6] Superseded by ARTAMONOV 00.

$m_{\psi(2S)} - m_{J/\psi(1S)}$

VALUE (MeV)	DOCUMENT ID		TECN	COMMENT
589.188±0.028 OUR AVERAGE				
589.194±0.027±0.011	[1] AULCHENKO	03	KEDR	$e^+e^- \to$ hadrons
589.7 ±1.2	LEMOIGNE	82	GOLI	185 π^-Be $\to \gamma\mu^+\mu^-$A
589.07 ±0.13	[1] ZHOLENTZ	80	OLYA	e^+e^-
588.7 ±0.8	LUTH	75	MRK1	
• • • We do not use the following data for averages, fits, limits, etc. • • •				
588 ±1	[2] BAI	98E	BES	e^+e^-

[1] Redundant with data in mass above.
[2] Systematic errors not evaluated.

$\psi(2S)$ WIDTH

VALUE (keV)	EVTS	DOCUMENT ID		TECN	COMMENT
293± 9 OUR FIT Error includes scale factor of 1.2.					
286±16 OUR AVERAGE					
358±88± 4		ABLIKIM	08B	BES2	$e^+e^- \to$ hadrons
290±25± 4	2.7k	ANDREOTTI	07	E835	$p\overline{p} \to e^+e^-$, $J/\psi X$
331±58± 2		ABLIKIM	06L	BES2	$e^+e^- \to$ hadrons
264±27		[1] BAI	02B	BES2	e^+e^-
287±37±16		[2] ARMSTRONG	93B	E760	$\overline{p}p \to e^+e^-$

[1] From a simultaneous fit to the hadronic and $\mu^+\mu^-$ cross section, assuming $\Gamma = \Gamma_h + \Gamma_e + \Gamma_\mu + \Gamma_\tau$ and lepton universality. Does not include vacuum polarization correction.
[2] The initial-state radiation correction reevaluated by ANDREOTTI 07 in its Ref. [4].

$\psi(2S)$ DECAY MODES

	Mode	Fraction (Γ_i/Γ)	Scale factor/ Confidence level
Γ_1	hadrons	(97.85 ±0.13) %	
Γ_2	virtual $\gamma \to$ hadrons	(1.79 ±0.04) %	
Γ_3	ggg	(10.6 ±1.6) %	
Γ_4	γgg	(1.03 ±0.29) %	
Γ_5	light hadrons	(15.4 ±1.5) %	
Γ_6	K^0_S anything	(16.1 ±1.1) %	
Γ_7	e^+e^-	(7.95 ±0.22) $\times 10^{-3}$	S=1.3
Γ_8	$\mu^+\mu^-$	(8.0 ±0.6) $\times 10^{-3}$	
Γ_9	$\tau^+\tau^-$	(3.1 ±0.4) $\times 10^{-3}$	
	Decays into $J/\psi(1S)$ and anything		
Γ_{10}	$J/\psi(1S)$ anything	(61.6 ±0.7) %	S=1.3
Γ_{11}	$J/\psi(1S)$ neutrals	(25.4 ±0.5) %	S=1.6
Γ_{12}	$J/\psi(1S)\pi^+\pi^-$	(34.78 ±0.33) %	S=1.1
Γ_{13}	$J/\psi(1S)\pi^0\pi^0$	(18.3 ±0.5) %	S=1.6
Γ_{14}	$J/\psi(1S)\eta$	(3.38 ±0.06) %	S=1.2
Γ_{15}	$J/\psi(1S)\pi^0$	(1.268±0.032) $\times 10^{-3}$	
	Hadronic decays		
Γ_{16}	$\pi^+\pi^-$	(7.8 ±2.6) $\times 10^{-6}$	
Γ_{17}	$\pi^+\pi^-\pi^0$	(2.01 ±0.17) $\times 10^{-4}$	S=1.7
Γ_{18}	$\rho(770)\pi \to \pi^+\pi^-\pi^0$	(3.2 ±1.2) $\times 10^{-5}$	S=1.8
Γ_{19}	$\rho(2150)\pi \to \pi^+\pi^-\pi^0$	(1.9 $^{+1.2}_{-0.4}$) $\times 10^{-4}$	
Γ_{20}	$2(\pi^+\pi^-)$	(2.4 ±0.6) $\times 10^{-4}$	S=2.2
Γ_{21}	$\rho^0\pi^+\pi^-$	(2.2 ±0.6) $\times 10^{-4}$	S=1.4
Γ_{22}	$2(\pi^+\pi^-)\pi^0$	(2.9 ±1.0) $\times 10^{-3}$	S=4.7
Γ_{23}	$\rho a_2(1320)$	(2.6 ±0.9) $\times 10^{-4}$	
Γ_{24}	$\pi^+\pi^-\pi^0\pi^0\pi^0$	(5.3 ±1.0) $\times 10^{-3}$	
Γ_{25}	$\rho^\pm\pi^\mp\pi^0\pi^0$	< 2.7 $\times 10^{-3}$	CL=90%
Γ_{26}	$\pi^+\pi^-4\pi^0$	(1.4 ±1.0) $\times 10^{-3}$	
Γ_{27}	$3(\pi^+\pi^-)$	(3.5 ±2.0) $\times 10^{-4}$	S=2.8
Γ_{28}	$2(\pi^+\pi^-\pi^0)$	(4.8 ±1.5) $\times 10^{-3}$	
Γ_{29}	$3(\pi^+\pi^-)\pi^0$	(3.5 ±1.6) $\times 10^{-3}$	
Γ_{30}	$2(\pi^+\pi^-)3\pi^0$	(1.42 ±0.31) %	
Γ_{31}	$\eta\pi^+\pi^-$	< 1.6 $\times 10^{-4}$	CL=90%
Γ_{32}	$\eta\pi^+\pi^-\pi^0$	(9.5 ±1.7) $\times 10^{-4}$	
Γ_{33}	$\eta 2(\pi^+\pi^-)$	(1.2 ±0.6) $\times 10^{-3}$	
Γ_{34}	$\eta\pi^+\pi^-\pi^0\pi^0$	< 4 $\times 10^{-4}$	CL=90%
Γ_{35}	$\eta\pi^+\pi^-3\pi^0$	< 2.1 $\times 10^{-3}$	CL=90%
Γ_{36}	$\eta 2(\pi^+\pi^-\pi^0)$	< 2.1 $\times 10^{-3}$	CL=90%
Γ_{37}	$\rho\eta$	(2.2 ±0.6) $\times 10^{-5}$	S=1.1
Γ_{38}	$\eta'\pi^+\pi^-\pi^0$	(4.5 ±2.1) $\times 10^{-4}$	
Γ_{39}	$\eta'\rho$	(1.9 $^{+1.7}_{-1.2}$) $\times 10^{-5}$	
Γ_{40}	$\omega\pi^0$	(2.1 ±0.6) $\times 10^{-5}$	
Γ_{41}	$\omega\pi^+\pi^-$	(7.3 ±1.2) $\times 10^{-4}$	S=2.1
Γ_{42}	$\omega\pi^+\pi^-2\pi^0$	(8.7 ±2.4) $\times 10^{-3}$	
Γ_{43}	$b_1^\pm\pi^\mp$	(4.0 ±0.6) $\times 10^{-4}$	S=1.1
Γ_{44}	$\omega f_2(1270)$	(2.2 ±0.4) $\times 10^{-4}$	
Γ_{45}	$\omega\pi^0\pi^0$	(1.11 ±0.35) $\times 10^{-3}$	
Γ_{46}	$\omega 3\pi^0$	< 8 $\times 10^{-4}$	CL=90%
Γ_{47}	$b_1^0\pi^0$	(2.4 ±0.6) $\times 10^{-4}$	
Γ_{48}	$\omega\eta$	< 1.1 $\times 10^{-5}$	CL=90%
Γ_{49}	$\omega\eta'$	(3.2 $^{+2.5}_{-2.1}$) $\times 10^{-5}$	
Γ_{50}	$\omega(782)\eta\eta$	(1.65 ±0.21) $\times 10^{-5}$	
Γ_{51}	$\phi\pi^0$	< 4 $\times 10^{-7}$	CL=90%
Γ_{52}	$\phi\pi^+\pi^-$	(1.18 ±0.26) $\times 10^{-4}$	S=1.5
Γ_{53}	$\phi f_0(980) \to \pi^+\pi^-$	(7.5 ±3.3) $\times 10^{-5}$	S=1.6
Γ_{54}	$\phi\eta$	(3.10 ±0.31) $\times 10^{-5}$	
Γ_{55}	$\eta\phi(2170)$, $\phi(2170) \to \phi f_0(980)$, $f_0 \to \pi^+\pi^-$	< 2.2 $\times 10^{-6}$	CL=90%
Γ_{56}	$\phi\eta'$	(1.54 ±0.20) $\times 10^{-5}$	
Γ_{57}	$\phi\eta\eta'$	(3.14 ±0.29) $\times 10^{-5}$	
Γ_{58}	$h_1(1900)\eta \to \phi\eta\eta'$	(3.8 ±2.1) $\times 10^{-6}$	
Γ_{59}	$\phi(2170)\eta \to \phi\eta\eta'$	(3.3 ±1.8) $\times 10^{-6}$	
Γ_{60}	$\phi(2170)\eta' \to \phi\eta\eta'$	(3.8 ±1.0) $\times 10^{-6}$	
Γ_{61}	$h_1(2300)\eta \to \phi\eta\eta'$	(2.2 ±1.0) $\times 10^{-6}$	
Γ_{62}	$h_1(2300)\eta' \to \phi\eta\eta'$	(4.8 ±1.5) $\times 10^{-6}$	
Γ_{63}	$\phi\phi\phi$	(1.46 ±0.18) $\times 10^{-5}$	
Γ_{64}	$\phi f_1(1285)$	(3.0 ±1.3) $\times 10^{-5}$	
Γ_{65}	$\phi\eta(1405) \to \phi\pi^+\pi^-\eta$	(8.5 ±1.7) $\times 10^{-6}$	
Γ_{66}	$\phi f'_2(1525)$	(4.4 ±1.6) $\times 10^{-5}$	
Γ_{67}	K^+K^-	(7.5 ±0.5) $\times 10^{-5}$	
Γ_{68}	$K^+K^-\pi^+\pi^-$	(7.3 ±0.5) $\times 10^{-4}$	
Γ_{69}	$K^+K^-\pi^0$	(4.07 ±0.31) $\times 10^{-5}$	
Γ_{70}	$K^0_S K^0_S$	< 1.1 $\times 10^{-8}$	CL=90%
Γ_{71}	$K^0_S K^0_L$	(5.34 ±0.33) $\times 10^{-5}$	
Γ_{72}	$K^0_S K^0_L \pi^0$	< 3.0 $\times 10^{-4}$	CL=90%
Γ_{73}	$K^+K^-\pi^0\pi^0$	(2.6 ±1.3) $\times 10^{-4}$	
Γ_{74}	$K^+K^-\pi^0\pi^0\pi^0$	(6.6 ±2.8) $\times 10^{-4}$	
Γ_{75}	$K^0_S K^\pm\pi^\mp\pi^0\pi^0$	(1.7 ±0.6) $\times 10^{-3}$	
Γ_{76}	$K^0_S K^\pm\pi^\mp\pi^+\pi^-$	(2.2 ±0.4) $\times 10^{-3}$	
Γ_{77}	$K^+K^-\pi^+\pi^-\pi^0$	(1.26 ±0.09) $\times 10^{-3}$	
Γ_{78}	$\omega f_0(1710) \to \omega K^+K^-$	(5.9 ±2.2) $\times 10^{-5}$	
Γ_{79}	$K^*(892)^0K^-\pi^+\pi^0$ + c.c.	(8.6 ±2.2) $\times 10^{-4}$	
Γ_{80}	$K^*(892)^+K^-\pi^+\pi^-$ + c.c.	(9.6 ±2.8) $\times 10^{-4}$	
Γ_{81}	$K^*(892)^+K^-\rho^0$ + c.c.	(7.3 ±2.6) $\times 10^{-4}$	
Γ_{82}	$K^*(892)^0K^-\rho^+$ + c.c.	(6.1 ±1.8) $\times 10^{-4}$	
Γ_{83}	$K^0_S K^0_S \pi^+\pi^-$	(2.2 ±0.4) $\times 10^{-4}$	
Γ_{84}	$K^0_S K^0_L \pi^0\pi^0$	(1.3 ±0.6) $\times 10^{-3}$	
Γ_{85}	$K^0_S K^*(892)^0\pi^0\pi^0$	(3.1 ±1.3) $\times 10^{-4}$	
Γ_{86}	$K^0_S K^\pm\rho(770)^\mp\pi^0$	< 7 $\times 10^{-4}$	CL=90%
Γ_{87}	$K^0_S K^\pm\pi^\mp\rho(770)^0$	< 7 $\times 10^{-4}$	CL=90%
Γ_{88}	$K^\mp K^*(892)^\pm\pi^0\pi^0$	(7.0 ±2.9) $\times 10^{-4}$	
Γ_{89}	$K^*(892)^+K^*(892)^-\pi^0$	(3.6 ±1.8) $\times 10^{-3}$	
Γ_{90}	$K^0_S K^0_L \eta$	(1.3 ±0.5) $\times 10^{-3}$	
Γ_{91}	$K^+K^-\rho^0$	(2.2 ±0.4) $\times 10^{-4}$	
Γ_{92}	$K^*(892)^0\overline{K}^*_2(1430)^0$	(1.9 ±0.5) $\times 10^{-4}$	
Γ_{93}	$K^+K^-\pi^+\pi^-\eta$	(1.3 ±0.7) $\times 10^{-3}$	
Γ_{94}	$K^+K^-2(\pi^+\pi^-)$	(1.9 ±0.9) $\times 10^{-3}$	
Γ_{95}	$K^+K^-2(\pi^+\pi^-)\pi^0$	(1.00 ±0.31) $\times 10^{-3}$	
Γ_{96}	$K^+K^*(892)^-$ + c.c.	(2.9 ±0.4) $\times 10^{-5}$	S=1.2
Γ_{97}	$2(K^+K^-)$	(6.3 ±1.3) $\times 10^{-5}$	
Γ_{98}	$2(K^+K^-)\pi^0$	(1.10 ±0.28) $\times 10^{-4}$	
Γ_{99}	$K^+K^-\phi$	(7.0 ±1.6) $\times 10^{-5}$	
Γ_{100}	$K^0_S K^0_S \phi$	(3.53 ±0.29) $\times 10^{-5}$	
Γ_{101}	$K_1(1270)^\pm K^\mp$	(1.00 ±0.28) $\times 10^{-3}$	
Γ_{102}	$K^+\overline{K}^*(892)^0\pi^-$ + c.c.	(6.7 ±2.5) $\times 10^{-4}$	
Γ_{103}	ηK^+K^-, no $\eta\phi$	(3.49 ±0.17) $\times 10^{-5}$	
Γ_{104}	ηK^+K^-	< 2.6 $\times 10^{-4}$	CL=90%
Γ_{105}	$X(1750)\eta \to K^+K^-\eta$	(4.8 ±2.8) $\times 10^{-6}$	
Γ_{106}	$K_1(1400)^\pm K^\mp$	< 3.1 $\times 10^{-4}$	CL=90%
Γ_{107}	$K^*_2(1430)^\pm K^\mp$	(7.1 $^{+1.3}_{-0.9}$) $\times 10^{-5}$	
Γ_{108}	$K^*(892)^0\overline{K}^0$ + c.c.	(1.09 ±0.20) $\times 10^{-4}$	
Γ_{109}	ωK^+K^-	(1.62 ±0.11) $\times 10^{-4}$	S=1.1
Γ_{110}	$\omega K^0_S K^0_S$	(7.0 ±0.5) $\times 10^{-5}$	
Γ_{111}	$\omega K^*(892)^+K^-$ + c.c.	(2.07 ±0.26) $\times 10^{-4}$	
Γ_{112}	$\omega K^*_2(1430)^+K^-$ + c.c.	(6.1 ±1.2) $\times 10^{-5}$	
Γ_{113}	$\omega\overline{K}^*(892)^0K^0$	(1.68 ±0.30) $\times 10^{-4}$	
Γ_{114}	$\omega\overline{K}^*_2(1430)^0K^0$	(5.8 ±2.2) $\times 10^{-5}$	
Γ_{115}	$\omega X(1440) \to \omega K^0_S K^-\pi^+$ + c.c.	(1.6 ±0.4) $\times 10^{-5}$	
Γ_{116}	$\omega X(1440) \to \omega K^+K^-\pi^0$	(1.09 ±0.26) $\times 10^{-5}$	
Γ_{117}	$\omega f_1(1285) \to \omega K^0_S K^-\pi^+$ + c.c.	(3.0 ±1.0) $\times 10^{-6}$	
Γ_{118}	$\omega f_1(1285) \to \omega K^+K^-\pi^0$	(1.2 ±0.7) $\times 10^{-6}$	
Γ_{119}	$p\overline{p}$	(2.95 ±0.09) $\times 10^{-4}$	S=1.3
Γ_{120}	$n\overline{n}$	(3.06 ±0.15) $\times 10^{-4}$	
Γ_{121}	$p\overline{p}\pi^0$	1.2×10^{-4} to 2.4×10^{-4}	
Γ_{122}	$N(940)\overline{p}$ + c.c. $\to p\overline{p}\pi^0$	(1.14 ±0.12) $\times 10^{-4}$	

Int. J. Mod. Phys. A 2026.41. Downloaded from www.worldscientific.com
by [redacted]LIFORNIA @ BERKELEY on 09/16/26. Re-use and distribution is strictly not permitted, except for Open Access articles.

Int. J. Mod. Phys. A 2026.41. Downloaded from www.worldscientific.com
by UNIVERSITY OF CALIFORNIA @ BERKELEY on 09/16/26. Re-use and distribution is strictly not permitted, except for Open Access articles.

Γ_{123}	$N(1440)\overline{p}+$ c.c. $\to p\overline{p}\pi^0$	$(7.5 \pm 1.1) \times 10^{-5}$		S=1.7
Γ_{124}	$N(1520)\overline{p}+$ c.c. $\to p\overline{p}\pi^0$	$(6.6 \pm 2.0) \times 10^{-6}$		
Γ_{125}	$N(1535)\overline{p}+$ c.c. $\to p\overline{p}\pi^0$	$(1.7 \pm 0.4) \times 10^{-5}$		
Γ_{126}	$N(1650)\overline{p}+$ c.c. $\to p\overline{p}\pi^0$	$(9.1 \pm 3.3) \times 10^{-6}$		
Γ_{127}	$N(1710)\overline{p}+$ c.c. $\to p\overline{p}\pi^0$	$(4 \pm 4) \times 10^{-6}$		
Γ_{128}	$N(1720)\overline{p}+$ c.c. $\to p\overline{p}\pi^0$	$(6.2 \pm 2.5) \times 10^{-6}$		
Γ_{129}	$N(2100)\overline{p}+$ c.c. $\to p\overline{p}\pi^0$	$(8 \pm 4) \times 10^{-6}$		
Γ_{130}	$N(2300)\overline{p}+$ c.c. $\to p\overline{p}\pi^0$	$(3.6 \pm 3.1) \times 10^{-6}$		
Γ_{131}	$N(2570)\overline{p}+$ c.c. $\to p\overline{p}\pi^0$	$(1.9 \pm 1.5) \times 10^{-5}$		
Γ_{132}	$p\overline{p}\pi^+\pi^-$	$(6.0 \pm 0.4) \times 10^{-4}$		
Γ_{133}	$p\overline{p}K^+K^-$	$(2.7 \pm 0.7) \times 10^{-5}$		
Γ_{134}	$p\overline{p}\eta$	5.5×10^{-5} to 9.1×10^{-5}		
Γ_{135}	$N(1535)\overline{p}+$ c.c. $\to p\overline{p}\eta$	$(4.7 \pm 0.5) \times 10^{-5}$		
Γ_{136}	$N(1710)\overline{p}+$ c.c. $\to p\overline{p}\eta$	$(7.8 \pm 3.2) \times 10^{-6}$		
Γ_{137}	$p\overline{p}\pi^+\pi^-\pi^0$	$(7.3 \pm 0.7) \times 10^{-4}$		
Γ_{138}	$p\overline{p}\rho^0$	$(5.0 \pm 2.2) \times 10^{-5}$		
Γ_{139}	$p\overline{p}\omega$	$(6.9 \pm 2.1) \times 10^{-5}$		
Γ_{140}	$p\overline{p}\eta'$	$(1.10 \pm 0.13) \times 10^{-5}$		
Γ_{141}	$p\overline{p}\phi$	$(6.1 \pm 0.6) \times 10^{-6}$		
Γ_{142}	$\phi X(1835) \to p\overline{p}\phi$	$< 1.82 \times 10^{-7}$		CL=90%
Γ_{143}	$p\overline{n}\pi^-$ or c.c.	$(2.48 \pm 0.17) \times 10^{-4}$		
Γ_{144}	$p\overline{n}\pi^-\pi^0$	$(3.2 \pm 0.7) \times 10^{-4}$		
Γ_{145}	$\Lambda\overline{\Lambda}$	$(3.81 \pm 0.13) \times 10^{-4}$		S=1.4
Γ_{146}	$\Lambda\overline{\Lambda}\pi^0$	$(1.4 \pm 0.7) \times 10^{-6}$		
Γ_{147}	$\Lambda\overline{\Lambda}\eta$	$(2.43 \pm 0.32) \times 10^{-5}$		
Γ_{148}	$\Lambda(1670)\overline{\Lambda} \to \Lambda\overline{\Lambda}\eta$	$(1.3 \pm 0.7) \times 10^{-5}$		
Γ_{149}	$\Lambda\overline{\Lambda}\eta'$	$(7.3 \pm 1.0) \times 10^{-6}$		
Γ_{150}	$\Lambda\overline{\Lambda}\omega(782)$	$(3.3 \pm 0.4) \times 10^{-5}$		
Γ_{151}	$\Lambda\overline{\Lambda}\pi^+\pi^-$	$(2.8 \pm 0.6) \times 10^{-4}$		
Γ_{152}	$\Lambda\overline{p}K^+$	$(1.00 \pm 0.14) \times 10^{-4}$		
Γ_{153}	$\Lambda\overline{p}K^*(892)^+$ + c.c.	$(6.3 \pm 0.7) \times 10^{-5}$		
Γ_{154}	$\Lambda\overline{p}K^+\pi^+\pi^-$	$(1.8 \pm 0.4) \times 10^{-4}$		
Γ_{155}	$\overline{\Lambda}nK^0_S$ + c.c.	$(8.1 \pm 1.8) \times 10^{-5}$		
Γ_{156}	$\Delta^{++}\overline{\Delta}^{--}$	$(1.28 \pm 0.35) \times 10^{-4}$		
Γ_{157}	$\Lambda\overline{\Sigma}^+\pi^-$ + c.c.	$(1.40 \pm 0.13) \times 10^{-4}$		
Γ_{158}	$\Lambda\overline{\Sigma}^-\pi^+$ + c.c.	$(1.54 \pm 0.14) \times 10^{-4}$		
Γ_{159}	$\Lambda\overline{\Sigma}^0$ + c.c.	$(1.6 \pm 0.7) \times 10^{-6}$		
Γ_{160}	$\Lambda\overline{\Sigma}^0$			
Γ_{161}	$\Lambda\overline{\Sigma}^0\pi^0$ + c.c.	$(1.54 \pm 0.07) \times 10^{-4}$		
Γ_{162}	$\Lambda(1520)\overline{\Xi}^+K^-$ + c.c., $\Lambda(1520) \to pK^-$	$(9.5 \pm 1.2) \times 10^{-7}$		
Γ_{163}	$\Sigma^0\overline{p}K^+$ + c.c.	$(1.67 \pm 0.18) \times 10^{-5}$		
Γ_{164}	$\Sigma^+\overline{\Sigma}^-$	$(2.43 \pm 0.10) \times 10^{-4}$		S=1.4
Γ_{165}	$\Sigma^0\overline{\Sigma}^0$	$(2.35 \pm 0.09) \times 10^{-4}$		S=1.1
Γ_{166}	$\Sigma^-\overline{\Sigma}^+$	$(2.82 \pm 0.09) \times 10^{-4}$		
Γ_{167}	$\Sigma^+\overline{\Sigma}^-\eta$	$(9.6 \pm 2.4) \times 10^{-6}$		
Γ_{168}	$\Sigma^+\overline{\Sigma}^-\omega$	$(1.89 \pm 0.28) \times 10^{-5}$		
Γ_{169}	$\Sigma^0\overline{\Sigma}^0\omega(782)$	$(1.24 \pm 0.19) \times 10^{-5}$		
Γ_{170}	$\Sigma^+\overline{\Sigma}^-\phi$	$(3.0 \pm 0.7) \times 10^{-6}$		
Γ_{171}	$\Sigma^0\overline{\Sigma}^0\phi$	$(2.64 \pm 0.34) \times 10^{-6}$		
Γ_{172}	$\Sigma(1385)^+\overline{\Sigma}(1385)^-$	$(8.5 \pm 0.7) \times 10^{-5}$		
Γ_{173}	$\Sigma(1385)^-\overline{\Sigma}(1385)^+$	$(8.5 \pm 0.8) \times 10^{-5}$		
Γ_{174}	$\Sigma(1385)^0\overline{\Sigma}(1385)^0$	$(6.9 \pm 0.7) \times 10^{-5}$		
Γ_{175}	$\Xi^-\overline{\Xi}^+$	$(2.87 \pm 0.11) \times 10^{-4}$		S=1.1
Γ_{176}	$\Xi^0\overline{\Xi}^0$	$(2.3 \pm 0.4) \times 10^{-4}$		S=4.2
Γ_{177}	$\Xi(1530)^0\overline{\Xi}(1530)^0$	$(6.8 \pm 0.4) \times 10^{-5}$		
Γ_{178}	$\Lambda\overline{\Xi}^+K^-$ + c.c.	$(3.67 \pm 0.22) \times 10^{-5}$		
Γ_{179}	$\Xi(1690)^-\overline{\Xi}^+ \to K^-\Lambda\overline{\Xi}^+$ + c.c.	$(6.2 \pm 2.1) \times 10^{-6}$		S=1.5
Γ_{180}	$\Xi(1820)^-\overline{\Xi}^+ \to K^-\Lambda\overline{\Xi}^+$ + c.c.	$(1.48 \pm 0.29) \times 10^{-5}$		S=1.2
Γ_{181}	$\Xi(1530)^-\overline{\Xi}(1530)^+$	$(1.15 \pm 0.07) \times 10^{-4}$		
Γ_{182}	$\Xi(1530)^-\overline{\Xi}^+$	$(7.0 \pm 1.2) \times 10^{-6}$		
Γ_{183}	$\Xi(1530)^0\overline{\Xi}^0$	$(5.3 \pm 0.5) \times 10^{-6}$		
Γ_{184}	$\Sigma^0\overline{\Xi}^+K^-$ + c.c.	$(3.7 \pm 0.4) \times 10^{-5}$		
Γ_{185}	$\Omega^-K^+\overline{\Xi}^0$ + c.c.	$(2.8 \pm 0.4) \times 10^{-6}$		
Γ_{186}	$\overline{\Omega}^+K^0_S\Xi^-$ + c.c.	$(2.9 \pm 0.6) \times 10^{-6}$		
Γ_{187}	$\Omega^-\overline{\Omega}^+$	$(5.66 \pm 0.30) \times 10^{-5}$		S=1.3
Γ_{188}	$\eta_c\pi^+\pi^-\pi^0$	$< 1.0 \times 10^{-3}$		CL=90%
Γ_{189}	$h_c(1P)\pi^0$	$(7.4 \pm 0.5) \times 10^{-4}$		
Γ_{190}	$\Lambda_c^+\overline{p}e^+e^-$ + c.c.	$< 1.7 \times 10^{-6}$		CL=90%
Γ_{191}	$\Theta(1540)\overline{\Theta}(1540) \to K^0_S pK^-\overline{n}$ + c.c.	[a] $< 8.8 \times 10^{-6}$		CL=90%
Γ_{192}	$\Theta(1540)K^-\overline{n} \to K^0_S pK^-\overline{n}$	[a] $< 1.0 \times 10^{-5}$		CL=90%
Γ_{193}	$\Theta(1540)K^0_S\overline{p} \to K^0_S\overline{p}K^+n$	[a] $< 7.0 \times 10^{-6}$		CL=90%
Γ_{194}	$\overline{\Theta}(1540)K^+n \to K^0_S\overline{p}K^+n$	[a] $< 2.6 \times 10^{-5}$		CL=90%
Γ_{195}	$\overline{\Theta}(1540)K^0_S p \to K^0_S pK^-\overline{n}$	[a] $< 6.0 \times 10^{-6}$		CL=90%
	Radiative decays			
Γ_{196}	$\gamma\chi_{c0}(1P)$	(10.06 ± 0.27) %		S=1.4
Γ_{197}	$\gamma\chi_{c1}(1P)$	(9.85 ± 0.26) %		S=1.2
Γ_{198}	$\gamma\chi_{c2}(1P)$	(9.63 ± 0.23) %		S=1.2
Γ_{199}	$\gamma\eta_c(1S)$	$(3.6 \pm 0.5) \times 10^{-3}$		S=1.3
Γ_{200}	$\gamma\eta_c(2S)$	$(5.4 {}^{+3.4}_{-2.9}) \times 10^{-4}$		
Γ_{201}	$\gamma\pi^0$			
Γ_{202}	$\gamma 2(\pi^+\pi^-)$	$(4.0 \pm 0.6) \times 10^{-4}$		
Γ_{203}	$\gamma 3(\pi^+\pi^-)$	$< 1.7 \times 10^{-4}$		CL=90%
Γ_{204}	$\gamma\eta'(958)$	$(1.24 \pm 0.04) \times 10^{-4}$		
Γ_{205}	$\gamma f_2(1270)$	$(2.73 {}^{+0.29}_{-0.25}) \times 10^{-4}$		S=1.8
Γ_{206}	$\gamma f_2(1270) \to \gamma K^0_S K^0_S$	$(2.1 \pm 0.9) \times 10^{-6}$		
Γ_{207}	$\gamma f_0(1370) \to \gamma K\overline{K}$	$(3.1 \pm 1.7) \times 10^{-5}$		
Γ_{208}	$\gamma f_0(1370) \to \gamma K^0_S K^0_S$	$(1.2 {}^{+3.2}_{-1.7}) \times 10^{-6}$		
Γ_{209}	$\gamma f_0(1500)$	$(9.3 \pm 1.9) \times 10^{-5}$		
Γ_{210}	$\gamma f_0(1500) \to \gamma K^0_S K^0_S$	$(1.7 {}^{+1.7}_{-1.2}) \times 10^{-6}$		
Γ_{211}	$\gamma f'_2(1525)$	$(3.3 \pm 0.8) \times 10^{-5}$		
Γ_{212}	$\gamma f'_2(1525) \to \gamma K^0_S K^0_S$	$(1.4 \pm 0.6) \times 10^{-6}$		
Γ_{213}	$\gamma f_0(1710)$	seen		
Γ_{214}	$\gamma f_0(1710) \to \gamma\pi\pi$	$(3.5 \pm 0.6) \times 10^{-5}$		
Γ_{215}	$\gamma f_0(1710) \to \gamma K\overline{K}$	$(6.6 \pm 0.7) \times 10^{-5}$		
Γ_{216}	$\gamma f_0(1710) \to \gamma K^0_S K^0_S$	$(1.83 {}^{+0.32}_{-0.27}) \times 10^{-5}$		
Γ_{217}	$\gamma f_2(1950) \to \gamma K^0_S K^0_S$	$(1.2 {}^{+1.0}_{-0.8}) \times 10^{-6}$		
Γ_{218}	$\gamma f_0(2020) \to \gamma K^0_S K^0_S$	$(4.6 \pm 1.5) \times 10^{-6}$		
Γ_{219}	$\gamma f_0(2100) \to \gamma\pi\pi$	$(4.8 \pm 1.0) \times 10^{-6}$		
Γ_{220}	$\gamma f_0(2200) \to \gamma K\overline{K}$	$(3.2 \pm 1.0) \times 10^{-6}$		
Γ_{221}	$\gamma f_J(2220) \to \gamma\pi\pi$	$< 5.8 \times 10^{-6}$		CL=90%
Γ_{222}	$\gamma f_J(2220) \to \gamma K\overline{K}$	$< 9.5 \times 10^{-6}$		CL=90%
Γ_{223}	$\gamma\eta$	$(9.2 \pm 1.8) \times 10^{-7}$		
Γ_{224}	$\gamma\eta\pi^+\pi^-$	$(8.7 \pm 2.1) \times 10^{-4}$		
Γ_{225}	$\gamma\eta(1405)$	seen		
Γ_{226}	$\gamma\eta(1405) \to \gamma K\overline{K}\pi$	$< 9 \times 10^{-5}$		CL=90%
Γ_{227}	$\gamma\eta(1405) \to \gamma\eta\pi^+\pi^-$	$(3.6 \pm 2.5) \times 10^{-5}$		
Γ_{228}	$\gamma\eta(1405) \to \gamma f_0(980)\pi^0 \to \gamma\pi^+\pi^-\pi^0$	$< 5.0 \times 10^{-7}$		CL=90%
Γ_{229}	$\gamma\eta(1475)$	seen		
Γ_{230}	$\gamma\eta(1475) \to \gamma K\overline{K}\pi$	$< 1.4 \times 10^{-4}$		CL=90%
Γ_{231}	$\gamma\eta(1475) \to \gamma\eta\pi^+\pi^-$	$< 8.8 \times 10^{-5}$		CL=90%
Γ_{232}	$\gamma K^{*0}K^+\pi^-$ + c.c.	$(3.7 \pm 0.9) \times 10^{-4}$		
Γ_{233}	$\gamma K^{*0}\overline{K}^{*0}$	$(2.4 \pm 0.7) \times 10^{-4}$		
Γ_{234}	$\gamma K^0_S K^+\pi^-$ + c.c.	$(2.6 \pm 0.5) \times 10^{-4}$		
Γ_{235}	$\gamma K^+K^-\pi^+\pi^-$	$(1.9 \pm 0.5) \times 10^{-4}$		
Γ_{236}	$\gamma K^+K^-2(\pi^+\pi^-)$	$< 2.2 \times 10^{-4}$		CL=90%
Γ_{237}	$\gamma 2(K^+K^-)$	$< 4 \times 10^{-5}$		CL=90%
Γ_{238}	$\gamma p\overline{p}$	$(3.9 \pm 0.5) \times 10^{-5}$		S=2.0
Γ_{239}	$\gamma f_2(1950) \to \gamma p\overline{p}$	$(1.20 \pm 0.22) \times 10^{-5}$		
Γ_{240}	$\gamma f_2(2150) \to \gamma p\overline{p}$	$(7.2 \pm 1.8) \times 10^{-6}$		
Γ_{241}	$\gamma X(1835) \to \gamma p\overline{p}$	$(4.6 {}^{+1.8}_{-4.0}) \times 10^{-6}$		
Γ_{242}	$\gamma X \to \gamma p\overline{p}$	[b] $< 2 \times 10^{-6}$		CL=90%
Γ_{243}	$\gamma p\overline{p}\pi^+\pi^-$	$(2.8 \pm 1.4) \times 10^{-5}$		
Γ_{244}	$\gamma\gamma$	$< 1.5 \times 10^{-4}$		CL=90%
Γ_{245}	$\gamma\gamma J/\psi$	$(3.1 {}^{+1.0}_{-1.2}) \times 10^{-4}$		
Γ_{246}	$e^+e^-\eta'$	$(1.90 \pm 0.26) \times 10^{-6}$		
Γ_{247}	$e^+e^-\eta_c(1S)$	$(3.8 \pm 0.4) \times 10^{-5}$		
Γ_{248}	$e^+e^-\chi_{c0}(1P)$	$(1.10 \pm 0.26) \times 10^{-3}$		
Γ_{249}	$e^+e^-\chi_{c1}(1P)$	$(8.6 \pm 0.7) \times 10^{-4}$		
Γ_{250}	$e^+e^-\chi_{c2}(1P)$	$(7.0 \pm 0.8) \times 10^{-4}$		
	Weak decays			
Γ_{251}	$D^0e^+e^-$ + c.c.	$< 1.4 \times 10^{-7}$		CL=90%
Γ_{252}	$\Lambda_c^+\overline{\Sigma}^-$ + c.c.	$< 1.4 \times 10^{-5}$		CL=90%
	Other decays			
Γ_{253}	invisible	< 1.6 %		CL=90%

[a] $\Theta(1540)$ is a hypothetical pentaquark state of 1.54 GeV/c^2 mass and a width of less than 25 MeV/c^2.

[b] For a narrow resonance in the range $2.2 < M(X) < 2.8$ GeV.

Int. J. Mod. Phys. A 2026.41. Downloaded from www.worldscientific.com
by CALIFORNIA @ BERKELEY on 09/16/26. Re-use and distribution is strictly not permitted, except for Open Access articles.

CONSTRAINED FIT INFORMATION

A multiparticle fit to $\chi_{c1}(1P)$, $\chi_{c0}(1P)$, $\chi_{c2}(1P)$, and $\psi(2S)$ with 4 total widths, a partial width, 27 combinations of partial widths obtained from integrated cross section, and 87 branching ratios uses 263 measurements to determine 50 parameters. The overall fit has a $\chi^2 = 435.4$ for 213 degrees of freedom.

The following *off-diagonal* array elements are the correlation coefficients $\langle \delta p_i \delta p_j \rangle / (\delta p_i \cdot \delta p_j)$, in percent, from the fit to parameters p_i, including the branching fractions, $x_i \equiv \Gamma_i/\Gamma_{total}$.

x_8	3									
x_9	0	0								
x_{12}	20	13	2							
x_{13}	22	4	1	28						
x_{14}	10	6	1	43	11					
x_{119}	0	0	0	3	2	1				
x_{196}	0	0	0	2	0	1	0			
x_{197}	1	0	0	3	0	1	0	0		
x_{198}	1	0	0	3	0	1	0	0	0	
Γ	−85	−4	−1	−29	−31	−15	−4	−1	−1	−1
	x_7	x_8	x_9	x_{12}	x_{13}	x_{14}	x_{119}	x_{196}	x_{197}	x_{198}

FIT INFORMATION

A multiparticle fit to $\eta_c(2S)$ and $\psi(2S)$ with 4 branching ratios uses 5 measurements to determine 3 parameters. The overall fit has a $\chi^2 = 2.6$ for 2 degrees of freedom.

FIT INFORMATION

A multiparticle fit to $\eta_c(1S)$, $J/\psi(1S)$, $\psi(2S)$, $h_c(1P)$, and $B^{\pm}$ with the total width, 10 combinations of partial widths obtained from integrated cross section, and 38 branching ratios uses 115 measurements to determine 19 parameters. The overall fit has a $\chi^2 = 215.4$ for 96 degrees of freedom.

$\psi(2S)$ PARTIAL WIDTHS

Γ(hadrons) — Γ_1

VALUE (keV)	DOCUMENT ID		TECN	COMMENT
• • • We do not use the following data for averages, fits, limits, etc. • • •				
258±26	BAI	02B	BES2	e^+e^-
224±56	LUTH	75	MRK1	e^+e^-

$\Gamma(e^+e^-)$ — Γ_7

VALUE (keV)	DOCUMENT ID		TECN	COMMENT
2.33 ±0.04 OUR FIT Error includes scale factor of 1.1.				
2.29 ±0.06 OUR AVERAGE				
2.22 ±0.10 ±0.02	[1] ABLIKIM	15V	BES3	4.0–4.4 $e^+e^- \to \pi^+\pi^- J/\psi$
2.338±0.037±0.096	ABLIKIM	08B	BES2	$e^+e^- \to$ hadrons
2.330±0.036±0.110	ABLIKIM	06L	BES2	$e^+e^- \to$ hadrons
2.44 ±0.21	[2] BAI	02B	BES2	e^+e^-
2.14 ±0.21	ALEXANDER	89	RVUE	See Υ mini-review
• • • We do not use the following data for averages, fits, limits, etc. • • •				
2.279±0.015±0.042	[3] ANASHIN	18	KEDR	e^+e^-
2.282±0.015±0.042	[4] ANASHIN	18	KEDR	e^+e^-
2.0 ±0.3	BRANDELIK	79C	DASP	e^+e^-
2.1 ±0.3	[5] LUTH	75	MRK1	e^+e^-

[1] ABLIKIM 15V reports 2.213 ± 0.018 ± 0.099 keV from a measurement of $[\Gamma(\psi(2S) \to e^+e^-)] \times [B(\psi(2S) \to J/\psi(1S)\pi^+\pi^-)]$ assuming $B(\psi(2S) \to J/\psi(1S)\pi^+\pi^-) = (34.95 \pm 0.45) \times 10^{-2}$, which we rescale to our best (shown rounded) value $B(\psi(2S) \to J/\psi(1S)\pi^+\pi^-) = (34.78 \pm 0.33) \times 10^{-2}$. Our first error is their experiment's error and our second error is the systematic error from using our best (shown rounded) value.

[2] From a simultaneous fit to e^+e^-, $\mu^+\mu^-$, and hadronic channel, assuming $\Gamma_e = \Gamma_\mu = \Gamma_\tau/0.38847$.

[3] Combining $\Gamma_{e^+e^-} \cdot B(\mu^+\mu^-)$ from ANASHIN 18 with $\Gamma_{e^+e^-} \cdot B$(hadrons) from ANASHIN 12 and assuming lepton universality.

[4] From the sum of $\Gamma_{e^+e^-} \cdot B$(hadrons) from ANASHIN 12, $\Gamma_{e^+e^-} \cdot B(e^+e^-)$ and $\Gamma_{e^+e^-} \cdot B(\mu^+\mu^-)$ from ANASHIN 18, and $\Gamma_{e^+e^-} \cdot B(\tau^+\tau^-)$ from ANASHIN 07.

[5] From a simultaneous fit to e^+e^-, $\mu^+\mu^-$, and hadronic channels assuming $\Gamma(e^+e^-) = \Gamma(\mu^+\mu^-)$.

$\Gamma(\gamma\gamma)$ — Γ_{244}

VALUE (eV)	CL%	DOCUMENT ID		TECN	COMMENT
<43	90	BRANDELIK	79C	DASP	e^+e^-

$\psi(2S)$ $\Gamma(i)\Gamma(e^+e^-)/\Gamma(\text{total})$

This combination of a partial width with the partial width into e^+e^- and with the total width is obtained from the integrated cross section into channel(i) in the e^+e^- annihilation. We list only data that have not been used to determine the partial width $\Gamma(i)$ or the branching ratio $\Gamma(i)$/total.

$\Gamma(\text{hadrons}) \times \Gamma(e^+e^-)/\Gamma_{total}$ — $\Gamma_1\Gamma_7/\Gamma$

VALUE (keV)	DOCUMENT ID		TECN	COMMENT
2.233±0.015±0.042	[1] ANASHIN	12	KEDR	$e^+e^- \to$ hadrons
• • • We do not use the following data for averages, fits, limits, etc. • • •				
2.2 ±0.4	ABRAMS	75	MRK1	e^+e^-

[1] ANASHIN 12 reports the value 2.233 ± 0.015 ± 0.037 ± 0.020 keV, where the third uncertainty is due to assumptions on the interference between the resonance and hadronic continuum. We combined the two systematic uncertainties.

$\Gamma(K^0_S \text{anything}) \times \Gamma(e^+e^-)/\Gamma_{total}$ — $\Gamma_6\Gamma_7/\Gamma$

VALUE (keV)	DOCUMENT ID		TECN	COMMENT
0.3738±0.0067±0.0200	ABLIKIM	21S	BES3	$e^+e^- \to K^0_S$ anything

$\Gamma(e^+e^-) \times \Gamma(e^+e^-)/\Gamma_{total}$ — $\Gamma_7\Gamma_7/\Gamma$

VALUE (eV)	DOCUMENT ID		TECN	COMMENT
21.2±0.7±1.2	[1] ANASHIN	18	KEDR	e^+e^-

[1] From the average of nine scans of the $\psi(2S)$.

$\Gamma(\mu^+\mu^-) \times \Gamma(e^+e^-)/\Gamma_{total}$ — $\Gamma_8\Gamma_7/\Gamma$

VALUE (eV)	DOCUMENT ID		TECN	COMMENT
19.3±0.3±0.5	[1] ANASHIN	18	KEDR	$\psi(2S) \to \mu^+\mu^-$

[1] From the average of nine scans of the $\psi(2S)$.

$\Gamma(\tau^+\tau^-) \times \Gamma(e^+e^-)/\Gamma_{total}$ — $\Gamma_9\Gamma_7/\Gamma$

VALUE (eV)	EVTS	DOCUMENT ID		TECN	COMMENT
• • • We do not use the following data for averages, fits, limits, etc. • • •					
9.0±2.6	79	[1] ANASHIN	07	KEDR	$e^+e^- \to \psi(2S) \to \tau^+\tau^-$

[1] Using $\psi(2S)$ total width of 337 ± 13 keV. Systematic errors not evaluated.

$\Gamma(J/\psi(1S)\pi^+\pi^-) \times \Gamma(e^+e^-)/\Gamma_{total}$ — $\Gamma_{12}\Gamma_7/\Gamma$

VALUE (keV)	EVTS	DOCUMENT ID		TECN	COMMENT
0.809±0.014 OUR FIT Error includes scale factor of 1.1.					
0.836±0.025 OUR AVERAGE Error includes scale factor of 1.3. See the ideogram below.					
0.78 ±0.12 ±0.07		[1] LEES	23	BABR	$e^+e^- \to \gamma_{ISR}$ hadrons
0.837±0.028±0.005		[2] LEES	12E	BABR	10.6 $e^+e^- \to 2\pi^+2\pi^-\gamma$
0.852±0.010±0.026	19.5k	ADAM	06	CLEO	3.773 $e^+e^- \to \gamma\psi(2S)$
0.68 ±0.09		[3] BAI	98E	BES	e^+e^-
• • • We do not use the following data for averages, fits, limits, etc. • • •					
0.93 ±0.08 ±0.03	256	[4] AUBERT	07AU	BABR	10.6 $e^+e^- \to J/\psi\pi^+\pi^-\gamma$
0.755±0.048±0.004	544	[5] AUBERT	05D	BABR	10.6 $e^+e^- \to \pi^+\pi^-\mu^+\mu^-\gamma$

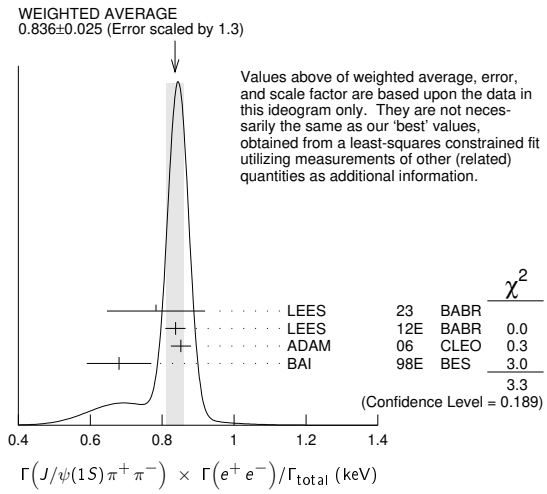

[1] LEES 23 reports $[\Gamma(\psi(2S) \to J/\psi(1S)\pi^+\pi^-) \times \Gamma(\psi(2S) \to e^+e^-)/\Gamma_{total}] \times [B(J/\psi(1S) \to K^0_S K^{\pm}\pi^{\mp})] = (4.14 \pm 0.55 \pm 0.29) \times 10^{-3}$ keV which we divide by our best (shown rounded) value $B(J/\psi(1S) \to K^0_S K^{\pm}\pi^{\mp}) = (5.3 \pm 0.5) \times 10^{-3}$. Our first error is their experiment's error and our second error is the systematic error from using our best (shown rounded) value.

[2] LEES 12E reports $[\Gamma(\psi(2S) \to J/\psi(1S)\pi^+\pi^-) \times \Gamma(\psi(2S) \to e^+e^-)/\Gamma_{total}] \times [B(J/\psi(1S) \to \mu^+\mu^-)] = (49.9 \pm 1.3 \pm 1.0) \times 10^{-3}$ keV which we divide by our best (shown rounded) value $B(J/\psi(1S) \to \mu^+\mu^-) = (5.961 \pm 0.033) \times 10^{-2}$. Our first error is their experiment's error and our second error is the systematic error from using our best (shown rounded) value.

Int. J. Mod. Phys. A 2026.41. Downloaded from www.worldscientific.com by UNIVERSITY OF CALIFORNIA @ BERKELEY on 09/16/26. Re-use and distribution is strictly not permitted, except for Open Access articles.

[3] The value of $\Gamma(e^+e^-)$ quoted in BAI 98E is derived using $B(\psi(2S) \to J/\psi(1S)\pi^+\pi^-) = (32.4 \pm 2.6) \times 10^{-2}$ and $B(J/\psi(1S) \to \ell^+\ell^-) = 0.1203 \pm 0.0038$. Recalculated by us using $B(J/\psi(1S) \to \ell^+\ell^-) = 0.1181 \pm 0.0020$.

[4] AUBERT 07AU reports $[\Gamma(\psi(2S) \to J/\psi(1S)\pi^+\pi^-) \times \Gamma(\psi(2S) \to e^+e^-)/\Gamma_{total}] \times [B(J/\psi(1S) \to \pi^+\pi^-\pi^0)] = 0.0186 \pm 0.0012 \pm 0.0011$ keV which we divide by our best (shown rounded) value $B(J/\psi(1S) \to \pi^+\pi^-\pi^0) = (2.00 \pm 0.07) \times 10^{-2}$. Our first error is their experiment's error and our second error is the systematic error from using our best (shown rounded) value.

[5] AUBERT 05D reports $[\Gamma(\psi(2S) \to J/\psi(1S)\pi^+\pi^-) \times \Gamma(\psi(2S) \to e^+e^-)/\Gamma_{total}] \times [B(J/\psi(1S) \to \mu^+\mu^-)] = 0.0450 \pm 0.0018 \pm 0.0022$ keV which we divide by our best (shown rounded) value $B(J/\psi(1S) \to \mu^+\mu^-) = (5.961 \pm 0.033) \times 10^{-2}$. Our first error is their experiment's error and our second error is the systematic error from using our best (shown rounded) value. Superseded by LEES 12E.

$\Gamma(J/\psi(1S)\pi^0\pi^0) \times \Gamma(e^+e^-)/\Gamma_{total}$ — $\Gamma_{13}\Gamma_7/\Gamma$

VALUE (keV)	EVTS	DOCUMENT ID		TECN	COMMENT
0.425±0.012 OUR FIT Error includes scale factor of 1.4.					
0.413±0.019 OUR AVERAGE					
0.45 ±0.13 ±0.02		[1] LEES	23	BABR	$e^+e^- \to \gamma_{ISR}$hadrons
0.45 ±0.12 ±0.04		[2] LEES	23	BABR	$e^+e^- \to \gamma_{ISR}$hadrons
0.411±0.008±0.018	3.6k	ADAM	06	CLEO	3.773 $e^+e^- \to \gamma\psi(2S)$
• • • We do not use the following data for averages, fits, limits, etc. • • •					
0.51 ±0.09 ±0.02	142	[3] LEES	18E	BABR	10.6 $e^+e^- \to J/\psi\pi^0\pi^0\gamma$

[1] LEES 23 reports $[\Gamma(\psi(2S) \to J/\psi(1S)\pi^0\pi^0) \times \Gamma(\psi(2S) \to e^+e^-)/\Gamma_{total}] \times [B(J/\psi(1S) \to K^+K^-\pi^0)] = (1.31 \pm 0.35 \pm 0.13) \times 10^{-3}$ keV which we divide by our best (shown rounded) value $B(J/\psi(1S) \to K^+K^-\pi^0) = (2.88 \pm 0.12) \times 10^{-3}$. Our first error is their experiment's error and our second error is the systematic error from using our best (shown rounded) value.

[2] LEES 23 reports $[\Gamma(\psi(2S) \to J/\psi(1S)\pi^0\pi^0) \times \Gamma(\psi(2S) \to e^+e^-)/\Gamma_{total}] \times [B(J/\psi(1S) \to K^0_S K^\pm\pi^\mp)] = (2.36 \pm 0.59 \pm 0.24) \times 10^{-3}$ keV which we divide by our best (shown rounded) value $B(J/\psi(1S) \to K^0_S K^\pm\pi^\mp) = (5.3 \pm 0.5) \times 10^{-3}$. Our first error is their experiment's error and our second error is the systematic error from using our best (shown rounded) value.

[3] LEES 18E reports $[\Gamma(\psi(2S) \to J/\psi(1S)\pi^0\pi^0) \times \Gamma(\psi(2S) \to e^+e^-)/\Gamma_{total}] \times [B(J/\psi(1S) \to \pi^+\pi^-\pi^0)] = 0.0101 \pm 0.0015 \pm 0.0011$ keV which we divide by our best (shown rounded) value $B(J/\psi(1S) \to \pi^+\pi^-\pi^0) = (2.00 \pm 0.07) \times 10^{-2}$. Our first error is their experiment's error and our second error is the systematic error from using our best (shown rounded) value.

$\Gamma(J/\psi(1S)\eta) \times \Gamma(e^+e^-)/\Gamma_{total}$ — $\Gamma_{14}\Gamma_7/\Gamma$

VALUE (eV)	EVTS	DOCUMENT ID		TECN	COMMENT
78.6± 1.8 OUR FIT Error includes scale factor of 1.1.					
87 ± 9 OUR AVERAGE					
83 ±25 ±5	14	[1] AUBERT	07AU	BABR	10.6 $e^+e^- \to J/\psi\pi^+\pi^-\pi^0\gamma$
88 ± 6 ±7	291 ± 24	ADAM	06	CLEO	3.773 $e^+e^- \to \gamma\psi(2S)$

[1] AUBERT 07AU quotes $\Gamma^{\psi(2S)}_{ee} \cdot B(\psi(2S) \to J/\psi\eta) \cdot B(J/\psi \to \mu^+\mu^-) \cdot B(\eta \to \pi^+\pi^-\pi^0) = 1.11 \pm 0.33 \pm 0.07$ eV.

$\Gamma(J/\psi(1S)\pi^0) \times \Gamma(e^+e^-)/\Gamma_{total}$ — $\Gamma_{15}\Gamma_7/\Gamma$

VALUE (eV)	CL%	EVTS	DOCUMENT ID		TECN	COMMENT
<8	90	<37	ADAM	06	CLEO	3.773 $e^+e^- \to \gamma\psi(2S)$

$\Gamma(2(\pi^+\pi^-)\pi^0) \times \Gamma(e^+e^-)/\Gamma_{total}$ — $\Gamma_{22}\Gamma_7/\Gamma$

VALUE (eV)	EVTS	DOCUMENT ID		TECN	COMMENT
29.7±2.2±1.8	410	AUBERT	07AU	BABR	10.6 $e^+e^- \to 2(\pi^+\pi^-)\pi^0\gamma$

$\Gamma(\pi^+\pi^-\pi^0\pi^0) \times \Gamma(e^+e^-)/\Gamma_{total}$ — $\Gamma_{24}\Gamma_7/\Gamma$

VALUE (eV)	EVTS	DOCUMENT ID		TECN	COMMENT
12.4±1.8±1.2	177	LEES	18E	BABR	10.6 $e^+e^- \to \pi^+\pi^-3\pi^0\gamma$

$\Gamma(\pi^+\pi^-4\pi^0) \times \Gamma(e^+e^-)/\Gamma_{total}$ — $\Gamma_{26}\Gamma_7/\Gamma$

VALUE (eV)	EVTS	DOCUMENT ID		TECN	COMMENT
3.3±2.3±0.5	18	LEES	21C	BABR	$e^+e^- \to \gamma_{ISR}(\pi^+\pi^-4\pi^0)$

$\Gamma(\rho^\pm\pi^\mp\pi^0\pi^0) \times \Gamma(e^+e^-)/\Gamma_{total}$ — $\Gamma_{25}\Gamma_7/\Gamma$

VALUE (eV)	CL%	DOCUMENT ID		TECN	COMMENT
<6.2	90	LEES	18E	BABR	10.6 $e^+e^- \to \pi^+\pi^-3\pi^0\gamma$

$\Gamma(2(\pi^+\pi^-\pi^0)) \times \Gamma(e^+e^-)/\Gamma_{total}$ — $\Gamma_{28}\Gamma_7/\Gamma$

VALUE (eV)	EVTS	DOCUMENT ID		TECN	COMMENT
11.2±3.3±1.3	43	AUBERT	06D	BABR	10.6 $e^+e^- \to 2(\pi^+\pi^-\pi^0)\gamma$

$\Gamma(2(\pi^+\pi^-)3\pi^0) \times \Gamma(e^+e^-)/\Gamma_{total}$ — $\Gamma_{30}\Gamma_7/\Gamma$

VALUE (eV)	EVTS	DOCUMENT ID		TECN	COMMENT
33±5±5	14k	LEES	21	BABR	10.6 $e^+e^- \to 2(\pi^+\pi^-)3\pi^0\gamma$

$\Gamma(\eta 2(\pi^+\pi^-)) \times \Gamma(e^+e^-)/\Gamma_{total}$ — $\Gamma_{33}\Gamma_7/\Gamma$

VALUE (eV)	CL%	EVTS	DOCUMENT ID		TECN	COMMENT
2.87±1.41±0.01		16	[1] AUBERT	07AU	BABR	10.6 $e^+e^- \to 2(\pi^+\pi^-)\eta\gamma$
• • • We do not use the following data for averages, fits, limits, etc. • • •						
<7	90	14k	[2] LEES	21	BABR	10.6 $e^+e^- \to 2(\pi^+\pi^-)3\pi^0\gamma$

[1] AUBERT 07AU reports $[\Gamma(\psi(2S) \to \eta 2(\pi^+\pi^-)) \times \Gamma(\psi(2S) \to e^+e^-)/\Gamma_{total}] \times [B(\eta \to 2\gamma)] = 1.13 \pm 0.55 \pm 0.08$ eV which we divide by our best (shown rounded) value $B(\eta \to 2\gamma) = (39.36 \pm 0.18) \times 10^{-2}$. Our first error is their experiment's error and our second error is the systematic error from using our best (shown rounded) value.

[2] LEES 21 reports $[\Gamma(\psi(2S) \to \eta 2(\pi^+\pi^-)) \times \Gamma(\psi(2S) \to e^+e^-)/\Gamma_{total}] \times [B(\eta \to 3\pi^0)] < 2.3$ eV which we divide by our best (shown rounded) value $B(\eta \to 3\pi^0) = 32.56 \times 10^{-2}$.

$\Gamma(\eta\pi^+\pi^-\pi^0\pi^0) \times \Gamma(e^+e^-)/\Gamma_{total}$ — $\Gamma_{34}\Gamma_7/\Gamma$

VALUE (eV)	CL%	DOCUMENT ID		TECN	COMMENT
<0.85	90	LEES	18E	BABR	10.6 $e^+e^- \to \pi^+\pi^-\pi^0\pi^0\eta\gamma$

$\Gamma(\eta\pi^+\pi^-3\pi^0) \times \Gamma(e^+e^-)/\Gamma_{total}$ — $\Gamma_{35}\Gamma_7/\Gamma$

VALUE (eV)	CL%	DOCUMENT ID		TECN	COMMENT
<5	90	[1] LEES	21C	BABR	$e^+e^- \to \gamma_{ISR}(\pi^+\pi^-3\pi^0\gamma\gamma)$

[1] LEES 21C reports $[\Gamma(\psi(2S) \to \eta\pi^+\pi^-3\pi^0) \times \Gamma(\psi(2S) \to e^+e^-)/\Gamma_{total}] \times [B(\eta \to 2\gamma)] < 1.9$ eV which we divide by our best (shown rounded) value $B(\eta \to 2\gamma) = 39.36 \times 10^{-2}$.

$\Gamma(\eta 2(\pi^+\pi^-\pi^0)) \times \Gamma(e^+e^-)/\Gamma_{total}$ — $\Gamma_{36}\Gamma_7/\Gamma$

VALUE (eV)	CL%	EVTS	DOCUMENT ID		TECN	COMMENT
<5	90	14k	[1] LEES	21	BABR	10.6 $e^+e^- \to 2(\pi^+\pi^-)3\pi^0\gamma$

[1] LEES 21 reports $[\Gamma(\psi(2S) \to \eta 2(\pi^+\pi^-\pi^0)) \times \Gamma(\psi(2S) \to e^+e^-)/\Gamma_{total}] \times [B(\eta \to 2\gamma)] < 1.9$ eV which we divide by our best (shown rounded) value $B(\eta \to 2\gamma) = 39.36 \times 10^{-2}$.

$\Gamma(\omega\pi^+\pi^-) \times \Gamma(e^+e^-)/\Gamma_{total}$ — $\Gamma_{41}\Gamma_7/\Gamma$

VALUE (eV)	EVTS	DOCUMENT ID		TECN	COMMENT
3.01±0.84±0.02	37	[1] AUBERT	07AU	BABR	10.6 $e^+e^- \to \omega\pi^+\pi^-\gamma$

[1] AUBERT 07AU reports $[\Gamma(\psi(2S) \to \omega\pi^+\pi^-) \times \Gamma(\psi(2S) \to e^+e^-)/\Gamma_{total}] \times [B(\omega(782) \to \pi^+\pi^-\pi^0)] = 2.69 \pm 0.73 \pm 0.16$ eV which we divide by our best (shown rounded) value $B(\omega(782) \to \pi^+\pi^-\pi^0) = (89.2 \pm 0.7) \times 10^{-2}$. Our first error is their experiment's error and our second error is the systematic error from using our best (shown rounded) value.

$\Gamma(\omega\pi^+\pi^-2\pi^0) \times \Gamma(e^+e^-)/\Gamma_{total}$ — $\Gamma_{42}\Gamma_7/\Gamma$

VALUE (eV)	EVTS	DOCUMENT ID		TECN	COMMENT
20.2±5.6±0.1	14k	[1] LEES	21	BABR	10.6 $e^+e^- \to 2(\pi^+\pi^-)3\pi^0\gamma$

[1] LEES 21 reports $[\Gamma(\psi(2S) \to \omega\pi^+\pi^-2\pi^0) \times \Gamma(\psi(2S) \to e^+e^-)/\Gamma_{total}] \times [B(\omega(782) \to \pi^+\pi^-\pi^0)] = 18 \pm 4 \pm 3$ eV which we divide by our best (shown rounded) value $B(\omega(782) \to \pi^+\pi^-\pi^0) = (89.2 \pm 0.7) \times 10^{-2}$. Our first error is their experiment's error and our second error is the systematic error from using our best (shown rounded) value.

$\Gamma(\omega\pi^0\pi^0) \times \Gamma(e^+e^-)/\Gamma_{total}$ — $\Gamma_{45}\Gamma_7/\Gamma$

VALUE (eV)	EVTS	DOCUMENT ID		TECN	COMMENT
2.58±0.82±0.02	33	[1] LEES	18E	BABR	10.6 $e^+e^- \to \pi^+\pi^-3\pi^0\gamma$

[1] LEES 18E reports $[\Gamma(\psi(2S) \to \omega\pi^0\pi^0) \times \Gamma(\psi(2S) \to e^+e^-)/\Gamma_{total}] \times [B(\omega(782) \to \pi^+\pi^-\pi^0)] = 2.3 \pm 0.7 \pm 0.2$ eV which we divide by our best (shown rounded) value $B(\omega(782) \to \pi^+\pi^-\pi^0) = (89.2 \pm 0.7) \times 10^{-2}$. Our first error is their experiment's error and our second error is the systematic error from using our best (shown rounded) value.

$\Gamma(\omega 3\pi^0) \times \Gamma(e^+e^-)/\Gamma_{total}$ — $\Gamma_{46}\Gamma_7/\Gamma$

VALUE (eV)	CL%	DOCUMENT ID		TECN	COMMENT
<1.8	90	[1] LEES	21C	BABR	$e^+e^- \to \gamma_{ISR}(\pi^+\pi^-4\pi^0)$

[1] LEES 21C reports $[\Gamma(\psi(2S) \to \omega 3\pi^0) \times \Gamma(\psi(2S) \to e^+e^-)/\Gamma_{total}] \times [B(\omega(782) \to \pi^+\pi^-\pi^0)] < 1.6$ eV which we divide by our best (shown rounded) value $B(\omega(782) \to \pi^+\pi^-\pi^0) = 89.2 \times 10^{-2}$.

$\Gamma(\phi\pi^+\pi^-) \times \Gamma(e^+e^-)/\Gamma_{total}$ — $\Gamma_{52}\Gamma_7/\Gamma$

VALUE (eV)	EVTS	DOCUMENT ID		TECN	COMMENT
0.54±0.18±0.01	19	[1] LEES	12F	BABR	10.6 $e^+e^- \to K^+K^-\pi^+\pi^-\gamma$
• • • We do not use the following data for averages, fits, limits, etc. • • •					
0.56±0.22±0.01	10	[2] AUBERT,BE	06D	BABR	10.6 $e^+e^- \to K^+K^-\pi^+\pi^-\gamma$

[1] LEES 12F reports $[\Gamma(\psi(2S) \to \phi\pi^+\pi^-) \times \Gamma(\psi(2S) \to e^+e^-)/\Gamma_{total}] \times [B(\phi(1020) \to K^+K^-)] = 0.27 \pm 0.09 \pm 0.02$ eV which we divide by our best (shown rounded) value $B(\phi(1020) \to K^+K^-) = (50.1 \pm 0.6) \times 10^{-2}$. Our first error is their experiment's error and our second error is the systematic error from using our best (shown rounded) value.

[2] Superseded by LEES 12F. AUBERT,BE 06D reports $[\Gamma(\psi(2S) \to \phi\pi^+\pi^-) \times \Gamma(\psi(2S) \to e^+e^-)/\Gamma_{total}] \times [B(\phi(1020) \to K^+K^-)] = 0.28 \pm 0.11 \pm 0.02$ eV which we divide by our best (shown rounded) value $B(\phi(1020) \to K^+K^-) = (50.1 \pm 0.6) \times 10^{-2}$. Our first error is their experiment's error and our second error is the systematic error from using our best (shown rounded) value.

$\Gamma(\phi f_0(980) \to \pi^+\pi^-) \times \Gamma(e^+e^-)/\Gamma_{total}$ — $\Gamma_{53}\Gamma_7/\Gamma$

VALUE (eV)	EVTS	DOCUMENT ID		TECN	COMMENT
0.339±0.126±0.004	12	[1] LEES	12F	BABR	10.6 $e^+e^- \to \pi^+\pi^-K^+K^-\gamma$
• • • We do not use the following data for averages, fits, limits, etc. • • •					
0.339±0.165±0.004	6 ± 3	[2] AUBERT	07AK	BABR	10.6 $e^+e^- \to \pi^+\pi^-K^+K^-\gamma$

[1] LEES 12F reports $[\Gamma(\psi(2S) \to \phi f_0(980) \to \pi^+\pi^-) \times \Gamma(\psi(2S) \to e^+e^-)/\Gamma_{total}] \times [B(\phi(1020) \to K^+K^-)] = 0.17 \pm 0.06 \pm 0.02$ eV which we divide by our best (shown rounded) value $B(\phi(1020) \to K^+K^-) = (50.1 \pm 0.6) \times 10^{-2}$. Our first error is their experiment's error and our second error is the systematic error from using our best (shown rounded) value.

[2] Superseded by LEES 12F. AUBERT 07AK reports $[\Gamma(\psi(2S) \to \phi f_0(980) \to \pi^+\pi^-) \times \Gamma(\psi(2S) \to e^+e^-)/\Gamma_{total}] \times [B(\phi(1020) \to K^+K^-)] = 0.17 \pm 0.08 \pm 0.02$ eV which we divide by our best (shown rounded) value $B(\phi(1020) \to K^+K^-) = (50.1 \pm 0.6) \times 10^{-2}$. Our first error is their experiment's error and our second error is the systematic error from using our best (shown rounded) value.

$\Gamma(K^+K^-) \times \Gamma(e^+e^-)/\Gamma_{total}$ — $\Gamma_{67}\Gamma_7/\Gamma$

VALUE (eV)	EVTS	DOCUMENT ID		TECN	COMMENT
• • • We do not use the following data for averages, fits, limits, etc. • • •					
$0.147 \pm 0.035 \pm 0.005$	66	[1] LEES	15J	BABR	$e^+e^- \to K^+K^-\gamma$
$0.197 \pm 0.035 \pm 0.005$	66	[2] LEES	15J	BABR	$e^+e^- \to K^+K^-\gamma$
$0.35 \pm 0.14 \pm 0.03$	11	[3] LEES	13Q	BABR	$e^+e^- \to K^+K^-\gamma$

[1] $\sin\phi > 0$.
[2] $\sin\phi < 0$.
[3] Interference with non-resonant K^+K^- production not taken into account.

$\Gamma(K^+K^-\pi^+\pi^-) \times \Gamma(e^+e^-)/\Gamma_{total}$ — $\Gamma_{68}\Gamma_7/\Gamma$

VALUE (eV)	EVTS	DOCUMENT ID		TECN	COMMENT
$1.92 \pm 0.30 \pm 0.06$	133	LEES	12F	BABR	$10.6\ e^+e^- \to \pi^+\pi^-K^+K^-\gamma$
• • • We do not use the following data for averages, fits, limits, etc. • • •					
$2.56 \pm 0.42 \pm 0.16$	85	[1] AUBERT	07AK	BABR	$10.6\ e^+e^- \to \pi^+\pi^-K^+K^-\gamma$

[1] Superseded by LEES 12F.

$\Gamma(K^0_S K^0_L \pi^0) \times \Gamma(e^+e^-)/\Gamma_{total}$ — $\Gamma_{72}\Gamma_7/\Gamma$

VALUE (eV)	CL%	EVTS	DOCUMENT ID		TECN	COMMENT
<0.7	90	8	LEES	17A	BABR	$e^+e^- \to K^0_S K^0_L \pi^0\gamma$

$\Gamma(K^+K^-\pi^0\pi^0) \times \Gamma(e^+e^-)/\Gamma_{total}$ — $\Gamma_{73}\Gamma_7/\Gamma$

VALUE (eV)	EVTS	DOCUMENT ID		TECN	COMMENT
$0.60 \pm 0.31 \pm 0.03$	17	LEES	12F	BABR	$10.6\ e^+e^- \to \pi^0\pi^0K^+K^-\gamma$

$\Gamma(K^+K^-\pi^0\pi^0\pi^0) \times \Gamma(e^+e^-)/\Gamma_{total}$ — $\Gamma_{74}\Gamma_7/\Gamma$

VALUE (eV)	DOCUMENT ID		TECN	COMMENT
$1.54 \pm 0.63 \pm 0.15$	LEES	23	BABR	$e^+e^- \to \gamma_{ISR}$hadrons

$\Gamma(K^0_S K^\pm\pi^\mp\pi^0\pi^0) \times \Gamma(e^+e^-)/\Gamma_{total}$ — $\Gamma_{75}\Gamma_7/\Gamma$

VALUE (eV)	DOCUMENT ID		TECN	COMMENT
$4.0 \pm 1.4 \pm 0.4$	LEES	23	BABR	$e^+e^- \to \gamma_{ISR}$hadrons

$\Gamma(K^0_S K^\pm\pi^\mp\pi^+\pi^-) \times \Gamma(e^+e^-)/\Gamma_{total}$ — $\Gamma_{76}\Gamma_7/\Gamma$

VALUE (eV)	DOCUMENT ID		TECN	COMMENT
$5.1 \pm 0.7 \pm 0.4$	LEES	23	BABR	$e^+e^- \to \gamma_{ISR}$hadrons

$\Gamma(K^+K^-\pi^+\pi^-\pi^0) \times \Gamma(e^+e^-)/\Gamma_{total}$ — $\Gamma_{77}\Gamma_7/\Gamma$

VALUE (eV)	EVTS	DOCUMENT ID		TECN	COMMENT
$4.4 \pm 1.3 \pm 0.3$	32	AUBERT	07AU	BABR	$10.6\ e^+e^- \to K^+K^-\pi^+\pi^-\pi^0\gamma$

$\Gamma(K^0_S K^0_L \pi^0\pi^0) \times \Gamma(e^+e^-)/\Gamma_{total}$ — $\Gamma_{84}\Gamma_7/\Gamma$

VALUE (eV)	EVTS	DOCUMENT ID		TECN	COMMENT
$2.92 \pm 1.27 \pm 0.15$	14	LEES	17A	BABR	$e^+e^- \to K^0_S K^0_L \pi^0\pi^0\gamma$

$\Gamma(K^0_S K^*(892)^0\pi^0\pi^0) \times \Gamma(e^+e^-)/\Gamma_{total}$ — $\Gamma_{85}\Gamma_7/\Gamma$

VALUE (eV)	DOCUMENT ID		TECN	COMMENT
$0.71 \pm 0.29 \pm 0.07$	LEES	23	BABR	$e^+e^- \to \gamma_{ISR}$hadrons

$\Gamma(K^0_S K^\pm\rho(770)^\mp\pi^0) \times \Gamma(e^+e^-)/\Gamma_{total}$ — $\Gamma_{86}\Gamma_7/\Gamma$

VALUE (eV)	CL%	DOCUMENT ID		TECN	COMMENT
<1.6	90	LEES	23	BABR	$e^+e^- \to \gamma_{ISR}$hadrons

$\Gamma(K^0_S K^\pm\pi^\mp\rho(770)^0) \times \Gamma(e^+e^-)/\Gamma_{total}$ — $\Gamma_{87}\Gamma_7/\Gamma$

VALUE (eV)	CL%	DOCUMENT ID		TECN	COMMENT
<1.6	90	LEES	23	BABR	$e^+e^- \to \gamma_{ISR}$hadrons

$\Gamma(K^*(892)^+K^*(892)^-\pi^0) \times \Gamma(e^+e^-)/\Gamma_{total}$ — $\Gamma_{89}\Gamma_7/\Gamma$

VALUE (eV)	DOCUMENT ID		TECN	COMMENT
$8.46 \pm 4.05 \pm 0.90$	LEES	23	BABR	$e^+e^- \to \gamma_{ISR}$hadrons

$\Gamma(K^\mp K^*(892)^\pm\pi^0\pi^0) \times \Gamma(e^+e^-)/\Gamma_{total}$ — $\Gamma_{88}\Gamma_7/\Gamma$

VALUE (eV)	DOCUMENT ID		TECN	COMMENT
$1.62 \pm 0.66 \pm 0.15$	LEES	23	BABR	$e^+e^- \to \gamma_{ISR}$hadrons

$\Gamma(K^0_S K^0_L \eta) \times \Gamma(e^+e^-)/\Gamma_{total}$ — $\Gamma_{90}\Gamma_7/\Gamma$

VALUE (eV)	EVTS	DOCUMENT ID		TECN	COMMENT
$3.14 \pm 1.08 \pm 0.16$	16	LEES	17A	BABR	$e^+e^- \to K^0_S K^0_L \eta\gamma$

$\Gamma(K^+K^-\pi^+\pi^-\eta) \times \Gamma(e^+e^-)/\Gamma_{total}$ — $\Gamma_{93}\Gamma_7/\Gamma$

VALUE (eV)	EVTS	DOCUMENT ID		TECN	COMMENT
$3.05 \pm 1.80 \pm 0.01$	7	[1] AUBERT	07AU	BABR	$10.6\ e^+e^- \to K^+K^-\pi^+\pi^-\eta\gamma$

[1] AUBERT 07AU reports $[\Gamma(\psi(2S) \to K^+K^-\pi^+\pi^-\eta) \times \Gamma(\psi(2S) \to e^+e^-)/\Gamma_{total}] \times [B(\eta \to 2\gamma)] = 1.2 \pm 0.7 \pm 0.1$ eV which we divide by our best (shown rounded) value $B(\eta \to 2\gamma) = (39.36 \pm 0.18) \times 10^{-2}$. Our first error is their experiment's error and our second error is the systematic error from using our best (shown rounded) value.

$\Gamma(K^+K^-2(\pi^+\pi^-)) \times \Gamma(e^+e^-)/\Gamma_{total}$ — $\Gamma_{94}\Gamma_7/\Gamma$

VALUE (eV)	EVTS	DOCUMENT ID		TECN	COMMENT
$4.4 \pm 2.1 \pm 0.3$	26	AUBERT	06D	BABR	$10.6\ e^+e^- \to K^+K^-2(\pi^+\pi^-)\gamma$

$\Gamma(2(K^+K^-)) \times \Gamma(e^+e^-)/\Gamma_{total}$ — $\Gamma_{97}\Gamma_7/\Gamma$

VALUE (eV)	EVTS	DOCUMENT ID		TECN	COMMENT
$0.22 \pm 0.10 \pm 0.02$	13	LEES	12F	BABR	$10.6\ e^+e^- \to K^+K^-K^+K^-\gamma$

$\Gamma(p\overline{p}) \times \Gamma(e^+e^-)/\Gamma_{total}$ — $\Gamma_{119}\Gamma_7/\Gamma$

VALUE (eV)	EVTS	DOCUMENT ID		TECN	COMMENT
0.685 ± 0.024 OUR FIT		Error includes scale factor of 1.2.			
0.63 ± 0.05 OUR AVERAGE		Error includes scale factor of 1.2.			
$0.67 \pm 0.12 \pm 0.02$	43	[1] LEES	13O	BABR	$e^+e^- \to p\overline{p}\gamma$
$0.74 \pm 0.07 \pm 0.04$	142	[2] LEES	13Y	BABR	$e^+e^- \to p\overline{p}\gamma$
$0.579 \pm 0.038 \pm 0.036$	2.7k	ANDREOTTI	07	E835	$p\overline{p} \to e^+e^-,\ J/\psi X$
• • • We do not use the following data for averages, fits, limits, etc. • • •					
$0.70 \pm 0.17 \pm 0.03$	22	[3] AUBERT	06B	BABR	$e^+e^- \to p\overline{p}\gamma$

[1] ISR photon reconstructed in the detector
[2] ISR photon undetected
[3] Superseded by LEES 13O

$\Gamma(\Lambda\overline{\Lambda}) \times \Gamma(e^+e^-)/\Gamma_{total}$ — $\Gamma_{145}\Gamma_7/\Gamma$

VALUE (eV)	DOCUMENT ID		TECN	COMMENT
$1.5 \pm 0.4 \pm 0.1$	AUBERT	07BD	BABR	$10.6\ e^+e^- \to \Lambda\overline{\Lambda}\gamma$

$\psi(2S)$ BRANCHING RATIOS

$\Gamma(\text{hadrons})/\Gamma_{total}$ — Γ_1/Γ

VALUE	DOCUMENT ID		TECN	COMMENT
0.9785 ± 0.0013 OUR AVERAGE				
0.9779 ± 0.0015	[1] BAI	02B	BES2	e^+e^-
0.981 ± 0.003	[1] LUTH	75	MRK1	e^+e^-

[1] Includes cascade decay into $J/\psi(1S)$.

$\Gamma(\text{virtual}\,\gamma \to \text{hadrons})/\Gamma_{total}$ — Γ_2/Γ

VALUE	DOCUMENT ID		TECN	COMMENT
0.0179 ± 0.0004	[1] LIAO	23	RVUE	e^+e^-
• • • We do not use the following data for averages, fits, limits, etc. • • •				
0.0166 ± 0.0010	[2,3] SETH	04	RVUE	e^+e^-
0.0199 ± 0.0019	[2] BAI	02B	BES2	e^+e^-
0.029 ± 0.004	[2] LUTH	75	MRK1	e^+e^-

[1] Using $B(\psi(2S) \to \ell^+\ell^-) = (0.794 \pm 0.017)\%$ and $R = 2.26 \pm 0.01$ determined by a fit to data from Mark-I, DM2, BESII, KEDR, and BESIII.
[2] Included in $\Gamma(\text{hadrons})/\Gamma_{total}$.
[3] Using $B(\psi(2S) \to \ell^+\ell^-) = (0.73 \pm 0.04)\%$ from RPP-2002 and $R = 2.28 \pm 0.04$ determined by a fit to data from BAI 00 and BAI 02C. Superseded by LIAO 23.

$\Gamma(ggg)/\Gamma_{total}$ — Γ_3/Γ

VALUE (units 10^{-2})	EVTS	DOCUMENT ID		TECN	COMMENT
10.58 ± 1.62	2.9 M	[1] LIBBY	09	CLEO	$\psi(2S) \to$ hadrons

[1] Calculated using $\Gamma(\gamma gg)/\Gamma(ggg) = 0.097 \pm 0.026 \pm 0.016$ from LIBBY 09, $B(\psi(2S) \to X\,J/\psi)$ relative and absolute branching fractions from MENDEZ 08, $B(\psi(2S) \to \gamma\eta_c)$ from MITCHELL 09, and $B(\psi(2S) \to$ virtual $\gamma \to$ hadrons), $B(\psi(2S) \to \gamma\chi_{c,J})$, and $B(\psi(2S) \to \ell^+\ell^-)$ from PDG 08. The statistical error is negligible and the systematic error is largely uncorrelated with that of $\Gamma(\gamma gg)/\Gamma_{total}$ LIBBY 09 measurement.

$\Gamma(\gamma gg)/\Gamma_{total}$ — Γ_4/Γ

VALUE (units 10^{-2})	EVTS	DOCUMENT ID		TECN	COMMENT
1.025 ± 0.288	200 k	[1] LIBBY	09	CLEO	$\psi(2S) \to \gamma +$ hadrons

[1] Calculated using $\Gamma(\gamma gg)/\Gamma(ggg) = 0.097 \pm 0.026 \pm 0.016$ from LIBBY 09. The statistical error is negligible and the systematic error is largely uncorrelated with that of $\Gamma(ggg)/\Gamma_{total}$ LIBBY 09 measurement.

$\Gamma(\gamma gg)/\Gamma(ggg)$ — Γ_4/Γ_3

VALUE (units 10^{-2})	EVTS	DOCUMENT ID		TECN	COMMENT
$9.7 \pm 2.6 \pm 1.6$	2.9 M	LIBBY	09	CLEO	$\psi(2S) \to (\gamma +)$ hadrons

$\Gamma(\text{light hadrons})/\Gamma_{total}$ — Γ_5/Γ

VALUE	DOCUMENT ID		TECN	COMMENT
0.154 ± 0.015	[1] MENDEZ	08	CLEO	$e^+e^- \to \psi(2S)$
• • • We do not use the following data for averages, fits, limits, etc. • • •				
0.169 ± 0.026	[2] ADAM	05A	CLEO	$e^+e^- \to \psi(2S)$

[1] Uses $B(\psi(2S) \to J/\psi X)$ from MENDEZ 08 and other branching fractions from PDG 07.
[2] Uses $B(J/\psi X)$ from ADAM 05A, $B(\chi_{c,J}\gamma)$, $B(\eta_c\gamma)$ from ATHAR 04 and $B(\ell^+\ell^-)$ from PDG 04. Superseded by MENDEZ 08.

Int. J. Mod. Phys. A 2026.41. Downloaded from www.worldscientific.com
by CALIFORNIA @ BERKELEY on 09/16/26. Re-use and distribution is strictly not permitted, except for Open Access articles.

Int. J. Mod. Phys. A 2026.41. Downloaded from www.worldscientific.com
by UNIVERSITY OF CALIFORNIA @ BERKELEY on 09/16/26. Re-use and distribution is strictly not permitted, except for Open Access articles.

$\Gamma(e^+e^-)/\Gamma_{total}$ — Γ_7/Γ

VALUE (units 10^{-4})	DOCUMENT ID		TECN	COMMENT
79.5 ± 2.2 OUR FIT Error includes scale factor of 1.3.				
• • • We do not use the following data for averages, fits, limits, etc. • • •				
88 ± 13	[1] FELDMAN	77	RVUE	e^+e^-

[1] From an overall fit assuming equal partial widths for e^+e^- and $\mu^+\mu^-$. For a measurement of the ratio see the entry $\Gamma(\mu^+\mu^-)/\Gamma(e^+e^-)$ below. Includes LUTH 75, HILGER 75, BURMESTER 77.

$\Gamma(\mu^+\mu^-)/\Gamma_{total}$ — Γ_8/Γ

VALUE (units 10^{-4})	DOCUMENT ID
80±6 OUR FIT	

$\Gamma(\mu^+\mu^-)/\Gamma(e^+e^-)$ — Γ_8/Γ_7

VALUE	DOCUMENT ID		TECN	COMMENT
1.00±0.08 OUR FIT				
• • • We do not use the following data for averages, fits, limits, etc. • • •				
0.89±0.16	BOYARSKI	75C	MRK1	e^+e^-

$\Gamma(\tau^+\tau^-)/\Gamma_{total}$ — Γ_9/Γ

VALUE (units 10^{-4})	DOCUMENT ID		TECN	COMMENT
31 ± 4 OUR FIT				
30.8±2.1±3.8	[1] ABLIKIM	06W	BES	$e^+e^- \to \psi(2S)$

[1] Computed using PDG 02 value of $B(\psi(2S) \to$ hadrons$) = 0.9810 \pm 0.0030$ to estimate the total number of $\psi(2S)$ events.

DECAYS INTO $J/\psi(1S)$ AND ANYTHING

$\Gamma(J/\psi(1S)\text{ anything})/\Gamma_{total}$ — $\Gamma_{10}/\Gamma = (\Gamma_{12}+\Gamma_{13}+\Gamma_{14}+0.339\Gamma_{197}+0.190\Gamma_{198})/\Gamma$

VALUE	EVTS	DOCUMENT ID		TECN	COMMENT
0.616 ± 0.007 OUR FIT Error includes scale factor of 1.3.					
0.55 ± 0.07 OUR AVERAGE					
0.51 ± 0.12		BRANDELIK	79C	DASP	$e^+e^- \to \mu^+\mu^- X$
0.57 ± 0.08		ABRAMS	75B	MRK1	$e^+e^- \to \mu^+\mu^- X$
• • • We do not use the following data for averages, fits, limits, etc. • • •					
0.644 ± 0.006 ± 0.016		[1] ABLIKIM	21Z	BES3	$e^+e^- \to \ell^+\ell^- X$
0.6254 ± 0.0016 ± 0.0155	1.1M	[2] MENDEZ	08	CLEO	$\psi(2S) \to \ell^+\ell^- X$
0.5950 ± 0.0015 ± 0.0190	151k	ADAM	05A	CLEO	Repl. by MENDEZ 08

[1] From a fit to the $e^+e^- \to J/\psi X$ cross section between 3.645 and 3.891 GeV, with $\Gamma(ee)$ and Γ fixed to the PDG 20 values of the cross particle fit which are correlated to "OUR FIT" value for $B(\psi(2S) \to J/\psi X)$.

[2] Not independent from other measurements of MENDEZ 08.

$\Gamma(e^+e^-)/\Gamma(J/\psi(1S)\text{ anything})$ — Γ_7/Γ_{10}

VALUE (units 10^{-2})	EVTS	DOCUMENT ID		TECN	COMMENT
1.291±0.035 OUR FIT Error includes scale factor of 1.3.					
1.28 ± 0.04 OUR AVERAGE Error includes scale factor of 1.6. See the ideogram below.					
1.22 ± 0.02 ± 0.05	5097 ± 73	[1] ANDREOTTI	05	E835	$p\overline{p} \to \psi(2S) \to e^+e^-$
1.28 ± 0.03 ± 0.02		[1] AMBROGIANI	00A	E835	$p\overline{p} \to \psi(2S)$
1.44 ± 0.08 ± 0.02		[1] ARMSTRONG	97	E760	$\overline{p}p \to \psi(2S)$

[1] Using $B(J/\psi(1S) \to e^+e^-) = 0.0593 \pm 0.0010$.

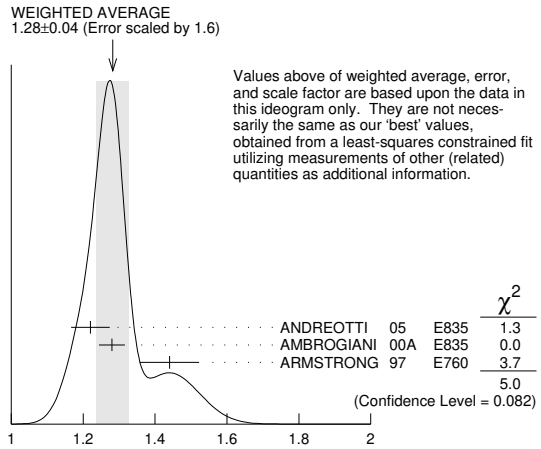

$\Gamma(\mu^+\mu^-)/\Gamma(J/\psi(1S)\text{ anything})$ — Γ_8/Γ_{10}

VALUE	DOCUMENT ID		TECN	COMMENT
0.0130±0.0010 OUR FIT				
0.014 ± 0.003	HILGER	75	SPEC	e^+e^-

$\Gamma(J/\psi(1S)\text{ neutrals})/\Gamma_{total}$ — Γ_{11}/Γ

VALUE	DOCUMENT ID
0.254±0.005 OUR FIT Error includes scale factor of 1.6.	

$\Gamma(J/\psi(1S)\pi^+\pi^-)/\Gamma_{total}$ — Γ_{12}/Γ

VALUE	EVTS	DOCUMENT ID		TECN	COMMENT
0.3478±0.0033 OUR FIT Error includes scale factor of 1.1.					
0.348 ± 0.005 OUR AVERAGE Error includes scale factor of 1.3. See the ideogram below.					
0.3498 ± 0.0002 ± 0.0045	20M	ABLIKIM	13R	BES3	$\psi(2S) \to J/\psi\pi^+\pi^-$
0.3504 ± 0.0007 ± 0.0077	565k	MENDEZ	08	CLEO	$\psi(2S) \to \ell^+\ell^-\pi^+\pi^-$
0.323 ± 0.014		BAI	02B	BES2	e^+e^-
0.32 ± 0.04		ABRAMS	75B	MRK1	$e^+e^- \to J/\psi\pi^+\pi^-$
• • • We do not use the following data for averages, fits, limits, etc. • • •					
0.3354 ± 0.0014 ± 0.0110	60k	[1] ADAM	05A	CLEO	Repl. by MENDEZ 08

[1] Not independent from other values reported by ADAM 05A.

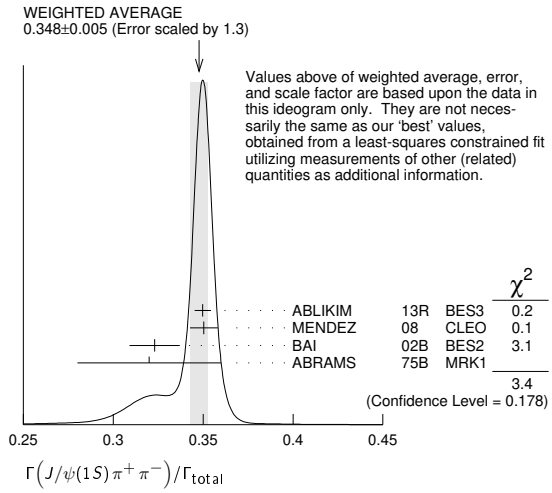

$\Gamma(e^+e^-)/\Gamma(J/\psi(1S)\pi^+\pi^-)$ — Γ_7/Γ_{12}

VALUE	DOCUMENT ID		TECN	COMMENT
0.0229±0.0006 OUR FIT Error includes scale factor of 1.3.				
0.0252±0.0028±0.0011	[1] AUBERT	02B	BABR	e^+e^-

[1] Using $B(J/\psi(1S) \to e^+e^-) = 0.0593 \pm 0.0010$.

$\Gamma(\mu^+\mu^-)/\Gamma(J/\psi(1S)\pi^+\pi^-)$ — Γ_8/Γ_{12}

VALUE	DOCUMENT ID		TECN	COMMENT
0.0230±0.0017 OUR FIT				
0.0228±0.0018 OUR AVERAGE				
0.0230 ± 0.0020 ± 0.0012	[1] AAIJ	16Y	LHCB	$\Lambda_b^0 \to \psi(2S)X$
0.0216 ± 0.0026 ± 0.0014	[2] AUBERT	02B	BABR	e^+e^-
0.0327 ± 0.0077 ± 0.0072	[2] GRIBUSHIN	96	FMPS	515 π^-Be $\to 2\mu X$

[1] Using $B(J/\psi(1S) \to \mu^+\mu^-) = (5.961 \pm 0.033) \times 10^{-2}$.

[2] Using $B(J/\psi(1S) \to \mu^+\mu^-) = (5.88 \pm 0.10) \times 10^{-2}$.

$\Gamma(\tau^+\tau^-)/\Gamma(J/\psi(1S)\pi^+\pi^-)$ — Γ_9/Γ_{12}

VALUE (units 10^{-3})	DOCUMENT ID		TECN	COMMENT
8.8 ± 1.1 OUR FIT				
8.73±1.39±1.57	BAI	02	BES	e^+e^-

$\Gamma(J/\psi(1S)\pi^+\pi^-)/\Gamma(J/\psi(1S)\text{ anything})$ — Γ_{12}/Γ_{10}

VALUE	EVTS	DOCUMENT ID		TECN	COMMENT
0.565 ± 0.004 OUR FIT Error includes scale factor of 1.7.					
0.554 ± 0.008 OUR AVERAGE Error includes scale factor of 1.3. See the ideogram below.					
0.5604 ± 0.0009 ± 0.0062	565k	MENDEZ	08	CLEO	$\psi(2S) \to \ell^+\ell^-\pi^+\pi^-$
0.525 ± 0.009 ± 0.022	4k	ANDREOTTI	05	E835	$\psi(2S) \to J/\psi X$
0.536 ± 0.007 ± 0.016	20k	[1,2] ABLIKIM	04B	BES	$\psi(2S) \to J/\psi X$
0.496 ± 0.037		ARMSTRONG	97	E760	$\overline{p}p \to \psi(2S)$
• • • We do not use the following data for averages, fits, limits, etc. • • •					
0.5637 ± 0.0027 ± 0.0046	60k	ADAM	05A	CLEO	Repl. by MENDEZ 08

[1] From a fit to the J/ψ recoil mass spectra.

[2] ABLIKIM 04B quotes $B(\psi(2S) \to J/\psi X)$ / $B(\psi(2S) \to J/\psi\pi^+\pi^-)$.

Int. J. Mod. Phys. A 2026.41. Downloaded from www.worldscientific.com
by CALIFORNIA @ BERKELEY on 09/16/26. Re-use and distribution is strictly not permitted, except for Open Access articles.

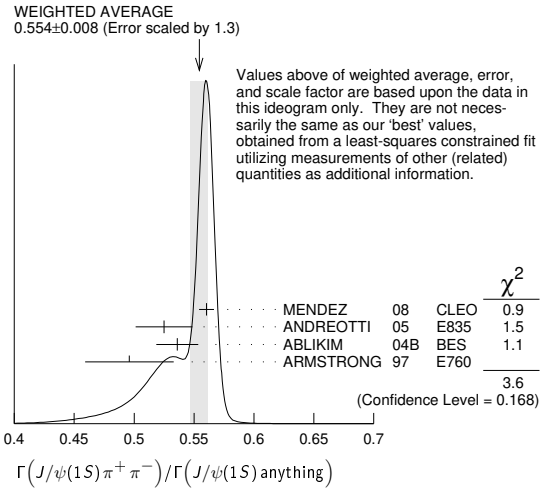

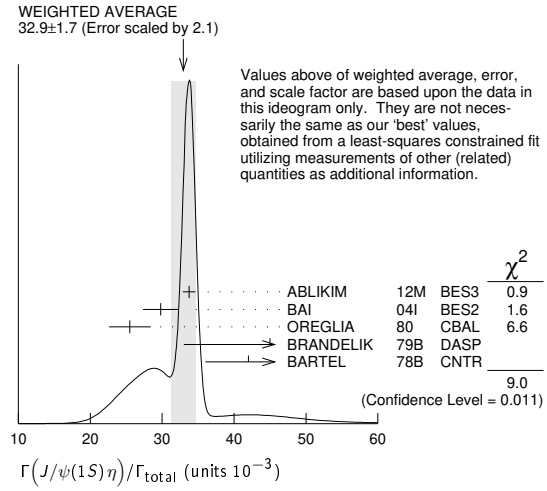

$\Gamma(J/\psi(1S)\,\text{neutrals})/\Gamma(J/\psi(1S)\pi^+\pi^-)$ Γ_{11}/Γ_{12}

$= (0.9761\Gamma_{13}+0.719\Gamma_{14}+0.339\Gamma_{197}+0.190\Gamma_{198})/\Gamma_{12}$

VALUE	DOCUMENT ID		TECN	COMMENT
0.732±0.014 OUR FIT Error includes scale factor of 1.7.				
0.73 ±0.09	TANENBAUM	76	MRK1	e^+e^-

$\Gamma(J/\psi(1S)\pi^0\pi^0)/\Gamma(J/\psi(1S)\,\text{anything})$ Γ_{13}/Γ_{10}

VALUE	EVTS	DOCUMENT ID		TECN	COMMENT
0.297 ±0.005 OUR FIT Error includes scale factor of 1.7.					
0.320 ±0.012 OUR AVERAGE					
0.300 ±0.008 ±0.022	1655 ± 44	ANDREOTTI	05	E835	$\psi(2S)\to J/\psi X$
0.328 ±0.013 ±0.008		AMBROGIANI	00A	E835	$p\overline{p}\to\psi(2S)$
0.323 ±0.033		ARMSTRONG	97	E760	$\overline{p}p\to\psi(2S)$
• • • We do not use the following data for averages, fits, limits, etc. • • •					
0.2829±0.0012±0.0056	61k	MENDEZ	08	CLEO	$\psi(2S)\to\ell^+\ell^-2\pi^0$
0.2776±0.0025±0.0043	13.4k	ADAM	05A	CLEO	Repl. by MENDEZ 08

$\Gamma(J/\psi(1S)\pi^0\pi^0)/\Gamma(J/\psi(1S)\pi^+\pi^-)$ Γ_{13}/Γ_{12}

VALUE	EVTS	DOCUMENT ID		TECN	COMMENT
0.526 ±0.013 OUR FIT Error includes scale factor of 1.7.					
0.513 ±0.022 OUR AVERAGE Error includes scale factor of 2.2.					
0.5047±0.0022±0.0102	61k	MENDEZ	08	CLEO	$\psi(2S)\to\ell^+\ell^-2\pi^0$
0.570 ±0.009 ±0.026	14k	[1] ABLIKIM	04B	BES	$\psi(2S)\to J/\psi X$
• • • We do not use the following data for averages, fits, limits, etc. • • •					
0.4924±0.0047±0.0086	73k	[2,3] ADAM	05A	CLEO	Repl. by MENDEZ 08
0.571 ±0.018 ±0.044		[4] ANDREOTTI	05	E835	$\psi(2S)\to J/\psi X$
0.53 ±0.06		TANENBAUM	76	MRK1	e^+e^-
0.64 ±0.15		[5] HILGER	75	SPEC	e^+e^-

[1] From a fit to the J/ψ recoil mass spectra.
[2] Not independent from other values reported by ADAM 05A.
[3] Using 13,217 $J/\psi\pi^0\pi^0$ and 60,010 $J/\psi\pi^+\pi^-$ events.
[4] Not independent from other values reported by ANDREOTTI 05.
[5] Ignoring the $J/\psi(1S)\eta$ and $J/\psi(1S)\gamma\gamma$ decays.

$\Gamma(J/\psi(1S)\eta)/\Gamma_{total}$ Γ_{14}/Γ

VALUE (units 10^{-3})	EVTS	DOCUMENT ID		TECN	COMMENT
33.8 ± 0.6 OUR FIT Error includes scale factor of 1.2.					
32.9 ± 1.7 OUR AVERAGE Error includes scale factor of 2.1. See the ideogram below.					
33.75± 0.17±0.86	68.2k	ABLIKIM	12M	BES3	$e^+e^-\to\ell^+\ell^-2\gamma$
29.8 ± 0.9 ±2.3	5.7k	BAI	04I	BES2	$\psi(2S)\to J/\psi\gamma\gamma$
25.5 ± 2.9	386	[1] OREGLIA	80	CBAL	$e^+e^-\to J/\psi 2\gamma$
45 ±12	17	[2] BRANDELIK	79B	DASP	$e^+e^-\to J/\psi 2\gamma$
42 ± 6	164	[2] BARTEL	78B	CNTR	e^+e^-
• • • We do not use the following data for averages, fits, limits, etc. • • •					
34.3 ± 0.4 ±0.9	18.4k	[3] MENDEZ	08	CLEO	$\psi(2S)\to\ell^+\ell^-\eta$
32.5 ± 0.6 ±1.1	2.8k	[4] ADAM	05A	CLEO	Repl. by MENDEZ 08
43 ± 8	44	TANENBAUM	76	MRK1	e^+e^-

[1] Recalculated by us using $B(J/\psi(1S)\to\ell^+\ell^-) = 0.1181 \pm 0.0020$.
[2] Recalculated by us using $B(J/\psi(1S)\to\mu^+\mu^-) = 0.0588 \pm 0.0010$.
[3] Not independent from other measurements of MENDEZ 08.
[4] Not independent from other values reported by ADAM 05A.

$\Gamma(J/\psi(1S)\eta)/\Gamma(J/\psi(1S)\,\text{anything})$ Γ_{14}/Γ_{10}

VALUE	EVTS	DOCUMENT ID		TECN	COMMENT
0.0548±0.0009 OUR FIT Error includes scale factor of 1.2.					
0.058 ±0.007 OUR AVERAGE Error includes scale factor of 1.4. See the ideogram below.					
0.050 ±0.006 ±0.003	298 ± 20	ANDREOTTI	05	E835	$\psi(2S)\to J/\psi X$
0.072 ±0.009		AMBROGIANI	00A	E835	$p\overline{p}\to\psi(2S)$
0.061 ±0.015		ARMSTRONG	97	E760	$\overline{p}p\to\psi(2S)$
• • • We do not use the following data for averages, fits, limits, etc. • • •					
0.0549±0.0006±0.0009	18.4k	[1] MENDEZ	08	CLEO	$\psi(2S)\to\ell^+\ell^-\eta$
0.0546±0.0010±0.0007	2.8k	ADAM	05A	CLEO	Repl. by MENDEZ 08

[1] Not independent from other measurements of MENDEZ 08.

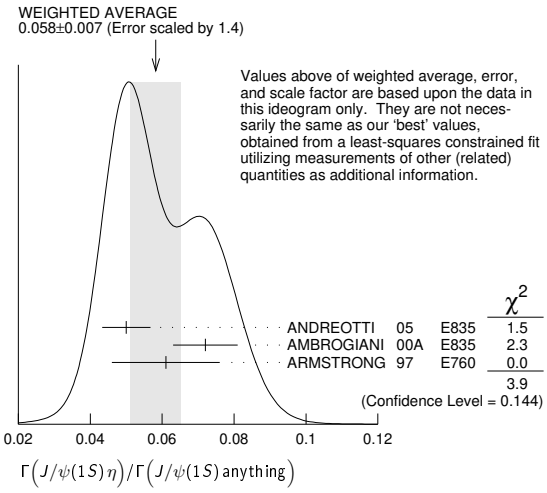

$\Gamma(J/\psi(1S)\eta)/\Gamma(J/\psi(1S)\pi^+\pi^-)$ Γ_{14}/Γ_{12}

VALUE	EVTS	DOCUMENT ID		TECN	COMMENT
0.0971±0.0016 OUR FIT Error includes scale factor of 1.1.					
0.0979±0.0018 OUR AVERAGE					
0.0979±0.0010±0.0015	18.4k	MENDEZ	08	CLEO	$\psi(2S)\to\ell^+\ell^-\eta$
0.098 ±0.005 ±0.010	2k	[1] ABLIKIM	04B	BES	$\psi(2S)\to J/\psi X$
0.091 ±0.021		[2] HIMEL	80	MRK2	$e^+e^-\to\psi(2S)X$
• • • We do not use the following data for averages, fits, limits, etc. • • •					
0.0968±0.0019±0.0013	2.8k	[3] ADAM	05A	CLEO	Repl. by MENDEZ 08
0.095 ±0.007 ±0.007		[4] ANDREOTTI	05	E835	$\psi(2S)\to J/\psi X$

[1] From a fit to the J/ψ recoil mass spectra.
[2] The value for $B(\psi(2S)\to J/\psi(1s)\eta)$ reported in HIMEL 80 is derived using $B(\psi(2S))\to J/\psi(1S)\pi^+\pi^-) = (33\pm3))\%$ and $B(J/\psi(1S)\to\ell^+\ell^-) = 0.138\pm0.018$. Calculated by us using $B(J/\psi(1S)\to\ell^+\ell^-) = (0.1181 \pm 0.0020)$.
[3] Not independent from other values reported by ADAM 05A.
[4] Not independent from other values reported by ANDREOTTI 05.

$\Gamma(J/\psi(1S)\pi^0)/\Gamma_{total}$ Γ_{15}/Γ

VALUE (units 10^{-4})	EVTS	DOCUMENT ID		TECN	COMMENT
12.68±0.32 OUR AVERAGE					
12.6 ±0.2 ±0.3	4.1k	ABLIKIM	12M	BES3	$e^+e^-\to\ell^+\ell^-2\gamma$
13.3 ±0.8 ±0.3	530	MENDEZ	08	CLEO	$\psi(2S)\to\ell^+\ell^-2\gamma$
14.3 ±1.4 ±1.2	280	BAI	04I	BES2	$\psi(2S)\to J/\psi\gamma\gamma$
14 ±6	7	HIMEL	80	MRK2	e^+e^-
9 ±2 ±1	23	[1] OREGLIA	80	CBAL	$\psi(2S)\to J/\psi 2\gamma$

Int. J. Mod. Phys. A 2026.41. Downloaded from www.worldscientific.com
by UNIVERSITY OF CALIFORNIA @ BERKELEY on 09/16/26. Re-use and distribution is strictly not permitted, except for Open Access articles.

• • • We do not use the following data for averages, fits, limits, etc. • • •

13 ±1 ±1	88	ADAM	05A	CLEO	Repl. by MENDEZ 08

[1] Recalculated by us using $B(J/\psi(1S) \to \ell^+\ell^-) = 0.1181 \pm 0.0020$.

$\Gamma(J/\psi(1S)\pi^0)/\Gamma(J/\psi(1S)\text{anything})$ $\Gamma_{15}/\Gamma_{10} = \Gamma_{15}/(\Gamma_{12}+\Gamma_{13}+\Gamma_{14}+0.339\Gamma_{197}+0.190\Gamma_{198})$

VALUE (units 10^{-2})	EVTS	DOCUMENT ID		TECN	COMMENT
• • • We do not use the following data for averages, fits, limits, etc. • • •					
0.213±0.012±0.003	527	[1] MENDEZ	08	CLEO	$e^+e^- \to J/\psi\gamma\gamma$
0.22 ±0.02 ±0.01		[2] ADAM	05A	CLEO	$e^+e^- \to \psi(2S) \to J/\psi\gamma\gamma$

[1] Not independent from other values reported by MENDEZ 08. Supersedes ADAM 05A.
[2] Not independent from other values reported by ADAM 05A.

$\Gamma(J/\psi(1S)\pi^0)/\Gamma(J/\psi(1S)\pi^+\pi^-)$ Γ_{15}/Γ_{12}

VALUE (units 10^{-2})	EVTS	DOCUMENT ID		TECN	COMMENT
• • • We do not use the following data for averages, fits, limits, etc. • • •					
0.380±0.022±0.005	527	[1] MENDEZ	08	CLEO	$e^+e^- \to J/\psi\gamma\gamma$
0.39 ±0.04 ±0.01		[2] ADAM	05A	CLEO	$e^+e^- \to \psi(2S) \to J/\psi\gamma\gamma$

[1] Not independent from other values reported by MENDEZ 08. Supersedes ADAM 05A.
[2] Not independent from other values reported by ADAM 05A.

HADRONIC DECAYS

$\Gamma(\pi^+\pi^-)/\Gamma_{total}$ Γ_{16}/Γ

VALUE (units 10^{-5})	CL%	EVTS	DOCUMENT ID		TECN	COMMENT
0.78±0.26 OUR AVERAGE						
0.76±0.25±0.06		30	[1] METREVELI	12		$\psi(2S) \to \pi^+\pi^-$
8 ±5			BRANDELIK	79C	DASP	e^+e^-
• • • We do not use the following data for averages, fits, limits, etc. • • •						
<2.1	90		DOBBS	06A	CLEO	$e^+e^- \to \psi(2S)$
<5	90		FELDMAN	77	MRK1	e^+e^-

[1] Obtained by analyzing CLEO-c data but not authored by the CLEO Collaboration. Using $\psi(3770) \to \pi^+\pi^-$ for continuum subtraction.

$\Gamma(\pi^+\pi^-\pi^0)/\Gamma_{total}$ Γ_{17}/Γ

VALUE (units 10^{-4})	EVTS	DOCUMENT ID		TECN	COMMENT
2.01±0.17 OUR AVERAGE Error includes scale factor of 1.7. See the ideogram below.					
$2.14\pm0.03^{+0.12}_{-0.11}$	7k	[1] ABLIKIM	12H	BES3	$e^+e^- \to \psi(2S)$
1.81±0.18±0.19	260 ± 19	[2] ABLIKIM	05J	BES2	$e^+e^- \to \psi(2S)$
$1.88^{+0.16}_{-0.15}\pm0.28$	194	ADAM	05	CLEO	$e^+e^- \to \psi(2S)$
0.85±0.46	4	FRANKLIN	83	MRK2	$e^+e^- \to$ hadrons

[1] From $\psi(2S) \to \pi^+\pi^-\pi^0$ events directly. The quoted systematic error includes a contribution of 4% (added in quadrature) from the uncertainty on the number of $\psi(2S)$ events.
[2] From a PW analysis of $\psi(2S) \to \pi^+\pi^-\pi^0$.

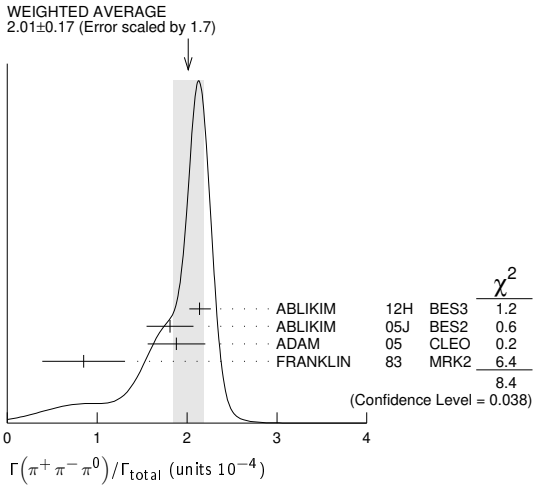

$\Gamma(\rho(770)\pi \to \pi^+\pi^-\pi^0)/\Gamma_{total}$ Γ_{18}/Γ

VALUE (units 10^{-4})	CL%	EVTS	DOCUMENT ID		TECN	COMMENT
0.32±0.12 OUR AVERAGE Error includes scale factor of 1.8.						
0.51±0.07±0.11			[1] ABLIKIM	05J	BES2	$\psi(2S) \to \rho(770)\pi \to \pi^+\pi^-\pi^0$
$0.24^{+0.08}_{-0.07}\pm0.02$		22	ADAM	05	CLEO	$e^+e^- \to \psi(2S)$
• • • We do not use the following data for averages, fits, limits, etc. • • •						
<0.83	90	1	FRANKLIN	83	MRK2	e^+e^-
<10	90		BARTEL	76	CNTR	e^+e^-
<10	90		[2] ABRAMS	75	MRK1	e^+e^-

[1] From a PW analysis of $\psi(2S) \to \pi^+\pi^-\pi^0$.
[2] Final state $\rho^0\pi^0$.

$\Gamma(\rho(2150)\pi \to \pi^+\pi^-\pi^0)/\Gamma_{total}$ Γ_{19}/Γ

VALUE (units 10^{-4})	DOCUMENT ID		TECN	COMMENT
$1.94\pm0.25^{+1.15}_{-0.34}$	[1] ABLIKIM	05J	BES2	$\psi(2S) \to \rho(2150)\pi \to \pi^+\pi^-\pi^0$

[1] From a PW analysis of $\psi(2S) \to \pi^+\pi^-\pi^0$.

$\Gamma(2(\pi^+\pi^-))/\Gamma_{total}$ Γ_{20}/Γ

VALUE (units 10^{-4})	EVTS	DOCUMENT ID		TECN	COMMENT
2.4±0.6 OUR AVERAGE Error includes scale factor of 2.2.					
2.2±0.2±0.2	308	BRIERE	05	CLEO	$e^+e^- \to \psi(2S) \to 2(\pi^+\pi^-)$
4.5±1.0		TANENBAUM	78	MRK1	e^+e^-

$\Gamma(\rho^0\pi^+\pi^-)/\Gamma_{total}$ Γ_{21}/Γ

VALUE (units 10^{-4})	EVTS	DOCUMENT ID		TECN	COMMENT
2.2±0.6 OUR AVERAGE Error includes scale factor of 1.4.					
2.0±0.2±0.4	285.5	BRIERE	05	CLEO	$e^+e^- \to \psi(2S) \to 2(\pi^+\pi^-)$
4.2±1.5		TANENBAUM	78	MRK1	e^+e^-

$\Gamma(2(\pi^+\pi^-)\pi^0)/\Gamma_{total}$ Γ_{22}/Γ

VALUE (units 10^{-4})	EVTS	DOCUMENT ID		TECN	COMMENT
29 ±10 OUR AVERAGE Error includes scale factor of 4.7. See the ideogram below.					
24.9± 0.7±3.6	2173	ABLIKIM	07D	BES2	$e^+e^- \to \psi(2S)$
128 ±12 ±2	410	[1] AUBERT	07AU	BABR	10.6 $e^+e^- \to 2(\pi^+\pi^-)\pi^0\gamma$
26.1± 0.7±3.0	1703	BRIERE	05	CLEO	$e^+e^- \to \psi(2S) \to 2(\pi^+\pi^-)\pi^0$
30 ± 8	42	FRANKLIN	83	MRK2	e^+e^-

[1] AUBERT 07AU reports $[\Gamma(\psi(2S) \to 2(\pi^+\pi^-)\pi^0)/\Gamma_{total}] \times [\Gamma(\psi(2S) \to e^+e^-)] = (297 \pm 22 \pm 18) \times 10^{-4}$ keV which we divide by our best (shown rounded) value $\Gamma(\psi(2S) \to e^+e^-) = 2.33 \pm 0.04$ keV. Our first error is their experiment's error and our second error is the systematic error from using our best (shown rounded) value.

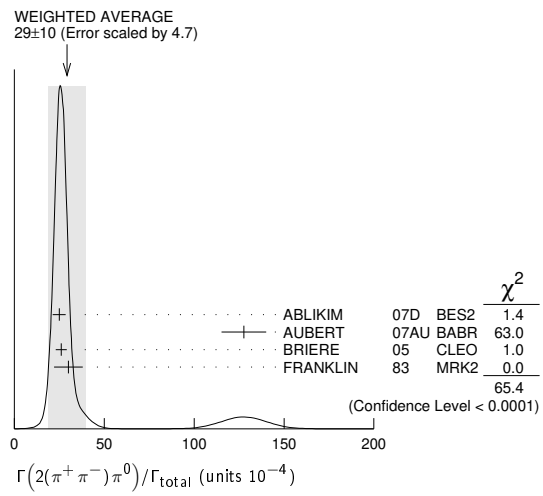

$\Gamma(\rho a_2(1320))/\Gamma_{total}$ Γ_{23}/Γ

VALUE (units 10^{-4})	CL%	EVTS	DOCUMENT ID		TECN	COMMENT
2.55±0.73±0.47		112 ± 31	BAI	04C	BES2	$\psi(2S) \to 2(\pi^+\pi^-)\pi^0$
• • • We do not use the following data for averages, fits, limits, etc. • • •						
<2.3	90		BAI	98J	BES	e^+e^-

$\Gamma(3(\pi^+\pi^-))/\Gamma_{total}$ Γ_{27}/Γ

VALUE (units 10^{-4})	EVTS	DOCUMENT ID		TECN	COMMENT
3.5 ±2.0 OUR AVERAGE Error includes scale factor of 2.8.					
5.45±0.42±0.87	671	ABLIKIM	05H	BES2	$e^+e^- \to \psi(2S) \to 3(\pi^+\pi^-)$
1.5 ±1.0		[1] TANENBAUM	78	MRK1	e^+e^-

[1] Assuming entirely strong decay.

$\Gamma(3(\pi^+\pi^-)\pi^0)/\Gamma_{total}$ Γ_{29}/Γ

VALUE (units 10^{-4})	EVTS	DOCUMENT ID		TECN	COMMENT
35±16	6	FRANKLIN	83	MRK2	$e^+e^- \to$ hadrons

$\Gamma(\eta\pi^+\pi^-)/\Gamma_{total}$ Γ_{31}/Γ

VALUE (units 10^{-4})	CL%	DOCUMENT ID		TECN	COMMENT
<1.6	90	BRIERE	05	CLEO	$e^+e^- \to \psi(2S) \to 2(\pi^+\pi^-)\pi^0$

$\Gamma(\eta\pi^+\pi^-\pi^0)/\Gamma_{total}$ Γ_{32}/Γ

VALUE (units 10^{-4})	EVTS	DOCUMENT ID		TECN	COMMENT
9.5±0.7±1.5		[1] BRIERE	05	CLEO	$e^+e^- \to \psi(2S) \to$ hadr

Int. J. Mod. Phys. A 2026.41. Downloaded from www.worldscientific.com by [redacted]LIFORNIA @ BERKELEY on 09/16/26. Re-use and distribution is strictly not permitted, except for Open Access articles.

• • • We do not use the following data for averages, fits, limits, etc. • • •

$10.3 \pm 0.8 \pm 1.4$	201.7	[2] BRIERE	05	CLEO	$e^+e^- \to \psi(2S) \to \eta 3\pi(\eta \to \gamma\gamma)$
$8.1 \pm 1.4 \pm 1.6$	50.0	[2] BRIERE	05	CLEO	$e^+e^- \to \psi(2S) \to \eta 3\pi(\eta \to 3\pi)$

[1] Average of $\eta \to \gamma\gamma$ and $\eta \to 3\pi$.
[2] Not independent from other values reported by BRIERE 05.

$\Gamma(\rho\eta)/\Gamma_{total}$ — Γ_{37}/Γ

VALUE (units 10^{-5})	EVTS	DOCUMENT ID		TECN	COMMENT
2.2 ±0.6 OUR AVERAGE Error includes scale factor of 1.1.					
$3.0\ ^{+1.1}_{-0.9} \pm 0.2$	18	ADAM	05	CLEO	$e^+e^- \to \psi(2S)$
$1.78\ ^{+0.67}_{-0.62} \pm 0.17$	13	ABLIKIM	04L	BES	$e^+e^- \to \psi(2S)$

$\Gamma(\eta'\pi^+\pi^-\pi^0)/\Gamma_{total}$ — Γ_{38}/Γ

VALUE (units 10^{-4})	EVTS	DOCUMENT ID		TECN	COMMENT
4.5±1.6±1.3	12.8	BRIERE	05	CLEO	$e^+e^- \to \psi(2S) \to$ hadr

$\Gamma(\eta'\rho)/\Gamma_{total}$ — Γ_{39}/Γ

VALUE (units 10^{-5})	EVTS	DOCUMENT ID		TECN	COMMENT
$1.87\ ^{+1.64}_{-1.11} \pm 0.33$	2	ABLIKIM	04L	BES	$e^+e^- \to \psi(2S)$
• • • We do not use the following data for averages, fits, limits, etc. • • •					
$1.02 \pm 0.11 \pm 0.24$	143	[1] ABLIKIM	17AK	BES3	$e^+e^- \to \psi(2S)$
$0.569 \pm 0.128 \pm 0.236$	80	[2] ABLIKIM	17AK	BES3	$e^+e^- \to \psi(2S)$

[1] Destructive-interference solution of a partial wave analysis of the decay $\psi(2S) \to \pi^+\pi^-\eta'$.
[2] Constructive-interference solution of a partial wave analysis of the decay $\psi(2S) \to \pi^+\pi^-\eta'$.

$\Gamma(\omega\pi^0)/\Gamma_{total}$ — Γ_{40}/Γ

VALUE (units 10^{-5})	EVTS	DOCUMENT ID		TECN	COMMENT
2.1 ±0.6 OUR AVERAGE					
$2.5\ ^{+1.2}_{-1.0} \pm 0.2$	14	ADAM	05	CLEO	$e^+e^- \to \psi(2S)$
$1.87\ ^{+0.68}_{-0.62} \pm 0.28$	14	ABLIKIM	04L	BES	$e^+e^- \to \psi(2S)$

$\Gamma(\omega\pi^+\pi^-)/\Gamma_{total}$ — Γ_{41}/Γ

VALUE (units 10^{-4})	EVTS	DOCUMENT ID		TECN	COMMENT
7.3±1.2 OUR AVERAGE Error includes scale factor of 2.1. See the ideogram below.					
$8.4 \pm 0.5 \pm 1.2$	386	ABLIKIM	07D	BES2	$e^+e^- \to \psi(2S)$
$12.2 \pm 2.2 \pm 0.7$	37	[1] AUBERT	07AU	BABR	$10.6\ e^+e^- \to \omega\pi^+\pi^-\gamma$
$8.2 \pm 0.5 \pm 0.7$	391	BRIERE	05	CLEO	$e^+e^- \to \psi(2S) \to 2(\pi^+\pi^-)\pi^0$
$4.8 \pm 0.6 \pm 0.7$	100 ± 22	[2] BAI	03B	BES	$\psi(2S) \to 2(\pi^+\pi^-)\pi^0$

[1] AUBERT 07AU quotes $\Gamma_{ee}^{\psi(2S)} \cdot B(\psi(2S) \to \omega\pi^+\pi^-) \cdot B(\omega \to 3\pi) = 2.69 \pm 0.73 \pm 0.16$ eV.
[2] Normalized to $B(\psi(2S) \to J/\psi\pi^+\pi^-) = 0.305 \pm 0.016$.

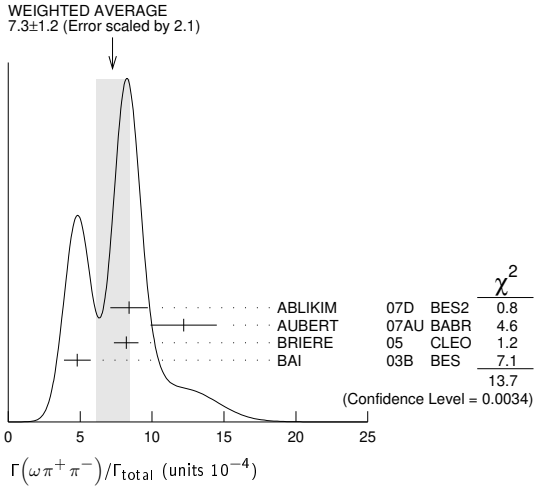

$\Gamma(b_1^\pm\pi^\mp)/\Gamma_{total}$ — Γ_{43}/Γ

VALUE (units 10^{-4})	EVTS	DOCUMENT ID		TECN	COMMENT
4.0 ±0.6 OUR AVERAGE Error includes scale factor of 1.1.					
$5.1 \pm 0.6 \pm 0.8$	202	ABLIKIM	07D	BES2	$e^+e^- \to \psi(2S)$
$4.18\ ^{+0.43}_{-0.42} \pm 0.92$	170	ADAM	05	CLEO	$e^+e^- \to \psi(2S)$
$3.2 \pm 0.6 \pm 0.5$	61 ± 11	[1,2] BAI	03B	BES	$\psi(2S) \to 2(\pi^+\pi^-)\pi^0$
• • • We do not use the following data for averages, fits, limits, etc. • • •					
$5.2 \pm 0.8 \pm 1.0$		[1] BAI	99C	BES	Repl. by BAI 03B

[1] Assuming $B(b_1 \to \omega\pi)=1$.
[2] Normalized to $B(\psi(2S) \to J/\psi\pi^+\pi^-) = 0.305 \pm 0.016$.

$\Gamma(\omega f_2(1270))/\Gamma_{total}$ — Γ_{44}/Γ

VALUE (units 10^{-4})	CL%	EVTS	DOCUMENT ID		TECN	COMMENT
2.2 ±0.4 OUR AVERAGE						
$2.3 \pm 0.5 \pm 0.4$		57	ABLIKIM	07D	BES2	$e^+e^- \to \psi(2S)$
$2.05 \pm 0.41 \pm 0.38$		62 ± 12	BAI	04C	BES2	$\psi(2S) \to 2(\pi^+\pi^-)\pi^0$
• • • We do not use the following data for averages, fits, limits, etc. • • •						
<1.5	90		[1] BAI	03B	BES	$\psi(2S) \to 2(\pi^+\pi^-)\pi^0$
<1.7	90		BAI	98J	BES	Repl. by BAI 03B

[1] Normalized to $B(\psi(2S) \to J/\psi\pi^+\pi^-) = 0.305 \pm 0.016$.

$\Gamma(b_1^0\pi^0)/\Gamma_{total}$ — Γ_{47}/Γ

VALUE (units 10^{-4})	EVTS	DOCUMENT ID		TECN	COMMENT
$2.35\ ^{+0.47}_{-0.42} \pm 0.40$	45	ADAM	05	CLEO	$e^+e^- \to \psi(2S)$

$\Gamma(\omega\eta)/\Gamma_{total}$ — Γ_{48}/Γ

VALUE (units 10^{-5})	CL%	DOCUMENT ID		TECN	COMMENT
<1.1	90	ADAM	05	CLEO	$e^+e^- \to \psi(2S)$
• • • We do not use the following data for averages, fits, limits, etc. • • •					
<3.1	90	ABLIKIM	04K	BES	$e^+e^- \to \psi(2S)$

$\Gamma(\omega\eta')/\Gamma_{total}$ — Γ_{49}/Γ

VALUE (units 10^{-5})	EVTS	DOCUMENT ID		TECN	COMMENT
$3.2\ ^{+2.4}_{-2.0} \pm 0.7$	4	[1] ABLIKIM	04K	BES	$e^+e^- \to \psi(2S)$

[1] Calculated combining $\eta' \to \gamma\rho$ and $\eta\pi^+\pi^-$ channels.

$\Gamma(\omega(782)\eta\eta)/\Gamma_{total}$ — Γ_{50}/Γ

VALUE (units 10^{-5})	EVTS	DOCUMENT ID	
1.65±0.02±0.21	1251	ABLIKIM	25BY

$\Gamma(\phi\pi^0)/\Gamma_{total}$ — Γ_{51}/Γ

VALUE (units 10^{-5})	CL%	DOCUMENT ID		TECN	COMMENT
<0.04	90	ABLIKIM	12L	BES3	$e^+e^- \to \psi(2S)$
• • • We do not use the following data for averages, fits, limits, etc. • • •					
<0.7	90	ADAM	05	CLEO	$e^+e^- \to \psi(2S)$
<0.4	90	ABLIKIM	04K	BES	$e^+e^- \to \psi(2S)$

$\Gamma(\phi\pi^+\pi^-)/\Gamma_{total}$ — Γ_{52}/Γ

VALUE (units 10^{-4})	EVTS	DOCUMENT ID		TECN	COMMENT
1.18±0.26 OUR AVERAGE Error includes scale factor of 1.5. See the ideogram below.					
$2.3 \pm 0.8 \pm 0.1$	19 ± 6	LEES	12F	BABR	$10.6\ e^+e^- \to \pi^+\pi^-K^+K^-\gamma$
$0.9 \pm 0.2 \pm 0.1$	47.6	BRIERE	05	CLEO	$e^+e^- \to \psi(2S) \to K^+K^-\pi^+\pi^-$
$1.5 \pm 0.2 \pm 0.2$	51.5 ± 8.3	[1] BAI	03B	BES	$\psi(2S) \to K^+K^-\pi^+\pi^-$
• • • We do not use the following data for averages, fits, limits, etc. • • •					
$2.45 \pm 0.96 \pm 0.04$	10 ± 4	[2,3] AUBERT	07AK	BABR	$10.6\ e^+e^- \to \pi^+\pi^-K^+K^-\gamma$

[1] Normalized to $B(\psi(2S) \to J/\psi\pi^+\pi^-) = 0.305 \pm 0.016$.
[2] Superseded by LEES 12F. AUBERT 07AK reports $[\Gamma(\psi(2S) \to \phi\pi^+\pi^-)/\Gamma_{total}] \times [\Gamma(\psi(2S) \to e^+e^-)] = (0.57 \pm 0.22 \pm 0.04) \times 10^{-3}$ keV which we divide by our best (shown rounded) value $\Gamma(\psi(2S) \to e^+e^-) = 2.33 \pm 0.04$ keV. Our first error is their experiment's error and our second error is the systematic error from using our best (shown rounded) value.
[3] Using $B(\phi \to K^+K^-) = (49.3 \pm 0.6)\%$.

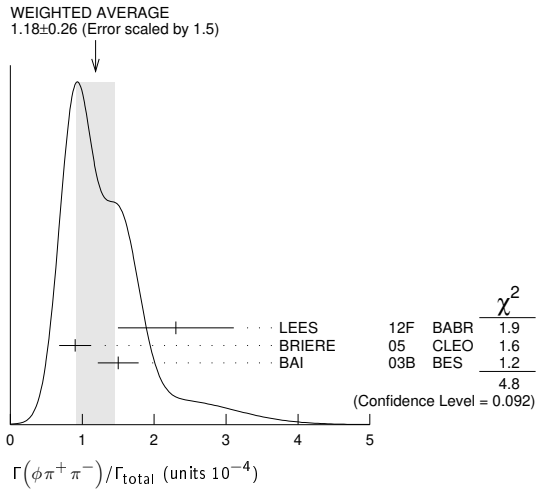

Int. J. Mod. Phys. A 2026.41. Downloaded from www.worldscientific.com
by UNIVERSITY OF CALIFORNIA @ BERKELEY on 09/16/26. Re-use and distribution is strictly not permitted, except for Open Access articles.

$\Gamma(\phi f_0(980) \to \pi^+\pi^-)/\Gamma_{total}$ — Γ_{53}/Γ

VALUE (units 10^{-4})	EVTS	DOCUMENT ID		TECN	COMMENT
0.75±0.33 OUR AVERAGE	Error includes scale factor of 1.6.				
1.5 ±0.5 ±0.1	12 ± 4	LEES	12F	BABR	10.6 $e^+e^- \to \pi^+\pi^-K^+K^-\gamma$
0.6 ±0.2 ±0.1	18.4 ± 6.4	[1] BAI	03B	BES	$\psi(2S) \to K^+K^-\pi^+\pi^-$
• • • We do not use the following data for averages, fits, limits, etc. • • •					
1.46±0.71±0.02	6 ± 3	[2,3] AUBERT	07AK	BABR	10.6 $e^+e^- \to \pi^+\pi^-K^+K^-\gamma$

[1] Normalized to $B(\psi(2S) \to J/\psi\pi^+\pi^-) = 0.305 \pm 0.016$.
[2] Superseded by LEES 12F. AUBERT 07AK reports $[\Gamma(\psi(2S) \to \phi f_0(980) \to \pi^+\pi^-)/\Gamma_{total}] \times [\Gamma(\psi(2S) \to e^+e^-)] = (0.34 \pm 0.16 \pm 0.04) \times 10^{-3}$ keV which we divide by our best (shown rounded) value $\Gamma(\psi(2S) \to e^+e^-) = 2.33 \pm 0.04$ keV. Our first error is their experiment's error and our second error is the systematic error from using our best (shown rounded) value.
[3] Using $B(\phi \to K^+K^-) = (49.3 \pm 0.6)\%$.

$\Gamma(\phi\eta)/\Gamma_{total}$ — Γ_{54}/Γ

VALUE (units 10^{-5})	EVTS	DOCUMENT ID		TECN	COMMENT
3.10±0.31 OUR AVERAGE					
3.14±0.23±0.23	0.2k	ABLIKIM	12L	BES3	$e^+e^- \to \psi(2S)$
$2.0\ ^{+1.5}_{-1.1}$ ±0.4	6	ADAM	05	CLEO	$e^+e^- \to \psi(2S)$
3.3 ±1.1 ±0.5	17	ABLIKIM	04K	BES	$e^+e^- \to \psi(2S)$

$\Gamma(\eta\phi(2170),\ \phi(2170) \to \phi f_0(980),\ f_0 \to \pi^+\pi^-)/\Gamma_{total}$ — Γ_{55}/Γ

VALUE	CL%	DOCUMENT ID		TECN	COMMENT
$<2.2 \times 10^{-6}$	90	ABLIKIM	19I	BES3	$e^+e^- \to \eta\phi f_0(980)$

$\Gamma(\phi\eta')/\Gamma_{total}$ — Γ_{56}/Γ

VALUE (units 10^{-5})	EVTS	DOCUMENT ID		TECN	COMMENT
1.54±0.20 OUR AVERAGE					
1.51±0.16±0.12	201	ABLIKIM	19BA	BES3	$e^+e^- \to \psi(2S)$
3.1 ±1.4 ±0.7	8	[1] ABLIKIM	04K	BES	$e^+e^- \to \psi(2S)$

[1] Calculated combining $\eta' \to \gamma\rho$ and $\eta\pi^+\pi^-$ channels.

$\Gamma(\phi\eta\eta')/\Gamma_{total}$ — Γ_{57}/Γ

VALUE (units 10^{-5})	EVTS	DOCUMENT ID		TECN	COMMENT
3.14±0.17±0.24	480	[1] ABLIKIM	25E	BES3	$e^+e^- \to \psi(2S)$

[1] The continuum is subtracted using data at 3.773 GeV. No interference between the $\psi(2S)$ and continuum amplitudes is assumed.

$\Gamma(h_1(1900)\eta \to \phi\eta\eta')/\Gamma_{total}$ — Γ_{58}/Γ

VALUE (units 10^{-6})	DOCUMENT ID		TECN	COMMENT
3.8±1.4±1.5	ABLIKIM	25E	BES3	$e^+e^- \to \psi(2S)$

$\Gamma(\phi(2170)\eta \to \phi\eta\eta')/\Gamma_{total}$ — Γ_{59}/Γ

VALUE (units 10^{-6})	DOCUMENT ID		TECN	COMMENT
3.3±1.4±1.2	ABLIKIM	25E	BES3	$e^+e^- \to \psi(2S)$

$\Gamma(\phi(2170)\eta' \to \phi\eta\eta')/\Gamma_{total}$ — Γ_{60}/Γ

VALUE (units 10^{-6})	DOCUMENT ID		TECN	COMMENT
3.8±0.9±0.5	ABLIKIM	25E	BES3	$e^+e^- \to \psi(2S)$

$\Gamma(h_1(2300)\eta \to \phi\eta\eta')/\Gamma_{total}$ — Γ_{61}/Γ

VALUE (units 10^{-6})	DOCUMENT ID		TECN	COMMENT
2.2±0.7±0.7	ABLIKIM	25E	BES3	$e^+e^- \to \psi(2S)$

$\Gamma(h_1(2300)\eta' \to \phi\eta\eta')/\Gamma_{total}$ — Γ_{62}/Γ

VALUE (units 10^{-6})	DOCUMENT ID		TECN	COMMENT
4.8±1.3±0.7	ABLIKIM	25E	BES3	$e^+e^- \to \psi(2S)$

$\Gamma(\phi\phi\phi)/\Gamma_{total}$ — Γ_{63}/Γ

VALUE (units 10^{-5})	EVTS	DOCUMENT ID		TECN	COMMENT
1.46±0.05±0.17	1.3k	[1] ABLIKIM	24O	BES3	$e^+e^- \to \psi(2S)$

[1] Data at 3.773 GeV assumed to be $e^+e^-(3.773) \to 3\phi$ events yield an estimate for the continuum amplitude at the $\psi(2S)$. No interference between the $\psi(2S)$ and continuum amplitudes is assumed.

$\Gamma(\phi f_1(1285))/\Gamma_{total}$ — Γ_{64}/Γ

VALUE (units 10^{-5})	EVTS	DOCUMENT ID		TECN	COMMENT
3.0±0.4±1.3	234	[1] ABLIKIM	19BA	BES3	$e^+e^- \to \psi(2S)$

[1] ABLIKIM 19BA reports $[\Gamma(\psi(2S) \to \phi f_1(1285))/\Gamma_{total}] \times [B(f_1(1285) \to \eta\pi^+\pi^-)] = (1.03 \pm 0.10 \pm 0.09) \times 10^{-5}$ which we divide by our best (shown rounded) value $B(f_1(1285) \to \eta\pi^+\pi^-) = (35 \pm 15) \times 10^{-2}$. Our first error is their experiment's error and our second error is the systematic error from using our best (shown rounded) value.

$\Gamma(\phi\eta(1405) \to \phi\pi^+\pi^-\eta)/\Gamma_{total}$ — Γ_{65}/Γ

VALUE (units 10^{-6})	EVTS	DOCUMENT ID		TECN	COMMENT
8.46±1.37±0.92	195	ABLIKIM	19BA	BES3	$e^+e^- \to \psi(2S)$

$\Gamma(\phi f_2'(1525))/\Gamma_{total}$ — Γ_{66}/Γ

VALUE (units 10^{-4})	CL%	EVTS	DOCUMENT ID		TECN	COMMENT
0.44±0.12±0.11		20 ± 6	BAI	04C		$\psi(2S) \to 2(K^+K^-)$
• • • We do not use the following data for averages, fits, limits, etc. • • •						
<0.45	90		BAI	98J	BES	$e^+e^- \to 2(K^+K^-)$

$\Gamma(K^+K^-)/\Gamma_{total}$ — Γ_{67}/Γ

VALUE (units 10^{-5})	CL%	EVTS	DOCUMENT ID		TECN	COMMENT
7.48±0.23±0.39		1.3k	[1] METREVELI	12		$\psi(2S) \to K^+K^-$
• • • We do not use the following data for averages, fits, limits, etc. • • •						
6.2 ±1.5 ±0.2		66	[2,3] LEES	15J	BABR	$e^+e^- \to K^+K^-\gamma$
8.3 ±1.5 ±0.2		66	[3,4] LEES	15J	BABR	$e^+e^- \to K^+K^-\gamma$
6.3 ±0.6 ±0.3			[5] DOBBS	06A	CLEO	e^+e^-
10 ±7			[5] BRANDELIK	79C	DASP	e^+e^-
< 5	90		FELDMAN	77	MRK1	e^+e^-

[1] Obtained by analyzing CLEO-c data but not authored by the CLEO Collaboration.
[2] $\sin\phi > 0$.
[3] Using $\Gamma(\psi(2S) \to e^+e^-) = (2.37 \pm 0.04)$ keV.
[4] $\sin\phi < 0$.
[5] Interference with non-resonant K^+K^- production not taken into account.

$\Gamma(K^+K^-\pi^+\pi^-)/\Gamma_{total}$ — Γ_{68}/Γ

VALUE (units 10^{-4})	EVTS	DOCUMENT ID		TECN	COMMENT
7.3±0.5 OUR AVERAGE					
8.1±1.3±0.3	133	LEES	12F	BABR	10.6 $e^+e^- \to \pi^+\pi^-K^+K^-\gamma$
7.1±0.3±0.4	817.2	BRIERE	05	CLEO	$e^+e^- \to \psi(2S) \to K^+K^-\pi^+\pi^-$
16 ±4		[1] TANENBAUM	78	MRK1	e^+e^-
• • • We do not use the following data for averages, fits, limits, etc. • • •					
11.0±1.9±0.2	85	[2] AUBERT	07AK	BABR	10.6 $e^+e^- \to \pi^+\pi^-K^+K^-\gamma$

[1] Assuming entirely strong decay.
[2] Superseded by LEES 12F. AUBERT 07AK reports $[\Gamma(\psi(2S) \to K^+K^-\pi^+\pi^-)/\Gamma_{total}] \times [\Gamma(\psi(2S) \to e^+e^-)] = (2.56 \pm 0.42 \pm 0.16) \times 10^{-3}$ keV which we divide by our best (shown rounded) value $\Gamma(\psi(2S) \to e^+e^-) = 2.33 \pm 0.04$ keV. Our first error is their experiment's error and our second error is the systematic error from using our best (shown rounded) value.

$\Gamma(K^+K^-\pi^0)/\Gamma_{total}$ — Γ_{69}/Γ

VALUE (units 10^{-5})	CL%	EVTS	DOCUMENT ID		TECN	COMMENT
4.07±0.16±0.26		0.9k	ABLIKIM	12L	BES3	$e^+e^- \to \psi(2S)$
• • • We do not use the following data for averages, fits, limits, etc. • • •						
<8.9	90	1	FRANKLIN	83	MRK2	$e^+e^- \to$ hadrons

$\Gamma(K^0_S K^0_S)/\Gamma_{total}$ — Γ_{70}/Γ

VALUE	CL%	DOCUMENT ID		TECN	COMMENT
$<1.1 \times 10^{-8}$	90	ABLIKIM	25CC	BES3	$\psi(2S) \to K^0_S K^0_S \to \pi^+\pi^-\pi^+\pi^-$
• • • We do not use the following data for averages, fits, limits, etc. • • •					
$<4.6 \times 10^{-6}$	95	[1] BAI	04D	BES	$e^+e^- \to \psi(2S) \to K^0_S K^0_S$

[1] Forbidden by *CP*.

$\Gamma(K^0_S K^0_L)/\Gamma_{total}$ — Γ_{71}/Γ

VALUE (units 10^{-5})	EVTS	DOCUMENT ID		TECN	COMMENT
5.34±0.33 OUR AVERAGE					
5.28±0.25±0.34	478 ± 23	[1] METREVELI	12		$\psi(2S) \to K^0_S K^0_L$
5.8 ±0.8 ±0.4		DOBBS	06A	CLEO	e^+e^-
5.24±0.47±0.48	156 ± 14	[2] BAI	04B	BES2	$\psi(2S) \to K^0_S K^0_L \to \pi^+\pi^-X$

[1] Obtained by analyzing CLEO-c data but not authored by the CLEO Collaboration.
[2] Using $B(K^0_S \to \pi^+\pi^-) = 0.6860 \pm 0.0027$.

$\Gamma(K^+K^-\pi^+\pi^-\pi^0)/\Gamma_{total}$ — Γ_{77}/Γ

VALUE (units 10^{-4})	EVTS	DOCUMENT ID		TECN	COMMENT
12.6±0.9 OUR AVERAGE					
18.9±5.7±0.3	32	[1] AUBERT	07AU	BABR	10.6 $e^+e^- \to K^+K^-\pi^+\pi^-\pi^0\gamma$
11.7±1.0±1.5	597	ABLIKIM	06G	BES2	$\psi(2S) \to K^+K^-\pi^+\pi^-\pi^0$
12.7±0.5±1.0	711.6	BRIERE	05	CLEO	$e^+e^- \to \psi(2S) \to K^+K^-\pi^+\pi^-\pi^0$

[1] AUBERT 07AU reports $[\Gamma(\psi(2S) \to K^+K^-\pi^+\pi^-\pi^0)/\Gamma_{total}] \times [\Gamma(\psi(2S) \to e^+e^-)] = (44 \pm 13 \pm 3) \times 10^{-4}$ keV which we divide by our best (shown rounded) value $\Gamma(\psi(2S) \to e^+e^-) = 2.33 \pm 0.04$ keV. Our first error is their experiment's error and our second error is the systematic error from using our best (shown rounded) value.

$\Gamma(\omega f_0(1710) \to \omega K^+K^-)/\Gamma_{total}$ — Γ_{78}/Γ

VALUE (units 10^{-5})	EVTS	DOCUMENT ID		TECN	COMMENT
5.9±2.0±0.9	19	ABLIKIM	06G	BES2	$\psi(2S) \to K^+K^-\pi^+\pi^-\pi^0$

Int. J. Mod. Phys. A 2026.41. Downloaded from www.worldscientific.com by CALIFORNIA @ BERKELEY on 09/16/26. Re-use and distribution is strictly not permitted, except for Open Access articles.

$\Gamma(K^*(892)^0 K^- \pi^+ \pi^0 + \text{c.c.})/\Gamma_{total}$ — Γ_{79}/Γ

VALUE (units 10^{-4})	EVTS	DOCUMENT ID		TECN	COMMENT
8.6±1.3±1.8	238	ABLIKIM	06G	BES2	$\psi(2S) \to K^+ K^- \pi^+ \pi^- \pi^0$

$\Gamma(K^*(892)^+ K^- \pi^+ \pi^- + \text{c.c.})/\Gamma_{total}$ — Γ_{80}/Γ

VALUE (units 10^{-4})	EVTS	DOCUMENT ID		TECN	COMMENT
9.6±2.2±1.7	133	ABLIKIM	06G	BES2	$\psi(2S) \to K^+ K^- \pi^+ \pi^- \pi^0$

$\Gamma(K^*(892)^+ K^- \rho^0 + \text{c.c.})/\Gamma_{total}$ — Γ_{81}/Γ

VALUE (units 10^{-4})	EVTS	DOCUMENT ID		TECN	COMMENT
7.3±2.2±1.4	78	ABLIKIM	06G	BES2	$\psi(2S) \to K^+ K^- \pi^+ \pi^- \pi^0$

$\Gamma(K^*(892)^0 K^- \rho^+ + \text{c.c.})/\Gamma_{total}$ — Γ_{82}/Γ

VALUE (units 10^{-4})	EVTS	DOCUMENT ID		TECN	COMMENT
6.1±1.3±1.2	125	ABLIKIM	06G	BES2	$\psi(2S) \to K^+ K^- \pi^+ \pi^- \pi^0$

$\Gamma(K^0_S K^0_S \pi^+ \pi^-)/\Gamma_{total}$ — Γ_{83}/Γ

VALUE (units 10^{-4})	EVTS	DOCUMENT ID		TECN	COMMENT
2.20±0.25±0.37	83 ± 9	ABLIKIM	05O	BES2	$e^+ e^- \to \psi(2S)$

$\Gamma(K^+ K^- \rho^0)/\Gamma_{total}$ — Γ_{91}/Γ

VALUE (units 10^{-4})	EVTS	DOCUMENT ID		TECN	COMMENT
2.2±0.2±0.4	223.8	BRIERE	05	CLEO	$e^+ e^- \to \psi(2S) \to K^+ K^- \pi^+ \pi^-$

$\Gamma(K^*(892)^0 \overline{K}^*_2(1430)^0)/\Gamma_{total}$ — Γ_{92}/Γ

VALUE (units 10^{-4})	CL%	EVTS	DOCUMENT ID		TECN	COMMENT
1.86±0.32±0.43		93 ± 16	BAI	04C		$\psi(2S) \to K^+ K^- \pi^+ \pi^-$
• • • We do not use the following data for averages, fits, limits, etc. • • •						
<1.2	90		BAI	98J	BES	$e^+ e^-$

$\Gamma(K^+ K^- \pi^+ \pi^- \eta)/\Gamma_{total}$ — Γ_{93}/Γ

VALUE (units 10^{-3})	EVTS	DOCUMENT ID		TECN	COMMENT
1.3±0.7±0.1	7	[1] AUBERT	07AU	BABR	$10.6\ e^+ e^- \to K^+ K^- \pi^+ \pi^- \eta\gamma$

[1] AUBERT 07AU quotes $\Gamma^{\psi(2S)}_{ee} \cdot B(\psi(2S) \to 2(\pi^+\pi^-)\eta) \cdot B(\eta \to \gamma\gamma) = 1.2 \pm 0.7 \pm 0.1$ eV.

$\Gamma(K^+ K^- 2(\pi^+ \pi^-) \pi^0)/\Gamma_{total}$ — Γ_{95}/Γ

VALUE (units 10^{-4})	EVTS	DOCUMENT ID		TECN	COMMENT
10.0±2.5±1.8	65	ABLIKIM	07D	BES2	$e^+ e^- \to \psi(2S)$

$\Gamma(K^+ K^*(892)^- + \text{c.c.})/\Gamma_{total}$ — Γ_{96}/Γ

VALUE (units 10^{-5})	CL%	EVTS	DOCUMENT ID		TECN	COMMENT
2.9 ±0.4 OUR AVERAGE Error includes scale factor of 1.2.						
$3.18 \pm 0.30^{+0.26}_{-0.31}$		0.2k	ABLIKIM	12L	BES3	$e^+ e^- \to \psi(2S)$
$2.9\ ^{+1.3}_{-1.7} \pm 0.4$		9.6 ± 4.2	ABLIKIM	05I	BES2	$e^+ e^- \to \psi(2S)$
$1.3\ ^{+1.0}_{-0.7} \pm 0.3$		7	ADAM	05	CLEO	$e^+ e^- \to \psi(2S)$
• • • We do not use the following data for averages, fits, limits, etc. • • •						
<5.4	90		FRANKLIN	83	MRK2	$e^+ e^- \to$ hadrons

$\Gamma(2(K^+ K^-))/\Gamma_{total}$ — Γ_{97}/Γ

VALUE (units 10^{-4})	EVTS	DOCUMENT ID		TECN	COMMENT
0.63±0.13 OUR AVERAGE					
0.9 ±0.4 ±0.1	13	LEES	12F	BABR	$10.6\ e^+ e^- \to 2(K^+ K^-)\gamma$
0.6 ±0.1 ±0.1	59.2	BRIERE	05	CLEO	$e^+ e^- \to \psi(2S) \to 2(K^+ K^-)$

$\Gamma(2(K^+ K^-)\pi^0)/\Gamma_{total}$ — Γ_{98}/Γ

VALUE (units 10^{-4})	EVTS	DOCUMENT ID		TECN	COMMENT
1.1±0.2±0.2	44.7	BRIERE	05	CLEO	$e^+ e^- \to \psi(2S) \to 2(K^+ K^-)\pi^0$

$\Gamma(K^+ K^- \phi)/\Gamma_{total}$ — Γ_{99}/Γ

VALUE (units 10^{-4})	EVTS	DOCUMENT ID		TECN	COMMENT
0.70±0.16 OUR AVERAGE					
0.8 ±0.2 ±0.1	36.8	BRIERE	05	CLEO	$e^+ e^- \to \psi(2S) \to 2(K^+ K^-)$
0.6 ±0.2 ±0.1	16.1 ± 5.0	[1] BAI	03B	BES	$\psi(2S) \to 2(K^+ K^-)$

[1] Normalized to $B(\psi(2S) \to J/\psi\pi^+\pi^-) = 0.305 \pm 0.016$.

$\Gamma(K^0_S K^0_S \phi)/\Gamma_{total}$ — Γ_{100}/Γ

VALUE (units 10^{-4})	EVTS	DOCUMENT ID		TECN	COMMENT
0.353±0.020±0.021	687	[1] ABLIKIM	23BA	BES3	$e^+ e^- \to \psi(2S) \to K^0_S K^0_S K^+ K^-$

[1] Solution with a constructive interference of the signal with the continuum background.

$\Gamma(K_1(1270)^\pm K^\mp)/\Gamma_{total}$ — Γ_{101}/Γ

VALUE (units 10^{-4})	DOCUMENT ID		TECN	COMMENT
10.0±1.8±2.1	[1] BAI	99C	BES	$e^+ e^-$

[1] Assuming $B(K_1(1270) \to K\rho) = 0.42 \pm 0.06$

$\Gamma(K^+ \overline{K}^*(892)^0 \pi^- + \text{c.c.})/\Gamma_{total}$ — Γ_{102}/Γ

VALUE (units 10^{-4})	DOCUMENT ID		TECN	COMMENT
6.7±2.5	TANENBAUM	78	MRK1	$e^+ e^-$

$\Gamma(\eta K^+ K^-, \text{no } \eta\phi)/\Gamma_{total}$ — Γ_{103}/Γ

VALUE (units 10^{-5})	CL%	EVTS	DOCUMENT ID		TECN	COMMENT
3.49±0.09±0.15		1.8k	[1] ABLIKIM	20F	BES3	$\psi(2S) \to K^+ K^- \gamma\gamma$
• • • We do not use the following data for averages, fits, limits, etc. • • •						
$3.08 \pm 0.29 \pm 0.25$		0.3k	[1,2] ABLIKIM	12L	BES3	$\psi(2S) \to K^+ K^- \gamma\gamma$
<13	90		BRIERE	05	CLEO	$e^+ e^- \to \psi(2S) \to K^+ K^- \pi^+ \pi^- \pi^0$

[1] Excluding $\eta\phi$.
[2] Superseded by ABLIKIM 20F.

$\Gamma(\eta K^+ K^-) \times \Gamma(e^+ e^-)/\Gamma_{total}$ — $\Gamma_{104}\Gamma_7/\Gamma$

VALUE (eV)	CL%	DOCUMENT ID		TECN	COMMENT
<0.6	90	[1] LEES	23	BABR	$e^+ e^- \to \gamma_{ISR}$hadrons

[1] LEES 23 reports $[\Gamma(\psi(2S) \to \eta K^+ K^-) \times \Gamma(\psi(2S) \to e^+ e^-)/\Gamma_{total}] \times [B(\eta \to 3\pi^0)] < 0.2$ eV which we divide by our best (shown rounded) value $B(\eta \to 3\pi^0) = 32.56 \times 10^{-2}$.

$\Gamma(X(1750)\eta \to K^+ K^- \eta)/\Gamma_{total}$ — Γ_{105}/Γ

VALUE (units 10^{-6})	DOCUMENT ID		TECN	COMMENT
4.8±1.0±2.6	ABLIKIM	20F	BES3	$\psi(2S) \to K^+ K^- \eta$

$\Gamma(K_1(1400)^\pm K^\mp)/\Gamma_{total}$ — Γ_{106}/Γ

VALUE (units 10^{-4})	CL%	DOCUMENT ID		TECN	COMMENT
<3.1	90	[1] BAI	99C	BES	$e^+ e^-$

[1] Assuming $B(K_1(1400) \to K^*\pi) = 0.94 \pm 0.06$

$\Gamma(K^*_2(1430)^\pm K^\mp)/\Gamma_{total}$ — Γ_{107}/Γ

VALUE (units 10^{-5})	EVTS	DOCUMENT ID		TECN	COMMENT
$\mathbf{7.12 \pm 0.62^{+1.13}_{-0.61}}$	251 ± 22	ABLIKIM	12L	BES3	$e^+ e^- \to \psi(2S)$

$\Gamma(K^*(892)^0 \overline{K}^0 + \text{c.c.})/\Gamma_{total}$ — Γ_{108}/Γ

VALUE (units 10^{-5})	EVTS	DOCUMENT ID		TECN	COMMENT
10.9±2.0 OUR AVERAGE					
$13.3^{+2.4}_{-2.8} \pm 1.7$	65.6 ± 9.0	ABLIKIM	05I	BES2	$e^+ e^- \to \psi(2S)$
$9.2^{+2.7}_{-2.2} \pm 0.9$	25	ADAM	05	CLEO	$e^+ e^- \to \psi(2S)$

$\Gamma(K^+ K^*(892)^- + \text{c.c.})/\Gamma(K^*(892)^0 \overline{K}^0 + \text{c.c.})$ — Γ_{96}/Γ_{108}

VALUE	DOCUMENT ID		TECN	COMMENT
0.16±0.06 OUR AVERAGE				
$0.22^{+0.10}_{-0.14}$	ABLIKIM	05I	BES2	$e^+ e^- \to \psi(2S)$
$0.14^{+0.08}_{-0.06}$	ADAM	05	CLEO	$e^+ e^- \to \psi(2S)$

$\Gamma(\omega K^+ K^-)/\Gamma_{total}$ — Γ_{109}/Γ

VALUE (units 10^{-4})	EVTS	DOCUMENT ID		TECN	COMMENT
1.62±0.11 OUR AVERAGE Error includes scale factor of 1.1.					
$1.56 \pm 0.04 \pm 0.11$	2.8k	ABLIKIM	14G	BES3	$\psi(2S) \to K^+ K^- \pi^+ \pi^- \pi^0$
$2.38 \pm 0.37 \pm 0.29$	78	ABLIKIM	06G	BES2	$\psi(2S) \to K^+ K^- \pi^+ \pi^- \pi^0$
1.9 ±0.3 ±0.3	76.8	BRIERE	05	CLEO	$e^+ e^- \to \psi(2S) \to K^+ K^- \pi^+ \pi^- \pi^0$
1.5 ±0.3 ±0.2	23	[1] BAI	03B	BES	$\psi(2S) \to K^+ K^- \pi^+ \pi^- \pi^0$

[1] Normalized to $B(\psi(2S) \to J/\psi\pi^+\pi^-) = 0.305 \pm 0.016$.

$\Gamma(\omega K^0_S K^0_S)/\Gamma_{total}$ — Γ_{110}/Γ

VALUE (units 10^{-5})	EVTS	DOCUMENT ID		TECN	COMMENT
7.04±0.39±0.36	1.5k	ABLIKIM	21AL	BES3	$\psi(2S) \to \pi^+ \pi^- \pi^0 K^0_S K^0_S$

$\Gamma(\omega K^*(892)^+ K^- + \text{c.c.})/\Gamma_{total}$ — Γ_{111}/Γ

VALUE (units 10^{-5})	EVTS	DOCUMENT ID		TECN	COMMENT
20.7±2.6 OUR AVERAGE					
$18.9 \pm 2.9 \pm 2.2$	396	ABLIKIM	13M	BES3	$\psi(2S) \to \omega K^0_S K^- \pi^+$
$22.6 \pm 3.0 \pm 2.4$	535	ABLIKIM	13M	BES3	$\psi(2S) \to \omega K^+ K^- \pi^0$

$\Gamma(\omega K^*_2(1430)^+ K^- + \text{c.c.})/\Gamma_{total}$ — Γ_{112}/Γ

VALUE (units 10^{-5})	EVTS	DOCUMENT ID		TECN	COMMENT
6.1 ±1.2 OUR AVERAGE					
$6.39 \pm 1.50 \pm 0.78$	128	ABLIKIM	13M	BES3	$\psi(2S) \to \omega K^0_S K^- \pi^+$
$5.86 \pm 1.61 \pm 0.83$	143	ABLIKIM	13M	BES3	$\psi(2S) \to \omega K^+ K^- \pi^0$

Int. J. Mod. Phys. A 2026.41. Downloaded from www.worldscientific.com
by UNIVERSITY OF CALIFORNIA @ BERKELEY on 09/16/26. Re-use and distribution is strictly not permitted, except for Open Access articles.

$\Gamma(\omega\overline{K}^*(892)^0 K^0)/\Gamma_{total}$ — Γ_{113}/Γ

VALUE (units 10^{-5})	EVTS	DOCUMENT ID		TECN	COMMENT
16.8±2.5±1.6	356	ABLIKIM	13M	BES3	$\psi(2S) \to \omega K^0_S K^- \pi^+$

$\Gamma(\omega\overline{K}^*_2(1430)^0 K^0)/\Gamma_{total}$ — Γ_{114}/Γ

VALUE (units 10^{-5})	EVTS	DOCUMENT ID		TECN	COMMENT
5.82±2.08±0.72	116	ABLIKIM	13M	BES3	$\psi(2S) \to \omega K^0_S K^- \pi^+$

$\Gamma(\omega X(1440) \to \omega K^0_S K^- \pi^+ + \text{c.c.})/\Gamma_{total}$ — Γ_{115}/Γ

VALUE (units 10^{-5})	EVTS	DOCUMENT ID		TECN	COMMENT
1.60±0.27±0.24	109	[1] ABLIKIM	13M	BES3	$\psi(2S) \to \omega K^0_S K^- \pi^+$

[1] $X(1440)$ compatible with $\eta(1405)$ and $\eta(1475)$. A $f_1(1420)$ is also possible.

$\Gamma(\omega X(1440) \to \omega K^+ K^- \pi^0)/\Gamma_{total}$ — Γ_{116}/Γ

VALUE (units 10^{-5})	EVTS	DOCUMENT ID		TECN	COMMENT
1.09±0.20±0.16	82	[1] ABLIKIM	13M	BES3	$\psi(2S) \to \omega K^+ K^- \pi^0$

[1] $X(1440)$ compatible with $\eta(1405)$ and $\eta(1475)$. A $f_1(1420)$ is also possible.

$\Gamma(\omega f_1(1285) \to \omega K^0_S K^- \pi^+ + \text{c.c.})/\Gamma_{total}$ — Γ_{117}/Γ

VALUE (units 10^{-5})	EVTS	DOCUMENT ID		TECN	COMMENT
0.302±0.098±0.027	22	[1] ABLIKIM	13M	BES3	$\psi(2S) \to \omega K^0_S K^- \pi^+$

[1] Statistical signficance 4.5 σ. This measurement is equivalent to a limit of $< 0.478\times10^{-5}$ at 90% C.L.

$\Gamma(\omega f_1(1285) \to \omega K^+ K^- \pi^0)/\Gamma_{total}$ — Γ_{118}/Γ

VALUE (units 10^{-5})	EVTS	DOCUMENT ID		TECN	COMMENT
0.125±0.070±0.013	10	[1] ABLIKIM	13M	BES3	$\psi(2S) \to \omega K^+ K^- \pi^0$

[1] Statistical signficance 3.2 σ. This measurement is equivalent to a limit of $< 0.221\times10^{-5}$ at 90% C.L.

$\Gamma(p\overline{p})/\Gamma_{total}$ — Γ_{119}/Γ

VALUE (units 10^{-4})	EVTS	DOCUMENT ID		TECN	COMMENT
2.95±0.09 OUR FIT	Error includes scale factor of 1.3.				
3.02±0.08 OUR AVERAGE					
3.05±0.02±0.12	19k	ABLIKIM	18T	BES3	$e^+e^- \to \psi(2S) \to p\overline{p}$
3.08±0.05±0.18	4.5k	[1] DOBBS	14		$e^+e^- \to \psi(2S) \to p\overline{p}$
3.36±0.09±0.25	1.6k	ABLIKIM	07C	BES	$e^+e^- \to \psi(2S) \to p\overline{p}$
2.87±0.12±0.15	557	PEDLAR	05	CLEO	$e^+e^- \to \psi(2S) \to p\overline{p}$
1.4 ±0.8	4	BRANDELIK	79C	DASP	$e^+e^- \to \psi(2S) \to p\overline{p}$
2.3 ±0.7		FELDMAN	77	MRK1	$e^+e^- \to \psi(2S) \to p\overline{p}$

[1] Using CLEO-c data but not authored by the CLEO Collaboration.

$\Gamma(p\overline{p})/\Gamma(J/\psi(1S)\pi^+\pi^-)$ — Γ_{119}/Γ_{12}

VALUE (units 10^{-4})	DOCUMENT ID		TECN	COMMENT
8.47±0.28 OUR FIT	Error includes scale factor of 1.3.			
6.98±0.49±0.97	BAI	01	BES	$e^+e^- \to \psi(2S) \to p\overline{p}$

$\Gamma(n\overline{n})/\Gamma_{total}$ — Γ_{120}/Γ

VALUE (units 10^{-4})	EVTS	DOCUMENT ID		TECN	COMMENT
3.06±0.06±0.14	6k	ABLIKIM	18T	BES3	$e^+e^- \to \psi(2S) \to n\overline{n}$

$\Gamma(p\overline{p}\pi^0)/\Gamma_{total}$ — Γ_{121}/Γ

The two different fit values of ABLIKIM 25M cannot be distinguished. Previous measurements did not consider the large uncertainty due to interference with the e^+e^- continuum.

VALUE (units 10^{-4})	EVTS	DOCUMENT ID		TECN	COMMENT
1.2 to 2.4 OUR EVALUATION					
1.339±0.112±0.023	188k	[1] ABLIKIM	25M	BES3	$\psi(2S) \to p\overline{p}\pi^0$
1.837±0.137±0.032	188k	[2] ABLIKIM	25M	BES3	$\psi(2S) \to p\overline{p}\pi^0$
• • • We do not use the following data for averages, fits, limits, etc. • • •					
1.65 ±0.03 ±0.15	4.5k	ABLIKIM	13A	BES3	$\psi(2S) \to p\overline{p}\pi^0$
1.54 ±0.06 ±0.06	948	ALEXANDER	10	CLEO	$\psi(2S) \to \pi^0 p\overline{p}$
1.32 ±0.10 ±0.15	256	[3] ABLIKIM	05E	BES2	$e^+e^- \to \psi(2S) \to p\overline{p}\gamma\gamma$
1.4 ±0.5	9	FRANKLIN	83	MRK2	e^+e^-

[1] Constructive-interference solution of a partial wave analysis of the decay $\psi(2S) \to p\overline{p}\pi^0$.
[2] Destructive-interference solution of a partial wave analysis of the decay $\psi(2S) \to p\overline{p}\pi^0$.
[3] Computed using $B(\pi^0 \to \gamma\gamma) = (98.80 \pm 0.03)\%$.

$\Gamma(N(940)\overline{p} + \text{c.c.} \to p\overline{p}\pi^0)/\Gamma_{total}$ — Γ_{122}/Γ

VALUE (units 10^{-5})	EVTS	DOCUMENT ID		TECN	COMMENT
11.39±0.31±1.19	121k	[1] ABLIKIM	25M	BES3	$\psi(2S) \to p\overline{p}\pi^0$
• • • We do not use the following data for averages, fits, limits, etc. • • •					
$6.42\pm0.20^{+1.78}_{-1.28}$	1.9k	[2] ABLIKIM	13A	BES3	$\psi(2S) \to p\overline{p}\pi^0$

[1] From a fit (PWA) of $\pi^0 p\overline{p}$ data to ten distinct intermediate $N\overline{p}$ resonant states.
[2] From a fit of $\pi^0 p\overline{p}$ data to eight distinct intermediate $N\overline{p}$ resonant states. Superseded by ABLIKIM 25M.

$\Gamma(N(1440)\overline{p} + \text{c.c.} \to p\overline{p}\pi^0)/\Gamma_{total}$ — Γ_{123}/Γ

VALUE (units 10^{-5})	EVTS	DOCUMENT ID		TECN	COMMENT
7.5 ±1.1 OUR AVERAGE	Error includes scale factor of 1.7.				
5.42±0.14±1.41	56k	[1] ABLIKIM	25M	BES3	$\psi(2S) \to p\overline{p}\pi^0$
8.1 ±0.7 ±0.3	474	[2] ALEXANDER	10	CLEO	$\psi(2S) \to \pi^0 p\overline{p}$
• • • We do not use the following data for averages, fits, limits, etc. • • •					
$3.58\pm0.25^{+1.59}_{-0.84}$	1.1k	[3] ABLIKIM	13A	BES3	$\psi(2S) \to p\overline{p}\pi^0$

[1] From a fit (PWA) of $\pi^0 p\overline{p}$ data to ten distinct intermediate $N\overline{p}$ resonant states.
[2] From a fit of the $p\overline{p}$ and $p\pi^0$ mass distributions to a combination of $N(1440)\overline{p}$, a broad $p\overline{p}$ enhancement around 2100 MeV, and two other broad, unestablished resonances.
[3] From a fit of $\pi^0 p\overline{p}$ data to eight distinct intermediate $N\overline{p}$ resonant states. Superseded by ABLIKIM 25M.

$\Gamma(N(1520)\overline{p} + \text{c.c.} \to p\overline{p}\pi^0)/\Gamma_{total}$ — Γ_{124}/Γ

VALUE (units 10^{-5})	EVTS	DOCUMENT ID		TECN	COMMENT
0.66±0.04±0.20	6749	[1] ABLIKIM	25M	BES3	$\psi(2S) \to p\overline{p}\pi^0$
• • • We do not use the following data for averages, fits, limits, etc. • • •					
$0.64\pm0.05^{+0.22}_{-0.17}$	0.2k	[2] ABLIKIM	13A	BES3	$\psi(2S) \to p\overline{p}\pi^0$

[1] From a fit (PWA) of $\pi^0 p\overline{p}$ data to ten distinct intermediate $N\overline{p}$ resonant states.
[2] From a fit of $\pi^0 p\overline{p}$ data to eight distinct intermediate $N\overline{p}$ resonant states. Superseded by ABLIKIM 25M.

$\Gamma(N(1535)\overline{p} + \text{c.c.} \to p\overline{p}\pi^0)/\Gamma_{total}$ — Γ_{125}/Γ

VALUE (units 10^{-5})	EVTS	DOCUMENT ID		TECN	COMMENT
1.75±0.07±0.36	19k	[1] ABLIKIM	25M	BES3	$\psi(2S) \to p\overline{p}\pi^0$
• • • We do not use the following data for averages, fits, limits, etc. • • •					
$2.47\pm0.28^{+0.99}_{-0.97}$	0.7k	[2] ABLIKIM	13A	BES3	$\psi(2S) \to p\overline{p}\pi^0$

[1] From a fit (PWA) of $\pi^0 p\overline{p}$ data to ten distinct intermediate $N\overline{p}$ resonant states.
[2] From a fit of $\pi^0 p\overline{p}$ data to eight distinct intermediate $N\overline{p}$ resonant states. Superseded by ABLIKIM 25M.

$\Gamma(N(1650)\overline{p} + \text{c.c.} \to p\overline{p}\pi^0)/\Gamma_{total}$ — Γ_{126}/Γ

VALUE (units 10^{-5})	EVTS	DOCUMENT ID		TECN	COMMENT
0.91±0.07±0.32	11k	[1] ABLIKIM	25M	BES3	$\psi(2S) \to p\overline{p}\pi^0$
• • • We do not use the following data for averages, fits, limits, etc. • • •					
$3.76\pm0.28^{+1.37}_{-1.66}$	1.1k	[2] ABLIKIM	13A	BES3	$\psi(2S) \to p\overline{p}\pi^0$

[1] From a fit (PWA) of $\pi^0 p\overline{p}$ data to ten distinct intermediate $N\overline{p}$ resonant states. Superseded by ABLIKIM 25M.
[2] From a fit of $\pi^0 p\overline{p}$ data to eight distinct intermediate $N\overline{p}$ resonant states.

$\Gamma(N(1710)\overline{p} + \text{c.c.} \to p\overline{p}\pi^0)/\Gamma_{total}$ — Γ_{127}/Γ

VALUE (units 10^{-6})	EVTS	DOCUMENT ID		TECN	COMMENT
4.2±0.5±4.0	4466	[1] ABLIKIM	25M	BES3	$\psi(2S) \to p\overline{p}\pi^0$

[1] From a fit (PWA) of $\pi^0 p\overline{p}$ data to ten distinct intermediate $N\overline{p}$ resonant states.

$\Gamma(N(1720)\overline{p} + \text{c.c.} \to p\overline{p}\pi^0)/\Gamma_{total}$ — Γ_{128}/Γ

VALUE (units 10^{-5})	EVTS	DOCUMENT ID		TECN	COMMENT
0.62±0.05±0.24	6644	[1] ABLIKIM	25M	BES3	$\psi(2S) \to p\overline{p}\pi^0$
• • • We do not use the following data for averages, fits, limits, etc. • • •					
$1.79\pm0.10^{+0.24}_{-0.71}$	0.5k	[2] ABLIKIM	13A	BES3	$\psi(2S) \to p\overline{p}\pi^0$

[1] From a fit (PWA) of $\pi^0 p\overline{p}$ data to ten distinct intermediate $N\overline{p}$ resonant states.
[2] From a fit of $\pi^0 p\overline{p}$ data to eight distinct intermediate $N\overline{p}$ resonant states. Superseded by ABLIKIM 25M.

$\Gamma(N(2100)\overline{p} + \text{c.c.} \to p\overline{p}\pi^0)/\Gamma_{total}$ — Γ_{129}/Γ

VALUE (units 10^{-6})	EVTS	DOCUMENT ID		TECN	COMMENT
8.5±0.9±3.8	10k	[1] ABLIKIM	25M	BES3	$\psi(2S) \to p\overline{p}\pi^0$

[1] From a fit (PWA) of $\pi^0 p\overline{p}$ data to ten distinct intermediate $N\overline{p}$ resonant states.

$\Gamma(N(2300)\overline{p} + \text{c.c.} \to p\overline{p}\pi^0)/\Gamma_{total}$ — Γ_{130}/Γ

VALUE (units 10^{-5})	EVTS	DOCUMENT ID		TECN	COMMENT
0.36±0.06±0.30	4235	[1] ABLIKIM	25M	BES3	$\psi(2S) \to p\overline{p}\pi^0$
• • • We do not use the following data for averages, fits, limits, etc. • • •					
$2.62\pm0.28^{+1.12}_{-0.64}$	0.9k	[2] ABLIKIM	13A	BES3	$\psi(2S) \to p\overline{p}\pi^0$

[1] From a fit (PWA) of $\pi^0 p\overline{p}$ data to ten distinct intermediate $N\overline{p}$ resonant states.
[2] From a fit of $\pi^0 p\overline{p}$ data to eight distinct intermediate $N\overline{p}$ resonant states. Superseded by ABLIKIM 25M.

$\Gamma(N(2570)\overline{p} + \text{c.c.} \to p\overline{p}\pi^0)/\Gamma_{total}$ — Γ_{131}/Γ

VALUE (units 10^{-5})	EVTS	DOCUMENT ID		TECN	COMMENT
1.95±0.09±1.45	24k	[1] ABLIKIM	25M	BES3	$\psi(2S) \to p\overline{p}\pi^0$
• • • We do not use the following data for averages, fits, limits, etc. • • •					
$2.13\pm0.08^{+0.40}_{-0.30}$	0.8k	[2] ABLIKIM	13A	BES3	$\psi(2S) \to p\overline{p}\pi^0$

[1] From a fit (PWA) of $\pi^0 p\overline{p}$ data to ten distinct intermediate $N\overline{p}$ resonant states.
[2] From a fit of $\pi^0 p\overline{p}$ data to eight distinct intermediate $N\overline{p}$ resonant states. Superseded by ABLIKIM 25M.

Int. J. Mod. Phys. A 2026.41. Downloaded from www.worldscientific.com by CALIFORNIA @ BERKELEY on 09/16/26. Re-use and distribution is strictly not permitted, except for Open Access articles.

$\Gamma(p\overline{p}\pi^+\pi^-)/\Gamma_{total}$ — Γ_{132}/Γ

VALUE (units 10^{-4})	EVTS	DOCUMENT ID		TECN	COMMENT
6.0±0.4 OUR AVERAGE					
5.9±0.2±0.4	904.5	BRIERE	05	CLEO	$e^+e^- \to \psi(2S) \to p\overline{p}\pi^+\pi^-$
8 ±2		[1] TANENBAUM	78	MRK1	e^+e^-

[1] Assuming entirely strong decay.

$\Gamma(p\overline{p}K^+K^-)/\Gamma_{total}$ — Γ_{133}/Γ

VALUE (units 10^{-5})	EVTS	DOCUMENT ID		TECN	COMMENT
2.7±0.6±0.4	30.1	BRIERE	05	CLEO	$e^+e^- \to \psi(2S) \to p\overline{p}K^+K^-$

$\Gamma(p\overline{p}\eta)/\Gamma_{total}$ — Γ_{134}/Γ

The two different fit values of ABLIKIM 25M cannot be distinguished. Previous measurements did not consider the large uncertainty due to interference with the e^+e^- continuum.

VALUE (units 10^{-5})	EVTS	DOCUMENT ID		TECN	COMMENT
5.5 to 9.1 OUR EVALUATION					
6.15±0.65±0.11	31k	[1] ABLIKIM	25M	BES3	$\psi(2S) \to p\overline{p}\eta$
8.44±0.69±0.14	31k	[2] ABLIKIM	25M	BES3	$\psi(2S) \to p\overline{p}\eta$
• • • We do not use the following data for averages, fits, limits, etc. • • •					
6.4 ±0.2 ±0.6	679	[3] ABLIKIM	13S	BES3	$\psi(2S) \to p\overline{p}\eta$
5.6 ±0.6 ±0.3	154	[3] ALEXANDER	10	CLEO	$\psi(2S) \to p\overline{p}\eta$
5.8 ±1.1 ±0.7	45	[4] ABLIKIM	05E	BES2	$e^+e^- \to \psi(2S) \to p\overline{p}\gamma\gamma$
8 ±3 ±3	9.8	BRIERE	05	CLEO	$e^+e^- \to \psi(2S) \to p\overline{p}\pi^+\pi^-\pi^0$

[1] Constructive-interference solution of a partial wave analysis of the decay $\psi(2S) \to p\overline{p}\eta$.
[2] Destructive-interference solution of a partial wave analysis of the decay $\psi(2S) \to p\overline{p}\eta$.
[3] With $N(1535)$ decaying to $p\eta$.
[4] Computed using $B(\eta \to \gamma\gamma) = (39.43 \pm 0.26)\%$.

$\Gamma(N(1535)\overline{p}+\text{c.c.} \to p\overline{p}\eta)/\Gamma_{total}$ — Γ_{135}/Γ

VALUE (units 10^{-5})	EVTS	DOCUMENT ID		TECN	COMMENT
4.7 ±0.5 OUR AVERAGE					
5.05±0.13±0.71	19k	[1] ABLIKIM	25M	BES3	$\psi(2S) \to p\overline{p}\eta$
4.4 ±0.6 ±0.3	123	[2] ALEXANDER	10	CLEO	$\psi(2S) \to \eta p\overline{p}$
• • • We do not use the following data for averages, fits, limits, etc. • • •					
5.2 ±0.3 $^{+3.2}_{-1.2}$	527	[3] ABLIKIM	13S	BES3	$\psi(2S) \to \eta p\overline{p}$

[1] From a fit (PWA) of $\eta p\overline{p}$ data to four distinct intermediate $N\overline{p}$ resonant states.
[2] From a fit of the $p\overline{p}$ and $p\eta$ distributions to a combination of $N^*(1535)\overline{p}$ and a broad $p\overline{p}$ enhancement around 2100 MeV.
[3] With $N(1535)$ decaying to $p\eta$. Superseded by ABLIKIM 25P.

$\Gamma(N(1710)\overline{p}+\text{c.c.} \to p\overline{p}\eta)/\Gamma_{total}$ — Γ_{136}/Γ

VALUE (units 10^{-6})	EVTS	DOCUMENT ID		TECN	COMMENT
7.8±0.7±3.1	3250	[1] ABLIKIM	25M	BES3	$\psi(2S) \to p\overline{p}\eta$

[1] From a fit (PWA) of $\eta p\overline{p}$ data to four distinct intermediate $N\overline{p}$ resonant states.

$\Gamma(p\overline{p}\pi^+\pi^-\pi^0)/\Gamma_{total}$ — Γ_{137}/Γ

VALUE (units 10^{-4})	EVTS	DOCUMENT ID		TECN	COMMENT
7.3±0.4±0.6	434.9	BRIERE	05	CLEO	$e^+e^- \to \psi(2S) \to p\overline{p}\pi^+\pi^-\pi^0$

$\Gamma(p\overline{p}\rho^0)/\Gamma_{total}$ — Γ_{138}/Γ

VALUE (units 10^{-4})	EVTS	DOCUMENT ID		TECN	COMMENT
0.5±0.1±0.2	61.1	BRIERE	05	CLEO	$e^+e^- \to \psi(2S) \to p\overline{p}\pi^+\pi^-$

$\Gamma(p\overline{p}\omega)/\Gamma_{total}$ — Γ_{139}/Γ

VALUE (units 10^{-4})	EVTS	DOCUMENT ID		TECN	COMMENT
0.69±0.21 OUR AVERAGE					
0.6 ±0.2 ±0.2	21.2	BRIERE	05	CLEO	$e^+e^- \to \psi(2S) \to p\overline{p}\pi^+\pi^-\pi^0$
0.8 ±0.3 ±0.1	14.9 ± 0.1	[1] BAI	03B	BES	$\psi(2S) \to p\overline{p}\pi^+\pi^-\pi^0$

[1] Normalized to $B(\psi(2S) \to J/\psi\pi^+\pi^-) = 0.305 \pm 0.016$.

$\Gamma(p\overline{p}\eta')/\Gamma_{total}$ — Γ_{140}/Γ

VALUE (units 10^{-5})	EVTS	DOCUMENT ID		TECN	COMMENT
1.10±0.10±0.08	491	[1] ABLIKIM	19N	BES3	$\psi(2S) \to \eta' p\overline{p}$

[1] From the combination of $p\overline{p}\eta' \to p\overline{p}\pi^+\pi^-\eta$ and $p\overline{p}\eta' \to p\overline{p}\pi^+\pi^-\gamma$ channels.

$\Gamma(p\overline{p}\phi)/\Gamma_{total}$ — Γ_{141}/Γ

VALUE (units 10^{-6})	CL%	EVTS	DOCUMENT ID		TECN	COMMENT
6.06±0.38±0.48		753	ABLIKIM	19AO	BES3	$e^+e^- \to \psi(2S) \to p\overline{p}K^+K^-$
• • • We do not use the following data for averages, fits, limits, etc. • • •						
<24	90		BRIERE	05	CLEO	$e^+e^- \to \psi(2S) \to p\overline{p}K^+K^-$
<26	90		[1] BAI	03B	BES	$\psi(2S) \to K^+K^-p\overline{p}$

[1] Normalized to $B(\psi(2S) \to J/\psi\pi^+\pi^-) = 0.305 \pm 0.016$.

$\Gamma(\phi X(1835) \to p\overline{p}\phi)/\Gamma_{total}$ — Γ_{142}/Γ

VALUE	CL%	DOCUMENT ID		TECN	COMMENT
<1.82 × 10^{-7}	90	ABLIKIM	19AO	BES3	$e^+e^- \to \psi(2S) \to p\overline{p}K^+K^-$

$\Gamma(p\overline{n}\pi^-\text{ or c.c.})/\Gamma_{total}$ — Γ_{143}/Γ

VALUE (units 10^{-4})	EVTS	DOCUMENT ID		TECN	COMMENT
2.48±0.17 OUR AVERAGE					
2.45±0.11±0.21	851	ABLIKIM	06I	BES2	$e^+e^- \to p\pi^-X$
2.52±0.12±0.22	849	ABLIKIM	06I	BES2	$e^+e^- \to \overline{p}\pi^+X$

$\Gamma(p\overline{n}\pi^-\pi^0)/\Gamma_{total}$ — Γ_{144}/Γ

VALUE (units 10^{-4})	EVTS	DOCUMENT ID		TECN	COMMENT
3.18±0.50±0.50	135 ± 21	ABLIKIM	06I	BES2	$e^+e^- \to p\pi^-\pi^0X$

$\Gamma(\Lambda\overline{\Lambda})/\Gamma_{total}$ — Γ_{145}/Γ

VALUE (units 10^{-4})	CL%	EVTS	DOCUMENT ID		TECN	COMMENT
3.81±0.13 OUR AVERAGE Error includes scale factor of 1.4. See the ideogram below.						
3.97±0.02±0.12		31k	ABLIKIM	17L	BES3	$e^+e^- \to \Lambda\overline{\Lambda}$
3.71±0.05±0.15		6.5k	[1] DOBBS	17		$e^+e^- \to \Lambda\overline{\Lambda}$
3.39±0.20±0.32		337	ABLIKIM	07C	BES	$e^+e^- \to \psi(2S) \to$ hadrons
6.4 ±1.8 ±0.1			[2] AUBERT	07BD	BABR	10.6 $e^+e^- \to \Lambda\overline{\Lambda}\gamma$
3.28±0.23±0.25		208	PEDLAR	05	CLEO	$e^+e^- \to \psi(2S) \to$ hadrons
• • • We do not use the following data for averages, fits, limits, etc. • • •						
3.75±0.09±0.23		1.9k	[1,3] DOBBS	14		$e^+e^- \to \Lambda\overline{\Lambda}$
1.81±0.20±0.27		80	[4] BAI	01	BES	$e^+e^- \to \psi(2S) \to$ hadrons
< 4	90		FELDMAN	77	MRK1	$e^+e^- \to \psi(2S) \to$ hadrons

[1] Using CLEO-c data but not authored by the CLEO Collaboration.
[2] AUBERT 07BD reports $[\Gamma(\psi(2S) \to \Lambda\overline{\Lambda})/\Gamma_{total}] \times [\Gamma(\psi(2S) \to e^+e^-)] = (15 \pm 4 \pm 1) \times 10^{-4}$ keV which we divide by our best (shown rounded) value $\Gamma(\psi(2S) \to e^+e^-) = 2.33 \pm 0.04$ keV. Our first error is their experiment's error and our second error is the systematic error from using our best (shown rounded) value.
[3] Superseded by DOBBS 17.
[4] Estimated using $B(\psi(2S) \to J/\psi\pi^+\pi^-) = 0.310 \pm 0.028$.

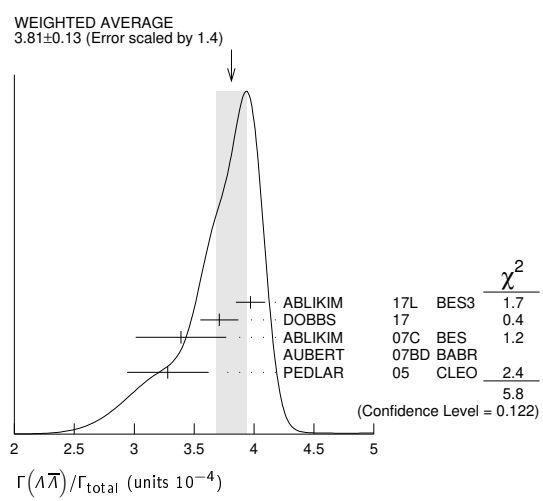

$\Gamma(\Lambda\overline{\Lambda}\pi^0)/\Gamma_{total}$ — Γ_{146}/Γ

VALUE (units 10^{-6})	CL%	EVTS	DOCUMENT ID		TECN	COMMENT
1.42±0.39±0.59		23	[1] ABLIKIM	22AP	BES3	$\psi(2S) \to p\overline{p}\pi^+\pi^-\gamma\gamma$
• • • We do not use the following data for averages, fits, limits, etc. • • •						
< 2.9	90		[2] ABLIKIM	13F	BES3	$\psi(2S) \to p\overline{p}\pi^+\pi^-\gamma\gamma$
<120	90		[3] ABLIKIM	07H	BES2	$e^+e^- \to \psi(2S)$

[1] With a significance of 3.7 σ. The corresponding 90% CL upper limit is 2.47×10^{-6}.
[2] Using $B(\Lambda \to \pi^-p) = 63.9\%$ and $B(\pi^0 \to \gamma\gamma) = 98.8\%$.
[3] Using $B(\Lambda \to \pi^-p) = 63.9\%$ and $B(\eta \to \gamma\gamma) = 39.4\%$.

$\Gamma(\Lambda\overline{\Lambda}\eta)/\Gamma_{total}$ — Γ_{147}/Γ

VALUE (units 10^{-5})	CL%	EVTS	DOCUMENT ID		TECN	COMMENT
2.43±0.32 OUR AVERAGE						
2.34±0.18±0.52		218	ABLIKIM	22AP	BES3	$\psi(2S) \to p\overline{p}\pi^+\pi^-\gamma\gamma$
2.48±0.34±0.19		60	[1] ABLIKIM	13F	BES3	$\psi(2S) \to p\overline{p}\pi^+\pi^-\gamma\gamma$
• • • We do not use the following data for averages, fits, limits, etc. • • •						
<4.9	90		[2] ABLIKIM	07H	BES2	$e^+e^- \to \psi(2S)$

[1] Using $B(\Lambda \to \pi^-p) = 63.9\%$ and $B(\eta \to \gamma\gamma) = 39.31\%$.
[2] Using $B(\Lambda \to \pi^-p) = 63.9\%$.

$\Gamma(\Lambda\overline{\Lambda}\eta')/\Gamma_{total}$ — Γ_{149}/Γ

VALUE (units 10^{-6})	EVTS	DOCUMENT ID		TECN	COMMENT
7.34±0.94±0.43	218	ABLIKIM	23BV	BES3	$\psi(2S) \to p\overline{p}2(\pi^+\pi^-)\gamma(\gamma)$

Int. J. Mod. Phys. A 2026.41. Downloaded from www.worldscientific.com
by UNIVERSITY OF CALIFORNIA @ BERKELEY on 09/16/26. Re-use and distribution is strictly not permitted, except for Open Access articles.

$\Gamma(\Lambda\overline{\Lambda}\omega(782))/\Gamma_{total}$ — Γ_{150}/Γ

VALUE (units 10^{-5})	EVTS	DOCUMENT ID		TECN	COMMENT
3.30±0.34±0.29	207	[1] ABLIKIM	22AZ	BES3	$e^+e^- \to \psi(2S)$

[1] Using $B(\Lambda \to \pi^- p) = 0.639$ and $B(\omega \to \pi^+\pi^-\pi^0) = 0.893$.

$\Gamma(\Lambda(1670)\overline{\Lambda} \to \Lambda\overline{\Lambda}\eta)/\Gamma_{total}$ — Γ_{148}/Γ

VALUE (units 10^{-5})	EVTS	DOCUMENT ID		TECN	COMMENT
1.29±0.31±0.62	116	[1] ABLIKIM	22AP	BES3	$\psi(2S) \to p\overline{p}\pi^+\pi^-\gamma\gamma$

[1] From a partial wave analysis of the $\Lambda\eta$ system.

$\Gamma(\Lambda\overline{\Lambda}\pi^+\pi^-)/\Gamma_{total}$ — Γ_{151}/Γ

VALUE (units 10^{-4})	EVTS	DOCUMENT ID		TECN	COMMENT
2.8±0.4±0.5	73.4	BRIERE	05	CLEO	$e^+e^- \to \psi(2S) \to p\overline{p}2(\pi^+\pi^-)$

$\Gamma(\Lambda\overline{p}K^+)/\Gamma_{total}$ — Γ_{152}/Γ

VALUE (units 10^{-4})	EVTS	DOCUMENT ID		TECN	COMMENT
1.0±0.1±0.1	74.0	BRIERE	05	CLEO	$e^+e^- \to \psi(2S) \to p\overline{p}K^+\pi^-$

$\Gamma(\Lambda\overline{p}K^*(892)^+ + c.c.)/\Gamma_{total}$ — Γ_{153}/Γ

VALUE (units 10^{-5})	EVTS	DOCUMENT ID		TECN	COMMENT
6.3±0.5±0.5	1011	ABLIKIM	19AU	BES3	$e^+e^- \to \psi(2S)$

$\Gamma(\Lambda\overline{p}K^+\pi^+\pi^-)/\Gamma_{total}$ — Γ_{154}/Γ

VALUE (units 10^{-4})	EVTS	DOCUMENT ID		TECN	COMMENT
1.8±0.3±0.3	45.8	BRIERE	05	CLEO	$e^+e^- \to \psi(2S) \to p\overline{p}K^+\pi^+\pi^-\pi^-$

$\Gamma(\overline{\Lambda}nK^0_S + c.c.)/\Gamma_{total}$ — Γ_{155}/Γ

VALUE (units 10^{-4})	EVTS	DOCUMENT ID		TECN	COMMENT
0.81±0.11±0.14	50	[1] ABLIKIM	08C	BES2	$e^+e^- \to J/\psi$

[1] Using $B(\overline{\Lambda} \to \overline{p}\pi^+) = 63.9\%$ and $B(K^0_S \to \pi^+\pi^-) = 69.2\%$.

$\Gamma(\Delta^{++}\overline{\Delta}^{--})/\Gamma_{total}$ — Γ_{156}/Γ

VALUE (units 10^{-5})	EVTS	DOCUMENT ID		TECN	COMMENT
12.8±1.0±3.4	157	[1] BAI	01	BES	$e^+e^- \to \psi(2S) \to$ hadrons

[1] Estimated using $B(\psi(2S) \to J/\psi\pi^+\pi^-) = 0.310 \pm 0.028$.

$\Gamma(\Lambda\overline{\Sigma}^+\pi^- + c.c.)/\Gamma_{total}$ — Γ_{157}/Γ

VALUE (units 10^{-4})	EVTS	DOCUMENT ID		TECN	COMMENT
1.40±0.03±0.13	2.8k	ABLIKIM	13W	BES3	$\psi(2S) \to$ hadrons

$\Gamma(\Lambda\overline{\Sigma}^-\pi^+ + c.c.)/\Gamma_{total}$ — Γ_{158}/Γ

VALUE (units 10^{-4})	EVTS	DOCUMENT ID		TECN	COMMENT
1.54±0.04±0.13	2.8k	ABLIKIM	13W	BES3	$\psi(2S) \to$ hadrons

$\Gamma(\Lambda\overline{\Sigma}^0 + c.c.)/\Gamma_{total}$ — Γ_{159}/Γ

VALUE (units 10^{-6})	EVTS	DOCUMENT ID		TECN	COMMENT
1.60±0.31±0.59	60	ABLIKIM	21L	BES3	$e^+e^- \to \psi(2S) \to$ hadrons

$\Gamma(\Lambda\overline{\Sigma}^0)/\Gamma_{total}$ — Γ_{160}/Γ

VALUE (units 10^{-5})	EVTS	DOCUMENT ID		COMMENT
• • • We do not use the following data for averages, fits, limits, etc. • • •				
1.23±0.23±0.08	30	[1] DOBBS	17	$e^+e^- \to \psi(2S) \to$ hadrons

[1] Using CLEO-c data but not authored by the CLEO Collaboration.

$\Gamma(\Lambda\overline{\Sigma}^0\pi^0 + c.c.)/\Gamma_{total}$ — Γ_{161}/Γ

VALUE (units 10^{-4})	EVTS	DOCUMENT ID		TECN	COMMENT
1.544±0.013±0.071	15.5k	[1] ABLIKIM	25AF	BES3	$e^+e^- \to \psi(2S)$

[1] Using $B(\Lambda \to pK^-)$, $B(\Sigma^0 \to \Lambda\gamma)$ and $B(\pi^0 \to \gamma\gamma)$ from PDG 22, together with a partial wave analysis of the intermediate $\Lambda\pi^0$ and $\Sigma^0\pi^0$ resonances, $\Lambda(1405, 1520, 1600, 1670, 1690, 1800, 1890, 2325)$ and $\Sigma^0(1385, 1660, 1670, 1750, 1910)$.

$\Gamma(\Lambda(1520)\overline{\Xi}^+K^- + c.c., \Lambda(1520) \to pK^-)/\Gamma_{total}$ — Γ_{162}/Γ

VALUE (units 10^{-7})	EVTS	DOCUMENT ID		TECN	COMMENT
9.47±0.75±0.97	190	ABLIKIM	25AG	BES3	$e^+e^- \to \psi(2S)$

$\Gamma(\Sigma^0\overline{p}K^+ + c.c.)/\Gamma_{total}$ — Γ_{163}/Γ

VALUE (units 10^{-5})	EVTS	DOCUMENT ID		TECN	COMMENT
1.67±0.13±0.12	276	[1] ABLIKIM	13D	BES3	$\psi(2S) \to \gamma\Lambda\overline{p}K^+$

[1] Using $B(\Lambda \to p\pi^-) = 63.9\%$, and $B(\Sigma^0 \to \Lambda\gamma) = 100\%$.

$\Gamma(\Sigma^+\overline{\Sigma}^-)/\Gamma_{total}$ — Γ_{164}/Γ

VALUE (units 10^{-4})	EVTS	DOCUMENT ID		TECN	COMMENT
2.43±0.10 OUR AVERAGE	Error includes scale factor of 1.4.				
2.52±0.04±0.09	5.4k	ABLIKIM	21AT	BES3	$\psi(2S) \to p\pi^0\overline{p}\pi^0$
2.31±0.06±0.10	1.9k	[1] DOBBS	17		$e^+e^- \to \psi(2S) \to$ hadrons
2.57±0.44±0.68	35	PEDLAR	05	CLEO	$e^+e^- \to \psi(2S) \to$ hadrons
• • • We do not use the following data for averages, fits, limits, etc. • • •					
2.51±0.15±0.16	281	[1,2] DOBBS	14		$e^+e^- \to \psi(2S) \to$ hadrons

[1] Using CLEO-c data but not authored by the CLEO Collaboration.
[2] Superseded by DOBBS 17.

$\Gamma(\Sigma^0\overline{\Sigma}^0)/\Gamma_{total}$ — Γ_{165}/Γ

VALUE (units 10^{-4})	EVTS	DOCUMENT ID		TECN	COMMENT
2.35±0.09 OUR AVERAGE	Error includes scale factor of 1.1.				
2.44±0.03±0.11	7k	ABLIKIM	17L	BES3	$e^+e^- \to \psi(2S) \to$ hadrons
2.22±0.05±0.11	2.6k	[1] DOBBS	17		$e^+e^- \to \psi(2S) \to$ hadrons
2.35±0.36±0.32	59	ABLIKIM	07C	BES	$e^+e^- \to \psi(2S) \to$ hadrons
2.63±0.35±0.21	58	PEDLAR	05	CLEO	$e^+e^- \to \psi(2S) \to$ hadrons
• • • We do not use the following data for averages, fits, limits, etc. • • •					
2.25±0.11±0.16	439	[1,2] DOBBS	14		$e^+e^- \to \psi(2S) \to$ hadrons
1.2 ±0.4 ±0.4	8	[3] BAI	01	BES	$e^+e^- \to \psi(2S) \to$ hadrons

[1] Using CLEO-c data but not authored by the CLEO Collaboration.
[2] Superseded by DOBBS 17.
[3] Estimated using $B(\psi(2S) \to J/\psi\pi^+\pi^-) = 0.310 \pm 0.028$.

$\Gamma(\Sigma^-\overline{\Sigma}^+)/\Gamma_{total}$ — Γ_{166}/Γ

VALUE (units 10^{-4})	EVTS	DOCUMENT ID		TECN	COMMENT
2.82±0.04±0.08	6.6k	ABLIKIM	22AV	BES3	$\psi(2S) \to n\pi^-\overline{n}\pi^+$

$\Gamma(\Sigma^+\overline{\Sigma}^-\eta)/\Gamma_{total}$ — Γ_{167}/Γ

VALUE (units 10^{-6})	EVTS	DOCUMENT ID		TECN	COMMENT
9.59±2.37±0.61	21	ABLIKIM	22AY	BES3	$\psi(2S) \to \Sigma^+\overline{\Sigma}^-\eta$

$\Gamma(\Sigma^+\overline{\Sigma}^-\omega)/\Gamma_{total}$ — Γ_{168}/Γ

VALUE (units 10^{-5})	EVTS	DOCUMENT ID		TECN	COMMENT
1.89±0.18±0.21	199	ABLIKIM	23BE	BES3	$e^+e^- \to \psi(2S) \to$ hadrons

$\Gamma(\Sigma^0\overline{\Sigma}^0\omega(782))/\Gamma_{total}$ — Γ_{169}/Γ

VALUE (units 10^{-5})	EVTS	DOCUMENT ID		TECN	COMMENT
1.24±0.16±0.11	172	ABLIKIM	25W	BES3	$e^+e^- \to \psi(2S)$

$\Gamma(\Sigma^+\overline{\Sigma}^-\phi)/\Gamma_{total}$ — Γ_{170}/Γ

VALUE (units 10^{-6})	EVTS	DOCUMENT ID		TECN	COMMENT
2.96±0.54±0.41	55	ABLIKIM	23BE	BES3	$e^+e^- \to \psi(2S) \to$ hadrons

$\Gamma(\Sigma^0\overline{\Sigma}^0\phi)/\Gamma_{total}$ — Γ_{171}/Γ

VALUE (units 10^{-6})	EVTS	DOCUMENT ID		TECN	COMMENT
2.64±0.32±0.12	108	[1] ABLIKIM	25Q	BES3	$e^+e^- \to \psi(2S)$

[1] ABLIKIM 25Q result is the first observation of this decay.

$\Gamma(\Sigma(1385)^+\overline{\Sigma}(1385)^-)/\Gamma_{total}$ — Γ_{172}/Γ

VALUE (units 10^{-5})	EVTS	DOCUMENT ID		TECN	COMMENT
8.5±0.7 OUR AVERAGE					
8.4±0.5±0.5	1.5k	ABLIKIM	16L	BES3	$\psi(2S) \to \Sigma(1385)^+\overline{\Sigma}(1385)^-$
11 ±3 ±3	14	[1] BAI	01	BES	$e^+e^- \to \psi(2S) \to$ hadrons

[1] Estimated using $B(\psi(2S) \to J/\psi\pi^+\pi^-) = 0.310 \pm 0.028$.

$\Gamma(\Sigma(1385)^-\overline{\Sigma}(1385)^+)/\Gamma_{total}$ — Γ_{173}/Γ

VALUE (units 10^{-5})	EVTS	DOCUMENT ID		TECN	COMMENT
8.5±0.6±0.6	1.4k	ABLIKIM	16L	BES3	$\psi(2S) \to \Sigma(1385)^-\overline{\Sigma}(1385)^+$

$\Gamma(\Sigma(1385)^0\overline{\Sigma}(1385)^0)/\Gamma_{total}$ — Γ_{174}/Γ

VALUE (units 10^{-4})	EVTS	DOCUMENT ID		TECN	COMMENT
0.69±0.05±0.05	2.2k	ABLIKIM	17E	BES3	$e^+e^- \to \psi(2S) \to$ hadrons

$\Gamma(\Xi^-\overline{\Xi}^+)/\Gamma_{total}$ — Γ_{175}/Γ

VALUE (units 10^{-4})	CL%	EVTS	DOCUMENT ID		TECN	COMMENT
2.87±0.11 OUR AVERAGE		Error includes scale factor of 1.1.				
3.03±0.05±0.14		3.6k	[1] DOBBS	17		$e^+e^- \to \psi(2S) \to$ hadrons
2.78±0.05±0.14		5k	ABLIKIM	16L	BES3	$\psi(2S) \to \Xi^-\overline{\Xi}^+$
3.03±0.40±0.32		67	ABLIKIM	07C	BES	$e^+e^- \to \psi(2S) \to$ hadrons
2.38±0.30±0.21		63	PEDLAR	05	CLEO	$e^+e^- \to \psi(2S) \to$ hadrons
• • • We do not use the following data for averages, fits, limits, etc. • • •						
2.66±0.12±0.20		548	[1,2] DOBBS	14		$e^+e^- \to \psi(2S) \to$ hadrons
0.94±0.27±0.15		12	[3] BAI	01	BES	$e^+e^- \to \psi(2S) \to$ hadrons
<2		90	FELDMAN	77	MRK1	$e^+e^- \to \psi(2S) \to$ hadrons

[1] Using CLEO-c data but not authored by the CLEO Collaboration.
[2] Superseded by DOBBS 17.
[3] Estimated using $B(\psi(2S) \to J/\psi\pi^+\pi^-) = 0.310 \pm 0.028$.

$\Gamma(\Xi^0\overline{\Xi}^0)/\Gamma_{total}$ — Γ_{176}/Γ

VALUE (units 10^{-4})	EVTS	DOCUMENT ID		TECN	COMMENT
2.3 ±0.4 OUR AVERAGE	Error includes scale factor of 4.2.				
2.73±0.03±0.13	11k	ABLIKIM	17E	BES3	$e^+e^- \to \psi(2S) \to$ hadrons
1.97±0.06±0.11	1.2k	[1] DOBBS	17		$e^+e^- \to \psi(2S) \to$ hadrons
2.75±0.64±0.61	19	PEDLAR	05	CLEO	$e^+e^- \to \psi(2S) \to$ hadrons

Int. J. Mod. Phys. A 2026.41. Downloaded from www.worldscientific.com by CALIFORNIA @ BERKELEY on 09/16/26. Re-use and distribution is strictly not permitted, except for Open Access articles.

• • • We do not use the following data for averages, fits, limits, etc. • • •

2.02±0.19±0.15	112	[1,2] DOBBS	14		$e^+e^- \to \psi(2S) \to$ hadrons

[1] Using CLEO-c data but not authored by the CLEO Collaboration.
[2] Superseded by DOBBS 17.

$\Gamma(\Xi(1530)^0\overline{\Xi}(1530)^0)/\Gamma_{total}$ — Γ_{177}/Γ

VALUE (units 10^{-5})	CL%	EVTS	DOCUMENT ID		TECN	COMMENT
6.77±0.14±0.39		2951	ABLIKIM	21AO	BES3	$e^+e^- \to \psi(2S) \to$ hadrons
• • • We do not use the following data for averages, fits, limits, etc. • • •						
<32	90		PEDLAR	05	CLEO	$e^+e^- \to \psi(2S) \to$ hadrons
< 8.1	90		[1] BAI	01	BES	$e^+e^- \to \psi(2S) \to$ hadrons

[1] Estimated using $B(\psi(2S) \to J/\psi\pi^+\pi^-) = 0.310 \pm 0.028$.

$\Gamma(\Lambda\overline{\Xi}^+K^- + c.c.)/\Gamma_{total}$ — Γ_{178}/Γ

VALUE (units 10^{-5})	EVTS	DOCUMENT ID		TECN	COMMENT
3.67±0.22 OUR AVERAGE					
3.60±0.10±0.24	1572	ABLIKIM	24N	BES3	$e^+e^- \to \psi(2S) \to K^-\Lambda\overline{\Xi}^+ +$ c.c.
3.86±0.27±0.32	236	ABLIKIM	15I	BES3	$e^+e^- \to \psi(2S) \to K^-\Lambda\overline{\Xi}^+ +$ c.c.

$\Gamma(\Xi(1530)^-\overline{\Xi}(1530)^+)/\Gamma_{total}$ — Γ_{181}/Γ

VALUE (units 10^{-5})	EVTS	DOCUMENT ID		TECN	COMMENT
11.45±0.40±0.59	5k	ABLIKIM	19AT	BES3	$e^+e^- \to \psi(2S) \to$ hadrons

$\Gamma(\Xi(1530)^-\overline{\Xi}^+)/\Gamma_{total}$ — Γ_{182}/Γ

VALUE (units 10^{-6})	EVTS	DOCUMENT ID		TECN	COMMENT
7.0±1.1±0.4	399	ABLIKIM	19AT	BES3	$e^+e^- \to \psi(2S) \to$ hadrons

$\Gamma(\Xi(1530)^0\overline{\Xi}^0)/\Gamma_{total}$ — Γ_{183}/Γ

VALUE (units 10^{-5})	EVTS	DOCUMENT ID		TECN	COMMENT
0.53±0.04±0.03	278	ABLIKIM	21AO	BES3	$e^+e^- \to \psi(2S) \to$ hadrons

$\Gamma(\Xi(1690)^-\overline{\Xi}^+ \to K^-\Lambda\overline{\Xi}^+ + c.c.)/\Gamma_{total}$ — Γ_{179}/Γ

VALUE (units 10^{-6})	EVTS	DOCUMENT ID		TECN	COMMENT
6.2 ±2.1 OUR AVERAGE Error includes scale factor of 1.5.					
10.6 ±1.0 ±3.1	464	ABLIKIM	24N	BES3	$e^+e^- \to \psi(2S) \to K^-\Lambda\overline{\Xi}^+ +$ c.c.
5.21±1.48±0.57	74	ABLIKIM	15I	BES3	$e^+e^- \to \psi(2S) \to K^-\Lambda\overline{\Xi}^+ +$ c.c.

$\Gamma(\Xi(1820)^-\overline{\Xi}^+ \to K^-\Lambda\overline{\Xi}^+ + c.c.)/\Gamma_{total}$ — Γ_{180}/Γ

VALUE (units 10^{-6})	EVTS	DOCUMENT ID		TECN	COMMENT
14.8 ±2.9 OUR AVERAGE Error includes scale factor of 1.2.					
17.8 ±1.0 ±3.2	776	ABLIKIM	24N	BES3	$e^+e^- \to \psi(2S) \to K^-\Lambda\overline{\Xi}^+ +$ c.c.
12.03±2.94±1.22	136	ABLIKIM	15I	BES3	$e^+e^- \to \psi(2S) \to K^-\Lambda\overline{\Xi}^+ +$ c.c.

$\Gamma(\Sigma^0\overline{\Xi}^+K^- + c.c.)/\Gamma_{total}$ — Γ_{184}/Γ

VALUE (units 10^{-5})	EVTS	DOCUMENT ID		TECN	COMMENT
3.67±0.33±0.28	142	ABLIKIM	15I	BES3	$e^+e^- \to \psi(2S) \to K^-\Sigma^0\overline{\Xi}^+ +$ c.c.

$\Gamma(\Omega^-K^+\overline{\Xi}^0 + c.c.)/\Gamma_{total}$ — Γ_{185}/Γ

VALUE (units 10^{-6})	EVTS	DOCUMENT ID		TECN	COMMENT
2.78±0.40±0.18	242	ABLIKIM	24AG	BES3	$e^+e^- \to \psi(2S)$

$\Gamma(\overline{\Omega}^+K^0_S\Xi^- + c.c.)/\Gamma_{total}$ — Γ_{186}/Γ

VALUE (units 10^{-6})	EVTS	DOCUMENT ID		TECN	COMMENT
2.91±0.47±0.33	224	ABLIKIM	25AJ	BES3	$e^+e^- \to \psi(2S)$

$\Gamma(\Omega^-\overline{\Omega}^+)/\Gamma_{total}$ — Γ_{187}/Γ

VALUE (units 10^{-5})	CL%	EVTS	DOCUMENT ID		TECN	COMMENT
5.66±0.30 OUR AVERAGE Error includes scale factor of 1.3.						
5.85±0.12±0.25		4k	[1] ABLIKIM	21E	BES3	$\psi(2S) \to \Omega^-\overline{\Omega}^+ \to \Lambda K^-\overline{\Lambda}K^+$
5.2 ±0.3 ±0.3		326	[1,2] DOBBS	17		$e^+e^- \to \psi(2S) \to$ hadrons
• • • We do not use the following data for averages, fits, limits, etc. • • •						
4.7 ±0.9 ±0.5		27	[1,2,3] DOBBS	14		$e^+e^- \to \psi(2S) \to$ hadrons
<15	90		ABLIKIM	12Q	BES2	$e^+e^- \to \psi(2S) \to$ hadrons
<16	90		PEDLAR	05	CLEO	$e^+e^- \to \psi(2S) \to$ hadrons
< 7.3	90		[4] BAI	01	BES	$e^+e^- \to \psi(2S) \to$ hadrons

[1] Using $B(\Omega^- \to \Lambda K^-) = (67.8 \pm 0.7)\%$ and $B(\Lambda \to p\pi^-) = (63.9 \pm 0.5)\%$.
[2] Using CLEO-c data but not authored by the CLEO Collaboration.
[3] Superseded by DOBBS 17.
[4] Estimated using $B(\psi(2S) \to J/\psi\pi^+\pi^-) = 0.310 \pm 0.028$.

$\Gamma(\eta_c\pi^+\pi^-\pi^0)/\Gamma_{total}$ — Γ_{188}/Γ

VALUE (units 10^{-3})	CL%	DOCUMENT ID		TECN	COMMENT
<1.0	90	PEDLAR	07	CLEO	$e^+e^- \to \psi(2S)$

$\Gamma(h_c(1P)\pi^0)/\Gamma_{total}$ — Γ_{189}/Γ

VALUE (units 10^{-4})	EVTS	DOCUMENT ID		TECN	COMMENT
7.4 ±0.5 OUR AVERAGE					
7.32±0.34±0.41	46k	ABLIKIM	22AQ	BES3	$\psi(2S) \to \pi^0$ hadrons
9.0 ±1.5 ±1.3	3k	[1] GE	11	CLEO	$\psi(2S) \to \pi^0$ anything
• • • We do not use the following data for averages, fits, limits, etc. • • •					
8.4 ±1.3 ±1.0	11k	[2] ABLIKIM	10B	BES3	$\psi(2S) \to \pi^0 h_c$
seen	92^{+23}_{-22}	ADAMS	09	CLEO	$\psi(2S) \to 2\pi^+2\pi^-2\pi^0$
seen	1282	DOBBS	08A	CLEO	$\psi(2S) \to \pi^0\eta_c\gamma$
seen	168 ± 40	ROSNER	05	CLEO	$\psi(2S) \to \pi^0\eta_c\gamma$

[1] Assuming a width $\Gamma(h_c(1P)) = 0.86$ MeV $\equiv \Gamma_0$, a measured dependence of the central value of $B = (7.6 +1.4 \times \Gamma(h_c(1P)/\Gamma_0) \times 10^{-4}$, and with a systematic error that accounts for the width variation range 0.43–1.29 MeV.
[2] Superseded by ABLIKIM 22AQ

$\Gamma(\Lambda_c^+\overline{p}e^+e^- + c.c.)/\Gamma_{total}$ — Γ_{190}/Γ

VALUE	CL%	EVTS	DOCUMENT ID		TECN	COMMENT
<1.7 × 10^{-6}	90	450M	ABLIKIM	18Q	BES3	$e^+e^- \to \psi(2S)$

$\Gamma(\Theta(1540)\overline{\Theta}(1540) \to K^0_S pK^-\overline{n} + c.c.)/\Gamma_{total}$ — Γ_{191}/Γ

VALUE (units 10^{-5})	CL%	DOCUMENT ID		TECN	COMMENT
<0.88	90	BAI	04G	BES2	e^+e^-

$\Gamma(\Theta(1540)K^-\overline{n} \to K^0_S pK^-\overline{n})/\Gamma_{total}$ — Γ_{192}/Γ

VALUE (units 10^{-5})	CL%	DOCUMENT ID		TECN	COMMENT
<1.0	90	BAI	04G	BES2	e^+e^-

$\Gamma(\Theta(1540)K^0_S\overline{p} \to K^0_S\overline{p}K^+n)/\Gamma_{total}$ — Γ_{193}/Γ

VALUE (units 10^{-5})	CL%	DOCUMENT ID		TECN	COMMENT
<0.70	90	BAI	04G	BES2	e^+e^-

$\Gamma(\overline{\Theta}(1540)K^+n \to K^0_S\overline{p}K^+n)/\Gamma_{total}$ — Γ_{194}/Γ

VALUE (units 10^{-5})	CL%	DOCUMENT ID		TECN	COMMENT
<2.6	90	BAI	04G	BES2	e^+e^-

$\Gamma(\overline{\Theta}(1540)K^0_S p \to K^0_S pK^-\overline{n})/\Gamma_{total}$ — Γ_{195}/Γ

VALUE (units 10^{-5})	CL%	DOCUMENT ID		TECN	COMMENT
<0.60	90	BAI	04G	BES2	e^+e^-

RADIATIVE DECAYS

$\Gamma(\gamma\chi_{c0}(1P))/\Gamma_{total}$ — Γ_{196}/Γ

VALUE (units 10^{-2})	EVTS	DOCUMENT ID		TECN	COMMENT
10.06 ±0.27 OUR FIT Error includes scale factor of 1.4.					
9.33 ±0.26 OUR AVERAGE					
9.389±0.014±0.332	4.7M	ABLIKIM	17U	BES3	$e^+e^- \to \gamma X$
9.22 ±0.11 ±0.46	72k	ATHAR	04	CLEO	$e^+e^- \to \gamma X$
9.9 ±0.5 ±0.8		[1] GAISER	86	CBAL	$e^+e^- \to \gamma X$
7.2 ±2.3		[1] BIDDICK	77	CNTR	$e^+e^- \to \gamma X$
7.5 ±2.6		[1] WHITAKER	76	MRK1	e^+e^-

[1] Angular distribution $(1+\cos^2\theta)$ assumed.

$\Gamma(\gamma\chi_{c1}(1P))/\Gamma_{total}$ — Γ_{197}/Γ

VALUE (units 10^{-2})	EVTS	DOCUMENT ID		TECN	COMMENT
9.85 ±0.26 OUR FIT Error includes scale factor of 1.2.					
9.54 ±0.29 OUR AVERAGE					
9.905±0.011±0.353	5.0M	ABLIKIM	17U	BES3	$e^+e^- \to \gamma X$
9.07 ±0.11 ±0.54	76k	ATHAR	04	CLEO	$e^+e^- \to \gamma X$
9.0 ±0.5 ±0.7		[1] GAISER	86	CBAL	$e^+e^- \to \gamma X$
7.1 ±1.9		[2] BIDDICK	77	CNTR	$e^+e^- \to \gamma X$

[1] Angular distribution $(1-0.189\cos^2\theta)$ assumed.
[2] Valid for isotropic distribution of the photon.

$\Gamma(\gamma\chi_{c0}(1P))/\Gamma(\gamma\chi_{c1}(1P))$ — $\Gamma_{196}/\Gamma_{197}$

VALUE	DOCUMENT ID		TECN	COMMENT
• • • We do not use the following data for averages, fits, limits, etc. • • •				
1.02±0.01±0.07	[1] ATHAR	04	CLEO	$e^+e^- \to \gamma X$

[1] Not independent from ATHAR 04 measurements of $B(\gamma\chi_{c,J})$.

$\Gamma(\gamma\chi_{c2}(1P))/\Gamma_{total}$ — Γ_{198}/Γ

VALUE (units 10^{-2})	EVTS	DOCUMENT ID		TECN	COMMENT
9.63 ±0.23 OUR FIT Error includes scale factor of 1.2.					
9.42 ±0.31 OUR AVERAGE Error includes scale factor of 1.3. See the ideogram below.					
9.621±0.013±0.272	4.2M	ABLIKIM	17U	BES3	$e^+e^- \to \gamma X$
9.33 ±0.14 ±0.61	79k	ATHAR	04	CLEO	$e^+e^- \to \gamma X$
8.0 ±0.5 ±0.7		[1] GAISER	86	CBAL	$e^+e^- \to \gamma X$
7.0 ±2.0		[2] BIDDICK	77	CNTR	$e^+e^- \to \gamma X$

Int. J. Mod. Phys. A 2026.41. Downloaded from www.worldscientific.com
by UNIVERSITY OF CALIFORNIA @ BERKELEY on 09/16/26. Re-use and distribution is strictly not permitted, except for Open Access articles.

[1] Angular distribution $(1-0.052\cos^2\theta)$ assumed.
[2] Valid for isotropic distribution of the photon.

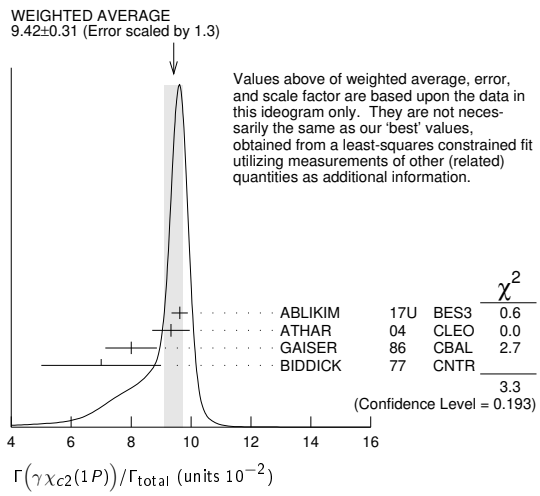

$[\Gamma(\gamma\chi_{c0}(1P)) + \Gamma(\gamma\chi_{c1}(1P)) + \Gamma(\gamma\chi_{c2}(1P))]/\Gamma_{total}$ — $(\Gamma_{196}+\Gamma_{197}+\Gamma_{198})/\Gamma$

VALUE	DOCUMENT ID		TECN	COMMENT
• • • We do not use the following data for averages, fits, limits, etc. • • •				
27.6±0.3±2.0	[1] ATHAR	04	CLEO	$e^+e^- \to \gamma X$

[1] Not independent from ATHAR 04 measurements of $B(\gamma\chi_{cJ})$.

$\Gamma(\gamma\chi_{c0}(1P))/\Gamma(\gamma\chi_{c2}(1P))$ — $\Gamma_{196}/\Gamma_{198}$

VALUE	DOCUMENT ID		TECN	COMMENT
• • • We do not use the following data for averages, fits, limits, etc. • • •				
0.99±0.02±0.08	[1] ATHAR	04	CLEO	$e^+e^- \to \gamma X$

[1] Not independent from ATHAR 04 measurements of $B(\gamma\chi_{cJ})$.

$\Gamma(\gamma\chi_{c2}(1P))/\Gamma(\gamma\chi_{c1}(1P))$ — $\Gamma_{198}/\Gamma_{197}$

VALUE	DOCUMENT ID		TECN	COMMENT
• • • We do not use the following data for averages, fits, limits, etc. • • •				
1.03±0.02±0.03	[1] ATHAR	04	CLEO	$e^+e^- \to \gamma X$

[1] Not independent from ATHAR 04 measurements of $B(\gamma\chi_{cJ})$.

$\Gamma(\gamma\eta_c(1S))/\Gamma_{total}$ — Γ_{199}/Γ

VALUE (units 10^{-2})	EVTS	DOCUMENT ID		TECN	COMMENT
0.36 ±0.05 OUR FIT Error includes scale factor of 1.3.					
0.34 ±0.05 OUR AVERAGE Error includes scale factor of 1.3. See the ideogram below.					
0.432±0.016±0.060		MITCHELL	09	CLEO	$e^+e^- \to \gamma X$
0.32 ±0.04 ±0.06	2.5k	[1] ATHAR	04	CLEO	$e^+e^- \to \gamma X$
0.28 ±0.06		[2] GAISER	86	CBAL	$e^+e^- \to \gamma X$

[1] ATHAR 04 used $\Gamma_{\eta_c(1S)} = 24.8 \pm 4.9$ MeV to obtain this result.
[2] GAISER 86 used $\Gamma_{\eta_c(1S)} = 11.5 \pm 4.5$ MeV to obtain this result.

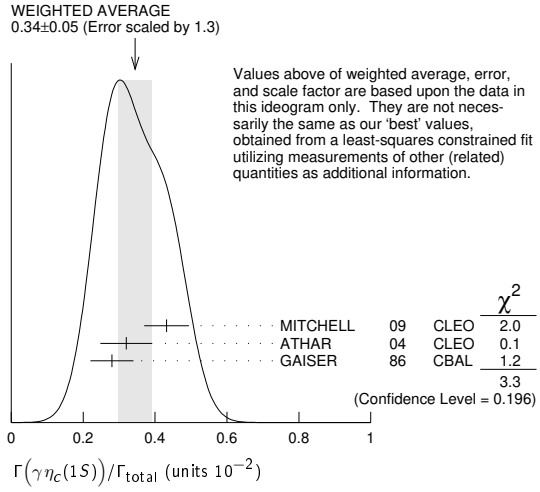

$\Gamma(\gamma\eta_c(2S))/\Gamma_{total}$ — Γ_{200}/Γ

VALUE (units 10^{-4})	CL%	EVTS	DOCUMENT ID		TECN	COMMENT
$5.4^{+3.4}_{-2.9}$ OUR FIT						
• • • We do not use the following data for averages, fits, limits, etc. • • •						
$5.1\pm0.6^{+2.7}_{-3.1}$		1.6k	[1] ABLIKIM	24J	BES3	$\psi(2S) \to \gamma\eta_c \to \gamma K\overline{K}\pi$
7 ±2 ±4			[2] ABLIKIM	12G	BES3	$\psi(2S) \to \gamma K^0 K\pi$, $KK\pi^0$
< 8	90		[3] CRONIN-HEN..	10	CLEO	$\psi(2S) \to \gamma K\overline{K}\pi$
<20	90		ATHAR	04	CLEO	$e^+e^- \to \gamma X$
20–130	95		EDWARDS	82C	CBAL	$e^+e^- \to \gamma X$

[1] ABLIKIM 24J reports $[\Gamma(\psi(2S) \to \gamma\eta_c(2S))/\Gamma_{total}] \times [B(\eta_c(2S) \to K\overline{K}\pi)] = (0.97 \pm 0.06 \pm 0.09) \times 10^{-5}$ which we divide by our best (shown rounded) value $B(\eta_c(2S) \to K\overline{K}\pi) = (1.9^{+1.2}_{-1.0}) \times 10^{-2}$. Our first error is their experiment's error and our second error is the systematic error from using our best (shown rounded) value.
[2] ABLIKIM 12G reports $[\Gamma(\psi(2S) \to \gamma\eta_c(2S))/\Gamma_{total}] \times [B(\eta_c(2S) \to K\overline{K}\pi)] = (1.30 \pm 0.20 \pm 0.30) \times 10^{-5}$ which we divide by our best (shown rounded) value $B(\eta_c(2S) \to K\overline{K}\pi) = (1.9^{+1.2}_{-1.0}) \times 10^{-2}$. Our first error is their experiment's error and our second error is the systematic error from using our best (shown rounded) value.
[3] CRONIN-HENNESSY 10 reports $[\Gamma(\psi(2S) \to \gamma\eta_c(2S))/\Gamma_{total}] \times [B(\eta_c(2S) \to K\overline{K}\pi)] < 14.5 \times 10^{-6}$ which we divide by our best (shown rounded) value $B(\eta_c(2S) \to K\overline{K}\pi) = 1.9 \times 10^{-2}$. This measurement assumes $\Gamma(\eta_c(2S)) = 14$ MeV. CRONIN-HENNESSY 10 gives the analytic dependence of limits on width.

$\Gamma(\gamma\pi^0)/\Gamma_{total}$ — Γ_{201}/Γ

VALUE (units 10^{-7})	CL%	EVTS	DOCUMENT ID		TECN	COMMENT
2.7 to 9.7	68		[1] ABLIKIM	24BS	BES3	$\psi(2S) \to \gamma\pi^0$
• • • We do not use the following data for averages, fits, limits, etc. • • •						
9.5±1.6±0.5		423	[2] ABLIKIM	17X	BES3	$\psi(2S) \to \gamma\pi^0$
15.8±4.0±1.3		37	[2] ABLIKIM	10F	BES3	$\psi(2S) \to \gamma\pi^0$
< 50	90		PEDLAR	09	CLE3	$\psi(2S) \to \gamma X$
< 54000	95		[3] LIBERMAN	75	SPEC	e^+e^-
<100000	90		WIIK	75	DASP	e^+e^-

[1] Taking into account interference between $\psi(2S)$ and continuum amplitudes. Range of the 1σ contour in the plane of $B(\psi(2S) \to \gamma\pi^0)$ versus ϕ, the relative phase of the amplitudes. The fit provides two solutions for $B(\psi(2S) \to \gamma\pi^0)$: 3.74×10^{-7} ($\phi = 3.93$ rad) and 7.87×10^{-7} ($\phi = 2.08$ rad).
[2] Interference between $\psi(2S)$ and the continuum is not taken into account.
[3] Restated by us using $B(\psi(2S) \to \mu^+\mu^-) = 0.0077$.

$\Gamma(\gamma 2(\pi^+\pi^-))/\Gamma_{total}$ — Γ_{202}/Γ

VALUE (units 10^{-5})	EVTS	DOCUMENT ID		TECN	COMMENT
39.6±2.8±5.0	583	ABLIKIM	07D	BES2	$e^+e^- \to \psi(2S)$

$\Gamma(\gamma 3(\pi^+\pi^-))/\Gamma_{total}$ — Γ_{203}/Γ

VALUE (units 10^{-5})	CL%	DOCUMENT ID		TECN	COMMENT
<17	90	ABLIKIM	07D	BES2	$e^+e^- \to \psi(2S)$

$\Gamma(\gamma\eta'(958))/\Gamma_{total}$ — Γ_{204}/Γ

VALUE (units 10^{-4})	CL%	EVTS	DOCUMENT ID		TECN	COMMENT
1.24 ±0.04 OUR AVERAGE						
1.251±0.022±0.062		56k	ABLIKIM	17X	BES3	$\psi(2S) \to \gamma\pi^+\pi^-\eta$, $\gamma\pi^0\pi^0\eta$
1.26 ±0.03 ±0.08		2226	[1] ABLIKIM	10F	BES3	$\psi(2S) \to 3\gamma\pi^+\pi^-$, $2\gamma\pi^+\pi^-$
1.19 ±0.08 ±0.03			PEDLAR	09	CLE3	$\psi(2S) \to \gamma X$
1.24 ±0.27 ±0.15		23	ABLIKIM	06R	BES2	$e^+e^- \to \psi(2S)$
1.54 ±0.31 ±0.20		∼ 43	BAI	98F	BES	$\psi(2S) \to \pi^+\pi^-2\gamma$, $\pi^+\pi^-3\gamma$
• • • We do not use the following data for averages, fits, limits, etc. • • •						
< 60	90		[2] BRAUNSCH...	77	DASP	e^+e^-
< 11	90		[3] BARTEL	76	CNTR	e^+e^-

[1] Combining the results from $\eta' \to \pi^+\pi^-\eta$ and $\eta' \to \pi^+\pi^-\gamma$ decay modes.
[2] Restated by us using total decay width 228 keV.
[3] The value is normalized to the branching ratio for $\Gamma(J/\psi(1S)\eta)/\Gamma_{total}$.

$\Gamma(\gamma f_2(1270))/\Gamma_{total}$ — Γ_{205}/Γ

VALUE (units 10^{-4})	EVTS	DOCUMENT ID		TECN	COMMENT
$2.73^{+0.29}_{-0.25}$ OUR AVERAGE Error includes scale factor of 1.8.					
$2.84\pm0.15^{+0.03}_{-0.10}$	1.9k	[1,2] DOBBS	15		$\psi(2S) \to \gamma\pi\pi$
2.12±0.19±0.32		[3,4] BAI	03C	BES	$\psi(2S) \to \gamma\pi\pi$
• • • We do not use the following data for averages, fits, limits, etc. • • •					
2.08±0.19±0.33	200.6 ± 18.8	[3] BAI	03C	BES	$\psi(2S) \to \gamma\pi^+\pi^-$
2.90±1.08±1.07	29.9 ± 11.1	[3] BAI	03C	BES	$\psi(2S) \to \gamma\pi^0\pi^0$

[1] Using CLEO-c data but not authored by the CLEO Collaboration.
[2] DOBBS 15 reports $[\Gamma(\psi(2S) \to \gamma f_2(1270))/\Gamma_{total}] \times [B(f_2(1270) \to \pi\pi)] = (2.39 \pm 0.09 \pm 0.09) \times 10^{-4}$ which we divide by our best (shown rounded) value $B(f_2(1270) \to \pi\pi) = (84.3^{+2.8}_{-1.0}) \times 10^{-2}$. Our first error is their experiment's error and our second error is the systematic error from using our best (shown rounded) value.
[3] Normalized to $B(\psi(2S) \to J/\psi\pi^+\pi^-) = 0.305 \pm 0.016$.
[4] Combining the results from $\pi^+\pi^-$ and $\pi^0\pi^0$ decay modes.

Int. J. Mod. Phys. A 2026.41. Downloaded from www.worldscientific.com
by CALIFORNIA @ BERKELEY on 09/16/26. Re-use and distribution is strictly not permitted, except for Open Access articles.

$\Gamma(\gamma f_2(1270) \to \gamma K^0_S K^0_S)/\Gamma_{total}$ — Γ_{206}/Γ

VALUE (units 10^{-6})	DOCUMENT ID		TECN	COMMENT
$2.1^{+0.4}_{-0.5} \pm 0.8$	ABLIKIM	25CD	BES3	$e^+e^- \to \psi(2S)$

$\Gamma(\gamma f_0(1370) \to \gamma K\overline{K})/\Gamma_{total}$ — Γ_{207}/Γ

VALUE (units 10^{-5})	EVTS	DOCUMENT ID		COMMENT
$3.1 \pm 1.0 \pm 1.4$	175	[1] DOBBS	15	$\psi(2S) \to \gamma K\overline{K}$

[1] Using CLEO-c data but not authored by the CLEO Collaboration.

$\Gamma(\gamma f_0(1370) \to \gamma K^0_S K^0_S)/\Gamma_{total}$ — Γ_{208}/Γ

VALUE (units 10^{-6})	DOCUMENT ID		TECN	COMMENT
$1.2^{+2.8}_{-0.7} \pm 1.6$	ABLIKIM	25CD	BES3	$e^+e^- \to \psi(2S)$

$\Gamma(\gamma f_0(1500))/\Gamma_{total}$ — Γ_{209}/Γ

VALUE (units 10^{-5})	EVTS	DOCUMENT ID		COMMENT
$9.3 \pm 1.8 \pm 0.6$	274	[1,2] DOBBS	15	$\psi(2S) \to \gamma\pi\pi$

[1] DOBBS 15 reports $[\Gamma(\psi(2S) \to \gamma f_0(1500))/\Gamma_{total}] \times [B(f_0(1500) \to \pi\pi)] = (3.2 \pm 0.6 \pm 0.2) \times 10^{-5}$ which we divide by our best (shown rounded) value $B(f_0(1500) \to \pi\pi) = (34.5 \pm 2.2) \times 10^{-2}$. Our first error is their experiment's error and our second error is the systematic error from using our best (shown rounded) value.
[2] Using CLEO-c data but not authored by the CLEO Collaboration.

$\Gamma(\gamma f_0(1500 \to \gamma K^0_S K^0_S)/\Gamma_{total}$ — Γ_{210}/Γ

VALUE (units 10^{-6})	DOCUMENT ID		TECN	COMMENT
$1.7^{+1.4}_{-0.7} \pm 1.0$	ABLIKIM	25CD	BES3	$e^+e^- \to \psi(2S)$

$\Gamma(\gamma f'_2(1525))/\Gamma_{total}$ — Γ_{211}/Γ

VALUE (units 10^{-5})	EVTS	DOCUMENT ID		COMMENT
$3.3 \pm 0.8 \pm 0.1$	136	[1,2] DOBBS	15	$\psi(2S) \to \gamma K\overline{K}$

[1] DOBBS 15 reports $[\Gamma(\psi(2S) \to \gamma f'_2(1525))/\Gamma_{total}] \times [B(f'_2(1525) \to K\overline{K})] = (2.9 \pm 0.6 \pm 0.3) \times 10^{-5}$ which we divide by our best (shown rounded) value $B(f'_2(1525) \to K\overline{K}) = (88.8 \pm 2.2) \times 10^{-2}$. Our first error is their experiment's error and our second error is the systematic error from using our best (shown rounded) value.
[2] Using CLEO-c data but not authored by the CLEO Collaboration.

$\Gamma(\gamma f'_2(1525) \to \gamma K^0_S K^0_S)/\Gamma_{total}$ — Γ_{212}/Γ

VALUE (units 10^{-6})	DOCUMENT ID		TECN	COMMENT
$1.4^{+0.5}_{-0.4} \pm 0.4$	ABLIKIM	25CD	BES3	$e^+e^- \to \psi(2S)$

$\Gamma(\gamma f_0(1710) \to \gamma\pi\pi)/\Gamma_{total}$ — Γ_{214}/Γ

VALUE (units 10^{-5})	EVTS	DOCUMENT ID		TECN	COMMENT
3.5 ±0.6 OUR AVERAGE					
$3.6 \pm 0.4 \pm 0.5$	290	[1] DOBBS	15		$\psi(2S) \to \gamma\pi\pi$
$3.01 \pm 0.41 \pm 1.24$	35.6 ± 4.8	[2] BAI	03C	BES	$\psi(2S) \to \gamma\pi^+\pi^-$

[1] Using CLEO-c data but not authored by the CLEO Collaboration.
[2] Normalized to $B(\psi(2S) \to J/\psi\pi^+\pi^-) = 0.305 \pm 0.016$.

$\Gamma(\gamma f_0(1710) \to \gamma K\overline{K})/\Gamma_{total}$ — Γ_{215}/Γ

VALUE (units 10^{-5})	CL%	EVTS	DOCUMENT ID		TECN	COMMENT
6.6 ±0.7 OUR AVERAGE						
$6.7 \pm 0.6 \pm 0.6$		375	[1] DOBBS	15		$\psi(2S) \to \gamma K\overline{K}$
$6.04 \pm 0.90 \pm 1.32$		39.6 ± 5.9	[2,3] BAI	03C	BES	$\psi(2S) \to \gamma K^+K^-$
• • • We do not use the following data for averages, fits, limits, etc. • • •						
< 15.6	90	6.8 ± 3.1	[2,3] BAI	03C	BES	$\psi(2S) \to \gamma K^0_S K^0_S$

[1] Using CLEO-c data but not authored by the CLEO Collaboration.
[2] Includes unknown branching fractions to K^+K^- or $K^0_S K^0_S$. We have multiplied the K^+K^- result by a factor of 2 and the $K^0_S K^0_S$ result by a factor of 4 to obtain the $K\overline{K}$ result.
[3] Normalized to $B(\psi(2S) \to J/\psi\pi^+\pi^-) = 0.305 \pm 0.016$.

$\Gamma(\gamma f_0(1710) \to \gamma K^0_S K^0_S)/\Gamma_{total}$ — Γ_{216}/Γ

VALUE (units 10^{-6})	DOCUMENT ID		TECN	COMMENT
$18.3^{+2.7}_{-2.0} \pm 1.8$	ABLIKIM	25CD	BES3	$e^+e^- \to \psi(2S)$

$\Gamma(\gamma f_2(1950) \to \gamma K^0_S K^0_S)/\Gamma_{total}$ — Γ_{217}/Γ

VALUE (units 10^{-6})	DOCUMENT ID		TECN	COMMENT
$1.2^{+0.8}_{-0.5} \pm 0.6$	ABLIKIM	25CD	BES3	$e^+e^- \to \psi(2S)$

$\Gamma(\gamma f_0(2020) \to \gamma K^0_S K^0_S)/\Gamma_{total}$ — Γ_{218}/Γ

VALUE (units 10^{-6})	DOCUMENT ID		TECN	COMMENT
$4.6^{+0.8}_{-0.7} \pm 1.3$	ABLIKIM	25CD	BES3	$e^+e^- \to \psi(2S)$

$\Gamma(\gamma f_0(2100) \to \gamma\pi\pi)/\Gamma_{total}$ — Γ_{219}/Γ

VALUE (units 10^{-6})	EVTS	DOCUMENT ID		COMMENT
$4.8 \pm 0.5 \pm 0.9$	373	[1] DOBBS	15	$\psi(2S) \to \gamma\pi\pi$

[1] Using CLEO-c data but not authored by the CLEO Collaboration.

$\Gamma(\gamma f_0(2200) \to \gamma K\overline{K})/\Gamma_{total}$ — Γ_{220}/Γ

VALUE (units 10^{-6})	EVTS	DOCUMENT ID		COMMENT
$3.2 \pm 0.6 \pm 0.8$	207	[1] DOBBS	15	$\psi(2S) \to \gamma K\overline{K}$

[1] Using CLEO-c data but not authored by the CLEO Collaboration.

$\Gamma(\gamma f_J(2220) \to \gamma\pi\pi)/\Gamma_{total}$ — Γ_{221}/Γ

VALUE	CL%	DOCUMENT ID		COMMENT
$<5.8 \times 10^{-6}$	90	[1,2] DOBBS	15	$\psi(2S) \to \gamma\pi\pi$

[1] Using CLEO-c data but not authored by the CLEO Collaboration.
[2] For $\Gamma = 20/50$ MeV, the 90% CL upper limits for $\pi^+\pi^-$ and $\pi^0\pi^0$ are $3.2/4.3 \times 10^{-6}$ and $2.6/4.0 \times 10^{-6}$, respectively.

$\Gamma(\gamma f_J(2220) \to \gamma K\overline{K})/\Gamma_{total}$ — Γ_{222}/Γ

VALUE	CL%	DOCUMENT ID		COMMENT
$<9.5 \times 10^{-6}$	90	[1,2] DOBBS	15	$\psi(2S) \to \gamma K\overline{K}$

[1] Using CLEO-c data but not authored by the CLEO Collaboration.
[2] For $\Gamma = 20/50$ MeV, the 90% CL upper limits for K^+K^- and $K^0_S K^0_S$ are $2.1/4.3 \times 10^{-6}$ and $3.7/5.5 \times 10^{-6}$, respectively.

$\Gamma(\gamma\eta)/\Gamma_{total}$ — Γ_{223}/Γ

VALUE (units 10^{-6})	CL%	EVTS	DOCUMENT ID		TECN	COMMENT
0.92±0.18 OUR AVERAGE						
$0.85 \pm 0.18 \pm 0.04$		382	[1] ABLIKIM	17X	BES3	$\psi(2S) \to \gamma\pi^+\pi^-\pi^0$, $\gamma 3\pi^0$
$1.38 \pm 0.48 \pm 0.09$		13	[1] ABLIKIM	10F	BES3	$\psi(2S) \to \gamma\pi^+\pi^-\pi^0$, $\gamma 3\pi^0$
• • • We do not use the following data for averages, fits, limits, etc. • • •						
< 2	90		PEDLAR	09	CLE3	$\psi(2S) \to \gamma X$
< 90	90		BAI	98F	BES	$\psi(2S) \to \pi^+\pi^- 3\gamma$
<200	90		YAMADA	77	DASP	$e^+e^- \to 3\gamma$

[1] Combining the results from $\eta \to \pi^+\pi^-\pi^0$ and $\eta \to 3\pi^0$ decay modes.

$\Gamma(\gamma\eta\pi^+\pi^-)/\Gamma_{total}$ — Γ_{224}/Γ

VALUE (units 10^{-4})	EVTS	DOCUMENT ID		TECN	COMMENT
$8.71 \pm 1.25 \pm 1.64$	418	ABLIKIM	06R	BES2	$\psi(2S) \to \gamma\eta\pi^+\pi^-$

$\Gamma(\gamma\eta(1405) \to \gamma K\overline{K}\pi)/\Gamma_{total}$ — Γ_{226}/Γ

VALUE (units 10^{-4})	CL%	DOCUMENT ID		TECN	COMMENT
<0.9	90	ABLIKIM	06R	BES2	$\psi(2S) \to \gamma K^0_S K^+\pi^- +$ c.c.
• • • We do not use the following data for averages, fits, limits, etc. • • •					
<1.3	90	ABLIKIM	06R	BES2	$\psi(2S) \to \gamma K^+K^-\pi^0$
<1.2	90	[1] SCHARRE	80	MRK1	e^+e^-

[1] Includes unknown branching fraction $\eta(1405) \to K\overline{K}\pi$.

$\Gamma(\gamma\eta(1405) \to \gamma\eta\pi^+\pi^-)/\Gamma_{total}$ — Γ_{227}/Γ

VALUE (units 10^{-4})	EVTS	DOCUMENT ID		TECN	COMMENT
$0.36 \pm 0.25 \pm 0.05$	10	ABLIKIM	06R	BES2	$\psi(2S) \to \gamma\eta\pi^+\pi^-$

$\Gamma(\gamma\eta(1405) \to \gamma f_0(980)\pi^0 \to \gamma\pi^+\pi^-\pi^0)/\Gamma_{total}$ — Γ_{228}/Γ

VALUE	CL%	DOCUMENT ID		TECN	COMMENT
$<5.0 \times 10^{-7}$	90	ABLIKIM	17AJ	BES3	$\psi(2S) \to \gamma\pi^+\pi^-\pi^0$

$\Gamma(\gamma\eta(1475) \to \gamma K\overline{K}\pi)/\Gamma_{total}$ — Γ_{230}/Γ

VALUE (units 10^{-4})	CL%	DOCUMENT ID		TECN	COMMENT
<1.4	90	ABLIKIM	06R	BES2	$\psi(2S) \to \gamma K^+K^-\pi^0$
• • • We do not use the following data for averages, fits, limits, etc. • • •					
<1.5	90	ABLIKIM	06R	BES2	$\psi(2S) \to \gamma K^0_S K^+\pi^- +$ c.c.

$\Gamma(\gamma\eta(1475) \to \gamma\eta\pi^+\pi^-)/\Gamma_{total}$ — Γ_{231}/Γ

VALUE (units 10^{-4})	CL%	DOCUMENT ID		TECN	COMMENT
<0.88	90	ABLIKIM	06R	BES2	$\psi(2S) \to \gamma\eta\pi^+\pi^-$

$\Gamma(\gamma K^{*0}K^+\pi^- +$ c.c.$)/\Gamma_{total}$ — Γ_{232}/Γ

VALUE (units 10^{-5})	EVTS	DOCUMENT ID		TECN	COMMENT
$37.0 \pm 6.1 \pm 7.2$	237	ABLIKIM	07D	BES2	$e^+e^- \to \psi(2S)$

$\Gamma(\gamma K^{*0}\overline{K}^{*0})/\Gamma_{total}$ — Γ_{233}/Γ

VALUE (units 10^{-5})	EVTS	DOCUMENT ID		TECN	COMMENT
$24.0 \pm 4.5 \pm 5.0$	41	ABLIKIM	07D	BES2	$e^+e^- \to \psi(2S)$

$\Gamma(\gamma K^0_S K^+\pi^- +$ c.c.$)/\Gamma_{total}$ — Γ_{234}/Γ

VALUE (units 10^{-5})	EVTS	DOCUMENT ID		TECN	COMMENT
$25.6 \pm 3.6 \pm 3.6$	115	ABLIKIM	07D	BES2	$e^+e^- \to \psi(2S)$

$\Gamma(\gamma K^+K^-\pi^+\pi^-)/\Gamma_{total}$ — Γ_{235}/Γ

VALUE (units 10^{-5})	EVTS	DOCUMENT ID		TECN	COMMENT
$19.1 \pm 2.7 \pm 4.3$	132	ABLIKIM	07D	BES2	$e^+e^- \to \psi(2S)$

Int. J. Mod. Phys. A 2026.41. Downloaded from www.worldscientific.com
by UNIVERSITY OF CALIFORNIA @ BERKELEY on 09/16/26. Re-use and distribution is strictly not permitted, except for Open Access articles.

$\Gamma(\gamma K^+ K^- 2(\pi^+\pi^-))/\Gamma_{total}$ — Γ_{236}/Γ

VALUE (units 10^{-5})	CL%	DOCUMENT ID		TECN	COMMENT
<22	90	ABLIKIM	07D	BES2	$e^+e^- \to \psi(2S)$

$\Gamma(\gamma 2(K^+K^-))/\Gamma_{total}$ — Γ_{237}/Γ

VALUE (units 10^{-5})	CL%	DOCUMENT ID		TECN	COMMENT
<4	90	ABLIKIM	07D	BES2	$e^+e^- \to \psi(2S)$

$\Gamma(\gamma p\overline{p})/\Gamma_{total}$ — Γ_{238}/Γ

VALUE (units 10^{-5})	EVTS	DOCUMENT ID		TECN	COMMENT
3.9 ±0.5 OUR AVERAGE Error includes scale factor of 2.0.					
4.18±0.26±0.18	348	[1] ALEXANDER	10	CLEO	$\psi(2S) \to \gamma p\overline{p}$
2.9 ±0.4 ±0.4	142	ABLIKIM	07D	BES2	$e^+e^- \to \psi(2S)$

[1] From a fit of the $p\overline{p}$ mass distribution to a combination of $\gamma f_2(1950)$, $\gamma f_2(2150)$, and $\gamma p\overline{p}$ phase space, for $M(p\overline{p} < 2.85$ GeV, and accounting for backgrounds from $\psi(2S) \to \pi^0 p\overline{p}$ and continuum.

$\Gamma(\gamma f_2(1950) \to \gamma p\overline{p})/\Gamma_{total}$ — Γ_{239}/Γ

VALUE (units 10^{-5})	EVTS	DOCUMENT ID		TECN	COMMENT
1.2±0.2±0.1	111	[1] ALEXANDER	10	CLEO	$\psi(2S) \to \gamma p\overline{p}$

[1] From a fit of the $p\overline{p}$ mass distribution to a combination of $\gamma f_2(1950)$, $\gamma f_2(2150)$, and $\gamma p\overline{p}$ phase space, for $M(p\overline{p} < 2.85$ GeV, and accounting for backgrounds from $\psi(2S) \to \pi^0 p\overline{p}$ and continuum.

$\Gamma(\gamma f_2(2150) \to \gamma p\overline{p})/\Gamma_{total}$ — Γ_{240}/Γ

VALUE (units 10^{-5})	EVTS	DOCUMENT ID		TECN	COMMENT
0.72±0.18±0.03	73	[1] ALEXANDER	10	CLEO	$\psi(2S) \to \gamma p\overline{p}$

[1] From a fit of the $p\overline{p}$ mass distribution to a combination of $\gamma f_2(1950)$, $\gamma f_2(2150)$, and $\gamma p\overline{p}$ phase space, for $M(p\overline{p} < 2.85$ GeV, and accounting for backgrounds from $\psi(2S) \to \pi^0 p\overline{p}$ and continuum.

$\Gamma(\gamma X(1835) \to \gamma p\overline{p})/\Gamma_{total}$ — Γ_{241}/Γ

VALUE (units 10^{-6})	CL%	DOCUMENT ID		TECN	COMMENT
$4.57\pm0.36^{+1.77}_{-4.26}$		ABLIKIM	12D	BES3	$J/\psi \to \gamma p\overline{p}$
• • • We do not use the following data for averages, fits, limits, etc. • • •					
<1.6	90	ALEXANDER	10	CLEO	$\psi(2S) \to \gamma p\overline{p}$
<5.4	90	ABLIKIM	07D	BES	$\psi(2S) \to \gamma p\overline{p}$

$\Gamma(\gamma X \to \gamma p\overline{p})/\Gamma_{total}$ — Γ_{242}/Γ

For a narrow resonance in the range $2.2 < M(X) < 2.8$ GeV.

VALUE (units 10^{-6})	CL%	DOCUMENT ID		TECN	COMMENT
<2	90	ALEXANDER	10	CLEO	$\psi(2S) \to \gamma p\overline{p}$

$\Gamma(\gamma p\overline{p}\pi^+\pi^-)/\Gamma_{total}$ — Γ_{243}/Γ

VALUE (units 10^{-5})	EVTS	DOCUMENT ID		TECN	COMMENT
2.8±1.2±0.7	17	ABLIKIM	07D	BES2	$e^+e^- \to \psi(2S)$

$\Gamma(\gamma\gamma J/\psi)/\Gamma_{total}$ — Γ_{245}/Γ

VALUE (units 10^{-4})	EVTS	DOCUMENT ID		TECN	COMMENT
$3.1\pm0.6^{+0.8}_{-1.0}$	1.1k	ABLIKIM	12O	BES3	$e^+e^- \to \psi(2S)$
• • • We do not use the following data for averages, fits, limits, etc. • • •					
3.2±0.6	1.1k	[1] ABLIKIM	17N	BES3	$\psi(2S) \to \gamma\gamma J/\psi$

[1] Uses B($J/\psi \to e^+e^-$) = (5.971 ± 0.032)% and B($J/\psi \to \mu^+\mu^-$) = (5.961 ± 0.033)%. No systematic error estimation.

$\Gamma(e^+e^-\eta')/\Gamma_{total}$ — Γ_{246}/Γ

VALUE (units 10^{-6})	EVTS	DOCUMENT ID		TECN	COMMENT
1.90±0.26 OUR AVERAGE					
1.99±0.33±0.12	57	ABLIKIM	18Z	BES3	$\psi(2S) \to \eta' e^+e^-$, $\eta' \to \gamma\pi^+\pi^-$
1.79±0.38±0.11	20	ABLIKIM	18Z	BES3	$\psi(2S) \to \eta' e^+e^-$, $\eta' \to \eta\pi^+\pi^-$

$\Gamma(e^+e^-\eta_c(1S))/\Gamma_{total}$ — Γ_{247}/Γ

VALUE (units 10^{-5})	EVTS	DOCUMENT ID		TECN	COMMENT
3.77±0.40±0.18	3k	[1] ABLIKIM	22AX	BES3	$e^+e^- \to \psi(2S)$

[1] From a fit to the recoil mass distribution of e^+e^- with inclusive $\eta_c(1S)$ decays.

$\Gamma(e^+e^-\chi_{c0}(1P))/\Gamma_{total}$ — Γ_{248}/Γ

VALUE (units 10^{-4})	EVTS	DOCUMENT ID		TECN	COMMENT
11.0±2.5±0.7	48	[1] ABLIKIM	17I	BES3	$\psi(2S) \to e^+e^-\gamma J/\psi$

[1] ABLIKIM 17I reports (11.7 ± 2.5 ± 1.0) × 10^{-4} from a measurement of [$\Gamma(\psi(2S) \to e^+e^-\chi_{c0}(1P))/\Gamma_{total}$] × [B($\chi_{c0}(1P) \to \gamma J/\psi(1S)$)] assuming B($\chi_{c0}(1P) \to \gamma J/\psi(1S)$) = (1.27 ± 0.06) × 10^{-2}, which we rescale to our best (shown rounded) value B($\chi_{c0}(1P) \to \gamma J/\psi(1S)$) = (1.35 ± 0.09) × 10^{-2}. Our first error is their experiment's error and our second error is the systematic error from using our best (shown rounded) value.

$\Gamma(e^+e^-\chi_{c0}(1P))/\Gamma(\gamma\chi_{c0}(1P))$ — $\Gamma_{248}/\Gamma_{196}$

VALUE (units 10^{-3})	EVTS	DOCUMENT ID		TECN	COMMENT
9.4±1.9±0.6	48	[1] ABLIKIM	17I	BES3	$\psi(2S) \to e^+e^-\gamma J/\psi$

[1] Uses B($\psi(2S) \to \gamma\chi_{c0}(1P)$) × B($\chi_{c0}(1P) \to \gamma J/\psi(1S)$) = (15.8±0.3±0.6)×$10^{-4}$ from ABLIKIM 17N and accounts for common systematic errors.

$\Gamma(e^+e^-\chi_{c1}(1P))/\Gamma_{total}$ — Γ_{249}/Γ

VALUE (units 10^{-4})	EVTS	DOCUMENT ID		TECN	COMMENT
8.6±0.3±0.6	873	[1] ABLIKIM	17I	BES3	$\psi(2S) \to e^+e^-\gamma J/\psi$

[1] ABLIKIM 17I reports (8.6 ± 0.3 ± 0.6) × 10^{-4} from a measurement of [$\Gamma(\psi(2S) \to e^+e^-\chi_{c1}(1P))/\Gamma_{total}$] × [B($\chi_{c1}(1P) \to \gamma J/\psi(1S)$)] assuming B($\chi_{c1}(1P) \to \gamma J/\psi(1S)$) = (33.9 ± 1.2) × 10^{-2}.

$\Gamma(e^+e^-\chi_{c1}(1P))/\Gamma(\gamma\chi_{c1}(1P))$ — $\Gamma_{249}/\Gamma_{197}$

VALUE (units 10^{-3})	EVTS	DOCUMENT ID		TECN	COMMENT
8.3±0.3±0.4	873	[1] ABLIKIM	17I	BES3	$\psi(2S) \to e^+e^-\gamma J/\psi$

[1] Uses B($\psi(2S) \to \gamma\chi_{c1}(1P)$) × B($\chi_{c1}(1P) \to \gamma J/\psi(1S)$) = (351.8 ± 1.0 ± 12.0) × 10^{-4} from ABLIKIM 17N and accounts for common systematic errors.

$\Gamma(e^+e^-\chi_{c2}(1P))/\Gamma_{total}$ — Γ_{250}/Γ

VALUE (units 10^{-4})	EVTS	DOCUMENT ID		TECN	COMMENT
7.0±0.7±0.3	227	[1] ABLIKIM	17I	BES3	$\psi(2S) \to e^+e^-\gamma J/\psi$

[1] ABLIKIM 17I reports (6.9 ± 0.5 ± 0.6) × 10^{-4} from a measurement of [$\Gamma(\psi(2S) \to e^+e^-\chi_{c2}(1P))/\Gamma_{total}$] × [B($\chi_{c2}(1P) \to \gamma J/\psi(1S)$)] assuming B($\chi_{c2}(1P) \to \gamma J/\psi(1S)$) = (19.2 ± 0.7) × 10^{-2}, which we rescale to our best (shown rounded) value B($\chi_{c2}(1P) \to \gamma J/\psi(1S)$) = (19.0 ± 0.8) × 10^{-2}. Our first error is their experiment's error and our second error is the systematic error from using our best (shown rounded) value.

$\Gamma(e^+e^-\chi_{c2}(1P))/\Gamma(\gamma\chi_{c2}(1P))$ — $\Gamma_{250}/\Gamma_{198}$

VALUE (units 10^{-3})	EVTS	DOCUMENT ID		TECN	COMMENT
6.6±0.5±0.4	227	[1] ABLIKIM	17I	BES3	$\psi(2S) \to e^+e^-\gamma J/\psi$

[1] Uses B($\psi(2S) \to \gamma\chi_{c2}(1P)$) × B($\chi_{c2}(1P) \to \gamma J/\psi(1S)$) = (199.6 ± 0.8 ± 7.0) × 10^{-4} from ABLIKIM 17N and accounts for common systematic errors.

WEAK DECAYS

$\Gamma(D^0 e^+e^- + c.c.)/\Gamma_{total}$ — Γ_{251}/Γ

VALUE	CL%	DOCUMENT ID		TECN	COMMENT
<1.4 × 10^{-7}	90	[1] ABLIKIM	17AF	BES3	$e^+e^- \to \psi(2S)$

[1] Using D^0 decays to $K^-\pi^+$, $K^-\pi^+\pi^0$, and $K^-\pi^+\pi^+\pi^-$.

$\Gamma(\Lambda_c^+\overline{\Sigma}^- + c.c.)/\Gamma_{total}$ — Γ_{252}/Γ

VALUE	CL%	DOCUMENT ID		TECN	COMMENT
<1.4 × 10^{-5}	90	[1] ABLIKIM	23	BES3	$e^+e^- \to \psi(2S)$

[1] Using $\Lambda_c^+ \to pK^-\pi^+$ and $\overline{\Sigma}^- \to \overline{p}\pi^0$.

OTHER DECAYS

$\Gamma(\text{invisible})/\Gamma(e^+e^-)$ — Γ_{253}/Γ_7

VALUE	CL%	DOCUMENT ID		TECN	COMMENT
<2.0	90	LEES	13I	BABR	$B \to K^{(*)}\psi(2S)$

$\psi(2S)$ CROSS-PARTICLE BRANCHING RATIOS

For measurements involving B($\psi(2S) \to \gamma\eta_c(2S)$)×B($\eta_c(2S) \to X$) see the corresponding entries in the $\eta_c(2S)$ sections.

MULTIPOLE AMPLITUDE RATIOS IN RADIATIVE DECAYS $\psi(2S) \to \gamma\chi_{cJ}(1P)$ and $\chi_{cJ} \to \gamma J/\psi(1S)$

$a_2(\chi_{c1})/a_2(\chi_{c2})$ Magnetic quadrupole transition amplitude ratio

VALUE (units 10^{-2})	EVTS	DOCUMENT ID		TECN	COMMENT
63 ± 7 OUR AVERAGE					
61.7± 8.3	253k	[1] ABLIKIM	17N	BES3	$\psi(2S) \to \gamma\gamma\ell^+\ell^-$
67^{+19}_{-13}	59k	[2] ARTUSO	09	CLEO	$\psi(2S) \to \gamma\gamma\ell^+\ell^-$

[1] Statistical and systematic errors combined.
[2] Statistical and systematic errors combined. Using values from fits with floating $M2$ amplitudes $a_2(\chi_{c1})$, $a_2(\chi_{c2})$, $b_2(\chi_{c1})$, $b_2(\chi_{c2})$ and fixed $E3$ amplitudes of $a_3(\chi_{c2}) = b_3(\chi_{c2}) = 0$. Not independent of values for $a_2(\chi_{c1}(1P))$ and $a_2(\chi_{c2}(1P))$ from ARTUSO 09.

$b_2(\chi_{c2})/b_2(\chi_{c1})$ Magnetic quadrupole transition amplitude ratio

VALUE (units 10^{-2})	EVTS	DOCUMENT ID		TECN	COMMENT
60±31 OUR AVERAGE					
74±40	253k	[1] ABLIKIM	17N	BES3	$\psi(2S) \to \gamma\gamma\ell^+\ell^-$
37^{+53}_{-47}	59k	[2] ARTUSO	09	CLEO	$\psi(2S) \to \gamma\gamma\ell^+\ell^-$

[1] Statistical and systematic errors combined. Derived from the reported measurement of $b_2(\chi_{c1})/b_2(\chi_{c2}) = 1.35 \pm 0.72$.
[2] Statistical and systematic errors combined. Using values from fits with floating $M2$ amplitudes $a_2(\chi_{c1})$, $a_2(\chi_{c2})$, $b_2(\chi_{c1})$, $b_2(\chi_{c2})$ and fixed $E3$ amplitudes of $a_3(\chi_{c2}) = b_3(\chi_{c2}) = 0$. Not independent of values for $b_2(\chi_{c1}(1P))$ and $b_2(\chi_{c2}(1P))$ from ARTUSO 09.

Int. J. Mod. Phys. A 2026.41. Downloaded from www.worldscientific.com
by CALIFORNIA @ BERKELEY on 09/16/26. Re-use and distribution is strictly not permitted, except for Open Access articles.

$\psi(2S)$ REFERENCES

ABLIKIM	25AF	JHEP 2502 212	M. Ablikim *et al.*	(BESIII Collab.)
ABLIKIM	25AG	JHEP 2503 145	M. Ablikim *et al.*	(BESIII Collab.)
ABLIKIM	25AJ	JHEP 2506 233	M. Ablikim *et al.*	(BESIII Collab.)
ABLIKIM	25BY	PR D112 112017	M. Ablikim *et al.*	(BESIII Collab.)
ABLIKIM	25CC	PR D112 052010	M. Ablikim *et al.*	(BESIII Collab.)
ABLIKIM	25CD	JHEP 2510 081	M. Ablikim *et al.*	(BESIII Collab.)
ABLIKIM	25E	PRL 134 191901	M. Ablikim *et al.*	(BESIII Collab.)
ABLIKIM	25M	PR D111 032011	M. Ablikim *et al.*	(BESIII Collab.)
ABLIKIM	25P	PR D111 052011	M. Ablikim *et al.*	(BESIII Collab.)
ABLIKIM	25Q	PR D111 052012	M. Ablikim *et al.*	(BESIII Collab.)
ABLIKIM	25W	PR D111 092007	M. Ablikim *et al.*	(BESIII Collab.)
ABLIKIM	24AG	JHEP 2404 013	M. Ablikim *et al.*	(BESIII Collab.)
ABLIKIM	24BS	PR D110 052011	M. Ablikim *et al.*	(BESIII Collab.)
ABLIKIM	24J	PR D109 032004	M. Ablikim *et al.*	(BESIII Collab.)
ABLIKIM	24N	PR D109 072008	M. Ablikim *et al.*	(BESIII Collab.)
ABLIKIM	24O	PR D109 072015	M. Ablikim *et al.*	(BESIII Collab.)
AAIJ	23AP	JHEP 2307 084	R. Aaij *et al.*	(LHCb Collab.)
ABLIKIM	23	CP C47 013002	M. Ablikim *et al.*	(BESIII Collab.)
ABLIKIM	23BA	PR D108 052001	M. Ablikim *et al.*	(BESIII Collab.)
ABLIKIM	23BE	PR D108 092011	M. Ablikim *et al.*	(BESIII Collab.)
ABLIKIM	23BV	PR D108 112014	M. Ablikim *et al.*	(BESIII Collab.)
LEES	23	PR D107 072001	J.P. Lees *et al.*	(BABAR Collab.)
LIAO	23	PR D107 112007	L. Liao *et al.*	
ABLIKIM	22AP	PR D106 072006	M. Ablikim *et al.*	(BESIII Collab.)
ABLIKIM	22AQ	PR D106 072007	M. Ablikim *et al.*	(BESIII Collab.)
ABLIKIM	22AV	JHEP 2212 016	M. Ablikim *et al.*	(BESIII Collab.)
ABLIKIM	22AX	PR D106 112002	M. Ablikim *et al.*	(BESIII Collab.)
ABLIKIM	22AY	PR D106 112007	M. Ablikim *et al.*	(BESIII Collab.)
ABLIKIM	22AZ	PR D106 112011	M. Ablikim *et al.*	(BESIII Collab.)
PDG	22	PTEP 2022 083C01	R.L. Workman *et al.*	(PDG Collab.)
ABLIKIM	21AL	PR D104 092003	M. Ablikim *et al.*	(BESIII Collab.)
ABLIKIM	21AO	PR D104 092012	M. Ablikim *et al.*	(BESIII Collab.)
ABLIKIM	21AT	JHEP 2111 226	M. Ablikim *et al.*	(BESIII Collab.)
ABLIKIM	21E	PRL 126 092002	M. Ablikim *et al.*	(BESIII Collab.)
ABLIKIM	21L	PR D103 112004	M. Ablikim *et al.*	(BESIII Collab.)
ABLIKIM	21S	PL B820 136576	M. Ablikim *et al.*	(BESIII Collab.)
ABLIKIM	21Z	PRL 127 082002	M. Ablikim *et al.*	(BESIII Collab.)
LEES	21	PR D103 092001	J.P. Lees *et al.*	(BABAR Collab.)
LEES	21C	PR D104 112004	J.P. Lees *et al.*	(BABAR Collab.)
ABLIKIM	20F	PR D101 032008	M. Ablikim *et al.*	(BESIII Collab.)
PDG	20	PTEP 2020 083C01	P.A. Zyla *et al.*	(PDG Collab.)
ABLIKIM	19AO	PR D99 112010	M. Ablikim *et al.*	(BESIII Collab.)
ABLIKIM	19AT	PR D100 051101	M. Ablikim *et al.*	(BESIII Collab.)
ABLIKIM	19AU	PR D100 052010	M. Ablikim *et al.*	(BESIII Collab.)
ABLIKIM	19BA	PR D100 092003	M. Ablikim *et al.*	(BESIII Collab.)
ABLIKIM	19I	PR D99 012014	M. Ablikim *et al.*	(BESIII Collab.)
ABLIKIM	19N	PR D99 032006	M. Ablikim *et al.*	(BESIII Collab.)
ABLIKIM	18Q	PR D97 091102	M. Ablikim *et al.*	(BESIII Collab.)
ABLIKIM	18T	PR D98 032006	M. Ablikim *et al.*	(BESIII Collab.)
ABLIKIM	18Z	PL B783 452	M. Ablikim *et al.*	(BESIII Collab.)
ANASHIN	18	PL B781 174	V.V. Anashin *et al.*	(KEDR Collab.)
LEES	18E	PR D98 112015	J.P. Lees *et al.*	(BABAR Collab.)
ABLIKIM	17AF	PR D96 111101	M. Ablikim *et al.*	(BESIII Collab.)
ABLIKIM	17AJ	PR D96 112008	M. Ablikim *et al.*	(BESIII Collab.)
ABLIKIM	17AK	PR D96 112012	M. Ablikim *et al.*	(BESIII Collab.)
ABLIKIM	17E	PL B770 217	M. Ablikim *et al.*	(BESIII Collab.)
ABLIKIM	17I	PRL 118 221802	M. Ablikim *et al.*	(BESIII Collab.)
ABLIKIM	17L	PR D95 052003	M. Ablikim *et al.*	(BESIII Collab.)
ABLIKIM	17N	PR D95 072004	M. Ablikim *et al.*	(BESIII Collab.)
ABLIKIM	17U	PR D96 032001	M. Ablikim *et al.*	(BESIII Collab.)
ABLIKIM	17X	PR D96 052003	M. Ablikim *et al.*	(BESIII Collab.)
DOBBS	17	PR D96 092004	S. Dobbs *et al.*	(NWES, WAYN)
LEES	17A	PR D95 052001	J.P. Lees *et al.*	(BABAR Collab.)
AAIJ	16Y	JHEP 1605 132	R. Aaij *et al.*	(LHCb Collab.)
ABLIKIM	16L	PR D93 072003	M. Ablikim *et al.*	(BESIII Collab.)
ABLIKIM	15I	PR D91 092006	M. Ablikim *et al.*	(BESIII Collab.)
ABLIKIM	15V	PL B749 414	M. Ablikim *et al.*	(BESIII Collab.)
ANASHIN	15	PL B749 50	V.V. Anashin *et al.*	(KEDR Collab.)
DOBBS	15	PR D91 052006	S. Dobbs *et al.*	(NWES)
LEES	15J	PR D92 072008	J.P. Lees *et al.*	(BABAR Collab.)
ABLIKIM	14G	PR D89 112006	M. Ablikim *et al.*	(BESIII Collab.)
DOBBS	14	PL B739 90	S. Dobbs *et al.*	(NWES, WAYN)
ABLIKIM	13A	PRL 110 022001	M. Ablikim *et al.*	(BESIII Collab.)
ABLIKIM	13D	PR D87 012007	M. Ablikim *et al.*	(BESIII Collab.)
ABLIKIM	13F	PR D87 052007	M. Ablikim *et al.*	(BESIII Collab.)
ABLIKIM	13M	PR D87 092006	M. Ablikim *et al.*	(BESIII Collab.)
ABLIKIM	13R	PR D88 032007	M. Ablikim *et al.*	(BESIII Collab.)
ABLIKIM	13S	PR D88 032010	M. Ablikim *et al.*	(BESIII Collab.)
ABLIKIM	13W	PR D88 112007	M. Ablikim *et al.*	(BESIII Collab.)
LEES	13I	PR D87 112005	J.P. Lees *et al.*	(BABAR Collab.)
LEES	13O	PR D87 092005	J.P. Lees *et al.*	(BABAR Collab.)
LEES	13Q	PR D88 032013	J.P. Lees *et al.*	(BABAR Collab.)
LEES	13Y	PR D88 072009	J.P. Lees *et al.*	(BABAR Collab.)
AAIJ	12H	EPJ C72 1972	R. Aaij *et al.*	(LHCb Collab.)
ABLIKIM	12D	PRL 108 112003	M. Ablikim *et al.*	(BESIII Collab.)
ABLIKIM	12G	PRL 109 042003	M. Ablikim *et al.*	(BESIII Collab.)
ABLIKIM	12H	PL B710 594	M. Ablikim *et al.*	(BESIII Collab.)
ABLIKIM	12L	PR D86 072011	M. Ablikim *et al.*	(BESIII Collab.)
ABLIKIM	12M	PR D86 092008	M. Ablikim *et al.*	(BESIII Collab.)
ABLIKIM	12O	PRL 109 172002	M. Ablikim *et al.*	(BESIII Collab.)
ABLIKIM	12Q	CP C36 1040	M. Ablikim *et al.*	(BES II Collab.)
ANASHIN	12	PL B711 280	V.V. Anashin *et al.*	(KEDR Collab.)
LEES	12E	PR D85 112009	J.P. Lees *et al.*	(BABAR Collab.)
LEES	12F	PR D86 012008	J.P. Lees *et al.*	(BABAR Collab.)
METREVELI	12	PR D85 092007	Z. Metreveli *et al.*	(NWES, FLOR, WAYN+)
GE	11	PR D84 032008	J.Y. Ge *et al.*	(CLEO Collab.)
ABLIKIM	10B	PRL 104 132002	M. Ablikim *et al.*	(BESIII Collab.)
ABLIKIM	10F	PRL 105 261801	M. Ablikim *et al.*	(BESIII Collab.)
ALEXANDER	10	PR D82 092002	J.P. Alexander *et al.*	(CLEO Collab.)
CRONIN-HEN...	10	PR D81 052002	D. Cronin-Hennessey *et al.*	(CLEO Collab.)
ADAMS	09	PR D80 051106	G.S. Adams *et al.*	(CLEO Collab.)
ARTUSO	09	PR D80 112003	M. Artuso *et al.*	(CLEO Collab.)
LIBBY	09	PR D80 072002	J. Libby *et al.*	(CLEO Collab.)
MITCHELL	09	PRL 102 011801	R.E. Mitchell *et al.*	(CLEO Collab.)
PEDLAR	09	PR D79 111101	T.K. Pedlar *et al.*	(CLEO Collab.)
ABLIKIM	08B	PL B659 74	M. Ablikim *et al.*	(BES Collab.)
ABLIKIM	08C	PL B659 789	M. Ablikim *et al.*	(BES Collab.)
DOBBS	08A	PRL 101 182003	S. Dobbs *et al.*	(CLEO Collab.)
MENDEZ	08	PR D78 011102	H. Mendez *et al.*	(CLEO Collab.)
PDG	08	PL B667 1	C. Amsler *et al.*	(PDG Collab.)
ABLIKIM	07C	PL B648 149	M. Ablikim *et al.*	(BES Collab.)
ABLIKIM	07D	PRL 99 011802	M. Ablikim *et al.*	(BES II Collab.)
ABLIKIM	07H	PR D76 092003	M. Ablikim *et al.*	(BES Collab.)
ANASHIN	07	JETPL 85 347	V.V. Anashin *et al.*	(KEDR Collab.)
		Translated from ZETFP 85 429.		
ANDREOTTI	07	PL B654 74	M. Andreotti *et al.*	(Femilab E835 Collab.)
AUBERT	07AK	PR D76 012008	B. Aubert *et al.*	(BABAR Collab.)
AUBERT	07AU	PR D76 092005	B. Aubert *et al.*	(BABAR Collab.)
Also		PR D77 119902E (errat.)	B. Aubert *et al.*	(BABAR Collab.)
AUBERT	07BD	PR D76 092006	B. Aubert *et al.*	(BABAR Collab.)
PDG	07	Unofficial 2007 WWW edition		(PDG Collab.)
PEDLAR	07	PR D75 011102	T.K. Pedlar *et al.*	(CLEO Collab.)
ABLIKIM	06G	PR D73 052004	M. Ablikim *et al.*	(BES Collab.)
ABLIKIM	06I	PR D74 012004	M. Ablikim *et al.*	(BES Collab.)
ABLIKIM	06L	PRL 97 121801	M. Ablikim *et al.*	(BES Collab.)
ABLIKIM	06R	PR D74 072001	M. Ablikim *et al.*	(BES Collab.)
ABLIKIM	06W	PR D74 112003	M. Ablikim *et al.*	(BES Collab.)
ADAM	06	PRL 96 082004	N.E. Adam *et al.*	(CLEO Collab.)
AUBERT	06B	PR D73 012005	B. Aubert *et al.*	(BABAR Collab.)
AUBERT	06D	PR D73 052003	B. Aubert *et al.*	(BABAR Collab.)
AUBERT,BE	06D	PR D74 091103	B. Aubert *et al.*	(BABAR Collab.)
DOBBS	06A	PR D74 011105	S. Dobbs *et al.*	(CLEO Collab.)
ABLIKIM	05E	PR D71 072006	M. Ablikim *et al.*	(BES Collab.)
ABLIKIM	05H	PR D72 012002	M. Ablikim *et al.*	(BES Collab.)
ABLIKIM	05I	PL B614 37	M. Ablikim *et al.*	(BES Collab.)
ABLIKIM	05J	PL B619 247	M. Ablikim *et al.*	(BES Collab.)
ABLIKIM	05O	PL B630 21	M. Ablikim *et al.*	(BES Collab.)
ADAM	05	PRL 94 012005	N.E. Adam *et al.*	(CLEO Collab.)
ADAM	05A	PRL 94 232002	N.E. Adam *et al.*	(CLEO Collab.)
ANDREOTTI	05	PR D71 032006	M. Andreotti *et al.*	(FNAL E835 Collab.)
AUBERT	05D	PR D71 052001	B. Aubert *et al.*	(BABAR Collab.)
BRIERE	05	PRL 95 062001	R.A. Briere *et al.*	(CLEO Collab.)
PEDLAR	05	PR D72 051108	T.K. Pedlar *et al.*	(CLEO Collab.)
ROSNER	05	PRL 95 102003	J.L. Rosner *et al.*	(CLEO Collab.)
ABLIKIM	04B	PR D70 012003	M. Ablikim *et al.*	(BES Collab.)
ABLIKIM	04K	PR D70 112003	M. Ablikim *et al.*	(BES Collab.)
ABLIKIM	04L	PR D70 112007	M. Ablikim *et al.*	(BES Collab.)
ATHAR	04	PR D70 112002	S.B. Athar *et al.*	(CLEO Collab.)
BAI	04B	PRL 92 052001	J.Z. Bai *et al.*	(BES Collab.)
BAI	04C	PR D69 072001	J.Z. Bai *et al.*	(BES Collab.)
BAI	04D	PL B589 7	J.Z. Bai *et al.*	(BES Collab.)
BAI	04G	PR D70 012004	J.Z. Bai *et al.*	(BES Collab.)
BAI	04I	PR D70 012006	J.Z. Bai *et al.*	(BES Collab.)
PDG	04	PL B592 1	S. Eidelman *et al.*	(PDG Collab.)
SETH	04	PR D69 097503	K.K. Seth	
AULCHENKO	03	PL B573 63	V.M. Aulchenko *et al.*	(KEDR Collab.)
BAI	03B	PR D67 052002	J.Z. Bai *et al.*	(BES Collab.)
BAI	03C	PR D67 032004	J.Z. Bai *et al.*	(BES Collab.)
AUBERT	02B	PR D65 031101	B. Aubert *et al.*	(BABAR Collab.)
BAI	02	PR D65 052004	J.Z. Bai *et al.*	(BES Collab.)
BAI	02B	PL B550 24	J.Z. Bai *et al.*	(BES Collab.)
BAI	02C	PRL 88 101802	J.Z. Bai *et al.*	(BES Collab.)
PDG	02	PR D66 010001	K. Hagiwara *et al.*	(PDG Collab.)
BAI	01	PR D63 032002	J.Z. Bai *et al.*	(BES Collab.)
AMBROGIANI	00A	PR D62 032004	M. Ambrogiani *et al.*	(FNAL E835 Collab.)
ARTAMONOV	00	PL B474 427	A.S. Artamonov *et al.*	
BAI	00	PRL 84 594	J.Z. Bai *et al.*	(BES Collab.)
BAI	99C	PRL 83 1918	J.Z. Bai *et al.*	(BES Collab.)
BAI	98E	PR D57 3854	J.Z. Bai *et al.*	(BES Collab.)
BAI	98F	PR D58 097101	J.Z. Bai *et al.*	(BES Collab.)
BAI	98J	PRL 81 5080	J.Z. Bai *et al.*	(BES Collab.)
ARMSTRONG	97	PR D55 1153	T.A. Armstrong *et al.*	(E760 Collab.)
GRIBUSHIN	96	PR D53 4723	A. Gribushin *et al.*	(E672 and E706 Collab.)
ARMSTRONG	93B	PR D47 772	T.A. Armstrong *et al.*	(FNAL E760 Collab.)
ALEXANDER	89	NP B320 45	J.P. Alexander *et al.*	(LBL, MICH, SLAC)
COHEN	87	RMP 59 1121	E.R. Cohen, B.N. Taylor	(RISC, NBS)
GAISER	86	PR D34 711	J. Gaiser *et al.*	(Crystal Ball Collab.)
KURAEV	85	SJNP 41 466	E.A. Kuraev, V.S. Fadin	(NOVO)
		Translated from YAF 41 733.		
FRANKLIN	83	PRL 51 963	M.E.B. Franklin *et al.*	(LBL, SLAC)
EDWARDS	82C	PRL 48 70	C. Edwards *et al.*	(CIT, HARV, PRIN+)
LEMOIGNE	82	PL 113B 509	Y. Lemoigne *et al.*	(SACL, LOIC, SHMP+)
HIMEL	80	PRL 44 920	T. Himel *et al.*	(LBL, SLAC)
OREGLIA	80	PRL 45 959	M.J. Oreglia *et al.*	(SLAC, CIT, HARV+)
SCHARRE	80	PL 97B 329	D.L. Scharre *et al.*	(SLAC, LBL)
ZHOLENTZ	80	PL 96B 214	A.A. Zholents *et al.*	(NOVO)
Also		SJNP 34 814	A.A. Zholents *et al.*	(NOVO)
		Translated from YAF 34 1471.		
BRANDELIK	79B	NP B160 426	R. Brandelik *et al.*	(DASP Collab.)
BRANDELIK	79C	ZPHY C1 233	R. Brandelik *et al.*	(DASP Collab.)
BARTEL	78B	PL 79B 492	W. Bartel *et al.*	(DESY, HEIDP)
TANENBAUM	78	PR D17 1731	W.M. Tanenbaum *et al.*	(SLAC, LBL)
BIDDICK	77	PRL 38 1324	C.J. Biddick *et al.*	(UCSD, UMD, PAVI+)
BRAUNSCH...	77	PL 67B 249	W. Braunschweig *et al.*	(DASP Collab.)
BURMESTER	77	PL 66B 395	J. Burmester *et al.*	(DESY, HAMB, SIEG+)
FELDMAN	77	PRPL 33C 285	G.J. Feldman, M.L. Perl	(LBL, SLAC)
YAMADA	77	Hamburg Conf. 69	S. Yamada	(DASP Collab.)
BARTEL	76	PL 64B 483	W. Bartel *et al.*	(DESY, HEIDP)
TANENBAUM	76	PRL 36 402	W.M. Tanenbaum *et al.*	(SLAC, LBL) IG
WHITAKER	76	PRL 37 1596	J.S. Whitaker *et al.*	(SLAC, LBL)
ABRAMS	75	Stanford Symp. 25	G.S. Abrams	(LBL)
ABRAMS	75B	PRL 34 1181	G.S. Abrams *et al.*	(LBL, SLAC)
BOYARSKI	75C	Palermo Conf. 54	A.M. Boyarski *et al.*	(SLAC, LBL)
HILGER	75	PRL 35 625	E. Hilger *et al.*	(STAN, PENN)
LIBERMAN	75	Stanford Symp. 55	A.D. Liberman	(STAN)
LUTH	75	PRL 35 1124	V. Luth *et al.*	(SLAC, LBL) JPC
WIIK	75	Stanford Symp. 69	B.H. Wiik	(DESY)

$\psi(3770)$

$I^G(J^{PC}) = 0^-(1^{--})$

$\psi(3770)$ MASS (MeV)

OUR FIT includes measurements of $m_{\psi(2S)}$, $m_{\psi(3770)}$, and $m_{\psi(3770)} - m_{\psi(2S)}$.

VALUE (MeV)	*EVTS*	*DOCUMENT ID*		*TECN*	*COMMENT*
3773.7±0.7 OUR FIT Error includes scale factor of 2.3.					
3778.1±0.7 OUR AVERAGE					
3778.1±0.7±0.6		[1] AAIJ	19M	LHCB	$pp \to D\overline{D}+$ anything
$3779.2^{+1.8+0.6}_{-1.7-0.8}$		[2] ANASHIN	12A	KEDR	$e^+e^- \to D\overline{D}$
3775.5±2.4±0.5	57	AUBERT	08B	BABR	$B \to D\overline{D}K$
3776 ±5 ±4	68	BRODZICKA	08	BELL	$B^+ \to D^0\overline{D}^0K^+$
3778.8±1.9±0.9		AUBERT	07BE	BABR	$e^+e^- \to D\overline{D}\gamma$
• • • We do not use the following data for averages, fits, limits, etc. • • •					
3778.8±0.3		[3] HANHART	24	RVUE	K-matrix formalism
3779.8±0.6		[4] SHAMOV	17	RVUE	$e^+e^- \to D\overline{D}$, hadrons
3772.0±1.9		[5,6] ABLIKIM	08D	BES2	$e^+e^- \to$ hadrons
3778.4±3.0±1.3	34	CHISTOV	04	BELL	Sup. by BRODZICKA 08

[1] Measured in prompt hadroproduction.
[2] Taking into account interference between the resonant and non-resonant $D\overline{D}$ production.
[3] Real part of pole location extracted using K-matrix formalism that includes two resonance poles, $\psi(2S)$ and $\psi(3770)$.
[4] From the joint analysis of the data on the $D\overline{D}$ and inclusive hadronic cross sections in the $\psi(3770)$ region from BaBar, Belle, BES-II, CLEO and KEDR.
[5] Reanalysis of data presented in BAI 02C. From a global fit over the center-of-mass energy region 3.7–5.0 GeV covering the $\psi(3770)$, $\psi(4040)$, $\psi(4160)$, and $\psi(4415)$ resonances. Phase angle fixed in the fit to $\delta = 0^\circ$.
[6] Interference between the resonant and non-resonant $D\overline{D}$ production not taken into account.

$m_{\psi(3770)} - m_{\psi(2S)}$

OUR FIT includes measurements of $m_{\psi(2S)}$, $m_{\psi(3770)}$, and $m_{\psi(3770)} - m_{\psi(2S)}$.

VALUE (MeV)	DOCUMENT ID		TECN	COMMENT
87.6±0.7 OUR FIT Error includes scale factor of 2.3.				
86.6±0.7 OUR AVERAGE Error includes scale factor of 2.0. See the ideogram below.				
86.9±0.4	[1] ABLIKIM	07E	BES2	$e^+e^- \to$ hadrons
86.7±0.7	ABLIKIM	06L	BES2	$e^+e^- \to$ hadrons
80 ±2	SCHINDLER	80	MRK2	e^+e^-
86 ±2	[2] BACINO	78	DLCO	e^+e^-
88 ±3	RAPIDIS	77	LGW	e^+e^-

[1] BES-II $\psi(2S)$ mass subtracted (see ABLIKIM 06L).
[2] SPEAR $\psi(2S)$ mass subtracted (see SCHINDLER 80).

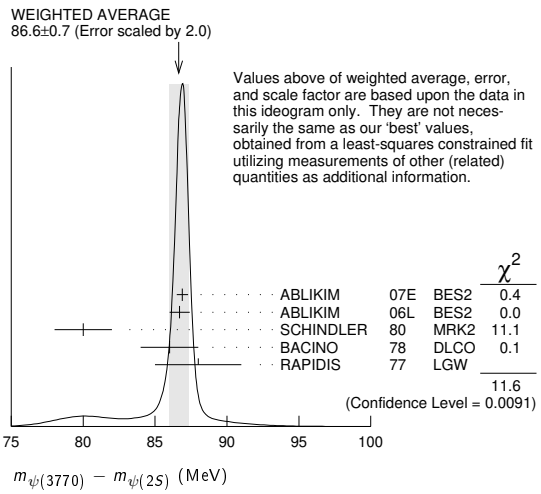

$\psi(3770)$ WIDTH

VALUE (MeV)	EVTS	DOCUMENT ID		TECN	COMMENT
27.2± 1.0 OUR FIT					
27.5± 0.9 OUR AVERAGE					
$24.9^{+4.6+0.5}_{-4.0-1.1}$		[1] ANASHIN	12A	KEDR	$e^+e^- \to D\overline{D}$
30.4± 8.5		[2,3] ABLIKIM	08D	BES2	$e^+e^- \to$ hadrons
27 ±10 ±5	68	BRODZICKA	08	BELL	$B^+ \to D^0\overline{D}^0K^+$
28.5± 1.2±0.2		[3] ABLIKIM	07E	BES2	$e^+e^- \to$ hadrons
23.5± 3.7±0.9		AUBERT	07BE	BABR	$e^+e^- \to D\overline{D}\gamma$
26.9± 2.4±0.3		[3] ABLIKIM	06L	BES2	$e^+e^- \to$ hadrons
24 ± 5		[3] SCHINDLER	80	MRK2	e^+e^-
24 ± 5		[3] BACINO	78	DLCO	e^+e^-
28 ± 5		[3] RAPIDIS	77	LGW	e^+e^-
• • • We do not use the following data for averages, fits, limits, etc. • • •					
25.0± 0.5		[4] HANHART	24	RVUE	K-matrix formalism
25.8± 1.3		[5] SHAMOV	17	RVUE	$e^+e^- \to D\overline{D}$, hadrons

[1] Taking into account interference between the resonant and non-resonant $D\overline{D}$ production.
[2] Reanalysis of data presented in BAI 02C. From a global fit over the center-of-mass energy region 3.7–5.0 GeV covering the $\psi(3770)$, $\psi(4040)$, $\psi(4160)$, and $\psi(4415)$ resonances. Phase angle fixed in the fit to $\delta = 0^\circ$.
[3] Interference between the resonant and non-resonant $D\overline{D}$ production not taken into account.
[4] $-2 \times$ imaginary part of pole location extracted using K-matrix formalism that includes two resonance poles, $\psi(2S)$ and $\psi(3770)$.
[5] From the joint analysis of the data on the $D\overline{D}$ and inclusive hadronic cross sections in the $\psi(3770)$ region from BaBar, Belle, BES-II, CLEO and KEDR.

$\psi(3770)$ DECAY MODES

	Mode	Fraction (Γ_i/Γ)	Scale factor/ Confidence level
Γ_1	$D\overline{D}$	$(93\ ^{+8}_{-9})$ %	S=2.0
Γ_2	$D^0\overline{D}^0$	$(52\ ^{+4}_{-5})$ %	S=2.0
Γ_3	D^+D^-	(41 ±4) %	S=2.0
Γ_4	$J/\psi X$	(5.0 ±2.2) $\times 10^{-3}$	
Γ_5	$J/\psi\pi^+\pi^-$	(1.93±0.28) $\times 10^{-3}$	
Γ_6	$J/\psi\pi^0\pi^0$	(8.0 ±3.0) $\times 10^{-4}$	
Γ_7	$J/\psi\eta$	(8.7 ±1.2) $\times 10^{-4}$	
Γ_8	$J/\psi\pi^0$	< 2.8 $\times 10^{-4}$	CL=90%
Γ_9	e^+e^-	(9.6 ±0.7) $\times 10^{-6}$	S=1.3
	Decays to light hadrons		
Γ_{10}	$b_1(1235)\pi$	< 1.4 $\times 10^{-5}$	CL=90%
Γ_{11}	$\phi\eta'$	< 2.3 $\times 10^{-5}$	CL=90%
Γ_{12}	$\omega\eta'$	< 4 $\times 10^{-4}$	CL=90%
Γ_{13}	$\rho^0\eta'$	< 6 $\times 10^{-4}$	CL=90%
Γ_{14}	$\phi\eta$	(3.1 ±0.7) $\times 10^{-4}$	
Γ_{15}	$\omega\eta$	< 1.4 $\times 10^{-5}$	CL=90%
Γ_{16}	$\rho^0\eta$	< 5 $\times 10^{-4}$	CL=90%
Γ_{17}	$\phi\pi^0$	< 3 $\times 10^{-5}$	CL=90%
Γ_{18}	$\omega\pi^0$	< 6 $\times 10^{-4}$	CL=90%
Γ_{19}	$\pi^+\pi^-\pi^0$	< 5 $\times 10^{-6}$	CL=90%
Γ_{20}	$\rho\pi$	< 5 $\times 10^{-6}$	CL=90%
Γ_{21}	K^+K^-	not seen	
Γ_{22}	$K^*(892)^+K^-$ + c.c.	< 1.4 $\times 10^{-5}$	CL=90%
Γ_{23}	$K^*(892)^0\overline{K}^0$ + c.c.	< 1.2 $\times 10^{-3}$	CL=90%
Γ_{24}	$K^0_SK^0_L$	$(2.6\ ^{+1.4}_{-1.6}) \times 10^{-5}$	
Γ_{25}	$2(\pi^+\pi^-)$	< 1.12 $\times 10^{-3}$	CL=90%
Γ_{26}	$2(\pi^+\pi^-)\pi^0$	< 1.06 $\times 10^{-3}$	CL=90%
Γ_{27}	$2(\pi^+\pi^-\pi^0)$	< 5.85 %	CL=90%
Γ_{28}	$\omega\pi^+\pi^-$	< 6.0 $\times 10^{-4}$	CL=90%
Γ_{29}	$3(\pi^+\pi^-)$	< 9.1 $\times 10^{-3}$	CL=90%
Γ_{30}	$3(\pi^+\pi^-)\pi^0$	< 1.37 %	CL=90%
Γ_{31}	$3(\pi^+\pi^-)2\pi^0$	< 11.74 %	CL=90%
Γ_{32}	$\eta\pi^+\pi^-$	< 1.24 $\times 10^{-3}$	CL=90%
Γ_{33}	$\pi^+\pi^-2\pi^0$	< 8.9 $\times 10^{-3}$	CL=90%
Γ_{34}	$\rho^0\pi^+\pi^-$	< 6.9 $\times 10^{-3}$	CL=90%
Γ_{35}	$\eta 3\pi$	< 1.34 $\times 10^{-3}$	CL=90%
Γ_{36}	$\eta 2(\pi^+\pi^-)$	< 2.43 %	CL=90%
Γ_{37}	$\eta\rho^0\pi^+\pi^-$	< 1.45 %	CL=90%
Γ_{38}	$\eta' 3\pi$	< 2.44 $\times 10^{-3}$	CL=90%
Γ_{39}	$K^+K^-\pi^+\pi^-$	< 9.0 $\times 10^{-4}$	CL=90%
Γ_{40}	$\phi\pi^+\pi^-$	< 4.1 $\times 10^{-4}$	CL=90%
Γ_{41}	$K^+K^-2\pi^0$	< 4.2 $\times 10^{-3}$	CL=90%
Γ_{42}	$4(\pi^+\pi^-)$	< 1.67 %	CL=90%
Γ_{43}	$4(\pi^+\pi^-)\pi^0$	< 3.06 %	CL=90%
Γ_{44}	$\phi f_0(980)$	< 4.5 $\times 10^{-4}$	CL=90%
Γ_{45}	$K^+K^-\pi^+\pi^-\pi^0$	< 2.36 $\times 10^{-3}$	CL=90%
Γ_{46}	$K^+K^-\rho^0\pi^0$	< 8 $\times 10^{-4}$	CL=90%
Γ_{47}	$K^+K^-\rho^+\pi^-$	< 1.46 %	CL=90%
Γ_{48}	ωK^+K^-	< 3.4 $\times 10^{-4}$	CL=90%
Γ_{49}	$\phi\pi^+\pi^-\pi^0$	< 3.8 $\times 10^{-3}$	CL=90%
Γ_{50}	$K^{*0}K^-\pi^+\pi^0$ + c.c.	< 1.62 %	CL=90%
Γ_{51}	$K^{*+}K^-\pi^+\pi^-$ + c.c.	< 3.23 %	CL=90%
Γ_{52}	$K^+K^-\pi^+\pi^-2\pi^0$	< 2.67 %	CL=90%
Γ_{53}	$K^+K^-2(\pi^+\pi^-)$	< 1.03 %	CL=90%
Γ_{54}	$K^+K^-2(\pi^+\pi^-)\pi^0$	< 3.60 %	CL=90%
Γ_{55}	ηK^+K^-	< 4.1 $\times 10^{-4}$	CL=90%
Γ_{56}	$\eta K^+K^-\pi^+\pi^-$	< 1.24 %	CL=90%
Γ_{57}	$\rho^0K^+K^-$	< 5.0 $\times 10^{-3}$	CL=90%
Γ_{58}	$2(K^+K^-)$	< 6.0 $\times 10^{-4}$	CL=90%
Γ_{59}	ϕK^+K^-	< 7.5 $\times 10^{-4}$	CL=90%
Γ_{60}	$2(K^+K^-)\pi^0$	< 2.9 $\times 10^{-4}$	CL=90%
Γ_{61}	$2(K^+K^-)\pi^+\pi^-$	< 3.2 $\times 10^{-3}$	CL=90%
Γ_{62}	$K^0_SK^-\pi^+$	< 3.2 $\times 10^{-3}$	CL=90%
Γ_{63}	$K^0_SK^-\pi^+\pi^0$	< 1.33 %	CL=90%
Γ_{64}	$K^0_SK^-\rho^+$	< 6.6 $\times 10^{-3}$	CL=90%
Γ_{65}	$K^0_SK^-2\pi^+\pi^-$	< 8.7 $\times 10^{-3}$	CL=90%
Γ_{66}	$K^0_SK^-\pi^+\rho^0$	< 1.6 %	CL=90%
Γ_{67}	$K^0_SK^-\pi^+\eta$	< 1.3 %	CL=90%
Γ_{68}	$K^0_SK^-2\pi^+\pi^-\pi^0$	< 4.18 %	CL=90%

Int. J. Mod. Phys. A 2026.41. Downloaded from www.worldscientific.com
by UNIVERSITY OF CALIFORNIA @ BERKELEY on 09/16/26. Re-use and distribution is strictly not permitted, except for Open Access articles.

Γ_{69}	$K^0_S K^- 2\pi^+ \pi^- \eta$	<	4.8	%	CL=90%
Γ_{70}	$K^0_S K^- \pi^+ 2(\pi^+ \pi^-)$	<	1.22	%	CL=90%
Γ_{71}	$K^0_S K^- \pi^+ 2\pi^0$	<	2.65	%	CL=90%
Γ_{72}	$K^0_S K^- K^+ K^- \pi^+$	<	4.9	$\times 10^{-3}$	CL=90%
Γ_{73}	$K^0_S K^- K^+ K^- \pi^+ \pi^0$	<	3.0	%	CL=90%
Γ_{74}	$K^0_S K^- K^+ K^- \pi^+ \eta$	<	2.2	%	CL=90%
Γ_{75}	$K^{*0} K^- \pi^+ +$ c.c.	<	9.7	$\times 10^{-3}$	CL=90%
Γ_{76}	$p\overline{p}$		not seen		
Γ_{77}	$p\overline{p}\pi^0$	<	4	$\times 10^{-5}$	CL=90%
Γ_{78}	$p\overline{p}\pi^+ \pi^-$	<	5.8	$\times 10^{-4}$	CL=90%
Γ_{79}	$\Lambda\overline{\Lambda}$	<	1.2	$\times 10^{-4}$	CL=90%
Γ_{80}	$p\overline{p}\pi^+ \pi^- \pi^0$	<	1.85	$\times 10^{-3}$	CL=90%
Γ_{81}	$\omega p\overline{p}$	<	2.9	$\times 10^{-4}$	CL=90%
Γ_{82}	$\Lambda\overline{\Lambda}\pi^0$	<	7	$\times 10^{-5}$	CL=90%
Γ_{83}	$p\overline{p}2(\pi^+ \pi^-)$	<	2.6	$\times 10^{-3}$	CL=90%
Γ_{84}	$\eta p\overline{p}$	<	5.4	$\times 10^{-4}$	CL=90%
Γ_{85}	$\eta p\overline{p}\pi^+ \pi^-$	<	3.3	$\times 10^{-3}$	CL=90%
Γ_{86}	$\rho^0 p\overline{p}$	<	1.7	$\times 10^{-3}$	CL=90%
Γ_{87}	$p\overline{p}K^+ K^-$	<	3.2	$\times 10^{-4}$	CL=90%
Γ_{88}	$\eta p\overline{p}K^+ K^-$	<	6.9	$\times 10^{-3}$	CL=90%
Γ_{89}	$\pi^0 p\overline{p}K^+ K^-$	<	1.2	$\times 10^{-3}$	CL=90%
Γ_{90}	$\phi p\overline{p}$	<	1.3	$\times 10^{-4}$	CL=90%
Γ_{91}	$\Lambda\overline{\Lambda}\pi^+ \pi^-$	<	2.5	$\times 10^{-4}$	CL=90%
Γ_{92}	$\Lambda\overline{p}K^+$	<	2.8	$\times 10^{-4}$	CL=90%
Γ_{93}	$\Lambda\overline{p}K^+ \pi^+ \pi^-$	<	6.3	$\times 10^{-4}$	CL=90%
Γ_{94}	$\Lambda\overline{\Lambda}\eta$	<	1.9	$\times 10^{-4}$	CL=90%
Γ_{95}	$\Sigma^+\overline{\Sigma}^-$	<	1.0	$\times 10^{-4}$	CL=90%
Γ_{96}	$\Sigma^0\overline{\Sigma}^0$	<	4	$\times 10^{-5}$	CL=90%
Γ_{97}	$\Xi^0\overline{\Xi}^0$	<	3.4	$\times 10^{-4}$	CL=90%
Γ_{98}	$\Xi^-\overline{\Xi}^+$	(	1.4 ±0.4)	$\times 10^{-4}$	
Γ_{99}	$\Lambda\overline{\Xi}^+ K^- +$ c.c.	<	1.0	$\times 10^{-4}$	CL=90%
Γ_{100}	$\Sigma^0\overline{\Xi}^+ K^- +$ c.c.	<	3.4	$\times 10^{-4}$	CL=90%
Γ_{101}	$pK^- K^-\overline{\Xi}^+ +$ c.c.	<	7	$\times 10^{-5}$	CL=90%

Radiative decays

Γ_{102}	$\gamma\chi_{c2}$	<	6.4	$\times 10^{-4}$	CL=90%
Γ_{103}	$\gamma\chi_{c1}$	(	2.49±0.23)	$\times 10^{-3}$	
Γ_{104}	$\gamma\chi_{c0}$	(	7.1 ±0.6)	$\times 10^{-3}$	
Γ_{105}	$\gamma\eta_c$	<	8	$\times 10^{-4}$	CL=90%
Γ_{106}	$\gamma\eta_c(2S)$	<	9	$\times 10^{-4}$	CL=90%
Γ_{107}	$\gamma\eta'$	<	1.8	$\times 10^{-4}$	CL=90%
Γ_{108}	$\gamma\eta$	<	1.5	$\times 10^{-4}$	CL=90%
Γ_{109}	$\gamma\pi^0$	<	2	$\times 10^{-4}$	CL=90%

FIT INFORMATION

An overall fit to the total width, a partial width, and 3 branching ratios uses 23 measurements to determine 4 parameters. The overall fit has a $\chi^2 = 20.1$ for 19 degrees of freedom.

The following *off-diagonal* array elements are the correlation coefficients $\langle \delta p_i \delta p_j \rangle / (\delta p_i \cdot \delta p_j)$, in percent, from the fit to parameters p_i, including the branching fractions, $x_i \equiv \Gamma_i/\Gamma_{total}$.

	x_2	x_3	x_9
x_3	99		
x_9	0	0	
Γ	0	0	−44

	Mode	Rate (MeV)	Scale factor
Γ_2	$D^0\overline{D}^0$	14.0 ±1.4	1.8
Γ_3	$D^+ D^-$	11.2 ±1.1	1.7
Γ_9	$e^+ e^-$	(2.62±0.18) $\times 10^{-4}$	1.4

$\psi(3770)$ PARTIAL WIDTHS

$\Gamma(e^+ e^-)$ — Γ_9

VALUE (keV)	EVTS	DOCUMENT ID		TECN	COMMENT
0.262±0.018 OUR FIT	Error includes scale factor of 1.4.				
0.256±0.016 OUR AVERAGE	Error includes scale factor of 1.2.				
$0.154^{+0.079}_{-0.058}{}^{+0.021}_{-0.027}$		[1,2] ANASHIN	12A	KEDR	$e^+ e^- \to D\overline{D}$
0.22 ±0.05		[3,4] ABLIKIM	08D	BES2	$e^+ e^- \to$ hadrons
0.277±0.011±0.013		[4] ABLIKIM	07E	BES2	$e^+ e^- \to$ hadrons
$0.203 \pm 0.003^{+0.041}_{-0.027}$	1.4M	[4,5] BESSON	06	CLEO	$e^+ e^- \to$ hadrons
0.276±0.050		[4] SCHINDLER	80	MRK2	$e^+ e^-$
0.18 ±0.06		[4] BACINO	78	DLCO	$e^+ e^-$
• • • We do not use the following data for averages, fits, limits, etc. • • •					
0.196±0.018		[6] SHAMOV	17	RVUE	$e^+ e^- \to D\overline{D}$, hadrons
$0.414^{+0.072}_{-0.080}{}^{+0.093}_{-0.028}$		[2,7] ANASHIN	12A	KEDR	$e^+ e^- \to D\overline{D}$
0.37 ±0.09		[8] RAPIDIS	77	LGW	$e^+ e^-$

[1] Solution I of the two solutions.
[2] Taking into account interference between the resonant and non-resonant $D\overline{D}$ production.
[3] Reanalysis of data presented in BAI 02C. From a global fit over the center-of-mass energy region 3.7–5.0 GeV covering the $\psi(3770)$, $\psi(4040)$, $\psi(4160)$, and $\psi(4415)$ resonances. Phase angle fixed in the fit to $\delta = 0^\circ$.
[4] Interference between the resonant and non-resonant $D\overline{D}$ production not taken into account.
[5] BESSON 06 (as corrected in BESSON 10) measure $\sigma(e^+ e^- \to \psi(3770) \to$ hadrons) $= 6.36 \pm 0.08^{+0.41}_{-0.30}$ nb at $\sqrt{s} = 3773 \pm 1$ MeV, and obtain Γ_{ee} from the Born-level cross section calculated using $\psi(3770)$ mass and width from our 2004 edition, PDG 04.
[6] From the joint analysis of the data on the $D\overline{D}$ and inclusive hadronic cross sections in the $\psi(3770)$ region from BaBar, Belle, BES-II, CLEO and KEDR.
[7] Solution II of the two solutions.
[8] See also $\Gamma(e^+ e^-)/\Gamma_{total}$ below.

$\psi(3770)$ $\Gamma(i) \times \Gamma(e^+ e^-)/\Gamma(total)$

$\Gamma(\Sigma^+\overline{\Sigma}^-) \times \Gamma(e^+ e^-)/\Gamma_{total}$ — $\Gamma_{95}\Gamma_9/\Gamma$

VALUE (eV)	CL%	DOCUMENT ID		TECN	COMMENT
<101.5 × 10⁻³	90	[1] ABLIKIM	24AH	BES3	$e^+ e^- \to \Sigma^+\overline{\Sigma}^-$

[1] Interference effect between resonance and continuum amplitudes is considered. Two solutions from the fit.

$\Gamma(\Sigma^0\overline{\Sigma}^0) \times \Gamma(e^+ e^-)/\Gamma_{total}$ — $\Gamma_{96}\Gamma_9/\Gamma$

VALUE (eV)	CL%	DOCUMENT ID		TECN	COMMENT
<29.2 × 10⁻³	90	[1] ABLIKIM	25U	BES3	$e^+ e^- \to \Sigma^0\overline{\Sigma}^0$

[1] Interference effect between resonance and continuum amplitudes is considered. Upper limit is for the larger of the two solutions from the fit.

$\Gamma(\Xi^0\overline{\Xi}^0) \times \Gamma(e^+ e^-)/\Gamma_{total}$ — $\Gamma_{97}\Gamma_9/\Gamma$

VALUE (eV)	CL%	DOCUMENT ID		TECN	COMMENT
<89.0 × 10⁻³	90	[1] ABLIKIM	24CD	BES3	$e^+ e^- \to \psi(3770)$

[1] From a fit to $e^+ e^- \to \Xi^0\overline{\Xi}^0$ cross sections.

$\Gamma(\Xi^-\overline{\Xi}^+) \times \Gamma(e^+ e^-)/\Gamma_{total}$ — $\Gamma_{98}\Gamma_9/\Gamma$

VALUE (eV)	DOCUMENT ID		TECN	COMMENT
(3.55±0.92) × 10⁻²	[1] ABLIKIM	23BK	BES3	$e^+ e^- \to \psi(3770)$

[1] From a fit to $e^+ e^- \to \Xi^-\overline{\Xi}^+$ cross sections. Signal significance is 4.5σ.

$\Gamma(\Lambda\overline{\Xi}^+ K^- +$ c.c.$) \times \Gamma(e^+ e^-)/\Gamma_{total}$ — $\Gamma_{99}\Gamma_9/\Gamma$

VALUE (eV)	CL%	DOCUMENT ID		TECN	COMMENT
<25.0 × 10⁻³	90	[1] ABLIKIM	24AL	BES3	$e^+ e^- \to \Lambda\overline{\Xi}^+ K^-$ + c.c.

[1] A fit to the Born cross section of $e^+ e^- \to \Lambda\overline{\Xi}^+ K^-$ + c.c. including interference with the continuum. Two solutions from the fit.

$\Gamma(\Sigma^0\overline{\Xi}^+ K^-$ + c.c.$) \times \Gamma(e^+ e^-)/\Gamma_{total}$ — $\Gamma_{100}\Gamma_9/\Gamma$

VALUE (eV)	CL%	DOCUMENT ID		TECN	COMMENT
<89.5 × 10⁻³	90	[1] ABLIKIM	24AL	BES3	$e^+ e^- \to \Sigma^0\overline{\Xi}^+ K^-$ + c.c.

[1] A fit to the Born cross section of $e^+ e^- \to \Sigma^0\overline{\Xi}^+ K^-$ + c.c. including interference with the continuum. Two solutions from the fit.

$\Gamma(e^+ e^-) \times \Gamma(pK^- K^-\overline{\Xi}^+$ + c.c.$)/\Gamma_{total}$ — $\Gamma_9\Gamma_{101}/\Gamma$

VALUE (eV)	CL%	DOCUMENT ID		TECN	COMMENT
<19.2 × 10⁻³	90	ABLIKIM	25CF	BES3	$e^+ e^- \to pK^- K^-\overline{\Xi}^+$ + c.c.

$\psi(3770)$ BRANCHING RATIOS

$\Gamma(D\overline{D})/\Gamma_{total}$ — $\Gamma_1/\Gamma = (\Gamma_2+\Gamma_3)/\Gamma$

VALUE	EVTS	DOCUMENT ID		TECN	COMMENT
$0.93^{+0.08}_{-0.09}$ OUR FIT	Error includes scale factor of 2.0.				
$0.93^{+0.08}_{-0.09}$ OUR AVERAGE	Error includes scale factor of 2.1.				
0.849±0.056±0.018		[1] ABLIKIM	08B	BES2	$e^+ e^- \to$ non-$D\overline{D}$
$1.033 \pm 0.014^{+0.048}_{-0.066}$	1.427M	[2] BESSON	06	CLEO	$e^+ e^- \to$ hadrons
• • • We do not use the following data for averages, fits, limits, etc. • • •					
0.836±0.049		[3] SHAMOV	17	RVUE	$e^+ e^- \to D\overline{D}$, hadrons
0.866±0.050±0.036		[4,5] ABLIKIM	07K	BES2	$e^+ e^- \to$ non-$D\overline{D}$
0.836±0.073±0.042		[5] ABLIKIM	06L	BES2	$e^+ e^- \to D\overline{D}$
0.855±0.017±0.058		[5,6] ABLIKIM	06N	BES2	$e^+ e^- \to D\overline{D}$

[1] Neglecting interference.
[2] Obtained by comparing a measurement of the total cross section (corrected in BESSON 10) with that of $D\overline{D}$ reported by CLEO in DOBBS 07.
[3] From the joint analysis of the data on the $D\overline{D}$ and inclusive hadronic cross sections in the $\psi(3770)$ region from BaBar, Belle, BES-II, CLEO and KEDR.
[4] Using $\sigma^{obs} = 7.07 \pm 0.58$ nb and neglecting interference.
[5] Not independent of ABLIKIM 08B.
[6] From a measurement of $\sigma(e^+ e^- \to D\overline{D})$ at $\sqrt{s} = 3773$ MeV, using the $\psi(3770)$ resonance parameters measured by ABLIKIM 06L.

Int. J. Mod. Phys. A 2026.41. Downloaded from www.worldscientific.com
by LIFORNIA @ BERKELEY on 09/16/26. Re-use and distribution is strictly not permitted, except for Open Access articles.

Int. J. Mod. Phys. A 2026.41. Downloaded from www.worldscientific.com
by UNIVERSITY OF CALIFORNIA @ BERKELEY on 09/16/26. Re-use and distribution is strictly not permitted, except for Open Access articles.

$\Gamma(D^0\overline{D}^0)/\Gamma_{total}$ — Γ_2/Γ

VALUE	DOCUMENT ID		TECN	COMMENT
$0.52\ ^{+0.04}_{-0.05}$ OUR FIT Error includes scale factor of 2.0.				
• • • We do not use the following data for averages, fits, limits, etc. • • •				
$0.467\pm0.047\pm0.023$	ABLIKIM	06L	BES2	$e^+e^-\to D^0\overline{D}^0$
$0.499\pm0.013\pm0.038$	[1] ABLIKIM	06N	BES2	$e^+e^-\to D^0\overline{D}^0$

[1] From a measurement of $\sigma(e^+e^-\to D\overline{D})$ at $\sqrt{s}$ = 3773 MeV, using the $\psi(3770)$ resonance parameters measured by ABLIKIM 06L.

$\Gamma(D^+D^-)/\Gamma_{total}$ — Γ_3/Γ

VALUE	DOCUMENT ID		TECN	COMMENT
$0.41\ \pm0.04$ OUR FIT Error includes scale factor of 2.0.				
• • • We do not use the following data for averages, fits, limits, etc. • • •				
$0.369\pm0.037\pm0.028$	ABLIKIM	06L	BES2	$e^+e^-\to D^+D^-$
$0.357\pm0.011\pm0.034$	[1] ABLIKIM	06N	BES2	$e^+e^-\to D^+D^-$

[1] From a measurement of $\sigma(e^+e^-\to D\overline{D})$ at $\sqrt{s}$ = 3773 MeV, using the $\psi(3770)$ resonance parameters measured by ABLIKIM 06L.

$\Gamma(D^0\overline{D}^0)/\Gamma(D^+D^-)$ — Γ_2/Γ_3

VALUE	EVTS	DOCUMENT ID		TECN	COMMENT
1.253 ± 0.016 OUR FIT					
1.253 ± 0.016 OUR AVERAGE					
$1.252\pm0.009\pm0.013$	5.3M	BONVICINI	14	CLEO	$e^+e^-\to D\overline{D}$
$1.39\ \pm0.31\ \pm0.12$		PAKHLOVA	08	BELL	$10.6\ e^+e^-\to D\overline{D}\gamma$
$1.78\ \pm0.33\ \pm0.24$		AUBERT	07BE	BABR	$e^+e^-\to D\overline{D}\gamma$
$1.27\ \pm0.12\ \pm0.08$		ABLIKIM	06L	BES2	$e^+e^-\to D\overline{D}$
$2.43\ \pm1.50\ \pm0.43$	34	[1] CHISTOV	04	BELL	$B^+\to\psi(3770)K^+$
• • • We do not use the following data for averages, fits, limits, etc. • • •					
$1.258\pm0.016\pm0.014$		[2] DOBBS	07	CLEO	$e^+e^-\to D\overline{D}$

[1] See ADLER 88C for older measurements of this quantity.
[2] Superseded by BONVICINI 14.

$\Gamma(J/\psi X)/\Gamma_{total}$ — Γ_4/Γ

VALUE (%)	DOCUMENT ID		TECN	COMMENT
$0.5\pm0.2\pm0.1$	[1] ABLIKIM	21Z	BES3	$e^+e^-\to\ell^+\ell^-X$

[1] From a fit to the $e^+e^-\to J/\psi X$ cross section between 3.645 and 3.891 GeV, with $\psi(2S)$ and $\psi(3770)$ masses, total widths and leptonic widths fixed to the values from the PDG 20. An alternative fit with an improved χ^2, corresponding to a significance of 5.3 σ, uses an additional resonance with a mass of 3766.2 $\pm$ 3.8 $\pm$ 0.4 MeV/c^2, a total width of 22.2 $\pm$ 5.9 $\pm$ 1.4 MeV, and Γ(e e)·B($J/\psi X$) = 79.4 $\pm$ 85.5 $\pm$ 11.7 eV, possibly compatible with the results of ABLIKIM 08H.

$\Gamma(J/\psi\pi^+\pi^-)/\Gamma_{total}$ — Γ_5/Γ

VALUE (units 10^{-3})	EVTS	DOCUMENT ID		TECN	COMMENT
1.93 ± 0.28 OUR AVERAGE					
$1.89\pm0.20\pm0.20$	231 ± 33	ADAM	06	CLEO	$e^+e^-\to\psi(3770)$
$3.4\ \pm1.4\ \pm0.9$	17.8 ± 4.8	BAI	05	BES2	$e^+e^-\to\psi(3770)$

$\Gamma(J/\psi\pi^0\pi^0)/\Gamma_{total}$ — Γ_6/Γ

VALUE (units 10^{-2})	EVTS	DOCUMENT ID		TECN	COMMENT
$0.080\pm0.025\pm0.016$	39 ± 14	ADAM	06	CLEO	$e^+e^-\to\psi(3770)$

$\Gamma(J/\psi\eta)/\Gamma_{total}$ — Γ_7/Γ

VALUE (units 10^{-4})	EVTS	DOCUMENT ID		TECN	COMMENT
8.7 ± 1.2 OUR AVERAGE					
$8.7\pm1.0\pm0.8$	232 ± 23	[1] ABLIKIM	23V	BES3	$e^+e^-\to\psi(3770)$
$8.7\pm3.3\pm2.2$	22 ± 10	ADAM	06	CLEO	$e^+e^-\to\psi(3770)$

[1] Incoherent fit. Alternate fits that include interference with background yield results between $(11.2\pm5.8\pm1.1)\times10^{-4}$ and $(11.6\pm6.0\pm1.1)\times10^{-4}$.

$\Gamma(J/\psi\pi^0)/\Gamma_{total}$ — Γ_8/Γ

VALUE (units 10^{-5})	CL%	EVTS	DOCUMENT ID		TECN	COMMENT
<28	90	<10	ADAM	06	CLEO	$e^+e^-\to\psi(3770)$

$\Gamma(e^+e^-)/\Gamma_{total}$ — Γ_9/Γ

VALUE (units 10^{-5})	DOCUMENT ID		TECN	COMMENT
0.96 ± 0.07 OUR FIT Error includes scale factor of 1.3.				
$1.3\ \pm0.2$	RAPIDIS	77	LGW	e^+e^-

DECAYS TO LIGHT HADRONS

$\Gamma(b_1(1235)\pi)/\Gamma_{total}$ — Γ_{10}/Γ

VALUE (units 10^{-5})	CL%	DOCUMENT ID		TECN	COMMENT
<1.4	90	[1] ADAMS	06	CLEO	$e^+e^-\to\psi(3770)$

[1] Comparing cross sections at $\sqrt{s}$ = 3.773 GeV and $\sqrt{s}$ = 3.671 GeV, neglecting interference, and using $\sigma(\psi(3770)\to D\overline{D})$ = 6.39 $\pm$ 0.20 nb.

$\Gamma(\phi\eta')/\Gamma_{total}$ — Γ_{11}/Γ

VALUE	CL%	DOCUMENT ID		TECN	COMMENT
$<2.3\times10^{-5}$	90	[1] ABLIKIM	23BC	BES3	$e^+e^-\to\psi(3770)$
• • • We do not use the following data for averages, fits, limits, etc. • • •					
$<7\ \times10^{-4}$	90	[2] ADAMS	06	CLEO	$e^+e^-\to\psi(3770)$

[1] ABLIKIM 23BC fit to $e^+e^-\to\phi\eta'$ cross sections between 3.508 and 4.951 GeV considering interference between continuum and $\psi(3770)$ amplitudes.
[2] ADAMS 06 compare cross sections at $\sqrt{s}$ = 3.773 GeV and $\sqrt{s}$ = 3.671 GeV, neglecting interference, and using $\sigma(\psi(3770)\to D\overline{D})$ = 6.39 $\pm$ 0.20 nb.

$\Gamma(\omega\eta')/\Gamma_{total}$ — Γ_{12}/Γ

VALUE (units 10^{-4})	CL%	DOCUMENT ID		TECN	COMMENT
<4	90	[1] ADAMS	06	CLEO	$e^+e^-\to\psi(3770)$

[1] Comparing cross sections at $\sqrt{s}$ = 3.773 GeV and $\sqrt{s}$ = 3.671 GeV, neglecting interference, and using $\sigma(\psi(3770)\to D\overline{D})$ = 6.39 $\pm$ 0.20 nb.

$\Gamma(\rho^0\eta')/\Gamma_{total}$ — Γ_{13}/Γ

VALUE (units 10^{-4})	CL%	DOCUMENT ID		TECN	COMMENT
<6	90	[1] ADAMS	06	CLEO	$e^+e^-\to\psi(3770)$

[1] Comparing cross sections at $\sqrt{s}$ = 3.773 GeV and $\sqrt{s}$ = 3.671 GeV, neglecting interference, and using $\sigma(\psi(3770)\to D\overline{D})$ = 6.39 $\pm$ 0.20 nb.

$\Gamma(\phi\eta)/\Gamma_{total}$ — Γ_{14}/Γ

VALUE (units 10^{-4})	CL%	DOCUMENT ID		TECN	COMMENT
$3.1\pm0.6\pm0.3$		[1] ADAMS	06	CLEO	3.773 $e^+e^-\to\phi\eta$
• • • We do not use the following data for averages, fits, limits, etc. • • •					
<19	90	[2] ABLIKIM	07B	BES2	$e^+e^-\to\psi(3770)$

[1] Comparing cross sections at $\sqrt{s}$ = 3.773 GeV and $\sqrt{s}$ = 3.671 GeV, neglecting interference, and using $\sigma(\psi(3770)\to D\overline{D})$ = 6.39 $\pm$ 0.20 nb.
[2] Assuming that interference effects between resonance and continuum can be neglected and using $\sigma^{obs}(e^+e^-\to\psi(3770))$ = 7.15 $\pm$ 0.38 nb.

$\Gamma(\omega\eta)/\Gamma_{total}$ — Γ_{15}/Γ

VALUE (units 10^{-5})	CL%	DOCUMENT ID		TECN	COMMENT
<1.4	90	[1] ADAMS	06	CLEO	$e^+e^-\to\psi(3770)$

[1] Comparing cross sections at $\sqrt{s}$ = 3.773 GeV and $\sqrt{s}$ = 3.671 GeV, neglecting interference, and using $\sigma(\psi(3770)\to D\overline{D})$ = 6.39 $\pm$ 0.20 nb.

$\Gamma(\rho^0\eta)/\Gamma_{total}$ — Γ_{16}/Γ

VALUE (units 10^{-4})	CL%	DOCUMENT ID		TECN	COMMENT
<5	90	[1] ADAMS	06	CLEO	$e^+e^-\to\psi(3770)$

[1] Comparing cross sections at $\sqrt{s}$ = 3.773 GeV and $\sqrt{s}$ = 3.671 GeV, neglecting interference, and using $\sigma(\psi(3770)\to D\overline{D})$ = 6.39 $\pm$ 0.20 nb.

$\Gamma(\phi\pi^0)/\Gamma_{total}$ — Γ_{17}/Γ

VALUE (units 10^{-5})	CL%	DOCUMENT ID		TECN	COMMENT
< 3	90	[1] ADAMS	06	CLEO	$e^+e^-\to\psi(3770)$
• • • We do not use the following data for averages, fits, limits, etc. • • •					
<50	90	[2] ABLIKIM	07B	BES2	$e^+e^-\to\psi(3770)$

[1] Comparing cross sections at $\sqrt{s}$ = 3.773 GeV and $\sqrt{s}$ = 3.671 GeV, neglecting interference, and using $\sigma(\psi(3770)\to D\overline{D})$ = 6.39 $\pm$ 0.20 nb.
[2] Assuming that interference effects between resonance and continuum can be neglected and using $\sigma^{obs}(e^+e^-\to\psi(3770))$ = 7.15 $\pm$ 0.38 nb.

$\Gamma(\omega\pi^0)/\Gamma_{total}$ — Γ_{18}/Γ

VALUE (units 10^{-4})	CL%	DOCUMENT ID		TECN	COMMENT
<6	90	[1] ADAMS	06	CLEO	$e^+e^-\to\psi(3770)$

[1] Comparing cross sections at $\sqrt{s}$ = 3.773 GeV and $\sqrt{s}$ = 3.671 GeV, neglecting interference, and using $\sigma(\psi(3770)\to D\overline{D})$ = 6.39 $\pm$ 0.20 nb.

$\Gamma(\pi^+\pi^-\pi^0)/\Gamma_{total}$ — Γ_{19}/Γ

VALUE (units 10^{-6})	CL%	DOCUMENT ID		TECN	COMMENT
<5	90	[1,2] ADAMS	06	CLEO	$e^+e^-\to\psi(3770)$

[1] Data suggest possible destructive interference with continuum.
[2] Comparing cross sections at $\sqrt{s}$ = 3.773 GeV and $\sqrt{s}$ = 3.671 GeV, neglecting interference, and using $\sigma(\psi(3770)\to D\overline{D})$ = 6.39 $\pm$ 0.20 nb.

$\Gamma(\rho\pi)/\Gamma_{total}$ — Γ_{20}/Γ

VALUE (units 10^{-6})	CL%	DOCUMENT ID		TECN	COMMENT
<5	90	[1,2] ADAMS	06	CLEO	$e^+e^-\to\psi(3770)$

[1] Comparing cross sections at $\sqrt{s}$ = 3.773 GeV and $\sqrt{s}$ = 3.671 GeV, neglecting interference, and using $\sigma(\psi(3770)\to D\overline{D})$ = 6.39 $\pm$ 0.20 nb.
[2] Data suggest possible destructive interference with continuum.

$\Gamma(K^+K^-)/\Gamma_{total}$ — Γ_{21}/Γ

VALUE	DOCUMENT ID		TECN	COMMENT
• • • We do not use the following data for averages, fits, limits, etc. • • •				
$\sim10^{-5}$	[1] DRUZHININ	15	RVUE	$e^+e^-\to\psi(3770)$

[1] DRUZHININ 15 uses BABAR and CLEO data takitaking into account interference of the processes $e^+e^-\to K^+K^-$ and $e^+e^-\to K^0_S K^0_L$.

$\Gamma(K^*(892)^+K^-+\text{c.c.})/\Gamma_{total}$ — Γ_{22}/Γ

VALUE (units 10^{-5})	CL%	DOCUMENT ID		TECN	COMMENT
<1.4	90	[1] ADAMS	06	CLEO	$e^+e^-\to\psi(3770)$

[1] Comparing cross sections at $\sqrt{s}$ = 3.773 GeV and $\sqrt{s}$ = 3.671 GeV, neglecting interference, and using $\sigma(\psi(3770)\to D\overline{D})$ = 6.39 $\pm$ 0.20 nb.

Int. J. Mod. Phys. A 2026.41. Downloaded from www.worldscientific.com by [redacted]LIFORNIA @ BERKELEY on 09/16/26. Re-use and distribution is strictly not permitted, except for Open Access articles.

$\Gamma(K^*(892)^0\overline{K}^0 + \text{c.c.})/\Gamma_{\text{total}}$ — Γ_{23}/Γ

VALUE (units 10^{-3})	CL%	DOCUMENT ID		TECN	COMMENT
<1.2	90	[1] ADAMS	06	CLEO	$e^+e^- \to \psi(3770)$

[1] Comparing cross sections at $\sqrt{s} = 3.773$ GeV and $\sqrt{s} = 3.671$ GeV, neglecting interference, and using $\sigma(\psi(3770) \to D\overline{D}) = 6.39 \pm 0.20$ nb.

$\Gamma(K^0_S K^0_L)/\Gamma_{\text{total}}$ — Γ_{24}/Γ

VALUE (units 10^{-5})	CL%	DOCUMENT ID		TECN	COMMENT
$2.63^{+1.40}_{-1.59}$		[1] ABLIKIM	24A	BES3	$e^+e \to K^0_S K^0_L (K^0_S \to \pi^+\pi^-)$
• • • We do not use the following data for averages, fits, limits, etc. • • •					
< 1.2	90	[2] CRONIN-HEN..	06	CLEO	$e^+e^- \to \psi(3770)$
<21	90	[3] ABLIKIM	04F	BES	$e^+e^- \to \psi(3770)$

[1] From the 1σ contour in the B.R. versus ϕ (relative phase between the continuum and $\psi(3770)$ amplitudes) likelihood scan. Mass, total width and electronic width of $\psi(3770)$ fixed at PDG 22 values.
[2] Using $\sigma(e^+e^- \to \psi(3770) \to \text{hadrons}) = (6.38 \pm 0.08^{+0.41}_{-0.30})$ nb from BESSON 06 and $B(K^0_S \to \pi^+\pi^-) = 0.6895 \pm 0.0014$.
[3] Using $B(K^0_S \to \pi^+\pi^-) = 0.6860 \pm 0.0027$.

$\Gamma(2(\pi^+\pi^-))/\Gamma_{\text{total}}$ — Γ_{25}/Γ

VALUE (units 10^{-4})	CL%	DOCUMENT ID		TECN	COMMENT
<11.2	90	[1] HUANG	06A	CLEO	$e^+e^- \to \psi(3770)$
• • • We do not use the following data for averages, fits, limits, etc. • • •					
<48	90	[2] ABLIKIM	07B	BES2	$e^+e^- \to \psi(3770)$

[1] Using $\sigma_{tot}(e^+e^- \to \psi(3770)) = 7.9 \pm 0.6$ nb at the resonance.
[2] Assuming that interference effects between resonance and continuum can be neglected and using $\sigma^{obs}(e^+e^- \to \psi(3770)) = 7.15 \pm 0.38$ nb.

$\Gamma(2(\pi^+\pi^-)\pi^0)/\Gamma_{\text{total}}$ — Γ_{26}/Γ

VALUE (units 10^{-4})	CL%	DOCUMENT ID		TECN	COMMENT
<10.6	90	[1] HUANG	06A	CLEO	$e^+e^- \to \psi(3770)$
• • • We do not use the following data for averages, fits, limits, etc. • • •					
<62	90	[2] ABLIKIM	07B	BES2	$e^+e^- \to \psi(3770)$

[1] Using $\sigma_{tot}(e^+e^- \to \psi(3770)) = 7.9 \pm 0.6$ nb at the resonance.
[2] Assuming that interference effects between resonance and continuum can be neglected and using $\sigma^{obs}(e^+e^- \to \psi(3770)) = 7.15 \pm 0.38$ nb.

$\Gamma(2(\pi^+\pi^-\pi^0))/\Gamma_{\text{total}}$ — Γ_{27}/Γ

VALUE (units 10^{-3})	CL%	EVTS	DOCUMENT ID		TECN	COMMENT
<58.5	90	305	ABLIKIM	08N	BES2	$e^+e^- \to \psi(3770)$

$\Gamma(\omega\pi^+\pi^-)/\Gamma_{\text{total}}$ — Γ_{28}/Γ

VALUE (units 10^{-4})	CL%	DOCUMENT ID		TECN	COMMENT
< 6.0	90	[1] HUANG	06A	CLEO	$e^+e^- \to \psi(3770)$
• • • We do not use the following data for averages, fits, limits, etc. • • •					
<55	90	[2] ABLIKIM	07I	BES2	3.77 e^+e^-

[1] Using $\sigma_{tot}(e^+e^- \to \psi(3770)) = 7.9 \pm 0.6$ nb at the resonance.
[2] Assuming that interference effects between resonance and continuum can be neglected and using $\sigma^{obs}(e^+e^- \to \psi(3770)) = 7.15 \pm 0.38$ nb.

$\Gamma(3(\pi^+\pi^-))/\Gamma_{\text{total}}$ — Γ_{29}/Γ

VALUE (units 10^{-4})	CL%	DOCUMENT ID		TECN	COMMENT
<91	90	[1] ABLIKIM	07B	BES2	$e^+e^- \to \psi(3770)$

[1] Assuming that interference effects between resonance and continuum can be neglected and using $\sigma^{obs}(e^+e^- \to \psi(3770)) = 7.15 \pm 0.38$ nb.

$\Gamma(3(\pi^+\pi^-)\pi^0)/\Gamma_{\text{total}}$ — Γ_{30}/Γ

VALUE (units 10^{-4})	CL%	DOCUMENT ID		TECN	COMMENT
<137	90	[1] ABLIKIM	07B	BES2	$e^+e^- \to \psi(3770)$

[1] Assuming that interference effects between resonance and continuum can be neglected and using $\sigma^{obs}(e^+e^- \to \psi(3770)) = 7.15 \pm 0.38$ nb.

$\Gamma(3(\pi^+\pi^-)2\pi^0)/\Gamma_{\text{total}}$ — Γ_{31}/Γ

VALUE (units 10^{-3})	CL%	EVTS	DOCUMENT ID		TECN	COMMENT
<117.4	90	59	ABLIKIM	08N	BES2	$e^+e^- \to \psi(3770)$

$\Gamma(\eta\pi^+\pi^-)/\Gamma_{\text{total}}$ — Γ_{32}/Γ

VALUE (units 10^{-3})	CL%	DOCUMENT ID		TECN	COMMENT
<1.24	90	[1] HUANG	06A	CLEO	$e^+e^- \to \psi(3770)$
• • • We do not use the following data for averages, fits, limits, etc. • • •					
<2.3	90	[2] ABLIKIM	10D	BES2	$e^+e^- \to \psi(3770)$

[1] Using $\sigma_{tot}(e^+e^- \to \psi(3770)) = 7.9 \pm 0.6$ nb at the resonance.
[2] Assuming that interference effects between resonance and continuum can be neglected and using $\sigma^{obs}(e^+e^- \to \psi(3770)) = 7.15 \pm 0.38$ nb.

$\Gamma(\pi^+\pi^-2\pi^0)/\Gamma_{\text{total}}$ — Γ_{33}/Γ

VALUE (units 10^{-3})	CL%	EVTS	DOCUMENT ID		TECN	COMMENT
<8.9	90	218	ABLIKIM	08N	BES2	$e^+e^- \to \psi(3770)$

$\Gamma(\rho^0\pi^+\pi^-)/\Gamma_{\text{total}}$ — Γ_{34}/Γ

VALUE (units 10^{-3})	CL%	DOCUMENT ID		TECN	COMMENT
<6.9	90	[1] ABLIKIM	07F	BES2	$e^+e^- \to \psi(3770)$

[1] Assuming that interference effects between resonance and continuum can be neglected and using $\sigma^{obs}(e^+e^- \to \psi(3770)) = 7.15 \pm 0.38$ nb.

$\Gamma(\eta 3\pi)/\Gamma_{\text{total}}$ — Γ_{35}/Γ

VALUE (units 10^{-4})	CL%	DOCUMENT ID		TECN	COMMENT
<13.4	90	[1] HUANG	06A	CLEO	$e^+e^- \to \psi(3770)$

[1] Using $\sigma_{tot}(e^+e^- \to \psi(3770)) = 7.9 \pm 0.6$ nb at the resonance.

$\Gamma(\eta 2(\pi^+\pi^-))/\Gamma_{\text{total}}$ — Γ_{36}/Γ

VALUE (units 10^{-4})	CL%	DOCUMENT ID		TECN	COMMENT
<243	90	[1] ABLIKIM	07B	BES2	$e^+e^- \to \psi(3770)$

[1] Assuming that interference effects between resonance and continuum can be neglected and using $\sigma^{obs}(e^+e^- \to \psi(3770)) = 7.15 \pm 0.38$ nb.

$\Gamma(\eta\rho^0\pi^+\pi^-)/\Gamma_{\text{total}}$ — Γ_{37}/Γ

VALUE (units 10^{-2})	CL%	DOCUMENT ID		TECN	COMMENT
<1.45	90	[1] ABLIKIM	10D	BES2	$e^+e^- \to \psi(3770)$

[1] Assuming that interference effects between resonance and continuum can be neglected and using $\sigma^{obs}(e^+e^- \to \psi(3770)) = 7.15 \pm 0.38$ nb.

$\Gamma(\eta' 3\pi)/\Gamma_{\text{total}}$ — Γ_{38}/Γ

VALUE (units 10^{-4})	CL%	DOCUMENT ID		TECN	COMMENT
<24.4	90	[1] HUANG	06A	CLEO	$e^+e^- \to \psi(3770)$

[1] Using $\sigma_{tot}(e^+e^- \to \psi(3770)) = 7.9 \pm 0.6$ nb at the resonance.

$\Gamma(K^+K^-\pi^+\pi^-)/\Gamma_{\text{total}}$ — Γ_{39}/Γ

VALUE (units 10^{-4})	CL%	DOCUMENT ID		TECN	COMMENT
< 9.0	90	[1] HUANG	06A	CLEO	$e^+e^- \to \psi(3770)$
• • • We do not use the following data for averages, fits, limits, etc. • • •					
<48	90	[2] ABLIKIM	07B	BES2	$e^+e^- \to \psi(3770)$

[1] Using $\sigma_{tot}(e^+e^- \to \psi(3770)) = 7.9 \pm 0.6$ nb at the resonance.
[2] Assuming that interference effects between resonance and continuum can be neglected and using $\sigma^{obs}(e^+e^- \to \psi(3770)) = 7.15 \pm 0.38$ nb.

$\Gamma(\phi\pi^+\pi^-)/\Gamma_{\text{total}}$ — Γ_{40}/Γ

VALUE (units 10^{-4})	CL%	DOCUMENT ID		TECN	COMMENT
< 4.1	90	[1] HUANG	06A	CLEO	$e^+e^- \to \psi(3770)$
• • • We do not use the following data for averages, fits, limits, etc. • • •					
<16	90	[2] ABLIKIM	07B	BES2	$e^+e^- \to \psi(3770)$

[1] Using $\sigma_{tot}(e^+e^- \to \psi(3770)) = 7.9 \pm 0.6$ nb at the resonance.
[2] Assuming that interference effects between resonance and continuum can be neglected and using $\sigma^{obs}(e^+e^- \to \psi(3770)) = 7.15 \pm 0.38$ nb.

$\Gamma(K^+K^-2\pi^0)/\Gamma_{\text{total}}$ — Γ_{41}/Γ

VALUE (units 10^{-3})	CL%	EVTS	DOCUMENT ID		TECN	COMMENT
<4.2	90	14	ABLIKIM	08N	BES2	$e^+e^- \to \psi(3770)$

$\Gamma(4(\pi^+\pi^-))/\Gamma_{\text{total}}$ — Γ_{42}/Γ

VALUE (units 10^{-3})	CL%	DOCUMENT ID		TECN	COMMENT
<16.7	90	[1] ABLIKIM	07F	BES2	$e^+e^- \to \psi(3770)$

[1] Assuming that interference effects between resonance and continuum can be neglected and using $\sigma^{obs}(e^+e^- \to \psi(3770)) = 7.15 \pm 0.38$ nb.

$\Gamma(4(\pi^+\pi^-)\pi^0)/\Gamma_{\text{total}}$ — Γ_{43}/Γ

VALUE (units 10^{-3})	CL%	DOCUMENT ID		TECN	COMMENT
<30.6	90	[1] ABLIKIM	07F	BES2	$e^+e^- \to \psi(3770)$

[1] Assuming that interference effects between resonance and continuum can be neglected and using $\sigma^{obs}(e^+e^- \to \psi(3770)) = 7.15 \pm 0.38$ nb.

$\Gamma(\phi f_0(980))/\Gamma_{\text{total}}$ — Γ_{44}/Γ

VALUE (units 10^{-4})	CL%	DOCUMENT ID		TECN	COMMENT
<4.5	90	[1] HUANG	06A	CLEO	$e^+e^- \to \psi(3770)$

[1] Using $\sigma_{tot}(e^+e^- \to \psi(3770)) = 7.9 \pm 0.6$ nb at the resonance.

$\Gamma(K^+K^-\pi^+\pi^-\pi^0)/\Gamma_{\text{total}}$ — Γ_{45}/Γ

VALUE (units 10^{-4})	CL%	DOCUMENT ID		TECN	COMMENT
< 23.6	90	[1] HUANG	06A	CLEO	$e^+e^- \to \psi(3770)$
• • • We do not use the following data for averages, fits, limits, etc. • • •					
<111	90	[2] ABLIKIM	07B	BES2	$e^+e^- \to \psi(3770)$

[1] Using $\sigma_{tot}(e^+e^- \to \psi(3770)) = 7.9 \pm 0.6$ nb at the resonance.
[2] Assuming that interference effects between resonance and continuum can be neglected and using $\sigma^{obs}(e^+e^- \to \psi(3770)) = 7.15 \pm 0.38$ nb.

$\Gamma(K^+K^-\rho^0\pi^0)/\Gamma_{\text{total}}$ — Γ_{46}/Γ

VALUE (units 10^{-4})	CL%	DOCUMENT ID		TECN	COMMENT
<8	90	[1] ABLIKIM	07I	BES2	3.77 e^+e^-

[1] Assuming that interference effects between resonance and continuum can be neglected and using $\sigma^{obs}(e^+e^- \to \psi(3770)) = 7.15 \pm 0.38$ nb.

Int. J. Mod. Phys. A 2026.41. Downloaded from www.worldscientific.com
by UNIVERSITY OF CALIFORNIA @ BERKELEY on 09/16/26. Re-use and distribution is strictly not permitted, except for Open Access articles.

$\Gamma(K^+K^-\rho^+\pi^-)/\Gamma_{total}$ — Γ_{47}/Γ

VALUE (units 10^{-4})	CL%	DOCUMENT ID		TECN	COMMENT
<146	90	[1] ABLIKIM	07I	BES2	3.77 e^+e^-

[1] Assuming that interference effects between resonance and continuum can be neglected and using $\sigma^{obs}(e^+e^- \to \psi(3770)) = 7.15 \pm 0.38$ nb.

$\Gamma(\omega K^+K^-)/\Gamma_{total}$ — Γ_{48}/Γ

VALUE (units 10^{-4})	CL%	DOCUMENT ID		TECN	COMMENT
< 3.4	90	[1] HUANG	06A	CLEO	$e^+e^- \to \psi(3770)$
• • • We do not use the following data for averages, fits, limits, etc. • • •					
<66	90	[2] ABLIKIM	07I	BES2	3.77 e^+e^-

[1] Using $\sigma_{tot}(e^+e^- \to \psi(3770)) = 7.9 \pm 0.6$ nb at the resonance.
[2] Assuming that interference effects between resonance and continuum can be neglected and using $\sigma^{obs}(e^+e^- \to \psi(3770)) = 7.15 \pm 0.38$ nb.

$\Gamma(\phi\pi^+\pi^-\pi^0)/\Gamma_{total}$ — Γ_{49}/Γ

VALUE (units 10^{-4})	CL%	DOCUMENT ID		TECN	COMMENT
<38	90	[1] ABLIKIM	07I	BES2	3.77 e^+e^-

[1] Assuming that interference effects between resonance and continuum can be neglected and using $\sigma^{obs}(e^+e^- \to \psi(3770)) = 7.15 \pm 0.38$ nb.

$\Gamma(K^{*0}K^-\pi^+\pi^0 + c.c.)/\Gamma_{total}$ — Γ_{50}/Γ

VALUE (units 10^{-4})	CL%	DOCUMENT ID		TECN	COMMENT
<162	90	[1] ABLIKIM	07I	BES2	3.77 e^+e^-

[1] Assuming that interference effects between resonance and continuum can be neglected and using $\sigma^{obs}(e^+e^- \to \psi(3770)) = 7.15 \pm 0.38$ nb.

$\Gamma(K^{*+}K^-\pi^+\pi^- + c.c.)/\Gamma_{total}$ — Γ_{51}/Γ

VALUE (units 10^{-4})	CL%	DOCUMENT ID		TECN	COMMENT
<323	90	[1] ABLIKIM	07I	BES2	3.77 e^+e^-

[1] Assuming that interference effects between resonance and continuum can be neglected and using $\sigma^{obs}(e^+e^- \to \psi(3770)) = 7.15 \pm 0.38$ nb.

$\Gamma(K^+K^-\pi^+\pi^-2\pi^0)/\Gamma_{total}$ — Γ_{52}/Γ

VALUE (units 10^{-3})	CL%	EVTS	DOCUMENT ID		TECN	COMMENT
<26.7	90	24	ABLIKIM	08N	BES2	$e^+e^- \to \psi(3770)$

$\Gamma(K^+K^-2(\pi^+\pi^-))/\Gamma_{total}$ — Γ_{53}/Γ

VALUE (units 10^{-3})	CL%	DOCUMENT ID		TECN	COMMENT
<10.3	90	[1] ABLIKIM	07F	BES2	$e^+e^- \to \psi(3770)$

[1] Assuming that interference effects between resonance and continuum can be neglected and using $\sigma^{obs}(e^+e^- \to \psi(3770)) = 7.15 \pm 0.38$ nb.

$\Gamma(K^+K^-2(\pi^+\pi^-)\pi^0)/\Gamma_{total}$ — Γ_{54}/Γ

VALUE (units 10^{-3})	CL%	DOCUMENT ID		TECN	COMMENT
<36.0	90	[1] ABLIKIM	07F	BES2	$e^+e^- \to \psi(3770)$

[1] Assuming that interference effects between resonance and continuum can be neglected and using $\sigma^{obs}(e^+e^- \to \psi(3770)) = 7.15 \pm 0.38$ nb.

$\Gamma(\eta K^+K^-)/\Gamma_{total}$ — Γ_{55}/Γ

VALUE (units 10^{-4})	CL%	DOCUMENT ID		TECN	COMMENT
< 4.1	90	[1] HUANG	06A	CLEO	$e^+e^- \to \psi(3770)$
• • • We do not use the following data for averages, fits, limits, etc. • • •					
<31	90	[2] ABLIKIM	10D	BES2	$e^+e^- \to \psi(3770)$

[1] Using $\sigma_{tot}(e^+e^- \to \psi(3770)) = 7.9 \pm 0.6$ nb at the resonance.
[2] Assuming that interference effects between resonance and continuum can be neglected and using $\sigma^{obs}(e^+e^- \to \psi(3770)) = 7.15 \pm 0.38$ nb.

$\Gamma(\eta K^+K^-\pi^+\pi^-)/\Gamma_{total}$ — Γ_{56}/Γ

VALUE (units 10^{-2})	CL%	DOCUMENT ID		TECN	COMMENT
<1.24	90	[1] ABLIKIM	10D	BES2	$e^+e^- \to \psi(3770)$

[1] Assuming that interference effects between resonance and continuum can be neglected and using $\sigma^{obs}(e^+e^- \to \psi(3770)) = 7.15 \pm 0.38$ nb.

$\Gamma(\rho^0K^+K^-)/\Gamma_{total}$ — Γ_{57}/Γ

VALUE (units 10^{-3})	CL%	DOCUMENT ID		TECN	COMMENT
<5.0	90	[1] ABLIKIM	07F	BES2	$e^+e^- \to \psi(3770)$

[1] Assuming that interference effects between resonance and continuum can be neglected and using $\sigma^{obs}(e^+e^- \to \psi(3770)) = 7.15 \pm 0.38$ nb.

$\Gamma(2(K^+K^-))/\Gamma_{total}$ — Γ_{58}/Γ

VALUE (units 10^{-4})	CL%	DOCUMENT ID		TECN	COMMENT
< 6.0	90	[1] HUANG	06A	CLEO	$e^+e^- \to \psi(3770)$
• • • We do not use the following data for averages, fits, limits, etc. • • •					
<17	90	[2] ABLIKIM	07B	BES2	$e^+e^- \to \psi(3770)$

[1] Using $\sigma_{tot}(e^+e^- \to \psi(3770)) = 7.9 \pm 0.6$ nb at the resonance.
[2] Assuming that interference effects between resonance and continuum can be neglected and using $\sigma^{obs}(e^+e^- \to \psi(3770)) = 7.15 \pm 0.38$ nb.

$\Gamma(\phi K^+K^-)/\Gamma_{total}$ — Γ_{59}/Γ

VALUE (units 10^{-4})	CL%	DOCUMENT ID		TECN	COMMENT
< 7.5	90	[1] HUANG	06A	CLEO	$e^+e^- \to \psi(3770)$
• • • We do not use the following data for averages, fits, limits, etc. • • •					
<24	90	[2] ABLIKIM	07B	BES2	$e^+e^- \to \psi(3770)$

[1] Using $\sigma_{tot}(e^+e^- \to \psi(3770)) = 7.9 \pm 0.6$ nb at the resonance.
[2] Assuming that interference effects between resonance and continuum can be neglected and using $\sigma^{obs}(e^+e^- \to \psi(3770)) = 7.15 \pm 0.38$ nb.

$\Gamma(2(K^+K^-)\pi^0)/\Gamma_{total}$ — Γ_{60}/Γ

VALUE (units 10^{-4})	CL%	DOCUMENT ID		TECN	COMMENT
< 2.9	90	[1] HUANG	06A	CLEO	$e^+e^- \to \psi(3770)$
• • • We do not use the following data for averages, fits, limits, etc. • • •					
<46	90	[2] ABLIKIM	07B	BES2	$e^+e^- \to \psi(3770)$

[1] Using $\sigma_{tot}(e^+e^- \to \psi(3770)) = 7.9 \pm 0.6$ nb at the resonance.
[2] Assuming that interference effects between resonance and continuum can be neglected and using $\sigma^{obs}(e^+e^- \to \psi(3770)) = 7.15 \pm 0.38$ nb.

$\Gamma(2(K^+K^-)\pi^+\pi^-)/\Gamma_{total}$ — Γ_{61}/Γ

VALUE (units 10^{-3})	CL%	DOCUMENT ID		TECN	COMMENT
<3.2	90	[1] ABLIKIM	07F	BES2	$e^+e^- \to \psi(3770)$

[1] Assuming that interference effects between resonance and continuum can be neglected and using $\sigma^{obs}(e^+e^- \to \psi(3770)) = 7.15 \pm 0.38$ nb.

$\Gamma(K^0_SK^-\pi^+)/\Gamma_{total}$ — Γ_{62}/Γ

VALUE (units 10^{-3})	CL%	EVTS	DOCUMENT ID		TECN	COMMENT
<3.2	90	18	ABLIKIM	08M	BES2	$e^+e^- \to \psi(3770)$

$\Gamma(K^0_SK^-\pi^+\pi^0)/\Gamma_{total}$ — Γ_{63}/Γ

VALUE (units 10^{-3})	CL%	EVTS	DOCUMENT ID		TECN	COMMENT
<13.3	90	40	ABLIKIM	08M	BES2	$e^+e^- \to \psi(3770)$

$\Gamma(K^0_SK^-\rho^+)/\Gamma_{total}$ — Γ_{64}/Γ

VALUE (units 10^{-3})	CL%	DOCUMENT ID		TECN	COMMENT
<6.6	90	ABLIKIM	09C	BES2	$e^+e^- \to \psi(3770)$

$\Gamma(K^0_SK^-2\pi^+\pi^-)/\Gamma_{total}$ — Γ_{65}/Γ

VALUE (units 10^{-3})	CL%	EVTS	DOCUMENT ID		TECN	COMMENT
<8.7	90	39	ABLIKIM	08M	BES2	$e^+e^- \to \psi(3770)$

$\Gamma(K^0_SK^-\pi^+\rho^0)/\Gamma_{total}$ — Γ_{66}/Γ

VALUE (units 10^{-2})	CL%	DOCUMENT ID		TECN	COMMENT
<1.6	90	ABLIKIM	09C	BES2	$e^+e^- \to \psi(3770)$

$\Gamma(K^0_SK^-\pi^+\eta)/\Gamma_{total}$ — Γ_{67}/Γ

VALUE (units 10^{-2})	CL%	DOCUMENT ID		TECN	COMMENT
<1.3	90	ABLIKIM	09C	BES2	$e^+e^- \to \psi(3770)$

$\Gamma(K^0_SK^-2\pi^+\pi^-\pi^0)/\Gamma_{total}$ — Γ_{68}/Γ

VALUE (units 10^{-3})	CL%	EVTS	DOCUMENT ID		TECN	COMMENT
<41.8	90	23	ABLIKIM	08M	BES2	$e^+e^- \to \psi(3770)$

$\Gamma(K^0_SK^-2\pi^+\pi^-\eta)/\Gamma_{total}$ — Γ_{69}/Γ

VALUE (units 10^{-2})	CL%	DOCUMENT ID		TECN	COMMENT
<4.8	90	ABLIKIM	09C	BES2	$e^+e^- \to \psi(3770)$

$\Gamma(K^0_SK^-\pi^+2(\pi^+\pi^-))/\Gamma_{total}$ — Γ_{70}/Γ

VALUE (units 10^{-3})	CL%	EVTS	DOCUMENT ID		TECN	COMMENT
<12.2	90	4	ABLIKIM	08M	BES2	$e^+e^- \to \psi(3770)$

$\Gamma(K^0_SK^-\pi^+2\pi^0)/\Gamma_{total}$ — Γ_{71}/Γ

VALUE (units 10^{-3})	CL%	EVTS	DOCUMENT ID		TECN	COMMENT
<26.5	90	17	ABLIKIM	08M	BES2	$e^+e^- \to \psi(3770)$

$\Gamma(K^0_SK^-K^+K^-\pi^+)/\Gamma_{total}$ — Γ_{72}/Γ

VALUE (units 10^{-3})	CL%	DOCUMENT ID		TECN	COMMENT
<4.9	90	ABLIKIM	09C	BES2	$e^+e^- \to \psi(3770)$

$\Gamma(K^0_SK^-K^+K^-\pi^+\pi^0)/\Gamma_{total}$ — Γ_{73}/Γ

VALUE (units 10^{-2})	CL%	DOCUMENT ID		TECN	COMMENT
<3.0	90	ABLIKIM	09C	BES2	$e^+e^- \to \psi(3770)$

$\Gamma(K^0_SK^-K^+K^-\pi^+\eta)/\Gamma_{total}$ — Γ_{74}/Γ

VALUE (units 10^{-2})	CL%	DOCUMENT ID		TECN	COMMENT
<2.2	90	ABLIKIM	09C	BES2	$e^+e^- \to \psi(3770)$

$\Gamma(K^{*0}K^-\pi^+ + c.c.)/\Gamma_{total}$ — Γ_{75}/Γ

VALUE (units 10^{-3})	CL%	DOCUMENT ID		TECN	COMMENT
<9.7	90	[1] ABLIKIM	07F	BES2	$e^+e^- \to \psi(3770)$

[1] Assuming that interference effects between resonance and continuum can be neglected and using $\sigma^{obs}(e^+e^- \to \psi(3770)) = 7.15 \pm 0.38$ nb.

Int. J. Mod. Phys. A 2026.41. Downloaded from www.worldscientific.com by CALIFORNIA @ BERKELEY on 09/16/26. Re-use and distribution is strictly not permitted, except for Open Access articles.

$\Gamma(p\overline{p})/\Gamma_{total}$ — Γ_{76}/Γ

VALUE (units 10^{-6})	EVTS	DOCUMENT ID		TECN	COMMENT
• • • We do not use the following data for averages, fits, limits, etc. • • •					
not seen		[1] AAIJ	17AD	LHCB	$pp \to B^+ X \to p\overline{p}K^+ X$
$7.1^{+8.6}_{-2.9}$	684	[2] ABLIKIM	14L	BES3	$e^+e^- \to \psi(3770)$
310 ± 30	684	[3] ABLIKIM	14L	BES3	$e^+e^- \to \psi(3770)$

[1] AAIJ 17AD reports $B(B^+ \to \psi(3770) K^+ \to p\overline{p}K^+)/B(B^+ \to J/\psi K^+ \to p\overline{p}K^+) < 0.09$ (0.10) at 90% (95%) CL.
[2] Solution I of two equivalent solutions in a fit with a resonance interfering with continuum.
[3] Solution II of two equivalent solutions in a fit with a resonance interfering with continuum.

$\Gamma(p\overline{p}\pi^0)/\Gamma_{total}$ — Γ_{77}/Γ

VALUE (units 10^{-4})	CL%	DOCUMENT ID		TECN	COMMENT
< 0.4	90	[1,2] ABLIKIM	14O	BES3	$e^+e^- \to \psi(3770)$
• • • We do not use the following data for averages, fits, limits, etc. • • •					
$59^{+3}_{-2} \pm 5$		[1,3] ABLIKIM	14O	BES3	$e^+e^- \to \psi(3770)$
<12	90	[4] ABLIKIM	07B	BES2	$e^+e^- \to \psi(3770)$

[1] Calculated by the authors using $\sigma(e^+e^- \to \psi(3770) \to \text{hadrons}) = 6.36 \pm 0.08^{+0.41}_{-0.30}$ nb from BESSON 10.
[2] Solution I of two equivalent solutions in a fit with a resonance interfering with continuum.
[3] Solution II of two equivalent solutions in a fit with a resonance interfering with continuum.
[4] Assuming that interference effects between resonance and continuum can be neglected and using $\sigma^{obs}(e^+e^- \to \psi(3770)) = 7.15 \pm 0.38$ nb.

$\Gamma(p\overline{p}\pi^+\pi^-)/\Gamma_{total}$ — Γ_{78}/Γ

VALUE (units 10^{-4})	CL%	DOCUMENT ID		TECN	COMMENT
< 5.8	90	[1] HUANG	06A	CLEO	$e^+e^- \to \psi(3770)$
• • • We do not use the following data for averages, fits, limits, etc. • • •					
<16	90	[2] ABLIKIM	07B	BES2	$e^+e^- \to \psi(3770)$

[1] Using $\sigma_{tot}(e^+e^- \to \psi(3770)) = 7.9 \pm 0.6$ nb at the resonance.
[2] Assuming that interference effects between resonance and continuum can be neglected and using $\sigma^{obs}(e^+e^- \to \psi(3770)) = 7.15 \pm 0.38$ nb.

$\Gamma(\Lambda\overline{\Lambda})/\Gamma_{total}$ — Γ_{79}/Γ

VALUE	CL%	DOCUMENT ID		TECN	COMMENT
$<1.2 \times 10^{-4}$	90	[1] HUANG	06A	CLEO	$e^+e^- \to \psi(3770)$
• • • We do not use the following data for averages, fits, limits, etc. • • •					
$<1.8 \times 10^{-4}$	90	[2] ABLIKIM	21AS	BES3	$e^+e^- \to \psi(3770)$
$<4 \times 10^{-4}$	90	[3] ABLIKIM	07F	BES2	$e^+e^- \to \psi(3770)$

[1] Using $\sigma_{tot}(e^+e^- \to \psi(3770)) = 7.9 \pm 0.6$ nb at the resonance.
[2] From a measurement of the $e^+e^- \to \Lambda\overline{\Lambda}$ cross section between 3.5 and 4.6 GeV. At a 90% CL the lower bound is $> 2.4 \times 10^{-6}$.
[3] Assuming that interference effects between resonance and continuum can be neglected and using $\sigma^{obs}(e^+e^- \to \psi(3770)) = 7.15 \pm 0.38$ nb.

$\Gamma(p\overline{p}\pi^+\pi^-\pi^0)/\Gamma_{total}$ — Γ_{80}/Γ

VALUE (units 10^{-4})	CL%	DOCUMENT ID		TECN	COMMENT
<18.5	90	[1] HUANG	06A	CLEO	$e^+e^- \to \psi(3770)$
• • • We do not use the following data for averages, fits, limits, etc. • • •					
<73	90	[2] ABLIKIM	07B	BES2	$e^+e^- \to \psi(3770)$

[1] Using $\sigma_{tot}(e^+e^- \to \psi(3770)) = 7.9 \pm 0.6$ nb at the resonance.
[2] Assuming that interference effects between resonance and continuum can be neglected and using $\sigma^{obs}(e^+e^- \to \psi(3770)) = 7.15 \pm 0.38$ nb.

$\Gamma(\omega p\overline{p})/\Gamma_{total}$ — Γ_{81}/Γ

VALUE (units 10^{-4})	CL%	DOCUMENT ID		TECN	COMMENT
< 2.9	90	[1] HUANG	06A	CLEO	$e^+e^- \to \psi(3770)$
• • • We do not use the following data for averages, fits, limits, etc. • • •					
<30	90	[2] ABLIKIM	07I	BES2	3.77 e^+e^-

[1] Using $\sigma_{tot}(e^+e^- \to \psi(3770)) = 7.9 \pm 0.6$ nb at the resonance.
[2] Using $\sigma^{obs} = 7.15 \pm 0.27 \pm 0.27$ nb and neglecting interference.

$\Gamma(\Lambda\overline{\Lambda}\pi^0)/\Gamma_{total}$ — Γ_{82}/Γ

VALUE (units 10^{-4})	CL%	DOCUMENT ID		TECN	COMMENT
< 0.7	90	[1] ABLIKIM	13Q	BES3	$e^+e^- \to \psi(3770)$
• • • We do not use the following data for averages, fits, limits, etc. • • •					
<12	90	[2] ABLIKIM	07I	BES2	3.77 e^+e^-

[1] Assuming that interference effects between resonance and continuum can be neglected.
[2] Assuming that interference effects between resonance and continuum can be neglected and using $\sigma^{obs}(e^+e^- \to \psi(3770)) = 7.15 \pm 0.38$ nb.

$\Gamma(p\overline{p}2(\pi^+\pi^-))/\Gamma_{total}$ — Γ_{83}/Γ

VALUE (units 10^{-3})	CL%	DOCUMENT ID		TECN	COMMENT
<2.6	90	[1] ABLIKIM	07F	BES2	$e^+e^- \to \psi(3770)$

[1] Assuming that interference effects between resonance and continuum can be neglected and using $\sigma^{obs}(e^+e^- \to \psi(3770)) = 7.15 \pm 0.38$ nb.

$\Gamma(\eta p\overline{p})/\Gamma_{total}$ — Γ_{84}/Γ

VALUE (units 10^{-4})	CL%	DOCUMENT ID		TECN	COMMENT
< 5.4	90	[1] HUANG	06A	CLEO	$e^+e^- \to \psi(3770)$
• • • We do not use the following data for averages, fits, limits, etc. • • •					
<11	90	[2] ABLIKIM	10D	BES2	$e^+e^- \to \psi(3770)$

[1] Using $\sigma_{tot}(e^+e^- \to \psi(3770)) = 7.9 \pm 0.6$ nb at the resonance.
[2] Assuming that interference effects between resonance and continuum can be neglected and using $\sigma^{obs}(e^+e^- \to \psi(3770)) = 7.15 \pm 0.38$ nb.

$\Gamma(\eta p\overline{p}\pi^+\pi^-)/\Gamma_{total}$ — Γ_{85}/Γ

VALUE (units 10^{-3})	CL%	DOCUMENT ID		TECN	COMMENT
<3.3	90	[1] ABLIKIM	10D	BES2	$e^+e^- \to \psi(3770)$

[1] Assuming that interference effects between resonance and continuum can be neglected and using $\sigma^{obs}(e^+e^- \to \psi(3770)) = 7.15 \pm 0.38$ nb.

$\Gamma(\rho^0 p\overline{p})/\Gamma_{total}$ — Γ_{86}/Γ

VALUE (units 10^{-3})	CL%	DOCUMENT ID		TECN	COMMENT
<1.7	90	[1] ABLIKIM	07F	BES2	$e^+e^- \to \psi(3770)$

[1] Assuming that interference effects between resonance and continuum can be neglected and using $\sigma^{obs}(e^+e^- \to \psi(3770)) = 7.15 \pm 0.38$ nb.

$\Gamma(p\overline{p}K^+K^-)/\Gamma_{total}$ — Γ_{87}/Γ

VALUE (units 10^{-4})	CL%	DOCUMENT ID		TECN	COMMENT
< 3.2	90	[1] HUANG	06A	CLEO	$e^+e^- \to \psi(3770)$
• • • We do not use the following data for averages, fits, limits, etc. • • •					
<11	90	[2] ABLIKIM	07B	BES2	$e^+e^- \to \psi(3770)$

[1] Using $\sigma_{tot}(e^+e^- \to \psi(3770)) = 7.9 \pm 0.6$ nb at the resonance.
[2] Assuming that interference effects between resonance and continuum can be neglected and using $\sigma^{obs}(e^+e^- \to \psi(3770)) = 7.15 \pm 0.38$ nb.

$\Gamma(\eta p\overline{p}K^+K^-)/\Gamma_{total}$ — Γ_{88}/Γ

VALUE (units 10^{-3})	CL%	DOCUMENT ID		TECN	COMMENT
<6.9	90	[1] ABLIKIM	10D	BES2	$e^+e^- \to \psi(3770)$

[1] Assuming that interference effects between resonance and continuum can be neglected and using $\sigma^{obs}(e^+e^- \to \psi(3770)) = 7.15 \pm 0.38$ nb.

$\Gamma(\pi^0 p\overline{p}K^+K^-)/\Gamma_{total}$ — Γ_{89}/Γ

VALUE (units 10^{-3})	CL%	DOCUMENT ID		TECN	COMMENT
<1.2	90	[1] ABLIKIM	10D	BES2	$e^+e^- \to \psi(3770)$

[1] Assuming that interference effects between resonance and continuum can be neglected and using $\sigma^{obs}(e^+e^- \to \psi(3770)) = 7.15 \pm 0.38$ nb.

$\Gamma(\phi p\overline{p})/\Gamma_{total}$ — Γ_{90}/Γ

VALUE (units 10^{-4})	CL%	DOCUMENT ID		TECN	COMMENT
<1.3	90	[1] HUANG	06A	CLEO	$e^+e^- \to \psi(3770)$
• • • We do not use the following data for averages, fits, limits, etc. • • •					
<9	90	[2] ABLIKIM	07B	BES2	$e^+e^- \to \psi(3770)$

[1] Using $\sigma_{tot}(e^+e^- \to \psi(3770)) = 7.9 \pm 0.6$ nb at the resonance.
[2] Assuming that interference effects between resonance and continuum can be neglected and using $\sigma^{obs}(e^+e^- \to \psi(3770)) = 7.15 \pm 0.38$ nb.

$\Gamma(\Lambda\overline{\Lambda}\pi^+\pi^-)/\Gamma_{total}$ — Γ_{91}/Γ

VALUE (units 10^{-4})	CL%	DOCUMENT ID		TECN	COMMENT
< 2.5	90	[1] HUANG	06A	CLEO	$e^+e^- \to \psi(3770)$
• • • We do not use the following data for averages, fits, limits, etc. • • •					
< 4.7	90	[2] ABLIKIM	13Q	BES3	$e^+e^- \to \psi(3770)$
<39	90	[3] ABLIKIM	07F	BES2	$e^+e^- \to \psi(3770)$

[1] Using $\sigma_{tot}(e^+e^- \to \psi(3770)) = 7.9 \pm 0.6$ nb at the resonance.
[2] Assuming that interference effects between resonance and continuum can be neglected.
[3] Assuming that interference effects between resonance and continuum can be neglected and using $\sigma^{obs}(e^+e^- \to \psi(3770)) = 7.15 \pm 0.38$ nb.

$\Gamma(\Lambda\overline{p}K^+)/\Gamma_{total}$ — Γ_{92}/Γ

VALUE (units 10^{-4})	CL%	DOCUMENT ID		TECN	COMMENT
<2.8	90	[1] HUANG	06A	CLEO	$e^+e^- \to \psi(3770)$

[1] Using $\sigma_{tot}(e^+e^- \to \psi(3770)) = 7.9 \pm 0.6$ nb at the resonance.

$\Gamma(\Lambda\overline{p}K^+\pi^+\pi^-)/\Gamma_{total}$ — Γ_{93}/Γ

VALUE (units 10^{-4})	CL%	DOCUMENT ID		TECN	COMMENT
<6.3	90	[1] HUANG	06A	CLEO	$e^+e^- \to \psi(3770)$

[1] Using $\sigma_{tot}(e^+e^- \to \psi(3770)) = 7.9 \pm 0.6$ nb at the resonance.

$\Gamma(\Lambda\overline{\Lambda}\eta)/\Gamma_{total}$ — Γ_{94}/Γ

VALUE (units 10^{-4})	CL%	DOCUMENT ID		TECN	COMMENT
<1.9	90	[1] ABLIKIM	13Q	BES3	$e^+e^- \to \psi(3770)$

[1] Assuming that interference effects between resonance and continuum can be neglected.

Int. J. Mod. Phys. A 2026.41. Downloaded from www.worldscientific.com
by UNIVERSITY OF CALIFORNIA @ BERKELEY on 09/16/26. Re-use and distribution is strictly not permitted, except for Open Access articles.

$\Gamma(\Sigma^+\overline{\Sigma}^-)/\Gamma_{total}$ — Γ_{95}/Γ

VALUE (units 10^{-4})	CL%	DOCUMENT ID		TECN	COMMENT
<1.0	90	[1] ABLIKIM	13Q	BES3	$e^+e^- \to \psi(3770)$

[1] Assuming that interference effects between resonance and continuum can be neglected.

$\Gamma(\Sigma^0\overline{\Sigma}^0)/\Gamma_{total}$ — Γ_{96}/Γ

VALUE (units 10^{-4})	CL%	DOCUMENT ID		TECN	COMMENT
<0.4	90	[1] ABLIKIM	13Q	BES3	$e^+e^- \to \psi(3770)$

[1] Assuming that interference effects between resonance and continuum can be neglected.

$\Gamma(\Xi^0\overline{\Xi}^0)/\Gamma_{total}$ — Γ_{97}/Γ

VALUE (units 10^{-4})	CL%	DOCUMENT ID		TECN	COMMENT
• • • We do not use the following data for averages, fits, limits, etc. • • •					
<1.4	90	[1] ABLIKIM	13Q	BES3	$e^+e^- \to \psi(3770)$

[1] Assuming that interference effects between resonance and continuum can be neglected.

$\Gamma(\Xi^-\overline{\Xi}^+)/\Gamma_{total}$ — Γ_{98}/Γ

VALUE (units 10^{-4})	CL%	DOCUMENT ID		TECN	COMMENT
• • • We do not use the following data for averages, fits, limits, etc. • • •					
<1.5	90	[1] ABLIKIM	13Q	BES3	$e^+e^- \to \psi(3770)$

[1] Assuming that interference effects between resonance and continuum can be neglected.

RADIATIVE DECAYS

$\Gamma(\gamma\chi_{c2})/\Gamma_{total}$ — Γ_{102}/Γ

VALUE (units 10^{-3})	CL%	DOCUMENT ID		TECN	COMMENT
<0.64	90	[1] ABLIKIM	15J	BES3	$e^+e^- \to \psi(3770) \to \gamma\gamma J/\psi$
• • • We do not use the following data for averages, fits, limits, etc. • • •					
<2.0	90	[2] BRIERE	06	CLEO	$e^+e^- \to \psi(3770) \to \gamma +$ hadrons
<0.9	90	[3] COAN	06A	CLEO	$e^+e^- \to \psi(3770) \to \gamma\gamma J/\psi$

[1] This limit is equivalent to $(0.25 \pm 0.21 \pm 0.18) \times 10^{-3}$ branching fraction value.
[2] Uses $B(\psi(2S) \to \gamma\chi_{c2}) = 9.22 \pm 0.11 \pm 0.46\,\%$ from ATHAR 04, $\psi(2S)$ mass and width from PDG 04, and $\Gamma_{ee}(\psi(2S)) = 2.54 \pm 0.03 \pm 0.11$ keV from ADAM 06.
[3] Using $\Gamma_{ee}(\psi(2S)) = (2.54 \pm 0.03 \pm 0.11)$ keV from ADAM 06 and taking $\sigma(e^+e^- \to D\overline{D})$ from HE 05 for $\sigma(e^+e^- \to \psi(3770))$.

$\Gamma(\gamma\chi_{c1})/\Gamma_{total}$ — Γ_{103}/Γ

VALUE (units 10^{-3})	EVTS	DOCUMENT ID		TECN	COMMENT
2.49±0.23 OUR AVERAGE					
2.0 ±0.8 ±0.1	202	[1] ABLIKIM	16B	BES3	$e^+e^- \to \psi(3770) \to \gamma +$ hadrons
2.48±0.15±0.23	0.6k	ABLIKIM	15J	BES3	$e^+e^- \to \psi(3770) \to \gamma\gamma J/\psi$
2.5 ±0.8 ±0.2		[2] ABLIKIM	14H	BES3	$e^+e^- \to \psi(3770) \to K^0_S K^\pm\pi^\mp$
2.9 ±0.5 ±0.4		[3] BRIERE	06	CLEO	$e^+e^- \to \psi(3770) \to \gamma +$ hadrons, $\gamma\gamma J/\psi$
• • • We do not use the following data for averages, fits, limits, etc. • • •					
3.9 ±1.4 ±0.6	54	[4] BRIERE	06	CLEO	$e^+e^- \to \psi(3770) \to \gamma +$ hadrons
2.8 ±0.5 ±0.4	53	[5] COAN	06A	CLEO	$e^+e^- \to \psi(3770) \to \gamma\gamma J/\psi$

[1] ABLIKIM 16B reports $(1.94 \pm 0.42 \pm 0.64) \times 10^{-3}$ from a measurement of $[\Gamma(\psi(3770) \to \gamma\chi_{c1})/\Gamma_{total}]$ / $[B(\psi(2S) \to \gamma\chi_{c1}(1P))]$ assuming $B(\psi(2S) \to \gamma\chi_{c1}(1P)) = (9.55 \pm 0.31) \times 10^{-2}$, which we rescale to our best (shown rounded) value $B(\psi(2S) \to \gamma\chi_{c1}(1P)) = (9.85 \pm 0.26) \times 10^{-2}$. Our first error is their experiment's error and our second error is the systematic error from using our best (shown rounded) value.
[2] ABLIKIM 14H reports $[\Gamma(\psi(3770) \to \gamma\chi_{c1})/\Gamma_{total}] \times [B(\chi_{c1}(1P) \to K^0_S K^\pm\pi^\mp)] = (8.51 \pm 2.39 \pm 1.42) \times 10^{-6}$ which we divide by our best (shown rounded) value $B(\chi_{c1}(1P) \to K^0_S K^\pm\pi^\mp) = 0.00346 \pm 0.00030$. Our first error is their experiment's error and our second error is the systematic error from using our best (shown rounded) value. We have calculated the best value of $B(\chi_{c1}(1P) \to K^0_S K^\pm\pi^\mp)$ as 1/2 of $B(\chi_{c1}(1P) \to \overline{K}^0 K^+\pi^- + \text{c.c.}) = (6.9 \pm 0.6) \times 10^{-3}$.
[3] Averages the two measurements from COAN 06A and BRIERE 06.
[4] Uses $B(\psi(2S) \to \gamma\chi_{c1}) = 9.07 \pm 0.11 \pm 0.54\,\%$ from ATHAR 04, $\psi(2S)$ mass and width from PDG 04, and $\Gamma_{ee}(\psi(2S)) = 2.54 \pm 0.03 \pm 0.11$ keV from ADAM 06.
[5] Using $\Gamma_{ee}(\psi(2S)) = (2.54 \pm 0.03 \pm 0.11)$ keV from ADAM 06 and taking $\sigma(e^+e^- \to D\overline{D})$ from HE 05 for $\sigma(e^+e^- \to \psi(3770))$.

$\Gamma(\gamma\chi_{c1})/\Gamma(J/\psi\pi^+\pi^-)$ — Γ_{103}/Γ_5

VALUE	EVTS	DOCUMENT ID		TECN	COMMENT
1.49±0.31±0.26	53 ± 10	[1] COAN	06A	CLEO	$e^+e^- \to \psi(3770) \to \gamma\gamma J/\psi$

[1] Using $B(\psi(3770) \to J/\psi\pi^+\pi^-) = (1.89 \pm 0.20 \pm 0.20) \times 10^{-3}$ from ADAM 06.

$\Gamma(\gamma\chi_{c0})/\Gamma_{total}$ — Γ_{104}/Γ

VALUE (units 10^{-3})	CL%	EVTS	DOCUMENT ID		TECN	COMMENT
7.1±0.6 OUR AVERAGE						
6.9±0.7±0.2		2.2k	[1] ABLIKIM	16B	BES3	$e^+e^- \to \psi(3770) \to \gamma +$ hadrons
7.3±0.7±0.6		274	BRIERE	06	CLEO	$e^+e^- \to \psi(3770) \to \gamma +$ hadrons
• • • We do not use the following data for averages, fits, limits, etc. • • •						
< 44	90		[2] COAN	06A	CLEO	$e^+e^- \to \psi(3770) \to \gamma\gamma J/\psi$

[1] ABLIKIM 16B reports $(6.88 \pm 0.28 \pm 0.67) \times 10^{-3}$ from a measurement of $[\Gamma(\psi(3770) \to \gamma\chi_{c0})/\Gamma_{total}]$ / $[B(\psi(2S) \to \gamma\chi_{c0}(1P))]$ assuming $B(\psi(2S) \to \gamma\chi_{c0}(1P)) = (9.99 \pm 0.27) \times 10^{-2}$, which we rescale to our best (shown rounded) value $B(\psi(2S) \to \gamma\chi_{c0}(1P)) = (10.06 \pm 0.27) \times 10^{-2}$. Our first error is their experiment's error and our second error is the systematic error from using our best (shown rounded) value.
[2] Using $\Gamma_{ee}(\psi(2S)) = (2.54 \pm 0.03 \pm 0.11)$ keV from ADAM 06 and taking $\sigma(e^+e^- \to D\overline{D})$ from HE 05 for $\sigma(e^+e^- \to \psi(3770))$.

$\Gamma(\gamma\chi_{c0})/\Gamma(\gamma\chi_{c2})$ — $\Gamma_{104}/\Gamma_{102}$

VALUE	CL%	DOCUMENT ID		TECN	COMMENT
• • • We do not use the following data for averages, fits, limits, etc. • • •					
>8	90	[1] BRIERE	06	CLEO	$e^+e^- \to \psi(3770)$

[1] Not independent of other results in BRIERE 06.

$\Gamma(\gamma\chi_{c0})/\Gamma(\gamma\chi_{c1})$ — $\Gamma_{104}/\Gamma_{103}$

VALUE	DOCUMENT ID		TECN	COMMENT
• • • We do not use the following data for averages, fits, limits, etc. • • •				
2.5±0.6	[1] BRIERE	06	CLEO	$e^+e^- \to \psi(3770)$

[1] Not independent of other results in BRIERE 06.

$\Gamma(\gamma\eta_c)/\Gamma_{total}$ — Γ_{105}/Γ

VALUE	CL%	DOCUMENT ID		TECN
<8 × 10^{-4}	90	[1] ABLIKIM	14H	BES3

[1] ABLIKIM 14H reports $[\Gamma(\psi(3770) \to \gamma\eta_c)/\Gamma_{total}] \times [B(\eta_c(1S) \to K^0_S K^\pm\pi^\mp)] < 16 \times 10^{-6}$ which we divide by our best (shown rounded) value $B(\eta_c(1S) \to K^0_S K^\pm\pi^\mp) = 1.97 \times 10^{-2}$. We have calculated the best value of $B(\eta_c(1S) \to K^0_S K^\pm\pi^\mp)$ as 1/3 of $B(\eta_c(1S) \to K\overline{K}\pi) = 5.9 \times 10^{-2}$.

$\Gamma(\gamma\eta_c(2S))/\Gamma_{total}$ — Γ_{106}/Γ

VALUE	CL%	DOCUMENT ID		TECN
<9 × 10^{-4}	90	[1] ABLIKIM	14H	BES3

[1] ABLIKIM 14H reports $[\Gamma(\psi(3770) \to \gamma\eta_c(2S))/\Gamma_{total}] \times [B(\eta_c(2S) \to K^0_S K^\pm\pi^\mp)] < 5.6 \times 10^{-6}$ which we divide by our best (shown rounded) value $B(\eta_c(2S) \to K^0_S K^\pm\pi^\mp) = 6.3 \times 10^{-3}$. We have calculated the best value of $B(\eta_c(2S) \to K^0_S K^\pm\pi^\mp)$ as 1/3 of $B(\eta_c(2S) \to K\overline{K}\pi) = 1.9 \times 10^{-2}$.

$\Gamma(\gamma\eta')/\Gamma_{total}$ — Γ_{107}/Γ

VALUE (units 10^{-4})	CL%	DOCUMENT ID		TECN	COMMENT
<1.8	90	[1] PEDLAR	09	CLE3	$\psi(2S) \to \gamma X$

[1] Assuming maximal destructive interference between $\psi(3770)$ and continuum sources.

$\Gamma(\gamma\eta)/\Gamma_{total}$ — Γ_{108}/Γ

VALUE (units 10^{-4})	CL%	DOCUMENT ID		TECN	COMMENT
<1.5	90	[1] PEDLAR	09	CLE3	$\psi(2S) \to \gamma X$

[1] Assuming maximal destructive interference between $\psi(3770)$ and continuum sources.

$\Gamma(\gamma\pi^0)/\Gamma_{total}$ — Γ_{109}/Γ

VALUE (units 10^{-4})	CL%	DOCUMENT ID		TECN	COMMENT
<2	90	PEDLAR	09	CLE3	$\psi(2S) \to \gamma X$

$\psi(3770)$ REFERENCES

ABLIKIM 25CF JHEP 2511 111 M. Ablikim et al. (BESIII Collab.)
ABLIKIM 25U PR D111 L051502 M. Ablikim et al. (BESIII Collab.)
ABLIKIM 24A PRL 132 131901 M. Ablikim et al. (BESIII Collab.)
ABLIKIM 24AH JHEP 2405 022 M. Ablikim et al. (BESIII Collab.)
ABLIKIM 24AL JHEP 2407 258 M. Ablikim et al. (BESIII Collab.)
ABLIKIM 24CD JHEP 2411 062 M. Ablikim et al. (BESIII Collab.)
HANHART 24 EPJ C84 483 C. Hanhart et al. (JULI, BONN, SIEG+)
ABLIKIM 23BC PR D108 052015 M. Ablikim et al. (BESIII Collab.)
ABLIKIM 23BK JHEP 2311 228 M. Ablikim et al. (BESIII Collab.)
ABLIKIM 23V PR D107 L091101 M. Ablikim et al. (BESIII Collab.)
PDG 22 PTEP 2022 083C01 R.L. Workman et al. (PDG Collab.)
ABLIKIM 21AS PR D104 L091104 M. Ablikim et al. (BESIII Collab.)
ABLIKIM 21Z PRL 127 082002 M. Ablikim et al. (BESIII Collab.)
PDG 20 PTEP 2020 083C01 P.A. Zyla et al. (PDG Collab.)
AAIJ 19M JHEP 1907 035 R. Aaij et al. (LHCb Collab.)
AAIJ 17AD PL B769 305 R. Aaij et al. (LHCb Collab.)
SHAMOV 17 PL B769 187 A.G. Shamov, K.Yu. Todyshev
ABLIKIM 16B PL B753 103 M. Ablikim et al. (BESIII Collab.)
ABLIKIM 15J PR D91 092009 M. Ablikim et al. (BESIII Collab.)
DRUZHININ 15 PR D92 054024 V.P. Druzhinin (NOVO)
ABLIKIM 14H PR D89 112005 M. Ablikim et al. (BESIII Collab.)
ABLIKIM 14L PL B735 101 M. Ablikim et al. (BESIII Collab.)
ABLIKIM 14O PR D90 032007 M. Ablikim et al. (BESIII Collab.)
BONVICINI 14 PR D89 072002 G. Bonvicini et al. (CLEO Collab.)
ABLIKIM 13Q PR D87 112011 M. Ablikim et al. (BESIII Collab.)
ANASHIN 12A PL B711 292 V.V. Anashin et al. (KEDR Collab.)
ABLIKIM 10D EPJ C66 11 M. Ablikim et al. (BES II Collab.)
BESSON 10 PRL 104 159901 (errat.) D. Besson et al. (CLEO Collab.)
ABLIKIM 09C EPJ C64 243 M. Ablikim et al. (BES Collab.)
PEDLAR 09 PR D79 111101 T.K. Pedlar et al. (CLEO Collab.)
ABLIKIM 08B PL B659 74 M. Ablikim et al. (BES Collab.)
ABLIKIM 08D PL B660 315 M. Ablikim et al. (BES Collab.)
ABLIKIM 08H PRL 101 102004 M. Ablikim et al. (BES Collab.)
ABLIKIM 08M PL B670 179 M. Ablikim et al. (BES Collab.)
ABLIKIM 08N PL B670 184 M. Ablikim et al. (BES Collab.)
AUBERT 08B PR D77 011102 B. Aubert et al. (BABAR Collab.)
BRODZICKA 08 PRL 100 092001 J. Brodzicka et al. (BELLE Collab.)

PAKHLOVA	08	PR D77 011103	G. Pakhlova *et al.*	(BELLE Collab.)
ABLIKIM	07B	PL B650 111	M. Ablikim *et al.*	(BES Collab.)
ABLIKIM	07E	PL B652 238	M. Ablikim *et al.*	(BES Collab.)
ABLIKIM	07F	PL B656 30	M. Ablikim *et al.*	(BES Collab.)
ABLIKIM	07I	EPJ C52 805	M. Ablikim *et al.*	(BES Collab.)
ABLIKIM	07K	PR D76 122002	M. Ablikim *et al.*	(BES Collab.)
AUBERT	07BE	PR D76 111105	B. Aubert *et al.*	(BABAR Collab.)
DOBBS	07	PR D76 112001	S. Dobbs *et al.*	(CLEO Collab.)
ABLIKIM	06L	PRL 97 121801	M. Ablikim *et al.*	(BES Collab.)
ABLIKIM	06N	PL B641 145	M. Ablikim *et al.*	(BES Collab.)
ADAM	06	PRL 96 082004	N.E. Adam *et al.*	(CLEO Collab.)
ADAMS	06	PR D73 012002	G.S. Adams *et al.*	(CLEO Collab.)
BESSON	06	PRL 96 092002	D. Besson *et al.*	(CLEO Collab.)
Also		PRL 104 159901 (errat.)	D. Besson *et al.*	(CLEO Collab.)
BRIERE	06	PR D74 031106	R.A. Briere *et al.*	(CLEO Collab.)
COAN	06A	PRL 96 182002	T.E. Coan *et al.*	(CLEO Collab.)
CRONIN-HEN...	06	PR D74 012005	D. Cronin-Hennessy *et al.*	(CLEO Collab.)
HUANG	06A	PRL 96 032003	G.S. Huang *et al.*	(CLEO Collab.)
BAI	05	PL B605 63	J.Z. Bai *et al.*	(BES Collab.)
HE	05	PRL 95 121801	Q. He *et al.*	(CLEO Collab.)
Also		PRL 96 199903 (errat.)	Q. He *et al.*	(CLEO Collab.)
ABLIKIM	04F	PR D70 077101	M. Ablikim *et al.*	(BES Collab.)
ATHAR	04	PR D70 112002	S.B. Athar *et al.*	(CLEO Collab.)
CHISTOV	04	PRL 93 051803	R. Chistov *et al.*	(BELLE Collab.)
PDG	04	PL B592 1	S. Eidelman *et al.*	(PDG Collab.)
BAI	02C	PRL 88 101802	J.Z. Bai *et al.*	(BES Collab.)
ADLER	88C	PRL 60 89	J. Adler *et al.*	(Mark III Collab.)
SCHINDLER	80	PR D21 2716	R.H. Schindler *et al.*	(Mark II Collab.)
BACINO	78	PRL 40 671	W.J. Bacino *et al.*	(SLAC, UCLA, UCI)
RAPIDIS	77	PRL 39 526	P.A. Rapidis *et al.*	(LGW Collab.)

$\psi_2(3823)$

$I^G(J^{PC}) = 0^-(2^{--})$
I, J, P need confirmation.

was $\psi(3823)$, $X(3823)$

Seen by BHARDWAJ 13 in $B \to \chi_{c1}\gamma K$ and ABLIKIM 15S in $e^+e^- \to \pi^+\pi^-\gamma\chi_{c1}$ decays as a narrow peak in the invariant mass distribution of the $\chi_{c1}\gamma$ system. Properties consistent with the $\psi_2(1^3D_2)$ $c\overline{c}$ state.

$\psi_2(3823)$ MASS

VALUE (MeV)	EVTS	DOCUMENT ID		TECN	COMMENT
3823.51 ± 0.34 OUR AVERAGE					
3824.5 ± 2.4 ± 1.0	30	[1] ABLIKIM	23J	BES3	$e^+e^- \to \pi^0\pi^0\chi_{c1}\gamma$
3823.12 ± 0.43 ± 0.13	120	ABLIKIM	22R	BES3	$e^+e^- \to \pi^+\pi^-\chi_{c1}\gamma$
3824.08 ± 0.53 ± 0.14	137	[2] AAIJ	20S	LHCB	$B^+ \to J/\psi\pi^+\pi^-K^+$
3823.1 ± 1.8 ± 0.7	33 ± 10	[3] BHARDWAJ	13	BELL	$B^\pm \to \chi_{c1}\gamma K^\pm$
• • • We do not use the following data for averages, fits, limits, etc. • • •					
3821.7 ± 1.3 ± 0.7	19 ± 5	[4] ABLIKIM	15S	BES3	$e^+e^- \to \pi^+\pi^-\chi_{c1}\gamma$

[1] Using the measured $m_{\psi_2(3823)} - m_{\psi(2S)}$ and assuming $m_{\psi(2S)} = 3686.097$ MeV from PDG 22.
[2] Using the measured $m_{\psi_2(3823)} - m_{\psi(2S)} = 137.98 \pm 0.53 \pm 0.14$ MeV.
[3] From a simultaneous fit to $B^\pm \to (\chi_{c1}\gamma)K^\pm$ and $B^0 \to (\chi_{c1}\gamma)K^0_S$ with significance 4.0σ including systematics. Corrected for the measured $\psi(2S)$ mass using $B \to \psi(2S)K \to (\gamma\chi_{c1})K$ decays.
[4] From a simultaneous unbinned maximum likelihood fit of $e^+e^- \to \pi^+\pi^-\chi_{c1}\gamma$ data (the $\pi^+\pi^-$ recoil mass) taken at $\sqrt{s}$ values of 4.23, 4.26, 4.36, 4.42, and 4.60 GeV to simulated events including both $\psi(2S) \to \chi_{c1}\gamma$ and $\psi_2(3823) \to \chi_{c1}\gamma$ together, with floating mass scale offset for $\psi(2S)$, floating $\psi_2(3823)$ mass, and zero $\psi_2(3823)$ width, resulting in a significance of 5.9σ when including systematic uncertainties. Superseded by ABLIKIM 22R.

$m_{\psi_2(3823)} - m_{\psi(2S)}$

VALUE (MeV)	EVTS	DOCUMENT ID		TECN	COMMENT
• • • We do not use the following data for averages, fits, limits, etc. • • •					
137.98 ± 0.53 ± 0.14	137	[1] AAIJ	20S	LHCB	$B^+ \to J/\psi\pi^+\pi^-K^+$

[1] AAIJ 20S also reports $m_{\chi_{c1}(3872)} - m_{\psi_2(3823)} = 47.50 \pm 0.53 \pm 0.13$ MeV.

$\psi_2(3823)$ WIDTH

VALUE (MeV)	CL%	EVTS	DOCUMENT ID		TECN	COMMENT
< 2.9	90	120	ABLIKIM	22R	BES3	$e^+e^- \to \pi^+\pi^-\chi_{c1}\gamma$
• • • We do not use the following data for averages, fits, limits, etc. • • •						
<18.8	90	30	[1] ABLIKIM	23J	BES3	$e^+e^- \to \pi^0\pi^0\chi_{c1}\gamma$
< 5.2	90		[2] AAIJ	20S	LHCB	$B^+ \to J/\psi\pi^+\pi^-K^+$
<16	90		[3] ABLIKIM	15S	BES3	$e^+e^- \to \pi^+\pi^-\chi_{c1}\gamma$
<24	90		[4] BHARDWAJ	13	BELL	$B^\pm \to \chi_{c1}\gamma K^\pm$

[1] From a fit of $e^+e^- \to \pi^0\pi^0\chi_{c1}\gamma$ data at $\sqrt{s}$ values from 4.23 to 4.70 GeV to a Breit-Wigner function with floating width, using the Bayesian approach.
[2] AAIJ 20S also provides a limit of < 6.6 MeV with 95% CL.
[3] From a fit of $e^+e^- \to \pi^+\pi^-\chi_{c1}\gamma$ data (the $\pi^+\pi^-$ recoil mass) taken at $\sqrt{s}$ values of 4.23, 4.26, 4.36, 4.42, and 4.60 GeV to a Breit-Wigner function with the mass fixed from the likelihood fit above, Gaussian resolution smearing, and floating width.
[4] From a simultaneous fit to $B^\pm \to (\chi_{c1}\gamma)K^\pm$ and $B^0 \to (\chi_{c1}\gamma)K^0_S$ with significance 4.0σ including systematics.

$\psi_2(3823)$ DECAY MODES

Branching fractions are given relative to the one **DEFINED AS 1**.

	Mode	Fraction (Γ_i/Γ)	Confidence level
Γ_1	$J/\psi(1S)\pi^+\pi^-$	<0.06	90%
Γ_2	$J/\psi(1S)\pi^0\pi^0$	<0.11	90%
Γ_3	$J/\psi(1S)\pi^0$	<0.030	90%
Γ_4	$J/\psi(1S)\eta$	<0.14	90%
Γ_5	$\chi_{c0}\gamma$	<0.24	90%
Γ_6	$\chi_{c1}\gamma$	**DEFINED AS 1**	
Γ_7	$\chi_{c2}\gamma$	$0.28\ ^{+0.14}_{-0.11}$	

$\psi_2(3823)$ BRANCHING RATIOS

$\Gamma(J/\psi(1S)\pi^+\pi^-)/\Gamma_{total}$ — Γ_1/Γ

VALUE	EVTS	DOCUMENT ID		TECN	COMMENT
• • • We do not use the following data for averages, fits, limits, etc. • • •					
not seen		[1] ABLIKIM	21O	BES3	$e^+e^- \to \pi^+\pi^-X$
seen	137 ± 26	AAIJ	20S	LHCB	$B^+ \to J/\psi\pi^+\pi^-K^+$

[1] From a simultaneous unbinned maximum likelihood fit of the $\pi^+\pi^-$ recoil mass distributions of seven decay channels in the process $e^+e^- \to \pi^+\pi^-X$.

$\Gamma(J/\psi(1S)\pi^+\pi^-)/\Gamma(\chi_{c1}\gamma)$ — Γ_1/Γ_6

VALUE	CL%	DOCUMENT ID		TECN	COMMENT
<0.06	90	[1] ABLIKIM	21O	BES3	$e^+e^- \to \pi^+\pi^-X$

[1] From a simultaneous unbinned maximum likelihood fit of the $\pi^+\pi^-$ recoil mass distributions of seven decay channels in the process $e^+e^- \to \pi^+\pi^-X$.

$\Gamma(J/\psi(1S)\pi^0\pi^0)/\Gamma(\chi_{c1}\gamma)$ — Γ_2/Γ_6

VALUE	CL%	DOCUMENT ID		TECN	COMMENT
<0.11	90	[1] ABLIKIM	21O	BES3	$e^+e^- \to \pi^+\pi^-X$

[1] From a simultaneous unbinned maximum likelihood fit of the $\pi^+\pi^-$ recoil mass distributions of seven decay channels in the process $e^+e^- \to \pi^+\pi^-X$.

$\Gamma(J/\psi(1S)\pi^0)/\Gamma(\chi_{c1}\gamma)$ — Γ_3/Γ_6

VALUE	CL%	DOCUMENT ID		TECN	COMMENT
<0.03	90	[1] ABLIKIM	21O	BES3	$e^+e^- \to \pi^+\pi^-X$

[1] From a simultaneous unbinned maximum likelihood fit of the $\pi^+\pi^-$ recoil mass distributions of seven decay channels in the process $e^+e^- \to \pi^+\pi^-X$.

$\Gamma(J/\psi(1S)\eta)/\Gamma(\chi_{c1}\gamma)$ — Γ_4/Γ_6

VALUE	CL%	DOCUMENT ID		TECN	COMMENT
<0.14	90	[1] ABLIKIM	21O	BES3	$e^+e^- \to \pi^+\pi^-X$

[1] From a simultaneous unbinned maximum likelihood fit of the $\pi^+\pi^-$ recoil mass distributions of seven decay channels in the process $e^+e^- \to \pi^+\pi^-X$.

$\Gamma(J/\psi(1S)\eta)/\Gamma(J/\psi(1S)\pi^+\pi^-)$ — Γ_4/Γ_1

VALUE	DOCUMENT ID		TECN	COMMENT
$\mathbf{4.4\ ^{+2.5}_{-1.9} \pm 0.9}$	[1] AAIJ	22D	LHCB	$B^+ \to J/\psi(1S)\eta K^+$

[1] Using the branching ratio for $B^+ \to \psi_2(3823)K^+$ with $\psi_2(3823) \to J/\psi(1S)\pi^+\pi^-$ from AAIJ 20S.

$\Gamma(\chi_{c0}\gamma)/\Gamma_{total}$ — Γ_5/Γ

VALUE	DOCUMENT ID		TECN	COMMENT
• • • We do not use the following data for averages, fits, limits, etc. • • •				
not seen	[1] ABLIKIM	21O	BES3	$e^+e^- \to \pi^+\pi^-X$

[1] From a simultaneous unbinned maximum likelihood fit of the $\pi^+\pi^-$ recoil mass distributions of seven decay channels in the process $e^+e^- \to \pi^+\pi^-X$.

$\Gamma(\chi_{c1}\gamma)/\Gamma_{total}$ — Γ_6/Γ

VALUE	EVTS	DOCUMENT ID		TECN	COMMENT
• • • We do not use the following data for averages, fits, limits, etc. • • •					
seen	120	[1] ABLIKIM	22R	BES3	$e^+e^- \to \pi^+\pi^-\chi_{c1}\gamma$
seen	63 ± 9	[2] ABLIKIM	21O	BES3	$e^+e^- \to \pi^+\pi^-X$
seen	16 ± 5	[3] ABLIKIM	21O	BES3	$e^+e^- \to \pi^0\pi^0X$
seen	33 ± 10	[4] BHARDWAJ	13	BELL	$B^\pm \to \chi_{c1}\gamma K^\pm$

[1] From a fit to the $e^+e^- \to \pi^+\pi^-\psi(3823)$ cross section between 4.23 and 4.70 GeV with two coherent Breit-Wigner resonances. The data is also consistent with a single peak R with mass 4417.5 ± 26.2 ± 3.5 MeV and width 245 ± 48 ± 13 MeV, which leads to $\Gamma(e+e-)\ B(R \to \pi^+\pi^-\psi_2(3823))\ B(\psi_2(3823) \to \chi_{c1}\gamma) = 0.57 \pm 0.08$ eV.
[2] From a simultaneous unbinned maximum likelihood fit of the $\pi^+\pi^-$ recoil mass distributions of seven decay channels in the process $e^+e^- \to \pi^+\pi^-X$. Signal has a 11.8 σ significance.
[3] From a fit of the invariant $\pi^0\pi^0$ recoil-mass distribution. Signal has a 4.3 σ significance.
[4] BHARDWAJ 13 reports $B(B^\pm \to \psi_2(3823)K^\pm) \times B(\psi_2(3823) \to \gamma\chi_{c1}) = (9.7 \pm 2.8 \pm 1.1) \times 10^{-6}$ with statistical significance 3.8 σ.

$\Gamma(\chi_{c0}\gamma)/\Gamma(\chi_{c1}\gamma)$ — Γ_5/Γ_6

VALUE	CL%	DOCUMENT ID		TECN	COMMENT
<0.24	90	[1] ABLIKIM	21O	BES3	$e^+e^- \to \pi^+\pi^-X$

[1] From a simultaneous unbinned maximum likelihood fit of the $\pi^+\pi^-$ recoil mass distributions of seven decay channels in the process $e^+e^- \to \pi^+\pi^-X$.

Int. J. Mod. Phys. A 2026.41. Downloaded from www.worldscientific.com
by CALIFORNIA @ BERKELEY on 09/16/26. Re-use and distribution is strictly not permitted, except for Open Access articles.

Int. J. Mod. Phys. A 2026.41. Downloaded from www.worldscientific.com
by UNIVERSITY OF CALIFORNIA @ BERKELEY on 09/16/26. Re-use and distribution is strictly not permitted, except for Open Access articles.

$\Gamma(\chi_{c2}\gamma)/\Gamma_{total}$ — Γ_7/Γ

VALUE	DOCUMENT ID		TECN	COMMENT
• • • We do not use the following data for averages, fits, limits, etc. • • •				
seen	[1] ABLIKIM	21O	BES3	$e^+e^- \to \pi^+\pi^- X$
not seen	[2] ABLIKIM	15S	BES3	$e^+e^- \to \pi^+\pi^-\chi_{c2}\gamma$
not seen	[3] BHARDWAJ	13	BELL	$B^\pm \to \chi_{c2}\gamma K^\pm$

[1] From a simultaneous unbinned maximum likelihood fit of the $\pi^+\pi^-$ recoil mass distributions of seven decay channels in the process $e^+e^- \to \pi^+\pi^- X$. Signal has a 3.2 σ significance.

[2] From a simultaneous unbinned maximum likelihood fit of $e^+e^- \to \pi^+\pi^-\chi_{c2}\gamma$ data (the $\pi^+\pi^-$ recoil mass) taken at $\sqrt{s}$ values of 4.23, 4.26, 4.36, 4.42, and 4.60 GeV to simulated events including both $\psi(2S) \to \chi_{c2}\gamma$ and $\psi_2(3823) \to \chi_{c2}\gamma$ together, with floating mass scale offset for $\psi(2S)$, $\psi_2(3823)$ mass floating (fixed to that above), and zero $\psi_2(3823)$ width.

[3] BHARDWAJ 13 reports $B(B^\pm \to \psi_2(3823)K^\pm) \times B(\psi_2(3823) \to \gamma\chi_{c2}) < 3.6 \times 10^{-6}$ at 90% CL.

$\Gamma(\chi_{c2}\gamma)/\Gamma(\chi_{c1}\gamma)$ — Γ_7/Γ_6

VALUE	CL%	EVTS	DOCUMENT ID		TECN	COMMENT
$0.28^{+0.14}_{-0.11} \pm 0.02$		9 ± 4	[1] ABLIKIM	21O	BES3	$e^+e^- \to \pi^+\pi^-\chi_{c2}\gamma$
• • • We do not use the following data for averages, fits, limits, etc. • • •						
<0.42	90		[2] ABLIKIM	15S	BES3	$e^+e^- \to \pi^+\pi^-\chi_{c2}\gamma$
<0.41	90		BHARDWAJ	13	BELL	$B^\pm \to \chi_{c1/c2}\gamma K^\pm$

[1] From a simultaneous unbinned maximum likelihood fit of the $\pi^+\pi^-$ recoil mass distributions of seven decay channels in the process $e^+e^- \to \pi^+\pi^- X$.

[2] From a simultaneous unbinned maximum likelihood fit of $e^+e^- \to \pi^+\pi^-\chi_{c1(2)}\gamma$ data (the $\pi^+\pi^-$ recoil mass) taken at $\sqrt{s}$ values of 4.23, 4.26, 4.36, 4.42, and 4.60 GeV to simulated events including both $\psi(2S) \to \chi_{c1(2)}\gamma$ and $\psi_2(3823) \to \chi_{c1(2)}\gamma$ together, with floating mass scale offset for $\psi(2S)$, $\psi_2(3823)$ mass floating (fixed to that above), and zero $\psi_2(3823)$ width.

$\psi_2(3823)$ REFERENCES

ABLIKIM	23J	JHEP 2302 171	M. Ablikim *et al.*	(BESIII Collab.)
AAIJ	22D	JHEP 2204 046	R. Aaij *et al.*	(LHCb Collab.)
ABLIKIM	22R	PRL 129 102003	M. Ablikim *et al.*	(BESIII Collab.)
PDG	22	PTEP 2022 083C01	R.L. Workman *et al.*	(PDG Collab.)
ABLIKIM	21O	PR D103 L091102	M. Ablikim *et al.*	(BESIII Collab.)
AAIJ	20S	JHEP 2008 123	R. Aaij *et al.*	(LHCb Collab.)
ABLIKIM	15S	PRL 115 011803	M. Ablikim *et al.*	(BESIII Collab.)
BHARDWAJ	13	PRL 111 032001	V. Bhardwaj *et al.*	(BELLE Collab.)

$\psi_3(3842)$

$I^G(J^{PC}) = 0^-(3^{--})$
J, P need confirmation.

J^P has not been measured, 3^- is the quark model prediction.

$\psi_3(3842)$ MASS

VALUE (MeV)	DOCUMENT ID		TECN	COMMENT
$3842.71 \pm 0.16 \pm 0.12$	AAIJ	19M	LHCB	$pp \to D\overline{D} +$ anything

$\psi_3(3842)$ WIDTH

VALUE (MeV)	DOCUMENT ID		TECN	COMMENT
$2.79 \pm 0.51 \pm 0.35$	AAIJ	19M	LHCB	$pp \to D\overline{D} +$ anything

$\psi_3(3842)$ DECAY MODES

	Mode	Fraction (Γ_i/Γ)
Γ_1	D^+D^-	seen
Γ_2	$D^0\overline{D}^0$	seen

$\psi_3(3842)$ BRANCHING RATIOS

$\Gamma(D^+D^-)/\Gamma_{total}$ — Γ_1/Γ

VALUE	DOCUMENT ID		TECN	COMMENT
seen	AAIJ	19M	LHCB	$pp \to D\overline{D} +$ anything
• • • We do not use the following data for averages, fits, limits, etc. • • •				
possibly seen	[1] ABLIKIM	22AL	BES3	$e^+e^- \to \pi^+\pi^- D^+D^-$

[1] From a fit to the $\pi^+\pi^-$ recoil mass for $e^+e^- \to D^+D^-\pi^+\pi^-$.

$\Gamma(D^0\overline{D}^0)/\Gamma_{total}$ — Γ_2/Γ

VALUE	DOCUMENT ID		TECN	COMMENT
seen	AAIJ	19M	LHCB	$pp \to D\overline{D} +$ anything

$\psi_3(3842)$ REFERENCES

ABLIKIM	22AL	PR D106 052012	M. Ablikim *et al.*	(BESIII Collab.)
AAIJ	19M	JHEP 1907 035	R. Aaij *et al.*	(LHCb Collab.)

$\chi_{c0}(3860)$

$I^G(J^{PC}) = 0^+(0^{++})$

OMITTED FROM SUMMARY TABLE

The assignment $J^P = 0^+$ is preferred over 2^+ by 2.5 sigma.

Observed by CHILIKIN 17 using full amplitude analysis of the process $e^+e^- \to J/\psi D\overline{D}$, where $D = D^0, D^+$. Not seen by AAIJ 20AI in the decay $B^+ \to D^+D^-K^+$.

$\chi_{c0}(3860)$ MASS

VALUE (MeV)	DOCUMENT ID		TECN	COMMENT
3862^{+26+40}_{-32-13}	CHILIKIN	17	BELL	$e^+e^- \to J/\psi D\overline{D}$

$\chi_{c0}(3860)$ WIDTH

VALUE (MeV)	DOCUMENT ID		TECN	COMMENT
$201^{+154+88}_{-67-82}$	CHILIKIN	17	BELL	$e^+e^- \to J/\psi D\overline{D}$

$\chi_{c0}(3860)$ DECAY MODES

	Mode	Fraction (Γ_i/Γ)
Γ_1	$D^0\overline{D}^0$	seen
Γ_2	D^+D^-	seen

$\chi_{c0}(3860)$ BRANCHING RATIOS

$\Gamma(D^0\overline{D}^0)/\Gamma_{total}$ — Γ_1/Γ

VALUE	DOCUMENT ID		TECN	COMMENT
seen	CHILIKIN	17	BELL	$e^+e^- \to J/\psi D^0\overline{D}^0$

$\Gamma(D^+D^-)/\Gamma_{total}$ — Γ_2/Γ

VALUE	DOCUMENT ID		TECN	COMMENT
seen	CHILIKIN	17	BELL	$e^+e^- \to J/\psi D^+D^-$

$\chi_{c0}(3860)$ REFERENCES

AAIJ	20AI	PR D102 112003	R. Aaij *et al.*	(LHCb Collab.)
CHILIKIN	17	PR D95 112003	K. Chilikin *et al.*	(BELLE Collab.) JPC

$\chi_{c1}(3872)$

$I^G(J^{PC}) = 0^+(1^{++})$

also known as $X(3872)$

This state shows properties different from a conventional $q\overline{q}$ state. A candidate for an exotic structure. See the review on non-$q\overline{q}$ states.

First observed by CHOI 03 in $B \to K\pi^+\pi^- J/\psi(1S)$ decays as a narrow peak in the invariant mass distribution of the $\pi^+\pi^- J/\psi(1S)$ final state. Isovector hypothesis excluded by AUBERT 05B and CHOI 11.

AAIJ 13Q perform a full five-dimensional amplitude analysis of the angular correlations between the decay products in $B^+ \to \chi_{c1}(3872)K^+$ decays, where $\chi_{c1}(3872) \to J/\psi\pi^+\pi^-$ and $J/\psi \to \mu^+\mu^-$, which unambiguously gives the $J^{PC} = 1^{++}$ assignment under the assumption that the $\pi^+\pi^-$ and J/ψ are in an S-wave. AAIJ 15AO extend this analysis with more data to limit D-wave contributions to $< 4\%$ at 95% CL.

See the review on "Spectroscopy of Mesons Containing Two Heavy Quarks."

$\chi_{c1}(3872)$ T-MATRIX POLE $\sqrt{s}$ relative to D^0D^{*+} threshold

VALUE (MeV)	DOCUMENT ID		TECN	COMMENT
$(0.01 \pm 0.15^{+0.07}_{-0.08} \pm 0.07) - i(0.19 \pm 0.08^{+0.14}_{-0.19})$ OUR ESTIMATE				
$(0.01 \pm 0.15^{+0.07}_{-0.08} \pm 0.07) - i(0.19 \pm 0.08^{+0.14}_{-0.19})$	[1,2] ABLIKIM	24C	BES3	$e^+e^- \to \gamma\chi_{c1}(3872)$

[1] From simultaneous line shape fits of $e^+e^- \to \gamma\chi_{c1}(3872) \to \gamma[D^0\overline{D}^0\pi^0]$ and $\gamma[J/\psi\pi^+\pi^-]$. The most prominent pole is reported at $7.04 \pm 0.15^{+0.07}_{-0.08}$ MeV above the $D^0\overline{D}^0\pi^0$ threshold of 3864.66 MeV on the first sheet with respect to the $D^{*0}\overline{D}^0$ channel. The uncertainty in the D^0 width is included in the uncertainty of the pole mass.

[2] The final uncertainty on the real part of the pole location comes from the uncertainty in the D^- and D^{*0} meson masses.

Int. J. Mod. Phys. A 2026.41. Downloaded from www.worldscientific.com
by CALIFORNIA @ BERKELEY on 09/16/26. Re-use and distribution is strictly not permitted, except for Open Access articles.

$\chi_{c1}(3872)$ T-MATRIX POLE $\sqrt{s}$

Note that $\Gamma = -2\,\mathrm{Im}(\sqrt{s})$.

VALUE (MeV)	DOCUMENT ID		TECN	COMMENT
$(3871.70 \pm 0.15^{+0.07}_{-0.08}) - i(0.19 \pm 0.08^{+0.14}_{-0.19})$ OUR ESTIMATE				
$(3871.70 \pm 0.15^{+0.07}_{-0.08}) - i(0.19 \pm 0.08^{+0.14}_{-0.19})$	[1] ABLIKIM	24C	BES3	$e^+e^- \to \gamma\chi_{c1}(3872)$

[1] From simultaneous line shape fits of $e^+e^- \to \gamma\chi_{c1}(3872) \to \gamma[D^0\overline{D}^0\pi^0]$ and $\gamma[J/\psi\pi^+\pi^-]$. The most prominent pole is reported at $7.04 \pm 0.15^{+0.07}_{-0.08}$ MeV above the $D^0\overline{D}^0\pi^0$ threshold of 3864.66 MeV on the first sheet with respect to the $D^{*0}\overline{D}^0$ channel. The uncertainty in the D^0 width is included in the uncertainty of the pole mass.

$\chi_{c1}(3872)$ MASS FROM $J/\psi X$ MODE

VALUE (MeV)	EVTS	DOCUMENT ID		TECN	COMMENT
3871.64 ± 0.06 OUR AVERAGE					
3870.2 ± 0.7 ± 0.3	24.6	ABLIKIM	23W	BES3	$e^+e^- \to J/\psi(1S)\pi^+\pi^-\omega$
3871.64 ± 0.06 ± 0.01	19.8k	[1] AAIJ	20S	LHCB	$B^+ \to J/\psi\pi^+\pi^-K^+$
3871.9 ± 0.7 ± 0.2	20	ABLIKIM	14	BES3	$e^+e^- \to J/\psi\pi^+\pi^-\gamma$
3871.95 ± 0.48 ± 0.12	0.6k	AAIJ	12H	LHCB	$pp \to J/\psi\pi^+\pi^-X$
3871.85 ± 0.27 ± 0.19	170	[2] CHOI	11	BELL	$B \to K\pi^+\pi^-J/\psi$
3873 $^{+1.8}_{-1.6}$ ± 1.3	27	[3] DEL-AMO-SA...	10B	BABR	$B \to \omega J/\psi K$
3871.61 ± 0.16 ± 0.19	6k	[3,4] AALTONEN	09AU	CDF2	$p\overline{p} \to J/\psi\pi^+\pi^-X$
3871.4 ± 0.6 ± 0.1	93.4	AUBERT	08Y	BABR	$B^+ \to K^+J/\psi\pi^+\pi^-$
3868.7 ± 1.5 ± 0.4	9.4	AUBERT	08Y	BABR	$B^0 \to K^0_S J/\psi\pi^+\pi^-$
3871.8 ± 3.1 ± 3.0	522	[3,5] ABAZOV	04F	D0	$p\overline{p} \to J/\psi\pi^+\pi^-X$
• • • We do not use the following data for averages, fits, limits, etc. • • •					
3871.57 ± 0.09	155	[6] AAIJ	23AP	LHCB	$B^0_s \to J/\psi 2(\pi^+\pi^-)$
3871.695 ± 0.067 ± 0.068	15.6k	[7] AAIJ	20AD	LHCB	$pp \to J/\psi\pi^+\pi^-X$
3871.59 ± 0.06 ± 0.03	4.2k	[8] AAIJ	20S	LHCB	$B^+ \to J/\psi\pi^+\pi^-K^+$
3873.3 ± 1.1 ± 1.0	45	[9] ABLIKIM	19V	BES	$e^+e^- \to \gamma\omega J/\psi$
3860.0 ± 10.4	13.6	[3,10] AGHASYAN	18A	COMP	$\gamma^* N \to X\pi^\pm N'$
3868.6 ± 1.2 ± 0.2	8	[11] AUBERT	06	BABR	$B^0 \to K^0_S J/\psi\pi^+\pi^-$
3871.3 ± 0.6 ± 0.1	61	[11] AUBERT	06	BABR	$B^- \to K^-J/\psi\pi^+\pi^-$
3873.4 ± 1.4	25	[12] AUBERT	05R	BABR	$B^+ \to K^+J/\psi\pi^+\pi^-$
3871.3 ± 0.7 ± 0.4	730	[3,13] ACOSTA	04	CDF2	$p\overline{p} \to J/\psi\pi^+\pi^-X$
3872.0 ± 0.6 ± 0.5	36	[14] CHOI	03	BELL	$B \to K\pi^+\pi^-J/\psi$
3836 ± 13	58	[3,15] ANTONIAZZI	94	E705	300 $\pi^\pm$Li $\to J/\psi\pi^+\pi^-X$

[1] Calculated from $m_{\chi_{c1}(3872)} - m_{\psi(2S)} = 185.54 \pm 0.06$ MeV obtained by combining the data with $\chi_{c1}(3872)$ produced in B^+ decays from AAIJ 20S and inclusive b-hadron decays from AAIJ 20AD and using $m_{\psi(2S)} = 3686.097$ MeV. Breit-Wigner parametrization.
[2] The mass difference for the $\chi_{c1}(3872)$ produced in B^+ and B^0 decays is $(-0.71 \pm 0.96 \pm 0.19)$ MeV.
[3] Width consistent with detector resolution.
[4] A possible equal mixture of two states with a mass difference greater than 3.6 MeV/c^2 is excluded at 95% CL.
[5] Calculated from the corresponding $m_{\chi_{c1}(3872)} - m_{J/\psi}$ using $m_{J/\psi}$=3096.916 MeV.
[6] From a fit of a relativistic S-wave Breit-Wigner convolved with the detector resolution. The width of $\chi_{c1}(3872)$ is constrained to the PDG 22 value. Systematic errors not evaluated.
[7] Using $\chi_{c1}(3872)$ produced in inclusive b-hadron decays and $m_{\psi(2S)} = 3686.097 \pm 0.010$ MeV. Breit-Wigner parametrization. Superseded by the combined value in AAIJ 20S.
[8] Using Breit-Wigner parametrization. Superseded by the combined value in AAIJ 20S.
[9] Fit with fixed width and including two resonances, $\chi_{c0}(3915)$ and $X(3960)$.
[10] Could be a different state.
[11] Calculated from the corresponding $m_{\chi_{c1}(3872)} - m_{\psi(2S)}$ using $m_{\psi(2S)} = 3686.093$ MeV. Superseded by AUBERT 08Y.
[12] Calculated from the corresponding $m_{\chi_{c1}(3872)} - m_{\psi(2S)}$ using $m_{\psi(2S)} = 3685.96$MeV. Superseded by AUBERT 06.
[13] Superseded by AALTONEN 09AU.
[14] Superseded by CHOI 11.
[15] A lower mass value can be due to an incorrect momentum scale for soft pions.

$\chi_{c1}(3872)$ MASS FROM $\overline{D}^{*0}D^0$ MODE

VALUE (MeV)	EVTS	DOCUMENT ID		TECN	COMMENT
• • • We do not use the following data for averages, fits, limits, etc. • • •					
$3873.71^{+0.56}_{-0.50} \pm 0.13$		[1] HIRATA	23	BELL	$B^0 \to D^0\overline{D}^{*0}K^0$, $B^+ \to D^0\overline{D}^{*0}K^+$
$3872.9^{+0.6}_{-0.4}{}^{+0.4}_{-0.5}$	50	[2,3] AUSHEV	10	BELL	$B \to \overline{D}^{*0}D^0K$
$3875.1^{+0.7}_{-0.5}$ ± 0.5	33 ± 6	[3] AUBERT	08B	BABR	$B \to \overline{D}^{*0}D^0K$
3875.2 ± 0.7 $^{+0.9}_{-1.8}$	24 ± 6	[3,4] GOKHROO	06	BELL	$B \to D^0\overline{D}^0\pi^0K$

[1] From a fit of a Breit-Wigner function with energy dependent width.
[2] Calculated from the measured $m_{\chi_{c1}(3872)} - m_{D^{*0}} - m_{\overline{D}^0} = 1.1^{+0.6}_{-0.4}{}^{+0.1}_{-0.3}$ MeV.
[3] Experiments report $D^{*0}\overline{D}^0$ invariant mass above $D^{*0}\overline{D}^0$ threshold because D^{*0} decay products are kinematically constrained to the D^{*0} mass, even though the D^{*0} may decay off-shell.
[4] Superseded by AUSHEV 10.

$m_{\chi_{c1}(3872)} - m_{J/\psi}$

VALUE (MeV)	EVTS	DOCUMENT ID		TECN	COMMENT
774.9±3.1±3.0	522	ABAZOV	04F	D0	$p\overline{p} \to J/\psi\pi^+\pi^-X$

$m_{\chi_{c1}(3872)} - m_{\psi(2S)}$

VALUE (MeV)	EVTS	DOCUMENT ID		TECN	COMMENT
• • • We do not use the following data for averages, fits, limits, etc. • • •					
185.598 ± 0.067 ± 0.068	15.6k	[1] AAIJ	20AD	LHCB	$pp \to J/\psi\pi^+\pi^-X$
185.54 ± 0.06	19.8k	[2] AAIJ	20S	LHCB	$pp \to J/\psi\pi^+\pi^-X$
187.4 ± 1.4	25	[3] AUBERT	05R	BABR	$B^+ \to K^+J/\psi\pi^+\pi^-$

[1] Using $\chi_{c1}(3872)$ produced in inclusive b-hadron decays. Breit-Wigner parametrization. Superseded by the combined value in AAIJ 20S.
[2] Combining $m_{\chi_{c1}(3872)} - m_{\psi(2S)} = 185.49 \pm 0.06 \pm 0.03$ MeV from AAIJ 20S and the measured mass difference from AAIJ 20AD. Breit-Wigner parametrization.
[3] Superseded by AUBERT 06.

$\chi_{c1}(3872)$ WIDTH

VALUE (MeV)	CL%	EVTS	DOCUMENT ID		TECN	COMMENT
1.19±0.21 OUR AVERAGE Error includes scale factor of 1.1.						
1.39 ± 0.24 ± 0.10		15.6k	[1] AAIJ	20AD	LHCB	$pp \to J/\psi\pi^+\pi^-X$
$0.96^{+0.19}_{-0.18}$ ± 0.21		4.2k	[2] AAIJ	20S	LHCB	$B^+ \to J/\psi\pi^+\pi^-K^+$
• • • We do not use the following data for averages, fits, limits, etc. • • •						
<2.4	90		ABLIKIM	14	BES3	$e^+e^- \to J/\psi\pi^+\pi^-\gamma$
<1.2	90		CHOI	11	BELL	$B \to K\pi^+\pi^-J/\psi$
<3.3	90		AUBERT	08Y	BABR	$B^+ \to K^+J/\psi\pi^+\pi^-$
<4.1	90	69	AUBERT	06	BABR	$B \to K\pi^+\pi^-J/\psi$
<2.3	90	36	[3] CHOI	03	BELL	$B \to K\pi^+\pi^-J/\psi$

[1] Using $\chi_{c1}(3872)$ produced in inclusive b-hadron decays. Breit-Wigner parametrization.
[2] Using Breit-Wigner parametrization. Partially overlapping dataset with that of AAIJ 20AD.
[3] Superseded by CHOI 11.

$\chi_{c1}(3872)$ WIDTH FROM $\overline{D}^{*0}D^0$ MODE

VALUE (MeV)	EVTS	DOCUMENT ID		TECN	COMMENT
• • • We do not use the following data for averages, fits, limits, etc. • • •					
$5.2^{+2.2}_{-1.5}$ ± 0.4		[1] HIRATA	23	BELL	$B^0 \to D^0\overline{D}^{*0}K^0$, $B^+ \to D^0\overline{D}^{*0}K^+$
$3.9^{+2.8}_{-1.4}{}^{+0.2}_{-1.1}$	50	[2] AUSHEV	10	BELL	$B \to \overline{D}^{*0}D^0K$
$3.0^{+1.9}_{-1.4}$ ± 0.9	33 ± 6	AUBERT	08B	BABR	$B \to \overline{D}^{*0}D^0K$

[1] From a fit of a Breit-Wigner function with energy dependent width.
[2] With a measured value of $B(B \to \chi_{c1}(3872)K) \times B(\chi_{c1}(3872) \to D^{*0}\overline{D}^0) = (0.80 \pm 0.20 \pm 0.10) \times 10^{-4}$, assumed to be equal for both charged and neutral modes.

$\chi_{c1}(3872)$ DECAY MODES

	Mode	Fraction (Γ_i/Γ)	Confidence level
Γ_1	e^+e^-	< 2.7 $\times 10^{-7}$	90%
Γ_2	$\pi^+\pi^-\pi^0$	< 1.0 %	90%
Γ_3	$\pi^+\pi^-J/\psi(1S)$	(4.3± 1.4) %	
Γ_4	$\pi^+\pi^-\pi^0J/\psi(1S)$	not seen	
Γ_5	$\omega\eta_c(1S)$	< 40 %	90%
Γ_6	$\rho(770)^0J/\psi(1S)$	(3.4± 1.1) %	
Γ_7	$\omega J/\psi(1S)$	(5.0± 1.9) %	
Γ_8	$\phi\phi$	not seen	
Γ_9	$D^0\overline{D}^0\pi^0$	(55 ±28) %	
Γ_{10}	$\overline{D}^{*0}D^0$	(46 ±16) %	
Γ_{11}	$\gamma\gamma$	< 13 %	90%
Γ_{12}	$D^0\overline{D}^0$	< 32 %	90%
Γ_{13}	D^+D^-	< 22 %	90%
Γ_{14}	$\pi^0\chi_{c2}$	< 5 %	90%
Γ_{15}	$\pi^0\chi_{c1}$	($3.8^{+1.9}_{-1.7}$) %	
Γ_{16}	$\pi^0\chi_{c0}$	< 16 %	90%
Γ_{17}	$\pi^+\pi^-\eta_c(1S)$	< 16 %	90%
Γ_{18}	$\pi^0\pi^0\chi_{c0}$	< 7 %	90%
Γ_{19}	$\pi^0\pi^0\chi_{c1}$	< 5 %	90%
Γ_{20}	$\pi^0\pi^0\chi_{c2}$	< 2.2 %	90%
Γ_{21}	$\pi^+\pi^-\chi_{c0}$	< 2.4 %	90%
Γ_{22}	$\pi^+\pi^-\chi_{c1}$	< 8 $\times 10^{-3}$	90%
Γ_{23}	$p\overline{p}$	< 2.7 $\times 10^{-5}$	95%
Γ_{24}	$\pi^+\pi^-\eta$	< 5 $\times 10^{-3}$	90%

Int. J. Mod. Phys. A 2026.41. Downloaded from www.worldscientific.com by UNIVERSITY OF CALIFORNIA @ BERKELEY on 09/16/26. Re-use and distribution is strictly not permitted, except for Open Access articles.

Radiative decays				
Γ_{25}	$\gamma D^+ D^-$	< 4	%	90%
Γ_{26}	$\gamma \overline{D}^0 D^0$	< 7	%	90%
Γ_{27}	$\gamma J/\psi$	$(10 \pm 4) \times 10^{-3}$		
Γ_{28}	$\gamma \chi_{c1}$	< 1.0	%	90%
Γ_{29}	$\gamma \chi_{c2}$	< 4	%	90%
Γ_{30}	$\gamma \psi(2S)$	possibly seen		
Γ_{31}	$\gamma \psi_2(3823)$	< 3.3	$\times 10^{-3}$	90%
***C*-violating decays**				
Γ_{32}	$\eta J/\psi$	< 2.1	%	90%

$\chi_{c1}(3872)$ PARTIAL WIDTHS

$\Gamma(e^+e^-)$ — Γ_1

VALUE (eV)	CL%	DOCUMENT ID		TECN	COMMENT
< 0.32	90	[1] ABLIKIM	23O	BES3	$e^+e^- \to \pi^+\pi^- J/\psi$
• • • We do not use the following data for averages, fits, limits, etc. • • •					
< 4.3	90	[2] ABLIKIM	15V	BES3	4.0–4.4 $e^+e^- \to \pi^+\pi^- J/\psi$
<280	90	[3] YUAN	04	RVUE	$e^+e^- \to \pi^+\pi^- J/\psi$

[1] Fit to cross section using a total width value of 1.19 ± 0.21 MeV and $B(\chi_{c1}(3872) \to \pi^+\pi^- J/\psi(1S)) = (3.8 \pm 1.2)\%$ from PDG 20.

[2] ABLIKIM 15V reports this limit from the measurement of $\Gamma(\chi_{c1}(3872) \to \pi^+\pi^- J/\psi(1S)) \times \Gamma(\chi_{c1}(3872) \to e^+e^-)/\Gamma < 0.13$ eV using $\Gamma(\chi_{c1}(3872) \to \pi^+\pi^- J/\psi(1S))/\Gamma = 3\%$.

[3] Using BAI 98E data on $e^+e^- \to \pi^+\pi^-\ell^+\ell^-$. Assuming that $\Gamma(\pi^+\pi^- J/\psi)$ of $\chi_{c1}(3872)$ is the same as that of $\psi(2S)$ (85.4 keV).

$\chi_{c1}(3872)$ $\Gamma(i)\Gamma(e^+e^-)/\Gamma(\text{total})$

$\Gamma(\pi^+\pi^- J/\psi(1S)) \times \Gamma(e^+e^-)/\Gamma_{\text{total}}$ — $\Gamma_3\Gamma_1/\Gamma$

VALUE (eV)	CL%	DOCUMENT ID		TECN	COMMENT
< 7.5 $\times 10^{-3}$	90	[1] ABLIKIM	23O	BES3	$e^+e^- \to \pi^+\pi^- J/\psi$
• • • We do not use the following data for averages, fits, limits, etc. • • •					
< 0.13	90	ABLIKIM	15V	BES3	4.0–4.4 $e^+e^- \to \pi^+\pi^- J/\psi$
< 6.2	90	[2,3] AUBERT	05D	BABR	10.6 $e^+e^- \to K^+K^-\pi^+\pi^-\gamma$
< 8.3	90	[3] DOBBS	05	CLE3	$e^+e^- \to \pi^+\pi^- J/\psi$
<10	90	[4] YUAN	04	RVUE	$e^+e^- \to \pi^+\pi^- J/\psi$

[1] Fit to cross section using a total width value of 1.19 ± 0.21 MeV from PDG 20.

[2] Using $B(\chi_{c1}(3872) \to J/\psi\pi^+\pi^-) \cdot B(J/\psi \to \mu^+\mu^-) \cdot \Gamma(\chi_{c1}(3872) \to e^+e^-) < 0.37$ eV from AUBERT 05D and $B(J/\psi \to \mu^+\mu^-) = 0.0588 \pm 0.0010$ from the PDG 04.

[3] Assuming $\chi_{c1}(3872)$ has $J^{PC} = 1^{--}$.

[4] Using BAI 98E data on $e^+e^- \to \pi^+\pi^-\ell^+\ell^-$. From theoretical calculation of the production cross section and using $B(J/\psi \to \mu^+\mu^-) = (5.88 \pm 0.10)\%$.

$\chi_{c1}(3872)$ $\Gamma(i)\Gamma(\gamma\gamma)/\Gamma(\text{total})$

$\Gamma(\pi^+\pi^- J/\psi(1S)) \times \Gamma(\gamma\gamma)/\Gamma_{\text{total}}$ — $\Gamma_3\Gamma_{11}/\Gamma$

VALUE (eV)	CL%	EVTS	DOCUMENT ID		TECN	COMMENT
• • • We do not use the following data for averages, fits, limits, etc. • • •						
$5.5^{+4.1}_{-3.8} \pm 0.7$		3	[1] TERAMOTO	21	BELL	$e^+e^- \to \gamma^*\gamma$ at $\Upsilon(nS)$
<12.9	90		[2] DOBBS	05	CLE3	$e^+e^- \to \pi^+\pi^- J/\psi\gamma$

[1] Measured in single-tag two-photon production assuming Q^2 dependence of a $c\overline{c}$ meson model. Here, $\Gamma(\chi_{c1}(3872) \to \gamma\gamma)$ is the reduced two-photon decay width, $\tilde{\Gamma}_{\gamma\gamma}$.

[2] Assuming $\chi_{c1}(3872)$ has positive C parity and spin 0.

$\Gamma(\omega J/\psi(1S)) \times \Gamma(\gamma\gamma)/\Gamma_{\text{total}}$ — $\Gamma_7\Gamma_{11}/\Gamma$

VALUE (eV)	CL%	DOCUMENT ID		TECN	COMMENT
• • • We do not use the following data for averages, fits, limits, etc. • • •					
<1.7	90	[1] LEES	12AD	BABR	$e^+e^- \to e^+e^-\omega J/\psi$

[1] Assuming $\chi_{c1}(3872)$ has spin 2.

$\Gamma(\pi^+\pi^-\eta_c(1S)) \times \Gamma(\gamma\gamma)/\Gamma_{\text{total}}$ — $\Gamma_{17}\Gamma_{11}/\Gamma$

VALUE (eV)	CL%	DOCUMENT ID		TECN	COMMENT
<11.1	90	LEES	12AE	BABR	$e^+e^- \to e^+e^-\pi^+\pi^-\eta_c$

$\chi_{c1}(3872)$ BRANCHING RATIOS

$\Gamma(\pi^+\pi^-\pi^0)/\Gamma_{\text{total}}$ — Γ_2/Γ

VALUE (%)	CL%	DOCUMENT ID		TECN	COMMENT
<1.0	90	[1,2] YIN	23	BELL	$B^+ \to \chi_{c1}(3872) K^+$
• • • We do not use the following data for averages, fits, limits, etc. • • •					
<1.3	90	[2,3] YIN	23	BELL	$B^0 \to \chi_{c1}(3872) K^0$

[1] YIN 23 reports $[\Gamma(\chi_{c1}(3872) \to \pi^+\pi^-\pi^0)/\Gamma_{\text{total}}] \times [B(B^+ \to \chi_{c1}(3872) K^+)] < 1.9 \times 10^{-6}$ which we divide by our best (shown rounded) value $B(B^+ \to \chi_{c1}(3872) K^+) = 1.9 \times 10^{-4}$.

[2] Assuming the decay products, $\pi^+\pi^-\pi^0$, are uniformly distributed in phase space. The limit is the 90% "credible" upper limit (i.e. Bayesian).

[3] YIN 23 reports $[\Gamma(\chi_{c1}(3872) \to \pi^+\pi^-\pi^0)/\Gamma_{\text{total}}] \times [B(B^0 \to \chi_{c1}(3872) K^0)] < 1.5 \times 10^{-6}$ which we divide by our best (shown rounded) value $B(B^0 \to \chi_{c1}(3872) K^0) = 1.1 \times 10^{-4}$.

$\Gamma(\pi^+\pi^- J/\psi(1S))/\Gamma_{\text{total}}$ — Γ_3/Γ

VALUE	EVTS	DOCUMENT ID		TECN	COMMENT
0.043±0.014 OUR AVERAGE					
0.043±0.002±0.013		[1] AAIJ	20S	LHCB	$B^+ \to J/\psi\pi^+\pi^- K^+$
0.047±0.005±0.015		[2] CHOI	11	BELL	$B^+ \to \pi^+\pi^- J/\psi K^+$
0.045±0.009±0.014	93	[3,4] AUBERT	08Y	BABR	$B \to \chi_{c1}(3872) K$
• • • We do not use the following data for averages, fits, limits, etc. • • •					
seen	151	[5] BALA	15	BELL	$B \to \chi_{c1}(3872) K\pi$
0.069±0.022±0.022	30	[6] AUBERT	05R	BABR	$B^+ \to K^+\pi^+\pi^- J/\psi$
0.074±0.016±0.023	36	[7] CHOI	03	BELL	$B^+ \to K^+\pi^+\pi^- J/\psi$

[1] AAIJ 20S reports $[\Gamma(\chi_{c1}(3872) \to \pi^+\pi^- J/\psi(1S))/\Gamma_{\text{total}}] \times [B(B^+ \to \chi_{c1}(3872) K^+)] = (7.95 \pm 0.15 \pm 0.33) \times 10^{-6}$ which we divide by our best (shown rounded) value $B(B^+ \to \chi_{c1}(3872) K^+) = (1.9 \pm 0.6) \times 10^{-4}$. Our first error is their experiment's error and our second error is the systematic error from using our best (shown rounded) value.

[2] CHOI 11 reports $[\Gamma(\chi_{c1}(3872) \to \pi^+\pi^- J/\psi(1S))/\Gamma_{\text{total}}] \times [B(B^+ \to \chi_{c1}(3872) K^+)] = (8.63 \pm 0.82 \pm 0.52) \times 10^{-6}$ which we divide by our best (shown rounded) value $B(B^+ \to \chi_{c1}(3872) K^+) = (1.9 \pm 0.6) \times 10^{-4}$. Our first error is their experiment's error and our second error is the systematic error from using our best (shown rounded) value.

[3] AUBERT 08Y reports $[\Gamma(\chi_{c1}(3872) \to \pi^+\pi^- J/\psi(1S))/\Gamma_{\text{total}}] \times [B(B^+ \to \chi_{c1}(3872) K^+)] = (8.4 \pm 1.5 \pm 0.7) \times 10^{-6}$ which we divide by our best (shown rounded) value $B(B^+ \to \chi_{c1}(3872) K^+) = (1.9 \pm 0.6) \times 10^{-4}$. Our first error is their experiment's error and our second error is the systematic error from using our best (shown rounded) value.

[4] superseded by LEES 20C

[5] BALA 15 reports $B(\chi_{c1}(3872) \to \pi^+\pi^- J/\psi) \times B(B^0 \to \chi_{c1}(3872) K^+\pi^-) = (7.9 \pm 1.3 \pm 0.4) \times 10^{-6}$ and $B(\chi_{c1}(3872) \to \pi^+\pi^- J/\psi) \times B(B^+ \to \chi_{c1}(3872) K^0\pi^+) = (10.6 \pm 3.0 \pm 0.9) \times 10^{-6}$.

[6] Superseded by AUBERT 08Y. AUBERT 05R reports $[\Gamma(\chi_{c1}(3872) \to \pi^+\pi^- J/\psi(1S))/\Gamma_{\text{total}}] \times [B(B^+ \to \chi_{c1}(3872) K^+)] = (1.28 \pm 0.41) \times 10^{-5}$ which we divide by our best (shown rounded) value $B(B^+ \to \chi_{c1}(3872) K^+) = (1.9 \pm 0.6) \times 10^{-4}$. Our first error is their experiment's error and our second error is the systematic error from using our best (shown rounded) value.

[7] CHOI 03 reports $[\Gamma(\chi_{c1}(3872) \to \pi^+\pi^- J/\psi(1S))/\Gamma_{\text{total}}] \times [B(B^+ \to \chi_{c1}(3872) K^+)] / [B(B^+ \to \psi(2S) K^+)] / [B(\psi(2S) \to J/\psi(1S)\pi^+\pi^-)] = 0.063 \pm 0.012 \pm 0.007$ which we multiply or divide by our best (shown rounded) values $B(B^+ \to \chi_{c1}(3872) K^+) = (1.9 \pm 0.6) \times 10^{-4}$, $B(B^+ \to \psi(2S) K^+) = (6.25 \pm 0.21) \times 10^{-4}$, $B(\psi(2S) \to J/\psi(1S)\pi^+\pi^-) = (34.78 \pm 0.33) \times 10^{-2}$. Our first error is their experiment's error and our second error is the systematic error from using our best (shown rounded) values.

$\Gamma(\pi^+\pi^-\pi^0 J/\psi(1S))/\Gamma_{\text{total}}$ — Γ_4/Γ

VALUE	DOCUMENT ID		TECN	COMMENT
not seen	[1] WANG	11B	BELL	$\Upsilon(2S) \to \gamma X$
not seen	[2] SHEN	10A	BELL	$\Upsilon(1S) \to \gamma X$

[1] WANG 11B reports $B(\Upsilon(2S) \to \gamma\chi_{c1}(3872)) \times B(\chi_{c1} \to \pi^+\pi^-\pi^0 J/\psi) < 2.4 \times 10^{-6}$ at 95% CL.

[2] SHEN 10A reports $B(\Upsilon(1S) \to \gamma\chi_{c1}(3872)) \times B(\chi_{c1} \to \pi^+\pi^-\pi^0 J/\psi) < 2.8 \times 10^{-6}$ at 95% CL.

$\Gamma(\omega\eta_c(1S))/\Gamma_{\text{total}}$ — Γ_5/Γ

VALUE	CL%	DOCUMENT ID		TECN	COMMENT
<0.4	90	[1] VINOKUROVA	15	BELL	$B^+ \to \omega\eta_c K^+$

[1] VINOKUROVA 15 reports $[\Gamma(\chi_{c1}(3872) \to \omega\eta_c(1S))/\Gamma_{\text{total}}] \times [B(B^+ \to \chi_{c1}(3872) K^+)] < 6.9 \times 10^{-5}$ which we divide by our best (shown rounded) value $B(B^+ \to \chi_{c1}(3872) K^+) = 1.9 \times 10^{-4}$.

$\Gamma(\rho(770)^0 J/\psi(1S))/\Gamma(\pi^+\pi^- J/\psi(1S))$ — Γ_6/Γ_3

VALUE (%)	DOCUMENT ID		TECN	COMMENT
78.6±2.3±2.0	[1] AAIJ	23S	LHCB	$B^+ \to K^+ J/\psi\pi^+\pi^-$

[1] Assuming pure ρ contribution only, i.e. excluding the contribution from ρ-ω interference. Using $B(\rho^0 \to \pi^+\pi^-) = 100\%$.

$\Gamma(\omega J/\psi(1S))/\Gamma_{\text{total}}$ — Γ_7/Γ

VALUE	EVTS	DOCUMENT ID		TECN	COMMENT
• • • We do not use the following data for averages, fits, limits, etc. • • •					
0.032±0.012±0.010	21 ± 7	[1] DEL-AMO-SA..10B		BABR	$B^+ \to \omega J/\psi K^+$

[1] DEL-AMO-SANCHEZ 10B reports $[\Gamma(\chi_{c1}(3872) \to \omega J/\psi(1S))/\Gamma_{\text{total}}] \times [B(B^+ \to \chi_{c1}(3872) K^+)] = (6 \pm 2 \pm 1) \times 10^{-6}$ which we divide by our best (shown rounded) value $B(B^+ \to \chi_{c1}(3872) K^+) = (1.9 \pm 0.6) \times 10^{-4}$. Our first error is their experiment's error and our second error is the systematic error from using our best (shown rounded) value. DEL-AMO-SANCHEZ 10B also reports $B(B^0 \to \chi_{c1}(3872) K^0) \times B(\chi_{c1}(3872) \to J/\psi\omega) = (6 \pm 3 \pm 1) \times 10^{-6}$.

Int. J. Mod. Phys. A 2026.41. Downloaded from www.worldscientific.com by CALIFORNIA @ BERKELEY on 09/16/26. Re-use and distribution is strictly not permitted, except for Open Access articles.

$\Gamma(\omega J/\psi(1S))/\Gamma(\pi^+\pi^- J/\psi(1S))$ — Γ_7/Γ_3

VALUE	DOCUMENT ID		TECN	COMMENT
1.16±0.24 OUR AVERAGE	Error includes scale factor of 1.2.			
1.24±0.33±0.10	[1,2] AAIJ	23S	LHCB	$B^+ \to K^+ J/\psi\pi^+\pi^-$
$1.6\ ^{+0.4}_{-0.3}\ \pm0.2$	[3] ABLIKIM	19V	BES	$e^+e^- \to \gamma\omega J/\psi$
0.8 ±0.3	[4] DEL-AMO-SA...	10B	BABR	$B \to \omega J/\psi K$

[1] AAIJ 23S reports $[\Gamma(\chi_{c1}(3872) \to \omega J/\psi(1S))/\Gamma(\chi_{c1}(3872) \to \pi^+\pi^- J/\psi(1S))] \times [B(\omega(782) \to \pi^+\pi^-)] = (1.9 \pm 0.4 \pm 0.3) \times 10^{-2}$ which we divide by our best (shown rounded) value $B(\omega(782) \to \pi^+\pi^-) = (1.53 \pm 0.12) \times 10^{-2}$. Our first error is their experiment's error and our second error is the systematic error from using our best (shown rounded) value.

[2] Excluding ρ-ω interference effects.

[3] Fit with fixed width and including two resonances, $\chi_{c0}(3915)$ and $X(3960)$.

[4] Statistical and systematic errors added in quadrature. Uses the values of $B(B \to \chi_{c1}(3872)K) \times B(\chi_{c1}(3872) \to J/\psi\pi^+\pi^-)$ reported in AUBERT 08Y, taking into account the common systematics.

$\Gamma(\phi\phi)/\Gamma_{total}$ — Γ_8/Γ

VALUE	DOCUMENT ID		TECN	COMMENT
not seen	[1] AAIJ	17BB	LHCB	pp at 7, 8 TeV

[1] AAIJ 17BB reports $B(b \to \chi_{c1}(3872)\,\text{anything}) \times B(\chi_{c1}(3872) \to \phi\phi) < 4.5 \times 10^{-7}$ at 95% CL.

$\Gamma(D^0\overline{D}^0\pi^0)/\Gamma_{total}$ — Γ_9/Γ

VALUE	CL%	EVTS	DOCUMENT ID		TECN	COMMENT
$\mathbf{0.55\ ^{+0.20}_{-0.23} \pm 0.17}$		17	[1] GOKHROO	06	BELL	$B^+ \to D^0\overline{D}^0\pi^0 K^+$
• • • We do not use the following data for averages, fits, limits, etc. • • •						
<0.32	90		[2] CHISTOV	04	BELL	Sup. by GOKHROO 06

[1] GOKHROO 06 reports $[\Gamma(\chi_{c1}(3872) \to D^0\overline{D}^0\pi^0)/\Gamma_{total}] \times [B(B^+ \to \chi_{c1}(3872)K^+)] = (1.02 \pm 0.31\ ^{+0.21}_{-0.29}) \times 10^{-4}$ which we divide by our best (shown rounded) value $B(B^+ \to \chi_{c1}(3872)K^+) = (1.9 \pm 0.6) \times 10^{-4}$. Our first error is their experiment's error and our second error is the systematic error from using our best (shown rounded) value.

[2] CHISTOV 04 reports $[\Gamma(\chi_{c1}(3872) \to D^0\overline{D}^0\pi^0)/\Gamma_{total}] \times [B(B^+ \to \chi_{c1}(3872)K^+)] < 0.6 \times 10^{-4}$ which we divide by our best (shown rounded) value $B(B^+ \to \chi_{c1}(3872)K^+) = 1.9 \times 10^{-4}$.

$\Gamma(D^0\overline{D}^0\pi^0)/\Gamma(\pi^+\pi^- J/\psi(1S))$ — Γ_9/Γ_3

VALUE	CL%	DOCUMENT ID	TECN	COMMENT
• • • We do not use the following data for averages, fits, limits, etc. • • •				
<1.16	90	ABLIKIM	20W	BES3 $e^+e^- \to \gamma\chi_{c1}(3872)$

$\Gamma(\overline{D}^{*0}D^0)/\Gamma_{total}$ — Γ_{10}/Γ

VALUE	EVTS	DOCUMENT ID		TECN	COMMENT
0.46±0.16 OUR AVERAGE					
$0.52\ ^{+0.13}_{-0.11} \pm 0.16$		[1,2] HIRATA	23	BELL	$e^+e^- \to \Upsilon(4S)$
$0.42 \pm 0.10 \pm 0.13$	$41\ ^{+9}_{-8}$	[3] AUSHEV	10	BELL	$B^+ \to D^{*0}\overline{D}^0 K^+$
• • • We do not use the following data for averages, fits, limits, etc. • • •					
$0.90 \pm 0.32 \pm 0.28$	27 ± 6	[4] AUBERT	08B	BABR	$B^+ \to \overline{D}^{*0}D^0 K^+$

[1] HIRATA 23 reports $[\Gamma(\chi_{c1}(3872) \to \overline{D}^{*0}D^0)/\Gamma_{total}] \times [B(B^+ \to \chi_{c1}(3872)K^+)] = (0.97\ ^{+0.21}_{-0.18} \pm 0.10) \times 10^{-4}$ which we divide by our best (shown rounded) value $B(B^+ \to \chi_{c1}(3872)K^+) = (1.9 \pm 0.6) \times 10^{-4}$. Our first error is their experiment's error and our second error is the systematic error from using our best (shown rounded) value.

[2] Assumes equal production of B^+ and B^0 at the $\Upsilon(4S)$.

[3] AUSHEV 10 reports $[\Gamma(\chi_{c1}(3872) \to \overline{D}^{*0}D^0)/\Gamma_{total}] \times [B(B^+ \to \chi_{c1}(3872)K^+)] = (0.77 \pm 0.16 \pm 0.10) \times 10^{-4}$ which we divide by our best (shown rounded) value $B(B^+ \to \chi_{c1}(3872)K^+) = (1.9 \pm 0.6) \times 10^{-4}$. Our first error is their experiment's error and our second error is the systematic error from using our best (shown rounded) value.

[4] AUBERT 08B reports $[\Gamma(\chi_{c1}(3872) \to \overline{D}^{*0}D^0)/\Gamma_{total}] \times [B(B^+ \to \chi_{c1}(3872)K^+)] = (1.67 \pm 0.36 \pm 0.47) \times 10^{-4}$ which we divide by our best (shown rounded) value $B(B^+ \to \chi_{c1}(3872)K^+) = (1.9 \pm 0.6) \times 10^{-4}$. Our first error is their experiment's error and our second error is the systematic error from using our best (shown rounded) value.

$\Gamma(\overline{D}^{*0}D^0)/\Gamma(\pi^+\pi^- J/\psi(1S))$ — Γ_{10}/Γ_3

VALUE	EVTS	DOCUMENT ID	TECN	COMMENT
11.77±3.09	50	ABLIKIM	20W	BES3 $e^+e^- \to \gamma\chi_{c1}(3872)$

$\Gamma(\gamma\gamma)/\Gamma_{total}$ — Γ_{11}/Γ

VALUE	CL%	DOCUMENT ID		TECN	COMMENT
<0.13	90	[1] WICHT	08	BELL	$e^+e^- \to \Upsilon(4S)$

[1] WICHT 08 reports $[\Gamma(\chi_{c1}(3872) \to \gamma\gamma)/\Gamma_{total}] \times [B(B^+ \to \chi_{c1}(3872)K^+)] < 2.4 \times 10^{-5}$ which we divide by our best (shown rounded) value $B(B^+ \to \chi_{c1}(3872)K^+) = 1.9 \times 10^{-4}$.

$\Gamma(D^0\overline{D}^0)/\Gamma_{total}$ — Γ_{12}/Γ

VALUE	CL%	DOCUMENT ID		TECN	COMMENT
<0.32	90	[1] CHISTOV	04	BELL	$B \to K D^0\overline{D}^0$

[1] CHISTOV 04 reports $[\Gamma(\chi_{c1}(3872) \to D^0\overline{D}^0)/\Gamma_{total}] \times [B(B^+ \to \chi_{c1}(3872)K^+)] < 6 \times 10^{-5}$ which we divide by our best (shown rounded) value $B(B^+ \to \chi_{c1}(3872)K^+) = 1.9 \times 10^{-4}$.

$\Gamma(D^+D^-)/\Gamma_{total}$ — Γ_{13}/Γ

VALUE	CL%	DOCUMENT ID		TECN	COMMENT
<0.22	90	[1] CHISTOV	04	BELL	$B \to K D^+D^-$

[1] CHISTOV 04 reports $[\Gamma(\chi_{c1}(3872) \to D^+D^-)/\Gamma_{total}] \times [B(B^+ \to \chi_{c1}(3872)K^+)] < 4 \times 10^{-5}$ which we divide by our best (shown rounded) value $B(B^+ \to \chi_{c1}(3872)K^+) = 1.9 \times 10^{-4}$.

$\Gamma(\pi^0\chi_{c2})/\Gamma(\pi^+\pi^- J/\psi(1S))$ — Γ_{14}/Γ_3

VALUE	CL%	DOCUMENT ID		TECN	COMMENT
<1.1	90	ABLIKIM	19U	BES3	$e^+e^- \to \gamma\chi_{c1}(3872)$

$\Gamma(\pi^0\chi_{c1})/\Gamma_{total}$ — Γ_{15}/Γ

VALUE	CL%	DOCUMENT ID		TECN	COMMENT
• • • We do not use the following data for averages, fits, limits, etc. • • •					
<0.04	90	[1] BHARDWAJ	19	BELL	$B^\pm \to \pi^0\chi_{c1}K^\pm$

[1] BHARDWAJ 19 reports $[\Gamma(\chi_{c1}(3872) \to \pi^0\chi_{c1})/\Gamma_{total}] \times [B(B^+ \to \chi_{c1}(3872)K^+)] < 8.1 \times 10^{-6}$ which we divide by our best (shown rounded) value $B(B^+ \to \chi_{c1}(3872)K^+) = 1.9 \times 10^{-4}$.

$\Gamma(\pi^0\chi_{c1})/\Gamma(\pi^+\pi^- J/\psi(1S))$ — Γ_{15}/Γ_3

VALUE (units 10^{-2})	EVTS	DOCUMENT ID		TECN	COMMENT
$\mathbf{88\ ^{+33}_{-27} \pm 10}$	10.8	ABLIKIM	19U	BES3	$e^+e^- \to \gamma\chi_{c1}(3872)$

$\Gamma(\pi^0\chi_{c0})/\Gamma(\pi^+\pi^- J/\psi(1S))$ — Γ_{16}/Γ_3

VALUE	CL%	DOCUMENT ID		TECN	COMMENT
< 3.6	90	ABLIKIM	22D	BES3	$e^+e^- \to \gamma\chi_{c1}(3872)$
• • • We do not use the following data for averages, fits, limits, etc. • • •					
<19	90	ABLIKIM	19U	BES3	$e^+e^- \to \gamma\chi_{c1}(3872)$

$\Gamma(\pi^+\pi^-\eta_c(1S))/\Gamma_{total}$ — Γ_{17}/Γ

VALUE	CL%	DOCUMENT ID		TECN	COMMENT
<0.16	90	[1] VINOKUROVA	15	BELL	$B^+ \to \pi^+\pi^-\eta_c K^+$

[1] VINOKUROVA 15 reports $[\Gamma(\chi_{c1}(3872) \to \pi^+\pi^-\eta_c(1S))/\Gamma_{total}] \times [B(B^+ \to \chi_{c1}(3872)K^+)] < 3.0 \times 10^{-5}$ which we divide by our best (shown rounded) value $B(B^+ \to \chi_{c1}(3872)K^+) = 1.9 \times 10^{-4}$.

$\Gamma(\pi^0\pi^0\chi_{c0})/\Gamma(\pi^+\pi^- J/\psi(1S))$ — Γ_{18}/Γ_3

VALUE	CL%	DOCUMENT ID		TECN	COMMENT
<1.7	90	ABLIKIM	22D	BES3	$e^+e^- \to \gamma\chi_{c1}(3872)$

$\Gamma(\pi^0\pi^0\chi_{c1})/\Gamma(\pi^+\pi^- J/\psi(1S))$ — Γ_{19}/Γ_3

VALUE	CL%	DOCUMENT ID		TECN	COMMENT
<1.1	90	ABLIKIM	24BU	BES3	$e^+e^- \to \gamma\chi_{c1}(3872)$

$\Gamma(\pi^0\pi^0\chi_{c2})/\Gamma(\pi^+\pi^- J/\psi(1S))$ — Γ_{20}/Γ_3

VALUE	CL%	DOCUMENT ID		TECN	COMMENT
<0.5	90	ABLIKIM	24BU	BES3	$e^+e^- \to \gamma\chi_{c1}(3872)$

$\Gamma(\pi^+\pi^-\chi_{c0})/\Gamma(\pi^+\pi^- J/\psi(1S))$ — Γ_{21}/Γ_3

VALUE	CL%	DOCUMENT ID		TECN	COMMENT
<0.56	90	ABLIKIM	22D	BES3	$e^+e^- \to \gamma\chi_{c1}(3872)$

$\Gamma(\pi^+\pi^-\chi_{c1})/\Gamma_{total}$ — Γ_{22}/Γ

VALUE	CL%	DOCUMENT ID		TECN	COMMENT
$<8 \times 10^{-3}$	90	[1] BHARDWAJ	16	BELL	$B^+ \to \pi^+\pi^-\chi_{c1}K^+$

[1] BHARDWAJ 16 reports $[\Gamma(\chi_{c1}(3872) \to \pi^+\pi^-\chi_{c1})/\Gamma_{total}] \times [B(B^+ \to \chi_{c1}(3872)K^+)] < 1.5 \times 10^{-6}$ which we divide by our best (shown rounded) value $B(B^+ \to \chi_{c1}(3872)K^+) = 1.9 \times 10^{-4}$.

$\Gamma(p\overline{p})/\Gamma_{total}$ — Γ_{23}/Γ

VALUE	CL%	DOCUMENT ID		TECN	COMMENT
$<2.7 \times 10^{-5}$	95	[1] AAIJ	17AD	LHCB	$B^+ \to p\overline{p}K^+$
• • • We do not use the following data for averages, fits, limits, etc. • • •					
$<9 \times 10^{-5}$	95	[2] AAIJ	13S	LHCB	$B^+ \to p\overline{p}K^+$

[1] AAIJ 17AD reports $[\Gamma(\chi_{c1}(3872) \to p\overline{p})/\Gamma_{total}] \times [B(B^+ \to \chi_{c1}(3872)K^+)] < 0.5 \times 10^{-8}$ which we divide by our best (shown rounded) value $B(B^+ \to \chi_{c1}(3872)K^+) = 1.9 \times 10^{-4}$.

[2] AAIJ 13S reports $[\Gamma(\chi_{c1}(3872) \to p\overline{p})/\Gamma_{total}] \times [B(B^+ \to \chi_{c1}(3872)K^+)] < 1.7 \times 10^{-8}$ which we divide by our best (shown rounded) value $B(B^+ \to \chi_{c1}(3872)K^+) = 1.9 \times 10^{-4}$.

$\Gamma(\pi^+\pi^-\eta)/\Gamma(\pi^+\pi^- J/\psi(1S))$ — Γ_{24}/Γ_3

VALUE	CL%	DOCUMENT ID		TECN	COMMENT
<0.12	90	ABLIKIM	24K	BES3	$e^+e^- \to \gamma\chi_{c1}(3872)$

Radiative decays

$\Gamma(\gamma D^+D^-)/\Gamma(\pi^+\pi^- J/\psi(1S))$ — Γ_{25}/Γ_3

VALUE	CL%	DOCUMENT ID		TECN	COMMENT
<0.99	90	ABLIKIM	20W	BES3	$e^+e^- \to \gamma\chi_{c1}(3872)$

Int. J. Mod. Phys. A 2026.41. Downloaded from www.worldscientific.com by UNIVERSITY OF CALIFORNIA @ BERKELEY on 09/16/26. Re-use and distribution is strictly not permitted, except for Open Access articles.

$\Gamma(\gamma \overline{D}^0 D^0)/\Gamma(\pi^+\pi^- J/\psi(1S))$ — Γ_{26}/Γ_3

VALUE	CL%	DOCUMENT ID		TECN	COMMENT
<1.58	90	ABLIKIM	20W	BES3	$e^+e^- \to \gamma\chi_{c1}(3872)$

$\Gamma(\gamma J/\psi)/\Gamma_{total}$ — Γ_{27}/Γ

VALUE (units 10^{-3})	EVTS	DOCUMENT ID		TECN	COMMENT
$9.6^{+2.7}_{-2.5}\pm3.0$		[1] BHARDWAJ	11	BELL	$B^\pm \to \gamma J/\psi K^\pm$
• • • We do not use the following data for averages, fits, limits, etc. • • •					
15 ±4 ±5	20	[2] AUBERT	09B	BABR	$B^+ \to \gamma J/\psi K^+$
18 ±6 ±6	19	[3] AUBERT,BE	06M	BABR	$B^+ \to \gamma J/\psi K^+$

[1] BHARDWAJ 11 reports $[\Gamma(\chi_{c1}(3872) \to \gamma J/\psi)/\Gamma_{total}] \times [B(B^+ \to \chi_{c1}(3872) K^+)] = (1.78^{+0.48}_{-0.44} \pm 0.12) \times 10^{-6}$ which we divide by our best (shown rounded) value $B(B^+ \to \chi_{c1}(3872) K^+) = (1.9 \pm 0.6) \times 10^{-4}$. Our first error is their experiment's error and our second error is the systematic error from using our best (shown rounded) value.

[2] AUBERT 09B reports $[\Gamma(\chi_{c1}(3872) \to \gamma J/\psi)/\Gamma_{total}] \times [B(B^+ \to \chi_{c1}(3872) K^+)] = (2.8 \pm 0.8 \pm 0.1) \times 10^{-6}$ which we divide by our best (shown rounded) value $B(B^+ \to \chi_{c1}(3872) K^+) = (1.9 \pm 0.6) \times 10^{-4}$. Our first error is their experiment's error and our second error is the systematic error from using our best (shown rounded) value.

[3] Superseded by AUBERT 09B. AUBERT,BE 06M reports $[\Gamma(\chi_{c1}(3872) \to \gamma J/\psi)/\Gamma_{total}] \times [B(B^+ \to \chi_{c1}(3872) K^+)] = (3.3 \pm 1.0 \pm 0.3) \times 10^{-6}$ which we divide by our best (shown rounded) value $B(B^+ \to \chi_{c1}(3872) K^+) = (1.9 \pm 0.6) \times 10^{-4}$. Our first error is their experiment's error and our second error is the systematic error from using our best (shown rounded) value.

$\Gamma(\gamma J/\psi)/\Gamma(\pi^+\pi^- J/\psi(1S))$ — Γ_{27}/Γ_3

VALUE	EVTS	DOCUMENT ID		TECN	COMMENT
0.52±0.19 OUR AVERAGE Error includes scale factor of 1.2.					
0.38±0.20±0.01	8 ± 4	ABLIKIM	24X	BES3	$e^+e^- \to \omega\chi_{c1}(3872)$
0.79±0.28		ABLIKIM	20W	BES3	$e^+e^- \to \gamma\chi_{c1}(3872)$

$\Gamma(\gamma\chi_{c1})/\Gamma_{total}$ — Γ_{28}/Γ

VALUE	CL%	DOCUMENT ID		TECN	COMMENT
<0.010	90	[1] BHARDWAJ	13	BELL	$B^\pm \to \chi_{c1}\gamma K^\pm$

[1] BHARDWAJ 13 reports $[\Gamma(\chi_{c1}(3872) \to \gamma\chi_{c1})/\Gamma_{total}] \times [B(B^+ \to \chi_{c1}(3872) K^+)] < 1.9 \times 10^{-6}$ which we divide by our best (shown rounded) value $B(B^+ \to \chi_{c1}(3872) K^+) = 1.9 \times 10^{-4}$.

$\Gamma(\gamma\chi_{c1})/\Gamma(\pi^+\pi^- J/\psi(1S))$ — Γ_{28}/Γ_3

VALUE	CL%	DOCUMENT ID		TECN	COMMENT
<0.89	90	CHOI	03	BELL	$B \to K\pi^+\pi^- J/\psi$

$\Gamma(\gamma\chi_{c2})/\Gamma_{total}$ — Γ_{29}/Γ

VALUE	CL%	DOCUMENT ID		TECN	COMMENT
<0.04	90	[1] BHARDWAJ	13	BELL	$B^\pm \to \chi_{c2}\gamma K^\pm$

[1] BHARDWAJ 13 reports $[\Gamma(\chi_{c1}(3872) \to \gamma\chi_{c2})/\Gamma_{total}] \times [B(B^+ \to \chi_{c1}(3872) K^+)] < 6.7 \times 10^{-6}$ which we divide by our best (shown rounded) value $B(B^+ \to \chi_{c1}(3872) K^+) = 1.9 \times 10^{-4}$.

$\Gamma(\gamma\psi(2S))/\Gamma_{total}$ — Γ_{30}/Γ

VALUE	EVTS	DOCUMENT ID		TECN	COMMENT
possibly seen	36 ± 9	[1] AAIJ	14AH	LHCB	$B^+ \to \gamma\psi(2S) K^+$
• • • We do not use the following data for averages, fits, limits, etc. • • •					
not seen		[2] BHARDWAJ	11	BELL	$B^+ \to \gamma\psi(2S) K^+$
0.051±0.015±0.016	25 ± 7	[3] AUBERT	09B	BABR	$B^+ \to \gamma\psi(2S) K^+$

[1] From 36.4 ± 9.0 events of $\chi_{c1}(3872) \to J/\psi\gamma$ decays with a statistical significance of 4.4σ.

[2] BHARDWAJ 11 reports $B(B^+ \to K^+\chi_{c1}(3872)) \times B(\chi_{c1} \to \gamma\psi(2S)) < 3.45 \times 10^{-6}$ at 90% CL.

[3] AUBERT 09B reports $[\Gamma(\chi_{c1}(3872) \to \gamma\psi(2S))/\Gamma_{total}] \times [B(B^+ \to \chi_{c1}(3872) K^+)] = (9.5 \pm 2.7 \pm 0.6) \times 10^{-6}$ which we divide by our best (shown rounded) value $B(B^+ \to \chi_{c1}(3872) K^+) = (1.9 \pm 0.6) \times 10^{-4}$. Our first error is their experiment's error and our second error is the systematic error from using our best (shown rounded) value.

$\Gamma(\gamma\psi(2S))/\Gamma(\pi^+\pi^- J/\psi(1S))$ — Γ_{30}/Γ_3

VALUE	CL%	DOCUMENT ID		TECN	COMMENT
<0.42	90	ABLIKIM	20W	BES3	$e^+e^- \to \gamma\chi_{c1}(3872)$

$\Gamma(\pi^+\pi^-\chi_{c1})/\Gamma(\pi^+\pi^- J/\psi(1S))$ — Γ_{22}/Γ_3

VALUE	CL%	DOCUMENT ID		TECN	COMMENT
<0.18	90	ABLIKIM	24S	BES3	$e^+e^- \to \gamma\chi_{c1}(3872)$

$\Gamma(\gamma\psi(2S))/\Gamma(\gamma J/\psi)$ — Γ_{30}/Γ_{27}

VALUE	CL%	EVTS	DOCUMENT ID		TECN	COMMENT
1.67±0.21±0.13			[1] AAIJ	24AD	LHCB	$B^+ \to \gamma\psi(2S) K^+$ and $\gamma J/\psi K^+$
• • • We do not use the following data for averages, fits, limits, etc. • • •						
<0.59	90		ABLIKIM	20W	BES3	$e^+e^- \to \gamma\chi_{c1}(3872)$
2.46±0.64±0.29		36 ± 9	[2] AAIJ	14AH	LHCB	$B^+ \to \gamma\psi(2S) K^+$
<2.1	90		BHARDWAJ	11	BELL	$B^+ \to \gamma\psi(2S) K^+$
3.4 ±1.4			AUBERT	09B	BABR	$B^+ \to \gamma c\overline{c} K'$

[1] AAIJ 24AD reports this ratio as 1.67 ± 0.21 ± 0.12 ± 0.04 where the last uncertainty is due to the uncertainties of the branching fractions of $\psi(2S)$ and J/ψ mesons. We have added the last two uncertainties in quadrature.

[2] From 36.4 ± 9.0 events of $\chi_{c1}(3872) \to J/\psi\gamma$ decays with a statistical significance of 4.4σ. Superseded by AAIJ 24AD.

$\Gamma(\gamma\psi_2(3823))/\Gamma(\pi^+\pi^- J/\psi(1S))$ — Γ_{31}/Γ_3

VALUE	CL%	DOCUMENT ID		TECN	COMMENT
<0.075	90	[1] ABLIKIM	24Z	BES3	$e^+e^- \to \gamma\psi_2(3823)$

[1] Using $B(\chi_{c1}(1P) \to \gamma J/\psi(1S)) = 0.343 \pm 0.010$. We have assumed that $B(\psi_2(3823) \to \gamma\chi_{c1}) = 1$.

C-violating decays

$\Gamma(\eta J/\psi)/\Gamma_{total}$ — Γ_{32}/Γ

VALUE	CL%	DOCUMENT ID		TECN	COMMENT
<0.021	90	[1,2] IWASHITA	14	BELL	$B \to K\eta J/\psi$
• • • We do not use the following data for averages, fits, limits, etc. • • •					
<0.04	90	[3] AUBERT	04Y	BABR	$B \to K\eta J/\psi$

[1] IWASHITA 14 reports $[\Gamma(\chi_{c1}(3872) \to \eta J/\psi)/\Gamma_{total}] \times [B(B^+ \to \chi_{c1}(3872) K^+)] < 3.8 \times 10^{-6}$ which we divide by our best (shown rounded) value $B(B^+ \to \chi_{c1}(3872) K^+) = 1.9 \times 10^{-4}$.

[2] IWASHITA 14 also scans the $\eta J/\psi$ mass range 3.8–4.75 GeV and sets upper limits for $B(B^\pm \to \chi_{c1}(3872) K^\pm) \times B(\chi_{c1}(3872) \to \eta J/\psi)$ in 5 MeV intervals.

[3] AUBERT 04Y reports $[\Gamma(\chi_{c1}(3872) \to \eta J/\psi)/\Gamma_{total}] \times [B(B^+ \to \chi_{c1}(3872) K^+)] < 7.7 \times 10^{-6}$ which we divide by our best (shown rounded) value $B(B^+ \to \chi_{c1}(3872) K^+) = 1.9 \times 10^{-4}$.

$\chi_{c1}(3872)$ REFERENCES

AAIJ	24AD	JHEP 2411 121	R. Aaij *et al.*	(LHCb Collab.)
ABLIKIM	24BU	PR D110 072015	M. Ablikim *et al.*	(BESIII Collab.)
ABLIKIM	24C	PRL 132 151903	M. Ablikim *et al.*	(BESIII Collab.)
ABLIKIM	24K	PR D109 L011102	M. Ablikim *et al.*	(BESIII Collab.)
ABLIKIM	24S	PR D109 L071101	M. Ablikim *et al.*	(BESIII Collab.)
ABLIKIM	24X	PR D110 012006	M. Ablikim *et al.*	(BESIII Collab.)
ABLIKIM	24Z	PR D110 012012	M. Ablikim *et al.*	(BESIII Collab.)
AAIJ	23AP	JHEP 2307 084	R. Aaij *et al.*	(LHCb Collab.)
AAIJ	23S	PR D108 L011103	R. Aaij *et al.*	(LHCb Collab.)
ABLIKIM	23O	PR D107 032007	M. Ablikim *et al.*	(BESIII Collab.)
ABLIKIM	23W	PRL 130 151904	M. Ablikim *et al.*	(BESIII Collab.)
HIRATA	23	PR D107 112011	H. Hirata *et al.*	(BELLE Collab.)
YIN	23	PR D107 052004	J.H. Yin *et al.*	(BELLE Collab.)
ABLIKIM	22D	PR D105 072009	M. Ablikim *et al.*	(BESIII Collab.)
PDG	22	PTEP 2022 083C01	R.L. Workman *et al.*	(PDG Collab.)
TERAMOTO	21	PRL 126 122001	Y. Teramoto *et al.*	(BELLE Collab.)
AAIJ	20AD	PR D102 092005	R. Aaij *et al.*	(LHCb Collab.)
AAIJ	20S	JHEP 2008 123	R. Aaij *et al.*	(LHCb Collab.)
ABLIKIM	20W	PRL 124 242001	M. Ablikim *et al.*	(BESIII Collab.)
LEES	20C	PRL 124 152001	J.P. Lees *et al.*	(BABAR Collab.)
PDG	20	PTEP 2020 083C01	P.A. Zyla *et al.*	(PDG Collab.)
ABLIKIM	19U	PRL 122 202001	M. Ablikim *et al.*	(BESIII Collab.)
ABLIKIM	19V	PRL 122 232002	M. Ablikim *et al.*	(BESIII Collab.)
BHARDWAJ	19	PR D99 111101	V. Bhardwaj *et al.*	(BELLE Collab.)
AGHASYAN	18A	PL B783 334	M. Aghasyan *et al.*	(COMPASS Collab.)
AAIJ	17AD	PL B769 305	R. Aaij *et al.*	(LHCb Collab.)
AAIJ	17BB	EPJ C77 609	R. Aaij *et al.*	(LHCb Collab.)
BHARDWAJ	16	PR D93 052016	V. Bhardwaj *et al.*	(BELLE Collab.)
AAIJ	15AO	PR D92 011102	R. Aaij *et al.*	(LHCb Collab.)
ABLIKIM	15V	PL B749 414	M. Ablikim *et al.*	(BESIII Collab.)
BALA	15	PR D91 051101	A. Bala *et al.*	(BELLE Collab.)
VINOKUROVA	15	JHEP 1506 132	A. Vinokurova *et al.*	(BELLE Collab.)
Also		JHEP 1702 088 (errat.)	A. Vinokurava *et al.*	(BELLE Collab.)
AAIJ	14AH	NP B886 665	R. Aaij *et al.*	(LHCb Collab.)
ABLIKIM	14	PRL 112 092001	M. Ablikim *et al.*	(BESIII Collab.)
IWASHITA	14	PTEP 2014 043C01	T. Iwashita *et al.*	(BELLE Collab.)
AAIJ	13Q	PRL 110 222001	R. Aaij *et al.*	(LHCb Collab.) JP
AAIJ	13S	EPJ C73 2462	R. Aaij *et al.*	(LHCb Collab.)
BHARDWAJ	13	PRL 111 032001	V. Bhardwaj *et al.*	(BELLE Collab.)
AAIJ	12H	EPJ C72 1972	R. Aaij *et al.*	(LHCb Collab.)
LEES	12AD	PR D86 072002	J.P. Lees *et al.*	(BABAR Collab.)
LEES	12AE	PR D86 092005	J.P. Lees *et al.*	(BABAR Collab.)
BHARDWAJ	11	PRL 107 091803	V. Bhardwaj *et al.*	(BELLE Collab.)
CHOI	11	PR D84 052004	S.-K. Choi *et al.*	(BELLE Collab.)
WANG	11B	PR D84 071107	X.L. Wang *et al.*	(BELLE Collab.)
AUSHEV	10	PR D81 031103	T. Aushev *et al.*	(BELLE Collab.)
DEL-AMO-SA...	10B	PR D82 011101	P. del Amo Sanchez *et al.*	(BABAR Collab.)
SHEN	10A	PR D82 051504	C.P. Shen *et al.*	(BELLE Collab.)
AALTONEN	09AU	PRL 103 152001	T. Aaltonen *et al.*	(CDF Collab.)
AUBERT	09B	PRL 102 132001	B. Aubert *et al.*	(BABAR Collab.)
AUBERT	08B	PR D77 011102	B. Aubert *et al.*	(BABAR Collab.)
AUBERT	08Y	PR D77 111101	B. Aubert *et al.*	(BABAR Collab.)
WICHT	08	PL B662 323	J. Wicht *et al.*	(BELLE Collab.)
AUBERT	06	PR D73 011101	B. Aubert *et al.*	(BABAR Collab.)
AUBERT,BE	06M	PR D74 071101	B. Aubert *et al.*	(BABAR Collab.)
GOKHROO	06	PRL 97 162002	G. Gokhroo *et al.*	(BELLE Collab.)
AUBERT	05B	PR D71 031501	B. Aubert *et al.*	(BABAR Collab.)
AUBERT	05D	PR D71 052001	B. Aubert *et al.*	(BABAR Collab.)
AUBERT	05R	PR D71 071103	B. Aubert *et al.*	(BABAR Collab.)
DOBBS	05	PRL 94 032004	S. Dobbs *et al.*	(CLEO Collab.)
ABAZOV	04F	PRL 93 162002	V.M. Abazov *et al.*	(D0 Collab.)
ACOSTA	04	PRL 93 072001	D. Acosta *et al.*	(CDF Collab.)
AUBERT	04Y	PRL 93 041801	B. Aubert *et al.*	(BABAR Collab.)
CHISTOV	04	PRL 93 051803	R. Chistov *et al.*	(BELLE Collab.)
PDG	04	PL B592 1	S. Eidelman *et al.*	(PDG Collab.)
YUAN	04	PL B579 74	C.Z. Yuan *et al.*	
CHOI	03	PRL 91 262001	S.-K. Choi *et al.*	(BELLE Collab.)
BAI	98E	PR D57 3854	J.Z. Bai *et al.*	(BES Collab.)
ANTONIAZZI	94	PR D50 4258	L. Antoniazzi *et al.*	(E705 Collab.)

Int. J. Mod. Phys. A 2026.41. Downloaded from www.worldscientific.com
by CALIFORNIA @ BERKELEY on 09/16/26. Re-use and distribution is strictly not permitted, except for Open Access articles.

$\chi_{c0}(3915)$

$I^G(J^{PC}) = 0^+(0^{++})$

was $X(3915)$

The $\chi_{c0}(3915)$ was originally seen by BELLE in its $\omega J/\psi$ decay mode and was produced in both B decays in CHOI 05 and $\gamma\gamma$ collisions in UEHARA 10. The J^{PC} was determined to be 0^{++} by BABAR in LEES 12AD but this assignment was questioned by ZHOU 15C. In AAIJ 20AI LHCb found the D^+D^- decay mode of the $\chi_{c0}(3915)$ using B decays and determined its J^{PC} to be 0^{++}. Based on their compatible mass, width, and J^{PC}, we assume the state decaying to $\omega J/\psi$ and the state decaying to D^+D^- are both the $\chi_{c0}(3915)$. See also the $\chi_{c2}(3930)$.

$\chi_{c0}(3915)$ MASS

VALUE (MeV)	EVTS	DOCUMENT ID		TECN	COMMENT
3922.1± 1.8 OUR AVERAGE		Error includes scale factor of 1.5. See the ideogram below.			
3956 ± 5 ±10	360	[1] AAIJ	23AA	LHCB	$B^+ \to D_s^+ D_s^- K^+$
3923.8± 1.5± 0.4	1.2k	[2] AAIJ	20AI	LHCB	$B^+ \to D^+ D^- K^+$
3919.4± 2.2± 1.6	59 ± 10	LEES	12AD	BABR	$e^+e^- \to e^+e^-\omega J/\psi$
$3919.1^{+3.8}_{-3.4}$± 2.0		DEL-AMO-SA...	10B	BABR	$B \to \omega J/\psi K$
3915 ± 3 ± 2	49 ± 15	UEHARA	10	BELL	10.6 $e^+e^- \to e^+e^-\omega J/\psi$
3943 ±11 ±13	58 ± 11	[3] CHOI	05	BELL	$B \to \omega J/\psi K$
• • • We do not use the following data for averages, fits, limits, etc. • • •					
3920.9± 0.9		[4] LI	24	RVUE	$\omega J/\psi$ invariant mass
3922.4± 6.5± 2.0		[5] WANG	22A	BELL	$\gamma\gamma \to \gamma\psi(2S)$
3926.4± 2.2± 1.2		[6] ABLIKIM	19V	BES	$e^+e^- \to \gamma\omega J/\psi$
$3914.6^{+3.8}_{-3.4}$± 2.0		[3] AUBERT	08W	BABR	Superseded by DEL-AMO-SANCHEZ 10B

[1] $D_s^+ D_s^-$ near-threshold enhancement parameterized with a Flatte-like function .
[2] Obtained from the full amplitude analysis. Parameterized with the relativistic Breit-Wigner line shape.
[3] $\omega J/\psi$ threshold enhancement fitted as an S-wave Breit-Wigner resonance.
[4] From a simultaneous χ^2 fit to the distributions of the $\omega J/\psi$ invariant mass measured by BaBar and Belle in the processes $\gamma\gamma \to \omega J/\psi$ and $B \to \omega J/\psi K$. LHCb results also taken into account as an additional constraint in the χ^2 calculation.
[5] Not distinguished from the $\chi_{c2}(3930)$.
[6] Could also be $X(3940)$. Significance 3.1σ. Fit with additional resonance at 3963.7 ± 5.7 MeV, significance 3.4σ.

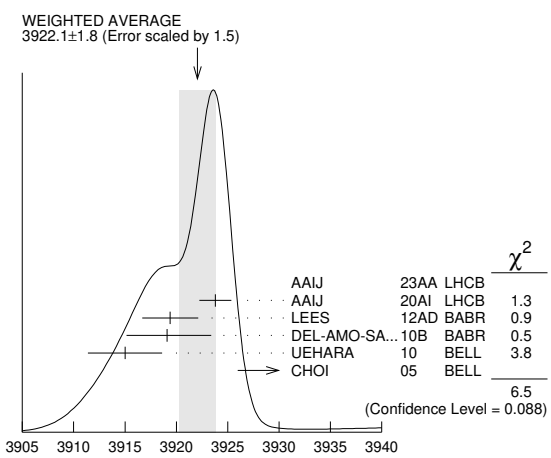

$\chi_{c0}(3915)$ MASS (MeV)

$\chi_{c0}(3915)$ WIDTH

VALUE (MeV)	EVTS	DOCUMENT ID		TECN	COMMENT
20 ± 4 OUR AVERAGE		Error includes scale factor of 1.1.			
43 ±13 ± 8	360	[1] AAIJ	23AA	LHCB	$B^+ \to D_s^+ D_s^- K^+$
17.4± 5.1± 0.8	1.2k	[2] AAIJ	20AI	LHCB	$B^+ \to D^+ D^- K^+$
13 ± 6 ± 3	59	LEES	12AD	BABR	$e^+e^- \to e^+e^-\omega J/\psi$
31^{+10}_{-8} ± 5		DEL-AMO-SA...	10B	BABR	$B \to \omega J/\psi K$
17 ±10 ± 3	49	UEHARA	10	BELL	10.6 $e^+e^- \to e^+e^-\omega J/\psi$
87 ±22 ±26	58	[3] CHOI	05	BELL	$B \to \omega J/\psi K$
• • • We do not use the following data for averages, fits, limits, etc. • • •					
18.2± 2.4		[4] LI	24	RVUE	$\omega J/\psi$ invariant mass
22 ±17 ± 4		[5] WANG	22A	BELL	$\gamma\gamma \to \gamma\psi(2S)$
3.8± 7.5± 2.6		[6] ABLIKIM	19V	BES	$e^+e^- \to \gamma\omega J/\psi$
34^{+12}_{-8} ± 5		[3] AUBERT	08W	BABR	Superseded by DEL-AMO-SANCHEZ 10B

[1] $D_s^+ D_s^-$ near-threshold enhancement parameterized with a Flatte-like function .
[2] Obtained from the full amplitude analysis. Parameterized with the relativistic Breit-Wigner line shape.
[3] $\omega J/\psi$ threshold enhancement fitted as an S-wave Breit-Wigner resonance.
[4] From a simultaneous χ^2 fit to the distributions of the $\omega J/\psi$ invariant mass measured by BaBar and Belle in the processes $\gamma\gamma \to \omega J/\psi$ and $B \to \omega J/\psi K$. LHCb results also taken into account as an additional constraint in the χ^2 calculation.
[5] Not distinguished from the $\chi_{c2}(3930)$.
[6] Could also be $X(3940)$. Significance 3.1σ. Fit with additional resonance at 3963.7 ± 5.7 MeV, significance 3.4σ.

$\chi_{c0}(3915)$ DECAY MODES

	Mode	Fraction (Γ_i/Γ)
Γ_1	$\omega J/\psi$	seen
Γ_2	$\overline{D}^{*0} D^0$	not seen
Γ_3	D^+D^-	seen
Γ_4	$D_s^+ D_s^-$	seen
Γ_5	$\pi^+\pi^-\eta_c(1S)$	not seen
Γ_6	$\eta_c\eta$	not seen
Γ_7	$\eta_c\pi^0$	not seen
Γ_8	$K\overline{K}$	not seen
Γ_9	$\gamma\gamma$	seen
Γ_{10}	$\gamma\psi(2S)$	not seen
Γ_{11}	$\pi^0\chi_{c1}$	not seen

$\chi_{c0}(3915)$ $\Gamma(i)\Gamma(\gamma\gamma)/\Gamma(\text{total})$

$\Gamma(\omega J/\psi) \times \Gamma(\gamma\gamma)/\Gamma_{\text{total}}$ — $\Gamma_1\Gamma_9/\Gamma$

VALUE (eV)	EVTS	DOCUMENT ID		TECN	COMMENT
54± 9 OUR AVERAGE					
52±10±3	59 ± 10	[1] LEES	12AD	BABR	$e^+e^- \to e^+e^-\omega J/\psi$
61±17±8	49 ± 15	[1] UEHARA	10	BELL	10.6 $e^+e^- \to e^+e^-\omega J/\psi$
• • • We do not use the following data for averages, fits, limits, etc. • • •					
18± 5±2	49 ± 15	[2] UEHARA	10	BELL	10.6 $e^+e^- \to e^+e^-\omega J/\psi$

[1] For $J^P = 0^+$.
[2] For $J^P = 2^+$, helicity-2.

$\Gamma(\gamma\psi(2S)) \times \Gamma(\gamma\gamma)/\Gamma_{\text{total}}$ — $\Gamma_{10}\Gamma_9/\Gamma$

VALUE (eV)	DOCUMENT ID		TECN	COMMENT
• • • We do not use the following data for averages, fits, limits, etc. • • •				
9.8±3.6±1.3	[1] WANG	22A	BELL	$\gamma\gamma \to \gamma\psi(2S)$

[1] Not distinguished from the $\chi_{c2}(3930)$.

$\Gamma(\pi^+\pi^-\eta_c(1S)) \times \Gamma(\gamma\gamma)/\Gamma_{\text{total}}$ — $\Gamma_5\Gamma_9/\Gamma$

VALUE (eV)	CL%	DOCUMENT ID		TECN	COMMENT
<16	90	LEES	12AE	BABR	$e^+e^- \to e^+e^-\pi^+\pi^-\eta_c$

$\Gamma(K\overline{K}) \times \Gamma(\gamma\gamma)/\Gamma_{\text{total}}$ — $\Gamma_8\Gamma_9/\Gamma$

VALUE (eV)	CL%	DOCUMENT ID		TECN	COMMENT
<1.96	90	UEHARA	13	BELL	$\gamma\gamma \to K_S^0 K_S^0$

$\chi_{c0}(3915)$ BRANCHING RATIOS

$\Gamma(\omega J/\psi)/\Gamma_{\text{total}}$ — Γ_1/Γ

VALUE	DOCUMENT ID		TECN	COMMENT
seen	[1] DEL-AMO-SA...	10B	BABR	$B \to \omega J/\psi K$
seen	[2] CHOI	05	BELL	$B \to \omega J/\psi K$

[1] DEL-AMO-SANCHEZ 10B reports $B(B^\pm \to \chi_{c0}(3915) K^\pm) \times B(\chi_{c0}(3915) \to J/\psi\omega) = (3.0^{+0.7+0.5}_{-0.6-0.3}) \times 10^{-5}$ and $B(B^0 \to \chi_{c0}(3915) K^0) \times B(\chi_{c0}(3915) \to J/\psi\omega) = (2.1 \pm 0.9 \pm 0.3) \times 10^{-5}$.
[2] CHOI 05 reports $B(B \to \chi_{c0}(3915) K) \times B(\chi_{c0}(3915) \to J/\psi\omega) = (7.1 \pm 1.3 \pm 3.1) \times 10^{-5}$.

$\Gamma(\omega J/\psi)/\Gamma(\overline{D}^{*0} D^0)$ — Γ_1/Γ_2

VALUE	CL%	DOCUMENT ID		TECN	COMMENT
>0.71	90	[1] AUSHEV	10	BELL	$B \to \overline{D}^{*0} D^0 K$

[1] By combining the upper limit $B(B \to \chi_{c0}(3915) K) \times B(\chi_{c0}(3915) \to D^{*0}\overline{D}^0) < 0.67 \times 10^{-4}$ from AUSHEV 10 with the average of CHOI 05 and AUBERT 08W measurements $B(B \to \chi_{c0}(3915) K) \times B(\chi_{c0}(3915) \to \omega J/\psi) = (0.51 \pm 0.11) \times 10^{-4}$.

$\Gamma(D^+D^-)/\Gamma_{\text{total}}$ — Γ_3/Γ

VALUE	DOCUMENT ID		TECN	COMMENT
seen	AAIJ	20AI	LHCB	$B^+ \to D^+D^-K^+$

$\Gamma(D^+D^-)/\Gamma(D_s^+ D_s^-)$ — Γ_3/Γ_4

VALUE	DOCUMENT ID		TECN	COMMENT
0.29±0.09±0.10±0.08	[1] AAIJ	23AA	LHCB	$B^+ \to D_s^+ D_s^- K^+$

[1] Assuming that AAIJ 20AI reporting on $B^+ \to D^+D^-K^+$ also refers to $\chi_{c0}(3915)$. The last uncertainty is due to the values of $B(D^+ \to K^-\pi^+\pi^+)$ and $B(D_s^+ \to K^-K^+\pi^+)$ from PDG 22.

Int. J. Mod. Phys. A 2026.41. Downloaded from www.worldscientific.com by UNIVERSITY OF CALIFORNIA @ BERKELEY on 09/16/26. Re-use and distribution is strictly not permitted, except for Open Access articles.

$\Gamma(\eta_c\eta)/\Gamma_{total}$ — Γ_6/Γ

VALUE	CL%	DOCUMENT ID		TECN	COMMENT
not seen	90	[1] VINOKUROVA	15	BELL	$B^+ \to K^+\eta_c\eta$

[1] VINOKUROVA 15 reports $B(B^+ \to K^+\chi_{c0}(3915)) \times B(\chi_{c0}(3915) \to \eta_c\eta) < 4.7\times10^{-5}$ at 90% CL.

$\Gamma(\eta_c\pi^0)/\Gamma_{total}$ — Γ_7/Γ

VALUE	CL%	DOCUMENT ID		TECN	COMMENT
not seen	90	[1] VINOKUROVA	15	BELL	$B^+ \to K^+\eta_c\pi^0$

[1] VINOKUROVA 15 reports $B(B^+ \to K^+\chi_{c0}(3915)^0) \times B(\chi_{c0}(3915) \to \eta_c\pi^0) < 1.7\times10^{-5}$ at 90% CL.

$\Gamma(\gamma\gamma)/\Gamma_{total}$ — Γ_9/Γ

VALUE	EVTS	DOCUMENT ID		TECN	COMMENT
seen	59 ± 10	LEES	12AD	BABR	$e^+e^- \to e^+e^-\omega J/\psi$
seen		UEHARA	10	BELL	$10.6\ e^+e^- \to e^+e^-\omega J/\psi$

$\Gamma(\pi^0\chi_{c1})/\Gamma_{total}$ — Γ_{11}/Γ

VALUE	EVTS	DOCUMENT ID		TECN	COMMENT
not seen	42 ± 14	[1] BHARDWAJ	19	BELL	$B^\pm \to \chi_{c1}\pi^0K^\pm$

[1] BHARDWAJ 19 reports $B(B^+ \to K^+\chi_{c0}(3915)) \times B(\chi_{c0}(3915) \to \chi_{c1}\pi^0) < 3.8\times10^{-5}$ at 90% CL. A signal significance 2.3 standard deviations.

$\chi_{c0}(3915)$ REFERENCES

LI	24	CP C48 063001	C. Li, X. Wang, C. Wu	(LNUDA)
AAIJ	23AA	PRL 131 071901	R. Aaij *et al.*	(LHCb Collab.)
PDG	22	PTEP 2022 083C01	R.L. Workman *et al.*	(PDG Collab.)
WANG	22A	PR D105 112011	X.L. Wang *et al.*	(BELLE Collab.)
AAIJ	20AI	PR D102 112003	R. Aaij *et al.*	(LHCb Collab.) JPC
ABLIKIM	19V	PRL 122 232002	M. Ablikim *et al.*	(BESIII Collab.)
BHARDWAJ	19	PR D99 111101	V. Bhardwaj *et al.*	(BELLE Collab.)
VINOKUROVA	15	JHEP 1506 132	A. Vinokurova *et al.*	(BELLE Collab.)
Also		JHEP 1702 088 (errat.)	A. Vinokurava *et al.*	(BELLE Collab.)
ZHOU	15C	PRL 115 022001	Z.-Y. Zhou, Z. Xiao, H.-Q. Zhou	(BEIJT, NANJ)
UEHARA	13	PTEP 2013 123C01	S. Uehara *et al.*	(BELLE Collab.)
LEES	12AD	PR D86 072002	J.P. Lees *et al.*	(BABAR Collab.)
LEES	12AE	PR D86 092005	J.P. Lees *et al.*	(BABAR Collab.)
AUSHEV	10	PR D81 031103	T. Aushev *et al.*	(BELLE Collab.)
DEL-AMO-SA...	10B	PR D82 011101	P. del Amo Sanchez *et al.*	(BABAR Collab.)
UEHARA	10	PRL 104 092001	S. Uehara *et al.*	(BELLE Collab.)
AUBERT	08W	PRL 101 082001	B. Aubert *et al.*	(BABAR Collab.)
CHOI	05	PRL 94 182002	S.-K. Choi *et al.*	(BELLE Collab.)

$\chi_{c2}(3930)$

$I^G(J^{PC}) = 0^+(2^{++})$

$\chi_{c2}(3930)$ MASS

VALUE (MeV)	EVTS	DOCUMENT ID		TECN	COMMENT
3922.5±1.0 OUR AVERAGE		Error includes scale factor of 1.7. See the ideogram below.			
$3926.8\pm2.4\pm0.8$	1.2k	[1] AAIJ	20AI	LHCB	$B^+ \to D^+D^-K^+$
$3921.9\pm0.6\pm0.2$		[2] AAIJ	19M	LHCB	$pp \to D\overline{D} +$ anything
$3926.7\pm2.7\pm1.1$	76 ± 17	AUBERT	10G	BABR	$10.6\ e^+e^- \to e^+e^-D\overline{D}$
$3929\ \pm5\ \pm2$	64	UEHARA	06	BELL	$10.6\ e^+e^- \to e^+e^-D\overline{D}$

[1] Obtained from the full amplitude analysis. Parameterized with the relativistic Breit-Wigner line shape. Previous measurements assumed a single state in this region. This analysis revealed the presence of $\chi_{c0}(3930)$ with the same mass.

[2] Measured in prompt hadroproduction.

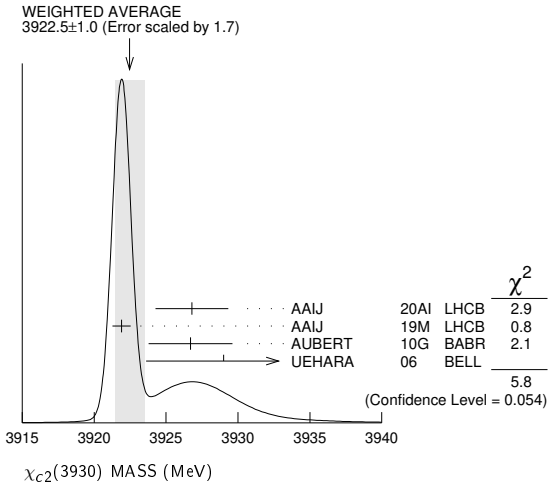

$\chi_{c2}(3930)$ WIDTH

VALUE (MeV)	EVTS	DOCUMENT ID		TECN	COMMENT
35.2± 2.2 OUR AVERAGE		Error includes scale factor of 1.2.			
$34.2\pm6.6\pm1.1$	1.2k	[1] AAIJ	20AI	LHCB	$B^+ \to D^+D^-K^+$
$36.6\pm1.9\pm0.9$		[2] AAIJ	19M	LHCB	$pp \to D\overline{D} +$ anything
$21.3\pm6.8\pm3.6$	76 ± 17	AUBERT	10G	BABR	$10.6\ e^+e^- \to e^+e^-D\overline{D}$
$29\ \pm10\ \pm2$	64	UEHARA	06	BELL	$10.6\ e^+e^- \to e^+e^-D\overline{D}$

[1] Obtained from the full amplitude analysis. Parameterized with the relativistic Breit-Wigner line shape. Previous measurements assumed a single state in this region. This analysis revealed the presence of $\chi_{c0}(3930)$ with the same mass.

[2] Measured in prompt hadroproduction.

$\chi_{c2}(3930)$ DECAY MODES

	Mode	Fraction (Γ_i/Γ)
Γ_1	$\gamma\gamma$	seen
Γ_2	$K\overline{K}\pi$	not seen
Γ_3	$K^+K^-\pi^+\pi^-\pi^0$	not seen
Γ_4	$D\overline{D}$	seen
Γ_5	D^+D^-	seen
Γ_6	$D^0\overline{D}^0$	seen
Γ_7	$\pi^+\pi^-\eta_c(1S)$	not seen
Γ_8	$K\overline{K}$	not seen

$\chi_{c2}(3930)$ PARTIAL WIDTHS

$\chi_{c2}(3930)\ \Gamma(i)\Gamma(\gamma\gamma)/\Gamma(total)$

$\Gamma(K\overline{K}\pi) \times \Gamma(\gamma\gamma)/\Gamma_{total}$ — $\Gamma_2\Gamma_1/\Gamma$

VALUE (eV)	CL%	DOCUMENT ID		TECN	COMMENT
<2.1	90	DEL-AMO-SA...	11M	BABR	$\gamma\gamma \to K^0_SK^\pm\pi^\mp$

$\Gamma(K^+K^-\pi^+\pi^-\pi^0) \times \Gamma(\gamma\gamma)/\Gamma_{total}$ — $\Gamma_3\Gamma_1/\Gamma$

VALUE (eV)	CL%	DOCUMENT ID		TECN	COMMENT
<3.4	90	DEL-AMO-SA...	11M	BABR	$\gamma\gamma \to K^+K^-\pi^+\pi^-\pi^0$

$\Gamma(D\overline{D}) \times \Gamma(\gamma\gamma)/\Gamma_{total}$ — $\Gamma_4\Gamma_1/\Gamma$

VALUE (keV)	EVTS	DOCUMENT ID		TECN	COMMENT
0.21±0.04 OUR AVERAGE					
$0.24\pm0.05\pm0.04$	76 ± 17	AUBERT	10G	BABR	$10.6\ e^+e^- \to e^+e^-D\overline{D}$
$0.18\pm0.05\pm0.03$	64	[1] UEHARA	06	BELL	$10.6\ e^+e^- \to e^+e^-D\overline{D}$

[1] Assuming $B(D^+D^-) = 0.89\ B(D^0\overline{D}^0)$.

$\Gamma(\pi^+\pi^-\eta_c(1S)) \times \Gamma(\gamma\gamma)/\Gamma_{total}$ — $\Gamma_7\Gamma_1/\Gamma$

VALUE (eV)	CL%	DOCUMENT ID		TECN	COMMENT
<18	90	LEES	12AE	BABR	$e^+e^- \to e^+e^-\pi^+\pi^-\eta_c$

$\Gamma(K\overline{K}) \times \Gamma(\gamma\gamma)/\Gamma_{total}$ — $\Gamma_8\Gamma_1/\Gamma$

VALUE (eV)	CL%	DOCUMENT ID		TECN	COMMENT
<0.256	90	UEHARA	13	BELL	$\gamma\gamma \to K^0_SK^0_S$

$\chi_{c2}(3930)$ BRANCHING RATIOS

$\Gamma(D^+D^-)/\Gamma(D^0\overline{D}^0)$ — Γ_5/Γ_6

VALUE	EVTS	DOCUMENT ID		TECN	COMMENT
0.74±0.43±0.16	64	UEHARA	06	BELL	$10.6\ e^+e^- \to e^+e^-D\overline{D}$

$\chi_{c2}(3930)$ REFERENCES

AAIJ	20AI	PR D102 112003	R. Aaij *et al.*	(LHCb Collab.)
AAIJ	19M	JHEP 1907 035	R. Aaij *et al.*	(LHCb Collab.)
UEHARA	13	PTEP 2013 123C01	S. Uehara *et al.*	(BELLE Collab.)
LEES	12AE	PR D86 092005	J.P. Lees *et al.*	(BABAR Collab.)
DEL-AMO-SA...	11M	PR D84 012004	P. del Amo Sanchez *et al.*	(BABAR Collab.)
AUBERT	10G	PR D81 092003	B. Aubert *et al.*	(BABAR Collab.)
UEHARA	06	PRL 96 082003	S. Uehara *et al.*	(BELLE Collab.)

$X(3940)$

$I^G(J^{PC}) = ?^?(?^{??})$

OMITTED FROM SUMMARY TABLE

Reported by ABE 07, observed in $e^+e^- \to J/\psi X$.

$X(3940)$ MASS

VALUE (MeV)	EVTS	DOCUMENT ID		TECN	COMMENT
3942± 9 OUR AVERAGE					
3945^{+28+37}_{-17-28}	1.6k	[1] AAIJ	24AB	LHCB	$B^+ \to D^{*\pm}D^\mp K^+$
$3942^{+7}_{-6}\pm6$	52	PAKHLOV	08	BELL	$e^+e^- \to J/\psi X$
• • • We do not use the following data for averages, fits, limits, etc. • • •					
$3943\pm6\pm6$	25	[2] ABE	07	BELL	$e^+e^- \to J/\psi X$
3936 ± 14	266	[3] ABE	07	BELL	$e^+e^- \to J/\psi(c\overline{c})$

[1] From a simultaneous amplitude analysis of $B^+ \to D^{*+} D^- K^+$, $B^+ \to D^{*-} D^+ K^+$ and their c.c.
[2] From a fit to $D^{*+} D^-$ and $D^{*0} \overline{D}^0$ events.
[3] From the inclusive fit. Not independent of the exclusive measurement by ABE 07.

$X(3940)$ WIDTH

VALUE (MeV)	CL%	EVTS	DOCUMENT ID		TECN	COMMENT
43^{+28}_{-18} OUR AVERAGE Error includes scale factor of 1.1.						
$130^{+92}_{-49}{}^{+101}_{-70}$		1.6k	[1] AAIJ	24AB	LHCB	$B^+ \to D^{*\pm} D^{\mp} K^+$
$37^{+26}_{-15} \pm 8$		52	PAKHLOV	08	BELL	$e^+ e^- \to J/\psi X$
• • • We do not use the following data for averages, fits, limits, etc. • • •						
< 52	90	25	ABE	07	BELL	$e^+ e^- \to J/\psi X$

[1] From a simultaneous amplitude analysis of $B^+ \to D^{*+} D^- K^+$, $B^+ \to D^{*-} D^+ K^+$ and their c.c.

$X(3940)$ DECAY MODES

	Mode	Fraction (Γ_i/Γ)
Γ_1	$D\overline{D}^* +$ c.c.	seen
Γ_2	$D\overline{D}$	not seen
Γ_3	$J/\psi\omega$	not seen

$X(3940)$ BRANCHING RATIOS

$\Gamma(D\overline{D}^* + \text{c.c.})/\Gamma_{total}$ — Γ_1/Γ

VALUE	CL%	EVTS	DOCUMENT ID		TECN	COMMENT
• • • We do not use the following data for averages, fits, limits, etc. • • •						
>0.45	90	25	[1,2] ABE	07	BELL	$e^+ e^- \to J/\psi X$

[1] For $X(3940)$ decaying to final states with more than two tracks.
[2] PAKHLOV 08 finds that the inclusive peak near 3940 MeV/c^2 may consist of several states.

$\Gamma(D\overline{D})/\Gamma_{total}$ — Γ_2/Γ

VALUE	CL%	DOCUMENT ID		TECN	COMMENT
• • • We do not use the following data for averages, fits, limits, etc. • • •					
<0.41	90	[1,2] ABE	07	BELL	$e^+ e^- \to J/\psi X$

[1] For $X(3940)$ decaying to final states with more than two tracks.
[2] PAKHLOV 08 finds that the inclusive peak near 3940 MeV/c^2 may consist of several states.

$\Gamma(J/\psi\omega)/\Gamma_{total}$ — Γ_3/Γ

VALUE	CL%	DOCUMENT ID		TECN	COMMENT
• • • We do not use the following data for averages, fits, limits, etc. • • •					
<0.26	90	[1,2] ABE	07	BELL	$e^+ e^- \to J/\psi X$

[1] For $X(3940)$ decaying to final states with more than two tracks.
[2] PAKHLOV 08 finds that the inclusive peak near 3940 MeV/c^2 may consist of several states.

$X(3940)$ REFERENCES

AAIJ	24AB	PRL 133 131902	R. Aaij *et al.*	(LHCb Collab.)
PAKHLOV	08	PRL 100 202001	P. Pakhlov *et al.*	(BELLE Collab.)
ABE	07	PRL 98 082001	K. Abe *et al.*	(BELLE Collab.)

$\psi(4040)$ [a]

$I^G(J^{PC}) = 0^-(1^{--})$

[a] J^{PC} known by production in $e^+ e^-$ via single photon annihilation. I^G is not known; interpretation of this state as a single resonance is unclear because of the expectation of substantial threshold effects in this energy region.

$\psi(4040)$ MASS

VALUE (MeV)	DOCUMENT ID		TECN	COMMENT
4039.6 ± 4.3	[1] ABLIKIM	08D	BES2	$e^+ e^- \to$ hadrons
• • • We do not use the following data for averages, fits, limits, etc. • • •				
4034 ± 6	[2] MO	10	RVUE	$e^+ e^- \to$ hadrons
4037 ± 2	[3] SETH	05A	RVUE	$e^+ e^- \to$ hadrons
4040 ± 1	[4] SETH	05A	RVUE	$e^+ e^- \to$ hadrons
4040 ± 10	BRANDELIK	78C	DASP	$e^+ e^-$

[1] Reanalysis of data presented in BAI 02C. From a global fit over the center-of-mass energy region 3.7–5.0 GeV covering the $\psi(3770)$, $\psi(4040)$, $\psi(4160)$, and $\psi(4415)$ resonances. Phase angle fixed in the fit to $\delta = (130 \pm 46)^\circ$.
[2] Reanalysis of data presented in BAI 00 and BAI 02C. From a global fit over the center-of-mass energy 3.8-4.8 GeV covering the $\psi(4040)$, $\psi(4160)$ and $\psi(4415)$ resonances and including interference effects.
[3] From a fit to Crystal Ball (OSTERHELD 86) data.
[4] From a fit to BES (BAI 02C) data.

$\psi(4040)$ WIDTH

VALUE (MeV)	DOCUMENT ID		TECN	COMMENT
84.5±12.3	[1] ABLIKIM	08D	BES2	$e^+ e^- \to$ hadrons
• • • We do not use the following data for averages, fits, limits, etc. • • •				
87 ± 11	[2] MO	10	RVUE	$e^+ e^- \to$ hadrons
85 ± 10	[3] SETH	05A	RVUE	$e^+ e^- \to$ hadrons
89 ± 6	[4] SETH	05A	RVUE	$e^+ e^- \to$ hadrons
52 ± 10	BRANDELIK	78C	DASP	$e^+ e^-$

[1] Reanalysis of data presented in BAI 02C. From a global fit over the center-of-mass energy region 3.7–5.0 GeV covering the $\psi(3770)$, $\psi(4040)$, $\psi(4160)$, and $\psi(4415)$ resonances. Phase angle fixed in the fit to $\delta = (130 \pm 46)^\circ$.
[2] Reanalysis of data presented in BAI 00 and BAI 02C. From a global fit over the center-of-mass energy 3.8-4.8 GeV covering the $\psi(4040)$, $\psi(4160)$ and $\psi(4415)$ resonances and including interference effects.
[3] From a fit to Crystal Ball (OSTERHELD 86) data.
[4] From a fit to BES (BAI 02C) data.

$\psi(4040)$ DECAY MODES

Due to the complexity of the $c\overline{c}$ threshold region, in this listing, "seen" ("not seen") means that a cross section for the mode in question has been measured at effective $\sqrt{s}$ near this particle's central mass value, more (less) than 2σ above zero, without regard to any peaking behavior in $\sqrt{s}$ or absence thereof. See mode listing(s) for details and references.

	Mode	Fraction (Γ_i/Γ)	Confidence level
Γ_1	$e^+ e^-$	$(1.02 \pm 0.17) \times 10^{-5}$	
Γ_2	$D\overline{D}$	seen	
Γ_3	$D^0\overline{D}^0$	seen	
Γ_4	$D^+ D^-$	seen	
Γ_5	$D^*\overline{D} +$ c.c.	seen	
Γ_6	$D^*(2007)^0\overline{D}^0 +$ c.c.	seen	
Γ_7	$D^*(2010)^+ D^- +$ c.c.	seen	
Γ_8	$D^*\overline{D}^*$	seen	
Γ_9	$D^*(2007)^0\overline{D}^*(2007)^0$	seen	
Γ_{10}	$D^*(2010)^+ D^*(2010)^-$	seen	
Γ_{11}	$D\overline{D}\pi$ (excl. $D^*\overline{D}$)	not seen	
Γ_{12}	$D^0 D^- \pi^+ +$c.c. (excl. $D^*(2010)^+ D^- +$c.c.)	not seen	
Γ_{13}	$D\overline{D}^*\pi$ (excl. $D^*\overline{D}^*$)	not seen	
Γ_{14}	$D^0\overline{D}^{*-}\pi^+ +$c.c. (excl. $D^*(2010)^+ D^*(2010)^-$)	seen	
Γ_{15}	$D_s^+ D_s^-$	seen	
Γ_{16}	$\pi^+\pi^+\pi^-\pi^-\pi^0$	seen	
Γ_{17}	$J/\psi(1S)$ hadrons	seen	
Γ_{18}	$J/\psi\pi^+\pi^-$	$< 4 \times 10^{-3}$	90%
Γ_{19}	$J/\psi\pi^0\pi^0$	$< 2 \times 10^{-3}$	90%
Γ_{20}	$J/\psi\eta$	$(5.2 \pm 0.7) \times 10^{-3}$	
Γ_{21}	$J/\psi\pi^0$	$< 2.8 \times 10^{-4}$	90%
Γ_{22}	$J/\psi\pi^+\pi^-\pi^0$	$< 2 \times 10^{-3}$	90%
Γ_{23}	$\chi_{c1}\gamma$	$< 3.4 \times 10^{-3}$	90%
Γ_{24}	$\chi_{c2}\gamma$	$< 5 \times 10^{-3}$	90%
Γ_{25}	$\chi_{c1}\pi^+\pi^-\pi^0$	< 1.1 %	90%
Γ_{26}	$\chi_{c2}\pi^+\pi^-\pi^0$	< 3.2 %	90%
Γ_{27}	$h_c(1P)\pi^+\pi^-$	$< 3 \times 10^{-3}$	90%
Γ_{28}	$\phi\pi^+\pi^-$	$< 3 \times 10^{-3}$	90%
Γ_{29}	$\Lambda\overline{\Lambda}\pi^+\pi^-$	$< 2.9 \times 10^{-4}$	90%
Γ_{30}	$\Lambda\overline{\Lambda}\pi^0$	$< 9 \times 10^{-5}$	90%
Γ_{31}	$\Lambda\overline{\Lambda}\eta$	$< 3.0 \times 10^{-4}$	90%
Γ_{32}	$\Lambda\overline{\Lambda}$	$< 6 \times 10^{-6}$	90%
Γ_{33}	$\Sigma^+\overline{\Sigma}^-$	$< 1.3 \times 10^{-4}$	90%
Γ_{34}	$\Sigma^0\overline{\Sigma}^0$	$< 7 \times 10^{-5}$	90%
Γ_{35}	$\Xi^+\overline{\Xi}^-$	$< 1.6 \times 10^{-4}$	90%
Γ_{36}	$\Xi^0\overline{\Xi}^0$	$< 1.8 \times 10^{-4}$	90%
Γ_{37}	$\Xi^-\overline{\Xi}^+$	$< 6 \times 10^{-5}$	90%
Γ_{38}	$\Lambda\overline{\Xi}^+ K^-$ + c.c.	$< 7 \times 10^{-5}$	90%
Γ_{39}	$\Sigma^0\overline{\Xi}^+ K^-$ + c.c.	$< 1.5 \times 10^{-5}$	90%
Γ_{40}	$p K^- K^- \overline{\Xi}^+$ + c.c.	$< 4 \times 10^{-5}$	90%
Γ_{41}	$\mu^+\mu^-$	$(9 \pm 6) \times 10^{-6}$	

$\psi(4040)$ PARTIAL WIDTHS

$\Gamma(e^+ e^-)$ — Γ_1

VALUE (keV)	DOCUMENT ID		TECN	COMMENT
0.86±0.07 OUR ESTIMATE				
0.83±0.20	[1] ABLIKIM	08D	BES2	$e^+ e^- \to$ hadrons

Int. J. Mod. Phys. A 2026.41. Downloaded from www.worldscientific.com
by LIFORNIA @ BERKELEY on 09/16/26. Re-use and distribution is strictly not permitted, except for Open Access articles.

Int. J. Mod. Phys. A 2026.41. Downloaded from www.worldscientific.com by UNIVERSITY OF CALIFORNIA @ BERKELEY on 09/16/26. Re-use and distribution is strictly not permitted, except for Open Access articles.

• • • We do not use the following data for averages, fits, limits, etc. • • •

0.6 to 1.4	[2] MO	10	RVUE	$e^+e^- \to$ hadrons
0.88 ± 0.11	[3] SETH	05A	RVUE	$e^+e^- \to$ hadrons
0.91 ± 0.13	[4] SETH	05A	RVUE	$e^+e^- \to$ hadrons
0.75 ± 0.15	BRANDELIK	78C	DASP	e^+e^-

[1] Reanalysis of data presented in BAI 02C. From a global fit over the center-of-mass energy region 3.7–5.0 GeV covering the $\psi(3770)$, $\psi(4040)$, $\psi(4160)$, and $\psi(4415)$ resonances. Phase angle fixed in the fit to $\delta = (130 \pm 46)^\circ$.

[2] Reanalysis of data presented in BAI 00 and BAI 02C. From a global fit over the center-of-mass energy 3.8-4.8 GeV covering the $\psi(4040)$, $\psi(4160)$ and $\psi(4415)$ resonances and including interference effects. Four sets of solutions are obtained with the same fit quality, mass and total width, but with different e^+e^- partial widths. We quote only the range of values.

[3] From a fit to Crystal Ball (OSTERHELD 86) data.

[4] From a fit to BES (BAI 02C) data.

$\Gamma(\mu^+\mu^-)$ — Γ_{41}

VALUE (keV)	DOCUMENT ID		TECN	COMMENT
0.73±0.48±0.12	[1,2] ABLIKIM	20AG	BES3	$e^+e^- \to \mu^+\mu^-$

[1] From a fit to the $e^+e^- \to \mu^+\mu^-$ cross section between 3.8 and 4.6 GeV to the coherent sum of four resonant amplitudes assuming $\Gamma(\mu^+\mu^-) = \Gamma(e^+e^-)$.

[2] From solution 1 of 8 with equal fit quality. Other solutions range from $0.58 \pm 0.52 \pm 0.10$ to $0.80 \pm 0.48 \pm 0.13$ keV.

$\psi(4040)$ $\Gamma(i) \times \Gamma(e^+e^-)/\Gamma(\text{total})$

$\Gamma(J/\psi\eta) \times \Gamma(e^+e^-)/\Gamma_{\text{total}}$ — $\Gamma_{20}\Gamma_1/\Gamma$

VALUE (eV)	DOCUMENT ID		TECN	COMMENT
• • • We do not use the following data for averages, fits, limits, etc. • • •				
$1.0 \pm 0.2 \pm 0.1$	[1] ABLIKIM	24T	BES3	$e^+e^- \to \eta J/\psi$
$7.1 \pm 0.6 \pm 0.9$	[2] ABLIKIM	24T	BES3	$e^+e^- \to \eta J/\psi$
$1.1 \pm 0.2 \pm 0.2$	[3] ABLIKIM	24T	BES3	$e^+e^- \to \eta J/\psi$
$7.8 \pm 0.6 \pm 1.1$	[4] ABLIKIM	24T	BES3	$e^+e^- \to \eta J/\psi$
1.5 ± 0.3	[5] ABLIKIM	20O	BES3	$e^+e^- \to \eta J/\psi$
1.4 ± 0.3	[6] ABLIKIM	20O	BES3	$e^+e^- \to \eta J/\psi$
7.0 ± 0.6	[7] ABLIKIM	20O	BES3	$e^+e^- \to \eta J/\psi$

[1] Solution 1 of 4. Supersedes ABLIKIM 20O.

[2] Solution 2 of 4. Supersedes ABLIKIM 20O.

[3] Solution 3 of 4. Supersedes ABLIKIM 20O.

[4] Solution 4 of 4. Supersedes ABLIKIM 20O.

[5] Solution 1 of three equivalent fit solutions using three resonant structures.

[6] Solution 2 of three equivalent fit solutions using three resonant structures.

[7] Solution 3 of three equivalent fit solutions using three resonant structures.

$\Gamma(\chi_{c1}\gamma) \times \Gamma(e^+e^-)/\Gamma_{\text{total}}$ — $\Gamma_{23}\Gamma_1/\Gamma$

VALUE (eV)	CL%	DOCUMENT ID		TECN	COMMENT
<2.9	90	[1] HAN	15	BELL	10.58 $e^+e^- \to \chi_{c1}\gamma$

[1] Using $B(\eta \to \gamma\gamma) = (39.41 \pm 0.21)\%$.

$\Gamma(\chi_{c2}\gamma) \times \Gamma(e^+e^-)/\Gamma_{\text{total}}$ — $\Gamma_{24}\Gamma_1/\Gamma$

VALUE (eV)	CL%	DOCUMENT ID		TECN	COMMENT
<4.6	90	[1] HAN	15	BELL	10.58 $e^+e^- \to \chi_{c2}\gamma$

[1] Using $B(\eta \to \gamma\gamma) = (39.41 \pm 0.21)\%$.

$\Gamma(\Lambda\overline{\Lambda}) \times \Gamma(e^+e^-)/\Gamma_{\text{total}}$ — $\Gamma_{32}\Gamma_1/\Gamma$

VALUE (eV)	CL%	DOCUMENT ID		TECN	COMMENT
$<5.5 \times 10^{-3}$	90	[1] ABLIKIM	21AS	BES3	$e^+e^- \to \psi(4040)$

[1] From a measurement of the $e^+e^- \to \Lambda\overline{\Lambda}$ cross section between 3.5 and 4.6 GeV.

$\Gamma(\Sigma^+\overline{\Sigma}^-) \times \Gamma(e^+e^-)/\Gamma_{\text{total}}$ — $\Gamma_{33}\Gamma_1/\Gamma$

VALUE (eV)	CL%	DOCUMENT ID		TECN	COMMENT
$<216.6 \times 10^{-3}$	90	[1] ABLIKIM	24AH	BES3	$e^+e^- \to \Sigma^+\overline{\Sigma}^-$

[1] Interference effect between resonance and continuum amplitudes is considered. Two solutions from the fit.

$\Gamma(\Sigma^0\overline{\Sigma}^0) \times \Gamma(e^+e^-)/\Gamma_{\text{total}}$ — $\Gamma_{34}\Gamma_1/\Gamma$

VALUE (eV)	CL%	DOCUMENT ID		TECN	COMMENT
$<66.1 \times 10^{-3}$	90	[1] ABLIKIM	25U	BES3	$e^+e^- \to \Sigma^0\overline{\Sigma}^0$

[1] Interference effect between resonance and continuum amplitudes is considered. Upper limit is for the larger of the two solutions from the fit.

$\Gamma(\Xi^0\overline{\Xi}^0) \times \Gamma(e^+e^-)/\Gamma_{\text{total}}$ — $\Gamma_{36}\Gamma_1/\Gamma$

VALUE (eV)	CL%	DOCUMENT ID		TECN	COMMENT
$<83.4 \times 10^{-3}$	90	[1] ABLIKIM	24CD	BES3	$e^+e^- \to \psi(4040)$

[1] From a fit to $e^+e^- \to \Xi^0\overline{\Xi}^0$ cross sections.

$\Gamma(\Xi^-\overline{\Xi}^+) \times \Gamma(e^+e^-)/\Gamma_{\text{total}}$ — $\Gamma_{37}\Gamma_1/\Gamma$

VALUE (eV)	CL%	DOCUMENT ID		TECN	COMMENT
$<51.9 \times 10^{-3}$	90	[1] ABLIKIM	23BK	BES3	$e^+e^- \to \psi(4040)$

[1] From a fit to $e^+e^- \to \Xi^-\overline{\Xi}^+$ cross sections.

$\Gamma(\Lambda\overline{\Xi}^+K^- + \text{c.c.}) \times \Gamma(e^+e^-)/\Gamma_{\text{total}}$ — $\Gamma_{38}\Gamma_1/\Gamma$

VALUE (eV)	CL%	DOCUMENT ID		TECN	COMMENT
$<62.0 \times 10^{-3}$	90	[1] ABLIKIM	24AL	BES3	$e^+e^- \to \Lambda\overline{\Xi}^+K^- +$ c.c.

[1] A fit to the Born cross section of $e^+e^- \to \Lambda\overline{\Xi}^+K^- +$ c.c. including interference with the continuum. Two solutions from the fit.

$\Gamma(\Sigma^0\overline{\Xi}^+K^- + \text{c.c.}) \times \Gamma(e^+e^-)/\Gamma_{\text{total}}$ — $\Gamma_{39}\Gamma_1/\Gamma$

VALUE (eV)	CL%	DOCUMENT ID		TECN	COMMENT
$<12.5 \times 10^{-3}$	90	[1] ABLIKIM	24AL	BES3	$e^+e^- \to \Sigma^0\overline{\Xi}^+K^- +$ c.c.

[1] A fit to the Born cross section of $e^+e^- \to \Sigma^0\overline{\Xi}^+K^- +$ c.c. including interference with the continuum. Two solutions from the fit.

$\Gamma(e^+e^-) \times \Gamma(pK^-K^-\overline{\Xi}^+ + \text{c.c.})/\Gamma_{\text{total}}$ — $\Gamma_1\Gamma_{40}/\Gamma$

VALUE (eV)	CL%	DOCUMENT ID		TECN	COMMENT
$<35.6 \times 10^{-3}$	90	ABLIKIM	25CF	BES3	$e^+e^- \to pK^-K^-\overline{\Xi}^+ +$ c.c.

$\psi(4040)$ $\Gamma(i) \times \Gamma(e^+e^-)/\Gamma^2(\text{total})$

$\Gamma(J/\psi\eta)/\Gamma_{\text{total}} \times \Gamma(e^+e^-)/\Gamma_{\text{total}}$ — $\Gamma_{20}/\Gamma \times \Gamma_1/\Gamma$

VALUE (units 10^{-8})	DOCUMENT ID		TECN	COMMENT
• • • We do not use the following data for averages, fits, limits, etc. • • •				
$5.1 \pm 1.4 \pm 1.5$	[1] WANG	13B	BELL	$e^+e^- \to J/\psi\eta\gamma$
$12.8 \pm 2.1 \pm 1.9$	[2] WANG	13B	BELL	$e^+e^- \to J/\psi\eta\gamma$

[1] Solution I of two equivalent solutions in a fit using two interfering resonances. Mass and width fixed at 4039 MeV and 80 MeV, respectively.

[2] Solution II of two equivalent solutions in a fit using two interfering resonances. Mass and width fixed at 4039 MeV and 80 MeV, respectively.

$\psi(4040)$ BRANCHING RATIOS

$\Gamma(e^+e^-)/\Gamma_{\text{total}}$ — Γ_1/Γ

VALUE (units 10^{-5})	DOCUMENT ID		TECN	COMMENT
• • • We do not use the following data for averages, fits, limits, etc. • • •				
~ 1.0	FELDMAN	77	MRK1	e^+e^-

$\Gamma(D^0\overline{D}^0)/\Gamma_{\text{total}}$ — Γ_3/Γ

VALUE	DOCUMENT ID		TECN	COMMENT
seen	[1] ABLIKIM	24BH	BES3	$e^+e^- \to D^0\overline{D}^0$
seen	AUBERT	09M	BABR	$e^+e^- \to D^0\overline{D}^0\gamma$
seen	CRONIN-HEN..	09	CLEO	$e^+e^- \to D^0\overline{D}^0$
seen	PAKHLOVA	08	BELL	$e^+e^- \to D^0\overline{D}^0\gamma$

[1] A precision measurement of the $e^+e^- \to D^0\overline{D}^0$ cross section shows complex structure in this mass region.

$\Gamma(D^+D^-)/\Gamma_{\text{total}}$ — Γ_4/Γ

VALUE	DOCUMENT ID		TECN	COMMENT
seen	[1] ABLIKIM	24BH	BES3	$e^+e^- \to D^+D^-$
seen	AUBERT	09M	BABR	$e^+e^- \to D^+D^-\gamma$
seen	CRONIN-HEN..	09	CLEO	$e^+e^- \to D^+D^-$
seen	PAKHLOVA	08	BELL	$e^+e^- \to D^+D^-\gamma$

[1] A precision measurement of the $e^+e^- \to D^+D^-$ cross section shows complex structure in this mass region.

$\Gamma(D\overline{D})/\Gamma(D^*\overline{D} + \text{c.c.})$ — Γ_2/Γ_5

VALUE	DOCUMENT ID		TECN	COMMENT
$0.24 \pm 0.05 \pm 0.12$	AUBERT	09M	BABR	$e^+e^- \to \gamma D^{(*)}\overline{D}$

$\Gamma(D^0\overline{D}^0)/\Gamma(D^*(2007)^0\overline{D}^0 + \text{c.c.})$ — Γ_3/Γ_6

VALUE	DOCUMENT ID		TECN	COMMENT
0.05 ± 0.03	[1] GOLDHABER	77	MRK1	e^+e^-

[1] Phase-space factor (p^3) explicitly removed.

$\Gamma(D^*(2007)^0\overline{D}^0 + \text{c.c.})/\Gamma_{\text{total}}$ — Γ_6/Γ

VALUE	DOCUMENT ID		TECN	COMMENT
seen	AUBERT	09M	BABR	$e^+e^- \to D^{*0}\overline{D}^0\gamma$
seen	CRONIN-HEN..	09	CLEO	$e^+e^- \to D^{*0}\overline{D}^0$

$\Gamma(D^*(2010)^+D^- + \text{c.c.})/\Gamma_{\text{total}}$ — Γ_7/Γ

VALUE	DOCUMENT ID		TECN	COMMENT
seen	[1] ZHUKOVA	18	BELL	$e^+e^- \to D^{*+}D^-\gamma$
seen	AUBERT	09M	BABR	$e^+e^- \to D^{*+}D^-\gamma$
seen	CRONIN-HEN..	09	CLEO	$e^+e^- \to D^{*+}D^-$
• • • We do not use the following data for averages, fits, limits, etc. • • •				
seen	PAKHLOVA	07	BELL	$e^+e^- \to D^{*+}D^-\gamma$

[1] Supersedes PAKHLOVA 07.

$\Gamma(D^*(2010)^+D^- + \text{c.c.})/\Gamma(D^*(2007)^0\overline{D}^0 + \text{c.c.})$ — Γ_7/Γ_6

VALUE	DOCUMENT ID		TECN	COMMENT
$0.95 \pm 0.09 \pm 0.10$	AUBERT	09M	BABR	$e^+e^- \to \gamma D^*\overline{D}$

Int. J. Mod. Phys. A 2026.41. Downloaded from www.worldscientific.com by CALIFORNIA @ BERKELEY on 09/16/26. Re-use and distribution is strictly not permitted, except for Open Access articles.

$\Gamma(D^*\overline{D}^*)/\Gamma(D^*\overline{D}+\text{c.c.})$ — Γ_8/Γ_5

VALUE	DOCUMENT ID		TECN	COMMENT
0.18±0.14±0.03	AUBERT	09M	BABR	$e^+e^- \to \gamma D^{(*)}\overline{D}^{(*)}$

$\Gamma(D^*(2007)^0\overline{D}^*(2007)^0)/\Gamma_{total}$ — Γ_9/Γ

VALUE	DOCUMENT ID		TECN	COMMENT
seen	AUBERT	09M	BABR	$e^+e^- \to D^{*0}\overline{D}^{*0}\gamma$
seen	CRONIN-HEN...	09	CLEO	$e^+e^- \to D^{*0}\overline{D}^{*0}$

$\Gamma(D^*(2007)^0\overline{D}^*(2007)^0)/\Gamma(D^*(2007)^0\overline{D}^0+\text{c.c.})$ — Γ_9/Γ_6

VALUE	DOCUMENT ID		TECN	COMMENT
32.0±12.0	[1] GOLDHABER	77	MRK1	e^+e^-

[1] Phase-space factor (p^3) explicitly removed.

$\Gamma(D^*(2010)^+D^*(2010)^-)/\Gamma_{total}$ — Γ_{10}/Γ

VALUE	DOCUMENT ID		TECN	COMMENT
seen	[1] ZHUKOVA	18	BELL	$e^+e^- \to D^{*+}D^{*-}\gamma$
seen	AUBERT	09M	BABR	$e^+e^- \to D^{*+}D^{*-}\gamma$
seen	CRONIN-HEN...	09	CLEO	$e^+e^- \to D^{*+}D^{*-}$
• • • We do not use the following data for averages, fits, limits, etc. • • •				
seen	PAKHLOVA	07	BELL	$e^+e^- \to D^{*+}D^{*-}\gamma$

[1] Supersedes PAKHLOVA 07.

$\Gamma(D^0D^-\pi^+ +\text{c.c. (excl. } D^*(2010)^+D^- +\text{c.c.}))/\Gamma_{total}$ — Γ_{12}/Γ

VALUE	DOCUMENT ID		TECN	COMMENT
not seen	PAKHLOVA	08A	BELL	$e^+e^- \to D^0D^-\pi^+\gamma$

$\Gamma(D\overline{D}^*\pi(\text{excl. } D^*\overline{D}^*))/\Gamma_{total}$ — Γ_{13}/Γ

VALUE	DOCUMENT ID		TECN	COMMENT
not seen	CRONIN-HEN...	09	CLEO	$e^+e^- \to D\overline{D}^*\pi$

$\Gamma(D^0\overline{D}^{*-}\pi^+ +\text{c.c. (excl. } D^*(2010)^+D^*(2010)^-))/\Gamma_{total}$ — Γ_{14}/Γ

VALUE	DOCUMENT ID		TECN	COMMENT
seen	PAKHLOVA	09	BELL	$e^+e^- \to D^0D^{*-}\pi^+\gamma$

$\Gamma(D_s^+D_s^-)/\Gamma_{total}$ — Γ_{15}/Γ

VALUE	DOCUMENT ID		TECN	COMMENT
seen	PAKHLOVA	11	BELL	$e^+e^- \to D_s^+D_s^-\gamma$
seen	DEL-AMO-SA...	10N	BABR	$e^+e^- \to D_s^+D_s^-\gamma$
seen	CRONIN-HEN...	09	CLEO	$e^+e^- \to D_s^+D_s^-$

$\Gamma(\pi^+\pi^+\pi^-\pi^-\pi^0)/\Gamma_{total}$ — Γ_{16}/Γ

VALUE	DOCUMENT ID		TECN	COMMENT
• • • We do not use the following data for averages, fits, limits, etc. • • •				
$(3.51\pm1.89\pm1.24)\times10^{-5}$	[1] ABLIKIM	21AW	BES3	$e^+e^- \to 2\pi^+2\pi^-\pi^0$
$(2.41\pm0.05\pm0.79)\times10^{-2}$	[2] ABLIKIM	21AW	BES3	$e^+e^- \to 2\pi^+2\pi^-\pi^0$

[1] Solution 1 of two solutions with equal fit quality. The significance of the $\psi(4040)$ signal is 3.6 σ.
[2] Solution 2 of two solutions with equal fit quality. The significance of the $\psi(4040)$ signal is 3.6 σ.

$\Gamma(J/\psi\pi^+\pi^-)/\Gamma_{total}$ — Γ_{18}/Γ

VALUE (units 10^{-3})	CL%	DOCUMENT ID		TECN	COMMENT
<4	90	COAN	06	CLEO	3.97–4.06 $e^+e^- \to$ hadrons

$\Gamma(J/\psi\pi^0\pi^0)/\Gamma_{total}$ — Γ_{19}/Γ

VALUE (units 10^{-3})	CL%	DOCUMENT ID		TECN	COMMENT
<2	90	COAN	06	CLEO	3.97–4.06 $e^+e^- \to$ hadrons

$\Gamma(J/\psi\eta)/\Gamma_{total}$ — Γ_{20}/Γ

VALUE (units 10^{-3})	CL%	DOCUMENT ID		TECN	COMMENT
5.2±0.5±0.5		[1] ABLIKIM	12K	BES3	$e^+e^- \to \ell^+\ell^-2\gamma$
• • • We do not use the following data for averages, fits, limits, etc. • • •					
<7	90	COAN	06	CLEO	3.97–4.06 $e^+e^- \to$ hadrons

[1] ABLIKIM 12K measure $\sigma(e^+e^- \to J/\psi\eta) = 32.1 \pm 2.8 \pm 1.3$ pb. They assume the $\eta J/\psi$ fully originates from $\psi(4040)$ decays. Also see ABLIKIM 24T.

$\Gamma(J/\psi\pi^0)/\Gamma_{total}$ — Γ_{21}/Γ

VALUE (units 10^{-3})	CL%	DOCUMENT ID		TECN	COMMENT
<0.28	90	[1] ABLIKIM	12K	BES3	$e^+e^- \to \ell^+\ell^-2\gamma$
• • • We do not use the following data for averages, fits, limits, etc. • • •					
<2	90	COAN	06	CLEO	3.97–4.06 $e^+e^- \to$ hadrons

[1] ABLIKIM 12K measure $\sigma(e^+e^- \to J/\psi\pi^0)$ <1.6 pb. They assume the $\eta J/\psi$ fully originates from $\psi(4040)$ decays.

$\Gamma(J/\psi\pi^+\pi^-\pi^0)/\Gamma_{total}$ — Γ_{22}/Γ

VALUE (units 10^{-3})	CL%	DOCUMENT ID		TECN	COMMENT
<2	90	COAN	06	CLEO	3.97–4.06 $e^+e^- \to$ hadrons

$\Gamma(\chi_{c1}\gamma)/\Gamma_{total}$ — Γ_{23}/Γ

VALUE (units 10^{-3})	CL%	DOCUMENT ID		TECN	COMMENT
• • • We do not use the following data for averages, fits, limits, etc. • • •					
<11	90	COAN	06	CLEO	3.97–4.06 $e^+e^- \to$ hadrons

$\Gamma(\chi_{c2}\gamma)/\Gamma_{total}$ — Γ_{24}/Γ

VALUE (units 10^{-3})	CL%	DOCUMENT ID		TECN	COMMENT
• • • We do not use the following data for averages, fits, limits, etc. • • •					
<17	90	COAN	06	CLEO	3.97–4.06 $e^+e^- \to$ hadrons

$\Gamma(\chi_{c1}\pi^+\pi^-\pi^0)/\Gamma_{total}$ — Γ_{25}/Γ

VALUE (units 10^{-3})	CL%	DOCUMENT ID		TECN	COMMENT
<11	90	COAN	06	CLEO	3.97–4.06 $e^+e^- \to$ hadrons

$\Gamma(\chi_{c2}\pi^+\pi^-\pi^0)/\Gamma_{total}$ — Γ_{26}/Γ

VALUE (units 10^{-3})	CL%	DOCUMENT ID		TECN	COMMENT
<32	90	COAN	06	CLEO	3.97–4.06 $e^+e^- \to$ hadrons

$\Gamma(h_c(1P)\pi^+\pi^-)/\Gamma_{total}$ — Γ_{27}/Γ

VALUE (units 10^{-3})	CL%	DOCUMENT ID		TECN	COMMENT
<3	90	[1] PEDLAR	11	CLEO	$e^+e^- \to h_c(1P)\pi^+\pi^-$

[1] From several values of $\sqrt{s}$ near the peak of the $\psi(4040)$, PEDLAR 11 measures $\sigma(e^+e^- \to h_c(1P)\pi^+\pi^-) = 1.0 \pm 8.0 \pm 5.4 \pm 0.2$ pb, where the errors are statistical, systematic, and due to uncertainty in $B(\psi(2S) \to \pi^0 h_c(1P))$, respectively.

$\Gamma(\phi\pi^+\pi^-)/\Gamma_{total}$ — Γ_{28}/Γ

VALUE (units 10^{-3})	CL%	DOCUMENT ID		TECN	COMMENT
<3	90	COAN	06	CLEO	3.97–4.06 $e^+e^- \to$ hadrons

$\Gamma(\Lambda\overline{\Lambda}\pi^+\pi^-)/\Gamma_{total}$ — Γ_{29}/Γ

VALUE (units 10^{-4})	CL%	DOCUMENT ID		TECN	COMMENT
<2.9	90	[1] ABLIKIM	13Q	BES3	$e^+e^- \to \psi(4040)$

[1] Assuming that interference effects between resonance and continuum can be neglected.

$\Gamma(\Lambda\overline{\Lambda}\pi^0)/\Gamma_{total}$ — Γ_{30}/Γ

VALUE (units 10^{-4})	CL%	DOCUMENT ID		TECN	COMMENT
<0.9	90	[1] ABLIKIM	13Q	BES3	$e^+e^- \to \psi(4040)$

[1] Assuming that interference effects between resonance and continuum can be neglected.

$\Gamma(\Lambda\overline{\Lambda}\eta)/\Gamma_{total}$ — Γ_{31}/Γ

VALUE (units 10^{-4})	CL%	DOCUMENT ID		TECN	COMMENT
<3.0	90	[1] ABLIKIM	13Q	BES3	$e^+e^- \to \psi(4040)$

[1] Assuming that interference effects between resonance and continuum can be neglected.

$\Gamma(\Sigma^+\overline{\Sigma}^-)/\Gamma_{total}$ — Γ_{33}/Γ

VALUE (units 10^{-4})	CL%	DOCUMENT ID		TECN	COMMENT
<1.3	90	[1] ABLIKIM	13Q	BES3	$e^+e^- \to \psi(4040)$

[1] Assuming that interference effects between resonance and continuum can be neglected.

$\Gamma(\Sigma^0\overline{\Sigma}^0)/\Gamma_{total}$ — Γ_{34}/Γ

VALUE (units 10^{-4})	CL%	DOCUMENT ID		TECN	COMMENT
<0.7	90	[1] ABLIKIM	13Q	BES3	$e^+e^- \to \psi(4040)$

[1] Assuming that interference effects between resonance and continuum can be neglected.

$\Gamma(\Xi^+\overline{\Xi}^-)/\Gamma_{total}$ — Γ_{35}/Γ

VALUE (units 10^{-4})	CL%	DOCUMENT ID		TECN	COMMENT
<1.6	90	[1] ABLIKIM	13Q	BES3	$e^+e^- \to \psi(4040)$

[1] Assuming that interference effects between resonance and continuum can be neglected.

$\Gamma(\Xi^0\overline{\Xi}^0)/\Gamma_{total}$ — Γ_{36}/Γ

VALUE (units 10^{-4})	CL%	DOCUMENT ID		TECN	COMMENT
<1.8	90	[1] ABLIKIM	13Q	BES3	$e^+e^- \to \psi(4040)$

[1] Assuming that interference effects between resonance and continuum can be neglected.

$\psi(4040)$ REFERENCES

ABLIKIM	25CF	JHEP 2511 111	M. Ablikim et al.	(BESIII Collab.)
ABLIKIM	25U	PR D111 L051502	M. Ablikim et al.	(BESIII Collab.)
ABLIKIM	24AH	JHEP 2405 022	M. Ablikim et al.	(BESIII Collab.)
ABLIKIM	24AL	JHEP 2407 258	M. Ablikim et al.	(BESIII Collab.)
ABLIKIM	24BH	PRL 133 081901	M. Ablikim et al.	(BESIII Collab.)
ABLIKIM	24CD	JHEP 2411 062	M. Ablikim et al.	(BESIII Collab.)
ABLIKIM	24T	PR D109 092012	M. Ablikim et al.	(BESIII Collab.)
ABLIKIM	23BK	JHEP 2311 228	M. Ablikim et al.	(BESIII Collab.)
ABLIKIM	21AS	PR D104 L091104	M. Ablikim et al.	(BESIII Collab.)
ABLIKIM	21AW	PR D104 112009	M. Ablikim et al.	(BESIII Collab.)
ABLIKIM	20AG	PR D102 112009	M. Ablikim et al.	(BESIII Collab.)
ABLIKIM	20O	PR D102 031101	M. Ablikim et al.	(BESIII Collab.)
ZHUKOVA	18	PR D97 012002	V. Zhukova et al.	(BELLE Collab.)
HAN	15	PR D92 012011	Y.L. Han et al.	(BELLE Collab.)
ABLIKIM	13Q	PR D87 112011	M. Ablikim et al.	(BESIII Collab.)
WANG	13B	PR D87 051101	X.L. Wang et al.	(BELLE Collab.)
ABLIKIM	12K	PR D86 071101	M. Ablikim et al.	(BESIII Collab.)
PAKHLOVA	11	PR D83 011101	G. Pakhlova et al.	(BELLE Collab.)

PEDLAR	11	PRL 107 041803	T. Pedlar *et al.*	(CLEO Collab.)
DEL-AMO-SA...	10N	PR D82 052004	P. del Amo Sanchez *et al.*	(BABAR Collab.)
MO	10	PR D82 077501	X.H. Mo, C.Z. Yuan, P. Wang	(BHEP)
AUBERT	09M	PR D79 092001	B. Aubert *et al.*	(BABAR Collab.)
CRONIN-HEN...	09	PR D80 072001	D. Cronin-Hennessy *et al.*	(CLEO Collab.)
PAKHLOVA	09	PR D80 091101	G. Pakhlova *et al.*	(BELLE Collab.)
ABLIKIM	08D	PL B660 315	M. Ablikim *et al.*	(BES Collab.)
PAKHLOVA	08	PR D77 011103	G. Pakhlova *et al.*	(BELLE Collab.)
PAKHLOVA	08A	PRL 100 062001	G. Pakhlova *et al.*	(BELLE Collab.)
PAKHLOVA	07	PRL 98 092001	G. Pakhlova *et al.*	(BELLE Collab.)
COAN	06	PRL 96 162003	T.E. Coan *et al.*	(CLEO Collab.)
SETH	05A	PR D72 017501	K.K. Seth	
BAI	02C	PRL 88 101802	J.Z. Bai *et al.*	(BES Collab.)
BAI	00	PRL 84 594	J.Z. Bai *et al.*	(BES Collab.)
OSTERHELD	86	SLAC-PUB-4160	A. Osterheld *et al.*	(SLAC Crystal Ball Collab.)
BRANDELIK	78C	PL 76B 361	R. Brandelik *et al.*	(DASP Collab.)
Also		ZPHY C1 233	R. Brandelik *et al.*	(DASP Collab.)
FELDMAN	77	PRPL 33C 285	G.J. Feldman, M.L. Perl	(LBL, SLAC)
GOLDHABER	77	PL 69B 503	G. Goldhaber *et al.*	(Mark I Collab.)

$\chi_{c1}(4140)$

$I^G(J^{PC}) = 0^+(1^{++})$

was $X(4140)$

This state shows properties different from a conventional $q\overline{q}$ state. A candidate for an exotic structure. See the review on non-$q\overline{q}$ states.

Seen by AALTONEN 09AH, ABAZOV 14A, CHATRCHYAN 14M, AAIJ 17C in $B^+ \to \chi_{c1} K^+$, $\chi_{c1} \to J/\psi\phi$, and by ABAZOV 15M separately in both prompt (4.7 σ) and non-prompt (5.6 σ) production in $p\overline{p} \to J/\psi\phi +$ anything. Not seen by SHEN 10 in $\gamma\gamma \to J/\psi\phi$ and ABLIKIM 15 in $e^+e^- \to \gamma J/\psi\phi$ at $\sqrt{s}$ = 4.23, 4.26, 4.36 GeV.

$\chi_{c1}(4140)$ MASS

VALUE (MeV)	EVTS	DOCUMENT ID		TECN	COMMENT
4146.5 ± 3.0 OUR AVERAGE					Error includes scale factor of 1.3. See the ideogram below.
$4118 \pm 11 \; ^{+19}_{-36}$	24k	[1] AAIJ	21E	LHCB	$B^+ \to J/\psi\phi K^+$
$4143.4 \; ^{+2.9}_{-3.0} \pm 0.6$	19	[2] AALTONEN	17	CDF	$B^+ \to J/\psi\phi K^+$
$4152.5 \pm 1.7 \; ^{+6.2}_{-5.4}$	616	[3] ABAZOV	15M	D0	$p\overline{p} \to J/\psi\phi +$ anything
$4159.0 \pm 4.3 \pm 6.6$	52	[4] ABAZOV	14A	D0	$B^+ \to J/\psi\phi K^+$
$4148.0 \pm 2.4 \pm 6.3$	0.3k	[5] CHATRCHYAN	14M	CMS	$B^+ \to J/\psi\phi K^+$
• • • We do not use the following data for averages, fits, limits, etc. • • •					
$4146.5 \pm 4.5 \; ^{+4.6}_{-2.8}$	4289	[6,7] AAIJ	17C	LHCB	$B^+ \to J/\psi\phi K^+$
$4143.0 \pm 2.9 \pm 1.2$	14	[8,9] AALTONEN	09AH	CDF	$B^+ \to J/\psi\phi K^+$

[1] From an amplitude analysis of the decay $B^+ \to J/\psi\phi K^+$ with a significance of 13 σ.
[2] Statistical significance of more than 5 σ.
[3] Statistical significance of more than 6 σ.
[4] Statistical significance of 3.1 σ.
[5] From a fit assuming an S-wave relativistic Breit-Wigner shape above a three-body phase-space non-resonant component with statistical significance of more than 5 σ.
[6] From an amplitude analysis of the decay $B^+ \to J/\psi\phi K^+$ with a significance of 8.4 σ.
[7] Superseded by AAIJ 21E.
[8] Statistical significance of 3.8 σ.
[9] Superseded by AALTONEN 17.

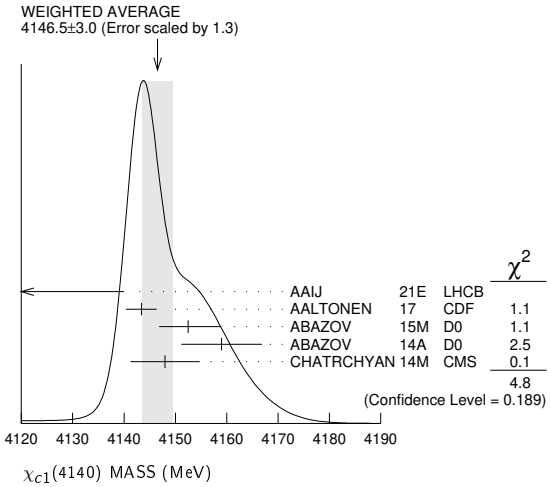

$\chi_{c1}(4140)$ WIDTH

VALUE (MeV)	EVTS	DOCUMENT ID		TECN	COMMENT
$19 \; ^{+7}_{-5}$ OUR AVERAGE					
$162 \pm 21 \; ^{+24}_{-49}$	24k	[1] AAIJ	21E	LHCB	$B^+ \to J/\psi\phi K^+$
$15.3 \; ^{+10.4}_{-6.1} \pm 2.5$	19	[2] AALTONEN	17	CDF	$B^+ \to J/\psi\phi K^+$
$16.3 \pm 5.6 \pm 11.4$	616	[3] ABAZOV	15M	D0	$p\overline{p} \to J/\psi\phi +$ anything
$20 \pm 13 \; ^{+3}_{-8}$	52	[4] ABAZOV	14A	D0	$B^+ \to J/\psi\phi K^+$
$28 \; ^{+15}_{-11} \pm 19$	0.3k	[5] CHATRCHYAN	14M	CMS	$B^+ \to J/\psi\phi K^+$
• • • We do not use the following data for averages, fits, limits, etc. • • •					
$83 \pm 21 \; ^{+21}_{-14}$	4289	[6,7] AAIJ	17C	LHCB	$B^+ \to J/\psi\phi K^+$
$11.7 \; ^{+8.3}_{-5.0} \pm 3.7$	14	[8,9] AALTONEN	09AH	CDF	$B^+ \to J/\psi\phi K^+$

[1] From an amplitude analysis of the decay $B^+ \to J/\psi\phi K^+$ with a significance of 13 σ.
[2] Statistical significance of more than 5 σ.
[3] Statistical significance of more than 6 σ.
[4] Statistical significance of 3.1 σ.
[5] From a fit assuming an S-wave relativistic Breit-Wigner shape above a three-body phase-space non-resonant component with statistical significance of more than 5 σ.
[6] From an amplitude analysis of the decay $B^+ \to J/\psi\phi K^+$ with a significance of 8.4 σ.
[7] Superseded by AAIJ 21E.
[8] Statistical significance of 3.8 σ.
[9] Superseded by AALTONEN 17.

$\chi_{c1}(4140)$ DECAY MODES

	Mode	Fraction (Γ_i/Γ)
Γ_1	$J/\psi\phi$	seen
Γ_2	$\gamma\gamma$	not seen

$\chi_{c1}(4140)$ $\Gamma(i)\Gamma(\gamma\gamma)/\Gamma(\text{total})$

$\Gamma(\gamma\gamma) \times \Gamma(J/\psi\phi)/\Gamma_{\text{total}}$ — $\Gamma_2\Gamma_1/\Gamma$

VALUE (eV)	CL%	DOCUMENT ID		TECN	COMMENT
<41	90	[1] SHEN	10	BELL	10.6 $e^+e^- \to e^+e^- J/\psi\phi$
• • • We do not use the following data for averages, fits, limits, etc. • • •					
< 6	90	[2] SHEN	10	BELL	10.6 $e^+e^- \to e^+e^- J/\psi\phi$

[1] For $J^P = 0^+$.
[2] For $J^P = 2^+$.

$\chi_{c1}(4140)$ BRANCHING RATIOS

$\Gamma(J/\psi\phi)/\Gamma_{\text{total}}$ — Γ_1/Γ

VALUE	EVTS	DOCUMENT ID		TECN	COMMENT
seen	24k	[1] AAIJ	21E	LHCB	$B^+ \to J/\psi\phi K^+$
seen	616	[2] ABAZOV	15M	D0	$p\overline{p} \to J/\psi\phi +$ anything
seen	52	[3] ABAZOV	14A	D0	$B^+ \to J/\psi\phi K^+$
seen	0.3k	[4] CHATRCHYAN	14M	CMS	$B^+ \to J/\psi\phi K^+$
seen	14	[5] AALTONEN	09AH	CDF	$B^+ \to J/\psi\phi K^+$
• • • We do not use the following data for averages, fits, limits, etc. • • •					
seen	4289	[6,7] AAIJ	17C	LHCB	$B^+ \to J/\psi\phi K^+$
not seen		[8] ABLIKIM	15	BES3	$e^+e^- \to \gamma\phi J/\psi$
not seen		[9] AAIJ	12AA	LHCB	$pp \to B^+X$ at 7 TeV

[1] From an amplitude analysis of the decay $B^+ \to J/\psi\phi K^+$ with a significance of 13 σ.
[2] Statistical significance of more than 6 σ.
[3] ABAZOV 14A reports $B(B^+ \to \chi_{c1}(4140) K^+ \to J/\psi\phi K^+)/B(B^+ \to J/\psi\phi K^+) = (19 \pm 7 \pm 4)\%$ with 3.1 σ signficance.
[4] From a fit assuming an S-wave relativistic Breit-Wigner shape above a three-body phase-space non-resonant component with statistical significance of more than 5 σ.
[5] Statistical significance of 3.8 σ.
[6] From an amplitude analysis of the decay $B^+ \to J/\psi\phi K^+$ with a significance of 8.4 σ.
[7] Superseded by AAIJ 21E.
[8] Reported $\sigma(e^+e^- \to \gamma\chi_{c1}(4140))\cdot B(\chi_{c1}(4140) \to J/\psi\phi) < 0.35$, 0.28, and 0.33 pb at 4.23, 4.26, and 4.36 GeV, respectively, at 90% CL.
[9] Reported $B(B^+ \to \chi_{c1}(4140) K^+)\cdot B(\chi_{c1}(4140) \to J/\psi\phi)/B(B^+ \to J/\psi\phi K^+) < 0.07$ at 90% CL.

$\Gamma(\gamma\gamma)/\Gamma_{\text{total}}$ — Γ_2/Γ

VALUE	DOCUMENT ID		TECN	COMMENT
not seen	SHEN	10	BELL	10.6 $e^+e^- \to e^+e^- J/\psi\phi$

$\chi_{c1}(4140)$ REFERENCES

AAIJ	21E	PRL 127 082001	R. Aaij *et al.*	(LHCb Collab.)
AAIJ	17C	PRL 118 022003	R. Aaij *et al.*	(LHCb Collab.) JP
Also		PR D95 012002	R. Aaij *et al.*	(LHCb Collab.)
AALTONEN	17	MPL A32 1750139	T. Aaltonen *et al.*	(CDF Collab.)
ABAZOV	15M	PRL 115 232001	V.M. Abazov *et al.*	(D0 Collab.)
ABLIKIM	15	PR D91 032002	M. Ablikim *et al.*	(BESIII Collab.)
ABAZOV	14A	PR D89 012004	V.M. Abazov *et al.*	(D0 Collab.)
CHATRCHYAN	14M	PL B734 261	S. Chatrchyan *et al.*	(CMS Collab.)
AAIJ	12AA	PR D85 091103	R. Aaij *et al.*	(LHCb Collab.)
SHEN	10	PRL 104 112004	C.P. Shen *et al.*	(BELLE Collab.)
AALTONEN	09AH	PRL 102 242002	T. Aaltonen *et al.*	(CDF Collab.)

Int. J. Mod. Phys. A 2026.41. Downloaded from www.worldscientific.com
by UNIVERSITY OF CALIFORNIA @ BERKELEY on 09/16/26. Re-use and distribution is strictly not permitted, except for Open Access articles.

Int. J. Mod. Phys. A 2026.41. Downloaded from www.worldscientific.com
by LIFORNIA @ BERKELEY on 09/16/26. Re-use and distribution is strictly not permitted, except for Open Access articles.

$\psi(4160)$ [a]

$I^G(J^{PC}) = 0^-(1^{--})$

[a] J^{PC} known by production in e^+e^- via single photon annihilation. I^G is not known; interpretation of this state as a single resonance is unclear because of the expectation of substantial threshold effects in this energy region.

$\psi(4160)$ MASS

VALUE (MeV)	DOCUMENT ID		TECN	COMMENT
4191 ± 5 OUR AVERAGE				
4186.8 ± 8.7 ± 30	[1] ABLIKIM	23BH	BES3	$e^+e^- \to D_s^{*+} D_s^{*-}$
4191^{+9}_{-8}	AAIJ	13BC	LHCB	$B^+ \to K^+\mu^+\mu^-$
4191.7 ± 6.5	[2] ABLIKIM	08D	BES2	$e^+e^- \to$ hadrons
• • • We do not use the following data for averages, fits, limits, etc. • • •				
4193 ± 7	[3] MO	10	RVUE	$e^+e^- \to$ hadrons
4151 ± 4	[4] SETH	05A	RVUE	$e^+e^- \to$ hadrons
4155 ± 5	[5] SETH	05A	RVUE	$e^+e^- \to$ hadrons
4159 ± 20	BRANDELIK	78C	DASP	e^+e^-

[1] Could also be the $\psi(4230)$.
[2] Reanalysis of data presented in BAI 02C. From a global fit over the center-of-mass energy region 3.7–5.0 GeV covering the $\psi(3770)$, $\psi(4040)$, $\psi(4160)$, and $\psi(4415)$ resonances. Phase angle fixed in the fit to $\delta = (293 \pm 57)^\circ$.
[3] Reanalysis of data presented in BAI 00 and BAI 02C. From a global fit over the center-of-mass energy 3.8–4.8 GeV covering the $\psi(4040)$, $\psi(4160)$ and $\psi(4415)$ resonances and including interference effects.
[4] From a fit to Crystal Ball (OSTERHELD 86) data.
[5] From a fit to BES (BAI 02C) data.

$\psi(4160)$ WIDTH

VALUE (MeV)	DOCUMENT ID		TECN	COMMENT
69 ±10 OUR AVERAGE				
55 ±15 ±53	[1] ABLIKIM	23BH	BES3	$e^+e^- \to D_s^{*+} D_s^{*-}$
65^{+22}_{-16}	AAIJ	13BC	LHCB	$B^+ \to K^+\mu^+\mu^-$
71.8 ± 12.3	[2] ABLIKIM	08D	BES2	$e^+e^- \to$ hadrons
• • • We do not use the following data for averages, fits, limits, etc. • • •				
79 ±14	[3] MO	10	RVUE	$e^+e^- \to$ hadrons
107 ±10	[4] SETH	05A	RVUE	$e^+e^- \to$ hadrons
107 ±16	[5] SETH	05A	RVUE	$e^+e^- \to$ hadrons
78 ±20	BRANDELIK	78C	DASP	e^+e^-

[1] Could also be the $\psi(4230)$.
[2] Reanalysis of data presented in BAI 02C. From a global fit over the center-of-mass energy region 3.7–5.0 GeV covering the $\psi(3770)$, $\psi(4040)$, $\psi(4160)$, and $\psi(4415)$ resonances. Phase angle fixed in the fit to $\delta = (293 \pm 57)^\circ$.
[3] Reanalysis of data presented in BAI 00 and BAI 02C. From a global fit over the center-of-mass energy 3.8–4.8 GeV covering the $\psi(4040)$, $\psi(4160)$ and $\psi(4415)$ resonances and including interference effects.
[4] From a fit to Crystal Ball (OSTERHELD 86) data.
[5] From a fit to BES (BAI 02C) data.

$\psi(4160)$ DECAY MODES

Due to the complexity of the $c\overline{c}$ threshold region, in this listing, "seen" ("not seen") means that a cross section for the mode in question has been measured at effective $\sqrt{s}$ near this particle's central mass value, more (less) than 2σ above zero, without regard to any peaking behavior in $\sqrt{s}$ or absence thereof. See mode listing(s) for details and references.

	Mode	Fraction (Γ_i/Γ)	Confidence level
Γ_1	e^+e^-	$(6.9 \pm 3.3) \times 10^{-6}$	
Γ_2	$\mu^+\mu^-$	seen	
Γ_3	$D\overline{D}$	seen	
Γ_4	$D^0\overline{D}^0$	seen	
Γ_5	D^+D^-	seen	
Γ_6	$D^*\overline{D}$ + c.c.	seen	
Γ_7	$D^*(2007)^0\overline{D}^0$ + c.c.	seen	
Γ_8	$D^*(2010)^+D^-$ + c.c.	seen	
Γ_9	$D^*\overline{D}^*$	seen	
Γ_{10}	$D^*(2007)^0\overline{D}^*(2007)^0$	seen	
Γ_{11}	$D^*(2010)^+D^*(2010)^-$	seen	
Γ_{12}	$D^0D^-\pi^+$ + c.c. (excl. $D^*(2010)^+D^-$ + c.c.)	not seen	
Γ_{13}	$D\overline{D}^*\pi$ + c.c. (excl. $D^*\overline{D}^*$)	seen	
Γ_{14}	$D^0D^{*-}\pi^+$ + c.c. (excl. $D^*(2010)^+D^*(2010)^-$)	not seen	
Γ_{15}	$D_s^+D_s^-$	not seen	
Γ_{16}	$D_s^{*+}D_s^-$ + c.c.	seen	
Γ_{17}	$J/\psi\pi^+\pi^-$	$< 3 \times 10^{-3}$	90%
Γ_{18}	$J/\psi\pi^0\pi^0$	$< 3 \times 10^{-3}$	90%
Γ_{19}	$J/\psi K^+K^-$	$< 2 \times 10^{-3}$	90%
Γ_{20}	$J/\psi\eta$	$< 8 \times 10^{-3}$	90%
Γ_{21}	$J/\psi\pi^0$	$< 1 \times 10^{-3}$	90%
Γ_{22}	$J/\psi\eta'$	$< 5 \times 10^{-3}$	90%
Γ_{23}	$J/\psi\pi^+\pi^-\pi^0$	$< 1 \times 10^{-3}$	90%
Γ_{24}	$\psi(2S)\pi^+\pi^-$	$< 4 \times 10^{-3}$	90%
Γ_{25}	$\chi_{c1}\gamma$	$< 5 \times 10^{-3}$	90%
Γ_{26}	$\chi_{c2}\gamma$	< 1.3 %	90%
Γ_{27}	$\chi_{c1}\pi^+\pi^-\pi^0$	$< 2 \times 10^{-3}$	90%
Γ_{28}	$\chi_{c2}\pi^+\pi^-\pi^0$	$< 8 \times 10^{-3}$	90%
Γ_{29}	$h_c(1P)\pi^+\pi^-$	$< 5 \times 10^{-3}$	90%
Γ_{30}	$h_c(1P)\pi^0\pi^0$	$< 2 \times 10^{-3}$	90%
Γ_{31}	$h_c(1P)\eta$	$< 2 \times 10^{-3}$	90%
Γ_{32}	$h_c(1P)\pi^0$	$< 4 \times 10^{-4}$	90%
Γ_{33}	$\omega\pi^+\pi^-$	seen	
Γ_{34}	$\phi\pi^+\pi^-$	$< 2 \times 10^{-3}$	90%
Γ_{35}	$\gamma\chi_{c1}(3872)$	$< 1.6 \times 10^{-3}$	90%
Γ_{36}	$\gamma\chi_{c0}(3915) \to \gamma J/\psi\pi^+\pi^-$	$< 1.36 \times 10^{-4}$	90%
Γ_{37}	$\gamma X(3930) \to \gamma J/\psi\pi^+\pi^-$	$< 1.18 \times 10^{-4}$	90%
Γ_{38}	$\gamma X(3940) \to \gamma J/\psi\pi^+\pi^-$	$< 1.47 \times 10^{-4}$	90%
Γ_{39}	$\gamma\chi_{c0}(3915) \to \gamma\gamma J/\psi$	$< 1.26 \times 10^{-4}$	90%
Γ_{40}	$\gamma X(3930) \to \gamma\gamma J/\psi$	$< 8.8 \times 10^{-5}$	90%
Γ_{41}	$\gamma X(3940) \to \gamma\gamma J/\psi$	$< 1.79 \times 10^{-4}$	90%
Γ_{42}	$\omega\pi^0$	not seen	
Γ_{43}	$\omega\eta$	not seen	
Γ_{44}	K^+K^-	not seen	
Γ_{45}	$K_S^0K^\pm\pi^\mp$	seen	
Γ_{46}	$p\overline{p}p\overline{p}$	not seen	
Γ_{47}	$\Lambda\overline{\Lambda}$	$< 1.5 \times 10^{-6}$	90%
Γ_{48}	$\Sigma^+\overline{\Sigma}^-$	$< 2.0 \times 10^{-4}$	90%
Γ_{49}	$\Sigma^0\overline{\Sigma}^0$	$< 5 \times 10^{-5}$	90%
Γ_{50}	$\Xi^0\overline{\Xi}^0$	$< 1.4 \times 10^{-4}$	90%
Γ_{51}	$\Xi^-\overline{\Xi}^+$	$< 8 \times 10^{-5}$	90%
Γ_{52}	$pK^-\overline{\Lambda}$ + c.c.	$< 6 \times 10^{-6}$	90%
Γ_{53}	$\Lambda\overline{\Xi}^+K^-$ + c.c.	seen	
Γ_{54}	$\Sigma^0\overline{\Xi}^+K^-$ + c.c.	$< 3.1 \times 10^{-6}$	90%
Γ_{55}	$pK^-K^-\overline{\Xi}^+$ + c.c.	$< 1.1 \times 10^{-4}$	90%

$\psi(4160)$ PARTIAL WIDTHS

$\Gamma(e^+e^-)$ — Γ_1

VALUE (keV)	DOCUMENT ID		TECN	COMMENT
0.48 ± 0.22	[1] ABLIKIM	08D	BES2	$e^+e^- \to$ hadrons
• • • We do not use the following data for averages, fits, limits, etc. • • •				
0.4 to 1.1	[2] MO	10	RVUE	$e^+e^- \to$ hadrons
0.83 ± 0.08	[3] SETH	05A	RVUE	$e^+e^- \to$ hadrons
0.84 ± 0.13	[4] SETH	05A	RVUE	$e^+e^- \to$ hadrons
0.77 ± 0.23	BRANDELIK	78C	DASP	e^+e^-

[1] Reanalysis of data presented in BAI 02C. From a global fit over the center-of-mass energy region 3.7–5.0 GeV covering the $\psi(3770)$, $\psi(4040)$, $\psi(4160)$, and $\psi(4415)$ resonances. Phase angle fixed in the fit to $\delta = (293 \pm 57)^\circ$.
[2] Reanalysis of data presented in BAI 00 and BAI 02C. From a global fit over the center-of-mass energy 3.8-4.8 GeV covering the $\psi(4040)$, $\psi(4160)$ and $\psi(4415)$ resonances and including interference effects. Four sets of solutions are obtained with the same fit quality, mass and total width, but with different e^+e^- partial widths. We quote only the range of values.
[3] From a fit to Crystal Ball (OSTERHELD 86) data.
[4] From a fit to BES (BAI 02C) data.

$\Gamma(\mu^+\mu^-)$ — Γ_2

VALUE (keV)	DOCUMENT ID		TECN	COMMENT
2.45 ± 1.24 ± 0.94	[1,2] ABLIKIM	20AG	BES3	$e^+e^- \to \mu^+\mu^-$

[1] From a fit to the $e^+e^- \to \mu^+\mu^-$ cross section between 3.8 and 4.6 GeV to the coherent sum of four resonant amplitudes assuming $\Gamma(\mu^+\mu^-) = \Gamma(e^+e^-)$.
[2] From solution 1 of 8 with equal fit quality. Other solutions range from 2.08 ± 0.99 ± 0.80 to 2.45 ± 1.24 ± 0.94 keV.

$\psi(4160)$ $\Gamma(i) \times \Gamma(e^+e^-)/\Gamma(\text{total})$

$\Gamma(J/\psi\eta') \times \Gamma(e^+e^-)/\Gamma_{\text{total}}$ — $\Gamma_{22}\Gamma_1/\Gamma$

VALUE (eV)	EVTS	DOCUMENT ID		TECN	COMMENT
• • • We do not use the following data for averages, fits, limits, etc. • • •					
0.17 ± 0.04	86	[1,2] ABLIKIM	20A	BES3	$e^+e^- \to \eta' J/\psi$
1.07 ± 0.09	86	[1,3] ABLIKIM	20A	BES3	$e^+e^- \to \eta' J/\psi$

[1] Based on a fit to $\sigma(e^+e^- \to \eta' J/\psi)$ from $\sqrt{s} = 4.18$ to 4.60 GeV assuming interfering $\psi(4160)$ and $\psi(4260)$ contributions. At $\sqrt{s} = 4.18$ GeV, $\sigma(e^+e^- \to \eta' J/\psi) = 2.4 \pm 0.3 \pm 0.2$ pb.
[2] Solution I of the fit, corresponding to a phase of -0.03 ± 0.44 rad.
[3] Solution II of the fit, corresponding to a phase of 2.54 ± 0.04 rad.

Int. J. Mod. Phys. A 2026.41. Downloaded from www.worldscientific.com by UNIVERSITY OF CALIFORNIA @ BERKELEY on 09/16/26. Re-use and distribution is strictly not permitted, except for Open Access articles.

$\Gamma(\chi_{c1}\gamma) \times \Gamma(e^+e^-)/\Gamma_{total}$ — $\Gamma_{25}\Gamma_1/\Gamma$

VALUE (eV)	CL%	DOCUMENT ID		TECN	COMMENT
<2.2	90	[1] HAN	15	BELL	10.58 $e^+e^- \to \chi_{c1}\gamma$

[1] Using $B(\eta \to \gamma\gamma) = (39.41 \pm 0.21)\%$.

$\Gamma(\chi_{c2}\gamma) \times \Gamma(e^+e^-)/\Gamma_{total}$ — $\Gamma_{26}\Gamma_1/\Gamma$

VALUE (eV)	CL%	DOCUMENT ID		TECN	COMMENT
• • • We do not use the following data for averages, fits, limits, etc. • • •					
<6.1	90	[1] HAN	15	BELL	10.58 $e^+e^- \to \chi_{c2}\gamma$

[1] Using $B(\eta \to \gamma\gamma) = (39.41 \pm 0.21)\%$.

$\Gamma(\omega\pi^+\pi^-) \times \Gamma(e^+e^-)/\Gamma_{total}$ — $\Gamma_{33}\Gamma_1/\Gamma$

VALUE (eV)	DOCUMENT ID		TECN	COMMENT
• • • We do not use the following data for averages, fits, limits, etc. • • •				
$0.0011 \pm 0.0008 \pm 0.0001$	[1,2] ABLIKIM	23AQ	BES3	fit to cross sections
$0.651 \pm 0.012 \pm 0.040$	[2,3] ABLIKIM	23AQ	BES3	fit to cross sections

[1] Solution I of the fit.
[2] From a fit to $e^+e^- \to \omega\pi^+\pi^-$ cross sections between 4 and 4.6 GeV. Recalculated from 12 π $\Gamma(e^+e^-)$ $B(\psi(4230) \to \omega\pi^+\pi^-)$. First uncertainty is from statistical and uncommon systematic uncertainties, and the second is a 6.2% common systematic uncertainty quoted in the paper.
[3] Solution II of the fit.

$\Gamma(K^0_S K^\pm\pi^\mp) \times \Gamma(e^+e^-)/\Gamma_{total}$ — $\Gamma_{45}\Gamma_1/\Gamma$

VALUE (eV)	DOCUMENT ID		TECN	COMMENT
• • • We do not use the following data for averages, fits, limits, etc. • • •				
$2.71 \pm 0.13 \pm 0.12$	[1] ABLIKIM	19AE	BES3	$e^+e^- \to K^0_S K^\pm\pi^\mp$
$0.0095 \pm 0.0088 \pm 0.0004$	[2] ABLIKIM	19AE	BES3	$e^+e^- \to K^0_S K^\pm\pi^\mp$

[1] Solution I of the fit including the $\psi(4160)$ with mass 4191 ± 5 MeV and width 70 ± 10 MeV from PDG 16 and the $\psi(4230)$ with mass $4219.6 \pm 3.3 \pm 5.1$ MeV and width $56.0 \pm 3.6 \pm 6.9$ MeV from GAO 17.
[2] Solution II of the fit including the $\psi(4160)$ with mass 4191 ± 5 MeV and width 70 ± 10 MeV from PDG 16 and the $\psi(4230)$ with mass $4219.6 \pm 3.3 \pm 5.1$ MeV and width $56.0 \pm 3.6 \pm 6.9$ MeV from GAO 17.

$\Gamma(\Lambda\overline{\Lambda}) \times \Gamma(e^+e^-)/\Gamma_{total}$ — $\Gamma_{47}\Gamma_1/\Gamma$

VALUE (eV)	CL%	DOCUMENT ID		TECN	COMMENT
$<0.7 \times 10^{-3}$	90	[1] ABLIKIM	21AS	BES3	$e^+e^- \to \psi(4160)$

[1] From a measurement of the $e^+e^- \to \Lambda\overline{\Lambda}$ cross section between 3.5 and 4.6 GeV.

$\Gamma(\Sigma^+\overline{\Sigma}^-) \times \Gamma(e^+e^-)/\Gamma_{total}$ — $\Gamma_{48}\Gamma_1/\Gamma$

VALUE (eV)	CL%	DOCUMENT ID		TECN	COMMENT
$<94.6 \times 10^{-3}$	90	[1] ABLIKIM	24AH	BES3	$e^+e^- \to \Sigma^+\overline{\Sigma}^-$

[1] Interference effect between resonance and continuum amplitudes is considered. Two solutions from the fit.

$\Gamma(\Sigma^0\overline{\Sigma}^0) \times \Gamma(e^+e^-)/\Gamma_{total}$ — $\Gamma_{49}\Gamma_1/\Gamma$

VALUE (eV)	CL%	DOCUMENT ID		TECN	COMMENT
$<22.7 \times 10^{-3}$	90	[1] ABLIKIM	25U	BES3	$e^+e^- \to \Sigma^0\overline{\Sigma}^0$

[1] Interference effect between resonance and continuum amplitudes is considered. Upper limit is for the larger of the two solutions from the fit.

$\Gamma(\Xi^0\overline{\Xi}^0) \times \Gamma(e^+e^-)/\Gamma_{total}$ — $\Gamma_{50}\Gamma_1/\Gamma$

VALUE (eV)	CL%	DOCUMENT ID		TECN	COMMENT
$<69.0 \times 10^{-3}$	90	[1] ABLIKIM	24CD	BES3	$e^+e^- \to \psi(4160)$

[1] From a fit to $e^+e^- \to \Xi^0\overline{\Xi}^0$ cross sections.

$\Gamma(\Xi^-\overline{\Xi}^+) \times \Gamma(e^+e^-)/\Gamma_{total}$ — $\Gamma_{51}\Gamma_1/\Gamma$

VALUE (eV)	CL%	DOCUMENT ID		TECN	COMMENT
$<37.2 \times 10^{-3}$	90	[1] ABLIKIM	23BK	BES3	$e^+e^- \to \psi(4160)$

[1] From a fit to $e^+e^- \to \Xi^-\overline{\Xi}^+$ cross sections.

$\Gamma(pK^-\overline{\Lambda} + \text{c.c.}) \times \Gamma(e^+e^-)/\Gamma_{total}$ — $\Gamma_{52}\Gamma_1/\Gamma$

VALUE (eV)	CL%	DOCUMENT ID		TECN	COMMENT
$<3.0 \times 10^{-3}$	90	[1] ABLIKIM	23BL	BES3	$e^+e^- \to \psi(4160)$

[1] From a fit to $e^+e^- \to pK^-\overline{\Lambda}$ + c.c. cross sections.

$\Gamma(\Lambda\overline{\Xi}^+K^- + \text{c.c.}) \times \Gamma(e^+e^-)/\Gamma_{total}$ — $\Gamma_{53}\Gamma_1/\Gamma$

VALUE (10^{-3} eV)	DOCUMENT ID		TECN	COMMENT
• • • We do not use the following data for averages, fits, limits, etc. • • •				
2.1 ± 0.2	[1] ABLIKIM	24AL	BES3	$e^+e^- \to \Lambda\overline{\Xi}^+K^-$ + c.c.
1.5 ± 0.4	[2] ABLIKIM	24AL	BES3	$e^+e^- \to \Lambda\overline{\Xi}^+K^-$ + c.c.

[1] A fit to the Born cross section of $e^+e^- \to \Lambda\overline{\Xi}^+K^-$ + c.c. including interference with the continuum. Significance is 4.4σ. Solution 1 of 2.
[2] A fit to the Born cross section of $e^+e^- \to \Lambda\overline{\Xi}^+K^-$ + c.c. including interference with the continuum. Significance is 4.4σ. Solution 2 of 2.

$\Gamma(\Sigma^0\overline{\Xi}^+K^- + \text{c.c.}) \times \Gamma(e^+e^-)/\Gamma_{total}$ — $\Gamma_{54}\Gamma_1/\Gamma$

VALUE (eV)	CL%	DOCUMENT ID		TECN	COMMENT
$<1.5 \times 10^{-3}$	90	[1] ABLIKIM	24AL	BES3	$e^+e^- \to \Sigma^0\overline{\Xi}^+K^-$ + c.c.

[1] A fit to the Born cross section of $e^+e^- \to \Sigma^0\overline{\Xi}^+K^-$ + c.c. including interference with the continuum. Two solutions from the fit.

$\Gamma(e^+e^-) \times \Gamma(pK^-K^-\overline{\Xi}^+ + \text{c.c.})/\Gamma_{total}$ — $\Gamma_1\Gamma_{55}/\Gamma$

VALUE (eV)	CL%	DOCUMENT ID		TECN	COMMENT
$<50.8 \times 10^{-3}$	90	ABLIKIM	25CF	BES3	$e^+e^- \to pK^-K^-\overline{\Xi}^+$ + c.c.

$\psi(4160)$ $\Gamma(i) \times \Gamma(e^+e^-)/\Gamma^2(total)$

$\Gamma(J/\psi\eta)/\Gamma_{total} \times \Gamma(e^+e^-)/\Gamma_{total}$ — $\Gamma_{20}/\Gamma \times \Gamma_1/\Gamma$

VALUE (units 10^{-8})	DOCUMENT ID		TECN	COMMENT
• • • We do not use the following data for averages, fits, limits, etc. • • •				
$2.8 \pm 0.9 \pm 0.9$	[1] WANG	13B	BELL	$e^+e^- \to J/\psi\eta\gamma$
$12.8 \pm 1.7 \pm 2.0$	[2] WANG	13B	BELL	$e^+e^- \to J/\psi\eta\gamma$

[1] Solution I of two equivalent solutions in a fit using two interfering resonances. Mass and width fixed at 4153 MeV and 103 MeV, respectively.
[2] Solution II of two equivalent solutions in a fit using two interfering resonances. Mass and width fixed at 4153 MeV and 103 MeV, respectively.

$\psi(4160)$ BRANCHING RATIOS

$\Gamma(\mu^+\mu^-)/\Gamma_{total}$ — Γ_2/Γ

VALUE	DOCUMENT ID		TECN	COMMENT
seen	[1] AAIJ	13BC	LHCB	$B^+ \to K^+\mu^+\mu^-$

[1] AAIJ 13BC report $B(B^+ \to K^+\psi(4160))\, B(\psi(4160) \to \mu^+\mu^-) = (3.5^{+0.9}_{-0.8}) \times 10^{-9}$.

$\Gamma(D\overline{D})/\Gamma(D^*\overline{D}^*)$ — Γ_3/Γ_9

VALUE	DOCUMENT ID		TECN	COMMENT
$0.02 \pm 0.03 \pm 0.02$	AUBERT	09M	BABR	$e^+e^- \to \gamma D^{(*)}\overline{D}^{(*)}$

$\Gamma(D^0\overline{D}^0)/\Gamma_{total}$ — Γ_4/Γ

VALUE	DOCUMENT ID		TECN	COMMENT
seen	[1] ABLIKIM	24BH	BES3	$e^+e^- \to D^0\overline{D}^0$
seen	CRONIN-HEN...	09	CLEO	$e^+e^- \to D^0\overline{D}^0$
seen	PAKHLOVA	08	BELL	$e^+e^- \to D^0\overline{D}^0\gamma$
• • • We do not use the following data for averages, fits, limits, etc. • • •				
not seen	AUBERT	09M	BABR	$e^+e^- \to D^0\overline{D}^0\gamma$

[1] A precision measurement of the $e^+e^- \to D^0\overline{D}^0$ cross section shows complex structure in this mass region.

$\Gamma(D^+D^-)/\Gamma_{total}$ — Γ_5/Γ

VALUE	DOCUMENT ID		TECN	COMMENT
seen	[1] ABLIKIM	24BH	BES3	$e^+e^- \to D^+D^-$
seen	CRONIN-HEN...	09	CLEO	$e^+e^- \to D^+D^-$
seen	PAKHLOVA	08	BELL	$e^+e^- \to D^+D^-\gamma$
• • • We do not use the following data for averages, fits, limits, etc. • • •				
not seen	AUBERT	09M	BABR	$e^+e^- \to D^+D^-\gamma$

[1] A precision measurement of the $e^+e^- \to D^+D^-$ cross section shows complex structure in this mass region.

$\Gamma(D^*(2007)^0\overline{D}^0 + \text{c.c.})/\Gamma_{total}$ — Γ_7/Γ

VALUE	DOCUMENT ID		TECN	COMMENT
seen	AUBERT	09M	BABR	$e^+e^- \to D^{*0}\overline{D}^0\gamma$
seen	CRONIN-HEN...	09	CLEO	$e^+e^- \to D^{*0}\overline{D}^0$

$\Gamma(D^*(2010)^+D^- + \text{c.c.})/\Gamma_{total}$ — Γ_8/Γ

VALUE	DOCUMENT ID		TECN	COMMENT
seen	[1] ZHUKOVA	18	BELL	$e^+e^- \to D^{*+}D^-\gamma$
seen	AUBERT	09M	BABR	$e^+e^- \to D^{*+}D^-\gamma$
seen	CRONIN-HEN...	09	CLEO	$e^+e^- \to D^{*+}D^-$
• • • We do not use the following data for averages, fits, limits, etc. • • •				
seen	PAKHLOVA	07	BELL	$e^+e^- \to D^{*+}D^-\gamma$

[1] Supersedes PAKHLOVA 07.

$\Gamma(D^*\overline{D} + \text{c.c.})/\Gamma(D^*\overline{D}^*)$ — Γ_6/Γ_9

VALUE	DOCUMENT ID		TECN	COMMENT
$0.34 \pm 0.14 \pm 0.05$	AUBERT	09M	BABR	$e^+e^- \to \gamma D^{(*)}\overline{D}^{(*)}$

$\Gamma(D^*(2007)^0\overline{D}^*(2007)^0)/\Gamma_{total}$ — Γ_{10}/Γ

VALUE	DOCUMENT ID		TECN	COMMENT
seen	AUBERT	09M	BABR	$e^+e^- \to D^{*0}\overline{D}^{*0}\gamma$
seen	CRONIN-HEN...	09	CLEO	$e^+e^- \to D^{*0}\overline{D}^{*0}$

$\Gamma(D^*(2010)^+D^*(2010)^-)/\Gamma_{total}$ — Γ_{11}/Γ

VALUE	DOCUMENT ID		TECN	COMMENT
seen	[1] ZHUKOVA	18	BELL	$e^+e^- \to D^{*+}D^{*-}\gamma$
seen	AUBERT	09M	BABR	$e^+e^- \to D^{*+}D^{*-}\gamma$
seen	CRONIN-HEN...	09	CLEO	$e^+e^- \to D^{*+}D^{*-}$
• • • We do not use the following data for averages, fits, limits, etc. • • •				
seen	PAKHLOVA	07	BELL	$e^+e^- \to D^{*+}D^{*-}\gamma$

[1] Supersedes PAKHLOVA 07.

$\Gamma(D^0D^-\pi^+ + \text{c.c. (excl. } D^*(2010)^+D^- + \text{c.c.}))/\Gamma_{total}$ — Γ_{12}/Γ

VALUE	DOCUMENT ID		TECN	COMMENT
not seen	PAKHLOVA	08A	BELL	$e^+e^- \to D^0D^-\pi^+\gamma$

Int. J. Mod. Phys. A 2026.41. Downloaded from www.worldscientific.com
by [redacted]LIFORNIA @ BERKELEY on 09/16/26. Re-use and distribution is strictly not permitted, except for Open Access articles.

$\Gamma(D\overline{D}^*\pi + \text{c.c. (excl. } D^*\overline{D}^*))/\Gamma_{\text{total}}$ — Γ_{13}/Γ

VALUE	DOCUMENT ID	TECN	COMMENT
seen	CRONIN-HEN...09	CLEO	$e^+e^- \to D\overline{D}^*\pi$

$\Gamma(D^0 D^{*-}\pi^+ + \text{c.c. (excl. } D^*(2010)^+ D^*(2010)^-))/\Gamma_{\text{total}}$ — Γ_{14}/Γ

VALUE	DOCUMENT ID	TECN	COMMENT
not seen	PAKHLOVA 09	BELL	$e^+e^- \to D^0 D^{*-}\pi^+\gamma$

$\Gamma(D_s^+ D_s^-)/\Gamma_{\text{total}}$ — Γ_{15}/Γ

VALUE	DOCUMENT ID	TECN	COMMENT
not seen	PAKHLOVA 11	BELL	$e^+e^- \to D_s^+ D_s^-\gamma$
not seen	DEL-AMO-SA...10N	BABR	$e^+e^- \to D_s^+ D_s^-\gamma$
not seen	CRONIN-HEN...09	CLEO	$e^+e^- \to D_s^+ D_s^-$

$\Gamma(D_s^{*+} D_s^- + \text{c.c.})/\Gamma_{\text{total}}$ — Γ_{16}/Γ

VALUE	DOCUMENT ID	TECN	COMMENT
seen	PAKHLOVA 11	BELL	$e^+e^- \to D_s^{*+} D_s^-\gamma$
seen	DEL-AMO-SA...10N	BABR	$e^+e^- \to D_s^{*+} D_s^-\gamma$
seen	CRONIN-HEN...09	CLEO	$e^+e^- \to D_s^{*+} D_s^-$

$\Gamma(J/\psi\pi^+\pi^-)/\Gamma_{\text{total}}$ — Γ_{17}/Γ

VALUE (units 10^{-3})	CL%	DOCUMENT ID	TECN	COMMENT
<3	90	COAN 06	CLEO	4.12–4.2 $e^+e^- \to$ hadrons

$\Gamma(J/\psi\pi^0\pi^0)/\Gamma_{\text{total}}$ — Γ_{18}/Γ

VALUE (units 10^{-3})	CL%	DOCUMENT ID	TECN	COMMENT
<3	90	COAN 06	CLEO	4.12–4.2 $e^+e^- \to$ hadrons

$\Gamma(J/\psi K^+K^-)/\Gamma_{\text{total}}$ — Γ_{19}/Γ

VALUE (units 10^{-3})	CL%	DOCUMENT ID	TECN	COMMENT
<2	90	COAN 06	CLEO	4.12–4.2 $e^+e^- \to$ hadrons

$\Gamma(J/\psi\eta)/\Gamma_{\text{total}}$ — Γ_{20}/Γ

VALUE (units 10^{-3})	CL%	DOCUMENT ID	TECN	COMMENT
<8	90	COAN 06	CLEO	4.12–4.2 $e^+e^- \to$ hadrons
• • • We do not use the following data for averages, fits, limits, etc. • • •				
possibly seen	[1] ABLIKIM 15L	BES3		$e^+e^- \to J/\psi\eta$
seen	WANG 13B	BELL		$e^+e^- \to J/\psi\eta\gamma$

[1] An enhancement around 4.2 GeV is observed.

$\Gamma(J/\psi\pi^0)/\Gamma_{\text{total}}$ — Γ_{21}/Γ

VALUE (units 10^{-3})	CL%	DOCUMENT ID	TECN	COMMENT
<1	90	COAN 06	CLEO	4.12–4.2 $e^+e^- \to$ hadrons

$\Gamma(J/\psi\eta')/\Gamma_{\text{total}}$ — Γ_{22}/Γ

VALUE (units 10^{-3})	CL%	DOCUMENT ID	TECN	COMMENT
<5	90	COAN 06	CLEO	4.12–4.2 $e^+e^- \to$ hadrons

$\Gamma(J/\psi\pi^+\pi^-\pi^0)/\Gamma_{\text{total}}$ — Γ_{23}/Γ

VALUE (units 10^{-3})	CL%	DOCUMENT ID	TECN	COMMENT
<1	90	COAN 06	CLEO	4.12–4.2 $e^+e^- \to$ hadrons

$\Gamma(\psi(2S)\pi^+\pi^-)/\Gamma_{\text{total}}$ — Γ_{24}/Γ

VALUE (units 10^{-3})	CL%	DOCUMENT ID	TECN	COMMENT
<4	90	COAN 06	CLEO	4.12–4.2 $e^+e^- \to$ hadrons

$\Gamma(\chi_{c1}\gamma)/\Gamma_{\text{total}}$ — Γ_{25}/Γ

VALUE (units 10^{-3})	CL%	DOCUMENT ID	TECN	COMMENT
• • • We do not use the following data for averages, fits, limits, etc. • • •				
<7	90	COAN 06	CLEO	4.12–4.2 $e^+e^- \to$ hadrons

$\Gamma(\chi_{c2}\gamma)/\Gamma_{\text{total}}$ — Γ_{26}/Γ

VALUE (units 10^{-3})	CL%	DOCUMENT ID	TECN	COMMENT
<13	90	COAN 06	CLEO	4.12–4.2 $e^+e^- \to$ hadrons

$\Gamma(\chi_{c1}\pi^+\pi^-\pi^0)/\Gamma_{\text{total}}$ — Γ_{27}/Γ

VALUE (units 10^{-3})	CL%	DOCUMENT ID	TECN	COMMENT
<2	90	COAN 06	CLEO	4.12–4.2 $e^+e^- \to$ hadrons

$\Gamma(\chi_{c2}\pi^+\pi^-\pi^0)/\Gamma_{\text{total}}$ — Γ_{28}/Γ

VALUE (units 10^{-3})	CL%	DOCUMENT ID	TECN	COMMENT
<8	90	COAN 06	CLEO	4.12–4.2 $e^+e^- \to$ hadrons

$\Gamma(h_c(1P)\pi^+\pi^-)/\Gamma_{\text{total}}$ — Γ_{29}/Γ

VALUE (units 10^{-3})	CL%	DOCUMENT ID	TECN	COMMENT
<5	90	[1] PEDLAR 11	CLEO	$e^+e^- \to h_c(1P)\pi^+\pi^-$

[1] At $\sqrt{s} = 4170$ MeV, PEDLAR 11 measures $\sigma(e^+e^- \to h_c(1P)\pi^+\pi^-) = 15.6 \pm 2.3 \pm 1.9 \pm 3.0$ pb, where the errors are statistical, systematic, and due to uncertainty in $B(\psi(2S) \to \pi^0 h_c(1P))$, respectively.

$\Gamma(h_c(1P)\pi^0\pi^0)/\Gamma_{\text{total}}$ — Γ_{30}/Γ

VALUE (units 10^{-3})	CL%	DOCUMENT ID	TECN	COMMENT
<2	90	[1] PEDLAR 11	CLEO	$e^+e^- \to h_c(1P)\pi^0\pi^0$

[1] At $\sqrt{s} = 4170$ MeV, PEDLAR 11 measures $\sigma(e^+e^- \to h_c(1P)\pi^0\pi^0) = 3.0 \pm 3.3 \pm 1.1 \pm 0.6$ pb, where the errors are statistical, systematic, and due to uncertainty in $B(\psi(2S) \to \pi^0 h_c(1P))$, respectively.

$\Gamma(h_c(1P)\eta)/\Gamma_{\text{total}}$ — Γ_{31}/Γ

VALUE (units 10^{-3})	CL%	EVTS	DOCUMENT ID	TECN	COMMENT
<2	90		[1] PEDLAR 11	CLEO	$e^+e^- \to h_c(1P)\eta$
• • • We do not use the following data for averages, fits, limits, etc. • • •					
possibly seen		41	[2] ABLIKIM 17R	BES3	$e^+e^- \to h_c(1P)\eta$

[1] At $\sqrt{s} = 4170$ MeV, PEDLAR 11 measures $\sigma(e^+e^- \to h_c(1P)\eta) = 4.7 \pm 1.7 \pm 1.0 \pm 0.9$ pb, where the errors are statistical, systematic, and due to uncertainty in $B(\psi(2S) \to \pi^0 h_c(1P))$, respectively.

[2] An enhancement around 4.2 GeV is observed.

$\Gamma(h_c(1P)\pi^0)/\Gamma_{\text{total}}$ — Γ_{32}/Γ

VALUE (units 10^{-3})	CL%	DOCUMENT ID	TECN	COMMENT
<0.4	90	[1] PEDLAR 11	CLEO	$e^+e^- \to h_c(1P)\pi^0$

[1] At $\sqrt{s} = 4170$ MeV, PEDLAR 11 measures $\sigma(e^+e^- \to h_c(1P)\pi^0) = -0.7 \pm 1.8 \pm 0.7 \pm 0.1$ pb, where the errors are statistical, systematic, and due to uncertainty in $B(\psi(2S) \to \pi^0 h_c(1P))$, respectively.

$\Gamma(\phi\pi^+\pi^-)/\Gamma_{\text{total}}$ — Γ_{34}/Γ

VALUE (units 10^{-3})	CL%	DOCUMENT ID	TECN	COMMENT
<2	90	COAN 06	CLEO	4.12–4.2 $e^+e^- \to$ hadrons

$\Gamma(\gamma\chi_{c1}(3872))/\Gamma_{\text{total}}$ — Γ_{35}/Γ

VALUE	CL%	DOCUMENT ID	COMMENT
$<1.6 \times 10^{-3}$	90	[1,2] XIAO 13	$\psi(4160) \to \gamma J/\psi\pi^+\pi^-$
• • • We do not use the following data for averages, fits, limits, etc. • • •			
<0.011	90	[1,3] XIAO 13	$\psi(4160) \to \gamma J/\psi\pi^+\pi^-$

[1] Obtained by analyzing CLEO data but not authored by the CLEO Collaboration.

[2] XIAO 13 reports $[\Gamma(\psi(4160) \to \gamma\chi_{c1}(3872))/\Gamma_{\text{total}}] \times [B(\chi_{c1}(3872) \to \pi^+\pi^- J/\psi(1S))] < 0.68 \times 10^{-4}$ which we divide by our best (shown rounded) value $B(\chi_{c1}(3872) \to \pi^+\pi^- J/\psi(1S)) = 4.3 \times 10^{-2}$.

[3] XIAO 13 reports $[\Gamma(\psi(4160) \to \gamma\chi_{c1}(3872))/\Gamma_{\text{total}}] \times [B(\chi_{c1}(3872) \to \gamma J/\psi)] < 1.05 \times 10^{-4}$ which we divide by our best (shown rounded) value $B(\chi_{c1}(3872) \to \gamma J/\psi) = 10 \times 10^{-3}$.

$\Gamma(\gamma\chi_{c0}(3915) \to \gamma J/\psi\pi^+\pi^-)/\Gamma_{\text{total}}$ — Γ_{36}/Γ

VALUE	CL%	DOCUMENT ID	COMMENT
$<1.36 \times 10^{-4}$	90	[1] XIAO 13	$\psi(4160) \to \gamma J/\psi\pi^+\pi^-$

[1] Obtained by analyzing CLEO data but not authored by the CLEO Collaboration.

$\Gamma(\gamma X(3930) \to \gamma J/\psi\pi^+\pi^-)/\Gamma_{\text{total}}$ — Γ_{37}/Γ

VALUE	CL%	DOCUMENT ID	COMMENT
$<1.18 \times 10^{-4}$	90	[1] XIAO 13	$\psi(4160) \to \gamma J/\psi\pi^+\pi^-$

[1] Obtained by analyzing CLEO data but not authored by the CLEO Collaboration.

$\Gamma(\gamma X(3940) \to \gamma J/\psi\pi^+\pi^-)/\Gamma_{\text{total}}$ — Γ_{38}/Γ

VALUE	CL%	DOCUMENT ID	COMMENT
$<1.47 \times 10^{-4}$	90	[1] XIAO 13	$\psi(4160) \to \gamma J/\psi\pi^+\pi^-$

[1] Obtained by analyzing CLEO data but not authored by the CLEO Collaboration.

$\Gamma(\gamma\chi_{c0}(3915) \to \gamma\gamma J/\psi)/\Gamma_{\text{total}}$ — Γ_{39}/Γ

VALUE	CL%	DOCUMENT ID	COMMENT
$<1.26 \times 10^{-4}$	90	[1] XIAO 13	$\psi(4160) \to \gamma\gamma J/\psi$

[1] Obtained by analyzing CLEO data but not authored by the CLEO Collaboration.

$\Gamma(\gamma X(3930) \to \gamma\gamma J/\psi)/\Gamma_{\text{total}}$ — Γ_{40}/Γ

VALUE	CL%	DOCUMENT ID	COMMENT
$<0.88 \times 10^{-4}$	90	[1] XIAO 13	$\psi(4160) \to \gamma\gamma J/\psi$

[1] Obtained by analyzing CLEO data but not authored by the CLEO Collaboration.

$\Gamma(\gamma X(3940) \to \gamma\gamma J/\psi)/\Gamma_{\text{total}}$ — Γ_{41}/Γ

VALUE	CL%	DOCUMENT ID	COMMENT
$<1.79 \times 10^{-4}$	90	[1] XIAO 13	$\psi(4160) \to \gamma\gamma J/\psi$

[1] Obtained by analyzing CLEO data but not authored by the CLEO Collaboration.

$\Gamma(\omega\pi^0)/\Gamma_{\text{total}}$ — Γ_{42}/Γ

VALUE	DOCUMENT ID	TECN	COMMENT
not seen	ABLIKIM 22K	BES3	$e^+e^- \to \omega\pi^0$

$\Gamma(\omega\eta)/\Gamma_{\text{total}}$ — Γ_{43}/Γ

VALUE	DOCUMENT ID	TECN	COMMENT
not seen	ABLIKIM 22K	BES3	$e^+e^- \to \omega\eta$

Int. J. Mod. Phys. A 2026.41. Downloaded from www.worldscientific.com by UNIVERSITY OF CALIFORNIA @ BERKELEY on 09/16/26. Re-use and distribution is strictly not permitted, except for Open Access articles.

$\Gamma(K^+K^-)/\Gamma_{total}$ — Γ_{44}/Γ

VALUE	CL%	DOCUMENT ID		TECN	COMMENT
• • • We do not use the following data for averages, fits, limits, etc. • • •					
$<2\times10^{-5}$	90	[1] DRUZHININ	15	RVUE	$e^+e^-\to\psi(3770)$

[1] DRUZHININ 15 uses BABAR and CLEO data taking into account interference of the processes $e^+e^-\to K^+K^-$ and $e^+e^-\to K^0_S K^0_L$.

$\Gamma(p\overline{p}p\overline{p})/\Gamma_{total}$ — Γ_{46}/Γ

VALUE	DOCUMENT ID		TECN	COMMENT
not seen	ABLIKIM	21D	BES3	4.0–4.6 $e^+e^-\to p\overline{p}p\overline{p}$

$\psi(4160)$ REFERENCES

ABLIKIM	25CF	JHEP 2511 111	M. Ablikim et al.	(BESIII Collab.)
ABLIKIM	25U	PR D111 L051502	M. Ablikim et al.	(BESIII Collab.)
ABLIKIM	24AH	JHEP 2405 022	M. Ablikim et al.	(BESIII Collab.)
ABLIKIM	24AL	JHEP 2407 258	M. Ablikim et al.	(BESIII Collab.)
ABLIKIM	24BH	PRL 133 081901	M. Ablikim et al.	(BESIII Collab.)
ABLIKIM	24CD	JHEP 2411 062	M. Ablikim et al.	(BESIII Collab.)
ABLIKIM	23AQ	JHEP 2308 159	M. Ablikim et al.	(BESIII Collab.)
ABLIKIM	23BH	PRL 131 151903	M. Ablikim et al.	(BESIII Collab.)
ABLIKIM	23BK	JHEP 2311 228	M. Ablikim et al.	(BESIII Collab.)
ABLIKIM	23BL	JHEP 2312 027	M. Ablikim et al.	(BESIII Collab.)
ABLIKIM	22K	JHEP 2207 064	M. Ablikim et al.	(BESIII Collab.)
ABLIKIM	21AS	PR D104 L091104	M. Ablikim et al.	(BESIII Collab.)
ABLIKIM	21D	PR D103 052003	M. Ablikim et al.	(BESIII Collab.)
ABLIKIM	20A	PR D101 012008	M. Ablikim et al.	(BESIII Collab.)
ABLIKIM	20AG	PR D102 112009	M. Ablikim et al.	(BESIII Collab.)
ABLIKIM	19AE	PR D99 072005	M. Ablikim et al.	(BESIII Collab.)
ZHUKOVA	18	PR D97 012002	V. Zhukova et al.	(BELLE Collab.)
ABLIKIM	17R	PR D96 012001	M. Ablikim et al.	(BESIII Collab.)
GAO	17	PR D95 092007	X.Y. Gao, C.P. Shen, C.Z. Yuan	
PDG	16	CP C40 100001	C. Patrignani et al.	(PDG Collab.)
ABLIKIM	15L	PR D91 112005	M. Ablikim et al.	(BESIII Collab.)
DRUZHININ	15	PR D92 054024	V.P. Druzhinin	(NOVO)
HAN	15	PR D92 012011	Y.L. Han et al.	(BELLE Collab.)
AAIJ	13BC	PRL 111 112003	R. Aaij et al.	(LHCb Collab.)
WANG	13B	PR D87 051101	X.L. Wang et al.	(BELLE Collab.)
XIAO	13	PR D87 057501	T. Xiao et al.	(NWES, WAYN)
PAKHLOVA	11	PR D83 011101	G. Pakhlova et al.	(BELLE Collab.)
PEDLAR	11	PRL 107 041803	T. Pedlar et al.	(CLEO Collab.)
DEL-AMO-SA...	10N	PR D82 052004	P. del Amo Sanchez et al.	(BABAR Collab.)
MO	10	PR D82 077501	X.H. Mo, C.Z. Yuan, P. Wang	(BHEP)
AUBERT	09M	PR D79 092001	B. Aubert et al.	(BABAR Collab.)
CRONIN-HEN...	09	PR D80 072001	D. Cronin-Hennessy et al.	(CLEO Collab.)
PAKHLOVA	09	PR D80 091101	G. Pakhlova et al.	(BELLE Collab.)
ABLIKIM	08D	PL B660 315	M. Ablikim et al.	(BES Collab.)
PAKHLOVA	08	PR D77 011103	G. Pakhlova et al.	(BELLE Collab.)
PAKHLOVA	08A	PRL 100 062001	G. Pakhlova et al.	(BELLE Collab.)
PAKHLOVA	07	PRL 98 092001	G. Pakhlova et al.	(BELLE Collab.)
COAN	06	PRL 96 162003	T.E. Coan et al.	(CLEO Collab.)
SETH	05A	PR D72 017501	K.K. Seth	
BAI	02C	PRL 88 101802	J.Z. Bai et al.	(BES Collab.)
BAI	00	PRL 84 594	J.Z. Bai et al.	(BES Collab.)
OSTERHELD	86	SLAC-PUB-4160	A. Osterheld et al.	(SLAC Crystal Ball Collab.)
BRANDELIK	78C	PL 76B 361	R. Brandelik et al.	(DASP Collab.)

$X(4160)$

$I^G(J^{PC}) = ?^?(?^{??})$

OMITTED FROM SUMMARY TABLE

Seen by PAKHLOV 08 in $e^+e^-\to J/\psi X$, $X\to D^*\overline{D}^*$

A state with consistent mass and width is seen by AAIJ 21E in $B^+\to X(4160)K^+$ with $X(4160)\to J/\psi\phi$ using an amplitude analysis of $B^+\to J/\psi\phi K^+$ with a significance (accounting for systematic uncertainties) of 4.8 σ. The $J^{PC}=2^{-+}$ assignment is favored over other assignments with a significance of more than 4 σ.

$X(4160)$ MASS

VALUE (MeV)	EVTS	DOCUMENT ID		TECN	COMMENT
4153^{+23}_{-21} OUR AVERAGE					
$4146\pm18\pm33$	24k	[1] AAIJ	21E	LHCB	$B^+\to J/\psi\phi K^+$
$4156^{+25}_{-20}\pm15$	24	PAKHLOV	08	BELL	$e^+e^-\to J/\psi X$

[1] From an amplitude analysis of the decay $B^+\to J/\psi\phi K^+$ with a significance of 4.8 σ.

$X(4160)$ WIDTH

VALUE (MeV)	EVTS	DOCUMENT ID		TECN	COMMENT
136^{+60}_{-35} OUR AVERAGE					
$135\pm28^{+59}_{-30}$	24k	[1] AAIJ	21E	LHCB	$B^+\to J/\psi\phi K^+$
$139^{+111}_{-61}\pm21$	24	PAKHLOV	08	BELL	$e^+e^-\to J/\psi X$

[1] From an amplitude analysis of the decay $B^+\to J/\psi\phi K^+$ with a significance of 4.8 σ.

$X(4160)$ DECAY MODES

	Mode	Fraction (Γ_i/Γ)
Γ_1	$D\overline{D}$	not seen
Γ_2	$D^*\overline{D}+$ c.c.	not seen
Γ_3	$D^*\overline{D}^*$	seen
Γ_4	$J/\psi\phi$	seen

$X(4160)$ BRANCHING RATIOS

$\Gamma(D\overline{D})/\Gamma(D^*\overline{D}^*)$ — Γ_1/Γ_3

VALUE	CL%	DOCUMENT ID		TECN	COMMENT
<0.09	90	PAKHLOV	08	BELL	$e^+e^-\to J/\psi X$

$\Gamma(D^*\overline{D}+\text{c.c.})/\Gamma(D^*\overline{D}^*)$ — Γ_2/Γ_3

VALUE	CL%	DOCUMENT ID		TECN	COMMENT
<0.22	90	PAKHLOV	08	BELL	$e^+e^-\to J/\psi X$

$\Gamma(J/\psi\phi)/\Gamma_{total}$ — Γ_4/Γ

VALUE	EVTS	DOCUMENT ID		TECN	COMMENT
seen	24k	[1] AAIJ	21E	LHCB	$B^+\to J/\psi\phi K^+$

[1] From an amplitude analysis of the decay $B^+\to J/\psi\phi K^+$ with a significance of 4.8 σ.

$X(4160)$ REFERENCES

AAIJ	21E	PRL 127 082001	R. Aaij et al.	(LHCb Collab.)
PAKHLOV	08	PRL 100 202001	P. Pakhlov et al.	(BELLE Collab.)

$\psi(4230)$

$I^G(J^{PC}) = 0^-(1^{--})$

also known as $Y(4230)$; was $\psi(4260)$

The original $\psi(4260)$ (also known as $Y(4260)$) was observed by AUBERT,B 05I as a peak in the energy dependence of the $e^+e^-\to\pi^+\pi^-J/\psi$ cross section and was confirmed by HE 06B, YUAN 07, LEES 12AC, and LIU 13B in the same process. A higher-statistics analysis by ABLIKIM 17B revealed an asymmetry in the cross section and resulted in a shift of the peak position to a lower mass. The $\psi(4260)$ was therefore renamed $\psi(4230)$. The energy-dependent cross sections for e^+e^- to other channels also exhibit peaks in the same mass region. The parameters corresponding to those peaks are also listed here, but the number of states in this region remains to be determined.

For details see the review on "Spectroscopy of mesons containing two heavy quarks."

$\psi(4230)$ MASS

VALUE (MeV)	EVTS	DOCUMENT ID		TECN	COMMENT
4221.7 ± 2.5 OUR AVERAGE Error includes scale factor of 1.9. See the ideogram below.					
$4223.6^{+3.6}_{-3.7}\pm^{2.6}_{2.9}$		[1] ABLIKIM	25B	BES3	$e^+e^-\to\pi^+\pi^-h_c(1P)$
$4188.8\pm4.7\pm8.0$		[2] ABLIKIM	25S	BES3	$e^+e^-\to\eta h_c$
$4219.7\pm2.5\pm4.5$		[3] ABLIKIM	24T	BES3	$e^+e^-\to\eta J/\psi$
$4226.9\pm6.6\pm22.0$		[4] ABLIKIM	23U	BES3	$e^+e^-\to K_S K_S J/\psi$
$4209.6\pm4.7\pm5.9$		[5] ABLIKIM	23X	BES3	$e^+e^-\to D^{*0}D^{*-}\pi^+$
$4221.4\pm1.5\pm2.0$		[6] ABLIKIM	22AM	BES3	$e^+e^-\to\pi^+\pi^-J/\psi$
$4225.3\pm2.3\pm21.5$		[7] ABLIKIM	22AU	BES3	$e^+e^-\to K^+K^-J/\psi$
$4234.4\pm3.2\pm0.2$		[8] ABLIKIM	21AJ	BES3	$e^+e^-\to\pi^+\pi^-\psi(2S)$
$4216.7\pm8.9\pm4.1$		[9] ABLIKIM	20AG	BES3	$e^+e^-\to\mu^+\mu^-$
$4220.4\pm2.4\pm2.3$		[10] ABLIKIM	20N	BES3	$e^+e^-\to\pi^0\pi^0J/\psi$
$4218.5\pm1.6\pm4.0$		[11] ABLIKIM	19AI	BES3	$e^+e^-\to\omega\chi_{c0}$
$4228.6\pm4.1\pm6.3$		ABLIKIM	19R	BES3	$e^+e^-\to\pi^+D^0D^{*-}+$ c.c.
$4200.6^{+7.9}_{-13.3}\pm3.0$		[12] ABLIKIM	19V	BES3	$e^+e^-\to\gamma\chi_{c1}(3872)$
$4218^{+5.5}_{-4.5}\pm0.9$		ABLIKIM	17G	BES3	$e^+e^-\to\pi^+\pi^-h_c$
• • • We do not use the following data for averages, fits, limits, etc. • • •					
$4225.7\pm4.1\pm3.4$		[13] ABLIKIM	25BU	BES3	$e^+e^-\to\pi^\pm Z_c(3900)^\mp$, $f_0(980)J/\psi$
$4231.9\pm5.3\pm4.9$		ABLIKIM	20N	BES3	$e^+e^-\to\pi^0T_{c\overline{c}1}(3900)^0$, $T^0_{c\overline{c}1}\to\pi^0J/\psi$
$4218.6\pm3.8\pm2.5$		[10] ABLIKIM	20O	BES3	$e^+e^-\to\eta J/\psi$
$4222.0\pm3.1\pm1.4$		[14] ABLIKIM	17B	BES3	$e^+e^-\to\pi^+\pi^-J/\psi$
$4209.5\pm7.4\pm1.4$		[15] ABLIKIM	17V	BES3	$e^+e^-\to\pi^+\pi^-\psi(2S)$
$4209.1\pm6.8\pm7.0$		[16] ZHANG	17B	RVUE	$e^+e^-\to\pi^+\pi^-\psi(2S)$
$4223.3\pm1.6\pm2.5$		[17] ZHANG	17C	RVUE	$e^+e^-\to\pi^+\pi^-J/\psi$ or $\psi(2S)$
$4230\pm8\pm6180$		[18] ABLIKIM	15C	BES3	$e^+e^-\to\omega\chi_{c0}$
$4258.6\pm8.3\pm12.1$		[19] LIU	13B	BELL	$e^+e^-\to\gamma\pi^+\pi^-J/\psi$
$4245\pm5\pm4$		[20] LEES	12AC	BABR	10.58 $e^+e^-\to\gamma\pi^+\pi^-J/\psi$
$4247\pm12^{+17}_{-32}$		[19,21] YUAN	07	BELL	10.58 $e^+e^-\to\gamma\pi^+\pi^-J/\psi$

$4284\ ^{+17}_{-16} \pm 413.6$	HE	06B	CLEO	9.4–10.6	$e^+e^- \to \gamma\pi^+\pi^- J/\psi$
$4259 \pm 8\ ^{+2}_{-6}\ 125$	[22] AUBERT,B	05I	BABR	10.58	$e^+e^- \to \gamma\pi^+\pi^- J/\psi$

[1] Using three coherent Breit-Wigner functions between 4.009 and 4.950 GeV.
[2] Also consistent with $\psi(4160)$.
[3] From a three-resonance fit to the Born cross section in the range $\sqrt{s}$ = 3.808–4.951 GeV. Supersedes ABLIKIM 20O.
[4] From a three-resonance fit to the dressed cross section in the range $\sqrt{s}$ = 4.128–4.950 GeV.
[5] From a cross-section measurement of $e^+e^- \to D^{*0}D^{*-}\pi^+$ between 4.189 and 4.951 GeV, assuming a coherent sum of 3 Breit-Wigner resonances plus a continuum amplitude. The two other resonances have masses (widths) 4675.3 ± 29.7 (218.3 ± 73.5) MeV and 4469.1 ± 26.4 (246.3 ± 37.9) MeV.
[6] From a three-resonance fit to the Born cross section in the range $\sqrt{s}$ = 3.7730–4.7008 GeV.
[7] From a two-resonance fit to the dressed cross section in the range $\sqrt{s}$ = 4.127–4.600 GeV. The second resonance has a mass of 4484.7 ± 13.3 ± 24.1 MeV and a total width of 111.1 ± 30.1 ± 15.2 MeV.
[8] From a three-resonance fit to the Born cross section in the range $\sqrt{s}$ = 4.008–4.698 GeV.
[9] Solution 1 of 8 with equal fit quality to the $e^+e^- \to \mu^+\mu^-$ cross section between 3.8 and 4.6 GeV to the coherent sum of four resonant amplitudes. Other solutions range from 4212.8 ± 7.2 ± 4.0 to 4219.4 ± 11.2 ± 4.1 MeV.
[10] From a fit of the measured cross section in the range $\sqrt{s}$ = 3.808–4.600 GeV.
[11] From a fit of the measured cross section from $\sqrt{s}$ = 4.178–4.278 GeV. Supersedes ABLIKIM 15C.
[12] Simultaneous fit to $\chi_{c1} \to \omega J/\psi$ and $\chi_{c1} \to \pi^+\pi^- J/\psi$.
[13] Average of the processes $\pi^\pm Z_c(3900)^\mp$ and $f_0(980)\,J/\psi$. Not independent from ABLIKIM 22AM.
[14] From a three-resonance fit. Superseded by ABLIKIM 22AM.
[15] From a fit to the cross section for $e^+e^- \to \pi^+\pi^-\psi(2S) \to 2(\pi^+\pi^-)\ell^+\ell^-$ obtained from 16 center-of-mass energies between 4.008 and 4.600 GeV and comprising 5.1 fb^{-1}. Superseded by ABLIKIM 21AJ.
[16] From a three-resonance fit.
[17] From a combined fit of BELLE, BABAR and BES3 $e^+e^- \to \pi^+\pi^- J/\psi$ and $e^+e^- \to \pi^+\pi^-\psi(2S)$ data.
[18] From a 3-parameter fit of measured cross sections from $\sqrt{s}$ = 4.21–4.42 GeV to a phase-space modified Breit-Wigner function, using the decays $\chi_{c0} \to \pi^+\pi^-$, $\chi_{c0} \to K^+K^-$, and $\omega \to \pi^+\pi^-\pi^0$.
[19] From a two-resonance fit.
[20] From a single-resonance fit. Supersedes AUBERT,B 05I.
[21] Superseded by LIU 13B.
[22] From a single-resonance fit. Two interfering resonances are not excluded. Superseded by LEES 12AC.

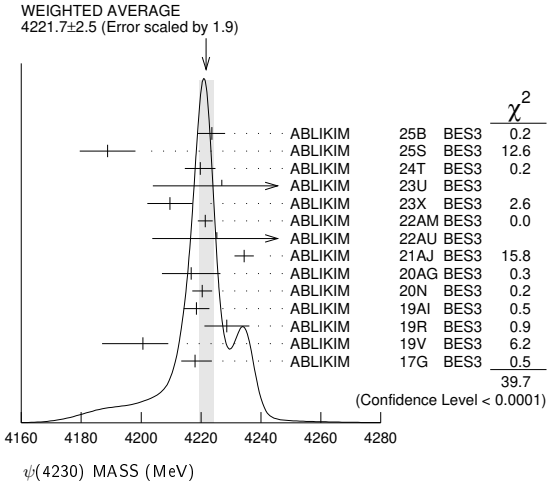

$\psi(4230)$ WIDTH

VALUE (MeV)	EVTS	DOCUMENT ID		TECN	COMMENT
51 ± 7 OUR AVERAGE		Error includes scale factor of 3.4. See the ideogram below.			
$58.5\ ^{+10.8}_{-11.4} \pm\ ^{6.7}_{6.5}$		[1] ABLIKIM	25B	BES3	$e^+e^- \to \pi^+\pi^- h_c(1P)$
$49 \pm 16 \pm 19$		[2] ABLIKIM	25S	BES3	$e^+e^- \to \eta h_c$
$80.7 \pm 4.4 \pm 1.4$		[3] ABLIKIM	24T	BES3	$e^+e^- \to \eta J/\psi$
$71.7 \pm 16.2 \pm 32.8$		[4] ABLIKIM	23U	BES3	$e^+e^- \to K_S K_S J/\psi$
$81.6 \pm 17.8 \pm 9.0$		[5] ABLIKIM	23X	BES3	$e^+e^- \to D^{*0}D^{*-}\pi^+$
$41.8 \pm 2.9 \pm 2.7$		[6] ABLIKIM	22AM	BES3	$e^+e^- \to \pi^+\pi^- J/\psi$
$72.9 \pm 6.1 \pm 30.8$		[7] ABLIKIM	22AU	BES3	$e^+e^- \to K^+K^- J/\psi$
$17.6 \pm 18.1 \pm 0.9$		[8] ABLIKIM	21AJ	BES3	$e^+e^- \to \pi^+\pi^-\psi(2S)$
$47.2 \pm 22.8 \pm 10.5$		[9] ABLIKIM	20AG	BES3	$e^+e^- \to \mu^+\mu^-$
$46.2 \pm 4.7 \pm 2.1$		[10] ABLIKIM	20N	BES3	$e^+e^- \to \pi^0\pi^0 J/\psi$
$28.2 \pm 3.9 \pm 1.6$		[11] ABLIKIM	19AI	BES3	$e^+e^- \to \omega\chi_{c0}$
$77.0 \pm 6.8 \pm 6.3$		ABLIKIM	19R	BES3	$e^+e^- \to \pi^+D^0D^{*-}$ + c.c.
$115\ ^{+38}_{-26} \pm 12$		[12] ABLIKIM	19V	BES3	$e^+e^- \to \gamma\chi_{c1}(3872)$
$66.0\ ^{+12.3}_{-8.3} \pm 0.4$		ABLIKIM	17G	BES3	$e^+e^- \to \pi^+\pi^- h_c$
• • • We do not use the following data for averages, fits, limits, etc. • • •					
$57.5 \pm 9.4 \pm 12.1$		[13] ABLIKIM	25BU	BES3	$e^+e^- \to \pi^\pm Z_c(3900)^\mp$, $f_0(980)\,J/\psi$
$41.2 \pm 16.0 \pm 16.4$		ABLIKIM	20N	BES3	$e^+e^- \to \pi^0 T_{c\bar{c}1}(3900)^0$, $T^0_{c\bar{c}1} \to \pi^0 J/\psi$
$82.0 \pm 5.7 \pm 0.4$		[10] ABLIKIM	20O	BES3	$e^+e^- \to \eta J/\psi$
$44.1 \pm 4.3 \pm 2.0$		[14] ABLIKIM	17B	BES3	$e^+e^- \to \pi^+\pi^- J/\psi$
$80.1 \pm 24.6 \pm 2.9$		[15] ABLIKIM	17V	BES3	$e^+e^- \to \pi^+\pi^-\psi(2S)$
$76.6 \pm 14.2 \pm 2.4$		[16] ZHANG	17B	RVUE	$e^+e^- \to \pi^+\pi^-\psi(2S)$
$54.2 \pm 2.6 \pm 1.0$		[17] ZHANG	17C	RVUE	$e^+e^- \to \pi^+\pi^- J/\psi$ or $\psi(2S)$
$38 \pm 12 \pm 2\ 180$		[18] ABLIKIM	15C	BES3	$e^+e^- \to \omega\chi_{c0}$
$134.1 \pm 16.4 \pm 5.5$		[19] LIU	13B	BELL	$e^+e^- \to \gamma\pi^+\pi^- J/\psi$
$114\ ^{+16}_{-15} \pm 7$		[20] LEES	12AC	BABR	10.58 $e^+e^- \to \gamma\pi^+\pi^- J/\psi$
$108 \pm 19 \pm 10$		[19,21] YUAN	07	BELL	10.58 $e^+e^- \to \gamma\pi^+\pi^- J/\psi$
$73\ ^{+39}_{-25} \pm 5\ 13.6$		HE	06B	CLEO	9.4–10.6 $e^+e^- \to \gamma\pi^+\pi^- J/\psi$
$88 \pm 23\ ^{+6}_{-4}\ 125$		[22] AUBERT,B	05I	BABR	10.58 $e^+e^- \to \gamma\pi^+\pi^- J/\psi$

[1] Using three coherent Breit-Wigner functions between 4.009 and 4.950 GeV.
[2] Also consistent with $\psi(4160)$.
[3] From a three-resonance fit to the Born cross section in the range $\sqrt{s}$ = 3.808–4.951 GeV. Supersedes ABLIKIM 20O.
[4] From a three-resonance fit to the dressed cross section in the range $\sqrt{s}$ = 4.128–4.950 GeV.
[5] From a cross-section measurement of $e^+e^- \to D^{*0}D^{*-}\pi^+$ between 4.189 and 4.951 GeV, assuming a coherent sum of 3 Breit-Wigner resonances plus a continuum amplitude. The two other resonances have masses (widths) 4675.3 ± 29.7 (218.3 ± 73.5) MeV and 4469.1 ± 26.4 (246.3 ± 37.9) MeV.
[6] From a three-resonance fit to the Born cross section in the range $\sqrt{s}$ = 3.7730–4.7008 GeV.
[7] From a two-resonance fit to the dressed cross section in the range $\sqrt{s}$ = 4.127–4.600 GeV. The second resonance has a mass of 4484.7 ± 13.3 ± 24.1 MeV and a total width of 111.1 ± 30.1 ± 15.2 MeV.
[8] From a three-resonance fit to the Born cross section in the range $\sqrt{s}$ = 4.008–4.698 GeV.
[9] Solution 1 of 8 with equal fit quality to the $e^+e^- \to \mu^+\mu^-$ cross section between 3.8 and 4.6 GeV to the coherent sum of four resonant amplitudes. Other solutions range from 36.4 ± 16.8 ± 8.1 to 49.6 ± 22.6 ± 11.0 MeV.
[10] From a fit of the measured cross section in the range $\sqrt{s}$ = 3.808–4.600 GeV.
[11] From a fit of the measured cross section from $\sqrt{s}$ = 4.178–4.278 GeV. Supersedes ABLIKIM 15C.
[12] Simultaneous fit to $\chi_{c1} \to \omega J/\psi$ and $\chi_{c1} \to \pi^+\pi^- J/\psi$.
[13] Average of the processes $\pi^\pm Z_c(3900)^\mp$ and $f_0(980)\,J/\psi$. Not independent from ABLIKIM 22AM.
[14] From a three-resonance fit. Superseded by ABLIKIM 22AM.
[15] From a fit to the cross section for $e^+e^- \to \pi^+\pi^-\psi(2S) \to 2(\pi^+\pi^-)\ell^+\ell^-$ obtained from 16 center-of-mass energies between 4.008 and 4.600 GeV and comprising 5.1 fb^{-1}. Superseded by ABLIKIM 21AJ.
[16] From a three-resonance fit.
[17] From a combined fit of BELLE, BABAR and BES3 $e^+e^- \to \pi^+\pi^- J/\psi$ and $e^+e^- \to \pi^+\pi^-\psi(2S)$ data.
[18] From a 3-parameter fit of measured cross sections from $\sqrt{s}$ = 4.21–4.42 GeV to a phase-space modified Breit-Wigner function, using the decays $\chi_{c0} \to \pi^+\pi^-$, $\chi_{c0} \to K^+K^-$, and $\omega \to \pi^+\pi^-\pi^0$.
[19] From a two-resonance fit.
[20] From a single-resonance fit. Supersedes AUBERT,B 05I.
[21] Superseded by LIU 13B.
[22] From a single-resonance fit. Two interfering resonances are not excluded. Superseded by LEES 12AC.

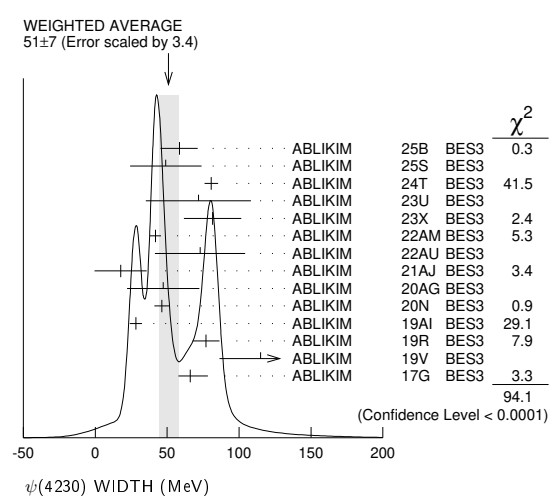

Int. J. Mod. Phys. A 2026.41. Downloaded from www.worldscientific.com
by LIFORNIA @ BERKELEY on 09/16/26. Re-use and distribution is strictly not permitted, except for Open Access articles.

Int. J. Mod. Phys. A 2026.41. Downloaded from www.worldscientific.com
by UNIVERSITY OF CALIFORNIA @ BERKELEY on 09/16/26. Re-use and distribution is strictly not permitted, except for Open Access articles.

$\psi(4230)$ DECAY MODES

	Mode	Fraction (Γ_i/Γ)
Γ_1	$e^+ e^-$	
Γ_2	$\mu^+ \mu^-$	$(3.0 \pm 2.7) \times 10^{-5}$
Γ_3	$\eta_c(1S)\pi^+\pi^-$	not seen
Γ_4	$\eta_c(1S)\pi^+\pi^-\pi^0$	seen
Γ_5	$J/\psi\pi^+\pi^-$	seen
Γ_6	$J/\psi f_0(980)$, $f_0(980) \to \pi^+\pi^-$	seen
Γ_7	$T_{c\overline{c}1}(3900)^{\pm}\pi^{\mp}$, $T^{\pm}_{c\overline{c}1} \to J/\psi\pi^{\pm}$	seen
Γ_8	$J/\psi\pi^0\pi^0$	seen
Γ_9	$J/\psi K^+ K^-$	seen
Γ_{10}	$J/\psi K^0_S K^0_S$	not seen
Γ_{11}	$J/\psi\eta$	seen
Γ_{12}	$J/\psi\pi^0$	not seen
Γ_{13}	$J/\psi\eta'$	seen
Γ_{14}	$J/\psi\pi^+\pi^-\pi^0$	not seen
Γ_{15}	$J/\psi\eta\pi^0$	not seen
Γ_{16}	$J/\psi\eta\eta$	not seen
Γ_{17}	$\psi(2S)\pi^+\pi^-$	seen
Γ_{18}	$\psi(2S)\eta$	not seen
Γ_{19}	$\chi_{c0}\omega$	seen
Γ_{20}	$\chi_{c1}\pi^+\pi^-\pi^0$	not seen
Γ_{21}	$\chi_{c2}\pi^+\pi^-\pi^0$	not seen
Γ_{22}	$h_c(1P)\pi^+\pi^-$	seen
Γ_{23}	$h_c(1P)\eta$	seen
Γ_{24}	$\phi\pi^+\pi^-$	not seen
Γ_{25}	$\phi f_0(980) \to \phi\pi^+\pi^-$	not seen
Γ_{26}	$\phi K^+ K^-$	not seen
Γ_{27}	$\phi K^0_S K^0_S$	not seen
Γ_{28}	$\phi\eta$	not seen
Γ_{29}	$\phi\eta'$	not seen
Γ_{30}	$D\overline{D}$	not seen
Γ_{31}	$D^0\overline{D}^0$	possibly seen
Γ_{32}	D^+D^-	possibly seen
Γ_{33}	$D^*\overline{D}$ + c.c.	not seen
Γ_{34}	$D^*(2007)^0\overline{D}^0$ + c.c.	not seen
Γ_{35}	$D^*(2010)^+D^-$ + c.c.	not seen
Γ_{36}	$D^*\overline{D}^*$	not seen
Γ_{37}	$D^*(2007)^0\overline{D}^*(2007)^0$	not seen
Γ_{38}	$D^*(2010)^+D^*(2010)^-$	not seen
Γ_{39}	$D\overline{D}\pi$ + c.c.	not seen
Γ_{40}	$D^0D^-\pi^+$ + c.c. (excl. $D^*(2007)^0\overline{D}^{*0}$ + c.c., $D^*(2010)^+D^-$ + c.c.)	not seen
Γ_{41}	$D\overline{D}^*\pi$ + c.c. (excl. $D^*\overline{D}^*$)	not seen
Γ_{42}	$D^0D^*(2010)^-\pi^+$ + c.c.	seen
Γ_{43}	$D_1(2420)\overline{D}$ + c.c.	not seen
Γ_{44}	$D^*\overline{D}^*\pi$	seen
Γ_{45}	$D^{*0}D^{*-}\pi^+$	seen
Γ_{46}	$D^+_s D^-_s$	not seen
Γ_{47}	$D^{*+}_s D^-_s$ + c.c.	not seen
Γ_{48}	$D^{*+}_s D^{*-}_s$	not seen
Γ_{49}	$p\overline{p}$	not seen
Γ_{50}	$p\overline{p}\pi^0$	not seen
Γ_{51}	$p\overline{p}\eta$	not seen
Γ_{52}	$\omega\pi^+\pi^-$	seen
Γ_{53}	$p\overline{p}\omega$	not seen
Γ_{54}	$\Xi^0\overline{\Xi}^0$	
Γ_{55}	$\Xi^-\overline{\Xi}^+$	not seen
Γ_{56}	$\pi^+\pi^+\pi^-\pi^-$	not seen
Γ_{57}	$\pi^+\pi^+\pi^-\pi^-\pi^0$	not seen
Γ_{58}	$\omega\pi^0$	not seen
Γ_{59}	$\omega\eta$	not seen
Γ_{60}	$K^0_S K^{\pm}\pi^{\mp}$	not seen
Γ_{61}	$K^0_S K^{\pm}\pi^{\mp}\pi^0$	not seen
Γ_{62}	$K^0_S K^{\pm}\pi^{\mp}\eta$	not seen
Γ_{63}	$K^+K^-\pi^0$	not seen
Γ_{64}	$K^+K^-\pi^+\pi^-$	not seen
Γ_{65}	$K^+K^-\pi^+\pi^-\pi^0$	not seen
Γ_{66}	$K^+K^+K^-K^-$	not seen
Γ_{67}	$K^+K^+K^-K^-\pi^0$	not seen
Γ_{68}	$p\overline{p}\pi^+\pi^-$	not seen
Γ_{69}	$p\overline{p}\pi^+\pi^-\pi^0$	not seen
Γ_{70}	$p\overline{p}p\overline{p}$	not seen
Γ_{71}	$\Lambda\overline{\Lambda}$	not seen
Γ_{72}	$\Sigma^+\overline{\Sigma}^-$	not seen
Γ_{73}	$\Sigma^0\overline{\Sigma}^0$	
Γ_{74}	$pK^-\overline{\Lambda}$ + c.c.	not seen
Γ_{75}	$\Lambda\overline{\Xi}^+K^-$ + c.c.	not seen
Γ_{76}	$\Sigma^0\overline{\Xi}^+K^-$ + c.c.	not seen
Γ_{77}	$pK^-K^-\overline{\Xi}^+$ + c.c.	
	Radiative decays	
Γ_{78}	$\eta_c(1S)\gamma$	possibly seen
Γ_{79}	$\eta_c(1S)\pi^0\gamma$	not seen
Γ_{80}	$\eta_c(1S)\eta\gamma$	not seen
Γ_{81}	$\eta_c(1S)\eta'\gamma$	not seen
Γ_{82}	$\chi_{c1}\gamma$	not seen
Γ_{83}	$\chi_{c2}\gamma$	not seen
Γ_{84}	$\chi_{c1}(3872)\gamma$	seen

$\psi(4230)$ PARTIAL WIDTHS

$\Gamma(\mu^+\mu^-)$ — Γ_2

VALUE (keV)		DOCUMENT ID		TECN	COMMENT
1.53±1.26±0.54	[1,2]	ABLIKIM	20AG	BES3	$e^+e^- \to \mu^+\mu^-$

[1] From a fit to the $e^+e^- \to \mu^+\mu^-$ cross section between 3.8 and 4.6 GeV to the coherent sum of four resonant amplitudes assuming $\Gamma(\mu^+\mu^-) = \Gamma(e^+e^-)$.
[2] From solution 1 of 8 with equal fit quality. Other solutions range from $1.09 \pm 0.84 \pm 0.39$ to $1.53 \pm 1.26 \pm 0.54$ keV.

$\psi(4230)$ $\Gamma(i) \times \Gamma(e^+e^-)/\Gamma(\text{total})$

$\Gamma(J/\psi\pi^+\pi^-) \times \Gamma(e^+e^-)/\Gamma_{\text{total}}$ — $\Gamma_5\Gamma_1/\Gamma$

VALUE (eV)	EVTS	DOCUMENT ID		TECN	COMMENT
9.2±1.0 OUR AVERAGE					
$9.2 \pm 0.8 \pm 0.7$		[1] LEES	12AC	BABR	$10.58\ e^+e^- \to \gamma\pi^+\pi^- J/\psi$
$8.9^{+3.9}_{-3.1} \pm 1.8$	8.1	HE	06B	CLEO	9.4–$10.6\ e^+e^- \to \gamma\pi^+\pi^- J/\psi$
• • • We do not use the following data for averages, fits, limits, etc. • • •					
$6.4 \pm 0.8 \pm 0.6$		[2] LIU	13B	BELL	$e^+e^- \to \gamma\pi^+\pi^- J/\psi$
$20.5 \pm 1.4 \pm 2.0$		[3] LIU	13B	BELL	$e^+e^- \to \gamma\pi^+\pi^- J/\psi$
$6.0 \pm 1.2^{+4.7}_{-0.5}$		[2,4] YUAN	07	BELL	$10.58\ e^+e^- \to \gamma\pi^+\pi^- J/\psi$
$20.6 \pm 2.3^{+9.1}_{-1.7}$		[3,4] YUAN	07	BELL	$10.58\ e^+e^- \to \gamma\pi^+\pi^- J/\psi$
$5.5 \pm 1.0^{+0.8}_{-0.7}$	125	[5] AUBERT,B	05I	BABR	$10.58\ e^+e^- \to \gamma\pi^+\pi^- J/\psi$

[1] From a single-resonance fit. Supersedes AUBERT,B 05I.
[2] Solution I of two equivalent solutions in a fit using two interfering resonances.
[3] Solution II of two equivalent solutions in a fit using two interfering resonances.
[4] Superseded by LIU 13B.
[5] From a single-resonance fit. Two interfering resonances are not excluded. Superseded by LEES 12AC.

$\Gamma(J/\psi K^+K^-) \times \Gamma(e^+e^-)/\Gamma_{\text{total}}$ — $\Gamma_9\Gamma_1/\Gamma$

VALUE (eV)	CL%	DOCUMENT ID		TECN	COMMENT
• • • We do not use the following data for averages, fits, limits, etc. • • •					
$0.42 \pm 0.04 \pm 0.15$		[1] ABLIKIM	22AU	BES3	$e^+e^- \to K^+K^- J/\psi$
$0.29 \pm 0.02 \pm 0.10$		[2] ABLIKIM	22AU	BES3	$e^+e^- \to K^+K^- J/\psi$
<1.7	90	[3] SHEN	14	BELL	9.4–$10.9\ e^+e^- \to \gamma K^+K^- J/\psi$
<1.2	90	[4] YUAN	08	BELL	$e^+e^- \to \gamma K^+K^- J/\psi$

[1] Solution I from a two-resonance fit to the dressed cross section in the range $\sqrt{s} =$ 4.127–4.600 GeV. The second resonance has a mass of $4484.7 \pm 13.3 \pm 24.1$ MeV, a total width of $111.1 \pm 30.1 \pm 15.2$ MeV, and $\Gamma_{ee} \cdot B = 1.35 \pm 0.14 \pm 0.07$ eV. The phase difference is $1.72 \pm 0.09 \pm 0.52$ rad.
[2] Solution II from a two-resonance fit to the dressed cross section in the range $\sqrt{s} =$ 4.127–4.600 GeV. The second resonance has a mass of $4484.7 \pm 13.3 \pm 24.1$ MeV, a total width of $111.1 \pm 30.1 \pm 15.2$ MeV, and $\Gamma_{ee} \cdot B = 0.41 \pm 0.08 \pm 0.13$ eV. The phase difference is $5.49 \pm 0.35 \pm 0.58$ rad.
[3] From a fit of the broad $K^+K^- J/\psi$ enhancement including a coherent $\psi(4260)$ amplitude with mass and width from LIU 13B. Supersedes YUAN 08. The shape of the cross section observed by ABLIKIM 18N between 4.2 and 4.3 GeV is incompatible with that of $e^+e^- \to \pi^+\pi^- J/\psi$ in ABLIKIM 13T and ABLIKIM 17B. They also observe a broad enhancement around 4.5 GeV.
[4] From a fit of the broad $K^+K^- J/\psi$ enhancement including a coherent $\psi(4260)$ amplitude with mass and width from YUAN 07.

$\Gamma(J/\psi K^0_S K^0_S) \times \Gamma(e^+e^-)/\Gamma_{\text{total}}$ — $\Gamma_{10}\Gamma_1/\Gamma$

VALUE (eV)	CL%	DOCUMENT ID		TECN	COMMENT
<0.85	90	[1] SHEN	14	BELL	9.4–$10.9\ e^+e^- \to \gamma K^0_S K^0_S J/\psi$
• • • We do not use the following data for averages, fits, limits, etc. • • •					
$0.13 \pm 0.02 \pm 0.05$		[2,3] ABLIKIM	23U	BES3	$e^+e^- \to K_S K_S J/\psi$
$0.14 \pm 0.03 \pm 0.06$		[2,4] ABLIKIM	23U	BES3	$e^+e^- \to K_S K_S J/\psi$
$0.18 \pm 0.05 \pm 0.07$		[2,5] ABLIKIM	23U	BES3	$e^+e^- \to K_S K_S J/\psi$
$0.20 \pm 0.04 \pm 0.07$		[2,6] ABLIKIM	23U	BES3	$e^+e^- \to K_S K_S J/\psi$

Int. J. Mod. Phys. A 2026.41. Downloaded from www.worldscientific.com by CALIFORNIA @ BERKELEY on 09/16/26. Re-use and distribution is strictly not permitted, except for Open Access articles.

[1] From a fit of the $K^0_S K^0_S J/\psi$ mass range from 4.4 to 5.5 GeV including a coherent $\psi(4260)$ amplitude with mass and width from LIU 13B.
[2] A three-resonance fit to the dressed cross section in the range $\sqrt{s}$ = 4.128–4.950 GeV.
[3] Solution I.
[4] Solution II.
[5] Solution III.
[6] Solution IV.

$\Gamma(J/\psi\eta) \times \Gamma(e^+e^-)/\Gamma_{total}$ — $\Gamma_{11}\Gamma_1/\Gamma$

VALUE (eV)	CL%	DOCUMENT ID		TECN	COMMENT
• • • We do not use the following data for averages, fits, limits, etc. • • •					
$4.0\pm0.5\pm0.1$		[1] ABLIKIM	24T	BES3	$e^+e^- \to \eta J/\psi$
$5.5\pm0.7\pm0.3$		[2] ABLIKIM	24T	BES3	$e^+e^- \to \eta J/\psi$
$8.7\pm1.0\pm0.4$		[3] ABLIKIM	24T	BES3	$e^+e^- \to \eta J/\psi$
$11.9\pm1.1\pm0.6$		[4] ABLIKIM	24T	BES3	$e^+e^- \to \eta J/\psi$
8.0 ± 1.7		[5] ABLIKIM	20O	BES3	$e^+e^- \to \eta J/\psi$
4.8 ± 1.0		[6] ABLIKIM	20O	BES3	$e^+e^- \to \eta J/\psi$
7.0 ± 1.5		[7] ABLIKIM	20O	BES3	$e^+e^- \to \eta J/\psi$
<14.2	90	WANG	13B	BELL	$e^+e^- \to J/\psi\eta\gamma$

[1] Solution 1 of 4. Supersedes ABLIKIM 20O.
[2] Solution 2 of 4. Supersedes ABLIKIM 20O.
[3] Solution 3 of 4. Supersedes ABLIKIM 20O.
[4] Solution 4 of 4. Supersedes ABLIKIM 20O.
[5] Solution 1 of three equivalent fit solutions using three resonant structures.
[6] Solution 2 of three equivalent fit solutions using three resonant structures.
[7] Solution 3 of three equivalent fit solutions using three resonant structures.

$\Gamma(J/\psi\eta') \times \Gamma(e^+e^-)/\Gamma_{total}$ — $\Gamma_{13}\Gamma_1/\Gamma$

VALUE (eV)	EVTS	DOCUMENT ID		TECN	COMMENT
• • • We do not use the following data for averages, fits, limits, etc. • • •					
0.06 ± 0.03	46	[1,2] ABLIKIM	20A	BES3	$e^+e^- \to \eta' J/\psi$
1.38 ± 0.11	46	[1,3] ABLIKIM	20A	BES3	$e^+e^- \to \eta' J/\psi$

[1] Based on a fit to $\sigma(e^+e^- \to \eta' J/\psi)$ from $\sqrt{s}$ = 4.18 to 4.60 GeV assuming interfering $\psi(4160)$ and $\psi(4260)$ contributions. At $\sqrt{s}$ = 4.23 GeV, $\sigma(e^+e^- \to \eta' J/\psi)$ = $3.6 \pm 0.6 \pm 0.3$ pb.
[2] Solution I of the fit, corresponding to a phase of -0.03 ± 0.44 rad.
[3] Solution II of the fit, corresponding to a phase of 2.54 ± 0.04 rad.

$\Gamma(\psi(2S)\pi^+\pi^-) \times \Gamma(e^+e^-)/\Gamma_{total}$ — $\Gamma_{17}\Gamma_1/\Gamma$

VALUE (eV)	CL%	DOCUMENT ID		TECN	COMMENT
• • • We do not use the following data for averages, fits, limits, etc. • • •					
1.59 ± 0.75		[1] ABLIKIM	21AJ	BES3	$e^+e^- \to \pi^+\pi^-\psi(2S)$
1.63 ± 0.78		[2] ABLIKIM	21AJ	BES3	$e^+e^- \to \pi^+\pi^-\psi(2S)$
0.02 ± 0.01		[3] ABLIKIM	21AJ	BES3	$e^+e^- \to \pi^+\pi^-\psi(2S)$
$1.6\ \pm1.3$		[4] ABLIKIM	19K	BES3	$e^+e^- \to \pi^+\pi^-\psi(2S)$
$1.8\ \pm1.4$		[5] ABLIKIM	19K	BES3	$e^+e^- \to \pi^+\pi^-\psi(2S)$
<4.3	90	[6] LIU	08H	RVUE	10.58 $e^+e^- \to \psi(2S)\pi^+\pi^-\gamma$
$7.4\ ^{+2.1}_{-1.7}$		[7] LIU	08H	RVUE	10.58 $e^+e^- \to \psi(2S)\pi^+\pi^-\gamma$

[1] Solution I of four equivalent solutions in a fit using three interfering resonances.
[2] Solution II of four equivalent solutions in a fit using three interfering resonances
[3] Solutions III and IV of four equivalent solutions in a fit using three interfering resonances.
[4] Solution I of two equivalent solutions in a fit using two interfering resonances.
[5] Solution II of two equivalent solutions in a fit using two interfering resonances.
[6] For constructive interference with the $\psi(4360)$ in a combined fit of AUBERT 07S and WANG 07D data with three resonances.
[7] For destructive interference with the $\psi(4360)$ in a combined fit of AUBERT 07S and WANG 07D data with three resonances.

$\Gamma(\chi_{c0}\omega) \times \Gamma(e^+e^-)/\Gamma_{total}$ — $\Gamma_{19}\Gamma_1/\Gamma$

VALUE (eV)	EVTS	DOCUMENT ID		TECN	COMMENT
$2.5\pm0.2\pm0.3$		[1] ABLIKIM	19AI	BES3	$e^+e^- \to \omega\chi_{c0}$
• • • We do not use the following data for averages, fits, limits, etc. • • •					
$2.7\pm0.5\pm0.4$	180	[2] ABLIKIM	15C	BES3	$e^+e^- \to \omega\chi_{c0}$

[1] From a fit of the measured cross section from $\sqrt{s}$ = 4.178–4.278 GeV. Supersedes ABLIKIM 15C.
[2] From a 3-parameter fit of measured cross sections from $\sqrt{s}$ = 4.21–4.42 GeV to a phase-space modified Breit-Wigner function, using the decays $\chi_{c0} \to \pi^+\pi^-$, $\chi_{c0} \to K^+K^-$, and $\omega \to \pi^+\pi^-\pi^0$.

$\Gamma(h_c(1P)\pi^+\pi^-) \times \Gamma(e^+e^-)/\Gamma_{total}$ — $\Gamma_{22}\Gamma_1/\Gamma$

VALUE (eV)	DOCUMENT ID		TECN	COMMENT
$8.4\ ^{+2.4}_{-2.0}$ OUR AVERAGE Error includes scale factor of 1.5.				
$10.2\ ^{+1.2}_{-1.5}\ ^{+1.4}_{-1.4}$	[1] ABLIKIM	25B	BES3	$e^+e^- \to \pi^+\pi^- h_c(1P)$
$4.6\ ^{+2.9}_{-1.4}\pm0.8$	ABLIKIM	17G	BES3	$e^+e^- \to \pi^+\pi^- h_c(1P)$

[1] Using three coherent Breit-Wigner functions between 4.009 and 4.950 GeV. Second solution: 0.9 ± 0.5 eV.

$\Gamma(h_c(1P)\eta) \times \Gamma(e^+e^-)/\Gamma_{total}$ — $\Gamma_{23}\Gamma_1/\Gamma$

VALUE (eV)	DOCUMENT ID		TECN	COMMENT
$0.80\pm0.19\pm0.45$	[1] ABLIKIM	25S	BES3	$e^+e^- \to \eta h_c$

[1] Also consistent with $\psi(4160)$.

$\Gamma(\phi\pi^+\pi^-) \times \Gamma(e^+e^-)/\Gamma_{total}$ — $\Gamma_{24}\Gamma_1/\Gamma$

VALUE (eV)	CL%	DOCUMENT ID		TECN	COMMENT
<0.4	90	AUBERT,BE	06D	BABR	10.6 $e^+e^- \to K^+K^-\pi^+\pi^-\gamma$

$\Gamma(\phi f_0(980) \to \phi\pi^+\pi^-) \times \Gamma(e^+e^-)/\Gamma_{total}$ — $\Gamma_{25}\Gamma_1/\Gamma$

VALUE (eV)	CL%	DOCUMENT ID		TECN	COMMENT
<0.28	90	[1] AUBERT	07AK	BABR	10.6 $e^+e^- \to \pi^+\pi^-K^+K^-\gamma$

[1] AUBERT 07AK reports $[\Gamma(\psi(4230) \to \phi f_0(980) \to \phi\pi^+\pi^-) \times \Gamma(\psi(4230) \to e^+e^-)/\Gamma_{total}] \times [B(\phi(1020) \to K^+K^-)] <$ 0.14 eV which we divide by our best (shown rounded) value $B(\phi(1020) \to K^+K^-) = 50.1 \times 10^{-2}$.

$\Gamma(\phi K^+K^-) \times \Gamma(e^+e^-)/\Gamma_{total}$ — $\Gamma_{26}\Gamma_1/\Gamma$

VALUE (eV)	CL%	DOCUMENT ID		TECN	COMMENT
<1.75	90	ABLIKIM	23AE	BES3	$e^+e^- \to \phi K^+K^-$

$\Gamma(\phi K^0_S K^0_S) \times \Gamma(e^+e^-)/\Gamma_{total}$ — $\Gamma_{27}\Gamma_1/\Gamma$

VALUE (eV)	CL%	DOCUMENT ID		TECN	COMMENT
<0.47	90	ABLIKIM	23AE	BES3	$e^+e^- \to \phi K^0_S K^0_S$

$\Gamma(\phi\eta') \times \Gamma(e^+e^-)/\Gamma_{total}$ — $\Gamma_{29}\Gamma_1/\Gamma$

VALUE (eV)	CL%	DOCUMENT ID		TECN	COMMENT
<0.53	90	ABLIKIM	23R	BES3	$e^+e^- \to \phi\eta'$

$\Gamma(D^{*0}D^{*-}\pi^+) \times \Gamma(e^+e^-)/\Gamma_{total}$ — $\Gamma_{45}\Gamma_1/\Gamma$

VALUE (eV)	DOCUMENT ID		TECN	COMMENT
• • • We do not use the following data for averages, fits, limits, etc. • • •				
5 to 22	[1] ABLIKIM	23X	BES3	$e^+e^- \to D^{*0}D^{*-}\pi^+$

[1] From a cross-section measurement of $e^+e^- \to D^{*0}D^{*-}\pi^+$ between 4.189 and 4.951 GeV, assuming a coherent sum of 3 Breit-Wigner resonances plus a continuum amplitude. Depending on solutions I – VIII with the same fit qualities.

$\Gamma(\omega\pi^+\pi^-) \times \Gamma(e^+e^-)/\Gamma_{total}$ — $\Gamma_{52}\Gamma_1/\Gamma$

VALUE (eV)	DOCUMENT ID		TECN	COMMENT
• • • We do not use the following data for averages, fits, limits, etc. • • •				
$0.487\ \pm0.008\ \pm0.030$	[1,2] ABLIKIM	23AQ	BES3	fit to cross sections
$0.0005\pm0.0003\pm0.0001$	[2,3] ABLIKIM	23AQ	BES3	fit to cross sections

[1] Solution I of the fit.
[2] From a fit to $e^+e^- \to \omega\pi^+\pi^-$ cross sections between 4 and 4.6 GeV. Recalculated from $12\ \pi\ \Gamma(e^+e^-)\ B(\psi(4230) \to \omega\pi^+\pi^-)$. First uncertainty is from statistical and uncommon systematic uncertainties, and the second is a 6.2% common systematic uncertainty quoted in the paper.
[3] Solution II of the fit.

$\Gamma(\pi^+\pi^+\pi^-\pi^-) \times \Gamma(e^+e^-)/\Gamma_{total}$ — $\Gamma_{56}\Gamma_1/\Gamma$

VALUE (eV)	CL%	DOCUMENT ID		TECN	COMMENT
<32	90	ABLIKIM	21AW	BES3	$e^+e^- \to 2\pi^+2\pi^-$

$\Gamma(\pi^+\pi^+\pi^-\pi^-\pi^0) \times \Gamma(e^+e^-)/\Gamma_{total}$ — $\Gamma_{57}\Gamma_1/\Gamma$

VALUE (eV)	CL%	DOCUMENT ID		TECN	COMMENT
<16	90	ABLIKIM	21AW	BES3	$e^+e^- \to 2\pi^+2\pi^-\pi^0$

$\Gamma(K^0_S K^\pm\pi^\mp) \times \Gamma(e^+e^-)/\Gamma_{total}$ — $\Gamma_{60}\Gamma_1/\Gamma$

VALUE (eV)	DOCUMENT ID		TECN	COMMENT
• • • We do not use the following data for averages, fits, limits, etc. • • •				
$2.04\ \ \pm0.19\ \ \pm0.09$	[1] ABLIKIM	19AE	BES3	$e^+e^- \to K^0_S K^\pm\pi^\mp$
$0.0027\pm0.0023\pm0.0001$	[2] ABLIKIM	19AE	BES3	$e^+e^- \to K^0_S K^\pm\pi^\mp$
< 0.5 at 90% CL	AUBERT	08S	BABR	10.6 $e^+e^- \to K^0_S K^\pm\pi^\mp\gamma$

[1] Solution I of the fit including the $\psi(4160)$ with mass 4191 ± 5 MeV and width 70 ± 10 MeV from PDG 16 and the $\psi(4230)$ with mass $4219.6 \pm 3.3 \pm 5.1$ MeV and width $56.0 \pm 3.6 \pm 6.9$ MeV from GAO 17.
[2] Solution II of the fit including the $\psi(4160)$ with mass 4191 ± 5 MeV and width 70 ± 10 MeV from PDG 16 and the $\psi(4230)$ with mass $4219.6 \pm 3.3 \pm 5.1$ MeV and width $56.0 \pm 3.6 \pm 6.9$ MeV from GAO 17.

$\Gamma(K^0_S K^\pm\pi^\mp\pi^0) \times \Gamma(e^+e^-)/\Gamma_{total}$ — $\Gamma_{61}\Gamma_1/\Gamma$

VALUE (eV)	CL%	DOCUMENT ID		TECN	COMMENT
<0.05	90	ABLIKIM	19	BES3	$e^+e^- \to K^0_S K^\pm\pi^\mp\pi^0$

$\Gamma(K^0_S K^\pm\pi^\mp\eta) \times \Gamma(e^+e^-)/\Gamma_{total}$ — $\Gamma_{62}\Gamma_1/\Gamma$

VALUE (eV)	CL%	DOCUMENT ID		TECN	COMMENT
<0.19	90	ABLIKIM	19	BES3	$e^+e^- \to K^0_S K^\pm\pi^\mp\eta$

$\Gamma(K^+K^-\pi^0) \times \Gamma(e^+e^-)/\Gamma_{total}$ — $\Gamma_{63}\Gamma_1/\Gamma$

VALUE (eV)	CL%	DOCUMENT ID		TECN	COMMENT
• • • We do not use the following data for averages, fits, limits, etc. • • •					
<0.6	90	AUBERT	08S	BABR	10.6 $e^+e^- \to K^+K^-\pi^0\gamma$

$\Gamma(K^+K^-\pi^+\pi^-) \times \Gamma(e^+e^-)/\Gamma_{total}$ — $\Gamma_{64}\Gamma_1/\Gamma$

VALUE (eV)	CL%	DOCUMENT ID		TECN	COMMENT
<20	90	ABLIKIM	21AW	BES3	$e^+e^- \to K^+K^-\pi^+\pi^-$

Int. J. Mod. Phys. A 2026.41. Downloaded from www.worldscientific.com
by UNIVERSITY OF CALIFORNIA @ BERKELEY on 09/16/26. Re-use and distribution is strictly not permitted, except for Open Access articles.

$\Gamma(K^+K^-\pi^+\pi^-\pi^0) \times \Gamma(e^+e^-)/\Gamma_{total}$ — $\Gamma_{65}\Gamma_1/\Gamma$

VALUE (eV)	CL%	DOCUMENT ID		TECN	COMMENT
<43	90	ABLIKIM	21AW	BES3	$e^+e^- \to K^+K^-\pi^+\pi^-\pi^0$

$\Gamma(K^+K^+K^-K^-) \times \Gamma(e^+e^-)/\Gamma_{total}$ — $\Gamma_{66}\Gamma_1/\Gamma$

VALUE (eV)	CL%	DOCUMENT ID		TECN	COMMENT
<3.8	90	ABLIKIM	21AW	BES3	$e^+e^- \to 2K^+2K^-$

$\Gamma(K^+K^+K^-K^-\pi^0) \times \Gamma(e^+e^-)/\Gamma_{total}$ — $\Gamma_{67}\Gamma_1/\Gamma$

VALUE (eV)	CL%	DOCUMENT ID		TECN	COMMENT
<2.1	90	ABLIKIM	21AW	BES3	$e^+e^- \to 2K^+2K^-\pi^0$

$\Gamma(p\overline{p}\pi^+\pi^-) \times \Gamma(e^+e^-)/\Gamma_{total}$ — $\Gamma_{68}\Gamma_1/\Gamma$

VALUE (eV)	CL%	DOCUMENT ID		TECN	COMMENT
<7.2	90	ABLIKIM	21AW	BES3	$e^+e^- \to p\overline{p}\pi^+\pi^-$

$\Gamma(p\overline{p}\pi^+\pi^-\pi^0) \times \Gamma(e^+e^-)/\Gamma_{total}$ — $\Gamma_{69}\Gamma_1/\Gamma$

VALUE (eV)	CL%	DOCUMENT ID		TECN	COMMENT
<15	90	ABLIKIM	21AW	BES3	$e^+e^- \to p\overline{p}\pi^+\pi^-\pi^0$

$\Gamma(\Lambda\overline{\Lambda}) \times \Gamma(e^+e^-)/\Gamma_{total}$ — $\Gamma_{71}\Gamma_1/\Gamma$

VALUE (eV)	CL%	DOCUMENT ID		TECN	COMMENT
$<0.8 \times 10^{-3}$	90	[1] ABLIKIM	21AS	BES3	$e^+e^- \to \psi(4260)$

[1] From a measurement of the $e^+e^- \to \Lambda\overline{\Lambda}$ cross section between 3.5 and 4.6 GeV.

$\Gamma(\Sigma^+\overline{\Sigma}^-) \times \Gamma(e^+e^-)/\Gamma_{total}$ — $\Gamma_{72}\Gamma_1/\Gamma$

VALUE (eV)	CL%	DOCUMENT ID		TECN	COMMENT
$<72.4 \times 10^{-3}$	90	[1] ABLIKIM	24AH	BES3	$e^+e^- \to \Sigma^+\overline{\Sigma}^-$

[1] Interference effect between resonance and continuum amplitudes is considered. Two solutions from the fit.

$\Gamma(\Sigma^0\overline{\Sigma}^0) \times \Gamma(e^+e^-)/\Gamma_{total}$ — $\Gamma_{73}\Gamma_1/\Gamma$

VALUE (eV)	CL%	DOCUMENT ID		TECN	COMMENT
$<14.7 \times 10^{-3}$	90	[1] ABLIKIM	25U	BES3	$e^+e^- \to \Sigma^0\overline{\Sigma}^0$

[1] Interference effect between resonance and continuum amplitudes is considered. Upper limit is for the larger of the two solutions from the fit.

$\Gamma(\Xi^0\overline{\Xi}^0) \times \Gamma(e^+e^-)/\Gamma_{total}$ — $\Gamma_{54}\Gamma_1/\Gamma$

VALUE (eV)	CL%	DOCUMENT ID		TECN	COMMENT
$<40.4 \times 10^{-3}$	90	[1] ABLIKIM	24CD	BES3	$e^+e^- \to \psi(4230)$

[1] From a fit to $e^+e^- \to \Xi^0\overline{\Xi}^0$ cross sections.

$\Gamma(\Xi^-\overline{\Xi}^+) \times \Gamma(e^+e^-)/\Gamma_{total}$ — $\Gamma_{55}\Gamma_1/\Gamma$

VALUE (eV)	CL%	DOCUMENT ID		TECN	COMMENT
$<25.1 \times 10^{-3}$	90	[1] ABLIKIM	23BK	BES3	$e^+e^- \to \psi(4230)$
• • • We do not use the following data for averages, fits, limits, etc. • • •					
$< 2.7 \times 10^{-4}$	90	[2] ABLIKIM	20C	BES3	$e^+e^- \to \Xi^-\overline{\Xi}^+$

[1] From a fit to $e^+e^- \to \Xi^-\overline{\Xi}^+$ cross sections.
[2] Superseded by ABLIKIM 23BK.

$\Gamma(pK^-\overline{\Lambda} + \text{c.c.}) \times \Gamma(e^+e^-)/\Gamma_{total}$ — $\Gamma_{74}\Gamma_1/\Gamma$

VALUE (eV)	CL%	DOCUMENT ID		TECN	COMMENT
$<1.3 \times 10^{-3}$	90	[1] ABLIKIM	23BL	BES3	$e^+e^- \to \psi(4230)$

[1] From a fit to $e^+e^- \to pK^-\overline{\Lambda}$ + c.c. cross sections.

$\Gamma(\Lambda\overline{\Xi}^+K^- + \text{c.c.}) \times \Gamma(e^+e^-)/\Gamma_{total}$ — $\Gamma_{75}\Gamma_1/\Gamma$

VALUE (eV)	CL%	DOCUMENT ID		TECN	COMMENT
$<24.9 \times 10^{-3}$	90	[1] ABLIKIM	24AL	BES3	$e^+e^- \to \Lambda\overline{\Xi}^+K^-$ + c.c.

[1] A fit to the Born cross section of $e^+e^- \to \Lambda\overline{\Xi}^+K^-$ + c.c. including interference with the continuum. Two solutions from the fit.

$\Gamma(\Sigma^0\overline{\Xi}^+K^- + \text{c.c.}) \times \Gamma(e^+e^-)/\Gamma_{total}$ — $\Gamma_{76}\Gamma_1/\Gamma$

VALUE (eV)	CL%	DOCUMENT ID		TECN	COMMENT
$<1.6 \times 10^{-3}$	90	[1] ABLIKIM	24AL	BES3	$e^+e^- \to \Sigma^0\overline{\Xi}^+K^-$ + c.c.

[1] A fit to the Born cross section of $e^+e^- \to \Sigma^0\overline{\Xi}^+K^-$ + c.c. including interference with the continuum. Two solutions from the fit.

$\Gamma(pK^-K^-\overline{\Xi}^+ + \text{c.c.}) \times \Gamma(e^+e^-)/\Gamma_{total}$ — $\Gamma_{77}\Gamma_1/\Gamma$

VALUE (eV)	CL%	DOCUMENT ID		TECN	COMMENT
$<35.6 \times 10^{-3}$	90	ABLIKIM	25CF	BES3	$e^+e^- \to pK^-K^-\overline{\Xi}^+$ + c.c.

$\Gamma(\chi_{c1}\gamma) \times \Gamma(e^+e^-)/\Gamma_{total}$ — $\Gamma_{82}\Gamma_1/\Gamma$

VALUE (eV)	CL%	DOCUMENT ID		TECN	COMMENT
<1.4	90	[1] HAN	15	BELL	10.58 $e^+e^- \to \chi_{c1}\gamma$

[1] Using $B(\eta \to \gamma\gamma) = (39.41 \pm 0.21)\%$.

$\Gamma(\chi_{c2}\gamma) \times \Gamma(e^+e^-)/\Gamma_{total}$ — $\Gamma_{83}\Gamma_1/\Gamma$

VALUE (eV)	CL%	DOCUMENT ID		TECN	COMMENT
<4.0	90	[1] HAN	15	BELL	10.58 $e^+e^- \to \chi_{c2}\gamma$

[1] Using $B(\eta \to \gamma\gamma) = (39.41 \pm 0.21)\%$.

$\psi(4230)$ $\Gamma(i) \times \Gamma(e^+e^-)/\Gamma^2(total)$

$\Gamma(D^0D^*(2010)^-\pi^+ + \text{c.c.})/\Gamma_{total} \times \Gamma(e^+e^-)/\Gamma_{total}$ — $\Gamma_{42}/\Gamma \times \Gamma_1/\Gamma$

VALUE	CL%	DOCUMENT ID		TECN	COMMENT
$<0.42 \times 10^{-6}$	90	[1] PAKHLOVA	09	BELL	$e^+e^- \to D^0D^{*-}\pi^+$

[1] Using 4263^{+8}_{-9} MeV for the mass of $\psi(4260)$.

$\psi(4230)$ BRANCHING RATIOS

$\Gamma(\eta_c(1S)\pi^+\pi^-)/\Gamma_{total}$ — Γ_3/Γ

VALUE	DOCUMENT ID		TECN	COMMENT
not seen	[1] ABLIKIM	21B	BES3	$e^+e^- \to \pi^+\pi^-\eta_c$

[1] Not seen in $e^+e^- \to \pi^+\pi^-\eta_c$ at $\sqrt{s} = 4.226$ GeV with a 90% C.L. upper limit on the cross section of 16.8 pb.

$\Gamma(\eta_c(1S)\pi^+\pi^-\pi^0)/\Gamma_{total}$ — Γ_4/Γ

VALUE	DOCUMENT ID		TECN	COMMENT
seen	[1] ABLIKIM	21B	BES3	$e^+e^- \to \pi^+\pi^-\pi^0\eta_c$

[1] Seen as a peak in the $e^+e^- \to \pi^+\pi^-\pi^0\eta_c$ cross section with a peak value of $46.1^{+9.5}_{-9.4} \pm 6.6$ pb at $\sqrt{s} = 4.226$ GeV.

$\Gamma(J/\psi\pi^+\pi^-)/\Gamma_{total}$ — Γ_5/Γ

VALUE	DOCUMENT ID		TECN	COMMENT
seen	[1] ABLIKIM	22AM	BES3	$e^+e^- \to \pi^+\pi^-J/\psi$
• • • We do not use the following data for averages, fits, limits, etc. • • •				
seen	[2] ABLIKIM	17B	BES3	$e^+e^- \to \pi^+\pi^-J/\psi$

[1] From a three-resonance fit to the Born cross section in the range $\sqrt{s} = 3.7730$–4.7008 GeV.
[2] From a three-resonance fit. Superseded by ABLIKIM 22AM.

$\Gamma(J/\psi f_0(980),\ f_0(980) \to \pi^+\pi^-)/\Gamma(J/\psi\pi^+\pi^-)$ — Γ_6/Γ_5

VALUE	DOCUMENT ID		TECN	COMMENT
• • • We do not use the following data for averages, fits, limits, etc. • • •				
0.17 ± 0.13	[1] LEES	12AC	BABR	10.58 $e^+e^- \to \gamma\pi^+\pi^-J/\psi$

[1] Systematic uncertainties not estimated.

$\Gamma(T_{c\overline{c}1}(3900)^\pm\pi^\mp,\ T^\pm_{c\overline{c}1} \to J/\psi\pi^\pm)/\Gamma(J/\psi\pi^+\pi^-)$ — Γ_7/Γ_5

VALUE	DOCUMENT ID		TECN	COMMENT
$0.215 \pm 0.033 \pm 0.075$	[1] ABLIKIM	13T	BES3	$e^+e^- \to \pi^+\pi^-J/\psi$
• • • We do not use the following data for averages, fits, limits, etc. • • •				
0.29 ± 0.08	[2] LIU	13B	BELL	$e^+e^- \to \gamma\pi^+\pi^-J/\psi$

[1] Assuming that the cross section of $e^+e^- \to \pi^+\pi^-J/\psi$ is fully due to the $\psi(4260)$.
[2] Systematic error not evaluated.

$\Gamma(J/\psi\pi^0\pi^0)/\Gamma_{total}$ — Γ_8/Γ

VALUE	DOCUMENT ID		TECN	COMMENT
seen	[1] ABLIKIM	20N	BES3	$e^+e^- \to \pi^0\pi^0J/\psi$

[1] From a fit to the cross section $e^+e^- \to \pi^0\pi^0J/\psi$ at center-of-mass energies between 3.808 and 4.600 GeV.

$\Gamma(J/\psi K^0_SK^0_S)/\Gamma_{total}$ — Γ_{10}/Γ

VALUE	DOCUMENT ID		TECN	COMMENT
not seen	SHEN	14	BELL	9.4–10.9 $e^+e^- \to \gamma K^0_SK^0_SJ/\psi$

$\Gamma(J/\psi\eta)/\Gamma_{total}$ — Γ_{11}/Γ

VALUE	DOCUMENT ID		TECN	COMMENT
seen	[1] ABLIKIM	24T	BES3	$e^+e^- \to \eta J/\psi$
• • • We do not use the following data for averages, fits, limits, etc. • • •				
seen	ABLIKIM	20O	BES3	$e^+e^- \to \eta J/\psi$

[1] Supersedes ABLIKIM 20O.

$\Gamma(J/\psi\eta\pi^0)/\Gamma_{total}$ — Γ_{15}/Γ

VALUE	DOCUMENT ID		TECN	COMMENT
not seen	ABLIKIM	15Q	BES3	4.0–4.6 $e^+e^- \to J/\psi\eta\pi^0$

$\Gamma(\psi(2S)\pi^+\pi^-)/\Gamma_{total}$ — Γ_{17}/Γ

VALUE	DOCUMENT ID		TECN	COMMENT
seen	[1] ABLIKIM	17V	BES3	$e^+e^- \to \pi^+\pi^-\psi(2S)$

[1] From a fit to the cross section for $e^+e^- \to \pi^+\pi^-\psi(2S) \to 2(\pi^+\pi^-)\ell^+\ell^-$ obtained from 16 center-of-mass energies between 4.008 and 4.600 GeV and comprising 5.1 fb^{-1}.

$\Gamma(\psi(2S)\pi^+\pi^-)/\Gamma(J/\psi\pi^+\pi^-)$ — Γ_{17}/Γ_5

VALUE	DOCUMENT ID		TECN	COMMENT
• • • We do not use the following data for averages, fits, limits, etc. • • •				
$(0.11 \pm 0.03 \pm 0.03)$ to $(0.55 \pm 0.18 \pm 0.19)$	[1] ZHANG	17C	RVUE	$e^+e^- \to \pi^+\pi^-J/\psi$ or $\psi(2S)$

[1] From a combined fit of BELLE, BABAR and BES3 $e^+e^- \to \pi^+\pi^-J/\psi$ and $e^+e^- \to \pi^+\pi^-\psi(2S)$ data.

Int. J. Mod. Phys. A 2026.41. Downloaded from www.worldscientific.com by [redacted]LIFORNIA @ BERKELEY on 09/16/26. Re-use and distribution is strictly not permitted, except for Open Access articles.

$\Gamma(\chi_{c0}\omega)/\Gamma_{total}$ — Γ_{19}/Γ

VALUE	EVTS	DOCUMENT ID		TECN	COMMENT
seen	180	[1] ABLIKIM	15C	BES3	$e^+e^- \to \omega\chi_{c0}$

[1] From a 3-parameter fit of measured cross sections from $\sqrt{s}$ = 4.21–4.42 GeV to a phase-space modified Breit-Wigner function, using the decays $\chi_{c0} \to \pi^+\pi^-$, $\chi_{c0} \to K^+K^-$, and $\omega \to \pi^+\pi^-\pi^0$.

$\Gamma(h_c(1P)\pi^+\pi^-)/\Gamma_{total}$ — Γ_{22}/Γ

VALUE	DOCUMENT ID		TECN	COMMENT
seen	ABLIKIM	17G	BES3	$e^+e^- \to \pi^+\pi^- h_c$

$\Gamma(h_c(1P)\pi^+\pi^-)/\Gamma(J/\psi\pi^+\pi^-)$ — Γ_{22}/Γ_5

VALUE	CL%	DOCUMENT ID		TECN	COMMENT
<1.0	90	[1] PEDLAR	11	CLEO	$e^+e^- \to h_c(1P)\pi^+\pi^-$

[1] At $\sqrt{s}$ = 4260 MeV, PEDLAR 11 measures $\sigma(e^+e^- \to h_c(1P)\pi^+\pi^-) = 32\pm17\pm6\pm6$ pb, where the errors are statistical, systematic, and due to uncertainty in $B(\psi(2S) \to \pi^0 h_c(1P))$, respectively.

$\Gamma(h_c(1P)\eta)/\Gamma_{total}$ — Γ_{23}/Γ

VALUE	DOCUMENT ID		TECN	COMMENT
seen	[1] ABLIKIM	25S	BES3	$e^+e^- \to \eta h_c$

[1] Also consistent with $\psi(4160)$.

$\Gamma(\phi\eta)/\Gamma_{total}$ — Γ_{28}/Γ

VALUE	DOCUMENT ID		TECN	COMMENT
not seen	ABLIKIM	23BT	BES3	$e^+e^- \to \phi\eta$

$\Gamma(D\overline{D})/\Gamma(J/\psi\pi^+\pi^-)$ — Γ_{30}/Γ_5

VALUE	CL%	DOCUMENT ID		TECN	COMMENT
<1.0	90	[1] AUBERT	07BE	BABR	$e^+e^- \to D\overline{D}\gamma$
• • • We do not use the following data for averages, fits, limits, etc. • • •					
<4.0	90	CRONIN-HEN...	09	CLEO	e^+e^-

[1] Using 4259 ± 10 MeV for the mass and 88 ± 24 MeV for the width of $\psi(4260)$.

$\Gamma(D^0\overline{D}^0)/\Gamma_{total}$ — Γ_{31}/Γ

VALUE	DOCUMENT ID		TECN	COMMENT
possibly seen	[1] ABLIKIM	24BH	BES3	$e^+e^- \to D^0\overline{D}^0$
• • • We do not use the following data for averages, fits, limits, etc. • • •				
not seen	AUBERT	09M	BABR	$e^+e^- \to D^0\overline{D}^0\gamma$
not seen	CRONIN-HEN...	09	CLEO	$e^+e^- \to D^0\overline{D}^0$
not seen	PAKHLOVA	08	BELL	$e^+e^- \to D^0\overline{D}^0\gamma$

[1] A precision measurement of the $e^+e^- \to D^0\overline{D}^0$ cross section shows complex structure in this mass region.

$\Gamma(D^+D^-)/\Gamma_{total}$ — Γ_{32}/Γ

VALUE	DOCUMENT ID		TECN	COMMENT
possibly seen	[1] ABLIKIM	24BH	BES3	$e^+e^- \to D^+D^-$
• • • We do not use the following data for averages, fits, limits, etc. • • •				
not seen	AUBERT	09M	BABR	$e^+e^- \to D^+D^-\gamma$
not seen	CRONIN-HEN...	09	CLEO	$e^+e^- \to D^+D^-$
not seen	PAKHLOVA	08	BELL	$e^+e^- \to D^+D^-\gamma$

[1] A precision measurement of the $e^+e^- \to D^+D^-$ cross section shows complex structure in this mass region.

$\Gamma(D^*\overline{D}+\text{c.c.})/\Gamma(J/\psi\pi^+\pi^-)$ — Γ_{33}/Γ_5

VALUE	CL%	DOCUMENT ID		TECN	COMMENT
<34	90	AUBERT	09M	BABR	$e^+e^- \to \gamma D^*\overline{D}$
• • • We do not use the following data for averages, fits, limits, etc. • • •					
<45	90	CRONIN-HEN...	09	CLEO	e^+e^-

$\Gamma(D^*(2007)^0\overline{D}^0+\text{c.c.})/\Gamma_{total}$ — Γ_{34}/Γ

VALUE	DOCUMENT ID		TECN	COMMENT
not seen	CRONIN-HEN...	09	CLEO	$e^+e^- \to D^{*0}\overline{D}^0$
• • • We do not use the following data for averages, fits, limits, etc. • • •				
not seen	AUBERT	09M	BABR	$e^+e^- \to D^{*0}\overline{D}^0\gamma$

$\Gamma(D^*(2010)^+D^-+\text{c.c.})/\Gamma_{total}$ — Γ_{35}/Γ

VALUE	DOCUMENT ID		TECN	COMMENT
not seen	CRONIN-HEN...	09	CLEO	$e^+e^- \to D^{*+}D^-$
not seen	PAKHLOVA	07	BELL	$e^+e^- \to D^{*+}D^-\gamma$
• • • We do not use the following data for averages, fits, limits, etc. • • •				
not seen	AUBERT	09M	BABR	$e^+e^- \to D^{*+}D^-\gamma$

$\Gamma(D^*\overline{D}^*)/\Gamma(J/\psi\pi^+\pi^-)$ — Γ_{36}/Γ_5

VALUE	CL%	DOCUMENT ID		TECN	COMMENT
<11	90	CRONIN-HEN...	09	CLEO	e^+e^-
• • • We do not use the following data for averages, fits, limits, etc. • • •					
<40	90	AUBERT	09M	BABR	$e^+e^- \to \gamma D^*\overline{D}^*$

$\Gamma(D^*(2007)^0\overline{D}^*(2007)^0)/\Gamma_{total}$ — Γ_{37}/Γ

VALUE	DOCUMENT ID		TECN	COMMENT
not seen	CRONIN-HEN...	09	CLEO	$e^+e^- \to D^{*0}\overline{D}^{*0}$
• • • We do not use the following data for averages, fits, limits, etc. • • •				
not seen	AUBERT	09M	BABR	$e^+e^- \to D^{*0}\overline{D}^{*0}\gamma$

$\Gamma(D^*(2010)^+D^*(2010)^-)/\Gamma_{total}$ — Γ_{38}/Γ

VALUE	DOCUMENT ID		TECN	COMMENT
not seen	CRONIN-HEN...	09	CLEO	$e^+e^- \to D^{*+}D^{*-}$
not seen	PAKHLOVA	07	BELL	$e^+e^- \to D^{*+}D^{*-}\gamma$
• • • We do not use the following data for averages, fits, limits, etc. • • •				
not seen	AUBERT	09M	BABR	$e^+e^- \to D^{*+}D^{*-}\gamma$

$\Gamma(D^0D^-\pi^++\text{c.c.}\ (\text{excl. } D^*(2007)^0\overline{D}^{*0}+\text{c.c.}, D^*(2010)^+D^-+\text{c.c.}))/\Gamma_{total}$ — Γ_{40}/Γ

VALUE	DOCUMENT ID		TECN	COMMENT
not seen	PAKHLOVA	08A	BELL	10.6 $e^+e^- \to D^0D^-\pi^+\gamma$

$\Gamma(D\overline{D}^*\pi+\text{c.c.}\ (\text{excl. } D^*\overline{D}^*))/\Gamma_{total}$ — Γ_{41}/Γ

VALUE	DOCUMENT ID		TECN	COMMENT
not seen	CRONIN-HEN...	09	CLEO	$e^+e^- \to D^*\overline{D}\pi$

$\Gamma(D\overline{D}^*\pi+\text{c.c.}\ (\text{excl. } D^*\overline{D}^*))/\Gamma(J/\psi\pi^+\pi^-)$ — Γ_{41}/Γ_5

VALUE	CL%	DOCUMENT ID		TECN	COMMENT
<15	90	CRONIN-HEN...	09	CLEO	e^+e^-

$\Gamma(D^0D^*(2010)^-\pi^++\text{c.c.})/\Gamma_{total}$ — Γ_{42}/Γ

VALUE	DOCUMENT ID		TECN	COMMENT
seen	ABLIKIM	19R	BES3	$e^+e^- \to \pi^+D^0D^{*-}$ + c.c.
• • • We do not use the following data for averages, fits, limits, etc. • • •				
not seen	PAKHLOVA	09	BELL	$e^+e^- \to D^0D^{*-}\pi^+\gamma$

$\Gamma(D^0D^*(2010)^-\pi^++\text{c.c.})/\Gamma(J/\psi\pi^+\pi^-)$ — Γ_{42}/Γ_5

VALUE	CL%	DOCUMENT ID		TECN	COMMENT
<9	90	PAKHLOVA	09	BELL	$e^+e^- \to D^0D^{*-}\pi^+$

$\Gamma(D_1(2420)\overline{D}+\text{c.c.})/\Gamma_{total}$ — Γ_{43}/Γ

VALUE	DOCUMENT ID		TECN	COMMENT
not seen	[1] ABLIKIM	19AR	BES3	$e^+e^- \to \pi^+\pi^-D\overline{D}$

[1] Results from a measurement of $\sigma(e^+e^- \to D_1(2420)\overline{D}+\text{c.c.})$ between $\sqrt{s}$ = 4.3 and 4.6 GeV.

$\Gamma(D^*\overline{D}^*\pi)/\Gamma_{total}$ — Γ_{44}/Γ

VALUE	DOCUMENT ID		TECN	COMMENT
seen	CRONIN-HEN...	09	CLEO	$e^+e^- \to D^*\overline{D}^*\pi$

$\Gamma(D^*\overline{D}^*\pi)/\Gamma(J/\psi\pi^+\pi^-)$ — Γ_{44}/Γ_5

VALUE	CL%	DOCUMENT ID		TECN	COMMENT
<8.2	90	CRONIN-HEN...	09	CLEO	e^+e^-

$\Gamma(D_s^+D_s^-)/\Gamma_{total}$ — Γ_{46}/Γ

VALUE	DOCUMENT ID		TECN	COMMENT
not seen	DEL-AMO-SA...	10N	BABR	$e^+e^- \to D_s^+D_s^-\gamma$
not seen	CRONIN-HEN...	09	CLEO	$e^+e^- \to D_s^+D_s^-$
• • • We do not use the following data for averages, fits, limits, etc. • • •				
not seen	PAKHLOVA	11	BELL	$e^+e^- \to D_s^+D_s^-\gamma$

$\Gamma(D_s^+D_s^-)/\Gamma(J/\psi\pi^+\pi^-)$ — Γ_{46}/Γ_5

VALUE	CL%	DOCUMENT ID		TECN	COMMENT
<0.7	95	DEL-AMO-SA...	10N	BABR	10.6 e^+e^-
• • • We do not use the following data for averages, fits, limits, etc. • • •					
<1.3	90	CRONIN-HEN...	09	CLEO	e^+e^-

$\Gamma(D_s^{*+}D_s^-+\text{c.c.})/\Gamma_{total}$ — Γ_{47}/Γ

VALUE	DOCUMENT ID		TECN	COMMENT
not seen	DEL-AMO-SA...	10N	BABR	$e^+e^- \to D_s^{*+}D_s^-\gamma$
not seen	CRONIN-HEN...	09	CLEO	$e^+e^- \to D_s^{*+}D_s^-$
• • • We do not use the following data for averages, fits, limits, etc. • • •				
not seen	PAKHLOVA	11	BELL	$e^+e^- \to D_s^{*+}D_s^-\gamma$

$\Gamma(D_s^{*+}D_s^-+\text{c.c.})/\Gamma(J/\psi\pi^+\pi^-)$ — Γ_{47}/Γ_5

VALUE	CL%	DOCUMENT ID		TECN	COMMENT
< 0.8	90	CRONIN-HEN...	09	CLEO	e^+e^-
• • • We do not use the following data for averages, fits, limits, etc. • • •					
<44	95	DEL-AMO-SA...	10N	BABR	10.6 e^+e^-

$\Gamma(D_s^{*+}D_s^{*-})/\Gamma_{total}$ — Γ_{48}/Γ

VALUE	DOCUMENT ID		TECN	COMMENT
not seen	CRONIN-HEN...	09	CLEO	$e^+e^- \to D_s^{*+}D_s^{*-}$
• • • We do not use the following data for averages, fits, limits, etc. • • •				
not seen	PAKHLOVA	11	BELL	$e^+e^- \to D_s^{*+}D_s^{*-}\gamma$
not seen	DEL-AMO-SA...	10N	BABR	$e^+e^- \to D_s^{*+}D_s^{*-}\gamma$

Int. J. Mod. Phys. A 2026.41. Downloaded from www.worldscientific.com by UNIVERSITY OF CALIFORNIA @ BERKELEY on 09/16/26. Re-use and distribution is strictly not permitted, except for Open Access articles.

$\Gamma(D_s^{*+} D_s^{*-})/\Gamma(J/\psi\pi^+\pi^-)$ — Γ_{48}/Γ_5

VALUE	CL%	DOCUMENT ID		TECN	COMMENT
< 9.5	90	CRONIN-HEN.	09	CLEO	e^+e^-
• • • We do not use the following data for averages, fits, limits, etc. • • •					
<30	95	DEL-AMO-SA.	10N	BABR	10.6 e^+e^-

$\Gamma(p\overline{p})/\Gamma(J/\psi\pi^+\pi^-)$ — Γ_{49}/Γ_5

VALUE	CL%	DOCUMENT ID		TECN	COMMENT
<0.13	90	[1] AUBERT	06B	BABR	$e^+e^- \to p\overline{p}\gamma$

[1] Using 4259 ± 10 MeV for the mass and 88 ± 24 MeV for the width of $\psi(4260)$.

$\Gamma(p\overline{p}\pi^0)/\Gamma(J/\psi\pi^+\pi^-)$ — Γ_{50}/Γ_5

VALUE	CL%	DOCUMENT ID		TECN	COMMENT
$<2\times10^{-4}$	90	ABLIKIM	17F	BES3	$e^+e^- \to \psi(4260) \to$ hadrons

$\Gamma(p\overline{p}\eta)/\Gamma_{total}$ — Γ_{51}/Γ

VALUE	DOCUMENT ID		TECN	COMMENT
not seen	ABLIKIM	21AN	BES3	$e^+e^- \to p\overline{p}\eta$

$\Gamma(p\overline{p}\omega)/\Gamma_{total}$ — Γ_{53}/Γ

VALUE	DOCUMENT ID		TECN	COMMENT
not seen	ABLIKIM	21AN	BES3	$e^+e^- \to p\overline{p}\omega$

$\Gamma(\omega\pi^0)/\Gamma_{total}$ — Γ_{58}/Γ

VALUE	DOCUMENT ID		TECN	COMMENT
not seen	ABLIKIM	22K	BES3	$e^+e^- \to \omega\pi^0$

$\Gamma(\omega\eta)/\Gamma_{total}$ — Γ_{59}/Γ

VALUE	DOCUMENT ID		TECN	COMMENT
not seen	ABLIKIM	22K	BES3	$e^+e^- \to \omega\eta$

$\Gamma(p\overline{p}p\overline{p})/\Gamma_{total}$ — Γ_{70}/Γ

VALUE	DOCUMENT ID		TECN	COMMENT
not seen	ABLIKIM	21D	BES3	4.0–4.6 $e^+e^- \to p\overline{p}p\overline{p}$

Radiative decays

$\Gamma(\eta_c(1S)\gamma)/\Gamma_{total}$ — Γ_{78}/Γ

VALUE	DOCUMENT ID		COMMENT
possibly seen	[1] ABLIKIM	17W	$e^+e^- \to \gamma\eta_c(1S)$

[1] Significance ranges from 4.2 σ to as low as 1.5 σ for a flat component plus $\psi(4260)$ spectrum. Needs confirmation.

$\Gamma(\eta_c(1S)\pi^0\gamma)/\Gamma_{total}$ — Γ_{79}/Γ

VALUE	DOCUMENT ID		TECN	COMMENT
not seen	[1] ABLIKIM	21B	BES3	$e^+e^- \to \gamma\pi^0\eta_c$

[1] Not seen in $e^+e^- \to \gamma\pi^0\eta_c$ at $\sqrt{s}$ = 4.226 GeV with a 90% C.L. upper limit on the cross section of 11.2 pb.

$\Gamma(\eta_c(1S)\eta\gamma)/\Gamma_{total}$ — Γ_{80}/Γ

VALUE	DOCUMENT ID		TECN	COMMENT
not seen	[1] ABLIKIM	25Y	BES3	$e^+e^- \to \gamma\eta\eta_c$

[1] Not seen in $e^+e^- \to \gamma\eta\eta_c$ at $\sqrt{s}$ = 4.258 GeV with a 90% C.L. upper limit on the cross section of 27.3 pb.

$\Gamma(\eta_c(1S)\eta'\gamma)/\Gamma_{total}$ — Γ_{81}/Γ

VALUE	DOCUMENT ID		TECN	COMMENT
not seen	[1] ABLIKIM	25Y	BES3	$e^+e^- \to \gamma\eta'\eta_c$

[1] Not seen in $e^+e^- \to \gamma\eta'\eta_c$ at $\sqrt{s}$ = 4.258 GeV with a 90% C.L. upper limit on the cross section of 51.2 pb.

$\Gamma(\chi_{c1}(3872)\gamma)/\Gamma_{total}$ — Γ_{84}/Γ

VALUE	EVTS	DOCUMENT ID		TECN	COMMENT
seen		ABLIKIM	19V	BES3	$e^+e^- \to \gamma\chi_{c1}(3872)$
seen	20 ± 5	ABLIKIM	14	BES3	$e^+e^- \to J/\psi\pi^+\pi^-\gamma$

$\psi(4230)$ REFERENCES

ABLIKIM	25B	PRL 135 071901	M. Ablikim *et al.*	(BESIII Collab.)
ABLIKIM	25BU	PR D112 092013	M. Ablikim *et al.*	(BESIII Collab.)
ABLIKIM	25CF	JHEP 2511 111	M. Ablikim *et al.*	(BESIII Collab.)
ABLIKIM	25S	PR D111 L011101	M. Ablikim *et al.*	(BESIII Collab.)
ABLIKIM	25U	PR D111 L051502	M. Ablikim *et al.*	(BESIII Collab.)
ABLIKIM	25Y	PR D111 112007	M. Ablikim *et al.*	(BESIII Collab.)
ABLIKIM	24AH	JHEP 2405 022	M. Ablikim *et al.*	(BESIII Collab.)
ABLIKIM	24AL	JHEP 2407 258	M. Ablikim *et al.*	(BESIII Collab.)
ABLIKIM	24BH	PRL 133 081901	M. Ablikim *et al.*	(BESIII Collab.)
ABLIKIM	24CD	JHEP 2411 062	M. Ablikim *et al.*	(BESIII Collab.)
ABLIKIM	24T	PR D109 092012	M. Ablikim *et al.*	(BESIII Collab.)
ABLIKIM	23AE	PR D108 032004	M. Ablikim *et al.*	(BESIII Collab.)
ABLIKIM	23AQ	JHEP 2308 159	M. Ablikim *et al.*	(BESIII Collab.)
ABLIKIM	23BK	JHEP 2311 228	M. Ablikim *et al.*	(BESIII Collab.)
ABLIKIM	23BL	JHEP 2312 027	M. Ablikim *et al.*	(BESIII Collab.)
ABLIKIM	23BT	PR D108 112011	M. Ablikim *et al.*	(BESIII Collab.)
ABLIKIM	23R	PR D107 072003	M. Ablikim *et al.*	(BESIII Collab.)
ABLIKIM	23U	PR D107 092005	M. Ablikim *et al.*	(BESIII Collab.)
ABLIKIM	23X	PRL 130 121901	M. Ablikim *et al.*	(BESIII Collab.)
ABLIKIM	22AM	PR D106 072001	M. Ablikim *et al.*	(BESIII Collab.)
ABLIKIM	22AU	CP C46 111002	M. Ablikim *et al.*	(BESIII Collab.)
ABLIKIM	22K	JHEP 2207 064	M. Ablikim *et al.*	(BESIII Collab.)
ABLIKIM	21AJ	PR D104 052012	M. Ablikim *et al.*	(BESIII Collab.)
ABLIKIM	21AN	PR D104 092008	M. Ablikim *et al.*	(BESIII Collab.)
ABLIKIM	21AS	PR D104 L091104	M. Ablikim *et al.*	(BESIII Collab.)
ABLIKIM	21AW	PR D104 112009	M. Ablikim *et al.*	(BESIII Collab.)
ABLIKIM	21B	PR D103 032006	M. Ablikim *et al.*	(BESIII Collab.)
ABLIKIM	21D	PR D103 052003	M. Ablikim *et al.*	(BESIII Collab.)
ABLIKIM	20A	PR D101 012008	M. Ablikim *et al.*	(BESIII Collab.)
ABLIKIM	20AG	PR D102 112009	M. Ablikim *et al.*	(BESIII Collab.)
ABLIKIM	20C	PRL 124 032002	M. Ablikim *et al.*	(BESIII Collab.)
ABLIKIM	20N	PR D102 012009	M. Ablikim *et al.*	(BESIII Collab.)
ABLIKIM	20O	PR D102 031101	M. Ablikim *et al.*	(BESIII Collab.)
ABLIKIM	19	PR D99 012003	M. Ablikim *et al.*	(BESIII Collab.)
ABLIKIM	19AE	PR D99 072005	M. Ablikim *et al.*	(BESIII Collab.)
ABLIKIM	19AI	PR D99 091103	M. Ablikim *et al.*	(BESIII Collab.)
ABLIKIM	19AR	PR D100 032005	M. Ablikim *et al.*	(BESIII Collab.)
ABLIKIM	19K	PR D99 019903 (errat.)	M. Ablikim *et al.*	(BESIII Collab.)
ABLIKIM	19R	PRL 122 102002	M. Ablikim *et al.*	(BESIII Collab.)
ABLIKIM	19V	PRL 122 232002	M. Ablikim *et al.*	(BESIII Collab.)
ABLIKIM	18N	PR D97 071101	M. Ablikim *et al.*	(BESIII Collab.)
ABLIKIM	17B	PRL 118 092001	M. Ablikim *et al.*	(BESIII Collab.)
ABLIKIM	17F	PL B771 45	M. Ablikim *et al.*	(BESIII Collab.)
ABLIKIM	17G	PRL 118 092002	M. Ablikim *et al.*	(BESIII Collab.)
ABLIKIM	17V	PR D96 032004	M. Ablikim *et al.*	(BESIII Collab.)
Also		PR D99 019903 (errat.)	M. Ablikim *et al.*	(BESIII Collab.)
ABLIKIM	17W	PR D96 051101	M. Ablikim *et al.*	(BESIII Collab.)
GAO	17	PR D95 092007	X.Y. Gao, C.P. Shen, C.Z. Yuan	
ZHANG	17B	PR D96 054008	J. Zhang, J. Zhang	
ZHANG	17C	EPJ C77 727	J. Zhang, L. Yuan	
PDG	16	CP C40 100001	C. Patrignani *et al.*	(PDG Collab.)
ABLIKIM	15C	PRL 114 092003	M. Ablikim *et al.*	(BESIII Collab.)
ABLIKIM	15Q	PR D92 012008	M. Ablikim *et al.*	(BESIII Collab.)
HAN	15	PR D92 012011	Y.L. Han *et al.*	(BELLE Collab.)
ABLIKIM	14	PRL 112 092001	M. Ablikim *et al.*	(BESIII Collab.)
SHEN	14	PR D89 072015	C.P. Shen *et al.*	(BELLE Collab.)
ABLIKIM	13T	PRL 110 252001	M. Ablikim *et al.*	(BESIII Collab.)
LIU	13B	PRL 110 252002	Z.Q. Liu *et al.*	(BELLE Collab.)
WANG	13B	PR D87 051101	X.L. Wang *et al.*	(BELLE Collab.)
LEES	12AC	PR D86 051102	J.P. Lees *et al.*	(BABAR Collab.)
PAKHLOVA	11	PR D83 011101	G. Pakhlova *et al.*	(BELLE Collab.)
PEDLAR	11	PRL 107 041803	T. Pedlar *et al.*	(CLEO Collab.)
DEL-AMO-SA.	10N	PR D82 052004	P. del Amo Sanchez *et al.*	(BABAR Collab.)
AUBERT	09M	PR D79 092001	B. Aubert *et al.*	(BABAR Collab.)
CRONIN-HEN.	09	PR D80 072001	D. Cronin-Hennessy *et al.*	(CLEO Collab.)
PAKHLOVA	09	PR D80 091101	G. Pakhlova *et al.*	(BELLE Collab.)
AUBERT	08S	PR D77 092002	B. Aubert *et al.*	(BABAR Collab.)
LIU	08H	PR D78 014032	Z.Q. Liu, X.S. Qin, C.Z. Yuan	
PAKHLOVA	08	PR D77 011103	G. Pakhlova *et al.*	(BELLE Collab.)
PAKHLOVA	08A	PRL 100 062001	G. Pakhlova *et al.*	(BELLE Collab.)
YUAN	08	PR D77 011105	C.Z. Yuan *et al.*	(BELLE Collab.)
AUBERT	07AK	PR D76 012008	B. Aubert *et al.*	(BABAR Collab.)
AUBERT	07BE	PR D76 111105	B. Aubert *et al.*	(BABAR Collab.)
AUBERT	07S	PRL 98 212001	B. Aubert *et al.*	(BABAR Collab.)
PAKHLOVA	07	PRL 98 092001	G. Pakhlova *et al.*	(BELLE Collab.)
WANG	07D	PRL 99 142002	X.L. Wang *et al.*	(BELLE Collab.)
YUAN	07	PRL 99 182004	C.Z. Yuan *et al.*	(BELLE Collab.)
AUBERT	06B	PR D73 012005	B. Aubert *et al.*	(BABAR Collab.)
AUBERT,BE	06D	PR D74 091103	B. Aubert *et al.*	(BABAR Collab.)
HE	06B	PR D74 091104	Q. He *et al.*	(CLEO Collab.)
AUBERT,B	05I	PRL 95 142001	B. Aubert *et al.*	(BABAR Collab.)

$\chi_{c1}(4274)$

$I^G(J^{PC}) = 0^+(1^{++})$

was $X(4274)$

See the review on the "Spectroscopy of Mesons Containing two Heavy Quarks."

$\chi_{c1}(4274)$ MASS

VALUE (MeV)	EVTS	DOCUMENT ID		TECN	COMMENT
4290 ±6 OUR AVERAGE	Error includes scale factor of 1.5. See the ideogram below.				
$4298 \pm 6^{+4}_{-5}$		[1] AAIJ	25B	LHCB	$pp \to p(J/\psi\phi)p$
$4294 \pm 4^{+3}_{-6}$	24k	[2] AAIJ	21E	LHCB	$B^+ \to J/\psi\phi K^+$
$4274.4^{+8.4}_{-6.7} \pm 1.9$	22	[3] AALTONEN	17	CDF	$B^+ \to J/\psi\phi K^+$
• • • We do not use the following data for averages, fits, limits, etc. • • •					
$4273.3 \pm 8.3^{+17.2}_{-3.6}$	4289	[4,5] AAIJ	17C	LHCB	$B^+ \to J/\psi\phi K^+$

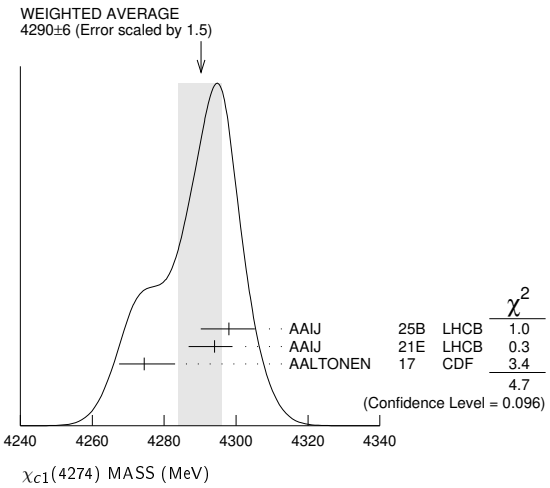

[1] From a fit using the five resonances reported in AAIJ 21E, described by relativistic Breit-Wigner distributions.
[2] From an amplitude analysis of the decay $B^+ \to J/\psi\phi K^+$ with a significance of 18 σ.
[3] From a fit to the invariant mass spectrum with a significance of 3.1 σ.
[4] From an amplitude analysis of the decay $B^+ \to J/\psi\phi K^+$ with a significance of 6.0 σ.
[5] Superseded by AAIJ 21E.

$\chi_{c1}(4274)$ WIDTH

VALUE (MeV)	EVTS	DOCUMENT ID		TECN	COMMENT
54 ± 8 OUR AVERAGE Error includes scale factor of 1.2.					
$92\ ^{+22}_{-18}\ ^{+33}_{-19}$		[1] AAIJ	25B	LHCB	$pp \to p(J/\psi\phi)p$
53 ± 5 ± 5	24k	[2] AAIJ	21E	LHCB	$B^+ \to J/\psi\phi K^+$
$32.3^{+21.9}_{-15.3} \pm 7.6$	22	[3] AALTONEN	17	CDF	$B^+ \to J/\psi\phi K^+$
• • • We do not use the following data for averages, fits, limits, etc. • • •					
$56 \pm 11\ ^{+8}_{-11}$	4289	[4,5] AAIJ	17C	LHCB	$B^+ \to J/\psi\phi K^+$

[1] From a fit using the five resonances reported in AAIJ 21E, described by relativistic Breit-Wigner distributions.
[2] From an amplitude analysis of the decay $B^+ \to J/\psi\phi K^+$ with a significance of 18 σ.
[3] From a fit to the invariant mass spectrum with a significance of 3.1 σ.
[4] From an amplitude analysis of the decay $B^+ \to J/\psi\phi K^+$ with a significance of 6.0 σ.
[5] Superseded by AAIJ 21E.

$\chi_{c1}(4274)$ DECAY MODES

	Mode	Fraction (Γ_i/Γ)
Γ_1	$J/\psi\phi$	seen

$\chi_{c1}(4274)$ BRANCHING RATIOS

$\Gamma(J/\psi\phi)/\Gamma_{total}$ — Γ_1/Γ

VALUE	EVTS	DOCUMENT ID		TECN	COMMENT
seen	24k	[1] AAIJ	21E	LHCB	$B^+ \to J/\psi\phi K^+$
• • • We do not use the following data for averages, fits, limits, etc. • • •					
seen	4289	[2,3] AAIJ	17C	LHCB	$B^+ \to J/\psi\phi K^+$

[1] From an amplitude analysis of the decay $B^+ \to J/\psi\phi K^+$ with a significance of 18 σ.
[2] From an amplitude analysis of the decay $B^+ \to J/\psi\phi K^+$ with a significance of 6.0 σ.
[3] Superseded by AAIJ 21E.

$\chi_{c1}(4274)$ REFERENCES

AAIJ	25B	PRL 134 031902	R. Aaij *et al.*	(LHCb Collab.)
AAIJ	21E	PRL 127 082001	R. Aaij *et al.*	(LHCb Collab.)
AAIJ	17C	PRL 118 022003	R. Aaij *et al.*	(LHCb Collab.) JP
Also		PR D95 012002	R. Aaij *et al.*	(LHCb Collab.)
AALTONEN	17	MPL A32 1750139	T. Altonen *et al.*	(CDF Collab.)

$X(4350)$

$I^G(J^{PC}) = 0^+(?^{?+})$

OMITTED FROM SUMMARY TABLE

Seen by SHEN 10 in the $\gamma\gamma \to J/\psi\phi$. Needs confirmation.

$X(4350)$ MASS

VALUE (MeV)	EVTS	DOCUMENT ID		TECN	COMMENT
$\mathbf{4350.6^{+4.6}_{-5.1} \pm 0.7}$	$8.8^{+4.2}_{-3.2}$	[1] SHEN	10	BELL	10.6 $e^+e^- \to e^+e^- J/\psi\phi$

[1] Statistical significance of 3.2 σ.

$X(4350)$ WIDTH

VALUE (MeV)	EVTS	DOCUMENT ID		TECN	COMMENT
$\mathbf{13^{+18}_{-9} \pm 4}$	$8.8^{+4.2}_{-3.2}$	[1] SHEN	10	BELL	10.6 $e^+e^- \to e^+e^- J/\psi\phi$

[1] Statistical significance of 3.2 σ.

$X(4350)$ DECAY MODES

	Mode	Fraction (Γ_i/Γ)
Γ_1	$J/\psi\phi$	seen
Γ_2	$\gamma\gamma$	seen

$X(4350)$ $\Gamma(i)\Gamma(\gamma\gamma)/\Gamma(total)$

$\Gamma(\gamma\gamma) \times \Gamma(J/\psi\phi)/\Gamma_{total}$ — $\Gamma_2\Gamma_1/\Gamma$

VALUE (eV)	EVTS	DOCUMENT ID		TECN	COMMENT
$\mathbf{6.7^{+3.2}_{-2.4} \pm 1.1}$	$8.8^{+4.2}_{-3.2}$	[1] SHEN	10	BELL	10.6 $e^+e^- \to e^+e^- J/\psi\phi$
• • • We do not use the following data for averages, fits, limits, etc. • • •					
$1.5^{+0.7}_{-0.6} \pm 0.3$	$8.8^{+4.2}_{-3.2}$	[2] SHEN	10	BELL	10.6 $e^+e^- \to e^+e^- J/\psi\phi$

[1] For $J^P = 0^+$. Statistical significance of 3.2 σ.
[2] For $J^P = 2^+$. Statistical significance of 3.2 σ.

$X(4350)$ BRANCHING RATIOS

$\Gamma(J/\psi\phi)/\Gamma_{total}$ — Γ_1/Γ

VALUE	DOCUMENT ID		TECN	COMMENT
seen	[1] SHEN	10	BELL	10.6 $e^+e^- \to e^+e^- J/\psi\phi$

[1] Statistical significance of 3.2 σ.

$\Gamma(\gamma\gamma)/\Gamma_{total}$ — Γ_2/Γ

VALUE	DOCUMENT ID		TECN	COMMENT
seen	[1] SHEN	10	BELL	10.6 $e^+e^- \to e^+e^- J/\psi\phi$

[1] Statistical significance of 3.2 σ.

$X(4350)$ REFERENCES

SHEN	10	PRL 104 112004	C.P. Shen *et al.*	(BELLE Collab.)

$\psi(4360)$

$I^G(J^{PC}) = 0^-(1^{--})$

also known as $Y(4360)$; was $X(4360)$

See the reviews on the "Spectroscopy of Mesons Containing two Heavy Quarks' and on "Heavy Non-qqbar Mesons."

$\psi(4360)$ MASS

VALUE (MeV)	EVTS	DOCUMENT ID		TECN	COMMENT
4373 ± 7 OUR AVERAGE Error includes scale factor of 2.3. See the ideogram below.					
$4327.4^{+20.1}_{-18.8}\ ^{+10.7}_{-9.3}$		[1] ABLIKIM	25B	BES3	$e^+e^- \to \pi^+\pi^- h_c(1P)$
4386 ± 13 ± 17		[2] ABLIKIM	24T	BES3	$e^+e^- \to \eta J/\psi$
4371.6 ± 2.5 ± 9.2		[3] ABLIKIM	22AL	BES3	$e^+e^- \to \pi^+\pi^- D^+D^-$
4298 ± 12 ± 26		[4] ABLIKIM	22AM	BES3	$e^+e^- \to \pi^+\pi^- J/\psi$
4390.3 ± 6.0 ± 0.7		[5] ABLIKIM	21AJ	BES3	$e^+e^- \to \pi^+\pi^- \psi(2S)$
4371.7 ± 7.5 ± 1.8		[6] ABLIKIM	21AK	BES3	$e^+e^- \to \gamma\chi_{c2} \to \gamma\gamma J/\psi$
$4391.5^{+6.3}_{-6.8} \pm 1.0$		ABLIKIM	17G	BES3	$e^+e^- \to \pi^+\pi^- h_c$
4347 ± 6 ± 3	279	[7] WANG	15A	BELL	10.58 $e^+e^- \to \gamma\pi^+\pi^-\psi(2S)$
4340 ± 16 ± 9	37	[8] LEES	14F	BABR	10.58 $e^+e^- \to \gamma\pi^+\pi^-\psi(2S)$
• • • We do not use the following data for averages, fits, limits, etc. • • •					
4406.9 ± 17.2 ± 4.5		[9] ABLIKIM	22R	BES3	$e^+e^- \to \pi^+\pi^-\chi_{c1}\gamma$
4382.0 ± 13.3 ± 1.7		[10] ABLIKIM	20O	BES3	$e^+e^- \to \eta J/\psi$
4320.0 ± 10.4 ± 7.0		[11] ABLIKIM	17B	BES3	$e^+e^- \to \pi^+\pi^- J/\psi$
4383.8 ± 4.2 ± 0.8		[12] ABLIKIM	17V	BES3	$e^+e^- \to \pi^+\pi^-\psi(2S)$
4383.7 ± 2.9 ± 6.2		[13] ZHANG	17B	RVUE	$e^+e^- \to \pi^+\pi^-\psi(2S)$
4386.4 ± 2.1 ± 6.4		[14] ZHANG	17C	RVUE	$e^+e^- \to \pi^+\pi^- J/\psi$ or $\psi(2S)$
$4355\ ^{+9}_{-10} \pm 9$	74	[15] LIU	08H	RVUE	10.58 $e^+e^- \to \gamma\pi^+\pi^-\psi(2S)$
4324 ± 24		[16] AUBERT	07S	BABR	10.58 $e^+e^- \to \gamma\pi^+\pi^-\psi(2S)$
4361 ± 9 ± 9	47	[8] WANG	07D	BELL	10.58 $e^+e^- \to \gamma\pi^+\pi^-\psi(2S)$

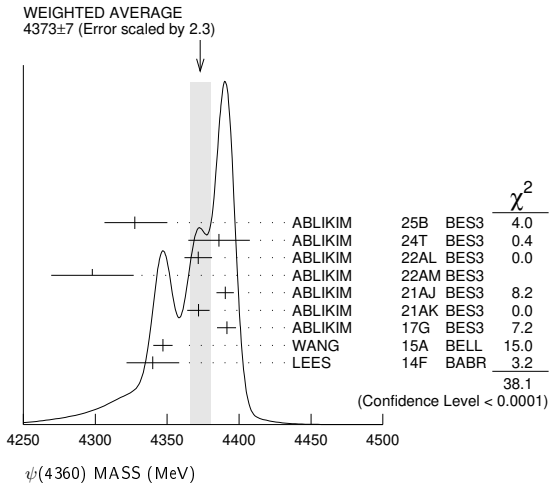

Int. J. Mod. Phys. A 2026.41. Downloaded from www.worldscientific.com
by CALIFORNIA @ BERKELEY on 09/16/26. Re-use and distribution is strictly not permitted, except for Open Access articles.

Int. J. Mod. Phys. A 2026.41. Downloaded from www.worldscientific.com
by UNIVERSITY OF CALIFORNIA @ BERKELEY on 09/16/26. Re-use and distribution is strictly not permitted, except for Open Access articles.

[1] Using three coherent Breit-Wigner functions between 4.009 and 4.950 GeV.
[2] From a three-resonance fit to the Born cross section in the range $\sqrt{s}$ = 3.808–4.951 GeV. Supersedes ABLIKIM 20O.
[3] From a fit to the cross section for $e^+e^- \to D^+D^-\pi^+\pi^-$ in the range $\sqrt{s}$ = 4.190–4.946 GeV.
[4] From a three-resonance fit to the Born cross section in the range $\sqrt{s}$ = 3.7730–4.7008 GeV. Parameters depend on the existence or non-existence of a state near 4.5 GeV.
[5] From a three-resonance fit to the Born cross section in the range $\sqrt{s}$ = 4.008–4.698 GeV.
[6] From a five-resonance fit to the cross section for $e^+e^- \to \gamma\gamma J/\psi \to \gamma\gamma\ell^+\ell^-$.
[7] From a two-resonance fit. Supersedes WANG 07D.
[8] From a two-resonance fit.
[9] From a fit to the $e^+e^- \to \pi^+\pi^-\psi(3823)$ cross section between 4.23 and 4.70 GeV with two coherent Breit-Wigner resonances. The data is also consistent with a single peak with mass 4417.5 ± 26.2 ± 3.5 MeV and width 245 ± 48 ± 13 MeV.
[10] From a fit of the measured cross section in the range $\sqrt{s}$ = 3.808–4.600 GeV.
[11] From a three-resonance fit. Superseded by ABLIKIM 22AM.
[12] From a fit to the cross section for $e^+e^- \to \pi^+\pi^-\psi(2S) \to 2(\pi^+\pi^-)\ell^+\ell^-$ obtained from 16 center-of-mass energies between 4.008 and 4.600 GeV and comprising 5.1 fb^{-1}. Superseded by ABLIKIM 21AJ.
[13] From a three-resonance fit.
[14] From a combined fit of BELLE, BABAR and BES3 $e^+e^- \to \pi^+\pi^- J/\psi$ and $e^+e^- \to \pi^+\pi^-\psi(2S)$ data.
[15] From a combined fit of AUBERT 07S and WANG 07D data with two resonances.
[16] From a single-resonance fit. Systematic errors not estimated.

$\psi(4360)$ WIDTH

VALUE (MeV)	EVTS	DOCUMENT ID		TECN	COMMENT
124 ±13 OUR AVERAGE		Error includes scale factor of 2.4. See the ideogram below.			
$244.1^{+34.0}_{-27.1}{}^{+24.2}_{-18.3}$		[1] ABLIKIM	25B	BES3	$e^+e^- \to \pi^+\pi^- h_c(1P)$
177 ±32 ±13		[2] ABLIKIM	24T	BES3	$e^+e^- \to \eta J/\psi$
167 ± 4 ±29		[3] ABLIKIM	22AL	BES3	$e^+e^- \to \pi^+\pi^- D^+D^-$
127 ±17 ±10		[4] ABLIKIM	22AM	BES3	$e^+e^- \to \pi^+\pi^- J/\psi$
143.3±10.0± 0.5		[5] ABLIKIM	21AJ	BES3	$e^+e^- \to \pi^+\pi^-\psi(2S)$
51.1±17.6± 1.9		[6] ABLIKIM	21AK	BES3	$e^+e^- \to \gamma\chi_{c2} \to \gamma\gamma J/\psi$
$139.5^{+16.2}_{-20.6}$± 0.6		ABLIKIM	17G	BES3	$e^+e^- \to \pi^+\pi^- h_c$
103 ± 9 ± 5	279	[7] WANG	15A	BELL	10.58 $e^+e^- \to \gamma\pi^+\pi^-\psi(2S)$
94 ±32 ±13	37	[8] LEES	14F	BABR	10.58 $e^+e^- \to \gamma\pi^+\pi^-\psi(2S)$
• • • We do not use the following data for averages, fits, limits, etc. • • •					
128.1±37.2± 2.3		[9] ABLIKIM	22R	BES3	$e^+e^- \to \pi^+\pi^-\chi_{c1}\gamma$
135.8±60.8±22.5		[10] ABLIKIM	20O	BES3	$e^+e^- \to \eta J/\psi$
$101.4^{+25.3}_{-19.7}$±10.2		[11] ABLIKIM	17B	BES3	$e^+e^- \to \pi^+\pi^- J/\psi$
84.2±12.5± 2.1		[12] ABLIKIM	17V	BES3	$e^+e^- \to \pi^+\pi^-\psi(2S)$
94.2± 7.3± 2.0		[13] ZHANG	17B	RVUE	$e^+e^- \to \pi^+\pi^-\psi(2S)$
96.0± 6.7± 2.7		[14] ZHANG	17C	RVUE	$e^+e^- \to \pi^+\pi^- J/\psi$ or $\psi(2S)$
103^{+17}_{-15} ±11	74	[15] LIU	08H	RVUE	10.58 $e^+e^- \to \gamma\pi^+\pi^-\psi(2S)$
172 ±33		[16] AUBERT	07S	BABR	10.58 $e^+e^- \to \gamma\pi^+\pi^-\psi(2S)$
74 ±15 ±10	47	[8] WANG	07D	BELL	10.58 $e^+e^- \to \gamma\pi^+\pi^-\psi(2S)$

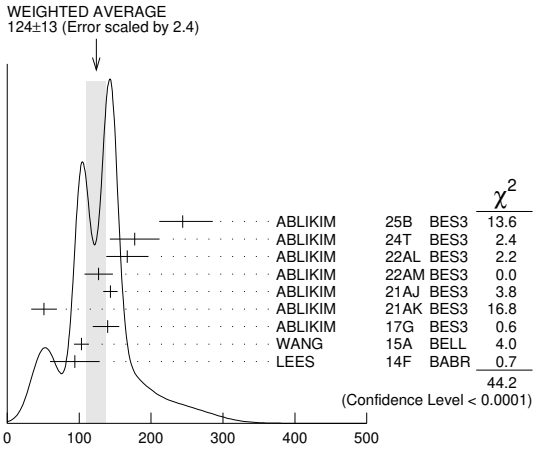

[1] Using three coherent Breit-Wigner functions between 4.009 and 4.950 GeV.
[2] From a three-resonance fit to the Born cross section in the range $\sqrt{s}$ = 3.808–4.951 GeV. Supersedes ABLIKIM 20O.
[3] From a fit to the cross section for $e^+e^- \to D^+D^-\pi^+\pi^-$ in the range $\sqrt{s}$ = 4.190–4.946 GeV.
[4] From a three-resonance fit to the Born cross section in the range $\sqrt{s}$ = 3.7730–4.7008 GeV. Parameters depend on the existence or non-existence of a state near 4.5 GeV.
[5] From a three-resonance fit to the Born cross section in the range $\sqrt{s}$ = 4.008–4.698 GeV.
[6] From a five-resonance fit to the cross section for $e^+e^- \to \gamma\gamma J/\psi \to \gamma\gamma\ell^+\ell^-$.
[7] From a two-resonance fit. Supersedes WANG 07D.
[8] From a two-resonance fit.
[9] From a fit to the $e^+e^- \to \pi^+\pi^-\psi(3823)$ cross section between 4.23 and 4.70 GeV with two coherent Breit-Wigner resonances. The data is also consistent with a single peak with mass 4417.5 ± 26.2 ± 3.5 MeV and width 245 ± 48 ± 13 MeV.
[10] From a fit of the measured cross section in the range $\sqrt{s}$ = 3.808–4.600 GeV.
[11] From a three-resonance fit. Superseded by ABLIKIM 22AM.
[12] From a fit to the cross section for $e^+e^- \to \pi^+\pi^-\psi(2S) \to 2(\pi^+\pi^-)\ell^+\ell^-$ obtained from 16 center-of-mass energies between 4.008 and 4.600 GeV and comprising 5.1 fb^{-1}. Superseded by ABLIKIM 21AJ.
[13] From a three-resonance fit.
[14] From a combined fit of BELLE, BABAR and BES3 $e^+e^- \to \pi^+\pi^- J/\psi$ and $e^+e^- \to \pi^+\pi^-\psi(2S)$ data.
[15] From a combined fit of AUBERT 07S and WANG 07D data with two resonances.
[16] From a single-resonance fit. Systematic errors not estimated.

$\psi(4360)$ DECAY MODES

	Mode	Fraction (Γ_i/Γ)
Γ_1	e^+e^-	seen
Γ_2	$h_c\pi^+\pi^-$	seen
Γ_3	$J/\psi\pi^+\pi^-$	seen
Γ_4	$\psi(2S)\pi^+\pi^-$	seen
Γ_5	$\psi(3770)\pi^+\pi^-$	possibly seen
Γ_6	$\psi_2(3823)\pi^+\pi^-$	seen
Γ_7	$J/\psi\eta$	seen
Γ_8	$D^0D^{*-}\pi^+$	not seen
Γ_9	$D^+D^-\pi^+\pi^-$	seen
Γ_{10}	$D_1(2420)\overline{D}+$ c.c.	possibly seen
Γ_{11}	$\phi\eta$	not seen
Γ_{12}	$\omega\pi^0$	not seen
Γ_{13}	$\omega\eta$	not seen
Γ_{14}	$p\overline{p}\eta$	not seen
Γ_{15}	$p\overline{p}\omega$	not seen
Γ_{16}	$\chi_{c1}\gamma$	not seen
Γ_{17}	$\chi_{c2}\gamma$	not seen
Γ_{18}	$\Sigma^+\overline{\Sigma}-$	not seen
Γ_{19}	$\Sigma^0\overline{\Sigma}^0$	
Γ_{20}	$\Xi^0\overline{\Xi}^0$	
Γ_{21}	$\Xi^-\overline{\Xi}^+$	not seen
Γ_{22}	$pK^-\overline{\Lambda}+$ c.c.	not seen
Γ_{23}	$\Lambda\overline{\Xi}^+K^-+$ c.c.	not seen
Γ_{24}	$\Sigma^0\overline{\Xi}^+K^-+$ c.c.	not seen
Γ_{25}	$pK^-K^-\overline{\Xi}^++$ c.c.	

$\psi(4360)$ $\Gamma(i) \times \Gamma(e^+e^-)/\Gamma(\text{total})$

$\Gamma(h_c\pi^+\pi^-) \times \Gamma(e^+e^-)/\Gamma_{\text{total}}$ — $\Gamma_2\Gamma_1/\Gamma$

VALUE (eV)	DOCUMENT ID		TECN	COMMENT
21 $^{+10}_{-8}$ OUR AVERAGE	Error includes scale factor of 2.4.			
$29.1^{+5.7}_{-3.9}{}^{+4.4}_{-3.4}$	[1] ABLIKIM	25B	BES3	$e^+e^- \to \pi^+\pi^- h_c(1P)$
$11.6^{+5.0}_{-4.4}$±1.9	ABLIKIM	17G	BES3	$e^+e^- \to \pi^+\pi^- h_c(1P)$

[1] Using three coherent Breit-Wigner functions between 4.009 and 4.950 GeV. Second solution: $10.8^{+3.1}_{-2.3}$ eV.

$\Gamma(\psi(2S)\pi^+\pi^-) \times \Gamma(e^+e^-)/\Gamma_{\text{total}}$ — $\Gamma_4\Gamma_1/\Gamma$

VALUE (eV)	EVTS	DOCUMENT ID		TECN	COMMENT
• • • We do not use the following data for averages, fits, limits, etc. • • •					
10.7±4.1		[1] ABLIKIM	21AJ	BES3	$e^+e^- \to \pi^+\pi^-\psi(2S)$
20.7±2.5		[2] ABLIKIM	21AJ	BES3	$e^+e^- \to \pi^+\pi^-\psi(2S)$
9.9±4.1		[3] ABLIKIM	21AJ	BES3	$e^+e^- \to \pi^+\pi^-\psi(2S)$
19.4±2.0		[4] ABLIKIM	21AJ	BES3	$e^+e^- \to \pi^+\pi^-\psi(2S)$
7.3±2.8		[5] ABLIKIM	19K	BES3	$e^+e^- \to \pi^+\pi^-\psi(2S)$
11.0±3.8		[6] ABLIKIM	19K	BES3	$e^+e^- \to \pi^+\pi^-\psi(2S)$
9.2±0.6±0.6	279	[7] WANG	15A	BELL	10.58 $e^+e^- \to \gamma\pi^+\pi^-\psi(2S)$
10.9±0.6±0.7	279	[8] WANG	15A	BELL	10.58 $e^+e^- \to \gamma\pi^+\pi^-\psi(2S)$
6.0±1.0±0.5	37	[5] LEES	14F	BABR	10.58 $e^+e^- \to \gamma\pi^+\pi^-\psi(2S)$
7.2±1.0±0.6	37	[6] LEES	14F	BABR	10.58 $e^+e^- \to \gamma\pi^+\pi^-\psi(2S)$
$11.1^{+1.3}_{-1.2}$	74	[9] LIU	08H	RVUE	10.58 $e^+e^- \to \gamma\pi^+\pi^-\psi(2S)$
12.3±1.2	74	[10] LIU	08H	RVUE	10.58 $e^+e^- \to \gamma\pi^+\pi^-\psi(2S)$
10.4±1.7±1.5	47	[5] WANG	07D	BELL	10.58 $e^+e^- \to \gamma\pi^+\pi^-\psi(2S)$
11.8±1.8±1.4	47	[6] WANG	07D	BELL	10.58 $e^+e^- \to \gamma\pi^+\pi^-\psi(2S)$

[1] Solution I of four equivalent solutions in a fit using three interfering resonances. Supersedes ABLIKIM 19K.
[2] Solution II of four equivalent solutions in a fit using three interfering resonances. Supersedes ABLIKIM 19K.
[3] Solution III of four equivalent solutions in a fit using three interfering resonances. Supersedes ABLIKIM 19K.
[4] Solution IV of four equivalent solutions in a fit using three interfering resonances. Supersedes ABLIKIM 19K.
[5] Solution I of two equivalent solutions in a fit using two interfering resonances.
[6] Solution II of two equivalent solutions in a fit using two interfering resonances.
[7] Solution I of two equivalent solutions from a fit using two interfering resonances. Supersedes WANG 07D.
[8] Solution II of two equivalent solutions from a fit using two interfering resonances. Supersedes WANG 07D.
[9] Solution I in a combined fit of AUBERT 07S and WANG 07D data with two resonances.
[10] Solution II in a combined fit of AUBERT 07S and WANG 07D data with two resonances.

$\Gamma(J/\psi\eta) \times \Gamma(e^+e^-)/\Gamma_{total}$ — $\Gamma_7\Gamma_1/\Gamma$

VALUE (eV)	CL%	DOCUMENT ID		TECN	COMMENT
• • • We do not use the following data for averages, fits, limits, etc. • • •					
$1.8 \pm 0.6 \pm 0.3$		[1] ABLIKIM	24T	BES3	$e^+e^- \to \eta J/\psi$
$2.1 \pm 0.7 \pm 0.3$		[2] ABLIKIM	24T	BES3	$e^+e^- \to \eta J/\psi$
$4.3 \pm 1.3 \pm 0.5$		[3] ABLIKIM	24T	BES3	$e^+e^- \to \eta J/\psi$
$5.0 \pm 1.5 \pm 0.5$		[4] ABLIKIM	24T	BES3	$e^+e^- \to \eta J/\psi$
3.4 ± 2.2		[5] ABLIKIM	20O	BES3	$e^+e^- \to \eta J/\psi$
1.5 ± 1.0		[6] ABLIKIM	20O	BES3	$e^+e^- \to \eta J/\psi$
1.7 ± 1.1		[7] ABLIKIM	20O	BES3	$e^+e^- \to \eta J/\psi$
<6.8	90	WANG	13B	BELL	$e^+e^- \to J/\psi\eta\gamma$

[1] Solution 1 of 4. Supersedes ABLIKIM 20O.
[2] Solution 2 of 4. Supersedes ABLIKIM 20O.
[3] Solution 3 of 4. Supersedes ABLIKIM 20O.
[4] Solution 4 of 4. Supersedes ABLIKIM 20O.
[5] Solution 1 of three equivalent fit solutions using three resonant structures.
[6] Solution 2 of three equivalent fit solutions using three resonant structures.
[7] Solution 3 of three equivalent fit solutions using three resonant structures.

$\Gamma(\chi_{c1}\gamma) \times \Gamma(e^+e^-)/\Gamma_{total}$ — $\Gamma_{16}\Gamma_1/\Gamma$

VALUE (eV)	CL%	DOCUMENT ID		TECN	COMMENT
<0.57	90	[1] HAN	15	BELL	10.58 $e^+e^- \to \chi_{c1}\gamma$

[1] Using $B(\eta \to \gamma\gamma) = (39.41 \pm 0.21)\%$.

$\Gamma(\chi_{c2}\gamma) \times \Gamma(e^+e^-)/\Gamma_{total}$ — $\Gamma_{17}\Gamma_1/\Gamma$

VALUE (eV)	CL%	DOCUMENT ID		TECN	COMMENT
<1.9	90	[1] HAN	15	BELL	10.58 $e^+e^- \to \chi_{c2}\gamma$

[1] Using $B(\eta \to \gamma\gamma) = (39.41 \pm 0.21)\%$.

$\Gamma(\Sigma^+\overline{\Sigma}^-) \times \Gamma(e^+e^-)/\Gamma_{total}$ — $\Gamma_{18}\Gamma_1/\Gamma$

VALUE (eV)	CL%	DOCUMENT ID		TECN	COMMENT
$<118.8 \times 10^{-3}$	90	[1] ABLIKIM	24AH	BES3	$e^+e^- \to \Sigma^+\overline{\Sigma}^-$

[1] Interference effect between resonance and continuum amplitudes is considered. Two solutions from the fit.

$\Gamma(\Sigma^0\overline{\Sigma}^0) \times \Gamma(e^+e^-)/\Gamma_{total}$ — $\Gamma_{19}\Gamma_1/\Gamma$

VALUE (eV)	CL%	DOCUMENT ID		TECN	COMMENT
$<29.3 \times 10^{-3}$	90	[1] ABLIKIM	25U	BES3	$e^+e^- \to \Sigma^0\overline{\Sigma}^0$

[1] Interference effect between resonance and continuum amplitudes is considered. Upper limit is for the larger of the two solutions from the fit.

$\Gamma(\Xi^0\overline{\Xi}^0) \times \Gamma(e^+e^-)/\Gamma_{total}$ — $\Gamma_{20}\Gamma_1/\Gamma$

VALUE (eV)	CL%	DOCUMENT ID		TECN	COMMENT
$<84.5 \times 10^{-3}$	90	[1] ABLIKIM	24CD	BES3	$e^+e^- \to \psi(4360)$

[1] From a fit to $e^+e^- \to \Xi^0\overline{\Xi}^0$ cross sections.

$\Gamma(\Xi^-\overline{\Xi}^+) \times \Gamma(e^+e^-)/\Gamma_{total}$ — $\Gamma_{21}\Gamma_1/\Gamma$

VALUE (eV)	CL%	DOCUMENT ID		TECN	COMMENT
$<44.8 \times 10^{-3}$	90	[1] ABLIKIM	23BK	BES3	$e^+e^- \to \psi(4360)$

[1] From a fit to $e^+e^- \to \Xi^-\overline{\Xi}^+$ cross sections.

$\Gamma(pK^-\overline{\Lambda} + \text{c.c.}) \times \Gamma(e^+e^-)/\Gamma_{total}$ — $\Gamma_{22}\Gamma_1/\Gamma$

VALUE (eV)	CL%	DOCUMENT ID		TECN	COMMENT
$<4.7 \times 10^{-3}$	90	[1] ABLIKIM	23BL	BES3	$e^+e^- \to \psi(4360)$

[1] From a fit to $e^+e^- \to pK^-\overline{\Lambda}$ + c.c. cross sections.

$\Gamma(\Lambda\overline{\Xi}^+K^- + \text{c.c.}) \times \Gamma(e^+e^-)/\Gamma_{total}$ — $\Gamma_{23}\Gamma_1/\Gamma$

VALUE (eV)	CL%	DOCUMENT ID		TECN	COMMENT
$<35.8 \times 10^{-3}$	90	[1] ABLIKIM	24AL	BES3	$e^+e^- \to \Lambda\overline{\Xi}^+K^-$ + c.c.

[1] A fit to the Born cross section of $e^+e^- \to \Lambda\overline{\Xi}^+K^-$ + c.c. including interference with the continuum. Two solutions from the fit.

$\Gamma(\Sigma^0\overline{\Xi}^+K^- + \text{c.c.}) \times \Gamma(e^+e^-)/\Gamma_{total}$ — $\Gamma_{24}\Gamma_1/\Gamma$

VALUE (eV)	CL%	DOCUMENT ID		TECN	COMMENT
$<2.8 \times 10^{-3}$	90	[1] ABLIKIM	24AL	BES3	$e^+e^- \to \Sigma^0\overline{\Xi}^+K^-$ + c.c.

[1] A fit to the Born cross section of $e^+e^- \to \Sigma^0\overline{\Xi}^+K^-$ + c.c. including interference with the continuum. Two solutions from the fit.

$\Gamma(e^+e^-) \times \Gamma(pK^-K^-\overline{\Xi}^+ + \text{c.c.})/\Gamma_{total}$ — $\Gamma_1\Gamma_{25}/\Gamma$

VALUE (eV)	CL%	DOCUMENT ID		TECN	COMMENT
$<66.6 \times 10^{-3}$	90	ABLIKIM	25CF	BES3	$e^+e^- \to pK^-K^-\overline{\Xi}^+$ + c.c.

$\psi(4360)$ BRANCHING RATIOS

$\Gamma(h_c\pi^+\pi^-)/\Gamma_{total}$ — Γ_2/Γ

VALUE	DOCUMENT ID		TECN	COMMENT
seen	ABLIKIM	17G	BES3	$e^+e^- \to \pi^+\pi^-h_c$

$\Gamma(\psi(2S)\pi^+\pi^-)/\Gamma_{total}$ — Γ_4/Γ

VALUE	DOCUMENT ID		TECN	COMMENT
seen	[1] ABLIKIM	17V	BES3	$e^+e^- \to \pi^+\pi^-\psi(2S)$

[1] From a fit to the cross section for $e^+e^- \to \pi^+\pi^-\psi(2S) \to 2(\pi^+\pi^-)\ell^+\ell^-$ obtained from 16 center-of-mass energies between 4.008 and 4.600 GeV and comprising 5.1 fb^{-1}.

$\Gamma(\psi(2S)\pi^+\pi^-)/\Gamma(J/\psi\pi^+\pi^-)$ — Γ_4/Γ_3

VALUE	DOCUMENT ID		TECN	COMMENT
• • • We do not use the following data for averages, fits, limits, etc. • • •				
$(0.81 \pm 0.12 \pm 0.13)$ to $(42 \pm 15 \pm 15)$	[1] ZHANG	17C	RVUE	$e^+e^- \to \pi^+\pi^-J/\psi$ or $\psi(2S)$

[1] From a combined fit of BELLE, BABAR and BES3 $e^+e^- \to \pi^+\pi^-J/\psi$ and $e^+e^- \to \pi^+\pi^-\psi(2S)$ data.

$\Gamma(\psi(3770)\pi^+\pi^-)/\Gamma_{total}$ — Γ_5/Γ

VALUE	DOCUMENT ID		TECN	COMMENT
possibly seen	[1] ABLIKIM	19AR	BES3	$e^+e^- \to \pi^+\pi^-D\overline{D}$

[1] Observe $e^+e^- \to \pi^+\pi^-\psi(3770)$ at $\sqrt{s}$ = 4.26, 4.36, and 4.42 GeV but cannot establish if continuum or resonant.

$\Gamma(\psi_2(3823)\pi^+\pi^-)/\Gamma_{total}$ — Γ_6/Γ

VALUE	EVTS	DOCUMENT ID		TECN	COMMENT
seen		[1] ABLIKIM	22R	BES3	$e^+e^- \to \pi^+\pi^-\chi_{c1}\gamma$
• • • We do not use the following data for averages, fits, limits, etc. • • •					
possibly seen	19	[2] ABLIKIM	15S	BES3	$e^+e^- \to \pi^+\pi^-\chi_{c1}\gamma$

[1] From a fit to the $e^+e^- \to \pi^+\pi^-\psi(3823)$ cross section between 4.23 and 4.70 GeV with two coherent Breit-Wigner resonances.
[2] From a fit of $e^+e^- \to \pi^+\pi^-\psi_2(3823)$, $\psi_2(3823) \to \chi_{c1}\gamma$ cross sections taken at $\sqrt{s}$ values of 4.23, 4.26, 4.36, 4.42, and 4.60 GeV to the $\psi(4360)$ line shape.

$\Gamma(J/\psi\eta)/\Gamma_{total}$ — Γ_7/Γ

VALUE	DOCUMENT ID		TECN	COMMENT
seen	[1] ABLIKIM	24T	BES3	$e^+e^- \to \eta J/\psi$
• • • We do not use the following data for averages, fits, limits, etc. • • •				
seen	[2] ABLIKIM	20O	BES3	$e^+e^- \to \eta J/\psi$

[1] Supersedes ABLIKIM 20O.
[2] With a significance of 6.0 σ.

$\Gamma(D^0D^{*-}\pi^+)/\Gamma_{total} \times \Gamma(e^+e^-)/\Gamma_{total}$ — $\Gamma_8/\Gamma \times \Gamma_1/\Gamma$

VALUE	CL%	DOCUMENT ID		TECN	COMMENT
$<0.72 \times 10^{-6}$	90	[1] PAKHLOVA	09	BELL	$e^+e^- \to \psi(4360) \to D^0D^{*-}\pi^+$

[1] Using $4355^{+9}_{-10} \pm 9$ MeV for the mass of $\psi(4360)$.

$\Gamma(D^0D^{*-}\pi^+)/\Gamma(\psi(2S)\pi^+\pi^-)$ — Γ_8/Γ_4

VALUE	CL%	DOCUMENT ID		TECN	COMMENT
<8	90	PAKHLOVA	09	BELL	$e^+e^- \to \psi(4360) \to D^0D^{*-}\pi^+$

$\Gamma(D^+D^-\pi^+\pi^-)/\Gamma_{total}$ — Γ_9/Γ

VALUE	DOCUMENT ID		TECN	COMMENT
seen	[1] ABLIKIM	22AL	BES3	$e^+e^- \to \pi^+\pi^-D^+D^-$

[1] From a fit to the cross section for $e^+e^- \to D^+D^-\pi^+\pi^-$ in the range $\sqrt{s}$ = 4.190–4.946 GeV.

$\Gamma(D_1(2420)\overline{D} + \text{c.c.})/\Gamma_{total}$ — Γ_{10}/Γ

VALUE	DOCUMENT ID		TECN	COMMENT
possibly seen	[1] ABLIKIM	19AR	BES3	$e^+e^- \to \pi^+\pi^-D\overline{D}$

[1] Evidence for $e^+e^- \to D_1(2420)\overline{D}$ + c.c. between $\sqrt{s}$ = 4.3 and 4.6 GeV, not necessarily resonant.

$\Gamma(\phi\eta)/\Gamma_{total}$ — Γ_{11}/Γ

VALUE	DOCUMENT ID		TECN	COMMENT
not seen	ABLIKIM	23BT	BES3	$e^+e^- \to \phi\eta$

$\Gamma(\omega\pi^0)/\Gamma_{total}$ — Γ_{12}/Γ

VALUE	DOCUMENT ID		TECN	COMMENT
not seen	ABLIKIM	22K	BES3	$e^+e^- \to \omega\pi^0$

$\Gamma(\omega\eta)/\Gamma_{total}$ — Γ_{13}/Γ

VALUE	DOCUMENT ID		TECN	COMMENT
not seen	ABLIKIM	22K	BES3	$e^+e^- \to \omega\eta$

Int. J. Mod. Phys. A 2026.41. Downloaded from www.worldscientific.com
by CALIFORNIA @ BERKELEY on 09/16/26. Re-use and distribution is strictly not permitted, except for Open Access articles.

Int. J. Mod. Phys. A 2026.41. Downloaded from www.worldscientific.com
by UNIVERSITY OF CALIFORNIA @ BERKELEY on 09/16/26. Re-use and distribution is strictly not permitted, except for Open Access articles.

$\Gamma(p\overline{p}\eta)/\Gamma_{total}$ — **Γ_{14}/Γ**

VALUE	DOCUMENT ID		TECN	COMMENT
not seen	ABLIKIM	21AN	BES3	$e^+e^- \to p\overline{p}\eta$

$\Gamma(p\overline{p}\omega)/\Gamma_{total}$ — **Γ_{15}/Γ**

VALUE	DOCUMENT ID		TECN	COMMENT
not seen	ABLIKIM	21AN	BES3	$e^+e^- \to p\overline{p}\omega$

$\psi(4360)$ REFERENCES

ABLIKIM	25B	PRL 135 071901	M. Ablikim et al.	(BESIII Collab.)
ABLIKIM	25CF	JHEP 2511 111	M. Ablikim et al.	(BESIII Collab.)
ABLIKIM	25U	PR D111 L051502	M. Ablikim et al.	(BESIII Collab.)
ABLIKIM	24AH	JHEP 2405 022	M. Ablikim et al.	(BESIII Collab.)
ABLIKIM	24AL	JHEP 2407 258	M. Ablikim et al.	(BESIII Collab.)
ABLIKIM	24CD	JHEP 2411 062	M. Ablikim et al.	(BESIII Collab.)
ABLIKIM	24T	PR D109 092012	M. Ablikim et al.	(BESIII Collab.)
ABLIKIM	23BK	JHEP 2311 228	M. Ablikim et al.	(BESIII Collab.)
ABLIKIM	23BL	JHEP 2312 027	M. Ablikim et al.	(BESIII Collab.)
ABLIKIM	23BT	PR D108 112011	M. Ablikim et al.	(BESIII Collab.)
ABLIKIM	22AL	PR D106 052012	M. Ablikim et al.	(BESIII Collab.)
ABLIKIM	22AM	PR D106 072001	M. Ablikim et al.	(BESIII Collab.)
ABLIKIM	22K	JHEP 2207 064	M. Ablikim et al.	(BESIII Collab.)
ABLIKIM	22R	PRL 129 102003	M. Ablikim et al.	(BESIII Collab.)
ABLIKIM	21AJ	PR D104 052012	M. Ablikim et al.	(BESIII Collab.)
ABLIKIM	21AK	PR D104 092001	M. Ablikim et al.	(BESIII Collab.)
ABLIKIM	21AN	PR D104 092008	M. Ablikim et al.	(BESIII Collab.)
ABLIKIM	20O	PR D102 031101	M. Ablikim et al.	(BESIII Collab.)
ABLIKIM	19AR	PR D100 032005	M. Ablikim et al.	(BESIII Collab.)
ABLIKIM	19K	PR D99 019903 (errat.)	M. Ablikim et al.	(BESIII Collab.)
ABLIKIM	17B	PRL 118 092001	M. Ablikim et al.	(BESIII Collab.)
ABLIKIM	17G	PRL 118 092002	M. Ablikim et al.	(BESIII Collab.)
ABLIKIM	17V	PR D96 032004	M. Ablikim et al.	(BESIII Collab.)
Also		PR D99 019903 (errat.)	M. Ablikim et al.	(BESIII Collab.)
ZHANG	17B	PR D96 054008	J. Zhang, J. Zhang	
ZHANG	17C	EPJ C77 727	J. Zhang, L. Yuan	
ABLIKIM	15S	PRL 115 011803	M. Ablikim et al.	(BESIII Collab.)
HAN	15	PR D92 012011	Y.L. Han et al.	(BELLE Collab.)
WANG	15A	PR D91 112007	X.L. Wang et al.	(BELLE Collab.)
LEES	14F	PR D89 111103	J.P. Lees et al.	(BABAR Collab.)
WANG	13B	PR D87 051101	X.L. Wang et al.	(BELLE Collab.)
PAKHLOVA	09	PR D80 091101	G. Pakhlova et al.	(BELLE Collab.)
LIU	08H	PR D78 014032	Z.Q. Liu, X.S. Qin, C.Z. Yuan	
AUBERT	07S	PRL 98 212001	B. Aubert et al.	(BABAR Collab.)
WANG	07D	PRL 99 142002	X.L. Wang et al.	(BELLE Collab.)

$\psi(4415)$ [a]

$I^G(J^{PC}) = 0^-(1^{--})$

[a] J^{PC} known by production in e^+e^- via single photon annihilation. I^G is not known; interpretation of this state as a single resonance is unclear because of the expectation of substantial threshold effects in this energy region.

$\psi(4415)$ MASS

VALUE (MeV)	DOCUMENT ID		TECN	COMMENT
4415 ± 5 OUR AVERAGE				
4413.6 ± 9.0 ± 0.8	[1] ABLIKIM	24D	BES3	$e^+e^- \to \omega\gamma J/\psi$
4414.6 ± 3.4 ± 6.1	ABLIKIM	23BH	BES3	$e^+e^- \to D_s^{*+}D_s^{*-}$
4415.1 ± 7.9	[2] ABLIKIM	08D	BES2	$e^+e^- \to$ hadrons
• • • We do not use the following data for averages, fits, limits, etc. • • •				
4412 ± 15	[3] MO	10	RVUE	$e^+e^- \to$ hadrons
4411 ± 7	[4] PAKHLOVA	08A	BELL	10.6 $e^+e^- \to D^0D^-\pi^+\gamma$
4425 ± 6	[5] SETH	05A	RVUE	$e^+e^- \to$ hadrons
4429 ± 9	[6] SETH	05A	RVUE	$e^+e^- \to$ hadrons
4417 ± 10	BRANDELIK	78C	DASP	e^+e^-
4414 ± 7	SIEGRIST	76	MRK1	e^+e^-

[1] Assuming one single Breit-Wigner resonance in $\omega\chi_{c2}(1P)$ ($\chi_{c2} \to \gamma J/\psi$).
[2] Reanalysis of data presented in BAI 02C. From a global fit over the center-of-mass energy region 3.7–5.0 GeV covering the $\psi(3770)$, $\psi(4040)$, $\psi(4160)$, and $\psi(4415)$ resonances. Phase angle fixed in the fit to $\delta = (234 \pm 88)^\circ$.
[3] Reanalysis of data presented in BAI 00 and BAI 02C. From a global fit over the center-of-mass energy 3.8-4.8 GeV covering the $\psi(4040)$, $\psi(4160)$ and $\psi(4415)$ resonances and including interference effects.
[4] Systematic uncertainties not estimated.
[5] From a fit to Crystal Ball (OSTERHELD 86) data.
[6] From a fit to BES (BAI 02C) data.

$\psi(4415)$ WIDTH

VALUE (MeV)	DOCUMENT ID		TECN	COMMENT
110 ± 13 OUR AVERAGE	Error includes scale factor of 1.6. See the ideogram below.			
110.5 ± 15.0 ± 2.9	[7] ABLIKIM	24D	BES3	$e^+e^- \to \omega\gamma J/\psi$
122.5 ± 7.5 ± 8.1	ABLIKIM	23BH	BES3	$e^+e^- \to D_s^{*+}D_s^{*-}$
71.5 ± 19.0	[8] ABLIKIM	08D	BES2	$e^+e^- \to$ hadrons
• • • We do not use the following data for averages, fits, limits, etc. • • •				
118 ± 32	[9] MO	10	RVUE	$e^+e^- \to$ hadrons
77 ± 20	[10] PAKHLOVA	08A	BELL	10.6 $e^+e^- \to D^0D^-\pi^+\gamma$
119 ± 16	[11] SETH	05A	RVUE	$e^+e^- \to$ hadrons
118 ± 35	[12] SETH	05A	RVUE	$e^+e^- \to$ hadrons
66 ± 15	BRANDELIK	78C	DASP	e^+e^-
33 ± 10	SIEGRIST	76	MRK1	e^+e^-

[7] Assuming one single Breit-Wigner resonance in $\omega\chi_{c2}(1P)$ ($\chi_{c2} \to \gamma J/\psi$).
[8] Reanalysis of data presented in BAI 02C. From a global fit over the center-of-mass energy region 3.7–5.0 GeV covering the $\psi(3770)$, $\psi(4040)$, $\psi(4160)$, and $\psi(4415)$ resonances. Phase angle fixed in the fit to $\delta = (234 \pm 88)^\circ$.
[9] Reanalysis of data presented in BAI 00 and BAI 02C. From a global fit over the center-of-mass energy 3.8-4.8 GeV covering the $\psi(4040)$, $\psi(4160)$ and $\psi(4415)$ resonances and including interference effects.
[10] Systematic uncertainties not estimated.
[11] From a fit to Crystal Ball (OSTERHELD 86) data.
[12] From a fit to BES (BAI 02C) data.

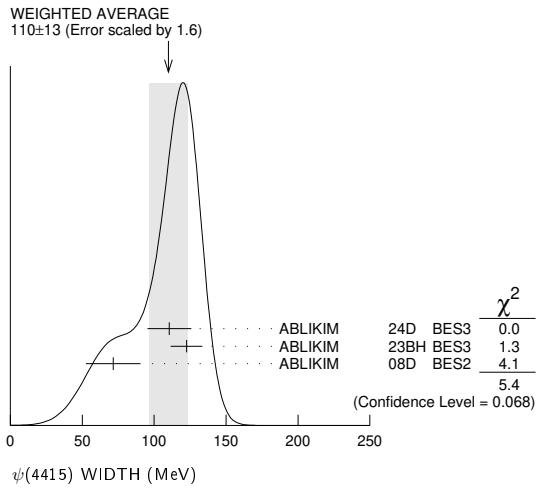

$\psi(4415)$ DECAY MODES

Due to the complexity of the $c\overline{c}$ threshold region, in this listing, "seen" ("not seen") means that a cross section for the mode in question has been measured at effective $\sqrt{s}$ near this particle's central mass value, more (less) than 2σ above zero, without regard to any peaking behavior in $\sqrt{s}$ or absence thereof. See mode listing(s) for details and references.

	Mode	Fraction (Γ_i/Γ)	Confidence level
Γ_1	$D\overline{D}$	seen	
Γ_2	$D^0\overline{D}^0$	seen	
Γ_3	D^+D^-	seen	
Γ_4	$D^*\overline{D}$ + c.c.	seen	
Γ_5	$D^*(2007)^0\overline{D}^0$ + c.c.	seen	
Γ_6	$D^*(2010)^+D^-$ + c.c.	seen	
Γ_7	$D^*\overline{D}^*$	seen	
Γ_8	$D^*(2007)^0\overline{D}^*(2007)^0$ + c.c.	seen	
Γ_9	$D^*(2010)^+D^*(2010)^-$ + c.c.	seen	
Γ_{10}	$D^0D^-\pi^+$ (excl. $D^*(2010)^+D^-$ +c.c.	< 2.3 %	90%
Γ_{11}	$D\overline{D}_2^*(2460) \to D^0D^-\pi^+$+c.c.	(10 ± 4) %	
Γ_{12}	$D^0D^{*-}\pi^+$+c.c.	< 31 %	90%
Γ_{13}	$D_1(2420)\overline{D}$+ c.c.	possibly seen	
Γ_{14}	$D_s^+D_s^-$	not seen	
Γ_{15}	$\omega\chi_{c2}$	$(9 \pm 4) \times 10^{-3}$	
Γ_{16}	$D_s^{*+}D_s^-$+c.c.	seen	
Γ_{17}	$D_s^{*+}D_s^{*-}$	seen	
Γ_{18}	$\psi_2(3823)\pi^+\pi^-$	possibly seen	
Γ_{19}	$\psi(3770)\pi^+\pi^-$	possibly seen	
Γ_{20}	$J/\psi\eta$	< 1.0 %	90%
Γ_{21}	$\chi_{c1}\gamma$	$< 1.3 \times 10^{-3}$	90%
Γ_{22}	$\chi_{c2}\gamma$	$< 7 \times 10^{-3}$	90%
Γ_{23}	$\Lambda\overline{\Lambda}$	$< 5 \times 10^{-6}$	90%
Γ_{24}	$\Sigma^+\overline{\Sigma}^-$	$< 1.8 \times 10^{-4}$	90%
Γ_{25}	$\Sigma^0\overline{\Sigma}^0$	$< 4 \times 10^{-5}$	90%
Γ_{26}	$\Xi^0\overline{\Xi}^0$	$< 1.4 \times 10^{-4}$	90%
Γ_{27}	$\Xi^-\overline{\Xi}^+$	$< 6 \times 10^{-5}$	90%
Γ_{28}	$pK^-\overline{\Lambda}$+ c.c.	$< 1.0 \times 10^{-5}$	90%
Γ_{29}	$\Lambda\overline{\Xi}^+K^-$+ c.c.	$< 4 \times 10^{-5}$	90%
Γ_{30}	$\Sigma^0\overline{\Xi}^+K^-$+ c.c.	$< 2.5 \times 10^{-4}$	90%
Γ_{31}	$pK^-K^-\overline{\Xi}^+$+ c.c.	$< 8 \times 10^{-5}$	90%
Γ_{32}	$\omega\pi^0$	not seen	
Γ_{33}	$\omega\eta$	not seen	
Γ_{34}	e^+e^-	$(3.2 \pm 1.2) \times 10^{-6}$	
Γ_{35}	$\mu^+\mu^-$	$(1.1 \pm 0.4) \times 10^{-5}$	

Int. J. Mod. Phys. A 2026.41. Downloaded from www.worldscientific.com by CALIFORNIA @ BERKELEY on 09/16/26. Re-use and distribution is strictly not permitted, except for Open Access articles.

$\psi(4415)$ PARTIAL WIDTHS

$\Gamma(e^+e^-)$ — Γ_{34}

VALUE (keV)	DOCUMENT ID		TECN	COMMENT
0.35±0.12	[13] ABLIKIM	08D	BES2	$e^+e^- \to$ hadrons
• • • We do not use the following data for averages, fits, limits, etc. • • •				
0.4 to 0.8	[14] MO	10	RVUE	$e^+e^- \to$ hadrons
0.72±0.11	[15] SETH	05A	RVUE	$e^+e^- \to$ hadrons
0.64±0.23	[16] SETH	05A	RVUE	$e^+e^- \to$ hadrons
0.49±0.13	BRANDELIK	78C	DASP	e^+e^-
0.44±0.14	SIEGRIST	76	MRK1	e^+e^-

[13] Reanalysis of data presented in BAI 02C. From a global fit over the center-of-mass energy region 3.7–5.0 GeV covering the $\psi(3770)$, $\psi(4040)$, $\psi(4160)$, and $\psi(4415)$ resonances. Phase angle fixed in the fit to $\delta = (234 \pm 88)^\circ$.

[14] Reanalysis of data presented in BAI 00 and BAI 02C. From a global fit over the center-of-mass energy 3.8-4.8 GeV covering the $\psi(4040)$, $\psi(4160)$ and $\psi(4415)$ resonances and including interference effects. Four sets of solutions are obtained with the same fit quality, mass and total width, but with different e^+e^- partial widths. We quote only the range of values.

[15] From a fit to Crystal Ball (OSTERHELD 86) data.

[16] From a fit to BES (BAI 02C) data.

$\Gamma(\mu^+\mu^-)$ — Γ_{35}

VALUE (keV)	DOCUMENT ID		TECN	COMMENT
1.25±0.28±0.35	[17,18] ABLIKIM	20AG	BES3	$e^+e^- \to \mu^+\mu^-$

[17] From a fit to the $e^+e^- \to \mu^+\mu^-$ cross section between 3.8 and 4.6 GeV to the coherent sum of four resonant amplitudes assuming $\Gamma(\mu^+\mu^-) = \Gamma(e^+e^-)$.

[18] From solution 1 of 8 with equal fit quality. Other solutions range from 1.24 ± 0.28 ± 0.35 to 1.27 ± 0.41 ± 0.36 keV.

$\psi(4415)$ $\Gamma(i) \times \Gamma(e^+e^-)/\Gamma(\text{total})$

$\Gamma(\omega\chi_{c2}) \times \Gamma(e^+e^-)/\Gamma_{\text{total}}$ — $\Gamma_{15}\Gamma_{34}/\Gamma$

VALUE (eV)	DOCUMENT ID		TECN	COMMENT
3.17±0.39±0.24	[19] ABLIKIM	24D	BES3	$e^+e^- \to \omega\gamma J/\psi$

[19] Assuming one single Breit-Wigner resonance in $\omega\chi_{c2}(1P)$ ($\chi_{c2} \to \gamma J/\psi$).

$\Gamma(J/\psi\eta) \times \Gamma(e^+e^-)/\Gamma_{\text{total}}$ — $\Gamma_{20}\Gamma_{34}/\Gamma$

VALUE (eV)	CL%	DOCUMENT ID		TECN	COMMENT
<3.6	90	WANG	13B	BELL	$e^+e^- \to J/\psi\eta\gamma$

$\Gamma(\chi_{c1}\gamma) \times \Gamma(e^+e^-)/\Gamma_{\text{total}}$ — $\Gamma_{21}\Gamma_{34}/\Gamma$

VALUE (eV)	CL%	DOCUMENT ID		TECN	COMMENT
<0.47	90	[20] HAN	15	BELL	10.58 $e^+e^- \to \chi_{c1}\gamma$

[20] Using $B(\eta \to \gamma\gamma) = (39.41 \pm 0.21)\%$.

$\Gamma(\chi_{c2}\gamma) \times \Gamma(e^+e^-)/\Gamma_{\text{total}}$ — $\Gamma_{22}\Gamma_{34}/\Gamma$

VALUE (eV)	CL%	DOCUMENT ID		TECN	COMMENT
<2.3	90	[21] HAN	15	BELL	10.58 $e^+e^- \to \chi_{c2}\gamma$

[21] Using $B(\eta \to \gamma\gamma) = (39.41 \pm 0.21)\%$.

$\Gamma(\Lambda\overline{\Lambda}) \times \Gamma(e^+e^-)/\Gamma_{\text{total}}$ — $\Gamma_{23}\Gamma_{34}/\Gamma$

VALUE (eV)	CL%	DOCUMENT ID		TECN	COMMENT
<1.8 × 10^{-3}	90	[22] ABLIKIM	21AS	BES3	$e^+e^- \to \psi(4415)$

[22] From a measurement of the $e^+e^- \to \Lambda\overline{\Lambda}$ cross section between 3.5 and 4.6 GeV.

$\Gamma(\Sigma^+\overline{\Sigma}^-) \times \Gamma(e^+e^-)/\Gamma_{\text{total}}$ — $\Gamma_{24}\Gamma_{34}/\Gamma$

VALUE (eV)	CL%	DOCUMENT ID		TECN	COMMENT
<62.1 × 10^{-3}	90	[23] ABLIKIM	24AH	BES3	$e^+e^- \to \Sigma^+\overline{\Sigma}^-$

[23] Interference effect between resonance and continuum amplitudes is considered. Two solutions from the fit.

$\Gamma(\Sigma^0\overline{\Sigma}^0) \times \Gamma(e^+e^-)/\Gamma_{\text{total}}$ — $\Gamma_{25}\Gamma_{34}/\Gamma$

VALUE (eV)	CL%	DOCUMENT ID		TECN	COMMENT
<14.0 × 10^{-3}	90	[24] ABLIKIM	25U	BES3	$e^+e^- \to \Sigma^0\overline{\Sigma}^0$

[24] Interference effect between resonance and continuum amplitudes is considered. Upper limit is for the larger of the two solutions from the fit.

$\Gamma(\Xi^0\overline{\Xi}^0) \times \Gamma(e^+e^-)/\Gamma_{\text{total}}$ — $\Gamma_{26}\Gamma_{34}/\Gamma$

VALUE (eV)	CL%	DOCUMENT ID		TECN	COMMENT
<48.0 × 10^{-3}	90	[25] ABLIKIM	24CD	BES3	$e^+e^- \to \psi(4415)$

[25] From a fit to $e^+e^- \to \Xi^0\overline{\Xi}^0$ cross sections.

$\Gamma(\Xi^-\overline{\Xi}^+) \times \Gamma(e^+e^-)/\Gamma_{\text{total}}$ — $\Gamma_{27}\Gamma_{34}/\Gamma$

VALUE (eV)	CL%	DOCUMENT ID		TECN	COMMENT
<21.7 × 10^{-3}	90	[26] ABLIKIM	23BK	BES3	$e^+e^- \to \psi(4415)$

[26] From a fit to $e^+e^- \to \Xi^-\overline{\Xi}^+$ cross sections.

$\Gamma(pK^-\overline{\Lambda}+\text{c.c.}) \times \Gamma(e^+e^-)/\Gamma_{\text{total}}$ — $\Gamma_{28}\Gamma_{34}/\Gamma$

VALUE (eV)	CL%	DOCUMENT ID		TECN	COMMENT
<3.4 × 10^{-3}	90	[27] ABLIKIM	23BL	BES3	$e^+e^- \to \psi(4415)$

[27] From a fit to $e^+e^- \to pK^-\overline{\Lambda}+$ c.c. cross sections.

$\Gamma(\Lambda\overline{\Xi}^+K^-+\text{c.c.}) \times \Gamma(e^+e^-)/\Gamma_{\text{total}}$ — $\Gamma_{29}\Gamma_{34}/\Gamma$

VALUE (eV)	CL%	DOCUMENT ID		TECN	COMMENT
<14.3 × 10^{-3}	90	[28] ABLIKIM	24AL	BES3	$e^+e^- \to \Lambda\overline{\Xi}^+K^-$ + c.c.

[28] A fit to the Born cross section of $e^+e^- \to \Lambda\overline{\Xi}^+K^-$ + c.c. including interference with the continuum. Two solutions from the fit.

$\Gamma(\Sigma^0\overline{\Xi}^+K^-+\text{c.c.}) \times \Gamma(e^+e^-)/\Gamma_{\text{total}}$ — $\Gamma_{30}\Gamma_{34}/\Gamma$

VALUE (eV)	CL%	DOCUMENT ID		TECN	COMMENT
<87.0 × 10^{-3}	90	[29] ABLIKIM	24AL	BES3	$e^+e^- \to \Sigma^0\overline{\Xi}^+K^-$ + c.c.

[29] A fit to the Born cross section of $e^+e^- \to \Sigma^0\overline{\Xi}^+K^-$ + c.c. including interference with the continuum. Two solutions from the fit.

$\Gamma(e^+e^-) \times \Gamma(pK^-K^-\overline{\Xi}^++\text{c.c.})/\Gamma_{\text{total}}$ — $\Gamma_{34}\Gamma_{31}/\Gamma$

VALUE (eV)	CL%	DOCUMENT ID		TECN	COMMENT
<29.4 × 10^{-3}	90	ABLIKIM	25CF	BES3	$e^+e^- \to pK^-K^-\overline{\Xi}^+$ + c.c.

$\psi(4415)$ $\Gamma(i) \times \Gamma(e^+e^-)/\Gamma^2(\text{total})$

$\Gamma(D^0D^{*-}\pi^++\text{c.c.})/\Gamma_{\text{total}} \times \Gamma(e^+e^-)/\Gamma_{\text{total}}$ — $\Gamma_{12}/\Gamma \times \Gamma_{34}/\Gamma$

VALUE	CL%	DOCUMENT ID		TECN	COMMENT
<0.99 × 10^{-6}	90	[30] PAKHLOVA	09	BELL	$e^+e^- \to D^0D^{*-}\pi^+$

[30] Using 4421 ± 4 MeV for the mass of $\psi(4415)$.

$\psi(4415)$ BRANCHING RATIOS

$\Gamma(D^0\overline{D}^0)/\Gamma_{\text{total}}$ — Γ_2/Γ

VALUE	DOCUMENT ID		TECN	COMMENT
seen	[31] ABLIKIM	24BH	BES3	$e^+e^- \to D^0\overline{D}^0$
seen	PAKHLOVA	08	BELL	$e^+e^- \to D^0\overline{D}^0\gamma$
• • • We do not use the following data for averages, fits, limits, etc. • • •				
not seen	AUBERT	09M	BABR	$e^+e^- \to D^0\overline{D}^0\gamma$

[31] A precision measurement of the $e^+e^- \to D^0\overline{D}^0$ cross section shows complex structure in this mass region.

$\Gamma(D^+D^-)/\Gamma_{\text{total}}$ — Γ_3/Γ

VALUE	DOCUMENT ID		TECN	COMMENT
seen	[32] ABLIKIM	24BH	BES3	$e^+e^- \to D^+D^-$
seen	PAKHLOVA	08	BELL	$e^+e^- \to D^+D^-\gamma$
• • • We do not use the following data for averages, fits, limits, etc. • • •				
not seen	AUBERT	09M	BABR	$e^+e^- \to D^+D^-\gamma$

[32] A precision measurement of the $e^+e^- \to D^+D^-$ cross section shows complex structure in this mass region.

$\Gamma(D^*(2007)^0\overline{D}^0+\text{c.c.})/\Gamma_{\text{total}}$ — Γ_5/Γ

VALUE	DOCUMENT ID		TECN	COMMENT
seen	AUBERT	09M	BABR	$e^+e^- \to D^{*0}\overline{D}^0\gamma$

$\Gamma(D^*(2010)^+D^-+\text{c.c.})/\Gamma_{\text{total}}$ — Γ_6/Γ

VALUE	DOCUMENT ID		TECN	COMMENT
seen	[33] ZHUKOVA	18	BELL	$e^+e^- \to D^{*+}D^-\gamma$
seen	AUBERT	09M	BABR	$e^+e^- \to D^{*+}D^-\gamma$
• • • We do not use the following data for averages, fits, limits, etc. • • •				
seen	PAKHLOVA	07	BELL	$e^+e^- \to D^{*+}D^-\gamma$

[33] Supersedes PAKHLOVA 07.

$\Gamma(D\overline{D})/\Gamma(D^*\overline{D}^*)$ — Γ_1/Γ_7

VALUE	DOCUMENT ID		TECN	COMMENT
0.14±0.12±0.03	AUBERT	09M	BABR	$e^+e^- \to \gamma D^{(*)}\overline{D}^{(*)}$

$\Gamma(D^*\overline{D}+\text{c.c.})/\Gamma(D^*\overline{D}^*)$ — Γ_4/Γ_7

VALUE	DOCUMENT ID		TECN	COMMENT
0.17±0.25±0.03	AUBERT	09M	BABR	$e^+e^- \to \gamma D^{(*)}\overline{D}^{(*)}$

$\Gamma(D^*(2007)^0\overline{D}^*(2007)^0+\text{c.c.})/\Gamma_{\text{total}}$ — Γ_8/Γ

VALUE	DOCUMENT ID		TECN	COMMENT
seen	AUBERT	09M	BABR	$e^+e^- \to D^{*0}\overline{D}^{*0}\gamma$

$\Gamma(D^*(2010)^+D^*(2010)^-+\text{c.c.})/\Gamma_{\text{total}}$ — Γ_9/Γ

VALUE	DOCUMENT ID		TECN	COMMENT
seen	[34] ZHUKOVA	18	BELL	$e^+e^- \to D^{*+}D^{*-}\gamma$
seen	AUBERT	09M	BABR	$e^+e^- \to D^{*+}D^{*-}\gamma$
• • • We do not use the following data for averages, fits, limits, etc. • • •				
seen	PAKHLOVA	07	BELL	$e^+e^- \to D^{*+}D^{*-}\gamma$

[34] Supersedes PAKHLOVA 07.

$\Gamma(D\overline{D}_2^*(2460) \to D^0D^-\pi^++\text{c.c.})/\Gamma_{\text{total}}$ — Γ_{11}/Γ

VALUE (units 10^{-2})	DOCUMENT ID		TECN	COMMENT
10.5±2.4±3.8	[35] PAKHLOVA	08A	BELL	10.6 $e^+e^- \to D^0D^-\pi^+\gamma$

[35] Using 4421 ± 4 MeV for the mass and 62 ± 20 MeV for the width of $\psi(4415)$.

Int. J. Mod. Phys. A 2026.41. Downloaded from www.worldscientific.com by UNIVERSITY OF CALIFORNIA @ BERKELEY on 09/16/26. Re-use and distribution is strictly not permitted, except for Open Access articles.

$\Gamma(D^0 D^- \pi^+$ (excl. $D^*(2010)^+ D^-$ +c.c.)$/\Gamma(D\overline{D}_2^*(2460) \to D^0 D^- \pi^+$ +c.c.) — Γ_{10}/Γ_{11}

VALUE	CL%	DOCUMENT ID		TECN	COMMENT
<0.22	90	[36] PAKHLOVA	08A	BELL	10.6 $e^+e^- \to D^0 D^- \pi^+ \gamma$

[36] Using 4421 ± 4 MeV for the mass and 62 ± 20 MeV for the width of $\psi(4415)$.

$\Gamma(D_1(2420)\overline{D}$ + c.c.$)/\Gamma_{total}$ — Γ_{13}/Γ

VALUE	DOCUMENT ID		TECN	COMMENT
possibly seen	[37] ABLIKIM	19AR	BES3	$e^+e^- \to \pi^+\pi^- D\overline{D}$

[37] Evidence for $e^+e^- \to D_1(2420)\overline{D}$ + c.c. between $\sqrt{s}$ = 4.3 and 4.6 GeV, not necessarily resonant.

$\Gamma(D_s^+ D_s^-)/\Gamma_{total}$ — Γ_{14}/Γ

VALUE	DOCUMENT ID		TECN	COMMENT
not seen	PAKHLOVA	11	BELL	$e^+e^- \to D_s^+ D_s^- \gamma$
not seen	DEL-AMO-SA...	10N	BABR	$e^+e^- \to D_s^+ D_s^- \gamma$

$\Gamma(D_s^{*+} D_s^-$ +c.c.$)/\Gamma_{total}$ — Γ_{16}/Γ

VALUE	DOCUMENT ID		TECN	COMMENT
seen	PAKHLOVA	11	BELL	$e^+e^- \to D_s^{*+} D_s^- \gamma$
seen	DEL-AMO-SA...	10N	BABR	$e^+e^- \to D_s^{*+} D_s^- \gamma$

$\Gamma(D_s^{*+} D_s^{*-})/\Gamma_{total}$ — Γ_{17}/Γ

VALUE	DOCUMENT ID		TECN	COMMENT
seen	ABLIKIM	23BH	BES3	$e^+e^- \to D_s^{*+} D_s^{*-}$
• • • We do not use the following data for averages, fits, limits, etc. • • •				
not seen	PAKHLOVA	11	BELL	$e^+e^- \to D_s^{*+} D_s^{*-} \gamma$
not seen	DEL-AMO-SA...	10N	BABR	$e^+e^- \to D_s^{*+} D_s^{*-} \gamma$

$\Gamma(\psi_2(3823)\pi^+\pi^-)/\Gamma_{total}$ — Γ_{18}/Γ

VALUE	EVTS	DOCUMENT ID		TECN	COMMENT
possibly seen	19	[38] ABLIKIM	15S	BES3	$e^+e^- \to \pi^+\pi^- \chi_{c1}\gamma$

[38] From a fit of $e^+e^- \to \pi^+\pi^-\psi_2(3823)$, $\psi_2(3823) \to \chi_{c1}\gamma$ cross sections taken at $\sqrt{s}$ values of 4.23, 4.26, 4.36, 4.42, and 4.60 GeV to the $\psi(4415)$ line shape.

$\Gamma(\psi(3770)\pi^+\pi^-)/\Gamma_{total}$ — Γ_{19}/Γ

VALUE	DOCUMENT ID		TECN	COMMENT
possibly seen	[39] ABLIKIM	19AR	BES3	$e^+e^- \to \pi^+\pi^- D\overline{D}$

[39] Observe $e^+e^- \to \pi^+\pi^-\psi(3770)$ at $\sqrt{s}$ = 4.26, 4.36, and 4.42 GeV but cannot establish if continuum or resonant.

$\Gamma(\omega\pi^0)/\Gamma_{total}$ — Γ_{32}/Γ

VALUE	DOCUMENT ID		TECN	COMMENT
not seen	ABLIKIM	22K	BES3	$e^+e^- \to \omega\pi^0$

$\Gamma(\omega\eta)/\Gamma_{total}$ — Γ_{33}/Γ

VALUE	DOCUMENT ID		TECN	COMMENT
not seen	ABLIKIM	22K	BES3	$e^+e^- \to \omega\eta$

$\psi(4415)$ REFERENCES

ABLIKIM	25CF	JHEP 2511 111	M. Ablikim *et al.*	(BESIII Collab.)
ABLIKIM	25U	PR D111 L051502	M. Ablikim *et al.*	(BESIII Collab.)
ABLIKIM	24AH	JHEP 2405 022	M. Ablikim *et al.*	(BESIII Collab.)
ABLIKIM	24AL	JHEP 2407 258	M. Ablikim *et al.*	(BESIII Collab.)
ABLIKIM	24BH	PRL 133 081901	M. Ablikim *et al.*	(BESIII Collab.)
ABLIKIM	24CD	JHEP 2411 062	M. Ablikim *et al.*	(BESIII Collab.)
ABLIKIM	24D	PRL 132 161901	M. Ablikim *et al.*	(BESIII Collab.)
ABLIKIM	23BH	PRL 131 151903	M. Ablikim *et al.*	(BESIII Collab.)
ABLIKIM	23BK	JHEP 2311 228	M. Ablikim *et al.*	(BESIII Collab.)
ABLIKIM	23BL	JHEP 2312 027	M. Ablikim *et al.*	(BESIII Collab.)
ABLIKIM	22K	JHEP 2207 064	M. Ablikim *et al.*	(BESIII Collab.)
ABLIKIM	21AS	PR D104 L091104	M. Ablikim *et al.*	(BESIII Collab.)
ABLIKIM	20AG	PR D102 112009	M. Ablikim *et al.*	(BESIII Collab.)
ABLIKIM	19AR	PR D100 032005	M. Ablikim *et al.*	(BESIII Collab.)
ZHUKOVA	18	PR D97 012002	V. Zhukova *et al.*	(BELLE Collab.)
ABLIKIM	15S	PRL 115 011803	M. Ablikim *et al.*	(BESIII Collab.)
HAN	15	PR D92 012011	Y.L. Han *et al.*	(BELLE Collab.)
WANG	13B	PR D87 051101	X.L. Wang *et al.*	(BELLE Collab.)
PAKHLOVA	11	PR D83 011101	G. Pakhlova *et al.*	(BELLE Collab.)
DEL-AMO-SA...	10N	PR D82 052004	P. del Amo Sanchez *et al.*	(BABAR Collab.)
MO	10	PR D82 077501	X.H. Mo, C.Z. Yuan, P. Wang	(BHEP)
AUBERT	09M	PR D79 092001	B. Aubert *et al.*	(BABAR Collab.)
PAKHLOVA	09	PR D80 091101	G. Pakhlova *et al.*	(BELLE Collab.)
ABLIKIM	08D	PL B660 315	M. Ablikim *et al.*	(BES Collab.)
PAKHLOVA	08	PR D77 011103	G. Pakhlova *et al.*	(BELLE Collab.)
PAKHLOVA	08A	PRL 100 062001	G. Pakhlova *et al.*	(BELLE Collab.)
PAKHLOVA	07	PRL 98 092001	G. Pakhlova *et al.*	(BELLE Collab.)
SETH	05A	PR D72 017501	K.K. Seth	
BAI	02C	PRL 88 101802	J.Z. Bai *et al.*	(BES Collab.)
BAI	00	PRL 84 594	J.Z. Bai *et al.*	(BES Collab.)
OSTERHELD	86	SLAC-PUB-4160	A. Osterheld *et al.*	(SLAC Crystal Ball Collab.)
BRANDELIK	78C	PL 76B 361	R. Brandelik *et al.*	(DASP Collab.)
SIEGRIST	76	PRL 36 700	J.L. Siegrist *et al.*	(LBL, SLAC)

$\chi_{c0}(4500)$

$I^G(J^{PC}) = 0^+(0^{++})$

was $X(4500)$

See the review on the "Spectroscopy of Mesons Containing two Heavy Quarks."

$\chi_{c0}(4500)$ MASS

VALUE (MeV)	EVTS	DOCUMENT ID		TECN	COMMENT
4484 ±12 OUR AVERAGE		Error includes scale factor of 3.4. See the ideogram below.			
$4512.5^{+6.0}_{-6.2}{}^{+3.2}_{-2.7}$		[1] AAIJ	25B	LHCB	$pp \to p(J/\psi\phi)p$
4475 ± 7 ±12		AAIJ	25Q	LHCB	$B^+ \to \psi(2S)K^+\pi^+\pi^-$
4474 ± 3 ± 3	24k	[2] AAIJ	21E	LHCB	$B^+ \to J/\psi\phi K^+$
• • • We do not use the following data for averages, fits, limits, etc. • • •					
4506 ±11 $^{+12}_{-15}$	4289	[3,4] AAIJ	17C	LHCB	$B^+ \to J/\psi\phi K^+$

[1] From a fit using the five resonances reported in AAIJ 21E, described by relativistic Breit-Wigner distributions.
[2] From an amplitude analysis of the decay $B^+ \to J/\psi\phi K^+$ with a significance of 20 σ.
[3] From an amplitude analysis of the decay $B^+ \to J/\psi\phi K^+$ with a significance of 6.1 σ.
[4] Superseded by AAIJ 21E.

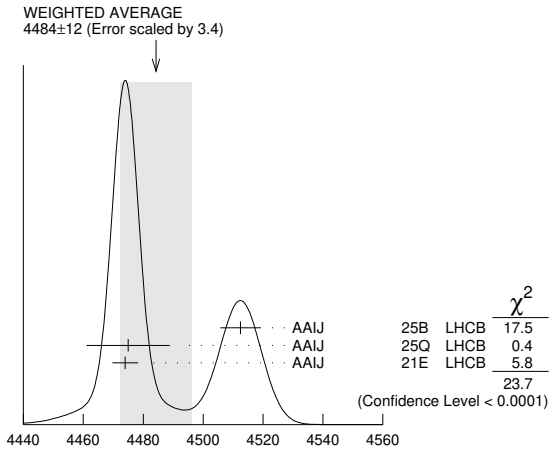

$\chi_{c0}(4500)$ WIDTH

VALUE (MeV)	EVTS	DOCUMENT ID		TECN	COMMENT
87^{+30}_{-24} OUR AVERAGE		Error includes scale factor of 2.9. See the ideogram below.			
$65^{+20}_{-16}{}^{+24}_{-9}$		[1] AAIJ	25B	LHCB	$pp \to p(J/\psi\phi)p$
231±19±32		AAIJ	25Q	LHCB	$B^+ \to \psi(2S)K^+\pi^+\pi^-$
77± $^{+10}_{-8}$	24k	[2] AAIJ	21E	LHCB	$B^+ \to J/\psi\phi K^+$
• • • We do not use the following data for averages, fits, limits, etc. • • •					
92±21$^{+21}_{-20}$	4289	[3,4] AAIJ	17C	LHCB	$B^+ \to J/\psi\phi K^+$

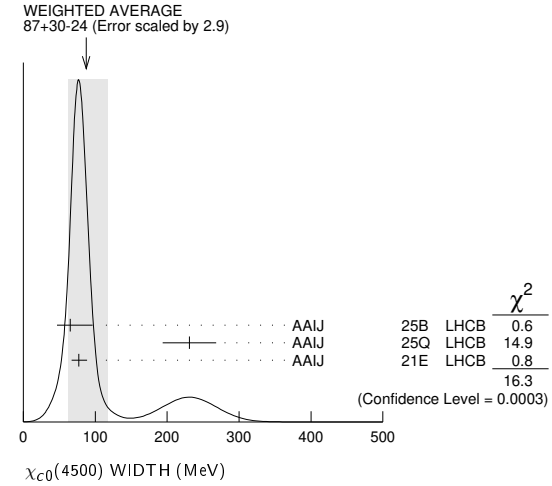

Int. J. Mod. Phys. A 2026.41. Downloaded from www.worldscientific.com by CALIFORNIA @ BERKELEY on 09/16/26. Re-use and distribution is strictly not permitted, except for Open Access articles.

[1] From a fit using the five resonances reported in AAIJ 21E, described by relativistic Breit-Wigner distributions.
[2] From an amplitude analysis of the decay $B^+ \to J/\psi\phi K^+$ with a significance of 20 σ.
[3] From an amplitude analysis of the decay $B^+ \to J/\psi\phi K^+$ with a significance of 6.1 σ.
[4] Superseded by AAIJ 21E.

$\chi_{c0}(4500)$ DECAY MODES

	Mode	Fraction (Γ_i/Γ)
Γ_1	$J/\psi\phi$	seen
Γ_2	$\psi(2S)\pi^+\pi^-$	seen

$\chi_{c0}(4500)$ BRANCHING RATIOS

$\Gamma(J/\psi\phi)/\Gamma_{total}$ — Γ_1/Γ

VALUE	EVTS	DOCUMENT ID		TECN	COMMENT
seen	24k	[1] AAIJ	21E	LHCB	$B^+ \to J/\psi\phi K^+$
• • • We do not use the following data for averages, fits, limits, etc. • • •					
seen	4289	[2,3] AAIJ	17C	LHCB	$B^+ \to J/\psi\phi K^+$

[1] From an amplitude analysis of the decay $B^+ \to J/\psi\phi K^+$ with a significance of 20 σ.
[2] From an amplitude analysis of the decay $B^+ \to J/\psi\phi K^+$ with a significance of 6.1 σ.
[3] Superseded by AAIJ 21E.

$\Gamma(\psi(2S)\pi^+\pi^-)/\Gamma_{total}$ — Γ_2/Γ

VALUE	DOCUMENT ID		TECN	COMMENT
seen	AAIJ	25Q	LHCB	$B^+ \to \psi(2S)K^+\pi^+\pi^-$

$\chi_{c0}(4500)$ REFERENCES

AAIJ	25B	PRL 134 031902	R. Aaij *et al.*	(LHCb Collab.)
AAIJ	25Q	JHEP 2501 054	R. Aaij *et al.*	(LHCb Collab.)
AAIJ	21E	PRL 127 082001	R. Aaij *et al.*	(LHCb Collab.)
AAIJ	17C	PRL 118 022003	R. Aaij *et al.*	(LHCb Collab.) JP
Also		PR D95 012002	R. Aaij *et al.*	(LHCb Collab.)

$X(4630)$

$I^G(J^{PC}) = 0^+(?^{?+})$

OMITTED FROM SUMMARY TABLE

This state shows properties different from a conventional $q\overline{q}$ state. A candidate for an exotic structure. See the review on "Heavy Non-$q\overline{q}$ Mesons."

Seen by AAIJ 21E in $B^+ \to X(4630)K^+$ with $X(4630) \to J/\psi\phi$ using an amplitude analysis of $B^+ \to J/\psi\phi K^+$ with a significance (accounting for systematic uncertainties) of 5.5 σ. The $J^P = 1^-$ assignment is favored over 2^- with a significance of 3 σ and other assignments are disfavored by more than 5 σ.

$X(4630)$ MASS

VALUE (MeV)	EVTS	DOCUMENT ID		TECN	COMMENT
4636^{+29}_{-100} OUR AVERAGE		Error includes scale factor of 1.2.			
$4785 \pm 37 \pm 119$		[1] AAIJ	25Q	LHCB	$B^+ \to \psi(2S)K^+\pi^+\pi^-$
$4626 \pm 16^{+18}_{-110}$	24k	[2] AAIJ	21E	LHCB	$B^+ \to J/\psi\phi K^+$

[1] $J^P = 1^-$.
[2] From an amplitude analysis of the decay $B^+ \to J/\psi\phi K^+$ with a significance of 5.5 σ.

$X(4630)$ WIDTH

VALUE (MeV)	EVTS	DOCUMENT ID		TECN	COMMENT
350^{+140}_{-100} OUR AVERAGE		Error includes scale factor of 1.6.			
$457 \pm 93 \pm 57$		[1] AAIJ	25Q	LHCB	$B^+ \to \psi(2S)K^+\pi^+\pi^-$
$174 \pm 27^{+134}_{-73}$	24k	[2] AAIJ	21E	LHCB	$B^+ \to J/\psi\phi K^+$

[1] $J^P = 1^-$.
[2] From an amplitude analysis of the decay $B^+ \to J/\psi\phi K^+$ with a significance of 5.5 σ.

$X(4630)$ DECAY MODES

	Mode	Fraction (Γ_i/Γ)
Γ_1	$J/\psi\phi$	seen
Γ_2	$\psi(2S)\pi^+\pi^-$	seen

$X(4630)$ BRANCHING RATIOS

$\Gamma(J/\psi\phi)/\Gamma_{total}$ — Γ_1/Γ

VALUE	EVTS	DOCUMENT ID		TECN	COMMENT
seen	24k	[1] AAIJ	21E	LHCB	$B^+ \to J/\psi\phi K^+$

[1] From an amplitude analysis of the decay $B^+ \to J/\psi\phi K^+$ with a significance of 5.5 σ.

$\Gamma(\psi(2S)\pi^+\pi^-)/\Gamma_{total}$ — Γ_2/Γ

VALUE	DOCUMENT ID		TECN	COMMENT
seen	AAIJ	25Q	LHCB	$B^+ \to \psi(2S)K^+\pi^+\pi^-$

$X(4630)$ REFERENCES

AAIJ	25Q	JHEP 2501 054	R. Aaij *et al.*	(LHCb Collab.)
AAIJ	21E	PRL 127 082001	R. Aaij *et al.*	(LHCb Collab.)

$\psi(4660)$

$I^G(J^{PC}) = 0^-(1^{--})$

also known as $Y(4660)$; was $X(4660)$

See the reviews on the "Spectroscopy of Mesons Containing two Heavy Quarks" and on "Heavy Non-qqbar Mesons."

$\psi(4660)$ MASS

VALUE (MeV)	EVTS	DOCUMENT ID		TECN	COMMENT
4623 ± 10 OUR AVERAGE		Error includes scale factor of 3.7. See the ideogram below.			
$4603.1 \pm 3.9 \pm 0.8$		[1] ABLIKIM	24BN	BES3	$e^+e^- \to D_s^+ D_{s2}^*(2573)^-$
$4584 \pm 14 \pm 80$		[2] ABLIKIM	24BN	BES3	$e^+e^- \to D_s^+ D_{s1}(2536)^-$
$4708 {}^{+17}_{-15} \pm 21$		[3] ABLIKIM	23BI	BES3	$e^+e^- \to K^+K^-J/\psi$
$4701.8 \pm 10.9 \pm 2.7$		[4] ABLIKIM	23H	BES3	$e^+e^- \to \phi\chi_{c2}$
$4675.3 \pm 29.5 \pm 3.5$		[5] ABLIKIM	23X	BES3	$e^+e^- \to D^{*0}D^{*-}\pi^+$
$4651.0 \pm 37.8 \pm 2.1$		[6] ABLIKIM	21AJ	BES3	$e^+e^- \to \pi^+\pi^-\psi(2S)$
$4619.8^{+8.9}_{-8.0} \pm 2.3$	66	[7] JIA	20	BELL	$e^+e^- \to \gamma D_s^+ D_{s2}^*(2573)^-$
$4625.9^{+6.2}_{-6.0} \pm 0.4$	89	[8] JIA	19A	BELL	$e^+e^- \to \gamma D_s^+ D_{s1}(2536)^-$
$4652 \pm 10 \pm 11$	279	[9] WANG	15A	BELL	10.58 $e^+e^- \to \gamma\pi^+\pi^-\psi(2S)$
$4669 \pm 21 \pm 3$	37	[10] LEES	14F	BABR	10.58 $e^+e^- \to \gamma\pi^+\pi^-\psi(2S)$
$4634 {}^{+8}_{-7} {}^{+5}_{-8}$	142	[11] PAKHLOVA	08B	BELL	$e^+e^- \to \Lambda_c^+\Lambda_c^-$
• • • We do not use the following data for averages, fits, limits, etc. • • •					
$4647.9 \pm 8.6 \pm 0.8$		[12] ABLIKIM	22R	BES3	$e^+e^- \to \pi^+\pi^-\chi_{c1}\gamma$
$4652.5 \pm 3.4 \pm 1.1$		[13] DAI	17	RVUE	$e^+e^- \to \Lambda_c^+\Lambda_c^-$
$4645.2 \pm 9.5 \pm 6.0$		[14] ZHANG	17B	RVUE	$e^+e^- \to \pi^+\pi^-\psi(2S)$
$4646.4 \pm 9.7 \pm 4.8$		[15] ZHANG	17C	RVUE	$e^+e^- \to \pi^+\pi^-J/\psi$ or $\psi(2S)$
$4661 {}^{+9}_{-8} \pm 6$	44	[16] LIU	08H	RVUE	10.58 $e^+e^- \to \gamma\pi^+\pi^-\psi(2S)$
$4664 \pm 11 \pm 5$	44	WANG	07D	BELL	10.58 $e^+e^- \to \gamma\pi^+\pi^-\psi(2S)$

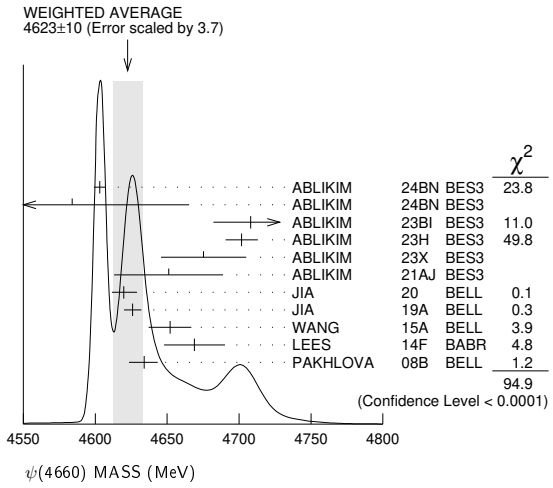

[1] Extracted in a fit that employs two BW resonances. The second one at about 4720 MeV shows low statistical significance of 2.7 σ.
[2] Extracted from a fit with two BW functions. The second one located at about 4750 MeV show a low statistical significance of 4.3 σ.
[3] Seen as a peak in the c.m. energy dependence of the $e^+e^- \to K^+K^-J/\psi$ cross section using 5.85 fb^{-1} of data at c.m. energies 4.61–4.95 GeV. Statistical significance is over 5σ.
[4] Fit model parameterized as the coherent sum of a Breit-Wigner resonance and a continuum amplitude term.
[5] From a cross-section measurement of $e^+e^- \to D^{*0}D^{*-}\pi^+$ between 4.189 and 4.951 GeV, assuming a coherent sum of 3 Breit-Wigner resonances plus a continuum amplitude. The two other resonances have masses (widths) 4209.6 ± 7.5 (81.6 ± 19.9) MeV and 4469.1 ± 26.4 (246.3 ± 37.9) MeV.
[6] From a three-resonance fit to the Born cross section in the range $\sqrt{s}$ = 4.008–4.698 GeV.
[7] Using $D_{s2}^*(2573)^- \to \overline{D}^0K^-$ decays.

Int. J. Mod. Phys. A 2026.41. Downloaded from www.worldscientific.com
by UNIVERSITY OF CALIFORNIA @ BERKELEY on 09/16/26. Re-use and distribution is strictly not permitted, except for Open Access articles.

[8] From a fit of a Breit-Wigner convolved with a Gaussian.
[9] From a two-resonance fit. Supersedes WANG 07D.
[10] From a two-resonance fit.
[11] The $\pi^+\pi^-\psi(2S)$ and $\Lambda_c^+\Lambda_c^-$ states are not necessarily the same.
[12] From a fit to the $e^+e^- \to \pi^+\pi^-\psi(3823)$ cross section between 4.23 and 4.70 GeV with two coherent Breit-Wigner resonances. The data is also consistent with a single peak with mass 4417.5 ± 26.2 ± 3.5 MeV and width 245 ± 48 ± 13 MeV.
[13] The pole parameters are extracted from the speed plot.
[14] From a three-resonance fit.
[15] From a combined fit of BELLE, BABAR and BES3 $e^+e^- \to \pi^+\pi^- J/\psi$ and $e^+e^- \to \pi^+\pi^-\psi(2S)$ data.
[16] From a combined fit of AUBERT 07S and WANG 07D data with two resonances.

$\psi(4660)$ WIDTH

VALUE (MeV)	EVTS	DOCUMENT ID		TECN	COMMENT
55 ± 9 OUR AVERAGE		Error includes scale factor of 1.9. See the ideogram below.			
57 ±12 ±219		[1] ABLIKIM	24BN	BES3	$e^+e^- \to D_s^+ D_{s1}(2536)^-$
45.2± 5.7± 0.7		[2] ABLIKIM	24BN	BES3	$e^+e^- \to D_s^+ D_{s2}^*(2573)^-$
126 $^{+27}_{-23}$ ± 30		[3] ABLIKIM	23BI	BES3	$e^+e^- \to K^+K^- J/\psi$
30.5±22.3± 14.6		[4] ABLIKIM	23H	BES3	$e^+e^- \to \phi\chi_{c2}$
218.3±72.9± 9.3		[5] ABLIKIM	23X	BES3	$e^+e^- \to D^{*0}D^{*-}\pi^+$
155.4±24.8± 0.8		[6] ABLIKIM	21AJ	BES3	$e^+e^- \to \pi^+\pi^-\psi(2S)$
47.0 $^{+31.3}_{-14.8}$ ± 4.6	66	[7] JIA	20	BELL	$e^+e^- \to \gamma D_s^+ D_{s2}^*(2573)^-$
49.8 $^{+13.9}_{-11.5}$ ± 4.0	89	[8] JIA	19A	BELL	$e^+e^- \to \gamma D_s^+ D_{s1}(2536)^-$
68 ±11 ± 5	279	[9] WANG	15A	BELL	10.58 $e^+e^- \to \gamma\pi^+\pi^-\psi(2S)$
104 ±48 ± 10	37	[10] LEES	14F	BABR	10.58 $e^+e^- \to \gamma\pi^+\pi^-\psi(2S)$
92 $^{+40}_{-24}$ ± 10 ± 21	142	[11] PAKHLOVA	08B	BELL	$e^+e^- \to \Lambda_c^+\Lambda_c^-$
• • • We do not use the following data for averages, fits, limits, etc. • • •					
33.1±18.6± 4.1		[12] ABLIKIM	22R	BES3	$e^+e^- \to \pi^+\pi^-\chi_{c1}\gamma$
62.6± 5.6± 4.3		[13] DAI	17	RVUE	$e^+e^- \to \Lambda_c^+\Lambda_c^-$
113.8±18.1± 3.4		[14] ZHANG	17B	RVUE	$e^+e^- \to \pi^+\pi^-\psi(2S)$
103.5±15.6± 4.0		[15] ZHANG	17C	RVUE	$e^+e^- \to \pi^+\pi^- J/\psi$ or $\psi(2S)$
42 $^{+17}_{-12}$ ± 6	44	[16] LIU	08H	RVUE	10.58 $e^+e^- \to \gamma\pi^+\pi^-\psi(2S)$
48 ±15 ± 3	44	WANG	07D	BELL	10.58 $e^+e^- \to \gamma\pi^+\pi^-\psi(2S)$

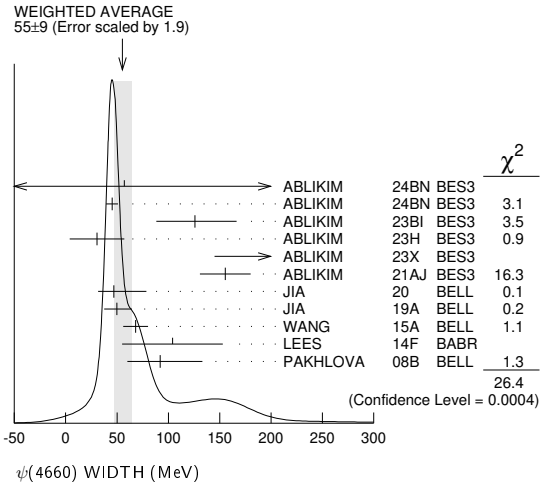

[1] Extracted from a fit with two BW functions. The second one located at about 4750 MeV show a low statistical significance of 4.3 σ.
[2] Extracted in a fit that employs two BW resonances. The second one at about 4720 MeV shows low statistical significance of 2.7 σ.
[3] Seen as a peak in the c.m. energy dependence of the $e^+e^- \to K^+K^- J/\psi$ cross section using 5.85 fb^{-1} of data at c.m. energies 4.61–4.95 GeV. Statistical significance is over 5σ.
[4] Fit model parameterized as the coherent sum of a Breit-Wigner resonance and a continuum amplitude term.
[5] From a cross-section measurement of $e^+e^- \to D^{*0}D^{*-}\pi^+$ between 4.189 and 4.951 GeV, assuming a coherent sum of 3 Breit-Wigner resonances plus a continuum amplitude. The two other resonances have masses (widths) 4209.6 ± 7.5 (81.6 ± 19.9) MeV and 4469.1 ± 26.4 (246.3 ± 37.9) MeV.
[6] From a three-resonance fit to the Born cross section in the range $\sqrt{s}$ = 4.008–4.698 GeV.
[7] Using $D_{s2}^*(2573)^- \to \overline{D}^0 K^-$ decays.
[8] From a fit of a Breit-Wigner convolved with a Gaussian.
[9] From a two-resonance fit. Supersedes WANG 07D.
[10] From a two-resonance fit.
[11] The $\pi^+\pi^-\psi(2S)$ and $\Lambda_c^+\Lambda_c^-$ states are not necessarily the same.
[12] From a fit to the $e^+e^- \to \pi^+\pi^-\psi(3823)$ cross section between 4.23 and 4.70 GeV with two coherent Breit-Wigner resonances. The data is also consistent with a single peak with mass 4417.5 ± 26.2 ± 3.5 MeV and width 245 ± 48 ± 13 MeV.
[13] The pole parameters are extracted from the speed plot.
[14] From a three-resonance fit.
[15] From a combined fit of BELLE, BABAR and BES3 $e^+e^- \to \pi^+\pi^- J/\psi$ and $e^+e^- \to \pi^+\pi^-\psi(2S)$ data.
[16] From a combined fit of AUBERT 07S and WANG 07D data with two resonances.

$\psi(4660)$ DECAY MODES

	Mode	Fraction (Γ_i/Γ)
Γ_1	e^+e^-	not seen
Γ_2	$\psi(2S)\pi^+\pi^-$	seen
Γ_3	$J/\psi\eta$	not seen
Γ_4	$D^0D^{*-}\pi^+$	not seen
Γ_5	$D^{*0}D^{*-}\pi^+$	seen
Γ_6	$\psi_2(3823)\pi^+\pi^-$	seen
Γ_7	$\chi_{c0}\phi$	not seen
Γ_8	$\chi_{c1}\gamma$	not seen
Γ_9	$\chi_{c1}\phi$	not seen
Γ_{10}	$\chi_{c2}\gamma$	not seen
Γ_{11}	$\chi_{c2}\phi$	seen
Γ_{12}	$\Lambda_c^+\Lambda_c^-$	seen
Γ_{13}	$D_s^+D_{s1}(2536)^-$	seen
Γ_{14}	$D_s^+D_{s2}^*(2573)^-$	seen
Γ_{15}	$\omega\pi^0$	not seen
Γ_{16}	$\omega\eta$	not seen
Γ_{17}	$\Sigma^+\overline{\Sigma}^-$	not seen
Γ_{18}	$\Sigma^0\overline{\Sigma}^0$	
Γ_{19}	$\Xi^0\overline{\Xi}^0$	not seen
Γ_{20}	$\Xi^-\overline{\Xi}^+$	not seen
Γ_{21}	$pK^-\overline{\Lambda}$ + c.c.	not seen
Γ_{22}	$\Lambda\overline{\Xi}^+K^-$ + c.c.	not seen
Γ_{23}	$\Sigma^0\overline{\Xi}^+K^-$ + c.c.	not seen
Γ_{24}	$pK^-K^-\overline{\Xi}^+$ + c.c.	

$\psi(4660)$ $\Gamma(i) \times \Gamma(e^+e^-)/\Gamma(\text{total})$

$\Gamma(\psi(2S)\pi^+\pi^-) \times \Gamma(e^+e^-)/\Gamma_{\text{total}}$ — $\Gamma_2\Gamma_1/\Gamma$

VALUE (eV)	EVTS	DOCUMENT ID		TECN	COMMENT
• • • We do not use the following data for averages, fits, limits, etc. • • •					
4.7±3.8		[1] ABLIKIM	21AJ	BES3	$e^+e^- \to \pi^+\pi^-\psi(2S)$
11.2±3.2		[2] ABLIKIM	21AJ	BES3	$e^+e^- \to \pi^+\pi^-\psi(2S)$
4.7±4.2		[3] ABLIKIM	21AJ	BES3	$e^+e^- \to \pi^+\pi^-\psi(2S)$
11.3±3.3		[4] ABLIKIM	21AJ	BES3	$e^+e^- \to \pi^+\pi^-\psi(2S)$
2.0±0.3±0.2	279	[5] WANG	15A	BELL	10.58 $e^+e^- \to \gamma\pi^+\pi^-\psi(2S)$
8.1±1.1±1.0	279	[6] WANG	15A	BELL	10.58 $e^+e^- \to \gamma\pi^+\pi^-\psi(2S)$
2.7±1.3±0.5	37	[7] LEES	14F	BABR	10.58 $e^+e^- \to \gamma\pi^+\pi^-\psi(2S)$
7.5±1.7±0.7	37	[8] LEES	14F	BABR	10.58 $e^+e^- \to \gamma\pi^+\pi^-\psi(2S)$
2.2 $^{+0.7}_{-0.6}$	44	[9] LIU	08H	RVUE	10.58 $e^+e^- \to \gamma\pi^+\pi^-\psi(2S)$
5.9±1.6	44	[10] LIU	08H	RVUE	10.58 $e^+e^- \to \gamma\pi^+\pi^-\psi(2S)$
3.0±0.9±0.3	44	[7] WANG	07D	BELL	10.58 $e^+e^- \to \gamma\pi^+\pi^-\psi(2S)$
7.6±1.8±0.8	44	[8] WANG	07D	BELL	10.58 $e^+e^- \to \gamma\pi^+\pi^-\psi(2S)$

[1] Solution I of four equivalent solutions in a fit using three interfering resonances.
[2] Solution II of four equivalent solutions in a fit using three interfering resonances.
[3] Solution III of four equivalent solutions in a fit using three interfering resonances.
[4] Solution IV of four equivalent solutions in a fit using three interfering resonances.
[5] Solution I of two equivalent solutions from a fit using two interfering resonances. Supersedes WANG 07D.
[6] Solution II of two equivalent solutions from a fit using two interfering resonances. Supersedes WANG 07D.
[7] Solution I of two equivalent solutions in a fit using two interfering resonances.
[8] Solution II of two equivalent solutions in a fit using two interfering resonances.
[9] Solution I in a combined fit of AUBERT 07S and WANG 07D data with two resonances.
[10] Solution II in a combined fit of AUBERT 07S and WANG 07D data with two resonances.

$\Gamma(J/\psi\eta) \times \Gamma(e^+e^-)/\Gamma_{\text{total}}$ — $\Gamma_3\Gamma_1/\Gamma$

VALUE (eV)	CL%	DOCUMENT ID		TECN	COMMENT
• • • We do not use the following data for averages, fits, limits, etc. • • •					
<0.94	90	WANG	13B	BELL	$e^+e^- \to J/\psi\eta\gamma$

$\Gamma(D^{*0}D^{*-}\pi^+) \times \Gamma(e^+e^-)/\Gamma_{\text{total}}$ — $\Gamma_5\Gamma_1/\Gamma$

VALUE (eV)	DOCUMENT ID		TECN	COMMENT
• • • We do not use the following data for averages, fits, limits, etc. • • •				
19 to 2005	[1] ABLIKIM	23X	BES3	$e^+e^- \to D^{*0}D^{*-}\pi^+$

[1] From a cross-section measurement of $e^+e^- \to D^{*0}D^{*-}\pi^+$ between 4.189 and 4.951 GeV, assuming a coherent sum of 3 Breit-Wigner resonances plus a continuum amplitude. Depending on solutions I – VIII with same fit qualities.

$\Gamma(\chi_{c0}\phi) \times \Gamma(e^+e^-)/\Gamma_{total}$ — $\Gamma_7\Gamma_1/\Gamma$

VALUE (eV)	CL%	DOCUMENT ID		TECN	COMMENT
<0.35	90	ABLIKIM	25J	BES3	$e^+e^- \to \phi\chi_{c0}$

$\Gamma(\chi_{c1}\gamma) \times \Gamma(e^+e^-)/\Gamma_{total}$ — $\Gamma_8\Gamma_1/\Gamma$

VALUE (eV)	CL%	DOCUMENT ID		TECN	COMMENT
<0.45	90	[1] HAN	15	BELL	10.58 $e^+e^- \to \chi_{c1}\gamma$

[1] Using $B(\eta \to \gamma\gamma) = (39.41 \pm 0.21)\%$.

$\Gamma(\chi_{c1}\phi) \times \Gamma(e^+e^-)/\Gamma_{total}$ — $\Gamma_9\Gamma_1/\Gamma$

VALUE (eV)	CL%	DOCUMENT ID		TECN	COMMENT
• • • We do not use the following data for averages, fits, limits, etc. • • •					
<0.04	90	[1] ABLIKIM	23H	BES3	$e^+e^- \to \phi\chi_{c1}$

[1] Fit model parameterized as the coherent sum of a Breit-Wigner resonance and a continuum amplitude term.

$\Gamma(\chi_{c2}\gamma) \times \Gamma(e^+e^-)/\Gamma_{total}$ — $\Gamma_{10}\Gamma_1/\Gamma$

VALUE (eV)	CL%	DOCUMENT ID		TECN	COMMENT
<2.1	90	[1] HAN	15	BELL	10.58 $e^+e^- \to \chi_{c2}\gamma$

[1] Using $B(\eta \to \gamma\gamma) = (39.41 \pm 0.21)\%$.

$\Gamma(\chi_{c2}\phi) \times \Gamma(e^+e^-)/\Gamma_{total}$ — $\Gamma_{11}\Gamma_1/\Gamma$

VALUE (eV)	DOCUMENT ID		TECN	COMMENT
• • • We do not use the following data for averages, fits, limits, etc. • • •				
0.13 ± 0.13	[1] ABLIKIM	23H	BES3	$e^+e^- \to \phi\chi_{c2}$

[1] Fit model parameterized as the coherent sum of a Breit-Wigner resonance and a continuum amplitude term. Constructive solution of the interference. Destructive solution gives 0.66 ± 0.41 eV.

$\Gamma(D_s^+ D_{s1}(2536)^-) \times \Gamma(e^+e^-)/\Gamma_{total}$ — $\Gamma_{13}\Gamma_1/\Gamma$

VALUE (eV)	EVTS	DOCUMENT ID		TECN	COMMENT
$\mathbf{14.3^{+2.8}_{-2.6} \pm 1.5}$	89	[1] JIA	19A	BELL	$e^+e^- \to \gamma D_s^+ D_{s1}(2536)^-$

[1] Assuming $B(D_{s1}(2536)^- \to \overline{D}^{*0}K^-) = 1$.

$\Gamma(D_s^+ D_{s2}^*(2573)^-) \times \Gamma(e^+e^-)/\Gamma_{total}$ — $\Gamma_{14}\Gamma_1/\Gamma$

VALUE (eV)	EVTS	DOCUMENT ID		TECN	COMMENT
$\mathbf{14.7^{+5.9}_{-4.5} \pm 3.6}$	66	[1] JIA	20	BELL	$e^+e^- \to \gamma D_s^+ D_{s2}^*(2573)^-$

[1] Assuming $B(D_{s2}^*(2573)^- \to \overline{D}^0K^-) = 1$.

$\Gamma(\Sigma^+\overline{\Sigma}^-) \times \Gamma(e^+e^-)/\Gamma_{total}$ — $\Gamma_{17}\Gamma_1/\Gamma$

VALUE (eV)	CL%	DOCUMENT ID		TECN	COMMENT
$\mathbf{<49.6 \times 10^{-3}}$	90	[1] ABLIKIM	24AH	BES3	$e^+e^- \to \Sigma^+\overline{\Sigma}^-$

[1] Interference effect between resonance and continuum amplitudes is considered. Two solutions from the fit.

$\Gamma(\Sigma^0\overline{\Sigma}^0) \times \Gamma(e^+e^-)/\Gamma_{total}$ — $\Gamma_{18}\Gamma_1/\Gamma$

VALUE (eV)	CL%	DOCUMENT ID		TECN	COMMENT
$\mathbf{<17.4 \times 10^{-3}}$	90	[1] ABLIKIM	25U	BES3	$e^+e^- \to \Sigma^0\overline{\Sigma}^0$

[1] Interference effect between resonance and continuum amplitudes is considered. Upper limit is for the larger of the two solutions from the fit.

$\Gamma(\Xi^0\overline{\Xi}^0) \times \Gamma(e^+e^-)/\Gamma_{total}$ — $\Gamma_{19}\Gamma_1/\Gamma$

VALUE (eV)	CL%	DOCUMENT ID		TECN	COMMENT
$\mathbf{<45.0 \times 10^{-3}}$	90	[1] ABLIKIM	24CD	BES3	$e^+e^- \to \psi(4660)$

[1] From a fit to $e^+e^- \to \Xi^0\overline{\Xi}^0$ cross sections.

$\Gamma(\Xi^-\overline{\Xi}^+) \times \Gamma(e^+e^-)/\Gamma_{total}$ — $\Gamma_{20}\Gamma_1/\Gamma$

VALUE (eV)	CL%	DOCUMENT ID		TECN	COMMENT
$\mathbf{<19.9 \times 10^{-3}}$	90	[1] ABLIKIM	23BK	BES3	$e^+e^- \to \psi(4660)$

[1] From a fit to $e^+e^- \to \Xi^-\overline{\Xi}^+$ cross sections.

$\Gamma(pK^-\overline{\Lambda} + c.c.) \times \Gamma(e^+e^-)/\Gamma_{total}$ — $\Gamma_{21}\Gamma_1/\Gamma$

VALUE (eV)	CL%	DOCUMENT ID		TECN	COMMENT
$\mathbf{<2.8 \times 10^{-3}}$	90	[1] ABLIKIM	23BL	BES3	$e^+e^- \to \psi(4660)$

[1] From a fit to $e^+e^- \to pK^-\overline{\Lambda}$ + c.c. cross sections.

$\Gamma(\Lambda\overline{\Xi}^+K^- + c.c.) \times \Gamma(e^+e^-)/\Gamma_{total}$ — $\Gamma_{22}\Gamma_1/\Gamma$

VALUE (eV)	CL%	DOCUMENT ID		TECN	COMMENT
$\mathbf{<13.0 \times 10^{-3}}$	90	[1] ABLIKIM	24AL	BES3	$e^+e^- \to \Lambda\overline{\Xi}^+K^-$ + c.c.

[1] A fit to the Born cross section of $e^+e^- \to \Lambda\overline{\Xi}^+K^-$ + c.c. including interference with the continuum. Two solutions from the fit.

$\Gamma(\Sigma^0\overline{\Xi}^+K^- + c.c.) \times \Gamma(e^+e^-)/\Gamma_{total}$ — $\Gamma_{23}\Gamma_1/\Gamma$

VALUE (eV)	CL%	DOCUMENT ID		TECN	COMMENT
$\mathbf{<77.3 \times 10^{-3}}$	90	[1] ABLIKIM	24AL	BES3	$e^+e^- \to \Sigma^0\overline{\Xi}^+K^-$ + c.c.

[1] A fit to the Born cross section of $e^+e^- \to \Sigma^0\overline{\Xi}^+K^-$ + c.c. including interference with the continuum. Two solutions from the fit.

$\Gamma(e^+e^-) \times \Gamma(pK^-K^-\overline{\Xi}^+ + c.c.)/\Gamma_{total}$ — $\Gamma_1\Gamma_{24}/\Gamma$

VALUE (eV)	CL%	DOCUMENT ID		TECN	COMMENT
$\mathbf{<46.2 \times 10^{-3}}$	90	ABLIKIM	25CF	BES3	$e^+e^- \to pK^-K^-\overline{\Xi}^+$ + c.c.

$\psi(4660)$ $\Gamma(i) \times \Gamma(e^+e^-)/\Gamma^2(total)$

$\Gamma(D^0D^{*-}\pi^+)/\Gamma_{total} \times \Gamma(e^+e^-)/\Gamma_{total}$ — $\Gamma_4/\Gamma \times \Gamma_1/\Gamma$

VALUE	CL%	DOCUMENT ID		TECN	COMMENT
$\mathbf{<0.37 \times 10^{-6}}$	90	[1] PAKHLOVA	09	BELL	$e^+e^- \to D^0D^{*-}\pi^+$

[1] Using $4664 \pm 11 \pm 5$ MeV for the mass of $\psi(4660)$.

$\Gamma(\Lambda_c^+\Lambda_c^-)/\Gamma_{total} \times \Gamma(e^+e^-)/\Gamma_{total}$ — $\Gamma_{12}/\Gamma \times \Gamma_1/\Gamma$

VALUE (units 10^{-6})	EVTS	DOCUMENT ID		TECN	COMMENT
$\mathbf{0.68^{+0.16}_{-0.15}{}^{+0.29}_{-0.30}}$	142	[1] PAKHLOVA	08B	BELL	$e^+e^- \to \Lambda_c^+\Lambda_c^-$

[1] The $\pi^+\pi^-\psi(2S)$ and $\Lambda_c^+\Lambda_c^-$ states are not necessarily the same.

$\psi(4660)$ BRANCHING RATIOS

$\Gamma(D^0D^{*-}\pi^+)/\Gamma(\psi(2S)\pi^+\pi^-)$ — Γ_4/Γ_2

VALUE	CL%	DOCUMENT ID		TECN	COMMENT
<10	90	PAKHLOVA	09	BELL	$e^+e^- \to D^0D^{*-}\pi^+$

$\Gamma(\psi_2(3823)\pi^+\pi^-)/\Gamma_{total}$ — Γ_6/Γ

VALUE	DOCUMENT ID		TECN	COMMENT
seen	[1] ABLIKIM	22R	BES3	$e^+e^- \to \pi^+\pi^-\chi_{c1}\gamma$

[1] From a fit to the $e^+e^- \to \pi^+\pi^-\psi(3823)$ cross section between 4.23 and 4.70 GeV with two coherent Breit-Wigner resonances.

$\Gamma(\omega\pi^0)/\Gamma_{total}$ — Γ_{15}/Γ

VALUE	DOCUMENT ID		TECN	COMMENT
not seen	ABLIKIM	22K	BES3	$e^+e^- \to \omega\pi^0$

$\Gamma(\omega\eta)/\Gamma_{total}$ — Γ_{16}/Γ

VALUE	DOCUMENT ID		TECN	COMMENT
not seen	ABLIKIM	22K	BES3	$e^+e^- \to \omega\eta$

$\psi(4660)$ REFERENCES

ABLIKIM	25CF	JHEP 2511 111	M. Ablikim *et al.*	(BESIII Collab.)
ABLIKIM	25J	PR D111 012016	M. Ablikim *et al.*	(BESIII Collab.)
ABLIKIM	25U	PR D111 L051502	M. Ablikim *et al.*	(BESIII Collab.)
ABLIKIM	24AH	JHEP 2405 022	M. Ablikim *et al.*	(BESIII Collab.)
ABLIKIM	24AL	JHEP 2407 258	M. Ablikim *et al.*	(BESIII Collab.)
ABLIKIM	24BN	PRL 133 171903	M. Ablikim *et al.*	(BESIII Collab.)
ABLIKIM	24CD	JHEP 2411 062	M. Ablikim *et al.*	(BESIII Collab.)
ABLIKIM	23BI	PRL 131 211902	M. Ablikim *et al.*	(BESIII Collab.)
ABLIKIM	23BK	JHEP 2311 228	M. Ablikim *et al.*	(BESIII Collab.)
ABLIKIM	23BL	JHEP 2312 027	M. Ablikim *et al.*	(BESIII Collab.)
ABLIKIM	23H	JHEP 2301 132	M. Ablikim *et al.*	(BESIII Collab.)
ABLIKIM	23X	PRL 130 121901	M. Ablikim *et al.*	(BESIII Collab.)
ABLIKIM	22K	JHEP 2207 064	M. Ablikim *et al.*	(BESIII Collab.)
ABLIKIM	22R	PRL 129 102003	M. Ablikim *et al.*	(BESIII Collab.)
ABLIKIM	21AJ	PR D104 052012	M. Ablikim *et al.*	(BESIII Collab.)
JIA	20	PR D101 091101	S. Jia *et al.*	(BELLE Collab.)
JIA	19A	PR D100 111103	S. Jia *et al.*	(BELLE Collab.)
DAI	17	PR D96 116001	L.-Y. Dai, J. Haidenbauer, U.-G. Meissner	(JULI+)
ZHANG	17B	PR D96 054008	J. Zhang, J. Zhang	
ZHANG	17C	EPJ C77 727	J. Zhang, L. Yuan	
HAN	15	PR D92 012011	Y.L. Han *et al.*	(BELLE Collab.)
WANG	15A	PR D91 112007	X.L. Wang *et al.*	(BELLE Collab.)
LEES	14F	PR D89 111103	J.P. Lees *et al.*	(BABAR Collab.)
WANG	13B	PR D87 051101	X.L. Wang *et al.*	(BELLE Collab.)
PAKHLOVA	09	PR D80 091101	G. Pakhlova *et al.*	(BELLE Collab.)
LIU	08H	PR D78 014032	Z.Q. Liu, X.S. Qin, C.Z. Yuan	
PAKHLOVA	08B	PRL 101 172001	C. Pakhlova *et al.*	(BELLE Collab.)
AUBERT	07S	PRL 98 212001	B. Aubert *et al.*	(BABAR Collab.)
WANG	07D	PRL 99 142002	X.L. Wang *et al.*	(BELLE Collab.)

$\chi_{c1}(4685)$

$I^G(J^{PC}) = 0^+(1^{++})$

OMITTED FROM SUMMARY TABLE

This state shows properties different from a conventional $q\overline{q}$ state. A candidate for an exotic structure. See the review on "Heavy Non-$q\overline{q}$ Mesons."

Seen by AAIJ 21E in $B^+ \to \chi_{c1}(4685)K^+$ with $\chi_{c1}(4685) \to J/\psi\phi$ using an amplitude analysis of $B^+ \to J/\psi\phi K^+$ with a significance (accounting for systematic uncertainties) of 15 σ. The $J^P = 1^+$ assignment is favored with high significance.

$\chi_{c1}(4685)$ MASS

VALUE (MeV)	EVTS	DOCUMENT ID		TECN	COMMENT
$\mathbf{4677^{+13}_{-15}}$ **OUR AVERAGE**					
$4653 \pm 14 \pm 27$		AAIJ	25Q	LHCB	$B^+ \to \psi(2S)K^+\pi^+\pi^-$
$4684 \pm 7^{+13}_{-16}$	24k	[1] AAIJ	21E	LHCB	$B^+ \to J/\psi\phi K^+$

Int. J. Mod. Phys. A 2026.41. Downloaded from www.worldscientific.com
by CALIFORNIA @ BERKELEY on 09/16/26. Re-use and distribution is strictly not permitted, except for Open Access articles.

[1] From an amplitude analysis of the decay $B^+ \to J/\psi\phi K^+$ with a significance of 15 σ.

$\chi_{c1}(4685)$ WIDTH

VALUE (MeV)	EVTS	DOCUMENT ID		TECN	COMMENT
180±50 OUR AVERAGE Error includes scale factor of 1.9.					
227±26±22		AAIJ	25Q	LHCB	$B^+ \to \psi(2S) K^+ \pi^+ \pi^-$
$126 \pm 15^{+37}_{-41}$	24k	[1] AAIJ	21E	LHCB	$B^+ \to J/\psi\phi K^+$

[1] From an amplitude analysis of the decay $B^+ \to J/\psi\phi K^+$ with a significance of 15 σ.

$\chi_{c1}(4685)$ DECAY MODES

	Mode	Fraction (Γ_i/Γ)
Γ_1	$J/\psi\phi$	seen
Γ_2	$\psi(2S)\pi^+\pi^-$	seen

$\chi_{c1}(4685)$ BRANCHING RATIOS

$\Gamma(J/\psi\phi)/\Gamma_{total}$ — **Γ_1/Γ**

VALUE	EVTS	DOCUMENT ID		TECN	COMMENT
seen	24k	[1] AAIJ	21E	LHCB	$B^+ \to J/\psi\phi K^+$

[1] From an amplitude analysis of the decay $B^+ \to J/\psi\phi K^+$ with a significance of 15 σ.

$\Gamma(\psi(2S)\pi^+\pi^-)/\Gamma_{total}$ — **Γ_2/Γ**

VALUE	DOCUMENT ID		TECN	COMMENT
seen	AAIJ	25Q	LHCB	$B^+ \to \psi(2S) K^+ \pi^+ \pi^-$

$\chi_{c1}(4685)$ REFERENCES

AAIJ	25Q	JHEP 2501 054	R. Aaij *et al.*	(LHCb Collab.)
AAIJ	21E	PRL 127 082001	R. Aaij *et al.*	(LHCb Collab.) JP

$\chi_{c0}(4700)$

$I^G(J^{PC}) = 0^+(0^{++})$

OMITTED FROM SUMMARY TABLE
was $X(4700)$
See the review on the "Spectroscopy of Mesons Containing two Heavy Quarks."

$\chi_{c0}(4700)$ MASS

VALUE (MeV)	EVTS	DOCUMENT ID		TECN	COMMENT
4708^{+6}_{-4} OUR AVERAGE					
4710± 4± 5		AAIJ	25Q	LHCB	$B^+ \to \psi(2S) K^+ \pi^+ \pi^-$
$4694 \pm 4^{+16}_{-3}$	24k	[1] AAIJ	21E	LHCB	$B^+ \to J/\psi\phi K^+$
• • • We do not use the following data for averages, fits, limits, etc. • • •					
4741± 6± 6	175	[2] AAIJ	21C	LHCB	$B^0_s \to J/\psi\phi\pi^+\pi^-$
$4704 \pm 10^{+14}_{-24}$	4289	[3,4] AAIJ	17C	LHCB	$B^+ \to J/\psi\phi K^+$

[1] From an amplitude analysis of the decay $B^+ \to J/\psi\phi K^+$ with a significance of 17 σ.
[2] From a 1D fit to the $J/\psi\phi$ mass distribution with a significance of 5.3 σ. The identification of this structure as the $\chi_{c0}(4700)$ needs confirmation.
[3] From an amplitude analysis of the decay $B^+ \to J/\psi\phi K^+$ with a significance of 5.6 σ.
[4] Superseded by AAIJ 21E.

$\chi_{c0}(4700)$ WIDTH

VALUE (MeV)	EVTS	DOCUMENT ID		TECN	COMMENT
78^{+15}_{-11} OUR AVERAGE Error includes scale factor of 1.4.					
64± 9±10		AAIJ	25Q	LHCB	$B^+ \to \psi(2S) K^+ \pi^+ \pi^-$
$87 \pm 8^{+16}_{-6}$	24k	[1] AAIJ	21E	LHCB	$B^+ \to J/\psi\phi K^+$
• • • We do not use the following data for averages, fits, limits, etc. • • •					
53±15±11	175	[2] AAIJ	21C	LHCB	$B^0_s \to J/\psi\phi\pi^+\pi^-$
$120 \pm 31^{+42}_{-33}$	4289	[3,4] AAIJ	17C	LHCB	$B^+ \to J/\psi\phi K^+$

[1] From an amplitude analysis of the decay $B^+ \to J/\psi\phi K^+$ with a significance of 17 σ.
[2] From a 1D fit to the $J/\psi\phi$ mass distribution with a significance of 5.3 σ. The identification of this structure as the $\chi_{c0}(4700)$ needs confirmation.
[3] From an amplitude analysis of the decay $B^+ \to J/\psi\phi K^+$ with a significance of 5.6 σ.
[4] Superseded by AAIJ 21E.

$\chi_{c0}(4700)$ DECAY MODES

	Mode	Fraction (Γ_i/Γ)
Γ_1	$J/\psi\phi$	seen
Γ_2	$\psi(2S)\pi^+\pi^-$	seen

$\chi_{c0}(4700)$ BRANCHING RATIOS

$\Gamma(J/\psi\phi)/\Gamma_{total}$ — **Γ_1/Γ**

VALUE	EVTS	DOCUMENT ID		TECN	COMMENT
seen	24k	[1] AAIJ	21E	LHCB	$B^+ \to J/\psi\phi K^+$
• • • We do not use the following data for averages, fits, limits, etc. • • •					
seen	175	[2] AAIJ	21C	LHCB	$B^0_s \to J/\psi\phi\pi^+\pi^-$
seen	4289	[3,4] AAIJ	17C	LHCB	$B^+ \to J/\psi\phi K^+$

[1] From an amplitude analysis of the decay $B^+ \to J/\psi\phi K^+$ with a significance of 17 σ.
[2] From a 1D fit to the $J/\psi\phi$ mass distribution with a significance of 5.3 σ. The identification of this structure as the $\chi_{c0}(4700)$ needs confirmation.
[3] From an amplitude analysis of the decay $B^+ \to J/\psi\phi K^+$ with a significance of 5.6 σ.
[4] Superseded by AAIJ 21E.

$\Gamma(\psi(2S)\pi^+\pi^-)/\Gamma_{total}$ — **Γ_2/Γ**

VALUE	DOCUMENT ID		TECN	COMMENT
seen	AAIJ	25Q	LHCB	$B^+ \to \psi(2S) K^+ \pi^+ \pi^-$

$\chi_{c0}(4700)$ REFERENCES

AAIJ	25Q	JHEP 2501 054	R. Aaij *et al.*	(LHCb Collab.)
AAIJ	21C	JHEP 2102 024	R. Aaij *et al.*	(LHCb Collab.)
AAIJ	21E	PRL 127 082001	R. Aaij *et al.*	(LHCb Collab.)
AAIJ	17C	PRL 118 022003	R. Aaij *et al.*	(LHCb Collab.) JP
Also		PR D95 012002	R. Aaij *et al.*	(LHCb Collab.)

Int. J. Mod. Phys. A 2026.41. Downloaded from www.worldscientific.com
by UNIVERSITY OF CALIFORNIA @ BERKELEY on 09/16/26. Re-use and distribution is strictly not permitted, except for Open Access articles.

$b\overline{b}$ MESONS (including possibly non-$q\overline{q}$ states)

Updated March 2024.

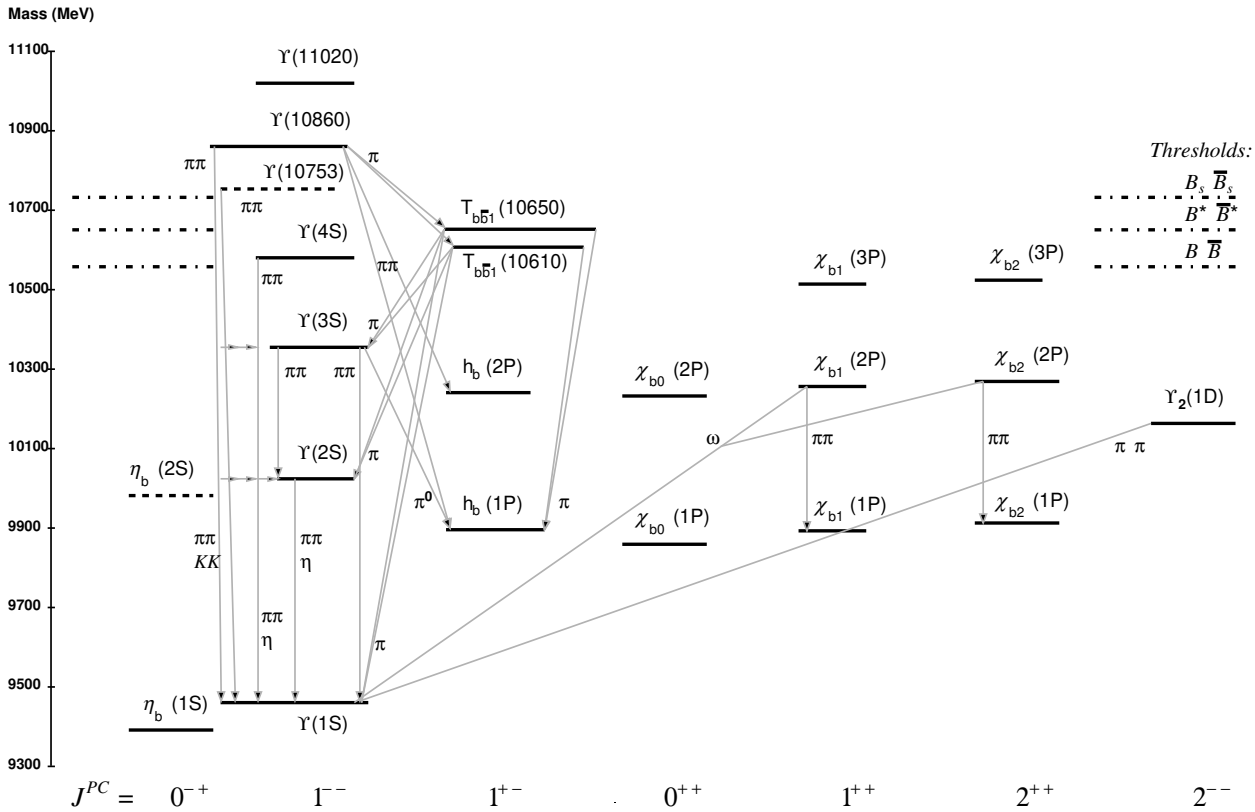

The level scheme of meson states containing a minimal quark content of $b\overline{b}$ and having $S = C = B = 0$. The name of a state is determined by its quantum numbers $I^G J^{PC}$ (see the review "Naming Scheme for Hadrons"). States included in the Summary Tables are shown with solid lines; those requiring confirmation are shown with dotted lines. The arrows indicate the most dominant hadronic transitions. Single photon transitions, including $\Upsilon(nS) \to \gamma\eta_b(mS)$, $\Upsilon(nS) \to \gamma\chi_{bJ}(mP)$, and $\chi_{bJ}(nP) \to \gamma\Upsilon(mS)$, are omitted for clarity. For orientation, the location of the thresholds related to a pair of ground state open bottom mesons is indicated in the figure. Decays to open flavour final states are not shown in the figure. The transitions $\Upsilon(10753) \to \omega\chi_{b1}(1P), \omega\chi_{b2}(1P)$ have also been reported.

WIDTH DETERMINATIONS OF THE Υ STATES

As is the case for the $J/\psi(1S)$ and $\psi(2S)$, the full widths of the $b\overline{b}$ states $\Upsilon(1S)$, $\Upsilon(2S)$, and $\Upsilon(3S)$ are not directly measurable, since they are much narrower than the energy resolution of the e^+e^- storage rings where these states are produced. The common indirect method to determine Γ starts from

$$\Gamma = \Gamma_{\ell\ell}/B_{\ell\ell} \ , \tag{1}$$

where $\Gamma_{\ell\ell}$ is one leptonic partial width and $B_{\ell\ell}$ is the corresponding branching fraction ($\ell = e,\ \mu,$ or τ). One then assumes e-μ-τ universality and uses

$$\Gamma_{\ell\ell} = \Gamma_{ee}$$

$$B_{\ell\ell} = \text{average of } B_{ee},\ B_{\mu\mu},\ \text{and } B_{\tau\tau} \ . \tag{2}$$

The electronic partial width Γ_{ee} is also not directly measurable at e^+e^- storage rings, only in the combination $\Gamma_{ee}\Gamma_{\rm had}/\Gamma$, where $\Gamma_{\rm had}$ is the hadronic partial width and

$$\Gamma_{\rm had} + 3\Gamma_{ee} = \Gamma \ . \tag{3}$$

This combination is obtained experimentally from the energy-integrated hadronic cross section

$$\int_{\rm resonance} \sigma(e^+e^- \to \Upsilon \to \text{hadrons})dE$$

$$= \frac{6\pi^2}{M^2}\frac{\Gamma_{ee}\Gamma_{\rm had}}{\Gamma}C_r = \frac{6\pi^2}{M^2}\frac{\Gamma_{ee}^{(0)}\Gamma_{\rm had}}{\Gamma}C_r^{(0)} \ , \tag{4}$$

where M is the Υ mass, and C_r and $C_r^{(0)}$ are radiative correction factors. C_r is used for obtaining Γ_{ee} as defined in Eq. (1), and

Int. J. Mod. Phys. A 2026.41. Downloaded from www.worldscientific.com
by LIFORNIA @ BERKELEY on 09/16/26. Re-use and distribution is strictly not permitted, except for Open Access articles.

Int. J. Mod. Phys. A 2026.41. Downloaded from www.worldscientific.com by UNIVERSITY OF CALIFORNIA @ BERKELEY on 09/16/26. Re-use and distribution is strictly not permitted, except for Open Access articles.

contains corrections from all orders of QED for describing $(b\bar{b}) \to e^+e^-$. The lowest order QED value $\Gamma_{ee}^{(0)}$, relevant for comparison with potential-model calculations, is defined by the lowest order QED graph (Born term) alone, and is about 7% lower than Γ_{ee}.

The Listings give experimental results on B_{ee}, $B_{\mu\mu}$, $B_{\tau\tau}$, and $\Gamma_{ee}\Gamma_{\rm had}/\Gamma$. The entries of the last quantity have been re-evaluated consistently using the correction procedure of KURAEV 85 [1]. The partial width Γ_{ee} is obtained from the average values for $\Gamma_{ee}\Gamma_{\rm had}/\Gamma$ and $B_{\ell\ell}$ using

$$\Gamma_{ee} = \frac{\Gamma_{ee}\Gamma_{\rm had}}{\Gamma(1-3B_{\ell\ell})} \ . \qquad (5)$$

The total width Γ is then obtained from Eq. (1). We do not list Γ_{ee} and Γ values of individual experiments. The Γ_{ee} values in the Meson Summary Table are also those defined in Eq. (1).

References

1. E.A. Kuraev, V.S. Fadin, Sov. J. Nucl. Phys. **41**, 466 (1985).

$\eta_b(1S)$

$I^G(J^{PC}) = 0^+(0^{-+})$

Quantum numbers shown are quark-model predictions. Observed in radiative decay of the $\Upsilon(3S)$, therefore $C = +$.

$\eta_b(1S)$ MASS

VALUE (MeV)	EVTS	DOCUMENT ID		TECN	COMMENT
9398.7± 2.0 OUR AVERAGE		Error includes scale factor of 1.5. See the ideogram below.			
$9394.8^{+2.7}_{-3.1}{}^{+4.5}_{-2.7}$	29k	FULSOM	18	BELL	$\Upsilon(2S) \to \gamma X$
9400.7± 1.7± 1.6	33.1k	TAMPONI	15	BELL	$e^+e^- \to \gamma\eta +$ hadrons
9402.4± 1.5± 1.8	34k	[1] MIZUK	12	BELL	$e^+e^- \to \gamma\pi^+\pi^- +$ hadrons
9391.8± 6.6± 2.0	2.3k	[2] BONVICINI	10	CLEO	$\Upsilon(3S) \to \gamma X$
$9394.2^{+4.8}_{-4.9}$± 2.0	13k	[2] AUBERT	09AQ	BABR	$\Upsilon(2S) \to \gamma X$
$9388.9^{+3.1}_{-2.3}$± 2.7	19k	[2] AUBERT	08V	BABR	$\Upsilon(3S) \to \gamma X$
• • • We do not use the following data for averages, fits, limits, etc. • • •					
9393.2± 3.4± 2.3	10	[2,3] DOBBS	12		$\Upsilon(2S) \to \gamma$ hadrons
9300 ±20 ±20		HEISTER	02D	ALEP	181–209 e^+e^-

[1] With floating width. Not independent of the corresponding mass difference measurement.
[2] Assuming $\Gamma_{\eta_b(1S)} = 10$ MeV. Not independent of the corresponding γ energy or mass difference measurements.
[3] Obtained by analyzing CLEO III data but not authored by the CLEO Collaboration.

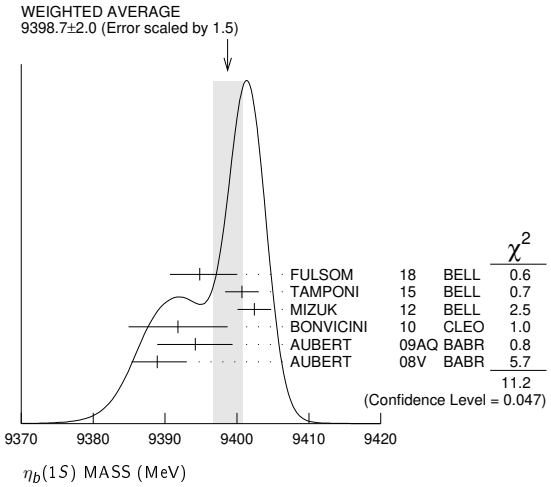

$m_{\Upsilon(1S)} - m_{\eta_b}$

VALUE (MeV)	EVTS	DOCUMENT ID		TECN	COMMENT
62.3±3.2 OUR AVERAGE		Error includes scale factor of 1.8. See the ideogram below.			
57.9±1.5±1.8	34k	[1] MIZUK	12	BELL	$e^+e^- \to \gamma\pi^+\pi^-$ + hadrons
68.5±6.6±2.0	2.3 ± 0.5k	[2] BONVICINI	10	CLEO	$\Upsilon(3S) \to \gamma X$
$66.1^{+4.8}_{-4.9}$±2.0	13 ± 5k	[2] AUBERT	09AQ	BABR	$\Upsilon(2S) \to \gamma X$
$71.4^{+2.3}_{-3.1}$±2.7	19 ± 3k	[2] AUBERT	08V	BABR	$\Upsilon(3S) \to \gamma X$
• • • We do not use the following data for averages, fits, limits, etc. • • •					
67.1±3.4±2.3	10^{+5}_{-4}	[2,3] DOBBS	12		$\Upsilon(2S) \to \gamma$ hadrons

[1] With floating width. Not independent of the corresponding mass measurement.
[2] Assuming $\Gamma_{\eta_b(1S)} = 10$ MeV. Not independent of the corresponding γ energy or mass measurements.
[3] Obtained by analyzing CLEO III data but not authored by the CLEO Collaboration.

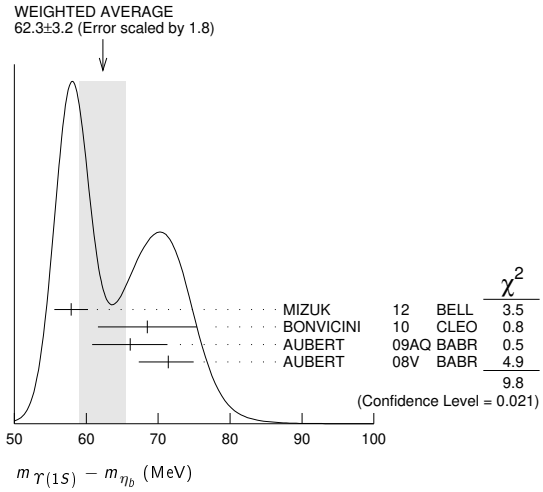

γ ENERGY IN $\Upsilon(3S)$ DECAY

VALUE (MeV)	EVTS	DOCUMENT ID		TECN	COMMENT
$920.6^{+2.8}_{-3.2}$ OUR AVERAGE					
918.6±6.0±1.9	2.3 ± 0.5k	[1] BONVICINI	10	CLEO	$\Upsilon(3S) \to \gamma X$
$921.2^{+2.1}_{-2.8}$±2.4	19 ± 3k	[1] AUBERT	08V	BABR	$\Upsilon(3S) \to \gamma X$

[1] Assuming $\Gamma_{\eta_b(1S)} = 10$ MeV. Not independent of the corresponding mass or mass difference measurements.

γ ENERGY IN $\Upsilon(2S)$ DECAY

VALUE (MeV)	EVTS	DOCUMENT ID		TECN	COMMENT
$609.3^{+4.6}_{-4.5}$±1.9	13 ± 5k	[1] AUBERT	09AQ	BABR	$\Upsilon(2S) \to \gamma X$

[1] Assuming $\Gamma_{\eta_b(1S)} = 10$ MeV. Not independent of the corresponding mass or mass difference measurements.

$\eta_b(1S)$ WIDTH

VALUE (MeV)	EVTS	DOCUMENT ID		TECN	COMMENT
10^{+5}_{-4} OUR AVERAGE					
8^{+6}_{-5} ±5	33.1k	[1] TAMPONI	15	BELL	$e^+e^- \to \gamma\eta +$ hadrons
$10.8^{+4.0}_{-3.7}{}^{+4.5}_{-2.0}$	34k	[1] MIZUK	12	BELL	$e^+e^- \to \gamma\pi^+\pi^- +$ hadrons

[1] With floating mass.

$\eta_b(1S)$ DECAY MODES

	Mode	Fraction (Γ_i/Γ)	Confidence level
Γ_1	hadrons	seen	
Γ_2	$3h^+3h^-$	not seen	
Γ_3	$2h^+2h^-$	not seen	
Γ_4	$4h^+4h^-$	not seen	
Γ_5	$\gamma\gamma$	not seen	
Γ_6	$\mu^+\mu^-$	$<9\times10^{-3}$	90%
Γ_7	$\tau^+\tau^-$	<8 %	90%

Int. J. Mod. Phys. A 2026.41. Downloaded from www.worldscientific.com by CALIFORNIA @ BERKELEY on 09/16/26. Re-use and distribution is strictly not permitted, except for Open Access articles.

$\eta_b(1S)$ Γ(i)Γ(γγ)/Γ(total)

$\Gamma(3h^+3h^-) \times \Gamma(\gamma\gamma)/\Gamma_{total}$ — $\Gamma_2\Gamma_5/\Gamma$

VALUE (eV)	CL%	DOCUMENT ID		TECN	COMMENT
• • • We do not use the following data for averages, fits, limits, etc. • • •					
<470	95	ABDALLAH	06	DLPH	161–209 e^+e^-
<132	95	HEISTER	02D	ALEP	181–209 e^+e^-

$\Gamma(2h^+2h^-) \times \Gamma(\gamma\gamma)/\Gamma_{total}$ — $\Gamma_3\Gamma_5/\Gamma$

VALUE (eV)	CL%	DOCUMENT ID		TECN	COMMENT
• • • We do not use the following data for averages, fits, limits, etc. • • •					
<190	95	ABDALLAH	06	DLPH	161–209 e^+e^-
< 48	95	HEISTER	02D	ALEP	181–209 e^+e^-

$\Gamma(4h^+4h^-) \times \Gamma(\gamma\gamma)/\Gamma_{total}$ — $\Gamma_4\Gamma_5/\Gamma$

VALUE (eV)	CL%	DOCUMENT ID		TECN	COMMENT
• • • We do not use the following data for averages, fits, limits, etc. • • •					
<660	95	ABDALLAH	06	DLPH	161–209 e^+e^-

$\eta_b(1S)$ BRANCHING RATIOS

$\Gamma(\text{hadrons})/\Gamma_{total}$ — Γ_1/Γ

VALUE	EVTS	DOCUMENT ID		TECN	COMMENT
seen	34k	MIZUK	12	BELL	$e^+e^- \to \gamma\pi^+\pi^-$ + hadrons

$\Gamma(\mu^+\mu^-)/\Gamma_{total}$ — Γ_6/Γ

VALUE	CL%	DOCUMENT ID		TECN	COMMENT
$<9\times10^{-3}$	90	[1] AUBERT	09Z	BABR	$e^+e^- \to \Upsilon(2S,3S) \to \gamma\eta_b$

[1] Obtained using $B(\Upsilon(2S) \to \gamma\eta_b) = (4.2^{+1.1}_{-1.0} \pm 0.9)\times10^{-4}$ and $B(\Upsilon(3S) \to \gamma\eta_b) = (4.8 \pm 0.5 \pm 0.6)\times10^{-4}$. This limit is equivalent to $B(\eta_b \to \mu^+\mu^-) = (-0.25 \pm 0.51 \pm 0.33)\%$ measurement.

$\Gamma(\tau^+\tau^-)/\Gamma_{total}$ — Γ_7/Γ

VALUE	CL%	DOCUMENT ID		TECN	COMMENT
$<8\times10^{-2}$	90	AUBERT	09P	BABR	$e^+e^- \to \gamma\tau^+\tau^-$

$\eta_b(1S)$ REFERENCES

FULSOM	18	PRL 121 232001	B.G. Fulsom *et al.*	(BELLE Collab.)
TAMPONI	15	PRL 115 142001	U. Tamponi *et al.*	(BELLE Collab.)
DOBBS	12	PRL 109 082001	S. Dobbs *et al.*	
MIZUK	12	PRL 109 232002	R. Mizuk *et al.*	(BELLE Collab.)
BONVICINI	10	PR D81 031104	G. Bonvicini *et al.*	(CLEO Collab.)
AUBERT	09AQ	PRL 103 161801	B. Aubert *et al.*	(BABAR Collab.)
AUBERT	09P	PRL 103 181801	B. Aubert *et al.*	(BABAR Collab.)
AUBERT	09Z	PRL 103 081803	B. Aubert *et al.*	(BABAR Collab.)
AUBERT	08V	PRL 101 071801	B. Aubert *et al.*	(BABAR Collab.)
ABDALLAH	06	PL B634 340	J.M. Abdallah *et al.*	(DELPHI Collab.)
HEISTER	02D	PL B530 56	A. Heister *et al.*	(ALEPH Collab.)

$\Upsilon(1S)$

$I^G(J^{PC}) = 0^-(1^{--})$

$\Upsilon(1S)$ MASS

VALUE (MeV)	EVTS	DOCUMENT ID		TECN	COMMENT
9460.40±0.10 OUR AVERAGE					
9460.37±0.01±2.85	15M	[1] AAIJ	24AC	LHCB	$\Upsilon(1S) \to \mu^+\mu^-$
9460.40±0.09±0.04		[2] SHAMOV	23	RVUE	$e^+e^- \to$ hadrons
• • • We do not use the following data for averages, fits, limits, etc. • • •					
9460.11±0.11±0.07		[3] SHAMOV	23	RVUE	$e^+e^- \to$ hadrons
9460.51±0.09±0.05		[4,5] ARTAMONOV	00	MD1	$e^+e^- \to$ hadrons
9460.60±0.09±0.05		[6,7] BARU	92B	MD1	$e^+e^- \to$ hadrons
9460.59±0.12		BARU	86	MD1	$e^+e^- \to$ hadrons
9460.6 ±0.4		[7,8] ARTAMONOV	84	MD1	$e^+e^- \to$ hadrons
9459.97±0.11±0.07		[9] MACKAY	84	CUSB	$e^+e^- \to$ hadrons

[1] Observed in prompt pp production.
[2] Reanalysis of MD1 data using the electron mass from COHEN 87, the radiative corrections from KURAEV 85 and interference effects.
[3] Obtained by reanalysing CUSB data (MACKAY 84), but not authored by the CUSB collaboration.
[4] Reanalysis of BARU 92B and ARTAMONOV 84 using new electron mass (COHEN 87).
[5] Superseded by SHAMOV 23.
[6] Supersedes BARU 86.
[7] Superseded by ARTAMONOV 00.
[8] Value includes data of ARTAMONOV 82.
[9] Reanalysed by SHAMOV 23.

$\Upsilon(1S)$ WIDTH

VALUE (keV)	DOCUMENT ID
54.02±1.25 OUR EVALUATION	See the Note on "Width Determinations of the Υ States"

$\Upsilon(1S)$ DECAY MODES

	Mode	Fraction (Γ_i/Γ)	Scale factor/ Confidence level
Γ_1	$\tau^+\tau^-$	(2.60 ±0.10) %	
Γ_2	e^+e^-	(2.39 ±0.08) %	
Γ_3	$\mu^+\mu^-$	(2.48 ±0.04) %	
	Hadronic decays		
Γ_4	ggg	(81.7 ±0.7) %	
Γ_5	γgg	(2.2 ±0.6) %	
Γ_6	$\eta'(958)$ anything	(2.94 ±0.24) %	
Γ_7	$J/\psi(1S)$ anything	(5.4 ±0.4) $\times10^{-4}$	S=1.4
Γ_8	$J/\psi(1S)\eta_c$	< 2.2 $\times10^{-6}$	CL=90%
Γ_9	$J/\psi(1S)\chi_{c0}$	< 3.4 $\times10^{-6}$	CL=90%
Γ_{10}	$J/\psi(1S)\chi_{c1}$	(3.9 ±1.2) $\times10^{-6}$	
Γ_{11}	$J/\psi(1S)\chi_{c2}$	< 1.4 $\times10^{-6}$	CL=90%
Γ_{12}	$J/\psi(1S)\eta_c(2S)$	< 2.2 $\times10^{-6}$	CL=90%
Γ_{13}	$J/\psi(1S)X(3940)$	< 5.4 $\times10^{-6}$	CL=90%
Γ_{14}	$J/\psi(1S)X(4160)$	< 5.4 $\times10^{-6}$	CL=90%
Γ_{15}	$X(4350)$ anything, $X \to J/\psi(1S)\phi$	< 8.1 $\times10^{-6}$	CL=90%
Γ_{16}	$T_{c\overline{c}1}(3900)^\pm$ anything, $T_{c\overline{c}1} \to J/\psi(1S)\pi^\pm$	< 1.3 $\times10^{-5}$	CL=90%
Γ_{17}	$T_{c\overline{c}1}(4200)^\pm$ anything, $Z_c \to J/\psi(1S)\pi^\pm$	< 6.0 $\times10^{-5}$	CL=90%
Γ_{18}	$T_{c\overline{c}1}(4430)^\pm$ anything, $T_{c\overline{c}1} \to J/\psi(1S)\pi^\pm$	< 4.9 $\times10^{-5}$	CL=90%
Γ_{19}	$P_{c\overline{c}s}(4459)/\overline{P}_{c\overline{c}s}(4459)$ anything	(3.5 ±2.0) $\times10^{-6}$	
Γ_{20}	$P_{c\overline{c}s}(4338)/\overline{P}_{c\overline{c}s}(4338)$ anything	< 1.8 $\times10^{-6}$	CL=90%
Γ_{21}	$P_c(4312)$ anything, $P_c(4312) \to pJ/\psi(1S)$	< 5.7 $\times10^{-6}$	CL=90%
Γ_{22}	$P_c(4440)$ anything, $P_c(4440) \to pJ/\psi(1S)$	< 1.00 $\times10^{-5}$	CL=90%
Γ_{23}	$P_c(4457)$ anything, $P_c(4457) \to pJ/\psi(1S)$	< 7.6 $\times10^{-6}$	CL=90%
Γ_{24}	$p/\overline{p}J/\psi(1S)$ anything	(8.1 ±0.8) $\times10^{-5}$	
Γ_{25}	$J/\psi(1S)\Lambda/\overline{\Lambda}$ anything	(3.7 ±0.6) $\times10^{-5}$	
Γ_{26}	$X_{cs}^\pm$ anything, $X \to J/\psi K^\pm$	< 5.7 $\times10^{-6}$	CL=90%
Γ_{27}	$\psi(4230)$ anything, $\psi \to J/\psi(1S)\pi^+\pi^-$	< 3.8 $\times10^{-5}$	CL=90%
Γ_{28}	$\psi(4230)$ anything, $\psi \to J/\psi(1S)K^+K^-$	< 7.5 $\times10^{-6}$	CL=90%
Γ_{29}	$\chi_{c1}(4140)$ anything, $\chi_{c1} \to J/\psi(1S)\phi$	< 5.2 $\times10^{-6}$	CL=90%
Γ_{30}	χ_{c0} anything	< 4 $\times10^{-3}$	CL=90%
Γ_{31}	χ_{c1} anything	(1.90 ±0.35) $\times10^{-4}$	
Γ_{32}	$\chi_{c1}(1P)X_{tetra}$	< 3.78 $\times10^{-5}$	CL=90%
Γ_{33}	χ_{c2} anything	(2.8 ±0.8) $\times10^{-4}$	
Γ_{34}	$\psi(2S)$ anything	(1.23 ±0.20) $\times10^{-4}$	
Γ_{35}	$\psi(2S)\eta_c$	< 3.6 $\times10^{-6}$	CL=90%
Γ_{36}	$\psi(2S)\chi_{c0}$	< 6.5 $\times10^{-6}$	CL=90%
Γ_{37}	$\psi(2S)\chi_{c1}$	< 4.5 $\times10^{-6}$	CL=90%
Γ_{38}	$\psi(2S)\chi_{c2}$	< 2.1 $\times10^{-6}$	CL=90%
Γ_{39}	$\psi(2S)\eta_c(2S)$	< 3.2 $\times10^{-6}$	CL=90%
Γ_{40}	$\psi(2S)X(3940)$	< 2.9 $\times10^{-6}$	CL=90%
Γ_{41}	$\psi(2S)X(4160)$	< 2.9 $\times10^{-6}$	CL=90%
Γ_{42}	$\psi(4230)$ anything, $\psi \to \psi(2S)\pi^+\pi^-$	< 7.9 $\times10^{-5}$	CL=90%
Γ_{43}	$\psi(4360)$ anything, $\psi \to \psi(2S)\pi^+\pi^-$	< 5.2 $\times10^{-5}$	CL=90%
Γ_{44}	$\psi(4660)$ anything, $\psi \to \psi(2S)\pi^+\pi^-$	< 2.2 $\times10^{-5}$	CL=90%
Γ_{45}	$T_{c\overline{c}}(4050)^\pm$ anything, $X \to \psi(2S)\pi^\pm$	< 8.8 $\times10^{-5}$	CL=90%
Γ_{46}	$T_{c\overline{c}1}(4430)^\pm$ anything, $T_{c\overline{c}1} \to \psi(2S)\pi^\pm$	< 6.7 $\times10^{-5}$	CL=90%
Γ_{47}	$\chi_{c1}(3872)$ anything	< 2.2 $\times10^{-4}$	CL=90%
Γ_{48}	$T_{c\overline{c}1}(4200)^+ T_{c\overline{c}1}(4200)^-$	< 2.23 $\times10^{-5}$	CL=90%
Γ_{49}	$T_{c\overline{c}1}(3900)^\pm T_{c\overline{c}1}(4200)^\mp$	< 8.1 $\times10^{-6}$	CL=90%
Γ_{50}	$T_{c\overline{c}1}(3900)^+ T_{c\overline{c}1}(3900)^-$	< 1.8 $\times10^{-6}$	CL=90%
Γ_{51}	$T_{c\overline{c}}(4050)^+ T_{c\overline{c}}(4050)^-$	< 1.58 $\times10^{-5}$	CL=90%
Γ_{52}	$T_{c\overline{c}}(4250)^+ T_{c\overline{c}}(4250)^-$	< 2.66 $\times10^{-5}$	CL=90%
Γ_{53}	$T_{c\overline{c}}(4050)^\pm T_{c\overline{c}}(4250)^\mp$	< 4.42 $\times10^{-5}$	CL=90%

Int. J. Mod. Phys. A 2026.41. Downloaded from www.worldscientific.com
by UNIVERSITY OF CALIFORNIA @ BERKELEY on 09/16/26. Re-use and distribution is strictly not permitted, except for Open Access articles.

Γ_{54}	$T_{c\overline{c}1}(4430)^+ T_{c\overline{c}1}(4430)^-$	$< 2.03 \times 10^{-5}$	CL=90%	
Γ_{55}	$T_{c\overline{c}}(4055)^\pm T_{c\overline{c}}(4055)^\mp$	$< 2.33 \times 10^{-5}$	CL=90%	
Γ_{56}	$T_{c\overline{c}}(4055)^\pm T_{c\overline{c}1}(4430)^\mp$	$< 4.55 \times 10^{-5}$	CL=90%	
Γ_{57}	$\rho\pi$	$< 3.68 \times 10^{-6}$	CL=90%	
Γ_{58}	$\omega\pi^0$	$< 3.90 \times 10^{-6}$	CL=90%	
Γ_{59}	$\pi^+\pi^-$	$< 5 \times 10^{-4}$	CL=90%	
Γ_{60}	K^+K^-	$< 5 \times 10^{-4}$	CL=90%	
Γ_{61}	$p\overline{p}$	$< 5 \times 10^{-4}$	CL=90%	
Γ_{62}	$\pi^+\pi^-\pi^0$	$(2.1 \pm 0.8) \times 10^{-6}$		
Γ_{63}	ϕK^+K^-	$(2.4 \pm 0.5) \times 10^{-6}$		
Γ_{64}	$\omega\pi^+\pi^-$	$(4.5 \pm 1.0) \times 10^{-6}$		
Γ_{65}	$K^*(892)^0 K^-\pi^+ +$ c.c.	$(4.4 \pm 0.8) \times 10^{-6}$		
Γ_{66}	$\phi f_2'(1525)$	$< 1.63 \times 10^{-6}$	CL=90%	
Γ_{67}	$\omega f_2(1270)$	$< 1.79 \times 10^{-6}$	CL=90%	
Γ_{68}	$\rho(770) a_2(1320)$	$< 2.24 \times 10^{-6}$	CL=90%	
Γ_{69}	$K^*(892)^0 \overline{K}_2^*(1430)^0 +$ c.c.	$(3.0 \pm 0.8) \times 10^{-6}$		
Γ_{70}	$K_1(1270)^\pm K^\mp$	$< 2.41 \times 10^{-6}$	CL=90%	
Γ_{71}	$K_1(1400)^\pm K^\mp$	$(1.0 \pm 0.4) \times 10^{-6}$		
Γ_{72}	$b_1(1235)^\pm \pi^\mp$	$< 1.25 \times 10^{-6}$	CL=90%	
Γ_{73}	$\pi^+\pi^-\pi^0\pi^0$	$(1.28 \pm 0.30) \times 10^{-5}$		
Γ_{74}	$K_S^0 K^+\pi^-+$ c.c.	$(1.6 \pm 0.4) \times 10^{-6}$		
Γ_{75}	$K^*(892)^0 \overline{K}^0 +$ c.c.	$(2.9 \pm 0.9) \times 10^{-6}$		
Γ_{76}	$K^*(892)^- K^+ +$ c.c.	$< 1.11 \times 10^{-6}$	CL=90%	
Γ_{77}	$f_1(1285)$ anything	$(4.6 \pm 3.1) \times 10^{-3}$		
Γ_{78}	$D^*(2010)^\pm$ anything	(2.52 ± 0.20) %		
Γ_{79}	$f_1(1285) X_{tetra}$	$< 6.24 \times 10^{-5}$	CL=90%	
Γ_{80}	^2H anything	$(2.85 \pm 0.25) \times 10^{-5}$		
Γ_{81}	Sum of 100 exclusive modes	(1.200 ± 0.017) %		

Radiative decays

Γ_{82}	$\gamma\pi^+\pi^-$	$(6.3 \pm 1.8) \times 10^{-5}$		
Γ_{83}	$\gamma\pi^0\pi^0$	$(1.7 \pm 0.7) \times 10^{-5}$		
Γ_{84}	$\gamma\pi\pi$ (S-wave)	$(4.6 \pm 0.7) \times 10^{-5}$		
Γ_{85}	$\gamma\pi^0\eta$	$< 2.4 \times 10^{-6}$	CL=90%	
Γ_{86}	γK^+K^-	[a] $(1.14 \pm 0.13) \times 10^{-5}$		
Γ_{87}	$\gamma p\overline{p}$	[b] $< 6 \times 10^{-6}$	CL=90%	
Γ_{88}	$\gamma 2h^+2h^-$	$(7.0 \pm 1.5) \times 10^{-4}$		
Γ_{89}	$\gamma 3h^+3h^-$	$(5.4 \pm 2.0) \times 10^{-4}$		
Γ_{90}	$\gamma 4h^+4h^-$	$(7.4 \pm 3.5) \times 10^{-4}$		
Γ_{91}	$\gamma\pi^+\pi^-K^+K^-$	$(2.9 \pm 0.9) \times 10^{-4}$		
Γ_{92}	$\gamma 2\pi^+2\pi^-$	$(2.5 \pm 0.9) \times 10^{-4}$		
Γ_{93}	$\gamma 3\pi^+3\pi^-$	$(2.5 \pm 1.2) \times 10^{-4}$		
Γ_{94}	$\gamma 2\pi^+2\pi^-K^+K^-$	$(2.4 \pm 1.2) \times 10^{-4}$		
Γ_{95}	$\gamma\pi^+\pi^-p\overline{p}$	$(1.5 \pm 0.6) \times 10^{-4}$		
Γ_{96}	$\gamma 2\pi^+2\pi^-p\overline{p}$	$(4 \pm 6) \times 10^{-5}$		
Γ_{97}	$\gamma 2K^+2K^-$	$(2.0 \pm 2.0) \times 10^{-5}$		
Γ_{98}	$\gamma\eta'(958)$	$< 1.9 \times 10^{-6}$	CL=90%	
Γ_{99}	$\gamma\eta$	$< 1.0 \times 10^{-6}$	CL=90%	
Γ_{100}	$\gamma f_0(980)$	$< 3 \times 10^{-5}$	CL=90%	
Γ_{101}	$\gamma f_2'(1525)$	$(2.9 \pm 0.6) \times 10^{-5}$		
Γ_{102}	$\gamma f_2(1270)$	$(1.01 \pm 0.06) \times 10^{-4}$		
Γ_{103}	$\gamma\eta(1405)$	$< 8.2 \times 10^{-5}$	CL=90%	
Γ_{104}	$\gamma f_0(1500)$	$< 1.5 \times 10^{-5}$	CL=90%	
Γ_{105}	$\gamma f_0(1500) \to \gamma K^+K^-$	$(1.0 \pm 0.4) \times 10^{-5}$		
Γ_{106}	$\gamma f_0(1710)$	$< 2.6 \times 10^{-4}$	CL=90%	
Γ_{107}	$\gamma f_0(1710) \to \gamma K^+K^-$	$(1.01 \pm 0.32) \times 10^{-5}$		
Γ_{108}	$\gamma f_0(1710) \to \gamma\pi^+\pi^-$	$(5.3 \pm 2.0) \times 10^{-6}$		
Γ_{109}	$\gamma f_0(1710) \to \gamma\pi^0\pi^0$	$< 1.4 \times 10^{-6}$	CL=90%	
Γ_{110}	$\gamma f_0(1710) \to \gamma\eta\eta$	$< 1.8 \times 10^{-6}$	CL=90%	
Γ_{111}	$\gamma f_4(2050)$	$< 5.3 \times 10^{-5}$	CL=90%	
Γ_{112}	$\gamma f_0(2200) \to \gamma K^+K^-$	$< 2 \times 10^{-4}$	CL=90%	
Γ_{113}	$\gamma f_J(2220) \to \gamma K^+K^-$	$< 8 \times 10^{-7}$	CL=90%	
Γ_{114}	$\gamma f_J(2220) \to \gamma\pi^+\pi^-$	$< 6 \times 10^{-7}$	CL=90%	
Γ_{115}	$\gamma f_J(2220) \to \gamma p\overline{p}$	$< 1.1 \times 10^{-6}$	CL=90%	
Γ_{116}	$\gamma\eta(2225) \to \gamma\phi\phi$	$< 3 \times 10^{-3}$	CL=90%	
Γ_{117}	$\gamma\eta_c(1S)$	$< 2.9 \times 10^{-5}$	CL=90%	
Γ_{118}	$\gamma\eta_c(2S)$	$< 4 \times 10^{-4}$	CL=90%	
Γ_{119}	$\gamma\chi_{c0}$	$< 6.6 \times 10^{-5}$	CL=90%	
Γ_{120}	$\gamma\chi_{c1}$	$(4.7 {}^{+2.4}_{-1.9}) \times 10^{-5}$		
Γ_{121}	$\gamma\chi_{c2}$	$< 7.6 \times 10^{-6}$	CL=90%	
Γ_{122}	$\gamma\chi_{c1}(3872)$	$< 4 \times 10^{-5}$	CL=90%	
Γ_{123}	$\gamma\chi_{c1}(3872)$, $\chi_{c1} \to \pi^+\pi^-\pi^0 J/\psi$	$< 2.8 \times 10^{-6}$	CL=90%	
Γ_{124}	$\gamma\chi_{c0}(3915) \to \omega J/\psi$	$< 3.0 \times 10^{-6}$	CL=90%	
Γ_{125}	$\gamma\chi_{c1}(4140) \to \phi J/\psi$	$< 2.2 \times 10^{-6}$	CL=90%	
Γ_{126}	$\gamma X\overline{X}(m_X < 3.1$ GeV)	[c] $< 1 \times 10^{-3}$	CL=90%	
Γ_{127}	$\gamma X\overline{X}(m_X < 4.5$ GeV)	[d] $< 2.4 \times 10^{-4}$	CL=90%	
Γ_{128}	$\gamma X \to \gamma + \geq 4$ prongs	[e] $< 1.78 \times 10^{-4}$	CL=95%	
Γ_{129}	γA^0	[f]		
Γ_{130}	$\gamma A^0 \to \gamma\mu^+\mu^-$	[g] $< 9 \times 10^{-6}$	CL=90%	
Γ_{131}	$\gamma A^0 \to \gamma\tau^+\tau^-$	[a] $< 1.30 \times 10^{-4}$	CL=90%	
Γ_{132}	$\gamma A^0 \to \gamma gg$	[h] < 1 %	CL=90%	
Γ_{133}	$\gamma A^0 \to \gamma s\overline{s}$	[h] $< 1 \times 10^{-3}$	CL=90%	

Lepton Family number (*LF*) violating modes

Γ_{134}	$e^\pm\mu^\mp$	*LF* $< 3.9 \times 10^{-7}$	CL=90%	
Γ_{135}	$\mu^\pm\tau^\mp$	*LF* $< 2.7 \times 10^{-6}$	CL=90%	
Γ_{136}	$e^\pm\tau^\mp$	*LF* $< 2.7 \times 10^{-6}$	CL=90%	
Γ_{137}	$\gamma e^\pm\mu^\mp$	*LF* $< 4.2 \times 10^{-7}$	CL=90%	
Γ_{138}	$\gamma\mu^\pm\tau^\mp$	*LF* $< 6.1 \times 10^{-6}$	CL=90%	
Γ_{139}	$\gamma e^\pm\tau^\mp$	*LF* $< 6.5 \times 10^{-6}$	CL=90%	

Other decays

Γ_{140}	invisible	$< 3.0 \times 10^{-4}$	CL=90%	
Γ_{141}	hadrons	(96 ± 4) %		

[a] $2m_\tau < M(\tau^+\tau^-) < 9.2$ GeV
[b] 2 GeV $< m_{K^+K^-} <$ 3 GeV
[c] $X\overline{X}$ = vectors with $m < 3.1$ GeV
[d] X and $\overline{X}$ = zero spin with $m < 4.5$ GeV
[e] 1.5 GeV $< m_X <$ 5.0 GeV
[f] A^0 = scalar with $m < 8.0$ GeV
[g] 201 MeV $< M(\mu^+\mu^-) <$ 3565 MeV
[h] 0.5 GeV $< m_X <$ 9.0 GeV, where m_X is the invariant mass of the hadronic final state.

$\Upsilon(1S)$ $\Gamma(i)\Gamma(e^+e^-)/\Gamma(\text{total})$

$\Gamma(\mu^+\mu^-) \times \Gamma(e^+e^-)/\Gamma_{total}$ — $\Gamma_3\Gamma_2/\Gamma$

VALUE (eV)	DOCUMENT ID		TECN	COMMENT
31.2±1.6±1.7	KOBEL	92	CBAL	$e^+e^- \to \mu^+\mu^-$

$\Gamma(\text{hadrons}) \times \Gamma(e^+e^-)/\Gamma_{total}$ — $\Gamma_{141}\Gamma_2/\Gamma$

VALUE (keV)	DOCUMENT ID		TECN	COMMENT
1.240±0.016 OUR AVERAGE				
1.252±0.004±0.019	[1] ROSNER	06	CLEO	9.5 $e^+e^- \to$ hadrons
1.187±0.023±0.031	[1] BARU	92B	MD1	$e^+e^- \to$ hadrons
1.23 ±0.02 ±0.05	[1] JAKUBOWSKI	88	CBAL	$e^+e^- \to$ hadrons
1.37 ±0.06 ±0.09	[2] GILES	84B	CLEO	$e^+e^- \to$ hadrons
1.23 ±0.08 ±0.04	[2] ALBRECHT	82	DASP	$e^+e^- \to$ hadrons
1.13 ±0.07 ±0.11	[2] NICZYPORUK	82	LENA	$e^+e^- \to$ hadrons
1.09 ±0.25	[2] BOCK	80	CNTR	$e^+e^- \to$ hadrons
1.35 ±0.14	[3] BERGER	79	PLUT	$e^+e^- \to$ hadrons

[1] Radiative corrections evaluated following KURAEV 85.
[2] Radiative corrections reevaluated by BUCHMUELLER 88 following KURAEV 85.
[3] Radiative corrections reevaluated by ALEXANDER 89 using $B(\mu\mu) = 0.026$.

$\Upsilon(1S)$ PARTIAL WIDTHS

$\Gamma(e^+e^-)$ — Γ_2

VALUE (keV)	DOCUMENT ID
1.340±0.018 OUR EVALUATION	

$\Upsilon(1S)$ BRANCHING RATIOS

$\Gamma(\tau^+\tau^-)/\Gamma_{total}$ — Γ_1/Γ

VALUE (units 10^{-2})	EVTS	DOCUMENT ID		TECN	COMMENT
2.60±0.10 OUR AVERAGE					
2.53±0.13±0.04	60k	[1] BESSON	07	CLEO	$e^+e^- \to \Upsilon(1S) \to \tau^+\tau^-$
$2.61\pm0.12{}^{+0.09}_{-0.13}$	25k	CINABRO	94B	CLE2	$e^+e^- \to \tau^+\tau^-$
2.7 ±0.4 ±0.2		[2] ALBRECHT	85C	ARG	$\Upsilon(2S) \to \pi^+\pi^-\tau^+\tau^-$
3.4 ±0.4 ±0.4		GILES	83	CLEO	$e^+e^- \to \tau^+\tau^-$

[1] BESSON 07 reports $[\Gamma(\Upsilon(1S) \to \tau^+\tau^-)/\Gamma_{total}] / [B(\Upsilon(1S) \to \mu^+\mu^-)] = 1.02 \pm 0.02 \pm 0.05$ which we multiply by our best (shown rounded) value $B(\Upsilon(1S) \to \mu^+\mu^-) = (2.48 \pm 0.04) \times 10^{-2}$. Our first error is their experiment's error and our second error is the systematic error from using our best (shown rounded) value.
[2] Using $B(\Upsilon(1S) \to ee) = B(\Upsilon(1S) \to \mu\mu) = 0.0256$; not used for width evaluations.

$\Gamma(e^+e^-)/\Gamma_{total}$ — Γ_2/Γ

VALUE (units 10^{-2})	EVTS	DOCUMENT ID		TECN	COMMENT
2.39±0.08 OUR AVERAGE					
2.40±0.01±0.12	191k	PATRA	22	BELL	$\Upsilon(2S) \to \pi^+\pi^-e^+e^-$
2.29±0.08±0.11		ALEXANDER	98	CLE2	$\Upsilon(2S) \to \pi^+\pi^-e^+e^-$
2.42±0.14±0.14	307	ALBRECHT	87	ARG	$\Upsilon(2S) \to \pi^+\pi^-e^+e^-$
2.8 ±0.3 ±0.2	826	BESSON	84	CLEO	$\Upsilon(2S) \to \pi^+\pi^-e^+e^-$
5.1 ±3.0		BERGER	80C	PLUT	$e^+e^- \to e^+e^-$

Int. J. Mod. Phys. A 2026.41. Downloaded from www.worldscientific.com by CALIFORNIA @ BERKELEY on 09/16/26. Re-use and distribution is strictly not permitted, except for Open Access articles.

$\Gamma(\mu^+\mu^-)/\Gamma_{total}$ — Γ_3/Γ

VALUE (units 10^{-2})	EVTS	DOCUMENT ID		TECN	COMMENT
2.48±0.04 OUR AVERAGE					
2.46±0.01±0.11	246k	PATRA	22	BELL	$\Upsilon(2S) \to \pi^+\pi^-\mu^+\mu^-$
2.49±0.02±0.07	345k	ADAMS	05	CLEO	$e^+e^- \to \mu^+\mu^-$
2.49±0.08±0.13		ALEXANDER	98	CLE2	$\Upsilon(2S) \to \pi^+\pi^-\mu^+\mu^-$
2.12±0.20±0.10		[1] BARU	92	MD1	$e^+e^- \to \mu^+\mu^-$
2.31±0.12±0.10		[1] KOBEL	92	CBAL	$e^+e^- \to \mu^+\mu^-$
2.52±0.07±0.07		CHEN	89B	CLEO	$e^+e^- \to \mu^+\mu^-$
2.61±0.09±0.11		KAARSBERG	89	CSB2	$e^+e^- \to \mu^+\mu^-$
2.30±0.25±0.13	86	ALBRECHT	87	ARG	$\Upsilon(2S) \to \pi^+\pi^-\mu^+\mu^-$
2.9 ±0.3 ±0.2	864	BESSON	84	CLEO	$\Upsilon(2S) \to \pi^+\pi^-\mu^+\mu^-$
2.7 ±0.3 ±0.3		ANDREWS	83	CLEO	$e^+e^- \to \mu^+\mu^-$
3.2 ±1.3 ±0.3		ALBRECHT	82	DASP	$e^+e^- \to \mu^+\mu^-$
3.8 ±1.5 ±0.2		NICZYPORUK	82	LENA	$e^+e^- \to \mu^+\mu^-$
$1.4\ ^{+3.4}_{-1.4}$		BOCK	80	CNTR	$e^+e^- \to \mu^+\mu^-$
2.2 ±2.0		BERGER	79	PLUT	$e^+e^- \to \mu^+\mu^-$

[1] Taking into account interference between the resonance and continuum.

$\Gamma(\tau^+\tau^-)/\Gamma(\mu^+\mu^-)$ — Γ_1/Γ_3

VALUE	EVTS	DOCUMENT ID		TECN	COMMENT
1.008±0.023 OUR AVERAGE					
1.005±0.013±0.022	0.7M	[1] DEL-AMO-SA...10C		BABR	$\Upsilon(3S) \to \pi^+\pi^-\Upsilon(1S)$
1.02 ±0.02 ±0.05	60k	BESSON	07	CLEO	$e^+e^- \to \Upsilon(1S)$

[1] Allows any number of extra photons with total energy < 500 MeV.

$\Gamma(ggg)/\Gamma_{total}$ — Γ_4/Γ

VALUE (units 10^{-2})	EVTS	DOCUMENT ID		TECN	COMMENT
81.7±0.7	20M	[1] BESSON	06A	CLEO	$\Upsilon(1S) \to$ hadrons

[1] Calculated using the value $\Gamma(\gamma gg)/\Gamma(ggg) = (2.70 \pm 0.01 \pm 0.13 \pm 0.24)\%$ from BESSON 06A and PDG 08 values of $B(\mu^+\mu^-) = (2.48 \pm 0.05)\%$ and $R_{hadrons} = 3.51$. The statistical error is negligible and the systematic error is partially correlated with that of $\Gamma(\gamma gg)/\Gamma_{total}$ measurement of BESSON 06A.

$\Gamma(\gamma gg)/\Gamma_{total}$ — Γ_5/Γ

VALUE (units 10^{-2})	EVTS	DOCUMENT ID		TECN	COMMENT
2.20±0.60	400k	[1] BESSON	06A	CLEO	$\Upsilon(1S) \to \gamma +$ hadrons

[1] Calculated using BESSON 06A values of $\Gamma(\gamma gg)/\Gamma(ggg) = (2.70 \pm 0.01 \pm 0.13 \pm 0.24)\%$ and $\Gamma(ggg)/\Gamma_{total}$. The statistical error is negligible and the systematic error is partially correlated with that of $\Gamma(ggg)/\Gamma_{total}$ measurement of BESSON 06A.

$\Gamma(\gamma gg)/\Gamma(ggg)$ — Γ_5/Γ_4

VALUE (units 10^{-2})	EVTS	DOCUMENT ID		TECN	COMMENT
2.70±0.01±0.27	20M	BESSON	06A	CLEO	$\Upsilon(1S) \to (\gamma +)$ hadrons

$\Gamma(\eta'(958)$ anything$)/\Gamma_{total}$ — Γ_6/Γ

VALUE	DOCUMENT ID		TECN	COMMENT
0.0294±0.0024 OUR AVERAGE				
0.030 ±0.002 ±0.002	AQUINES	06A	CLE3	$\Upsilon(1S) \to \eta'$ anything
0.028 ±0.004 ±0.002	ARTUSO	03	CLE2	$\Upsilon(1S) \to \eta'$ anything

$\Gamma(J/\psi(1S)$ anything$)/\Gamma_{total}$ — Γ_7/Γ

VALUE (units 10^{-4})	CL%	EVTS	DOCUMENT ID		TECN	COMMENT
5.4 ±0.4 OUR FIT Error includes scale factor of 1.4.						
5.4 ±0.4 OUR AVERAGE Error includes scale factor of 1.5.						
5.25±0.13±0.25		3k	SHEN	16	BELL	$e^+e^- \to J/\psi X$
6.4 ±0.4 ±0.6		730	BRIERE	04	CLEO	$e^+e^- \to J/\psi X$
11 ±4 ±2			[1] FULTON	89	CLEO	$e^+e^- \to \mu^+\mu^- X$
• • • We do not use the following data for averages, fits, limits, etc. • • •						
<6.8	90		ALBRECHT	92J	ARG	$e^+e^- \to e^+e^- X$, $\mu^+\mu^- X$
<17	90		MASCHMANN	90	CBAL	$e^+e^- \to$ hadrons
<200	90		NICZYPORUK	83	LENA	

[1] Using $B((J/\psi) \to \mu^+\mu^-) = (6.9 \pm 0.9)\%$.

$\Gamma(J/\psi(1S)\eta_c)/\Gamma_{total}$ — Γ_8/Γ

VALUE	CL%	DOCUMENT ID		TECN	COMMENT
$<2.2 \times 10^{-6}$	90	YANG	14	BELL	$e^+e^- \to J/\psi X$

$\Gamma(J/\psi(1S)\chi_{c0})/\Gamma_{total}$ — Γ_9/Γ

VALUE	CL%	DOCUMENT ID		TECN	COMMENT
$<3.4 \times 10^{-6}$	90	YANG	14	BELL	$e^+e^- \to J/\psi X$

$\Gamma(J/\psi(1S)\chi_{c1})/\Gamma_{total}$ — Γ_{10}/Γ

VALUE (units 10^{-6})	EVTS	DOCUMENT ID		TECN	COMMENT
3.90±1.21±0.23	20	YANG	14	BELL	$e^+e^- \to J/\psi X$

$\Gamma(J/\psi(1S)\chi_{c2})/\Gamma_{total}$ — Γ_{11}/Γ

VALUE	CL%	DOCUMENT ID		TECN	COMMENT
$<1.4 \times 10^{-6}$	90	YANG	14	BELL	$e^+e^- \to J/\psi X$

$\Gamma(J/\psi(1S)\eta_c(2S))/\Gamma_{total}$ — Γ_{12}/Γ

VALUE	CL%	DOCUMENT ID		TECN	COMMENT
$<2.2 \times 10^{-6}$	90	YANG	14	BELL	$e^+e^- \to J/\psi X$

$\Gamma(J/\psi(1S)X(3940))/\Gamma_{total}$ — Γ_{13}/Γ

VALUE	CL%	DOCUMENT ID		TECN	COMMENT
$<5.4 \times 10^{-6}$	90	YANG	14	BELL	$e^+e^- \to J/\psi X$

$\Gamma(J/\psi(1S)X(4160))/\Gamma_{total}$ — Γ_{14}/Γ

VALUE	CL%	DOCUMENT ID		TECN	COMMENT
$<5.4 \times 10^{-6}$	90	YANG	14	BELL	$e^+e^- \to J/\psi X$

$\Gamma(X(4350)$ anything, $X \to J/\psi(1S)\phi)/\Gamma_{total}$ — Γ_{15}/Γ

VALUE	CL%	DOCUMENT ID		TECN	COMMENT
$<8.1 \times 10^{-6}$	90	SHEN	16	BELL	$\Upsilon(1S) \to J/\psi K^+K^- X$

$\Gamma(T_{c\bar{c}1}(3900)^\pm$ anything, $T_{c\bar{c}1} \to J/\psi(1S)\pi^\pm)/\Gamma_{total}$ — Γ_{16}/Γ

VALUE	CL%	DOCUMENT ID		TECN	COMMENT
$<1.3 \times 10^{-5}$	90	SHEN	16	BELL	$\Upsilon(1S) \to J/\psi\pi^\pm X$

$\Gamma(T_{c\bar{c}1}(4200)^\pm$ anything, $Z_c \to J/\psi(1S)\pi^\pm)/\Gamma_{total}$ — Γ_{17}/Γ

VALUE	CL%	DOCUMENT ID		TECN	COMMENT
$<6.0 \times 10^{-5}$	90	SHEN	16	BELL	$\Upsilon(1S) \to J/\psi\pi^\pm X$

$\Gamma(T_{c\bar{c}1}(4430)^\pm$ anything, $T_{c\bar{c}1} \to J/\psi(1S)\pi^\pm)/\Gamma_{total}$ — Γ_{18}/Γ

VALUE	CL%	DOCUMENT ID		TECN	COMMENT
$<4.9 \times 10^{-5}$	90	SHEN	16	BELL	$\Upsilon(1S) \to J/\psi\pi^\pm X$

$\Gamma(P_{c\bar{c}s}(4459)/\overline{P}_{c\bar{c}s}(4459)$ anything$)/\Gamma_{total}$ — Γ_{19}/Γ

VALUE (units 10^{-6})	EVTS	DOCUMENT ID		TECN	COMMENT
3.5±2.0±0.2	21	[1] ADACHI	25A	BELL	$e^+e^- \to \Upsilon(1S)$

[1] 21 ± 5 corresponds to the number of $P_{c\bar{c}s}(4459)$ events in the combined $\Upsilon(1S)$ and $\Upsilon(2S)$ samples.

$\Gamma(P_{c\bar{c}s}(4338)/\overline{P}_{c\bar{c}s}(4338)$ anything$)/\Gamma_{total}$ — Γ_{20}/Γ

VALUE	CL%	DOCUMENT ID		TECN	COMMENT
$<1.8 \times 10^{-6}$	90	ADACHI	25A	BELL	$e^+e^- \to \Upsilon(1S)$

$\Gamma(P_c(4312)$ anything, $P_c(4312) \to pJ/\psi(1S))/\Gamma_{total}$ — Γ_{21}/Γ

VALUE	CL%	DOCUMENT ID		TECN	COMMENT
$<5.7 \times 10^{-6}$	90	DONG	25	BELL	$e^+e^- \to \Upsilon(1S)$

$\Gamma(P_c(4440)$ anything, $P_c(4440) \to pJ/\psi(1S))/\Gamma_{total}$ — Γ_{22}/Γ

VALUE	CL%	DOCUMENT ID		TECN	COMMENT
$<10.0 \times 10^{-6}$	90	DONG	25	BELL	$e^+e^- \to \Upsilon(1S)$

$\Gamma(P_c(4457)$ anything, $P_c(4457) \to pJ/\psi(1S))/\Gamma_{total}$ — Γ_{23}/Γ

VALUE	CL%	DOCUMENT ID		TECN	COMMENT
$<7.6 \times 10^{-6}$	90	DONG	25	BELL	$e^+e^- \to \Upsilon(1S)$

$\Gamma(p/\overline{p}J/\psi(1S)$ anything$)/\Gamma_{total}$ — Γ_{24}/Γ

VALUE (units 10^{-5})	EVTS	DOCUMENT ID		TECN	COMMENT
8.1±0.6±0.5	377	DONG	25	BELL	$e^+e^- \to \Upsilon(1S)$

$\Gamma(J/\psi(1S)\Lambda/\overline{\Lambda}$ anything$)/\Gamma_{total}$ — Γ_{25}/Γ

VALUE (units 10^{-6})	EVTS	DOCUMENT ID		TECN	COMMENT
36.9±5.3±2.4	84	ADACHI	25A	BELL	$e^+e^- \to \Upsilon(1S)$

$\Gamma(X_{cs}^\pm$ anything, $X \to J/\psi K^\pm)/\Gamma_{total}$ — Γ_{26}/Γ

VALUE	CL%	DOCUMENT ID		TECN	COMMENT
$<5.7 \times 10^{-6}$	90	SHEN	16	BELL	$\Upsilon(1S) \to J/\psi K^- X$

$\Gamma(\psi(4230)$ anything, $\psi \to J/\psi(1S)\pi^+\pi^-)/\Gamma_{total}$ — Γ_{27}/Γ

VALUE	CL%	DOCUMENT ID		TECN	COMMENT
$<3.8 \times 10^{-5}$	90	SHEN	16	BELL	$\Upsilon(1S) \to J/\psi\pi^+\pi^- X$

$\Gamma(\psi(4230)$ anything, $\psi \to J/\psi(1S)K^+K^-)/\Gamma_{total}$ — Γ_{28}/Γ

VALUE	CL%	DOCUMENT ID		TECN	COMMENT
$<7.5 \times 10^{-6}$	90	SHEN	16	BELL	$\Upsilon(1S) \to J/\psi K^+K^- X$

$\Gamma(\chi_{c1}(4140)$ anything, $\chi_{c1} \to J/\psi(1S)\phi)/\Gamma_{total}$ — Γ_{29}/Γ

VALUE	CL%	DOCUMENT ID		TECN	COMMENT
$<5.2 \times 10^{-6}$	90	SHEN	16	BELL	$\Upsilon(1S) \to J/\psi K^+K^- X$

$\Gamma(\chi_{c0}$ anything$)/\Gamma(J/\psi(1S)$ anything$)$ — Γ_{30}/Γ_7

VALUE	CL%	DOCUMENT ID		TECN	COMMENT
<7.4	90	BRIERE	04	CLEO	$e^+e^- \to J/\psi X$

Int. J. Mod. Phys. A 2026.41. Downloaded from www.worldscientific.com
by UNIVERSITY OF CALIFORNIA @ BERKELEY on 09/16/26. Re-use and distribution is strictly not permitted, except for Open Access articles.

$\Gamma(\chi_{c1}\text{ anything})/\Gamma_{\text{total}}$ — Γ_{31}/Γ

VALUE (units 10^{-4})	EVTS	DOCUMENT ID		TECN	COMMENT
1.90±0.35 OUR FIT					
1.90±0.43±0.14	215	JIA	17	BELL	$\Upsilon(1S) \to \gamma J/\psi(1S)$

$\Gamma(\chi_{c1}\text{ anything})/\Gamma(J/\psi(1S)\text{ anything})$ — Γ_{31}/Γ_{7}

VALUE	EVTS	DOCUMENT ID		TECN	COMMENT
0.35±0.07 OUR FIT					
0.35±0.08±0.06	52 ± 12	BRIERE	04	CLEO	$e^+e^- \to J/\psi X$

$\Gamma(\chi_{c1}(1P)X_{tetra})/\Gamma_{\text{total}}$ — Γ_{32}/Γ

VALUE	CL%	DOCUMENT ID		TECN	COMMENT
<37.8 × 10^{-6}	90	[1] JIA	17A	BELL	$e^+e^- \to$ hadrons

[1] For a tetraquark state X_{tetra}, with mass in the range 1.16–2.46 GeV and width in the range 0–0.3 GeV. Measured 90% CL limits as a function of X_{tetra} mass and width range from 4.4 × 10^{-6} to 37.8 × 10^{-6}.

$\Gamma(\chi_{c2}\text{ anything})/\Gamma(J/\psi(1S)\text{ anything})$ — Γ_{33}/Γ_{7}

VALUE	EVTS	DOCUMENT ID		TECN	COMMENT
0.52±0.12±0.09	47 ± 11	BRIERE	04	CLEO	$e^+e^- \to J/\psi X$

$\Gamma(\psi(2S)\text{ anything})/\Gamma_{\text{total}}$ — Γ_{34}/Γ

VALUE (units 10^{-4})	EVTS	DOCUMENT ID		TECN	COMMENT
1.23±0.17±0.11	215	SHEN	16	BELL	$e^+e^- \to \psi(2S)X$

$\Gamma(\psi(2S)\text{ anything})/\Gamma(J/\psi(1S)\text{ anything})$ — Γ_{34}/Γ_{7}

VALUE	EVTS	DOCUMENT ID		TECN	COMMENT
0.41±0.11±0.08	42 ± 11	BRIERE	04	CLEO	$e^+e^- \to J/\psi\pi^+\pi^-X$

$\Gamma(\psi(2S)\eta_c)/\Gamma_{\text{total}}$ — Γ_{35}/Γ

VALUE	CL%	DOCUMENT ID		TECN	COMMENT
<3.6 × 10^{-6}	90	YANG	14	BELL	$e^+e^- \to \psi(2S)X$

$\Gamma(\psi(2S)\chi_{c0})/\Gamma_{\text{total}}$ — Γ_{36}/Γ

VALUE	CL%	DOCUMENT ID		TECN	COMMENT
<6.5 × 10^{-6}	90	YANG	14	BELL	$e^+e^- \to \psi(2S)X$

$\Gamma(\psi(2S)\chi_{c1})/\Gamma_{\text{total}}$ — Γ_{37}/Γ

VALUE	CL%	DOCUMENT ID		TECN	COMMENT
<4.5 × 10^{-6}	90	YANG	14	BELL	$e^+e^- \to \psi(2S)X$

$\Gamma(\psi(2S)\chi_{c2})/\Gamma_{\text{total}}$ — Γ_{38}/Γ

VALUE	CL%	DOCUMENT ID		TECN	COMMENT
<2.1 × 10^{-6}	90	YANG	14	BELL	$e^+e^- \to \psi(2S)X$

$\Gamma(\psi(2S)\eta_c(2S))/\Gamma_{\text{total}}$ — Γ_{39}/Γ

VALUE	CL%	DOCUMENT ID		TECN	COMMENT
<3.2 × 10^{-6}	90	YANG	14	BELL	$e^+e^- \to \psi(2S)X$

$\Gamma(\psi(2S)X(3940))/\Gamma_{\text{total}}$ — Γ_{40}/Γ

VALUE	CL%	DOCUMENT ID		TECN	COMMENT
<2.9 × 10^{-6}	90	YANG	14	BELL	$e^+e^- \to \psi(2S)X$

$\Gamma(\psi(2S)X(4160))/\Gamma_{\text{total}}$ — Γ_{41}/Γ

VALUE	CL%	DOCUMENT ID		TECN	COMMENT
<2.9 × 10^{-6}	90	YANG	14	BELL	$e^+e^- \to \psi(2S)X$

$\Gamma(\psi(4230)\text{ anything}, \psi \to \psi(2S)\pi^+\pi^-)/\Gamma_{\text{total}}$ — Γ_{42}/Γ

VALUE	CL%	DOCUMENT ID		TECN	COMMENT
<7.9 × 10^{-5}	90	SHEN	16	BELL	$\Upsilon(1S) \to \psi(2S)\pi^+\pi^-X$

$\Gamma(\psi(4360)\text{ anything}, \psi \to \psi(2S)\pi^+\pi^-)/\Gamma_{\text{total}}$ — Γ_{43}/Γ

VALUE	CL%	DOCUMENT ID		TECN	COMMENT
<5.2 × 10^{-5}	90	SHEN	16	BELL	$\Upsilon(1S) \to \psi(2S)\pi^+\pi^-X$

$\Gamma(\psi(4660)\text{ anything}, \psi \to \psi(2S)\pi^+\pi^-)/\Gamma_{\text{total}}$ — Γ_{44}/Γ

VALUE	CL%	DOCUMENT ID		TECN	COMMENT
<2.2 × 10^{-5}	90	SHEN	16	BELL	$\Upsilon(1S) \to \psi(2S)\pi^+\pi^-X$

$\Gamma(T_{c\overline{c}}(4050)^{\pm}\text{ anything}, X \to \psi(2S)\pi^{\pm})/\Gamma_{\text{total}}$ — Γ_{45}/Γ

VALUE	CL%	DOCUMENT ID		TECN	COMMENT
<8.8 × 10^{-5}	90	SHEN	16	BELL	$\Upsilon(1S) \to \psi(2S)\pi^{\pm}X$

$\Gamma(T_{c\overline{c}1}(4430)^{\pm}\text{ anything}, T_{c\overline{c}1} \to \psi(2S)\pi^{\pm})/\Gamma_{\text{total}}$ — Γ_{46}/Γ

VALUE	CL%	DOCUMENT ID		TECN	COMMENT
<6.7 × 10^{-5}	90	SHEN	16	BELL	$\Upsilon(1S) \to \psi(2S)\pi^{\pm}X$

$\Gamma(\chi_{c1}(3872)\text{ anything})/\Gamma_{\text{total}}$ — Γ_{47}/Γ

VALUE	CL%	DOCUMENT ID		TECN	COMMENT
<2.2 × 10^{-4}	90	[1] SHEN	16	BELL	$\Upsilon(1S) \to J/\psi\pi^+\pi^-X$

[1] SHEN 16 reports $[\Gamma(\Upsilon(1S) \to \chi_{c1}(3872)\text{anything})/\Gamma_{\text{total}}] \times [B(\chi_{c1}(3872) \to \pi^+\pi^- J/\psi(1S))] < 9.5 \times 10^{-6}$ which we divide by our best (shown rounded) value $B(\chi_{c1}(3872) \to \pi^+\pi^- J/\psi(1S)) = 4.3 \times 10^{-2}$.

$\Gamma(T_{c\overline{c}1}(4200)^+ T_{c\overline{c}1}(4200)^-)/\Gamma_{\text{total}}$ — Γ_{48}/Γ

VALUE	CL%	DOCUMENT ID		TECN	COMMENT
<22.3 × 10^{-6}	90	[1] JIA	18	BELL	$\Upsilon(1S) \to J/\psi\pi^{\pm}X$

[1] Assuming $B(T_{c\overline{c}1}(4200)^{\pm} \to J/\psi\pi^{\pm}) = 1$.

$\Gamma(T_{c\overline{c}1}(3900)^{\pm} T_{c\overline{c}1}(4200)^{\mp})/\Gamma_{\text{total}}$ — Γ_{49}/Γ

VALUE	CL%	DOCUMENT ID		TECN	COMMENT
<8.1 × 10^{-6}	90	[1] JIA	18	BELL	$\Upsilon(1S) \to J/\psi\pi^{\pm}X$

[1] Assuming $B(T_{c\overline{c}1}(4200)^{\pm} \to J/\psi\pi^{\pm}) = 1 = B(T_{c\overline{c}1}(3900)^{\pm} \to J/\psi\pi^{\pm})$.

$\Gamma(T_{c\overline{c}1}(3900)^+ T_{c\overline{c}1}(3900)^-)/\Gamma_{\text{total}}$ — Γ_{50}/Γ

VALUE	CL%	DOCUMENT ID		TECN	COMMENT
<1.8 × 10^{-6}	90	[1] JIA	18	BELL	$\Upsilon(1S) \to J/\psi\pi^{\pm}X$

[1] Assuming $B(T_{c\overline{c}1}(3900)^{\pm} \to J/\psi\pi^{\pm}) = 1$

$\Gamma(T_{c\overline{c}}(4050)^+ T_{c\overline{c}}(4050)^-)/\Gamma_{\text{total}}$ — Γ_{51}/Γ

VALUE	CL%	DOCUMENT ID		TECN	COMMENT
<15.8 × 10^{-6}	90	[1] JIA	18	BELL	$\Upsilon(1S) \to \chi_{c1}(1P)\pi^{\pm}X$

[1] Assuming $B(T_{c\overline{c}}(4050)^{\pm} \to \chi_{c1}(1P)\pi^{\pm}) = 1$

$\Gamma(T_{c\overline{c}}(4250)^+ T_{c\overline{c}}(4250)^-)/\Gamma_{\text{total}}$ — Γ_{52}/Γ

VALUE	CL%	DOCUMENT ID		TECN	COMMENT
<26.6 × 10^{-6}	90	[1] JIA	18	BELL	$\Upsilon(1S) \to \chi_{c1}(1P)\pi^{\pm}X$

[1] Assuming $B(T_{c\overline{c}}(4250)^{\pm} \to \chi_{c1}(1P)\pi^{\pm}) = 1$

$\Gamma(T_{c\overline{c}}(4050)^{\pm} T_{c\overline{c}}(4250)^{\mp})/\Gamma_{\text{total}}$ — Γ_{53}/Γ

VALUE	CL%	DOCUMENT ID		TECN	COMMENT
<44.2 × 10^{-6}	90	[1] JIA	18	BELL	$\Upsilon(1S) \to \chi_{c1}(1P)\pi^{\pm}X$

[1] Assuming $B(T_{c\overline{c}}(4050)^{\pm} \to \chi_{c1}(1P)\pi^{\pm}) = 1 = B(T_{c\overline{c}}(4250)^{\pm} \to \chi_{c1}(1P)\pi^{\pm})$

$\Gamma(T_{c\overline{c}1}(4430)^+ T_{c\overline{c}1}(4430)^-)/\Gamma_{\text{total}}$ — Γ_{54}/Γ

VALUE	CL%	DOCUMENT ID		TECN	COMMENT
<20.3 × 10^{-6}	90	[1] JIA	18	BELL	$\Upsilon(2S) \to \psi(2S)\pi^{\pm}X$

[1] Assuming $B(T_{c\overline{c}1}(4430)^{\pm} \to \psi(2S)\pi^{\pm}) = 1$

$\Gamma(T_{c\overline{c}}(4055)^{\pm} T_{c\overline{c}}(4055)^{\mp})/\Gamma_{\text{total}}$ — Γ_{55}/Γ

VALUE	CL%	DOCUMENT ID		TECN	COMMENT
<23.3 × 10^{-6}	90	[1] JIA	18	BELL	$\Upsilon(1S) \to \psi(2S)\pi^{\pm}X$

[1] Assuming $B(T_{c\overline{c}}(4055)^{\pm} \to \psi(2S)\pi^{\pm}) = 1$

$\Gamma(T_{c\overline{c}}(4055)^{\pm} T_{c\overline{c}1}(4430)^{\mp})/\Gamma_{\text{total}}$ — Γ_{56}/Γ

VALUE	CL%	DOCUMENT ID		TECN	COMMENT
<45.5 × 10^{-6}	90	[1] JIA	18	BELL	$\Upsilon(1S) \to \psi(2S)\pi^{\pm}X$

[1] Assuming $B(T_{c\overline{c}}(4055)^{\pm} \to \psi(2S)\pi^{\pm}) = 1 = B(T_{c\overline{c}1}(4430)^{\pm} \to \psi(2S)\pi^{\pm})$

$\Gamma(\rho\pi)/\Gamma_{\text{total}}$ — Γ_{57}/Γ

VALUE (units 10^{-6})	CL%	DOCUMENT ID		TECN	COMMENT
<3.68	90	SHEN	13	BELL	$\Upsilon(1S) \to \pi^+\pi^-\pi^0$
• • • We do not use the following data for averages, fits, limits, etc. • • •					
<1 × 10^3	90	BLINOV	90	MD1	$\Upsilon(1S) \to \rho^0\pi^0$
<2 × 10^2	90	FULTON	90B		$\Upsilon(1S) \to \rho^0\pi^0$
<2.1 × 10^3	90	NICZYPORUK	83	LENA	$\Upsilon(1S) \to \rho^0\pi^0$

$\Gamma(\omega\pi^0)/\Gamma_{\text{total}}$ — Γ_{58}/Γ

VALUE (units 10^{-6})	CL%	DOCUMENT ID		TECN	COMMENT
<3.90	90	SHEN	13	BELL	$\Upsilon(1S) \to \pi^+\pi^-\pi^0\pi^0$

$\Gamma(\pi^+\pi^-)/\Gamma_{\text{total}}$ — Γ_{59}/Γ

VALUE (units 10^{-4})	CL%	DOCUMENT ID		TECN	COMMENT
<5	90	BARU	92	MD1	$\Upsilon(1S) \to \pi^+\pi^-$

$\Gamma(K^+K^-)/\Gamma_{\text{total}}$ — Γ_{60}/Γ

VALUE (units 10^{-4})	CL%	DOCUMENT ID		TECN	COMMENT
<5	90	BARU	92	MD1	$\Upsilon(1S) \to K^+K^-$

$\Gamma(p\overline{p})/\Gamma_{\text{total}}$ — Γ_{61}/Γ

VALUE (units 10^{-4})	CL%	DOCUMENT ID		TECN	COMMENT
<5	90	[1] BARU	96	MD1	$\Upsilon(1S) \to p\overline{p}$

[1] Supersedes BARU 92 in this node.

$\Gamma(\pi^+\pi^-\pi^0)/\Gamma_{\text{total}}$ — Γ_{62}/Γ

VALUE (units 10^{-6})	CL%	EVTS	DOCUMENT ID		TECN	COMMENT
2.14±0.72±0.34		26 ± 9	SHEN	13	BELL	$\Upsilon(1S) \to \pi^+\pi^-\pi^0$
• • • We do not use the following data for averages, fits, limits, etc. • • •						
<18.4	90		ANASTASSOV	99	CLE2	$e^+e^- \to$ hadrons

$\Gamma(\phi K^+K^-)/\Gamma_{\text{total}}$ — Γ_{63}/Γ

VALUE (units 10^{-6})	EVTS	DOCUMENT ID		TECN	COMMENT
2.36±0.37±0.29	56	SHEN	12A	BELL	$\Upsilon(1S) \to 2(K^+K^-)$

Int. J. Mod. Phys. A 2026.41. Downloaded from www.worldscientific.com by CALIFORNIA @ BERKELEY on 09/16/26. Re-use and distribution is strictly not permitted, except for Open Access articles.

$\Gamma(\omega\pi^+\pi^-)/\Gamma_{total}$ — Γ_{64}/Γ

VALUE (units 10^{-6})	EVTS	DOCUMENT ID		TECN	COMMENT
4.46±0.67±0.72	64	SHEN	12A	BELL	$\Upsilon(1S) \to 2(\pi^+\pi^-)\pi^0$

$\Gamma(K^*(892)^0 K^-\pi^+ + \text{c.c.})/\Gamma_{total}$ — Γ_{65}/Γ

VALUE (units 10^{-6})	EVTS	DOCUMENT ID		TECN	COMMENT
4.42±0.50±0.58	173	SHEN	12A	BELL	$\Upsilon(1S) \to K^+K^-\pi^+\pi^-$

$\Gamma(\phi f_2'(1525))/\Gamma_{total}$ — Γ_{66}/Γ

VALUE (units 10^{-6})	CL%	DOCUMENT ID		TECN	COMMENT
<1.63	90	SHEN	12A	BELL	$\Upsilon(1S) \to 2(K^+K^-)$

$\Gamma(\omega f_2(1270))/\Gamma_{total}$ — Γ_{67}/Γ

VALUE (units 10^{-6})	CL%	DOCUMENT ID		TECN	COMMENT
<1.79	90	SHEN	12A	BELL	$\Upsilon(1S) \to 2(\pi^+\pi^-)\pi^0$

$\Gamma(\rho(770)a_2(1320))/\Gamma_{total}$ — Γ_{68}/Γ

VALUE (units 10^{-6})	CL%	DOCUMENT ID		TECN	COMMENT
<2.24	90	SHEN	12A	BELL	$\Upsilon(1S) \to 2(\pi^+\pi^-)\pi^0$

$\Gamma(K^*(892)^0\overline{K}_2^*(1430)^0 + \text{c.c.})/\Gamma_{total}$ — Γ_{69}/Γ

VALUE (units 10^{-6})	EVTS	DOCUMENT ID		TECN	COMMENT
3.02±0.68±0.34	42	SHEN	12A	BELL	$\Upsilon(1S) \to K^+K^-\pi^+\pi^-$

$\Gamma(K_1(1270)^\pm K^\mp)/\Gamma_{total}$ — Γ_{70}/Γ

VALUE (units 10^{-6})	CL%	DOCUMENT ID		TECN	COMMENT
<2.41	90	SHEN	12A	BELL	$\Upsilon(1S) \to K^+K^-\pi^+\pi^-$

$\Gamma(K_1(1400)^\pm K^\mp)/\Gamma_{total}$ — Γ_{71}/Γ

VALUE (units 10^{-6})	EVTS	DOCUMENT ID		TECN	COMMENT
1.02±0.35±0.22	24	SHEN	12A	BELL	$\Upsilon(1S) \to K^+K^-\pi^+\pi^-$

$\Gamma(b_1(1235)^\pm\pi^\mp)/\Gamma_{total}$ — Γ_{72}/Γ

VALUE (units 10^{-6})	CL%	DOCUMENT ID		TECN	COMMENT
<1.25	90	SHEN	12A	BELL	$\Upsilon(1S) \to 2(\pi^+\pi^-)\pi^0$

$\Gamma(\pi^+\pi^-\pi^0\pi^0)/\Gamma_{total}$ — Γ_{73}/Γ

VALUE (units 10^{-6})	EVTS	DOCUMENT ID		TECN	COMMENT
12.8±2.0±2.3	143 ± 22	SHEN	13	BELL	$\Upsilon(1S) \to \pi^+\pi^-\pi^0\pi^0$

$\Gamma(K_S^0 K^+\pi^- + \text{c.c.})/\Gamma_{total}$ — Γ_{74}/Γ

VALUE (units 10^{-6})	CL%	EVTS	DOCUMENT ID		TECN	COMMENT
1.59±0.33±0.18		37 ± 8	SHEN	13	BELL	$\Upsilon(1S) \to K_S^0 K^-\pi^+$
• • • We do not use the following data for averages, fits, limits, etc. • • •						
<3.4	90		[1] DOBBS	12A		$\Upsilon(1S) \to K_S^0 K^-\pi^+$

[1] Obtained by analyzing CLEO III data but not authored by the CLEO Collaboration.

$\Gamma(K^*(892)^0\overline{K}^0 + \text{c.c.})/\Gamma_{total}$ — Γ_{75}/Γ

VALUE (units 10^{-6})	EVTS	DOCUMENT ID		TECN	COMMENT
2.92±0.85±0.37	16 ± 5	SHEN	13	BELL	$\Upsilon(1S) \to K_S^0 K^-\pi^+$

$\Gamma(K^*(892)^- K^+ + \text{c.c.})/\Gamma_{total}$ — Γ_{76}/Γ

VALUE (units 10^{-6})	CL%	DOCUMENT ID		TECN	COMMENT
<1.11	90	SHEN	13	BELL	$\Upsilon(1S) \to K_S^0 K^-\pi^+$

$\Gamma(f_1(1285)\text{ anything})/\Gamma_{total}$ — Γ_{77}/Γ

VALUE (units 10^{-3})	EVTS	DOCUMENT ID		TECN	COMMENT
4.6±2.8±1.3	3.1k	JIA	17A	BELL	$e^+e^- \to$ hadrons

$\Gamma(D^*(2010)^\pm\text{ anything})/\Gamma_{total}$ — Γ_{78}/Γ

VALUE (units 10^{-3})	CL%	EVTS	DOCUMENT ID		TECN	COMMENT
25.2±1.3±1.5		≈ 2k	[1] AUBERT	10C	BABR	$\Upsilon(2S) \to \pi^+\pi^-\Upsilon(1S)$
• • • We do not use the following data for averages, fits, limits, etc. • • •						
<19	90		[2] ALBRECHT	92J	ARG	$e^+e^- \to D^0\pi^\pm X$

[1] For $x_p > 0.1$.
[2] For $x_p > 0.2$.

$\Gamma(f_1(1285)X_{tetra})/\Gamma_{total}$ — Γ_{79}/Γ

VALUE	CL%	DOCUMENT ID		TECN	COMMENT
<62.4 × 10^{-6}	90	[1] JIA	17A	BELL	$e^+e^- \to$ hadrons

[1] For a tetraquark state X_{tetra}, with mass in the range 1.16–2.46 GeV and width in the range 0–0.3 GeV. Measured 90% CL limits as a function of X_{tetra} mass and width range from 4.6 × 10^{-6} to 62.4 × 10^{-6}.

$\Gamma(\overline{^2H}\text{ anything})/\Gamma_{total}$ — Γ_{80}/Γ

VALUE (units 10^{-5})	EVTS	DOCUMENT ID		TECN	COMMENT
2.85±0.25 OUR AVERAGE					
$2.81 \pm 0.49^{+0.20}_{-0.24}$		LEES	14G	BABR	$e^+e^- \to \overline{^2H}X$
2.86±0.19±0.21	455	ASNER	07	CLEO	$e^+e^- \to \overline{^2H}X$

$\Gamma(\text{Sum of 100 exclusive modes})/\Gamma_{total}$ — Γ_{81}/Γ

VALUE (units 10^{-2})	DOCUMENT ID		COMMENT
1.200±0.017	[1,2] DOBBS	12A	$\Upsilon(1S) \to$ hadrons

[1] DOBBS 12A presents individual exclusive branching fractions or upper limits for 100 modes of four to ten pions, kaons, or protons.
[2] Obtained by analyzing CLEO III data but not authored by the CLEO Collaboration.

$\Gamma(ggg, \gamma gg \to \overline{d}\text{ anything})/\Gamma(ggg, \gamma gg \to \text{anything})$

VALUE (units 10^{-5})	EVTS	DOCUMENT ID		TECN	COMMENT
3.36±0.23±0.25	455	ASNER	07	CLEO	$e^+e^- \to \overline{d}X$

$\Gamma(\gamma\pi^+\pi^-)/\Gamma_{total}$ — Γ_{82}/Γ

VALUE (units 10^{-5})	DOCUMENT ID		TECN	COMMENT
6.3±1.2±1.3	[1] ANASTASSOV	99	CLE2	$e^+e^- \to$ hadrons

[1] For $m_{\pi\pi} > 1$ GeV.

$\Gamma(\gamma\pi^0\pi^0)/\Gamma_{total}$ — Γ_{83}/Γ

VALUE (units 10^{-5})	DOCUMENT ID		TECN	COMMENT
1.7±0.6±0.3	[1] ANASTASSOV	99	CLE2	$e^+e^- \to$ hadrons

[1] For $m_{\pi\pi} > 1$ GeV.

$\Gamma(\gamma\pi\pi\text{ (S-wave)})/\Gamma_{total}$ — Γ_{84}/Γ

VALUE (units 10^{-5})	DOCUMENT ID		TECN	COMMENT
4.63±0.56±0.48	LEES	18A	BABR	$\Upsilon(1S) \to \gamma\pi^+\pi^-$

$\Gamma(\gamma\pi^0\eta)/\Gamma_{total}$ — Γ_{85}/Γ

VALUE (units 10^{-6})	CL%	DOCUMENT ID		TECN	COMMENT
<2.4	90	[1] BESSON	07A	CLEO	$e^+e^- \to \Upsilon(1S)$

[1] BESSON 07A obtained this limit for $0.7 < m_{\pi^0\eta} < 3$ GeV.

$\Gamma(\gamma K^+K^-)/\Gamma_{total}$ — Γ_{86}/Γ
($2 < m_{K^+K^-} < 3$ GeV)

VALUE (units 10^{-5})	CL%	DOCUMENT ID		TECN	COMMENT
1.14±0.08±0.10	90	ATHAR	06	CLE3	$\Upsilon(1S) \to \gamma K^+K^-$

$\Gamma(\gamma p\overline{p})/\Gamma_{total}$ — Γ_{87}/Γ
($2 < m_{p\overline{p}} < 3$ GeV)

VALUE (units 10^{-5})	CL%	DOCUMENT ID		TECN	COMMENT
<0.6	90	ATHAR	06	CLE3	$\Upsilon(1S) \to \gamma p\overline{p}$

$\Gamma(\gamma 2h^+2h^-)/\Gamma_{total}$ — Γ_{88}/Γ

VALUE (units 10^{-4})	EVTS	DOCUMENT ID		TECN	COMMENT
7.0±1.1±1.0	80 ± 12	FULTON	90B	CLEO	$e^+e^- \to$ hadrons

$\Gamma(\gamma 3h^+3h^-)/\Gamma_{total}$ — Γ_{89}/Γ

VALUE (units 10^{-4})	EVTS	DOCUMENT ID		TECN	COMMENT
5.4±1.5±1.3	39 ± 11	FULTON	90B	CLEO	$e^+e^- \to$ hadrons

$\Gamma(\gamma 4h^+4h^-)/\Gamma_{total}$ — Γ_{90}/Γ

VALUE (units 10^{-4})	EVTS	DOCUMENT ID		TECN	COMMENT
7.4±2.5±2.5	36 ± 12	FULTON	90B	CLEO	$e^+e^- \to$ hadrons

$\Gamma(\gamma\pi^+\pi^-K^+K^-)/\Gamma_{total}$ — Γ_{91}/Γ

VALUE (units 10^{-4})	EVTS	DOCUMENT ID		TECN	COMMENT
2.9±0.7±0.6	29 ± 8	FULTON	90B	CLEO	$e^+e^- \to$ hadrons

$\Gamma(\gamma 2\pi^+2\pi^-)/\Gamma_{total}$ — Γ_{92}/Γ

VALUE (units 10^{-4})	EVTS	DOCUMENT ID		TECN	COMMENT
2.5±0.7±0.5	26 ± 7	FULTON	90B	CLEO	$e^+e^- \to$ hadrons

$\Gamma(\gamma 3\pi^+3\pi^-)/\Gamma_{total}$ — Γ_{93}/Γ

VALUE (units 10^{-4})	EVTS	DOCUMENT ID		TECN	COMMENT
2.5±0.9±0.8	17 ± 5	FULTON	90B	CLEO	$e^+e^- \to$ hadrons

$\Gamma(\gamma 2\pi^+2\pi^-K^+K^-)/\Gamma_{total}$ — Γ_{94}/Γ

VALUE (units 10^{-4})	EVTS	DOCUMENT ID		TECN	COMMENT
2.4±0.9±0.8	18 ± 7	FULTON	90B	CLEO	$e^+e^- \to$ hadrons

$\Gamma(\gamma\pi^+\pi^-p\overline{p})/\Gamma_{total}$ — Γ_{95}/Γ

VALUE (units 10^{-4})	EVTS	DOCUMENT ID		TECN	COMMENT
1.5±0.5±0.3	22 ± 6	FULTON	90B	CLEO	$e^+e^- \to$ hadrons

$\Gamma(\gamma 2\pi^+2\pi^-p\overline{p})/\Gamma_{total}$ — Γ_{96}/Γ

VALUE (units 10^{-4})	EVTS	DOCUMENT ID		TECN	COMMENT
0.4±0.4±0.4	7 ± 6	FULTON	90B	CLEO	$e^+e^- \to$ hadrons

$\Gamma(\gamma 2K^+2K^-)/\Gamma_{total}$ — Γ_{97}/Γ

VALUE (units 10^{-4})	EVTS	DOCUMENT ID		TECN	COMMENT
0.2±0.2	2 ± 2	FULTON	90B	CLEO	$e^+e^- \to$ hadrons

Int. J. Mod. Phys. A 2026.41. Downloaded from www.worldscientific.com
by UNIVERSITY OF CALIFORNIA @ BERKELEY on 09/16/26. Re-use and distribution is strictly not permitted, except for Open Access articles.

$\Gamma(\gamma\eta'(958))/\Gamma_{total}$ — Γ_{98}/Γ

VALUE (units 10^{-6})	CL%	DOCUMENT ID		TECN	COMMENT
< 1.9	90	ATHAR	07A	CLEO	$\Upsilon(1S) \to \gamma\eta' \to \gamma\pi^+\pi^-\eta, \gamma\rho$
• • • We do not use the following data for averages, fits, limits, etc. • • •					
<16	90	RICHICHI	01B	CLE2	$\Upsilon(1S) \to \gamma\eta' \to \gamma\eta\pi^+\pi^-$

$\Gamma(\gamma\eta)/\Gamma_{total}$ — Γ_{99}/Γ

VALUE (units 10^{-6})	CL%	DOCUMENT ID		TECN	COMMENT
< 1.0	90	ATHAR	07A	CLEO	$\Upsilon(1S) \to \gamma\eta \to \gamma\gamma\gamma, \gamma\pi^+\pi^-\pi^0, \gamma 3\pi^0$
• • • We do not use the following data for averages, fits, limits, etc. • • •					
<21	90	MASEK	02	CLEO	$\Upsilon(1S) \to \gamma\eta$

$\Gamma(\gamma f_0(980))/\Gamma_{total}$ — Γ_{100}/Γ

VALUE (units 10^{-5})	CL%	DOCUMENT ID		TECN	COMMENT
<3	90	[1] ATHAR	06	CLE3	$\Upsilon(1S) \to \gamma\pi^+\pi^-$

[1] Assuming $B(f_0(980) \to \pi\pi) = 1$.

$\Gamma(\gamma f_2'(1525))/\Gamma_{total}$ — Γ_{101}/Γ

VALUE (units 10^{-5})	CL%	EVTS	DOCUMENT ID		TECN	COMMENT
2.9 ±0.6 OUR AVERAGE						
$2.13 \pm 0.28 \pm 0.72$			[1] LEES	18A	BABR	$\Upsilon(1S) \to \gamma K^+K^-$
$4.0 \pm 1.4 \pm 0.1$		17	[2] BESSON	11	CLEO	$\Upsilon(1S) \to \gamma K^0_S K^0_S$
$3.7\ ^{+0.9}_{-0.7} \pm 0.8$			ATHAR	06	CLE3	$\Upsilon(1S) \to \gamma K^+K^-$
• • • We do not use the following data for averages, fits, limits, etc. • • •						
<14	90		[3] FULTON	90B	CLEO	$\Upsilon(1S) \to \gamma K^+K^-$
<19.4	90		[3] ALBRECHT	89	ARG	$\Upsilon(1S) \to \gamma K^+K^-$

[1] Using $B(f_2'(1525) \to K\overline{K}) = 0.887 \pm 0.022$ and $B(K^0\overline{K}^0) = 1/2\ B(K\overline{K})$.

[2] BESSON 11 reports $(4.0 \pm 1.3 \pm 0.6) \times 10^{-5}$ from a measurement of $[\Gamma(\Upsilon(1S) \to \gamma f_2'(1525))/\Gamma_{total}] \times [B(f_2'(1525) \to K\overline{K})]$ assuming $B(f_2'(1525) \to K\overline{K}) = (88.8 \pm 3.1) \times 10^{-2}$, which we rescale to our best (shown rounded) value $B(f_2'(1525) \to K\overline{K}) = (88.8 \pm 2.2) \times 10^{-2}$. Our first error is their experiment's error and our second error is the systematic error from using our best (shown rounded) value. The result also assumes $B(K^0_S \to \pi^+\pi^-) = (69.20 \pm 0.05)\%$ and $B(f_2'(1525) \to K\overline{K}) = 4\ B(f_2'(1525) \to K^0_S K^0_S)$.

[3] Assuming $B(f_2'(1525) \to K\overline{K}) = 0.71$.

$\Gamma(\gamma f_2(1270))/\Gamma_{total}$ — Γ_{102}/Γ

VALUE (units 10^{-5})	CL%	DOCUMENT ID		TECN	COMMENT
10.1 ±0.6 OUR AVERAGE					
$10.15 \pm 0.59\ ^{+0.54}_{-0.43}$		[1] LEES	18A	BABR	$\Upsilon(1S) \to \gamma\pi^+\pi^-$
$10.5 \pm 1.6\ ^{+1.9}_{-1.8}$		[2] BESSON	07A	CLE3	$\Upsilon(1S) \to \gamma\pi^0\pi^0$
$10.2 \pm 0.8 \pm 0.7$		ATHAR	06	CLE3	$\Upsilon(1S) \to \gamma\pi^+\pi^-$
$8.1 \pm 2.3\ ^{+2.9}_{-2.7}$		[3] ANASTASSOV	99	CLE2	$e^+e^- \to$ hadrons
• • • We do not use the following data for averages, fits, limits, etc. • • •					
<21	90	[3] FULTON	90B	CLEO	$\Upsilon(1S) \to \gamma\pi^+\pi^-$
<13	90	[3] ALBRECHT	89	ARG	$\Upsilon(1S) \to \gamma\pi^+\pi^-$
<81	90	SCHMITT	88	CBAL	$\Upsilon(1S) \to \gamma X$

[1] Using $B(f_2(1270) \to \pi^0\pi^0) = 1/3\ B(f_2(1270) \to \pi\pi)$ and $B(f_2(1270) \to \pi\pi) = (84.2\ ^{+2.9}_{-0.9})\%$.

[2] Using $B(f_2(1270) \to \pi^0\pi^0) = B(f_2(1270) \to \pi\pi)/3$ and $B(f_2(1270) \to \pi\pi) = (84.7\ ^{+2.5}_{-1.2})\%$.

[3] Using $B(f_2(1270) \to \pi\pi) = 0.84$.

$\Gamma(\gamma\eta(1405))/\Gamma_{total}$ — Γ_{103}/Γ

VALUE (units 10^{-5})	CL%	DOCUMENT ID		TECN	COMMENT
<8.2	90	[1] FULTON	90B	CLEO	$\Upsilon(1S) \to \gamma K^\pm\pi^\mp K^0_S$

[1] Includes unknown branching ratio of $\eta(1405) \to K^\pm\pi^\mp K^0_S$.

$\Gamma(\gamma f_0(1500))/\Gamma_{total}$ — Γ_{104}/Γ

VALUE (units 10^{-5})	CL%	DOCUMENT ID		TECN	COMMENT
<1.5	90	[1] BESSON	07A	CLEO	$e^+e^- \to \Upsilon(1S) \to \gamma\pi^0\pi^0$
• • • We do not use the following data for averages, fits, limits, etc. • • •					
<6.1	90	[2] BESSON	07A	CLEO	$e^+e^- \to \Upsilon(1S) \to \gamma\eta\eta$

[1] Using $B(f_0(1500) \to \pi^0\pi^0) = B(f_0(1500) \to \pi\pi)/3$ and $B(f_0(1500) \to \pi\pi) = (0.349 \pm 0.023)\%$.

[2] Calculated by us using $B(f_0(1500) \to \eta\eta) = (5.1 \pm 0.9)\%$.

$\Gamma(\gamma f_0(1500) \to \gamma K^+K^-)/\Gamma_{total}$ — Γ_{105}/Γ

VALUE (units 10^{-5})	DOCUMENT ID		TECN	COMMENT
1.04±0.14±0.33	[1] LEES	18A	BABR	$e^+e^- \to \Upsilon(1S) \to \gamma K^+K^-$

[1] LEES 18A quotes $B(\Upsilon(1S) \to \gamma f_0(1500) \to \gamma K\overline{K}) = (2.08 \pm 0.27 \pm 0.65) \times 10^{-5}$ assuming $B(K^0\overline{K}^0) = 1/2\ B(K\overline{K})$.

$\Gamma(\gamma f_0(1710))/\Gamma_{total}$ — Γ_{106}/Γ

VALUE (units 10^{-4})	CL%	DOCUMENT ID		TECN	COMMENT
< 2.6	90	[1] ALBRECHT	89	ARG	$\Upsilon(1S) \to \gamma K^+K^-$
• • • We do not use the following data for averages, fits, limits, etc. • • •					
< 6.3	90	[1] FULTON	90B	CLEO	$\Upsilon(1S) \to \gamma K^+K^-$
<19	90	[1] FULTON	90B	CLEO	$\Upsilon(1S) \to \gamma K^0_S K^0_S$
< 8	90	[2] ALBRECHT	89	ARG	$\Upsilon(1S) \to \gamma\pi^+\pi^-$
<24	90	[3] SCHMITT	88	CBAL	$\Upsilon(1S) \to \gamma X$

[1] Assuming $B(f_0(1710) \to K\overline{K}) = 0.38$.

[2] Assuming $B(f_0(1710) \to \pi\pi) = 0.04$.

[3] Assuming $B(f_0(1710) \to \eta\eta) = 0.18$.

$\Gamma(\gamma f_0(1710) \to \gamma K^+K^-)/\Gamma_{total}$ — Γ_{107}/Γ

VALUE (units 10^{-5})	CL%	DOCUMENT ID		TECN	COMMENT
1.01±0.26±0.18		[1] LEES	18A	BABR	$e^+e^- \to \Upsilon(1S) \to \gamma K^+K^-$
• • • We do not use the following data for averages, fits, limits, etc. • • •					
<0.7	90	ATHAR	06	CLEO	$e^+e^- \to \Upsilon(1S) \to \gamma K^+K^-$

[1] LEES 18A quotes $B(\Upsilon(1S) \to \gamma f_0(1710) \to \gamma K\overline{K}) = (2.02 \pm 0.51 \pm 0.35) \times 10^{-5}$ assuming $B(K^0\overline{K}^0) = 1/2\ B(K\overline{K})$.

$\Gamma(\gamma f_0(1710) \to \gamma\pi^+\pi^-)/\Gamma_{total}$ — Γ_{108}/Γ

VALUE (units 10^{-5})	DOCUMENT ID		TECN	COMMENT
0.53±0.17±0.11	[1] LEES	18A	BABR	$\Upsilon(1S) \to \gamma\pi^+\pi^-$

[1] LEES 18A quotes $B(\Upsilon(1S) \to \gamma f_0(1710) \to \gamma\pi\pi) = (0.79 \pm 0.26 \pm 0.17) \times 10^{-5}$ assuming $B(\pi^0\pi^0) = 1/3\ B(\pi\pi)$.

$\Gamma(\gamma f_0(1710) \to \gamma\pi^0\pi^0)/\Gamma_{total}$ — Γ_{109}/Γ

VALUE (units 10^{-6})	CL%	DOCUMENT ID		TECN	COMMENT
<1.4	90	BESSON	07A	CLEO	$e^+e^- \to \Upsilon(1S) \to \gamma\pi^0\pi^0$

$\Gamma(\gamma f_0(1710) \to \gamma\eta\eta)/\Gamma_{total}$ — Γ_{110}/Γ

VALUE (units 10^{-6})	CL%	DOCUMENT ID		TECN	COMMENT
<1.8	90	BESSON	07A	CLEO	$e^+e^- \to \Upsilon(1S) \to \gamma\eta\eta$

$\Gamma(\gamma f_4(2050))/\Gamma_{total}$ — Γ_{111}/Γ

VALUE (units 10^{-5})	CL%	DOCUMENT ID		TECN	COMMENT
<5.3	90	[1] ATHAR	06	CLE3	$\Upsilon(1S) \to \gamma\pi^+\pi^-$

[1] Assuming $B(f_4(2050) \to \pi\pi) = 0.17$.

$\Gamma(\gamma f_0(2200) \to \gamma K^+K^-)/\Gamma_{total}$ — Γ_{112}/Γ

VALUE	CL%	DOCUMENT ID		TECN	COMMENT
<0.0002	90	BARU	89	MD1	$\Upsilon(1S) \to \gamma K^+K^-$

$\Gamma(\gamma f_J(2220) \to \gamma K^+K^-)/\Gamma_{total}$ — Γ_{113}/Γ

VALUE (units 10^{-7})	CL%	DOCUMENT ID		TECN	COMMENT
< 8	90	ATHAR	06	CLE3	$\Upsilon(1S) \to \gamma K^+K^-$
• • • We do not use the following data for averages, fits, limits, etc. • • •					
< 160	90	MASEK	02	CLEO	$\Upsilon(1S) \to \gamma K^+K^-$
< 150	90	FULTON	90B	CLEO	$\Upsilon(1S) \to \gamma K^+K^-$
< 290	90	ALBRECHT	89	ARG	$\Upsilon(1S) \to \gamma K^+K^-$
<2000	90	BARU	89	MD1	$\Upsilon(1S) \to \gamma K^+K^-$

$\Gamma(\gamma f_J(2220) \to \gamma\pi^+\pi^-)/\Gamma_{total}$ — Γ_{114}/Γ

VALUE (units 10^{-7})	CL%	DOCUMENT ID		TECN	COMMENT
< 6	90	ATHAR	06	CLE3	$\Upsilon(1S) \to \gamma\pi^+\pi^-$
• • • We do not use the following data for averages, fits, limits, etc. • • •					
<120	90	MASEK	02	CLEO	$\Upsilon(1S) \to \gamma\pi^+\pi^-$

$\Gamma(\gamma f_J(2220) \to \gamma p\overline{p})/\Gamma_{total}$ — Γ_{115}/Γ

VALUE (units 10^{-7})	CL%	DOCUMENT ID		TECN	COMMENT
< 11	90	ATHAR	06	CLE3	$\Upsilon(1S) \to \gamma p\overline{p}$
• • • We do not use the following data for averages, fits, limits, etc. • • •					
<160	90	MASEK	02	CLEO	$\Upsilon(1S) \to \gamma p\overline{p}$

$\Gamma(\gamma\eta(2225) \to \gamma\phi\phi)/\Gamma_{total}$ — Γ_{116}/Γ

VALUE	CL%	DOCUMENT ID		TECN	COMMENT
<0.003	90	BARU	89	MD1	$\Upsilon(1S) \to \gamma K^+K^-K^+K^-$

$\Gamma(\gamma\eta_c(1S))/\Gamma_{total}$ — Γ_{117}/Γ

VALUE	CL%	DOCUMENT ID		TECN	COMMENT
$<2.9 \times 10^{-5}$	90	[1] KATRENKO	20	BELL	$e^+e^- \to \gamma +$ hadrons
• • • We do not use the following data for averages, fits, limits, etc. • • •					
$<5.7 \times 10^{-5}$	90	SHEN	10A	BELL	$\Upsilon(1S) \to \gamma X$

[1] Using $\Upsilon(2S) \to \Upsilon(1S)\pi^+\pi^-$ decays.

$\Gamma(\gamma\eta_c(2S))/\Gamma_{total}$ — Γ_{118}/Γ

VALUE	CL%	DOCUMENT ID		TECN	COMMENT
$<4 \times 10^{-4}$	90	[1] KATRENKO	20	BELL	$e^+e^- \to \gamma +$ hadrons

[1] Using $\Upsilon(2S) \to \Upsilon(1S)\pi^+\pi^-$ decays.

Int. J. Mod. Phys. A 2026.41. Downloaded from www.worldscientific.com by CALIFORNIA @ BERKELEY on 09/16/26. Re-use and distribution is strictly not permitted, except for Open Access articles.

$\Gamma(\gamma\chi_{c0})/\Gamma_{total}$ — Γ_{119}/Γ

VALUE	CL%	DOCUMENT ID		TECN	COMMENT
$<6.6\times10^{-5}$	90	[1] KATRENKO	20	BELL	$\Upsilon(1S)\to\gamma+$ hadrons
• • • We do not use the following data for averages, fits, limits, etc. • • •					
$<6.5\times10^{-4}$	90	SHEN	10A	BELL	$\Upsilon(1S)\to\gamma X$

[1] Using $\Upsilon(2S)\to\Upsilon(1S)\pi^+\pi^-$ decays.

$\Gamma(\gamma\chi_{c1})/\Gamma_{total}$ — Γ_{120}/Γ

VALUE (units 10^{-5})	CL%	EVTS	DOCUMENT ID		TECN	COMMENT
$4.7^{+2.4}_{-1.8}{}^{+0.4}_{-0.5}$		5	[1] KATRENKO	20	BELL	$\Upsilon(1S)\to\gamma+$ hadrons
• • • We do not use the following data for averages, fits, limits, etc. • • •						
<2.3	90		SHEN	10A	BELL	$\Upsilon(1S)\to\gamma X$

[1] Using $\Upsilon(2S)\to\Upsilon(1S)\pi^+\pi^-$ decays.

$\Gamma(\gamma\chi_{c2})/\Gamma_{total}$ — Γ_{121}/Γ

VALUE	CL%	DOCUMENT ID		TECN	COMMENT
$<7.6\times10^{-6}$	90	SHEN	10A	BELL	$\Upsilon(1S)\to\gamma X$
• • • We do not use the following data for averages, fits, limits, etc. • • •					
$<3.3\times10^{-5}$	90	[1] KATRENKO	20	BELL	$\Upsilon(1S)\to\gamma+$ hadrons

[1] Using $\Upsilon(2S)\to\Upsilon(1S)\pi^+\pi^-$ decays.

$\Gamma(\gamma\chi_{c1}(3872))/\Gamma_{total}$ — Γ_{122}/Γ

VALUE	CL%	DOCUMENT ID		TECN	COMMENT
$<4\times10^{-5}$	90	[1] SHEN	10A	BELL	$\Upsilon(1S)\to\gamma X$

[1] SHEN 10A reports $[\Gamma(\Upsilon(1S)\to\gamma\chi_{c1}(3872))/\Gamma_{total}]\times[B(\chi_{c1}(3872)\to\pi^+\pi^-J/\psi(1S))]<1.6\times10^{-6}$ which we divide by our best (shown rounded) value $B(\chi_{c1}(3872)\to\pi^+\pi^-J/\psi(1S))=4.3\times10^{-2}$.

$\Gamma(\gamma\chi_{c1}(3872),\ \chi_{c1}\to\pi^+\pi^-\pi^0J/\psi)/\Gamma_{total}$ — Γ_{123}/Γ

VALUE	CL%	DOCUMENT ID		TECN	COMMENT
$<2.8\times10^{-6}$	90	SHEN	10A	BELL	$\Upsilon(1S)\to\gamma X$

$\Gamma(\gamma\chi_{c0}(3915)\to\omega J/\psi)/\Gamma_{total}$ — Γ_{124}/Γ

VALUE (units 10^{-6})	CL%	DOCUMENT ID		TECN	COMMENT
<3.0	90	SHEN	10A	BELL	$\Upsilon(1S)\to\gamma X$

$\Gamma(\gamma\chi_{c1}(4140)\to\phi J/\psi)/\Gamma_{total}$ — Γ_{125}/Γ

VALUE (units 10^{-6})	CL%	DOCUMENT ID		TECN	COMMENT
<2.2	90	SHEN	10A	BELL	$\Upsilon(1S)\to\gamma X$

$\Gamma(\gamma X\overline{X}(m_X<3.1\text{ GeV}))/\Gamma_{total}$ — Γ_{126}/Γ

($X\overline{X}$ = vectors with $m<3.1$ GeV)

VALUE (units 10^{-3})	CL%	DOCUMENT ID		TECN	COMMENT
<1	90	[1] BALEST	95	CLEO	$e^+e^-\to\gamma+X\overline{X}$

[1] For a noninteracting vector X with mass <3.1 GeV.

$\Gamma(\gamma X\overline{X}(m_X<4.5\text{ GeV}))/\Gamma_{total}$ — Γ_{127}/Γ

X and $\overline{X}$ = zero spin with $m<4.5$ GeV

VALUE (units 10^{-5})	CL%	DOCUMENT ID		TECN	COMMENT
<24	90	[1] DEL-AMO-SA...	11J	BABR	$e^+e^-\to\gamma+X\overline{X}$

[1] For a noninteracting scalar X with mass $m<4.5$ GeV.

$\Gamma(\gamma X\to\gamma+\geq4\text{ prongs})/\Gamma_{total}$ — Γ_{128}/Γ

($1.5\text{ GeV}<m_X<5.0$ GeV)

VALUE (units 10^{-4})	CL%	DOCUMENT ID		TECN	COMMENT
<1.78	95	ROSNER	07A	CLEO	$e^+e^-\to\gamma X$

$\Gamma(\gamma A^0)/\Gamma_{total}$ — Γ_{129}/Γ

(A^0 = scalar with $m<8.0$ GeV)

VALUE	CL%	DOCUMENT ID		TECN	COMMENT
• • • We do not use the following data for averages, fits, limits, etc. • • •					
$<4.5\times10^{-6}$	90	[1] DEL-AMO-SA...	11J	BABR	$e^+e^-\to\gamma+X$
$<3\times10^{-5}$	90	[2] BALEST	95	CLEO	$e^+e^-\to\gamma+X$
$<5.6\times10^{-5}$	90	[2] ANTREASYAN	90C	CBAL	$e^+e^-\to\gamma+X$

[1] For a non-interacting scalar or pseudoscalar, A^0, with mass $m_{A^0}<8.0$ GeV. 90% CL upper limits range from 1.9×10^{-6} to 4.5×10^{-6}.
[2] For any non-interacting long-lived particle with mass <7.2 GeV.

$\Gamma(\gamma A^0\to\gamma\mu^+\mu^-)/\Gamma_{total}$ — Γ_{130}/Γ

($201<M(\mu^+\mu^-)<3565$ MeV)

VALUE (units 10^{-6})	CL%	DOCUMENT ID		TECN	COMMENT
<9	90	[1] LOVE	08	CLEO	$e^+e^-\to\gamma A^0\to\gamma\mu^+\mu^-$
• • • We do not use the following data for averages, fits, limits, etc. • • •					
<16	90	[2] JIA	22	BELL	$\Upsilon(2S)\to\gamma\mu^+\mu^-\pi^+\pi^-$
<9.7	90	[3] LEES	13C	BABR	$e^+e^-\to\gamma A^0\to\gamma\mu^+\mu^-$

[1] For a narrow scalar or pseudoscalar, A^0, with $201<M(\mu^+\mu^-)<3565$ MeV, excluding J/ψ. Measured 90% CL limits as a function of $M(\mu^+\mu^-)$ range from $1\text{–}9\times10^{-6}$.
[2] For a narrow scalar or pseudoscalar, A^0, with $0.22<M(A^0)<9.2$ GeV, resulting in 90% CL upper limits ranging from 3.1×10^{-7} at $M(A^0)=0.22$ GeV to 1.6×10^{-5} at $M(A^0)=9.2$ GeV.
[3] For a narrow scalar or pseudoscalar, A^0, with mass in the range 0.212–9.2 GeV, excluding J/ψ and $\psi(2S)$. Measured 90% CL limits as a function of m_{A^0} are in the range $0.28\text{–}9.7\times10^{-6}$.

$\Gamma(\gamma A^0\to\gamma\tau^+\tau^-)/\Gamma_{total}$ — Γ_{131}/Γ

($2m_\tau<M(\tau^+\tau^-)<9.2$ GeV)

VALUE (units 10^{-6})	CL%	DOCUMENT ID		TECN	COMMENT
<130	90	[1] LEES	13R	BABR	$\Upsilon(2S)\to\gamma\tau^+\tau^-\pi^+\pi^-$
• • • We do not use the following data for averages, fits, limits, etc. • • •					
<150	90	[2] JIA	22	BELL	$\Upsilon(2S)\to\gamma\tau^+\tau^-\pi^+\pi^-$
<50	90	[3] LOVE	08	CLEO	$e^+e^-\to\gamma A^0\to\gamma\tau^+\tau^-$

[1] For a narrow scalar or pseudoscalar, A^0, with $2m_\tau<M(A^0)<9.2$ GeV, resulting in 90% CL upper limits of 0.9×10^{-5} at $M(A^0)=2m_\tau$, $\approx1.5\times10^{-5}$ at $M(A^0)=7.5$ GeV, and 13×10^{-5} at $M(A^0)=9.2$ GeV.
[2] For a narrow scalar or pseudoscalar, A^0, with $2m_\tau<M(A^0)<9.2$ GeV, resulting in 90% CL upper limits ranging from 3.8×10^{-6} at $M(A^0)=2m_\tau$ to 1.5×10^{-4} at $M(A^0)=9.2$ GeV.
[3] For a narrow scalar or pseudoscalar, A^0, with $2m_\tau<M(A^0)<7.5$ GeV, resulting in 90% CL limits ranging from 1×10^{-5} at $M(A^0)=2m_\tau$ to 5×10^{-5} at $M(A^0)=7.5$ GeV.

$\Gamma(\gamma A^0\to\gamma gg)/\Gamma_{total}$ — Γ_{132}/Γ

($0.5\text{ GeV}<m<9.0$ GeV)

VALUE	CL%	DOCUMENT ID		TECN	COMMENT
$<1\times10^{-2}$	90	[1] LEES	13L	BABR	$\Upsilon(1S)\to\gamma X$

[1] For a narrow, CP-odd pseudoscalar, A^0, searched for in 26 hadronic decay modes with invariant mass $0.5\text{ GeV}<m_{A^0}<9.0$ GeV. Measured 90% CL limits as a function of m_{A^0} range from 10^{-6} to 10^{-2}.

$\Gamma(\gamma A^0\to\gamma s\overline{s})/\Gamma_{total}$ — Γ_{133}/Γ

($0.5\text{ GeV}<m<9.0$ GeV)

VALUE	CL%	DOCUMENT ID		TECN	COMMENT
$<1\times10^{-3}$	90	[1] LEES	13L	BABR	$\Upsilon(1S)\to\gamma X$

[1] For a narrow, CP-odd pseudoscalar, A^0, searched for in 14 hadronic decay modes with invariant mass $1.5\text{ GeV}<m_{A^0}<9.0$ GeV. Measured 90% CL limits as a function of m_{A^0} range from 10^{-5} to 10^{-3}.

LEPTON FAMILY NUMBER (LF) VIOLATING MODES

$\Gamma(e^\pm\mu^\mp)/\Gamma_{total}$ — Γ_{134}/Γ

VALUE (units 10^{-7})	CL%	DOCUMENT ID		TECN	COMMENT
<3.9	90	PATRA	22	BELL	$\Upsilon(2S)\to\pi^+\pi^-e^\pm\mu^\mp$

$\Gamma(\mu^\pm\tau^\mp)/\Gamma_{total}$ — Γ_{135}/Γ

VALUE	CL%	DOCUMENT ID		TECN	COMMENT
$<2.7\times10^{-6}$	90	PATRA	22	BELL	$\Upsilon(2S)\to\pi^+\pi^-\mu^\pm\tau^\mp$
• • • We do not use the following data for averages, fits, limits, etc. • • •					
$<6.0\times10^{-6}$	95	LOVE	08A	CLEO	$e^+e^-\to\mu^\pm\tau^\mp$

$\Gamma(e^\pm\tau^\mp)/\Gamma_{total}$ — Γ_{136}/Γ

VALUE (units 10^{-6})	CL%	DOCUMENT ID		TECN	COMMENT
<2.7	90	PATRA	22	BELL	$\Upsilon(2S)\to\pi^+\pi^-e^\pm\tau^\mp$

$\Gamma(\gamma e^\pm\mu^\mp)/\Gamma_{total}$ — Γ_{137}/Γ

VALUE (units 10^{-7})	CL%	DOCUMENT ID		TECN	COMMENT
<4.2	90	PATRA	22	BELL	$\Upsilon(2S)\to\pi^+\pi^-\gamma e^\pm\mu^\mp$

$\Gamma(\gamma\mu^\pm\tau^\mp)/\Gamma_{total}$ — Γ_{138}/Γ

VALUE (units 10^{-6})	CL%	DOCUMENT ID		TECN	COMMENT
<6.1	90	PATRA	22	BELL	$\Upsilon(2S)\to\pi^+\pi^-\gamma\mu^\pm\tau^\mp$

$\Gamma(\gamma e^\pm\tau^\mp)/\Gamma_{total}$ — Γ_{139}/Γ

VALUE (units 10^{-6})	CL%	DOCUMENT ID		TECN	COMMENT
<6.5	90	PATRA	22	BELL	$\Upsilon(2S)\to\pi^+\pi^-\gamma e^\pm\tau^\mp$

OTHER DECAYS

$\Gamma(\text{invisible})/\Gamma_{total}$ — Γ_{140}/Γ

VALUE (units 10^{-4})	CL%	DOCUMENT ID		TECN	COMMENT
<3.0	90	AUBERT	09AX	BABR	$\Upsilon(3S)\to\pi^+\pi^-\Upsilon(1S)$
• • • We do not use the following data for averages, fits, limits, etc. • • •					
<39	90	RUBIN	07	CLEO	$\Upsilon(2S)\to\pi^+\pi^-\Upsilon(1S)$
<25	90	TAJIMA	07	BELL	$\Upsilon(3S)\to\pi^+\pi^-\Upsilon(1S)$

Int. J. Mod. Phys. A 2026.41. Downloaded from www.worldscientific.com
by UNIVERSITY OF CALIFORNIA @ BERKELEY on 09/16/26. Re-use and distribution is strictly not permitted, except for Open Access articles.

$\Upsilon(1S)$ REFERENCES

ADACHI	25A	PRL 135 041901	I. Adachi *et al.*	(BELLE and BELLE II Collab.)
DONG	25	JHEP 2509 048	X. Dong *et al.*	(BELLE Collab.)
AAIJ	24AC	JHEP 2410 122	R. Aaij *et al.*	(LHCb Collab.)
SHAMOV	23	PL B839 137766	A.G. Shamov, O.L. Rezanova	(NOVO, NOVOU)
JIA	22	PRL 128 081804	S. Jia *et al.*	(BELLE Collab.)
PATRA	22	JHEP 2205 095	S. Patra *et al.*	(BELLE Collab.)
KATRENKO	20	PRL 124 122001	P. Katrenko *et al.*	(BELLE Collab.)
JIA	18	PR D97 112004	S. Jia *et al.*	(BELLE Collab.)
LEES	18A	PR D97 112006	J.P. Lees *et al.*	(BABAR Collab.)
JIA	17	PR D95 012001	S. Jia *et al.*	(BELLE Collab.)
JIA	17A	PR D96 112002	S. Jia *et al.*	(BELLE Collab.)
SHEN	16	PR D93 112013	C.P. Shen *et al.*	(BELLE Collab.)
LEES	14G	PR D89 111102	J.P. Lees *et al.*	(BABAR Collab.)
YANG	14	PR D90 112008	S.D. Yang *et al.*	(BELLE Collab.)
LEES	13C	PR D87 031102	J.P. Lees *et al.*	(BABAR Collab.)
LEES	13L	PR D88 031701	J.P. Lees *et al.*	(BABAR Collab.)
LEES	13R	PR D88 071102	J.P. Lees *et al.*	(BABAR Collab.)
SHEN	13	PR D88 011102	C.P. Shen *et al.*	(BELLE Collab.)
DOBBS	12A	PR D86 052003	S. Dobbs *et al.*	
SHEN	12A	PR D86 031102	C.P. Shen *et al.*	(BELLE Collab.)
BESSON	11	PR D83 037101	D. Besson *et al.*	(CLEO Collab.)
DEL-AMO-SA...	11J	PRL 107 021804	P. del Amo Sanchez *et al.*	(BABAR Collab.)
AUBERT	10C	PR D81 011102	B. Aubert *et al.*	(BABAR Collab.)
DEL-AMO-SA...	10C	PRL 104 191801	P. del Amo Sanchez *et al.*	(BABAR Collab.)
SHEN	10A	PR D82 051504	C.P. Shen *et al.*	(BELLE Collab.)
AUBERT	09AX	PRL 103 251801	B. Aubert *et al.*	(BABAR Collab.)
LOVE	08	PRL 101 151802	W. Love *et al.*	(CLEO Collab.)
LOVE	08A	PRL 101 201601	W. Love *et al.*	(CLEO Collab.)
PDG	08	PL B667 1	C. Amsler *et al.*	(PDG Collab.)
ASNER	07	PR D75 012009	D.M. Asner *et al.*	(CLEO Collab.)
ATHAR	07A	PR D76 072003	S.B. Athar *et al.*	(CLEO Collab.)
BESSON	07	PRL 98 052002	D. Besson *et al.*	(CLEO Collab.)
BESSON	07A	PR D75 072001	D. Besson *et al.*	(CLEO Collab.)
ROSNER	07A	PR D76 117102	J.L. Rosner *et al.*	(CLEO Collab.)
RUBIN	07	PR D75 031104	P. Rubin *et al.*	(CLEO Collab.)
TAJIMA	07	PRL 98 132001	O. Tajima *et al.*	(BELLE Collab.)
AQUINES	06A	PR D74 092006	O. Aquines *et al.*	(CLEO Collab.)
ATHAR	06	PR D73 032001	S.B. Athar *et al.*	(CLEO Collab.)
BESSON	06A	PR D74 012003	D. Besson *et al.*	(CLEO Collab.)
ROSNER	06	PRL 96 092003	J.L. Rosner *et al.*	(CLEO Collab.)
ADAMS	05	PRL 94 012001	G.S. Adams *et al.*	(CLEO Collab.)
BRIERE	04	PR D70 072001	R.A. Briere *et al.*	(CLEO Collab.)
ARTUSO	03	PR D67 052003	M. Artuso *et al.*	(CLEO Collab.)
MASEK	02	PR D65 072002	G. Masek *et al.*	(CLEO Collab.)
RICHICHI	01B	PRL 87 141801	S.J. Richichi *et al.*	(CLEO Collab.)
ARTAMONOV	00	PL B474 427	A.S. Artamonov *et al.*	
ANASTASSOV	99	PRL 82 286	A. Anastassov *et al.*	(CLEO Collab.)
ALEXANDER	98	PR D58 052004	J.P. Alexander *et al.*	(CLEO Collab.)
BARU	96	PRPL 267 71	S.E. Baru *et al.*	(NOVO)
BALEST	95	PR D51 2053	R. Balest *et al.*	(CLEO Collab.)
CINABRO	94B	PL B340 129	D. Cinabro *et al.*	(CLEO Collab.)
ALBRECHT	92J	ZPHY C55 25	H. Albrecht *et al.*	(ARGUS Collab.)
BARU	92	ZPHY C54 229	S.E. Baru *et al.*	(NOVO)
BARU	92B	ZPHY C56 547	S.E. Baru *et al.*	(NOVO)
KOBEL	92	ZPHY C53 193	M. Kobel *et al.*	(Crystal Ball Collab.)
ANTREASYAN	90C	PL B251 204	D. Antreasyan *et al.*	(Crystal Ball Collab.)
BLINOV	90	PL B245 311	A.E. Blinov *et al.*	(NOVO)
FULTON	90B	PR D41 1401	R. Fulton *et al.*	(CLEO Collab.)
MASCHMANN	90	ZPHY C46 555	W.S. Maschmann *et al.*	(Crystal Ball Collab.)
ALBRECHT	89	ZPHY C42 349	H. Albrecht *et al.*	(ARGUS Collab.)
ALEXANDER	89	NP B320 45	J.P. Alexander *et al.*	(LBL, MICH, SLAC)
BARU	89	ZPHY C42 505	S.E. Baru *et al.*	(NOVO)
CHEN	89B	PR D39 3528	W.Y. Chen *et al.*	(CLEO Collab.)
FULTON	89	PL B224 445	R. Fulton *et al.*	(CLEO Collab.)
KAARSBERG	89	PRL 62 2077	T.M. Kaarsberg *et al.*	(CUSB Collab.)
BUCHMUEL...	88	HE e^+e^- Physics 412 Editors: A. Ali and P. Soeding, World Scientific, Singapore	W. Buchmueller, S. Cooper	(HANN, DESY, MIT)
JAKUBOWSKI	88	ZPHY C40 49	Z. Jakubowski *et al.*	(Crystal Ball Collab.) IGJPC
SCHMITT	88	ZPHY C40 199	P. Schmitt *et al.*	(Crystal Ball Collab.)
ALBRECHT	87	ZPHY C35 283	H. Albrecht *et al.*	(ARGUS Collab.)
COHEN	87	RMP 59 1121	E.R. Cohen, B.N. Taylor	(RISC, NBS)
BARU	86	ZPHY C30 551	S.E. Baru *et al.*	(NOVO)
ALBRECHT	85C	PL 154B 452	H. Albrecht *et al.*	(ARGUS Collab.)
KURAEV	85	SJNP 41 466 Translated from YAF 41 733.	E.A. Kuraev, V.S. Fadin	(NOVO)
ARTAMONOV	84	PL 137B 272	A.S. Artamonov *et al.*	(NOVO)
BESSON	84	PR D30 1433	D. Besson *et al.*	(CLEO Collab.)
GILES	84B	PR D29 1285	R. Giles *et al.*	(CLEO Collab.)
MACKAY	84	PR D29 2483	W.W. MacKay *et al.*	(CUSB Collab.)
ANDREWS	83	PRL 50 807	D.E. Andrews *et al.*	(CLEO Collab.)
GILES	83	PRL 50 877	R. Giles *et al.*	(HARV, OSU, ROCH, RUTG+)
NICZYPORUK	83	ZPHY C17 197	B. Niczyporuk *et al.*	(LENA Collab.)
ALBRECHT	82	PL 116B 383	H. Albrecht *et al.*	(DESY, DORT, HEIDH+)
ARTAMONOV	82	PL 118B 225	A.S. Artamonov *et al.*	(NOVO)
NICZYPORUK	82	ZPHY C15 299	B. Niczyporuk *et al.*	(LENA Collab.)
BERGER	80C	PL 93B 497	C. Berger *et al.*	(PLUTO Collab.)
BOCK	80	ZPHY C6 125	P. Bock *et al.*	(HEIDP, MPIM, DESY, HAMB)
BERGER	79	ZPHY C1 343	C. Berger *et al.*	(PLUTO Collab.)

$\chi_{b0}(1P)$

$I^G(J^{PC}) = 0^+(0^{++})$

J needs confirmation.

Observed in radiative decay of the $\Upsilon(2S)$, therefore $C = +$. Branching ratio requires E1 transition, M1 is strongly disfavored, therefore $P = +$.

$\chi_{b0}(1P)$ MASS

VALUE (MeV)	DOCUMENT ID
9859.44±0.42±0.31 OUR EVALUATION	From average γ energy below, using $\Upsilon(2S)$ mass = 10023.26 ± 0.31 MeV

$m_{\chi_{b1}(1P)} - m_{\chi_{b0}(1P)}$

VALUE (MeV)	DOCUMENT ID		TECN	COMMENT
32.49±0.93	LEES	14M	BABR	$\Upsilon(2S) \to \gamma\gamma\mu^+\mu^-$

γ ENERGY IN $\Upsilon(2S)$ DECAY

VALUE (MeV)	DOCUMENT ID		TECN	COMMENT
162.5 ±0.4 OUR AVERAGE				
162.56±0.19±0.42	ARTUSO	05	CLEO	$\Upsilon(2S) \to \gamma X$
162.0 ±0.8 ±1.2	EDWARDS	99	CLE2	$\Upsilon(2S) \to \gamma\chi(1P)$
162.1 ±0.5 ±1.4	ALBRECHT	85E	ARG	$\Upsilon(2S) \to$ conv. γX
163.8 ±1.6 ±2.7	NERNST	85	CBAL	$\Upsilon(2S) \to \gamma X$
158.0 ±7 ±1	HAAS	84	CLEO	$\Upsilon(2S) \to$ conv. γX
• • • We do not use the following data for averages, fits, limits, etc. • • •				
149.4 ±0.7 ±5.0	KLOPFEN...	83	CUSB	$\Upsilon(2S) \to \gamma X$

$\chi_{b0}(1P)$ DECAY MODES

	Mode	Fraction (Γ_i/Γ)	Confidence level
Γ_1	$\gamma\,\Upsilon(1S)$	(1.94±0.27) %	
Γ_2	$D^0 X$	< 10.4 %	90%
Γ_3	$\pi^+\pi^-K^+K^-\pi^0$	< 1.6 $\times 10^{-4}$	90%
Γ_4	$2\pi^+\pi^-K^-K^0_S$	< 5 $\times 10^{-5}$	90%
Γ_5	$2\pi^+\pi^-K^-K^0_S 2\pi^0$	< 5 $\times 10^{-4}$	90%
Γ_6	$2\pi^+2\pi^-2\pi^0$	< 2.1 $\times 10^{-4}$	90%
Γ_7	$2\pi^+2\pi^-K^+K^-$	(1.1 ±0.6) $\times 10^{-4}$	
Γ_8	$2\pi^+2\pi^-K^+K^-\pi^0$	< 2.7 $\times 10^{-4}$	90%
Γ_9	$2\pi^+2\pi^-K^+K^-2\pi^0$	< 5 $\times 10^{-4}$	90%
Γ_{10}	$3\pi^+2\pi^-K^-K^0_S\pi^0$	< 1.6 $\times 10^{-4}$	90%
Γ_{11}	$3\pi^+3\pi^-$	< 8 $\times 10^{-5}$	90%
Γ_{12}	$3\pi^+3\pi^-2\pi^0$	< 6 $\times 10^{-4}$	90%
Γ_{13}	$3\pi^+3\pi^-K^+K^-$	(2.4 ±1.2) $\times 10^{-4}$	
Γ_{14}	$3\pi^+3\pi^-K^+K^-\pi^0$	< 1.0 $\times 10^{-3}$	90%
Γ_{15}	$4\pi^+4\pi^-$	< 8 $\times 10^{-5}$	90%
Γ_{16}	$4\pi^+4\pi^-2\pi^0$	< 2.1 $\times 10^{-3}$	90%
Γ_{17}	$J/\psi J/\psi$	< 7 $\times 10^{-5}$	90%
Γ_{18}	$J/\psi\psi(2S)$	< 1.2 $\times 10^{-4}$	90%
Γ_{19}	$\psi(2S)\psi(2S)$	< 3.1 $\times 10^{-5}$	90%
Γ_{20}	$J/\psi(1S)$anything	< 2.3 $\times 10^{-3}$	90%

$\chi_{b0}(1P)$ BRANCHING RATIOS

$\Gamma(\gamma\,\Upsilon(1S))/\Gamma_{total}$ — Γ_1/Γ

VALUE (%)	CL%	EVTS	DOCUMENT ID		TECN	COMMENT
1.94±0.27 OUR AVERAGE						
2.07±0.24±0.21			[1,2] LEES	14M	BABR	$\Upsilon(2S) \to \gamma\gamma\mu^+\mu^-$
1.76±0.30±0.18		87	[3,4] KORNICER	11	CLEO	$e^+e^- \to \gamma\gamma\ell^+\ell^-$
• • • We do not use the following data for averages, fits, limits, etc. • • •						
< 4.6	90		[5] LEES	11J	BABR	$\Upsilon(2S) \to X\gamma$
< 6	90		WALK	86	CBAL	$\Upsilon(2S) \to \gamma\gamma\ell^+\ell^-$
<11	90		PAUSS	83	CUSB	$\Upsilon(2S) \to \gamma\gamma\ell^+\ell^-$

[1] LEES 14M quotes $\Gamma(\chi_{b0}(1P) \to \gamma\,\Upsilon(1S))/\Gamma_{total} \times \Gamma(\Upsilon(2S) \to \gamma\chi_{b0}(1P))/\Gamma_{total} = (7.75 \pm 0.91) \times 10^{-4}$ combining the results from samples of $\Upsilon(2S) \to \gamma\gamma\mu^+\mu^-$ with and without converted photons. Assumes $B(\Upsilon(1S) \to \mu^+\mu^-) = (2.48 \pm 0.05)\%$.

[2] LEES 14M reports $[\Gamma(\chi_{b0}(1P) \to \gamma\,\Upsilon(1S))/\Gamma_{total}] \times [B(\Upsilon(2S) \to \gamma\chi_{b0}(1P))] = (7.75 \pm 0.91) \times 10^{-4}$ which we divide by our best (shown rounded) value $B(\Upsilon(2S) \to \gamma\chi_{b0}(1P)) = (3.8 \pm 0.4) \times 10^{-2}$. Our first error is their experiment's error and our second error is the systematic error from using our best (shown rounded) value.

[3] Assuming $B(\Upsilon(1S) \to \ell^+\ell^-) = (2.48 \pm 0.05)\%$.

[4] KORNICER 11 reports $[\Gamma(\chi_{b0}(1P) \to \gamma\,\Upsilon(1S))/\Gamma_{total}] \times [B(\Upsilon(2S) \to \gamma\chi_{b0}(1P))] = (6.59 \pm 0.96 \pm 0.60) \times 10^{-4}$ which we divide by our best (shown rounded) value $B(\Upsilon(2S) \to \gamma\chi_{b0}(1P)) = (3.8 \pm 0.4) \times 10^{-2}$. Our first error is their experiment's error and our second error is the systematic error from using our best (shown rounded) value.

[5] LEES 11J quotes a central value of $\Gamma(\chi_{b0}(1P) \to \gamma\,\Upsilon(1S))/\Gamma_{total} \times \Gamma(\Upsilon(2S) \to \gamma\chi_{b0}(1P))/\Gamma_{total} = (8.3 \pm 5.6^{+3.7}_{-2.6}) \times 10^{-4}$.

$\Gamma(D^0X)/\Gamma_{total}$ — Γ_2/Γ

VALUE	CL%	DOCUMENT ID		TECN	COMMENT
<10.4 × 10^{-2}	90	[6,7] BRIERE	08	CLEO	$\Upsilon(2S) \to \gamma D^0 X$

[6] For $p_{D^0} > 2.5$ GeV/c.

[7] The authors also present their result as $(5.6 \pm 3.6 \pm 0.5) \times 10^{-2}$.

$\Gamma(\pi^+\pi^-K^+K^-\pi^0)/\Gamma_{total}$ — Γ_3/Γ

VALUE (units 10^{-4})	CL%	DOCUMENT ID		TECN	COMMENT
<1.6	90	[8] ASNER	08A	CLEO	$\Upsilon(2S) \to \gamma\pi^+\pi^-K^+K^-\pi^0$

[8] ASNER 08A reports $[\Gamma(\chi_{b0}(1P) \to \pi^+\pi^-K^+K^-\pi^0)/\Gamma_{total}] \times [B(\Upsilon(2S) \to \gamma\chi_{b0}(1P))] < 6\times10^{-6}$ which we divide by our best (shown rounded) value $B(\Upsilon(2S) \to \gamma\chi_{b0}(1P)) = 3.8 \times 10^{-2}$.

Int. J. Mod. Phys. A 2026.41. Downloaded from www.worldscientific.com by CALIFORNIA @ BERKELEY on 09/16/26. Re-use and distribution is strictly not permitted, except for Open Access articles.

$\Gamma(2\pi^+\pi^-K^-K^0_S)/\Gamma_{total}$ — Γ_4/Γ

VALUE (units 10^{-4})	CL%	DOCUMENT ID		TECN	COMMENT
<0.5	90	[9] ASNER	08A	CLEO	$\Upsilon(2S) \to \gamma 2\pi^+\pi^-K^-K^0_S$

[9] ASNER 08A reports $[\Gamma(\chi_{b0}(1P) \to 2\pi^+\pi^-K^-K^0_S)/\Gamma_{total}] \times [B(\Upsilon(2S) \to \gamma\chi_{b0}(1P))] < 2\times10^{-6}$ which we divide by our best (shown rounded) value $B(\Upsilon(2S) \to \gamma\chi_{b0}(1P)) = 3.8\times10^{-2}$.

$\Gamma(2\pi^+\pi^-K^-K^0_S2\pi^0)/\Gamma_{total}$ — Γ_5/Γ

VALUE (units 10^{-4})	CL%	DOCUMENT ID		TECN	COMMENT
<5	90	[10] ASNER	08A	CLEO	$\Upsilon(2S) \to \gamma 2\pi^+\pi^-K^-2\pi^0$

[10] ASNER 08A reports $[\Gamma(\chi_{b0}(1P) \to 2\pi^+\pi^-K^-K^0_S2\pi^0)/\Gamma_{total}] \times [B(\Upsilon(2S) \to \gamma\chi_{b0}(1P))] < 18\times10^{-6}$ which we divide by our best (shown rounded) value $B(\Upsilon(2S) \to \gamma\chi_{b0}(1P)) = 3.8\times10^{-2}$.

$\Gamma(2\pi^+2\pi^-2\pi^0)/\Gamma_{total}$ — Γ_6/Γ

VALUE (units 10^{-4})	CL%	DOCUMENT ID		TECN	COMMENT
<2.1	90	[11] ASNER	08A	CLEO	$\Upsilon(2S) \to \gamma 2\pi^+2\pi^-2\pi^0$

[11] ASNER 08A reports $[\Gamma(\chi_{b0}(1P) \to 2\pi^+2\pi^-2\pi^0)/\Gamma_{total}] \times [B(\Upsilon(2S) \to \gamma\chi_{b0}(1P))] < 8\times10^{-6}$ which we divide by our best (shown rounded) value $B(\Upsilon(2S) \to \gamma\chi_{b0}(1P)) = 3.8\times10^{-2}$.

$\Gamma(2\pi^+2\pi^-K^+K^-)/\Gamma_{total}$ — Γ_7/Γ

VALUE (units 10^{-4})	EVTS	DOCUMENT ID		TECN	COMMENT
1.1±0.6±0.1	7	[12] ASNER	08A	CLEO	$\Upsilon(2S) \to \gamma 2\pi^+2\pi^-K^+K^-$

[12] ASNER 08A reports $[\Gamma(\chi_{b0}(1P) \to 2\pi^+2\pi^-K^+K^-)/\Gamma_{total}] \times [B(\Upsilon(2S) \to \gamma\chi_{b0}(1P))] = (4 \pm 2 \pm 1)\times10^{-6}$ which we divide by our best (shown rounded) value $B(\Upsilon(2S) \to \gamma\chi_{b0}(1P)) = (3.8 \pm 0.4)\times10^{-2}$. Our first error is their experiment's error and our second error is the systematic error from using our best (shown rounded) value.

$\Gamma(2\pi^+2\pi^-K^+K^-\pi^0)/\Gamma_{total}$ — Γ_8/Γ

VALUE (units 10^{-4})	CL%	DOCUMENT ID		TECN	COMMENT
<2.7	90	[13] ASNER	08A	CLEO	$\Upsilon(2S) \to \gamma 2\pi^+2\pi^-K^+K^-\pi^0$

[13] ASNER 08A reports $[\Gamma(\chi_{b0}(1P) \to 2\pi^+2\pi^-K^+K^-\pi^0)/\Gamma_{total}] \times [B(\Upsilon(2S) \to \gamma\chi_{b0}(1P))] < 10\times10^{-6}$ which we divide by our best (shown rounded) value $B(\Upsilon(2S) \to \gamma\chi_{b0}(1P)) = 3.8\times10^{-2}$.

$\Gamma(2\pi^+2\pi^-K^+K^-2\pi^0)/\Gamma_{total}$ — Γ_9/Γ

VALUE (units 10^{-4})	CL%	DOCUMENT ID		TECN	COMMENT
<5	90	[14] ASNER	08A	CLEO	$\Upsilon(2S) \to \gamma 2\pi^+2\pi^-K^+K^-2\pi^0$

[14] ASNER 08A reports $[\Gamma(\chi_{b0}(1P) \to 2\pi^+2\pi^-K^+K^-2\pi^0)/\Gamma_{total}] \times [B(\Upsilon(2S) \to \gamma\chi_{b0}(1P))] < 20\times10^{-6}$ which we divide by our best (shown rounded) value $B(\Upsilon(2S) \to \gamma\chi_{b0}(1P)) = 3.8\times10^{-2}$.

$\Gamma(3\pi^+2\pi^-K^-K^0_S\pi^0)/\Gamma_{total}$ — Γ_{10}/Γ

VALUE (units 10^{-4})	CL%	DOCUMENT ID		TECN	COMMENT
<1.6	90	[15] ASNER	08A	CLEO	$\Upsilon(2S) \to \gamma 3\pi^+2\pi^-K^-K^0_S\pi^0$

[15] ASNER 08A reports $[\Gamma(\chi_{b0}(1P) \to 3\pi^+2\pi^-K^-K^0_S\pi^0)/\Gamma_{total}] \times [B(\Upsilon(2S) \to \gamma\chi_{b0}(1P))] < 6\times10^{-6}$ which we divide by our best (shown rounded) value $B(\Upsilon(2S) \to \gamma\chi_{b0}(1P)) = 3.8\times10^{-2}$.

$\Gamma(3\pi^+3\pi^-)/\Gamma_{total}$ — Γ_{11}/Γ

VALUE (units 10^{-4})	CL%	DOCUMENT ID		TECN	COMMENT
<0.8	90	[16] ASNER	08A	CLEO	$\Upsilon(2S) \to \gamma 3\pi^+3\pi^-$

[16] ASNER 08A reports $[\Gamma(\chi_{b0}(1P) \to 3\pi^+3\pi^-)/\Gamma_{total}] \times [B(\Upsilon(2S) \to \gamma\chi_{b0}(1P))] < 3\times10^{-6}$ which we divide by our best (shown rounded) value $B(\Upsilon(2S) \to \gamma\chi_{b0}(1P)) = 3.8\times10^{-2}$.

$\Gamma(3\pi^+3\pi^-2\pi^0)/\Gamma_{total}$ — Γ_{12}/Γ

VALUE (units 10^{-4})	CL%	DOCUMENT ID		TECN	COMMENT
<6	90	[17] ASNER	08A	CLEO	$\Upsilon(2S) \to \gamma 3\pi^+3\pi^-2\pi^0$

[17] ASNER 08A reports $[\Gamma(\chi_{b0}(1P) \to 3\pi^+3\pi^-2\pi^0)/\Gamma_{total}] \times [B(\Upsilon(2S) \to \gamma\chi_{b0}(1P))] < 22\times10^{-6}$ which we divide by our best (shown rounded) value $B(\Upsilon(2S) \to \gamma\chi_{b0}(1P)) = 3.8\times10^{-2}$.

$\Gamma(3\pi^+3\pi^-K^+K^-)/\Gamma_{total}$ — Γ_{13}/Γ

VALUE (units 10^{-4})	EVTS	DOCUMENT ID		TECN	COMMENT
2.4±1.2±0.2	9	[18] ASNER	08A	CLEO	$\Upsilon(2S) \to \gamma 3\pi^+3\pi^-K^+K^-$

[18] ASNER 08A reports $[\Gamma(\chi_{b0}(1P) \to 3\pi^+3\pi^-K^+K^-)/\Gamma_{total}] \times [B(\Upsilon(2S) \to \gamma\chi_{b0}(1P))] = (9 \pm 4 \pm 2)\times10^{-6}$ which we divide by our best (shown rounded) value $B(\Upsilon(2S) \to \gamma\chi_{b0}(1P)) = (3.8 \pm 0.4)\times10^{-2}$. Our first error is their experiment's error and our second error is the systematic error from using our best (shown rounded) value.

$\Gamma(3\pi^+3\pi^-K^+K^-\pi^0)/\Gamma_{total}$ — Γ_{14}/Γ

VALUE (units 10^{-4})	CL%	DOCUMENT ID		TECN	COMMENT
<10	90	[19] ASNER	08A	CLEO	$\Upsilon(2S) \to \gamma 3\pi^+3\pi^-K^+K^-\pi^0$

[19] ASNER 08A reports $[\Gamma(\chi_{b0}(1P) \to 3\pi^+3\pi^-K^+K^-\pi^0)/\Gamma_{total}] \times [B(\Upsilon(2S) \to \gamma\chi_{b0}(1P))] < 37\times10^{-6}$ which we divide by our best (shown rounded) value $B(\Upsilon(2S) \to \gamma\chi_{b0}(1P)) = 3.8\times10^{-2}$.

$\Gamma(4\pi^+4\pi^-)/\Gamma_{total}$ — Γ_{15}/Γ

VALUE (units 10^{-4})	CL%	DOCUMENT ID		TECN	COMMENT
<0.8	90	[20] ASNER	08A	CLEO	$\Upsilon(2S) \to \gamma 4\pi^+4\pi^-$

[20] ASNER 08A reports $[\Gamma(\chi_{b0}(1P) \to 4\pi^+4\pi^-)/\Gamma_{total}] \times [B(\Upsilon(2S) \to \gamma\chi_{b0}(1P))] < 3\times10^{-6}$ which we divide by our best (shown rounded) value $B(\Upsilon(2S) \to \gamma\chi_{b0}(1P)) = 3.8\times10^{-2}$.

$\Gamma(4\pi^+4\pi^-2\pi^0)/\Gamma_{total}$ — Γ_{16}/Γ

VALUE (units 10^{-4})	CL%	DOCUMENT ID		TECN	COMMENT
<21	90	[21] ASNER	08A	CLEO	$\Upsilon(2S) \to \gamma 4\pi^+4\pi^-2\pi^0$

[21] ASNER 08A reports $[\Gamma(\chi_{b0}(1P) \to 4\pi^+4\pi^-2\pi^0)/\Gamma_{total}] \times [B(\Upsilon(2S) \to \gamma\chi_{b0}(1P))] < 77\times10^{-6}$ which we divide by our best (shown rounded) value $B(\Upsilon(2S) \to \gamma\chi_{b0}(1P)) = 3.8\times10^{-2}$.

$\Gamma(J/\psi J/\psi)/\Gamma_{total}$ — Γ_{17}/Γ

VALUE (units 10^{-5})	CL%	DOCUMENT ID		TECN	COMMENT
<7	90	[22] SHEN	12	BELL	$\Upsilon(2S) \to \gamma\psi X$

[22] SHEN 12 reports $< 7.1\times10^{-5}$ from a measurement of $[\Gamma(\chi_{b0}(1P) \to J/\psi J/\psi)/\Gamma_{total}] \times [B(\Upsilon(2S) \to \gamma\chi_{b0}(1P))]$ assuming $B(\Upsilon(2S) \to \gamma\chi_{b0}(1P)) = (3.8 \pm 0.4)\times10^{-2}$.

$\Gamma(J/\psi\psi(2S))/\Gamma_{total}$ — Γ_{18}/Γ

VALUE (units 10^{-5})	CL%	DOCUMENT ID		TECN	COMMENT
<12	90	[23] SHEN	12	BELL	$\Upsilon(2S) \to \gamma\psi X$

[23] SHEN 12 reports $< 12\times10^{-5}$ from a measurement of $[\Gamma(\chi_{b0}(1P) \to J/\psi\psi(2S))/\Gamma_{total}] \times [B(\Upsilon(2S) \to \gamma\chi_{b0}(1P))]$ assuming $B(\Upsilon(2S) \to \gamma\chi_{b0}(1P)) = (3.8 \pm 0.4)\times10^{-2}$.

$\Gamma(\psi(2S)\psi(2S))/\Gamma_{total}$ — Γ_{19}/Γ

VALUE (units 10^{-5})	CL%	DOCUMENT ID		TECN	COMMENT
<3.1	90	[24] SHEN	12	BELL	$\Upsilon(2S) \to \gamma\psi X$

[24] SHEN 12 reports $< 3.1\times10^{-5}$ from a measurement of $[\Gamma(\chi_{b0}(1P) \to \psi(2S)\psi(2S))/\Gamma_{total}] \times [B(\Upsilon(2S) \to \gamma\chi_{b0}(1P))]$ assuming $B(\Upsilon(2S) \to \gamma\chi_{b0}(1P)) = (3.8 \pm 0.4)\times10^{-2}$.

$\Gamma(J/\psi(1S)\text{anything})/\Gamma_{total}$ — Γ_{20}/Γ

VALUE	CL%	DOCUMENT ID		TECN	COMMENT
$<2.3\times10^{-3}$	90	JIA	17A	BELL	$e^+e^- \to$ hadrons

$\chi_{b0}(1P)$ CROSS-PARTICLE BRANCHING RATIOS

$\Gamma(\chi_{b0}(1P) \to \gamma\Upsilon(1S))/\Gamma_{total} \times \Gamma(\Upsilon(2S) \to \gamma\chi_{b0}(1P))/\Gamma_{total}$ — $\Gamma_1/\Gamma \times \Gamma^{\Upsilon(2S)}_{80}/\Gamma^{\Upsilon(2S)}$

VALUE	CL%	DOCUMENT ID		TECN	COMMENT
$<1.7\times10^{-3}$	90	[25] LEES	11J	BABR	$\Upsilon(2S) \to X\gamma$

[25] LEES 11J quotes a central value of $\Gamma(\chi_{b0}(1P) \to \gamma\Upsilon(1S))/\Gamma_{total} \times \Gamma(\Upsilon(2S) \to \gamma\chi_{b0}(1P))/\Gamma_{total} = (8.3 \pm 5.6^{+3.7}_{-2.6})\times10^{-4}$ and derives a 90% CL upper limit of $\Gamma(\gamma\Upsilon(1S))/\Gamma_{total} < 4.6\%$ using $B(\Upsilon(2S) \to \gamma\chi_{b0}(1P)) = (3.8 \pm 0.4)\%$.

$B(\chi_{b0}(1P) \to \gamma\Upsilon(1S)) \times B(\Upsilon(2S) \to \gamma\chi_{b0}(1P)) \times B(\Upsilon(1S) \to \ell^+\ell^-)$

VALUE (units 10^{-5})	EVTS	DOCUMENT ID		TECN	COMMENT
1.67±0.28 OUR AVERAGE					
$2.9\ ^{+1.7}_{-1.4}\ ^{+0.1}_{-0.8}$		[26] LEES	14M	BABR	$\Upsilon(2S) \to \gamma\gamma\mu^+\mu^-$
1.63±0.24±0.15	87	KORNICER	11	CLEO	$e^+e^- \to \gamma\gamma\ell^+\ell^-$

[26] From a sample of $\Upsilon(2S) \to \gamma\gamma\mu^+\mu^-$ with one converted photon.

$[B(\chi_{b0}(1P) \to \gamma\Upsilon(1S)) \times B(\Upsilon(2S) \to \gamma\chi_{b0}(1P))]$ / $[B(\chi_{b1}(1P) \to \gamma\Upsilon(1S)) \times B(\Upsilon(2S) \to \gamma\chi_{b1}(1P))]$

VALUE (%)	DOCUMENT ID		TECN	COMMENT
3.28±0.37	[27] LEES	14M	BABR	$\Upsilon(2S) \to \gamma\gamma\mu^+\mu^-$

[27] From a sample of $\Upsilon(2S) \to \gamma\gamma\mu^+\mu^-$ without converted photons.

$\chi_{b0}(1P)$ REFERENCES

JIA	17A	PR D96 112002	S. Jia *et al.*	(BELLE Collab.)
LEES	14M	PR D90 112010	J.P. Lees *et al.*	(BABAR Collab.)
SHEN	12	PR D85 071102	C.P. Shen *et al.*	(BELLE Collab.)
KORNICER	11	PR D83 054003	M. Kornicer *et al.*	(CLEO Collab.)
LEES	11J	PR D84 072002	J.P. Lees *et al.*	(BABAR Collab.)
ASNER	08A	PR D78 091103	D.M. Asner *et al.*	(CLEO Collab.)
BRIERE	08	PR D78 092007	R.A. Briere *et al.*	(CLEO Collab.)
ARTUSO	05	PRL 94 032001	M. Artuso *et al.*	(CLEO Collab.)
EDWARDS	99	PR D59 032003	K.W. Edwards *et al.*	(CLEO Collab.)
WALK	86	PR D34 2611	W.S. Walk *et al.*	(Crystal Ball Collab.)
ALBRECHT	85E	PL 160B 331	H. Albrecht *et al.*	(ARGUS Collab.)
NERNST	85	PRL 54 2195	R. Nernst *et al.*	(Crystal Ball Collab.)
HAAS	84	PRL 52 799	J. Haas *et al.*	(CLEO Collab.)
KLOPFEN...	83	PRL 51 160	C. Klopfenstein *et al.*	(CUSB Collab.)
PAUSS	83	PL 130B 439	F. Pauss *et al.*	(MPIM, COLU, CORN, LSU+)

Int. J. Mod. Phys. A 2026.41. Downloaded from www.worldscientific.com by UNIVERSITY OF CALIFORNIA @ BERKELEY on 09/16/26. Re-use and distribution is strictly not permitted, except for Open Access articles.

$\chi_{b1}(1P)$

$I^G(J^{PC}) = 0^+(1^{++})$
J needs confirmation.

Observed in radiative decay of the $\Upsilon(2S)$, therefore $C = +$. Branching ratio requires E1 transition, M1 is strongly disfavored, therefore $P = +$. $J = 1$ from SKWARNICKI 87.

$\chi_{b1}(1P)$ MASS

VALUE (MeV)	DOCUMENT ID
9892.78±0.26±0.31 OUR EVALUATION	From average γ energy below, using $\Upsilon(2S)$ mass = 10023.26 ± 0.31 MeV

$m_{\chi_{b1}(1P)} - m_{\Upsilon(1S)}$

VALUE (MeV)	EVTS	DOCUMENT ID		TECN	COMMENT
432.10±0.26±0.10	50	[1] AAIJ	24AC	LHCB	$\chi_{b1}(1P) \to \Upsilon(1S)\mu^+\mu^-$

[1] Observed in prompt pp production.

γ ENERGY IN $\Upsilon(2S)$ DECAY

VALUE (MeV)	DOCUMENT ID		TECN	COMMENT
129.63±0.33 OUR AVERAGE	Error includes scale factor of 1.3.			See the ideogram below.
129.58±0.09±0.29	ARTUSO	05	CLEO	$\Upsilon(2S) \to \gamma X$
128.8 ±0.4 ±0.6	EDWARDS	99	CLE2	$\Upsilon(2S) \to \gamma\chi(1P)$
131.7 ±0.9 ±1.3	WALK	86	CBAL	$\Upsilon(2S) \to \gamma\gamma\ell^+\ell^-$
131.7 ±0.3 ±1.1	ALBRECHT	85E	ARG	$\Upsilon(2S) \to$ conv.γX
130.6 ±0.8 ±2.4	NERNST	85	CBAL	$\Upsilon(2S) \to \gamma X$
129 ±0.8 ±1	HAAS	84	CLEO	$\Upsilon(2S) \to$ conv.γX
128.1 ±0.4 ±3.0	KLOPFEN...	83	CUSB	$\Upsilon(2S) \to \gamma X$
130.6 ±3.0	PAUSS	83	CUSB	$\Upsilon(2S) \to \gamma\gamma\ell^+\ell^-$

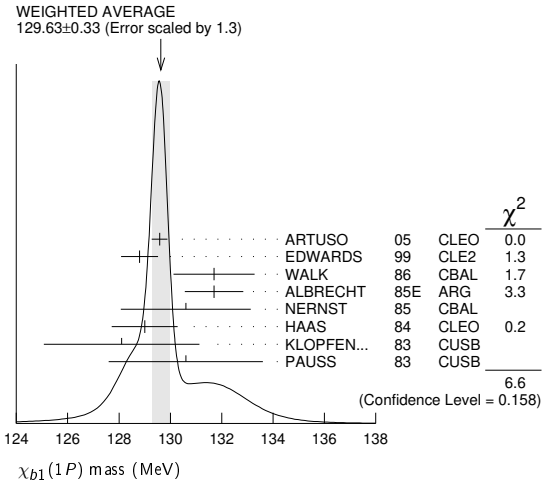

$\chi_{b1}(1P)$ DECAY MODES

	Mode	Fraction (Γ_i/Γ)	Confidence level
Γ_1	$\gamma\Upsilon(1S)$	(35.2 ±2.0) %	
Γ_2	D^0X	(12.6 ±2.2) %	
Γ_3	$\pi^+\pi^-K^+K^-\pi^0$	$(2.0 \pm 0.6) \times 10^{-4}$	
Γ_4	$2\pi^+\pi^-K^-K^0_S$	$(1.3 \pm 0.5) \times 10^{-4}$	
Γ_5	$2\pi^+\pi^-K^-K^0_S2\pi^0$	$< 6 \times 10^{-4}$	90%
Γ_6	$2\pi^+2\pi^-2\pi^0$	$(8.0 \pm 2.5) \times 10^{-4}$	
Γ_7	$2\pi^+2\pi^-K^+K^-$	$(1.5 \pm 0.5) \times 10^{-4}$	
Γ_8	$2\pi^+2\pi^-K^+K^-\pi^0$	$(3.5 \pm 1.2) \times 10^{-4}$	
Γ_9	$2\pi^+2\pi^-K^+K^-2\pi^0$	$(8.6 \pm 3.2) \times 10^{-4}$	
Γ_{10}	$3\pi^+2\pi^-K^-K^0_S\pi^0$	$(9.3 \pm 3.3) \times 10^{-4}$	
Γ_{11}	$3\pi^+3\pi^-$	$(1.9 \pm 0.6) \times 10^{-4}$	
Γ_{12}	$3\pi^+3\pi^-2\pi^0$	$(1.7 \pm 0.5) \times 10^{-3}$	
Γ_{13}	$3\pi^+3\pi^-K^+K^-$	$(2.6 \pm 0.8) \times 10^{-4}$	
Γ_{14}	$3\pi^+3\pi^-K^+K^-\pi^0$	$(7.5 \pm 2.6) \times 10^{-4}$	
Γ_{15}	$4\pi^+4\pi^-$	$(2.6 \pm 0.9) \times 10^{-4}$	
Γ_{16}	$4\pi^+4\pi^-2\pi^0$	$(1.4 \pm 0.6) \times 10^{-3}$	
Γ_{17}	ωanything	(4.9 ±1.4) %	
Γ_{18}	ωX_{tetra}	$< 4.44 \times 10^{-4}$	90%
Γ_{19}	$J/\psi J/\psi$	$< 2.7 \times 10^{-5}$	90%
Γ_{20}	$J/\psi\psi(2S)$	$< 1.7 \times 10^{-5}$	90%
Γ_{21}	$\psi(2S)\psi(2S)$	$< 6 \times 10^{-5}$	90%
Γ_{22}	$J/\psi(1S)$anything	$< 1.1 \times 10^{-3}$	90%
Γ_{23}	$J/\psi(1S)X_{tetra}$	$< 2.27 \times 10^{-4}$	90%

$\chi_{b1}(1P)$ BRANCHING RATIOS

$\Gamma(\gamma\Upsilon(1S))/\Gamma_{total}$ — Γ_1/Γ

VALUE	EVTS	DOCUMENT ID		TECN	COMMENT
0.352±0.020 OUR AVERAGE					
$0.356^{+0.016}_{-0.022}\pm0.019$	964k	[1] FULSOM	18	BELL	$\Upsilon(2S) \to \gamma X$
0.364±0.017±0.019		[2,3,4] LEES	14M	BABR	$\Upsilon(2S) \to \gamma\gamma\mu^+\mu^-$
0.331±0.018±0.017	3222	[4,5] KORNICER	11	CLEO	$e^+e^- \to \gamma\gamma\ell^+\ell^-$
0.350±0.023±0.018	13k	[6] LEES	11J	BABR	$\Upsilon(2S) \to X\gamma$
0.34 ±0.07 ±0.02	53	[4,7,8] WALK	86	CBAL	$\Upsilon(2S) \to \gamma\gamma\ell^+\ell^-$
0.47 ±0.18		KLOPFEN...	83	CUSB	$\Upsilon(2S) \to \gamma\gamma\ell^+\ell^-$

[1] FULSOM 18 reports $[\Gamma(\chi_{b1}(1P) \to \gamma\Upsilon(1S))/\Gamma_{total}] \times [B(\Upsilon(2S) \to \gamma\chi_{b1}(1P))] = (2.45 \pm 0.02^{+0.11}_{-0.15}) \times 10^{-2}$ which we divide by our best (shown rounded) value $B(\Upsilon(2S) \to \gamma\chi_{b1}(1P)) = (6.9 \pm 0.4) \times 10^{-2}$. Our first error is their experiment's error and our second error is the systematic error from using our best (shown rounded) value.

[2] LEES 14M quotes $\Gamma(\chi_{b1}(1P) \to \gamma\Upsilon(1S))/\Gamma_{total} \times \Gamma(\Upsilon(2S) \to \gamma\chi_{b1}(1P))/\Gamma_{total} = (2.51 \pm 0.12)$ % combining the results from samples of $\Upsilon(2S) \to \gamma\gamma\mu^+\mu^-$ with and without converted photons.

[3] LEES 14M reports $[\Gamma(\chi_{b1}(1P) \to \gamma\Upsilon(1S))/\Gamma_{total}] \times [B(\Upsilon(2S) \to \gamma\chi_{b1}(1P))] = (2.51 \pm 0.12) \times 10^{-2}$ which we divide by our best (shown rounded) value $B(\Upsilon(2S) \to \gamma\chi_{b1}(1P)) = (6.9 \pm 0.4) \times 10^{-2}$. Our first error is their experiment's error and our second error is the systematic error from using our best (shown rounded) value.

[4] Assuming $B(\Upsilon(1S) \to \mu^+\mu^-) = (2.48 \pm 0.05)$%.

[5] KORNICER 11 reports $[\Gamma(\chi_{b1}(1P) \to \gamma\Upsilon(1S))/\Gamma_{total}] \times [B(\Upsilon(2S) \to \gamma\chi_{b1}(1P))] = (22.8 \pm 0.4 \pm 1.2) \times 10^{-3}$ which we divide by our best (shown rounded) value $B(\Upsilon(2S) \to \gamma\chi_{b1}(1P)) = (6.9 \pm 0.4) \times 10^{-2}$. Our first error is their experiment's error and our second error is the systematic error from using our best (shown rounded) value.

[6] LEES 11J reports $[\Gamma(\chi_{b1}(1P) \to \gamma\Upsilon(1S))/\Gamma_{total}] \times [B(\Upsilon(2S) \to \gamma\chi_{b1}(1P))] = (24.1 \pm 0.6 \pm 1.5) \times 10^{-3}$ which we divide by our best (shown rounded) value $B(\Upsilon(2S) \to \gamma\chi_{b1}(1P)) = (6.9 \pm 0.4) \times 10^{-2}$. Our first error is their experiment's error and our second error is the systematic error from using our best (shown rounded) value.

[7] WALK 86 quotes $B(\Upsilon(2S) \to \gamma\chi_{b1}(1P)) \times B(\chi_{b1}(1P) \to \gamma\Upsilon(1S)) \times B(\Upsilon(1S) \to \ell^+\ell^-) = (5.8 \pm 0.9 \pm 0.7)$ %.

[8] WALK 86 reports $[\Gamma(\chi_{b1}(1P) \to \gamma\Upsilon(1S))/\Gamma_{total}] \times [B(\Upsilon(2S) \to \gamma\chi_{b1}(1P))] = (23.4 \pm 3.63 \pm 2.82) \times 10^{-3}$ which we divide by our best (shown rounded) value $B(\Upsilon(2S) \to \gamma\chi_{b1}(1P)) = (6.9 \pm 0.4) \times 10^{-2}$. Our first error is their experiment's error and our second error is the systematic error from using our best (shown rounded) value.

$\Gamma(D^0X)/\Gamma_{total}$ — Γ_2/Γ

VALUE (units 10^{-2})	EVTS	DOCUMENT ID		TECN	COMMENT
12.6±1.9±1.1	2310	[1] BRIERE	08	CLEO	$\Upsilon(2S) \to \gamma D^0X$

[1] For $p_{D^0} > 2.5$ GeV/c.

$\Gamma(\pi^+\pi^-K^+K^-\pi^0)/\Gamma_{total}$ — Γ_3/Γ

VALUE (units 10^{-4})	EVTS	DOCUMENT ID		TECN	COMMENT
2.0±0.6±0.1	18	[1] ASNER	08A	CLEO	$\Upsilon(2S) \to \gamma\pi^+\pi^-K^+K^-\pi^0$

[1] ASNER 08A reports $[\Gamma(\chi_{b1}(1P) \to \pi^+\pi^-K^+K^-\pi^0)/\Gamma_{total}] \times [B(\Upsilon(2S) \to \gamma\chi_{b1}(1P))] = (14 \pm 3 \pm 3) \times 10^{-6}$ which we divide by our best (shown rounded) value $B(\Upsilon(2S) \to \gamma\chi_{b1}(1P)) = (6.9 \pm 0.4) \times 10^{-2}$. Our first error is their experiment's error and our second error is the systematic error from using our best (shown rounded) value.

$\Gamma(2\pi^+\pi^-K^-K^0_S)/\Gamma_{total}$ — Γ_4/Γ

VALUE (units 10^{-4})	EVTS	DOCUMENT ID		TECN	COMMENT
1.3±0.5±0.1	11	[1] ASNER	08A	CLEO	$\Upsilon(2S) \to \gamma 2\pi^+\pi^-K^-K^0_S$

[1] ASNER 08A reports $[\Gamma(\chi_{b1}(1P) \to 2\pi^+\pi^-K^-K^0_S)/\Gamma_{total}] \times [B(\Upsilon(2S) \to \gamma\chi_{b1}(1P))] = (9 \pm 3 \pm 2) \times 10^{-6}$ which we divide by our best (shown rounded) value $B(\Upsilon(2S) \to \gamma\chi_{b1}(1P)) = (6.9 \pm 0.4) \times 10^{-2}$. Our first error is their experiment's error and our second error is the systematic error from using our best (shown rounded) value.

$\Gamma(2\pi^+\pi^-K^-K^0_S2\pi^0)/\Gamma_{total}$ — Γ_5/Γ

VALUE (units 10^{-4})	CL%	DOCUMENT ID		TECN	COMMENT
<6	90	[1] ASNER	08A	CLEO	$\Upsilon(2S) \to \gamma 2\pi^+\pi^-K^-2\pi^0$

[1] ASNER 08A reports $[\Gamma(\chi_{b1}(1P) \to 2\pi^+\pi^-K^-K^0_S2\pi^0)/\Gamma_{total}] \times [B(\Upsilon(2S) \to \gamma\chi_{b1}(1P))] < 42 \times 10^{-6}$ which we divide by our best (shown rounded) value $B(\Upsilon(2S) \to \gamma\chi_{b1}(1P)) = 6.9 \times 10^{-2}$.

$\Gamma(2\pi^+2\pi^-2\pi^0)/\Gamma_{total}$ — Γ_6/Γ

VALUE (units 10^{-4})	EVTS	DOCUMENT ID		TECN	COMMENT
8.0±2.4±0.4	46	[1] ASNER	08A	CLEO	$\Upsilon(2S) \to \gamma 2\pi^+2\pi^-2\pi^0$

[1] ASNER 08A reports $[\Gamma(\chi_{b1}(1P) \to 2\pi^+2\pi^-2\pi^0)/\Gamma_{total}] \times [B(\Upsilon(2S) \to \gamma\chi_{b1}(1P))] = (55 \pm 9 \pm 14) \times 10^{-6}$ which we divide by our best (shown rounded) value $B(\Upsilon(2S) \to \gamma\chi_{b1}(1P)) = (6.9 \pm 0.4) \times 10^{-2}$. Our first error is their experiment's error and our second error is the systematic error from using our best (shown rounded) value.

$\Gamma(2\pi^+2\pi^-K^+K^-)/\Gamma_{total}$ — Γ_7/Γ

VALUE (units 10^{-4})	EVTS	DOCUMENT ID		TECN	COMMENT
1.5±0.5±0.1	18	[1] ASNER	08A	CLEO	$\Upsilon(2S) \to \gamma 2\pi^+2\pi^-K^+K^-$

[1] ASNER 08A reports $[\Gamma(\chi_{b1}(1P) \to 2\pi^+2\pi^-K^+K^-)/\Gamma_{total}] \times [B(\Upsilon(2S) \to \gamma\chi_{b1}(1P))] = (10 \pm 3 \pm 2) \times 10^{-6}$ which we divide by our best (shown rounded) value $B(\Upsilon(2S) \to \gamma\chi_{b1}(1P)) = (6.9 \pm 0.4) \times 10^{-2}$. Our first error is their experiment's error and our second error is the systematic error from using our best (shown rounded) value.

$\Gamma(2\pi^+2\pi^-K^+K^-\pi^0)/\Gamma_{total}$ — Γ_8/Γ

VALUE (units 10^{-4})	EVTS	DOCUMENT ID		TECN	COMMENT
3.5±1.2±0.2	22	[1] ASNER	08A	CLEO	$\Upsilon(2S) \to \gamma 2\pi^+2\pi^-K^+K^-\pi^0$

[1] ASNER 08A reports $[\Gamma(\chi_{b1}(1P) \to 2\pi^+2\pi^-K^+K^-\pi^0)/\Gamma_{total}] \times [B(\Upsilon(2S) \to \gamma\chi_{b1}(1P))] = (24 \pm 6 \pm 6) \times 10^{-6}$ which we divide by our best (shown rounded) value $B(\Upsilon(2S) \to \gamma\chi_{b1}(1P)) = (6.9 \pm 0.4) \times 10^{-2}$. Our first error is their experiment's error and our second error is the systematic error from using our best (shown rounded) value.

$\Gamma(2\pi^+2\pi^-K^+K^-2\pi^0)/\Gamma_{total}$ — Γ_9/Γ

VALUE (units 10^{-4})	EVTS	DOCUMENT ID		TECN	COMMENT
8.6±3.2±0.4	26	[1] ASNER	08A	CLEO	$\Upsilon(2S) \to \gamma 2\pi^+2\pi^-K^+K^-2\pi^0$

[1] ASNER 08A reports $[\Gamma(\chi_{b1}(1P) \to 2\pi^+2\pi^-K^+K^-2\pi^0)/\Gamma_{total}] \times [B(\Upsilon(2S) \to \gamma\chi_{b1}(1P))] = (59 \pm 14 \pm 17) \times 10^{-6}$ which we divide by our best (shown rounded) value $B(\Upsilon(2S) \to \gamma\chi_{b1}(1P)) = (6.9 \pm 0.4) \times 10^{-2}$. Our first error is their experiment's error and our second error is the systematic error from using our best (shown rounded) value.

$\Gamma(3\pi^+2\pi^-K^-K^0_S\pi^0)/\Gamma_{total}$ — Γ_{10}/Γ

VALUE (units 10^{-4})	EVTS	DOCUMENT ID		TECN	COMMENT
9.3±3.3±0.5	21	[1] ASNER	08A	CLEO	$\Upsilon(2S) \to \gamma 3\pi^+2\pi^-K^-K^0_S\pi^0$

[1] ASNER 08A reports $[\Gamma(\chi_{b1}(1P) \to 3\pi^+2\pi^-K^-K^0_S\pi^0)/\Gamma_{total}] \times [B(\Upsilon(2S) \to \gamma\chi_{b1}(1P))] = (64 \pm 16 \pm 16) \times 10^{-6}$ which we divide by our best (shown rounded) value $B(\Upsilon(2S) \to \gamma\chi_{b1}(1P)) = (6.9 \pm 0.4) \times 10^{-2}$. Our first error is their experiment's error and our second error is the systematic error from using our best (shown rounded) value.

$\Gamma(3\pi^+3\pi^-)/\Gamma_{total}$ — Γ_{11}/Γ

VALUE (units 10^{-4})	EVTS	DOCUMENT ID		TECN	COMMENT
1.9±0.6±0.1	25	[1] ASNER	08A	CLEO	$\Upsilon(2S) \to \gamma 3\pi^+3\pi^-$

[1] ASNER 08A reports $[\Gamma(\chi_{b1}(1P) \to 3\pi^+3\pi^-)/\Gamma_{total}] \times [B(\Upsilon(2S) \to \gamma\chi_{b1}(1P))] = (13 \pm 3 \pm 3) \times 10^{-6}$ which we divide by our best (shown rounded) value $B(\Upsilon(2S) \to \gamma\chi_{b1}(1P)) = (6.9 \pm 0.4) \times 10^{-2}$. Our first error is their experiment's error and our second error is the systematic error from using our best (shown rounded) value.

$\Gamma(3\pi^+3\pi^-2\pi^0)/\Gamma_{total}$ — Γ_{12}/Γ

VALUE (units 10^{-4})	EVTS	DOCUMENT ID		TECN	COMMENT
17±5±1	56	[1] ASNER	08A	CLEO	$\Upsilon(2S) \to \gamma 3\pi^+3\pi^-2\pi^0$

[1] ASNER 08A reports $[\Gamma(\chi_{b1}(1P) \to 3\pi^+3\pi^-2\pi^0)/\Gamma_{total}] \times [B(\Upsilon(2S) \to \gamma\chi_{b1}(1P))] = (119 \pm 18 \pm 32) \times 10^{-6}$ which we divide by our best (shown rounded) value $B(\Upsilon(2S) \to \gamma\chi_{b1}(1P)) = (6.9 \pm 0.4) \times 10^{-2}$. Our first error is their experiment's error and our second error is the systematic error from using our best (shown rounded) value.

$\Gamma(3\pi^+3\pi^-K^+K^-)/\Gamma_{total}$ — Γ_{13}/Γ

VALUE (units 10^{-4})	EVTS	DOCUMENT ID		TECN	COMMENT
2.6±0.8±0.1	21	[1] ASNER	08A	CLEO	$\Upsilon(2S) \to \gamma 3\pi^+3\pi^-K^+K^-$

[1] ASNER 08A reports $[\Gamma(\chi_{b1}(1P) \to 3\pi^+3\pi^-K^+K^-)/\Gamma_{total}] \times [B(\Upsilon(2S) \to \gamma\chi_{b1}(1P))] = (18 \pm 4 \pm 4) \times 10^{-6}$ which we divide by our best (shown rounded) value $B(\Upsilon(2S) \to \gamma\chi_{b1}(1P)) = (6.9 \pm 0.4) \times 10^{-2}$. Our first error is their experiment's error and our second error is the systematic error from using our best (shown rounded) value.

$\Gamma(3\pi^+3\pi^-K^+K^-\pi^0)/\Gamma_{total}$ — Γ_{14}/Γ

VALUE (units 10^{-4})	EVTS	DOCUMENT ID		TECN	COMMENT
7.5±2.6±0.4	28	[1] ASNER	08A	CLEO	$\Upsilon(2S) \to \gamma 3\pi^+3\pi^-K^+K^-\pi^0$

[1] ASNER 08A reports $[\Gamma(\chi_{b1}(1P) \to 3\pi^+3\pi^-K^+K^-\pi^0)/\Gamma_{total}] \times [B(\Upsilon(2S) \to \gamma\chi_{b1}(1P))] = (52 \pm 11 \pm 14) \times 10^{-6}$ which we divide by our best (shown rounded) value $B(\Upsilon(2S) \to \gamma\chi_{b1}(1P)) = (6.9 \pm 0.4) \times 10^{-2}$. Our first error is their experiment's error and our second error is the systematic error from using our best (shown rounded) value.

$\Gamma(4\pi^+4\pi^-)/\Gamma_{total}$ — Γ_{15}/Γ

VALUE (units 10^{-4})	EVTS	DOCUMENT ID		TECN	COMMENT
2.6±0.9±0.1	24	[1] ASNER	08A	CLEO	$\Upsilon(2S) \to \gamma 4\pi^+4\pi^-$

[1] ASNER 08A reports $[\Gamma(\chi_{b1}(1P) \to 4\pi^+4\pi^-)/\Gamma_{total}] \times [B(\Upsilon(2S) \to \gamma\chi_{b1}(1P))] = (18 \pm 4 \pm 5) \times 10^{-6}$ which we divide by our best (shown rounded) value $B(\Upsilon(2S) \to \gamma\chi_{b1}(1P)) = (6.9 \pm 0.4) \times 10^{-2}$. Our first error is their experiment's error and our second error is the systematic error from using our best (shown rounded) value.

$\Gamma(4\pi^+4\pi^-2\pi^0)/\Gamma_{total}$ — Γ_{16}/Γ

VALUE (units 10^{-4})	EVTS	DOCUMENT ID		TECN	COMMENT
14±5±1	26	[1] ASNER	08A	CLEO	$\Upsilon(2S) \to \gamma 4\pi^+4\pi^-2\pi^0$

[1] ASNER 08A reports $[\Gamma(\chi_{b1}(1P) \to 4\pi^+4\pi^-2\pi^0)/\Gamma_{total}] \times [B(\Upsilon(2S) \to \gamma\chi_{b1}(1P))] = (96 \pm 24 \pm 29) \times 10^{-6}$ which we divide by our best (shown rounded) value $B(\Upsilon(2S) \to \gamma\chi_{b1}(1P)) = (6.9 \pm 0.4) \times 10^{-2}$. Our first error is their experiment's error and our second error is the systematic error from using our best (shown rounded) value.

$\Gamma(\omega\,\text{anything})/\Gamma_{total}$ — Γ_{17}/Γ

VALUE (units 10^{-2})	EVTS	DOCUMENT ID		TECN	COMMENT
4.9±1.3±0.6	51k	JIA	17A	BELL	$e^+e^- \to$ hadrons

$\Gamma(\omega X_{tetra})/\Gamma_{total}$ — Γ_{18}/Γ

VALUE	CL%	DOCUMENT ID		TECN	COMMENT
<44.4 × 10^{-5}	90	[1] JIA	17A	BELL	$e^+e^- \to$ hadrons

[1] For a tetraquark state X_{tetra}, with mass in the range 1.16–2.46 GeV and width in the range 0–0.3 GeV. Measured 90% CL limits as a function of X_{tetra} mass and width range from 3.3×10^{-5} to 44.4×10^{-5}.

$\Gamma(J/\psi J/\psi)/\Gamma_{total}$ — Γ_{19}/Γ

VALUE (units 10^{-5})	CL%	DOCUMENT ID		TECN	COMMENT
<2.7	90	[1] SHEN	12	BELL	$\Upsilon(2S) \to \gamma\psi X$

[1] SHEN 12 reports $< 2.7 \times 10^{-5}$ from a measurement of $[\Gamma(\chi_{b1}(1P) \to J/\psi J/\psi)/\Gamma_{total}] \times [B(\Upsilon(2S) \to \gamma\chi_{b1}(1P))]$ assuming $B(\Upsilon(2S) \to \gamma\chi_{b1}(1P)) = (6.9 \pm 0.4) \times 10^{-2}$.

$\Gamma(J/\psi\psi(2S))/\Gamma_{total}$ — Γ_{20}/Γ

VALUE (units 10^{-5})	CL%	DOCUMENT ID		TECN	COMMENT
<1.7	90	[1] SHEN	12	BELL	$\Upsilon(2S) \to \gamma\psi X$

[1] SHEN 12 reports $< 1.7 \times 10^{-5}$ from a measurement of $[\Gamma(\chi_{b1}(1P) \to J/\psi\psi(2S))/\Gamma_{total}] \times [B(\Upsilon(2S) \to \gamma\chi_{b1}(1P))]$ assuming $B(\Upsilon(2S) \to \gamma\chi_{b1}(1P)) = (6.9 \pm 0.4) \times 10^{-2}$.

$\Gamma(\psi(2S)\psi(2S))/\Gamma_{total}$ — Γ_{21}/Γ

VALUE (units 10^{-5})	CL%	DOCUMENT ID		TECN	COMMENT
<6	90	[1] SHEN	12	BELL	$\Upsilon(2S) \to \gamma\psi X$

[1] SHEN 12 reports $< 6.2 \times 10^{-5}$ from a measurement of $[\Gamma(\chi_{b1}(1P) \to \psi(2S)\psi(2S))/\Gamma_{total}] \times [B(\Upsilon(2S) \to \gamma\chi_{b1}(1P))]$ assuming $B(\Upsilon(2S) \to \gamma\chi_{b1}(1P)) = (6.9 \pm 0.4) \times 10^{-2}$.

$\Gamma(J/\psi(1S)\,\text{anything})/\Gamma_{total}$ — Γ_{22}/Γ

VALUE	CL%	DOCUMENT ID		TECN	COMMENT
<1.1 × 10^{-3}	90	JIA	17A	BELL	$e^+e^- \to$ hadrons

$\Gamma(J/\psi(1S)X_{tetra})/\Gamma_{total}$ — Γ_{23}/Γ

VALUE	CL%	DOCUMENT ID		TECN	COMMENT
<22.7 × 10^{-5}	90	[1] JIA	17A	BELL	$e^+e^- \to$ hadrons

[1] For a tetraquark state X_{tetra}, with mass in the range 1.16–2.46 GeV and width in the range 0–0.3 GeV. Measured 90% CL limits as a function of X_{tetra} mass and width range from 1.8×10^{-5} to 22.7×10^{-5}.

$\chi_{b1}(1P)$ Cross-Particle Branching Ratios

$\Gamma(\chi_{b1}(1P) \to \gamma\Upsilon(1S))/\Gamma_{total} \times \Gamma(\Upsilon(2S) \to \gamma\chi_{b1}(1P))/\Gamma_{total}$ — $\Gamma_1/\Gamma \times \Gamma_{78}^{\Upsilon(2S)}/\Gamma^{\Upsilon(2S)}$

VALUE (units 10^{-3})	EVTS	DOCUMENT ID		TECN	COMMENT
24.1±0.6±1.5	13k	LEES	11J	BABR	$\Upsilon(2S) \to X\gamma$

$B(\chi_{b1}(1P) \to \gamma\Upsilon(1S)) \times B(\Upsilon(2S) \to \gamma\chi_{b1}(1P)) \times B(\Upsilon(1S) \to \ell^+\ell^-)$

VALUE (units 10^{-4})	EVTS	DOCUMENT ID		TECN	COMMENT
5.90±0.34 OUR AVERAGE	Error includes scale factor of 1.3. See the ideogram below.				
$6.86^{+0.47+0.44}_{-0.45-0.35}$		[1] LEES	14M	BABR	$\Upsilon(2S) \to \gamma\gamma\mu^+\mu^-$
5.65±0.11±0.27	3222	KORNICER	11	CLEO	$e^+e^- \to \gamma\gamma\ell^+\ell^-$
5.8 ±0.9 ±0.7	53	WALK	86	CBAL	$\Upsilon(2S) \to \gamma\gamma\ell^+\ell^-$

[1] From a sample of $\Upsilon(2S) \to \gamma\gamma\mu^+\mu^-$ with one converted photon.

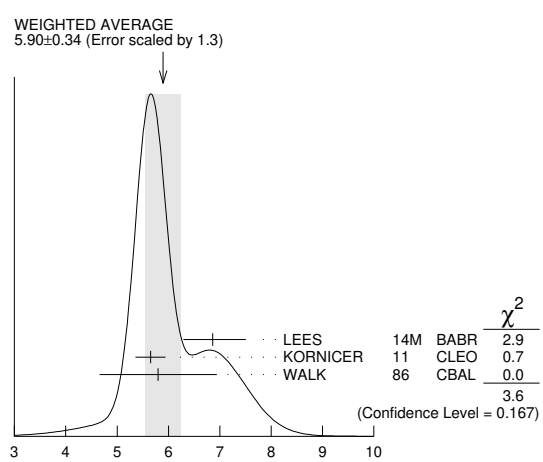

Int. J. Mod. Phys. A 2026.41. Downloaded from www.worldscientific.com
by CALIFORNIA @ BERKELEY on 09/16/26. Re-use and distribution is strictly not permitted, except for Open Access articles.

Int. J. Mod. Phys. A 2026.41. Downloaded from www.worldscientific.com by UNIVERSITY OF CALIFORNIA @ BERKELEY on 09/16/26. Re-use and distribution is strictly not permitted, except for Open Access articles.

$B(\chi_{b1}(1P) \to \gamma\Upsilon(1S)) \times B(\Upsilon(3S) \to \gamma\chi_{b1}(1P)) \times B(\Upsilon(1S) \to \ell^+\ell^-)$

VALUE (units 10^{-5})	EVTS	DOCUMENT ID		TECN	COMMENT
1.30±0.34 OUR AVERAGE					
$1.16^{+0.78}_{-0.67}{}^{+0.14}_{-0.16}$		[1] LEES	14M	BABR	$\Upsilon(3S) \to \gamma\gamma\mu^+\mu^-$
1.33±0.30±0.23	50	KORNICER	11	CLEO	$e^+e^- \to \gamma\gamma\ell^+\ell^-$

[1] From a sample of $\Upsilon(3S) \to \gamma\gamma\mu^+\mu^-$ with converted photons.

$B(\chi_{b2}(1P) \to pX + \bar{p}X)/B(\chi_{b1}(1P) \to pX + \bar{p}X)$

VALUE	DOCUMENT ID		TECN	COMMENT
1.068±0.010±0.040	BRIERE	07	CLEO	$\Upsilon(2S) \to \gamma\chi_{bJ}(1P)$

$B(\chi_{b0}(1P) \to pX + \bar{p}X)/B(\chi_{b1}(1P) \to pX + \bar{p}X)$

VALUE	DOCUMENT ID		TECN	COMMENT
1.11±0.15±0.20	BRIERE	07	CLEO	$\Upsilon(2S) \to \gamma\chi_{bJ}(1P)$

$\chi_{b1}(1P)$ REFERENCES

AAIJ	24AC	JHEP 2410 122	R. Aaij et al.	(LHCb Collab.)
FULSOM	18	PRL 121 232001	B.G. Fulsom et al.	(BELLE Collab.)
JIA	17A	PR D96 112002	S. Jia et al.	(BELLE Collab.)
LEES	14M	PR D90 112010	J.P. Lees et al.	(BABAR Collab.)
SHEN	12	PR D85 071102	C.P. Shen et al.	(BELLE Collab.)
KORNICER	11	PR D83 054003	M. Kornicer et al.	(CLEO Collab.)
LEES	11J	PR D84 072002	J.P. Lees et al.	(BABAR Collab.)
ASNER	08A	PR D78 091103	D.M. Asner et al.	(CLEO Collab.)
BRIERE	08	PR D78 092007	R.A. Briere et al.	(CLEO Collab.)
BRIERE	07	PR D76 012005	R.A. Briere et al.	(CLEO Collab.)
ARTUSO	05	PRL 94 032001	M. Artuso et al.	(CLEO Collab.)
EDWARDS	99	PR D59 032003	K.W. Edwards et al.	(CLEO Collab.)
SKWARNICKI	87	PRL 58 972	T. Skwarnicki et al.	(Crystal Ball Collab.) J
WALK	86	PR D34 2611	W.S. Walk et al.	(Crystal Ball Collab.)
ALBRECHT	85E	PL 160B 331	H. Albrecht et al.	(ARGUS Collab.)
NERNST	85	PRL 54 2195	R. Nernst et al.	(Crystal Ball Collab.)
HAAS	84	PRL 52 799	J. Haas et al.	(CLEO Collab.)
KLOPFEN...	83	PRL 51 160	C. Klopfenstein et al.	(CUSB Collab.)
PAUSS	83	PL 130B 439	F. Pauss et al.	(MPIM, COLU, CORN, LSU+)

$h_b(1P)$

$I^G(J^{PC}) = 0^-(1^{+-})$

Quantum numbers are quark model predictions, $C = -$ established by $\eta_b\gamma$ decay.

$h_b(1P)$ MASS

VALUE (MeV)	EVTS	DOCUMENT ID		TECN	COMMENT
9899.3±0.8 OUR AVERAGE					
9899.3±0.4±1.0	112k	TAMPONI	15	BELL	$e^+e^- \to \gamma\eta +$ hadrons
9899.1±0.4±1.0	70k	MIZUK	12	BELL	$e^+e^- \to \pi^+\pi^-$ hadrons
9902 ±4 ±2	10.8k	LEES	11K	BABR	$\Upsilon(3S) \to \eta_b\gamma\pi^0$
• • • We do not use the following data for averages, fits, limits, etc. • • •					
$9898.2^{+1.1}_{-1.0}{}^{+1.0}_{-1.1}$	50.0k	[1] ADACHI	12	BELL	10.86 $e^+e^- \to \pi^+\pi^-$ MM

[1] Superseded by MIZUK 12.

$h_b(1P)$ DECAY MODES

	Mode	Fraction (Γ_i/Γ)	Confidence level
Γ_1	$\eta_b(1S)\gamma$	$(52\ ^{+6}_{-5})$ %	
Γ_2	$\Upsilon(1S)\pi^0$	$< 1.8 \times 10^{-3}$	90%

$h_b(1P)$ BRANCHING RATIOS

$\Gamma(\eta_b(1S)\gamma)/\Gamma_{total}$ — Γ_1/Γ

VALUE (units 10^{-2})	EVTS	DOCUMENT ID		TECN	COMMENT
$52\ ^{+6}_{-5}$ OUR AVERAGE					
56 ±8 ±4	33.1k	[1] TAMPONI	15	BELL	$e^+e^- \to \gamma\eta +$ hadrons
$49.2 \pm 5.7^{+5.6}_{-3.3}$	24k	MIZUK	12	BELL	$e^+e^- \to (\gamma)\pi^+\pi^-$ hadrons
• • • We do not use the following data for averages, fits, limits, etc. • • •					
seen	10.8k	LEES	11K	BABR	$\Upsilon(3S) \to \eta_b\gamma\pi^0$

[1] Using $B(\eta \to 2\gamma) = (39.41 \pm 0.20)$%.

$\Gamma(\Upsilon(1S)\pi^0)/\Gamma_{total}$ — Γ_2/Γ

VALUE	CL%	EVTS	DOCUMENT ID		TECN	COMMENT
$<1.8 \times 10^{-3}$	90	0.43	KOVALENKO	24	BELL	$e^+e^- \to \Upsilon(5S)$

$h_b(1P)$ REFERENCES

KOVALENKO	24	PRL 133 261901	E. Kovalenko et al.	(BELLE Collab.)
TAMPONI	15	PRL 115 142001	U. Tamponi et al.	(BELLE Collab.)
ADACHI	12	PRL 108 032001	I. Adachi et al.	(BELLE Collab.)
MIZUK	12	PRL 109 232002	R. Mizuk et al.	(BELLE Collab.)
LEES	11K	PR D84 091101	J.P. Lees et al.	(BABAR Collab.)

$\chi_{b2}(1P)$

$I^G(J^{PC}) = 0^+(2^{++})$

J needs confirmation.

Observed in radiative decay of the $\Upsilon(2S)$, therefore $C = +$. Branching ratio requires E1 transition, M1 is strongly disfavored, therefore $P = +$. $J = 2$ from SKWARNICKI 87.

$\chi_{b2}(1P)$ MASS

VALUE (MeV)	DOCUMENT ID
9912.21±0.26±0.31 OUR EVALUATION	From average γ energy below, using $\Upsilon(2S)$ mass = 10023.26 ± 0.31 MeV

$m_{\chi_{b2}(1P)} - m_{\chi_{b1}(1P)}$

VALUE (MeV)	EVTS	DOCUMENT ID		TECN	COMMENT
19.17±0.20 OUR AVERAGE					
19.4 ±0.4	50	[1] AAIJ	24AC	LHCB	$\chi_b(1P) \to \Upsilon(1S)\mu^+\mu^-$
19.81±0.65±0.20		[2] AAIJ	14BG	LHCB	$pp \to \gamma\mu^+\mu^-X$
19.01±0.24		LEES	14M	BABR	$\Upsilon(2S) \to \gamma\gamma\mu^+\mu^-$

[1] Observed in prompt pp production.

[2] From the $\chi_{bj}(1P) \to \Upsilon(1S)\gamma$ transition.

γ ENERGY IN $\Upsilon(2S)$ DECAY

VALUE (MeV)	DOCUMENT ID		TECN	COMMENT
110.44±0.29 OUR AVERAGE	Error includes scale factor of 1.1.			
110.58±0.08±0.30	ARTUSO	05	CLEO	$\Upsilon(2S) \to \gamma X$
110.8 ±0.3 ±0.6	EDWARDS	99	CLE2	$\Upsilon(2S) \to \gamma\chi(1P)$
107.0 ±1.1 ±1.3	WALK	86	CBAL	$\Upsilon(2S) \to \gamma\gamma\ell^+\ell^-$
110.6 ±0.3 ±0.9	ALBRECHT	85E	ARG	$\Upsilon(2S) \to$ conv.γX
110.4 ±0.8 ±2.2	NERNST	85	CBAL	$\Upsilon(2S) \to \gamma X$
109.5 ±0.7 ±1.0	HAAS	84	CLEO	$\Upsilon(2S) \to$ conv.γX
108.2 ±0.3 ±2.0	KLOPFEN...	83	CUSB	$\Upsilon(2S) \to \gamma X$
108.8 ±4.0	PAUSS	83	CUSB	$\Upsilon(2S) \to \gamma\gamma\ell^+\ell^-$

$\chi_{b2}(1P)$ DECAY MODES

	Mode	Fraction (Γ_i/Γ)	Confidence level
Γ_1	$\gamma\Upsilon(1S)$	(18.0±1.0) %	
Γ_2	D^0X	< 7.9 %	90%
Γ_3	$\pi^+\pi^-K^+K^-\pi^0$	$(8 \pm 5) \times 10^{-5}$	
Γ_4	$2\pi^+\pi^-K^-K^0_S$	$< 1.0 \times 10^{-4}$	90%
Γ_5	$2\pi^+\pi^-K^-K^0_S2\pi^0$	$(5.3\pm2.4) \times 10^{-4}$	
Γ_6	$2\pi^+2\pi^-2\pi^0$	$(3.5\pm1.4) \times 10^{-4}$	
Γ_7	$2\pi^+2\pi^-K^+K^-$	$(1.1\pm0.4) \times 10^{-4}$	
Γ_8	$2\pi^+2\pi^-K^+K^-\pi^0$	$(2.1\pm0.9) \times 10^{-4}$	
Γ_9	$2\pi^+2\pi^-K^+K^-2\pi^0$	$(3.9\pm1.8) \times 10^{-4}$	
Γ_{10}	$3\pi^+2\pi^-K^-K^0_S\pi^0$	$< 5 \times 10^{-4}$	90%
Γ_{11}	$3\pi^+3\pi^-$	$(7.0\pm3.1) \times 10^{-5}$	
Γ_{12}	$3\pi^+3\pi^-2\pi^0$	$(1.0\pm0.4) \times 10^{-3}$	
Γ_{13}	$3\pi^+3\pi^-K^+K^-$	$< 8 \times 10^{-5}$	90%
Γ_{14}	$3\pi^+3\pi^-K^+K^-\pi^0$	$(3.6\pm1.5) \times 10^{-4}$	
Γ_{15}	$4\pi^+4\pi^-$	$(8 \pm 4) \times 10^{-5}$	
Γ_{16}	$4\pi^+4\pi^-2\pi^0$	$(1.8\pm0.7) \times 10^{-3}$	
Γ_{17}	$J/\psi J/\psi$	$< 4 \times 10^{-5}$	90%
Γ_{18}	$J/\psi\psi(2S)$	$< 5 \times 10^{-5}$	90%
Γ_{19}	$\psi(2S)\psi(2S)$	$< 1.6 \times 10^{-5}$	90%
Γ_{20}	$J/\psi(1S)$anything	$(1.5\pm0.4) \times 10^{-3}$	

$\chi_{b2}(1P)$ BRANCHING RATIOS

$\Gamma(\gamma\Upsilon(1S))/\Gamma_{total}$ — Γ_1/Γ

VALUE	EVTS	DOCUMENT ID		TECN	COMMENT
0.180±0.010 OUR AVERAGE					
$0.164^{+0.009}_{-0.010}\pm0.008$	503k	[1] FULSOM	18	BELL	$\Upsilon(2S) \to \gamma X$
0.185±0.008±0.009		[2,3,4] LEES	14M	BABR	$\Upsilon(2S) \to \gamma\gamma\mu^+\mu^-$
0.186±0.011±0.009	1770	[4,5] KORNICER	11	CLEO	$e^+e^- \to \gamma\gamma\ell^+\ell^-$
$0.194^{+0.014}_{-0.017}\pm0.009$	8k	[6] LEES	11J	BABR	$\Upsilon(2S) \to X\gamma$
0.25 ±0.06 ±0.01	35	[4,7,8] WALK	86	CBAL	$\Upsilon(2S) \to \gamma\gamma\ell^+\ell^-$
0.20 ±0.05		KLOPFEN...	83	CUSB	$\Upsilon(2S) \to \gamma\gamma\ell^+\ell^-$

[1] FULSOM 18 reports $[\Gamma(\chi_{b2}(1P) \to \gamma\Upsilon(1S))/\Gamma_{total}] \times [B(\Upsilon(2S) \to \gamma\chi_{b2}(1P))] = (1.17 \pm 0.01^{+0.06}_{-0.07}) \times 10^{-2}$ which we divide by our best (shown rounded) value $B(\Upsilon(2S) \to \gamma\chi_{b2}(1P)) = (7.15 \pm 0.35) \times 10^{-2}$. Our first error is their experiment's error and our second error is the systematic error from using our best (shown rounded) value.

[2] LEES 14M quotes $\Gamma(\chi_{b2}(1P) \to \gamma\Upsilon(1S))/\Gamma_{total} \times \Gamma(\Upsilon(2S) \to \gamma\chi_{b2}(1P))/\Gamma_{total} = (1.32 \pm 0.06)$% combining the results from samples of $\Upsilon(2S) \to \gamma\gamma\mu^+\mu^-$ with and without converted photons.

[3] LEES 14M reports $[\Gamma(\chi_{b2}(1P) \to \gamma\Upsilon(1S))/\Gamma_{total}] \times [B(\Upsilon(2S) \to \gamma\chi_{b2}(1P))] = (1.32 \pm 0.06) \times 10^{-2}$ which we divide by our best (shown rounded) value $B(\Upsilon(2S) \to \gamma\chi_{b2}(1P)) = (7.15 \pm 0.35) \times 10^{-2}$. Our first error is their experiment's error and our second error is the systematic error from using our best (shown rounded) value.

[4] Assuming $B(\Upsilon(1S) \to \mu^+\mu^-) = (2.48 \pm 0.05)\%$.

[5] KORNICER 11 reports $[\Gamma(\chi_{b2}(1P) \to \gamma\Upsilon(1S))/\Gamma_{total}] \times [B(\Upsilon(2S) \to \gamma\chi_{b2}(1P))] = (1.33 \pm 0.04 \pm 0.07) \times 10^{-2}$ which we divide by our best (shown rounded) value $B(\Upsilon(2S) \to \gamma\chi_{b2}(1P)) = (7.15 \pm 0.35) \times 10^{-2}$. Our first error is their experiment's error and our second error is the systematic error from using our best (shown rounded) value.

[6] LEES 11J reports $[\Gamma(\chi_{b2}(1P) \to \gamma\Upsilon(1S))/\Gamma_{total}] \times [B(\Upsilon(2S) \to \gamma\chi_{b2}(1P))] = (13.9 \pm 0.5 {}^{+0.9}_{-1.1}) \times 10^{-3}$ which we divide by our best (shown rounded) value $B(\Upsilon(2S) \to \gamma\chi_{b2}(1P)) = (7.15 \pm 0.35) \times 10^{-2}$. Our first error is their experiment's error and our second error is the systematic error from using our best (shown rounded) value.

[7] WALK 86 quotes $B(\Upsilon(2S) \to \gamma\chi_{b2}(1P)) \times B(\chi_{b2}(1P) \to \gamma\Upsilon(1S)) \times B(\Upsilon(1S) \to \ell^+\ell^-) = (4.4 \pm 0.9 \pm 0.5)$ %.

[8] WALK 86 reports $[\Gamma(\chi_{b2}(1P) \to \gamma\Upsilon(1S))/\Gamma_{total}] \times [B(\Upsilon(2S) \to \gamma\chi_{b2}(1P))] = (17.7 \pm 3.6 \pm 2.0) \times 10^{-3}$ which we divide by our best (shown rounded) value $B(\Upsilon(2S) \to \gamma\chi_{b2}(1P)) = (7.15 \pm 0.35) \times 10^{-2}$. Our first error is their experiment's error and our second error is the systematic error from using our best (shown rounded) value.

$\Gamma(D^0 X)/\Gamma_{total}$ — Γ_2/Γ

VALUE	CL%	DOCUMENT ID		TECN	COMMENT
$<7.9 \times 10^{-2}$	90	[1,2] BRIERE	08	CLEO	$\Upsilon(2S) \to \gamma D^0 X$

[1] For $p_{D^0} > 2.5$ GeV/c.

[2] The authors also present their result as $(5.4 \pm 1.9 \pm 0.5) \times 10^{-2}$.

$\Gamma(\pi^+\pi^-K^+K^-\pi^0)/\Gamma_{total}$ — Γ_3/Γ

VALUE (units 10^{-4})	EVTS	DOCUMENT ID		TECN	COMMENT
0.84±0.50±0.04	8	[1] ASNER	08A	CLEO	$\Upsilon(2S) \to \gamma\pi^+\pi^-K^+K^-\pi^0$

[1] ASNER 08A reports $[\Gamma(\chi_{b2}(1P) \to \pi^+\pi^-K^+K^-\pi^0)/\Gamma_{total}] \times [B(\Upsilon(2S) \to \gamma\chi_{b2}(1P))] = (6 \pm 3 \pm 2) \times 10^{-6}$ which we divide by our best (shown rounded) value $B(\Upsilon(2S) \to \gamma\chi_{b2}(1P)) = (7.15 \pm 0.35) \times 10^{-2}$. Our first error is their experiment's error and our second error is the systematic error from using our best (shown rounded) value.

$\Gamma(2\pi^+\pi^-K^-K^0_S)/\Gamma_{total}$ — Γ_4/Γ

VALUE (units 10^{-4})	CL%	DOCUMENT ID		TECN	COMMENT
<1.0	90	[1] ASNER	08A	CLEO	$\Upsilon(2S) \to \gamma 2\pi^+\pi^-K^-K^0_S$

[1] ASNER 08A reports $[\Gamma(\chi_{b2}(1P) \to 2\pi^+\pi^-K^-K^0_S)/\Gamma_{total}] \times [B(\Upsilon(2S) \to \gamma\chi_{b2}(1P))] < 7 \times 10^{-6}$ which we divide by our best (shown rounded) value $B(\Upsilon(2S) \to \gamma\chi_{b2}(1P)) = 7.15 \times 10^{-2}$.

$\Gamma(2\pi^+\pi^-K^-K^0_S 2\pi^0)/\Gamma_{total}$ — Γ_5/Γ

VALUE (units 10^{-4})	EVTS	DOCUMENT ID		TECN	COMMENT
5.3±2.4±0.3	11	[1] ASNER	08A	CLEO	$\Upsilon(2S) \to \gamma 2\pi^+\pi^-K^-2\pi^0$

[1] ASNER 08A reports $[\Gamma(\chi_{b2}(1P) \to 2\pi^+\pi^-K^-K^0_S 2\pi^0)/\Gamma_{total}] \times [B(\Upsilon(2S) \to \gamma\chi_{b2}(1P))] = (38 \pm 14 \pm 10) \times 10^{-6}$ which we divide by our best (shown rounded) value $B(\Upsilon(2S) \to \gamma\chi_{b2}(1P)) = (7.15 \pm 0.35) \times 10^{-2}$. Our first error is their experiment's error and our second error is the systematic error from using our best (shown rounded) value.

$\Gamma(2\pi^+2\pi^-2\pi^0)/\Gamma_{total}$ — Γ_6/Γ

VALUE (units 10^{-4})	EVTS	DOCUMENT ID		TECN	COMMENT
3.5±1.4±0.2	19	[1] ASNER	08A	CLEO	$\Upsilon(2S) \to \gamma 2\pi^+2\pi^-2\pi^0$

[1] ASNER 08A reports $[\Gamma(\chi_{b2}(1P) \to 2\pi^+2\pi^-2\pi^0)/\Gamma_{total}] \times [B(\Upsilon(2S) \to \gamma\chi_{b2}(1P))] = (25 \pm 8 \pm 6) \times 10^{-6}$ which we divide by our best (shown rounded) value $B(\Upsilon(2S) \to \gamma\chi_{b2}(1P)) = (7.15 \pm 0.35) \times 10^{-2}$. Our first error is their experiment's error and our second error is the systematic error from using our best (shown rounded) value.

$\Gamma(2\pi^+2\pi^-K^+K^-)/\Gamma_{total}$ — Γ_7/Γ

VALUE (units 10^{-4})	EVTS	DOCUMENT ID		TECN	COMMENT
1.1±0.4±0.1	14	[1] ASNER	08A	CLEO	$\Upsilon(2S) \to \gamma 2\pi^+2\pi^-K^+K^-$

[1] ASNER 08A reports $[\Gamma(\chi_{b2}(1P) \to 2\pi^+2\pi^-K^+K^-)/\Gamma_{total}] \times [B(\Upsilon(2S) \to \gamma\chi_{b2}(1P))] = (8 \pm 2 \pm 2) \times 10^{-6}$ which we divide by our best (shown rounded) value $B(\Upsilon(2S) \to \gamma\chi_{b2}(1P)) = (7.15 \pm 0.35) \times 10^{-2}$. Our first error is their experiment's error and our second error is the systematic error from using our best (shown rounded) value.

$\Gamma(2\pi^+2\pi^-K^+K^-\pi^0)/\Gamma_{total}$ — Γ_8/Γ

VALUE (units 10^{-4})	EVTS	DOCUMENT ID		TECN	COMMENT
2.1±0.9±0.1	13	[1] ASNER	08A	CLEO	$\Upsilon(2S) \to \gamma 2\pi^+2\pi^-K^+K^-\pi^0$

[1] ASNER 08A reports $[\Gamma(\chi_{b2}(1P) \to 2\pi^+2\pi^-K^+K^-\pi^0)/\Gamma_{total}] \times [B(\Upsilon(2S) \to \gamma\chi_{b2}(1P))] = (15 \pm 5 \pm 4) \times 10^{-6}$ which we divide by our best (shown rounded) value $B(\Upsilon(2S) \to \gamma\chi_{b2}(1P)) = (7.15 \pm 0.35) \times 10^{-2}$. Our first error is their experiment's error and our second error is the systematic error from using our best (shown rounded) value.

$\Gamma(2\pi^+2\pi^-K^+K^-2\pi^0)/\Gamma_{total}$ — Γ_9/Γ

VALUE (units 10^{-4})	EVTS	DOCUMENT ID		TECN	COMMENT
3.9±1.8±0.2	11	[1] ASNER	08A	CLEO	$\Upsilon(2S) \to \gamma 2\pi^+2\pi^-K^+K^-2\pi^0$

[1] ASNER 08A reports $[\Gamma(\chi_{b2}(1P) \to 2\pi^+2\pi^-K^+K^-2\pi^0)/\Gamma_{total}] \times [B(\Upsilon(2S) \to \gamma\chi_{b2}(1P))] = (28 \pm 11 \pm 7) \times 10^{-6}$ which we divide by our best (shown rounded) value $B(\Upsilon(2S) \to \gamma\chi_{b2}(1P)) = (7.15 \pm 0.35) \times 10^{-2}$. Our first error is their experiment's error and our second error is the systematic error from using our best (shown rounded) value.

$\Gamma(3\pi^+2\pi^-K^-K^0_S\pi^0)/\Gamma_{total}$ — Γ_{10}/Γ

VALUE (units 10^{-4})	CL%	DOCUMENT ID		TECN	COMMENT
<5	90	[1] ASNER	08A	CLEO	$\Upsilon(2S) \to \gamma 3\pi^+2\pi^-K^-K^0_S\pi^0$

[1] ASNER 08A reports $[\Gamma(\chi_{b2}(1P) \to 3\pi^+2\pi^-K^-K^0_S\pi^0)/\Gamma_{total}] \times [B(\Upsilon(2S) \to \gamma\chi_{b2}(1P))] < 36 \times 10^{-6}$ which we divide by our best (shown rounded) value $B(\Upsilon(2S) \to \gamma\chi_{b2}(1P)) = 7.15 \times 10^{-2}$.

$\Gamma(3\pi^+3\pi^-)/\Gamma_{total}$ — Γ_{11}/Γ

VALUE (units 10^{-4})	EVTS	DOCUMENT ID		TECN	COMMENT
0.70±0.31±0.03	9	[1] ASNER	08A	CLEO	$\Upsilon(2S) \to \gamma 3\pi^+3\pi^-$

[1] ASNER 08A reports $[\Gamma(\chi_{b2}(1P) \to 3\pi^+3\pi^-)/\Gamma_{total}] \times [B(\Upsilon(2S) \to \gamma\chi_{b2}(1P))] = (5 \pm 2 \pm 1) \times 10^{-6}$ which we divide by our best (shown rounded) value $B(\Upsilon(2S) \to \gamma\chi_{b2}(1P)) = (7.15 \pm 0.35) \times 10^{-2}$. Our first error is their experiment's error and our second error is the systematic error from using our best (shown rounded) value.

$\Gamma(3\pi^+3\pi^-2\pi^0)/\Gamma_{total}$ — Γ_{12}/Γ

VALUE (units 10^{-4})	EVTS	DOCUMENT ID		TECN	COMMENT
10.2±3.6±0.5	34	[1] ASNER	08A	CLEO	$\Upsilon(2S) \to \gamma 3\pi^+3\pi^-2\pi^0$

[1] ASNER 08A reports $[\Gamma(\chi_{b2}(1P) \to 3\pi^+3\pi^-2\pi^0)/\Gamma_{total}] \times [B(\Upsilon(2S) \to \gamma\chi_{b2}(1P))] = (73 \pm 16 \pm 20) \times 10^{-6}$ which we divide by our best (shown rounded) value $B(\Upsilon(2S) \to \gamma\chi_{b2}(1P)) = (7.15 \pm 0.35) \times 10^{-2}$. Our first error is their experiment's error and our second error is the systematic error from using our best (shown rounded) value.

$\Gamma(3\pi^+3\pi^-K^+K^-)/\Gamma_{total}$ — Γ_{13}/Γ

VALUE (units 10^{-4})	CL%	DOCUMENT ID		TECN	COMMENT
<0.8	90	[1] ASNER	08A	CLEO	$\Upsilon(2S) \to \gamma 3\pi^+3\pi^-K^+K^-$

[1] ASNER 08A reports $[\Gamma(\chi_{b2}(1P) \to 3\pi^+3\pi^-K^+K^-)/\Gamma_{total}] \times [B(\Upsilon(2S) \to \gamma\chi_{b2}(1P))] < 6 \times 10^{-6}$ which we divide by our best (shown rounded) value $B(\Upsilon(2S) \to \gamma\chi_{b2}(1P)) = 7.15 \times 10^{-2}$.

$\Gamma(3\pi^+3\pi^-K^+K^-\pi^0)/\Gamma_{total}$ — Γ_{14}/Γ

VALUE (units 10^{-4})	EVTS	DOCUMENT ID		TECN	COMMENT
3.6±1.5±0.2	14	[1] ASNER	08A	CLEO	$\Upsilon(2S) \to \gamma 3\pi^+3\pi^-K^+K^-\pi^0$

[1] ASNER 08A reports $[\Gamma(\chi_{b2}(1P) \to 3\pi^+3\pi^-K^+K^-\pi^0)/\Gamma_{total}] \times [B(\Upsilon(2S) \to \gamma\chi_{b2}(1P))] = (26 \pm 8 \pm 7) \times 10^{-6}$ which we divide by our best (shown rounded) value $B(\Upsilon(2S) \to \gamma\chi_{b2}(1P)) = (7.15 \pm 0.35) \times 10^{-2}$. Our first error is their experiment's error and our second error is the systematic error from using our best (shown rounded) value.

$\Gamma(4\pi^+4\pi^-)/\Gamma_{total}$ — Γ_{15}/Γ

VALUE (units 10^{-4})	EVTS	DOCUMENT ID		TECN	COMMENT
0.84±0.40±0.04	7	[1] ASNER	08A	CLEO	$\Upsilon(2S) \to \gamma 4\pi^+4\pi^-$

[1] ASNER 08A reports $[\Gamma(\chi_{b2}(1P) \to 4\pi^+4\pi^-)/\Gamma_{total}] \times [B(\Upsilon(2S) \to \gamma\chi_{b2}(1P))] = (6 \pm 2 \pm 2) \times 10^{-6}$ which we divide by our best (shown rounded) value $B(\Upsilon(2S) \to \gamma\chi_{b2}(1P)) = (7.15 \pm 0.35) \times 10^{-2}$. Our first error is their experiment's error and our second error is the systematic error from using our best (shown rounded) value.

$\Gamma(4\pi^+4\pi^-2\pi^0)/\Gamma_{total}$ — Γ_{16}/Γ

VALUE (units 10^{-4})	EVTS	DOCUMENT ID		TECN	COMMENT
18±7±1	29	[1] ASNER	08A	CLEO	$\Upsilon(2S) \to \gamma 4\pi^+4\pi^-2\pi^0$

[1] ASNER 08A reports $[\Gamma(\chi_{b2}(1P) \to 4\pi^+4\pi^-2\pi^0)/\Gamma_{total}] \times [B(\Upsilon(2S) \to \gamma\chi_{b2}(1P))] = (132 \pm 31 \pm 40) \times 10^{-6}$ which we divide by our best (shown rounded) value $B(\Upsilon(2S) \to \gamma\chi_{b2}(1P)) = (7.15 \pm 0.35) \times 10^{-2}$. Our first error is their experiment's error and our second error is the systematic error from using our best (shown rounded) value.

$\Gamma(J/\psi J/\psi)/\Gamma_{total}$ — Γ_{17}/Γ

VALUE (units 10^{-5})	CL%	DOCUMENT ID		TECN	COMMENT
<5	90	[1] SHEN	12	BELL	$\Upsilon(2S) \to \gamma\psi X$

[1] SHEN 12 reports $< 4.5 \times 10^{-5}$ from a measurement of $[\Gamma(\chi_{b2}(1P) \to J/\psi J/\psi)/\Gamma_{total}] \times [B(\Upsilon(2S) \to \gamma\chi_{b2}(1P))]$ assuming $B(\Upsilon(2S) \to \gamma\chi_{b2}(1P)) = (7.15 \pm 0.35) \times 10^{-2}$.

$\Gamma(J/\psi\psi(2S))/\Gamma_{total}$ — Γ_{18}/Γ

VALUE (units 10^{-5})	CL%	DOCUMENT ID		TECN	COMMENT
<5	90	[1] SHEN	12	BELL	$\Upsilon(2S) \to \gamma\psi X$

[1] SHEN 12 reports $< 4.9 \times 10^{-5}$ from a measurement of $[\Gamma(\chi_{b2}(1P) \to J/\psi\psi(2S))/\Gamma_{total}] \times [B(\Upsilon(2S) \to \gamma\chi_{b2}(1P))]$ assuming $B(\Upsilon(2S) \to \gamma\chi_{b2}(1P)) = (7.15 \pm 0.35) \times 10^{-2}$.

Int. J. Mod. Phys. A 2026.41. Downloaded from www.worldscientific.com
by LIFORNIA @ BERKELEY on 09/16/26. Re-use and distribution is strictly not permitted, except for Open Access articles.

Int. J. Mod. Phys. A 2026.41. Downloaded from www.worldscientific.com by UNIVERSITY OF CALIFORNIA @ BERKELEY on 09/16/26. Re-use and distribution is strictly not permitted, except for Open Access articles.

$\Gamma(\psi(2S)\psi(2S))/\Gamma_{total}$ — Γ_{19}/Γ

VALUE (units 10^{-5})	CL%	DOCUMENT ID		TECN	COMMENT
<1.6	90	[1] SHEN	12	BELL	$\Upsilon(2S) \to \gamma\psi X$

[1] SHEN 12 reports $< 1.6 \times 10^{-5}$ from a measurement of $[\Gamma(\chi_{b2}(1P) \to \psi(2S)\psi(2S))/\Gamma_{total}] \times [B(\Upsilon(2S) \to \gamma\chi_{b2}(1P))]$ assuming $B(\Upsilon(2S) \to \gamma\chi_{b2}(1P)) = (7.15 \pm 0.35) \times 10^{-2}$.

$\Gamma(J/\psi(1S)\,\text{anything})/\Gamma_{total}$ — Γ_{20}/Γ

VALUE (units 10^{-3})	EVTS	DOCUMENT ID		TECN	COMMENT
1.50±0.34±0.22	462	JIA	17A	BELL	$e^+e^- \to$ hadrons

$\chi_{b2}(1P)$ Cross-Particle Branching Ratios

$\Gamma(\chi_{b2}(1P) \to \gamma\Upsilon(1S))/\Gamma_{total} \times \Gamma(\Upsilon(2S) \to \gamma\chi_{b2}(1P))/\Gamma_{total}$ — $\Gamma_1/\Gamma \times \Gamma_{79}^{\Upsilon(2S)}/\Gamma^{\Upsilon(2S)}$

VALUE (units 10^{-3})	EVTS	DOCUMENT ID		TECN	COMMENT
$13.9 \pm 0.5^{+0.9}_{-1.1}$	8k	LEES	11J	BABR	$\Upsilon(2S) \to X\gamma$

$B(\chi_{b2}(1P) \to \gamma\Upsilon(1S)) \times B(\Upsilon(2S) \to \gamma\chi_{b2}(1P)) \times B(\Upsilon(1S) \to \ell^+\ell^-)$

VALUE (units 10^{-4})	EVTS	DOCUMENT ID		TECN	COMMENT
3.38±0.16 OUR AVERAGE					
$3.63^{+0.36}_{-0.34} \pm 0.18^{+0.18}_{-0.19}$		[1] LEES	14M	BABR	$\Upsilon(2S) \to \gamma\gamma\mu^+\mu^-$
3.29±0.09±0.16	1770	KORNICER	11	CLEO	$e^+e^- \to \gamma\gamma\ell^+\ell^-$
4.4 ±0.9 ±0.5	35	WALK	86	CBAL	$\Upsilon(2S) \to \gamma\gamma\ell^+\ell^-$

[1] From a sample of $\Upsilon(2S) \to \gamma\gamma\mu^+\mu^-$ with converted photons.

$[B(\chi_{b2}(1P) \to \gamma\Upsilon(1S)) \times B(\Upsilon(2S) \to \gamma\chi_{b2}(1P))] / [B(\chi_{b1}(1P) \to \gamma\Upsilon(1S)) \times B(\Upsilon(2S) \to \gamma\chi_{b1}(1P))]$

VALUE (%)	DOCUMENT ID		TECN	COMMENT
55.6±1.6	[1] LEES	14M	BABR	$\Upsilon(2S) \to \gamma\gamma\mu^+\mu^-$

[1] From a sample of $\Upsilon(2S) \to \gamma\gamma\mu^+\mu^-$ events without converted photons.

$B(\chi_{b2}(1P) \to \gamma\Upsilon(1S)) \times B(\Upsilon(3S) \to \gamma\chi_{b2}(1P)) \times B(\Upsilon(1S) \to \ell^+\ell^-)$

VALUE (units 10^{-5})	EVTS	DOCUMENT ID		TECN	COMMENT
3.8 ±0.5 OUR AVERAGE					
$4.68^{+0.99}_{-0.92} \pm 0.37$		[1] LEES	14M	BABR	$\Upsilon(3S) \to \gamma\gamma\mu^+\mu^-$
3.56±0.40±0.41	126	KORNICER	11	CLEO	$e^+e^- \to \gamma\gamma\ell^+\ell^-$

[1] From a sample of $\Upsilon(3S) \to \gamma\gamma\mu^+\mu^-$ with converted photons.

$\chi_{b2}(1P)$ REFERENCES

AAIJ	24AC	JHEP 2410 122	R. Aaij *et al.*	(LHCb Collab.)
FULSOM	18	PRL 121 232001	B.G. Fulsom *et al.*	(BELLE Collab.)
JIA	17A	PR D96 112002	S. Jia *et al.*	(BELLE Collab.)
AAIJ	14BG	JHEP 1410 088	R. Aaij *et al.*	(LHCb Collab.)
LEES	14M	PR D90 112010	J.P. Lees *et al.*	(BABAR Collab.)
SHEN	12	PR D85 071102	C.P. Shen *et al.*	(BELLE Collab.)
KORNICER	11	PR D83 054003	M. Kornicer *et al.*	(CLEO Collab.)
LEES	11J	PR D84 072002	J.P. Lees *et al.*	(BABAR Collab.)
ASNER	08A	PR D78 091103	D.M. Asner *et al.*	(CLEO Collab.)
BRIERE	08	PR D78 092007	R.A. Briere *et al.*	(CLEO Collab.)
ARTUSO	05	PRL 94 032001	M. Artuso *et al.*	(CLEO Collab.)
EDWARDS	99	PR D59 032003	K.W. Edwards *et al.*	(CLEO Collab.)
SKWARNICKI	87	PRL 58 972	T. Skwarnicki *et al.*	(Crystal Ball Collab.) J
WALK	86	PR D34 2611	W.S. Walk *et al.*	(Crystal Ball Collab.)
ALBRECHT	85E	PL 160B 331	H. Albrecht *et al.*	(ARGUS Collab.)
NERNST	85	PRL 54 2195	R. Nernst *et al.*	(Crystal Ball Collab.)
HAAS	84	PRL 52 799	J. Haas *et al.*	(CLEO Collab.)
KLOPFEN...	83	PRL 51 160	C. Klopfenstein *et al.*	(CUSB Collab.)
PAUSS	83	PL 130B 439	F. Pauss *et al.*	(MPIM, COLU, CORN, LSU+)

$\eta_b(2S)$

$I^G(J^{PC}) = 0^+(0^{-+})$

OMITTED FROM SUMMARY TABLE

Quantum numbers shown are quark-model predictions.

$\eta_b(2S)$ MASS

VALUE (MeV)	EVTS	DOCUMENT ID		TECN	COMMENT
$9999.0 \pm 3.5^{+2.8}_{-1.9}$	26k	[1] MIZUK	12	BELL	$e^+e^- \to \gamma\pi^+\pi^-$ + hadrons
• • • We do not use the following data for averages, fits, limits, etc. • • •					
9974.6±2.3±2.1	11 ± 4	[2,3,4] DOBBS	12		$\Upsilon(2S) \to \gamma$ hadrons

[1] Assuming $\Gamma_{\eta_b(2S)} = 4.9$ MeV. Not independent of the corresponding mass difference measurement.

[2] SANDILYA 13 (Belle Collab.) search for such a state reconstructed in the same 26 exclusive hadronic final states as DOBBS 12 using a sample of $(157.8 \pm 3.6) \times 10^6$ $\Upsilon(2S)$ decays or about 17 times larger and find no evidence for a signal. Their 90% C.L. upper limit on the branching fraction $B(\Upsilon(2S) \to \eta_b(2S)\gamma) \times \sum_i B(\eta_b(2S) \to X_i) < 4.9 \times 10^{-6}$, summed over the exclusive hadronic final states X_i, is an order of magnitude smaller than that reported by DOBBS 12.

[3] Obtained by analyzing CLEO III data but not authored by the CLEO Collaboration.

[4] Assuming $\Gamma_{\eta_b(2S)} = 5$ MeV. Not independent of the corresponding mass difference measurement.

$m_{\Upsilon(2S)} - m_{\eta_b(2S)}$

VALUE (MeV)	EVTS	DOCUMENT ID		TECN	COMMENT
$24.3 \pm 3.5^{+2.8}_{-1.9}$	26k	[5] MIZUK	12	BELL	$e^+e^- \to \gamma\pi^+\pi^-$ + hadrons
• • • We do not use the following data for averages, fits, limits, etc. • • •					
48.7±2.3±2.1	11 ± 4	[6,7,8] DOBBS	12		$\Upsilon(2S) \to \gamma$ hadrons

[5] Assuming $\Gamma_{\eta_b(2S)} = 4.9$ MeV. Not independent of the corresponding mass measurement.

[6] SANDILYA 13 (Belle Collab.) search for such a state reconstructed in the same 26 exclusive hadronic final states as DOBBS 12 using a sample of $(157.8 \pm 3.6) \times 10^6$ $\Upsilon(2S)$ decays or about 17 times larger and find no evidence for a signal. Their 90% C.L. upper limit on the branching fraction $B(\Upsilon(2S) \to \eta_b(2S)\gamma) \times \sum_i B(\eta_b(2S) \to X_i) < 4.9 \times 10^{-6}$, summed over the exclusive hadronic final states X_i, is an order of magnitude smaller than that reported by DOBBS 12.

[7] Obtained by analyzing CLEO III data but not authored by the CLEO Collaboration.

[8] Assuming $\Gamma_{\eta_b(2S)} = 5$ MeV. Not independent of the corresponding mass measurement.

$\eta_b(2S)$ WIDTH

VALUE (MeV)	CL%	DOCUMENT ID		TECN	COMMENT
<24	90	MIZUK	12	BELL	$e^+e^- \to \gamma\pi^+\pi^-$ hadrons

$\eta_b(2S)$ DECAY MODES

	Mode	Fraction (Γ_i/Γ)
Γ_1	hadrons	seen

$\eta_b(2S)$ BRANCHING RATIOS

$\Gamma(\text{hadrons})/\Gamma_{total}$ — Γ_1/Γ

VALUE	EVTS	DOCUMENT ID		TECN	COMMENT
seen	26k	MIZUK	12	BELL	$e^+e^- \to \gamma\pi^+\pi^-$ hadrons
• • • We do not use the following data for averages, fits, limits, etc. • • •					
seen		[9,10] DOBBS	12		$\Upsilon(2S) \to \gamma$ hadrons

[9] SANDILYA 13 (Belle Collab.) search for such a state reconstructed in the same 26 exclusive hadronic final states as DOBBS 12 using a sample of $(157.8 \pm 3.6) \times 10^6$ $\Upsilon(2S)$ decays or about 17 times larger and find no evidence for a signal. Their 90% C.L. upper limit on the branching fraction $B(\Upsilon(2S) \to \eta_b(2S)\gamma) \times \sum_i B(\eta_b(2S) \to X_i) < 4.9 \times 10^{-6}$, summed over the exclusive hadronic final states X_i, is an order of magnitude smaller than that reported by DOBBS 12.

[10] Obtained by analyzing CLEO III data but not authored by the CLEO Collaboration.

$\eta_b(2S)$ REFERENCES

SANDILYA	13	PRL 111 112001	S. Sandilya *et al.*	(BELLE Collab.)
DOBBS	12	PRL 109 082001	S. Dobbs *et al.*	
MIZUK	12	PRL 109 232002	R. Mizuk *et al.*	(BELLE Collab.)

$\Upsilon(2S)$

$I^G(J^{PC}) = 0^-(1^{--})$

$\Upsilon(2S)$ MASS

VALUE (MeV)	DOCUMENT ID		TECN	COMMENT
10023.4±0.5	[1] SHAMOV	23	RVUE	$e^+e^- \to$ hadrons
• • • We do not use the following data for averages, fits, limits, etc. • • •				
10022.7±0.4	[2] SHAMOV	23	RVUE	$e^+e^- \to$ hadrons
10023.5±0.5	[3,4] ARTAMONOV	00	MD1	$e^+e^- \to$ hadrons
10023.6±0.5	[5,6] BARU	86B	MD1	$e^+e^- \to$ hadrons
10023.1±0.4	[7] BARBER	84	ARG	$e^+e^- \to$ hadrons

[1] Reanalysis of MD1 data using the electron mass from COHEN 87, the radiative corrections from KURAEV 85 and interference effects.

[2] Obtained by reanalysing ARGUS and Crystal Ball data (BARBER 84), but not authored by the ARGUS and Crystal Ball collaboration.

[3] Reanalysis of BARU 86B using new electron mass (COHEN 87).

[4] Superseded by SHAMOV 23.

[5] Reanalysis of ARTAMONOV 84.

[6] Superseded by ARTAMONOV 00.

[7] Reanalysed by SHAMOV 23.

$m_{\Upsilon(2S)} - m_{\Upsilon(1S)}$

VALUE (MeV)	EVTS	DOCUMENT ID		TECN	COMMENT
562.81±0.11 OUR AVERAGE					
562.71±0.04±0.20	3.7M	[1] AAIJ	24AC	LHCB	$\Upsilon \to \mu^+\mu^-$
562.85±0.03±0.12	89k	[1] AAIJ	24AC	LHCB	$\Upsilon(2S) \to \Upsilon(1S)\pi^+\pi^-$

[1] Observed in prompt pp production.

$\Upsilon(2S)$ WIDTH

VALUE (keV)	DOCUMENT ID
31.98±2.63 OUR EVALUATION	See the Note on "Width Determinations of the Υ States"

Int. J. Mod. Phys. A 2026.41. Downloaded from www.worldscientific.com by CALIFORNIA @ BERKELEY on 09/16/26. Re-use and distribution is strictly not permitted, except for Open Access articles.

$\Upsilon(2S)$ DECAY MODES

	Mode	Fraction (Γ_i/Γ)	Scale factor/ Confidence level
Γ_1	$\Upsilon(1S)\pi^+\pi^-$	(17.85 ± 0.26) %	
Γ_2	$\Upsilon(1S)\pi^0\pi^0$	(8.6 ± 0.4) %	
Γ_3	$\tau^+\tau^-$	(2.00 ± 0.21) %	
Γ_4	$\mu^+\mu^-$	(1.93 ± 0.17) %	S=2.2
Γ_5	e^+e^-	(1.91 ± 0.16) %	
Γ_6	$\Upsilon(1S)\pi^0$	$< 4 \times 10^{-5}$	CL=90%
Γ_7	$\Upsilon(1S)\eta$	$(2.9 \pm 0.4) \times 10^{-4}$	S=2.0
Γ_8	$J/\psi(1S)$ anything	$< 6 \times 10^{-3}$	CL=90%
Γ_9	$J/\psi(1S)\eta_c$	$< 5.4 \times 10^{-6}$	CL=90%
Γ_{10}	$J/\psi(1S)\chi_{c0}$	$< 3.4 \times 10^{-6}$	CL=90%
Γ_{11}	$J/\psi(1S)\chi_{c1}$	$< 1.2 \times 10^{-6}$	CL=90%
Γ_{12}	$J/\psi(1S)\chi_{c2}$	$< 2.0 \times 10^{-6}$	CL=90%
Γ_{13}	$J/\psi(1S)\eta_c(2S)$	$< 2.5 \times 10^{-6}$	CL=90%
Γ_{14}	$J/\psi(1S)X(3940)$	$< 2.0 \times 10^{-6}$	CL=90%
Γ_{15}	$J/\psi(1S)X(4160)$	$< 2.0 \times 10^{-6}$	CL=90%
Γ_{16}	χ_{c1} anything	$(2.2 \pm 0.5) \times 10^{-4}$	
Γ_{17}	$\chi_{c1}(1P)^0 X_{tetra}$	$< 3.67 \times 10^{-5}$	CL=90%
Γ_{18}	χ_{c2} anything	$(2.3 \pm 0.8) \times 10^{-4}$	
Γ_{19}	$\psi(2S)\eta_c$	$< 5.1 \times 10^{-6}$	CL=90%
Γ_{20}	$\psi(2S)\chi_{c0}$	$< 4.7 \times 10^{-6}$	CL=90%
Γ_{21}	$\psi(2S)\chi_{c1}$	$< 2.5 \times 10^{-6}$	CL=90%
Γ_{22}	$\psi(2S)\chi_{c2}$	$< 1.9 \times 10^{-6}$	CL=90%
Γ_{23}	$\psi(2S)\eta_c(2S)$	$< 3.3 \times 10^{-6}$	CL=90%
Γ_{24}	$\psi(2S)X(3940)$	$< 3.9 \times 10^{-6}$	CL=90%
Γ_{25}	$\psi(2S)X(4160)$	$< 3.9 \times 10^{-6}$	CL=90%
Γ_{26}	$T_{c\overline{c}1}(3900)^+ T_{c\overline{c}1}(3900)^-$	$< 1.0 \times 10^{-6}$	CL=90%
Γ_{27}	$T_{c\overline{c}1}(4200)^+ T_{c\overline{c}1}(4200)^-$	$< 1.67 \times 10^{-5}$	CL=90%
Γ_{28}	$T_{c\overline{c}1}(3900)^\pm T_{c\overline{c}1}(4200)^\mp$	$< 7.3 \times 10^{-6}$	CL=90%
Γ_{29}	$T_{c\overline{c}}(4050)^+ T_{c\overline{c}}(4050)^-$	$< 1.35 \times 10^{-5}$	CL=90%
Γ_{30}	$T_{c\overline{c}}(4250)^+ T_{c\overline{c}}(4250)^-$	$< 2.67 \times 10^{-5}$	CL=90%
Γ_{31}	$T_{c\overline{c}}(4050)^\pm T_{c\overline{c}}(4250)^\mp$	$< 2.72 \times 10^{-5}$	CL=90%
Γ_{32}	$T_{c\overline{c}1}(4430)^+ T_{c\overline{c}1}(4430)^-$	$< 2.03 \times 10^{-5}$	CL=90%
Γ_{33}	$T_{c\overline{c}}(4055)^\pm T_{c\overline{c}}(4055)^\mp$	$< 1.11 \times 10^{-5}$	CL=90%
Γ_{34}	$T_{c\overline{c}}(4055)^\pm T_{c\overline{c}1}(4430)^\mp$	$< 2.11 \times 10^{-5}$	CL=90%
Γ_{35}	$P_{c\overline{c}s}(4459)/\overline{P}_{c\overline{c}s}(4459)$ anything	$(2.9 \pm 1.7) \times 10^{-6}$	
Γ_{36}	$P_{c\overline{c}s}(4338)/\overline{P}_{c\overline{c}s}(4338)$ anything	$< 1.6 \times 10^{-6}$	CL=90%
Γ_{37}	$P_c(4457)$ anything, $P_c(4457) \to pJ/\psi(1S)$	$< 4.6 \times 10^{-6}$	CL=90%
Γ_{38}	$P_c(4440)$ anything, $P_c(4440) \to pJ/\psi(1S)$	$< 1.18 \times 10^{-5}$	CL=90%
Γ_{39}	$P_c(4312)$ anything, $P_c(4312) \to pJ/\psi(1S)$	$< 7.2 \times 10^{-6}$	CL=90%
Γ_{40}	$p/\overline{p}J/\psi(1S)$ anything	$(4.3 \pm 0.6) \times 10^{-5}$	
Γ_{41}	$J/\psi(1S)\Lambda/\overline{\Lambda}$ anything	$(2.2 \pm 0.6) \times 10^{-5}$	
Γ_{42}	$\overline{^2H}$ anything	$(2.78^{+0.30}_{-0.26}) \times 10^{-5}$	S=1.2
Γ_{43}	hadrons	(94 ± 11) %	
Γ_{44}	ggg	(58.8 ± 1.2) %	
Γ_{45}	γgg	(1.87 ± 0.28) %	
Γ_{46}	ϕK^+K^-	$(1.6 \pm 0.4) \times 10^{-6}$	
Γ_{47}	$\omega\pi^+\pi^-$	$< 2.58 \times 10^{-6}$	CL=90%
Γ_{48}	$K^*(892)^0 K^-\pi^+ +$ c.c.	$(2.3 \pm 0.7) \times 10^{-6}$	
Γ_{49}	$\phi f_2'(1525)$	$< 1.33 \times 10^{-6}$	CL=90%
Γ_{50}	$\omega f_2(1270)$	$< 5.7 \times 10^{-7}$	CL=90%
Γ_{51}	$\rho(770)a_2(1320)$	$< 8.8 \times 10^{-7}$	CL=90%
Γ_{52}	$K^*(892)^0\overline{K}_2^*(1430)^0 +$ c.c.	$(1.5 \pm 0.6) \times 10^{-6}$	
Γ_{53}	$K_1(1270)^\pm K^\mp$	$< 3.22 \times 10^{-6}$	CL=90%
Γ_{54}	$K_1(1400)^\pm K^\mp$	$< 8.3 \times 10^{-7}$	CL=90%
Γ_{55}	$b_1(1235)^\pm\pi^\mp$	$< 4.0 \times 10^{-7}$	CL=90%
Γ_{56}	$\rho\pi$	$< 1.16 \times 10^{-6}$	CL=90%
Γ_{57}	$\pi^+\pi^-\pi^0$	$< 8.0 \times 10^{-7}$	CL=90%
Γ_{58}	$\omega\pi^0$	$< 1.63 \times 10^{-6}$	CL=90%
Γ_{59}	$\pi^+\pi^-\pi^0\pi^0$	$(1.30 \pm 0.28) \times 10^{-5}$	
Γ_{60}	$K_S^0 K^+\pi^- +$ c.c.	$(1.14 \pm 0.33) \times 10^{-6}$	
Γ_{61}	$K^*(892)^0\overline{K}^0 +$ c.c.	$< 4.22 \times 10^{-6}$	CL=90%
Γ_{62}	$K^*(892)^- K^+ +$ c.c.	$< 1.45 \times 10^{-6}$	CL=90%
Γ_{63}	$f_1(1285)$ anything	$(2.2 \pm 1.6) \times 10^{-3}$	
Γ_{64}	$f_1(1285)X_{tetra}$	$< 6.47 \times 10^{-5}$	CL=90%
Γ_{65}	$D_s^+ D_{s1}(2536)^-$		
Γ_{66}	$D_s^+ D_{s1}(2536)^-$, $D_{s1}^- \to K^- D^*(2007)^0$	$(1.6 \pm 0.4) \times 10^{-5}$	
Γ_{67}	$D_s^+ D_{s1}(2536)^-$, $D_{s1}^- \to K_S^0 D^*(2010)^-$	$(8.4 \pm 2.3) \times 10^{-6}$	
Γ_{68}	$D_s^{*+} D_{s1}(2536)^-$		
Γ_{69}	$D_s^{*+} D_{s1}(2536)^-$, $D_{s1}^- \to K^- D^*(2007)^0$	$(1.4 \pm 0.4) \times 10^{-5}$	
Γ_{70}	$D_s^{*+} D_{s1}(2536)^-$, $D_{s1}^- \to K_S^0 D^*(2010)^-$	$(8.2 \pm 3.1) \times 10^{-6}$	
Γ_{71}	$D_s^+ D_{s2}^*(2573)^-$		
Γ_{72}	$D_s^+ D_{s2}^*(2573)^-$, $D_{s2}^{*-} \to K^- D^0$	$(1.4 \pm 0.4) \times 10^{-5}$	
Γ_{73}	$D_s^+ D_{s2}^*(2573)^-$, $D_{s2}^{*-} \to K_S^0 D^-$	$(6.9 \pm 3.0) \times 10^{-6}$	
Γ_{74}	$D_s^{*+} D_{s2}^*(2573)^-$		
Γ_{75}	$D_s^{*+} D_{s2}^*(2573)^-$, $D_{s2}^{*-} \to K^- D^0$	$(9 \pm 5) \times 10^{-6}$	
Γ_{76}	$D_s^{*+} D_{s2}^*(2573)^-$, $D_{s2}^{*-} \to K_S^0 D^-$	$(5 \pm 6) \times 10^{-6}$	
Γ_{77}	Sum of 100 exclusive modes	$(2.90 \pm 0.30) \times 10^{-3}$	

Radiative decays

Γ_{78}	$\gamma\chi_{b1}(1P)$	(6.9 ± 0.4) %	
Γ_{79}	$\gamma\chi_{b2}(1P)$	(7.15 ± 0.35) %	
Γ_{80}	$\gamma\chi_{b0}(1P)$	(3.8 ± 0.4) %	
Γ_{81}	$\gamma f_0(1710)$	$< 5.9 \times 10^{-4}$	CL=90%
Γ_{82}	$\gamma f_2'(1525)$	$< 5.3 \times 10^{-4}$	CL=90%
Γ_{83}	$\gamma f_2(1270)$	$< 2.41 \times 10^{-4}$	CL=90%
Γ_{84}	$\gamma f_J(2220)$		
Γ_{85}	$\gamma\eta_c(1S)$	$< 2.7 \times 10^{-5}$	CL=90%
Γ_{86}	$\gamma\chi_{c0}$	$< 1.0 \times 10^{-4}$	CL=90%
Γ_{87}	$\gamma\chi_{c1}$	$< 3.6 \times 10^{-6}$	CL=90%
Γ_{88}	$\gamma\chi_{c2}$	$< 1.5 \times 10^{-5}$	CL=90%
Γ_{89}	$\gamma\chi_{c1}(3872)$	$< 1.8 \times 10^{-5}$	CL=90%
Γ_{90}	$\gamma\chi_{c1}(3872)$, $\chi_{c1} \to \pi^+\pi^-\pi^0 J/\psi$	$< 2.4 \times 10^{-6}$	CL=90%
Γ_{91}	$\gamma\chi_{c0}(3915) \to \omega J/\psi$	$< 2.8 \times 10^{-6}$	CL=90%
Γ_{92}	$\gamma\chi_{c1}(4140) \to \phi J/\psi$	$< 1.2 \times 10^{-6}$	CL=90%
Γ_{93}	$\gamma X(4350) \to \phi J/\psi$	$< 1.3 \times 10^{-6}$	CL=90%
Γ_{94}	$\gamma\eta_b(1S)$	$(5.5 {}^{+1.1}_{-0.9}) \times 10^{-4}$	S=1.2
Γ_{95}	$\gamma\eta_b(1S) \to \gamma$ Sum of 26 exclusive modes	$< 3.7 \times 10^{-6}$	CL=90%
Γ_{96}	$\gamma X_{b\overline{b}} \to \gamma$ Sum of 26 exclusive modes	$< 4.9 \times 10^{-6}$	CL=90%
Γ_{97}	$\gamma X \to \gamma + \geq 4$ prongs	[a] $< 1.95 \times 10^{-4}$	CL=95%
Γ_{98}	$\gamma A^0 \to \gamma$ hadrons	$< 8 \times 10^{-5}$	CL=90%
Γ_{99}	$\gamma A^0 \to \gamma\mu^+\mu^-$	$< 8.3 \times 10^{-6}$	CL=90%

Lepton Family number (*LF*) violating modes

Γ_{100}	$e^\pm\tau^\mp$ *LF*	$< 1.12 \times 10^{-6}$	CL=90%
Γ_{101}	$\mu^\pm\tau^\mp$ *LF*	$< 2.3 \times 10^{-7}$	CL=90%

[a] 1.5 GeV $< m_X <$ 5.0 GeV

FIT INFORMATION

An overall fit to 3 branching ratios uses 13 measurements to determine 2 parameters. The overall fit has a $\chi^2 = 11.8$ for 11 degrees of freedom.

The following *off-diagonal* array elements are the correlation coefficients $\langle \delta x_i \delta x_j \rangle / (\delta x_i \cdot \delta x_j)$, in percent, from the fit to the branching fractions, $x_i \equiv \Gamma_i/\Gamma_{\text{total}}$.

x_7 2
x_1

$\Upsilon(2S)$ $\Gamma(i)\Gamma(e^+e^-)/\Gamma(\text{total})$

$\Gamma(\mu^+\mu^-) \times \Gamma(e^+e^-)/\Gamma_{\text{total}}$ — $\Gamma_4\Gamma_5/\Gamma$

VALUE (eV)	DOCUMENT ID		TECN	COMMENT
6.5 ± 1.5 ± 1.0	KOBEL	92	CBAL	$e^+e^- \to \mu^+\mu^-$

$\Gamma(\Upsilon(1S)\pi^+\pi^-) \times \Gamma(e^+e^-)/\Gamma_{\text{total}}$ — $\Gamma_1\Gamma_5/\Gamma$

VALUE (eV)	EVTS	DOCUMENT ID		TECN	COMMENT
105.4 ± 1.0 ± 4.2	11.8k	[1] AUBERT	08BP	BABR	10.58 $e^+e^- \to \gamma\pi^+\pi^-\ell^+\ell^-$

[1] Using B($\Upsilon(1S) \to e^+e^-$) = (2.38 ± 0.11)% and B($\Upsilon(1S) \to \mu^+\mu^-$) = (2.48 ± 0.05)%.

$\Gamma(\text{hadrons}) \times \Gamma(e^+e^-)/\Gamma_{\text{total}}$ — $\Gamma_{43}\Gamma_5/\Gamma$

VALUE (keV)	DOCUMENT ID		TECN	COMMENT
0.577±0.009 OUR AVERAGE				
0.581±0.004±0.009	[1] ROSNER	06	CLEO	10.0 $e^+e^- \to$ hadrons
0.552±0.031±0.017	[1] BARU	96	MD1	$e^+e^- \to$ hadrons
0.54 ±0.04 ±0.02	[1] JAKUBOWSKI	88	CBAL	$e^+e^- \to$ hadrons
0.58 ±0.03 ±0.04	[2] GILES	84B	CLEO	$e^+e^- \to$ hadrons
0.60 ±0.12 ±0.07	[2] ALBRECHT	82	DASP	$e^+e^- \to$ hadrons
0.54 ±0.07 $^{+0.09}_{-0.05}$	[2] NICZYPORUK	81C	LENA	$e^+e^- \to$ hadrons
0.41 ±0.18	[2] BOCK	80	CNTR	$e^+e^- \to$ hadrons

[1] Radiative corrections evaluated following KURAEV 85.
[2] Radiative corrections reevaluated by BUCHMUELLER 88 following KURAEV 85.

$\Upsilon(2S)$ PARTIAL WIDTHS

$\Gamma(e^+e^-)$ — Γ_5

VALUE (keV)	DOCUMENT ID
0.612±0.011 OUR EVALUATION	

$\Upsilon(2S)$ BRANCHING RATIOS

$\Gamma(\Upsilon(1S)\pi^+\pi^-)/\Gamma_{\text{total}}$ — Γ_1/Γ

Abbreviation MM in the *COMMENT* field below stands for missing mass.

VALUE (units 10^{-2})	EVTS	DOCUMENT ID		TECN	COMMENT
17.85±0.26 OUR FIT					
17.92±0.26 OUR AVERAGE					
16.8 ±1.1 ±1.3	906k	[1] LEES	11C	BABR	$e^+e^- \to \pi^+\pi^- X$
17.80±0.05±0.37	170k	[2] LEES	11L	BABR	$\Upsilon(2S) \to \pi^+\pi^-\mu^+\mu^-$
18.02±0.02±0.61	851k	[3] BHARI	09	CLEO	$e^+e^- \to \pi^+\pi^-$ MM
17.22±0.17±0.75	11.8k	[4] AUBERT	08BP	BABR	$e^+e^- \to \gamma\pi^+\pi^-\ell^+\ell^-$
19.2 ±0.2 ±1.0	52.6k	[5] ALEXANDER	98	CLE2	$\pi^+\pi^-\ell^+\ell^-$, $\pi^+\pi^-$ MM
18.1 ±0.5 ±1.0	11.6k	ALBRECHT	87	ARG	$e^+e^- \to \pi^+\pi^-$ MM
16.9 ±4.0		GELPHMAN	85	CBAL	$e^+e^- \to e^+e^-\pi^+\pi^-$
19.1 ±1.2 ±0.6		BESSON	84	CLEO	$\pi^+\pi^-$ MM
18.9 ±2.6		FONSECA	84	CUSB	$e^+e^- \to \ell^+\ell^-\pi^+\pi^-$
21 ±7	7	NICZYPORUK	81B	LENA	$e^+e^- \to \ell^+\ell^-\pi^+\pi^-$

[1] LEES 11C reports [$\Gamma(\Upsilon(2S) \to \Upsilon(1S)\pi^+\pi^-)/\Gamma_{\text{total}}$] × [B($\Upsilon(3S) \to \Upsilon(2S)$anything)] = (1.78 ± 0.02 ± 0.11) × 10^{-2} which we divide by our best (shown rounded) value B($\Upsilon(3S) \to \Upsilon(2S)$anything) = (10.6 ± 0.8) × 10^{-2}. Our first error is their experiment's error and our second error is the systematic error from using our best (shown rounded) value.
[2] Using B($\Upsilon(1S) \to \mu^+\mu^-$) = (2.48 ± 0.05)%.
[3] A weighted average of the inclusive and exclusive results.
[4] Using B($\Upsilon(2S) \to e^+e^-$) = (1.91 ± 0.16)%, B($\Upsilon(2S) \to \mu^+\mu^-$) = (1.93 ± 0.17)% and, $\Gamma_{ee}(\Upsilon(2S))$ = 0.612 ± 0.011 keV.
[5] Using B($\Upsilon(1S) \to e^+e^-$) = (2.52 ± 0.17)% and B($\Upsilon(1S) \to \mu^+\mu^-$) = (2.48 ± 0.07)%.

$\Gamma(\Upsilon(1S)\pi^0\pi^0)/\Gamma_{\text{total}}$ — Γ_2/Γ

VALUE (units 10^{-2})	EVTS	DOCUMENT ID		TECN	COMMENT
8.6 ±0.4 OUR AVERAGE					
8.43±0.16±0.42	38k	[1] BHARI	09	CLEO	$e^+e^- \to \pi^0\pi^0\ell^+\ell^-$
9.2 ±0.6 ±0.8	275	[2] ALEXANDER	98	CLE2	$e^+e^- \to \pi^0\pi^0\ell^+\ell^-$
9.5 ±1.9 ±1.9	25	ALBRECHT	87	ARG	$e^+e^- \to \pi^0\pi^0\ell^+\ell^-$
8.0 ±1.5		GELPHMAN	85	CBAL	$e^+e^- \to \pi^0\pi^0\ell^+\ell^-$
10.3 ±2.3		FONSECA	84	CUSB	$e^+e^- \to \pi^0\pi^0\ell^+\ell^-$

[1] Authors assume B($\Upsilon(1S) \to e^+e^-$) + B($\Upsilon(1S) \to \mu^+\mu^-$) = 4.96%.
[2] Using B($\Upsilon(1S) \to e^+e^-$) = (2.52 ± 0.17)% and B($\Upsilon(1S) \to \mu^+\mu^-$) = (2.48 ± 0.07)%.

$\Gamma(\Upsilon(1S)\pi^0\pi^0)/\Gamma(\Upsilon(1S)\pi^+\pi^-)$ — Γ_2/Γ_1

VALUE	DOCUMENT ID		TECN	COMMENT
• • • We do not use the following data for averages, fits, limits, etc. • • •				
0.462±0.037	[1] BHARI	09	CLEO	$e^+e^- \to \Upsilon(2S)$

[1] Not independent of other values reported by BHARI 09.

$\Gamma(\tau^+\tau^-)/\Gamma_{\text{total}}$ — Γ_3/Γ

VALUE (units 10^{-2})	EVTS	DOCUMENT ID		TECN	COMMENT
2.00±0.21 OUR AVERAGE					
2.00±0.12±0.18	22k	[1] BESSON	07	CLEO	$e^+e^- \to \Upsilon(2S) \to \tau^+\tau^-$
1.7 ±1.5 ±0.6		HAAS	84B	CLEO	$e^+e^- \to \tau^+\tau^-$

[1] BESSON 07 reports [$\Gamma(\Upsilon(2S) \to \tau^+\tau^-)/\Gamma_{\text{total}}$] / [B($\Upsilon(2S) \to \mu^+\mu^-$)] = 1.04 ± 0.04 ± 0.05 which we multiply by our best (shown rounded) value B($\Upsilon(2S) \to \mu^+\mu^-$) = (1.93 ± 0.17) × 10^{-2}. Our first error is their experiment's error and our second error is the systematic error from using our best (shown rounded) value.

$\Gamma(\mu^+\mu^-)/\Gamma_{\text{total}}$ — Γ_4/Γ

VALUE	CL%	EVTS	DOCUMENT ID		TECN	COMMENT
0.0193±0.0017 OUR AVERAGE Error includes scale factor of 2.2. See the ideogram below.						
0.0203±0.0003±0.0008		120k	ADAMS	05	CLEO	$e^+e^- \to \mu^+\mu^-$
0.0122±0.0028±0.0019			[1] KOBEL	92	CBAL	$e^+e^- \to \mu^+\mu^-$
0.0138±0.0025±0.0015			KAARSBERG	89	CSB2	$e^+e^- \to \mu^+\mu^-$
0.009 ±0.006 ±0.006			[2] ALBRECHT	85	ARG	$e^+e^- \to \mu^+\mu^-$
0.018 ±0.008 ±0.005			HAAS	84B	CLEO	$e^+e^- \to \mu^+\mu^-$
• • • We do not use the following data for averages, fits, limits, etc. • • •						
<0.038		90	NICZYPORUK	81C	LENA	$e^+e^- \to \mu^+\mu^-$

[1] Taking into account interference between the resonance and continuum.
[2] Re-evaluated using B($\Upsilon(1S) \to \mu^+\mu^-$) = 0.026.

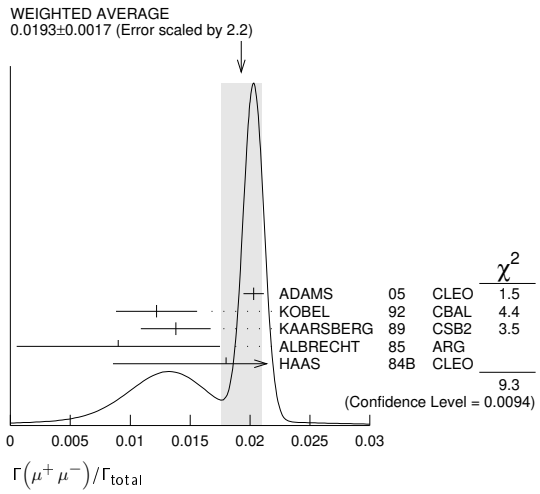

$\Gamma(\tau^+\tau^-)/\Gamma(\mu^+\mu^-)$ — Γ_3/Γ_4

VALUE	EVTS	DOCUMENT ID		TECN	COMMENT
1.04±0.04±0.05	22k	BESSON	07	CLEO	$e^+e^- \to \Upsilon(2S)$

$\Gamma(\Upsilon(1S)\pi^0)/\Gamma_{\text{total}}$ — Γ_6/Γ

VALUE (units 10^{-5})	CL%	DOCUMENT ID		TECN	COMMENT
• • • We do not use the following data for averages, fits, limits, etc. • • •					
< 4	90	[1] TAMPONI	13	BELL	$e^+e^- \to \Upsilon(1S)\pi^0$
< 18	90	[2] HE	08A	CLEO	$e^+e^- \to \ell^+\ell^-\gamma\gamma$
<110	90	ALEXANDER	98	CLE2	$e^+e^- \to \ell^+\ell^-\gamma\gamma$
<800	90	LURZ	87	CBAL	$e^+e^- \to \ell^+\ell^-\gamma\gamma$

[1] TAMPONI 13 reports [$\Gamma(\Upsilon(2S) \to \Upsilon(1S)\pi^0)/\Gamma_{\text{total}}$] / [B($\Upsilon(2S) \to \Upsilon(1S)\pi^+\pi^-$)] < 2.3 × 10^{-4} which we multiply by our best (shown rounded) value B($\Upsilon(2S) \to \Upsilon(1S)\pi^+\pi^-$) = 17.85 × 10^{-2}.
[2] Authors assume B($\Upsilon(1S) \to e^+e^-$) + B($\Upsilon(1S) \to \mu^+\mu^-$) = 4.96%.

$\Gamma(\Upsilon(1S)\pi^0)/\Gamma(\Upsilon(1S)\pi^+\pi^-)$ — Γ_6/Γ_1

VALUE (units 10^{-4})	CL%	DOCUMENT ID		TECN	COMMENT
<2.3	90	TAMPONI	13	BELL	$e^+e^- \to \Upsilon(1S)\pi^0$

$\Gamma(\Upsilon(1S)\eta)/\Gamma_{\text{total}}$ — Γ_7/Γ

VALUE (units 10^{-4})	CL%	EVTS	DOCUMENT ID		TECN	COMMENT
2.9 ±0.4 OUR FIT Error includes scale factor of 2.0.						
2.9 ±0.4 OUR AVERAGE Error includes scale factor of 1.9. See the ideogram below.						
2.39±0.31±0.14		112	[1] LEES	11L	BABR	$\Upsilon(2S) \to \ell^+\ell^-\eta$
2.1 $^{+0.7}_{-0.6}$ ±0.3		14	[2] HE	08A	CLEO	$e^+e^- \to \ell^+\ell^-\eta$
• • • We use the following data for averages but not for fits. • • •						
3.55±0.32±0.05		241	[3] TAMPONI	13	BELL	$e^+e^- \to \Upsilon(1S)\eta$
• • • We do not use the following data for averages, fits, limits, etc. • • •						
< 9	90		[1,4] AUBERT	08BP	BABR	$e^+e^- \to \gamma\pi^+\pi^-\pi^0\ell^+\ell^-$
< 28	90		ALEXANDER	98	CLE2	$e^+e^- \to \ell^+\ell^-\eta$
< 50	90		ALBRECHT	87	ARG	$e^+e^- \to \pi^+\pi^-\ell^+\ell^-$ MM
< 70	90		LURZ	87	CBAL	$e^+e^- \to \ell^+\ell^-(\gamma\gamma, 3\pi^0)$
< 100	90		BESSON	84	CLEO	$e^+e^- \to \pi^+\pi^-\ell^+\ell^-$ MM
< 20	90		FONSECA	84	CUSB	$e^+e^- \to \ell^+\ell^-(\gamma\gamma, \pi^+\pi^-\pi^0)$

[1] Using B($\Upsilon(1S) \to e^+e^-$) = (2.38 ± 0.11)% and B($\Upsilon(1S) \to \mu^+\mu^-$) = (2.48 ± 0.05)%.
[2] Authors assume B($\Upsilon(1S) \to e^+e^-$) + B($\Upsilon(1S) \to \mu^+\mu^-$) = 4.96%.
[3] TAMPONI 13 reports [$\Gamma(\Upsilon(2S) \to \Upsilon(1S)\eta)/\Gamma_{\text{total}}$] / [B($\Upsilon(2S) \to \Upsilon(1S)\pi^+\pi^-$)] = (1.99 ± 0.14 ± 0.11) × 10^{-3} which we multiply by our best (shown rounded) value B($\Upsilon(2S) \to \Upsilon(1S)\pi^+\pi^-$) = (17.85 ± 0.26) × 10^{-2}. Our first error is their experiment's error and our second error is the systematic error from using our best (shown rounded) value.
[4] Using $\Gamma_{ee}(\Upsilon(2S))$ = 0.612 ± 0.011 keV.

Int. J. Mod. Phys. A 2026.41. Downloaded from www.worldscientific.com
by UNIVERSITY OF CALIFORNIA @ BERKELEY on 09/16/26. Re-use and distribution is strictly not permitted, except for Open Access articles.

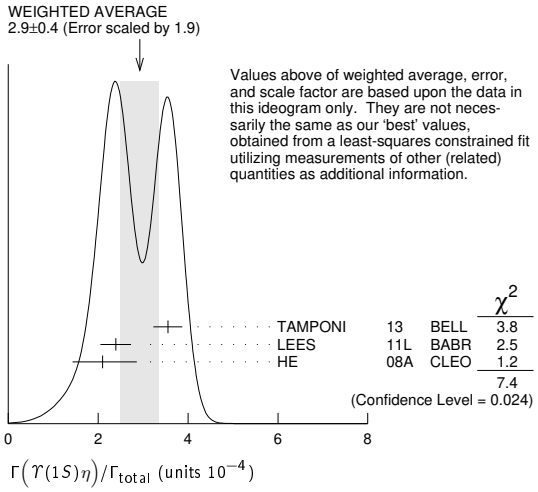

$\Gamma(\Upsilon(1S)\eta)/\Gamma(\Upsilon(1S)\pi^+\pi^-)$ — Γ_7/Γ_1

VALUE (units 10^{-3})	CL%	EVTS	DOCUMENT ID		TECN	COMMENT
1.64±0.25 OUR FIT			Error includes scale factor of 2.0.			
1.99±0.14±0.11		241	TAMPONI	13	BELL	$e^+e^- \to \Upsilon(1S)\eta$
• • • We do not use the following data for averages, fits, limits, etc. • • •						
1.35±0.17±0.08			[1] LEES	11L	BABR	$\Upsilon(2S) \to (\pi^+\pi^-)(\gamma\gamma)\mu^+\mu^-$
< 5.2	90		[2] AUBERT	08BP	BABR	$e^+e^- \to \gamma\pi^+\pi^-(\pi^0)\ell^+\ell^-$

[1] Not independent of other values reported by LEES 11L.
[2] Not independent of other values reported by AUBERT 08BP.

$\Gamma(\Upsilon(1S)\pi^0)/\Gamma(\Upsilon(1S)\eta)$ — Γ_6/Γ_7

VALUE	CL%	DOCUMENT ID		TECN	COMMENT
• • • We do not use the following data for averages, fits, limits, etc. • • •					
<0.13	90	TAMPONI	13	BELL	$e^+e^- \to \Upsilon(1S)\pi^0$

$\Gamma(J/\psi(1S)\text{ anything})/\Gamma_{total}$ — Γ_8/Γ

VALUE	CL%	DOCUMENT ID		TECN	COMMENT
<0.006	90	MASCHMANN	90	CBAL	$e^+e^- \to$ hadrons

$\Gamma(J/\psi(1S)\eta_c)/\Gamma_{total}$ — Γ_9/Γ

VALUE	CL%	DOCUMENT ID		TECN	COMMENT
<5.4 × 10⁻⁶	90	YANG	14	BELL	$e^+e^- \to J/\psi X$

$\Gamma(J/\psi(1S)\chi_{c0})/\Gamma_{total}$ — Γ_{10}/Γ

VALUE	CL%	DOCUMENT ID		TECN	COMMENT
<3.4 × 10⁻⁶	90	YANG	14	BELL	$e^+e^- \to J/\psi X$

$\Gamma(J/\psi(1S)\chi_{c1})/\Gamma_{total}$ — Γ_{11}/Γ

VALUE	CL%	DOCUMENT ID		TECN	COMMENT
<1.2 × 10⁻⁶	90	YANG	14	BELL	$e^+e^- \to J/\psi X$

$\Gamma(J/\psi(1S)\chi_{c2})/\Gamma_{total}$ — Γ_{12}/Γ

VALUE	CL%	DOCUMENT ID		TECN	COMMENT
<2.0 × 10⁻⁶	90	YANG	14	BELL	$e^+e^- \to J/\psi X$

$\Gamma(J/\psi(1S)\eta_c(2S))/\Gamma_{total}$ — Γ_{13}/Γ

VALUE	CL%	DOCUMENT ID		TECN	COMMENT
<2.5 × 10⁻⁶	90	YANG	14	BELL	$e^+e^- \to J/\psi X$

$\Gamma(J/\psi(1S)X(3940))/\Gamma_{total}$ — Γ_{14}/Γ

VALUE	CL%	DOCUMENT ID		TECN	COMMENT
<2.0 × 10⁻⁶	90	YANG	14	BELL	$e^+e^- \to J/\psi X$

$\Gamma(J/\psi(1S)X(4160))/\Gamma_{total}$ — Γ_{15}/Γ

VALUE	CL%	DOCUMENT ID		TECN	COMMENT
<2.0 × 10⁻⁶	90	YANG	14	BELL	$e^+e^- \to J/\psi X$

$\Gamma(\chi_{c1}\text{ anything})/\Gamma_{total}$ — Γ_{16}/Γ

VALUE (units 10^{-4})	EVTS	DOCUMENT ID		TECN	COMMENT
2.24±0.44±0.20	376	JIA	17	BELL	$\Upsilon(2S) \to \gamma J/\psi(1S)$

$\Gamma(\chi_{c1}(1P)^0 X_{tetra})/\Gamma_{total}$ — Γ_{17}/Γ

VALUE	CL%	DOCUMENT ID		TECN	COMMENT
<36.7 × 10⁻⁶	90	[1] JIA	17A	BELL	$e^+e^- \to$ hadrons

[1] For a tetraquark state X_{tetra}, with mass in the range 1.16–2.46 GeV and width in the range 0–0.3 GeV. Measured 90% CL limits as a function of X_{tetra} mass and width range from 4.4×10^{-6} to 36.7×10^{-6}.

$\Gamma(\chi_{c2}\text{ anything})/\Gamma_{total}$ — Γ_{18}/Γ

VALUE (units 10^{-4})	DOCUMENT ID		TECN	COMMENT
2.28±0.73±0.34	JIA	17	BELL	$\Upsilon(2S) \to \gamma J/\psi(1S)$

$\Gamma(\psi(2S)\eta_c)/\Gamma_{total}$ — Γ_{19}/Γ

VALUE	CL%	DOCUMENT ID		TECN	COMMENT
<5.1 × 10⁻⁶	90	YANG	14	BELL	$e^+e^- \to \psi(2S)X$

$\Gamma(\psi(2S)\chi_{c0})/\Gamma_{total}$ — Γ_{20}/Γ

VALUE	CL%	DOCUMENT ID		TECN	COMMENT
<4.7 × 10⁻⁶	90	YANG	14	BELL	$e^+e^- \to \psi(2S)X$

$\Gamma(\psi(2S)\chi_{c1})/\Gamma_{total}$ — Γ_{21}/Γ

VALUE	CL%	DOCUMENT ID		TECN	COMMENT
<2.5 × 10⁻⁶	90	YANG	14	BELL	$e^+e^- \to \psi(2S)X$

$\Gamma(\psi(2S)\chi_{c2})/\Gamma_{total}$ — Γ_{22}/Γ

VALUE	CL%	DOCUMENT ID		TECN	COMMENT
<1.9 × 10⁻⁶	90	YANG	14	BELL	$e^+e^- \to \psi(2S)X$

$\Gamma(\psi(2S)\eta_c(2S))/\Gamma_{total}$ — Γ_{23}/Γ

VALUE	CL%	DOCUMENT ID		TECN	COMMENT
<3.3 × 10⁻⁶	90	YANG	14	BELL	$e^+e^- \to \psi(2S)X$

$\Gamma(\psi(2S)X(3940))/\Gamma_{total}$ — Γ_{24}/Γ

VALUE	CL%	DOCUMENT ID		TECN	COMMENT
<3.9 × 10⁻⁶	90	YANG	14	BELL	$e^+e^- \to \psi(2S)X$

$\Gamma(\psi(2S)X(4160))/\Gamma_{total}$ — Γ_{25}/Γ

VALUE	CL%	DOCUMENT ID		TECN	COMMENT
<3.9 × 10⁻⁶	90	YANG	14	BELL	$e^+e^- \to \psi(2S)X$

$\Gamma(T_{c\overline{c}1}(3900)^+ T_{c\overline{c}1}(3900)^-)/\Gamma_{total}$ — Γ_{26}/Γ

VALUE	CL%	DOCUMENT ID		TECN	COMMENT
<1.0 × 10⁻⁶	90	[1] JIA	18	BELL	$\Upsilon(2S) \to J/\psi\pi^\pm X$

[1] Assuming $B(T_{c\overline{c}1}(3900)^\pm \to J/\psi\pi^\pm) = 1$.

$\Gamma(T_{c\overline{c}1}(4200)^+ T_{c\overline{c}1}(4200)^-)/\Gamma_{total}$ — Γ_{27}/Γ

VALUE	CL%	DOCUMENT ID		TECN	COMMENT
<16.7 × 10⁻⁶	90	[1] JIA	18	BELL	$\Upsilon(1S) \to J/\psi\pi^\pm X$

[1] Assuming $B(T_{c\overline{c}1}(4200)^\pm \to J/\psi\pi^\pm) = 1$

$\Gamma(T_{c\overline{c}1}(3900)^\pm T_{c\overline{c}1}(4200)^\mp)/\Gamma_{total}$ — Γ_{28}/Γ

VALUE	CL%	DOCUMENT ID		TECN	COMMENT
<7.3 × 10⁻⁶	90	[1] JIA	18	BELL	$\Upsilon(2S) \to J/\psi\pi^\pm X$

[1] Assuming $B(T_{c\overline{c}1}(4200)^\pm \to J/\psi\pi^\pm) = 1 = B(T_{c\overline{c}1}(3900)^\pm \to J/\psi\pi^\pm)$.

$\Gamma(T_{c\overline{c}}(4050)^+ T_{c\overline{c}}(4050)^-)/\Gamma_{total}$ — Γ_{29}/Γ

VALUE	CL%	DOCUMENT ID		TECN	COMMENT
<13.5 × 10⁻⁶	90	[1] JIA	18	BELL	$\Upsilon(2S) \to \chi_{c1}(1P)\pi^\pm X$

[1] Assuming $B(T_{c\overline{c}}(4050)^\pm \to \chi_{c1}(1P)\pi^\pm)$

$\Gamma(T_{c\overline{c}}(4250)^+ T_{c\overline{c}}(4250)^-)/\Gamma_{total}$ — Γ_{30}/Γ

VALUE	CL%	DOCUMENT ID		TECN	COMMENT
<26.7 × 10⁻⁶	90	[1] JIA	18	BELL	$\Upsilon(2S) \to \chi_{c1}(1P)\pi^\pm X$

[1] Assuming $B(T_{c\overline{c}}(4250)^\pm \to \chi_{c1}(1P)\pi^\pm) = 1$

$\Gamma(T_{c\overline{c}}(4050)^\pm T_{c\overline{c}}(4250)^\mp)/\Gamma_{total}$ — Γ_{31}/Γ

VALUE	CL%	DOCUMENT ID		TECN	COMMENT
<27.2 × 10⁻⁶	90	[1] JIA	18	BELL	$\Upsilon(2S) \to \chi_{c1}(1P)\pi^\pm X$

[1] Assuming $B(T_{c\overline{c}}(4050)^\pm \to \chi_{c1}(1P)\pi^\pm) = 1 = B(T_{c\overline{c}}(4250)^\pm \to \chi_{c1}(1P)\pi^\pm)$

$\Gamma(T_{c\overline{c}1}(4430)^+ T_{c\overline{c}1}(4430)^-)/\Gamma_{total}$ — Γ_{32}/Γ

VALUE	CL%	DOCUMENT ID		TECN	COMMENT
<20.3 × 10⁻⁶	90	[1] JIA	18	BELL	$\Upsilon(2S) \to \psi(2S)\pi^\pm X$

[1] Assuming $B(T_{c\overline{c}1}(4430)^\pm \to \psi(2P)\pi^\pm) = 1$

$\Gamma(T_{c\overline{c}}(4055)^\pm T_{c\overline{c}}(4055)^\mp)/\Gamma_{total}$ — Γ_{33}/Γ

VALUE	CL%	DOCUMENT ID		TECN	COMMENT
<11.1 × 10⁻⁶	90	[1] JIA	18	BELL	$\Upsilon(2S) \to \psi(2S)\pi^\pm X$

[1] Assuming $B(T_{c\overline{c}}(4055)^\pm \to \psi(2S)\pi^\pm) = 1$

$\Gamma(T_{c\overline{c}}(4055)^\pm T_{c\overline{c}1}(4430)^\mp)/\Gamma_{total}$ — Γ_{34}/Γ

VALUE	CL%	DOCUMENT ID		TECN	COMMENT
<21.1 × 10⁻⁶	90	[1] JIA	18	BELL	$\Upsilon(2S) \to \psi(2S)\pi^\pm X$

[1] Assuming $B(T_{c\overline{c}}(4055)^\pm \to \psi(2S)\pi^\pm) = 1 = B(T_{c\overline{c}1}(4430)^\pm \to \psi(2S)\pi^\pm)$

Int. J. Mod. Phys. A 2026.41. Downloaded from www.worldscientific.com
by [redacted]LIFORNIA @ BERKELEY on 09/16/26. Re-use and distribution is strictly not permitted, except for Open Access articles.

Int. J. Mod. Phys. A 2026.41. Downloaded from www.worldscientific.com
by UNIVERSITY OF CALIFORNIA @ BERKELEY on 09/16/26. Re-use and distribution is strictly not permitted, except for Open Access articles.

$\Gamma(P_{c\bar{c}s}(4459)/\overline{P}_{c\bar{c}s}(4459)\,\text{anything})/\Gamma_{\text{total}}$ — Γ_{35}/Γ

VALUE (units 10^{-6})	EVTS	DOCUMENT ID		TECN	COMMENT
2.9±1.7±0.4	21	[1] ADACHI	25A	BELL	$e^+e^- \to \Upsilon(2S)$

[1] 21 ± 5 corresponds to the number of $P_{c\bar{c}s}(4459)$ events in the combined $\Upsilon(1S)$ and $\Upsilon(2S)$ samples.

$\Gamma(P_{c\bar{c}s}(4338)/\overline{P}_{c\bar{c}s}(4338)\,\text{anything})/\Gamma_{\text{total}}$ — Γ_{36}/Γ

VALUE	CL%	DOCUMENT ID		TECN	COMMENT
<1.6 × 10^{-6}	90	ADACHI	25A	BELL	$e^+e^- \to \Upsilon(2S)$

$\Gamma(P_c(4457)\,\text{anything},\ P_c(4457) \to pJ/\psi(1S))/\Gamma_{\text{total}}$ — Γ_{37}/Γ

VALUE	CL%	DOCUMENT ID		TECN	COMMENT
<4.6 × 10^{-6}	90	DONG	25	BELL	$e^+e^- \to \Upsilon(2S)$

$\Gamma(P_c(4440)\,\text{anything},\ P_c(4440) \to pJ/\psi(1S))/\Gamma_{\text{total}}$ — Γ_{38}/Γ

VALUE	CL%	DOCUMENT ID		TECN	COMMENT
<11.8 × 10^{-6}	90	DONG	25	BELL	$e^+e^- \to \Upsilon(2S)$

$\Gamma(P_c(4312)\,\text{anything},\ P_c(4312) \to pJ/\psi(1S))/\Gamma_{\text{total}}$ — Γ_{39}/Γ

VALUE	CL%	DOCUMENT ID		TECN	COMMENT
<7.2 × 10^{-6}	90	DONG	25	BELL	$e^+e^- \to \Upsilon(2S)$

$\Gamma(p/\overline{p}J/\psi(1S)\,\text{anything})/\Gamma_{\text{total}}$ — Γ_{40}/Γ

VALUE (units 10^{-5})	EVTS	DOCUMENT ID		TECN	COMMENT
4.3±0.5±0.4	564	[1] DONG	25	BELL	$e^+e^- \to \Upsilon(2S)$

[1] The contribution from cascade $\Upsilon(1S)$ decays has been removed.

$\Gamma(J/\psi(1S)\Lambda/\overline{\Lambda}\,\text{anything})/\Gamma_{\text{total}}$ — Γ_{41}/Γ

VALUE (units 10^{-6})	EVTS	DOCUMENT ID		TECN	COMMENT
22.3±5.7±3.1	140	ADACHI	25A	BELL	$e^+e^- \to \Upsilon(2S)$

$\Gamma(\overline{^2H}\ \text{anything})/\Gamma_{\text{total}}$ — Γ_{42}/Γ

VALUE (units 10^{-5})	EVTS	DOCUMENT ID		TECN	COMMENT
$2.78^{+0.30}_{-0.26}$ OUR AVERAGE Error includes scale factor of 1.2.					
$2.64 \pm 0.11^{+0.26}_{-0.21}$		LEES	14G	BABR	$e^+e^- \to \overline{^2H}\,X$
$3.37 \pm 0.50 \pm 0.25$	58	ASNER	07	CLEO	$e^+e^- \to \overline{^2H}\,X$

$\Gamma(ggg)/\Gamma_{\text{total}}$ — Γ_{44}/Γ

VALUE (units 10^{-2})	EVTS	DOCUMENT ID		TECN	COMMENT
58.8±1.2	6M	[1] BESSON	06A	CLEO	$\Upsilon(2S) \to$ hadrons

[1] Calculated using the value $\Gamma(\gamma gg)/\Gamma(ggg) = (3.18 \pm 0.04 \pm 0.22 \pm 0.41)\%$ from BESSON 06A and PDG 08 values of $B(\pi^+\pi^-\Upsilon(1S)) = (18.1 \pm 0.4)\%$, $B(\pi^0\pi^0\Upsilon(1S)) = (8.6 \pm 0.4)\%$, $B(\mu^+\mu^-) = (1.93 \pm 0.17)\%$, and $R_{\text{hadrons}} = 3.51$. The statistical error is negligible and the systematic error is partially correlated with that of $\Gamma(\gamma gg)/\Gamma_{\text{total}}$ measurement of BESSON 06A.

$\Gamma(\gamma gg)/\Gamma(ggg)$ — Γ_{45}/Γ_{44}

VALUE (units 10^{-2})	EVTS	DOCUMENT ID		TECN	COMMENT
3.18±0.04±0.47	6M	BESSON	06A	CLEO	$\Upsilon(2S) \to (\gamma\ +)$ hadrons

$\Gamma(\phi K^+K^-)/\Gamma_{\text{total}}$ — Γ_{46}/Γ

VALUE (units 10^{-6})	EVTS	DOCUMENT ID		TECN	COMMENT
1.58±0.33±0.18	58	SHEN	12A	BELL	$\Upsilon(1S) \to 2(K^+K^-)$

$\Gamma(\omega\pi^+\pi^-)/\Gamma_{\text{total}}$ — Γ_{47}/Γ

VALUE (units 10^{-6})	CL%	DOCUMENT ID		TECN	COMMENT
<2.58	90	SHEN	12A	BELL	$\Upsilon(1S) \to 2(\pi^+\pi^-)\pi^0$

$\Gamma(K^*(892)^0K^-\pi^+ + \text{c.c.})/\Gamma_{\text{total}}$ — Γ_{48}/Γ

VALUE (units 10^{-6})	EVTS	DOCUMENT ID		TECN	COMMENT
2.32±0.40±0.54	135	SHEN	12A	BELL	$\Upsilon(1S) \to K^+K^-\pi^+\pi^-$

$\Gamma(\phi f_2'(1525))/\Gamma_{\text{total}}$ — Γ_{49}/Γ

VALUE (units 10^{-6})	CL%	DOCUMENT ID		TECN	COMMENT
<1.33	90	SHEN	12A	BELL	$\Upsilon(1S) \to 2(K^+K^-)$

$\Gamma(\omega f_2(1270))/\Gamma_{\text{total}}$ — Γ_{50}/Γ

VALUE (units 10^{-6})	CL%	DOCUMENT ID		TECN	COMMENT
<0.57	90	SHEN	12A	BELL	$\Upsilon(1S) \to 2(\pi^+\pi^-)\pi^0$

$\Gamma(\rho(770)a_2(1320))/\Gamma_{\text{total}}$ — Γ_{51}/Γ

VALUE (units 10^{-6})	CL%	DOCUMENT ID		TECN	COMMENT
<0.88	90	SHEN	12A	BELL	$\Upsilon(1S) \to 2(\pi^+\pi^-)\pi^0$

$\Gamma(K^*(892)^0\overline{K}_2^*(1430)^0 + \text{c.c.})/\Gamma_{\text{total}}$ — Γ_{52}/Γ

VALUE (units 10^{-6})	EVTS	DOCUMENT ID		TECN	COMMENT
1.53±0.52±0.19	32	SHEN	12A	BELL	$\Upsilon(1S) \to K^+K^-\pi^+\pi^-$

$\Gamma(K_1(1270)^\pm K^\mp)/\Gamma_{\text{total}}$ — Γ_{53}/Γ

VALUE (units 10^{-6})	CL%	DOCUMENT ID		TECN	COMMENT
<3.22	90	SHEN	12A	BELL	$\Upsilon(1S) \to K^+K^-\pi^+\pi^-$

$\Gamma(K_1(1400)^\pm K^\mp)/\Gamma_{\text{total}}$ — Γ_{54}/Γ

VALUE (units 10^{-6})	CL%	DOCUMENT ID		TECN	COMMENT
<0.83	90	SHEN	12A	BELL	$\Upsilon(1S) \to K^+K^-\pi^+\pi^-$

$\Gamma(b_1(1235)^\pm\pi^\mp)/\Gamma_{\text{total}}$ — Γ_{55}/Γ

VALUE (units 10^{-6})	CL%	DOCUMENT ID		TECN	COMMENT
<0.40	90	SHEN	12A	BELL	$\Upsilon(1S) \to 2(\pi^+\pi^-)\pi^0$

$\Gamma(\rho\pi)/\Gamma_{\text{total}}$ — Γ_{56}/Γ

VALUE (units 10^{-6})	CL%	DOCUMENT ID		TECN	COMMENT
<1.16	90	SHEN	13	BELL	$\Upsilon(2S) \to \pi^+\pi^-\pi^0$

$\Gamma(\pi^+\pi^-\pi^0)/\Gamma_{\text{total}}$ — Γ_{57}/Γ

VALUE (units 10^{-6})	CL%	DOCUMENT ID		TECN	COMMENT
<0.80	90	SHEN	13	BELL	$\Upsilon(2S) \to \pi^+\pi^-\pi^0$

$\Gamma(\omega\pi^0)/\Gamma_{\text{total}}$ — Γ_{58}/Γ

VALUE (units 10^{-6})	CL%	DOCUMENT ID		TECN	COMMENT
<1.63	90	SHEN	13	BELL	$\Upsilon(2S) \to \pi^+\pi^-\pi^0\pi^0$

$\Gamma(\pi^+\pi^-\pi^0\pi^0)/\Gamma_{\text{total}}$ — Γ_{59}/Γ

VALUE (units 10^{-6})	EVTS	DOCUMENT ID		TECN	COMMENT
13.0±1.9±2.1	261 ± 37	SHEN	13	BELL	$\Upsilon(2S) \to \pi^+\pi^-\pi^0\pi^0$

$\Gamma(K_S^0K^+\pi^- + \text{c.c.})/\Gamma_{\text{total}}$ — Γ_{60}/Γ

VALUE (units 10^{-6})	CL%	EVTS	DOCUMENT ID		TECN	COMMENT
1.14±0.30±0.13		40 ± 10	SHEN	13	BELL	$\Upsilon(2S) \to K_S^0K^-\pi^+$
• • • We do not use the following data for averages, fits, limits, etc. • • •						
<3.2	90		[1] DOBBS	12A		$\Upsilon(2S) \to K_S^0K^-\pi^+$

[1] Obtained by analyzing CLEO III data but not authored by the CLEO Collaboration.

$\Gamma(K^*(892)^0\overline{K}^0 + \text{c.c.})/\Gamma_{\text{total}}$ — Γ_{61}/Γ

VALUE (units 10^{-6})	CL%	DOCUMENT ID		TECN	COMMENT
<4.22	90	SHEN	13	BELL	$\Upsilon(2S) \to K_S^0K^-\pi^+$

$\Gamma(K^*(892)^-K^+ + \text{c.c.})/\Gamma_{\text{total}}$ — Γ_{62}/Γ

VALUE (units 10^{-6})	CL%	DOCUMENT ID		TECN	COMMENT
<1.45	90	SHEN	13	BELL	$\Upsilon(2S) \to K_S^0K^-\pi^+$

$\Gamma(f_1(1285)\,\text{anything})/\Gamma_{\text{total}}$ — Γ_{63}/Γ

VALUE (units 10^{-3})	EVTS	DOCUMENT ID		TECN	COMMENT
2.20±1.50±0.63	2.9k	JIA	17A	BELL	$e^+e^- \to$ hadrons

$\Gamma(f_1(1285)X_{tetra})/\Gamma_{\text{total}}$ — Γ_{64}/Γ

VALUE	CL%	DOCUMENT ID		TECN	COMMENT
<64.7 × 10^{-6}	90	[1] JIA	17A	BELL	$e^+e^- \to$ hadrons

[1] For a tetraquark state X_{tetra}, with mass in the range 1.16–2.46 GeV and width in the range 0–0.3 GeV. Measured 90% CL limits as a function of X_{tetra} mass and width range from 7.8×10^{-6} to 64.7×10^{-6}.

$\Gamma(D_s^+D_{s1}(2536)^-,\ D_{s1}^- \to K^-D^*(2007)^0)/\Gamma_{\text{total}}$ — Γ_{66}/Γ

VALUE (units 10^{-5})	DOCUMENT ID		TECN	COMMENT
1.6±0.3±0.2	GAO	23	BELL	e^+e^- at 10.52 GeV

$\Gamma(D_s^+D_{s1}(2536)^-,\ D_{s1}^- \to K_S^0D^*(2010)^-)/\Gamma_{\text{total}}$ — Γ_{67}/Γ

VALUE (units 10^{-5})	DOCUMENT ID		TECN	COMMENT
0.84±0.18±0.15	GAO	23	BELL	e^+e^- at 10.52 GeV

$\Gamma(D_s^{*+}D_{s1}(2536)^-,\ D_{s1}^- \to K^-D^*(2007)^0)/\Gamma_{\text{total}}$ — Γ_{69}/Γ

VALUE (units 10^{-5})	DOCUMENT ID		TECN	COMMENT
1.4±0.4±0.2	GAO	23	BELL	e^+e^- at 10.52 GeV

$\Gamma(D_s^{*+}D_{s1}(2536)^-,\ D_{s1}^- \to K_S^0D^*(2010)^-)/\Gamma_{\text{total}}$ — Γ_{70}/Γ

VALUE (units 10^{-5})	DOCUMENT ID		TECN	COMMENT
0.82±0.25±0.19	GAO	23	BELL	e^+e^- at 10.52 GeV

$\Gamma(D_s^+D_{s2}^*(2573)^-,\ D_{s2}^{*-} \to K^-D^0)/\Gamma_{\text{total}}$ — Γ_{72}/Γ

VALUE (units 10^{-5})	DOCUMENT ID		TECN	COMMENT
1.4±0.4±0.2	GAO	23	BELL	e^+e^- at 10.52 GeV

$\Gamma(D_s^+D_{s2}^*(2573)^-,\ D_{s2}^{*-} \to K_S^0D^-)/\Gamma_{\text{total}}$ — Γ_{73}/Γ

VALUE (units 10^{-5})	DOCUMENT ID		TECN	COMMENT
0.69±0.20±0.22	GAO	23	BELL	e^+e^- at 10.52 GeV

Int. J. Mod. Phys. A 2026.41. Downloaded from www.worldscientific.com by CALIFORNIA @ BERKELEY on 09/16/26. Re-use and distribution is strictly not permitted, except for Open Access articles.

$\Gamma(D_s^{*+} D_{s2}^*(2573)^-,\ D_{s2}^{*-} \to K^- D^0)/\Gamma_{total}$ — Γ_{75}/Γ

VALUE (units 10^{-5})	DOCUMENT ID		TECN	COMMENT
0.9±0.5±0.2	GAO	23	BELL	e^+e^- at 10.52 GeV

$\Gamma(D_s^{*+} D_{s2}^*(2573)^-,\ D_{s2}^{*-} \to K_S^0 D^-)/\Gamma_{total}$ — Γ_{76}/Γ

VALUE (units 10^{-5})	DOCUMENT ID		TECN	COMMENT
0.54±0.31±0.47	GAO	23	BELL	e^+e^- at 10.52 GeV

Γ(Sum of 100 exclusive modes)$/\Gamma_{total}$ — Γ_{77}/Γ

VALUE (units 10^{-2})	DOCUMENT ID		COMMENT
0.29±0.03	[1,2] DOBBS	12A	$\Upsilon(2S) \to$ hadrons

[1] DOBBS 12A presents individual exclusive branching fractions or upper limits for 100 modes of four to ten pions, kaons, or protons.
[2] Obtained by analyzing CLEO III data but not authored by the CLEO Collaboration.

$\Gamma(\gamma\chi_{b1}(1P))/\Gamma_{total}$ — Γ_{78}/Γ

VALUE	EVTS	DOCUMENT ID		TECN	COMMENT
0.069 ±0.004 OUR AVERAGE					
0.0693±0.0012±0.0041	407k	ARTUSO	05	CLEO	$e^+e^- \to \gamma X$
0.069 ±0.005 ±0.009		EDWARDS	99	CLE2	$\Upsilon(2S) \to \gamma\chi(1P)$
0.091 ±0.018 ±0.022		ALBRECHT	85E	ARG	$e^+e^- \to \gamma$conv. X
0.065 ±0.007 ±0.012		NERNST	85	CBAL	$e^+e^- \to \gamma X$
0.080 ±0.017 ±0.016		HAAS	84	CLEO	$e^+e^- \to \gamma$conv. X
0.059 ±0.014		KLOPFEN...	83	CUSB	$e^+e^- \to \gamma X$

$\Gamma(\gamma\chi_{b2}(1P))/\Gamma_{total}$ — Γ_{79}/Γ

VALUE	EVTS	DOCUMENT ID		TECN	COMMENT
0.0715±0.0035 OUR AVERAGE					
0.0724±0.0011±0.0040	410k	ARTUSO	05	CLEO	$e^+e^- \to \gamma X$
0.074 ±0.005 ±0.008		EDWARDS	99	CLE2	$\Upsilon(2S) \to \gamma\chi(1P)$
0.098 ±0.021 ±0.024		ALBRECHT	85E	ARG	$e^+e^- \to \gamma$conv. X
0.058 ±0.007 ±0.010		NERNST	85	CBAL	$e^+e^- \to \gamma X$
0.102 ±0.018 ±0.021		HAAS	84	CLEO	$e^+e^- \to \gamma$conv. X
0.061 ±0.014		KLOPFEN...	83	CUSB	$e^+e^- \to \gamma X$

$\Gamma(\gamma\chi_{b0}(1P))/\Gamma_{total}$ — Γ_{80}/Γ

VALUE	EVTS	DOCUMENT ID		TECN	COMMENT
0.038 ±0.004 OUR AVERAGE					
0.0375±0.0012±0.0047	198k	ARTUSO	05	CLEO	$e^+e^- \to \gamma X$
0.034 ±0.005 ±0.006		EDWARDS	99	CLE2	$\Upsilon(2S) \to \gamma\chi(1P)$
0.064 ±0.014 ±0.016		ALBRECHT	85E	ARG	$e^+e^- \to \gamma$conv. X
0.036 ±0.008 ±0.009		NERNST	85	CBAL	$e^+e^- \to \gamma X$
0.044 ±0.023 ±0.009		HAAS	84	CLEO	$e^+e^- \to \gamma$conv. X
• • • We do not use the following data for averages, fits, limits, etc. • • •					
0.035 ±0.014		KLOPFEN...	83	CUSB	$e^+e^- \to \gamma X$

$\Gamma(\gamma f_0(1710))/\Gamma_{total}$ — Γ_{81}/Γ

VALUE (units 10^{-5})	CL%	DOCUMENT ID		TECN	COMMENT
<59	90	[1] ALBRECHT	89	ARG	$\Upsilon(2S) \to \gamma K^+K^-$
• • • We do not use the following data for averages, fits, limits, etc. • • •					
< 5.9	90	[2] ALBRECHT	89	ARG	$\Upsilon(2S) \to \gamma\pi^+\pi^-$

[1] Re-evaluated assuming $B(f_0(1710) \to K^+K^-) = 0.19$.
[2] Includes unknown branching ratio of $f_0(1710) \to \pi^+\pi^-$.

$\Gamma(\gamma f_2'(1525))/\Gamma_{total}$ — Γ_{82}/Γ

VALUE (units 10^{-5})	CL%	DOCUMENT ID		TECN	COMMENT
<53	90	[1] ALBRECHT	89	ARG	$\Upsilon(2S) \to \gamma K^+K^-$

[1] Re-evaluated assuming $B(f_2'(1525) \to K\overline{K}) = 0.71$.

$\Gamma(\gamma f_2(1270))/\Gamma_{total}$ — Γ_{83}/Γ

VALUE (units 10^{-5})	CL%	DOCUMENT ID		TECN	COMMENT
<24.1	90	[1] ALBRECHT	89	ARG	$\Upsilon(2S) \to \gamma\pi^+\pi^-$

[1] Using $B(f_2(1270) \to \pi\pi) = 0.84$.

$\Gamma(\gamma f_J(2220))/\Gamma_{total}$ — Γ_{84}/Γ

VALUE (units 10^{-5})	CL%	DOCUMENT ID		TECN	COMMENT
• • • We do not use the following data for averages, fits, limits, etc. • • •					
<6.8	90	[1] ALBRECHT	89	ARG	$\Upsilon(2S) \to \gamma K^+K^-$

[1] Includes unknown branching ratio of $f_J(2220) \to K^+K^-$.

$\Gamma(\gamma\eta_c(1S))/\Gamma_{total}$ — Γ_{85}/Γ

VALUE	CL%	DOCUMENT ID		TECN	COMMENT
$<2.7\times10^{-5}$	90	WANG	11B	BELL	$\Upsilon(2S) \to \gamma X$

$\Gamma(\gamma\chi_{c0})/\Gamma_{total}$ — Γ_{86}/Γ

VALUE	CL%	DOCUMENT ID		TECN	COMMENT
$<1.0\times10^{-4}$	90	WANG	11B	BELL	$\Upsilon(2S) \to \gamma X$

$\Gamma(\gamma\chi_{c1})/\Gamma_{total}$ — Γ_{87}/Γ

VALUE	CL%	DOCUMENT ID		TECN	COMMENT
$<3.6\times10^{-6}$	90	WANG	11B	BELL	$\Upsilon(2S) \to \gamma X$

$\Gamma(\gamma\chi_{c2})/\Gamma_{total}$ — Γ_{88}/Γ

VALUE	CL%	DOCUMENT ID		TECN	COMMENT
$<1.5\times10^{-5}$	90	WANG	11B	BELL	$\Upsilon(2S) \to \gamma X$

$\Gamma(\gamma\chi_{c1}(3872))/\Gamma_{total}$ — Γ_{89}/Γ

VALUE	CL%	DOCUMENT ID		TECN	COMMENT
$<1.8\times10^{-5}$	90	[1] WANG	11B	BELL	$\Upsilon(2S) \to \gamma X$

[1] WANG 11B reports $[\Gamma(\Upsilon(2S) \to \gamma\chi_{c1}(3872))/\Gamma_{total}] \times [B(\chi_{c1}(3872) \to \pi^+\pi^- J/\psi(1S))] < 0.8\times10^{-6}$ which we divide by our best (shown rounded) value $B(\chi_{c1}(3872) \to \pi^+\pi^- J/\psi(1S)) = 4.3\times10^{-2}$.

$\Gamma(\gamma\chi_{c1}(3872),\ \chi_{c1} \to \pi^+\pi^-\pi^0 J/\psi)/\Gamma_{total}$ — Γ_{90}/Γ

VALUE	CL%	DOCUMENT ID		TECN	COMMENT
$<2.4\times10^{-6}$	90	WANG	11B	BELL	$\Upsilon(2S) \to \gamma X$

$\Gamma(\gamma\chi_{c0}(3915) \to \omega J/\psi)/\Gamma_{total}$ — Γ_{91}/Γ

VALUE	CL%	DOCUMENT ID		TECN	COMMENT
$<2.8\times10^{-6}$	90	WANG	11B	BELL	$\Upsilon(2S) \to \gamma X$

$\Gamma(\gamma\chi_{c1}(4140) \to \phi J/\psi)/\Gamma_{total}$ — Γ_{92}/Γ

VALUE	CL%	DOCUMENT ID		TECN	COMMENT
$<1.2\times10^{-6}$	90	WANG	11B	BELL	$\Upsilon(2S) \to \gamma X$

$\Gamma(\gamma X(4350) \to \phi J/\psi)/\Gamma_{total}$ — Γ_{93}/Γ

VALUE	CL%	DOCUMENT ID		TECN	COMMENT
$<1.3\times10^{-6}$	90	WANG	11B	BELL	$\Upsilon(2S) \to \gamma X$

$\Gamma(\gamma\eta_b(1S))/\Gamma_{total}$ — Γ_{94}/Γ

VALUE (units 10^{-4})	CL%	EVTS	DOCUMENT ID		TECN	COMMENT
$5.5^{+1.1}_{-0.9}$ OUR AVERAGE Error includes scale factor of 1.2.						
$6.1^{+0.6+0.9}_{-0.7-0.6}$		29k	FULSOM	18	BELL	$\Upsilon(2S) \to \gamma X$
$3.9\pm1.1^{+1.1}_{-0.9}$		13 ± 5k	[1] AUBERT	09AQ	BABR	$\Upsilon(2S) \to \gamma X$
• • • We do not use the following data for averages, fits, limits, etc. • • •						
<21	90		LEES	11J	BABR	$\Upsilon(2S) \to X\gamma$
< 8.4	90		[1] BONVICINI	10	CLEO	$\Upsilon(2S) \to \gamma X$
< 5.1	90		[2] ARTUSO	05	CLEO	$e^+e^- \to \gamma X$

[1] Assuming $\Gamma_{\eta_b(1S)} = 10$ MeV.
[2] Superseded by BONVICINI 10.

$\Gamma(\gamma\eta_b(1S) \to \gamma$Sum of 26 exclusive modes$)/\Gamma_{total}$ — Γ_{95}/Γ

VALUE	CL%	DOCUMENT ID		TECN	COMMENT
$<3.7\times10^{-6}$	90	SANDILYA	13	BELL	$\Upsilon(2S) \to \gamma$ hadrons

$\Gamma(\gamma X_{b\overline{b}} \to \gamma$Sum of 26 exclusive modes$)/\Gamma_{total}$ — Γ_{96}/Γ

VALUE (units 10^{-6})	CL%	EVTS	DOCUMENT ID		TECN	COMMENT
< 4.9	90		SANDILYA	13	BELL	$\Upsilon(2S) \to \gamma$ hadrons
• • • We do not use the following data for averages, fits, limits, etc. • • •						
$46.2^{+29.7}_{-14.2}\pm10.6$		10	[1] DOBBS	12		$\Upsilon(2S) \to \gamma$ hadrons

[1] Obtained by analyzing CLEO III data but not authored by the CLEO Collaboration.

$\Gamma(\gamma X \to \gamma + \geq 4$ prongs$)/\Gamma_{total}$ — Γ_{97}/Γ
(1.5 GeV $< m_X <$ 5.0 GeV)

VALUE (units 10^{-4})	CL%	DOCUMENT ID		TECN	COMMENT
<1.95	95	ROSNER	07A	CLEO	$e^+e^- \to \gamma X$

$\Gamma(\gamma A^0 \to \gamma$hadrons$)/\Gamma_{total}$ — Γ_{98}/Γ
(0.3 GeV $< m_{A^0} <$ 7 GeV)

VALUE	CL%	DOCUMENT ID		TECN	COMMENT
$<8\times10^{-5}$	90	[1] LEES	11H	BABR	$\Upsilon(2S) \to \gamma$ hadrons

[1] For a narrow scalar or pseudoscalar, A^0, excluding known resonances, with mass in the range 0.3–7 GeV. Measured 90% CL limits as a function of m_{A^0} range from 1×10^{-6} to 8×10^{-5}.

$\Gamma(\gamma A^0 \to \gamma\mu^+\mu^-)/\Gamma_{total}$ — Γ_{99}/Γ

VALUE (units 10^{-6})	CL%	DOCUMENT ID		TECN	COMMENT
<8.3	90	[1] AUBERT	09Z	BABR	$e^+e^- \to A^0 \to \gamma\mu^+\mu^-$

[1] For a narrow scalar or pseudoscalar, A^0, with mass in the range 212–9300 MeV, excluding J/ψ and $\psi(2S)$. Measured 90% CL limits as a function of m_{A^0} range from 0.26–8.3×10^{-6}.

LEPTON FAMILY NUMBER (*LF*) VIOLATING MODES

$\Gamma(e^\pm\tau^\mp)/\Gamma_{total}$ — Γ_{100}/Γ

VALUE (units 10^{-6})	CL%	DOCUMENT ID		TECN	COMMENT
<1.12	90	DHAMIJA	24	BELL	$e^+e^- \to e^\pm\tau^\mp$
• • • We do not use the following data for averages, fits, limits, etc. • • •					
<3.2	90	LEES	10B	BABR	$e^+e^- \to e^\pm\tau^\mp$

Int. J. Mod. Phys. A 2026.41. Downloaded from www.worldscientific.com by UNIVERSITY OF CALIFORNIA @ BERKELEY on 09/16/26. Re-use and distribution is strictly not permitted, except for Open Access articles.

$\Gamma(\mu^\pm\tau^\mp)/\Gamma_{total}$ — Γ_{101}/Γ

VALUE (units 10^{-6})	CL%	DOCUMENT ID		TECN	COMMENT
< 0.23	90	DHAMIJA	24	BELL	$e^+e^- \to \mu^\pm\tau^\mp$
• • • We do not use the following data for averages, fits, limits, etc. • • •					
< 3.3	90	LEES	10B	BABR	$e^+e^- \to \mu^\pm\tau^\mp$
<14.4	95	LOVE	08A	CLEO	$e^+e^- \to \mu^\pm\tau^\mp$

$\Upsilon(2S)$ Cross-Particle Branching Ratios

$B(\Upsilon(2S) \to \pi^+\pi^-) \times B(\Upsilon(3S) \to \Upsilon(2S)X)$

VALUE (units 10^{-2})	EVTS	DOCUMENT ID		TECN	COMMENT
1.78±0.02±0.11	906k	LEES	11C	BABR	$e^+e^- \to \pi^+\pi^- X$

$\Upsilon(2S)$ REFERENCES

ADACHI	25A	PRL 135 041901	I. Adachi et al.	(BELLE and BELLE II Collab.)
DONG	25	JHEP 2509 048	X. Dong et al.	(BELLE Collab.)
AAIJ	24AC	JHEP 2410 122	R. Aaij et al.	(LHCb Collab.)
DHAMIJA	24	JHEP 2402 187	R. Dhamija et al.	(BELLE Collab.)
GAO	23	PR D108 112015	B.S. Gao et al.	(BELLE Collab.)
SHAMOV	23	PL B839 137766	A.G. Shamov, O.L. Rezanova	(NOVO, NOVOU)
FULSOM	18	PRL 121 232001	B.G. Fulsom et al.	(BELLE Collab.)
JIA	18	PR D97 112004	S. Jia et al.	(BELLE Collab.)
JIA	17	PR D95 012001	S. Jia et al.	(BELLE Collab.)
JIA	17A	PR D96 112002	S. Jia et al.	(BELLE Collab.)
LEES	14G	PR D89 111102	J.P. Lees et al.	(BABAR Collab.)
YANG	14	PR D90 112008	S.D. Yang et al.	(BELLE Collab.)
SANDILYA	13	PRL 111 112001	S. Sandilya et al.	(BELLE Collab.)
SHEN	13	PR D88 011102	C.P. Shen et al.	(BELLE Collab.)
TAMPONI	13	PR D87 011104	U. Tamponi et al.	(BELLE Collab.)
DOBBS	12	PRL 109 082001	S. Dobbs et al.	
DOBBS	12A	PR D86 052003	S. Dobbs et al.	
SHEN	12A	PR D86 031102	C.P. Shen et al.	(BELLE Collab.)
LEES	11C	PR D84 011104	J.P. Lees et al.	(BABAR Collab.)
LEES	11H	PRL 107 221803	J.P. Lees et al.	(BABAR Collab.)
LEES	11J	PR D84 072002	J.P. Lees et al.	(BABAR Collab.)
LEES	11L	PR D84 092003	J.P. Lees et al.	(BABAR Collab.)
WANG	11B	PR D84 071107	X.L. Wang et al.	(BELLE Collab.)
BONVICINI	10	PR D81 031104	G. Bonvicini et al.	(CLEO Collab.)
LEES	10B	PRL 104 151802	J.P. Lees et al.	(BABAR Collab.)
AUBERT	09AQ	PRL 103 161801	B. Aubert et al.	(BABAR Collab.)
AUBERT	09Z	PRL 103 081803	B. Aubert et al.	(BABAR Collab.)
BHARI	09	PR D79 011103	S.R. Bhari et al.	(CLEO Collab.)
AUBERT	08BP	PR D78 112002	B. Aubert et al.	(BABAR Collab.)
HE	08A	PRL 101 192001	Q. He et al.	(CLEO Collab.)
LOVE	08A	PRL 101 201601	W. Love et al.	(CLEO Collab.)
PDG	08	PL B667 1	C. Amsler et al.	(PDG Collab.)
ASNER	07	PR D75 012009	D.M. Asner et al.	(CLEO Collab.)
BESSON	07	PRL 98 052002	D. Besson et al.	(CLEO Collab.)
ROSNER	07A	PR D76 117102	J.L. Rosner et al.	(CLEO Collab.)
BESSON	06A	PR D74 012003	D. Besson et al.	(CLEO Collab.)
ROSNER	06	PRL 96 092003	J.L. Rosner et al.	(CLEO Collab.)
ADAMS	05	PRL 94 012001	G.S. Adams et al.	(CLEO Collab.)
ARTUSO	05	PRL 94 032001	M. Artuso et al.	(CLEO Collab.)
ARTAMONOV	00	PL B474 427	A.S. Artamonov et al.	
EDWARDS	99	PR D59 032003	K.W. Edwards et al.	(CLEO Collab.)
ALEXANDER	98	PR D58 052004	J.P. Alexander et al.	(CLEO Collab.)
BARU	96	PRPL 267 71	S.E. Baru et al.	(NOVO)
KOBEL	92	ZPHY C53 193	M. Kobel et al.	(Crystal Ball Collab.)
MASCHMANN	90	ZPHY C46 555	W.S. Maschmann et al.	(Crystal Ball Collab.)
ALBRECHT	89	ZPHY C42 349	H. Albrecht et al.	(ARGUS Collab.)
KAARSBERG	89	PRL 62 2077	T.M. Kaarsberg et al.	(CUSB Collab.)
BUCHMUEL...	88	HE e^+e^- Physics 412 Editors: A. Ali and P. Soeding, World Scientific, Singapore	W. Buchmueller, S. Cooper	(HANN, DESY, MIT)
JAKUBOWSKI	88	ZPHY C40 49	Z. Jakubowski et al.	(Crystal Ball Collab.) IGJPC
ALBRECHT	87	ZPHY C35 283	H. Albrecht et al.	(ARGUS Collab.)
COHEN	87	RMP 59 1121	E.R. Cohen, B.N. Taylor	(RISC, NBS)
LURZ	87	ZPHY C36 383	B. Lurz et al.	(Crystal Ball Collab.)
BARU	86B	ZPHY C32 622 (errat.)	S.E. Baru et al.	(NOVO)
ALBRECHT	85	ZPHY C28 45	H. Albrecht et al.	(ARGUS Collab.)
ALBRECHT	85E	PL 160B 331	H. Albrecht et al.	(ARGUS Collab.)
GELPHMAN	85	PR D32 2893	D. Gelphman et al.	(Crystal Ball Collab.)
KURAEV	85	SJNP 41 466 Translated from YAF 41 733.	E.A. Kuraev, V.S. Fadin	(NOVO)
NERNST	85	PRL 54 2195	R. Nernst et al.	(Crystal Ball Collab.)
ARTAMONOV	84	PL 137B 272	A.S. Artamonov et al.	(NOVO)
BARBER	84	PL 135B 498	D.P. Barber et al.	
BESSON	84	PR D30 1433	D. Besson et al.	(CLEO Collab.)
FONSECA	84	NP B242 31	V. Fonseca et al.	(CUSB Collab.)
GILES	84B	PR D29 1285	R. Giles et al.	(CLEO Collab.)
HAAS	84	PRL 52 799	J. Haas et al.	(CLEO Collab.)
HAAS	84B	PR D30 1996	J. Haas et al.	(CLEO Collab.)
KLOPFEN...	83	PRL 51 160	C. Klopfenstein et al.	(CUSB Collab.)
ALBRECHT	82	PL 116B 383	H. Albrecht et al.	(DESY, DORT, HEIDH+)
NICZYPORUK	81B	PL 100B 95	B. Niczyporuk et al.	(LENA Collab.)
NICZYPORUK	81C	PL 99B 169	B. Niczyporuk et al.	(LENA Collab.)
BOCK	80	ZPHY C6 125	P. Bock et al.	(HEIDP, MPIM, DESY, HAMB)

$\Upsilon_2(1D)$

$I^G(J^{PC}) = 0^-(2^{--})$

was $\Upsilon(1D)$

First observed by BONVICINI 04 in the decay to $\gamma\gamma\Upsilon(1S)$ and confirmed by DEL-AMO-SANCHEZ 10R in the decay to $\pi^+\pi^-\Upsilon(1S)$. Data consistent with $J^P = 2^-$. The states with $J = 1$ and 3 also possibly seen, but need confirmation.

$\Upsilon_2(1D)$ MASS

VALUE (MeV)	EVTS	DOCUMENT ID		TECN	COMMENT
10163.7±1.4 OUR AVERAGE		Error includes scale factor of 1.7.			
10164.5±0.8±0.5		DEL-AMO-SA...10R		BABR	$\Upsilon(3S) \to \gamma\gamma\pi^+\pi^-\ell^+\ell^-$
10161.1±0.6±1.6	38	BONVICINI	04	CLE3	$\Upsilon(3S) \to 4\gamma\ell^+\ell^-$

$\Upsilon_2(1D)$ DECAY MODES

	Mode	Fraction (Γ_i/Γ)
Γ_1	$\gamma\gamma\Upsilon(1S)$	seen
Γ_2	$\gamma\chi_{bJ}(1P)$	seen
Γ_3	$\eta\Upsilon(1S)$	not seen
Γ_4	$\pi^+\pi^-\Upsilon(1S)$	$(6.6\pm1.6)\times10^{-3}$

$\Upsilon_2(1D)$ BRANCHING RATIOS

$\Gamma(\eta\Upsilon(1S))/\Gamma(\gamma\gamma\Upsilon(1S))$ — Γ_3/Γ_1

VALUE	CL%	DOCUMENT ID		TECN	COMMENT
<0.25	90	BONVICINI	04	CLE3	$\Upsilon(3S) \to 4\gamma\ell^+\ell^-$

$\Gamma(\pi^+\pi^-\Upsilon(1S))/\Gamma_{total}$ — Γ_4/Γ

VALUE (units 10^{-2})	DOCUMENT ID		TECN	COMMENT
$0.66^{+0.15}_{-0.14}\pm0.06$	[1] DEL-AMO-SA...10R		BABR	$\Upsilon(3S) \to \gamma\gamma\pi^+\pi^-\ell^+\ell^-$

[1] Using theoretical predictions for $B(\chi_{bJ}(2P) \to \gamma\Upsilon_2(1D))$.

$\Gamma(\pi^+\pi^-\Upsilon(1S))/\Gamma(\gamma\gamma\Upsilon(1S))$ — Γ_4/Γ_1

VALUE	CL%	DOCUMENT ID		TECN	COMMENT
<1.2	90	[2] BONVICINI	04	CLE3	$\Upsilon(3S) \to 4\gamma\ell^+\ell^-$

[2] Assuming $J = 2$.

$\Upsilon_2(1D)$ REFERENCES

DEL-AMO-SA...	10R	PR D82 111102	P. del Amo Sanchez et al.	(BABAR Collab.)
BONVICINI	04	PR D70 032001	G. Bonvicini et al.	(CLEO Collab.)

$\chi_{b0}(2P)$

$I^G(J^{PC}) = 0^+(0^{++})$

J needs confirmation.

Observed in radiative decay of the $\Upsilon(3S)$, therefore $C = +$. Branching ratio requires E1 transition, M1 is strongly disfavored, therefore $P = +$.

$\chi_{b0}(2P)$ MASS

VALUE (MeV)	DOCUMENT ID
10232.5±0.4±0.5 OUR EVALUATION	From γ energy below, using $\Upsilon(3S)$ mass = 10355.2 ± 0.5 MeV

$m_{\chi_{b1}(2P)} - m_{\chi_{b0}(2P)}$

VALUE (MeV)	DOCUMENT ID		TECN	COMMENT
23.8±1.7	LEES	14M	BABR	$\Upsilon(3S) \to \gamma\gamma\mu^+\mu^-$

γ ENERGY IN $\Upsilon(3S)$ DECAY

VALUE (MeV)	EVTS	DOCUMENT ID		TECN	COMMENT
121.9 ±0.4 OUR EVALUATION		Treating systematic errors as correlated			
122.2 ±0.5 OUR AVERAGE		Error includes scale factor of 1.4. See the ideogram below.			
121.55±0.16±0.46		ARTUSO	05	CLEO	$\Upsilon(3S) \to \gamma X$
123.0 ±0.8	4959	[1] HEINTZ	92	CSB2	$e^+e^- \to \gamma X$
124.6 ±1.4	17	[2] HEINTZ	92	CSB2	$e^+e^- \to \ell^+\ell^-\gamma\gamma$
122.3 ±0.3 ±0.6	9903	MORRISON	91	CLE2	$e^+e^- \to \gamma X$

[1] A systematic uncertainty on the energy scale of 0.9% not included. Supersedes NARAIN 91.

[2] A systematic uncertainty on the energy scale of 0.9% not included. Supersedes HEINTZ 91.

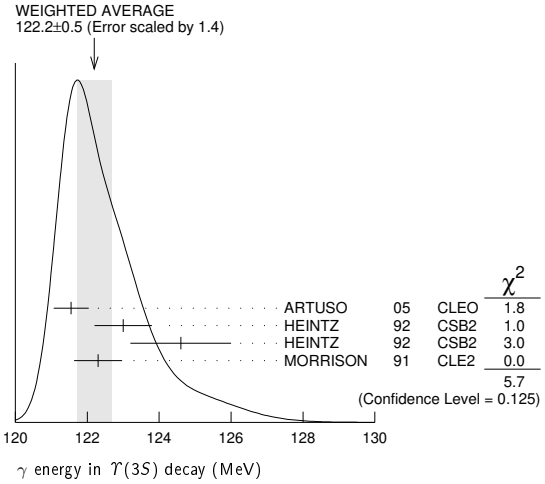

Int. J. Mod. Phys. A 2026.41. Downloaded from www.worldscientific.com by CALIFORNIA @ BERKELEY on 09/16/26. Re-use and distribution is strictly not permitted, except for Open Access articles.

$\chi_{b0}(2P)$ DECAY MODES

	Mode	Fraction (Γ_i/Γ)	Confidence level
Γ_1	$\gamma\,\Upsilon(2S)$	(1.38 ± 0.30) %	
Γ_2	$\omega\,\Upsilon(1S)$	$(5.5\ \pm2.0\ )\times10^{-3}$	
Γ_3	$\gamma\,\Upsilon(1S)$	$(3.8\ \pm1.7\ )\times10^{-3}$	
Γ_4	D^0X	<8.2 %	90%
Γ_5	$\pi^+\pi^-K^+K^-\pi^0$	$<3.4\times10^{-5}$	90%
Γ_6	$2\pi^+\pi^-K^-K^0_S$	$<5\times10^{-5}$	90%
Γ_7	$2\pi^+\pi^-K^-K^0_S2\pi^0$	$<2.2\times10^{-4}$	90%
Γ_8	$2\pi^+2\pi^-2\pi^0$	$<2.4\times10^{-4}$	90%
Γ_9	$2\pi^+2\pi^-K^+K^-$	$<1.5\times10^{-4}$	90%
Γ_{10}	$2\pi^+2\pi^-K^+K^-\pi^0$	$<2.2\times10^{-4}$	90%
Γ_{11}	$2\pi^+2\pi^-K^+K^-2\pi^0$	$<1.1\times10^{-3}$	90%
Γ_{12}	$3\pi^+2\pi^-K^-K^0_S\pi^0$	$<7\times10^{-4}$	90%
Γ_{13}	$3\pi^+3\pi^-$	$<7\times10^{-5}$	90%
Γ_{14}	$3\pi^+3\pi^-2\pi^0$	$<1.2\times10^{-3}$	90%
Γ_{15}	$3\pi^+3\pi^-K^+K^-$	$<1.5\times10^{-4}$	90%
Γ_{16}	$3\pi^+3\pi^-K^+K^-\pi^0$	$<7\times10^{-4}$	90%
Γ_{17}	$4\pi^+4\pi^-$	$<1.7\times10^{-4}$	90%
Γ_{18}	$4\pi^+4\pi^-2\pi^0$	$<6\times10^{-4}$	90%

$\chi_{b0}(2P)$ BRANCHING RATIOS

$\Gamma(\gamma\,\Upsilon(2S))/\Gamma_{total}$ — Γ_1/Γ

VALUE (%)	CL%	DOCUMENT ID		TECN	COMMENT
1.38±0.30 OUR AVERAGE					
$1.31\pm0.27^{+0.13}_{-0.12}$		[3,4] LEES	14M	BABR	$\Upsilon(3S)\to\gamma\gamma\mu^+\mu^-$
$3.6\ \pm1.6\ \pm0.3$		[3,5] HEINTZ	92	CSB2	$e^+e^-\to\ell^+\ell^-\gamma\gamma$
• • • We do not use the following data for averages, fits, limits, etc. • • •					
<2.8	90	[6] LEES	11J	BABR	$\Upsilon(3S)\to X\gamma$
<8.9	90	[7] CRAWFORD	92B	CLE2	$e^+e^-\to\ell^+\ell^-\gamma\gamma$

[3] Assuming $B(\Upsilon(2S)\to\mu^+\mu^-)=(1.93\pm0.17)$%.
[4] LEES 14M reports $[\Gamma(\chi_{b0}(2P)\to\gamma\,\Upsilon(2S))/\Gamma_{total}]\times[B(\Upsilon(3S)\to\gamma\chi_{b0}(2P))]=(7.7\pm1.6)\times10^{-4}$ which we divide by our best (shown rounded) value $B(\Upsilon(3S)\to\gamma\chi_{b0}(2P))=(5.9\pm0.6)\times10^{-2}$. Our first error is their experiment's error and our second error is the systematic error from using our best (shown rounded) value.
[5] Recalculated by us. HEINTZ 92 quotes $B(\Upsilon(3S)\to\gamma\chi_{b0}(2P))\times B(\chi_{b0}(2P)\to\gamma\,\Upsilon(2S))=(0.28\pm0.12\pm0.03)$% using $B(\Upsilon(2S)\to\mu^+\mu^-)=(1.44\pm0.10)$%. Supersedes HEINTZ 91.
[6] LEES 11J quotes a central value of $\Gamma(\chi_{b0}(2P)\to\gamma\,\Upsilon(2S))/\Gamma_{total}\times\Gamma(\Upsilon(3S)\to\gamma\chi_{b0}(2P))/\Gamma_{total}=(-0.3\pm0.2^{+0.5}_{-0.4})$%.
[7] Using $B(\Upsilon(2S)\to\mu^+\mu^-)=(1.37\pm0.26)$%, $B(\Upsilon(3S)\to\gamma\gamma\,\Upsilon(2S))\times2\,B(\Upsilon(2S)\to\mu^+\mu^-)<1.19\times10^{-4}$, and $B(\Upsilon(3S)\to\chi_{b0}(2P)\gamma)=0.049$.

$\Gamma(\omega\,\Upsilon(1S))/\Gamma_{total}$ — Γ_2/Γ

VALUE (%)	EVTS	DOCUMENT ID		TECN	COMMENT
0.55±0.19±0.07	32	[8] STOTTLER	25	BELL	$\Upsilon(3S)\to\gamma\omega\,\Upsilon(1S)$

[8] STOTTLER 25 reports $0.55\pm0.19\pm0.07$ % from a measurement of $[\Gamma(\chi_{b0}(2P)\to\omega\,\Upsilon(1S))/\Gamma_{total}]\times[B(\Upsilon(3S)\to\gamma\chi_{b0}(2P))]$ assuming $B(\Upsilon(3S)\to\gamma\chi_{b0}(2P))=(5.9\pm0.6)\times10^{-2}$.

$\Gamma(\gamma\,\Upsilon(1S))/\Gamma_{total}$ — Γ_3/Γ

VALUE (%)	CL%	DOCUMENT ID		TECN	COMMENT
0.38±0.17 OUR AVERAGE					
$0.36\pm0.17\pm0.03$		[9,10,11] LEES	14M	BABR	$\Upsilon(3S)\to\gamma\gamma\mu^+\mu^-$
$0.9\ \pm0.7\ \pm0.1$		[10,12] HEINTZ	92	CSB2	$e^+e^-\to\ell^+\ell^-\gamma\gamma$
• • • We do not use the following data for averages, fits, limits, etc. • • •					
<1.2	90	[13] LEES	11J	BABR	$\Upsilon(3S)\to X\gamma$
<2.5	90	[14] CRAWFORD	92B	CLE2	$e^+e^-\to\ell^+\ell^-\gamma\gamma$

[9] LEES 14M quotes $\Gamma(\chi_{b0}(2P)\to\gamma\,\Upsilon(1S))/\Gamma_{total}\times\Gamma(\Upsilon(3S)\to\gamma\chi_{b0}(2P))/\Gamma_{total}=(2.1\pm1.0)\times10^{-4}$ combining the results from $\Upsilon(3S)\to\gamma\gamma\mu^+\mu^-$ samples with and without photon conversions.
[10] Assuming $B(\Upsilon(1S)\to\mu^+\mu^-)=(2.48\pm0.05)$%.
[11] LEES 14M reports $[\Gamma(\chi_{b0}(2P)\to\gamma\,\Upsilon(1S))/\Gamma_{total}]\times[B(\Upsilon(3S)\to\gamma\chi_{b0}(2P))]=(2.1\pm1.0)\times10^{-4}$ which we divide by our best (shown rounded) value $B(\Upsilon(3S)\to\gamma\chi_{b0}(2P))=(5.9\pm0.6)\times10^{-2}$. Our first error is their experiment's error and our second error is the systematic error from using our best (shown rounded) value.
[12] Recalculated by us. HEINTZ 92 quotes $B(\Upsilon(3S)\to\gamma\chi_{b0}(2P))\times B(\chi_{b0}(2P)\to\gamma\,\Upsilon(1S))=(0.05\pm0.04\pm0.01)$% using $B(\Upsilon(1S)\to\mu^+\mu^-)=(2.57\pm0.05)$%. Supersedes HEINTZ 91.
[13] LEES 11J quotes a central value of $\Gamma(\chi_{b0}(2P)\to\gamma\,\Upsilon(1S))/\Gamma_{total}\times\Gamma(\Upsilon(3S)\to\gamma\chi_{b0}(2P))/\Gamma_{total}=(3.9\pm2.2^{+1.2}_{-0.6})\times10^{-4}$.
[14] Using $B(\Upsilon(1S)\to\mu^+\mu^-)=(2.57\pm0.07)$%, $B(\Upsilon(3S)\to\gamma\gamma\,\Upsilon(1S))\times2\,B(\Upsilon(1S)\to\mu^+\mu^-)<0.63\times10^{-4}$, and $B(\Upsilon(3S)\to\chi_{b0}(2P)\gamma)=0.049$.

$\Gamma(D^0X)/\Gamma_{total}$ — Γ_4/Γ

VALUE	CL%	DOCUMENT ID		TECN	COMMENT
$\mathbf{<8.2\times10^{-2}}$	90	[15,16] BRIERE	08	CLEO	$\Upsilon(3S)\to\gamma D^0X$

[15] For $p_{D^0}>2.5$ GeV/c.
[16] The authors also present their result as $(4.1\pm3.0\pm0.4)\times10^{-2}$.

$\Gamma(\pi^+\pi^-K^+K^-\pi^0)/\Gamma_{total}$ — Γ_5/Γ

VALUE (units 10^{-4})	CL%	DOCUMENT ID		TECN	COMMENT
<0.34	90	[17] ASNER	08A	CLEO	$\Upsilon(3S)\to\gamma\pi^+\pi^-K^+K^-\pi^0$

[17] ASNER 08A reports $[\Gamma(\chi_{b0}(2P)\to\pi^+\pi^-K^+K^-\pi^0)/\Gamma_{total}]\times[B(\Upsilon(3S)\to\gamma\chi_{b0}(2P))]<2\times10^{-6}$ which we divide by our best (shown rounded) value $B(\Upsilon(3S)\to\gamma\chi_{b0}(2P))=5.9\times10^{-2}$.

$\Gamma(2\pi^+\pi^-K^-K^0_S)/\Gamma_{total}$ — Γ_6/Γ

VALUE (units 10^{-4})	CL%	DOCUMENT ID		TECN	COMMENT
<0.5	90	[18] ASNER	08A	CLEO	$\Upsilon(3S)\to\gamma2\pi^+\pi^-K^-K^0_S$

[18] ASNER 08A reports $[\Gamma(\chi_{b0}(2P)\to2\pi^+\pi^-K^-K^0_S)/\Gamma_{total}]\times[B(\Upsilon(3S)\to\gamma\chi_{b0}(2P))]<3\times10^{-6}$ which we divide by our best (shown rounded) value $B(\Upsilon(3S)\to\gamma\chi_{b0}(2P))=5.9\times10^{-2}$.

$\Gamma(2\pi^+\pi^-K^-K^0_S2\pi^0)/\Gamma_{total}$ — Γ_7/Γ

VALUE (units 10^{-4})	CL%	DOCUMENT ID		TECN	COMMENT
<2.2	90	[19] ASNER	08A	CLEO	$\Upsilon(3S)\to\gamma2\pi^+\pi^-K^-2\pi^0$

[19] ASNER 08A reports $[\Gamma(\chi_{b0}(2P)\to2\pi^+\pi^-K^-K^0_S2\pi^0)/\Gamma_{total}]\times[B(\Upsilon(3S)\to\gamma\chi_{b0}(2P))]<13\times10^{-6}$ which we divide by our best (shown rounded) value $B(\Upsilon(3S)\to\gamma\chi_{b0}(2P))=5.9\times10^{-2}$.

$\Gamma(2\pi^+2\pi^-2\pi^0)/\Gamma_{total}$ — Γ_8/Γ

VALUE (units 10^{-4})	CL%	DOCUMENT ID		TECN	COMMENT
<2.4	90	[20] ASNER	08A	CLEO	$\Upsilon(3S)\to\gamma2\pi^+2\pi^-2\pi^0$

[20] ASNER 08A reports $[\Gamma(\chi_{b0}(2P)\to2\pi^+2\pi^-2\pi^0)/\Gamma_{total}]\times[B(\Upsilon(3S)\to\gamma\chi_{b0}(2P))]<14\times10^{-6}$ which we divide by our best (shown rounded) value $B(\Upsilon(3S)\to\gamma\chi_{b0}(2P))=5.9\times10^{-2}$.

$\Gamma(2\pi^+2\pi^-K^+K^-)/\Gamma_{total}$ — Γ_9/Γ

VALUE (units 10^{-4})	CL%	DOCUMENT ID		TECN	COMMENT
<1.5	90	[21] ASNER	08A	CLEO	$\Upsilon(3S)\to\gamma2\pi^+2\pi^-K^+K^-$

[21] ASNER 08A reports $[\Gamma(\chi_{b0}(2P)\to2\pi^+2\pi^-K^+K^-)/\Gamma_{total}]\times[B(\Upsilon(3S)\to\gamma\chi_{b0}(2P))]<9\times10^{-6}$ which we divide by our best (shown rounded) value $B(\Upsilon(3S)\to\gamma\chi_{b0}(2P))=5.9\times10^{-2}$.

$\Gamma(2\pi^+2\pi^-K^+K^-\pi^0)/\Gamma_{total}$ — Γ_{10}/Γ

VALUE (units 10^{-4})	CL%	DOCUMENT ID		TECN	COMMENT
<2.2	90	[22] ASNER	08A	CLEO	$\Upsilon(3S)\to\gamma2\pi^+2\pi^-K^+K^-\pi^0$

[22] ASNER 08A reports $[\Gamma(\chi_{b0}(2P)\to2\pi^+2\pi^-K^+K^-\pi^0)/\Gamma_{total}]\times[B(\Upsilon(3S)\to\gamma\chi_{b0}(2P))]<13\times10^{-6}$ which we divide by our best (shown rounded) value $B(\Upsilon(3S)\to\gamma\chi_{b0}(2P))=5.9\times10^{-2}$.

$\Gamma(2\pi^+2\pi^-K^+K^-2\pi^0)/\Gamma_{total}$ — Γ_{11}/Γ

VALUE (units 10^{-4})	CL%	DOCUMENT ID		TECN	COMMENT
<11	90	[23] ASNER	08A	CLEO	$\Upsilon(3S)\to\gamma2\pi^+2\pi^-K^+K^-2\pi^0$

[23] ASNER 08A reports $[\Gamma(\chi_{b0}(2P)\to2\pi^+2\pi^-K^+K^-2\pi^0)/\Gamma_{total}]\times[B(\Upsilon(3S)\to\gamma\chi_{b0}(2P))]<63\times10^{-6}$ which we divide by our best (shown rounded) value $B(\Upsilon(3S)\to\gamma\chi_{b0}(2P))=5.9\times10^{-2}$.

$\Gamma(3\pi^+2\pi^-K^-K^0_S\pi^0)/\Gamma_{total}$ — Γ_{12}/Γ

VALUE (units 10^{-4})	CL%	DOCUMENT ID		TECN	COMMENT
<7	90	[24] ASNER	08A	CLEO	$\Upsilon(3S)\to\gamma3\pi^+2\pi^-K^-K^0_S\pi^0$

[24] ASNER 08A reports $[\Gamma(\chi_{b0}(2P)\to3\pi^+2\pi^-K^-K^0_S\pi^0)/\Gamma_{total}]\times[B(\Upsilon(3S)\to\gamma\chi_{b0}(2P))]<39\times10^{-6}$ which we divide by our best (shown rounded) value $B(\Upsilon(3S)\to\gamma\chi_{b0}(2P))=5.9\times10^{-2}$.

$\Gamma(3\pi^+3\pi^-)/\Gamma_{total}$ — Γ_{13}/Γ

VALUE (units 10^{-4})	CL%	DOCUMENT ID		TECN	COMMENT
<0.7	90	[25] ASNER	08A	CLEO	$\Upsilon(3S)\to\gamma3\pi^+3\pi^-$

[25] ASNER 08A reports $[\Gamma(\chi_{b0}(2P)\to3\pi^+3\pi^-)/\Gamma_{total}]\times[B(\Upsilon(3S)\to\gamma\chi_{b0}(2P))]<4\times10^{-6}$ which we divide by our best (shown rounded) value $B(\Upsilon(3S)\to\gamma\chi_{b0}(2P))=5.9\times10^{-2}$.

$\Gamma(3\pi^+3\pi^-2\pi^0)/\Gamma_{total}$ — Γ_{14}/Γ

VALUE (units 10^{-4})	CL%	DOCUMENT ID		TECN	COMMENT
<12	90	[26] ASNER	08A	CLEO	$\Upsilon(3S)\to\gamma3\pi^+3\pi^-2\pi^0$

[26] ASNER 08A reports $[\Gamma(\chi_{b0}(2P)\to3\pi^+3\pi^-2\pi^0)/\Gamma_{total}]\times[B(\Upsilon(3S)\to\gamma\chi_{b0}(2P))]<72\times10^{-6}$ which we divide by our best (shown rounded) value $B(\Upsilon(3S)\to\gamma\chi_{b0}(2P))=5.9\times10^{-2}$.

$\Gamma(3\pi^+3\pi^-K^+K^-)/\Gamma_{total}$ — Γ_{15}/Γ

VALUE (units 10^{-4})	CL%	DOCUMENT ID		TECN	COMMENT
<1.5	90	[27] ASNER	08A	CLEO	$\Upsilon(3S)\to\gamma3\pi^+3\pi^-K^+K^-$

[27] ASNER 08A reports $[\Gamma(\chi_{b0}(2P)\to3\pi^+3\pi^-K^+K^-)/\Gamma_{total}]\times[B(\Upsilon(3S)\to\gamma\chi_{b0}(2P))]<9\times10^{-6}$ which we divide by our best (shown rounded) value $B(\Upsilon(3S)\to\gamma\chi_{b0}(2P))=5.9\times10^{-2}$.

Int. J. Mod. Phys. A 2026.41. Downloaded from www.worldscientific.com
by UNIVERSITY OF CALIFORNIA @ BERKELEY on 09/16/26. Re-use and distribution is strictly not permitted, except for Open Access articles.

$\Gamma(3\pi^+3\pi^-K^+K^-\pi^0)/\Gamma_{total}$ — Γ_{16}/Γ

VALUE (units 10^{-4})	CL%	DOCUMENT ID		TECN	COMMENT
<7	90	[28] ASNER	08A	CLEO	$\Upsilon(3S) \to \gamma 3\pi^+3\pi^-K^+K^-\pi^0$

[28] ASNER 08A reports $[\Gamma(\chi_{b0}(2P) \to 3\pi^+3\pi^-K^+K^-\pi^0)/\Gamma_{total}] \times [B(\Upsilon(3S) \to \gamma\chi_{b0}(2P))] < 43 \times 10^{-6}$ which we divide by our best (shown rounded) value $B(\Upsilon(3S) \to \gamma\chi_{b0}(2P)) = 5.9 \times 10^{-2}$.

$\Gamma(4\pi^+4\pi^-)/\Gamma_{total}$ — Γ_{17}/Γ

VALUE (units 10^{-4})	CL%	DOCUMENT ID		TECN	COMMENT
<1.7	90	[29] ASNER	08A	CLEO	$\Upsilon(3S) \to \gamma 4\pi^+4\pi^-$

[29] ASNER 08A reports $[\Gamma(\chi_{b0}(2P) \to 4\pi^+4\pi^-)/\Gamma_{total}] \times [B(\Upsilon(3S) \to \gamma\chi_{b0}(2P))] < 10 \times 10^{-6}$ which we divide by our best (shown rounded) value $B(\Upsilon(3S) \to \gamma\chi_{b0}(2P)) = 5.9 \times 10^{-2}$.

$\Gamma(4\pi^+4\pi^-2\pi^0)/\Gamma_{total}$ — Γ_{18}/Γ

VALUE (units 10^{-4})	CL%	DOCUMENT ID		TECN	COMMENT
<6	90	[30] ASNER	08A	CLEO	$\Upsilon(3S) \to \gamma 4\pi^+4\pi^-2\pi^0$

[30] ASNER 08A reports $[\Gamma(\chi_{b0}(2P) \to 4\pi^+4\pi^-2\pi^0)/\Gamma_{total}] \times [B(\Upsilon(3S) \to \gamma\chi_{b0}(2P))] < 38 \times 10^{-6}$ which we divide by our best (shown rounded) value $B(\Upsilon(3S) \to \gamma\chi_{b0}(2P)) = 5.9 \times 10^{-2}$.

$\Gamma(\chi_{b0}(2P) \to \gamma\Upsilon(1S))/\Gamma_{total} \times \Gamma(\Upsilon(3S) \to \gamma\chi_{b0}(2P))/\Gamma_{total}$ — $\Gamma_3/\Gamma \times \Gamma_{22}^{\Upsilon(3S)}/\Gamma^{\Upsilon(3S)}$

VALUE (units 10^{-4})	CL%	DOCUMENT ID		TECN	COMMENT
<8.2	90	[31] LEES	11J	BABR	$\Upsilon(3S) \to X\gamma$

[31] LEES 11J quotes a central value of $\Gamma(\chi_{b0}(2P) \to \gamma\Upsilon(1S))/\Gamma_{total} \times \Gamma(\Upsilon(3S) \to \gamma\chi_{b0}(2P))/\Gamma_{total} = (3.9 \pm 2.2^{+1.2}_{-0.6}) \times 10^{-4}$ and derives a 90% CL upper limit of $B(\chi_{b0}(2P) \to \gamma\Upsilon(1S)) < 1.2\%$ using $B(\Upsilon(3S) \to \gamma\chi_{b0}(2P)) = (5.9 \pm 0.6)\%$.

$B(\chi_{b0}(2P) \to \gamma\Upsilon(1S)) \times B(\Upsilon(3S) \to \gamma\chi_{b0}(2P)) \times B(\Upsilon(1S) \to \ell^+\ell^-)$

VALUE (units 10^{-5})	DOCUMENT ID		TECN	COMMENT
1.4±0.9 OUR AVERAGE				
$1.7^{+1.5}_{-1.4}{}^{+0.1}_{-1.2}$	[32] LEES	14M	BABR	$\Upsilon(3S) \to \gamma\gamma\mu^+\mu^-$
1.3±1.0±0.3	[33] HEINTZ	92	CSB2	$\Upsilon(3S) \to \gamma\gamma\ell^+\ell^-$

[32] From a sample of $\Upsilon(3S) \to \gamma\gamma\mu^+\mu^-$ with one converted photon.

[33] Calculated by us. HEINTZ 92 quotes $B(\Upsilon(3S) \to \gamma\chi_{b0}(2P)) \times B(\chi_{b0}(2P) \to \gamma\Upsilon(1S)) = (0.05 \pm 0.04 \pm 0.01)\%$ using $B(\Upsilon(1S) \to \mu^+\mu^-) = (2.57 \pm 0.05)\%$.

$[B(\chi_{b0}(2P) \to \gamma\Upsilon(1S)) \times B(\Upsilon(3S) \to \gamma\chi_{b0}(2P))] / [B(\chi_{b1}(2P) \to \gamma\Upsilon(1S)) \times B(\Upsilon(3S) \to \gamma\chi_{b1}(2P))]$

VALUE (%)	DOCUMENT ID		TECN	COMMENT
1.71±0.80	[34] LEES	14M	BABR	$\Upsilon(3S) \to \gamma\gamma\mu^+\mu^-$

[34] From a sample of $\Upsilon(3S) \to \gamma\gamma\mu^+\mu^-$ without converted photons.

$\Gamma(\chi_{b0}(2P) \to \gamma\Upsilon(2S))/\Gamma_{total} \times \Gamma(\Upsilon(3S) \to \gamma\chi_{b0}(2P))/\Gamma_{total}$ — $\Gamma_1/\Gamma \times \Gamma_{22}^{\Upsilon(3S)}/\Gamma^{\Upsilon(3S)}$

VALUE (units 10^{-3})	CL%	DOCUMENT ID		TECN	COMMENT
<1.6	90	[35] LEES	11J	BABR	$\Upsilon(3S) \to X\gamma$

[35] LEES 11J quotes a central value of $\Gamma(\chi_{b0}(2P) \to \gamma\Upsilon(2S))/\Gamma_{total} \times \Gamma(\Upsilon(3S) \to \gamma\chi_{b0}(2P))/\Gamma_{total} = (-0.3 \pm 0.2^{+0.5}_{-0.4})\%$ and derives a 90% CL upper limit of $B(\chi_{b0}(2P) \to \gamma\Upsilon(2S)) < 2.8\%$ using $B(\Upsilon(3S) \to \gamma\chi_{b0}(2P)) = (5.9 \pm 0.6)\%$.

$B(\chi_{b0}(2P) \to \gamma\Upsilon(2S)) \times B(\Upsilon(3S) \to \gamma\chi_{b0}(2P)) \times B(\Upsilon(2S) \to \ell^+\ell^-)$

VALUE (units 10^{-5})	DOCUMENT ID		TECN	COMMENT
4.4±1.6 OUR AVERAGE				
$6.6^{+4.9}_{-4.0}{}^{+2.0}_{-0.3}$	[36] LEES	14M	BABR	$\Upsilon(3S) \to \gamma\gamma\mu^+\mu^-$
4.0±1.7±0.3	[37] HEINTZ	92	CSB2	$\Upsilon(3S) \to \gamma\gamma\ell^+\ell^-$

[36] From a sample of $\Upsilon(3S) \to \gamma\gamma\mu^+\mu^-$ with one converted photon.

[37] Calculated by us. HEINTZ 92 quotes $B(\Upsilon(3S) \to \gamma\chi_{b0}(2P)) \times B(\chi_{b0}(2P) \to \gamma\Upsilon(2S)) = (0.28 \pm 0.12 \pm 0.03)\%$ using $B(\Upsilon(2S) \to \mu^+\mu^-) = (1.44 \pm 0.10)\%$.

$[B(\chi_{b0}(2P) \to \gamma\Upsilon(2S)) \times B(\Upsilon(3S) \to \gamma\chi_{b0}(2P))] / [B(\chi_{b1}(2P) \to \gamma\Upsilon(2S)) \times B(\Upsilon(3S) \to \gamma\chi_{b1}(2P))]$

VALUE (%)	DOCUMENT ID		TECN	COMMENT
3.31±0.56	[38] LEES	14M	BABR	$\Upsilon(3S) \to \gamma\gamma\mu^+\mu^-$

[38] From a sample of $\Upsilon(3S) \to \gamma\gamma\mu^+\mu^-$ without converted photons.

$\chi_{b0}(2P)$ REFERENCES

STOTTLER	25	PRL 135 121902	Z.S. Stottler *et al.*	(BELLE Collab.)
LEES	14M	PR D90 112010	J.P. Lees *et al.*	(BABAR Collab.)
LEES	11J	PR D84 072002	J.P. Lees *et al.*	(BABAR Collab.)
ASNER	08A	PR D78 091103	D.M. Asner *et al.*	(CLEO Collab.)
BRIERE	08	PR D78 092007	R.A. Briere *et al.*	(CLEO Collab.)
ARTUSO	05	PRL 94 032001	M. Artuso *et al.*	(CLEO Collab.)
CRAWFORD	92B	PL B294 139	G. Crawford *et al.*	(CLEO Collab.)
HEINTZ	92	PR D46 1928	U. Heintz *et al.*	(CUSB II Collab.)
HEINTZ	91	PRL 66 1563	U. Heintz *et al.*	(CUSB Collab.)
MORRISON	91	PRL 67 1696	R.J. Morrison *et al.*	(CLEO Collab.)
NARAIN	91	PRL 66 3113	M. Narain *et al.*	(CUSB Collab.)

$\chi_{b1}(2P)$

$I^G(J^{PC}) = 0^+(1^{++})$
J needs confirmation.

Observed in radiative decay of the $\Upsilon(3S)$, therefore $C = +$. Branching ratio requires E1 transition, M1 is strongly disfavored, therefore $P = +$.

$\chi_{b1}(2P)$ MASS

VALUE (MeV)	DOCUMENT ID
10255.46±0.22±0.50 OUR EVALUATION	From γ energy below, using $\Upsilon(3S)$ mass = 10355.2 ± 0.5 MeV

$m_{\chi_{b1}(2P)} - m_{\chi_{b0}(2P)}$

VALUE (MeV)	DOCUMENT ID		TECN	COMMENT
23.5±0.7±0.7	[1] HEINTZ	92	CSB2	$e^+e^- \to \gamma X, \ell^+\ell^-\gamma\gamma$

[1] From the average photon energy for inclusive and exclusive events. Supersedes NARAIN 91.

$m_{\chi_{b1}(2P)} - m_{\Upsilon(1S)}$

VALUE (MeV)	EVTS	DOCUMENT ID		TECN	COMMENT
793.57±0.75±0.22	50	[2] AAIJ	24AC	LHCB	$\chi_{b1}(2P) \to \Upsilon(1S)\mu^+\mu^-$

[2] Observed in prompt pp production.

γ ENERGY IN $\Upsilon(3S)$ DECAY

VALUE (MeV)	EVTS	DOCUMENT ID		TECN	COMMENT
99.26±0.22 OUR EVALUATION		Treating systematic errors as correlated			
99.53±0.23 OUR AVERAGE		Error includes scale factor of 1.3. See the ideogram below.			
99.15±0.07±0.25		ARTUSO	05	CLEO	$\Upsilon(3S) \to \gamma X$
99 ±1	169	CRAWFORD	92B	CLE2	$e^+e^- \to \ell^+\ell^-\gamma\gamma$
100.1 ±0.4	11147	[3] HEINTZ	92	CSB2	$e^+e^- \to \gamma X$
100.2 ±0.5	223	[4] HEINTZ	92	CSB2	$e^+e^- \to \ell^+\ell^-\gamma\gamma$
99.5 ±0.1 ±0.5	25759	MORRISON	91	CLE2	$e^+e^- \to \gamma X$

[3] A systematic uncertainty on the energy scale of 0.9% not included. Supersedes NARAIN 91.

[4] A systematic uncertainty on the energy scale of 0.9% not included. Supersedes HEINTZ 91.

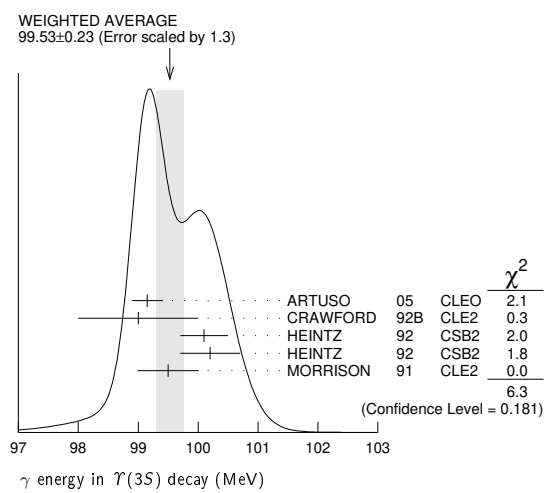

$\chi_{b1}(2P)$ DECAY MODES

	Mode	Fraction (Γ_i/Γ)	Scale factor
Γ_1	$\omega\Upsilon(1S)$	(2.1±0.4) %	1.6
Γ_2	$\gamma\Upsilon(2S)$	(18.1±1.9) %	
Γ_3	$\gamma\Upsilon(1S)$	(9.9±1.0) %	
Γ_4	$\pi\pi\chi_{b1}(1P)$	$(9.1\pm1.3) \times 10^{-3}$	
Γ_5	D^0X	(8.8±1.7) %	
Γ_6	$\pi^+\pi^-K^+K^-\pi^0$	$(3.1\pm1.0) \times 10^{-4}$	
Γ_7	$2\pi^+\pi^-K^-K^0_S$	$(1.1\pm0.5) \times 10^{-4}$	
Γ_8	$2\pi^+\pi^-K^-K^0_S2\pi^0$	$(7.7\pm3.2) \times 10^{-4}$	
Γ_9	$2\pi^+2\pi^-2\pi^0$	$(5.9\pm2.0) \times 10^{-4}$	
Γ_{10}	$2\pi^+2\pi^-K^+K^-$	$(10 \pm4) \times 10^{-5}$	
Γ_{11}	$2\pi^+2\pi^-K^+K^-\pi^0$	$(5.5\pm1.8) \times 10^{-4}$	
Γ_{12}	$2\pi^+2\pi^-K^+K^-2\pi^0$	$(10 \pm4) \times 10^{-4}$	
Γ_{13}	$3\pi^+2\pi^-K^-K^0_S\pi^0$	$(6.7\pm2.6) \times 10^{-4}$	
Γ_{14}	$3\pi^+3\pi^-$	$(1.2\pm0.4) \times 10^{-4}$	
Γ_{15}	$3\pi^+3\pi^-2\pi^0$	$(1.2\pm0.4) \times 10^{-3}$	
Γ_{16}	$3\pi^+3\pi^-K^+K^-$	$(2.0\pm0.8) \times 10^{-4}$	

Γ_{17}	$3\pi^+3\pi^-K^+K^-\pi^0$	$(6.1\pm2.2)\times10^{-4}$
Γ_{18}	$4\pi^+4\pi^-$	$(1.7\pm0.6)\times10^{-4}$
Γ_{19}	$4\pi^+4\pi^-2\pi^0$	$(1.9\pm0.7)\times10^{-3}$

$\chi_{b1}(2P)$ BRANCHING RATIOS

$\Gamma(\omega\Upsilon(1S))/\Gamma_{total}$ — Γ_1/Γ

VALUE (units 10^{-2})	EVTS	DOCUMENT ID		TECN	COMMENT
2.1 ±0.4 OUR AVERAGE Error includes scale factor of 1.6.					
$2.39^{+0.20}_{-0.19}\pm0.24$	304	[5] STOTTLER	25	BELL	$\Upsilon(3S)\to\gamma\omega\Upsilon(1S)$
$1.46^{+0.34}_{-0.30}\pm0.13$	$32.6^{+6.9}_{-6.1}$	[6] CRONIN-HEN.	04	CLE3	$\Upsilon(3S)\to\gamma\omega\Upsilon(1S)$

[5] STOTTLER 25 reports $(2.39^{+0.20}_{-0.19}\pm0.24)\times10^{-2}$ from a measurement of $[\Gamma(\chi_{b1}(2P)\to\omega\Upsilon(1S))/\Gamma_{total}]\times[B(\Upsilon(3S)\to\gamma\chi_{b1}(2P))]$ assuming $B(\Upsilon(3S)\to\gamma\chi_{b1}(2P))=(12.6\pm1.2)\times10^{-2}$.

[6] CRONIN-HENNESSY 04 reports $(1.63^{+0.35+0.16}_{-0.31-0.15})\times10^{-2}$ from a measurement of $[\Gamma(\chi_{b1}(2P)\to\omega\Upsilon(1S))/\Gamma_{total}]\times[B(\Upsilon(3S)\to\gamma\chi_{b1}(2P))]$ assuming $B(\Upsilon(3S)\to\gamma\chi_{b1}(2P))=(11.3\pm0.6)\times10^{-2}$, which we rescale to our best (shown rounded) value $B(\Upsilon(3S)\to\gamma\chi_{b1}(2P))=(12.6\pm1.2)\times10^{-2}$. Our first error is their experiment's error and our second error is the systematic error from using our best (shown rounded) value.

$\Gamma(\gamma\Upsilon(2S))/\Gamma_{total}$ — Γ_2/Γ

VALUE	EVTS	DOCUMENT ID		TECN	COMMENT
0.181±0.019 OUR AVERAGE					
$0.211\pm0.017\pm0.019$		[7,8,9] LEES	14M	BABR	$\Upsilon(3S)\to\gamma\gamma\mu^+\mu^-$
$0.190\pm0.018\pm0.017$	4.3k	[10] LEES	11J	BABR	$\Upsilon(3S)\to X\gamma$
$0.206\pm0.035\pm0.019$		[7,11] CRAWFORD	92B	CLE2	$e^+e^-\to\ell^+\ell^-\gamma\gamma$
$0.132\pm0.018\pm0.012$		[7,12] HEINTZ	92	CSB2	$e^+e^-\to\ell^+\ell^-\gamma\gamma$

[7] Assuming $B(\Upsilon(2S)\to\mu^+\mu^-)=(1.93\pm0.17)\%$.

[8] LEES 14M quotes $\Gamma(\chi_{b1}(2P)\to\gamma\Upsilon(2S))/\Gamma_{total}\times\Gamma(\Upsilon(3S)\to\gamma\chi_{b1}(2P))/\Gamma_{total}=(2.66\pm0.22)\%$ combining the results from $\Upsilon(3S)\to\gamma\gamma\mu^+\mu^-$ samples with and without photon conversions.

[9] LEES 14M reports $[\Gamma(\chi_{b1}(2P)\to\gamma\Upsilon(2S))/\Gamma_{total}]\times[B(\Upsilon(3S)\to\gamma\chi_{b1}(2P))]=(2.66\pm0.22)\times10^{-2}$ which we divide by our best (shown rounded) value $B(\Upsilon(3S)\to\gamma\chi_{b1}(2P))=(12.6\pm1.2)\times10^{-2}$. Our first error is their experiment's error and our second error is the systematic error from using our best (shown rounded) value.

[10] LEES 11J reports $[\Gamma(\chi_{b1}(2P)\to\gamma\Upsilon(2S))/\Gamma_{total}]\times[B(\Upsilon(3S)\to\gamma\chi_{b1}(2P))]=(2.4\pm0.1\pm0.2)\times10^{-2}$ which we divide by our best (shown rounded) value $B(\Upsilon(3S)\to\gamma\chi_{b1}(2P))=(12.6\pm1.2)\times10^{-2}$. Our first error is their experiment's error and our second error is the systematic error from using our best (shown rounded) value.

[11] CRAWFORD 92B quotes $B(\Upsilon(3S)\to\gamma\chi_{b1}(2P))\times B(\chi_{b1}(2P)\to\gamma\Upsilon(2S))\times2\,B(\Upsilon(2S)\to\ell^+\ell^-)=(10.23\pm1.20\pm1.26)\,10^{-4}$.

[12] Recalculated by us. HEINTZ 92 quotes $B(\Upsilon(3S)\to\gamma\chi_{b1}(2P))\times B(\chi_{b1}(2P)\to\gamma\Upsilon(2S))=(2.29\pm0.23\pm0.21)$ % using $B(\Upsilon(2S)\to\mu^+\mu^-)=(1.44\pm0.10)\%$. Supersedes HEINTZ 91.

$\Gamma(\gamma\Upsilon(1S))/\Gamma_{total}$ — Γ_3/Γ

VALUE	EVTS	DOCUMENT ID		TECN	COMMENT
0.099±0.010 OUR AVERAGE					
$0.107\pm0.006\pm0.010$		[13,14,15] LEES	14M	BABR	$\Upsilon(3S)\to\gamma\gamma\mu^+\mu^-$
$0.098\pm0.005\pm0.009$	15k	[16] LEES	11J	BABR	$\Upsilon(3S)\to X\gamma$
$0.103\pm0.023\pm0.009$		[13,17] CRAWFORD	92B	CLE2	$e^+e^-\to\ell^+\ell^-\gamma\gamma$
$0.075\pm0.010\pm0.007$		[13,18] HEINTZ	92	CSB2	$e^+e^-\to\ell^+\ell^-\gamma\gamma$

[13] Assuming $B(\Upsilon(1S)\to\mu^+\mu^-)=(2.48\pm0.05)\%$.

[14] LEES 14M quotes $\Gamma(\chi_{b1}(2P)\to\gamma\Upsilon(1S))/\Gamma_{total}\times\Gamma(\Upsilon(3S)\to\gamma\chi_{b1}(2P))/\Gamma_{total}=(13.48\pm0.72)\times10^{-3}$ combining the results from samples of $\Upsilon(3S)\to\gamma\gamma\mu^+\mu^-$ with and without converted photons.

[15] LEES 14M reports $[\Gamma(\chi_{b1}(2P)\to\gamma\Upsilon(1S))/\Gamma_{total}]\times[B(\Upsilon(3S)\to\gamma\chi_{b1}(2P))]=(13.48\pm0.72)\times10^{-3}$ which we divide by our best (shown rounded) value $B(\Upsilon(3S)\to\gamma\chi_{b1}(2P))=(12.6\pm1.2)\times10^{-2}$. Our first error is their experiment's error and our second error is the systematic error from using our best (shown rounded) value.

[16] LEES 11J reports $[\Gamma(\chi_{b1}(2P)\to\gamma\Upsilon(1S))/\Gamma_{total}]\times[B(\Upsilon(3S)\to\gamma\chi_{b1}(2P))]=(12.4\pm0.3\pm0.6)\times10^{-3}$ which we divide by our best (shown rounded) value $B(\Upsilon(3S)\to\gamma\chi_{b1}(2P))=(12.6\pm1.2)\times10^{-2}$. Our first error is their experiment's error and our second error is the systematic error from using our best (shown rounded) value.

[17] CRAWFORD 92B quotes $B(\Upsilon(3S)\to\gamma\chi_{b1}(2P))\times B(\chi_{b1}(2P)\to\gamma\Upsilon(1S))\times2\,B(\Upsilon(1S)\to\ell^+\ell^-)=(6.47\pm1.12\pm0.82)\,10^{-4}$.

[18] Recalculated by us. HEINTZ 92 quotes $B(\Upsilon(3S)\to\gamma\chi_{b1}(2P))\times B(\chi_{b1}(2P)\to\gamma\Upsilon(1S))=(0.91\pm0.11\pm0.06)\%$ using $B(\Upsilon(1S)\to\mu^+\mu^-)=(2.57\pm0.05)\%$. Supersedes HEINTZ 91.

$\Gamma(\pi\pi\chi_{b1}(1P))/\Gamma_{total}$ — Γ_4/Γ

VALUE (units 10^{-3})	EVTS	DOCUMENT ID		TECN	COMMENT
9.1±1.3 OUR AVERAGE					
$9.2\pm1.1\pm0.8$	31k	[19] LEES	11C	BABR	$e^+e^-\to\pi^+\pi^-X$
$8.6\pm2.3\pm2.1$		[20] CAWLFIELD	06	CLE3	$\Upsilon(3S)\to2(\gamma\pi\ell)$

[19] LEES 11C measures $B(\Upsilon(3S)\to\chi_{b1}(2P)X)\times B(\chi_{b1}(2P)\to\chi_{b1}(1P)\pi^+\pi^-)=(1.16\pm0.07\pm0.12)\times10^{-3}$. We derive the value assuming $B(\Upsilon(3S)\to\chi_{b1}(2P)X)=B(\Upsilon(3S)\to\chi_{b1}(2P)\gamma)=(12.6\pm1.2)\times10^{-2}$.

[20] CAWLFIELD 06 quote $\Gamma(\chi_b(2P)\to\pi\pi\chi_b(1P))=0.83\pm0.22\pm0.08\pm0.19$ keV assuming l-spin conservation, no D-wave contribution, $\Gamma(\chi_{b1}(2P))=96\pm16$keV, and $\Gamma(\chi_{b2}(2P))=138\pm19$ keV.

$\Gamma(D^0X)/\Gamma_{total}$ — Γ_5/Γ

VALUE (units 10^{-2})	EVTS	DOCUMENT ID		TECN	COMMENT
8.8±1.5±0.8	2243	[21] BRIERE	08	CLEO	$\Upsilon(3S)\to\gamma D^0X$

[21] For $p_{D^0}>2.5$ GeV/c.

$\Gamma(\pi^+\pi^-K^+K^-\pi^0)/\Gamma_{total}$ — Γ_6/Γ

VALUE (units 10^{-4})	EVTS	DOCUMENT ID		TECN	COMMENT
3.1±1.0±0.3	30	[22] ASNER	08A	CLEO	$\Upsilon(3S)\to\gamma\pi^+\pi^-K^+K^-\pi^0$

[22] ASNER 08A reports $[\Gamma(\chi_{b1}(2P)\to\pi^+\pi^-K^+K^-\pi^0)/\Gamma_{total}]\times[B(\Upsilon(3S)\to\gamma\chi_{b1}(2P))]=(39\pm8\pm9)\times10^{-6}$ which we divide by our best (shown rounded) value $B(\Upsilon(3S)\to\gamma\chi_{b1}(2P))=(12.6\pm1.2)\times10^{-2}$. Our first error is their experiment's error and our second error is the systematic error from using our best (shown rounded) value.

$\Gamma(2\pi^+\pi^-K^-K^0_S)/\Gamma_{total}$ — Γ_7/Γ

VALUE (units 10^{-4})	EVTS	DOCUMENT ID		TECN	COMMENT
1.1±0.5±0.1	10	[23] ASNER	08A	CLEO	$\Upsilon(3S)\to\gamma2\pi^+\pi^-K^-K^0_S$

[23] ASNER 08A reports $[\Gamma(\chi_{b1}(2P)\to2\pi^+\pi^-K^-K^0_S)/\Gamma_{total}]\times[B(\Upsilon(3S)\to\gamma\chi_{b1}(2P))]=(14\pm5\pm3)\times10^{-6}$ which we divide by our best (shown rounded) value $B(\Upsilon(3S)\to\gamma\chi_{b1}(2P))=(12.6\pm1.2)\times10^{-2}$. Our first error is their experiment's error and our second error is the systematic error from using our best (shown rounded) value.

$\Gamma(2\pi^+\pi^-K^-K^0_S2\pi^0)/\Gamma_{total}$ — Γ_8/Γ

VALUE (units 10^{-4})	EVTS	DOCUMENT ID		TECN	COMMENT
7.7±3.1±0.7	15	[24] ASNER	08A	CLEO	$\Upsilon(3S)\to\gamma2\pi^+\pi^-K^-2\pi^0$

[24] ASNER 08A reports $[\Gamma(\chi_{b1}(2P)\to2\pi^+\pi^-K^-K^0_S2\pi^0)/\Gamma_{total}]\times[B(\Upsilon(3S)\to\gamma\chi_{b1}(2P))]=(97\pm30\pm26)\times10^{-6}$ which we divide by our best (shown rounded) value $B(\Upsilon(3S)\to\gamma\chi_{b1}(2P))=(12.6\pm1.2)\times10^{-2}$. Our first error is their experiment's error and our second error is the systematic error from using our best (shown rounded) value.

$\Gamma(2\pi^+2\pi^-2\pi^0)/\Gamma_{total}$ — Γ_9/Γ

VALUE (units 10^{-4})	EVTS	DOCUMENT ID		TECN	COMMENT
5.9±2.0±0.5	36	[25] ASNER	08A	CLEO	$\Upsilon(3S)\to\gamma2\pi^+2\pi^-2\pi^0$

[25] ASNER 08A reports $[\Gamma(\chi_{b1}(2P)\to2\pi^+2\pi^-2\pi^0)/\Gamma_{total}]\times[B(\Upsilon(3S)\to\gamma\chi_{b1}(2P))]=(74\pm16\pm19)\times10^{-6}$ which we divide by our best (shown rounded) value $B(\Upsilon(3S)\to\gamma\chi_{b1}(2P))=(12.6\pm1.2)\times10^{-2}$. Our first error is their experiment's error and our second error is the systematic error from using our best (shown rounded) value.

$\Gamma(2\pi^+2\pi^-K^+K^-)/\Gamma_{total}$ — Γ_{10}/Γ

VALUE (units 10^{-4})	EVTS	DOCUMENT ID		TECN	COMMENT
1.0±0.4±0.1	12	[26] ASNER	08A	CLEO	$\Upsilon(3S)\to\gamma2\pi^+2\pi^-K^+K^-$

[26] ASNER 08A reports $[\Gamma(\chi_{b1}(2P)\to2\pi^+2\pi^-K^+K^-)/\Gamma_{total}]\times[B(\Upsilon(3S)\to\gamma\chi_{b1}(2P))]=(12\pm4\pm3)\times10^{-6}$ which we divide by our best (shown rounded) value $B(\Upsilon(3S)\to\gamma\chi_{b1}(2P))=(12.6\pm1.2)\times10^{-2}$. Our first error is their experiment's error and our second error is the systematic error from using our best (shown rounded) value.

$\Gamma(2\pi^+2\pi^-K^+K^-\pi^0)/\Gamma_{total}$ — Γ_{11}/Γ

VALUE (units 10^{-4})	EVTS	DOCUMENT ID		TECN	COMMENT
5.5±1.7±0.5	38	[27] ASNER	08A	CLEO	$\Upsilon(3S)\to\gamma2\pi^+2\pi^-K^+K^-\pi^0$

[27] ASNER 08A reports $[\Gamma(\chi_{b1}(2P)\to2\pi^+2\pi^-K^+K^-\pi^0)/\Gamma_{total}]\times[B(\Upsilon(3S)\to\gamma\chi_{b1}(2P))]=(69\pm13\pm17)\times10^{-6}$ which we divide by our best (shown rounded) value $B(\Upsilon(3S)\to\gamma\chi_{b1}(2P))=(12.6\pm1.2)\times10^{-2}$. Our first error is their experiment's error and our second error is the systematic error from using our best (shown rounded) value.

$\Gamma(2\pi^+2\pi^-K^+K^-2\pi^0)/\Gamma_{total}$ — Γ_{12}/Γ

VALUE (units 10^{-4})	EVTS	DOCUMENT ID		TECN	COMMENT
9.6±3.5±0.9	27	[28] ASNER	08A	CLEO	$\Upsilon(3S)\to\gamma2\pi^+2\pi^-K^+K^-2\pi^0$

[28] ASNER 08A reports $[\Gamma(\chi_{b1}(2P)\to2\pi^+2\pi^-K^+K^-2\pi^0)/\Gamma_{total}]\times[B(\Upsilon(3S)\to\gamma\chi_{b1}(2P))]=(121\pm29\pm33)\times10^{-6}$ which we divide by our best (shown rounded) value $B(\Upsilon(3S)\to\gamma\chi_{b1}(2P))=(12.6\pm1.2)\times10^{-2}$. Our first error is their experiment's error and our second error is the systematic error from using our best (shown rounded) value.

$\Gamma(3\pi^+2\pi^-K^-K^0_S\pi^0)/\Gamma_{total}$ — Γ_{13}/Γ

VALUE (units 10^{-4})	EVTS	DOCUMENT ID		TECN	COMMENT
6.7±2.5±0.6	17	[29] ASNER	08A	CLEO	$\Upsilon(3S)\to\gamma3\pi^+2\pi^-K^-K^0_S\pi^0$

[29] ASNER 08A reports $[\Gamma(\chi_{b1}(2P)\to3\pi^+2\pi^-K^-K^0_S\pi^0)/\Gamma_{total}]\times[B(\Upsilon(3S)\to\gamma\chi_{b1}(2P))]=(85\pm23\pm22)\times10^{-6}$ which we divide by our best (shown rounded) value $B(\Upsilon(3S)\to\gamma\chi_{b1}(2P))=(12.6\pm1.2)\times10^{-2}$. Our first error is their experiment's error and our second error is the systematic error from using our best (shown rounded) value.

$\Gamma(3\pi^+3\pi^-)/\Gamma_{total}$ — Γ_{14}/Γ

VALUE (units 10^{-4})	EVTS	DOCUMENT ID		TECN	COMMENT
1.2±0.4±0.1	18	[30] ASNER	08A	CLEO	$\Upsilon(3S)\to\gamma3\pi^+3\pi^-$

Int. J. Mod. Phys. A 2026.41. Downloaded from www.worldscientific.com
by CALIFORNIA @ BERKELEY on 09/16/26. Re-use and distribution is strictly not permitted, except for Open Access articles.

[30] ASNER 08A reports $[\Gamma(\chi_{b1}(2P) \to 3\pi^+3\pi^-)/\Gamma_{total}] \times [B(\Upsilon(3S) \to \gamma\chi_{b1}(2P))] = (15 \pm 4 \pm 3) \times 10^{-6}$ which we divide by our best (shown rounded) value $B(\Upsilon(3S) \to \gamma\chi_{b1}(2P)) = (12.6 \pm 1.2) \times 10^{-2}$. Our first error is their experiment's error and our second error is the systematic error from using our best (shown rounded) value.

$\Gamma(3\pi^+3\pi^-2\pi^0)/\Gamma_{total}$ — Γ_{15}/Γ

VALUE (units 10^{-4})	EVTS	DOCUMENT ID		TECN	COMMENT
12±4±1	44	[31] ASNER	08A	CLEO	$\Upsilon(3S) \to \gamma 3\pi^+3\pi^-2\pi^0$

[31] ASNER 08A reports $[\Gamma(\chi_{b1}(2P) \to 3\pi^+3\pi^-2\pi^0)/\Gamma_{total}] \times [B(\Upsilon(3S) \to \gamma\chi_{b1}(2P))] = (150 \pm 30 \pm 40) \times 10^{-6}$ which we divide by our best (shown rounded) value $B(\Upsilon(3S) \to \gamma\chi_{b1}(2P)) = (12.6 \pm 1.2) \times 10^{-2}$. Our first error is their experiment's error and our second error is the systematic error from using our best (shown rounded) value.

$\Gamma(3\pi^+3\pi^-K^+K^-)/\Gamma_{total}$ — Γ_{16}/Γ

VALUE (units 10^{-4})	EVTS	DOCUMENT ID		TECN	COMMENT
2.0±0.7±0.2	16	[32] ASNER	08A	CLEO	$\Upsilon(3S) \to \gamma 3\pi^+3\pi^-K^+K^-$

[32] ASNER 08A reports $[\Gamma(\chi_{b1}(2P) \to 3\pi^+3\pi^-K^+K^-)/\Gamma_{total}] \times [B(\Upsilon(3S) \to \gamma\chi_{b1}(2P))] = (25 \pm 7 \pm 6) \times 10^{-6}$ which we divide by our best (shown rounded) value $B(\Upsilon(3S) \to \gamma\chi_{b1}(2P)) = (12.6 \pm 1.2) \times 10^{-2}$. Our first error is their experiment's error and our second error is the systematic error from using our best (shown rounded) value.

$\Gamma(3\pi^+3\pi^-K^+K^-\pi^0)/\Gamma_{total}$ — Γ_{17}/Γ

VALUE (units 10^{-4})	EVTS	DOCUMENT ID		TECN	COMMENT
6.1±2.1±0.6	25	[33] ASNER	08A	CLEO	$\Upsilon(3S) \to \gamma 3\pi^+3\pi^-K^+K^-\pi^0$

[33] ASNER 08A reports $[\Gamma(\chi_{b1}(2P) \to 3\pi^+3\pi^-K^+K^-\pi^0)/\Gamma_{total}] \times [B(\Upsilon(3S) \to \gamma\chi_{b1}(2P))] = (77 \pm 17 \pm 21) \times 10^{-6}$ which we divide by our best (shown rounded) value $B(\Upsilon(3S) \to \gamma\chi_{b1}(2P)) = (12.6 \pm 1.2) \times 10^{-2}$. Our first error is their experiment's error and our second error is the systematic error from using our best (shown rounded) value.

$\Gamma(4\pi^+4\pi^-)/\Gamma_{total}$ — Γ_{18}/Γ

VALUE (units 10^{-4})	EVTS	DOCUMENT ID		TECN	COMMENT
1.7±0.6±0.2	16	[34] ASNER	08A	CLEO	$\Upsilon(3S) \to \gamma 4\pi^+4\pi^-$

[34] ASNER 08A reports $[\Gamma(\chi_{b1}(2P) \to 4\pi^+4\pi^-)/\Gamma_{total}] \times [B(\Upsilon(3S) \to \gamma\chi_{b1}(2P))] = (22 \pm 6 \pm 5) \times 10^{-6}$ which we divide by our best (shown rounded) value $B(\Upsilon(3S) \to \gamma\chi_{b1}(2P)) = (12.6 \pm 1.2) \times 10^{-2}$. Our first error is their experiment's error and our second error is the systematic error from using our best (shown rounded) value.

$\Gamma(4\pi^+4\pi^-2\pi^0)/\Gamma_{total}$ — Γ_{19}/Γ

VALUE (units 10^{-4})	EVTS	DOCUMENT ID		TECN	COMMENT
19±7±2	41	[35] ASNER	08A	CLEO	$\Upsilon(3S) \to \gamma 4\pi^+4\pi^-2\pi^0$

[35] ASNER 08A reports $[\Gamma(\chi_{b1}(2P) \to 4\pi^+4\pi^-2\pi^0)/\Gamma_{total}] \times [B(\Upsilon(3S) \to \gamma\chi_{b1}(2P))] = (241 \pm 47 \pm 72) \times 10^{-6}$ which we divide by our best (shown rounded) value $B(\Upsilon(3S) \to \gamma\chi_{b1}(2P)) = (12.6 \pm 1.2) \times 10^{-2}$. Our first error is their experiment's error and our second error is the systematic error from using our best (shown rounded) value.

$\chi_{b1}(2P)$ Cross-Particle Branching Ratios

$\Gamma(\chi_{b1}(2P) \to \gamma\Upsilon(1S))/\Gamma_{total} \times \Gamma(\Upsilon(3S) \to \gamma\chi_{b1}(2P))/\Gamma_{total}$ — $\Gamma_3/\Gamma \times \Gamma_{21}^{\Upsilon(3S)}/\Gamma^{\Upsilon(3S)}$

VALUE (units 10^{-3})	EVTS	DOCUMENT ID		TECN	COMMENT
12.4±0.3±0.6	15k	LEES	11J	BABR	$\Upsilon(3S) \to X\gamma$

$B(\chi_{b1}(2P) \to \gamma\Upsilon(1S)) \times B(\Upsilon(3S) \to \gamma\chi_{b1}(2P)) \times B(\Upsilon(1S) \to \ell^+\ell^-)$

VALUE (units 10^{-4})	EVTS	DOCUMENT ID		TECN	COMMENT
2.9 ±0.4 OUR AVERAGE	Error includes scale factor of 1.9. See the ideogram below.				
$3.52^{+0.28}_{-0.27}{}^{+0.17}_{-0.18}$		[36] LEES	14M	BABR	$\Upsilon(3S) \to \gamma\gamma\mu^+\mu^-$
$3.24 \pm 0.56 \pm 0.41$	58	[37] CRAWFORD	92B	CLE2	$\Upsilon(3S) \to \gamma\gamma\ell^+\ell^-$
$2.34 \pm 0.28 \pm 0.15$		[38] HEINTZ	92	CSB2	$\Upsilon(3S) \to \gamma\gamma\ell^+\ell^-$

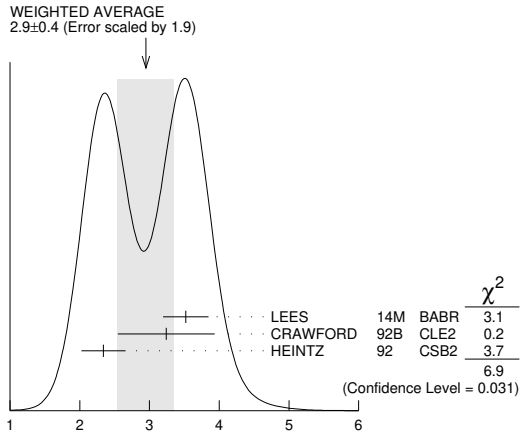

$B(\chi_{b1}(2P) \to \gamma\Upsilon(1S)) \times B(\Upsilon(3S) \to \gamma\chi_{b1}(2P)) \times B(\Upsilon(1S) \to \ell^+\ell^-)$ (units 10^{-4})

[36] From a sample of $\Upsilon(3S) \to \gamma\gamma\mu^+\mu^-$ with one converted photon.

[37] CRAWFORD 92B quotes $2 \times B(\Upsilon(3S) \to \gamma\chi_{bJ}(2P))\ B(\chi_{bJ}(2P) \to \gamma\Upsilon(nS))\ B(\Upsilon(nS) \to \ell^+\ell^-)$.

[38] Calculated by us. HEINTZ 92 quotes $B(\Upsilon(3S) \to \gamma\chi_{b1}(2P)) \times B(\chi_{b1}(2P) \to \gamma\Upsilon(1S)) = (0.91 \pm 0.11 \pm 0.06)\%$ using $B(\Upsilon(1S) \to \mu^+\mu^-) = (2.57 \pm 0.05)\%$.

$\Gamma(\chi_{b1}(2P) \to \gamma\Upsilon(2S))/\Gamma_{total} \times \Gamma(\Upsilon(3S) \to \gamma\chi_{b1}(2P))/\Gamma_{total}$ — $\Gamma_2/\Gamma \times \Gamma_{21}^{\Upsilon(3S)}/\Gamma^{\Upsilon(3S)}$

VALUE (units 10^{-2})	EVTS	DOCUMENT ID		TECN	COMMENT
2.4±0.1±0.2	4.3k	LEES	11J	BABR	$\Upsilon(3S) \to X\gamma$

$B(\chi_{b1}(2P) \to \gamma\Upsilon(2S)) \times B(\Upsilon(3S) \to \gamma\chi_{b1}(2P)) \times B(\Upsilon(2S) \to \ell^+\ell^-)$

VALUE (units 10^{-4})	EVTS	DOCUMENT ID		TECN	COMMENT
3.8 ±0.6 OUR AVERAGE	Error includes scale factor of 1.8. See the ideogram below.				
$4.95^{+0.75}_{-0.70}{}^{+1.01}_{-0.24}$		[39] LEES	14M	BABR	$\Upsilon(3S) \to \gamma\gamma\mu^+\mu^-$
$5.12 \pm 0.60 \pm 0.63$	111	[40] CRAWFORD	92B	CLE2	$\Upsilon(3S) \to \gamma\gamma\ell^+\ell^-$
$3.30 \pm 0.33 \pm 0.20$		[41] HEINTZ	92	CSB2	$\Upsilon(3S) \to \gamma\gamma\ell^+\ell^-$

[39] From a sample of $\Upsilon(3S) \to \gamma\gamma\mu^+\mu^-$ with one converted photon.

[40] CRAWFORD 92B quotes $2 \times B(\Upsilon(3S) \to \gamma\chi_{bJ}(2P))\ B(\chi_{bJ}(2P) \to \gamma\Upsilon(nS))\ B(\Upsilon(nS) \to \ell^+\ell^-)$.

[41] Calculated by us. HEINTZ 92 quotes $B(\Upsilon(3S) \to \gamma\chi_{b1}(2P)) \times B(\chi_{b1}(2P) \to \gamma\Upsilon(2S)) = (2.29 \pm 0.23 \pm 0.21)$ % using $B(\Upsilon(2S) \to \mu^+\mu^-) = (1.44 \pm 0.10)\%$.

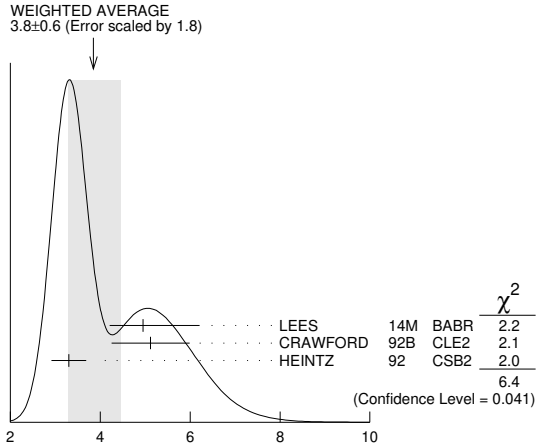

$B(\chi_{b1}(2P) \to \gamma\Upsilon(2S)) \times B(\Upsilon(3S) \to \gamma\chi_{b1}(2P)) \times B(\Upsilon(2S) \to \ell^+\ell^-)$ (units 10^{-4})

$B(\chi_{b1}(2P) \to \chi_{b1}(1P)\pi^+\pi^-) \times B(\Upsilon(3S) \to \chi_{b1}(2P)X)$

VALUE (units 10^{-3})	EVTS	DOCUMENT ID		TECN	COMMENT
1.16±0.07±0.12	31k	LEES	11C	BABR	$e^+e^- \to \pi^+\pi^-X$

$B(\chi_{b2}(2P) \to pX + \bar{p}X)/B(\chi_{b1}(2P) \to pX + \bar{p}X)$

VALUE	DOCUMENT ID		TECN	COMMENT
1.109±0.007±0.040	BRIERE	07	CLEO	$\Upsilon(3S) \to \gamma\chi_{bJ}(2P)$

$B(\chi_{b0}(2P) \to pX + \bar{p}X)/B(\chi_{b1}(2P) \to pX + \bar{p}X)$

VALUE	DOCUMENT ID		TECN	COMMENT
1.082±0.025±0.060	BRIERE	07	CLEO	$\Upsilon(3S) \to \gamma\chi_{bJ}(2P)$

$\chi_{b1}(2P)$ REFERENCES

STOTTLER	25	PRL 135 121902	Z.S. Stottler *et al.*	(BELLE Collab.)
AAIJ	24AC	JHEP 2410 122	R. Aaij *et al.*	(LHCb Collab.)
LEES	14M	PR D90 112010	J.P. Lees *et al.*	(BABAR Collab.)
LEES	11C	PR D84 011104	J.P. Lees *et al.*	(BABAR Collab.)
LEES	11J	PR D84 072002	J.P. Lees *et al.*	(BABAR Collab.)
ASNER	08A	PR D78 091103	D.M. Asner *et al.*	(CLEO Collab.)
BRIERE	08	PR D78 092007	R.A. Briere *et al.*	(CLEO Collab.)
BRIERE	07	PR D76 012005	R.A. Briere *et al.*	(CLEO Collab.)
CAWLFIELD	06	PR D73 012003	C. Cawlfield *et al.*	(CLEO Collab.)
ARTUSO	05	PRL 94 032001	M. Artuso *et al.*	(CLEO Collab.)
CRONIN-HEN...	04	PRL 92 222002	D. Cronin-Hennessy *et al.*	(CLEO Collab.)
CRAWFORD	92B	PL B294 139	G. Crawford *et al.*	(CLEO Collab.)
HEINTZ	92	PR D46 1928	U. Heintz *et al.*	(CUSB II Collab.)
HEINTZ	91	PRL 66 1563	U. Heintz *et al.*	(CUSB Collab.)
MORRISON	91	PRL 67 1696	R.J. Morrison *et al.*	(CLEO Collab.)
NARAIN	91	PRL 66 3113	M. Narain *et al.*	(CUSB Collab.)

Int. J. Mod. Phys. A 2026.41. Downloaded from www.worldscientific.com
by UNIVERSITY OF CALIFORNIA @ BERKELEY on 09/16/26. Re-use and distribution is strictly not permitted, except for Open Access articles.

Int. J. Mod. Phys. A 2026.41. Downloaded from www.worldscientific.com
by [redacted]LIFORNIA @ BERKELEY on 09/16/26. Re-use and distribution is strictly not permitted, except for Open Access articles.

$h_b(2P)$

$I^G(J^{PC}) = 0^-(1^{+-})$

Quantum numbers are quark model predictions. $C = -$ established by $\eta_b\gamma$ decay.

$h_b(2P)$ MASS

VALUE (MeV)	EVTS	DOCUMENT ID		TECN	COMMENT
10259.8±0.5±1.1	90k	[1] MIZUK	12	BELL	$e^+e^- \to \pi^+\pi^-$ hadrons
• • • We do not use the following data for averages, fits, limits, etc. • • •					
$10259.8\pm0.6^{+1.4}_{-1.0}$	83.9k	[2] ADACHI	12	BELL	10.86 $e^+e^- \to \pi^+\pi^-$ MM

[1] Observed with 9 standard deviations significance.
[2] Superseded by MIZUK 12.

$h_b(2P)$ DECAY MODES

	Mode	Fraction (Γ_i/Γ)	Confidence level
Γ_1	hadrons	not seen	
Γ_2	$\eta_b(1S)\gamma$	(22 ± 5) %	
Γ_3	$\eta_b(2S)\gamma$	(48 ±13) %	
Γ_4	$\Upsilon(1S)\eta$	$(7.1^{+4.0}_{-3.3})\times10^{-3}$	
Γ_5	$\Upsilon(1S)\pi^0$	$< 1.8 \times10^{-3}$	90%
Γ_6	$\gamma\chi_{b0}(1P)$	< 27 %	90%
Γ_7	$\gamma\chi_{b1}(1P)$	$< 5.4 \times10^{-3}$	90%
Γ_8	$\gamma\chi_{b2}(1P)$	< 1.3 %	90%

$h_b(2P)$ BRANCHING RATIOS

$\Gamma(\text{hadrons})/\Gamma_{\text{total}}$ — Γ_1/Γ

VALUE	EVTS	DOCUMENT ID		TECN	COMMENT
not seen	83.9k	ADACHI	12	BELL	10.86 $e^+e^- \to \pi^+\pi^-$ MM

$\Gamma(\eta_b(1S)\gamma)/\Gamma_{\text{total}}$ — Γ_2/Γ

VALUE (units 10^{-2})	EVTS	DOCUMENT ID		TECN	COMMENT
$22.3\pm3.8^{+3.1}_{-3.3}$	10k	MIZUK	12	BELL	$e^+e^- \to (\gamma)\pi^+\pi^-$ hadrons

$\Gamma(\eta_b(2S)\gamma)/\Gamma_{\text{total}}$ — Γ_3/Γ

VALUE (units 10^{-2})	EVTS	DOCUMENT ID		TECN	COMMENT
$47.5\pm10.5^{+6.8}_{-7.7}$	26k	MIZUK	12	BELL	$e^+e^- \to (\gamma)\pi^+\pi^-$ hadrons

$\Gamma(\Upsilon(1S)\eta)/\Gamma_{\text{total}}$ — Γ_4/Γ

VALUE (units 10^{-3})	EVTS	DOCUMENT ID		TECN	COMMENT
$7.1^{+3.7}_{-3.2}\pm0.8$	3.8	KOVALENKO	24	BELL	$e^+e^- \to \Upsilon(5S)$

$\Gamma(\Upsilon(1S)\pi^0)/\Gamma_{\text{total}}$ — Γ_5/Γ

VALUE	CL%	EVTS	DOCUMENT ID		TECN	COMMENT
$<1.8\times10^{-3}$	90	0.1	KOVALENKO	24	BELL	$e^+e^- \to \Upsilon(5S)$

$\Gamma(\gamma\chi_{b0}(1P))/\Gamma_{\text{total}}$ — Γ_6/Γ

VALUE	CL%	DOCUMENT ID		TECN	COMMENT
$<2.7\times10^{-1}$	90	BOSCHETTI	25	BELL	$\Upsilon(10860) \to h_b(2P)\pi^+\pi^-$

$\Gamma(\gamma\chi_{b1}(1P))/\Gamma_{\text{total}}$ — Γ_7/Γ

VALUE	CL%	DOCUMENT ID		TECN	COMMENT
$<5.4\times10^{-3}$	90	BOSCHETTI	25	BELL	$\Upsilon(10860) \to h_b(2P)\pi^+\pi^-$

$\Gamma(\gamma\chi_{b2}(1P))/\Gamma_{\text{total}}$ — Γ_8/Γ

VALUE	CL%	DOCUMENT ID		TECN	COMMENT
$<1.3\times10^{-2}$	90	BOSCHETTI	25	BELL	$\Upsilon(10860) \to h_b(2P)\pi^+\pi^-$

$h_b(2P)$ REFERENCES

BOSCHETTI	25	PR D111 L011102	A. Boschetti *et al.*	(BELLE Collab.)
KOVALENKO	24	PRL 133 261901	E. Kovalenko *et al.*	(BELLE Collab.)
ADACHI	12	PRL 108 032001	I. Adachi *et al.*	(BELLE Collab.)
MIZUK	12	PRL 109 232002	R. Mizuk *et al.*	(BELLE Collab.)

$\chi_{b2}(2P)$

$I^G(J^{PC}) = 0^+(2^{++})$
J needs confirmation.

Observed in radiative decay of the $\Upsilon(3S)$, therefore $C = +$. Branching ratio requires E1 transition, M1 is strongly disfavored, therefore $P = +$.

$\chi_{b2}(2P)$ MASS

VALUE (MeV)	DOCUMENT ID
10268.65±0.22±0.50 OUR EVALUATION	From γ energy below, using $\Upsilon(3S)$ mass = 10355.2 ± 0.5 MeV

$m_{\chi_{b2}(2P)} - m_{\chi_{b1}(2P)}$

VALUE (MeV)	EVTS	DOCUMENT ID		TECN	COMMENT
13.2 ±0.4 OUR AVERAGE		Error includes scale factor of 1.8. See the ideogram below.			
15.7 ±1.0	50	[1] AAIJ	24AC	LHCB	$\chi_b(2P) \to \Upsilon(1S)\mu^+\mu^-$
12.3 ±2.6 ±0.6		[2] AAIJ	14BG	LHCB	$pp \to \gamma\mu^+\mu^-X$
13.04±0.26		LEES	14M	BABR	$\Upsilon(3S) \to \gamma\gamma\mu^+\mu^-$
13.5 ±0.4 ±0.5		[3] HEINTZ	92	CSB2	$e^+e^- \to \gamma X, \ell^+\ell^-\gamma\gamma$

[1] Observed in prompt pp production.
[2] From the $\chi_{bj}(2P) \to \Upsilon(1S)\gamma$ transition.
[3] From the average photon energy for inclusive and exclusive events. Supersedes NARAIN 91.

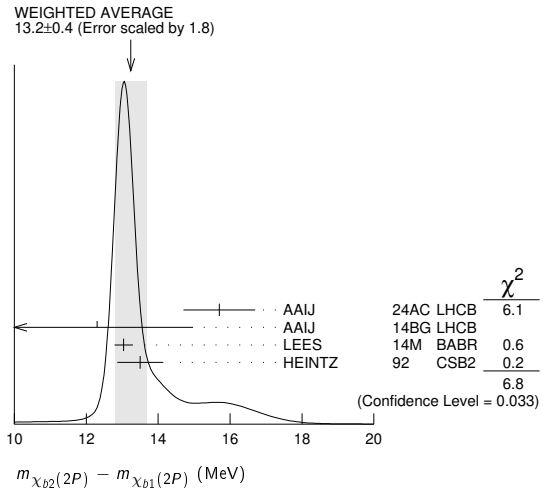

γ ENERGY IN $\Upsilon(3S)$ DECAY

VALUE (MeV)	EVTS	DOCUMENT ID		TECN	COMMENT
86.19±0.22 OUR EVALUATION		Treating systematic errors as correlated			
86.40±0.18 OUR AVERAGE					
86.04±0.06±0.27		ARTUSO	05	CLEO	$\Upsilon(3S) \to \gamma X$
86 ±1	101	CRAWFORD	92B	CLE2	$e^+e^- \to \ell^+\ell^-\gamma\gamma$
86.7 ±0.4	10319	[4] HEINTZ	92	CSB2	$e^+e^- \to \gamma X$
86.9 ±0.4	157	[5] HEINTZ	92	CSB2	$e^+e^- \to \ell^+\ell^-\gamma\gamma$
86.4 ±0.1 ±0.4	30741	MORRISON	91	CLE2	$e^+e^- \to \gamma X$

[4] A systematic uncertainty on the energy scale of 0.9% not included. Supersedes NARAIN 91.
[5] A systematic uncertainty on the energy scale of 0.9% not included. Supersedes HEINTZ 91.

$\chi_{b2}(2P)$ DECAY MODES

	Mode	Fraction (Γ_i/Γ)	Scale factor/ Confidence level
Γ_1	$\omega\Upsilon(1S)$	$(5.7\pm2.0)\times10^{-3}$	S=1.5
Γ_2	$\gamma\Upsilon(2S)$	(8.9±1.2) %	
Γ_3	$\gamma\Upsilon(1S)$	(6.6±0.8) %	
Γ_4	$\pi\pi\chi_{b2}(1P)$	$(5.1\pm0.9)\times10^{-3}$	
Γ_5	D^0X	< 2.4 %	CL=90%
Γ_6	$\pi^+\pi^-K^+K^-\pi^0$	$< 1.1 \times10^{-4}$	CL=90%
Γ_7	$2\pi^+\pi^-K^-K^0_S$	$< 9 \times10^{-5}$	CL=90%
Γ_8	$2\pi^+\pi^-K^-K^0_S2\pi^0$	$< 7 \times10^{-4}$	CL=90%
Γ_9	$2\pi^+2\pi^-2\pi^0$	$(3.9\pm1.6)\times10^{-4}$	
Γ_{10}	$2\pi^+2\pi^-K^+K^-$	$(9 \pm4)\times10^{-5}$	
Γ_{11}	$2\pi^+2\pi^-K^+K^-\pi^0$	$(2.4\pm1.1)\times10^{-4}$	
Γ_{12}	$2\pi^+2\pi^-K^+K^-2\pi^0$	$(4.7\pm2.3)\times10^{-4}$	
Γ_{13}	$3\pi^+2\pi^-K^-K^0_S\pi^0$	$< 4 \times10^{-4}$	CL=90%
Γ_{14}	$3\pi^+3\pi^-$	$(9 \pm4)\times10^{-5}$	
Γ_{15}	$3\pi^+3\pi^-2\pi^0$	$(1.2\pm0.4)\times10^{-3}$	
Γ_{16}	$3\pi^+3\pi^-K^+K^-$	$(1.4\pm0.7)\times10^{-4}$	
Γ_{17}	$3\pi^+3\pi^-K^+K^-\pi^0$	$(4.2\pm1.7)\times10^{-4}$	
Γ_{18}	$4\pi^+4\pi^-$	$(9 \pm5)\times10^{-5}$	
Γ_{19}	$4\pi^+4\pi^-2\pi^0$	$(1.3\pm0.5)\times10^{-3}$	

Int. J. Mod. Phys. A 2026.41. Downloaded from www.worldscientific.com
by UNIVERSITY OF CALIFORNIA @ BERKELEY on 09/16/26. Re-use and distribution is strictly not permitted, except for Open Access articles.

$\chi_{b2}(2P)$ BRANCHING RATIOS

$\Gamma(\omega\Upsilon(1S))/\Gamma_{total}$ — Γ_1/Γ

VALUE (units 10^{-2})	EVTS	DOCUMENT ID		TECN	COMMENT
0.57±0.20 OUR AVERAGE		Error includes scale factor of 1.5.			
$0.47^{+0.13}_{-0.12}\pm0.06$	62	[6] STOTTLER	25	BELL	$\Upsilon(3S)\to\gamma\omega\Upsilon(1S)$
$0.96^{+0.29}_{-0.25}\pm0.12$	$20.1^{+5.8}_{-5.1}$	[7] CRONIN-HEN.	04	CLE3	$\Upsilon(3S)\to\gamma\omega\Upsilon(1S)$

[6] STOTTLER 25 reports $(0.47^{+0.13}_{-0.12}\pm0.06)\times10^{-2}$ from a measurement of $[\Gamma(\chi_{b2}(2P)\to\omega\Upsilon(1S))/\Gamma_{total}]\times[B(\Upsilon(3S)\to\gamma\chi_{b2}(2P))]$ assuming $B(\Upsilon(3S)\to\gamma\chi_{b2}(2P))=(13.1\pm1.6)\times10^{-2}$.

[7] CRONIN-HENNESSY 04 reports $(1.10^{+0.32+0.11}_{-0.28-0.10})\times10^{-2}$ from a measurement of $[\Gamma(\chi_{b2}(2P)\to\omega\Upsilon(1S))/\Gamma_{total}]\times[B(\Upsilon(3S)\to\gamma\chi_{b2}(2P))]$ assuming $B(\Upsilon(3S)\to\gamma\chi_{b2}(2P))=(11.4\pm0.8)\times10^{-2}$, which we rescale to our best (shown rounded) value $B(\Upsilon(3S)\to\gamma\chi_{b2}(2P))=(13.1\pm1.6)\times10^{-2}$. Our first error is their experiment's error and our second error is the systematic error from using our best (shown rounded) value.

$\Gamma(\gamma\Upsilon(2S))/\Gamma_{total}$ — Γ_2/Γ

VALUE	EVTS	DOCUMENT ID		TECN	COMMENT
0.089±0.012 OUR AVERAGE					
$0.085\pm0.010\pm0.010$		[8,9,10] LEES	14M	BABR	$\Upsilon(3S)\to\gamma\gamma\mu^+\mu^-$
$0.084\pm0.011\pm0.010$	2.5k	[11] LEES	11J	BABR	$\Upsilon(3S)\to X\gamma$
$0.096\pm0.022\pm0.012$		[9,12] CRAWFORD	92B	CLE2	$e^+e^-\to\ell^+\ell^-\gamma\gamma$
$0.106\pm0.016\pm0.013$		[9,13] HEINTZ	92	CSB2	$e^+e^-\to\ell^+\ell^-\gamma\gamma$

[8] LEES 14M quotes $\Gamma(\chi_{b2}(2P)\to\gamma\Upsilon(2S))/\Gamma_{total}\times\Gamma(\Upsilon(3S)\to\gamma\chi_{b2}(2P))/\Gamma_{total}=(1.12\pm0.13)\%$ combining the results from samples of $\Upsilon(3S)\to\gamma\gamma\mu^+\mu^-$ with and without converted photons.

[9] Assuming $B(\Upsilon(2S)\to\mu^+\mu^-)=(1.93\pm0.17)\%$.

[10] LEES 14M reports $[\Gamma(\chi_{b2}(2P)\to\gamma\Upsilon(2S))/\Gamma_{total}]\times[B(\Upsilon(3S)\to\gamma\chi_{b2}(2P))]=(1.12\pm0.13)\times10^{-2}$ which we divide by our best (shown rounded) value $B(\Upsilon(3S)\to\gamma\chi_{b2}(2P))=(13.1\pm1.6)\times10^{-2}$. Our first error is their experiment's error and our second error is the systematic error from using our best (shown rounded) value.

[11] LEES 11J reports $[\Gamma(\chi_{b2}(2P)\to\gamma\Upsilon(2S))/\Gamma_{total}]\times[B(\Upsilon(3S)\to\gamma\chi_{b2}(2P))]=(1.1\pm0.1\pm0.1)\times10^{-2}$ which we divide by our best (shown rounded) value $B(\Upsilon(3S)\to\gamma\chi_{b2}(2P))=(13.1\pm1.6)\times10^{-2}$. Our first error is their experiment's error and our second error is the systematic error from using our best (shown rounded) value.

[12] CRAWFORD 92B quotes $B(\Upsilon(3S)\to\gamma\chi_{b1}(2P))\times B(\chi_{b2}(2P)\to\gamma\Upsilon(2S))\times2\,B(\Upsilon(2S)\to\ell^+\ell^-)=(4.98\pm0.94\pm0.62)\,10^{-4}$.

[13] Recalculated by us. HEINTZ 92 quotes $B(\Upsilon(3S)\to\gamma\chi_{b2}(2P))\times B(\chi_{b2}(2P)\to\gamma\Upsilon(2S))=(1.90\pm0.23\pm0.18)\%$ using $B(\Upsilon(2S)\to\mu^+\mu^-)=(1.44\pm0.10)\%$. Supersedes HEINTZ 91.

$\Gamma(\gamma\Upsilon(1S))/\Gamma_{total}$ — Γ_3/Γ

VALUE	EVTS	DOCUMENT ID		TECN	COMMENT
0.066±0.008 OUR AVERAGE					
$0.061\pm0.004\pm0.007$		[14,15,16] LEES	14M	BABR	$\Upsilon(3S)\to\gamma\gamma\mu^+\mu^-$
$0.070\pm0.004\pm0.008$	11k	[17] LEES	11J	BABR	$\Upsilon(3S)\to X\gamma$
$0.077\pm0.018\pm0.009$		[15,18] CRAWFORD	92B	CLE2	$e^+e^-\to\ell^+\ell^-\gamma\gamma$
$0.061\pm0.009\pm0.007$		[15,19] HEINTZ	92	CSB2	$e^+e^-\to\ell^+\ell^-\gamma\gamma$

[14] LEES 14M quotes $\Gamma(\chi_{b2}(2P)\to\gamma\Upsilon(1S))/\Gamma_{total}\times\Gamma(\Upsilon(3S)\to\gamma\chi_{b2}(2P))/\Gamma_{total}=(8.03\pm0.50)\times10^{-3}$ combining the results from samples of $\Upsilon(3S)\to\gamma\gamma\mu^+\mu^-$ with and without converted photons.

[15] Assuming $B(\Upsilon(1S)\to\mu^+\mu^-)=(2.48\pm0.05)\%$.

[16] LEES 14M reports $[\Gamma(\chi_{b2}(2P)\to\gamma\Upsilon(1S))/\Gamma_{total}]\times[B(\Upsilon(3S)\to\gamma\chi_{b2}(2P))]=(8.03\pm0.50)\times10^{-3}$ which we divide by our best (shown rounded) value $B(\Upsilon(3S)\to\gamma\chi_{b2}(2P))=(13.1\pm1.6)\times10^{-2}$. Our first error is their experiment's error and our second error is the systematic error from using our best (shown rounded) value.

[17] LEES 11J reports $[\Gamma(\chi_{b2}(2P)\to\gamma\Upsilon(1S))/\Gamma_{total}]\times[B(\Upsilon(3S)\to\gamma\chi_{b2}(2P))]=(9.2\pm0.3\pm0.4)\times10^{-3}$ which we divide by our best (shown rounded) value $B(\Upsilon(3S)\to\gamma\chi_{b2}(2P))=(13.1\pm1.6)\times10^{-2}$. Our first error is their experiment's error and our second error is the systematic error from using our best (shown rounded) value.

[18] CRAWFORD 92B quotes $B(\Upsilon(3S)\to\gamma\chi_{b2}(2P))\times B(\chi_{b2}(2P)\to\gamma\Upsilon(1S))\times2\,B(\Upsilon(1S)\to\ell^+\ell^-)=(5.03\pm0.94\pm0.63)\,10^{-4}$.

[19] Recalculated by us. HEINTZ 92 quotes $B(\Upsilon(3S)\to\gamma\chi_{b2}(2P))\times B(\chi_{b2}(2P)\to\gamma\Upsilon(1S))=(0.77\pm0.11\pm0.05)\%$ using $B(\Upsilon(1S)\to\mu^+\mu^-)=(2.57\pm0.05)\%$. Supersedes HEINTZ 91.

$\Gamma(\pi\pi\chi_{b2}(1P))/\Gamma_{total}$ — Γ_4/Γ

VALUE (units 10^{-3})	EVTS	DOCUMENT ID		TECN	COMMENT
5.1±0.9 OUR AVERAGE					
$4.9\pm0.7\pm0.6$	17k	[20] LEES	11C	BABR	$e^+e^-\to\pi^+\pi^-X$
$6.0\pm1.6\pm1.4$		[21] CAWLFIELD	06	CLE3	$\Upsilon(3S)\to2(\gamma\pi\ell)$

[20] $(0.64\pm0.05\pm0.08)\times10^{-3}$. We derive the value assuming $B(\Upsilon(3S)\to\chi_{b2}(2P)X)=B(\Upsilon(3S)\to\chi_{b2}(2P)\gamma)=(13.1\pm1.6)\times10^{-2}$.

[21] CAWLFIELD 06 quote $\Gamma(\chi_b(2P)\to\pi\pi\chi_b(1P))=0.83\pm0.22\pm0.08\pm0.19$ keV assuming I-spin conservation, no D-wave contribution, $\Gamma(\chi_{b1}(2P))=96\pm16$keV, and $\Gamma(\chi_{b2}(2P))=138\pm19$ keV.

$\Gamma(D^0X)/\Gamma_{total}$ — Γ_5/Γ

VALUE	CL%	DOCUMENT ID		TECN	COMMENT
<2.4 × 10^{-2}	90	[22,23] BRIERE	08	CLEO	$\Upsilon(3S)\to\gamma D^0X$

[22] For $p_{D^0}>2.5$ GeV/c.

[23] The authors also present their result as $(0.2\pm1.4\pm0.1)\times10^{-2}$.

$\Gamma(\pi^+\pi^-K^+K^-\pi^0)/\Gamma_{total}$ — Γ_6/Γ

VALUE (units 10^{-4})	CL%	DOCUMENT ID		TECN	COMMENT
<1.1	90	[24] ASNER	08A	CLEO	$\Upsilon(3S)\to\gamma\pi^+\pi^-K^+K^-\pi^0$

[24] ASNER 08A reports $[\Gamma(\chi_{b2}(2P)\to\pi^+\pi^-K^+K^-\pi^0)/\Gamma_{total}]\times[B(\Upsilon(3S)\to\gamma\chi_{b2}(2P))]<14\times10^{-6}$ which we divide by our best (shown rounded) value $B(\Upsilon(3S)\to\gamma\chi_{b2}(2P))=13.1\times10^{-2}$.

$\Gamma(2\pi^+\pi^-K^-K^0_S)/\Gamma_{total}$ — Γ_7/Γ

VALUE (units 10^{-4})	CL%	DOCUMENT ID		TECN	COMMENT
<0.9	90	[25] ASNER	08A	CLEO	$\Upsilon(3S)\to\gamma2\pi^+\pi^-K^-K^0_S$

[25] ASNER 08A reports $[\Gamma(\chi_{b2}(2P)\to2\pi^+\pi^-K^-K^0_S)/\Gamma_{total}]\times[B(\Upsilon(3S)\to\gamma\chi_{b2}(2P))]<12\times10^{-6}$ which we divide by our best (shown rounded) value $B(\Upsilon(3S)\to\gamma\chi_{b2}(2P))=13.1\times10^{-2}$.

$\Gamma(2\pi^+\pi^-K^-K^0_S2\pi^0)/\Gamma_{total}$ — Γ_8/Γ

VALUE (units 10^{-4})	CL%	DOCUMENT ID		TECN	COMMENT
<7	90	[26] ASNER	08A	CLEO	$\Upsilon(3S)\to\gamma2\pi^+\pi^-K^-2\pi^0$

[26] ASNER 08A reports $[\Gamma(\chi_{b2}(2P)\to2\pi^+\pi^-K^-K^0_S2\pi^0)/\Gamma_{total}]\times[B(\Upsilon(3S)\to\gamma\chi_{b2}(2P))]<87\times10^{-6}$ which we divide by our best (shown rounded) value $B(\Upsilon(3S)\to\gamma\chi_{b2}(2P))=13.1\times10^{-2}$.

$\Gamma(2\pi^+2\pi^-2\pi^0)/\Gamma_{total}$ — Γ_9/Γ

VALUE (units 10^{-4})	EVTS	DOCUMENT ID		TECN	COMMENT
3.9±1.6±0.5	23	[27] ASNER	08A	CLEO	$\Upsilon(3S)\to\gamma2\pi^+2\pi^-2\pi^0$

[27] ASNER 08A reports $[\Gamma(\chi_{b2}(2P)\to2\pi^+2\pi^-2\pi^0)/\Gamma_{total}]\times[B(\Upsilon(3S)\to\gamma\chi_{b2}(2P))]=(51\pm16\pm13)\times10^{-6}$ which we divide by our best (shown rounded) value $B(\Upsilon(3S)\to\gamma\chi_{b2}(2P))=(13.1\pm1.6)\times10^{-2}$. Our first error is their experiment's error and our second error is the systematic error from using our best (shown rounded) value.

$\Gamma(2\pi^+2\pi^-K^+K^-)/\Gamma_{total}$ — Γ_{10}/Γ

VALUE (units 10^{-4})	EVTS	DOCUMENT ID		TECN	COMMENT
0.9±0.4±0.1	11	[28] ASNER	08A	CLEO	$\Upsilon(3S)\to\gamma2\pi^+2\pi^-K^+K^-$

[28] ASNER 08A reports $[\Gamma(\chi_{b2}(2P)\to2\pi^+2\pi^-K^+K^-)/\Gamma_{total}]\times[B(\Upsilon(3S)\to\gamma\chi_{b2}(2P))]=(12\pm4\pm3)\times10^{-6}$ which we divide by our best (shown rounded) value $B(\Upsilon(3S)\to\gamma\chi_{b2}(2P))=(13.1\pm1.6)\times10^{-2}$. Our first error is their experiment's error and our second error is the systematic error from using our best (shown rounded) value.

$\Gamma(2\pi^+2\pi^-K^+K^-\pi^0)/\Gamma_{total}$ — Γ_{11}/Γ

VALUE (units 10^{-4})	EVTS	DOCUMENT ID		TECN	COMMENT
2.4±1.0±0.3	16	[29] ASNER	08A	CLEO	$\Upsilon(3S)\to\gamma2\pi^+2\pi^-K^+K^-\pi^0$

[29] ASNER 08A reports $[\Gamma(\chi_{b2}(2P)\to2\pi^+2\pi^-K^+K^-\pi^0)/\Gamma_{total}]\times[B(\Upsilon(3S)\to\gamma\chi_{b2}(2P))]=(32\pm11\pm8)\times10^{-6}$ which we divide by our best (shown rounded) value $B(\Upsilon(3S)\to\gamma\chi_{b2}(2P))=(13.1\pm1.6)\times10^{-2}$. Our first error is their experiment's error and our second error is the systematic error from using our best (shown rounded) value.

$\Gamma(2\pi^+2\pi^-K^+K^-2\pi^0)/\Gamma_{total}$ — Γ_{12}/Γ

VALUE (units 10^{-4})	EVTS	DOCUMENT ID		TECN	COMMENT
4.7±2.2±0.6	14	[30] ASNER	08A	CLEO	$\Upsilon(3S)\to\gamma2\pi^+2\pi^-K^+K^-2\pi^0$

[30] ASNER 08A reports $[\Gamma(\chi_{b2}(2P)\to2\pi^+2\pi^-K^+K^-2\pi^0)/\Gamma_{total}]\times[B(\Upsilon(3S)\to\gamma\chi_{b2}(2P))]=(62\pm23\pm17)\times10^{-6}$ which we divide by our best (shown rounded) value $B(\Upsilon(3S)\to\gamma\chi_{b2}(2P))=(13.1\pm1.6)\times10^{-2}$. Our first error is their experiment's error and our second error is the systematic error from using our best (shown rounded) value.

$\Gamma(3\pi^+2\pi^-K^-K^0_S\pi^0)/\Gamma_{total}$ — Γ_{13}/Γ

VALUE (units 10^{-4})	CL%	DOCUMENT ID		TECN	COMMENT
<4	90	[31] ASNER	08A	CLEO	$\Upsilon(3S)\to\gamma3\pi^+2\pi^-K^-K^0_S\pi^0$

[31] ASNER 08A reports $[\Gamma(\chi_{b2}(2P)\to3\pi^+2\pi^-K^-K^0_S\pi^0)/\Gamma_{total}]\times[B(\Upsilon(3S)\to\gamma\chi_{b2}(2P))]<58\times10^{-6}$ which we divide by our best (shown rounded) value $B(\Upsilon(3S)\to\gamma\chi_{b2}(2P))=13.1\times10^{-2}$.

$\Gamma(3\pi^+3\pi^-)/\Gamma_{total}$ — Γ_{14}/Γ

VALUE (units 10^{-4})	EVTS	DOCUMENT ID		TECN	COMMENT
0.9±0.4±0.1	14	[32] ASNER	08A	CLEO	$\Upsilon(3S)\to\gamma3\pi^+3\pi^-$

[32] ASNER 08A reports $[\Gamma(\chi_{b2}(2P)\to3\pi^+3\pi^-)/\Gamma_{total}]\times[B(\Upsilon(3S)\to\gamma\chi_{b2}(2P))]=(12\pm4\pm3)\times10^{-6}$ which we divide by our best (shown rounded) value $B(\Upsilon(3S)\to\gamma\chi_{b2}(2P))=(13.1\pm1.6)\times10^{-2}$. Our first error is their experiment's error and our second error is the systematic error from using our best (shown rounded) value.

$\Gamma(3\pi^+3\pi^-2\pi^0)/\Gamma_{total}$ — Γ_{15}/Γ

VALUE (units 10^{-4})	EVTS	DOCUMENT ID		TECN	COMMENT
12±4±1	45	[33] ASNER	08A	CLEO	$\Upsilon(3S)\to\gamma3\pi^+3\pi^-2\pi^0$

[33] ASNER 08A reports $[\Gamma(\chi_{b2}(2P)\to3\pi^+3\pi^-2\pi^0)/\Gamma_{total}]\times[B(\Upsilon(3S)\to\gamma\chi_{b2}(2P))]=(159\pm33\pm43)\times10^{-6}$ which we divide by our best (shown rounded) value $B(\Upsilon(3S)\to\gamma\chi_{b2}(2P))=(13.1\pm1.6)\times10^{-2}$. Our first error is their experiment's error and our second error is the systematic error from using our best (shown rounded) value.

Int. J. Mod. Phys. A 2026.41. Downloaded from www.worldscientific.com by CALIFORNIA @ BERKELEY on 09/16/26. Re-use and distribution is strictly not permitted, except for Open Access articles.

$\Gamma(3\pi^+3\pi^-K^+K^-)/\Gamma_{total}$ — Γ_{16}/Γ

VALUE (units 10^{-4})	EVTS	DOCUMENT ID		TECN	COMMENT
1.4±0.7±0.2	12	[34] ASNER	08A	CLEO	$\Upsilon(3S) \to \gamma 3\pi^+3\pi^-K^+K^-$

[34] ASNER 08A reports $[\Gamma(\chi_{b2}(2P) \to 3\pi^+3\pi^-K^+K^-)/\Gamma_{total}] \times [B(\Upsilon(3S) \to \gamma\chi_{b2}(2P))] = (19 \pm 7 \pm 5) \times 10^{-6}$ which we divide by our best (shown rounded) value $B(\Upsilon(3S) \to \gamma\chi_{b2}(2P)) = (13.1 \pm 1.6) \times 10^{-2}$. Our first error is their experiment's error and our second error is the systematic error from using our best (shown rounded) value.

$\Gamma(3\pi^+3\pi^-K^+K^-\pi^0)/\Gamma_{total}$ — Γ_{17}/Γ

VALUE (units 10^{-4})	EVTS	DOCUMENT ID		TECN	COMMENT
4.2±1.7±0.5	16	[35] ASNER	08A	CLEO	$\Upsilon(3S) \to \gamma 3\pi^+3\pi^-K^+K^-\pi^0$

[35] ASNER 08A reports $[\Gamma(\chi_{b2}(2P) \to 3\pi^+3\pi^-K^+K^-\pi^0)/\Gamma_{total}] \times [B(\Upsilon(3S) \to \gamma\chi_{b2}(2P))] = (55 \pm 16 \pm 15) \times 10^{-6}$ which we divide by our best (shown rounded) value $B(\Upsilon(3S) \to \gamma\chi_{b2}(2P)) = (13.1 \pm 1.6) \times 10^{-2}$. Our first error is their experiment's error and our second error is the systematic error from using our best (shown rounded) value.

$\Gamma(4\pi^+4\pi^-)/\Gamma_{total}$ — Γ_{18}/Γ

VALUE (units 10^{-4})	EVTS	DOCUMENT ID		TECN	COMMENT
0.9±0.4±0.1	9	[36] ASNER	08A	CLEO	$\Upsilon(3S) \to \gamma 4\pi^+4\pi^-$

[36] ASNER 08A reports $[\Gamma(\chi_{b2}(2P) \to 4\pi^+4\pi^-)/\Gamma_{total}] \times [B(\Upsilon(3S) \to \gamma\chi_{b2}(2P))] = (12 \pm 5 \pm 3) \times 10^{-6}$ which we divide by our best (shown rounded) value $B(\Upsilon(3S) \to \gamma\chi_{b2}(2P)) = (13.1 \pm 1.6) \times 10^{-2}$. Our first error is their experiment's error and our second error is the systematic error from using our best (shown rounded) value.

$\Gamma(4\pi^+4\pi^-2\pi^0)/\Gamma_{total}$ — Γ_{19}/Γ

VALUE (units 10^{-4})	EVTS	DOCUMENT ID		TECN	COMMENT
13±5±2	27	[37] ASNER	08A	CLEO	$\Upsilon(3S) \to \gamma 4\pi^+4\pi^-2\pi^0$

[37] ASNER 08A reports $[\Gamma(\chi_{b2}(2P) \to 4\pi^+4\pi^-2\pi^0)/\Gamma_{total}] \times [B(\Upsilon(3S) \to \gamma\chi_{b2}(2P))] = (165 \pm 46 \pm 50) \times 10^{-6}$ which we divide by our best (shown rounded) value $B(\Upsilon(3S) \to \gamma\chi_{b2}(2P)) = (13.1 \pm 1.6) \times 10^{-2}$. Our first error is their experiment's error and our second error is the systematic error from using our best (shown rounded) value.

$\chi_{b2}(2P)$ Cross-Particle Branching Ratios

$\Gamma(\chi_{b2}(2P) \to \gamma\Upsilon(1S))/\Gamma_{total} \times \Gamma(\Upsilon(3S) \to \gamma\chi_{b2}(2P))/\Gamma_{total}$ — $\Gamma_3/\Gamma \times \Gamma_{20}^{\Upsilon(3S)}/\Gamma^{\Upsilon(3S)}$

VALUE (units 10^{-3})	EVTS	DOCUMENT ID		TECN	COMMENT
9.2±0.3±0.4	11k	LEES	11J	BABR	$\Upsilon(3S) \to X\gamma$

$\Gamma(\chi_{b2}(2P) \to \gamma\Upsilon(2S))/\Gamma_{total} \times \Gamma(\Upsilon(3S) \to \gamma\chi_{b2}(2P))/\Gamma_{total}$ — $\Gamma_2/\Gamma \times \Gamma_{20}^{\Upsilon(3S)}/\Gamma^{\Upsilon(3S)}$

VALUE (units 10^{-2})	EVTS	DOCUMENT ID		TECN	COMMENT
1.1±0.1±0.1	2.5k	LEES	11J	BABR	$\Upsilon(3S) \to X\gamma$

$B(\chi_{b2}(2P) \to \chi_{b2}(1P)\pi^+\pi^-) \times B(\Upsilon(3S) \to \chi_{b2}(2P)X)$

VALUE (units 10^{-3})	EVTS	DOCUMENT ID		TECN	COMMENT
0.64±0.05±0.08	17k	LEES	11C	BABR	$e^+e^- \to \pi^+\pi^-X$

$B(\chi_{b2}(2P) \to \gamma\Upsilon(1S)) \times B(\Upsilon(3S) \to \gamma\chi_{b2}(2P)) \times B(\Upsilon(1S) \to \ell^+\ell^-)$

VALUE (units 10^{-4})	EVTS	DOCUMENT ID		TECN	COMMENT
2.02±0.18 OUR AVERAGE					
$1.95^{+0.22+0.10}_{-0.21-0.16}$		[38] LEES	14M	BABR	$\Upsilon(3S) \to \gamma\gamma\mu^+\mu^-$
2.52±0.47±0.32	48	[39] CRAWFORD	92B	CLE2	$\Upsilon(3S) \to \gamma\gamma\ell^+\ell^-$
1.98±0.28±0.12		[40] HEINTZ	92	CSB2	$\Upsilon(3S) \to \gamma\gamma\ell^+\ell^-$

[38] From a sample of $\Upsilon(3S) \to \gamma\gamma\mu^+\mu^-$ with converted photons.

[39] CRAWFORD 92B quotes $2\times B(\Upsilon(3S) \to \gamma\chi_{bJ}(2P))\ B(\chi_{bJ}(2P) \to \gamma\Upsilon(nS))\ B(\Upsilon(nS) \to \ell^+\ell^-)$.

[40] Calculated by us. HEINTZ 92 quotes $B(\Upsilon(3S) \to \gamma\chi_{b2}(2P)) \times B(\chi_{b2}(2P) \to \gamma\Upsilon(1S)) = (0.77 \pm 0.11 \pm 0.05)\%$ using $B(\Upsilon(1S) \to \mu^+\mu^-) = (2.57 \pm 0.05)\%$.

$[B(\chi_{b2}(2P) \to \gamma\Upsilon(1S)) \times B(\Upsilon(3S) \to \gamma\chi_{b2}(2P))] / [B(\chi_{b1}(2P) \to \gamma\Upsilon(1S)) \times B(\Upsilon(3S) \to \gamma\chi_{b1}(2P))]$

VALUE (%)	DOCUMENT ID		TECN	COMMENT
66.6±3.0	[41] LEES	14M	BABR	$\Upsilon(3S) \to \gamma\gamma\mu^+\mu^-$

[41] From a sample of $\Upsilon(3S) \to \gamma\gamma\mu^+\mu^-$ events without converted photons.

$B(\chi_{b2}(2P) \to \gamma\Upsilon(2S)) \times B(\Upsilon(3S) \to \gamma\chi_{b2}(2P)) \times B(\Upsilon(2S) \to \ell^+\ell^-)$

VALUE (units 10^{-4})	EVTS	DOCUMENT ID		TECN	COMMENT
2.74±0.29 OUR AVERAGE					
$3.22^{+0.58+0.16}_{-0.53-0.71}$		[42] LEES	14M	BABR	$\Upsilon(3S) \to \gamma\gamma\mu^+\mu^-$
2.49±0.47±0.31	53	[43] CRAWFORD	92B	CLE2	$\Upsilon(3S) \to \gamma\gamma\ell^+\ell^-$
2.74±0.33±0.18		[44] HEINTZ	92	CSB2	$\Upsilon(3S) \to \gamma\gamma\ell^+\ell^-$

[42] From a sample of $\Upsilon(3S) \to \gamma\gamma\mu^+\mu^-$ with converted photons.

[43] CRAWFORD 92B quotes $2\times B(\Upsilon(3S) \to \gamma\chi_{bJ}(2P))\ B(\chi_{bJ}(2P) \to \gamma\Upsilon(nS))\ B(\Upsilon(nS) \to \ell^+\ell^-)$.

[44] Calculated by us. HEINTZ 92 quotes $B(\Upsilon(3S) \to \gamma\chi_{b2}(2P)) \times B(\chi_{b2}(2P) \to \gamma\Upsilon(2S)) = (1.90 \pm 0.23 \pm 0.18)\%$ using $B(\Upsilon(2S) \to \mu^+\mu^-) = (1.44 \pm 0.10)\%$.

$[B(\chi_{b2}(2P) \to \gamma\Upsilon(2S)) \times B(\Upsilon(3S) \to \gamma\chi_{b2}(2P))] / [B(\chi_{b1}(2P) \to \gamma\Upsilon(2S)) \times B(\Upsilon(3S) \to \gamma\chi_{b1}(2P))]$

VALUE (%)	DOCUMENT ID		TECN	COMMENT
46.9±2.0	[45] LEES	14M	BABR	$\Upsilon(3S) \to \gamma\gamma\mu^+\mu^-$

[45] From a sample of $\Upsilon(3S) \to \gamma\gamma\mu^+\mu^-$ without converted photons.

$\chi_{b2}(2P)$ REFERENCES

STOTTLER	25	PRL 135 121902	Z.S. Stottler *et al.*	(BELLE Collab.)
AAIJ	24AC	JHEP 2410 122	R. Aaij *et al.*	(LHCb Collab.)
AAIJ	14BG	JHEP 1410 088	R. Aaij *et al.*	(LHCb Collab.)
LEES	14M	PR D90 112010	J.P. Lees *et al.*	(BABAR Collab.)
LEES	11C	PR D84 011104	J.P. Lees *et al.*	(BABAR Collab.)
LEES	11J	PR D84 072002	J.P. Lees *et al.*	(BABAR Collab.)
ASNER	08A	PR D78 091103	D.M. Asner *et al.*	(CLEO Collab.)
BRIERE	08	PR D78 092007	R.A. Briere *et al.*	(CLEO Collab.)
CAWLFIELD	06	PR D73 012003	C. Cawlfield *et al.*	(CLEO Collab.)
ARTUSO	05	PRL 94 032001	M. Artuso *et al.*	(CLEO Collab.)
CRONIN-HEN...	04	PRL 92 222002	D. Cronin-Hennessy *et al.*	(CLEO Collab.)
CRAWFORD	92B	PL B294 139	G. Crawford *et al.*	(CLEO Collab.)
HEINTZ	92	PR D46 1928	U. Heintz *et al.*	(CUSB II Collab.)
HEINTZ	91	PRL 66 1563	U. Heintz *et al.*	(CUSB Collab.)
MORRISON	91	PRL 67 1696	R.J. Morrison *et al.*	(CLEO Collab.)
NARAIN	91	PRL 66 3113	M. Narain *et al.*	(CUSB Collab.)

$\Upsilon(3S)$

$I^G(J^{PC}) = 0^-(1^{--})$

$\Upsilon(3S)$ MASS

VALUE (MeV)	DOCUMENT ID		TECN	COMMENT
10355.1±0.5	[1] SHAMOV	23	RVUE	$e^+e^- \to$ hadrons
• • • We do not use the following data for averages, fits, limits, etc. • • •				
10355.2±0.5	[2,3] ARTAMONOV	00	MD1	$e^+e^- \to$ hadrons
10355.3±0.5	[4,5] BARU	86B	MD1	$e^+e^- \to$ hadrons

[1] Reanalysis of MD1 data using the electron mass from COHEN 87, the radiative corrections from KURAEV 85 and interference effects.

[2] Reanalysis of BARU 86B using new electron mass (COHEN 87).

[3] Superseded by SHAMOV 23.

[4] Reanalysis of ARTAMONOV 84.

[5] Superseded by ARTAMONOV 00.

$m_{\Upsilon(3S)} - m_{\Upsilon(2S)}$

VALUE (MeV)	EVTS	DOCUMENT ID		TECN	COMMENT
331.82±0.08 OUR AVERAGE	Error includes scale factor of 1.9. See the ideogram below.				
331.77±0.07±0.10	1.8M	[6] AAIJ	24AC	LHCB	$\Upsilon \to \mu^+\mu^-$
331.88±0.03±0.04	1.5k	[6] AAIJ	24AC	LHCB	$\Upsilon(3S) \to \Upsilon(2S)\pi^+\pi^-$
331.50±0.02±0.13		LEES	11C	BABR	$e^+e^- \to \pi^+\pi^-X$

[6] Observed in prompt pp production.

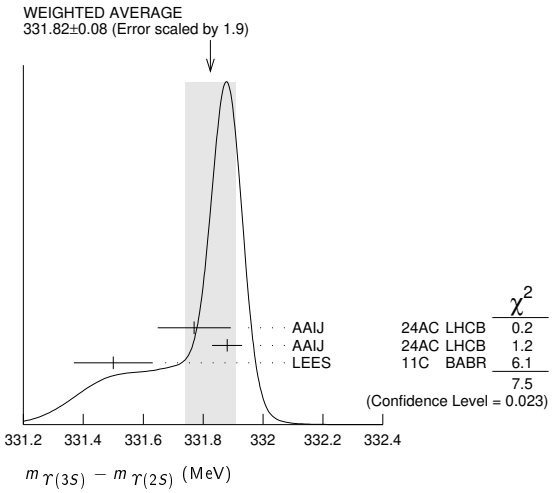

$\Upsilon(3S)$ WIDTH

VALUE (keV)	DOCUMENT ID
20.32±1.85 OUR EVALUATION	See the Note on "Width Determinations of the Υ States"

Int. J. Mod. Phys. A 2026.41. Downloaded from www.worldscientific.com
by UNIVERSITY OF CALIFORNIA @ BERKELEY on 09/16/26. Re-use and distribution is strictly not permitted, except for Open Access articles.

$\Upsilon(3S)$ DECAY MODES

	Mode	Fraction (Γ_i/Γ)	Scale factor/ Confidence level
Γ_1	$\Upsilon(2S)$ anything	(10.6 ± 0.8) %	
Γ_2	$\Upsilon(2S)\pi^+\pi^-$	(2.82 ± 0.18) %	S=1.6
Γ_3	$\Upsilon(2S)\pi^0\pi^0$	(1.85 ± 0.14) %	
Γ_4	$\Upsilon(2S)\gamma\gamma$	(5.0 ± 0.7) %	
Γ_5	$\Upsilon(2S)\pi^0$	$< 5.1 \times 10^{-4}$	CL=90%
Γ_6	$\Upsilon(1S)\pi^+\pi^-$	(4.37 ± 0.08) %	
Γ_7	$\Upsilon(1S)\pi^0\pi^0$	(2.20 ± 0.13) %	
Γ_8	$\Upsilon(1S)\eta$	$< 1 \times 10^{-4}$	CL=90%
Γ_9	$\Upsilon(1S)\pi^0$	$< 7 \times 10^{-5}$	CL=90%
Γ_{10}	$h_b(1P)\pi^0$	$< 1.2 \times 10^{-3}$	CL=90%
Γ_{11}	$h_b(1P)\pi^0 \to \gamma\eta_b(1S)\pi^0$	$(4.3 \pm 1.4) \times 10^{-4}$	
Γ_{12}	$h_b(1P)\pi^+\pi^-$	$< 1.2 \times 10^{-4}$	CL=90%
Γ_{13}	$\tau^+\tau^-$	(2.29 ± 0.30) %	
Γ_{14}	$\mu^+\mu^-$	(2.18 ± 0.21) %	S=2.1
Γ_{15}	e^+e^-	(2.18 ± 0.20) %	
Γ_{16}	hadrons	(93 ± 12) %	
Γ_{17}	ggg	(35.7 ± 2.6) %	
Γ_{18}	$\underline{\gamma gg}$	$(9.7 \pm 1.8) \times 10^{-3}$	
Γ_{19}	^2H anything	$(2.33 \pm 0.33) \times 10^{-5}$	
	Radiative decays		
Γ_{20}	$\gamma\chi_{b2}(2P)$	(13.1 ± 1.6) %	S=3.4
Γ_{21}	$\gamma\chi_{b1}(2P)$	(12.6 ± 1.2) %	S=2.4
Γ_{22}	$\gamma\chi_{b0}(2P)$	(5.9 ± 0.6) %	S=1.4
Γ_{23}	$\gamma\chi_{b2}(1P)$	$(10.0 \pm 1.0) \times 10^{-3}$	S=1.7
Γ_{24}	$\gamma\chi_{b1}(1P)$	$(9 \pm 5) \times 10^{-4}$	S=1.8
Γ_{25}	$\gamma\chi_{b0}(1P)$	$(2.7 \pm 0.4) \times 10^{-3}$	
Γ_{26}	$\gamma\eta_b(2S)$	$< 6.2 \times 10^{-4}$	CL=90%
Γ_{27}	$\gamma\eta_b(1S)$	$(5.1 \pm 0.7) \times 10^{-4}$	
Γ_{28}	$\gamma A^0 \to \gamma$ hadrons	$< 8 \times 10^{-5}$	CL=90%
Γ_{29}	$\gamma X \to \gamma + \geq 4$ prongs	[a] $< 2.2 \times 10^{-4}$	CL=95%
Γ_{30}	$\gamma A^0 \to \gamma\mu^+\mu^-$	$< 5.5 \times 10^{-6}$	CL=90%
Γ_{31}	$\gamma A^0 \to \gamma\tau^+\tau^-$	[b] $< 1.6 \times 10^{-4}$	CL=90%
	Lepton Family number (*LF*) violating modes		
Γ_{32}	$e^\pm\tau^\mp$ *LF*	$< 4.2 \times 10^{-6}$	CL=90%
Γ_{33}	$e^\pm\mu^\mp$ *LF*	$< 3.6 \times 10^{-7}$	CL=90%
Γ_{34}	$\mu^\pm\tau^\mp$ *LF*	$< 3.1 \times 10^{-6}$	CL=90%

[a] 1.5 GeV $< m_X <$ 5.0 GeV

[b] For $m_{\tau^+\tau^-}$ in the ranges 4.03–9.52 and 9.61–10.10 GeV.

$\Upsilon(3S)$ $\Gamma(i)\Gamma(e^+e^-)/\Gamma(\text{total})$

$\Gamma(\text{hadrons}) \times \Gamma(e^+e^-)/\Gamma_{\text{total}}$ — $\Gamma_{16}\Gamma_{15}/\Gamma$

VALUE (keV)	DOCUMENT ID		TECN	COMMENT
0.414±0.007 OUR AVERAGE				
0.413±0.004±0.006	ROSNER	06	CLEO	10.4 $e^+e^- \to$ hadrons
0.45 ±0.03 ±0.03	[7] GILES	84B	CLEO	$e^+e^- \to$ hadrons

[7] Radiative corrections reevaluated by BUCHMUELLER 88 following KURAEV 85.

$\Gamma(\Upsilon(1S)\pi^+\pi^-) \times \Gamma(e^+e^-)/\Gamma_{\text{total}}$ — $\Gamma_6\Gamma_{15}/\Gamma$

VALUE (eV)	EVTS	DOCUMENT ID		TECN	COMMENT
18.46±0.27±0.77	6.4k	[8] AUBERT	08BP	BABR	$e^+e^- \to \gamma\pi^+\pi^-\ell^+\ell^-$

[8] Using B($\Upsilon(1S) \to e^+e^-$) = (2.38 ± 0.11)% and B($\Upsilon(1S) \to \mu^+\mu^-$) = (2.48 ± 0.05)%.

$\Upsilon(3S)$ PARTIAL WIDTHS

$\Gamma(e^+e^-)$ — Γ_{15}

VALUE (keV)	DOCUMENT ID
0.443±0.008 OUR EVALUATION	

$\Upsilon(3S)$ BRANCHING RATIOS

$\Gamma(\Upsilon(2S)\text{anything})/\Gamma_{\text{total}}$ — Γ_1/Γ

VALUE	EVTS	DOCUMENT ID		TECN	COMMENT
0.106 ±0.008 OUR AVERAGE					
0.1023±0.0105	4625	[9,10,11] BUTLER	94B	CLE2	$e^+e^- \to \ell^+\ell^-$X
0.111 ±0.012	4891	[10,11,12] BROCK	91	CLEO	$e^+e^- \to \pi^+\pi^-$X, $\pi^+\pi^-\ell^+\ell^-$

[9] Using B($\Upsilon(2S) \to \Upsilon(1S)\gamma\gamma$) = (0.038 ± 0.007)%, and B($\Upsilon(2S) \to \Upsilon(1S)\pi^0\pi^0$) = (1/2)B($\Upsilon(2S) \to \Upsilon(1S)\pi^+\pi^-$).

[10] Using B($\Upsilon(1S) \to \mu^+\mu^-$) = (2.48 ± 0.06)%. With the assumption of $e\mu$ universality.

[11] Using B($\Upsilon(2S) \to \Upsilon(1S)\pi^+\pi^-$) = (18.5 ± 0.8)%.

[12] Using B($\Upsilon(2S) \to \mu^+\mu^-$) = (1.31 ± 0.21)%, B($\Upsilon(2S) \to \Upsilon(1S)\gamma\gamma$)×2B($\Upsilon(1S) \to \mu^+\mu^-$) = (0.188 ± 0.035)%, and B($\Upsilon(2S) \to \Upsilon(1S)\pi^0\pi^0$)×2B($\Upsilon(1S) \to \mu^+\mu^-$) = (0.436 ± 0.056)%. With the assumption of $e\mu$ universality.

$\Gamma(\Upsilon(2S)\pi^+\pi^-)/\Gamma_{\text{total}}$ — Γ_2/Γ

VALUE (units 10^{-2})	EVTS	DOCUMENT ID		TECN	COMMENT
2.82±0.18 OUR AVERAGE	Error includes scale factor of 1.6. See the ideogram below.				
3.00±0.02±0.14	543k	LEES	11C	BABR	$e^+e^- \to \pi^+\pi^-X$
2.40±0.10±0.26	800	[13] AUBERT	08BP	BABR	$e^+e^- \to \gamma\pi^+\pi^-e^+e^-$
3.12±0.49	980	[14,15] BUTLER	94B	CLE2	$e^+e^- \to \pi^+\pi^-\ell^+\ell^-$
2.13±0.38	974	[16] BROCK	91	CLEO	$e^+e^- \to \pi^+\pi^-$X, $\pi^+\pi^-\ell^+\ell^-$
• • • We do not use the following data for averages, fits, limits, etc. • • •					
4.82±0.65±0.53	138	[16] WU	93	CUSB	$\Upsilon(3S) \to \pi^+\pi^-\ell^+\ell^-$
3.1 ±2.0	5	MAGERAS	82	CUSB	$\Upsilon(3S) \to \pi^+\pi^-\ell^+\ell^-$

[13] Using B($\Upsilon(1S) \to e^+e^-$) = (2.38 ± 0.11)%, B($\Upsilon(1S) \to \mu^+\mu^-$) = (2.48 ± 0.05)%, and $\Gamma_{ee}(\Upsilon(3S))$ = 0.443 ± 0.008 keV.

[14] From the exclusive mode.

[15] Using B($\Upsilon(2S) \to \Upsilon(1S)\gamma\gamma$) = (0.038 ± 0.007)%, and B($\Upsilon(2S) \to \Upsilon(1S)\pi^0\pi^0$) = (1/2)B($\Upsilon(2S) \to \Upsilon(1S)\pi^+\pi^-$).

[16] Using B($\Upsilon(2S) \to \mu^+\mu^-$) = (1.31 ± 0.21)%, B($\Upsilon(2S) \to \Upsilon(1S)\gamma\gamma$)×2B($\Upsilon(1S) \to \mu^+\mu^-$) = (0.188 ± 0.035)%, and B($\Upsilon(2S) \to \Upsilon(1S)\pi^0\pi^0$)×2B($\Upsilon(1S) \to \mu^+\mu^-$) = (0.436 ± 0.056)%. With the assumption of $e\mu$ universality.

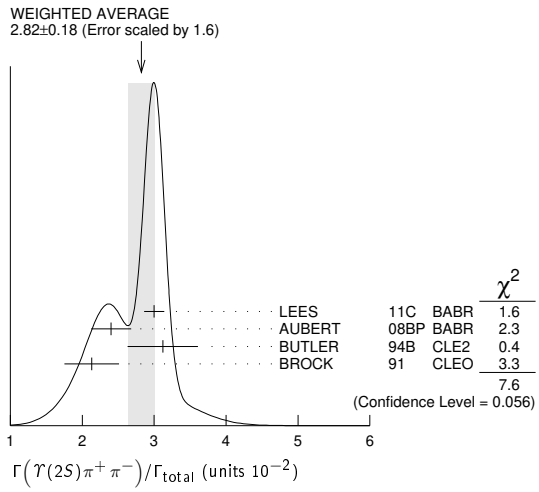

$\Gamma(\Upsilon(2S)\pi^0\pi^0)/\Gamma_{\text{total}}$ — Γ_3/Γ

VALUE (units 10^{-2})	EVTS	DOCUMENT ID		TECN	COMMENT
1.85±0.14 OUR AVERAGE					
1.82±0.09±0.12	4391	[17] BHARI	09	CLEO	$e^+e^- \to \pi^0\pi^0\ell^+\ell^-$
2.16±0.39		[18,19] BUTLER	94B	CLE2	$e^+e^- \to \pi^0\pi^0\ell^+\ell^-$
1.7 ±0.5 ±0.2	10	[20] HEINTZ	92	CSB2	$e^+e^- \to \pi^0\pi^0\ell^+\ell^-$

[17] Authors assume B($\Upsilon(1S) \to e^+e^-$) + B($\Upsilon(1S) \to \mu^+\mu^-$) = 4.06%.

[18] B($\Upsilon(2S) \to \mu^+\mu^-$) = (1.31 ± 0.21)% and assuming $e\mu$ universality.

[19] From the exclusive mode.

[20] B($\Upsilon(2S) \to \mu^+\mu^-$) = (1.44 ± 0.10)% and assuming $e\mu$ universality. Supersedes HEINTZ 91.

$\Gamma(\Upsilon(2S)\gamma\gamma)/\Gamma_{\text{total}}$ — Γ_4/Γ

VALUE	DOCUMENT ID		TECN	COMMENT
0.0502±0.0069	[21] BUTLER	94B	CLE2	$e^+e^- \to \ell^+\ell^-2\gamma$

[21] From the exclusive mode.

$\Gamma(\Upsilon(2S)\pi^0)/\Gamma_{\text{total}}$ — Γ_5/Γ

VALUE (units 10^{-3})	CL%	DOCUMENT ID		TECN	COMMENT
<0.51	90	[22] HE	08A	CLEO	$e^+e^- \to \ell^+\ell^-\gamma\gamma$

[22] Authors assume B($\Upsilon(2S) \to e^+e^-$) + B($\Upsilon(1S) \to \mu^+\mu^-$) = 4.06%.

$\Gamma(\Upsilon(1S)\pi^+\pi^-)/\Gamma_{\text{total}}$ — Γ_6/Γ

Abbreviation MM in the *COMMENT* field below stands for missing mass.

VALUE (units 10^{-2})	EVTS	DOCUMENT ID		TECN	COMMENT
4.37±0.08 OUR AVERAGE					
4.32±0.07±0.13	90k	[23] LEES	11L	BABR	$\Upsilon(3S) \to \pi^+\pi^-\ell^+\ell^-$
4.46±0.01±0.13	190k	[24] BHARI	09	CLEO	$e^+e^- \to \pi^+\pi^-$ MM
4.17±0.06±0.19	6.4k	[25] AUBERT	08BP	BABR	10.58 $e^+e^- \to \gamma\pi^+\pi^-\ell^+\ell^-$
4.52±0.35	11830	[26] BUTLER	94B	CLE2	$e^+e^- \to \pi^+\pi^-$X, $\pi^+\pi^-\ell^+\ell^-$
4.46±0.34±0.50	451	[26] WU	93	CUSB	$\Upsilon(3S) \to \pi^+\pi^-\ell^+\ell^-$
4.46±0.30	11221	[26] BROCK	91	CLEO	$e^+e^- \to \pi^+\pi^-$X, $\pi^+\pi^-\ell^+\ell^-$
• • • We do not use the following data for averages, fits, limits, etc. • • •					
4.9 ±1.0	22	GREEN	82	CLEO	$\Upsilon(3S) \to \pi^+\pi^-\ell^+\ell^-$
3.9 ±1.3	26	MAGERAS	82	CUSB	$\Upsilon(3S) \to \pi^+\pi^-\ell^+\ell^-$

[23] Using B($\Upsilon(1S) \to e^+e^-$) = (2.38 ± 0.11)% and B($\Upsilon(1S) \to \mu^+\mu^-$) = (2.48 ± 0.05)%.

[24] A weighted average of the inclusive and exclusive results.

[25] Using B($\Upsilon(2S) \to e^+e^-$) = (1.91 ± 0.16)%, B($\Upsilon(2S) \to \mu^+\mu^-$) = (1.93 ± 0.17)%, and $\Gamma_{ee}(\Upsilon(3S))$ = 0.443 ± 0.008 keV.

[26] Using B($\Upsilon(1S) \to \mu^+\mu^-$) = (2.48 ± 0.06)%. With the assumption of $e\mu$ universality.

Int. J. Mod. Phys. A 2026.41. Downloaded from www.worldscientific.com by CALIFORNIA @ BERKELEY on 09/16/26. Re-use and distribution is strictly not permitted, except for Open Access articles.

$\Gamma(\Upsilon(2S)\pi^+\pi^-)/\Gamma(\Upsilon(1S)\pi^+\pi^-)$ — Γ_2/Γ_6

VALUE	EVTS	DOCUMENT ID		TECN	COMMENT
• • • We do not use the following data for averages, fits, limits, etc. • • •					
$0.577\pm0.026\pm0.060$	800	[27] AUBERT	08BP	BABR	$e^+e^- \to \gamma\pi^+\pi^-\ell^+\ell^-$

[27] Using $B(\Upsilon(1S) \to e^+e^-) = (2.38\pm0.11)\%$, $B(\Upsilon(1S) \to \mu^+\mu^-) = (2.48\pm0.05)\%$, $B(\Upsilon(2S) \to e^+e^-) = (1.91\pm0.16)\%$, and $B(\Upsilon(2S) \to \mu^+\mu^-) = (1.93\pm0.17)\%$. Not independent of other values reported by AUBERT 08BP.

$\Gamma(\Upsilon(1S)\pi^0\pi^0)/\Gamma_{total}$ — Γ_7/Γ

VALUE (units 10^{-2})	EVTS	DOCUMENT ID		TECN	COMMENT
2.20±0.13 OUR AVERAGE					
$2.24\pm0.09\pm0.11$	6584	[28] BHARI	09	CLEO	$e^+e^- \to \pi^0\pi^0\ell^+\ell^-$
1.99 ± 0.34	56	[29] BUTLER	94B	CLE2	$e^+e^- \to \pi^0\pi^0\ell^+\ell^-$
$2.2\ \pm0.4\ \pm0.3$	33	[30] HEINTZ	92	CSB2	$e^+e^- \to \pi^0\pi^0\ell^+\ell^-$

[28] Authors assume $B(\Upsilon(1S) \to e^+e^-) + B(\Upsilon(1S) \to \mu^+\mu^-) = 4.96\%$.
[29] Using $B(\Upsilon(1S) \to \mu^+\mu^-) = (2.48\pm0.06)\%$ and assuming $e\mu$ universality.
[30] Using $B(\Upsilon(1S) \to \mu^+\mu^-) = (2.57\pm0.07)\%$ and assuming $e\mu$ universality. Supersedes HEINTZ 91.

$\Gamma(\Upsilon(1S)\pi^0\pi^0)/\Gamma(\Upsilon(1S)\pi^+\pi^-)$ — Γ_7/Γ_6

VALUE	DOCUMENT ID		TECN	COMMENT
• • • We do not use the following data for averages, fits, limits, etc. • • •				
0.501 ± 0.043	[31] BHARI	09	CLEO	$e^+e^- \to \Upsilon(3S)$

[31] Not independent of other values reported by BHARI 09.

$\Gamma(\Upsilon(1S)\eta)/\Gamma_{total}$ — Γ_8/Γ

VALUE (units 10^{-3})	CL%	DOCUMENT ID		TECN	COMMENT
<0.1	90	[32] LEES	11L	BABR	$\Upsilon(3S) \to (\pi^+\pi^-)(\gamma\gamma)\ell^+\ell^-$
• • • We do not use the following data for averages, fits, limits, etc. • • •					
<0.8	90	[32,33] AUBERT	08BP	BABR	$e^+e^- \to \gamma\pi^+\pi^-\pi^0\ell^+\ell^-$
<0.18	90	[34] HE	08A	CLEO	$e^+e^- \to \ell^+\ell^-\eta$
<2.2	90	BROCK	91	CLEO	$e^+e^- \to \ell^+\ell^-\eta$

[32] Using $B(\Upsilon(1S) \to e^+e^-) = (2.38\pm0.11)\%$, $B(\Upsilon(1S) \to \mu^+\mu^-) = (2.48\pm0.05)\%$.
[33] Using $\Gamma_{ee}(\Upsilon(3S)) = 0.443\pm0.008$ keV.
[34] Authors assume $B(\Upsilon(1S) \to e^+e^-) + B(\Upsilon(1S) \to \mu^+\mu^-) = 4.96\%$.

$\Gamma(\Upsilon(1S)\eta)/\Gamma(\Upsilon(1S)\pi^+\pi^-)$ — Γ_8/Γ_6

VALUE (units 10^{-2})	CL%	DOCUMENT ID		TECN	COMMENT
<0.23	90	[35] LEES	11L	BABR	$\Upsilon(3S) \to (\pi^+\pi^-)(\gamma\gamma)\ell^+\ell^-$
• • • We do not use the following data for averages, fits, limits, etc. • • •					
<1.9	90	[36] AUBERT	08BP	BABR	$e^+e^- \to \gamma\pi^+\pi^-(\pi^0)\ell^+\ell^-$

[35] Not independent of other values reported by LEES 11L.
[36] Not independent of other values reported by AUBERT 08BP.

$\Gamma(\Upsilon(1S)\pi^0)/\Gamma_{total}$ — Γ_9/Γ

VALUE (units 10^{-3})	CL%	DOCUMENT ID		TECN	COMMENT
<0.07	90	[37] HE	08A	CLEO	$e^+e^- \to \ell^+\ell^-\gamma\gamma$

[37] Authors assume $B(\Upsilon(1S) \to e^+e^-) + B(\Upsilon(1S) \to \mu^+\mu^-) = 4.96\%$.

$\Gamma(h_b(1P)\pi^0)/\Gamma_{total}$ — Γ_{10}/Γ

VALUE	CL%	DOCUMENT ID		TECN	COMMENT
$<1.2\times10^{-3}$	90	[38] GE	11	CLEO	$\Upsilon(3S) \to \pi^0$ anything

[38] Assuming $M(h_b(1P)) = 9900$ MeV and $\Gamma(h_b(1P)) = 0$ MeV, and allowing $B(h_b(1P) \to \gamma\eta_b(1S))$ to vary from 0–100%.

$\Gamma(h_b(1P)\pi^0 \to \gamma\eta_b(1S)\pi^0)/\Gamma_{total}$ — Γ_{11}/Γ

VALUE (units 10^{-4})	DOCUMENT ID		TECN	COMMENT
4.3±1.1±0.9	LEES	11K	BABR	$\Upsilon(3S) \to \eta_b\gamma\pi^0$

$\Gamma(h_b(1P)\pi^+\pi^-)/\Gamma_{total}$ — Γ_{12}/Γ

VALUE (units 10^{-4})	CL%	DOCUMENT ID		TECN	COMMENT
< 1.2	90	[39] LEES	11C	BABR	$e^+e^- \to \pi^+\pi^-X$
• • • We do not use the following data for averages, fits, limits, etc. • • •					
<18		[39] BUTLER	94B	CLE2	$e^+e^- \to \pi^+\pi^-X$
<15		[39] BROCK	91	CLEO	$e^+e^- \to \pi^+\pi^-X$

[39] For $M(h_b(1P)) = 9900$ MeV.

$\Gamma(\tau^+\tau^-)/\Gamma_{total}$ — Γ_{13}/Γ

VALUE (units 10^{-2})	EVTS	DOCUMENT ID		TECN	COMMENT
2.29±0.21±0.22	15k	[40] BESSON	07	CLEO	$e^+e^- \to \Upsilon(3S) \to \tau^+\tau^-$

[40] BESSON 07 reports $[\Gamma(\Upsilon(3S) \to \tau^+\tau^-)/\Gamma_{total}] / [B(\Upsilon(3S) \to \mu^+\mu^-)] = 1.05\pm0.08\pm0.05$ which we multiply by our best (shown rounded) value $B(\Upsilon(3S) \to \mu^+\mu^-) = (2.18\pm0.21)\times10^{-2}$. Our first error is their experiment's error and our second error is the systematic error from using our best (shown rounded) value.

$\Gamma(\tau^+\tau^-)/\Gamma(\mu^+\mu^-)$ — Γ_{13}/Γ_{14}

VALUE	EVTS	DOCUMENT ID		TECN	COMMENT
0.968±0.016 OUR AVERAGE					
$0.966\pm0.008\pm0.014$	2.2M	LEES	20E	BABR	$e^+e^- \to \Upsilon(3S)$
$1.05\ \pm0.08\ \pm0.05$	15k	BESSON	07	CLEO	$e^+e^- \to \Upsilon(3S)$

$\Gamma(\mu^+\mu^-)/\Gamma_{total}$ — Γ_{14}/Γ

VALUE	EVTS	DOCUMENT ID		TECN	COMMENT
0.0218±0.0021 OUR AVERAGE Error includes scale factor of 2.1. See the ideogram below.					
$0.0239\pm0.0007\pm0.0010$	81k	ADAMS	05	CLEO	$e^+e^- \to \mu^+\mu^-$
$0.0202\pm0.0019\pm0.0033$		CHEN	89B	CLEO	$e^+e^- \to \mu^+\mu^-$
$0.0173\pm0.0015\pm0.0011$		KAARSBERG	89	CSB2	$e^+e^- \to \mu^+\mu^-$
$0.033\ \pm0.013\ \pm0.007$	1096	ANDREWS	83	CLEO	$e^+e^- \to \mu^+\mu^-$

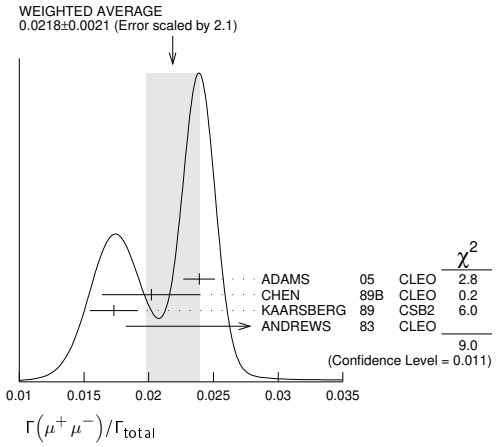

$\Gamma(ggg)/\Gamma_{total}$ — Γ_{17}/Γ

VALUE (units 10^{-2})	EVTS	DOCUMENT ID		TECN	COMMENT
35.7±2.6	3M	[41] BESSON	06A	CLEO	$\Upsilon(3S) \to$ hadrons

[41] Calculated using BESSON 06A value of $\Gamma(\gamma gg)/\Gamma(ggg) = (2.72\pm0.06\pm0.32\pm0.37)\%$ and the PDG 08 values of $B(\Upsilon(2S) + \text{anything}) = (10.6\pm0.8)\%$, $B(\pi^+\pi^-\Upsilon(1S)) = (4.40\pm0.10)\%$, $B(\pi^0\pi^0\Upsilon(1S)) = (2.20\pm0.13)\%$, $B(\gamma\chi_{b2}(2P)) = (13.1\pm1.6)\%$, $B(\gamma\chi_{b1}(2P)) = (12.6\pm1.2)\%$, $B(\gamma\chi_{b0}(2P)) = (5.9\pm0.6)\%$, $B(\gamma\chi_{b0}(1P)) = (0.30\pm0.11)\%$, $B(\mu^+\mu^-) = (2.18\pm0.21)\%$, and $R_{hadrons} = 3.51$. The statistical error is negligible and the systematic error is partially correlated with $\Gamma(\gamma gg)/\Gamma_{total}$ BESSON 06A value.

$\Gamma(\gamma gg)/\Gamma_{total}$ — Γ_{18}/Γ

VALUE (units 10^{-2})	EVTS	DOCUMENT ID		TECN	COMMENT
0.97±0.18	60k	[42] BESSON	06A	CLEO	$\Upsilon(3S) \to \gamma +$ hadrons

[42] Calculated using BESSON 06A values of $\Gamma(\gamma gg)/\Gamma(ggg) = (2.72\pm0.06\pm0.32\pm0.37)\%$ and $\Gamma(ggg)/\Gamma_{total}$. The statistical error is negligible and the systematic error is partially correlated with $\Gamma(ggg)/\Gamma_{total}$ BESSON 06A value.

$\Gamma(\gamma gg)/\Gamma(ggg)$ — Γ_{18}/Γ_{17}

VALUE (units 10^{-2})	EVTS	DOCUMENT ID		TECN	COMMENT
2.72±0.06±0.49	3M	BESSON	06A	CLEO	$\Upsilon(3S) \to (\gamma +)$ hadrons

$\Gamma(\overline{^2H}\text{ anything})/\Gamma_{total}$ — Γ_{19}/Γ

VALUE (units 10^{-5})	DOCUMENT ID		TECN	COMMENT
$2.33\pm0.15^{+0.31}_{-0.28}$	LEES	14G	BABR	$e^+e^- \to \overline{^2H}X$

$\Gamma(\gamma\chi_{b2}(2P))/\Gamma_{total}$ — Γ_{20}/Γ

VALUE	EVTS	DOCUMENT ID		TECN	COMMENT
0.131 ±0.016 OUR AVERAGE Error includes scale factor of 3.4. See the ideogram below.					
$0.1579\pm0.0017\pm0.0073$	568k	ARTUSO	05	CLEO	$e^+e^- \to \gamma X$
$0.111\ \pm0.005\ \pm0.004$	10319	[43] HEINTZ	92	CSB2	$e^+e^- \to \gamma X$
$0.135\ \pm0.003\ \pm0.017$	30741	MORRISON	91	CLE2	$e^+e^- \to \gamma X$

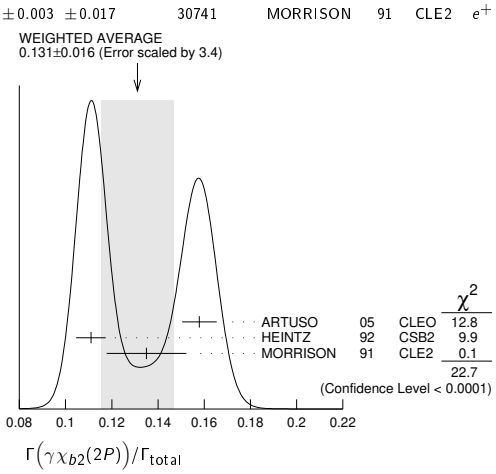

Int. J. Mod. Phys. A 2026.41. Downloaded from www.worldscientific.com by UNIVERSITY OF CALIFORNIA @ BERKELEY on 09/16/26. Re-use and distribution is strictly not permitted, except for Open Access articles.

[43] Supersedes NARAIN 91.

$\Gamma(\gamma\chi_{b1}(2P))/\Gamma_{total}$ — Γ_{21}/Γ

VALUE	EVTS	DOCUMENT ID		TECN	COMMENT
0.126 ±0.012 OUR AVERAGE Error includes scale factor of 2.4. See the ideogram below.					
0.1454±0.0018±0.0073	537k	ARTUSO	05	CLEO	$e^+e^- \to \gamma X$
0.115 ±0.005 ±0.005	11147	[44] HEINTZ	92	CSB2	$e^+e^- \to \gamma X$
0.105 $^{+0.003}_{-0.002}$ ±0.013	25759	MORRISON	91	CLE2	$e^+e^- \to \gamma X$

[44] Supersedes NARAIN 91.

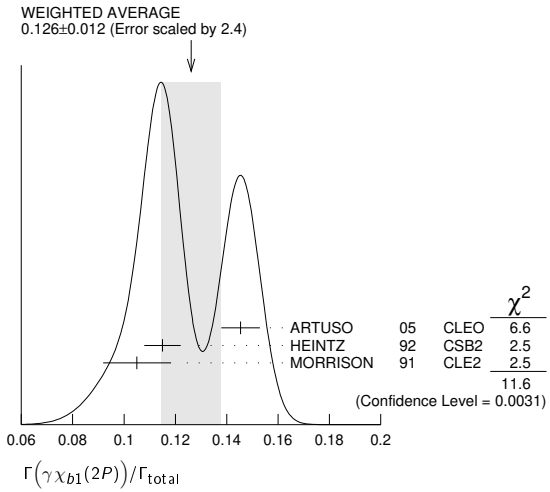

$\Gamma(\gamma\chi_{b0}(2P))/\Gamma_{total}$ — Γ_{22}/Γ

VALUE	EVTS	DOCUMENT ID		TECN	COMMENT
0.059 ±0.006 OUR AVERAGE Error includes scale factor of 1.4. See the ideogram below.					
0.0677±0.0020±0.0065	225k	ARTUSO	05	CLEO	$e^+e^- \to \gamma X$
0.060 ±0.004 ±0.006	4959	[45] HEINTZ	92	CSB2	$e^+e^- \to \gamma X$
0.049 $^{+0.003}_{-0.004}$ ±0.006	9903	MORRISON	91	CLE2	$e^+e^- \to \gamma X$

[45] Supersedes NARAIN 91.

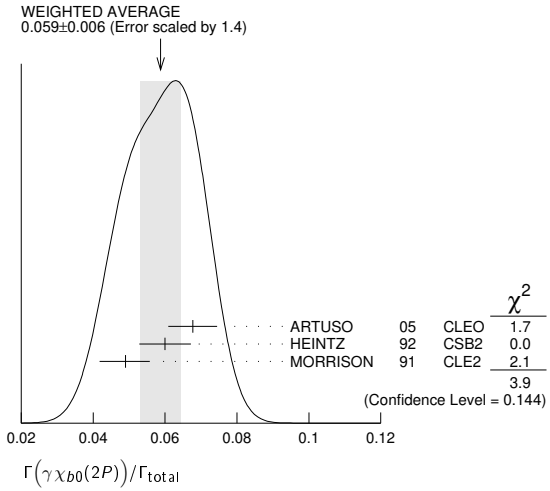

$\Gamma(\gamma\chi_{b2}(1P))/\Gamma_{total}$ — Γ_{23}/Γ

VALUE (units 10^{-3})	CL%	EVTS	DOCUMENT ID		TECN	COMMENT
10.0±1.0 OUR AVERAGE Error includes scale factor of 1.7.						
8.0±1.3±0.4		126	[46,47] KORNICER	11	CLEO	$e^+e^- \to \gamma\gamma\ell^+\ell^-$
10.5±0.3$^{+0.7}_{-0.6}$		9.7k	LEES	11J	BABR	$\Upsilon(3S) \to X\gamma$
• • • We do not use the following data for averages, fits, limits, etc. • • •						
<19	90		[48] ASNER	08A	CLEO	$\Upsilon(3S) \to \gamma +$ hadrons
seen			[49] HEINTZ	92	CSB2	$e^+e^- \to \gamma\gamma\ell^+\ell^-$

[46] Assuming $B(\Upsilon(1S) \to \ell^+\ell^-) = (2.48 \pm 0.05)\%$.

[47] KORNICER 11 reports $[\Gamma(\Upsilon(3S) \to \gamma\chi_{b2}(1P))/\Gamma_{total}] \times [B(\chi_{b2}(1P) \to \gamma\Upsilon(1S))] = (1.435 \pm 0.162 \pm 0.169) \times 10^{-3}$ which we divide by our best (shown rounded) value $B(\chi_{b2}(1P) \to \gamma\Upsilon(1S)) = (18.0 \pm 1.0) \times 10^{-2}$. Our first error is their experiment's error and our second error is the systematic error from using our best (shown rounded) value.

[48] ASNER 08A reports $[\Gamma(\Upsilon(3S) \to \gamma\chi_{b2}(1P))/\Gamma_{total}]$ / $[B(\Upsilon(2S) \to \gamma\chi_{b2}(1P))]$ $< 27.1 \times 10^{-2}$ which we multiply by our best (shown rounded) value $B(\Upsilon(2S) \to \gamma\chi_{b2}(1P)) = 7.15 \times 10^{-2}$.

[49] HEINTZ 92, while unable to distinguish between different J states, measures $\sum_J B(\Upsilon(3S) \to \gamma\chi_{bJ}) \times B(\chi_{bJ} \to \gamma\Upsilon(1S)) = (1.7 \pm 0.4 \pm 0.6) \times 10^{-3}$ for $J = 0,1,2$ using inclusive $\Upsilon(1S)$ decays and $(1.2^{+0.4}_{-0.3} \pm 0.09) \times 10^{-3}$ for $J = 1,2$ using $\Upsilon(1S) \to \ell^+\ell^-$.

$\Gamma(\gamma\chi_{b1}(1P))/\Gamma_{total}$ — Γ_{24}/Γ

VALUE (units 10^{-3})	CL%	EVTS	DOCUMENT ID		TECN	COMMENT
0.9±0.5 OUR AVERAGE Error includes scale factor of 1.8.						
1.5±0.4±0.1		50	[50,51] KORNICER	11	CLEO	$e^+e^- \to \gamma\gamma\ell^+\ell^-$
0.5±0.3$^{+0.2}_{-0.1}$			LEES	11J	BABR	$\Upsilon(3S) \to X\gamma$
• • • We do not use the following data for averages, fits, limits, etc. • • •						
<1.7	90		[52] ASNER	08A	CLEO	$\Upsilon(3S) \to \gamma +$ hadrons
seen			[53] HEINTZ	92	CSB2	$e^+e^- \to \gamma\gamma\ell^+\ell^-$

[50] Assuming $B(\Upsilon(1S) \to \ell^+\ell^-) = (2.48 \pm 0.05)\%$.

[51] KORNICER 11 reports $[\Gamma(\Upsilon(3S) \to \gamma\chi_{b1}(1P))/\Gamma_{total}] \times [B(\chi_{b1}(1P) \to \gamma\Upsilon(1S))] = (5.38 \pm 1.20 \pm 0.95) \times 10^{-4}$ which we divide by our best (shown rounded) value $B(\chi_{b1}(1P) \to \gamma\Upsilon(1S)) = (35.2 \pm 2.0) \times 10^{-2}$. Our first error is their experiment's error and our second error is the systematic error from using our best (shown rounded) value.

[52] ASNER 08A reports $[\Gamma(\Upsilon(3S) \to \gamma\chi_{b1}(1P))/\Gamma_{total}]$ / $[B(\Upsilon(2S) \to \gamma\chi_{b1}(1P))]$ $< 2.5 \times 10^{-2}$ which we multiply by our best (shown rounded) value $B(\Upsilon(2S) \to \gamma\chi_{b1}(1P)) = 6.9 \times 10^{-2}$.

[53] HEINTZ 92, while unable to distinguish between different J states, measures $\sum_J B(\Upsilon(3S) \to \gamma\chi_{bJ}) \times B(\chi_{bJ} \to \gamma\Upsilon(1S)) = (1.7 \pm 0.4 \pm 0.6) \times 10^{-3}$ for $J = 0,1,2$ using inclusive $\Upsilon(1S)$ decays and $(1.2^{+0.4}_{-0.3} \pm 0.09) \times 10^{-3}$ for $J = 1,2$ using $\Upsilon(1S) \to \ell^+\ell^-$.

$\Gamma(\gamma\chi_{b0}(1P))/\Gamma_{total}$ — Γ_{25}/Γ

VALUE (units 10^{-2})	CL%	EVTS	DOCUMENT ID		TECN	COMMENT
0.27±0.04 OUR AVERAGE						
0.27±0.04±0.02		2.3k	LEES	11J	BABR	$\Upsilon(3S) \to X\gamma$
0.30±0.04±0.10		8.7k	ARTUSO	05	CLEO	$e^+e^- \to \gamma X$
• • • We do not use the following data for averages, fits, limits, etc. • • •						
<0.8	90		[54] ASNER	08A	CLEO	$\Upsilon(3S) \to \gamma +$ hadrons

[54] ASNER 08A reports $[\Gamma(\Upsilon(3S) \to \gamma\chi_{b0}(1P))/\Gamma_{total}]$ / $[B(\Upsilon(2S) \to \gamma\chi_{b0}(1P))]$ $< 21.9 \times 10^{-2}$ which we multiply by our best (shown rounded) value $B(\Upsilon(2S) \to \gamma\chi_{b0}(1P)) = 3.8 \times 10^{-2}$.

$\Gamma(\gamma\eta_b(2S))/\Gamma_{total}$ — Γ_{26}/Γ

VALUE (units 10^{-4})	CL%	DOCUMENT ID		TECN	COMMENT
< 6.2	90	ARTUSO	05	CLEO	$e^+e^- \to \gamma X$
• • • We do not use the following data for averages, fits, limits, etc. • • •					
<19	90	LEES	11J	BABR	$\Upsilon(3S) \to X\gamma$

$\Gamma(\gamma\eta_b(1S))/\Gamma_{total}$ — Γ_{27}/Γ

VALUE (units 10^{-4})	CL%	EVTS	DOCUMENT ID		TECN	COMMENT
5.1±0.7 OUR AVERAGE						
7.1±1.8±1.3		2.3±0.5k	[55] BONVICINI	10	CLEO	$\Upsilon(3S) \to \gamma X$
4.8±0.5±0.6		19 ± 3k	[55] AUBERT	09AQ	BABR	$\Upsilon(3S) \to \gamma X$
• • • We do not use the following data for averages, fits, limits, etc. • • •						
<8.5	90		LEES	11J	BABR	$\Upsilon(3S) \to X\gamma$
4.8±0.5±1.2		19 ± 3k	[55,56] AUBERT	08V	BABR	$\Upsilon(3S) \to \gamma X$
<4.3	90		[57] ARTUSO	05	CLEO	$e^+e^- \to \gamma X$

[55] Assuming $\Gamma_{\eta_b(1S)} = 10$ MeV.

[56] Systematic error re-evaluated by AUBERT 09AQ.

[57] Superseded by BONVICINI 10.

$\Gamma(\gamma A^0 \to \gamma\text{hadrons})/\Gamma_{total}$ — Γ_{28}/Γ

(0.3 GeV $< m_{A^0} <$ 7 GeV)

VALUE	CL%	DOCUMENT ID		TECN	COMMENT
<8 × 10^{-5}	90	[58] LEES	11H	BABR	$\Upsilon(3S) \to \gamma$ hadrons

[58] For a narrow scalar or pseudoscalar, A^0, excluding known resonances, with mass in the range 0.3–7 GeV. Measured 90% CL limits as a function of m_{A^0} range from 1×10^{-6} to 8×10^{-5}.

$\Gamma(\gamma X \to \gamma + \geq 4\text{ prongs})/\Gamma_{total}$ — Γ_{29}/Γ

(1.5 GeV $< m_X <$ 5.0 GeV)

VALUE (units 10^{-4})	CL%	DOCUMENT ID		TECN	COMMENT
<2.2	95	ROSNER	07A	CLEO	$e^+e^- \to \gamma X$

$\Gamma(\gamma A^0 \to \gamma\mu^+\mu^-)/\Gamma_{total}$ — Γ_{30}/Γ

VALUE (units 10^{-6})	CL%	DOCUMENT ID		TECN	COMMENT
<5.5	90	[59] AUBERT	09Z	BABR	$e^+e^- \to \gamma A^0 \to \gamma\mu^+\mu^-$

[59] For a narrow scalar or pseudoscalar, A^0, with mass in the range 212–9300 MeV, excluding J/ψ and $\psi(2S)$. Measured 90% CL limits as a function of m_{A^0} range from 0.27–5.5 × 10^{-6}.

Meson Particle Listings

$\Upsilon(3S)$, $\chi_{b1}(3P)$, $\chi_{b2}(3P)$

$\Gamma(\gamma A^0 \to \gamma\tau^+\tau^-)/\Gamma_{total}$ — Γ_{31}/Γ

VALUE	CL%	DOCUMENT ID		TECN	COMMENT
$<1.6 \times 10^{-4}$	90	[60] AUBERT	09P	BABR	$e^+e^- \to \gamma A^0 \to \gamma\tau^+\tau^-$

[60] For a narrow scalar or pseudoscalar, A^0, with $M(\tau^+\tau^-)$ in the ranges 4.03–9.52 and 9.61–10.10 GeV. Measured 90% CL limits as a function of $M(\tau^+\tau^-)$ range from $1.5–16 \times 10^{-5}$.

LEPTON FAMILY NUMBER (*LF*) VIOLATING MODES

$\Gamma(e^\pm\tau^\mp)/\Gamma_{total}$ — Γ_{32}/Γ

VALUE (units 10^{-6})	CL%	DOCUMENT ID		TECN	COMMENT
<4.2	90	LEES	10B	BABR	$e^+e^- \to e^\pm\tau^\mp$

$\Gamma(e^\pm\mu^\mp)/\Gamma_{total}$ — Γ_{33}/Γ

VALUE	CL%	DOCUMENT ID		TECN	COMMENT
$<3.6 \times 10^{-7}$	90	LEES	22A	BABR	$e^+e^- \to e^\pm\mu^\mp$

$\Gamma(\mu^\pm\tau^\mp)/\Gamma_{total}$ — Γ_{34}/Γ

VALUE (units 10^{-6})	CL%	DOCUMENT ID		TECN	COMMENT
< 3.1	90	LEES	10B	BABR	$e^+e^- \to \mu^\pm\tau^\mp$
• • • We do not use the following data for averages, fits, limits, etc. • • •					
<20.3	95	LOVE	08A	CLEO	$e^+e^- \to \mu^\pm\tau^\mp$

$\Upsilon(3S)$ REFERENCES

AAIJ	24AC	JHEP 2410 122	R. Aaij *et al.*	(LHCb Collab.)
SHAMOV	23	PL B839 137766	A.G. Shamov, O.L. Rezanova	(NOVO, NOVOU)
LEES	22A	PRL 128 091804	J.P. Lees *et al.*	(BABAR Collab.)
LEES	20E	PRL 125 241801	J.P. Lees *et al.*	(BABAR Collab.)
LEES	14G	PR D89 111102	J.P. Lees *et al.*	(BABAR Collab.)
GE	11	PR D84 032008	J.Y. Ge *et al.*	(CLEO Collab.)
KORNICER	11	PR D83 054003	M. Kornicer *et al.*	(CLEO Collab.)
LEES	11C	PR D84 011104	J.P. Lees *et al.*	(BABAR Collab.)
LEES	11H	PRL 107 221803	J.P. Lees *et al.*	(BABAR Collab.)
LEES	11J	PR D84 072002	J.P. Lees *et al.*	(BABAR Collab.)
LEES	11K	PR D84 091101	J.P. Lees *et al.*	(BABAR Collab.)
LEES	11L	PR D84 092003	J.P. Lees *et al.*	(BABAR Collab.)
BONVICINI	10	PR D81 031104	G. Bonvicini *et al.*	(CLEO Collab.)
LEES	10B	PRL 104 151802	J.P. Lees *et al.*	(BABAR Collab.)
AUBERT	09AQ	PRL 103 161801	B. Aubert *et al.*	(BABAR Collab.)
AUBERT	09P	PRL 103 181801	B. Aubert *et al.*	(BABAR Collab.)
AUBERT	09Z	PRL 103 081803	B. Aubert *et al.*	(BABAR Collab.)
BHARI	09	PR D79 011103	S.R. Bhari *et al.*	(CLEO Collab.)
ASNER	08A	PR D78 091103	D.M. Asner *et al.*	(CLEO Collab.)
AUBERT	08BP	PR D78 112002	B. Aubert *et al.*	(BABAR Collab.)
AUBERT	08V	PRL 101 071801	B. Aubert *et al.*	(BABAR Collab.)
HE	08A	PRL 101 192001	Q. He *et al.*	(CLEO Collab.)
LOVE	08A	PRL 101 201601	W. Love *et al.*	(CLEO Collab.)
PDG	08	PL B667 1	C. Amsler *et al.*	(PDG Collab.)
BESSON	07	PRL 98 052002	D. Besson *et al.*	(CLEO Collab.)
ROSNER	07A	PR D76 117102	J.L. Rosner *et al.*	(CLEO Collab.)
BESSON	06A	PR D74 012003	D. Besson *et al.*	(CLEO Collab.)
ROSNER	06	PRL 96 092003	J.L. Rosner *et al.*	(CLEO Collab.)
ADAMS	05	PRL 94 012001	G.S. Adams *et al.*	(CLEO Collab.)
ARTUSO	05	PRL 94 032001	M. Artuso *et al.*	(CLEO Collab.)
ARTAMONOV	00	PL B474 427	A.S. Artamonov *et al.*	
BUTLER	94B	PR D49 40	F. Butler *et al.*	(CLEO Collab.)
WU	93	PL B301 307	Q.W. Wu *et al.*	(CUSB Collab.)
HEINTZ	92	PR D46 1928	U. Heintz *et al.*	(CUSB II Collab.)
BROCK	91	PR D43 1448	I.C. Brock *et al.*	(CLEO Collab.)
HEINTZ	91	PRL 66 1563	U. Heintz *et al.*	(CUSB Collab.)
MORRISON	91	PRL 67 1696	R.J. Morrison *et al.*	(CLEO Collab.)
NARAIN	91	PRL 66 3113	M. Narain *et al.*	(CUSB Collab.)
CHEN	89B	PR D39 3528	W.Y. Chen *et al.*	(CLEO Collab.)
KAARSBERG	89	PRL 62 2077	T.M. Kaarsberg *et al.*	(CUSB Collab.)
BUCHMUEL...	88	HE e^+e^- Physics 412	W. Buchmueller, S. Cooper	(HANN, DESY, MIT)
Editors: A. Ali and P. Soeding, World Scientific, Singapore				
COHEN	87	RMP 59 1121	E.R. Cohen, B.N. Taylor	(RISC, NBS)
BARU	86B	ZPHY C32 622 (errat.)	S.E. Baru *et al.*	(NOVO)
KURAEV	85	SJNP 41 466	E.A. Kuraev, V.S. Fadin	(NOVO)
		Translated from YAF 41 733.		
ARTAMONOV	84	PL 137B 272	A.S. Artamonov *et al.*	(NOVO)
GILES	84B	PR D29 1285	R. Giles *et al.*	(CLEO Collab.)
ANDREWS	83	PRL 50 807	D.E. Andrews *et al.*	(CLEO Collab.)
GREEN	82	PRL 49 617	J. Green *et al.*	(CLEO Collab.)
MAGERAS	82	PL 118B 453	G. Mageras *et al.*	(COLU, CORN, LSU+)

$\chi_{b1}(3P)$

$I^G(J^{PC}) = 0^+(1^{++})$
J needs confirmation.

Observed in the radiative decay to $\Upsilon(1S, 2S, 3S)$, therefore $C = +$.

$\chi_{b1}(3P)$ MASS

VALUE (MeV)	EVTS	DOCUMENT ID		TECN	COMMENT
10513.42± 0.41± 0.53		[1] SIRUNYAN	18N	CMS	$pp \to \gamma\mu^+\mu^- X$
• • • We do not use the following data for averages, fits, limits, etc. • • •					
$10515.7 \; {}^{+2.2}_{-3.9} \; {}^{+1.5}_{-2.1}$	169	[2] AAIJ	14BG	LHCB	$pp \to \gamma\mu^+\mu^- X$
10512.1 ± 2.1 ± 0.9	351	[3] AAIJ	14BG	LHCB	$pp \to \gamma\mu^+\mu^- X$
10511.3 ± 1.7 ± 2.5	182	[4] AAIJ	14BI	LHCB	$pp \to \gamma\mu^+\mu^- X$
10530 ± 5 ± 9		[5] AAD	12A	ATLS	$pp \to \gamma\mu^+\mu^- X$
10551 ±14 ±17		[5] ABAZOV	12Q	D0	$p\overline{p} \to \gamma\mu^+\mu^- X$

[1] Systematic error includes an additional 0.5 MeV for the uncertainty on the $\Upsilon(3S)$ mass. Also measures $m_{\chi_{b2}(3P)} - m_{\chi_{b1}(3P)} = 10.60 \pm 0.64 \pm 0.17$ MeV. A total of 372 $\chi_{b1}(3P)$ and $\chi_{b2}(3P)$ events was observed.

[2] From $\chi_{b1}(3P) \to \Upsilon(1S,2S)\gamma$ transitions assuming $m_{\chi_{b2}(3P)} - m_{\chi_{b1}(3P)} = 10.5 \pm 1.5$ MeV and allowing for ±30% variation in the $\chi_{b2}(3P)$ production rate relative to that of $\chi_{b1}(3P)$.

[3] The mass of the $\chi_{b1}(3P)$ state obtained by combining the results of AAIJ 14BG with that of AAIJ 14BI. The first uncertainty is experimental and the second attributable to the unknown mass splitting, assumed to be $m_{\chi_{b2}(3P)} - m_{\chi_{b1}(3P)} = 10.5 \pm 1.5$ MeV.

[4] From $\chi_{b1}(3P) \to \Upsilon(3S)\gamma$ transition assuming $m_{\chi_{b2}(3P)} - m_{\chi_{b1}(3P)} = 10.5 \pm 1.5$ MeV.

[5] The mass barycenter of the merged lineshapes from the $J = 1$ and 2 states.

$\chi_{b1}(3P)$ DECAY MODES

	Mode	Fraction (Γ_i/Γ)
Γ_1	$\Upsilon(1S)\gamma$	seen
Γ_2	$\Upsilon(2S)\gamma$	seen
Γ_3	$\Upsilon(3S)\gamma$	seen

$\chi_{b1}(3P)$ BRANCHING RATIOS

$\Gamma(\Upsilon(1S)\gamma)/\Gamma_{total}$ — Γ_1/Γ

VALUE	EVTS	DOCUMENT ID		TECN	COMMENT
seen	169	[1] AAIJ	14BG	LHCB	$pp \to \gamma\mu^+\mu^- X$
• • • We do not use the following data for averages, fits, limits, etc. • • •					
seen		AAD	12A	ATLS	$pp \to \gamma\mu^+\mu^- X$
seen		ABAZOV	12Q	D0	$p\overline{p} \to \gamma\mu^+\mu^- X$

[1] From $\chi_{b1}(3P) \to \Upsilon(1S,2S)\gamma$ transitions assuming $m_{\chi_{b2}(3P)} - m_{\chi_{b1}(3P)} = 10.5 \pm 1.5$ MeV and allowing for ±30% variation in the $\chi_{b2}(3P)$ production rate relative to that of $\chi_{b1}(3P)$.

$\Gamma(\Upsilon(2S)\gamma)/\Gamma_{total}$ — Γ_2/Γ

VALUE	EVTS	DOCUMENT ID		TECN	COMMENT
seen	169	[1] AAIJ	14BG	LHCB	$pp \to \gamma\mu^+\mu^- X$
• • • We do not use the following data for averages, fits, limits, etc. • • •					
seen		AAD	12A	ATLS	$pp \to \gamma\mu^+\mu^- X$

[1] From $\chi_{b1}(3P) \to \Upsilon(1S,2S)\gamma$ transitions assuming $m_{\chi_{b2}(3P)} - m_{\chi_{b1}(3P)} = 10.5 \pm 1.5$ MeV and allowing for ±30% variation in the $\chi_{b2}(3P)$ production rate relative to that of $\chi_{b1}(3P)$.

$\Gamma(\Upsilon(3S)\gamma)/\Gamma_{total}$ — Γ_3/Γ

VALUE	EVTS	DOCUMENT ID		TECN	COMMENT
seen		SIRUNYAN	18N	CMS	$pp \to \gamma\mu^+\mu^- X$
seen	182	AAIJ	14BI	LHCB	$pp \to \gamma\mu^+\mu^- X$

$\chi_{b1}(3P)$ REFERENCES

SIRUNYAN	18N	PRL 121 092002	A.M. Sirunyan *et al.*	(CMS Collab.)
AAIJ	14BG	JHEP 1410 088	R. Aaij *et al.*	(LHCb Collab.)
AAIJ	14BI	EPJ C74 3092	R. Aaij *et al.*	(LHCb Collab.)
AAD	12A	PRL 108 152001	G. Aad *et al.*	(ATLAS Collab.)
ABAZOV	12Q	PR D86 031103	V.M. Abazov *et al.*	(D0 Collab.)

$\chi_{b2}(3P)$

$I^G(J^{PC}) = 0^+(2^{++})$
J needs confirmation.

Observed in the radiative decay to $\Upsilon(3S)$, therefore $C = +$.

$\chi_{b2}(3P)$ MASS

VALUE (MeV)	DOCUMENT ID		TECN	COMMENT
10524.02±0.57±0.53	[1] SIRUNYAN	18N	CMS	$pp \to \gamma\mu^+\mu^- X$
• • • We do not use the following data for averages, fits, limits, etc. • • •				
10530 ±5 ±9	[2] AAD	12A	ATLS	$pp \to \gamma\mu^+\mu^- X$

[1] Systematic error includes an additional 0.5 MeV for the uncertainty on the $\Upsilon(3S)$ mass. Also measures $m_{\chi_{b2}(3P)} - m_{\chi_{b1}(3P)} = 10.60 \pm 0.64 \pm 0.17$ MeV. A total of 372 $\chi_{b1}(3P)$ and $\chi_{b2}(3P)$ events was observed.

[2] The mass barycenter of the merged lineshapes from the $J = 1$ and 2 states.

$\chi_{b2}(3P)$ DECAY MODES

	Mode	Fraction (Γ_i/Γ)
Γ_1	$\Upsilon(3S)\gamma$	seen

$\chi_{b2}(3P)$ BRANCHING RATIOS

$\Gamma(\Upsilon(3S)\gamma)/\Gamma_{total}$ — Γ_1/Γ

VALUE	DOCUMENT ID		TECN	COMMENT
seen	SIRUNYAN	18N	CMS	$pp \to \gamma\mu^+\mu^- X$

$\chi_{b2}(3P)$ REFERENCES

SIRUNYAN	18N	PRL 121 092002	A.M. Sirunyan *et al.*	(CMS Collab.)
AAD	12A	PRL 108 152001	G. Aad *et al.*	(ATLAS Collab.)

Int. J. Mod. Phys. A 2026.41. Downloaded from www.worldscientific.com by CALIFORNIA @ BERKELEY on 09/16/26. Re-use and distribution is strictly not permitted, except for Open Access articles.

See key on page 1227

Int. J. Mod. Phys. A 2026.41. Downloaded from www.worldscientific.com
by UNIVERSITY OF CALIFORNIA @ BERKELEY on 09/16/26. Re-use and distribution is strictly not permitted, except for Open Access articles.

$\Upsilon(4S)$

$I^G(J^{PC}) = 0^-(1^{--})$

also known as $\Upsilon(10580)$

$\Upsilon(4S)$ MASS

VALUE (MeV)	DOCUMENT ID		TECN	COMMENT
10579.4±1.2 OUR AVERAGE				
10579.3±0.4±1.2	AUBERT	05Q	BABR	$e^+e^- \to$ hadrons
10580.0±3.5	[1] BEBEK	87	CLEO	$e^+e^- \to$ hadrons
• • • We do not use the following data for averages, fits, limits, etc. • • •				
10577.4±1.0	[2] LOVELOCK	85	CUSB	$e^+e^- \to$ hadrons

[1] Reanalysis of BESSON 85.
[2] No systematic error given.

$\Upsilon(4S)$ WIDTH

VALUE (MeV)	DOCUMENT ID		TECN	COMMENT
20.5±2.5 OUR AVERAGE				
20.7±1.6±2.5	AUBERT	05Q	BABR	$e^+e^- \to$ hadrons
20 ±2 ±4	BESSON	85	CLEO	$e^+e^- \to$ hadrons
• • • We do not use the following data for averages, fits, limits, etc. • • •				
25 ±2.5	LOVELOCK	85	CUSB	$e^+e^- \to$ hadrons

$\Upsilon(4S)$ DECAY MODES

	Mode	Fraction (Γ_i/Γ)	Confidence level
Γ_1	$B\overline{B}$	> 96 %	95%
Γ_2	B^+B^-	$(51.1 \pm^{0.7}_{1.1})$ %	
Γ_3	D_s^+ anything + c.c.	(17.8 ± 2.6) %	
Γ_4	$B^0\overline{B}^0$	(48.6 ± 0.8) %	
Γ_5	$J/\psi K^0_S + (J/\psi, \eta_c) K^0_S$	$< 4 \times 10^{-7}$	90%
Γ_6	non-$B\overline{B}$	$(2.64 \pm^{13.00}_{0.20}) \times 10^{-3}$	
Γ_7	e^+e^-	$(1.57 \pm 0.08) \times 10^{-5}$	
Γ_8	$\rho^+\rho^-$	$< 5.7 \times 10^{-6}$	90%
Γ_9	$K^*(892)^0\overline{K}^0$	$< 2.0 \times 10^{-6}$	90%
Γ_{10}	$J/\psi(1S)$ anything	$< 1.9 \times 10^{-4}$	95%
Γ_{11}	D^{*+} anything + c.c.	< 7.4 %	90%
Γ_{12}	ϕ anything	(7.1 ± 0.6) %	
Γ_{13}	$\phi\eta$	$< 1.8 \times 10^{-6}$	90%
Γ_{14}	$\phi\eta'$	$< 4.3 \times 10^{-6}$	90%
Γ_{15}	$\rho\eta$	$< 1.3 \times 10^{-6}$	90%
Γ_{16}	$\rho\eta'$	$< 2.5 \times 10^{-6}$	90%
Γ_{17}	$\Upsilon(1S)$ anything	$< 4 \times 10^{-3}$	90%
Γ_{18}	$\Upsilon(1S)\pi^+\pi^-$	$(8.2 \pm 0.4) \times 10^{-5}$	
Γ_{19}	$\Upsilon(1S)\eta$	$(1.81 \pm 0.18) \times 10^{-4}$	
Γ_{20}	$\Upsilon(1S)\eta'$	$(3.4 \pm 0.9) \times 10^{-5}$	
Γ_{21}	$\Upsilon(2S)\pi^+\pi^-$	$(8.2 \pm 0.8) \times 10^{-5}$	
Γ_{22}	$h_b(1P)\pi^+\pi^-$	not seen	
Γ_{23}	$h_b(1P)\eta$	$(2.18 \pm 0.21) \times 10^{-3}$	
Γ_{24}	$\eta_b(1S)\omega$	$< 1.8 \times 10^{-4}$	90%
Γ_{25}	^2H anything	$< 1.3 \times 10^{-5}$	90%
	Double Radiative Decays		
Γ_{26}	$\gamma\gamma\,\Upsilon(D) \to \gamma\gamma\eta\,\Upsilon(1S)$	$< 2.3 \times 10^{-5}$	90%

$\Upsilon(4S)$ PARTIAL WIDTHS

$\Gamma(e^+e^-)$ — Γ_7

VALUE (keV)	DOCUMENT ID		TECN	COMMENT
0.272±0.029 OUR AVERAGE	Error includes scale factor of 1.5.			See the ideogram below.
0.321±0.017±0.029	AUBERT	05Q	BABR	$e^+e^- \to$ hadrons
0.28 ±0.05 ±0.01	[1] ALBRECHT	95E	ARG	$e^+e^- \to$ hadrons
0.192±0.007±0.038	BESSON	85	CLEO	$e^+e^- \to$ hadrons
0.283±0.037	LOVELOCK	85	CUSB	$e^+e^- \to$ hadrons

[1] Using LEYAOUANC 77 parametrization of $\Gamma(s)$.

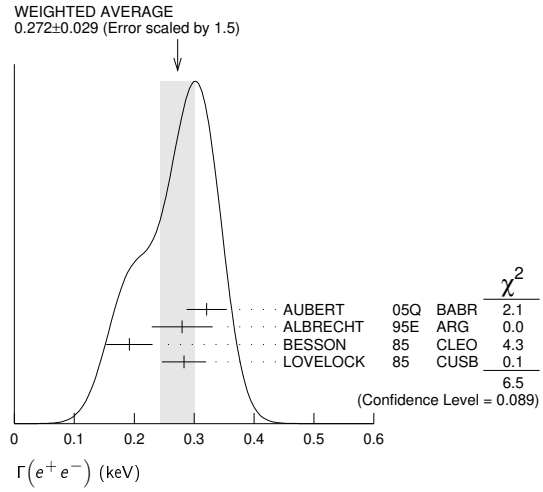

$\Upsilon(4S)$ BRANCHING RATIOS

$B\overline{B}$ DECAYS

$\Gamma(B^+B^-)/\Gamma_{total}$ — Γ_2/Γ

VALUE	DOCUMENT ID		TECN
$\mathbf{0.5113^{+0.0073}_{-0.0108}}$	[1] BANERJEE	26	RVUE

[1] The quantities $\Gamma(B^+B^-)/\Gamma_{total}$, $\Gamma(B^0\overline{B}^0)/\Gamma_{total}$, $\Gamma(B^+B^-)/\Gamma(B^0\overline{B}^0)$ and $\Gamma(\text{non-}B\overline{B})/\Gamma_{total}$ produced by the Heavy Flavor Averaging Group (HFLAV) are correlated.

$\Gamma(D_s^+ \text{ anything} + \text{c.c.})/\Gamma_{total}$ — Γ_3/Γ

VALUE	DOCUMENT ID		TECN	COMMENT
0.178±0.021±0.016	[1] ARTUSO	05B	CLE3	$e^+e^- \to D_X X$

[1] ARTUSO 05B reports $[\Gamma(\Upsilon(4S) \to D_s^+ \text{ anything} + \text{c.c.})/\Gamma_{total}] \times [B(D_s^+ \to \phi\pi^+)] = (8.0 \pm 0.2 \pm 0.9) \times 10^{-3}$ which we divide by our best (shown rounded) value $B(D_s^+ \to \phi\pi^+) = (4.5 \pm 0.4) \times 10^{-2}$. Our first error is their experiment's error and our second error is the systematic error from using our best (shown rounded) value.

$\Gamma(B^0\overline{B}^0)/\Gamma_{total}$ — Γ_4/Γ

VALUE	DOCUMENT ID		TECN	COMMENT
$\mathbf{0.4861^{+0.0074}_{-0.0080}}$	[1] BANERJEE	26	RVUE	
• • • We do not use the following data for averages, fits, limits, etc. • • •				
0.487 ±0.010 ±0.008	[2] AUBERT,B	05H	BABR	$\Upsilon(4S) \to \overline{B}B \to D^*\ell\nu_\ell$

[1] The quantities $\Gamma(B^+B^-)/\Gamma_{total}$, $\Gamma(B^0\overline{B}^0)/\Gamma_{total}$, $\Gamma(B^+B^-)/\Gamma(B^0\overline{B}^0)$ and $\Gamma(\text{non-}B\overline{B})/\Gamma_{total}$ produced by the Heavy Flavor Averaging Group (HFLAV) are correlated.
[2] Direct measurement. This value is averaged with the value extracted from the $\Gamma(B^+B^-)$ / $\Gamma(B^0\overline{B}^0)$ measurements.

$\Gamma(B^+B^-)/\Gamma(B^0\overline{B}^0)$ — Γ_2/Γ_4

VALUE	DOCUMENT ID		TECN	COMMENT
1.052±0.031	[1] BANERJEE	26	RVUE	
• • • We do not use the following data for averages, fits, limits, etc. • • •				
1.065±0.012±0.051	[2] CHOUDHURY	23	BELL	$\Upsilon(4S) \to B\overline{B} \to J/\psi K$
1.006±0.036±0.031	[3] AUBERT	04F	BABR	$\Upsilon(4S) \to B\overline{B} \to J/\psi K$
1.01 ±0.03 ±0.09	[3] HASTINGS	03	BELL	$\Upsilon(4S) \to B\overline{B} \to$ dileptons
1.058±0.084±0.136	[4] ATHAR	02	CLEO	$\Upsilon(4S) \to B\overline{B} \to D^*\ell\nu$
1.10 ±0.06 ±0.05	[5] AUBERT	02	BABR	$\Upsilon(4S) \to B\overline{B} \to (c\overline{c})K^*$
1.04 ±0.07 ±0.04	[6] ALEXANDER	01	CLEO	$\Upsilon(4S) \to B\overline{B} \to J/\psi K^*$

[1] The quantities $\Gamma(B^+B^-)/\Gamma_{total}$, $\Gamma(B^0\overline{B}^0)/\Gamma_{total}$, $\Gamma(B^+B^-)/\Gamma(B^0\overline{B}^0)$ and $\Gamma(\text{non-}B\overline{B})/\Gamma_{total}$ produced by the Heavy Flavor Averaging Group (HFLAV) are correlated.
[2] CHOUDHURY 23 includes uncertainty due to the isospin symmetry assumption in $B \to J/\psi K$ decays.
[3] HASTINGS 03 and AUBERT 04F assume $\tau(B^+)$ / $\tau(B^0) = 1.083 \pm 0.017$.
[4] ATHAR 02 assumes $\tau(B^+)$ / $\tau(B^0) = 1.074 \pm 0.028$. Supersedes BARISH 95.
[5] AUBERT 02 assumes $\tau(B^+)$ / $\tau(B^0) = 1.062 \pm 0.029$.
[6] ALEXANDER 01 assumes $\tau(B^+)$ / $\tau(B^0) = 1.066 \pm 0.024$.

$[\Gamma(J/\psi K^0_S) + \Gamma((J/\psi, \eta_c)K^0_S)]/\Gamma_{total}$ — Γ_5/Γ

Forbidden by CP invariance.

VALUE (units 10^{-7})	CL%	DOCUMENT ID		TECN	COMMENT
<4	90	[1] TAJIMA	07A	BELL	$\Upsilon(4S) \to B^0\overline{B}^0$

[1] $\Upsilon(4S)$ with $CP = +1$ decays to the final state with $CP = -1$.

Int. J. Mod. Phys. A 2026.41. Downloaded from www.worldscientific.com by LIFORNIA @ BERKELEY on 09/16/26. Re-use and distribution is strictly not permitted, except for Open Access articles.

non-$B\overline{B}$ DECAYS

$\Gamma(\text{non-}B\overline{B})/\Gamma_{\text{total}}$ — Γ_6/Γ

VALUE (units 10^{-2})	CL%	DOCUMENT ID		TECN	COMMENT
$0.26^{+1.25}_{-0.02}$		[1] BANERJEE	26	RVUE	
• • • We do not use the following data for averages, fits, limits, etc. • • •					
<4	95	BARISH	96B	CLEO	e^+e^-

[1] The quantities $\Gamma(B^+B^-)/\Gamma_{\text{total}}$, $\Gamma(B^0\overline{B}^0)/\Gamma_{\text{total}}$, $\Gamma(B^+B^-)/\Gamma(B^0\overline{B}^0)$ and $\Gamma(\text{non-}B\overline{B})/\Gamma_{\text{total}}$ produced by the Heavy Flavor Averaging Group (HFLAV) are correlated.

$\Gamma(e^+e^-)/\Gamma_{\text{total}}$ — Γ_7/Γ

VALUE (units 10^{-5})	DOCUMENT ID		TECN	COMMENT
1.57±0.08 OUR AVERAGE				
1.55±0.04±0.07	AUBERT	05Q	BABR	$e^+e^- \to$ hadrons
2.77±0.50±0.49	[1] ALBRECHT	95E	ARG	$e^+e^- \to$ hadrons

[1] Using LEYAOUANC 77 parametrization of $\Gamma(s)$.

$\Gamma(\rho^+\rho^-)/\Gamma_{\text{total}}$ — Γ_8/Γ

VALUE	CL%	DOCUMENT ID		TECN	COMMENT
$<5.7\times10^{-6}$	90	AUBERT	08BO	BABR	$e^+e^- \to \pi^+\pi^-2\pi^0$

$\Gamma(K^*(892)^0\overline{K}^0)/\Gamma_{\text{total}}$ — Γ_9/Γ

VALUE	CL%	DOCUMENT ID		TECN	COMMENT
$<2.0\times10^{-6}$	90	SHEN	13A	BELL	$e^+e^- \to K^*(892)^0\overline{K}^0$

$\Gamma(J/\psi(1S)\text{ anything})/\Gamma_{\text{total}}$ — Γ_{10}/Γ

VALUE (units 10^{-4})	CL%	DOCUMENT ID		TECN	COMMENT
<1.9	95	[1] ABE	02D	BELL	$e^+e^- \to J/\psi X \to \ell^+\ell^- X$
• • • We do not use the following data for averages, fits, limits, etc. • • •					
<4.7	90	[1] AUBERT	01C	BABR	$e^+e^- \to J/\psi X \to \ell^+\ell^- X$

[1] Uses $B(J/\psi \to e^+e^-) = 0.0593 \pm 0.0010$ and $B(J/\psi \to \mu^+\mu^-) = 0.0588 \pm 0.0010$.

$\Gamma(D^{*+}\text{ anything} + \text{c.c.})/\Gamma_{\text{total}}$ — Γ_{11}/Γ

VALUE	CL%	DOCUMENT ID		TECN	COMMENT
<0.074	90	[1] ALEXANDER	90C	CLEO	e^+e^-

[1] For $x > 0.473$.

$\Gamma(\phi\text{ anything})/\Gamma_{\text{total}}$ — Γ_{12}/Γ

VALUE (units 10^{-2})	CL%	DOCUMENT ID		TECN	COMMENT
7.1 ±0.1±0.6		HUANG	07	CLEO	$\Upsilon(4S) \to \phi X$
• • • We do not use the following data for averages, fits, limits, etc. • • •					
<0.23	90	[1] ALEXANDER	90C	CLEO	e^+e^-

[1] For $x > 0.52$.

$\Gamma(\phi\eta)/\Gamma_{\text{total}}$ — Γ_{13}/Γ

VALUE (units 10^{-6})	CL%	DOCUMENT ID		TECN	COMMENT
<1.8	90	[1] BELOUS	09	BELL	$e^+e^- \to \phi\eta$
• • • We do not use the following data for averages, fits, limits, etc. • • •					
<2.5	90	AUBERT,BE	06F	BABR	$e^+e^- \to \phi\eta$

[1] Using all intermedite branching fraction values from PDG 08.

$\Gamma(\phi\eta')/\Gamma_{\text{total}}$ — Γ_{14}/Γ

VALUE (units 10^{-6})	CL%	DOCUMENT ID		TECN	COMMENT
<4.3	90	[1] BELOUS	09	BELL	$e^+e^- \to \phi\eta'$

[1] Using all intermedite branching fraction values from PDG 08.

$\Gamma(\rho\eta)/\Gamma_{\text{total}}$ — Γ_{15}/Γ

VALUE (units 10^{-6})	CL%	DOCUMENT ID		TECN	COMMENT
<1.3	90	[1] BELOUS	09	BELL	$e^+e^- \to \rho\eta$

[1] Using all intermedite branching fraction values from PDG 08.

$\Gamma(\rho\eta')/\Gamma_{\text{total}}$ — Γ_{16}/Γ

VALUE (units 10^{-6})	CL%	DOCUMENT ID		TECN	COMMENT
<2.5	90	[1] BELOUS	09	BELL	$e^+e^- \to \rho\eta'$

[1] Using all intermedite branching fraction values from PDG 08.

$\Gamma(\Upsilon(1S)\text{ anything})/\Gamma_{\text{total}}$ — Γ_{17}/Γ

VALUE	CL%	DOCUMENT ID		TECN	COMMENT
<0.004	90	ALEXANDER	90C	CLEO	e^+e^-

$\Gamma(\Upsilon(1S)\pi^+\pi^-)/\Gamma_{\text{total}}$ — Γ_{18}/Γ

VALUE (units 10^{-5})	CL%	EVTS	DOCUMENT ID		TECN	COMMENT
8.2 ±0.4 OUR AVERAGE						
8.2 ±0.5 ±0.4		515	GUIDO	17	BELL	$\Upsilon(4S) \to \pi^+\pi^-\mu^+\mu^-$
8.5 ±1.3 ±0.1		113 ± 16	[1] SOKOLOV	09	BELL	$e^+e^- \to \pi^+\pi^-\mu^+\mu^-$
8.00±0.64±0.27		430	[2] AUBERT	08BP	BABR	$\Upsilon(4S) \to \pi^+\pi^-\ell^+\ell^-$
• • • We do not use the following data for averages, fits, limits, etc. • • •						
17.8 ±4.0 ±0.3			[3,4] SOKOLOV	07	BELL	$e^+e^- \to \pi^+\pi^-\mu^+\mu^-$
9.0 ±1.5 ±0.2		167 ± 19	[5] AUBERT	06R	BABR	$e^+e^- \to \pi^+\pi^-\mu^+\mu^-$
<12	90		GLENN	99	CLE2	e^+e^-

[1] SOKOLOV 09 reports $[\Gamma(\Upsilon(4S) \to \Upsilon(1S)\pi^+\pi^-)/\Gamma_{\text{total}}] \times [B(\Upsilon(1S) \to \mu^+\mu^-)] = (0.211 \pm 0.030 \pm 0.014) \times 10^{-5}$ which we divide by our best (shown rounded) value $B(\Upsilon(1S) \to \mu^+\mu^-) = (2.48 \pm 0.04) \times 10^{-2}$. Our first error is their experiment's error and our second error is the systematic error from using our best (shown rounded) value.

[2] Using $B(\Upsilon(1S) \to e^+e^-) = (2.38 \pm 0.11)\%$ and $B(\Upsilon(1S) \to \mu^+\mu^-) = (2.48 \pm 0.05)\%$.

[3] SOKOLOV 07 reports $[\Gamma(\Upsilon(4S) \to \Upsilon(1S)\pi^+\pi^-)/\Gamma_{\text{total}}] \times [B(\Upsilon(1S) \to \mu^+\mu^-)] = (4.42 \pm 0.81 \pm 0.56) \times 10^{-6}$ which we divide by our best (shown rounded) value $B(\Upsilon(1S) \to \mu^+\mu^-) = (2.48 \pm 0.04) \times 10^{-2}$. Our first error is their experiment's error and our second error is the systematic error from using our best (shown rounded) value.

[4] According to the authors, systematic errors were underestimated.

[5] Superseded by AUBERT 08BP. AUBERT 06R reports $[\Gamma(\Upsilon(4S) \to \Upsilon(1S)\pi^+\pi^-)/\Gamma_{\text{total}}] \times [B(\Upsilon(1S) \to \mu^+\mu^-)] = (2.23 \pm 0.25 \pm 0.27) \times 10^{-6}$ which we divide by our best (shown rounded) value $B(\Upsilon(1S) \to \mu^+\mu^-) = (2.48 \pm 0.04) \times 10^{-2}$. Our first error is their experiment's error and our second error is the systematic error from using our best (shown rounded) value.

$\Gamma(\Upsilon(1S)\eta)/\Gamma_{\text{total}}$ — Γ_{19}/Γ

VALUE (units 10^{-4})	CL%	EVTS	DOCUMENT ID		TECN	COMMENT
1.81±0.18 OUR AVERAGE						
1.70±0.23±0.08		49	GUIDO	17	BELL	$\Upsilon(4S) \to \pi^+\pi^-\pi^0\mu^+\mu^-$
1.96±0.26±0.09		56	[1] AUBERT	08BP	BABR	$\Upsilon(4S) \to \pi^+\pi^-\pi^0\ell^+\ell^-$
• • • We do not use the following data for averages, fits, limits, etc. • • •						
<2.7	90		[2] TAMPONI	15	BELL	$e^+e^- \to \gamma\eta +$ hadrons

[1] Using $B(\Upsilon(1S) \to e^+e^-) = (2.38 \pm 0.11)\%$ and $B(\Upsilon(1S) \to \mu^+\mu^-) = (2.48 \pm 0.05)\%$.

[2] Using $B(\eta \to 2\gamma) = (39.41 \pm 0.20)\%$.

$\Gamma(\Upsilon(1S)\eta')/\Gamma_{\text{total}}$ — Γ_{20}/Γ

VALUE (units 10^{-5})	EVTS	DOCUMENT ID		TECN	COMMENT
3.43±0.88±0.21	27	GUIDO	18	BELL	$\Upsilon(4S) \to (\rho^0\gamma, \pi^+\pi^-\eta)\mu^+\mu^-$

$\Gamma(\Upsilon(1S)\eta)/\Gamma(\Upsilon(1S)\pi^+\pi^-)$ — Γ_{19}/Γ_{18}

VALUE	EVTS	DOCUMENT ID		TECN	COMMENT
• • • We do not use the following data for averages, fits, limits, etc. • • •					
2.41±0.40±0.12	56	[1] AUBERT	08BP	BABR	$\Upsilon(4S) \to \pi^+\pi^-(\pi^0)\ell^+\ell^-$

[1] Not independent of other values reported by AUBERT 08BP.

$\Gamma(\Upsilon(2S)\pi^+\pi^-)/\Gamma_{\text{total}}$ — Γ_{21}/Γ

VALUE (units 10^{-5})	CL%	EVTS	DOCUMENT ID		TECN	COMMENT
8.2±0.8 OUR AVERAGE						
7.9±1.0±0.4		181	GUIDO	17	BELL	$\Upsilon(4S) \to \pi^+\pi^-\mu^+\mu^-$
8.6±1.1±0.7		220	[1] AUBERT	08BP	BABR	$\Upsilon(4S) \to \pi^+\pi^-\ell^+\ell^-$
• • • We do not use the following data for averages, fits, limits, etc. • • •						
8.8±1.7±0.8		97 ± 15	[2] AUBERT	06R	BABR	$e^+e^- \to \pi^+\pi^-\mu^+\mu^-$
<3.9	90		GLENN	99	CLE2	e^+e^-

[1] Using $B(\Upsilon(2S) \to e^+e^-) = (1.91 \pm 0.16)\%$ and $B(\Upsilon(2S) \to \mu^+\mu^-) = (1.93 \pm 0.17)\%$.

[2] Superseded by AUBERT 08BP. AUBERT 06R reports $[\Gamma(\Upsilon(4S) \to \Upsilon(2S)\pi^+\pi^-)/\Gamma_{\text{total}}] \times [B(\Upsilon(2S) \to \mu^+\mu^-)] = (1.69 \pm 0.26 \pm 0.20) \times 10^{-6}$ which we divide by our best (shown rounded) value $B(\Upsilon(2S) \to \mu^+\mu^-) = (1.93 \pm 0.17) \times 10^{-2}$. Our first error is their experiment's error and our second error is the systematic error from using our best (shown rounded) value.

$\Gamma(\Upsilon(2S)\pi^+\pi^-)/\Gamma(\Upsilon(1S)\pi^+\pi^-)$ — Γ_{21}/Γ_{18}

VALUE	EVTS	DOCUMENT ID		TECN	COMMENT
• • • We do not use the following data for averages, fits, limits, etc. • • •					
1.16±0.16±0.14	220	[1] AUBERT	08BP	BABR	$\Upsilon(4S) \to \pi^+\pi^-\ell^+\ell^-$

[1] Using $B(\Upsilon(1S) \to e^+e^-) = (2.38 \pm 0.11)\%$, $B(\Upsilon(1S) \to \mu^+\mu^-) = (2.48 \pm 0.05)\%$, $B(\Upsilon(2S) \to e^+e^-) = (1.91 \pm 0.16)\%$, and $B(\Upsilon(2S) \to \mu^+\mu^-) = (1.93 \pm 0.17)\%$. Not independent of other values reported by AUBERT 08BP.

$\Gamma(h_b(1P)\pi^+\pi^-)/\Gamma_{\text{total}}$ — Γ_{22}/Γ

VALUE	EVTS	DOCUMENT ID		TECN	COMMENT
not seen	(35^{+32}_{-26})k	[1] ADACHI	12	BELL	10.58 $e^+e^- \to h_b(1P)\pi^+\pi^-$

[1] From the upper limit on the ratio of $\sigma(e^+e^- \to h_b(1P)\pi^+\pi^-)$ at the $\Upsilon(4S)$ to that at the $\Upsilon(5S)$ of 0.27.

$\Gamma(h_b(1P)\eta)/\Gamma_{\text{total}}$ — Γ_{23}/Γ

VALUE (units 10^{-3})	EVTS	DOCUMENT ID		TECN	COMMENT
2.18±0.11±0.18	112k	[1] TAMPONI	15	BELL	$e^+e^- \to h_b(1P)\eta$

[1] Using $B(\eta \to 2\gamma) = (39.41 \pm 0.20)\%$.

$\Gamma(\eta_b(1S)\omega)/\Gamma_{\text{total}}$ — Γ_{24}/Γ

VALUE	CL%	DOCUMENT ID		TECN	COMMENT
$<8.4\times10^{-4}$	90	OSKIN	20	BELL	$e^+e^- \to \omega X$

$\Gamma(\eta_b(1S)\omega)/\Gamma(h_b(1P)\eta)$ — Γ_{24}/Γ_{23}

VALUE	CL%	DOCUMENT ID		TECN	COMMENT
$<8.4\times10^{-2}$	90	[1] OSKIN	20	BELL	$e^+e^- \to \omega X$

[1] Using $B(\Upsilon(4S) \to h_b(1P)\eta) = (2.18 \pm 0.11 \pm 0.18) \times 10^{-3}$ from TAMPONI 15.

Int. J. Mod. Phys. A 2026.41. Downloaded from www.worldscientific.com by UNIVERSITY OF CALIFORNIA @ BERKELEY on 09/16/26. Re-use and distribution is strictly not permitted, except for Open Access articles.

$\Gamma(\overline{2H}\text{ anything})/\Gamma_{total}$ — Γ_{25}/Γ

VALUE (units 10^{-5})	CL%	DOCUMENT ID		TECN	COMMENT
<1.3	90	ASNER	07	CLEO	$e^+e^- \to \overline{d}X$

Double Radiative Decays

$\Gamma(\gamma\gamma\Upsilon(D) \to \gamma\gamma\eta\Upsilon(1S))/\Gamma_{total}$ — Γ_{26}/Γ

VALUE	CL%	DOCUMENT ID		TECN	COMMENT
$<2.3\times10^{-5}$	90	GUIDO	17	BELL	$\Upsilon(4S) \to \gamma\gamma\pi^+\pi^-\pi^0\mu^+\mu^-$

$\Upsilon(4S)$ REFERENCES

BANERJEE	26	PR D113 012008	Sw. Banerjee *et al.*	(HFLAV Collab.)
CHOUDHURY	23	PR D107 L031102	S. Choudhury *et al.*	(BELLE Collab.)
OSKIN	20	PR D102 092011	P. Oskin *et al.*	(BELLE Collab.)
GUIDO	18	PRL 121 062001	E. Guido *et al.*	(BELLE Collab.)
GUIDO	17	PR D96 052005	E. Guido *et al.*	(BELLE Collab.)
TAMPONI	15	PRL 115 142001	U. Tamponi *et al.*	(BELLE Collab.)
SHEN	13A	PR D88 052019	C.P. Shen *et al.*	(BELLE Collab.)
ADACHI	12	PRL 108 032001	I. Adachi *et al.*	(BELLE Collab.)
BELOUS	09	PL B681 400	K. Belous *et al.*	(BELLE Collab.)
SOKOLOV	09	PR D79 051103	A. Sokolov *et al.*	(BELLE Collab.)
AUBERT	08BO	PR D78 071103	B. Aubert *et al.*	(BABAR Collab.)
AUBERT	08BP	PR D78 112002	B. Aubert *et al.*	(BABAR Collab.)
PDG	08	PL B667 1	C. Amsler *et al.*	(PDG Collab.)
ASNER	07	PR D75 012009	D.M. Asner *et al.*	(CLEO Collab.)
HUANG	07	PR D75 012002	G.S. Huang *et al.*	(CLEO Collab.)
SOKOLOV	07	PR D75 071103	A. Sokolov *et al.*	(BELLE Collab.)
TAJIMA	07A	PRL 99 211601	O. Tajima *et al.*	(BELLE Collab.)
AUBERT	06R	PRL 96 232001	B. Aubert *et al.*	(BABAR Collab.)
AUBERT,BE	06F	PR D74 111103	B. Aubert *et al.*	(BABAR Collab.)
ARTUSO	05B	PRL 95 261801	M. Artuso *et al.*	(CLEO Collab.)
AUBERT	05Q	PR D72 032005	B. Aubert *et al.*	(BABAR Collab.)
AUBERT,B	05H	PRL 95 042001	B. Aubert *et al.*	(BABAR Collab.)
AUBERT	04F	PR D69 071101	B. Aubert *et al.*	(BABAR Collab.)
HASTINGS	03	PR D67 052004	N.C. Hastings *et al.*	(BELLE Collab.)
ABE	02D	PRL 88 052001	K. Abe *et al.*	(BELLE Collab.)
ATHAR	02	PR D66 052003	S.B. Athar *et al.*	(CLEO Collab.)
AUBERT	02	PR D65 032001	B. Aubert *et al.*	(BABAR Collab.)
ALEXANDER	01	PRL 86 2737	J.P. Alexander *et al.*	(CLEO Collab.)
AUBERT	01C	PRL 87 162002	B. Aubert *et al.*	(BABAR Collab.)
GLENN	99	PR D59 052003	S. Glenn *et al.*	
BARISH	96B	PRL 76 1570	B.C. Barish *et al.*	(CLEO Collab.)
ALBRECHT	95E	ZPHY C65 619	H. Albrecht *et al.*	(ARGUS Collab.)
BARISH	95	PR D51 1014	B.C. Barish *et al.*	(CLEO Collab.)
ALEXANDER	90C	PRL 64 2226	J. Alexander *et al.*	(CLEO Collab.)
BEBEK	87	PR D36 1289	C. Bebek *et al.*	(CLEO Collab.)
BESSON	85	PRL 54 381	D. Besson *et al.*	(CLEO Collab.)
LOVELOCK	85	PRL 54 377	D.M.J. Lovelock *et al.*	(CUSB Collab.)
LEYAOUANC	77	PL B71 397	A. Le Yaouanc *et al.*	(ORSAY)

$\Upsilon(10753)$

$I^G(J^{PC}) = ?^?(1^{--})$

A candidate for $\Upsilon(3D)$ state or an exotic structure.

$\Upsilon(10753)$ MASS

VALUE (MeV)	DOCUMENT ID		TECN	COMMENT
10756.6±2.7±0.9	[1] ADACHI	24V	BELL	$e^+e^- \to \Upsilon(nS)\pi^+\pi^-$
• • • We do not use the following data for averages, fits, limits, etc. • • •				
10761 ±2	[2] DONG	20A		$e^+e^- \to b\overline{b}$
$10752.7\pm5.9^{+0.7}_{-1.1}$	[3] MIZUK	19	BELL	$e^+e^- \to \Upsilon(nS)\pi^+\pi^-$

[1] From a simultaneous fit to the $\Upsilon(1S,2S,3S)\pi^+\pi^-$ cross section.
[2] From a fit to the dressed cross sections of AUBERT 09E by BaBar and SANTEL 16 by Belle above 10.68 GeV with a coherent sum of a continuum amplitude and three Breit-Wigner functions with constant widths.
[3] From a simultaneous fit to the $\Upsilon(nS)\pi^+\pi^-$, n = 1, 2, 3, cross sections at 28 energy points within $\sqrt{s}$ = 10.63–11.02 GeV, including the initial-state radiation at $\Upsilon(10860)$. Superseded by ADACHI 24V.

$\Upsilon(10753)$ WIDTH

VALUE (MeV)	DOCUMENT ID		TECN	COMMENT
29.0± 8.8±1.2	[1] ADACHI	24V	BELL	$e^+e^- \to \Upsilon(nS)\pi^+\pi^-$
• • • We do not use the following data for averages, fits, limits, etc. • • •				
48.5± 3.0	[2] DONG	20A		$e^+e^- \to b\overline{b}$
$35.5^{+17.6+3.9}_{-11.3-3.3}$	[3] MIZUK	19	BELL	$e^+e^- \to \Upsilon(nS)\pi^+\pi^-$

[1] From a simultaneous fit to the $\Upsilon(1S,2S,3S)\pi^+\pi^-$ cross section.
[2] From a fit to the dressed cross sections of AUBERT 09E by BaBar and SANTEL 16 by Belle above 10.68 GeV with a coherent sum of a continuum amplitude and three Breit-Wigner functions with constant widths.
[3] From a simultaneous fit to the $\Upsilon(nS)\pi^+\pi^-$, n = 1, 2, 3, cross sections at 28 energy points within $\sqrt{s}$ = 10.63–11.02 GeV, including the initial-state radiation at $\Upsilon(10860)$. Superseded by ADACHI 24V.

$\Upsilon(10753)$ DECAY MODES

	Mode
Γ_1	$\Upsilon(1S)\pi^+\pi^-$
Γ_2	$\Upsilon(2S)\pi^+\pi^-$
Γ_3	$\Upsilon(3S)\pi^+\pi^-$
Γ_4	$\omega\chi_{b1}(1P)$
Γ_5	$\omega\chi_{b2}(1P)$
Γ_6	e^+e^-

$\Upsilon(10753)$ $\Gamma(i)\Gamma(e^+e^-)/\Gamma(total)$

$\Gamma(\Upsilon(1S)\pi^+\pi^-) \times \Gamma(e^+e^-)/\Gamma_{total}$ — $\Gamma_1\Gamma_6/\Gamma$

VALUE (eV)	DOCUMENT ID		TECN	COMMENT
• • • We do not use the following data for averages, fits, limits, etc. • • •				
0.295±0.175	[1,2] MIZUK	19	BELL	$e^+e^- \to \Upsilon(nS)\pi^+\pi^-$

[1] From a simultaneous fit to the $\Upsilon(nS)\pi^+\pi^-$, n = 1, 2, 3, cross sections at 28 energy points within $\sqrt{s}$ = 10.63–11.02 GeV, including the initial-state radiation at $\Upsilon(10860)$.
[2] Reported as the range 0.12–0.47 eV obtained from multiple solutions of an amplitude fit within a model composed as a sum of Breit-Wigner functions.

$\Gamma(\Upsilon(2S)\pi^+\pi^-) \times \Gamma(e^+e^-)/\Gamma_{total}$ — $\Gamma_2\Gamma_6/\Gamma$

VALUE (eV)	DOCUMENT ID		TECN	COMMENT
• • • We do not use the following data for averages, fits, limits, etc. • • •				
0.875±0.345	[1,2] MIZUK	19	BELL	$e^+e^- \to \Upsilon(nS)\pi^+\pi^-$

[1] From a simultaneous fit to the $\Upsilon(nS)\pi^+\pi^-$, n = 1, 2, 3, cross sections at 28 energy points within $\sqrt{s}$ = 10.63–11.02 GeV, including the initial-state radiation at $\Upsilon(10860)$.
[2] Reported as the range 0.53–1.22 eV obtained from multiple solutions of an amplitude fit within a model composed as a sum of Breit-Wigner functions.

$\Gamma(\Upsilon(3S)\pi^+\pi^-) \times \Gamma(e^+e^-)/\Gamma_{total}$ — $\Gamma_3\Gamma_6/\Gamma$

VALUE (eV)	DOCUMENT ID		TECN	COMMENT
• • • We do not use the following data for averages, fits, limits, etc. • • •				
0.235±0.025	[1,2] MIZUK	19	BELL	$e^+e^- \to \Upsilon(nS)\pi^+\pi^-$

[1] From a simultaneous fit to the $\Upsilon(nS)\pi^+\pi^-$, n = 1, 2, 3, cross sections at 28 energy points within $\sqrt{s}$ = 10.63–11.02 GeV, including the initial-state radiation at $\Upsilon(10860)$.
[2] Reported as the range 0.21–0.26 eV obtained from multiple solutions of an amplitude fit within a model composed as a sum of Breit-Wigner functions.

$\Gamma(\omega\chi_{b1}(1P)) \times \Gamma(e^+e^-)/\Gamma_{total}$ — $\Gamma_4\Gamma_6/\Gamma$

VALUE (eV)	CL%	DOCUMENT ID		TECN	COMMENT
0.63±0.39±0.20	68	[1] ADACHI	23	BELL	$e^+e^- \to \pi^+\pi^-\pi^0\gamma\Upsilon(1S)$

[1] A fit solution with constructive interference. The other solution corresponding to destructive interference gives a value of 2.01 ± 0.38 ± 0.76 eV.

$\Gamma(\omega\chi_{b2}(1P)) \times \Gamma(e^+e^-)/\Gamma_{total}$ — $\Gamma_5\Gamma_6/\Gamma$

VALUE (eV)	CL%	DOCUMENT ID		TECN	COMMENT
0.53±0.46±0.15	68	[1] ADACHI	23	BELL	$e^+e^- \to \pi^+\pi^-\pi^0\gamma\Upsilon(1S)$

[1] A fit solution with constructive interference. The other solution corresponding to destructive interference gives a value of 1.32 ± 0.44 ± 0.55 eV.

$\Upsilon(10753)$ REFERENCES

ADACHI	24V	JHEP 2407 116	I. Adachi *et al.*	(BELLE II Collab.)
ADACHI	23	PRL 130 091902	I. Adachi *et al.*	(BELLE II Collab.)
DONG	20A	CP C44 083001	X.-K. Dong *et al.*	
MIZUK	19	JHEP 1910 220	R. Mizuk *et al.*	(BELLE Collab.)
SANTEL	16	PR D93 011101	D. Santel *et al.*	(BELLE Collab.)
AUBERT	09E	PRL 102 012001	B. Aubert *et al.*	(BABAR Collab.)

$\Upsilon(10860)$

$I^G(J^{PC}) = 0^-(1^{--})$

$\Upsilon(10860)$ MASS

VALUE (MeV)	DOCUMENT ID		TECN	COMMENT
$10885.2^{+2.6}_{-1.6}$ OUR AVERAGE				
$10885.3\pm1.5^{+2.2}_{-0.9}$	[1] MIZUK	19	BELL	$e^+e^- \to \Upsilon(nS)\pi^+\pi^-$
$10884.7^{+3.6+8.9}_{-3.4-1.0}$	[2] MIZUK	16	BELL	$e^+e^- \to h_b(1P,2P)\pi^+\pi^-$
• • • We do not use the following data for averages, fits, limits, etc. • • •				
10882 ± 1	[3] DONG	20A		$e^+e^- \to b\overline{b}$
$10881.8^{+1.0}_{-1.1}\pm1.2$	[4,5] SANTEL	16	BELL	$e^+e^- \to$ hadrons
$10891.1\pm3.2^{+1.2}_{-2.0}$	[6,7] SANTEL	16	BELL	$e^+e^- \to \Upsilon(1S,2S,3S)\pi^+\pi^-$
10879 ± 3	[8,9] CHEN	10	BELL	$e^+e^- \to$ hadrons
$10888.4^{+2.7}_{-2.6}\pm1.2$	[10] CHEN	10	BELL	$e^+e^- \to \Upsilon(1S,2S,3S)\pi^+\pi^-$
10876 ± 2	[8] AUBERT	09E	BABR	$e^+e^- \to$ hadrons
10869 ± 2	[11] AUBERT	09E	BABR	$e^+e^- \to$ hadrons
10868 ± 6 ±5	[12] BESSON	85	CLEO	$e^+e^- \to$ hadrons
10845 ±20	[13] LOVELOCK	85	CUSB	$e^+e^- \to$ hadrons

[1] From a simultaneous fit to the $\Upsilon(nS)\pi^+\pi^-$, n = 1, 2, 3, cross sections at 28 energy points within $\sqrt{s}$ = 10.6–11.05 GeV, including the initial-state radiation at $\Upsilon(10860)$.
[2] From a simultaneous fit to the $h_b(nP)\pi^+\pi^-$, n = 1, 2 cross sections at 22 energy points within $\sqrt{s}$ = 10.77–11.02 GeV to a pair of interfering Breit-Wigner amplitudes modified by phase space factors, with eight resonance parameters (a mass and width for each of $\Upsilon(10860)$ and $\Upsilon(11020)$, a single relative phase, a single relative amplitude,

and two overall normalization factors, one for each n). The systematic error estimate is dominated by possible interference with a small nonresonant continuum amplitude.

[3] From a fit to the dressed cross sections of AUBERT 09E by BaBar and SANTEL 16 by Belle above 10.68 GeV with a coherent sum of a continuum amplitude and three Breit-Wigner functions with constant widths.

[4] From a fit to the total hadronic cross sections measured at 60 energy points within $\sqrt{s}$ = 10.82–11.05 GeV to a pair of interfering Breit-Wigner amplitudes and two floating continuum amplitudes with $1/\sqrt{s}$ dependence, one coherent with the resonances and one incoherent, with six resonance parameters (a mass, width, and an amplitude for each of $\Upsilon(10860)$ and $\Upsilon(11020)$, one relative phase, and one decoherence coefficient).

[5] Not including uncertain and potentially large systematic errors due to assumed continuum amplitude $1/\sqrt{s}$ dependence and related interference contributions.

[6] From a simultaneous fit to the $\Upsilon(\mathrm{nS})\pi^+\pi^-$, n = 1, 2, 3, cross sections at 25energy points within $\sqrt{s}$ = 10.6–11.05 GeV to a pair of interfering Breit-Wigner amplitudesmodified by phase space factors, with fourteen resonance parameters (a mass, width, and threeamplitudes for each of $\Upsilon(10860)$ and $\Upsilon(11020)$, a single universal relativephase, and three decoherence coefficients, one for each n). Continuum contributions weremeasured (and therefore fixed) to be zero.

[7] Superseded by MIZUK 19.

[8] In a model where a flat non-resonant $b\overline{b}$-continuum is incoherently added to a second flat component interfering with two Breit-Wigner resonances. Systematic uncertainties not estimated.

[9] The parameters of the $\Upsilon(11020)$ are fixed to those in AUBERT 09E.

[10] In a model where a flat nonresonant $\Upsilon(1S, 2S, 3S)\pi^+\pi^-$ continuum interferes with a single Breit-Wigner resonance.

[11] In a model where a non-resonant $b\overline{b}$-continuum represented by a threshold function at $\sqrt{s}$=$2m_B$ is incoherently added to a flat component interfering with two Breit-Wigner resonances. Not independent of other AUBERT 09E results. Systematic uncertainties not estimated.

[12] Assuming four Gaussians with radiative tails and a single step in R.

[13] In a coupled-channel model with three resonances and a smooth step in R.

$\Upsilon(10860)$ WIDTH

VALUE (MeV)	DOCUMENT ID		TECN	COMMENT
37 ± 4 OUR AVERAGE				
$36.6^{+4.5}_{-3.9}{}^{+0.5}_{-1.1}$	[1] MIZUK	19	BELL	$e^+e^- \to \Upsilon(\mathrm{nS})\pi^+\pi^-$
$40.6^{+12.7}_{-8.0}{}^{+1.1}_{-19.1}$	[2] MIZUK	16	BELL	$e^+e^- \to h_b(1\mathrm{P},2\mathrm{P})\pi^+\pi^-$
• • • We do not use the following data for averages, fits, limits, etc. • • •				
49.5 ± 1.5	[3] DONG	20A		$e^+e^- \to b\overline{b}$
$48.5^{+1.9}_{-1.8}{}^{+2.0}_{-2.8}$	[4,5] SANTEL	16	BELL	$e^+e^- \to$ hadrons
$53.7^{+7.1}_{-5.6}{}^{+1.3}_{-5.4}$	[6,7] SANTEL	16	BELL	$e^+e^- \to \Upsilon(1S,2S,3S)\pi^+\pi^-$
46^{+9}_{-7}	[8,9] CHEN	10	BELL	$e^+e^- \to$ hadrons
$30.7^{+8.3}_{-7.0} \pm 3.1$	[10] CHEN	10	BELL	$e^+e^- \to \Upsilon(1S,2S,3S)\pi^+\pi^-$
43 ± 4	[8] AUBERT	09E	BABR	$e^+e^- \to$ hadrons
74 ± 4	[11] AUBERT	09E	BABR	$e^+e^- \to$ hadrons
112 ±17 ±23	[12] BESSON	85	CLEO	$e^+e^- \to$ hadrons
110 ±15	[13] LOVELOCK	85	CUSB	$e^+e^- \to$ hadrons

[1] From a simultaneous fit to the $\Upsilon(\mathrm{nS})\pi^+\pi^-$, n = 1, 2, 3, cross sections at 28 energy points within $\sqrt{s}$ = 10.6–11.05 GeV, including the initial-state radiation at $\Upsilon(10860)$.

[2] From a simultaneous fit to the $h_b(\mathrm{nP})\pi^+\pi^-$, n = 1, 2 cross sections at 22 energy points within $\sqrt{s}$ = 10.77–11.02 GeV to a pair of interfering Breit-Wigner amplitudes modified by phase space factors, with eight resonance parameters (a mass and width for each of $\Upsilon(10860)$ and $\Upsilon(11020)$, a single relative phase, a single relative amplitude, and two overall normalization factors, one for each n). The systematic error estimate is dominated by possible interference with a small nonresonant continuum amplitude.

[3] From a fit to the dressed cross sections of AUBERT 09E by BaBar and SANTEL 16 by Belle above 10.68 GeV with a coherent sum of a continuum amplitude and three Breit-Wigner functions with constant widths.

[4] From a fit to the total hadronic cross sections measured at 60 energy points within $\sqrt{s}$ = 10.82–11.05 GeV to a pair of interfering Breit-Wigner amplitudes and two floating continuum amplitudes with $1/\sqrt{s}$ dependence, one coherent with the resonances and one incoherent, with six resonance parameters (a mass, width, and an amplitude for each of $\Upsilon(10860)$ and $\Upsilon(11020)$, one relative phase, and one decoherence coefficient).

[5] Not including uncertain and potentially large systematic errors due to assumed continuum amplitude $1/\sqrt{s}$ dependence and related interference contributions.

[6] From a simultaneous fit to the $\Upsilon(\mathrm{nS})\pi^+\pi^-$, n = 1, 2, 3, cross sections at 25energy points within $\sqrt{s}$ = 10.6–11.05 GeV to a pair of interfering Breit-Wigner amplitudesmodified by phase space factors, with fourteen resonance parameters (a mass, width, and threeamplitudes for each of $\Upsilon(10860)$ and $\Upsilon(11020)$, a single universal relativephase, and three decoherence coefficients, one for each n). Continuum contributions weremeasured (and therefore fixed) to be zero.

[7] Superseded by MIZUK 19.

[8] In a model where a flat non-resonant $b\overline{b}$-continuum is incoherently added to a second flat component interfering with two Breit-Wigner resonances. Systematic uncertainties not estimated.

[9] The parameters of the $\Upsilon(11020)$ are fixed to those in AUBERT 09E.

[10] In a model where a flat nonresonant $\Upsilon(1S, 2S, 3S)\pi^+\pi^-$ continuum interferes with a single Breit-Wigner resonance.

[11] In a model where a non-resonant $b\overline{b}$-continuum represented by a threshold function at $\sqrt{s}$=$2m_B$ is incoherently added to a flat component interfering with two Breit-Wigner resonances. Not independent of other AUBERT 09E results. Systematic uncertainties not estimated.

[12] Assuming four Gaussians with radiative tails and a single step in R.

[13] In a coupled-channel model with three resonances and a smooth step in R.

$\Upsilon(10860)$ DECAY MODES

	Mode	Fraction (Γ_i/Γ)	Confidence level
Γ_1	$B\overline{B}X$	$(73.5\ ^{+1.5}_{-2.8})$ %	
Γ_2	$B\overline{B}$	(5.5 ± 1.0) %	
Γ_3	$B\overline{B}^* +$ c.c.	(13.7 ± 1.6) %	
Γ_4	$B^*\overline{B}^*$	(38.1 ± 3.4) %	
Γ_5	$B\overline{B}^{(*)}\pi$	< 19.7 %	90%
Γ_6	$B\overline{B}\pi$	(0.0 ± 1.2) %	
Γ_7	$B^*\overline{B}\pi + B\overline{B}^*\pi$	(7.3 ± 2.3) %	
Γ_8	$B^*\overline{B}^*\pi$	(1.0 ± 1.4) %	
Γ_9	$B\overline{B}\pi\pi$	< 8.9 %	90%
Γ_{10}	$B_s^{(*)}\overline{B}_s^{(*)}$	(21.3 ± 1.5) %	
Γ_{11}	$B_s\overline{B}_s$	$(6 \pm 5) \times 10^{-3}$	
Γ_{12}	$B_s\overline{B}_s^* +$ c.c.	(1.44 ± 0.28) %	
Γ_{13}	$B_s^*\overline{B}_s^*$	(18.7 ± 1.3) %	
Γ_{14}	no open-bottom	$(4.8\ ^{+4.0}_{-0.5})$ %	
Γ_{15}	e^+e^-	$(8.3 \pm 2.1) \times 10^{-6}$	
Γ_{16}	$K^*(892)^0\overline{K}^0$	$< 1.0 \times 10^{-5}$	90%
Γ_{17}	$\Upsilon(1S)\pi^+\pi^-$	$(5.3 \pm 0.6) \times 10^{-3}$	
Γ_{18}	$\Upsilon(1S)\eta$	$(8.5 \pm 1.7) \times 10^{-4}$	
Γ_{19}	$\Upsilon(1S)\eta'$	$< 6.9 \times 10^{-5}$	90%
Γ_{20}	$\Upsilon(2S)\pi^+\pi^-$	$(7.8 \pm 1.3) \times 10^{-3}$	
Γ_{21}	$\Upsilon(2S)\eta$	$(4.1 \pm 0.6) \times 10^{-3}$	
Γ_{22}	$\Upsilon(3S)\pi^+\pi^-$	$(4.8\ ^{+1.9}_{-1.7}) \times 10^{-3}$	
Γ_{23}	$\Upsilon(1S)K^+K^-$	$(6.1 \pm 1.8) \times 10^{-4}$	
Γ_{24}	$\eta\Upsilon_J(1D)$	$(4.8 \pm 1.1) \times 10^{-3}$	
Γ_{25}	$h_b(1P)\pi^+\pi^-$	$(3.5\ ^{+1.0}_{-1.3}) \times 10^{-3}$	
Γ_{26}	$h_b(2P)\pi^+\pi^-$	$(5.7\ ^{+1.7}_{-2.1}) \times 10^{-3}$	
Γ_{27}	$\chi_{bJ}(1P)\pi^+\pi^-\pi^0$	$(2.5 \pm 2.3) \times 10^{-3}$	
Γ_{28}	$\chi_{b0}(1P)\pi^+\pi^-\pi^0$	$< 6.3 \times 10^{-3}$	90%
Γ_{29}	$\chi_{b0}(1P)\omega$	$< 3.9 \times 10^{-3}$	90%
Γ_{30}	$\chi_{b0}(1P)(\pi^+\pi^-\pi^0)_{\mathrm{non}-\omega}$	$< 4.8 \times 10^{-3}$	90%
Γ_{31}	$\chi_{b1}(1P)\pi^+\pi^-\pi^0$	$(1.85 \pm 0.33) \times 10^{-3}$	
Γ_{32}	$\chi_{b1}(1P)\omega$	$(1.57 \pm 0.30) \times 10^{-3}$	
Γ_{33}	$\chi_{b1}(1P)(\pi^+\pi^-\pi^0)_{\mathrm{non}-\omega}$	$(5.2 \pm 1.9) \times 10^{-4}$	
Γ_{34}	$\chi_{b2}(1P)\pi^+\pi^-\pi^0$	$(1.17 \pm 0.30) \times 10^{-3}$	
Γ_{35}	$\chi_{b2}(1P)\omega$	$(6.0 \pm 2.7) \times 10^{-4}$	
Γ_{36}	$\chi_{b2}(1P)(\pi^+\pi^-\pi^0)_{\mathrm{non}-\omega}$	$(6 \pm 4) \times 10^{-4}$	
Γ_{37}	$\gamma X_b \to \gamma\Upsilon(1S)\omega$	$< 3.8 \times 10^{-5}$	90%
Γ_{38}	$\eta_b(1S)\omega$	$< 1.3 \times 10^{-3}$	90%
Γ_{39}	$\eta_b(2S)\omega$	$< 5.6 \times 10^{-3}$	90%

Inclusive Decays.

These decay modes are submodes of one or more of the decay modes above.

Γ_{40}	ϕ anything	$(13.8\ ^{+2.4}_{-1.7})$ %	
Γ_{41}	D^0 anything + c.c.	(112 ± 6) %	
Γ_{42}	D_s anything + c.c.	(44.7 ± 2.6) %	
Γ_{43}	J/ψ anything	(2.06 ± 0.21) %	
Γ_{44}	B^0 anything + c.c.	(77 ± 8) %	
Γ_{45}	B^+ anything + c.c.	(72 ± 6) %	

$\Upsilon(10860)$ PARTIAL WIDTHS

$\Gamma(e^+e^-)$ — Γ_{15}

VALUE (keV)	DOCUMENT ID		TECN	COMMENT
0.31 ±0.07 OUR AVERAGE	Error includes scale factor of 1.3.			
0.22 ±0.05 ±0.07	BESSON	85	CLEO	$e^+e^- \to$ hadrons
0.365 ±0.070	LOVELOCK	85	CUSB	$e^+e^- \to$ hadrons

$\Gamma(e^+e^-) \times \Gamma(\Upsilon(1S)\pi^+\pi^-)/\Gamma_{\mathrm{total}}$ — $\Gamma_{15}\Gamma_{17}/\Gamma$

VALUE (eV)	DOCUMENT ID		TECN	COMMENT
• • • We do not use the following data for averages, fits, limits, etc. • • •				
1.09±0.34	[1,2] MIZUK	19	BELL	$e^+e^- \to \Upsilon(\mathrm{nS})\pi^+\pi^-$

[1] From a simultaneous fit to the $\Upsilon(\mathrm{nS})\pi^+\pi^-$, n = 1, 2, 3, cross sections at 28 energy points within $\sqrt{s}$ = 10.6–11.05 GeV, including the initial-state radiation at $\Upsilon(10860)$.

[2] Reported as the range 0.75–1.43 eV obtained from multiple solutions of an amplitude fit within a model composed as a sum of Breit-Wigner functions.

Int. J. Mod. Phys. A 2026.41. Downloaded from www.worldscientific.com
by LIFORNIA @ BERKELEY on 09/16/26. Re-use and distribution is strictly not permitted, except for Open Access articles.

Int. J. Mod. Phys. A 2026.41. Downloaded from www.worldscientific.com
by UNIVERSITY OF CALIFORNIA @ BERKELEY on 09/16/26. Re-use and distribution is strictly not permitted, except for Open Access articles.

$\Gamma(e^+e^-) \times \Gamma(\Upsilon(2S)\pi^+\pi^-)/\Gamma_{total}$ — $\Gamma_{15}\Gamma_{20}/\Gamma$

VALUE (eV)	DOCUMENT ID		TECN	COMMENT
• • • We do not use the following data for averages, fits, limits, etc. • • •				
2.58±1.22	[1,2] MIZUK	19	BELL	$e^+e^- \to \Upsilon(nS)\pi^+\pi^-$

[1] From a simultaneous fit to the $\Upsilon(nS)\pi^+\pi^-$, $n = 1, 2, 3$, cross sections at 28 energy points within $\sqrt{s} = 10.6$–11.05 GeV, including the initial-state radiation at $\Upsilon(10860)$.
[2] Reported as the range 1.35–3.80 eV obtained from multiple solutions of an amplitude fit within a model composed as a sum of Breit-Wigner functions.

$\Gamma(e^+e^-) \times \Gamma(\Upsilon(3S)\pi^+\pi^-)/\Gamma_{total}$ — $\Gamma_{15}\Gamma_{22}/\Gamma$

VALUE (eV)	DOCUMENT ID		TECN	COMMENT
• • • We do not use the following data for averages, fits, limits, etc. • • •				
0.73±0.30	[1,2] MIZUK	19	BELL	$e^+e^- \to \Upsilon(nS)\pi^+\pi^-$

[1] From a simultaneous fit to the $\Upsilon(nS)\pi^+\pi^-$, $n = 1, 2, 3$, cross sections at 28 energy points within $\sqrt{s} = 10.6$–11.05 GeV, including the initial-state radiation at $\Upsilon(10860)$.
[2] Reported as the range 0.43–1.03 eV obtained from multiple solutions of an amplitude fit within a model composed as a sum of Breit-Wigner functions.

$\Upsilon(10860)$ BRANCHING RATIOS

$\Gamma(B\overline{B}X)/\Gamma_{total}$ — Γ_1/Γ

VALUE	EVTS	DOCUMENT ID		TECN	COMMENT
$0.735^{+0.015}_{-0.028}$ OUR AVERAGE					
$0.738^{+0.015}_{-0.029}$		ADACHI	25O	BELL	$e^+e^- \to \Upsilon(5S)$
0.589±0.100±0.092		[1] HUANG	07	CLEO	$\Upsilon(5S) \to$ hadrons
• • • We do not use the following data for averages, fits, limits, etc. • • •					
0.737±0.032±0.051	1063	[2] DRUTSKOY	10	BELL	$\Upsilon(5S) \to B^+X,\ B^0X$

[1] Using measurements or limits from AQUINES 06.
[2] Not independent of DRUTSKOY 10 values for $\Upsilon(5S) \to B^{\pm,0}$ anything. Superseded by ADACHI 25O.

$\Gamma(B\overline{B})/\Gamma_{total}$ — Γ_2/Γ

VALUE (units 10^{-2})	CL%	DOCUMENT ID		TECN	COMMENT
$5.5^{+1.0}_{-0.9}$±0.4		[1] DRUTSKOY	10	BELL	$\Upsilon(5S) \to B^+X,\ B^0X$
• • • We do not use the following data for averages, fits, limits, etc. • • •					
<13.8	90	[2] HUANG	07	CLEO	$\Upsilon(5S) \to$ hadrons

[1] Assuming isospin conservation.
[2] Using measurements or limits from AQUINES 06.

$\Gamma(B\overline{B})/\Gamma(B\overline{B}X)$ — Γ_2/Γ_1

VALUE	CL%	DOCUMENT ID		TECN	COMMENT
<0.22	90	AQUINES	06	CLE3	$\Upsilon(5S) \to$ hadrons

$\Gamma(B\overline{B}^* + c.c.)/\Gamma_{total}$ — Γ_3/Γ

VALUE	DOCUMENT ID		TECN	COMMENT
0.137±0.016 OUR AVERAGE				
0.137±0.013±0.011	[1] DRUTSKOY	10	BELL	$\Upsilon(5S) \to B^+X,\ B^0X$
0.143±0.053±0.027	[2] HUANG	07	CLEO	$\Upsilon(5S) \to$ hadrons

[1] Assuming isospin conservation.
[2] Using measurements or limits from AQUINES 06.

$\Gamma(B\overline{B}^* + c.c.)/\Gamma(B\overline{B}X)$ — Γ_3/Γ_1

VALUE	EVTS	DOCUMENT ID		TECN	COMMENT
0.24±0.09±0.03	10	AQUINES	06	CLE3	$\Upsilon(5S) \to$ hadrons

$\Gamma(B^*\overline{B}^*)/\Gamma_{total}$ — Γ_4/Γ

VALUE	DOCUMENT ID		TECN	COMMENT
0.381±0.034 OUR AVERAGE				
$0.375^{+0.021}_{-0.019}$±0.030	[1] DRUTSKOY	10	BELL	$\Upsilon(5S) \to B^+X,\ B^0X$
0.436±0.083±0.072	[2] HUANG	07	CLEO	$\Upsilon(5S) \to$ hadrons

[1] Assuming isospin conservation.
[2] Using measurements or limits from AQUINES 06.

$\Gamma(B^*\overline{B}^*)/\Gamma(B\overline{B}X)$ — Γ_4/Γ_1

VALUE	EVTS	DOCUMENT ID		TECN	COMMENT
0.74±0.15±0.08	31	AQUINES	06	CLE3	$\Upsilon(5S) \to$ hadrons

$\Gamma(B\overline{B}^{(*)}\pi)/\Gamma_{total}$ — Γ_5/Γ

VALUE	CL%	DOCUMENT ID		TECN	COMMENT
<0.197	90	[1] HUANG	07	CLEO	$\Upsilon(5S) \to$ hadrons

[1] Using measurements or limits from AQUINES 06.

$\Gamma(B\overline{B}^{(*)}\pi)/\Gamma(B\overline{B}X)$ — Γ_5/Γ_1

VALUE	CL%	DOCUMENT ID		TECN	COMMENT
<0.32	90	AQUINES	06	CLE3	$\Upsilon(5S) \to$ hadrons

$\Gamma(B\overline{B}\pi)/\Gamma_{total}$ — Γ_6/Γ

VALUE (units 10^{-2})	EVTS	DOCUMENT ID		TECN	COMMENT
0.0±1.2±0.3	0	[1] DRUTSKOY	10	BELL	$\Upsilon(5S) \to B^{+,0}\pi^-X$

[1] Assuming isospin conservation.

$[\Gamma(B^*\overline{B}\pi) + \Gamma(B\overline{B}^*\pi)]/\Gamma_{total}$ — Γ_7/Γ

VALUE (units 10^{-2})	EVTS	DOCUMENT ID		TECN	COMMENT
$7.3^{+2.3}_{-2.1}$±0.8	38	[1] DRUTSKOY	10	BELL	$\Upsilon(5S) \to B^{+,0}\pi^-X$

[1] Assuming isospin conservation.

$\Gamma(B^*\overline{B}^*\pi)/\Gamma_{total}$ — Γ_8/Γ

VALUE (units 10^{-2})	EVTS	DOCUMENT ID		TECN	COMMENT
$1.0^{+1.4}_{-1.3}$±0.4	5	[1] DRUTSKOY	10	BELL	$\Upsilon(5S) \to B^{+,0}\pi^-X$

[1] Assuming isospin conservation.

$\Gamma(B\overline{B}\pi\pi)/\Gamma_{total}$ — Γ_9/Γ

VALUE	CL%	DOCUMENT ID		TECN	COMMENT
<0.089	90	[1] HUANG	07	CLEO	$\Upsilon(5S) \to$ hadrons

[1] Using measurements or limits from AQUINES 06.

$\Gamma(B\overline{B}\pi\pi)/\Gamma(B\overline{B}X)$ — Γ_9/Γ_1

VALUE	CL%	DOCUMENT ID		TECN	COMMENT
<0.14	90	AQUINES	06	CLE3	$\Upsilon(5S) \to$ hadrons

$\Gamma(B_s^{(*)}\overline{B}_s^{(*)})/\Gamma_{total}$ — $\Gamma_{10}/\Gamma = (\Gamma_{11}+\Gamma_{12}+\Gamma_{13})/\Gamma$

VALUE	DOCUMENT ID		TECN	COMMENT
0.213±0.015 OUR AVERAGE				
$0.214^{+0.015}_{-0.017}$	ADACHI	25O	BELL	$e^+e^- \to \Upsilon(5S)$
$0.21^{+0.06}_{-0.03}$	[1] HUANG	07	CLEO	$\Upsilon(5S) \to D_sX$
• • • We do not use the following data for averages, fits, limits, etc. • • •				
0.172±0.030	[2] ESEN	13	BELL	$\Upsilon(5S) \to D^0X,\ D_sX$
0.180±0.013±0.032	[3] DRUTSKOY	07	BELL	$\Upsilon(5S) \to D^0X,\ D_sX$
0.160±0.026±0.058	[4] ARTUSO	05B	CLEO	$e^+e^- \to D_XX$

[1] Supersedes ARTUSO 05B. Combining inclusive ϕ, D_s, and B measurements. Using $B(D_s^+ \to \phi\pi^+) = 4.4 \pm 0.6\%$ from PDG 06.
[2] Superseded by ADACHI 25O.
[3] Using $B(D_s^+ \to \phi\pi^+) = (4.4 \pm 0.6)\%$ from PDG 06. Superseded by ESEN 13
[4] Uses a model-dependent estimate $B(B_s \to D_sX) = (92 \pm 11)\%$.

$\Gamma(B_s^{(*)}\overline{B}_s^{(*)})/\Gamma(B\overline{B}X)$ — Γ_{10}/Γ_1

VALUE	DOCUMENT ID
$0.264^{+0.052}_{-0.045}$ OUR EVALUATION	

$\Gamma(B_s^*\overline{B}_s^*)/\Gamma(B_s^{(*)}\overline{B}_s^{(*)})$ — $\Gamma_{13}/\Gamma_{10} = \Gamma_{13}/(\Gamma_{11}+\Gamma_{12}+\Gamma_{13})$

VALUE (units 10^{-2})	EVTS	DOCUMENT ID		TECN	COMMENT
87.8±1.5 OUR AVERAGE					
87.0±1.7		[1,2] ESEN	13	BELL	$B_s^0 \to D_s^-\pi^+$
90.5±3.2±0.1	227	[2,3] LI	12	BELL	$B_s^0 \to J/\psi\eta^{(\prime)}$
• • • We do not use the following data for averages, fits, limits, etc. • • •					
$90.1^{+3.8}_{-4.0}$±0.2		[4] LOUVOT	09	BELL	10.86 $e^+e^- \to B_s^{(*)}\overline{B}_s^{(*)}$
93^{+7}_{-9} ±1		[4] DRUTSKOY	07A	BELL	Superseded by LOUVOT 09

[1] Supersedes LOUVOT 09.
[2] With $N(B_s^{(*)}\overline{B}_s^{(*)}) = (7.11 \pm 1.30) \times 10^6$.
[3] The ratios $N(B_s^*\overline{B}_s^*)$ / $N(B_s^{(*)}\overline{B}_s^{(*)})$ and $N(B_s^*\overline{B}_s^0)$ / $N(B_s^{(*)}\overline{B}_s^{(*)})$ are measured with a correlation coefficient of −0.72.
[4] From a measurement of $\sigma(e^+e^- \to B_s^*\overline{B}_s^*)$ / $\sigma(e^+e^- \to B_s^{(*)}\overline{B}_s^{(*)})$ at $\sqrt{s} = 10.86$ GeV.

$\Gamma(B_s\overline{B}_s)/\Gamma(B_s^{(*)}\overline{B}_s^{(*)})$ — $\Gamma_{11}/\Gamma_{10} = \Gamma_{11}/(\Gamma_{11}+\Gamma_{12}+\Gamma_{13})$

VALUE (units 10^{-2})	DOCUMENT ID		TECN	COMMENT
$2.6^{+2.6}_{-2.5}$	LOUVOT	09	BELL	10.86 $e^+e^- \to B_s^{(*)}\overline{B}_s^{(*)}$

$\Gamma(B_s\overline{B}_s)/\Gamma(B_s^*\overline{B}_s^*)$ — Γ_{11}/Γ_{13}

VALUE	CL%	DOCUMENT ID		TECN	COMMENT
<0.16	90	BONVICINI	06	CLE3	e^+e^-

$\Gamma(B_s\overline{B}_s^* + c.c.)/\Gamma(B_s^{(*)}\overline{B}_s^{(*)})$ — $\Gamma_{12}/\Gamma_{10} = \Gamma_{12}/(\Gamma_{11}+\Gamma_{12}+\Gamma_{13})$

VALUE (units 10^{-2})	EVTS	DOCUMENT ID		TECN	COMMENT
6.7±1.2 OUR AVERAGE					
7.3±1.4		[1,2] ESEN	13	BELL	$B_s^0 \to D_s^-\pi^+$
4.9±2.5±0.0	227	[2,3] LI	12	BELL	$B_s^0 \to J/\psi\eta^{(\prime)}$
• • • We do not use the following data for averages, fits, limits, etc. • • •					
$7.3^{+3.3}_{-3.0}$±0.1		LOUVOT	09	BELL	10.86 $e^+e^- \to B_s^{(*)}\overline{B}_s^{(*)}$

[1] Supersedes LOUVOT 09.
[2] With $N(B_s^{(*)}\overline{B}_s^{(*)}) = (7.11 \pm 1.30) \times 10^6$.
[3] The ratios $N(B_s^*\overline{B}_s^*)$ / $N(B_s^{(*)}\overline{B}_s^{(*)})$ and $N(B_s^*\overline{B}_s^0)$ / $N(B_s^{(*)}\overline{B}_s^{(*)})$ are measured with a correlation coefficient of −0.72.

Int. J. Mod. Phys. A 2026.41. Downloaded from www.worldscientific.com by [redacted]LIFORNIA @ BERKELEY on 09/16/26. Re-use and distribution is strictly not permitted, except for Open Access articles.

$\Gamma(B_s\overline{B}_s^* + \text{c.c.})/\Gamma(B_s^*\overline{B}_s^*)$ — Γ_{12}/Γ_{13}

VALUE	CL%	DOCUMENT ID		TECN	COMMENT
<0.16	90	BONVICINI	06	CLE3	e^+e^-

$\Gamma(\text{no open-bottom})/\Gamma_{\text{total}}$ — Γ_{14}/Γ

VALUE	DOCUMENT ID		TECN	COMMENT
$\mathbf{0.048^{+0.036}_{-0.005}}$	ADACHI	25O	BELL	$e^+e^- \to \Upsilon(5S)$

$\Gamma(K^*(892)^0\overline{K}^0)/\Gamma_{\text{total}}$ — Γ_{16}/Γ

VALUE	CL%	DOCUMENT ID		TECN	COMMENT
$\mathbf{<1.0\times10^{-5}}$	90	SHEN	13A	BELL	$e^+e^- \to K^*(892)^0\overline{K}^0$

$\Gamma(\eta\,\Upsilon_J(1D))/\Gamma_{\text{total}}$ — Γ_{24}/Γ

VALUE (units 10^{-3})	DOCUMENT ID		TECN	COMMENT
4.82±0.92±0.67	[1] TAMPONI	18	BELL	$e^+e^- \to \Upsilon(5S) \to \eta X$

[1] Mainly $J=2$, assumes no continuum contribution under $\Upsilon(5S)$.

$\Gamma(\Upsilon(1S)\pi^+\pi^-)/\Gamma_{\text{total}}$ — Γ_{17}/Γ

VALUE (units 10^{-3})	EVTS	DOCUMENT ID		TECN	COMMENT
5.3±0.3±0.5	325	[1] CHEN	08	BELL	10.87 $e^+e^- \to \Upsilon(1S)\pi^+\pi^-$

[1] Assuming that the observed events are solely due to the $\Upsilon(5S)$ resonance.

$\Gamma(\Upsilon(1S)\eta)/\Gamma_{\text{total}}$ — Γ_{18}/Γ

VALUE (units 10^{-3})	DOCUMENT ID		TECN	COMMENT
0.85±0.15±0.08	[1,2] KOVALENKO	21	BELL	$e^+e^- \to \Upsilon(5S)$

[1] Assuming that the observed events are solely due to the $\Upsilon(5S)$ resonance.
[2] Using a data sample of 118.3 fb^{-1} of e^+e^- collisions at $\sqrt{s}=10.866$ GeV.

$\Gamma(\Upsilon(1S)\eta')/\Gamma_{\text{total}}$ — Γ_{19}/Γ

VALUE	CL%	DOCUMENT ID		TECN	COMMENT
$\mathbf{<6.9\times10^{-5}}$	90	[1,2] KOVALENKO	21	BELL	$e^+e^- \to \Upsilon(5S)$

[1] Assuming that the observed events are solely due to the $\Upsilon(5S)$ resonance.
[2] Using a data sample of 118.3 fb^{-1} of e^+e^- collisions at $\sqrt{s}=10.866$ GeV.

$\Gamma(\Upsilon(2S)\pi^+\pi^-)/\Gamma_{\text{total}}$ — Γ_{20}/Γ

VALUE (units 10^{-3})	EVTS	DOCUMENT ID		TECN	COMMENT
7.8±0.6±1.1	186	[1] CHEN	08	BELL	10.87 $e^+e^- \to \Upsilon(2S)\pi^+\pi^-$

[1] Assuming that the observed events are solely due to the $\Upsilon(5S)$ resonance.

$\Gamma(\Upsilon(2S)\eta)/\Gamma_{\text{total}}$ — Γ_{21}/Γ

VALUE (units 10^{-3})	DOCUMENT ID		TECN	COMMENT
4.13±0.41±0.37	[1,2] KOVALENKO	21	BELL	$e^+e^- \to \Upsilon(5S)$

[1] Assuming that the observed events are solely due to the $\Upsilon(5S)$ resonance.
[2] Using a data sample of 118.3 fb^{-1} of e^+e^- collisions at $\sqrt{s}=10.866$ GeV.

$\Gamma(\Upsilon(3S)\pi^+\pi^-)/\Gamma_{\text{total}}$ — Γ_{22}/Γ

VALUE (units 10^{-3})	EVTS	DOCUMENT ID		TECN	COMMENT
$\mathbf{4.8^{+1.8}_{-1.5}\pm0.7}$	10	[1] CHEN	08	BELL	10.87 $e^+e^- \to \Upsilon(3S)\pi^+\pi^-$

[1] Assuming that the observed events are solely due to the $\Upsilon(5S)$ resonance.

$\Gamma(\Upsilon(1S)K^+K^-)/\Gamma_{\text{total}}$ — Γ_{23}/Γ

VALUE (units 10^{-4})	EVTS	DOCUMENT ID		TECN	COMMENT
$\mathbf{6.1^{+1.6}_{-1.4}\pm1.0}$	20	[1] CHEN	08	BELL	10.87 $e^+e^- \to \Upsilon(1S)K^+K^-$

[1] Assuming that the observed events are solely due to the $\Upsilon(5S)$ resonance.

$\Gamma(h_b(1P)\pi^+\pi^-)/\Gamma(\Upsilon(2S)\pi^+\pi^-)$ — Γ_{25}/Γ_{20}

VALUE	DOCUMENT ID		TECN	COMMENT
$\mathbf{0.45\pm0.08^{+0.07}_{-0.12}}$	ADACHI	12	BELL	10.86 $e^+e^- \to$ hadrons

$\Gamma(h_b(2P)\pi^+\pi^-)/\Gamma(\Upsilon(2S)\pi^+\pi^-)$ — Γ_{26}/Γ_{20}

VALUE	DOCUMENT ID		TECN	COMMENT
$\mathbf{0.77\pm0.08^{+0.22}_{-0.17}}$	ADACHI	12	BELL	10.86 $e^+e^- \to$ hadrons

$\Gamma(h_b(1P)\pi^+\pi^-)/\Gamma(h_b(2P)\pi^+\pi^-)$ — Γ_{25}/Γ_{26}

VALUE	DOCUMENT ID		TECN	COMMENT
0.616±0.052±0.017	MIZUK	16	BELL	$e^+e^- \to h_b(1P,2P)\pi^+\pi^-$

$\Gamma(\chi_{bJ}(1P)\pi^+\pi^-\pi^0)/\Gamma_{\text{total}}$ — Γ_{27}/Γ

VALUE (units 10^{-3})	DOCUMENT ID		TECN	COMMENT
2.5±0.6±2.2	YIN	18	BELL	$e^+e^- \to$ hadrons

$\Gamma(\chi_{b0}(1P)\pi^+\pi^-\pi^0)/\Gamma_{\text{total}}$ — Γ_{28}/Γ

VALUE	CL%	DOCUMENT ID		TECN	COMMENT
$\mathbf{<6.3\times10^{-3}}$	90	[1] HE	14	BELL	$\Upsilon(5S) \to \pi^+\pi^-\pi^0\gamma\,\Upsilon(1S)$

[1] Assuming that all the $b\overline{b}$ events are from $\Upsilon(5S)$ resonance decays and using $\sigma(e^+e^- \to b\overline{b}) = 0.340 \pm 0.016$ nb from ESEN 13. Correlated with other results from HE 14.

$\Gamma(\chi_{b0}(1P)\omega)/\Gamma_{\text{total}}$ — Γ_{29}/Γ

VALUE	CL%	DOCUMENT ID		TECN	COMMENT
$\mathbf{<3.9\times10^{-3}}$	90	[1] HE	14	BELL	$\Upsilon(5S) \to \pi^+\pi^-\pi^0\gamma\,\Upsilon(1S)$

[1] Assuming that all the $b\overline{b}$ events are from $\Upsilon(5S)$ resonance decays and using $\sigma(e^+e^- \to b\overline{b}) = 0.340 \pm 0.016$ nb from ESEN 13. Correlated with other results from HE 14.

$\Gamma(\chi_{b0}(1P)(\pi^+\pi^-\pi^0)_{\text{non}-\omega})/\Gamma_{\text{total}}$ — Γ_{30}/Γ

VALUE	CL%	DOCUMENT ID		TECN	COMMENT
$\mathbf{<4.8\times10^{-3}}$	90	[1] HE	14	BELL	$\Upsilon(5S) \to \pi^+\pi^-\pi^0\gamma\,\Upsilon(1S)$

[1] Assuming that all the $b\overline{b}$ events are from $\Upsilon(5S)$ resonance decays and using $\sigma(e^+e^- \to b\overline{b}) = 0.340 \pm 0.016$ nb from ESEN 13. Correlated with other results from HE 14.

$\Gamma(\chi_{b1}(1P)\pi^+\pi^-\pi^0)/\Gamma_{\text{total}}$ — Γ_{31}/Γ

VALUE (units 10^{-3})	EVTS	DOCUMENT ID		TECN	COMMENT
1.85±0.23±0.23	80	[1] HE	14	BELL	$\Upsilon(5S) \to \pi^+\pi^-\pi^0\gamma\,\Upsilon(1S)$

[1] Assuming that all the $b\overline{b}$ events are from $\Upsilon(5S)$ resonance decays and using $\sigma(e^+e^- \to b\overline{b}) = 0.340 \pm 0.016$ nb from ESEN 13. Correlated with other results from HE 14.

$\Gamma(\chi_{b1}(1P)\omega)/\Gamma_{\text{total}}$ — Γ_{32}/Γ

VALUE (units 10^{-3})	EVTS	DOCUMENT ID		TECN	COMMENT
1.57±0.22±0.21	60	[1] HE	14	BELL	$\Upsilon(5S) \to \pi^+\pi^-\pi^0\gamma\,\Upsilon(1S)$

[1] Assuming that all the $b\overline{b}$ events are from $\Upsilon(5S)$ resonance decays and using $\sigma(e^+e^- \to b\overline{b}) = 0.340 \pm 0.016$ nb from ESEN 13. Correlated with other results from HE 14.

$\Gamma(\chi_{b1}(1P)(\pi^+\pi^-\pi^0)_{\text{non}-\omega})/\Gamma_{\text{total}}$ — Γ_{33}/Γ

VALUE (units 10^{-3})	EVTS	DOCUMENT ID		TECN	COMMENT
0.52±0.15±0.11	24	[1] HE	14	BELL	$\Upsilon(5S) \to \pi^+\pi^-\pi^0\gamma\,\Upsilon(1S)$

[1] Assuming that all the $b\overline{b}$ events are from $\Upsilon(5S)$ resonance decays and using $\sigma(e^+e^- \to b\overline{b}) = 0.340 \pm 0.016$ nb from ESEN 13. Correlated with other results from HE 14.

$\Gamma(\chi_{b2}(1P)\pi^+\pi^-\pi^0)/\Gamma_{\text{total}}$ — Γ_{34}/Γ

VALUE (units 10^{-3})	EVTS	DOCUMENT ID		TECN	COMMENT
1.17±0.27±0.14	29	[1] HE	14	BELL	$\Upsilon(5S) \to \pi^+\pi^-\pi^0\gamma\,\Upsilon(1S)$

[1] Assuming that all the $b\overline{b}$ events are from $\Upsilon(5S)$ resonance decays and using $\sigma(e^+e^- \to b\overline{b}) = 0.340 \pm 0.016$ nb from ESEN 13. Correlated with other results from HE 14.

$\Gamma(\chi_{b2}(1P)\omega)/\Gamma_{\text{total}}$ — Γ_{35}/Γ

VALUE (units 10^{-3})	EVTS	DOCUMENT ID		TECN	COMMENT
0.60±0.23±0.15	13	[1] HE	14	BELL	$\Upsilon(5S) \to \pi^+\pi^-\pi^0\gamma\,\Upsilon(1S)$

[1] Assuming that all the $b\overline{b}$ events are from $\Upsilon(5S)$ resonance decays and using $\sigma(e^+e^- \to b\overline{b}) = 0.340 \pm 0.016$ nb from ESEN 13. Correlated with other results from HE 14.

$\Gamma(\chi_{b2}(1P)\omega)/\Gamma(\chi_{b1}(1P)\omega)$ — Γ_{35}/Γ_{32}

VALUE	DOCUMENT ID		TECN	COMMENT
• • • We do not use the following data for averages, fits, limits, etc. • • •				
0.38±0.16±0.09	[1] HE	14	BELL	$\Upsilon(5S) \to \pi^+\pi^-\pi^0\gamma\,\Upsilon(1S)$

[1] Accounting for correlated systematics.

$\Gamma(\chi_{b2}(1P)(\pi^+\pi^-\pi^0)_{\text{non}-\omega})/\Gamma_{\text{total}}$ — Γ_{36}/Γ

VALUE (units 10^{-3})	EVTS	DOCUMENT ID		TECN	COMMENT
0.61±0.22±0.28	16	[1] HE	14	BELL	$\Upsilon(5S) \to \pi^+\pi^-\pi^0\gamma\,\Upsilon(1S)$

[1] Assuming that all the $b\overline{b}$ events are from $\Upsilon(5S)$ resonance decays and using $\sigma(e^+e^- \to b\overline{b}) = 0.340 \pm 0.016$ nb from ESEN 13. Correlated with other results from HE 14.

$\Gamma(\chi_{b2}(1P)(\pi^+\pi^-\pi^0)_{\text{non}-\omega})/\Gamma(\chi_{b1}(1P)(\pi^+\pi^-\pi^0)_{\text{non}-\omega})$ — Γ_{36}/Γ_{33}

VALUE	DOCUMENT ID		TECN	COMMENT
• • • We do not use the following data for averages, fits, limits, etc. • • •				
1.20±0.55±0.65	[1] HE	14	BELL	$\Upsilon(5S) \to \pi^+\pi^-\pi^0\gamma\,\Upsilon(1S)$

[1] Accounting for correlated systematics.

$\Gamma(\eta_b(1S)\omega)/\Gamma_{\text{total}}$ — Γ_{38}/Γ

VALUE	CL%	DOCUMENT ID		TECN	COMMENT
$\mathbf{<1.3\times10^{-3}}$	90	[1] OSKIN	20	BELL	$e^+e^- \to \omega X$

[1] Using $\sigma_{b\overline{b}} = 0.340 \pm 0.016$ nb from TAMPONI 15.

$\Gamma(\eta_b(2S)\omega)/\Gamma_{\text{total}}$ — Γ_{39}/Γ

VALUE	CL%	DOCUMENT ID		TECN	COMMENT
$\mathbf{<5.6\times10^{-3}}$	90	[1] OSKIN	20	BELL	$e^+e^- \to \omega X$

[1] Using $\sigma_{b\overline{b}} = 0.340 \pm 0.016$ nb from TAMPONI 15.

$\Gamma(\gamma X_b \to \gamma\,\Upsilon(1S)\omega)/\Gamma_{\text{total}}$ — Γ_{37}/Γ

VALUE	CL%	DOCUMENT ID		TECN	COMMENT
$\mathbf{<3.8\times10^{-5}}$	90	[1] HE	14	BELL	$\Upsilon(5S) \to \pi^+\pi^-\pi^0\gamma\,\Upsilon(1S)$

[1] Assuming that all the $b\overline{b}$ events are from $\Upsilon(5S)$ resonance decays and using $\sigma(e^+e^- \to b\overline{b}) = 0.340 \pm 0.016$ nb from ESEN 13. Correlated with other results from HE 14. For a state X_b with mass between 10.55 GeV/c^2 and 10.65 GeV/c^2, the obtained 90% upper limit as a function of m_{X_b} varies from 2.6×10^{-5} to 3.8×10^{-5}.

Int. J. Mod. Phys. A 2026.41. Downloaded from www.worldscientific.com
by UNIVERSITY OF CALIFORNIA @ BERKELEY on 09/16/26. Re-use and distribution is strictly not permitted, except for Open Access articles.

$\Gamma(\phi \text{ anything})/\Gamma_{total}$ — Γ_{40}/Γ

VALUE	DOCUMENT ID		TECN	COMMENT
$0.138 \pm 0.007^{+0.023}_{-0.015}$	HUANG	07	CLEO	$\Upsilon(5S) \to \phi X$

$\Gamma(D^0 \text{ anything} + \text{c.c.})/\Gamma_{total}$ — Γ_{41}/Γ

VALUE	DOCUMENT ID		TECN	COMMENT
$1.117 \pm 0.005 \pm 0.060$	[1] ZHUKOVA	23	BELL	$\Upsilon(5S) \to D^0 X$, $\overline{D}^0 X$
• • • We do not use the following data for averages, fits, limits, etc. • • •				
$1.076 \pm 0.040 \pm 0.068$	DRUTSKOY	07	BELL	$\Upsilon(5S) \to D^0 X$, $\overline{D}^0 X$

[1] Supersedes DRUTSKOY 07.

$\Gamma(D_s \text{ anything} + \text{c.c.})/\Gamma_{total}$ — Γ_{42}/Γ

VALUE	DOCUMENT ID		TECN	COMMENT
0.447 ± 0.026 OUR AVERAGE				
$0.447 \pm 0.003 \pm 0.027$	[1] ZHUKOVA	23	BELL	$\Upsilon(5S) \to D_s^{\pm} X$
$0.44 \pm 0.09 \pm 0.04$	[2] ARTUSO	05B	CLE3	$\Upsilon(5S) \to D_s^{\pm} X$
• • • We do not use the following data for averages, fits, limits, etc. • • •				
$0.472 \pm 0.024 \pm 0.072$	[3] DRUTSKOY	07	BELL	$\Upsilon(5S) \to D_s^{\pm} X$

[1] Supersedes DRUTSKOY 07.

[2] ARTUSO 05B reports $[\Gamma(\Upsilon(10860) \to D_s \text{ anything} + \text{c.c.})/\Gamma_{total}] \times [B(D_s^+ \to \phi\pi^+)] = 0.0198 \pm 0.0019 \pm 0.0038$ which we divide by our best (shown rounded) value $B(D_s^+ \to \phi\pi^+) = (4.5 \pm 0.4) \times 10^{-2}$. Our first error is their experiment's error and our second error is the systematic error from using our best (shown rounded) value.

[3] Using $B(D_s^+ \to \phi\pi^+) = (4.4 \pm 0.6)\%$ from PDG 06.

$\Gamma(J/\psi \text{ anything})/\Gamma_{total}$ — Γ_{43}/Γ

VALUE (units 10^{-2})	DOCUMENT ID		TECN	COMMENT
$2.060 \pm 0.160 \pm 0.134$	DRUTSKOY	07	BELL	$\Upsilon(5S) \to J/\psi X$

$\Gamma(B^0 \text{ anything} + \text{c.c.})/\Gamma_{total}$ — Γ_{44}/Γ

VALUE	EVTS	DOCUMENT ID		TECN	COMMENT
$0.770^{+0.058}_{-0.056} \pm 0.061$	352	DRUTSKOY	10	BELL	$\Upsilon(5S) \to B^0 X$

$\Gamma(B^+ \text{ anything} + \text{c.c.})/\Gamma_{total}$ — Γ_{45}/Γ

VALUE	EVTS	DOCUMENT ID		TECN	COMMENT
$0.721^{+0.039}_{-0.038} \pm 0.050$	711	DRUTSKOY	10	BELL	$\Upsilon(5S) \to B^+ X$

$\Upsilon(10860)$ REFERENCES

ADACHI	25O	JHEP 2504 114	I. Adachi *et al.*	(BELLE and BELLEII Collab.)
ZHUKOVA	23	JHEP 2308 131	V. Zhukova *et al.*	(BELLE Collab.)
KOVALENKO	21	PR D104 112006	E. Kovalenko *et al.*	(BELLE Collab.)
DONG	20A	CP C44 083001	X.-K. Dong *et al.*	
OSKIN	20	PR D102 092011	P. Oskin *et al.*	(BELLE Collab.)
MIZUK	19	JHEP 1910 220	R. Mizuk *et al.*	(BELLE Collab.)
TAMPONI	18	EPJ C78 633	U. Tamponi *et al.*	(BELLE Collab.)
YIN	18	PR D98 091102	J.H. Yin *et al.*	(BELLE Collab.)
MIZUK	16	PRL 117 142001	R. Mizuk *et al.*	(BELLE Collab.)
SANTEL	16	PR D93 011101	D. Santel *et al.*	(BELLE Collab.)
TAMPONI	15	PRL 115 142001	U. Tamponi *et al.*	(BELLE Collab.)
HE	14	PRL 113 142001	X.H. He *et al.*	(BELLE Collab.)
ESEN	13	PR D87 031101	S. Esen *et al.*	(BELLE Collab.)
SHEN	13A	PR D88 052019	C.P. Shen *et al.*	(BELLE Collab.)
ADACHI	12	PRL 108 032001	I. Adachi *et al.*	(BELLE Collab.)
LI	12	PRL 108 181808	J. Li *et al.*	(BELLE Collab.)
CHEN	10	PR D82 091106	K.-F. Chen *et al.*	(BELLE Collab.)
DRUTSKOY	10	PR D81 112003	A. Drutskoy *et al.*	(BELLE Collab.)
AUBERT	09E	PRL 102 012001	B. Aubert *et al.*	(BABAR Collab.)
LOUVOT	09	PRL 102 021801	R. Louvot *et al.*	(BELLE Collab.)
CHEN	08	PRL 100 112001	K.-F. Chen *et al.*	(BELLE Collab.)
DRUTSKOY	07	PRL 98 052001	A. Drutskoy *et al.*	(BELLE Collab.)
DRUTSKOY	07A	PR D76 012002	A. Drutskoy *et al.*	(BELLE Collab.)
HUANG	07	PR D75 012002	G.S. Huang *et al.*	(CLEO Collab.)
AQUINES	06	PRL 96 152001	O. Aquines *et al.*	(CLEO Collab.)
BONVICINI	06	PRL 96 022002	G. Bonvicini *et al.*	(CLEO Collab.)
PDG	06	JP G33 1	W.-M. Yao *et al.*	(PDG Collab.)
ARTUSO	05B	PRL 95 261801	M. Artuso *et al.*	(CLEO Collab.)
BESSON	85	PRL 54 381	D. Besson *et al.*	(CLEO Collab.)
LOVELOCK	85	PRL 54 377	D.M.J. Lovelock *et al.*	(CUSB Collab.)

$\Upsilon(11020)$

$I^G(J^{PC}) = 0^-(1^{--})$

$\Upsilon(11020)$ MASS

VALUE (MeV)	DOCUMENT ID		TECN	COMMENT
11000 ± 4 OUR AVERAGE				
$11000.0^{+4.0}_{-4.5} {}^{+1.0}_{-1.3}$	[1] MIZUK	19	BELL	$e^+e^- \to \Upsilon(1S,2S,3S)\pi^+\pi^-$
$10999.0^{+7.3}_{-7.8} {}^{+16.9}_{-1.0}$	[2] MIZUK	16	BELL	$e^+e^- \to h_b(1P,2P)\pi^+\pi^-$
• • • We do not use the following data for averages, fits, limits, etc. • • •				
11001 ± 1	[3] DONG	20A		$e^+e^- \to b\overline{b}$
$11003.0 \pm 1.1^{+0.9}_{-1.0}$	[4,5] SANTEL	16	BELL	$e^+e^- \to$ hadrons
$10987.5^{+6.4}_{-2.5} {}^{+9.1}_{-2.3}$	[6,7] SANTEL	16	BELL	$e^+e^- \to \Upsilon(1S,2S,3S)\pi^+\pi^-$
10996 ± 2	[8] AUBERT	09E	BABR	$e^+e^- \to$ hadrons
$11019 \pm 5 \pm 7$	BESSON	85	CLEO	$e^+e^- \to$ hadrons
11020 ± 30	LOVELOCK	85	CUSB	$e^+e^- \to$ hadrons

[1] From a simultaneous fit to the $\Upsilon(nS)\pi^+\pi^-$, $n = 1, 2, 3$, cross sections at 28 energy points within $\sqrt{s} = 10.6$–11.05 GeV, including the initial-state radiation at $\Upsilon(10860)$.

[2] From a simultaneous fit to the $h_b(nP)\pi^+\pi^-$, $n = 1, 2$ cross sections at 22 energy points within $\sqrt{s} = 10.77$–11.02 GeV to a pair of interfering Breit-Wigner amplitudes modified by phase space factors, with eight resonance parameters (a mass and width for each of $\Upsilon(10860)$ and $\Upsilon(11020)$, a single relative phase, a single relative amplitude, and two overall normalization factors, one for each n). The systematic error estimate is dominated by possible interference with a small nonresonant continuum amplitude.

[3] From a fit to the dressed cross sections of AUBERT 09E by BaBar and SANTEL 16 by Belle above 10.68 GeV with a coherent sum of a continuum amplitude and three Breit-Wigner functions with constant widths.

[4] From a fit to the total hadronic cross sections measured at 60 energy points within $\sqrt{s} = 10.82$–11.05 GeV to a pair of interfering Breit-Wigner amplitudes and two floating continuum amplitudes with $1/\sqrt{s}$ dependence, one coherent with the resonances and one incoherent, with six resonance parameters (a mass, width, and an amplitude for each of $\Upsilon(10860)$ and $\Upsilon(11020)$, one relative phase, and one decoherence coefficient).

[5] Not including uncertain and potentially large systematic errors due to assumed continuum amplitude $1/\sqrt{s}$ dependence and related interference contributions.

[6] From a simultaneous fit to the $\Upsilon(nS)\pi^+\pi^-$, $n = 1, 2, 3$, cross sections at 25energy points within $\sqrt{s} = 10.6$–11.05 GeV to a pair of interfering Breit-Wigner amplitudesmodified by phase space factors, with fourteen resonance parameters (a mass, width, and threeamplitudes for each of $\Upsilon(10860)$ and $\Upsilon(11020)$, a single universal relativephase, and three decoherence coefficients, one for each n). Continuum contributions weremeasured (and therefore fixed) to be zero.

[7] Superseded by MIZUK 19.

[8] In a model where a flat non-resonant $b\overline{b}$-continuum is incoherently added to a second flat component interfering with two Breit-Wigner resonances. Systematic uncertainties not estimated.

$\Upsilon(11020)$ WIDTH

VALUE (MeV)	DOCUMENT ID		TECN	COMMENT
24^{+8}_{-6} OUR AVERAGE				
$23.8^{+8.0}_{-6.8} {}^{+0.7}_{-1.8}$	[1] MIZUK	19	BELL	$e^+e^- \to \Upsilon(nS)\pi^+\pi^-$
$27^{+27}_{-11} {}^{+5}_{-12}$	[2] MIZUK	16	BELL	$e^+e^- \to h_b(1P,2P)\pi^+\pi^-$
• • • We do not use the following data for averages, fits, limits, etc. • • •				
35.1 ± 1.2	[3] DONG	20A		$e^+e^- \to b\overline{b}$
$39.3^{+1.7}_{-1.6} {}^{+1.3}_{-2.4}$	[4,5] SANTEL	16	BELL	$e^+e^- \to$ hadrons
$61^{+9}_{-19} {}^{+2}_{-20}$	[6,7] SANTEL	16	BELL	$e^+e^- \to \Upsilon(1S,2S,3S)\pi^+\pi^-$
37 ± 3	[8] AUBERT	09E	BABR	$e^+e^- \to$ hadrons
$61 \pm 13 \pm 22$	BESSON	85	CLEO	$e^+e^- \to$ hadrons
90 ± 20	LOVELOCK	85	CUSB	$e^+e^- \to$ hadrons

[1] From a simultaneous fit to the $\Upsilon(nS)\pi^+\pi^-$, $n = 1, 2, 3$, cross sections at 28 energy points within $\sqrt{s} = 10.6$–11.05 GeV, including the initial-state radiation at $\Upsilon(10860)$.

[2] From a simultaneous fit to the $h_b(nP)\pi^+\pi^-$, $n = 1, 2$ cross sections at 22 energy points within $\sqrt{s} = 10.77$–11.02 GeV to a pair of interfering Breit-Wigner amplitudes modified by phase space factors, with eight resonance parameters (a mass and width for each of $\Upsilon(10860)$ and $\Upsilon(11020)$, a single relative phase, a single relative amplitude, and two overall normalization factors, one for each n). The systematic error estimate is dominated by possible interference with a small nonresonant continuum amplitude.

[3] From a fit to the dressed cross sections of AUBERT 09E by BaBar and SANTEL 16 by Belle above 10.68 GeV with a coherent sum of a continuum amplitude and three Breit-Wigner functions with constant widths.

[4] From a fit to the total hadronic cross sections measured at 60 energy points within $\sqrt{s} = 10.82$–11.05 GeV to a pair of interfering Breit-Wigner amplitudes and two floating continuum amplitudes with $1/\sqrt{s}$ dependence, one coherent with the resonances and one incoherent, with six resonance parameters (a mass, width, and an amplitude for each of $\Upsilon(10860)$ and $\Upsilon(11020)$, one relative phase, and one decoherence coefficient).

[5] Not including uncertain and potentially large systematic errors due to assumed continuum amplitude $1/\sqrt{s}$ dependence and related interference contributions.

[6] From a simultaneous fit to the $\Upsilon(nS)\pi^+\pi^-$, n=1, 2, 3, cross sections at 25energy points within $\sqrt{s} = 10.6$–11.05 GeV to a pair of interfering Breit-Wigner amplitudesmodified by phase space factors, with fourteen resonance parameters (a mass, width, and threeamplitudes for each of $\Upsilon(10860)$ and $\Upsilon(11020)$, a single universal relativephase, and three decoherence coefficients, one for each n). Continuum contributions weremeasured (and therefore fixed) to be zero.

[7] Superseded by MIZUK 19.

[8] In a model where a flat non-resonant $b\overline{b}$-continuum is incoherently added to a second flat component interfering with two Breit-Wigner resonances. Systematic uncertainties not estimated.

$\Upsilon(11020)$ DECAY MODES

	Mode	Fraction (Γ_i/Γ)
Γ_1	e^+e^-	$(5.4^{+1.9}_{-2.1}) \times 10^{-6}$
Γ_2	$\Upsilon(1S)\pi^+\pi^-$	
Γ_3	$\Upsilon(2S)\pi^+\pi^-$	
Γ_4	$\Upsilon(3S)\pi^+\pi^-$	
Γ_5	$\chi_{bJ}(1P)\pi^+\pi^-\pi^0$	$(9^{+9}_{-8}) \times 10^{-3}$
Γ_6	$\chi_{b1}(1P)\pi^+\pi^-\pi^0$	seen
Γ_7	$\chi_{b2}(1P)\pi^+\pi^-\pi^0$	seen

$\Upsilon(11020)$ PARTIAL WIDTHS

$\Gamma(e^+e^-)$ — Γ_1

VALUE (keV)	DOCUMENT ID		TECN	COMMENT
0.130±0.030 OUR AVERAGE				
0.095±0.03 ±0.035	BESSON	85	CLEO	$e^+e^- \to$ hadrons
0.156±0.040	LOVELOCK	85	CUSB	$e^+e^- \to$ hadrons

$\Gamma(e^+e^-) \times \Gamma(\Upsilon(1S)\pi^+\pi^-)/\Gamma_{total}$ — $\Gamma_1\Gamma_2/\Gamma$

VALUE (eV)	DOCUMENT ID		TECN	COMMENT
• • • We do not use the following data for averages, fits, limits, etc. • • •				
0.46±0.08	[1,2] MIZUK	19	BELL	$e^+e^- \to \Upsilon(nS)\pi^+\pi^-$

[1] From a simultaneous fit to the $\Upsilon(nS)\pi^+\pi^-$, n = 1, 2, 3, cross sections at 28 energy points within $\sqrt{s}$ = 10.6–11.05 GeV, including the initial-state radiation at $\Upsilon(10860)$.
[2] Reported as the range 0.38–0.54 eV obtained from multiple solutions of an amplitude fit within a model composed as a sum of Breit-Wigner functions.

$\Gamma(e^+e^-) \times \Gamma(\Upsilon(2S)\pi^+\pi^-)/\Gamma_{total}$ — $\Gamma_1\Gamma_3/\Gamma$

VALUE (eV)	DOCUMENT ID		TECN	COMMENT
• • • We do not use the following data for averages, fits, limits, etc. • • •				
0.65±0.52	[1,2] MIZUK	19	BELL	$e^+e^- \to \Upsilon(nS)\pi^+\pi^-$

[1] From a simultaneous fit to the $\Upsilon(nS)\pi^+\pi^-$, n = 1, 2, 3, cross sections at 28 energy points within $\sqrt{s}$ = 10.6–11.05 GeV, including the initial-state radiation at $\Upsilon(10860)$.
[2] Reported as the range 0.13–1.16 eV obtained from multiple solutions of an amplitude fit within a model composed as a sum of Breit-Wigner functions.

$\Gamma(e^+e^-) \times \Gamma(\Upsilon(3S)\pi^+\pi^-)/\Gamma_{total}$ — $\Gamma_1\Gamma_4/\Gamma$

VALUE (eV)	DOCUMENT ID		TECN	COMMENT
• • • We do not use the following data for averages, fits, limits, etc. • • •				
0.33±0.16	[1,2] MIZUK	19	BELL	$e^+e^- \to \Upsilon(nS)\pi^+\pi^-$

[1] From a simultaneous fit to the $\Upsilon(nS)\pi^+\pi^-$, n = 1, 2, 3, cross sections at 28 energy points within $\sqrt{s}$ = 10.6–11.05 GeV, including the initial-state radiation at $\Upsilon(10860)$.
[2] Reported as the range 0.17–0.49 eV obtained from multiple solutions of an amplitude fit within a model composed as a sum of Breit-Wigner functions.

$\Gamma(\chi_{bJ}(1P)\pi^+\pi^-\pi^0)/\Gamma_{total}$ — Γ_5/Γ

VALUE (units 10^{-3})	DOCUMENT ID		TECN	COMMENT
$8.7\pm4.3^{+7.6}_{-6.6}$	YIN	18	BELL	$e^+e^- \to$ hadrons

$\Gamma(\chi_{b1}(1P)\pi^+\pi^-\pi^0)/\Gamma_{total}$ — Γ_6/Γ

VALUE	DOCUMENT ID		TECN	COMMENT
seen	YIN	18	BELL	$e^+e^- \to$ hadrons

$\Gamma(\chi_{b2}(1P)\pi^+\pi^-\pi^0)/\Gamma_{total}$ — Γ_7/Γ

VALUE	DOCUMENT ID		TECN	COMMENT
seen	YIN	18	BELL	$e^+e^- \to$ hadrons

$\Gamma(\chi_{b2}(1P)\pi^+\pi^-\pi^0)/\Gamma(\chi_{b1}(1P)\pi^+\pi^-\pi^0)$ — Γ_7/Γ_6

VALUE	DOCUMENT ID		TECN	COMMENT
0.4±0.2	YIN	18	BELL	$e^+e^- \to$ hadrons

$\Upsilon(11020)$ REFERENCES

DONG	20A	CP C44 083001	X.-K. Dong *et al.*	
MIZUK	19	JHEP 1910 220	R. Mizuk *et al.*	(BELLE Collab.)
YIN	18	PR D98 091102	J.H. Yin *et al.*	(BELLE Collab.)
MIZUK	16	PRL 117 142001	R. Mizuk *et al.*	(BELLE Collab.)
SANTEL	16	PR D93 011101	D. Santel *et al.*	(BELLE Collab.)
AUBERT	09E	PRL 102 012001	B. Aubert *et al.*	(BABAR Collab.)
BESSON	85	PRL 54 381	D. Besson *et al.*	(CLEO Collab.)
LOVELOCK	85	PRL 54 377	D.M.J. Lovelock *et al.*	(CUSB Collab.)

Int. J. Mod. Phys. A 2026.41. Downloaded from www.worldscientific.com
by [redacted]LIFORNIA @ BERKELEY on 09/16/26. Re-use and distribution is strictly not permitted, except for Open Access articles.

OTHER MESONS

$T^*_{\overline{c}s0}(2870)^0$

$I(J^P) = ?(0^+)$

OMITTED FROM SUMMARY TABLE

was $X_0(2900)$

An exotic state with minimal quark content $\overline{c}d\overline{s}u$. Observed by AAIJ 20AI using full amplitude analysis of $B^+ \to D^+D^-K^+$ decays.

$T^*_{\overline{c}s0}(2870)^0$ MASS

VALUE (MeV)	EVTS	DOCUMENT ID		TECN	COMMENT
2874±11 OUR AVERAGE	Error includes scale factor of 1.8. See the ideogram below.				
2883±11± 8	1.6k	[1] AAIJ	25C	LHCB	$B^+ \to D^+\overline{D}^0K^0_S$
2914±11±15	1.6k	[2] AAIJ	24AB	LHCB	$B^+ \to D^{*+}D^-K^+$
2866± 7± 2	1.2k	[3] AAIJ	20AI	LHCB	$B^+ \to D^+D^-K^+$

[1] Obtained from the amplitude analysis. Parameterized with the relativistic Breit-Wigner line shape.
[2] From a simultaneous amplitude analysis of $B^+ \to D^{*+}D^-K^+$, $B^+ \to D^{*-}D^+K^+$ and their c.c.
[3] Obtained from the full amplitude analysis. Parameterized with the relativistic Breit-Wigner line shape. Also confirmed by the model-independent analysis of AAIJ 20AF.

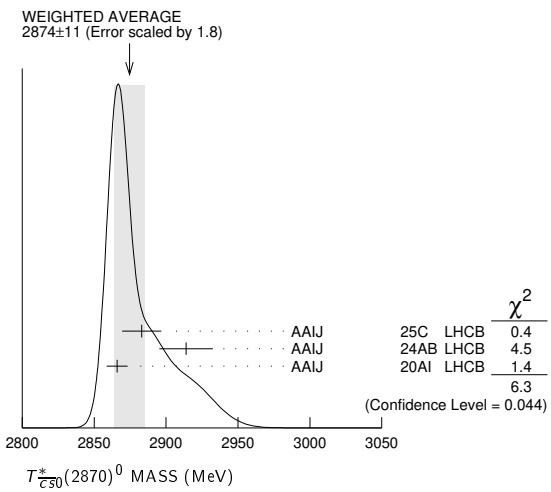

$T^*_{\overline{c}s0}(2870)^0$ WIDTH

VALUE (MeV)	EVTS	DOCUMENT ID		TECN	COMMENT
68±17 OUR AVERAGE	Error includes scale factor of 1.5. See the ideogram below.				
87^{+22}_{-47}±17	1.5k	[1] AAIJ	25C	LHCB	$B^+ \to D^+\overline{D}^0K^0_S$
128±22±23	1.6k	[2] AAIJ	24AB	LHCB	$B^+ \to D^{*+}D^-K^+$
57±12± 4	1.2k	[3] AAIJ	20AI	LHCB	$B^+ \to D^+D^-K^+$

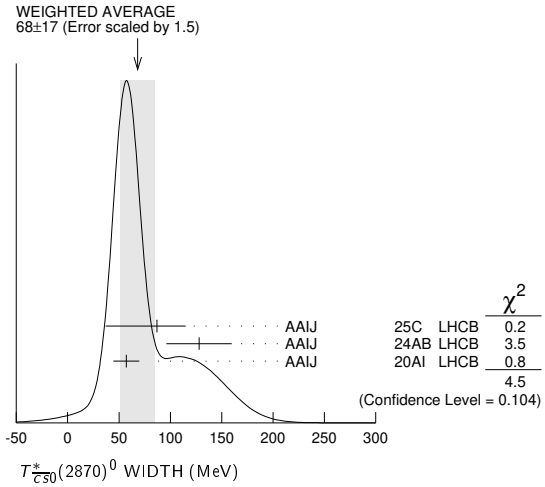

[1] Obtained from the amplitude analysis. Parameterized with the relativistic Breit-Wigner line shape.
[2] From a simultaneous amplitude analysis of $B^+ \to D^{*+}D^-K^+$, $B^+ \to D^{*-}D^+K^+$ and their c.c.
[3] Obtained from the full amplitude analysis. Parameterized with the relativistic Breit-Wigner line shape. Also confirmed by the model-independent analysis of AAIJ 20AF.

$T^*_{\overline{c}s0}(2870)^0$ DECAY MODES

	Mode	Fraction (Γ_i/Γ)
Γ_1	D^-K^+	seen
Γ_2	$\overline{D}^0K^0_S$	seen

$T^*_{\overline{c}s0}(2870)^0$ BRANCHING RATIOS

$\Gamma(D^-K^+)/\Gamma_{total}$ — Γ_1/Γ

VALUE	DOCUMENT ID		TECN	COMMENT
seen	AAIJ	20AI	LHCB	$B^+ \to D^+D^-K^+$

$\Gamma(\overline{D}^0K^0_S)/\Gamma(D^-K^+)$ — Γ_2/Γ_1

VALUE	EVTS	DOCUMENT ID		TECN	COMMENT
3.3±1.1±1.6	1.5k	[1] AAIJ	25C	LHCB	$B^+ \to D^+\overline{D}^0K^0_S$, $D^+D^-K^+$

[1] Obtained from fit fractions based an amplitude analyses. Parameterized with the relativistic Breit-Wigner line shape. The last error includes uncertainties from $B(B^+ \to D^+\overline{D}^0K^0_S)$ and $B(B^+ \to D^+D^-K^+)$ values.

$T^*_{\overline{c}s0}(2870)^0$ REFERENCES

AAIJ	25C	PRL 134 101901	R. Aaij *et al.*	(LHCb Collab.)
AAIJ	24AB	PRL 133 131902	R. Aaij *et al.*	(LHCb Collab.)
AAIJ	20AF	PRL 125 242001	R. Aaij *et al.*	(LHCb Collab.)
AAIJ	20AI	PR D102 112003	R. Aaij *et al.*	(LHCb Collab.)

$T^*_{\overline{c}s1}(2900)^0$

$I(J^P) = ?(1^-)$

OMITTED FROM SUMMARY TABLE

was $X_1(2900)$

An exotic state with minimal quark content $\overline{c}d\overline{s}u$. Observed by AAIJ 20AI using full amplitude analysis of $B^+ \to D^+D^-K^+$ decays.

$T^*_{\overline{c}s1}(2900)^0$ MASS

VALUE (MeV)	EVTS	DOCUMENT ID		TECN	COMMENT
2887 +- 8 + 7	1.6k	[1] AAIJ	24AB	LHCB	$B^+ \to D^{*+}D^-K^+$
2904±5±1	1.2k	[2] AAIJ	20AI	LHCB	$B^+ \to D^+D^-K^+$

[1] From a simultaneous amplitude analysis of $B^+ \to D^{*+}D^-K^+$, $B^+ \to D^{*-}D^+K^+$ and their c.c.
[2] Obtained from the full amplitude analysis. Parameterized with the relativistic Breit-Wigner line shape. Also confirmed by the model-independent analysis of AAIJ 20AF.

$T^*_{\overline{c}s1}(2900)^0$ WIDTH

VALUE (MeV)	EVTS	DOCUMENT ID		TECN	COMMENT
106±10 OUR AVERAGE					
92±16±16	1.6k	[1] AAIJ	24AB	LHCB	$B^+ \to D^{*+}D^-K^+$
110±11± 4	1.2k	[2] AAIJ	20AI	LHCB	$B^+ \to D^+D^-K^+$

[1] From a simultaneous amplitude analysis of $B^+ \to D^{*+}D^-K^+$, $B^+ \to D^{*-}D^+K^+$ and their c.c.
[2] Obtained from the full amplitude analysis. Parameterized with the relativistic Breit-Wigner line shape. Also confirmed by the model-independent analysis of AAIJ 20AF.

$T^*_{\overline{c}s1}(2900)^0$ DECAY MODES

	Mode	Fraction (Γ_i/Γ)
Γ_1	D^-K^+	seen

$T^*_{\overline{c}s1}(2900)^0$ BRANCHING RATIOS

$\Gamma(D^-K^+)/\Gamma_{total}$ — Γ_1/Γ

VALUE	DOCUMENT ID		TECN	COMMENT
seen	AAIJ	20AI	LHCB	$B^+ \to D^+D^-K^+$

$T^*_{\overline{c}s1}(2900)^0$ REFERENCES

AAIJ	24AB	PRL 133 131902	R. Aaij *et al.*	(LHCb Collab.)
AAIJ	20AF	PRL 125 242001	R. Aaij *et al.*	(LHCb Collab.)
AAIJ	20AI	PR D102 112003	R. Aaij *et al.*	(LHCb Collab.)

Int. J. Mod. Phys. A 2026.41. Downloaded from www.worldscientific.com
by UNIVERSITY OF CALIFORNIA @ BERKELEY on 09/16/26. Re-use and distribution is strictly not permitted, except for Open Access articles.

Meson Particle Listings

$T^*_{c\bar{s}0}(2900)$, $T_{cc}(3875)^+$, $T_{c\bar{c}1}(3900)$

$T^*_{c\bar{s}0}(2900)$

$I(J^P) = 1(0^+)$

OMITTED FROM SUMMARY TABLE

Observed by LHCb in AAIJ 23B using a simultaneous amplitude analysis of $B^0 \to \overline{D}^0 D_s^+ \pi^-$ and $B^+ \to D^- D_s^+ \pi^+$. The $T^*_{c\bar{s}0}(2900)^0 \to D_s^+ \pi^-$ and $T^*_{c\bar{s}0}(2900)^{++} \to D_s^+ \pi^+$ decays are observed with 8.0 and 6.5 σ significance, respectively.

$T^*_{c\bar{s}0}(2900)^0$ MASS

VALUE (MeV)	DOCUMENT ID		TECN	COMMENT
2892±14±15	[1] AAIJ	23C	LHCB	$B^0 \to \overline{D}^0 D_s^+ \pi^-$

[1] From an amplitude analysis of $B^0 \to \overline{D}^0 D_s^+ \pi^-$. A simultaneous fit to $B^0 \to \overline{D}^0 D_s^+ \pi^-$ and $B^- \to D^- D_s^+ \pi^+$ assuming isospin symmetry yields a mass of 2908 ± 11 ± 20 MeV.

$T^*_{c\bar{s}0}(2900)^{++}$ MASS

VALUE (MeV)	DOCUMENT ID		TECN	COMMENT
2921±17±20	[2] AAIJ	23C	LHCB	$B^- \to D^- D_s^+ \pi^+$

[2] From an amplitude analysis of $B^- \to D^- D_s^+ \pi^+$. A simultaneous fit to $B^0 \to \overline{D}^0 D_s^+ \pi^-$ and $B^- \to D^- D_s^+ \pi^+$ assuming isospin symmetry yields a mass of 2908 ± 11 ± 20 MeV.

$T^*_{c\bar{s}0}(2900)^0$ WIDTH

VALUE (MeV)	DOCUMENT ID		TECN	COMMENT
119±26±13	[3] AAIJ	23C	LHCB	$B^0 \to \overline{D}^0 D_s^+ \pi^-$

[3] From an amplitude analysis of $B^0 \to \overline{D}^0 D_s^+ \pi^-$. A simultaneous fit to $B^0 \to \overline{D}^0 D_s^+ \pi^-$ and $B^- \to D^- D_s^+ \pi^+$ assuming isospin symmetry yields a width of 136 ± 23 ± 13 MeV.

$T^*_{c\bar{s}0}(2900)^{++}$ WIDTH

VALUE (MeV)	DOCUMENT ID		TECN	COMMENT
137±32±17	[4] AAIJ	23C	LHCB	$B^- \to D^- D_s^+ \pi^+$

[4] From an amplitude analysis of $B^- \to D^- D_s^+ \pi^+$. A simultaneous fit to $B^0 \to \overline{D}^0 D_s^+ \pi^-$ and $B^- \to D^- D_s^+ \pi^+$ assuming isospin symmetry yields a width of 136 ± 23 ± 13 MeV.

$T^*_{c\bar{s}0}(2900)$ DECAY MODES

	Mode	Fraction (Γ_i/Γ)
Γ_1	$D_s^+ \pi^-$	seen
Γ_2	$D_s^+ \pi^+$	seen

$T^*_{c\bar{s}0}(2900)$ BRANCHING RATIOS

$\Gamma(D_s^+ \pi^-)/\Gamma_{total}$ — Γ_1/Γ

VALUE	DOCUMENT ID		TECN	COMMENT
seen	AAIJ	23C	LHCB	$B^0 \to \overline{D}^0 D_s^+ \pi^-$

$\Gamma(D_s^+ \pi^+)/\Gamma_{total}$ — Γ_2/Γ

VALUE	DOCUMENT ID		TECN	COMMENT
seen	AAIJ	23C	LHCB	$B^- \to D^- D_s^+ \pi^+$

$T^*_{c\bar{s}0}(2900)$ REFERENCES

AAIJ	23B	PR D108 012017	R. Aaij *et al.*	(LHCb Collab.)
AAIJ	23C	PRL 131 041902	R. Aaij *et al.*	(LHCb Collab.)

$T_{cc}(3875)^+$

$I(J^P) = ?(?^?)$

OMITTED FROM SUMMARY TABLE

Observed with large significance by AAIJ 22E in the doubly-charmed (C = 2) decay mode $D^0 D^0 \pi^+$ using inclusive pp collisions at 7, 8, and 13 TeV.

$T_{cc}(3875)^+$ T-Matrix Pole $\sqrt{s}$ relative to $D^0 D^{*+}$ threshold

VALUE (keV)	EVTS	DOCUMENT ID		TECN	COMMENT
$(-360 \pm 40^{+4}_{-0}) - i(24 \pm 1^{+0}_{-7})$	117	[1] AAIJ	22Z	LHCB	$pp \to D^0 D^0 \pi^+ X$
• • • We do not use the following data for averages, fits, limits, etc. • • •					
$(-356^{+39}_{-38}) - i(28 \pm 1)$		[2] DU	22	RVUE	

[1] The fit uses a coupled channel model accounting for the $D^0 D^{*+}$ threshold. The real part is given relative to the $D^0 D^{*+}$ threshold.

[2] The study provides fits results of three different coupled-channel calculations of increasing levels of sophistication to the LHCb data of AAIJ 22Z. We quote the result of the most advanced calculation with full three-body unitarity. The real part is given relative to the $D^0 D^{*+}$ threshold.

$T_{cc}(3875)^+$ T-Matrix Pole $\sqrt{s}$

VALUE (MeV)	DOCUMENT ID
$(3874.75 \pm 0.10) - i(0.024^{+0.001}_{-0.007})$ OUR EVALUATION	

$T_{cc}(3875)^+$ WIDTH

VALUE (MeV)	EVTS	DOCUMENT ID		TECN	COMMENT
$0.048 \pm 0.002^{+0.000}_{-0.014}$	117	[1] AAIJ	22Z	LHCB	$pp \to D^0 D^0 \pi^+ X$
• • • We do not use the following data for averages, fits, limits, etc. • • •					
$0.410 \pm 0.165^{+0.047}_{-0.057}$	117	[2] AAIJ	22E	LHCB	$pp \to D^0 D^0 \pi^+ X$

[1] Fit uses coupled channel model accounting for $D^0 D^{*+}$ threshold.

[2] The fit uses a relativistic P-wave Breit-Wigner function without taking into account the $D^0 D^{*+}$ threshold. The fit uses a relativistic P-wave Breit-Wigner function. Parameters are shown to be biased in AAIJ 22z.

$T_{cc}(3875)^+$ DECAY MODES

	Mode	Fraction (Γ_i/Γ)
Γ_1	$D^0 D^0 \pi^+$	seen

$T_{cc}(3875)^+$ BRANCHING RATIOS

$\Gamma(D^0 D^0 \pi^+)/\Gamma_{total}$ — Γ_1/Γ

VALUE	EVTS	DOCUMENT ID		TECN	COMMENT
seen	117	AAIJ	22E	LHCB	$pp \to D^0 D^0 \pi^+ X$

$T_{cc}(3875)^+$ REFERENCES

AAIJ	22E	NATP 18 751	R. Aaij *et al.*	(LHCb Collab.)
AAIJ	22Z	NATC 13 3351	R. Aaij *et al.*	(LHCb Collab.)
DU	22	PR D105 014024	M.-L. Du *et al.*	(VALE, IFIC, BOCH, KIAE+)

$T_{c\bar{c}1}(3900)$

$I^G(J^{PC}) = 1^+(1^{+-})$

was $Z_c(3900)$, $X(3900)$

Properties incompatible with a $q\overline{q}$ structure (exotic state). See the review on non-$q\overline{q}$ states.

Charged $T_{c\bar{c}1}(3900)^\pm$ seen as a peak in the invariant mass distribution of the $J/\psi\pi^\pm$ system by BES III (ABLIKIM 13T) in $e^+e^- \to \pi^+\pi^- J/\psi$ at c.m. energy of 4.26 GeV and by radiative return from e^+e^- collisions at $\sqrt{s}$ from 9.46 to 10.86 GeV at Belle (LIU 13B). Partial wave analysis of ABLIKIM 17J determines $J^P = 1^+$ with more than 7 σ significance. Neutral $T_{c\bar{c}1}(3900)^0$ seen in the $J/\psi\pi^0$ invariant mass distribution in $e^+e^- \to \pi^0\pi^0 J/\psi$ at c.m. energies of 4.23, 4.26, and 4.36 GeV by BES III (ABLIKIM 15U) and at 4.17 GeV by XIAO 13A. Peaks in $(D\overline{D}^*)^{0,\pm}$ reported by BES III (ABLIKIM 14A, ABLIKIM 15AB) are assumed to be related.

$T_{c\bar{c}1}(3900)$ MASS

VALUE (MeV)	EVTS	DOCUMENT ID		TECN	CHG	COMMENT
3886.7±2.3 OUR AVERAGE		Error includes scale factor of 1.7. See the ideogram below.				
3884.6±0.7± 3.3		[1] ABLIKIM	25BU	BES3	±	$e^+e^- \to \pi^+\pi^- J/\psi$
3893.1±2.2± 3.0		[1] ABLIKIM	20N	BES3	0	$e^+e^- \to \pi^0\pi^0 J/\psi$
$3902.6^{+5.2}_{-5.0} \pm 3.3 \pm 1.4$		[2,3] ABAZOV	19	D0	±	1.96 TeV $p\overline{p} \to J/\psi\pi^+\pi^- X$
$3885.7^{+4.3}_{-5.7} \pm 8.4$		[2,4] ABLIKIM	15AB	BES3	0	$e^+e^- \to \pi^0(D\overline{D}^*)^0$
3881.7±1.6± 1.6	1.2k	[2,4] ABLIKIM	15AC	BES3	±	$e^+e^- \to \pi^\pm(D\overline{D}^*)^\mp$
3883.9±1.5± 4.2	1.2k	[2,4] ABLIKIM	14A	BES3	±	$e^+e^- \to \pi^\pm(D\overline{D}^*)^\mp$
3894.5±6.6± 4.5	159	[2] LIU	13B	BELL	±	$e^+e^- \to \gamma\pi^+\pi^- J/\psi$
3886 ±4 ± 2	81	[2,5] XIAO	13A		±	4.17 $e^+e^- \to \pi^+\pi^- J/\psi$
3904 ±9 ± 5	25	[2,5] XIAO	13A		0	4.17 $e^+e^- \to \pi^0\pi^0 J/\psi$
• • • We do not use the following data for averages, fits, limits, etc. • • •						
$3895.0 \pm 5.2^{+4.0}_{-2.7}$	502	[2,6] ABAZOV	18B	D0	±	1.96 TeV $p\overline{p} \to J/\psi\pi^+\pi^- X$
3881.2±4.2±52.7	6k	[4,7] ABLIKIM	17J	BES3	±	$e^+e^- \to \pi^+\pi^- J/\psi$
3894.8±2.3± 3.2	356	[2,8] ABLIKIM	15U	BES3	0	$e^+e^- \to \pi^0\pi^0 J/\psi$
3899.0±3.6± 4.9	307	[2,9] ABLIKIM	13T	BES3	±	$e^+e^- \to \pi^+\pi^- J/\psi$

Int. J. Mod. Phys. A 2026.41. Downloaded from www.worldscientific.com by CALIFORNIA @ BERKELEY on 09/16/26. Re-use and distribution is strictly not permitted, except for Open Access articles.

Int. J. Mod. Phys. A 2026.41. Downloaded from www.worldscientific.com
by UNIVERSITY OF CALIFORNIA @ BERKELEY on 09/16/26. Re-use and distribution is strictly not permitted, except for Open Access articles.

[1] Pole mass obtained from a fit to a relativistic Breit-Wigner.
[2] Neglecting interference between the $T_{c\overline{c}1}(3900)$ and other processes.
[3] Measured in weak decays of b-flavored hadrons (nonprompt).
[4] Pole mass obtained from a fit to a Flatte-like formula.
[5] For $M^2(\pi^+\pi^-) < 0.65$ GeV^2. Obtained by analyzing CLEO-c data but not authored by the CLEO Collaboration.
[6] The signal of the $T_{c\overline{c}1}(3900)$ is correlated with a parent $J/\psi\pi^+\pi^-$ system in the invariant mass range 4.2–4.7 GeV. Superseded by ABAZOV 19.
[7] Superseded by ABLIKIM 25BU.
[8] Superseded by ABLIKIM 20N.
[9] Superseded by ABLIKIM 17J.

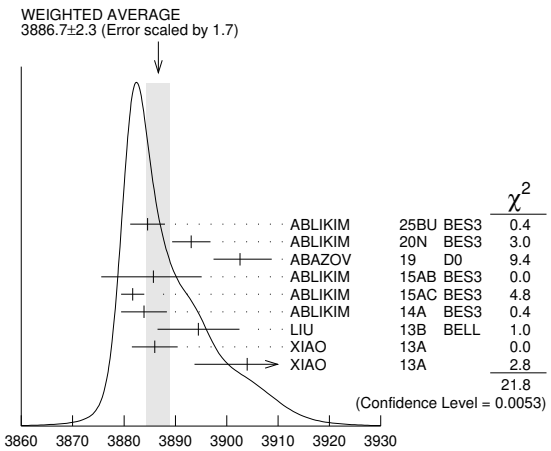

$T_{c\overline{c}1}(3900)$ WIDTH

VALUE (MeV)	EVTS	DOCUMENT ID		TECN	CHG	COMMENT
29.5± 2.4 OUR AVERAGE						
37.2± 1.3± 6.6		[1] ABLIKIM	25BU	BES3	±	$e^+e^- \to \pi^+\pi^- J/\psi$
44.4± 5.2±14.0		[1] ABLIKIM	20N	BES3	0	$e^+e^- \to \pi^0\pi^0 J/\psi$
$32\ ^{+28}_{-21}\ ^{+26}_{-7}$		[2,3] ABAZOV	19	D0	±	1.96 TeV $p\overline{p} \to \pi^+\pi^- J/\psi X$ (nonprompt)
$35\ ^{+11}_{-12}\ \pm15$		[2,4] ABLIKIM	15AB	BES3	0	$e^+e^- \to \pi^0(D\overline{D}^*)^0$
26.6± 2.0± 2.1	1248	[2,4] ABLIKIM	15AC	BES3	±	$e^+e^- \to \pi^\pm(D\overline{D}^*)^\mp$
24.8± 3.3±11.0	1212	[2,4] ABLIKIM	14A	BES3	±	$e^+e^- \to \pi^\pm(D\overline{D}^*)^\mp$
63 ±24 ±26	159	[2] LIU	13B	BELL	±	$e^+e^- \to \gamma\pi^+\pi^- J/\psi$
37 ± 4 ± 8	81	[2,5] XIAO	13A		±	4.17 $e^+e^- \to \pi^+\pi^- J/\psi$
• • • We do not use the following data for averages, fits, limits, etc. • • •						
51.8± 4.6±36.0	6 k	[4,6] ABLIKIM	17J	BES3	±	$e^+e^- \to \pi^+\pi^- J/\psi$
29.6± 8.2± 8.2	356	[2,7] ABLIKIM	15U	BES3	0	$e^+e^- \to \pi^0\pi^0 J/\psi$
46 ±10 ±20	307	[2,8] ABLIKIM	13T	BES3	±	$e^+e^- \to \pi^+\pi^- J/\psi$

[1] Pole width obtained from a fit to a relativistic Breit-Wigner.
[2] Neglecting interference between the $T_{c\overline{c}1}(3900)$ and other processes.
[3] Measured in weak decays of b-flavored hadrons (nonprompt).
[4] Pole width obtained from a fit to a Flatte-like formula.
[5] For $M^2(\pi^+\pi^-) < 0.65$ GeV^2. Obtained by analyzing CLEO-c data but not authored by the CLEO Collaboration.
[6] Superseded by ABLIKIM 25BU.
[7] Superseded by ABLIKIM 20N.
[8] Superseded by ABLIKIM 17J.

$T_{c\overline{c}1}(3900)$ DECAY MODES

	Mode	Fraction (Γ_i/Γ)
Γ_1	$J/\psi\pi$	seen
Γ_2	$h_c\pi^\pm$	not seen
Γ_3	$\eta_c\pi^+\pi^-$	not seen
Γ_4	$\eta_c(1S)\rho(770)^\pm$	seen
Γ_5	$(D\overline{D}^*)^\pm$	seen
Γ_6	D^0D^{*-} + c.c.	seen
Γ_7	D^-D^{*0} + c.c.	seen
Γ_8	$\omega\pi^\pm$	not seen
Γ_9	$J/\psi\eta$	not seen
Γ_{10}	D^+D^{*-} + c.c	seen
Γ_{11}	$D^0\overline{D}^{*0}$ + c.c	seen

$T_{c\overline{c}1}(3900)$ BRANCHING RATIOS

$\Gamma(J/\psi\pi)/\Gamma_{total}$ — Γ_1/Γ

VALUE	EVTS	DOCUMENT ID		TECN	CHG	COMMENT
seen		ABLIKIM	20N	BES3	0	$e^+e^- \to \pi^0\pi^0 J/\psi$
seen		[1] ABAZOV	19	D0	±	1.96 TeV $p\overline{p} \to \pi^+\pi^- J/\psi X$ (prompt)
seen		ABLIKIM	17J	BES3	±	$e^+e^- \to \pi^+\pi^- J/\psi$
seen	356	ABLIKIM	15U	BES3	0	$e^+e^- \to \pi^0\pi^0 J/\psi$
not seen		[2] ADOLPH	15D	COMP	±	$\gamma N \to J/\psi\pi^\pm N$
seen	307	ABLIKIM	13T	BES3	±	$e^+e^- \to \pi^+\pi^- J/\psi$
seen	25	[3] XIAO	13A		0	4.17 $e^+e^- \to \pi^0\pi^0 J/\psi$

[1] But not seen in the "prompt" sample (no b-hadron enhancement).
[2] ADOLPH 15D measure $B(T_{c\overline{c}1}(3900)^\pm \to J/\psi\pi^\pm)\ \sigma(\gamma N \to T_{c\overline{c}1}(3900)^\pm N)/\sigma(\gamma N \to J/\psi N) < 3.7\times10^{-3}$ at 90% CL.
[3] Obtained by analyzing CLEO-c data but not authored by the CLEO Collaboration.

$\Gamma(h_c\pi^\pm)/\Gamma_{total}$ — Γ_2/Γ

VALUE	DOCUMENT ID		TECN	CHG	COMMENT
not seen	ABLIKIM	13X	BES3	±	$e^+e^- \to h_c\pi^+\pi^-$

$\Gamma(\eta_c\pi^+\pi^-)/\Gamma_{total}$ — Γ_3/Γ

VALUE	DOCUMENT ID		TECN	CHG	COMMENT
not seen	[1] VINOKUROVA	15	BELL	0	$B^+ \to K^+\eta_c\pi^+\pi^-$

[1] VINOKUROVA 15 reports $B(B^+ \to K^+ Z_c(3900)^0) \times B(X \to \eta_c\pi^+\pi^-) < 4.7\times10^{-5}$ at 90% CL.

$\Gamma(\eta_c(1S)\rho(770)^\pm)/\Gamma(J/\psi\pi)$ — Γ_4/Γ_1

VALUE	EVTS	DOCUMENT ID		TECN	COMMENT
2.3±0.8	332	[1] ABLIKIM	19BC	BES3	$e^+e^- \to \pi^+\pi^-\pi^0\eta_c(1S)$

[1] Using $e^+e^- \to \pi^\mp(T_{c\overline{c}1}(3900)^\pm \to J/\psi\pi^\pm)$ cross section at 4.23 and 4.26 GeV from ABLIKIM 17J.

$\Gamma((D\overline{D}^*)^\pm)/\Gamma(J/\psi\pi)$ — Γ_5/Γ_1

VALUE	DOCUMENT ID		TECN	CHG	COMMENT
6.2±1.1±2.7	[1] ABLIKIM	14A	BES3	±	$e^+e^- \to \pi^\pm(D\overline{D}^*)^\mp$

[1] Assuming the same origin of the $(D\overline{D}^*)^\pm$ and $\pi^\pm J/\psi$ decay modes.

$\Gamma(D^0D^{*-}$ + c.c.$)/\Gamma_{total}$ — Γ_6/Γ

VALUE	DOCUMENT ID		TECN	CHG	COMMENT
seen	ABLIKIM	15AC	BES3	±	$e^+e^- \to \pi^+D^0D^{*-}$ + c.c.
seen	ABLIKIM	14A	BES3	±	$e^+e^- \to \pi^+D^0D^{*-}$ + c.c.

$\Gamma(D^-D^{*0}$ + c.c.$)/\Gamma_{total}$ — Γ_7/Γ

VALUE	DOCUMENT ID		TECN	CHG	COMMENT
seen	ABLIKIM	15AC	BES3	±	$e^+e^- \to \pi^+D^-D^{*0}$ + c.c.
seen	ABLIKIM	14A	BES3	±	$e^+e^- \to \pi^+D^-D^{*0}$ + c.c.

$\Gamma(\omega\pi^\pm)/\Gamma_{total}$ — Γ_8/Γ

VALUE	DOCUMENT ID		TECN	CHG	COMMENT
not seen	ABLIKIM	15R	BES3	±	$e^+e^- \to \omega\pi^+\pi^-$

$\Gamma(J/\psi\eta)/\Gamma_{total}$ — Γ_9/Γ

VALUE	DOCUMENT ID		TECN	CHG	COMMENT
not seen	ABLIKIM	15Q	BES3	0	4.0–4.6 $e^+e^- \to J/\psi\eta\pi^0$

$\Gamma(J/\psi\eta)/\Gamma(J/\psi\pi)$ — Γ_9/Γ_1

VALUE	CL%	DOCUMENT ID		TECN	CHG	COMMENT
<0.15	90	ABLIKIM	15Q	BES3	0	4.226 $e^+e^- \to J/\psi\eta\pi^0$
• • • We do not use the following data for averages, fits, limits, etc. • • •						
<0.65	90	ABLIKIM	15Q	BES3	0	4.257 $e^+e^- \to J/\psi\eta\pi^0$

$\Gamma(D^+D^{*-}$ + c.c$)/\Gamma_{total}$ — Γ_{10}/Γ

VALUE	DOCUMENT ID		TECN	CHG	COMMENT
seen	ABLIKIM	15AB	BES3	0	$e^+e^- \to \pi^0(D\overline{D}^*)^0$

$\Gamma(D^0\overline{D}^{*0}$ + c.c$)/\Gamma_{total}$ — Γ_{11}/Γ

VALUE	DOCUMENT ID		TECN	CHG	COMMENT
seen	ABLIKIM	15AB	BES3	0	$e^+e^- \to \pi^0(D\overline{D}^*)^0$

$\Gamma(D^+D^{*-}$ + c.c$)/\Gamma(D^0\overline{D}^{*0}$ + c.c$)$ — Γ_{10}/Γ_{11}

VALUE	DOCUMENT ID		TECN	CHG	COMMENT
0.96±0.18±0.12	ABLIKIM	15AB	BES3	0	$e^+e^- \to \pi^0(D\overline{D}^*)^0$

$T_{c\overline{c}1}(3900)$ REFERENCES

ABLIKIM 25BU PR D112 092013 M. Ablikim et al. (BESIII Collab.)
ABLIKIM 20N PR D102 012009 M. Ablikim et al. (BESIII Collab.) JP
ABAZOV 19 PR D100 012005 V.M. Abazov et al. (D0 Collab.)
ABLIKIM 19BC PR D100 111102 M. Ablikim et al. (BESIII Collab.)
ABAZOV 18B PR D98 052010 V.M. Abazov et al. (D0 Collab.)
ABLIKIM 17J PRL 119 072001 M. Ablikim et al. (BESIII Collab.) JP
ABLIKIM 15AB PRL 115 222002 M. Ablikim et al. (BESIII Collab.)
ABLIKIM 15AC PR D92 092006 M. Ablikim et al. (BESIII Collab.) JP
ABLIKIM 15Q PR D92 012008 M. Ablikim et al. (BESIII Collab.)

ABLIKIM	15R	PR D92 032009	M. Ablikim *et al.*	(BESIII Collab.)
ABLIKIM	15U	PRL 115 112003	M. Ablikim *et al.*	(BESIII Collab.)
ADOLPH	15D	PL B742 330	C. Adolph *et al.*	(COMPASS Collab.)
VINOKUROVA	15	JHEP 1506 132	A. Vinokurova *et al.*	(BELLE Collab.)
Also		JHEP 1702 088 (errat.)	A. Vinokurava *et al.*	(BELLE Collab.)
ABLIKIM	14A	PRL 112 022001	M. Ablikim *et al.*	(BESIII Collab.) JP
ABLIKIM	13T	PRL 110 252001	M. Ablikim *et al.*	(BESIII Collab.)
ABLIKIM	13X	PRL 111 242001	M. Ablikim *et al.*	(BESIII Collab.)
LIU	13B	PRL 110 252002	Z.Q. Liu *et al.*	(BELLE Collab.)
XIAO	13A	PL B727 366	T. Xiao *et al.*	(NWES)

$T_{c\overline{c}s1}(4000)$

$I(J^P) = \frac{1}{2}(1^+)$

OMITTED FROM SUMMARY TABLE

was $Z_{cs}(4000)$

Properties incompatible with a $q\overline{q}$ structure (exotic state). See the review on "Heavy Non-$q\overline{q}$ Mesons."

Seen by AAIJ 21E in $B^+ \to T_{c\overline{c}s1}(4000)^+ \phi$ with $T_{c\overline{c}s1}(4000)^+ \to J/\psi K^+$ using an amplitude analysis of $B^+ \to J/\psi \phi K^+$ with a significance (accounting for systematic uncertainties) of 15 σ. The $J^P = 1^+$ assignment is favored with high significance. ABLIKIM 21G also reports a $J^P = 1^+$ $T_{c\overline{c}s}$ state in this mass region using $e^+e^- \to K^+(D_s^- D^{*0} + D_s^{*-} D^0)$ with a significance of 5.3 σ. The incompatible values for the widths reported by AAIJ 21E and ABLIKIM 21G could either indicate the existence of two separate states or possibly be explained in a coupled channel model (see ORTEGA 21).

$T_{c\overline{c}s1}(4000)$ MASS

VALUE (MeV)	EVTS	DOCUMENT ID		TECN	COMMENT
3980–4010 OUR EVALUATION					
3988 ± 5 OUR AVERAGE		Error includes scale factor of 2.7.			
$3991\ ^{+12}_{-10}\ ^{+9}_{-17}$		[1] AAIJ	23AQ	LHCB	$B^0 \to J/\psi \phi K^0_S$
$3992.2 \pm 1.7 \pm 1.6$		[2] ABLIKIM	22AE	BES3	$e^+e^- \to K^0_S(D_s^- D^{*+} + D_s^{*-} D^+)$
$4003 \pm 6\ ^{+4}_{-14}$	24k	[3] AAIJ	21E	LHCB	$B^+ \to J/\psi \phi K^+$
$3982.5\ ^{+1.8}_{-2.6} \pm 2.1$		[4] ABLIKIM	21G	BES3	$e^+e^- \to K^+(D_s^- D^{*0} + D_s^{*-} D^0)$

[1] From an amplitude analysis of the decay $B^0 \to J/\psi \phi K^0_S$ with a significance of 4.0 σ. The mass difference with respect to the charged partner in AAIJ 21E is $-12\ ^{+11}_{-10}\ ^{+6}_{-4}$ MeV.
[2] Pole mass for a mass-, width-dependent Breit-Wigner fit to the mass spectrum recoiling against K^0_S at center of mass energies between 4.628 and 4.699 GeV, with a significance of 4.6 σ.
[3] From an amplitude analysis of the decay $B^+ \to J/\psi \phi K^+$ with a significance of 15 σ.
[4] Pole mass for a mass-dependent Breit-Wigner fit to the mass spectrum recoiling against K^+ at center of mass energies between 4.628 and 4.698 GeV, with a significance of 5.3 σ.

$T_{c\overline{c}s1}(4000)$ WIDTH

VALUE (MeV)	EVTS	DOCUMENT ID		TECN	COMMENT
5–150 OUR EVALUATION					
14 ± 4 OUR AVERAGE		Error includes scale factor of 1.1.			
$105\ ^{+29}_{-25}\ ^{+17}_{-23}$		[1] AAIJ	23AQ	LHCB	$B^0 \to J/\psi \phi K^0_S$
$7.7\ ^{+4.1}_{-3.8} \pm 4.3$		[2] ABLIKIM	22AE	BES3	$e^+e^- \to K^0_S(D_s^- D^{*+} + D_s^{*-} D^+)$
$131 \pm 15 \pm 26$	24k	[3] AAIJ	21E	LHCB	$B^+ \to J/\psi \phi K^+$
$12.8\ ^{+5.3}_{-4.4} \pm 3.0$		[4] ABLIKIM	21G	BES3	$e^+e^- \to K^+(D_s^- D^{*0} + D_s^{*-} D^0)$

[1] From an amplitude analysis of the decay $B^0 \to J/\psi \phi K^0_S$ with a significance of 4.0 σ.
[2] Pole width for a mass-, width-dependent Breit-Wigner fit to the mass spectrum recoiling against K^0_S at center of mass energies between 4.628 and 4.699 GeV, with a significance of 4.6 σ.
[3] From an amplitude analysis of the decay $B^+ \to J/\psi \phi K^+$ with a significance of 15 σ.
[4] Pole width for a mass-dependent Breit-Wigner fit to the mass spectrum recoiling against K^+ at center of mass energies between 4.628 and 4.698 GeV, with a significance of 5.3 σ.

$T_{c\overline{c}s1}(4000)$ DECAY MODES

	Mode	Fraction (Γ_i/Γ)
Γ_1	$J/\psi K^+$	seen
Γ_2	$J/\psi K^0_S$	seen
Γ_3	$D_s^+ \overline{D}^{*0}$ or $D_s^{*+} \overline{D}^0$	seen
Γ_4	$D_s^+ D^{*-}$ or $D_s^{*+} D^-$	seen

$T_{c\overline{c}s1}(4000)$ BRANCHING RATIOS

$\Gamma(J/\psi K^+)/\Gamma_{total}$ — Γ_1/Γ

VALUE	EVTS	DOCUMENT ID		TECN	COMMENT
seen	24k	[1] AAIJ	21E	LHCB	$B^+ \to J/\psi \phi K^+$

[1] From an amplitude analysis of the decay $B^+ \to J/\psi \phi K^+$ with a significance of 15 σ.

$\Gamma(J/\psi K^0_S)/\Gamma_{total}$ — Γ_2/Γ

VALUE	DOCUMENT ID		TECN	COMMENT
seen	[1] AAIJ	23AQ	LHCB	$B^0 \to J/\psi \phi K^0_S$

[1] From an amplitude analysis of the decay $B^0 \to J/\psi \phi K^0_S$ with a significance of 4.0 σ.

$\Gamma(D_s^+ \overline{D}^{*0}$ or $D_s^{*+} \overline{D}^0)/\Gamma_{total}$ — Γ_3/Γ

VALUE	DOCUMENT ID		TECN	COMMENT
seen	[1] ABLIKIM	21G	BES3	$e^+e^- \to K^+(D_s^- D^{*0} + D_s^{*-} D^0)$

[1] Seen in the spectrum recoiling against K^+ in $e^+e^- \to K^+(D_s^- D^{*0} + D_s^{*-} D^0)$ collisions at center of mass energies between 4.628 and 4.698 GeV, with a significance of 5.3 σ.

$\Gamma(J/\psi K^+)/\Gamma(D_s^+ \overline{D}^{*0}$ or $D_s^{*+} \overline{D}^0)$ — Γ_1/Γ_3

VALUE	CL%	DOCUMENT ID		TECN	COMMENT
<0.03	90	ABLIKIM	23BI	BES3	$e^+e^- \to K^+K^- J/\psi$

$\Gamma(D_s^+ D^{*-}$ or $D_s^{*+} D^-)/\Gamma_{total}$ — Γ_4/Γ

VALUE	DOCUMENT ID		TECN	COMMENT
seen	[1] ABLIKIM	22AE	BES3	$e^+e^- \to K^0_S(D_s^- D^{*+} + D_s^{*-} D^+)$

[1] Seen in the mass spectrum recoiling against K^0_S at center of mass energies between 4.628 and 4.699 GeV, with a significance of 4.6 σ.

$T_{c\overline{c}s1}(4000)$ REFERENCES

AAIJ	23AQ	PRL 131 131901	R. Aaij *et al.*	(LHCb Collab.)
ABLIKIM	23BI	PRL 131 211902	M. Ablikim *et al.*	(BESIII Collab.)
ABLIKIM	22AE	PRL 129 112003	M. Ablikim *et al.*	(BESIII Collab.)
AAIJ	21E	PRL 127 082001	R. Aaij *et al.*	(LHCb Collab.) JP
ABLIKIM	21G	PRL 126 102001	M. Ablikim *et al.*	(BESIII Collab.)
ORTEGA	21	PL B818 136382	P.G. Ortega, D.R. Entem, F. Fernandez	

$T_{c\overline{c}}(4020)$

$I^G(J^{PC}) = 1^+(?^{?-})$

was $X(4020)$

Properties incompatible with a $q\overline{q}$ structure (exotic state). See the review on non-$q\overline{q}$ states.

Charged $T_{c\overline{c}}(4020)$ seen by ABLIKIM 13X from $e^+e^- \to \pi^+\pi^- h_c(1P)$ at c.m. energy from 3.90 to 4.42 GeV as a peak in the invariant mass distribution of the $\pi^\pm h_c(1P)$ system, and by ABLIKIM 14B from $e^+e^- \to (D^*\overline{D}^*)^\pm \pi^\mp$ events in $(D^*\overline{D}^*)^\pm$ mass. A neutral $T_{c\overline{c}}(4020)$ seen by ABLIKIM 14P at three c.m. energies in the same range in $e^+e^- \to \pi^0\pi^0 h_c(1P)$ as a peak in the larger of the two masses recoiling against a π^0. ABLIKIM 15AA observes a 5.9 σ signal in $(D^*\overline{D}^*)^0$ in $e^+e^- \to (D^*\overline{D}^*)^0 \pi^0$ events using collisions at two c.m. energies. Production rates and mass values support grouping neutral and charged $T_{c\overline{c}}(4020)$ together as manifestations of a single $I = 1$ particle.

$T_{c\overline{c}}(4020)$ MASS

VALUE (MeV)	EVTS	DOCUMENT ID		TECN	CHG	COMMENT
4024.1±1.9 OUR AVERAGE						
$4025.5\ ^{+2.0}_{-4.7} \pm 3.1$	116	[1] ABLIKIM	15AA	BES3	0	$e^+e^- \to (D^*\overline{D}^*)^0 \pi^0$
$4026.3 \pm 2.6 \pm 3.7$	401	[1] ABLIKIM	14B	BES3	±	$e^+e^- \to (D^*\overline{D}^*)^\pm \pi^\mp$
$4023.9 \pm 2.2 \pm 3.8$	61	[1,2] ABLIKIM	14P	BES3	0	$e^+e^- \to \pi^0\pi^0 h_c$
$4022.9 \pm 0.8 \pm 2.7$	253	[1] ABLIKIM	13X	BES3	±	$e^+e^- \to \pi^+\pi^- h_c$

[1] Neglecting interference between the $T_{c\overline{c}}(4020)$ and non-resonant continuum.
[2] Assuming $J^P = 1^+$ and width of 7.9 ± 2.6 MeV.

$T_{c\overline{c}}(4020)$ WIDTH

VALUE (MeV)	EVTS	DOCUMENT ID		TECN	CHG	COMMENT
13 ±5 OUR AVERAGE		Error includes scale factor of 1.7. See the ideogram below.				
$23.0 \pm 6.0 \pm 1.0$	116	[1] ABLIKIM	15AA	BES3	0	$e^+e^- \to (D^*\overline{D}^*)^0 \pi^0$
$24.8 \pm 5.6 \pm 7.7$	401	[1] ABLIKIM	14B	BES3	±	$e^+e^- \to (D^*\overline{D}^*)^\pm \pi^\mp$
$7.9 \pm 2.7 \pm 2.6$	253	[1] ABLIKIM	13X	BES3	±	$e^+e^- \to \pi^+\pi^- h_c$

[1] Neglecting interference between the $T_{c\overline{c}}(4020)$ and non-resonant continuum.

Int. J. Mod. Phys. A 2026.41. Downloaded from www.worldscientific.com
by CALIFORNIA @ BERKELEY on 09/16/26. Re-use and distribution is strictly not permitted, except for Open Access articles.

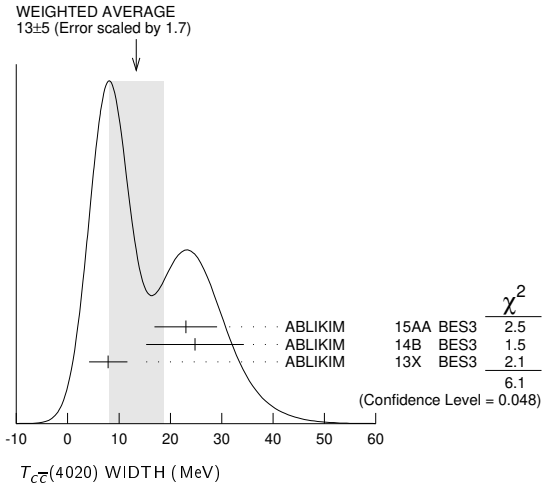

$T_{c\overline{c}}(4020)$ DECAY MODES

	Mode	Fraction (Γ_i/Γ)
Γ_1	$h_c(1P)\pi$	seen
Γ_2	$D^*\overline{D}^*$	seen
Γ_3	$D\overline{D}^*$ + c.c.	not seen
Γ_4	$\eta_c\pi^+\pi^-$	not seen
Γ_5	$\eta_c(1S)\rho(770)^\pm$	not seen
Γ_6	$J/\psi(1S)\pi^\pm$	not seen

$T_{c\overline{c}}(4020)$ BRANCHING RATIOS

$\Gamma(h_c(1P)\pi)/\Gamma_{total}$ — Γ_1/Γ

VALUE	EVTS	DOCUMENT ID		TECN	CHG	COMMENT
seen	61	ABLIKIM	14P	BES3	0	$e^+e^- \to \pi^0\pi^0 h_c$
seen	253	ABLIKIM	13X	BES3	$\pm$	$e^+e^- \to \pi^+\pi^- h_c$

$\Gamma(D^*\overline{D}^*)/\Gamma_{total}$ — Γ_2/Γ

VALUE	EVTS	DOCUMENT ID		TECN	CHG	COMMENT
seen	116	[1] ABLIKIM	15AA	BES3	0	$e^+e^- \to (D^*\overline{D}^*)^0\pi^0$
seen	401	[1] ABLIKIM	14B	BES3	$\pm$	$e^+e^- \to (D^*\overline{D}^*)^\pm\pi^\mp$

[1] Neglecting interference between the $T_{c\overline{c}}(4020)$ and non-resonant continuum.

$\Gamma(D\overline{D}^*$ + c.c.$)/\Gamma_{total}$ — Γ_3/Γ

VALUE	DOCUMENT ID		TECN	CHG	COMMENT
not seen	ABLIKIM	15AC	BES3	$\pm$	$e^+e^- \to \pi^\pm(D\overline{D}^*)^\mp$

$\Gamma(\eta_c\pi^+\pi^-)/\Gamma_{total}$ — Γ_4/Γ

VALUE	DOCUMENT ID		TECN	COMMENT
not seen	[1] VINOKUROVA	15	BELL	$B^+ \to K^+\eta_c\pi^+\pi^-$

[1] VINOKUROVA 15 reports $B(B^+ \to K^+ T_{c\overline{c}}(4020)^0) \times B(T_{c\overline{c}} \to \eta_c\pi^+\pi^-) < 1.6\times10^{-5}$ at 90% CL.

$\Gamma(\eta_c(1S)\rho(770)^\pm)/\Gamma(h_c(1P)\pi)$ — Γ_5/Γ_1

VALUE	CL%	DOCUMENT ID		TECN	COMMENT
<1.2	90	[1] ABLIKIM	19BC	BES3	$e^+e^- \to \pi^+\pi^-\pi^0\eta_c(1S)$

[1] Using $e^+e^- \to \pi^\mp(Z_c(4020)^\pm \to h_c(1P)\pi^\pm)$ cross section at 4.23, 4.26 and 4.36 GeV from ABLIKIM 13X.

$\Gamma(J/\psi(1S)\pi^\pm)/\Gamma_{total}$ — Γ_6/Γ

VALUE	DOCUMENT ID		TECN	COMMENT
not seen	[1] ABLIKIM	17J	BES3	$e^+e^- \to \pi^+\pi^- J/\psi$

[1] From Partial Wave Analysis assuming $J^P = 1^+$.

$T_{c\overline{c}}(4020)$ REFERENCES

ABLIKIM	19BC	PR D100 111102	M. Ablikim *et al.*	(BESIII Collab.)
ABLIKIM	17J	PRL 119 072001	M. Ablikim *et al.*	(BESIII Collab.)
ABLIKIM	15AA	PRL 115 182002	M. Ablikim *et al.*	(BESIII Collab.)
ABLIKIM	15AC	PR D92 092006	M. Ablikim *et al.*	(BESIII Collab.)
VINOKUROVA	15	JHEP 1506 132	A. Vinokurova *et al.*	(BELLE Collab.)
Also		JHEP 1702 088 (errat.)	A. Vinokurava *et al.*	(BELLE Collab.)
ABLIKIM	14B	PRL 112 132001	M. Ablikim *et al.*	(BESIII Collab.)
ABLIKIM	14P	PRL 113 212002	M. Ablikim *et al.*	(BESIII Collab.)
ABLIKIM	13X	PRL 111 242001	M. Ablikim *et al.*	(BESIII Collab.)

$T_{c\overline{c}}(4050)^+$

$I^G(J^{PC}) = 1^-(?^{?+})$
I, G, C need confirmation.

OMITTED FROM SUMMARY TABLE
was $X(4050)$

Properties incompatible with a $q\overline{q}$ structure (exotic state). See the review on non-$q\overline{q}$ states.

Observed by MIZUK 08 in the $\pi^+\chi_{c1}(1P)$ invariant mass distribution in $\overline{B}^0 \to K^-\pi^+\chi_{c1}(1P)$ decays. Not seen by LEES 12B in this same mode after accounting for $K\pi$ resonant mass and angular structure.

$T_{c\overline{c}}(4050)^+$ MASS

VALUE (MeV)	DOCUMENT ID		TECN	COMMENT
$4051\pm14^{+20}_{-41}$	[1] MIZUK	08	BELL	$\overline{B}^0 \to K^-\pi^+\chi_{c1}(1P)$

[1] From a Dalitz plot analysis with two Breit-Wigner amplitudes.

$T_{c\overline{c}}(4050)^+$ WIDTH

VALUE (MeV)	DOCUMENT ID		TECN	COMMENT
82^{+21+47}_{-17-22}	[1] MIZUK	08	BELL	$\overline{B}^0 \to K^-\pi^+\chi_{c1}(1P)$

[1] From a Dalitz plot analysis with two Breit-Wigner amplitudes.

$T_{c\overline{c}}(4050)^+$ DECAY MODES

	Mode	Fraction (Γ_i/Γ)
Γ_1	$\pi^+\chi_{c1}(1P)$	seen
Γ_2	$\pi^\pm\psi(3770)$	not seen
Γ_3	$\pi^\pm\chi_{c0}(1P)$	not seen
Γ_4	$\pi^\pm\chi_{c2}(1P)$	not seen

$T_{c\overline{c}}(4050)^+$ BRANCHING RATIOS

$\Gamma(\pi^+\chi_{c1}(1P))/\Gamma_{total}$ — Γ_1/Γ

VALUE	EVTS	DOCUMENT ID		TECN	COMMENT
seen		[1] MIZUK	08	BELL	$\overline{B}^0 \to K^-\pi^+\chi_{c1}(1P)$
• • • We do not use the following data for averages, fits, limits, etc. • • •					
not seen	16	[2] ABLIKIM	21W	BES3	$e^+e^- \to \chi_{cJ}\pi^+\pi^+$
not seen		[3] LEES	12B	BABR	$B \to K\pi\chi_{c1}(1P)$

[1] With a product branching fraction measurement of $B(\overline{B}^0 \to K^- T_{c\overline{c}}(4050)^+) \times B(T_{c\overline{c}}(4050)^+ \to \pi^+\chi_{c1}(1P)) = (3.0^{+1.5+3.7}_{-0.8-1.6})\times10^{-5}$.
[2] ABLIKIM 21W measurement is limited by statistics.
[3] With a product branching fraction limit of $B(\overline{B}^0 \to T_{c\overline{c}}(4050)^+K^-) \times B(T_{c\overline{c}}(4050)^+ \to \chi_{c1}\pi^+) < 1.8\times10^{-5}$ at 90% CL.

$\Gamma(\pi^\pm\chi_{c0}(1P))/\Gamma_{total}$ — Γ_3/Γ

VALUE	EVTS	DOCUMENT ID		TECN	COMMENT
not seen	18	[1] ABLIKIM	21W	BES3	$e^+e^- \to \chi_{cJ}\pi^+\pi^+$

[1] ABLIKIM 21W measurement is limited by statistics.

$\Gamma(\pi^\pm\chi_{c2}(1P))/\Gamma_{total}$ — Γ_4/Γ

VALUE	EVTS	DOCUMENT ID		TECN	COMMENT
not seen	14	[1] ABLIKIM	21W	BES3	$e^+e^- \to \chi_{cJ}\pi^+\pi^+$

[1] ABLIKIM 21W measurement is limited by statistics.

$\Gamma(\pi^\pm\psi(3770))/\Gamma_{total}$ — Γ_2/Γ

VALUE	DOCUMENT ID		TECN	COMMENT
not seen	[1] ABLIKIM	19AR	BES3	$e^+e^- \to \pi^+\pi^- D\overline{D}$

[1] From a measurement of $\sigma(e^+e^- \to \pi^+\pi^- D\overline{D})$ between $\sqrt{s} = 4.08$ and 4.6 GeV.

$T_{c\overline{c}}(4050)^+$ REFERENCES

ABLIKIM	21W	PR D103 052010	M. Ablikim *et al.*	(BESIII Collab.)
ABLIKIM	19AR	PR D100 032005	M. Ablikim *et al.*	(BESIII Collab.)
LEES	12B	PR D85 052003	J.P. Lees *et al.*	(BABAR Collab.)
MIZUK	08	PR D78 072004	R. Mizuk *et al.*	(BELLE Collab.)

Int. J. Mod. Phys. A 2026.41. Downloaded from www.worldscientific.com
by UNIVERSITY OF CALIFORNIA @ BERKELEY on 09/16/26. Re-use and distribution is strictly not permitted, except for Open Access articles.

Int. J. Mod. Phys. A 2026.41. Downloaded from www.worldscientific.com
by CALIFORNIA @ BERKELEY on 09/16/26. Re-use and distribution is strictly not permitted, except for Open Access articles.

$T_{c\overline{c}}(4055)^+$

$I^G(J^{PC}) = 1^+(?^{?-})$
I, G, C need confirmation.

OMITTED FROM SUMMARY TABLE
was $X(4055)^\pm$

Properties incompatible with a $q\overline{q}$ structure (exotic state). See the review on non-$q\overline{q}$ states.

Needs confirmation. Seen by WANG 15A in the $\psi(2S)\pi^+$ invariant mass distribution in $\psi(4360) \to \psi(2S)\pi^+\pi^-$ decay.

$T_{c\overline{c}}(4055)^+$ MASS

VALUE (MeV)	DOCUMENT ID		TECN	COMMENT
4054 ±3 ±1	[1] WANG	15A	BELL	10.58 $e^+e^- \to \gamma\pi^+\pi^-\psi(2S)$
• • • We do not use the following data for averages, fits, limits, etc. • • •				
4039.3±6.0	[2] ABLIKIM	18K	BES3	$e^+e^- \to \pi^0\pi^0\psi(2S)$
4032.1±2.4	[3] ABLIKIM	17V	BES3	$e^+e^- \to \pi^+\pi^-\psi(2S)$

[1] Statistical significance of 3.5 σ.
[2] Statistical error only, with significance of 5.9 σ (from a fit with a 19% CL). Identified as the same structure observed in ABLIKIM 17V in $e^+e^- \to \pi^+\pi^-\psi(2S)$ decays.
[3] Statistical error only, with significance of 9.2 σ. From an unbinned maximum likelihood fit of the $\pi^+\pi^-\psi(2S)$ Dalitz plot from data collected at $\sqrt{s} = 4.416$ GeV for a $J^C = 1^+$ state. The fit does not match the detailed structure of the data, having a C.L. of only 8%.

$T_{c\overline{c}}(4055)^+$ WIDTH

VALUE (MeV)	DOCUMENT ID		TECN	COMMENT
45 ±11 ±6	[1] WANG	15A	BELL	10.58 $e^+e^- \to \gamma\pi^+\pi^-\psi(2S)$
• • • We do not use the following data for averages, fits, limits, etc. • • •				
31.9±14.8	[2] ABLIKIM	18K	BES3	$e^+e^- \to \pi^0\pi^0\psi(2S)$
26.1± 5.3	[3] ABLIKIM	17V	BES3	$e^+e^- \to \pi^+\pi^-\psi(2S)$

[1] Statistical significance of 3.5 σ.
[2] Statistical error only, with significance of 5.9 σ (from a fit with a 19% CL). Identified as the same structure observed in ABLIKIM 17V in $e^+e^- \to \pi^+\pi^-\psi(2S)$ decays.
[3] Statistical error only, with significance of 9.2 σ. From an unbinned maximum likelihood fit of the $\pi^+\pi^-\psi(2S)$ Dalitz plot from data collected at $\sqrt{s} = 4.416$ GeV for a $J^C = 1^+$ state. The fit does not match the detailed structure of the data, having a C.L. of only 8%.

$T_{c\overline{c}}(4055)^+$ DECAY MODES

	Mode	Fraction (Γ_i/Γ)
Γ_1	$\pi^+\psi(2S)$	seen
Γ_2	$\pi^+\psi(3770)$	not seen

$T_{c\overline{c}}(4055)^+$ BRANCHING RATIOS

$\Gamma(\pi^+\psi(2S))/\Gamma_{total}$ — **Γ_1/Γ**

VALUE	DOCUMENT ID		TECN	COMMENT
seen	[1] WANG	15A	BELL	10.58 $e^+e^- \to \gamma\pi^+\pi^-\psi(2S)$

[1] Statistical significance of 3.5 σ.

$\Gamma(\pi^+\psi(3770))/\Gamma_{total}$ — **Γ_2/Γ**

VALUE	DOCUMENT ID		TECN	COMMENT
not seen	[1] ABLIKIM	19AR	BES3	$e^+e^- \to \pi^+\pi^- D\overline{D}$

[1] From a measurement of $\sigma(e^+e^- \to \pi^+\pi^- D\overline{D})$ between $\sqrt{s} = 4.08$ and 4.6 GeV.

$T_{c\overline{c}}(4055)^+$ REFERENCES

ABLIKIM	19AR	PR D100 032005	M. Ablikim *et al.*	(BESIII Collab.)
ABLIKIM	18K	PR D97 052001	M. Ablikim *et al.*	(BESIII Collab.)
ABLIKIM	17V	PR D96 032004	M. Ablikim *et al.*	(BESIII Collab.)
Also		PR D99 019903 (errat.)	M. Ablikim *et al.*	(BESIII Collab.)
WANG	15A	PR D91 112007	X.L. Wang *et al.*	(BELLE Collab.)

$T_{c\overline{c}}(4100)^+$

$I^G(J^{PC}) = 1^-(?^{?+})$

OMITTED FROM SUMMARY TABLE
was $X(4100)^\pm$

Properties incompatible with a $q\overline{q}$ structure (exotic state). See the review on non-$q\overline{q}$ states.

Reported by AAIJ 18AN in the $\eta_c(1S)\pi^+$ invariant mass distribution in $\overline{B}^0 \to \eta_c(1S)K^-\pi^+$ decays with a significance of 3.4σ. $J^P = 0^+$ or 1^- assignment consistent with data.

$T_{c\overline{c}}(4100)^+$ MASS

VALUE (MeV)	DOCUMENT ID		TECN	COMMENT
$4096 \pm 20^{+18}_{-22}$	AAIJ	18AN	LHCB	$B^0 \to \eta_c(1S)K^+\pi^-$

$T_{c\overline{c}}(4100)^+$ WIDTH

VALUE (MeV)	DOCUMENT ID		TECN	COMMENT
$152 \pm 58^{+60}_{-35}$	AAIJ	18AN	LHCB	$B^0 \to \eta_c(1S)K^+\pi^-$

$T_{c\overline{c}}(4100)^+$ DECAY MODES

	Mode	Fraction (Γ_i/Γ)
Γ_1	$\pi^+\eta_c(1S)$	seen
Γ_2	$\pi^+\psi(3770)$	not seen

$T_{c\overline{c}}(4100)^+$ BRANCHING RATIOS

$\Gamma(\pi^+\eta_c(1S))/\Gamma_{total}$ — **Γ_1/Γ**

VALUE	DOCUMENT ID		TECN	COMMENT
seen	[1] AAIJ	18AN	LHCB	$B^0 \to \eta_c(1S)K^+\pi^-$

[1] AAIJ 18AN quotes a fit fraction for $B^0 \to T_{c\overline{c}}(4100)^- K^+ \to \eta_c(1S)\pi^- K^+$ of $(3.3 \pm 1.1^{+1.2}_{-1.1})$% from an amplitude analysis.

$\Gamma(\pi^+\psi(3770))/\Gamma_{total}$ — **Γ_2/Γ**

VALUE	DOCUMENT ID		TECN	COMMENT
not seen	[1] ABLIKIM	19AR	BES3	$e^+e^- \to \pi^+\pi^- D\overline{D}$

[1] From a measurement of $\sigma(e^+e^- \to \pi^+\pi^- D\overline{D})$ between $\sqrt{s} = 4.08$ and 4.6 GeV.

$T_{c\overline{c}}(4100)^+$ REFERENCES

ABLIKIM	19AR	PR D100 032005	M. Ablikim *et al.*	(BESIII Collab.)
AAIJ	18AN	EPJ C78 1019	R. Aaij *et al.*	(LHCb Collab.)

$T_{c\overline{c}1}(4200)^+$

$I^G(J^{PC}) = 1^+(1^{+-})$
I, G, C need confirmation.

OMITTED FROM SUMMARY TABLE
was $Z_c(4200)$, $X(4200)^\pm$

This state shows properties different from a conventional $q\overline{q}$ state. A candidate for an exotic structure. See the review on non-$q\overline{q}$ states.

Reported by CHILIKIN 14 in $J/\psi\pi^+$ at a significance of 6.2σ. Assignments of 0^-, 1^-, 2^-, and 2^+ excluded at 6.1σ, 7.4σ, 4.4σ, and 7.0σ level, respectively. Needs confirmation.

$T_{c\overline{c}1}(4200)^+$ MASS

VALUE (MeV)	DOCUMENT ID		TECN	COMMENT
4242±26 OUR AVERAGE	Error includes scale factor of 1.5.			
4257±11±17	AAIJ	25Q	LHCB	$B^+ \to \psi(2S)K^+\pi^+\pi^-$
$4196^{+31}_{-29}{}^{+17}_{-13}$	CHILIKIN	14	BELL	$\overline{B}^0 \to J/\psi K^-\pi^+$

$T_{c\overline{c}1}(4200)^+$ WIDTH

VALUE (MeV)	DOCUMENT ID		TECN	COMMENT
310±40 OUR AVERAGE				
308±20± 32	AAIJ	25Q	LHCB	$B^+ \to \psi(2S)K^+\pi^+\pi^-$
$370 \pm 70^{+70}_{-132}$	CHILIKIN	14	BELL	$\overline{B}^0 \to J/\psi K^-\pi^+$

$T_{c\overline{c}1}(4200)^+$ DECAY MODES

	Mode	Fraction (Γ_i/Γ)
Γ_1	$J/\psi\pi^+$	seen
Γ_2	$\psi(2S)\pi^+$	seen

$T_{c\overline{c}1}(4200)^+$ BRANCHING RATIOS

$\Gamma(J/\psi\pi^+)/\Gamma_{total}$ — **Γ_1/Γ**

VALUE	DOCUMENT ID		TECN	COMMENT
seen	CHILIKIN	14	BELL	$\overline{B}^0 \to J/\psi K^-\pi^+$
• • • We do not use the following data for averages, fits, limits, etc. • • •				
possibly seen	[1] AAIJ	19R	LHCB	$B^0 \to K^+\pi^- J/\psi$ + c.c.

[1] From a model-independent analysis.

Int. J. Mod. Phys. A 2026.41. Downloaded from www.worldscientific.com by UNIVERSITY OF CALIFORNIA @ BERKELEY on 09/16/26. Re-use and distribution is strictly not permitted, except for Open Access articles.

$\Gamma(\psi(2S)\pi^+)/\Gamma_{total}$ — **Γ_2/Γ**

VALUE	DOCUMENT ID		TECN	COMMENT
seen	AAIJ	25Q	LHCB	$B^+ \to \psi(2S) K^+ \pi^+ \pi^-$

$T_{c\overline{c}1}(4200)^+$ REFERENCES

AAIJ	25Q	JHEP 2501 054	R. Aaij *et al.*	(LHCb Collab.)
AAIJ	19R	PRL 122 152002	R. Aaij *et al.*	(LHCb Collab.)
CHILIKIN	14	PR D90 112009	K. Chilikin *et al.*	(BELLE Collab.)

$T_{c\overline{c}s1}(4220)^+$

$I(J^P) = \frac{1}{2}(1^+)$

OMITTED FROM SUMMARY TABLE

was $Z_{cs}(4220)^+$

Properties incompatible with a $q\overline{q}$ structure (exotic state). See the review on "Heavy Non-$q\overline{q}$ Mesons."

Seen by AAIJ 21E in $B^+ \to T_{c\overline{c}s1}(4220)^+ \phi$ with $T_{c\overline{c}s1}(4220)^+ \to J/\psi K^+$ using an amplitude analysis of $B^+ \to J/\psi \phi K^+$ with a significance (accounting for systematic uncertainties) of 5.9 σ. The $J^P = 1^+$ assignment is favored over 1^- with a significance of 2 σ and other assignments are disfavored by 4.9 σ.

$T_{c\overline{c}s1}(4220)^+$ MASS

VALUE (MeV)	EVTS	DOCUMENT ID		TECN	COMMENT
$\mathbf{4216 \pm 24^{+43}_{-30}}$	24k	[1] AAIJ	21E	LHCB	$B^+ \to J/\psi \phi K^+$

[1] From an amplitude analysis of the decay $B^+ \to J/\psi \phi K^+$ with a significance of 5.9 σ.

$T_{c\overline{c}s1}(4220)^+$ WIDTH

VALUE (MeV)	EVTS	DOCUMENT ID		TECN	COMMENT
$\mathbf{233 \pm 52^{+97}_{-73}}$	24k	[1] AAIJ	21E	LHCB	$B^+ \to J/\psi \phi K^+$

[1] From an amplitude analysis of the decay $B^+ \to J/\psi \phi K^+$ with a significance of 5.9 σ.

$T_{c\overline{c}s1}(4220)^+$ DECAY MODES

	Mode	Fraction (Γ_i/Γ)
Γ_1	$J/\psi K^+$	seen

$T_{c\overline{c}s1}(4220)^+$ BRANCHING RATIOS

$\Gamma(J/\psi K^+)/\Gamma_{total}$ — **Γ_1/Γ**

VALUE	EVTS	DOCUMENT ID		TECN	COMMENT
seen	24k	[1] AAIJ	21E	LHCB	$B^+ \to J/\psi \phi K^+$

[1] From an amplitude analysis of the decay $B^+ \to J/\psi \phi K^+$ with a significance of 5.9 σ.

$T_{c\overline{c}s1}(4220)^+$ REFERENCES

AAIJ	21E	PRL 127 082001	R. Aaij *et al.*	(LHCb Collab.) JP

$T_{c\overline{c}0}(4240)^+$

$I^G(J^{PC}) = 1^+(0^{--})$

I, G, C need confirmation.

OMITTED FROM SUMMARY TABLE

was $R_{c0}(4240)$, $X(4240)^\pm$

Properties incompatible with a $q\overline{q}$ structure (exotic state). See the review on non-$q\overline{q}$ states.

Spin and parity assignment $J^P = 0^-$ is favored over 1^-, 2^-, and 2^+ by 8 σ and over 1^+ by 1 σ, according to the four-dimensional amplitude analysis of AAIJ 14AG.

$T_{c\overline{c}0}(4240)^+$ MASS

VALUE (MeV)	DOCUMENT ID		TECN	COMMENT
$\mathbf{4239 \pm 18^{+45}_{-10}}$	[1] AAIJ	14AG	LHCB	$\overline{B}^0 \to K^- \pi^+ \psi(2S)$

[1] From a 4-dimensional analysis when a second, lower mass resonance is allowed in the $T_{c\overline{c}1}(4430)$ fit, with significance 6 σ including systematic variations.

$T_{c\overline{c}0}(4240)^+$ WIDTH

VALUE (MeV)	DOCUMENT ID		TECN	COMMENT
$\mathbf{220 \pm 47^{+108}_{-74}}$	[1] AAIJ	14AG	LHCB	$\overline{B}^0 \to K^- \pi^+ \psi(2S)$

[1] From a 4-dimensional analysis when a second, lower mass resonance is allowed in the $T_{c\overline{c}1}(4430)$ fit, with significance 6 σ including systematic variations.

$T_{c\overline{c}0}(4240)^+$ DECAY MODES

	Mode	Fraction (Γ_i/Γ)
Γ_1	$\pi^+ \psi(2S)$	seen

$T_{c\overline{c}0}(4240)^+$ BRANCHING RATIOS

$\Gamma(\pi^+ \psi(2S))/\Gamma_{total}$ — **Γ_1/Γ**

VALUE	DOCUMENT ID		TECN	COMMENT
seen	[1] AAIJ	14AG	LHCB	$\overline{B}^0 \to K^- \pi^+ \psi(2S)$

[1] From a 4-dimensional analysis when a second, lower mass resonance is allowed in the $T_{c\overline{c}1}(4430)$ fit. No partial branching fraction quoted.

$T_{c\overline{c}0}(4240)^+$ REFERENCES

AAIJ	14AG	PRL 112 222002	R. Aaij *et al.*	(LHCb Collab.)

$T_{c\overline{c}}(4250)^+$

$I^G(J^{PC}) = 1^-(?^{?+})$

I, G, C need confirmation.

OMITTED FROM SUMMARY TABLE

was $X(4250)^\pm$

Properties incompatible with a $q\overline{q}$ structure (exotic state). See the review on non-$q\overline{q}$ states.

Observed by MIZUK 08 in the $\pi^+ \chi_{c1}(1P)$ invariant mass distribution in $\overline{B}^0 \to K^- \pi^+ \chi_{c1}(1P)$ decays. Not seen by LEES 12B in this same mode after accounting for $K\pi$ resonant mass and angular structure.

$T_{c\overline{c}}(4250)^+$ MASS

VALUE (MeV)	DOCUMENT ID		TECN	COMMENT
$\mathbf{4248^{+44}_{-29}{}^{+180}_{-35}}$	[1] MIZUK	08	BELL	$\overline{B}^0 \to K^- \pi^+ \chi_{c1}(1P)$

[1] From a Dalitz plot analysis with two Breit-Wigner amplitudes.

$T_{c\overline{c}}(4250)^+$ WIDTH

VALUE (MeV)	DOCUMENT ID		TECN	COMMENT
$\mathbf{177^{+54}_{-39}{}^{+316}_{-61}}$	[1] MIZUK	08	BELL	$\overline{B}^0 \to K^- \pi^+ \chi_{c1}(1P)$

[1] From a Dalitz plot analysis with two Breit-Wigner amplitudes.

$T_{c\overline{c}}(4250)^+$ DECAY MODES

	Mode	Fraction (Γ_i/Γ)
Γ_1	$\pi^+ \chi_{c1}(1P)$	seen

$T_{c\overline{c}}(4250)^+$ BRANCHING RATIOS

$\Gamma(\pi^+ \chi_{c1}(1P))/\Gamma_{total}$ — **Γ_1/Γ**

VALUE	DOCUMENT ID		TECN	COMMENT
seen	[1] MIZUK	08	BELL	$\overline{B}^0 \to K^- \pi^+ \chi_{c1}(1P)$
• • • We do not use the following data for averages, fits, limits, etc. • • •				
not seen	[2] LEES	12B	BABR	$B \to K \pi \chi_{c1}(1P)$

[1] With a product branching fraction measurement of $B(\overline{B}^0 \to K^- T_{c\overline{c}}(4250)^+) \times B(T_{c\overline{c}}(4250)^+ \to \pi^+ \chi_{c1}(1P)) = (4.0^{+2.3}_{-0.9}{}^{+19.7}_{-0.5}) \times 10^{-5}$.

[2] With a product branching fraction limit of $B(\overline{B}^0 \to T_{c\overline{c}}(4250)^+ K^-) \times B(T_{c\overline{c}}(4250)^+ \to \chi_{c1} \pi^+) < 4.0 \times 10^{-5}$ at 90% CL.

$T_{c\overline{c}}(4250)^+$ REFERENCES

LEES	12B	PR D85 052003	J.P. Lees *et al.*	(BABAR Collab.)
MIZUK	08	PR D78 072004	R. Mizuk *et al.*	(BELLE Collab.)

$T_{c\overline{c}1}(4430)^+$

$I^G(J^{PC}) = 1^+(1^{+-})$

G, C need confirmation.

was $Z_c(4430)$, $X(4430)^\pm$

Properties incompatible with a $q\overline{q}$ structure (exotic state). See the review on non-$q\overline{q}$ states.

First seen by CHOI 08 in $B \to K \pi^+ \psi(2S)$ decays, confirmed by AAIJ 14AG, and confirmed in a model-independent way by AAIJ 15BH. Also seen by CHILIKIN 14 in $B \to K^+ \pi J/\psi$ decays. J^P was determined by CHILIKIN 13 and AAIJ 14AG.

Int. J. Mod. Phys. A 2026.41. Downloaded from www.worldscientific.com by CALIFORNIA @ BERKELEY on 09/16/26. Re-use and distribution is strictly not permitted, except for Open Access articles.

$T_{c\overline{c}1}(4430)^+$ MASS

VALUE (MeV)	DOCUMENT ID		TECN	COMMENT
4478^{+15}_{-17} OUR AVERAGE				
$4468 \pm 21 \pm 80$	AAIJ	25Q	LHCB	$B^+ \to \psi(2S) K^+ \pi^+ \pi^-$
$4475 \pm 7^{+15}_{-25}$	[1] AAIJ	14AG	LHCB	$\overline{B}^0 \to K^- \pi^+ \psi(2S)$
$4485 \pm 22^{+28}_{-11}$	[1] CHILIKIN	13	BELL	$B^0 \to K^+ \pi^- \psi(2S)$
• • • We do not use the following data for averages, fits, limits, etc. • • •				
$4443^{+15}_{-12}{}^{+19}_{-13}$	[2] MIZUK	09	BELL	$B \to K \pi^+ \psi(2S)$
$4433 \pm 4 \pm 2$	[3] CHOI	08	BELL	$B \to K \pi^+ \psi(2S)$

[1] From a four-dimensional amplitude analysis.
[2] From a Dalitz plot analysis. Superseded by CHILIKIN 13.
[3] Superseded by MIZUK 09 and CHILIKIN 13.

$T_{c\overline{c}1}(4430)^+$ WIDTH

VALUE (MeV)	DOCUMENT ID		TECN	COMMENT
189 ± 29 OUR AVERAGE				
$251 \pm 42 \pm 82$	AAIJ	25Q	LHCB	$B^+ \to \psi(2S) K^+ \pi^+ \pi^-$
$172 \pm 13^{+37}_{-34}$	[1] AAIJ	14AG	LHCB	$\overline{B}^0 \to K^- \pi^+ \psi(2S)$
$200^{+41}_{-46}{}^{+26}_{-35}$	[1] CHILIKIN	13	BELL	$B^0 \to K^+ \pi^- \psi(2S)$
• • • We do not use the following data for averages, fits, limits, etc. • • •				
$107^{+86}_{-43}{}^{+74}_{-56}$	[2] MIZUK	09	BELL	$B \to K \pi^+ \psi(2S)$
$45^{+18}_{-13}{}^{+30}_{-13}$	[3] CHOI	08	BELL	$B \to K \pi^+ \psi(2S)$

[1] From a four-dimensional amplitude analysis.
[2] From a Dalitz plot analysis. Superseded by CHILIKIN 13.
[3] Superseded by MIZUK 09 and CHILIKIN 13.

$T_{c\overline{c}1}(4430)^+$ DECAY MODES

	Mode	Fraction (Γ_i/Γ)
Γ_1	$\pi^+ \psi(2S)$	seen
Γ_2	$\pi^+ J/\psi$	seen

$T_{c\overline{c}1}(4430)^+$ BRANCHING RATIOS

$\Gamma(\pi^+ \psi(2S))/\Gamma_{total}$ — **Γ_1/Γ**

VALUE	DOCUMENT ID		TECN	COMMENT
seen	AAIJ	25Q	LHCB	$B^+ \to \psi(2S) K^+ \pi^+ \pi^-$
seen	[1] AAIJ	14AG	LHCB	$\overline{B}^0 \to K^- \pi^+ \psi(2S)$
seen	[2] CHILIKIN	13	BELL	$B^0 \to K^+ \pi^- \psi(2S)$
• • • We do not use the following data for averages, fits, limits, etc. • • •				
not seen	[3] AUBERT	09AA	BABR	$B \to K \pi^+ \psi(2S)$
seen	[4] MIZUK	09	BELL	$B \to K \pi^+ \psi(2S)$

[1] From a four-dimensional amplitude analysis. No product of branching fractions quoted.
[2] From a four-dimensional amplitude analysis. Measured a product of branching fractions $B(B^0 \to T_{c\overline{c}1}(4430)^- K^+) \times B(T_{c\overline{c}1}(4430)^- \to \psi(2S)\pi^-) = (6.0^{+1.7}_{-2.0}{}^{+2.5}_{-1.4}) \times 10^{-5}$.
[3] AUBERT 09AA quotes $B(B^+ \to \overline{K}^0 T_{c\overline{c}1}(4430)^+) \times B(T_{c\overline{c}1}(4430)^+ \to \pi^+ \psi(2S)) < 4.7 \times 10^{-5}$ and $B(\overline{B}^0 \to K^- T_{c\overline{c}1}(4430)^+) \times B(T_{c\overline{c}1}(4430)^+ \to \pi^+ \psi(2S)) < 3.1 \times 10^{-5}$ at 95% CL.
[4] Measured a product of branching fractions $B(\overline{B}^0 \to K^- T_{c\overline{c}1}(4430)^+) \times B(T_{c\overline{c}1}(4430)^+ \to \pi^+ \psi(2S)) = (3.2^{+1.8}_{-0.9}{}^{+5.3}_{-1.6}) \times 10^{-5}$. Superseded by CHILIKIN 13.

$\Gamma(\pi^+ J/\psi)/\Gamma_{total}$ — **Γ_2/Γ**

VALUE	DOCUMENT ID		TECN	COMMENT
seen	[1,2] CHILIKIN	14	BELL	$\overline{B}^0 \to K^- \pi^+ J/\psi$
• • • We do not use the following data for averages, fits, limits, etc. • • •				
not seen	[3] AUBERT	09AA	BABR	$B \to K \pi^+ J/\psi$

[1] CHILIKIN 14 reports $B(\overline{B}^0 \to T_{c\overline{c}1}(4430)^+ K^-) \times B(T_{c\overline{c}1}(4430)^+ \to J/\psi \pi^+) = (5.4^{+4.0}_{-1.0}{}^{+1.1}_{-0.9}) \times 10^{-6}$.
[2] A broad enhancement seen by AAIJ 19R in the decays $B^0 \to J/\psi \pi^+ K^-$ at 4600 MeV can be due to an interplay of $T_{c\overline{c}1}(4430)$, $T_{c\overline{c}1}(4200)$ and the fitting polynomials.
[3] AUBERT 09AA quotes $B(B^+ \to \overline{K}^0 T_{c\overline{c}1}(4430)^+) \times B(T_{c\overline{c}1}(4430)^+ \to \pi^+ J/\psi) < 1.5 \times 10^{-5}$ and $B(\overline{B}^0 \to K^- T_{c\overline{c}1}(4430)^+) \times B(T_{c\overline{c}1}(4430)^+ \to \pi^+ J/\psi) < 0.4 \times 10^{-5}$ at 95% CL.

$T_{c\overline{c}1}(4430)^+$ REFERENCES

AAIJ	25Q	JHEP 2501 054	R. Aaij *et al.*	(LHCb Collab.)
AAIJ	19R	PRL 122 152002	R. Aaij *et al.*	(LHCb Collab.)
AAIJ	15BH	PR D92 112009	R. Aaij *et al.*	(LHCb Collab.)
AAIJ	14AG	PRL 112 222002	R. Aaij *et al.*	(LHCb Collab.) JP
CHILIKIN	14	PR D90 112009	K. Chilikin *et al.*	(BELLE Collab.)
CHILIKIN	13	PR D88 074026	K. Chilikin *et al.*	(BELLE Collab.) JP
AUBERT	09AA	PR D79 112001	B. Aubert *et al.*	(BABAR Collab.)
MIZUK	09	PR D80 031104	R. Mizuk *et al.*	(BELLE Collab.)
CHOI	08	PRL 100 142001	S.-K. Choi *et al.*	(BELLE Collab.)

$T_{b\overline{s}}(5568)^+$

$I(J^P) = 1(?^?)$

OMITTED FROM SUMMARY TABLE
was $X(5568)^\pm$

Seen as a peak in the $B_s \pi^\pm$ mass spectrum with a significance of more than 3σ by ABAZOV 16E and ABAZOV 18A in inclusive $p\overline{p}$ collisions at 1.96 TeV. Not seen by AAIJ 16AI, AABOUD 18L, AALTONEN 18A, and SIRUNYAN 18J. Needs confirmation.

$T_{b\overline{s}}(5568)^+$ MASS

VALUE (MeV)	EVTS	DOCUMENT ID		TECN	COMMENT
$5566.9^{+3.2}_{-3.1}{}^{+0.6}_{-1.2}$	278	[1] ABAZOV	18A	D0	$p\overline{p} \to B_s^0 \pi^\pm X$
• • • We do not use the following data for averages, fits, limits, etc. • • •					
$5567.8 \pm 2.9^{+0.9}_{-1.9}$	133	[2] ABAZOV	16E	D0	$p\overline{p} \to B_s^0 \pi^\pm X$

[1] From the combined analysis of $B_s^0 \to J/\psi\phi$ and $B_s^0 \to D_s^\pm \mu^\mp X$ decays.
[2] Assumes $T_{b\overline{s}}(5568)^\pm \to B_s \pi^\pm$ decay. If $T_{b\overline{s}}(5568)^\pm \to B_s^* \pi^\pm$ decay is assumed, the mass shifts upward by 49 MeV.

$T_{b\overline{s}}(5568)^+$ WIDTH

VALUE (MeV)	EVTS	DOCUMENT ID		TECN	COMMENT
$18.6^{+7.9}_{-6.1}{}^{+3.5}_{-3.8}$	278	[1] ABAZOV	18A	D0	$p\overline{p} \to B_s \pi^\pm X$
• • • We do not use the following data for averages, fits, limits, etc. • • •					
$21.9 \pm 6.4^{+5.0}_{-2.5}$	133	ABAZOV	16E	D0	$p\overline{p} \to B_s \pi^\pm X$

[1] From the combined analysis of $B_s^0 \to J/\psi\phi$ and $B_s^0 \to D_s^\pm \mu^\mp X$ decays.

$T_{b\overline{s}}(5568)^+$ DECAY MODES

	Mode	Fraction (Γ_i/Γ)
Γ_1	$B_s \pi^+$	seen

$T_{b\overline{s}}(5568)^+$ BRANCHING RATIOS

$\Gamma(B_s \pi^+)/\Gamma_{total}$ — **Γ_1/Γ**

VALUE	EVTS	DOCUMENT ID		TECN	COMMENT
seen	145	[1] ABAZOV	18A	D0	$p\overline{p} \to B_s^0 \pi^\pm X$
seen	133	[2] ABAZOV	16E	D0	$p\overline{p} \to B_s^0 \pi^\pm X$
• • • We do not use the following data for averages, fits, limits, etc. • • •					
not seen		[3] AABOUD	18L	ATLS	$pp \to B_s^0 \pi^\pm X$
not seen		[4] AALTONEN	18A	CDF	$p\overline{p} \to B_s^0 \pi^\pm X$
not seen		[5] SIRUNYAN	18J	CMS	$pp \to B_s^0 \pi^\pm X$
not seen		[6] AAIJ	16AI	LHCB	$pp \to B_s^0 \pi^\pm X$

[1] With B_s mesons reconstructed in decays to $D_s^\pm \mu^\mp X$.
[2] Seen in $p\overline{p}$ collisions at 1.96 TeV at a rate of $(8.6 \pm 1.9 \pm 1.4)\%$ relative to inclusive B_s production in the kinematic region $10 < p_T(B_s) < 30$ GeV/c, with B_s mesons reconstructed in decays to $J/\psi\phi$.An alternative possibility, $T_{b\overline{s}}(5568)^\pm \to B_s^* \pi^\pm$ with a missing γ, could not be ruled out.
[3] Not seen in 24.4 fb^{-1} of pp collision data at $\sqrt{s} = 7$ and 8 TeV with B_s mesons reconstructed in decays to $J/\psi\phi$. An upper limit on the production rate times branching fraction for $T_{b\overline{s}}(5568)^\pm \to B_s \pi^\pm$ relative to inclusive B_s production is less than 1.5% at $p_T(B_s) > 10$ GeV/c and less than 1.6% at $p_T(B_s) > 15$ GeV/c at 95% CL.
[4] Not seen in 9.6 fb^{-1} of $p\overline{p}$ collision data at $\sqrt{s} = 1.96$ TeV with B_s mesons reconstructed in decays to $J/\psi\phi$. An upper limit on the production rate times branching fraction for $T_{b\overline{s}}(5568)^\pm \to B_s \pi^\pm$ relative to inclusive B_s production is less than 6.7% at 95% CL.
[5] Not seen in 19.7 fb^{-1} of pp collisions data at $\sqrt{s} = 8$ TeV with B_s mesons reconstructed in decays to $J/\psi\phi$. An upper limit on the production rate times branching fraction for $T_{b\overline{s}}(5568)^\pm \to B_s \pi^\pm$ relative to inclusive B_s production is less than 1.1% at $p_T(B_s) > 10$ GeV/c and less than 1.0% at $p_T(B_s) > 15$ GeV/c at 95%CL.
[6] Not seen in 3 fb^{-1} of pp collision data at $\sqrt{s} = 7$ and 8 TeV in a scan over the $T_{b\overline{s}}(5568)$ mass and width, with B_s mesons reconstructed in decays to $D_s^- \pi^+$ or $J/\psi\phi$. An upper limit on the production rate times branching fraction for $T_{b\overline{s}}(5568)^\pm \to B_s \pi^\pm$ relative to inclusive B_s production is less than 2.1% at $p_T(B_s) > 10$ GeV/c at 90% CL.

$T_{b\overline{s}}(5568)^+$ REFERENCES

AABOUD	18L	PRL 120 202007	M. Aaboud *et al.*	(ATLAS Collab.)
AALTONEN	18A	PRL 120 202006	T. Aaltonen *et al.*	(CDF Collab.)
ABAZOV	18A	PR D97 092004	V.M. Abazov *et al.*	(D0 Collab.)
SIRUNYAN	18J	PRL 120 202005	A.M. Sirunyan *et al.*	(CMS Collab.)
AAIJ	16AI	PRL 117 152003	R. Aaij *et al.*	(LHCb Collab.)
ABAZOV	16E	PRL 117 022003	V.M. Abazov *et al.*	(D0 Collab.)

Int. J. Mod. Phys. A 2026.41. Downloaded from www.worldscientific.com by UNIVERSITY OF CALIFORNIA @ BERKELEY on 09/16/26. Re-use and distribution is strictly not permitted, except for Open Access articles.

$T_{cc\overline{cc}}(6600)$

$I^G(J^{PC}) = 0^+(2^{++})$

OMITTED FROM SUMMARY TABLE

Assuming that all structures seen in the $J/\psi J/\psi$ final state have the same quantum numbers, CMS determined those to $J^{PC} = 2^{++}$ (HAYRAPETYAN 25AG). State incompatible with a $q\overline{q}$ structure. Needs confirmation. See the review on "Heavy Non-$q\overline{q}$ Mesons."

$T_{cc\overline{cc}}(6600)$ MASS

VALUE (MeV)	DOCUMENT ID		TECN	COMMENT
6646^{+28}_{-25} OUR AVERAGE				
$6638^{+43}_{-38}{}^{+16}_{-31}$	[1] HAYRAPETY...24		CMS	$pp \to J/\psi J/\psi X$
$6650 \pm 20^{+30}_{-20}$	[2] AAD	23BL	ATLS	$pp \to J/\psi J/\psi X$

[1] In a model with three resonances described by interfering relativistic Breit-Wigner functions above background from non-resonant single and double parton scattering and a threshold enhancement.
[2] In a model with two resonances, with the $T_{cc\overline{cc}}(6600)$ interfering with single parton scattering, and a non-interfering $T_{cc\overline{cc}}(6900)$.

$T_{cc\overline{cc}}(6600)$ WIDTH

VALUE (MeV)	DOCUMENT ID		TECN	COMMENT
440 ± 70 OUR AVERAGE				
$440^{+230}_{-200}{}^{+110}_{-240}$	[1] HAYRAPETY...24		CMS	$pp \to J/\psi J/\psi X$
$440 \pm 50^{+60}_{-50}$	[2] AAD	23BL	ATLS	$pp \to J/\psi J/\psi X$

[1] In a model with three resonances described by interfering relativistic Breit-Wigner functions above background from non-resonant single and double parton scattering and a threshold enhancement.
[2] In a model with two resonances, with the $T_{cc\overline{cc}}(6600)$ interfering with single parton scattering, and a non-interfering $T_{cc\overline{cc}}(6900)$.

$T_{cc\overline{cc}}(6600)$ DECAY MODES

	Mode	Fraction (Γ_i/Γ)
Γ_1	$J/\psi J/\psi$	seen

$T_{cc\overline{cc}}(6600)$ BRANCHING RATIOS

$\Gamma(J/\psi J/\psi)/\Gamma_{total}$ — Γ_1/Γ

VALUE	DOCUMENT ID	TECN	COMMENT
seen	HAYRAPETY...24	CMS	$pp \to J/\psi J/\psi X$

$T_{cc\overline{cc}}(6600)$ REFERENCES

HAYRAPETY... 25AG NAT 648 58 A. Hayrapetyan *et al.* (CMS Collab.) JPC
HAYRAPETY... 24 PRL 132 111901 A. Hayrapetyan *et al.* (CMS Collab.)
AAD 23BL PRL 131 151902 G. Aad *et al.* (ATLAS Collab.)

$T_{cc\overline{cc}}(6900)^0$

$I^G(J^{PC}) = 0^+(2^{++})$

was $X(6900)$

Assuming that all structures seen in the $J/\psi J/\psi$ final state have the same quantum numbers, CMS determined those to $J^{PC} = 2^{++}$ (HAYRAPETYAN 25AG). State incompatible with a $q\overline{q}$ structure. See the review on "Heavy Non-$q\overline{q}$ Mesons."

$T_{cc\overline{cc}}(6900)^0$ MASS

VALUE (MeV)	DOCUMENT ID		TECN	COMMENT
6898 ± 12 OUR AVERAGE Error includes scale factor of 1.2.				
$6847^{+44}_{-28}{}^{+48}_{-20}$	[1] HAYRAPETY...24		CMS	$pp \to J/\psi J/\psi X$
$6910 \pm 10 \pm 10$	[2] AAD	23BL	ATLS	$pp \to J/\psi J/\psi X$
$6886 \pm 11 \pm 11$	[3] AAIJ	20AY	LHCB	$pp \to J/\psi J/\psi X$
• • • We do not use the following data for averages, fits, limits, etc. • • •				
$6960 \pm 50 \pm 30$	[4] AAD	23BL	ATLS	$pp \to J/\psi \psi(2S) X$

[1] In a model with three resonances described by interfering relativistic Breit-Wigner functions above background from non-resonant single and double parton scattering and a threshold enhancement.
[2] In a model with two resonances, with the $T_{cc\overline{cc}}(6600)$ interfering with single parton scattering, and a non-interfering $T_{cc\overline{cc}}(6900)$.
[3] In a model where the broad structure above threshold interferes with non-resonant single parton scattering. Without interference the mass is $6905 \pm 11 \pm 7$ MeV.
[4] Assuming a single resonance (could be another state). A 3σ signal is observed for an additional resonance with mass $7220 \pm 30^{+10}_{-40}$ MeV and width $90 \pm 60^{+60}_{-50}$ MeV.

$T_{cc\overline{cc}}(6900)^0$ WIDTH

VALUE (MeV)	DOCUMENT ID		TECN	COMMENT
161 ± 26 OUR AVERAGE				
$191^{+66}_{-49}{}^{+25}_{-17}$	[1] HAYRAPETY...24		CMS	$pp \to J/\psi J/\psi X$
$150 \pm 30 \pm 10$	[2] AAD	23BL	ATLS	$pp \to J/\psi J/\psi X$
$168 \pm 33 \pm 69$	[3] AAIJ	20AY	LHCB	$pp \to J/\psi J/\psi X$
• • • We do not use the following data for averages, fits, limits, etc. • • •				
$510 \pm 170^{+110}_{-100}$	[4] AAD	23BL	ATLS	$pp \to J/\psi \psi(2S) X$

[1] In a model with three resonances described by interfering relativistic Breit-Wigner functions above background from non-resonant single and double parton scattering and a threshold enhancement.
[2] In a model with two resonances, with the $T_{cc\overline{cc}}(6600)$ interfering with single parton scattering, and a non-interfering $T_{cc\overline{cc}}(6900)$.
[3] In a model where the broad structure above threshold interferes with non-resonant single parton scattering. Without interference the width is 80 ± 38 MeV.
[4] Assuming a single resonance (could be another state). A 3σ signal is observed for an additional resonance with mass $7220 \pm 30^{+10}_{-40}$ MeV and width $90 \pm 60^{+60}_{-50}$ MeV.

$T_{cc\overline{cc}}(6900)^0$ DECAY MODES

	Mode	Fraction (Γ_i/Γ)
Γ_1	$J/\psi J/\psi$	seen

$T_{cc\overline{cc}}(6900)^0$ BRANCHING RATIOS

$\Gamma(J/\psi J/\psi)/\Gamma_{total}$ — Γ_1/Γ

VALUE	DOCUMENT ID		TECN	COMMENT
seen	HAYRAPETY...24		CMS	$pp \to J/\psi J/\psi X$
seen	AAD	23BL	ATLS	$pp \to J/\psi J/\psi X$
seen	AAIJ	20AY	LHCB	$pp \to J/\psi J/\psi X$

$T_{cc\overline{cc}}(6900)^0$ REFERENCES

HAYRAPETY... 25AG NAT 648 58 A. Hayrapetyan *et al.* (CMS Collab.) JPC
HAYRAPETY... 24 PRL 132 111901 A. Hayrapetyan *et al.* (CMS Collab.)
AAD 23BL PRL 131 151902 G. Aad *et al.* (ATLAS Collab.)
AAIJ 20AY SCIB 65 1983 R. Aaij *et al.* (LHCb Collab.)

$T_{cc\overline{cc}}(7100)$

$I^G(J^{PC}) = 0^+(2^{++})$

OMITTED FROM SUMMARY TABLE

Assuming that all structures seen in the $J/\psi J/\psi$ final state have the same quantum numbers, CMS determined those to $J^{PC} = 2^{++}$ (HAYRAPETYAN 25AG). State incompatible with a $q\overline{q}$ structure. Needs confirmation. See the review on "Heavy Non-$q\overline{q}$ Mesons."

$T_{cc\overline{cc}}(7100)$ MASS

VALUE (MeV)	DOCUMENT ID		TECN	COMMENT
$7134^{+48}_{-25}{}^{+41}_{-15}$	[1] HAYRAPETY...24		CMS	$pp \to J/\psi J/\psi X$

[1] In a model with three resonances described by interfering relativistic Breit-Wigner functions above background from non-resonant single and double parton scattering and a threshold enhancement.

$T_{cc\overline{cc}}(7100)$ WIDTH

VALUE (MeV)	DOCUMENT ID		TECN	COMMENT
$97^{+40}_{-29}{}^{+29}_{-26}$	[1] HAYRAPETY...24		CMS	$pp \to J/\psi J/\psi X$

[1] In a model with three resonances described by interfering relativistic Breit-Wigner functions above background from non-resonant single and double parton scattering and a threshold enhancement.

$T_{cc\overline{cc}}(7100)$ DECAY MODES

	Mode	Fraction (Γ_i/Γ)
Γ_1	$J/\psi J/\psi$	seen

$T_{cc\overline{cc}}(7100)$ BRANCHING RATIOS

$\Gamma(J/\psi J/\psi)/\Gamma_{total}$ — Γ_1/Γ

VALUE	DOCUMENT ID	TECN	COMMENT
seen	HAYRAPETY...24	CMS	$pp \to J/\psi J/\psi X$

$T_{cc\overline{cc}}(7100)$ REFERENCES

HAYRAPETY... 25AG NAT 648 58 A. Hayrapetyan *et al.* (CMS Collab.) JPC
HAYRAPETY... 24 PRL 132 111901 A. Hayrapetyan *et al.* (CMS Collab.)

Int. J. Mod. Phys. A 2026.41. Downloaded from www.worldscientific.com
by [redacted]LIFORNIA @ BERKELEY on 09/16/26. Re-use and distribution is strictly not permitted, except for Open Access articles.

$T_{b\bar{b}1}(10610)$

$I^G(J^{PC}) = 1^+(1^{+-})$

was $Z_b(10610)$, $X(10610)$

Properties incompatible with a $q\bar{q}$ structure (exotic state). See the review on non-$q\bar{q}$ states.

Observed by BONDAR 12 in $\Upsilon(5S)$ decays to $\Upsilon(\mathrm{nS})\pi^+\pi^-$ (n = 1, 2, 3) and $h_b(\mathrm{mP})\pi^+\pi^-$ (m = 1, 2). $J^P = 1^+$ is favored from angular analyses.

$T_{b\bar{b}1}(10610)^\pm$ MASS

VALUE (MeV)	DOCUMENT ID		TECN	COMMENT
10607.2±2.0	[1] BONDAR	12	BELL	$e^+e^- \to$ hadrons
• • • We do not use the following data for averages, fits, limits, etc. • • •				
$10608.5 \pm 3.4^{+3.7}_{-1.4}$	[2] GARMASH	15	BELL	$e^+e^- \to \Upsilon(1S)\pi^+\pi^-$
$10608.1 \pm 1.2^{+1.5}_{-0.2}$	[2] GARMASH	15	BELL	$e^+e^- \to \Upsilon(2S)\pi^+\pi^-$
$10607.4 \pm 1.5^{+0.8}_{-0.2}$	[2] GARMASH	15	BELL	$e^+e^- \to \Upsilon(3S)\pi^+\pi^-$
$10611 \pm 4 \pm 3$	[3] BONDAR	12	BELL	$e^+e^- \to \Upsilon(1S)\pi^+\pi^-$
$10609 \pm 2 \pm 3$	[3] BONDAR	12	BELL	$e^+e^- \to \Upsilon(2S)\pi^+\pi^-$
$10608 \pm 2 \pm 3$	[3] BONDAR	12	BELL	$e^+e^- \to \Upsilon(3S)\pi^+\pi^-$
$10605 \pm 2 {}^{+3}_{-1}$	[3] BONDAR	12	BELL	$e^+e^- \to h_b(1P)\pi^+\pi^-$
$10599 {}^{+6}_{-3} {}^{+5}_{-4}$	[3] BONDAR	12	BELL	$e^+e^- \to h_b(2P)\pi^+\pi^-$

[1] Average of the BONDAR 12 measurements in separate channels.
[2] Correlated with the corresponding result from BONDAR 12.
[3] Superseded by the average measurement of BONDAR 12.

$T_{b\bar{b}1}(10610)^0$ MASS

VALUE (MeV)	DOCUMENT ID		TECN	COMMENT
10609±4±4	[1] KROKOVNY	13	BELL	$e^+e^- \to \Upsilon(2S)/\Upsilon(3S)\pi^0\pi^0$

[1] From a simultaneous fit to the KROKOVNY 13 Dalitz analysis of $e^+e^- \to \Upsilon(2S)/\Upsilon(3S)\pi^0\pi^0$ decays with fixed width $\Gamma(T_{b\bar{b}1}(10610)^0) = 18.4$ MeV.

$T_{b\bar{b}1}(10610)^\pm$ WIDTH

VALUE (MeV)	DOCUMENT ID		TECN	COMMENT
18.4± 2.4	[1] BONDAR	12	BELL	$e^+e^- \to$ hadrons
• • • We do not use the following data for averages, fits, limits, etc. • • •				
$18.5 \pm 5.3^{+6.1}_{-2.3}$	[2] GARMASH	15	BELL	$e^+e^- \to \Upsilon(1S)\pi^+\pi^-$
$20.8 \pm 2.5^{+0.3}_{-2.1}$	[2] GARMASH	15	BELL	$e^+e^- \to \Upsilon(2S)\pi^+\pi^-$
$18.7 \pm 3.4^{+2.5}_{-1.3}$	[2] GARMASH	15	BELL	$e^+e^- \to \Upsilon(3S)\pi^+\pi^-$
$22.3 \pm 7.7^{+3.0}_{-4.0}$	[3] BONDAR	12	BELL	$e^+e^- \to \Upsilon(1S)\pi^+\pi^-$
$24.2 \pm 3.1^{+2.0}_{-3.0}$	[3] BONDAR	12	BELL	$e^+e^- \to \Upsilon(2S)\pi^+\pi^-$
$17.6 \pm 3.0 \pm 3.0$	[3] BONDAR	12	BELL	$e^+e^- \to \Upsilon(3S)\pi^+\pi^-$
$11.4 {}^{+4.5}_{-3.9} {}^{+2.1}_{-1.2}$	[3] BONDAR	12	BELL	$e^+e^- \to h_b(1P)\pi^+\pi^-$
$13 {}^{+10}_{-8} {}^{+9}_{-7}$	[3] BONDAR	12	BELL	$e^+e^- \to h_b(2P)\pi^+\pi^-$

[1] Average of the BONDAR 12 measurements in separate channels.
[2] Correlated with the corresponding result from BONDAR 12.
[3] Superseded by the average measurement of BONDAR 12.

$T_{b\bar{b}1}(10610)$ DECAY MODES

	Mode	Fraction (Γ_i/Γ)
Γ_1	$\Upsilon(1S)\pi^+$	$(5.4^{+1.9}_{-1.5}) \times 10^{-3}$
Γ_2	$\Upsilon(1S)\pi^0$	not seen
Γ_3	$\Upsilon(2S)\pi^+$	$(3.6^{+1.1}_{-0.8})$ %
Γ_4	$\Upsilon(2S)\pi^0$	seen
Γ_5	$\Upsilon(3S)\pi^+$	$(2.1^{+0.8}_{-0.6})$ %
Γ_6	$\Upsilon(3S)\pi^0$	seen
Γ_7	$h_b(1P)\pi^+$	$(3.5^{+1.2}_{-0.9})$ %
Γ_8	$h_b(2P)\pi^+$	$(4.7^{+1.7}_{-1.3})$ %
Γ_9	$B^+\overline{B}^0$	not seen
Γ_{10}	$B^+\overline{B}^{*0} + B^{*+}\overline{B}^0$	$(85.6^{+2.1}_{-2.9})$ %

$T_{b\bar{b}1}(10610)$ BRANCHING RATIOS

$\Gamma(\Upsilon(1S)\pi^+)/\Gamma_{\text{total}}$ — Γ_1/Γ

VALUE (units 10^{-3})	DOCUMENT ID		TECN	COMMENT
$\mathbf{5.4^{+1.6}_{-1.3}{}^{+1.1}_{-0.8}}$	[1] GARMASH	16	BELL	$e^+e^- \to \pi^-B^+\overline{B}^{*0}$, $\pi^-\overline{B}^0B^{*+}$
• • • We do not use the following data for averages, fits, limits, etc. • • •				
seen	GARMASH	15	BELL	$e^+e^- \to \Upsilon(1S)\pi^+\pi^-$
seen	BONDAR	12	BELL	$e^+e^- \to \Upsilon(1S)\pi^+\pi^-$

[1] Assuming the $T_{b\bar{b}1}(10610)$ decay width is saturated by the channels $\pi^+\Upsilon(1S,2S,3S)$, $\pi^+h_b(1P,2P)$, and $B^+\overline{B}^{*0} + \overline{B}^0B^{*+}$, and using the results from BONDAR 12 and MIZUK 16.

$\Gamma(\Upsilon(1S)\pi^0)/\Gamma_{\text{total}}$ — Γ_2/Γ

VALUE	DOCUMENT ID		TECN	COMMENT
not seen	KROKOVNY	13	BELL	$e^+e^- \to \Upsilon(1S)\pi^0\pi^0$

$\Gamma(\Upsilon(2S)\pi^+)/\Gamma_{\text{total}}$ — Γ_3/Γ

VALUE (units 10^{-2})	DOCUMENT ID		TECN	COMMENT
$\mathbf{3.62^{+0.76}_{-0.59}{}^{+0.79}_{-0.53}}$	[1] GARMASH	16	BELL	$e^+e^- \to \pi^-B^+\overline{B}^{*0}$, $\pi^-\overline{B}^0B^{*+}$
• • • We do not use the following data for averages, fits, limits, etc. • • •				
seen	GARMASH	15	BELL	$e^+e^- \to \Upsilon(2S)\pi^+\pi^-$
seen	BONDAR	12	BELL	$e^+e^- \to \Upsilon(2S)\pi^+\pi^-$

[1] Assuming the $T_{b\bar{b}1}(10610)$ decay width is saturated by the channels $\pi^+\Upsilon(1S,2S,3S)$, $\pi^+h_b(1P,2P)$, and $B^+\overline{B}^{*0} + \overline{B}^0B^{*+}$, and using the results from BONDAR 12 and MIZUK 16.

$\Gamma(\Upsilon(2S)\pi^0)/\Gamma_{\text{total}}$ — Γ_4/Γ

VALUE	DOCUMENT ID		TECN	COMMENT
seen	[1] KROKOVNY	13	BELL	$e^+e^- \to \Upsilon(2S)\pi^0\pi^0$

[1] Combined significance in $e^+e^- \to \Upsilon(2S)/\Upsilon(3S)\pi^0\pi^0$, including systematics, of 6.5σ.

$\Gamma(\Upsilon(3S)\pi^+)/\Gamma_{\text{total}}$ — Γ_5/Γ

VALUE (units 10^{-2})	DOCUMENT ID		TECN	COMMENT
$\mathbf{2.15^{+0.55}_{-0.42}{}^{+0.60}_{-0.43}}$	[1] GARMASH	16	BELL	$e^+e^- \to \pi^-B^+\overline{B}^{*0}$, $\pi^-\overline{B}^0B^{*+}$
• • • We do not use the following data for averages, fits, limits, etc. • • •				
seen	GARMASH	15	BELL	$e^+e^- \to \Upsilon(3S)\pi^+\pi^-$
seen	BONDAR	12	BELL	$e^+e^- \to \Upsilon(3S)\pi^+\pi^-$

[1] Assuming the $T_{b\bar{b}1}(10610)$ decay width is saturated by the channels $\pi^+\Upsilon(1S,2S,3S)$, $\pi^+h_b(1P,2P)$, and $B^+\overline{B}^{*0} + \overline{B}^0B^{*+}$, and using the results from BONDAR 12 and MIZUK 16.

$\Gamma(\Upsilon(3S)\pi^0)/\Gamma_{\text{total}}$ — Γ_6/Γ

VALUE	DOCUMENT ID		TECN	COMMENT
seen	[1] KROKOVNY	13	BELL	$e^+e^- \to \Upsilon(3S)\pi^0\pi^0$

[1] Combined significance in $e^+e^- \to \Upsilon(2S)/\Upsilon(3S)\pi^0\pi^0$, including systematics, of 6.5σ.

$\Gamma(h_b(1P)\pi^+)/\Gamma_{\text{total}}$ — Γ_7/Γ

VALUE (units 10^{-2})	DOCUMENT ID		TECN	COMMENT
$\mathbf{3.45^{+0.87}_{-0.71}{}^{+0.86}_{-0.63}}$	[1] GARMASH	16	BELL	$e^+e^- \to \pi^-B^+\overline{B}^{*0}$, $\pi^-\overline{B}^0B^{*+}$
• • • We do not use the following data for averages, fits, limits, etc. • • •				
possibly seen	[2] MIZUK	16	BELL	$e^+e^- \to h_b(1P)\pi^+\pi^-$
seen	[3] BONDAR	12	BELL	$e^+e^- \to h_b(1P)\pi^+\pi^-$

[1] Assuming the $T_{b\bar{b}1}(10610)$ decay width is saturated by the channels $\pi^+\Upsilon(1S,2S,3S)$, $\pi^+h_b(1P,2P)$, and $B^+\overline{B}^{*0} + \overline{B}^0B^{*+}$, and using the results from BONDAR 12 and MIZUK 16.
[2] Using e^+e^- energies near the $\Upsilon(11020)$.
[3] Using e^+e^- energies near the $\Upsilon(10860)$.

$\Gamma(h_b(2P)\pi^+)/\Gamma_{\text{total}}$ — Γ_8/Γ

VALUE (units 10^{-2})	DOCUMENT ID		TECN	COMMENT
$\mathbf{4.67^{+1.24}_{-1.00}{}^{+1.18}_{-0.89}}$	[1] GARMASH	16	BELL	$e^+e^- \to \pi^-B^+\overline{B}^{*0}$, $\pi^-\overline{B}^0B^{*+}$
• • • We do not use the following data for averages, fits, limits, etc. • • •				
possibly seen	[2] MIZUK	16	BELL	$e^+e^- \to h_b(2P)\pi^+\pi^-$
seen	[3] BONDAR	12	BELL	$e^+e^- \to h_b(2P)\pi^+\pi^-$

[1] Assuming the $T_{b\bar{b}1}(10610)$ decay width is saturated by the channels $\pi^+\Upsilon(1S,2S,3S)$, $\pi^+h_b(1P,2P)$, and $B^+\overline{B}^{*0} + \overline{B}^0B^{*+}$, and using the results from BONDAR 12 and MIZUK 16.
[2] Using e^+e^- energies near the $\Upsilon(11020)$.
[3] Using e^+e^- energies near the $\Upsilon(10860)$.

$\Gamma(B^+\overline{B}^0)/\Gamma_{\text{total}}$ — Γ_9/Γ

VALUE	DOCUMENT ID		TECN	COMMENT
not seen	GARMASH	16	BELL	$e^+e^- \to \pi^-B^+\overline{B}^0$

Int. J. Mod. Phys. A 2026.41. Downloaded from www.worldscientific.com by UNIVERSITY OF CALIFORNIA @ BERKELEY on 09/16/26. Re-use and distribution is strictly not permitted, except for Open Access articles.

$[\Gamma(B^+\overline{B}^{*0})+\Gamma(B^{*+}\overline{B}^0)]/\Gamma_{total}$ — Γ_{10}/Γ

VALUE (units 10^{-2})	EVTS	DOCUMENT ID		TECN	COMMENT
$85.6^{+1.5}_{-2.0}{}^{+1.5}_{-2.1}$	357	[1] GARMASH	16	BELL	$e^+e^-\to\pi^-B^+\overline{B}^{*0}$, $\pi^-B^{*+}\overline{B}^0$

[1] Assuming the $T_{b\overline{b}1}(10610)$ decay width is saturated by the channels $\pi^+\Upsilon(1S,2S,3S)$, $\pi^+h_b(1P,2P)$, and $B^+\overline{B}^{*0}+B^{*+}\overline{B}^0$, and using the results from BONDAR 12 and MIZUK 16. Using the mass and width of the $T_{b\overline{b}1}(10610)$ from BONDAR 12.

$[\Gamma(B^+\overline{B}^{*0})+\Gamma(B^{*+}\overline{B}^0)]/[\Gamma(\Upsilon(1S)\pi^+)+\Gamma(\Upsilon(2S)\pi^+)+\Gamma(\Upsilon(3S)\pi^+)+\Gamma(h_b(1P)\pi^+)+\Gamma(h_b(2P)\pi^+)]$ — $\Gamma_{10}/(\Gamma_1+\Gamma_3+\Gamma_5+\Gamma_7+\Gamma_8)$

VALUE (units 10^{-2})	EVTS	DOCUMENT ID		TECN	COMMENT
• • • We do not use the following data for averages, fits, limits, etc. • • •					
$5.93^{+0.99}_{-0.69}{}^{+1.01}_{-0.73}$	357	[1] GARMASH	16	BELL	$e^+e^-\to\pi^-B^+\overline{B}^{*0}$, $\pi^-\overline{B}^0B^{*+}$

[1] Combined with the results of BONDAR 12 and MIZUK 16. Not independent from $T_{b\overline{b}1}(10610)$ branching fractions to $\pi^+\Upsilon(1S,2S,3S)$, $\pi^+h_b(1P,2P)$, and $B^+\overline{B}^{*0}+\overline{B}^0B^{*+}$.

$T_{b\overline{b}1}(10610)$ REFERENCES

GARMASH	16	PRL 116 212001	A. Garmash *et al.*	(BELLE Collab.)
MIZUK	16	PRL 117 142001	R. Mizuk *et al.*	(BELLE Collab.)
GARMASH	15	PR D91 072003	A. Garmash *et al.*	(BELLE Collab.)
KROKOVNY	13	PR D88 052016	P. Krokovny *et al.*	(BELLE Collab.)
BONDAR	12	PRL 108 122001	A. Bondar *et al.*	(BELLE Collab.)

$T_{b\overline{b}1}(10650)$

$I^G(J^{PC}) = 1^+(1^{+-})$
I, G, C need confirmation.

was $Z_b(10650)$, $X(10650)^\pm$

Properties incompatible with a $q\overline{q}$ structure (exotic state). See the review on non-$q\overline{q}$ states.

Observed by BONDAR 12 in $\Upsilon(5S)$ decays to $\Upsilon(nS)\pi^+\pi^-$ (n = 1, 2, 3) and $h_b(mP)\pi^+\pi^-$ (m = 1, 2). $J^P=1^+$ is favored from angular analyses.

$T_{b\overline{b}1}(10650)^+$ MASS

VALUE (MeV)	DOCUMENT ID		TECN	COMMENT
10652.2±1.5	[1] BONDAR	12	BELL	$e^+e^-\to$ hadrons
• • • We do not use the following data for averages, fits, limits, etc. • • •				
$10656.7\pm5.0^{+1.1}_{-3.1}$	[2] GARMASH	15	BELL	$e^+e^-\to\Upsilon(1S)\pi^+\pi^-$
$10650.7\pm1.5^{+0.5}_{-0.2}$	[2] GARMASH	15	BELL	$e^+e^-\to\Upsilon(2S)\pi^+\pi^-$
$10651.2\pm1.0^{+0.4}_{-0.3}$	[2] GARMASH	15	BELL	$e^+e^-\to\Upsilon(3S)\pi^+\pi^-$
$10657\pm6\pm3$	[3] BONDAR	12	BELL	$e^+e^-\to\Upsilon(1S)\pi^+\pi^-$
$10651\pm2\pm3$	[3] BONDAR	12	BELL	$e^+e^-\to\Upsilon(2S)\pi^+\pi^-$
$10652\pm1\pm2$	[3] BONDAR	12	BELL	$e^+e^-\to\Upsilon(3S)\pi^+\pi^-$
$10654\pm3\,^{+1}_{-2}$	[3] BONDAR	12	BELL	$e^+e^-\to h_b(1P)\pi^+\pi^-$
$10651\,^{+2}_{-3}\,^{+3}_{-2}$	[3] BONDAR	12	BELL	$e^+e^-\to h_b(2P)\pi^+\pi^-$

[1] Average of the BONDAR 12 measurements in separate channels.
[2] Correlated with the corresponding result from BONDAR 12.
[3] Superseded by the average measurement of BONDAR 12.

$T_{b\overline{b}1}(10650)^+$ WIDTH

VALUE (MeV)	DOCUMENT ID		TECN	COMMENT
11.5± 2.2	[1] BONDAR	12	BELL	$e^+e^-\to$ hadrons
• • • We do not use the following data for averages, fits, limits, etc. • • •				
$12.1^{+11.3}_{-4.8}\pm2.7\,^{+2.7}_{-0.6}$	[2] GARMASH	15	BELL	$e^+e^-\to\Upsilon(1S)\pi^+\pi^-$
$14.2\pm3.7^{+0.9}_{-0.4}$	[2] GARMASH	15	BELL	$e^+e^-\to\Upsilon(2S)\pi^+\pi^-$
$9.3\pm2.2^{+0.3}_{-0.5}$	[2] GARMASH	15	BELL	$e^+e^-\to\Upsilon(3S)\pi^+\pi^-$
$16.3\pm9.8^{+6.0}_{-2.0}$	[3] BONDAR	12	BELL	$e^+e^-\to\Upsilon(1S)\pi^+\pi^-$
$13.3\pm3.3^{+4.0}_{-3.0}$	[3] BONDAR	12	BELL	$e^+e^-\to\Upsilon(2S)\pi^+\pi^-$
$8.4\pm2.0\pm2.0$	[3] BONDAR	12	BELL	$e^+e^-\to\Upsilon(3S)\pi^+\pi^-$
$20.9^{+5.4}_{-4.7}\pm2.1\,^{+2.1}_{-5.7}$	[3] BONDAR	12	BELL	$e^+e^-\to h_b(1P)\pi^+\pi^-$
$19\pm7\,^{+11}_{-7}$	[3] BONDAR	12	BELL	$e^+e^-\to h_b(2P)\pi^+\pi^-$

[1] Average of the BONDAR 12 measurements in separate channels.
[2] Correlated with the corresponding result from BONDAR 12.
[3] Superseded by the average measurement of BONDAR 12.

$T_{b\overline{b}1}(10650)$ DECAY MODES

	Mode	Fraction (Γ_i/Γ)
Γ_1	$\Upsilon(1S)\pi^+$	$(1.7^{+0.8}_{-0.6})\times10^{-3}$
Γ_2	$\Upsilon(2S)\pi^+$	$(1.4^{+0.6}_{-0.4})$ %
Γ_3	$\Upsilon(3S)\pi^+$	$(1.6^{+0.7}_{-0.5})$ %
Γ_4	$h_b(1P)\pi^+$	$(8.4^{+2.9}_{-2.4})$ %
Γ_5	$h_b(2P)\pi^+$	(15 ± 4) %
Γ_6	$B^+\overline{B}^0$	not seen
Γ_7	$B^+\overline{B}^{*0}+B^{*+}\overline{B}^0$	not seen
Γ_8	$B^{*+}\overline{B}^{*0}$	$(74\,^{+4}_{-6})$ %

$T_{b\overline{b}1}(10650)$ BRANCHING RATIOS

$\Gamma(\Upsilon(1S)\pi^+)/\Gamma_{total}$ — Γ_1/Γ

VALUE (units 10^{-3})	DOCUMENT ID		TECN	COMMENT
$1.7^{+0.7}_{-0.6}{}^{+0.3}_{-0.2}$	[1] GARMASH	16	BELL	$e^+e^-\to\pi^-B^{*+}\overline{B}^{*0}$
• • • We do not use the following data for averages, fits, limits, etc. • • •				
seen	GARMASH	15	BELL	$e^+e^-\to\Upsilon(1S)\pi^+\pi^-$
seen	BONDAR	12	BELL	$e^+e^-\to\Upsilon(1S)\pi^+\pi^-$

[1] Assuming the $T_{b\overline{b}1}(10650)$ decay width is saturated by the channels $\pi^+\Upsilon(1S,2S,3S)$, $\pi^+h_b(1P,2P)$, and $B^{*+}\overline{B}^{*0}$, and using the results from BONDAR 12 and MIZUK 16.

$\Gamma(\Upsilon(2S)\pi^+)/\Gamma_{total}$ — Γ_2/Γ

VALUE (units 10^{-2})	DOCUMENT ID		TECN	COMMENT
$1.39^{+0.48}_{-0.38}{}^{+0.34}_{-0.23}$	[1] GARMASH	16		$e^+e^-\to\pi^-B^{*+}\overline{B}^{*0}$
• • • We do not use the following data for averages, fits, limits, etc. • • •				
seen	GARMASH	15	BELL	$e^+e^-\to\Upsilon(2S)\pi^+\pi^-$
seen	BONDAR	12	BELL	$e^+e^-\to\Upsilon(2S)\pi^+\pi^-$

[1] Assuming the $T_{b\overline{b}1}(10650)$ decay width is saturated by the channels $\pi^+\Upsilon(1S,2S,3S)$, $\pi^+h_b(1P,2P)$, and $B^{*+}\overline{B}^{*0}$, and using the results from BONDAR 12 and MIZUK 16.

$\Gamma(\Upsilon(3S)\pi^+)/\Gamma_{total}$ — Γ_3/Γ

VALUE (units 10^{-2})	DOCUMENT ID		TECN	COMMENT
$1.63^{+0.53}_{-0.42}{}^{+0.39}_{-0.28}$	[1] GARMASH	16	BELL	$e^+e^-\to\pi^-B^{*+}\overline{B}^{*0}$
• • • We do not use the following data for averages, fits, limits, etc. • • •				
seen	GARMASH	15	BELL	$e^+e^-\to\Upsilon(3S)\pi^+\pi^-$
seen	BONDAR	12	BELL	$e^+e^-\to\Upsilon(3S)\pi^+\pi^-$

[1] Assuming the $T_{b\overline{b}1}(10650)$ decay width is saturated by the channels $\pi^+\Upsilon(1S,2S,3S)$, $\pi^+h_b(1P,2P)$, and $B^{*+}\overline{B}^{*0}$, and using the results from BONDAR 12 and MIZUK 16.

$\Gamma(h_b(1P)\pi^+)/\Gamma_{total}$ — Γ_4/Γ

VALUE (units 10^{-2})	DOCUMENT ID		TECN	COMMENT
$8.41^{+2.43}_{-2.12}{}^{+1.49}_{-1.06}$	[1] GARMASH	16	BELL	$e^+e^-\to\pi^-B^{*+}\overline{B}^{*0}$
• • • We do not use the following data for averages, fits, limits, etc. • • •				
seen	[2] MIZUK	16	BELL	$e^+e^-\to h_b(1P)\pi^+\pi^-$
seen	[3] BONDAR	12	BELL	$e^+e^-\to h_b(1P)\pi^+\pi^-$

[1] Assuming the $T_{b\overline{b}1}(10650)$ decay width is saturated by the channels $\pi^+\Upsilon(1S,2S,3S)$, $\pi^+h_b(1P,2P)$, and $B^{*+}\overline{B}^{*0}$, and using the results from BONDAR 12 and MIZUK 16.
[2] Using e^+e^- energies near the $\Upsilon(11020)$.
[3] Using e^+e^- energies near the $\Upsilon(10860)$.

$\Gamma(h_b(2P)\pi^+)/\Gamma_{total}$ — Γ_5/Γ

VALUE (units 10^{-2})	DOCUMENT ID		TECN	COMMENT
$14.7^{+3.2}_{-2.8}{}^{+2.8}_{-2.3}$	[1] GARMASH	16	BELL	$e^+e^-\to\pi^-B^{*+}\overline{B}^{*0}$
• • • We do not use the following data for averages, fits, limits, etc. • • •				
possibly seen	[2] MIZUK	16	BELL	$e^+e^-\to h_b(2P)\pi^+\pi^-$
seen	[3] BONDAR	12	BELL	$e^+e^-\to h_b(2P)\pi^+\pi^-$

[1] Assuming the $T_{b\overline{b}1}(10650)$ decay width is saturated by the channels $\pi^+\Upsilon(1S,2S,3S)$, $\pi^+h_b(1P,2P)$, and $B^{*+}\overline{B}^{*0}$, and using the results from BONDAR 12 and MIZUK 16.
[2] Using e^+e^- energies near the $\Upsilon(11020)$.
[3] Using e^+e^- energies near the $\Upsilon(10860)$.

$\Gamma(B^+\overline{B}^0)/\Gamma_{total}$ — Γ_6/Γ

VALUE	DOCUMENT ID		TECN	COMMENT
not seen	GARMASH	16	BELL	$e^+e^-\to\pi^-B^+\overline{B}^0$

$[\Gamma(B^+\overline{B}^{*0})+\Gamma(B^{*+}\overline{B}^0)]/\Gamma_{total}$ — Γ_7/Γ

VALUE	DOCUMENT ID		TECN	COMMENT
not seen	GARMASH	16	BELL	$e^+e^-\to\pi^-B^+\overline{B}^{*0}$, $\pi^-\overline{B}^0B^{*+}$

Int. J. Mod. Phys. A 2026.41. Downloaded from www.worldscientific.com
by CALIFORNIA @ BERKELEY on 09/16/26. Re-use and distribution is strictly not permitted, except for Open Access articles.

$\Gamma(B^{*+}\overline{B}^{*0})/\Gamma_{total}$ — **Γ_8/Γ**

VALUE (units 10^{-2})	EVTS	DOCUMENT ID		TECN	COMMENT
$73.7^{+3.4}_{-4.4}{}^{+2.7}_{-3.5}$	161	[1] GARMASH	16	BELL	$e^+e^- \to \pi^- B^{*+}\overline{B}^{*0}$

[1] Assuming the $T_{b\bar{b}1}(10650)$ decay width is saturated by the channels $\pi^+\Upsilon(1S,2S,3S)$, $\pi^+ h_b(1P,2P)$, and $B^{*+}\overline{B}^{*0}$, and using the results from BONDAR 12 and MIZUK 16. Using the mass and width of the $T_{b\bar{b}1}(10650)$ from BONDAR 12.

$\Gamma(B^{*+}\overline{B}^{*0})/[\Gamma(\Upsilon(1S)\pi^+)+\Gamma(\Upsilon(2S)\pi^+)+\Gamma(\Upsilon(3S)\pi^+)+\Gamma(h_b(1P)\pi^+)+\Gamma(h_b(2P)\pi^+)]$ — **$\Gamma_8/(\Gamma_1+\Gamma_2+\Gamma_3+\Gamma_4+\Gamma_5)$**

VALUE (units 10^{-2})	EVTS	DOCUMENT ID		TECN	COMMENT
• • • We do not use the following data for averages, fits, limits, etc. • • •					
$2.80^{+0.69}_{-0.40}{}^{+0.54}_{-0.36}$	161	[1] GARMASH	16	BELL	$e^+e^- \to \pi^- B^{*+}\overline{B}^{*0}$

[1] Combined with the results of BONDAR 12 and MIZUK 16. Not independent from $T_{b\bar{b}1}(10650)$ branching fractions to $\pi^+\Upsilon(1S,2S,3S)$, $\pi^+ h_b(1P,2P)$, and $B^{*+}\overline{B}^{*0}$.

$T_{b\bar{b}1}(10650)$ REFERENCES

GARMASH	16	PRL 116 212001	A. Garmash *et al.*	(BELLE Collab.)
MIZUK	16	PRL 117 142001	R. Mizuk *et al.*	(BELLE Collab.)
GARMASH	15	PR D91 072003	A. Garmash *et al.*	(BELLE Collab.)
BONDAR	12	PRL 108 122001	A. Bondar *et al.*	(BELLE Collab.)

Further States

OMITTED FROM SUMMARY TABLE

This section contains states observed by a single group or states poorly established that thus need confirmation.

QUANTUM NUMBERS, MASSES, WIDTHS, AND BRANCHING RATIOS

$X(360)$ $I^G(J^{PC}) = ?^?(?^{?+})$

MASS (MeV)	WIDTH (MeV)	EVTS	DOCUMENT ID		TECN	COMMENT
$360\pm7\pm9$	64 ± 18	2.3k	[1] ABRAAMYAN	09	CNTR	2.75 $dC \to \gamma\gamma X$

[1] Not seen in $pC \to \gamma\gamma X$ at 5.5 GeV/c.

$X(1070)$ $I^G(J^{PC}) = ?^?(0^{++})$

MASS (MeV)	WIDTH (MeV)	DOCUMENT ID		COMMENT
1072 ± 1	3.5 ± 0.5	[1] VLADIMIRSK...	08	$40\ \pi^- p \to K^0_S K^0_S n + m\pi^0$

[1] Supersedes GRIGOR'EV 05.

$X(1110)$ $I^G(J^{PC}) = 0^+(\text{even}^{++})$

MASS (MeV)	WIDTH (MeV)	DOCUMENT ID		TECN	COMMENT
1107 ± 4	$111\pm8\pm15$	DAFTARI	87	DBC	0. $\overline{p}n \to \rho^-\pi^+\pi^-$

$f_0(1200\text{–}1600)$ $I^G(J^{PC}) = 0^+(0^{++})$

MASS (MeV)	WIDTH (MeV)	DOCUMENT ID		TECN	COMMENT
1323 ± 8	237 ± 20	VLADIMIRSK...	06	SPEC	$40\ \pi^- p \to K^0_S K^0_S n$
1480^{+100}_{-150}	1030^{+80}_{-170}	[1] ANISOVICH	03	SPEC	
1530^{+90}_{-250}	560 ± 40	[2] ANISOVICH	03	SPEC	

[1] K-matrix pole from combined analysis of $\pi^- p \to \pi^0\pi^0 n$, $\pi^- p \to K\overline{K}n$, $\pi^+\pi^- \to \pi^+\pi^-$, $\overline{p}p \to \pi^0\pi^0\pi^0$, $\pi^0\eta\eta$, $\pi^0\pi^0\eta$, $\pi^+\pi^-\pi^0$, $K^+K^-\pi^0$, $K^0_S K^0_S \pi^0$, $K^+K^0_S\pi^-$ at rest, $\overline{p}n \to \pi^-\pi^-\pi^+$, $K^0_S K^-\pi^0$, $K^0_S K^0_S \pi^-$ at rest.

[2] K-matrix pole from combined analysis of $\pi^- p \to \pi^0\pi^0 n$, $\pi^- p \to K\overline{K}n$, $\overline{p}p \to \pi^0\pi^0\pi^0$, $\pi^0\eta\eta$, $\pi^0\pi^0\eta$ at rest.

$X(1420)$ $I^G(J^{PC}) = 2^+(0^{++})$

MASS (MeV)	WIDTH (MeV)	DOCUMENT ID		TECN	COMMENT
1420 ± 20	160 ± 10	FILIPPI	00	OBLX	$0\ \overline{n}p \to \pi^+\pi^+\pi^-$

$X(1545)$ $I^G(J^{PC}) = ?^?(?^{++})$

MASS (MeV)	WIDTH (MeV)	DOCUMENT ID		COMMENT
1545 ± 3	6.0 ± 2.5	[1] VLADIMIRSK...	08	$40\ \pi^- p \to K^0_S K^0_S n + m\pi^0$

[1] Supersedes VLADIMIRSKII 00.

$X(1575)$ $I^G(J^{PC}) = ?^?(1^{--})$

MASS (MeV)	WIDTH (MeV)	DOCUMENT ID		TECN	COMMENT
$1576^{+49}_{-55}{}^{+98}_{-91}$	$818^{+22}_{-23}{}^{+64}_{-133}$	[1] ABLIKIM	06S	BES	$J/\psi \to K^+K^-\pi^0$

[1] A broad peak observed at K^+K^- invariant mass. Mass and width above are its pole position. The observed branching ratio is $B(J/\psi \to X\pi^0)\ B(X \to K^+K^-) = (8.5 \pm 0.6^{+2.7}_{-3.6}) \times 10^{-4}$.

$X(1600)$ $I^G(J^{PC}) = 2^+(2^{++})$

MASS (MeV)	WIDTH (MeV)	DOCUMENT ID		TECN	COMMENT
1600 ± 100	400 ± 200	[1] ALBRECHT	91F	ARG	$10.2\ e^+e^- \to e^+e^-2(\pi^+\pi^-)$

[1] Our estimate.

$X(1650)$ $I^G(J^{PC}) = 0^-(?^{?-})$

MASS (MeV)	WIDTH (MeV)	EVTS	DOCUMENT ID		TECN	COMMENT
1652 ± 7	<50	100	PROKOSHKIN	96	GAM2	$32,38\ \pi p \to \omega\eta n$

$X(1730)$ $I^G(J^{PC}) = ?^?(?^{?+})$

MASS (MeV)	WIDTH (MeV)	EVTS	DOCUMENT ID		TECN	COMMENT
$1731.0\pm1.2\pm2.0$	$3.2\pm0.8\pm1.3$	58	VLADIMIRSK...	07	SPEC	$40\ \pi^- p \to K^0_S K^0_S X$

$f_2(1750)$ $I^G(J^{PC}) = 0^+(2^{++})$

MASS (MeV)	WIDTH (MeV)	EVTS	DOCUMENT ID		TECN	COMMENT
1755 ± 10	67 ± 12	870	[1] SCHEGELSKY	06A	RVUE	$\gamma\gamma \to K^0_S K^0_S$

$\Gamma(K\overline{K})$

VALUE (MeV)	EVTS	DOCUMENT ID		TECN	COMMENT
17 ± 5	870	[2] SCHEGELSKY	06A	RVUE	$\gamma\gamma \to K^0_S K^0_S$

$\Gamma(\gamma\gamma)$

VALUE (keV)	EVTS	DOCUMENT ID		TECN	COMMENT
0.13 ± 0.04	870	[2] SCHEGELSKY	06A	RVUE	$\gamma\gamma \to K^0_S K^0_S$

$\Gamma(\pi\pi)$

VALUE (MeV)	EVTS	DOCUMENT ID		TECN	COMMENT
1.3 ± 1.0	870	[2] SCHEGELSKY	06A	RVUE	$\gamma\gamma \to K^0_S K^0_S$

$\Gamma(\eta\eta)$

VALUE (MeV)	EVTS	DOCUMENT ID		TECN	COMMENT
2.0 ± 0.5	870	[2] SCHEGELSKY	06A	RVUE	$\gamma\gamma \to K^0_S K^0_S$

[1] From analysis of L3 data at 91 and 183–209 GeV.
[2] From analysis of L3 data at 91 and 183–209 GeV and using SU(3) relations.

$X(1775)$ $I^G(J^{PC}) = 1^-(?^{-+})$

MASS (MeV)	WIDTH (MeV)	DOCUMENT ID		TECN	COMMENT
1763 ± 20	192 ± 60	CONDO	91	SHF	$\gamma p \to (p\pi^+)(\pi^+\pi^-\pi^-)$
1787 ± 18	118 ± 60	CONDO	91	SHF	$\gamma p \to n\pi^+\pi^+\pi^-$

$X(1850 - 3100)$ $I^G(J^{PC}) = ?^?(1^{--})$

$\Gamma(e^+e^-)B(X \to hadrons)$ (eV)	CL%	DOCUMENT ID		TECN	COMMENT
<120	90	[1] ANASHIN	11	KEDR	$e^+e^- \to$ hadrons

[1] This limit is center-of-mass energy dependent. We quote the most stringent one.

$X(1855)$ $I^G(J^{PC}) = ?^?(?^{??})$

MASS (MeV)	WIDTH (MeV)	DOCUMENT ID		TECN	COMMENT
1856.6 ± 5	20 ± 5	BRIDGES	86D	SPEC	0. $\overline{p}d \to \pi\pi N$

$X(1870)$ $I^G(J^{PC}) = ?^?(2^{??})$

MASS (MeV)	WIDTH (MeV)	DOCUMENT ID		TECN	COMMENT
1870 ± 40	250 ± 30	ALDE	86D	GAM4	$100\ \pi^- p \to 2\eta X$

$a_3(1875)$ $I^G(J^{PC}) = 1^-(3^{++})$

MASS (MeV)	WIDTH (MeV)	DOCUMENT ID		TECN	COMMENT
$1874\pm43\pm96$	$385\pm121\pm114$	CHUNG	02	B852	$18.3\ \pi^- p \to \pi^+\pi^-\pi^- p$

$B(a_3(1875) \to f_2(1270)\pi)/B(a_3(1875) \to \rho\pi)$

VALUE	DOCUMENT ID		TECN	COMMENT
0.8 ± 0.2	[1] CHUNG	02	B852	$18.3\ \pi^- p \to \pi^+\pi^-\pi^- p$

[1] Using the observable fractions of 50.0% $\rho\pi$, 56.5% $f_2\pi$, and 11.8% $\rho_3\pi$.

$B(a_3(1875) \to \rho_3(1690)\pi)/B(a_3(1875) \to \rho\pi)$

VALUE	DOCUMENT ID		TECN	COMMENT
0.9 ± 0.3	[1] CHUNG	02	B852	$18.3\ \pi^- p \to \pi^+\pi^-\pi^- p$

[1] Using the observable fractions of 50.0% $\rho\pi$, 56.5% $f_2\pi$, and 11.8% $\rho_3\pi$.

Int. J. Mod. Phys. A 2026.41. Downloaded from www.worldscientific.com
by UNIVERSITY OF CALIFORNIA @ BERKELEY on 09/16/26. Re-use and distribution is strictly not permitted, except for Open Access articles.

$h_1(1900)$ $I^G(J^{PC}) = 0^-(1^{+-})$

MASS (MeV)	WIDTH (MeV)	DOCUMENT ID	TECN	COMMENT
$1908 \pm 6^{+8}_{-4}$	$175 \pm 13^{+7}_{-16}$	ABLIKIM	24CB BES3	$J/\psi \to \phi\eta\pi^0$

$a_1(1930)$ $I^G(J^{PC}) = 1^-(1^{++})$

MASS (MeV)	WIDTH (MeV)	DOCUMENT ID	TECN	COMMENT
1930^{+30}_{-70}	155 ± 45	ANISOVICH 01F	SPEC	2.0 $\overline{p}p \to 3\pi^0, \pi^0\eta, \pi^0\eta'$

$X(1935)$ $I^G(J^{PC}) = 1^+(1^{-?})$

MASS (MeV)	WIDTH (MeV)	DOCUMENT ID	TECN	COMMENT
1935 ± 20	215 ± 30	EVANGELIS... 79	OMEG	10,16 $\pi^- p \to \overline{p}pn$

$\rho_2(1940)$ $I^G(J^{PC}) = 1^+(2^{--})$

MASS (MeV)	WIDTH (MeV)	DOCUMENT ID	TECN	COMMENT
1940 ± 40	155 ± 40	[1] ANISOVICH 02	SPEC	0.6–1.9 $p\overline{p} \to \omega\pi^0, \omega\eta\pi^0, \pi^+\pi^-$

[1] From the combined analysis of ANISOVICH 00J, ANISOVICH 01D, ANISOVICH 01E, and ANISOVICH 02.

$\omega_3(1945)$ $I^G(J^{PC}) = 0^-(3^{--})$

MASS (MeV)	WIDTH (MeV)	DOCUMENT ID	TECN	COMMENT
1945 ± 20	115 ± 22	[1] ANISOVICH 02B	SPEC	0.6–1.9 $p\overline{p} \to \omega\eta, \omega\pi^0\pi^0$

[1] From the combined analysis of ANISOVICH 00D, ANISOVICH 01C, and ANISOVICH 02B.

$a_2(1950)$ $I^G(J^{PC}) = 1^-(2^{++})$

MASS (MeV)	WIDTH (MeV)	DOCUMENT ID	TECN	COMMENT
1950^{+30}_{-70}	180^{+30}_{-70}	[1] ANISOVICH 01F	SPEC	1.96–2.41 $\overline{p}p$

[1] From the combined analysis of ANISOVICH 99C, ANISOVICH 99E, and ANISOVICH 01F.

$\omega(1960)$ $I^G(J^{PC}) = 0^-(1^{--})$

MASS (MeV)	WIDTH (MeV)	DOCUMENT ID	TECN	COMMENT
1960 ± 25	195 ± 60	[1] ANISOVICH 02B	SPEC	0.6–1.9 $p\overline{p} \to \omega\eta, \omega\pi^0\pi^0$

[1] From the combined analysis of ANISOVICH 00D, ANISOVICH 01C, and ANISOVICH 02B.

$b_1(1960)$ $I^G(J^{PC}) = 1^+(1^{+-})$

MASS (MeV)	WIDTH (MeV)	DOCUMENT ID	TECN	COMMENT
1960 ± 35	230 ± 50	[1] ANISOVICH 02	SPEC	0.6–1.9 $p\overline{p} \to \omega\pi^0, \omega\eta\pi^0, \pi^+\pi^-$

[1] From the combined analysis of ANISOVICH 00J, ANISOVICH 01D, ANISOVICH 01E, and ANISOVICH 02.

$h_1(1965)$ $I^G(J^{PC}) = 0^-(1^{+-})$

MASS (MeV)	WIDTH (MeV)	DOCUMENT ID	TECN	COMMENT
1965 ± 45	345 ± 75	[1] ANISOVICH 02B	SPEC	0.6–1.9 $p\overline{p} \to \omega\eta, \omega\pi^0\pi^0$

[1] From the combined analysis of ANISOVICH 00D, ANISOVICH 01C, and ANISOVICH 02B.

$f_1(1970)$ $I^G(J^{PC}) = 0^+(1^{++})$

MASS (MeV)	WIDTH (MeV)	DOCUMENT ID	TECN
1971 ± 15	240 ± 45	ANISOVICH 00J	SPEC

$X(1970)$ $I^G(J^{PC}) = ?^?(?^{??})$

MASS (MeV)	WIDTH (MeV)	DOCUMENT ID	TECN	COMMENT
1970 ± 10	40 ± 20	CHLIAPNIK... 80	HBC	32 $K^+p \to 2K^0_S 2\pi X$

$X(1975)$ $I^G(J^{PC}) = ?^?(?^{??})$

MASS (MeV)	WIDTH (MeV)	EVTS	DOCUMENT ID	TECN	COMMENT
1973 ± 15	80	30	CASO 70	HBC	11.2 $\pi^- p \to \rho 2\pi$

$\omega_2(1975)$ $I^G(J^{PC}) = 0^-(2^{--})$

MASS (MeV)	WIDTH (MeV)	DOCUMENT ID	TECN	COMMENT
1975 ± 20	175 ± 25	[1] ANISOVICH 02B	SPEC	0.6–1.9 $p\overline{p} \to \omega\eta, \omega\pi^0\pi^0$

[1] From the combined analysis of ANISOVICH 00D, ANISOVICH 01C, and ANISOVICH 02B.

$a_2(1990)$ $I^G(J^{PC}) = 1^-(2^{++})$

MASS (MeV)	WIDTH (MeV)	EVTS	DOCUMENT ID	TECN	COMMENT
$2050 \pm 10 \pm 40$	$190 \pm 22 \pm 100$	18k	[1] SCHEGELSKY 06	RVUE	$\gamma\gamma \to \pi^+\pi^-\pi^0$
$2003 \pm 10 \pm 19$	$249 \pm 23 \pm 32$		LU 05	B852	18 $\pi^- p \to \omega\pi^-\pi^0 p$

[1] From analysis of L3 data at 183–209 GeV.

$\Gamma(\gamma\gamma)\ \Gamma(\pi^+\pi^-\pi^0)\ /\ \Gamma(\text{total})$

VALUE (keV)	EVTS	DOCUMENT ID	TECN	COMMENT
$0.11 \pm 0.04 \pm 0.05$	18k	[1] SCHEGELSKY 06	RVUE	$\gamma\gamma \to \pi^+\pi^-\pi^0$

[1] From analysis of L3 data at 183–209 GeV.

$\rho(2000)$ $I^G(J^{PC}) = 1^+(1^{--})$

MASS (MeV)	WIDTH (MeV)	DOCUMENT ID	TECN	COMMENT
2000 ± 30	260 ± 45	[1] BUGG 04C	RVUE	Compilation
~ 1988	~ 244	HASAN 94	RVUE	$\overline{p}p \to \pi\pi$

[1] From the combined analysis of ANISOVICH 00J, ANISOVICH 01D, ANISOVICH 01E, and ANISOVICH 02.

$f_2(2000)$ $I^G(J^{PC}) = 0^+(2^{++})$

MASS (MeV)	WIDTH (MeV)	DOCUMENT ID	TECN	COMMENT
2001 ± 10	312 ± 32	ANISOVICH 00J	SPEC	
~ 1996	~ 134	HASAN 94	RVUE	$\overline{p}p \to \pi\pi$

$X(2000)$ $I^G(J^{PC}) = 1^-(?^{?+})$

MASS (MeV)	WIDTH (MeV)	DOCUMENT ID	TECN	CHG	COMMENT
1964 ± 35	225 ± 50	[1] ARMSTRONG 93D	E760		$\overline{p}p \to 3\pi^0 \to 6\gamma$
~ 2100	~ 500	[1] ANTIPOV 77	CIBS	$-$	25 $\pi^- p \to p\pi^-\rho_3$
2214 ± 15	355 ± 21	[2] BALTAY 77	HBC	0	15 $\pi^- p \to \Delta^{++}3\pi$
2080 ± 40	340 ± 80	KALELKAR 75	HBC	$+$	15 $\pi^+ p \to p\pi^+\rho_3$

[1] Cannot determine spin to be 3.
[2] BALTAY 77 favors $J^P = ,3^+$.

$X(2000)$ $I^G(J^{PC}) = ?^?(4^{++})$

MASS (MeV)	WIDTH (MeV)	DOCUMENT ID	TECN	COMMENT
$1998 \pm 3 \pm 5$	<15	VLADIMIRSK...03	SPEC	$\pi^- p \to K^0_S K^0_S MM$

$X(2000)$ $I^G(J^{PC}) = 0^-(1^{--})$

MASS (MeV)	WIDTH (MeV)	DOCUMENT ID	TECN	COMMENT
$1992 \pm 12^{+15}_{-6}$	$132 \pm 22^{+17}_{-4}$	ABLIKIM	24CB BES3	$J/\psi \to \phi\eta\pi^0$

$\eta(2010)$ $I^G(J^{PC}) = 0^+(0^{-+})$

MASS (MeV)	WIDTH (MeV)	DOCUMENT ID	TECN
2010^{+35}_{-60}	270 ± 60	ANISOVICH 00J	SPEC

$\pi_1(2015)$ $I^G(J^{PC}) = 1^-(1^{-+})$

MASS (MeV)	WIDTH (MeV)	EVTS	DOCUMENT ID	TECN	COMMENT
$2014 \pm 20 \pm 16$	$230 \pm 32 \pm 73$	145k	LU 05	B852	18 $\pi^- p \to \omega\pi^-\pi^0 p$
$2001 \pm 30 \pm 92$	$333 \pm 52 \pm 49$	69k	KUHN 04	B852	18 $\pi^- p \to \eta\pi^+\pi^-\pi^- p$

$a_0(2020)$ $I^G(J^{PC}) = 1^-(0^{++})$

MASS (MeV)	WIDTH (MeV)	DOCUMENT ID	TECN
2025 ± 30	330 ± 75	ANISOVICH 99C	SPEC

$X(2020)$ $I^G(J^{PC}) = ?^?(?^{??})$

MASS (MeV)	WIDTH (MeV)	DOCUMENT ID	TECN	COMMENT
2015 ± 3	10 ± 4	FERRER 99	RVUE	$\pi p \to pp\overline{p}\pi(\pi)$

$h_3(2025)$ $I^G(J^{PC}) = 0^-(3^{+-})$

MASS (MeV)	WIDTH (MeV)	DOCUMENT ID	TECN	COMMENT
2025 ± 20	145 ± 30	[1] ANISOVICH 02B	SPEC	0.6–1.9 $p\overline{p} \to \omega\eta, \omega\pi^0\pi^0$

[1] From the combined analysis of ANISOVICH 00D, ANISOVICH 01C, and ANISOVICH 02B.

$b_3(2030)$ $I^G(J^{PC}) = 1^+(3^{+-})$

MASS (MeV)	WIDTH (MeV)	DOCUMENT ID	TECN	COMMENT
2032 ± 12	117 ± 11	[1] ANISOVICH 02	SPEC	0.6–1.9 $p\overline{p} \to \omega\pi^0, \omega\eta\pi^0, \pi^+\pi^-$

[1] From the combined analysis of ANISOVICH 00J, ANISOVICH 01D, ANISOVICH 01E, and ANISOVICH 02.

$a_2(2030)$ $I^G(J^{PC}) = 1^-(2^{++})$

MASS (MeV)	WIDTH (MeV)	DOCUMENT ID	TECN	COMMENT
2030 ± 20	205 ± 30	[1] ANISOVICH 01F	SPEC	1.96–2.41 $\overline{p}p$

[1] From the combined analysis of ANISOVICH 99C, ANISOVICH 99E, and ANISOVICH 01F.

$a_3(2030)$ $I^G(J^{PC}) = 1^-(3^{++})$

MASS (MeV)	WIDTH (MeV)	DOCUMENT ID	TECN	COMMENT
2031 ± 12	150 ± 18	[1] ANISOVICH 01F	SPEC	1.96–2.41 $\overline{p}p$

[1] From the combined analysis of ANISOVICH 99C, ANISOVICH 99E, and ANISOVICH 01F.

$\eta_2(2030)$ $I^G(J^{PC}) = 0^+(2^{-+})$

MASS (MeV)	WIDTH (MeV)	DOCUMENT ID		TECN
$2030 \pm 5 \pm 15$	$205 \pm 10 \pm 15$	ANISOVICH	00E	SPEC

$B(a_2\pi)_{L=0}/B(a_2\pi)_{L=2}$

VALUE	DOCUMENT ID		TECN	COMMENT
0.05 ± 0.03	[1] ANISOVICH	11	SPEC	0.9–1.94 $p\overline{p}$

[1] Reanalysis of ADOMEIT 96 and ANISOVICH 00E.

$B(a_0\pi)/B(a_2\pi)_{L=2}$

VALUE	DOCUMENT ID		TECN	COMMENT
0.10 ± 0.08	[1] ANISOVICH	11	SPEC	0.9–1.94 $p\overline{p}$

[1] Reanalysis of ADOMEIT 96 and ANISOVICH 00E.

$B(f_2\eta)/B(a_2\pi)_{L=2}$

VALUE	DOCUMENT ID		TECN	COMMENT
0.13 ± 0.06	[1] ANISOVICH	11	SPEC	0.9–1.94 $p\overline{p}$

[1] Reanalysis of ADOMEIT 96 and ANISOVICH 00E.

$f_3(2050)$ $I^G(J^{PC}) = 0^+(3^{++})$

MASS (MeV)	WIDTH (MeV)	DOCUMENT ID		TECN	COMMENT
2048 ± 8	213 ± 34	ANISOVICH	00J	SPEC	2.0 $p\overline{p} \to \eta\pi^0\pi^0$

$f_0(2060)$ $I^G(J^{PC}) = 0^+(0^{++})$

MASS (MeV)	WIDTH (MeV)	DOCUMENT ID		TECN	COMMENT
~ 2050	~ 120	[1] OAKDEN	94	RVUE	0.36–1.55 $\overline{p}p \to \pi\pi$
~ 2060	~ 50	[1] OAKDEN	94	RVUE	0.36–1.55 $\overline{p}p \to \pi\pi$

[1] See SEMENOV 99 and KLOET 96.

$\pi(2070)$ $I^G(J^{PC}) = 1^-(0^{-+})$

MASS (MeV)	WIDTH (MeV)	DOCUMENT ID		TECN	COMMENT
2070 ± 35	310^{+100}_{-50}	ANISOVICH	01F	SPEC	2.0 $\overline{p}p \to 3\pi^0, \pi^0\eta, \pi^0\eta'$

$X(2080)$ $I^G(J^{PC}) = ?^?(?^{??})$

MASS (MeV)	WIDTH (MeV)	DOCUMENT ID		TECN	COMMENT
2080 ± 10	110 ± 20	KREYMER	80	STRC	13 $\pi^- d \to p\overline{p}n(n_s)$

$X(2080)$ $I^G(J^{PC}) = ?^?(3^{-?})$

MASS (MeV)	WIDTH (MeV)	DOCUMENT ID		TECN	COMMENT
2080 ± 10	190 ± 15	ROZANSKA	80	SPRK	18 $\pi^- p \to p\overline{p}n$

$K_1(2085)$ $I^G(J^{PC}) = ?^?(1^{+?})$

MASS (MeV)	WIDTH (MeV)	DOCUMENT ID		TECN	COMMENT
$2084^{+4}_{-2} \pm 9$	$58^{+4}_{-3} \pm 25$	[1,2] ABLIKIM	23BG	BES3	$e^+e^- \to pK^-\overline{\Lambda}$
$2075 \pm 12 \pm 5$	$90 \pm 35 \pm 9$	[3] ABLIKIM	04J	BES2	$J/\psi \to K^-p\overline{\Lambda}$

[1] The reported mass and width are the pole positions in the complex (M, Γ) plane.
[2] Signal observed with a statistical significance $>20\sigma$ comes from 3883 candidate events. Spin parity determined to be $J^P = 1^+$ with a statistical significance $>5\sigma$ over 0^-, 1^-, 2^+ hypotheses, and in the range within 3.1–7.5 σ with respect to 2^-.
[3] From a fit in the region $M_{p\overline{\Lambda}} - M_p - M_\Lambda < 150$ MeV. S-wave in the $p\overline{\Lambda}$ system preferred. A similar near-threshold enhancement in the $p\overline{\Lambda}$ system is observed in $B^+ \to p\overline{\Lambda}D^0$ by CHEN 11F.

$a_1(2095)$ $I^G(J^{PC}) = 1^-(1^{++})$

MASS (MeV)	WIDTH (MeV)	EVTS	DOCUMENT ID		TECN	COMMENT
$2096 \pm 17 \pm 121$	$451 \pm 41 \pm 81$	69k	KUHN	04	B852	18 $\pi^- p \to \eta\pi^+\pi^-\pi^- p$

$B(a_1(2095) \to f_1(1285)\pi)$ / $B(a_1(2095) \to a_1(1260))$

VALUE	EVTS	DOCUMENT ID		TECN	COMMENT
3.18 ± 0.64	69k	KUHN	04	B852	18 $\pi^- p \to \eta\pi^+\pi^-\pi^- p$

$\eta(2100)$ $I^G(J^{PC}) = 0^+(0^{-+})$

MASS (MeV)	WIDTH (MeV)	EVTS	DOCUMENT ID		TECN	COMMENT
$2050^{+30}_{-24} \pm 75^{+26}_{-30} \pm 164$			[1] ABLIKIM	16N	BES3	$J/\psi \to \gamma K^+K^-K^+K^-$
2103 ± 50	187 ± 75	586	[2] BISELLO	89B	DM2	$J/\psi \to 4\pi\gamma$

[1] From a partial wave analysis of $J/\psi \to \gamma\phi\phi$, for which the primary signal is $\eta(2225) \to \phi\phi$, and that also finds significant signals for for 0^{-+} phase space, $f_0(2100)$, $f_2(2010)$, $f_2(2300)$, $f_2(2340)$, and a previously unseen 0^{-+} state $X(2500)$ ($M = 2470^{+15}_{-19} \pm 101^{+101}_{-23}$ MeV, $\Gamma = 230^{+64}_{-35} \pm 56^{+56}_{-33}$ MeV).
[2] ASTON 81B sees no peak, has 850 events in Ajinenko+Barth bins. ARESTOV 80 sees no peak.

$X(2100)$ $I^G(J^{PC}) = ?^?(0^{??})$

MASS (MeV)	WIDTH (MeV)	DOCUMENT ID		TECN	COMMENT
2100 ± 40	250 ± 40	ALDE	86D	GAM4	100 $\pi^- p \to 2\eta X$

$X(2110)$ $I^G(J^{PC}) = 1^+(3^{-?})$

MASS (MeV)	WIDTH (MeV)	DOCUMENT ID		TECN	COMMENT
2110 ± 10	330 ± 20	EVANGELIS...	79	OMEG	10,16 $\pi^- p \to \overline{p}pn$

$X(2120)$ $I^G(J^{PC}) = ?^?(0^{??})$

MASS (MeV)	WIDTH (MeV)	EVTS	DOCUMENT ID		TECN	COMMENT
$2122.4 \pm 6.7^{+4.7}_{-2.7}$	$83 \pm 16^{+31}_{-11}$	647	ABLIKIM	11C	BES3	$J/\psi \to \gamma\pi^+\pi^-\eta'$

$\omega(2120)$ or **$\phi(2120)$** $I^G(J^{PC}) = 0^-(?^{--})$

MASS (MeV)	WIDTH (MeV)	DOCUMENT ID		TECN	COMMENT
$2119 \pm 11 \pm 15$	$69 \pm 30 \pm 5$	[1] ABLIKIM	24AA	BES3	$e^+e^- \to \pi^+\pi^-\pi^0$

[1] From a fit with more than 5σ to the Born cross section line shapes of $e^+e^- \to \rho\pi$ and $e^+e^- \to \rho(1450)\pi$.

$f_2(2140)$ $I^G(J^{PC}) = 0^+(2^{++})$

MASS (MeV)	WIDTH (MeV)	EVTS	DOCUMENT ID		TECN	COMMENT
2141 ± 12	49 ± 28	389	GREEN	86	MPSF	400 $pA \to 4KX$

$X(2150)$ $I^G(J^{PC}) = ?^?(2^{+?})$

MASS (MeV)	WIDTH (MeV)	DOCUMENT ID		TECN	COMMENT
2150 ± 10	260 ± 10	ROZANSKA	80	SPRK	18 $\pi^- p \to p\overline{p}n$

$a_2(2175)$ $I^G(J^{PC}) = 1^-(2^{++})$

MASS (MeV)	WIDTH (MeV)	DOCUMENT ID		TECN	COMMENT
2175 ± 40	310^{+90}_{-45}	ANISOVICH	01F	SPEC	2.0 $\overline{p}p \to 3\pi^0, \pi^0\eta, \pi^0\eta'$

$\eta(2190)$ $I^G(J^{PC}) = 0^+(0^{-+})$

MASS (MeV)	WIDTH (MeV)	DOCUMENT ID		TECN
2190 ± 50	850 ± 100	BUGG	99	BES

$\omega_2(2195)$ $I^G(J^{PC}) = 0^-(2^{--})$

MASS (MeV)	WIDTH (MeV)	DOCUMENT ID		TECN	COMMENT
2195 ± 30	225 ± 40	[1] ANISOVICH	02B	SPEC	0.6–1.9 $p\overline{p} \to \omega\eta, \omega\pi^0\pi^0$

[1] From the combined analysis of ANISOVICH 00D, ANISOVICH 01C, and ANISOVICH 02B.

$X(2210)$ $I^G(J^{PC}) = ?^?(?^{??})$

MASS (MeV)	WIDTH (MeV)	DOCUMENT ID		TECN	COMMENT
2210^{+79}_{-21}	203^{+437}_{-87}	EVANGELIS...	79B	OMEG	10 $\pi^- p \to K^+K^-n$
2207 ± 22	130	CASO	70	HBC	11.2 $\pi^- p$

$X_2(2210)$ $I^G(J^{PC}) = 0^+(2^{++})$

MASS (MeV)	WIDTH (MeV)	DOCUMENT ID		TECN	COMMENT
2210 ± 60	360 ± 120	[1] KLEMPT	22	RVUE	$J/\psi \to \gamma\pi^0\pi^0$, $\gamma K^0_S K^0_S$

[1] Fit of the tensor partial waves from BES3 in the multipole basis. Might be a cluster of $J^{PC} = 2^{++}$ resonances. The ratio of decay widths $KK^-/\pi\pi$ is 0.23 ± 0.05.

$h_1(2215)$ $I^G(J^{PC}) = 0^-(1^{+-})$

MASS (MeV)	WIDTH (MeV)	DOCUMENT ID		TECN	COMMENT
2215 ± 40	325 ± 55	[1] ANISOVICH	02B	SPEC	0.6–1.9 $p\overline{p} \to \omega\eta, \omega\pi^0\pi^0$

[1] From the combined analysis of ANISOVICH 00D, ANISOVICH 01C, and ANISOVICH 02B.

$\rho_2(2225)$ $I^G(J^{PC}) = 1^+(2^{--})$

MASS (MeV)	WIDTH (MeV)	DOCUMENT ID		TECN	COMMENT
2225 ± 35	335^{+100}_{-50}	[1] ANISOVICH	02	SPEC	0.6–1.9 $p\overline{p} \to \omega\pi^0$, $\omega\eta\pi^0$, $\pi^+\pi^-$

[1] From the combined analysis of ANISOVICH 00J, ANISOVICH 01D, ANISOVICH 01E, and ANISOVICH 02.

$\rho_4(2230)$ $I^G(J^{PC}) = 1^+(4^{--})$

MASS (MeV)	WIDTH (MeV)	DOCUMENT ID		TECN	COMMENT
2230 ± 25	210 ± 30	[1] ANISOVICH	02	SPEC	0.6–1.9 $p\overline{p} \to \omega\pi^0$, $\omega\eta\pi^0$, $\pi^+\pi^-$

Int. J. Mod. Phys. A 2026.41. Downloaded from www.worldscientific.com by LIFORNIA @ BERKELEY on 09/16/26. Re-use and distribution is strictly not permitted, except for Open Access articles.

Int. J. Mod. Phys. A 2026.41. Downloaded from www.worldscientific.com
by UNIVERSITY OF CALIFORNIA @ BERKELEY on 09/16/26. Re-use and distribution is strictly not permitted, except for Open Access articles.

[1] From the combined analysis of ANISOVICH 00J, ANISOVICH 01D, ANISOVICH 01E, and ANISOVICH 02.

$b_1(2240)$ $I^G(J^{PC}) = 1^+(1^{+-})$

MASS (MeV)	WIDTH (MeV)	DOCUMENT ID		TECN	COMMENT
2240 ± 35	320 ± 85	[1] ANISOVICH	02	SPEC	0.6–1.9 $p\overline{p} \to \omega\pi^0$, $\omega\eta\pi^0$, $\pi^+\pi^-$

[1] From the combined analysis of ANISOVICH 00J, ANISOVICH 01D, ANISOVICH 01E, and ANISOVICH 02.

$f_2(2240)$ $I^G(J^{PC}) = 0^+(2^{++})$

MASS (MeV)	WIDTH (MeV)	DOCUMENT ID		TECN	COMMENT
2240 ± 15	241 ± 30	[1] ANISOVICH	00J	SPEC	1.92–2.41 $p\overline{p}$
• • • We do not use the following data for averages, fits, limits, etc. • • •					
∼ 2226	∼ 226	HASAN	94	RVUE	$p\overline{p} \to \pi\pi$

[1] From the combined analysis of ANISOVICH 99C, ANISOVICH 99F, ANISOVICH 99J, ANISOVICH 99K, and ANISOVICH 00B. See also ANISOVICH 12.

$b_3(2245)$ $I^G(J^{PC}) = 1^+(3^{+-})$

MASS (MeV)	WIDTH (MeV)	DOCUMENT ID		TECN
2245 ± 50	320 ± 70	[1] BUGG	04C	RVUE

[1] From the combined analysis of ANISOVICH 00J, ANISOVICH 01D, ANISOVICH 01E, and ANISOVICH 02.

$\eta_2(2250)$ $I^G(J^{PC}) = 0^+(2^{-+})$

MASS (MeV)	WIDTH (MeV)	DOCUMENT ID		TECN
2248 ± 20	280 ± 20	ANISOVICH	00I	SPEC
2267 ± 14	290 ± 50	ANISOVICH	00J	SPEC

$\pi_4(2250)$ $I^G(J^{PC}) = 1^-(4^{-+})$

MASS (MeV)	WIDTH (MeV)	DOCUMENT ID		TECN	COMMENT
2250 ± 15	215 ± 25	ANISOVICH	01F	SPEC	2.0 $\overline{p}p \to 3\pi^0$, $\pi^0\eta$, $\pi^0\eta'$

$\omega_4(2250)$ $I^G(J^{PC}) = 0^-(4^{--})$

MASS (MeV)	WIDTH (MeV)	DOCUMENT ID		TECN	COMMENT
2250 ± 30	150 ± 50	[1] ANISOVICH	02B	SPEC	0.6–1.9 $p\overline{p} \to \omega\eta$, $\omega\pi^0\pi^0$

[1] From the combined analysis of ANISOVICH 00D, ANISOVICH 01C, and ANISOVICH 02B.

$\omega_5(2250)$ $I^G(J^{PC}) = 0^-(5^{--})$

MASS (MeV)	WIDTH (MeV)	DOCUMENT ID		TECN
2250 ± 70	320 ± 95	[1] BUGG	04	RVUE

[1] From the combined analysis of ANISOVICH 00D, ANISOVICH 01C, and ANISOVICH 02B.

$\omega_3(2255)$ $I^G(J^{PC}) = 0^-(3^{--})$

MASS (MeV)	WIDTH (MeV)	DOCUMENT ID		TECN	COMMENT
2255 ± 15	175 ± 30	[1] ANISOVICH	02B	SPEC	0.6–1.9 $p\overline{p} \to \omega\eta$, $\omega\pi^0\pi^0$

[1] From the combined analysis of ANISOVICH 00D, ANISOVICH 01C, and ANISOVICH 02B.

$a_4(2255)$ $I^G(J^{PC}) = 1^-(4^{++})$

MASS (MeV)	WIDTH (MeV)	DOCUMENT ID		TECN	COMMENT
2237 ± 5	291 ± 12	UMAN	06	E835	5.2 $\overline{p}p \to \eta\eta\pi^0$
2255 ± 40	330^{+110}_{-50}	[1] ANISOVICH	01F	SPEC	1.96–2.41 $\overline{p}p$

[1] From the combined analysis of ANISOVICH 99C, ANISOVICH 99E, and ANISOVICH 01F.

$a_2(2255)$ $I^G(J^{PC}) = 1^-(2^{++})$

MASS (MeV)	WIDTH (MeV)	DOCUMENT ID		TECN	COMMENT
2255 ± 20	230 ± 15	[1] ANISOVICH	01G	SPEC	1.96–2.41 $\overline{p}p$

[1] From the combined analysis of ANISOVICH 99C, ANISOVICH 99E, ANISOVICH 01F, and ANISOVICH 01G.

$X(2260)$ $I^G(J^{PC}) = 0^+(4^{+?})$

MASS (MeV)	WIDTH (MeV)	DOCUMENT ID		TECN	COMMENT
2260 ± 20	400 ± 100	EVANGELIS...	79	OMEG	10,16 $\pi^-p \to \overline{p}pn$

$\rho(2270)$ $I^G(J^{PC}) = 1^+(1^{--})$

MASS (MeV)	WIDTH (MeV)	DOCUMENT ID		TECN	COMMENT
2265 ± 40	325 ± 80	[1] ANISOVICH	02	SPEC	0.6–1.9 $p\overline{p} \to \omega\pi^0$, $\omega\eta\pi^0$, $\pi^+\pi^-$
2280 ± 50	440 ± 110	ATKINSON	85	OMEG	20–70 $\gamma p \to p\omega\pi^+\pi^-\pi^0$

[1] From the combined analysis of ANISOVICH 00J, ANISOVICH 01D, ANISOVICH 01E, and ANISOVICH 02.

$a_1(2270)$ $I^G(J^{PC}) = 1^-(1^{++})$

MASS (MeV)	WIDTH (MeV)	DOCUMENT ID		TECN	COMMENT
2270^{+55}_{-40}	305^{+70}_{-40}	ANISOVICH	01F	SPEC	2.0 $\overline{p}p \to 3\pi^0$, $\pi^0\eta$, $\pi^0\eta'$

$h_3(2275)$ $I^G(J^{PC}) = 0^-(3^{+-})$

MASS (MeV)	WIDTH (MeV)	DOCUMENT ID		TECN	COMMENT
2275 ± 25	190 ± 45	[1] ANISOVICH	02B	SPEC	0.6–1.9 $p\overline{p} \to \omega\eta$, $\omega\pi^0\pi^0$

[1] From the combined analysis of ANISOVICH 00D, ANISOVICH 01C, and ANISOVICH 02B.

$a_3(2275)$ $I^G(J^{PC}) = 1^-(3^{++})$

MASS (MeV)	WIDTH (MeV)	DOCUMENT ID		TECN	COMMENT
2275 ± 35	350^{+100}_{-50}	[1] ANISOVICH	01G	SPEC	1.96–2.41 $\overline{p}p$

[1] From the combined analysis of ANISOVICH 99C, ANISOVICH 99E, ANISOVICH 01F, and ANISOVICH 01G.

$\pi_2(2285)$ $I^G(J^{PC}) = 1^-(2^{-+})$

MASS (MeV)	WIDTH (MeV)	DOCUMENT ID		TECN	COMMENT
2285 ± 20 ± 25	250 ± 20 ± 25	[1] ANISOVICH	11	SPEC	0.9–1.94 $p\overline{p}$

[1] Reanalysis of ADOMEIT 96 and ANISOVICH 00E.

$\omega_3(2285)$ $I^G(J^{PC}) = 0^-(3^{--})$

MASS (MeV)	WIDTH (MeV)	DOCUMENT ID		TECN	COMMENT
2278 ± 28	224 ± 50	[1] BUGG	04A	RVUE	
2285 ± 60	230 ± 40	[2] ANISOVICH	02B	SPEC	0.6–1.9 $p\overline{p} \to \omega\eta$, $\omega\pi^0\pi^0$

[1] Partial wave analysis of the data on $p\overline{p} \to \overline{\Lambda}\Lambda$ from BARNES 00.
[2] From the combined analysis of ANISOVICH 00D, ANISOVICH 01C, and ANISOVICH 02B.

$\omega(2290)$ $I^G(J^{PC}) = 0^-(1^{--})$

MASS (MeV)	WIDTH (MeV)	DOCUMENT ID		TECN
2290 ± 20	275 ± 35	[1] BUGG	04A	RVUE

[1] Partial wave analysis of the data on $p\overline{p} \to \overline{\Lambda}\Lambda$ from BARNES 00.

$f_2(2295)$ $I^G(J^{PC}) = 0^+(2^{++})$

MASS (MeV)	WIDTH (MeV)	DOCUMENT ID		TECN	COMMENT
2293 ± 13	216 ± 37	[1] ANISOVICH	00J	SPEC	1.92–2.41 $p\overline{p}$

[1] From the combined analysis of ANISOVICH 99C, ANISOVICH 99F, ANISOVICH 99J, ANISOVICH 99K, and ANISOVICH 00B. See also ANISOVICH 12.

$f_3(2300)$ $I^G(J^{PC}) = 0^+(3^{++})$

MASS (MeV)	WIDTH (MeV)	DOCUMENT ID		TECN
2334 ± 25	200 ± 20	[1] BUGG	04A	RVUE

[1] Partial wave analysis of the data on $p\overline{p} \to \overline{\Lambda}\Lambda$ from BARNES 00.

$h_1(2300)$ $I^G(J^{PC}) = 0^-(1^{+-})$

MASS (MeV)	WIDTH (MeV)	DOCUMENT ID		TECN
2316 ± 9 ± 30	89 ± 15 ± 26	[1] ABLIKIM	25E	BES3

[1] From a partial wave analysis of $\psi(2S) \to \phi\eta\eta'$. Reported in $\psi(2S) \to h_1(2300)\eta'$ with 9.6σ significance and in $\psi(2S) \to h_1(2300)\eta$ at 5.6σ.

$f_1(2310)$ $I^G(J^{PC}) = 0^+(1^{++})$

MASS (MeV)	WIDTH (MeV)	DOCUMENT ID		TECN
2310 ± 60	255 ± 70	ANISOVICH	00J	SPEC

$\eta(2320)$ $I^G(J^{PC}) = 0^+(0^{-+})$

MASS (MeV)	WIDTH (MeV)	DOCUMENT ID		TECN
2320 ± 15	230 ± 35	[1] ANISOVICH	00M	SPEC

[1] From the combined analysis of $\overline{p}p \to \eta\eta\eta$ from ANISOVICH 00M and $\overline{p}p \to \eta\pi^0\pi^0$ from ANISOVICH 00J.

$\eta_4(2330)$ $I^G(J^{PC}) = 0^+(4^{-+})$

MASS (MeV)	WIDTH (MeV)	DOCUMENT ID		TECN	COMMENT
2328 ± 38	240 ± 90	ANISOVICH	00J	SPEC	2.0 $p\overline{p} \to \eta\pi^0\pi^0$

$\omega(2330)$ $I^G(J^{PC}) = 0^-(1^{--})$

MASS (MeV)	WIDTH (MeV)	DOCUMENT ID		TECN	COMMENT
2330 ± 30	435 ± 75	ATKINSON	88	OMEG	25–50 $\gamma p \to \rho^\pm\rho^0\pi^\mp$

Int. J. Mod. Phys. A 2026.41. Downloaded from www.worldscientific.com by CALIFORNIA @ BERKELEY on 09/16/26. Re-use and distribution is strictly not permitted, except for Open Access articles.

$T^*_{c\bar{s}0}(2330)$ $I(J^P) = 1(0^+)$

MASS (MeV)	WIDTH (MeV)	DOCUMENT ID		TECN	COMMENT
$2327 \pm 13 \pm 13$	$96 \pm 16^{+170}_{-23}$	[1] AAIJ	24AQ	LHCB	$D_{s1}(2460)^+ \to D_s^+ \pi^+ \pi^-$

[1] From a K-matrix model analysis including $f_0(500)$ and $T^*_{c\bar{s}0}$. The $T^*_{c\bar{s}0}$ resonance is claimed by one experiment only.

$X(2340)$ $I^G(J^{PC}) = ?^?(?^{??})$

MASS (MeV)	WIDTH (MeV)	EVTS	DOCUMENT ID		TECN	COMMENT
2340 ± 20	180 ± 60	126	[1] BALTAY	75	HBC	$15\ \pi^+ p \to p 5\pi$

[1] Dominant decay into $\rho^0 \rho^0 \pi^+$. BALTAY 78 finds confirmation in $2\pi^+\pi^-2\pi^0$ events which contain $\rho^+\rho^0\pi^0$ and $2\rho^+\pi^-$.

$\pi(2360)$ $I^G(J^{PC}) = 1^-(0^{-+})$

MASS (MeV)	WIDTH (MeV)	DOCUMENT ID		TECN	COMMENT
2360 ± 25	300^{+100}_{-50}	ANISOVICH	01F	SPEC	$2.0\ \bar{p}p \to 3\pi^0, \pi^0\eta, \pi^0\eta'$

$X(2360)$ $I^G(J^{PC}) = ?^?(4^{+?})$

MASS (MeV)	WIDTH (MeV)	DOCUMENT ID		TECN	COMMENT
2360 ± 10	430 ± 30	ROZANSKA	80	SPRK	$18\ \pi^- p \to p\bar{p}n$
• • • We do not use the following data for averages, fits, limits, etc. • • •					
$2356 \pm 7 \pm 15$	$304 \pm 28 \pm 54$	[1] ABLIKIM	23AY	BES3	$e^+e^- \to (\Lambda\bar{\Lambda})\eta$

[1] Assuming $J^{PC} = 1^{--}$.

$X(2440)$ $I^G(J^{PC}) = ?^?(5^{-?})$

MASS (MeV)	WIDTH (MeV)	DOCUMENT ID		TECN	COMMENT
2440 ± 10	310 ± 20	ROZANSKA	80	SPRK	$18\ \pi^- p \to p\bar{p}n$

$a_6(2450)$ $I^G(J^{PC}) = 1^-(6^{++})$

MASS (MeV)	WIDTH (MeV)	DOCUMENT ID		TECN	COMMENT
2450 ± 130	400 ± 250	CLELAND	82B	SPEC	$50\ \pi p \to K^0_S K^\pm p$

$X(2540)$ $I^G(J^{PC}) = 0^+(0^{++})$

MASS (MeV)	WIDTH (MeV)	DOCUMENT ID		TECN	COMMENT
$2539 \pm 14^{+38}_{-14}$	$274^{+77}_{-61} \pm 163$	UEHARA	13	BELL	$\gamma\gamma \to K^0_S K^0_S$

$\Gamma(\gamma\gamma) \times B(K\overline{K})$

VALUE (eV)	DOCUMENT ID		TECN	COMMENT
$40^{+9}_{-7} \pm 40$	UEHARA	13	BELL	$\gamma\gamma \to K^0_S K^0_S$

$X(2600)$ $I^G(J^{PC}) = ?^?(?^{??})$

MASS (MeV)	WIDTH (MeV)	DOCUMENT ID		TECN	COMMENT
$2618.3 \pm 2.0^{+16.3}_{-1.4}$	$195 \pm 5^{+26}_{-17}$	ABLIKIM	22G	BES3	$J/\psi \to \gamma\pi^+\pi^-\eta'$

$B(J/\psi \to \gamma X(2600)) \times B(X(2600) \to f_0(1500)\eta') \times B(f_0(1500) \to \pi^+\pi^-)$

VALUE (units 10^{-5})	DOCUMENT ID		TECN	COMMENT
$3.09 \pm 0.21^{+1.14}_{-0.77}$	[1] ABLIKIM	22G	BES3	$J/\psi \to \gamma\pi^+\pi^-\eta'$

[1] The $\pi^+\pi^-$ mass spectrum is described by a coherent sum of two Breit-Wigner resonances, $f_0(1500)$ and a new $X(1540)$ with mass $1540.2 \pm 7.0^{+36.3}_{-6.1}$ MeV and width $157 \pm 19^{+11}_{-77}$ MeV.

$B(J/\psi \to \gamma X(2600)) \times B(X(2600) \to X(1540)\eta') \times B(X(1540) \to \pi^+\pi^-)$

VALUE (units 10^{-5})	DOCUMENT ID		TECN	COMMENT
$2.69 \pm 0.19^{+0.38}_{-1.21}$	[1] ABLIKIM	22G	BES3	$J/\psi \to \gamma\pi^+\pi^-\eta'$

[1] The $\pi^+\pi^-$ mass spectrum is described by a coherent sum of two Breit-Wigner resonances, $f_0(1500)$ and a new $X(1540)$ with mass $1540.2 \pm 7.0^{+36.3}_{-6.1}$ MeV and width $157 \pm 19^{+11}_{-77}$ MeV.

$K^*_0(2600)$ $I(J^P) = 1/2(0^+)$

MASS (MeV)	WIDTH (MeV)	DOCUMENT ID		TECN	COMMENT
$2662 \pm 59 \pm 201$	$480 \pm 47 \pm 72$	[1] AAIJ	23AH	LHCB	$B^+ \to K^+(K^0_S K\pi)$

[1] From Dalitz plot analyses of $\eta_c(1S, 2S) \to K^0_S K^+\pi^-$ + c.c..

$X(2632)$ $I^G(J^{PC}) = ?^?(?^{??})$

MASS (MeV)	WIDTH (MeV)	DOCUMENT ID		TECN	COMMENT
2635.2 ± 3.3		[1] EVDOKIMOV	04	SELX	$X(2632) \to D^+_S \eta$
2631.6 ± 2.1	< 17	[2] EVDOKIMOV	04	SELX	$X(2632) \to D^0 K^+$

[1] From a mass difference to D^+_S of 666.9 ± 3.3 MeV.
[2] From a mass difference to D^0 of 767.0 ± 2.0 MeV.

$B(X(2632) \to D^0 K^+)/B(X(2632) \to D^+_s \eta)$

VALUE	DOCUMENT ID		TECN
0.14 ± 0.06	[1] EVDOKIMOV	04	SELX

[1] Possible interpretation of this decay pattern is discussed by YASUI 07.

$X(2680)$ $I^G(J^{PC}) = ?^?(?^{??})$

MASS (MeV)	WIDTH (MeV)	DOCUMENT ID		TECN	COMMENT
2676 ± 27	150	CASO	70	HBC	$11.2\ \pi^- p \to \rho^-\pi^+\pi^- p$

$X(2710)$ $I^G(J^{PC}) = ?^?(6^{+?})$

MASS (MeV)	WIDTH (MeV)	DOCUMENT ID		TECN	COMMENT
2710 ± 20	170 ± 40	ROZANSKA	80	SPRK	$18\ \pi^- p \to p\bar{p}n$

$X(2750)$ $I^G(J^{PC}) = ?^?(7^{-?})$

MASS (MeV)	WIDTH (MeV)	DOCUMENT ID		TECN	COMMENT
2747 ± 32	195 ± 75	DENNEY	83	LASS	$10\ \pi^+ p \to K^+K^-\pi^+ p$

$f_6(3100)$ $I^G(J^{PC}) = 0^+(6^{++})$

MASS (MeV)	WIDTH (MeV)	DOCUMENT ID		TECN	COMMENT
3100 ± 100	700 ± 130	BINON	05	GAMS	$33\ \pi^- p \to \eta\eta n$

$X(3250)$ $I^G(J^{PC}) = ?^?(?^{??})$ 3-Body Decays

MASS (MeV)	WIDTH (MeV)	DOCUMENT ID		TECN	COMMENT
$3250 \pm 8 \pm 20$	45 ± 18	ALEEV	93	BIS2	$X(3250) \to \Lambda\bar{p}K^+$
$3265 \pm 7 \pm 20$	40 ± 18	ALEEV	93	BIS2	$X(3250) \to \bar{\Lambda}pK^-$

$X(3250)$ $I^G(J^{PC}) = ?^?(?^{??})$ 4-Body Decays

MASS (MeV)	WIDTH (MeV)	DOCUMENT ID		TECN	COMMENT
$3245 \pm 8 \pm 20$	25 ± 11	ALEEV	93	BIS2	$X(3250) \to \Lambda\bar{p}K^+\pi^\pm$
$3250 \pm 9 \pm 20$	50 ± 20	ALEEV	93	BIS2	$X(3250) \to \bar{\Lambda}pK^-\pi^\mp$
$3270 \pm 8 \pm 20$	25 ± 11	ALEEV	93	BIS2	$X(3250) \to K^0_S p\bar{p}K^\pm$

$X(3350)$ $I^G(J^{PC}) = ?^?(?^{??})$

MASS (MeV)	WIDTH (MeV)	EVTS	DOCUMENT ID		TECN	COMMENT
$3350^{+10}_{-20} \pm 20$	$70^{+40}_{-30} \pm 40$	50 ± 10	[1] GABYSHEV	06A	BELL	$B^- \to \Lambda_c^+\bar{p}\pi^-$

[1] A similar enhancement in the $\Lambda_c^+\bar{p}$ final state is also reported by BABAR collaboration in AUBERT 10H.

$\psi(3760)$ $I^G(J^{PC}) = ?^?(1^{--})$

MASS (MeV)	DOCUMENT ID		TECN	COMMENT
$3751.9 \pm 3.8 \pm 2.8$	[1] ABLIKIM	24BO	BES3	$e^+e^- \to$ hadrons
~ 3740	[1] ABLIKIM	24E	BES3	$e^+e^- \to$ light hadrons

[1] Fit to cross sections for $\sqrt{s} = 3645$ to 3871 MeV.

$\psi(3780)$ $I^G(J^{PC}) = ?^?(1^{--})$

MASS (MeV)	DOCUMENT ID		TECN	COMMENT
$3778.7 \pm 0.5 \pm 0.3$	[1] ABLIKIM	24BO	BES3	$e^+e^- \to$ hadrons
~ 3780	[1] ABLIKIM	24E	BES3	$e^+e^- \to$ light hadrons

[1] Fit to cross sections for $\sqrt{s} = 3645$ to 3871 MeV.

$\psi(3810)$ $I^G(J^{PC}) = ?^?(1^{--})$

MASS (MeV)	DOCUMENT ID		TECN	COMMENT
$3804.5 \pm 0.9 \pm 0.9$	[1] ABLIKIM	24BO	BES3	$e^+e^- \to$ hadrons
~ 3806	[1] ABLIKIM	24E	BES3	$e^+e^- \to$ light hadrons

[1] Fit to cross sections for $\sqrt{s} = 3645$ to 3871 MeV.

$h_c(4000)$ $I^G(J^{PC}) = 0^-(1^{+-})$

MASS (MeV)	WIDTH (MeV)	EVTS	DOCUMENT ID		TECN	COMMENT
$4000^{+17}_{-14} \pm 29_{-22}$	$184^{+71}_{-45} \pm 97_{-61}$	1.6k	[1] AAIJ	24AB	LHCB	$B^+ \to D^{*\pm}D^\mp K^+$

[1] From a simultaneous amplitude analysis of $B^+ \to D^{*+}D^-K^+$, $B^+ \to D^{*-}D^+K^+$ and their c.c.

$\chi_{c1}(4010)$ $I^G(J^{PC}) = 0^+(1^{++})$

MASS (MeV)	WIDTH (MeV)	EVTS	DOCUMENT ID		TECN	COMMENT
$4012.5^{+3.6}_{-3.9} \pm 4.1_{-3.7}$	$62.7^{+7.0}_{-6.4} \pm 6.6$	1.6k	[1] AAIJ	24AB	LHCB	$B^+ \to D^{*\pm}D^\mp K^+$

[1] From a simultaneous amplitude analysis of $B^+ \to D^{*+}D^-K^+$, $B^+ \to D^{*-}D^+K^+$ and their c.c.

$h_c(4300)$ $I^G(J^{PC}) = 0^-(1^{+-})$

MASS (MeV)	WIDTH (MeV)	EVTS	DOCUMENT ID		TECN	COMMENT
$4307.3^{+6.4}_{-6.6} \pm 3.3_{-4.1}$	$58^{+28}_{-16} \pm 28_{-25}$	1.6k	[1] AAIJ	24AB	LHCB	$B^+ \to D^{*\pm}D^\mp K^+$

[1] From a simultaneous amplitude analysis of $B^+ \to D^{*+} D^- K^+$, $B^+ \to D^{*-} D^+ K^+$ and their c.c.

$\psi(4500)$ $I^G(J^{PC}) = 0^-(1^{--})$

MASS (MeV)	WIDTH (MeV)	DOCUMENT ID	TECN	COMMENT
$4467.4^{+7.2}_{-5.4}{}^{+3.2}_{-2.7}$	$62.8^{+19.2}_{-14.4}{}^{+9.9}_{-7.0}$	[1] ABLIKIM 25B	BES3	$e^+e^- \to \pi^+\pi^- h_c(1P)$
$4544.2 \pm 18.7 \pm 1.7$	$116.1 \pm 33.5 \pm 1.7$	[2] ABLIKIM 24D	BES3	$e^+e^- \to \omega\gamma J/\psi$
$4469.1 \pm 26.2 \pm 3.6$	$246.3 \pm 36.7 \pm 9.4$	[3] ABLIKIM 23X	BES3	$e^+e^- \to D^{*0} D^{*-} \pi^+$
$4484.7 \pm 13.3 \pm 24.1$	$111.1 \pm 30 \pm 15.2$	[4] ABLIKIM 22AU	BES3	$e^+e^- \to K^+K^- J/\psi$

[1] Using three coherent Breit-Wigner functions between 4.009 and 4.950 GeV.

[2] Assuming one single Breit-Wigner resonance in $\omega\chi_{c2}(1P)$ ($\chi_{c2} \to \gamma J/\psi$). Measured $\Gamma_{ee} \cdot B(\omega\chi_{c1}(1P)) = 1.86 \pm 0.32 \pm 0.13$ eV.

[3] From a cross-section measurement of $e^+e^- \to D^{*0} D^{*-} \pi^+$ between 4.189 and 4.951 GeV, assuming a coherent sum of 3 Breit-Wigner resonances plus a continuum amplitude. $\Gamma(e^+e^-) \cdot B(D^{*0} D^{*-} \pi^+) = 107$–$1744$ eV depending on solutions I – VIII with the same fit qualities. The two other resonances have masses (widths) 4209.6 ± 7.5 (81.6 ± 19.9) MeV and 4675.3 ± 29.7 (218.3 ± 73.5) MeV.

[4] ABLIKIM 22AU cross sections analysis of the process $e^+e^- \to K^+K^- J/\psi$ at c.m. energies 4.127–4.600 GeV from 15.6 fb^{-1} of data.

$T_{c\bar{c}s\bar{1}}(4600)^0$ $I^G(J^{PC}) = 1/2^?(1^{+?})$

MASS (MeV)	WIDTH (MeV)	DOCUMENT ID	TECN	COMMENT
$4578 \pm 10 \pm 18$	$133 \pm 28 \pm 69$	AAIJ 25Q	LHCB	$B^+ \to \psi(2S) K^+ \pi^+ \pi^-$

$T_{c\bar{c}s\bar{1}}(4900)^0$ $I^G(J^{PC}) = 1/2^?(1^{+?})$

MASS (MeV)	WIDTH (MeV)	DOCUMENT ID	TECN	COMMENT
$4925 \pm 22 \pm 47$	$255 \pm 55 \pm 127$	AAIJ 25Q	LHCB	$B^+ \to \psi(2S) K^+ \pi^+ \pi^-$

$T_{c\bar{c}s\bar{1}}(5200)^0$ $I^G(J^{PC}) = 1/2^?(1^{-?})$

MASS (MeV)	WIDTH (MeV)	DOCUMENT ID	TECN	COMMENT
$5225 \pm 86 \pm 181$	$226 \pm 76 \pm 374$	AAIJ 25Q	LHCB	$B^+ \to \psi(2S) K^+ \pi^+ \pi^-$

REFERENCES for Further States

AAIJ 25Q JHEP 2501 054 R. Aaij et al. (LHCb Collab.)
ABLIKIM 25B PRL 135 071901 M. Ablikim et al. (BESIII Collab.)
ABLIKIM 25E PRL 134 191901 M. Ablikim et al. (BESIII Collab.)
AAIJ 24AB PRL 133 131902 R. Aaij et al. (LHCb Collab.)
AAIJ 24AQ SCIB 70 1432 R. Aaij et al. (LHCb Collab.)
ABLIKIM 24AA PR D110 032005 M. Ablikim et al. (BESIII Collab.)
ABLIKIM 24BO PRL 133 241902 M. Ablikim et al. (BESIII Collab.)
ABLIKIM 24CB PR D110 112014 M. Ablikim et al. (BESIII Collab.)
ABLIKIM 24D PRL 132 161901 M. Ablikim et al. (BESIII Collab.)
ABLIKIM 24E PRL 132 191902 M. Ablikim et al. (BESIII Collab.)
AAIJ 23AH PR D108 032010 R. Aaij et al. (LHCb Collab.)
ABLIKIM 23AY PR D107 112001 M. Ablikim et al. (BESIII Collab.)
ABLIKIM 23BG PRL 131 151901 M. Ablikim et al. (BESIII Collab.)
ABLIKIM 23X PRL 130 121901 M. Ablikim et al. (BESIII Collab.)
ABLIKIM 22AU CP C46 111002 M. Ablikim et al. (BESIII Collab.)
ABLIKIM 22G PRL 129 042001 M. Ablikim et al. (BESIII Collab.)
KLEMPT 22 PL B830 137171 E. Klempt et al. (BONN)
ABLIKIM 16N PR D93 112011 M. Ablikim (BESIII Collab.)
UEHARA 13 PTEP 2013 123C01 S. Uehara et al. (BELLE Collab.)
ANISOVICH 12 PR D85 014001 A.V. Anisovich et al.
ABLIKIM 11C PRL 106 072002 M. Ablikim et al. (BESIII Collab.)
ANASHIN 11 PL B703 543 V.V. Anashin et al. (KEDR Collab.)
ANISOVICH 11 EPJ C71 1511 A.V. Anisovich et al. (LOQM, RAL, PNPI)
CHEN 11F PR D84 071501 P. Chen et al. (BELLE Collab.)
AUBERT 10H PR D82 031102 B. Aubert et al. (BABAR Collab.)
ABRAAMYAN 09 PR C80 034001 Kh.U. Abraamyan et al.
VLADIMIRSK... 08 PAN 71 2129 V.V. Vladimirsky et al. (ITEP)
Translated from YAF 71 2166.
VLADIMIRSK... 07 PAN 70 1706 V. Vladimirsky et al.
Translated from YAF 70 1751.
YASUI 07 PR D76 034009 S. Yasui, M. Oka
ABLIKIM 06S PRL 97 142002 M. Ablikim et al. (BES Collab.)
GABYSHEV 06A PRL 97 242001 N. Gabyshev et al. (BELLE Collab.)
SCHEGELSKY 06 EPJ A27 199 V.A. Schegelsky et al.
SCHEGELSKY 06A EPJ A27 207 V.A. Schegelsky et al.
UMAN 06 PR D73 052009 I. Uman et al. (FNAL E835)
VLADIMIRSK... 06 PAN 69 493 V.V. Vladimirsky et al. (ITEP, Moscow)
Translated from YAF 69 515.
BINON 05 PAN 68 960 F. Binon et al.
Translated from YAF 68 998.
GRIGOR'EV 05 PAN 68 1271 V.K. Grigor'ev et al. (ITEP)
Translated from YAF 68 1324.
LU 05 PRL 94 032002 M. Lu et al. (BNL E852 Collab.)
ABLIKIM 04J PRL 93 112002 M. Ablikim et al. (BES Collab.)
BUGG 04 PL B595 556 (errat.) D.V. Bugg
BUGG 04A EPJ C36 161 D.V. Bugg
BUGG 04C PRPL 397 257 D.V. Bugg
EVDOKIMOV 04 PRL 93 242001 A.V. Evdokimov et al. (SELEX Collab.)
KUHN 04 PL B595 109 J. Kuhn et al. (BNL E852 Collab.)
ANISOVICH 03 EPJ A16 229 V.V. Anisovich et al.
VLADIMIRSK... 03 PAN 66 700 V.V. Vladimirsky et al.
Translated from YAF 66 729.
ANISOVICH 02 PL B542 8 A.V. Anisovich et al.
ANISOVICH 02B PL B542 19 A.V. Anisovich et al.
CHUNG 02 PR D65 072001 S.U. Chung et al. (BNL E852 Collab.)
ANISOVICH 01C PL B507 23 A.V. Anisovich et al.
ANISOVICH 01D PL B508 6 A.V. Anisovich et al.
ANISOVICH 01E PL B513 281 A.V. Anisovich et al.
ANISOVICH 01F PL B517 261 A.V. Anisovich et al.
ANISOVICH 01G PL B517 273 A.V. Anisovich et al.
ANISOVICH 00B NP A662 319 A.V. Anisovich et al.
ANISOVICH 00D PL B476 15 A.V. Anisovich et al.
ANISOVICH 00E PL B477 19 A.V. Anisovich et al.
ANISOVICH 00I PL B491 40 A.V. Anisovich et al.
ANISOVICH 00J PL B491 47 A.V. Anisovich et al. (RAL, LOQM, PNPI+)
ANISOVICH 00M PL B496 145 A.V. Anisovich et al.
BARNES 00 PR C62 055203 P.D. Barnes et al.
FILIPPI 00 PL B495 284 A. Filippi et al. (OBELIX Experiment)
VLADIMIRSKII 00 JETPL 72 486 V.V. Vladimirskii et al.
Translated from ZETFP 72 698.
ANISOVICH 99C PL B452 173 A.V. Anisovich et al.
ANISOVICH 99E PL B452 187 A.V. Anisovich et al.
ANISOVICH 99F NP A651 253 A.V. Anisovich et al.
ANISOVICH 99J PL B471 271 A.V. Anisovich et al.
ANISOVICH 99K PL B468 309 A.V. Anisovich et al.
BUGG 99 PL B458 511 D.V. Bugg et al.
FERRER 99 EPJ C10 249 A. Ferrer et al.
SEMENOV 99 SPU 42 847 S.V. Semenov
Translated from UFN 42 937.
ADOMEIT 96 ZPHY C71 227 J. Adomeit et al. (Crystal Barrel Collab.)
KLOET 96 PR D53 6120 W.M. Kloet, F. Myhrer (RUTG, NORD)
PROKOSHKIN 96 PD 41 247 Y.D. Prokoshkin, V.D. Samoilenko (SERP)
Translated from DANS 348 481.
HASAN 94 PL B334 215 A. Hasan, D.V. Bugg (LOQM)
OAKDEN 94 NP A574 731 M.N. Oakden, M.R. Pennington (DURH)
ALEEV 93 PAN 56 1358 A.N. Aleev et al. (BIS-2 Collab.)
Translated from YAF 56 100.
ARMSTRONG 93D PL B307 399 T.A. Armstrong et al. (FNAL, FERR, GENO+)
ALBRECHT 91F ZPHY C50 1 H. Albrecht et al. (ARGUS Collab.)
CONDO 91 PR D43 2787 G.T. Condo et al. (SLAC Hybrid Collab.)
BISELLO 89B PR D39 701 G. Busetto et al. (DM2 Collab.)
ATKINSON 88 ZPHY C38 535 M. Atkinson et al. (BONN, CERN, GLAS+)
DAFTARI 87 PRL 58 859 I.K. Daftari et al. (SYRA)
ALDE 86D NP B269 485 D.M. Alde et al. (BELG, LAPP, SERP, CERN+)
BRIDGES 86D PL B180 313 D.L. Bridges et al. (SYRA, BNL, CASE+)
GREEN 86 PRL 56 1639 D.R. Green et al. (FNAL, ARIZ, FSU+)
ATKINSON 85 ZPHY C29 333 M. Atkinson et al. (BONN, CERN, GLAS+)
DENNEY 83 PR D28 2726 D.L. Denney et al. (IOWA, MICH)
CLELAND 82B NP B208 228 W.E. Cleland et al. (DURH, GEVA, LAUS+)
ASTON 81B NP B189 205 D. Aston et al. (BONN, CERN, EPOL, GLAS+)
ARESTOV 80 IHEP 80-165 Y.I. Arestov et al. (SERP)
CHLIAPNIK... 80 ZPHY C3 285 P.V. Chliapnikov et al. (SERP, BRUX, MONS)
KREYMER 80 PR D22 36 A.E. Kreymer et al. (IND, PURD, SLAC+)
ROZANSKA 80 NP B162 505 M. Rozanska et al. (MPIM, CERN)
EVANGELIS... 79 NP B153 253 C. Evangelista et al. (BARI, BONN, CERN+)
EVANGELIS... 79B NP B154 381 C. Evangelista et al. (BARI, BONN, CERN+)
BALTAY 78 PR D17 52 C. Baltay et al. (COLU, BING)
ANTIPOV 77 NP B119 45 Y.M. Antipov et al. (SERP, GEVA)
BALTAY 77 PRL 39 591 C. Baltay, C.V. Cautis, M. Kalelkar (COLU)
BALTAY 75 PRL 35 891 C. Baltay et al. (COLU, BING)
KALELKAR 75 Thesis Nevis 207 M.S. Kalelkar (COLU)
CASO 70 LNC 3 707 C. Caso et al. (GENO, HAMB, MILA, SACL)

Int. J. Mod. Phys. A 2026.41. Downloaded from www.worldscientific.com
by UNIVERSITY OF CALIFORNIA @ BERKELEY on 09/16/26. Re-use and distribution is strictly not permitted, except for Open Access articles.

Meson Particle Listings

Int. J. Mod. Phys. A 2026.41. Downloaded from www.worldscientific.com
by [redacted]LIFORNIA @ BERKELEY on 09/16/26. Re-use and distribution is strictly not permitted, except for Open Access articles.

Int. J. Mod. Phys. A 2026.41. Downloaded from www.worldscientific.com
by UNIVERSITY OF CALIFORNIA @ BERKELEY on 09/16/26. Re-use and distribution is strictly not permitted, except for Open Access articles.

N BARYONS ($S = 0, I = 1/2$)

p 2203
n 2213
N resonances 2219

Δ BARYONS ($S = 0, I = 3/2$)

Δ resonances 2263

Λ BARYONS ($S = -1, I = 0$)

Λ 2289
Λ resonances 2292

Σ BARYONS ($S = -1, I = 1$)

Σ^+ 2315
Σ^0 2317
Σ^- 2318
Σ resonances 2320

Ξ BARYONS ($S = -2, I = 1/2$)

Ξ^0 2347
Ξ^- 2350
Ξ resonances 2353

Ω BARYONS ($S = -3, I = 0$)

Ω^- 2361
Ω resonances 2363

CHARMED BARYONS ($C = +1$)

Λ_c^+ 2364
$\Lambda_c(2595)^+$ 2375
$\Lambda_c(2625)^+$ 2376
$\Lambda_c(2765)^+$ aka $\Sigma_c(2765)$ 2376
$\Lambda_c(2860)^+$ 2377
$\Lambda_c(2880)^+$ 2377
$\Lambda_c(2910)^+$ 2377
$\Lambda_c(2940)^+$ 2378
$\Sigma_c(2455)$ 2378
$\Sigma_c(2520)$ 2379
$\Sigma_c(2800)$ 2380
Ξ_c^+ 2381
Ξ_c^0 2383
$\Xi_c^{\prime +}$ 2385
$\Xi_c^{\prime 0}$ 2386
$\Xi_c(2645)$ 2386
$\Xi_c(2790)$ 2386
$\Xi_c(2815)$ 2387
$\Xi_c(2882)$ 2388
$\Xi_c(2923)$ 2388
$\Xi_c(2930)$ 2388
$\Xi_c(2970)$ was $\Xi_c(2980)$ 2389
$\Xi_c(3055)$ 2390
$\Xi_c(3080)$ 2391
$\Xi_c(3123)$ 2391
Ω_c^0 2391
$\Omega_c(2770)^0$ 2393
$\Omega_c(3000)^0$ 2393
$\Omega_c(3050)^0$ 2394
$\Omega_c(3065)^0$ 2394
$\Omega_c(3090)^0$ 2394
$\Omega_c(3120)^0$ 2395
$\Omega_c(3185)^0$ 2395
$\Omega_c(3327)^0$ 2395
Ξ_{cc}^+ 2396
Ξ_{cc}^{++} 2396

BOTTOM (BEAUTY) BARYONS ($B = -1$)

Λ_b^0 2398
$\Lambda_b(5912)^0$ 2408
$\Lambda_b(5920)^0$ 2409
$\Lambda_b(6070)^0$ 2409
$\Lambda_b(6146)^0$ 2409
$\Lambda_b(6152)^0$ 2410
Σ_b 2410
Σ_b^* 2411
$\Sigma_b(6097)^+$ 2411
$\Sigma_b(6097)^-$ 2411
Ξ_b^- 2412
Ξ_b^0 2414
$\Xi_b^{\prime}(5935)^-$ 2416
$\Xi_b(5945)^0$ 2416
$\Xi_b(5955)^-$ 2416
$\Xi_b(6087)^0$ 2417
$\Xi_b(6095)^0$ 2417
$\Xi_b(6100)^-$ 2417
$\Xi_b(6227)^-$ 2417
$\Xi_b(6227)^0$ 2418
$\Xi_b(6327)^0$ 2418
$\Xi_b(6333)^0$ 2418
Ξ_{bc}^0 2418
Ω_b^- 2419
$\Omega_b(6316)^-$ 2420
$\Omega_b(6330)^-$ 2420
$\Omega_b(6340)^-$ 2420
$\Omega_b(6350)^-$ 2420
b-baryon ADMIXTURE (Λ_b, Ξ_b, Ω_b) 2421

EXOTIC BARYONS

$P_{c\bar{c}}(4312)^+$ 2423
$P_{c\bar{c}s}(4338)^0$ 2423
$P_{c\bar{c}}(4380)^+$ 2423
$P_{c\bar{c}}(4440)^+$ 2424
$P_{c\bar{c}}(4457)^+$ was $P_c(4450)$ 2424
$P_{c\bar{c}s}(4459)^0$ 2425

Notes in the Listings

Radiative hyperon decays 2348
Ξ and Ω resonances (rev.) 2352

Related Reviews in Volume 1

79. Baryon decay parameters 1046
80. N and Δ resonances 1047
81. Λ and Σ resonances 1052
82. Pole structure of the $\Lambda(1405)$ region (rev.) 1055
83. Pentaquarks (rev.) 1057

Int. J. Mod. Phys. A 2026.41. Downloaded from www.worldscientific.com
UNIVERSITY OF CALIFORNIA @ BERKELEY on 09/16/26. Re-use and distribution is strictly not permitted, except for Open Access articles.

Int. J. Mod. Phys. A 2026.41. Downloaded from www.worldscientific.com
by UNIVERSITY OF CALIFORNIA @ BERKELEY on 09/16/26. Re-use and distribution is strictly not permitted, except for Open Access articles.

N BARYONS
($S = 0$, $I = 1/2$)

p, $N^+ = uud$; n, $N^0 = udd$

p

$I(J^P) = \frac{1}{2}(\frac{1}{2}^+)$ Status: ****

p MASS (atomic mass units u)

The mass is known more precisely in u (atomic mass units) than in MeV. See the next data block.

VALUE (u)		DOCUMENT ID		TECN	COMMENT
1.007276466578 9±0.0000000000083		**OUR EVALUATION**	2022 CODATA		
1.007276466578 9±0.0000000000083		MOHR	25	RVUE	2022 CODATA value
• • • We do not use the following data for averages, fits, limits, etc. • • •					
1.007276466574	±0.000000000010	[1] FINK	21	SPEC	Penning trap
1.007276466621	±0.000000000053	[2] TIESINGA	21	RVUE	2018 CODATA value
1.007276466598	±0.000000000033	[3] HEISSE	19	SPEC	Penning Trap
1.007276466583	±0.000000000032	[4] HEISSE	17	SPEC	See HEISSE 19
1.007276466879	±0.000000000091	MOHR	16	RVUE	2014 CODATA value
1.007276466812	±0.000000000090	MOHR	12	RVUE	2010 CODATA value
1.00727646677	±0.00000000010	MOHR	08	RVUE	2006 CODATA value
1.00727646688	±0.00000000013	MOHR	05	RVUE	2002 CODATA value
1.00727646688	±0.00000000013	MOHR	99	RVUE	1998 CODATA value
1.007276470	±0.000000012	COHEN	87	RVUE	1986 CODATA value

[1] FINK 21 simultaneously measure the cyclotron frequencies of an H_2^+ ion and a deuteron in a coupled magnetron orbit. The proton mass is extracted using the precise deuteron mass value.

[2] The 2018 CODATA combination in TIESINGA 21 includes data from HEISSE 17, but does not include updates in HEISSE 19, which superseded HEISSE 17. Consequently, we do not average HEISSE 19 and TIESINGA 21. Updating the 2018 CODATA combination to use HEISSE 19 would shift the central value for the proton mass upwards by less than half a standard deviation. Therefore, we take the 2018 CODATA result in TIESINGA 21 as the recommended value for the proton mass.

[3] The value is an update of HEISSE 17; the result is shifted by 1.5×10^{-11} u, corresponding to 0.45 σ due to the corrected motional temperatures of the particles. The statistical and total systematic uncertainties are given as 16 and 29 in the last two digits.

[4] The statistical and systematic errors are 15 and 29 in the last two places of the value. Superseded by HEISSE 19.

p MASS (MeV)

The mass is known more precisely in u (atomic mass units) than in MeV. The conversion is: 1 u = 931.494 103 72(29) MeV/c^2 (2022 CODATA value, MOHR 25).

VALUE (MeV)		DOCUMENT ID		TECN	COMMENT
938.27208943±0.00000029		**OUR EVALUATION**	2022 CODATA		
938.27208943±0.00000029		MOHR	25	RVUE	2022 CODATA value
• • • We do not use the following data for averages, fits, limits, etc. • • •					
938.27208812	±0.00000029	FINK	21	SPEC	Penning trap
938.27208816	±0.00000029	TIESINGA	21	RVUE	2018 CODATA value
938.2720813	±0.0000058	MOHR	16	RVUE	2014 CODATA value
938.272046	±0.000021	MOHR	12	RVUE	2010 CODATA value
938.272013	±0.000023	MOHR	08	RVUE	2006 CODATA value
938.272029	±0.000080	MOHR	05	RVUE	2002 CODATA value
938.271998	±0.000038	MOHR	99	RVUE	1998 CODATA value
938.27231	±0.00028	COHEN	87	RVUE	1986 CODATA value
938.2796	±0.0027	COHEN	73	RVUE	1973 CODATA value

$|m_p - m_{\overline{p}}|/m_p$

A test of CPT invariance. Note that the comparison of the $\overline{p}$ and p charge-to-mass ratio, given in the next data block, is much better determined.

VALUE	CL%	DOCUMENT ID		TECN	COMMENT
<7 $\times 10^{-10}$	90	[1] HORI	11	SPEC	$\overline{p}e^-$He atom
• • • We do not use the following data for averages, fits, limits, etc. • • •					
$<2 \times 10^{-9}$	90	[1] HORI	06	SPEC	$\overline{p}e^-$He atom
$<1.0 \times 10^{-8}$	90	[1] HORI	03	SPEC	$\overline{p}e^-$ ^{4}He, $\overline{p}e^-$ ^{3}He
$<6 \times 10^{-8}$	90	[1] HORI	01	SPEC	$\overline{p}e^-$He atom
$<5 \times 10^{-7}$		[2] TORII	99	SPEC	$\overline{p}e^-$He atom

[1] HORI 01, HORI 03, HORI 06, and HORI 11 use the more-precisely-known constraint on the $\overline{p}$ charge-to-mass ratio of GABRIELSE 99 (see below) to get their results. Their results are not independent of the HORI 01, HORI 03, HORI 06, and HORI 11 values for $|q_p + q_{\overline{p}}|/e$, below.

[2] TORII 99 uses the more-precisely-known constraint on the $\overline{p}$ charge-to-mass ratio of GABRIELSE 95 (see below) to get this result. This is not independent of the TORII 99 value for $|q_p + q_{\overline{p}}|/e$, below.

$\overline{p}/p$ CHARGE-TO-MASS RATIO, $|\frac{q_{\overline{p}}}{m_{\overline{p}}}|/(\frac{q_p}{m_p})$

A test of CPT invariance. Listed here are measurements involving the *inertial* masses. For a discussion of what may be inferred about the ratio of $\overline{p}$ and p *gravitational* masses, see ERICSON 90; they obtain an upper bound of 10^{-6}–10^{-7} for violation of the equivalence principle for $\overline{p}$'s.

VALUE	DOCUMENT ID		TECN	COMMENT
1.000000000003±0.000000000016	**OUR AVERAGE**			
1.000000000003±0.000000000016	BORCHERT	22	TRAP	Penning trap
1.000000000001±0.000000000069	ULMER	15	TRAP	Penning trap
• • • We do not use the following data for averages, fits, limits, etc. • • •				
0.99999999991 ±0.00000000009	GABRIELSE	99	TRAP	Penning trap
1.0000000015 ±0.0000000011	[1] GABRIELSE	95	TRAP	Penning trap
1.000000023 ±0.000000042	[2] GABRIELSE	90	TRAP	Penning trap

[1] Equation (2) of GABRIELSE 95 should read $M(\overline{p})/M(p) = 0.999\,999\,998\underline{5}$ (11) (G. Gabrielse, private communication).

[2] GABRIELSE 90 also measures $m_{\overline{p}}/m_{e^-} = 1836.152660 \pm 0.000083$ and $m_p/m_{e^-} = 1836.152680 \pm 0.000088$. Both are completely consistent with the 1986 CODATA (COHEN 87) value for m_p/m_{e^-} of 1836.152701 ± 0.000037.

$(|\frac{q_{\overline{p}}}{m_{\overline{p}}}| - \frac{q_p}{m_p})/\frac{q_p}{m_p}$

A test of CPT invariance. Taken from the $\overline{p}/p$ charge-to-mass ratio, above.

VALUE	DOCUMENT ID
(0.3±1.6) $\times 10^{-11}$	**OUR EVALUATION**

$|q_p + q_{\overline{p}}|/e$

A test of CPT invariance. Note that the comparison of the $\overline{p}$ and p charge-to-mass ratios given above is much better determined. See also a similar test involving the electron.

VALUE	CL%	DOCUMENT ID		TECN	COMMENT
<7 $\times 10^{-10}$	90	[1] HORI	11	SPEC	$\overline{p}e^-$He atom
• • • We do not use the following data for averages, fits, limits, etc. • • •					
$<2 \times 10^{-9}$	90	[1] HORI	06	SPEC	$\overline{p}e^-$He atom
$<1.0 \times 10^{-8}$	90	[1] HORI	03	SPEC	$\overline{p}e^-$ ^{4}He, $\overline{p}e^-$ ^{3}He
$<6 \times 10^{-8}$	90	[1] HORI	01	SPEC	$\overline{p}e^-$He atom
$<5 \times 10^{-7}$		[2] TORII	99	SPEC	$\overline{p}e^-$He atom
$<2 \times 10^{-5}$		[3] HUGHES	92	RVUE	

[1] HORI 01, HORI 03, HORI 06, and HORI 11 use the more-precisely-known constraint on the $\overline{p}$ charge-to-mass ratio of GABRIELSE 99 (see above) to get their results. Their results are not independent of the HORI 01, HORI 03, HORI 06, and HORI 11 values for $|m_p - m_{\overline{p}}|/m_p$, above.

[2] TORII 99 uses the more-precisely-known constraint on the $\overline{p}$ charge-to-mass ratio of GABRIELSE 95 (see above) to get this result. This is not independent of the TORII 99 value for $|m_p - m_{\overline{p}}|/m_p$, above.

[3] HUGHES 92 uses recent measurements of Rydberg-energy and cyclotron-frequency ratios.

$|q_p + q_e|/e$

See BRESSI 11 for a summary of experiments on the neutrality of matter. See also "n CHARGE" in the neutron Listings.

VALUE	DOCUMENT ID		COMMENT
<1 $\times 10^{-21}$	[1] BRESSI	11	Neutrality of SF_6
• • • We do not use the following data for averages, fits, limits, etc. • • •			
$<3.2 \times 10^{-20}$	[2] SENGUPTA	00	binary pulsar
$<0.8 \times 10^{-21}$	MARINELLI	84	Magnetic levitation
$<1.0 \times 10^{-21}$	[1] DYLLA	73	Neutrality of SF_6

[1] BRESSI 11 uses the method of DYLLA 73 but finds serious errors in that experiment that greatly reduce its accuracy. The BRESSI 11 limit assumes that $n \to p e^- \nu_e$ conserves charge. Thus the limit applies equally to the charge of the neutron.

[2] SENGUPTA 00 uses the difference between the observed rate of of rotational energy loss by the binary pulsar PSR B1913+16 and the rate predicted by general relativity to set this limit. See the paper for assumptions.

p MAGNETIC MOMENT

See the "Quark Model" review.

VALUE (μ_N)	DOCUMENT ID		TECN	COMMENT
2.79284734463±0.00000000082	MOHR	25	RVUE	2022 CODATA value
• • • We do not use the following data for averages, fits, limits, etc. • • •				
2.79284734463±0.00000000082	TIESINGA	21	RVUE	2018 CODATA value
2.79284734462±0.00000000082	SCHNEIDER	17	TRAP	Double Penning trap
2.7928473508 ±0.0000000085	MOHR	16	RVUE	2014 CODATA value
2.792847356 ±0.000000023	MOHR	12	RVUE	2010 CODATA value
2.792847356 ±0.000000023	MOHR	08	RVUE	2006 CODATA value
2.792847351 ±0.000000028	MOHR	05	RVUE	2002 CODATA value

2.792847337	±0.000000029	MOHR	99	RVUE	1998 CODATA value
2.792847386	±0.000000063	COHEN	87	RVUE	1986 CODATA value

$\overline{p}$ MAGNETIC MOMENT

A few early results have been omitted.

VALUE (μ_N)		DOCUMENT ID		TECN	COMMENT
−2.7928473441±0.0000000042		SMORRA	17	TRAP	Hot/cold $\overline{p}$ frequencies, Penning traps
• • • We do not use the following data for averages, fits, limits, etc. • • •					
−2.7928465	±0.0000023	NAGAHAMA	17	TRAP	Single $\overline{p}$, Penning trap
−2.792845	±0.000012	DISCIACCA	13	TRAP	Single $\overline{p}$, Penning trap
−2.7862	±0.0083	PASK	09	CNTR	$\overline{p}$ He^+ hyperfine structure
−2.8005	±0.0090	KREISSL	88	CNTR	$\overline{p}$ ^{208}Pb 11→ 10 X-ray
−2.817	±0.048	ROBERTS	78	CNTR	
−2.791	±0.021	HU	75	CNTR	Exotic atoms

$(\mu_p + \mu_{\overline{p}}) / \mu_p$

A test of *CPT* invariance.

VALUE (units 10^{-6})	DOCUMENT ID		TECN	COMMENT
0.002±0.004	SMORRA	17	TRAP	Hot/cold $\overline{p}$ frequencies, Penning traps
• • • We do not use the following data for averages, fits, limits, etc. • • •				
0.3 ±0.8	NAGAHAMA	17	TRAP	Single $\overline{p}$, Penning trap
0 ±5	DISCIACCA	13	TRAP	Single $\overline{p}$, Penning trap

p ELECTRIC DIPOLE MOMENT

A nonzero value is forbidden by both *T* invariance and *P* invariance.

VALUE (10^{-23} *e* cm)	DOCUMENT ID		TECN	COMMENT
< 0.021	[1] SAHOO	17		Theory plus ^{199}Hg atom EDM
• • • We do not use the following data for averages, fits, limits, etc. • • •				
< 0.54	[1] DMITRIEV	03		Theory plus ^{199}Hg atom EDM
− 3.7 ± 6.3	CHO	89	NMR	Tl F molecules
< 400	DZUBA	85	THEO	Uses ^{129}Xe moment
130 ± 200	[2] WILKENING	84		
900 ±1400	[3] WILKENING	84		
700 ± 900	HARRISON	69	MBR	Molecular beam

[1] SAHOO 17 and DMITRIEV 03 are not direct measurements of the proton electric dipole moment. They use theory to calculate this limit from the limit on the electric dipole moment of the ^{199}Hg atom.
[2] This WILKENING 84 value includes a finite-size effect and a magnetic effect.
[3] This WILKENING 84 value is more cautious than the other and excludes the finite-size effect, which relies on uncertain nuclear integrals.

p ELECTRIC POLARIZABILITY α_p

For a very complete review of the "polarizability of the nucleon and Compton scattering," see SCHUMACHER 05, updated in SCHUMACHER 19.

See LI 22D and therein for measurements of the mean square proton electric polarizability radius.

VALUE (10^{-4} fm^3)	DOCUMENT ID		TECN	COMMENT
11.5 ±0.4 OUR AVERAGE Error includes scale factor of 1.1.				
12.7 ±0.8 ±0.1	[1] MORNACCHI	22	FIT	Fit of RCS data sets
10.65±0.35±0.36	MCGOVERN	13	RVUE	χEFT + Compton scattering
12.1 ±1.1 ±0.5	[2] BEANE	03		EFT + γp
11.82±0.98$^{+0.52}_{-0.98}$	[3] BLANPIED	01	LEGS	$p(\vec{\gamma},\gamma)$, $p(\vec{\gamma},\pi^0)$, $p(\vec{\gamma},\pi^+)$
11.9 ±0.5 ±1.3	[4] OLMOSDEL...	01	CNTR	γp Compton scattering
12.1 ±0.8 ±0.5	[5] MACGIBBON	95	RVUE	global average
• • • We do not use the following data for averages, fits, limits, etc. • • •				
12.03$^{+0.48}_{-0.54}$	[6] PASQUINI	19		fit of RCS data sets
11.7 ±0.8 ±0.7	[7] BARANOV	01	RVUE	Global average
12.5 ±0.6 ±0.9	MACGIBBON	95	CNTR	γp Compton scattering
9.8 ±0.4 ±1.1	HALLIN	93	CNTR	γp Compton scattering
10.62$^{+1.25}_{-1.19}$ $^{+1.07}_{-1.03}$	ZIEGER	92	CNTR	γp Compton scattering
10.9 ±2.2 ±1.3	[8] FEDERSPIEL	91	CNTR	γp Compton scattering

[1] MORNACCHI 22 perform the first simultaneous extraction of the six leading-order proton polarizabilities using fixed-t subtracted dispersion relations and a bootstrap-based fitting technique.
[2] BEANE 03 uses effective field theory and low-energy γp and γd Compton-scattering data. It also gets for the isoscalar polarizabilities (see the erratum) $\alpha_N = (13.0 \pm 1.9^{+3.9}_{-1.5}) \times 10^{-4}$ fm^3 and $\beta_N = (-1.8 \pm 1.9^{+2.1}_{-0.9}) \times 10^{-4}$ fm^3.
[3] BLANPIED 01 gives $\alpha_p + \beta_p$ and $\alpha_p - \beta_p$. The separate α_p and β_p are provided to us by A. Sandorfi. The first error above is statistics plus systematics; the second is from the model.
[4] This OLMOSDELEON 01 result uses the TAPS data alone, and does not use the (re-evaluated) sum-rule constraint that $\alpha + \beta = (13.8 \pm 0.4) \times 10^{-4}$ fm^3. See the paper for a discussion.
[5] MACGIBBON 95 combine the results of ZIEGER 92, FEDERSPIEL 91, and their own experiment to get a "global average" in which model errors and systematic errors are treated in a consistent way. See MACGIBBON 95 for a discussion.
[6] PASQUINI 19 fit data sets for the unpolarized proton RCS cross section, using fixed-t subtracted dispersion relations and a bootstrap-based fitting technique.
[7] BARANOV 01 combines the results of 10 experiments from 1958 through 1995 to get a global average that takes into account both systematic and model errors and does not use the theoretical constraint on the sum $\alpha_p + \beta_p$.
[8] FEDERSPIEL 91 obtains for the (static) electric polarizability α_p, defined in terms of the induced electric dipole moment by $\mathbf{D} = 4\pi\epsilon_0\alpha_p\mathbf{E}$, the value $(7.0 \pm 2.2 \pm 1.3) \times 10^{-4}$ fm^3.

p MAGNETIC POLARIZABILITY β_p

The electric and magnetic polarizabilities are subject to a dispersion sum-rule constraint $\overline{\alpha} + \overline{\beta} = (14.2 \pm 0.5) \times 10^{-4}$ fm^3. Errors here are anticorrelated with those on $\overline{\alpha}_p$ due to this constraint.

See LI 22D and therein for measurements of the mean square proton magnetic polarizability radius.

VALUE (10^{-4} fm^3)	DOCUMENT ID		TECN	COMMENT
2.31±0.29 OUR AVERAGE Error includes scale factor of 1.1.				
2.4 ±0.6 ±0.1	[1] MORNACCHI	22	FIT	Fit of RCS data sets
1.77$^{+0.52}_{-0.54}$	[2] PASQUINI	19	FIT	fit of RCS data sets
3.15±0.35±0.36	MCGOVERN	13	RVUE	χEFT + Compton scattering
3.4 ±1.1 ±0.1	[3] BEANE	03		EFT + γp
1.43±0.98$^{+0.52}_{-0.98}$	[4] BLANPIED	01	LEGS	$p(\vec{\gamma},\gamma)$, $p(\vec{\gamma},\pi^0)$, $p(\vec{\gamma},\pi^+)$
1.2 ±0.7 ±0.5	[5] OLMOSDEL...	01	CNTR	γp Compton scattering
2.1 ±0.8 ±0.5	[6] MACGIBBON	95	RVUE	global average
• • • We do not use the following data for averages, fits, limits, etc. • • •				
2.3 ±0.9 ±0.7	[7] BARANOV	01	RVUE	Global average
1.7 ±0.6 ±0.9	MACGIBBON	95	CNTR	γp Compton scattering
4.4 ±0.4 ±1.1	HALLIN	93	CNTR	γp Compton scattering
3.58$^{+1.19}_{-1.25}$ $^{+1.03}_{-1.07}$	ZIEGER	92	CNTR	γp Compton scattering
3.3 ±2.2 ±1.3	FEDERSPIEL	91	CNTR	γp Compton scattering

[1] MORNACCHI 22 perform the first simultaneous extraction of the six leading-order proton polarizabilities using fixed-t subtracted dispersion relations and a bootstrap-based fitting technique.
[2] PASQUINI 19 fit data sets for the unpolarized proton RCS cross section, using fixed-t subtracted dispersion relations and a bootstrap-based fitting technique.
[3] BEANE 03 uses effective field theory and low-energy γp and γd Compton-scattering data. It also gets for the isoscalar polarizabilities (see the erratum) $\alpha_N = (13.0 \pm 1.9^{+3.9}_{-1.5}) \times 10^{-4}$ fm^3 and $\beta_N = (-1.8 \pm 1.9^{+2.1}_{-0.9}) \times 10^{-4}$ fm^3.
[4] BLANPIED 01 gives $\alpha_p + \beta_p$ and $\alpha_p - \beta_p$. The separate α_p and β_p are provided to us by A. Sandorfi. The first error above is statistics plus systematics; the second is from the model.
[5] This OLMOSDELEON 01 result uses the TAPS data alone, and does not use the (re-evaluated) sum-rule constraint that $\alpha + \beta = (13.8 \pm 0.4) \times 10^{-4}$ fm^3. See the paper for a discussion.
[6] MACGIBBON 95 combine the results of ZIEGER 92, FEDERSPIEL 91, and their own experiment to get a "global average" in which model errors and systematic errors are treated in a consistent way. See MACGIBBON 95 for a discussion.
[7] BARANOV 01 combines the results of 10 experiments from 1958 through 1995 to get a global average that takes into account both systematic and model errors and does not use the theoretical constraint on the sum $\alpha_p + \beta_p$.

p SPIN POLARIZABILITY γ_{E1E1}

VALUE (10^{-4} fm^4)	DOCUMENT ID		TECN	COMMENT
−3.0±0.6±0.4	[1] MORNACCHI	22	FIT	Fit of RCS data sets

[1] MORNACCHI 22 perform the first simultaneous extraction of the six leading-order proton polarizabilities using fixed-t subtracted dispersion relations and a bootstrap-based fitting technique.

p SPIN POLARIZABILITY γ_{M1M1}

VALUE (10^{-4} fm^4)	DOCUMENT ID		TECN	COMMENT
3.7±0.5±0.1	[1] MORNACCHI	22	FIT	Fit of RCS data sets

[1] MORNACCHI 22 perform the first simultaneous extraction of the six leading-order proton polarizabilities using fixed-t subtracted dispersion relations and a bootstrap-based fitting technique.

p SPIN POLARIZABILITY γ_{E1M2}

VALUE (10^{-4} fm^4)	DOCUMENT ID		TECN	COMMENT
−1.2±1.0±0.3	[1] MORNACCHI	22	FIT	Fit of RCS data sets

[1] MORNACCHI 22 perform the first simultaneous extraction of the six leading-order proton polarizabilities using fixed-t subtracted dispersion relations and a bootstrap-based fitting technique.

p SPIN POLARIZABILITY γ_{M1E2}

VALUE (10^{-4} fm^4)	DOCUMENT ID		TECN	COMMENT
2.0±0.7±0.4	[1] MORNACCHI	22	FIT	Fit of RCS data sets

[1] MORNACCHI 22 perform the first simultaneous extraction of the six leading-order proton polarizabilities using fixed-t subtracted dispersion relations and a bootstrap-based fitting technique.

Int. J. Mod. Phys. A 2026.41. Downloaded from www.worldscientific.com
UNIVERSITY OF CALIFORNIA @ BERKELEY on 09/16/26. Re-use and distribution is strictly not permitted, except for Open Access articles.

Int. J. Mod. Phys. A 2026.41. Downloaded from www.worldscientific.com
by UNIVERSITY OF CALIFORNIA @ BERKELEY on 09/16/26. Re-use and distribution is strictly not permitted, except for Open Access articles.

p CHARGE RADIUS

This is the rms electric charge radius, $\sqrt{\langle r_E^2 \rangle}$.

There are three kinds of measurements of the proton radius: via transitions in atomic hydrogen; via electron scattering off hydrogen; and via muonic hydrogen Lamb shift. Most measurements of the radius of the proton involve electron-proton interactions, the most recent of which is the electron scattering measurement XIONG 19, and the atomic-hydrogen result BEZGINOV 19. These can be compared to another atomic-hydrogen value BEYER 17 and with the best measurement using muonic hydrogen Lamb shift ANTOGNINI 13, that is far more precise.

The latest 2022 CODATA recommendation (MOHR 25) is based on much improved theory descriptions for muonic hydrogen Lamb shift and the atomic-hydrogen transitions. MOHR 25 do not include the electron scattering data because of a lack of consensus as to how the electron-scattering data should be analyzed, and there remains some tension between the different r_p measurements. See GAO 22A for an updated discussion.

See our 2014 edition (Chinese Physics **C38** 070001 (2014)) for values published before 2003.

VALUE (fm)			DOCUMENT ID		TECN	COMMENT
0.84075 ± 0.00064			[1] MOHR	25	RVUE	2022 CODATA
• • • We do not use the following data for averages, fits, limits, etc. • • •						
0.847	±0.008		[2] CUI	21	FIT	use existing ep data
0.878	±0.011	±0.031	[3] MIHOVILOVIC	21		ISR $ep \to ep$ reanalysis
0.833	±0.010		[4] BEZGINOV	19	LASR	2S-2P transition in H
0.831	±0.007	±0.012	[5] XIONG	19	SPEC	$ep \to ep$ form factor
0.877	±0.013		[6] FLEURBAEY	18	LASR	1S-3S transition in H
0.8335	±0.0095		[7] BEYER	17	LASR	2S-4P transition in H
0.8751	±0.0061		MOHR	16	RVUE	2014 CODATA value
0.895	±0.014	±0.014	[8] LEE	15	SPEC	Just 2010 Mainz data
0.916	±0.024		LEE	15	SPEC	World data, no Mainz
0.84087	±0.00026	±0.00029	ANTOGNINI	13	LASR	μp-atom Lamb shift
0.8775	±0.0051		MOHR	12	RVUE	2010 CODATA, ep data
0.875	±0.008	±0.006	ZHAN	11	SPEC	Recoil polarimetry
0.879	±0.005	±0.006	BERNAUER	10	SPEC	$ep \to ep$ form factor
0.912	±0.009	±0.007	BORISYUK	10		reanalyzes old ep data
0.871	±0.009	±0.003	HILL	10		z-expansion reanalysis
0.84184	±0.00036	±0.00056	POHL	10	LASR	See ANTOGNINI 13
0.8768	±0.0069		MOHR	08	RVUE	2006 CODATA value
0.844	$^{+0.008}_{-0.004}$		BELUSHKIN	07		Dispersion analysis
0.897	±0.018		BLUNDEN	05		SICK 03 + 2γ correction
0.8750	±0.0068		MOHR	05	RVUE	2002 CODATA value
0.895	±0.010	±0.013	SICK	03		$ep \to ep$ reanalysis

[1] MOHR 25 do not include the electron scattering data.
[2] CUI 21 employ a new mathematical procedure (statistical SPM, Schlessinger point method) based on form-unbiased interpolations of existing ep scattering data.
[3] MIHOVILOVIC 21 reports a value of 0.878 ± 0.011 ± 0.031 ± 0.002 fm where the last uncertainty comes from the dependence on the model form factor function.
[4] BEZGINOV 19 measures the $2S_{1/2}$ to $2P_{1/2}$ transition frequency in atomic hydrogen using the frequency-offset separated oscillatory field (FOSOF) technique. The result agrees well with the muonic hydrogen Lamb shift value.
[5] The XIONG 19 value from $ep \to ep$ scattering and supports the muonic hydrogen Lamb shift value.
[6] FLEURBAEY 18 measures the 1S-3S transition frequency in hydrogen and in combination with the 1S-2S transition frequency deduces the proton radius and the Rydberg constant.
[7] The BEYER 17 result is 3.3 combined standard deviations below the MOHR 16 (2014 CODATA) value. The experiment measures the 2S-4P transition in hydrogen and gets the proton radius and the Rydberg constant.
[8] Authors also provide values for combinations of all available data.

p MAGNETIC RADIUS

This is the rms magnetic radius, $\sqrt{\langle r_M^2 \rangle}$.

VALUE (fm)	DOCUMENT ID		TECN	COMMENT
0.851 ± 0.026	[1] LEE	15		Combination of world and Mainz data
• • • We do not use the following data for averages, fits, limits, etc. • • •				
0.817 ± 0.027	[2] CUI	21B	FIT	use existing ep data
0.87 ± 0.02	EPSTEIN	14		Using ep, en, $\pi\pi$ data
0.867 ± 0.009 ± 0.018	ZHAN	11	SPEC	Recoil polarimetry
0.777 ± 0.013 ± 0.010	BERNAUER	10	SPEC	$ep \to ep$ form factor
0.876 ± 0.010 ± 0.016	BORISYUK	10		Reanalyzes old $ep \to ep$ data
0.854 ± 0.005	BELUSHKIN	07		Dispersion analysis

[1] In a consistent reanalysis LEE 2015 extract values separately for the Mainz 2010 data only (0.776+-0.034+-0.017) fm and for the world data without Mainz data (0.914+-0.035) fm. The quoted value is a simple combination of the two, which ignores possible discrepancies and unknown correlations and should be considered with caution.
[2] CUI 21B employ a new mathematical procedure (statistical SPM, Schlessinger point method) based on form-unbiased interpolations of existing ep scattering data.

p MEAN LIFE

A test of baryon conservation. See the "p Partial Mean Lives" section below for limits for identified final states. The limits here are to "anything" or are for "disappearance" modes of a bound proton (p) or (n). See also the 3ν modes in the "Partial Mean Lives" section. Table 1 of BACK 03 is a nice summary.

LIMIT (years)	PARTICLE	CL%	DOCUMENT ID		TECN	COMMENT
>0.96 × 10^30	**p**	90	[1] ALLEGA	22	SNO+	$p \to$ invisible
>0.9 × 10^30	**n**	90	[2] ALLEGA	22	SNO+	$n \to$ invisible
• • • We do not use the following data for averages, fits, limits, etc. • • •						
>1.3 × 10^24	p	90	[3] AGOSTINI	24A	HPGE	$p \to$ invisible
>1.5 × 10^24	n	90	[4] AGOSTINI	24A	HPGE	$n \to$ invisible
>3.6 × 10^29	p	90	[5] ANDERSON	19A	SNO+	$p \to$ invisible
>2.5 × 10^29	n	90	[5] ANDERSON	19A	SNO+	$n \to$ invisible
>5.8 × 10^29	n	90	[6] ARAKI	06	KLND	$n \to$ invisible
>2.1 × 10^29	p	90	[5] AHMED	04	SNO	$p \to$ invisible
>1.9 × 10^29	n	90	[5] AHMED	04	SNO	$n \to$ invisible
>1.8 × 10^25	n	90	[7] BACK	03	BORX	
>1.1 × 10^26	p	90	[7] BACK	03	BORX	
>3.5 × 10^28	p	90	[8] ZDESENKO	03		$p \to$ invisible
>1 × 10^28	p	90	[9] AHMAD	02	SNO	$p \to$ invisible
>4 × 10^23	p	95	TRETYAK	01		$d \to n$ + ?
>1.9 × 10^24	p	90	[10] BERNABEI	00B	DAMA	
>1.6 × 10^25	p, n		[11,12] EVANS	77		
>3 × 10^23	p		[12] DIX	70	CNTR	
>3 × 10^23	p, n		[12,13] FLEROV	58		

[1] ALLEGA 22 look for γ rays from the de-excitation of a residual ^{15}N* following the disappearance of p in ^{16}O.
[2] ALLEGA 22 look for γ rays from the de-excitation of a residual ^{15}O* following the disappearance of n in ^{16}O.
[3] AGOSTINI 24A look for γ rays from the de-excitation of a residual ^{75}As* following the disappearance of p in ^{76}Ge (through the transition chain ^{76}Ge $\to$ ^{75}Ga $\to$ ^{75}Ge $\to$ ^{75}As).
[4] AGOSTINI 24A look for γ rays from the de-excitation of a residual ^{75}As* following the disappearance of n in ^{76}Ge (through the transition chain ^{76}Ge $\to$ ^{75}Ge $\to$ ^{75}As).
[5] AHMED 04 and ANDERSON 19A look for γ rays from the de-excitation of a residual ^{15}O* or ^{15}N* following the disappearance of a neutron or proton in ^{16}O.
[6] ARAKI 06 looks for signs of de-excitation of the residual nucleus after disappearance of a neutron from the s shell of ^{12}C.
[7] BACK 03 looks for decays of unstable nuclides left after N decays of parent ^{12}C, ^{13}C, ^{16}O nuclei. These are "invisible channel" limits.
[8] ZDESENKO 03 gets this limit on proton disappearance in deuterium by analyzing SNO data in AHMAD 02.
[9] AHMAD 02 (see its footnote 7) looks for neutrons left behind after the disappearance of the proton in deuterons.
[10] BERNABEI 00B looks for the decay of a $^{128}_{53}$I nucleus following the disappearance of a proton in the otherwise-stable $^{129}_{54}$Xe nucleus.
[11] EVANS 77 looks for the daughter nuclide ^{129}Xe from possible ^{130}Te decays in ancient Te ore samples.
[12] This mean-life limit has been obtained from a half-life limit by dividing the latter by ln(2) = 0.693.
[13] FLEROV 58 looks for the spontaneous fission of a ^{232}Th nucleus after the disappearance of one of its nucleons.

$\overline{p}$ MEAN LIFE

Of the two astrophysical limits here, that of GEER 00D involves considerably more refinements in its modeling. The other limits come from direct observations of stored antiprotons. See also "$\overline{p}$ Partial Mean Lives" after "p Partial Mean Lives," below, for exclusive-mode limits. The best (lifetime/branching fraction) limit there is 7×10^5 years, for $\overline{p} \to e^- \gamma$. We advance only the exclusive-mode limits to our Summary Tables.

LIMIT (years)	CL%	EVTS	DOCUMENT ID		TECN	COMMENT
• • • We do not use the following data for averages, fits, limits, etc. • • •						
>5.0	90		SELLNER	17	TRAP	Penning trap
>8 × 10^5	90		[1] GEER	00D		$\overline{p}/p$ ratio, cosmic rays
>0.28			GABRIELSE	90	TRAP	Penning trap
>0.08	90	1	BELL	79	CNTR	Storage ring
>1 × 10^7			GOLDEN	79	SPEC	$\overline{p}/p$ ratio, cosmic rays
>3.7 × 10^−3			BREGMAN	78	CNTR	Storage ring

[1] GEER 00D uses agreement between a model of galactic $\overline{p}$ production and propagation and the observed $\overline{p}/p$ cosmic-ray spectrum to set this limit.

p DECAY MODES

See the "Note on Nucleon Decay" in our 1994 edition (Phys. Rev. **D50**, 1173) for a short review.

The "partial mean life" limits tabulated here are the limits on τ/B_i, where τ is the total mean life and B_i is the branching fraction for the mode in question. For N decays, p and n indicate proton and neutron partial lifetimes.

Int. J. Mod. Phys. A 2026.41. Downloaded from www.worldscientific.com
UNIVERSITY OF CALIFORNIA @ BERKELEY on 09/16/26. Re-use and distribution is strictly not permitted, except for Open Access articles.

	Mode	Partial mean life (10^{30} years)	Confidence level
	Antilepton + meson		
τ_1	$N \to e^+ \pi$	> 5300 (n), > 24000 (p)	90%
τ_2	$N \to \mu^+ \pi$	> 3500 (n), > 16000 (p)	90%
τ_3	$N \to \nu \pi$	> 1100 (n), > 390 (p)	90%
τ_4	$p \to e^+ \eta$	> 10000	90%
τ_5	$p \to \mu^+ \eta$	> 4700	90%
τ_6	$n \to \nu \eta$	> 158	90%
τ_7	$N \to e^+ \rho$	> 217 (n), > 720 (p)	90%
τ_8	$N \to \mu^+ \rho$	> 228 (n), > 570 (p)	90%
τ_9	$N \to \nu \rho$	> 19 (n), > 162 (p)	90%
τ_{10}	$p \to e^+ \omega$	> 1600	90%
τ_{11}	$p \to \mu^+ \omega$	> 2800	90%
τ_{12}	$n \to \nu \omega$	> 108	90%
τ_{13}	$N \to e^+ K$	> 17 (n), > 1000 (p)	90%
τ_{14}	$p \to e^+ K^0_S$		
τ_{15}	$p \to e^+ K^0_L$		
τ_{16}	$N \to \mu^+ K$	> 26 (n), > 4500 (p)	90%
τ_{17}	$p \to \mu^+ K^0_S$		
τ_{18}	$p \to \mu^+ K^0_L$		
τ_{19}	$N \to \nu K$	> 86 (n), > 5900 (p)	90%
τ_{20}	$n \to \nu K^0_S$	> 1560	90%
τ_{21}	$p \to e^+ K^*(892)^0$	> 84	90%
τ_{22}	$N \to \nu K^*(892)$	> 78 (n), > 51 (p)	90%
	Antilepton + mesons		
τ_{23}	$p \to e^+ \pi^+ \pi^-$	> 82	90%
τ_{24}	$p \to e^+ \pi^0 \pi^0$	> 147	90%
τ_{25}	$n \to e^+ \pi^- \pi^0$	> 52	90%
τ_{26}	$p \to \mu^+ \pi^+ \pi^-$	> 133	90%
τ_{27}	$p \to \mu^+ \pi^0 \pi^0$	> 101	90%
τ_{28}	$n \to \mu^+ \pi^- \pi^0$	> 74	90%
τ_{29}	$n \to e^+ K^0 \pi^-$	> 18	90%
	Lepton + meson		
τ_{30}	$n \to e^- \pi^+$	> 65	90%
τ_{31}	$n \to \mu^- \pi^+$	> 49	90%
τ_{32}	$n \to e^- \rho^+$	> 62	90%
τ_{33}	$n \to \mu^- \rho^+$	> 7	90%
τ_{34}	$n \to e^- K^+$	> 32	90%
τ_{35}	$n \to \mu^- K^+$	> 57	90%
	Lepton + mesons		
τ_{36}	$p \to e^- \pi^+ \pi^+$	> 30	90%
τ_{37}	$n \to e^- \pi^+ \pi^0$	> 29	90%
τ_{38}	$p \to \mu^- \pi^+ \pi^+$	> 17	90%
τ_{39}	$n \to \mu^- \pi^+ \pi^0$	> 34	90%
τ_{40}	$p \to e^- \pi^+ K^+$	> 75	90%
τ_{41}	$p \to \mu^- \pi^+ K^+$	> 245	90%
	Antilepton + photon(s)		
τ_{42}	$p \to e^+ \gamma$	> 670	90%
τ_{43}	$p \to \mu^+ \gamma$	> 478	90%
τ_{44}	$n \to \nu \gamma$	> 550	90%
τ_{45}	$p \to e^+ \gamma \gamma$	> 100	90%
τ_{46}	$n \to \nu \gamma \gamma$	> 219	90%
	Antilepton + single massless		
τ_{47}	$p \to e^+ X$	> 790	90%
τ_{48}	$p \to \mu^+ X$	> 410	90%
	Three (or more) leptons		
τ_{49}	$p \to e^+ e^+ e^-$	> 34000	90%
τ_{50}	$p \to e^+ \mu^+ \mu^-$	> 9200	90%
τ_{51}	$p \to e^+ \nu \nu$	> 170	90%
τ_{52}	$n \to e^+ e^- \nu$	> 257	90%
τ_{53}	$n \to \mu^+ e^- \nu$	> 83	90%
τ_{54}	$n \to \mu^+ \mu^- \nu$	> 79	90%
τ_{55}	$p \to \mu^+ e^+ e^-$	> 23000	90%
τ_{56}	$p \to \mu^- e^+ e^+$	> 19000	90%
τ_{57}	$p \to \mu^+ \mu^+ \mu^-$	> 10000	90%
τ_{58}	$p \to \mu^+ \nu \nu$	> 220	90%
τ_{59}	$p \to e^- \mu^+ \mu^+$	> 11000	90%
τ_{60}	$n \to 3\nu$	$> 5 \times 10^{-4}$	90%
τ_{61}	$n \to 5\nu$		
	Inclusive modes		
τ_{62}	$N \to e^+$ anything	> 0.6 (n, p)	90%
τ_{63}	$N \to \mu^+$ anything	> 12 (n, p)	90%
τ_{64}	$N \to \nu$ anything		
τ_{65}	$N \to e^+ \pi^0$ anything	> 0.6 (n, p)	90%
τ_{66}	$N \to$ 2 bodies, ν-free		
	$\Delta B = 2$ dinucleon modes		
	The following are lifetime limits per iron nucleus.		
τ_{67}	$p p \to \pi^+ \pi^+$	> 72.2	90%
τ_{68}	$p n \to \pi^+ \pi^0$	> 170	90%
τ_{69}	$n n \to \pi^+ \pi^-$	> 0.7	90%
τ_{70}	$n n \to \pi^0 \pi^0$	> 404	90%
τ_{71}	$p p \to K^+ K^+$	> 170	90%
τ_{72}	$p p \to e^+ e^+$	> 5.8	90%
τ_{73}	$p p \to e^+ \mu^+$	> 3.6	90%
τ_{74}	$p p \to \mu^+ \mu^+$	> 1.7	90%
τ_{75}	$p n \to e^+ \overline{\nu}$	> 260	90%
τ_{76}	$p n \to \mu^+ \overline{\nu}$	> 200	90%
τ_{77}	$p n \to \tau^+ \overline{\nu}_\tau$	> 29	90%
τ_{78}	$n n \to$ invisible	> 1.4	90%
τ_{79}	$n n \to \nu_e \overline{\nu}_e$	> 1.4	90%
τ_{80}	$n n \to \nu_\mu \overline{\nu}_\mu$	> 1.4	90%
τ_{81}	$p n \to$ invisible	> 0.06	90%
τ_{82}	$p p \to$ invisible	> 0.11	90%

$\overline{p}$ DECAY MODES

	Mode	Partial mean life (years)	Confidence level
τ_{83}	$\overline{p} \to e^- \gamma$	$> 7 \times 10^5$	90%
τ_{84}	$\overline{p} \to \mu^- \gamma$	$> 5 \times 10^4$	90%
τ_{85}	$\overline{p} \to e^- \pi^0$	$> 4 \times 10^5$	90%
τ_{86}	$\overline{p} \to \mu^- \pi^0$	$> 5 \times 10^4$	90%
τ_{87}	$\overline{p} \to e^- \eta$	$> 2 \times 10^4$	90%
τ_{88}	$\overline{p} \to \mu^- \eta$	$> 8 \times 10^3$	90%
τ_{89}	$\overline{p} \to e^- K^0_S$	> 900	90%
τ_{90}	$\overline{p} \to \mu^- K^0_S$	$> 4 \times 10^3$	90%
τ_{91}	$\overline{p} \to e^- K^0_L$	$> 9 \times 10^3$	90%
τ_{92}	$\overline{p} \to \mu^- K^0_L$	$> 7 \times 10^3$	90%
τ_{93}	$\overline{p} \to e^- \gamma \gamma$	$> 2 \times 10^4$	90%
τ_{94}	$\overline{p} \to \mu^- \gamma \gamma$	$> 2 \times 10^4$	90%
τ_{95}	$\overline{p} \to e^- \omega$	> 200	90%

p PARTIAL MEAN LIVES

The "partial mean life" limits tabulated here are the limits on τ/B_i, where τ is the total mean life for the proton and B_i is the branching fraction for the mode in question.

Decaying particle: p = proton, n = bound neutron. The same event may appear under more than one partial decay mode. Background estimates may be accurate to a factor of two.

Antilepton + meson

$\tau(N \to e^+ \pi)$ — τ_1

LIMIT (10^{30} years)	PARTICLE	CL%	EVTS	BKGD EST	DOCUMENT ID		TECN
>24000	***p***	**90**	**0**	**0.59**	[1] TAKENAKA	20	SKAM
> 5300	***n***	**90**	**0**	**0.41**	ABE	17D	SKAM
• • • We do not use the following data for averages, fits, limits, etc. • • •							
>16000	p	90	0	0.61	ABE	17	SKAM
> 2000	n	90	0	0.27	NISHINO	12	SKAM
> 8200	p	90	0	0.3	NISHINO	09	SKAM
> 540	p	90	0	0.2	MCGREW	99	IMB3
> 158	n	90	3	5	MCGREW	99	IMB3
> 1600	p	90	0	0.1	SHIOZAWA	98	SKAM
> 70	p	90	0	0.5	BERGER	91	FREJ
> 70	n	90	0	≤ 0.1	BERGER	91	FREJ
> 550	p	90	0	0.7	[2] BECKER-SZ...	90	IMB3
> 260	p	90	0	<0.04	HIRATA	89C	KAMI
> 130	n	90	0	<0.2	HIRATA	89C	KAMI
> 310	p	90	0	0.6	SEIDEL	88	IMB
> 100	n	90	0	1.6	SEIDEL	88	IMB
> 1.3	n	90	0		BARTELT	87	SOUD
> 1.3	p	90	0		BARTELT	87	SOUD
> 250	p	90	0	0.3	HAINES	86	IMB
> 31	n	90	8	9	HAINES	86	IMB
> 64	p	90	0	<0.4	ARISAKA	85	KAMI
> 26	n	90	0	<0.7	ARISAKA	85	KAMI
> 82	p (free)	90	0	0.2	BLEWITT	85	IMB
> 250	p	90	0	0.2	BLEWITT	85	IMB
> 25	n	90	4	4	PARK	85	IMB

> 15	p, n	90	0		BATTISTONI	84	NUSX
> 0.5	p	90	1	0.3	[3] BARTELT	83	SOUD
> 0.5	n	90	1	0.3	[3] BARTELT	83	SOUD
> 5.8	p	90	2		[4] KRISHNA...	82	KOLR
> 5.8	n	90	2		[4] KRISHNA...	82	KOLR
> 0.1	n	90			[5] GURR	67	CNTR

[1] TAKENAKA 20 includes data of ABE 17, and thus supersedes ABE 17.
[2] This BECKER-SZENDY 90 result includes data from SEIDEL 88.
[3] Limit based on zero events.
[4] We have calculated 90% CL limit from 1 confined event.
[5] We have converted half-life to 90% CL mean life.

$\tau(N \to \mu^+ \pi)$ — τ_2

LIMIT (10^{30} years)	PARTICLE	CL%	EVTS	BKGD EST	DOCUMENT ID		TECN
>16000	**p**	**90**	**1**	**0.94**	[1] TAKENAKA	20	SKAM
> 3500	**n**	**90**	**1**	**0.77**	ABE	17D	SKAM
• • • We do not use the following data for averages, fits, limits, etc. • • •							
> 7700	p	90	2	0.87	ABE	17	SKAM
> 1000	n	90	1	0.43	NISHINO	12	SKAM
> 6600	p	90	0	0.3	NISHINO	09	SKAM
> 473	p	90	0	0.6	MCGREW	99	IMB3
> 90	n	90	1	1.9	MCGREW	99	IMB3
> 81	p	90	0	0.2	BERGER	91	FREJ
> 35	n	90	1	1.0	BERGER	91	FREJ
> 230	p	90	0	<0.07	HIRATA	89C	KAMI
> 100	n	90	0	<0.2	HIRATA	89C	KAMI
> 270	p	90	0	0.5	SEIDEL	88	IMB
> 63	n	90	0	0.5	SEIDEL	88	IMB
> 76	p	90	2	1	HAINES	86	IMB
> 23	n	90	8	7	HAINES	86	IMB
> 46	p	90	0	<0.7	ARISAKA	85	KAMI
> 20	n	90	0	<0.4	ARISAKA	85	KAMI
> 59	p (free)	90	0	0.2	BLEWITT	85	IMB
> 100	p	90	1	0.4	BLEWITT	85	IMB
> 38	n	90	1	4	PARK	85	IMB
> 10	p, n	90	0		BATTISTONI	84	NUSX
> 1.3	p, n	90	0		ALEKSEEV	81	BAKS

[1] TAKENAKA 20 includes the data of ABE 17 and thus supersedes ABE 17.

$\tau(N \to \nu \pi)$ — τ_3

LIMIT (10^{30} years)	PARTICLE	CL%	EVTS	BKGD EST	DOCUMENT ID		TECN
> 390	**p**	**90**	**52.8**		ABE	14E	SKAM
>1100	**n**	**90**	**19.1**		ABE	14E	SKAM
• • • We do not use the following data for averages, fits, limits, etc. • • •							
> 16	p	90	6	6.7	WALL	00B	SOU2
> 39	n	90	4	3.8	WALL	00B	SOU2
> 10	p	90	15	20.3	MCGREW	99	IMB3
> 112	n	90	6	6.6	MCGREW	99	IMB3
> 13	n	90	1	1.2	BERGER	89	FREJ
> 10	p	90	11	14	BERGER	89	FREJ
> 25	p	90	32	32.8	[1] HIRATA	89C	KAMI
> 100	n	90	1	3	HIRATA	89C	KAMI
> 6	n	90	73	60	HAINES	86	IMB
> 2	p	90	16	13	KAJITA	86	KAMI
> 40	n	90	0	1	KAJITA	86	KAMI
> 7	n	90	28	19	PARK	85	IMB
> 7	n	90	0		BATTISTONI	84	NUSX
> 2	p	90	≤ 3		BATTISTONI	84	NUSX
> 5.8	p	90	1		[2] KRISHNA...	82	KOLR
> 0.3	p	90	2		[3] CHERRY	81	HOME
> 0.1	p	90			[4] GURR	67	CNTR

[1] In estimating the background, this HIRATA 89C limit (as opposed to the later limits of WALL 00B and MCGREW 99) does not take into account present understanding that the flux of ν_μ originating in the upper atmosphere is depleted. Doing so would reduce the background and thus also would reduce the limit here.
[2] We have calculated 90% CL limit from 1 confined event.
[3] We have converted 2 possible events to 90% CL limit.
[4] We have converted half-life to 90% CL mean life.

$\tau(p \to e^+ \eta)$ — τ_4

LIMIT (10^{30} years)	PARTICLE	CL%	EVTS	BKGD EST	DOCUMENT ID		TECN
>14000	**p**	**90**	**0**	**0.42**	[1] TANIUCHI	24	SKAM
• • • We do not use the following data for averages, fits, limits, etc. • • •							
>10000	p	90	0	0.78	ABE	17D	SKAM
> 4200	p	90	0	0.44	NISHINO	12	SKAM
> 81	p	90	1	1.7	WALL	00B	SOU2
> 313	p	90	0	0.2	MCGREW	99	IMB3
> 44	p	90	0	0.1	BERGER	91	FREJ
> 140	p	90	0	<0.04	HIRATA	89C	KAMI
> 100	p	90	0	0.6	SEIDEL	88	IMB
> 200	p	90	5	3.3	HAINES	86	IMB
> 64	p	90	0	<0.8	ARISAKA	85	KAMI
> 64	p (free)	90	5	6.5	BLEWITT	85	IMB
> 200	p	90	5	4.7	BLEWITT	85	IMB
> 1.2	p	90	2		[2] CHERRY	81	HOME

[1] TANIUCHI 24 includes the ABE 17D dataset and thus supersedes ABE 17D entries.
[2] We have converted 2 possible events to 90% CL limit.

$\tau(p \to \mu^+ \eta)$ — τ_5

LIMIT (10^{30} years)	PARTICLE	CL%	EVTS	BKGD EST	DOCUMENT ID		TECN
>7300	**p**	**90**	**2**	**0.93**	[1] TANIUCHI	24	SKAM
• • • We do not use the following data for averages, fits, limits, etc. • • •							
>4700	p	90	2	0.85	ABE	17D	SKAM
>1300	p	90	2	0.49	NISHINO	12	SKAM
> 89	p	90	0	1.6	WALL	00B	SOU2
> 126	p	90	3	2.8	MCGREW	99	IMB3
> 26	p	90	1	0.8	BERGER	91	FREJ
> 69	p	90	1	<0.08	HIRATA	89C	KAMI
> 1.3	p	90	0	0.7	PHILLIPS	89	HPW
> 34	p	90	1	1.5	SEIDEL	88	IMB
> 46	p	90	7	6	HAINES	86	IMB
> 26	p	90	1	<0.8	ARISAKA	85	KAMI
> 17	p (free)	90	6	6	BLEWITT	85	IMB
> 46	p	90	7	8	BLEWITT	85	IMB

[1] TANIUCHI 24 includes the ABE 17D dataset and thus supersedes ABE 17D entries.

$\tau(n \to \nu \eta)$ — τ_6

LIMIT (10^{30} years)	PARTICLE	CL%	EVTS	BKGD EST	DOCUMENT ID		TECN
>158	**n**	**90**	**0**	**1.2**	MCGREW	99	IMB3
• • • We do not use the following data for averages, fits, limits, etc. • • •							
> 71	n	90	2	3.7	WALL	00B	SOU2
> 29	n	90	0	0.9	BERGER	89	FREJ
> 54	n	90	2	0.9	HIRATA	89C	KAMI
> 16	n	90	3	2.1	SEIDEL	88	IMB
> 25	n	90	7	6	HAINES	86	IMB
> 30	n	90	0	0.4	KAJITA	86	KAMI
> 18	n	90	4	3	PARK	85	IMB
> 0.6	n	90	2		[1] CHERRY	81	HOME

[1] We have converted 2 possible events to 90% CL limit.

$\tau(N \to e^+ \rho)$ — τ_7

LIMIT (10^{30} years)	PARTICLE	CL%	EVTS	BKGD EST	DOCUMENT ID		TECN
>720	**p**	**90**	**2**	**0.64**	ABE	17D	SKAM
>217	**n**	**90**	**4**	**4.8**	MCGREW	99	IMB3
• • • We do not use the following data for averages, fits, limits, etc. • • •							
> 30	n	90	4	0.87	ABE	17D	SKAM
>710	p	90	0	0.35	NISHINO	12	SKAM
> 70	n	90	1	0.38	NISHINO	12	SKAM
> 29	p	90	0	2.2	BERGER	91	FREJ
> 41	n	90	0	1.4	BERGER	91	FREJ
> 75	p	90	2	2.7	HIRATA	89C	KAMI
> 58	n	90	0	1.9	HIRATA	89C	KAMI
> 38	n	90	2	4.1	SEIDEL	88	IMB
> 1.2	p	90	0		BARTELT	87	SOUD
> 1.5	n	90	0		BARTELT	87	SOUD
> 17	p	90	7	7	HAINES	86	IMB
> 14	n	90	9	4	HAINES	86	IMB
> 12	p	90	0	<1.2	ARISAKA	85	KAMI
> 6	n	90	2	<1	ARISAKA	85	KAMI
> 6.7	p (free)	90	6	6	BLEWITT	85	IMB
> 17	p	90	7	7	BLEWITT	85	IMB
> 12	n	90	4	2	PARK	85	IMB
> 0.6	n	90	1	0.3	[1] BARTELT	83	SOUD
> 0.5	p	90	1	0.3	[1] BARTELT	83	SOUD
> 9.8	p	90	1		[2] KRISHNA...	82	KOLR
> 0.8	p	90	2		[3] CHERRY	81	HOME

[1] Limit based on zero events.
[2] We have calculated 90% CL limit from 0 confined events.
[3] We have converted 2 possible events to 90% CL limit.

$\tau(N \to \mu^+ \rho)$ — τ_8

LIMIT (10^{30} years)	PARTICLE	CL%	EVTS	BKGD EST	DOCUMENT ID		TECN
>570	**p**	**90**	**1**	**1.30**	ABE	17D	SKAM
>228	**n**	**90**	**3**	**9.5**	MCGREW	99	IMB3
• • • We do not use the following data for averages, fits, limits, etc. • • •							
> 60	n	90	1	0.96	ABE	17D	SKAM
>160	p	90	1	0.42	NISHINO	12	SKAM
> 36	n	90	0	0.29	NISHINO	12	SKAM
> 12	p	90	0	0.5	BERGER	91	FREJ
> 22	n	90	0	1.1	BERGER	91	FREJ
>110	p	90	0	1.7	HIRATA	89C	KAMI
> 23	n	90	1	1.8	HIRATA	89C	KAMI
> 4.3	p	90	0	0.7	PHILLIPS	89	HPW
> 30	p	90	0	0.5	SEIDEL	88	IMB
> 11	n	90	1	1.1	SEIDEL	88	IMB
> 16	p	90	4	4.5	HAINES	86	IMB
> 7	n	90	6	5	HAINES	86	IMB
> 12	p	90	0	<0.7	ARISAKA	85	KAMI

Int. J. Mod. Phys. A 2026.41. Downloaded from www.worldscientific.com
by UNIVERSITY OF CALIFORNIA @ BERKELEY on 09/16/26. Re-use and distribution is strictly not permitted, except for Open Access articles.

> 5	*n*	90	1	<1.2	ARISAKA	85	KAMI
> 5.5	*p* (free)	90	4	5	BLEWITT	85	IMB
> 16	*p*	90	4	5	BLEWITT	85	IMB
> 9	*n*	90	1	2	PARK	85	IMB

$\tau(N \to \nu\rho)$ — τ_9

LIMIT (10^{30} years)	PARTICLE	CL%	EVTS	BKGD EST	DOCUMENT ID		TECN
>162	***p***	**90**	**18**	**21.7**	MCGREW	99	IMB3
> 19	***n***	**90**	**0**	**0.5**	SEIDEL	88	IMB
• • • We do not use the following data for averages, fits, limits, etc. • • •							
> 9	*n*	90	4	2.4	BERGER	89	FREJ
> 24	*p*	90	0	0.9	BERGER	89	FREJ
> 27	*p*	90	5	1.5	HIRATA	89C	KAMI
> 13	*n*	90	4	3.6	HIRATA	89C	KAMI
> 13	*p*	90	1	1.1	SEIDEL	88	IMB
> 8	*p*	90	6	5	HAINES	86	IMB
> 2	*n*	90	15	10	HAINES	86	IMB
> 11	*p*	90	2	1	KAJITA	86	KAMI
> 4	*n*	90	2	2	KAJITA	86	KAMI
> 4.1	*p* (free)	90	6	7	BLEWITT	85	IMB
> 8.4	*p*	90	6	5	BLEWITT	85	IMB
> 2	*n*	90	7	3	PARK	85	IMB
> 0.9	*p*	90	2		[1] CHERRY	81	HOME
> 0.6	*n*	90	2		[1] CHERRY	81	HOME

[1] We have converted 2 possible events to 90% CL limit.

$\tau(p \to e^+\omega)$ — τ_{10}

LIMIT (10^{30} years)	PARTICLE	CL%	EVTS	BKGD EST	DOCUMENT ID		TECN
>1600	***p***	**90**	**1**	**1.35**	ABE	17D	SKAM
• • • We do not use the following data for averages, fits, limits, etc. • • •							
> 320	*p*	90	1	0.53	NISHINO	12	SKAM
> 107	*p*	90	7	10.8	MCGREW	99	IMB3
> 17	*p*	90	0	1.1	BERGER	91	FREJ
> 45	*p*	90	2	1.45	HIRATA	89C	KAMI
> 26	*p*	90	1	1.0	SEIDEL	88	IMB
> 1.5	*p*	90	0		BARTELT	87	SOUD
> 37	*p*	90	6	5.3	HAINES	86	IMB
> 25	*p*	90	1	<1.4	ARISAKA	85	KAMI
> 12	*p* (free)	90	6	7.5	BLEWITT	85	IMB
> 37	*p*	90	6	5.7	BLEWITT	85	IMB
> 0.6	*p*	90	1	0.3	[1] BARTELT	83	SOUD
> 9.8	*p*	90	1		[2] KRISHNA...	82	KOLR
> 2.8	*p*	90	2		[3] CHERRY	81	HOME

[1] Limit based on zero events.
[2] We have calculated 90% CL limit from 0 confined events.
[3] We have converted 2 possible events to 90% CL limit.

$\tau(p \to \mu^+\omega)$ — τ_{11}

LIMIT (10^{30} years)	PARTICLE	CL%	EVTS	BKGD EST	DOCUMENT ID		TECN
>2800	***p***	**90**	**0**	**1.09**	ABE	17D	SKAM
• • • We do not use the following data for averages, fits, limits, etc. • • •							
> 780	*p*	90	0	0.48	NISHINO	12	SKAM
> 117	*p*	90	11	12.1	MCGREW	99	IMB3
> 11	*p*	90	0	1.0	BERGER	91	FREJ
> 57	*p*	90	2	1.9	HIRATA	89C	KAMI
> 4.4	*p*	90	0	0.7	PHILLIPS	89	HPW
> 10	*p*	90	2	1.3	SEIDEL	88	IMB
> 23	*p*	90	2	1	HAINES	86	IMB
> 6.5	*p* (free)	90	9	8.7	BLEWITT	85	IMB
> 23	*p*	90	8	7	BLEWITT	85	IMB

$\tau(n \to \nu\omega)$ — τ_{12}

LIMIT (10^{30} years)	PARTICLE	CL%	EVTS	BKGD EST	DOCUMENT ID		TECN
>108	***n***	**90**	**12**	**22.5**	MCGREW	99	IMB3
• • • We do not use the following data for averages, fits, limits, etc. • • •							
> 17	*n*	90	1	0.7	BERGER	89	FREJ
> 43	*n*	90	3	2.7	HIRATA	89C	KAMI
> 6	*n*	90	2	1.3	SEIDEL	88	IMB
> 12	*n*	90	6	6	HAINES	86	IMB
> 18	*n*	90	2	2	KAJITA	86	KAMI
> 16	*n*	90	1	2	PARK	85	IMB
> 2.0	*n*	90	2		[1] CHERRY	81	HOME

[1] We have converted 2 possible events to 90% CL limit.

$\tau(N \to e^+K)$ — τ_{13}

LIMIT (10^{30} years)	PARTICLE	CL%	EVTS	BKGD EST	DOCUMENT ID		TECN
>1000	***p***	**90**	**6**	**4.7**	KOBAYASHI	05	SKAM
> 17	***n***	**90**	**35**	**29.4**	MCGREW	99	IMB3
• • • We do not use the following data for averages, fits, limits, etc. • • •							
> 85	*p*	90	3	4.9	WALL	00	SOU2
> 31	*p*	90	23	25.2	MCGREW	99	IMB3
> 60	*p*	90	0		BERGER	91	FREJ
> 150	*p*	90	0	<0.27	HIRATA	89C	KAMI
> 70	*p*	90	0	1.8	SEIDEL	88	IMB
> 77	*p*	90	5	4.5	HAINES	86	IMB
> 38	*p*	90	0	<0.8	ARISAKA	85	KAMI
> 24	*p* (free)	90	7	8.5	BLEWITT	85	IMB
> 77	*p*	90	5	4	BLEWITT	85	IMB
> 1.3	*p*	90	0		ALEKSEEV	81	BAKS
> 1.3	*n*	90	0		ALEKSEEV	81	BAKS

$\tau(p \to e^+K^0_S)$ — τ_{14}

LIMIT (10^{30} years)	PARTICLE	CL%	EVTS	BKGD EST	DOCUMENT ID		TECN
• • • We do not use the following data for averages, fits, limits, etc. • • •							
>120	*p*	90	1	1.3	WALL	00	SOU2
> 76	*p*	90	0	0.5	BERGER	91	FREJ

$\tau(p \to e^+K^0_L)$ — τ_{15}

LIMIT (10^{30} years)	PARTICLE	CL%	EVTS	BKGD EST	DOCUMENT ID		TECN
• • • We do not use the following data for averages, fits, limits, etc. • • •							
>51	*p*	90	2	3.5	WALL	00	SOU2
>44	*p*	90	0	≤ 0.1	BERGER	91	FREJ

$\tau(N \to \mu^+K)$ — τ_{16}

LIMIT (10^{30} years)	PARTICLE	CL%	EVTS	BKGD EST	DOCUMENT ID		TECN
>4500	***p***	**90**	**1**	**3.08**	[1] MATSUMOTO	22	SKAM
> 26	***n***	**90**	**20**	**28.4**	MCGREW	99	IMB3
• • • We do not use the following data for averages, fits, limits, etc. • • •							
>3600	*p*	90	14	16.3	[2] MATSUMOTO	22	SKAM
>1600	*p*	90	13	13.2	REGIS	12	SKAM
>1300	p	90	3	3.9	KOBAYASHI	05	SKAM
> 120	*p*	90	0	<1.2	WALL	00	SOU2
> 120	*p*	90	4	7.2	MCGREW	99	IMB3
> 54	*p*	90	0		BERGER	91	FREJ
> 120	*p*	90	1	0.4	HIRATA	89C	KAMI
> 3.0	*p*	90	0	0.7	PHILLIPS	89	HPW
> 19	*p*	90	3	2.5	SEIDEL	88	IMB
> 1.5	*p*	90	0		[3] BARTELT	87	SOUD
> 1.1	*n*	90	0		BARTELT	87	SOUD
> 40	*p*	90	7	6	HAINES	86	IMB
> 19	*p*	90	1	<1.1	ARISAKA	85	KAMI
> 6.7	*p* (free)	90	11	13	BLEWITT	85	IMB
> 40	*p*	90	7	8	BLEWITT	85	IMB
> 6	*p*	90	1		BATTISTONI	84	NUSX
> 0.6	*p*	90	0		[4] BARTELT	83	SOUD
> 0.4	*n*	90	0		[4] BARTELT	83	SOUD
> 5.8	*p*	90	2		[5] KRISHNA...	82	KOLR
> 2.0	*p*	90	0		CHERRY	81	HOME
> 0.2	*n*	90			[6] GURR	67	CNTR

[1] MATSUMOTO 22 limit $> 4500 \times 10^{30}$ is derived from the latest dataset SKA IV phase (from 2008 to 2018) with 0.20 Mton-years of exposure.
[2] MATSUMOTO 22 limit $> 3600 \times 10^{30}$ is derived from a combination of all datasets SKA I,II, III and IV phase (from 1996 to 2018) with a total of 0.37 Mton-years of exposure. Note, the limit from only SKA IV is stronger, because there were some events observed in SKA II.
[3] BARTELT 87 limit applies to $p \to \mu^+ K^0_S$.
[4] Limit based on zero events.
[5] We have calculated 90% CL limit from 1 confined event.
[6] We have converted half-life to 90% CL mean life.

$\tau(p \to \mu^+K^0_S)$ — τ_{17}

LIMIT (10^{30} years)	PARTICLE	CL%	EVTS	BKGD EST	DOCUMENT ID		TECN
• • • We do not use the following data for averages, fits, limits, etc. • • •							
>150	*p*	90	0	<0.8	WALL	00	SOU2
> 64	*p*	90	0	1.2	BERGER	91	FREJ

$\tau(p \to \mu^+K^0_L)$ — τ_{18}

LIMIT (10^{30} years)	PARTICLE	CL%	EVTS	BKGD EST	DOCUMENT ID		TECN
• • • We do not use the following data for averages, fits, limits, etc. • • •							
>83	*p*	90	0	0.4	WALL	00	SOU2
>44	*p*	90	0	≤ 0.1	BERGER	91	FREJ

$\tau(N \to \nu K)$ — τ_{19}

LIMIT (10^{30} years)	PARTICLE	CL%	EVTS	BKGD EST	DOCUMENT ID		TECN
>5900	***p***	**90**	**0**	**1.0**	ABE	14G	SKAM
> 86	***n***	**90**	**0**	**2.4**	HIRATA	89C	KAMI
• • • We do not use the following data for averages, fits, limits, etc. • • •							
> 540	*p*	90	0	0.9	ASAKURA	15	KLND
>2300	*p*	90	0	1.3	KOBAYASHI	05	SKAM
> 26	*n*	90	16	9.1	WALL	00	SOU2
> 670	*p*	90			HAYATO	99	SKAM

Int. J. Mod. Phys. A 2026.41. Downloaded from www.worldscientific.com
UNIVERSITY OF CALIFORNIA @ BERKELEY on 09/16/26. Re-use and distribution is strictly not permitted, except for Open Access articles.

> 151	p	90	15	21.4		MCGREW	99	IMB3
> 30	n	90	34	34.1		MCGREW	99	IMB3
> 43	p	90	1	1.54	[1]	ALLISON	98	SOU2
> 15	n	90	1	1.8		BERGER	89	FREJ
> 15	p	90	1	1.8		BERGER	89	FREJ
> 100	p	90	9	7.3		HIRATA	89C	KAMI
> 0.28	p	90	0	0.7		PHILLIPS	89	HPW
> 0.3	p	90	0			BARTELT	87	SOUD
> 0.75	n	90	0		[2]	BARTELT	87	SOUD
> 10	p	90	6	5		HAINES	86	IMB
> 15	n	90	3	5		HAINES	86	IMB
> 28	p	90	3	3		KAJITA	86	KAMI
> 32	n	90	0	1.4		KAJITA	86	KAMI
> 1.8	p (free)	90	6	11		BLEWITT	85	IMB
> 9.6	p	90	6	5		BLEWITT	85	IMB
> 10	n	90	2	2		PARK	85	IMB
> 5	n	90	0			BATTISTONI	84	NUSX
> 2	p	90	0			BATTISTONI	84	NUSX
> 0.3	n	90	0		[3]	BARTELT	83	SOUD
> 0.1	p	90	0		[3]	BARTELT	83	SOUD
> 5.8	p	90	1		[4]	KRISHNA...	82	KOLR
> 0.3	n	90	2		[5]	CHERRY	81	HOME

[1] This ALLISON 98 limit is with no background subtraction; with subtraction the limit becomes $> 46 \times 10^{30}$ years.
[2] BARTELT 87 limit applies to $n \to \nu K^0_S$.
[3] Limit based on zero events.
[4] We have calculated 90% CL limit from 1 confined event.
[5] We have converted 2 possible events to 90% CL limit.

$\tau(n \to \nu K^0_S)$ — τ_{20}

LIMIT (10^{30} years)	PARTICLE	CL%	EVTS	BKGD EST		DOCUMENT ID		TECN
>1560	**n**	**90**	**198**	**166**	[1]	YAMAUCHI	25	SKAM
• • • We do not use the following data for averages, fits, limits, etc. • • •								
> 260	n	90	34	30	[2]	KOBAYASHI	05	SKAM
> 51	n	90	16	9.1		WALL	00	SOU2

[1] We have doubled the $n \to \nu K^0$ limit given in YAMAUCHI 25 to obtain this $n \to \nu K^0_S$ limit. The result is based on the full 0.401 Mton-year exposure of all pure water phases.
[2] Superseded by YAMAUCHI 25. We have doubled the $n \to \nu K^0$ limit given in KOBAYASHI 05 to obtain this $n \to \nu K^0_S$ limit.

$\tau(p \to e^+ K^*(892)^0)$ — τ_{21}

LIMIT (10^{30} years)	PARTICLE	CL%	EVTS	BKGD EST	DOCUMENT ID		TECN
>84	**p**	**90**	**38**	**52.0**	MCGREW	99	IMB3
• • • We do not use the following data for averages, fits, limits, etc. • • •							
>10	p	90	0	0.8	BERGER	91	FREJ
>52	p	90	2	1.55	HIRATA	89C	KAMI
>10	p	90	1	<1	ARISAKA	85	KAMI

$\tau(N \to \nu K^*(892))$ — τ_{22}

LIMIT (10^{30} years)	PARTICLE	CL%	EVTS	BKGD EST	DOCUMENT ID		TECN
>51	**p**	**90**	**7**	**9.1**	MCGREW	99	IMB3
>78	**n**	**90**	**40**	**50**	MCGREW	99	IMB3
• • • We do not use the following data for averages, fits, limits, etc. • • •							
>22	n	90	0	2.1	BERGER	89	FREJ
>17	p	90	0	2.4	BERGER	89	FREJ
>20	p	90	5	2.1	HIRATA	89C	KAMI
>21	n	90	4	2.4	HIRATA	89C	KAMI
>10	p	90	7	6	HAINES	86	IMB
> 5	n	90	8	7	HAINES	86	IMB
> 8	p	90	3	2	KAJITA	86	KAMI
> 6	n	90	2	1.6	KAJITA	86	KAMI
> 5.8	p (free)	90	10	16	BLEWITT	85	IMB
> 9.6	p	90	7	6	BLEWITT	85	IMB
> 7	n	90	1	4	PARK	85	IMB
> 2.1	p	90	1		[1] BATTISTONI	82	NUSX

[1] We have converted 1 possible event to 90% CL limit.

Antilepton + mesons

$\tau(p \to e^+ \pi^+ \pi^-)$ — τ_{23}

LIMIT (10^{30} years)	PARTICLE	CL%	EVTS	BKGD EST	DOCUMENT ID		TECN
>82	**p**	**90**	**16**	**23.1**	MCGREW	99	IMB3
• • • We do not use the following data for averages, fits, limits, etc. • • •							
>21	p	90	0	2.2	BERGER	91	FREJ

$\tau(p \to e^+ \pi^0 \pi^0)$ — τ_{24}

LIMIT (10^{30} years)	PARTICLE	CL%	EVTS	BKGD EST	DOCUMENT ID		TECN
>147	**p**	**90**	**2**	**0.8**	MCGREW	99	IMB3
• • • We do not use the following data for averages, fits, limits, etc. • • •							
> 38	p	90	1	0.5	BERGER	91	FREJ

$\tau(n \to e^+ \pi^- \pi^0)$ — τ_{25}

LIMIT (10^{30} years)	PARTICLE	CL%	EVTS	BKGD EST	DOCUMENT ID		TECN
>52	**n**	**90**	**38**	**34.2**	MCGREW	99	IMB3
• • • We do not use the following data for averages, fits, limits, etc. • • •							
>32	n	90	1	0.8	BERGER	91	FREJ

$\tau(p \to \mu^+ \pi^+ \pi^-)$ — τ_{26}

LIMIT (10^{30} years)	PARTICLE	CL%	EVTS	BKGD EST	DOCUMENT ID		TECN
>133	**p**	**90**	**25**	**38.0**	MCGREW	99	IMB3
• • • We do not use the following data for averages, fits, limits, etc. • • •							
> 17	p	90	1	2.6	BERGER	91	FREJ
> 3.3	p	90	0	0.7	PHILLIPS	89	HPW

$\tau(p \to \mu^+ \pi^0 \pi^0)$ — τ_{27}

LIMIT (10^{30} years)	PARTICLE	CL%	EVTS	BKGD EST	DOCUMENT ID		TECN
>101	**p**	**90**	**3**	**1.6**	MCGREW	99	IMB3
• • • We do not use the following data for averages, fits, limits, etc. • • •							
> 33	p	90	1	0.9	BERGER	91	FREJ

$\tau(n \to \mu^+ \pi^- \pi^0)$ — τ_{28}

LIMIT (10^{30} years)	PARTICLE	CL%	EVTS	BKGD EST	DOCUMENT ID		TECN
>74	**n**	**90**	**17**	**20.8**	MCGREW	99	IMB3
• • • We do not use the following data for averages, fits, limits, etc. • • •							
>33	n	90	0	1.1	BERGER	91	FREJ

$\tau(n \to e^+ K^0 \pi^-)$ — τ_{29}

LIMIT (10^{30} years)	PARTICLE	CL%	EVTS	BKGD EST	DOCUMENT ID		TECN
>18	**n**	**90**	**1**	**0.2**	BERGER	91	FREJ

Lepton + meson

$\tau(n \to e^- \pi^+)$ — τ_{30}

LIMIT (10^{30} years)	PARTICLE	CL%	EVTS	BKGD EST	DOCUMENT ID		TECN
>65	**n**	**90**	**0**	**1.6**	SEIDEL	88	IMB
• • • We do not use the following data for averages, fits, limits, etc. • • •							
>55	n	90	0	1.09	BERGER	91B	FREJ
>16	n	90	9	7	HAINES	86	IMB
>25	n	90	2	4	PARK	85	IMB

$\tau(n \to \mu^- \pi^+)$ — τ_{31}

LIMIT (10^{30} years)	PARTICLE	CL%	EVTS	BKGD EST	DOCUMENT ID		TECN
>49	**n**	**90**	**0**	**0.5**	SEIDEL	88	IMB
• • • We do not use the following data for averages, fits, limits, etc. • • •							
>33	n	90	0	1.40	BERGER	91B	FREJ
> 2.7	n	90	0	0.7	PHILLIPS	89	HPW
>25	n	90	7	6	HAINES	86	IMB
>27	n	90	2	3	PARK	85	IMB

$\tau(n \to e^- \rho^+)$ — τ_{32}

LIMIT (10^{30} years)	PARTICLE	CL%	EVTS	BKGD EST	DOCUMENT ID		TECN
>62	**n**	**90**	**2**	**4.1**	SEIDEL	88	IMB
• • • We do not use the following data for averages, fits, limits, etc. • • •							
>12	n	90	13	6	HAINES	86	IMB
>12	n	90	5	3	PARK	85	IMB

$\tau(n \to \mu^- \rho^+)$ — τ_{33}

LIMIT (10^{30} years)	PARTICLE	CL%	EVTS	BKGD EST	DOCUMENT ID		TECN
>7	**n**	**90**	**1**	**1.1**	SEIDEL	88	IMB
• • • We do not use the following data for averages, fits, limits, etc. • • •							
>2.6	n	90	0	0.7	PHILLIPS	89	HPW
>9	n	90	7	5	HAINES	86	IMB
>9	n	90	2	2	PARK	85	IMB

$\tau(n \to e^- K^+)$ — τ_{34}

LIMIT (10^{30} years)	PARTICLE	CL%	EVTS	BKGD EST	DOCUMENT ID		TECN
>32	**n**	**90**	**3**	**2.96**	BERGER	91B	FREJ
• • • We do not use the following data for averages, fits, limits, etc. • • •							
> 0.23	n	90	0	0.7	PHILLIPS	89	HPW

$\tau(n \to \mu^- K^+)$ — τ_{35}

LIMIT (10^{30} years)	PARTICLE	CL%	EVTS	BKGD EST	DOCUMENT ID		TECN
>57	**n**	**90**	**0**	**2.18**	BERGER	91B	FREJ
• • • We do not use the following data for averages, fits, limits, etc. • • •							
> 4.7	n	90	0	0.7	PHILLIPS	89	HPW

Int. J. Mod. Phys. A 2026.41. Downloaded from www.worldscientific.com
by UNIVERSITY OF CALIFORNIA @ BERKELEY on 09/16/26. Re-use and distribution is strictly not permitted, except for Open Access articles.

Int. J. Mod. Phys. A 2026.41. Downloaded from www.worldscientific.com
UNIVERSITY OF CALIFORNIA @ BERKELEY on 09/16/26. Re-use and distribution is strictly not permitted, except for Open Access articles.

Lepton + mesons

$\tau(p \to e^- \pi^+ \pi^+)$ — τ_{36}

LIMIT (10^{30} years)	PARTICLE	CL%	EVTS	BKGD EST	DOCUMENT ID		TECN
>30	***p***	**90**	**1**	**2.50**	BERGER	91B	FREJ
• • • We do not use the following data for averages, fits, limits, etc. • • •							
> 2.0	*p*	90	0	0.7	PHILLIPS	89	HPW

$\tau(n \to e^- \pi^+ \pi^0)$ — τ_{37}

LIMIT (10^{30} years)	PARTICLE	CL%	EVTS	BKGD EST	DOCUMENT ID		TECN
>29	***n***	**90**	**1**	**0.78**	BERGER	91B	FREJ

$\tau(p \to \mu^- \pi^+ \pi^+)$ — τ_{38}

LIMIT (10^{30} years)	PARTICLE	CL%	EVTS	BKGD EST	DOCUMENT ID		TECN
>17	***p***	**90**	**1**	**1.72**	BERGER	91B	FREJ
• • • We do not use the following data for averages, fits, limits, etc. • • •							
> 7.8	*p*	90	0	0.7	PHILLIPS	89	HPW

$\tau(n \to \mu^- \pi^+ \pi^0)$ — τ_{39}

LIMIT (10^{30} years)	PARTICLE	CL%	EVTS	BKGD EST	DOCUMENT ID		TECN
>34	***n***	**90**	**0**	**0.78**	BERGER	91B	FREJ

$\tau(p \to e^- \pi^+ K^+)$ — τ_{40}

LIMIT (10^{30} years)	PARTICLE	CL%	EVTS	BKGD EST	DOCUMENT ID		TECN
>75	***p***	**90**	**81**	**127.2**	MCGREW	99	IMB3
• • • We do not use the following data for averages, fits, limits, etc. • • •							
>20	*p*	90	3	2.50	BERGER	91B	FREJ

$\tau(p \to \mu^- \pi^+ K^+)$ — τ_{41}

LIMIT (10^{30} years)	PARTICLE	CL%	EVTS	BKGD EST	DOCUMENT ID		TECN
>245	***p***	**90**	**3**	**4.0**	MCGREW	99	IMB3
• • • We do not use the following data for averages, fits, limits, etc. • • •							
> 5	*p*	90	2	0.78	BERGER	91B	FREJ

Antilepton + photon(s)

$\tau(p \to e^+ \gamma)$ — τ_{42}

LIMIT (10^{30} years)	PARTICLE	CL%	EVTS	BKGD EST	DOCUMENT ID		TECN
>670	***p***	**90**	**0**	**0.1**	MCGREW	99	IMB3
• • • We do not use the following data for averages, fits, limits, etc. • • •							
>133	*p*	90	0	0.3	BERGER	91	FREJ
>460	*p*	90	0	0.6	SEIDEL	88	IMB
>360	*p*	90	0	0.3	HAINES	86	IMB
> 87	*p* (free)	90	0	0.2	BLEWITT	85	IMB
>360	*p*	90	0	0.2	BLEWITT	85	IMB
> 0.1	*p*	90		[1]	GURR	67	CNTR

[1] We have converted half-life to 90% CL mean life.

$\tau(p \to \mu^+ \gamma)$ — τ_{43}

LIMIT (10^{30} years)	PARTICLE	CL%	EVTS	BKGD EST	DOCUMENT ID		TECN
>478	***p***	**90**	**0**	**0.1**	MCGREW	99	IMB3
• • • We do not use the following data for averages, fits, limits, etc. • • •							
>155	*p*	90	0	0.1	BERGER	91	FREJ
>380	*p*	90	0	0.5	SEIDEL	88	IMB
> 97	*p*	90	3	2	HAINES	86	IMB
> 61	*p* (free)	90	0	0.2	BLEWITT	85	IMB
>280	*p*	90	0	0.6	BLEWITT	85	IMB
> 0.3	*p*	90		[1]	GURR	67	CNTR

[1] We have converted half-life to 90% CL mean life.

$\tau(n \to \nu\gamma)$ — τ_{44}

LIMIT (10^{30} years)	PARTICLE	CL%	EVTS	BKGD EST	DOCUMENT ID		TECN
>550		**90**			TAKHISTOV	15	SKAM
• • • We do not use the following data for averages, fits, limits, etc. • • •							
> 28	*n*	90	163	144.7	MCGREW	99	IMB3
> 24	*n*	90	10	6.86	BERGER	91B	FREJ
> 9	*n*	90	73	60	HAINES	86	IMB
> 11	*n*	90	28	19	PARK	85	IMB

$\tau(p \to e^+ \gamma\gamma)$ — τ_{45}

LIMIT (10^{30} years)	PARTICLE	CL%	EVTS	BKGD EST	DOCUMENT ID		TECN
>100	***p***	**90**	**1**	**0.8**	BERGER	91	FREJ

$\tau(n \to \nu\gamma\gamma)$ — τ_{46}

LIMIT (10^{30} years)	PARTICLE	CL%	EVTS	BKGD EST	DOCUMENT ID		TECN
>219	***n***	**90**	**5**	**7.5**	MCGREW	99	IMB3

Antilepton + single massless

$\tau(p \to e^+ X)$ — τ_{47}

VALUE (10^{30} years)	CL%	DOCUMENT ID		TECN
>790	90	TAKHISTOV	15	SKAM

$\tau(p \to \mu^+ X)$ — τ_{48}

VALUE (10^{30} years)	CL%	DOCUMENT ID		TECN
>410	90	TAKHISTOV	15	SKAM

Three (or more) leptons

$\tau(p \to e^+ e^+ e^-)$ — τ_{49}

LIMIT (10^{30} years)	PARTICLE	CL%	EVTS	BKGD EST	DOCUMENT ID		TECN
>34000	***p***	**90**	**0**	**0.58**	TANAKA	20	SKAM
• • • We do not use the following data for averages, fits, limits, etc. • • •							
> 793	*p*	90	0	0.5	MCGREW	99	IMB3
> 147	*p*	90	0	0.1	BERGER	91	FREJ
> 510	*p*	90	0	0.3	HAINES	86	IMB
> 89	*p* (free)	90	0	0.5	BLEWITT	85	IMB
> 510	*p*	90	0	0.7	BLEWITT	85	IMB

$\tau(p \to e^+ \mu^+ \mu^-)$ — τ_{50}

LIMIT (10^{30} years)	PARTICLE	CL%	EVTS	BKGD EST	DOCUMENT ID		TECN
>9200	***p***	**90**	**1**	**0.27**	TANAKA	20	SKAM
• • • We do not use the following data for averages, fits, limits, etc. • • •							
> 359	*p*	90	1	0.9	MCGREW	99	IMB3
> 81	*p*	90	0	0.16	BERGER	91	FREJ
> 5.0	*p*	90	0	0.7	PHILLIPS	89	HPW

$\tau(p \to e^+ \nu\nu)$ — τ_{51}

LIMIT (10^{30} years)	PARTICLE	CL%	EVTS	BKGD EST	DOCUMENT ID		TECN
>170	***p***	**90**			[1] TAKHISTOV	14	SKAM
• • • We do not use the following data for averages, fits, limits, etc. • • •							
> 17	*p*	90	152	153.7	MCGREW	99	IMB3
> 11	*p*	90	11	6.08	BERGER	91B	FREJ

[1] Allowed events at 90% CL are 459.

$\tau(n \to e^+ e^- \nu)$ — τ_{52}

LIMIT (10^{30} years)	PARTICLE	CL%	EVTS	BKGD EST	DOCUMENT ID		TECN
>257	***n***	**90**	**5**	**7.5**	MCGREW	99	IMB3
• • • We do not use the following data for averages, fits, limits, etc. • • •							
> 74	*n*	90	0	< 0.1	BERGER	91B	FREJ
> 45	*n*	90	5	5	HAINES	86	IMB
> 26	*n*	90	4	3	PARK	85	IMB

$\tau(n \to \mu^+ e^- \nu)$ — τ_{53}

LIMIT (10^{30} years)	PARTICLE	CL%	EVTS	BKGD EST	DOCUMENT ID		TECN
>83	***n***	**90**	**25**	**29.4**	MCGREW	99	IMB3
• • • We do not use the following data for averages, fits, limits, etc. • • •							
>47	*n*	90	0	< 0.1	BERGER	91B	FREJ

$\tau(n \to \mu^+ \mu^- \nu)$ — τ_{54}

LIMIT (10^{30} years)	PARTICLE	CL%	EVTS	BKGD EST	DOCUMENT ID		TECN
>79	***n***	**90**	**100**	**145**	MCGREW	99	IMB3
• • • We do not use the following data for averages, fits, limits, etc. • • •							
>42	*n*	90	0	1.4	BERGER	91B	FREJ
> 5.1	*n*	90	0	0.7	PHILLIPS	89	HPW
>16	*n*	90	14	7	HAINES	86	IMB
>19	*n*	90	4	7	PARK	85	IMB

$\tau(p \to \mu^+ e^+ e^-)$ — τ_{55}

LIMIT (10^{30} years)	PARTICLE	CL%	EVTS	BKGD EST	DOCUMENT ID		TECN
>23000	***p***	**90**	**0**	**0.5**	TANAKA	20	SKAM
• • • We do not use the following data for averages, fits, limits, etc. • • •							
> 529	*p*	90	0	1.0	MCGREW	99	IMB3
> 91	*p*	90	0	≤ 0.1	BERGER	91	FREJ

$\tau(p \to \mu^- e^+ e^+)$ — τ_{56}

LIMIT (10^{30} years)	PARTICLE	CL%	EVTS	BKGD EST	DOCUMENT ID		TECN
>19000	***p***	**90**	**0**	**0.5**	TANAKA	20	SKAM

$\tau(p \to \mu^+ \mu^+ \mu^-)$ — τ_{57}

LIMIT (10^{30} years)	PARTICLE	CL%	EVTS	BKGD EST	DOCUMENT ID		TECN
>10000	***p***	**90**	**1**	**0.4**	TANAKA	20	SKAM

Int. J. Mod. Phys. A 2026.41. Downloaded from www.worldscientific.com
by UNIVERSITY OF CALIFORNIA @ BERKELEY on 09/16/26. Re-use and distribution is strictly not permitted, except for Open Access articles.

• • • We do not use the following data for averages, fits, limits, etc. • • •

> 675	p	90	0	0.3	MCGREW	99	IMB3
> 119	p	90	0	0.2	BERGER	91	FREJ
> 10.5	p	90	0	0.7	PHILLIPS	89	HPW
> 190	p	90	1	0.1	HAINES	86	IMB
> 44	p (free)	90	1	0.7	BLEWITT	85	IMB
> 190	p	90	1	0.9	BLEWITT	85	IMB
> 2.1	p	90	1		[1] BATTISTONI	82	NUSX

[1] We have converted 1 possible event to 90% CL limit.

$\tau(p \to \mu^+ \nu\nu)$ — τ_{58}

LIMIT (10^{30} years)	PARTICLE	CL%	EVTS	BKGD EST	DOCUMENT ID		TECN
>220	**p**	**90**			[1] TAKHISTOV	14	SKAM

• • • We do not use the following data for averages, fits, limits, etc. • • •

> 21	p	90	7	11.23	BERGER	91B	FREJ

[1] Allowed events at 90% CL are 286.

$\tau(p \to e^- \mu^+ \mu^+)$ — τ_{59}

LIMIT (10^{30} years)	PARTICLE	CL%	EVTS	BKGD EST	DOCUMENT ID		TECN
>11000	**p**	**90**	**1**	**0.27**	TANAKA	20	SKAM

• • • We do not use the following data for averages, fits, limits, etc. • • •

> 6.0	p	90	0	0.7	PHILLIPS	89	HPW

$\tau(n \to 3\nu)$ — τ_{60}

See also the "to anything" and "disappearance" limits for bound nucleons in the "p Mean Life" data block just in front of the list of possible p decay modes. Such modes could of course be to three (or five) neutrinos, and the limits are stronger, but we do not repeat them here.

LIMIT (10^{30} years)	PARTICLE	CL%	EVTS	BKGD EST	DOCUMENT ID		TECN
>0.00049	**n**	**90**	**2**	**2**	[1] SUZUKI	93B	KAMI

• • • We do not use the following data for averages, fits, limits, etc. • • •

>0.0023	n	90			[2] GLICENSTEIN	97	KAMI
>0.00003	n	90	11	6.1	[3] BERGER	91B	FREJ
>0.00012	n	90	7	11.2	[3] BERGER	91B	FREJ
>0.0005	n	90	0		LEARNED	79	RVUE

[1] The SUZUKI 93B limit applies to any of $\nu_e \nu_e \overline{\nu}_e$, $\nu_\mu \nu_\mu \overline{\nu}_\mu$, or $\nu_\tau \nu_\tau \overline{\nu}_\tau$.
[2] GLICENSTEIN 97 uses Kamioka data and the idea that the disappearance of the neutron's magnetic moment should produce radiation.
[3] The first BERGER 91B limit is for $n \to \nu_e \nu_e \overline{\nu}_e$, the second is for $n \to \nu_\mu \nu_\mu \overline{\nu}_\mu$.

$\tau(n \to 5\nu)$ — τ_{61}

See the note on $\tau(n \to 3\nu)$ on the previous data block.

LIMIT (10^{30} years)	PARTICLE	CL%	EVTS	BKGD EST	DOCUMENT ID		TECN

• • • We do not use the following data for averages, fits, limits, etc. • • •

>0.0017	n	90			[1] GLICENSTEIN	97	KAMI

[1] GLICENSTEIN 97 uses Kamioka data and the idea that the disappearance of the neutron's magnetic moment should produce radiation.

Inclusive modes

$\tau(N \to e^+ \text{anything})$ — τ_{62}

LIMIT (10^{30} years)	PARTICLE	CL%	EVTS	BKGD EST	DOCUMENT ID		TECN
>0.6	**p, n**	**90**			[1] LEARNED	79	RVUE

[1] The electron may be primary or secondary.

$\tau(N \to \mu^+ \text{anything})$ — τ_{63}

LIMIT (10^{30} years)	PARTICLE	CL%	EVTS	BKGD EST	DOCUMENT ID		TECN
>12	**p, n**	**90**	**2**		[1,2] CHERRY	81	HOME

• • • We do not use the following data for averages, fits, limits, etc. • • •

> 1.8	p, n	90			[2] COWSIK	80	CNTR
> 6	p, n	90			[2] LEARNED	79	RVUE

[1] We have converted 2 possible events to 90% CL limit.
[2] The muon may be primary or secondary.

$\tau(N \to \nu \text{anything})$ — τ_{64}

Anything = π, ρ, K, etc.

LIMIT (10^{30} years)	PARTICLE	CL%	EVTS	BKGD EST	DOCUMENT ID		TECN

• • • We do not use the following data for averages, fits, limits, etc. • • •

>0.0002	p, n	90	0		LEARNED	79	RVUE

$\tau(N \to e^+ \pi^0 \text{anything})$ — τ_{65}

LIMIT (10^{30} years)	PARTICLE	CL%	EVTS	BKGD EST	DOCUMENT ID		TECN
>0.6	**p, n**	**90**	**0**		LEARNED	79	RVUE

$\tau(N \to 2 \text{ bodies}, \nu\text{-free})$ — τ_{66}

LIMIT (10^{30} years)	PARTICLE	CL%	EVTS	BKGD EST	DOCUMENT ID		TECN

• • • We do not use the following data for averages, fits, limits, etc. • • •

>1.3	p, n	90	0		ALEKSEEV	81	BAKS

$\Delta B = 2$ dinucleon modes

$\tau(pp \to \pi^+ \pi^+)$ — τ_{67}

LIMIT (10^{30} years)	CL%	EVTS	BKGD EST	DOCUMENT ID		TECN	COMMENT
>72.2	**90**	**2**	**4.45**	GUSTAFSON	15	SKAM	per oxygen nucleus

• • • We do not use the following data for averages, fits, limits, etc. • • •

> 0.7	90	4	2.34	BERGER	91B	FREJ	per iron nucleus

$\tau(pn \to \pi^+ \pi^0)$ — τ_{68}

LIMIT (10^{30} years)	CL%	EVTS	BKGD EST	DOCUMENT ID		TECN	COMMENT
>170	**90**			GUSTAFSON	15	SKAM	per oxygen nucleus

• • • We do not use the following data for averages, fits, limits, etc. • • •

> 2.0	90	0	0.31	BERGER	91B	FREJ	per iron nucleus

$\tau(nn \to \pi^+ \pi^-)$ — τ_{69}

LIMIT (10^{30} years)	CL%	EVTS	BKGD EST	DOCUMENT ID		TECN	COMMENT
>0.7	**90**	**4**	**2.18**	BERGER	91B	FREJ	τ per iron nucleus

$\tau(nn \to \pi^0 \pi^0)$ — τ_{70}

LIMIT (10^{30} years)	CL%	EVTS	BKGD EST	DOCUMENT ID		TECN	COMMENT
>404	**90**			GUSTAFSON	15	SKAM	per oxygen nucleus

• • • We do not use the following data for averages, fits, limits, etc. • • •

> 3.4	90	0	0.78	BERGER	91B	FREJ	per iron nucleus

$\tau(pp \to K^+ K^+)$ — τ_{71}

LIMIT (10^{30} years)	CL%	EVTS	BKGD EST	DOCUMENT ID		TECN	COMMENT
>170	**90**	**0**	**0.28**	LITOS	14	SKAM	τ per oxygen nucleus

$\tau(pp \to e^+ e^+)$ — τ_{72}

LIMIT (10^{30} years)	CL%	EVTS	BKGD EST	DOCUMENT ID		TECN	COMMENT
>5.8	**90**	**0**	**<0.1**	BERGER	91B	FREJ	τ per iron nucleus

$\tau(pp \to e^+ \mu^+)$ — τ_{73}

LIMIT (10^{30} years)	CL%	EVTS	BKGD EST	DOCUMENT ID		TECN	COMMENT
>3.6	**90**	**0**	**<0.1**	BERGER	91B	FREJ	τ per iron nucleus

$\tau(pp \to \mu^+ \mu^+)$ — τ_{74}

LIMIT (10^{30} years)	CL%	EVTS	BKGD EST	DOCUMENT ID		TECN	COMMENT
>1.7	**90**	**0**	**0.62**	BERGER	91B	FREJ	τ per iron nucleus

$\tau(pn \to e^+ \overline{\nu})$ — τ_{75}

LIMIT (10^{30} years)	CL%	EVTS	BKGD EST	DOCUMENT ID		TECN	COMMENT
>260	**90**			TAKHISTOV	15	SKAM	

• • • We do not use the following data for averages, fits, limits, etc. • • •

> 2.8	90	5	9.67	BERGER	91B	FREJ	τ per iron nucleus

$\tau(pn \to \mu^+ \overline{\nu})$ — τ_{76}

LIMIT (10^{30} years)	CL%	EVTS	BKGD EST	DOCUMENT ID		TECN	COMMENT
>200	**90**			TAKHISTOV	15	SKAM	

• • • We do not use the following data for averages, fits, limits, etc. • • •

> 1.6	90	4	4.37	BERGER	91B	FREJ	τ per iron nucleus

$\tau(pn \to \tau^+ \overline{\nu}_\tau)$ — τ_{77}

LIMIT (10^{30} years)	CL%	EVTS	BKGD EST	DOCUMENT ID		TECN
>29	**90**			TAKHISTOV	15	SKAM

• • • We do not use the following data for averages, fits, limits, etc. • • •

> 1	90			[1] BRYMAN	14	CHER

[1] BRYMAN 14 uses a MCGREW 99 limit on the $p \to e^+ \nu\nu$ lifetime to extract this value.

$\tau(nn \to \text{invisible})$ — τ_{78}

LIMIT (10^{30} years)	CL%	EVTS	BKGD EST	DOCUMENT ID		TECN	COMMENT
>1.4	**90**			[1] ARAKI	06	KLND	$nn \to$ invisible

• • • We do not use the following data for averages, fits, limits, etc. • • •

>0.015	90		[2,3] ALLEGA	22	SNO+	$nn \to$ invisible
>0.013	90		[2] ANDERSON	19A	SNO+	$nn \to$ invisible
>0.000042	90		[4] TRETYAK	04	CNTR	$nn \to$ invisible
>0.000049	90		[5] BACK	03	BORX	$nn \to$ invisible
>0.000012	90		[6] BERNABEI	00B	DAMA	$nn \to$ invisible

[1] ARAKI 06 looks for signs of de-excitation of the residual nucleus after disappearance of two neutrons from the s shell of ^{12}C.
[2] ALLEGA 22 and ANDERSON 19A look for γ rays from the de-excitation of a residual ^{14}O* following the disappearance of nn in ^{16}O.
[3] ALLEGA 22 replaces the previous SNO+ value of ANDERSON 19A.

Int. J. Mod. Phys. A 2026.41. Downloaded from www.worldscientific.com
UNIVERSITY OF CALIFORNIA @ BERKELEY on 09/16/26. Re-use and distribution is strictly not permitted, except for Open Access articles.

[4] TRETYAK 04 uses data from an old Homestake-mine radiochemical experiment on limits for invisible decays of ^{39}K to ^{37}Ar.
[5] BACK 03 looks for decays of unstable nuclides left after NN decays of parent ^{12}C, ^{13}C, ^{16}O nuclei. These are "invisible channel" limits.
[6] BERNABEI 00B looks for the decay of a $^{127}_{54}$Xe nucleus following the disappearance of an nn pair in the otherwise-stable $^{129}_{54}$Xe nucleus. The limit here applies as well to $nn \to \nu_\mu \overline{\nu}_\mu$, $nn \to \nu_\tau \overline{\nu}_\tau$, or any "disappearance" mode.

$\tau(nn \to \nu_e \overline{\nu}_e)$ — τ_{79}

LIMIT (10^{30} years)	CL%	EVTS	BKGD EST	DOCUMENT ID		TECN	COMMENT
>0.000012	**90**	**5**	**9.7**	BERGER	91B	FREJ	τ per iron nucleus

$\tau(nn \to \nu_\mu \overline{\nu}_\mu)$ — τ_{80}

See the proceeding data block. "Invisible modes" would include any multi-neutrino mode.

LIMIT (10^{30} years)	CL%	EVTS	BKGD EST	DOCUMENT ID		TECN	COMMENT
> 1.4 (CL=90%) OUR LIMIT							
• • • We do not use the following data for averages, fits, limits, etc. • • •							
>0.000006	90	4	4.4	BERGER	91B	FREJ	τ per iron nucleus

$\tau(pn \to$ invisible$)$ — τ_{81}

This violates charge conservation as well as baryon number conservation.

VALUE (10^{30} years)	CL%	DOCUMENT ID		TECN
>0.06	90	[1,2] ALLEGA	22	SNO+
• • • We do not use the following data for averages, fits, limits, etc. • • •				
>0.026	90	[1] ANDERSON	19A	SNO+
>0.000021	90	[3] TRETYAK	04	CNTR

[1] ALLEGA 22 and ANDERSON 19A look for γ rays from the de-excitation of a residual ^{14}N* following the disappearance of pn in ^{16}O.
[2] ALLEGA 22 replaces the previous SNO+ value of ANDERSON 19A.
[3] TRETYAK 04 uses data from an old Homestake-mine radiochemical experiment on limits for invisible decays of ^{39}K to ^{37}Ar.

$\tau(pp \to$ invisible$)$ — τ_{82}

This violates charge conservation as well as baryon number conservation.

VALUE (10^{30} years)	CL%	DOCUMENT ID		TECN
>0.11	90	[1] ALLEGA	22	SNO+
• • • We do not use the following data for averages, fits, limits, etc. • • •				
>0.047	90	[1] ANDERSON	19A	SNO+
>0.00005	90	[2] BACK	03	BORX
>0.00000055	90	[3] BERNABEI	00B	DAMA

[1] ALLEGA 22 look for γ rays from the de-excitation of a residual ^{14}C* following the disappearance of pp in ^{16}O. Supersedes ANDERSON 19A result.
[2] BACK 03 looks for decays of unstable nuclides left after NN decays of parent ^{12}C, ^{13}C, ^{16}O nuclei. These are "invisible channel" limits.
[3] BERNABEI 00B looks for the decay of a $^{127}_{52}$Te nucleus following the disappearance of a pp pair in the otherwise-stable $^{129}_{54}$Xe nucleus.

$\Delta B = 1$

$\overline{p}$ PARTIAL MEAN LIVES

The "partial mean life" limits tabulated here are the limits on $\overline{\tau}/B_i$, where $\overline{\tau}$ is the total mean life for the antiproton and B_i is the branching fraction for the mode in question.

$\tau(\overline{p} \to e^- \gamma)$ — τ_{83}

VALUE (years)	CL%	DOCUMENT ID		TECN	COMMENT
> 7×10^5	90	GEER	00	APEX	8.9 GeV/c $\overline{p}$ beam
• • • We do not use the following data for averages, fits, limits, etc. • • •					
>1848	95	GEER	94	CALO	8.9 GeV/c $\overline{p}$ beam

$\tau(\overline{p} \to \mu^- \gamma)$ — τ_{84}

VALUE (years)	CL%	DOCUMENT ID		TECN	COMMENT
>5 $\times 10^4$	90	GEER	00	APEX	8.9 GeV/c $\overline{p}$ beam
• • • We do not use the following data for averages, fits, limits, etc. • • •					
>5.0×10^4	90	HU	98B	APEX	8.9 GeV/c $\overline{p}$ beam

$\tau(\overline{p} \to e^- \pi^0)$ — τ_{85}

VALUE (years)	CL%	DOCUMENT ID		TECN	COMMENT
> 4×10^5	90	GEER	00	APEX	8.9 GeV/c $\overline{p}$ beam
• • • We do not use the following data for averages, fits, limits, etc. • • •					
>554	95	GEER	94	CALO	8.9 GeV/c $\overline{p}$ beam

$\tau(\overline{p} \to \mu^- \pi^0)$ — τ_{86}

VALUE (years)	CL%	DOCUMENT ID		TECN	COMMENT
>5 $\times 10^4$	90	GEER	00	APEX	8.9 GeV/c $\overline{p}$ beam
• • • We do not use the following data for averages, fits, limits, etc. • • •					
>4.8×10^4	90	HU	98B	APEX	8.9 GeV/c $\overline{p}$ beam

$\tau(\overline{p} \to e^- \eta)$ — τ_{87}

VALUE (years)	CL%	DOCUMENT ID		TECN	COMMENT
> 2×10^4	90	GEER	00	APEX	8.9 GeV/c $\overline{p}$ beam
• • • We do not use the following data for averages, fits, limits, etc. • • •					
>171	95	GEER	94	CALO	8.9 GeV/c $\overline{p}$ beam

$\tau(\overline{p} \to \mu^- \eta)$ — τ_{88}

VALUE (years)	CL%	DOCUMENT ID		TECN	COMMENT
>8 $\times 10^3$	90	GEER	00	APEX	8.9 GeV/c $\overline{p}$ beam
• • • We do not use the following data for averages, fits, limits, etc. • • •					
>7.9×10^3	90	HU	98B	APEX	8.9 GeV/c $\overline{p}$ beam

$\tau(\overline{p} \to e^- K^0_S)$ — τ_{89}

VALUE (years)	CL%	DOCUMENT ID		TECN	COMMENT
>900	90	GEER	00	APEX	8.9 GeV/c $\overline{p}$ beam
• • • We do not use the following data for averages, fits, limits, etc. • • •					
> 29	95	GEER	94	CALO	8.9 GeV/c $\overline{p}$ beam

$\tau(\overline{p} \to \mu^- K^0_S)$ — τ_{90}

VALUE (years)	CL%	DOCUMENT ID		TECN	COMMENT
>4 $\times 10^3$	90	GEER	00	APEX	8.9 GeV/c $\overline{p}$ beam
• • • We do not use the following data for averages, fits, limits, etc. • • •					
>4.3×10^3	90	HU	98B	APEX	8.9 GeV/c $\overline{p}$ beam

$\tau(\overline{p} \to e^- K^0_L)$ — τ_{91}

VALUE (years)	CL%	DOCUMENT ID		TECN	COMMENT
>9 $\times 10^3$	90	GEER	00	APEX	8.9 GeV/c $\overline{p}$ beam
• • • We do not use the following data for averages, fits, limits, etc. • • •					
>9	95	GEER	94	CALO	8.9 GeV/c $\overline{p}$ beam

$\tau(\overline{p} \to \mu^- K^0_L)$ — τ_{92}

VALUE (years)	CL%	DOCUMENT ID		TECN	COMMENT
>7 $\times 10^3$	90	GEER	00	APEX	8.9 GeV/c $\overline{p}$ beam
• • • We do not use the following data for averages, fits, limits, etc. • • •					
>6.5×10^3	90	HU	98B	APEX	8.9 GeV/c $\overline{p}$ beam

$\tau(\overline{p} \to e^- \gamma\gamma)$ — τ_{93}

VALUE (years)	CL%	DOCUMENT ID		TECN	COMMENT
>2 $\times 10^4$	90	GEER	00	APEX	8.9 GeV/c $\overline{p}$ beam

$\tau(\overline{p} \to \mu^- \gamma\gamma)$ — τ_{94}

VALUE (years)	CL%	DOCUMENT ID		TECN	COMMENT
>2 $\times 10^4$	90	GEER	00	APEX	8.9 GeV/c $\overline{p}$ beam
• • • We do not use the following data for averages, fits, limits, etc. • • •					
>2.3×10^4	90	HU	98B	APEX	8.9 GeV/c $\overline{p}$ beam

$\tau(\overline{p} \to e^- \omega)$ — τ_{95}

VALUE (years)	CL%	DOCUMENT ID		TECN	COMMENT
>200	90	GEER	00	APEX	8.9 GeV/c $\overline{p}$ beam

p REFERENCES

MOHR 25 RMP 97 025002 P.J. Mohr et al. (NIST)
YAMAUCHI 25 PR D112 092004 K. Yamauchi et al. (Super-Kamiokande Collab.)
AGOSTINI 24A EPJ C84 940 M. Agostini et al. (GERDA Collab.)
TANIUCHI 24 PR D110 112011 N. Taniuchi et al. (Super-Kamiokande Collab.)
ALLEGA 22 PR D105 112012 A. Allega et al. (SNO+ Collab.)
BORCHERT 22 NAT 601 53 M.J. Borchert et al. (BASE Collab.)
GAO 22A RMP 94 015002 H. Gao, M. Vanderhaeghen (DUKE, MAINZ)
LI 22D NAT 611 265 R. Li et al.
MATSUMOTO 22 PR D106 072003 R. Matsumoto et al. (Super-Kamiokande Collab.)
MORNACCHI 22 PRL 129 102501 E. Mornacchi et al. (MAINZ, REGE, PAVI+)
CUI 21 PRL 127 092001 Z.-F. Cui et al. (NJU, ECT, HZDR)
CUI 21B CPL 38 121401 Z.-F. Cui et al. (NJU, ECT, HZDR)
FINK 21 PRL 127 243001 D.J. Fink, E.G. Myers (FSU)
MIHOVILOVIC 21 EPJ A57 107 M. Mihovilovic et al. (LJUB, MAINZ, MIT+)
TIESINGA 21 RMP 93 025010 E. Tiesinga et al. (NIST)
TAKENAKA 20 PR D102 112011 A. Takenaka et al. (Super-Kamiokande Collab.)
TANAKA 20 PR D101 052011 M. Tanaka et al. (Super-Kamiokande Collab.)
ANDERSON 19A PR D99 032008 M. Anderson et al. (SNO+ Collab.)
BEZGINOV 19 SCI 365 1007 N. Bezginov et al. (YORKC, TNTO)
HEISSE 19 PR A100 022518 F. Heisse et al. (MPIK, GSI, MAINZ)
PASQUINI 19 JP G46 104001 B. Pasquini, P. Pedroni, S. Sconfietti (PAVI)
SCHUMACHER 19 LHEP 4 4 M. Schumacher (GOET)
XIONG 19 NAT 575 147 W. Xiong et al. (PRad Collab.)
FLEURBAEY 18 PRL 120 183001 H. Fleurbaey et al. (SORB)
ABE 17 PR D95 012004 K. Abe et al. (Super-Kamiokande Collab.)
ABE 17D PR D96 012003 K. Abe et al. (Super-Kamiokande Collab.)
BEYER 17 SCI 358 79 A. Beyer et al. (MPQG Collab.)
HEISSE 17 PRL 119 033001 F. Heisse et al. (MPIK, GSI, MAINZ, RIKEN)
NAGAHAMA 17 NATC 8 14084 H. Nagahama et al. (RIKEN, TOKY, CERN+)
SAHOO 17 PR D95 013002 B.K. Sahoo (AHMEB)
SCHNEIDER 17 SCI 358 1081 G. Schneider et al. (MAINZ, RIKEN, +)
SELLNER 17 NJP 19 083023 S. Sellner et al. (RIKEN, MPIK, +)
SMORRA 17 NAT 550 371 C. Smorra et al. (RIKEN, CERN, +)
MOHR 16 RMP 88 035009 P.J. Mohr, D.B. Newell, B.N. Taylor (NIST)
ASAKURA 15 PR D92 052006 K. Asakura et al. (KamLAND Collab.)
GUSTAFSON 15 PR D91 072009 J. Gustafson et al. (Super-Kamiokande Collab.)
LEE 15 PR D92 013013 G. Lee, J.R. Arrington, R.J. Hill (ANL, EFI+)
TAKHISTOV 15 PRL 115 121803 V. Takhistov et al. (Super-Kamiokande Collab.)
ULMER 15 NAT 524 196 S. Ulmer et al. (RIKEN, CERN, MPIK, +)
ABE 14E PRL 113 121802 K. Abe et al. (Super-Kamiokande Collab.)
ABE 14G PR D90 072005 K. Abe et al. (Super-Kamiokande Collab.)
BRYMAN 14 PL B733 190 D. Bryman (BRCO)
EPSTEIN 14 PR D90 074027 Z. Epstein, G. Paz, J. Roy (UMD, WAYN)

Int. J. Mod. Phys. A 2026.41. Downloaded from www.worldscientific.com
by UNIVERSITY OF CALIFORNIA @ BERKELEY on 09/16/26. Re-use and distribution is strictly not permitted, except for Open Access articles.

LITOS	14	PRL 112 131803	M. Litos *et al.*	(Super-Kamiokande Collab.)
PDG	14	CP C38 070001	K. Olive *et al.*	(PDG Collab.)
TAKHISTOV	14	PRL 113 101801	V. Takhistov *et al.*	(Super-Kamiokande Collab.)
ANTOGNINI	13	SCI 339 417	A. Antognini *et al.*	(MPIM, ETH, UPMC+)
DISCIACCA	13	PRL 110 130801	J. DiSciacca *et al.*	(ATRAP Collab.)
MCGOVERN	13	EPJ A49 12	J.A. McGovern, D.R. Phillips, H.W. Griesshammer	
MOHR	12	RMP 84 1527	P.J. Mohr, B.N. Taylor, D.B. Newell	(NIST)
NISHINO	12	PR D85 112001	H. Nishino *et al.*	(Super-Kamiokande Collab.)
REGIS	12	PR D86 012006	C. Regis *et al.*	(Super-Kamiokande Collab.)
BRESSI	11	PR A83 052101	G. Bressi *et al.*	(LEGN, PAVII, PADO, TRST+)
HORI	11	NAT 475 484	M. Hori *et al.*	(MPIG, TOKY, BUDA, +)
ZHAN	11	PL B705 59	X. Zhan *et al.*	(JLAB-Hall A Collab.)
BERNAUER	10	PRL 105 242001	J.C. Bernauer *et al.*	(MAMI A1 Collab.)
Also		PR C90 015206	J.C. Bernauer *et al.*	(MAMI A1 Collab.)
BORISYUK	10	NP A843 59	D. Borisyuk	(KIEV)
HILL	10	PR D82 113005	R.J. Hill, G. Paz	(CHIC)
POHL	10	NAT 466 213	R. Pohl *et al.*	(MPIQ, ENSP, COIM, +)
NISHINO	09	PRL 102 141801	H. Nishino *et al.*	(Super-Kamiokande Collab.)
PASK	09	PL B678 55	T. Pask *et al.*	(Stefan Meyer Inst., Vienna, TOKY+)
MOHR	08	RMP 80 633	P.J. Mohr, B.N. Taylor, D.B. Newell	(NIST)
BELUSHKIN	07	PR C75 035202	M.A. Belushkin, H.W. Hammer, U.-G. Meissner	(BONN+)
ARAKI	06	PRL 96 101802	T. Araki *et al.*	(KamLAND Collab.)
HORI	06	PRL 96 243401	M. Hori *et al.*	(CERN, TOKYO+)
BLUNDEN	05	PR C72 057601	P.G. Blunden, I. Sick	(MANI, BASL)
KOBAYASHI	05	PR D72 052007	K. Kobayashi *et al.*	(Super-Kamiokande Collab.)
MOHR	05	RMP 77 1	P.J. Mohr, B.N. Taylor	(NIST)
SCHUMACHER	05	PPNP 55 567	M. Schumacher	(GOET)
AHMED	04	PRL 92 102004	S.N. Ahmed *et al.*	(SNO Collab.)
TRETYAK	04	JETPL 79 106	V.I. Tretyak, V.Yu. Denisov, Yu.G. Zdesenko	(KIEV)
		Translated from ZETFP 79 136.		
BACK	03	PL B563 23	H.O. Back *et al.*	(Borexino Collab.)
BEANE	03	PL B567 200	S.R. Beane *et al.*	
Also		PL B607 320 (errat.)	S.R. Beane *et al.*	
DMITRIEV	03	PRL 91 212303	V.F. Dmitriev, R.A. Senkov	(NOVO)
HORI	03	PRL 91 123401	M. Hori *et al.*	(CERN ASACUSA Collab.)
SICK	03	PL B576 62	I. Sick	(BASL)
ZDESENKO	03	PL B553 135	Yu.G. Zdesenko, V.I. Tretyak	(KIEV)
AHMAD	02	PRL 89 011301	Q.R. Ahmad *et al.*	(SNO Collab.)
BARANOV	01	PPN 32 376	P.S. Baranov *et al.*	
		Translated from FECAY 32 699.		
BLANPIED	01	PR C64 025203	G. Blanpied *et al.*	(BNL LEGS Collab.)
HORI	01	PRL 87 093401	M. Hori *et al.*	(CERN ASACUSA Collab.)
OLMOSDEL...	01	EPJ A10 207	V. Olmos de Leon *et al.*	(MAMI TAPS Collab.)
TRETYAK	01	PL B505 59	V.I. Tretyak, Yu.G. Zdesenko	(KIEV)
BERNABEI	00B	PL B493 12	R. Bernabei *et al.*	(Gran Sasso DAMA Collab.)
GEER	00	PRL 84 590	S. Geer *et al.*	(FNAL APEX Collab.)
Also		PR D62 052004	S. Geer *et al.*	(FNAL APEX Collab.)
Also		PRL 85 3546 (errat.)	S. Geer *et al.*	(FNAL APEX Collab.)
GEER	00D	APJ 532 648	S.H. Geer, D.C. Kennedy	
SENGUPTA	00	PL B484 275	S. Sengupta	
WALL	00	PR D61 072004	D. Wall *et al.*	(Soudan-2 Collab.)
WALL	00B	PR D62 092003	D. Wall *et al.*	(Soudan-2 Collab.)
GABRIELSE	99	PRL 82 3198	G. Gabrielse *et al.*	
HAYATO	99	PRL 83 1529	Y. Hayato *et al.*	(Super-Kamiokande Collab.)
MCGREW	99	PR D59 052004	C. McGrew *et al.*	(IMB-3 Collab.)
MOHR	99	JPCRD 28 1713	P.J. Mohr, B.N. Taylor	(NIST)
Also		RMP 72 351	P.J. Mohr, B.N. Taylor	(NIST)
TORII	99	PR A59 223	H.A. Torii *et al.*	(CERN PS-205 Collab.)
ALLISON	98	PL B427 217	W.W.M. Allison *et al.*	(Soudan-2 Collab.)
HU	98B	PR D58 111101	M. Hu *et al.*	(FNAL APEX Collab.)
SHIOZAWA	98	PRL 81 3319	M. Shiozawa *et al.*	(Super-Kamiokande Collab.)
GLICENSTEIN	97	PL B411 326	J.F. Glicenstein	(SACL)
GABRIELSE	95	PRL 74 3544	G. Gabrielse *et al.*	(HARV, MAINZ, SEOUL)
MACGIBBON	95	PR C52 2097	B.E. MacGibbon *et al.*	(ILL, SASK, INRM)
GEER	94	PRL 72 1596	S. Geer *et al.*	(FNAL, UCLA, PSU)
HALLIN	93	PR C48 1497	E.L. Hallin *et al.*	(SASK, BOST, ILL)
SUZUKI	93B	PL B311 357	Y. Suzuki *et al.*	(Kamiokande Collab.)
HUGHES	92	PRL 69 578	R.J. Hughes, B.I. Deutch	(LANL, AARH)
ZIEGER	92	PL B278 34	A. Zieger *et al.*	(MPCM)
Also		PL B281 417 (errat.)	A. Zieger *et al.*	(MPCM)
BERGER	91	ZPHY C50 385	C. Berger *et al.*	(FREJUS Collab.)
BERGER	91B	PL B269 227	C. Berger *et al.*	(FREJUS Collab.)
FEDERSPIEL	91	PRL 67 1511	F.J. Federspiel *et al.*	(ILL)
BECKER-SZ...	90	PR D42 2974	R.A. Becker-Szendy *et al.*	(IMB-3 Collab.)
ERICSON	90	EPL 11 295	T.E.O. Ericson, A. Richter	(CERN, DARM)
GABRIELSE	90	PRL 65 1317	G. Gabrielse *et al.*	(HARV, MAINZ, WASH+)
BERGER	89	NP B313 509	C. Berger *et al.*	(FREJUS Collab.)
CHO	89	PRL 63 2559	D. Cho, K. Sangster, E.A. Hinds	(YALE)
HIRATA	89C	PL B220 308	K.S. Hirata *et al.*	(Kamiokande Collab.)
PHILLIPS	89	PL B224 348	T.J. Phillips *et al.*	(HPW Collab.)
KREISSL	88	ZPHY C37 557	A. Kreissl *et al.*	(CERN PS176 Collab.)
SEIDEL	88	PRL 61 2522	S. Seidel *et al.*	(IMB Collab.)
BARTELT	87	PR D36 1990	J.E. Bartelt *et al.*	(Soudan Collab.)
Also		PR D40 1701 (errat.)	J.E. Bartelt *et al.*	(Soudan Collab.)
COHEN	87	RMP 59 1121	E.R. Cohen, B.N. Taylor	(RISC, NBS)
HAINES	86	PRL 57 1986	T.J. Haines *et al.*	(IMB Collab.)
KAJITA	86	JPSJ 55 711	T. Kajita *et al.*	(Kamiokande Collab.)
ARISAKA	85	JPSJ 54 3213	K. Arisaka *et al.*	(Kamiokande Collab.)
BLEWITT	85	PRL 55 2114	G.B. Blewitt *et al.*	(IMB Collab.)
DZUBA	85	PL 154B 93	V.A. Dzuba, V.V. Flambaum, P.G. Silvestrov	(NOVO)
PARK	85	PRL 54 22	H.S. Park *et al.*	(IMB Collab.)
BATTISTONI	84	PL 133B 454	G. Battistoni *et al.*	(NUSEX Collab.)
MARINELLI	84	PL 137B 439	M. Marinelli, G. Morpurgo	(GENO)
WILKENING	84	PR A29 425	D.A. Wilkening, N.F. Ramsey, D.J. Larson	(HARV+)
BARTELT	83	PRL 50 651	J.E. Bartelt *et al.*	(MINN, ANL)
BATTISTONI	82	PL 118B 461	G. Battistoni *et al.*	(NUSEX Collab.)
KRISHNA...	82	PL 115B 349	M.R. Krishnaswamy *et al.*	(TATA, OSKC+)
ALEKSEEV	81	JETPL 33 651	E.N. Alekseev *et al.*	(PNPI)
		Translated from ZETFP 33 664.		
CHERRY	81	PRL 47 1507	M.L. Cherry *et al.*	(PENN, BNL)
COWSIK	80	PR D22 2204	R. Cowsik, V.S. Narasimham	(TATA)
BELL	79	PL 86B 215	M. Bell *et al.*	(CERN)
GOLDEN	79	PRL 43 1196	R.L. Golden *et al.*	(NASA, PSLL)
LEARNED	79	PRL 43 907	J.G. Learned, F. Reines, A. Soni	(UCI)
BREGMAN	78	PL 78B 174	M. Bregman *et al.*	(CERN)
ROBERTS	78	PR D17 358	B.L. Roberts	(WILL, RHEL)
EVANS	77	SCI 197 989	J.C. Evans Jr., R.I. Steinberg	(BNL, PENN)
HU	75	NP A254 403	E. Hu *et al.*	(COLU, YALE)
COHEN	73	JPCRD 2 664	E.R. Cohen, B.N. Taylor	(RISC, NBS)
DYLLA	73	PR A7 1224	H.F. Dylla, J.G. King	(MIT)
DIX	70	Thesis Case	F.W. Dix	(CASE)
HARRISON	69	PRL 22 1263	G.E. Harrison, P.G.H. Sandars, S.J. Wright	(OXF)
GURR	67	PR 158 1321	H.S. Gurr *et al.*	(CASE, WITW)
FLEROV	58	DOKL 3 79	G.N. Flerov *et al.*	(ASCI)

n

$I(J^P) = \frac{1}{2}(\frac{1}{2}^+)$ Status: ****

We have omitted some results that have been superseded by later experiments. See our earlier editions.

Anyone interested in the neutron should look at these two review articles: D. Dubbers and M.G. Schmidt, "The neutron and its role in cosmology and particle physics," Reviews of Modern Physics **83** 1111 (2011); and F.E. Wietfeldt and G.L. Greene, "The neutron lifetime," Reviews of Modern Physics **83** 1173 (2011).

n MASS (atomic mass units u)

The mass is known much more precisely in u (atomic mass units) than in MeV. See the next data block.

VALUE (u)	*DOCUMENT ID*		*TECN*	*COMMENT*
1.00866491606±0.00000000040	MOHR	25	RVUE	2022 CODATA value
• • • We do not use the following data for averages, fits, limits, etc. • • •				
1.00866491595±0.00000000049	TIESINGA	21	RVUE	2018 CODATA value
1.00866491588±0.00000000049	MOHR	16	RVUE	2014 CODATA value
1.00866491600±0.00000000043	MOHR	12	RVUE	2010 CODATA value
1.00866491597±0.00000000043	MOHR	08	RVUE	2006 CODATA value
1.00866491560±0.00000000055	MOHR	05	RVUE	2002 CODATA value
1.00866491578±0.00000000055	MOHR	99	RVUE	1998 CODATA value
1.008665904 ±0.000000014	COHEN	87	RVUE	1986 CODATA value

n MASS (MeV)

The mass is known more precisely in u (atomic mass units) than in MeV. The conversion is: 1 u = 931.494 103 72(29) MeV/c^2 (2022 CODATA value, MOHR 25).

VALUE (MeV)		*DOCUMENT ID*		*TECN*	*COMMENT*
939.56542194±0.00000048		MOHR	25	RVUE	2022 CODATA value
• • • We do not use the following data for averages, fits, limits, etc. • • •					
939.56542052±0.00000054		TIESINGA	21	RVUE	2018 CODATA value
939.5654133 ±0.0000058		MOHR	16	RVUE	2014 CODATA value
939.565379 ±0.000021		MOHR	12	RVUE	2010 CODATA value
939.565346 ±0.000023		MOHR	08	RVUE	2006 CODATA value
939.565360 ±0.000081		MOHR	05	RVUE	2002 CODATA value
939.565331 ±0.000037	[1]	KESSLER	99	SPEC	$np \to d\gamma$
939.565330 ±0.000038		MOHR	99	RVUE	1998 CODATA value
939.56565 ±0.00028	[2,3]	DIFILIPPO	94	TRAP	Penning trap
939.56563 ±0.00028		COHEN	87	RVUE	1986 CODATA value
939.56564 ±0.00028	[3,4]	GREENE	86	SPEC	$np \to d\gamma$
939.5731 ±0.0027	[3]	COHEN	73	RVUE	1973 CODATA value

[1] We use the 1998 CODATA u-to-MeV conversion factor (see the heading above) to get this mass in MeV from the much more precisely measured KESSLER 99 value of 1.00866491637 ± 0.00000000082 u.

[2] The mass is known much more precisely in u: m = 1.0086649235 ± 0.0000000023 u. We use the 1986 CODATA conversion factor to get the mass in MeV.

[3] These determinations are not independent of the $m_n - m_p$ measurements below.

[4] The mass is known much more precisely in u: m = 1.008664919 ± 0.000000014 u.

$\overline{n}$ MASS

VALUE (MeV)	*EVTS*		*DOCUMENT ID*		*TECN*	*COMMENT*
939.485±0.051	59	[1]	CRESTI	86	HBC	$\overline{p}p \to \overline{n}n$

[1] This is a corrected result (see the erratum). The error is statistical. The maximum systematic error is 0.029 MeV.

$(m_n - m_{\overline{n}})/ m_n$

A test of CPT invariance. Calculated from the n and $\overline{n}$ masses, above.

VALUE	*DOCUMENT ID*
(9±5) × 10^{-5} OUR EVALUATION	

$m_n - m_p$

VALUE (MeV)		*DOCUMENT ID*		*TECN*	*COMMENT*
1.29333251±0.00000038		MOHR	25	RVUE	2022 CODATA value
• • • We do not use the following data for averages, fits, limits, etc. • • •					
1.29333236±0.00000046	[1]	TIESINGA	21	RVUE	2018 CODATA value
1.29333205±0.00000051	[2]	MOHR	16	RVUE	2014 CODATA value
1.29333217±0.00000042	[3]	MOHR	12	RVUE	2010 CODATA value
1.29333214±0.00000043	[4]	MOHR	08	RVUE	2006 CODATA value
1.2933317 ±0.0000005	[5]	MOHR	05	RVUE	2002 CODATA value
1.2933318 ±0.0000005	[6]	MOHR	99	RVUE	1998 CODATA value
1.293318 ±0.000009	[7]	COHEN	87	RVUE	1986 CODATA value
1.2933328 ±0.0000072		GREENE	86	SPEC	$np \to d\gamma$
1.293429 ±0.000036		COHEN	73	RVUE	1973 CODATA value

[1] The 2018 CODATA mass difference in u is $m_n - m_p = 1.388\,449\,33(49) \times 10^{-3} u$.

[2] The 2014 CODATA mass difference in u is $m_n - m_p = 1.388\,449\,00(51) \times 10^{-3} u$.

[3] The 2010 CODATA mass difference in u is $m_n - m_p = 1.388\,449\,19(45) \times 10^{-3} u$.

[4] Calculated by us from the MOHR 08 ratio $m_n/m_p = 1.00137841918(46)$. In u, $m_n - m_p = 1.38844920(46) \times 10^{-3}$ u.

[5] Calculated by us from the MOHR 05 ratio $m_n/m_p = 1.00137841870 \pm 0.00000000058$. In u, $m_n - m_p = (1.3884487 \pm 0.0000006) \times 10^{-3}$ u.

[6] Calculated by us from the MOHR 99 ratio $m_n/m_p = 1.00137841887 \pm 0.00000000058$. In u, $m_n - m_p = (1.3884489 \pm 0.0000006) \times 10^{-3}$ u.

[7] Calculated by us from the COHEN 87 ratio $m_n/m_p = 1.001378404 \pm 0.000000009$. In u, $m_n - m_p = 0.001388434 \pm 0.000000009$ u.

n MEAN LIFE

Limits on lifetimes for *bound* neutrons are given in the section "p PARTIAL MEAN LIVES."

We average eight of the best nine measurements, those made with ultra-cold neutrons (UCN's). If we include the one in-beam measurement with a comparable error (YUE 13), we get 878.6 ± 0.6 s, where the scale factor is now 2.2.

For a recent discussion of the long-standing disagreement between in-beam and UCN results, see CZARNECKI 18 (Physical Review Letters **120** 202002 (2018)). For a full review of all matters concerning the neutron lifetime until about 2010, see WIETFELDT 11, F.E. Wietfeldt and G.L. Greene, "The neutron lifetime," Reviews of Modern Physics **83** 1173 (2011).

VALUE (s)	DOCUMENT ID		TECN	COMMENT
878.3 ± 0.4 OUR AVERAGE	Error includes scale factor of 1.8. See the ideogram below.			
$877.82 \pm 0.22^{+0.20}_{-0.17}$	[1] MUSEDINOVIC	25	CNTR	UCN magneto-gravit. trap
878.3 ± 1.6 ± 1.0	EZHOV	18	CNTR	UCN magneto-gravit. trap
$877.7 \pm 0.7^{+0.4}_{-0.2}$	[2] PATTIE	18	CNTR	UCN asym. magnetic trap
881.5 ± 0.7 ± 0.6	SEREBROV	18	CNTR	UCN gravitational trap
880.2 ± 1.2	[3] ARZUMANOV	15	CNTR	UCN double bottle
882.5 ± 1.4 ± 1.5	[4] STEYERL	12	CNTR	UCN material bottle
880.7 ± 1.3 ± 1.2	PICHLMAIER	10	CNTR	UCN material bottle
878.5 ± 0.7 ± 0.3	SEREBROV	05	CNTR	UCN gravitational trap
• • • We do not use the following data for averages, fits, limits, etc. • • •				
$877.75 \pm 0.28^{+0.22}_{-0.16}$	[5] GONZALEZ	21	CNTR	UCN asym. magnetic trap
$887 \pm 14^{+7}_{-3}$	[6] WILSON	21	CNTR	space-based n rate
887.7 ± 1.2 ± 1.9	[7] YUE	13	CNTR	In-beam n, trapped p
881.6 ± 0.8 ± 1.9	[8] ARZUMANOV	12	CNTR	See ARZUMANOV 15
886.3 ± 1.2 ± 3.2	NICO	05	CNTR	See YUE 13
886.8 ± 1.2 ± 3.2	DEWEY	03	CNTR	See NICO 05
885.4 ± 0.9 ± 0.4	ARZUMANOV	00	CNTR	See ARZUMANOV 12
889.2 ± 3.0 ± 3.8	BYRNE	96	CNTR	Penning trap
882.6 ± 2.7	[9] MAMPE	93	CNTR	UCN material bottle
888.4 ± 3.1 ± 1.1	[10] NESVIZHEV...	92	CNTR	UCN material bottle
888.4 ± 2.9	ALFIMENKOV	90	CNTR	See NESVIZHEVSKII 92
893.6 ± 3.8 ± 3.7	BYRNE	90	CNTR	See BYRNE 96
878 ± 27 ± 14	KOSSAKOW...	89	TPC	Pulsed beam
887.6 ± 3.0	MAMPE	89	CNTR	See STEYERL 12
877 ± 10	PAUL	89	CNTR	Magnetic storage ring
876 ± 10 ± 19	LAST	88	SPEC	Pulsed beam
891 ± 9	SPIVAK	88	CNTR	Beam
903 ± 13	KOSVINTSEV	86	CNTR	UCN material bottle
937 ± 18	[11] BYRNE	80	CNTR	
875 ± 95	KOSVINTSEV	80	CNTR	
881 ± 8	BONDAREN...	78	CNTR	See SPIVAK 88
918 ± 14	CHRISTENSEN	72	CNTR	

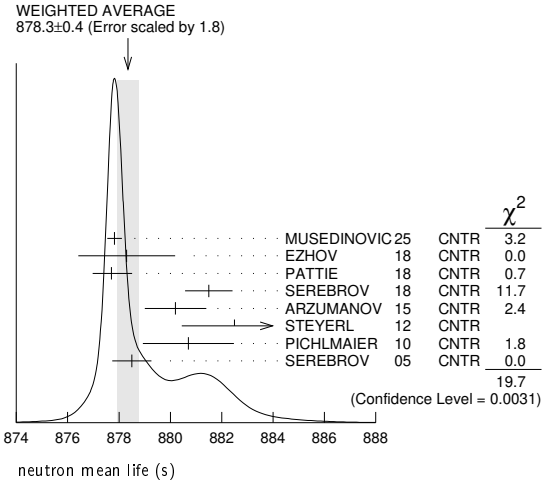

[1] MUSEDINOVIC 25 result is the average value of the previously published data of 2018–2019 in GONZALEZ 21 with the new 2020–2022 data. The new data alone yields a value of 877.96 ± 0.37 s. GONZALEZ 21 results are thus superseded.

[2] PATTIE 18 uses a new technique, with a semi-toroidal magneto-gravitational asymmetric trap and a novel in situ n-detector.

[3] ARZUMANOV 15 is a reanalysis of their 2008–2010 dataset, with improved systematic corrections of of ARZUMANOV 00 and ARZUMANOV 12.

[4] STEYERL 12 is a detailed reanalysis of neutron storage loss corrections to the raw data of MAMPE 89, and it replaces that value.

[5] Superseded by MUSEDINOVIC 25.

[6] WILSON 21 extract the value from the flux of n escaping the moon using data from the Lunar Prospector Neutron Spectrometer.

[7] YUE 13 differs from NICO 05 in that a different and better method was used to measure the neutron density in the fiducial volume. This shifted the lifetime by +1.4 seconds and reduced the previously largest source of systematic uncertainty by a factor of five.

[8] ARZUMANOV 12 reanalyzes its systematic corrections in ARZUMANOV 00 and obtains this corrected value.

[9] IGNATOVICH 95 calls into question some of the corrections and averaging procedures used by MAMPE 93. The response, BONDARENKO 96, denies the validity of the criticisms.

[10] The NESVIZHEVSKII 92 measurement has been withdrawn by A. Serebrov.

[11] The BYRNE 80 measurement has been withdrawn (J. Byrne, private communication, 1990).

n MAGNETIC MOMENT

See the "Quark Model" review.

VALUE (μ_N)	DOCUMENT ID		TECN	COMMENT
−1.91304276±0.00000045	MOHR	25	RVUE	2022 CODATA value
• • • We do not use the following data for averages, fits, limits, etc. • • •				
−1.91304273±0.00000045	TIESINGA	21	RVUE	2018 CODATA value
−1.91304273±0.00000045	MOHR	16	RVUE	2014 CODATA value
−1.91304272±0.00000045	MOHR	12	RVUE	2010 CODATA value
−1.91304273±0.00000045	MOHR	08	RVUE	2006 CODATA value
−1.91304273±0.00000045	MOHR	05	RVUE	2002 CODATA value
−1.91304272±0.00000045	MOHR	99	RVUE	1998 CODATA value
−1.91304275±0.00000045	COHEN	87	RVUE	1986 CODATA value
−1.91304277±0.00000048	[1] GREENE	82	MRS	

[1] GREENE 82 measures the moment to be $(1.04187564 \pm 0.00000026) \times 10^{-3}$ Bohr magnetons. The value above is obtained by multiplying this by $m_p/m_e = 1836.152701 \pm 0.000037$ (the 1986 CODATA value from COHEN 87).

n ELECTRIC DIPOLE MOMENT

A nonzero value is forbidden by both T invariance and P invariance. A number of early results have been omitted. See RAMSEY 90, GOLUB 94, and LAMOREAUX 09 for reviews.

The results are upper limits on $|d_n|$.

VALUE (10^{-25} $e$cm)	CL%	DOCUMENT ID		TECN	COMMENT
< 0.18	90	[1] ABEL	20	MRS	UCN
• • • We do not use the following data for averages, fits, limits, etc. • • •					
< 0.22	95	[2] SAHOO	17		^{199}Hg atom EDM + theory
< 0.16	95	GRANER	16	MRS	^{199}Hg atom EDM + theory
< 0.30	90	[3] PENDLEBURY	15	MRS	Supersedes BAKER 06
< 0.55	90	SEREBROV	15	MRS	UCN's, $h\nu = 2\mu_n B \pm 2d_n E$
< 0.55	90	[4] SEREBROV	14	MRS	See SEREBROV 15
< 0.29	90	[5] BAKER	06	MRS	See PENDLEBURY 15
< 0.63	90	[6] HARRIS	99	MRS	$d = (-0.1 \pm 0.36) \times 10^{-25}$
< 0.97	90	ALTAREV	96	MRS	See SEREBROV 14
< 1.1	95	ALTAREV	92	MRS	See ALTAREV 96
< 1.2	95	SMITH	90	MRS	See HARRIS 99
< 2.6	95	ALTAREV	86	MRS	$d = (-1.4 \pm 0.6) \times 10^{-25}$
0.3 ±4.8		PENDLEBURY	84	MRS	Ultracold neutrons
< 6	90	ALTAREV	81	MRS	$d = (2.1 \pm 2.4) \times 10^{-25}$
<16	90	ALTAREV	79	MRS	$d = (4.0 \pm 7.5) \times 10^{-25}$

[1] ABEL 20 reports $d = (0.0 \pm 1.1 \pm 0.2) \times 10^{-26}$ $e$cm value corresponding to the listed limit.

[2] SAHOO 17 develops theory to calculate this limit from the measured limit by GRANER 16 of the ^{199}Hg atom EDM.

[3] PENDLEBURY 15 reports $d = (-0.21 \pm 1.82) \times 10^{-26}$ $e$cm value corresponding to the listed limit.

[4] SEREBROV 14 includes the data of ALTAREV 96.

[5] LAMOREAUX 07 faults BAKER 06 for not including in the estimate of systematic error an effect due to the Earth's rotation. BAKER 07 replies (1) that the effect was included implicitly in the analysis and (2) that further analysis confirms that the BAKER 06 limit is correct as is. See also SILENKO 07.

[6] This HARRIS 99 result includes the result of SMITH 90. However, the averaging of the results of these two experiments has been criticized by LAMOREAUX 00.

n MEAN-SQUARE CHARGE RADIUS

The mean-square charge radius of the neutron, $\langle r_n^2 \rangle$, is related to the neutron-electron scattering length b_{ne} by $\langle r_n^2 \rangle = 3(m_e a_0/m_n) b_{ne}$, where m_e and m_n are the masses of the electron and neutron, and a_0 is the Bohr radius. Numerically, $\langle r_n^2 \rangle = 86.34\, b_{ne}$, if we use a_0 for a nucleus with infinite mass.

Int. J. Mod. Phys. A 2026.41. Downloaded from www.worldscientific.com
UNIVERSITY OF CALIFORNIA @ BERKELEY on 09/16/26. Re-use and distribution is strictly not permitted, except for Open Access articles.

Int. J. Mod. Phys. A 2026.41. Downloaded from www.worldscientific.com
by UNIVERSITY OF CALIFORNIA @ BERKELEY on 09/16/26. Re-use and distribution is strictly not permitted, except for Open Access articles.

VALUE (fm^2)	DOCUMENT ID		COMMENT
−0.1155±0.0017 OUR AVERAGE			
−0.115 ±0.002 ±0.003	KOPECKY	97	*ne* scattering (Pb)
−0.124 ±0.003 ±0.005	KOPECKY	97	*ne* scattering (Bi)
−0.114 ±0.003	KOESTER	95	*ne* scattering (Pb, Bi)
−0.115 ±0.003	[1] KROHN	73	*ne* scattering (Ne, Ar, Kr, Xe)
• • • We do not use the following data for averages, fits, limits, etc. • • •			
−0.1101±0.0089	[2] HEACOCK	21	*n* interferometry
−0.106 $^{+0.007}_{-0.005}$	[3] FILIN	20	chiral EFT analysis
−0.117 $^{+0.007}_{-0.011}$	BELUSHKIN	07	Dispersion analysis
−0.113 ±0.003 ±0.004	KOPECKY	95	*ne* scattering (Pb)
−0.134 ±0.009	ALEKSANDR...	86	*ne* scattering (Bi)
−0.114 ±0.003	KOESTER	86	*ne* scattering (Pb, Bi)
−0.118 ±0.002	KOESTER	76	*ne* scattering (Pb)
−0.120 ±0.002	KOESTER	76	*ne* scattering (Bi)
−0.116 ±0.003	KROHN	66	*ne* scattering (Ne, Ar, Kr, Xe)

[1] KROHN 73 measured −0.112 ± 0.003 fm^2. This value is as corrected by KOESTER 76.
[2] HEACOCK 21 extract the value from Pendelloesung interferometry to measure the neutron structure factors of silicon. This value is strongly anti-correlated with the mean-square thermal atomic displacement.
[3] FILIN 20 extract the value based on their chiral-EFT calculation of the deuteron structure radius and use as input the atomic data for the difference of the deuteron and proton charge radii.

n MAGNETIC RADIUS

This is the rms magnetic radius, $\sqrt{\langle r_M^2 \rangle}$.

VALUE (fm)	DOCUMENT ID		COMMENT
0.864 $^{+0.009}_{-0.008}$ OUR AVERAGE			
0.89 ±0.03	EPSTEIN	14	Using *ep*, *en*, $\pi\pi$ data
0.862 $^{+0.009}_{-0.008}$	BELUSHKIN	07	Dispersion analysis

n ELECTRIC POLARIZABILITY α_n

Following is the electric polarizability α_n defined in terms of the induced electric dipole moment by $\mathbf{D} = 4\pi\epsilon_0\alpha_n\mathbf{E}$. For a review, see SCHMIEDMAYER 89.

For a very complete reviews of the polarizability of the nucleon and Compton scattering, see SCHUMACHER 05, updated in SCHUMACHER 19, and GRIESSHAMMER 12.

VALUE (10^{-4} fm^3)	DOCUMENT ID		TECN	COMMENT
11.8 ± 1.1 OUR AVERAGE				
11.55 ± 1.25 ± 0.8	MYERS	14	CNTR	$\gamma d \to \gamma d$
12.5 ± 1.8 $^{+1.6}_{-1.3}$	[1] KOSSERT	03	CNTR	$\gamma d \to \gamma p n$
12.0 ± 1.5 ±2.0	SCHMIEDM...	91	CNTR	*n* Pb transmission
10.7 $^{+3.3}_{-10.7}$	ROSE	90B	CNTR	$\gamma d \to \gamma n p$
• • • We do not use the following data for averages, fits, limits, etc. • • •				
8.8 ± 2.4 ±3.0	[2] LUNDIN	03	CNTR	$\gamma d \to \gamma d$
13.6	[3] KOLB	00	CNTR	$\gamma d \to \gamma n p$
0.0 ± 5.0	[4] KOESTER	95	CNTR	*n* Pb, *n* Bi transmission
11.7 $^{+4.3}_{-11.7}$	ROSE	90	CNTR	See ROSE 90B
8 ±10	KOESTER	88	CNTR	*n* Pb, *n* Bi transmission
12 ±10	SCHMIEDM...	88	CNTR	*n* Pb, *n* C transmission

[1] KOSSERT 03 gets $\alpha_n - \beta_n$ =(9.8 ± 3.6$^{+2.1}_{-1.1}$ ± 2.2) × 10^{-4} fm^3, and uses $\alpha_n + \beta_n$ = (15.2 ± 0.5) × 10^{-4} fm^3 from LEVCHUK 00. Thus the errors on α_n and β_n are anti-correlated.
[2] LUNDIN 03 measures $\alpha_N - \beta_N$ = (6.4 ± 2.4) × 10^{-4} fm^3 and uses accurate values for α_p and α_p and a precise sum-rule result for $\alpha_n + \beta_n$. The second error is a model uncertainty, and errors on α_n and β_n are anticorrelated. The data from this paper aer included in the analysis of MYERS 14.
[3] KOLB 00 obtains this value with a lower limit of 7.6 × 10^{-4} fm^3 but no upper limit from this experiment alone. Combined with results of ROSE 90, the 1-σ range is (7.6–14.0) × 10^{-4} fm^3.
[4] KOESTER 95 uses natural Pb and the isotopes 208, 207, and 206. See this paper for a discussion of methods used by various groups to extract α_n from data.

n MAGNETIC POLARIZABILITY β_n

VALUE (10^{-4} fm^3)	DOCUMENT ID		TECN	COMMENT
3.7 ±1.2 OUR AVERAGE				
3.65 ± 1.25 ± 0.8	MYERS	14	CNTR	$\gamma d \to \gamma d$
2.7 ±1.8 $^{+1.3}_{-1.6}$	[1] KOSSERT	03	CNTR	$\gamma d \to \gamma p n$
6.5 ±2.4 ±3.0	[2] LUNDIN	03	CNTR	$\gamma d \to \gamma d$
• • • We do not use the following data for averages, fits, limits, etc. • • •				
1.6	[3] KOLB	00	CNTR	$\gamma d \to \gamma n p$

[1] KOSSERT 03 gets $\alpha_n - \beta_n$ =(9.8 ± 3.6$^{+2.1}_{-1.1}$ ± 2.2) × 10^{-4} fm^3, and uses $\alpha_n + \beta_n$ = (15.2 ± 0.5) × 10^{-4} fm^3 from LEVCHUK 00. Thus the errors on α_n and β_n are anti-correlated.
[2] LUNDIN 03 measures $\alpha_N - \beta_N$ = (6.4 ± 2.4) × 10^{-4} fm^3 and uses accurate values for α_p and α_p and a precise sum-rule result for $\alpha_n + \beta_n$. The second error is a model uncertainty, and errors on α_n and β_n are anticorrelated.
[3] KOLB 00 obtains this value with an upper limit of 7.6×10^{-4} fm^3 but no lower limit from this experiment alone. Combined with results of ROSE 90, the 1-σ range is (1.2–7.6) × 10^{-4} fm^3.

n CHARGE

See also "$|q_p + q_e|/e$" in the proton Listings.

VALUE (10^{-21} *e*)	DOCUMENT ID		TECN	COMMENT
− 0.2± 0.8 OUR AVERAGE				
− 0.1± 1.1	[1] BRESSI	11		Neutrality of SF_6
− 0.4± 1.1	[2] BAUMANN	88		Cold *n* deflection
• • • We do not use the following data for averages, fits, limits, etc. • • •				
−15 ±22	[3] GAEHLER	82	CNTR	Cold *n* deflection

[1] As a limit, this BRESSI 11 value is $< 1 \times 10^{-21}$ *e*.
[2] The BAUMANN 88 error ±1.1 gives the 68% CL limits about the the value −0.4.
[3] The GAEHLER 82 error ±22 gives the 90% CL limits about the the value −15.

LIMIT ON $n\overline{n}$ OSCILLATIONS

Mean Time for $n\overline{n}$ Transition

A test of ΔB=2 baryon number nonconservation. MOHAPATRA 80 and MOHAPATRA 89 discuss the theoretical motivations for looking for $n\overline{n}$ oscillations. DOVER 83 and DOVER 85 give phenomenological analyses. The best limits come from looking for the decay of neutrons bound in nuclei. However, these analyses require model-dependent corrections for nuclear effects. See KABIR 83, DOVER 89, ALBERICO 91, and GAL 00 for discussions. Direct searches for $n \to \overline{n}$ transitions using reactor neutrons are cleaner but give somewhat poorer limits. We include limits for both free and bound neutrons in the Summary Table. See MOHAPATRA 09 and PHILLIPS 16 for recent reviews.

VALUE (s)	CL%	DOCUMENT ID		TECN	COMMENT
>4.7 × 10^8	90	[1] ABE	21	CNTR	*n* bound in oxygen
>8.6 × 10^7	90	BALDO-...	94	CNTR	Reactor (free) neutrons
• • • We do not use the following data for averages, fits, limits, etc. • • •					
>1.37 × 10^8	90	[2] AHARMIM	17	SNO	*n* bound in deuteron
>2.7 × 10^8	90	ABE	15C	CNTR	*n* bound in oxygen
>1.3 × 10^8	90	CHUNG	02B	SOU2	*n* bound in iron
>1 × 10^7	90	BALDO-...	90	CNTR	See BALDO-CEOLIN 94
>1.2 × 10^8	90	BERGER	90	FREJ	*n* bound in iron
>4.9 × 10^5	90	BRESSI	90	CNTR	Reactor neutrons
>4.7 × 10^5	90	BRESSI	89	CNTR	See BRESSI 90
>1.2 × 10^8	90	TAKITA	86	CNTR	*n* bound in oxygen
>1 × 10^6	90	FIDECARO	85	CNTR	Reactor neutrons
>8.8 × 10^7	90	PARK	85B	CNTR	
>3 × 10^7		BATTISTONI	84	NUSX	
> 0.27–1.1 × 10^8		JONES	84	CNTR	
>2 × 10^7		CHERRY	83	CNTR	

[1] ABE 21 supersedes ABE 15C.
[2] The AHARMIM 17 value is an unbounded limit (it does not assume a positive lifetime). The bounded limit is 1.23 × 10^8 sec.

LIMIT ON nn' OSCILLATIONS

Lee and Yang (LEE 56) proposed the existence of mirror world in an attempt to restore global parity symmetry. A possible candidate for dark matter. Limits depend on assumptions about fields B and B'. See the papers for details. See BEREZHIANI 18 for a recent discussion.

VALUE (s)	CL%	DOCUMENT ID		TECN	COMMENT
>448	90	SEREBROV	09A	CNTR	Assumes $B' < 100$ nT
• • • We do not use the following data for averages, fits, limits, etc. • • •					
> 1	95	[1] BAN	23	CNTR	UCN, scan of B field
		[2] ALMAZAN	22	CNTR	STEREO, hidden neutron search $\lvert m_n - m_{n'} \rvert \geq 0$.
> 9	95	[3] ABEL	21	CNTR	UCN, scan of B field
> 17	95	[4] BEREZHIANI	18	CNTR	UCN, scan of B field
> 12	95	[5] ALTAREV	09A	CNTR	UCN, scan $0 \leq B \leq 12.5$ μT
>414	90	SEREBROV	08	CNTR	UCN, B field on & off
>103	95	BAN	07	CNTR	UCN, B field on & off

[1] BAN 23 determine limits on the oscillation time for the $|\delta m(nn')|$ range of 2–59 peV. The quoted value is $\tau_{nn'}/\sqrt{cos(\beta)} > 1$ sec. for B in 30–1143 μT, for the case $\beta = 0$.
[2] ALMAZAN 22 reports an experimental constraint on the probability for neutron conversion into a hidden neutron, $p < 3.1 \times 10^{-11}$ at 95% CL, which may be used to set a limit on the nn' oscillation time.
[3] ABEL 21 determine several limits on the oscillation time as a function of the mirror magnetic field B', and of the fixed angle, β, between the applied magnetic field and B'. The latter is assumed to be bound to Earth. Two values are quoted from two analysis methods: (i) $\tau_{nn'}/\sqrt{cos(\beta)} > 9$ sec for B' in 5–25.4 μT, and (ii) for any angle β, $\tau_{nn'} > 6$ sec for B' in 0.4–25.7 μT. The authors also quote a limit of 352 sec for the case $B' = 0$ T.

[4] The B field was set to (0.09, 0.12, 0.21) G. Limits on oscillation time are valid for any mirror field B' in (0.08–0.17) G, and for aligned fields B and B'. For larger values of B', the limits are significantly reduced.

[5] Losses of neutrons due to oscillations to mirror neutrons would be maximal when the magnetic fields B and B' in the two worlds were equal. Hence the scan over B by ALTAREV 09A: the limit applies for any B' over the given range. At $B' = 0$, the limit is 141 s (95% CL).

n DECAY MODES

See the proton listings for many other neutron decay modes.

	Mode		Fraction (Γ_i/Γ)	Confidence level
Γ_1	$p e^- \overline{\nu}_e$		100 %	
Γ_2	$p e^- \overline{\nu}_e \gamma$	[a]	$(9.2 \pm 0.7) \times 10^{-3}$	
Γ_3	hydrogen-atom $\overline{\nu}_e$		$< 2.7 \times 10^{-3}$	95%
	Charge conservation (Q) violating mode			
Γ_4	$p \nu_e \overline{\nu}_e$	Q	$< 8 \times 10^{-27}$	68%
	Baryon number violating decay			
Γ_5	$e^+ e^-$ invisible			
Γ_6	γ invisible			

[a] This limit is for γ energies between 0.4 and 782 keV.

n BRANCHING RATIOS

$\Gamma(p e^- \overline{\nu}_e \gamma)/\Gamma_{total}$ — Γ_2/Γ

VALUE (units 10^{-3})	CL%	DOCUMENT ID		TECN	COMMENT
9.17±0.24±0.64		[1] BALES	16	RDK2	Two different set-ups
• • • We do not use the following data for averages, fits, limits, etc. • • •					
3.09±0.11±0.30		[2] COOPER	10	CNTR	See BALES 16
3.13±0.11±0.33		NICO	06	CNTR	See COOPER 10
<6.9	90	[3] BECK	02	CNTR	γ, p, e^- coincidence

[1] BALES 16 gets a branching fraction of $(5.82 \pm 0.23 \pm 0.62) \times 10^{-3}$ for a photon energy range 0.4 to 14.0 keV, and with a different detector array, $(3.35 \pm 0.05 \pm 0.15) \times 10^{-3}$ for 14.1 to 782 keV. Our result above is the sum; the error on the sum is completely dominated by the error on the lower range.

[2] This COOPER 10 result is for γ energies between 15 and 340 keV.

[3] This BECK 02 limit is for γ energies between 35 and 100 keV.

$\Gamma(\text{hydrogen-atom } \overline{\nu}_e)/\Gamma_{total}$ — Γ_3/Γ

VALUE	CL%	DOCUMENT ID		TECN	COMMENT
$<0.27 \times 10^{-2}$	95	[1] CZARNECKI	18		Lifetime analysis
• • • We do not use the following data for averages, fits, limits, etc. • • •					
$<3 \times 10^{-2}$	95	[2] GREEN	90	RVUE	

[1] CZARNECKI 18 limit from an analysis of experimental discrepancies on the neutron lifetime and axial coupling applies as well to other possible exotic neutron decays.

[2] GREEN 90 infers that $\tau(\text{hydrogen-atom}\,\overline{\nu}_e) > 3 \times 10^4$ s by comparing neutron lifetime measurements made in storage experiments with those made in β-decay experiments. However, the result depends sensitively on the lifetime measurements, and does not of course take into account more recent measurements of same.

$\Gamma(p \nu_e \overline{\nu}_e)/\Gamma_{total}$ — Γ_4/Γ

Forbidden by charge conservation.

VALUE	CL%	DOCUMENT ID		TECN	COMMENT
$<8 \times 10^{-27}$	68	[1] NORMAN	96	RVUE	^{71}Ga $\rightarrow$ ^{71}Ge neutrals
• • • We do not use the following data for averages, fits, limits, etc. • • •					
$<9.7 \times 10^{-18}$	90	ROY	83	CNTR	^{113}Cd $\rightarrow$ ^{113m}In neut.
$<7.9 \times 10^{-21}$		VAIDYA	83	CNTR	^{87}Rb $\rightarrow$ ^{87m}Sr neut.
$<9 \times 10^{-24}$	90	BARABANOV	80	CNTR	^{71}Ga $\rightarrow$ ^{71}GeX
$<3 \times 10^{-19}$		NORMAN	79	CNTR	^{87}Rb $\rightarrow$ ^{87m}Sr neut.

[1] NORMAN 96 gets this limit by attributing SAGE and GALLEX counting rates to the charge-nonconserving transition ^{71}Ga $\rightarrow$ ^{71}Ge+neutrals rather than to solar-neutrino reactions.

$\Gamma(e^+ e^- \text{invisible})/\Gamma_{total}$ — Γ_5/Γ

Baryon number violating decay

VALUE	CL%	DOCUMENT ID		TECN	COMMENT
• • • We do not use the following data for averages, fits, limits, etc. • • •					
<0.01	90	[1] KLOPF	19	CNTR	re-interpretation of MUND 13
$<1 \times 10^{-4}$	90	[2] SUN	18	SPEC	Ultracold n, polarized

[1] KLOPF 19 value is for baryon number violating decay of neutron to electrons plus an invisible state, χ. The limit is valid for KE($e^+ e^-$) range between 32 keV and 664 keV, strengthening to few $\times 10^{-4}$ above approximately 100 keV.

[2] SUN 18 value is for baryon number violating decay of neutron to electrons plus an invisible state, χ. The limit is valid for 100 keV $<$ KE($e^+ e^-$) $<$ 644 keV. Assuming this decay $\chi e e$ is the only allowed χ decay channel, a 0.01 BR is ruled out for 100 keV $<$ E($e^+ e^-$) $<$ 644 keV at over 5σ.

$\Gamma(\gamma \text{invisible})/\Gamma_{total}$ — Γ_6/Γ

VALUE	DOCUMENT ID		TECN	COMMENT
• • • We do not use the following data for averages, fits, limits, etc. • • •				
not seen	[1] LE-JOUBIOUX	24	SPEC	^{6}He $\rightarrow$ ^{4}He + n
not seen	[2] TANG	18	SPEC	Ultracold n, in NiP-coated bottle

[1] LE-JOUBIOUX 24 search for the baryon number violating decay of n to invisible dark matter candidate, using the ^{6}He $\rightarrow$ ^{4}He + n + χ reaction, looking for a coincident neutron signal.

[2] TANG 18 search for the baryon number violating decay of n to γ plus an invisible dark matter candidate. They exclude the presence of a monoenergetic γ ray in the E(γ) range 782–1664 keV with branching ratio $\simeq$ 1% at 97% CL or greater.

See the related review(s):
Baryon Decay Parameters

$n \rightarrow p e^- \overline{\nu}_e$ DECAY PARAMETERS

See the above "Note on Baryon Decay Parameters." For discussions of recent results, see the references cited at the beginning of the section on the neutron mean life. For discussions of the values of the weak coupling constants g_A and g_V obtained using the neutron lifetime and asymmetry parameter A, comparisons with other methods of obtaining these constants, and implications for particle physics and for astrophysics, see DUBBERS 91 and WOOLCOCK 91. For tests of the $V-A$ theory of neutron decay, see EROZOLIMSKII 91B, MOSTOVOI 96, NICO 05, SEVERIJNS 06, and ABELE 08.

$\lambda \equiv g_A / g_V$

In the Standard Model $\lambda \equiv g_A/g_V$ is related to parameter a, e-$\overline{\nu}_e$ angular correlation coefficient, by $a = (1 - \lambda^2) / (1 + 3\lambda^2)$; this assumes that g_A and g_V are real. The relationship between a and λ is further modified once recoil corrections are included, see WIETFELDT 24.

VALUE	DOCUMENT ID		TECN	COMMENT
−1.2753 ±0.0013 OUR AVERAGE	Error includes scale factor of 2.7. See the ideogram below.			
−1.2712 ±0.0061	[1] WIETFELDT	24	SPEC	Cold n, unpolarized
−1.2677 ±0.0028	[2] BECK	20	SPEC	Proton recoil spectrum
−1.27641±0.00045±0.00033	[3] MAERKISCH	19	SPEC	pulsed cold n, polarized
−1.2772 ±0.0020	[4] BROWN	18	UCNA	Ultracold n, polarized
−1.2748 ±0.0008 $^{+0.0010}_{-0.0011}$	[5] MUND	13	SPEC	Cold n, polarized
−1.275 ±0.006 ±0.015	SCHUMANN	08	CNTR	Cold n, polarized
−1.2686 ±0.0046 ±0.0007	[6] MOSTOVOI	01	CNTR	A and B × polarizations
−1.266 ±0.004	LIAUD	97	TPC	Cold n, polarized, A
−1.2594 ±0.0038	[7] YEROZLIM...	97	CNTR	Cold n, polarized, A
−1.262 ±0.005	BOPP	86	SPEC	Cold n, polarized, A
• • • We do not use the following data for averages, fits, limits, etc. • • •				
−1.2796 ±0.0062	[8] HASSAN	21	SPEC	Cold n, unpolarized
−1.27607±0.00068	[9] SAUL	20	SPEC	Cold n, polarized, A
−1.284 ±0.014	[10] DARIUS	17	SPEC	Cold n, unpolarized
−1.2755 ±0.0030	[11] MENDENHALL	13	UCNA	See BROWN 18
−1.27590±0.00239 $^{+0.00331}_{-0.00377}$	[12] PLASTER	12	UCNA	See MENDENHALL 13
−1.27590 $^{+0.00409}_{-0.00445}$	LIU	10	UCNA	See PLASTER 12
−1.2739 ±0.0019	[13] ABELE	02	SPEC	See MUND 13
−1.274 ±0.003	ABELE	97D	SPEC	Cold n, polarized, A
−1.266 ±0.004	SCHRECK...	95	TPC	See LIAUD 97
−1.2544 ±0.0036	EROZOLIM...	91	CNTR	See YEROZOLIMSKY 97
−1.226 ±0.042	MOSTOVOY	83	RVUE	
−1.261 ±0.012	EROZOLIM...	79	CNTR	Cold n, polarized, A
−1.259 ±0.017	[14] STRATOWA	78	CNTR	p recoil spectrum, a
−1.263 ±0.015	EROZOLIM...	77	CNTR	See EROZOLIMSKII 79
−1.250 ±0.036	[14] DOBROZE...	75	CNTR	See STRATOWA 78
−1.258 ±0.015	[15] KROHN	75	CNTR	Cold n, polarized, A
−1.263 ±0.016	[16] KROPF	74	RVUE	n decay alone
−1.250 ±0.009	[16] KROPF	74	RVUE	n decay + nuclear ft

[1] WIETFELDT 24 updates HASSAN 21, see footnote to HASSAN 21. The value is extracted from the angular correlation coefficient.

[2] BECK 20 calculates this value from the measurement of the β-decay e–$\overline{\nu}_e$ angular correlation coefficient a.

[3] MAERKISCH 19 gets $A = -0.11985 \pm 0.00017 \pm 0.00012$.

[4] BROWN 18 gets $A = -0.12054 \pm 0.00044 \pm 0.00068$ and $\lambda = -1.2783 \pm 0.0022$. We quote the combined values that include the earlier UCNA measurements (MENDENHALL 13).

[5] This MUND 13 value includes earlier PERKEO II measurements (ABELE 02 and ABELE 97D).

[6] MOSTOVOI 01 measures the two P-odd correlations A and B, or rather SA and SB, where S is the n polarization, in free neutron decay.

[7] YEROZOLIMSKY 97 makes a correction to the EROZOLIMSKII 91 value.

[8] HASSAN 21 include earlier data of DARIUS 17. The value is extracted from the angular correlation coefficient a.

[9] SAUL 20 quote this value of λ under the SM assumption of the Fierz term $b = 0$. In a combined fit authors extract a value of $\lambda = -1.2792 \pm 0.0060$.

[10] DARIUS 17 calculates this value from the measurement of the a parameter (see below). Data is included in HASSAN 21.

[11] MENDENHALL 13 gets $A = -0.11954 \pm 0.00055 \pm 0.00098$ and $\lambda = -1.2756 \pm 0.0030$. We quote the nearly identical values that include the earlier UCNA measurement (PLASTER 12), with a correction to that result.

[12] This PLASTER 12 value is identical with that given in LIU 10, but the experiment is now described in detail.

[13] This is the combined result of ABELE 02 and ABELE 97D.

[14] These experiments measure the absolute value of g_A/g_V only.

[15] KROHN 75 includes events of CHRISTENSEN 70.

[16] KROPF 74 reviews all data through 1972.

Int. J. Mod. Phys. A 2026.41. Downloaded from www.worldscientific.com
by UNIVERSITY OF CALIFORNIA @ BERKELEY on 09/16/26. Re-use and distribution is strictly not permitted, except for Open Access articles.

Int. J. Mod. Phys. A 2026.41. Downloaded from www.worldscientific.com
by UNIVERSITY OF CALIFORNIA @ BERKELEY on 09/16/26. Re-use and distribution is strictly not permitted, except for Open Access articles.

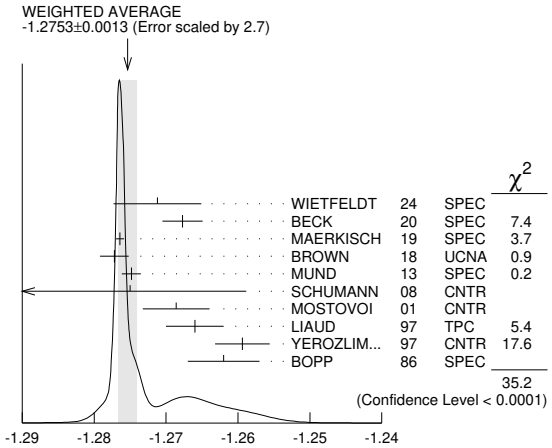

e^- ASYMMETRY PARAMETER A

This is the neutron-spin electron-momentum correlation coefficient. The coefficient itself is not well defined in any measurement once higher-order radiative and recoil corrections, which are experiment dependent, are included. By contrast, measurements of the ratio $\lambda \equiv g_A/g_V$ (see data block above) incorporate such higher-order effects. For this reason, and in order to meaningfully compare results from different measurements, we list here the zero-recoil-order A-coefficient, which in the Standard Model and at zero recoil order, is related to $\lambda \equiv g_A/g_V$ by $A = -2\,\lambda\,(\lambda+1)\,/\,(1+3\lambda^2)$; this assumes that g_A and g_V are real. See e.g. MAERKISCH 19 and BROWN 18.

VALUE	DOCUMENT ID		TECN	COMMENT
−0.11958±0.00021 OUR AVERAGE	Error includes scale factor of 1.2. See the ideogram below.			
−0.11985±0.00017±0.00012	[1] MAERKISCH	19	SPEC	pulsed cold n, polarized
−0.12015±0.00034±0.00063	[2] BROWN	18	UCNA	Ultracold n, polarized
$-0.11926\pm0.00031^{+0.00036}_{-0.00042}$	[3] MUND	13	SPEC	Cold n, polarized
−0.1160 ±0.0009 ±0.0012	LIAUD	97	TPC	Cold n, polarized
−0.1135 ±0.0014	[4] YEROZLIM...	97	CNTR	Cold n, polarized
−0.1146 ±0.0019	BOPP	86	SPEC	Cold n, polarized
• • • We do not use the following data for averages, fits, limits, etc. • • •				
−0.11972±0.00025	[5] SAUL	20	SPEC	Cold n, polarized
−0.11952±0.00110	[6] MENDENHALL	13	UCNA	See BROWN 18
$-0.11966\pm0.00089^{+0.00123}_{-0.00140}$	[7] PLASTER	12	UCNA	See MENDENHALL 13
$-0.11966\pm0.00089^{+0.00123}_{-0.00140}$	LIU	10	UCNA	See PLASTER 12
−0.1138 ±0.0046 ±0.0021	PATTIE	09	SPEC	Ultracold n, polarized
−0.1189 ±0.0007	[8] ABELE	02	SPEC	See MUND 13
−0.1168 ±0.0017	[9] MOSTOVOI	01	CNTR	Inferred
−0.1189 ±0.0012	ABELE	97D	SPEC	Cold n, polarized
−0.1160 ±0.0009 ±0.0011	SCHRECK...	95	TPC	See LIAUD 97
−0.1116 ±0.0014	EROZOLIM...	91	CNTR	See YEROZOLIMSKY 97
−0.114 ±0.005	[10] EROZOLIM...	79	CNTR	Cold n, polarized
−0.113 ±0.006	[10] KROHN	75	CNTR	Cold n, polarized

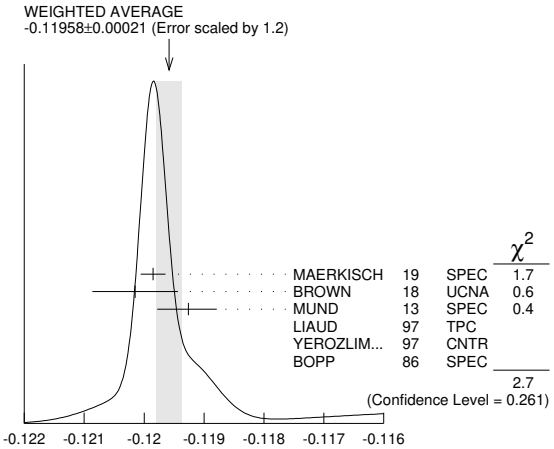

[1] MAERKISCH 19 further derive a value for the CKM-element $|V_{ud}| = 0.97351 \pm 0.00060$, using $\tau_n = 879.7(8)$ sec and the relation from CZARNECKI 18.

[2] BROWN 18 gets $A = -0.12054 \pm 0.00044 \pm 0.00068$ and $\lambda = -1.2783 \pm 0.0022$. We quote the combined values that include the earlier UCNA measurements (MENDENHALL 13).

[3] This MUND 13 value includes earlier PERKEO II measurements (ABELE 02 and ABELE 97D), with a correction to those results.

[4] YEROZOLIMSKY 97 makes a correction to the EROZOLIMSKII 91 value.

[5] Under the SM assumption that the Fierz term $b = 0$, SAUL 20 obtain the quoted asymmetry parameter A and $\lambda = -1.27607 \pm 0.00068$. In a combined fit authors extract the values $A = -0.1209 \pm 0.0015$, $\lambda = -1.2792 \pm 0.0060$, and $b = 0.017 \pm 0.021$.

[6] MENDENHALL 13 gets $A = -0.11954 \pm 0.00055 \pm 0.00098$ and $\lambda = -1.2756 \pm 0.0030$. We quote the nearly identical values that include the earlier UCNA measurement (PLASTER 12), with a correction to that result.

[7] This PLASTER 12 value is identical with that given in LIU 10, but the experiment is now described in detail.

[8] This is the combined result of ABELE 02 and ABELE 97D.

[9] MOSTOVOI 01 calculates this from its measurement of $\lambda = g_A/g_V$ above.

[10] These results are not corrected for radiative effects and weak magnetism, but the corrections are small compared to the errors.

$\overline{\nu}_e$ ASYMMETRY PARAMETER B

This is the neutron-spin antineutrino-momentum correlation coefficient. In the Standard Model, B is related to $\lambda \equiv g_A/g_V$ by $B = 2\lambda(\lambda-1)\,/\,(1+3\lambda^2)$; this assumes that g_A and g_V are real.

VALUE	DOCUMENT ID		TECN	COMMENT
0.9807±0.0030 OUR AVERAGE				
0.9802±0.0034±0.0036	SCHUMANN	07	CNTR	Cold n, polarized
0.967 ±0.006 ±0.010	KREUZ	05	CNTR	Cold n, polarized
0.9801±0.0046	SEREBROV	98	CNTR	Cold n, polarized
0.9894±0.0083	KUZNETSOV	95	CNTR	Cold n, polarized
1.00 ±0.05	CHRISTENSEN	70	CNTR	Cold n, polarized
0.995 ±0.034	EROZOLIM...	70C	CNTR	Cold n, polarized
• • • We do not use the following data for averages, fits, limits, etc. • • •				
0.9876±0.0004	[1] MOSTOVOI	01	CNTR	Inferred

[1] MOSTOVOI 01 calculates this from its measurement of $\lambda = g_A/g_V$ above.

PROTON ASYMMETRY PARAMETER C

Describes the correlation between the neutron spin and the proton momentum. In the Standard Model, C is related to $\lambda \equiv g_A/g_V$ by $C = -x_c\,(A+B) = x_c\,4\lambda/(1+3\lambda^2)$, where $x_c = 0.27484$ is a kinematic factor; this assumes that g_A and g_V are real.

VALUE	DOCUMENT ID		TECN	COMMENT
−0.2377±0.0010±0.0024	SCHUMANN	08	CNTR	Cold n, polarized

e-$\overline{\nu}_e$ ANGULAR CORRELATION COEFFICIENT a_0

For a review of past measurements of the a-coefficient, see WIETFELDT 05. The a-coefficient itself is not well defined in any measurement once higher-order radiative and recoil corrections, which are experiment dependent, are included. By contrast, measurements of the ratio $\lambda \equiv g_A/g_V$ (see data block above) incorporate such higher-order effects. For this reason, and in order to meaningfully compare results for the angular correlation coefficient from measurements of different observables, we list here the zero-recoil-order a-coefficient, denoted a_0, which in the Standard Model and at zero recoil order, is related to λ by $a_0 = (1-\lambda^2)\,/\,(1+3\lambda^2)$; this assumes that g_A and g_V are real. See also the discussion in WIETFELDT 24.

VALUE	DOCUMENT ID		TECN	COMMENT
−0.1044 ±0.0007 OUR AVERAGE				
−0.1053 ±0.0018	[1] WIETFELDT	24	SPEC	Cold n, unpolarized
−0.10430±0.00084	BECK	20	SPEC	Proton recoil spectrum
−0.1054 ±0.0055	BYRNE	02	SPEC	Proton recoil spectrum
−0.1017 ±0.0051	STRATOWA	78	CNTR	Proton recoil spectrum
−0.091 ±0.039	GRIGOREV	68	SPEC	Proton recoil spectrum
• • • We do not use the following data for averages, fits, limits, etc. • • •				
−0.10782±0.00124±0.00133	[2] HASSAN	21	SPEC	Cold n, unpolarized
−0.1090 ±0.0030 ±0.0028	[3] DARIUS	17	SPEC	Cold n, unpolarized
−0.1045 ±0.0014	[4] MOSTOVOI	01	CNTR	Inferred

[1] WIETFELDT 24 updates HASSAN 21. Includes radiative and recoil corrections to first order, and is averaged over the full Fermi neutron beta spectrum. Supersedes HASSAN 21.

[2] HASSAN 21 includes the data of DARIUS 17. Uses the asymmetry in time-of-flight between the beta electron and recoil proton in delayed coincidence. Supersedes DARIUS 17.

[3] DARIUS 17 exploits a "wishbone" correlation, where the p time of flight is correlated with the momentum of the electron in delayed coincidence. Data is included in HASSAN 21.

[4] MOSTOVOI 01 calculates this from its measurement of $\lambda = g_A/g_V$ above.

ϕ_{AV}, PHASE OF g_A RELATIVE TO g_V

Time reversal invariance requires this to be 0 or 180°. This is related to D given in the next data block and $\lambda \equiv g_A/g_V$ by $\sin(\phi_{AV}) \equiv D(1+3\lambda^2)/2|\lambda|$; this assumes that g_A and g_V are real.

VALUE (°)	CL%	DOCUMENT ID		TECN	COMMENT
180.017±0.026 OUR AVERAGE					
180.012±0.028	68	CHUPP	12	CNTR	Cold n, polarized > 91%
180.04 ±0.09		SOLDNER	04	CNTR	Cold n, polarized
180.08 ±0.13		LISING	00	CNTR	Polarized > 93%
• • • We do not use the following data for averages, fits, limits, etc. • • •					
180.013±0.028		MUMM	11	CNTR	See CHUPP 12
179.71 ±0.39		EROZOLIM...	78	CNTR	Cold n, polarized
180.35 ±0.43		EROZOLIM...	74	CNTR	Cold n, polarized
181.1 ±1.3		[1] KROPF	74	RVUE	n decay
180.14 ±0.22		STEINBERG	74	CNTR	Cold n, polarized

[1] KROPF 74 reviews all data through 1972.

Int. J. Mod. Phys. A 2026.41. Downloaded from www.worldscientific.com
UNIVERSITY OF CALIFORNIA @ BERKELEY on 09/16/26. Re-use and distribution is strictly not permitted, except for Open Access articles.

TRIPLE CORRELATION COEFFICIENT *D*

These are measurements of the component of *n* spin perpendicular to the decay plane in β decay. Should be zero if *T* invariance is not violated.

VALUE (units 10^{-4})	*DOCUMENT ID*		*TECN*	*COMMENT*
− 1.2 ± 2.0 OUR AVERAGE				
− 0.94 ± 1.89 ± 0.97	CHUPP	12	CNTR	Cold *n*, polarized > 91%
− 2.8 ± 6.4 ± 3.0	SOLDNER	04	CNTR	Cold *n*, polarized
− 6 ± 12 ± 5	LISING	00	CNTR	Polarized > 93%
• • • We do not use the following data for averages, fits, limits, etc. • • •				
− 0.96 ± 1.89 ± 1.01	MUMM	11	CNTR	See CHUPP 12
+ 22 ± 30	EROZOLIM...	78	CNTR	Cold *n*, polarized
− 27 ± 50	[1] EROZOLIM...	74	CNTR	Cold *n*, polarized
− 11 ± 17	STEINBERG	74	CNTR	Cold *n*, polarized

[1] EROZOLIMSKII 78 says asymmetric proton losses and nonuniform beam polarization may give a systematic error up to 30×10^{-4}, thus increasing the EROZOLIMSKII 74 error to 50×10^{-4}. STEINBERG 74 and STEINBERG 76 estimate these systematic errors to be insignificant in their experiment.

TRIPLE CORRELATION COEFFICIENT *R*

Another test of time-reversal invariance. *R* measures the polarization of the electron in the direction perpendicular to the plane defined by the neutron spin and the electron momentum. $R = 0$ for T invariance.

VALUE	*DOCUMENT ID*		*TECN*	*COMMENT*
+0.004 ± 0.012 ± 0.005	[1] KOZELA	12	CNTR	Mott polarimeter
• • • We do not use the following data for averages, fits, limits, etc. • • •				
+ 0.008 ± 0.015 ± 0.005	KOZELA	09	CNTR	See KOZELA 12

[1] KOZELA 12 also measures the polarization of the electron along the direction of the neutron spin. This is nonzero in the Standard Model; the correlation coefficient is $N = +0.067 \pm 0.011 \pm 0.004$.

FIERZ INTERFERENCE TERM *b*

The coefficient of the Fierz interference term, *b*, probes additional contributions to the differential decay rate of the neutron from scalar or tensor current interactions, beyond the Standard Model.

VALUE	*DOCUMENT ID*		*TECN*	*COMMENT*
0.017 ± 0.020 ± 0.003	[1] SAUL	20	SPEC	Cold *n*, polarized

[1] In a combined fit SAUL 20 extract this best fit value of the Fierz interference term *b* and the values $A = -0.1209 \pm 0.0015$ and $\lambda = -1.2792 \pm 0.0060$. For *b* it translates into a 90% CL region of $-0.018 \leq b \leq 0.052$ as a function of *A*.

n REFERENCES

We have omitted some papers that have been superseded by later experiments. See our earlier editions.

MOHR	25	RMP 97 025002	P.J. Mohr *et al.*	(NIST)
MUSEDINOVIC	25	PR C111 045501	R. Musedinovic *et al.*	(UCNtau Collab.)
LE-JOUBIOUX	24	PRL 132 132501	M. Le Joubioux *et al.*	(GANIL)
WIETFELDT	24	PR C110 015502	F.E. Wietfeldt *et al.*	(aCORN Collab)
BAN	23	PRL 131 191801	G. Ban *et al.*	(CAEN, ZURI, ISNG, SORB+)
ALMAZAN	22	PRL 128 061801	H. Almazan *et al.*	(STEREO Collab.)
ABE	21	PR D103 012008	K. Abe *et al.*	(Super-Kamiokande Collab.)
ABEL	21	PL B812 135993	C. Abel *et al.*	(nEDM Collab.)
GONZALEZ	21	PRL 127 162501	F.M. Gonzalez *et al.*	(UCNtau Collab.)
HASSAN	21	PR C103 045502	M.T. Hassan *et al.*	(aCORN Collab)
HEACOCK	21	SCI 373 1239	B. Heacock *et al.*	(NIST, RIKEN, NAGO+)
TIESINGA	21	RMP 93 025010	E. Tiesinga *et al.*	(NIST)
WILSON	21	PR C104 045501	J.T. Wilson *et al.*	(JHU, DURH)
ABEL	20	PRL 124 081803	C. Abel *et al.*	(nEDM Collab.)
BECK	20	PR C101 055506	M. Beck *et al.*	(aSPECT Collab.)
FILIN	20	PRL 124 082501	A.A. Filin *et al.*	
SAUL	20	PRL 125 112501	H. Saul *et al.*	(PERKEO III Collab.)
KLOPF	19	PRL 122 222503	M. Klopf *et al.*	(PERKEO II Collab.)
MAERKISCH	19	PRL 122 242501	B. Maerkisch *et al.*	(TUM, ILL, +)
SCHUMACHER	19	LHEP 4 4	M. Schumacher	(GOET)
BEREZHIANI	18	EPJ C78 717	Z. Berezhiani *et al.*	(AQUI, INFN, ILLG+)
BROWN	18	PR C97 035505	M.A.-P. Brown *et al.*	(UCNA Collab.)
CZARNECKI	18	PRL 120 202002	A. Czarnecki, W.J. Marciano, A. Sirlin	(ALBE+)
EZHOV	18	JETPL 107 671	V.F. Ezhov *et al.*	(PNPI, LENSU, CAEN+)
PATTIE	18	SCI 360 627	R.W. Pattie Jr. *et al.*	(LASL, IND, NCSU+)
SEREBROV	18	PR C97 055503	A.P. Serebrov *et al.*	(PNPI, ILLG, RAL)
Also		JETPL 106 623	A.P. Serebrov *et al.*	(PNPI, ILLG, RAL)
SUN	18	PR C97 052501	X. Sun *et al.*	(UCNA Collab.)
TANG	18	PRL 121 022505	Z. Tang *et al.*	(Los Alamos UCNtau Collab.)
AHARMIM	17	PR D96 092005	B. Aharmin *et al.*	(SNO Collab.)
DARIUS	17	PRL 119 042502	G. Darius *et al.*	(aCORN at NIST)
SAHOO	17	PR D95 013002	B.K. Sahoo	(AHMEB)
BALES	16	PRL 116 242501	M.J. Bales *et al.*	(RDK II Collab.)
GRANER	16	PRL 116 161601	B. Graner *et al.*	(WASH)
Also		PRL 119 119901 (errat.)	B. Graner *et al.*	(WASH)
MOHR	16	RMP 88 035009	P.J. Mohr, D.B. Newell, B.N. Taylor	(NIST)
PHILLIPS	16	PRPL 612 1	D.G. Phillips II *et al.*	
ABE	15C	PR D91 072006	K. Abe *et al.*	(Super-Kamiokande Collab.)
ARZUMANOV	15	PL B745 79	S. Arzumanov *et al.*	(ILLG, KIAE)
PENDLEBURY	15	PR D92 092003	J.M. Pendlebury *et al.*	(ETHZ, PSI, SUSS)
SEREBROV	15	PR C92 055501	A.P. Serebrov *et al.*	(PNPI, ILLG, IOFF)
EPSTEIN	14	PR D90 074027	Z. Epstein, G. Paz, J. Roy	(UMD, WAYN)
MYERS	14	PRL 113 262506	L.S. Myers *et al.*	(COMPTON/MAX-lab Collab.)
SEREBROV	14	JETPL 99 4	A.P. Serebrov *et al.*	(PNPI, ILL, IOFF)
MENDENHALL	13	PR C87 032501	M.P. Mendenhall *et al.*	(UCNA Collab.)
MUND	13	PRL 110 172502	D. Mund *et al.*	(HEID, ILLG)
YUE	13	PRL 111 222501	A.T. Yue *et al.*	(UMD, NIST, TENN, ORNL+)
ARZUMANOV	12	JETPL 95 224	S.S. Arzumanov *et al.*	(KIAE)
		Translated from ZETFP 95 248.		
CHUPP	12	PR C86 035505	T.E. Chupp *et al.*	(MICH, UCB, WASH+)
GRIESSHAM...	12	PPNP 67 841	H.W. Griesshammer *et al.*	(GWU, MCHS+)
KOZELA	12	PR C85 045501	A. Kozela *et al.*	(nTRV Collab.)
MOHR	12	RMP 84 1527	P.J. Mohr, B.N. Taylor, D.B. Newell	(NIST)
PLASTER	12	PR C86 055501	B. Plaster *et al.*	(UCNA Collab.)
STEYERL	12	PR C85 065503	A. Steyerl *et al.*	(URI, SUSS)
BRESSI	11	PR A83 052101	G. Bressi *et al.*	(LEGN, PAVII, PADO, TRST+)
DUBBERS	11	RMP 83 1111	D. Dubbers, M.G. Schmidt	(HEID)
MUMM	11	PRL 107 102301	H.P. Mumm *et al.*	(NIST, WASH, MICH, LBL+)
WIETFELDT	11	RMP 83 1173	F.E. Wietfeldt, G.L. Greene	(TULA, TENN)
COOPER	10	PR C81 035503	R.L. Cooper *et al.*	(MICH, NIST, TULA+)
LIU	10	PRL 105 181803	J. Liu *et al.*	(UCNA Collab.)
Also		PRL 105 219903 (errat.)	J. Liu *et al.*	(UCNA Collab.)
PICHLMAIER	10	PL B693 221	A. Pichlmaier *et al.*	(TUM, PNPI, ILLG)
ALTAREV	09A	PR D80 032003	I. Altarev *et al.*	(TUM, RAL, CAEN+)
KOZELA	09	PRL 102 172301	A. Kozela *et al.*	(JAGL, CRAC, PSI, CAEN+)
LAMOREAUX	09	JP G36 104002	S.K. Lamoreaux, R. Golub	(YALE, NCSU)
MOHAPATRA	09	JP G36 104006	R.N. Mohapatra	(UMD)
PATTIE	09	PRL 102 012301	R.W. Pattie Jr. *et al.*	(Los Alamos UCNA Collab.)
SEREBROV	09A	NIM A611 137	A.P. Serebrov *et al.*	(PNPI, IOFF, ILLG+)
ABELE	08	PPNP 60 1	H. Abele	(HEID)
MOHR	08	RMP 80 633	P.J. Mohr, B.N. Taylor, D.B. Newell	(NIST)
SCHUMANN	08	PRL 100 151801	M. Schumann *et al.*	(HEID, ILLG, KARL+)
SEREBROV	08	PL B663 181	A.P. Serebrov *et al.*	(PNPI, IOFF, ILLG+)
BAKER	07	PRL 98 149102	C.A. Baker *et al.*	(RAL, SUSS, ILLG)
BAN	07	PRL 99 161603	G. Ban *et al.*	(CAEN, JAGL, PSI, JINR+)
BELUSHKIN	07	PR C75 035202	M.A. Belushkin, H.W. Hammer, U.-G. Meissner	(BONN+)
LAMOREAUX	07	PRL 98 149101	S.K. Lamoreaux, R. Golub	(YALE, NCSU)
SCHUMANN	07	PRL 99 191803	M. Schumann *et al.*	(HEID, ILLG, KARL+)
SILENKO	07	PPNL 4 468	A.Ya. Silenko	(Belarussian U.)
		Translated from PFECAY 6 784.		
BAKER	06	PRL 97 131801	C.A. Baker *et al.*	(RAL, SUSS, ILLG)
NICO	06	NAT 444 1059	J.S. Nico *et al.*	(NIST, TULN, MICH, UMD+)
SEVERIJNS	06	RMP 78 991	N. Severijns, M. Beck, O. Naviliat-Cuncic	(LEUV+)
KREUZ	05	PL B619 263	M. Kreuz *et al.*	(HEID, ILLG, MAINZ, KARL+)
MOHR	05	RMP 77 1	P.J. Mohr, B.N. Taylor	(NIST)
NICO	05	PR C71 055502	J.S. Nico *et al.*	(NIST, TULN, IND, TENN+)
SCHUMACHER	05	PPNP 55 567	M. Schumacher	(GOET)
SEREBROV	05	PL B605 72	A.P. Serebrov *et al.*	(PNPI, JINR, ILLG)
Also		SPU 48 867	A.P. Serebrov *et al.*	(PPNI, JINR, ILLG)
		Translated from UFN 175 905.		
WIETFELDT	05	MPL A20 1783	F.E. Wietfeldt	(TULN)
SOLDNER	04	PL B581 49	T. Soldner *et al.*	(ILLG, TUM)
DEWEY	03	PRL 91 152302	M.S. Dewey *et al.*	(NIST, TULN, IND+)
KOSSERT	03	EPJ A16 259	K. Kossert *et al.*	(Mainz MAMI Collab.)
Also		PRL 88 162301	K. Kossert *et al.*	(Mainz MAMI Collab.)
LUNDIN	03	PRL 90 192501	M. Lundin *et al.*	
ABELE	02	PRL 88 211801	H. Abele *et al.*	(PERKEO-II Collab.)
BECK	02	JETPL 76 332	M. Beck *et al.*	(LEUV, SUSS, KIAE, PNPI)
		Translated from ZETFP 76 392.		
BYRNE	02	JP G28 1325	J. Byrne *et al.*	
CHUNG	02B	PR D66 032004	J. Chung *et al.*	(SOUDAN-2 Collab.)
MOSTOVOI	01	PAN 64 1955	Yu.A. Mostovoi *et al.*	
		Translated from YAF 64 2040.		
ARZUMANOV	00	PL B483 15	S. Arzumanov *et al.*	
GAL	00	PR C61 028201	A. Gal	
KOLB	00	PRL 85 1388	N.R. Kolb *et al.*	
LAMOREAUX	00	PR D61 051301	S.K. Lamoreaux, R. Golub	
LEVCHUK	00	NP A674 449	M.I. Levchuk, A.I. L'vov	(BELA, LEBD)
LISING	00	PR C62 055501	L.J. Lising *et al.*	(NIST emiT Collab.)
HARRIS	99	PRL 82 904	P.G. Harris *et al.*	
KESSLER	99	PL A255 221	E.G. Kessler Jr *et al.*	
MOHR	99	JPCRD 28 1713	P.J. Mohr, B.N. Taylor	(NIST)
Also		RMP 72 351	P.J. Mohr, B.N. Taylor	(NIST)
SEREBROV	98	JETP 86 1074	A.P. Serebrov *et al.*	
		Translated from ZETF 113 1963.		
ABELE	97D	PL B407 212	H. Abele *et al.*	(HEIDP, ILLG)
KOPECKY	97	PR C56 2229	S. Kopecky *et al.*	
LIAUD	97	NP A612 53	P. Liaud *et al.*	(ILLG, LAPP)
YEROZLIM...	97	PL B412 240	B.G. Erozolimsky *et al.*	(HARV, PNPI, KIAE)
ALTAREV	96	PAN 59 1152	I.S. Altarev *et al.*	(PNPI)
		Translated from YAF 59 1204.		
BONDAREN...	96	JETPL 64 416	L.N. Bondarenko *et al.*	(KIAE)
		Translated from ZETFP 64 382.		
BYRNE	96	EPL 33 187	J. Byrne *et al.*	(SUSS, ILLG)
MOSTOVOI	96	PAN 59 968	Y.A. Mostovoy	(KIAE)
		Translated from YAF 59 1013.		
NORMAN	96	PR D53 4086	E.B. Norman, J.N. Bahcall, M. Goldhaber	(LBL+)
IGNATOVICH	95	JETPL 62 1	V.K. Ignatovich	(JINR)
		Translated from ZETFP 62 3.		
KOESTER	95	PR C51 3363	L. Koester *et al.*	(TUM, JINR, LATV)
KOPECKY	95	PRL 74 2427	S. Kopecky *et al.*	
KUZNETSOV	95	PRL 75 794	I.A. Kuznetsov *et al.*	(PNPI, KIAE, HARV+)
SCHRECK...	95	PL B349 427	K. Schreckenbach *et al.*	(TUM, ILLG, LAPP)
BALDO-...	94	ZPHY C63 409	M. Baldo-Ceolin *et al.*	(HEID, ILLG, PADO+)
DIFILIPPO	94	PRL 73 1481	F. DiFilippo *et al.*	(MIT)
Also		PRL 71 1998	V. Natarajan *et al.*	(MIT)
GOLUB	94	PRPL 237C 1	R. Golub, K. Lamoreaux	(HAHN, WASH)
MAMPE	93	JETPL 57 82	B. Mampe *et al.*	(KIAE)
		Translated from ZETFP 57 77.		
ALTAREV	92	PL B276 242	I.S. Altarev *et al.*	(PNPI)
NESVIZHEV...	92	JETP 75 405	V.V. Nesvizhevsky *et al.*	(PNPI, JINR)
		Translated from ZETF 102 740.		
ALBERICO	91	NP A523 488	W.M. Alberico, A. de Pace, M. Pignone	(TORI)
DUBBERS	91	NP A527 239c	D. Dubbers	(ILLG)
Also		EPL 11 195	D. Dubbers, W. Mampe, J. Dohner	(ILLG, HEID)
EROZOLIM...	91	PL B263 33	B.G. Erozolimsky *et al.*	(PNPI, KIAE)
Also		SJNP 52 999	B.G. Erozolimsky *et al.*	(PNPI, KIAE)
		Translated from YAF 52 1583.		
EROZOLIM...	91B	SJNP 53 260	B.G. Erozolimsky, Y.A. Mostovoy	(KIAE)
		Translated from YAF 53 418.		
SCHMIEDM...	91	PRL 66 1015	J. Schmiedmayer *et al.*	(TUW, ORNL)
WOOLCOCK	91	MPL A6 2579	W.S. Woolcock	(CANB)
ALFIMENKOV	90	JETPL 52 373	V.P. Alfimenkov *et al.*	(PNPI, JINR)
		Translated from ZETFP 52 984.		
BALDO-...	90	PL B236 95	M. Baldo-Ceolin *et al.*	(PADO, PAVI, HEIDP+)
BERGER	90	PL B240 237	C. Berger *et al.*	(FREJUS Collab.)
BRESSI	90	NC 103A 731	G. Bressi *et al.*	(PAVI, ROMA, MILA)
BYRNE	90	PRL 65 289	J. Byrne *et al.*	(SUSS, NBS, SCOT, CBNM)
GREEN	90	JP G16 L75	K. Green, D. Thompson	(RAL)
RAMSEY	90	ARNPS 40 1	N.F. Ramsey	(HARV)
ROSE	90	PL B234 460	K.W. Rose *et al.*	(GOET, MPCM, MAINZ)
ROSE	90B	NP A514 621	K.W. Rose *et al.*	(GOET, MPCM)
SMITH	90	PL B234 191	K.F. Smith *et al.*	(SUSS, RAL, HARV+)
BRESSI	89	ZPHY C43 175	G. Bressi *et al.*	(INFN, MILA, PAVI, ROMA)
DOVER	89	NIM A284 13	C.B. Dover, A. Gal, J.M. Richard	(BNL, HEBR+)
KOSSAKOW...	89	NP A503 473	R. Kossakowski *et al.*	(LAPP, SAVO, ISNG+)
MAMPE	89	PRL 63 593	W. Mampe *et al.*	(ILLG, RISL, SUSS, URI)
MOHAPATRA	89	NIM A284 1	R.N. Mohapatra	(UMD)
PAUL	89	ZPHY C45 25	W. Paul *et al.*	(BONN, WUPP, MPIK, ILLG)
SCHMIEDM...	89	NIM A284 137	J. Schmiedmayer, H. Rauch, P. Riehs	(WIEN)
BAUMANN	88	PR D37 3107	J. Baumann *et al.*	(BAYR, MUNI, ILLG)
KOESTER	88	ZPHY A329 229	L. Koester, W. Waschkowski, J. Meier	(MUNI, TUM)
LAST	88	PRL 60 995	I. Last *et al.*	(HEIDP, ILLG, ANL)
SCHMIEDM...	88	PRL 61 1065	J. Schmiedmayer, H. Rauch, P. Riehs	(TUW)
Also		PRL 61 2509 (errat.)	J. Schmiedmayer, H. Rauch, P. Riehs	(TUW)
SPIVAK	88	JETP 67 1735	P.E. Spivak	(KIAE)
		Translated from ZETF 94 1.		
COHEN	87	RMP 59 1121	E.R. Cohen, B.N. Taylor	(RISC, NBS)
ALEKSANDR...	86	SJNP 44 900	Yu.A. Aleksandrov *et al.*	
		Translated from YAF 44 1384.		
ALTAREV	86	JETPL 44 460	I.S. Altarev *et al.*	(PNPI)
		Translated from ZETFP 44 360.		
BOPP	86	PRL 56 919	P. Bopp *et al.*	(HEIDP, ANL, ILLG)
Also		ZPHY C37 179	E. Klempt *et al.*	(HEIDP, ANL, ILLG)
CRESTI	86	PL B177 206	M. Cresti *et al.*	(PADO)
Also		PL B200 587 (errat.)	M. Cresti *et al.*	(PADO)

Int. J. Mod. Phys. A 2026.41. Downloaded from www.worldscientific.com by UNIVERSITY OF CALIFORNIA @ BERKELEY on 09/16/26. Re-use and distribution is strictly not permitted, except for Open Access articles.

GREENE	86	PRL 56 819	G.L. Greene *et al.*	(NBS, ILLG)
KOESTER	86	Physica B137 282	L. Koester *et al.*	
KOSVINTSEV	86	JETPL 44 571	Y.Y. Kosvintsev, V.I. Morozov, G.I. Terekhov	(KIAE)
		Translated from ZETFP 44 444.		
TAKITA	86	PR D34 902	M. Takita *et al.*	(KEK, TOKY+)
DOVER	85	PR C31 1423	C.B. Dover, A. Gal, J.M. Richard	(BNL)
FIDECARO	85	PL 156B 122	G. Fidecaro *et al.*	(CERN, ILLG, PADO+)
PARK	85B	NP B252 261	H.S. Park *et al.*	(IMB Collab.)
BATTISTONI	84	PL 133B 454	G. Battistoni *et al.*	(NUSEX Collab.)
JONES	84	PRL 52 720	T.W. Jones *et al.*	(IMB Collab.)
PENDLEBURY	84	PL 136B 327	J.M. Pendlebury *et al.*	(SUSS, HARV, RAL+)
CHERRY	83	PRL 50 1354	M.L. Cherry *et al.*	(PENN, BNL)
DOVER	83	PR D27 1090	C.B. Dover, A. Gal, J.M. Richard	(BNL)
KABIR	83	PRL 51 231	P.K. Kabir	(HARV)
MOSTOVOY	83	JETPL 37 196	Y.A. Mostovoy	(KIAE)
		Translated from ZETFP 37 162.		
ROY	83	PR D28 1770	A. Roy *et al.*	(TATA)
VAIDYA	83	PR D27 486	S.C. Vaidya *et al.*	(TATA)
GAEHLER	82	PR D25 2887	R. Gahler, J. Kalus, W. Mampe	(BAYR, ILLG)
GREENE	82	Metrologia 18 93	G.L. Greene *et al.*	(YALE, HARV, ILLG+)
ALTAREV	81	PL 102B 13	I.S. Altarev *et al.*	(PNPI)
BARABANOV	80	JETPL 32 359	I.R. Barabanov *et al.*	(PNPI)
		Translated from ZETFP 32 384.		
BYRNE	80	PL 92B 274	J. Byrne *et al.*	(SUSS, RL)
KOSVINTSEV	80	JETPL 31 236	Y.Y. Kosvintsev *et al.*	(JINR)
		Translated from ZETFP 31 257.		
MOHAPATRA	80	PRL 44 1316	R.N. Mohapatra, R.E. Marshak	(CUNY, VPI)
ALTAREV	79	JETPL 29 730	I.S. Altarev *et al.*	(PNPI)
		Translated from ZETFP 29 794.		
EROZOLIM...	79	SJNP 30 356	B.G. Erozolimsky *et al.*	(KIAE)
		Translated from YAF 30 692.		
NORMAN	79	PRL 43 1226	E.B. Norman, A.G. Seamster	(WASH)
BONDAREN...	78	JETPL 28 303	L.N. Bondarenko *et al.*	(KIAE)
		Translated from ZETFP 28 328.		
Also		Smolenice Conf.	P.G. Bondarenko	(KIAE)
EROZOLIM...	78	SJNP 28 48	B.G. Erozolimsky *et al.*	(KIAE)
		Translated from YAF 28 98.		
STRATOWA	78	PR D18 3970	C. Stratowa, R. Dobrozemsky, P. Weinzierl	(SEIB)
EROZOLIM...	77	JETPL 23 663	B.G. Erozolimsky *et al.*	(KIAE)
		Translated from ZETFP 23 720.		
KOESTER	76	PRL 36 1021	L. Koester *et al.*	
STEINBERG	76	PR D13 2469	R.I. Steinberg *et al.*	(YALE, ISNG)
DOBROZE...	75	PR D11 510	R. Dobrozemsky *et al.*	(SEIB)
KROHN	75	PL 55B 175	V.E. Krohn, G.R. Ringo	(ANL)
EROZOLIM...	74	JETPL 20 345	B.G. Erozolimsky *et al.*	(KIAE)
		Translated from ZETFP 20 745.		
KROPF	74	ZPHY 267 129	H. Kropf, E. Paul	(LINZ)
Also		NP A154 160	H. Paul	(VIEN)
STEINBERG	74	PRL 33 41	R.I. Steinberg *et al.*	(YALE, ISNG)
COHEN	73	JPCRD 2 664	E.R. Cohen, B.N. Taylor	(RISC, NBS)
KROHN	73	PR D8 1305	V.E. Krohn, G.R. Ringo	
CHRISTENSEN	72	PR D5 1628	C.J. Christensen *et al.*	(RISO)
CHRISTENSEN	70	PR C1 1693	C.J. Christensen, V.E. Krohn, G.R. Ringo	(ANL)
EROZOLIM...	70C	PL 33B 351	B.G. Erozolimsky *et al.*	(KIAE)
GRIGOREV	68	SJNP 6 239	V.K. Grigoriev *et al.*	(ITEP)
		Translated from YAF 6 329.		
KROHN	66	PR 148 1303	V.E. Krohn, G.R. Ringo	
LEE	56	PR 104 254	T.D. Lee, C.N. Yang	(COLU, BNL)

See the related review(s):
N and Δ Resonances

$N(1440)\ 1/2^+$

$I(J^P) = \frac{1}{2}(\frac{1}{2}^+)$ Status: ****

Older and obsolete values are listed and referenced in the 2014 edition, Chinese Physics **C38** 070001 (2014).

$N(1440)$ POLE POSITION

REAL PART

VALUE (MeV)	DOCUMENT ID		TECN	COMMENT
1360 to 1380 (≈ 1370) OUR ESTIMATE				
1366± 3	SARANTSEV	25	DPWA	Multichannel
1374± 3±4	[1] HOFERICHT...	24	RVUE	$\pi N \to \pi N$
1353± 1	ROENCHEN	22	DPWA	Multichannel
1363± 2±2	[2] SVARC	14	L+P	$\pi N \to \pi N$
1375±30	CUTKOSKY	80	IPWA	$\pi N \to \pi N$
• • • We do not use the following data for averages, fits, limits, etc. • • •				
1360	HUNT	19	DPWA	Multichannel
1355	ROENCHEN	15A	DPWA	Multichannel
1369± 3	SOKHOYAN	15A	DPWA	Multichannel
1386	SHKLYAR	13	DPWA	Multichannel
1363±11	BATINIC	10	DPWA	$\pi N \to N\pi,\ N\eta$
1359	ARNDT	06	DPWA	$\pi N \to \pi N,\ \eta N$
1383	VRANA	00	DPWA	Multichannel
1385	HOEHLER	93	SPED	$\pi N \to \pi N$

[1] Roy-Steiner equations and Pade methods applied to πN scattering amplitudes and pionic atom data.
[2] Fit to the amplitudes of HOEHLER 79.

−2×IMAGINARY PART

VALUE (MeV)	DOCUMENT ID		TECN	COMMENT
180 to 205 (≈ 190) OUR ESTIMATE				
192± 4	SARANTSEV	25	DPWA	Multichannel
215±18±8	[1] HOFERICHT...	24	RVUE	$\pi N \to \pi N$
203± 2	ROENCHEN	22	DPWA	Multichannel
180± 4±5	[2] SVARC	14	L+P	$\pi N \to \pi N$
180±40	CUTKOSKY	80	IPWA	$\pi N \to \pi N$
• • • We do not use the following data for averages, fits, limits, etc. • • •				
186	HUNT	19	DPWA	Multichannel
215	ROENCHEN	15A	DPWA	Multichannel
189± 5	SOKHOYAN	15A	DPWA	Multichannel
277	SHKLYAR	13	DPWA	Multichannel
151±13	BATINIC	10	DPWA	$\pi N \to N\pi,\ N\eta$
162	ARNDT	06	DPWA	$\pi N \to \pi N,\ \eta N$
316	VRANA	00	DPWA	Multichannel
164	HOEHLER	93	SPED	$\pi N \to \pi N$

[1] Roy-Steiner equations and Pade methods applied to πN scattering amplitudes and pionic atom data.
[2] Fit to the amplitudes of HOEHLER 79.

$N(1440)$ ELASTIC POLE RESIDUE

MODULUS $|r|$

VALUE (MeV)	DOCUMENT ID		TECN	COMMENT
50 to 60 (≈ 55) OUR ESTIMATE				
58±15±17	[1] HOFERICHT...	24	RVUE	$\pi N \to \pi N$
59± 1	ROENCHEN	22	DPWA	Multichannel
49± 3	SOKHOYAN	15A	DPWA	Multichannel
50± 1± 2	[2] SVARC	14	L+P	$\pi N \to \pi N$
52± 5	CUTKOSKY	80	IPWA	$\pi N \to \pi N$
• • • We do not use the following data for averages, fits, limits, etc. • • •				
62	ROENCHEN	15A	DPWA	Multichannel
126	SHKLYAR	13	DPWA	Multichannel
48± 3	ANISOVICH	12A	DPWA	Multichannel
44	BATINIC	10	DPWA	$\pi N \to N\pi,\ N\eta$
38	ARNDT	06	DPWA	$\pi N \to \pi N,\ \eta N$
40	HOEHLER	93	SPED	$\pi N \to \pi N$

[1] Roy-Steiner equations and Pade methods applied to πN scattering amplitudes and pionic atom data.
[2] Fit to the amplitudes of HOEHLER 79.

PHASE θ

VALUE (°)	DOCUMENT ID		TECN	COMMENT
−100 to −80 (≈ −90) OUR ESTIMATE				
− 65± 2±11	[1] HOFERICHT...	24	RVUE	$\pi N \to \pi N$
−104± 2	ROENCHEN	22	DPWA	Multichannel
− 82± 5	SOKHOYAN	15A	DPWA	Multichannel
− 88± 1± 2	[2] SVARC	14	L+P	$\pi N \to \pi N$
−100±35	CUTKOSKY	80	IPWA	$\pi N \to \pi N$
• • • We do not use the following data for averages, fits, limits, etc. • • •				
− 98	ROENCHEN	15A	DPWA	Multichannel
− 60	SHKLYAR	13	DPWA	Multichannel
− 78± 4	ANISOVICH	12A	DPWA	Multichannel
− 88	BATINIC	10	DPWA	$\pi N \to N\pi,\ N\eta$
− 98	ARNDT	06	DPWA	$\pi N \to \pi N,\ \eta N$

[1] Roy-Steiner equations and Pade methods applied to πN scattering amplitudes and pionic atom data.
[2] Fit to the amplitudes of HOEHLER 79.

$N(1440)$ INELASTIC POLE RESIDUE

The "normalized residue" is the residue divided by $\Gamma_{pole}/2$.

Normalized residue in $N\pi \to N(1440) \to N\eta$

MODULUS	PHASE (°)	DOCUMENT ID		TECN	COMMENT
0.084±0.002	−28 ± 2	ROENCHEN	22	DPWA	Multichannel
• • • We do not use the following data for averages, fits, limits, etc. • • •					
0.078	−27	ROENCHEN	15A	DPWA	Multichannel

Normalized residue in $N\pi \to N(1440) \to \Delta\pi$, P-wave

MODULUS	PHASE (°)	DOCUMENT ID		TECN	COMMENT
0.27±0.02	38 ± 5	SOKHOYAN	15A	DPWA	Multichannel
• • • We do not use the following data for averages, fits, limits, etc. • • •					
0.27±0.02	40 ± 5	ANISOVICH	12A	DPWA	Multichannel

Normalized residue in $N\pi \to N(1440) \to \Lambda K$

MODULUS	PHASE (°)	DOCUMENT ID		TECN	COMMENT
0.025±0.005	−92 ± 43	ROENCHEN	22	DPWA	Multichannel
• • • We do not use the following data for averages, fits, limits, etc. • • •					
0.016	145	ROENCHEN	15A	DPWA	Multichannel

Normalized residue in $N\pi \to N(1440) \to \Sigma K$

MODULUS	PHASE (°)	DOCUMENT ID		TECN	COMMENT
0.002±0.003	−32 ± 77	ROENCHEN	22	DPWA	Multichannel
• • • We do not use the following data for averages, fits, limits, etc. • • •					
0.027	113	ROENCHEN	15A	DPWA	Multichannel

Normalized residue in $N\pi \to N(1440) \to N\ (\pi\pi)^{I=0}_{S-wave}$

MODULUS	PHASE (°)	DOCUMENT ID		TECN	COMMENT
0.21±0.04	−136 ± 4	SOKHOYAN	15A	DPWA	Multichannel
• • • We do not use the following data for averages, fits, limits, etc. • • •					
0.21±0.05	−135 ± 7	ANISOVICH	12A	DPWA	Multichannel

Int. J. Mod. Phys. A 2026.41. Downloaded from www.worldscientific.com
UNIVERSITY OF CALIFORNIA @ BERKELEY on 09/16/26. Re-use and distribution is strictly not permitted, except for Open Access articles.

$N(1440)$ BREIT-WIGNER MASS

VALUE (MeV)	DOCUMENT ID		TECN	COMMENT
1410 to 1470 (≈ 1440) OUR ESTIMATE				
1410 ±10	SARANTSEV	25	DPWA	Multichannel
1417 ± 4	[1] HUNT	19	DPWA	Multichannel
1515 ±15	[1] SHKLYAR	13	DPWA	Multichannel
1485.0± 1.2	[1] ARNDT	06	DPWA	$\pi N \to \pi N$, ηN
1440 ±30	CUTKOSKY	80	IPWA	$\pi N \to \pi N$
1410 ±12	HOEHLER	79	IPWA	$\pi N \to \pi N$
• • • We do not use the following data for averages, fits, limits, etc. • • •				
1430 ±10	SOKHOYAN	15A	DPWA	Multichannel
1412 ± 2	[1] SHRESTHA	12A	DPWA	Multichannel
1439 ±19	BATINIC	10	DPWA	$\pi N \to N\pi$, $N\eta$
1518 ± 5	PENNER	02C	DPWA	Multichannel
1479 ±80	VRANA	00	DPWA	Multichannel

[1] Statistical error only.

$N(1440)$ BREIT-WIGNER WIDTH

VALUE (MeV)	DOCUMENT ID		TECN	COMMENT
250 to 450 (≈ 350) OUR ESTIMATE				
290± 30	SARANTSEV	25	DPWA	Multichannel
257± 11	[1] HUNT	19	DPWA	Multichannel
605± 90	[1] SHKLYAR	13	DPWA	Multichannel
284± 18	[1] ARNDT	06	DPWA	$\pi N \to \pi N$, ηN
340± 70	CUTKOSKY	80	IPWA	$\pi N \to \pi N$
135± 10	HOEHLER	79	IPWA	$\pi N \to \pi N$
• • • We do not use the following data for averages, fits, limits, etc. • • •				
360± 30	SOKHOYAN	15A	DPWA	Multichannel
248± 5	[1] SHRESTHA	12A	DPWA	Multichannel
437±141	BATINIC	10	DPWA	$\pi N \to N\pi$, $N\eta$
668± 41	PENNER	02C	DPWA	Multichannel
490±120	VRANA	00	DPWA	Multichannel

[1] Statistical error only.

$N(1440)$ DECAY MODES

The following branching fractions are our estimates, not fits or averages.

	Mode	Fraction (Γ_i/Γ)
Γ_1	$N\pi$	55–75 %
Γ_2	$N\eta$	< 1 %
Γ_3	$N\pi\pi$	17–50 %
Γ_4	$\Delta(1232)\pi$	6–27 %
Γ_5	$N\rho$	(18±6) %
Γ_6	$N\rho$, $S=1/2$	(9±4) %
Γ_7	$N\rho$, $S=3/2$	(9±4) %
Γ_8	$N\sigma$	11–23 %
Γ_9	$p\gamma$, helicity=1/2	0.035–0.048 %
Γ_{10}	$n\gamma$, helicity=1/2	0.02–0.04 %

$N(1440)$ BRANCHING RATIOS

$\Gamma(N\pi)/\Gamma_{total}$ — Γ_1/Γ

VALUE (%)	DOCUMENT ID		TECN	COMMENT
55 to 75 (≈ 65) OUR ESTIMATE				
66 ±3	SEIFEN	25	DPWA	Multichannel
59 ±2	[1] HUNT	19	DPWA	Multichannel
56 ±2	[1] SHKLYAR	13	DPWA	Multichannel
78.7±1.6	[1] ARNDT	06	DPWA	$\pi N \to \pi N$, ηN
68 ±4	CUTKOSKY	80	IPWA	$\pi N \to \pi N$
51 ±5	HOEHLER	79	IPWA	$\pi N \to \pi N$
• • • We do not use the following data for averages, fits, limits, etc. • • •				
63 ±2	SOKHOYAN	15A	DPWA	Multichannel
64.8±0.9	[1] SHRESTHA	12A	DPWA	Multichannel
62 ±4	BATINIC	10	DPWA	$\pi N \to N\pi$, $N\eta$
57 ±1	PENNER	02C	DPWA	Multichannel
72 ±5	VRANA	00	DPWA	Multichannel

[1] Statistical error only.

$\Gamma(N\eta)/\Gamma_{total}$ — Γ_2/Γ

VALUE (%)	DOCUMENT ID		TECN	COMMENT
• • • We do not use the following data for averages, fits, limits, etc. • • •				
0±1	VRANA	00	DPWA	Multichannel

$\Gamma(\Delta(1232)\pi)/\Gamma_{total}$ — Γ_4/Γ

VALUE (%)	DOCUMENT ID		TECN	COMMENT
6 to 27 (≈ 15) OUR ESTIMATE				
15 ±7	SARANTSEV	25	DPWA	Multichannel
10 ±6	SEIFEN	25	DPWA	Multichannel
22 ±4	[1] HUNT	19	DPWA	Multichannel
12^{+5}_{-3}	SHKLYAR	16	DPWA	Multichannel
• • • We do not use the following data for averages, fits, limits, etc. • • •				
20 ±7	SOKHOYAN	15A	DPWA	Multichannel
6.5±0.8	[1] SHRESTHA	12A	DPWA	Multichannel
16 ±1	VRANA	00	DPWA	Multichannel

[1] Statistical error only.

$\Gamma(N\rho)/\Gamma_{total}$ — Γ_5/Γ

VALUE (%)	DOCUMENT ID		TECN	COMMENT
18±6	SARANTSEV	25	DPWA	Multichannel

$\Gamma(N\rho, S=1/2)/\Gamma_{total}$ — Γ_6/Γ

VALUE (%)	DOCUMENT ID		TECN	COMMENT
9±4	SARANTSEV	25	DPWA	Multichannel

$\Gamma(N\rho, S=3/2)/\Gamma_{total}$ — Γ_7/Γ

VALUE (%)	DOCUMENT ID		TECN	COMMENT
9±4	SARANTSEV	25	DPWA	Multichannel

$\Gamma(N\sigma)/\Gamma_{total}$ — Γ_8/Γ

VALUE (%)	DOCUMENT ID		TECN	COMMENT
15±5	SARANTSEV	25	DPWA	Multichannel
17±6	SEIFEN	25	DPWA	Multichannel
16±3	[1] HUNT	19	DPWA	Multichannel
27^{+4}_{-9}	SHKLYAR	16	DPWA	Multichannel
• • • We do not use the following data for averages, fits, limits, etc. • • •				
17±6	SOKHOYAN	15A	DPWA	Multichannel
27±1	[1] SHRESTHA	12A	DPWA	Multichannel
12±1	VRANA	00	DPWA	Multichannel

[1] Statistical error only.

$N(1440)$ PHOTON DECAY AMPLITUDES AT THE POLE

$N(1440) \to p\gamma$, helicity-1/2 amplitude $A_{1/2}$

MODULUS ($GeV^{-1/2}$)	PHASE (°)	DOCUMENT ID		TECN	COMMENT
−0.060±0.006	−30 ± 7	SARANTSEV	25	DPWA	Multichannel
−0.090±0.007	−30 ± 3	ROENCHEN	22	DPWA	Multichannel
• • • We do not use the following data for averages, fits, limits, etc. • • •					
−0.060	−23	ROENCHEN	15A	DPWA	Multichannel
−0.044±0.005	−40 ± 8	SOKHOYAN	15A	DPWA	Multichannel

$N(1440) \to n\gamma$, helicity-1/2 amplitude $A_{1/2}$

MODULUS ($GeV^{-1/2}$)	PHASE (°)	DOCUMENT ID		TECN	COMMENT
0.041±0.005	23 ± 10	ANISOVICH	17E	DPWA	Multichannel

$N(1440)$ BREIT-WIGNER PHOTON DECAY AMPLITUDES

$N(1440) \to p\gamma$, helicity-1/2 amplitude $A_{1/2}$

VALUE ($GeV^{-1/2}$)	DOCUMENT ID		TECN	COMMENT
−0.080 to −0.050 (≈ −0.065) OUR ESTIMATE				
−0.076±0.008	SARANTSEV	25	DPWA	Multichannel
−0.091±0.007	[1] HUNT	19	DPWA	Multichannel
−0.085±0.003	[1] SHKLYAR	13	DPWA	Multichannel
−0.056±0.001	[1] WORKMAN	12A	DPWA	$\gamma N \to N\pi$
−0.051±0.002	[1] DUGGER	07	DPWA	$\gamma N \to \pi N$
• • • We do not use the following data for averages, fits, limits, etc. • • •				
−0.061±0.006	SOKHOYAN	15A	DPWA	Multichannel
−0.084±0.003	[1] SHRESTHA	12A	DPWA	Multichannel
−0.061	DRECHSEL	07	DPWA	$\gamma N \to \pi N$
−0.087	PENNER	02D	DPWA	Multichannel

[1] Statistical error only.

$N(1440) \to n\gamma$, helicity-1/2 amplitude $A_{1/2}$

VALUE ($GeV^{-1/2}$)	DOCUMENT ID		TECN	COMMENT
0.035 to 0.055 (≈ 0.045) OUR ESTIMATE				
0.013±0.012	[1] HUNT	19	DPWA	Multichannel
0.053±0.007	ANISOVICH	17E	DPWA	Multichannel
0.048±0.004	[1] CHEN	12A	DPWA	$\gamma N \to \pi N$
• • • We do not use the following data for averages, fits, limits, etc. • • •				
0.043±0.012	ANISOVICH	13B	DPWA	Multichannel
0.040±0.005	[1] SHRESTHA	12A	DPWA	Multichannel
0.054	DRECHSEL	07	DPWA	$\gamma N \to \pi N$
0.121	PENNER	02D	DPWA	Multichannel

[1] Statistical error only.

$N(1440)$ REFERENCES

For early references, see Physics Letters **111B** 1 (1982).

SARANTSEV	25	PR C112 015202	A.V. Sarantsev *et al.*	(Bonn-Gatchina Collab.)
SEIFEN	25	EPJ A61 173	T. Seifen *et al.*	(CBELSA/TAPS Collab.)
HOFERICHT...	24	PL B853 138698	M. Hoferichter *et al.*	(BERN, MADU, BONN+)
ROENCHEN	22	EPJ A58 229	D. Roenchen *et al.*	(JULI, GWU, BONN+)

Int. J. Mod. Phys. A 2026.41. Downloaded from www.worldscientific.com by UNIVERSITY OF CALIFORNIA @ BERKELEY on 09/16/26. Re-use and distribution is strictly not permitted, except for Open Access articles.

HUNT	19	PR C99 055205	B.C. Hunt, D.M. Manley	
ANISOVICH	17E	PR C96 055202	A.V. Anisovich *et al.*	(BONN, PNPI, JLAB+)
SHKLYAR	16	PR C93 045206	V. Shklyar, H. Lenske, U. Mosel	(GIES)
ROENCHEN	15A	EPJ A51 70	D. Roenchen *et al.*	
SOKHOYAN	15A	EPJ A51 95	V. Sokhoyan *et al.*	(CBELSA/TAPS Collab.)
PDG	14	CP C38 070001	K. Olive *et al.*	(PDG Collab.)
SVARC	14	PR C89 045205	A. Svarc *et al.*	(RBI Zagreb, UNI Tuzla)
ANISOVICH	13B	EPJ A49 67	A.V. Anisovich *et al.*	
SHKLYAR	13	PR C87 015201	V. Shklyar, H. Lenske, U. Mosel	(GIES)
ANISOVICH	12A	EPJ A48 15	A.V. Anisovich *et al.*	(BONN, PNPI)
CHEN	12A	PR C86 015206	W. Chen *et al.*	(DUKE, GWU, MSST, ITEP+)
SHRESTHA	12A	PR C86 055203	M. Shrestha, D.M. Manley	(KSU)
WORKMAN	12A	PR C86 015202	R. Workman *et al.*	(GWU)
BATINIC	10	PR C82 038203	M. Batinic *et al.*	(ZAGR)
DRECHSEL	07	EPJ A34 69	D. Drechsel, S.S. Kamalov, L. Tiator	(MAINZ, JINR)
DUGGER	07	PR C76 025211	M. Dugger *et al.*	(JLab CLAS Collab.)
ARNDT	06	PR C74 045205	R.A. Arndt *et al.*	(GWU)
PENNER	02C	PR C66 055211	G. Penner, U. Mosel	(GIES)
PENNER	02D	PR C66 055212	G. Penner, U. Mosel	(GIES)
VRANA	00	PRPL 328 181	T.P. Vrana, S.A. Dytman, T.-S.H. Lee	(PITT, ANL)
HOEHLER	93	πN Newsletter 9 1	G. Hohler	(KARL)
CUTKOSKY	80	PR D20 1475	R.E. Cutkosky *et al.*	(CMU, LBL) IJP
Also		PR D20 2839	R.E. Cutkosky *et al.*	(CMU, LBL) IJP
HOEHLER	79	PDAT 12-1	G. Hohler *et al.*	(KARLT) IJP
Also		Toronto Conf. 3	R. Koch	(KARLT) IJP

$N(1520)\ 3/2^-$

$I(J^P) = \frac{1}{2}(\frac{3}{2}^-)$ Status: ****

Older and obsolete values are listed and referenced in the 2014 edition, Chinese Physics **C38** 070001 (2014).

$N(1520)$ POLE POSITION

REAL PART

VALUE (MeV)	DOCUMENT ID		TECN	COMMENT
1505 to 1515 (≈ 1510) OUR ESTIMATE				
1506±2	SARANTSEV	25	DPWA	Multichannel
1482±3	ROENCHEN	22	DPWA	Multichannel
1506±1±1	[1] SVARC	14	L+P	$\pi N \to \pi N$
1510±5	CUTKOSKY	80	IPWA	$\pi N \to \pi N$
• • • We do not use the following data for averages, fits, limits, etc. • • •				
1500	HUNT	19	DPWA	Multichannel
1512	ROENCHEN	15A	DPWA	Multichannel
1507±2	SOKHOYAN	15A	DPWA	Multichannel
1492	SHKLYAR	13	DPWA	Multichannel
1506±9	BATINIC	10	DPWA	$\pi N \to N\pi,\ N\eta$
1515	ARNDT	06	DPWA	$\pi N \to \pi N,\ \eta N$
1504	VRANA	00	DPWA	Multichannel
1510	HOEHLER	93	ARGD	$\pi N \to \pi N$

[1] Fit to the amplitudes of HOEHLER 79.

−2×IMAGINARY PART

VALUE (MeV)	DOCUMENT ID		TECN	COMMENT
105 to 120 (≈ 110) OUR ESTIMATE				
112± 3	SARANTSEV	25	DPWA	Multichannel
126± 9	ROENCHEN	22	DPWA	Multichannel
115± 2±1	[1] SVARC	14	L+P	$\pi N \to \pi N$
114±10	CUTKOSKY	80	IPWA	$\pi N \to \pi N$
• • • We do not use the following data for averages, fits, limits, etc. • • •				
117	HUNT	19	DPWA	Multichannel
89	ROENCHEN	15A	DPWA	Multichannel
111± 3	SOKHOYAN	15A	DPWA	Multichannel
94	SHKLYAR	13	DPWA	Multichannel
122± 9	BATINIC	10	DPWA	$\pi N \to N\pi,\ N\eta$
113	ARNDT	06	DPWA	$\pi N \to \pi N,\ \eta N$
112	VRANA	00	DPWA	Multichannel
120	HOEHLER	93	ARGD	$\pi N \to \pi N$

[1] Fit to the amplitudes of HOEHLER 79.

$N(1520)$ ELASTIC POLE RESIDUE

MODULUS $|r|$

VALUE (MeV)	DOCUMENT ID		TECN	COMMENT
32 to 38 (≈ 35) OUR ESTIMATE				
27±11	ROENCHEN	22	DPWA	Multichannel
36± 2	SOKHOYAN	15A	DPWA	Multichannel
33± 1±1	[1] SVARC	14	L+P	$\pi N \to \pi N$
35± 2	CUTKOSKY	80	IPWA	$\pi N \to \pi N$
• • • We do not use the following data for averages, fits, limits, etc. • • •				
37	ROENCHEN	15A	DPWA	Multichannel
27	SHKLYAR	13	DPWA	Multichannel
36± 3	ANISOVICH	12A	DPWA	Multichannel
35	BATINIC	10	DPWA	$\pi N \to N\pi,\ N\eta$
38	ARNDT	06	DPWA	$\pi N \to \pi N,\ \eta N$
32	HOEHLER	93	ARGD	$\pi N \to \pi N$

[1] Fit to the amplitudes of HOEHLER 79.

PHASE θ

VALUE (°)	DOCUMENT ID		TECN	COMMENT
−15 to −5 (≈ −10) OUR ESTIMATE				
−36±24	ROENCHEN	22	DPWA	Multichannel
−14± 3	SOKHOYAN	15A	DPWA	Multichannel
−15± 1±1	[1] SVARC	14	L+P	$\pi N \to \pi N$
−12± 5	CUTKOSKY	80	IPWA	$\pi N \to \pi N$
• • • We do not use the following data for averages, fits, limits, etc. • • •				
− 6	ROENCHEN	15A	DPWA	Multichannel
−35	SHKLYAR	13	DPWA	Multichannel
−14± 3	ANISOVICH	12A	DPWA	Multichannel
− 7	BATINIC	10	DPWA	$\pi N \to N\pi,\ N\eta$
− 5	ARNDT	06	DPWA	$\pi N \to \pi N,\ \eta N$
− 8	HOEHLER	93	ARGD	$\pi N \to \pi N$

[1] Fit to the amplitudes of HOEHLER 79.

$N(1520)$ INELASTIC POLE RESIDUE

The "normalized residue" is the residue divided by $\Gamma_{pole}/2$.

Normalized residue in $N\pi \to N(1520) \to \Delta\pi$, S-wave

MODULUS	PHASE (°)	DOCUMENT ID		TECN	COMMENT
0.33±0.04	155 ± 15	SOKHOYAN	15A	DPWA	Multichannel
• • • We do not use the following data for averages, fits, limits, etc. • • •					
0.33±0.05	150 ± 20	ANISOVICH	12A	DPWA	Multichannel

Normalized residue in $N\pi \to N(1520) \to \Delta\pi$, D-wave

MODULUS	PHASE (°)	DOCUMENT ID		TECN	COMMENT
0.25±0.03	105 ± 18	SOKHOYAN	15A	DPWA	Multichannel
• • • We do not use the following data for averages, fits, limits, etc. • • •					
0.25±0.03	100 ± 20	ANISOVICH	12A	DPWA	Multichannel

Normalized residue in $N\pi \to N(1520) \to N\eta$

MODULUS	PHASE (°)	DOCUMENT ID		TECN	COMMENT
0.021±0.009	34 ± 27	ROENCHEN	22	DPWA	Multichannel
• • • We do not use the following data for averages, fits, limits, etc. • • •					
0.026	95	ROENCHEN	15A	DPWA	Multichannel

Normalized residue in $N\pi \to N(1520) \to \Lambda K$

MODULUS	PHASE (°)	DOCUMENT ID		TECN	COMMENT
0.026±0.010	127 ± 24	ROENCHEN	22	DPWA	Multichannel
• • • We do not use the following data for averages, fits, limits, etc. • • •					
0.069	158	ROENCHEN	15A	DPWA	Multichannel

Normalized residue in $N\pi \to N(1520) \to \Sigma K$

MODULUS	PHASE (°)	DOCUMENT ID		TECN	COMMENT
0.010±0.006	94 ± 34	ROENCHEN	22	DPWA	Multichannel
• • • We do not use the following data for averages, fits, limits, etc. • • •					
0.049	−41	ROENCHEN	15A	DPWA	Multichannel

Normalized residue in $N\pi \to N(1520) \to N\sigma$

MODULUS	PHASE (°)	DOCUMENT ID		TECN	COMMENT
0.08±0.03	−45 ± 25	SOKHOYAN	15A	DPWA	Multichannel

$N(1520)$ BREIT-WIGNER MASS

VALUE (MeV)	DOCUMENT ID		TECN	COMMENT
1510 to 1520 (≈ 1515) OUR ESTIMATE				
1515 ± 3	SARANTSEV	25	DPWA	Multichannel
1512.0± 1.5	[1] HUNT	19	DPWA	Multichannel
1505 ± 4	[1] SHKLYAR	13	DPWA	Multichannel
1514.5± 0.2	[1] ARNDT	06	DPWA	$\pi N \to \pi N,\ \eta N$
1525 ±10	CUTKOSKY	80	IPWA	$\pi N \to \pi N$
1519 ± 4	HOEHLER	79	IPWA	$\pi N \to \pi N$
• • • We do not use the following data for averages, fits, limits, etc. • • •				
1516 ± 2	SOKHOYAN	15A	DPWA	Multichannel
1512.6± 0.5	[1] SHRESTHA	12A	DPWA	Multichannel
1522 ± 8	BATINIC	10	DPWA	$\pi N \to N\pi,\ N\eta$
1509 ± 1	PENNER	02C	DPWA	Multichannel
1518 ± 3	VRANA	00	DPWA	Multichannel

[1] Statistical error only.

$N(1520)$ BREIT-WIGNER WIDTH

VALUE (MeV)	DOCUMENT ID		TECN	COMMENT
100 to 120 (≈ 110) OUR ESTIMATE				
114 ± 4	SARANTSEV	25	DPWA	Multichannel
121 ± 3	[1] HUNT	19	DPWA	Multichannel
100 ± 2	[1] SHKLYAR	13	DPWA	Multichannel
103.6± 0.4	[1] ARNDT	06	DPWA	$\pi N \to \pi N,\ \eta N$
120 ±15	CUTKOSKY	80	IPWA	$\pi N \to \pi N$
114 ± 7	HOEHLER	79	IPWA	$\pi N \to \pi N$
• • • We do not use the following data for averages, fits, limits, etc. • • •				
113 ± 4	SOKHOYAN	15A	DPWA	Multichannel
117 ± 1	[1] SHRESTHA	12A	DPWA	Multichannel
132 ±11	BATINIC	10	DPWA	$\pi N \to N\pi,\ N\eta$
100 ± 2	PENNER	02C	DPWA	Multichannel
124 ± 4	VRANA	00	DPWA	Multichannel

[1] Statistical error only.

Int. J. Mod. Phys. A 2026.41. Downloaded from www.worldscientific.com
UNIVERSITY OF CALIFORNIA @ BERKELEY on 09/16/26. Re-use and distribution is strictly not permitted, except for Open Access articles.

$N(1520)$ DECAY MODES

The following branching fractions are our estimates, not fits or averages.

	Mode	Fraction (Γ_i/Γ)
Γ_1	$N\pi$	55–65 %
Γ_2	$N\eta$	0.07–0.09 %
Γ_3	$N\pi\pi$	25–35 %
Γ_4	$\Delta(1232)\pi$	22–34 %
Γ_5	$\Delta(1232)\pi$, S-wave	15–23 %
Γ_6	$\Delta(1232)\pi$, D-wave	7–11 %
Γ_7	$N\rho$	10–16 %
Γ_8	$N\rho$, $S=1/2$	0.2–0.4 %
Γ_9	$N\rho$, $S=3/2$, S-wave	10–16 %
Γ_{10}	$N\rho$, $S=3/2$, D-wave	<1 %
Γ_{11}	$N\sigma$	<10 %
Γ_{12}	$N(1440)\pi$	
Γ_{13}	$p\gamma$	0.31–0.52 %
Γ_{14}	$p\gamma$, helicity=1/2	0.01–0.02 %
Γ_{15}	$p\gamma$, helicity=3/2	0.30–0.50 %
Γ_{16}	$n\gamma$	0.30–0.53 %
Γ_{17}	$n\gamma$, helicity=1/2	0.04–0.10 %
Γ_{18}	$n\gamma$, helicity=3/2	0.25–0.45 %

$N(1520)$ BRANCHING RATIOS

$\Gamma(N\pi)/\Gamma_{total}$ — Γ_1/Γ

VALUE (%)	DOCUMENT ID		TECN	COMMENT
55 to 65 (≈ 60) OUR ESTIMATE				
61 ±3	SEIFEN	25	DPWA	Multichannel
58.3±1.5	[1] HUNT	19	DPWA	Multichannel
57 ±2	[1] SHKLYAR	13	DPWA	Multichannel
63.2±0.1	[1] ARNDT	06	DPWA	$\pi N \to \pi N, \eta N$
58 ±3	CUTKOSKY	80	IPWA	$\pi N \to \pi N$
54 ±3	HOEHLER	79	IPWA	$\pi N \to \pi N$
• • • We do not use the following data for averages, fits, limits, etc. • • •				
61 ±2	SOKHOYAN	15A	DPWA	Multichannel
62.7±0.5	[1] SHRESTHA	12A	DPWA	Multichannel
55 ±5	BATINIC	10	DPWA	$\pi N \to N\pi, N\eta$
56 ±1	PENNER	02C	DPWA	Multichannel
63 ±2	VRANA	00	DPWA	Multichannel

[1] Statistical error only.

$\Gamma(N\eta)/\Gamma_{total}$ — Γ_2/Γ

VALUE (%)	DOCUMENT ID		TECN	COMMENT
<0.1	MUELLER	20	DPWA	Multichannel
0.03±0.01	[1] HUNT	19	DPWA	Multichannel
0.08±0.01	TIATOR	99	DPWA	$\gamma p \to p\eta$
• • • We do not use the following data for averages, fits, limits, etc. • • •				
<1	SHKLYAR	13	DPWA	Multichannel
0.1 ±0.1	BATINIC	10	DPWA	$\pi N \to N\pi, N\eta$
0.2 ±0.1	THOMA	08	DPWA	Multichannel
0.08 to 0.12	ARNDT	05	DPWA	Multichannel
0.23±0.04	PENNER	02C	DPWA	Multichannel
0 ±1	VRANA	00	DPWA	Multichannel

[1] Statistical error only.

$\Gamma(\Delta(1232)\pi)/\Gamma_{total}$ — Γ_4/Γ

VALUE (%)	DOCUMENT ID		TECN	COMMENT
26±6	SARANTSEV	25	DPWA	Multichannel

$\Gamma(\Delta(1232)\pi, S\text{-wave})/\Gamma_{total}$ — Γ_5/Γ

VALUE (%)	DOCUMENT ID		TECN	COMMENT
12 ±4	SARANTSEV	25	DPWA	Multichannel
10 ±4	SEIFEN	25	DPWA	Multichannel
12.1±2.1	ADAMCZEW...	20	DPWA	Multichannel
21 ±2	[1] HUNT	19	DPWA	Multichannel
• • • We do not use the following data for averages, fits, limits, etc. • • •				
19 ±4	SOKHOYAN	15A	DPWA	Multichannel
9.3±0.7	[1] SHRESTHA	12A	DPWA	Multichannel
15 ±2	VRANA	00	DPWA	Multichannel

[1] Statistical error only.

$\Gamma(\Delta(1232)\pi, D\text{-wave})/\Gamma_{total}$ — Γ_6/Γ

VALUE (%)	DOCUMENT ID		TECN	COMMENT
14 ±4	SARANTSEV	25	DPWA	Multichannel
10 ±3	SEIFEN	25	DPWA	Multichannel
6 ±2	ADAMCZEW...	20	DPWA	Multichannel
6 ±1	[1] HUNT	19	DPWA	Multichannel
• • • We do not use the following data for averages, fits, limits, etc. • • •				
9 ±2	SOKHOYAN	15A	DPWA	Multichannel
6.3±0.5	[1] SHRESTHA	12A	DPWA	Multichannel
11 ±2	VRANA	00	DPWA	Multichannel

[1] Statistical error only.

$\Gamma(N\rho)/\Gamma_{total}$ — Γ_7/Γ

VALUE (%)	DOCUMENT ID		TECN	COMMENT
28±4	SARANTSEV	25	DPWA	Multichannel

$\Gamma(N\rho, S=1/2)/\Gamma_{total}$ — Γ_8/Γ

VALUE (%)	DOCUMENT ID		TECN	COMMENT
0.2–0.4 % OUR EVALUATION				
4 ±3	SARANTSEV	25	DPWA	Multichannel
0.4±0.2	ADAMCZEW...	20	DPWA	Multichannel

$\Gamma(N\rho, S=3/2, S\text{-wave})/\Gamma_{total}$ — Γ_9/Γ

VALUE (%)	DOCUMENT ID		TECN	COMMENT
10–16 % OUR EVALUATION				
24 ±3	SARANTSEV	25	DPWA	Multichannel
11.8±1.9	ADAMCZEW...	20	DPWA	Multichannel
14.1±1.5	[1] HUNT	19	DPWA	Multichannel

[1] Statistical error only

$\Gamma(N\rho, S=3/2, D\text{-wave})/\Gamma_{total}$ — Γ_{10}/Γ

VALUE (%)	DOCUMENT ID		TECN	COMMENT
<1	SARANTSEV	25	DPWA	Multichannel

$\Gamma(N\sigma)/\Gamma_{total}$ — Γ_{11}/Γ

VALUE (%)	DOCUMENT ID		TECN	COMMENT
<10 % OUR ESTIMATE				
<2	SARANTSEV	25	DPWA	Multichannel
<2	SEIFEN	25	DPWA	Multichannel
7 ±3	ADAMCZEW...	20	DPWA	Multichannel
<0.7	[1] HUNT	19	DPWA	Multichannel
• • • We do not use the following data for averages, fits, limits, etc. • • •				
<2	SOKHOYAN	15A	DPWA	Multichannel
<1	[1] SHRESTHA	12A	DPWA	Multichannel
<4	THOMA	08	DPWA	Multichannel
1 ±1	VRANA	00	DPWA	Multichannel

[1] Statistical error only.

$\Gamma(N(1440)\pi)/\Gamma_{total}$ — Γ_{12}/Γ

VALUE (%)	DOCUMENT ID		TECN	COMMENT
<1	SEIFEN	25	DPWA	Multichannel

$N(1520)$ PHOTON DECAY AMPLITUDES AT THE POLE

$N(1520) \to p\gamma$, helicity-1/2 amplitude $A_{1/2}$

MODULUS ($GeV^{-1/2}$)	PHASE (°)	DOCUMENT ID		TECN	COMMENT
−0.028±0.005	−17 ± 8	SARANTSEV	25	DPWA	Multichannel
−0.043±0.013	−47 ± 10	ROENCHEN	22	DPWA	Multichannel
• • • We do not use the following data for averages, fits, limits, etc. • • •					
−0.031	−17	ROENCHEN	15A	DPWA	Multichannel
−0.023±0.004	−6 ± 5	SOKHOYAN	15A	DPWA	Multichannel

$N(1520) \to p\gamma$, helicity-3/2 amplitude $A_{3/2}$

MODULUS ($GeV^{-1/2}$)	PHASE (°)	DOCUMENT ID		TECN	COMMENT
0.134±0.007	7 ± 4	SARANTSEV	25	DPWA	Multichannel
0.112±0.032	1.8 ± 19	ROENCHEN	22	DPWA	Multichannel
• • • We do not use the following data for averages, fits, limits, etc. • • •					
0.075	1.7	ROENCHEN	15A	DPWA	Multichannel
0.131±0.006	4 ± 4	SOKHOYAN	15A	DPWA	Multichannel

$N(1520) \to n\gamma$, helicity-1/2 amplitude $A_{1/2}$

MODULUS ($GeV^{-1/2}$)	PHASE (°)	DOCUMENT ID		TECN	COMMENT
−0.045±0.005	−5 ± 4	ANISOVICH	17E	DPWA	Multichannel

$N(1520) \to n\gamma$, helicity-3/2 amplitude $A_{3/2}$

MODULUS ($GeV^{-1/2}$)	PHASE (°)	DOCUMENT ID		TECN	COMMENT
−0.119±0.005	5 ± 4	ANISOVICH	17E	DPWA	Multichannel

$N(1520)$ BREIT-WIGNER PHOTON DECAY AMPLITUDES

$N(1520) \to p\gamma$, helicity-1/2 amplitude $A_{1/2}$

VALUE ($GeV^{-1/2}$)	DOCUMENT ID		TECN	COMMENT
−0.030 to −0.015 (≈ −0.025) OUR ESTIMATE				
−0.029±0.004	SARANTSEV	25	DPWA	Multichannel
−0.034±0.003	[1] HUNT	19	DPWA	Multichannel
−0.015±0.001	[1] SHKLYAR	13	DPWA	Multichannel
−0.019±0.002	[1] WORKMAN	12A	DPWA	$\gamma N \to N\pi$
−0.028±0.002	[1] DUGGER	07	DPWA	$\gamma N \to \pi N$
−0.038±0.003	[1] AHRENS	02	DPWA	$\gamma N \to \pi N$
• • • We do not use the following data for averages, fits, limits, etc. • • •				
−0.024±0.004	SOKHOYAN	15A	DPWA	Multichannel

Int. J. Mod. Phys. A 2026.41. Downloaded from www.worldscientific.com
by UNIVERSITY OF CALIFORNIA @ BERKELEY on 09/16/26. Re-use and distribution is strictly not permitted, except for Open Access articles.

−0.034±0.001	[1] SHRESTHA	12A	DPWA	Multichannel
−0.027	DRECHSEL	07	DPWA	$\gamma N \to \pi N$
−0.003	PENNER	02D	DPWA	Multichannel
−0.052±0.010±0.007	[1] MUKHOPAD...	98		$\gamma p \to \eta p$

[1] Statistical error only.

$N(1520) \to p\gamma$, helicity-3/2 amplitude $A_{3/2}$

VALUE (GeV$^{-1/2}$)	DOCUMENT ID		TECN	COMMENT
0.135 to 0.145 (≈ 0.140) OUR ESTIMATE				
0.133±0.006	SARANTSEV	25	DPWA	Multichannel
0.142±0.003	[1] HUNT	19	DPWA	Multichannel
0.146±0.001	[1] SHKLYAR	13	DPWA	Multichannel
0.141±0.002	[1] WORKMAN	12A	DPWA	$\gamma N \to N\pi$
0.143±0.002	[1] DUGGER	07	DPWA	$\gamma N \to \pi N$
0.147±0.010	[1] AHRENS	02	DPWA	$\gamma N \to \pi N$
• • • We do not use the following data for averages, fits, limits, etc. • • •				
0.130±0.006	SOKHOYAN	15A	DPWA	Multichannel
0.127±0.003	[1] SHRESTHA	12A	DPWA	Multichannel
0.161	DRECHSEL	07	DPWA	$\gamma N \to \pi N$
0.151	PENNER	02D	DPWA	Multichannel
0.130±0.020±0.015	[1] MUKHOPAD...	98		$\gamma p \to \eta p$

[1] Statistical error only.

$N(1520) \to n\gamma$, helicity-1/2 amplitude $A_{1/2}$

VALUE (GeV$^{-1/2}$)	DOCUMENT ID		TECN	COMMENT
−0.055 to −0.040 (≈ −0.050) OUR ESTIMATE				
−0.072±0.003	[1] HUNT	19	DPWA	Multichannel
−0.046±0.005	ANISOVICH	17E	DPWA	Multichannel
−0.046±0.006	[1] CHEN	12A	DPWA	$\gamma N \to \pi N$
• • • We do not use the following data for averages, fits, limits, etc. • • •				
−0.049±0.008	ANISOVICH	13B	DPWA	Multichannel
−0.038±0.003	[1] SHRESTHA	12A	DPWA	Multichannel
−0.077	DRECHSEL	07	DPWA	$\gamma N \to \pi N$
−0.084	PENNER	02D	DPWA	Multichannel

[1] Statistical error only.

$N(1520) \to n\gamma$, helicity-3/2 amplitude $A_{3/2}$

VALUE (GeV$^{-1/2}$)	DOCUMENT ID		TECN	COMMENT
−0.120 to −0.100 (≈ −0.115) OUR ESTIMATE				
−0.123±0.006	[1] HUNT	19	DPWA	Multichannel
−0.118±0.005	ANISOVICH	17E	DPWA	Multichannel
−0.115±0.005	[1] CHEN	12A	DPWA	$\gamma N \to \pi N$
• • • We do not use the following data for averages, fits, limits, etc. • • •				
−0.113±0.012	ANISOVICH	13B	DPWA	Multichannel
−0.101±0.004	[1] SHRESTHA	12A	DPWA	Multichannel
−0.154	DRECHSEL	07	DPWA	$\gamma N \to \pi N$
−0.159	PENNER	02D	DPWA	Multichannel

[1] Statistical error only.

$N(1520)$ REFERENCES

For early references, see Physics Letters **111B** 1 (1982). For very early references, see Reviews of Modern Physics **37** 633 (1965).

SARANTSEV	25	PR C112 015202	A.V. Sarantsev *et al.*	(Bonn-Gatchina Collab.)
SEIFEN	25	EPJ A61 173	T. Seifen *et al.*	(CBELSA/TAPS Collab.)
ROENCHEN	22	EPJ A58 229	D. Roenchen *et al.*	(JULI, GWU, BONN+)
ADAMCZEW...	20	PR C102 024001	J. Adamczewski-Musch *et al.*	(HADES Collab.)
MUELLER	20	PL B803 135323	J. Mueller *et al.*	(CBELSA/TAPS Collab.)
HUNT	19	PR C99 055205	B.C. Hunt, D.M. Manley	
ANISOVICH	17E	PR C96 055202	A.V. Anisovich *et al.*	(BONN, PNPI, JLAB+)
ROENCHEN	15A	EPJ A51 70	D. Roenchen *et al.*	
SOKHOYAN	15A	EPJ A51 95	V. Sokhoyan *et al.*	(CBELSA/TAPS Collab.)
PDG	14	CP C38 070001	K. Olive *et al.*	(PDG Collab.)
SVARC	14	PR C89 045205	A. Svarc *et al.*	(RBI Zagreb, UNI Tuzla)
ANISOVICH	13B	EPJ A49 67	A.V. Anisovich *et al.*	
SHKLYAR	13	PR C87 015201	V. Shklyar, H. Lenske, U. Mosel	(GIES)
ANISOVICH	12A	EPJ A48 15	A.V. Anisovich *et al.*	(BONN, PNPI)
CHEN	12A	PR C86 015206	W. Chen *et al.*	(DUKE, GWU, MSST, ITEP+)
SHRESTHA	12A	PR C86 055203	M. Shrestha, D.M. Manley	(KSU)
WORKMAN	12A	PR C86 015202	R. Workman *et al.*	(GWU)
BATINIC	10	PR C82 038203	M. Batinic *et al.*	(ZAGR)
THOMA	08	PL B659 87	U. Thoma *et al.*	(CB-ELSA Collab.)
DRECHSEL	07	EPJ A34 69	D. Drechsel, S.S. Kamalov, L. Tiator	(MAINZ, JINR)
DUGGER	07	PR C76 025211	M. Dugger *et al.*	(JLab CLAS Collab.)
ARNDT	06	PR C74 045205	R.A. Arndt *et al.*	(GWU)
ARNDT	05	PR C72 045202	R.A. Arndt *et al.*	(GWU, PNPI)
AHRENS	02	PRL 88 232002	J. Ahrens *et al.*	(Mainz MAMI GDH/A2 Collab.)
PENNER	02C	PR C66 055211	G. Penner, U. Mosel	(GIES)
PENNER	02D	PR C66 055212	G. Penner, U. Mosel	(GIES)
VRANA	00	PRPL 328 181	T.P. Vrana, S.A. Dytman, T.-S.H. Lee	(PITT, ANL)
TIATOR	99	PR C60 035210	L. Tiator *et al.*	
MUKHOPAD...	98	PL B444 7	N.C. Mukhopadhyay, N. Mathur	
HOEHLER	93	πN Newsletter 9 1	G. Hohler	(KARL)
CUTKOSKY	80	Toronto Conf. 19	R.E. Cutkosky *et al.*	(CMU, LBL) IJP
Also		PR D20 2839	R.E. Cutkosky *et al.*	(CMU, LBL) IJP
HOEHLER	79	PDAT 12-1	G. Hohler *et al.*	(KARLT) IJP
Also		Toronto Conf. 3	R. Koch	(KARLT) IJP

$N(1535)\ 1/2^-$

$I(J^P) = \frac{1}{2}(\frac{1}{2}^-)$ Status: ****

Older and obsolete values are listed and referenced in the 2014 edition, Chinese Physics **C38** 070001 (2014).

$N(1535)$ POLE POSITION

REAL PART

VALUE (MeV)	DOCUMENT ID		TECN	COMMENT
1500 to 1520 (≈ 1510) OUR ESTIMATE				
1494± 7	SARANTSEV	25	DPWA	Multichannel
1504± 0	ROENCHEN	22	DPWA	Multichannel
1496± 4	AFZAL	20	DPWA	Multichannel
1509± 4±2	[1] SVARC	14	L+P	$\pi N \to \pi N$
1510±50	CUTKOSKY	80	IPWA	$\pi N \to \pi N$
• • • We do not use the following data for averages, fits, limits, etc. • • •				
1496	HUNT	19	DPWA	Multichannel
1499	ROENCHEN	15A	DPWA	Multichannel
1500± 4	SOKHOYAN	15A	DPWA	Multichannel
1490	SHKLYAR	13	DPWA	Multichannel
1521±14	BATINIC	10	DPWA	$\pi N \to N\pi$, $N\eta$
1502	ARNDT	06	DPWA	$\pi N \to \pi N$, ηN
1525	VRANA	00	DPWA	Multichannel
1487	HOEHLER	93	SPED	$\pi N \to \pi N$

[1] Fit to the amplitudes of HOEHLER 79.

−2×IMAGINARY PART

VALUE (MeV)	DOCUMENT ID		TECN	COMMENT
80 to 130 (≈ 110) OUR ESTIMATE				
115±10	SARANTSEV	25	DPWA	Multichannel
74± 1	ROENCHEN	22	DPWA	Multichannel
125± 6	AFZAL	20	DPWA	Multichannel
118± 9±2	[2] SVARC	14	L+P	$\pi N \to \pi N$
260±80	CUTKOSKY	80	IPWA	$\pi N \to \pi N$
• • • We do not use the following data for averages, fits, limits, etc. • • •				
119	HUNT	19	DPWA	Multichannel
104	ROENCHEN	15A	DPWA	Multichannel
128± 9	SOKHOYAN	15A	DPWA	Multichannel
100	SHKLYAR	13	DPWA	Multichannel
190±28	BATINIC	10	DPWA	$\pi N \to N\pi$, $N\eta$
95	ARNDT	06	DPWA	$\pi N \to \pi N$, ηN
102	VRANA	00	DPWA	Multichannel

[2] Fit to the amplitudes of HOEHLER 79.

$N(1535)$ ELASTIC POLE RESIDUE

MODULUS $|r|$

VALUE (MeV)	DOCUMENT ID		TECN	COMMENT
15 to 35 (≈ 25) OUR ESTIMATE				
18± 1	ROENCHEN	22	DPWA	Multichannel
29± 4	SOKHOYAN	15A	DPWA	Multichannel
22± 2±0.4	[3] SVARC	14	L+P	$\pi N \to \pi N$
120±40	CUTKOSKY	80	IPWA	$\pi N \to \pi N$
• • • We do not use the following data for averages, fits, limits, etc. • • •				
22	ROENCHEN	15A	DPWA	Multichannel
15	SHKLYAR	13	DPWA	Multichannel
31± 4	ANISOVICH	12A	DPWA	Multichannel
68	BATINIC	10	DPWA	$\pi N \to N\pi$, $N\eta$
16	ARNDT	06	DPWA	$\pi N \to \pi N$, ηN

[3] Fit to the amplitudes of HOEHLER 79.

PHASE θ

VALUE (°)	DOCUMENT ID		TECN	COMMENT
−40 to 0 (≈ −20) OUR ESTIMATE				
−37± 2	ROENCHEN	22	DPWA	Multichannel
−20±10	SOKHOYAN	15A	DPWA	Multichannel
− 5± 5±3	[4] SVARC	14	L+P	$\pi N \to \pi N$
+15±45	CUTKOSKY	80	IPWA	$\pi N \to \pi N$
• • • We do not use the following data for averages, fits, limits, etc. • • •				
−46	ROENCHEN	15A	DPWA	Multichannel
−51	SHKLYAR	13	DPWA	Multichannel
−29± 5	ANISOVICH	12A	DPWA	Multichannel
12	BATINIC	10	DPWA	$\pi N \to N\pi$, $N\eta$
−16	ARNDT	06	DPWA	$\pi N \to \pi N$, ηN

[4] Fit to the amplitudes of HOEHLER 79.

$N(1535)$ INELASTIC POLE RESIDUE

The "normalized residue" is the residue divided by $\Gamma_{pole}/2$.

Normalized residue in $N\pi \to N(1535) \to N\eta$

MODULUS	PHASE (°)	DOCUMENT ID		TECN	COMMENT
0.50±0.02	118 ± 1	ROENCHEN	22	DPWA	Multichannel
0.43±0.03	−76 ± 5	ANISOVICH	12A	DPWA	Multichannel
• • • We do not use the following data for averages, fits, limits, etc. • • •					
0.51	112	ROENCHEN	15A	DPWA	Multichannel

Int. J. Mod. Phys. A 2026.41. Downloaded from www.worldscientific.com
UNIVERSITY OF CALIFORNIA @ BERKELEY on 09/16/26. Re-use and distribution is strictly not permitted, except for Open Access articles.

Normalized residue in $N\pi \to N(1535) \to \Lambda K$

MODULUS	PHASE (°)	DOCUMENT ID		TECN	COMMENT
0.26±0.01	−67 ± 2	ROENCHEN	22	DPWA	Multichannel
• • • We do not use the following data for averages, fits, limits, etc. • • •					
0.05	32	ROENCHEN	15A	DPWA	Multichannel

Normalized residue in $N\pi \to N(1535) \to \Sigma K$

MODULUS	PHASE (°)	DOCUMENT ID		TECN	COMMENT
0.28±0.01	92 ± 2	ROENCHEN	22	DPWA	Multichannel
• • • We do not use the following data for averages, fits, limits, etc. • • •					
0.05	−69	ROENCHEN	15A	DPWA	Multichannel

Normalized residue in $N\pi \to N(1535) \to \Delta\pi$, D-wave

MODULUS	PHASE (°)	DOCUMENT ID		TECN	COMMENT
0.11±0.02	160 ± 20	SOKHOYAN	15A	DPWA	Multichannel
• • • We do not use the following data for averages, fits, limits, etc. • • •					
0.12±0.03	145 ± 17	ANISOVICH	12A	DPWA	Multichannel

Normalized residue in $N\pi \to N(1535) \to N\sigma$

MODULUS	PHASE (°)	DOCUMENT ID		TECN	COMMENT
0.16±0.07	25 ± 40	SOKHOYAN	15A	DPWA	Multichannel

Normalized residue in $N\pi \to N(1535) \to N(1440)\pi$

MODULUS	PHASE (°)	DOCUMENT ID		TECN	COMMENT
0.21±0.14	−45 ± 50	SOKHOYAN	15A	DPWA	Multichannel

$N(1535)$ BREIT-WIGNER MASS

VALUE (MeV)	DOCUMENT ID		TECN	COMMENT
1515 to 1545 (≈ 1530) OUR ESTIMATE				
1517 ± 4	SARANTSEV	25	DPWA	Multichannel
1525 ± 2	[5] HUNT	19	DPWA	Multichannel
1528 ± 6	KASHEVAROV	17	DPWA	$\gamma p \to \eta p, \eta' p$
1517 ± 4	SOKHOYAN	15A	DPWA	Multichannel
1526 ± 2	[5] SHKLYAR	13	DPWA	Multichannel
1547.0± 0.7	[5] ARNDT	06	DPWA	$\pi N \to \pi N, \eta N$
1550 ±40	CUTKOSKY	80	IPWA	$\pi N \to \pi N$
1526 ± 7	HOEHLER	79	IPWA	$\pi N \to \pi N$
• • • We do not use the following data for averages, fits, limits, etc. • • •				
1519 ± 5	ANISOVICH	12A	DPWA	Multichannel
1538 ± 1	[5] SHRESTHA	12A	DPWA	Multichannel
1553 ± 8	BATINIC	10	DPWA	$\pi N \to N\pi, N\eta$
1546.7± 2.2	ARNDT	04	DPWA	$\pi N \to \pi N, \eta N$
1526 ± 2	PENNER	02C	DPWA	Multichannel
1530 ±10	BAI	01B	BES	$J/\psi \to p\overline{p}\eta$
1522 ±11	THOMPSON	01	CLAS	$\gamma^* p \to p\eta$
1542 ± 3	VRANA	00	DPWA	Multichannel
1532 ± 5	ARMSTRONG	99B	DPWA	$\gamma^* p \to p\eta$

[5] Statistical error only.

$N(1535)$ BREIT-WIGNER WIDTH

VALUE (MeV)	DOCUMENT ID		TECN	COMMENT
125 to 175 (≈ 150) OUR ESTIMATE				
115 ± 7	SARANTSEV	25	DPWA	Multichannel
147 ± 5	[6] HUNT	19	DPWA	Multichannel
163 ±25	KASHEVAROV	17	DPWA	$\gamma p \to \eta p, \eta' p$
120 ±10	SOKHOYAN	15A	DPWA	Multichannel
131 ±12	[6] SHKLYAR	13	DPWA	Multichannel
188.4± 3.8	[6] ARNDT	06	DPWA	$\pi N \to \pi N, \eta N$
240 ±80	CUTKOSKY	80	IPWA	$\pi N \to \pi N$
120 ±20	HOEHLER	79	IPWA	$\pi N \to \pi N$
• • • We do not use the following data for averages, fits, limits, etc. • • •				
128 ±14	ANISOVICH	12A	DPWA	Multichannel
141 ± 4	[6] SHRESTHA	12A	DPWA	Multichannel
182 ±25	BATINIC	10	DPWA	$\pi N \to N\pi, N\eta$
129 ± 8	PENNER	02C	DPWA	Multichannel
95 ±25	BAI	01B	BES	$J/\psi \to p\overline{p}\eta$
143 ±18	THOMPSON	01	CLAS	$\gamma^* p \to p\eta$
112 ±19	VRANA	00	DPWA	Multichannel
154 ±20	ARMSTRONG	99B	DPWA	$\gamma^* p \to p\eta$

[6] Statistical error only.

$N(1535)$ DECAY MODES

The following branching fractions are our estimates, not fits or averages.

	Mode	Fraction (Γ_i/Γ)
Γ_1	$N\pi$	32–52 %
Γ_2	$N\eta$	30–55 %
Γ_3	$N\pi\pi$	4–31 %
Γ_4	$\Delta(1232)\pi$	1–4 %
Γ_5	$N\rho$	2–17 %
Γ_6	$N\rho$, S=1/2	2–16 %
Γ_7	$N\rho$, S=3/2	<1 %
Γ_8	$N\sigma$	2–10 %
Γ_9	$N(1440)\pi$	5–12 %
Γ_{10}	$p\gamma$, helicity=1/2	0.15–0.30 %
Γ_{11}	$n\gamma$, helicity=1/2	0.01–0.25 %

$N(1535)$ BRANCHING RATIOS

$\Gamma(N\pi)/\Gamma_{total}$ — Γ_1/Γ

VALUE (%)	DOCUMENT ID		TECN	COMMENT
32–52 % OUR ESTIMATE				
46 ± 5	SEIFEN	25	DPWA	Multichannel
42 ± 2	[7] HUNT	19	DPWA	Multichannel
35 ± 3	[7] SHKLYAR	13	DPWA	Multichannel
35.5± 0.2	[7] ARNDT	06	DPWA	$\pi N \to \pi N, \eta N$
50 ±10	CUTKOSKY	80	IPWA	$\pi N \to \pi N$
38 ± 4	HOEHLER	79	IPWA	$\pi N \to \pi N$
• • • We do not use the following data for averages, fits, limits, etc. • • •				
52 ± 5	SOKHOYAN	15A	DPWA	Multichannel
37 ± 1	[7] SHRESTHA	12A	DPWA	Multichannel
46 ± 7	BATINIC	10	DPWA	$\pi N \to N\pi, N\eta$
36 ± 1	PENNER	02C	DPWA	Multichannel
35 ± 8	VRANA	00	DPWA	Multichannel

[7] Statistical error only.

$\Gamma(N\eta)/\Gamma_{total}$ — Γ_2/Γ

VALUE (%)	DOCUMENT ID		TECN	COMMENT
30–55 % OUR ESTIMATE				
41±4	MUELLER	20	DPWA	Multichannel
43±3	[8] HUNT	19	DPWA	Multichannel
41±4	[9] KASHEVAROV	17	DPWA	$\gamma p \to \eta p, \eta' p$
58±4	[8] SHKLYAR	13	DPWA	Multichannel
33±5	ANISOVICH	12A	DPWA	Multichannel
53±1	PENNER	02C	DPWA	Multichannel
51±5	VRANA	00	DPWA	Multichannel
• • • We do not use the following data for averages, fits, limits, etc. • • •				
41±2	[8] SHRESTHA	12A	DPWA	Multichannel
50±7	BATINIC	10	DPWA	$\pi N \to N\pi, N\eta$

[8] Statistical error only.
[9] Assuming $A_{1/2} = 0.115$ GeV$^{-1/2}$.

$\Gamma(N\eta)/\Gamma(N\pi)$ — Γ_2/Γ_1

VALUE	DOCUMENT ID		TECN	COMMENT
• • • We do not use the following data for averages, fits, limits, etc. • • •				
0.99±0.05±0.19	ABLIKIM	25M	BES3	$\psi(3686) \to p\overline{p}\pi^0, p\overline{p}\eta$
0.95±0.03	AZNAURYAN	09	CLAS	π, η electroproduction

$\Gamma(\Delta(1232)\pi)/\Gamma_{total}$ — Γ_4/Γ

VALUE (%)	DOCUMENT ID		TECN	COMMENT
1–4 % OUR ESTIMATE				
5 ±3	SARANTSEV	25	DPWA	Multichannel
5 ±3	SEIFEN	25	DPWA	Multichannel
3 ±1	ADAMCZEW...	20	DPWA	Multichannel
<1.1	[10] HUNT	19	DPWA	Multichannel
• • • We do not use the following data for averages, fits, limits, etc. • • •				
2.5±1.5	SOKHOYAN	15A	DPWA	Multichannel
1.8±0.8	[10] SHRESTHA	12A	DPWA	Multichannel
1 ±1	VRANA	00	DPWA	Multichannel

[10] Statistical error only.

$\Gamma(N\rho, S{=}1/2)/\Gamma_{total}$ — Γ_6/Γ

VALUE (%)	DOCUMENT ID		TECN	COMMENT
2–16 % OUR ESTIMATE				
< 1	SARANTSEV	25	DPWA	Multichannel
2.7±0.6	ADAMCZEW...	20	DPWA	Multichannel
14 ±2	[11] HUNT	19	DPWA	Multichannel

[11] Statistical error only.

$\Gamma(N\rho, S{=}3/2)/\Gamma_{total}$ — Γ_7/Γ

VALUE (%)	DOCUMENT ID		TECN	COMMENT
<1 % OUR ESTIMATE				
0.5±0.5	ADAMCZEW...	20	DPWA	Multichannel
<0.3	[12] HUNT	19	DPWA	Multichannel

[12] Statistical error only.

$\Gamma(N\sigma)/\Gamma_{total}$ — Γ_8/Γ

VALUE (%)	DOCUMENT ID		TECN	COMMENT
2–10 % OUR ESTIMATE				
6 ±3	SARANTSEV	25	DPWA	Multichannel
4 ±2	SEIFEN	25	DPWA	Multichannel
<1	[13] HUNT	19	DPWA	Multichannel

Int. J. Mod. Phys. A 2026.41. Downloaded from www.worldscientific.com by UNIVERSITY OF CALIFORNIA @ BERKELEY on 09/16/26. Re-use and distribution is strictly not permitted, except for Open Access articles.

• • • We do not use the following data for averages, fits, limits, etc. • • •

6 ±4	SOKHOYAN	15A	DPWA	Multichannel
1.5±0.5	[13] SHRESTHA	12A	DPWA	Multichannel
2 ±1	VRANA	00	DPWA	Multichannel

[13] Statistical error only.

$\Gamma(N(1440)\pi)/\Gamma_{total}$ — Γ_9/Γ

VALUE (%)	DOCUMENT ID		TECN	COMMENT
5–12 % OUR ESTIMATE				
6 ±5	SEIFEN	25	DPWA	Multichannel
< 0.01	[14] HUNT	19	DPWA	Multichannel
8 ±2	[14] STAROSTIN	03		$\pi^- p \to n 3\pi^0$
• • • We do not use the following data for averages, fits, limits, etc. • • •				
12 ±8	SOKHOYAN	15A	DPWA	Multichannel
< 1	[14] SHRESTHA	12A	DPWA	Multichannel
10 ±9	VRANA	00	DPWA	Multichannel

[14] This value is an estimate made using simplest assumptions.

$N(1535)$ PHOTON DECAY AMPLITUDES AT THE POLE

$N(1535) \to p\gamma$, helicity-1/2 amplitude $A_{1/2}$

MODULUS ($GeV^{-1/2}$)	PHASE (°)	DOCUMENT ID		TECN	COMMENT
0.110±0.006	0 ± 5	SARANTSEV	25	DPWA	Multichannel
0.084±0.002	−12 ± 2	ROENCHEN	22	DPWA	Multichannel
• • • We do not use the following data for averages, fits, limits, etc. • • •					
0.106	5.2	ROENCHEN	15A	DPWA	Multichannel
0.114±0.008	10 ± 5	SOKHOYAN	15A	DPWA	Multichannel

$N(1535) \to n\gamma$, helicity-1/2 amplitude $A_{1/2}$

MODULUS ($GeV^{-1/2}$)	PHASE (°)	DOCUMENT ID		TECN	COMMENT
−0.088±0.004	**5 ± 4**	ANISOVICH	17D	DPWA	Multichannel
• • • We do not use the following data for averages, fits, limits, etc. • • •					
−0.095±0.006	8 ± 5	ANISOVICH	15A	DPWA	Multichannel

$N(1535)$ BREIT-WIGNER PHOTON DECAY AMPLITUDES

$N(1535) \to p\gamma$, helicity-1/2 amplitude $A_{1/2}$

VALUE ($GeV^{-1/2}$)	DOCUMENT ID		TECN	COMMENT
0.090 to 0.120 (≈ 0.105) OUR ESTIMATE				
0.102±0.008	SARANTSEV	25	DPWA	Multichannel
0.107±0.003	[15] HUNT	19	DPWA	Multichannel
0.091±0.004	[15] SHKLYAR	13	DPWA	Multichannel
0.128±0.004	[15] WORKMAN	12A	DPWA	$\gamma N \to N\pi$
0.091±0.002	[15] DUGGER	07	DPWA	$\gamma N \to \pi N$
• • • We do not use the following data for averages, fits, limits, etc. • • •				
0.101±0.007	SOKHOYAN	15A	DPWA	Multichannel
0.059±0.003	[15] SHRESTHA	12A	DPWA	Multichannel
0.066	DRECHSEL	07	DPWA	$\gamma N \to \pi N$
0.090	PENNER	02D	DPWA	Multichannel

[15] Statistical error only.

$N(1535) \to n\gamma$, helicity-1/2 amplitude $A_{1/2}$

VALUE ($GeV^{-1/2}$)	DOCUMENT ID		TECN	COMMENT
−0.095 to −0.055 (≈ − 0.075) OUR ESTIMATE				
−0.055±0.006	[16] HUNT	19	DPWA	Multichannel
−0.081±0.006	ANISOVICH	17E	DPWA	Multichannel
−0.058±0.006	[16] CHEN	12A	DPWA	$\gamma N \to \pi N$
• • • We do not use the following data for averages, fits, limits, etc. • • •				
−0.093±0.011	ANISOVICH	13B	DPWA	Multichannel
−0.049±0.003	[16] SHRESTHA	12A	DPWA	Multichannel
−0.051	DRECHSEL	07	DPWA	$\gamma N \to \pi N$
−0.024	PENNER	02D	DPWA	Multichannel

[16] Statistical error only.

$N(1535) \to N\gamma$, ratio $A^n_{1/2}/A^p_{1/2}$

VALUE ($GeV^{-1/2}$)	DOCUMENT ID		TECN
• • • We do not use the following data for averages, fits, limits, etc. • • •			
−0.84±0.15	MUKHOPAD...	95B	IPWA

$N(1535)$ REFERENCES

For early references, see Physics Letters **111B** 1 (1982).

ABLIKIM	25M	PR D111 032011	M. Ablikim *et al.*	(BESIII Collab.)
SARANTSEV	25	PR C112 015202	A.V. Sarantsev *et al.*	(Bonn-Gatchina Collab.)
SEIFEN	25	EPJ A61 173	T. Seifen *et al.*	(CBELSA/TAPS Collab.)
ROENCHEN	22	EPJ A58 229	D. Roenchen *et al.*	(JULI, GWU, BONN+)
ADAMCZEW...	20	PR C102 024001	J. Adamczewski-Musch *et al.*	(HADES Collab.)
AFZAL	20	PRL 125 152002	F. Afzal *et al.*	(CBELSA/TAPS Collab.)
MUELLER	20	PL B803 135323	J. Mueller *et al.*	(CBELSA/TAPS Collab.)
HUNT	19	PR C99 055205	B.C. Hunt, D.M. Manley	
ANISOVICH	17D	PR C95 035211	A.V. Anisovich *et al.*	
ANISOVICH	17E	PR C96 055202	A.V. Anisovich *et al.*	(BONN, PNPI, JLAB+)
KASHEVAROV	17	PRL 118 212001	V.L. Kashevarov *et al.*	(A2/MAMI Collab.)
ANISOVICH	15A	EPJ A51 72	A.V. Anisovich *et al.*	
ROENCHEN	15A	EPJ A51 70	D. Roenchen *et al.*	
SOKHOYAN	15A	EPJ A51 95	V. Sokhoyan *et al.*	(CBELSA/TAPS Collab.)
PDG	14	CP C38 070001	K. Olive *et al.*	(PDG Collab.)
SVARC	14	PR C89 045205	A. Svarc *et al.*	(RBI Zagreb, UNI Tuzla)
ANISOVICH	13B	EPJ A49 67	A.V. Anisovich *et al.*	
SHKLYAR	13	PR C87 015201	V. Shklyar, H. Lenske, U. Mosel	(GIES)
ANISOVICH	12A	EPJ A48 15	A.V. Anisovich *et al.*	(BONN, PNPI)
CHEN	12A	PR C86 015206	W. Chen *et al.*	(DUKE, GWU, MSST, ITEP+)
SHRESTHA	12A	PR C86 055203	M. Shrestha, D.M. Manley	(KSU)
WORKMAN	12A	PR C86 015202	R. Workman *et al.*	(GWU)
BATINIC	10	PR C82 038203	M. Batinic *et al.*	(ZAGR)
AZNAURYAN	09	PR C80 055203	I.G. Aznauryan *et al.*	(JLab CLAS Collab.)
DRECHSEL	07	EPJ A34 69	D. Drechsel, S.S. Kamalov, L. Tiator	(MAINZ, JINR)
DUGGER	07	PR C76 025211	M. Dugger *et al.*	(JLab CLAS Collab.)
ARNDT	06	PR C74 045205	R.A. Arndt *et al.*	(GWU)
ARNDT	04	PR C69 035213	R.A. Arndt *et al.*	(GWU, TRIU)
STAROSTIN	03	PR C67 068201	A. Starostin *et al.*	(BNL Crystal Ball Collab.)
PENNER	02C	PR C66 055211	G. Penner, U. Mosel	(GIES)
PENNER	02D	PR C66 055212	G. Penner, U. Mosel	(GIES)
BAI	01B	PL B510 75	J.Z. Bai *et al.*	(BES Collab.)
THOMPSON	01	PRL 86 1702	R. Thompson *et al.*	(JLab CLAS Collab.)
VRANA	00	PRPL 328 181	T.P. Vrana, S.A. Dytman, T.-S.H. Lee	(PITT, ANL)
ARMSTRONG	99B	PR D60 052004	C.S. Armstrong *et al.*	
MUKHOPAD...	95B	PL B364 1	N.C. Mukhopadhyay, J.F. Zhang, M. Benmerrouche	
HOEHLER	93	πN Newsletter 9 1	G. Hohler	(KARL)
CUTKOSKY	80	Toronto Conf. 19	R.E. Cutkosky *et al.*	(CMU, LBL) IJP
Also		PR D20 2839	R.E. Cutkosky *et al.*	(CMU, LBL) IJP
HOEHLER	79	PDAT 12-1	G. Hohler *et al.*	(KARLT) IJP
Also		Toronto Conf. 3	R. Koch	(KARLT) IJP

$N(1650)$ $1/2^-$

$I(J^P) = \frac{1}{2}(\frac{1}{2}^-)$ Status: ****

Older and obsolete values are listed and referenced in the 2014 edition, Chinese Physics **C38** 070001 (2014).

$N(1650)$ POLE POSITION

REAL PART

VALUE (MeV)	DOCUMENT ID		TECN	COMMENT
1650 to 1680 (≈ 1665) OUR ESTIMATE				
1664±10	SARANTSEV	25	DPWA	Multichannel
1678± 2	ROENCHEN	22	DPWA	Multichannel
1664± 4	AFZAL	20	DPWA	Multichannel
1660± 5	[1] ANISOVICH	17A	L+P	γp, $\pi^- p \to K\Lambda$
1660± 3.5±1	[2] SVARC	14	L+P	$\pi N \to \pi N$
1640±20	CUTKOSKY	80	IPWA	$\pi N \to \pi N$
• • • We do not use the following data for averages, fits, limits, etc. • • •				
1656	HUNT	19	DPWA	Multichannel
1672	ROENCHEN	15A	DPWA	Multichannel
1652± 7	SOKHOYAN	15A	DPWA	Multichannel
1650	SHKLYAR	13	DPWA	Multichannel
1646± 8	BATINIC	10	DPWA	$\pi N \to N\pi$, $N\eta$
1648	ARNDT	06	DPWA	$\pi N \to \pi N$, ηN
1663	VRANA	00	DPWA	Multichannel
1670	HOEHLER	93	ARGD	$\pi N \to \pi N$

[1] Statistical error only.
[2] Fit to the amplitudes of HOEHLER 79.

−2×IMAGINARY PART

VALUE (MeV)	DOCUMENT ID		TECN	COMMENT
100 to 170 (≈ 135) OUR ESTIMATE				
105± 6	SARANTSEV	25	DPWA	Multichannel
127± 2	ROENCHEN	22	DPWA	Multichannel
98± 6	AFZAL	20	DPWA	Multichannel
59±16	[1] ANISOVICH	17A	L+P	γp, $\pi^- p \to K\Lambda$
167± 8±2	[2] SVARC	14	L+P	$\pi N \to \pi N$
150±30	CUTKOSKY	80	IPWA	$\pi N \to \pi N$
• • • We do not use the following data for averages, fits, limits, etc. • • •				
130	HUNT	19	DPWA	Multichannel
137	ROENCHEN	15A	DPWA	Multichannel
102± 8	SOKHOYAN	15A	DPWA	Multichannel
89	SHKLYAR	13	DPWA	Multichannel
204±17	BATINIC	10	DPWA	$\pi N \to N\pi$, $N\eta$
80	ARNDT	06	DPWA	$\pi N \to \pi N$, ηN
240	VRANA	00	DPWA	Multichannel
163	HOEHLER	93	ARGD	$\pi N \to \pi N$

[1] Statistical error only.
[2] Fit to the amplitudes of HOEHLER 79.

$N(1650)$ ELASTIC POLE RESIDUE

MODULUS $|r|$

VALUE (MeV)	DOCUMENT ID		TECN	COMMENT
25 to 55 (≈ 45) OUR ESTIMATE				
59±11	ROENCHEN	22	DPWA	Multichannel
27± 6	SOKHOYAN	15A	DPWA	Multichannel
47± 3±1	[1] SVARC	14	L+P	$\pi N \to \pi N$
60±10	CUTKOSKY	80	IPWA	$\pi N \to \pi N$
• • • We do not use the following data for averages, fits, limits, etc. • • •				
37	ROENCHEN	15A	DPWA	Multichannel
19	SHKLYAR	13	DPWA	Multichannel
24± 3	ANISOVICH	12A	DPWA	Multichannel
100	BATINIC	10	DPWA	$\pi N \to N\pi$, $N\eta$
14	ARNDT	06	DPWA	$\pi N \to \pi N$, ηN
39	HOEHLER	93	ARGD	$\pi N \to \pi N$

[1] Fit to the amplitudes of HOEHLER 79.

PHASE θ

VALUE (°)	DOCUMENT ID		TECN	COMMENT
−80 to −50 (≈ −70) OUR ESTIMATE				
−18±23	ROENCHEN	22	DPWA	Multichannel
−60±20	SOKHOYAN	15A	DPWA	Multichannel
−47± 3±1	[1] SVARC	14	L+P	$\pi N \to \pi N$
−75±25	CUTKOSKY	80	IPWA	$\pi N \to \pi N$
• • • We do not use the following data for averages, fits, limits, etc. • • •				
−59	ROENCHEN	15A	DPWA	Multichannel
−46	SHKLYAR	13	DPWA	Multichannel
−75±12	ANISOVICH	12A	DPWA	Multichannel
−65	BATINIC	10	DPWA	$\pi N \to N\pi$, $N\eta$
−69	ARNDT	06	DPWA	$\pi N \to \pi N$, ηN
−37	HOEHLER	93	ARGD	$\pi N \to \pi N$

[1] Fit to the amplitudes of HOEHLER 79.

$N(1650)$ INELASTIC POLE RESIDUE

The "normalized residue" is the residue divided by $\Gamma_{pole}/2$.

Normalized residue in $N\pi \to N(1650) \to N\eta$

MODULUS	PHASE (°)	DOCUMENT ID		TECN	COMMENT
0.34±0.06	71 ± 23	ROENCHEN	22	DPWA	Multichannel
0.29±0.03	134 ± 10	ANISOVICH	12A	DPWA	Multichannel
• • • We do not use the following data for averages, fits, limits, etc. • • •					
0.21	48	ROENCHEN	15A	DPWA	Multichannel

Normalized residue in $N\pi \to N(1650) \to \Lambda K$

MODULUS	PHASE (°)	DOCUMENT ID		TECN	COMMENT
0.26±0.05	−40 ± 23	ROENCHEN	22	DPWA	Multichannel
0.26±0.10	110 ± 20	ANISOVICH	17A	DPWA	Multichannel
0.10±0.10	95 ± 33	[1] ANISOVICH	17A	L+P	$\gamma p, \pi^- p \to K\Lambda$
• • • We do not use the following data for averages, fits, limits, etc. • • •					
0.20	−54	ROENCHEN	15A	DPWA	Multichannel
0.23±0.09	85 ± 9	ANISOVICH	12A	DPWA	Multichannel

[1] Statistical error only.

Normalized residue in $N\pi \to N(1650) \to \Sigma K$

MODULUS	PHASE (°)	DOCUMENT ID		TECN	COMMENT
0.41 ±0.07	−21 ± 24	ROENCHEN	22	DPWA	Multichannel
• • • We do not use the following data for averages, fits, limits, etc. • • •					
0.026	−74	ROENCHEN	15A	DPWA	Multichannel

Normalized residue in $N\pi \to N(1650) \to \Delta\pi$, D-wave

MODULUS	PHASE (°)	DOCUMENT ID		TECN	COMMENT
0.19±0.06	−30 ± 20	SOKHOYAN	15A	DPWA	Multichannel
• • • We do not use the following data for averages, fits, limits, etc. • • •					
0.23±0.04	−30 ± 20	ANISOVICH	12A	DPWA	Multichannel

Normalized residue in $N\pi \to N(1650) \to N\sigma$

MODULUS	PHASE (°)	DOCUMENT ID		TECN	COMMENT
0.20±0.15	undefined	SOKHOYAN	15A	DPWA	Multichannel

Normalized residue in $N\pi \to N(1650) \to N(1440)\pi$

MODULUS	PHASE (°)	DOCUMENT ID		TECN	COMMENT
0.30±0.17	undefined	SOKHOYAN	15A	DPWA	Multichannel

$N(1650)$ BREIT-WIGNER MASS

VALUE (MeV)	DOCUMENT ID		TECN	COMMENT
1635 to 1665 (≈ 1650) OUR ESTIMATE				
1670 ± 6	SARANTSEV	25	DPWA	Multichannel
1657 ± 6	GOLOVATCH	19	DPWA	$\gamma p \to \pi^+\pi^- p$
1666 ± 3	[1] HUNT	19	DPWA	Multichannel
1634 ± 5	KASHEVAROV	17	DPWA	$\gamma p \to \eta p$, $\eta' p$
1665 ± 2	[1] SHKLYAR	13	DPWA	Multichannel
1634.7± 1.1	[1] ARNDT	06	DPWA	$\pi N \to \pi N$, ηN
1650 ±30	CUTKOSKY	80	IPWA	$\pi N \to \pi N$
1670 ± 8	HOEHLER	79	IPWA	$\pi N \to \pi N$
• • • We do not use the following data for averages, fits, limits, etc. • • •				
1654 ± 6	SOKHOYAN	15A	DPWA	Multichannel
1664 ± 2	[1] SHRESTHA	12A	DPWA	Multichannel
1652 ± 9	BATINIC	10	DPWA	$\pi N \to N\pi$, $N\eta$
1665 ± 2	PENNER	02C	DPWA	Multichannel
1647 ±20	BAI	01B	BES	$J/\psi \to p\overline{p}\eta$
1689 ±12	VRANA	00	DPWA	Multichannel

[1] Statistical error only.

$N(1650)$ BREIT-WIGNER WIDTH

VALUE (MeV)	DOCUMENT ID		TECN	COMMENT
100 to 150 (≈ 125) OUR ESTIMATE				
110 ± 7	SARANTSEV	25	DPWA	Multichannel
154 ±28	GOLOVATCH	19	DPWA	$\gamma p \to \pi^+\pi^- p$
133 ± 7	[1] HUNT	19	DPWA	Multichannel
128 ±16	KASHEVAROV	17	DPWA	$\gamma p \to \eta p$, $\eta' p$
147 ±14	[1] SHKLYAR	13	DPWA	Multichannel
115.4± 2.8	[1] ARNDT	06	DPWA	$\pi N \to \pi N$, ηN
150 ±40	CUTKOSKY	80	IPWA	$\pi N \to \pi N$
180 ±20	HOEHLER	79	IPWA	$\pi N \to \pi N$
• • • We do not use the following data for averages, fits, limits, etc. • • •				
102 ± 8	SOKHOYAN	15A	DPWA	Multichannel
126 ± 3	[1] SHRESTHA	12A	DPWA	Multichannel
202 ±16	BATINIC	10	DPWA	$\pi N \to N\pi$, $N\eta$
138 ± 7	PENNER	02C	DPWA	Multichannel
145 $^{+80}_{-45}$	BAI	01B	BES	$J/\psi \to p\overline{p}\eta$
202 ±40	VRANA	00	DPWA	Multichannel

[1] Statistical error only.

$N(1650)$ DECAY MODES

The following branching fractions are our estimates, not fits or averages.

	Mode	Fraction (Γ_i/Γ)
Γ_1	$N\pi$	50–70 %
Γ_2	$N\eta$	15–35 %
Γ_3	ΛK	5–15 %
Γ_4	$N\pi\pi$	20–58 %
Γ_5	$\Delta(1232)\pi$	6–18 %
Γ_6	$N\rho$	12–22 %
Γ_7	$N\rho$, $S=1/2$	<4 %
Γ_8	$N\rho$, $S=3/2$	12–18 %
Γ_9	$N\sigma$	2–18 %
Γ_{10}	$N(1440)\pi$	6–26 %
Γ_{11}	$p\gamma$, helicity=1/2	0.04–0.20 %
Γ_{12}	$n\gamma$, helicity=1/2	0.003–0.17 %

$N(1650)$ BRANCHING RATIOS

$\Gamma(N\pi)/\Gamma_{total}$ — Γ_1/Γ

VALUE (%)	DOCUMENT ID		TECN	COMMENT
50 to 70 (≈ 60) OUR ESTIMATE				
48± 4	SEIFEN	25	DPWA	Multichannel
64± 4	[1] HUNT	19	DPWA	Multichannel
74± 3	[1] SHKLYAR	13	DPWA	Multichannel
65±10	CUTKOSKY	80	IPWA	$\pi N \to \pi N$
61± 4	HOEHLER	79	IPWA	$\pi N \to \pi N$
• • • We do not use the following data for averages, fits, limits, etc. • • •				
51± 4	SOKHOYAN	15A	DPWA	Multichannel
57± 2	[1] SHRESTHA	12A	DPWA	Multichannel
79± 6	BATINIC	10	DPWA	$\pi N \to N\pi$, $N\eta$
100	ARNDT	06	DPWA	$\pi N \to \pi N$, ηN
65± 4	PENNER	02C	DPWA	Multichannel
74± 2	VRANA	00	DPWA	Multichannel

[1] Statistical error only.

$\Gamma(N\eta)/\Gamma_{total}$ — Γ_2/Γ

VALUE (%)	DOCUMENT ID		TECN	COMMENT
15 to 35 (≈ 25) OUR ESTIMATE				
33 ± 4	MUELLER	20	DPWA	Multichannel
0.8± 0.6	[1] HUNT	19	DPWA	Multichannel
28 ±11	[2] KASHEVAROV	17	DPWA	$\gamma p \to \eta p$, $\eta' p$
< 3	SHKLYAR	13	DPWA	Multichannel
18 ± 4	ANISOVICH	12A	DPWA	Multichannel
• • • We do not use the following data for averages, fits, limits, etc. • • •				
21 ± 2	[1] SHRESTHA	12A	DPWA	Multichannel
13 ± 5	BATINIC	10	DPWA	$\pi N \to N\pi$, $N\eta$
1.0± 0.6	PENNER	02C	DPWA	Multichannel
6 ± 1	VRANA	00	DPWA	Multichannel

[1] Statistical error only.
[2] Assuming $A_{1/2} = 0.045$ GeV$^{-1/2}$.

$\Gamma(\Lambda K)/\Gamma_{total}$ — Γ_3/Γ

VALUE (%)	DOCUMENT ID		TECN	COMMENT
5 to 15 (≈ 10) OUR ESTIMATE				
3.5±0.2	[1] HUNT	19	DPWA	Multichannel
10 ±5	ANISOVICH	12A	DPWA	Multichannel
4 ±1	[1] SHKLYAR	05	DPWA	Multichannel
• • • We do not use the following data for averages, fits, limits, etc. • • •				
8 ±1	[1] SHRESTHA	12A	DPWA	Multichannel
2.7±0.4	PENNER	02C	DPWA	Multichannel

Int. J. Mod. Phys. A 2026.41. Downloaded from www.worldscientific.com
UNIVERSITY OF CALIFORNIA @ BERKELEY on 09/16/26. Re-use and distribution is strictly not permitted, except for Open Access articles.

[1] Statistical error only.

$\Gamma(N\pi\pi)/\Gamma_{total}$ — Γ_4/Γ

VALUE	DOCUMENT ID		TECN	COMMENT
0.12±0.02	GOLOVATCH	19	DPWA	$\gamma p \to \pi^+\pi^- p$

$\Gamma(\Delta(1232)\pi)/\Gamma_{total}$ — Γ_5/Γ

VALUE (%)	DOCUMENT ID		TECN	COMMENT
6 ±5	SARANTSEV	25	DPWA	Multichannel
6 ±3	SEIFEN	25	DPWA	Multichannel
< 0.2	[1] HUNT	19	DPWA	Multichannel
• • • We do not use the following data for averages, fits, limits, etc. • • •				
12 ±6	SOKHOYAN	15A	DPWA	Multichannel
7 ±2	[1] SHRESTHA	12A	DPWA	Multichannel
2 ±1	VRANA	00	DPWA	Multichannel

[1] Statistical error only.

$\Gamma(N\rho)/\Gamma_{total}$ — Γ_6/Γ

VALUE (%)	DOCUMENT ID		TECN	COMMENT
17±6	SARANTSEV	25	DPWA	Multichannel

$\Gamma(N\rho, S{=}1/2)/\Gamma_{total}$ — Γ_7/Γ

VALUE (%)	DOCUMENT ID		TECN	COMMENT
12 ±5	SARANTSEV	25	DPWA	Multichannel
1.8±1.7	[1] HUNT	19	DPWA	Multichannel

[1] Statistical error only.

$\Gamma(N\rho, S{=}3/2)/\Gamma_{total}$ — Γ_8/Γ

VALUE (%)	DOCUMENT ID		TECN	COMMENT
5±3	SARANTSEV	25	DPWA	Multichannel
15±3	[1] HUNT	19	DPWA	Multichannel

[1] Statistical error only.

$\Gamma(N\sigma)/\Gamma_{total}$ — Γ_9/Γ

VALUE (%)	DOCUMENT ID		TECN	COMMENT
3±2	SARANTSEV	25	DPWA	Multichannel
3±2	SEIFEN	25	DPWA	Multichannel
12±4	[1] HUNT	19	DPWA	Multichannel
• • • We do not use the following data for averages, fits, limits, etc. • • •				
10±8	SOKHOYAN	15A	DPWA	Multichannel
< 1	[1] SHRESTHA	12A	DPWA	Multichannel
1±1	VRANA	00	DPWA	Multichannel

[1] Statistical error only.

$\Gamma(N(1440)\pi)/\Gamma_{total}$ — Γ_{10}/Γ

VALUE (%)	DOCUMENT ID		TECN	COMMENT
5± 3	SEIFEN	25	DPWA	Multichannel
2± 1	[1] HUNT	19	DPWA	Multichannel
• • • We do not use the following data for averages, fits, limits, etc. • • •				
16±10	SOKHOYAN	15A	DPWA	Multichannel
< 1	[1] SHRESTHA	12A	DPWA	Multichannel
3± 1	VRANA	00	DPWA	Multichannel

[1] Statistical error only.

$N(1650)$ PHOTON DECAY AMPLITUDES AT THE POLE

$N(1650) \to p\gamma$, helicity-1/2 amplitude $A_{1/2}$

MODULUS ($GeV^{-1/2}$)	PHASE (°)	DOCUMENT ID		TECN	COMMENT
0.031±0.005	2 ± 5	SARANTSEV	25	DPWA	Multichannel
0.039±0.005	−0.2 ± 14	ROENCHEN	22	DPWA	Multichannel
• • • We do not use the following data for averages, fits, limits, etc. • • •					
0.059	−14	ROENCHEN	15A	DPWA	Multichannel
0.032±0.006	−2 ± 11	SOKHOYAN	15A	DPWA	Multichannel

$N(1650) \to n\gamma$, helicity-1/2 amplitude $A_{1/2}$

MODULUS ($GeV^{-1/2}$)	PHASE (°)	DOCUMENT ID		TECN	COMMENT
0.016±0.004	−28 ± 10	ANISOVICH	17D	DPWA	Multichannel
• • • We do not use the following data for averages, fits, limits, etc. • • •					
0.019±0.006	0 ± 15	ANISOVICH	15A	DPWA	Multichannel

$N(1650)$ BREIT-WIGNER PHOTON DECAY AMPLITUDES

$N(1650) \to p\gamma$, helicity-1/2 amplitude $A_{1/2}$

VALUE ($GeV^{-1/2}$)	DOCUMENT ID		TECN	COMMENT
0.035 to 0.055 (≈ 0.045) OUR ESTIMATE				
0.031 ±0.004	SARANTSEV	25	DPWA	Multichannel
0.0605±0.0077	GOLOVATCH	19	DPWA	$\gamma p \to \pi^+\pi^- p$
0.048 ±0.003	[1] HUNT	19	DPWA	Multichannel
0.063 ±0.006	[1] SHKLYAR	13	DPWA	Multichannel
0.055 ±0.030	[1] WORKMAN	12A	DPWA	$\gamma N \to N\pi$
0.022 ±0.007	[1] DUGGER	07	DPWA	$\gamma N \to \pi N$
• • • We do not use the following data for averages, fits, limits, etc. • • •				
0.032 ±0.006	SOKHOYAN	15A	DPWA	Multichannel
0.030 ±0.003	[1] SHRESTHA	12A	DPWA	Multichannel
0.033	DRECHSEL	07	DPWA	$\gamma N \to \pi N$
0.049	PENNER	02D	DPWA	Multichannel

[1] Statistical error only.

$N(1650) \to n\gamma$, helicity-1/2 amplitude $A_{1/2}$

VALUE ($GeV^{-1/2}$)	DOCUMENT ID		TECN	COMMENT
−0.040 to 0.030 (≈ −0.010) OUR ESTIMATE				
0.001±0.006	[1] HUNT	19	DPWA	Multichannel
0.016±0.005	ANISOVICH	17E	DPWA	Multichannel
−0.040±0.010	[1] CHEN	12A	DPWA	$\gamma N \to \pi N$
• • • We do not use the following data for averages, fits, limits, etc. • • •				
0.025±0.020	ANISOVICH	13B	DPWA	Multichannel
0.011±0.002	[1] SHRESTHA	12A	DPWA	Multichannel
0.009	DRECHSEL	07	DPWA	$\gamma N \to \pi N$
−0.011	PENNER	02D	DPWA	Multichannel

[1] Statistical error only.

$N(1650)$ REFERENCES

For early references, see Physics Letters **111B** 1 (1982).

SARANTSEV	25	PR C112 015202	A.V. Sarantsev *et al.*	(Bonn-Gatchina Collab.)
SEIFEN	25	EPJ A61 173	T. Seifen *et al.*	(CBELSA/TAPS Collab.)
ROENCHEN	22	EPJ A58 229	D. Roenchen *et al.*	(JULI, GWU, BONN+)
AFZAL	20	PRL 125 152002	F. Afzal *et al.*	(CBELSA/TAPS Collab.)
MUELLER	20	PL B803 135323	J. Mueller *et al.*	(CBELSA/TAPS Collab.)
GOLOVATCH	19	PL B788 371	E. Golovatch *et al.*	(CLAS Collab.)
HUNT	19	PR C99 055205	B.C. Hunt, D.M. Manley	
ANISOVICH	17A	PRL 119 062004	A.V. Anisovich *et al.*	
ANISOVICH	17D	PR C95 035211	A.V. Anisovich *et al.*	
ANISOVICH	17E	PR C96 055202	A.V. Anisovich *et al.*	(BONN, PNPI, JLAB+)
KASHEVAROV	17	PRL 118 212001	V.L. Kashevarov *et al.*	(A2/MAMI Collab.)
ANISOVICH	15A	EPJ A51 72	A.V. Anisovich *et al.*	
ROENCHEN	15A	EPJ A51 70	D. Roenchen *et al.*	
SOKHOYAN	15A	EPJ A51 95	V. Sokhoyan *et al.*	(CBELSA/TAPS Collab.)
PDG	14	CP C38 070001	K. Olive *et al.*	(PDG Collab.)
SVARC	14	PR C89 045205	A. Svarc *et al.*	(RBI Zagreb, UNI Tuzla)
ANISOVICH	13B	EPJ A49 67	A.V. Anisovich *et al.*	
SHKLYAR	13	PR C87 015201	V. Shklyar, H. Lenske, U. Mosel	(GIES)
ANISOVICH	12A	EPJ A48 15	A.V. Anisovich *et al.*	(BONN, PNPI)
CHEN	12A	PR C86 015206	W. Chen *et al.*	(DUKE, GWU, MSST, ITEP+)
SHRESTHA	12A	PR C86 055203	M. Shrestha, D.M. Manley	(KSU)
WORKMAN	12A	PR C86 015202	R. Workman *et al.*	(GWU)
BATINIC	10	PR C82 038203	M. Batinic *et al.*	(ZAGR)
DRECHSEL	07	EPJ A34 69	D. Drechsel, S.S. Kamalov, L. Tiator	(MAINZ, JINR)
DUGGER	07	PR C76 025211	M. Dugger *et al.*	(JLab CLAS Collab.)
ARNDT	06	PR C74 045205	R.A. Arndt *et al.*	(GWU)
SHKLYAR	05	PR C72 015210	V. Shklyar, H. Lenske, U. Mosel	(GIES)
PENNER	02C	PR C66 055211	G. Penner, U. Mosel	(GIES)
PENNER	02D	PR C66 055212	G. Penner, U. Mosel	(GIES)
BAI	01B	PL B510 75	J.Z. Bai *et al.*	(BES Collab.)
VRANA	00	PRPL 328 181	T.P. Vrana, S.A. Dytman, T.-S.H. Lee	(PITT, ANL)
HOEHLER	93	πN Newsletter 9 1	G. Hohler	(KARL)
CUTKOSKY	80	Toronto Conf. 19	R.E. Cutkosky *et al.*	(CMU, LBL) IJP
Also		PR D20 2839	R.E. Cutkosky *et al.*	(CMU, LBL) IJP
HOEHLER	79	PDAT 12-1	G. Hohler *et al.*	(KARLT) IJP
Also		Toronto Conf. 3	R. Koch	(KARLT) IJP

$N(1675)\ 5/2^-$

$I(J^P) = \frac{1}{2}(\frac{5}{2}^-)$ Status: ****

Older and obsolete values are listed and referenced in the 2014 edition, Chinese Physics **C38** 070001 (2014).

$N(1675)$ POLE POSITION

REAL PART

VALUE (MeV)	DOCUMENT ID		TECN	COMMENT
1650 to 1660 (≈ 1655) OUR ESTIMATE				
1662± 5	SARANTSEV	25	DPWA	Multichannel
1652± 2	ROENCHEN	22	DPWA	Multichannel
1654± 2	[1] SVARC	14	L+P	$\pi N \to \pi N$
1660±10	CUTKOSKY	80	IPWA	$\pi N \to \pi N$
• • • We do not use the following data for averages, fits, limits, etc. • • •				
1646	HUNT	19	DPWA	Multichannel
1646	ROENCHEN	15A	DPWA	Multichannel
1655± 4	SOKHOYAN	15A	DPWA	Multichannel
1640	SHKLYAR	13	DPWA	Multichannel
1658± 9	BATINIC	10	DPWA	$\pi N \to N\pi$, $N\eta$
1657	ARNDT	06	DPWA	$\pi N \to \pi N$, ηN
1674	VRANA	00	DPWA	Multichannel
1656	HOEHLER	93	ARGD	$\pi N \to \pi N$

[1] Fit to the amplitudes of HOEHLER 79.

−2×IMAGINARY PART

VALUE (MeV)	DOCUMENT ID		TECN	COMMENT
120 to 150 (≈ 135) OUR ESTIMATE				
130± 8	SARANTSEV	25	DPWA	Multichannel
119± 1	ROENCHEN	22	DPWA	Multichannel
125± 3±1	[1] SVARC	14	L+P	$\pi N \to \pi N$
140±10	CUTKOSKY	80	IPWA	$\pi N \to \pi N$

Int. J. Mod. Phys. A 2026.41. Downloaded from www.worldscientific.com
by UNIVERSITY OF CALIFORNIA @ BERKELEY on 09/16/26. Re-use and distribution is strictly not permitted, except for Open Access articles.

Int. J. Mod. Phys. A 2026.41. Downloaded from www.worldscientific.com
UNIVERSITY OF CALIFORNIA @ BERKELEY on 09/16/26. Re-use and distribution is strictly not permitted, except for Open Access articles.

• • • We do not use the following data for averages, fits, limits, etc. • • •

146	HUNT	19	DPWA	Multichannel
125	ROENCHEN	15A	DPWA	Multichannel
147± 5	SOKHOYAN	15A	DPWA	Multichannel
108	SHKLYAR	13	DPWA	Multichannel
137± 7	BATINIC	10	DPWA	$\pi N \to N\pi$, $N\eta$
139	ARNDT	06	DPWA	$\pi N \to \pi N$, ηN
120	VRANA	00	DPWA	Multichannel
126	HOEHLER	93	ARGD	$\pi N \to \pi N$

[1] Fit to the amplitudes of HOEHLER 79.

$N(1675)$ ELASTIC POLE RESIDUE

MODULUS $|r|$

VALUE (MeV)	DOCUMENT ID		TECN	COMMENT
22 to 32 (≈ 26) OUR ESTIMATE				
22±1	ROENCHEN	22	DPWA	Multichannel
28±1	SOKHOYAN	15A	DPWA	Multichannel
23±1	[1] SVARC	14	L+P	$\pi N \to \pi N$
31±5	CUTKOSKY	80	IPWA	$\pi N \to \pi N$
• • • We do not use the following data for averages, fits, limits, etc. • • •				
24	ROENCHEN	15A	DPWA	Multichannel
20	SHKLYAR	13	DPWA	Multichannel
28±1	ANISOVICH	12A	DPWA	Multichannel
25	BATINIC	10	DPWA	$\pi N \to N\pi$, $N\eta$
27	ARNDT	06	DPWA	$\pi N \to \pi N$, ηN
23	HOEHLER	93	ARGD	$\pi N \to \pi N$

[1] Fit to the amplitudes of HOEHLER 79.

PHASE θ

VALUE (°)	DOCUMENT ID		TECN	COMMENT
−27 to −17 (≈ −22) OUR ESTIMATE				
−17± 1	ROENCHEN	22	DPWA	Multichannel
−24± 4	SOKHOYAN	15A	DPWA	Multichannel
−25± 2	[1] SVARC	14	L+P	$\pi N \to \pi N$
−30±10	CUTKOSKY	80	IPWA	$\pi N \to \pi N$
• • • We do not use the following data for averages, fits, limits, etc. • • •				
−22	ROENCHEN	15A	DPWA	Multichannel
−49	SHKLYAR	13	DPWA	Multichannel
−26± 4	ANISOVICH	12A	DPWA	Multichannel
−16	BATINIC	10	DPWA	$\pi N \to N\pi$, $N\eta$
−21	ARNDT	06	DPWA	$\pi N \to \pi N$, ηN
−22	HOEHLER	93	ARGD	$\pi N \to \pi N$

[1] Fit to the amplitudes of HOEHLER 79.

$N(1675)$ INELASTIC POLE RESIDUE

The "normalized residue" is the residue divided by $\Gamma_{pole}/2$.

Normalized residue in $N\pi \to N(1675) \to \Delta\pi$, D-wave

MODULUS	PHASE (°)	DOCUMENT ID		TECN	COMMENT
0.33±0.04	90 ± 15	SOKHOYAN	15A	DPWA	Multichannel
• • • We do not use the following data for averages, fits, limits, etc. • • •					
0.33±0.05	82 ± 10	ANISOVICH	12A	DPWA	Multichannel

Normalized residue in $N\pi \to N(1675) \to N\eta$

MODULUS	PHASE (°)	DOCUMENT ID		TECN	COMMENT
0.063±0.005	−39 ± 1	ROENCHEN	22	DPWA	Multichannel
• • • We do not use the following data for averages, fits, limits, etc. • • •					
0.044	−43	ROENCHEN	15A	DPWA	Multichannel

Normalized residue in $N\pi \to N(1675) \to \Lambda K$

MODULUS	PHASE (°)	DOCUMENT ID		TECN	COMMENT
0.001±0.001	174 ± 80	ROENCHEN	22	DPWA	Multichannel
• • • We do not use the following data for averages, fits, limits, etc. • • •					
0.001	100	ROENCHEN	15A	DPWA	Multichannel

Normalized residue in $N\pi \to N(1675) \to \Sigma K$

MODULUS	PHASE (°)	DOCUMENT ID		TECN	COMMENT
0.024±0.001	−166 ± 3	ROENCHEN	22	DPWA	Multichannel
• • • We do not use the following data for averages, fits, limits, etc. • • •					
0.031	−175	ROENCHEN	15A	DPWA	Multichannel

Normalized residue in $N\pi \to N(1675) \to N\sigma$

MODULUS	PHASE (°)	DOCUMENT ID		TECN	COMMENT
0.13±0.03	125 ± 20	SOKHOYAN	15A	DPWA	Multichannel
• • • We do not use the following data for averages, fits, limits, etc. • • •					
0.15±0.04	132 ± 18	ANISOVICH	12A	DPWA	Multichannel

$N(1675)$ BREIT-WIGNER MASS

VALUE (MeV)	DOCUMENT ID		TECN	COMMENT
1665 to 1680 (≈ 1675) OUR ESTIMATE				
1668 ± 4	SARANTSEV	25	DPWA	Multichannel
1669 ± 2	[1] HUNT	19	DPWA	Multichannel
1666 ± 2	[1] SHKLYAR	13	DPWA	Multichannel
1674.1± 0.2	[1] ARNDT	06	DPWA	$\pi N \to \pi N$, ηN
1675 ±10	CUTKOSKY	80	IPWA	$\pi N \to \pi N$
1679 ± 8	HOEHLER	79	IPWA	$\pi N \to \pi N$
• • • We do not use the following data for averages, fits, limits, etc. • • •				
1663 ± 4	SOKHOYAN	15A	DPWA	Multichannel
1679 ± 1	[1] SHRESTHA	12A	DPWA	Multichannel
1679 ± 9	BATINIC	10	DPWA	$\pi N \to N\pi$, $N\eta$
1685 ± 4	VRANA	00	DPWA	Multichannel

[1] Statistical error only.

$N(1675)$ BREIT-WIGNER WIDTH

VALUE (MeV)	DOCUMENT ID		TECN	COMMENT
130 to 160 (≈ 145) OUR ESTIMATE				
130 ± 8	SARANTSEV	25	DPWA	Multichannel
161 ± 8	[1] HUNT	19	DPWA	Multichannel
148 ± 1	[1] SHKLYAR	13	DPWA	Multichannel
146.5± 1.0	[1] ARNDT	06	DPWA	$\pi N \to \pi N$, ηN
160 ±20	CUTKOSKY	80	IPWA	$\pi N \to \pi N$
120 ±15	HOEHLER	79	IPWA	$\pi N \to \pi N$
• • • We do not use the following data for averages, fits, limits, etc. • • •				
146 ± 6	SOKHOYAN	15A	DPWA	Multichannel
145 ± 4	[1] SHRESTHA	12A	DPWA	Multichannel
152 ± 8	BATINIC	10	DPWA	$\pi N \to N\pi$, $N\eta$
131 ±10	VRANA	00	DPWA	Multichannel

[1] Statistical error only.

$N(1675)$ DECAY MODES

The following branching fractions are our estimates, not fits or averages.

	Mode	Fraction (Γ_i/Γ)
Γ_1	$N\pi$	38–42 %
Γ_2	$N\eta$	< 1 %
Γ_3	ΛK	<0.04 %
Γ_4	$N\pi\pi$	25–45 %
Γ_5	$\Delta(1232)\pi$	(19±4) %
Γ_6	$\Delta(1232)\pi$, D-wave	23–37 %
Γ_7	$N\rho$	0.1–0.9 %
Γ_8	$N\rho$, S=1/2	<0.2 %
Γ_9	$N\rho$, S=3/2 , D-wave	0.1–0.7 %
Γ_{10}	$N\sigma$	3–7 %
Γ_{11}	$p\gamma$	0–0.02 %
Γ_{12}	$p\gamma$, helicity=1/2	0–0.01 %
Γ_{13}	$p\gamma$, helicity=3/2	0–0.01 %
Γ_{14}	$n\gamma$	0–0.15 %
Γ_{15}	$n\gamma$, helicity=1/2	0–0.05 %
Γ_{16}	$n\gamma$, helicity=3/2	0–0.10 %

$N(1675)$ BRANCHING RATIOS

$\Gamma(N\pi)/\Gamma_{total}$ — Γ_1/Γ

VALUE (%)	DOCUMENT ID		TECN	COMMENT
38 to 42 (≈ 40) OUR ESTIMATE				
40 ±1	SEIFEN	25	DPWA	Multichannel
33 ±1	[1] HUNT	19	DPWA	Multichannel
41 ±1	[1] SHKLYAR	13	DPWA	Multichannel
39.3±0.1	[1] ARNDT	06	DPWA	$\pi N \to \pi N$, ηN
38 ±5	CUTKOSKY	80	IPWA	$\pi N \to \pi N$
38 ±3	HOEHLER	79	IPWA	$\pi N \to \pi N$
• • • We do not use the following data for averages, fits, limits, etc. • • •				
41 ±2	SOKHOYAN	15A	DPWA	Multichannel
38.6±0.6	[1] SHRESTHA	12A	DPWA	Multichannel
35 ±4	BATINIC	10	DPWA	$\pi N \to N\pi$, $N\eta$
35 ±1	VRANA	00	DPWA	Multichannel

[1] Statistical error only.

$\Gamma(N\eta)/\Gamma_{total}$ — Γ_2/Γ

VALUE (%)	DOCUMENT ID		TECN	COMMENT
0.5±0.5	MUELLER	20	DPWA	Multichannel
2.0±0.3	[1] HUNT	19	DPWA	Multichannel
<1	SHKLYAR	13	DPWA	Multichannel
• • • We do not use the following data for averages, fits, limits, etc. • • •				
<1	[1] SHRESTHA	12A	DPWA	Multichannel
0.1±0.1	BATINIC	10	DPWA	$\pi N \to N\pi$, $N\eta$

Int. J. Mod. Phys. A 2026.41. Downloaded from www.worldscientific.com
by UNIVERSITY OF CALIFORNIA @ BERKELEY on 09/16/26. Re-use and distribution is strictly not permitted, except for Open Access articles.

3 ±3	THOMA	08	DPWA	Multichannel
0 ±1	VRANA	00	DPWA	Multichannel

[1] Statistical error only.

$\Gamma(\Lambda K)/\Gamma_{total}$ — Γ_3/Γ

VALUE (%)	DOCUMENT ID		TECN	COMMENT
<0.04 % OUR ESTIMATE				
<0.04	[1] HUNT	19	DPWA	Multichannel

[1] Statistical error only.

$\Gamma(\Delta(1232)\pi)/\Gamma_{total}$ — Γ_5/Γ

VALUE (%)	DOCUMENT ID		TECN	COMMENT
19±4	SARANTSEV	25	DPWA	Multichannel

$\Gamma(\Delta(1232)\pi, D\text{-wave})/\Gamma_{total}$ — Γ_6/Γ

VALUE (%)	DOCUMENT ID		TECN	COMMENT
19 ±4	SARANTSEV	25	DPWA	Multichannel
19 ±3	SEIFEN	25	DPWA	Multichannel
58.3±0.2	[1] HUNT	19	DPWA	Multichannel
• • • We do not use the following data for averages, fits, limits, etc. • • •				
30 ±7	SOKHOYAN	15A	DPWA	Multichannel
46 ±1	[1] SHRESTHA	12A	DPWA	Multichannel
63 ±2	VRANA	00	DPWA	Multichannel

[1] Statistical error only.

$\Gamma(N\rho)/\Gamma_{total}$ — Γ_7/Γ

VALUE (%)	DOCUMENT ID		TECN	COMMENT
30±9	SARANTSEV	25	DPWA	Multichannel

$\Gamma(N\rho, S=1/2)/\Gamma_{total}$ — Γ_8/Γ

VALUE (%)	DOCUMENT ID		TECN	COMMENT
<0.2 % OUR ESTIMATE				
20 ±7	SARANTSEV	25	DPWA	Multichannel
< 0.2	[1] HUNT	19	DPWA	Multichannel

[1] Statistical error only.

$\Gamma(N\rho, S=3/2, D\text{-wave})/\Gamma_{total}$ — Γ_9/Γ

VALUE (%)	DOCUMENT ID		TECN	COMMENT
0.1–0.7 % OUR ESTIMATE				
10 ±5	SARANTSEV	25	DPWA	Multichannel
0.4±0.3	[1] HUNT	19	DPWA	Multichannel

[1] Statistical error only.

$\Gamma(N\sigma)/\Gamma_{total}$ — Γ_{10}/Γ

VALUE (%)	DOCUMENT ID		TECN	COMMENT
5±3	SARANTSEV	25	DPWA	Multichannel
1±1	SEIFEN	25	DPWA	Multichannel
• • • We do not use the following data for averages, fits, limits, etc. • • •				
5±2	SOKHOYAN	15A	DPWA	Multichannel

N(1675) PHOTON DECAY AMPLITUDES AT THE POLE

$N(1675) \to p\gamma$, helicity-1/2 amplitude $A_{1/2}$

MODULUS ($GeV^{-1/2}$)	PHASE (°)	DOCUMENT ID		TECN	COMMENT
0.021±0.004	30 ± 15	SARANTSEV	25	DPWA	Multichannel
0.025±0.002	−1.2 ± 3.9	ROENCHEN	22	DPWA	Multichannel
• • • We do not use the following data for averages, fits, limits, etc. • • •					
0.032	36	ROENCHEN	15A	DPWA	Multichannel
0.022±0.003	−12 ± 7	SOKHOYAN	15A	DPWA	Multichannel

$N(1675) \to p\gamma$, helicity-3/2 amplitude $A_{3/2}$

MODULUS ($GeV^{-1/2}$)	PHASE (°)	DOCUMENT ID		TECN	COMMENT
0.030±0.004	−25 ± 10	SARANTSEV	25	DPWA	Multichannel
0.051±0.002	−1.0 ± 1.9	ROENCHEN	22	DPWA	Multichannel
• • • We do not use the following data for averages, fits, limits, etc. • • •					
0.051	−9.3	ROENCHEN	15A	DPWA	Multichannel
0.028±0.006	−17 ± 6	SOKHOYAN	15A	DPWA	Multichannel

$N(1675) \to n\gamma$, helicity-1/2 amplitude $A_{1/2}$

MODULUS ($GeV^{-1/2}$)	PHASE (°)	DOCUMENT ID		TECN	COMMENT
−0.053±0.004	−3 ± 5	ANISOVICH	17E	DPWA	Multichannel

$N(1675) \to n\gamma$, helicity-3/2 amplitude $A_{3/2}$

MODULUS ($GeV^{-1/2}$)	PHASE (°)	DOCUMENT ID		TECN	COMMENT
−0.073±0.005	−12 ± 5	ANISOVICH	17E	DPWA	Multichannel

N(1675) BREIT-WIGNER PHOTON DECAY AMPLITUDES

$N(1675) \to p\gamma$, helicity-1/2 amplitude $A_{1/2}$

VALUE ($GeV^{-1/2}$)	DOCUMENT ID		TECN	COMMENT
0.010 to 0.025 (≈ 0.018) OUR ESTIMATE				
0.022±0.004	SARANTSEV	25	DPWA	Multichannel
0.026±0.002	[1] HUNT	19	DPWA	Multichannel
0.009±0.001	[1] SHKLYAR	13	DPWA	Multichannel
0.013±0.001	[1] WORKMAN	12A	DPWA	$\gamma N \to N\pi$
0.018±0.002	[1] DUGGER	07	DPWA	$\gamma N \to \pi N$
• • • We do not use the following data for averages, fits, limits, etc. • • •				
0.022±0.003	SOKHOYAN	15A	DPWA	Multichannel
0.011±0.001	[1] SHRESTHA	12A	DPWA	Multichannel
0.015	DRECHSEL	07	DPWA	$\gamma N \to \pi N$

[1] Statistical error only.

$N(1675) \to p\gamma$, helicity-3/2 amplitude $A_{3/2}$

VALUE ($GeV^{-1/2}$)	DOCUMENT ID		TECN	COMMENT
0.015 to 0.030 (≈ 0.022) OUR ESTIMATE				
0.030±0.005	SARANTSEV	25	DPWA	Multichannel
0.005±0.002	[1] HUNT	19	DPWA	Multichannel
0.021±0.001	[1] SHKLYAR	13	DPWA	Multichannel
0.016±0.001	[1] WORKMAN	12A	DPWA	$\gamma N \to N\pi$
0.021±0.001	[1] DUGGER	07	DPWA	$\gamma N \to \pi N$
• • • We do not use the following data for averages, fits, limits, etc. • • •				
0.027±0.006	SOKHOYAN	15A	DPWA	Multichannel
0.020±0.001	[1] SHRESTHA	12A	DPWA	Multichannel
0.022	DRECHSEL	07	DPWA	$\gamma N \to \pi N$

[1] Statistical error only.

$N(1675) \to n\gamma$, helicity-1/2 amplitude $A_{1/2}$

VALUE ($GeV^{-1/2}$)	DOCUMENT ID		TECN	COMMENT
−0.065 to −0.055 (≈ −0.060) OUR ESTIMATE				
−0.069±0.005	[1] HUNT	19	DPWA	Multichannel
−0.053±0.004	ANISOVICH	17E	DPWA	Multichannel
−0.058±0.002	[1] CHEN	12A	DPWA	$\gamma N \to \pi N$
• • • We do not use the following data for averages, fits, limits, etc. • • •				
−0.060±0.007	ANISOVICH	13B	DPWA	Multichannel
−0.040±0.004	[1] SHRESTHA	12A	DPWA	Multichannel
−0.062	DRECHSEL	07	DPWA	$\gamma N \to \pi N$

[1] Statistical error only.

$N(1675) \to n\gamma$, helicity-3/2 amplitude $A_{3/2}$

VALUE ($GeV^{-1/2}$)	DOCUMENT ID		TECN	COMMENT
−0.095 to −0.075 (≈ −0.085) OUR ESTIMATE				
−0.031±0.005	[1] HUNT	19	DPWA	Multichannel
−0.072±0.005	ANISOVICH	17E	DPWA	Multichannel
−0.080±0.005	[1] CHEN	12A	DPWA	$\gamma N \to \pi N$
• • • We do not use the following data for averages, fits, limits, etc. • • •				
−0.088±0.010	ANISOVICH	13B	DPWA	Multichannel
−0.068±0.004	[1] SHRESTHA	12A	DPWA	Multichannel
−0.084	DRECHSEL	07	DPWA	$\gamma N \to \pi N$

[1] Statistical error only.

N(1675) REFERENCES

For early references, see Physics Letters **111B** 1 (1982).

SARANTSEV	25	PR C112 015202	A.V. Sarantsev *et al.*	(Bonn-Gatchina Collab.)
SEIFEN	25	EPJ A61 173	T. Seifen *et al.*	(CBELSA/TAPS Collab.)
ROENCHEN	22	EPJ A58 229	D. Roenchen *et al.*	(JULI, GWU, BONN+)
MUELLER	20	PL B803 135323	J. Mueller *et al.*	(CBELSA/TAPS Collab.)
HUNT	19	PR C99 055205	B.C. Hunt, D.M. Manley	
ANISOVICH	17E	PR C96 055202	A.V. Anisovich *et al.*	(BONN, PNPI, JLAB+)
ROENCHEN	15A	EPJ A51 70	D. Roenchen *et al.*	
SOKHOYAN	15A	EPJ A51 95	V. Sokhoyan *et al.*	(CBELSA/TAPS Collab.)
PDG	14	CP C38 070001	K. Olive *et al.*	(PDG Collab.)
SVARC	14	PR C89 045205	A. Svarc *et al.*	(RBI Zagreb, UNI Tuzla)
ANISOVICH	13B	EPJ A49 67	A.V. Anisovich *et al.*	
SHKLYAR	13	PR C87 015201	V. Shklyar, H. Lenske, U. Mosel	(GIES)
ANISOVICH	12A	EPJ A48 15	A.V. Anisovich *et al.*	(BONN, PNPI)
CHEN	12A	PR C86 015206	W. Chen *et al.*	(DUKE, GWU, MSST, ITEP+)
SHRESTHA	12A	PR C86 055203	M. Shrestha, D.M. Manley	(KSU)
WORKMAN	12A	PR C86 015202	R. Workman *et al.*	(GWU)
BATINIC	10	PR C82 038203	M. Batinic *et al.*	(ZAGR)
THOMA	08	PL B659 87	U. Thoma *et al.*	(CB-ELSA Collab.)
DRECHSEL	07	EPJ A34 69	D. Drechsel, S.S. Kamalov, L. Tiator	(MAINZ, JINR)
DUGGER	07	PR C76 025211	M. Dugger *et al.*	(JLab CLAS Collab.)
ARNDT	06	PR C74 045205	R.A. Arndt *et al.*	(GWU)
VRANA	00	PRPL 328 181	T.P. Vrana, S.A. Dytman, T.-S.H. Lee	(PITT, ANL)
HOEHLER	93	πN Newsletter 9 1	G. Hohler	(KARL)
CUTKOSKY	80	Toronto Conf. 19	R.E. Cutkosky *et al.*	(CMU, LBL) IJP
Also		PR D20 2839	R.E. Cutkosky *et al.*	(CMU, LBL) IJP
HOEHLER	79	PDAT 12-1	G. Hohler *et al.*	(KARLT) IJP
Also		Toronto Conf. 3	R. Koch	(KARLT) IJP

Int. J. Mod. Phys. A 2026.41. Downloaded from www.worldscientific.com
UNIVERSITY OF CALIFORNIA @ BERKELEY on 09/16/26. Re-use and distribution is strictly not permitted, except for Open Access articles.

$N(1680)\ 5/2^+$

$I(J^P) = \frac{1}{2}(\frac{5}{2}^+)$ Status: ****

Older and obsolete values are listed and referenced in the 2014 edition, Chinese Physics **C38** 070001 (2014).

$N(1680)$ POLE POSITION

REAL PART

VALUE (MeV)	DOCUMENT ID		TECN	COMMENT
1660 to 1680 (≈ 1670) OUR ESTIMATE				
1676±6	SARANTSEV	25	DPWA	Multichannel
1657±2	ROENCHEN	22	DPWA	Multichannel
1674±2±1	[1] SVARC	14	L+P	$\pi N \to \pi N$
1667±5	CUTKOSKY	80	IPWA	$\pi N \to \pi N$
• • • We do not use the following data for averages, fits, limits, etc. • • •				
1668	HUNT	19	DPWA	Multichannel
1669	ROENCHEN	15A	DPWA	Multichannel
1678±5	SOKHOYAN	15A	DPWA	Multichannel
1660	SHKLYAR	13	DPWA	Multichannel
1666±8	BATINIC	10	DPWA	$\pi N \to N\pi,\ N\eta$
1674	ARNDT	06	DPWA	$\pi N \to \pi N,\ \eta N$
1667	VRANA	00	DPWA	Multichannel
1673	HOEHLER	93	ARGD	$\pi N \to \pi N$

[1] Fit to the amplitudes of HOEHLER 79.

−2×IMAGINARY PART

VALUE (MeV)	DOCUMENT ID		TECN	COMMENT
110 to 135 (≈ 120) OUR ESTIMATE				
117± 4	SARANTSEV	25	DPWA	Multichannel
120± 1	ROENCHEN	22	DPWA	Multichannel
129± 3±1	[1] SVARC	14	L+P	$\pi N \to \pi N$
110±10	CUTKOSKY	80	IPWA	$\pi N \to \pi N$
• • • We do not use the following data for averages, fits, limits, etc. • • •				
118	HUNT	19	DPWA	Multichannel
100	ROENCHEN	15A	DPWA	Multichannel
113± 4	SOKHOYAN	15A	DPWA	Multichannel
98	SHKLYAR	13	DPWA	Multichannel
135± 6	BATINIC	10	DPWA	$\pi N \to N\pi,\ N\eta$
115	ARNDT	06	DPWA	$\pi N \to \pi N,\ \eta N$
122	VRANA	00	DPWA	Multichannel
135	HOEHLER	93	ARGD	$\pi N \to \pi N$

[1] Fit to the amplitudes of HOEHLER 79.

$N(1680)$ ELASTIC POLE RESIDUE

MODULUS $|r|$

VALUE (MeV)	DOCUMENT ID		TECN	COMMENT
35 to 45 (≈ 40) OUR ESTIMATE				
36±1	ROENCHEN	22	DPWA	Multichannel
45±4	SOKHOYAN	15A	DPWA	Multichannel
44±1±1	[1] SVARC	14	L+P	$\pi N \to \pi N$
34±2	CUTKOSKY	80	IPWA	$\pi N \to \pi N$
• • • We do not use the following data for averages, fits, limits, etc. • • •				
34	ROENCHEN	15A	DPWA	Multichannel
33	SHKLYAR	13	DPWA	Multichannel
43±4	ANISOVICH	12A	DPWA	Multichannel
44	BATINIC	10	DPWA	$\pi N \to N\pi,\ N\eta$
42	ARNDT	06	DPWA	$\pi N \to \pi N,\ \eta N$
44	HOEHLER	93	ARGD	$\pi N \to \pi N$

[1] Fit to the amplitudes of HOEHLER 79.

PHASE θ

VALUE (°)	DOCUMENT ID		TECN	COMMENT
−30 to −10 (≈ −20) OUR ESTIMATE				
−31± 1	ROENCHEN	22	DPWA	Multichannel
5±10	SOKHOYAN	15A	DPWA	Multichannel
−16± 1±1	[1] SVARC	14	L+P	$\pi N \to \pi N$
−25± 5	CUTKOSKY	80	IPWA	$\pi N \to \pi N$
• • • We do not use the following data for averages, fits, limits, etc. • • •				
−19	ROENCHEN	15A	DPWA	Multichannel
−32	SHKLYAR	13	DPWA	Multichannel
− 2±10	ANISOVICH	12A	DPWA	Multichannel
−19	BATINIC	10	DPWA	$\pi N \to N\pi,\ N\eta$
− 4	ARNDT	06	DPWA	$\pi N \to \pi N,\ \eta N$
−17	HOEHLER	93	ARGD	$\pi N \to \pi N$

[1] Fit to the amplitudes of HOEHLER 79.

$N(1680)$ INELASTIC POLE RESIDUE

The "normalized residue" is the residue divided by $\Gamma_{pole}/2$.

Normalized residue in $N\pi \to N(1680) \to \Delta\pi$, P-wave

MODULUS	PHASE (°)	DOCUMENT ID		TECN	COMMENT
0.15±0.03	−60 ± 30	SOKHOYAN	15A	DPWA	Multichannel
• • • We do not use the following data for averages, fits, limits, etc. • • •					
0.15±0.03	−70 ± 45	ANISOVICH	12A	DPWA	Multichannel

Normalized residue in $N\pi \to N(1680) \to \Delta\pi$, F-wave

MODULUS	PHASE (°)	DOCUMENT ID		TECN	COMMENT
0.23±0.04	90 ± 12	SOKHOYAN	15A	DPWA	Multichannel
• • • We do not use the following data for averages, fits, limits, etc. • • •					
0.23±0.04	85 ± 15	ANISOVICH	12A	DPWA	Multichannel

Normalized residue in $N\pi \to N(1680) \to N\eta$

MODULUS	PHASE (°)	DOCUMENT ID		TECN	COMMENT
0.006±0.004	118 ± 1	ROENCHEN	22	DPWA	Multichannel
• • • We do not use the following data for averages, fits, limits, etc. • • •					
0.027	136	ROENCHEN	15A	DPWA	Multichannel

Normalized residue in $N\pi \to N(1680) \to \Lambda K$

MODULUS	PHASE (°)	DOCUMENT ID		TECN	COMMENT
0.006±0.001	−119 ± 2	ROENCHEN	22	DPWA	Multichannel
• • • We do not use the following data for averages, fits, limits, etc. • • •					
0.001	90	ROENCHEN	15A	DPWA	Multichannel

Normalized residue in $N\pi \to N(1680) \to \Sigma K$

MODULUS	PHASE (°)	DOCUMENT ID		TECN	COMMENT
0.001±0.001	−46 ± 15	ROENCHEN	22	DPWA	Multichannel
• • • We do not use the following data for averages, fits, limits, etc. • • •					
0.004	148	ROENCHEN	15A	DPWA	Multichannel

Normalized residue in $N\pi \to N(1680) \to N\,(\pi\pi)^{I=0}_{S-wave}$

MODULUS	PHASE (°)	DOCUMENT ID		TECN	COMMENT
0.29±0.06	−45 ± 15	SOKHOYAN	15A	DPWA	Multichannel
• • • We do not use the following data for averages, fits, limits, etc. • • •					
0.26±0.04	−56 ± 15	ANISOVICH	12A	DPWA	Multichannel

$N(1680)$ BREIT-WIGNER MASS

VALUE (MeV)	DOCUMENT ID		TECN	COMMENT
1680 to 1690 (≈ 1685) OUR ESTIMATE				
1689 ± 5	SARANTSEV	25	DPWA	Multichannel
1686 ± 5	GOLOVATCH	19	DPWA	$\gamma p \to \pi^+\pi^- p$
1681.0± 0.1	[1] HUNT	19	DPWA	Multichannel
1676 ± 2	[1] SHKLYAR	13	DPWA	Multichannel
1680.1± 0.2	[1] ARNDT	06	DPWA	$\pi N \to \pi N,\ \eta N$
1680 ±10	CUTKOSKY	80	IPWA	$\pi N \to \pi N$
1684 ± 3	HOEHLER	79	IPWA	$\pi N \to \pi N$
• • • We do not use the following data for averages, fits, limits, etc. • • •				
1690 ± 5	SOKHOYAN	15A	DPWA	Multichannel
1682.7± 0.5	[1] SHRESTHA	12A	DPWA	Multichannel
1680 ± 7	BATINIC	10	DPWA	$\pi N \to N\pi,\ N\eta$
1679 ± 3	VRANA	00	DPWA	Multichannel

[1] Statistical error only.

$N(1680)$ BREIT-WIGNER WIDTH

VALUE (MeV)	DOCUMENT ID		TECN	COMMENT
115 to 130 (≈ 120) OUR ESTIMATE				
122 ± 5	SARANTSEV	25	DPWA	Multichannel
118 ±20	GOLOVATCH	19	DPWA	$\gamma p \to \pi^+\pi^- p$
123 ± 3	[1] HUNT	19	DPWA	Multichannel
115 ± 1	[1] SHKLYAR	13	DPWA	Multichannel
128.0± 1.1	[1] ARNDT	06	DPWA	$\pi N \to \pi N,\ \eta N$
120 ±10	CUTKOSKY	80	IPWA	$\pi N \to \pi N$
128 ± 8	HOEHLER	79	IPWA	$\pi N \to \pi N$
• • • We do not use the following data for averages, fits, limits, etc. • • •				
119 ± 4	SOKHOYAN	15A	DPWA	Multichannel
126 ± 1	[1] SHRESTHA	12A	DPWA	Multichannel
142 ± 7	BATINIC	10	DPWA	$\pi N \to N\pi,\ N\eta$
128 ± 9	VRANA	00	DPWA	Multichannel

[1] Statistical error only.

$N(1680)$ DECAY MODES

The following branching fractions are our estimates, not fits or averages.

	Mode	Fraction (Γ_i/Γ)
Γ_1	$N\pi$	60–70 %
Γ_2	$N\eta$	<1 %
Γ_3	$N\pi\pi$	28–53 %
Γ_4	$\Delta(1232)\pi$	11–23 %
Γ_5	$\Delta(1232)\pi$, P-wave	4–10 %
Γ_6	$\Delta(1232)\pi$, F-wave	1–13 %
Γ_7	$N\rho$	8–11 %
Γ_8	$N\rho$, $S=3/2$, P-wave	6–8 %
Γ_9	$N\rho$, $S=3/2$, F-wave	2–3 %
Γ_{10}	$N(1520)\pi$, D-wave	

Γ_{11}	$N\sigma$	9–19 %
Γ_{12}	$p\gamma$	0.21–0.32 %
Γ_{13}	$p\gamma$, helicity=1/2	0.001–0.011 %
Γ_{14}	$p\gamma$, helicity=3/2	0.20–0.32 %
Γ_{15}	$n\gamma$	0.021–0.046 %
Γ_{16}	$n\gamma$, helicity=1/2	0.004–0.029 %
Γ_{17}	$n\gamma$, helicity=3/2	0.01–0.024 %

$N(1680)$ BRANCHING RATIOS

$\Gamma(N\pi)/\Gamma_{total}$ — Γ_1/Γ

VALUE (%)	DOCUMENT ID		TECN	COMMENT
60 to 70 (≈ 65) OUR ESTIMATE				
68 ±8	SEIFEN	25	DPWA	Multichannel
68.0±0.1	[1] HUNT	19	DPWA	Multichannel
68 ±1	[1] SHKLYAR	13	DPWA	Multichannel
70.1±0.1	[1] ARNDT	06	DPWA	$\pi N \to \pi N, \eta N$
62 ±5	CUTKOSKY	80	IPWA	$\pi N \to \pi N$
65 ±2	HOEHLER	79	IPWA	$\pi N \to \pi N$
• • • We do not use the following data for averages, fits, limits, etc. • • •				
62 ±4	SOKHOYAN	15A	DPWA	Multichannel
68.0±0.5	[1] SHRESTHA	12A	DPWA	Multichannel
67 ±3	BATINIC	10	DPWA	$\pi N \to N\pi, N\eta$
69 ±2	VRANA	00	DPWA	Multichannel

[1] Statistical error only.

$\Gamma(N\eta)/\Gamma_{total}$ — Γ_2/Γ

VALUE (%)	DOCUMENT ID		TECN	COMMENT
0.2 ±0.1	MUELLER	20	DPWA	Multichannel
0.09±0.02	[1] HUNT	19	DPWA	Multichannel
<1	SHKLYAR	13	DPWA	Multichannel
$0.15^{+0.35}_{-0.10}$	TIATOR	99	DPWA	$\gamma p \to p\eta$
• • • We do not use the following data for averages, fits, limits, etc. • • •				
1.0 ±0.3	[1] SHRESTHA	12A	DPWA	Multichannel
0.4 ±0.2	BATINIC	10	DPWA	$\pi N \to N\pi, N\eta$
<1	THOMA	08	DPWA	Multichannel
0 ±1	VRANA	00	DPWA	Multichannel

[1] Statistical error only.

$\Gamma(N\pi\pi)/\Gamma_{total}$ — Γ_3/Γ

VALUE (%)	DOCUMENT ID		TECN	COMMENT
28–53 % OUR ESTIMATE				
24±4	GOLOVATCH	19	DPWA	$\gamma p \to \pi^+\pi^- p$

$\Gamma(\Delta(1232)\pi)/\Gamma_{total}$ — Γ_4/Γ

VALUE (%)	DOCUMENT ID		TECN	COMMENT
23±7	SARANTSEV	25	DPWA	Multichannel

$\Gamma(\Delta(1232)\pi, P\text{-wave})/\Gamma_{total}$ — Γ_5/Γ

VALUE (%)	DOCUMENT ID		TECN	COMMENT
9 ±3	SARANTSEV	25	DPWA	Multichannel
8 ±4	SEIFEN	25	DPWA	Multichannel
13 ±1	[1] HUNT	19	DPWA	Multichannel
• • • We do not use the following data for averages, fits, limits, etc. • • •				
7 ±3	SOKHOYAN	15A	DPWA	Multichannel
10.5±0.9	[1] SHRESTHA	12A	DPWA	Multichannel
14 ±3	VRANA	00	DPWA	Multichannel

[1] Statistical error only.

$\Gamma(\Delta(1232)\pi, F\text{-wave})/\Gamma_{total}$ — Γ_6/Γ

VALUE (%)	DOCUMENT ID		TECN	COMMENT
14 ±6	SARANTSEV	25	DPWA	Multichannel
8 ±4	SEIFEN	25	DPWA	Multichannel
< 0.3	[1] HUNT	19	DPWA	Multichannel
• • • We do not use the following data for averages, fits, limits, etc. • • •				
10 ±3	SOKHOYAN	15A	DPWA	Multichannel
1.0±0.1	[1] SHRESTHA	12A	DPWA	Multichannel
1 ±1	VRANA	00	DPWA	Multichannel

[1] Statistical error only.

$\Gamma(N\rho)/\Gamma_{total}$ — Γ_7/Γ

VALUE (%)	DOCUMENT ID		TECN	COMMENT
9±4	SARANTSEV	25	DPWA	Multichannel

$\Gamma(N\rho, S=3/2, P\text{-wave})/\Gamma_{total}$ — Γ_8/Γ

VALUE (%)	DOCUMENT ID		TECN	COMMENT
6–8 % OUR ESTIMATE				
9±4	SARANTSEV	25	DPWA	Multichannel
7±1	[1] HUNT	19	DPWA	Multichannel

[1] Statistical error only.

$\Gamma(N\rho, S=3/2, F\text{-wave})/\Gamma_{total}$ — Γ_9/Γ

VALUE (%)	DOCUMENT ID		TECN	COMMENT
2–3 % OUR ESTIMATE				
2.4±0.4	[1] HUNT	19	DPWA	Multichannel

[1] Statistical error only.

$\Gamma(N\sigma)/\Gamma_{total}$ — Γ_{11}/Γ

VALUE (%)	DOCUMENT ID		TECN	COMMENT
8 ±4	SEIFEN	25	DPWA	Multichannel
8.7±1.5	[1] HUNT	19	DPWA	Multichannel
• • • We do not use the following data for averages, fits, limits, etc. • • •				
14 ±5	SOKHOYAN	15A	DPWA	Multichannel
9.4±0.8	[1] SHRESTHA	12A	DPWA	Multichannel
9 ±1	VRANA	00	DPWA	Multichannel

[1] Statistical error only.

$\Gamma(N(1520)\pi, D\text{-wave})/\Gamma_{total}$ — Γ_{10}/Γ

VALUE (%)	DOCUMENT ID		TECN	COMMENT
<1	SEIFEN	25	DPWA	Multichannel

$N(1680)$ PHOTON DECAY AMPLITUDES AT THE POLE

$N(1680) \to p\gamma$, helicity-1/2 amplitude $A_{1/2}$

MODULUS ($GeV^{-1/2}$)	PHASE (°)	DOCUMENT ID		TECN	COMMENT
−0.016±0.004	−35 ± 15	SARANTSEV	25	DPWA	Multichannel
−0.017±0.003	70 ± 7	ROENCHEN	22	DPWA	Multichannel
• • • We do not use the following data for averages, fits, limits, etc. • • •					
−0.022	−28	ROENCHEN	15A	DPWA	Multichannel
−0.013±0.003	−20 ± 17	SOKHOYAN	15A	DPWA	Multichannel

$N(1680) \to p\gamma$, helicity-3/2 amplitude $A_{3/2}$

MODULUS ($GeV^{-1/2}$)	PHASE (°)	DOCUMENT ID		TECN	COMMENT
0.134±0.005	2 ± 5	SARANTSEV	25	DPWA	Multichannel
0.095±0.003	−57 ± 4	ROENCHEN	22	DPWA	Multichannel
• • • We do not use the following data for averages, fits, limits, etc. • • •					
0.102	−11	ROENCHEN	15A	DPWA	Multichannel
0.135±0.005	1 ± 3	SOKHOYAN	15A	DPWA	Multichannel

$N(1680) \to n\gamma$, helicity-1/2 amplitude $A_{1/2}$

MODULUS ($GeV^{-1/2}$)	PHASE (°)	DOCUMENT ID		TECN	COMMENT
0.032±0.003	−7 ± 5	ANISOVICH	17E	DPWA	Multichannel

$N(1680) \to n\gamma$, helicity-3/2 amplitude $A_{3/2}$

MODULUS ($GeV^{-1/2}$)	PHASE (°)	DOCUMENT ID		TECN	COMMENT
−0.063±0.004	−10 ± 5	ANISOVICH	17E	DPWA	Multichannel

$N(1680)$ BREIT-WIGNER PHOTON DECAY AMPLITUDES

$N(1680) \to p\gamma$, helicity-1/2 amplitude $A_{1/2}$

VALUE ($GeV^{-1/2}$)	DOCUMENT ID		TECN	COMMENT
−0.018 to −0.005 (≈ −0.010) OUR ESTIMATE				
−0.016 ±0.004	SARANTSEV	25	DPWA	Multichannel
−0.0278±0.0036	GOLOVATCH	19	DPWA	$\gamma p \to \pi^+\pi^- p$
−0.026 ±0.004	[1] HUNT	19	DPWA	Multichannel
0.003 ±0.001	[1] SHKLYAR	13	DPWA	Multichannel
−0.007 ±0.002	[1] WORKMAN	12A	DPWA	$\gamma N \to N\pi$
−0.017 ±0.001	[1] DUGGER	07	DPWA	$\gamma N \to \pi N$
• • • We do not use the following data for averages, fits, limits, etc. • • •				
−0.015 ±0.002	SOKHOYAN	15A	DPWA	Multichannel
−0.017 ±0.001	[1] SHRESTHA	12A	DPWA	Multichannel
−0.025	DRECHSEL	07	DPWA	$\gamma N \to \pi N$

[1] Statistical error only.

$N(1680) \to p\gamma$, helicity-3/2 amplitude $A_{3/2}$

VALUE ($GeV^{-1/2}$)	DOCUMENT ID		TECN	COMMENT
0.130 to 0.140 (≈ 0.135) OUR ESTIMATE				
0.133±0.005	SARANTSEV	25	DPWA	Multichannel
0.128±0.011	GOLOVATCH	19	DPWA	$\gamma p \to \pi^+\pi^- p$
0.112±0.005	[1] HUNT	19	DPWA	Multichannel
0.116±0.001	[1] SHKLYAR	13	DPWA	Multichannel
0.140±0.002	[1] WORKMAN	12A	DPWA	$\gamma N \to N\pi$
0.134±0.002	[1] DUGGER	07	DPWA	$\gamma N \to \pi N$
• • • We do not use the following data for averages, fits, limits, etc. • • •				
0.136±0.005	SOKHOYAN	15A	DPWA	Multichannel
0.136±0.001	[1] SHRESTHA	12A	DPWA	Multichannel
0.134	DRECHSEL	07	DPWA	$\gamma N \to \pi N$

[1] Statistical error only.

Int. J. Mod. Phys. A 2026.41. Downloaded from www.worldscientific.com
by UNIVERSITY OF CALIFORNIA @ BERKELEY on 09/16/26. Re-use and distribution is strictly not permitted, except for Open Access articles.

Int. J. Mod. Phys. A 2026.41. Downloaded from www.worldscientific.com
UNIVERSITY OF CALIFORNIA @ BERKELEY on 09/16/26. Re-use and distribution is strictly not permitted, except for Open Access articles.

$N(1680) \rightarrow n\gamma$, helicity-1/2 amplitude $A_{1/2}$

VALUE ($GeV^{-1/2}$)	DOCUMENT ID		TECN	COMMENT
0.020 to 0.040 (≈ 0.030) OUR ESTIMATE				
0.005±0.004	[1] HUNT	19	DPWA	Multichannel
0.033±0.003	ANISOVICH	17E	DPWA	Multichannel
0.026±0.004	[1] CHEN	12A	DPWA	$\gamma N \rightarrow \pi N$
• • • We do not use the following data for averages, fits, limits, etc. • • •				
0.034±0.006	ANISOVICH	13B	DPWA	Multichannel
0.029±0.002	[1] SHRESTHA	12A	DPWA	Multichannel
0.028	DRECHSEL	07	DPWA	$\gamma N \rightarrow \pi N$

[1] Statistical error only.

$N(1680) \rightarrow n\gamma$, helicity-3/2 amplitude $A_{3/2}$

VALUE ($GeV^{-1/2}$)	DOCUMENT ID		TECN	COMMENT
−0.050 to −0.025 (≈ −0.035) OUR ESTIMATE				
−0.061±0.004	[1] HUNT	19	DPWA	Multichannel
−0.063±0.004	ANISOVICH	17E	DPWA	Multichannel
−0.029±0.002	[1] CHEN	12A	DPWA	$\gamma N \rightarrow \pi N$
• • • We do not use the following data for averages, fits, limits, etc. • • •				
−0.044±0.009	ANISOVICH	13B	DPWA	Multichannel
−0.059±0.002	[1] SHRESTHA	12A	DPWA	Multichannel
−0.038	DRECHSEL	07	DPWA	$\gamma N \rightarrow \pi N$

[1] Statistical error only.

$N(1680)$ REFERENCES

For early references, see Physics Letters **111B** 1 (1982). For very early references, see Reviews of Modern Physics **37** 633 (1965).

SARANTSEV	25	PR C112 015202	A.V. Sarantsev *et al.*	(Bonn-Gatchina Collab.)
SEIFEN	25	EPJ A61 173	T. Seifen *et al.*	(CBELSA/TAPS Collab.)
ROENCHEN	22	EPJ A58 229	D. Roenchen *et al.*	(JULI, GWU, BONN+)
MUELLER	20	PL B803 135323	J. Mueller *et al.*	(CBELSA/TAPS Collab.)
GOLOVATCH	19	PL B788 371	E. Golovatch *et al.*	(CLAS Collab.)
HUNT	19	PR C99 055205	B.C. Hunt, D.M. Manley	
ANISOVICH	17E	PR C96 055202	A.V. Anisovich *et al.*	(BONN, PNPI, JLAB+)
ROENCHEN	15A	EPJ A51 70	D. Roenchen *et al.*	
SOKHOYAN	15A	EPJ A51 95	V. Sokhoyan *et al.*	(CBELSA/TAPS Collab.)
PDG	14	CP C38 070001	K. Olive *et al.*	(PDG Collab.)
SVARC	14	PR C89 045205	A. Svarc *et al.*	(RBI Zagreb, UNI Tuzla)
ANISOVICH	13B	EPJ A49 67	A.V. Anisovich *et al.*	
SHKLYAR	13	PR C87 015201	V. Shklyar, H. Lenske, U. Mosel	(GIES)
ANISOVICH	12A	EPJ A48 15	A.V. Anisovich *et al.*	(BONN, PNPI)
CHEN	12A	PR C86 015206	W. Chen *et al.*	(DUKE, GWU, MSST, ITEP+)
SHRESTHA	12A	PR C86 055203	M. Shrestha, D.M. Manley	(KSU)
WORKMAN	12A	PR C86 015202	R. Workman *et al.*	(GWU)
BATINIC	10	PR C82 038203	M. Batinic *et al.*	(ZAGR)
THOMA	08	PL B659 87	U. Thoma *et al.*	(CB-ELSA Collab.)
DRECHSEL	07	EPJ A34 69	D. Drechsel, S.S. Kamalov, L. Tiator	(MAINZ, JINR)
DUGGER	07	PR C76 025211	M. Dugger *et al.*	(JLab CLAS Collab.)
ARNDT	06	PR C74 045205	R.A. Arndt *et al.*	(GWU)
VRANA	00	PRPL 328 181	T.P. Vrana, S.A. Dytman, T.-S.H. Lee	(PITT, ANL)
TIATOR	99	PR C60 035210	L. Tiator *et al.*	
HOEHLER	93	πN Newsletter 9 1	G. Hohler	(KARL)
CUTKOSKY	80	Toronto Conf. 19	R.E. Cutkosky *et al.*	(CMU, LBL) IJP
Also		PR D20 2839	R.E. Cutkosky *et al.*	(CMU, LBL) IJP
HOEHLER	79	PDAT 12-1	G. Hohler *et al.*	(KARLT) IJP
Also		Toronto Conf. 3	R. Koch	(KARLT) IJP

$N(1700)\ 3/2^-$

$I(J^P) = \frac{1}{2}(\frac{3}{2}^-)$ Status: ***

Older and obsolete values are listed and referenced in the 2014 edition, Chinese Physics **C38** 070001 (2014).

$N(1700)$ POLE POSITION

REAL PART

VALUE (MeV)	DOCUMENT ID		TECN	COMMENT
1650 to 1750 (≈ 1700) OUR ESTIMATE				
1745±40	SARANTSEV	25	DPWA	Multichannel
1757± 4±1	[1] SVARC	14	L+P	$\pi N \rightarrow \pi N$
1660±30	CUTKOSKY	80	IPWA	$\pi N \rightarrow \pi N$
• • • We do not use the following data for averages, fits, limits, etc. • • •				
1647	HUNT	19	DPWA	Multichannel
1780±35	SOKHOYAN	15A	DPWA	Multichannel
1806±23	BATINIC	10	DPWA	$\pi N \rightarrow N\pi,\ N\eta$
1704	VRANA	00	DPWA	Multichannel
1700	HOEHLER	93	SPED	$\pi N \rightarrow \pi N$

[1] Fit to the amplitudes of HOEHLER 79.

−2×IMAGINARY PART

VALUE (MeV)	DOCUMENT ID		TECN	COMMENT
100 to 300 (≈ 200) OUR ESTIMATE				
420± 50	SARANTSEV	25	DPWA	Multichannel
136± 7±4	[1] SVARC	14	L+P	$\pi N \rightarrow \pi N$
90± 40	CUTKOSKY	80	IPWA	$\pi N \rightarrow \pi N$
• • • We do not use the following data for averages, fits, limits, etc. • • •				
79	HUNT	19	DPWA	Multichannel
420±140	SOKHOYAN	15A	DPWA	Multichannel
129± 33	BATINIC	10	DPWA	$\pi N \rightarrow N\pi,\ N\eta$
156	VRANA	00	DPWA	Multichannel
120	HOEHLER	93	SPED	$\pi N \rightarrow \pi N$

[1] Fit to the amplitudes of HOEHLER 79.

$N(1700)$ ELASTIC POLE RESIDUE

MODULUS $|r|$

VALUE (MeV)	DOCUMENT ID		TECN	COMMENT
5 to 50 (≈ 10) OUR ESTIMATE				
60±30	SOKHOYAN	15A	DPWA	Multichannel
7± 1±1	[1] SVARC	14	L+P	$\pi N \rightarrow \pi N$
6± 3	CUTKOSKY	80	IPWA	$\pi N \rightarrow \pi N$
• • • We do not use the following data for averages, fits, limits, etc. • • •				
50±40	ANISOVICH	12A	DPWA	Multichannel
7	BATINIC	10	DPWA	$\pi N \rightarrow N\pi,\ N\eta$
5	HOEHLER	93	SPED	$\pi N \rightarrow \pi N$

[1] Fit to the amplitudes of HOEHLER 79.

PHASE θ

VALUE (°)	DOCUMENT ID		TECN	COMMENT
−120 to 0 (≈ −90) OUR ESTIMATE				
−115±30	SOKHOYAN	15A	DPWA	Multichannel
−113± 4±2	[1] SVARC	14	L+P	$\pi N \rightarrow \pi N$
0±50	CUTKOSKY	80	IPWA	$\pi N \rightarrow \pi N$
• • • We do not use the following data for averages, fits, limits, etc. • • •				
−100±40	ANISOVICH	12A	DPWA	Multichannel
− 34	BATINIC	10	DPWA	$\pi N \rightarrow N\pi,\ N\eta$

[1] Fit to the amplitudes of HOEHLER 79.

$N(1700)$ INELASTIC POLE RESIDUE

The "normalized residue" is the residue divided by $\Gamma_{pole}/2$.

Normalized residue in $N\pi \rightarrow N(1700) \rightarrow \Delta\pi$, S-wave

MODULUS	PHASE (°)	DOCUMENT ID		TECN	COMMENT
0.33±0.10	−70 ± 25	SOKHOYAN	15A	DPWA	Multichannel
• • • We do not use the following data for averages, fits, limits, etc. • • •					
0.34±0.21	−60 ± 40	ANISOVICH	12A	DPWA	Multichannel

Normalized residue in $N\pi \rightarrow N(1700) \rightarrow \Delta\pi$, D-wave

MODULUS	PHASE (°)	DOCUMENT ID		TECN	COMMENT
0.10±0.06	75 ± 30	SOKHOYAN	15A	DPWA	Multichannel
• • • We do not use the following data for averages, fits, limits, etc. • • •					
0.08±0.06	90 ± 35	ANISOVICH	12A	DPWA	Multichannel

Normalized residue in $N\pi \rightarrow N(1700) \rightarrow N\sigma$

MODULUS	PHASE (°)	DOCUMENT ID		TECN	COMMENT
0.13±0.08	−100 ± 35	SOKHOYAN	15A	DPWA	Multichannel

Normalized residue in $N\pi \rightarrow N(1700) \rightarrow N(1440)\pi$

MODULUS	PHASE (°)	DOCUMENT ID		TECN	COMMENT
0.13±0.05	40 ± 35	SOKHOYAN	15A	DPWA	Multichannel

Normalized residue in $N\pi \rightarrow N(1700) \rightarrow N(1520)\pi$, P-wave

MODULUS	PHASE (°)	DOCUMENT ID		TECN	COMMENT
0.07±0.03	160 ± 45	SOKHOYAN	15A	DPWA	Multichannel

$N(1700)$ BREIT-WIGNER MASS

VALUE (MeV)	DOCUMENT ID		TECN	COMMENT
1650 to 1800 (≈ 1720) OUR ESTIMATE				
1770±30	SARANTSEV	25	DPWA	Multichannel
1653± 5	[1] HUNT	19	DPWA	Multichannel
1675±25	CUTKOSKY	80	IPWA	$\pi N \rightarrow \pi N$
1731±15	HOEHLER	79	IPWA	$\pi N \rightarrow \pi N$
• • • We do not use the following data for averages, fits, limits, etc. • • •				
1800±35	SOKHOYAN	15A	DPWA	Multichannel
1665± 3	[1] SHRESTHA	12A	DPWA	Multichannel
1817±22	BATINIC	10	DPWA	$\pi N \rightarrow N\pi,\ N\eta$
1736±33	VRANA	00	DPWA	Multichannel

[1] Statistical error only.

$N(1700)$ BREIT-WIGNER WIDTH

VALUE (MeV)	DOCUMENT ID		TECN	COMMENT
100 to 300 (≈ 200) OUR ESTIMATE				
400± 50	SARANTSEV	25	DPWA	Multichannel
81± 13	[1] HUNT	19	DPWA	Multichannel
90± 40	CUTKOSKY	80	IPWA	$\pi N \rightarrow \pi N$
110± 30	HOEHLER	79	IPWA	$\pi N \rightarrow \pi N$
• • • We do not use the following data for averages, fits, limits, etc. • • •				
400±100	SOKHOYAN	15A	DPWA	Multichannel
56± 8	[1] SHRESTHA	12A	DPWA	Multichannel
134± 37	BATINIC	10	DPWA	$\pi N \rightarrow N\pi,\ N\eta$
175±133	VRANA	00	DPWA	Multichannel

[1] Statistical error only.

Int. J. Mod. Phys. A 2026.41. Downloaded from www.worldscientific.com
by UNIVERSITY OF CALIFORNIA @ BERKELEY on 09/16/26. Re-use and distribution is strictly not permitted, except for Open Access articles.

N(1700) DECAY MODES

The following branching fractions are our estimates, not fits or averages.

	Mode	Fraction (Γ_i/Γ)
Γ_1	$N\pi$	7–17 %
Γ_2	$N\eta$	1–2 %
Γ_3	$N\omega$	10–34 %
Γ_4	ΛK	1–2 %
Γ_5	$N\pi\pi$	>89 %
Γ_6	$\Delta(1232)\pi$	55–85 %
Γ_7	$\Delta(1232)\pi$, S-wave	50–80 %
Γ_8	$\Delta(1232)\pi$, D-wave	4–14 %
Γ_9	$N\rho$	(21 ±9) %
Γ_{10}	$N\rho$, $S=1/2$	(5.0±3.0) %
Γ_{11}	$N\rho$, $S=3/2$, S-wave	32–44 %
Γ_{12}	$N\rho$, $S=3/2$, D-wave	(16 ±8) %
Γ_{13}	$N\sigma$	2–14 %
Γ_{14}	$N(1440)\pi$	3–11 %
Γ_{15}	$N(1520)\pi$	<4 %
Γ_{16}	$N(1535)\pi$	< 1 %
Γ_{17}	$p\gamma$	0.01–0.05 %
Γ_{18}	$p\gamma$, helicity=1/2	0.0–0.024 %
Γ_{19}	$p\gamma$, helicity=3/2	0.002–0.026 %
Γ_{20}	$n\gamma$	0.01–0.13 %
Γ_{21}	$n\gamma$, helicity=1/2	0.0–0.09 %
Γ_{22}	$n\gamma$, helicity=3/2	0.01–0.05 %

N(1700) BRANCHING RATIOS

$\Gamma(N\pi)/\Gamma_{total}$ — Γ_1/Γ

VALUE (%)	DOCUMENT ID		TECN	COMMENT
7 to 17 (≈ 12) OUR ESTIMATE				
20 ±8	SEIFEN	25	DPWA	Multichannel
3.7±0.1	[1] HUNT	19	DPWA	Multichannel
11 ±5	CUTKOSKY	80	IPWA	$\pi N \to \pi N$
8 ±3	HOEHLER	79	IPWA	$\pi N \to \pi N$
• • • We do not use the following data for averages, fits, limits, etc. • • •				
15 ±6	SOKHOYAN	15A	DPWA	Multichannel
2.8±0.5	[1] SHRESTHA	12A	DPWA	Multichannel
9 ±6	BATINIC	10	DPWA	$\pi N \to N\pi$, $N\eta$
4 ±2	VRANA	00	DPWA	Multichannel

[1] Statistical error only.

$\Gamma(N\eta)/\Gamma_{total}$ — Γ_2/Γ

VALUE (%)	DOCUMENT ID		TECN	COMMENT
1–2 % OUR ESTIMATE				
1 ±1	MUELLER	20	DPWA	Multichannel
1.1±0.6	[1] HUNT	19	DPWA	Multichannel
• • • We do not use the following data for averages, fits, limits, etc. • • •				
14 ±5	BATINIC	10	DPWA	$\pi N \to N\pi$, $N\eta$
10 ±5	THOMA	08	DPWA	Multichannel
0 ±1	VRANA	00	DPWA	Multichannel

[1] Statistical error only.

$\Gamma(N\omega)/\Gamma_{total}$ — Γ_3/Γ

VALUE (%)	DOCUMENT ID		TECN	COMMENT
22±12	DENISENKO	16	DPWA	Multichannel

$\Gamma(\Lambda K)/\Gamma_{total}$ — Γ_4/Γ

VALUE (%)	DOCUMENT ID		TECN	COMMENT
1–2 % OUR ESTIMATE				
1.3±0.7	[1] HUNT	19	DPWA	Multichannel

[1] Statistical error only.

$\Gamma(\Delta(1232)\pi)/\Gamma_{total}$ — Γ_6/Γ

VALUE (%)	DOCUMENT ID		TECN	COMMENT
58±8	SARANTSEV	25	DPWA	Multichannel

$\Gamma(\Delta(1232)\pi, S\text{-wave})/\Gamma_{total}$ — Γ_7/Γ

VALUE (%)	DOCUMENT ID		TECN	COMMENT
54± 8	SARANTSEV	25	DPWA	Multichannel
66±17	SEIFEN	25	DPWA	Multichannel
11± 8	[1] HUNT	19	DPWA	Multichannel
• • • We do not use the following data for averages, fits, limits, etc. • • •				
65±15	SOKHOYAN	15A	DPWA	Multichannel
31± 9	[1] SHRESTHA	12A	DPWA	Multichannel
11± 1	VRANA	00	DPWA	Multichannel

[1] Statistical error only.

$\Gamma(\Delta(1232)\pi, D\text{-wave})/\Gamma_{total}$ — Γ_8/Γ

VALUE (%)	DOCUMENT ID		TECN	COMMENT
4± 2	SARANTSEV	25	DPWA	Multichannel
7± 4	SEIFEN	25	DPWA	Multichannel
13± 5	[1] HUNT	19	DPWA	Multichannel
• • • We do not use the following data for averages, fits, limits, etc. • • •				
9± 5	SOKHOYAN	15A	DPWA	Multichannel
3± 2	[1] SHRESTHA	12A	DPWA	Multichannel
79±56	VRANA	00	DPWA	Multichannel

[1] Statistical error only.

$\Gamma(N\rho)/\Gamma_{total}$ — Γ_9/Γ

VALUE (%)	DOCUMENT ID		TECN	COMMENT
21±9	SARANTSEV	25	DPWA	Multichannel

$\Gamma(N\rho, S=1/2)/\Gamma_{total}$ — Γ_{10}/Γ

VALUE (%)	DOCUMENT ID		TECN	COMMENT
5±3	SARANTSEV	25	DPWA	Multichannel

$\Gamma(N\rho, S=3/2, S\text{-wave})/\Gamma_{total}$ — Γ_{11}/Γ

VALUE (%)	DOCUMENT ID		TECN	COMMENT
7.5±3.6	[1] HUNT	19	DPWA	Multichannel
• • • We do not use the following data for averages, fits, limits, etc. • • •				
38 ±6	[1] SHRESTHA	12A	DPWA	Multichannel
7 ±1	VRANA	00	DPWA	Multichannel

[1] Statistical error only.

$\Gamma(N\rho, S=3/2, D\text{-wave})/\Gamma_{total}$ — Γ_{12}/Γ

VALUE (%)	DOCUMENT ID		TECN	COMMENT
16±8	SARANTSEV	25	DPWA	Multichannel

$\Gamma(N\sigma)/\Gamma_{total}$ — Γ_{13}/Γ

VALUE (%)	DOCUMENT ID		TECN	COMMENT
2± 2	SARANTSEV	25	DPWA	Multichannel
6± 4	SEIFEN	25	DPWA	Multichannel
62± 9	[1] HUNT	19	DPWA	Multichannel
• • • We do not use the following data for averages, fits, limits, etc. • • •				
8± 6	SOKHOYAN	15A	DPWA	Multichannel
24± 6	[1] SHRESTHA	12A	DPWA	Multichannel
18±12	THOMA	08	DPWA	Multichannel
0± 1	VRANA	00	DPWA	Multichannel

[1] Statistical error only.

$\Gamma(N(1440)\pi)/\Gamma_{total}$ — Γ_{14}/Γ

VALUE (%)	DOCUMENT ID		TECN	COMMENT
9±5	SEIFEN	25	DPWA	Multichannel
• • • We do not use the following data for averages, fits, limits, etc. • • •				
7±4	SOKHOYAN	15A	DPWA	Multichannel

$\Gamma(N(1520)\pi)/\Gamma_{total}$ — Γ_{15}/Γ

VALUE (%)	DOCUMENT ID		TECN	COMMENT
<2	SEIFEN	25	DPWA	Multichannel
• • • We do not use the following data for averages, fits, limits, etc. • • •				
<4	SOKHOYAN	15A	DPWA	Multichannel

$\Gamma(N(1535)\pi)/\Gamma_{total}$ — Γ_{16}/Γ

VALUE (%)	DOCUMENT ID		TECN	COMMENT
<1	SEIFEN	25	DPWA	Multichannel

N(1700) PHOTON DECAY AMPLITUDES AT THE POLE

$N(1700) \to p\gamma$, helicity-1/2 amplitude $A_{1/2}$

MODULUS ($GeV^{-1/2}$)	PHASE (°)	DOCUMENT ID		TECN	COMMENT
0.035±0.014	−20 ± 35	SARANTSEV	25	DPWA	Multichannel
• • • We do not use the following data for averages, fits, limits, etc. • • •					
0.047±0.016	75 ± 30	SOKHOYAN	15A	DPWA	Multichannel

$N(1700) \to p\gamma$, helicity-3/2 amplitude $A_{3/2}$

MODULUS ($GeV^{-1/2}$)	PHASE (°)	DOCUMENT ID		TECN	COMMENT
−0.100±0.030	5 ± 20	SARANTSEV	25	DPWA	Multichannel
• • • We do not use the following data for averages, fits, limits, etc. • • •					
−0.041±0.014	0 ± 20	SOKHOYAN	15A	DPWA	Multichannel

N(1700) BREIT-WIGNER PHOTON DECAY AMPLITUDES

$N(1700) \to p\gamma$, helicity-1/2 amplitude $A_{1/2}$

VALUE ($GeV^{-1/2}$)	DOCUMENT ID		TECN	COMMENT
0.032±0.013	SARANTSEV	25	DPWA	Multichannel
0.032±0.005	[1] HUNT	19	DPWA	Multichannel
• • • We do not use the following data for averages, fits, limits, etc. • • •				
0.041±0.017	ANISOVICH	12A	DPWA	Multichannel
0.021±0.005	[1] SHRESTHA	12A	DPWA	Multichannel

[1] Statistical error only.

Int. J. Mod. Phys. A 2026.41. Downloaded from www.worldscientific.com
UNIVERSITY OF CALIFORNIA @ BERKELEY on 09/16/26. Re-use and distribution is strictly not permitted, except for Open Access articles.

$N(1700) \to p\gamma$, helicity-3/2 amplitude $A_{3/2}$

VALUE (GeV$^{-1/2}$)	DOCUMENT ID		TECN	COMMENT
-0.090 ± 0.025	SARANTSEV	25	DPWA	Multichannel
0.034 ± 0.006	[1] HUNT	19	DPWA	Multichannel
• • • We do not use the following data for averages, fits, limits, etc. • • •				
-0.037 ± 0.014	SOKHOYAN	15A	DPWA	Multichannel
0.050 ± 0.009	[1] SHRESTHA	12A	DPWA	Multichannel

[1] Statistical error only.

$N(1700) \to n\gamma$, helicity-1/2 amplitude $A_{1/2}$

VALUE (GeV$^{-1/2}$)	DOCUMENT ID		TECN	COMMENT
0.005 ± 0.011	[1] HUNT	19	DPWA	Multichannel
0.025 ± 0.010	ANISOVICH	13B	DPWA	Multichannel
• • • We do not use the following data for averages, fits, limits, etc. • • •				
-0.049 ± 0.008	[1] SHRESTHA	12A	DPWA	Multichannel

[1] Statistical error only.

$N(1700) \to n\gamma$, helicity-3/2 amplitude $A_{3/2}$

VALUE (GeV$^{-1/2}$)	DOCUMENT ID		TECN	COMMENT
-0.094 ± 0.017	[1] HUNT	19	DPWA	Multichannel
-0.032 ± 0.018	ANISOVICH	13B	DPWA	Multichannel
• • • We do not use the following data for averages, fits, limits, etc. • • •				
-0.092 ± 0.014	[1] SHRESTHA	12A	DPWA	Multichannel

[1] Statistical error only.

$N(1700)$ REFERENCES

For early references, see Physics Letters **111B** 1 (1982).

SARANTSEV	25	PR C112 015202	A.V. Sarantsev *et al.*	(Bonn-Gatchina Collab.)
SEIFEN	25	EPJ A61 173	T. Seifen *et al.*	(CBELSA/TAPS Collab.)
MUELLER	20	PL B803 135323	J. Mueller *et al.*	(CBELSA/TAPS Collab.)
HUNT	19	PR C99 055205	B.C. Hunt, D.M. Manley	
DENISENKO	16	PL B755 97	I. Denisenko *et al.*	
SOKHOYAN	15A	EPJ A51 95	V. Sokhoyan *et al.*	(CBELSA/TAPS Collab.)
PDG	14	CP C38 070001	K. Olive *et al.*	(PDG Collab.)
SVARC	14	PR C89 045205	A. Svarc *et al.*	(RBI Zagreb, UNI Tuzla)
ANISOVICH	13B	EPJ A49 67	A.V. Anisovich *et al.*	
ANISOVICH	12A	EPJ A48 15	A.V. Anisovich *et al.*	(BONN, PNPI)
SHRESTHA	12A	PR C86 055203	M. Shrestha, D.M. Manley	(KSU)
BATINIC	10	PR C82 038203	M. Batinic *et al.*	(ZAGR)
THOMA	08	PL B659 87	U. Thoma *et al.*	(CB-ELSA Collab.)
VRANA	00	PRPL 328 181	T.P. Vrana, S.A. Dytman, T.-S.H. Lee	(PITT, ANL)
HOEHLER	93	πN Newsletter 9 1	G. Hohler	(KARL)
CUTKOSKY	80	Toronto Conf. 19	R.E. Cutkosky *et al.*	(CMU, LBL) IJP
Also		PR D20 2839	R.E. Cutkosky *et al.*	(CMU, LBL) IJP
HOEHLER	79	PDAT 12-1	G. Hohler *et al.*	(KARL) IJP
Also		Toronto Conf. 3	R. Koch	(KARL) IJP

$N(1710)\ 1/2^+$

$I(J^P) = \frac{1}{2}(\frac{1}{2}^+)$ Status: ****

Older and obsolete values are listed and referenced in the 2014 edition, Chinese Physics **C38** 070001 (2014).

$N(1710)$ POLE POSITION

REAL PART

VALUE (MeV)	DOCUMENT ID		TECN	COMMENT
1650 to 1750 ($\approx$ 1700) OUR ESTIMATE				
1696 ± 10	SARANTSEV	25	DPWA	Multichannel
1605 ± 7	ROENCHEN	22	DPWA	Multichannel
1697 ± 23	[1] ANISOVICH	17A	L+P	$\gamma p, \pi^- p \to K\Lambda$
$1770 \pm 5 \pm 2$	[2] SVARC	14	L+P	$\pi N \to \pi N$
1690 ± 20	CUTKOSKY	80	IPWA	$\pi N \to \pi N$
• • • We do not use the following data for averages, fits, limits, etc. • • •				
1615	HUNT	19	DPWA	Multichannel
1651	ROENCHEN	15A	DPWA	Multichannel
1690 ± 15	SOKHOYAN	15A	DPWA	Multichannel
1690 ± 15	GUTZ	14	DPWA	Multichannel
1670	SHKLYAR	13	DPWA	Multichannel
1711 ± 15	[3] BATINIC	10	DPWA	$\pi N \to N\pi, N\eta$
1679	VRANA	00	DPWA	Multichannel
1690	HOEHLER	93	SPED	$\pi N \to \pi N$
1698	CUTKOSKY	90	IPWA	$\pi N \to \pi N$

[1] Statistical error only.
[2] Fit to the amplitudes of HOEHLER 79.
[3] BATINIC 10 finds evidence for a second P_{11} state with all parameters except for the phase of the pole residue very similar to the parameters we give here.

$-2\times$IMAGINARY PART

VALUE (MeV)	DOCUMENT ID		TECN	COMMENT
80 to 160 ($\approx$ 120) OUR ESTIMATE				
155 ± 15	SARANTSEV	25	DPWA	Multichannel
115 ± 5	ROENCHEN	22	DPWA	Multichannel
84 ± 34	[1] ANISOVICH	17A	L+P	$\gamma p, \pi^- p \to K\Lambda$
$98 \pm 8 \pm 5$	[2] SVARC	14	L+P	$\pi N \to \pi N$
80 ± 20	CUTKOSKY	80	IPWA	$\pi N \to \pi N$
• • • We do not use the following data for averages, fits, limits, etc. • • •				
169	HUNT	19	DPWA	Multichannel
155 ± 25	ANISOVICH	17A	DPWA	Multichannel
121	ROENCHEN	15A	DPWA	Multichannel
170 ± 20	SOKHOYAN	15A	DPWA	Multichannel
170 ± 20	GUTZ	14	DPWA	Multichannel
159	SHKLYAR	13	DPWA	Multichannel
174 ± 16	[3] BATINIC	10	DPWA	$\pi N \to N\pi, N\eta$
132	VRANA	00	DPWA	Multichannel
200	HOEHLER	93	SPED	$\pi N \to \pi N$
88	CUTKOSKY	90	IPWA	$\pi N \to \pi N$

[1] Statistical error only.
[2] Fit to the amplitudes of HOEHLER 79.
[3] BATINIC 10 finds evidence for a second P_{11} state with all parameters except for the phase of the pole residue very similar to the parameters we give here.

$N(1710)$ ELASTIC POLE RESIDUE

MODULUS $|r|$

VALUE (MeV)	DOCUMENT ID		TECN	COMMENT
4 to 10 ($\approx$ 7) OUR ESTIMATE				
5.5 ± 2.4	ROENCHEN	22	DPWA	Multichannel
6 ± 3	SOKHOYAN	15A	DPWA	Multichannel
$5 \pm 1 \pm 1$	[1] SVARC	14	L+P	$\pi N \to \pi N$
8 ± 2	CUTKOSKY	80	IPWA	$\pi N \to \pi N$
• • • We do not use the following data for averages, fits, limits, etc. • • •				
3.2	ROENCHEN	15A	DPWA	Multichannel
6 ± 3	GUTZ	14	DPWA	Multichannel
11	SHKLYAR	13	DPWA	Multichannel
6 ± 4	ANISOVICH	12A	DPWA	Multichannel
24	[2] BATINIC	10	DPWA	$\pi N \to N\pi, N\eta$
15	HOEHLER	93	SPED	$\pi N \to \pi N$
9	CUTKOSKY	90	IPWA	$\pi N \to \pi N$

[1] Fit to the amplitudes of HOEHLER 79.
[2] BATINIC 10 finds evidence for a second P_{11} state with all parameters except for the phase of the pole residue very similar to the parameters we give here.

PHASE θ

VALUE (°)	DOCUMENT ID		TECN	COMMENT
120 to 270 ($\approx$ 190) OUR ESTIMATE				
-114 ± 29	ROENCHEN	22	DPWA	Multichannel
130 ± 35	SOKHOYAN	15A	DPWA	Multichannel
$-104 \pm 7 \pm 3$	[1] SVARC	14	L+P	$\pi N \to \pi N$
175 ± 35	CUTKOSKY	80	IPWA	$\pi N \to \pi N$
• • • We do not use the following data for averages, fits, limits, etc. • • •				
55	ROENCHEN	15A	DPWA	Multichannel
120 ± 45	GUTZ	14	DPWA	Multichannel
9	SHKLYAR	13	DPWA	Multichannel
120 ± 70	ANISOVICH	12A	DPWA	Multichannel
20	[2] BATINIC	10	DPWA	$\pi N \to N\pi, N\eta$
-167	CUTKOSKY	90	IPWA	$\pi N \to \pi N$

[1] Fit to the amplitudes of HOEHLER 79.
[2] BATINIC 10 finds evidence for a second P_{11} state with all parameters except for the phase of the pole residue very similar to the parameters we give here.

$N(1710)$ INELASTIC POLE RESIDUE

The "normalized residue" is the residue divided by $\Gamma_{pole}/2$.

Normalized residue in $N\pi \to N(1710) \to N\eta$

MODULUS	PHASE (°)	DOCUMENT ID		TECN	COMMENT
0.28 ± 0.13	91 ± 32	ROENCHEN	22	DPWA	Multichannel
0.12 ± 0.04	0 ± 45	ANISOVICH	12A	DPWA	Multichannel
• • • We do not use the following data for averages, fits, limits, etc. • • •					
0.16	-180	ROENCHEN	15A	DPWA	Multichannel

Normalized residue in $N\pi \to N(1710) \to \Lambda K$

MODULUS	PHASE (°)	DOCUMENT ID		TECN	COMMENT
0.20 ± 0.10	-144 ± 39	ROENCHEN	22	DPWA	Multichannel
0.16 ± 0.05	-160 ± 25	ANISOVICH	17A	DPWA	Multichannel
$0.12^{+0.24}_{-0.12}$	-119 ± 83	[1] ANISOVICH	17A	L+P	$\gamma p, \pi^- p \to K\Lambda$
• • • We do not use the following data for averages, fits, limits, etc. • • •					
0.12	-32	ROENCHEN	15A	DPWA	Multichannel
0.17 ± 0.06	-110 ± 20	ANISOVICH	12A	DPWA	Multichannel

[1] Statistical error only.

Normalized residue in $N\pi \to N(1710) \to \Sigma K$

MODULUS	PHASE (°)	DOCUMENT ID		TECN	COMMENT
0.055 ± 0.024	162 ± 153	ROENCHEN	22	DPWA	Multichannel
• • • We do not use the following data for averages, fits, limits, etc. • • •					
0.004	-43	ROENCHEN	15A	DPWA	Multichannel

Normalized residue in $N\pi \to N(1710) \to N(1535)\pi$

MODULUS	PHASE (°)	DOCUMENT ID		TECN	COMMENT
0.10 ± 0.04	140 ± 40	GUTZ	14	DPWA	Multichannel

Int. J. Mod. Phys. A 2026.41. Downloaded from www.worldscientific.com
by UNIVERSITY OF CALIFORNIA @ BERKELEY on 09/16/26. Re-use and distribution is strictly not permitted, except for Open Access articles.

$N(1710)$ BREIT-WIGNER MASS

VALUE (MeV)	DOCUMENT ID		TECN	COMMENT
1680 to 1740 (≈ 1710) OUR ESTIMATE				
1710 ± 8	SARANTSEV	25	DPWA	Multichannel
1648 ± 16	[1] HUNT	19	DPWA	Multichannel
1737 ± 17	[1] SHKLYAR	13	DPWA	Multichannel
1700 ± 50	CUTKOSKY	80	IPWA	$\pi N \to \pi N$
1723 ± 9	HOEHLER	79	IPWA	$\pi N \to \pi N$
• • • We do not use the following data for averages, fits, limits, etc. • • •				
1715 ± 20	SOKHOYAN	15A	DPWA	Multichannel
1715 ± 20	GUTZ	14	DPWA	Multichannel
1662 ± 7	[1] SHRESTHA	12A	DPWA	Multichannel
1729 ± 16	[2] BATINIC	10	DPWA	$\pi N \to N\pi$, $N\eta$
1752 ± 3	PENNER	02C	DPWA	Multichannel
1699 ± 65	VRANA	00	DPWA	Multichannel

[1] Statistical error only.
[2] BATINIC 10 finds evidence for a second P_{11} state with all parameters except for the phase of the pole residue very similar to the parameters we give here.

$N(1710)$ BREIT-WIGNER WIDTH

VALUE (MeV)	DOCUMENT ID		TECN	COMMENT
80 to 200 (≈ 140) OUR ESTIMATE				
155 ± 14	SARANTSEV	25	DPWA	Multichannel
195 ± 46	[1] HUNT	19	DPWA	Multichannel
368 ± 120	[1] SHKLYAR	13	DPWA	Multichannel
93 ± 30	CUTKOSKY	90	IPWA	$\pi N \to \pi N$
90 ± 30	CUTKOSKY	80	IPWA	$\pi N \to \pi N$
120 ± 15	HOEHLER	79	IPWA	$\pi N \to \pi N$
• • • We do not use the following data for averages, fits, limits, etc. • • •				
175 ± 15	SOKHOYAN	15A	DPWA	Multichannel
175 ± 15	GUTZ	14	DPWA	Multichannel
116 ± 17	[1] SHRESTHA	12A	DPWA	Multichannel
180 ± 17	[2] BATINIC	10	DPWA	$\pi N \to N\pi$, $N\eta$
386 ± 59	PENNER	02C	DPWA	Multichannel
143 ± 100	VRANA	00	DPWA	Multichannel

[1] Statistical error only.
[2] BATINIC 10 finds evidence for a second P_{11} state with all parameters except for the phase of the pole residue very similar to the parameters we give here.

$N(1710)$ DECAY MODES

The following branching fractions are our estimates, not fits or averages.

	Mode	Fraction (Γ_i/Γ)
Γ_1	$N\pi$	5–20 %
Γ_2	$N\eta$	10–50 %
Γ_3	$N\omega$	1–5 %
Γ_4	ΛK	5–25 %
Γ_5	ΣK	seen
Γ_6	$N\pi\pi$	14–48 %
Γ_7	$\Delta(1232)\pi$	3–9 %
Γ_8	$N\rho$	(17 ± 4) %
Γ_9	$N\rho$, $S=1/2$	11–23 %
Γ_{10}	$N\rho$, $S=3/2$	(11.0 ± 3.0) %
Γ_{11}	$N\sigma$	<16 %
Γ_{12}	$N(1440)\pi$	(22 ± 12) %
Γ_{13}	$N(1520)\pi$	< 2 %
Γ_{14}	$N(1535)\pi$	9–21 %
Γ_{15}	$p\gamma$, helicity=1/2	0.002–0.08 %
Γ_{16}	$n\gamma$, helicity=1/2	0.0–0.02%

$N(1710)$ BRANCHING RATIOS

$\Gamma(N\pi)/\Gamma_{total}$ — Γ_1/Γ

VALUE (%)	DOCUMENT ID		TECN	COMMENT
5 to 20 (≈ 10) OUR ESTIMATE				
5 ± 3	SEIFEN	25	DPWA	Multichannel
12 ± 6	[1] HUNT	19	DPWA	Multichannel
2 ± 2	[1] SHKLYAR	13	PWA	Multichannel
20 ± 4	CUTKOSKY	80	IPWA	$\pi N \to \pi N$
12 ± 4	HOEHLER	79	IPWA	$\pi N \to \pi N$
• • • We do not use the following data for averages, fits, limits, etc. • • •				
5 ± 3	SOKHOYAN	15A	DPWA	Multichannel
5 ± 3	GUTZ	14	DPWA	Multichannel
15 ± 4	[1] SHRESTHA	12A	DPWA	Multichannel
22 ± 24	[2] BATINIC	10	DPWA	$\pi N \to N\pi$, $N\eta$
14 ± 8	PENNER	02C	DPWA	Multichannel
27 ± 13	VRANA	00	DPWA	Multichannel

[1] Statistical error only.
[2] BATINIC 10 finds evidence for a second P_{11} state with all parameters except for the phase of the pole residue very similar to the parameters we give here.

$\Gamma(N\eta)/\Gamma_{total}$ — Γ_2/Γ

VALUE (%)	DOCUMENT ID		TECN	COMMENT
10 to 50 (≈ 30) OUR ESTIMATE				
18 ± 10	MUELLER	20	DPWA	Multichannel
17 ± 8	[1] HUNT	19	DPWA	Multichannel
45 ± 4	[1] SHKLYAR	13	DPWA	Multichannel
17 ± 10	ANISOVICH	12A	DPWA	Multichannel
• • • We do not use the following data for averages, fits, limits, etc. • • •				
11 ± 7	[1] SHRESTHA	12A	DPWA	Multichannel
6 ± 8	[2] BATINIC	10	DPWA	$\pi N \to N\pi$, $N\eta$
36 ± 11	PENNER	02C	DPWA	Multichannel
6 ± 1	VRANA	00	DPWA	Multichannel

[1] Statistical error only.
[2] BATINIC 10 finds evidence for a second P_{11} state with all parameters except for the phase of the pole residue very similar to the parameters we give here.

$\Gamma(N\omega)/\Gamma_{total}$ — Γ_3/Γ

VALUE (%)	DOCUMENT ID		TECN	COMMENT
1 to 5 (≈ 3) OUR ESTIMATE				
2 ± 2	DENISENKO	16	DPWA	Multichannel
3 ± 2	[1] SHKLYAR	13	DPWA	Multichannel
• • • We do not use the following data for averages, fits, limits, etc. • • •				
13 ± 2	PENNER	02C	DPWA	Multichannel

[1] Statistical error only.

$\Gamma(\Lambda K)/\Gamma_{total}$ — Γ_4/Γ

VALUE (%)	DOCUMENT ID		TECN	COMMENT
5 to 25 (≈ 15) OUR ESTIMATE				
1.8 ± 1.5	[1] HUNT	19	DPWA	Multichannel
23 ± 7	ANISOVICH	12A	DPWA	Multichannel
5 ± 3	SHKLYAR	05	DPWA	Multichannel
• • • We do not use the following data for averages, fits, limits, etc. • • •				
8 ± 4	[1] SHRESTHA	12A	DPWA	Multichannel
5 ± 2	PENNER	02C	DPWA	Multichannel
10 ± 10	VRANA	00	DPWA	Multichannel

[1] Statistical error only.

$\Gamma(\Sigma K)/\Gamma_{total}$ — Γ_5/Γ

VALUE (%)	DOCUMENT ID		TECN	COMMENT
• • • We do not use the following data for averages, fits, limits, etc. • • •				
7 ± 7	PENNER	02C	DPWA	Multichannel

$\Gamma(\Delta(1232)\pi)/\Gamma_{total}$ — Γ_7/Γ

VALUE (%)	DOCUMENT ID		TECN	COMMENT
3–9 % OUR ESTIMATE				
7 ± 4	SARANTSEV	25	DPWA	Multichannel
6 ± 4	SEIFEN	25	DPWA	Multichannel
28 ± 9	[1] HUNT	19	DPWA	Multichannel
• • • We do not use the following data for averages, fits, limits, etc. • • •				
6 ± 3	[1] SHRESTHA	12A	DPWA	Multichannel
39 ± 8	VRANA	00	DPWA	Multichannel

[1] Statistical error only.

$\Gamma(N\rho)/\Gamma_{total}$ — Γ_8/Γ

VALUE (%)	DOCUMENT ID		TECN	COMMENT
17 ± 4	SARANTSEV	25	DPWA	Multichannel

$\Gamma(N\rho, S=1/2)/\Gamma_{total}$ — Γ_9/Γ

VALUE (%)	DOCUMENT ID		TECN	COMMENT
11–23 % OUR ESTIMATE				
6 ± 2	SARANTSEV	25	DPWA	Multichannel
17 ± 9	[1] HUNT	19	DPWA	Multichannel
• • • We do not use the following data for averages, fits, limits, etc. • • •				
17 ± 6	[1] SHRESTHA	12A	DPWA	Multichannel
17 ± 1	VRANA	00	DPWA	Multichannel

[1] Statistical error only.

$\Gamma(N\rho, S=3/2)/\Gamma_{total}$ — Γ_{10}/Γ

VALUE (%)	DOCUMENT ID		TECN	COMMENT
11 ± 3	SARANTSEV	25	DPWA	Multichannel

$\Gamma(N\sigma)/\Gamma_{total}$ — Γ_{11}/Γ

VALUE (%)	DOCUMENT ID		TECN	COMMENT
<16 % OUR ESTIMATE				
11 ± 4	SARANTSEV	25	DPWA	Multichannel
14 ± 6	SEIFEN	25	DPWA	Multichannel
<16	[1] HUNT	19	DPWA	Multichannel

[1] Statistical error only.

$\Gamma(N(1440)\pi)/\Gamma_{total}$ — Γ_{12}/Γ

VALUE (%)	DOCUMENT ID		TECN	COMMENT
22 ± 12	SEIFEN	25	DPWA	Multichannel

Int. J. Mod. Phys. A 2026.41. Downloaded from www.worldscientific.com
UNIVERSITY OF CALIFORNIA @ BERKELEY on 09/16/26. Re-use and distribution is strictly not permitted, except for Open Access articles.

$\Gamma(N(1520)\pi)/\Gamma_{total}$ — Γ_{13}/Γ

VALUE (%)	DOCUMENT ID		TECN	COMMENT
<2	SEIFEN	25	DPWA	Multichannel

$\Gamma(N(1535)\pi)/\Gamma_{total}$ — Γ_{14}/Γ

VALUE (%)	DOCUMENT ID		TECN	COMMENT
4±4	SEIFEN	25	DPWA	Multichannel
15±6	GUTZ	14	DPWA	Multichannel

$N(1710)$ PHOTON DECAY AMPLITUDES AT THE POLE

$N(1710) \to p\gamma$, helicity-1/2 amplitude $A_{1/2}$

MODULUS ($GeV^{-1/2}$)	PHASE (°)	DOCUMENT ID		TECN	COMMENT
0.045±0.012	−30 ± 20	SARANTSEV	25	DPWA	Multichannel
−0.018±0.010	40 ± 55	ROENCHEN	22	DPWA	Multichannel
• • • We do not use the following data for averages, fits, limits, etc. • • •					
0.020	−83	ROENCHEN	15A	DPWA	Multichannel

$N(1710) \to n\gamma$, helicity-1/2 amplitude $A_{1/2}$

MODULUS ($GeV^{-1/2}$)	PHASE (°)	DOCUMENT ID		TECN	COMMENT
0.029±0.007	80 ± 20	ANISOVICH	17E	DPWA	Multichannel

$N(1710)$ BREIT-WIGNER PHOTON DECAY AMPLITUDES

$N(1710) \to p\gamma$, helicity-1/2 amplitude $A_{1/2}$

VALUE ($GeV^{-1/2}$)	DOCUMENT ID		TECN	COMMENT
0.049±0.008	SARANTSEV	25	DPWA	Multichannel
0.014±0.008	[1] HUNT	19	DPWA	Multichannel
−0.050±0.001	[1] SHKLYAR	13	DPWA	Multichannel
• • • We do not use the following data for averages, fits, limits, etc. • • •				
0.050±0.010	SOKHOYAN	15A	DPWA	Multichannel
0.05 ±0.01	GUTZ	14	DPWA	Multichannel
−0.008±0.003	[1] SHRESTHA	12A	DPWA	Multichannel
0.044	PENNER	02D	DPWA	Multichannel

[1] Statistical error only.

$N(1710) \to n\gamma$, helicity-1/2 amplitude $A_{1/2}$

VALUE ($GeV^{-1/2}$)	DOCUMENT ID		TECN	COMMENT
0.0053±0.0003	[1] HUNT	19	DPWA	Multichannel
−0.040 ±0.020	ANISOVICH	13B	DPWA	Multichannel
• • • We do not use the following data for averages, fits, limits, etc. • • •				
0.017 ±0.003	[1] SHRESTHA	12A	DPWA	Multichannel
−0.024	PENNER	02D	DPWA	Multichannel

[1] Statistical error only.

$N(1710)$ REFERENCES

For early references, see Physics Letters **111B** 1 (1982).

SARANTSEV	25	PR C112 015202	A.V. Sarantsev *et al.*	(Bonn-Gatchina Collab.)
SEIFEN	25	EPJ A61 173	T. Seifen *et al.*	(CBELSA/TAPS Collab.)
ROENCHEN	22	EPJ A58 229	D. Roenchen *et al.*	(JULI, GWU, BONN+)
MUELLER	20	PL B803 135323	J. Mueller *et al.*	(CBELSA/TAPS Collab.)
HUNT	19	PR C99 055205	B.C. Hunt, D.M. Manley	
ANISOVICH	17A	PRL 119 062004	A.V. Anisovich *et al.*	
ANISOVICH	17E	PR C96 055202	A.V. Anisovich *et al.*	(BONN, PNPI, JLAB+)
DENISENKO	16	PL B755 97	I. Denisenko *et al.*	
ROENCHEN	15A	EPJ A51 70	D. Roenchen *et al.*	
SOKHOYAN	15A	EPJ A51 95	V. Sokhoyan *et al.*	(CBELSA/TAPS Collab.)
GUTZ	14	EPJ A50 74	E. Gutz *et al.*	(CBELSA/TAPS Collab.)
PDG	14	CP C38 070001	K. Olive *et al.*	(PDG Collab.)
SVARC	14	PR C89 045205	A. Svarc *et al.*	(RBI Zagreb, UNI Tuzla)
ANISOVICH	13B	EPJ A49 67	A.V. Anisovich *et al.*	
SHKLYAR	13	PR C87 015201	V. Shklyar, H. Lenske, U. Mosel	(GIES)
ANISOVICH	12A	EPJ A48 15	A.V. Anisovich *et al.*	(BONN, PNPI)
SHRESTHA	12A	PR C86 055203	M. Shrestha, D.M. Manley	(KSU)
BATINIC	10	PR C82 038203	M. Batinic *et al.*	(ZAGR)
SHKLYAR	05	PR C72 015210	V. Shklyar, H. Lenske, U. Mosel	(GIES)
PENNER	02C	PR C66 055211	G. Penner, U. Mosel	(GIES)
PENNER	02D	PR C66 055212	G. Penner, U. Mosel	(GIES)
VRANA	00	PRPL 328 181	T.P. Vrana, S.A. Dytman, T.-S.H. Lee	(PITT, ANL)
HOEHLER	93	πN Newsletter 9 1	G. Hohler	(KARL)
CUTKOSKY	90	PR D42 235	R.E. Cutkosky, S. Wang	(CMU)
CUTKOSKY	80	Toronto Conf. 19	R.E. Cutkosky *et al.*	(CMU, LBL) IJP
Also		PR D20 2839	R.E. Cutkosky *et al.*	(CMU, LBL) IJP
HOEHLER	79	PDAT 12-1	G. Hohler *et al.*	(KARLT) IJP
Also		Toronto Conf. 3	R. Koch	(KARLT) IJP

$N(1720)\ 3/2^+$

$I(J^P) = \frac{1}{2}(\frac{3}{2}^+)$ Status: ****

Older and obsolete values are listed and referenced in the 2014 edition, Chinese Physics **C38** 070001 (2014).

$N(1720)$ POLE POSITION

REAL PART

VALUE (MeV)	DOCUMENT ID		TECN	COMMENT
1660 to 1710 (≈ 1680) OUR ESTIMATE				
1710±20	SARANTSEV	25	DPWA	Multichannel
1726± 4	ROENCHEN	22	DPWA	Multichannel
1677± 4±1	[1] SVARC	14	L+P	$\pi N \to \pi N$
1680±30	CUTKOSKY	80	IPWA	$\pi N \to \pi N$
• • • We do not use the following data for averages, fits, limits, etc. • • •				
1654	HUNT	19	DPWA	Multichannel
1710	ROENCHEN	15A	DPWA	Multichannel
1670±25	SOKHOYAN	15A	DPWA	Multichannel
1670	SHKLYAR	13	DPWA	Multichannel
1691±23	BATINIC	10	DPWA	$\pi N \to N\pi, N\eta$
1666	ARNDT	06	DPWA	$\pi N \to \pi N, \eta N$
1692	VRANA	00	DPWA	Multichannel
1686	HOEHLER	93	SPED	$\pi N \to \pi N$

[1] Fit to the amplitudes of HOEHLER 79.

−2×IMAGINARY PART

VALUE (MeV)	DOCUMENT ID		TECN	COMMENT
150 to 300 (≈ 200) OUR ESTIMATE				
180± 30	SARANTSEV	25	DPWA	Multichannel
185± 6	ROENCHEN	22	DPWA	Multichannel
184± 8±1	[1] SVARC	14	L+P	$\pi N \to \pi N$
120± 40	CUTKOSKY	80	IPWA	$\pi N \to \pi N$
• • • We do not use the following data for averages, fits, limits, etc. • • •				
100	HUNT	19	DPWA	Multichannel
219	ROENCHEN	15A	DPWA	Multichannel
430±100	SOKHOYAN	15A	DPWA	Multichannel
118	SHKLYAR	13	DPWA	Multichannel
233± 23	BATINIC	10	DPWA	$\pi N \to N\pi, N\eta$
355	ARNDT	06	DPWA	$\pi N \to \pi N, \eta N$
94	VRANA	00	DPWA	Multichannel
187	HOEHLER	93	SPED	$\pi N \to \pi N$

[1] Fit to the amplitudes of HOEHLER 79.

$N(1720)$ ELASTIC POLE RESIDUE

MODULUS $|r|$

VALUE (MeV)	DOCUMENT ID		TECN	COMMENT
10 to 25 (≈ 15) OUR ESTIMATE				
15 ± 1	ROENCHEN	22	DPWA	Multichannel
26 ±10	SOKHOYAN	15A	DPWA	Multichannel
13 ± 1	[1] SVARC	14	L+P	$\pi N \to \pi N$
8 ± 2	CUTKOSKY	80	IPWA	$\pi N \to \pi N$
• • • We do not use the following data for averages, fits, limits, etc. • • •				
4.2	ROENCHEN	15A	DPWA	Multichannel
12	SHKLYAR	13	DPWA	Multichannel
22 ± 8	ANISOVICH	12A	DPWA	Multichannel
20	BATINIC	10	DPWA	$\pi N \to N\pi, N\eta$
25	ARNDT	06	DPWA	$\pi N \to \pi N, \eta N$
15	HOEHLER	93	SPED	$\pi N \to \pi N$

[1] Fit to the amplitudes of HOEHLER 79.

PHASE θ

VALUE (°)	DOCUMENT ID		TECN	COMMENT
−160 to −60 (≈ − 110) OUR ESTIMATE				
− 60± 3	ROENCHEN	22	DPWA	Multichannel
−100±25	SOKHOYAN	15A	DPWA	Multichannel
−115± 3±2	[1] SVARC	14	L+P	$\pi N \to \pi N$
−160±30	CUTKOSKY	80	IPWA	$\pi N \to \pi N$
• • • We do not use the following data for averages, fits, limits, etc. • • •				
− 47	ROENCHEN	15A	DPWA	Multichannel
− 45	SHKLYAR	13	DPWA	Multichannel
−115±30	ANISOVICH	12A	DPWA	Multichannel
−109	BATINIC	10	DPWA	$\pi N \to N\pi, N\eta$
− 94	ARNDT	06	DPWA	$\pi N \to \pi N, \eta N$

[1] Fit to the amplitudes of HOEHLER 79.

$N(1720)$ INELASTIC POLE RESIDUE

The "normalized residue" is the residue divided by $\Gamma_{pole}/2$.

Normalized residue in $N\pi \to N(1720) \to N\eta$

MODULUS	PHASE (°)	DOCUMENT ID		TECN	COMMENT
0.049±0.005	64 ± 5	ROENCHEN	22	DPWA	Multichannel
0.03 ±0.02		ANISOVICH	12A	DPWA	Multichannel
• • • We do not use the following data for averages, fits, limits, etc. • • •					
0.007	106	ROENCHEN	15A	DPWA	Multichannel

Normalized residue in $N\pi \to N(1720) \to \Lambda K$

MODULUS	PHASE (°)	DOCUMENT ID		TECN	COMMENT
0.034±0.002	−101 ± 4	ROENCHEN	22	DPWA	Multichannel
0.06 ±0.04	−150 ± 45	ANISOVICH	12A	DPWA	Multichannel
• • • We do not use the following data for averages, fits, limits, etc. • • •					
0.011	−70	ROENCHEN	15A	DPWA	Multichannel

Normalized residue in $N\pi \to N(1720) \to \Sigma K$

MODULUS	PHASE (°)	DOCUMENT ID		TECN	COMMENT
0.059±0.005	**82 ± 3**	ROENCHEN	22	DPWA	Multichannel

Int. J. Mod. Phys. A 2026.41. Downloaded from www.worldscientific.com
by UNIVERSITY OF CALIFORNIA @ BERKELEY on 09/16/26. Re-use and distribution is strictly not permitted, except for Open Access articles.

• • • We do not use the following data for averages, fits, limits, etc. • • •

0.002	79	ROENCHEN	15A	DPWA	Multichannel

Normalized residue in $N\pi \to N(1720) \to \Delta\pi$, P-wave

MODULUS	PHASE (°)	DOCUMENT ID		TECN	COMMENT
0.28±0.09	95 ± 30	SOKHOYAN	15A	DPWA	Multichannel
• • • We do not use the following data for averages, fits, limits, etc. • • •					
0.29±0.08	80 ± 40	ANISOVICH	12A	DPWA	Multichannel

Normalized residue in $N\pi \to N(1720) \to \Delta\pi$, F-wave

MODULUS	PHASE (°)	DOCUMENT ID		TECN	COMMENT
0.07±0.05		SOKHOYAN	15A	DPWA	Multichannel
• • • We do not use the following data for averages, fits, limits, etc. • • •					
0.03±0.03		ANISOVICH	12A	DPWA	Multichannel

Normalized residue in $N\pi \to N(1720) \to N\sigma$

MODULUS	PHASE (°)	DOCUMENT ID		TECN	COMMENT
0.08±0.04	−110 ± 35	SOKHOYAN	15A	DPWA	Multichannel

Normalized residue in $N\pi \to N(1720) \to N(1520)\pi$, S-wave

MODULUS	PHASE (°)	DOCUMENT ID		TECN	COMMENT
0.05±0.04	undefined	SOKHOYAN	15A	DPWA	Multichannel

N(1720) BREIT-WIGNER MASS

VALUE (MeV)	DOCUMENT ID		TECN	COMMENT
1680 to 1750 (≈ 1720) OUR ESTIMATE				
1716 ± 18	SARANTSEV	25	DPWA	Multichannel
1745 ± 6	GOLOVATCH	19	DPWA	$\gamma p \to \pi^+\pi^- p$
1711 ± 4	[1] HUNT	19	DPWA	Multichannel
1700 ± 10	[1] SHKLYAR	13	DPWA	Multichannel
1763.8± 4.6	ARNDT	06	DPWA	$\pi N \to \pi N, \eta N$
1700 ± 50	CUTKOSKY	80	IPWA	$\pi N \to \pi N$
1710 ± 20	HOEHLER	79	IPWA	$\pi N \to \pi N$
• • • We do not use the following data for averages, fits, limits, etc. • • •				
1748 ± 5	[2] MOKEEV	20	DPWA	$\gamma p \to \pi^+\pi^- p$
1725 ± 10	[3] MOKEEV	20	DPWA	$\gamma p \to \pi^+\pi^- p$
1690 ± 30	SOKHOYAN	15A	DPWA	Multichannel
1720 ± 5	[1] SHRESTHA	12A	DPWA	Multichannel
1720 ± 18	BATINIC	10	DPWA	$\pi N \to N\pi, N\eta$
1705 ± 10	PENNER	02C	DPWA	Multichannel
1716 ±112	VRANA	00	DPWA	Multichannel

[1] Statistical error only.
[2] State a) of two states seen by the CLAS collaboration.
[3] State b) of two states seen by the CLAS collaboration.

N(1720) BREIT-WIGNER WIDTH

VALUE (MeV)	DOCUMENT ID		TECN	COMMENT
150 to 400 (≈ 250) OUR ESTIMATE				
180±25	SARANTSEV	25	DPWA	Multichannel
116±27	GOLOVATCH	19	DPWA	$\gamma p \to \pi^+\pi^- p$
229±22	[1] HUNT	19	DPWA	Multichannel
152± 2	[1] SHKLYAR	13	DPWA	Multichannel
210±22	ARNDT	06	DPWA	$\pi N \to \pi N, \eta N$
125±70	CUTKOSKY	80	IPWA	$\pi N \to \pi N$
190±30	HOEHLER	79	IPWA	$\pi N \to \pi N$
• • • We do not use the following data for averages, fits, limits, etc. • • •				
114± 6	[2] MOKEEV	20	DPWA	$\gamma p \to \pi^+\pi^- p$
120± 6	[3] MOKEEV	20	DPWA	$\gamma p \to \pi^+\pi^- p$
420±80	SOKHOYAN	15A	DPWA	Multichannel
200±20	[1] SHRESTHA	12A	DPWA	Multichannel
244±28	BATINIC	10	DPWA	$\pi N \to N\pi, N\eta$
237±73	PENNER	02C	DPWA	Multichannel
121±39	VRANA	00	DPWA	Multichannel

[1] Statistical error only.
[2] State a) of two states seen by the CLAS collaboration.
[3] State b) of two states seen by the CLAS collaboration.

N(1720) DECAY MODES

The following branching fractions are our estimates, not fits or averages.

	Mode	Fraction (Γ_i/Γ)
Γ_1	$N\pi$	8–14 %
Γ_2	$N\eta$	1–5 %
Γ_3	$N\omega$	12–40 %
Γ_4	ΛK	4–19 %
Γ_5	$N\pi\pi$	>50 %
Γ_6	$\Delta(1232)\pi$	47–89 %
Γ_7	$\Delta(1232)\pi$, P-wave	47–77 %
Γ_8	$\Delta(1232)\pi$, F-wave	<12 %
Γ_9	$N\rho$	(29 ±8) %
Γ_{10}	$N\rho$, S=1/2	1–2 %
Γ_{11}	$N\rho$, S=3/2 , P-wave	(17 ±6) %
Γ_{12}	$N\sigma$	2–14 %
Γ_{13}	$N(1440)\pi$	<2 %
Γ_{14}	$N(1520)\pi$, S-wave	1–5 %
Γ_{15}	$N(1535)\pi$	(4.0±2.0) %
Γ_{16}	$p\gamma$	0.05–0.25 %
Γ_{17}	$p\gamma$, helicity=1/2	0.05–0.15 %
Γ_{18}	$p\gamma$, helicity=3/2	0.002–0.16 %
Γ_{19}	$n\gamma$	0.0–0.016 %
Γ_{20}	$n\gamma$, helicity=1/2	0.0–0.01 %
Γ_{21}	$n\gamma$, helicity=3/2	0.0–0.015 %

N(1720) BRANCHING RATIOS

$\Gamma(N\pi)/\Gamma_{total}$ — Γ_1/Γ

VALUE (%)	DOCUMENT ID		TECN	COMMENT
8 to 14 (≈ 11) OUR ESTIMATE				
13 ±5	SEIFEN	25	DPWA	Multichannel
18 ±2	[1] HUNT	19	DPWA	Multichannel
17 ±2	[1] SHKLYAR	13	DPWA	Multichannel
9.4±0.5	ARNDT	06	DPWA	$\pi N \to \pi N, \eta N$
10 ±4	CUTKOSKY	80	IPWA	$\pi N \to \pi N$
14 ±3	HOEHLER	79	IPWA	$\pi N \to \pi N$
• • • We do not use the following data for averages, fits, limits, etc. • • •				
11 ±4	SOKHOYAN	15A	DPWA	Multichannel
13.6±0.6	[1] SHRESTHA	12A	DPWA	Multichannel
18 ±3	BATINIC	10	DPWA	$\pi N \to N\pi, N\eta$
17 ±2	PENNER	02C	DPWA	Multichannel
5 ±5	VRANA	00	DPWA	Multichannel

[1] Statistical error only.

$\Gamma(N\eta)/\Gamma_{total}$ — Γ_2/Γ

VALUE (%)	DOCUMENT ID		TECN	COMMENT
1 to 5 (≈ 3) OUR ESTIMATE				
3 ±2	MUELLER	20	DPWA	Multichannel
3.8±0.5	[1] HUNT	19	DPWA	Multichannel
< 1	SHKLYAR	13	DPWA	Multichannel
3 ±2	ANISOVICH	12A	DPWA	Multichannel
• • • We do not use the following data for averages, fits, limits, etc. • • •				
< 1	[1] SHRESTHA	12A	DPWA	Multichannel
0 ±1	BATINIC	10	DPWA	$\pi N \to N\pi, N\eta$
10 ±7	THOMA	08	DPWA	Multichannel
0.2±0.2	PENNER	02C	DPWA	Multichannel
4 ±1	VRANA	00	DPWA	Multichannel

[1] Statistical error only.

$\Gamma(N\omega)/\Gamma_{total}$ — Γ_3/Γ

VALUE (%)	DOCUMENT ID		TECN	COMMENT
26±14	DENISENKO	16	DPWA	Multichannel

$\Gamma(\Lambda K)/\Gamma_{total}$ — Γ_4/Γ

VALUE (%)	DOCUMENT ID		TECN	COMMENT
4–19 % OUR ESTIMATE				
16 ±3	[1] HUNT	19	DPWA	Multichannel
4.3±0.4	SHKLYAR	05	DPWA	Multichannel
• • • We do not use the following data for averages, fits, limits, etc. • • •				
2.8±0.4	[1] SHRESTHA	12A	DPWA	Multichannel
12 ±9	THOMA	08	DPWA	Multichannel
9 ±3	PENNER	02C	DPWA	Multichannel

[1] Statistical error only.

$\Gamma(N\pi\pi)/\Gamma_{total}$ — Γ_5/Γ

VALUE (%)	DOCUMENT ID		TECN	COMMENT
>50 % OUR ESTIMATE				
84±16	GOLOVATCH	19	DPWA	$\gamma p \to \pi^+\pi^- p$

$\Gamma(\Delta(1232)\pi)/\Gamma_{total}$ — Γ_6/Γ

VALUE (%)	DOCUMENT ID		TECN	COMMENT
20±7	SARANTSEV	25	DPWA	Multichannel
• • • We do not use the following data for averages, fits, limits, etc. • • •				
45±8	[1] MOKEEV	20	DPWA	$\gamma p \to \pi^+\pi^- p$
54±8	[2] MOKEEV	20	DPWA	$\gamma p \to \pi^+\pi^- p$

[1] State a) of two states seen by the CLAS collaboration.
[2] State b) of two states seen by the CLAS collaboration.

$\Gamma(\Delta(1232)\pi$, P-wave$)/\Gamma_{total}$ — Γ_7/Γ

VALUE (%)	DOCUMENT ID		TECN	COMMENT
9± 5	SARANTSEV	25	DPWA	Multichannel
15± 7	SEIFEN	25	DPWA	Multichannel
• • • We do not use the following data for averages, fits, limits, etc. • • •				
62±15	SOKHOYAN	15A	DPWA	Multichannel

Int. J. Mod. Phys. A 2026.41. Downloaded from www.worldscientific.com
UNIVERSITY OF CALIFORNIA @ BERKELEY on 09/16/26. Re-use and distribution is strictly not permitted, except for Open Access articles.

$\Gamma(\Delta(1232)\pi, F\text{-wave})/\Gamma_{total}$ — Γ_8/Γ

VALUE (%)	DOCUMENT ID		TECN	COMMENT
11 ± 5	SARANTSEV	25	DPWA	Multichannel
6 ± 6	SEIFEN	25	DPWA	Multichannel
• • • We do not use the following data for averages, fits, limits, etc. • • •				
6 ± 6	SOKHOYAN	15A	DPWA	Multichannel

$\Gamma(N\rho)/\Gamma_{total}$ — Γ_9/Γ

VALUE (%)	DOCUMENT ID		TECN	COMMENT
29±8	SARANTSEV	25	DPWA	Multichannel
• • • We do not use the following data for averages, fits, limits, etc. • • •				
38 ± 8	[1] MOKEEV	20	DPWA	$\gamma p \to \pi^+\pi^- p$
7 ± 3	[2] MOKEEV	20	DPWA	$\gamma p \to \pi^+\pi^- p$

[1] State a) of two states seen by the CLAS collaboration.
[2] State b) of two states seen by the CLAS collaboration.

$\Gamma(N\rho, S{=}1/2)/\Gamma_{total}$ — Γ_{10}/Γ

VALUE (%)	DOCUMENT ID		TECN	COMMENT
$12\ \pm5$	SARANTSEV	25	DPWA	Multichannel
1.4 ± 0.5	[1] SHRESTHA	12A	DPWA	Multichannel
• • • We do not use the following data for averages, fits, limits, etc. • • •				
$91\ \pm1$	VRANA	00	DPWA	Multichannel

[1] Statistical error only.

$\Gamma(N\rho, S{=}3/2, P\text{-wave})/\Gamma_{total}$ — Γ_{11}/Γ

VALUE (%)	DOCUMENT ID		TECN	COMMENT
17±6	SARANTSEV	25	DPWA	Multichannel

$\Gamma(N\sigma)/\Gamma_{total}$ — Γ_{12}/Γ

VALUE (%)	DOCUMENT ID		TECN	COMMENT
$25\pm\ 6$	SARANTSEV	25	DPWA	Multichannel
20 ± 10	SEIFEN	25	DPWA	Multichannel
• • • We do not use the following data for averages, fits, limits, etc. • • •				
$8\pm\ 6$	SOKHOYAN	15A	DPWA	Multichannel

$\Gamma(N(1440)\pi)/\Gamma_{total}$ — Γ_{13}/Γ

VALUE (%)	DOCUMENT ID		TECN	COMMENT
6 ± 5	SEIFEN	25	DPWA	Multichannel
• • • We do not use the following data for averages, fits, limits, etc. • • •				
<2	SOKHOYAN	15A	DPWA	Multichannel

$\Gamma(N(1520)\pi, S\text{-wave})/\Gamma_{total}$ — Γ_{14}/Γ

VALUE (%)	DOCUMENT ID		TECN	COMMENT
7 ± 3	SEIFEN	25	DPWA	Multichannel
• • • We do not use the following data for averages, fits, limits, etc. • • •				
3 ± 2	SOKHOYAN	15A	DPWA	Multichannel

$\Gamma(N(1535)\pi)/\Gamma_{total}$ — Γ_{15}/Γ

VALUE (%)	DOCUMENT ID		TECN	COMMENT
4±2	SEIFEN	25	DPWA	Multichannel

$N(1720)$ PHOTON DECAY AMPLITUDES AT THE POLE

$N(1720) \to p\gamma$, helicity-1/2 amplitude $A_{1/2}$

MODULUS ($GeV^{-1/2}$)	PHASE (°)	DOCUMENT ID		TECN	COMMENT
0.100 ± 0.025	$-5\ \pm30$	SARANTSEV	25	DPWA	Multichannel
0.039 ± 0.004	$60\ \pm5$	ROENCHEN	22	DPWA	Multichannel
• • • We do not use the following data for averages, fits, limits, etc. • • •					
0.039	5.3	ROENCHEN	15A	DPWA	Multichannel
0.115 ± 0.045	$0\ \pm35$	SOKHOYAN	15A	DPWA	Multichannel

$N(1720) \to p\gamma$, helicity-3/2 amplitude $A_{3/2}$

MODULUS ($GeV^{-1/2}$)	PHASE (°)	DOCUMENT ID		TECN	COMMENT
0.045 ± 0.020	$120\ \pm30$	SARANTSEV	25	DPWA	Multichannel
-0.025 ± 0.004	$-5.7\ \pm7$	ROENCHEN	22	DPWA	Multichannel
• • • We do not use the following data for averages, fits, limits, etc. • • •					
0.032	66	ROENCHEN	15A	DPWA	Multichannel
0.140 ± 0.040	$65\ \pm35$	SOKHOYAN	15A	DPWA	Multichannel

$N(1720) \to n\gamma$, helicity-1/2 amplitude $A_{1/2}$

MODULUS ($GeV^{-1/2}$)	PHASE (°)	DOCUMENT ID		TECN	COMMENT
$-0.025^{+0.015}_{-0.040}$	$-75\ \pm35$	ANISOVICH	17E	DPWA	Multichannel

$N(1720) \to n\gamma$, helicity-3/2 amplitude $A_{3/2}$

MODULUS ($GeV^{-1/2}$)	PHASE (°)	DOCUMENT ID		TECN	COMMENT
0.100 ± 0.035	$-80\ \pm35$	ANISOVICH	17E	DPWA	Multichannel

$N(1720)$ BREIT-WIGNER PHOTON DECAY AMPLITUDES

$N(1720) \to p\gamma$, helicity-1/2 amplitude $A_{1/2}$

VALUE ($GeV^{-1/2}$)	DOCUMENT ID		TECN	COMMENT
0.080 to 0.120 (≈ 0.100) OUR ESTIMATE				
$0.100\ \pm0.025$	SARANTSEV	25	DPWA	Multichannel
0.0809 ± 0.0115	GOLOVATCH	19	DPWA	$\gamma p \to \pi^+\pi^- p$
$0.068\ \pm0.004$	[1] HUNT	19	DPWA	Multichannel
$-0.065\ \pm0.002$	[1] SHKLYAR	13	DPWA	Multichannel
$0.095\ \pm0.002$	WORKMAN	12A	DPWA	$\gamma N \to N\pi$
• • • We do not use the following data for averages, fits, limits, etc. • • •				
$0.115\ \pm0.045$	SOKHOYAN	15A	DPWA	Multichannel
$0.057\ \pm0.003$	[1] SHRESTHA	12A	DPWA	Multichannel
0.073	DRECHSEL	07	DPWA	$\gamma N \to \pi N$
$0.097\ \pm0.003$	DUGGER	07	DPWA	$\gamma N \to \pi N$
-0.053	PENNER	02D	DPWA	Multichannel

[1] Statistical error only.

$N(1720) \to p\gamma$, helicity-3/2 amplitude $A_{3/2}$

VALUE ($GeV^{-1/2}$)	DOCUMENT ID		TECN	COMMENT
-0.041 ± 0.020	SARANTSEV	25	DPWA	Multichannel
-0.034 ± 0.0076	GOLOVATCH	19	DPWA	$\gamma p \to \pi^+\pi^- p$
0.028 ± 0.003	[1] HUNT	19	DPWA	Multichannel
0.035 ± 0.002	[1] SHKLYAR	13	DPWA	Multichannel
-0.048 ± 0.002	WORKMAN	12A	DPWA	$\gamma N \to N\pi$
• • • We do not use the following data for averages, fits, limits, etc. • • •				
0.135 ± 0.040	SOKHOYAN	15A	DPWA	Multichannel
-0.019 ± 0.002	[1] SHRESTHA	12A	DPWA	Multichannel
-0.011	DRECHSEL	07	DPWA	$\gamma N \to \pi N$
-0.039 ± 0.003	DUGGER	07	DPWA	$\gamma N \to \pi N$
0.027	PENNER	02D	DPWA	Multichannel

[1] Statistical error only.

$N(1720) \to n\gamma$, helicity-1/2 amplitude $A_{1/2}$

VALUE ($GeV^{-1/2}$)	DOCUMENT ID		TECN	COMMENT
-0.064 ± 0.006	[1] HUNT	19	DPWA	Multichannel
$-0.028^{+0.015}_{-0.040}$	ANISOVICH	17E	DPWA	Multichannel
• • • We do not use the following data for averages, fits, limits, etc. • • •				
-0.080 ± 0.050	ANISOVICH	13B	DPWA	Multichannel
-0.002 ± 0.001	[1] SHRESTHA	12A	DPWA	Multichannel
-0.003	DRECHSEL	07	DPWA	$\gamma N \to \pi N$
-0.004	PENNER	02D	DPWA	Multichannel

[1] Statistical error only.

$N(1720) \to n\gamma$, helicity-3/2 amplitude $A_{3/2}$

VALUE ($GeV^{-1/2}$)	DOCUMENT ID		TECN	COMMENT
-0.004 ± 0.006	[1] HUNT	19	DPWA	Multichannel
-0.140 ± 0.065	ANISOVICH	13B	DPWA	Multichannel
• • • We do not use the following data for averages, fits, limits, etc. • • •				
-0.001 ± 0.002	[1] SHRESTHA	12A	DPWA	Multichannel
-0.031	DRECHSEL	07	DPWA	$\gamma N \to \pi N$
0.003	PENNER	02D	DPWA	Multichannel

[1] Statistical error only.

$N(1720)$ REFERENCES

For early references, see Physics Letters **111B** 1 (1982).

SARANTSEV	25	PR C112 015202	A.V. Sarantsev *et al.*	(Bonn-Gatchina Collab.)
SEIFEN	25	EPJ A61 173	T. Seifen *et al.*	(CBELSA/TAPS Collab.)
ROENCHEN	22	EPJ A58 229	D. Roenchen *et al.*	(JULI, GWU, BONN+)
MOKEEV	20	PL B805 135457	V.I. Mokeev *et al.*	(CLAS Collab.)
MUELLER	20	PL B803 135323	J. Mueller *et al.*	(CBELSA/TAPS Collab.)
GOLOVATCH	19	PL B788 371	E. Golovatch *et al.*	(CLAS Collab.)
HUNT	19	PR C99 055205	B.C. Hunt, D.M. Manley	
ANISOVICH	17E	PR C96 055202	A.V. Anisovich *et al.*	(BONN, PNPI, JLAB+)
DENISENKO	16	PL B755 97	I. Denisenko *et al.*	
ROENCHEN	15A	EPJ A51 70	D. Roenchen *et al.*	
SOKHOYAN	15A	EPJ A51 95	V. Sokhoyan *et al.*	(CBELSA/TAPS Collab.)
PDG	14	CP C38 070001	K. Olive *et al.*	(PDG Collab.)
SVARC	14	PR C89 045205	A. Svarc *et al.*	(RBI Zagreb, UNI Tuzla)
ANISOVICH	13B	EPJ A49 67	A.V. Anisovich *et al.*	
SHKLYAR	13	PR C87 015201	V. Shklyar, H. Lenske, U. Mosel	(GIES)
ANISOVICH	12A	EPJ A48 15	A.V. Anisovich *et al.*	(BONN, PNPI)
SHRESTHA	12A	PR C86 055203	M. Shrestha, D.M. Manley	(KSU)
WORKMAN	12A	PR C86 015202	R. Workman *et al.*	(GWU)
BATINIC	10	PR C82 038203	M. Batinic *et al.*	(ZAGR)
THOMA	08	PL B659 87	U. Thoma *et al.*	(CB-ELSA Collab.)
DRECHSEL	07	EPJ A34 69	D. Drechsel, S.S. Kamalov, L. Tiator	(MAINZ, JINR)
DUGGER	07	PR C76 025211	M. Dugger *et al.*	(JLab CLAS Collab.)
ARNDT	06	PR C74 045205	R.A. Arndt *et al.*	(GWU)
SHKLYAR	05	PR C72 015210	V. Shklyar, H. Lenske, U. Mosel	(GIES)
PENNER	02C	PR C66 055211	G. Penner, U. Mosel	(GIES)
PENNER	02D	PR C66 055212	G. Penner, U. Mosel	(GIES)
VRANA	00	PRPL 328 181	T.P. Vrana, S.A. Dytman, T.-S.H. Lee	(PITT, ANL)
HOEHLER	93	πN Newsletter 9 1	G. Hohler	(KARL)
CUTKOSKY	80	Toronto Conf. 19	R.E. Cutkosky *et al.*	(CMU, LBL) IJP
Also		PR D20 2839	R.E. Cutkosky *et al.*	(CMU, LBL) IJP
HOEHLER	79	PDAT 12-1	G. Hohler *et al.*	(KARLT) IJP
Also		Toronto Conf. 3	R. Koch	(KARLT) IJP

Int. J. Mod. Phys. A 2026.41. Downloaded from www.worldscientific.com
by UNIVERSITY OF CALIFORNIA @ BERKELEY on 09/16/26. Re-use and distribution is strictly not permitted, except for Open Access articles.

N(1860) 5/2+

$I(J^P) = \frac{1}{2}(\frac{5}{2}^+)$ Status: **

OMITTED FROM SUMMARY TABLE

Before the 2012 *Review*, all the evidence for a $J^P = 5/2^+$ state with a mass above 1800 MeV was filed under a two-star N(2000). There is now some evidence from ANISOVICH 12A for two $5/2^+$ states in this region, so we have split the older data (according to mass) between two two-star $5/2^+$ states, an N(1860) and an N(2000).

N(1860) POLE POSITION

REAL PART

VALUE (MeV)	DOCUMENT ID		TECN	COMMENT
1870± 25	SARANTSEV	25	DPWA	Multichannel
1834± 19±6	[1] SVARC	14	L+P	$\pi N \to \pi N$
• • • We do not use the following data for averages, fits, limits, etc. • • •				
1871	HUNT	19	DPWA	Multichannel
1830^{+120}_{-60}	ANISOVICH	12A	DPWA	Multichannel
1807	ARNDT	06	DPWA	$\pi N \to \pi N, \eta N$

[1] Fit to the amplitudes of HOEHLER 79.

−2×IMAGINARY PART

VALUE (MeV)	DOCUMENT ID		TECN	COMMENT
290± 40	SARANTSEV	25	DPWA	Multichannel
122± 34±7	[2] SVARC	14	L+P	$\pi N \to \pi N$
• • • We do not use the following data for averages, fits, limits, etc. • • •				
337	HUNT	19	DPWA	Multichannel
250^{+150}_{-50}	ANISOVICH	12A	DPWA	Multichannel
109	ARNDT	06	DPWA	$\pi N \to \pi N, \eta N$

[2] Fit to the amplitudes of HOEHLER 79.

N(1860) ELASTIC POLE RESIDUE

MODULUS |r|

VALUE (MeV)	DOCUMENT ID		TECN	COMMENT
4± 1±1	[3] SVARC	14	L+P	$\pi N \to \pi N$
50±20	ANISOVICH	12A	DPWA	Multichannel
• • • We do not use the following data for averages, fits, limits, etc. • • •				
60	ARNDT	06	DPWA	$\pi N \to \pi N, \eta N$

[3] Fit to the amplitudes of HOEHLER 79.

PHASE θ

VALUE (°)	DOCUMENT ID		TECN	COMMENT
−39±18±9	[4] SVARC	14	L+P	$\pi N \to \pi N$
−80±40	ANISOVICH	12A	DPWA	Multichannel
• • • We do not use the following data for averages, fits, limits, etc. • • •				
−67	ARNDT	06	DPWA	$\pi N \to \pi N, \eta N$

[4] Fit to the amplitudes of HOEHLER 79.

N(1860) BREIT-WIGNER MASS

VALUE (MeV)	DOCUMENT ID		TECN	COMMENT
1920 ± 25	SARANTSEV	25	DPWA	Multichannel
1928 ± 21	[5] HUNT	19	DPWA	Multichannel
1882 ± 10	HOEHLER	79	IPWA	$\pi N \to \pi N$
• • • We do not use the following data for averages, fits, limits, etc. • • •				
1860^{+120}_{-60}	ANISOVICH	12A	DPWA	Multichannel
1900 ± 7	[5] SHRESTHA	12A	DPWA	Multichannel
1817.7	ARNDT	06	DPWA	$\pi N \to \pi N, \eta N$

[5] Statistical error only.

N(1860) BREIT-WIGNER WIDTH

VALUE (MeV)	DOCUMENT ID		TECN	COMMENT
300 ± 35	SARANTSEV	25	DPWA	Multichannel
376 ± 58	[6] HUNT	19	DPWA	Multichannel
95 ± 20	HOEHLER	79	IPWA	$\pi N \to \pi N$
• • • We do not use the following data for averages, fits, limits, etc. • • •				
270^{+140}_{-50}	ANISOVICH	12A	DPWA	Multichannel
219 ± 23	[6] SHRESTHA	12A	DPWA	Multichannel
117.6	ARNDT	06	DPWA	$\pi N \to \pi N, \eta N$

[6] Statistical error only.

N(1860) DECAY MODES

	Mode	Fraction (Γ_i/Γ)
Γ_1	$N\pi$	4–20 %
Γ_2	$N\eta$	0–6 %
Γ_3	ΛK	<0.01 %
Γ_4	$N\pi\pi$	>61 %
Γ_5	$\Delta\pi$	20–54 %
Γ_6	$\Delta\pi$, P-wave	4–16 %
Γ_7	$\Delta\pi$, F-wave	16–38 %
Γ_8	$N\rho$	<8.6 %
Γ_9	$N\rho$, S=1/2	(16±9) %
Γ_{10}	$N\rho$, S=3/2 , P-wave	<8.5 %
Γ_{11}	$N\rho$, S=3/2 , F-wave	<0.1 %
Γ_{12}	$N\sigma$	41–61 %
Γ_{13}	$p\gamma$	
Γ_{14}	$p\gamma$, helicity=1/2	seen
Γ_{15}	$p\gamma$, helicity=3/2	seen
Γ_{16}	$n\gamma$	0.0017–0.062 %
Γ_{17}	$n\gamma$, helicity=1/2	0.0003–0.019 %
Γ_{18}	$n\gamma$, helicity=3/2	0.0014–0.043 %

N(1860) BRANCHING RATIOS

$\Gamma(N\pi)/\Gamma_{total}$ — Γ_1/Γ

VALUE (%)	DOCUMENT ID		TECN	COMMENT
4–20 % OUR ESTIMATE				
12 ±4	SEIFEN	25	DPWA	Multichannel
8.0±0.1	[7] HUNT	19	DPWA	Multichannel
4 ±2	HOEHLER	79	IPWA	$\pi N \to \pi N$
• • • We do not use the following data for averages, fits, limits, etc. • • •				
20 ±6	ANISOVICH	12A	DPWA	Multichannel
17 ±1	[7] SHRESTHA	12A	DPWA	Multichannel
12.7	ARNDT	06	DPWA	$\pi N \to \pi N, \eta N$

[7] Statistical error only.

$\Gamma(N\eta)/\Gamma_{total}$ — Γ_2/Γ

VALUE (%)	DOCUMENT ID		TECN	COMMENT
0–6 % OUR ESTIMATE				
0.11±0.09	[8] HUNT	19	DPWA	Multichannel
• • • We do not use the following data for averages, fits, limits, etc. • • •				
4 ±2	[8] SHRESTHA	12A	DPWA	Multichannel

[8] Statistical error only.

$\Gamma(\Lambda K)/\Gamma_{total}$ — Γ_3/Γ

VALUE (%)	DOCUMENT ID		TECN	COMMENT
<0.01 % OUR ESTIMATE				
<0.01	[9] HUNT	19	DPWA	Multichannel

[9] Statistical error only.

$\Gamma(\Delta\pi)/\Gamma_{total}$ — Γ_5/Γ

VALUE (%)	DOCUMENT ID		TECN	COMMENT
7±3	SARANTSEV	25	DPWA	Multichannel

$\Gamma(\Delta\pi, P\text{-wave})/\Gamma_{total}$ — Γ_6/Γ

VALUE (%)	DOCUMENT ID		TECN	COMMENT
4–16 % OUR ESTIMATE				
2±2	SARANTSEV	25	DPWA	Multichannel
2±2	SEIFEN	25	DPWA	Multichannel
10±6	[10] HUNT	19	DPWA	Multichannel

[10] Statistical error only.

$\Gamma(\Delta\pi, F\text{-wave})/\Gamma_{total}$ — Γ_7/Γ

VALUE (%)	DOCUMENT ID		TECN	COMMENT
16–38 % OUR ESTIMATE				
5± 2	SARANTSEV	25	DPWA	Multichannel
4± 2	SEIFEN	25	DPWA	Multichannel
27±11	[11] HUNT	19	DPWA	Multichannel

[11] Statistical error only.

$\Gamma(N\rho)/\Gamma_{total}$ — Γ_8/Γ

VALUE (%)	DOCUMENT ID		TECN	COMMENT
54±16	SARANTSEV	25	DPWA	Multichannel

$\Gamma(N\rho, S=1/2)/\Gamma_{total}$ — Γ_9/Γ

VALUE (%)	DOCUMENT ID		TECN	COMMENT
16±9	SARANTSEV	25	DPWA	Multichannel

Int. J. Mod. Phys. A 2026.41. Downloaded from www.worldscientific.com
UNIVERSITY OF CALIFORNIA @ BERKELEY on 09/16/26. Re-use and distribution is strictly not permitted, except for Open Access articles.

$\Gamma(N\rho, S{=}3/2, P\text{-wave})/\Gamma_{total}$ — Γ_{10}/Γ

VALUE (%)	DOCUMENT ID		TECN	COMMENT
<8.5 % OUR ESTIMATE				
13 ±5	SARANTSEV	25	DPWA	Multichannel
< 8.5	[12] HUNT	19	DPWA	Multichannel

[12] Statistical error only.

$\Gamma(N\rho, S{=}3/2, F\text{-wave})/\Gamma_{total}$ — Γ_{11}/Γ

VALUE (%)	DOCUMENT ID		TECN	COMMENT
<0.1 % OUR ESTIMATE				
25 ±12	SARANTSEV	25	DPWA	Multichannel
< 0.1	[13] HUNT	19	DPWA	Multichannel

[13] Statistical error only.

$\Gamma(N\sigma)/\Gamma_{total}$ — Γ_{12}/Γ

VALUE (%)	DOCUMENT ID		TECN	COMMENT
41–61 % OUR ESTIMATE				
9± 3	SARANTSEV	25	DPWA	Multichannel
4± 4	SEIFEN	25	DPWA	Multichannel
51±10	[14] HUNT	19	DPWA	Multichannel
• • • We do not use the following data for averages, fits, limits, etc. • • •				
41± 6	[14] SHRESTHA	12A	DPWA	Multichannel

[14] Statistical error only.

$N(1860)$ PHOTON DECAY AMPLITUDES AT THE POLE

$N(1860) \to p\gamma$, helicity-1/2 amplitude $A_{1/2}$

MODULUS ($GeV^{-1/2}$)	PHASE (°)	DOCUMENT ID		TECN	COMMENT
0.020±0.006	85 ± 25	SARANTSEV	25	DPWA	Multichannel

$N(1860) \to p\gamma$, helicity-3/2 amplitude $A_{3/2}$

MODULUS ($GeV^{-1/2}$)	PHASE (°)	DOCUMENT ID		TECN	COMMENT
0.062±0.015	−5 ± 15	SARANTSEV	25	DPWA	Multichannel

$N(1860)$ BREIT-WIGNER PHOTON DECAY AMPLITUDES

$N(1860) \to p\gamma$, helicity-1/2 amplitude $A_{1/2}$

VALUE ($GeV^{-1/2}$)	DOCUMENT ID		TECN	COMMENT
0.022±0.006	[15] SARANTSEV	25	DPWA	Multichannel
−0.022±0.020	[16] HUNT	19	DPWA	Multichannel
• • • We do not use the following data for averages, fits, limits, etc. • • •				
−0.017±0.003	[16] SHRESTHA	12A	DPWA	Multichannel

[15] Sign is undetermined.
[16] Statistical error only.

$N(1860) \to p\gamma$, helicity-3/2 amplitude $A_{3/2}$

VALUE	DOCUMENT ID		TECN	COMMENT
0.063±0.013	SARANTSEV	25	DPWA	Multichannel
−0.032±0.034	[17] HUNT	19	DPWA	Multichannel
• • • We do not use the following data for averages, fits, limits, etc. • • •				
0.029±0.004	[17] SHRESTHA	12A	DPWA	Multichannel

[17] Statistical error only.

$N(1860) \to n\gamma$, helicity-1/2 amplitude $A_{1/2}$

VALUE ($GeV^{-1/2}$)	DOCUMENT ID		TECN	COMMENT
0.021±0.029	[18] HUNT	19	DPWA	Multichannel
0.021±0.013	ANISOVICH	13B	DPWA	Multichannel
• • • We do not use the following data for averages, fits, limits, etc. • • •				
0.010±0.005	[18] SHRESTHA	12A	DPWA	Multichannel

[18] Statistical error only.

$N(1860) \to n\gamma$, helicity-3/2 amplitude $A_{3/2}$

VALUE ($GeV^{-1/2}$)	DOCUMENT ID		TECN	COMMENT
0.070±0.035	[19] HUNT	19	DPWA	Multichannel
0.034±0.017	ANISOVICH	13B	DPWA	Multichannel
• • • We do not use the following data for averages, fits, limits, etc. • • •				
−0.009±0.005	[19] SHRESTHA	12A	DPWA	Multichannel

[19] Statistical error only.

$N(1860)$ REFERENCES

SARANTSEV	25	PR C112 015202	A.V. Sarantsev *et al.*	(Bonn-Gatchina Collab.)
SEIFEN	25	EPJ A61 173	T. Seifen *et al.*	(CBELSA/TAPS Collab.)
HUNT	19	PR C99 055205	B.C. Hunt, D.M. Manley	
SVARC	14	PR C89 045205	A. Svarc *et al.*	(RBI Zagreb, UNI Tuzla)
ANISOVICH	13B	EPJ A49 67	A.V. Anisovich *et al.*	
ANISOVICH	12A	EPJ A48 15	A.V. Anisovich *et al.*	(BONN, PNPI)
SHRESTHA	12A	PR C86 055203	M. Shrestha, D.M. Manley	(KSU)
ARNDT	06	PR C74 045205	R.A. Arndt *et al.*	(GWU)
HOEHLER	79	PDAT 12-1	G. Hohler *et al.*	(KARLT)

$N(1875)\ 3/2^-$

$I(J^P) = \frac{1}{2}(\frac{3}{2}^-)$ Status: ***

was $N(2080)$

Before the 2012 *Review*, all the evidence for a $J^P = 3/2^-$ state with a mass above 1800 MeV was filed under a two-star $N(2080)$. There is now evidence from ANISOVICH 12A for two $3/2^-$ states in this region, so we have split the older data (according to mass) between a three-star $N(1875)$ and a two-star $N(2120)$.

$N(1875)$ POLE POSITION

REAL PART

VALUE (MeV)	DOCUMENT ID		TECN	COMMENT
1850 to 1950 (≈ 1900) OUR ESTIMATE				
1855± 17	SARANTSEV	25	DPWA	Multichannel
1880±100	CUTKOSKY	80	IPWA	$\pi N \to \pi N$ (lower m)
• • • We do not use the following data for averages, fits, limits, etc. • • •				
1993	HUNT	19	DPWA	Multichannel
1870± 20	SOKHOYAN	15A	DPWA	Multichannel
1810	SHKLYAR	13	DPWA	Multichannel
1957± 49	BATINIC	10	DPWA	$\pi N \to N\pi$, $N\eta$
1824	VRANA	00	DPWA	Multichannel

−2×IMAGINARY PART

VALUE (MeV)	DOCUMENT ID		TECN	COMMENT
100 to 220 (≈ 160) OUR ESTIMATE				
260± 20	SARANTSEV	25	DPWA	Multichannel
160± 80	CUTKOSKY	80	IPWA	$\pi N \to \pi N$ (lower m)
• • • We do not use the following data for averages, fits, limits, etc. • • •				
319	HUNT	19	DPWA	Multichannel
200± 15	SOKHOYAN	15A	DPWA	Multichannel
98	SHKLYAR	13	DPWA	Multichannel
467±106	BATINIC	10	DPWA	$\pi N \to N\pi$, $N\eta$
614	VRANA	00	DPWA	Multichannel

$N(1875)$ ELASTIC POLE RESIDUE

MODULUS $|r|$

VALUE (MeV)	DOCUMENT ID		TECN	COMMENT
3 to 12 (≈ 10) OUR ESTIMATE				
3 ±1.5	SOKHOYAN	15A	DPWA	Multichannel
10 ±5	CUTKOSKY	80	IPWA	$\pi N \to \pi N$ (lower m)
• • • We do not use the following data for averages, fits, limits, etc. • • •				
3	SHKLYAR	13	DPWA	Multichannel
2.5±1.0	ANISOVICH	12A	DPWA	Multichannel
53	BATINIC	10	DPWA	$\pi N \to N\pi$, $N\eta$

PHASE θ

VALUE (°)	DOCUMENT ID		TECN	COMMENT
50 to 200 (≈ 100) OUR ESTIMATE				
160±50	SOKHOYAN	15A	DPWA	Multichannel
100±80	CUTKOSKY	80	IPWA	$\pi N \to \pi N$ (lower m)
• • • We do not use the following data for averages, fits, limits, etc. • • •				
− 76	SHKLYAR	13	DPWA	Multichannel
− 65	BATINIC	10	DPWA	$\pi N \to N\pi$, $N\eta$

$N(1875)$ INELASTIC POLE RESIDUE

The "normalized residue" is the residue divided by $\Gamma_{pole}/2$.

Normalized residue in $N\pi \to N(1875) \to \Lambda K$

MODULUS	PHASE (°)	DOCUMENT ID		TECN	COMMENT
0.015±0.005		ANISOVICH	12A	DPWA	Multichannel

Normalized residue in $N\pi \to N(1875) \to \Sigma K$

MODULUS	PHASE (°)	DOCUMENT ID		TECN	COMMENT
0.04±0.02		ANISOVICH	12A	DPWA	Multichannel

Normalized residue in $N\pi \to N(1875) \to N\sigma$

MODULUS	PHASE (°)	DOCUMENT ID		TECN	COMMENT
0.09±0.03	−175 ± 45	SOKHOYAN	15A	DPWA	Multichannel
• • • We do not use the following data for averages, fits, limits, etc. • • •					
0.08±0.03	−170 ± 65	ANISOVICH	12A	DPWA	Multichannel

Normalized residue in $N\pi \to N(1875) \to \Delta(1232)\pi$, S-wave

MODULUS	PHASE (°)	DOCUMENT ID		TECN	COMMENT
0.05±0.03	undefined	SOKHOYAN	15A	DPWA	Multichannel

Normalized residue in $N\pi \to N(1875) \to \Delta(1232)\pi$, D-wave

MODULUS	PHASE (°)	DOCUMENT ID		TECN	COMMENT
0.04±0.02	undefined	SOKHOYAN	15A	DPWA	Multichannel

Int. J. Mod. Phys. A 2026.41. Downloaded from www.worldscientific.com
by UNIVERSITY OF CALIFORNIA @ BERKELEY on 09/16/26. Re-use and distribution is strictly not permitted, except for Open Access articles.

Normalized residue in $N\pi \to N(1875) \to N(1440)\pi$

MODULUS	PHASE (°)	DOCUMENT ID		TECN	COMMENT
0.03±0.02	undefined	SOKHOYAN	15A	DPWA	Multichannel

$N(1875)$ BREIT-WIGNER MASS

VALUE (MeV)	DOCUMENT ID		TECN	COMMENT
1850 to 1920 (≈ 1875) OUR ESTIMATE				
1885± 15	SARANTSEV	25	DPWA	Multichannel
2005± 12	[1] HUNT	19	DPWA	Multichannel
1934± 10	[1] SHKLYAR	13	DPWA	Multichannel
1880±100	CUTKOSKY	80	IPWA	$\pi N \to \pi N$
• • • We do not use the following data for averages, fits, limits, etc. • • •				
1875± 20	SOKHOYAN	15A	DPWA	Multichannel
1951± 27	[1] SHRESTHA	12A	DPWA	Multichannel
2048± 65	BATINIC	10	DPWA	$\pi N \to N\pi$, $N\eta$
1946± 1	PENNER	02C	DPWA	Multichannel
1895	MART	00	DPWA	$\gamma p \to \Lambda K^+$
2003± 18	VRANA	00	DPWA	Multichannel

[1] Statistical error only.

$N(1875)$ BREIT-WIGNER WIDTH

VALUE (MeV)	DOCUMENT ID		TECN	COMMENT
120 to 250 (≈ 200) OUR ESTIMATE				
270± 20	SARANTSEV	25	DPWA	Multichannel
321± 21	[1] HUNT	19	DPWA	Multichannel
857±100	[1] SHKLYAR	13	DPWA	Multichannel
180± 60	CUTKOSKY	80	IPWA	$\pi N \to \pi N$ (lower m)
• • • We do not use the following data for averages, fits, limits, etc. • • •				
200± 25	SOKHOYAN	15A	DPWA	Multichannel
500± 45	[1] SHRESTHA	12A	DPWA	Multichannel
529±128	BATINIC	10	DPWA	$\pi N \to N\pi$, $N\eta$
859± 7	PENNER	02C	DPWA	Multichannel
372	MART	00	DPWA	$\gamma p \to \Lambda K^+$
1070±858	VRANA	00	DPWA	Multichannel

[1] Statistical error only.

$N(1875)$ DECAY MODES

	Mode	Fraction (Γ_i/Γ)
Γ_1	$N\pi$	3–11 %
Γ_2	$N\eta$	3–16 %
Γ_3	$N\omega$	15–25 %
Γ_4	ΛK	1–2 %
Γ_5	ΣK	0.3–1.1 %
Γ_6	$N\pi\pi$	>56 %
Γ_7	$\Delta(1232)\pi$	4–44 %
Γ_8	$\Delta(1232)\pi$, S-wave	2–21 %
Γ_9	$\Delta(1232)\pi$, D-wave	2–23 %
Γ_{10}	$N\rho$, S=3/2, S-wave	36–56 %
Γ_{11}	$N\sigma$	16–60 %
Γ_{12}	$N(1440)\pi$	2–8 %
Γ_{13}	$N(1520)\pi$	<2 %
Γ_{14}	$N(1535)\pi$	(2.0±2.0) %
Γ_{15}	$\Lambda K^*(892)$	<0.2 %
Γ_{16}	$p\gamma$	0.001–0.025 %
Γ_{17}	$p\gamma$, helicity=1/2	0.001–0.021 %
Γ_{18}	$p\gamma$, helicity=3/2	<0.003 %
Γ_{19}	$n\gamma$	<0.040 %
Γ_{20}	$n\gamma$, helicity=1/2	<0.007 %
Γ_{21}	$n\gamma$, helicity=3/2	<0.033 %

$N(1875)$ BRANCHING RATIOS

$\Gamma(N\pi)/\Gamma_{total}$ — Γ_1/Γ

VALUE (%)	DOCUMENT ID		TECN	COMMENT
3 to 11 (≈ 7) OUR ESTIMATE				
3 ±2	SEIFEN	25	DPWA	Multichannel
7.5±0.1	[1] HUNT	19	DPWA	Multichannel
11 ±1	[1] SHKLYAR	13	DPWA	Multichannel
10 ±4	CUTKOSKY	80	IPWA	$\pi N \to \pi N$ (lower m)
• • • We do not use the following data for averages, fits, limits, etc. • • •				
4 ±2	SOKHOYAN	15A	DPWA	Multichannel
7 ±2	[1] SHRESTHA	12A	DPWA	Multichannel
17 ±7	BATINIC	10	DPWA	$\pi N \to N\pi$, $N\eta$
12 ±2	PENNER	02C	DPWA	Multichannel
13 ±3	VRANA	00	DPWA	Multichannel

[1] Statistical error only.

$\Gamma(N\eta)/\Gamma_{total}$ — Γ_2/Γ

VALUE (%)	DOCUMENT ID		TECN	COMMENT
3–16 % OUR ESTIMATE				
10 ±6	MUELLER	20	DPWA	Multichannel
3.3±0.8	[1] HUNT	19	DPWA	Multichannel
< 1	SHKLYAR	13	DPWA	Multichannel
• • • We do not use the following data for averages, fits, limits, etc. • • •				
8 ±3	BATINIC	10	DPWA	$\pi N \to N\pi$, $N\eta$
7 ±2	PENNER	02C	DPWA	Multichannel
0 ±2	VRANA	00	DPWA	Multichannel

[1] Statistical error only.

$\Gamma(N\omega)/\Gamma_{total}$ — Γ_3/Γ

VALUE (%)	DOCUMENT ID		TECN	COMMENT
13±7	DENISENKO	16	DPWA	Multichannel
20±5	[1] SHKLYAR	13	DPWA	Multichannel
• • • We do not use the following data for averages, fits, limits, etc. • • •				
21±7	PENNER	02C	DPWA	Multichannel

[1] Statistical error only.

$\Gamma(\Lambda K)/\Gamma_{total}$ — Γ_4/Γ

VALUE (%)	DOCUMENT ID		TECN	COMMENT
1–2 % OUR ESTIMATE				
1.1±0.4	[1] HUNT	19	DPWA	Multichannel
• • • We do not use the following data for averages, fits, limits, etc. • • •				
0.2±0.2	PENNER	02C	DPWA	Multichannel

[1] Statistical error only.

$\Gamma(\Sigma K)/\Gamma_{total}$ — Γ_5/Γ

VALUE (%)	DOCUMENT ID		TECN	COMMENT
0.3–1.1 % OUR ESTIMATE				
0.7±0.4	PENNER	02C	DPWA	Multichannel

$\Gamma(\Delta(1232)\pi)/\Gamma_{total}$ — Γ_7/Γ

VALUE (%)	DOCUMENT ID		TECN	COMMENT
14^{+15}_{-10}	SARANTSEV	25	DPWA	Multichannel

$\Gamma(\Delta(1232)\pi, S\text{-wave})/\Gamma_{total}$ — Γ_8/Γ

VALUE (%)	DOCUMENT ID		TECN	COMMENT
2–21 % OUR ESTIMATE				
10^{+15}_{-10}	SARANTSEV	25	DPWA	Multichannel
6± 4	SEIFEN	25	DPWA	Multichannel
< 2	[1] HUNT	19	DPWA	Multichannel
• • • We do not use the following data for averages, fits, limits, etc. • • •				
14± 7	SOKHOYAN	15A	DPWA	Multichannel
87± 3	[1] SHRESTHA	12A	DPWA	Multichannel
40±10	VRANA	00	DPWA	Multichannel

[1] Statistical error only.

$\Gamma(\Delta(1232)\pi, D\text{-wave})/\Gamma_{total}$ — Γ_9/Γ

VALUE (%)	DOCUMENT ID		TECN	COMMENT
2–23 % OUR ESTIMATE				
4± 2	SARANTSEV	25	DPWA	Multichannel
4± 3	SEIFEN	25	DPWA	Multichannel
17± 6	[1] HUNT	19	DPWA	Multichannel
• • • We do not use the following data for averages, fits, limits, etc. • • •				
7± 5	SOKHOYAN	15A	DPWA	Multichannel
< 6	[1] SHRESTHA	12A	DPWA	Multichannel
17±10	VRANA	00	DPWA	Multichannel

[1] Statistical error only.

$\Gamma(N\rho, S=3/2, S\text{-wave})/\Gamma_{total}$ — Γ_{10}/Γ

VALUE (%)	DOCUMENT ID		TECN	COMMENT
36–56 % OUR ESTIMATE				
46±10	[1] HUNT	19	DPWA	Multichannel
• • • We do not use the following data for averages, fits, limits, etc. • • •				
< 5	[1] SHRESTHA	12A	DPWA	Multichannel
6± 6	VRANA	00	DPWA	Multichannel

[1] Statistical error only.

$\Gamma(N\sigma)/\Gamma_{total}$ — Γ_{11}/Γ

VALUE (%)	DOCUMENT ID		TECN	COMMENT
16–60 % OUR ESTIMATE				
33 ±20	SARANTSEV	25	DPWA	Multichannel
50 ±20	SEIFEN	25	DPWA	Multichannel
24.3± 8.6	[1] HUNT	19	DPWA	Multichannel
• • • We do not use the following data for averages, fits, limits, etc. • • •				
45 ±15	SOKHOYAN	15A	DPWA	Multichannel
< 4	[1] SHRESTHA	12A	DPWA	Multichannel
24 ±24	VRANA	00	DPWA	Multichannel

[1] Statistical error only.

Int. J. Mod. Phys. A 2026.41. Downloaded from www.worldscientific.com
UNIVERSITY OF CALIFORNIA @ BERKELEY on 09/16/26. Re-use and distribution is strictly not permitted, except for Open Access articles.

$\Gamma(N(1440)\pi)/\Gamma_{total}$ — Γ_{12}/Γ

VALUE (%)	DOCUMENT ID		TECN	COMMENT
11 ± 5	SEIFEN	25	DPWA	Multichannel
• • • We do not use the following data for averages, fits, limits, etc. • • •				
5 ± 3	SOKHOYAN	15A	DPWA	Multichannel

$\Gamma(N(1520)\pi)/\Gamma_{total}$ — Γ_{13}/Γ

VALUE (%)	DOCUMENT ID		TECN	COMMENT
4 ± 4	SEIFEN	25	DPWA	Multichannel
• • • We do not use the following data for averages, fits, limits, etc. • • •				
<2	SOKHOYAN	15A	DPWA	Multichannel

$\Gamma(N(1535)\pi)/\Gamma_{total}$ — Γ_{14}/Γ

VALUE (%)	DOCUMENT ID		TECN	COMMENT
2 ± 2	SEIFEN	25	DPWA	Multichannel

$\Gamma(\Lambda K^*(892))/\Gamma_{total}$ — Γ_{15}/Γ

VALUE (%)	DOCUMENT ID		TECN	COMMENT
<0.2 % OUR ESTIMATE				
<0.2	ANISOVICH	17B	DPWA	Multichannel

$N(1875)$ PHOTON DECAY AMPLITUDES AT THE POLE

$N(1875) \to p\gamma$, helicity-1/2 amplitude $A_{1/2}$

MODULUS ($GeV^{-1/2}$)	PHASE (°)	DOCUMENT ID		TECN	COMMENT
0.012 ± 0.006	-140 ± 30	SARANTSEV	25	DPWA	Multichannel
• • • We do not use the following data for averages, fits, limits, etc. • • •					
0.017 ± 0.009	-110 ± 40	SOKHOYAN	15A	DPWA	Multichannel

$N(1875) \to p\gamma$, helicity-3/2 amplitude $A_{3/2}$

MODULUS ($GeV^{-1/2}$)	PHASE (°)	DOCUMENT ID		TECN	COMMENT
0.014 ± 0.006	175 ± 30	SARANTSEV	25	DPWA	Multichannel
• • • We do not use the following data for averages, fits, limits, etc. • • •					
0.008 ± 0.004	180 ± 40	SOKHOYAN	15A	DPWA	Multichannel

$N(1875) \to n\gamma$, helicity-1/2 amplitude $A_{1/2}$

MODULUS ($GeV^{-1/2}$)	PHASE (°)	DOCUMENT ID		TECN	COMMENT
0.004 ± 0.003	-85 ± 35	ANISOVICH	17E	DPWA	Multichannel

$N(1875) \to n\gamma$, helicity-3/2 amplitude $A_{3/2}$

MODULUS ($GeV^{-1/2}$)	PHASE (°)	DOCUMENT ID		TECN	COMMENT
-0.006 ± 0.004	-85 ± 45	ANISOVICH	17E	DPWA	Multichannel

$N(1875)$ BREIT-WIGNER PHOTON DECAY AMPLITUDES

$N(1875) \to p\gamma$, helicity-1/2 amplitude $A_{1/2}$

VALUE ($GeV^{-1/2}$)	DOCUMENT ID		TECN	COMMENT
0.010 to 0.025 ($\approx$ 0.015) OUR ESTIMATE				
-0.013 ± 0.006	SARANTSEV	25	DPWA	Multichannel
-0.013 ± 0.008	[1] HUNT	19	DPWA	Multichannel
0.011 ± 0.001	[1] SHKLYAR	13	DPWA	Multichannel
• • • We do not use the following data for averages, fits, limits, etc. • • •				
0.018 ± 0.010	ANISOVICH	12A	DPWA	Multichannel
0.007 ± 0.008	[1] SHRESTHA	12A	DPWA	Multichannel
0.012	PENNER	02D	DPWA	Multichannel

[1] Statistical error only.

$N(1875) \to p\gamma$, helicity-3/2 amplitude $A_{3/2}$

VALUE ($GeV^{-1/2}$)	DOCUMENT ID		TECN	COMMENT
-0.010 to 0.025 (≈ -0.005) OUR ESTIMATE				
-0.015 ± 0.006	SARANTSEV	25	DPWA	Multichannel
-0.093 ± 0.009	[1] HUNT	19	DPWA	Multichannel
0.026 ± 0.001	[1] SHKLYAR	13	DPWA	Multichannel
• • • We do not use the following data for averages, fits, limits, etc. • • •				
-0.007 ± 0.004	SOKHOYAN	15A	DPWA	Multichannel
0.043 ± 0.022	[1] SHRESTHA	12A	DPWA	Multichannel
-0.010	PENNER	02D	DPWA	Multichannel

[1] Statistical error only.

$N(1875) \to n\gamma$, helicity-1/2 amplitude $A_{1/2}$

VALUE ($GeV^{-1/2}$)	DOCUMENT ID		TECN	COMMENT
0.050 ± 0.009	[1] HUNT	19	DPWA	Multichannel
0.010 ± 0.006	ANISOVICH	13B	DPWA	Multichannel
• • • We do not use the following data for averages, fits, limits, etc. • • •				
0.055 ± 0.021	[1] SHRESTHA	12A	DPWA	Multichannel
0.023	PENNER	02D	DPWA	Multichannel

[1] Statistical error only.

$N(1875) \to n\gamma$, helicity-3/2 amplitude $A_{3/2}$

VALUE ($GeV^{-1/2}$)	DOCUMENT ID		TECN	COMMENT
0.141 ± 0.022	[1] HUNT	19	DPWA	Multichannel
-0.020 ± 0.015	ANISOVICH	13B	DPWA	Multichannel
• • • We do not use the following data for averages, fits, limits, etc. • • •				
-0.085 ± 0.031	[1] SHRESTHA	12A	DPWA	Multichannel
-0.009	PENNER	02D	DPWA	Multichannel

[1] Statistical error only.

$N(1875)$ REFERENCES

For early references, see Physics Letters **111B** 1 (1982).

SARANTSEV	25	PR C112 015202	A.V. Sarantsev *et al.*	(Bonn-Gatchina Collab.)
SEIFEN	25	EPJ A61 173	T. Seifen *et al.*	(CBELSA/TAPS Collab.)
MUELLER	20	PL B803 135323	J. Mueller *et al.*	(CBELSA/TAPS Collab.)
HUNT	19	PR C99 055205	B.C. Hunt, D.M. Manley	
ANISOVICH	17B	PL B771 142	A.V. Anisovich *et al.*	
ANISOVICH	17E	PR C96 055202	A.V. Anisovich *et al.*	(BONN, PNPI, JLAB+)
DENISENKO	16	PL B755 97	I. Denisenko *et al.*	
SOKHOYAN	15A	EPJ A51 95	V. Sokhoyan *et al.*	(CBELSA/TAPS Collab.)
ANISOVICH	13B	EPJ A49 67	A.V. Anisovich *et al.*	
SHKLYAR	13	PR C87 015201	V. Shklyar, H. Lenske, U. Mosel	(GIES)
ANISOVICH	12A	EPJ A48 15	A.V. Anisovich *et al.*	(BONN, PNPI)
SHRESTHA	12A	PR C86 055203	M. Shrestha, D.M. Manley	(KSU)
BATINIC	10	PR C82 038203	M. Batinic *et al.*	(ZAGR)
PENNER	02C	PR C66 055211	G. Penner, U. Mosel	(GIES)
PENNER	02D	PR C66 055212	G. Penner, U. Mosel	(GIES)
MART	00	PR C61 012201	T. Mart, C. Bennhold	
VRANA	00	PRPL 328 181	T.P. Vrana, S.A. Dytman, T.-S.H. Lee	(PITT, ANL)
CUTKOSKY	80	Toronto Conf. 19	R.E. Cutkosky *et al.*	(CMU, LBL) IJP
Also		PR D20 2839	R.E. Cutkosky *et al.*	(CMU, LBL) IJP

$N(1880)\ 1/2^+$

$I(J^P) = \frac{1}{2}(\frac{1}{2}^+)$ Status: ***

$N(1880)$ POLE POSITION

REAL PART

VALUE (MeV)	DOCUMENT ID		TECN	COMMENT
1820 to 1900 ($\approx$ 1860) OUR ESTIMATE				
1860 ± 25	SARANTSEV	25	DPWA	Multichannel
• • • We do not use the following data for averages, fits, limits, etc. • • •				
1880	HUNT	19	DPWA	Multichannel
1875 ± 11	ANISOVICH	17A	L+P	γp, $\pi^- p \to K\Lambda$
1870 ± 40	SOKHOYAN	15A	DPWA	Multichannel
1870 ± 40	GUTZ	14	DPWA	Multichannel

$-2\times$IMAGINARY PART

VALUE (MeV)	DOCUMENT ID		TECN	COMMENT
180 to 280 ($\approx$ 230) OUR ESTIMATE				
270 ± 30	SARANTSEV	25	DPWA	Multichannel
• • • We do not use the following data for averages, fits, limits, etc. • • •				
429	HUNT	19	DPWA	Multichannel
33 ± 9	[1] ANISOVICH	17A	L+P	γp, $\pi^- p \to K\Lambda$
220 ± 50	SOKHOYAN	15A	DPWA	Multichannel
220 ± 50	GUTZ	14	DPWA	Multichannel

[1] Statistical error only.

$N(1880)$ ELASTIC POLE RESIDUE

MODULUS $|r|$

VALUE (MeV)	DOCUMENT ID		TECN	COMMENT
6 ± 4	SOKHOYAN	15A	DPWA	Multichannel
• • • We do not use the following data for averages, fits, limits, etc. • • •				
6 ± 4	GUTZ	14	DPWA	Multichannel
6 ± 4	ANISOVICH	12A	DPWA	Multichannel

PHASE θ

VALUE (°)	DOCUMENT ID		TECN	COMMENT
70 ± 60	SOKHOYAN	15A	DPWA	Multichannel
• • • We do not use the following data for averages, fits, limits, etc. • • •				
70 ± 60	GUTZ	14	DPWA	Multichannel
80 ± 65	ANISOVICH	12A	DPWA	Multichannel

$N(1880)$ INELASTIC POLE RESIDUE

The "normalized residue" is the residue divided by $\Gamma_{pole}/2$.

Normalized residue in $N\pi \to N(1880) \to N\eta$

MODULUS	PHASE (°)	DOCUMENT ID		TECN	COMMENT
0.11 ± 0.07	-75 ± 55	ANISOVICH	12A	DPWA	Multichannel

Normalized residue in $N\pi \to N(1880) \to \Lambda K$

MODULUS	PHASE (°)	DOCUMENT ID		TECN	COMMENT
0.05 ± 0.02	27 ± 30	ANISOVICH	17A	DPWA	γp, $\pi^- p \to K\Lambda$
• • • We do not use the following data for averages, fits, limits, etc. • • •					
0.3 ± 0.1	82 ± 9	[2] ANISOVICH	17A	L+P	γp, $\pi^- p \to K\Lambda$
0.03 ± 0.02	40 ± 40	ANISOVICH	12A	DPWA	Multichannel

[2] Statistical error only.

Int. J. Mod. Phys. A 2026.41. Downloaded from www.worldscientific.com
by UNIVERSITY OF CALIFORNIA @ BERKELEY on 09/16/26. Re-use and distribution is strictly not permitted, except for Open Access articles.

Normalized residue in $N\pi \to N(1880) \to \Sigma K$

MODULUS	PHASE (°)	DOCUMENT ID		TECN	COMMENT
• • • We do not use the following data for averages, fits, limits, etc. • • •					
0.11±0.06	95 ± 40	ANISOVICH	12A	DPWA	Multichannel

Normalized residue in $N\pi \to N(1880) \to \Delta\pi$, P-wave

MODULUS	PHASE (°)	DOCUMENT ID		TECN	COMMENT
0.14±0.08	−150 ± 55	SOKHOYAN	15A	DPWA	Multichannel
• • • We do not use the following data for averages, fits, limits, etc. • • •					
0.20±0.08	−150 ± 50	ANISOVICH	12A	DPWA	Multichannel

Normalized residue in $N\pi \to N(1880) \to N(1535)\pi$

MODULUS	PHASE (°)	DOCUMENT ID		TECN	COMMENT
0.09±0.05	130 ± 60	GUTZ	14	DPWA	Multichannel

Normalized residue in $N\pi \to N(1880) \to Na_0(980)$

MODULUS	PHASE (°)	DOCUMENT ID		TECN	COMMENT
0.04±0.03	40 ± 65	GUTZ	14	DPWA	Multichannel

Normalized residue in $N\pi \to N(1880) \to N\sigma$

MODULUS	PHASE (°)	DOCUMENT ID		TECN	COMMENT
0.10±0.05	−140 ± 55	SOKHOYAN	15A	DPWA	Multichannel

$N(1880)$ BREIT-WIGNER MASS

VALUE (MeV)	DOCUMENT ID		TECN	COMMENT
1830 to 1930 (≈ 1880) OUR ESTIMATE				
1865±25	SARANTSEV	25	DPWA	Multichannel
1967±20	[3] HUNT	19	DPWA	Multichannel
• • • We do not use the following data for averages, fits, limits, etc. • • •				
1875±40	SOKHOYAN	15A	DPWA	Multichannel
1875±40	GUTZ	14	DPWA	Multichannel
1900±36	[3] SHRESTHA	12A	DPWA	Multichannel

[3] Statistical error only.

$N(1880)$ BREIT-WIGNER WIDTH

VALUE (MeV)	DOCUMENT ID		TECN	COMMENT
200 to 400 (≈ 300) OUR ESTIMATE				
275± 30	SARANTSEV	25	DPWA	Multichannel
500± 77	[4] HUNT	19	DPWA	Multichannel
• • • We do not use the following data for averages, fits, limits, etc. • • •				
230± 50	SOKHOYAN	15A	DPWA	Multichannel
230± 50	GUTZ	14	DPWA	Multichannel
485±142	[4] SHRESTHA	12A	DPWA	Multichannel

[4] Statistical error only.

$N(1880)$ DECAY MODES

	Mode	Fraction (Γ_i/Γ)
Γ_1	$N\pi$	3–31 %
Γ_2	$N\eta$	1–55 %
Γ_3	$N\omega$	12–28 %
Γ_4	ΛK	1–3 %
Γ_5	ΣK	10–24 %
Γ_6	$N\pi\pi$	>32 %
Γ_7	$\Delta(1232)\pi$	5–42 %
Γ_8	$N\rho$	(28 ±7) %
Γ_9	$N\rho$, $S=1/2$	19–45 %
Γ_{10}	$N\rho$, $S=3/2$	(8.0±3.0) %
Γ_{11}	$N\sigma$	8–40 %
Γ_{12}	$N(1535)\pi$	4–12 %
Γ_{13}	$Na_0(980)$	1–5 %
Γ_{14}	$\Lambda K^*(892)$	0.5–1.1 %
Γ_{15}	$p\gamma$, helicity=1/2	seen
Γ_{16}	$n\gamma$, helicity=1/2	0.002–0.63 %

$N(1880)$ BRANCHING RATIOS

$\Gamma(N\pi)/\Gamma_{total}$ — Γ_1/Γ

VALUE (%)	DOCUMENT ID		TECN	COMMENT
3–31 % OUR ESTIMATE				
11±6	SEIFEN	25	DPWA	Multichannel
25±6	[5] HUNT	19	DPWA	Multichannel
• • • We do not use the following data for averages, fits, limits, etc. • • •				
6±3	SOKHOYAN	15A	DPWA	Multichannel
6±3	GUTZ	14	DPWA	Multichannel
15±5	[5] SHRESTHA	12A	DPWA	Multichannel

[5] Statistical error only.

$\Gamma(N\eta)/\Gamma_{total}$ — Γ_2/Γ

VALUE (%)	DOCUMENT ID		TECN	COMMENT
1–55 % OUR ESTIMATE				
18± 8	MUELLER	20	DPWA	Multichannel
2± 1	[6] HUNT	19	DPWA	Multichannel
25^{+30}_{-20}	ANISOVICH	12A	DPWA	Multichannel
• • • We do not use the following data for averages, fits, limits, etc. • • •				
16± 7	[6] SHRESTHA	12A	DPWA	Multichannel

[6] Statistical error only.

$\Gamma(N\omega)/\Gamma_{total}$ — Γ_3/Γ

VALUE (%)	DOCUMENT ID		TECN	COMMENT
12–28 % OUR ESTIMATE				
20±8	DENISENKO	16	DPWA	Multichannel

$\Gamma(\Lambda K)/\Gamma_{total}$ — Γ_4/Γ

VALUE (%)	DOCUMENT ID		TECN	COMMENT
1–3 % OUR ESTIMATE				
2± 1	[7] HUNT	19	DPWA	Multichannel
2± 1	ANISOVICH	12A	DPWA	Multichannel
• • • We do not use the following data for averages, fits, limits, etc. • • •				
32±10	[7] SHRESTHA	12A	DPWA	Multichannel

[7] Statistical error only.

$\Gamma(\Sigma K)/\Gamma_{total}$ — Γ_5/Γ

VALUE (%)	DOCUMENT ID		TECN	COMMENT
10–24 % OUR ESTIMATE				
17±7	ANISOVICH	12A	DPWA	Multichannel

$\Gamma(\Delta(1232)\pi)/\Gamma_{total}$ — Γ_7/Γ

VALUE (%)	DOCUMENT ID		TECN	COMMENT
5–42 % OUR ESTIMATE				
6± 3	SARANTSEV	25	DPWA	Multichannel
4± 2	SEIFEN	25	DPWA	Multichannel
11± 6	[8] HUNT	19	DPWA	Multichannel
• • • We do not use the following data for averages, fits, limits, etc. • • •				
30±12	SOKHOYAN	15A	DPWA	Multichannel
< 2	[8] SHRESTHA	12A	DPWA	Multichannel

[8] Statistical error only.

$\Gamma(N\rho)/\Gamma_{total}$ — Γ_8/Γ

VALUE (%)	DOCUMENT ID		TECN	COMMENT
28±7	SARANTSEV	25	DPWA	Multichannel

$\Gamma(N\rho, S=1/2)/\Gamma_{total}$ — Γ_9/Γ

VALUE (%)	DOCUMENT ID		TECN	COMMENT
19–45 % OUR ESTIMATE				
20± 6	SARANTSEV	25	DPWA	Multichannel
32±13	[9] HUNT	19	DPWA	Multichannel

[9] Statistical error only.

$\Gamma(N\rho, S=3/2)/\Gamma_{total}$ — Γ_{10}/Γ

VALUE (%)	DOCUMENT ID		TECN	COMMENT
8±3	SARANTSEV	25	DPWA	Multichannel

$\Gamma(N\sigma)/\Gamma_{total}$ — Γ_{11}/Γ

VALUE (%)	DOCUMENT ID		TECN	COMMENT
8–40 % OUR ESTIMATE				
20± 4	SARANTSEV	25	DPWA	Multichannel
22±13	SEIFEN	25	DPWA	Multichannel
< 9	[10] HUNT	19	DPWA	Multichannel
• • • We do not use the following data for averages, fits, limits, etc. • • •				
25±15	SOKHOYAN	15A	DPWA	Multichannel
8± 5	[10] SHRESTHA	12A	DPWA	Multichannel

[10] Statistical error only.

$\Gamma(N(1535)\pi)/\Gamma_{total}$ — Γ_{12}/Γ

VALUE (%)	DOCUMENT ID		TECN	COMMENT
4–12 % OUR ESTIMATE				
6±3	SEIFEN	25	DPWA	Multichannel
8±4	GUTZ	14	DPWA	Multichannel

$\Gamma(Na_0(980))/\Gamma_{total}$ — Γ_{13}/Γ

VALUE (%)	DOCUMENT ID		TECN	COMMENT
1–5 % OUR ESTIMATE				
3±2	GUTZ	14	DPWA	Multichannel

$\Gamma(\Lambda K^*(892))/\Gamma_{total}$ — Γ_{14}/Γ

VALUE (%)	DOCUMENT ID		TECN	COMMENT
0.5–1.1 % OUR ESTIMATE				
0.8±0.3	ANISOVICH	17B	DPWA	Multichannel

Int. J. Mod. Phys. A 2026.41. Downloaded from www.worldscientific.com
UNIVERSITY OF CALIFORNIA @ BERKELEY on 09/16/26. Re-use and distribution is strictly not permitted, except for Open Access articles.

$N(1880)$ PHOTON DECAY AMPLITUDES AT THE POLE

$N(1880) \to p\gamma$, helicity-1/2 amplitude $A_{1/2}$

MODULUS ($GeV^{-1/2}$)	PHASE (°)	DOCUMENT ID		TECN	COMMENT
0.015 ± 0.005	-10 ± 20	SARANTSEV	25	DPWA	Multichannel

$N(1880) \to n\gamma$, helicity-1/2 amplitude $A_{1/2}$

MODULUS ($GeV^{-1/2}$)	PHASE (°)	DOCUMENT ID		TECN	COMMENT
0.072 ± 0.024	-30 ± 30	ANISOVICH	17E	DPWA	Multichannel

$N(1880)$ BREIT-WIGNER PHOTON DECAY AMPLITUDES

$N(1880) \to p\gamma$, helicity-1/2 amplitude $A_{1/2}$

VALUE ($GeV^{-1/2}$)	DOCUMENT ID		TECN	COMMENT
0.016 ± 0.005	SARANTSEV	25	DPWA	Multichannel
0.119 ± 0.015	[11] HUNT	19	DPWA	Multichannel
• • • We do not use the following data for averages, fits, limits, etc. • • •				
0.021 ± 0.006	[11] SHRESTHA	12A	DPWA	Multichannel

[11] Statistical error only.

$N(1880) \to n\gamma$, helicity-1/2 amplitude $A_{1/2}$

VALUE ($GeV^{-1/2}$)	DOCUMENT ID		TECN	COMMENT
0.016 ± 0.010	[12] HUNT	19	DPWA	Multichannel
0.070 ± 0.022	ANISOVICH	17E	DPWA	Multichannel
• • • We do not use the following data for averages, fits, limits, etc. • • •				
-0.060 ± 0.050	ANISOVICH	13B	DPWA	Multichannel
0.014 ± 0.007	[12] SHRESTHA	12A	DPWA	Multichannel

[12] Statistical error only.

$N(1880)$ REFERENCES

SARANTSEV	25	PR C112 015202	A.V. Sarantsev *et al.*	(Bonn-Gatchina Collab.)
SEIFEN	25	EPJ A61 173	T. Seifen *et al.*	(CBELSA/TAPS Collab.)
MUELLER	20	PL B803 135323	J. Mueller *et al.*	(CBELSA/TAPS Collab.)
HUNT	19	PR C99 055205	B.C. Hunt, D.M. Manley	
ANISOVICH	17A	PRL 119 062004	A.V. Anisovich *et al.*	
ANISOVICH	17B	PL B771 142	A.V. Anisovich *et al.*	
ANISOVICH	17E	PR C96 055202	A.V. Anisovich *et al.*	(BONN, PNPI, JLAB+)
DENISENKO	16	PL B755 97	I. Denisenko *et al.*	
SOKHOYAN	15A	EPJ A51 95	V. Sokhoyan *et al.*	(CBELSA/TAPS Collab.)
GUTZ	14	EPJ A50 74	E. Gutz *et al.*	(CBELSA/TAPS Collab.)
ANISOVICH	13B	EPJ A49 67	A.V. Anisovich *et al.*	
ANISOVICH	12A	EPJ A48 15	A.V. Anisovich *et al.*	(BONN, PNPI)
SHRESTHA	12A	PR C86 055203	M. Shrestha, D.M. Manley	(KSU)

$N(1895)\ 1/2^-$

$I(J^P) = \frac{1}{2}(\frac{1}{2}^-)$ Status: ****

was $N(2090)$

Before our 2012 *Review*, this state appeared in our Listings as the $N(2090)$. Any structure in the S_{11} wave above 1800 MeV is listed here. A few early results that are now obsolete have been omitted.

$N(1895)$ POLE POSITION

REAL PART

VALUE (MeV)	DOCUMENT ID		TECN	COMMENT
1890 to 1930 (≈ 1910) OUR ESTIMATE				
1905 ± 15	SARANTSEV	25	DPWA	Multichannel
1907 ± 10	AFZAL	20	DPWA	Multichannel
1906 ± 17	[1] ANISOVICH	17A	L+P	$\gamma p, \pi^- p \to K\Lambda$
$1917 \pm 19 \pm 1$	[2] SVARC	14	L+P	$\pi N \to \pi N$
• • • We do not use the following data for averages, fits, limits, etc. • • •				
1956	HUNT	19	DPWA	Multichannel
1907 ± 10	SOKHOYAN	15A	DPWA	Multichannel
1797 ± 26	BATINIC	10	DPWA	$\pi N \to N\pi, N\eta$
1795	VRANA	00	DPWA	Multichannel
2150 ± 70	CUTKOSKY	80	IPWA	$\pi N \to \pi N$

[1] Statistical error only.
[2] Fit to the amplitudes of HOEHLER 79.

$-2\times$IMAGINARY PART

VALUE (MeV)	DOCUMENT ID		TECN	COMMENT
80 to 140 (≈ 110) OUR ESTIMATE				
185 ± 25	SARANTSEV	25	DPWA	Multichannel
100^{+40}_{-10}	AFZAL	20	DPWA	Multichannel
100 ± 10	[1] ANISOVICH	17A	L+P	$\gamma p, \pi^- p \to K\Lambda$
$101 \pm 36 \pm 1$	[1,2] SVARC	14	L+P	$\pi N \to \pi N$
• • • We do not use the following data for averages, fits, limits, etc. • • •				
449	HUNT	19	DPWA	Multichannel
100^{+40}_{-15}	SOKHOYAN	15A	DPWA	Multichannel
420 ± 45	BATINIC	10	DPWA	$\pi N \to N\pi, N\eta$
220	VRANA	00	DPWA	Multichannel
350 ± 100	CUTKOSKY	80	IPWA	$\pi N \to \pi N$

[1] Statistical error only.
[2] Fit to the amplitudes of HOEHLER 79.

$N(1895)$ ELASTIC POLE RESIDUE

MODULUS $|r|$

VALUE (MeV)	DOCUMENT ID		TECN	COMMENT
1 to 5 (≈ 3) OUR ESTIMATE				
3 ± 2	SOKHOYAN	15A	DPWA	Multichannel
3.1 ± 1.4	[1] SVARC	14	L+P	$\pi N \to \pi N$
• • • We do not use the following data for averages, fits, limits, etc. • • •				
1 ± 1	ANISOVICH	12A	DPWA	Multichannel
60	BATINIC	10	DPWA	$\pi N \to N\pi, N\eta$
40 ± 20	CUTKOSKY	80	IPWA	$\pi N \to \pi N$

[1] Fit to the amplitudes of HOEHLER 79.

PHASE θ

VALUE (°)	DOCUMENT ID		TECN	COMMENT
125 ± 45	SOKHOYAN	15A	DPWA	Multichannel
$-107 \pm 23 \pm 2$	[1] SVARC	14	L+P	$\pi N \to \pi N$
0 ± 90	CUTKOSKY	80	IPWA	$\pi N \to \pi N$
• • • We do not use the following data for averages, fits, limits, etc. • • •				
-164	BATINIC	10	DPWA	$\pi N \to N\pi, N\eta$

[1] Fit to the amplitudes of HOEHLER 79.

$N(1895)$ INELASTIC POLE RESIDUE

The "normalized residue" is the residue divided by $\Gamma_{pole}/2$.

Normalized residue in $N\pi \to N(1895) \to \Lambda K$

MODULUS	PHASE (°)	DOCUMENT ID		TECN	COMMENT
0.09 ± 0.03	8 ± 30	ANISOVICH	17A	DPWA	Multichannel
0.06 ± 0.02	87 ± 27	[1] ANISOVICH	17A	L+P	$\gamma p, \pi^- p \to K\Lambda$
• • • We do not use the following data for averages, fits, limits, etc. • • •					
0.05 ± 0.02	-90 ± 30	ANISOVICH	12A	DPWA	Multichannel

[1] Statistical error only.

Normalized residue in $N\pi \to N(1895) \to \Sigma K$

MODULUS	PHASE (°)	DOCUMENT ID		TECN	COMMENT
0.06 ± 0.02	40 ± 30	ANISOVICH	12A	DPWA	Multichannel

Normalized residue in $N\pi \to N(1895) \to \Delta(1232)\pi$

MODULUS	PHASE (°)	DOCUMENT ID		TECN	COMMENT
0.05 ± 0.025	-100 ± 45	SOKHOYAN	15A	DPWA	Multichannel

Normalized residue in $N\pi \to N(1895) \to N(1440)\pi$

MODULUS	PHASE (°)	DOCUMENT ID		TECN	COMMENT
0.05 ± 0.025	-100 ± 45	SOKHOYAN	15A	DPWA	Multichannel

$N(1895)$ BREIT-WIGNER MASS

VALUE (MeV)	DOCUMENT ID		TECN	COMMENT
1870 to 1920 (≈ 1895) OUR ESTIMATE				
1907 ± 15	SARANTSEV	25	DPWA	Multichannel
2000 ± 29	[1] HUNT	19	DPWA	Multichannel
1890^{+9}_{-23}	KASHEVAROV	17	DPWA	$\gamma p \to \eta p, \eta' p$
1880 ± 20	HOEHLER	79	IPWA	$\pi N \to \pi N$
• • • We do not use the following data for averages, fits, limits, etc. • • •				
1905 ± 12	SOKHOYAN	15A	DPWA	Multichannel
1910 ± 15	[1] SHRESTHA	12A	DPWA	Multichannel
1812 ± 25	BATINIC	10	DPWA	$\pi N \to N\pi, N\eta$
1822 ± 43	VRANA	00	DPWA	Multichannel
2180 ± 80	CUTKOSKY	80	IPWA	$\pi N \to \pi N$

[1] Statistical error only.

$N(1895)$ BREIT-WIGNER WIDTH

VALUE (MeV)	DOCUMENT ID		TECN	COMMENT
80 to 200 (≈ 120) OUR ESTIMATE				
195 ± 20	SARANTSEV	25	DPWA	Multichannel
466 ± 72	[1] HUNT	19	DPWA	Multichannel
150 ± 57	KASHEVAROV	17	DPWA	$\gamma p \to \eta p, \eta' p$
95 ± 30	HOEHLER	79	IPWA	$\pi N \to \pi N$
• • • We do not use the following data for averages, fits, limits, etc. • • •				
100^{+30}_{-10}	SOKHOYAN	15A	DPWA	Multichannel
502 ± 47	[1] SHRESTHA	12A	DPWA	Multichannel
405 ± 40	BATINIC	10	DPWA	$\pi N \to N\pi, N\eta$
248 ± 185	VRANA	00	DPWA	Multichannel
350 ± 100	CUTKOSKY	80	IPWA	$\pi N \to \pi N$

[1] Statistical error only.

Int. J. Mod. Phys. A 2026.41. Downloaded from www.worldscientific.com
by UNIVERSITY OF CALIFORNIA @ BERKELEY on 09/16/26. Re-use and distribution is strictly not permitted, except for Open Access articles.

N(1895) DECAY MODES

	Mode	Fraction (Γ_i/Γ)
Γ_1	$N\pi$	2–18 %
Γ_2	$N\eta$	15–45 %
Γ_3	$N\eta'$	10–40 %
Γ_4	$N\omega$	16–40 %
Γ_5	ΛK	3–23 %
Γ_6	ΣK	6–20 %
Γ_7	$N\pi\pi$	17–74 %
Γ_8	$\Delta(1232)\pi$	3–11 %
Γ_9	$N\rho$	14–50 %
Γ_{10}	$N\rho$, $S=1/2$	<18 %
Γ_{11}	$N\rho$, $S=3/2$	14–32 %
Γ_{12}	$N\sigma$	<13 %
Γ_{13}	$N(1440)\pi$	2–12 %
Γ_{14}	$\Lambda K^*(892)$	4–9 %
Γ_{15}	$p\gamma$, helicity=1/2	0.01–0.06 %
Γ_{16}	$n\gamma$, helicity=1/2	0.003–0.05 %

N(1895) BRANCHING RATIOS

$\Gamma(N\pi)/\Gamma_{total}$ — Γ_1/Γ

VALUE (%)	DOCUMENT ID		TECN	COMMENT
2–18 % OUR ESTIMATE				
6 ±4	SEIFEN	25	DPWA	Multichannel
8 ±4	[1] HUNT	19	DPWA	Multichannel
9 ±5	HOEHLER	79	IPWA	$\pi N \to \pi N$
• • • We do not use the following data for averages, fits, limits, etc. • • •				
2.5±1.5	SOKHOYAN	15A	DPWA	Multichannel
17 ±2	[1] SHRESTHA	12A	DPWA	Multichannel
32 ±6	BATINIC	10	DPWA	$\pi N \to N\pi$, $N\eta$
17 ±3	VRANA	00	DPWA	Multichannel
18 ±8	CUTKOSKY	80	IPWA	$\pi N \to \pi N$

[1] Statistical error only.

$\Gamma(N\eta)/\Gamma_{total}$ — Γ_2/Γ

VALUE (%)	DOCUMENT ID		TECN	COMMENT
15–45 % OUR ESTIMATE				
10± 5	MUELLER	20	DPWA	Multichannel
37± 9	[1] HUNT	19	DPWA	Multichannel
10± 5	ANISOVICH	17C	DPWA	Multichannel
20± 6	[2] KASHEVAROV	17	DPWA	$\gamma p \to \eta p$, $\eta' p$
• • • We do not use the following data for averages, fits, limits, etc. • • •				
21± 6	ANISOVICH	12A	DPWA	Multichannel
40± 4	[1] SHRESTHA	12A	DPWA	Multichannel
22±10	BATINIC	10	DPWA	$\pi N \to N\pi$, $N\eta$
41± 4	VRANA	00	DPWA	Multichannel

[1] Statistical error only.
[2] Assuming $A_{1/2} = -0.030$ GeV$^{-1/2}$.

$\Gamma(N\eta')/\Gamma_{total}$ — Γ_3/Γ

VALUE (%)	DOCUMENT ID		TECN	COMMENT
10–40 % OUR ESTIMATE				
13± 5	ANISOVICH	17C	DPWA	Multichannel
38±20	[1] KASHEVAROV	17	DPWA	$\gamma p \to \eta p$, $\eta' p$

[1] Assuming $A_{1/2} = -0.030$ GeV$^{-1/2}$.

$\Gamma(N\omega)/\Gamma_{total}$ — Γ_4/Γ

VALUE (%)	DOCUMENT ID		TECN	COMMENT
16–40 % OUR ESTIMATE				
28±12	DENISENKO	16	DPWA	Multichannel

$\Gamma(\Lambda K)/\Gamma_{total}$ — Γ_5/Γ

VALUE (%)	DOCUMENT ID		TECN	COMMENT
3–23 % OUR ESTIMATE				
7 ±4	[1] HUNT	19	DPWA	Multichannel
18 ±5	ANISOVICH	12A	DPWA	Multichannel
• • • We do not use the following data for averages, fits, limits, etc. • • •				
1.8±0.8	[1] SHRESTHA	12A	DPWA	Multichannel

[1] Statistical error only.

$\Gamma(\Sigma K)/\Gamma_{total}$ — Γ_6/Γ

VALUE (%)	DOCUMENT ID		TECN	COMMENT
6–20 % OUR ESTIMATE				
13±7	ANISOVICH	12A	DPWA	Multichannel

$\Gamma(\Delta(1232)\pi)/\Gamma_{total}$ — Γ_8/Γ

VALUE (%)	DOCUMENT ID		TECN	COMMENT
3–11 % OUR ESTIMATE				
8±3	SARANTSEV	25	DPWA	Multichannel
5±3	SEIFEN	25	DPWA	Multichannel
<10	[1] HUNT	19	DPWA	Multichannel
• • • We do not use the following data for averages, fits, limits, etc. • • •				
7±4	SOKHOYAN	15A	DPWA	Multichannel
7±3	[1] SHRESTHA	12A	DPWA	Multichannel
1±1	VRANA	00	DPWA	Multichannel

[1] Statistical error only.

$\Gamma(N\rho)/\Gamma_{total}$ — Γ_9/Γ

VALUE (%)	DOCUMENT ID		TECN	COMMENT
43±15	SARANTSEV	25	DPWA	Multichannel

$\Gamma(N\rho, S=1/2)/\Gamma_{total}$ — Γ_{10}/Γ

VALUE (%)	DOCUMENT ID		TECN	COMMENT
<18 % OUR ESTIMATE				
18±5	SARANTSEV	25	DPWA	Multichannel
<18	[1] HUNT	19	DPWA	Multichannel
• • • We do not use the following data for averages, fits, limits, etc. • • •				
< 2	[1] SHRESTHA	12A	DPWA	Multichannel
36±1	VRANA	00	DPWA	Multichannel

[1] Statistical error only.

$\Gamma(N\rho, S=3/2)/\Gamma_{total}$ — Γ_{11}/Γ

VALUE (%)	DOCUMENT ID		TECN	COMMENT
14–32 % OUR ESTIMATE				
25±14	SARANTSEV	25	DPWA	Multichannel
23± 9	[1] HUNT	19	DPWA	Multichannel
• • • We do not use the following data for averages, fits, limits, etc. • • •				
9± 3	[1] SHRESTHA	12A	DPWA	Multichannel
1± 1	VRANA	00	DPWA	Multichannel

[1] Statistical error only.

$\Gamma(N\sigma)/\Gamma_{total}$ — Γ_{12}/Γ

VALUE (%)	DOCUMENT ID		TECN	COMMENT
<13 % OUR ESTIMATE				
18±6	SARANTSEV	25	DPWA	Multichannel
11±7	SEIFEN	25	DPWA	Multichannel
<13	[1] HUNT	19	DPWA	Multichannel
• • • We do not use the following data for averages, fits, limits, etc. • • •				
< 2	[1] SHRESTHA	12A	DPWA	Multichannel
2±1	VRANA	00	DPWA	Multichannel

[1] Statistical error only.

$\Gamma(N(1440)\pi)/\Gamma_{total}$ — Γ_{13}/Γ

VALUE (%)	DOCUMENT ID		TECN	COMMENT
2–12 % OUR ESTIMATE				
2 ±2	SEIFEN	25	DPWA	Multichannel
7 ±5	[1] HUNT	19	DPWA	Multichannel
• • • We do not use the following data for averages, fits, limits, etc. • • •				
2.5±1.5	SOKHOYAN	15A	DPWA	Multichannel
24 ±4	[1] SHRESTHA	12A	DPWA	Multichannel
2 ±1	VRANA	00	DPWA	Multichannel

[1] Statistical error only.

$\Gamma(\Lambda K^*(892))/\Gamma_{total}$ — Γ_{14}/Γ

VALUE (%)	DOCUMENT ID		TECN	COMMENT
4–9 % OUR ESTIMATE				
6.3±2.5	ANISOVICH	17B	DPWA	Multichannel

N(1895) PHOTON DECAY AMPLITUDES AT THE POLE

$N(1895) \to p\gamma$, helicity-1/2 amplitude $A_{1/2}$

MODULUS (GeV$^{-1/2}$)	PHASE (°)	DOCUMENT ID		TECN	COMMENT
0.021±0.006	150 ± 30	SARANTSEV	25	DPWA	Multichannel
• • • We do not use the following data for averages, fits, limits, etc. • • •					
0.015±0.006	145 ± 35	SOKHOYAN	15A	DPWA	Multichannel

$N(1895) \to n\gamma$, helicity-1/2 amplitude $A_{1/2}$

MODULUS (GeV$^{-1/2}$)	PHASE (°)	DOCUMENT ID		TECN	COMMENT
−0.015±0.010	60 ± 25	ANISOVICH	17E	DPWA	Multichannel

N(1895) BREIT-WIGNER PHOTON DECAY AMPLITUDES

$N(1895) \to p\gamma$, helicity-1/2 amplitude $A_{1/2}$

VALUE (GeV$^{-1/2}$)	DOCUMENT ID		TECN	COMMENT
−0.021±0.008	SARANTSEV	25	DPWA	Multichannel
0.017±0.005	[1] HUNT	19	DPWA	Multichannel
• • • We do not use the following data for averages, fits, limits, etc. • • •				
−0.016±0.006	SOKHOYAN	15A	DPWA	Multichannel
0.012±0.006	[1] SHRESTHA	12A	DPWA	Multichannel

[1] Statistical error only.

Int. J. Mod. Phys. A 2026.41. Downloaded from www.worldscientific.com
UNIVERSITY OF CALIFORNIA @ BERKELEY on 09/16/26. Re-use and distribution is strictly not permitted, except for Open Access articles.

$N(1895) \to n\gamma$, helicity-1/2 amplitude $A_{1/2}$

VALUE ($GeV^{-1/2}$)	DOCUMENT ID		TECN	COMMENT
0.002±0.013	[1] HUNT	19	DPWA	Multichannel
−0.014±0.010	ANISOVICH	17E	DPWA	Multichannel
• • • We do not use the following data for averages, fits, limits, etc. • • •				
0.013±0.006	ANISOVICH	13B	DPWA	Multichannel
0.003±0.007	[1] SHRESTHA	12A	DPWA	Multichannel

[1] Statistical error only.

$N(1895)$ REFERENCES

SARANTSEV	25	PR C112 015202	A.V. Sarantsev *et al.*	(Bonn-Gatchina Collab.)
SEIFEN	25	EPJ A61 173	T. Seifen *et al.*	(CBELSA/TAPS Collab.)
AFZAL	20	PRL 125 152002	F. Afzal *et al.*	(CBELSA/TAPS Collab.)
MUELLER	20	PL B803 135323	J. Mueller *et al.*	(CBELSA/TAPS Collab.)
HUNT	19	PR C99 055205	B.C. Hunt, D.M. Manley	
ANISOVICH	17A	PRL 119 062004	A.V. Anisovich *et al.*	
ANISOVICH	17B	PL B771 142	A.V. Anisovich *et al.*	
ANISOVICH	17C	PL B772 247	A.V. Anisovich *et al.*	
ANISOVICH	17E	PR C96 055202	A.V. Anisovich *et al.*	(BONN, PNPI, JLAB+)
KASHEVAROV	17	PRL 118 212001	V.L. Kashevarov *et al.*	(A2/MAMI Collab.)
DENISENKO	16	PL B755 97	I. Denisenko *et al.*	
SOKHOYAN	15A	EPJ A51 95	V. Sokhoyan *et al.*	(CBELSA/TAPS Collab.)
SVARC	14	PR C89 045205	A. Svarc *et al.*	(RBI Zagreb, UNI Tuzla)
ANISOVICH	13B	EPJ A49 67	A.V. Anisovich *et al.*	
ANISOVICH	12A	EPJ A48 15	A.V. Anisovich *et al.*	(BONN, PNPI)
SHRESTHA	12A	PR C86 055203	M. Shrestha, D.M. Manley	(KSU)
BATINIC	10	PR C82 038203	M. Batinic *et al.*	(ZAGR)
VRANA	00	PRPL 328 181	T.P. Vrana, S.A. Dytman, T.-S.H. Lee	(PITT, ANL)
CUTKOSKY	80	Toronto Conf. 19	R.E. Cutkosky *et al.*	(CMU, LBL) IJP
Also		PR D20 2839	R.E. Cutkosky *et al.*	(CMU, LBL)
HOEHLER	79	PDAT 12-1	G. Hohler *et al.*	(KARLT) IJP
Also		Toronto Conf. 3	R. Koch	(KARLT) IJP

$N(1900)$ $3/2^+$

$I(J^P) = \frac{1}{2}(\frac{3}{2}^+)$ Status: ****

$N(1900)$ POLE POSITION

REAL PART

VALUE (MeV)	DOCUMENT ID		TECN	COMMENT
1900 to 1940 (≈ 1920) OUR ESTIMATE				
1925±25	SARANTSEV	25	DPWA	Multichannel
1905± 2	ROENCHEN	22	DPWA	Multichannel
1928±18±2	[1] SVARC	14	L+P	$\pi N \to \pi N$
• • • We do not use the following data for averages, fits, limits, etc. • • •				
1856	HUNT	19	DPWA	Multichannel
1912±30	[2] ANISOVICH	17A	L+P	$\gamma p, \pi^- p \to K\Lambda$
1910±30	SOKHOYAN	15A	DPWA	Multichannel
1910±30	GUTZ	14	DPWA	Multichannel
1910	SHKLYAR	13	DPWA	Multichannel

[1] Fit to the amplitudes of HOEHLER 79.
[2] Statistical error only.

−2×IMAGINARY PART

VALUE (MeV)	DOCUMENT ID		TECN	COMMENT
90 to 160 (≈ 130) OUR ESTIMATE				
270±30	SARANTSEV	25	DPWA	Multichannel
93± 2	ROENCHEN	22	DPWA	Multichannel
152±40±9	[1] SVARC	14	L+P	$\pi N \to \pi N$
• • • We do not use the following data for averages, fits, limits, etc. • • •				
241	HUNT	19	DPWA	Multichannel
166±30	[2] ANISOVICH	17A	L+P	$\gamma p, \pi^- p \to K\Lambda$
280±50	SOKHOYAN	15A	DPWA	Multichannel
280±50	GUTZ	14	DPWA	Multichannel
173	SHKLYAR	13	DPWA	Multichannel

[1] Fit to the amplitudes of HOEHLER 79.
[2] Statistical error only.

$N(1900)$ ELASTIC POLE RESIDUE

MODULUS $|r|$

VALUE (MeV)	DOCUMENT ID		TECN	COMMENT
2 to 6 (≈ 4) OUR ESTIMATE				
1.6±0.2	ROENCHEN	22	DPWA	Multichannel
4 ±2	SOKHOYAN	15A	DPWA	Multichannel
4 ±1 ±1	[1] SVARC	14	L+P	$\pi N \to \pi N$
• • • We do not use the following data for averages, fits, limits, etc. • • •				
4 ±2	GUTZ	14	DPWA	Multichannel
10	SHKLYAR	13	DPWA	Multichannel
3 ±2	ANISOVICH	12A	DPWA	Multichannel

[1] Fit to the amplitudes of HOEHLER 79.

PHASE θ

VALUE (°)	DOCUMENT ID		TECN	COMMENT
−40 to 20 (≈ −10) OUR ESTIMATE				
44±11	ROENCHEN	22	DPWA	Multichannel
−10±40	SOKHOYAN	15A	DPWA	Multichannel
−29±15±2	[1] SVARC	14	L+P	$\pi N \to \pi N$
• • • We do not use the following data for averages, fits, limits, etc. • • •				
−10±40	GUTZ	14	DPWA	Multichannel
−64	SHKLYAR	13	DPWA	Multichannel
10±35	ANISOVICH	12A	DPWA	Multichannel

[1] Fit to the amplitudes of HOEHLER 79.

$N(1900)$ INELASTIC POLE RESIDUE

The "normalized residue" is the residue divided by $\Gamma_{pole}/2$.

Normalized residue in $N\pi \to N(1900) \to N\eta$

MODULUS	PHASE (°)	DOCUMENT ID		TECN	COMMENT
0.010±0.002	55 ± 15	ROENCHEN	22	DPWA	Multichannel
0.05 ±0.02	70 ± 60	ANISOVICH	12A	DPWA	Multichannel

Normalized residue in $N\pi \to N(1900) \to \Lambda K$

MODULUS	PHASE (°)	DOCUMENT ID		TECN	COMMENT
0.029±0.003	5.4 ± 9.3	ROENCHEN	22	DPWA	Multichannel
0.03 ±0.02	90 ± 40	ANISOVICH	17A	DPWA	Multichannel
• • • We do not use the following data for averages, fits, limits, etc. • • •					
0.07 ±0.03	135 ± 25	ANISOVICH	12A	DPWA	Multichannel

Normalized residue in $N\pi \to N(1900) \to \Sigma K$

MODULUS	PHASE (°)	DOCUMENT ID		TECN	COMMENT
0.013±0.002	−40 ± 9	ROENCHEN	22	DPWA	Multichannel
0.04 ±0.02	110 ± 30	ANISOVICH	12A	DPWA	Multichannel

Normalized residue in $N\pi \to N(1900) \to N(1535)\pi$

MODULUS	PHASE (°)	DOCUMENT ID		TECN	COMMENT
0.04±0.01	170 ± 30	GUTZ	14	DPWA	Multichannel

Normalized residue in $N\pi \to N(1900) \to \Delta(1232)\pi$, P-wave

MODULUS	PHASE (°)	DOCUMENT ID		TECN	COMMENT
0.07±0.04	−65 ± 30	SOKHOYAN	15A	DPWA	Multichannel

Normalized residue in $N\pi \to N(1900) \to \Delta(1232)\pi$, F-wave

MODULUS	PHASE (°)	DOCUMENT ID		TECN	COMMENT
0.10±0.05	80 ± 30	SOKHOYAN	15A	DPWA	Multichannel

Normalized residue in $N\pi \to N(1900) \to N(1520)\pi$

MODULUS	PHASE (°)	DOCUMENT ID		TECN	COMMENT
0.07±0.04	−105 ± 35	SOKHOYAN	15A	DPWA	Multichannel

Normalized residue in $N\pi \to N(1900) \to N\sigma$

MODULUS	PHASE (°)	DOCUMENT ID		TECN	COMMENT
0.03±0.02	−110 ± 35	SOKHOYAN	15A	DPWA	Multichannel

$N(1900)$ BREIT-WIGNER MASS

VALUE (MeV)	DOCUMENT ID		TECN	COMMENT
1890 to 1950 (≈ 1920) OUR ESTIMATE				
1930±15	SARANTSEV	25	DPWA	Multichannel
1911± 6	[1] HUNT	19	DPWA	Multichannel
1998± 3	[1] SHKLYAR	13	DPWA	Multichannel
• • • We do not use the following data for averages, fits, limits, etc. • • •				
1910±30	SOKHOYAN	15A	DPWA	Multichannel
1910±30	GUTZ	14	DPWA	Multichannel
1900± 8	[1] SHRESTHA	12A	DPWA	Multichannel
1951±53	PENNER	02C	DPWA	Multichannel

[1] Statistical error only.

$N(1900)$ BREIT-WIGNER WIDTH

VALUE (MeV)	DOCUMENT ID		TECN	COMMENT
100 to 320 (≈ 200) OUR ESTIMATE				
270±20	SARANTSEV	25	DPWA	Multichannel
292±16	[1] HUNT	19	DPWA	Multichannel
359±10	[1] SHKLYAR	13	DPWA	Multichannel
• • • We do not use the following data for averages, fits, limits, etc. • • •				
270±50	SOKHOYAN	15A	DPWA	Multichannel
270±50	GUTZ	14	DPWA	Multichannel
101±15	[1] SHRESTHA	12A	DPWA	Multichannel
622±42	PENNER	02C	DPWA	Multichannel

[1] Statistical error only.

Int. J. Mod. Phys. A 2026.41. Downloaded from www.worldscientific.com
by UNIVERSITY OF CALIFORNIA @ BERKELEY on 09/16/26. Re-use and distribution is strictly not permitted, except for Open Access articles.

N(1900) DECAY MODES

	Mode	Fraction (Γ_i/Γ)
Γ_1	$N\pi$	1–20 %
Γ_2	$N\eta$	2–14 %
Γ_3	$N\eta'$	4–8 %
Γ_4	$N\omega$	7–13 %
Γ_5	ΛK	2–20 %
Γ_6	ΣK	3–7 %
Γ_7	$N\pi\pi$	>56 %
Γ_8	$\Delta(1232)\pi$	30–70 %
Γ_9	$\Delta(1232)\pi$, P-wave	9–25 %
Γ_{10}	$\Delta(1232)\pi$, F-wave	21–45 %
Γ_{11}	$N\rho$	(46 ±13) %
Γ_{12}	$N\rho$, $S=1/2$	25–40 %
Γ_{13}	$N\rho$, $S=3/2$, P-wave	(9.0± 3.0) %
Γ_{14}	$N\rho$, $S=3/2$, F-wave	(30 ±12) %
Γ_{15}	$N\sigma$	1–7 %
Γ_{16}	$N(1440)\pi$	(9 ± 6) %
Γ_{17}	$N(1520)\pi$, S-wave	7–23 %
Γ_{18}	$N(1535)\pi$	4–10 %
Γ_{19}	$\Lambda K^*(892)$	< 0.2 %
Γ_{20}	$p\gamma$	0.001–0.025 %
Γ_{21}	$p\gamma$, helicity=1/2	0.001–0.021 %
Γ_{22}	$p\gamma$, helicity=3/2	<0.003 %
Γ_{23}	$n\gamma$	<0.040 %
Γ_{24}	$n\gamma$, helicity=1/2	<0.007 %
Γ_{25}	$n\gamma$, helicity=3/2	<0.033 %

N(1900) BRANCHING RATIOS

$\Gamma(N\pi)/\Gamma_{total}$ — Γ_1/Γ

VALUE (%)	DOCUMENT ID		TECN	COMMENT
1–20 % OUR ESTIMATE				
4 ±3	SEIFEN	25	DPWA	Multichannel
1.9±0.1	[1] HUNT	19	DPWA	Multichannel
25 ±1	[1] SHKLYAR	13	DPWA	Multichannel
• • • We do not use the following data for averages, fits, limits, etc. • • •				
3 ±2	SOKHOYAN	15A	DPWA	Multichannel
3 ±2	GUTZ	14	DPWA	Multichannel
7 ±4	[1] SHRESTHA	12A	DPWA	Multichannel
16 ±2	PENNER	02C	DPWA	Multichannel

[1] Statistical error only.

$\Gamma(N\eta)/\Gamma_{total}$ — Γ_2/Γ

VALUE (%)	DOCUMENT ID		TECN	COMMENT
2 ±2	MUELLER	20	DPWA	Multichannel
1.3±0.5	[1] HUNT	19	DPWA	Multichannel
2 ±2	[1] SHKLYAR	13	DPWA	Multichannel
10 ±4	ANISOVICH	12A	DPWA	Multichannel
• • • We do not use the following data for averages, fits, limits, etc. • • •				
< 1	[1] SHRESTHA	12A	DPWA	Multichannel
14 ±5	PENNER	02C	DPWA	Multichannel

[1] Statistical error only.

$\Gamma(N\eta')/\Gamma_{total}$ — Γ_3/Γ

VALUE (%)	DOCUMENT ID		TECN	COMMENT
4–8 % OUR ESTIMATE				
6±2	ANISOVICH	17C	DPWA	Multichannel

$\Gamma(N\omega)/\Gamma_{total}$ — Γ_4/Γ

VALUE (%)	DOCUMENT ID		TECN	COMMENT
15±8	DENISENKO	16	DPWA	Multichannel
10±3	[1] SHKLYAR	13	DPWA	Multichannel
• • • We do not use the following data for averages, fits, limits, etc. • • •				
39±9	PENNER	02C	DPWA	Multichannel

[1] Statistical error only.

$\Gamma(\Lambda K)/\Gamma_{total}$ — Γ_5/Γ

VALUE (%)	DOCUMENT ID		TECN	COMMENT
13.7±0.3	[1] HUNT	19	DPWA	Multichannel
16 ±5	ANISOVICH	12A	DPWA	Multichannel
2.4±0.3	[1] SHKLYAR	05	DPWA	Multichannel
• • • We do not use the following data for averages, fits, limits, etc. • • •				
14 ±5	[1] SHRESTHA	12A	DPWA	Multichannel
5 to 15	NIKONOV	08	DPWA	Multichannel
0.1±0.1	PENNER	02C	DPWA	Multichannel

[1] Statistical error only.

$\Gamma(\Sigma K)/\Gamma_{total}$ — Γ_6/Γ

VALUE (%)	DOCUMENT ID		TECN	COMMENT
5±2	ANISOVICH	12A	DPWA	Multichannel
• • • We do not use the following data for averages, fits, limits, etc. • • •				
1±1	PENNER	02C	DPWA	Multichannel

$\Gamma(\Delta(1232)\pi)/\Gamma_{total}$ — Γ_8/Γ

VALUE (%)	DOCUMENT ID		TECN	COMMENT
13±5	SARANTSEV	25	DPWA	Multichannel

$\Gamma(\Delta(1232)\pi$, P-wave$)/\Gamma_{total}$ — Γ_9/Γ

VALUE (%)	DOCUMENT ID		TECN	COMMENT
8±4	SARANTSEV	25	DPWA	Multichannel
9±6	SEIFEN	25	DPWA	Multichannel
• • • We do not use the following data for averages, fits, limits, etc. • • •				
17±8	SOKHOYAN	15A	DPWA	Multichannel

$\Gamma(\Delta(1232)\pi$, F-wave$)/\Gamma_{total}$ — Γ_{10}/Γ

VALUE (%)	DOCUMENT ID		TECN	COMMENT
5± 3	SARANTSEV	25	DPWA	Multichannel
4± 3	SEIFEN	25	DPWA	Multichannel
• • • We do not use the following data for averages, fits, limits, etc. • • •				
33±12	SOKHOYAN	15A	DPWA	Multichannel

$\Gamma(N\rho)/\Gamma_{total}$ — Γ_{11}/Γ

VALUE (%)	DOCUMENT ID		TECN	COMMENT
46±13	SARANTSEV	25	DPWA	Multichannel

$\Gamma(N\rho, S=1/2)/\Gamma_{total}$ — Γ_{12}/Γ

VALUE (%)	DOCUMENT ID		TECN	COMMENT
25–40 % OUR ESTIMATE				
7±4	SARANTSEV	25	DPWA	Multichannel
32±7	[1] HUNT	19	DPWA	Multichannel

[1] Statistical error only.

$\Gamma(N\rho, S=3/2$, P-wave$)/\Gamma_{total}$ — Γ_{13}/Γ

VALUE (%)	DOCUMENT ID		TECN	COMMENT
9±3	SARANTSEV	25	DPWA	Multichannel

$\Gamma(N\rho, S=3/2$, F-wave$)/\Gamma_{total}$ — Γ_{14}/Γ

VALUE (%)	DOCUMENT ID		TECN	COMMENT
30±12	SARANTSEV	25	DPWA	Multichannel

$\Gamma(N\sigma)/\Gamma_{total}$ — Γ_{15}/Γ

VALUE (%)	DOCUMENT ID		TECN	COMMENT
10±3	SARANTSEV	25	DPWA	Multichannel
9±4	SEIFEN	25	DPWA	Multichannel
• • • We do not use the following data for averages, fits, limits, etc. • • •				
4±3	SOKHOYAN	15A	DPWA	Multichannel

$\Gamma(N(1440)\pi)/\Gamma_{total}$ — Γ_{16}/Γ

VALUE (%)	DOCUMENT ID		TECN	COMMENT
9±6	SEIFEN	25	DPWA	Multichannel

$\Gamma(N(1520)\pi$, S-wave$)/\Gamma_{total}$ — Γ_{17}/Γ

VALUE (%)	DOCUMENT ID		TECN	COMMENT
< 2	SEIFEN	25	DPWA	Multichannel
15±8	SOKHOYAN	15A	DPWA	Multichannel

$\Gamma(N(1535)\pi)/\Gamma_{total}$ — Γ_{18}/Γ

VALUE (%)	DOCUMENT ID		TECN	COMMENT
15±6	SEIFEN	25	DPWA	Multichannel
7±3	GUTZ	14	DPWA	Multichannel

$\Gamma(\Lambda K^*(892))/\Gamma_{total}$ — Γ_{19}/Γ

VALUE (%)	DOCUMENT ID		TECN	COMMENT
< 0.2 % OUR ESTIMATE				
<0.2	ANISOVICH	17B	DPWA	Multichannel

N(1900) PHOTON DECAY AMPLITUDES AT THE POLE

$N(1900) \to p\gamma$, helicity-1/2 amplitude $A_{1/2}$

MODULUS ($GeV^{-1/2}$)	PHASE (°)	DOCUMENT ID		TECN	COMMENT
−0.050 ±0.012	40 ± 40	SARANTSEV	25	DPWA	Multichannel
0.0091±0.0014	80 ± 12	ROENCHEN	22	DPWA	Multichannel
• • • We do not use the following data for averages, fits, limits, etc. • • •					
0.026 ±0.014	60 ± 35	SOKHOYAN	15A	DPWA	Multichannel

$N(1900) \to p\gamma$, helicity-3/2 amplitude $A_{3/2}$

MODULUS ($GeV^{-1/2}$)	PHASE (°)	DOCUMENT ID		TECN	COMMENT
−0.044 ±0.012	35 ± 20	SARANTSEV	25	DPWA	Multichannel
−0.0077±0.0017	−42 ± 12	ROENCHEN	22	DPWA	Multichannel
• • • We do not use the following data for averages, fits, limits, etc. • • •					
−0.070 ±0.030	70 ± 50	SOKHOYAN	15A	DPWA	Multichannel

Int. J. Mod. Phys. A 2026.41. Downloaded from www.worldscientific.com
UNIVERSITY OF CALIFORNIA @ BERKELEY on 09/16/26. Re-use and distribution is strictly not permitted, except for Open Access articles.

$N(1900) \to n\gamma$, helicity-1/2 amplitude $A_{1/2}$

MODULUS ($GeV^{-1/2}$)	PHASE (°)	DOCUMENT ID		TECN	COMMENT
-0.098 ± 0.020	-13 ± 20	ANISOVICH	17E	DPWA	Multichannel

$N(1900) \to n\gamma$, helicity-3/2 amplitude $A_{3/2}$

MODULUS ($GeV^{-1/2}$)	PHASE (°)	DOCUMENT ID		TECN	COMMENT
0.074 ± 0.015	5 ± 15	ANISOVICH	17E	DPWA	Multichannel

$N(1900)$ BREIT-WIGNER PHOTON DECAY AMPLITUDES

$N(1900) \to p\gamma$, helicity-1/2 amplitude $A_{1/2}$

VALUE ($GeV^{-1/2}$)	DOCUMENT ID		TECN	COMMENT
-0.050 ± 0.012	SARANTSEV	25	DPWA	Multichannel
0.040 ± 0.004	[1] HUNT	19	DPWA	Multichannel
-0.008 ± 0.001	[1] SHKLYAR	13	DPWA	Multichannel
• • • We do not use the following data for averages, fits, limits, etc. • • •				
0.024 ± 0.014	SOKHOYAN	15A	DPWA	Multichannel
0.024 ± 0.014	GUTZ	14	DPWA	Multichannel
0.041 ± 0.008	[1] SHRESTHA	12A	DPWA	Multichannel
-0.017	PENNER	02D	DPWA	Multichannel

[1] Statistical error only.

$N(1900) \to p\gamma$, helicity-3/2 amplitude $A_{3/2}$

VALUE ($GeV^{-1/2}$)	DOCUMENT ID		TECN	COMMENT
-0.044 ± 0.014	SARANTSEV	25	DPWA	Multichannel
-0.094 ± 0.007	[1] HUNT	19	DPWA	Multichannel
< 0.001	SHKLYAR	13	DPWA	Multichannel
• • • We do not use the following data for averages, fits, limits, etc. • • •				
-0.067 ± 0.030	SOKHOYAN	15A	DPWA	Multichannel
-0.067 ± 0.030	GUTZ	14	DPWA	Multichannel
-0.004 ± 0.006	[1] SHRESTHA	12A	DPWA	Multichannel
0.031	PENNER	02D	DPWA	Multichannel

[1] Statistical error only.

$N(1900) \to n\gamma$, helicity-1/2 amplitude $A_{1/2}$

VALUE ($GeV^{-1/2}$)	DOCUMENT ID		TECN	COMMENT
0.007 ± 0.014	[1] HUNT	19	DPWA	Multichannel
-0.102 ± 0.020	ANISOVICH	17E	DPWA	Multichannel
• • • We do not use the following data for averages, fits, limits, etc. • • •				
0.000 ± 0.030	ANISOVICH	13B	DPWA	Multichannel
-0.010 ± 0.004	[1] SHRESTHA	12A	DPWA	Multichannel
-0.016	PENNER	02D	DPWA	Multichannel

[1] Statistical error only.

$N(1900) \to n\gamma$, helicity-3/2 amplitude $A_{3/2}$

VALUE ($GeV^{-1/2}$)	DOCUMENT ID		TECN	COMMENT
0.007 ± 0.011	[1] HUNT	19	DPWA	Multichannel
0.073 ± 0.015	ANISOVICH	17E	DPWA	Multichannel
• • • We do not use the following data for averages, fits, limits, etc. • • •				
-0.060 ± 0.045	ANISOVICH	13B	DPWA	Multichannel
-0.011 ± 0.007	[1] SHRESTHA	12A	DPWA	Multichannel
-0.002	PENNER	02D	DPWA	Multichannel

[1] Statistical error only.

$N(1900)$ REFERENCES

SARANTSEV	25	PR C112 015202	A.V. Sarantsev *et al.*	(Bonn-Gatchina Collab.)
SEIFEN	25	EPJ A61 173	T. Seifen *et al.*	(CBELSA/TAPS Collab.)
ROENCHEN	22	EPJ A58 229	D. Roenchen *et al.*	(JULI, GWU, BONN+)
MUELLER	20	PL B803 135323	J. Mueller *et al.*	(CBELSA/TAPS Collab.)
HUNT	19	PR C99 055205	B.C. Hunt, D.M. Manley	
ANISOVICH	17A	PRL 119 062004	A.V. Anisovich *et al.*	
ANISOVICH	17B	PL B771 142	A.V. Anisovich *et al.*	
ANISOVICH	17C	PL B772 247	A.V. Anisovich *et al.*	
ANISOVICH	17E	PR C96 055202	A.V. Anisovich *et al.*	(BONN, PNPI, JLAB+)
DENISENKO	16	PL B755 97	I. Denisenko *et al.*	
SOKHOYAN	15A	EPJ A51 95	V. Sokhoyan *et al.*	(CBELSA/TAPS Collab.)
GUTZ	14	EPJ A50 74	E. Gutz *et al.*	(CBELSA/TAPS Collab.)
SVARC	14	PR C89 045205	A. Svarc *et al.*	(RBI Zagreb, UNI Tuzla)
ANISOVICH	13B	EPJ A49 67	A.V. Anisovich *et al.*	
SHKLYAR	13	PR C87 015201	V. Shklyar, H. Lenske, U. Mosel	(GIES)
ANISOVICH	12A	EPJ A48 15	A.V. Anisovich *et al.*	(BONN, PNPI)
SHRESTHA	12A	PR C86 055203	M. Shrestha, D.M. Manley	(KSU)
NIKONOV	08	PL B662 245	V.A. Nikonov *et al.*	(Bonn, Gatchina)
SHKLYAR	05	PR C72 015210	V. Shklyar, H. Lenske, U. Mosel	(GIES)
PENNER	02C	PR C66 055211	G. Penner, U. Mosel	(GIES)
PENNER	02D	PR C66 055212	G. Penner, U. Mosel	(GIES)
HOEHLER	79	PDAT 12-1	G. Hohler *et al.*	(KARLT)

$N(1990)\ 7/2^+$

$I(J^P) = \frac{1}{2}(\frac{7}{2}^+)$ Status: **

OMITTED FROM SUMMARY TABLE

Older and obsolete values are listed and referenced in the 2014 edition, Chinese Physics **C38** 070001 (2014).

$N(1990)$ POLE POSITION

REAL PART

VALUE (MeV)	DOCUMENT ID		TECN	COMMENT
2005 ± 25	SARANTSEV	25	DPWA	Multichannel
1861 ± 5	ROENCHEN	22	DPWA	Multichannel
1900 ± 30	CUTKOSKY	80	IPWA	$\pi N \to \pi N$
• • • We do not use the following data for averages, fits, limits, etc. • • •				
1913	HUNT	19	DPWA	Multichannel
1738	ROENCHEN	15A	DPWA	Multichannel
2030 ± 65	ANISOVICH	12A	DPWA	Multichannel
2301	VRANA	00	DPWA	Multichannel

$-2\times$IMAGINARY PART

VALUE (MeV)	DOCUMENT ID		TECN	COMMENT
270 ± 30	SARANTSEV	25	DPWA	Multichannel
72 ± 3	ROENCHEN	22	DPWA	Multichannel
260 ± 60	CUTKOSKY	80	IPWA	$\pi N \to \pi N$
• • • We do not use the following data for averages, fits, limits, etc. • • •				
163	HUNT	19	DPWA	Multichannel
188	ROENCHEN	15A	DPWA	Multichannel
240 ± 60	ANISOVICH	12A	DPWA	Multichannel
202	VRANA	00	DPWA	Multichannel

$N(1990)$ ELASTIC POLE RESIDUE

MODULUS $|r|$

VALUE (MeV)	DOCUMENT ID		TECN	COMMENT
0.16 ± 0.01	ROENCHEN	22	DPWA	Multichannel
2 ± 1	ANISOVICH	12A	DPWA	Multichannel
9 ± 3	CUTKOSKY	80	IPWA	$\pi N \to \pi N$
• • • We do not use the following data for averages, fits, limits, etc. • • •				
4.3	ROENCHEN	15A	DPWA	Multichannel

PHASE θ

VALUE (°)	DOCUMENT ID		TECN	COMMENT
-119 ± 2	ROENCHEN	22	DPWA	Multichannel
125 ± 65	ANISOVICH	12A	DPWA	Multichannel
-60 ± 30	CUTKOSKY	80	IPWA	$\pi N \to \pi N$
• • • We do not use the following data for averages, fits, limits, etc. • • •				
-70	ROENCHEN	15A	DPWA	Multichannel

$\Delta(1990)$ INELASTIC POLE RESIDUE

The "normalized residue" is the residue divided by $\Gamma_{pole}/2$.

Normalized residue in $N\pi \to N(1990) \to N\eta$

MODULUS	PHASE (°)	DOCUMENT ID		TECN	COMMENT
0.048 ± 0.001	**-43 ± 2**	ROENCHEN	22	DPWA	Multichannel
• • • We do not use the following data for averages, fits, limits, etc. • • •					
0.013	-82	ROENCHEN	15A	DPWA	Multichannel

Normalized residue in $N\pi \to N(1990) \to \Lambda K$

MODULUS	PHASE (°)	DOCUMENT ID		TECN	COMMENT
0.004 ± 0.001	**133 ± 2**	ROENCHEN	22	DPWA	Multichannel
• • • We do not use the following data for averages, fits, limits, etc. • • •					
0.022	-111	ROENCHEN	15A	DPWA	Multichannel

Normalized residue in $N\pi \to N(1990) \to \Sigma K$

MODULUS	PHASE (°)	DOCUMENT ID		TECN	COMMENT
0.010 ± 0.002	-54 ± 2	ROENCHEN	22	DPWA	Multichannel
• • • We do not use the following data for averages, fits, limits, etc. • • •					
0.005	24	ROENCHEN	15A	DPWA	Multichannel

$N(1990)$ BREIT-WIGNER MASS

VALUE (MeV)	DOCUMENT ID		TECN	COMMENT
1950 to 2100 ($\approx$ 2020) OUR ESTIMATE				
2020 ± 25	SARANTSEV	25	DPWA	Multichannel
2028 ± 19	[1] HUNT	19	DPWA	Multichannel
1970 ± 50	CUTKOSKY	80	IPWA	$\pi N \to \pi N$
2005 ± 150	HOEHLER	79	IPWA	$\pi N \to \pi N$
• • • We do not use the following data for averages, fits, limits, etc. • • •				
2060 ± 65	ANISOVICH	12A	DPWA	Multichannel
1990 ± 45	[1] SHRESTHA	12A	DPWA	Multichannel
2311 ± 16	VRANA	00	DPWA	Multichannel

[1] Statistical error only.

Int. J. Mod. Phys. A 2026.41. Downloaded from www.worldscientific.com
by UNIVERSITY OF CALIFORNIA @ BERKELEY on 09/16/26. Re-use and distribution is strictly not permitted, except for Open Access articles.

N(1990) BREIT-WIGNER WIDTH

VALUE (MeV)	DOCUMENT ID		TECN	COMMENT
200 to 400 (≈ 300) OUR ESTIMATE				
280 ± 30	SARANTSEV	25	DPWA	Multichannel
490 ± 110	[1] HUNT	19	DPWA	Multichannel
350 ± 120	CUTKOSKY	80	IPWA	$\pi N \to \pi N$
350 ± 100	HOEHLER	79	IPWA	$\pi N \to \pi N$
• • • We do not use the following data for averages, fits, limits, etc. • • •				
240 ± 50	ANISOVICH	12A	DPWA	Multichannel
203 ± 161	[1] SHRESTHA	12A	DPWA	Multichannel
205 ± 72	VRANA	00	DPWA	Multichannel

[1] Statistical error only.

N(1990) DECAY MODES

	Mode	Fraction (Γ_i/Γ)
Γ_1	$N\pi$	2–6 %
Γ_2	$N\eta$	<3 %
Γ_3	ΛK	5.9–6.1 %
Γ_4	$N\pi\pi$	
Γ_5	$\Delta\pi$	(72 ±15) %
Γ_6	$\Delta\pi$, F-wave	
Γ_7	$N\rho$	(10 ± 5) %
Γ_8	$N\rho$, S=1/2	(8 ± 4) %
Γ_9	$N\rho$, S=3/2 , F-wave	(2.0± 2.0) %
Γ_{10}	$N(1440)\pi$	< 2 %
Γ_{11}	$N(1520)\pi$, P-wave	< 2 %
Γ_{12}	$N(1535)\pi$	< 2 %
Γ_{13}	$p\gamma$	0.01–0.12%
Γ_{14}	$p\gamma$, helicity=1/2	0.003–0.042%
Γ_{15}	$p\gamma$, helicity=3/2	0.009–0.075 %
Γ_{16}	$n\gamma$	0.01–0.16 %
Γ_{17}	$n\gamma$, helicity=1/2	0.003–0.066 %
Γ_{18}	$n\gamma$, helicity=3/2	0.003–0.098 %

N(1990) BRANCHING RATIOS

$\Gamma(N\pi)/\Gamma_{total}$ — Γ_1/Γ

VALUE (%)	DOCUMENT ID		TECN	COMMENT
2–6 % OUR ESTIMATE				
1 ± 1	SEIFEN	25	DPWA	Multichannel
1.9 ± 0.4	[1] HUNT	19	DPWA	Multichannel
6 ± 2	CUTKOSKY	80	IPWA	$\pi N \to \pi N$
4 ± 2	HOEHLER	79	IPWA	$\pi N \to \pi N$
• • • We do not use the following data for averages, fits, limits, etc. • • •				
2 ± 1	ANISOVICH	12A	DPWA	Multichannel
2 ± 1	[1] SHRESTHA	12A	DPWA	Multichannel
22 ±11	VRANA	00	DPWA	Multichannel

[1] Statistical error only.

$\Gamma(N\eta)/\Gamma_{total}$ — Γ_2/Γ

VALUE (%)	DOCUMENT ID		TECN	COMMENT
<3 % OUR ESTIMATE				
1 ±1	MUELLER	20	DPWA	Multichannel
1.7 ± 0.9	[1] HUNT	19	DPWA	Multichannel

[1] Statistical error only.

$\Gamma(\Lambda K)/\Gamma_{total}$ — Γ_3/Γ

VALUE (%)	DOCUMENT ID		TECN	COMMENT
5.9–6.1 % OUR ESTIMATE				
6.0 ± 0.1	[1] HUNT	19	DPWA	Multichannel

[1] Statistical error only.

$\Gamma(\Delta\pi)/\Gamma_{total}$ — Γ_5/Γ

VALUE (%)	DOCUMENT ID		TECN	COMMENT
72±15	SARANTSEV	25	DPWA	Multichannel

$\Gamma(\Delta\pi, F\text{-wave})/\Gamma_{total}$ — Γ_6/Γ

VALUE (%)	DOCUMENT ID		TECN	COMMENT
72 ± 15	SARANTSEV	25	DPWA	Multichannel
65 ± 20	SEIFEN	25	DPWA	Multichannel

$\Gamma(N\rho)/\Gamma_{total}$ — Γ_7/Γ

VALUE (%)	DOCUMENT ID		TECN	COMMENT
10±5	SARANTSEV	25	DPWA	Multichannel

$\Gamma(N\rho, S=1/2)/\Gamma_{total}$ — Γ_8/Γ

VALUE (%)	DOCUMENT ID		TECN	COMMENT
8±4	SARANTSEV	25	DPWA	Multichannel

$\Gamma(N\rho, S=3/2, F\text{-wave})/\Gamma_{total}$ — Γ_9/Γ

VALUE (%)	DOCUMENT ID		TECN	COMMENT
2±2	SARANTSEV	25	DPWA	Multichannel

$\Gamma(N(1440)\pi)/\Gamma_{total}$ — Γ_{10}/Γ

VALUE (%)	DOCUMENT ID		TECN	COMMENT
<2	SEIFEN	25	DPWA	Multichannel

$\Gamma(N(1520)\pi, P\text{-wave})/\Gamma_{total}$ — Γ_{11}/Γ

VALUE (%)	DOCUMENT ID		TECN	COMMENT
<2	SEIFEN	25	DPWA	Multichannel

$\Gamma(N(1535)\pi)/\Gamma_{total}$ — Γ_{12}/Γ

VALUE (%)	DOCUMENT ID		TECN	COMMENT
<2	SEIFEN	25	DPWA	Multichannel

N(1990) PHOTON DECAY AMPLITUDES AT THE POLE

N(1990) → $p\gamma$, helicity-1/2 amplitude $A_{1/2}$

MODULUS ($GeV^{-1/2}$)	PHASE (°)	DOCUMENT ID		TECN	COMMENT
0.011 ± 0.006	40 ± 20	SARANTSEV	25	DPWA	Multichannel
−0.030 ± 0.008	−135 ± 13	ROENCHEN	22	DPWA	Multichannel
• • • We do not use the following data for averages, fits, limits, etc. • • •					
0.029	67	ROENCHEN	15A	DPWA	Multichannel

N(1990) → $p\gamma$, helicity-3/2 amplitude $A_{3/2}$

MODULUS ($GeV^{-1/2}$)	PHASE (°)	DOCUMENT ID		TECN	COMMENT
0.017 ± 0.008	90 ± 25	SARANTSEV	25	DPWA	Multichannel
−0.018 ± 0.006	53 ± 16	ROENCHEN	22	DPWA	Multichannel
• • • We do not use the following data for averages, fits, limits, etc. • • •					
0.033	39	ROENCHEN	15A	DPWA	Multichannel

N(1990) → $n\gamma$, helicity-1/2 amplitude $A_{1/2}$

MODULUS ($GeV^{-1/2}$)	PHASE (°)	DOCUMENT ID		TECN	COMMENT
−0.032 ± 0.015	5 ± 20	ANISOVICH	17E	DPWA	Multichannel

N(1990) → $n\gamma$, helicity-3/2 amplitude $A_{3/2}$

MODULUS ($GeV^{-1/2}$)	PHASE (°)	DOCUMENT ID		TECN	COMMENT
−0.070 ± 0.025	0 ± 20	ANISOVICH	17E	DPWA	Multichannel

N(1990) BREIT-WIGNER PHOTON DECAY AMPLITUDES

N(1990) → $p\gamma$, helicity-1/2 amplitude $A_{1/2}$

VALUE ($GeV^{-1/2}$)	DOCUMENT ID		TECN	COMMENT
0.012 ± 0.010	SARANTSEV	25	DPWA	Multichannel
0.006 ± 0.003	[1] HUNT	19	DPWA	Multichannel
• • • We do not use the following data for averages, fits, limits, etc. • • •				
0.040 ± 0.012	ANISOVICH	12A	DPWA	Multichannel

[1] Statistical error only.

N(1990) → $p\gamma$, helicity-3/2 amplitude $A_{3/2}$

VALUE ($GeV^{-1/2}$)	DOCUMENT ID		TECN	COMMENT
0.017 ± 0.008	[1] SARANTSEV	25	DPWA	Multichannel
−0.055 ± 0.008	[2] HUNT	19	DPWA	Multichannel
• • • We do not use the following data for averages, fits, limits, etc. • • •				
0.057 ± 0.012	ANISOVICH	12A	DPWA	Multichannel

[1] Sign is undetermined.
[2] Statistical error only.

N(1990) → $n\gamma$, helicity-1/2 amplitude $A_{1/2}$

VALUE ($GeV^{-1/2}$)	DOCUMENT ID		TECN	COMMENT
−0.027 ± 0.024	[1] HUNT	19	DPWA	Multichannel
−0.032 ± 0.015	ANISOVICH	17E	DPWA	Multichannel
• • • We do not use the following data for averages, fits, limits, etc. • • •				
−0.045 ± 0.020	ANISOVICH	13B	DPWA	Multichannel

[1] Statistical error only.

N(1990) → $n\gamma$, helicity-3/2 amplitude $A_{3/2}$

VALUE ($GeV^{-1/2}$)	DOCUMENT ID		TECN	COMMENT
0.051 ± 0.020	[1] HUNT	19	DPWA	Multichannel
−0.072 ± 0.025	ANISOVICH	17E	DPWA	Multichannel
• • • We do not use the following data for averages, fits, limits, etc. • • •				
−0.052 ± 0.027	ANISOVICH	13B	DPWA	Multichannel

[1] Statistical error only.

Int. J. Mod. Phys. A 2026.41. Downloaded from www.worldscientific.com
UNIVERSITY OF CALIFORNIA @ BERKELEY on 09/16/26. Re-use and distribution is strictly not permitted, except for Open Access articles.

$N(1990)$ REFERENCES

For early references, see Physics Letters **111B** 1 (1982).

SARANTSEV	25	PR C112 015202	A.V. Sarantsev *et al.*	(Bonn-Gatchina Collab.)
SEIFEN	25	EPJ A61 173	T. Seifen *et al.*	(CBELSA/TAPS Collab.)
ROENCHEN	22	EPJ A58 229	D. Roenchen *et al.*	(JULI, GWU, BONN+)
MUELLER	20	PL B803 135323	J. Mueller *et al.*	(CBELSA/TAPS Collab.)
HUNT	19	PR C99 055205	B.C. Hunt, D.M. Manley	
ANISOVICH	17E	PR C96 055202	A.V. Anisovich *et al.*	(BONN, PNPI, JLAB+)
ROENCHEN	15A	EPJ A51 70	D. Roenchen *et al.*	
PDG	14	CP C38 070001	K. Olive *et al.*	(PDG Collab.)
ANISOVICH	13B	EPJ A49 67	A.V. Anisovich *et al.*	
ANISOVICH	12A	EPJ A48 15	A.V. Anisovich *et al.*	(BONN, PNPI)
SHRESTHA	12A	PR C86 055203	M. Shrestha, D.M. Manley	(KSU)
VRANA	00	PRPL 328 181	T.P. Vrana, S.A. Dytman, T.-S.H. Lee	(PITT, ANL)
CUTKOSKY	80	Toronto Conf. 19	R.E. Cutkosky *et al.*	(CMU, LBL) IJP
Also		PR D20 2839	R.E. Cutkosky *et al.*	(CMU, LBL) IJP
HOEHLER	79	PDAT 12-1	G. Hohler *et al.*	(KARLT) IJP
Also		Toronto Conf. 3	R. Koch	(KARLT) IJP

$N(2000)$ $5/2^+$

$I(J^P) = \frac{1}{2}(\frac{5}{2}^+)$ Status: **

OMITTED FROM SUMMARY TABLE
was $N(1900)$

Before the 2012 *Review*, all the evidence for a $J^P = 5/2^+$ state with a mass above 1800 MeV was filed under a two-star $N(2000)$. There is now some evidence from ANISOVICH 12A for two $5/2^+$ states in this region, so we have split the older data (according to mass) between two two-star $5/2^+$ states, an $N(1860)$ and an $N(2000)$.

$N(2000)$ POLE POSITION

REAL PART

VALUE (MeV)	DOCUMENT ID		TECN	COMMENT
1990±40	SARANTSEV	25	DPWA	Multichannel
• • • We do not use the following data for averages, fits, limits, etc. • • •				
2030±40	SOKHOYAN	15A	DPWA	Multichannel
1900	SHKLYAR	13	DPWA	Multichannel

−2×IMAGINARY PART

VALUE (MeV)	DOCUMENT ID		TECN	COMMENT
480±60	SARANTSEV	25	DPWA	Multichannel
• • • We do not use the following data for averages, fits, limits, etc. • • •				
380±60	SOKHOYAN	15A	DPWA	Multichannel
123	SHKLYAR	13	DPWA	Multichannel

$N(2000)$ ELASTIC POLE RESIDUE

MODULUS $|r|$

VALUE (MeV)	DOCUMENT ID		TECN	COMMENT
18± 8	SOKHOYAN	15A	DPWA	Multichannel
• • • We do not use the following data for averages, fits, limits, etc. • • •				
11	SHKLYAR	13	DPWA	Multichannel
35^{+80}_{-15}	ANISOVICH	12A	DPWA	Multichannel

PHASE θ

VALUE (°)	DOCUMENT ID		TECN	COMMENT
−150±40	SOKHOYAN	15A	DPWA	Multichannel
• • • We do not use the following data for averages, fits, limits, etc. • • •				
− 6	SHKLYAR	13	DPWA	Multichannel
−100±40	ANISOVICH	12A	DPWA	Multichannel

$N(2000)$ INELASTIC POLE RESIDUE

The "normalized residue" is the residue divided by $\Gamma_{pole}/2$.

Normalized residue in $N\pi \to N(2000) \to \Delta(1232)\pi$, P-wave

MODULUS	PHASE (°)	DOCUMENT ID		TECN	COMMENT
0.16±0.06	100 ± 50	SOKHOYAN	15A	DPWA	Multichannel

Normalized residue in $N\pi \to N(2000) \to \Delta(1232)\pi$, F-wave

MODULUS	PHASE (°)	DOCUMENT ID		TECN	COMMENT
0.20±0.10	−20 ± 45	SOKHOYAN	15A	DPWA	Multichannel

Normalized residue in $N\pi \to N(2000) \to N\sigma$

MODULUS	PHASE (°)	DOCUMENT ID		TECN	COMMENT
0.12±0.06	80 ± 40	SOKHOYAN	15A	DPWA	Multichannel

Normalized residue in $N\pi \to N(2000) \to N(1520)\pi$, D-wave

MODULUS	PHASE (°)	DOCUMENT ID		TECN	COMMENT
0.17±0.09	−60 ± 35	SOKHOYAN	15A	DPWA	Multichannel

$N(2000)$ BREIT-WIGNER MASS

VALUE (MeV)	DOCUMENT ID		TECN	COMMENT
2050±40	SARANTSEV	25	DPWA	Multichannel
1946± 4 [1]	SHKLYAR	13	DPWA	Multichannel
• • • We do not use the following data for averages, fits, limits, etc. • • •				
2060±30	SOKHOYAN	15A	DPWA	Multichannel

[1] Statistical error only.

$N(2000)$ BREIT-WIGNER WIDTH

VALUE (MeV)	DOCUMENT ID		TECN	COMMENT
500±60	SARANTSEV	25	DPWA	Multichannel
198± 2 [2]	SHKLYAR	13	DPWA	Multichannel
• • • We do not use the following data for averages, fits, limits, etc. • • •				
390±55	SOKHOYAN	15A	DPWA	Multichannel

[2] Statistical error only.

$N(2000)$ DECAY MODES

	Mode	Fraction (Γ_i/Γ)
Γ_1	$N\pi$	6–10 %
Γ_2	$N\eta$	<4 %
Γ_3	$N\omega$	<2 %
Γ_4	$N\pi\pi$	35–90 %
Γ_5	$\Delta(1232)\pi$	30–80 %
Γ_6	$\Delta(1232)\pi$, P-wave	12–32 %
Γ_7	$\Delta(1232)\pi$, F-wave	19–49 %
Γ_8	$N\rho$	(15 ±4) %
Γ_9	$N\rho$, S=1/2	(8.0±3.0) %
Γ_{10}	$N\rho$, S=3/2 , P-wave	(7.0±3.0) %
Γ_{11}	$N\sigma$	5–15 %
Γ_{12}	$N(1520)\pi$, D-wave	11–31 %
Γ_{13}	$N(1680)\pi$, P-wave	17–25 %
Γ_{14}	$\Lambda K^*(892)$	1–3 %
Γ_{15}	$p\gamma$	0.01–0.08 %
Γ_{16}	$p\gamma$, helicity=1/2	0.003–0.031 %
Γ_{17}	$p\gamma$, helicity=3/2	0.008–0.048 %
Γ_{18}	$n\gamma$	0.002–0.07 %
Γ_{19}	$n\gamma$, helicity=1/2	<0.017 %
Γ_{20}	$n\gamma$, helicity=3/2	0.001–0.056 %

$N(2000)$ BRANCHING RATIOS

$\Gamma(N\pi)/\Gamma_{total}$ — Γ_1/Γ

VALUE (%)	DOCUMENT ID		TECN	COMMENT
6 to 10 (≈ 8) OUR ESTIMATE				
11±5	SEIFEN	25	DPWA	Multichannel
10±1 [3]	SHKLYAR	13	DPWA	Multichannel
• • • We do not use the following data for averages, fits, limits, etc. • • •				
8±4	SOKHOYAN	15A	DPWA	Multichannel

[3] Statistical error only.

$\Gamma(N\eta)/\Gamma_{total}$ — Γ_2/Γ

VALUE (%)	DOCUMENT ID		TECN	COMMENT
2±2	MUELLER	20	DPWA	Multichannel
2±2 [4]	SHKLYAR	13	DPWA	Multichannel

[4] Statistical error only.

$\Gamma(N\omega)/\Gamma_{total}$ — Γ_3/Γ

VALUE (%)	DOCUMENT ID		TECN	COMMENT
18±8	DENISENKO	16	DPWA	Multichannel
1±1 [5]	SHKLYAR	13	DPWA	Multichannel

[5] Statistical error only.

$\Gamma(\Delta(1232)\pi)/\Gamma_{total}$ — Γ_5/Γ

VALUE (%)	DOCUMENT ID		TECN	COMMENT
25±6	SARANTSEV	25	DPWA	Multichannel

$\Gamma(\Delta(1232)\pi, P\text{-wave})/\Gamma_{total}$ — Γ_6/Γ

VALUE (%)	DOCUMENT ID		TECN	COMMENT
8± 4	SARANTSEV	25	DPWA	Multichannel
9± 4	SEIFEN	25	DPWA	Multichannel
• • • We do not use the following data for averages, fits, limits, etc. • • •				
22±10	SOKHOYAN	15A	DPWA	Multichannel

Int. J. Mod. Phys. A 2026.41. Downloaded from www.worldscientific.com
by UNIVERSITY OF CALIFORNIA @ BERKELEY on 09/16/26. Re-use and distribution is strictly not permitted, except for Open Access articles.

$\Gamma(\Delta(1232)\pi, F\text{-wave})/\Gamma_{total}$ — Γ_7/Γ

VALUE (%)	DOCUMENT ID		TECN	COMMENT
17± 4	SARANTSEV	25	DPWA	Multichannel
16± 4	SEIFEN	25	DPWA	Multichannel
• • • We do not use the following data for averages, fits, limits, etc. • • •				
34±15	SOKHOYAN	15A	DPWA	Multichannel

$\Gamma(N\rho)/\Gamma_{total}$ — Γ_8/Γ

VALUE (%)	DOCUMENT ID		TECN	COMMENT
15±4	SARANTSEV	25	DPWA	Multichannel

$\Gamma(N\rho, S=1/2)/\Gamma_{total}$ — Γ_9/Γ

VALUE (%)	DOCUMENT ID		TECN	COMMENT
8±3	SARANTSEV	25	DPWA	Multichannel

$\Gamma(N\rho, S=3/2, P\text{-wave})/\Gamma_{total}$ — Γ_{10}/Γ

VALUE (%)	DOCUMENT ID		TECN	COMMENT
7±3	SARANTSEV	25	DPWA	Multichannel

$\Gamma(N\sigma)/\Gamma_{total}$ — Γ_{11}/Γ

VALUE (%)	DOCUMENT ID		TECN	COMMENT
28±10	SARANTSEV	25	DPWA	Multichannel
28±15	SEIFEN	25	DPWA	Multichannel
• • • We do not use the following data for averages, fits, limits, etc. • • •				
10± 5	SOKHOYAN	15A	DPWA	Multichannel

$\Gamma(N(1520)\pi, D\text{-wave})/\Gamma_{total}$ — Γ_{12}/Γ

VALUE (%)	DOCUMENT ID		TECN	COMMENT
2± 2	SEIFEN	25	DPWA	Multichannel
• • • We do not use the following data for averages, fits, limits, etc. • • •				
21±10	SOKHOYAN	15A	DPWA	Multichannel

$\Gamma(N(1680)\pi, P\text{-wave})/\Gamma_{total}$ — Γ_{13}/Γ

VALUE (%)	DOCUMENT ID		TECN	COMMENT
28±9	SEIFEN	25	DPWA	Multichannel
• • • We do not use the following data for averages, fits, limits, etc. • • •				
16±9	SOKHOYAN	15A	DPWA	Multichannel

$\Gamma(\Lambda K^*(892))/\Gamma_{total}$ — Γ_{14}/Γ

VALUE (%)	DOCUMENT ID		TECN	COMMENT
1–3 % OUR EVALUATION				
2.2±1.0	ANISOVICH	17B	DPWA	Multichannel

N(2000) PHOTON DECAY AMPLITUDES AT THE POLE

$N(2000) \to p\gamma$, helicity-1/2 amplitude $A_{1/2}$

MODULUS ($GeV^{-1/2}$)	PHASE (°)	DOCUMENT ID		TECN	COMMENT
0.033±0.006	35 ± 25	SARANTSEV	25	DPWA	Multichannel
• • • We do not use the following data for averages, fits, limits, etc. • • •					
0.033±0.010	15 ± 25	SOKHOYAN	15A	DPWA	Multichannel

$N(2000) \to p\gamma$, helicity-3/2 amplitude $A_{3/2}$

MODULUS ($GeV^{-1/2}$)	PHASE (°)	DOCUMENT ID		TECN	COMMENT
0.043±0.012	−100 ± 30	SARANTSEV	25	DPWA	Multichannel
• • • We do not use the following data for averages, fits, limits, etc. • • •					
0.045±0.008	−140 ± 25	SOKHOYAN	15A	DPWA	Multichannel

$N(2000) \to n\gamma$, helicity-1/2 amplitude $A_{1/2}$

MODULUS ($GeV^{-1/2}$)	PHASE (°)	DOCUMENT ID		TECN	COMMENT
0.019±0.010	−80 ± 40	ANISOVICH	17E	DPWA	Multichannel

$N(2000) \to n\gamma$, helicity-3/2 amplitude $A_{3/2}$

MODULUS ($GeV^{-1/2}$)	PHASE (°)	DOCUMENT ID		TECN	COMMENT
0.011±0.005	82 ± 30	ANISOVICH	17E	DPWA	Multichannel

N(2000) BREIT-WIGNER PHOTON DECAY AMPLITUDES

$N(2000) \to p\gamma$, helicity-1/2 amplitude $A_{1/2}$

VALUE ($GeV^{-1/2}$)	DOCUMENT ID		TECN	COMMENT
0.033±0.006	SARANTSEV	25	DPWA	Multichannel
0.011±0.001	[6] SHKLYAR	13	DPWA	Multichannel
• • • We do not use the following data for averages, fits, limits, etc. • • •				
0.031±0.010	SOKHOYAN	15A	DPWA	Multichannel

[6] Statistical error only.

$N(2000) \to p\gamma$, helicity-3/2 amplitude $A_{3/2}$

VALUE ($GeV^{-1/2}$)	DOCUMENT ID		TECN	COMMENT
−0.044±0.012	SARANTSEV	25	DPWA	Multichannel
0.025±0.001	[7] SHKLYAR	13	DPWA	Multichannel
• • • We do not use the following data for averages, fits, limits, etc. • • •				
−0.043±0.008	SOKHOYAN	15A	DPWA	Multichannel

[7] Statistical error only.

$N(2000) \to n\gamma$, helicity-1/2 amplitude $A_{1/2}$

VALUE ($GeV^{-1/2}$)	DOCUMENT ID		TECN	COMMENT
−0.018±0.012	ANISOVICH	13B	DPWA	Multichannel

$N(2000) \to n\gamma$, helicity-3/2 amplitude $A_{3/2}$

VALUE ($GeV^{-1/2}$)	DOCUMENT ID		TECN	COMMENT
−0.035±0.020	ANISOVICH	13B	DPWA	Multichannel

N(2000) REFERENCES

SARANTSEV	25	PR C112 015202	A.V. Sarantsev *et al.*	(Bonn-Gatchina Collab.)
SEIFEN	25	EPJ A61 173	T. Seifen *et al.*	(CBELSA/TAPS Collab.)
MUELLER	20	PL B803 135323	J. Mueller *et al.*	(CBELSA/TAPS Collab.)
ANISOVICH	17B	PL B771 142	A.V. Anisovich *et al.*	
ANISOVICH	17E	PR C96 055202	A.V. Anisovich *et al.*	(BONN, PNPI, JLAB+)
DENISENKO	16	PL B755 97	I. Denisenko *et al.*	
SOKHOYAN	15A	EPJ A51 95	V. Sokhoyan *et al.*	(CBELSA/TAPS Collab.)
ANISOVICH	13B	EPJ A49 67	A.V. Anisovich *et al.*	
SHKLYAR	13	PR C87 015201	V. Shklyar, H. Lenske, U. Mosel	(GIES)
ANISOVICH	12A	EPJ A48 15	A.V. Anisovich *et al.*	(BONN, PNPI)

N(2040) 3/2+

$J^P = \frac{3}{2}^+$ Status: *

OMITTED FROM SUMMARY TABLE

N(2040) MASS

VALUE (MeV)	DOCUMENT ID		TECN	COMMENT
$2040^{+3}_{-4} \pm 25$	ABLIKIM	09B	BES2	$J/\psi \to p\overline{p}\pi^0$
$2068 \pm 3^{+15}_{-40}$	ABLIKIM	06K	BES2	$J/\psi \to p\overline{n}\pi^-, n\overline{p}\pi^+$
• • • We do not use the following data for averages, fits, limits, etc. • • •				
2244±30	[1,2] HUNT	19	DPWA	Multichannel

[1] Statistical error only.
[2] We list here candidates for high-mass 3/2+ states.

N(2040) WIDTH

VALUE (MeV)	DOCUMENT ID		TECN	COMMENT
230± 8±52	ABLIKIM	09B	BES2	$J/\psi \to p\overline{p}\pi^0$
165±14±40	ABLIKIM	06K	BES2	$J/\psi \to p\overline{n}\pi^-, n\overline{p}\pi^+$
• • • We do not use the following data for averages, fits, limits, etc. • • •				
530±89	[3,4] HUNT	19	DPWA	Multichannel

[3] Statistical error only.
[4] We list here candidates for high-mass 3/2+ states.

N(2040) REFERENCES

HUNT	19	PR C99 055205	B.C. Hunt, D.M. Manley	
ABLIKIM	09B	PR D80 052004	M. Ablikim *et al.*	(BES II Collab.)
ABLIKIM	06K	PRL 97 062001	M. Ablikim *et al.*	(BES II Collab.)

N(2060) 5/2−

$I(J^P) = \frac{1}{2}(\frac{5}{2}^-)$ Status: ***

was N(2200)

Before our 2012 *Review*, this state appeared in our Listings as the N(2200).

N(2060) POLE POSITION

REAL PART

VALUE (MeV)	DOCUMENT ID		TECN	COMMENT
2020 to 2130 (≈ 2070) OUR ESTIMATE				
2020±30	SARANTSEV	25	DPWA	Multichannel
2119±11±1	[1] SVARC	14	L+P	$\pi N \to \pi N$
2100±60	CUTKOSKY	80	IPWA	$\pi N \to \pi N$
• • • We do not use the following data for averages, fits, limits, etc. • • •				
2010	HUNT	19	DPWA	Multichannel
2030±15	SOKHOYAN	15A	DPWA	Multichannel
2144±31	BATINIC	10	DPWA	$\pi N \to N\pi, N\eta$

[1] Fit to the amplitudes of HOEHLER 79.

−2×IMAGINARY PART

VALUE (MeV)	DOCUMENT ID		TECN	COMMENT
350 to 430 (≈ 400) OUR ESTIMATE				
410±50	SARANTSEV	25	DPWA	Multichannel
370±20±5	[1] SVARC	14	L+P	$\pi N \to \pi N$
360±80	CUTKOSKY	80	IPWA	$\pi N \to \pi N$
• • • We do not use the following data for averages, fits, limits, etc. • • •				
395	HUNT	19	DPWA	Multichannel
400±35	SOKHOYAN	15A	DPWA	Multichannel
438±13	BATINIC	10	DPWA	$\pi N \to N\pi, N\eta$

[1] Fit to the amplitudes of HOEHLER 79.

Int. J. Mod. Phys. A 2026.41. Downloaded from www.worldscientific.com
UNIVERSITY OF CALIFORNIA @ BERKELEY on 09/16/26. Re-use and distribution is strictly not permitted, except for Open Access articles.

$N(2060)$ ELASTIC POLE RESIDUE

MODULUS $|r|$

VALUE (MeV)	DOCUMENT ID		TECN	COMMENT
15 to 30 (≈ 20) OUR ESTIMATE				
25 ± 8	SOKHOYAN	15A	DPWA	Multichannel
19 ± 1 ± 1	[1] SVARC	14	L+P	$\pi N \to \pi N$
20 ± 10	CUTKOSKY	80	IPWA	$\pi N \to \pi N$
• • • We do not use the following data for averages, fits, limits, etc. • • •				
19 ± 5	ANISOVICH	12A	DPWA	Multichannel
26	BATINIC	10	DPWA	$\pi N \to N\pi$, $N\eta$

[1] Fit to the amplitudes of HOEHLER 79.

PHASE θ

VALUE (°)	DOCUMENT ID		TECN	COMMENT
−130 to −90 (≈ −110) OUR ESTIMATE				
−130 ± 20	SOKHOYAN	15A	DPWA	Multichannel
− 94 ± 5 ± 1	[1] SVARC	14	L+P	$\pi N \to \pi N$
− 90 ± 50	CUTKOSKY	80	IPWA	$\pi N \to \pi N$
• • • We do not use the following data for averages, fits, limits, etc. • • •				
−125 ± 20	ANISOVICH	12A	DPWA	Multichannel
− 71	BATINIC	10	DPWA	$\pi N \to N\pi$, $N\eta$

[1] Fit to the amplitudes of HOEHLER 79.

$N(2060)$ INELASTIC POLE RESIDUE

The "normalized residue" is the residue divided by $\Gamma_{pole}/2$.

Normalized residue in $N\pi \to N(2060) \to N\eta$

MODULUS	PHASE (°)	DOCUMENT ID		TECN	COMMENT
0.05 ± 0.03	40 ± 25	ANISOVICH	12A	DPWA	Multichannel

Normalized residue in $N\pi \to N(2060) \to \Lambda K$

MODULUS	DOCUMENT ID		TECN	COMMENT
0.01 ± 0.005	ANISOVICH	12A	DPWA	Multichannel

Normalized residue in $N\pi \to N(2060) \to \Sigma K$

MODULUS	PHASE (°)	DOCUMENT ID		TECN	COMMENT
0.04 ± 0.02	−70 ± 30	ANISOVICH	12A	DPWA	Multichannel

Normalized residue in $N\pi \to N(2060) \to \Delta(1232)\pi$, D-wave

MODULUS	PHASE (°)	DOCUMENT ID		TECN	COMMENT
0.06 ± 0.03	−90 ± 40	SOKHOYAN	15A	DPWA	Multichannel

Normalized residue in $N\pi \to N(2060) \to N\sigma$

MODULUS	PHASE (°)	DOCUMENT ID		TECN	COMMENT
0.12 ± 0.06	80 ± 40	SOKHOYAN	15A	DPWA	Multichannel

Normalized residue in $N\pi \to N(2060) \to N(1440)\pi$

MODULUS	PHASE (°)	DOCUMENT ID		TECN	COMMENT
0.17 ± 0.09	−60 ± 35	SOKHOYAN	15A	DPWA	Multichannel

Normalized residue in $N\pi \to N(2060) \to N(1520)\pi$, P-wave

MODULUS	PHASE (°)	DOCUMENT ID		TECN	COMMENT
0.14 ± 0.06	−45 ± 15	SOKHOYAN	15A	DPWA	Multichannel

$N(2060)$ BREIT-WIGNER MASS

VALUE (MeV)	DOCUMENT ID		TECN	COMMENT
2030 to 2200 (≈ 2100) OUR ESTIMATE				
2040 ± 30	SARANTSEV	25	DPWA	Multichannel
2111 ± 17	[1] HUNT	19	DPWA	Multichannel
2180 ± 80	CUTKOSKY	80	IPWA	$\pi N \to \pi N$
2228 ± 30	HOEHLER	79	IPWA	$\pi N \to \pi N$
• • • We do not use the following data for averages, fits, limits, etc. • • •				
2045 ± 15	SOKHOYAN	15A	DPWA	Multichannel
2116 ± 21	[1] SHRESTHA	12A	DPWA	Multichannel
2217 ± 27	BATINIC	10	DPWA	$\pi N \to N\pi$, $N\eta$

[1] Statistical error only.

$N(2060)$ BREIT-WIGNER WIDTH

VALUE (MeV)	DOCUMENT ID		TECN	COMMENT
300 to 450 (≈ 400) OUR ESTIMATE				
420 ± 50	SARANTSEV	25	DPWA	Multichannel
499 ± 70	[1] HUNT	19	DPWA	Multichannel
400 ± 100	CUTKOSKY	80	IPWA	$\pi N \to \pi N$
310 ± 50	HOEHLER	79	IPWA	$\pi N \to \pi N$
• • • We do not use the following data for averages, fits, limits, etc. • • •				
420 ± 30	SOKHOYAN	15A	DPWA	Multichannel
307 ± 112	[1] SHRESTHA	12A	DPWA	Multichannel
481 ± 17	BATINIC	10	DPWA	$\pi N \to N\pi$, $N\eta$

[1] Statistical error only.

$N(2060)$ DECAY MODES

	Mode	Fraction (Γ_i/Γ)
Γ_1	$N\pi$	7–12 %
Γ_2	$N\eta$	2–38 %
Γ_3	$N\omega$	1–7 %
Γ_4	ΛK	10–20 %
Γ_5	ΣK	1–5 %
Γ_6	$N\pi\pi$	12–52 %
Γ_7	$\Delta(1232)\pi$	(12.0 ± 3.0) %
Γ_8	$\Delta(1232)\pi$, D-wave	4–10 %
Γ_9	$N\rho$	5–33 %
Γ_{10}	$N\rho$, $S=1/2$	
Γ_{11}	$N\rho$, $S=3/2$, D-wave	5–23 %
Γ_{12}	$N\sigma$	3–9 %
Γ_{13}	$N(1440)\pi$	4–14 %
Γ_{14}	$N(1520)\pi$, P-wave	9–21 %
Γ_{15}	$N(1680)\pi$, S-wave	8–22 %
Γ_{16}	$\Lambda K^*(892)$	0.3–1.3 %
Γ_{17}	$p\gamma$	0.03–0.19 %
Γ_{18}	$p\gamma$, helicity=1/2	0.02–0.08 %
Γ_{19}	$p\gamma$, helicity=3/2	0.01–0.10 %
Γ_{20}	$n\gamma$	0.003–0.07 %
Γ_{21}	$n\gamma$, helicity=1/2	0.001–0.02 %
Γ_{22}	$n\gamma$, helicity=3/2	0.002–0.05 %

$N(2060)$ BRANCHING RATIOS

$\Gamma(N\pi)/\Gamma_{total}$ — Γ_1/Γ

VALUE (%)	DOCUMENT ID		TECN	COMMENT
7 to 12 (≈ 10) OUR ESTIMATE				
11 ± 2	SEIFEN	25	DPWA	Multichannel
5.3 ± 1.4	[1] HUNT	19	DPWA	Multichannel
10 ± 3	CUTKOSKY	80	IPWA	$\pi N \to \pi N$
7 ± 2	HOEHLER	79	IPWA	$\pi N \to \pi N$
• • • We do not use the following data for averages, fits, limits, etc. • • •				
11 ± 2	SOKHOYAN	15A	DPWA	Multichannel
9 ± 2	[1] SHRESTHA	12A	DPWA	Multichannel
13 ± 4	BATINIC	10	DPWA	$\pi N \to N\pi$, $N\eta$

[1] Statistical error only.

$\Gamma(N\eta)/\Gamma_{total}$ — Γ_2/Γ

VALUE (%)	DOCUMENT ID		TECN	COMMENT
2–38 % OUR ESTIMATE				
6 ± 2	MUELLER	20	DPWA	Multichannel
30 ± 8	[1] HUNT	19	DPWA	Multichannel
4 ± 2	ANISOVICH	12A	DPWA	Multichannel
• • • We do not use the following data for averages, fits, limits, etc. • • •				
< 1	[1] SHRESTHA	12A	DPWA	Multichannel
0.2 ± 1.0	BATINIC	10	DPWA	$\pi N \to N\pi$, $N\eta$

[1] Statistical error only.

$\Gamma(N\omega)/\Gamma_{total}$ — Γ_3/Γ

VALUE (%)	DOCUMENT ID		TECN	COMMENT
4 ± 3	DENISENKO	16	DPWA	Multichannel

$\Gamma(\Lambda K)/\Gamma_{total}$ — Γ_4/Γ

VALUE (%)	DOCUMENT ID		TECN	COMMENT
10–20 % OUR ESTIMATE				
15 ± 5	[1] HUNT	19	DPWA	Multichannel

[1] Statistical error only.

$\Gamma(\Sigma K)/\Gamma_{total}$ — Γ_5/Γ

VALUE (%)	DOCUMENT ID		TECN	COMMENT
3 ± 2	ANISOVICH	12A	DPWA	Multichannel

$\Gamma(\Delta(1232)\pi)/\Gamma_{total}$ — Γ_7/Γ

VALUE (%)	DOCUMENT ID		TECN	COMMENT
12 ± 3	SARANTSEV	25	DPWA	Multichannel

$\Gamma(\Delta(1232)\pi, D\text{-wave})/\Gamma_{total}$ — Γ_8/Γ

VALUE (%)	DOCUMENT ID		TECN	COMMENT
4–10 % OUR ESTIMATE				
12 ± 3	SARANTSEV	25	DPWA	Multichannel
9 ± 3	SEIFEN	25	DPWA	Multichannel
15 ± 6	[1] HUNT	19	DPWA	Multichannel
• • • We do not use the following data for averages, fits, limits, etc. • • •				
7 ± 3	SOKHOYAN	15A	DPWA	Multichannel
40 ± 13	[1] SHRESTHA	12A	DPWA	Multichannel

[1] Statistical error only.

Int. J. Mod. Phys. A 2026.41. Downloaded from www.worldscientific.com
by UNIVERSITY OF CALIFORNIA @ BERKELEY on 09/16/26. Re-use and distribution is strictly not permitted, except for Open Access articles.

$\Gamma(N\rho)/\Gamma_{total}$ — Γ_9/Γ

VALUE (%)	DOCUMENT ID		TECN	COMMENT
28±11	SARANTSEV	25	DPWA	Multichannel

$\Gamma(N\rho, S=1/2)/\Gamma_{total}$ — Γ_{10}/Γ

VALUE (%)	DOCUMENT ID		TECN	COMMENT
24±10	SARANTSEV	25	DPWA	Multichannel
<10	[1] HUNT	19	DPWA	Multichannel
• • • We do not use the following data for averages, fits, limits, etc. • • •				
21±15	[1] SHRESTHA	12A	DPWA	Multichannel

[1] Statistical error only.

$\Gamma(N\rho, S=3/2, D\text{-wave})/\Gamma_{total}$ — Γ_{11}/Γ

VALUE (%)	DOCUMENT ID		TECN	COMMENT
5–23 % OUR ESTIMATE				
4±4	SARANTSEV	25	DPWA	Multichannel
14±9	[1] HUNT	19	DPWA	Multichannel

[1] Statistical error only.

$\Gamma(N\sigma)/\Gamma_{total}$ — Γ_{12}/Γ

VALUE (%)	DOCUMENT ID		TECN	COMMENT
3±2	SARANTSEV	25	DPWA	Multichannel
5±3	SEIFEN	25	DPWA	Multichannel
• • • We do not use the following data for averages, fits, limits, etc. • • •				
6±3	SOKHOYAN	15A	DPWA	Multichannel

$\Gamma(N(1440)\pi)/\Gamma_{total}$ — Γ_{13}/Γ

VALUE (%)	DOCUMENT ID		TECN	COMMENT
8±5	SEIFEN	25	DPWA	Multichannel
• • • We do not use the following data for averages, fits, limits, etc. • • •				
9±5	SOKHOYAN	15A	DPWA	Multichannel

$\Gamma(N(1520)\pi, P\text{-wave})/\Gamma_{total}$ — Γ_{14}/Γ

VALUE (%)	DOCUMENT ID		TECN	COMMENT
13±7	SEIFEN	25	DPWA	Multichannel
• • • We do not use the following data for averages, fits, limits, etc. • • •				
15±6	SOKHOYAN	15A	DPWA	Multichannel

$\Gamma(N(1680)\pi, S\text{-wave})/\Gamma_{total}$ — Γ_{15}/Γ

VALUE (%)	DOCUMENT ID		TECN	COMMENT
14±5	SEIFEN	25	DPWA	Multichannel
• • • We do not use the following data for averages, fits, limits, etc. • • •				
15±7	SOKHOYAN	15A	DPWA	Multichannel

$\Gamma(\Lambda K^*(892))/\Gamma_{total}$ — Γ_{16}/Γ

VALUE (%)	DOCUMENT ID		TECN	COMMENT
0.3–1.3 % OUR ESTIMATE				
0.8±0.5	ANISOVICH	17B	DPWA	Multichannel

$N(2060)$ PHOTON DECAY AMPLITUDES AT THE POLE

$N(2060) \to p\gamma$, helicity-1/2 amplitude $A_{1/2}$

MODULUS ($GeV^{-1/2}$)	PHASE (°)	DOCUMENT ID		TECN	COMMENT
0.065±0.015	20 ± 10	SARANTSEV	25	DPWA	Multichannel
• • • We do not use the following data for averages, fits, limits, etc. • • •					
0.064±0.010	12 ± 8	SOKHOYAN	15A	DPWA	Multichannel

$N(2060) \to p\gamma$, helicity-3/2 amplitude $A_{3/2}$

MODULUS ($GeV^{-1/2}$)	PHASE (°)	DOCUMENT ID		TECN	COMMENT
0.030±0.020	160 ± 30	SARANTSEV	25	DPWA	Multichannel
• • • We do not use the following data for averages, fits, limits, etc. • • •					
0.060±0.020	13 ± 10	SOKHOYAN	15A	DPWA	Multichannel

$N(2060) \to n\gamma$, helicity-1/2 amplitude $A_{1/2}$

MODULUS ($GeV^{-1/2}$)	PHASE (°)	DOCUMENT ID		TECN	COMMENT
0.052±0.025	−5 ± 20	ANISOVICH	17E	DPWA	Multichannel

$N(2060) \to n\gamma$, helicity-3/2 amplitude $A_{3/2}$

MODULUS ($GeV^{-1/2}$)	PHASE (°)	DOCUMENT ID		TECN	COMMENT
0.012±0.007	−40 ± 35	ANISOVICH	17E	DPWA	Multichannel

$N(2060)$ BREIT-WIGNER PHOTON DECAY AMPLITUDES

$N(2060) \to p\gamma$, helicity-1/2 amplitude $A_{1/2}$

VALUE ($GeV^{-1/2}$)	DOCUMENT ID		TECN	COMMENT
0.065±0.015	SARANTSEV	25	DPWA	Multichannel
−0.019±0.005	[1] HUNT	19	DPWA	Multichannel
• • • We do not use the following data for averages, fits, limits, etc. • • •				
0.062±0.010	SOKHOYAN	15A	DPWA	Multichannel
0.018±0.004	[1] SHRESTHA	12A	DPWA	Multichannel

[1] Statistical error only.

$N(2060) \to p\gamma$, helicity-3/2 amplitude $A_{3/2}$

VALUE ($GeV^{-1/2}$)	DOCUMENT ID		TECN	COMMENT
−0.030±0.020	SARANTSEV	25	DPWA	Multichannel
0.039±0.005	[1] HUNT	19	DPWA	Multichannel
• • • We do not use the following data for averages, fits, limits, etc. • • •				
0.062±0.020	SOKHOYAN	15A	DPWA	Multichannel
0.010±0.004	[1] SHRESTHA	12A	DPWA	Multichannel

[1] Statistical error only.

$N(2060) \to n\gamma$, helicity-1/2 amplitude $A_{1/2}$

VALUE ($GeV^{-1/2}$)	DOCUMENT ID		TECN	COMMENT
0.069±0.017	[1] HUNT	19	DPWA	Multichannel
0.052±0.024	ANISOVICH	17E	DPWA	Multichannel
• • • We do not use the following data for averages, fits, limits, etc. • • •				
0.025±0.011	ANISOVICH	13B	DPWA	Multichannel
−0.012±0.017	[1] SHRESTHA	12A	DPWA	Multichannel

[1] Statistical error only.

$N(2060) \to n\gamma$, helicity-3/2 amplitude $A_{3/2}$

VALUE ($GeV^{-1/2}$)	DOCUMENT ID		TECN	COMMENT
−0.023±0.020	[1] HUNT	19	DPWA	Multichannel
0.012±0.007	ANISOVICH	17E	DPWA	Multichannel
• • • We do not use the following data for averages, fits, limits, etc. • • •				
−0.037±0.017	ANISOVICH	13B	DPWA	Multichannel
−0.023±0.023	[1] SHRESTHA	12A	DPWA	Multichannel

[1] Statistical error only.

$N(2060)$ REFERENCES

SARANTSEV	25	PR C112 015202	A.V. Sarantsev *et al.*	(Bonn-Gatchina Collab.)
SEIFEN	25	EPJ A61 173	T. Seifen *et al.*	(CBELSA/TAPS Collab.)
MUELLER	20	PL B803 135323	J. Mueller *et al.*	(CBELSA/TAPS Collab.)
HUNT	19	PR C99 055205	B.C. Hunt, D.M. Manley	
ANISOVICH	17B	PL B771 142	A.V. Anisovich *et al.*	
ANISOVICH	17E	PR C96 055202	A.V. Anisovich *et al.*	(BONN, PNPI, JLAB+)
DENISENKO	16	PL B755 97	I. Denisenko *et al.*	
SOKHOYAN	15A	EPJ A51 95	V. Sokhoyan *et al.*	(CBELSA/TAPS Collab.)
SVARC	14	PR C89 045205	A. Svarc *et al.*	(RBI Zagreb, UNI Tuzla)
ANISOVICH	13B	EPJ A49 67	A.V. Anisovich *et al.*	
ANISOVICH	12A	EPJ A48 15	A.V. Anisovich *et al.*	(BONN, PNPI)
SHRESTHA	12A	PR C86 055203	M. Shrestha, D.M. Manley	(KSU)
BATINIC	10	PR C82 038203	M. Batinic *et al.*	(ZAGR)
CUTKOSKY	80	Toronto Conf. 19	R.E. Cutkosky *et al.*	(CMU, LBL) IJP
Also		PR D20 2839	R.E. Cutkosky *et al.*	(CMU, LBL)
HOEHLER	79	PDAT 12-1	G. Hohler *et al.*	(KARLT) IJP
Also		Toronto Conf. 3	R. Koch	(KARLT) IJP

$N(2100)\ 1/2^+$

$I(J^P) = \frac{1}{2}(\frac{1}{2}^+)$ Status: ***

$N(2100)$ POLE POSITION

REAL PART

VALUE (MeV)	DOCUMENT ID		TECN	COMMENT
2050 to 2150 (≈ 2100) OUR ESTIMATE				
2055±25	SARANTSEV	25	DPWA	Multichannel
2052± 6±3	[1] SVARC	14	L+P	$\pi N \to \pi N$
2120±40	CUTKOSKY	80	IPWA	$\pi N \to \pi N$
• • • We do not use the following data for averages, fits, limits, etc. • • •				
2217	HUNT	19	DPWA	Multichannel
2120±25	SOKHOYAN	15A	DPWA	Multichannel
2120±47	BATINIC	10	DPWA	$\pi N \to N\pi$, $N\eta$
1810	VRANA	00	DPWA	Multichannel

[1] Fit to the amplitudes of HOEHLER 79.

−2×IMAGINARY PART

VALUE (MeV)	DOCUMENT ID		TECN	COMMENT
240 to 340 (≈ 300) OUR ESTIMATE				
430±65	SARANTSEV	25	DPWA	Multichannel
337±10±4	[1] SVARC	14	L+P	$\pi N \to \pi N$
240±80	CUTKOSKY	80	IPWA	$\pi N \to \pi N$
• • • We do not use the following data for averages, fits, limits, etc. • • •				
545	HUNT	19	DPWA	Multichannel
290±30	SOKHOYAN	15A	DPWA	Multichannel
346±80	BATINIC	10	DPWA	$\pi N \to N\pi$, $N\eta$
622	VRANA	00	DPWA	Multichannel

[1] Fit to the amplitudes of HOEHLER 79.

$N(2100)$ ELASTIC POLE RESIDUE

MODULUS $|r|$

VALUE (MeV)	DOCUMENT ID		TECN	COMMENT
15 to 30 (≈ 20) OUR ESTIMATE				
23±5	SOKHOYAN	15A	DPWA	Multichannel
30±1±1	[1] SVARC	14	L+P	$\pi N \to \pi N$
14±7	CUTKOSKY	80	IPWA	$\pi N \to \pi N$
• • • We do not use the following data for averages, fits, limits, etc. • • •				
33	BATINIC	10	DPWA	$\pi N \to N\pi$, $N\eta$

[1] Fit to the amplitudes of HOEHLER 79.

Int. J. Mod. Phys. A 2026.41. Downloaded from www.worldscientific.com
UNIVERSITY OF CALIFORNIA @ BERKELEY on 09/16/26. Re-use and distribution is strictly not permitted, except for Open Access articles.

PHASE θ

VALUE (°)	DOCUMENT ID		TECN	COMMENT
−100 to −60 (≈ −80) OUR ESTIMATE				
−70±25	SOKHOYAN	15A	DPWA	Multichannel
−92± 3±2	[1] SVARC	14	L+P	$\pi N \to \pi N$
35±25	CUTKOSKY	80	IPWA	$\pi N \to \pi N$
• • • We do not use the following data for averages, fits, limits, etc. • • •				
−59	BATINIC	10	DPWA	$\pi N \to N\pi,\ N\eta$

[1] Fit to the amplitudes of HOEHLER 79.

$N(2100)$ INELASTIC POLE RESIDUE

Normalized residue in $N\pi \to N(2100) \to \Delta(1232)\pi$

MODULUS	PHASE (°)	DOCUMENT ID		TECN	COMMENT
0.11±0.05	20 ± 60	SOKHOYAN	15A	DPWA	Multichannel

Normalized residue in $N\pi \to N(2100) \to N\sigma$

MODULUS	PHASE (°)	DOCUMENT ID		TECN	COMMENT
0.18±0.06	125 ± 25	SOKHOYAN	15A	DPWA	Multichannel

Normalized residue in $N\pi \to N(2100) \to N(1535)\pi$

MODULUS	PHASE (°)	DOCUMENT ID		TECN	COMMENT
0.22±0.06	−40 ± 25	SOKHOYAN	15A	DPWA	Multichannel

$N(2100)$ BREIT-WIGNER MASS

VALUE (MeV)	DOCUMENT ID		TECN	COMMENT
2050 to 2150 (≈ 2100) OUR ESTIMATE				
2070±35	SARANTSEV	25	DPWA	Multichannel
2221±92	[1] HUNT	19	DPWA	Multichannel
2125±75	CUTKOSKY	80	IPWA	$\pi N \to \pi N$
2050±20	HOEHLER	79	IPWA	$\pi N \to \pi N$
• • • We do not use the following data for averages, fits, limits, etc. • • •				
2115±20	SOKHOYAN	15A	DPWA	Multichannel
2157±42	BATINIC	10	DPWA	$\pi N \to N\pi,\ N\eta$
$2068\pm 3^{+15}_{-40}$	ABLIKIM	06K	BES2	$J/\psi \to (p\pi^-)\overline{n}$
2084±93	VRANA	00	DPWA	Multichannel

[1] Statistical error only.

$N(2100)$ BREIT-WIGNER WIDTH

VALUE (MeV)	DOCUMENT ID		TECN	COMMENT
200 to 320 (≈ 260) OUR ESTIMATE				
450± 60	SARANTSEV	25	DPWA	Multichannel
545±170	[1] HUNT	19	DPWA	Multichannel
260±100	CUTKOSKY	80	IPWA	$\pi N \to \pi N$
200± 30	HOEHLER	79	IPWA	$\pi N \to \pi N$
• • • We do not use the following data for averages, fits, limits, etc. • • •				
290± 20	SOKHOYAN	15A	DPWA	Multichannel
355± 88	BATINIC	10	DPWA	$\pi N \to N\pi,\ N\eta$
165± 14±40	ABLIKIM	06K	BES2	$J/\psi \to (p\pi^-)\overline{n}$
1077±643	VRANA	00	DPWA	Multichannel

[1] Statistical error only.

$N(2100)$ DECAY MODES

	Mode	Fraction (Γ_i/Γ)
Γ_1	$N\pi$	8–32 %
Γ_2	$N\eta$	5–45 %
Γ_3	$N\eta'$	5–11 %
Γ_4	$N\omega$	10–25 %
Γ_5	ΛK	<1.0 %
Γ_6	$N\pi\pi$	>55 %
Γ_7	$\Delta(1232)\pi$	6–14 %
Γ_8	$N\rho$	(17 ±6) %
Γ_9	$N\rho,\ S=1/2$	35–70 %
Γ_{10}	$N\rho,\ S=3/2$	(5.0±3.0) %
Γ_{11}	$N\sigma$	14–35 %
Γ_{12}	$N(1535)\pi$	26–34 %
Γ_{13}	$N(1520)\pi$, D-wave	< 2 %
Γ_{14}	$\Lambda K^*(892)$	3–11 %
Γ_{15}	$p\gamma$, helicity=1/2	0.001–0.13 %
Γ_{16}	$n\gamma$, helicity=1/2	0.004–0.09 %

$N(2100)$ BRANCHING RATIOS

$\Gamma(N\pi)/\Gamma_{total}$ — Γ_1/Γ

VALUE (%)	DOCUMENT ID		TECN	COMMENT
8–32 % OUR ESTIMATE				
17± 7	SEIFEN	25	DPWA	Multichannel
21±11	[1] HUNT	19	DPWA	Multichannel
12± 3	CUTKOSKY	80	IPWA	$\pi N \to \pi N$
10± 4	HOEHLER	79	IPWA	$\pi N \to \pi N$
• • • We do not use the following data for averages, fits, limits, etc. • • •				
16± 5	SOKHOYAN	15A	DPWA	Multichannel
16± 5	BATINIC	10	DPWA	$\pi N \to N\pi,\ N\eta$
2± 5	VRANA	00	DPWA	Multichannel

[1] Statistical error only.

$\Gamma(N\eta)/\Gamma_{total}$ — Γ_2/Γ

VALUE (%)	DOCUMENT ID		TECN	COMMENT
5–45 % OUR ESTIMATE				
30 ±15	MUELLER	20	DPWA	Multichannel
< 4.7	[1] HUNT	19	DPWA	Multichannel
• • • We do not use the following data for averages, fits, limits, etc. • • •				
83 ± 5	BATINIC	10	DPWA	$\pi N \to N\pi,\ N\eta$
61 ±61	VRANA	00	DPWA	Multichannel

[1] Statistical error only.

$\Gamma(N\eta')/\Gamma_{total}$ — Γ_3/Γ

VALUE (%)	DOCUMENT ID		TECN	COMMENT
5–11 % OUR ESTIMATE				
8±3	ANISOVICH	17C	DPWA	Multichannel

$\Gamma(N\omega)/\Gamma_{total}$ — Γ_4/Γ

VALUE (%)	DOCUMENT ID		TECN	COMMENT
10–25 % OUR ESTIMATE				
15±10	DENISENKO	16	DPWA	Multichannel

$\Gamma(\Lambda K)/\Gamma_{total}$ — Γ_5/Γ

VALUE (%)	DOCUMENT ID		TECN	COMMENT
<1.0 % OUR ESTIMATE				
< 1.0	[1] HUNT	19	DPWA	Multichannel
• • • We do not use the following data for averages, fits, limits, etc. • • •				
21 ±20	VRANA	00	DPWA	Multichannel

[1] Statistical error only.

$\Gamma(\Delta(1232)\pi)/\Gamma_{total}$ — Γ_7/Γ

VALUE (%)	DOCUMENT ID		TECN	COMMENT
6–14 % OUR ESTIMATE				
10 ±4	SARANTSEV	25	DPWA	Multichannel
12 ±6	SEIFEN	25	DPWA	Multichannel
< 7.5	[1] HUNT	19	DPWA	Multichannel
10 ±4	SOKHOYAN	15A	DPWA	Multichannel
• • • We do not use the following data for averages, fits, limits, etc. • • •				
2 ±1	VRANA	00	DPWA	Multichannel

[1] Statistical error only.

$\Gamma(N\rho)/\Gamma_{total}$ — Γ_8/Γ

VALUE (%)	DOCUMENT ID		TECN	COMMENT
17±6	SARANTSEV	25	DPWA	Multichannel

$\Gamma(N\rho, S=1/2)/\Gamma_{total}$ — Γ_9/Γ

VALUE (%)	DOCUMENT ID		TECN	COMMENT
35–70 % OUR ESTIMATE				
12± 6	SARANTSEV	25	DPWA	Multichannel
52±19	[1] HUNT	19	DPWA	Multichannel
• • • We do not use the following data for averages, fits, limits, etc. • • •				
4± 1	VRANA	00	DPWA	Multichannel

[1] Statistical error only.

$\Gamma(N\rho, S=3/2)/\Gamma_{total}$ — Γ_{10}/Γ

VALUE (%)	DOCUMENT ID		TECN	COMMENT
5±3	SARANTSEV	25	DPWA	Multichannel

$\Gamma(N\sigma)/\Gamma_{total}$ — Γ_{11}/Γ

VALUE (%)	DOCUMENT ID		TECN	COMMENT
14–35 % OUR ESTIMATE				
28±6	SARANTSEV	25	DPWA	Multichannel
28±7	SEIFEN	25	DPWA	Multichannel
<35	[1] HUNT	19	DPWA	Multichannel
• • • We do not use the following data for averages, fits, limits, etc. • • •				
20±6	SOKHOYAN	15A	DPWA	Multichannel
10±1	VRANA	00	DPWA	Multichannel

[1] Statistical error only.

$\Gamma(N(1535)\pi)/\Gamma_{total}$ — Γ_{12}/Γ

VALUE (%)	DOCUMENT ID		TECN	COMMENT
26–34 % OUR ESTIMATE				
< 1	SEIFEN	25	DPWA	Multichannel
30±4	SOKHOYAN	15A	DPWA	Multichannel

$\Gamma(N(1520)\pi,\ D\text{-wave})/\Gamma_{total}$ — Γ_{13}/Γ

VALUE (%)	DOCUMENT ID		TECN	COMMENT
<2	SEIFEN	25	DPWA	Multichannel

Int. J. Mod. Phys. A 2026.41. Downloaded from www.worldscientific.com
by UNIVERSITY OF CALIFORNIA @ BERKELEY on 09/16/26. Re-use and distribution is strictly not permitted, except for Open Access articles.

$\Gamma(\Lambda K^*(892))/\Gamma_{total}$ — Γ_{14}/Γ

VALUE (%)	DOCUMENT ID		TECN	COMMENT
3–11 % OUR ESTIMATE				
7±4	ANISOVICH	17B	DPWA	Multichannel

$N(2100)$ PHOTON DECAY AMPLITUDES AT THE POLE

$N(2100) \to p\gamma$, helicity-1/2 amplitude $A_{1/2}$

MODULUS ($GeV^{-1/2}$)	PHASE (°)	DOCUMENT ID		TECN	COMMENT
0.020±0.008	65 ± 20	SARANTSEV	25	DPWA	Multichannel
• • • We do not use the following data for averages, fits, limits, etc. • • •					
0.011±0.004	65 ± 30	SOKHOYAN	15A	DPWA	Multichannel

$N(2100) \to n\gamma$, helicity-1/2 amplitude $A_{1/2}$

MODULUS	PHASE (°)	DOCUMENT ID		TECN	COMMENT
0.029±0.009	35 ± 20	ANISOVICH	17E	DPWA	Multichannel

$N(2100)$ BREIT-WIGNER PHOTON DECAY AMPLITUDES

$N(2100) \to p\gamma$, helicity-1/2 amplitude $A_{1/2}$

VALUE ($GeV^{-1/2}$)	DOCUMENT ID		TECN	COMMENT
0.021±0.007	SARANTSEV	25	DPWA	Multichannel
0.032±0.014	[1] HUNT	19	DPWA	Multichannel
• • • We do not use the following data for averages, fits, limits, etc. • • •				
0.010±0.004	SOKHOYAN	15A	DPWA	Multichannel

[1] Statistical error only.

$N(2100) \to n\gamma$, helicity-1/2 amplitude $A_{1/2}$

VALUE ($GeV^{-1/2}$)	DOCUMENT ID		TECN	COMMENT
0.026±0.013	[1] HUNT	19	DPWA	Multichannel
0.029±0.010	ANISOVICH	17E	DPWA	Multichannel

[1] Statistical error only.

$N(2100)$ REFERENCES

SARANTSEV	25	PR C112 015202	A.V. Sarantsev *et al.*	(Bonn-Gatchina Collab.)
SEIFEN	25	EPJ A61 173	T. Seifen *et al.*	(CBELSA/TAPS Collab.)
MUELLER	20	PL B803 135323	J. Mueller *et al.*	(CBELSA/TAPS Collab.)
HUNT	19	PR C99 055205	B.C. Hunt, D.M. Manley	
ANISOVICH	17B	PL B771 142	A.V. Anisovich *et al.*	
ANISOVICH	17C	PL B772 247	A.V. Anisovich *et al.*	
ANISOVICH	17E	PR C96 055202	A.V. Anisovich *et al.*	(BONN, PNPI, JLAB+)
DENISENKO	16	PL B755 97	I. Denisenko *et al.*	
SOKHOYAN	15A	EPJ A51 95	V. Sokhoyan *et al.*	(CBELSA/TAPS Collab.)
SVARC	14	PR C89 045205	A. Svarc *et al.*	(RBI Zagreb, UNI Tuzla)
BATINIC	10	PR C82 038203	M. Batinic *et al.*	(ZAGR)
ABLIKIM	06K	PRL 97 062001	M. Ablikim *et al.*	(BES II Collab.)
VRANA	00	PRPL 328 181	T.P. Vrana, S.A. Dytman, T.-S.H. Lee	(PITT, ANL)
CUTKOSKY	80	Toronto Conf. 19	R.E. Cutkosky *et al.*	(CMU, LBL) IJP
Also		PR D20 2839	R.E. Cutkosky *et al.*	(CMU, LBL)
HOEHLER	79	PDAT 12-1	G. Hohler *et al.*	(KARLT) IJP
Also		Toronto Conf. 3	R. Koch	(KARLT) IJP

$N(2120)\ 3/2^-$

$I(J^P) = \frac{1}{2}(\frac{3}{2}^-)$ Status: ***

Before the 2012 *Review*, all the evidence for a $J^P = 3/2^-$ state with a mass above 1800 MeV was filed under a two-star $N(2080)$. There is now evidence from ANISOVICH 12A for two $3/2^-$ states in this region, so we have split the older data (according to mass) between a three-star $N(1875)$ and a two-star $N(2120)$.

$N(2120)$ POLE POSITION

REAL PART

VALUE (MeV)	DOCUMENT ID		TECN	COMMENT
2050 to 2150 (≈ 2100) OUR ESTIMATE				
2130±40	SARANTSEV	25	DPWA	Multichannel
2094± 7±11	SVARC	14	L+P	$\pi N \to \pi N$
2050±70	CUTKOSKY	80	IPWA	$\pi N \to \pi N$ (higher m)
• • • We do not use the following data for averages, fits, limits, etc. • • •				
2357	HUNT	19	DPWA	Multichannel
2115±40	SOKHOYAN	15A	DPWA	Multichannel
2115±40	GUTZ	14	DPWA	Multichannel

−2×IMAGINARY PART

VALUE (MeV)	DOCUMENT ID		TECN	COMMENT
200 to 360 (≈ 280) OUR ESTIMATE				
350±35	SARANTSEV	25	DPWA	Multichannel
296±15±4	SVARC	14	L+P	$\pi N \to \pi N$
200±80	CUTKOSKY	80	IPWA	$\pi N \to \pi N$ (higher m)
• • • We do not use the following data for averages, fits, limits, etc. • • •				
503	HUNT	19	DPWA	Multichannel
345±35	SOKHOYAN	15A	DPWA	Multichannel
345±35	GUTZ	14	DPWA	Multichannel

$N(2120)$ ELASTIC POLE RESIDUE

MODULUS $|r|$

VALUE (MeV)	DOCUMENT ID		TECN	COMMENT
10 to 30 (≈ 20) OUR ESTIMATE				
11± 6	SOKHOYAN	15A	DPWA	Multichannel
13± 1±1	SVARC	14	L+P	$\pi N \to \pi N$
30±20	CUTKOSKY	80	IPWA	$\pi N \to \pi N$ (higher m)
• • • We do not use the following data for averages, fits, limits, etc. • • •				
11± 6	GUTZ	14	DPWA	Multichannel
13± 3	ANISOVICH	12A	DPWA	Multichannel

PHASE θ

VALUE (°)	DOCUMENT ID		TECN	COMMENT
−40 to 20 (≈ −10) OUR ESTIMATE				
−30± 20	SOKHOYAN	15A	DPWA	Multichannel
− 2± 4±9	SVARC	14	L+P	$\pi N \to \pi N$
0±100	CUTKOSKY	80	IPWA	$\pi N \to \pi N$ (higher m)
• • • We do not use the following data for averages, fits, limits, etc. • • •				
−30± 20	GUTZ	14	DPWA	Multichannel
−20± 10	ANISOVICH	12A	DPWA	Multichannel

$N(2120)$ INELASTIC POLE RESIDUE

The "normalized residue" is the residue divided by $\Gamma_{pole}/2$.

Normalized residue in $N\pi \to N(2120) \to \Lambda K$

MODULUS	PHASE (°)	DOCUMENT ID		TECN	COMMENT
0.03±0.01	100 ± 30	ANISOVICH	12A	DPWA	Multichannel

Normalized residue in $N\pi \to N(2120) \to \Sigma K$

MODULUS	PHASE (°)	DOCUMENT ID		TECN	COMMENT
0.02±0.015	−50 ± 40	ANISOVICH	12A	DPWA	Multichannel

Normalized residue in $N\pi \to N(2120) \to N(1535)\pi$

MODULUS	PHASE (°)	DOCUMENT ID		TECN	COMMENT
0.15±0.08	−90 ± 40	GUTZ	14	DPWA	Multichannel

Normalized residue in $N\pi \to N(2120) \to \Delta(1232)\pi$, S-wave

MODULUS	PHASE (°)	DOCUMENT ID		TECN	COMMENT
0.25±0.10	undefined	SOKHOYAN	15A	DPWA	Multichannel

Normalized residue in $N\pi \to N(2120) \to \Delta(1232)\pi$, D-wave

MODULUS	PHASE (°)	DOCUMENT ID		TECN	COMMENT
0.15±0.06	−35 ± 30	SOKHOYAN	15A	DPWA	Multichannel

Normalized residue in $N\pi \to N(2120) \to N\sigma$

MODULUS	PHASE (°)	DOCUMENT ID		TECN	COMMENT
0.09±0.05	−80 ± 50	SOKHOYAN	15A	DPWA	Multichannel

$N(2120)$ BREIT-WIGNER MASS

VALUE (MeV)	DOCUMENT ID		TECN	COMMENT
2060 to 2160 (≈ 2120) OUR ESTIMATE				
2140±35	SARANTSEV	25	DPWA	Multichannel
2353±29	[1] HUNT	19	DPWA	Multichannel
2060±80	CUTKOSKY	80	IPWA	$\pi N \to \pi N$
2081±20	HOEHLER	79	IPWA	$\pi N \to \pi N$
• • • We do not use the following data for averages, fits, limits, etc. • • •				
2120±45	SOKHOYAN	15A	DPWA	Multichannel
2120±35	GUTZ	14	DPWA	Multichannel

[1] Statistical error only.

$N(2120)$ BREIT-WIGNER WIDTH

VALUE (MeV)	DOCUMENT ID		TECN	COMMENT
260 to 360 (≈ 300) OUR ESTIMATE				
360± 35	SARANTSEV	25	DPWA	Multichannel
503± 62	[1] HUNT	19	DPWA	Multichannel
300±100	CUTKOSKY	80	IPWA	$\pi N \to \pi N$ (higher m)
265± 40	HOEHLER	79	IPWA	$\pi N \to \pi N$
• • • We do not use the following data for averages, fits, limits, etc. • • •				
340± 35	SOKHOYAN	15A	DPWA	Multichannel
340± 35	GUTZ	14	DPWA	Multichannel

[1] Statistical error only.

$N(2120)$ DECAY MODES

	Mode	Fraction (Γ_i/Γ)
Γ_1	$N\pi$	5–15 %
Γ_2	$N\eta$	1–5 %
Γ_3	$N\eta'$	2–6 %
Γ_4	$N\omega$	4–20 %
Γ_5	ΛK	6–11 %

Γ_6	$N\pi\pi$	>27 %
Γ_7	$\Delta(1232)\pi$	>23 %
Γ_8	$\Delta(1232)\pi$, S-wave	15–70 %
Γ_9	$\Delta(1232)\pi$, D-wave	8–45 %
Γ_{10}	$N\rho$	(28 ±6) %
Γ_{11}	$N\rho$, S=1/2	(4.0±2.0) %
Γ_{12}	$N\rho$, S=3/2 , S-wave	< 3 %
Γ_{13}	$N\rho$, S=3/2 , D-wave	(5.0±3.0) %
Γ_{14}	$N\sigma$	4–15 %
Γ_{15}	$N(1440)\pi$	(6 ±6) %
Γ_{16}	$N(1520)\pi$, P-wave	(10 ±5) %
Γ_{17}	$N(1535)\pi$	7–23 %
Γ_{18}	$\Lambda K^*(892)$	< 0.2 %
Γ_{19}	$p\gamma$	0.16–2.1 %
Γ_{20}	$p\gamma$, helicity=1/2	0.07–0.80 %
Γ_{21}	$p\gamma$, helicity=3/2	0.09–1.3 %
Γ_{22}	$n\gamma$	0.04–0.72 %
Γ_{23}	$n\gamma$, helicity=1/2	0.04–0.60 %
Γ_{24}	$n\gamma$, helicity=3/2	0.001–0.12 %

$N(2120)$ BRANCHING RATIOS

$\Gamma(N\pi)/\Gamma_{total}$ — Γ_1/Γ

VALUE (%)	DOCUMENT ID		TECN	COMMENT
5–15 % OUR ESTIMATE				
5±2	SEIFEN	25	DPWA	Multichannel
19±2	[1] HUNT	19	DPWA	Multichannel
14±7	CUTKOSKY	80	IPWA	$\pi N \to \pi N$ (higher m)
6±2	HOEHLER	79	IPWA	$\pi N \to \pi N$
• • • We do not use the following data for averages, fits, limits, etc. • • •				
5±3	SOKHOYAN	15A	DPWA	Multichannel
5±3	GUTZ	14	DPWA	Multichannel

[1] Statistical error only.

$\Gamma(N\eta)/\Gamma_{total}$ — Γ_2/Γ

VALUE (%)	DOCUMENT ID		TECN	COMMENT
1–5 % OUR ESTIMATE				
<1	MUELLER	20	DPWA	Multichannel
3.1±2.4	[1] HUNT	19	DPWA	Multichannel

[1] Statistical error only.

$\Gamma(N\eta')/\Gamma_{total}$ — Γ_3/Γ

VALUE (%)	DOCUMENT ID		TECN	COMMENT
2–6 % OUR ESTIMATE				
4±2	ANISOVICH	17C	DPWA	Multichannel

$\Gamma(N\omega)/\Gamma_{total}$ — Γ_4/Γ

VALUE (%)	DOCUMENT ID		TECN	COMMENT
4–20 % OUR ESTIMATE				
12±8	DENISENKO	16	DPWA	Multichannel

$\Gamma(\Lambda K)/\Gamma_{total}$ — Γ_5/Γ

VALUE (%)	DOCUMENT ID		TECN	COMMENT
6–11 % OUR ESTIMATE				
8.5±2.5	[1] HUNT	19	DPWA	Multichannel

[1] Statistical error only.

$\Gamma(\Delta(1232)\pi)/\Gamma_{total}$ — Γ_7/Γ

VALUE (%)	DOCUMENT ID		TECN	COMMENT
19±5	SARANTSEV	25	DPWA	Multichannel

$\Gamma(\Delta(1232)\pi, S\text{-wave})/\Gamma_{total}$ — Γ_8/Γ

VALUE (%)	DOCUMENT ID		TECN	COMMENT
15–70 % OUR ESTIMATE				
8± 3	SARANTSEV	25	DPWA	Multichannel
10± 5	SEIFEN	25	DPWA	Multichannel
25±11	[1] HUNT	19	DPWA	Multichannel
• • • We do not use the following data for averages, fits, limits, etc. • • •				
50±20	SOKHOYAN	15A	DPWA	Multichannel

[1] Statistical error only.

$\Gamma(\Delta(1232)\pi, D\text{-wave})/\Gamma_{total}$ — Γ_9/Γ

VALUE (%)	DOCUMENT ID		TECN	COMMENT
8–45 % OUR ESTIMATE				
11± 4	SARANTSEV	25	DPWA	Multichannel
14± 7	SEIFEN	25	DPWA	Multichannel
34±11	[1] HUNT	19	DPWA	Multichannel
• • • We do not use the following data for averages, fits, limits, etc. • • •				
20±12	SOKHOYAN	15A	DPWA	Multichannel

[1] Statistical error only.

$\Gamma(N\rho)/\Gamma_{total}$ — Γ_{10}/Γ

VALUE (%)	DOCUMENT ID		TECN	COMMENT
28±6	SARANTSEV	25	DPWA	Multichannel

$\Gamma(N\rho, S=1/2)/\Gamma_{total}$ — Γ_{11}/Γ

VALUE (%)	DOCUMENT ID		TECN	COMMENT
4±2	SARANTSEV	25	DPWA	Multichannel

$\Gamma(N\rho, S=3/2, S\text{-wave})/\Gamma_{total}$ — Γ_{12}/Γ

VALUE (%)	DOCUMENT ID		TECN	COMMENT
< 3 % OUR ESTIMATE				
19±5	SARANTSEV	25	DPWA	Multichannel
< 3	[1] HUNT	19	DPWA	Multichannel

[1] Statistical error only.

$\Gamma(N\rho, S=3/2, D\text{-wave})/\Gamma_{total}$ — Γ_{13}/Γ

VALUE (%)	DOCUMENT ID		TECN	COMMENT
5±3	SARANTSEV	25	DPWA	Multichannel

$\Gamma(N\sigma)/\Gamma_{total}$ — Γ_{14}/Γ

VALUE (%)	DOCUMENT ID		TECN	COMMENT
4–15 % OUR ESTIMATE				
5±3	SARANTSEV	25	DPWA	Multichannel
4±3	SEIFEN	25	DPWA	Multichannel
9±5	[1] HUNT	19	DPWA	Multichannel
• • • We do not use the following data for averages, fits, limits, etc. • • •				
11±4	SOKHOYAN	15A	DPWA	Multichannel

[1] Statistical error only.

$\Gamma(N(1440)\pi)/\Gamma_{total}$ — Γ_{15}/Γ

VALUE (%)	DOCUMENT ID		TECN	COMMENT
6±6	SEIFEN	25	DPWA	Multichannel

$\Gamma(N(1520)\pi, P\text{-wave})/\Gamma_{total}$ — Γ_{16}/Γ

VALUE (%)	DOCUMENT ID		TECN	COMMENT
10±5	SEIFEN	25	DPWA	Multichannel

$\Gamma(N(1535)\pi)/\Gamma_{total}$ — Γ_{17}/Γ

VALUE (%)	DOCUMENT ID		TECN	COMMENT
7–23 % OUR ESTIMATE				
< 2	SEIFEN	25	DPWA	Multichannel
15±8	GUTZ	14	DPWA	Multichannel

$\Gamma(\Lambda K^*(892))/\Gamma_{total}$ — Γ_{18}/Γ

VALUE (%)	DOCUMENT ID		TECN	COMMENT
< 0.2 % OUR ESTIMATE				
<0.2	ANISOVICH	17B	DPWA	Multichannel

$N(2120)$ PHOTON DECAY AMPLITUDES AT THE POLE

$N(2120) \to p\gamma$, helicity-1/2 amplitude $A_{1/2}$

MODULUS ($GeV^{-1/2}$)	PHASE (°)	DOCUMENT ID		TECN	COMMENT
−0.025±0.015	40 ± 25	SARANTSEV	25	DPWA	Multichannel
• • • We do not use the following data for averages, fits, limits, etc. • • •					
0.130±0.045	−40 ± 25	SOKHOYAN	15A	DPWA	Multichannel

$N(2120) \to p\gamma$, helicity-3/2 amplitude $A_{3/2}$

MODULUS ($GeV^{-1/2}$)	PHASE (°)	DOCUMENT ID		TECN	COMMENT
−0.045±0.015	25 ± 25	SARANTSEV	25	DPWA	Multichannel
• • • We do not use the following data for averages, fits, limits, etc. • • •					
0.160±0.060	−30 ± 15	SOKHOYAN	15A	DPWA	Multichannel

$N(2120) \to n\gamma$, helicity-1/2 amplitude $A_{1/2}$

MODULUS ($GeV^{-1/2}$)	PHASE (°)	DOCUMENT ID		TECN	COMMENT
0.080±0.030	15 ± 25	ANISOVICH	17E	DPWA	Multichannel

$N(2120) \to n\gamma$, helicity-3/2 amplitude $A_{3/2}$

MODULUS ($GeV^{-1/2}$)	PHASE (°)	DOCUMENT ID		TECN	COMMENT
−0.033±0.020	−60 ± 35	ANISOVICH	17E	DPWA	Multichannel

$N(2120)$ BREIT-WIGNER PHOTON DECAY AMPLITUDES

$N(2120) \to p\gamma$, helicity-1/2 amplitude $A_{1/2}$

VALUE ($GeV^{-1/2}$)	DOCUMENT ID		TECN	COMMENT
0.026±0.015	SARANTSEV	25	DPWA	Multichannel
0.047±0.009	[1] HUNT	19	DPWA	Multichannel
• • • We do not use the following data for averages, fits, limits, etc. • • •				
0.130±0.050	SOKHOYAN	15A	DPWA	Multichannel
0.130±0.050	GUTZ	14	DPWA	Multichannel

[1] Statistical error only.

Int. J. Mod. Phys. A 2026.41. Downloaded from www.worldscientific.com
UNIVERSITY OF CALIFORNIA @ BERKELEY on 09/16/26. Re-use and distribution is strictly not permitted, except for Open Access articles.

Int. J. Mod. Phys. A 2026.41. Downloaded from www.worldscientific.com
by UNIVERSITY OF CALIFORNIA @ BERKELEY on 09/16/26. Re-use and distribution is strictly not permitted, except for Open Access articles.

$N(2120) \to p\gamma$, helicity-3/2 amplitude $A_{3/2}$

VALUE (GeV$^{-1/2}$)	DOCUMENT ID		TECN	COMMENT
0.047±0.015	SARANTSEV	25	DPWA	Multichannel
0.001±0.007	[1] HUNT	19	DPWA	Multichannel
• • • We do not use the following data for averages, fits, limits, etc. • • •				
0.160±0.065	SOKHOYAN	15A	DPWA	Multichannel
0.160±0.065	GUTZ	14	DPWA	Multichannel

[1] Statistical error only.

$N(2120) \to n\gamma$, helicity-1/2 amplitude $A_{1/2}$

VALUE (GeV$^{-1/2}$)	DOCUMENT ID		TECN	COMMENT
−0.020±0.013	[1] HUNT	19	DPWA	Multichannel
0.081±0.030	ANISOVICH	17E	DPWA	Multichannel
• • • We do not use the following data for averages, fits, limits, etc. • • •				
0.110±0.045	ANISOVICH	13B	DPWA	Multichannel

[1] Statistical error only.

$N(2120) \to n\gamma$, helicity-3/2 amplitude $A_{3/2}$

VALUE (GeV$^{-1/2}$)	DOCUMENT ID		TECN	COMMENT
−0.00 ±0.02	[1] HUNT	19	DPWA	Multichannel
−0.032±0.020	ANISOVICH	17E	DPWA	Multichannel
• • • We do not use the following data for averages, fits, limits, etc. • • •				
0.040±0.030	ANISOVICH	13B	DPWA	Multichannel

[1] Statistical error only.

$N(2120)$ REFERENCES

SARANTSEV	25	PR C112 015202	A.V. Sarantsev *et al.*	(Bonn-Gatchina Collab.)
SEIFEN	25	EPJ A61 173	T. Seifen *et al.*	(CBELSA/TAPS Collab.)
MUELLER	20	PL B803 135323	J. Mueller *et al.*	(CBELSA/TAPS Collab.)
HUNT	19	PR C99 055205	B.C. Hunt, D.M. Manley	
ANISOVICH	17B	PL B771 142	A.V. Anisovich *et al.*	
ANISOVICH	17C	PL B772 247	A.V. Anisovich *et al.*	
ANISOVICH	17E	PR C96 055202	A.V. Anisovich *et al.*	(BONN, PNPI, JLAB+)
DENISENKO	16	PL B755 97	I. Denisenko *et al.*	
SOKHOYAN	15A	EPJ A51 95	V. Sokhoyan *et al.*	(CBELSA/TAPS Collab.)
GUTZ	14	EPJ A50 74	E. Gutz *et al.*	(CBELSA/TAPS Collab.)
SVARC	14	PR C89 045205	A. Svarc *et al.*	(RBI Zagreb, UNI Tuzla)
ANISOVICH	13B	EPJ A49 67	A.V. Anisovich *et al.*	
ANISOVICH	12A	EPJ A48 15	A.V. Anisovich *et al.*	(BONN, PNPI)
CUTKOSKY	80	Toronto Conf. 19	R.E. Cutkosky *et al.*	(CMU, LBL)
HOEHLER	79	PDAT 12-1	G. Hohler *et al.*	(KARLT)

$N(2190)\ 7/2^-$

$I(J^P) = \frac{1}{2}(\frac{7}{2}^-)$ Status: ****

Older and obsolete values are listed and referenced in the 2014 edition, Chinese Physics **C38** 070001 (2014).

$N(2190)$ POLE POSITION

REAL PART

VALUE (MeV)	DOCUMENT ID		TECN	COMMENT
1950 to 2150 (≈ 2050) OUR ESTIMATE				
2130±35	SARANTSEV	25	DPWA	Multichannel
1965± 6	ROENCHEN	22	DPWA	Multichannel
2140±20	AFZAL	20	DPWA	Multichannel
2079± 4±9	[1] SVARC	14	L+P	$\pi N \to \pi N$
2100±50	CUTKOSKY	80	IPWA	$\pi N \to \pi N$
• • • We do not use the following data for averages, fits, limits, etc. • • •				
2162	HUNT	19	DPWA	Multichannel
2074	ROENCHEN	15A	DPWA	Multichannel
2150±25	SOKHOYAN	15A	DPWA	Multichannel
2063±32	BATINIC	10	DPWA	$\pi N \to N\pi$, $N\eta$
2070	ARNDT	06	DPWA	$\pi N \to \pi N$, ηN
2107	VRANA	00	DPWA	Multichannel
2042	HOEHLER	93	SPED	$\pi N \to \pi N$

[1] Fit to the amplitudes of HOEHLER 79.

−2×IMAGINARY PART

VALUE (MeV)	DOCUMENT ID		TECN	COMMENT
300 to 500 (≈ 400) OUR ESTIMATE				
370± 45	SARANTSEV	25	DPWA	Multichannel
287± 33	ROENCHEN	22	DPWA	Multichannel
420^{+120}_{-40}	AFZAL	20	DPWA	Multichannel
509± 7±16	[1] SVARC	14	L+P	$\pi N \to \pi N$
400±160	CUTKOSKY	80	IPWA	$\pi N \to \pi N$
• • • We do not use the following data for averages, fits, limits, etc. • • •				
407	HUNT	19	DPWA	Multichannel
327	ROENCHEN	15A	DPWA	Multichannel
325± 25	SOKHOYAN	15A	DPWA	Multichannel
330±101	BATINIC	10	DPWA	$\pi N \to N\pi$, $N\eta$
520	ARNDT	06	DPWA	$\pi N \to \pi N$, ηN
380	VRANA	00	DPWA	Multichannel
482	HOEHLER	93	SPED	$\pi N \to \pi N$

[1] Fit to the amplitudes of HOEHLER 79.

$N(2190)$ ELASTIC POLE RESIDUE

MODULUS $|r|$

VALUE (MeV)	DOCUMENT ID		TECN	COMMENT
20 to 60 (≈ 40) OUR ESTIMATE				
18± 4	ROENCHEN	22	DPWA	Multichannel
30± 4	SOKHOYAN	15A	DPWA	Multichannel
54± 1±3	[1] SVARC	14	L+P	$\pi N \to \pi N$
25±10	CUTKOSKY	80	IPWA	$\pi N \to \pi N$
• • • We do not use the following data for averages, fits, limits, etc. • • •				
35	ROENCHEN	15A	DPWA	Multichannel
30± 5	ANISOVICH	12A	DPWA	Multichannel
34	BATINIC	10	DPWA	$\pi N \to N\pi$, $N\eta$
72	ARNDT	06	DPWA	$\pi N \to \pi N$, ηN
45	HOEHLER	93	SPED	$\pi N \to \pi N$

[1] Fit to the amplitudes of HOEHLER 79.

PHASE θ

VALUE (°)	DOCUMENT ID		TECN	COMMENT
−30 to 30 (≈ 0) OUR ESTIMATE				
−45±14	ROENCHEN	22	DPWA	Multichannel
28±10	SOKHOYAN	15A	DPWA	Multichannel
−18± 1±3	[1] SVARC	14	L+P	$\pi N \to \pi N$
−30±50	CUTKOSKY	80	IPWA	$\pi N \to \pi N$
• • • We do not use the following data for averages, fits, limits, etc. • • •				
−40	ROENCHEN	15A	DPWA	Multichannel
30±10	ANISOVICH	12A	DPWA	Multichannel
−19	BATINIC	10	DPWA	$\pi N \to N\pi$, $N\eta$
−32	ARNDT	06	DPWA	$\pi N \to \pi N$, ηN

[1] Fit to the amplitudes of HOEHLER 79.

$N(2190)$ INELASTIC POLE RESIDUE

The "normalized residue" is the residue divided by $\Gamma_{pole}/2$.

Normalized residue in $N\pi \to N(2190) \to \Lambda K$

MODULUS	PHASE (°)	DOCUMENT ID		TECN	COMMENT
0.026±0.007	−78 ± 15	ROENCHEN	22	DPWA	Multichannel
0.03 ±0.01	20 ± 15	ANISOVICH	12A	DPWA	Multichannel
• • • We do not use the following data for averages, fits, limits, etc. • • •					
0.005	−51	ROENCHEN	15A	DPWA	Multichannel

Normalized residue in $N\pi \to N(2190) \to \Sigma K$

MODULUS	PHASE (°)	DOCUMENT ID		TECN	COMMENT
0.005±0.001	−92 ± 16	ROENCHEN	22	DPWA	Multichannel
• • • We do not use the following data for averages, fits, limits, etc. • • •					
0.013	−69	ROENCHEN	15A	DPWA	Multichannel

Normalized residue in $N\pi \to N(2190) \to N\eta$

MODULUS	PHASE (°)	DOCUMENT ID		TECN	COMMENT
0.021±0.005	−65 ± 15	ROENCHEN	22	DPWA	Multichannel
• • • We do not use the following data for averages, fits, limits, etc. • • •					
0.016	129	ROENCHEN	15A	DPWA	Multichannel

Normalized residue in $N\pi \to N(2190) \to \Delta(1232)\pi$, D-wave

MODULUS	PHASE (°)	DOCUMENT ID		TECN	COMMENT
0.27±0.04	−165 ± 20	SOKHOYAN	15A	DPWA	Multichannel

Normalized residue in $N\pi \to N(2190) \to N\sigma$

MODULUS	PHASE (°)	DOCUMENT ID		TECN	COMMENT
0.13±0.05	50 ± 15	SOKHOYAN	15A	DPWA	Multichannel

$N(2190)$ BREIT-WIGNER MASS

VALUE (MeV)	DOCUMENT ID		TECN	COMMENT
2140 to 2220 (≈ 2180) OUR ESTIMATE				
2170 ±25	SARANTSEV	25	DPWA	Multichannel
2222 ±15	[1] HUNT	19	DPWA	Multichannel
2152.4± 1.4	[1] ARNDT	06	DPWA	$\pi N \to \pi N$, ηN
2200 ±70	CUTKOSKY	80	IPWA	$\pi N \to \pi N$
2140 ±12	HOEHLER	79	IPWA	$\pi N \to \pi N$
• • • We do not use the following data for averages, fits, limits, etc. • • •				
2205 ±18	SOKHOYAN	15A	DPWA	Multichannel
2150 ±26	[1] SHRESTHA	12A	DPWA	Multichannel
2125 ±61	BATINIC	10	DPWA	$\pi N \to N\pi$, $N\eta$
2168 ±18	VRANA	00	DPWA	Multichannel

[1] Statistical error only.

$N(2190)$ BREIT-WIGNER WIDTH

VALUE (MeV)	DOCUMENT ID		TECN	COMMENT
300 to 500 (≈ 400) OUR ESTIMATE				
420± 45	SARANTSEV	25	DPWA	Multichannel
442± 40	[1] HUNT	19	DPWA	Multichannel
484± 13	[1] ARNDT	06	DPWA	$\pi N \to \pi N$, ηN
500±150	CUTKOSKY	80	IPWA	$\pi N \to \pi N$
390± 30	HOEHLER	79	IPWA	$\pi N \to \pi N$

Int. J. Mod. Phys. A 2026.41. Downloaded from www.worldscientific.com
UNIVERSITY OF CALIFORNIA @ BERKELEY on 09/16/26. Re-use and distribution is strictly not permitted, except for Open Access articles.

• • • We do not use the following data for averages, fits, limits, etc. • • •

355 ± 30	SOKHOYAN	15A	DPWA	Multichannel
500 ± 74	[1] SHRESTHA	12A	DPWA	Multichannel
381 ± 160	BATINIC	10	DPWA	$\pi N \to N\pi$, $N\eta$
453 ± 101	VRANA	00	DPWA	Multichannel

[1] Statistical error only.

$N(2190)$ DECAY MODES

The following branching fractions are our estimates, not fits or averages.

	Mode	Fraction (Γ_i/Γ)
Γ_1	$N\pi$	10–20 %
Γ_2	$N\eta$	1–5 %
Γ_3	$N\omega$	8–20 %
Γ_4	ΛK	0.2–0.8 %
Γ_5	$N\pi\pi$	22–51 %
Γ_6	$\Delta\pi$	(4.0 ± 2.0) %
Γ_7	$\Delta(1232)\pi$, D-wave	19–31 %
Γ_8	$N\rho$	(8 ± 7) %
Γ_9	$N\rho$, $S=3/2$, D-wave	<11 %
Γ_{10}	$N\sigma$	3–9 %
Γ_{11}	$\Lambda K^*(892)$	0.2–0.8 %
Γ_{12}	$p\gamma$	<0.08 %
Γ_{13}	$p\gamma$, helicity=1/2	<0.06 %
Γ_{14}	$p\gamma$, helicity=3/2	<0.02 %
Γ_{15}	$n\gamma$	<0.04 %
Γ_{16}	$n\gamma$, helicity=1/2	<0.01 %
Γ_{17}	$n\gamma$, helicity=3/2	<0.03 %

$N(2190)$ BRANCHING RATIOS

$\Gamma(N\pi)/\Gamma_{total}$ — Γ_1/Γ

VALUE (%)	DOCUMENT ID		TECN	COMMENT
10–20 % OUR ESTIMATE				
15 ± 3	SEIFEN	25	DPWA	Multichannel
22.9 ± 0.6	[1] HUNT	19	DPWA	Multichannel
23.8 ± 0.1	[1] ARNDT	06	DPWA	$\pi N \to \pi N$, ηN
12 ± 6	CUTKOSKY	80	IPWA	$\pi N \to \pi N$
14 ± 2	HOEHLER	79	IPWA	$\pi N \to \pi N$
• • • We do not use the following data for averages, fits, limits, etc. • • •				
16 ± 2	SOKHOYAN	15A	DPWA	Multichannel
20 ± 1	[1] SHRESTHA	12A	DPWA	Multichannel
18 ± 12	BATINIC	10	DPWA	$\pi N \to N\pi$, $N\eta$
20 ± 4	VRANA	00	DPWA	Multichannel

[1] Statistical error only.

$\Gamma(N\eta)/\Gamma_{total}$ — Γ_2/Γ

VALUE (%)	DOCUMENT ID		TECN	COMMENT
1–5 % OUR ESTIMATE				
4 ± 2	MUELLER	20	DPWA	Multichannel
2.7 ± 2.2	[1] HUNT	19	DPWA	Multichannel
• • • We do not use the following data for averages, fits, limits, etc. • • •				
2 ± 1	[1] SHRESTHA	12A	DPWA	Multichannel
0.1 ± 0.3	BATINIC	10	DPWA	$\pi N \to N\pi$, $N\eta$
0 ± 1	VRANA	00	DPWA	Multichannel

[1] Statistical error only.

$\Gamma(N\omega)/\Gamma_{total}$ — Γ_3/Γ

VALUE (%)	DOCUMENT ID		TECN	COMMENT
8–20 % OUR ESTIMATE				
14 ± 6	DENISENKO	16	DPWA	Multichannel
• • • We do not use the following data for averages, fits, limits, etc. • • •				
seen	WILLIAMS	09	IPWA	$\gamma p \to p\omega$

$\Gamma(\Lambda K)/\Gamma_{total}$ — Γ_4/Γ

VALUE (%)	DOCUMENT ID		TECN	COMMENT
0.2–0.8 % OUR ESTIMATE				
0.6 ± 0.1	[1] HUNT	19	DPWA	Multichannel
0.5 ± 0.3	ANISOVICH	12A	DPWA	Multichannel
• • • We do not use the following data for averages, fits, limits, etc. • • •				
<1	[1] SHRESTHA	12A	DPWA	Multichannel

[1] Statistical error only.

$\Gamma(\Delta\pi)/\Gamma_{total}$ — Γ_6/Γ

VALUE (%)	DOCUMENT ID		TECN	COMMENT
4 ± 2	SARANTSEV	25	DPWA	Multichannel

$\Gamma(\Delta(1232)\pi, D\text{-wave})/\Gamma_{total}$ — Γ_7/Γ

VALUE (%)	DOCUMENT ID		TECN	COMMENT
19–31 % OUR ESTIMATE				
4 ± 2	SEIFEN	25	DPWA	Multichannel
• • • We do not use the following data for averages, fits, limits, etc. • • •				
25 ± 6	SOKHOYAN	15A	DPWA	Multichannel

$\Gamma(N\rho)/\Gamma_{total}$ — Γ_8/Γ

VALUE (%)	DOCUMENT ID		TECN	COMMENT
8 ± 7	SARANTSEV	25	DPWA	Multichannel

$\Gamma(N\rho, S=3/2, D\text{-wave})/\Gamma_{total}$ — Γ_9/Γ

VALUE (%)	DOCUMENT ID		TECN	COMMENT
<11 % OUR ESTIMATE				
8 ± 7	SARANTSEV	25	DPWA	Multichannel
<11	[1] HUNT	19	DPWA	Multichannel
• • • We do not use the following data for averages, fits, limits, etc. • • •				
29 ± 28	VRANA	00	DPWA	Multichannel

[1] Statistical error only.

$\Gamma(N\sigma)/\Gamma_{total}$ — Γ_{10}/Γ

VALUE (%)	DOCUMENT ID		TECN	COMMENT
3–9 % OUR ESTIMATE				
6 ± 3	SEIFEN	25	DPWA	Multichannel
• • • We do not use the following data for averages, fits, limits, etc. • • •				
6 ± 3	SOKHOYAN	15A	DPWA	Multichannel

$\Gamma(\Lambda K^*(892))/\Gamma_{total}$ — Γ_{11}/Γ

VALUE (%)	DOCUMENT ID		TECN	COMMENT
0.2–0.8 % OUR ESTIMATE				
0.5 ± 0.3	ANISOVICH	17B	DPWA	Multichannel

$N(2190)$ PHOTON DECAY AMPLITUDES AT THE POLE

$N(2190) \to p\gamma$, helicity-1/2 amplitude $A_{1/2}$

MODULUS ($GeV^{-1/2}$)	PHASE (°)	DOCUMENT ID		TECN	COMMENT
0.060 ± 0.012	150 ± 25	SARANTSEV	25	DPWA	Multichannel
−0.015 ± 0.004	111 ± 9	ROENCHEN	22	DPWA	Multichannel
• • • We do not use the following data for averages, fits, limits, etc. • • •					
−0.041	−21	ROENCHEN	15A	DPWA	Multichannel
0.068 ± 0.005	−170 ± 12	SOKHOYAN	15A	DPWA	Multichannel

$N(2190) \to p\gamma$, helicity-3/2 amplitude $A_{3/2}$

MODULUS ($GeV^{-1/2}$)	PHASE (°)	DOCUMENT ID		TECN	COMMENT
0.050 ± 0.015	−10 ± 25	SARANTSEV	25	DPWA	Multichannel
0.062 ± 0.011	179 ± 13	ROENCHEN	22	DPWA	Multichannel
• • • We do not use the following data for averages, fits, limits, etc. • • •					
0.085	−22	ROENCHEN	15A	DPWA	Multichannel
0.025 ± 0.010	22 ± 10	SOKHOYAN	15A	DPWA	Multichannel

$N(2190) \to n\gamma$, helicity-1/2 amplitude $A_{1/2}$

MODULUS ($GeV^{-1/2}$)	PHASE (°)	DOCUMENT ID		TECN	COMMENT
0.030 ± 0.007	5 ± 15	ANISOVICH	17E	DPWA	Multichannel

$N(2190) \to n\gamma$, helicity-3/2 amplitude $A_{3/2}$

MODULUS ($GeV^{-1/2}$)	PHASE (°)	DOCUMENT ID		TECN	COMMENT
−0.023 ± 0.008	13 ± 20	ANISOVICH	17E	DPWA	Multichannel

$N(2190)$ BREIT-WIGNER PHOTON DECAY AMPLITUDES

$N(2190) \to p\gamma$, helicity-1/2 amplitude $A_{1/2}$

VALUE ($GeV^{-1/2}$)	DOCUMENT ID		TECN	COMMENT
−0.060 ± 0.010	SARANTSEV	25	DPWA	Multichannel
0.001 ± 0.002	[1] HUNT	19	DPWA	Multichannel
• • • We do not use the following data for averages, fits, limits, etc. • • •				
−0.071 ± 0.006	SOKHOYAN	15A	DPWA	Multichannel

[1] Statistical error only.

$N(2190) \to p\gamma$, helicity-3/2 amplitude $A_{3/2}$

VALUE ($GeV^{-1/2}$)	DOCUMENT ID		TECN	COMMENT
0.051 ± 0.006	SARANTSEV	25	DPWA	Multichannel
0.015 ± 0.003	[1] HUNT	19	DPWA	Multichannel
• • • We do not use the following data for averages, fits, limits, etc. • • •				
0.027 ± 0.010	SOKHOYAN	15A	DPWA	Multichannel

[1] Statistical error only.

$N(2190) \to p\gamma$, ratio of helicity amplitudes $A_{3/2}/A_{1/2}$

VALUE	DOCUMENT ID		TECN	COMMENT
• • • We do not use the following data for averages, fits, limits, etc. • • •				
−0.17 ± 0.15	WILLIAMS	09	IPWA	$\gamma p \to p\omega$

$N(2190) \to n\gamma$, helicity-1/2 amplitude $A_{1/2}$

VALUE ($GeV^{-1/2}$)	DOCUMENT ID		TECN	COMMENT
−0.01 ± 0.02	[1] HUNT	19	DPWA	Multichannel
0.030 ± 0.007	ANISOVICH	17E	DPWA	Multichannel
• • • We do not use the following data for averages, fits, limits, etc. • • •				
−0.015 ± 0.013	ANISOVICH	13B	DPWA	Multichannel

[1] Statistical error only.

Int. J. Mod. Phys. A 2026.41. Downloaded from www.worldscientific.com by UNIVERSITY OF CALIFORNIA @ BERKELEY on 09/16/26. Re-use and distribution is strictly not permitted, except for Open Access articles.

$N(2190) \to n\gamma$, helicity-3/2 amplitude $A_{3/2}$

VALUE (GeV$^{-1/2}$)	DOCUMENT ID		TECN	COMMENT
-0.023 ± 0.022	[1] HUNT	19	DPWA	Multichannel
-0.023 ± 0.008	ANISOVICH	17E	DPWA	Multichannel
• • • We do not use the following data for averages, fits, limits, etc. • • •				
-0.034 ± 0.022	ANISOVICH	13B	DPWA	Multichannel

[1] Statistical error only.

$N(2190)$ REFERENCES

For early references, see Physics Letters **111B** 1 (1982).

SARANTSEV	25	PR C112 015202	A.V. Sarantsev *et al.*	(Bonn-Gatchina Collab.)
SEIFEN	25	EPJ A61 173	T. Seifen *et al.*	(CBELSA/TAPS Collab.)
ROENCHEN	22	EPJ A58 229	D. Roenchen *et al.*	(JULI, GWU, BONN+)
AFZAL	20	PRL 125 152002	F. Afzal *et al.*	(CBELSA/TAPS Collab.)
MUELLER	20	PL B803 135323	J. Mueller *et al.*	(CBELSA/TAPS Collab.)
HUNT	19	PR C99 055205	B.C. Hunt, D.M. Manley	
ANISOVICH	17B	PL B771 142	A.V. Anisovich *et al.*	
ANISOVICH	17E	PR C96 055202	A.V. Anisovich *et al.*	(BONN, PNPI, JLAB+)
DENISENKO	16	PL B755 97	I. Denisenko *et al.*	
ROENCHEN	15A	EPJ A51 70	D. Roenchen *et al.*	
SOKHOYAN	15A	EPJ A51 95	V. Sokhoyan *et al.*	(CBELSA/TAPS Collab.)
PDG	14	CP C38 070001	K. Olive *et al.*	(PDG Collab.)
SVARC	14	PR C89 045205	A. Svarc *et al.*	(RBI Zagreb, UNI Tuzla)
ANISOVICH	13B	EPJ A49 67	A.V. Anisovich *et al.*	
ANISOVICH	12A	EPJ A48 15	A.V. Anisovich *et al.*	(BONN, PNPI)
SHRESTHA	12A	PR C86 055203	M. Shrestha, D.M. Manley	(KSU)
BATINIC	10	PR C82 038203	M. Batinic *et al.*	(ZAGR)
WILLIAMS	09	PR C80 065209	M. Williams *et al.*	(JLab CLAS Collab.)
ARNDT	06	PR C74 045205	R.A. Arndt *et al.*	(GWU)
VRANA	00	PRPL 328 181	T.P. Vrana, S.A. Dytman, T.-S.H. Lee	(PITT, ANL)
HOEHLER	93	πN Newsletter 9 1	G. Hohler	(KARL)
CUTKOSKY	80	Toronto Conf. 19	R.E. Cutkosky *et al.*	(CMU, LBL) IJP
Also		PR D20 2839	R.E. Cutkosky *et al.*	(CMU, LBL) IJP
HOEHLER	79	PDAT 12-1	G. Hohler *et al.*	(KARLT) IJP
Also		Toronto Conf. 3	R. Koch	(KARLT) IJP

$N(2220)\ 9/2^+$

$I(J^P) = \frac{1}{2}(\frac{9}{2}^+)$ Status: ****

Older and obsolete values are listed and referenced in the 2014 edition, Chinese Physics **C38** 070001 (2014).

$N(2220)$ POLE POSITION

REAL PART

VALUE (MeV)	DOCUMENT ID		TECN	COMMENT
2130 to 2200 (≈ 2150) OUR ESTIMATE				
2165 ± 30	SARANTSEV	25	DPWA	Multichannel
2131 ± 6	ROENCHEN	22	DPWA	Multichannel
$2127 \pm 3 \pm 24$	[1] SVARC	14	L+P	$\pi N \to \pi N$
2160 ± 80	CUTKOSKY	80	IPWA	$\pi N \to \pi N$
• • • We do not use the following data for averages, fits, limits, etc. • • •				
2171	ROENCHEN	15A	DPWA	Multichannel
2150 ± 35	ANISOVICH	12A	DPWA	Multichannel
2199	ARNDT	06	DPWA	$\pi N \to \pi N, \eta N$
2135	HOEHLER	93	ARGD	$\pi N \to \pi N$

[1] Fit to the amplitudes of HOEHLER 79.

$-2\times$IMAGINARY PART

VALUE (MeV)	DOCUMENT ID		TECN	COMMENT
360 to 480 (≈ 400) OUR ESTIMATE				
440 ± 40	SARANTSEV	25	DPWA	Multichannel
388 ± 6	ROENCHEN	22	DPWA	Multichannel
$380 \pm 7 \pm 22$	[1] SVARC	14	L+P	$\pi N \to \pi N$
480 ± 100	CUTKOSKY	80	IPWA	$\pi N \to \pi N$
• • • We do not use the following data for averages, fits, limits, etc. • • •				
593	ROENCHEN	15A	DPWA	Multichannel
440 ± 40	ANISOVICH	12A	DPWA	Multichannel
372	ARNDT	06	DPWA	$\pi N \to \pi N, \eta N$
400	HOEHLER	93	ARGD	$\pi N \to \pi N$

[1] Fit to the amplitudes of HOEHLER 79.

$N(2220)$ ELASTIC POLE RESIDUE

MODULUS $|r|$

VALUE (MeV)	DOCUMENT ID		TECN	COMMENT
35 to 60 (≈ 45) OUR ESTIMATE				
48 ± 5	ROENCHEN	22	DPWA	Multichannel
$38 \pm 1 \pm 5$	[1] SVARC	14	L+P	$\pi N \to \pi N$
60 ± 12	ANISOVICH	12A	DPWA	Multichannel
45 ± 20	CUTKOSKY	80	IPWA	$\pi N \to \pi N$
• • • We do not use the following data for averages, fits, limits, etc. • • •				
62	ROENCHEN	15A	DPWA	Multichannel
33	ARNDT	06	DPWA	$\pi N \to \pi N, \eta N$
40	HOEHLER	93	ARGD	$\pi N \to \pi N$

[1] Fit to the amplitudes of HOEHLER 79.

PHASE θ

VALUE (°)	DOCUMENT ID		TECN	COMMENT
-60 to -10 (≈ -40) OUR ESTIMATE				
-13 ± 2	ROENCHEN	22	DPWA	Multichannel
$-52 \pm 1 \pm 14$	[1] SVARC	14	L+P	$\pi N \to \pi N$
-58 ± 12	ANISOVICH	12A	DPWA	Multichannel
-45 ± 25	CUTKOSKY	80	IPWA	$\pi N \to \pi N$
• • • We do not use the following data for averages, fits, limits, etc. • • •				
-59	ROENCHEN	15A	DPWA	Multichannel
-33	ARNDT	06	DPWA	$\pi N \to \pi N, \eta N$
-50	HOEHLER	93	ARGD	$\pi N \to \pi N$

[1] Fit to the amplitudes of HOEHLER 79.

$N(2220)$ INELASTIC POLE RESIDUE

The "normalized residue" is the residue divided by $\Gamma_{pole}/2$.

Normalized residue in $N\pi \to N(2220) \to N\eta$

MODULUS	PHASE (°)	DOCUMENT ID		TECN	COMMENT
0.042 ± 0.006	-48 ± 2	ROENCHEN	22	DPWA	Multichannel
• • • We do not use the following data for averages, fits, limits, etc. • • •					
0.004	-101	ROENCHEN	15A	DPWA	Multichannel

Normalized residue in $N\pi \to N(2220) \to \Lambda K$

MODULUS	PHASE (°)	DOCUMENT ID		TECN	COMMENT
0.020 ± 0.003	-60 ± 2	ROENCHEN	22	DPWA	Multichannel
• • • We do not use the following data for averages, fits, limits, etc. • • •					
0.007	62	ROENCHEN	15A	DPWA	Multichannel

Normalized residue in $N\pi \to N(2220) \to \Sigma K$

MODULUS	PHASE (°)	DOCUMENT ID		TECN	COMMENT
0.003 ± 0.008	-70 ± 2	ROENCHEN	22	DPWA	Multichannel
• • • We do not use the following data for averages, fits, limits, etc. • • •					
0.009	-128	ROENCHEN	15A	DPWA	Multichannel

$N(2220)$ BREIT-WIGNER MASS

VALUE (MeV)	DOCUMENT ID		TECN	COMMENT
2200 to 2300 (≈ 2250) OUR ESTIMATE				
2230 ± 30	SARANTSEV	25	DPWA	Multichannel
2316.3 ± 2.9	[1] ARNDT	06	DPWA	$\pi N \to \pi N, \eta N$
2230 ± 80	CUTKOSKY	80	IPWA	$\pi N \to \pi N$
2205 ± 10	HOEHLER	79	IPWA	$\pi N \to \pi N$

[1] Statistical error only.

$N(2220)$ BREIT-WIGNER WIDTH

VALUE (MeV)	DOCUMENT ID		TECN	COMMENT
350 to 500 (≈ 400) OUR ESTIMATE				
500 ± 40	SARANTSEV	25	DPWA	Multichannel
633 ± 17	[1] ARNDT	06	DPWA	$\pi N \to \pi N, \eta N$
500 ± 150	CUTKOSKY	80	IPWA	$\pi N \to \pi N$
365 ± 30	HOEHLER	79	IPWA	$\pi N \to \pi N$

[1] Statistical error only.

$N(2220)$ DECAY MODES

The following branching fractions are our estimates, not fits or averages.

	Mode	Fraction (Γ_i/Γ)
Γ_1	$N\pi$	15–30 %
Γ_2	$N\pi\pi$	
Γ_3	$\Delta\pi$	(15 ± 10) %
Γ_4	$\Delta\pi$, F-wave	(15 ± 10) %
Γ_5	$N\rho$	(10 ± 10) %
Γ_6	$N\rho$, $S=3/2$, F-wave	(10 ± 10) %
Γ_7	$N\sigma$	(5 ± 5) %

$N(2220)$ BRANCHING RATIOS

$\Gamma(N\pi)/\Gamma_{total}$ — Γ_1/Γ

VALUE (%)	DOCUMENT ID		TECN	COMMENT
15 to 30 (≈ 25) OUR ESTIMATE				
24 ± 5	ANISOVICH	12A	DPWA	Multichannel
24.6 ± 0.1	[1] ARNDT	06	DPWA	$\pi N \to \pi N, \eta N$
15 ± 3	CUTKOSKY	80	IPWA	$\pi N \to \pi N$
18.0 ± 1.5	HOEHLER	79	IPWA	$\pi N \to \pi N$

[1] Statistical error only.

$\Gamma(\Delta\pi)/\Gamma_{total}$ — Γ_3/Γ

VALUE (%)	DOCUMENT ID		TECN	COMMENT
15 ± 10	SARANTSEV	25	DPWA	Multichannel

Int. J. Mod. Phys. A 2026.41. Downloaded from www.worldscientific.com
UNIVERSITY OF CALIFORNIA @ BERKELEY on 09/16/26. Re-use and distribution is strictly not permitted, except for Open Access articles.

$\Gamma(\Delta\pi, F\text{-wave})/\Gamma_{total}$ — Γ_4/Γ

VALUE (%)	DOCUMENT ID		TECN	COMMENT
15±10	SARANTSEV	25	DPWA	Multichannel

$\Gamma(N\rho)/\Gamma_{total}$ — Γ_5/Γ

VALUE (%)	DOCUMENT ID		TECN	COMMENT
10±10	SARANTSEV	25	DPWA	Multichannel

$\Gamma(N\rho, S=3/2, F\text{-wave})/\Gamma_{total}$ — Γ_6/Γ

VALUE (%)	DOCUMENT ID		TECN	COMMENT
10±10	SARANTSEV	25	DPWA	Multichannel

$\Gamma(N\sigma)/\Gamma_{total}$ — Γ_7/Γ

VALUE (%)	DOCUMENT ID		TECN	COMMENT
5±5	SARANTSEV	25	DPWA	Multichannel

$N(2220)$ PHOTON DECAY AMPLITUDES AT THE POLE

$N(2220) \to p\gamma$, helicity-1/2 amplitude $A_{1/2}$

MODULUS ($GeV^{-1/2}$)	PHASE (°)	DOCUMENT ID		TECN	COMMENT
0.015±0.010	90 ± 30	SARANTSEV	25	DPWA	Multichannel
0.357±0.020	−91 ± 4	ROENCHEN	22	DPWA	Multichannel
• • • We do not use the following data for averages, fits, limits, etc. • • •					
0.135	114	ROENCHEN	15A	DPWA	Multichannel

$N(2220) \to p\gamma$, helicity-3/2 amplitude $A_{3/2}$

MODULUS ($GeV^{-1/2}$)	PHASE (°)	DOCUMENT ID		TECN	COMMENT
0.018±0.010	−20 ± 30	SARANTSEV	25	DPWA	Multichannel
−0.273±0.025	−102 ± 3	ROENCHEN	22	DPWA	Multichannel
• • • We do not use the following data for averages, fits, limits, etc. • • •					
0.082	−41	ROENCHEN	15A	DPWA	Multichannel

$N(2220)$ BREIT-WIGNER PHOTON DECAY AMPLITUDES

$N(2220) \to p\gamma$, helicity-1/2 amplitude $A_{1/2}$

VALUE ($GeV^{-1/2}$)	DOCUMENT ID		TECN	COMMENT
0.017±0.010	[1] SARANTSEV	25	DPWA	Multichannel

[1] Sign is undetermined

$N(2220) \to p\gamma$, helicity-3/2 amplitude $A_{3/2}$

VALUE ($GeV^{-1/2}$)	DOCUMENT ID		TECN	COMMENT
0.020±0.010	SARANTSEV	25	DPWA	Multichannel

$N(2220)$ REFERENCES

For early references, see Physics Letters **111B** 1 (1982).

SARANTSEV	25	PR C112 015202	A.V. Sarantsev *et al.*	(Bonn-Gatchina Collab.)
ROENCHEN	22	EPJ A58 229	D. Roenchen *et al.*	(JULI, GWU, BONN+)
ROENCHEN	15A	EPJ A51 70	D. Roenchen *et al.*	
PDG	14	CP C38 070001	K. Olive *et al.*	(PDG Collab.)
SVARC	14	PR C89 045205	A. Svarc *et al.*	(RBI Zagreb, UNI Tuzla)
ANISOVICH	12A	EPJ A48 15	A.V. Anisovich *et al.*	(BONN, PNPI)
ARNDT	06	PR C74 045205	R.A. Arndt *et al.*	(GWU)
HOEHLER	93	πN Newsletter 9 1	G. Hohler	(KARL)
CUTKOSKY	80	Toronto Conf. 19	R.E. Cutkosky *et al.*	(CMU, LBL) IJP
Also		PR D20 2839	R.E. Cutkosky *et al.*	(CMU, LBL) IJP
HOEHLER	79	PDAT 12-1	G. Hohler *et al.*	(KARLT) IJP
Also		Toronto Conf. 3	R. Koch	(KARLT) IJP

$N(2250)\ 9/2^-$

$I(J^P) = \frac{1}{2}(\frac{9}{2}^-)$ Status: ****

Older and obsolete values are listed and referenced in the 2014 edition, Chinese Physics **C38** 070001 (2014).

$N(2250)$ POLE POSITION

REAL PART

VALUE (MeV)	DOCUMENT ID		TECN	COMMENT
2100 to 2200 (≈ 2150) OUR ESTIMATE				
2220±40	SARANTSEV	25	DPWA	Multichannel
2095±10	ROENCHEN	22	DPWA	Multichannel
2195±45	AFZAL	20	DPWA	Multichannel
2157± 3±14	[1] SVARC	14	L+P	$\pi N \to \pi N$
2150±50	CUTKOSKY	80	IPWA	$\pi N \to \pi N$
• • • We do not use the following data for averages, fits, limits, etc. • • •				
2127	HUNT	19	DPWA	Multichannel
2062	ROENCHEN	15A	DPWA	Multichannel
2195±45	ANISOVICH	12A	DPWA	Multichannel
2217	ARNDT	06	DPWA	$\pi N \to \pi N, \eta N$
2187	HOEHLER	93	SPED	$\pi N \to \pi N$

[1] Fit to the amplitudes of HOEHLER 79.

−2×IMAGINARY PART

VALUE (MeV)	DOCUMENT ID		TECN	COMMENT
350 to 500 (≈ 420) OUR ESTIMATE				
470± 40	SARANTSEV	25	DPWA	Multichannel
422± 13	ROENCHEN	22	DPWA	Multichannel
470± 50	AFZAL	20	DPWA	Multichannel
412± 7±44	[1] SVARC	14	L+P	$\pi N \to \pi N$
360±100	CUTKOSKY	80	IPWA	$\pi N \to \pi N$
• • • We do not use the following data for averages, fits, limits, etc. • • •				
262	HUNT	19	DPWA	Multichannel
403	ROENCHEN	15A	DPWA	Multichannel
470± 50	ANISOVICH	12A	DPWA	Multichannel
431	ARNDT	06	DPWA	$\pi N \to \pi N, \eta N$
388	HOEHLER	93	SPED	$\pi N \to \pi N$

[1] Fit to the amplitudes of HOEHLER 79.

$N(2250)$ ELASTIC POLE RESIDUE

MODULUS $|r|$

VALUE (MeV)	DOCUMENT ID		TECN	COMMENT
15 to 30 (≈ 25) OUR ESTIMATE				
14 ±1	ROENCHEN	22	DPWA	Multichannel
24 ±1±5	[1] SVARC	14	L+P	$\pi N \to \pi N$
26 ±5	ANISOVICH	12A	DPWA	Multichannel
20 ±6	CUTKOSKY	80	IPWA	$\pi N \to \pi N$
• • • We do not use the following data for averages, fits, limits, etc. • • •				
8.2	ROENCHEN	15A	DPWA	Multichannel
21	ARNDT	06	DPWA	$\pi N \to \pi N, \eta N$
21	HOEHLER	93	SPED	$\pi N \to \pi N$

[1] Fit to the amplitudes of HOEHLER 79.

PHASE θ

VALUE (°)	DOCUMENT ID		TECN	COMMENT
−60 to −20 (≈ −40) OUR ESTIMATE				
−67± 9	ROENCHEN	22	DPWA	Multichannel
−62± 1±11	[1] SVARC	14	L+P	$\pi N \to \pi N$
−38±25	ANISOVICH	12A	DPWA	Multichannel
−50±20	CUTKOSKY	80	IPWA	$\pi N \to \pi N$
• • • We do not use the following data for averages, fits, limits, etc. • • •				
−64	ROENCHEN	15A	DPWA	Multichannel
−20	ARNDT	06	DPWA	$\pi N \to \pi N, \eta N$

[1] Fit to the amplitudes of HOEHLER 79.

$N(2250)$ INELASTIC POLE RESIDUE

The "normalized residue" is the residue divided by $\Gamma_{pole}/2$.

Normalized residue in $N\pi \to N(2250) \to N\eta$

MODULUS	PHASE (°)	DOCUMENT ID		TECN	COMMENT
0.018±0.001	−89 ± 5	ROENCHEN	22	DPWA	Multichannel
• • • We do not use the following data for averages, fits, limits, etc. • • •					
0.017	−89	ROENCHEN	15A	DPWA	Multichannel

Normalized residue in $N\pi \to N(2250) \to \Lambda K$

MODULUS	PHASE (°)	DOCUMENT ID		TECN	COMMENT
0.003±0.001	80 ± 5	ROENCHEN	22	DPWA	Multichannel
• • • We do not use the following data for averages, fits, limits, etc. • • •					
0.006	−101	ROENCHEN	15A	DPWA	Multichannel

Normalized residue in $N\pi \to N(2250) \to \Sigma K$

MODULUS	PHASE (°)	DOCUMENT ID		TECN	COMMENT
0.004±0.002	−111 ± 5	ROENCHEN	22	DPWA	Multichannel
• • • We do not use the following data for averages, fits, limits, etc. • • •					
0.002	70	ROENCHEN	15A	DPWA	Multichannel

$N(2250)$ BREIT-WIGNER MASS

VALUE (MeV)	DOCUMENT ID		TECN	COMMENT
2250 to 2320 (≈ 2280) OUR ESTIMATE				
2310±40	SARANTSEV	25	DPWA	Multichannel
2200±10	[1] HUNT	19	DPWA	Multichannel
2302± 6	[1] ARNDT	06	DPWA	$\pi N \to \pi N, \eta N$
2250±80	CUTKOSKY	80	IPWA	$\pi N \to \pi N$
2268±15	HOEHLER	79	IPWA	$\pi N \to \pi N$
• • • We do not use the following data for averages, fits, limits, etc. • • •				
2280±40	ANISOVICH	12A	DPWA	Multichannel

[1] Statistical error only.

Int. J. Mod. Phys. A 2026.41. Downloaded from www.worldscientific.com
by UNIVERSITY OF CALIFORNIA @ BERKELEY on 09/16/26. Re-use and distribution is strictly not permitted, except for Open Access articles.

$N(2250)$ BREIT-WIGNER WIDTH

VALUE (MeV)	DOCUMENT ID		TECN	COMMENT
300 to 600 (≈ 500) OUR ESTIMATE				
520± 50	SARANTSEV	25	DPWA	Multichannel
343± 51	[1] HUNT	19	DPWA	Multichannel
628± 28	[1] ARNDT	06	DPWA	$\pi N \to \pi N, \eta N$
480±120	CUTKOSKY	80	IPWA	$\pi N \to \pi N$
300± 40	HOEHLER	79	IPWA	$\pi N \to \pi N$
• • • We do not use the following data for averages, fits, limits, etc. • • •				
520± 50	ANISOVICH	12A	DPWA	Multichannel

[1] Statistical error only.

$N(2250)$ DECAY MODES

The following branching fractions are our estimates, not fits or averages.

	Mode	Fraction (Γ_i/Γ)
Γ_1	$N\pi$	5–15 %
Γ_2	$N\eta$	<5 %
Γ_3	ΛK	1–3 %
Γ_4	$N\pi\pi$	
Γ_5	$\Delta\pi$	(10±7) %
Γ_6	$\Delta\pi$, G-wave	(10±7) %
Γ_7	$N\rho$	(11±7) %
Γ_8	$N\rho$, S=1/2	(5±5) %
Γ_9	$N\rho$, S=3/2 , G-wave	(6±4) %

$N(2250)$ BRANCHING RATIOS

$\Gamma(N\pi)/\Gamma_{total}$ — Γ_1/Γ

VALUE (%)	DOCUMENT ID		TECN	COMMENT
5–15 % OUR ESTIMATE				
8.5±0.4	[1] HUNT	19	DPWA	Multichannel
12 ±4	ANISOVICH	12A	DPWA	Multichannel
8.9±0.1	[1] ARNDT	06	DPWA	$\pi N \to \pi N, \eta N$
10 ±2	CUTKOSKY	80	IPWA	$\pi N \to \pi N$
10 ±2	HOEHLER	79	IPWA	$\pi N \to \pi N$

[1] Statistical error only.

$\Gamma(N\eta)/\Gamma_{total}$ — Γ_2/Γ

VALUE (%)	DOCUMENT ID		TECN	COMMENT
<5 % OUR ESTIMATE				
<5	[1] HUNT	19	DPWA	Multichannel

[1] Statistical error only.

$\Gamma(\Lambda K)/\Gamma_{total}$ — Γ_3/Γ

VALUE (%)	DOCUMENT ID		TECN	COMMENT
1–3 % OUR ESTIMATE				
2.0±0.6	[1] HUNT	19	DPWA	Multichannel

[1] Statistical error only.

$\Gamma(\Delta\pi)/\Gamma_{total}$ — Γ_5/Γ

VALUE (%)	DOCUMENT ID		TECN	COMMENT
10±7	SARANTSEV	25	DPWA	Multichannel

$\Gamma(\Delta\pi, G\text{-wave})/\Gamma_{total}$ — Γ_6/Γ

VALUE (%)	DOCUMENT ID		TECN	COMMENT
10±7	SARANTSEV	25	DPWA	Multichannel

$\Gamma(N\rho)/\Gamma_{total}$ — Γ_7/Γ

VALUE (%)	DOCUMENT ID		TECN	COMMENT
11±7	SARANTSEV	25	DPWA	Multichannel

$\Gamma(N\rho, S=1/2)/\Gamma_{total}$ — Γ_8/Γ

VALUE (%)	DOCUMENT ID		TECN	COMMENT
5±5	SARANTSEV	25	DPWA	Multichannel

$\Gamma(N\rho, S=3/2, G\text{-wave})/\Gamma_{total}$ — Γ_9/Γ

VALUE (%)	DOCUMENT ID		TECN	COMMENT
6±4	SARANTSEV	25	DPWA	Multichannel

$N(2250)$ PHOTON DECAY AMPLITUDES AT THE POLE

$N(2250) \to p\gamma$, helicity-1/2 amplitude $A_{1/2}$

MODULUS ($GeV^{-1/2}$)	PHASE (°)	DOCUMENT ID		TECN	COMMENT
0.020±0.010	−10 ± 30	SARANTSEV	25	DPWA	Multichannel
−0.108±0.007	112 ± 4	ROENCHEN	22	DPWA	Multichannel
• • • We do not use the following data for averages, fits, limits, etc. • • •					
0.026	−26	ROENCHEN	15A	DPWA	Multichannel

$N(2250) \to p\gamma$, helicity-3/2 amplitude $A_{3/2}$

MODULUS ($GeV^{-1/2}$)	PHASE (°)	DOCUMENT ID		TECN	COMMENT
0.025±0.009	−10 ± 20	SARANTSEV	25	DPWA	Multichannel
0.050±0.011	69 ± 8	ROENCHEN	22	DPWA	Multichannel
• • • We do not use the following data for averages, fits, limits, etc. • • •					
0.119	−42	ROENCHEN	15A	DPWA	Multichannel

$N(2250)$ BREIT-WIGNER PHOTON DECAY AMPLITUDES

$N(2250) \to p\gamma$, helicity-1/2 amplitude $A_{1/2}$

VALUE ($GeV^{-1/2}$)	DOCUMENT ID		TECN	COMMENT
0.015 ±0.008	SARANTSEV	25	DPWA	Multichannel
0.0006±0.0037	[1] HUNT	19	DPWA	Multichannel

[1] Statistical error only.

$N(2250) \to p\gamma$, helicity-3/2 amplitude $A_{3/2}$

VALUE ($GeV^{-1/2}$)	DOCUMENT ID		TECN	COMMENT
0.025±0.008	SARANTSEV	25	DPWA	Multichannel
0.013±0.004	[1] HUNT	19	DPWA	Multichannel

[1] Statistical error only.

$N(2250)$ REFERENCES

SARANTSEV	25	PR C112 015202	A.V. Sarantsev *et al.*	(Bonn-Gatchina Collab.)
ROENCHEN	22	EPJ A58 229	D. Roenchen *et al.*	(JULI, GWU, BONN+)
AFZAL	20	PRL 125 152002	F. Afzal *et al.*	(CBELSA/TAPS Collab.)
HUNT	19	PR C99 055205	B.C. Hunt, D.M. Manley	
ROENCHEN	15A	EPJ A51 70	D. Roenchen *et al.*	
PDG	14	CP C38 070001	K. Olive *et al.*	(PDG Collab.)
SVARC	14	PR C89 045205	A. Svarc *et al.*	(RBI Zagreb, UNI Tuzla)
ANISOVICH	12A	EPJ A48 15	A.V. Anisovich *et al.*	(BONN, PNPI)
ARNDT	06	PR C74 045205	R.A. Arndt *et al.*	(GWU)
HOEHLER	93	πN Newsletter 9 1	G. Hohler	(KARL)
CUTKOSKY	80	Toronto Conf. 19	R.E. Cutkosky *et al.*	(CMU, LBL) IJP
Also		PR D20 2839	R.E. Cutkosky *et al.*	(CMU, LBL) IJP
HOEHLER	79	PDAT 12-1	G. Hohler *et al.*	(KARLT) IJP
Also		Toronto Conf. 3	R. Koch	(KARLT) IJP

$N(2300)$ $1/2^+$

$I(J^P) = \frac{1}{2}(\frac{1}{2}^+)$ Status: **

OMITTED FROM SUMMARY TABLE

$N(2300)$ MASS

VALUE (MeV)	DOCUMENT ID		TECN	COMMENT
$2300^{+40}_{-30}{}^{+109}_{-\ 0}$	ABLIKIM	13A	BES3	$\psi(2S) \to p\overline{p}\pi^0$

$N(2300)$ WIDTH

VALUE (MeV)	DOCUMENT ID		TECN	COMMENT
$340\pm30^{+110}_{-\ 58}$	ABLIKIM	13A	BES3	$\psi(2S) \to p\overline{p}\pi^0$

$N(2300)$ REFERENCES

ABLIKIM	13A	PRL 110 022001	M. Ablikim *et al.*	(BESIII Collab.)

$N(2570)$ $5/2^-$

$I(J^P) = \frac{1}{2}(\frac{5}{2}^-)$ Status: **

OMITTED FROM SUMMARY TABLE

$N(2570)$ MASS

VALUE (MeV)	DOCUMENT ID		TECN	COMMENT
$2570^{+19}_{-10}{}^{+34}_{-10}$	ABLIKIM	13A	BES3	$\psi(2S) \to p\overline{p}\pi^0$

$N(2570)$ WIDTH

VALUE (MeV)	DOCUMENT ID		TECN	COMMENT
$250^{+14}_{-24}{}^{+69}_{-21}$	ABLIKIM	13A	BES3	$\psi(2S) \to p\overline{p}\pi^0$

$N(2570)$ REFERENCES

ABLIKIM	13A	PRL 110 022001	M. Ablikim *et al.*	(BESIII Collab.)

Int. J. Mod. Phys. A 2026.41. Downloaded from www.worldscientific.com
UNIVERSITY OF CALIFORNIA @ BERKELEY on 09/16/26. Re-use and distribution is strictly not permitted, except for Open Access articles.

$N(2600)\ 11/2^-$

$I(J^P) = \frac{1}{2}(\frac{11}{2}^-)$ Status: ***

$N(2600)$ BREIT-WIGNER MASS

VALUE (MeV)	DOCUMENT ID		TECN	COMMENT
2550 to 2750 (≈ 2600) OUR ESTIMATE				
2623±197	ARNDT	06	DPWA	$\pi N \to \pi N, \eta N$
2577± 50	HOEHLER	79	IPWA	$\pi N \to \pi N$

$N(2600)$ BREIT-WIGNER WIDTH

VALUE (MeV)	DOCUMENT ID		TECN	COMMENT
500 to 800 (≈ 650) OUR ESTIMATE				
1311±996	ARNDT	06	DPWA	$\pi N \to \pi N, \eta N$
400±100	HOEHLER	79	IPWA	$\pi N \to \pi N$

$N(2600)$ DECAY MODES

	Mode	Fraction (Γ_i/Γ)
Γ_1	$N\pi$	3–8 %

$N(2600)$ BRANCHING RATIOS

$\Gamma(N\pi)/\Gamma_{total}$ — Γ_1/Γ

VALUE (%)	DOCUMENT ID		TECN	COMMENT
3 to 8 (≈ 5) OUR ESTIMATE				
5.0±1.8	ARNDT	06	DPWA	$\pi N \to \pi N, \eta N$
5 ±1	HOEHLER	79	IPWA	$\pi N \to \pi N$

$N(2600)$ REFERENCES

ARNDT	06	PR C74 045205	R.A. Arndt *et al.*	(GWU)
HOEHLER	79	PDAT 12-1	G. Hohler *et al.*	(KARLT) IJP
Also		Toronto Conf. 3	R. Koch	(KARLT) IJP

$N(2700)\ 13/2^+$

$I(J^P) = \frac{1}{2}(\frac{13}{2}^+)$ Status: **

OMITTED FROM SUMMARY TABLE

$N(2700)$ BREIT-WIGNER MASS

VALUE (MeV)	DOCUMENT ID		TECN	COMMENT
2612±45	HOEHLER	79	IPWA	$\pi N \to \pi N$

$N(2700)$ BREIT-WIGNER WIDTH

VALUE (MeV)	DOCUMENT ID		TECN	COMMENT
350±50	HOEHLER	79	IPWA	$\pi N \to \pi N$

$N(2700)$ DECAY MODES

	Mode	Fraction (Γ_i/Γ)
Γ_1	$N\pi$	3–5 %

$N(2700)$ BRANCHING RATIOS

$\Gamma(N\pi)/\Gamma_{total}$ — Γ_1/Γ

VALUE (%)	DOCUMENT ID		TECN	COMMENT
4±1	HOEHLER	79	IPWA	$\pi N \to \pi N$

$N(2700)$ REFERENCES

HOEHLER	79	PDAT 12-1	G. Hohler *et al.*	(KARLT) IJP
Also		Toronto Conf. 3	R. Koch	(KARLT) IJP

$N(\sim 3000$ Region) Partial-Wave Analyses

OMITTED FROM SUMMARY TABLE

We list here miscellaneous high-mass candidates for isospin-1/2 resonances found in partial-wave analyses.

Our 1982 edition had an $N(3245)$, an $N(3690)$, and an $N(3755)$, each a narrow peak seen in a production experiment. Since nothing has been heard from them since the 1960's, we declare them to be dead. There was also an $N(3030)$, deduced from total cross-section and 180° elastic cross-section measurements; it is the KOCH 80 $L_{1,15}$ state below.

$N(\sim 3000)$ BREIT-WIGNER MASS

VALUE (MeV)	DOCUMENT ID		TECN	COMMENT
≈ 3000 OUR ESTIMATE				
2600	KOCH	80	IPWA	$\pi N \to \pi N\ D_{13}$
3100	KOCH	80	IPWA	$\pi N \to \pi N\ L_{1,15}$ wave
3500	KOCH	80	IPWA	$\pi N \to \pi N\ M_{1,17}$ wave
3500 to 4000	KOCH	80	IPWA	$\pi N \to \pi N\ N_{1,19}$ wave
3500±200	HENDRY	78	MPWA	$\pi N \to \pi N\ L_{1,15}$ wave
3800±200	HENDRY	78	MPWA	$\pi N \to \pi N\ M_{1,17}$ wave
4100±200	HENDRY	78	MPWA	$\pi N \to \pi N\ N_{1,19}$ wave

$N(\sim 3000)$ BREIT-WIGNER WIDTH

VALUE (MeV)	DOCUMENT ID		TECN	COMMENT
1300±200	HENDRY	78	MPWA	$\pi N \to \pi N\ L_{1,15}$ wave
1600±200	HENDRY	78	MPWA	$\pi N \to \pi N\ M_{1,17}$ wave
1900±300	HENDRY	78	MPWA	$\pi N \to \pi N\ N_{1,19}$ wave

$N(\sim 3000)$ DECAY MODES

	Mode	Fraction (Γ_i/Γ)
Γ_1	$N\pi$	2–8 %

$N(\sim 3000)$ BRANCHING RATIOS

$\Gamma(N\pi)/\Gamma_{total}$ — Γ_1/Γ

VALUE (%)	DOCUMENT ID		TECN	COMMENT
2–8 % OUR ESTIMATE				
6 ±2	HENDRY	78	MPWA	$\pi N \to \pi N\ L_{1,15}$ wave
4.0±1.5	HENDRY	78	MPWA	$\pi N \to \pi N\ M_{1,17}$ wave
3.0±1.5	HENDRY	78	MPWA	$\pi N \to \pi N\ N_{1,19}$ wave

$N(\sim 3000)$ REFERENCES

KOCH	80	Toronto Conf. 3	R. Koch	(KARLT) IJP
HENDRY	78	PRL 41 222	A.W. Hendry	(IND, LBL) IJP
Also		ANP 136 1	A.W. Hendry	(IND) IJP

Int. J. Mod. Phys. A 2026.41. Downloaded from www.worldscientific.com
by UNIVERSITY OF CALIFORNIA @ BERKELEY on 09/16/26. Re-use and distribution is strictly not permitted, except for Open Access articles.

Δ BARYONS
($S = 0$, $I = 3/2$)

$\Delta^{++} = uuu$, $\Delta^{+} = uud$, $\Delta^{0} = udd$, $\Delta^{-} = ddd$

$\Delta(1232)\ 3/2^+$

$I(J^P) = \frac{3}{2}(\frac{3}{2}^+)$ Status: ****

Older and obsolete values are listed and referenced in the 2014 edition, Chinese Physics **C38** 070001 (2014).

$\Delta(1232)$ POLE POSITIONS

REAL PART, MIXED CHARGES

VALUE (MeV)	DOCUMENT ID		TECN	COMMENT
1209 to 1211 (≈ 1210) OUR ESTIMATE				
1210 ±1	SARANTSEV	25	DPWA	Multichannel
1209.5 ±1.1	[1] HOFERICHT...	24	RVUE	$\pi N \to \pi N$
1215 ±1	ROENCHEN	22	DPWA	Multichannel
1211 ±1 ±1	[2] SVARC	14	L+P	$\pi N \to \pi N$
1210 ±1	CUTKOSKY	80	IPWA	$\pi N \to \pi N$
• • • We do not use the following data for averages, fits, limits, etc. • • •				
1212.4	HUNT	19	DPWA	Multichannel
1218	ROENCHEN	15A	DPWA	Multichannel
1210.5 ±1.0	ANISOVICH	12A	DPWA	Multichannel
1211	ARNDT	06	DPWA	$\pi N \to \pi N, \eta N$
1210	ARNDT	04	DPWA	$\pi N \to \pi N, \eta N$
1209	[3] HOEHLER	93	ARGD	$\pi N \to \pi N$

[1] Roy-Steiner equations applied to πN scattering amplitudes and pionic atom data
[2] Fit to the amplitudes of HOEHLER 79.
[3] See HOEHLER 93 for a detailed discussion of the evidence for and the pole parameters of N and Δ resonances as determined from Argand diagrams of πN elastic partial-wave amplitudes and from plots of the speeds with which the amplitudes traverse the diagrams.

−2×IMAGINARY PART, MIXED CHARGES

VALUE (MeV)	DOCUMENT ID		TECN	COMMENT
98 to 102 (≈ 100) OUR ESTIMATE				
101 ±2	SARANTSEV	25	DPWA	Multichannel
98.5 ±1.2	[1] HOFERICHT...	24	RVUE	$\pi N \to \pi N$
93 ±1	ROENCHEN	22	DPWA	Multichannel
98 ±2 ±1	[2] SVARC	14	L+P	$\pi N \to \pi N$
100 ±2	CUTKOSKY	80	IPWA	$\pi N \to \pi N$
• • • We do not use the following data for averages, fits, limits, etc. • • •				
96.8	HUNT	19	DPWA	Multichannel
92	ROENCHEN	15A	DPWA	Multichannel
99 ±2	ANISOVICH	12A	DPWA	Multichannel
99	ARNDT	06	DPWA	$\pi N \to \pi N, \eta N$
100	ARNDT	04	DPWA	$\pi N \to \pi N, \eta N$
100	[3] HOEHLER	93	ARGD	$\pi N \to \pi N$

[1] Roy-Steiner equations applied to πN scattering amplitudes and pionic atom data.
[2] Fit to the amplitudes of HOEHLER 79.
[3] See HOEHLER 93 for a detailed discussion of the evidence for and the pole parameters of N and Δ resonances as determined from Argand diagrams of πN elastic partial-wave amplitudes and from plots of the speeds with which the amplitudes traverse the diagrams.

REAL PART, $\Delta(1232)^{++}$

VALUE (MeV)	DOCUMENT ID		COMMENT
• • • We do not use the following data for averages, fits, limits, etc. • • •			
1212.50 ±0.24	BERNICHA	96	Fit to PEDRONI 78

−2×IMAGINARY PART, $\Delta(1232)^{++}$

VALUE (MeV)	DOCUMENT ID		COMMENT
• • • We do not use the following data for averages, fits, limits, etc. • • •			
97.37 ±0.42	BERNICHA	96	Fit to PEDRONI 78

REAL PART, $\Delta(1232)^{+}$

VALUE (MeV)	DOCUMENT ID		TECN	COMMENT
• • • We do not use the following data for averages, fits, limits, etc. • • •				
1211 ±1 to 1212 ± 1	HANSTEIN	96	DPWA	$\gamma N \to \pi N$
1206.9 ±0.9 to 1210.5 ± 1.8	MIROSHNIC...	79		Fit photoproduction

−2×IMAGINARY PART, $\Delta(1232)^{+}$

VALUE (MeV)	DOCUMENT ID		TECN	COMMENT
• • • We do not use the following data for averages, fits, limits, etc. • • •				
102 ±2 to 99 ± 2	[1] HANSTEIN	96	DPWA	$\gamma N \to \pi N$
111.2 ±2.0 to 116.6 ± 2.2	MIROSHNIC...	79		Fit photoproduction

[1] The second (lower) value of HANSTEIN 96 here goes with the second (higher) value of the real part in the preceding data block.

REAL PART, $\Delta(1232)^{0}$

VALUE (MeV)	DOCUMENT ID		COMMENT
• • • We do not use the following data for averages, fits, limits, etc. • • •			
1213.20 ±0.66	BERNICHA	96	Fit to PEDRONI 78

−2×IMAGINARY PART, $\Delta(1232)^{0}$

VALUE (MeV)	DOCUMENT ID		COMMENT
• • • We do not use the following data for averages, fits, limits, etc. • • •			
104.10 ±1.01	BERNICHA	96	Fit to PEDRONI 78

$\Delta(1232)$ ELASTIC POLE RESIDUES

ABSOLUTE VALUE, MIXED CHARGES

VALUE (MeV)	DOCUMENT ID		TECN	COMMENT
49 to 52 (≈ 50) OUR ESTIMATE				
51.3 ±0.9	[1] HOFERICHT...	24	RVUE	$\pi N \to \pi N$
50 ±1	ROENCHEN	22	DPWA	Multichannel
50 ±1 ±1	[2] SVARC	14	L+P	$\pi N \to \pi N$
51.6 ±0.6	ANISOVICH	12A	DPWA	Multichannel
53 ±2	CUTKOSKY	80	IPWA	$\pi N \to \pi N$
• • • We do not use the following data for averages, fits, limits, etc. • • •				
46	ROENCHEN	15A	DPWA	Multichannel
52	ARNDT	06	DPWA	$\pi N \to \pi N, \eta N$
53	ARNDT	04	DPWA	$\pi N \to \pi N, \eta N$
50	HOEHLER	93	ARGD	$\pi N \to \pi N$

[1] Roy-Steiner equations applied to πN scattering amplitudes and pionic atom data.
[2] Fit to the amplitudes of HOEHLER 79.

PHASE, MIXED CHARGES

VALUE (°)	DOCUMENT ID		TECN	COMMENT
−48 to −45 (≈ −46) OUR ESTIMATE				
−47.4 ±0.4	[1] HOFERICHT...	24	RVUE	$\pi N \to \pi N$
−39 ±1	ROENCHEN	22	DPWA	Multichannel
−46 ±1 ±1	[2] SVARC	14	L+P	$\pi N \to \pi N$
−46 ±1	ANISOVICH	12A	DPWA	Multichannel
−47 ±1	CUTKOSKY	80	IPWA	$\pi N \to \pi N$
• • • We do not use the following data for averages, fits, limits, etc. • • •				
−36	ROENCHEN	15A	DPWA	Multichannel
−47	ARNDT	06	DPWA	$\pi N \to \pi N, \eta N$
−47	ARNDT	04	DPWA	$\pi N \to \pi N, \eta N$
−48	HOEHLER	93	ARGD	$\pi N \to \pi N$

[1] Roy-Steiner equations applied to πN scattering amplitudes and pionic atom data.
[2] Fit to the amplitudes of HOEHLER 79.

$\Delta(1232)$ BREIT-WIGNER MASSES

MIXED CHARGES

VALUE (MeV)	DOCUMENT ID		TECN	COMMENT
1230 to 1234 (≈ 1232) OUR ESTIMATE				
1230 ±1	SARANTSEV	25	DPWA	Multichannel
1230.8 ±0.4	[1] HUNT	19	DPWA	Multichannel
1233.4 ±0.4	[1] ARNDT	06	DPWA	$\pi N \to \pi N, \eta N$
1232 ±3	CUTKOSKY	80	IPWA	$\pi N \to \pi N$
1233 ±2	HOEHLER	79	IPWA	$\pi N \to \pi N$
• • • We do not use the following data for averages, fits, limits, etc. • • •				
1228 ±2	ANISOVICH	12A	DPWA	Multichannel
1231.1 ±0.2	[1] SHRESTHA	12A	DPWA	Multichannel
1232.9 ±1.2	ARNDT	04	DPWA	$\pi N \to \pi N, \eta N$
1228 ±1	PENNER	02C	DPWA	Multichannel

[1] Statistical error only.

$\Delta(1232)^{++}$ MASS

VALUE (MeV)	DOCUMENT ID		TECN	COMMENT
• • • We do not use the following data for averages, fits, limits, etc. • • •				
1230.55 ±0.20	GRIDNEV	06	DPWA	$\pi N \to \pi N$
1231.88 ±0.29	BERNICHA	96		Fit to PEDRONI 78
1230.5 ±0.2	ABAEV	95	IPWA	$\pi N \to \pi N$
1230.9 ±0.3	KOCH	80B	IPWA	$\pi N \to \pi N$
1231.1 ±0.2	PEDRONI	78		$\pi N \to \pi N$ 70–370 MeV

$\Delta(1232)^{+}$ MASS

VALUE (MeV)	DOCUMENT ID		COMMENT
• • • We do not use the following data for averages, fits, limits, etc. • • •			
1234.9 ±1.4	MIROSHNIC...	79	Fit photoproduction

$\Delta(1232)^{0}$ MASS

VALUE (MeV)	DOCUMENT ID		TECN	COMMENT
• • • We do not use the following data for averages, fits, limits, etc. • • •				
1231.3 ±0.6	BREITSCHOP...	06	CNTR	Using new CHEX data
1233.40 ±0.22	GRIDNEV	06	DPWA	$\pi N \to \pi N$
1234.35 ±0.75	BERNICHA	96		Fit to PEDRONI 78
1233.1 ±0.3	ABAEV	95	IPWA	$\pi N \to \pi N$
1233.6 ±0.5	KOCH	80B	IPWA	$\pi N \to \pi N$
1233.8 ±0.2	PEDRONI	78		$\pi N \to \pi N$ 70–370 MeV

Int. J. Mod. Phys. A 2026.41. Downloaded from www.worldscientific.com
UNIVERSITY OF CALIFORNIA @ BERKELEY on 09/16/26. Re-use and distribution is strictly not permitted, except for Open Access articles.

$m_{\Delta^0} - m_{\Delta^{++}}$

VALUE (MeV)	DOCUMENT ID		TECN	COMMENT
• • • We do not use the following data for averages, fits, limits, etc. • • •				
2.86±0.30	GRIDNEV	06	DPWA	$\pi N \to \pi N$
2.25±0.68	BERNICHA	96		Fit to PEDRONI 78
2.6 ±0.4	ABAEV	95	IPWA	$\pi N \to \pi N$
2.7 ±0.3	[1] PEDRONI	78		See the masses

[1] Using $\pi^{\pm} d$ as well, PEDRONI 78 determine $(M^- - M^{++}) + (M^0 - M^+)/3 = 4.6 \pm 0.2$ MeV.

$\Delta(1232)$ BREIT-WIGNER WIDTHS

MIXED CHARGES

VALUE (MeV)	DOCUMENT ID		TECN	COMMENT
114 to 120 (≈ 117) OUR ESTIMATE				
116 ±2	SARANTSEV	25	DPWA	Multichannel
110.9±0.8	[1] HUNT	19	DPWA	Multichannel
118.7±0.6	[1] ARNDT	06	DPWA	$\pi N \to \pi N, \eta N$
120 ±5	CUTKOSKY	80	IPWA	$\pi N \to \pi N$
116 ±5	HOEHLER	79	IPWA	$\pi N \to \pi N$
• • • We do not use the following data for averages, fits, limits, etc. • • •				
110 ±3	ANISOVICH	12A	DPWA	Multichannel
113.0±0.5	[1] SHRESTHA	12A	DPWA	Multichannel
118.0±2.2	ARNDT	04	DPWA	$\pi N \to \pi N, \eta N$
106 ±1	PENNER	02C	DPWA	Multichannel

[1] Statistical error only.

$\Delta(1232)^{++}$ WIDTH

VALUE (MeV)	DOCUMENT ID		TECN	COMMENT
• • • We do not use the following data for averages, fits, limits, etc. • • •				
112.2 ±0.7	GRIDNEV	06	DPWA	$\pi N \to \pi N$
109.07±0.48	BERNICHA	96		Fit to PEDRONI 78
111.0 ±1.0	KOCH	80B	IPWA	$\pi N \to \pi N$
111.3 ±0.5	PEDRONI	78		$\pi N \to \pi N$ 70–370 MeV

$\Delta(1232)^{+}$ WIDTH

VALUE (MeV)	DOCUMENT ID		COMMENT
• • • We do not use the following data for averages, fits, limits, etc. • • •			
131.1±2.4	MIROSHNIC...	79	Fit photoproduction

$\Delta(1232)^{0}$ WIDTH

VALUE (MeV)	DOCUMENT ID		TECN	COMMENT
• • • We do not use the following data for averages, fits, limits, etc. • • •				
112.5 ±1.9	BREITSCHOP...	06	CNTR	Using new CHEX data
116.9 ±0.7	GRIDNEV	06	DPWA	$\pi N \to \pi N$
117.58±1.16	BERNICHA	96		Fit to PEDRONI 78
113.0 ±1.5	KOCH	80B	IPWA	$\pi N \to \pi N$
117.9 ±0.9	PEDRONI	78		$\pi N \to \pi N$ 70–370 MeV

Δ^0-Δ^{++} WIDTH DIFFERENCE

VALUE (MeV)	DOCUMENT ID		TECN	COMMENT
• • • We do not use the following data for averages, fits, limits, etc. • • •				
4.66±1.0	GRIDNEV	06	DPWA	$\pi N \to \pi N$
8.45±1.11	BERNICHA	96		Fit to PEDRONI 78
5.1 ±1.0	ABAEV	95	IPWA	$\pi N \to \pi N$
6.6 ±1.0	PEDRONI	78		See the widths

$\Delta(1232)$ DECAY MODES

The following branching fractions are our estimates, not fits or averages.

	Mode	Fraction (Γ_i/Γ)
Γ_1	$N\pi$	99.4 %
Γ_2	$N\gamma$	0.55–0.65 %
Γ_3	$N\gamma$, helicity=1/2	0.11–0.13 %
Γ_4	$N\gamma$, helicity=3/2	0.44–0.52 %
Γ_5	$p e^+ e^-$	$(4.2\pm0.7)\times10^{-5}$

$\Delta(1232)$ BRANCHING RATIOS

$\Gamma(N\pi)/\Gamma_{total}$ — Γ_1/Γ

VALUE	DOCUMENT ID		TECN	COMMENT
0.994 OUR ESTIMATE				
0.9939±0.0001	[1] HUNT	19	DPWA	Multichannel
1.00	ARNDT	06	DPWA	$\pi N \to \pi N, \eta N$
1.0	CUTKOSKY	80	IPWA	$\pi N \to \pi N$
1.0	HOEHLER	79	IPWA	$\pi N \to \pi N$
• • • We do not use the following data for averages, fits, limits, etc. • • •				
0.994	SHRESTHA	12A	DPWA	Multichannel
1.0	ANISOVICH	10	DPWA	Multichannel
1.000	ARNDT	04	DPWA	$\pi N \to \pi N, \eta N$
1.00	PENNER	02C	DPWA	Multichannel

[1] Statistical error only.

$\Gamma(p e^+ e^-)/\Gamma_{total}$ — Γ_5/Γ

VALUE (units 10^{-5})	DOCUMENT ID
4.19±0.34±0.62	[1] ADAMCZEW... 17

[1] The systematic uncertainty includes the model dependence.

$\Delta(1232)$ PHOTON DECAY AMPLITUDES AT THE POLE

$\Delta(1232) \to N\gamma$, helicity-1/2 amplitude $A_{1/2}$

MODULUS ($GeV^{-1/2}$)	PHASE (°)	DOCUMENT ID		TECN	COMMENT
−0.133±0.003	−17 ± 2	SARANTSEV	25	DPWA	Multichannel
−0.126±0.002	−18 ± 2	ROENCHEN	22	DPWA	Multichannel
• • • We do not use the following data for averages, fits, limits, etc. • • •					
−0.117	−6.6	ROENCHEN	15A	DPWA	Multichannel

$\Delta(1232) \to N\gamma$, helicity-3/2 amplitude $A_{3/2}$

MODULUS ($GeV^{-1/2}$)	PHASE (°)	DOCUMENT ID		TECN	COMMENT
−0.255±0.005	−10 ± 2	SARANTSEV	25	DPWA	Multichannel
−0.245±0.004	−0.7 ± 0.9	ROENCHEN	22	DPWA	Multichannel
• • • We do not use the following data for averages, fits, limits, etc. • • •					
−0.226	2.8	ROENCHEN	15A	DPWA	Multichannel

$\Delta(1232)$ BREIT-WIGNER PHOTON DECAY AMPLITUDES

Papers on γN amplitudes predating 1981 may be found in our 2006 edition, Journal of Physics **G33** 1 (2006).

$\Delta(1232) \to N\gamma$, helicity-1/2 amplitude $A_{1/2}$

VALUE ($GeV^{-1/2}$)	DOCUMENT ID		TECN	COMMENT
−0.142 to −0.129 (≈ −0.135) OUR ESTIMATE				
−0.135 ±0.003	SARANTSEV	25	DPWA	Multichannel
−0.146 ±0.002	[1] HUNT	19	DPWA	Multichannel
−0.139 ±0.002	[1] WORKMAN	12A	DPWA	$\gamma N \to N\pi$
−0.139 ±0.004	[1] DUGGER	07	DPWA	$\gamma N \to \pi N$
−0.137 ±0.005	AHRENS	04A	DPWA	$\vec{\gamma}\vec{p} \to N\pi$
−0.1357±0.0013±0.0037	BLANPIED	01	LEGS	$\gamma p \to p\gamma, p\pi^0, n\pi^+$
−0.131 ±0.001	[1] BECK	00	IPWA	$\vec{\gamma}p \to p\pi^0, n\pi^+$
−0.140 ±0.005	KAMALOV	99	DPWA	$\gamma N \to \pi N$
−0.1294±0.0013	HANSTEIN	98	IPWA	$\gamma N \to \pi N$
−0.1278±0.0012	DAVIDSON	97	DPWA	$\gamma N \to \pi N$
• • • We do not use the following data for averages, fits, limits, etc. • • •				
−0.131 ±0.004	ANISOVICH	12A	DPWA	Multichannel
−0.137 ±0.001	[1] SHRESTHA	12A	DPWA	Multichannel
−0.140	DRECHSEL	07	DPWA	$\gamma N \to \pi N$
−0.129 ±0.001	ARNDT	02	DPWA	$\gamma p \to N\pi$
−0.128	PENNER	02D	DPWA	Multichannel
−0.1312	HANSTEIN	98	DPWA	$\gamma N \to \pi N$

[1] Statistical error only.

$\Delta(1232) \to N\gamma$, helicity-3/2 amplitude $A_{3/2}$

VALUE ($GeV^{-1/2}$)	DOCUMENT ID		TECN	COMMENT
−0.262 to −0.248 (≈ −0.255) OUR ESTIMATE				
−0.259 ±0.005	SARANTSEV	25	DPWA	Multichannel
−0.250 ±0.002	[1] HUNT	19	DPWA	Multichannel
−0.262 ±0.003	WORKMAN	12A	DPWA	$\gamma N \to N\pi$
−0.258 ±0.005	DUGGER	07	DPWA	$\gamma N \to \pi N$
−0.256 ±0.003	AHRENS	04A	DPWA	$\vec{\gamma}\vec{p} \to N\pi$
−0.2669±0.0016±0.0078	BLANPIED	01	LEGS	$\gamma p \to p\gamma, p\pi^0, n\pi^+$
−0.251 ±0.001	BECK	00	IPWA	$\vec{\gamma}p \to p\pi^0, n\pi^+$
−0.258 ±0.006	KAMALOV	99	DPWA	$\gamma N \to \pi N$
−0.2466±0.0013	HANSTEIN	98	IPWA	$\gamma N \to \pi N$
−0.2524±0.0013	DAVIDSON	97	DPWA	$\gamma N \to \pi N$
• • • We do not use the following data for averages, fits, limits, etc. • • •				
−0.254 ±0.005	ANISOVICH	12A	DPWA	Multichannel
−0.251 ±0.001	[1] SHRESTHA	12A	DPWA	Multichannel
−0.265	DRECHSEL	07	DPWA	$\gamma N \to \pi N$
−0.243 ±0.001	ARNDT	02	DPWA	$\gamma p \to N\pi$
−0.247	PENNER	02D	DPWA	Multichannel
−0.2522	HANSTEIN	98	DPWA	$\gamma N \to \pi N$

[1] Statistical error only.

$\Delta(1232) \to N\gamma$, E_2/M_1 ratio

VALUE	DOCUMENT ID		TECN	COMMENT
−0.028 to −0.022 (≈ −0.025) OUR ESTIMATE				
−0.0238±0.0016±0.0010	MORNACCHI	24	DPWA	$\vec{\gamma}\vec{p} \to N\pi$
−0.0274±0.0003±0.0030	AHRENS	04A	DPWA	$\vec{\gamma}\vec{p} \to N\pi$
−0.020 ±0.002	ARNDT	02	DPWA	$\gamma p \to N\pi$
−0.0307±0.0026±0.0024	BLANPIED	01	LEGS	$\gamma p \to p\gamma, p\pi^0, n\pi^+$
−0.016 ±0.004 ±0.002	GALLER	01	DPWA	$\gamma p \to \gamma p$
−0.025 ±0.001 ±0.002	BECK	00	IPWA	$\vec{\gamma}p \to p\pi^0, n\pi^+$
−0.0233±0.0017	HANSTEIN	98	IPWA	$\gamma N \to \pi N$
−0.015 ±0.005	[1] ARNDT	97	IPWA	$\gamma N \to \pi N$
−0.0319±0.0024	DAVIDSON	97	DPWA	$\gamma N \to \pi N$
• • • We do not use the following data for averages, fits, limits, etc. • • •				
−0.022	DRECHSEL	07	DPWA	$\gamma N \to \pi N$

−0.026	PENNER	02D	DPWA	Multichannel
−0.0254±0.0010	HANSTEIN	98	DPWA	$\gamma N \to \pi N$
−0.025 ±0.002 ±0.002	BECK	97	IPWA	$\gamma N \to \pi N$
−0.030 ±0.003 ±0.002	BLANPIED	97	DPWA	$\gamma N \to \pi N, \gamma N$

[1] This ARNDT 97 value is very sensitive to the database being fitted. The result is from a fit to the full pion photoproduction database, apart from the BLANPIED 97 cross-section measurements.

$\Delta(1232) \to N\gamma$, absolute value of E_2/M_1 ratio at pole

VALUE	DOCUMENT ID		TECN	COMMENT
• • • We do not use the following data for averages, fits, limits, etc. • • •				
0.065±0.007	ARNDT	97	DPWA	$\gamma N \to \pi N$
0.058	HANSTEIN	96	DPWA	$\gamma N \to \pi N$

$\Delta(1232) \to N\gamma$, phase of E_2/M_1 ratio at pole

VALUE	DOCUMENT ID		TECN	COMMENT
• • • We do not use the following data for averages, fits, limits, etc. • • •				
−122 ±5	ARNDT	97	DPWA	$\gamma N \to \pi N$
−127.2	HANSTEIN	96	DPWA	$\gamma N \to \pi N$

$\Delta(1232)$ MAGNETIC MOMENTS

$\Delta(1232)^{++}$ MAGNETIC MOMENT

The values are extracted from UCLA and SIN data on $\pi^+ p$ bremsstrahlung using a variety of different theoretical approximations and methods. Our estimate is *only* a rough guess of the range we expect the moment to lie within.

VALUE (μ_N)	DOCUMENT ID		TECN	COMMENT
• • • We do not use the following data for averages, fits, limits, etc. • • •				
6.14±0.51	LOPEZCAST...	01	DPWA	$\pi^+ p \to \pi^+ p\gamma$
4.52±0.50±0.45	BOSSHARD	91		$\pi^+ p \to \pi^+ p\gamma$ (SIN data)
3.7 to 4.2	LIN	91B		$\pi^+ p \to \pi^+ p\gamma$ (from UCLA data)
4.6 to 4.9	LIN	91B		$\pi^+ p \to \pi^+ p\gamma$ (from SIN data)
5.6 to 7.5	WITTMAN	88		$\pi^+ p \to \pi^+ p\gamma$ (from UCLA data)
6.9 to 9.8	HELLER	87		$\pi^+ p \to \pi^+ p\gamma$ (from UCLA data)
4.7 to 6.7	NEFKENS	78		$\pi^+ p \to \pi^+ p\gamma$ (UCLA data)

$\Delta(1232)^{+}$ MAGNETIC MOMENT

VALUE (μ_N)	DOCUMENT ID		COMMENT
• • • We do not use the following data for averages, fits, limits, etc. • • •			
$2.7^{+1.0}_{-1.3} \pm 1.5 \pm 3$	[1] KOTULLA	02	$\gamma p \to p\pi^0\gamma'$

[1] The second error is systematic, the third is an estimate of theoretical uncertainties.

$\Delta(1232)$ REFERENCES

For early references, see Physics Letters **111B** 1 (1982).

SARANTSEV	25	PR C112 015202	A.V. Sarantsev *et al.*	(Bonn-Gatchina Collab.)
HOFERICHT...	24	PL B853 138698	M. Hoferichter *et al.*	(BERN, MADU, BONN+)
MORNACCHI	24	PR C109 055201	E. Mornacchi *et al.*	(A2 Collab. at MAMI)
ROENCHEN	22	EPJ A58 229	D. Roenchen *et al.*	(JULI, GWU, BONN+)
HUNT	19	PR C99 055205	B.C. Hunt, D.M. Manley	
ADAMCZEW...	17	PR C95 065205	J. Adamczewski-Musch *et al.*	(HADES Collab.)
ROENCHEN	15A	EPJ A51 70	D. Roenchen *et al.*	
PDG	14	CP C38 070001	K. Olive *et al.*	(PDG Collab.)
SVARC	14	PR C89 045205	A. Svarc *et al.*	(RBI Zagreb, UNI Tuzla)
ANISOVICH	12A	EPJ A48 15	A.V. Anisovich *et al.*	(BONN, PNPI)
SHRESTHA	12A	PR C86 055203	M. Shrestha, D.M. Manley	(KSU)
WORKMAN	12A	PR C86 015202	R. Workman *et al.*	(GWU)
ANISOVICH	10	EPJ A44 203	A.V. Anisovich *et al.*	(BONN, PNPI)
DRECHSEL	07	EPJ A34 69	D. Drechsel, S.S. Kamalov, L. Tiator	(MAINZ, JINR)
DUGGER	07	PR C76 025211	M. Dugger *et al.*	(JLab CLAS Collab.)
ARNDT	06	PR C74 045205	R.A. Arndt *et al.*	(GWU)
BREITSCHOP...	06	PL B639 424	J. Breitschopf *et al.*	(TUBIN, HEBR, CSUS)
GRIDNEV	06	PAN 69 1542	A.B. Gridnev *et al.*	(PNPI, BONN, GWU)
PDG	06	JP G33 1	W.-M. Yao *et al.*	(PDG Collab.)
AHRENS	04A	EPJ A21 323	J. Ahrens *et al.*	(A2 Collab.)
ARNDT	04	PR C69 035213	R.A. Arndt *et al.*	(GWU, TRIU)
ARNDT	02	PR C66 055213	R. A. Arndt *et al.*	(GWU)
KOTULLA	02	PRL 89 272001	M. Kotulla *et al.*	(MAMI TAPS Collab.)
PENNER	02C	PR C66 055211	G. Penner, U. Mosel	(GIES)
PENNER	02D	PR C66 055212	G. Penner, U. Mosel	(GIES)
BLANPIED	01	PR C64 025203	G. Blanpied *et al.*	(BNL LEGS Collab.)
GALLER	01	PL B503 245	G. Galler *et al.*	(Mainz LARA Collab.)
LOPEZCAST...	01	PL B517 339	G. Lopez Castro, A. Mariano	
Also		NP A697 440	G. Lopez Castro, A. Mariano	
BECK	00	PR C61 035204	R. Beck *et al.*	(Mainz Microtron DAPHNE Col.)
KAMALOV	99	PRL 83 4494	S.S. Kamalov, S.N. Yang	(Taiwan U.)
HANSTEIN	98	NP A632 561	O. Hanstein, D. Drechsel, L. Tiator	
ARNDT	97	PR C56 577	R.A. Arndt, I.I. Strakovsky, R.L. Workman	(VPI)
BECK	97	PRL 78 606	R. Beck *et al.*	(MAINZ, SACL, PAVI, GLAS)
Also		PRL 79 4510	R.L. Beck, H.P. Krahn	(MAINZ)
Also		PRL 79 4512	R.L. Beck, H.P. Krahn	(MAINZ)
Also		PRL 79 4515 (errat.)	R.L. Beck *et al.*	(MAINZ, SACL, PAVI, GLAS)
BLANPIED	97	PRL 79 4337	G.S. Blanpied *et al.*	(LEGS Collab.)
DAVIDSON	97	PRL 79 4509	R.M. Davidson, N.C.A. Mukhopadhyay	(RPI)
BERNICHA	96	NP A597 623	A. Bernicha, G. Lopez Castro, J. Pestieau	(LOUV+)
HANSTEIN	96	PL B385 45	O. Hanstein, D. Drechsel, L. Tiator	(MAINZ)
ABAEV	95	ZPHY A352 85	V.V. Abaev, S.P. Kruglov	(PNPI)
HOEHLER	93	πN Newsletter 9 1	G. Hohler	(KARL)
BOSSHARD	91	PR D44 1962	A. Bosshard *et al.*	(ZURI, LBL, VILL+)
Also		PRL 64 2619	A. Bosshard *et al.*	(CATH, LAUS, LBL+)
LIN	91B	PR C44 1819	D.H. Lin, M.K. Liou, Z.M. Ding	(CUNY, CSOK)
Also		PR C43 R930	D. Lin, M.K. Liou	(CUNY)
WITTMAN	88	PR C37 2075	R. Wittman	(TRIU)
HELLER	87	PR C35 718	L. Heller *et al.*	(LANL, MIT, ILL)
CUTKOSKY	80	Toronto Conf. 19	R.E. Cutkosky *et al.*	(CMU, LBL) IJP
Also		PR D20 2839	R.E. Cutkosky *et al.*	(CMU, LBL)
KOCH	80B	NP A336 331	R. Koch, E. Pietarinen	(KARLT) IJP
HOEHLER	79	PDAT 12-1	G. Hohler *et al.*	(KARLT) IJP
Also		Toronto Conf. 3	R. Koch	(KARLT) IJP
MIROSHNIC...	79	SJNP 29 94	I.I. Miroshnichenko *et al.*	(KFTI) IJP
		Translated from YAF 29 188.		
NEFKENS	78	PR D18 3911	B.M.K. Nefkens *et al.*	(UCLA, CATH) IJP
PEDRONI	78	NP A300 321	E. Pedroni *et al.*	(SIN, ISNG, KARLE+) IJP

$\Delta(1600)\ 3/2^+$

$I(J^P) = \frac{3}{2}(\frac{3}{2}^+)$ Status: ****

Older and obsolete values are listed and referenced in the 2014 edition, Chinese Physics **C38** 070001 (2014).

$\Delta(1600)$ POLE POSITION

REAL PART

VALUE (MeV)	DOCUMENT ID		TECN	COMMENT
1470 to 1590 (≈ 1520) OUR ESTIMATE				
1550±15	SARANTSEV	25	DPWA	Multichannel
1590± 1	ROENCHEN	22	DPWA	Multichannel
1469±10±5	[1] SVARC	14	L+P	$\pi N \to \pi N$
1550±40	CUTKOSKY	80	IPWA	$\pi N \to \pi N$
• • • We do not use the following data for averages, fits, limits, etc. • • •				
1619	HUNT	19	DPWA	Multichannel
1552	ROENCHEN	15A	DPWA	Multichannel
1515±20	SOKHOYAN	15A	DPWA	Multichannel
1457	ARNDT	06	DPWA	$\pi N \to \pi N, \eta N$
1599	VRANA	00	DPWA	Multichannel
1550	HOEHLER	93	SPED	$\pi N \to \pi N$

[1] Fit to the amplitudes of HOEHLER 79.

−2×IMAGINARY PART

VALUE (MeV)	DOCUMENT ID		TECN	COMMENT
150 to 320 (≈ 280) OUR ESTIMATE				
260±20	SARANTSEV	25	DPWA	Multichannel
136± 1	ROENCHEN	22	DPWA	Multichannel
314±18±8	[1] SVARC	14	L+P	$\pi N \to \pi N$
200±60	CUTKOSKY	80	IPWA	$\pi N \to \pi N$
• • • We do not use the following data for averages, fits, limits, etc. • • •				
295	HUNT	19	DPWA	Multichannel
350	ROENCHEN	15A	DPWA	Multichannel
250±30	SOKHOYAN	15A	DPWA	Multichannel
400	ARNDT	06	DPWA	$\pi N \to \pi N, \eta N$
312	VRANA	00	DPWA	Multichannel

[1] Fit to the amplitudes of HOEHLER 79.

$\Delta(1600)$ ELASTIC POLE RESIDUE

MODULUS $|r|$

VALUE (MeV)	DOCUMENT ID		TECN	COMMENT
10 to 40 (≈ 25) OUR ESTIMATE				
11±1	ROENCHEN	22	DPWA	Multichannel
13±3	SOKHOYAN	15A	DPWA	Multichannel
38±2±2	[1] SVARC	14	L+P	$\pi N \to \pi N$
17±4	CUTKOSKY	80	IPWA	$\pi N \to \pi N$
• • • We do not use the following data for averages, fits, limits, etc. • • •				
23	ROENCHEN	15A	DPWA	Multichannel
11±6	ANISOVICH	12A	DPWA	Multichannel
44	ARNDT	06	DPWA	$\pi N \to \pi N, \eta N$

[1] Fit to the amplitudes of HOEHLER 79.

PHASE θ

VALUE (°)	DOCUMENT ID		TECN	COMMENT
180 to 250 (≈ 210) OUR ESTIMATE				
−106± 1	ROENCHEN	22	DPWA	Multichannel
−155±20	SOKHOYAN	15A	DPWA	Multichannel
173± 5±5	[1] SVARC	14	L+P	$\pi N \to \pi N$
−150±30	CUTKOSKY	80	IPWA	$\pi N \to \pi N$
• • • We do not use the following data for averages, fits, limits, etc. • • •				
−155	ROENCHEN	15A	DPWA	Multichannel
−160±33	ANISOVICH	12A	DPWA	Multichannel
+147	ARNDT	06	DPWA	$\pi N \to \pi N, \eta N$

[1] Fit to the amplitudes of HOEHLER 79.

$\Delta(1600)$ INELASTIC POLE RESIDUE

The "normalized residue" is the residue divided by $\Gamma_{pole}/2$.

Normalized residue in $N\pi \to \Delta(1600) \to \Delta\pi$, P-wave

MODULUS	PHASE (°)	DOCUMENT ID		TECN	COMMENT
0.30±0.02	87 ± 2	ROENCHEN	22	DPWA	Multichannel
0.15±0.04	30 ± 35	SOKHOYAN	15A	DPWA	Multichannel
• • • We do not use the following data for averages, fits, limits, etc. • • •					
0.31	31	ROENCHEN	15A	DPWA	Multichannel
0.14±0.10	154 ± 40	ANISOVICH	12A	DPWA	Multichannel

Normalized residue in $N\pi \to \Delta(1600) \to \Delta\pi$, F-wave

MODULUS	PHASE (°)	DOCUMENT ID		TECN	COMMENT
0.004±0.0002	−62 ± 5	ROENCHEN	22	DPWA	Multichannel

Int. J. Mod. Phys. A 2026.41. Downloaded from www.worldscientific.com
by UNIVERSITY OF CALIFORNIA @ BERKELEY on 09/16/26. Re-use and distribution is strictly not permitted, except for Open Access articles.

Int. J. Mod. Phys. A 2026.41. Downloaded from www.worldscientific.com
UNIVERSITY OF CALIFORNIA @ BERKELEY on 09/16/26. Re-use and distribution is strictly not permitted, except for Open Access articles.

0.010±0.005		SOKHOYAN	15A	DPWA	Multichannel
• • • We do not use the following data for averages, fits, limits, etc. • • •					
0.013	29	ROENCHEN	15A	DPWA	Multichannel
0.010±0.005		ANISOVICH	12A	DPWA	Multichannel

Normalized residue in $N\pi \to \Delta(1600) \to \Sigma K$

MODULUS	PHASE (°)	DOCUMENT ID		TECN	COMMENT
0.14±0.01	14 ± 1	ROENCHEN	22	DPWA	Multichannel
• • • We do not use the following data for averages, fits, limits, etc. • • •					
0.13	−5.6	ROENCHEN	15A	DPWA	Multichannel

$\Delta(1600)$ BREIT-WIGNER MASS

VALUE (MeV)	DOCUMENT ID		TECN	COMMENT
1500 to 1640 (≈ 1570) OUR ESTIMATE				
1575±15	SARANTSEV	25	DPWA	Multichannel
1664±16	[1] HUNT	19	DPWA	Multichannel
1600±50	CUTKOSKY	80	IPWA	$\pi N \to \pi N$
1522±13	HOEHLER	79	IPWA	$\pi N \to \pi N$
• • • We do not use the following data for averages, fits, limits, etc. • • •				
1520±20	SOKHOYAN	15A	DPWA	Multichannel
1626± 8	[1] SHRESTHA	12A	DPWA	Multichannel
1667± 1	PENNER	02C	DPWA	Multichannel
1687±44	VRANA	00	DPWA	Multichannel

[1] Statistical error only.

$\Delta(1600)$ BREIT-WIGNER WIDTH

VALUE (MeV)	DOCUMENT ID		TECN	COMMENT
200 to 300 (≈ 250) OUR ESTIMATE				
290± 25	SARANTSEV	25	DPWA	Multichannel
322± 46	[1] HUNT	19	DPWA	Multichannel
300±100	CUTKOSKY	80	IPWA	$\pi N \to \pi N$
220± 40	HOEHLER	79	IPWA	$\pi N \to \pi N$
• • • We do not use the following data for averages, fits, limits, etc. • • •				
235± 30	SOKHOYAN	15A	DPWA	Multichannel
225± 18	[1] SHRESTHA	12A	DPWA	Multichannel
397± 10	PENNER	02C	DPWA	Multichannel
493± 75	VRANA	00	DPWA	Multichannel

[1] Statistical error only.

$\Delta(1600)$ DECAY MODES

The following branching fractions are our estimates, not fits or averages.

	Mode	Fraction (Γ_i/Γ)
Γ_1	$N\pi$	8–24%
Γ_2	$N\pi\pi$	58–84 %
Γ_3	$\Delta(1232)\pi$	58–82 %
Γ_4	$\Delta(1232)\pi$, P-wave	72–82%
Γ_5	$\Delta(1232)\pi$, F-wave	<2%
Γ_6	$N\rho$	(7 ±4) %
Γ_7	$N\rho$, S=1/2	(2.0±2.0) %
Γ_8	$N\rho$, S=3/2 , P-wave	(5.0±3.0) %
Γ_9	$N(1440)\pi$	17–27%
Γ_{10}	$N\gamma$	0.001–0.035 %
Γ_{11}	$N\gamma$, helicity=1/2	0.0–0.02 %
Γ_{12}	$N\gamma$, helicity=3/2	0.001–0.015 %

$\Delta(1600)$ BRANCHING RATIOS

$\Gamma(N\pi)/\Gamma_{total}$ — Γ_1/Γ

VALUE (%)	DOCUMENT ID		TECN	COMMENT
8–24% OUR ESTIMATE				
17 ±4	SEIFEN	25	DPWA	Multichannel
10.7±1.9	[1] HUNT	19	DPWA	Multichannel
14 ±4	SOKHOYAN	15A	DPWA	Multichannel
18 ±4	CUTKOSKY	80	IPWA	$\pi N \to \pi N$
21 ±6	HOEHLER	79	IPWA	$\pi N \to \pi N$
• • • We do not use the following data for averages, fits, limits, etc. • • •				
8 ±2	[1] SHRESTHA	12A	DPWA	Multichannel
13 ±1	PENNER	02C	DPWA	Multichannel
28 ±5	VRANA	00	DPWA	Multichannel

[1] Statistical error only.

$\Gamma(\Delta(1232)\pi)/\Gamma_{total}$ — Γ_3/Γ

VALUE (%)	DOCUMENT ID		TECN	COMMENT
44±7	SARANTSEV	25	DPWA	Multichannel

$\Gamma(\Delta(1232)\pi, P\text{-wave})/\Gamma_{total}$ — Γ_4/Γ

VALUE (%)	DOCUMENT ID		TECN	COMMENT
72–82% OUR ESTIMATE				
40± 6	SARANTSEV	25	DPWA	Multichannel
70± 6	SEIFEN	25	DPWA	Multichannel
64± 6	[1] HUNT	19	DPWA	Multichannel
• • • We do not use the following data for averages, fits, limits, etc. • • •				
77± 5	SOKHOYAN	15A	DPWA	Multichannel
70± 3	[1] SHRESTHA	12A	DPWA	Multichannel
59±10	VRANA	00	DPWA	Multichannel

[1] Statistical error only.

$\Gamma(\Delta(1232)\pi, F\text{-wave})/\Gamma_{total}$ — Γ_5/Γ

VALUE (%)	DOCUMENT ID		TECN	COMMENT
<2% OUR ESTIMATE				
4±3	SARANTSEV	25	DPWA	Multichannel
<2	SEIFEN	25	DPWA	Multichannel
• • • We do not use the following data for averages, fits, limits, etc. • • •				
<2	SOKHOYAN	15A	DPWA	Multichannel

$\Gamma(N\rho)/\Gamma_{total}$ — Γ_6/Γ

VALUE (%)	DOCUMENT ID		TECN	COMMENT
7±4	SARANTSEV	25	DPWA	Multichannel

$\Gamma(N\rho, S=1/2)/\Gamma_{total}$ — Γ_7/Γ

VALUE (%)	DOCUMENT ID		TECN	COMMENT
2±2	SARANTSEV	25	DPWA	Multichannel

$\Gamma(N\rho, S=3/2, P\text{-wave})/\Gamma_{total}$ — Γ_8/Γ

VALUE (%)	DOCUMENT ID		TECN	COMMENT
5±3	SARANTSEV	25	DPWA	Multichannel

$\Gamma(N(1440)\pi)/\Gamma_{total}$ — Γ_9/Γ

VALUE (%)	DOCUMENT ID		TECN	COMMENT
17–27% OUR ESTIMATE				
< 1	SEIFEN	25	DPWA	Multichannel
22±5	[1] HUNT	19	DPWA	Multichannel
• • • We do not use the following data for averages, fits, limits, etc. • • •				
22±3	[1] SHRESTHA	12A	DPWA	Multichannel
13±4	VRANA	00	DPWA	Multichannel

[1] Statistical error only.

$\Delta(1600)$ PHOTON DECAY AMPLITUDES AT THE POLE

$\Delta(1600) \to N\gamma$, helicity-1/2 amplitude $A_{1/2}$

MODULUS ($GeV^{-1/2}$)	PHASE (°)	DOCUMENT ID		TECN	COMMENT
0.040±0.008	120 ± 20	SARANTSEV	25	DPWA	Multichannel
0.025±0.005	0.5 ± 3.0	ROENCHEN	22	DPWA	Multichannel
• • • We do not use the following data for averages, fits, limits, etc. • • •					
−0.230	−42	ROENCHEN	15A	DPWA	Multichannel
0.053±0.010	130 ± 15	SOKHOYAN	15A	DPWA	Multichannel

$\Delta(1600) \to N\gamma$, helicity-3/2 amplitude $A_{3/2}$

MODULUS ($GeV^{-1/2}$)	PHASE (°)	DOCUMENT ID		TECN	COMMENT
0.038±0.012	155 ± 20	SARANTSEV	25	DPWA	Multichannel
−0.006±0.0013	62 ± 32	ROENCHEN	22	DPWA	Multichannel
• • • We do not use the following data for averages, fits, limits, etc. • • •					
0.332	−71	ROENCHEN	15A	DPWA	Multichannel
0.055±0.010	152 ± 15	SOKHOYAN	15A	DPWA	Multichannel

$\Delta(1600)$ BREIT-WIGNER PHOTON DECAY AMPLITUDES

$\Delta(1600) \to N\gamma$, helicity-1/2 amplitude $A_{1/2}$

VALUE ($GeV^{-1/2}$)	DOCUMENT ID		TECN	COMMENT
−0.060 to −0.030 (≈ −0.045) OUR ESTIMATE				
−0.042 ±0.010	SARANTSEV	25	DPWA	Multichannel
0.0082±0.0014	[1] HUNT	19	DPWA	Multichannel
−0.018 ±0.015	[1] ARNDT	96	IPWA	$\gamma N \to \pi N$
• • • We do not use the following data for averages, fits, limits, etc. • • •				
−0.051 ±0.010	SOKHOYAN	15A	DPWA	Multichannel
0.006 ±0.005	[1] SHRESTHA	12A	DPWA	Multichannel
0.0	PENNER	02D	DPWA	Multichannel

[1] Statistical error only.

$\Delta(1600) \to N\gamma$, helicity-3/2 amplitude $A_{3/2}$

VALUE ($GeV^{-1/2}$)	DOCUMENT ID		TECN	COMMENT
−0.050 to −0.020 (≈ −0.035) OUR ESTIMATE				
−0.039±0.008	SARANTSEV	25	DPWA	Multichannel
0.048±0.014	[1] HUNT	19	DPWA	Multichannel
−0.025±0.015	[1] ARNDT	96	IPWA	$\gamma N \to \pi N$
• • • We do not use the following data for averages, fits, limits, etc. • • •				
−0.055±0.010	SOKHOYAN	15A	DPWA	Multichannel

Int. J. Mod. Phys. A 2026.41. Downloaded from www.worldscientific.com
by UNIVERSITY OF CALIFORNIA @ BERKELEY on 09/16/26. Re-use and distribution is strictly not permitted, except for Open Access articles.

0.052±0.008	[1] SHRESTHA	12A	DPWA	Multichannel
−0.024	PENNER	02D	DPWA	Multichannel

[1] Statistical error only.

$\Delta(1600)$ REFERENCES

For early references, see Physics Letters **111B** 1 (1982).

SARANTSEV	25	PR C112 015202	A.V. Sarantsev *et al.*	(Bonn-Gatchina Collab.)
SEIFEN	25	EPJ A61 173	T. Seifen *et al.*	(CBELSA/TAPS Collab.)
ROENCHEN	22	EPJ A58 229	D. Roenchen *et al.*	(JULI, GWU, BONN+)
HUNT	19	PR C99 055205	B.C. Hunt, D.M. Manley	
ROENCHEN	15A	EPJ A51 70	D. Roenchen *et al.*	
SOKHOYAN	15A	EPJ A51 95	V. Sokhoyan *et al.*	(CBELSA/TAPS Collab.)
PDG	14	CP C38 070001	K. Olive *et al.*	(PDG Collab.)
SVARC	14	PR C89 045205	A. Svarc *et al.*	(RBI Zagreb, UNI Tuzla)
ANISOVICH	12A	EPJ A48 15	A.V. Anisovich *et al.*	(BONN, PNPI)
SHRESTHA	12A	PR C86 055203	M. Shrestha, D.M. Manley	(KSU)
ARNDT	06	PR C74 045205	R.A. Arndt *et al.*	(GWU)
PENNER	02C	PR C66 055211	G. Penner, U. Mosel	(GIES)
PENNER	02D	PR C66 055212	G. Penner, U. Mosel	(GIES)
VRANA	00	PRPL 328 181	T.P. Vrana, S.A. Dytman, T.-S.H. Lee	(PITT, ANL)
ARNDT	96	PR C53 430	R.A. Arndt, I.I. Strakovsky, R.L. Workman	(VPI)
HOEHLER	93	πN Newsletter 9 1	G. Hohler	(KARL)
CUTKOSKY	80	Toronto Conf. 19	R.E. Cutkosky *et al.*	(CMU, LBL) IJP
Also		PR D20 2839	R.E. Cutkosky *et al.*	(CMU, LBL) IJP
HOEHLER	79	PDAT 12-1	G. Hohler *et al.*	(KARLT) IJP
Also		Toronto Conf. 3	R. Koch	(KARLT) IJP

$\Delta(1620)\ 1/2^-$

$I(J^P) = \frac{3}{2}(\frac{1}{2}^-)$ Status: ****

Older and obsolete values are listed and referenced in the 2014 edition, Chinese Physics **C38** 070001 (2014).

$\Delta(1620)$ POLE POSITION

REAL PART

VALUE (MeV)	DOCUMENT ID		TECN	COMMENT
1590 to 1610 (≈ 1600) OUR ESTIMATE				
1598± 7	SARANTSEV	25	DPWA	Multichannel
1607± 2	ROENCHEN	22	DPWA	Multichannel
1603± 7±2	[1] SVARC	14	L+P	$\pi N \to \pi N$
1600±15	CUTKOSKY	80	IPWA	$\pi N \to \pi N$
• • • We do not use the following data for averages, fits, limits, etc. • • •				
1577	HUNT	19	DPWA	Multichannel
1600	ROENCHEN	15A	DPWA	Multichannel
1597± 5	SOKHOYAN	15A	DPWA	Multichannel
1595	ARNDT	06	DPWA	$\pi N \to \pi N, \eta N$
1607	VRANA	00	DPWA	Multichannel
1608	HOEHLER	93	SPED	$\pi N \to \pi N$

[1] Fit to the amplitudes of HOEHLER 79.

−2×IMAGINARY PART

VALUE (MeV)	DOCUMENT ID		TECN	COMMENT
80 to 140 (≈ 110) OUR ESTIMATE				
130±10	SARANTSEV	25	DPWA	Multichannel
85± 3	ROENCHEN	22	DPWA	Multichannel
114±12±4	[1] SVARC	14	L+P	$\pi N \to \pi N$
120±20	CUTKOSKY	80	IPWA	$\pi N \to \pi N$
• • • We do not use the following data for averages, fits, limits, etc. • • •				
101	HUNT	19	DPWA	Multichannel
65	ROENCHEN	15A	DPWA	Multichannel
134± 8	SOKHOYAN	15A	DPWA	Multichannel
135	ARNDT	06	DPWA	$\pi N \to \pi N, \eta N$
148	VRANA	00	DPWA	Multichannel
116	HOEHLER	93	SPED	$\pi N \to \pi N$

[1] Fit to the amplitudes of HOEHLER 79.

$\Delta(1620)$ ELASTIC POLE RESIDUE

MODULUS $|r|$

VALUE (MeV)	DOCUMENT ID		TECN	COMMENT
10 to 20 (≈ 15) OUR ESTIMATE				
12±1	ROENCHEN	22	DPWA	Multichannel
20±3	SOKHOYAN	15A	DPWA	Multichannel
17±2±1	[1] SVARC	14	L+P	$\pi N \to \pi N$
15±2	CUTKOSKY	80	IPWA	$\pi N \to \pi N$
• • • We do not use the following data for averages, fits, limits, etc. • • •				
16	ROENCHEN	15A	DPWA	Multichannel
18±2	ANISOVICH	12A	DPWA	Multichannel
15	ARNDT	06	DPWA	$\pi N \to \pi N, \eta N$
19	HOEHLER	93	SPED	$\pi N \to \pi N$

[1] Fit to the amplitudes of HOEHLER 79.

PHASE θ

VALUE (°)	DOCUMENT ID		TECN	COMMENT
−120 to −80 (≈ −100) OUR ESTIMATE				
126± 2	ROENCHEN	22	DPWA	Multichannel
− 90±15	SOKHOYAN	15A	DPWA	Multichannel
−106±10±4	[1] SVARC	14	L+P	$\pi N \to \pi N$
−110±20	CUTKOSKY	80	IPWA	$\pi N \to \pi N$
• • • We do not use the following data for averages, fits, limits, etc. • • •				
−104	ROENCHEN	15A	DPWA	Multichannel
−100± 5	ANISOVICH	12A	DPWA	Multichannel
− 92	ARNDT	06	DPWA	$\pi N \to \pi N, \eta N$
− 95	HOEHLER	93	SPED	$\pi N \to \pi N$

[1] Fit to the amplitudes of HOEHLER 79.

$\Delta(1620)$ INELASTIC POLE RESIDUE

The "normalized residue" is the residue divided by $\Gamma_{pole}/2$.

Normalized residue in $N\pi \to \Delta(1620) \to \Delta\pi$, D-wave

MODULUS	PHASE (°)	DOCUMENT ID		TECN	COMMENT
0.32±0.01	81 ± 1	ROENCHEN	22	DPWA	Multichannel
0.42±0.06	−90 ± 20	SOKHOYAN	15A	DPWA	Multichannel
• • • We do not use the following data for averages, fits, limits, etc. • • •					
0.57	105	ROENCHEN	15A	DPWA	Multichannel
0.38±0.09	−85 ± 30	ANISOVICH	12A	DPWA	Multichannel

Normalized residue in $N\pi \to \Delta(1620) \to \Sigma K$

MODULUS	PHASE (°)	DOCUMENT ID		TECN	COMMENT
0.11±0.01	−120 ± 3	ROENCHEN	22	DPWA	Multichannel
• • • We do not use the following data for averages, fits, limits, etc. • • •					
0.22	−105	ROENCHEN	15A	DPWA	Multichannel

Normalized residue in $N\pi \to \Delta(1620) \to N(1440)\pi$

MODULUS	PHASE (°)	DOCUMENT ID		TECN	COMMENT
0.10±0.06	−65 ± 30	SOKHOYAN	15A	DPWA	Multichannel

$\Delta(1620)$ BREIT-WIGNER MASS

VALUE (MeV)	DOCUMENT ID		TECN	COMMENT
1590 to 1630 (≈ 1610) OUR ESTIMATE				
1600 ± 8	SARANTSEV	25	DPWA	Multichannel
1635 ± 8	GOLOVATCH	19	DPWA	$\gamma p \to \pi^+\pi^- p$
1589 ± 3	[1] HUNT	19	DPWA	Multichannel
1615.2± 0.4	[1] ARNDT	06	DPWA	$\pi N \to \pi N, \eta N$
1620 ±20	CUTKOSKY	80	IPWA	$\pi N \to \pi N$
1610 ± 7	HOEHLER	79	IPWA	$\pi N \to \pi N$
• • • We do not use the following data for averages, fits, limits, etc. • • •				
1595 ± 8	SOKHOYAN	15A	DPWA	Multichannel
1600 ± 1	[1] SHRESTHA	12A	DPWA	Multichannel
1612 ± 2	PENNER	02C	DPWA	Multichannel
1617 ±15	VRANA	00	DPWA	Multichannel

[1] Statistical error only.

$\Delta(1620)$ BREIT-WIGNER WIDTH

VALUE (MeV)	DOCUMENT ID		TECN	COMMENT
110 to 150 (≈ 130) OUR ESTIMATE				
135 ±10	SARANTSEV	25	DPWA	Multichannel
144 ±16	GOLOVATCH	19	DPWA	$\gamma p \to \pi^+\pi^- p$
107 ± 7	[1] HUNT	19	DPWA	Multichannel
146.9± 1.9	[1] ARNDT	06	DPWA	$\pi N \to \pi N, \eta N$
140 ±20	CUTKOSKY	80	IPWA	$\pi N \to \pi N$
139 ±18	HOEHLER	79	IPWA	$\pi N \to \pi N$
• • • We do not use the following data for averages, fits, limits, etc. • • •				
135 ± 9	SOKHOYAN	15A	DPWA	Multichannel
112 ± 2	[1] SHRESTHA	12A	DPWA	Multichannel
202 ± 7	PENNER	02C	DPWA	Multichannel
143 ±42	VRANA	00	DPWA	Multichannel

[1] Statistical error only.

$\Delta(1620)$ DECAY MODES

The following branching fractions are our estimates, not fits or averages.

	Mode	Fraction (Γ_i/Γ)
Γ_1	$N\pi$	25–35 %
Γ_2	$N\pi\pi$	>67 %
Γ_3	$\Delta(1232)\pi$	44–72 %
Γ_4	$N\rho$	23–32%
Γ_5	$N\rho$, S=1/2	23–32%
Γ_6	$N\rho$, S=3/2	<0.04%
Γ_7	$N(1440)\pi$	<9 %
Γ_8	$N\gamma$, helicity=1/2	0.03–0.10 %

$\Delta(1620)$ BRANCHING RATIOS

$\Gamma(N\pi)/\Gamma_{total}$ — Γ_1/Γ

VALUE (%)	DOCUMENT ID		TECN	COMMENT
25 to 35 (≈ 30) OUR ESTIMATE				
30 ±5	SEIFEN	25	DPWA	Multichannel
24 ±2	[1] HUNT	19	DPWA	Multichannel

Int. J. Mod. Phys. A 2026.41. Downloaded from www.worldscientific.com
UNIVERSITY OF CALIFORNIA @ BERKELEY on 09/16/26. Re-use and distribution is strictly not permitted, except for Open Access articles.

31.5 ± 0.1	[1] ARNDT	06	DPWA	$\pi N \to \pi N, \eta N$
25 ± 3	CUTKOSKY	80	IPWA	$\pi N \to \pi N$
35 ± 6	HOEHLER	79	IPWA	$\pi N \to \pi N$
• • • We do not use the following data for averages, fits, limits, etc. • • •				
28 ± 3	SOKHOYAN	15A	DPWA	Multichannel
33 ± 2	[1] SHRESTHA	12A	DPWA	Multichannel
34 ± 1	PENNER	02C	DPWA	Multichannel
45 ± 5	VRANA	00	DPWA	Multichannel

[1] Statistical error only.

$\Gamma(N\pi\pi)/\Gamma_{total}$ — Γ_2/Γ

VALUE	DOCUMENT ID		TECN	COMMENT
0.90±0.10	GOLOVATCH	19	DPWA	$\gamma p \to \pi^+\pi^- p$

$\Gamma(\Delta(1232)\pi)/\Gamma_{total}$ — Γ_3/Γ

VALUE (%)	DOCUMENT ID		TECN	COMMENT
28±11	SARANTSEV	25	DPWA	Multichannel
28±15	SEIFEN	25	DPWA	Multichannel
48± 4	[1] HUNT	19	DPWA	Multichannel
• • • We do not use the following data for averages, fits, limits, etc. • • •				
62±10	SOKHOYAN	15A	DPWA	Multichannel
32± 2	[1] SHRESTHA	12A	DPWA	Multichannel
39± 2	VRANA	00	DPWA	Multichannel

[1] Statistical error only.

$\Gamma(N\rho)/\Gamma_{total}$ — Γ_4/Γ

VALUE (%)	DOCUMENT ID		TECN	COMMENT
52±17	SARANTSEV	25	DPWA	Multichannel

$\Gamma(N\rho, S=1/2)/\Gamma_{total}$ — Γ_5/Γ

VALUE (%)	DOCUMENT ID		TECN	COMMENT
30±12	SARANTSEV	25	DPWA	Multichannel
27± 4	[1] HUNT	19	DPWA	Multichannel
• • • We do not use the following data for averages, fits, limits, etc. • • •				
26± 2	[1] SHRESTHA	12A	DPWA	Multichannel
14± 3	VRANA	00	DPWA	Multichannel

[1] Statistical error only.

$\Gamma(N\rho, S=3/2)/\Gamma_{total}$ — Γ_6/Γ

VALUE (%)	DOCUMENT ID		TECN	COMMENT
22 ±12	SARANTSEV	25	DPWA	Multichannel
< 0.04	[1] HUNT	19	DPWA	Multichannel
• • • We do not use the following data for averages, fits, limits, etc. • • •				
2 ± 1	VRANA	00	DPWA	Multichannel

[1] Statistical error only.

$\Gamma(N(1440)\pi)/\Gamma_{total}$ — Γ_7/Γ

VALUE (%)	DOCUMENT ID		TECN	COMMENT
15 ±8	SEIFEN	25	DPWA	Multichannel
< 0.02	[1] HUNT	19	DPWA	Multichannel
6 ±3	SOKHOYAN	15A	DPWA	Multichannel
• • • We do not use the following data for averages, fits, limits, etc. • • •				
9 ±1	[1] SHRESTHA	12A	DPWA	Multichannel
0 ±1	VRANA	00	DPWA	Multichannel

[1] Statistical error only.

$\Delta(1620)$ PHOTON DECAY AMPLITUDES AT THE POLE

$\Delta(1620) \to N\gamma$, helicity-1/2 amplitude $A_{1/2}$

MODULUS ($GeV^{-1/2}$)	PHASE (°)	DOCUMENT ID		TECN	COMMENT
0.047±0.007	10 ± 15	SARANTSEV	25	DPWA	Multichannel
0.011±0.002	57 ± 12	ROENCHEN	22	DPWA	Multichannel
• • • We do not use the following data for averages, fits, limits, etc. • • •					
0.014	26	ROENCHEN	15A	DPWA	Multichannel
0.054±0.007	−6 ± 7	SOKHOYAN	15A	DPWA	Multichannel

$\Delta(1620)$ BREIT-WIGNER PHOTON DECAY AMPLITUDES

$\Delta(1620) \to N\gamma$, helicity-1/2 amplitude $A_{1/2}$

VALUE ($GeV^{-1/2}$)	DOCUMENT ID		TECN	COMMENT
0.030 to 0.060 (≈ 0.050) OUR ESTIMATE				
0.048 ±0.007	SARANTSEV	25	DPWA	Multichannel
0.029 ±0.0062	GOLOVATCH	19	DPWA	$\gamma p \to \pi^+\pi^- p$
0.0124±0.0007	[1] HUNT	19	DPWA	Multichannel
0.029 ±0.003	[1] WORKMAN	12A	DPWA	$\gamma N \to N\pi$
0.050 ±0.002	[1] DUGGER	07	DPWA	$\gamma N \to \pi N$
• • • We do not use the following data for averages, fits, limits, etc. • • •				
0.055 ±0.007	SOKHOYAN	15A	DPWA	Multichannel
−0.003 ±0.003	[1] SHRESTHA	12A	DPWA	Multichannel
0.066	DRECHSEL	07	DPWA	$\gamma N \to \pi N$
−0.050	PENNER	02D	DPWA	Multichannel

[1] Statistical error only.

$\Delta(1620)$ REFERENCES

For early references, see Physics Letters **111B** 1 (1982).

SARANTSEV	25	PR C112 015202	A.V. Sarantsev *et al.*	(Bonn-Gatchina Collab.)
SEIFEN	25	EPJ A61 173	T. Seifen *et al.*	(CBELSA/TAPS Collab.)
ROENCHEN	22	EPJ A58 229	D. Roenchen *et al.*	(JULI, GWU, BONN+)
GOLOVATCH	19	PL B788 371	E. Golovatch *et al.*	(CLAS Collab.)
HUNT	19	PR C99 055205	B.C. Hunt, D.M. Manley	
ROENCHEN	15A	EPJ A51 70	D. Roenchen *et al.*	
SOKHOYAN	15A	EPJ A51 95	V. Sokhoyan *et al.*	(CBELSA/TAPS Collab.)
PDG	14	CP C38 070001	K. Olive *et al.*	(PDG Collab.)
SVARC	14	PR C89 045205	A. Svarc *et al.*	(RBI Zagreb, UNI Tuzla)
ANISOVICH	12A	EPJ A48 15	A.V. Anisovich *et al.*	(BONN, PNPI)
SHRESTHA	12A	PR C86 055203	M. Shrestha, D.M. Manley	(KSU)
WORKMAN	12A	PR C86 015202	R. Workman *et al.*	(GWU)
DRECHSEL	07	EPJ A34 69	D. Drechsel, S.S. Kamalov, L. Tiator	(MAINZ, JINR)
DUGGER	07	PR C76 025211	M. Dugger *et al.*	(JLab CLAS Collab.)
ARNDT	06	PR C74 045205	R.A. Arndt *et al.*	(GWU)
PENNER	02C	PR C66 055211	G. Penner, U. Mosel	(GIES)
PENNER	02D	PR C66 055212	G. Penner, U. Mosel	(GIES)
VRANA	00	PRPL 328 181	T.P. Vrana, S.A. Dytman, T.-S.H. Lee	(PITT, ANL)
HOEHLER	93	πN Newsletter 9 1	G. Hohler	(KARL)
CUTKOSKY	80	Toronto Conf. 19	R.E. Cutkosky *et al.*	(CMU, LBL) IJP
Also		PR D20 2839	R.E. Cutkosky *et al.*	(CMU, LBL) IJP
HOEHLER	79	PDAT 12-1	G. Hohler *et al.*	(KARLT) IJP
Also		Toronto Conf. 3	R. Koch	(KARLT) IJP

$\Delta(1700)\ 3/2^-$

$I(J^P) = \frac{3}{2}(\frac{3}{2}^-)$ Status: ****

Older and obsolete values are listed and referenced in the 2014 edition, Chinese Physics **C38** 070001 (2014).

$\Delta(1700)$ POLE POSITION

REAL PART

VALUE (MeV)	DOCUMENT ID		TECN	COMMENT
1640 to 1690 (≈ 1665) OUR ESTIMATE				
1655±15	SARANTSEV	25	DPWA	Multichannel
1637±32	ROENCHEN	22	DPWA	Multichannel
1643± 6±3	[1] SVARC	14	L+P	$\pi N \to \pi N$
1675±25	CUTKOSKY	80	IPWA	$\pi N \to \pi N$
• • • We do not use the following data for averages, fits, limits, etc. • • •				
1693	HUNT	19	DPWA	Multichannel
1677	ROENCHEN	15A	DPWA	Multichannel
1685±10	SOKHOYAN	15A	DPWA	Multichannel
1685±10	GUTZ	14	DPWA	Multichannel
1632	ARNDT	06	DPWA	$\pi N \to \pi N, \eta N$
1726	VRANA	00	DPWA	Multichannel
1651	HOEHLER	93	SPED	$\pi N \to \pi N$

[1] Fit to the amplitudes of HOEHLER 79.

−2×IMAGINARY PART

VALUE (MeV)	DOCUMENT ID		TECN	COMMENT
200 to 300 (≈ 250) OUR ESTIMATE				
300±15	SARANTSEV	25	DPWA	Multichannel
295±29	ROENCHEN	22	DPWA	Multichannel
217±10±8	[1] SVARC	14	L+P	$\pi N \to \pi N$
220±40	CUTKOSKY	80	IPWA	$\pi N \to \pi N$
• • • We do not use the following data for averages, fits, limits, etc. • • •				
213	HUNT	19	DPWA	Multichannel
305	ROENCHEN	15A	DPWA	Multichannel
300±15	SOKHOYAN	15A	DPWA	Multichannel
300±15	GUTZ	14	DPWA	Multichannel
253	ARNDT	06	DPWA	$\pi N \to \pi N, \eta N$
118	VRANA	00	DPWA	Multichannel
159	HOEHLER	93	SPED	$\pi N \to \pi N$

[1] Fit to the amplitudes of HOEHLER 79.

$\Delta(1700)$ ELASTIC POLE RESIDUE

MODULUS $|r|$

VALUE (MeV)	DOCUMENT ID		TECN	COMMENT
10 to 40 (≈ 25) OUR ESTIMATE				
15±12	ROENCHEN	22	DPWA	Multichannel
40± 6	SOKHOYAN	15A	DPWA	Multichannel
13± 1±1	[1] SVARC	14	L+P	$\pi N \to \pi N$
13± 3	CUTKOSKY	80	IPWA	$\pi N \to \pi N$
• • • We do not use the following data for averages, fits, limits, etc. • • •				
24	ROENCHEN	15A	DPWA	Multichannel
40± 6	GUTZ	14	DPWA	Multichannel
42± 7	ANISOVICH	12A	DPWA	Multichannel
18	ARNDT	06	DPWA	$\pi N \to \pi N, \eta N$
10	HOEHLER	93	SPED	$\pi N \to \pi N$

[1] Fit to the amplitudes of HOEHLER 79.

PHASE θ

VALUE (°)	DOCUMENT ID		TECN	COMMENT
−40 to 0 (≈ −20) OUR ESTIMATE				
−13 ±74	ROENCHEN	22	DPWA	Multichannel
− 1 ±10	SOKHOYAN	15A	DPWA	Multichannel
−30 ± 4±3	[1] SVARC	14	L+P	$\pi N \to \pi N$
−40	ARNDT	06	DPWA	$\pi N \to \pi N, \eta N$
−20 ±25	CUTKOSKY	80	IPWA	$\pi N \to \pi N$

Int. J. Mod. Phys. A 2026.41. Downloaded from www.worldscientific.com
by UNIVERSITY OF CALIFORNIA @ BERKELEY on 09/16/26. Re-use and distribution is strictly not permitted, except for Open Access articles.

• • • We do not use the following data for averages, fits, limits, etc. • • •

− 7.3	ROENCHEN	15A	DPWA	Multichannel
− 1 ±10	GUTZ	14	DPWA	Multichannel
− 3 ±15	ANISOVICH	12A	DPWA	Multichannel

[1] Fit to the amplitudes of HOEHLER 79.

$\Delta(1700)$ INELASTIC POLE RESIDUE

The "normalized residue" is the residue divided by $\Gamma_{pole}/2$.

Normalized residue in $N\pi \to \Delta(1700) \to \Delta\eta$

MODULUS	PHASE (°)	DOCUMENT ID		TECN	COMMENT
0.12±0.02	−60 ± 12	GUTZ	14	DPWA	Multichannel
• • • We do not use the following data for averages, fits, limits, etc. • • •					
0.12±0.03	−60 ± 15	ANISOVICH	12A	DPWA	Multichannel

Normalized residue in $N\pi \to \Delta(1700) \to \Sigma K$

MODULUS	PHASE (°)	DOCUMENT ID		TECN	COMMENT
0.007±0.008	**−176 ± 160**	ROENCHEN	22	DPWA	Multichannel
• • • We do not use the following data for averages, fits, limits, etc. • • •					
0.011	−147	ROENCHEN	15A	DPWA	Multichannel

Normalized residue in $N\pi \to \Delta(1700) \to N(1535)\pi$

MODULUS	PHASE (°)	DOCUMENT ID		TECN	COMMENT
0.035±0.015	−75 ± 30	GUTZ	14	DPWA	Multichannel

Normalized residue in $N\pi \to \Delta(1700) \to \Delta(1232)\pi$, S-wave

MODULUS	PHASE (°)	DOCUMENT ID		TECN	COMMENT
0.20±0.15	146 ± 133	ROENCHEN	22	DPWA	Multichannel
0.25±0.12	135 ± 45	SOKHOYAN	15A	DPWA	Multichannel
• • • We do not use the following data for averages, fits, limits, etc. • • •					
0.39	151	ROENCHEN	15A	DPWA	Multichannel

Normalized residue in $N\pi \to \Delta(1700) \to \Delta(1232)\pi$, D-wave

MODULUS	PHASE (°)	DOCUMENT ID		TECN	COMMENT
0.038±0.039	127 ± 127	ROENCHEN	22	DPWA	Multichannel
0.12 ±0.06	−160 ± 30	SOKHOYAN	15A	DPWA	Multichannel
• • • We do not use the following data for averages, fits, limits, etc. • • •					
0.054	166	ROENCHEN	15A	DPWA	Multichannel

Normalized residue in $N\pi \to \Delta(1700) \to N(1520)\pi$, P-wave

MODULUS	PHASE (°)	DOCUMENT ID		TECN	COMMENT
0.10±0.03	−10 ± 20	SOKHOYAN	15A	DPWA	Multichannel

$\Delta(1700)$ BREIT-WIGNER MASS

VALUE (MeV)	DOCUMENT ID		TECN	COMMENT
1690 to 1730 (≈ 1710) OUR ESTIMATE				
1690 ±15	SARANTSEV	25	DPWA	Multichannel
1704 ± 8	GOLOVATCH	19	DPWA	$\gamma p \to \pi^+\pi^- p$
1720 ± 5	[1] HUNT	19	DPWA	Multichannel
1695.0± 1.3	[1] ARNDT	06	DPWA	$\pi N \to \pi N, \eta N$
1710 ±30	CUTKOSKY	80	IPWA	$\pi N \to \pi N$
1680 ±70	HOEHLER	79	IPWA	$\pi N \to \pi N$
• • • We do not use the following data for averages, fits, limits, etc. • • •				
1715 ±20	SOKHOYAN	15A	DPWA	Multichannel
1715 ±20	GUTZ	14	DPWA	Multichannel
1691 ± 4	[1] SHRESTHA	12A	DPWA	Multichannel
1678 ± 1	PENNER	02C	DPWA	Multichannel
1732 ±23	VRANA	00	DPWA	Multichannel

[1] Statistical error only.

$\Delta(1700)$ BREIT-WIGNER WIDTH

VALUE (MeV)	DOCUMENT ID		TECN	COMMENT
220 to 380 (≈ 300) OUR ESTIMATE				
310 ±15	SARANTSEV	25	DPWA	Multichannel
295 ±35	GOLOVATCH	19	DPWA	$\gamma p \to \pi^+\pi^- p$
226 ±14	[1] HUNT	19	DPWA	Multichannel
375.5± 7.0	[1] ARNDT	06	DPWA	$\pi N \to \pi N, \eta N$
280 ±80	CUTKOSKY	80	IPWA	$\pi N \to \pi N$
230 ±80	HOEHLER	79	IPWA	$\pi N \to \pi N$
• • • We do not use the following data for averages, fits, limits, etc. • • •				
300 ±25	SOKHOYAN	15A	DPWA	Multichannel
300 ±25	GUTZ	14	DPWA	Multichannel
248 ± 9	[1] SHRESTHA	12A	DPWA	Multichannel
606 ±15	PENNER	02C	DPWA	Multichannel
119 ±70	VRANA	00	DPWA	Multichannel

[1] Statistical error only.

$\Delta(1700)$ DECAY MODES

The following branching fractions are our estimates, not fits or averages.

	Mode	Fraction (Γ_i/Γ)
Γ_1	$N\pi$	10–20 %
Γ_2	$N\pi\pi$	>31 %
Γ_3	$\Delta(1232)\pi$	9–70 %
Γ_4	$\Delta(1232)\pi$, S-wave	5–54 %
Γ_5	$\Delta(1232)\pi$, D-wave	4–16 %
Γ_6	$N\rho$	(15 ±4) %
Γ_7	$N\rho$, S=3/2, S-wave	22–32%
Γ_8	$N(1440)\pi$	(3.0±2.0) %
Γ_9	$N(1520)\pi$, P-wave	1–5 %
Γ_{10}	$N(1535)\pi$	0.5–1.5 %
Γ_{11}	$\Delta(1232)\eta$	3–7 %
Γ_{12}	$N\gamma$	0.22–0.60 %
Γ_{13}	$N\gamma$, helicity=1/2	0.12–0.30 %
Γ_{14}	$N\gamma$, helicity=3/2	0.10–0.30 %

$\Delta(1700)$ BRANCHING RATIOS

$\Gamma(N\pi)/\Gamma_{total}$ — Γ_1/Γ

VALUE (%)	DOCUMENT ID		TECN	COMMENT
10 to 20 OUR ESTIMATE				
22 ±6	SEIFEN	25	DPWA	Multichannel
15 ±2	[1] HUNT	19	DPWA	Multichannel
15.6±0.1	[1] ARNDT	06	DPWA	$\pi N \to \pi N, \eta N$
12 ±3	CUTKOSKY	80	IPWA	$\pi N \to \pi N$
20 ±3	HOEHLER	79	IPWA	$\pi N \to \pi N$
• • • We do not use the following data for averages, fits, limits, etc. • • •				
22 ±4	SOKHOYAN	15A	DPWA	Multichannel
22 ±4	GUTZ	14	DPWA	Multichannel
14 ±1	[1] SHRESTHA	12A	DPWA	Multichannel
14 ±1	PENNER	02C	DPWA	Multichannel
5 ±1	VRANA	00	DPWA	Multichannel

[1] Statistical error only.

$\Gamma(N\pi\pi)/\Gamma_{total}$ — Γ_2/Γ

VALUE	DOCUMENT ID		TECN	COMMENT
0.89±0.11	GOLOVATCH	19	DPWA	$\gamma p \to \pi^+\pi^- p$

$\Gamma(\Delta(1232)\pi)/\Gamma_{total}$ — Γ_3/Γ

VALUE (%)	DOCUMENT ID		TECN	COMMENT
35±13	SARANTSEV	25	DPWA	Multichannel

$\Gamma(\Delta(1232)\pi, S\text{-wave})/\Gamma_{total}$ — Γ_4/Γ

VALUE (%)	DOCUMENT ID		TECN	COMMENT
23±13	SARANTSEV	25	DPWA	Multichannel
16±15	SEIFEN	25	DPWA	Multichannel
49± 5	[1] HUNT	19	DPWA	Multichannel
• • • We do not use the following data for averages, fits, limits, etc. • • •				
20±15	SOKHOYAN	15A	DPWA	Multichannel
54± 3	[1] SHRESTHA	12A	DPWA	Multichannel
90± 2	VRANA	00	DPWA	Multichannel

[1] Statistical error only.

$\Gamma(\Delta(1232)\pi, D\text{-wave})/\Gamma_{total}$ — Γ_5/Γ

VALUE (%)	DOCUMENT ID		TECN	COMMENT
12 ±8	SARANTSEV	25	DPWA	Multichannel
8 ±6	SEIFEN	25	DPWA	Multichannel
7.6±0.3	[1] HUNT	19	DPWA	Multichannel
• • • We do not use the following data for averages, fits, limits, etc. • • •				
10 ±6	SOKHOYAN	15A	DPWA	Multichannel
1 ±1	[1] SHRESTHA	12A	DPWA	Multichannel
4 ±1	VRANA	00	DPWA	Multichannel

[1] Statistical error only.

$\Gamma(N\rho)/\Gamma_{total}$ — Γ_6/Γ

VALUE (%)	DOCUMENT ID		TECN	COMMENT
15±4	SARANTSEV	25	DPWA	Multichannel

$\Gamma(N\rho, S\text{=}3/2, S\text{-wave})/\Gamma_{total}$ — Γ_7/Γ

VALUE (%)	DOCUMENT ID		TECN	COMMENT
15±4	SARANTSEV	25	DPWA	Multichannel
27±5	[1] HUNT	19	DPWA	Multichannel
• • • We do not use the following data for averages, fits, limits, etc. • • •				
30±3	[1] SHRESTHA	12A	DPWA	Multichannel
1±1	VRANA	00	DPWA	Multichannel

[1] Statistical error only.

Int. J. Mod. Phys. A 2026.41. Downloaded from www.worldscientific.com
UNIVERSITY OF CALIFORNIA @ BERKELEY on 09/16/26. Re-use and distribution is strictly not permitted, except for Open Access articles.

$\Gamma(N(1440)\pi)/\Gamma_{total}$ — Γ_8/Γ

VALUE (%)	DOCUMENT ID		TECN	COMMENT
3±2	SEIFEN	25	DPWA	Multichannel

$\Gamma(N(1520)\pi, P\text{-wave})/\Gamma_{total}$ — Γ_9/Γ

VALUE (%)	DOCUMENT ID		TECN	COMMENT
<1	SEIFEN	25	DPWA	Multichannel
• • • We do not use the following data for averages, fits, limits, etc. • • •				
3±2	SOKHOYAN	15A	DPWA	Multichannel

$\Gamma(N(1535)\pi)/\Gamma_{total}$ — Γ_{10}/Γ

VALUE (%)	DOCUMENT ID		TECN	COMMENT
<1	SEIFEN	25	DPWA	Multichannel
1.0±0.5	GUTZ	14	DPWA	Multichannel
• • • We do not use the following data for averages, fits, limits, etc. • • •				
4 ±2	HORN	08A	DPWA	Multichannel

$\Gamma(\Delta(1232)\eta)/\Gamma_{total}$ — Γ_{11}/Γ

VALUE (%)	DOCUMENT ID		TECN	COMMENT
5±2	GUTZ	14	DPWA	Multichannel
• • • We do not use the following data for averages, fits, limits, etc. • • •				
5±2	ANISOVICH	12A	DPWA	Multichannel

$\Gamma(N(1535)\pi)/\Gamma(\Delta(1232)\eta)$ — Γ_{10}/Γ_{11}

VALUE	DOCUMENT ID		TECN	COMMENT
• • • We do not use the following data for averages, fits, limits, etc. • • •				
0.67	KASHEVAROV	09	CBAL	$\gamma p \to p\pi^0\eta$

$\Delta(1700)$ PHOTON DECAY AMPLITUDES AT THE POLE

$\Delta(1700) \to N\gamma$, helicity-1/2 amplitude $A_{1/2}$

MODULUS ($GeV^{-1/2}$)	PHASE (°)	DOCUMENT ID		TECN	COMMENT
0.150±0.020	30 ± 15	SARANTSEV	25	DPWA	Multichannel
0.163±0.060	−4.4 ± 39	ROENCHEN	22	DPWA	Multichannel
• • • We do not use the following data for averages, fits, limits, etc. • • •					
0.123	1.1	ROENCHEN	15A	DPWA	Multichannel
0.175±0.020	50 ± 10	SOKHOYAN	15A	DPWA	Multichannel

$\Delta(1700) \to N\gamma$, helicity-3/2 amplitude $A_{3/2}$

MODULUS ($GeV^{-1/2}$)	PHASE (°)	DOCUMENT ID		TECN	COMMENT
0.155±0.020	40 ± 15	SARANTSEV	25	DPWA	Multichannel
0.221±0.093	−12 ± 40	ROENCHEN	22	DPWA	Multichannel
• • • We do not use the following data for averages, fits, limits, etc. • • •					
0.124	22	ROENCHEN	15A	DPWA	Multichannel
0.180±0.020	45 ± 10	SOKHOYAN	15A	DPWA	Multichannel

$\Delta(1700)$ BREIT-WIGNER PHOTON DECAY AMPLITUDES

$\Delta(1700) \to N\gamma$, helicity-1/2 amplitude $A_{1/2}$

VALUE ($GeV^{-1/2}$)	DOCUMENT ID		TECN	COMMENT
0.100 to 0.160 (≈ 0.130) OUR ESTIMATE				
0.153 ±0.018	SARANTSEV	25	DPWA	Multichannel
0.0872±0.0189	GOLOVATCH	19	DPWA	$\gamma p \to \pi^+\pi^- p$
0.156 ±0.017	[1] HUNT	19	DPWA	Multichannel
0.132 ±0.005	[1] DUGGER	13	DPWA	$\gamma N \to \pi N$
0.105 ±0.005	[1] WORKMAN	12A	DPWA	$\gamma N \to \pi N$
• • • We do not use the following data for averages, fits, limits, etc. • • •				
0.165 ±0.020	SOKHOYAN	15A	DPWA	Multichannel
0.165 ±0.020	GUTZ	14	DPWA	Multichannel
0.058 ±0.010	[1] SHRESTHA	12A	DPWA	Multichannel
0.226	DRECHSEL	07	DPWA	$\gamma N \to \pi N$
0.125 ±0.003	DUGGER	07	DPWA	$\gamma N \to \pi N$
0.096	PENNER	02D	DPWA	Multichannel

[1] Statistical error only.

$\Delta(1700) \to N\gamma$, helicity-3/2 amplitude $A_{3/2}$

VALUE ($GeV^{-1/2}$)	DOCUMENT ID		TECN	COMMENT
0.090 to 0.170 (≈ 0.130) OUR ESTIMATE				
0.158 ±0.017	SARANTSEV	25	DPWA	Multichannel
0.0872±0.0164	GOLOVATCH	19	DPWA	$\gamma p \to \pi^+\pi^- p$
0.0125±0.0016	[1] HUNT	19	DPWA	Multichannel
0.108 ±0.005	[1] DUGGER	13	DPWA	$\gamma N \to \pi N$
0.092 ±0.004	[1] WORKMAN	12A	DPWA	$\gamma N \to \pi N$
• • • We do not use the following data for averages, fits, limits, etc. • • •				
0.170 ±0.025	SOKHOYAN	15A	DPWA	Multichannel
0.170 ±0.025	GUTZ	14	DPWA	Multichannel
0.097 ±0.008	[1] SHRESTHA	12A	DPWA	Multichannel
0.210	DRECHSEL	07	DPWA	$\gamma N \to \pi N$
0.105 ±0.003	DUGGER	07	DPWA	$\gamma N \to \pi N$
0.154	PENNER	02D	DPWA	Multichannel

[1] Statistical error only.

$\Delta(1700)$ REFERENCES

For early references, see Physics Letters **111B** 1 (1982).

SARANTSEV	25	PR C112 015202	A.V. Sarantsev *et al.*	(Bonn-Gatchina Collab.)
SEIFEN	25	EPJ A61 173	T. Seifen *et al.*	(CBELSA/TAPS Collab.)
ROENCHEN	22	EPJ A58 229	D. Roenchen *et al.*	(JULI, GWU, BONN+)
GOLOVATCH	19	PL B788 371	E. Golovatch *et al.*	(CLAS Collab.)
HUNT	19	PR C99 055205	B.C. Hunt, D.M. Manley	
ROENCHEN	15A	EPJ A51 70	D. Roenchen *et al.*	
SOKHOYAN	15A	EPJ A51 95	V. Sokhoyan *et al.*	(CBELSA/TAPS Collab.)
GUTZ	14	EPJ A50 74	E. Gutz *et al.*	(CBELSA/TAPS Collab.)
PDG	14	CP C38 070001	K. Olive *et al.*	(PDG Collab.)
SVARC	14	PR C89 045205	A. Svarc *et al.*	(RBI Zagreb, UNI Tuzla)
DUGGER	13	PR C88 065203	M. Dugger *et al.*	(JLab CLAS Collab.)
ANISOVICH	12A	EPJ A48 15	A.V. Anisovich *et al.*	(BONN, PNPI)
SHRESTHA	12A	PR C86 055203	M. Shrestha, D.M. Manley	(KSU)
WORKMAN	12A	PR C86 015202	R. Workman *et al.*	(GWU)
KASHEVAROV	09	EPJ A42 141	V.L. Kashevarov *et al.*	(MAMI Crystal Ball/TAPS)
HORN	08A	EPJ A38 173	I. Horn *et al.*	(CB-ELSA Collab.)
Also		PRL 101 202002	I. Horn *et al.*	(CB-ELSA Collab.)
DRECHSEL	07	EPJ A34 69	D. Drechsel, S.S. Kamalov, L. Tiator	(MAINZ, JINR)
DUGGER	07	PR C76 025211	M. Dugger *et al.*	(JLab CLAS Collab.)
ARNDT	06	PR C74 045205	R.A. Arndt *et al.*	(GWU)
PENNER	02C	PR C66 055211	G. Penner, U. Mosel	(GIES)
PENNER	02D	PR C66 055212	G. Penner, U. Mosel	(GIES)
VRANA	00	PRPL 328 181	T.P. Vrana, S.A. Dytman, T.-S.H. Lee	(PITT, ANL)
HOEHLER	93	πN Newsletter 9 1	G. Hohler	(KARL)
CUTKOSKY	80	Toronto Conf. 19	R.E. Cutkosky *et al.*	(CMU, LBL) IJP
Also		PR D20 2839	R.E. Cutkosky *et al.*	(CMU, LBL) IJP
HOEHLER	79	PDAT 12-1	G. Hohler *et al.*	(KARLT) IJP
Also		Toronto Conf. 3	R. Koch	(KARLT) IJP

$\Delta(1750)\ 1/2^+$

$I(J^P) = \frac{3}{2}(\frac{1}{2}^+)$ Status: *

OMITTED FROM SUMMARY TABLE

$\Delta(1750)$ POLE POSITION

REAL PART

VALUE (MeV)	DOCUMENT ID		TECN	COMMENT
• • • We do not use the following data for averages, fits, limits, etc. • • •				
1748	ARNDT	04	DPWA	$\pi N \to \pi N, \eta N$
1714	VRANA	00	DPWA	Multichannel

−2×IMAGINARY PART

VALUE (MeV)	DOCUMENT ID		TECN	COMMENT
• • • We do not use the following data for averages, fits, limits, etc. • • •				
524	ARNDT	04	DPWA	$\pi N \to \pi N, \eta N$
68	VRANA	00	DPWA	Multichannel

$\Delta(1750)$ ELASTIC POLE RESIDUE

MODULUS $|r|$

VALUE (MeV)	DOCUMENT ID		TECN	COMMENT
• • • We do not use the following data for averages, fits, limits, etc. • • •				
48	ARNDT	04	DPWA	$\pi N \to \pi N, \eta N$

PHASE θ

VALUE (°)	DOCUMENT ID		TECN	COMMENT
• • • We do not use the following data for averages, fits, limits, etc. • • •				
158	ARNDT	04	DPWA	$\pi N \to \pi N, \eta N$

$\Delta(1750)$ BREIT-WIGNER MASS

VALUE (MeV)	DOCUMENT ID		TECN	COMMENT
• • • We do not use the following data for averages, fits, limits, etc. • • •				
1712± 1	PENNER	02C	DPWA	Multichannel
1721±61	VRANA	00	DPWA	Multichannel

$\Delta(1750)$ BREIT-WIGNER WIDTH

VALUE (MeV)	DOCUMENT ID		TECN	COMMENT
• • • We do not use the following data for averages, fits, limits, etc. • • •				
643±17	PENNER	02C	DPWA	Multichannel
70±50	VRANA	00	DPWA	Multichannel

$\Delta(1750)$ DECAY MODES

	Mode	Fraction (Γ_i/Γ)
Γ_1	$N\pi$	seen
Γ_2	$N(1440)\pi$	seen
Γ_3	ΣK	seen

$\Delta(1750)$ BRANCHING RATIOS

$\Gamma(N\pi)/\Gamma_{total}$ — Γ_1/Γ

VALUE (%)	DOCUMENT ID		TECN	COMMENT
• • • We do not use the following data for averages, fits, limits, etc. • • •				
1±1	PENNER	02C	DPWA	Multichannel
6±9	VRANA	00	DPWA	Multichannel

Int. J. Mod. Phys. A 2026.41. Downloaded from www.worldscientific.com
by UNIVERSITY OF CALIFORNIA @ BERKELEY on 09/16/26. Re-use and distribution is strictly not permitted, except for Open Access articles.

$\Gamma(N(1440)\pi)/\Gamma_{total}$ — Γ_2/Γ

VALUE (%)	DOCUMENT ID		TECN	COMMENT
• • • We do not use the following data for averages, fits, limits, etc. • • •				
83±1	VRANA	00	DPWA	Multichannel

$\Gamma(\Sigma K)/\Gamma_{total}$ — Γ_3/Γ

VALUE (%)	DOCUMENT ID		TECN	COMMENT
• • • We do not use the following data for averages, fits, limits, etc. • • •				
0.1±0.1	PENNER	02C	DPWA	Multichannel

$\Delta(1750)$ BREIT-WIGNER PHOTON DECAY AMPLITUDES

Papers on γN amplitudes predating 1981 may be found in our 2006 edition, Journal of Physics **G33** 1 (2006).

$\Delta(1750) \to N\gamma$, helicity-1/2 amplitude $A_{1/2}$

VALUE (GeV$^{-1/2}$)	DOCUMENT ID		TECN	COMMENT
• • • We do not use the following data for averages, fits, limits, etc. • • •				
0.053	PENNER	02D	DPWA	Multichannel

$\Delta(1750)$ REFERENCES

PDG	06	JP G33 1	W.-M. Yao *et al.*	(PDG Collab.)
ARNDT	04	PR C69 035213	R.A. Arndt *et al.*	(GWU, TRIU)
PENNER	02C	PR C66 055211	G. Penner, U. Mosel	(GIES)
PENNER	02D	PR C66 055212	G. Penner, U. Mosel	(GIES)
VRANA	00	PRPL 328 181	T.P. Vrana, S.A. Dytman, T.-S.H. Lee	(PITT, ANL)

$\Delta(1900)\ 1/2^-$

$I(J^P) = \frac{3}{2}(\frac{1}{2}^-)$ Status: ***

Older and obsolete values are listed and referenced in the 2014 edition, Chinese Physics **C38** 070001 (2014).

$\Delta(1900)$ POLE POSITION

REAL PART

VALUE (MeV)	DOCUMENT ID		TECN	COMMENT
1830 to 1900 (≈ 1865) OUR ESTIMATE				
1815±20	SARANTSEV	25	DPWA	Multichannel
1865±35±19	[1] SVARC	14	L+P	$\pi N \to \pi N$
1870±40	CUTKOSKY	80	IPWA	$\pi N \to \pi N$
• • • We do not use the following data for averages, fits, limits, etc. • • •				
1957	HUNT	19	DPWA	Multichannel
1845±20	SOKHOYAN	15A	DPWA	Multichannel
1845±20	GUTZ	14	DPWA	Multichannel
1795	VRANA	00	DPWA	Multichannel
1780	HOEHLER	93	SPED	$\pi N \to \pi N$

[1] Fit to the amplitudes of HOEHLER 79.

−2×IMAGINARY PART

VALUE (MeV)	DOCUMENT ID		TECN	COMMENT
180 to 300 (≈ 240) OUR ESTIMATE				
340±35	SARANTSEV	25	DPWA	Multichannel
187±50±19	[1] SVARC	14	L+P	$\pi N \to \pi N$
180±50	CUTKOSKY	80	IPWA	$\pi N \to \pi N$
• • • We do not use the following data for averages, fits, limits, etc. • • •				
447	HUNT	19	DPWA	Multichannel
295±35	SOKHOYAN	15A	DPWA	Multichannel
295±35	GUTZ	14	DPWA	Multichannel
58	VRANA	00	DPWA	Multichannel

[1] Fit to the amplitudes of HOEHLER 79.

$\Delta(1900)$ ELASTIC POLE RESIDUE

MODULUS $|r|$

VALUE (MeV)	DOCUMENT ID		TECN	COMMENT
8 to 14 (≈ 11) OUR ESTIMATE				
11±2	SOKHOYAN	15A	DPWA	Multichannel
11±4±2	[1] SVARC	14	L+P	$\pi N \to \pi N$
10±3	CUTKOSKY	80	IPWA	$\pi N \to \pi N$
• • • We do not use the following data for averages, fits, limits, etc. • • •				
11±2	GUTZ	14	DPWA	Multichannel
10±3	ANISOVICH	12A	DPWA	Multichannel

[1] Fit to the amplitudes of HOEHLER 79.

PHASE θ

VALUE (°)	DOCUMENT ID		TECN	COMMENT
−115±20	SOKHOYAN	15A	DPWA	Multichannel
20±27±19	[1] SVARC	14	L+P	$\pi N \to \pi N$
+ 20±40	CUTKOSKY	80	IPWA	$\pi N \to \pi N$
• • • We do not use the following data for averages, fits, limits, etc. • • •				
−115±20	GUTZ	14	DPWA	Multichannel
−125±20	ANISOVICH	12A	DPWA	Multichannel

[1] Fit to the amplitudes of HOEHLER 79.

$\Delta(1900)$ INELASTIC POLE RESIDUE

The "normalized residue" is the residue divided by $\Gamma_{pole}/2$.

Normalized residue in $N\pi \to \Delta(1900) \to \Sigma K$

MODULUS	PHASE (°)	DOCUMENT ID		TECN	COMMENT
0.07±0.02	−50 ± 30	ANISOVICH	12A	DPWA	Multichannel

Normalized residue in $N\pi \to \Delta(1900) \to \Delta\pi$, D-wave

MODULUS	PHASE (°)	DOCUMENT ID		TECN	COMMENT
0.18±0.10	105 ± 25	SOKHOYAN	15A	DPWA	Multichannel
• • • We do not use the following data for averages, fits, limits, etc. • • •					
$0.12^{+0.08}_{-0.05}$	110 ± 20	ANISOVICH	12A	DPWA	Multichannel

Normalized residue in $N\pi \to \Delta(1900) \to \Delta(1232)\eta$

MODULUS	PHASE (°)	DOCUMENT ID		TECN	COMMENT
0.013±0.006	undefined	GUTZ	14	DPWA	Multichannel

Normalized residue in $N\pi \to \Delta(1900) \to N(1440)\pi$

MODULUS	PHASE (°)	DOCUMENT ID		TECN	COMMENT
0.11±0.06	115 ± 30	SOKHOYAN	15A	DPWA	Multichannel

Normalized residue in $N\pi \to \Delta(1900) \to N(1520)\pi$

MODULUS	PHASE (°)	DOCUMENT ID		TECN	COMMENT
0.06±0.03	undefined	SOKHOYAN	15A	DPWA	Multichannel

$\Delta(1900)$ BREIT-WIGNER MASS

VALUE (MeV)	DOCUMENT ID		TECN	COMMENT
1840 to 1920 (≈ 1860) OUR ESTIMATE				
1825±20	SARANTSEV	25	DPWA	Multichannel
1989±22	[1] HUNT	19	DPWA	Multichannel
1890±50	CUTKOSKY	80	IPWA	$\pi N \to \pi N$
1908±30	HOEHLER	79	IPWA	$\pi N \to \pi N$
• • • We do not use the following data for averages, fits, limits, etc. • • •				
1840±20	SOKHOYAN	15A	DPWA	Multichannel
1840±20	GUTZ	14	DPWA	Multichannel
1868±12	[1] SHRESTHA	12A	DPWA	Multichannel
1802±87	VRANA	00	DPWA	Multichannel

[1] Statistical error only.

$\Delta(1900)$ BREIT-WIGNER WIDTH

VALUE (MeV)	DOCUMENT ID		TECN	COMMENT
180 to 320 (≈ 250) OUR ESTIMATE				
360±35	SARANTSEV	25	DPWA	Multichannel
457±60	[1] HUNT	19	DPWA	Multichannel
170±50	CUTKOSKY	80	IPWA	$\pi N \to \pi N$
140±40	HOEHLER	79	IPWA	$\pi N \to \pi N$
• • • We do not use the following data for averages, fits, limits, etc. • • •				
295±30	SOKHOYAN	15A	DPWA	Multichannel
295±30	GUTZ	14	DPWA	Multichannel
234±27	[1] SHRESTHA	12A	DPWA	Multichannel
48±45	VRANA	00	DPWA	Multichannel

[1] Statistical error only.

$\Delta(1900)$ DECAY MODES

The following branching fractions are our estimates, not fits or averages.

	Mode	Fraction (Γ_i/Γ)
Γ_1	$N\pi$	4–12%
Γ_2	ΣK	seen
Γ_3	$N\pi\pi$	> 52%
Γ_4	$\Delta(1232)\pi$	30–70%
Γ_5	$N\rho$	22–60 %
Γ_6	$N\rho$, S=1/2	11–35%
Γ_7	$N\rho$, S=3/2	11–25%
Γ_8	$N(1440)\pi$	3–32%
Γ_9	$N(1520)\pi$	2–10%
Γ_{10}	$\Delta(1232)\eta$	< 2%
Γ_{11}	$N\gamma$, helicity=1/2	0.06–0.43 %

$\Delta(1900)$ BRANCHING RATIOS

$\Gamma(N\pi)/\Gamma_{total}$ — Γ_1/Γ

VALUE (%)	DOCUMENT ID		TECN	COMMENT
4–12% OUR ESTIMATE				
4 ± 4	SEIFEN	25	DPWA	Multichannel
3.7± 0.8	[1] HUNT	19	DPWA	Multichannel
10 ± 3	CUTKOSKY	80	IPWA	$\pi N \to \pi N$
8 ± 4	HOEHLER	79	IPWA	$\pi N \to \pi N$

Int. J. Mod. Phys. A 2026.41. Downloaded from www.worldscientific.com
UNIVERSITY OF CALIFORNIA @ BERKELEY on 09/16/26. Re-use and distribution is strictly not permitted, except for Open Access articles.

• • • We do not use the following data for averages, fits, limits, etc. • • •

7 ± 2	SOKHOYAN	15A	DPWA	Multichannel
7 ± 2	GUTZ	14	DPWA	Multichannel
8 ± 1	[1] SHRESTHA	12A	DPWA	Multichannel
33 ±10	VRANA	00	DPWA	Multichannel

[1] Statistical error only.

$\Gamma(\Delta(1232)\pi)/\Gamma_{total}$ — Γ_4/Γ

VALUE (%)	DOCUMENT ID		TECN	COMMENT
30–70% OUR ESTIMATE				
64±15	SARANTSEV	25	DPWA	Multichannel
60±25	SEIFEN	25	DPWA	Multichannel
42± 8	[1] HUNT	19	DPWA	Multichannel
• • • We do not use the following data for averages, fits, limits, etc. • • •				
50±20	SOKHOYAN	15A	DPWA	Multichannel
56± 6	[1] SHRESTHA	12A	DPWA	Multichannel
28± 1	VRANA	00	DPWA	Multichannel

[1] Statistical error only.

$\Gamma(N\rho)/\Gamma_{total}$ — Γ_5/Γ

VALUE (%)	DOCUMENT ID		TECN	COMMENT
38±13	SARANTSEV	25	DPWA	Multichannel

$\Gamma(N\rho, S{=}1/2)/\Gamma_{total}$ — Γ_6/Γ

VALUE (%)	DOCUMENT ID		TECN	COMMENT
11–35% OUR ESTIMATE				
18± 8	SARANTSEV	25	DPWA	Multichannel
23±12	[1] HUNT	19	DPWA	Multichannel
• • • We do not use the following data for averages, fits, limits, etc. • • •				
12± 4	[1] SHRESTHA	12A	DPWA	Multichannel
30± 2	VRANA	00	DPWA	Multichannel

[1] Statistical error only.

$\Gamma(N\rho, S{=}3/2)/\Gamma_{total}$ — Γ_7/Γ

VALUE (%)	DOCUMENT ID		TECN	COMMENT
11–25% OUR ESTIMATE				
20±10	SARANTSEV	25	DPWA	Multichannel
18± 7	[1] HUNT	19	DPWA	Multichannel
• • • We do not use the following data for averages, fits, limits, etc. • • •				
23± 5	[1] SHRESTHA	12A	DPWA	Multichannel
5± 1	VRANA	00	DPWA	Multichannel

[1] Statistical error only.

$\Gamma(N(1440)\pi)/\Gamma_{total}$ — Γ_8/Γ

VALUE (%)	DOCUMENT ID		TECN	COMMENT
3–32% OUR ESTIMATE				
15±12	SEIFEN	25	DPWA	Multichannel
12± 9	[1] HUNT	19	DPWA	Multichannel
• • • We do not use the following data for averages, fits, limits, etc. • • •				
20±12	SOKHOYAN	15A	DPWA	Multichannel
< 1	[1] SHRESTHA	12A	DPWA	Multichannel
4± 1	VRANA	00	DPWA	Multichannel

[1] Statistical error only.

$\Gamma(N(1520)\pi)/\Gamma_{total}$ — Γ_9/Γ

VALUE (%)	DOCUMENT ID		TECN	COMMENT
2–10% OUR ESTIMATE				
10±7	SEIFEN	25	DPWA	Multichannel
• • • We do not use the following data for averages, fits, limits, etc. • • •				
6±4	SOKHOYAN	15A	DPWA	Multichannel

$\Gamma(\Delta(1232)\eta)/\Gamma_{total}$ — Γ_{10}/Γ

VALUE (%)	DOCUMENT ID		TECN	COMMENT
< 2% OUR ESTIMATE				
1±1	GUTZ	14	DPWA	Multichannel

$\Delta(1900)$ PHOTON DECAY AMPLITUDES AT THE POLE

$\Delta(1900) \to N\gamma$, helicity-1/2 amplitude $A_{1/2}$

MODULUS ($GeV^{-1/2}$)	PHASE (°)	DOCUMENT ID		TECN	COMMENT
0.075±0.015	−65 ± 25	SARANTSEV	25	DPWA	Multichannel
• • • We do not use the following data for averages, fits, limits, etc. • • •					
0.064±0.015	60 ± 20	SOKHOYAN	15A	DPWA	Multichannel

$\Delta(1900)$ BREIT-WIGNER PHOTON DECAY AMPLITUDES

$\Delta(1900) \to N\gamma$, helicity-1/2 amplitude $A_{1/2}$

VALUE ($GeV^{-1/2}$)	DOCUMENT ID		TECN	COMMENT
0.075±0.015	SARANTSEV	25	DPWA	Multichannel
0.212±0.029	[1] HUNT	19	DPWA	Multichannel
• • • We do not use the following data for averages, fits, limits, etc. • • •				
0.065±0.015	SOKHOYAN	15A	DPWA	Multichannel
0.057±0.014	GUTZ	14	DPWA	Multichannel
−0.082±0.009	[1] SHRESTHA	12A	DPWA	Multichannel

[1] Statistical error only.

$\Delta(1900)$ REFERENCES

For early references, see Physics Letters **111B** 1 (1982).

SARANTSEV	25	PR C112 015202	A.V. Sarantsev *et al.*	(Bonn-Gatchina Collab.)
SEIFEN	25	EPJ A61 173	T. Seifen *et al.*	(CBELSA/TAPS Collab.)
HUNT	19	PR C99 055205	B.C. Hunt, D.M. Manley	
SOKHOYAN	15A	EPJ A51 95	V. Sokhoyan *et al.*	(CBELSA/TAPS Collab.)
GUTZ	14	EPJ A50 74	E. Gutz *et al.*	(CBELSA/TAPS Collab.)
PDG	14	CP C38 070001	K. Olive *et al.*	(PDG Collab.)
SVARC	14	PR C89 045205	A. Svarc *et al.*	(RBI Zagreb, UNI Tuzla)
ANISOVICH	12A	EPJ A48 15	A.V. Anisovich *et al.*	(BONN, PNPI)
SHRESTHA	12A	PR C86 055203	M. Shrestha, D.M. Manley	(KSU)
VRANA	00	PRPL 328 181	T.P. Vrana, S.A. Dytman, T.-S.H. Lee	(PITT, ANL)
HOEHLER	93	πN Newsletter 9 1	G. Hohler	(KARL)
CUTKOSKY	80	Toronto Conf. 19	R.E. Cutkosky *et al.*	(CMU, LBL) IJP
Also		PR D20 2839	R.E. Cutkosky *et al.*	(CMU, LBL) IJP
HOEHLER	79	PDAT 12-1	G. Hohler *et al.*	(KARLT) IJP
Also		Toronto Conf. 3	R. Koch	(KARLT) IJP

$\Delta(1905)\ 5/2^+$

$I(J^P) = \frac{3}{2}(\frac{5}{2}^+)$ Status: ****

Older and obsolete values are listed and referenced in the 2014 edition, Chinese Physics **C38** 070001 (2014).

$\Delta(1905)$ POLE POSITION

REAL PART

VALUE (MeV)	DOCUMENT ID		TECN	COMMENT
1750 to 1800 (≈ 1770) OUR ESTIMATE				
1795 ±20	SARANTSEV	25	DPWA	Multichannel
1707± 1	ROENCHEN	22	DPWA	Multichannel
1752± 3±2	[1] SVARC	14	L+P	$\pi N \to \pi N$
1830±40	CUTKOSKY	80	IPWA	$\pi N \to \pi N$
• • • We do not use the following data for averages, fits, limits, etc. • • •				
1819	HUNT	19	DPWA	Multichannel
1795	ROENCHEN	15A	DPWA	Multichannel
1800± 6	SOKHOYAN	15A	DPWA	Multichannel
1800± 6	GUTZ	14	DPWA	Multichannel
1819	ARNDT	06	DPWA	$\pi N \to \pi N, \eta N$
1793	VRANA	00	DPWA	Multichannel
1829	HOEHLER	93	SPED	$\pi N \to \pi N$

[1] Fit to the amplitudes of HOEHLER 79.

−2×IMAGINARY PART

VALUE (MeV)	DOCUMENT ID		TECN	COMMENT
260 to 340 (≈ 300) OUR ESTIMATE				
280±20	SARANTSEV	25	DPWA	Multichannel
127± 4	ROENCHEN	22	DPWA	Multichannel
346± 6±2	[1] SVARC	14	L+P	$\pi N \to \pi N$
280±60	CUTKOSKY	80	IPWA	$\pi N \to \pi N$
• • • We do not use the following data for averages, fits, limits, etc. • • •				
253	HUNT	19	DPWA	Multichannel
247	ROENCHEN	15A	DPWA	Multichannel
290±15	SOKHOYAN	15A	DPWA	Multichannel
290±15	GUTZ	14	DPWA	Multichannel
247	ARNDT	06	DPWA	$\pi N \to \pi N, \eta N$
302	VRANA	00	DPWA	Multichannel
303	HOEHLER	93	SPED	$\pi N \to \pi N$

[1] Fit to the amplitudes of HOEHLER 79.

$\Delta(1905)$ ELASTIC POLE RESIDUE

MODULUS $|r|$

VALUE (MeV)	DOCUMENT ID		TECN	COMMENT
15 to 25 (≈ 20) OUR ESTIMATE				
3.7±1.0	ROENCHEN	22	DPWA	Multichannel
19 ±2	SOKHOYAN	15A	DPWA	Multichannel
24 ±1 ±1	[1] SVARC	14	L+P	$\pi N \to \pi N$
25 ±8	CUTKOSKY	80	IPWA	$\pi N \to \pi N$
• • • We do not use the following data for averages, fits, limits, etc. • • •				
5.3	ROENCHEN	15A	DPWA	Multichannel
19 ±2	GUTZ	14	DPWA	Multichannel
20 ±2	ANISOVICH	12A	DPWA	Multichannel
15	ARNDT	06	DPWA	$\pi N \to \pi N, \eta N$
25	HOEHLER	93	SPED	$\pi N \to \pi N$

[1] Fit to the amplitudes of HOEHLER 79.

PHASE θ

VALUE (°)	DOCUMENT ID		TECN	COMMENT
−120 to −30 (≈ −45) OUR ESTIMATE				
− 92± 6	ROENCHEN	22	DPWA	Multichannel
− 45± 4	SOKHOYAN	15A	DPWA	Multichannel
−114± 1±2	[1] SVARC	14	L+P	$\pi N \to \pi N$
− 50±20	CUTKOSKY	80	IPWA	$\pi N \to \pi N$
• • • We do not use the following data for averages, fits, limits, etc. • • •				
− 89	ROENCHEN	15A	DPWA	Multichannel
− 45± 4	GUTZ	14	DPWA	Multichannel

Int. J. Mod. Phys. A 2026.41. Downloaded from www.worldscientific.com
by UNIVERSITY OF CALIFORNIA @ BERKELEY on 09/16/26. Re-use and distribution is strictly not permitted, except for Open Access articles.

− 44± 5	ANISOVICH	12A	DPWA	Multichannel
− 30	ARNDT	06	DPWA	$\pi N \to \pi N, \eta N$

[1] Fit to the amplitudes of HOEHLER 79.

$\Delta(1905)$ INELASTIC POLE RESIDUE

The "normalized residue" is the residue divided by $\Gamma_{pole}/2$.

Normalized residue in $N\pi \to \Delta(1905) \to \Delta\pi$, P-wave

MODULUS	PHASE (°)	DOCUMENT ID		TECN	COMMENT
0.10 ±0.01	−109 ± 7	ROENCHEN	22	DPWA	Multichannel
0.19 ±0.07	10 ± 30	SOKHOYAN	15A	DPWA	Multichannel
• • • We do not use the following data for averages, fits, limits, etc. • • •					
0.0870	72	ROENCHEN	15A	DPWA	Multichannel
0.25 ±0.06	0 ± 15	ANISOVICH	12A	DPWA	Multichannel

Normalized residue in $N\pi \to \Delta(1905) \to \Delta\pi$, F-wave

MODULUS	PHASE (°)	DOCUMENT ID		TECN	COMMENT
0.017±0.002	18 ± 8	ROENCHEN	22	DPWA	Multichannel
• • • We do not use the following data for averages, fits, limits, etc. • • •					
0.009	64	ROENCHEN	15A	DPWA	Multichannel

Normalized residue in $N\pi \to \Delta(1905) \to \Sigma K$

MODULUS	PHASE (°)	DOCUMENT ID		TECN	COMMENT
0.0020±0.0002	154 ± 6	ROENCHEN	22	DPWA	Multichannel
• • • We do not use the following data for averages, fits, limits, etc. • • •					
0.001	−155	ROENCHEN	15A	DPWA	Multichannel

Normalized residue in $N\pi \to \Delta(1905) \to N(1535)\pi$

MODULUS	PHASE (°)	DOCUMENT ID		TECN	COMMENT
0.025±0.010	130 ± 35	GUTZ	14	DPWA	Multichannel

Normalized residue in $N\pi \to \Delta(1905) \to \Delta(1232)\eta$

MODULUS	PHASE (°)	DOCUMENT ID		TECN	COMMENT
0.07±0.02	40 ± 20	GUTZ	14	DPWA	Multichannel

$\Delta(1905)$ BREIT-WIGNER MASS

VALUE (MeV)	DOCUMENT ID		TECN	COMMENT
1855 to 1910 (≈ 1880) OUR ESTIMATE				
1845 ±20	SARANTSEV	25	DPWA	Multichannel
1883 ±19	GOLOVATCH	19	DPWA	$\gamma p \to \pi^+\pi^- p$
1866 ± 9	[1] HUNT	19	DPWA	Multichannel
1857.8± 1.6	[1] ARNDT	06	DPWA	$\pi N \to \pi N, \eta N$
1910 ±30	CUTKOSKY	80	IPWA	$\pi N \to \pi N$
1905 ±20	HOEHLER	79	IPWA	$\pi N \to \pi N$
• • • We do not use the following data for averages, fits, limits, etc. • • •				
1856 ± 6	SOKHOYAN	15A	DPWA	Multichannel
1856 ± 6	GUTZ	14	DPWA	Multichannel
1818 ± 8	[1] SHRESTHA	12A	DPWA	Multichannel
1873 ±77	VRANA	00	DPWA	Multichannel

[1] Statistical error only.

$\Delta(1905)$ BREIT-WIGNER WIDTH

VALUE (MeV)	DOCUMENT ID		TECN	COMMENT
270 to 400 (≈ 330) OUR ESTIMATE				
315 ± 20	SARANTSEV	25	DPWA	Multichannel
327 ± 69	GOLOVATCH	19	DPWA	$\gamma p \to \pi^+\pi^- p$
289 ± 20	[1] HUNT	19	DPWA	Multichannel
320.6± 8.6	[1] ARNDT	06	DPWA	$\pi N \to \pi N, \eta N$
400 ±100	CUTKOSKY	80	IPWA	$\pi N \to \pi N$
260 ± 20	HOEHLER	79	IPWA	$\pi N \to \pi N$
• • • We do not use the following data for averages, fits, limits, etc. • • •				
325 ± 15	SOKHOYAN	15A	DPWA	Multichannel
325 ± 15	GUTZ	14	DPWA	Multichannel
278 ± 18	[1] SHRESTHA	12A	DPWA	Multichannel
461 ±111	VRANA	00	DPWA	Multichannel

[1] Statistical error only.

$\Delta(1905)$ DECAY MODES

The following branching fractions are our estimates, not fits or averages.

	Mode	Fraction (Γ_i/Γ)
Γ_1	$N\pi$	9–15%
Γ_2	$N\pi\pi$	>65%
Γ_3	$\Delta(1232)\pi$	>48%
Γ_4	$\Delta(1232)\pi$, P-wave	8–43%
Γ_5	$\Delta(1232)\pi$, F-wave	40–58%
Γ_6	$N\rho$	(25±10) %
Γ_7	$N\rho$, S=3/2, P-wave	17–35%
Γ_8	$N(1535)\pi$	< 1 %
Γ_9	$N(1680)\pi$, P-wave	5–15%
Γ_{10}	$\Delta(1232)\eta$	2–6%
Γ_{11}	$N\gamma$	0.012–0.036 %
Γ_{12}	$N\gamma$, helicity=1/2	0.002–0.006 %
Γ_{13}	$N\gamma$, helicity=3/2	0.01–0.03 %

$\Delta(1905)$ BRANCHING RATIOS

$\Gamma(N\pi)/\Gamma_{total}$ — Γ_1/Γ

VALUE (%)	DOCUMENT ID		TECN	COMMENT
9–15% OUR ESTIMATE				
13 ±4	SEIFEN	25	DPWA	Multichannel
17 ±1	[1] HUNT	19	DPWA	Multichannel
12.2±0.1	[1] ARNDT	06	DPWA	$\pi N \to \pi N, \eta N$
8 ±3	CUTKOSKY	80	IPWA	$\pi N \to \pi N$
15 ±2	HOEHLER	79	IPWA	$\pi N \to \pi N$
• • • We do not use the following data for averages, fits, limits, etc. • • •				
13 ±2	SOKHOYAN	15A	DPWA	Multichannel
13 ±2	GUTZ	14	DPWA	Multichannel
6 ±1	[1] SHRESTHA	12A	DPWA	Multichannel
9 ±1	VRANA	00	DPWA	Multichannel

[1] Statistical error only.

$\Gamma(N\pi\pi)/\Gamma_{total}$ — Γ_2/Γ

VALUE	DOCUMENT ID		TECN	COMMENT
>65% OUR ESTIMATE				
0.85±0.15	GOLOVATCH	19	DPWA	$\gamma p \to \pi^+\pi^- p$

$\Gamma(\Delta(1232)\pi)/\Gamma_{total}$ — Γ_3/Γ

VALUE (%)	DOCUMENT ID		TECN	COMMENT
19±8	SARANTSEV	25	DPWA	Multichannel

$\Gamma(\Delta(1232)\pi, P\text{-wave})/\Gamma_{total}$ — Γ_4/Γ

VALUE (%)	DOCUMENT ID		TECN	COMMENT
8–43% OUR ESTIMATE				
14 ± 7	SARANTSEV	25	DPWA	Multichannel
20 ±12	SEIFEN	25	DPWA	Multichannel
8.4± 0.5	[1] HUNT	19	DPWA	Multichannel
• • • We do not use the following data for averages, fits, limits, etc. • • •				
33 ±10	SOKHOYAN	15A	DPWA	Multichannel
28 ± 7	[1] SHRESTHA	12A	DPWA	Multichannel
23 ± 1	VRANA	00	DPWA	Multichannel

[1] Statistical error only.

$\Gamma(\Delta(1232)\pi, F\text{-wave})/\Gamma_{total}$ — Γ_5/Γ

VALUE (%)	DOCUMENT ID		TECN	COMMENT
40–58% OUR ESTIMATE				
5±3	SARANTSEV	25	DPWA	Multichannel
49±9	[1] HUNT	19	DPWA	Multichannel
• • • We do not use the following data for averages, fits, limits, etc. • • •				
64±8	[1] SHRESTHA	12A	DPWA	Multichannel
44±1	VRANA	00	DPWA	Multichannel

[1] Statistical error only.

$\Gamma(N\rho)/\Gamma_{total}$ — Γ_6/Γ

VALUE (%)	DOCUMENT ID		TECN	COMMENT
25±10	SARANTSEV	25	DPWA	Multichannel

$\Gamma(N\rho, S=3/2, P\text{-wave})/\Gamma_{total}$ — Γ_7/Γ

VALUE (%)	DOCUMENT ID		TECN	COMMENT
17–35% OUR ESTIMATE				
25±10	SARANTSEV	25	DPWA	Multichannel
26± 9	[1] HUNT	19	DPWA	Multichannel
• • • We do not use the following data for averages, fits, limits, etc. • • •				
< 6	[1] SHRESTHA	12A	DPWA	Multichannel
24± 1	VRANA	00	DPWA	Multichannel

[1] Statistical error only.

$\Gamma(N(1535)\pi)/\Gamma_{total}$ — Γ_8/Γ

VALUE (%)	DOCUMENT ID		TECN	COMMENT
< 1 % OUR ESTIMATE				
<1	SEIFEN	25	DPWA	Multichannel
<1	GUTZ	14	DPWA	Multichannel

$\Gamma(N(1680)\pi, P\text{-wave})/\Gamma_{total}$ — Γ_9/Γ

VALUE (%)	DOCUMENT ID		TECN	COMMENT
5–15% OUR ESTIMATE				
6±2	SEIFEN	25	DPWA	Multichannel
• • • We do not use the following data for averages, fits, limits, etc. • • •				
10±5	SOKHOYAN	15A	DPWA	Multichannel

Int. J. Mod. Phys. A 2026.41. Downloaded from www.worldscientific.com
UNIVERSITY OF CALIFORNIA @ BERKELEY on 09/16/26. Re-use and distribution is strictly not permitted, except for Open Access articles.

$\Gamma(\Delta(1232)\eta)/\Gamma_{total}$ — Γ_{10}/Γ

VALUE (%)	DOCUMENT ID		TECN	COMMENT
2–6% OUR ESTIMATE				
4±2	GUTZ	14	DPWA	Multichannel

$\Delta(1905)$ PHOTON DECAY AMPLITUDES AT THE POLE

$\Delta(1905) \to N\gamma$, helicity-1/2 amplitude $A_{1/2}$

MODULUS ($GeV^{-1/2}$)	PHASE (°)	DOCUMENT ID		TECN	COMMENT
0.030±0.007	−35 ± 15	SARANTSEV	25	DPWA	Multichannel
0.055±0.004	−159 ± 2	ROENCHEN	22	DPWA	Multichannel
• • • We do not use the following data for averages, fits, limits, etc. • • •					
0.053	89	ROENCHEN	15A	DPWA	Multichannel
0.025±0.005	−28 ± 12	SOKHOYAN	15A	DPWA	Multichannel

$\Delta(1905) \to N\gamma$, helicity-3/2 amplitude $A_{3/2}$

MODULUS ($GeV^{-1/2}$)	PHASE (°)	DOCUMENT ID		TECN	COMMENT
−0.072±0.010	−10 ± 20	SARANTSEV	25	DPWA	Multichannel
−0.168±0.020	172 ± 0.9	ROENCHEN	22	DPWA	Multichannel
• • • We do not use the following data for averages, fits, limits, etc. • • •					
−0.030	80	ROENCHEN	15A	DPWA	Multichannel
−0.050±0.004	5 ± 10	SOKHOYAN	15A	DPWA	Multichannel

$\Delta(1905)$ BREIT-WIGNER PHOTON DECAY AMPLITUDES

$\Delta(1905) \to N\gamma$, helicity-1/2 amplitude $A_{1/2}$

VALUE ($GeV^{-1/2}$)	DOCUMENT ID		TECN	COMMENT
0.017 to 0.027 (≈ 0.022) OUR ESTIMATE				
0.032±0.008	SARANTSEV	25	DPWA	Multichannel
0.019±0.0076	GOLOVATCH	19	DPWA	$\gamma p \to \pi^+\pi^- p$
0.077±0.010	[1] HUNT	19	DPWA	Multichannel
0.020±0.002	[1] DUGGER	13	DPWA	$\gamma N \to \pi N$
0.019±0.002	[1] WORKMAN	12A	DPWA	$\gamma N \to \pi N$
• • • We do not use the following data for averages, fits, limits, etc. • • •				
0.025±0.005	SOKHOYAN	15A	DPWA	Multichannel
0.025±0.005	GUTZ	14	DPWA	Multichannel
0.066±0.018	[1] SHRESTHA	12A	DPWA	Multichannel
0.018	DRECHSEL	07	DPWA	$\gamma N \to \pi N$

[1] Statistical error only.

$\Delta(1905) \to N\gamma$, helicity-3/2 amplitude $A_{3/2}$

VALUE ($GeV^{-1/2}$)	DOCUMENT ID		TECN	COMMENT
−0.055 to −0.035 (≈ −0.045) OUR ESTIMATE				
−0.075 ±0.010	SARANTSEV	25	DPWA	Multichannel
−0.0432±0.0173	GOLOVATCH	19	DPWA	$\gamma p \to \pi^+\pi^- p$
−0.053 ±0.029	[1] HUNT	19	DPWA	Multichannel
−0.049 ±0.005	[1] DUGGER	13	DPWA	$\gamma N \to \pi N$
−0.038 ±0.004	WORKMAN	12A	DPWA	$\gamma N \to \pi N$
• • • We do not use the following data for averages, fits, limits, etc. • • •				
−0.050 ±0.005	SOKHOYAN	15A	DPWA	Multichannel
−0.050 ±0.005	GUTZ	14	DPWA	Multichannel
−0.223 ±0.029	[1] SHRESTHA	12A	DPWA	Multichannel
−0.028	DRECHSEL	07	DPWA	$\gamma N \to \pi N$

[1] Statistical error only.

$\Delta(1905)$ REFERENCES

For early references, see Physics Letters **11B** 1 (1982).

SARANTSEV	25	PR C112 015202	A.V. Sarantsev *et al.*	(Bonn-Gatchina Collab.)
SEIFEN	25	EPJ A61 173	T. Seifen *et al.*	(CBELSA/TAPS Collab.)
ROENCHEN	22	EPJ A58 229	D. Roenchen *et al.*	(JULI, GWU, BONN+)
GOLOVATCH	19	PL B788 371	E. Golovatch *et al.*	(CLAS Collab.)
HUNT	19	PR C99 055205	B.C. Hunt, D.M. Manley	
ROENCHEN	15A	EPJ A51 70	D. Roenchen *et al.*	
SOKHOYAN	15A	EPJ A51 95	V. Sokhoyan *et al.*	(CBELSA/TAPS Collab.)
GUTZ	14	EPJ A50 74	E. Gutz *et al.*	(CBELSA/TAPS Collab.)
PDG	14	CP C38 070001	K. Olive *et al.*	(PDG Collab.)
SVARC	14	PR C89 045205	A. Svarc *et al.*	(RBI Zagreb, UNI Tuzla)
DUGGER	13	PR C88 065203	M. Dugger *et al.*	(JLab CLAS Collab.)
ANISOVICH	12A	EPJ A48 15	A.V. Anisovich *et al.*	(BONN, PNPI)
SHRESTHA	12A	PR C86 055203	M. Shrestha, D.M. Manley	(KSU)
WORKMAN	12A	PR C86 015202	R. Workman *et al.*	(GWU)
DRECHSEL	07	EPJ A34 69	D. Drechsel, S.S. Kamalov, L. Tiator	(MAINZ, JINR)
ARNDT	06	PR C74 045205	R.A. Arndt *et al.*	(GWU)
VRANA	00	PRPL 328 181	T.P. Vrana, S.A. Dytman, T.-S.H. Lee	(PITT, ANL)
HOEHLER	93	πN Newsletter 9 1	G. Hohler	(KARL)
CUTKOSKY	80	Toronto Conf. 19	R.E. Cutkosky *et al.*	(CMU, LBL) IJP
Also		PR D20 2839	R.E. Cutkosky *et al.*	(CMU, LBL) IJP
HOEHLER	79	PDAT 12-1	G. Hohler *et al.*	(KARLT) IJP
Also		Toronto Conf. 3	R. Koch	(KARLT) IJP

$\Delta(1910)\ 1/2^+$

$I(J^P) = \frac{3}{2}(\frac{1}{2}^+)$ Status: ****

Older and obsolete values are listed and referenced in the 2014 edition, Chinese Physics **C38** 070001 (2014).

$\Delta(1910)$ POLE POSITION

REAL PART

VALUE (MeV)	DOCUMENT ID		TECN	COMMENT
1800 to 1900 (≈ 1850) OUR ESTIMATE				
1880±20	SARANTSEV	25	DPWA	Multichannel
1802± 6	ROENCHEN	22	DPWA	Multichannel
1896±11	[1] SVARC	14	L+P	$\pi N \to \pi N$
1880±30	CUTKOSKY	80	IPWA	$\pi N \to \pi N$
• • • We do not use the following data for averages, fits, limits, etc. • • •				
1801	HUNT	19	DPWA	Multichannel
1799	ROENCHEN	15A	DPWA	Multichannel
1840±40	SOKHOYAN	15A	DPWA	Multichannel
1840±40	GUTZ	14	DPWA	Multichannel
1771	ARNDT	06	DPWA	$\pi N \to \pi N, \eta N$
1880	VRANA	00	DPWA	Multichannel
1874	HOEHLER	93	SPED	$\pi N \to \pi N$

[1] Fit to the amplitudes of HOEHLER 79.

−2×IMAGINARY PART

VALUE (MeV)	DOCUMENT ID		TECN	COMMENT
200 to 500 (≈ 350) OUR ESTIMATE				
480±65	SARANTSEV	25	DPWA	Multichannel
550±11	ROENCHEN	22	DPWA	Multichannel
302±22	[1] SVARC	14	L+P	$\pi N \to \pi N$
200±40	CUTKOSKY	80	IPWA	$\pi N \to \pi N$
• • • We do not use the following data for averages, fits, limits, etc. • • •				
224	HUNT	19	DPWA	Multichannel
648	ROENCHEN	15A	DPWA	Multichannel
370±60	SOKHOYAN	15A	DPWA	Multichannel
370±60	GUTZ	14	DPWA	Multichannel
479	ARNDT	06	DPWA	$\pi N \to \pi N, \eta N$
496	VRANA	00	DPWA	Multichannel
283	HOEHLER	93	SPED	$\pi N \to \pi N$

[1] Fit to the amplitudes of HOEHLER 79.

$\Delta(1910)$ ELASTIC POLE RESIDUE

MODULUS $|r|$

VALUE (MeV)	DOCUMENT ID		TECN	COMMENT
20 to 30 (≈ 25) OUR ESTIMATE				
35±13	ROENCHEN	22	DPWA	Multichannel
25± 6	SOKHOYAN	15A	DPWA	Multichannel
29± 2	[1] SVARC	14	L+P	$\pi N \to \pi N$
20± 4	CUTKOSKY	80	IPWA	$\pi N \to \pi N$
• • • We do not use the following data for averages, fits, limits, etc. • • •				
90	ROENCHEN	15A	DPWA	Multichannel
25± 6	GUTZ	14	DPWA	Multichannel
24± 6	ANISOVICH	12A	DPWA	Multichannel
45	ARNDT	06	DPWA	$\pi N \to \pi N, \eta N$
38	HOEHLER	93	SPED	$\pi N \to \pi N$

[1] Fit to the amplitudes of HOEHLER 79.

PHASE θ

VALUE (°)	DOCUMENT ID		TECN	COMMENT
−180 to 90 (≈ −90) OUR ESTIMATE				
93± 7	ROENCHEN	22	DPWA	Multichannel
−155±30	SOKHOYAN	15A	DPWA	Multichannel
− 83± 4±1	[1] SVARC	14	L+P	$\pi N \to \pi N$
− 90±30	CUTKOSKY	80	IPWA	$\pi N \to \pi N$
• • • We do not use the following data for averages, fits, limits, etc. • • •				
− 83	ROENCHEN	15A	DPWA	Multichannel
−155±30	GUTZ	14	DPWA	Multichannel
−145±30	ANISOVICH	12A	DPWA	Multichannel
+172	ARNDT	06	DPWA	$\pi N \to \pi N, \eta N$

[1] Fit to the amplitudes of HOEHLER 79.

$\Delta(1910)$ INELASTIC POLE RESIDUE

The "normalized residue" is the residue divided by $\Gamma_{pole}/2$.

Normalized residue in $N\pi \to \Delta(1910) \to \Sigma K$

MODULUS	PHASE (°)	DOCUMENT ID		TECN	COMMENT
0.002±0.002	138 ± 10	ROENCHEN	22	DPWA	Multichannel
0.07 ±0.02	−110 ± 30	ANISOVICH	12A	DPWA	Multichannel
• • • We do not use the following data for averages, fits, limits, etc. • • •					
0.019	−123	ROENCHEN	15A	DPWA	Multichannel

Int. J. Mod. Phys. A 2026.41. Downloaded from www.worldscientific.com
by UNIVERSITY OF CALIFORNIA @ BERKELEY on 09/16/26. Re-use and distribution is strictly not permitted, except for Open Access articles.

Normalized residue in $N\pi \to \Delta(1910) \to \Delta\pi$, P-wave

MODULUS	PHASE (°)	DOCUMENT ID		TECN	COMMENT
0.24±0.09	−42 ± 7	ROENCHEN	22	DPWA	Multichannel
0.24±0.10	85 ± 35	SOKHOYAN	15A	DPWA	Multichannel
• • • We do not use the following data for averages, fits, limits, etc. • • •					
0.58	131	ROENCHEN	15A	DPWA	Multichannel
0.16±0.09	95 ± 40	ANISOVICH	12A	DPWA	Multichannel

Normalized residue in $N\pi \to \Delta(1910) \to \Delta(1232)\eta$

MODULUS	PHASE (°)	DOCUMENT ID		TECN	COMMENT
0.11±0.04	−150 ± 50	GUTZ	14	DPWA	Multichannel

Normalized residue in $N\pi \to \Delta(1910) \to N(1440)\pi$

MODULUS	PHASE (°)	DOCUMENT ID		TECN	COMMENT
0.06±0.03	170 ± 45	SOKHOYAN	15A	DPWA	Multichannel

$\Delta(1910)$ BREIT-WIGNER MASS

VALUE (MeV)	DOCUMENT ID		TECN	COMMENT
1850 to 1950 (≈ 1900) OUR ESTIMATE				
1890 ±20	SARANTSEV	25	DPWA	Multichannel
1846 ±18	[1] HUNT	19	DPWA	Multichannel
2067.9± 1.7	[1] ARNDT	06	DPWA	$\pi N \to \pi N, \eta N$
1910 ±40	CUTKOSKY	80	IPWA	$\pi N \to \pi N$
1888 ±20	HOEHLER	79	IPWA	$\pi N \to \pi N$
• • • We do not use the following data for averages, fits, limits, etc. • • •				
1845 ±40	SOKHOYAN	15A	DPWA	Multichannel
1845 ±40	GUTZ	14	DPWA	Multichannel
1934 ± 5	[1] SHRESTHA	12A	DPWA	Multichannel
1995 ±12	VRANA	00	DPWA	Multichannel

[1] Statistical error only.

$\Delta(1910)$ BREIT-WIGNER WIDTH

VALUE (MeV)	DOCUMENT ID		TECN	COMMENT
200 to 400 (≈ 300) OUR ESTIMATE				
520± 60	SARANTSEV	25	DPWA	Multichannel
260± 57	[1] HUNT	19	DPWA	Multichannel
543± 10	[1] ARNDT	06	DPWA	$\pi N \to \pi N, \eta N$
225± 50	CUTKOSKY	80	IPWA	$\pi N \to \pi N$
280± 50	HOEHLER	79	IPWA	$\pi N \to \pi N$
• • • We do not use the following data for averages, fits, limits, etc. • • •				
360± 60	SOKHOYAN	15A	DPWA	Multichannel
360± 60	GUTZ	14	DPWA	Multichannel
211± 11	[1] SHRESTHA	12A	DPWA	Multichannel
713±465	VRANA	00	DPWA	Multichannel

[1] Statistical error only.

$\Delta(1910)$ DECAY MODES

The following branching fractions are our estimates, not fits or averages.

	Mode	Fraction (Γ_i/Γ)
Γ_1	$N\pi$	10–30%
Γ_2	ΣK	4–14%
Γ_3	$N\pi\pi$	
Γ_4	$\Delta(1232)\pi$	34–66%
Γ_5	$N\rho$	(10 ±4) %
Γ_6	$N\rho$, $S=1/2$	(5.0±3.0) %
Γ_7	$N\rho$, $S=3/2$	(5.0±3.0) %
Γ_8	$N(1440)\pi$	3–45%
Γ_9	$N(1535)\pi$	(4.0±2.0) %
Γ_{10}	$\Delta(1232)\eta$	5–13%
Γ_{11}	$N\gamma$, helicity=1/2	0.0–0.02 %

$\Delta(1910)$ BRANCHING RATIOS

$\Gamma(N\pi)/\Gamma_{total}$ — Γ_1/Γ

VALUE (%)	DOCUMENT ID		TECN	COMMENT
10–30% OUR ESTIMATE				
16 ± 6	SEIFEN	25	DPWA	Multichannel
13 ± 3	[1] HUNT	19	DPWA	Multichannel
23.9± 0.1	[1] ARNDT	06	DPWA	$\pi N \to \pi N, \eta N$
19 ± 3	CUTKOSKY	80	IPWA	$\pi N \to \pi N$
24 ± 6	HOEHLER	79	IPWA	$\pi N \to \pi N$
• • • We do not use the following data for averages, fits, limits, etc. • • •				
12 ± 3	SOKHOYAN	15A	DPWA	Multichannel
12 ± 3	GUTZ	14	DPWA	Multichannel
17 ± 1	[1] SHRESTHA	12A	DPWA	Multichannel
29 ±21	VRANA	00	DPWA	Multichannel

[1] Statistical error only.

$\Gamma(\Sigma K)/\Gamma_{total}$ — Γ_2/Γ

VALUE (%)	DOCUMENT ID		TECN	COMMENT
4–14% OUR ESTIMATE				
9±5	ANISOVICH	12A	DPWA	Multichannel

$\Gamma(\Delta(1232)\pi)/\Gamma_{total}$ — Γ_4/Γ

VALUE (%)	DOCUMENT ID		TECN	COMMENT
34–66% OUR ESTIMATE				
74±10	SARANTSEV	25	DPWA	Multichannel
17± 9	SEIFEN	25	DPWA	Multichannel
• • • We do not use the following data for averages, fits, limits, etc. • • •				
50±16	SOKHOYAN	15A	DPWA	Multichannel

$\Gamma(N\rho)/\Gamma_{total}$ — Γ_5/Γ

VALUE (%)	DOCUMENT ID		TECN	COMMENT
10±4	SARANTSEV	25	DPWA	Multichannel

$\Gamma(N\rho, S=1/2)/\Gamma_{total}$ — Γ_6/Γ

VALUE (%)	DOCUMENT ID		TECN	COMMENT
5±3	SARANTSEV	25	DPWA	Multichannel

$\Gamma(N\rho, S=3/2)/\Gamma_{total}$ — Γ_7/Γ

VALUE (%)	DOCUMENT ID		TECN	COMMENT
5±3	SARANTSEV	25	DPWA	Multichannel

$\Gamma(N(1440)\pi)/\Gamma_{total}$ — Γ_8/Γ

VALUE (%)	DOCUMENT ID		TECN	COMMENT
3–45% OUR ESTIMATE				
40±15	SEIFEN	25	DPWA	Multichannel
33±12	[1] HUNT	19	DPWA	Multichannel
• • • We do not use the following data for averages, fits, limits, etc. • • •				
6± 3	SOKHOYAN	15A	DPWA	Multichannel
47± 6	[1] SHRESTHA	12A	DPWA	Multichannel
56± 7	VRANA	00	DPWA	Multichannel

[1] Statistical error only.

$\Gamma(N(1535)\pi)/\Gamma_{total}$ — Γ_9/Γ

VALUE (%)	DOCUMENT ID		TECN	COMMENT
4±2	SEIFEN	25	DPWA	Multichannel

$\Gamma(\Delta(1232)\eta)/\Gamma_{total}$ — Γ_{10}/Γ

VALUE (%)	DOCUMENT ID		TECN	COMMENT
5–13% OUR ESTIMATE				
9±4	GUTZ	14	DPWA	Multichannel

$\Delta(1910)$ PHOTON DECAY AMPLITUDES AT THE POLE

$\Delta(1910) \to N\gamma$, helicity-1/2 amplitude $A_{1/2}$

MODULUS ($GeV^{-1/2}$)	PHASE (°)	DOCUMENT ID		TECN	COMMENT
0.090±0.009	40 ± 40	SARANTSEV	25	DPWA	Multichannel
−0.446±0.036	−70 ± 11	ROENCHEN	22	DPWA	Multichannel
• • • We do not use the following data for averages, fits, limits, etc. • • •					
0.321	39	ROENCHEN	15A	DPWA	Multichannel
0.027±0.009	−30 ± 60	SOKHOYAN	15A	DPWA	Multichannel

$\Delta(1910)$ BREIT-WIGNER PHOTON DECAY AMPLITUDES

$\Delta(1910) \to N\gamma$, helicity-1/2 amplitude $A_{1/2}$

VALUE ($GeV^{-1/2}$)	DOCUMENT ID		TECN	COMMENT
0.010 to 0.030 (≈ 0.020) OUR ESTIMATE				
0.100±0.040	SARANTSEV	25	DPWA	Multichannel
0.203±0.056	[1] HUNT	19	DPWA	Multichannel
−0.002±0.008	[1] ARNDT	96	IPWA	$\gamma N \to \pi N$
• • • We do not use the following data for averages, fits, limits, etc. • • •				
0.026±0.008	SOKHOYAN	15A	DPWA	Multichannel
0.026±0.008	GUTZ	14	DPWA	Multichannel
0.030±0.002	[1] SHRESTHA	12A	DPWA	Multichannel

[1] Statistical error only.

$\Delta(1910)$ REFERENCES

For early references, see Physics Letters **111B** 1 (1982).

SARANTSEV	25	PR C112 015202	A.V. Sarantsev *et al.*	(Bonn-Gatchina Collab.)
SEIFEN	25	EPJ A61 173	T. Seifen *et al.*	(CBELSA/TAPS Collab.)
ROENCHEN	22	EPJ A58 229	D. Roenchen *et al.*	(JULI, GWU, BONN+)
HUNT	19	PR C99 055205	B.C. Hunt, D.M. Manley	
ROENCHEN	15A	EPJ A51 70	D. Roenchen *et al.*	
SOKHOYAN	15A	EPJ A51 95	V. Sokhoyan *et al.*	(CBELSA/TAPS Collab.)
GUTZ	14	EPJ A50 74	E. Gutz *et al.*	(CBELSA/TAPS Collab.)
PDG	14	CP C38 070001	K. Olive *et al.*	(PDG Collab.)
SVARC	14	PR C89 045205	A. Svarc *et al.*	(RBI Zagreb, UNI Tuzla)

ANISOVICH	12A	EPJ A48 15	A.V. Anisovich *et al.*	(BONN, PNPI)
SHRESTHA	12A	PR C86 055203	M. Shrestha, D.M. Manley	(KSU)
ARNDT	06	PR C74 045205	R.A. Arndt *et al.*	(GWU)
VRANA	00	PRPL 328 181	T.P. Vrana, S.A. Dytman, T.-S.H. Lee	(PITT, ANL)
ARNDT	96	PR C53 430	R.A. Arndt, I.I. Strakovsky, R.L. Workman	(VPI)
HOEHLER	93	πN Newsletter 9 1	G. Hohler	(KARL)
CUTKOSKY	80	Toronto Conf. 19	R.E. Cutkosky *et al.*	(CMU, LBL) IJP
Also		PR D20 2839	R.E. Cutkosky *et al.*	(CMU, LBL) IJP
HOEHLER	79	PDAT 12-1	G. Hohler *et al.*	(KARLT) IJP
Also		Toronto Conf. 3	R. Koch	(KARLT) IJP

$\Delta(1920)\ 3/2^+$

$I(J^P) = \frac{3}{2}(\frac{3}{2}^+)$ Status: ***

Older and obsolete values are listed and referenced in the 2014 edition, Chinese Physics **C38** 070001 (2014).

$\Delta(1920)$ POLE POSITION

REAL PART

VALUE (MeV)	DOCUMENT ID		TECN	COMMENT
1850 to 1950 (≈ 1900) OUR ESTIMATE				
1880±30	SARANTSEV	25	DPWA	Multichannel
1883± 2	ROENCHEN	22	DPWA	Multichannel
1906±10±2	[1] SVARC	14	L+P	$\pi N \to \pi N$
1900±80	CUTKOSKY	80	IPWA	$\pi N \to \pi N$
• • • We do not use the following data for averages, fits, limits, etc. • • •				
1910	HUNT	19	DPWA	Multichannel
1715	ROENCHEN	15A	DPWA	Multichannel
1875±30	SOKHOYAN	15A	DPWA	Multichannel
1875±30	GUTZ	14	DPWA	Multichannel
1880	VRANA	00	DPWA	Multichannel
1900	HOEHLER	93	SPED	$\pi N \to \pi N$

[1] Fit to the amplitudes of HOEHLER 79.

−2×IMAGINARY PART

VALUE (MeV)	DOCUMENT ID		TECN	COMMENT
200 to 400 (≈ 300) OUR ESTIMATE				
260± 40	SARANTSEV	25	DPWA	Multichannel
844± 5	ROENCHEN	22	DPWA	Multichannel
310± 20±11	[1] SVARC	14	L+P	$\pi N \to \pi N$
300±100	CUTKOSKY	80	IPWA	$\pi N \to \pi N$
• • • We do not use the following data for averages, fits, limits, etc. • • •				
472	HUNT	19	DPWA	Multichannel
882	ROENCHEN	15A	DPWA	Multichannel
300± 40	SOKHOYAN	15A	DPWA	Multichannel
300± 40	GUTZ	14	DPWA	Multichannel
120	VRANA	00	DPWA	Multichannel

[1] Fit to the amplitudes of HOEHLER 79.

$\Delta(1920)$ ELASTIC POLE RESIDUE

MODULUS $|r|$

VALUE (MeV)	DOCUMENT ID		TECN	COMMENT
15 to 35 (≈ 25) OUR ESTIMATE				
41±3	ROENCHEN	22	DPWA	Multichannel
16±6	SOKHOYAN	15A	DPWA	Multichannel
26±3±2	[1] SVARC	14	L+P	$\pi N \to \pi N$
24±4	CUTKOSKY	80	IPWA	$\pi N \to \pi N$
• • • We do not use the following data for averages, fits, limits, etc. • • •				
38	ROENCHEN	15A	DPWA	Multichannel
16±6	GUTZ	14	DPWA	Multichannel
17±8	ANISOVICH	12A	DPWA	Multichannel

[1] Fit to the amplitudes of HOEHLER 79.

PHASE θ

VALUE (°)	DOCUMENT ID		TECN	COMMENT
−150 to −50 (≈ − 100) OUR ESTIMATE				
11± 4	ROENCHEN	22	DPWA	Multichannel
− 50±25	SOKHOYAN	15A	DPWA	Multichannel
−130± 5±3	[1] SVARC	14	L+P	$\pi N \to \pi N$
−150±30	CUTKOSKY	80	IPWA	$\pi N \to \pi N$
• • • We do not use the following data for averages, fits, limits, etc. • • •				
146	ROENCHEN	15A	DPWA	Multichannel
− 50±25	GUTZ	14	DPWA	Multichannel
− 40±20	ANISOVICH	12A	DPWA	Multichannel

[1] Fit to the amplitudes of HOEHLER 79.

$\Delta(1920)$ INELASTIC POLE RESIDUE

The "normalized residue" is the residue divided by $\Gamma_{pole}/2$.

Normalized residue in $N\pi \to \Delta(1920) \to \Delta\eta$

MODULUS	PHASE (°)	DOCUMENT ID		TECN	COMMENT
0.15±0.04	70 ± 20	GUTZ	14	DPWA	Multichannel
• • • We do not use the following data for averages, fits, limits, etc. • • •					
0.17±0.08	70 ± 20	ANISOVICH	12A	DPWA	Multichannel

Normalized residue in $N\pi \to \Delta(1920) \to \Sigma K$

MODULUS	PHASE (°)	DOCUMENT ID		TECN	COMMENT
0.20±0.01	104 ± 2	ROENCHEN	22	DPWA	Multichannel
0.09±0.03	80 ± 40	ANISOVICH	12A	DPWA	Multichannel
• • • We do not use the following data for averages, fits, limits, etc. • • •					
0.17	−35	ROENCHEN	15A	DPWA	Multichannel

Normalized residue in $N\pi \to \Delta(1920) \to \Delta\pi$, P-wave

MODULUS	PHASE (°)	DOCUMENT ID		TECN	COMMENT
0.057±0.003	−48 ± 3	ROENCHEN	22	DPWA	Multichannel
0.20 ±0.08	−105 ± 25	SOKHOYAN	15A	DPWA	Multichannel
• • • We do not use the following data for averages, fits, limits, etc. • • •					
0.069	131	ROENCHEN	15A	DPWA	Multichannel
0.20 ±0.12	−120 ± 30	ANISOVICH	12A	DPWA	Multichannel

Normalized residue in $N\pi \to \Delta(1920) \to \Delta\pi$, F-wave

MODULUS	PHASE (°)	DOCUMENT ID		TECN	COMMENT
0.020±0.002	147 ± 4	ROENCHEN	22	DPWA	Multichannel
0.37 ±0.10	−90 ± 20	SOKHOYAN	15A	DPWA	Multichannel
• • • We do not use the following data for averages, fits, limits, etc. • • •					
0.013	−115	ROENCHEN	15A	DPWA	Multichannel
0.28 ±0.07	−95 ± 35	ANISOVICH	12A	DPWA	Multichannel

Normalized residue in $N\pi \to \Delta(1920) \to N(1535)\pi$

MODULUS	PHASE (°)	DOCUMENT ID		TECN	COMMENT
0.03±0.02	35 ± 45	GUTZ	14	DPWA	Multichannel

Normalized residue in $N\pi \to \Delta(1920) \to N a_0(980)$

MODULUS	PHASE (°)	DOCUMENT ID		TECN	COMMENT
0.03±0.02	−85 ± 45	GUTZ	14	DPWA	Multichannel

Normalized residue in $N\pi \to \Delta(1920) \to N(1440)\pi$

MODULUS	PHASE (°)	DOCUMENT ID		TECN	COMMENT
0.04±0.03	undefined	SOKHOYAN	15A	DPWA	Multichannel

Normalized residue in $N\pi \to \Delta(1920) \to N(1520)\pi$, S-wave

MODULUS	PHASE (°)	DOCUMENT ID		TECN	COMMENT
0.05±0.05	undefined	SOKHOYAN	15A	DPWA	Multichannel

$\Delta(1920)$ BREIT-WIGNER MASS

VALUE (MeV)	DOCUMENT ID		TECN	COMMENT
1870 to 1970 (≈ 1920) OUR ESTIMATE				
1890± 25	SARANTSEV	25	DPWA	Multichannel
1976± 49	HUNT	19	DPWA	Multichannel
2146± 32	[1] SHRESTHA	12A	DPWA	Multichannel
1920± 80	CUTKOSKY	80	IPWA	$\pi N \to \pi N$
1868± 10	HOEHLER	79	IPWA	$\pi N \to \pi N$
• • • We do not use the following data for averages, fits, limits, etc. • • •				
1880± 30	SOKHOYAN	15A	DPWA	Multichannel
1880± 30	GUTZ	14	DPWA	Multichannel
2057± 1	PENNER	02C	DPWA	Multichannel
1889±100	VRANA	00	DPWA	Multichannel

[1] Statistical error only.

$\Delta(1920)$ BREIT-WIGNER WIDTH

VALUE (MeV)	DOCUMENT ID		TECN	COMMENT
240 to 360 (≈ 300) OUR ESTIMATE				
280± 40	SARANTSEV	25	DPWA	Multichannel
509±170	HUNT	19	DPWA	Multichannel
400± 80	[1] SHRESTHA	12A	DPWA	Multichannel
300±100	CUTKOSKY	80	IPWA	$\pi N \to \pi N$
220± 80	HOEHLER	79	IPWA	$\pi N \to \pi N$
• • • We do not use the following data for averages, fits, limits, etc. • • •				
300± 40	SOKHOYAN	15A	DPWA	Multichannel
300± 40	GUTZ	14	DPWA	Multichannel
525± 32	PENNER	02C	DPWA	Multichannel
123± 53	VRANA	00	DPWA	Multichannel

[1] Statistical error only.

$\Delta(1920)$ DECAY MODES

The following branching fractions are our estimates, not fits or averages.

	Mode	Fraction (Γ_i/Γ)
Γ_1	$N\pi$	5–20 %
Γ_2	ΣK	2–6 %
Γ_3	$N\pi\pi$	>46 %
Γ_4	$\Delta(1232)\pi$	(38±15) %
Γ_5	$\Delta(1232)\pi$, P-wave	2–28 %
Γ_6	$\Delta(1232)\pi$, F-wave	44–72 %
Γ_7	$N\rho$	(57± 8) %

Int. J. Mod. Phys. A 2026.41. Downloaded from www.worldscientific.com
UNIVERSITY OF CALIFORNIA @ BERKELEY on 09/16/26. Re-use and distribution is strictly not permitted, except for Open Access articles.

Γ_8	$N\rho$, $S=1/2$	(8± 4) %
Γ_9	$N\rho$, $S=3/2$, P-wave	(14± 5) %
Γ_{10}	$N\rho$, $S=3/2$, F-wave	(35± 6) %
Γ_{11}	$N(1440)\pi$, P-wave	4–86 %
Γ_{12}	$N(1520)\pi$, S-wave	< 5 %
Γ_{13}	$N(1535)\pi$	< 2 %
Γ_{14}	$N a_0(980)$	seen
Γ_{15}	$\Delta(1232)\eta$	5–17 %
Γ_{16}	$N\gamma$	0.01–0.84 %
Γ_{17}	$N\gamma$, helicity=1/2	0.0–0.42 %
Γ_{18}	$N\gamma$, helicity=3/2	0.01–0.42 %

$\Delta(1920)$ BRANCHING RATIOS

$\Gamma(N\pi)/\Gamma_{total}$ — Γ_1/Γ

VALUE (%)	DOCUMENT ID		TECN	COMMENT
5–20 % OUR ESTIMATE				
12 ±6	SEIFEN	25	DPWA	Multichannel
10.5±3.0	[1] HUNT	19	DPWA	Multichannel
20 ±5	CUTKOSKY	80	IPWA	$\pi N \to \pi N$
14 ±4	HOEHLER	79	IPWA	$\pi N \to \pi N$
• • • We do not use the following data for averages, fits, limits, etc. • • •				
8 ±4	SOKHOYAN	15A	DPWA	Multichannel
8 ±4	GUTZ	14	DPWA	Multichannel
16 ±4	[1] SHRESTHA	12A	DPWA	Multichannel
15 ±1	PENNER	02C	DPWA	Multichannel
5 ±4	VRANA	00	DPWA	Multichannel

[1] Statistical error only.

$\Gamma(\Sigma K)/\Gamma_{total}$ — Γ_2/Γ

VALUE (%)	DOCUMENT ID		TECN	COMMENT
2–6 % OUR ESTIMATE				
4 ±2	ANISOVICH	12A	DPWA	Multichannel
• • • We do not use the following data for averages, fits, limits, etc. • • •				
2.1±0.3	PENNER	02C	DPWA	Multichannel

$\Gamma(\Delta(1232)\pi)/\Gamma_{total}$ — Γ_4/Γ

VALUE (%)	DOCUMENT ID		TECN	COMMENT
38±15	SARANTSEV	25	DPWA	Multichannel

$\Gamma(\Delta(1232)\pi, P\text{-wave})/\Gamma_{total}$ — Γ_5/Γ

VALUE (%)	DOCUMENT ID		TECN	COMMENT
2–28 % OUR ESTIMATE				
6 ± 4	SARANTSEV	25	DPWA	Multichannel
5 ± 4	SEIFEN	25	DPWA	Multichannel
< 1.6	[1] HUNT	19	DPWA	Multichannel
• • • We do not use the following data for averages, fits, limits, etc. • • •				
18 ±10	SOKHOYAN	15A	DPWA	Multichannel
7 ± 5	[1] SHRESTHA	12A	DPWA	Multichannel
41 ± 3	VRANA	00	DPWA	Multichannel

[1] Statistical error only.

$\Gamma(\Delta(1232)\pi, F\text{-wave})/\Gamma_{total}$ — Γ_6/Γ

VALUE (%)	DOCUMENT ID		TECN	COMMENT
44–72 % OUR ESTIMATE				
32±15	SARANTSEV	25	DPWA	Multichannel
40±20	SEIFEN	25	DPWA	Multichannel
• • • We do not use the following data for averages, fits, limits, etc. • • •				
58±14	SOKHOYAN	15A	DPWA	Multichannel

$\Gamma(N\rho)/\Gamma_{total}$ — Γ_7/Γ

VALUE (%)	DOCUMENT ID		TECN	COMMENT
57±8	SARANTSEV	25	DPWA	Multichannel

$\Gamma(N\rho, S=1/2)/\Gamma_{total}$ — Γ_8/Γ

VALUE (%)	DOCUMENT ID		TECN	COMMENT
8±4	SARANTSEV	25	DPWA	Multichannel

$\Gamma(N\rho, S=3/2, P\text{-wave})/\Gamma_{total}$ — Γ_9/Γ

VALUE (%)	DOCUMENT ID		TECN	COMMENT
14±5	SARANTSEV	25	DPWA	Multichannel

$\Gamma(N\rho, S=3/2, F\text{-wave})/\Gamma_{total}$ — Γ_{10}/Γ

VALUE (%)	DOCUMENT ID		TECN	COMMENT
35±6	SARANTSEV	25	DPWA	Multichannel

$\Gamma(N(1440)\pi, P\text{-wave})/\Gamma_{total}$ — Γ_{11}/Γ

VALUE (%)	DOCUMENT ID		TECN	COMMENT
4–86 % OUR ESTIMATE				
9±6	SEIFEN	25	DPWA	Multichannel
77±9	[1] HUNT	19	DPWA	Multichannel
• • • We do not use the following data for averages, fits, limits, etc. • • •				
< 4	SOKHOYAN	15A	DPWA	Multichannel
<20	[1] SHRESTHA	12A	DPWA	Multichannel
53±8	VRANA	00	DPWA	Multichannel

[1] Statistical error only.

$\Gamma(N(1520)\pi, S\text{-wave})/\Gamma_{total}$ — Γ_{12}/Γ

VALUE (%)	DOCUMENT ID		TECN	COMMENT
< 5 OUR ESTIMATE				
10±8	SEIFEN	25	DPWA	Multichannel
• • • We do not use the following data for averages, fits, limits, etc. • • •				
< 5	SOKHOYAN	15A	DPWA	Multichannel

$\Gamma(N(1535)\pi)/\Gamma_{total}$ — Γ_{13}/Γ

VALUE (%)	DOCUMENT ID		TECN	COMMENT
<2 OUR ESTIMATE				
5±5	SEIFEN	25	DPWA	Multichannel
<2	GUTZ	14	DPWA	Multichannel

$\Gamma(N a_0(980))/\Gamma_{total}$ — Γ_{14}/Γ

VALUE (%)	DOCUMENT ID		TECN	COMMENT
seen OUR ESTIMATE				
• • • We do not use the following data for averages, fits, limits, etc. • • •				
4±2	HORN	08A	DPWA	Multichannel

$\Gamma(\Delta(1232)\eta)/\Gamma_{total}$ — Γ_{15}/Γ

VALUE (%)	DOCUMENT ID		TECN	COMMENT
5–17 % OUR ESTIMATE				
11±6	GUTZ	14	DPWA	Multichannel
• • • We do not use the following data for averages, fits, limits, etc. • • •				
15±8	ANISOVICH	12A	DPWA	Multichannel

$\Delta(1920)$ PHOTON DECAY AMPLITUDES AT THE POLE

$\Delta(1920) \to N\gamma$, helicity-1/2 amplitude $A_{1/2}$

MODULUS ($GeV^{-1/2}$)	PHASE (°)	DOCUMENT ID		TECN	COMMENT
0.040±0.025	−30 ± 25	SARANTSEV	25	DPWA	Multichannel
0.138±0.006	−8.9 ± 2.0	ROENCHEN	22	DPWA	Multichannel
• • • We do not use the following data for averages, fits, limits, etc. • • •					
−0.192	46	ROENCHEN	15A	DPWA	Multichannel
0.110±0.030	−50 ± 20	SOKHOYAN	15A	DPWA	Multichannel

$\Delta(1920) \to N\gamma$, helicity-3/2 amplitude $A_{3/2}$

MODULUS ($GeV^{-1/2}$)	PHASE (°)	DOCUMENT ID		TECN	COMMENT
0.055±0.025	−50 ± 35	SARANTSEV	25	DPWA	Multichannel
0.252±0.007	14 ± 2	ROENCHEN	22	DPWA	Multichannel
• • • We do not use the following data for averages, fits, limits, etc. • • •					
0.522	67	ROENCHEN	15A	DPWA	Multichannel
−0.100±0.040	0 ± 20	SOKHOYAN	15A	DPWA	Multichannel

$\Delta(1920)$ BREIT-WIGNER PHOTON DECAY AMPLITUDES

$\Delta(1920) \to N\gamma$, helicity-1/2 amplitude $A_{1/2}$

VALUE ($GeV^{-1/2}$)	DOCUMENT ID		TECN	COMMENT
0.043±0.025	SARANTSEV	25	DPWA	Multichannel
−0.028±0.010	[1] HUNT	19	DPWA	Multichannel
• • • We do not use the following data for averages, fits, limits, etc. • • •				
0.110±0.030	SOKHOYAN	15A	DPWA	Multichannel
0.110±0.030	GUTZ	14	DPWA	Multichannel
0.051±0.010	[1] SHRESTHA	12A	DPWA	Multichannel
−0.007	PENNER	02D	DPWA	Multichannel

[1] Statistical error only.

$\Delta(1920) \to N\gamma$, helicity-3/2 amplitude $A_{3/2}$

VALUE ($GeV^{-1/2}$)	DOCUMENT ID		TECN	COMMENT
0.058±0.030	SARANTSEV	25	DPWA	Multichannel
−0.043±0.014	[1] HUNT	19	DPWA	Multichannel
• • • We do not use the following data for averages, fits, limits, etc. • • •				
−0.105±0.035	SOKHOYAN	15A	DPWA	Multichannel
−0.105±0.035	GUTZ	14	DPWA	Multichannel
0.017±0.015	[1] SHRESTHA	12A	DPWA	Multichannel
−0.001	PENNER	02D	DPWA	Multichannel

[1] Statistical error only.

Int. J. Mod. Phys. A 2026.41. Downloaded from www.worldscientific.com
by UNIVERSITY OF CALIFORNIA @ BERKELEY on 09/16/26. Re-use and distribution is strictly not permitted, except for Open Access articles.

Int. J. Mod. Phys. A 2026.41. Downloaded from www.worldscientific.com
UNIVERSITY OF CALIFORNIA @ BERKELEY on 09/16/26. Re-use and distribution is strictly not permitted, except for Open Access articles.

$\Delta(1920)$ REFERENCES

For early references, see Physics Letters **111B** 1 (1982).

SARANTSEV	25	PR C112 015202	A.V. Sarantsev *et al.*	(Bonn-Gatchina Collab.)
SEIFEN	25	EPJ A61 173	T. Seifen *et al.*	(CBELSA/TAPS Collab.)
ROENCHEN	22	EPJ A58 229	D. Roenchen *et al.*	(JULI, GWU, BONN+)
HUNT	19	PR C99 055205	B.C. Hunt, D.M. Manley	
ROENCHEN	15A	EPJ A51 70	D. Roenchen *et al.*	
SOKHOYAN	15A	EPJ A51 95	V. Sokhoyan *et al.*	(CBELSA/TAPS Collab.)
GUTZ	14	EPJ A50 74	E. Gutz *et al.*	(CBELSA/TAPS Collab.)
PDG	14	CP C38 070001	K. Olive *et al.*	(PDG Collab.)
SVARC	14	PR C89 045205	A. Svarc *et al.*	(RBI Zagreb, UNI Tuzla)
ANISOVICH	12A	EPJ A48 15	A.V. Anisovich *et al.*	(BONN, PNPI)
SHRESTHA	12A	PR C86 055203	M. Shrestha, D.M. Manley	(KSU)
HORN	08A	EPJ A38 173	I. Horn *et al.*	(CB-ELSA Collab.)
Also		PRL 101 202002	I. Horn *et al.*	(CB-ELSA Collab.)
PENNER	02C	PR C66 055211	G. Penner, U. Mosel	(GIES)
PENNER	02D	PR C66 055212	G. Penner, U. Mosel	(GIES)
VRANA	00	PRPL 328 181	T.P. Vrana, S.A. Dytman, T.-S.H. Lee	(PITT, ANL)
HOEHLER	93	πN Newsletter 9 1	G. Hohler	(KARL)
CUTKOSKY	80	Toronto Conf. 19	R.E. Cutkosky *et al.*	(CMU, LBL) IJP
Also		PR D20 2839	R.E. Cutkosky *et al.*	(CMU, LBL) IJP
HOEHLER	79	PDAT 12-1	G. Hohler *et al.*	(KARLT) IJP
Also		Toronto Conf. 3	R. Koch	(KARLT) IJP

$\Delta(1930)\ 5/2^-$

$I(J^P) = \frac{3}{2}(\frac{5}{2}^-)$ Status: ***

Older and obsolete values are listed and referenced in the 2014 edition, Chinese Physics **C38** 070001 (2014).

$\Delta(1930)$ POLE POSITION

REAL PART

VALUE (MeV)	DOCUMENT ID		TECN	COMMENT
1820 to 1880 ($\approx$ 1850) OUR ESTIMATE				
1812±10	SARANTSEV	25	DPWA	Multichannel
1821± 2	ROENCHEN	22	DPWA	Multichannel
1848± 9±19	[1] SVARC	14	L+P	$\pi N \to \pi N$
1890±50	CUTKOSKY	80	IPWA	$\pi N \to \pi N$
• • • We do not use the following data for averages, fits, limits, etc. • • •				
1863	HUNT	19	DPWA	Multichannel
1836	ROENCHEN	15A	DPWA	Multichannel
2001	ARNDT	06	DPWA	$\pi N \to \pi N, \eta N$
1883	VRANA	00	DPWA	Multichannel
1850	HOEHLER	93	SPED	$\pi N \to \pi N$

[1] Fit to the amplitudes of HOEHLER 79.

−2×IMAGINARY PART

VALUE (MeV)	DOCUMENT ID		TECN	COMMENT
300 to 450 ($\approx$ 320) OUR ESTIMATE				
420±25	SARANTSEV	25	DPWA	Multichannel
447± 7	ROENCHEN	22	DPWA	Multichannel
321±17±7	[1] SVARC	14	L+P	$\pi N \to \pi N$
260±60	CUTKOSKY	80	IPWA	$\pi N \to \pi N$
• • • We do not use the following data for averages, fits, limits, etc. • • •				
260	HUNT	19	DPWA	Multichannel
724	ROENCHEN	15A	DPWA	Multichannel
387	ARNDT	06	DPWA	$\pi N \to \pi N, \eta N$
250	VRANA	00	DPWA	Multichannel
180	HOEHLER	93	SPED	$\pi N \to \pi N$

[1] Fit to the amplitudes of HOEHLER 79.

$\Delta(1930)$ ELASTIC POLE RESIDUE

MODULUS $|r|$

VALUE (MeV)	DOCUMENT ID		TECN	COMMENT
8 to 20 ($\approx$ 14) OUR ESTIMATE				
15±2	ROENCHEN	22	DPWA	Multichannel
9±1±1	[1] SVARC	14	L+P	$\pi N \to \pi N$
18±6	CUTKOSKY	80	IPWA	$\pi N \to \pi N$
• • • We do not use the following data for averages, fits, limits, etc. • • •				
34	ROENCHEN	15A	DPWA	Multichannel
7	ARNDT	06	DPWA	$\pi N \to \pi N, \eta N$
20	HOEHLER	93	SPED	$\pi N \to \pi N$

[1] Fit to the amplitudes of HOEHLER 79.

PHASE θ

VALUE (°)	DOCUMENT ID		TECN	COMMENT
−100 to −10 ($\approx$ −50) OUR ESTIMATE				
−108± 5	ROENCHEN	22	DPWA	Multichannel
− 37± 3±7	[1] SVARC	14	L+P	$\pi N \to \pi N$
− 20±40	CUTKOSKY	80	IPWA	$\pi N \to \pi N$
• • • We do not use the following data for averages, fits, limits, etc. • • •				
−155	ROENCHEN	15A	DPWA	Multichannel
− 12	ARNDT	06	DPWA	$\pi N \to \pi N, \eta N$

[1] Fit to the amplitudes of HOEHLER 79.

$\Delta(1930)$ INELASTIC POLE RESIDUE

The "normalized residue" is the residue divided by $\Gamma_{pole}/2$.

Normalized residue in $N\pi \to \Delta(1930) \to \Sigma K$

MODULUS	PHASE (°)	DOCUMENT ID		TECN	COMMENT
0.010±0.001	**49 ± 5**	ROENCHEN	22	DPWA	Multichannel
• • • We do not use the following data for averages, fits, limits, etc. • • •					
0.043	−0.5	ROENCHEN	15A	DPWA	Multichannel

Normalized residue in $N\pi \to \Delta(1930) \to \Delta\pi$, D-wave

MODULUS	PHASE (°)	DOCUMENT ID		TECN	COMMENT
0.12±0.02	**64 ± 4**	ROENCHEN	22	DPWA	Multichannel
• • • We do not use the following data for averages, fits, limits, etc. • • •					
0.15	30	ROENCHEN	15A	DPWA	Multichannel

Normalized residue in $N\pi \to \Delta(1930) \to \Delta\pi$, G-wave

MODULUS	PHASE (°)	DOCUMENT ID		TECN	COMMENT
0.008±0.001	**148 ± 2**	ROENCHEN	22	DPWA	Multichannel
• • • We do not use the following data for averages, fits, limits, etc. • • •					
0.009	121	ROENCHEN	15A	DPWA	Multichannel

$\Delta(1930)$ BREIT-WIGNER MASS

VALUE (MeV)	DOCUMENT ID		TECN	COMMENT
1900 to 2000 ($\approx$ 1950) OUR ESTIMATE				
1834± 10	SARANTSEV	25	DPWA	Multichannel
1988± 32	[1] HUNT	19	DPWA	Multichannel
2233± 53	[1] ARNDT	06	DPWA	$\pi N \to \pi N, \eta N$
1940± 30	CUTKOSKY	80	IPWA	$\pi N \to \pi N$
1901± 15	HOEHLER	79	IPWA	$\pi N \to \pi N$
• • • We do not use the following data for averages, fits, limits, etc. • • •				
1930± 12	[1] SHRESTHA	12A	DPWA	Multichannel
1932±100	VRANA	00	DPWA	Multichannel

[1] Statistical error only.

$\Delta(1930)$ BREIT-WIGNER WIDTH

VALUE (MeV)	DOCUMENT ID		TECN	COMMENT
200 to 400 ($\approx$ 300) OUR ESTIMATE				
425± 25	SARANTSEV	25	DPWA	Multichannel
500±160	[1] HUNT	19	DPWA	Multichannel
773±187	ARNDT	06	DPWA	$\pi N \to \pi N, \eta N$
320± 60	CUTKOSKY	80	IPWA	$\pi N \to \pi N$
195± 60	HOEHLER	79	IPWA	$\pi N \to \pi N$
• • • We do not use the following data for averages, fits, limits, etc. • • •				
235± 39	[1] SHRESTHA	12A	DPWA	Multichannel
316±237	VRANA	00	DPWA	Multichannel

[1] Statistical error only.

$\Delta(1930)$ DECAY MODES

The following branching fractions are our estimates, not fits or averages.

	Mode	Fraction (Γ_i/Γ)
Γ_1	$N\pi$	5–15 %
Γ_2	$N\pi\pi$	
Γ_3	$\Delta(1232)\pi$	(33 ±9) %
Γ_4	$\Delta(1232)\pi$, D-wave	(28 ±7) %
Γ_5	$\Delta(1232)\pi$, G-wave	(5 ±5) %
Γ_6	$N\rho$	(33 ±8) %
Γ_7	$N\rho$, S=1/2	(3.0±2.0) %
Γ_8	$N\rho$, S=3/2 , G-wave	(30 ±8) %
Γ_9	$N\gamma$	0.0–0.01 %
Γ_{10}	$N\gamma$, helicity=1/2	0.0–0.005 %
Γ_{11}	$N\gamma$, helicity=3/2	0.0–0.004 %

$\Delta(1930)$ BRANCHING RATIOS

$\Gamma(N\pi)/\Gamma_{total}$ — Γ_1/Γ

VALUE (%)	DOCUMENT ID		TECN	COMMENT
5 to 15 ($\approx$ 10) OUR ESTIMATE				
9.5±0.1	[1] HUNT	19	DPWA	Multichannel
8.1±1.2	[1] ARNDT	06	DPWA	$\pi N \to \pi N, \eta N$
14 ±4	CUTKOSKY	80	IPWA	$\pi N \to \pi N$
4 ±3	HOEHLER	79	IPWA	$\pi N \to \pi N$
• • • We do not use the following data for averages, fits, limits, etc. • • •				
7.9±0.4	[1] SHRESTHA	12A	DPWA	Multichannel
9 ±8	VRANA	00	DPWA	Multichannel

[1] Statistical error only.

Int. J. Mod. Phys. A 2026.41. Downloaded from www.worldscientific.com
by UNIVERSITY OF CALIFORNIA @ BERKELEY on 09/16/26. Re-use and distribution is strictly not permitted, except for Open Access articles.

$\Gamma(\Delta(1232)\pi)/\Gamma_{total}$ — Γ_3/Γ

VALUE (%)	DOCUMENT ID		TECN	COMMENT
33±9	SARANTSEV	25	DPWA	Multichannel

$\Gamma(\Delta(1232)\pi, D\text{-wave})/\Gamma_{total}$ — Γ_4/Γ

VALUE (%)	DOCUMENT ID		TECN	COMMENT
28±7	SARANTSEV	25	DPWA	Multichannel

$\Gamma(\Delta(1232)\pi, G\text{-wave})/\Gamma_{total}$ — Γ_5/Γ

VALUE (%)	DOCUMENT ID		TECN	COMMENT
5±5	SARANTSEV	25	DPWA	Multichannel

$\Gamma(N\rho)/\Gamma_{total}$ — Γ_6/Γ

VALUE (%)	DOCUMENT ID		TECN	COMMENT
33±8	SARANTSEV	25	DPWA	Multichannel

$\Gamma(N\rho, S=1/2)/\Gamma_{total}$ — Γ_7/Γ

VALUE (%)	DOCUMENT ID		TECN	COMMENT
3±2	SARANTSEV	25	DPWA	Multichannel

$\Gamma(N\rho, S=3/2, G\text{-wave})/\Gamma_{total}$ — Γ_8/Γ

VALUE (%)	DOCUMENT ID		TECN	COMMENT
30±8	SARANTSEV	25	DPWA	Multichannel

$\Delta(1930)$ PHOTON DECAY AMPLITUDES AT THE POLE

$\Delta(1930) \to N\gamma$, helicity-1/2 amplitude $A_{1/2}$

MODULUS ($GeV^{-1/2}$)	PHASE (°)	DOCUMENT ID		TECN	COMMENT
0.036±0.008	117 ± 30	SARANTSEV	25	DPWA	Multichannel
0.104±0.009	129 ± 8	ROENCHEN	22	DPWA	Multichannel
• • • We do not use the following data for averages, fits, limits, etc. • • •					
−0.270	33	ROENCHEN	15A	DPWA	Multichannel

$\Delta(1930) \to N\gamma$, helicity-3/2 amplitude $A_{3/2}$

MODULUS ($GeV^{-1/2}$)	PHASE (°)	DOCUMENT ID		TECN	COMMENT
0.020±0.008	−150 ± 30	SARANTSEV	25	DPWA	Multichannel
0.322±0.022	142 ± 4	ROENCHEN	22	DPWA	Multichannel
• • • We do not use the following data for averages, fits, limits, etc. • • •					
0.153	81	ROENCHEN	15A	DPWA	Multichannel

$\Delta(1930)$ BREIT-WIGNER PHOTON DECAY AMPLITUDES

$\Delta(1930) \to N\gamma$, helicity-1/2 amplitude $A_{1/2}$

VALUE ($GeV^{-1/2}$)	DOCUMENT ID		TECN	COMMENT
−0.037±0.008	SARANTSEV	25	DPWA	Multichannel
−0.043±0.008	[1] HUNT	19	DPWA	Multichannel
−0.007±0.010	[1] ARNDT	96	IPWA	$\gamma N \to \pi N$
• • • We do not use the following data for averages, fits, limits, etc. • • •				
0.011±0.003	[1] SHRESTHA	12A	DPWA	Multichannel

[1] Statistical error only.

$\Delta(1930) \to N\gamma$, helicity-3/2 amplitude $A_{3/2}$

VALUE ($GeV^{-1/2}$)	DOCUMENT ID		TECN	COMMENT
−0.020±0.008	SARANTSEV	25	DPWA	Multichannel
−0.020±0.017	[1] HUNT	19	DPWA	Multichannel
0.005±0.010	[1] ARNDT	96	IPWA	$\gamma N \to \pi N$
• • • We do not use the following data for averages, fits, limits, etc. • • •				
0.002±0.002	[1] SHRESTHA	12A	DPWA	Multichannel

[1] Statistical error only.

$\Delta(1930)$ REFERENCES

For early references, see Physics Letters **111B** 1 (1982).

SARANTSEV	25	PR C112 015202	A.V. Sarantsev *et al.*	(Bonn-Gatchina Collab.)
ROENCHEN	22	EPJ A58 229	D. Roenchen *et al.*	(JULI, GWU, BONN+)
HUNT	19	PR C99 055205	B.C. Hunt, D.M. Manley	
ROENCHEN	15A	EPJ A51 70	D. Roenchen *et al.*	
PDG	14	CP C38 070001	K. Olive *et al.*	(PDG Collab.)
SVARC	14	PR C89 045205	A. Svarc *et al.*	(RBI Zagreb, UNI Tuzla)
SHRESTHA	12A	PR C86 055203	M. Shrestha, D.M. Manley	(KSU)
ARNDT	06	PR C74 045205	R.A. Arndt *et al.*	(GWU)
VRANA	00	PRPL 328 181	T.P. Vrana, S.A. Dytman, T.-S.H. Lee	(PITT, ANL)
ARNDT	96	PR C53 430	R.A. Arndt, I.I. Strakovsky, R.L. Workman	(VPI)
HOEHLER	93	πN Newsletter 9 1	G. Hohler	(KARL)
CUTKOSKY	80	Toronto Conf. 19	R.E. Cutkosky *et al.*	(CMU, LBL) IJP
Also		PR D20 2839	R.E. Cutkosky *et al.*	(CMU, LBL) IJP
HOEHLER	79	PDAT 12-1	G. Hohler *et al.*	(KARLT) IJP
Also		Toronto Conf. 3	R. Koch	(KARLT) IJP

$\Delta(1940)\ 3/2^-$

$I(J^P) = \frac{3}{2}(\frac{3}{2}^-)$ Status: **

OMITTED FROM SUMMARY TABLE

$\Delta(1940)$ POLE POSITION

REAL PART

VALUE (MeV)	DOCUMENT ID		TECN	COMMENT
1850 to 2050 (≈ 1950) OUR ESTIMATE				
2040± 40	SARANTSEV	25	DPWA	Multichannel
1878± 11±5.5	[1] SVARC	14	L+P	$\pi N \to \pi N$
1900±100	CUTKOSKY	80	IPWA	$\pi N \to \pi N$
• • • We do not use the following data for averages, fits, limits, etc. • • •				
2139	HUNT	19	DPWA	Multichannel
2040± 50	SOKHOYAN	15A	DPWA	Multichannel
2040± 50	GUTZ	14	DPWA	Multichannel

[1] Fit to the amplitudes of HOEHLER 79.

−2×IMAGINARY PART

VALUE (MeV)	DOCUMENT ID		TECN	COMMENT
200 to 500 (≈ 350) OUR ESTIMATE				
450±50	SARANTSEV	25	DPWA	Multichannel
212±21±6	[1] SVARC	14	L+P	$\pi N \to \pi N$
200±60	CUTKOSKY	80	IPWA	$\pi N \to \pi N$
• • • We do not use the following data for averages, fits, limits, etc. • • •				
400	HUNT	19	DPWA	Multichannel
450±90	SOKHOYAN	15A	DPWA	Multichannel
450±90	GUTZ	14	DPWA	Multichannel

[1] Fit to the amplitudes of HOEHLER 79.

$\Delta(1940)$ ELASTIC POLE RESIDUE

MODULUS $|r|$

VALUE (MeV)	DOCUMENT ID		TECN	COMMENT
4 to 10 (≈ 7) OUR ESTIMATE				
6±3	SOKHOYAN	15A	DPWA	Multichannel
9±1±1	[1] SVARC	14	L+P	$\pi N \to \pi N$
8±3	CUTKOSKY	80	IPWA	$\pi N \to \pi N$
• • • We do not use the following data for averages, fits, limits, etc. • • •				
4±3	GUTZ	14	DPWA	Multichannel
4±4	ANISOVICH	12A	DPWA	Multichannel

[1] Fit to the amplitudes of HOEHLER 79.

PHASE θ

VALUE (°)	DOCUMENT ID		TECN	COMMENT
150 to 250 (≈ 200) OUR ESTIMATE				
− 90±35	SOKHOYAN	15A	DPWA	Multichannel
140± 7±7	[1] SVARC	14	L+P	$\pi N \to \pi N$
135±45	CUTKOSKY	80	IPWA	$\pi N \to \pi N$
• • • We do not use the following data for averages, fits, limits, etc. • • •				
− 50±35	GUTZ	14	DPWA	Multichannel

[1] Fit to the amplitudes of HOEHLER 79.

$\Delta(1940)$ INELASTIC POLE RESIDUE

The "normalized residue" is the residue divided by $\Gamma_{pole}/2$.

Normalized residue in $N\pi \to \Delta(1940) \to \Delta(1232)\eta$

MODULUS	PHASE (°)	DOCUMENT ID		TECN	COMMENT
<0.01	undefined	GUTZ	14	DPWA	Multichannel

Normalized residue in $N\pi \to \Delta(1940) \to N(1535)\pi$

MODULUS	PHASE (°)	DOCUMENT ID		TECN	COMMENT
<0.03	undefined	GUTZ	14	DPWA	Multichannel

Normalized residue in $N\pi \to \Delta(1940) \to \Delta(1232)\pi$, S-wave

MODULUS	PHASE (°)	DOCUMENT ID		TECN	COMMENT
0.12±0.06	120 ± 45	SOKHOYAN	15A	DPWA	Multichannel

Normalized residue in $N\pi \to \Delta(1940) \to \Delta(1232)\pi$, D-wave

MODULUS	PHASE (°)	DOCUMENT ID		TECN	COMMENT
0.06±0.04	−80 ± 35	SOKHOYAN	15A	DPWA	Multichannel

$\Delta(1940)$ BREIT-WIGNER MASS

VALUE (MeV)	DOCUMENT ID		TECN	COMMENT
1940 to 2060 (≈ 2000) OUR ESTIMATE				
2060± 40	SARANTSEV	25	DPWA	Multichannel
2137± 13	[1] HUNT	19	DPWA	Multichannel
1940±100	CUTKOSKY	80	IPWA	$\pi N \to \pi N$
• • • We do not use the following data for averages, fits, limits, etc. • • •				
2050± 40	SOKHOYAN	15A	DPWA	Multichannel
2050± 40	GUTZ	14	DPWA	Multichannel

[1] Statistical error only.

$\Delta(1940)$ BREIT-WIGNER WIDTH

VALUE (MeV)	DOCUMENT ID		TECN	COMMENT
300 to 500 ($\approx$ 400) OUR ESTIMATE				
460 ± 50	SARANTSEV	25	DPWA	Multichannel
400 ± 43	[1] HUNT	19	DPWA	Multichannel
200 ± 100	CUTKOSKY	80	IPWA	$\pi N \to \pi N$
• • • We do not use the following data for averages, fits, limits, etc. • • •				
450 ± 70	SOKHOYAN	15A	DPWA	Multichannel
450 ± 70	GUTZ	14	DPWA	Multichannel

[1] Statistical error only.

$\Delta(1940)$ DECAY MODES

	Mode	Fraction (Γ_i/Γ)
Γ_1	$N\pi$	1–20 %
Γ_2	$N\pi\pi$	>81 %
Γ_3	$\Delta(1232)\pi$	(38±10) %
Γ_4	$\Delta(1232)\pi$, S-wave	1–65 %
Γ_5	$\Delta(1232)\pi$, D-wave	5–20 %
Γ_6	$N\rho$	(24± 6) %
Γ_7	$N\rho$, S=1/2	(6± 4) %
Γ_8	$N\rho$, S=3/2 , S-wave	75–85 %
Γ_9	$N\rho$, S=3/2 , D-wave	(8± 4) %
Γ_{10}	$N(1440)\pi$	(5± 5) %
Γ_{11}	$N(1520)\pi$, P-wave	(7± 5) %
Γ_{12}	$N(1535)\pi$	2–14 %
Γ_{13}	$N a_0(980)$	seen
Γ_{14}	$\Delta(1232)\eta$	4–16 %
Γ_{15}	$N\gamma$	0.06–2.53 %
Γ_{16}	$N\gamma$, helicity=1/2	0.06–1.51 %
Γ_{17}	$N\gamma$, helicity=3/2	0–1.02 %

$\Delta(1940)$ BRANCHING RATIOS

$\Gamma(N\pi)/\Gamma_{total}$ — Γ_1/Γ

VALUE (%)	DOCUMENT ID		TECN	COMMENT
1–20 % OUR ESTIMATE				
13±6	SEIFEN	25	DPWA	Multichannel
16±4	[1] HUNT	19	DPWA	Multichannel
5±2	CUTKOSKY	80	IPWA	$\pi N \to \pi N$
• • • We do not use the following data for averages, fits, limits, etc. • • •				
2±1	SOKHOYAN	15A	DPWA	Multichannel
2±1	GUTZ	14	DPWA	Multichannel

[1] Statistical error only.

$\Gamma(\Delta(1232)\pi)/\Gamma_{total}$ — Γ_3/Γ

VALUE (%)	DOCUMENT ID		TECN	COMMENT
38±10	SARANTSEV	25	DPWA	Multichannel

$\Gamma(\Delta(1232)\pi, S\text{-wave})/\Gamma_{total}$ — Γ_4/Γ

VALUE (%)	DOCUMENT ID		TECN	COMMENT
1–65 % OUR ESTIMATE				
21 ± 8	SARANTSEV	25	DPWA	Multichannel
16 ± 6	SEIFEN	25	DPWA	Multichannel
< 0.9	[1] HUNT	19	DPWA	Multichannel
• • • We do not use the following data for averages, fits, limits, etc. • • •				
46 ±20	SOKHOYAN	15A	DPWA	Multichannel

[1] Statistical error only.

$\Gamma(\Delta(1232)\pi, D\text{-wave})/\Gamma_{total}$ — Γ_5/Γ

VALUE (%)	DOCUMENT ID		TECN	COMMENT
5–20 % OUR ESTIMATE				
17 ± 9	SARANTSEV	25	DPWA	Multichannel
30 ±12	SEIFEN	25	DPWA	Multichannel
< 6.3	[1] HUNT	19	DPWA	Multichannel
• • • We do not use the following data for averages, fits, limits, etc. • • •				
12 ± 7	SOKHOYAN	15A	DPWA	Multichannel

[1] Statistical error only.

$\Gamma(N\rho)/\Gamma_{total}$ — Γ_6/Γ

VALUE (%)	DOCUMENT ID		TECN	COMMENT
24±6	SARANTSEV	25	DPWA	Multichannel

$\Gamma(N\rho, S=1/2)/\Gamma_{total}$ — Γ_7/Γ

VALUE (%)	DOCUMENT ID		TECN	COMMENT
6±4	SARANTSEV	25	DPWA	Multichannel

$\Gamma(N\rho, S=3/2, S\text{-wave})/\Gamma_{total}$ — Γ_8/Γ

VALUE (%)	DOCUMENT ID		TECN	COMMENT
75–85 % OUR ESTIMATE				
10±5	SARANTSEV	25	DPWA	Multichannel
80±5	[1] HUNT	19	DPWA	Multichannel

[1] Statistical error only.

$\Gamma(N\rho, S=3/2, D\text{-wave})/\Gamma_{total}$ — Γ_9/Γ

VALUE (%)	DOCUMENT ID		TECN	COMMENT
8±4	SARANTSEV	25	DPWA	Multichannel

$\Gamma(N(1440)\pi)/\Gamma_{total}$ — Γ_{10}/Γ

VALUE (%)	DOCUMENT ID		TECN	COMMENT
5±5	SEIFEN	25	DPWA	Multichannel

$\Gamma(N(1520)\pi, P\text{-wave})/\Gamma_{total}$ — Γ_{11}/Γ

VALUE (%)	DOCUMENT ID		TECN	COMMENT
7±5	SEIFEN	25	DPWA	Multichannel

$\Gamma(N(1535)\pi)/\Gamma_{total}$ — Γ_{12}/Γ

VALUE (%)	DOCUMENT ID		TECN	COMMENT
2–14 % OUR ESTIMATE				
20±13	SEIFEN	25	DPWA	Multichannel
8± 6	GUTZ	14	DPWA	Multichannel
• • • We do not use the following data for averages, fits, limits, etc. • • •				
2± 1	HORN	08A	DPWA	Multichannel

$\Gamma(N a_0(980))/\Gamma_{total}$ — Γ_{13}/Γ

VALUE (%)	DOCUMENT ID		TECN	COMMENT
seen OUR ESTIMATE				
• • • We do not use the following data for averages, fits, limits, etc. • • •				
2±1	HORN	08A	DPWA	Multichannel

$\Gamma(\Delta(1232)\eta)/\Gamma_{total}$ — Γ_{14}/Γ

VALUE (%)	DOCUMENT ID		TECN	COMMENT
4–16 % OUR ESTIMATE				
10±6	GUTZ	14	DPWA	Multichannel
• • • We do not use the following data for averages, fits, limits, etc. • • •				
4±2	HORN	08A	DPWA	Multichannel

$\Delta(1940)$ PHOTON DECAY AMPLITUDES AT THE POLE

$\Delta(1940) \to N\gamma$, helicity-1/2 amplitude $A_{1/2}$

MODULUS ($GeV^{-1/2}$)	PHASE (°)	DOCUMENT ID		TECN	COMMENT
0.045±0.025	−40 ± 30	SARANTSEV	25	DPWA	Multichannel
• • • We do not use the following data for averages, fits, limits, etc. • • •					
$0.170^{+0.120}_{-0.100}$	−10 ± 30	SOKHOYAN	15A	DPWA	Multichannel

$\Delta(1940) \to N\gamma$, helicity-3/2 amplitude $A_{3/2}$

MODULUS ($GeV^{-1/2}$)	PHASE (°)	DOCUMENT ID		TECN	COMMENT
0.080±0.030	−75 ± 30	SARANTSEV	25	DPWA	Multichannel
• • • We do not use the following data for averages, fits, limits, etc. • • •					
0.150±0.080	−10 ± 30	SOKHOYAN	15A	DPWA	Multichannel

$\Delta(1940)$ BREIT-WIGNER PHOTON DECAY AMPLITUDES

$\Delta(1940) \to N\gamma$, helicity-1/2 amplitude $A_{1/2}$

VALUE ($GeV^{-1/2}$)	DOCUMENT ID		TECN	COMMENT
0.052 ±0.025	SARANTSEV	25	DPWA	Multichannel
0.1614±0.0031	[1] HUNT	19	DPWA	Multichannel
• • • We do not use the following data for averages, fits, limits, etc. • • •				
$0.170\ ^{+0.110}_{-0.080}$	SOKHOYAN	15A	DPWA	Multichannel
$0.170\ ^{+0.110}_{-0.080}$	GUTZ	14	DPWA	Multichannel

[1] Statistical error only.

$\Delta(1940) \to N\gamma$, helicity-3/2 amplitude $A_{3/2}$

VALUE ($GeV^{-1/2}$)	DOCUMENT ID		TECN	COMMENT
0.095±0.030	SARANTSEV	25	DPWA	Multichannel
−0.209±0.023	[1] HUNT	19	DPWA	Multichannel
• • • We do not use the following data for averages, fits, limits, etc. • • •				
0.150±0.080	SOKHOYAN	15A	DPWA	Multichannel
0.150±0.080	GUTZ	14	DPWA	Multichannel

[1] Statistical error only.

Int. J. Mod. Phys. A 2026.41. Downloaded from www.worldscientific.com
UNIVERSITY OF CALIFORNIA @ BERKELEY on 09/16/26. Re-use and distribution is strictly not permitted, except for Open Access articles.

Int. J. Mod. Phys. A 2026.41. Downloaded from www.worldscientific.com
by UNIVERSITY OF CALIFORNIA @ BERKELEY on 09/16/26. Re-use and distribution is strictly not permitted, except for Open Access articles.

$\Delta(1940)$ REFERENCES

SARANTSEV	25	PR C112 015202	A.V. Sarantsev *et al.*	(Bonn-Gatchina Collab.)
SEIFEN	25	EPJ A61 173	T. Seifen *et al.*	(CBELSA/TAPS Collab.)
HUNT	19	PR C99 055205	B.C. Hunt, D.M. Manley	
SOKHOYAN	15A	EPJ A51 95	V. Sokhoyan *et al.*	(CBELSA/TAPS Collab.)
GUTZ	14	EPJ A50 74	E. Gutz *et al.*	(CBELSA/TAPS Collab.)
SVARC	14	PR C89 045205	A. Svarc *et al.*	(RBI Zagreb, UNI Tuzla)
ANISOVICH	12A	EPJ A48 15	A.V. Anisovich *et al.*	(BONN, PNPI)
HORN	08A	EPJ A38 173	I. Horn *et al.*	(CB-ELSA Collab.)
Also		PRL 101 202002	I. Horn *et al.*	(CB-ELSA Collab.)
CUTKOSKY	80	Toronto Conf. 19	R.E. Cutkosky *et al.*	(CMU, LBL) IJP
Also		PR D20 2839	R.E. Cutkosky *et al.*	(CMU, LBL)
HOEHLER	79	PDAT 12-1	G. Hohler *et al.*	(KARLT)

$\Delta(1950)\ 7/2^+$

$I(J^P) = \frac{3}{2}(\frac{7}{2}^+)$ Status: ****

Older and obsolete values are listed and referenced in the 2014 edition, Chinese Physics **C38** 070001 (2014).

$\Delta(1950)$ POLE POSITION

REAL PART

VALUE (MeV)	DOCUMENT ID		TECN	COMMENT
1870 to 1890 (≈ 1880) OUR ESTIMATE				
1892± 5	SARANTSEV	25	DPWA	Multichannel
1875± 1	ROENCHEN	22	DPWA	Multichannel
1877± 2±1	[1] SVARC	14	L+P	$\pi N \to \pi N$
1890±15	CUTKOSKY	80	IPWA	$\pi N \to \pi N$
• • • We do not use the following data for averages, fits, limits, etc. • • •				
1871	HUNT	19	DPWA	Multichannel
1874	ROENCHEN	15A	DPWA	Multichannel
1888± 4	SOKHOYAN	15A	DPWA	Multichannel
1888± 4	GUTZ	14	DPWA	Multichannel
1876	ARNDT	06	DPWA	$\pi N \to \pi N, \eta N$
1910	VRANA	00	DPWA	Multichannel
1878	HOEHLER	93	ARGD	$\pi N \to \pi N$

[1] Fit to the amplitudes of HOEHLER 79.

−2×IMAGINARY PART

VALUE (MeV)	DOCUMENT ID		TECN	COMMENT
220 to 260 (≈ 240) OUR ESTIMATE				
250±10	SARANTSEV	25	DPWA	Multichannel
166± 2	ROENCHEN	22	DPWA	Multichannel
223± 4±1	[1] SVARC	14	L+P	$\pi N \to \pi N$
260±40	CUTKOSKY	80	IPWA	$\pi N \to \pi N$
• • • We do not use the following data for averages, fits, limits, etc. • • •				
206	HUNT	19	DPWA	Multichannel
239	ROENCHEN	15A	DPWA	Multichannel
245± 8	SOKHOYAN	15A	DPWA	Multichannel
245± 8	GUTZ	14	DPWA	Multichannel
227	ARNDT	06	DPWA	$\pi N \to \pi N, \eta N$
230	VRANA	00	DPWA	Multichannel
230	HOEHLER	93	ARGD	$\pi N \to \pi N$

[1] Fit to the amplitudes of HOEHLER 79.

$\Delta(1950)$ ELASTIC POLE RESIDUE

MODULUS $|r|$

VALUE (MeV)	DOCUMENT ID		TECN	COMMENT
44 to 60 (≈ 52) OUR ESTIMATE				
27±1	ROENCHEN	22	DPWA	Multichannel
58±2	SOKHOYAN	15A	DPWA	Multichannel
44±1	[1] SVARC	14	L+P	$\pi N \to \pi N$
50±7	CUTKOSKY	80	IPWA	$\pi N \to \pi N$
• • • We do not use the following data for averages, fits, limits, etc. • • •				
56	ROENCHEN	15A	DPWA	Multichannel
58±2	GUTZ	14	DPWA	Multichannel
58±2	ANISOVICH	12A	DPWA	Multichannel
53	ARNDT	06	DPWA	$\pi N \to \pi N, \eta N$
47	HOEHLER	93	ARGD	$\pi N \to \pi N$

[1] Fit to the amplitudes of HOEHLER 79.

PHASE θ

VALUE (°)	DOCUMENT ID		TECN	COMMENT
−40 to −24 (≈ −32) OUR ESTIMATE				
1.1±1.0	ROENCHEN	22	DPWA	Multichannel
−24 ±3	SOKHOYAN	15A	DPWA	Multichannel
−39 ±1 ±1	[1] SVARC	14	L+P	$\pi N \to \pi N$
−33 ±8	CUTKOSKY	80	IPWA	$\pi N \to \pi N$
• • • We do not use the following data for averages, fits, limits, etc. • • •				
−33	ROENCHEN	15A	DPWA	Multichannel
−24 ±3	GUTZ	14	DPWA	Multichannel
−24 ±3	ANISOVICH	12A	DPWA	Multichannel
−31	ARNDT	06	DPWA	$\pi N \to \pi N, \eta N$
−32	HOEHLER	93	ARGD	$\pi N \to \pi N$

[1] Fit to the amplitudes of HOEHLER 79.

$\Delta(1950)$ INELASTIC POLE RESIDUE

The "normalized residue" is the residue divided by $\Gamma_{pole}/2$.

Normalized residue in $N\pi \to \Delta(1950) \to \Sigma K$

MODULUS	PHASE (°)	DOCUMENT ID		TECN	COMMENT
0.020±0.002	−40 ± 4	ROENCHEN	22	DPWA	Multichannel
0.05 ±0.01	−65 ± 25	ANISOVICH	12A	DPWA	Multichannel
• • • We do not use the following data for averages, fits, limits, etc. • • •					
0.031	−87	ROENCHEN	15A	DPWA	Multichannel

Normalized residue in $N\pi \to \Delta(1950) \to \Delta\pi$, F-wave

MODULUS	PHASE (°)	DOCUMENT ID		TECN	COMMENT
0.30±0.27	166 ± 1	ROENCHEN	22	DPWA	Multichannel
0.12±0.04	undefined	SOKHOYAN	15A	DPWA	Multichannel
• • • We do not use the following data for averages, fits, limits, etc. • • •					
0.54	131	ROENCHEN	15A	DPWA	Multichannel
0.12±0.04	12 ± 10	ANISOVICH	12A	DPWA	Multichannel

Normalized residue in $N\pi \to \Delta(1950) \to \Delta\pi$, H-wave

MODULUS	PHASE (°)	DOCUMENT ID		TECN	COMMENT
0.051±0.004	−11 ± 1	ROENCHEN	22	DPWA	Multichannel
• • • We do not use the following data for averages, fits, limits, etc. • • •					
0.033	−97	ROENCHEN	15A	DPWA	Multichannel

Normalized residue in $N\pi \to \Delta(1950) \to \Delta(1232)\eta$

MODULUS	PHASE (°)	DOCUMENT ID		TECN	COMMENT
0.035±0.005	90 ± 25	GUTZ	14	DPWA	Multichannel

$\Delta(1950)$ BREIT-WIGNER MASS

VALUE (MeV)	DOCUMENT ID		TECN	COMMENT
1915 to 1950 (≈ 1930) OUR ESTIMATE				
1919 ± 5	SARANTSEV	25	DPWA	Multichannel
1943 ±18	GOLOVATCH	19	DPWA	$\gamma p \to \pi^+\pi^- p$
1913 ± 4	[1] HUNT	19	DPWA	Multichannel
1921.3± 0.2	[1] ARNDT	06	DPWA	$\pi N \to \pi N, \eta N$
1950 ±15	CUTKOSKY	80	IPWA	$\pi N \to \pi N$
1913 ± 8	HOEHLER	79	IPWA	$\pi N \to \pi N$
• • • We do not use the following data for averages, fits, limits, etc. • • •				
1917 ± 4	SOKHOYAN	15A	DPWA	Multichannel
1917 ± 4	GUTZ	14	DPWA	Multichannel
1918 ± 1	[1] SHRESTHA	12A	DPWA	Multichannel
1936 ± 5	VRANA	00	DPWA	Multichannel

[1] Statistical error only.

$\Delta(1950)$ BREIT-WIGNER WIDTH

VALUE (MeV)	DOCUMENT ID		TECN	COMMENT
235 to 335 (≈ 285) OUR ESTIMATE				
258 ± 8	SARANTSEV	25	DPWA	Multichannel
230 ±88	GOLOVATCH	19	DPWA	$\gamma p \to \pi^+\pi^- p$
241 ±10	[1] HUNT	19	DPWA	Multichannel
271.1± 1.1	[1] ARNDT	06	DPWA	$\pi N \to \pi N, \eta N$
340 ±50	CUTKOSKY	80	IPWA	$\pi N \to \pi N$
224 ±10	HOEHLER	79	IPWA	$\pi N \to \pi N$
• • • We do not use the following data for averages, fits, limits, etc. • • •				
251 ± 8	SOKHOYAN	15A	DPWA	Multichannel
251 ± 8	GUTZ	14	DPWA	Multichannel
259 ± 4	[1] SHRESTHA	12A	DPWA	Multichannel
245 ±12	VRANA	00	DPWA	Multichannel

[1] Statistical error only.

$\Delta(1950)$ DECAY MODES

The following branching fractions are our estimates, not fits or averages.

	Mode	Fraction (Γ_i/Γ)
Γ_1	$N\pi$	35–45 %
Γ_2	ΣK	0.3–0.5 %
Γ_3	$N\pi\pi$	37–77 %
Γ_4	$\Delta(1232)\pi$	(4.0±3.0) %
Γ_5	$\Delta(1232)\pi$, F-wave	1–9 %
Γ_6	$N\rho$	(10 ±5) %
Γ_7	$N\rho$, S=1/2	(10 ±5) %
Γ_8	$N(1680)\pi$, P-wave	3–9 %
Γ_9	$\Delta(1232)\eta$	< 0.6 %
Γ_{10}	$N\gamma$	0.06–0.14 %
Γ_{11}	$N\gamma$, helicity=1/2	0.03–0.05 %
Γ_{12}	$N\gamma$, helicity=3/2	0.04–0.09 %

Int. J. Mod. Phys. A 2026.41. Downloaded from www.worldscientific.com
UNIVERSITY OF CALIFORNIA @ BERKELEY on 09/16/26. Re-use and distribution is strictly not permitted, except for Open Access articles.

$\Delta(1950)$ BRANCHING RATIOS

$\Gamma(N\pi)/\Gamma_{total}$ — Γ_1/Γ

VALUE (%)	DOCUMENT ID		TECN	COMMENT
35–45 % OUR ESTIMATE				
46 ±4	SEIFEN	25	DPWA	Multichannel
38 ±2	[1] HUNT	19	DPWA	Multichannel
47.1 ±0.1	[1] ARNDT	06	DPWA	$\pi N \to \pi N, \eta N$
39 ±4	CUTKOSKY	80	IPWA	$\pi N \to \pi N$
38 ±2	HOEHLER	79	IPWA	$\pi N \to \pi N$
• • • We do not use the following data for averages, fits, limits, etc. • • •				
0.046±0.002	SOKHOYAN	15A	DPWA	Multichannel
46 ±2	GUTZ	14	DPWA	Multichannel
45.6 ±0.4	[1] SHRESTHA	12A	DPWA	Multichannel
44 ±1	VRANA	00	DPWA	Multichannel

[1] Statistical error only.

$\Gamma(N\pi\pi)/\Gamma_{total}$ — Γ_3/Γ

VALUE (%)	DOCUMENT ID		TECN	COMMENT
57±20	GOLOVATCH	19	DPWA	$\gamma p \to \pi^+\pi^- p$

$\Gamma(\Sigma K)/\Gamma_{total}$ — Γ_2/Γ

VALUE (%)	DOCUMENT ID		TECN	COMMENT
0.6±0.2	ANISOVICH	17	DPWA	Multichannel
• • • We do not use the following data for averages, fits, limits, etc. • • •				
0.4±0.1	ANISOVICH	12A	DPWA	Multichannel

$\Gamma(\Delta(1232)\pi)/\Gamma_{total}$ — Γ_4/Γ

VALUE (%)	DOCUMENT ID		TECN	COMMENT
4±3	SARANTSEV	25	DPWA	Multichannel

$\Gamma(\Delta(1232)\pi, F\text{-wave})/\Gamma_{total}$ — Γ_5/Γ

VALUE (%)	DOCUMENT ID		TECN	COMMENT
4±3	SARANTSEV	25	DPWA	Multichannel
5±4	SEIFEN	25	DPWA	Multichannel
8±1	[1] SHRESTHA	12A	DPWA	Multichannel
• • • We do not use the following data for averages, fits, limits, etc. • • •				
5±4	SOKHOYAN	15A	DPWA	Multichannel
36±1	VRANA	00	DPWA	Multichannel

[1] Statistical error only.

$\Gamma(N\rho)/\Gamma_{total}$ — Γ_6/Γ

VALUE (%)	DOCUMENT ID		TECN	COMMENT
10±5	SARANTSEV	25	DPWA	Multichannel

$\Gamma(N\rho, S=1/2)/\Gamma_{total}$ — Γ_7/Γ

VALUE (%)	DOCUMENT ID		TECN	COMMENT
10±5	SARANTSEV	25	DPWA	Multichannel

$\Gamma(N(1680)\pi, P\text{-wave})/\Gamma_{total}$ — Γ_8/Γ

VALUE (%)	DOCUMENT ID		TECN	COMMENT
3±2	SEIFEN	25	DPWA	Multichannel
• • • We do not use the following data for averages, fits, limits, etc. • • •				
6±3	SOKHOYAN	15A	DPWA	Multichannel

$\Gamma(\Delta(1232)\eta)/\Gamma_{total}$ — Γ_9/Γ

VALUE (%)	DOCUMENT ID		TECN	COMMENT
0.3±0.3	ANISOVICH	17	DPWA	Multichannel
• • • We do not use the following data for averages, fits, limits, etc. • • •				
<1	GUTZ	14	DPWA	Multichannel

$\Delta(1950)$ PHOTON DECAY AMPLITUDES AT THE POLE

$\Delta(1950) \to N\gamma$, helicity-1/2 amplitude $A_{1/2}$

MODULUS ($GeV^{-1/2}$)	PHASE (°)	DOCUMENT ID		TECN	COMMENT
−0.076±0.006	−10 ± 5	SARANTSEV	25	DPWA	Multichannel
−0.031±0.002	−81 ± 4	ROENCHEN	22	DPWA	Multichannel
• • • We do not use the following data for averages, fits, limits, etc. • • •					
−0.068	−19	ROENCHEN	15A	DPWA	Multichannel
−0.067±0.004	−10 ± 5	SOKHOYAN	15A	DPWA	Multichannel

$\Delta(1950) \to N\gamma$, helicity-3/2 amplitude $A_{3/2}$

MODULUS ($GeV^{-1/2}$)	PHASE (°)	DOCUMENT ID		TECN	COMMENT
−0.092±0.004	−10 ± 5	SARANTSEV	25	DPWA	Multichannel
−0.045±0.002	−89 ± 2	ROENCHEN	22	DPWA	Multichannel
• • • We do not use the following data for averages, fits, limits, etc. • • •					
−0.084	−19	ROENCHEN	15A	DPWA	Multichannel
−0.095±0.004	−10 ± 5	SOKHOYAN	15A	DPWA	Multichannel

$\Delta(1950)$ BREIT-WIGNER PHOTON DECAY AMPLITUDES

$\Delta(1950) \to N\gamma$, helicity-1/2 amplitude $A_{1/2}$

VALUE ($GeV^{-1/2}$)	DOCUMENT ID		TECN	COMMENT
−0.075 to −0.065 (≈ −0.070) OUR ESTIMATE				
−0.077 ±0.006	SARANTSEV	25	DPWA	Multichannel
−0.0698±0.0141	GOLOVATCH	19	DPWA	$\gamma p \to \pi^+\pi^- p$
−0.047 ±0.002	[1] HUNT	19	DPWA	Multichannel
−0.083 ±0.004	WORKMAN	12A	DPWA	$\gamma N \to N\pi$
• • • We do not use the following data for averages, fits, limits, etc. • • •				
−0.067 ±0.005	SOKHOYAN	15A	DPWA	Multichannel
−0.067 ±0.005	GUTZ	14	DPWA	Multichannel
−0.065 ±0.001	[1] SHRESTHA	12A	DPWA	Multichannel
−0.094	DRECHSEL	07	DPWA	$\gamma N \to \pi N$

[1] Statistical error only.

$\Delta(1950) \to N\gamma$, helicity-3/2 amplitude $A_{3/2}$

VALUE ($GeV^{-1/2}$)	DOCUMENT ID		TECN	COMMENT
−0.100 to −0.080 (≈ −0.090) OUR ESTIMATE				
−0.094 ±0.004	SARANTSEV	25	DPWA	Multichannel
−0.1181±0.0193	GOLOVATCH	19	DPWA	$\gamma p \to \pi^+\pi^- p$
−0.074 ±0.002	[1] HUNT	19	DPWA	Multichannel
−0.096 ±0.004	WORKMAN	12A	DPWA	$\gamma N \to N\pi$
• • • We do not use the following data for averages, fits, limits, etc. • • •				
−0.094 ±0.004	SOKHOYAN	15A	DPWA	Multichannel
−0.094 ±0.004	GUTZ	14	DPWA	Multichannel
−0.083 ±0.001	[1] SHRESTHA	12A	DPWA	Multichannel
−0.121	DRECHSEL	07	DPWA	$\gamma N \to \pi N$

[1] Statistical error only.

$\Delta(1950)$ REFERENCES

SARANTSEV	25	PR C112 015202	A.V. Sarantsev *et al.*	(Bonn-Gatchina Collab.)
SEIFEN	25	EPJ A61 173	T. Seifen *et al.*	(CBELSA/TAPS Collab.)
ROENCHEN	22	EPJ A58 229	D. Roenchen *et al.*	(JULI, GWU, BONN+)
GOLOVATCH	19	PL B788 371	E. Golovatch *et al.*	(CLAS Collab.)
HUNT	19	PR C99 055205	B.C. Hunt, D.M. Manley	
ANISOVICH	17	PL B766 357	A.V. Anisovich *et al.*	
ROENCHEN	15A	EPJ A51 70	D. Roenchen *et al.*	
SOKHOYAN	15A	EPJ A51 95	V. Sokhoyan *et al.*	(CBELSA/TAPS Collab.)
GUTZ	14	EPJ A50 74	E. Gutz *et al.*	(CBELSA/TAPS Collab.)
PDG	14	CP C38 070001	K. Olive *et al.*	(PDG Collab.)
SVARC	14	PR C89 045205	A. Svarc *et al.*	(RBI Zagreb, UNI Tuzla)
ANISOVICH	12A	EPJ A48 15	A.V. Anisovich *et al.*	(BONN, PNPI)
SHRESTHA	12A	PR C86 055203	M. Shrestha, D.M. Manley	(KSU)
WORKMAN	12A	PR C86 015202	R. Workman *et al.*	(GWU)
DRECHSEL	07	EPJ A34 69	D. Drechsel, S.S. Kamalov, L. Tiator	(MAINZ, JINR)
ARNDT	06	PR C74 045205	R.A. Arndt *et al.*	(GWU)
VRANA	00	PRPL 328 181	T.P. Vrana, S.A. Dytman, T.-S.H. Lee	(PITT, ANL)
HOEHLER	93	πN Newsletter 9 1	G. Hohler	(KARL)
CUTKOSKY	80	Toronto Conf. 19	R.E. Cutkosky *et al.*	(CMU, LBL) IJP
Also		PR D20 2839	R.E. Cutkosky *et al.*	(CMU, LBL) IJP
HOEHLER	79	PDAT 12-1	G. Hohler *et al.*	(KARLT) IJP
Also		Toronto Conf. 3	R. Koch	(KARLT) IJP

$\Delta(2000)\ 5/2^+$

$I(J^P) = \frac{3}{2}(\frac{5}{2}^+)$ Status: **

OMITTED FROM SUMMARY TABLE

$\Delta(2000)$ POLE POSITION

REAL PART

VALUE (MeV)	DOCUMENT ID		TECN	COMMENT
1998± 4±4	[1] SVARC	14	L+P	$\pi N \to \pi N$
1976	SHRESTHA	12A	DPWA	Multichannel
2150±100	CUTKOSKY	80	IPWA	$\pi N \to \pi N$
• • • We do not use the following data for averages, fits, limits, etc. • • •				
1697	VRANA	00	DPWA	Multichannel

[1] Fit to the amplitudes of HOEHLER 79.

−2×IMAGINARY PART

VALUE (MeV)	DOCUMENT ID		TECN	COMMENT
404± 10±4	[1] SVARC	14	L+P	$\pi N \to \pi N$
350±100	CUTKOSKY	80	IPWA	$\pi N \to \pi N$
• • • We do not use the following data for averages, fits, limits, etc. • • •				
488	SHRESTHA	12A	DPWA	Multichannel
112	VRANA	00	DPWA	Multichannel

[1] Fit to the amplitudes of HOEHLER 79.

$\Delta(2000)$ ELASTIC POLE RESIDUE

MODULUS $|r|$

VALUE (MeV)	DOCUMENT ID		TECN	COMMENT
34±1±1	[1] SVARC	14	L+P	$\pi N \to \pi N$
16±5	CUTKOSKY	80	IPWA	$\pi N \to \pi N$

[1] Fit to the amplitudes of HOEHLER 79.

Int. J. Mod. Phys. A 2026.41. Downloaded from www.worldscientific.com
by UNIVERSITY OF CALIFORNIA @ BERKELEY on 09/16/26. Re-use and distribution is strictly not permitted, except for Open Access articles.

PHASE θ

VALUE (°)	DOCUMENT ID		TECN	COMMENT
110± 1±3	[1] SVARC	14	L+P	$\pi N \to \pi N$
150±90	CUTKOSKY	80	IPWA	$\pi N \to \pi N$

[1] Fit to the amplitudes of HOEHLER 79.

$\Delta(2000)$ BREIT-WIGNER MASS

VALUE (MeV)	DOCUMENT ID		TECN	COMMENT
2015± 24	[1] SHRESTHA	12A	DPWA	Multichannel
2200±125	CUTKOSKY	80	IPWA	$\pi N \to \pi N$
• • • We do not use the following data for averages, fits, limits, etc. • • •				
1724± 61	VRANA	00	DPWA	Multichannel
1752± 32	MANLEY	92	IPWA	$\pi N \to \pi N$ & $N\pi\pi$

[1] Statistical error only.

$\Delta(2000)$ BREIT-WIGNER WIDTH

VALUE (MeV)	DOCUMENT ID		TECN	COMMENT
500± 52	[1] SHRESTHA	12A	DPWA	Multichannel
400±125	CUTKOSKY	80	IPWA	$\pi N \to \pi N$
• • • We do not use the following data for averages, fits, limits, etc. • • •				
138± 68	VRANA	00	DPWA	Multichannel
251± 93	MANLEY	92	IPWA	$\pi N \to \pi N$ & $N\pi\pi$

[1] Statistical error only.

$\Delta(2000)$ DECAY MODES

	Mode	Fraction (Γ_i/Γ)
Γ_1	$N\pi$	3–11 %
Γ_2	$N\pi\pi$	>87 %
Γ_3	$\Delta(1232)\pi$	<9 %
Γ_4	$\Delta(1232)\pi$, P-wave	<6 %
Γ_5	$\Delta(1232)\pi$, F-wave	<3 %
Γ_6	$N\rho$, S=3/2, P-wave	seen
Γ_7	$N(1440)\pi$	
Γ_8	$N(1520)\pi$, S-wave	
Γ_9	$N(1535)\pi$	
Γ_{10}	$N\gamma$	
Γ_{11}	$N\gamma$, helicity=1/2	seen
Γ_{12}	$N\gamma$, helicity=3/2	seen

$\Delta(2000)$ BRANCHING RATIOS

$\Gamma(N\pi)/\Gamma_{total}$ — Γ_1/Γ

VALUE (%)	DOCUMENT ID		TECN	COMMENT
11±5	SEIFEN	25	DPWA	Multichannel
7±1	[1] SHRESTHA	12A	DPWA	Multichannel
7±4	CUTKOSKY	80	IPWA	$\pi N \to \pi N$
• • • We do not use the following data for averages, fits, limits, etc. • • •				
0±1	VRANA	00	DPWA	Multichannel
2±1	MANLEY	92	IPWA	$\pi N \to \pi N$ & $N\pi\pi$

[1] Statistical error only.

$\Gamma(\Delta(1232)\pi, P\text{-wave})/\Gamma_{total}$ — Γ_4/Γ

VALUE (%)	DOCUMENT ID		TECN	COMMENT
14±6	SEIFEN	25	DPWA	Multichannel
3±3	[1] SHRESTHA	12A	DPWA	Multichannel
• • • We do not use the following data for averages, fits, limits, etc. • • •				
0±1	VRANA	00	DPWA	Multichannel

[1] Statistical error only.

$\Gamma(\Delta(1232)\pi, F\text{-wave})/\Gamma_{total}$ — Γ_5/Γ

VALUE (%)	DOCUMENT ID		TECN	COMMENT
3±2	SEIFEN	25	DPWA	Multichannel
< 3	SHRESTHA	12A	DPWA	Multichannel
• • • We do not use the following data for averages, fits, limits, etc. • • •				
40±1	VRANA	00	DPWA	Multichannel

$\Gamma(N\rho, S=3/2, P\text{-wave})/\Gamma_{total}$ — Γ_6/Γ

VALUE (%)	DOCUMENT ID		TECN	COMMENT
90± 3	[1] SHRESTHA	12A	DPWA	Multichannel
• • • We do not use the following data for averages, fits, limits, etc. • • •				
60±60	VRANA	00	DPWA	Multichannel

[1] Statistical error only.

$\Gamma(N(1440)\pi)/\Gamma_{total}$ — Γ_7/Γ

VALUE (%)	DOCUMENT ID		TECN	COMMENT
9±6	SEIFEN	25	DPWA	Multichannel

$\Gamma(N(1520)\pi, S\text{-wave})/\Gamma_{total}$ — Γ_8/Γ

VALUE (%)	DOCUMENT ID		TECN	COMMENT
<1	SEIFEN	25	DPWA	Multichannel

$\Gamma(N(1535)\pi)/\Gamma_{total}$ — Γ_9/Γ

VALUE (%)	DOCUMENT ID		TECN	COMMENT
<1	SEIFEN	25	DPWA	Multichannel

$\Delta(2000)$ BREIT-WIGNER PHOTON DECAY AMPLITUDES

$\Delta(2000) \to p\gamma$, helicity-1/2 amplitude $A_{1/2}$

VALUE (GeV$^{-1/2}$)	DOCUMENT ID		TECN	COMMENT
• • • We do not use the following data for averages, fits, limits, etc. • • •				
−0.061±0.018	[1] SHRESTHA	12A	DPWA	Multichannel

[1] Statistical error only.

$\Delta(2000) \to p\gamma$, helicity-3/2 amplitude $A_{3/2}$

VALUE (GeV$^{-1/2}$)	DOCUMENT ID		TECN	COMMENT
• • • We do not use the following data for averages, fits, limits, etc. • • •				
0.158±0.032	[1] SHRESTHA	12A	DPWA	Multichannel

[1] Statistical error only.

$\Delta(2000)$ REFERENCES

SEIFEN	25	EPJ A61 173	T. Seifen *et al.*	(CBELSA/TAPS Collab.)
SVARC	14	PR C89 045205	A. Svarc *et al.*	(RBI Zagreb, UNI Tuzla)
SHRESTHA	12A	PR C86 055203	M. Shrestha, D.M. Manley	(KSU)
VRANA	00	PRPL 328 181	T.P. Vrana, S.A. Dytman, T.-S.H. Lee	(PITT, ANL)
MANLEY	92	PR D45 4002	D.M. Manley, E.M. Saleski	(KSA) IJP
Also		PR D30 904	D.M. Manley *et al.*	(VPI)
CUTKOSKY	80	Toronto Conf. 19	R.E. Cutkosky *et al.*	(CMU, LBL)
Also		PR D20 2839	R.E. Cutkosky *et al.*	(CMU, LBL)
HOEHLER	79	PDAT 12-1	G. Höhler *et al.*	(KARLT)

$\Delta(2150)\ 1/2^-$

$I(J^P) = \frac{3}{2}(\frac{1}{2}^-)$ Status: *

OMITTED FROM SUMMARY TABLE

$\Delta(2150)$ POLE POSITION

REAL PART

VALUE (MeV)	DOCUMENT ID		TECN	COMMENT
2140±80	CUTKOSKY	80	IPWA	$\pi N \to \pi N$

−2×IMAGINARY PART

VALUE (MeV)	DOCUMENT ID		TECN	COMMENT
200±80	CUTKOSKY	80	IPWA	$\pi N \to \pi N$

$\Delta(2150)$ ELASTIC POLE RESIDUE

MODULUS $|r|$

VALUE (MeV)	DOCUMENT ID		TECN	COMMENT
7±2	CUTKOSKY	80	IPWA	$\pi N \to \pi N$

PHASE θ

VALUE (°)	DOCUMENT ID		TECN	COMMENT
−60±90	CUTKOSKY	80	IPWA	$\pi N \to \pi N$

$\Delta(2150)$ BREIT-WIGNER MASS

VALUE (MeV)	DOCUMENT ID		TECN	COMMENT
2150±100	CUTKOSKY	80	IPWA	$\pi N \to \pi N$

$\Delta(2150)$ BREIT-WIGNER WIDTH

VALUE (MeV)	DOCUMENT ID		TECN	COMMENT
200±100	CUTKOSKY	80	IPWA	$\pi N \to \pi N$

$\Delta(2150)$ DECAY MODES

	Mode	Fraction (Γ_i/Γ)
Γ_1	$N\pi$	6–10 %

$\Delta(2150)$ BRANCHING RATIOS

$\Gamma(N\pi)/\Gamma_{total}$ — Γ_1/Γ

VALUE (%)	DOCUMENT ID		TECN	COMMENT
8±2	CUTKOSKY	80	IPWA	$\pi N \to \pi N$

$\Delta(2150)$ REFERENCES

CUTKOSKY	80	Toronto Conf. 19	R.E. Cutkosky *et al.*	(CMU, LBL) IJP
Also		PR D20 2839	R.E. Cutkosky *et al.*	(CMU, LBL)

Int. J. Mod. Phys. A 2026.41. Downloaded from www.worldscientific.com
UNIVERSITY OF CALIFORNIA @ BERKELEY on 09/16/26. Re-use and distribution is strictly not permitted, except for Open Access articles.

$\Delta(2200)\ 7/2^-$

$I(J^P) = \frac{3}{2}(\frac{7}{2}^-)$ Status: ***

$\Delta(2200)$ POLE POSITION

REAL PART

VALUE (MeV)	DOCUMENT ID		TECN	COMMENT
2050 to 2150 (≈ 2100) OUR ESTIMATE				
2090±20	SARANTSEV	25	DPWA	Multichannel
1963± 1	ROENCHEN	22	DPWA	Multichannel
2100±50	CUTKOSKY	80	IPWA	$\pi N \to \pi N$
• • • We do not use the following data for averages, fits, limits, etc. • • •				
2142	ROENCHEN	15A	DPWA	Multichannel

−2×IMAGINARY PART

VALUE (MeV)	DOCUMENT ID		TECN	COMMENT
260 to 420 (≈ 340) OUR ESTIMATE				
360±35	SARANTSEV	25	DPWA	Multichannel
328± 2	ROENCHEN	22	DPWA	Multichannel
340±80	CUTKOSKY	80	IPWA	$\pi N \to \pi N$
• • • We do not use the following data for averages, fits, limits, etc. • • •				
486	ROENCHEN	15A	DPWA	Multichannel

$\Delta(2200)$ ELASTIC POLE RESIDUE

MODULUS $|r|$

VALUE (MeV)	DOCUMENT ID		TECN	COMMENT
6.8±0.3	ROENCHEN	22	DPWA	Multichannel
8 ±3	CUTKOSKY	80	IPWA	$\pi N \to \pi N$
• • • We do not use the following data for averages, fits, limits, etc. • • •				
17	ROENCHEN	15A	DPWA	Multichannel

PHASE θ

VALUE (°)	DOCUMENT ID		TECN	COMMENT
−80± 1	ROENCHEN	22	DPWA	Multichannel
−70±40	CUTKOSKY	80	IPWA	$\pi N \to \pi N$
• • • We do not use the following data for averages, fits, limits, etc. • • •				
−56	ROENCHEN	15A	DPWA	Multichannel

$\Delta(2200)$ INELASTIC POLE RESIDUE

The "normalized residue" is the residue divided by $\Gamma_{pole}/2$.

Normalized residue in $N\pi \to \Delta(2200) \to \Sigma K$

MODULUS	PHASE (°)	DOCUMENT ID		TECN	COMMENT
0.001±0.002	−123 ± 1	ROENCHEN	22	DPWA	Multichannel
• • • We do not use the following data for averages, fits, limits, etc. • • •					
0.005	−103	ROENCHEN	15A	DPWA	Multichannel

Normalized residue in $N\pi \to \Delta(2200) \to \Delta\pi$, D-wave

MODULUS	PHASE (°)	DOCUMENT ID		TECN	COMMENT
0.16±0.01	100 ± 1	ROENCHEN	22	DPWA	Multichannel
• • • We do not use the following data for averages, fits, limits, etc. • • •					
0.23	107	ROENCHEN	15A	DPWA	Multichannel

Normalized residue in $N\pi \to \Delta(2200) \to \Delta\pi$, G-wave

MODULUS	PHASE (°)	DOCUMENT ID		TECN	COMMENT
0.003±0.001	152 ± 3	ROENCHEN	22	DPWA	Multichannel
• • • We do not use the following data for averages, fits, limits, etc. • • •					
0.022	−151	ROENCHEN	15A	DPWA	Multichannel

$\Delta(2200)$ BREIT-WIGNER MASS

VALUE (MeV)	DOCUMENT ID		TECN	COMMENT
2150 to 2250 (≈ 2200) OUR ESTIMATE				
2180±30	SARANTSEV	25	DPWA	Multichannel
2200±80	CUTKOSKY	80	IPWA	$\pi N \to \pi N$
2215±60	HOEHLER	79	IPWA	$\pi N \to \pi N$
• • • We do not use the following data for averages, fits, limits, etc. • • •				
2176±40	ANISOVICH	17	DPWA	Multichannel

$\Delta(2200)$ BREIT-WIGNER WIDTH

VALUE (MeV)	DOCUMENT ID		TECN	COMMENT
200 to 500 (≈ 350) OUR ESTIMATE				
420± 50	SARANTSEV	25	DPWA	Multichannel
450±100	CUTKOSKY	80	IPWA	$\pi N \to \pi N$
400±100	HOEHLER	79	IPWA	$\pi N \to \pi N$
• • • We do not use the following data for averages, fits, limits, etc. • • •				
210± 70	ANISOVICH	17	DPWA	Multichannel

$\Delta(2200)$ DECAY MODES

	Mode	Fraction (Γ_i/Γ)
Γ_1	$N\pi$	2–8 %
Γ_2	ΣK	1–7 %
Γ_3	$N\pi\pi$	>45 %
Γ_4	$\Delta\pi$	>45 %
Γ_5	$\Delta\pi$, D-wave	(70±30) %
Γ_6	$\Delta\pi$, G-wave	5–25 %
Γ_7	$\Delta\eta$	
Γ_8	$\Delta\eta$, D-wave	seen

$\Delta(2200)$ BRANCHING RATIOS

$\Gamma(N\pi)/\Gamma_{total}$ — Γ_1/Γ

VALUE (%)	DOCUMENT ID		TECN	COMMENT
2–8 % OUR ESTIMATE				
3.5±1.5	ANISOVICH	17	DPWA	Multichannel
6 ±2	CUTKOSKY	80	IPWA	$\pi N \to \pi N$
5 ±2	HOEHLER	79	IPWA	$\pi N \to \pi N$

$\Gamma(\Sigma K)/\Gamma_{total}$ — Γ_2/Γ

VALUE (%)	DOCUMENT ID		TECN	COMMENT
4±3	ANISOVICH	17	DPWA	Multichannel

$\Gamma(\Delta\pi)/\Gamma_{total}$ — Γ_4/Γ

VALUE (%)	DOCUMENT ID		TECN	COMMENT
2±2	SARANTSEV	25	DPWA	Multichannel

$\Gamma(\Delta\pi, D\text{-wave})/\Gamma_{total}$ — Γ_5/Γ

VALUE (%)	DOCUMENT ID		TECN	COMMENT
70±30	ANISOVICH	17	DPWA	Multichannel

$\Gamma(\Delta\pi, G\text{-wave})/\Gamma_{total}$ — Γ_6/Γ

VALUE (%)	DOCUMENT ID		TECN	COMMENT
1± 1	SARANTSEV	25	DPWA	Multichannel
• • • We do not use the following data for averages, fits, limits, etc. • • •				
15±10	ANISOVICH	17	DPWA	Multichannel

$\Gamma(\Delta\eta, D\text{-wave})/\Gamma_{total}$ — Γ_8/Γ

VALUE (%)	DOCUMENT ID		TECN	COMMENT
∼ 1	ANISOVICH	17	DPWA	Multichannel

$\Delta(2200)$ PHOTON DECAY AMPLITUDES AT THE POLE

$\Delta(2200) \to N\gamma$, helicity-1/2 amplitude $A_{1/2}$

MODULUS ($GeV^{-1/2}$)	PHASE (°)	DOCUMENT ID		TECN	COMMENT
0.120±0.015	−35 ± 20	SARANTSEV	25	DPWA	Multichannel
0.104±0.011	−139 ± 2	ROENCHEN	22	DPWA	Multichannel
• • • We do not use the following data for averages, fits, limits, etc. • • •					
0.106	−23	ROENCHEN	15A	DPWA	Multichannel

$\Delta(2200) \to N\gamma$, helicity-3/2 amplitude $A_{3/2}$

MODULUS ($GeV^{-1/2}$)	PHASE (°)	DOCUMENT ID		TECN	COMMENT
0.073±0.012	−30 ± 20	SARANTSEV	25	DPWA	Multichannel
0.021±0.013	−180 ± 20	ROENCHEN	22	DPWA	Multichannel
• • • We do not use the following data for averages, fits, limits, etc. • • •					
0.157	−60	ROENCHEN	15A	DPWA	Multichannel

$\Delta(2200)$ BREIT-WIGNER PHOTON DECAY AMPLITUDES

$\Delta(2200) \to N\gamma$, helicity-1/2 amplitude $A_{1/2}$

VALUE ($GeV^{-1/2}$)	DOCUMENT ID		TECN	COMMENT
0.125±0.016	SARANTSEV	25	DPWA	Multichannel

$\Delta(2200) \to N\gamma$, helicity-3/2 amplitude $A_{3/2}$

VALUE ($GeV^{-1/2}$)	DOCUMENT ID		TECN	COMMENT
0.075±0.012	SARANTSEV	25	DPWA	Multichannel

$\Delta(2200)$ REFERENCES

SARANTSEV	25	PR C112 015202	A.V. Sarantsev *et al.*	(Bonn-Gatchina Collab.)
ROENCHEN	22	EPJ A58 229	D. Roenchen *et al.*	(JULI, GWU, BONN+)
ANISOVICH	17	PL B766 357	A.V. Anisovich *et al.*	
ROENCHEN	15A	EPJ A51 70	D. Roenchen *et al.*	
CUTKOSKY	80	Toronto Conf. 19	R.E. Cutkosky *et al.*	(CMU, LBL) IJP
Also		PR D20 2839	R.E. Cutkosky *et al.*	(CMU, LBL) IJP
HOEHLER	79	PDAT 12-1	G. Hohler *et al.*	(KARLT) IJP
Also		Toronto Conf. 3	R. Koch	(KARLT) IJP

Int. J. Mod. Phys. A 2026.41. Downloaded from www.worldscientific.com by UNIVERSITY OF CALIFORNIA @ BERKELEY on 09/16/26. Re-use and distribution is strictly not permitted, except for Open Access articles.

$\Delta(2300)\ 9/2^+$

$I(J^P) = \frac{3}{2}(\frac{9}{2}^+)$ Status: **

OMITTED FROM SUMMARY TABLE

$\Delta(2300)$ POLE POSITION

REAL PART

VALUE (MeV)	DOCUMENT ID		TECN	COMMENT
2370±80	CUTKOSKY	80	IPWA	$\pi N \to \pi N$

−2×IMAGINARY PART

VALUE (MeV)	DOCUMENT ID		TECN	COMMENT
420±160	CUTKOSKY	80	IPWA	$\pi N \to \pi N$

$\Delta(2300)$ ELASTIC POLE RESIDUE

MODULUS $|r|$

VALUE (MeV)	DOCUMENT ID		TECN	COMMENT
10±4	CUTKOSKY	80	IPWA	$\pi N \to \pi N$

PHASE θ

VALUE (°)	DOCUMENT ID		TECN	COMMENT
−20±30	CUTKOSKY	80	IPWA	$\pi N \to \pi N$

$\Delta(2300)$ BREIT-WIGNER MASS

VALUE (MeV)	DOCUMENT ID		TECN	COMMENT
2400±125	CUTKOSKY	80	IPWA	$\pi N \to \pi N$
2217± 80	HOEHLER	79	IPWA	$\pi N \to \pi N$

$\Delta(2300)$ BREIT-WIGNER WIDTH

VALUE (MeV)	DOCUMENT ID		TECN	COMMENT
425±150	CUTKOSKY	80	IPWA	$\pi N \to \pi N$
300±100	HOEHLER	79	IPWA	$\pi N \to \pi N$

$\Delta(2300)$ DECAY MODES

	Mode	Fraction (Γ_i/Γ)
Γ_1	$N\pi$	1–8 %

$\Delta(2300)$ BRANCHING RATIOS

$\Gamma(N\pi)/\Gamma_{total}$ — Γ_1/Γ

VALUE (%)	DOCUMENT ID		TECN	COMMENT
6±2	CUTKOSKY	80	IPWA	$\pi N \to \pi N$
3±2	HOEHLER	79	IPWA	$\pi N \to \pi N$

$\Delta(2300)$ REFERENCES

CUTKOSKY	80	Toronto Conf. 19	R.E. Cutkosky *et al.*	(CMU, LBL) IJP
Also		PR D20 2839	R.E. Cutkosky *et al.*	(CMU, LBL)
HOEHLER	79	PDAT 12-1	G. Hohler *et al.*	(KARLT) IJP
Also		Toronto Conf. 3	R. Koch	(KARLT) IJP

$\Delta(2350)\ 5/2^-$

$I(J^P) = \frac{3}{2}(\frac{5}{2}^-)$ Status: *

OMITTED FROM SUMMARY TABLE

$\Delta(2350)$ POLE POSITION

REAL PART

VALUE (MeV)	DOCUMENT ID		TECN	COMMENT
2400±125	CUTKOSKY	80	IPWA	$\pi N \to \pi N$
• • • We do not use the following data for averages, fits, limits, etc. • • •				
2427	VRANA	00	DPWA	Multichannel

−2×IMAGINARY PART

VALUE (MeV)	DOCUMENT ID		TECN	COMMENT
400±150	CUTKOSKY	80	IPWA	$\pi N \to \pi N$
• • • We do not use the following data for averages, fits, limits, etc. • • •				
458	VRANA	00	DPWA	Multichannel

$\Delta(2350)$ ELASTIC POLE RESIDUE

MODULUS $|r|$

VALUE (MeV)	DOCUMENT ID		TECN	COMMENT
15±8	CUTKOSKY	80	IPWA	$\pi N \to \pi N$

PHASE θ

VALUE (°)	DOCUMENT ID		TECN	COMMENT
−70±70	CUTKOSKY	80	IPWA	$\pi N \to \pi N$

$\Delta(2350)$ BREIT-WIGNER MASS

VALUE (MeV)	DOCUMENT ID		TECN	COMMENT
2400±125	CUTKOSKY	80	IPWA	$\pi N \to \pi N$
2305± 26	HOEHLER	79	IPWA	$\pi N \to \pi N$
• • • We do not use the following data for averages, fits, limits, etc. • • •				
2459±100	VRANA	00	DPWA	Multichannel

$\Delta(2350)$ BREIT-WIGNER WIDTH

VALUE (MeV)	DOCUMENT ID		TECN	COMMENT
400±150	CUTKOSKY	80	IPWA	$\pi N \to \pi N$
300± 70	HOEHLER	79	IPWA	$\pi N \to \pi N$
• • • We do not use the following data for averages, fits, limits, etc. • • •				
480±360	VRANA	00	DPWA	Multichannel

$\Delta(2350)$ DECAY MODES

	Mode	Fraction (Γ_i/Γ)
Γ_1	$N\pi$	4–30 %

$\Delta(2350)$ BRANCHING RATIOS

$\Gamma(N\pi)/\Gamma_{total}$ — Γ_1/Γ

VALUE (%)	DOCUMENT ID		TECN	COMMENT
20±10	CUTKOSKY	80	IPWA	$\pi N \to \pi N$
4± 2	HOEHLER	79	IPWA	$\pi N \to \pi N$
• • • We do not use the following data for averages, fits, limits, etc. • • •				
7±14	VRANA	00	DPWA	Multichannel

$\Delta(2350)$ REFERENCES

VRANA	00	PRPL 328 181	T.P. Vrana, S.A. Dytman, T.-S.H. Lee	(PITT, ANL)
CUTKOSKY	80	Toronto Conf. 19	R.E. Cutkosky *et al.*	(CMU, LBL) IJP
Also		PR D20 2839	R.E. Cutkosky *et al.*	(CMU, LBL)
HOEHLER	79	PDAT 12-1	G. Hohler *et al.*	(KARLT) IJP
Also		Toronto Conf. 3	R. Koch	(KARLT) IJP

$\Delta(2390)\ 7/2^+$

$I(J^P) = \frac{3}{2}(\frac{7}{2}^+)$ Status: *

OMITTED FROM SUMMARY TABLE

$\Delta(2390)$ POLE POSITION

REAL PART

VALUE (MeV)	DOCUMENT ID		TECN	COMMENT
2223± 15±19	[1] SVARC	14	L+P	$\pi N \to \pi N$
2350±100	CUTKOSKY	80	IPWA	$\pi N \to \pi N$

−2×IMAGINARY PART

VALUE (MeV)	DOCUMENT ID		TECN	COMMENT
431± 26±7	[1] SVARC	14	L+P	$\pi N \to \pi N$
260±100	CUTKOSKY	80	IPWA	$\pi N \to \pi N$

$\Delta(2390)$ ELASTIC POLE RESIDUE

MODULUS $|r|$

VALUE (MeV)	DOCUMENT ID		TECN	COMMENT
26±2±1	[1] SVARC	14	L+P	$\pi N \to \pi N$
12±6	CUTKOSKY	80	IPWA	$\pi N \to \pi N$

PHASE θ

VALUE (°)	DOCUMENT ID		TECN	COMMENT
−160± 5±11	[1] SVARC	14	L+P	$\pi N \to \pi N$
− 90±60	CUTKOSKY	80	IPWA	$\pi N \to \pi N$

$\Delta(2390)$ BREIT-WIGNER MASS

VALUE (MeV)	DOCUMENT ID		TECN	COMMENT
2350±100	CUTKOSKY	80	IPWA	$\pi N \to \pi N$
2425± 60	HOEHLER	79	IPWA	$\pi N \to \pi N$

$\Delta(2390)$ BREIT-WIGNER WIDTH

VALUE (MeV)	DOCUMENT ID		TECN	COMMENT
300±100	CUTKOSKY	80	IPWA	$\pi N \to \pi N$
300± 80	HOEHLER	79	IPWA	$\pi N \to \pi N$

Int. J. Mod. Phys. A 2026.41. Downloaded from www.worldscientific.com
UNIVERSITY OF CALIFORNIA @ BERKELEY on 09/16/26. Re-use and distribution is strictly not permitted, except for Open Access articles.

$\Delta(2390)$ DECAY MODES

	Mode	Fraction (Γ_i/Γ)
Γ_1	$N\pi$	3–12 %

$\Delta(2390)$ BRANCHING RATIOS

$\Gamma(N\pi)/\Gamma_{total}$ — Γ_1/Γ

VALUE (%)	DOCUMENT ID		TECN	COMMENT
8±4	CUTKOSKY	80	IPWA	$\pi N \to \pi N$
7±4	HOEHLER	79	IPWA	$\pi N \to \pi N$

$\Delta(2390)$ FOOTNOTES

[1] Fit to the amplitudes of HOEHLER 79.

$\Delta(2390)$ REFERENCES

SVARC	14	PR C89 045205	A. Svarc *et al.*	(RBI Zagreb, UNI Tuzla)
CUTKOSKY	80	Toronto Conf. 19	R.E. Cutkosky *et al.*	(CMU, LBL) IJP
Also		PR D20 2839	R.E. Cutkosky *et al.*	(CMU, LBL)
HOEHLER	79	PDAT 12-1	G. Hohler *et al.*	(KARLT) IJP
Also		Toronto Conf. 3	R. Koch	(KARLT) IJP

$\Delta(2400)\ 9/2^-$

$I(J^P) = \frac{3}{2}(\frac{9}{2}^-)$ Status: **

OMITTED FROM SUMMARY TABLE

$\Delta(2400)$ POLE POSITION

REAL PART

VALUE (MeV)	DOCUMENT ID		TECN	COMMENT
2458± 2	ROENCHEN	22	DPWA	Multichannel
2260±60	CUTKOSKY	80	IPWA	$\pi N \to \pi N$
• • • We do not use the following data for averages, fits, limits, etc. • • •				
1931	ROENCHEN	15A	DPWA	Multichannel
1983	ARNDT	06	DPWA	$\pi N \to \pi N, \eta N$

−2×IMAGINARY PART

VALUE (MeV)	DOCUMENT ID		TECN	COMMENT
280± 2	ROENCHEN	22	DPWA	Multichannel
320±160	CUTKOSKY	80	IPWA	$\pi N \to \pi N$
• • • We do not use the following data for averages, fits, limits, etc. • • •				
442	ROENCHEN	15A	DPWA	Multichannel
878	ARNDT	06	DPWA	$\pi N \to \pi N, \eta N$

$\Delta(2400)$ ELASTIC POLE RESIDUE

MODULUS $|r|$

VALUE (MeV)	DOCUMENT ID		TECN	COMMENT
5.4±2.7	ROENCHEN	22	DPWA	Multichannel
8 ±4	CUTKOSKY	80	IPWA	$\pi N \to \pi N$
• • • We do not use the following data for averages, fits, limits, etc. • • •				
13	ROENCHEN	15A	DPWA	Multichannel
24	ARNDT	06	DPWA	$\pi N \to \pi N, \eta N$

PHASE θ

VALUE (°)	DOCUMENT ID		TECN	COMMENT
8.4±17	ROENCHEN	22	DPWA	Multichannel
− 25 ±15	CUTKOSKY	80	IPWA	$\pi N \to \pi N$
• • • We do not use the following data for averages, fits, limits, etc. • • •				
− 96	ROENCHEN	15A	DPWA	Multichannel
−139	ARNDT	06	DPWA	$\pi N \to \pi N, \eta N$

$\Delta(2400)$ INELASTIC POLE RESIDUE

The "normalized residue" is the residue divided by $\Gamma_{pole}/2$.

Normalized residue in $N\pi \to \Delta(2400) \to \Sigma K$

MODULUS	PHASE (°)	DOCUMENT ID		TECN	COMMENT
0.004±0.003	17 ± 15	ROENCHEN	22	DPWA	Multichannel
• • • We do not use the following data for averages, fits, limits, etc. • • •					
0.009	25	ROENCHEN	15A	DPWA	Multichannel

Normalized residue in $N\pi \to \Delta(2400) \to \Delta\pi$, G-wave

MODULUS	PHASE (°)	DOCUMENT ID		TECN	COMMENT
0.10±0.05	17 ± 11	ROENCHEN	22	DPWA	Multichannel
• • • We do not use the following data for averages, fits, limits, etc. • • •					
0.18	−110	ROENCHEN	15A	DPWA	Multichannel

Normalized residue in $N\pi \to \Delta(2400) \to \Delta\pi$, I-wave

MODULUS	PHASE (°)	DOCUMENT ID		TECN	COMMENT
0.019±0.003	−120 ± 25	ROENCHEN	22	DPWA	Multichannel
• • • We do not use the following data for averages, fits, limits, etc. • • •					
0.012	−1.0	ROENCHEN	15A	DPWA	Multichannel

$\Delta(2400)$ BREIT-WIGNER MASS

VALUE (MeV)	DOCUMENT ID		TECN	COMMENT
2643±141	[1] ARNDT	06	DPWA	$\pi N \to \pi N, \eta N$
2300±100	CUTKOSKY	80	IPWA	$\pi N \to \pi N$
2468± 50	HOEHLER	79	IPWA	$\pi N \to \pi N$

[1] Statistical error only.

$\Delta(2400)$ BREIT-WIGNER WIDTH

VALUE (MeV)	DOCUMENT ID		TECN	COMMENT
895±432	[2] ARNDT	06	DPWA	$\pi N \to \pi N, \eta N$
330±100	CUTKOSKY	80	IPWA	$\pi N \to \pi N$
480±100	HOEHLER	79	IPWA	$\pi N \to \pi N$

[2] Statistical error only.

$\Delta(2400)$ DECAY MODES

	Mode	Fraction (Γ_i/Γ)
Γ_1	$N\pi$	3–9 %

$\Delta(2400)$ BRANCHING RATIOS

$\Gamma(N\pi)/\Gamma_{total}$ — Γ_1/Γ

VALUE (%)	DOCUMENT ID		TECN	COMMENT
6.4±2.2	[3] ARNDT	06	DPWA	$\pi N \to \pi N, \eta N$
5 ±2	CUTKOSKY	80	IPWA	$\pi N \to \pi N$
6 ±3	HOEHLER	79	IPWA	$\pi N \to \pi N$

[3] Statistical error only.

$\Delta(2400)$ PHOTON DECAY AMPLITUDES AT THE POLE

$\Delta(2400) \to N\gamma$, helicity-1/2 amplitude $A_{1/2}$

MODULUS ($GeV^{-1/2}$)	PHASE (°)	DOCUMENT ID		TECN	COMMENT
0.021±0.007	−67 ± 12	ROENCHEN	22	DPWA	Multichannel
• • • We do not use the following data for averages, fits, limits, etc. • • •					
−0.034	63	ROENCHEN	15A	DPWA	Multichannel

$\Delta(2400) \to N\gamma$, helicity-3/2 amplitude $A_{3/2}$

MODULUS ($GeV^{-1/2}$)	PHASE (°)	DOCUMENT ID		TECN	COMMENT
0.022±0.007	122 ± 7	ROENCHEN	22	DPWA	Multichannel
• • • We do not use the following data for averages, fits, limits, etc. • • •					
0.054	−75	ROENCHEN	15A	DPWA	Multichannel

$\Delta(2400)$ REFERENCES

ROENCHEN	22	EPJ A58 229	D. Roenchen *et al.*	(JULI, GWU, BONN+)
ROENCHEN	15A	EPJ A51 70	D. Roenchen *et al.*	
ARNDT	06	PR C74 045205	R.A. Arndt *et al.*	(GWU)
CUTKOSKY	80	Toronto Conf. 19	R.E. Cutkosky *et al.*	(CMU, LBL) IJP
Also		PR D20 2839	R.E. Cutkosky *et al.*	(CMU, LBL)
HOEHLER	79	PDAT 12-1	G. Hohler *et al.*	(KARLT) IJP
Also		Toronto Conf. 3	R. Koch	(KARLT) IJP

$\Delta(2420)\ 11/2^+$

$I(J^P) = \frac{3}{2}(\frac{11}{2}^+)$ Status: ****

Older and obsolete values are listed and referenced in the 2014 edition, Chinese Physics **C38** 070001 (2014).

$\Delta(2420)$ POLE POSITION

REAL PART

VALUE (MeV)	DOCUMENT ID		TECN	COMMENT
2300 to 2500 (≈ 2400) OUR ESTIMATE				
2454± 4±11	[1] SVARC	14	L+P	$\pi N \to \pi N$
2360±100	CUTKOSKY	80	IPWA	$\pi N \to \pi N$
• • • We do not use the following data for averages, fits, limits, etc. • • •				
2529	ARNDT	06	DPWA	$\pi N \to \pi N, \eta N$
2300	HOEHLER	93	ARGD	$\pi N \to \pi N$

[1] Fit to the amplitudes of HOEHLER 79.

Int. J. Mod. Phys. A 2026.41. Downloaded from www.worldscientific.com by UNIVERSITY OF CALIFORNIA @ BERKELEY on 09/16/26. Re-use and distribution is strictly not permitted, except for Open Access articles.

−2×IMAGINARY PART

VALUE (MeV)	DOCUMENT ID		TECN	COMMENT
350 to 550 (≈ 450) OUR ESTIMATE				
462± 8±50	[1] SVARC	14	L+P	$\pi N \to \pi N$
420±100	CUTKOSKY	80	IPWA	$\pi N \to \pi N$
• • • We do not use the following data for averages, fits, limits, etc. • • •				
621	ARNDT	06	DPWA	$\pi N \to \pi N, \eta N$
620	HOEHLER	93	ARGD	$\pi N \to \pi N$

[1] Fit to the amplitudes of HOEHLER 79.

$\Delta(2420)$ ELASTIC POLE RESIDUE

MODULUS $|r|$

VALUE (MeV)	DOCUMENT ID		TECN	COMMENT
20 to 40 (≈ 30) OUR ESTIMATE				
30±1±7	[1] SVARC	14	L+P	$\pi N \to \pi N$
18±6	CUTKOSKY	80	IPWA	$\pi N \to \pi N$
• • • We do not use the following data for averages, fits, limits, etc. • • •				
33	ARNDT	06	DPWA	$\pi N \to \pi N, \eta N$
39	HOEHLER	93	ARGD	$\pi N \to \pi N$

[1] Fit to the amplitudes of HOEHLER 79.

PHASE θ

VALUE (°)	DOCUMENT ID		TECN	COMMENT
−60 to 20 (≈ −20) OUR ESTIMATE				
11± 1±8	[1] SVARC	14	L+P	$\pi N \to \pi N$
−30±40	CUTKOSKY	80	IPWA	$\pi N \to \pi N$
• • • We do not use the following data for averages, fits, limits, etc. • • •				
−45	ARNDT	06	DPWA	$\pi N \to \pi N, \eta N$
−60	HOEHLER	93	ARGD	$\pi N \to \pi N$

[1] Fit to the amplitudes of HOEHLER 79.

$\Delta(2420)$ BREIT-WIGNER MASS

VALUE (MeV)	DOCUMENT ID		TECN	COMMENT
2300 to 2600 (≈ 2450) OUR ESTIMATE				
2633± 29	[1] ARNDT	06	DPWA	$\pi N \to \pi N, \eta N$
2400±125	CUTKOSKY	80	IPWA	$\pi N \to \pi N$
2416± 17	HOEHLER	79	IPWA	$\pi N \to \pi N$

[1] Statistical error only.

$\Delta(2420)$ BREIT-WIGNER WIDTH

VALUE (MeV)	DOCUMENT ID		TECN	COMMENT
300 to 700 (≈ 500) OUR ESTIMATE				
692± 47	[1] ARNDT	06	DPWA	$\pi N \to \pi N, \eta N$
450±150	CUTKOSKY	80	IPWA	$\pi N \to \pi N$
340± 28	HOEHLER	79	IPWA	$\pi N \to \pi N$

[1] Statistical error only.

$\Delta(2420)$ DECAY MODES

The following branching fractions are our estimates, not fits or averages.

	Mode	Fraction (Γ_i/Γ)
Γ_1	$N\pi$	5–10 %

$\Delta(2420)$ BRANCHING RATIOS

$\Gamma(N\pi)/\Gamma_{total}$ — Γ_1/Γ

VALUE (%)	DOCUMENT ID		TECN	COMMENT
5 to 10 (≈ 8) OUR ESTIMATE				
8.5±0.8	[1] ARNDT	06	DPWA	$\pi N \to \pi N, \eta N$
8 ±3	CUTKOSKY	80	IPWA	$\pi N \to \pi N$
8.0±1.5	HOEHLER	79	IPWA	$\pi N \to \pi N$

[1] Statistical error only.

$\Delta(2420)$ REFERENCES

PDG	14	CP C38 070001	K. Olive *et al.*	(PDG Collab.)
SVARC	14	PR C89 045205	A. Svarc *et al.*	(RBI Zagreb, UNI Tuzla)
ARNDT	06	PR C74 045205	R.A. Arndt *et al.*	(GWU)
HOEHLER	93	πN Newsletter 9 1	G. Hohler	(KARL)
CUTKOSKY	80	Toronto Conf. 19	R.E. Cutkosky *et al.*	(CMU, LBL) IJP
Also		PR D20 2839	R.E. Cutkosky *et al.*	(CMU, LBL)
HOEHLER	79	PDAT 12-1	G. Hohler *et al.*	(KARLT) IJP
Also		Toronto Conf. 3	R. Koch	(KARLT) IJP

$\Delta(2750)\ 13/2^-$

$I(J^P) = \frac{3}{2}(\frac{13}{2}^-)$ Status: **

OMITTED FROM SUMMARY TABLE

$\Delta(2750)$ BREIT-WIGNER MASS

VALUE (MeV)	DOCUMENT ID		TECN	COMMENT
2794±80	HOEHLER	79	IPWA	$\pi N \to \pi N$

$\Delta(2750)$ BREIT-WIGNER WIDTH

VALUE (MeV)	DOCUMENT ID		TECN	COMMENT
350±100	HOEHLER	79	IPWA	$\pi N \to \pi N$

$\Delta(2750)$ DECAY MODES

	Mode	Fraction (Γ_i/Γ)
Γ_1	$N\pi$	2–6 %

$\Delta(2750)$ BRANCHING RATIOS

$\Gamma(N\pi)/\Gamma_{total}$ — Γ_1/Γ

VALUE (%)	DOCUMENT ID		TECN	COMMENT
4.0±1.5	HOEHLER	79	IPWA	$\pi N \to \pi N$

$\Delta(2750)$ REFERENCES

HOEHLER	79	PDAT 12-1	G. Hohler *et al.*	(KARLT) IJP
Also		Toronto Conf. 3	R. Koch	(KARLT) IJP

$\Delta(2950)\ 15/2^+$

$I(J^P) = \frac{3}{2}(\frac{15}{2}^+)$ Status: **

OMITTED FROM SUMMARY TABLE

$\Delta(2950)$ BREIT-WIGNER MASS

VALUE (MeV)	DOCUMENT ID		TECN	COMMENT
2990±100	HOEHLER	79	IPWA	$\pi N \to \pi N$

$\Delta(2950)$ BREIT-WIGNER WIDTH

VALUE (MeV)	DOCUMENT ID		TECN	COMMENT
330±100	HOEHLER	79	IPWA	$\pi N \to \pi N$

$\Delta(2950)$ DECAY MODES

	Mode	Fraction (Γ_i/Γ)
Γ_1	$N\pi$	2–6 %

$\Delta(2950)$ BRANCHING RATIOS

$\Gamma(N\pi)/\Gamma_{total}$ — Γ_1/Γ

VALUE (%)	DOCUMENT ID		TECN	COMMENT
4±2	HOEHLER	79	IPWA	$\pi N \to \pi N$

$\Delta(2950)$ REFERENCES

HOEHLER	79	PDAT 12-1	G. Hohler *et al.*	(KARLT) IJP
Also		Toronto Conf. 3	R. Koch	(KARLT) IJP

$\Delta(\sim 3000$ Region) Partial-Wave Analyses

OMITTED FROM SUMMARY TABLE

We list here miscellaneous high-mass candidates for isospin-3/2 resonances found in partial-wave analyses.

Our 1982 edition also had a $\Delta(2850)$ and a $\Delta(3230)$. The evidence for them was deduced from total cross-section and 180° elastic cross-section measurements. The $\Delta(2850)$ has been resolved into the $\Delta(2750)$ $I_{3,13}$ and $\Delta(2950)$ $K_{3,15}$. The $\Delta(3230)$ is perhaps related to the $K_{3,13}$ of HENDRY 78 and to the $L_{3,17}$ of KOCH 80.

$\Delta(\sim 3000)$ BREIT-WIGNER MASS

VALUE (MeV)	DOCUMENT ID		TECN	COMMENT
3300	[1] KOCH	80	IPWA	$\pi N \to \pi N$ $L_{3,17}$ wave
3500	[1] KOCH	80	IPWA	$\pi N \to \pi N$ $M_{3,19}$ wave
2850±150	HENDRY	78	MPWA	$\pi N \to \pi N$ $I_{3,11}$ wave
3200±200	HENDRY	78	MPWA	$\pi N \to \pi N$ $K_{3,13}$ wave
3300±200	HENDRY	78	MPWA	$\pi N \to \pi N$ $L_{3,17}$ wave
3700±200	HENDRY	78	MPWA	$\pi N \to \pi N$ $M_{3,19}$ wave
4100±300	HENDRY	78	MPWA	$\pi N \to \pi N$ $N_{3,21}$ wave

$\Delta(\sim 3000)$ BREIT-WIGNER WIDTH

VALUE (MeV)	DOCUMENT ID		TECN	COMMENT
700±200	HENDRY	78	MPWA	$\pi N \to \pi N$ $I_{3,11}$ wave
1000±300	HENDRY	78	MPWA	$\pi N \to \pi N$ $K_{3,13}$ wave
1100±300	HENDRY	78	MPWA	$\pi N \to \pi N$ $L_{3,17}$ wave
1300±400	HENDRY	78	MPWA	$\pi N \to \pi N$ $M_{3,19}$ wave
1600±500	HENDRY	78	MPWA	$\pi N \to \pi N$ $N_{3,21}$ wave

$\Delta(\sim 3000)$ DECAY MODES

	Mode	Fraction (Γ_i/Γ)
Γ_1	$N\pi$	1–8%

$\Delta(\sim 3000)$ BRANCHING RATIOS

$\Gamma(N\pi)/\Gamma_{total}$ — Γ_1/Γ

VALUE (%)	DOCUMENT ID		TECN	COMMENT
1–8% OUR ESTIMATE				
6±2	HENDRY	78	MPWA	$\pi N \to \pi N$ $I_{3,11}$ wave
5±2	HENDRY	78	MPWA	$\pi N \to \pi N$ $K_{3,13}$ wave
3±1	HENDRY	78	MPWA	$\pi N \to \pi N$ $L_{3,17}$ wave
3±1	HENDRY	78	MPWA	$\pi N \to \pi N$ $M_{3,19}$ wave
2±1	HENDRY	78	MPWA	$\pi N \to \pi N$ $N_{3,21}$ wave

$\Delta(\sim 3000)$ FOOTNOTES

[1] In addition, KOCH 80 reports some evidence for an S_{31} $\Delta(2700)$ and a P_{33} $\Delta(2800)$.

$\Delta(\sim 3000)$ REFERENCES

KOCH 80 Toronto Conf. 3 R. Koch (KARLT) IJP
HENDRY 78 PRL 41 222 A.W. Hendry (IND, LBL) IJP
Also ANP 136 1 A.W. Hendry (IND)

Int. J. Mod. Phys. A 2026.41. Downloaded from www.worldscientific.com
UNIVERSITY OF CALIFORNIA @ BERKELEY on 09/16/26. Re-use and distribution is strictly not permitted, except for Open Access articles.

Int. J. Mod. Phys. A 2026.41. Downloaded from www.worldscientific.com
by UNIVERSITY OF CALIFORNIA @ BERKELEY on 09/16/26. Re-use and distribution is strictly not permitted, except for Open Access articles.

Λ BARYONS
($S = -1$, $I = 0$)

$\Lambda^0 = uds$

Λ

$I(J^P) = 0(\frac{1}{2}^+)$ Status: ****

We have omitted some results that have been superseded by later experiments. See our earlier editions.

Λ MASS

The fit uses Λ, Σ^+, Σ^0, Σ^- mass and mass-difference measurements.

VALUE (MeV)	EVTS	DOCUMENT ID		TECN	COMMENT
1115.683±0.006 OUR FIT					
1115.683±0.006 OUR AVERAGE					
1115.678±0.006±0.006	20k	HARTOUNI	94	SPEC	pp 27.5 GeV/c
1115.690±0.008±0.006	18k	[1] HARTOUNI	94	SPEC	pp 27.5 GeV/c
• • • We do not use the following data for averages, fits, limits, etc. • • •					
1115.59 ±0.08	935	HYMAN	72	HEBC	
1115.39 ±0.12	195	MAYEUR	67	EMUL	
1115.6 ±0.4		LONDON	66	HBC	
1115.65 ±0.07	488	[2] SCHMIDT	65	HBC	
1115.44 ±0.12		[3] BHOWMIK	63	RVUE	

[1] We assume CPT invariance: this is the $\overline{\Lambda}$ mass as measured by HARTOUNI 94. See below for the fractional mass difference, testing CPT.
[2] The SCHMIDT 65 masses have been reevaluated using our April 1973 proton and $K^\pm$ and $\pi^\pm$ masses. P. Schmidt, private communication (1974).
[3] The mass has been raised 35 keV to take into account a 46 keV increase in the proton mass and an 11 keV decrease in the $\pi^\pm$ mass (note added Reviews of Modern Physics **39** 1 (1967)).

$(m_\Lambda - m_{\overline{\Lambda}}) / m_\Lambda$

A test of CPT invariance.

VALUE (units 10^{-5})	EVTS	DOCUMENT ID		TECN	COMMENT
− 0.1 ± 1.1 OUR AVERAGE	Error includes scale factor of 1.6.				
+ 1.3 ± 1.2	31k	[1] RYBICKI	96	NA32	π^- Cu, 230 GeV
− 1.08 ± 0.90		HARTOUNI	94	SPEC	pp 27.5 GeV/c
4.5 ± 5.4		CHIEN	66	HBC	6.9 GeV/c $\overline{p}p$
• • • We do not use the following data for averages, fits, limits, etc. • • •					
−26 ±13		BADIER	67	HBC	2.4 GeV/c $\overline{p}p$

[1] RYBICKI 96 is an analysis of old ACCMOR (NA32) data.

Λ MEAN LIFE

Measurements with an error $\geq 0.1 \times 10^{-10}$ s have been omitted altogether, and only the highest-statistics are used.

VALUE (10^{-10} s)	EVTS	DOCUMENT ID		TECN	COMMENT
2.617 ±0.010 OUR AVERAGE	Error includes scale factor of 1.5. See the ideogram below.				
2.6107±0.0037±0.0072	188M	ACHARYA	23	ALCE	Pb-Pb → ΛX or $\overline{\Lambda} X$ at 5.02 TeV
2.69 ±0.03	53k	ZECH	77	SPEC	Neutral hyperon beam
2.611 ±0.020	34k	CLAYTON	75	HBC	0.96–1.4 GeV/c K^-p
2.626 ±0.020	36k	POULARD	73	HBC	0.4–2.3 GeV/c K^-p
• • • We do not use the following data for averages, fits, limits, etc. • • •					
2.69 ±0.05	6582	ALTHOFF	73B	OSPK	$\pi^+ n \to \Lambda K^+$
2.54 ±0.04	4572	BALTAY	71B	HBC	K^-p at rest
2.535 ±0.035	8342	GRIMM	68	HBC	
2.47 ±0.08	2600	HEPP	68	HBC	
2.35 ±0.09	916	BURAN	66	HLBC	
$2.452^{+0.056}_{-0.054}$	2213	ENGELMANN	66	HBC	
2.59 ±0.09	794	HUBBARD	64	HBC	
2.59 ±0.07	1378	SCHWARTZ	64	HBC	
2.36 ±0.06	2239	BLOCK	63	HEBC	

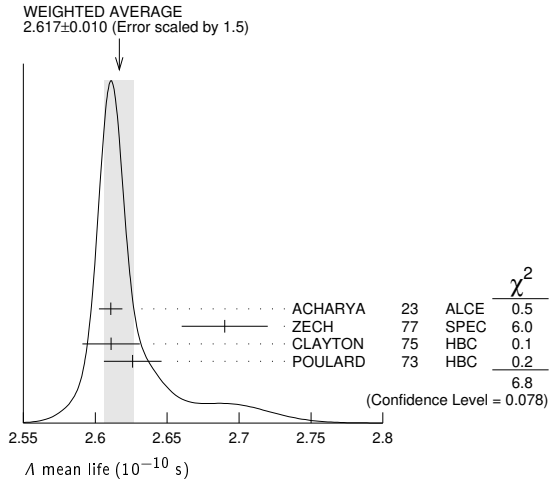

$(\tau_\Lambda - \tau_{\overline{\Lambda}}) / \tau_\Lambda$

A test of CPT invariance.

VALUE (units 10^{-3})	EVTS	DOCUMENT ID		TECN	COMMENT
0.9± 3.2 OUR AVERAGE					
1.3± 2.8±2.1	188M	ACHARYA	23	ALCE	Pb-Pb → ΛX or $\overline{\Lambda} X$ at 5.02 TeV
− 1.8± 6.6±5.6		BARNES	96	CNTR	LEAR $\overline{p}p \to \overline{\Lambda}\Lambda$
44 ±85		BADIER	67	HBC	2.4 GeV/c $\overline{p}p$

Λ MAGNETIC MOMENT

See the "Quark Model" review. Measurements with an error $\geq 0.15\ \mu_N$ have been omitted.

VALUE (μ_N)	EVTS	DOCUMENT ID		TECN	COMMENT
−0.613 ±0.004 OUR AVERAGE					
−0.606 ±0.015	200k	COX	81	SPEC	
−0.6138±0.0047	3M	SCHACHIN...	78	SPEC	
−0.59 ±0.07	350k	HELLER	77	SPEC	
−0.57 ±0.05	1.2M	BUNCE	76	SPEC	
−0.66 ±0.07	1300	DAHL-JENSEN	71	EMUL	200 kG field

Λ ELECTRIC DIPOLE MOMENT

A nonzero value is forbidden by both T invariance and P invariance.

VALUE (10^{-16} ecm)	CL%	DOCUMENT ID		TECN
< 1.5	95	[1] PONDROM	81	SPEC
• • • We do not use the following data for averages, fits, limits, etc. • • •				
<100	95	[2] BARONI	71	EMUL
<500	95	GIBSON	66	EMUL

[1] PONDROM 81 measures $(-3.0 \pm 7.4) \times 10^{-17}$ e-cm.
[2] BARONI 71 measures $(-5.9 \pm 2.9) \times 10^{-15}$ e-cm.

Λ DECAY MODES

	Mode		Fraction (Γ_i/Γ)	Confidence level
Γ_1	$p\pi^-$		(64.1 ±0.5) %	
Γ_2	$n\pi^0$		(35.9 ±0.5) %	
Γ_3	$n\gamma$		(8.3 ±0.7) $\times 10^{-4}$	
Γ_4	$p\pi^-\gamma$	[a]	(8.5 ±1.4) $\times 10^{-4}$	
Γ_5	$pe^-\overline{\nu}_e$		(8.34±0.14) $\times 10^{-4}$	
Γ_6	$p\mu^-\overline{\nu}_\mu$		(1.51±0.19) $\times 10^{-4}$	
	Lepton (L) and/or Baryon (B) number violating decay modes			
Γ_7	$\pi^+ e^-$	L,B	< 6 $\times 10^{-7}$	90%
Γ_8	$\pi^+ \mu^-$	L,B	< 6 $\times 10^{-7}$	90%
Γ_9	$\pi^- e^+$	L,B	< 4 $\times 10^{-7}$	90%
Γ_{10}	$\pi^- \mu^+$	L,B	< 6 $\times 10^{-7}$	90%
Γ_{11}	$K^+ e^-$	L,B	< 2 $\times 10^{-6}$	90%
Γ_{12}	$K^+ \mu^-$	L,B	< 3 $\times 10^{-6}$	90%
Γ_{13}	$K^- e^+$	L,B	< 2 $\times 10^{-6}$	90%
Γ_{14}	$K^- \mu^+$	L,B	< 3 $\times 10^{-6}$	90%
Γ_{15}	$K^0_S \nu$	L,B	< 2 $\times 10^{-5}$	90%
Γ_{16}	$\overline{p}\pi^+$	B	< 9 $\times 10^{-7}$	90%
Γ_{17}	invisible		< 7.4 $\times 10^{-5}$	90%

[a] See the Listings below for the pion momentum range used in this measurement.

Int. J. Mod. Phys. A 2026.41. Downloaded from www.worldscientific.com
UNIVERSITY OF CALIFORNIA @ BERKELEY on 09/16/26. Re-use and distribution is strictly not permitted, except for Open Access articles.

CONSTRAINED FIT INFORMATION

An overall fit to 4 branching ratios uses 11 measurements and one constraint to determine 3 parameters. The overall fit has a $\chi^2 = 6.9$ for 9 degrees of freedom.

The following *off-diagonal* array elements are the correlation coefficients $\langle \delta x_i \delta x_j \rangle / (\delta x_i \cdot \delta x_j)$, in percent, from the fit to the branching fractions, $x_i \equiv \Gamma_i/\Gamma_{total}$. The fit constrains the x_i whose labels appear in this array to sum to one.

	x_1	x_2
x_2	−100	
x_6	0	0

Λ BRANCHING RATIOS

$\Gamma(p\pi^-)/\Gamma(N\pi)$ — $\Gamma_1/(\Gamma_1+\Gamma_2)$

VALUE	EVTS	DOCUMENT ID		TECN	COMMENT
0.641±0.005 OUR FIT					
0.640±0.005 OUR AVERAGE					
0.646±0.008	4572	BALTAY	71B	HBC	K^-p at rest
0.635±0.007	6736	DOYLE	69	HBC	$\pi^-p \to \Lambda K^0$
0.643±0.016	903	HUMPHREY	62	HBC	
0.624±0.030		CRAWFORD	59B	HBC	$\pi^-p \to \Lambda K^0$

$\Gamma(n\pi^0)/\Gamma(N\pi)$ — $\Gamma_2/(\Gamma_1+\Gamma_2)$

VALUE	EVTS	DOCUMENT ID		TECN
0.359±0.005 OUR FIT				
0.310±0.028 OUR AVERAGE				
0.35 ±0.05		BROWN	63	HLBC
0.291±0.034	75	CHRETIEN	63	HLBC

$\Gamma(n\gamma)/\Gamma_{total}$ — Γ_3/Γ

VALUE (units 10^{-3})	EVTS	DOCUMENT ID		TECN	COMMENT
0.832±0.038±0.054	1221	[1] ABLIKIM	22AJ	BES3	$J/\psi \to \Lambda\overline{\Lambda}$
• • • We do not use the following data for averages, fits, limits, etc. • • •					
1.75 ±0.15	1816	LARSON	93	SPEC	K^-p at rest
1.78 ±0.24 $^{+0.14}_{-0.16}$	287	NOBLE	92	SPEC	See LARSON 93

[1] This ABLIKIM 22AJ value is a factor of 2.1 smaller and differs by 5.6σ from the previous LARSON 93 value.

$\Gamma(n\gamma)/\Gamma(n\pi^0)$ — Γ_3/Γ_2

VALUE (units 10^{-3})	EVTS	DOCUMENT ID		TECN	COMMENT
• • • We do not use the following data for averages, fits, limits, etc. • • •					
2.86±0.74±0.57	24	BIAGI	86	SPEC	SPS hyperon beam

$\Gamma(p\pi^-\gamma)/\Gamma(p\pi^-)$ — Γ_4/Γ_1

VALUE (units 10^{-3})	EVTS	DOCUMENT ID		TECN	COMMENT
1.32±0.22	72	BAGGETT	72C	HBC	$\pi^- < 95$ MeV/c

$\Gamma(pe^-\overline{\nu}_e)/\Gamma(p\pi^-)$ — Γ_5/Γ_1

VALUE (units 10^{-3})	EVTS	DOCUMENT ID		TECN	COMMENT
1.301±0.019 OUR AVERAGE					
1.335±0.056	7111	BOURQUIN	83	SPEC	SPS hyperon beam
1.313±0.024	10k	WISE	80	SPEC	
1.23 ±0.11	544	LINDQUIST	77	SPEC	$\pi^-p \to K^0\Lambda$
1.27 ±0.07	1089	KATZ	73	HBC	
1.31 ±0.06	1078	ALTHOFF	71	OSPK	
1.17 ±0.13	86	[1] CANTER	71	HBC	K^-p at rest
1.20 ±0.12	143	[2] MALONEY	69	HBC	
1.17 ±0.18	120	[2] BAGLIN	64	FBC	K^- freon 1.45 GeV/c
1.23 ±0.20	150	[2] ELY	63	FBC	
• • • We do not use the following data for averages, fits, limits, etc. • • •					
1.32 ±0.15	218	[1] LINDQUIST	71	OSPK	See LINDQUIST 77

[1] Changed by us from $\Gamma(pe^-\overline{\nu}_e)/\Gamma(N\pi)$ assuming the authors used $\Gamma(\Lambda \to p\pi^-)/\Gamma(\text{total}) = 2/3$.

[2] Changed by us from $\Gamma(pe^-\overline{\nu}_e)/\Gamma(N\pi)$ because $\Gamma(pe^-\nu)/\Gamma(p\pi^-)$ is the directly measured quantity.

$\Gamma(p\mu^-\overline{\nu}_\mu)/\Gamma_{total}$ — Γ_6/Γ

VALUE (units 10^{-4})	EVTS	DOCUMENT ID		TECN	COMMENT
1.51±0.19 OUR FIT					
1.48±0.21±0.08	64	[1] ABLIKIM	21AG	BES3	$J/\psi \to \Lambda\overline{\Lambda}$

[1] ABLIKIM 21AG use $\overline{\Lambda} \to \overline{p}\pi^+$ decay mode as the double tag identifier and thus as indirect normalization.

$\Gamma(p\mu^-\overline{\nu}_\mu)/\Gamma(N\pi)$ — $\Gamma_6/(\Gamma_1+\Gamma_2)$

VALUE (units 10^{-4})	EVTS	DOCUMENT ID		TECN	COMMENT
1.51±0.19 OUR FIT					
1.57±0.35 OUR AVERAGE					
1.4 ±0.5	14	BAGGETT	72B	HBC	K^-p at rest
2.4 ±0.8	9	CANTER	71B	HBC	K^-p at rest
1.3 ±0.7	3	LIND	64	RVUE	
1.5 ±1.2	2	RONNE	64	FBC	

Lepton (L) and/or Baryon (B) number violating decay modes

$\Gamma(\pi^+e^-)/\Gamma_{total}$ — Γ_7/Γ

VALUE	CL%	DOCUMENT ID		TECN	COMMENT
<6 × 10^{-7}	90	[1] MCCRACKEN	15	CLAS	$\gamma p \to K^+\Lambda$

[1] Uses B($\Lambda \to p\pi^-$) = (63.9 ± 0.5)% for normalization mode.

$\Gamma(\pi^+\mu^-)/\Gamma_{total}$ — Γ_8/Γ

VALUE	CL%	DOCUMENT ID		TECN	COMMENT
<6 × 10^{-7}	90	[1] MCCRACKEN	15	CLAS	$\gamma p \to K^+\Lambda$

[1] Uses B($\Lambda \to p\pi^-$) = (63.9 ± 0.5)% for normalization mode.

$\Gamma(\pi^-e^+)/\Gamma_{total}$ — Γ_9/Γ

VALUE	CL%	DOCUMENT ID		TECN	COMMENT
<4 × 10^{-7}	90	[1] MCCRACKEN	15	CLAS	$\gamma p \to K^+\Lambda$

[1] Uses B($\Lambda \to p\pi^-$) = (63.9 ± 0.5)% for normalization mode.

$\Gamma(\pi^-\mu^+)/\Gamma_{total}$ — Γ_{10}/Γ

VALUE	CL%	DOCUMENT ID		TECN	COMMENT
<6 × 10^{-7}	90	[1] MCCRACKEN	15	CLAS	$\gamma p \to K^+\Lambda$

[1] Uses B($\Lambda \to p\pi^-$) = (63.9 ± 0.5)% for normalization mode.

$\Gamma(K^+e^-)/\Gamma_{total}$ — Γ_{11}/Γ

VALUE	CL%	DOCUMENT ID		TECN	COMMENT
<2 × 10^{-6}	90	[1] MCCRACKEN	15	CLAS	$\gamma p \to K^+\Lambda$

[1] Uses B($\Lambda \to p\pi^-$) = (63.9 ± 0.5)% for normalization mode.

$\Gamma(K^+\mu^-)/\Gamma_{total}$ — Γ_{12}/Γ

VALUE	CL%	DOCUMENT ID		TECN	COMMENT
<3 × 10^{-6}	90	[1] MCCRACKEN	15	CLAS	$\gamma p \to K^+\Lambda$

[1] Uses B($\Lambda \to p\pi^-$) = (63.9 ± 0.5)% for normalization mode.

$\Gamma(K^-e^+)/\Gamma_{total}$ — Γ_{13}/Γ

VALUE	CL%	DOCUMENT ID		TECN	COMMENT
<2 × 10^{-6}	90	[1] MCCRACKEN	15	CLAS	$\gamma p \to K^+\Lambda$

[1] Uses B($\Lambda \to p\pi^-$) = (63.9 ± 0.5)% for normalization mode.

$\Gamma(K^-\mu^+)/\Gamma_{total}$ — Γ_{14}/Γ

VALUE	CL%	DOCUMENT ID		TECN	COMMENT
<3 × 10^{-6}	90	[1] MCCRACKEN	15	CLAS	$\gamma p \to K^+\Lambda$

[1] Uses B($\Lambda \to p\pi^-$) = (63.9 ± 0.5)% for normalization mode.

$\Gamma(K^0_S\nu)/\Gamma_{total}$ — Γ_{15}/Γ

VALUE	CL%	DOCUMENT ID		TECN	COMMENT
<2 × 10^{-5}	90	[1] MCCRACKEN	15	CLAS	$\gamma p \to K^+\Lambda$

[1] Uses B($\Lambda \to p\pi^-$) = (63.9 ± 0.5)% for normalization mode.

$\Gamma(\overline{p}\pi^+)/\Gamma_{total}$ — Γ_{16}/Γ

VALUE	CL%	DOCUMENT ID		TECN	COMMENT
<9 × 10^{-7}	90	[1] MCCRACKEN	15	CLAS	$\gamma p \to K^+\Lambda$

[1] Uses B($\Lambda \to p\pi^-$) = (63.9 ± 0.5)% for normalization mode.

$\Gamma(\text{invisible})/\Gamma_{total}$ — Γ_{17}/Γ

VALUE	CL%	DOCUMENT ID		TECN	COMMENT
<7.4 × 10^{-5}	90	ABLIKIM	22P	BES3	$J/\psi \to \Lambda\overline{\Lambda}$

Λ CP-violating decay-rate asymmetries

This is the difference between Λ and $\overline{\Lambda}$ decay rates to state f and $\overline{f}$ divided by the sum of the rates:
$A_{CP}(f) = [(B(\Lambda \to f)) - (B(\overline{\Lambda} \to \overline{f}))]/\text{Sum}$.

$A_{CP}(p\mu^-\overline{\nu}_\mu)$ in $\Lambda \to p\mu^-\overline{\nu}_\mu, \overline{\Lambda} \to \overline{p}\mu^+\nu_\mu$

VALUE	DOCUMENT ID		TECN	COMMENT
0.02±0.14±0.02	ABLIKIM	21AG	BES3	$J/\psi \to \Lambda\overline{\Lambda}$

Limit on $\overline{\Lambda}\Lambda$ oscillations

Upper limit for the oscillation rate of ($\overline{\Lambda} \to \Lambda$) hyperons. A test of baryon number nonconservation. We quote the oscillation parameter $\delta m_{\overline{\Lambda}\Lambda}$, deduced from the oscillation rate P(Λ) and the hyperon lifetime τ_Λ, as $(\delta m_{\overline{\Lambda}\Lambda})^2 = P(\Lambda) / 2\tau_\Lambda^2$.

VALUE (GeV)	CL%	DOCUMENT ID		TECN	COMMENT
<2.1 × 10^{-18}	90	[1] ABLIKIM	25AT	BES3	$J/\psi \to \Lambda\overline{\Lambda} \to (p\pi^-)(\overline{p}\pi^+)$
<3.8 × 10^{-18}	90	[2] ABLIKIM	23BM	BES3	$J/\psi \to pK^-\overline{\Lambda}$

[1] ABLIKIM 25AT quote the oscillation rate limit P(Λ) < 1.4 × 10^{-6} and calculate the oscillation parameter $\delta m_{\overline{\Lambda}\Lambda}$ given here.

[2] ABLIKIM 23BM quote the oscillation rate limit P(Λ) < 4.4 × 10^{-6} and calculate the oscillation parameter $\delta m_{\overline{\Lambda}\Lambda}$ given here.

Int. J. Mod. Phys. A 2026.41. Downloaded from www.worldscientific.com by UNIVERSITY OF CALIFORNIA @ BERKELEY on 09/16/26. Re-use and distribution is strictly not permitted, except for Open Access articles.

Λ DECAY PARAMETERS

See the "Note on Baryon Decay Parameters" in the neutron Listings. Some early results have been omitted.

α_- FOR $\Lambda \to p\pi^-$

OUR FIT value is obtained from measurements of $\alpha(\Xi^-)$, $\alpha_-(\Lambda)$, and $\alpha(\Xi^-)\alpha_-(\Lambda)$.

VALUE	EVTS	DOCUMENT ID	TECN	COMMENT
0.748 ±0.008 OUR FIT Error includes scale factor of 2.4.				
0.746 ±0.008 OUR AVERAGE Error includes scale factor of 2.4. See the ideogram below.				
0.717 ±0.017 ±0.009	27k	AAIJ	24AH LHCB	$\Lambda_b \to \Lambda_c \to \Lambda h^+$
0.764 ±0.008 $^{+0.005}_{-0.006}$	144k	ABLIKIM	24AR BES3	$J/\psi \to \Xi\overline{\Xi} \to \Lambda\overline{\Lambda}\pi\pi$
0.730 ±0.051 ±0.011	1.1M	ABLIKIM	24CE BES3	$J/\psi \to \Sigma\overline{\Sigma} \to \Lambda\overline{\Lambda}\gamma\gamma$
0.7519±0.0036±0.0024	3.2M	ABLIKIM	22AG BES3	$J/\psi \to \Lambda\overline{\Lambda}$
0.721 ±0.006 ±0.005		[1] IRELAND	19 CLAS	K production
• • • We do not use the following data for averages, fits, limits, etc. • • •				
0.757 ±0.011 ±0.008	73k	ABLIKIM	22AD BES3	$J/\psi \to \Xi\overline{\Xi} \to \Lambda\overline{\Lambda}\pi\pi$
0.74 $^{+0.04}_{-0.03}$		AAIJ	20O LHCB	$\Lambda_b \to J/\psi\Lambda$
0.750 ±0.009 ±0.004	420k	ABLIKIM	19BJ BES3	$J/\psi \to \Lambda\overline{\Lambda}$
0.584 ±0.046	8500	ASTBURY	75 SPEC	
0.649 ±0.023	10325	CLELAND	72 OSPK	
0.67 ±0.06	3520	DAUBER	69 HBC	From Ξ decay
0.645 ±0.017	10130	OVERSETH	67 OSPK	Λ from $\pi^- p$
0.62 ±0.07	1156	CRONIN	63 CNTR	Λ from $\pi^- p$

[1] This is a new analysis based on existing kaon photoproduction data of the CLAS collaboration and using spin algebra constraints.

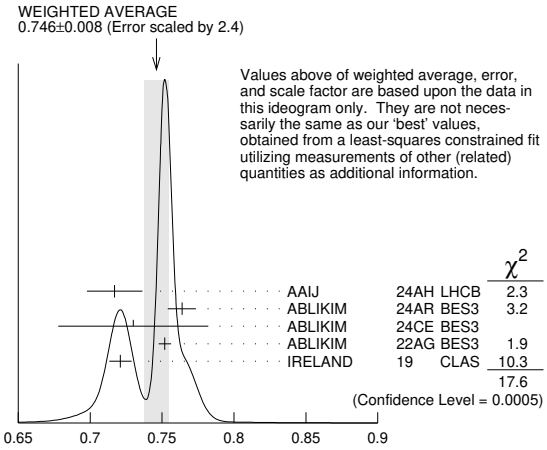

α_- FOR $\Lambda \to p\pi^-$

α_+ FOR $\overline{\Lambda} \to \overline{p}\pi^+$

VALUE	EVTS	DOCUMENT ID	TECN	COMMENT
−0.758 ±0.005 OUR AVERAGE Error includes scale factor of 1.2.				
−0.748 ±0.016 ±0.007	27k	AAIJ	24AH LHCB	$\Lambda_b \to \Lambda_c \to \Lambda h^+$
−0.774 ±0.009 $^{+0.005}_{-0.005}$	123k	ABLIKIM	24AR BES3	$J/\psi \to \Xi\overline{\Xi} \to \Lambda\overline{\Lambda}\pi\pi$
−0.776 ±0.054 ±0.010	1.1M	ABLIKIM	24CE BES3	$J/\psi \to \Sigma\overline{\Sigma} \to \Lambda\overline{\Lambda}\gamma\gamma$
−0.7559±0.0036±0.0030	3.2M	ABLIKIM	22AG BES3	$J/\psi \to \Lambda\overline{\Lambda}$
• • • We do not use the following data for averages, fits, limits, etc. • • •				
−0.763 ±0.011 ±0.007	73k	ABLIKIM	22AD BES3	$J/\psi \to \Xi\overline{\Xi} \to \Lambda\overline{\Lambda}\pi\pi$
−0.758 ±0.010 ±0.007	420k	ABLIKIM	19BJ BES3	$J/\psi \to \Lambda\overline{\Lambda}$
−0.755 ±0.083 ±0.063	8.7k	ABLIKIM	10 BES	$J/\psi \to \Lambda\overline{\Lambda}$
−0.63 ±0.13	770	TIXIER	88 DM2	$J/\psi \to \Lambda\overline{\Lambda}$

$\overline{\alpha}_0$ FOR $\overline{\Lambda} \to \overline{n}\pi^0$

VALUE	EVTS	DOCUMENT ID	TECN	COMMENT
−0.675±0.011 OUR AVERAGE Error includes scale factor of 1.2.				
−0.668±0.008$^{+0.006}_{-0.008}$	123k	ABLIKIM	24AR BES3	$J/\psi \to \Xi\overline{\Xi} \to \Lambda\overline{\Lambda}\pi\pi$
−0.692±0.016±0.006	47k	ABLIKIM	19BJ BES3	J/ψ to $\Lambda\overline{\Lambda}$

α_0 FOR $\Lambda \to n\pi^0$

VALUE	EVTS	DOCUMENT ID	TECN	COMMENT
0.670±0.009$^{+0.009}_{-0.008}$	144k	ABLIKIM	24AR BES3	$J/\psi \to \Xi\overline{\Xi} \to \Lambda\overline{\Lambda}\pi\pi$

α_γ FOR $\Lambda \to n\gamma$

VALUE	EVTS	DOCUMENT ID	TECN	COMMENT
−0.16±0.10±0.05	13889	ABLIKIM	22AJ BES3	$J/\psi \to \Lambda\overline{\Lambda}$

ϕ ANGLE FOR $\Lambda \to p\pi^-$ ($\tan\phi = \beta / \gamma$)

VALUE (°)	EVTS	DOCUMENT ID	TECN	COMMENT
− 6.5± 3.5 OUR AVERAGE				
− 7.0± 4.5	10325	CLELAND	72 OSPK	Λ from $\pi^- p$
− 8.0± 6.0	10130	OVERSETH	67 OSPK	Λ from $\pi^- p$
13.0±17.0	1156	CRONIN	63 OSPK	Λ from $\pi^- p$

$\alpha_0 / \alpha_- = \alpha(\Lambda \to n\pi^0) / \alpha(\Lambda \to p\pi^-)$

VALUE	EVTS	DOCUMENT ID	TECN	COMMENT
0.888$^{+0.034}_{-0.030}$ OUR AVERAGE Error includes scale factor of 1.7.				
0.877±0.015$^{+0.014}_{-0.010}$	144k	ABLIKIM	24AR BES3	$J/\psi \to \Xi\overline{\Xi} \to \Lambda\overline{\Lambda}\pi\pi$
1.000±0.068	4760	[1] OLSEN	70 OSPK	$\pi^+ n \to \Lambda K^+$
1.10 ±0.27		CORK	60 CNTR	

[1] OLSEN 70 compares proton and neutron distributions from Λ decay.

$\overline{\alpha}_0 / \alpha_+$ in $\overline{\Lambda} \to \overline{n}\pi^0$, $\overline{\Lambda} \to \overline{p}\pi^+$

VALUE	EVTS	DOCUMENT ID	TECN	COMMENT
0.876$^{+0.022}_{-0.020}$ OUR AVERAGE Error includes scale factor of 1.4.				
0.863±0.014$^{+0.012}_{-0.008}$	123k	ABLIKIM	24AR BES3	$J/\psi \to \Xi\overline{\Xi} \to \Lambda\overline{\Lambda}\pi\pi$
0.913±0.028±0.012	47k	ABLIKIM	19BJ BES3	J/ψ to $\Lambda\overline{\Lambda}$

$(\alpha_- + \alpha_+)/(\alpha_- - \alpha_+)$ in $\Lambda \to p\pi^-$, $\overline{\Lambda} \to \overline{p}\pi^+$

Zero if CP is conserved; α_- and α_+ are the asymmetry parameters for $\Lambda \to p\pi^-$ and $\overline{\Lambda} \to \overline{p}\pi^+$ decay. See also the Ξ^- for a similar test involving the decay chain $\Xi^- \to \Lambda\pi^-$, $\Lambda \to p\pi^-$ and the corresponding antiparticle chain.

VALUE (units 10^{-2})	EVTS	DOCUMENT ID	TECN	COMMENT
−0.3 ± 0.4 OUR AVERAGE				
−2.2 ± 1.6 ±0.7	27k	AAIJ	24AH LHCB	$\Lambda_b \to \Lambda_c \to \Lambda h^+$
−0.7 ± 0.8 $^{+0.2}_{-0.3}$	267k	ABLIKIM	24AR BES3	$J/\psi \to \Xi\overline{\Xi} \to \Lambda\overline{\Lambda}\pi\pi$
3.0 ± 6.9 ±1.5	1.1M	ABLIKIM	24CE BES3	$J/\psi/\psi(2S) \to \Sigma\overline{\Sigma} \to \Lambda\overline{\Lambda}\gamma\gamma$
1.3 ± 0.7 ±1.1	369k	[1] LI	23C BELL	$J/\psi \to \Xi\overline{\Xi} \to \Lambda\overline{\Lambda}\pi\pi$
−0.25± 0.46±0.12	3.2M	ABLIKIM	22AG BES3	$J/\psi \to \Lambda\overline{\Lambda}$
−8.1 ± 5.5 ±5.9	8.7k	ABLIKIM	10 BES	$J/\psi \to \Lambda\overline{\Lambda}$
1.3 ± 2.2	96k	BARNES	96 CNTR	LEAR $\overline{p}p \to \overline{\Lambda}\Lambda$
1 ±10	770	TIXIER	88 DM2	$J/\psi \to \Lambda\overline{\Lambda}$
−2 ±14	10k	[2] CHAUVAT	85 CNTR	pp, $\overline{p}p$ ISR
• • • We do not use the following data for averages, fits, limits, etc. • • •				
−0.4 ± 1.2 ±0.9	73k	ABLIKIM	22AD BES3	$J/\psi \to \Xi\overline{\Xi} \to \Lambda\overline{\Lambda}\pi\pi$
−0.6 ± 1.2 ±0.7	420k	[3] ABLIKIM	19BJ BES3	$J/\psi \to \Lambda\overline{\Lambda}$
−7 ± 9	4063	BARNES	87 CNTR	See BARNES 96

[1] LI 23C quote the average Λ-hyperon asymmetry A^{α}_{CP} from 264k $\Lambda_c^+ \to \Lambda\pi^+$ decays and 105k $\Lambda_c^+ \to \Sigma^0\pi^+$ decays, under the assumption of no CP violation in the SM for Λ_c^+, i.e. $\alpha_{\Lambda_c^+} = -\alpha_{\overline{\Lambda}_c^-}$.

[2] CHAUVAT 85 actually gives $\alpha_+(\overline{\Lambda})/\alpha_-(\Lambda) = -1.04 \pm 0.29$. Assumes polarization is same in $\overline{p}p \to \overline{\Lambda}X$ and $pp \to \Lambda X$. Tests of this assumption, based on C-invariance and fragmentation, are satisfied by the data.

[3] Superseded by ABLIKIM 22AG.

$(\alpha_0 + \overline{\alpha}_0)/(\alpha_0 - \overline{\alpha}_0)$ in $\Lambda \to n\pi^0$, $\overline{\Lambda} \to \overline{n}\pi^0$

VALUE (units 10^{-2})	EVTS	DOCUMENT ID	TECN	COMMENT
0.1±0.9$^{+0.5}_{-0.7}$	267k	ABLIKIM	24AR BES3	$J/\psi \to \Xi\overline{\Xi} \to \Lambda\overline{\Lambda}\pi\pi$

$R = |G_E/G_M|$ in $\Lambda \to p\pi^-$, $\overline{\Lambda} \to \overline{p}\pi^+$

VALUE	EVTS	DOCUMENT ID	TECN	COMMENT
• • • We do not use the following data for averages, fits, limits, etc. • • •				
0.91±0.08±0.02		[1,2] ABLIKIM	25BQ BES3	$e^+e^- \to \overline{\Lambda}\Lambda$ at $\sqrt{s}$ = 2.396 GeV
0.47±0.08±0.05	2.2k	[3] ABLIKIM	25CK BES3	$e^+e^- \to \overline{\Lambda}\Lambda$ at $\sqrt{s}$ = 3.773 GeV
0.96±0.14±0.02		[4] ABLIKIM	19BF BES3	$e^+e^- \to \overline{\Lambda}\Lambda$ at $\sqrt{s}$ = 2.396 GeV

[1] ABLIKIM 25BQ provides values in a range of $\sqrt{s}$ energies of 2.396–2.90 GeV. We quote their most precise value at 2.396 GeV.

[2] Determined using asymmetry parameter value $\alpha = 0.754$.

[3] Determined using asymmetry parameter value $\alpha = 0.7542$.

[4] Determined using asymmetry parameter value $\alpha = 0.750 \pm 0.010$.

$\Delta\Phi = \Phi_E - \Phi_M$ in $\Lambda \to p\pi^-$, $\overline{\Lambda} \to \overline{p}\pi^+$

Relative phase between G_E and G_M.

VALUE (degrees)	EVTS	DOCUMENT ID	TECN	COMMENT
• • • We do not use the following data for averages, fits, limits, etc. • • •				
42 ±10 ±2		[1,2] ABLIKIM	25BQ BES3	$e^+e^- \to \overline{\Lambda}\Lambda$ at $\sqrt{s}$ = 2.396 GeV
87.7±20.6±1.7	2.2k	[3] ABLIKIM	25CK BES3	$e^+e^- \to \overline{\Lambda}\Lambda$ at $\sqrt{s}$ = 3.773 GeV
37 ±12 ±6		[4] ABLIKIM	19BF BES3	$e^+e^- \to \overline{\Lambda}\Lambda$ at $\sqrt{s}$ = 2.396 GeV

[1] ABLIKIM 25BQ provides values in a range of $\sqrt{s}$ energies of 2.396–2.90 GeV. We quote their most precise value at 2.396 GeV.

[2] Determined using asymmetry parameter value $\alpha = 0.754$.

[3] Determined using asymmetry parameter value $\alpha = 0.7542$.

[4] Determined using asymmetry parameter value $\alpha = 0.750 \pm 0.010$.

Int. J. Mod. Phys. A 2026.41. Downloaded from www.worldscientific.com by UNIVERSITY OF CALIFORNIA @ BERKELEY on 09/16/26. Re-use and distribution is strictly not permitted, except for Open Access articles.

g_A / g_V FOR $\Lambda \to pe^-\overline{\nu}_e$

Measurements with fewer than 500 events have been omitted. Where necessary, signs have been changed to agree with our conventions, which are given in the "Note on Baryon Decay Parameters" in the neutron Listings. The measurements all assume that the form factor $g_2 = 0$. See also the footnote on DWORKIN 90.

VALUE	EVTS	DOCUMENT ID		TECN	COMMENT
-0.718 ± 0.015 OUR AVERAGE					
$-0.719 \pm 0.016 \pm 0.012$	37k	[1] DWORKIN	90	SPEC	$e\nu$ angular corr.
-0.70 ± 0.03	7111	BOURQUIN	83	SPEC	$\Xi \to \Lambda\pi^-$
-0.734 ± 0.031	10k	[2] WISE	81	SPEC	$e\nu$ angular correl.
• • • We do not use the following data for averages, fits, limits, etc. • • •					
-0.63 ± 0.06	817	ALTHOFF	73	OSPK	Polarized Λ

[1] The tabulated result assumes the weak-magnetism coupling $w \equiv g_W(0)/g_V(0)$ to be 0.97, as given by the CVC hypothesis and as assumed by the other listed measurements. However, DWORKIN 90 *measures* w to be 0.15 ± 0.30, and then $g_A/g_V = -0.731 \pm 0.016$.

[2] This experiment measures only the absolute value of g_A/g_V.

Λ REFERENCES

We have omitted some papers that have been superseded by later experiments. See our earlier editions.

ABLIKIM	25AT	PR D111 052014	M. Ablikim *et al.*	(BESIII Collab.)
ABLIKIM	25BQ	PRL 135 191902	M. Ablikim *et al.*	(BESIII Collab.)
ABLIKIM	25CK	PR D112 L051102	M. Ablikim *et al.*	(BESIII Collab.)
AAIJ	24AH	PRL 133 261804	R. Aaij *et al.*	(LHCb Collab.)
ABLIKIM	24AR	PRL 132 101801	M. Ablikim *et al.*	(BESIII Collab.)
ABLIKIM	24CE	PRL 133 101902	M. Ablikim *et al.*	(BESIII Collab.)
ABLIKIM	23BM	PRL 131 121801	M. Ablikim *et al.*	(BESIII Collab.)
ACHARYA	23	PR D108 032009	S. Acharya *et al.*	(ALICE Collab.)
LI	23C	SCIB 68 583	L.K. Li *et al.*	(BELLE Collab.)
ABLIKIM	22AD	NAT 606 64	M. Ablikim *et al.*	(BESIII Collab.)
ABLIKIM	22AG	PRL 129 131801	M. Ablikim *et al.*	(BESIII Collab.)
ABLIKIM	22AJ	PRL 129 212002	M. Ablikim *et al.*	(BESIII Collab.)
ABLIKIM	22P	PR D105 L071101	M. Ablikim *et al.*	(BESIII Collab.)
ABLIKIM	21AG	PRL 127 121802	M. Ablikim *et al.*	(BESIII Collab.)
AAIJ	20O	JHEP 2006 110	R. Aaij *et al.*	(LHCb Collab.)
ABLIKIM	19BF	PRL 123 122003	M. Ablikim *et al.*	(BESIII Collab.)
ABLIKIM	19BJ	NATP 15 631	M. Ablikim *et al.*	(BESIII Collab.)
IRELAND	19	PRL 123 182301	D.G. Ireland *et al.*	(GLAS, GWU, JULI+)
MCCRACKEN	15	PR D92 072002	M.E. McCracken *et al.*	(JLab CLAS Collab.)
ABLIKIM	10	PR D81 012003	M. Ablikim *et al.*	(BES Collab.)
BARNES	96	PR C54 1877	P.D. Barnes *et al.*	(CERN PS-185 Collab.)
RYBICKI	96	APP B27 2155	K. Rybicki	
HARTOUNI	94	PRL 72 1322	E.P. Hartouni *et al.*	(BNL E766 Collab.)
Also		PRL 72 2821 (errat.)	E.P. Hartouni *et al.*	(BNL E766 Collab.)
LARSON	93	PR D47 799	K.D. Larson *et al.*	(BNL-811 Collab.)
NOBLE	92	PRL 69 414	A.J. Noble *et al.*	(BIRM, BOST, BRCO+)
DWORKIN	90	PR D41 780	J. Dworkin *et al.*	(MICH, WISC, RUTG+)
TIXIER	88	PL B212 523	M.H. Tixier *et al.*	(DM2 Collab.)
BARNES	87	PL B199 147	P.D. Barnes *et al.*	(CMU, SACL, LANL+)
BIAGI	86	ZPHY C30 201	S.F. Biagi *et al.*	(BRIS, CERN, GEVA+)
CHAUVAT	85	PL 163B 273	P. Chauvat *et al.*	(CERN, CLER, UCLA+)
BOURQUIN	83	ZPHY C21 1	M.H. Bourquin *et al.*	(BRIS, GEVA, HEIDP+)
COX	81	PRL 46 877	P.T. Cox *et al.*	(MICH, WISC, RUTG, MINN+)
PONDROM	81	PR D23 814	L. Pondrom *et al.*	(WISC, MICH, RUTG+)
WISE	81	PL 98B 123	J.E. Wise *et al.*	(MASA, BNL)
WISE	80	PL 91B 165	J.E. Wise *et al.*	(MASA, BNL)
SCHACHIN...	78	PRL 41 1348	L. Schachinger *et al.*	(MICH, RUTG, WISC)
HELLER	77	PL 68B 480	K. Heller *et al.*	(MICH, WISC, HEIDH)
LINDQUIST	77	PR D16 2104	J. Lindquist *et al.*	(EFI, OSU, ANL)
Also		JP G2 L211	J. Lindquist *et al.*	(EFI, WUSL, OSU+)
ZECH	77	NP B124 413	G. Zech *et al.*	(SIEG, CERN, DORT, HEIDH)
BUNCE	76	PRL 36 1113	G.R.M. Bunce *et al.*	(WISC, MICH, RUTG)
ASTBURY	75	NP B99 30	P. Astbury *et al.*	(LOIC, CERN, ETH+)
CLAYTON	75	NP B95 130	E.F. Clayton *et al.*	(LOIC, RHEL)
ALTHOFF	73	PL 43B 237	K.H. Althoff *et al.*	(CERN, HEID)
ALTHOFF	73B	NP B66 29	K.H. Althoff *et al.*	(CERN, HEID)
KATZ	73	Thesis MDDP-TR-74-044	C.N. Katz	(UMD)
POULARD	73	PL 46B 135	G. Poulard, A. Givernaud, A.C. Borg	(SACL)
BAGGETT	72B	ZPHY 252 362	M.J. Baggett *et al.*	(HEID)
BAGGETT	72C	PL 42B 379	M.J. Baggett *et al.*	(HEID)
CLELAND	72	NP B40 221	W.E. Cleland *et al.*	(CERN, GEVA, LUND)
HYMAN	72	PR D5 1063	L.G. Hyman *et al.*	(ANL, CMU)
ALTHOFF	71	PL 37B 531	K.H. Althoff *et al.*	(CERN, HEID)
BALTAY	71B	PR D4 670	C. Baltay *et al.*	(COLU, BING)
BARONI	71	LNC 2 1256	G. Baroni, S. Petrera, G. Romano	(ROMA)
CANTER	71	PRL 26 868	J. Canter *et al.*	(STON, COLU)
CANTER	71B	PRL 27 59	J. Canter *et al.*	(STON, COLU)
DAHL-JENSEN	71	NC 3A 1	E. Dahl-Jensen *et al.*	(CERN, ANKA, LAUS+)
LINDQUIST	71	PRL 27 612	J. Lindquist *et al.*	(EFI, WUSL, OSU+)
OLSEN	70	PRL 24 843	S.L. Olsen *et al.*	(WISC, MICH)
DAUBER	69	PR 179 1262	P.M. Dauber *et al.*	(LRL)
DOYLE	69	Thesis UCRL 18139	J.C. Doyle	(LRL)
MALONEY	69	PRL 23 425	J.E. Maloney, B. Sechi-Zorn	(UMD)
GRIMM	68	NC 54A 187	H.J. Grimm	(HEID)
HEPP	68	ZPHY 214 71	V. Hepp, H. Schleich	(HEID)
BADIER	67	PL 25B 152	J. Badier *et al.*	(EPOL)
MAYEUR	67	U.Libr.Brux.Bul. 32	C. Mayeur, E. Tompa, J.H. Wickens	(BELG, LOUC)
OVERSETH	67	PRL 19 391	O.E. Overseth, R.F. Roth	(MICH, PRIN)
PDG	67	RMP 39 1	A.H. Rosenfeld *et al.*	(LRL, CERN, YALE)
BURAN	66	PL 20 318	T. Buran *et al.*	(OSLO)
CHIEN	66	PR 152 1171	C.Y. Chien *et al.*	(YALE, BNL)
ENGELMANN	66	NC 45A 1038	R. Engelmann *et al.*	(HEID, REHO)
GIBSON	66	NC 45A 882	W.M. Gibson, K. Green	(BRIS)
LONDON	66	PR 143 1034	G.W. London *et al.*	(BNL, SYRA)
SCHMIDT	65	PR 140 B1328	P. Schmidt	(COLU)
BAGLIN	64	NC 35 977	C. Baglin *et al.*	(EPOL, CERN, LOUC, RHEL+)
HUBBARD	64	PR 135 B183	J.R. Hubbard *et al.*	(LRL)
LIND	64	PR 135 B1483	V.G. Lind *et al.*	(WISC)
RONNE	64	PL 11 357	B.E. Ronne *et al.*	(CERN, EPOL, LOUC+)
SCHWARTZ	64	Thesis UCRL 11360	J.A. Schwartz	(LRL)
BHOWMIK	63	NC 28 1494	B. Bhowmik, D.P. Goyal	(DELH)
BLOCK	63	PR 130 766	M.M. Block *et al.*	(NWES, BGNA, SYRA+)
BROWN	63	PR 130 769	J.L. Brown *et al.*	(LRL, MICH)
CHRETIEN	63	PR 131 2208	M. Chretien *et al.*	(BRAN, BROW, HARV+)
CRONIN	63	PR 129 1795	J.W. Cronin, O.E. Overseth	(PRIN)
ELY	63	PR 131 868	R.P. Ely *et al.*	(LRL)
HUMPHREY	62	PR 127 1305	W.E. Humphrey, R.R. Ross	(LRL)
CORK	60	PR 120 1000	B. Cork *et al.*	(LRL, PRIN, BNL)
CRAWFORD	59B	PRL 2 266	F.S. Crawford *et al.*	(LRL)

See the related review(s):
Λ and Σ Resonances

$\Lambda(1380)\ 1/2^-$

$J^P = \frac{1}{2}^-$ Status: $**$

OMITTED FROM SUMMARY TABLE

See the related review on "Pole Structure of the $\Lambda(1405)$ Region."

$\Lambda(1380)$ POLE POSITION

REAL PART

VALUE (MeV)	DOCUMENT ID		TECN
• • • We do not use the following data for averages, fits, limits, etc. • • •			
1325 ± 15	[1] MAI	15	DPWA
1330^{+4}_{-5}	[2] MAI	15	DPWA
1388 ± 9	GUO	13	DPWA
1381^{+18}_{-6}	IKEDA	12	DPWA

[1] Solution number 4.
[2] Solution number 2.

$-2\times$IMAGINARY PART

VALUE (MeV)	DOCUMENT ID		TECN
• • • We do not use the following data for averages, fits, limits, etc. • • •			
180^{+24}_{-36}	[1] MAI	15	DPWA
112^{+34}_{-22}	[2] MAI	15	DPWA
228^{+48}_{-50}	GUO	13	DPWA
162^{+38}_{-16}	IKEDA	12	DPWA

[1] Solution number 4.
[2] Solution number 2.

$\Lambda(1380)$ REFERENCES

MAI	15	EPJ A51 30	M. Mai, U.-G. Meissner	(BONN, JULI)
GUO	13	PR C87 035202	Z.-H. Guo, J. Oller	
IKEDA	12	NP A881 98	Y. Ikeda, T. Hyodo, W. Weise	(TUM, RIKEN, TINT)

$\Lambda(1405)\ 1/2^-$

$I(J^P) = 0(\frac{1}{2}^-)$ Status: $****$

In the 1998 Note on the $\Lambda(1405)$ in PDG 98, R.H. Dalitz discussed the S-shaped cusp behavior of the intensity at the N-$\overline{K}$ threshold observed in THOMAS 73 and HEMINGWAY 85. He commented that this behavior "is characteristic of S-wave coupling; the other below threshold hyperon, the $\Sigma(1385)$, has no such threshold distortion because its N-$\overline{K}$ coupling is P-wave. For $\Lambda(1405)$ this asymmetry is the sole direct evidence that $J^P = 1/2^-$."

A recent measurement by the CLAS collaboration, MORIYA 14, definitively established the long-assumed $J^P = 1/2^-$ spin-parity assignment of the $\Lambda(1405)$. The experiment produced the $\Lambda(1405)$ spin-polarized in the photoproduction process $\gamma p \to K^+\Lambda(1405)$ and measured the decay of the $\Lambda(1405)$(polarized) $\to \Sigma^+$(polarized)π^-. The observed isotropic decay of $\Lambda(1405)$ is consistent with spin $J = 1/2$. The polarization transfer to the Σ^+(polarized) direction revealed negative parity, and thus established $J^P = 1/2^-$.

See the related review(s):
Pole Structure of the $\Lambda(1405)$ Region

$\Lambda(1405)$ POLE POSITION

REAL PART

VALUE (MeV)	DOCUMENT ID		TECN
• • • We do not use the following data for averages, fits, limits, etc. • • •			
$1417.7^{+6.0+1.1}_{-7.4-1.0}$	AIKAWA	23	DPWA
1429^{+8}_{-7}	[1] MAI	15	DPWA
1434 ± 2	[2] MAI	15	DPWA
1421^{+3}_{-2}	GUO	13	DPWA
1424^{+7}_{-23}	IKEDA	12	DPWA

[1] Solution number 4.
[2] Solution number 2.

Int. J. Mod. Phys. A 2026.41. Downloaded from www.worldscientific.com
by UNIVERSITY OF CALIFORNIA @ BERKELEY on 09/16/26. Re-use and distribution is strictly not permitted, except for Open Access articles.

−2×IMAGINARY PART

VALUE (MeV)	DOCUMENT ID		TECN
• • • We do not use the following data for averages, fits, limits, etc. • • •			
$52.2^{+12.0}_{-15.8}{}^{+3.4}_{-4.0}$	AIKAWA	23	DPWA
24^{+4}_{-6}	[1] MAI	15	DPWA
20^{+4}_{-2}	[2] MAI	15	DPWA
38^{+16}_{-10}	GUO	13	DPWA
52^{+6}_{-28}	IKEDA	12	DPWA

[1] Solution number 4.
[2] Solution number 2.

$\Lambda(1405)$ MASS

PRODUCTION EXPERIMENTS

VALUE (MeV)	EVTS	DOCUMENT ID		TECN	COMMENT
$1405.1^{+1.3}_{-1.0}$ OUR AVERAGE					
1405^{+11}_{-9}		HASSANVAND	13	SPEC	$pp \to p\Lambda(1405)K^+$
$1405^{+1.4}_{-1.0}$		ESMAILI	10	RVUE	^{4}He $K^- \to \Sigma^\pm\pi^\mp X$ at rest
1406.5 ± 4.0		[1] DALITZ	91		M-matrix fit
• • • We do not use the following data for averages, fits, limits, etc. • • •					
1391 ± 1	700	[1] HEMINGWAY	85	HBC	K^-p 4.2 GeV/c
~ 1405	400	[2] THOMAS	73	HBC	π^-p 1.69 GeV/c
1405	120	BARBARO-...	68B	DBC	K^-d 2.1–2.7 GeV/c
1400 ± 5	67	BIRMINGHAM	66	HBC	K^-p 3.5 GeV/c
1382 ± 8		ENGLER	65	HDBC	π^-p, π^+d 1.68 GeV/c
1400 ± 24		MUSGRAVE	65	HBC	$\bar{p}p$ 3–4 GeV/c
1410		ALEXANDER	62	HBC	π^-p 2.1 GeV/c
1405		ALSTON	62	HBC	K^-p 1.2–0.5 GeV/c
1405		ALSTON	61B	HBC	K^-p 1.15 GeV/c

[1] DALITZ 91 fits the HEMINGWAY 85 data.
[2] THOMAS 73 data is fit by CHAO 73 (see next section).

EXTRAPOLATIONS BELOW $N\overline{K}$ THRESHOLD

VALUE (MeV)	DOCUMENT ID		TECN	COMMENT
• • • We do not use the following data for averages, fits, limits, etc. • • •				
1407.56 or 1407.50	[1] KIMURA	00		potential model
1411	[2] MARTIN	81		K-matrix fit
1406	[3] CHAO	73	DPWA	0–range fit (sol. B)
1421	MARTIN	70	RVUE	Constant K-matrix
1416 ± 4	MARTIN	69	HBC	Constant K-matrix
1403 ± 3	KIM	67	HBC	K-matrix fit
1407.5 ± 1.2	[4] KITTEL	66	HBC	0–effective-range fit
1410.7 ± 1.0	KIM	65	HBC	0–effective-range fit
1409.6 ± 1.7	[4] SAKITT	65	HBC	0–effective-range fit

[1] The KIMURA 00 values are from fits A and B from a coupled-channel potential model using low-energy $\overline{K}N$ and $\Sigma\pi$ data, kaonic-hydrogen x-ray measurements, and our $\Lambda(1405)$ mass and width. The results bear mainly on the *nature* of the $\Lambda(1405)$: three-quark state or $\overline{K}N$ bound state.
[2] The MARTIN 81 fit includes the $K^\pm p$ forward scattering amplitudes and the dispersion relations they must satisfy.
[3] See also the accompanying paper of THOMAS 73.
[4] Data of SAKITT 65 are used in the fit by KITTEL 66.

$\Lambda(1405)$ WIDTH

PRODUCTION EXPERIMENTS

VALUE (MeV)	EVTS	DOCUMENT ID		TECN	COMMENT
50.5 ± 2.0 OUR AVERAGE					
62 ± 10		HASSANVAND	13	SPEC	$pp \to p\Lambda(1405)K^+$
50 ± 2		[1] DALITZ	91		M-matrix fit
• • • We do not use the following data for averages, fits, limits, etc. • • •					
24^{+4}_{-3}		ESMAILI	10	RVUE	^{4}He $K^- \to \Sigma^\pm\pi^\mp X$ at rest
32 ± 1	700	[1] HEMINGWAY	85	HBC	K^-p 4.2 GeV/c
45 to 55	400	[2] THOMAS	73	HBC	π^-p 1.69 GeV/c
35	120	BARBARO-...	68B	DBC	K^-d 2.1–2.7 GeV/c
50 ± 10	67	BIRMINGHAM	66	HBC	K^-p 3.5 GeV/c
89 ± 20		ENGLER	65	HDBC	
60 ± 20		MUSGRAVE	65	HBC	
35 ± 5		ALEXANDER	62	HBC	
50		ALSTON	62	HBC	
20		ALSTON	61B	HBC	

[1] DALITZ 91 fits the HEMINGWAY 85 data.
[2] THOMAS 73 data is fit by CHAO 73 (see next section).

EXTRAPOLATIONS BELOW $N\overline{K}$ THRESHOLD

VALUE (MeV)	DOCUMENT ID		TECN	COMMENT
• • • We do not use the following data for averages, fits, limits, etc. • • •				
50.24 or 50.26	[1] KIMURA	00		potential model
30	[2] MARTIN	81		K-matrix fit
55	[3,4] CHAO	73	DPWA	0–range fit (sol. B)
20	MARTIN	70	RVUE	Constant K-matrix
29 ± 6	MARTIN	69	HBC	Constant K-matrix
50 ± 5	KIM	67	HBC	K-matrix fit
34.1 ± 4.1	[5] KITTEL	66	HBC	
37.0 ± 3.2	KIM	65	HBC	
28.2 ± 4.1	[5] SAKITT	65	HBC	

[1] The KIMURA 00 values are from fits A and B from a coupled-channel potential model using low-energy $\overline{K}N$ and $\Sigma\pi$ data, kaonic-hydrogen x-ray measurements, and our $\Lambda(1405)$ mass and width. The results bear mainly on the *nature* of the $\Lambda(1405)$: three-quark state or $\overline{K}N$ bound state.
[2] The MARTIN 81 fit includes the $K^\pm p$ forward scattering amplitudes and the dispersion relations they must satisfy.
[3] An asymmetric shape, with $\Gamma/2 = 41$ MeV below resonance, 14 MeV above.
[4] See also the accompanying paper of THOMAS 73.
[5] Data of SAKITT 65 are used in the fit by KITTEL 66.

$\Lambda(1405)$ DECAY MODES

	Mode	Fraction (Γ_i/Γ)
Γ_1	$\Sigma\pi$	100 %
Γ_2	$\Lambda\gamma$	
Γ_3	$\Sigma^0\gamma$	
Γ_4	$N\overline{K}$	

$\Lambda(1405)$ PARTIAL WIDTHS

$\Gamma(\Lambda\gamma)$ — Γ_2

VALUE (keV)	DOCUMENT ID	COMMENT
• • • We do not use the following data for averages, fits, limits, etc. • • •		
27 ± 8	BURKHARDT 91	Isobar model fit

$\Gamma(\Sigma^0\gamma)$ — Γ_3

VALUE (keV)	DOCUMENT ID	COMMENT
• • • We do not use the following data for averages, fits, limits, etc. • • •		
10 ± 4 or 23 ± 7	BURKHARDT 91	Isobar model fit

$\Lambda(1405)$ BRANCHING RATIOS

$\Gamma(N\overline{K})/\Gamma(\Sigma\pi)$ — Γ_4/Γ_1

VALUE	CL%	DOCUMENT ID		TECN	COMMENT
• • • We do not use the following data for averages, fits, limits, etc. • • •					
<3	95	HEMINGWAY	85	HBC	K^-p 4.2 GeV/c

$\Lambda(1405)$ REFERENCES

AIKAWA	23	PL B837 137637	S. Aikawa *et al.*	(J-PARC E31 Collab.)
MAI	15	EPJ A51 30	M. Mai, U.-G. Meissner	(BONN, JULI)
MORIYA	14	PRL 112 082004	K. Moriya *et al.*	(CLAS Collab.) JP
GUO	13	PR C87 035202	Z.-H. Guo, J. Oller	
HASSANVAND	13	PR C87 055202	M. Hassanvand *et al.*	
Also		PR C88 019905 (errat.)	M. Hassanvand *et al.*	
IKEDA	12	NP A881 98	Y. Ikeda, T. Hyodo, W. Weise	(TUM, RIKEN, TINT)
ESMAILI	10	PL B686 23	J. Esmaili, Y. Akaishi, T. Yamazaki	(RIKEN, ISUT+)
KIMURA	00	PR C62 015206	M. Kimura *et al.*	
PDG	98	EPJ C3 1	C. Caso *et al.*	(PDG Collab.)
BURKHARDT	91	PR C44 607	H. Burkhardt, J. Lowe	(NOTT, UNM, BIRM)
DALITZ	91	JP G17 289	R.H. Dalitz, A. Deloff	(OXFTP, WINR)
HEMINGWAY	85	NP B253 742	R.J. Hemingway	(CERN) J
MARTIN	81	NP B179 33	A.D. Martin	(DURH)
CHAO	73	NP B56 46	Y.A. Chao *et al.*	(RHEL, CMU, LOUC)
THOMAS	73	NP B56 15	D.W. Thomas *et al.*	(CMU) J
MARTIN	70	NP B16 479	A.D. Martin, G.G. Ross	(DURH)
MARTIN	69	PR 183 1352	B.R. Martin, M. Sakitt	(LOUC, BNL)
Also		PR 183 1345	B.R. Martin, M. Sakitt	(LOUC, BNL)
BARBARO-...	68B	PRL 21 573	A. Barbaro-Galtieri *et al.*	(LRL, SLAC)
KIM	67	PRL 19 1074	J.K. Kim	(YALE)
BIRMINGHAM	66	PR 152 1148	M. Haque *et al.*	(BIRM, GLAS, LOIC, OXF+)
KITTEL	66	PL 21 349	W. Kittel, G. Otter, I. Wacek	(VIEN)
ENGLER	65	PRL 15 224	A. Engler *et al.*	(CMU, BNL) IJ
KIM	65	PRL 14 29	J.K. Kim	(COLU)
MUSGRAVE	65	NC 35 735	B. Musgrave *et al.*	(BIRM, CERN, EPOL+)
SAKITT	65	PR 139 B719	M. Sakitt *et al.*	(UMD, LRL)
ALEXANDER	62	PRL 8 447	G. Alexander *et al.*	(LRL) I
ALSTON	62	CERN Conf. 311	M.H. Alston *et al.*	(LRL) I
ALSTON	61B	PRL 6 698	M.H. Alston *et al.*	(LRL) I

OTHER RELATED PAPERS

IWASAKI	97	PRL 78 3067	M. Iwasaki *et al.*	(KEK 228 Collab.)
FINK	90	PR C41 2720	P.J.Jr. Fink *et al.*	(IBMY, ORST, ANSM)
LEINWEBER	90	ANP 198 203	D.B. Leinweber	(MCMS)
MUELLER-GR...	90	NP A513 557	A. Mueller-Groeling, K. Holinde, J. Speth	(JULI)
BARRETT	89	NC 102A 179	R.C. Barrett	(SURR)
BATTY	89	NC 102A 255	C.J. Batty, A. Gal	(RAL, HEBR)
CAPSTICK	89	Excited Baryons 88, p.32	S. Capstick	(GUEL)
LOWE	89	NC 102A 167	J. Lowe	(BIRM)
WHITEHOUSE	89	PRL 63 1352	D.A. Whitehouse *et al.*	(BIRM, BOST, BRCO+)
SIEGEL	88	PR C38 2221	P.B. Siegel, W. Weise	(REGE)
WORKMAN	88	PR D37 3117	R.L. Workman, H.W. Fearing	(TRIU)
SCHNICK	87	PRL 58 1719	J. Schnick, R.H. Landau	(ORST)
CAPSTICK	86	PR D34 2809	S. Capstick, N. Isgur	(TNTO)
JENNINGS	86	PL B176 229	B.K. Jennings	(TRIU)
MALTMAN	86	PR D34 1372	K. Maltman, N. Isgur	(LANL, TNTO)
ZHONG	86	PL B171 471	Y.S. Zhong *et al.*	(ADLD, TRIU, SURR)
BURKHARDT	85	NP A440 653	H. Burkhardt, J. Lowe, A.S. Rosenthal	(NOTT+)
DAREWYCH	85	PR D32 1765	J.W. Darewych, R. Koniuk, N. Isgur	(YORKC, TNTO)
VEIT	85	PR D31 1033	E.A. Veit *et al.*	(TRIU, ADLD, SURR)

KIANG	84	PR C30 1638	D. Kiang *et al.*	(DALH, MCMS)
MILLER	84	Conference paper	D.J. Miller	(LOUC)
Conf. Intersections between Particle and Nuclear Physics, p. 783				
VANDIJK	84	PR D30 937	W. van Dijk	(MCMS)
VEIT	84	PL 137B 415	E.A. Veit *et al.*	(TRIU, SURR, CERN)
DALITZ	82	Heid. Conf.	R.H. Dalitz *et al.*	(OXFTP)
Heidelberg Conf., p. 201				
DALITZ	81	Kaon Conf.	R.H. Dalitz, J.G. McGinley	(OXFTP)
Low and Intermediate Energy Kaon-Nucleon Physics, p.381				
MARTIN	81B	Kaon Conf.	A.D. Martin	(DURH)
Low and Intermediate Energy Kaon-Nucelon Physics, p. 97				
OADES	77	NC 42A 462	G.C. Oades, G. Rasche	(AARH, ZURI)
SHAW	73	Purdue Conf. 417	G.L. Shaw	(UCI)
BARBARO-...	72	LBL-555	A. Barbaro-Galtieri	(LBL)
DOBSON	72	PR D6 3256	P.N. Dobson, R. McElhaney	(HAWA)
RAJASEKA...	72	PR D5 610	G. Rajasekaran	(TATA)
Earlier papers also cited in RAJASEKARAN 72.				
CLINE	71	PRL 26 1194	D. Cline, R. Laumann, J. Mapp	(WISC)
MARTIN	71	PL 35B 62	A.D. Martin, A.D. Martin, G.G. Ross	(DURH, LOUC+)
DALITZ	67	PR 153 1617	R.H. Dalitz, T.C. Wong, G. Rajasekaran	(OXFTP+)
DONALD	66	PL 22 711	R.A. Donald *et al.*	(LIVP)
KADYK	66	PRL 17 599	J.A. Kadyk *et al.*	(LRL)
ABRAMS	65	PR 139 B454	G.S. Abrams, B. Sechi-Zorn	(UMD)

$\Lambda(1520)$ $3/2^-$

$I(J^P) = 0(\frac{3}{2}^-)$ Status: ****

Discovered by FERRO-LUZZI 62; the elaboration in WATSON 63 is the classic paper on the Breit-Wigner analysis of a multichannel resonance.

The measurements of the mass, width, and elasticity published before 1975 are now obsolete and have been omitted. They were last listed in our 1982 edition Physics Letters **111B** 1 (1982).

Production and formation experiments agree quite well, so they are listed together here.

$\Lambda(1520)$ POLE POSITION

REAL PART

VALUE (MeV)	DOCUMENT ID		TECN	COMMENT
1517 to 1518 (≈ 1517.5) OUR ESTIMATE				
1517.5 ± 0.4 OUR AVERAGE				
1517.5 ± 0.4	SARANTSEV	19	DPWA	$\overline{K}N$ multichannel
1517 $^{+4}_{-4}$	[1] KAMANO	15	DPWA	$\overline{K}N$ multichannel
• • • We do not use the following data for averages, fits, limits, etc. • • •				
1518	ZHANG	13A	DPWA	$\overline{K}N$ multichannel
1518.8	QIANG	10	SPEC	$ep \to e'K^+X$ (fit to X)

[1] From the preferred solution A in KAMANO 15.

−2×IMAGINARY PART

VALUE (MeV)	DOCUMENT ID		TECN	COMMENT
14 to 18 (≈ 16) OUR ESTIMATE				
15.3 ± 0.9 OUR AVERAGE				
15.3 ± 0.9	SARANTSEV	19	DPWA	$\overline{K}N$ multichannel
15 $^{+10}_{-8}$	[1] KAMANO	15	DPWA	$\overline{K}N$ multichannel
• • • We do not use the following data for averages, fits, limits, etc. • • •				
16	ZHANG	13A	DPWA	$\overline{K}N$ multichannel
17.2	QIANG	10	SPEC	$ep \to e'K^+X$ (fit to X)

[1] From the preferred solution A in KAMANO 15.

$\Lambda(1520)$ POLE RESIDUES

The normalized residue is the residue divided by $\Gamma_{pole}/2$.

Normalized residue in $N\overline{K} \to \Lambda(1520) \to N\overline{K}$

MODULUS	PHASE (°)	DOCUMENT ID		TECN	COMMENT
0.45 ± 0.01	**−10 ± 3**	SARANTSEV	19	DPWA	$\overline{K}N$ multichannel
• • • We do not use the following data for averages, fits, limits, etc. • • •					
0.431	−11	[1] KAMANO	15	DPWA	$\overline{K}N$ multichannel

[1] From the preferred solution A in KAMANO 15.

Normalized residue in $N\overline{K} \to \Lambda(1520) \to \Sigma\pi$

MODULUS	PHASE (°)	DOCUMENT ID		TECN	COMMENT
0.44 ± 0.01	**−15 ± 3**	SARANTSEV	19	DPWA	$\overline{K}N$ multichannel
• • • We do not use the following data for averages, fits, limits, etc. • • •					
0.435	−10	[1] KAMANO	15	DPWA	$\overline{K}N$ multichannel

[1] From the preferred solution A in KAMANO 15.

Normalized residue in $N\overline{K} \to \Lambda(1520) \to \Lambda\eta$

MODULUS	PHASE (°)	DOCUMENT ID		TECN	COMMENT
0.013 ± 0.003	**116 ± 3**	SARANTSEV	19	DPWA	$\overline{K}N$ multichannel

Normalized residue in $N\overline{K} \to \Lambda(1520) \to \Sigma(1385)\pi$, S-wave

MODULUS	PHASE (°)	DOCUMENT ID		TECN	COMMENT
• • • We do not use the following data for averages, fits, limits, etc. • • •					
0.431	−123	[1] KAMANO	15	DPWA	$\overline{K}N$ multichannel

[1] From the preferred solution A in KAMANO 15.

Normalized residue in $N\overline{K} \to \Lambda(1520) \to \Sigma(1385)\pi$, D-wave

MODULUS	PHASE (°)	DOCUMENT ID		TECN	COMMENT
• • • We do not use the following data for averages, fits, limits, etc. • • •					
0.0141	122	[1] KAMANO	15	DPWA	$\overline{K}N$ multichannel

[1] From the preferred solution A in KAMANO 15.

$\Lambda(1520)$ MASS

VALUE (MeV)	EVTS	DOCUMENT ID		TECN	COMMENT
1518 to 1520 (≈ 1519) OUR ESTIMATE					
1519.42 ± 0.19 OUR AVERAGE Error includes scale factor of 1.2.					
1519.9 ± 1.6 ± 4.8		ABLIKIM	25AF	BES3	$\psi(3686) \to \Lambda\overline{\Sigma}^0\pi^0 +$ c.c. (PWA)
1518.5 ± 0.5		SARANTSEV	19	DPWA	$\overline{K}N$ multichannel
1519.6 ± 0.5		ZHANG	13A	DPWA	$\overline{K}N$ multichannel
1520.4 ± 0.6 ± 1.5		QIANG	10	SPEC	$ep \to e'K^+X$ (fit to X)
1517.3 ± 1.5	300	BARBER	80D	SPEC	$\gamma p \to \Lambda(1520)K^+$
1517.8 ± 1.2	5k	BARLAG	79	HBC	K^-p 4.2 GeV/c
1520.0 ± 0.5		ALSTON-...	78	DPWA	$\overline{K}N \to \overline{K}N$
1519.7 ± 0.3	4k	CAMERON	77	HBC	K^-p 0.96–1.36 GeV/c
1519 ± 1		GOPAL	77	DPWA	$\overline{K}N$ multichannel
1519.4 ± 0.3	2000	CORDEN	75	DBC	K^-d 1.4–1.8 GeV/c

$\Lambda(1520)$ WIDTH

VALUE (MeV)	EVTS	DOCUMENT ID		TECN	COMMENT
15 to 17 (≈ 16) OUR ESTIMATE					
15.80 ± 0.32 OUR AVERAGE Error includes scale factor of 1.3. See the ideogram below.					
20.6 ± 1.9 ± 0.6		ABLIKIM	25AF	BES3	$\psi(3686) \to \Lambda\overline{\Sigma}^0\pi^0 +$ c.c. (PWA)
15.7 ± 1.0		SARANTSEV	19	DPWA	$\overline{K}N$ multichannel
17 ± 1		ZHANG	13A	DPWA	$\overline{K}N$ multichannel
18.6 ± 1.9 ± 1.0		QIANG	10	SPEC	$ep \to e'K^+X$ (fit to X)
16.3 ± 3.3	300	BARBER	80D	SPEC	$\gamma p \to \Lambda(1520)K^+$
16 ± 1		GOPAL	80	DPWA	$\overline{K}N \to \overline{K}N$
14 ± 3	677	[1] BARLAG	79	HBC	K^-p 4.2 GeV/c
15.4 ± 0.5		ALSTON-...	78	DPWA	$\overline{K}N \to \overline{K}N$
16.3 ± 0.5	4k	CAMERON	77	HBC	K^-p 0.96–1.36 GeV/c
15.0 ± 0.5		GOPAL	77	DPWA	$\overline{K}N$ multichannel
15.5 ± 1.6	2000	CORDEN	75	DBC	K^-d 1.4–1.8 GeV/c

[1] From the best-resolution sample of $\Lambda\pi\pi$ events only.

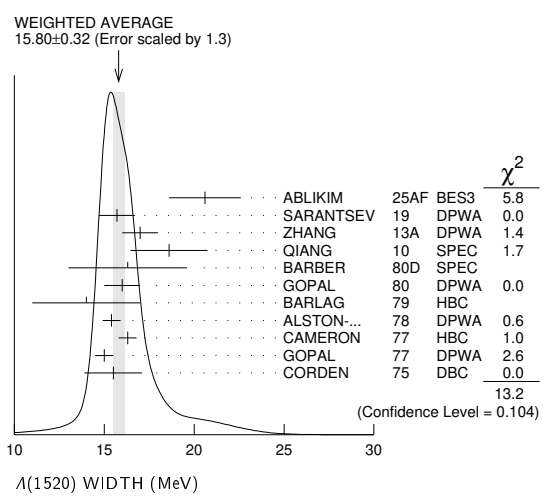

$\Lambda(1520)$ DECAY MODES

	Mode	Fraction (Γ_i/Γ)
Γ_1	$N\overline{K}$	(45 ± 1) %
Γ_2	$\Sigma\pi$	(42 ± 1) %
Γ_3	$\Lambda\pi\pi$	(10 ± 1) %
Γ_4	$\Sigma(1385)\pi$, S-wave	
Γ_5	$\Sigma(1385)\pi$, D-wave	
Γ_6	$\Sigma(1385)\pi$	(4.1 ± 0.5) %
Γ_7	$\Sigma(1385)\pi(\to \Lambda\pi\pi)$	
Γ_8	$\Lambda(\pi\pi)_{S\text{-wave}}$	(2.0 ± 0.8) %
Γ_9	$\Sigma\pi\pi$	(0.9 ± 0.1) %
Γ_{10}	$\Lambda\gamma$	(0.85 ± 0.15) %
Γ_{11}	$\Sigma^0\gamma$	(2.00 ± 0.35) %

Int. J. Mod. Phys. A 2026.41. Downloaded from www.worldscientific.com
UNIVERSITY OF CALIFORNIA @ BERKELEY on 09/16/26. Re-use and distribution is strictly not permitted, except for Open Access articles.

Int. J. Mod. Phys. A 2026.41. Downloaded from www.worldscientific.com by UNIVERSITY OF CALIFORNIA @ BERKELEY on 09/16/26. Re-use and distribution is strictly not permitted, except for Open Access articles.

$\Lambda(1520)$ BRANCHING RATIOS

See "Sign conventions for resonance couplings" in the Note on Λ and Σ Resonances.

$\Gamma(N\overline{K})/\Gamma_{total}$ — Γ_1/Γ

VALUE	DOCUMENT ID		TECN	COMMENT
0.45 to 0.47 OUR ESTIMATE				
0.45 ±0.01	SARANTSEV	19	DPWA	$\overline{K}N$ multichannel
0.47 ±0.04	ZHANG	13A	DPWA	$\overline{K}N$ multichannel
0.47 ±0.02	GOPAL	80	DPWA	$\overline{K}N \to \overline{K}N$
0.45 ±0.03	ALSTON-...	78	DPWA	$\overline{K}N \to \overline{K}N$
0.448±0.014	CORDEN	75	DBC	$K^- d$ 1.4–1.8 GeV/c
• • • We do not use the following data for averages, fits, limits, etc. • • •				
0.43	[1] KAMANO	15	DPWA	$\overline{K}N$ multichannel
0.47 ±0.01	GOPAL	77	DPWA	See GOPAL 80
0.42	MAST	76	HBC	$K^- p \to \overline{K}^0 n$

[1] From the preferred solution A in KAMANO 15.

$\Gamma(\Sigma\pi)/\Gamma_{total}$ — Γ_2/Γ

VALUE	DOCUMENT ID		TECN	COMMENT
0.42 to 0.46 OUR ESTIMATE				
0.43 ±0.01	SARANTSEV	19	DPWA	$\overline{K}N$ multichannel
0.47 ±0.05	ZHANG	13A	DPWA	$\overline{K}N$ multichannel
0.426±0.014	CORDEN	75	DBC	$K^- d$ 1.4–1.8 GeV/c
0.418±0.017	BARBARO-...	69B	HBC	$K^- p$ 0.28–0.45 GeV/c
• • • We do not use the following data for averages, fits, limits, etc. • • •				
0.446	[1] KAMANO	15	DPWA	$\overline{K}N$ multichannel
0.46	KIM	71	DPWA	K-matrix analysis

[1] From the preferred solution A in KAMANO 15.

$\Gamma(\Sigma\pi)/\Gamma(N\overline{K})$ — Γ_2/Γ_1

VALUE	DOCUMENT ID		TECN	COMMENT
0.9 to 1.0 OUR ESTIMATE				
0.98±0.03	[1] GOPAL	77	DPWA	$\overline{K}N$ multichannel
0.82±0.08	BURKHARDT	69	HBC	$K^- p$ 0.8–1.2 GeV/c
1.06±0.14	SCHEUER	68	DBC	$K^- N$ 3 GeV/c
0.96±0.20	DAHL	67	HBC	$\pi^- p$ 1.6–4 GeV/c
0.73±0.11	DAUBER	67	HBC	$K^- p$ 2 GeV/c
• • • We do not use the following data for averages, fits, limits, etc. • • •				
1.06±0.12	BERTHON	74	HBC	Quasi-2-body σ
1.72±0.78	MUSGRAVE	65	HBC	

[1] The $\overline{K}N \to \Sigma\pi$ amplitude at resonance is $+0.46 \pm 0.01$.

$\Gamma(\Lambda\pi\pi)/\Gamma_{total}$ — Γ_3/Γ

VALUE	DOCUMENT ID		TECN	COMMENT
0.09 to 0.11 OUR ESTIMATE				
0.091±0.006	CORDEN	75	DBC	$K^- d$ 1.4–1.8 GeV/c
0.11 ±0.01	[1] MAST	73B	IPWA	$K^- p \to \Lambda\pi\pi$

[1] Assumes $\Gamma(N\overline{K})/\Gamma_{total} = 0.46 \pm 0.02$.

$\Gamma(\Lambda\pi\pi)/\Gamma(N\overline{K})$ — Γ_3/Γ_1

VALUE	DOCUMENT ID		TECN	COMMENT
0.18 to 0.22 OUR ESTIMATE				
0.22±0.03	BURKHARDT	69	HBC	$K^- p$ 0.8–1.2 GeV/c
0.19±0.04	SCHEUER	68	DBC	$K^- N$ 3 GeV/c
0.17±0.05	DAHL	67	HBC	$\pi^- p$ 1.6–4 GeV/c
0.21±0.18	DAUBER	67	HBC	$K^- p$ 2 GeV/c
• • • We do not use the following data for averages, fits, limits, etc. • • •				
0.27±0.13	BERTHON	74	HBC	Quasi-2-body σ
0.2	KIM	71	DPWA	K-matrix analysis

$\Gamma(\Sigma\pi)/\Gamma(\Lambda\pi\pi)$ — Γ_2/Γ_3

VALUE	DOCUMENT ID		TECN	COMMENT
3.4 to 4.4 OUR ESTIMATE				
3.9±1.0	UHLIG	67	HBC	$K^- p$ 0.9–1.0 GeV/c
3.3±1.1	BIRMINGHAM	66	HBC	$K^- p$ 3.5 GeV/c
4.5±1.0	ARMENTEROS	65C	HBC	

$\Gamma(\Sigma(1385)\pi, S\text{-wave})/\Gamma_{total}$ — Γ_4/Γ

VALUE	DOCUMENT ID		TECN	COMMENT
• • • We do not use the following data for averages, fits, limits, etc. • • •				
0.121	[1] KAMANO	15	DPWA	$\overline{K}N$ multichannel

[1] From the preferred solution A in KAMANO 15.

$\Gamma(\Sigma(1385)\pi, D\text{-wave})/\Gamma_{total}$ — Γ_5/Γ

VALUE	DOCUMENT ID		TECN	COMMENT
• • • We do not use the following data for averages, fits, limits, etc. • • •				
0.003	[1] KAMANO	15	DPWA	Multichannel

[1] From the preferred solution A in KAMANO 15.

$\Gamma(\Sigma(1385)\pi)/\Gamma_{total}$ — Γ_6/Γ

VALUE	DOCUMENT ID		TECN	COMMENT
0.041±0.005	CHAN	72	HBC	$K^- p \to \Lambda\pi\pi$

$\Gamma(\Sigma(1385)\pi(\to \Lambda\pi\pi))/\Gamma(\Lambda\pi\pi)$ — Γ_7/Γ_3

The $\Lambda\pi\pi$ mode is largely due to $\Sigma(1385)\pi$. Only the values of $(\Sigma(1385)\pi)$ / $(\Lambda 2\pi)$ given by MAST 73B and CORDEN 75 are based on real 3-body partial-wave analyses. The discrepancy between the two results is essentially due to the different hypotheses made concerning the shape of the $(\pi\pi)_{S\text{-wave}}$ state.

VALUE	CL%	DOCUMENT ID		TECN	COMMENT
0.58±0.22		CORDEN	75	DBC	$K^- d$ 1.4–1.8 GeV/c
0.82±0.10		[1] MAST	73B	IPWA	$K^- p \to \Lambda\pi\pi$
• • • We do not use the following data for averages, fits, limits, etc. • • •					
<0.44	90	WIELAND	11	SPHR	$\gamma p \to K^+\Lambda(1520)$
0.39±0.10		[2] BURKHARDT	71	HBC	$K^- p \to (\Lambda\pi\pi)\pi$

[1] Both $\Sigma(1385)\pi$ DS_{03} and $\Sigma(\pi\pi)$ DP_{03} contribute.

[2] The central bin (1514–1524 MeV) gives 0.74 ± 0.10; other bins are lower by 2-to-5 standard deviations.

$\Gamma(\Lambda(\pi\pi)_{S\text{-wave}})/\Gamma(\Lambda\pi\pi)$ — Γ_8/Γ_3

VALUE	DOCUMENT ID		TECN	COMMENT
0.20±0.08	CORDEN	75	DBC	$K^- d$ 1.4–1.8 GeV/c

$\Gamma(\Sigma\pi\pi)/\Gamma_{total}$ — Γ_9/Γ

VALUE	DOCUMENT ID		TECN	COMMENT
0.007 to 0.011 OUR ESTIMATE				
0.007 ±0.002	[1] CORDEN	75	DBC	$K^- d$ 1.4–1.8 GeV/c
0.0085±0.0006	[2] MAST	73	MPWA	$K^- p \to \Sigma\pi\pi$
0.010 ±0.0015	BARBARO-...	69B	HBC	$K^- p$ 0.28–0.45 GeV/c

[1] Much of the $\Sigma\pi\pi$ decay proceeds via $\Sigma(1385)\pi$.

[2] Assumes $\Gamma(N\overline{K})/\Gamma_{total} = 0.46$.

$\Gamma(\Lambda\gamma)/\Gamma_{total}$ — Γ_{10}/Γ

VALUE (units 10^{-3})	EVTS	DOCUMENT ID		TECN	COMMENT
7 to 11 OUR ESTIMATE					
$10.7\pm2.9^{+1.5}_{-0.4}$	32	TAYLOR	05	CLAS	$\gamma p \to K^+\Lambda\gamma$
10.2±2.1±1.5	290	ANTIPOV	04A	SPNX	$pN(C) \to \Lambda(1520)K^+N(C)$
8.0±1.4	238	MAST	68B	HBC	Using $\Gamma(N\overline{K})/\Gamma_{total} = 0.45$

$\Gamma(\Sigma^0\gamma)/\Gamma_{total}$ — Γ_{11}/Γ

VALUE	DOCUMENT ID		TECN	COMMENT
0.02±0.0035	[1] MAST	68B	HBC	Not measured; see note

[1] Calculated from $\Gamma(\Lambda\gamma)/\Gamma_{total}$, assuming SU(3). Needed to constrain the sum of all the branching ratios to be unity.

$\Lambda(1520)$ REFERENCES

ABLIKIM	25AF	JHEP 2502 212	M. Ablikim et al.	(BESIII Collab.)
SARANTSEV	19	EPJ A55 180	A.V. Sarantsev et al.	(BONN, PNPI)
KAMANO	15	PR C92 025205	H. Kamano et al.	(ANL, OSAK)
ZHANG	13A	PR C88 035205	H. Zhang et al.	(KSU)
WIELAND	11	EPJ A47 47	F. Wieland et al.	(ELSA SAPHIR Collab.)
QIANG	10	PL B694 123	Y. Qiang et al.	(DUKE, JEFF, PNPI, GWU+)
TAYLOR	05	PR C71 054609	S. Taylor et al.	(JLab CLAS Collab.)
Also		PR C72 039902 (errat.)	S. Taylor et al.	(JLab CLAS Collab.)
ANTIPOV	04A	PL B604 22	Yu.M. Antipov et al.	(IHEP SPHINX Collab.)
PDG	82	PL 111B 1	M. Roos et al.	(HELS, CIT, CERN)
BARBER	80D	ZPHY C7 17	D.P. Barber et al.	(DARE, LANC, SHEF)
GOPAL	80	Toronto Conf. 159	G.P. Gopal	(RHEL) IJP
BARLAG	79	NP B149 220	S.J.M. Barlag et al.	(AMST, CERN, NIJM+)
ALSTON-...	78	PR D18 182	M. Alston-Garnjost et al.	(LBL, MTHO+) IJP
Also		PRL 38 1007	M. Alston-Garnjost et al.	(LBL, MTHO+) IJP
CAMERON	77	NP B131 399	W. Cameron et al.	(RHEL, LOIC) IJP
GOPAL	77	NP B119 362	G.P. Gopal et al.	(LOIC, RHEL) IJP
MAST	76	PR D14 13	T.S. Mast et al.	(LBL)
CORDEN	75	NP B84 306	M.J. Corden et al.	(BIRM)
BERTHON	74	NC 21A 146	A. Berthon et al.	(CDEF, RHEL, SACL+)
MAST	73	PR D7 3212	T.S. Mast et al.	(LBL) IJP
MAST	73B	PR D7 5	T.S. Mast et al.	(LBL) IJP
CHAN	72	PRL 28 256	S.B. Chan et al.	(MASA, YALE)
BURKHARDT	71	NP B27 64	E. Burkhardt et al.	(HEID, CERN, SACL)
KIM	71	PRL 27 356	J.K. Kim	(HARV) IJP
Also		Duke Conf. 161	J.K. Kim	(HARV) IJP
Hyperon Resonances, 1970				
BARBARO-...	69B	Lund Conf. 352	A. Barbaro-Galtieri et al.	(LRL)
Also		Duke Conf. 95	R.D. Tripp	(LRL)
Hyperon Resonances 1970				
BURKHARDT	69	NP B14 106	E. Burkhardt et al.	(HEID, EFI, CERN+)
MAST	68B	PRL 21 1715	T.S. Mast et al.	(LRL)
SCHEUER	68	NP B8 503	J.C. Scheuer et al.	(SABRE Collab.)
DAHL	67	PR 163 1377	O.I. Dahl et al.	(LRL)
DAUBER	67	PL 24B 525	P.M. Dauber et al.	(UCLA)
UHLIG	67	PR 155 1448	R.P. Uhlig et al.	(UMD, NRL)
BIRMINGHAM	66	PR 152 1148	M. Haque et al.	(BIRM, GLAS, LOIC, OXF+)
ARMENTEROS	65C	PL 19 338	R. Armenteros et al.	(CERN, HEID, SACL)
MUSGRAVE	65	NC 35 735	B. Musgrave et al.	(BIRM, CERN, EPOL+)
WATSON	63	PR 131 2248	M.B. Watson, M. Ferro-Luzzi, R.D. Tripp	(LRL) IJP
FERRO-LUZZI	62	PRL 8 28	M. Ferro-Luzzi, R.D. Tripp, M.B. Watson	(LRL) IJP

$\Lambda(1600)$ $1/2^+$

$I(J^P) = 0(\frac{1}{2}^+)$ Status: ****

$\Lambda(1600)$ POLE POSITION

REAL PART

VALUE (MeV)	DOCUMENT ID		TECN	COMMENT
1540 to 1560 (≈ 1550) OUR ESTIMATE				
1546±6 OUR AVERAGE Error includes scale factor of 2.1.				
1562±8	SARANTSEV	19	DPWA	$\overline{K}N$ multichannel
1544^{+3}_{-3}	[1] KAMANO	15	DPWA	Multichannel

Int. J. Mod. Phys. A 2026.41. Downloaded from www.worldscientific.com
UNIVERSITY OF CALIFORNIA @ BERKELEY on 09/16/26. Re-use and distribution is strictly not permitted, except for Open Access articles.

• • • We do not use the following data for averages, fits, limits, etc. • • •

1572	ZHANG	13A	DPWA	Multichannel

[1] From the preferred solution A in KAMANO 15.

−2×IMAGINARY PART

VALUE (MeV)	DOCUMENT ID		TECN	COMMENT
120 to 240 (≈ 180) OUR ESTIMATE				
159^{+60}_{-12} OUR AVERAGE Error includes scale factor of 6.2.				
232±15	SARANTSEV	19	DPWA	$\overline{K}N$ multichannel
112^{+12}_{-2}	[1] KAMANO	15	DPWA	Multichannel
• • • We do not use the following data for averages, fits, limits, etc. • • •				
138	ZHANG	13A	DPWA	Multichannel

[1] From the preferred solution A in KAMANO 15.

$\Lambda(1600)$ POLE RESIDUES

The normalized residue is the residue divided by $\Gamma_{pole}/2$.

Normalized residue in $N\overline{K} \to \Lambda(1600) \to N\overline{K}$

MODULUS	PHASE (°)	DOCUMENT ID		TECN	COMMENT
0.36 ±0.07	**−63 ± 10**	SARANTSEV	19	DPWA	$\overline{K}N$ multichannel
• • • We do not use the following data for averages, fits, limits, etc. • • •					
0.105	−80	[1] KAMANO	15	DPWA	Multichannel

[1] From the preferred solution A in KAMANO 15.

Normalized residue in $N\overline{K} \to \Lambda(1600) \to \Sigma\pi$

MODULUS	PHASE (°)	DOCUMENT ID		TECN	COMMENT
0.39 ±0.08	**148 ± 10**	SARANTSEV	19	DPWA	$\overline{K}N$ multichannel
• • • We do not use the following data for averages, fits, limits, etc. • • •					
0.232	108	[1] KAMANO	15	DPWA	Multichannel

[1] From the preferred solution A in KAMANO 15.

Normalized residue in $N\overline{K} \to \Lambda(1600) \to \Lambda\eta$

MODULUS	PHASE (°)	DOCUMENT ID		TECN	COMMENT
0.22±0.13	**180 ± 20**	SARANTSEV	19	DPWA	$\overline{K}N$ multichannel

Normalized residue in $N\overline{K} \to \Lambda(1600) \to \Lambda\sigma$

MODULUS	PHASE (°)	DOCUMENT ID		TECN	COMMENT
0.30±0.06	**−70 ± 10**	SARANTSEV	19	DPWA	$\overline{K}N$ multichannel

Normalized residue in $N\overline{K} \to \Lambda(1600) \to \Sigma(1385)\pi$

MODULUS	PHASE (°)	DOCUMENT ID		TECN	COMMENT
0.37 ±0.07	**103 ± 12**	SARANTSEV	19	DPWA	$\overline{K}N$ multichannel
• • • We do not use the following data for averages, fits, limits, etc. • • •					
0.183	77	[1] KAMANO	15	DPWA	Multichannel

[1] From the preferred solution A in KAMANO 15.

Normalized residue in $N\overline{K} \to \Lambda(1600) \to N\overline{K}^*(892)$, S=1/2, P-wave

MODULUS	PHASE (°)	DOCUMENT ID		TECN	COMMENT
0.02±0.01	**126 ± 45**	SARANTSEV	19	DPWA	$\overline{K}N$ multichannel

Normalized residue in $N\overline{K} \to \Lambda(1600) \to N\overline{K}^*(892)$, S=3/2, P-wave

MODULUS	PHASE (°)	DOCUMENT ID		TECN	COMMENT
0.02±0.01	**−135 ± 45**	SARANTSEV	19	DPWA	$\overline{K}N$ multichannel

$\Lambda(1600)$ MASS

VALUE (MeV)	DOCUMENT ID		TECN	COMMENT
1570 to 1630 (≈ 1600) OUR ESTIMATE				
1570.5± 4.6±12.1	ABLIKIM	25AF	BES3	$\psi(3686) \to \Lambda\overline{\Sigma}^0\pi^0 +$ c.c. (PWA)
1605 ± 8	SARANTSEV	19	DPWA	$\overline{K}N$ multichannel
1592 ± 10	ZHANG	13A	DPWA	Multichannel
1568 ± 20	GOPAL	80	DPWA	$\overline{K}N \to \overline{K}N$
1703 ±100	ALSTON-...	78	DPWA	$\overline{K}N \to \overline{K}N$
1573 ± 25	GOPAL	77	DPWA	$\overline{K}N$ multichannel
1596 ± 6	KANE	74	DPWA	$K^-p \to \Sigma\pi$
1620 ± 10	LANGBEIN	72	IPWA	$\overline{K}N$ multichannel
• • • We do not use the following data for averages, fits, limits, etc. • • •				
1572 or 1617	[1] MARTIN	77	DPWA	$\overline{K}N$ multichannel
1646 ± 7	[2] CARROLL	76	DPWA	Isospin-0 total σ
1570	KIM	71	DPWA	K-matrix analysis

[1] The two MARTIN 77 values are from a T-matrix pole and from a Breit-Wigner fit.
[2] A total cross-section bump with $(J+1/2)\ \Gamma_{el}\ /\ \Gamma_{total} = 0.04$.

$\Lambda(1600)$ WIDTH

VALUE (MeV)	DOCUMENT ID		TECN	COMMENT
150 to 250 (≈ 200) OUR ESTIMATE				
228.1± 11.9±34.8	ABLIKIM	25AF	BES3	$\psi(3686) \to \Lambda\overline{\Sigma}^0\pi^0 +$ c.c. (PWA)
245 ± 15	SARANTSEV	19	DPWA	$\overline{K}N$ multichannel
150 ± 28	ZHANG	13A	DPWA	Multichannel
116 ± 20	GOPAL	80	DPWA	$\overline{K}N \to \overline{K}N$
593 ±200	ALSTON-...	78	DPWA	$\overline{K}N \to \overline{K}N$
147 ± 50	GOPAL	77	DPWA	$\overline{K}N$ multichannel
175 ± 20	KANE	74	DPWA	$K^-p \to \Sigma\pi$
60 ± 10	LANGBEIN	72	IPWA	$\overline{K}N$ multichannel
• • • We do not use the following data for averages, fits, limits, etc. • • •				
247 or 271	[1] MARTIN	77	DPWA	$\overline{K}N$ multichannel
20	[2] CARROLL	76	DPWA	Isospin-0 total σ
50	KIM	71	DPWA	K-matrix analysis

[1] The two MARTIN 77 values are from a T-matrix pole and from a Breit-Wigner fit.
[2] A total cross-section bump with $(J+1/2)\ \Gamma_{el}\ /\ \Gamma_{total} = 0.04$.

$\Lambda(1600)$ DECAY MODES

	Mode	Fraction (Γ_i/Γ)
Γ_1	$N\overline{K}$	15–30 %
Γ_2	$\Sigma\pi$	10–60 %
Γ_3	$\Lambda\sigma$	(19±4) %
Γ_4	$\Sigma(1385)\pi$	(9±4) %

$\Lambda(1600)$ BRANCHING RATIOS

See "Sign conventions for resonance couplings" in the Note on Λ and Σ Resonances.

$\Gamma(N\overline{K})/\Gamma_{total}$ — Γ_1/Γ

VALUE	DOCUMENT ID		TECN	COMMENT
0.14 to 0.28 OUR ESTIMATE				
0.29 ±0.06	SARANTSEV	19	DPWA	$\overline{K}N$ multichannel
0.14 ±0.04	ZHANG	13A	DPWA	Multichannel
0.23 ±0.04	GOPAL	80	DPWA	$\overline{K}N \to \overline{K}N$
0.14 ±0.05	ALSTON-...	78	DPWA	$\overline{K}N \to \overline{K}N$
0.25 ±0.15	LANGBEIN	72	IPWA	$\overline{K}N$ multichannel
• • • We do not use the following data for averages, fits, limits, etc. • • •				
0.064	[1] KAMANO	15	DPWA	Multichannel
0.24 ±0.04	GOPAL	77	DPWA	See GOPAL 80
0.30 or 0.29	[2] MARTIN	77	DPWA	$\overline{K}N$ multichannel

[1] From the preferred solution A in KAMANO 15.
[2] The two MARTIN 77 values are from a T-matrix pole and from a Breit-Wigner fit.

$\Gamma(\Sigma\pi)/\Gamma_{total}$ — Γ_2/Γ

VALUE	DOCUMENT ID		TECN	COMMENT
0.37 ±0.07	SARANTSEV	19	DPWA	$\overline{K}N$ multichannel
• • • We do not use the following data for averages, fits, limits, etc. • • •				
0.851	[1] KAMANO	15	DPWA	Multichannel

[1] From the preferred solution A in KAMANO 15.

$\Gamma(\Lambda\sigma)/\Gamma_{total}$ — Γ_3/Γ

VALUE	DOCUMENT ID		TECN	COMMENT
0.19±0.04	SARANTSEV	19	DPWA	$\overline{K}N$ multichannel

$\Gamma(\Sigma(1385)\pi)/\Gamma_{total}$ — Γ_4/Γ

VALUE	DOCUMENT ID		TECN	COMMENT
0.09 ±0.04	SARANTSEV	19	DPWA	$\overline{K}N$ multichannel
• • • We do not use the following data for averages, fits, limits, etc. • • •				
0.085	[1] KAMANO	15	DPWA	Multichannel

[1] From the preferred solution A in KAMANO 15.

$(\Gamma_i\Gamma_f)^{1/2}/\Gamma_{total}$ in $N\overline{K} \to \Lambda(1600) \to \Sigma\pi$ — $(\Gamma_1\Gamma_2)^{1/2}/\Gamma$

VALUE	DOCUMENT ID		TECN	COMMENT
−0.23±0.03	ZHANG	13A	DPWA	Multichannel
−0.16±0.04	GOPAL	77	DPWA	$\overline{K}N$ multichannel
−0.33±0.11	KANE	74	DPWA	$K^-p \to \Sigma\pi$
0.28±0.09	LANGBEIN	72	IPWA	$\overline{K}N$ multichannel
• • • We do not use the following data for averages, fits, limits, etc. • • •				
−0.39 or −0.39	[1] MARTIN	77	DPWA	$\overline{K}N$ multichannel
not seen	HEPP	76B	DPWA	$K^-N \to \Sigma\pi$

[1] The two MARTIN 77 values are from a T-matrix pole and from a Breit-Wigner fit.

Int. J. Mod. Phys. A 2026.41. Downloaded from www.worldscientific.com
by UNIVERSITY OF CALIFORNIA @ BERKELEY on 09/16/26. Re-use and distribution is strictly not permitted, except for Open Access articles.

$\Lambda(1600)$ REFERENCES

ABLIKIM	25AF	JHEP 2502 212	M. Ablikim *et al.*	(BESIII Collab.)
SARANTSEV	19	EPJ A55 180	A.V. Sarantsev *et al.*	(BONN, PNPI)
KAMANO	15	PR C92 025205	H. Kamano *et al.*	(ANL, OSAK)
ZHANG	13A	PR C88 035205	H. Zhang *et al.*	(KSU)
GOPAL	80	Toronto Conf. 159	G.P. Gopal	(RHEL) IJP
ALSTON-...	78	PR D18 182	M. Alston-Garnjost *et al.*	(LBL, MTHO+) IJP
Also		PRL 38 1007	M. Alston-Garnjost *et al.*	(LBL, MTHO+) IJP
GOPAL	77	NP B119 362	G.P. Gopal *et al.*	(LOIC, RHEL) IJP
MARTIN	77	NP B127 349	B.R. Martin, M.K. Pidcock, R.G. Moorhouse	(LOUC+) IJP
Also		NP B126 266	B.R. Martin, M.K. Pidcock	(LOUC)
Also		NP B126 285	B.R. Martin, M.K. Pidcock	(LOUC) IJP
CARROLL	76	PRL 37 806	A.S. Carroll *et al.*	(BNL) I
HEPP	76B	PL 65B 487	V. Hepp *et al.*	(CERN, HEIDH, MPIM) IJP
KANE	74	LBL-2452	D.F. Kane	(LBL) IJP
LANGBEIN	72	NP B47 477	W. Langbein, F. Wagner	(MPIM) IJP
KIM	71	PRL 27 356	J.K. Kim	(HARV) IJP

$\Lambda(1670)\ 1/2^-$

$I(J^P) = 0(\frac{1}{2}^-)$ Status: ****

The measurements of the mass, width, and elasticity published before 1974 are now obsolete and have been omitted. They were last listed in our 1982 edition Physics Letters **111B** 1 (1982).

$\Lambda(1670)$ POLE POSITIONS

REAL PART

VALUE (MeV)	DOCUMENT ID		TECN	COMMENT
1670 to 1678 (≈ 1674) OUR ESTIMATE				
1676 ±2	SARANTSEV	19	DPWA	$\overline{K}N$ multichannel
1669 $^{+3}_{-8}$	[1] KAMANO	15	DPWA	$\overline{K}N$ multichannel
1677.5 ±0.8	GARCIA-REC...	03	DPWA	$\overline{K}N$ multichannel
• • • We do not use the following data for averages, fits, limits, etc. • • •				
1667	ZHANG	13A	DPWA	$\overline{K}N$ multichannel

[1] From the preferred solution A in KAMANO 15.

−2×IMAGINARY PART

VALUE (MeV)	DOCUMENT ID		TECN	COMMENT
28 to 36 (≈ 32) OUR ESTIMATE				
33 ± 4	SARANTSEV	19	DPWA	$\overline{K}N$ multichannel
19 $^{+18}_{-2}$	[1] KAMANO	15	DPWA	$\overline{K}N$ multichannel
29.2± 1.4	GARCIA-REC...	03	DPWA	$\overline{K}N$ multichannel
• • • We do not use the following data for averages, fits, limits, etc. • • •				
26	ZHANG	13A	DPWA	$\overline{K}N$ multichannel

[1] From the preferred solution A in KAMANO 15.

$\Lambda(1670)$ POLE RESIDUES

The normalized residue is the residue divided by $\Gamma_{pole}/2$.

Normalized residue in $\overline{K}N \to \Lambda(1670) \to \overline{K}N$

MODULUS	PHASE (°)	DOCUMENT ID		TECN	COMMENT
0.30 ±0.06	**−145 ± 11**	SARANTSEV	19	DPWA	$\overline{K}N$ multichannel
• • • We do not use the following data for averages, fits, limits, etc. • • •					
0.351	164	[1] KAMANO	15	DPWA	$\overline{K}N$ multichannel

[1] From the preferred solution A in KAMANO 15.

Normalized residue in $N\overline{K} \to \Lambda(1670) \to \Sigma\pi$

MODULUS	PHASE (°)	DOCUMENT ID		TECN	COMMENT
0.19 ±0.06	**145 ± 14**	SARANTSEV	19	DPWA	$\overline{K}N$ multichannel
• • • We do not use the following data for averages, fits, limits, etc. • • •					
0.327	125	[1] KAMANO	15	DPWA	$\overline{K}N$ multichannel

[1] From the preferred solution A in KAMANO 15.

Normalized residue in $N\overline{K} \to \Lambda(1670) \to \Lambda\eta$

MODULUS	PHASE (°)	DOCUMENT ID		TECN	COMMENT
0.26 ±0.09	**104 ± 14**	SARANTSEV	19	DPWA	$\overline{K}N$ multichannel
• • • We do not use the following data for averages, fits, limits, etc. • • •					
0.474	59	[1] KAMANO	15	DPWA	Multichannel

[1] From the preferred solution A in KAMANO 15.

Normalized residue in $N\overline{K} \to \Lambda(1670) \to \Xi K$

MODULUS	PHASE (°)	DOCUMENT ID		TECN	COMMENT
0.02±0.02	**100 ± 25**	SARANTSEV	19	DPWA	$\overline{K}N$ multichannel

Normalized residue in $N\overline{K} \to \Lambda(1670) \to \Lambda\omega$, S=1/2, S-wave

MODULUS	PHASE (°)	DOCUMENT ID		TECN	COMMENT
0.09±0.04	**−60 ± 35**	SARANTSEV	19	DPWA	$\overline{K}N$ multichannel

Normalized residue in $N\overline{K} \to \Lambda(1670) \to \Lambda\omega$, S=3/2, D-wave

MODULUS	PHASE (°)	DOCUMENT ID		TECN	COMMENT
0.05±0.04		SARANTSEV	19	DPWA	$\overline{K}N$ multichannel

Normalized residue in $N\overline{K} \to \Lambda(1670) \to N\overline{K}^*(892)$, S=1/2, S-wave

MODULUS	PHASE (°)	DOCUMENT ID		TECN	COMMENT
0.31±0.14	**100 ± 45**	SARANTSEV	19	DPWA	$\overline{K}N$ multichannel

Normalized residue in $N\overline{K} \to \Lambda(1670) \to N\overline{K}^*(892)$, S=3/2, D-wave

MODULUS	PHASE (°)	DOCUMENT ID		TECN	COMMENT
0.06±0.03	**−85 ± 40**	SARANTSEV	19	DPWA	$\overline{K}N$ multichannel

Normalized residue in $N\overline{K} \to \Lambda(1670) \to \Lambda\sigma$

MODULUS	PHASE (°)	DOCUMENT ID		TECN	COMMENT
0.25±0.08	**160 ± 15**	SARANTSEV	19	DPWA	$\overline{K}N$ multichannel

Normalized residue in $N\overline{K} \to \Lambda(1670) \to \Sigma(1385)\pi$

MODULUS	PHASE (°)	DOCUMENT ID		TECN	COMMENT
0.13 ±0.06	**110 ± 12**	SARANTSEV	19	DPWA	$\overline{K}N$ multichannel
• • • We do not use the following data for averages, fits, limits, etc. • • •					
0.0988	−104	[1] KAMANO	15	DPWA	Multichannel

[1] From the preferred solution A in KAMANO 15.

$\Lambda(1670)$ MASS

VALUE (MeV)	DOCUMENT ID		TECN	COMMENT
1670 to 1678 (≈ 1674) OUR ESTIMATE				
1667.5 ±2.3±3.6	ABLIKIM	25AF	BES3	$\psi(3686) \to \Lambda\overline{\Sigma}^0\pi^0$ + c.c. (PWA)
1674.3 ±0.8±4.9	LEE	21A	BELL	$\Lambda_c^+ \to \Lambda(1670)\pi^+$
1677 ±2	SARANTSEV	19	DPWA	$\overline{K}N$ multichannel
1672 ±3	ZHANG	13A	DPWA	Multichannel
1670.8 ±1.7	KOISO	85	DPWA	$K^-p \to \Sigma\pi$
1667 ±5	GOPAL	80	DPWA	$\overline{K}N \to \overline{K}N$
1671 ±3	ALSTON-...	78	DPWA	$\overline{K}N \to \overline{K}N$
1675 ±2	HEPP	76B	DPWA	$K^-N \to \Sigma\pi$
1679 ±1	KANE	74	DPWA	$K^-p \to \Sigma\pi$
1665 ±5	PREVOST	74	DPWA	$K^-N \to \Sigma(1385)\pi$
• • • We do not use the following data for averages, fits, limits, etc. • • •				
1673 ±2	MANLEY	02	DPWA	$\overline{K}N$ multichannel
1668.9 ±2.0	ABAEV	96	DPWA	$K^-p \to \Lambda\eta$
1670 ±5	GOPAL	77	DPWA	$\overline{K}N$ multichannel
1664	[1] MARTIN	77	DPWA	$\overline{K}N$ multichannel

[1] MARTIN 77 obtains identical resonance parameters from a T-matrix pole and from a Breit-Wigner fit.

$\Lambda(1670)$ WIDTH

VALUE (MeV)	DOCUMENT ID		TECN	COMMENT
25 to 35 (≈ 30) OUR ESTIMATE				
30.2± 4.2±8.7	ABLIKIM	25AF	BES3	$\psi(3686) \to \Lambda\overline{\Sigma}^0\pi^0$ + c.c. (PWA)
36.1± 2.4±4.8	LEE	21A	BELL	$\Lambda_c^+ \to \Lambda(1670)\pi^+$
33 ± 4	SARANTSEV	19	DPWA	$\overline{K}N$ multichannel
29 ± 5	ZHANG	13A	DPWA	$\overline{K}N$ multichannel
34.1± 3.7	KOISO	85	DPWA	$K^-p \to \Sigma\pi$
29 ± 5	GOPAL	80	DPWA	$\overline{K}N \to \overline{K}N$
29 ± 5	ALSTON-...	78	DPWA	$\overline{K}N \to \overline{K}N$
46 ± 5	HEPP	76B	DPWA	$K^-N \to \Sigma\pi$
40 ± 3	KANE	74	DPWA	$K^-p \to \Sigma\pi$
19 ± 5	PREVOST	74	DPWA	$K^-N \to \Sigma(1385)\pi$
• • • We do not use the following data for averages, fits, limits, etc. • • •				
23 ± 6	MANLEY	02	DPWA	$\overline{K}N$ multichannel
21.1± 3.6	ABAEV	96	DPWA	$K^-p \to \Lambda\eta$
45 ±10	GOPAL	77	DPWA	$\overline{K}N$ multichannel
12	[1] MARTIN	77	DPWA	$\overline{K}N$ multichannel

[1] MARTIN 77 obtains identical resonance parameters from a T-matrix pole and from a Breit-Wigner fit.

$\Lambda(1670)$ DECAY MODES

	Mode	Fraction (Γ_i/Γ)
Γ_1	$N\overline{K}$	20–30 %
Γ_2	$\Sigma\pi$	25–55 %
Γ_3	$\Lambda\eta$	10–25 %
Γ_4	$\Sigma(1385)\pi$, D-wave	(6.0±2.0) %
Γ_5	$N\overline{K}^*(892)$, S=1/2, S-wave	
Γ_6	$N\overline{K}^*(892)$, S=3/2, D-wave	(5 ±4) %
Γ_7	$\Lambda\sigma$	(20 ±8) %

Int. J. Mod. Phys. A 2026.41. Downloaded from www.worldscientific.com
UNIVERSITY OF CALIFORNIA @ BERKELEY on 09/16/26. Re-use and distribution is strictly not permitted, except for Open Access articles.

$\Lambda(1670)$ BRANCHING RATIOS

See "Sign conventions for resonance couplings" in the Note on Λ and Σ Resonances.

$\Gamma(N\overline{K})/\Gamma_{total}$ — Γ_1/Γ

VALUE	DOCUMENT ID		TECN	COMMENT
0.20 to 0.30 OUR ESTIMATE				
0.33 ±0.07	SARANTSEV	19	DPWA	$\overline{K}N$ multichannel
0.26 ±0.25	ZHANG	13A	DPWA	$\overline{K}N$ multichannel
0.18 ±0.03	GOPAL	80	DPWA	$\overline{K}N \to \overline{K}N$
0.17 ±0.03	ALSTON-...	78	DPWA	$\overline{K}N \to \overline{K}N$
• • • We do not use the following data for averages, fits, limits, etc. • • •				
0.318	[1] KAMANO	15	DPWA	$\overline{K}N$ multichannel
0.37 ±0.07	MANLEY	02	DPWA	$\overline{K}N$ multichannel
0.20 ±0.03	GOPAL	77	DPWA	See GOPAL 80
0.15	[2] MARTIN	77	DPWA	$\overline{K}N$ multichannel

[1] From the preferred solution A in KAMANO 15.
[2] MARTIN 77 obtains identical resonance parameters from a T-matrix pole and from a Breit-Wigner fit.

$\Gamma(\Sigma\pi)/\Gamma_{total}$ — Γ_2/Γ

VALUE	DOCUMENT ID		TECN	COMMENT
0.12 ±0.03	SARANTSEV	19	DPWA	$\overline{K}N$ multichannel
• • • We do not use the following data for averages, fits, limits, etc. • • •				
0.289	[1] KAMANO	15	DPWA	Multichannel

[1] From the preferred solution A in KAMANO 15.

$\Gamma(\Lambda\eta)/\Gamma_{total}$ — Γ_3/Γ

VALUE	DOCUMENT ID		TECN	COMMENT
0.20 ±0.08	SARANTSEV	19	DPWA	$\overline{K}N$ multichannel
• • • We do not use the following data for averages, fits, limits, etc. • • •				
0.373	KAMANO	15	DPWA	Multichannel
0.30 ±0.08	ABAEV	96	DPWA	$K^-p \to \Lambda\eta$

$\Gamma(\Sigma(1385)\pi, D\text{-wave})/\Gamma_{total}$ — Γ_4/Γ

VALUE	DOCUMENT ID		TECN	COMMENT
0.06 ±0.02	SARANTSEV	19	DPWA	$\overline{K}N$ multichannel
• • • We do not use the following data for averages, fits, limits, etc. • • •				
0.019	KAMANO	15	DPWA	Multi-channel

$\Gamma(\Lambda\sigma)/\Gamma_{total}$ — Γ_7/Γ

VALUE	DOCUMENT ID		TECN	COMMENT
0.20±0.08	SARANTSEV	19	DPWA	$\overline{K}N$ multichannel

$\Gamma(N\overline{K}^*(892), S=1/2, S\text{-wave})/\Gamma_{total}$ — Γ_5/Γ

VALUE	DOCUMENT ID		TECN	COMMENT
• • • We do not use the following data for averages, fits, limits, etc. • • •				
not seen	[1] KAMANO	15	DPWA	Multichannel

[1] Not seen in the preferred solution A in KAMANO 15.

$\Gamma(N\overline{K}^*(892), S=3/2, D\text{-wave})/\Gamma_{total}$ — Γ_6/Γ

VALUE	DOCUMENT ID		TECN	COMMENT
0.05±0.04	ZHANG	13A	DPWA	Multichannel
• • • We do not use the following data for averages, fits, limits, etc. • • •				
not seen	[1] KAMANO	15	DPWA	Multichannel

[1] Not seen in the preferred solution A in KAMANO 15.

$(\Gamma_i\Gamma_f)^{1/2}/\Gamma_{total}$ in $N\overline{K} \to \Lambda(1670) \to \Sigma\pi$ — $(\Gamma_1\Gamma_2)^{1/2}/\Gamma$

VALUE	DOCUMENT ID		TECN	COMMENT
−0.29±0.06	ZHANG	13A	DPWA	Multichannel
−0.26±0.02	KOISO	85	DPWA	$K^-p \to \Sigma\pi$
−0.31±0.03	GOPAL	77	DPWA	$\overline{K}N$ multichannel
−0.29±0.03	HEPP	76B	DPWA	$K^-N \to \Sigma\pi$
−0.23±0.03	LONDON	75	HLBC	$K^-p \to \Sigma^0\pi^0$
−0.27±0.02	KANE	74	DPWA	$K^-p \to \Sigma\pi$
• • • We do not use the following data for averages, fits, limits, etc. • • •				
−0.38±0.03	MANLEY	02	DPWA	$\overline{K}N$ multichannel
−0.13	[1] MARTIN	77	DPWA	$\overline{K}N$ multichannel

[1] MARTIN 77 obtains identical resonance parameters from a T-matrix pole and from a Breit-Wigner fit.

$(\Gamma_i\Gamma_f)^{1/2}/\Gamma_{total}$ in $N\overline{K} \to \Lambda(1670) \to \Lambda\eta$ — $(\Gamma_1\Gamma_3)^{1/2}/\Gamma$

VALUE	DOCUMENT ID		TECN	COMMENT
−0.30±0.10	ZHANG	13A	DPWA	Multichannel
+0.20±0.05	BAXTER	73	DPWA	$K^-p \to$ neutrals
• • • We do not use the following data for averages, fits, limits, etc. • • •				
+0.24±0.04	MANLEY	02	DPWA	$\overline{K}N$ multichannel
0.24	KIM	71	DPWA	K-matrix analysis
0.26	ARMENTEROS	69C	HBC	
0.20 or 0.23	BERLEY	65	HBC	

$(\Gamma_i\Gamma_f)^{1/2}/\Gamma_{total}$ in $N\overline{K} \to \Lambda(1670) \to \Sigma(1385)\pi$, D-wave — $(\Gamma_1\Gamma_4)^{1/2}/\Gamma$

VALUE	DOCUMENT ID		TECN	COMMENT
−0.17±0.06	MANLEY	02	DPWA	$\overline{K}N$ multichannel
−0.18±0.05	PREVOST	74	DPWA	$K^-N \to \Sigma(1385)\pi$

$\Lambda(1670)$ REFERENCES

ABLIKIM	25AF	JHEP 2502 212	M. Ablikim *et al.*	(BESIII Collab.)
LEE	21A	PR D103 052005	J.Y. Lee *et al.*	(BELLE Collab.)
SARANTSEV	19	EPJ A55 180	A.V. Sarantsev *et al.*	(BONN, PNPI)
KAMANO	15	PR C92 025205	H. Kamano *et al.*	(ANL, OSAK)
ZHANG	13A	PR C88 035205	H. Zhang *et al.*	(KSU)
GARCIA-REC...	03	PR D67 076009	C. Garcia-Recio *et al.*	(GRAN, VALE)
MANLEY	02	PRL 88 012002	D.M. Manley *et al.*	(BNL Crystal Ball Collab.)
ABAEV	96	PR C53 385	V.V. Abaev, B.M.K. Nefkens	(UCLA)
KOISO	85	NP A433 619	H. Koiso *et al.*	(TOKY, MASA)
PDG	82	PL 111B 1	M. Roos *et al.*	(HELS, CIT, CERN)
GOPAL	80	Toronto Conf. 159	G.P. Gopal	(RHEL) IJP
ALSTON-...	78	PR D18 182	M. Alston-Garnjost *et al.*	(LBL, MTHO+) IJP
Also		PRL 38 1007	M. Alston-Garnjost *et al.*	(LBL, MTHO+) IJP
GOPAL	77	NP B119 362	G.P. Gopal *et al.*	(LOIC, RHEL) IJP
MARTIN	77	NP B127 349	B.R. Martin, M.K. Pidcock, R.G. Moorhouse	(LOUC+) IJP
Also		NP B126 266	B.R. Martin, M.K. Pidcock	(LOUC)
Also		NP B126 285	B.R. Martin, M.K. Pidcock	(LOUC) IJP
HEPP	76B	PL 65B 487	V. Hepp *et al.*	(CERN, HEIDH, MPIM) IJP
LONDON	75	NP B85 289	G.W. London *et al.*	(BNL, CERN, EPOL+)
KANE	74	LBL-2452	D.F. Kane	(LBL) IJP
PREVOST	74	NP B69 246	J. Prevost *et al.*	(SACL, CERN, HEID)
BAXTER	73	NP B67 125	D.F. Baxter *et al.*	(OXF) IJP
KIM	71	PRL 27 356	J.K. Kim	(HARV) IJP
Also		Duke Conf. 161	J.K. Kim	(HARV) IJP
Hyperon Resonances, 1970				
ARMENTEROS	69C	Lund Paper 229	R. Armenteros *et al.*	(CERN, HEID, SACL) IJP
Values are quoted in LEVI-SETTI 69.				
BERLEY	65	PRL 15 641	D. Berley *et al.*	(BNL) IJP

$\Lambda(1690)\ 3/2^-$

$I(J^P) = 0(\frac{3}{2}^-)$ Status: ****

The measurements of the mass, width, and elasticity published before 1974 are now obsolete and have been omitted. They were last listed in our 1982 edition Physics Letters **111B** 1 (1982).

$\Lambda(1690)$ POLE POSITION

REAL PART

VALUE (MeV)	DOCUMENT ID		TECN	COMMENT
1680 to 1700 (≈ 1690) OUR ESTIMATE				
1683±3	SARANTSEV	19	DPWA	$\overline{K}N$ multichannel
1697^{+6}_{-6}	[1] KAMANO	15	DPWA	$\overline{K}N$ multichannel
• • • We do not use the following data for averages, fits, limits, etc. • • •				
1689	ZHANG	13A	DPWA	$\overline{K}N$ multichannel

[1] From the preferred solution A in KAMANO 15.

−2×IMAGINARY PART

VALUE (MeV)	DOCUMENT ID		TECN	COMMENT
60 to 80 (≈ 70) OUR ESTIMATE				
72± 5	SARANTSEV	19	DPWA	$\overline{K}N$ multichannel
65±14	[1] KAMANO	15	DPWA	$\overline{K}N$ multichannel
• • • We do not use the following data for averages, fits, limits, etc. • • •				
53	ZHANG	13A	DPWA	$\overline{K}N$ multichannel

[1] From the preferred solution A in KAMANO 15.

$\Lambda(1690)$ POLE RESIDUES

The normalized residue is the residue divided by $\Gamma_{pole}/2$.

Normalized residue in $N\overline{K} \to \Lambda(1690) \to N\overline{K}$

MODULUS	PHASE (°)	DOCUMENT ID		TECN	COMMENT
0.24 ±0.05	**−28 ± 5**	SARANTSEV	19	DPWA	$\overline{K}N$ multichannel
• • • We do not use the following data for averages, fits, limits, etc. • • •					
0.251	3	[1] KAMANO	15	DPWA	Multichannel

[1] From the preferred solution A in KAMANO 15.

Normalized residue in $N\overline{K} \to \Lambda(1690) \to \Sigma\pi$

MODULUS	PHASE (°)	DOCUMENT ID		TECN	COMMENT
0.35 ±0.07	**175 ± 6**	SARANTSEV	19	DPWA	$\overline{K}N$ multichannel
• • • We do not use the following data for averages, fits, limits, etc. • • •					
0.315	−173	[1] KAMANO	15	DPWA	$\overline{K}N$ multichannel

[1] From the preferred solution A in KAMANO 15.

Normalized residue in $N\overline{K} \to \Lambda(1690) \to \Lambda\eta$

MODULUS	PHASE (°)	DOCUMENT ID		TECN	COMMENT
0.05 ±0.02	**88 ± 8**	SARANTSEV	19	DPWA	$\overline{K}N$ multichannel
• • • We do not use the following data for averages, fits, limits, etc. • • •					
0.00567	81	[1] KAMANO	15	DPWA	Multichannel

[1] From the preferred solution A in KAMANO 15.

Int. J. Mod. Phys. A 2026.41. Downloaded from www.worldscientific.com
by UNIVERSITY OF CALIFORNIA @ BERKELEY on 09/16/26. Re-use and distribution is strictly not permitted, except for Open Access articles.

Normalized residue in $N\overline{K} \to \Lambda(1690) \to \Lambda\sigma$

MODULUS	PHASE (°)	DOCUMENT ID		TECN	COMMENT
0.08±0.02	**−10 ± 6**	SARANTSEV	19	DPWA	$\overline{K}N$ multichannel

Normalized residue in $N\overline{K} \to \Lambda(1690) \to \Sigma(1385)\pi$, S-wave

MODULUS	PHASE (°)	DOCUMENT ID		TECN	COMMENT
0.11 ±0.06	**170 ± 70**	SARANTSEV	19	DPWA	$\overline{K}N$ multichannel
• • • We do not use the following data for averages, fits, limits, etc. • • •					
0.134	168	[1] KAMANO	15	DPWA	$\overline{K}N$ multichannel

[1] From the preferred solution A in KAMANO 15.

Normalized residue in $N\overline{K} \to \Lambda(1690) \to \Sigma(1385)\pi$, D-wave

MODULUS	PHASE (°)	DOCUMENT ID		TECN	COMMENT
0.06 ±0.04	**164 ± 15**	SARANTSEV	19	DPWA	$\overline{K}N$ multichannel
• • • We do not use the following data for averages, fits, limits, etc. • • •					
0.319	−22	[1] KAMANO	15	DPWA	$\overline{K}N$ multichannel

[1] From the preferred solution A in KAMANO 15.

Normalized residue in $N\overline{K} \to \Lambda(1690) \to N\overline{K}^*(892)$, S-wave

VALUE	DOCUMENT ID		TECN	COMMENT
0.05±0.04	SARANTSEV	19	DPWA	$\overline{K}N$ multichannel

Normalized residue in $N\overline{K} \to \Lambda(1690) \to N\overline{K}^*(892)$, D-wave

VALUE	DOCUMENT ID		TECN	COMMENT
0.18+-0.050-110+-45	SARANTSEV	19	DPWA	$\overline{K}N$ multichannel

$\Lambda(1690)$ MASS

VALUE (MeV)	DOCUMENT ID		TECN	COMMENT
1685 to 1695 (≈ 1690) OUR ESTIMATE				
1691.1±4.4±15.7	ABLIKIM	25AF	BES3	$\psi(3686) \to \Lambda\overline{\Sigma}^0\pi^0$ + c.c. (PWA)
1689 ±3	SARANTSEV	19	DPWA	$\overline{K}N$ multichannel
1691 ±3	ZHANG	13A	DPWA	$\overline{K}N$ multichannel
1695.7±2.6	KOISO	85	DPWA	$K^-p \to \Sigma\pi$
1690 ±5	GOPAL	80	DPWA	$\overline{K}N \to \overline{K}N$
1692 ±5	ALSTON-...	78	DPWA	$\overline{K}N \to \overline{K}N$
1690 ±3	HEPP	76B	DPWA	$K^-N \to \Sigma\pi$
1689 ±1	KANE	74	DPWA	$K^-p \to \Sigma\pi$
• • • We do not use the following data for averages, fits, limits, etc. • • •				
1690 ±5	GOPAL	77	DPWA	$\overline{K}N$ multichannel
1687 or 1689	[1] MARTIN	77	DPWA	$\overline{K}N$ multichannel
1692 ±4	CARROLL	76	DPWA	Isospin-0 total σ

[1] The two MARTIN 77 values are from a T-matrix pole and from a Breit-Wigner fit. Another D_{03} Λ at 1966 MeV is also suggested by MARTIN 77, but is very uncertain.

$\Lambda(1690)$ WIDTH

VALUE (MeV)	DOCUMENT ID		TECN	COMMENT
60 to 80 (≈ 70) OUR ESTIMATE				
72.3± 4.7±18.3	ABLIKIM	25AF	BES3	$\psi(3686) \to \Lambda\overline{\Sigma}^0\pi^0$ + c.c. (PWA)
75 ± 5	SARANTSEV	19	DPWA	$\overline{K}N$ multichannel
54 ± 5	ZHANG	13A	DPWA	$\overline{K}N$ multichannel
67.2± 5.6	KOISO	85	DPWA	$K^-p \to \Sigma\pi$
61 ± 5	GOPAL	80	DPWA	$\overline{K}N \to \overline{K}N$
64 ±10	ALSTON-...	78	DPWA	$\overline{K}N \to \overline{K}N$
82 ± 8	HEPP	76B	DPWA	$K^-N \to \Sigma\pi$
60 ± 4	KANE	74	DPWA	$K^-p \to \Sigma\pi$
• • • We do not use the following data for averages, fits, limits, etc. • • •				
60 ± 5	GOPAL	77	DPWA	$\overline{K}N$ multichannel
62 or 62	[1] MARTIN	77	DPWA	$\overline{K}N$ multichannel
38	CARROLL	76	DPWA	Isospin-0 total σ

[1] The two MARTIN 77 values are from a T-matrix pole and from a Breit-Wigner fit. Another D_{03} Λ at 1966 MeV is also suggested by MARTIN 77, but is very uncertain.

$\Lambda(1690)$ DECAY MODES

	Mode	Fraction (Γ_i/Γ)
Γ_1	$N\overline{K}$	20–30 %
Γ_2	$\Sigma\pi$	20–40 %
Γ_3	$\Lambda\sigma$	(5.0±2.0) %
Γ_4	$\Lambda\pi\pi$	∼ 25 %
Γ_5	$\Sigma\pi\pi$	∼ 20 %
Γ_6	$\Lambda\eta$	
Γ_7	$\Sigma(1385)\pi$, S-wave	(9 ±5) %
Γ_8	$\Sigma(1385)\pi$, D-wave	(3.0±2.0) %
Γ_9	$N\overline{K}^*(892)$, S=1/2, D-wave	
Γ_{10}	$N\overline{K}^*(892)$, S=3/2, S-wave	
Γ_{11}	$N\overline{K}^*(892)$, S=3/2, D-wave	

$\Lambda(1690)$ BRANCHING RATIOS

$\Gamma(N\overline{K})/\Gamma_{total}$ — Γ_1/Γ

VALUE	DOCUMENT ID		TECN	COMMENT
0.20 to 0.28 OUR ESTIMATE				
0.23 ±0.05	SARANTSEV	19	DPWA	$\overline{K}N$ multichannel
0.25 ±0.04	ZHANG	13A	DPWA	$\overline{K}N$ multichannel
0.23 ±0.03	GOPAL	80	DPWA	$\overline{K}N \to \overline{K}N$
0.22 ±0.03	ALSTON-...	78	DPWA	$\overline{K}N \to \overline{K}N$
• • • We do not use the following data for averages, fits, limits, etc. • • •				
0.239	[1] KAMANO	15	DPWA	$\overline{K}N$ multichannel
0.24 ±0.03	GOPAL	77	DPWA	See GOPAL 80
0.28 or 0.26	[2] MARTIN	77	DPWA	$\overline{K}N$ multichannel

[1] From the preferred solution A in KAMANO 15.
[2] The two MARTIN 77 values are from a T-matrix pole and from a Breit-Wigner fit. Another D_{03} Λ at 1966 MeV is also suggested by MARTIN 77, but is very uncertain.

$\Gamma(\Sigma\pi)/\Gamma_{total}$ — Γ_2/Γ

VALUE	DOCUMENT ID		TECN	COMMENT
0.50 ±0.10	SARANTSEV	19	DPWA	$\overline{K}N$ multichannel
• • • We do not use the following data for averages, fits, limits, etc. • • •				
0.387	[1] KAMANO	15	DPWA	$\overline{K}N$ multichannel

[1] From the preferred solution A in KAMANO 15.

$\Gamma(\Lambda\eta)/\Gamma_{total}$ — Γ_6/Γ

VALUE	DOCUMENT ID		TECN	COMMENT
∼ 0.01	SARANTSEV	19	DPWA	$\overline{K}N$ multichannel
• • • We do not use the following data for averages, fits, limits, etc. • • •				
not seen	[1] KAMANO	15	DPWA	Multichannel

[1] From the preferred solution A in KAMANO 15.

$\Gamma(\Lambda\sigma)/\Gamma_{total}$ — Γ_3/Γ

VALUE	DOCUMENT ID		TECN	COMMENT
0.05±0.02	SARANTSEV	19	DPWA	$\overline{K}N$ multichannel

$\Gamma(\Sigma(1385)\pi$, S-wave$)/\Gamma_{total}$ — Γ_7/Γ

VALUE	DOCUMENT ID		TECN	COMMENT
0.09 ±0.05	SARANTSEV	19	DPWA	$\overline{K}N$ multichannel
• • • We do not use the following data for averages, fits, limits, etc. • • •				
0.062	[1] KAMANO	15	DPWA	$\overline{K}N$ multichannel

[1] From the preferred solution A in KAMANO 15.

$\Gamma(\Sigma(1385)\pi$, D-wave$)/\Gamma_{total}$ — Γ_8/Γ

VALUE	DOCUMENT ID		TECN	COMMENT
0.03 ±0.02	SARANTSEV	19	DPWA	$\overline{K}N$ multichannel
• • • We do not use the following data for averages, fits, limits, etc. • • •				
0.308	[1] KAMANO	15	DPWA	$\overline{K}N$ multichannel

[1] From the preferred solution A in KAMANO 15.

$\Gamma(N\overline{K}^*(892)$, S=1/2, D-wave$)/\Gamma_{total}$ — Γ_9/Γ

VALUE	DOCUMENT ID		TECN	COMMENT
• • • We do not use the following data for averages, fits, limits, etc. • • •				
not seen	SARANTSEV	19	DPWA	$\overline{K}N$ multichannel
not seen	[1] KAMANO	15	DPWA	$\overline{K}N$ multichannel

[1] From the preferred solution A in KAMANO 15.

$\Gamma(N\overline{K}^*(892)$, S=3/2, S-wave$)/\Gamma_{total}$ — Γ_{10}/Γ

VALUE	DOCUMENT ID		TECN	COMMENT
• • • We do not use the following data for averages, fits, limits, etc. • • •				
0.003	KAMANO	15	DPWA	Multichannel

$\Gamma(N\overline{K}^*(892)$, S=3/2, D-wave$)/\Gamma_{total}$ — Γ_{11}/Γ

VALUE	DOCUMENT ID		TECN	COMMENT
• • • We do not use the following data for averages, fits, limits, etc. • • •				
not seen	[1] KAMANO	15	DPWA	Multichannel

[1] From the preferred solution A in KAMANO 15.

$(\Gamma_i\Gamma_f)^{1/2}/\Gamma_{total}$ in $N\overline{K} \to \Lambda(1690) \to \Sigma\pi$ — $(\Gamma_1\Gamma_2)^{1/2}/\Gamma$

VALUE	DOCUMENT ID		TECN	COMMENT
−0.27±0.03	ZHANG	13A	DPWA	Multichannel
−0.34±0.02	KOISO	85	DPWA	$K^-p \to \Sigma\pi$
−0.25±0.03	GOPAL	77	DPWA	$\overline{K}N$ multichannel
−0.29±0.03	HEPP	76B	DPWA	$K^-N \to \Sigma\pi$
−0.28±0.03	LONDON	75	HLBC	$K^-p \to \Sigma^0\pi^0$
−0.28±0.02	KANE	74	DPWA	$K^-p \to \Sigma\pi$
• • • We do not use the following data for averages, fits, limits, etc. • • •				
−0.30 or −0.28	[1] MARTIN	77	DPWA	$\overline{K}N$ multichannel

[1] The two MARTIN 77 values are from a T-matrix pole and from a Breit-Wigner fit. Another D_{03} Λ at 1966 MeV is also suggested by MARTIN 77, but is very uncertain.

Int. J. Mod. Phys. A 2026.41. Downloaded from www.worldscientific.com
UNIVERSITY OF CALIFORNIA @ BERKELEY on 09/16/26. Re-use and distribution is strictly not permitted, except for Open Access articles.

$(\Gamma_i\Gamma_f)^{1/2}/\Gamma_{total}$ in $N\overline{K} \to \Lambda(1690) \to \Lambda\pi\pi$ — $(\Gamma_1\Gamma_4)^{1/2}/\Gamma$

VALUE	DOCUMENT ID		TECN	COMMENT
• • • We do not use the following data for averages, fits, limits, etc. • • •				
0.25 ± 0.02	[1] BARTLEY	68	HDBC	$K^-p \to \Lambda\pi\pi$

[1] BARTLEY 68 uses only cross-section data. The enhancement is not seen by PREVOST 71.

$(\Gamma_i\Gamma_f)^{1/2}/\Gamma_{total}$ in $N\overline{K} \to \Lambda(1690) \to \Sigma\pi\pi$ — $(\Gamma_1\Gamma_5)^{1/2}/\Gamma$

VALUE	DOCUMENT ID		TECN	COMMENT
0.21	ARMENTEROS	68C	HDBC	$K^-N \to \Sigma\pi\pi$

$(\Gamma_i\Gamma_f)^{1/2}/\Gamma_{total}$ in $N\overline{K} \to \Lambda(1690) \to \Lambda\eta$ — $(\Gamma_1\Gamma_6)^{1/2}/\Gamma$

VALUE	DOCUMENT ID		TECN	COMMENT
0.00 ± 0.03	BAXTER	73	DPWA	$K^-p \to$ neutrals

$(\Gamma_i\Gamma_f)^{1/2}/\Gamma_{total}$ in $N\overline{K} \to \Lambda(1690) \to \Sigma(1385)\pi$, S-wave — $(\Gamma_1\Gamma_7)^{1/2}/\Gamma$

VALUE	DOCUMENT ID		TECN	COMMENT
-0.28 ± 0.06	ZHANG	13A	DPWA	Multichannel
$+0.27\pm0.04$	PREVOST	74	DPWA	$K^-N \to \Sigma(1385)\pi$

$\Lambda(1690)$ REFERENCES

ABLIKIM	25AF	JHEP 2502 212	M. Ablikim *et al.*	(BESIII Collab.)
SARANTSEV	19	EPJ A55 180	A.V. Sarantsev *et al.*	(BONN, PNPI)
KAMANO	15	PR C92 025205	H. Kamano *et al.*	(ANL, OSAK)
ZHANG	13A	PR C88 035205	H. Zhang *et al.*	(KSU)
KOISO	85	NP A433 619	H. Koiso *et al.*	(TOKY, MASA)
PDG	82	PL 111B 1	M. Roos *et al.*	(HELS, CIT, CERN)
GOPAL	80	Toronto Conf. 159	G.P. Gopal	(RHEL) IJP
ALSTON-...	78	PR D18 182	M. Alston-Garnjost *et al.*	(LBL, MTHO+) IJP
Also		PRL 38 1007	M. Alston-Garnjost *et al.*	(LBL, MTHO+) IJP
GOPAL	77	NP B119 362	G.P. Gopal *et al.*	(LOIC, RHEL) IJP
MARTIN	77	NP B127 349	B.R. Martin, M.K. Pidcock, R.G. Moorhouse	(LOUC+) IJP
Also		NP B126 266	B.R. Martin, M.K. Pidcock	(LOUC)
Also		NP B126 285	B.R. Martin, M.K. Pidcock	(LOUC) IJP
CARROLL	76	PRL 37 806	A.S. Carroll *et al.*	(BNL) I
HEPP	76B	PL 65B 487	V. Hepp *et al.*	(CERN, HEIDH, MPIM) IJP
LONDON	75	NP B85 289	G.W. London *et al.*	(BNL, CERN, EPOL+)
KANE	74	LBL-2452	D.F. Kane	(LBL) IJP
PREVOST	74	NP B69 246	J. Prevost *et al.*	(SACL, CERN, HEID)
BAXTER	73	NP B67 125	D.F. Baxter *et al.*	(OXF) IJP
PREVOST	71	Amsterdam Conf.	J. Prevost	(CERN, HEID, SACL)
ARMENTEROS	68C	NP B8 216	R. Armenteros *et al.*	(CERN, HEID, SACL) I
BARTLEY	68	PRL 21 1111	J.H. Bartley *et al.*	(TUFTS, FSU, BRAN) I

$\Lambda(1710)\ 1/2^+$

$I(J^P) = 0(\frac{1}{2}^+)$ Status: *

OMITTED FROM SUMMARY TABLE

$\Lambda(1710)$ MASS

VALUE (MeV)	DOCUMENT ID		TECN	COMMENT
1713±13	ZHANG	13A	DPWA	Multichannel

$\Lambda(1710)$ WIDTH

VALUE (MeV)	DOCUMENT ID		TECN	COMMENT
180±42	ZHANG	13A	DPWA	Multichannel

$\Lambda(1710)$ DECAY MODES

	Mode	Fraction (Γ_i/Γ)
Γ_1	$N\overline{K}$	(43 ± 4) %
Γ_2	$\Sigma\pi$	(21 ± 5) %
Γ_3	$\Sigma^*(1385)\pi$, P-wave	(20 ± 8) %
Γ_4	$N\overline{K}^*(892)$	
Γ_5	$N\overline{K}^*(892)$, $S=1/2$	(5 ± 4) %
Γ_6	$N\overline{K}^*(892)$, $S=3/2$, P-wave	(10 ± 8) %

$\Lambda(1710)$ BRANCHING RATIOS

$\Gamma(N\overline{K})/\Gamma_{total}$ — Γ_1/Γ

VALUE	DOCUMENT ID		TECN	COMMENT
0.43±0.04	ZHANG	13A	DPWA	Multichannel

$\Gamma(\Sigma\pi)/\Gamma_{total}$ — Γ_2/Γ

VALUE	DOCUMENT ID		TECN	COMMENT
0.21±0.05	ZHANG	13A	DPWA	Multichannel

$\Gamma(\Sigma^*(1385)\pi, P\text{-wave})/\Gamma_{total}$ — Γ_3/Γ

VALUE	DOCUMENT ID		TECN	COMMENT
0.20±0.08	ZHANG	13A	DPWA	Multichannel

$\Gamma(N\overline{K}^*(892), S=1/2)/\Gamma_{total}$ — Γ_5/Γ

VALUE	DOCUMENT ID		TECN	COMMENT
0.05±0.04	ZHANG	13A	DPWA	Multichannel

$\Gamma(N\overline{K}^*(892), S=3/2, P\text{-wave})/\Gamma_{total}$ — Γ_6/Γ

VALUE	DOCUMENT ID		TECN	COMMENT
0.10±0.08	ZHANG	13A	DPWA	Multichannel

$\Lambda(1710)$ REFERENCES

ZHANG	13A	PR C88 035205	H. Zhang *et al.*	(KSU)

$\Lambda(1800)\ 1/2^-$

$I(J^P) = 0(\frac{1}{2}^-)$ Status: ***

$\Lambda(1800)$ POLE POSITION

REAL PART

VALUE (MeV)	DOCUMENT ID		TECN	COMMENT
1809±9	SARANTSEV	19	DPWA	$\overline{K}N$ multichannel
• • • We do not use the following data for averages, fits, limits, etc. • • •				
1729	ZHANG	13A	DPWA	Multichannel

−2×IMAGINARY PART

VALUE (MeV)	DOCUMENT ID		TECN	COMMENT
205±16	SARANTSEV	19	DPWA	$\overline{K}N$ multichannel
• • • We do not use the following data for averages, fits, limits, etc. • • •				
198	ZHANG	13A	DPWA	Multichannel

$\Lambda(1800)$ POLE RESIDUES

The normalized residue is the residue divided by $\Gamma_{pole}/2$.

Normalized residue in $N\overline{K} \to \Lambda(1800) \to N\overline{K}$

MODULUS	PHASE (°)	DOCUMENT ID		TECN	COMMENT
0.34±0.07	**103 ± 8**	SARANTSEV	19	DPWA	$\overline{K}N$ multichannel

Normalized residue in $N\overline{K} \to \Lambda(1800) \to \Sigma\pi$

MODULUS	PHASE (°)	DOCUMENT ID		TECN	COMMENT
0.30±0.06	**−123 ± 8**	SARANTSEV	19	DPWA	$\overline{K}N$ multichannel

Normalized residue in $N\overline{K} \to \Lambda(1800) \to \Lambda\eta$

MODULUS	PHASE (°)	DOCUMENT ID		TECN	COMMENT
0.06±0.03	**75 ± 10**	SARANTSEV	19	DPWA	$\overline{K}N$ multichannel

Normalized residue in $N\overline{K} \to \Lambda(1800) \to \Lambda\sigma$

MODULUS	PHASE (°)	DOCUMENT ID		TECN	COMMENT
0.24±0.05	**25 ± 10**	SARANTSEV	19	DPWA	$\overline{K}N$ multichannel

Normalized residue in $N\overline{K} \to \Lambda(1800) \to \Lambda\omega$, $S=1/2$, S-wave

MODULUS	PHASE (°)	DOCUMENT ID		TECN	COMMENT
0.12±0.04	**−114 ± 30**	SARANTSEV	19	DPWA	$\overline{K}N$ multichannel

Normalized residue in $N\overline{K} \to \Lambda(1800) \to \Lambda\omega$, $S=3/2$, D-wave

MODULUS	PHASE (°)	DOCUMENT ID		TECN	COMMENT
0.08±0.03	**−90 ± 17**	SARANTSEV	19	DPWA	$\overline{K}N$ multichannel

Normalized residue in $N\overline{K} \to \Lambda(1800) \to \Sigma(1385)\pi$

MODULUS	PHASE (°)	DOCUMENT ID		TECN	COMMENT
0.16±0.06	**−140 ± 35**	SARANTSEV	19	DPWA	$\overline{K}N$ multichannel

Normalized residue in $N\overline{K} \to \Lambda(1800) \to N\overline{K}^*(892)$, $S=1/2$, S-wave

MODULUS	PHASE (°)	DOCUMENT ID		TECN	COMMENT
0.18±0.06	**65 ± 40**	SARANTSEV	19	DPWA	$\overline{K}N$ multichannel

Normalized residue in $N\overline{K} \to \Lambda(1800) \to N\overline{K}^*(892)$, $S=3/2$, D-wave

MODULUS	PHASE (°)	DOCUMENT ID		TECN	COMMENT
0.09±0.07		SARANTSEV	19	DPWA	$\overline{K}N$ multichannel

$\Lambda(1800)$ MASS

VALUE (MeV)	DOCUMENT ID		TECN	COMMENT
1750 to 1850 (≈ 1800) OUR ESTIMATE				
$1800.9\pm13.3\pm12.6$	ABLIKIM	25AF	BES3	$\psi(3686) \to \Lambda\overline{\Sigma}^0\pi^0 +$ c.c. (PWA)
1811 ±10	SARANTSEV	19	DPWA	$\overline{K}N$ multichannel
1783 ±19	ZHANG	13A	DPWA	$\overline{K}N$ multichannel
1841 ±10	GOPAL	80	DPWA	$\overline{K}N \to \overline{K}N$
1725 ±20	ALSTON-...	78	DPWA	$\overline{K}N \to \overline{K}N$
1830 ±20	LANGBEIN	72	IPWA	$\overline{K}N$ multichannel
• • • We do not use the following data for averages, fits, limits, etc. • • •				
1845 ±10	MANLEY	02	DPWA	$\overline{K}N$ multichannel
1825 ±20	GOPAL	77	DPWA	$\overline{K}N$ multichannel
1767 or 1842	[1] MARTIN	77	DPWA	$\overline{K}N$ multichannel
1780	KIM	71	DPWA	K-matrix analysis
1872 ±10	BRICMAN	70B	DPWA	$\overline{K}N \to \overline{K}N$

Int. J. Mod. Phys. A 2026.41. Downloaded from www.worldscientific.com by UNIVERSITY OF CALIFORNIA @ BERKELEY on 09/16/26. Re-use and distribution is strictly not permitted, except for Open Access articles.

$\Lambda(1800)$ WIDTH

VALUE (MeV)	DOCUMENT ID		TECN	COMMENT
150 to 250 (≈ 200) OUR ESTIMATE				
208.8±14.5±36.7	ABLIKIM	25AF	BES3	$\psi(3686) \to \Lambda\overline{\Sigma}^0\pi^0 +$ c.c. (PWA)
209 ±18	SARANTSEV	19	DPWA	$\overline{K}N$ multichannel
256 ±35	ZHANG	13A	DPWA	$\overline{K}N$ multichannel
228 ±20	GOPAL	80	DPWA	$\overline{K}N \to \overline{K}N$
185 ±20	ALSTON-...	78	DPWA	$\overline{K}N \to \overline{K}N$
70 ±15	LANGBEIN	72	IPWA	$\overline{K}N$ multichannel
• • • We do not use the following data for averages, fits, limits, etc. • • •				
518 ±84	MANLEY	02	DPWA	$\overline{K}N$ multichannel
230 ±20	GOPAL	77	DPWA	$\overline{K}N$ multichannel
435 or 473	[1] MARTIN	77	DPWA	$\overline{K}N$ multichannel
40	KIM	71	DPWA	K-matrix analysis
100 ±20	BRICMAN	70B	DPWA	$\overline{K}N \to \overline{K}N$

$\Lambda(1800)$ DECAY MODES

	Mode	Fraction (Γ_i/Γ)
Γ_1	$N\overline{K}$	25–40 %
Γ_2	$\Sigma\pi$	(27 ±6) %
Γ_3	$\Lambda\sigma$	(15 ±4) %
Γ_4	$\Sigma(1385)\pi$	(9 ±4) %
Γ_5	$\Lambda\eta$	0.01 to 0.10
Γ_6	$N\overline{K}^*(892)$	seen
Γ_7	$N\overline{K}^*(892)$, S=1/2, S-wave	
Γ_8	$N\overline{K}^*(892)$, S=3/2, D-wave	

$\Lambda(1800)$ BRANCHING RATIOS

See "Sign conventions for resonance couplings" in the Note on Λ and Σ Resonances.

$\Gamma(N\overline{K})/\Gamma_{total}$ — Γ_1/Γ

VALUE	DOCUMENT ID		TECN	COMMENT
0.25 to 0.40 OUR ESTIMATE				
0.35±0.07	SARANTSEV	19	DPWA	$\overline{K}N$ multichannel
0.13±0.06	ZHANG	13A	DPWA	$\overline{K}N$ multichannel
0.36±0.04	GOPAL	80	DPWA	$\overline{K}N \to \overline{K}N$
0.28±0.05	ALSTON-...	78	DPWA	$\overline{K}N \to \overline{K}N$
0.35±0.15	LANGBEIN	72	IPWA	$\overline{K}N$ multichannel
• • • We do not use the following data for averages, fits, limits, etc. • • •				
0.24±0.10	MANLEY	02	DPWA	$\overline{K}N$ multichannel
0.37±0.05	GOPAL	77	DPWA	See GOPAL 80
1.21 or 0.70	[1] MARTIN	77	DPWA	$\overline{K}N$ multichannel
0.80	KIM	71	DPWA	K-matrix analysis
0.18±0.02	BRICMAN	70B	DPWA	$\overline{K}N \to \overline{K}N$

$\Gamma(\Sigma\pi)/\Gamma_{total}$ — Γ_2/Γ

VALUE	DOCUMENT ID		TECN	COMMENT
0.27±0.06	SARANTSEV	19	DPWA	$\overline{K}N$ multichannel

$\Gamma(\Lambda\sigma)/\Gamma_{total}$ — Γ_3/Γ

VALUE	DOCUMENT ID		TECN	COMMENT
0.15±0.04	SARANTSEV	19	DPWA	$\overline{K}N$ multichannel

$\Gamma(\Sigma(1385)\pi)/\Gamma_{total}$ — Γ_4/Γ

VALUE	DOCUMENT ID		TECN	COMMENT
0.09±0.04	SARANTSEV	19	DPWA	$\overline{K}N$ multichannel

$\Gamma(\Lambda\eta)/\Gamma_{total}$ — Γ_5/Γ

VALUE	DOCUMENT ID		TECN	COMMENT
0.01 to 0.10 OUR ESTIMATE				
0.010±0.005	SARANTSEV	19	DPWA	$\overline{K}N$ multichannel
0.06 ±0.05	ZHANG	13A	DPWA	Multichannel

$(\Gamma_i\Gamma_f)^{1/2}/\Gamma_{total}$ in $N\overline{K} \to \Lambda(1800) \to \Sigma\pi$ — $(\Gamma_1\Gamma_2)^{1/2}/\Gamma$

VALUE	DOCUMENT ID		TECN	COMMENT
−0.07±0.02	ZHANG	13A	DPWA	Multichannel
−0.08±0.05	GOPAL	77	DPWA	$\overline{K}N$ multichannel
• • • We do not use the following data for averages, fits, limits, etc. • • •				
−0.74 or −0.43	[1] MARTIN	77	DPWA	$\overline{K}N$ multichannel
0.24	KIM	71	DPWA	K-matrix analysis

$(\Gamma_i\Gamma_f)^{1/2}/\Gamma_{total}$ in $N\overline{K} \to \Lambda(1800) \to \Sigma(1385)\pi$ — $(\Gamma_1\Gamma_4)^{1/2}/\Gamma$

VALUE	DOCUMENT ID		TECN	COMMENT
−0.09 ±0.05	ZHANG	13A	DPWA	Multichannel
+0.056±0.028	[2] CAMERON	78	DPWA	$K^-p \to \Sigma(1385)\pi$

$(\Gamma_i\Gamma_f)^{1/2}/\Gamma_{total}$ in $N\overline{K} \to \Lambda(1800) \to N\overline{K}^*(892)$, S=1/2, S-wave — $(\Gamma_1\Gamma_7)^{1/2}/\Gamma$

VALUE	DOCUMENT ID		TECN	COMMENT
−0.13±0.02	ZHANG	13A	DPWA	Multichannel
−0.17±0.03	[2] CAMERON	78B	DPWA	$K^-p \to N\overline{K}^*$

$(\Gamma_i\Gamma_f)^{1/2}/\Gamma_{total}$ in $N\overline{K} \to \Lambda(1800) \to N\overline{K}^*(892)$, S=3/2, D-wave — $(\Gamma_1\Gamma_8)^{1/2}/\Gamma$

VALUE	DOCUMENT ID		TECN	COMMENT
−0.13±0.04	CAMERON	78B	DPWA	$K^-p \to N\overline{K}^*$

$\Lambda(1800)$ FOOTNOTES

[1] The two MARTIN 77 values are from a T-matrix pole and from a Breit-Wigner fit.
[2] The published sign has been changed to be in accord with the baryon-first convention.

$\Lambda(1800)$ REFERENCES

ABLIKIM	25AF	JHEP 2502 212	M. Ablikim *et al.*	(BESIII Collab.)
SARANTSEV	19	EPJ A55 180	A.V. Sarantsev *et al.*	(BONN, PNPI)
ZHANG	13A	PR C88 035205	H. Zhang *et al.*	(KSU)
MANLEY	02	PRL 88 012002	D.M. Manley *et al.*	(BNL Crystal Ball Collab.)
GOPAL	80	Toronto Conf. 159	G.P. Gopal	(RHEL) IJP
ALSTON-...	78	PR D18 182	M. Alston-Garnjost *et al.*	(LBL, MTHO+) IJP
Also		PRL 38 1007	M. Alston-Garnjost *et al.*	(LBL, MTHO+) IJP
CAMERON	78	NP B143 189	W. Cameron *et al.*	(RHEL, LOIC) IJP
CAMERON	78B	NP B146 327	W. Cameron *et al.*	(RHEL, LOIC) IJP
GOPAL	77	NP B119 362	G.P. Gopal *et al.*	(LOIC, RHEL) IJP
MARTIN	77	NP B127 349	B.R. Martin, M.K. Pidcock, R.G. Moorhouse	(LOUC+) IJP
Also		NP B126 266	B.R. Martin, M.K. Pidcock	(LOUC)
Also		NP B126 285	B.R. Martin, M.K. Pidcock	(LOUC) IJP
LANGBEIN	72	NP B47 477	W. Langbein, F. Wagner	(MPIM) IJP
KIM	71	PRL 27 356	J.K. Kim	(HARV) IJP
Also		Duke Conf. 161	J.K. Kim	(HARV) IJP
Hyperon Resonances, 1970				
BRICMAN	70B	PL 33B 511	C. Bricman, M. Ferro-Luzzi, J.P. Lagnaux	(CERN) IJP

$\Lambda(1810)\ 1/2^+$

$I(J^P) = 0(\frac{1}{2}^+)$ Status: ***

$\Lambda(1810)$ POLE POSITION

REAL PART

VALUE (MeV)	DOCUMENT ID		TECN	COMMENT
1773± 7	SARANTSEV	19	DPWA	$\overline{K}N$ multichannel
• • • We do not use the following data for averages, fits, limits, etc. • • •				
2097^{+40}_{-1}	[1] KAMANO	15	DPWA	Multichannel
1780	ZHANG	13A	DPWA	Multichannel

[1] From the preferred solution A in KAMANO 15. Solution B reports M = 1841^{+3}_{-4} MeV.

−2×IMAGINARY PART

VALUE (MeV)	DOCUMENT ID		TECN	COMMENT
38±14	SARANTSEV	19	DPWA	$\overline{K}N$ multichannel
• • • We do not use the following data for averages, fits, limits, etc. • • •				
166^{+64}_{-12}	[1] KAMANO	15	DPWA	Multichannel
64	ZHANG	13A	DPWA	Multichannel

[1] From the preferred solution A in KAMANO 15. Solution B Reports Γ = 62^{+6}_{-4} MeV.

$\Lambda(1810)$ POLE RESIDUES

The normalized residue is the residue divided by $\Gamma_{pole}/2$.

Normalized residue in $N\overline{K} \to \Lambda(1810) \to N\overline{K}$

MODULUS	PHASE (°)	DOCUMENT ID		TECN	COMMENT
0.018±0.008	**65 ± 26**	SARANTSEV	19	DPWA	$\overline{K}N$ multichannel
• • • We do not use the following data for averages, fits, limits, etc. • • •					
0.205	−63	[1] KAMANO	15	DPWA	Multichannel

[1] From the preferred solution A in KAMANO 15.

Normalized residue in $N\overline{K} \to \Lambda(1810) \to \Sigma\pi$

MODULUS	PHASE (°)	DOCUMENT ID		TECN	COMMENT
0.045 ±0.020	**−143 ± 24**	SARANTSEV	19	DPWA	$\overline{K}N$ multichannel
• • • We do not use the following data for averages, fits, limits, etc. • • •					
0.0325	29	[1] KAMANO	15	DPWA	Multichannel

[1] From the preferred solution A in KAMANO 15.

Normalized residue in $N\overline{K} \to \Lambda(1810) \to \Lambda\eta$

MODULUS	PHASE (°)	DOCUMENT ID		TECN	COMMENT
• • • We do not use the following data for averages, fits, limits, etc. • • •					
0.155	165	[1] KAMANO	15	DPWA	Multichannel

[1] From the preferred solution A in KAMANO 15.

Normalized residue in $N\overline{K} \to \Lambda(1810) \to \Lambda\sigma$

MODULUS	PHASE (°)	DOCUMENT ID		TECN	COMMENT
0.055±0.020	**30 ± 16**	SARANTSEV	19	DPWA	$\overline{K}N$ multichannel

Int. J. Mod. Phys. A 2026.41. Downloaded from www.worldscientific.com
UNIVERSITY OF CALIFORNIA @ BERKELEY on 09/16/26. Re-use and distribution is strictly not permitted, except for Open Access articles.

Normalized residue in $N\overline{K} \to \Lambda(1810) \to \Xi K$

MODULUS	PHASE (°)	DOCUMENT ID		TECN	COMMENT
• • • We do not use the following data for averages, fits, limits, etc. • • •					
0.0937	−64	[1] KAMANO	15	DPWA	Multichannel

[1] From the preferred solution A in KAMANO 15.

Normalized residue in $N\overline{K} \to \Lambda(1810) \to \Sigma(1385)\pi$

MODULUS	PHASE (°)	DOCUMENT ID		TECN	COMMENT
0.08 ±0.03	**−50 ± 30**	SARANTSEV	19	DPWA	$\overline{K}N$ multichannel
• • • We do not use the following data for averages, fits, limits, etc. • • •					
0.244	−10	[1] KAMANO	15	DPWA	Multichannel

[1] From the preferred solution A in KAMANO 15.

Normalized residue in $N\overline{K} \to \Lambda(1810) \to N\overline{K}^*(892)$, S=1/2, P-wave

MODULUS	PHASE (°)	DOCUMENT ID		TECN	COMMENT
0.03 ±0.03		SARANTSEV	19	DPWA	$\overline{K}N$ multichannel
• • • We do not use the following data for averages, fits, limits, etc. • • •					
0.159	−97	[1] KAMANO	15	DPWA	Multichannel

[1] From the preferred solution A in KAMANO 15.

Normalized residue in $N\overline{K} \to \Lambda(1810) \to N\overline{K}^*(892)$, S=3/2, P-wave

MODULUS	PHASE (°)	DOCUMENT ID		TECN	COMMENT
0.05 ±0.04		SARANTSEV	19	DPWA	$\overline{K}N$ multichannel
• • • We do not use the following data for averages, fits, limits, etc. • • •					
0.0497	2	[1] KAMANO	15	DPWA	Multichannel

[1] From the preferred solution A in KAMANO 15.

$\Lambda(1810)$ MASS

VALUE (MeV)	DOCUMENT ID		TECN	COMMENT
1740 to 1840 (≈ 1790) OUR ESTIMATE				
1773 ± 7	SARANTSEV	19	DPWA	$\overline{K}N$ multichannel
1821 ± 10	ZHANG	13A	DPWA	Multichannel
1841 ± 20	GOPAL	80	DPWA	$\overline{K}N \to \overline{K}N$
1735 ± 5	CARROLL	76	DPWA	Isospin-0 total σ
1746 ± 10	PREVOST	74	DPWA	$K^-N \to \Sigma(1385)\pi$
1780 ± 20	LANGBEIN	72	IPWA	$\overline{K}N$ multichannel
• • • We do not use the following data for averages, fits, limits, etc. • • •				
1853 ± 20	GOPAL	77	DPWA	$\overline{K}N$ multichannel
1861 or 1953	[1] MARTIN	77	DPWA	$\overline{K}N$ multichannel
1755	KIM	71	DPWA	K-matrix analysis
1800	ARMENTEROS70		HBC	$\overline{K}N \to \overline{K}N$
1750	ARMENTEROS70		HBC	$\overline{K}N \to \Sigma\pi$
1690 ± 10	BARBARO-...	70	HBC	$\overline{K}N \to \Sigma\pi$
1740	BAILEY	69	DPWA	$\overline{K}N \to \overline{K}N$
1745	ARMENTEROS68B		HBC	$\overline{K}N \to \overline{K}N$

[1] The two MARTIN 77 values are from a T-matrix pole and from a Breit-Wigner fit.

$\Lambda(1810)$ WIDTH

VALUE (MeV)	DOCUMENT ID		TECN	COMMENT
50 to 170 (≈ 110) OUR ESTIMATE				
39 ± 15	SARANTSEV	19	DPWA	$\overline{K}N$ multichannel
174 ± 50	ZHANG	13A	DPWA	Multichannel
164 ± 20	GOPAL	80	DPWA	$\overline{K}N \to \overline{K}N$
90 ± 20	CAMERON	78B	DPWA	$K^-p \to N\overline{K}^*$
46 ± 20	PREVOST	74	DPWA	$K^-N \to \Sigma(1385)\pi$
120 ± 10	LANGBEIN	72	IPWA	$\overline{K}N$ multichannel
• • • We do not use the following data for averages, fits, limits, etc. • • •				
166 ± 20	GOPAL	77	DPWA	$\overline{K}N$ multichannel
535 or 585	[1] MARTIN	77	DPWA	$\overline{K}N$ multichannel
28	CARROLL	76	DPWA	Isospin-0 total σ
35	KIM	71	DPWA	K-matrix analysis
30	ARMENTEROS70		HBC	$\overline{K}N \to \overline{K}N$
70	ARMENTEROS70		HBC	$\overline{K}N \to \Sigma\pi$
22	BARBARO-...	70	HBC	$\overline{K}N \to \Sigma\pi$
300	BAILEY	69	DPWA	$\overline{K}N \to \overline{K}N$
147	ARMENTEROS68B		HBC	

[1] The two MARTIN 77 values are from a T-matrix pole and from a Breit-Wigner fit.

$\Lambda(1810)$ DECAY MODES

	Mode	Fraction (Γ_i/Γ)
Γ_1	$N\overline{K}$	0.05 to 0.35
Γ_2	$\Sigma\pi$	(16 ± 5) %
Γ_3	$\Lambda\eta$	
Γ_4	ΞK	
Γ_5	$\Sigma(1385)\pi$	(40 ±15) %
Γ_6	$N\overline{K}^*(892)$	30–60 %
Γ_7	$N\overline{K}^*(892)$, S=1/2, P-wave	
Γ_8	$N\overline{K}^*(892)$, S=3/2, P-wave	

$\Lambda(1810)$ BRANCHING RATIOS

$\Gamma(N\overline{K})/\Gamma_{total}$ — Γ_1/Γ

VALUE	DOCUMENT ID		TECN	COMMENT
0.05 to 0.35 OUR ESTIMATE				
0.025 ± 0.013	SARANTSEV	19	DPWA	$\overline{K}N$ multichannel
0.19 ± 0.08	ZHANG	13A	DPWA	$\overline{K}N$ multichannel
0.24 ± 0.04	GOPAL	80	DPWA	$\overline{K}N \to \overline{K}N$
0.36 ± 0.05	LANGBEIN	72	IPWA	$\overline{K}N$ multichannel
• • • We do not use the following data for averages, fits, limits, etc. • • •				
0.225	[1] KAMANO	15	DPWA	$\overline{K}N$ multichannel
0.21 ± 0.04	GOPAL	77	DPWA	See GOPAL 80
0.52 or 0.49	[2] MARTIN	77	DPWA	$\overline{K}N$ multichannel
0.30	KIM	71	DPWA	K-matrix analysis
0.15	ARMENTEROS70		DPWA	$\overline{K}N \to \overline{K}N$
0.55	BAILEY	69	DPWA	$\overline{K}N \to \overline{K}N$
0.4	ARMENTEROS68B		DPWA	$\overline{K}N \to \overline{K}N$

[1] From the preferred solution A in KAMANO 15.
[2] The two MARTIN 77 values are from a T-matrix pole and from a Breit-Wigner fit.

$\Gamma(\Sigma\pi)/\Gamma_{total}$ — Γ_2/Γ

VALUE	DOCUMENT ID		TECN	COMMENT
0.16 ±0.05	SARANTSEV	19	DPWA	$\overline{K}N$ multichannel
• • • We do not use the following data for averages, fits, limits, etc. • • •				
0.009	[1] KAMANO	15	DPWA	Multichannel

[1] From the preferred solution A in KAMANO 15.

$\Gamma(\Lambda\eta)/\Gamma_{total}$ — Γ_3/Γ

VALUE	DOCUMENT ID		TECN	COMMENT
• • • We do not use the following data for averages, fits, limits, etc. • • •				
0.111	[1] KAMANO	15	DPWA	Multichannel

[1] From the preferred solution A in KAMANO 15.

$\Gamma(\Xi K)/\Gamma_{total}$ — Γ_4/Γ

VALUE	DOCUMENT ID		TECN	COMMENT
• • • We do not use the following data for averages, fits, limits, etc. • • •				
0.051	[1] KAMANO	15	DPWA	Multichannel

[1] From the preferred solution A in KAMANO 15.

$\Gamma(\Sigma(1385)\pi)/\Gamma_{total}$ — Γ_5/Γ

VALUE	DOCUMENT ID		TECN	COMMENT
0.40 ±0.15	SARANTSEV	19	DPWA	$\overline{K}N$ multichannel
• • • We do not use the following data for averages, fits, limits, etc. • • •				
0.600	[1] KAMANO	15	DPWA	Multichannel

[1] From the preferred solution A in KAMANO 15.

$\Gamma(N\overline{K}^*(892), S=1/2, P\text{-wave})/\Gamma_{total}$ — Γ_7/Γ

VALUE	DOCUMENT ID		TECN	COMMENT
• • • We do not use the following data for averages, fits, limits, etc. • • •				
0.003	[1] KAMANO	15	DPWA	Multichannel

[1] From the preferred solution A in KAMANO 15.

$(\Gamma_i\Gamma_f)^{1/2}/\Gamma_{total}$ in $N\overline{K} \to \Lambda(1810) \to \Sigma\pi$ — $(\Gamma_1\Gamma_2)^{1/2}/\Gamma$

VALUE	DOCUMENT ID		TECN	COMMENT
−0.08 ± 0.05	ZHANG	13A	DPWA	Multichannel
−0.24 ± 0.04	GOPAL	77	DPWA	$\overline{K}N$ multichannel
• • • We do not use the following data for averages, fits, limits, etc. • • •				
+0.25 or +0.23	[1] MARTIN	77	DPWA	$\overline{K}N$ multichannel
< 0.01	LANGBEIN	72	IPWA	$\overline{K}N$ multichannel
0.17	KIM	71	DPWA	K-matrix analysis
+0.20	[2] ARMENTEROS70		DPWA	$\overline{K}N \to \Sigma\pi$
−0.13 ± 0.03	BARBARO-...	70	DPWA	$\overline{K}N \to \Sigma\pi$

[1] The two MARTIN 77 values are from a T-matrix pole and from a Breit-Wigner fit.
[2] The published sign has been changed to be in accord with the baryon-first convention.

$(\Gamma_i\Gamma_f)^{1/2}/\Gamma_{total}$ in $N\overline{K} \to \Lambda(1810) \to \Sigma(1385)\pi$ — $(\Gamma_1\Gamma_5)^{1/2}/\Gamma$

VALUE	DOCUMENT ID		TECN	COMMENT
+0.18 ± 0.10	PREVOST	74	DPWA	$K^-N \to \Sigma(1385)\pi$

$(\Gamma_i\Gamma_f)^{1/2}/\Gamma_{total}$ in $N\overline{K} \to \Lambda(1810) \to N\overline{K}^*(892)$, S=1/2, P-wave — $(\Gamma_1\Gamma_7)^{1/2}/\Gamma$

VALUE	DOCUMENT ID		TECN	COMMENT
−0.14 ± 0.03	[1] CAMERON	78B	DPWA	$K^-p \to N\overline{K}^*$

[1] The published sign has been changed to be in accord with the baryon-first convention.

$(\Gamma_i\Gamma_f)^{1/2}/\Gamma_{total}$ in $N\overline{K} \to \Lambda(1810) \to N\overline{K}^*(892)$, S=3/2, P-wave — $(\Gamma_1\Gamma_8)^{1/2}/\Gamma$

VALUE	DOCUMENT ID		TECN	COMMENT
+0.38 ± 0.06	ZHANG	13A	DPWA	Multichannel
+0.35 ± 0.06	CAMERON	78B	DPWA	$K^-p \to N\overline{K}^*$

Int. J. Mod. Phys. A 2026.41. Downloaded from www.worldscientific.com
by UNIVERSITY OF CALIFORNIA @ BERKELEY on 09/16/26. Re-use and distribution is strictly not permitted, except for Open Access articles.

$\Lambda(1810)$ REFERENCES

SARANTSEV	19	EPJ A55 180	A.V. Sarantsev *et al.*	(BONN, PNPI)
KAMANO	15	PR C92 025205	H. Kamano *et al.*	(ANL, OSAK)
ZHANG	13A	PR C88 035205	H. Zhang *et al.*	(KSU)
GOPAL	80	Toronto Conf. 159	G.P. Gopal	(RHEL) IJP
CAMERON	78B	NP B146 327	W. Cameron *et al.*	(RHEL, LOIC) IJP
GOPAL	77	NP B119 362	G.P. Gopal *et al.*	(LOIC, RHEL) IJP
MARTIN	77	NP B127 349	B.R. Martin, M.K. Pidcock, R.G. Moorhouse	(LOUC+) IJP
Also		NP B126 266	B.R. Martin, M.K. Pidcock	(LOUC)
Also		NP B126 285	B.R. Martin, M.K. Pidcock	(LOUC) IJP
CARROLL	76	PRL 37 806	A.S. Carroll *et al.*	(BNL) I
PREVOST	74	NP B69 246	J. Prevost *et al.*	(SACL, CERN, HEID)
LANGBEIN	72	NP B47 477	W. Langbein, F. Wagner	(MPIM) IJP
KIM	71	PRL 27 356	J.K. Kim	(HARV) IJP
Also		Duke Conf. 161	J.K. Kim	(HARV) IJP
Hyperon Resonances, 1970				
ARMENTEROS	70	Duke Conf. 123	R. Armenteros *et al.*	(CERN, HEID, SACL) IJP
Hyperon Resonances, 1970				
BARBARO-...	70	Duke Conf. 173	A. Barbaro-Galtieri	(LRL) IJP
Hyperon Resonances, 1970				
BAILEY	69	Thesis UCRL 50617	J.M. Bailey	(LLL) IJP
ARMENTEROS	68B	NP B8 195	R. Armenteros *et al.*	(CERN, HEID, SACL) IJP

$\Lambda(1820)\ 5/2^+$

$I(J^P) = 0(\frac{5}{2}^+)$ Status: ****

This resonance is the cornerstone for all partial-wave analyses in this region. Most of the results published before 1973 are now obsolete and have been omitted. They may be found in our 1982 edition Physics Letters **111B** 1 (1982).

$\Lambda(1820)$ POLE POSITION

REAL PART

VALUE (MeV)	DOCUMENT ID		TECN	COMMENT
1812 to 1825 ($\approx$ 1818) OUR ESTIMATE				
1813 ± 3	SARANTSEV	19	DPWA	$\overline{K}N$ multichannel
1824^{+2}_{-1}	[1] KAMANO	15	DPWA	$\overline{K}N$ multichannel
• • • We do not use the following data for averages, fits, limits, etc. • • •				
1814	ZHANG	13A	DPWA	$\overline{K}N$ multichannel

[1] From the preferred solution A in KAMANO 15.

$-2\times$IMAGINARY PART

VALUE (MeV)	DOCUMENT ID		TECN	COMMENT
75 to 80 ($\approx$ 77) OUR ESTIMATE				
78 ± 7	SARANTSEV	19	DPWA	$\overline{K}N$ multichannel
77 ± 2	[1] KAMANO	15	DPWA	$\overline{K}N$ multichannel
• • • We do not use the following data for averages, fits, limits, etc. • • •				
85	ZHANG	13A	DPWA	$\overline{K}N$ multichannel

[1] From the preferred solution A in KAMANO 15.

$\Lambda(1820)$ POLE RESIDUES

The normalized residue is the residue divided by $\Gamma_{pole}/2$.

Normalized residue in $N\overline{K} \to \Lambda(1820) \to N\overline{K}$

MODULUS	PHASE (°)	DOCUMENT ID		TECN	COMMENT
0.60 ±0.12	**−22 ± 5**	SARANTSEV	19	DPWA	$\overline{K}N$ multichannel
• • • We do not use the following data for averages, fits, limits, etc. • • •					
0.558	−13	[1] KAMANO	15	DPWA	$\overline{K}N$ multichannel

[1] From the preferred solution A in KAMANO 15.

Normalized residue in $N\overline{K} \to \Lambda(1820) \to \Sigma\pi$

MODULUS	PHASE (°)	DOCUMENT ID		TECN	COMMENT
0.34 ±0.07	**174 ± 5**	SARANTSEV	19	DPWA	$\overline{K}N$ multichannel
• • • We do not use the following data for averages, fits, limits, etc. • • •					
0.357	168	[1] KAMANO	15	DPWA	$\overline{K}N$ multichannel

[1] From the preferred solution A in KAMANO 15.

Normalized residue in $N\overline{K} \to \Lambda(1820) \to \Lambda\eta$

MODULUS	PHASE (°)	DOCUMENT ID		TECN	COMMENT
• • • We do not use the following data for averages, fits, limits, etc. • • •					
0.0184	−3	[1] KAMANO	15	DPWA	$\overline{K}N$ multichannel

[1] From the preferred solution A in KAMANO 15.

Normalized residue in $N\overline{K} \to \Lambda(1820) \to \Xi K$

MODULUS	PHASE (°)	DOCUMENT ID		TECN	COMMENT
~ 0		SARANTSEV	19	DPWA	$\overline{K}N$ multichannel
• • • We do not use the following data for averages, fits, limits, etc. • • •					
0.00111	70	[1] KAMANO	15	DPWA	$\overline{K}N$ multichannel

[1] From the preferred solution A in KAMANO 15.

Normalized residue in $N\overline{K} \to \Lambda(1820) \to \Sigma(1385)\pi$, P-wave

MODULUS	PHASE (°)	DOCUMENT ID		TECN	COMMENT
0.07 ±0.02	**−60 ± 50**	SARANTSEV	19	DPWA	$\overline{K}N$ multichannel
• • • We do not use the following data for averages, fits, limits, etc. • • •					
0.340	161	[1] KAMANO	15	DPWA	$\overline{K}N$ multichannel

[1] From the preferred solution A in KAMANO 15.

Normalized residue in $N\overline{K} \to \Lambda(1820) \to \Sigma(1385)\pi$, F-wave

MODULUS	PHASE (°)	DOCUMENT ID		TECN	COMMENT
0.11 ±0.04	**5 ± 45**	SARANTSEV	19	DPWA	$\overline{K}N$ multichannel
• • • We do not use the following data for averages, fits, limits, etc. • • •					
0.201	151	[1] KAMANO	15	DPWA	$\overline{K}N$ multichannel

[1] From the preferred solution A in KAMANO 15.

Normalized residue in $N\overline{K} \to \Lambda(1820) \to N\overline{K}^*(892)$, $S=1/2$, F-wave

MODULUS	PHASE (°)	DOCUMENT ID		TECN	COMMENT
0.02 ±0.02		SARANTSEV	19	DPWA	$\overline{K}N$ multichannel
• • • We do not use the following data for averages, fits, limits, etc. • • •					
0.00750	41	[1] KAMANO	15	DPWA	$\overline{K}N$ multichannel

[1] From the preferred solution A in KAMANO 15.

Normalized residue in $N\overline{K} \to \Lambda(1820) \to N\overline{K}^*(892)$, $S=3/2$, P-wave

MODULUS	PHASE (°)	DOCUMENT ID		TECN	COMMENT
0.35 ±0.15	**−30 ± 45**	SARANTSEV	19	DPWA	$\overline{K}N$ multichannel
• • • We do not use the following data for averages, fits, limits, etc. • • •					
0.171	−139	[1] KAMANO	15	DPWA	$\overline{K}N$ multichannel

[1] From the preferred solution A in KAMANO 15.

Normalized residue in $N\overline{K} \to \Lambda(1820) \to N\overline{K}^*(892)$, $S=3/2$, F-wave

MODULUS	PHASE (°)	DOCUMENT ID		TECN	COMMENT
0.02 ±0.02		SARANTSEV	19	DPWA	$\overline{K}N$ multichannel
• • • We do not use the following data for averages, fits, limits, etc. • • •					
0.000517	161	[1] KAMANO	15	DPWA	$\overline{K}N$ multichannel

[1] From the preferred solution A in KAMANO 15.

$\Lambda(1820)$ MASS

VALUE (MeV)	DOCUMENT ID		TECN	COMMENT
1815 to 1825 ($\approx$ 1820) OUR ESTIMATE				
$1822\ \pm4$	SARANTSEV	19	DPWA	$\overline{K}N$ multichannel
1823.5 ± 0.8	ZHANG	13A	DPWA	$\overline{K}N$ multichannel
$1823\ \pm3$	GOPAL	80	DPWA	$\overline{K}N \to \overline{K}N$
$1819\ \pm2$	ALSTON-...	78	DPWA	$\overline{K}N \to \overline{K}N$
$1821\ \pm2$	KANE	74	DPWA	$K^-p \to \Sigma\pi$
• • • We do not use the following data for averages, fits, limits, etc. • • •				
1830	DECLAIS	77	DPWA	$\overline{K}N \to \overline{K}N$
$1822\ \pm2$	GOPAL	77	DPWA	$\overline{K}N$ multichannel
1817 or 1819	[1] MARTIN	77	DPWA	$\overline{K}N$ multichannel

[1] The two MARTIN 77 values are from a T-matrix pole and from a Breit-Wigner fit.

$\Lambda(1820)$ WIDTH

VALUE (MeV)	DOCUMENT ID		TECN	COMMENT
70 to 90 ($\approx$ 80) OUR ESTIMATE				
80 ± 8	SARANTSEV	19	DPWA	$\overline{K}N$ multichannel
89 ± 2	ZHANG	13A	DPWA	$\overline{K}N$ multichannel
77 ± 5	GOPAL	80	DPWA	$\overline{K}N \to \overline{K}N$
72 ± 5	ALSTON-...	78	DPWA	$\overline{K}N \to \overline{K}N$
87 ± 3	KANE	74	DPWA	$K^-p \to \Sigma\pi$
• • • We do not use the following data for averages, fits, limits, etc. • • •				
82	DECLAIS	77	DPWA	$\overline{K}N \to \overline{K}N$
81 ± 5	GOPAL	77	DPWA	$\overline{K}N$ multichannel
76 or 76	[1] MARTIN	77	DPWA	$\overline{K}N$ multichannel

[1] The two MARTIN 77 values are from a T-matrix pole and from a Breit-Wigner fit.

$\Lambda(1820)$ DECAY MODES

	Mode	Fraction (Γ_i/Γ)
Γ_1	$N\overline{K}$	55–65 %
Γ_2	$\Sigma\pi$	8–14 %
Γ_3	$\Sigma(1385)\pi$	5–10 %
Γ_4	$\Sigma(1385)\pi$, P-wave	
Γ_5	$\Sigma(1385)\pi$, F-wave	(2.0 ± 1.0) %
Γ_6	$\Lambda\eta$	
Γ_7	ΞK	
Γ_8	$\Sigma\pi\pi$	
Γ_9	$N\overline{K}^*(892)$, $S=1/2$, F-wave	
Γ_{10}	$N\overline{K}^*(892)$, $S=3/2$, P-wave	(3.0 ± 1.0) %
Γ_{11}	$N\overline{K}^*(892)$, $S=3/2$, F-wave	

Int. J. Mod. Phys. A 2026.41. Downloaded from www.worldscientific.com
UNIVERSITY OF CALIFORNIA @ BERKELEY on 09/16/26. Re-use and distribution is strictly not permitted, except for Open Access articles.

$\Lambda(1820)$ BRANCHING RATIOS

Errors quoted do not include uncertainties in the parametrizations used in the partial-wave analyses and are thus too small. See also "Sign conventions for resonance couplings" in the Note on Λ and Σ Resonances.

$\Gamma(N\overline{K})/\Gamma_{total}$ — Γ_1/Γ

VALUE	DOCUMENT ID		TECN	COMMENT
0.55 to 0.65 OUR ESTIMATE				
0.58 ±0.12	SARANTSEV	19	DPWA	$\overline{K}N$ multichannel
0.54 ±0.01	ZHANG	13A	DPWA	$\overline{K}N$ multichannel
0.58 ±0.02	GOPAL	80	DPWA	$\overline{K}N \to \overline{K}N$
0.60 ±0.03	ALSTON-...	78	DPWA	$\overline{K}N \to \overline{K}N$
• • • We do not use the following data for averages, fits, limits, etc. • • •				
0.547	[1] KAMANO	15	DPWA	$\overline{K}N$ multichannel
0.51	DECLAIS	77	DPWA	$\overline{K}N \to \overline{K}N$
0.57 ±0.02	GOPAL	77	DPWA	See GOPAL 80
0.59 or 0.58	[2] MARTIN	77	DPWA	$\overline{K}N$ multichannel

[1] From the preferred solution A in KAMANO 15.
[2] The two MARTIN 77 values are from a T-matrix pole and from a Breit-Wigner fit.

$\Gamma(\Sigma\pi)/\Gamma_{total}$ — Γ_2/Γ

VALUE	DOCUMENT ID		TECN	COMMENT
0.19 ±0.04	SARANTSEV	19	DPWA	$\overline{K}N$ multichannel
• • • We do not use the following data for averages, fits, limits, etc. • • •				
0.218	[1] KAMANO	15	DPWA	$\overline{K}N$ multichannel

[1] From the preferred solution A in KAMANO 15.

$\Gamma(\Sigma(1385)\pi, P\text{-wave})/\Gamma_{total}$ — Γ_4/Γ

VALUE	DOCUMENT ID		TECN	COMMENT
~ 0.01	SARANTSEV	19	DPWA	$\overline{K}N$ multichannel
• • • We do not use the following data for averages, fits, limits, etc. • • •				
0.173	[1] KAMANO	15	DPWA	$\overline{K}N$ multichannel

[1] From the preferred solution A in KAMANO 15.

$\Gamma(\Sigma(1385)\pi, F\text{-wave})/\Gamma_{total}$ — Γ_5/Γ

VALUE	DOCUMENT ID		TECN	COMMENT
0.02 ±0.01	SARANTSEV	19	DPWA	$\overline{K}N$ multichannel
• • • We do not use the following data for averages, fits, limits, etc. • • •				
0.055	[1] KAMANO	15	DPWA	$\overline{K}N$ multichannel

[1] From the preferred solution A in KAMANO 15.

$\Gamma(\Lambda\eta)/\Gamma_{total}$ — Γ_6/Γ

VALUE	DOCUMENT ID		TECN	COMMENT
• • • We do not use the following data for averages, fits, limits, etc. • • •				
0.001	[1] KAMANO	15	DPWA	Multichannel

[1] From the preferred solution A in KAMANO 15.

$\Gamma(\Xi K)/\Gamma_{total}$ — Γ_7/Γ

VALUE	DOCUMENT ID		TECN	COMMENT
• • • We do not use the following data for averages, fits, limits, etc. • • •				
not seen	[1] KAMANO	15	DPWA	Multichannel

[1] From the preferred solution A in KAMANO 15.

$\Gamma(\Sigma\pi\pi)/\Gamma_{total}$ — Γ_8/Γ

VALUE	DOCUMENT ID		TECN	COMMENT
no clear signal	[1] ARMENTEROS	68C	HDBC	$K^- N \to \Sigma\pi\pi$

[1] There is a suggestion of a bump, enough to be consistent with what is expected from $\Sigma(1385) \to \Sigma\pi$ decay.

$\Gamma(N\overline{K}^*(892), S{=}1/2, F\text{-wave})/\Gamma_{total}$ — Γ_9/Γ

VALUE	DOCUMENT ID		TECN	COMMENT
• • • We do not use the following data for averages, fits, limits, etc. • • •				
not seen	[1] KAMANO	15	DPWA	Multichannel

[1] From the preferred solution A in KAMANO 15.

$\Gamma(N\overline{K}^*(892), S{=}3/2, P\text{-wave})/\Gamma_{total}$ — Γ_{10}/Γ

VALUE	DOCUMENT ID		TECN	COMMENT
0.03 ±0.01	ZHANG	13A	DPWA	Multichannel
• • • We do not use the following data for averages, fits, limits, etc. • • •				
0.006	[1] KAMANO	15	DPWA	Multichannel

[1] From the preferred solution A in KAMANO 15.

$\Gamma(N\overline{K}^*(892), S{=}3/2, F\text{-wave})/\Gamma_{total}$ — Γ_{11}/Γ

VALUE	DOCUMENT ID		TECN	COMMENT
• • • We do not use the following data for averages, fits, limits, etc. • • •				
not seen	[1] KAMANO	15	DPWA	Multichannel

[1] From the preferred solution A in KAMANO 15.

$(\Gamma_i\Gamma_f)^{1/2}/\Gamma_{total}$ in $N\overline{K} \to \Lambda(1820) \to \Sigma\pi$ — $(\Gamma_1\Gamma_2)^{1/2}/\Gamma$

VALUE	DOCUMENT ID		TECN	COMMENT
−0.28±0.01	ZHANG	13A	DPWA	Multichannel
−0.28±0.03	GOPAL	77	DPWA	$\overline{K}N$ multichannel
−0.28±0.01	KANE	74	DPWA	$K^- p \to \Sigma\pi$
• • • We do not use the following data for averages, fits, limits, etc. • • •				
−0.25 or −0.25	[1] MARTIN	77	DPWA	$\overline{K}N$ multichannel

[1] The two MARTIN 77 values are from a T-matrix pole and from a Breit-Wigner fit.

$(\Gamma_i\Gamma_f)^{1/2}/\Gamma_{total}$ in $N\overline{K} \to \Lambda(1820) \to \Sigma(1385)\pi$, P-wave — $(\Gamma_1\Gamma_4)^{1/2}/\Gamma$

VALUE	DOCUMENT ID		TECN	COMMENT
−0.20 ±0.02	ZHANG	13A	DPWA	Multichannel
−0.167±0.054	[1] CAMERON	78	DPWA	$K^- p \to \Sigma(1385)\pi$
+0.27 ±0.03	PREVOST	74	DPWA	$K^- N \to \Sigma(1385)\pi$

[1] The published sign has been changed to be in accord with the baryon-first convention.

$(\Gamma_i\Gamma_f)^{1/2}/\Gamma_{total}$ in $N\overline{K} \to \Lambda(1820) \to \Sigma(1385)\pi$, F-wave — $(\Gamma_1\Gamma_5)^{1/2}/\Gamma$

VALUE	DOCUMENT ID		TECN	COMMENT
+0.065±0.029	[1] CAMERON	78	DPWA	$K^- p \to \Sigma(1385)\pi$

[1] The published sign has been changed to be in accord with the baryon-first convention.

$(\Gamma_i\Gamma_f)^{1/2}/\Gamma_{total}$ in $N\overline{K} \to \Lambda(1820) \to \Lambda\eta$ — $(\Gamma_1\Gamma_6)^{1/2}/\Gamma$

VALUE	DOCUMENT ID		TECN
$-0.096^{+0.040}_{-0.020}$	RADER	73	MPWA

$\Lambda(1820)$ REFERENCES

SARANTSEV	19	EPJ A55 180	A.V. Sarantsev *et al.*	(BONN, PNPI)
KAMANO	15	PR C92 025205	H. Kamano *et al.*	(ANL, OSAK)
ZHANG	13A	PR C88 035205	H. Zhang *et al.*	(KSU)
PDG	82	PL 111B 1	M. Roos *et al.*	(HELS, CIT, CERN)
GOPAL	80	Toronto Conf. 159	G.P. Gopal	(RHEL) IJP
ALSTON-...	78	PR D18 182	M. Alston-Garnjost *et al.*	(LBL, MTHO+) IJP
Also		PRL 38 1007	M. Alston-Garnjost *et al.*	(LBL, MTHO+) IJP
CAMERON	78	NP B143 189	W. Cameron *et al.*	(RHEL, LOIC) IJP
DECLAIS	77	CERN 77-16	Y. Declais *et al.*	(CAEN, CERN) IJP
GOPAL	77	NP B119 362	G.P. Gopal *et al.*	(LOIC, RHEL) IJP
MARTIN	77	NP B127 349	B.R. Martin, M.K. Pidcock, R.G. Moorhouse	(LOUC+) IJP
Also		NP B126 266	B.R. Martin, M.K. Pidcock	(LOUC)
Also		NP B126 285	B.R. Martin, M.K. Pidcock	(LOUC) IJP
KANE	74	LBL-2452	D.F. Kane	(LBL) IJP
PREVOST	74	NP B69 246	J. Prevost *et al.*	(SACL, CERN, HEID)
RADER	73	NC 16A 178	R.K. Rader *et al.*	(SACL, HEID, CERN+)
ARMENTEROS	68C	NP B8 216	R. Armenteros *et al.*	(CERN, HEID, SACL) I

$\Lambda(1830)$ $5/2^-$

$I(J^P) = 0(\frac{5}{2}^-)$ Status: ****

For results published before 1973 (they are now obsolete), see our 1982 edition Physics Letters **111B** 1 (1982).

The best evidence for this resonance is in the $\Sigma\pi$ channel.

$\Lambda(1830)$ POLE POSITION

REAL PART

VALUE (MeV)	DOCUMENT ID		TECN	COMMENT
1800 to 1860 (≈ 1830) OUR ESTIMATE				
1819.5 ± 3.0	SARANTSEV	19	DPWA	$\overline{K}N$ multichannel
1899^{+35}_{-37}	[1] KAMANO	15	DPWA	Multichannel
• • • We do not use the following data for averages, fits, limits, etc. • • •				
1766^{+37}_{-34}	[2] KAMANO	15	DPWA	Multichannel
1809	ZHANG	13A	DPWA	Multichannel

[1] The preferred solution A in KAMANO 15 reports two poles. This entry is from the preferred solution A.
[2] From the preferred solution A in KAMANO 15. Not seen in solution B.

−2×IMAGINARY PART

VALUE (MeV)	DOCUMENT ID		TECN	COMMENT
50 to 80 (≈ 65) OUR ESTIMATE				
62± 5	SARANTSEV	19	DPWA	$\overline{K}N$ multichannel
80^{+100}_{-34}	[1] KAMANO	15	DPWA	Multichannel
• • • We do not use the following data for averages, fits, limits, etc. • • •				
212^{+94}_{-62}	[2] KAMANO	15	DPWA	Multichannel
109	ZHANG	13A	DPWA	Multichannel

[1] The preferred solution A in KAMANO 15 reports two poles. This entry is from the preferred solution A.
[2] From the preferred solution A in KAMANO 15. Not seen in solution B.

Int. J. Mod. Phys. A 2026.41. Downloaded from www.worldscientific.com
by UNIVERSITY OF CALIFORNIA @ BERKELEY on 09/16/26. Re-use and distribution is strictly not permitted, except for Open Access articles.

$\Lambda(1830)$ POLE RESIDUES

The normalized residue is the residue divided by $\Gamma_{pole}/2$.

Normalized residue in $N\overline{K} \to \Lambda(1830) \to N\overline{K}$

MODULUS	PHASE (°)	DOCUMENT ID		TECN	COMMENT
0.055 ±0.010	**20 ± 14**	SARANTSEV	19	DPWA	$\overline{K}N$ multichannel
• • • We do not use the following data for averages, fits, limits, etc. • • •					
0.00502	−80	[1] KAMANO	15	DPWA	Multichannel

[1] From the preferred solution A in KAMANO 15.

Normalized residue in $N\overline{K} \to \Lambda(1830) \to \Sigma\pi$

MODULUS	PHASE (°)	DOCUMENT ID		TECN	COMMENT
0.15 ±0.03	**180 ± 10**	SARANTSEV	19	DPWA	$\overline{K}N$ multichannel
• • • We do not use the following data for averages, fits, limits, etc. • • •					
0.00581	179	[1] KAMANO	15	DPWA	Multichannel

[1] From the preferred solution A in KAMANO 15.

Normalized residue in $N\overline{K} \to \Lambda(1830) \to \Lambda\eta$

MODULUS	PHASE (°)	DOCUMENT ID		TECN	COMMENT
• • • We do not use the following data for averages, fits, limits, etc. • • •					
0.00941	−65	[1] KAMANO	15	DPWA	Multichannel

[1] From the preferred solution A in KAMANO 15.

Normalized residue in $N\overline{K} \to \Lambda(1830) \to \Xi K$

MODULUS	PHASE (°)	DOCUMENT ID		TECN	COMMENT
0.010 ±0.005	**65 ± 20**	SARANTSEV	19	DPWA	$\overline{K}N$ multichannel
• • • We do not use the following data for averages, fits, limits, etc. • • •					
0.0477	94	[1] KAMANO	15	DPWA	Multichannel

[1] From the preferred solution A in KAMANO 15.

Normalized residue in $N\overline{K} \to \Lambda(1830) \to \Sigma(1385)\pi$, D-wave

MODULUS	PHASE (°)	DOCUMENT ID		TECN	COMMENT
0.10 ±0.04	**10 ± 25**	SARANTSEV	19	DPWA	$\overline{K}N$ multichannel
• • • We do not use the following data for averages, fits, limits, etc. • • •					
0.0237	113	[1] KAMANO	15	DPWA	Multichannel

[1] From the preferred solution A in KAMANO 15.

Normalized residue in $N\overline{K} \to \Lambda(1830) \to \Sigma(1385)\pi$, G-wave

MODULUS	PHASE (°)	DOCUMENT ID		TECN	COMMENT
0.03 ±0.02		SARANTSEV	19	DPWA	$\overline{K}N$ multichannel
• • • We do not use the following data for averages, fits, limits, etc. • • •					
0.000726	127	[1] KAMANO	15	DPWA	Multichannel

[1] From the preferred solution A in KAMANO 15.

Normalized residue in $N\overline{K} \to \Lambda(1830) \to N\overline{K}^*(892)$, S=1/2 , D-wave

MODULUS	PHASE (°)	DOCUMENT ID		TECN	COMMENT
• • • We do not use the following data for averages, fits, limits, etc. • • •					
0.0278	−177	[1] KAMANO	15	DPWA	Multichannel

[1] From the preferred solution A in KAMANO 15.

Normalized residue in $N\overline{K} \to \Lambda(1830) \to N\overline{K}^*(892)$, S=3/2 , D-wave

MODULUS	PHASE (°)	DOCUMENT ID		TECN	COMMENT
• • • We do not use the following data for averages, fits, limits, etc. • • •					
0.0255	3	[1] KAMANO	15	DPWA	Multichannel

[1] From the preferred solution A in KAMANO 15.

Normalized residue in $N\overline{K} \to \Lambda(1830) \to N\overline{K}^*(892)$, S=3/2 , G-wave

MODULUS	PHASE (°)	DOCUMENT ID		TECN	COMMENT
• • • We do not use the following data for averages, fits, limits, etc. • • •					
0.00773	−17	[1] KAMANO	15	DPWA	Multichannel

[1] From the preferred solution A in KAMANO 15.

Normalized residue in $N\overline{K} \to \Lambda(1830) \to \Lambda\omega$, S=1/2 , D-wave

MODULUS	PHASE (°)	DOCUMENT ID		TECN	COMMENT
0.04±0.03		SARANTSEV	19	DPWA	$\overline{K}N$ multichannel

Normalized residue in $N\overline{K} \to \Lambda(1830) \to \Lambda\omega$, S=3/2 , D-wave

MODULUS	PHASE (°)	DOCUMENT ID		TECN	COMMENT
0.05±0.03	**−110 ± 35**	SARANTSEV	19	DPWA	$\overline{K}N$ multichannel

$\Lambda(1830)$ MASS

VALUE (MeV)	DOCUMENT ID		TECN	COMMENT
1820 to 1830 (≈ 1825) OUR ESTIMATE				
1821 ± 3	SARANTSEV	19	DPWA	$\overline{K}N$ multichannel
1820 ± 4	ZHANG	13A	DPWA	Multichannel
1831 ± 10	GOPAL	80	DPWA	$\overline{K}N \to \overline{K}N$
1825 ± 10	GOPAL	77	DPWA	$\overline{K}N$ multichannel
1825 ± 1	KANE	74	DPWA	$K^-p \to \Sigma\pi$
• • • We do not use the following data for averages, fits, limits, etc. • • •				
1817 or 1818	[1] MARTIN	77	DPWA	$\overline{K}N$ multichannel

[1] The two MARTIN 77 values are from a T-matrix pole and from a Breit-Wigner fit.

$\Lambda(1830)$ WIDTH

VALUE (MeV)	DOCUMENT ID		TECN	COMMENT
60 to 120 (≈ 90) OUR ESTIMATE				
64 ± 7	SARANTSEV	19	DPWA	$\overline{K}N$ multichannel
114 ± 10	ZHANG	13A	DPWA	Multichannel
100 ± 10	GOPAL	80	DPWA	$\overline{K}N \to \overline{K}N$
94 ± 10	GOPAL	77	DPWA	$\overline{K}N$ multichannel
119 ± 3	KANE	74	DPWA	$K^-p \to \Sigma\pi$
• • • We do not use the following data for averages, fits, limits, etc. • • •				
56 or 56	[1] MARTIN	77	DPWA	$\overline{K}N$ multichannel

[1] The two MARTIN 77 values are from a T-matrix pole and from a Breit-Wigner fit.

$\Lambda(1830)$ DECAY MODES

	Mode	Fraction (Γ_i/Γ)	Scale factor
Γ_1	$N\overline{K}$	0.04 to 0.08	
Γ_2	$\Sigma\pi$	35–75 %	
Γ_3	ΞK		
Γ_4	$\Sigma(1385)\pi$	>15 %	
Γ_5	$\Sigma(1385)\pi$, D-wave	(40 ±15) %	3.2
Γ_6	$\Sigma(1385)\pi$, G-wave		
Γ_7	$\Lambda\eta$		
Γ_8	$N\overline{K}^*(892)$, S=1/2, D-wave		
Γ_9	$N\overline{K}^*(892)$, S=3/2, D-wave		
Γ_{10}	$N\overline{K}^*(892)$, S=3/2, G-wave		

$\Lambda(1830)$ BRANCHING RATIOS

See "Sign conventions for resonance couplings" in the Note on Λ and Σ Resonances.

$\Gamma(N\overline{K})/\Gamma_{total}$ — Γ_1/Γ

VALUE	DOCUMENT ID		TECN	COMMENT
0.04 to 0.08 OUR ESTIMATE				
0.055 ± 0.010	SARANTSEV	19	DPWA	$\overline{K}N$ multichannel
0.041 ± 0.005	ZHANG	13A	DPWA	Multichannel
0.08 ± 0.03	GOPAL	80	DPWA	$\overline{K}N \to \overline{K}N$
0.02 ± 0.02	ALSTON-...	78	DPWA	$\overline{K}N \to \overline{K}N$
• • • We do not use the following data for averages, fits, limits, etc. • • •				
0.006	[1] KAMANO	15	DPWA	Multichannel
0.04 ± 0.03	GOPAL	77	DPWA	See GOPAL 80
0.04 or 0.04	[2] MARTIN	77	DPWA	$\overline{K}N$ multichannel

[1] From the preferred solution A in KAMANO 15.
[2] The two MARTIN 77 values are from a T-matrix pole and from a Breit-Wigner fit.

$\Gamma(\Sigma\pi)/\Gamma_{total}$ — Γ_2/Γ

VALUE	DOCUMENT ID		TECN	COMMENT
0.42 ±0.08	SARANTSEV	19	DPWA	$\overline{K}N$ multichannel
• • • We do not use the following data for averages, fits, limits, etc. • • •				
0.017	[1] KAMANO	15	DPWA	Multichannel

[1] From the preferred solution A in KAMANO 15.

$\Gamma(\Xi K)/\Gamma_{total}$ — Γ_3/Γ

VALUE	DOCUMENT ID		TECN	COMMENT
• • • We do not use the following data for averages, fits, limits, etc. • • •				
0.562	[1] KAMANO	15	DPWA	Multichannel

[1] From the preferred solution A in KAMANO 15.

$\Gamma(\Sigma(1385)\pi, D\text{-wave})/\Gamma_{total}$ — Γ_5/Γ

VALUE	DOCUMENT ID		TECN	COMMENT
0.40 ±0.15 OUR AVERAGE Error includes scale factor of 3.2.				
0.20 ± 0.08	SARANTSEV	19	DPWA	$\overline{K}N$ multichannel
0.52 ± 0.06	ZHANG	13A	DPWA	Multichannel
• • • We do not use the following data for averages, fits, limits, etc. • • •				
0.134	[1] KAMANO	15	DPWA	Multichannel

[1] From the preferred solution A in KAMANO 15.

$\Gamma(\Sigma(1385)\pi, G\text{-wave})/\Gamma_{total}$ — Γ_6/Γ

VALUE	DOCUMENT ID		TECN	COMMENT
0.020 ± 0.015	SARANTSEV	19	DPWA	$\overline{K}N$ multichannel

$\Gamma(\Lambda\eta)/\Gamma_{total}$ — Γ_7/Γ

VALUE	DOCUMENT ID		TECN	COMMENT
• • • We do not use the following data for averages, fits, limits, etc. • • •				
0.024	[1] KAMANO	15	DPWA	Multichannel

[1] From the preferred solution A in KAMANO 15.

Int. J. Mod. Phys. A 2026.41. Downloaded from www.worldscientific.com
UNIVERSITY OF CALIFORNIA @ BERKELEY on 09/16/26. Re-use and distribution is strictly not permitted, except for Open Access articles.

$\Gamma(N\overline{K}^*(892), S=1/2, D\text{-wave})/\Gamma_{total}$ — Γ_8/Γ

VALUE	DOCUMENT ID		TECN	COMMENT
• • • We do not use the following data for averages, fits, limits, etc. • • •				
0.134	[1] KAMANO	15	DPWA	Multichannel

[1] From the preferred solution A in KAMANO 15.

$\Gamma(N\overline{K}^*(892), S=3/2, D\text{-wave})/\Gamma_{total}$ — Γ_9/Γ

VALUE	DOCUMENT ID		TECN	COMMENT
• • • We do not use the following data for averages, fits, limits, etc. • • •				
0.115	[1] KAMANO	15	DPWA	Multichannel

[1] From the preferred solution A in KAMANO 15.

$\Gamma(N\overline{K}^*(892), S=3/2, G\text{-wave})/\Gamma_{total}$ — Γ_{10}/Γ

VALUE	DOCUMENT ID		TECN	COMMENT
• • • We do not use the following data for averages, fits, limits, etc. • • •				
0.009	[1] KAMANO	15	DPWA	Multichannel

[1] From the preferred solution A in KAMANO 15.

$(\Gamma_i\Gamma_f)^{1/2}/\Gamma_{total}$ in $N\overline{K} \to \Lambda(1830) \to \Sigma\pi$ — $(\Gamma_1\Gamma_2)^{1/2}/\Gamma$

VALUE	DOCUMENT ID		TECN	COMMENT
-0.13 ± 0.01	ZHANG	13A	DPWA	Multichannel
-0.17 ± 0.03	GOPAL	77	DPWA	$\overline{K}N$ multichannel
-0.15 ± 0.01	KANE	74	DPWA	$K^-p \to \Sigma\pi$
• • • We do not use the following data for averages, fits, limits, etc. • • •				
-0.17 or -0.17	[1] MARTIN	77	DPWA	$\overline{K}N$ multichannel

[1] The two MARTIN 77 values are from a T-matrix pole and from a Breit-Wigner fit.

$(\Gamma_i\Gamma_f)^{1/2}/\Gamma_{total}$ in $N\overline{K} \to \Lambda(1830) \to \Sigma(1385)\pi$ — $(\Gamma_1\Gamma_4)^{1/2}/\Gamma$

VALUE	DOCUMENT ID		TECN	COMMENT
0.20 to 0.50 OUR ESTIMATE				
$+0.141\pm0.014$	[1] CAMERON	78	DPWA	$K^-p \to \Sigma(1385)\pi$
$+0.13\pm0.03$	PREVOST	74	DPWA	$K^-N \to \Sigma(1385)\pi$

[1] The CAMERON 78 upper limit on G-wave decay is 0.03. The published sign has been changed to be in accord with the baryon-first convention.

$(\Gamma_i\Gamma_f)^{1/2}/\Gamma_{total}$ in $N\overline{K} \to \Lambda(1830) \to \Lambda\eta$ — $(\Gamma_1\Gamma_7)^{1/2}/\Gamma$

VALUE	DOCUMENT ID		TECN
-0.044 ± 0.020	RADER	73	MPWA

$\Lambda(1830)$ REFERENCES

SARANTSEV	19	EPJ A55 180	A.V. Sarantsev *et al.*	(BONN, PNPI)
KAMANO	15	PR C92 025205	H. Kamano *et al.*	(ANL, OSAK)
ZHANG	13A	PR C88 035205	H. Zhang *et al.*	(KSU)
PDG	82	PL 111B 1	M. Roos *et al.*	(HELS, CIT, CERN)
GOPAL	80	Toronto Conf. 159	G.P. Gopal	(RHEL) IJP
ALSTON-...	78	PR D18 182	M. Alston-Garnjost *et al.*	(LBL, MTHO+) IJP
Also		PRL 38 1007	M. Alston-Garnjost *et al.*	(LBL, MTHO+) IJP
CAMERON	78	NP B143 189	W. Cameron *et al.*	(RHEL, LOIC) IJP
GOPAL	77	NP B119 362	G.P. Gopal *et al.*	(LOIC, RHEL) IJP
MARTIN	77	NP B127 349	B.R. Martin, M.K. Pidcock, R.G. Moorhouse	(LOUC+) IJP
Also		NP B126 266	B.R. Martin, M.K. Pidcock	(LOUC)
Also		NP B126 285	B.R. Martin, M.K. Pidcock	(LOUC) IJP
KANE	74	LBL-2452	D.F. Kane	(LBL) IJP
PREVOST	74	NP B69 246	J. Prevost *et al.*	(SACL, CERN, HEID)
RADER	73	NC 16A 178	R.K. Rader *et al.*	(SACL, HEID, CERN+)

$\Lambda(1890)\ 3/2^+$

$I(J^P) = 0(\frac{3}{2}^+)$ Status: ****

For results published before 1974 (they are now obsolete), see our 1982 edition Physics Letters **111B** 1 (1982).

$\Lambda(1890)$ POLE POSITION

REAL PART

VALUE (MeV)	DOCUMENT ID		TECN	COMMENT
1872±5	SARANTSEV	19	DPWA	$\overline{K}N$ multichannel
• • • We do not use the following data for averages, fits, limits, etc. • • •				
1859^{+5}_{-7}	[1] KAMANO	15	DPWA	Multichannel
1876	ZHANG	13A	DPWA	Multichannel

[1] From the preferred solution A in KAMANO 15, incompatible with solution B.

$-2\times$IMAGINARY PART

VALUE (MeV)	DOCUMENT ID		TECN	COMMENT
101±10	SARANTSEV	19	DPWA	$\overline{K}N$ multichannel
• • • We do not use the following data for averages, fits, limits, etc. • • •				
113^{+20}_{-4}	[1] KAMANO	15	DPWA	$\overline{K}N$ multichannel
145	ZHANG	13A	DPWA	$\overline{K}N$ multichannel

[1] From the preferred solution A in KAMANO 15, incompatible with solution B.

$\Lambda(1890)$ POLE RESIDUE

The "normalized residue" is the residue divided by $\Gamma_{pole}/2$.

Normalized residue in $KN \to \Lambda(1890) \to KN$

MODULUS	PHASE (°)	DOCUMENT ID		TECN	COMMENT
0.30 ±0.06	**0 ± 10**	SARANTSEV	19	DPWA	$\overline{K}N$ multichannel
• • • We do not use the following data for averages, fits, limits, etc. • • •					
0.241	−23	[1] KAMANO	15	DPWA	$\overline{K}N$ multichannel

[1] From the preferred solution A in KAMANO 15.

Normalized residue in $N\overline{K} \to \Lambda(1890) \to \Sigma\pi$

MODULUS	PHASE (°)	DOCUMENT ID		TECN	COMMENT
0.14 ±0.05	**148 ± 12**	SARANTSEV	19	DPWA	$\overline{K}N$ multichannel
• • • We do not use the following data for averages, fits, limits, etc. • • •					
0.101	104	[1] KAMANO	15	DPWA	$\overline{K}N$ multichannel

[1] From the preferred solution A in KAMANO 15.

Normalized residue in $N\overline{K} \to \Lambda(1890) \to \Lambda\eta$

MODULUS	PHASE (°)	DOCUMENT ID		TECN	COMMENT
• • • We do not use the following data for averages, fits, limits, etc. • • •					
0.0485	−54	[1] KAMANO	15	DPWA	Multichannel

[1] From the preferred solution A in KAMANO 15.

Normalized residue in $N\overline{K} \to \Lambda(1890) \to \Xi K$

MODULUS	PHASE (°)	DOCUMENT ID		TECN	COMMENT
0.065 ±0.020	**160 ± 30**	SARANTSEV	19	DPWA	$\overline{K}N$ multichannel
• • • We do not use the following data for averages, fits, limits, etc. • • •					
0.0562	−85	[1] KAMANO	15	DPWA	$\overline{K}N$ multichannel

[1] From the preferred solution A in KAMANO 15.

Normalized residue in $N\overline{K} \to \Lambda(1890) \to \Sigma(1385)\pi$, P-wave

MODULUS	PHASE (°)	DOCUMENT ID		TECN	COMMENT
0.11 ±0.05	**−160 ± 45**	SARANTSEV	19	DPWA	$\overline{K}N$ multichannel
• • • We do not use the following data for averages, fits, limits, etc. • • •					
0.295	−40	[1] KAMANO	15	DPWA	$\overline{K}N$ multichannel

[1] From the preferred solution A in KAMANO 15.

Normalized residue in $N\overline{K} \to \Lambda(1890) \to \Sigma(1385)\pi$, F-wave

MODULUS	PHASE (°)	DOCUMENT ID		TECN	COMMENT
0.10 ±0.04	**10 ± 50**	SARANTSEV	19	DPWA	$\overline{K}N$ multichannel
• • • We do not use the following data for averages, fits, limits, etc. • • •					
0.064	127	[1] KAMANO	15	DPWA	$\overline{K}N$ multichannel

[1] From the preferred solution A in KAMANO 15.

Normalized residue in $N\overline{K} \to \Lambda(1890) \to N\overline{K}^*(892)$, $S=1/2$, P-wave

MODULUS	PHASE (°)	DOCUMENT ID		TECN	COMMENT
0.03 ±0.03		SARANTSEV	19	DPWA	$\overline{K}N$ multichannel
• • • We do not use the following data for averages, fits, limits, etc. • • •					
0.188	−160	[1] KAMANO	15	DPWA	$\overline{K}N$ multichannel

[1] From the preferred solution A in KAMANO 15.

Normalized residue in $N\overline{K} \to \Lambda(1890) \to N\overline{K}^*(892)$, $S=3/2$, P-wave

MODULUS	PHASE (°)	DOCUMENT ID		TECN	COMMENT
0.05 ±0.03	**180 ± 40**	SARANTSEV	19	DPWA	$\overline{K}N$ multichannel
• • • We do not use the following data for averages, fits, limits, etc. • • •					
0.209	15	[1] KAMANO	15	DPWA	$\overline{K}N$ multichannel

[1] From the preferred solution A in KAMANO 15.

Normalized residue in $N\overline{K} \to \Lambda(1890) \to N\overline{K}^*(892)$, $S=3/2$, F-wave

MODULUS	PHASE (°)	DOCUMENT ID		TECN	COMMENT
• • • We do not use the following data for averages, fits, limits, etc. • • •					
0.0141	129	[1] KAMANO	15	DPWA	Multichannel

[1] From the preferred solution A in KAMANO 15.

Normalized residue in $N\overline{K} \to \Lambda(1890) \to \Lambda\omega$, $S=1/2$, P-wave

MODULUS	PHASE (°)	DOCUMENT ID		TECN	COMMENT
0.24±0.06	**15 ± 20**	SARANTSEV	19	DPWA	$\overline{K}N$ multichannel

Normalized residue in $N\overline{K} \to \Lambda(1890) \to \Lambda\omega$, $S=3/2$, P-wave

MODULUS	PHASE (°)	DOCUMENT ID		TECN	COMMENT
0.15±0.08	**−165 ± 20**	SARANTSEV	19	DPWA	$\overline{K}N$ multichannel

$\Lambda(1890)$ MASS

VALUE (MeV)	DOCUMENT ID		TECN	COMMENT
1870 to 1910 (≈ 1890) OUR ESTIMATE				
1897.2± 9.6±6.2	ABLIKIM	25AF	BES3	$\psi(3686) \to \Lambda\overline{\Sigma}^0\pi^0$ + c.c. (PWA)
1873 ± 5	SARANTSEV	19	DPWA	$\overline{K}N$ multichannel
1900 ± 5	ZHANG	13A	DPWA	$\overline{K}N$ multichannel
1897 ± 5	GOPAL	80	DPWA	$\overline{K}N \to \overline{K}N$
1908 ±10	ALSTON-...	78	DPWA	$\overline{K}N \to \overline{K}N$
1894 ±10	HEMINGWAY	75	DPWA	$K^-p \to \overline{K}N$

Int. J. Mod. Phys. A 2026.41. Downloaded from www.worldscientific.com
by UNIVERSITY OF CALIFORNIA @ BERKELEY on 09/16/26. Re-use and distribution is strictly not permitted, except for Open Access articles.

• • • We do not use the following data for averages, fits, limits, etc. • • •

1900 ± 5	GOPAL	77	DPWA	$\overline{K}N$ multichannel
1856 or 1868	[1] MARTIN	77	DPWA	$\overline{K}N$ multichannel
1900	[2] NAKKASYAN	75	DPWA	$K^-p \to \Lambda\omega$

[1] The two MARTIN 77 values are from a T-matrix pole and from a Breit-Wigner fit.
[2] Found in one of two best solutions.

$\Lambda(1890)$ WIDTH

VALUE (MeV)	DOCUMENT ID		TECN	COMMENT
80 to 160 (≈ 120) OUR ESTIMATE				
149.2±13.5±4.1	ABLIKIM	25AF	BES3	$\psi(3686) \to \Lambda\overline{\Sigma}^0\pi^0$ + c.c. (PWA)
103 ±10	SARANTSEV	19	DPWA	$\overline{K}N$ multichannel
161 ±15	ZHANG	13A	DPWA	$\overline{K}N$ multichannel
74 ±10	GOPAL	80	DPWA	$\overline{K}N \to \overline{K}N$
119 ±20	ALSTON-...	78	DPWA	$\overline{K}N \to \overline{K}N$
107 ±10	HEMINGWAY	75	DPWA	$K^-p \to \overline{K}N$
• • • We do not use the following data for averages, fits, limits, etc. • • •				
72 ±10	GOPAL	77	DPWA	$\overline{K}N$ multichannel
191 or 193	[1] MARTIN	77	DPWA	$\overline{K}N$ multichannel
100	[2] NAKKASYAN	75	DPWA	$K^-p \to \Lambda\omega$

[1] The two MARTIN 77 values are from a T-matrix pole and from a Breit-Wigner fit.
[2] Found in one of two best solutions.

$\Lambda(1890)$ DECAY MODES

	Mode	Fraction (Γ_i/Γ)
Γ_1	$N\overline{K}$	0.24 to 0.36
Γ_2	$\Sigma\pi$	3–10 %
Γ_3	$\Lambda\eta$	
Γ_4	ΞK	
Γ_5	$\Sigma(1385)\pi$	seen
Γ_6	$\Sigma(1385)\pi$, P-wave	(6.0 ±3.0) %
Γ_7	$\Sigma(1385)\pi$, F-wave	(4.0 ±2.0) %
Γ_8	$N\overline{K}^*(892)$	seen
Γ_9	$N\overline{K}^*(892)$, $S=1/2$	
Γ_{10}	$N\overline{K}^*(892)$, $S=1/2$, P-wave	
Γ_{11}	$N\overline{K}^*(892)$, $S=3/2$, P-wave	
Γ_{12}	$N\overline{K}^*(892)$, $S=3/2$, F-wave	
Γ_{13}	$\Lambda\omega$	

$\Lambda(1890)$ BRANCHING RATIOS

See "Sign conventions for resonance couplings" in the Note on Λ and Σ Resonances.

$\Gamma(N\overline{K})/\Gamma_{total}$ — Γ_1/Γ

VALUE	DOCUMENT ID		TECN	COMMENT
0.24 to 0.36 OUR ESTIMATE				
0.30 ±0.06	SARANTSEV	19	DPWA	$\overline{K}N$ multichannel
0.37 ±0.03	ZHANG	13A	DPWA	$\overline{K}N$ multichannel
0.20 ±0.02	GOPAL	80	DPWA	$\overline{K}N \to \overline{K}N$
0.34 ±0.05	ALSTON-...	78	DPWA	$\overline{K}N \to \overline{K}N$
0.24 ±0.04	HEMINGWAY	75	DPWA	$K^-p \to \overline{K}N$
• • • We do not use the following data for averages, fits, limits, etc. • • •				
0.305	[1] KAMANO	15	DPWA	$\overline{K}N$ multichannel
0.18 ±0.02	GOPAL	77	DPWA	See GOPAL 80
0.36 or 0.34	[2] MARTIN	77	DPWA	$\overline{K}N$ multichannel

[1] From the preferred solution A in KAMANO 15.
[2] The two MARTIN 77 values are from a T-matrix pole and from a Breit-Wigner fit.

$\Gamma(\Sigma\pi)/\Gamma_{total}$ — Γ_2/Γ

VALUE	DOCUMENT ID		TECN	COMMENT
6 ±2	SARANTSEV	19	DPWA	$\overline{K}N$ multichannel
<0.03	LANGBEIN	72	IPWA	$\overline{K}N$ multichannel
• • • We do not use the following data for averages, fits, limits, etc. • • •				
0.04	[1] KAMANO	15	DPWA	$\overline{K}N$ multichannel

[1] From the preferred solution A in KAMANO 15.

$\Gamma(\Lambda\eta)/\Gamma_{total}$ — Γ_3/Γ

VALUE	DOCUMENT ID		TECN	COMMENT
• • • We do not use the following data for averages, fits, limits, etc. • • •				
0.012	[1] KAMANO	15	DPWA	$\overline{K}N$ multichannel

[1] From the preferred solution A in KAMANO 15.

$\Gamma(\Xi K)/\Gamma_{total}$ — Γ_4/Γ

VALUE	DOCUMENT ID		TECN	COMMENT
∼ 0.01	SARANTSEV	19	DPWA	$\overline{K}N$ multichannel
• • • We do not use the following data for averages, fits, limits, etc. • • •				
0.009	[1] KAMANO	15	DPWA	$\overline{K}N$ multichannel

[1] From the preferred solution A in KAMANO 15.

$\Gamma(\Sigma(1385)\pi, P\text{-wave})/\Gamma_{total}$ — Γ_6/Γ

VALUE	DOCUMENT ID		TECN	COMMENT
0.06 ±0.03	SARANTSEV	19	DPWA	$\overline{K}N$ multichannel
• • • We do not use the following data for averages, fits, limits, etc. • • •				
0.453	[1] KAMANO	15	DPWA	$\overline{K}N$ multichannel

[1] From the preferred solution A in KAMANO 15.

$\Gamma(\Sigma(1385)\pi, F\text{-wave})/\Gamma_{total}$ — Γ_7/Γ

VALUE	DOCUMENT ID		TECN	COMMENT
0.04 ±0.02	SARANTSEV	19	DPWA	$\overline{K}N$ multichannel
• • • We do not use the following data for averages, fits, limits, etc. • • •				
0.019	[1] KAMANO	15	DPWA	$\overline{K}N$ multichannel

[1] From the preferred solution A in KAMANO 15.

$\Gamma(N\overline{K}^*(892), S=1/2, P\text{-wave})/\Gamma_{total}$ — Γ_{10}/Γ

VALUE	DOCUMENT ID		TECN	COMMENT
<0.01	SARANTSEV	19	DPWA	$\overline{K}N$ multichannel
• • • We do not use the following data for averages, fits, limits, etc. • • •				
0.073	[1] KAMANO	15	DPWA	$\overline{K}N$ multichannel

[1] From the preferred solution A in KAMANO 15.

$\Gamma(N\overline{K}^*(892), S=3/2, P\text{-wave})/\Gamma_{total}$ — Γ_{11}/Γ

VALUE	DOCUMENT ID		TECN	COMMENT
∼ 0.01	SARANTSEV	19	DPWA	$\overline{K}N$ multichannel
• • • We do not use the following data for averages, fits, limits, etc. • • •				
0.088	[1] KAMANO	15	DPWA	$\overline{K}N$ multichannel

[1] From the preferred solution A in KAMANO 15.

$\Gamma(N\overline{K}^*(892), S=3/2, F\text{-wave})/\Gamma_{total}$ — Γ_{12}/Γ

VALUE	DOCUMENT ID		TECN	COMMENT
• • • We do not use the following data for averages, fits, limits, etc. • • •				
0.001	[1] KAMANO	15	DPWA	$\overline{K}N$ multichannel

[1] From the preferred solution A in KAMANO 15.

$(\Gamma_i\Gamma_f)^{1/2}/\Gamma_{total}$ in $N\overline{K} \to \Lambda(1890) \to \Sigma\pi$ — $(\Gamma_1\Gamma_2)^{1/2}/\Gamma$

VALUE	DOCUMENT ID		TECN	COMMENT
−0.09±0.02	ZHANG	13A	DPWA	$\overline{K}N$ multichannel
−0.09±0.03	GOPAL	77	DPWA	$\overline{K}N$ multichannel
• • • We do not use the following data for averages, fits, limits, etc. • • •				
+0.15 or +0.14	[1] MARTIN	77	DPWA	$\overline{K}N$ multichannel

[1] The two MARTIN 77 values are from a T-matrix pole and from a Breit-Wigner fit.

$(\Gamma_i\Gamma_f)^{1/2}/\Gamma_{total}$ in $N\overline{K} \to \Lambda(1890) \to \Sigma(1385)\pi$, P-wave — $(\Gamma_1\Gamma_6)^{1/2}/\Gamma$

VALUE	DOCUMENT ID		TECN	COMMENT
<0.03	CAMERON	78	DPWA	$K^-p \to \Sigma(1385)\pi$

$(\Gamma_i\Gamma_f)^{1/2}/\Gamma_{total}$ in $N\overline{K} \to \Lambda(1890) \to \Sigma(1385)\pi$, F-wave — $(\Gamma_1\Gamma_7)^{1/2}/\Gamma$

VALUE	DOCUMENT ID		TECN	COMMENT
−0.31 ±0.04	ZHANG	13A	DPWA	$\overline{K}N$ multichannel
−0.126±0.055	[1] CAMERON	78	DPWA	$K^-p \to \Sigma(1385)\pi$

[1] The published sign has been changed to be in accord with the baryon-first convention.

$(\Gamma_i\Gamma_f)^{1/2}/\Gamma_{total}$ in $N\overline{K} \to \Lambda(1890) \to N\overline{K}^*(892)$, $S=1/2$ — $(\Gamma_1\Gamma_9)^{1/2}/\Gamma$

VALUE	DOCUMENT ID		TECN	COMMENT
−0.17±0.05	ZHANG	13A	DPWA	$\overline{K}N$ multichannel
−0.07±0.03	[1,2] CAMERON	78B	DPWA	$K^-p \to N\overline{K}^*$

[1] Upper limits on the P_3 and F_3 waves are each 0.03.
[2] The published sign has been changed to be in accord with the baryon-first convention.

$(\Gamma_i\Gamma_f)^{1/2}/\Gamma_{total}$ in $N\overline{K} \to \Lambda(1890) \to N\overline{K}^*(892)$, $S=3/2$, F-wave — $(\Gamma_1\Gamma_{12})^{1/2}/\Gamma$

VALUE	DOCUMENT ID		TECN	COMMENT
−0.11±0.03	ZHANG	13A	DPWA	$\overline{K}N$ multichannel

$(\Gamma_i\Gamma_f)^{1/2}/\Gamma_{total}$ in $N\overline{K} \to \Lambda(1890) \to \Lambda\omega$ — $(\Gamma_1\Gamma_{13})^{1/2}/\Gamma$

VALUE	DOCUMENT ID		TECN	COMMENT
seen	BACCARI	77	IPWA	$K^-p \to \Lambda\omega$
0.032	[1] NAKKASYAN	75	DPWA	$K^-p \to \Lambda\omega$

[1] Found in one of two best solutions.

$\Lambda(1890)$ REFERENCES

ABLIKIM	25AF	JHEP 2502 212	M. Ablikim *et al.*	(BESIII Collab.)
SARANTSEV	19	EPJ A55 180	A.V. Sarantsev *et al.*	(BONN, PNPI)
KAMANO	15	PR C92 025205	H. Kamano *et al.*	(ANL, OSAK)
ZHANG	13A	PR C88 035205	H. Zhang *et al.*	(KSU)
PDG	82	PL 111B 1	M. Roos *et al.*	(HELS, CIT, CERN)
GOPAL	80	Toronto Conf. 159	G.P. Gopal	(RHEL) IJP
ALSTON-...	78	PR D18 182	M. Alston-Garnjost *et al.*	(LBL, MTHO+) IJP
Also		PRL 38 1007	M. Alston-Garnjost *et al.*	(LBL, MTHO+) IJP
CAMERON	78	NP B143 189	W. Cameron *et al.*	(RHEL, LOIC) IJP

CAMERON	78B	NP B146 327	W. Cameron *et al.*	(RHEL, LOIC) IJP
BACCARI	77	NC 41A 96	B. Baccari *et al.*	(SACL, CDEF) IJP
GOPAL	77	NP B119 362	G.P. Gopal *et al.*	(LOIC, RHEL) IJP
MARTIN	77	NP B127 349	B.R. Martin, M.K. Pidcock, R.G. Moorhouse	(LOUC+) IJP
Also		NP B126 266	B.R. Martin, M.K. Pidcock	(LOUC)
Also		NP B126 285	B.R. Martin, M.K. Pidcock	(LOUC) IJP
HEMINGWAY	75	NP B91 12	R.J. Hemingway *et al.*	(CERN, HEIDH, MPIM) IJP
NAKKASYAN	75	NP B93 85	A. Nakkasyan	(CERN) IJP
LANGBEIN	72	NP B47 477	W. Langbein, F. Wagner	(MPIM) IJP

$\Lambda(2000)\ 1/2^-$

$I(J^P) = 0(\frac{1}{2}^-)$ Status: *

OMITTED FROM SUMMARY TABLE

BARBARO-GALTIERI 70 (in $\Sigma\pi$) and BRANDSTETTER 72 (in $\Lambda\omega$) proposed a state at about this mass. Those analyses are considered to be obsolete, see NAKKASYAN 75 and PDG 18.

$\Lambda(2000)$ MASS

VALUE (MeV)	DOCUMENT ID		TECN	COMMENT
≈ 2000 OUR ESTIMATE				
2020±16	ZHANG	13A	DPWA	Multichannel
2030±30	CAMERON	78B	DPWA	$K^-p \to N\overline{K}^*$

$\Lambda(2000)$ WIDTH

VALUE (MeV)	DOCUMENT ID		TECN	COMMENT
255±63	ZHANG	13A	DPWA	Multichannel
125±25	CAMERON	78B	DPWA	$K^-p \to N\overline{K}^*$

$\Lambda(2000)$ DECAY MODES

	Mode	Fraction (Γ_i/Γ)
Γ_1	$N\overline{K}$	(27±6) %
Γ_2	$\Sigma\pi$	
Γ_3	$\Lambda\eta$	(16±7) %
Γ_4	$N\overline{K}^*(892)$, S=1/2, S-wave	
Γ_5	$N\overline{K}^*(892)$, S=3/2, D-wave	

$\Lambda(2000)$ BRANCHING RATIOS

See "Sign conventions for resonance couplings" in the Note on Λ and Σ Resonances.

$\Gamma(N\overline{K})/\Gamma_{total}$ — Γ_1/Γ

VALUE	DOCUMENT ID		TECN	COMMENT
0.27±0.06	ZHANG	13A	DPWA	Multichannel

$(\Gamma_i\Gamma_f)^{1/2}/\Gamma_{total}$ in $N\overline{K} \to \Lambda(2000) \to \Sigma\pi$ — $(\Gamma_1\Gamma_2)^{1/2}/\Gamma$

VALUE	DOCUMENT ID		TECN	COMMENT
−0.07±0.03	ZHANG	13A	DPWA	Multichannel

$\Gamma(\Lambda\eta)/\Gamma_{total}$ — Γ_3/Γ

VALUE	DOCUMENT ID		TECN	COMMENT
0.16±0.07	ZHANG	13A	DPWA	Multichannel

$(\Gamma_i\Gamma_f)^{1/2}/\Gamma_{total}$ in $N\overline{K} \to \Lambda(2000) \to N\overline{K}^*(892)$, S=1/2, S-wave — $(\Gamma_1\Gamma_4)^{1/2}/\Gamma$

VALUE	DOCUMENT ID		TECN	COMMENT
−0.12±0.03	[1] CAMERON	78B	DPWA	$K^-p \to N\overline{K}^*$

[1] The published sign has been changed to be in accord with the baryon-first convention.

$(\Gamma_i\Gamma_f)^{1/2}/\Gamma_{total}$ in $N\overline{K} \to \Lambda(2000) \to N\overline{K}^*(892)$, S=3/2, D-wave — $(\Gamma_1\Gamma_5)^{1/2}/\Gamma$

VALUE	DOCUMENT ID		TECN	COMMENT
+0.34±0.05	ZHANG	13A	DPWA	Multichannel
+0.09±0.03	CAMERON	78B	DPWA	$K^-p \to N\overline{K}^*$

$\Lambda(2000)$ REFERENCES

PDG	18	PR D98 030001	M. Tanabashi *et al.*	(PDG Collab.)
ZHANG	13A	PR C88 035205	H. Zhang *et al.*	(KSU)
CAMERON	78B	NP B146 327	W. Cameron *et al.*	(RHEL, LOIC) IJP
NAKKASYAN	75	NP B93 85	A. Nakkasyan	(CERN) IJP
BRANDSTETT...	72	NP B39 13	A.A. Brandstetter *et al.*	(RHEL, CDEF+)
BARBARO-...	70	Duke Conf. 173 Hyperon Resonances, 1970	A. Barbaro-Galtieri	(LRL) IJP

$\Lambda(2050)\ 3/2^-$

$I(J^P) = 0(\frac{3}{2}^-)$ Status: *

OMITTED FROM SUMMARY TABLE

$\Lambda(2050)$ MASS

VALUE (MeV)	DOCUMENT ID		TECN	COMMENT
2056±22	ZHANG	13A	DPWA	Multichannel

$\Lambda(2050)$ WIDTH

VALUE (MeV)	DOCUMENT ID		TECN	COMMENT
493±61	ZHANG	13A	DPWA	Multichannel

$\Lambda(2050)$ DECAY MODES

	Mode	Fraction (Γ_i/Γ)
Γ_1	$N\overline{K}$	(19 ±4) %
Γ_2	$\Sigma\pi$	(6.0±3.0) %
Γ_3	$\Sigma^*(1385)\pi$, S-wave	(8 ±6) %
Γ_4	$\Sigma^*(1385)\pi$, D-wave	(4.0±3.0) %
Γ_5	$N\overline{K}^*(892)$, S=1/2	(23 ±7) %

$\Lambda(2050)$ BRANCHING RATIOS

$\Gamma(N\overline{K})/\Gamma_{total}$ — Γ_1/Γ

VALUE	DOCUMENT ID		TECN	COMMENT
0.19±0.04	ZHANG	13A	DPWA	Multichannel

$\Gamma(\Sigma\pi)/\Gamma_{total}$ — Γ_2/Γ

VALUE	DOCUMENT ID		TECN	COMMENT
0.06±0.03	ZHANG	13A	DPWA	Multichannel

$\Gamma(\Sigma^*(1385)\pi$, S-wave$)/\Gamma_{total}$ — Γ_3/Γ

VALUE	DOCUMENT ID		TECN	COMMENT
0.08±0.06	ZHANG	13A	DPWA	Multichannel

$\Gamma(\Sigma^*(1385)\pi$, D-wave$)/\Gamma_{total}$ — Γ_4/Γ

VALUE	DOCUMENT ID		TECN	COMMENT
0.04±0.03	ZHANG	13A	DPWA	Multichannel

$\Gamma(N\overline{K}^*(892), S=1/2)/\Gamma_{total}$ — Γ_5/Γ

VALUE	DOCUMENT ID		TECN	COMMENT
0.23±0.07	ZHANG	13A	DPWA	Multichannel

$\Lambda(2050)$ REFERENCES

ZHANG	13A	PR C88 035205	H. Zhang *et al.*	(KSU)

$\Lambda(2070)\ 3/2^+$

$J^P = \frac{3}{2}^+$ Status: *

OMITTED FROM SUMMARY TABLE

$\Lambda(2070)$ POLE POSITION

REAL PART

VALUE (MeV)	DOCUMENT ID		TECN	COMMENT
2044±20	SARANTSEV	19	DPWA	$\overline{K}N$ multichannel

−2×IMAGINARY PART

VALUE (MeV)	DOCUMENT ID		TECN	COMMENT
360±45	SARANTSEV	19	DPWA	$\overline{K}N$ multichannel

$\Lambda(2070)$ POLE RESIDUES

Normalized residue in $N\overline{K} \to \Lambda(2070) \to N\overline{K}$

MODULUS	PHASE (°)	DOCUMENT ID		TECN	COMMENT
0.15±0.05	**−37 ± 10**	SARANTSEV	19	DPWA	$\overline{K}N$ multichannel

Normalized residue in $N\overline{K} \to \Lambda(2070) \to \Sigma\pi$

MODULUS	PHASE (°)	DOCUMENT ID		TECN	COMMENT
0.10±0.03	**−47 ± 8**	SARANTSEV	19	DPWA	$\overline{K}N$ multichannel

Normalized residue in $N\overline{K} \to \Lambda(2070) \to \Xi K$

MODULUS	PHASE (°)	DOCUMENT ID		TECN	COMMENT
0.11±0.03	**0 ± 25**	SARANTSEV	19	DPWA	$\overline{K}N$ multichannel

Normalized residue in $N\overline{K} \to \Lambda(2070) \to \Lambda\omega$, S=1/2 , P-wave

MODULUS	PHASE (°)	DOCUMENT ID		TECN	COMMENT
0.10±0.04	**150 ± 17**	SARANTSEV	19	DPWA	$\overline{K}N$ multichannel

Normalized residue in $N\overline{K} \to \Lambda(2070) \to \Lambda\omega$, S=3/2 , P-wave

MODULUS	PHASE (°)	DOCUMENT ID		TECN	COMMENT
0.08±0.04	**20 ± 30**	SARANTSEV	19	DPWA	$\overline{K}N$ multichannel

Normalized residue in $N\overline{K} \to \Lambda(2070) \to \Lambda\omega$, S=3/2 , F-wave

MODULUS	PHASE (°)	DOCUMENT ID		TECN	COMMENT
0.04±0.02	**−175 ± 35**	SARANTSEV	19	DPWA	$\overline{K}N$ multichannel

Int. J. Mod. Phys. A 2026.41. Downloaded from www.worldscientific.com
UNIVERSITY OF CALIFORNIA @ BERKELEY on 09/16/26. Re-use and distribution is strictly not permitted, except for Open Access articles.

Int. J. Mod. Phys. A 2026.41. Downloaded from www.worldscientific.com
by UNIVERSITY OF CALIFORNIA @ BERKELEY on 09/16/26. Re-use and distribution is strictly not permitted, except for Open Access articles.

Normalized residue in $N\overline{K} \to \Lambda(2070) \to \Sigma(1385)\pi$, P-wave

MODULUS	PHASE (°)	DOCUMENT ID	TECN	COMMENT
0.12±0.07	−160 ± 55	SARANTSEV 19	DPWA	$\overline{K}N$ multichannel

Normalized residue in $N\overline{K} \to \Lambda(2070) \to \Sigma(1385)\pi$, F-wave

MODULUS	PHASE (°)	DOCUMENT ID	TECN	COMMENT
0.07±0.04	−145 ± 50	SARANTSEV 19	DPWA	$\overline{K}N$ multichannel

Normalized residue in $N\overline{K} \to \Lambda(2070) \to N\overline{K}^*(892)$, S=1/2 , P-wave

MODULUS	PHASE (°)	DOCUMENT ID	TECN	COMMENT
0.36±0.07	−45 ± 30	SARANTSEV 19	DPWA	$\overline{K}N$ multichannel

Normalized residue in $N\overline{K} \to \Lambda(2070) \to N\overline{K}^*(892)$, S=3/2 , P-wave

MODULUS	PHASE (°)	DOCUMENT ID	TECN	COMMENT
0.16±0.05	150 ± 35	SARANTSEV 19	DPWA	$\overline{K}N$ multichannel

Normalized residue in $N\overline{K} \to \Lambda(2070) \to N\overline{K}^*(892)$, S=3/2 , F-wave

MODULUS	PHASE (°)	DOCUMENT ID	TECN	COMMENT
0.14±0.08	−50 ± 30	SARANTSEV 19	DPWA	$\overline{K}N$ multichannel

$\Lambda(2070)$ MASS

VALUE (MeV)	DOCUMENT ID	TECN	COMMENT
2070±24	SARANTSEV 19	DPWA	$\overline{K}N$ multichannel

$\Lambda(2070)$ WIDTH

VALUE (MeV)	DOCUMENT ID	TECN	COMMENT
370±50	SARANTSEV 19	DPWA	$\overline{K}N$ multichannel

$\Lambda(2070)$ DECAY MODES

	Mode	Fraction (Γ_i/Γ)
Γ_1	$N\overline{K}$	(12 ±5) %
Γ_2	$\Sigma\pi$	(7.0±3.0) %
Γ_3	ΞK	(7.0±3.0) %
Γ_4	$\Lambda\omega$, S=1/2 , P-wave	(7 ±4) %
Γ_5	$\Lambda\omega$, S=3/2 , P-wave	(3.0±2.0) %
Γ_6	$\Lambda\omega$, S=3/2 , F-wave	(1.0±1.0) %
Γ_7	$\Sigma(1385)\pi$, P-wave	(10 ±5) %
Γ_8	$\Sigma(1385)\pi$, F-wave	(2.0±2.0) %
Γ_9	$N\overline{K}^*(892)$, S=1/2 , P-wave	(42 ±8) %
Γ_{10}	$N\overline{K}^*(892)$, S=3/2 , P-wave	(14 ±6) %
Γ_{11}	$N\overline{K}^*(892)$, S=3/2 , F-wave	(10 ±6) %

$\Lambda(2070)$ BRANCHING RATIOS

$\Gamma(N\overline{K})/\Gamma_{total}$ — Γ_1/Γ

VALUE	DOCUMENT ID	TECN	COMMENT
0.12±0.05	SARANTSEV 19	DPWA	$\overline{K}N$ multichannel

$\Gamma(\Sigma\pi)/\Gamma_{total}$ — Γ_2/Γ

VALUE	DOCUMENT ID	TECN	COMMENT
0.07±0.03	SARANTSEV 19	DPWA	$\overline{K}N$ multichannel

$\Gamma(\Xi K)/\Gamma_{total}$ — Γ_3/Γ

VALUE	DOCUMENT ID	TECN	COMMENT
0.07±0.03	SARANTSEV 19	DPWA	$\overline{K}N$ multichannel

$\Gamma(\Lambda\omega$, S=1/2 , P-wave$)/\Gamma_{total}$ — Γ_4/Γ

VALUE	DOCUMENT ID	TECN	COMMENT
0.07±0.04	SARANTSEV 19	DPWA	$\overline{K}N$ multichannel

$\Gamma(\Lambda\omega$, S=3/2 , P-wave$)/\Gamma_{total}$ — Γ_5/Γ

VALUE	DOCUMENT ID	TECN	COMMENT
0.03±0.02	SARANTSEV 19	DPWA	$\overline{K}N$ multichannel

$\Gamma(\Lambda\omega$, S=3/2 , F-wave$)/\Gamma_{total}$ — Γ_6/Γ

VALUE	DOCUMENT ID	TECN	COMMENT
0.01±0.01	SARANTSEV 19	DPWA	$\overline{K}N$ multichannel

$\Gamma(\Sigma(1385)\pi$, P-wave$)/\Gamma_{total}$ — Γ_7/Γ

VALUE	DOCUMENT ID	TECN	COMMENT
0.10±0.05	SARANTSEV 19	DPWA	$\overline{K}N$ multichannel

$\Gamma(\Sigma(1385)\pi$, F-wave$)/\Gamma_{total}$ — Γ_8/Γ

VALUE	DOCUMENT ID	TECN	COMMENT
0.02±0.02	SARANTSEV 19	DPWA	$\overline{K}N$ multichannel

$\Gamma(N\overline{K}^*(892)$, S=1/2 , P-wave$)/\Gamma_{total}$ — Γ_9/Γ

VALUE	DOCUMENT ID	TECN	COMMENT
0.42±0.08	SARANTSEV 19	DPWA	$\overline{K}N$ multichannel

$\Gamma(N\overline{K}^*(892)$, S=3/2 , P-wave$)/\Gamma_{total}$ — Γ_{10}/Γ

VALUE	DOCUMENT ID	TECN	COMMENT
0.14±0.06	SARANTSEV 19	DPWA	$\overline{K}N$ multichannel

$\Gamma(N\overline{K}^*(892)$, S=3/2 , F-wave$)/\Gamma_{total}$ — Γ_{11}/Γ

VALUE	DOCUMENT ID	TECN	COMMENT
0.10±0.06	SARANTSEV 19	DPWA	$\overline{K}N$ multichannel

$\Lambda(2070)$ REFERENCES

SARANTSEV 19 EPJ A55 180 A.V. Sarantsev *et al.* (BONN, PNPI)

$\Lambda(2080)$ $5/2^-$

$J^P = \frac{5}{2}^-$ Status: *

OMITTED FROM SUMMARY TABLE

$\Lambda(2080)$ POLE POSITION

REAL PART

VALUE (MeV)	DOCUMENT ID	TECN	COMMENT
2070±15	SARANTSEV 19	DPWA	$\overline{K}N$ multichannel

−2×IMAGINARY PART

VALUE (MeV)	DOCUMENT ID	TECN	COMMENT
172±28	SARANTSEV 19	DPWA	$\overline{K}N$ multichannel

$\Lambda(2080)$ POLE RESIDUES

Normalized residue in $N\overline{K} \to \Lambda(2080) \to N\overline{K}$

MODULUS	PHASE (°)	DOCUMENT ID	TECN	COMMENT
0.12±0.03	−35 ± 22	SARANTSEV 19	DPWA	$\overline{K}N$ multichannel

Normalized residue in $N\overline{K} \to \Lambda(2080) \to \Sigma\pi$

MODULUS	PHASE (°)	DOCUMENT ID	TECN	COMMENT
0.07±0.03	11 ± 16	SARANTSEV 19	DPWA	$\overline{K}N$ multichannel

Normalized residue in $N\overline{K} \to \Lambda(2080) \to \Xi K$

MODULUS	PHASE (°)	DOCUMENT ID	TECN	COMMENT
0.06±0.02	115 ± 20	SARANTSEV 19	DPWA	$\overline{K}N$ multichannel

Normalized residue in $N\overline{K} \to \Lambda(2080) \to \Lambda\omega$, S=1/2, D-wave

MODULUS	PHASE (°)	DOCUMENT ID	TECN	COMMENT
0.06±0.03	115 ± 25	SARANTSEV 19	DPWA	$\overline{K}N$ multichannel

Normalized residue in $N\overline{K} \to \Lambda(2080) \to \Lambda\omega$, S=3/2 , D-wave

MODULUS	PHASE (°)	DOCUMENT ID	TECN	COMMENT
0.09±0.03	−10 ± 35	SARANTSEV 19	DPWA	$\overline{K}N$ multichannel

Normalized residue in $N\overline{K} \to \Lambda(2080) \to \Sigma(1385)\pi$, D-wave

MODULUS	PHASE (°)	DOCUMENT ID	TECN	COMMENT
0.14±0.04	155 ± 45	SARANTSEV 19	DPWA	$\overline{K}N$ multichannel

Normalized residue in $N\overline{K} \to \Lambda(2080) \to \Sigma(1385)\pi$, G-wave

MODULUS	PHASE (°)	DOCUMENT ID	COMMENT
0.05±0.03	30 ± 45	SARANTSEV 19	$\overline{K}N$ multichannel

Normalized residue in $N\overline{K} \to \Lambda(2080) \to N\overline{K}^*(892)$, S=1/2 , D-wave

MODULUS	PHASE (°)	DOCUMENT ID	TECN	COMMENT
0.16±0.08	−120 ± 50	SARANTSEV 19	DPWA	$\overline{K}N$ multichannel

Normalized residue in $N\overline{K} \to \Lambda(2080) \to N\overline{K}^*(892)$, S=3/2 , D-wave

MODULUS	PHASE (°)	DOCUMENT ID	TECN	COMMENT
0.20±0.14	60 ± 50	SARANTSEV 19	DPWA	$\overline{K}N$ multichannel

$\Lambda(2080)$ MASS

VALUE (MeV)	DOCUMENT ID	TECN	COMMENT
2082±13	SARANTSEV 19	DPWA	$\overline{K}N$ multichannel

$\Lambda(2080)$ WIDTH

VALUE (MeV)	DOCUMENT ID	TECN	COMMENT
181±29	SARANTSEV 19	DPWA	$\overline{K}N$ multichannel

$\Lambda(2080)$ DECAY MODES

	Mode	Fraction (Γ_i/Γ)
Γ_1	$N\overline{K}$	(11.0± 3.0) %
Γ_2	$\Sigma\pi$	(5.0± 2.0) %
Γ_3	ΞK	(4.0± 1.0) %
Γ_4	$\Lambda\omega$, S=1/2, D-wave	(4.0± 2.0) %

Int. J. Mod. Phys. A 2026.41. Downloaded from www.worldscientific.com
UNIVERSITY OF CALIFORNIA @ BERKELEY on 09/16/26. Re-use and distribution is strictly not permitted, except for Open Access articles.

Γ_5	$\Lambda\omega$, S=3/2, D-wave	(8.0± 3.0) %
Γ_6	$\Sigma(1385)\pi$, D-wave	(15 ± 5) %
Γ_7	$\Sigma(1385)\pi$, G-wave	(3.0± 2.0) %
Γ_8	$N\overline{K}^*(892)$, S=1/2, D-wave	(17 ± 9) %
Γ_9	$N\overline{K}^*(892)$, S=3/2, D-wave	(25 ±16) %

$\Lambda(2080)$ BRANCHING RATIOS

$\Gamma(N\overline{K})/\Gamma_{total}$ — Γ_1/Γ

VALUE	DOCUMENT ID		TECN	COMMENT
0.11±0.03	SARANTSEV	19	DPWA	$\overline{K}N$ multichannel

$\Gamma(\Sigma\pi)/\Gamma_{total}$ — Γ_2/Γ

VALUE	DOCUMENT ID		TECN	COMMENT
0.05±0.02	SARANTSEV	19	DPWA	$\overline{K}N$ multichannel

$\Gamma(\Xi K)/\Gamma_{total}$ — Γ_3/Γ

VALUE	DOCUMENT ID		TECN	COMMENT
0.04±0.01	SARANTSEV	19	DPWA	$\overline{K}N$ multichannel

$\Gamma(\Lambda\omega$, S=1/2, D-wave$)/\Gamma_{total}$ — Γ_4/Γ

VALUE	DOCUMENT ID		TECN	COMMENT
0.04±0.02	SARANTSEV	19	DPWA	$\overline{K}N$ multichannel

$\Gamma(\Lambda\omega$, S=3/2, D-wave$)/\Gamma_{total}$ — Γ_5/Γ

VALUE	DOCUMENT ID		TECN	COMMENT
0.08±0.03	SARANTSEV	19	DPWA	$\overline{K}N$ multichannel

$\Gamma(\Sigma(1385)\pi$, D-wave$)/\Gamma_{total}$ — Γ_6/Γ

VALUE	DOCUMENT ID		TECN	COMMENT
0.15±0.05	SARANTSEV	19	DPWA	$\overline{K}N$ multichannel

$\Gamma(\Sigma(1385)\pi$, G-wave$)/\Gamma_{total}$ — Γ_7/Γ

VALUE	DOCUMENT ID		TECN	COMMENT
0.03±0.02	SARANTSEV	19	DPWA	$\overline{K}N$ multichannel

$\Gamma(N\overline{K}^*(892)$, S=1/2, D-wave$)/\Gamma_{total}$ — Γ_8/Γ

VALUE	DOCUMENT ID		TECN	COMMENT
0.17±0.09	SARANTSEV	19	DPWA	$\overline{K}N$ multichannel

$\Gamma(N\overline{K}^*(892)$, S=3/2, D-wave$)/\Gamma_{total}$ — Γ_9/Γ

VALUE	DOCUMENT ID		TECN	COMMENT
0.25±0.16	SARANTSEV	19	DPWA	$\overline{K}N$ multichannel

$\Lambda(2080)$ REFERENCES

SARANTSEV 19 EPJ A55 180 A.V. Sarantsev *et al.* (BONN, PNPI)

$\Lambda(2085)$ $7/2^+$

$I(J^P) = 0(\frac{7}{2}^+)$ Status: **

OMITTED FROM SUMMARY TABLE
was $\Lambda(2020)$

In LITCHFIELD 71, need for the state rests solely on a possibly inconsistent polarization measurement at 1.784 GeV/c. HEMINGWAY 75 does not require this state. GOPAL 77 does not need it in either $N\overline{K}$ or $\Sigma\pi$. With new K^-n angular distributions included, DECLAIS 77 sees it. However, this and other new data are included in GOPAL 80 and the state is not required. BACCARI 77 weakly supports it.

$\Lambda(2085)$ POLE POSITION

REAL PART

VALUE	DOCUMENT ID		TECN	COMMENT
• • • We do not use the following data for averages, fits, limits, etc. • • •				
1757	[1] KAMANO	15	DPWA	Multichannel

[1] From the preferred solution A in KAMANO 15. Solution B reports M = 2041^{+80}_{-82} MeV.

−2×IMAGINARY PART

VALUE	DOCUMENT ID		TECN	COMMENT
• • • We do not use the following data for averages, fits, limits, etc. • • •				
146	[1] KAMANO	15	DPWA	Multichannel

[1] From the preferred solution A in KAMANO 15. Solution B reports M = 238^{+114}_{-34} MeV.

$\Lambda(2085)$ POLE RESIDUES

The normalized residue is the residue divided by $\Gamma_{pole}/2$.

Normalized residue in $N\overline{K} \to \Lambda(2085) \to N\overline{K}$

MODULUS	PHASE (°)	DOCUMENT ID		TECN	COMMENT
• • • We do not use the following data for averages, fits, limits, etc. • • •					
0.000145	−77	[1] KAMANO	15	DPWA	Multichannel

[1] From the preferred solution A in KAMANO 15.

Normalized residue in $N\overline{K} \to \Lambda(2085) \to \Sigma\pi$

MODULUS	PHASE (°)	DOCUMENT ID		TECN	COMMENT
• • • We do not use the following data for averages, fits, limits, etc. • • •					
0.0112	120	[1] KAMANO	15	DPWA	Multichannel

[1] From the preferred solution A in KAMANO 15.

Normalized residue in $N\overline{K} \to \Lambda(2085) \to \Lambda\eta$

MODULUS	PHASE (°)	DOCUMENT ID		TECN	COMMENT
• • • We do not use the following data for averages, fits, limits, etc. • • •					
0.000786	−100	[1] KAMANO	15	DPWA	Multichannel

[1] From the preferred solution A in KAMANO 15.

Normalized residue in $N\overline{K} \to \Lambda(2085) \to \Sigma(1385)\pi$, F-wave

MODULUS	PHASE (°)	DOCUMENT ID		TECN	COMMENT
• • • We do not use the following data for averages, fits, limits, etc. • • •					
0.00451	−82	[1] KAMANO	15	DPWA	Multichannel

[1] From the preferred solution A in KAMANO 15.

Normalized residue in $N\overline{K} \to \Lambda(2085) \to \Sigma(1385)\pi$, H-wave

MODULUS	PHASE (°)	DOCUMENT ID		TECN	COMMENT
• • • We do not use the following data for averages, fits, limits, etc. • • •					
0.0000298	−128	[1] KAMANO	15	DPWA	Multichannel

[1] From the preferred solution A in KAMANO 15.

$\Lambda(2085)$ MASS

VALUE (MeV)	DOCUMENT ID		TECN	COMMENT
≈ 2020 OUR ESTIMATE				
2043±22	ZHANG	13A	DPWA	Multichannel
2140	BACCARI	77	DPWA	$K^-p \to \Lambda\omega$
2117	DECLAIS	77	DPWA	$\overline{K}N \to \overline{K}N$
2100±30	LITCHFIELD	71	DPWA	$K^-p \to \overline{K}N$
2020±20	BARBARO-...	70	DPWA	$K^-p \to \Sigma\pi$

$\Lambda(2085)$ WIDTH

VALUE (MeV)	DOCUMENT ID		TECN	COMMENT
200±75	ZHANG	13A	DPWA	Multichannel
128	BACCARI	77	DPWA	$K^-p \to \Lambda\omega$
167	DECLAIS	77	DPWA	$\overline{K}N \to \overline{K}N$
120±30	LITCHFIELD	71	DPWA	$K^-p \to \overline{K}N$
160±30	BARBARO-...	70	DPWA	$K^-p \to \Sigma\pi$

$\Lambda(2085)$ DECAY MODES

	Mode	Fraction (Γ_i/Γ)
Γ_1	$N\overline{K}$	
Γ_2	$\Sigma\pi$	
Γ_3	$\Lambda\eta$	
Γ_4	$\Sigma(1385)\pi$, F-wave	
Γ_5	$\Sigma(1385)\pi$, H-wave	
Γ_6	$N\overline{K}^*(892)$, S=1/2	(30±9) %
Γ_7	$N\overline{K}^*(892)$, S=1/2, F-wave	
Γ_8	$N\overline{K}^*(892)$, S=3/2, F-wave	
Γ_9	$N\overline{K}^*(892)$, S=3/2, H-wave	
Γ_{10}	$\Lambda\omega$	

$\Lambda(2085)$ BRANCHING RATIOS

See "Sign conventions for resonance couplings" in the Note on Λ and Σ Resonances.

$\Gamma(N\overline{K})/\Gamma_{total}$ — Γ_1/Γ

VALUE	DOCUMENT ID		TECN	COMMENT
0.028±0.005	ZHANG	13A	DPWA	Multichannel
0.05	DECLAIS	77	DPWA	$\overline{K}N \to \overline{K}N$
0.05 ±0.02	LITCHFIELD	71	DPWA	$K^-p \to \overline{K}N$
• • • We do not use the following data for averages, fits, limits, etc. • • •				
not seen	[1] KAMANO	15	DPWA	Multichannel

[1] From the preferred solution A in KAMANO 15.

$\Gamma(\Sigma\pi)/\Gamma_{total}$ — Γ_2/Γ

VALUE	DOCUMENT ID		TECN	COMMENT
• • • We do not use the following data for averages, fits, limits, etc. • • •				
0.891	[1] KAMANO	15	DPWA	Multichannel

[1] From the preferred solution A in KAMANO 15.

Int. J. Mod. Phys. A 2026.41. Downloaded from www.worldscientific.com
by UNIVERSITY OF CALIFORNIA @ BERKELEY on 09/16/26. Re-use and distribution is strictly not permitted, except for Open Access articles.

$\Gamma(\Lambda\eta)/\Gamma_{total}$ — Γ_3/Γ

VALUE	DOCUMENT ID		TECN	COMMENT
• • • We do not use the following data for averages, fits, limits, etc. • • •				
0.002	[1] KAMANO	15	DPWA	Multichannel

[1] From the preferred solution A in KAMANO 15.

$\Gamma(\Sigma(1385)\pi$, F-wave$)/\Gamma_{total}$ — Γ_4/Γ

VALUE	DOCUMENT ID		TECN	COMMENT
• • • We do not use the following data for averages, fits, limits, etc. • • •				
0.105	[1] KAMANO	15	DPWA	Multichannel

[1] From the preferred solution A in KAMANO 15.

$\Gamma(\Sigma(1385)\pi$, H-wave$)/\Gamma_{total}$ — Γ_5/Γ

VALUE	DOCUMENT ID		TECN	COMMENT
• • • We do not use the following data for averages, fits, limits, etc. • • •				
not seen	[1] KAMANO	15	DPWA	Multichannel

[1] From the preferred solution A in KAMANO 15.

$\Gamma(N\overline{K}^*(892), S=1/2, F$-wave$)/\Gamma_{total}$ — Γ_7/Γ

VALUE	DOCUMENT ID		TECN	COMMENT
• • • We do not use the following data for averages, fits, limits, etc. • • •				
not seen	[1] KAMANO	15	DPWA	Multichannel

[1] From the preferred solution A in KAMANO 15.

$\Gamma(N\overline{K}^*(892), S=3/2, F$-wave$)/\Gamma_{total}$ — Γ_8/Γ

VALUE	DOCUMENT ID		TECN	COMMENT
• • • We do not use the following data for averages, fits, limits, etc. • • •				
0.001	[1] KAMANO	15	DPWA	Multichannel

[1] From the preferred solution A in KAMANO 15.

$\Gamma(N\overline{K}^*(892), S=3/2, H$-wave$)/\Gamma_{total}$ — Γ_9/Γ

VALUE	DOCUMENT ID		TECN	COMMENT
• • • We do not use the following data for averages, fits, limits, etc. • • •				
not seen	[1] KAMANO	15	DPWA	Multichannel

[1] From the preferred solution A in KAMANO 15.

$\Gamma(N\overline{K}^*(892), S=1/2)/\Gamma_{total}$ — Γ_6/Γ

VALUE	DOCUMENT ID		TECN	COMMENT
0.30±0.09	ZHANG	13A	DPWA	Multichannel

$(\Gamma_i\Gamma_f)^{1/2}/\Gamma_{total}$ in $N\overline{K} \to \Lambda(2085) \to \Sigma\pi$ — $(\Gamma_1\Gamma_2)^{1/2}/\Gamma$

VALUE	DOCUMENT ID		TECN	COMMENT
+0.02±0.01	ZHANG	13A	DPWA	Multichannel
−0.15±0.02	BARBARO-...	70	DPWA	$K^-p \to \Sigma\pi$

$(\Gamma_i\Gamma_f)^{1/2}/\Gamma_{total}$ in $N\overline{K} \to \Lambda(2085) \to \Lambda\omega$ — $(\Gamma_1\Gamma_{10})^{1/2}/\Gamma$

VALUE	DOCUMENT ID		TECN	COMMENT
<0.05	BACCARI	77	DPWA	$K^-p \to \Lambda\omega$

$\Lambda(2085)$ REFERENCES

KAMANO	15	PR C92 025205	H. Kamano *et al.*	(ANL, OSAK)
ZHANG	13A	PR C88 035205	H. Zhang *et al.*	(KSU)
GOPAL	80	Toronto Conf. 159	G.P. Gopal	(RHEL)
BACCARI	77	NC 41A 96	B. Baccari *et al.*	(SACL, CDEF) IJP
DECLAIS	77	CERN 77-16	Y. Declais *et al.*	(CAEN, CERN) IJP
GOPAL	77	NP B119 362	G.P. Gopal *et al.*	(LOIC, RHEL)
HEMINGWAY	75	NP B91 12	R.J. Hemingway *et al.*	(CERN, HEIDH, MPIM) IJP
LITCHFIELD	71	NP B30 125	P.J. Litchfield *et al.*	(RHEL, CDEF, SACL) IJP
BARBARO-...	70	Duke Conf. 173 Hyperon Resonances, 1970	A. Barbaro-Galtieri	(LRL) IJP

$\Lambda(2100)\ 7/2^-$

$I(J^P) = 0(\frac{7}{2}^-)$ Status: ****

Most of the results published before 1973 are now obsolete and have been omitted. They may be found in our 1982 edition Physics Letters **111B** 1 (1982).

This entry only includes results from partial-wave analyses. Parameters of peaks seen in cross sections and in invariant-mass distributions around 2100 MeV used to be listed in a separate entry immediately following. It may be found in our 1986 edition Physics Letters **170B** 1 (1986).

$\Lambda(2100)$ POLE POSITION

REAL PART

VALUE (MeV)	DOCUMENT ID		TECN	COMMENT
2040±14	SARANTSEV	19	DPWA	$\overline{K}N$ multichannel
• • • We do not use the following data for averages, fits, limits, etc. • • •				
2023	ZHANG	13A	DPWA	Multichannel

−2×IMAGINARY PART

VALUE (MeV)	DOCUMENT ID		TECN	COMMENT
215±29	SARANTSEV	19	DPWA	$\overline{K}N$ multichannel
• • • We do not use the following data for averages, fits, limits, etc. • • •				
239	ZHANG	13A	DPWA	Multichannel

$\Lambda(2100)$ POLE RESIDUE

The "normalized residue" is the residue divided by $\Gamma_{pole}/2$.

Normalized residue in $N\overline{K} \to \Lambda(2100) \to N\overline{K}$

MODULUS	PHASE (°)	DOCUMENT ID		TECN	COMMENT
0.28±0.06	**−40 ± 10**	SARANTSEV	19	DPWA	$\overline{K}N$ multichannel

Normalized residue in $N\overline{K} \to \Lambda(2100) \to \Sigma\pi$

MODULUS	PHASE (°)	DOCUMENT ID		TECN	COMMENT
0.09±0.02	**−35 ± 15**	SARANTSEV	19	DPWA	$\overline{K}N$ multichannel

Normalized residue in $N\overline{K} \to \Lambda(2100) \to \Sigma(1385)\pi$, D-wave

MODULUS	PHASE (°)	DOCUMENT ID		TECN	COMMENT
0.04±0.03		SARANTSEV	19	DPWA	$\overline{K}N$ multichannel

Normalized residue in $N\overline{K} \to \Lambda(2100) \to \Sigma(1385)\pi$, G-wave

MODULUS	PHASE (°)	DOCUMENT ID		TECN	COMMENT
0.06±0.03	**−45 ± 15**	SARANTSEV	19	DPWA	$\overline{K}N$ multichannel

Normalized residue in $N\overline{K} \to \Lambda(2100) \to N\overline{K}^*(892)$, $S=3/2$, D-wave

MODULUS	PHASE (°)	DOCUMENT ID		TECN	COMMENT
0.11±0.06	**−30 ± 30**	SARANTSEV	19	DPWA	$\overline{K}N$ multichannel

$\Lambda(2100)$ MASS

VALUE (MeV)	DOCUMENT ID		TECN	COMMENT
2090 to 2110 (≈ 2100) OUR ESTIMATE				
2090±15	SARANTSEV	19	DPWA	$\overline{K}N$ multichannel
2086± 6	ZHANG	13A	DPWA	Multichannel
2104±10	GOPAL	80	DPWA	$\overline{K}N \to \overline{K}N$
2106±30	DEBELLEFON	78	DPWA	$\overline{K}N \to \overline{K}N$
2110±10	GOPAL	77	DPWA	$\overline{K}N$ multichannel
2105±10	HEMINGWAY	75	DPWA	$K^-p \to \overline{K}N$
2115±10	KANE	74	DPWA	$K^-p \to \Sigma\pi$
• • • We do not use the following data for averages, fits, limits, etc. • • •				
2094	BACCARI	77	DPWA	$K^-p \to \Lambda\omega$
2094	DECLAIS	77	DPWA	$\overline{K}N \to \overline{K}N$
2110 or 2089	[1] NAKKASYAN	75	DPWA	$K^-p \to \Lambda\omega$

$\Lambda(2100)$ WIDTH

VALUE (MeV)	DOCUMENT ID		TECN	COMMENT
100 to 250 (≈ 200) OUR ESTIMATE				
290±30	SARANTSEV	19	DPWA	$\overline{K}N$ multichannel
305±16	ZHANG	13A	DPWA	Multichannel
157±40	DEBELLEFON	78	DPWA	$\overline{K}N \to \overline{K}N$
250±30	GOPAL	77	DPWA	$\overline{K}N$ multichannel
241±30	HEMINGWAY	75	DPWA	$K^-p \to \overline{K}N$
152±15	KANE	74	DPWA	$K^-p \to \Sigma\pi$
• • • We do not use the following data for averages, fits, limits, etc. • • •				
98	BACCARI	77	DPWA	$K^-p \to \Lambda\omega$
250	DECLAIS	77	DPWA	$\overline{K}N \to \overline{K}N$
244 or 302	[1] NAKKASYAN	75	DPWA	$K^-p \to \Lambda\omega$

$\Lambda(2100)$ DECAY MODES

	Mode	Fraction (Γ_i/Γ)
Γ_1	$N\overline{K}$	25–35 %
Γ_2	$\Sigma\pi$	∼ 5 %
Γ_3	$\Lambda\eta$	<3 %
Γ_4	ΞK	<3 %
Γ_5	$\Lambda\omega$	<8 %
Γ_6	$\Sigma(1385)\pi$, D-wave	
Γ_7	$\Sigma(1385)\pi$, G-wave	(1.0±1.0) %
Γ_8	$N\overline{K}^*(892)$	10–20 %
Γ_9	$N\overline{K}^*(892)$, $S=3/2$, D-wave	(4.0±2.0) %
Γ_{10}	$N\overline{K}^*(892)$, $S=1/2$, G-wave	
Γ_{11}	$N\overline{K}^*(892)$, $S=3/2$, G-wave	

Int. J. Mod. Phys. A 2026.41. Downloaded from www.worldscientific.com
UNIVERSITY OF CALIFORNIA @ BERKELEY on 09/16/26. Re-use and distribution is strictly not permitted, except for Open Access articles.

$\Lambda(2100)$ BRANCHING RATIOS

See "Sign conventions for resonance couplings" in the Note on Λ and Σ Resonances.

$\Gamma(N\overline{K})/\Gamma_{total}$ — Γ_1/Γ

VALUE	DOCUMENT ID		TECN	COMMENT
0.25 to 0.35 ($\approx$ 0.30) OUR ESTIMATE				
0.24±0.05	SARANTSEV	19	DPWA	$\overline{K}N$ multichannel
0.23±0.01	ZHANG	13A	DPWA	Multichannel
0.34±0.03	GOPAL	80	DPWA	$\overline{K}N \to \overline{K}N$
0.24±0.06	DEBELLEFON	78	DPWA	$\overline{K}N \to \overline{K}N$
0.31±0.03	HEMINGWAY	75	DPWA	$K^-p \to \overline{K}N$
• • • We do not use the following data for averages, fits, limits, etc. • • •				
0.29	DECLAIS	77	DPWA	$\overline{K}N \to \overline{K}N$
0.30±0.03	GOPAL	77	DPWA	See GOPAL 80

$\Gamma(\Sigma\pi)/\Gamma_{total}$ — Γ_2/Γ

VALUE	DOCUMENT ID		TECN	COMMENT
0.030±0.015	SARANTSEV	19	DPWA	$\overline{K}N$ multichannel

$\Gamma(\Sigma(1385)\pi$, D-wave$)/\Gamma_{total}$ — Γ_6/Γ

VALUE	DOCUMENT ID		TECN	COMMENT
<0.01	SARANTSEV	19	DPWA	$\overline{K}N$ multichannel

$\Gamma(\Sigma(1385)\pi$, G-wave$)/\Gamma_{total}$ — Γ_7/Γ

VALUE	DOCUMENT ID		TECN	COMMENT
0.01±0.01	SARANTSEV	19	DPWA	$\overline{K}N$ multichannel

$\Gamma(N\overline{K}^*(892), S=3/2, D$-wave$)/\Gamma_{total}$ — Γ_9/Γ

VALUE	DOCUMENT ID		TECN	COMMENT
0.04±0.02	SARANTSEV	19	DPWA	$\overline{K}N$ multichannel

$(\Gamma_i\Gamma_f)^{1/2}/\Gamma_{total}$ in $N\overline{K} \to \Lambda(2100) \to \Sigma\pi$ — $(\Gamma_1\Gamma_2)^{1/2}/\Gamma$

VALUE	DOCUMENT ID		TECN	COMMENT
+0.03±0.01	ZHANG	13A	DPWA	Multichannel
+0.12±0.04	GOPAL	77	DPWA	$\overline{K}N$ multichannel
+0.11±0.01	KANE	74	DPWA	$K^-p \to \Sigma\pi$

$(\Gamma_i\Gamma_f)^{1/2}/\Gamma_{total}$ in $N\overline{K} \to \Lambda(2100) \to \Lambda\eta$ — $(\Gamma_1\Gamma_3)^{1/2}/\Gamma$

VALUE	DOCUMENT ID		TECN	COMMENT
−0.050±0.020	RADER	73	MPWA	$K^-p \to \Lambda\eta$

$(\Gamma_i\Gamma_f)^{1/2}/\Gamma_{total}$ in $N\overline{K} \to \Lambda(2100) \to \Xi K$ — $(\Gamma_1\Gamma_4)^{1/2}/\Gamma$

VALUE	DOCUMENT ID		TECN	COMMENT
0.035±0.018	LITCHFIELD	71	DPWA	$K^-p \to \Xi K$
• • • We do not use the following data for averages, fits, limits, etc. • • •				
0.003	MULLER	69B	DPWA	$K^-p \to \Xi K$
0.05	TRIPP	67	RVUE	$K^-p \to \Xi K$

$(\Gamma_i\Gamma_f)^{1/2}/\Gamma_{total}$ in $N\overline{K} \to \Lambda(2100) \to \Lambda\omega$ — $(\Gamma_1\Gamma_5)^{1/2}/\Gamma$

VALUE	DOCUMENT ID		TECN	COMMENT
−0.070	[2] BACCARI	77	DPWA	GD_{37} wave
+0.011	[2] BACCARI	77	DPWA	GG_{17} wave
+0.008	[2] BACCARI	77	DPWA	GG_{37} wave
0.122 or 0.154	[1] NAKKASYAN	75	DPWA	$K^-p \to \Lambda\omega$

$(\Gamma_i\Gamma_f)^{1/2}/\Gamma_{total}$ in $N\overline{K} \to \Lambda(2100) \to N\overline{K}^*(892)$, $S=3/2$, D-wave — $(\Gamma_1\Gamma_9)^{1/2}/\Gamma$

VALUE	DOCUMENT ID		TECN	COMMENT
+0.16±0.02	ZHANG	13A	DPWA	Multichannel
+0.21±0.04	CAMERON	78B	DPWA	$K^-p \to N\overline{K}^*$

$(\Gamma_i\Gamma_f)^{1/2}/\Gamma_{total}$ in $N\overline{K} \to \Lambda(2100) \to N\overline{K}^*(892)$, $S=1/2$, G-wave — $(\Gamma_1\Gamma_{10})^{1/2}/\Gamma$

VALUE	DOCUMENT ID		TECN	COMMENT
−0.03±0.02	ZHANG	13A	DPWA	Multichannel
−0.04±0.03	[3] CAMERON	78B	DPWA	$K^-p \to N\overline{K}^*$

$(\Gamma_i\Gamma_f)^{1/2}/\Gamma_{total}$ in $N\overline{K} \to \Lambda(2100) \to N\overline{K}^*(892)$, $S=3/2$, G-wave — $(\Gamma_1\Gamma_{11})^{1/2}/\Gamma$

VALUE	DOCUMENT ID		TECN	COMMENT
+0.08±0.02	ZHANG	13A	DPWA	Multichannel

$\Lambda(2100)$ FOOTNOTES

[1] The NAKKASYAN 75 values are from the two best solutions found. Each has the $\Lambda(2100)$ and one additional resonance (P_3 or F_5).

[2] Note that the three for BACCARI 77 entries are for three different waves.

[3] The published sign has been changed to be in accord with the baryon-first convention. The upper limit on the G_3 wave is 0.03.

$\Lambda(2100)$ REFERENCES

SARANTSEV	19	EPJ A55 180	A.V. Sarantsev *et al.*	(BONN, PNPI)
ZHANG	13A	PR C88 035205	H. Zhang *et al.*	(KSU)
PDG	86	PL 170B 1	M. Aguilar-Benitez *et al.*	(CERN, CIT+)
PDG	82	PL 111B 1	M. Roos *et al.*	(HELS, CIT, CERN)
GOPAL	80	Toronto Conf. 159	G.P. Gopal	(RHEL) IJP
CAMERON	78B	NP B146 327	W. Cameron *et al.*	(RHEL, LOIC) IJP
DEBELLEFON	78	NC 42A 403	A. de Bellefon *et al.*	(CDEF, SACL) IJP
BACCARI	77	NC 41A 96	B. Baccari *et al.*	(SACL, CDEF) IJP
DECLAIS	77	CERN 77-16	Y. Declais *et al.*	(CAEN, CERN) IJP
GOPAL	77	NP B119 362	G.P. Gopal *et al.*	(LOIC, RHEL) IJP
HEMINGWAY	75	NP B91 12	R.J. Hemingway *et al.*	(CERN, HEIDH, MPIM) IJP
NAKKASYAN	75	NP B93 85	A. Nakkasyan	(CERN) IJP
KANE	74	LBL-2452	D.F. Kane	(LBL) IJP
RADER	73	NC 16A 178	R.K. Rader *et al.*	(SACL, HEID, CERN+)
LITCHFIELD	71	NP B30 125	P.J. Litchfield *et al.*	(RHEL, CDEF, SACL) IJP
MULLER	69B	Thesis UCRL 19372	R.A. Muller	(LRL)
TRIPP	67	NP B3 10	R.D. Tripp *et al.*	(LRL, SLAC, CERN+)

$\Lambda(2110)\ 5/2^+$

$I(J^P) = 0(\frac{5}{2}^+)$ Status: ***

For results published before 1974 (they are now obsolete), see our 1982 edition Physics Letters **111B** 1 (1982). All the references have been retained.

This resonance is in the Baryon Summary Table, but the evidence for it could be better.

$\Lambda(2110)$ POLE POSITION

REAL PART

VALUE (MeV)	DOCUMENT ID		TECN	COMMENT
2048±10	SARANTSEV	19	DPWA	$\overline{K}N$ multichannel
• • • We do not use the following data for averages, fits, limits, etc. • • •				
1970	ZHANG	13A	DPWA	$\overline{K}N$ multichannel

−2×IMAGINARY PART

VALUE (MeV)	DOCUMENT ID		TECN	COMMENT
255±20	SARANTSEV	19	DPWA	$\overline{K}N$ multichannel
• • • We do not use the following data for averages, fits, limits, etc. • • •				
350	ZHANG	13A	DPWA	$\overline{K}N$ multichannel

$\Lambda(2110)$ POLE RESIDUE

The "normalized residue" is the residue divided by $\Gamma_{pole}/2$.

Normalized residue in $N\overline{K} \to \Lambda(2110) \to N\overline{K}$

MODULUS	PHASE (°)	DOCUMENT ID		TECN	COMMENT
0.020±0.005	**5 ± 15**	SARANTSEV	19	DPWA	$\overline{K}N$ multichannel

Normalized residue in $N\overline{K} \to \Lambda(2110) \to \Sigma\pi$

MODULUS	PHASE (°)	DOCUMENT ID		TECN	COMMENT
0.13±0.03	**0 ± 15**	SARANTSEV	19	DPWA	$\overline{K}N$ multichannel

Normalized residue in $N\overline{K} \to \Lambda(2110) \to \Xi K$

MODULUS	PHASE (°)	DOCUMENT ID		TECN	COMMENT
0.005±0.005		SARANTSEV	19	DPWA	$\overline{K}N$ multichannel

Normalized residue in $N\overline{K} \to \Lambda(2110) \to \Lambda\omega$, $S=1/2$, P-wave

MODULUS	PHASE (°)	DOCUMENT ID		TECN	COMMENT
0.01±0.01		SARANTSEV	19	DPWA	$\overline{K}N$ multichannel

Normalized residue in $N\overline{K} \to \Lambda(2110) \to \Lambda\omega$, $S=3/2$, P-wave

MODULUS	PHASE (°)	DOCUMENT ID		TECN	COMMENT
0.03±0.01	**−7 ± 16**	SARANTSEV	19	DPWA	$\overline{K}N$ multichannel

Normalized residue in $N\overline{K} \to \Lambda(2110) \to \Lambda\omega$, $S=3/2$, F-wave

MODULUS	PHASE (°)	DOCUMENT ID		TECN	COMMENT
0.01±0.01		SARANTSEV	19	DPWA	$\overline{K}N$ multichannel

$\Lambda(2110)$ MASS

VALUE (MeV)	DOCUMENT ID		TECN	COMMENT
2050 to 2130 ($\approx$ 2090) OUR ESTIMATE				
2086±12	SARANTSEV	19	DPWA	$\overline{K}N$ multichannel
2036±13	ZHANG	13A	DPWA	$\overline{K}N$ multichannel
2092±25	GOPAL	80	DPWA	$\overline{K}N \to \overline{K}N$
2125±25	CAMERON	78B	DPWA	$K^-p \to N\overline{K}^*$
2106±50	DEBELLEFON	78	DPWA	$\overline{K}N \to \overline{K}N$
2140±20	DEBELLEFON	77	DPWA	$K^-p \to \Sigma\pi$
2100±50	GOPAL	77	DPWA	$\overline{K}N$ multichannel
2112± 7	KANE	74	DPWA	$K^-p \to \Sigma\pi$
• • • We do not use the following data for averages, fits, limits, etc. • • •				
2137	BACCARI	77	DPWA	$K^-p \to \Lambda\omega$
2103	[1] NAKKASYAN	75	DPWA	$K^-p \to \Lambda\omega$

Int. J. Mod. Phys. A 2026.41. Downloaded from www.worldscientific.com
by UNIVERSITY OF CALIFORNIA @ BERKELEY on 09/16/26. Re-use and distribution is strictly not permitted, except for Open Access articles.

$\Lambda(2110)$ WIDTH

VALUE (MeV)	DOCUMENT ID		TECN	COMMENT
200 to 300 (≈ 250) OUR ESTIMATE				
274±25	SARANTSEV	19	DPWA	$\overline{K}N$ multichannel
400±38	ZHANG	13A	DPWA	$\overline{K}N$ multichannel
245±25	GOPAL	80	DPWA	$\overline{K}N \to \overline{K}N$
160±30	CAMERON	78B	DPWA	$K^-p \to N\overline{K}^*$
251±50	DEBELLEFON	78	DPWA	$\overline{K}N \to \overline{K}N$
140±20	DEBELLEFON	77	DPWA	$K^-p \to \Sigma\pi$
200±50	GOPAL	77	DPWA	$\overline{K}N$ multichannel
190±30	KANE	74	DPWA	$K^-p \to \Sigma\pi$
• • • We do not use the following data for averages, fits, limits, etc. • • •				
132	BACCARI	77	DPWA	$K^-p \to \Lambda\omega$
391	[1] NAKKASYAN	75	DPWA	$K^-p \to \Lambda\omega$

$\Lambda(2110)$ DECAY MODES

	Mode	Fraction (Γ_i/Γ)
Γ_1	$N\overline{K}$	5–25 %
Γ_2	$\Sigma\pi$	10–40 %
Γ_3	$\Lambda\omega$	seen
Γ_4	$\Lambda\omega$, $S=1/2$, P-wave	
Γ_5	$\Lambda\omega$, $S=3/2$, P-wave	(5.0±2.0) %
Γ_6	$\Lambda\omega$, $S=3/2$, F-wave	
Γ_7	ΞK	
Γ_8	$\Sigma(1385)\pi$	seen
Γ_9	$\Sigma(1385)\pi$, P-wave	
Γ_{10}	$N\overline{K}^*(892)$	10–60 %
Γ_{11}	$N\overline{K}^*(892)$, $S=1/2$	
Γ_{12}	$N\overline{K}^*(892)$, $S=3/2$, P-wave	

$\Lambda(2110)$ BRANCHING RATIOS

See "Sign conventions for resonance couplings" in the Note on Λ and Σ Resonances.

$\Gamma(N\overline{K})/\Gamma_{total}$ — Γ_1/Γ

VALUE	DOCUMENT ID		TECN	COMMENT
0.05 to 0.25 OUR ESTIMATE				
0.020±0.005	SARANTSEV	19	DPWA	$\overline{K}N$ multichannel
0.083±0.005	ZHANG	13A	DPWA	$\overline{K}N$ multichannel
0.07 ±0.03	GOPAL	80	DPWA	$\overline{K}N \to \overline{K}N$
0.27 ±0.06	[2] DEBELLEFON	78	DPWA	$\overline{K}N \to \overline{K}N$
• • • We do not use the following data for averages, fits, limits, etc. • • •				
0.07 ±0.03	GOPAL	77	DPWA	See GOPAL 80

$\Gamma(\Sigma\pi)/\Gamma_{total}$ — Γ_2/Γ

VALUE	DOCUMENT ID		TECN	COMMENT
0.88±0.20	SARANTSEV	19	DPWA	$\overline{K}N$ multichannel

$\Gamma(\Lambda\omega, S=1/2, P\text{-wave})/\Gamma_{total}$ — Γ_4/Γ

VALUE	DOCUMENT ID		TECN	COMMENT
<0.01	SARANTSEV	19	DPWA	$\overline{K}N$ multichannel

$\Gamma(\Lambda\omega, S=3/2, P\text{-wave})/\Gamma_{total}$ — Γ_5/Γ

VALUE	DOCUMENT ID		TECN	COMMENT
0.05±0.02	SARANTSEV	19	DPWA	$\overline{K}N$ multichannel

$\Gamma(\Lambda\omega, S=3/2, F\text{-wave})/\Gamma_{total}$ — Γ_6/Γ

VALUE	DOCUMENT ID		TECN	COMMENT
<0.01	SARANTSEV	19	DPWA	$\overline{K}N$ multichannel

$\Gamma(\Xi K)/\Gamma_{total}$ — Γ_7/Γ

VALUE	DOCUMENT ID		TECN	COMMENT
∼ 0	SARANTSEV	19	DPWA	$\overline{K}N$ multichannel

$(\Gamma_i\Gamma_f)^{1/2}/\Gamma_{total}$ in $N\overline{K} \to \Lambda(2110) \to \Sigma\pi$ — $(\Gamma_1\Gamma_2)^{1/2}/\Gamma$

VALUE	DOCUMENT ID		TECN	COMMENT
+0.04±0.01	ZHANG	13A	DPWA	Multichannel
+0.14±0.01	DEBELLEFON	77	DPWA	$K^-p \to \Sigma\pi$
+0.20±0.03	KANE	74	DPWA	$K^-p \to \Sigma\pi$
• • • We do not use the following data for averages, fits, limits, etc. • • •				
+0.10±0.03	GOPAL	77	DPWA	$\overline{K}N$ multichannel

$(\Gamma_i\Gamma_f)^{1/2}/\Gamma_{total}$ in $N\overline{K} \to \Lambda(2110) \to \Lambda\omega$ — $(\Gamma_1\Gamma_3)^{1/2}/\Gamma$

VALUE	DOCUMENT ID		TECN	COMMENT
<0.05	BACCARI	77	DPWA	$K^-p \to \Lambda\omega$
0.112	[1] NAKKASYAN	75	DPWA	$K^-p \to \Lambda\omega$

$(\Gamma_i\Gamma_f)^{1/2}/\Gamma_{total}$ in $N\overline{K} \to \Lambda(2110) \to \Sigma(1385)\pi$, P-wave — $(\Gamma_1\Gamma_9)^{1/2}/\Gamma$

VALUE	DOCUMENT ID		TECN	COMMENT
+0.04 ±0.01	ZHANG	13A	DPWA	Multichannel
+0.071±0.025	[3] CAMERON	78	DPWA	$K^-p \to \Sigma(1385)\pi$

$(\Gamma_i\Gamma_f)^{1/2}/\Gamma_{total}$ in $N\overline{K} \to \Lambda(2110) \to N\overline{K}^*(892)$, $S=1/2$ — $(\Gamma_1\Gamma_{11})^{1/2}/\Gamma$

VALUE	DOCUMENT ID		TECN	COMMENT
−0.09±0.01	ZHANG	13A	DPWA	Multichannel
−0.17±0.04	[4] CAMERON	78B	DPWA	$K^-p \to N\overline{K}^*$

$(\Gamma_i\Gamma_f)^{1/2}/\Gamma_{total}$ in $N\overline{K} \to \Lambda(2110) \to N\overline{K}^*(892)$, $S=3/2$, P-wave — $(\Gamma_1\Gamma_{12})^{1/2}/\Gamma$

VALUE	DOCUMENT ID		TECN	COMMENT
0.24±0.01	ZHANG	13A	DPWA	Multichannel

$\Lambda(2110)$ FOOTNOTES

[1] Found in one of two best solutions.
[2] The published error of 0.6 was a misprint.
[3] The CAMERON 78 upper limit on F-wave decay is 0.03. The sign here has been changed to be in accord with the baryon-first convention.
[4] The published sign has been changed to be in accord with the baryon-first convention. The CAMERON 78B upper limits on the P_3 and F_3 waves are each 0.03.

$\Lambda(2110)$ REFERENCES

SARANTSEV	19	EPJ A55 180	A.V. Sarantsev *et al.*	(BONN, PNPI)
ZHANG	13A	PR C88 035205	H. Zhang *et al.*	(KSU)
PDG	82	PL 111B 1	M. Roos *et al.*	(HELS, CIT, CERN)
GOPAL	80	Toronto Conf. 159	G.P. Gopal	(RHEL) IJP
CAMERON	78	NP B143 189	W. Cameron *et al.*	(RHEL, LOIC) IJP
CAMERON	78B	NP B146 327	W. Cameron *et al.*	(RHEL, LOIC) IJP
DEBELLEFON	78	NC 42A 403	A. de Bellefon *et al.*	(CDEF, SACL) IJP
BACCARI	77	NC 41A 96	B. Baccari *et al.*	(SACL, CDEF) IJP
DEBELLEFON	77	NC 37A 175	A. de Bellefon *et al.*	(CDEF, SACL) IJP
GOPAL	77	NP B119 362	G.P. Gopal *et al.*	(LOIC, RHEL) IJP
NAKKASYAN	75	NP B93 85	A. Nakkasyan	(CERN) IJP
KANE	74	LBL-2452	D.F. Kane	(LBL) IJP

$\Lambda(2325)\ 3/2^-$

$I(J^P) = 0(\frac{3}{2}^-)$ Status: *

OMITTED FROM SUMMARY TABLE

BACCARI 77 finds this state with either $J^P = 3/2^-$ or $3/2^+$ in a energy-dependent partial-wave analyses of $K^-p \to \Lambda\omega$ from 2070 to 2436 MeV. A subsequent semi-energy-independent analysis from threshold to 2436 MeV selects $3/2^-$. DEBELLEFON 78 (same group) also sees this state in an energy-dependent partial-wave analysis of $K^-p \to \overline{K}N$ data, and finds $J^P = 3/2^-$ or $3/2^+$. They again prefer $J^P = 3/2^-$, but only on the basis of model-dependent considerations.

$\Lambda(2325)$ MASS

VALUE (MeV)	DOCUMENT ID		TECN	COMMENT
≈ 2325 OUR ESTIMATE				
2306.5± 6.3±17.1	ABLIKIM	25AF	BES3	$\psi(3686) \to \Lambda\overline{\Sigma}^0\pi^0$ + c.c. (PWA)
2342 ±30	DEBELLEFON	78	DPWA	$\overline{K}N \to \overline{K}N$
2327 ±20	BACCARI	77	DPWA	$K^-p \to \Lambda\omega$

$\Lambda(2325)$ WIDTH

VALUE (MeV)	DOCUMENT ID		TECN	COMMENT
227.1±12.2±47.8	ABLIKIM	25AF	BES3	$\psi(3686) \to \Lambda\overline{\Sigma}^0\pi^0$ + c.c. (PWA)
177 ±40	DEBELLEFON	78	DPWA	$\overline{K}N \to \overline{K}N$
160 ±40	BACCARI	77	IPWA	$K^-p \to \Lambda\omega$

$\Lambda(2325)$ DECAY MODES

	Mode
Γ_1	$N\overline{K}$
Γ_2	$\Lambda\omega$

$\Lambda(2325)$ BRANCHING RATIOS

$\Gamma(N\overline{K})/\Gamma_{total}$ — Γ_1/Γ

VALUE	DOCUMENT ID		TECN	COMMENT
0.19±0.06	DEBELLEFON	78	DPWA	$\overline{K}N \to \overline{K}N$

$(\Gamma_i\Gamma_f)^{1/2}/\Gamma_{total}$ in $N\overline{K} \to \Lambda(2325) \to \Lambda\omega$ — $(\Gamma_1\Gamma_2)^{1/2}/\Gamma$

VALUE	DOCUMENT ID		TECN	COMMENT
0.06±0.02	[1] BACCARI	77	IPWA	DS_{33} wave
0.05±0.02	[1] BACCARI	77	DPWA	DD_{13} wave
0.08±0.03	[1] BACCARI	77	DPWA	DD_{33} wave

Int. J. Mod. Phys. A 2026.41. Downloaded from www.worldscientific.com
UNIVERSITY OF CALIFORNIA @ BERKELEY on 09/16/26. Re-use and distribution is strictly not permitted, except for Open Access articles.

Λ(2325) FOOTNOTES

[1] Note that the three BACCARI 77 entries are for three different waves.

Λ(2325) REFERENCES

ABLIKIM	25AF	JHEP 2502 212	M. Ablikim *et al.*	(BESIII Collab.)
DEBELLEFON	78	NC 42A 403	A. de Bellefon *et al.*	(CDEF, SACL) IJP
BACCARI	77	NC 41A 96	B. Baccari *et al.*	(SACL, CDEF) IJP

Λ(2350) $9/2^+$

$I(J^P) = 0(\frac{9}{2}^+)$ Status: ***

DAUM 68 favors $J^P = 7/2^-$ or $9/2^+$. BRICMAN 70 favors $9/2^+$. LASINSKI 71 suggests three states in this region using a Pomeron + resonances model. There are now also three formation experiments from the College de France-Saclay group, DEBELLEFON 77, BACCARI 77, and DEBELLEFON 78, which find $9/2^+$ in energy-dependent partial-wave analyses of $\overline{K}N \to \Sigma\pi$, $\Lambda\omega$, and $N\overline{K}$.

Λ(2350) MASS

VALUE (MeV)	DOCUMENT ID		TECN	COMMENT
2340 to 2370 (≈ 2350) OUR ESTIMATE				
2370±50	DEBELLEFON	78	DPWA	$\overline{K}N \to \overline{K}N$
2365±20	DEBELLEFON	77	DPWA	$K^-p \to \Sigma\pi$
2358± 6	BRICMAN	70	CNTR	Total, charge exchange
• • • We do not use the following data for averages, fits, limits, etc. • • •				
2372	BACCARI	77	DPWA	$K^-p \to \Lambda\omega$
2344±15	COOL	70	CNTR	K^-p, K^-d total
2360±20	LU	70	CNTR	$\gamma p \to K^+Y^*$
2340± 7	BUGG	68	CNTR	K^-p, K^-d total

Λ(2350) WIDTH

VALUE (MeV)	DOCUMENT ID		TECN	COMMENT
100 to 250 (≈ 150) OUR ESTIMATE				
204±50	DEBELLEFON	78	DPWA	$\overline{K}N \to \overline{K}N$
110±20	DEBELLEFON	77	DPWA	$K^-p \to \Sigma\pi$
324±30	BRICMAN	70	CNTR	Total, charge exchange
• • • We do not use the following data for averages, fits, limits, etc. • • •				
257	BACCARI	77	DPWA	$K^-p \to \Lambda\omega$
190	COOL	70	CNTR	K^-p, K^-d total
55	LU	70	CNTR	$\gamma p \to K^+Y^*$
140±20	BUGG	68	CNTR	K^-p, K^-d total

Λ(2350) DECAY MODES

	Mode	Fraction (Γ_i/Γ)
Γ_1	$N\overline{K}$	~ 12 %
Γ_2	$\Sigma\pi$	~ 10 %
Γ_3	$\Lambda\omega$	

Λ(2350) BRANCHING RATIOS

See "Sign conventions for resonance couplings" in the Note on Λ and Σ Resonances.

$\Gamma(N\overline{K})/\Gamma_{total}$ — Γ_1/Γ

VALUE	DOCUMENT ID		TECN	COMMENT
~ 0.12 OUR ESTIMATE				
0.12±0.04	DEBELLEFON	78	DPWA	$\overline{K}N \to \overline{K}N$

$(\Gamma_i\Gamma_f)^{1/2}/\Gamma_{total}$ in $N\overline{K} \to \Lambda(2350) \to \Sigma\pi$ — $(\Gamma_1\Gamma_2)^{1/2}/\Gamma$

VALUE	DOCUMENT ID		TECN	COMMENT
−0.11±0.02	DEBELLEFON	77	DPWA	$K^-p \to \Sigma\pi$

$(\Gamma_i\Gamma_f)^{1/2}/\Gamma_{total}$ in $N\overline{K} \to \Lambda(2350) \to \Lambda\omega$ — $(\Gamma_1\Gamma_3)^{1/2}/\Gamma$

VALUE	DOCUMENT ID		TECN	COMMENT
<0.05	BACCARI	77	DPWA	$K^-p \to \Lambda\omega$

Λ(2350) REFERENCES

DEBELLEFON	78	NC 42A 403	A. de Bellefon *et al.*	(CDEF, SACL) IJP
BACCARI	77	NC 41A 96	B. Baccari *et al.*	(SACL, CDEF) IJP
DEBELLEFON	77	NC 37A 175	A. de Bellefon *et al.*	(CDEF, SACL) IJP
LASINSKI	71	NP B29 125	T.A. Lasinski	(EFI) IJP
BRICMAN	70	PL 31B 152	C. Bricman *et al.*	(CERN, CAEN, SACL)
COOL	70	PR D1 1887	R.L. Cool *et al.*	(BNL) I
Also		PRL 16 1228	R.L. Cool *et al.*	(BNL) I
LU	70	PR D2 1846	D.C. Lu *et al.*	(YALE)
BUGG	68	PR 168 1466	D.V. Bugg *et al.*	(RHEL, BIRM, CAVE) I
DAUM	68	NP B7 19	C. Daum *et al.*	(CERN) JP

Λ(2585) Bumps

$I(J^P) = 0(?^?)$ Status: *

OMITTED FROM SUMMARY TABLE

Λ(2585) MASS (BUMPS)

VALUE (MeV)	DOCUMENT ID		TECN	COMMENT
≈ 2585 OUR ESTIMATE				
2585±45	ABRAMS	70	CNTR	K^-p, K^-d total
2530±25	LU	70	CNTR	$\gamma p \to K^+Y^*$

Λ(2585) WIDTH (BUMPS)

VALUE (MeV)	DOCUMENT ID		TECN	COMMENT
300	ABRAMS	70	CNTR	K^-p, K^-d total
150	LU	70	CNTR	$\gamma p \to K^+Y^*$

Λ(2585) DECAY MODES (BUMPS)

	Mode
Γ_1	$N\overline{K}$

Λ(2585) BRANCHING RATIOS (BUMPS)

$(J+\frac{1}{2})\times\Gamma(N\overline{K})/\Gamma_{total}$ — Γ_1/Γ

J is not known, so only $(J+\frac{1}{2})\times\Gamma(N\overline{K})/\Gamma_{total}$ can be given.

VALUE	DOCUMENT ID		TECN	COMMENT
1	ABRAMS	70	CNTR	K^-p, K^-d total
0.12±0.12	[1] BRICMAN	70	CNTR	Total, charge exchange

Λ(2585) FOOTNOTES (BUMPS)

[1] The resonance is at the end of the region analyzed — no clear signal.

Λ(2585) REFERENCES (BUMPS)

ABRAMS	70	PR D1 1917	R.J. Abrams *et al.*	(BNL) I
Also		PRL 16 1228	R.L. Cool *et al.*	(BNL) I
BRICMAN	70	PL 31B 152	C. Bricman *et al.*	(CERN, CAEN, SACL)
LU	70	PR D2 1846	D.C. Lu *et al.*	(YALE)

Int. J. Mod. Phys. A 2026.41. Downloaded from www.worldscientific.com
by UNIVERSITY OF CALIFORNIA @ BERKELEY on 09/16/26. Re-use and distribution is strictly not permitted, except for Open Access articles.

Σ BARYONS
($S = -1$, $I = 1$)

$\Sigma^+ = uus$, $\Sigma^0 = uds$, $\Sigma^- = dds$

Σ^+

$I(J^P) = 1(\frac{1}{2}^+)$ Status: ****

We have omitted some results that have been superseded by later experiments. See our earlier editions.

Σ^+ MASS

The fit uses Σ^+, Σ^0, Σ^-, and Λ mass and mass-difference measurements.

VALUE (MeV)	EVTS	DOCUMENT ID		TECN	COMMENT
1189.37±0.07 OUR FIT Error includes scale factor of 2.2.					
1189.37±0.06 OUR AVERAGE Error includes scale factor of 1.8. See the ideogram below.					
1189.33±0.04	607	[1] BOHM	72	EMUL	
1189.16±0.12		HYMAN	67	HEBC	
1189.61±0.08	4205	SCHMIDT	65	HBC	See note with Λ mass
1189.48±0.22	58	[2] BHOWMIK	64	EMUL	
1189.38±0.15	144	[2] BARKAS	63	EMUL	

[1] BOHM 72 is updated with our 1973 K^-, π^-, and π^0 masses (Reviews of Modern Physics **45** S1 (1973)).

[2] These masses have been raised 30 keV to take into account a 46 keV increase in the proton mass and a 21 keV decrease in the π^0 mass (note added 1967 edition, Reviews of Modern Physics **39** 1 (1967)).

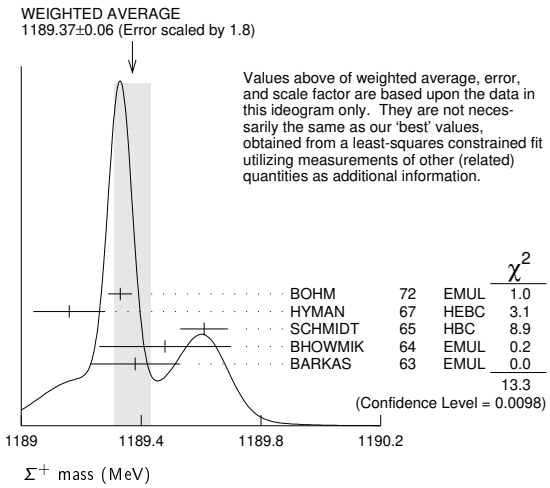

Σ^+ MEAN LIFE

Measurements with fewer than 1000 events have been omitted.

VALUE (10^{-10} s)	EVTS	DOCUMENT ID		TECN	COMMENT
0.8018±0.0026 OUR AVERAGE					
0.8038±0.0040±0.0014		BARBOSA	00	E761	hyperons, 375 GeV
0.8043±0.0080±0.0014		[1] BARBOSA	00	E761	hyperons, 375 GeV
0.798 ±0.005	30k	MARRAFFINO	80	HBC	K^-p 0.42–0.5 GeV/c
0.807 ±0.013	5719	CONFORTO	76	HBC	K^-p 1–1.4 GeV/c
0.795 ±0.010	20k	EISELE	70	HBC	K^-p at rest
0.803 ±0.008	10664	BARLOUTAUD	69	HBC	K^-p 0.4–1.2 GeV/c
0.83 ±0.032	1300	[2] CHANG	66	HBC	

[1] This is a measurement of the $\overline{\Sigma}^-$ lifetime. Here we assume CPT invariance; see below for the fractional Σ^+-$\overline{\Sigma}^-$ lifetime difference obtained by BARBOSA 00.

[2] We have increased the CHANG 66 error of 0.018; see our 1970 edition, Reviews of Modern Physics **42** 87 (1970).

$(\tau_{\Sigma^+} - \tau_{\overline{\Sigma}^-}) / \tau_{\Sigma^+}$

A test of CPT invariance.

VALUE	DOCUMENT ID		TECN	COMMENT
$(-6\pm12)\times10^{-4}$	BARBOSA	00	E761	hyperons, 375 GeV

Σ^+ MAGNETIC MOMENT

See the "Quark Model" review. Measurements with an error $\geq 0.1\ \mu_N$ have been omitted.

VALUE (μ_N)	EVTS	DOCUMENT ID		TECN	COMMENT
2.458 ±0.010 OUR AVERAGE Error includes scale factor of 2.1. See the ideogram below.					
2.4613±0.0034±0.0040	250k	MORELOS	93	SPEC	pCu 800 GeV
2.428 ±0.036 ±0.007	12k	[1] MORELOS	93	SPEC	pCu 800 GeV
2.479 ±0.012 ±0.022	137k	WILKINSON	87	SPEC	pBe 400 GeV
2.4040±0.0198	44k	[2] ANKENBRA...	83	CNTR	pCu 400 GeV

[1] We assume CPT invariance: this is (minus) the $\overline{\Sigma}^-$ magnetic moment as measured by MORELOS 93. See below for the moment difference testing CPT.

[2] ANKENBRANDT 83 gives the value 2.38 ± 0.02μ_N. MORELOS 93 uses the same hyperon magnet and channel and claims to determine the field integral better, leading to the revised value given here.

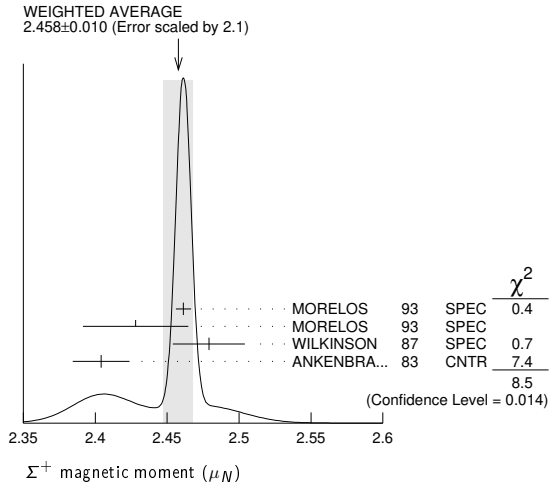

$(\mu_{\Sigma^+} + \mu_{\overline{\Sigma}^-}) / \mu_{\Sigma^+}$

A test of CPT invariance.

VALUE	DOCUMENT ID		TECN	COMMENT
0.014±0.015	[1] MORELOS	93	SPEC	pCu 800 GeV

[1] This is our calculation from the MORELOS 93 measurements of the Σ^+ and $\overline{\Sigma}^-$ magnetic moments given above. The statistical error on $\mu_{\overline{\Sigma}^-}$ dominates the error here.

Σ^+ DECAY MODES

	Mode		Fraction (Γ_i/Γ)	Scale factor/ Confidence level
Γ_1	$p\pi^0$		(51.47±0.30) %	
Γ_2	$n\pi^+$		(48.43±0.30) %	
Γ_3	$p\gamma$		$(1.04\pm0.06)\times10^{-3}$	S=2.4
Γ_4	$n\pi^+\gamma$	[a]	$(4.5\pm0.5)\times10^{-4}$	
Γ_5	$\Lambda e^+\nu_e$		$(2.3\pm0.4)\times10^{-5}$	
	$\Delta S = \Delta Q$ (SQ) violating modes or $\Delta S = 1$ weak neutral current ($S1$) modes			
Γ_6	$n e^+\nu_e$	SQ	$< 5\times10^{-6}$	CL=90%
Γ_7	$n\mu^+\nu_\mu$	SQ	$< 3.0\times10^{-5}$	CL=90%
Γ_8	$p e^+ e^-$	$S1$	$< 7\times10^{-6}$	
Γ_9	$p\mu^+\mu^-$	$S1$	$(1.09\pm0.17)\times10^{-8}$	
Γ_{10}	$p\gamma_{dark}$		$< 3.2\times10^{-5}$	CL=90%

[a] See the Listings below for the pion momentum range used in this measurement.

CONSTRAINED FIT INFORMATION

An overall fit to 3 branching ratios uses 15 measurements and one constraint to determine 3 parameters. The overall fit has a χ^2 = 22.0 for 13 degrees of freedom.

The following *off-diagonal* array elements are the correlation coefficients $\langle \delta x_i \delta x_j \rangle / (\delta x_i \cdot \delta x_j)$, in percent, from the fit to the branching fractions, $x_i \equiv \Gamma_i/\Gamma_{total}$. The fit constrains the x_i whose labels appear in this array to sum to one.

x_2	−100	
x_3	5	−7
	x_1	x_2

Σ^+ BRANCHING RATIOS

$\Gamma(n\pi^+)/\Gamma(N\pi)$ — $\Gamma_2/(\Gamma_1+\Gamma_2)$

VALUE	EVTS	DOCUMENT ID		TECN	COMMENT
0.4848±0.0030 OUR FIT					
0.4836±0.0030 OUR AVERAGE					
0.4828±0.0036	10k	[1] MARRAFFINO	80	HBC	K^-p 0.42–0.5 GeV/c
0.488 ±0.008	1861	NOWAK	78	HBC	
0.484 ±0.015	537	TOVEE	71	EMUL	
0.488 ±0.010	1331	BARLOUTAUD	69	HBC	K^-p 0.4–1.2 GeV/c
0.46 ±0.02	534	CHANG	66	HBC	
0.490 ±0.024	308	HUMPHREY	62	HBC	

[1] MARRAFFINO 80 actually gives $\Gamma(p\pi^0)/\Gamma(\text{total}) = 0.5172 \pm 0.0036$.

$\Gamma(p\gamma)/\Gamma(p\pi^0)$ — Γ_3/Γ_1

VALUE (units 10^{-3})	EVTS	DOCUMENT ID		TECN	COMMENT
2.03±0.11 OUR FIT Error includes scale factor of 2.4.					
2.38±0.10 OUR AVERAGE					
2.32±0.11±0.10	32k	TIMM	95	E761	Σ^+ 375 GeV
$2.81\pm0.39^{+0.21}_{-0.43}$	408	HESSEY	89	CNTR	$K^-p \to \Sigma^+\pi^-$ at rest
2.52±0.28	190	[1] KOBAYASHI	87	CNTR	$\pi^+p \to \Sigma^+K^+$
$2.46^{+0.30}_{-0.35}$	155	BIAGI	85	CNTR	CERN hyperon beam
2.11±0.38	46	MANZ	80	HBC	$K^-p \to \Sigma^+\pi^-$
2.1 ±0.3	45	ANG	69B	HBC	K^-p at rest
2.76±0.51	31	GERSHWIN	69B	HBC	$K^-p \to \Sigma^+\pi^-$
3.7 ±0.8	24	BAZIN	65	HBC	K^-p at rest

[1] KOBAYASHI 87 actually gives $\Gamma(p\gamma)/\Gamma(\text{total}) = (1.30 \pm 0.15) \times 10^{-3}$.

$\Gamma(p\gamma)/\Gamma_{\text{total}}$ — Γ_3/Γ

VALUE (units 10^{-3})	EVTS	DOCUMENT ID		TECN	COMMENT
1.04 ±0.06 OUR FIT Error includes scale factor of 2.4.					
0.996±0.021±0.018	2.5k	[1] ABLIKIM	23Y	BES3	$e^+e^- \to J/\psi \to \Sigma\overline{\Sigma}$

[1] This value is quoted by ABLIKIM 23Y for the simultaneous fit to $\Sigma \to p\gamma$ and $\overline{\Sigma} \to \overline{p}\gamma$ assuming no CP violation. Individual values for the branching fractions are given as $(1.005 \pm 0.032) \times 10^{-3}$ and $(0.993 \pm 0.030) \times 10^{-3}$, respectively.

$\Gamma(n\pi^+\gamma)/\Gamma(n\pi^+)$ — Γ_4/Γ_2

The π^+ momentum cuts differ, so we do not average the results but simply use the latest value in the Summary Table.

VALUE (units 10^{-3})	EVTS	DOCUMENT ID		TECN	COMMENT
0.93±0.10	180	EBENHOH	73	HBC	$\pi^+ < 150$ MeV/c
• • • We do not use the following data for averages, fits, limits, etc. • • •					
0.27±0.05	29	ANG	69B	HBC	$\pi^+ < 110$ MeV/c
∼ 1.8		BAZIN	65B	HBC	$\pi^+ < 116$ MeV/c

$\Gamma(\Lambda e^+\nu_e)/\Gamma_{\text{total}}$ — Γ_5/Γ

VALUE (units 10^{-5})	EVTS	DOCUMENT ID		TECN	COMMENT
2.3 ±0.4 OUR AVERAGE					
2.93±0.74±0.13	16	ABLIKIM	23AA	BES3	$e^+e^- \to J/\psi \to \Sigma\overline{\Sigma}$
1.6 ±0.7	5	BALTAY	69	HBC	K^-p at rest
2.9 ±1.0	10	EISELE	69	HBC	K^-p at rest
2.0 ±0.8	6	BARASH	67	HBC	K^-p at rest

$\Gamma(ne^+\nu_e)/\Gamma(n\pi^+)$ — Γ_6/Γ_2

Test of $\Delta S = \Delta Q$ rule. Experiments with an effective denominator less than 100,000 have been omitted.

EFFECTIVE DENOM.	EVTS	DOCUMENT ID		TECN	COMMENT
$< 1.1 \times 10^{-5}$ OUR LIMIT Our 90% CL limit = (2.3 events)/(effective denominator sum). [Number of events increased to 2.3 for a 90% confidence level.]					
111000	0	[1] EBENHOH	74	HBC	K^-p at rest
105000	0	[1] SECHI-ZORN	73	HBC	K^-p at rest

[1] Effective denominator calculated by us.

$\Gamma(n\mu^+\nu_\mu)/\Gamma(n\pi^+)$ — Γ_7/Γ_2

Test of $\Delta S = \Delta Q$ rule.

EFFECTIVE DENOM.	EVTS	DOCUMENT ID		TECN
$< 6.2 \times 10^{-5}$ OUR LIMIT Our 90% CL limit = (6.7 events)/(effective denominator sum). [Number of events increased to 6.7 for a 90% confidence level.]				
33800	0	BAGGETT	69B	HBC
62000	2	[1] EISELE	69B	HBC
10150	0	[2] COURANT	64	HBC
1710	0	[2] NAUENBERG	64	HBC
120	1	GALTIERI	62	EMUL

[1] Effective denominator calculated by us.
[2] Effective denominator taken from EISELE 67.

$\Gamma(pe^+e^-)/\Gamma_{\text{total}}$ — Γ_8/Γ

VALUE (units 10^{-6})	DOCUMENT ID		TECN	COMMENT
<7	[1] ANG	69B	HBC	K^-p at rest

[1] ANG 69B found three pe^+e^- events in agreement with $\gamma \to e^+e^-$ conversion from $\Sigma^+ \to p\gamma$. The limit given here is for neutral currents.

$\Gamma(p\mu^+\mu^-)/\Gamma_{\text{total}}$ — Γ_9/Γ

A test for a $\Delta S = 1$ weak neutral current, but also allowed by higher-order electroweak interactions.

VALUE (units 10^{-8})	EVTS	DOCUMENT ID		TECN	COMMENT
1.09±0.17	0.25k	[1] AAIJ	25D	LHCB	pp at 7, 8, 13 TeV
• • • We do not use the following data for averages, fits, limits, etc. • • •					
1.08±0.17	237	[2] AAIJ	25D	LHCB	pp at 13 TeV
$2.2\ ^{+0.9}_{-0.8}\ ^{+1.5}_{-1.1}$	10.2	[3] AAIJ	18E	LHCB	pp at 7, 8 TeV
$8.6\ ^{+6.6}_{-5.4} \pm 5.5$	3	[4] PARK	05	HYCP	p Cu, 800 GeV

[1] Combination of AAIJ 18E (Run 1) and AAIJ 25D (Run 2) results.
[2] Uses $B(\Sigma^+ \to p\pi^0) = (51.57 \pm 0.30) \times 10^{-2}$.
[3] AAIJ 18E sees no structure in the dimuon mass distribution, contrary to PARK 05.
[4] The masses of the three dimuons of PARK 05 are within 1 MeV of one another, perhaps indicating the existence of a new state P^0 with mass 214.3 ± 0.5 MeV. In that case, the decay is $\Sigma^+ \to pP^0$, $P^0 \to \mu^+\mu^-$, with a branching fraction of $(3.1\ ^{+2.4}_{-1.9} \pm 1.5) \times 10^{-8}$.

$\Gamma(p\gamma_{dark})/\Gamma_{\text{total}}$ — Γ_{10}/Γ

VALUE	CL%	DOCUMENT ID		TECN	COMMENT
$<3.2 \times 10^{-5}$	90	[1] ABLIKIM	24AF	BES3	$J/\psi, \psi(2S) \to \Sigma^+\overline{\Sigma}^-$

[1] FCNC search for invisible massless particles (dark photons) using missing energy in Σ hyperon decays to a proton. For a QCD axion scenario, a competitive lower limit can be derived for the axial-vector part of the s-d flavor-violating axion-fermion effective decay constant $F^A_{sd} > 2.8 \times 10^7$ GeV.

$\Gamma(\Sigma^+ \to ne^+\nu_e)/\Gamma(\Sigma^- \to ne^-\overline{\nu}_e)$ — $\Gamma_6/\Gamma_3^{\Sigma^-}$

VALUE	CL%	EVTS	DOCUMENT ID		TECN	COMMENT
<0.009 OUR LIMIT Our 90% CL limit, using $\Gamma(ne^+\nu_e)/\Gamma(n\pi^+)$ above.						
• • • We do not use the following data for averages, fits, limits, etc. • • •						
<0.019	90	0	EBENHOH	74	HBC	K^-p at rest
<0.018	90	0	SECHI-ZORN	73	HBC	K^-p at rest
<0.12	95	0	COLE	71	HBC	K^-p at rest
<0.03	90	0	EISELE	69B	HBC	See EBENHOH 74

$\Gamma(\Sigma^+ \to n\mu^+\nu_\mu)/\Gamma(\Sigma^- \to n\mu^-\overline{\nu}_\mu)$ — $\Gamma_7/\Gamma_4^{\Sigma^-}$

VALUE	EVTS	DOCUMENT ID		TECN	COMMENT
<0.12 OUR LIMIT Our 90% CL limit, using $\Gamma(n\mu^+\nu_\mu)/\Gamma(n\pi^+)$ above.					
• • • We do not use the following data for averages, fits, limits, etc. • • •					
$0.06^{+0.045}_{-0.03}$	2	EISELE	69B	HBC	K^-p at rest

$\Gamma(\Sigma^+ \to n\ell^+\nu)/\Gamma(\Sigma^- \to n\ell^-\overline{\nu}_\ell)$ — $(\Gamma_6+\Gamma_7)/(\Gamma_3^{\Sigma^-}+\Gamma_4^{\Sigma^-})$

Test of $\Delta S = \Delta Q$ rule.

VALUE	EVTS	DOCUMENT ID		TECN
<0.043 OUR LIMIT Our 90% CL limit, using $[\Gamma(\Sigma^+ \to n\mu^+\nu_\mu) + \Gamma(\Sigma^+ \to ne^+\nu_e)]/\Gamma(\Sigma^+ \to n\pi^+)$.				
• • • We do not use the following data for averages, fits, limits, etc. • • •				
<0.08	1	NORTON	69	HBC
<0.034	0	BAGGETT	67	HBC

Σ^+ DECAY PARAMETERS

See the "Note on Baryon Decay Parameters" in the neutron Listings. A few early results have been omitted.

α_0 FOR $\Sigma^+ \to p\pi^0$

VALUE	EVTS	DOCUMENT ID		TECN	COMMENT
−0.977±0.009 OUR FIT					
−0.977±0.009 OUR AVERAGE					
−0.975±0.011±0.002	1.07M	[1] ABLIKIM	25BT	BES3	$J/\psi/\psi(2S) \to \Sigma^+\overline{\Sigma}^-$
$-0.945^{+0.055}_{-0.042}$	1259	[2] LIPMAN	73	OSPK	$\pi^+p \to \Sigma^+$
−0.940±0.045	16k	BELLAMY	72	ASPK	$\pi^+p \to \Sigma^+K^+$
$-0.98\ ^{+0.05}_{-0.02}$	1335	[3] HARRIS	70	OSPK	$\pi^+p \to \Sigma^+K^+$
−0.999±0.022	32k	BANGERTER	69	HBC	K^-p 0.4 GeV/c
• • • We do not use the following data for averages, fits, limits, etc. • • •					
−0.998±0.037±0.009	93k	[4] ABLIKIM	20X	BES3	$J/\psi/\psi(2S) \to \Sigma^+\overline{\Sigma}^-$

[1] ABLIKIM 25BT uses production through $e^+e \to J/\psi \to \Sigma^+\overline{\Sigma}^-$ and $e^+e \to \psi(2S) \to \Sigma^+\overline{\Sigma}^-$, with 1016678 ± 1398 and 53293 ± 299 events, respectively.
[2] Decay protons scattered off aluminum.
[3] Decay protons scattered off carbon.
[4] ABLIKIM 20X uses production through $e^+e \to J/\psi \to \Sigma^+\overline{\Sigma}^-$ and $e^+e \to \psi(2S) \to \Sigma^+\overline{\Sigma}^-$, with 87,815 and 5,327 events, respectively. Note that the reported values of decay parameters α_0 of Σ^+ and $\overline{\alpha}_0$ of $\overline{\Sigma}^-$ are correlated.

$\overline{\alpha}_0$ FOR $\overline{\Sigma}^- \to \overline{p}\pi^0$

VALUE	EVTS	DOCUMENT ID		TECN	COMMENT
0.999±0.011±0.004	1.07M	[1] ABLIKIM	25BT	BES3	$J/\psi/\psi(2S) \to \Sigma^+\overline{\Sigma}^-$
• • • We do not use the following data for averages, fits, limits, etc. • • •					
0.990±0.037±0.011	93k	[2] ABLIKIM	20X	BES3	$J/\psi/\psi(2S) \to \Sigma^+\overline{\Sigma}^-$

Int. J. Mod. Phys. A 2026.41. Downloaded from www.worldscientific.com
UNIVERSITY OF CALIFORNIA @ BERKELEY on 09/16/26. Re-use and distribution is strictly not permitted, except for Open Access articles.

[1] ABLIKIM 25BT uses production through $e^+e^- \to J/\psi \to \Sigma^+\overline{\Sigma}^-$ and $e^+e^- \to \psi(2S) \to \Sigma^+\overline{\Sigma}^-$, with 1016678 ± 1398 and 53293 ± 299 events, respectively.
[2] ABLIKIM 20X uses production through $e^+e^- \to J/\psi \to \Sigma^+\overline{\Sigma}^-$ and $e^+e^- \to \psi(2S) \to \Sigma^+\overline{\Sigma}^-$, with 87,815 and 5,327 events, respectively. Note that the reported values of decay parameters α_0 of Σ^+ and $\overline{\alpha}_0$ of $\overline{\Sigma}^-$ are correlated.

$(\alpha_0 + \overline{\alpha}_0) / (\alpha_0 - \overline{\alpha}_0)$

Test of *CP* violation.

VALUE (units 10^{-2})	EVTS	DOCUMENT ID		TECN	COMMENT
−1.18±0.83±0.28	1.07M	[1] ABLIKIM	25BT	BES3	$J/\psi/\psi(2S) \to \Sigma^+\overline{\Sigma}^-$
• • • We do not use the following data for averages, fits, limits, etc. • • •					
0.4 ±3.7 ±1.0	93k	[2] ABLIKIM	20X	BES3	$J/\psi/\psi(2S) \to \Sigma^+\overline{\Sigma}^-$

[1] ABLIKIM 25BT uses production through $e^+e^- \to J/\psi \to \Sigma^+\overline{\Sigma}^-$ and $e^+e^- \to \psi(2S) \to \Sigma^+\overline{\Sigma}^-$, with 1016678 ± 1398 and 53293 ± 299 events, respectively.
[2] ABLIKIM 20X uses production through $e^+e^- \to J/\psi \to \Sigma^+\overline{\Sigma}^-$ and $e^+e^- \to \psi(2S) \to \Sigma^+\overline{\Sigma}^-$, with 87,815 and 5,327 events, respectively. Note that the reported values of decay parameters α_0 of Σ^+ and $\overline{\alpha}_0$ of $\overline{\Sigma}^-$ are correlated.

$(\alpha_0 - \overline{\alpha}_0)/2$

Average decay parameter assuming *CP* conservation.

VALUE	EVTS	DOCUMENT ID		TECN	COMMENT
−0.9869±0.0011±0.0016	1.07M	[1] ABLIKIM	25BT	BES3	$J/\psi/\psi(2S) \to \Sigma^+\overline{\Sigma}^-$

[1] ABLIKIM 25BT uses production through $e^+e^- \to J/\psi \to \Sigma^+\overline{\Sigma}^-$ and $e^+e^- \to \psi(2S) \to \Sigma^+\overline{\Sigma}^-$, with 1016678 ± 1398 and 53293 ± 299 events, respectively.

ϕ_0 ANGLE FOR $\Sigma^+ \to p\pi^0$ $(\tan\phi_0 = \beta/\gamma)$

VALUE (°)	EVTS	DOCUMENT ID		TECN	COMMENT
36 ±34 OUR AVERAGE					
$38.1^{+35.7}_{-37.1}$	1259	[1] LIPMAN	73	OSPK	$\pi^+p \to \Sigma^+K^+$
22 ±90		[2] HARRIS	70	OSPK	$\pi^+p \to \Sigma^+K^+$

[1] Decay proton scattered off aluminum.
[2] Decay protons scattered off carbon.

α_+ / α_0

Older results have been omitted.

VALUE (units 10^{-2})	EVTS	DOCUMENT ID		TECN	COMMENT
−4.99±0.27 OUR FIT					
−5.0 ±0.4 OUR AVERAGE					
−4.90±0.32±0.21	754k	[1] ABLIKIM	23BN	BES3	$J/\psi \to \Sigma^+\overline{\Sigma}^-$
−7.3 ±2.1	23k	MARRAFFINO	80	HBC	K^-p 0.42–0.5 GeV/c

[1] ABLIKIM 23BN uses production through $e^+e^- \to J/\psi \to \Sigma^+\overline{\Sigma}^-$ with 10G J/ψ events.

α_+ FOR $\Sigma^+ \to n\pi^+$

VALUE (units 10^{-2})	EVTS	DOCUMENT ID		TECN	COMMENT
4.88±0.26 OUR FIT					
4.9 ±0.4 OUR AVERAGE Error includes scale factor of 1.2.					
4.81±0.31±0.19	754k	[1] ABLIKIM	23BN	BES3	$J/\psi \to \Sigma^+\overline{\Sigma}^-$
3.7 ±4.9	4101	BERLEY	70B	HBC	
6.9 ±1.7	35k	BANGERTER	69	HBC	K^-p 0.4 GeV/c

[1] ABLIKIM 23BN uses production through $e^+e^- \to J/\psi \to \Sigma^+\overline{\Sigma}^-$ with 10G J/ψ events.

ϕ_+ ANGLE FOR $\Sigma^+ \to n\pi^+$ $(\tan\phi_+ = \beta/\gamma)$

VALUE (°)	EVTS	DOCUMENT ID		TECN	COMMENT
167±20 OUR AVERAGE Error includes scale factor of 1.1.					
184±24	1054	[1] BERLEY	70B	HBC	
143±29	560	BANGERTER	69B	HBC	K^-p 0.4 GeV/c

[1] Changed from 176 to 184° to agree with our sign convention.

$\overline{\alpha}_- $ FOR $\overline{\Sigma}^- \to \overline{n}\pi^-$

VALUE (units 10^{-2})	EVTS	DOCUMENT ID		TECN	COMMENT
−5.65±0.47±0.22	1.1M	[1] ABLIKIM	23BN	BES3	$J/\psi \to \Sigma^+\overline{\Sigma}^-$

[1] ABLIKIM 23BN uses production through $e^+e^- \to J/\psi \to \Sigma^+\overline{\Sigma}^-$ with 10G J/ψ events.

$\overline{\alpha}_- / \overline{\alpha}_0$

VALUE (units 10^{-2})	DOCUMENT ID		TECN	COMMENT
−5.71±0.53±0.32	ABLIKIM	23BN	BES3	$J/\psi \to \Sigma^+\overline{\Sigma}^-$

$(\alpha_+ + \overline{\alpha}_-) / (\alpha_+ - \overline{\alpha}_-)$

VALUE (units 10^{-2})	DOCUMENT ID		TECN	COMMENT
−8.0±5.2±2.8	ABLIKIM	23BN	BES3	$J/\psi \to \Sigma^+\overline{\Sigma}^-$

α_γ FOR $\Sigma^+ \to p\gamma$

VALUE	EVTS	DOCUMENT ID		TECN	COMMENT
−0.69 ±0.05 OUR AVERAGE					
−0.652±0.056±0.020	2.5k	[1] ABLIKIM	23Y	BES3	$e^+e^- \to J/\psi \to \Sigma\overline{\Sigma}$
−0.720±0.086±0.045	35k	[2] FOUCHER	92	SPEC	Σ^+ 375 GeV
−0.86 ±0.13 ±0.04	190	KOBAYASHI	87	CNTR	$\pi^+p \to \Sigma^+K^+$
$-0.53\ ^{+0.38}_{-0.36}$	46	MANZ	80	HBC	$K^-p \to \Sigma^+\pi^-$
$-1.03\ ^{+0.52}_{-0.42}$	61	GERSHWIN	69B	HBC	$K^-p \to \Sigma^+\pi^-$

[1] This value is quoted by ABLIKIM 23Y for the simultaneous fit to $\Sigma \to p\gamma$ and $\overline{\Sigma} \to \overline{p}\gamma$ assuming no *CP* violation. Individual values are given as −0.587 ± 0.082 and 0.710 ± 0.076, respectively.
[2] See TIMM 95 for a detailed description of the analysis.

Σ^+ REFERENCES

We have omitted some papers that have been superseded by later experiments. See our earlier editions.

AAIJ	25D	PRL 135 051801	R. Aaij *et al.*	(LHCb Collab.)
ABLIKIM	25BT	PRL 135 141804	M. Ablikim *et al.*	(BESIII Collab.)
ABLIKIM	24AF	PL B852 138614	M. Ablikim *et al.*	(BESIII Collab.)
ABLIKIM	23AA	PR D107 072010	M. Ablikim *et al.*	(BESIII Collab.)
ABLIKIM	23BN	PRL 131 191802	M. Ablikim *et al.*	(BESIII Collab.)
ABLIKIM	23Y	PRL 130 211901	M. Ablikim *et al.*	(BESIII Collab.)
ABLIKIM	20X	PRL 125 052004	M. Ablikim *et al.*	(BESIII Collab.)
AAIJ	18E	PRL 120 221803	R. Aaij *et al.*	(LHCb Collab.)
PARK	05	PRL 94 021801	H.K. Park *et al.*	(FNAL HyperCP Collab.)
BARBOSA	00	PR D61 031101	R.F. Barbosa *et al.*	(FNAL E761 Collab.)
TIMM	95	PR D51 4638	S. Timm *et al.*	(FNAL E761 Collab.)
MORELOS	93	PRL 71 3417	A. Morelos *et al.*	(FNAL E761 Collab.)
FOUCHER	92	PRL 68 3004	M. Foucher *et al.*	(FNAL E761 Collab.)
HESSEY	89	ZPHY C42 175	N.P. Hessey *et al.*	(BNL-811 Collab.)
KOBAYASHI	87	PRL 59 868	M. Kobayashi *et al.*	(KYOT)
WILKINSON	87	PRL 58 855	C.A. Wilkinson *et al.*	(WISC, MICH, RUTG+)
BIAGI	85	ZPHY C28 495	S.F. Biagi *et al.*	(CERN WA62 Collab.)
ANKENBRA...	83	PRL 51 863	C.M. Ankenbrandt *et al.*	(FNAL, IOWA, ISU+)
MANZ	80	PL 96B 217	A. Manz *et al.*	(MPIM, VAND)
MARRAFFINO	80	PR D21 2501	J. Marraffino *et al.*	(VAND, MPIM)
NOWAK	78	NP B139 61	R.J. Nowak *et al.*	(LOUC, BELG, DURH+)
CONFORTO	76	NP B105 189	B. Conforto *et al.*	(RHEL, LOIC)
EBENHOH	74	ZPHY 266 367	H. Ebenhoh *et al.*	(HEIDT)
EBENHOH	73	ZPHY 264 413	W. Ebenhoh *et al.*	(HEIDT)
LIPMAN	73	PL 43B 89	N.H. Lipman *et al.*	(RHEL, SUSS, LOWC)
PDG	73	RMP 45 S1	T.A. Lasinski *et al.*	(LBL, BRAN, CERN+)
SECHI-ZORN	73	PR D8 12	B. Sechi-Zorn, G.A. Snow	(UMD)
BELLAMY	72	PL 39B 299	E.H. Bellamy *et al.*	(LOWC, RHEL, SUSS)
BOHM	72	NP B48 1	G. Bohm *et al.*	(BERL, KIDR, BRUX, IASD+)
Also		IIHE-73.2 Nov	G. Bohm	(BERL, KIDR, BRUX, IASD, DUUC+)
COLE	71	PR D4 631	J. Cole *et al.*	(STON, COLU)
TOVEE	71	NP B33 493	D.N. Tovee *et al.*	(LOUC, KIDR, BERL+)
BERLEY	70B	PR D1 2015	D. Berley *et al.*	(BNL, MASA, YALE)
EISELE	70	ZPHY 238 372	F. Eisele *et al.*	(HEID)
HARRIS	70	PRL 24 165	F. Harris *et al.*	(MICH, WISC)
PDG	70	RMP 42 87	A. Barbaro-Galtieri *et al.*	(LRL, BRAN+)
ANG	69B	ZPHY 228 151	G. Ang *et al.*	(HEID)
BAGGETT	69B	Thesis MDDP-TR-973	N.V. Baggett	(UMD)
BALTAY	69	PRL 22 615	C. Baltay *et al.*	(COLU, STON)
BANGERTER	69	Thesis UCRL 19244	R.O. Bangerter	(LRL)
BANGERTER	69B	PR 187 1821	R.O. Bangerter *et al.*	(LRL)
BARLOUTAUD	69	NP B14 153	R. Barloutaud *et al.*	(SACL, CERN, HEID)
EISELE	69	ZPHY 221 1	F. Eisele *et al.*	(HEID)
Also		PRL 13 291	W. Willis *et al.*	(BNL, CERN, HEID, UMD)
EISELE	69B	ZPHY 221 401	F. Eisele *et al.*	(HEID)
GERSHWIN	69B	PR 188 2077	L.K. Gershwin *et al.*	(LRL)
Also		Thesis UCRL 19246	L.K. Gershwin	(LRL)
NORTON	69	Thesis Nevis 175	H. Norton	(COLU)
BAGGETT	67	PRL 19 1458	N. Baggett *et al.*	(UMD)
Also		Vienna Abs. 374	N.V. Baggett, B. Kehoe	(UMD)
Also		Private Comm.	N.V. Baggett	(UMD)
BARASH	67	PRL 19 181	N. Barash *et al.*	(UMD)
EISELE	67	ZPHY 205 409	F. Eisele *et al.*	(HEID)
HYMAN	67	PL 25B 376	L.G. Hyman *et al.*	(ANL, CMU, NWES)
PDG	67	RMP 39 1	A.H. Rosenfeld *et al.*	(LRL, CERN, YALE)
CHANG	66	PR 151 1081	C.Y. Chang	(COLU)
Also		Thesis Nevis 145	C.Y. Chang	(COLU)
BAZIN	65	PRL 14 154	M. Bazin *et al.*	(PRIN, COLU)
BAZIN	65B	PR 140 B1358	M. Bazin *et al.*	(PRIN, RUTG, COLU)
SCHMIDT	65	PR 140 B1328	P. Schmidt	(COLU)
BHOWMIK	64	NP 53 22	B. Bhowmik *et al.*	(DELH)
COURANT	64	PR 136 B1791	H. Courant *et al.*	(CERN, HEID, UMD+)
NAUENBERG	64	PRL 12 679	U. Nauenberg *et al.*	(COLU, RUTG, PRIN)
BARKAS	63	PRL 11 26	W.H. Barkas, J.N. Dyer, H.H. Heckman	(LRL)
Also		Thesis UCRL 9450	J.N. Dyer	(LRL)
GALTIERI	62	PRL 9 26	A. Barbaro-Galtieri *et al.*	(LRL)
HUMPHREY	62	PR 127 1305	W.E. Humphrey, R.R. Ross	(LRL)

Σ^0

$I(J^P) = 1(\frac{1}{2}^+)$ Status: ****

COURANT 63 and ALFF 65, using $\Sigma^0 \to \Lambda e^+e^-$ decays (Dalitz decays), determined the Σ^0 parity to be positive, given that $J = 1/2$ and that certain very reasonable assumptions about form factors are true. The results of experiments involving the Primakoff effect, from which the Σ^0 mean life and $\Sigma^0 \to \Lambda$ transition magnetic moment come (see below), strongly support $J = 1/2$.

Σ^0 MASS

The fit uses Σ^+, Σ^0, Σ^-, and Λ mass and mass-difference measurements.

VALUE (MeV)	EVTS	DOCUMENT ID		TECN	COMMENT
1192.642±0.024 OUR FIT					
• • • We do not use the following data for averages, fits, limits, etc. • • •					
1192.65 ±0.020±0.014	3327	[1] WANG	97	SPEC	$\Sigma^0 \to \Lambda\gamma \to (p\pi^-)(e^+e^-)$

[1] This WANG 97 result is redundant with the Σ^0-Λ mass-difference measurement below.

$m_{\Sigma^-} - m_{\Sigma^0}$

VALUE (MeV)	EVTS	DOCUMENT ID		TECN	COMMENT
4.807±0.035 OUR FIT Error includes scale factor of 1.1.					
4.86 ±0.08 OUR AVERAGE Error includes scale factor of 1.2.					
4.87 ±0.12	37	DOSCH	65	HBC	
5.01 ±0.12	12	SCHMIDT	65	HBC	See note with Λ mass
4.75 ±0.1	18	BURNSTEIN	64	HBC	

Int. J. Mod. Phys. A 2026.41. Downloaded from www.worldscientific.com
by UNIVERSITY OF CALIFORNIA @ BERKELEY on 09/16/26. Re-use and distribution is strictly not permitted, except for Open Access articles.

Int. J. Mod. Phys. A 2026.41. Downloaded from www.worldscientific.com
UNIVERSITY OF CALIFORNIA @ BERKELEY on 09/16/26. Re-use and distribution is strictly not permitted, except for Open Access articles.

$m_{\Sigma^0} - m_\Lambda$

VALUE (MeV)	EVTS	DOCUMENT ID		TECN	COMMENT
76.959±0.023 OUR FIT					
76.966±0.020±0.013	3327	WANG	97	SPEC	$\Sigma^0 \to \Lambda\gamma \to (p\pi^-)(e^+e^-)$
• • • We do not use the following data for averages, fits, limits, etc. • • •					
76.23 ±0.55	109	COLAS	75	HLBC	$\Sigma^0 \to \Lambda\gamma$
76.63 ±0.28	208	SCHMIDT	65	HBC	See note with Λ mass

Σ^0 MEAN LIFE

These lifetimes are deduced from measurements of the cross sections for the Primakoff process $\Lambda \to \Sigma^0$ in nuclear Coulomb fields. An alternative expression of the same information is the Σ^0-Λ transition magnetic moment given in the following section. The relation is $(\mu_{\Sigma\Lambda}/\mu_N)^2\,\tau = 1.92951 \times 10^{-19}$ s (see DEVLIN 86).

VALUE (10^{-20} s)	DOCUMENT ID		TECN	COMMENT
7.4±0.7 OUR EVALUATION	Using $\mu_{\Sigma\Lambda}$ (see the above note).			
$6.5^{+1.7}_{-1.1}$	[2] DEVLIN	86	SPEC	Primakoff effect
7.6±0.5±0.7	[3] PETERSEN	86	SPEC	Primakoff effect
• • • We do not use the following data for averages, fits, limits, etc. • • •				
5.8±1.3	[2] DYDAK	77	SPEC	See DEVLIN 86

[2] DEVLIN 86 is a recalculation of the results of DYDAK 77 removing a numerical approximation made in that work.
[3] An additional uncertainty of the Primakoff formalism is estimated to be < 5%.

$|\mu(\Sigma^0 \to \Lambda)|$ TRANSITION MAGNETIC MOMENT

See the note in the Σ^0 mean-life section above. Also, See the "Quark Model" review.

VALUE (μ_N)	DOCUMENT ID		TECN	COMMENT
1.61±0.08 OUR AVERAGE				
$1.72^{+0.17}_{-0.19}$	[4] DEVLIN	86	SPEC	Primakoff effect
1.59±0.05±0.07	[5] PETERSEN	86	SPEC	Primakoff effect
• • • We do not use the following data for averages, fits, limits, etc. • • •				
$1.82^{+0.25}_{-0.18}$	[4] DYDAK	77	SPEC	See DEVLIN 86

[4] DEVLIN 86 is a recalculation of the results of DYDAK 77 removing a numerical approximation made in that work.
[5] An additional uncertainty of the Primakoff formalism is estimated to be < 2.5%.

Σ^0 DECAY MODES

	Mode	Fraction (Γ_i/Γ)	Confidence level
Γ_1	$\Lambda\gamma$	100 %	
Γ_2	$\Lambda\gamma\gamma$	< 3 %	90%
Γ_3	$\Lambda e^+ e^-$	[a] 5×10^{-3}	

[a] A theoretical value using QED.

Σ^0 BRANCHING RATIOS

$\Gamma(\Lambda\gamma\gamma)/\Gamma_{total}$ — Γ_2/Γ

VALUE	CL%	DOCUMENT ID		TECN
<0.03	90	COLAS	75	HLBC

$\Gamma(\Lambda e^+ e^-)/\Gamma_{total}$ — Γ_3/Γ

See COURANT 63 and ALFF 65 for measurements of the invariant-mass spectrum of the Dalitz pairs.

VALUE	DOCUMENT ID		COMMENT
0.00545	FEINBERG	58	Theoretical QED calculation

Σ^0 DECAY PARAMETERS

α for $\Sigma^0 \to \Lambda\gamma$

VALUE (units 10^{-3})	EVTS	DOCUMENT ID		TECN	COMMENT
−1.7±2.1±1.8	1.1M	ABLIKIM	24CE	BES3	$J/\psi/\psi(2S) \to \Sigma\overline{\Sigma} \to \Lambda\overline{\Lambda}\gamma\gamma$

$\overline{\alpha}$ for $\overline{\Sigma}^0 \to \overline{\Lambda}\gamma$

VALUE (units 10^{-3})	EVTS	DOCUMENT ID		TECN	COMMENT
2.1±2.0±2.2	1.1M	ABLIKIM	24CE	BES3	$J/\psi/\psi(2S) \to \Sigma\overline{\Sigma} \to \Lambda\overline{\Lambda}\gamma\gamma$

$\alpha + \overline{\alpha}$ in $\Sigma \to \Lambda\gamma$ and $\overline{\Sigma} \to \overline{\Lambda}\gamma$

VALUE (units 10^{-3})	EVTS	DOCUMENT ID		TECN	COMMENT
0.4±2.9±1.3	1.1M	ABLIKIM	24CE	BES3	$J/\psi/\psi(2S) \to \Sigma\overline{\Sigma} \to \Lambda\overline{\Lambda}\gamma\gamma$

Σ^0 REFERENCES

ABLIKIM	24CE	PRL 133 101902	M. Ablikim *et al.*	(BESIII Collab.)
WANG	97	PR D56 2544	M.H.L.S. Wang *et al.*	(BNL-E766 Collab.)
DEVLIN	86	PR D34 1626	T. Devlin, P.C. Petersen, A. Beretvas	(RUTG)
PETERSEN	86	PRL 57 949	P.C. Petersen *et al.*	(RUTG, WISC, MICH+)
DYDAK	77	NP B118 1	F. Dydak *et al.*	(CERN, DORT, HEIDH)
COLAS	75	NP B91 253	J. Colas *et al.*	(ORSAY)
ALFF	65	PR 137 B1105	C. Alff *et al.*	(COLU, RUTG, BNL) P
DOSCH	65	PL 14 239	H.C. Dosch *et al.*	(HEID)
SCHMIDT	65	PR 140 B1328	P. Schmidt	(COLU)
BURNSTEIN	64	PRL 13 66	R.A. Burnstein *et al.*	(UMD)
COURANT	63	PRL 10 409	H. Courant *et al.*	(CERN, UMD) P
FEINBERG	58	PR 109 1019	G. Feinberg	(BNL)

Σ^-

$I(J^P) = 1(\frac{1}{2}^+)$ Status: ****

We have omitted some results that have been superseded by later experiments. See our earlier editions.

Σ^- MASS

The fit uses Σ^+, Σ^0, Σ^-, and Λ mass and mass-difference measurements.

VALUE (MeV)	EVTS	DOCUMENT ID		TECN	COMMENT
1197.449±0.029 OUR FIT	Error includes scale factor of 1.1.				
1197.45 ±0.04 OUR AVERAGE	Error includes scale factor of 1.2.				
1197.417±0.040		GUREV	93	SPEC	Σ^-C atom, crystal diff.
1197.532±0.057		GALL	88	CNTR	Σ^-Pb, Σ^-W atoms
1197.43 ±0.08	3000	SCHMIDT	65	HBC	See note with Λ mass
• • • We do not use the following data for averages, fits, limits, etc. • • •					
1197.24 ±0.15		[1] DUGAN	75	CNTR	Exotic atoms

[1] GALL 88 concludes that the DUGAN 75 mass needs to be reevaluated.

$m_{\Sigma^-} - m_{\Sigma^+}$

VALUE (MeV)	EVTS	DOCUMENT ID		TECN
8.08±0.08 OUR FIT	Error includes scale factor of 1.9.			
8.09±0.16 OUR AVERAGE				
7.91±0.23	86	BOHM	72	EMUL
8.25±0.25	2500	DOSCH	65	HBC
8.25±0.40	87	BARKAS	63	EMUL

$m_{\Sigma^-} - m_\Lambda$

VALUE (MeV)	EVTS	DOCUMENT ID		TECN	COMMENT
81.766±0.029 OUR FIT	Error includes scale factor of 1.1.				
81.69 ±0.07 OUR AVERAGE					
81.64 ±0.09	2279	HEPP	68	HBC	
81.80 ±0.13	85	SCHMIDT	65	HBC	See note with Λ mass
81.70 ±0.19		BURNSTEIN	64	HBC	

Σ^- MEAN LIFE

Measurements with an error $\geq 0.2 \times 10^{-10}$ s have been omitted.

VALUE (10^{-10} s)	EVTS	DOCUMENT ID		TECN	COMMENT
1.479±0.011 OUR AVERAGE	Error includes scale factor of 1.3.				See the ideogram below.
1.480±0.014	16k	MARRAFFINO	80	HBC	K^-p 0.42–0.5 GeV/c
1.49 ±0.03	8437	CONFORTO	76	HBC	K^-p 1–1.4 GeV/c
1.463±0.039	2400	ROBERTSON	72	HBC	K^-p 0.25 GeV/c
1.42 ±0.05	1383	BAKKER	71	DBC	$K^-N \to \Sigma^-\pi\pi$
$1.41^{+0.09}_{-0.08}$		TOVEE	71	EMUL	
1.485±0.022	100k	EISELE	70	HBC	K^-p at rest
1.472±0.016	10k	BARLOUTAUD	69	HBC	K^-p 0.4–1.2 GeV/c
1.38 ±0.07	506	WHITESIDE	68	HBC	K^-p at rest
1.666±0.075	3267	[1] CHANG	66	HBC	K^-p at rest
1.58 ±0.06	1208	HUMPHREY	62	HBC	K^-p at rest

[1] We have increased the CHANG 66 error of 0.026; see our 1970 edition, Reviews of Modern Physics **42** 87 (1970).

Int. J. Mod. Phys. A 2026.41. Downloaded from www.worldscientific.com
by UNIVERSITY OF CALIFORNIA @ BERKELEY on 09/16/26. Re-use and distribution is strictly not permitted, except for Open Access articles.

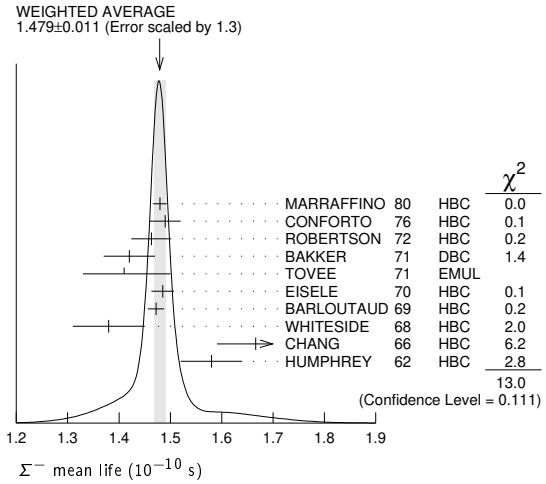

Σ^- MAGNETIC MOMENT

See the "Quark Model" review. Measurements with an error $\geq 0.3\ \mu_N$ have been omitted.

VALUE (μ_N)	EVTS	DOCUMENT ID		TECN	COMMENT
−1.160±0.025 OUR AVERAGE		Error includes scale factor of 1.7. See the ideogram below.			
−1.105±0.029±0.010		HERTZOG	88	CNTR	Σ^-Pb, Σ^-W atoms
−1.166±0.014±0.010	671k	ZAPALAC	86	SPEC	$ne^-\nu$, $n\pi^-$ decays
−1.23 ±0.03 ±0.03		WAH	85	CNTR	pCu → Σ^-X
• • • We do not use the following data for averages, fits, limits, etc. • • •					
−0.89 ±0.14	516k	DECK	83	SPEC	pBe → Σ^-X

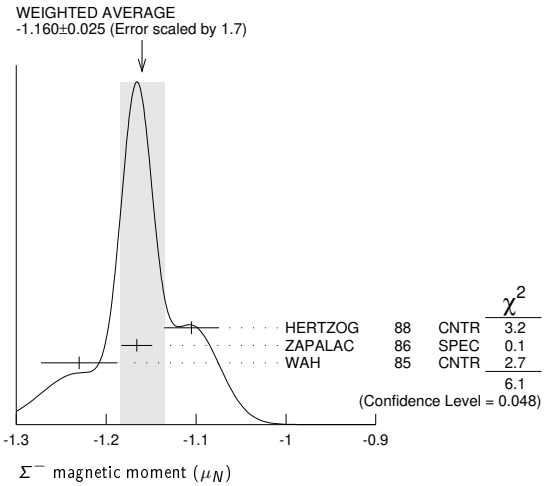

Σ^- CHARGE RADIUS

VALUE (fm)	DOCUMENT ID		TECN	COMMENT
0.780±0.080±0.060	[1] ESCHRICH	01	SELX	$\Sigma^-e \to \Sigma^-e$

[1] ESCHRICH 01 actually gives $\langle r^2 \rangle = (0.61 \pm 0.12 \pm 0.09)$ fm^2.

Σ^- DECAY MODES

	Mode		Fraction (Γ_i/Γ)	Confidence level
Γ_1	$n\pi^-$		(99.848±0.005) %	
Γ_2	$n\pi^-\gamma$	[a]	(4.6 ±0.6) × 10^{-4}	
Γ_3	$ne^-\overline{\nu}_e$		(1.017±0.034) × 10^{-3}	
Γ_4	$n\mu^-\overline{\nu}_\mu$		(4.5 ±0.4) × 10^{-4}	
Γ_5	$\Lambda e^-\overline{\nu}_e$		(5.73 ±0.27) × 10^{-5}	
Γ_6	Σ^+X		< 1.2 × 10^{-4}	90%
	Lepton number (L) violating modes			
Γ_7	pe^-e^-	L	< 6.7 × 10^{-5}	90%

[a] See the Listings below for the pion momentum range used in this measurement.

CONSTRAINED FIT INFORMATION

An overall fit to 3 branching ratios uses 16 measurements and one constraint to determine 4 parameters. The overall fit has a χ^2 = 8.7 for 13 degrees of freedom.

The following *off-diagonal* array elements are the correlation coefficients $\langle \delta x_i \delta x_j \rangle / (\delta x_i \cdot \delta x_j)$, in percent, from the fit to the branching fractions, $x_i \equiv \Gamma_i/\Gamma_{total}$. The fit constrains the x_i whose labels appear in this array to sum to one.

	x_1	x_3	x_4
x_3	−64		
x_4	−77	0	
x_5	−5	0	0

Σ^- BRANCHING RATIOS

$\Gamma(n\pi^-\gamma)/\Gamma(n\pi^-)$ — Γ_2/Γ_1

The π^+ momentum cuts differ, so we do not average the results but simply use the latest value for the Summary Table.

VALUE (units 10^{-3})	EVTS	DOCUMENT ID		TECN	COMMENT
0.46±0.06	292	EBENHOH	73	HBC	π^+ < 150 MeV/c
• • • We do not use the following data for averages, fits, limits, etc. • • •					
0.10±0.02	23	ANG	69B	HBC	π^- < 110 MeV/c
∼ 1.1		BAZIN	65B	HBC	π^- < 166 MeV/c

$\Gamma(ne^-\overline{\nu}_e)/\Gamma(n\pi^-)$ — Γ_3/Γ_1

Measurements with an error $\geq 0.2 \times 10^{-3}$ have been omitted.

VALUE (units 10^{-3})	EVTS	DOCUMENT ID		TECN	COMMENT
1.019±0.035 OUR FIT					
$1.019^{+0.031}_{-0.040}$ OUR AVERAGE					
0.96 ±0.05	2847	BOURQUIN	83C	SPEC	SPS hyperon beam
$1.09\ ^{+0.06}_{-0.08}$	601	[1] EBENHOH	74	HBC	K^-p at rest
$1.05\ ^{+0.07}_{-0.13}$	455	[1] SECHI-ZORN	73	HBC	K^-p at rest
0.97 ±0.15	57	COLE	71	HBC	K^-p at rest
1.11 ±0.09	180	BIERMAN	68	HBC	

[1] An additional negative systematic error is included for internal radiative corrections and latest form factors; see BOURQUIN 83C.

$\Gamma(n\mu^-\overline{\nu}_\mu)/\Gamma(n\pi^-)$ — Γ_4/Γ_1

VALUE (units 10^{-3})	EVTS	DOCUMENT ID		TECN	COMMENT
0.45±0.04 OUR FIT					
0.45±0.04 OUR AVERAGE					
0.38±0.11	13	COLE	71	HBC	K^-p at rest
0.43±0.06	72	ANG	69	HBC	K^-p at rest
0.43±0.09	56	BAGGETT	69	HBC	K^-p at rest
0.56±0.20	11	BAZIN	65B	HBC	K^-p at rest
0.66±0.15	22	COURANT	64	HBC	

$\Gamma(\Lambda e^-\overline{\nu}_e)/\Gamma(n\pi^-)$ — Γ_5/Γ_1

VALUE (units 10^{-4})	EVTS	DOCUMENT ID		TECN	COMMENT
0.574±0.027 OUR FIT					
0.574±0.027 OUR AVERAGE					
0.561±0.031	1620	[1] BOURQUIN	82	SPEC	SPS hyperon beam
0.63 ±0.11	114	THOMPSON	80	ASPK	Hyperon beam
0.52 ±0.09	31	BALTAY	69	HBC	K^-p at rest
0.69 ±0.12	31	EISELE	69	HBC	K^-p at rest
0.64 ±0.12	35	BARASH	67	HBC	K^-p at rest
0.75 ±0.28	11	COURANT	64	HBC	K^-p at rest

[1] The value is from BOURQUIN 83B, and includes radiation corrections and new acceptance.

$\Gamma(\Sigma^+X)/\Gamma_{total}$ — Γ_6/Γ

Here mode X can be any particle combination.

VALUE	CL%	DOCUMENT ID		TECN	COMMENT
<1.2 × 10^{-4}	90	ABLIKIM	21F	BES	1,311 M J/ψ decays

Lepton number (L) violating modes

$\Gamma(pe^-e^-)/\Gamma_{total}$ — Γ_7/Γ

This decay violates lepton number conservation with $\Delta Q = \Delta L = 2$.

VALUE	CL%	DOCUMENT ID		TECN	COMMENT
<6.7 × 10^{-5}	90	ABLIKIM	21F	BES	1,311 M J/ψ decays

Σ^- DECAY PARAMETERS

See the "Note on Baryon Decay Parameters" in the neutron Listings. Older, outdated results have been omitted.

α_- FOR $\Sigma^- \to n\pi^-$

VALUE	EVTS	DOCUMENT ID		TECN	COMMENT
−0.068±0.008 OUR AVERAGE					
−0.062±0.024	28k	HANSL	78	HBC	$K^-p \to \Sigma^-\pi^+$

Int. J. Mod. Phys. A 2026.41. Downloaded from www.worldscientific.com
UNIVERSITY OF CALIFORNIA @ BERKELEY on 09/16/26. Re-use and distribution is strictly not permitted, except for Open Access articles.

-0.067 ± 0.011	60k	BOGERT	70	HBC	$K^- p$ 0.4 GeV/c
-0.071 ± 0.012	51k	BANGERTER	69	HBC	$K^- p$ 0.4 GeV/c

ϕ ANGLE FOR $\Sigma^- \to n\pi^-$ ($\tan\phi = \beta / \gamma$)

VALUE (°)	EVTS	DOCUMENT ID		TECN	COMMENT
10±15 OUR AVERAGE					
$+5 \pm 23$	1092	[1] BERLEY	70B	HBC	n rescattering
14 ± 19	1385	BANGERTER	69B	HBC	$K^- p$ 0.4 GeV/c

[1] BERLEY 70B changed from -5 to $+5°$ to agree with our sign convention.

g_A/g_V FOR $\Sigma^- \to n e^- \overline{\nu}_e$

Measurements with fewer than 500 events have been omitted. Where necessary, signs have been changed to agree with our conventions, which are given in the "Note on Baryon Decay Parameters" in the neutron Listings. What is actually listed is $|g_1/f_1 - 0.237 g_2/f_1|$. This reduces to $g_A/g_V \equiv g_1(0)/f_1(0)$ on making the usual assumption that $g_2 = 0$. See also the note on HSUEH 88.

VALUE	EVTS	DOCUMENT ID		TECN	COMMENT
0.340±0.017 OUR AVERAGE					
$+0.327 \pm 0.007 \pm 0.019$	50k	[1] HSUEH	88	SPEC	Σ^- 250 GeV
$+0.34 \pm 0.05$	4456	[2] BOURQUIN	83C	SPEC	SPS hyperon beam
0.385 ± 0.037	3507	[3] TANENBAUM	74	ASPK	
• • • We do not use the following data for averages, fits, limits, etc. • • •					
0.29 ± 0.07	25k	HSUEH	85	SPEC	See HSUEH 88
$0.17 {}^{+0.07}_{-0.09}$	519	DECAMP	77	ELEC	Hyperon beam

[1] The sign is, *with our conventions*, unambiguously positive. The value assumes, as usual, that $g_2 = 0$. If g_2 is included in the fit, than (with our sign convention) $g_2 = -0.56 \pm 0.37$, with a corresponding reduction of g_A/g_V to $+0.20 \pm 0.08$.

[2] BOURQUIN 83C favors the positive sign by at least 2.6 standard deviations.

[3] TANENBAUM 74 gives 0.435 ± 0.035, assuming no q^2 dependence in g_A and g_V. The listed result allows q^2 dependence, and is taken from HSUEH 88.

$f_2(0)/f_1(0)$ FOR $\Sigma^- \to n e^- \overline{\nu}_e$

The signs have been changed to be in accord with our conventions, given in the "Note on Baryon Decay Parameters" in the neutron Listings.

VALUE	EVTS	DOCUMENT ID		TECN	COMMENT
0.97±0.14 OUR AVERAGE					
$+0.96 \pm 0.07 \pm 0.13$	50k	HSUEH	88	SPEC	Σ^- 250 GeV
$+1.02 \pm 0.34$	4456	BOURQUIN	83C	SPEC	SPS hyperon beam

TRIPLE CORRELATION COEFFICIENT D for $\Sigma^- \to n e^- \overline{\nu}_e$

The coefficient D of the term $D\ \mathbf{P}\cdot(\hat{\mathbf{p}}_e \times \hat{\mathbf{p}}_\nu)$ in the $\Sigma^- \to n e^- \overline{\nu}$ decay angular distribution. A nonzero value would indicate a violation of time-reversal invariance.

VALUE	EVTS	DOCUMENT ID		TECN	COMMENT
0.11±0.10	50k	HSUEH	88	SPEC	Σ^- 250 GeV

g_V/g_A FOR $\Sigma^- \to \Lambda e^- \overline{\nu}_e$

For the sign convention, see the "Note on Baryon Decay Parameters" in the neutron Listings. The value is predicted to be zero by conserved vector current theory. The values averaged assume CVC-SU(3) weak magnetism term.

VALUE	EVTS	DOCUMENT ID		TECN	COMMENT
0.01 ±0.10 OUR AVERAGE Error includes scale factor of 1.5. See the ideogram below.					
-0.034 ± 0.080	1620	[1] BOURQUIN	82	SPEC	SPS hyperon beam
-0.29 ± 0.29	114	THOMPSON	80	ASPK	BNL hyperon beam
-0.17 ± 0.35	55	TANENBAUM	75B	SPEC	BNL hyperon beam
$+0.45 \pm 0.20$	186	[1,2] FRANZINI	72	HBC	

[1] The sign has been changed to agree with our convention.

[2] The FRANZINI 72 value includes the events of earlier papers.

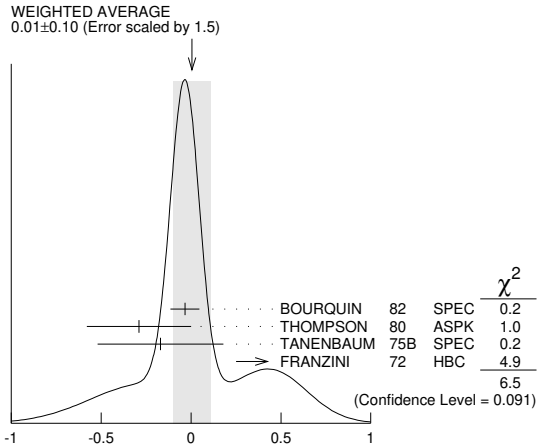

g_V/g_A for $\Sigma^- \to \Lambda e^- \overline{\nu}_e$

g_{WM}/g_A FOR $\Sigma^- \to \Lambda e^- \overline{\nu}_e$

The values quoted assume the CVC prediction $g_V = 0$.

VALUE	EVTS	DOCUMENT ID		TECN	COMMENT
2.4 ±1.7 OUR AVERAGE					
1.75 ± 3.5	114	THOMPSON	80	ASPK	BNL hyperon beam
3.5 ± 4.5	55	TANENBAUM	75B	SPEC	BNL hyperon beam
2.4 ± 2.1	186	FRANZINI	72	HBC	

Σ^- REFERENCES

We have omitted some papers that have been superseded by later experiments. See our earlier editions.

ABLIKIM	21F	PR D103 052011	M. Ablikim *et al.* (BESIII Collab.)
ESCHRICH	01	PL B522 233	I. Eschrich *et al.* (FNAL SELEX Collab.)
GUREV	93	JETPL 57 400 Translated from ZETFP 57 389.	M.P. Gurev *et al.* (PNPI)
GALL	88	PRL 60 186	K.P. Gall *et al.* (BOST, MIT, WILL, CIT+)
HERTZOG	88	PR D37 1142	D.W. Hertzog *et al.* (WILL, BOST, MIT+)
HSUEH	88	PR D38 2056	S.Y. Hsueh *et al.* (CHIC, ELMT, FNAL+)
ZAPALAC	86	PRL 57 1526	G. Zapalac *et al.* (EFI, ELMT, FNAL+)
HSUEH	85	PRL 54 2399	S.Y. Hsueh *et al.* (CHIC, ELMT, FNAL+)
WAH	85	PRL 55 2551	Y.W. Wah *et al.* (FNAL, IOWA, ISU)
BOURQUIN	83B	ZPHY C21 27	M.H. Bourquin *et al.* (BRIS, GEVA, HEIDP+)
BOURQUIN	83C	ZPHY C21 17	M.H. Bourquin *et al.* (BRIS, GEVA, HEIDP+)
DECK	83	PR D28 1	L. Deck *et al.* (RUTG, WISC, MICH, MINN)
BOURQUIN	82	ZPHY C12 307	M.H. Bourquin *et al.* (BRIS, GEVA, HEIDP+)
MARRAFFINO	80	PR D21 2501	J. Marraffino *et al.* (VAND, MPIM)
THOMPSON	80	PR D21 25	J.A. Thompson *et al.* (PITT, BNL)
HANSL	78	NP B132 45	T. Hansl *et al.* (MPIM, VAND)
DECAMP	77	PL 66B 295	D. Decamp *et al.* (LALO, EPOL)
CONFORTO	76	NP B105 189	B. Conforto *et al.* (RHEL, LOIC)
DUGAN	75	NP A254 396	G. Dugan *et al.* (COLU, YALE)
TANENBAUM	75B	PR D12 1871	W. Tanenbaum *et al.* (YALE, FNAL, BNL)
EBENHOH	74	ZPHY 266 367	H. Ebenhoh *et al.* (HEIDT)
TANENBAUM	74	PRL 33 175	W. Tanenbaum *et al.* (YALE, FNAL, BNL)
EBENHOH	73	ZPHY 264 413	W. Ebenhoh *et al.* (HEIDT)
SECHI-ZORN	73	PR D8 12	B. Sechi-Zorn, G.A. Snow (UMD)
BOHM	72	NP B48 1	G. Bohm *et al.* (BERL, KIDR, BRUX, IASD+)
FRANZINI	72	PR D6 2417	P. Franzini *et al.* (COLU, HEID, UMD+)
ROBERTSON	72	Thesis UMI 78-00877	R.M. Robertson (IIT)
BAKKER	71	LNC 1 37	A.M. Bakker *et al.* (SABRE Collab.)
COLE	71	PR D4 631	J. Cole *et al.* (STON, COLU)
Also		Thesis Nevis 175	H. Norton (COLU)
TOVEE	71	NP B33 493	D.N. Tovee *et al.* (LOUC, KIDR, BERL+)
BERLEY	70B	PR D1 2015	D. Berley *et al.* (BNL, MASA, YALE)
BOGERT	70	PR D2 6	D.V. Bogert *et al.* (BNL, MASA, YALE)
EISELE	70	ZPHY 238 372	F. Eisele *et al.* (HEID)
PDG	70	RMP 42 87	A. Barbaro-Galtieri *et al.* (LRL, BRAN+)
ANG	69	ZPHY 223 103	G. Ang *et al.* (HEID)
ANG	69B	ZPHY 228 151	G. Ang *et al.* (HEID)
BAGGETT	69	PRL 23 249	N.V. Baggett, B. Kehoe, G.A. Snow (UMD)
BALTAY	69	PRL 22 615	C. Baltay *et al.* (COLU, STON)
BANGERTER	69	Thesis UCRL 19244	R.O. Bangerter (LRL)
BANGERTER	69B	PR 187 1821	R.O. Bangerter *et al.* (LRL)
BARLOUTAUD	69	NP B14 153	R. Barloutaud *et al.* (SACL, CERN, HEID)
EISELE	69	ZPHY 221 1	F. Eisele *et al.* (HEID)
BIERMAN	68	PRL 20 1459	E. Bierman *et al.* (PRIN)
HEPP	68	ZPHY 214 71	V. Hepp, H. Schleich (HEID)
WHITESIDE	68	NC 54A 537	H. Whiteside, J. Gollub (OBER)
BARASH	67	PRL 19 181	N. Barash *et al.* (UMD)
CHANG	66	PR 151 1081	C.Y. Chang (COLU)
BAZIN	65B	PR 140 B1358	M. Bazin *et al.* (PRIN, RUTG, COLU)
DOSCH	65	PL 14 239	H.C. Dosch *et al.* (HEID)
Also		PR 151 1081	C.Y. Chang (COLU)
SCHMIDT	65	PR 140 B1328	P. Schmidt (COLU)
BURNSTEIN	64	PRL 13 66	R.A. Burnstein *et al.* (UMD)
COURANT	64	PR 136 B1791	H. Courant *et al.* (CERN, HEID, UMD+)
BARKAS	63	PRL 11 26	W.H. Barkas, J.N. Dyer, H.H. Heckman (LRL)
HUMPHREY	62	PR 127 1305	W.E. Humphrey, R.R. Ross (LRL)

$\Sigma(1385)\ 3/2^+$

$I(J^P) = 1(\frac{3}{2}^+)$ Status: ****

Discovered by ALSTON 60. Early measurements of the mass and width for combined charge states have been omitted. They may be found in our 1984 edition Reviews of Modern Physics **56** S1 (1984).

We average only the most significant determinations. We do not average results from inclusive experiments with large backgrounds or results which are not accompanied by some discussion of experimental resolution. Nevertheless systematic differences between experiments remain. (See the ideograms in the Listings below.) These differences could arise from interference effects that change with production mechanism and/or beam momentum. They can also be accounted for in part by differences in the parametrizations employed. (See BORENSTEIN 74 for a discussion on this point.) Thus BORENSTEIN 74 uses a Breit-Wigner with energy-independent width, since a P-wave was found to give unsatisfactory fits. CAMERON 78 uses the same form. On the other hand HOLMGREN 77 obtains a good fit to their $\Lambda\pi$ spectrum with a P-wave Breit-Wigner, but includes the partial width for the $\Sigma\pi$ decay mode in the parametrization. AGUILAR-BENITEZ 81D gives masses and widths for five different Breit-Wigner shapes. The results vary considerably. Only the best-fit S-wave results are given here.

$\Sigma(1385)$ POLE POSITIONS

$\Sigma(1385)^+$ REAL PART

VALUE	DOCUMENT ID	COMMENT
1379 ± 1	LICHTENBERG74	Extrapolates HABIBI 73

See key on page 1227

Int. J. Mod. Phys. A 2026.41. Downloaded from www.worldscientific.com
by UNIVERSITY OF CALIFORNIA @ BERKELEY on 09/16/26. Re-use and distribution is strictly not permitted, except for Open Access articles.

$\Sigma(1385)^+$ –IMAGINARY PART

VALUE	DOCUMENT ID	COMMENT
17.5±1.5	LICHTENBERG74	Extrapolates HABIBI 73

$\Sigma(1385)^-$ REAL PART

VALUE	DOCUMENT ID	COMMENT
1383±1	LICHTENBERG74	Extrapolates HABIBI 73

$\Sigma(1385)^-$ –IMAGINARY PART

VALUE	DOCUMENT ID	COMMENT
22.5±1.5	LICHTENBERG74	Extrapolates HABIBI 73

$\Sigma(1385)$ MASSES

$\Sigma(1385)^+$ MASS

VALUE (MeV)	EVTS	DOCUMENT ID		TECN	COMMENT
1382.83±0.34 OUR AVERAGE		Error includes scale factor of 1.9. See the ideogram below.			
1384.8 ±0.3 ±1.4		LEE	21A	BELL	$\Lambda_c^+ \to \eta\Sigma(1385)^+$
1383.2 ±0.9 $^{+0.1}_{-1.5}$		AGAKISHIEV	12	SPEC	$pp \to \Sigma(1385)^+ K^+ n$, 3.5 GeV
1384.1 ±0.7	1897	BAUBILLIER	84	HBC	$K^- p$ 8.25 GeV/c
1384.5 ±0.5	5256	AGUILAR-...	81D	HBC	$K^- p \to \Lambda\pi\pi$ 4.2 GeV/c
1383.0 ±0.4	9361	AGUILAR-...	81D	HBC	$K^- p \to \Lambda 3\pi$ 4.2 GeV/c
1381.9 ±0.3	6900	CAMERON	78	HBC	$K^- p$ 0.96–1.36 GeV/c
1381 ±1	6846	BORENSTEIN	74	HBC	$K^- p$ 2.18 GeV/c
1383.5 ±0.85	2300	HABIBI	73	HBC	$K^- p \to \Lambda\pi\pi$
1382 ±2	400	AGUILAR-...	72B	HBC	$K^- p \to \Lambda\pi$'s
1384.4 ±1.0	1260	SIEGEL	67	HBC	$K^- p$ 2.1 GeV/c
1382 ±1	750	ARMENTEROS	65B	HBC	$K^- p$ 0.9–1.2 GeV/c
1381.0 ±1.6	859	HUWE	64	HBC	$K^- p$ 1.22 GeV/c
• • • We do not use the following data for averages, fits, limits, etc. • • •					
1385.1 ±1.2	600	BAKER	80	HYBR	$\pi^+ p$ 7 GeV/c
1383.2 ±1.0	750	BAKER	80	HYBR	$K^- p$ 7 GeV/c
1381 ±2	7k	[1] BAUBILLIER	79B	HBC	$K^- p$ 8.25 GeV/c
1391 ±2	2k	CAUTIS	79	HYBR	$\pi^+ p/K^- p$ 11.5 GeV
1390 ±2	100	[1] SUGAHARA	79B	HBC	$\pi^- p$ 6 GeV/c
1385 ±3	22k	[1,2] BARREIRO	77B	HBC	$K^- p$ 4.2 GeV/c
1385 ±1	2594	HOLMGREN	77	HBC	See AGUILAR-BENITEZ 81D
1380 ±2		[1] BARDADIN-...	75	HBC	$K^- p$ 14.3 GeV/c
1382 ±1	3740	[3] BERTHON	74	HBC	$K^- p$ 1263–1843 MeV/c
1390 ±6	46	AGUILAR-...	70B	HBC	$K^- p \to \Sigma\pi$'s 4 GeV/c
1383 ±8	62	[4] BIRMINGHAM	66	HBC	$K^- p$ 3.5 GeV/c
1378 ±5	135	LONDON	66	HBC	$K^- p$ 2.24 GeV/c
1384.3 ±1.9	250	[4] SMITH	65	HBC	$K^- p$ 1.8 GeV/c
1382.6 ±2.1	250	[4] SMITH	65	HBC	$K^- p$ 1.95 GeV/c
1375.0 ±3.9	170	COOPER	64	HBC	$K^- p$ 1.45 GeV/c
1376.0 ±3.9	154	[4] ELY	61	HLBC	$K^- p$ 1.11 GeV/c

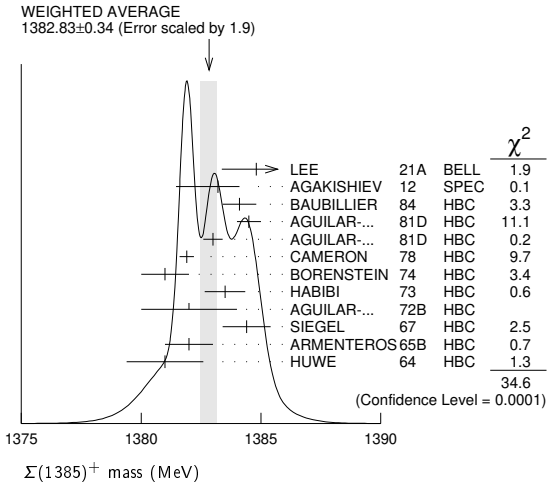

$\Sigma(1385)^0$ MASS

VALUE (MeV)	EVTS	DOCUMENT ID		TECN	COMMENT
1383.8±0.9 OUR AVERAGE		Error includes scale factor of 1.3. See the ideogram below.			
1388.2±1.9±3.3		ABLIKIM	25AF	BES3	$\psi(3686) \to \Lambda\overline{\Sigma}^0\pi^0 +$ c.c. (PWA)
1384.1±0.8	5722	AGUILAR-...	81D	HBC	$K^- p \to \Lambda 3\pi$ 4.2 GeV/c
1380 ±2	3100	[5] BORENSTEIN	74	HBC	$K^- p \to \Lambda 3\pi$ 2.18 GeV/c
1385.1±2.5	240	[4] THOMAS	73	HBC	$\pi^- p \to \Lambda\pi^0 K^0$
• • • We do not use the following data for averages, fits, limits, etc. • • •					
1389 ±3	500	[6] BAUBILLIER	79B	HBC	$K^- p$ 8.25 GeV/c

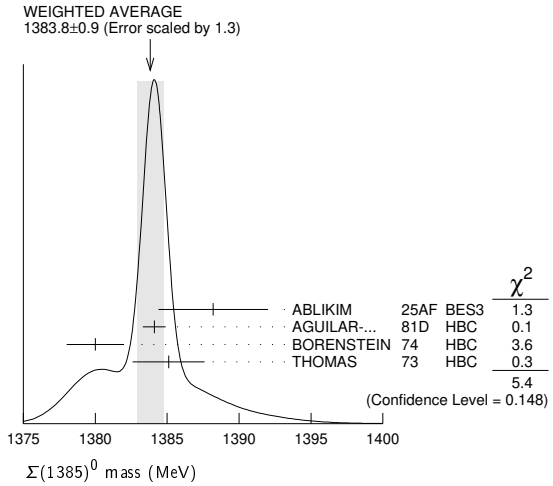

$\Sigma(1385)^-$ MASS

VALUE (MeV)	EVTS	DOCUMENT ID		TECN	COMMENT
1387.2±0.5 OUR AVERAGE		Error includes scale factor of 2.2. See the ideogram below.			
1388.3±1.7	620	AGUILAR-...	81D	HBC	$K^- p \to \Lambda\pi\pi$ 4.2 GeV/c
1384.9±0.8	3346	AGUILAR-...	81D	HBC	$K^- p \to \Lambda 3\pi$ 4.2 GeV/c
1387.6±0.3	9720	CAMERON	78	HBC	$K^- p$ 0.96–1.36 GeV/c
1383 ±2	2303	BORENSTEIN	74	HBC	$K^- p$ 2.18 GeV/c
1390.7±1.2	1900	HABIBI	73	HBC	$K^- p \to \Lambda\pi\pi$
1387.1±1.9	630	[4] THOMAS	73	HBC	$\pi^- p \to \Lambda\pi^- K^+$
1390.7±2.0	370	SIEGEL	67	HBC	$K^- p$ 2.1 GeV/c
1384 ±1	1380	ARMENTEROS	65B	HBC	$K^- p$ 0.9–1.2 GeV/c
1385.3±1.9	1086	[4] HUWE	64	HBC	$K^- p$ 1.15–1.30 GeV/c
• • • We do not use the following data for averages, fits, limits, etc. • • •					
1383 ±1	4.5k	[1] BAUBILLIER	79B	HBC	$K^- p$ 8.25 GeV/c
1380 ±6	150	[1] SUGAHARA	79B	HBC	$\pi^- p$ 6 GeV/c
1387 ±3	12k	[1,2] BARREIRO	77B	HBC	$K^- p$ 4.2 GeV/c
1391 ±3	193	HOLMGREN	77	HBC	See AGUILAR-BENITEZ 81D
1383 ±2		[1] BARDADIN-...	75	HBC	$K^- p$ 14.3 GeV/c
1389 ±1	3060	[3] BERTHON	74	HBC	$K^- p$ 1263–1843 MeV/c
1389 ±9	15	LONDON	66	HBC	$K^- p$ 2.24 GeV/c
1391.5±2.6	120	[4] SMITH	65	HBC	$K^- p$ 1.8 GeV/c
1399.8±2.2	58	[4] SMITH	65	HBC	$K^- p$ 1.95 GeV/c
1392.0±6.2	200	COOPER	64	HBC	$K^- p$ 1.45 GeV/c
1382 ±3	93	DAHL	61	DBC	$K^- d$ 0.45 GeV/c
1376.0±4.4	224	[4] ELY	61	HLBC	$K^- p$ 1.11 GeV/c

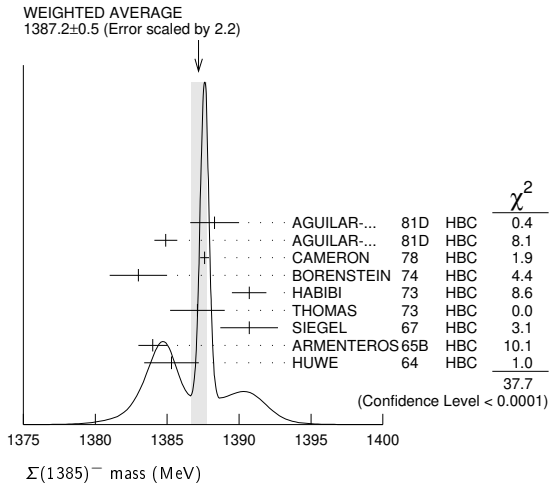

$m_{\Sigma(1385)^-} - m_{\Sigma(1385)^+}$

VALUE (MeV)	CL%	DOCUMENT ID		TECN	COMMENT
• • • We do not use the following data for averages, fits, limits, etc. • • •					
−2 to +6	95	[7] BORENSTEIN	74	HBC	$K^- p$ 2.18 GeV/c
7.2±1.4		[7] HABIBI	73	HBC	$K^- p \to \Lambda\pi\pi$
6.3±2.0		[7] SIEGEL	67	HBC	$K^- p$ 2.1 GeV/c
11 ±9		[7] LONDON	66	HBC	$K^- p$ 2.24 GeV/c
9 ±6		LONDON	66	HBC	$\Lambda 3\pi$ events
2.0±1.5		[7] ARMENTEROS	65B	HBC	$K^- p$ 0.9–1.2 GeV/c

7.2±2.1	[7] SMITH	65	HBC	$K^- p$ 1.8 GeV/c
17.2±2.0	[7] SMITH	65	HBC	$K^- p$ 1.95 GeV/c
17 ±7	[7] COOPER	64	HBC	$K^- p$ 1.45 GeV/c
4.3±2.2	[7] HUWE	64	HBC	$K^- p$ 1.22 GeV/c
0.0±4.2	[7] ELY	61	HLBC	$K^- p$ 1.11 GeV/c

$m_{\Sigma(1385)^0} - m_{\Sigma(1385)^+}$

VALUE (MeV)	CL%	DOCUMENT ID		TECN	COMMENT
• • • We do not use the following data for averages, fits, limits, etc. • • •					
−4 to +4	95	[7] BORENSTEIN	74	HBC	$K^- p$ 2.18 GeV/c

$m_{\Sigma(1385)^-} - m_{\Sigma(1385)^0}$

VALUE (MeV)	DOCUMENT ID		TECN	COMMENT
• • • We do not use the following data for averages, fits, limits, etc. • • •				
2.0±2.4	[7] THOMAS	73	HBC	$\pi^- p \to \Lambda \pi^- K^+$

$\Sigma(1385)$ WIDTHS

$\Sigma(1385)^+$ WIDTH

VALUE (MeV)	EVTS	DOCUMENT ID		TECN	COMMENT
36.2± 0.7 OUR AVERAGE					
38.1± 1.5±2.1		LEE	21A	BELL	$\Lambda_c^+ \to \eta \Sigma(1385)^+$
40.2± 2.1 $^{+1.2}_{-2.8}$		AGAKISHIEV	12	SPEC	$pp \to \Sigma(1385)^+ K^+ n$, 3.5 GeV
37.2± 2.0	1897	BAUBILLIER	84	HBC	$K^- p$ 8.25 GeV/c
35.1± 1.7	5256	AGUILAR-...	81D	HBC	$K^- p \to \Lambda \pi \pi$ 4.2 GeV/c
37.5± 2.0	9361	AGUILAR-...	81D	HBC	$K^- p \to \Lambda 3\pi$ 4.2 GeV/c
35.5± 1.9	6900	CAMERON	78	HBC	$K^- p$ 0.96–1.36 GeV/c
34.0± 1.6	6846	[8] BORENSTEIN	74	HBC	$K^- p$ 2.18 GeV/c
38.3± 3.2	2300	[9] HABIBI	73	HBC	$K^- p \to \Lambda \pi \pi$
32.5± 6.0	400	AGUILAR-...	72B	HBC	$K^- p \to \Lambda \pi$'s
36 ± 4	1260	[9] SIEGEL	67	HBC	$K^- p$ 2.1 GeV/c
32.0± 4.7	750	[9] ARMENTEROS	65B	HBC	$K^- p$ 0.95–1.20 GeV/c
46.5± 6.4	859	[9] HUWE	64	HBC	$K^- p$ 1.15–1.30 GeV/c
• • • We do not use the following data for averages, fits, limits, etc. • • •					
40 ± 3	600	BAKER	80	HYBR	$\pi^+ p$ 7 GeV/c
37 ± 2	750	BAKER	80	HYBR	$K^- p$ 7 GeV/c
37 ± 2	7k	[1] BAUBILLIER	79B	HBC	$K^- p$ 8.25 GeV/c
30 ± 4	2k	CAUTIS	79	HYBR	$\pi^+ p / K^- p$ 11.5 GeV
30 ± 6	100	[1] SUGAHARA	79B	HBC	$\pi^- p$ 6 GeV/c
43 ± 5	22k	[1,2] BARREIRO	77B	HBC	$K^- p$ 4.2 GeV/c
34 ± 2	2594	HOLMGREN	77	HBC	See AGUILAR-BENITEZ 81D
40.0± 3.2		[1] BARDADIN-...	75	HBC	$K^- p$ 14.3 GeV/c
48 ± 3	3740	[3] BERTHON	74	HBC	$K^- p$ 1263–1843 MeV/c
33 ±20	46	[9] AGUILAR-...	70B	HBC	$K^- p \to \Sigma \pi$'s 4 GeV/c
25 ±32	62	[9] BIRMINGHAM	66	HBC	$K^- p$ 3.5 GeV/c
30.3± 7.5	250	[9] SMITH	65	HBC	$K^- p$ 1.8 GeV/c
33.1± 8.3	250	[9] SMITH	65	HBC	$K^- p$ 1.95 GeV/c
51 ±16	170	[9] COOPER	64	HBC	$K^- p$ 1.45 GeV/c
48 ±16	154	[9] ELY	61	HLBC	$K^- p$ 1.11 GeV/c

$\Sigma(1385)^0$ WIDTH

VALUE (MeV)	EVTS	DOCUMENT ID		TECN	COMMENT
44 ± 8 OUR AVERAGE	Error includes scale factor of 2.0. See the ideogram below.				
60.5± 3.6±6.3		ABLIKIM	25AF	BES3	$\psi(3686) \to \Lambda \overline{\Sigma}^0 \pi^0 +$ c.c. (PWA)
34.8± 5.6	5722	AGUILAR-...	81D	HBC	$K^- p \to \Lambda 3\pi$ 4.2 GeV/c
39.3±10.2	240	[9] THOMAS	73	HBC	$\pi^- p \to \Lambda \pi^0 K^0$
• • • We do not use the following data for averages, fits, limits, etc. • • •					
53 ± 8	3100	[10] BORENSTEIN	74	HBC	$K^- p \to \Lambda 3\pi$ 2.18 GeV/c
30 ± 9	106	CURTIS	63	OSPK	$\pi^- p$ 1.5 GeV/c

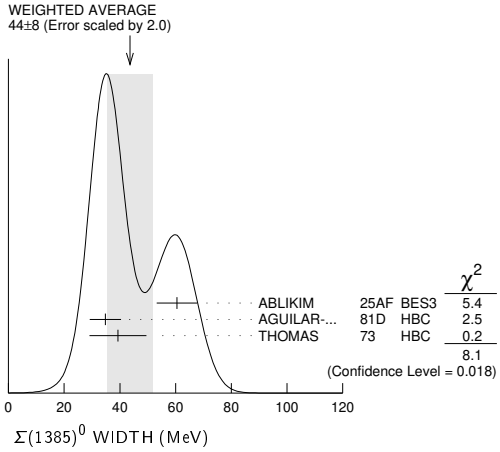

$\Sigma(1385)^-$ WIDTH

VALUE (MeV)	EVTS	DOCUMENT ID		TECN	COMMENT
39.4± 2.1 OUR AVERAGE	Error includes scale factor of 1.7. See the ideogram below.				
38.4±10.7	620	AGUILAR-...	81D	HBC	$K^- p \to \Lambda \pi \pi$ 4.2 GeV/c
34.6± 4.2	3346	AGUILAR-...	81D	HBC	$K^- p \to \Lambda 3\pi$ 4.2 GeV/c
39.2± 1.7	9720	CAMERON	78	HBC	$K^- p$ 0.96–1.36 GeV/c
35 ± 3	2303	[8] BORENSTEIN	74	HBC	$K^- p$ 2.18 GeV/c
51.9± 4.8	1900	[9] HABIBI	73	HBC	$K^- p \to \Lambda \pi \pi$
48.2± 7.7	630	[9] THOMAS	73	HBC	$\pi^- p \to \Lambda \pi^- K^0$
31.0± 6.5	370	[9] SIEGEL	67	HBC	$K^- p$ 2.1 GeV/c
38.0± 4.1	1382	[9] ARMENTEROS	65B	HBC	$K^- p$ 0.95–1.20 GeV/c
62 ± 7	1086	HUWE	64	HBC	$K^- p$ 1.15–1.30 GeV/c
• • • We do not use the following data for averages, fits, limits, etc. • • •					
44 ± 4	4.5k	[1] BAUBILLIER	79B	HBC	$K^- p$ 8.25 GeV/c
58 ± 4	150	[1] SUGAHARA	79B	HBC	$\pi^- p$ 6 GeV/c
45 ± 5	12k	[1,2] BARREIRO	77B	HBC	$K^- p$ 4.2 GeV/c
35 ±10	193	HOLMGREN	77	HBC	See AGUILAR-BENITEZ 81D
47 ± 6		[1] BARDADIN-...	75	HBC	$K^- p$ 14.3 GeV/c
40 ± 3	3060	[3] BERTHON	74	HBC	$K^- p$ 1263–1843 MeV/c
29.2±10.6	120	[9] SMITH	65	HBC	$K^- p$ 1.80 GeV/c
17.1± 8.9	58	[9] SMITH	65	HBC	$K^- p$ 1.95 GeV/c
88 ±24	200	[9] COOPER	64	HBC	$K^- p$ 1.45 GeV/c
40		DAHL	61	DBC	$K^- d$ 0.45 GeV/c
66 ±18	224	[9] ELY	61	HLBC	$K^- p$ 1.11 GeV/c

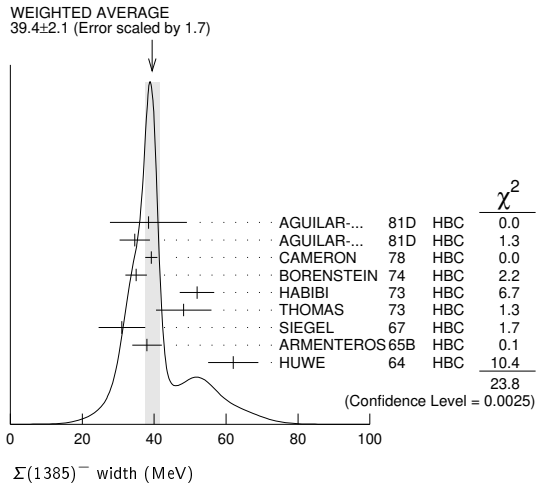

$\Sigma(1385)$ DECAY MODES

	Mode	Fraction (Γ_i/Γ)	Confidence level
Γ_1	$\Lambda \pi$	(87.0 ±1.5) %	
Γ_2	$\Sigma \pi$	(11.7 ±1.5) %	
Γ_3	$\Lambda \gamma$	($1.25^{+0.13}_{-0.12}$) %	
Γ_4	$\Sigma^+ \gamma$	(7.0 ±1.7) $\times 10^{-3}$	
Γ_5	$\Sigma^- \gamma$	< 2.4 $\times 10^{-4}$	90%
Γ_6	$N \overline{K}$		

$\Sigma(1385)$ BRANCHING RATIOS

$\Gamma(\Sigma\pi)/\Gamma(\Lambda\pi)$ — Γ_2/Γ_1

VALUE	DOCUMENT ID		TECN	CHG	COMMENT
0.135±0.011 OUR AVERAGE					
0.20 ±0.06	DIONISI	78B	HBC	±	$K^- p \to Y^* K \overline{K}$
0.16 ±0.03	BERTHON	74	HBC	+	$K^- p$ 1.26–1.84 GeV/c
0.11 ±0.02	BERTHON	74	HBC	−	$K^- p$ 1.26–1.84 GeV/c
0.21 ±0.05	BORENSTEIN	74	HBC	+	$K^- p \to \Lambda \pi^+ \pi^-$, $\Sigma^0 \pi^+ \pi^-$
0.18 ±0.04	MAST	73	MPWA	±	$K^- p \to \Lambda \pi^+ \pi^-$, $\Sigma^0 \pi^+ \pi^-$
0.10 ±0.05	THOMAS	73	HBC	−	$\pi^- p \to \Lambda K \pi$, $\Sigma K \pi$
0.16 ±0.07	AGUILAR-...	72B	HBC	+	$K^- p$ 3.9, 4.6 GeV/c
0.13 ±0.04	COLLEY	71B	DBC	−0	$K^- N$ 1.5 GeV/c
0.13 ±0.04	PAN	69	HBC	+	$\pi^+ p \to \Lambda K \pi$, $\Sigma K \pi$
0.08 ±0.06	LONDON	66	HBC	+	$K^- p$ 2.24 GeV/c
0.163±0.041	ARMENTEROS	65B	HBC	±	$K^- p$ 0.95–1.20 GeV/c
0.09 ±0.04	HUWE	64	HBC	±	$K^- p$ 1.2–1.7 GeV
• • • We do not use the following data for averages, fits, limits, etc. • • •					
<0.04	ALSTON	62	HBC	±0	$K^- p$ 1.15 GeV/c
0.04 ±0.04	BASTIEN	61	HBC	±	

Int. J. Mod. Phys. A 2026.41. Downloaded from www.worldscientific.com
UNIVERSITY OF CALIFORNIA @ BERKELEY on 09/16/26. Re-use and distribution is strictly not permitted, except for Open Access articles.

Int. J. Mod. Phys. A 2026.41. Downloaded from www.worldscientific.com by UNIVERSITY OF CALIFORNIA @ BERKELEY on 09/16/26. Re-use and distribution is strictly not permitted, except for Open Access articles.

$\Gamma(\Lambda\gamma)/\Gamma(\Lambda\pi)$ — Γ_3/Γ_1

This ratio is of course for $\Sigma(1385)^0 \to \Lambda\gamma$ and $\Lambda\pi^0$.

VALUE (units 10^{-2})	EVTS	DOCUMENT ID		TECN	COMMENT
$1.43^{+0.15}_{-0.13}$ OUR AVERAGE					
$1.42\pm0.12^{+0.11}_{-0.07}$	624 ± 25	KELLER	11	CLAS	$\gamma p \to K^+\Lambda\gamma$, E_γ 1.6–3.8 GeV
$1.53\pm0.39^{+0.15}_{-0.24}$	61	TAYLOR	05	CLAS	$\gamma p \to K^+\Lambda\gamma$

$\Gamma(\Sigma^+\gamma)/\Gamma(\Sigma\pi)$ — Γ_4/Γ_2

This ratio is for $\Sigma(1385)^+ \to \Sigma^+\gamma$ over $\Sigma(1385)^+ \to \Sigma\pi$.

VALUE (%)	DOCUMENT ID		TECN	COMMENT
$5.98\pm1.11^{+0.27}_{-0.61}$	[11] KELLER	12	CLAS	$\gamma p \to K^0\Sigma(1385)^+$

$\Gamma(\Sigma^-\gamma)/\Gamma_{total}$ — Γ_5/Γ

VALUE	CL%	DOCUMENT ID		TECN	CHG	COMMENT
$<2.4\times10^{-4}$	90	[12] MOLCHANOV	04	SELX	–	Σ^- Pb $\to \Sigma(1385)^-$ Pb, 600 GeV
• • • We do not use the following data for averages, fits, limits, etc. • • •						
$<6.1\times10^{-4}$	90	[13] ARIK	77	SPEC	–	Σ^- Pb $\to \Sigma(1385)^-$ Pb, 23 GeV

$(\Gamma_i\Gamma_f)^{1/2}/\Gamma_{total}$ in $N\overline{K} \to \Sigma(1385) \to \Lambda\pi$ — $(\Gamma_6\Gamma_1)^{1/2}/\Gamma$

VALUE	DOCUMENT ID		CHG	COMMENT
$+0.586\pm0.319$	[14] DEVENISH	74B	0	Fixed-t dispersion rel.

$\Sigma(1385)$ FOOTNOTES

[1] From fit to inclusive $\Lambda\pi$ spectrum.
[2] Includes data of HOLMGREN 77.
[3] The errors are statistical only. The resolution is not unfolded.
[4] The error is enlarged to $\Gamma/\sqrt{N}$. See the note on the $K^*(892)$ mass in the 1984 edition.
[5] From a fit to $\Lambda\pi^0$ with the width fixed at 34 MeV.
[6] From fit to inclusive $\Lambda\pi^0$ spectrum with the width fixed at 40 MeV.
[7] Redundant with data in the mass Listings.
[8] Results from $\Lambda\pi^+\pi^-$ and $\Lambda\pi^+\pi^-\pi^0$ combined by us.
[9] The error is enlarged to $4\Gamma/\sqrt{N}$. See the note on the $K^*(892)$ mass in the 1984 edition.
[10] Consistent with +, 0, and − widths equal.
[11] KELLER 12 gives $\Gamma(\Sigma^+\gamma)/\Gamma(\Sigma^+\pi^0) = (11.95 \pm 2.21^{+0.53}_{-1.21})\%$, using 1/2 our total $\Sigma(1385) \to \Sigma\pi$ fraction for $\Sigma^+\pi^0$. We divide the KELLER 12 value by two.
[12] We calculate this from the MOLCHANOV 04 upper limit of 9.5 keV on the $\Sigma^-\gamma$ width.
[13] We calculate this from the ARIK 77 upper limit of 24 keV on the $\Sigma^-\gamma$ width.
[14] An extrapolation of the parametrized amplitude below threshold.

$\Sigma(1385)$ REFERENCES

ABLIKIM	25AF	JHEP 2502 212	M. Ablikim *et al.*	(BESIII Collab.)
LEE	21A	PR D103 052005	J.Y. Lee *et al.*	(BELLE Collab.)
AGAKISHIEV	12	PR C85 035203	G. Agakishiev *et al.*	(HADES Collab.)
KELLER	12	PR D85 052004	D. Keller *et al.*	(JLab CLAS Collab.)
KELLER	11	PR D83 072004	D. Keller *et al.*	(JLab CLAS Collab.)
TAYLOR	05	PR C71 054609	S. Taylor *et al.*	(JLab CLAS Collab.)
Also		PR C72 039902 (errat.)	S. Taylor *et al.*	(JLab CLAS Collab.)
MOLCHANOV	04	PL B590 161	V.V. Molchanov *et al.*	(FNAL SELEX Collab.)
BAUBILLIER	84	ZPHY C23 213	M. Baubillier *et al.*	(BIRM, CERN, GLAS+)
PDG	84	RMP 56 S1	C.G. Wohl *et al.*	(LBL, CIT, CERN)
AGUILAR-...	81D	AFIS A77 144	M. Aguilar-Benitez, J. Salicio	(MADR)
BAKER	80	NP B166 207	P.A. Baker *et al.*	(LOIC)
BAUBILLIER	79B	NP B148 18	M. Baubillier *et al.*	(BIRM, CERN, GLAS+)
CAUTIS	79	NP B156 507	C.V. Cautis *et al.*	(SLAC)
SUGAHARA	79B	NP B156 237	R. Sugahara *et al.*	(KEK, OSKC, KINK)
CAMERON	78	NP B143 189	W. Cameron *et al.*	(RHEL, LOIC)
DIONISI	78B	PL 78B 154	C. Dionisi, R. Armenteros, J. Diaz	(CERN, AMST+)
ARIK	77	PRL 38 1000	E. Arik *et al.*	(PITT, BNL, MASA)
BARREIRO	77B	NP B126 319	F. Barreiro *et al.*	(CERN, AMST, NIJM)
HOLMGREN	77	NP B119 261	S.O. Holmgren *et al.*	(CERN, AMST, NIJM)
BARDADIN-...	75	NP B98 418	M. Bardadin-Otwinowska *et al.*	(SACL, EPOL+)
BERTHON	74	NC 21A 146	A. Berthon *et al.*	(CDEF, RHEL, SACL+)
BORENSTEIN	74	PR D9 3006	S.R. Borenstein *et al.*	(BNL, MICH)
DEVENISH	74B	NP B81 330	R.C.E. Devenish, C.D. Froggatt, B.R. Martin	(DESY+)
LICHTENBERG	74	PR D10 3865	D.B. Lichtenberg	(IND)
Also		Private Comm.	D.B. Lichtenberg	(IND)
HABIBI	73	Thesis Nevis 199	M. Habibi	(COLU)
Also		Purdue Conf. 387	C. Baltay *et al.*	(COLU, BING)
MAST	73	PR D7 3212	T.S. Mast *et al.*	(LBL) IJP
Also		PR D7 5	T.S. Mast *et al.*	(LBL) IJP
THOMAS	73	NP B56 15	D.W. Thomas *et al.*	(CMU) JP
AGUILAR-...	72B	PR D6 29	M. Aguilar-Benitez *et al.*	(BNL)
COLLEY	71B	NP B31 61	D.C. Colley *et al.*	(BIRM, EDIN, GLAS+)
AGUILAR-...	70B	PRL 25 58	M. Aguilar-Benitez *et al.*	(BNL, SYRA)
PAN	69	PRL 23 808	Y.L. Pan, F.L. Forman	(PENN) I
SIEGEL	67	Thesis UCRL 18041	D.M. Siegel	(LRL)
BIRMINGHAM	66	PR 152 1148	M. Haque *et al.*	(BIRM, GLAS, LOIC, OXF+)
LONDON	66	PR 143 1034	G.W. London *et al.*	(BNL, SYRA) J
ARMENTEROS	65B	PL 19 75	R. Armenteros *et al.*	(CERN, HEID, SACL)
SMITH	65	Thesis UCLA	L.T. Smith	(UCLA)
COOPER	64	PL 8 365	W.A. Cooper *et al.*	(CERN, AMST)
HUWE	64	Thesis UCRL 11291	D.O. Huwe	(LRL) JP
Also		PR 181 1824	D.O. Huwe	(LRL)
CURTIS	63	PR 132 1771	L.J. Curtis *et al.*	(MICH) J
ALSTON	62	CERN Conf. 311	M.H. Alston *et al.*	(LRL)
BASTIEN	61	PRL 6 702	P.L. Bastien, M. Ferro-Luzzi, A.H. Rosenfeld	(LRL)
DAHL	61	PRL 6 142	O.I. Dahl *et al.*	(LRL)
ELY	61	PRL 7 461	R.P. Ely *et al.*	(LRL) J
ALSTON	60	PRL 5 520	M.H. Alston *et al.*	(LRL) I

$\Sigma(1580)\ 3/2^-$

$I(J^P) = 1(\frac{3}{2}^-)$ Status: *

OMITTED FROM SUMMARY TABLE

Seen in the isospin-1 $\overline{K}N$ cross section at BNL (LI 73, CARROLL 76) and in a partial-wave analysis of $K^-p \to \Lambda\pi^0$ for c.m. energies 1560–1600 MeV by LITCHFIELD 74. LITCHFIELD 74 finds $J^P = 3/2^-$. Not seen by ENGLER 78, CAMERON 78C, OLMSTED 04, nor by PRAKHOV 04.

Neither ZHANG 13A nor SARANTSEV 19 see any evidence for this state.

$\Sigma(1580)$ POLE POSITION

REAL PART

VALUE (MeV)	DOCUMENT ID		TECN	COMMENT
• • • We do not use the following data for averages, fits, limits, etc. • • •				
1607^{+13}_{-11}	[1] KAMANO	15	DPWA	Multichannel

[1] From the preferred solution A in KAMANO 15. Solution B reports $M = 1492^{+4}_{-7}$ MeV.

−2×IMAGINARY PART

VALUE (MeV)	DOCUMENT ID		TECN	COMMENT
• • • We do not use the following data for averages, fits, limits, etc. • • •				
253^{+30}_{-18}	[2] KAMANO	15	DPWA	Multichannel

[2] From the preferred solution A in KAMANO 15. Solution B reports $M = 138^{+8}_{-14}$ MeV.

$\Sigma(1580)$ POLE RESIDUES

The "normalized residue" is the residue divided by $\Gamma_{pole}/2$.

Normalized residue in $N\overline{K} \to \Sigma(1580) \to N\overline{K}$

MODULUS	PHASE (°)	DOCUMENT ID		TECN	COMMENT
• • • We do not use the following data for averages, fits, limits, etc. • • •					
0.00778	51	[3] KAMANO	15	DPWA	Multichannel

[3] From the preferred solution A in KAMANO 15.

Normalized residue in $N\overline{K} \to \Sigma(1580) \to \Sigma\pi$

MODULUS	PHASE (°)	DOCUMENT ID		TECN	COMMENT
• • • We do not use the following data for averages, fits, limits, etc. • • •					
0.0625	−6	[4] KAMANO	15	DPWA	Multichannel

[4] From the preferred solution A in KAMANO 15.

Normalized residue in $N\overline{K} \to \Sigma(1580) \to \Lambda\pi$

MODULUS	PHASE (°)	DOCUMENT ID		TECN	COMMENT
• • • We do not use the following data for averages, fits, limits, etc. • • •					
0.059	156	[5] KAMANO	15	DPWA	Multichannel

[5] From the preferred solution A in KAMANO 15.

Normalized residue in $N\overline{K} \to \Sigma(1580) \to \Sigma(1385)\pi$, S-wave

MODULUS	PHASE (°)	DOCUMENT ID		TECN	COMMENT
• • • We do not use the following data for averages, fits, limits, etc. • • •					
0.0368	−18	[6] KAMANO	15	DPWA	Multichannel

[6] From the preferred solution A in KAMANO 15.

Normalized residue in $N\overline{K} \to \Sigma(1580) \to \Sigma(1385)\pi$, D-wave

MODULUS	PHASE (°)	DOCUMENT ID		TECN	COMMENT
• • • We do not use the following data for averages, fits, limits, etc. • • •					
0.0103	123	[7] KAMANO	15	DPWA	Multichannel

[7] From the preferred solution A in KAMANO 15.

$\Sigma(1580)$ MASS

VALUE (MeV)	DOCUMENT ID		TECN	COMMENT
≈ 1580 OUR ESTIMATE				
1583 ± 4	[8] CARROLL	76	DPWA	Isospin-1 total σ
1582 ± 4	[9] LITCHFIELD	74	DPWA	$K^-p \to \Lambda\pi^0$

[8] CARROLL 76 sees a total-cross-section bump with $(J+1/2)\ \Gamma_{el}\ /\ \Gamma_{total} = 0.06$.
[9] The main effect observed by LITCHFIELD 74 is in the $\Lambda\pi$ final state; the $\overline{K}N$ and $\Sigma\pi$ couplings are estimated from a multichannel fit including total-cross-section data of LI 73.

$\Sigma(1580)$ WIDTH

VALUE (MeV)	DOCUMENT ID		TECN	COMMENT
15	[10] CARROLL	76	DPWA	Isospin-1 total σ
11 ± 4	[11] LITCHFIELD	74	DPWA	$K^-p \to \Lambda\pi^0$

[10] CARROLL 76 sees a total-cross-section bump with $(J+1/2)\ \Gamma_{el}\ /\ \Gamma_{total} = 0.06$.
[11] The main effect observed by LITCHFIELD 74 is in the $\Lambda\pi$ final state; the $\overline{K}N$ and $\Sigma\pi$ couplings are estimated from a multichannel fit including total-cross-section data of LI 73.

Int. J. Mod. Phys. A 2026.41. Downloaded from www.worldscientific.com
UNIVERSITY OF CALIFORNIA @ BERKELEY on 09/16/26. Re-use and distribution is strictly not permitted, except for Open Access articles.

$\Sigma(1580)$ DECAY MODES

	Mode
Γ_1	$N\overline{K}$
Γ_2	$\Lambda\pi$
Γ_3	$\Sigma\pi$
Γ_4	$\Sigma(1385)\pi$, S-wave
Γ_5	$\Sigma(1385)\pi$, D-wave
Γ_6	$N\overline{K}^*(892)$, S=1/2, D-wave
Γ_7	$N\overline{K}^*(892)$, S=3/2, S-wave
Γ_8	$N\overline{K}^*(892)$, S=3/2, D-wave

$\Sigma(1580)$ BRANCHING RATIOS

See "Sign conventions for resonance couplings" in the Note on Λ and Σ Resonances.

$\Gamma(N\overline{K})/\Gamma_{total}$ — Γ_1/Γ

VALUE	DOCUMENT ID		TECN	COMMENT
$+0.03 \pm 0.01$	[12] LITCHFIELD	74	DPWA	$\overline{K}N$ multichannel
• • • We do not use the following data for averages, fits, limits, etc. • • •				
0.003	[13] KAMANO	15	DPWA	Multichannel

[12] The main effect observed by LITCHFIELD 74 is in the $\Lambda\pi$ final state; the $\overline{K}N$ and $\Sigma\pi$ couplings are estimated from a multichannel fit including total-cross-section data of LI 73.
[13] From the preferred solution A in KAMANO 15.

$\Gamma(\Lambda\pi)/\Gamma_{total}$ — Γ_2/Γ

VALUE	DOCUMENT ID		TECN	COMMENT
• • • We do not use the following data for averages, fits, limits, etc. • • •				
0.490	[14] KAMANO	15	DPWA	Multichannel

[14] From the preferred solution A in KAMANO 15.

$\Gamma(\Sigma\pi)/\Gamma_{total}$ — Γ_3/Γ

VALUE	DOCUMENT ID		TECN	COMMENT
• • • We do not use the following data for averages, fits, limits, etc. • • •				
0.387	[15] KAMANO	15	DPWA	Multichannel

[15] From the preferred solution A in KAMANO 15.

$\Gamma(\Sigma(1385)\pi, S\text{-wave})/\Gamma_{total}$ — Γ_4/Γ

VALUE	DOCUMENT ID		TECN	COMMENT
• • • We do not use the following data for averages, fits, limits, etc. • • •				
0.12	[16] KAMANO	15	DPWA	Multichannel

[16] From the preferred solution A in KAMANO 15.

$\Gamma(\Sigma(1385)\pi, D\text{-wave})/\Gamma_{total}$ — Γ_5/Γ

VALUE	DOCUMENT ID		TECN	COMMENT
• • • We do not use the following data for averages, fits, limits, etc. • • •				
0.001	[17] KAMANO	15	DPWA	Multichannel

[17] From the preferred solution A in KAMANO 15.

$\Gamma(N\overline{K}^*(892), S=1/2, D\text{-wave})/\Gamma_{total}$ — Γ_6/Γ

VALUE	DOCUMENT ID		TECN	COMMENT
• • • We do not use the following data for averages, fits, limits, etc. • • •				
not seen	[18] KAMANO	15	DPWA	Multichannel

[18] From the preferred solution A in KAMANO 15.

$\Gamma(N\overline{K}^*(892), S=3/2, S\text{-wave})/\Gamma_{total}$ — Γ_7/Γ

VALUE	DOCUMENT ID		TECN	COMMENT
• • • We do not use the following data for averages, fits, limits, etc. • • •				
not seen	[19] KAMANO	15	DPWA	Multichannel

[19] From the preferred solution A in KAMANO 15.

$\Gamma(N\overline{K}^*(892), S=3/2, D\text{-wave})/\Gamma_{total}$ — Γ_8/Γ

VALUE	DOCUMENT ID		TECN	COMMENT
• • • We do not use the following data for averages, fits, limits, etc. • • •				
not seen	[20] KAMANO	15	DPWA	Multichannel

[20] From the preferred solution A in KAMANO 15.

$(\Gamma_i\Gamma_f)^{1/2}/\Gamma_{total}$ in $N\overline{K} \to \Sigma(1580) \to \Lambda\pi$ — $(\Gamma_1\Gamma_2)^{1/2}/\Gamma$

VALUE	DOCUMENT ID		TECN	COMMENT
not seen	CAMERON	78C	HBC	$K^0_L p \to \Lambda\pi^+$
not seen	ENGLER	78	HBC	$K^0_L p \to \Lambda\pi^+$
$+0.10 \pm 0.02$	[21] LITCHFIELD	74	DPWA	$K^- p \to \Lambda\pi^0$

[21] The main effect observed by LITCHFIELD 74 is in the $\Lambda\pi$ final state; the $\overline{K}N$ and $\Sigma\pi$ couplings are estimated from a multichannel fit including total-cross-section data of LI 73.

$(\Gamma_i\Gamma_f)^{1/2}/\Gamma_{total}$ in $N\overline{K} \to \Sigma(1580) \to \Sigma\pi$ — $(\Gamma_1\Gamma_3)^{1/2}/\Gamma$

VALUE	DOCUMENT ID		TECN	COMMENT
not seen	CAMERON	78C	HBC	$K^0_L p \to \Sigma^0\pi^+$
not seen	ENGLER	78	HBC	$K^0_L p \to \Sigma^0\pi^+$
$+0.03 \pm 0.04$	[22] LITCHFIELD	74	DPWA	$\overline{K}N$ multichannel

[22] The main effect observed by LITCHFIELD 74 is in the $\Lambda\pi$ final state; the $\overline{K}N$ and $\Sigma\pi$ couplings are estimated from a multichannel fit including total-cross-section data of LI 73.

$\Sigma(1580)$ REFERENCES

SARANTSEV	19	EPJ A55 180	A.V. Sarantsev *et al.*	(BONN, PNPI)
KAMANO	15	PR C92 025205	H. Kamano *et al.*	(ANL, OSAK)
ZHANG	13A	PR C88 035205	H. Zhang *et al.*	(KSU)
OLMSTED	04	PL B588 29	J. Olmsted *et al.*	(BNL Crystal Ball Collab.)
PRAKHOV	04	PR C69 042202	S. Prakhov *et al.*	(BNL Crystal Ball Collab.)
CAMERON	78C	NP B132 189	W. Cameron *et al.*	(BGNA, EDIN, GLAS+) I
ENGLER	78	PR D18 3061	A. Engler *et al.*	(CMU, ANL)
CARROLL	76	PRL 37 806	A.S. Carroll *et al.*	(BNL) I
LITCHFIELD	74	PL 51B 509	P.J. Litchfield	(CERN) IJP
LI	73	Purdue Conf. 283	K.K. Li	(BNL) I

$\Sigma(1620)\ 1/2^-$

$I(J^P) = 1(\frac{1}{2}^-)$ Status: *

OMITTED FROM SUMMARY TABLE

The S_{11} state at 1697 MeV reported by VANHORN 75 is tentatively listed under the $\Sigma(1750)$. CARROLL 76 sees two bumps in the isospin-1 total cross section near this mass. GAO 12 sees no evidence for this resonance.

Production experiments are listed separately in the next entry.

$\Sigma(1620)$ POLE POSITION

REAL PART

VALUE (MeV)	DOCUMENT ID		TECN	COMMENT
1680±8	SARANTSEV	19	DPWA	$\overline{K}N$ multichannel
• • • We do not use the following data for averages, fits, limits, etc. • • •				
1501	ZHANG	13A	DPWA	$\overline{K}N$ multichannel

−2×IMAGINARY PART

VALUE (MeV)	DOCUMENT ID		TECN	COMMENT
39±11	SARANTSEV	19	DPWA	$\overline{K}N$ multichannel
• • • We do not use the following data for averages, fits, limits, etc. • • •				
171	ZHANG	13A	DPWA	$\overline{K}N$ multichannel

$\Sigma(1620)$ POLE RESIDUE

The "normalized residue" is the residue divided by $\Gamma_{pole}/2$.

Normalized residue in $N\overline{K} \to \Sigma(1620) \to \Sigma\pi$

MODULUS	PHASE (°)	DOCUMENT ID		TECN	COMMENT
0.14±0.03	**−90 ± 25**	SARANTSEV	19	DPWA	$\overline{K}N$ multichannel

Normalized residue in $N\overline{K} \to \Sigma(1620) \to \Lambda\pi$

MODULUS	PHASE (°)	DOCUMENT ID		TECN	COMMENT
0.10±0.03	**75 ± 20**	SARANTSEV	19	DPWA	$\overline{K}N$ multichannel

Normalized residue in $N\overline{K} \to \Sigma(1620) \to \Xi K$

MODULUS	PHASE (°)	DOCUMENT ID		TECN	COMMENT
0.02±0.01	**120 ± 20**	SARANTSEV	19	DPWA	$\overline{K}N$ multichannel

Normalized residue in $N\overline{K} \to \Sigma(1620) \to \Lambda(1520)\pi$

MODULUS	PHASE (°)	DOCUMENT ID		TECN	COMMENT
0.12±0.05	**140 ± 40**	SARANTSEV	19	DPWA	$\overline{K}N$ multichannel

Normalized residue in $N\overline{K} \to \Sigma(1620) \to \Sigma(1385)\pi$

MODULUS	PHASE (°)	DOCUMENT ID		TECN	COMMENT
0.015±0.010	**155 ± 40**	SARANTSEV	19	DPWA	$\overline{K}N$ multichannel

Normalized residue in $N\overline{K} \to \Sigma(1620) \to N\overline{K}^*(892)$, S-wave

MODULUS	PHASE (°)	DOCUMENT ID		TECN	COMMENT
0.05±0.04		SARANTSEV	19	DPWA	$\overline{K}N$ multichannel

Normalized residue in $N\overline{K} \to \Sigma(1620) \to N\overline{K}^*(892)$, D-wave

MODULUS	PHASE (°)	DOCUMENT ID		TECN	COMMENT
0.01±0.01		SARANTSEV	19	DPWA	$\overline{K}N$ multichannel

Normalized residue in $N\overline{K} \to \Sigma(1620) \to N\overline{K}$

MODULUS	PHASE (°)	DOCUMENT ID		TECN	COMMENT
0.11±0.03	**43 ± 20**	SARANTSEV	19	DPWA	$\overline{K}N$ multichannel

Int. J. Mod. Phys. A 2026.41. Downloaded from www.worldscientific.com by UNIVERSITY OF CALIFORNIA @ BERKELEY on 09/16/26. Re-use and distribution is strictly not permitted, except for Open Access articles.

$\Sigma(1620)$ MASS

VALUE (MeV)	DOCUMENT ID		TECN	COMMENT
1600 to 1650 (≈ 1620) OUR ESTIMATE				
1681 ± 6	SARANTSEV	19	DPWA	$\overline{K}N$ multichannel
1600 ± 15	ZHANG	13A	DPWA	$\overline{K}N$ multichannel
1600 ± 6	[1] MORRIS	78	DPWA	$K^- n \to \Lambda\pi^-$
1608 ± 5	[2] CARROLL	76	DPWA	Isospin-1 total σ
1630 ± 10	LANGBEIN	72	IPWA	$\overline{K}N$ multichannel
1620	KIM	71	DPWA	K-matrix analysis
• • • We do not use the following data for averages, fits, limits, etc. • • •				
1633 ± 10	[3] CARROLL	76	DPWA	Isospin-1 total σ

$\Sigma(1620)$ WIDTH

VALUE (MeV)	DOCUMENT ID		TECN	COMMENT
40 to 100 (≈ 70) OUR ESTIMATE				
40 ± 12	SARANTSEV	19	DPWA	$\overline{K}N$ multichannel
400 ± 152	ZHANG	13A	DPWA	$\overline{K}N$ multichannel
87 ± 19	[1] MORRIS	78	DPWA	$K^- n \to \Lambda\pi^-$
15	[2] CARROLL	76	DPWA	Isospin-1 total σ
65 ± 20	LANGBEIN	72	IPWA	$\overline{K}N$ multichannel
40	KIM	71	DPWA	K-matrix analysis
• • • We do not use the following data for averages, fits, limits, etc. • • •				
10	[3] CARROLL	76	DPWA	Isospin-1 total σ

$\Sigma(1620)$ DECAY MODES

	Mode	Fraction (Γ_i/Γ)
Γ_1	$N\overline{K}$	0.10 to 0.60
Γ_2	$\Lambda\pi$	(9.0 ± 3.0) %
Γ_3	$\Sigma\pi$	(17 ± 5) %
Γ_4	ΞK	
Γ_5	$\Lambda(1520)\pi$	(10 ± 5) %
Γ_6	$\Sigma(1385)\pi$	

$\Sigma(1620)$ BRANCHING RATIOS

$\Gamma(N\overline{K})/\Gamma_{total}$ — Γ_1/Γ

VALUE	DOCUMENT ID		TECN	COMMENT
0.10 to 0.60 OUR ESTIMATE				
0.11 ± 0.03	SARANTSEV	19	DPWA	$\overline{K}N$ multichannel
0.59 ± 0.10	ZHANG	13A	DPWA	$\overline{K}N$ multichannel
0.22 ± 0.02	LANGBEIN	72	IPWA	$\overline{K}N$ multichannel
0.05	KIM	71	DPWA	K-matrix analysis

$\Gamma(\Sigma\pi)/\Gamma_{total}$ — Γ_3/Γ

VALUE	DOCUMENT ID		TECN	COMMENT
0.17 ± 0.05	SARANTSEV	19	DPWA	$\overline{K}N$ multichannel

$\Gamma(\Lambda\pi)/\Gamma_{total}$ — Γ_2/Γ

VALUE	DOCUMENT ID		TECN	COMMENT
0.09 ± 0.03	SARANTSEV	19	DPWA	$\overline{K}N$ multichannel

$\Gamma(\Xi K)/\Gamma_{total}$ — Γ_4/Γ

VALUE	DOCUMENT ID		TECN	COMMENT
∼ 0	SARANTSEV	19	DPWA	$\overline{K}N$ multichannel

$\Gamma(\Lambda(1520)\pi)/\Gamma_{total}$ — Γ_5/Γ

VALUE	DOCUMENT ID		TECN	COMMENT
0.10 ± 0.05	SARANTSEV	19	DPWA	$\overline{K}N$ multichannel

$\Gamma(\Sigma(1385)\pi)/\Gamma_{total}$ — Γ_6/Γ

VALUE	DOCUMENT ID		TECN	COMMENT
<0.01	SARANTSEV	19	DPWA	$\overline{K}N$ multichannel

$(\Gamma_i\Gamma_f)^{1/2}/\Gamma_{total}$ in $N\overline{K} \to \Sigma(1620) \to \Lambda\pi$ — $(\Gamma_1\Gamma_2)^{1/2}/\Gamma$

VALUE	DOCUMENT ID		TECN	COMMENT
0.12 ± 0.02	[1] MORRIS	78	DPWA	$K^- n \to \Lambda\pi^-$
not seen	BAILLON	75	IPWA	$\overline{K}N \to \Lambda\pi$
0.15	KIM	71	DPWA	K-matrix analysis

$(\Gamma_i\Gamma_f)^{1/2}/\Gamma_{total}$ in $N\overline{K} \to \Sigma(1620) \to \Sigma\pi$ — $(\Gamma_1\Gamma_3)^{1/2}/\Gamma$

VALUE	DOCUMENT ID		TECN	COMMENT
+ 0.32 ± 0.03	ZHANG	13A	DPWA	Multichannel
not seen	HEPP	76B	DPWA	$K^- N \to \Sigma\pi$
+ 0.40 ± 0.06	LANGBEIN	72	IPWA	$\overline{K}N$ multichannel
+ 0.08	KIM	71	DPWA	K-matrix analysis

$\Sigma(1620)$ FOOTNOTES

[1] MORRIS 78 obtains an equally good fit without including this resonance.
[2] Total cross-section bump with $(J+1/2)\ \Gamma_{el}\ /\ \Gamma_{total}$ is 0.06 seen by CARROLL 76.
[3] Total cross-section bump with $(J+1/2)\ \Gamma_{el}\ /\ \Gamma_{total}$ is 0.04 seen by CARROLL 76.

$\Sigma(1620)$ REFERENCES

SARANTSEV	19	EPJ A55 180	A.V. Sarantsev *et al.*	(BONN, PNPI)
ZHANG	13A	PR C88 035205	H. Zhang *et al.*	(KSU)
GAO	12	PR C86 025201	P. Gao, J. Shi, B.S. Zou	(BHEP, BEIJT)
Also		NP A867 41	P. Gao, B.S. Zou, A. Sibirtsev	(BHEP, BEIJT+)
MORRIS	78	PR D17 55	W.A. Morris *et al.*	(FSU) IJP
CARROLL	76	PRL 37 806	A.S. Carroll *et al.*	(BNL) I
HEPP	76B	PL 65B 487	V. Hepp *et al.*	(CERN, HEIDH, MPIM) IJP
BAILLON	75	NP B94 39	P.H. Baillon, P.J. Litchfield	(CERN, RHEL) IJP
VANHORN	75	NP B87 145	A.J. van Horn	(LBL) IJP
Also		NP B87 157	A.J. van Horn	(LBL) IJP
LANGBEIN	72	NP B47 477	W. Langbein, F. Wagner	(MPIM) IJP
KIM	71	PRL 27 356	J.K. Kim	(HARV) IJP
Also		Duke Conf. 161 Hyperon Resonances, 1970	J.K. Kim	(HARV) IJP

$\Sigma(1660)\ 1/2^+$

$I(J^P) = 1(\frac{1}{2}^+)$ Status: ***

For results published before 1974 (they are now obsolete), see our 1982 edition Physics Letters **111B** 1 (1982).

$\Sigma(1660)$ POLE POSITION

REAL PART

VALUE (MeV)	DOCUMENT ID		TECN	COMMENT
1585 ± 20	SARANTSEV	19	DPWA	$\overline{K}N$ multichannel
• • • We do not use the following data for averages, fits, limits, etc. • • •				
1547^{+111}_{-59}	[1] KAMANO	15	DPWA	$\overline{K}N$ multichannel

[1] From the preferred solution A in KAMANO 15. Solution B reports $M = 1457^{+5}_{-1}$ MeV.

−2×IMAGINARY PART

VALUE (MeV)	DOCUMENT ID		TECN	COMMENT
290^{+140}_{-40}	SARANTSEV	19	DPWA	$\overline{K}N$ multichannel
• • • We do not use the following data for averages, fits, limits, etc. • • •				
183^{+86}_{-78}	[1] KAMANO	15	DPWA	$\overline{K}N$ multichannel

[1] From the preferred solution A in KAMANO 15. Solution B reports $\Gamma = 78^{+2}_{-8}$ MeV.

$\Sigma(1660)$ POLE RESIDUES

The normalized residue is the residue divided by $\Gamma_{pole}/2$.

Normalized residue in $N\overline{K} \to \Sigma(1660) \to N\overline{K}$

MODULUS	PHASE (°)	DOCUMENT ID		TECN	COMMENT
0.07 ± 0.03	**−165 ± 35**	SARANTSEV	19	DPWA	$\overline{K}N$ multichannel
• • • We do not use the following data for averages, fits, limits, etc. • • •					
0.0247	168	[1] KAMANO	15	DPWA	$\overline{K}N$ multichannel

[1] From the preferred solution A in KAMANO 15.

Normalized residue in $N\overline{K} \to \Sigma(1660) \to \Sigma\pi$

MODULUS	PHASE (°)	DOCUMENT ID		TECN	COMMENT
0.17 ± 0.04	**150 ± 20**	SARANTSEV	19	DPWA	$\overline{K}N$ multichannel
• • • We do not use the following data for averages, fits, limits, etc. • • •					
0.16	78	[1] KAMANO	15	DPWA	$\overline{K}N$ multichannel

[1] From the preferred solution A in KAMANO 15.

Normalized residue in $N\overline{K} \to \Sigma(1660) \to \Lambda\pi$

MODULUS	PHASE (°)	DOCUMENT ID		TECN	COMMENT
0.16 ± 0.05	**0 ± 25**	SARANTSEV	19	DPWA	$\overline{K}N$ multichannel
• • • We do not use the following data for averages, fits, limits, etc. • • •					
0.0614	−84	[1] KAMANO	15	DPWA	$\overline{K}N$ multichannel

[1] From the preferred solution A in KAMANO 15.

Normalized residue in $N\overline{K} \to \Sigma(1660) \to \Sigma\sigma$

MODULUS	PHASE (°)	DOCUMENT ID		TECN	COMMENT
0.14 ± 0.06	**−150 ± 30**	SARANTSEV	19	DPWA	$\overline{K}N$ multichannel

Normalized residue in $N\overline{K} \to \Sigma(1660) \to \Sigma(1385)\pi$

MODULUS	PHASE (°)	DOCUMENT ID		TECN	COMMENT
• • • We do not use the following data for averages, fits, limits, etc. • • •					
0.0513	−44	[1] KAMANO	15	DPWA	Multichannel

[1] From the preferred solution A in KAMANO 15.

Normalized residue in $N\overline{K} \to \Sigma(1660) \to \Lambda(1405)\pi$

MODULUS	PHASE (°)	DOCUMENT ID		TECN	COMMENT
0.06 ± 0.03	**−90 ± 25**	SARANTSEV	19	DPWA	$\overline{K}N$ multichannel

Normalized residue in $N\overline{K} \to \Sigma(1660) \to \Lambda(1520)\pi$

MODULUS	PHASE (°)	DOCUMENT ID		TECN	COMMENT
0.04 ± 0.02	**5 ± 20**	SARANTSEV	19	DPWA	$\overline{K}N$ multichannel

Int. J. Mod. Phys. A 2026.41. Downloaded from www.worldscientific.com
UNIVERSITY OF CALIFORNIA @ BERKELEY on 09/16/26. Re-use and distribution is strictly not permitted, except for Open Access articles.

$\Sigma(1660)$ MASS

VALUE (MeV)	DOCUMENT ID		TECN	COMMENT
1640 to 1680 (≈ 1660) OUR ESTIMATE				
1643.2 ± 4.5 ± 7.6	ABLIKIM	25AF	BES3	$\psi(3686) \to \Lambda\overline{\Sigma}^0\pi^0$ + c.c. (PWA)
1665 ± 20	SARANTSEV	19	DPWA	$\overline{K}N$ multichannel
1633 ± 3	GAO	12	DPWA	$\overline{K}N \to \Lambda\pi$
1665.1 ± 11.2	[1] KOISO	85	DPWA	$K^-p \to \Sigma\pi$
1670 ± 10	GOPAL	80	DPWA	$\overline{K}N \to \overline{K}N$
1679 ± 10	ALSTON-...	78	DPWA	$\overline{K}N \to \overline{K}N$
1668 ± 25	VANHORN	75	DPWA	$K^-p \to \Lambda\pi^0$
1670 ± 20	KANE	74	DPWA	$K^-p \to \Sigma\pi$
• • • We do not use the following data for averages, fits, limits, etc. • • •				
1676 ± 15	GOPAL	77	DPWA	$\overline{K}N$ multichannel
1565 or 1597	[2] MARTIN	77	DPWA	$\overline{K}N$ multichannel
1660 ± 30	[3] BAILLON	75	IPWA	$\overline{K}N \to \Lambda\pi$
1671 ± 2	[4] PONTE	75	DPWA	$K^-p \to \Lambda\pi^0$

[1] The evidence of KOISO 85 is weak.
[2] The two MARTIN 77 values are from a T-matrix pole and from a Breit-Wigner fit.
[3] From solution 1 of BAILLON 75; not present in solution 2.
[4] From solution 2 of PONTE 75; not present in solution 1.

$\Sigma(1660)$ WIDTH

VALUE (MeV)	DOCUMENT ID		TECN	COMMENT
100 to 300 (≈ 200) OUR ESTIMATE				
221.3 ± 13.1 ± 41.1	ABLIKIM	25AF	BES3	$\psi(3686) \to \Lambda\overline{\Sigma}^0\pi^0$ + c.c. (PWA)
300^{+140}_{-40}	SARANTSEV	19	DPWA	$\overline{K}N$ multichannel
121^{+4}_{-7}	GAO	12	DPWA	$\overline{K}N \to \Lambda\pi$
81.5 ± 22.2	[1] KOISO	85	DPWA	$K^-p \to \Sigma\pi$
152 ± 20	GOPAL	80	DPWA	$\overline{K}N \to \overline{K}N$
38 ± 10	ALSTON-...	78	DPWA	$\overline{K}N \to \overline{K}N$
230^{+165}_{-60}	VANHORN	75	DPWA	$K^-p \to \Lambda\pi^0$
250 ± 110	KANE	74	DPWA	$K^-p \to \Sigma\pi$
• • • We do not use the following data for averages, fits, limits, etc. • • •				
120 ± 20	GOPAL	77	DPWA	$\overline{K}N$ multichannel
202 or 217	[2] MARTIN	77	DPWA	$\overline{K}N$ multichannel
80 ± 40	[3] BAILLON	75	IPWA	$\overline{K}N \to \Lambda\pi$
81 ± 10	[4] PONTE	75	DPWA	$K^-p \to \Lambda\pi^0$

[1] The evidence of KOISO 85 is weak.
[2] The two MARTIN 77 values are from a T-matrix pole and from a Breit-Wigner fit.
[3] From solution 1 of BAILLON 75; not present in solution 2.
[4] From solution 2 of PONTE 75; not present in solution 1.

$\Sigma(1660)$ DECAY MODES

	Mode	Fraction (Γ_i/Γ)
Γ_1	$N\overline{K}$	0.05 to 0.15 (≈ 0.10)
Γ_2	$\Lambda\pi$	(35 ± 12) %
Γ_3	$\Sigma\pi$	(37 ± 10) %
Γ_4	$\Sigma\sigma$	(20 ± 8) %
Γ_5	$\Sigma(1385)\pi$	
Γ_6	$\Lambda(1405)\pi$	(4.0 ± 2.0) %
Γ_7	$\Lambda(1520)\pi$	

$\Sigma(1660)$ BRANCHING RATIOS

See "Sign conventions for resonance couplings" in the Note on Λ and Σ Resonances.

$\Gamma(N\overline{K})/\Gamma_{total}$ — Γ_1/Γ

VALUE	DOCUMENT ID		TECN	COMMENT
0.05 to 0.15 (≈ 0.10) OUR ESTIMATE				
0.07 ± 0.03	SARANTSEV	19	DPWA	$\overline{K}N$ multichannel
0.12 ± 0.03	GOPAL	80	DPWA	$\overline{K}N \to \overline{K}N$
0.10 ± 0.05	ALSTON-...	78	DPWA	$\overline{K}N \to \overline{K}N$
• • • We do not use the following data for averages, fits, limits, etc. • • •				
0.005	[1] KAMANO	15	DPWA	$\overline{K}N$ multichannel
<0.04	GOPAL	77	DPWA	See GOPAL 80
0.27 or 0.29	[2] MARTIN	77	DPWA	$\overline{K}N$ multichannel

[1] From the preferred solution A in KAMANO 15.
[2] The two MARTIN 77 values are from a T-matrix pole and from a Breit-Wigner fit.

$\Gamma(\Lambda\pi)/\Gamma_{total}$ — Γ_2/Γ

VALUE	DOCUMENT ID		TECN	COMMENT
0.35 ± 0.12	SARANTSEV	19	DPWA	$\overline{K}N$ multichannel
• • • We do not use the following data for averages, fits, limits, etc. • • •				
0.128	[1] KAMANO	15	DPWA	$\overline{K}N$ multichannel

[1] From the preferred solution A in KAMANO 15.

$\Gamma(\Sigma\pi)/\Gamma_{total}$ — Γ_3/Γ

VALUE	DOCUMENT ID		TECN	COMMENT
0.37 ± 0.10	SARANTSEV	19	DPWA	$\overline{K}N$ multichannel
• • • We do not use the following data for averages, fits, limits, etc. • • •				
0.865	[1] KAMANO	15	DPWA	$\overline{K}N$ multichannel

[1] From the preferred solution A in KAMANO 15.

$\Gamma(\Sigma\sigma)/\Gamma_{total}$ — Γ_4/Γ

VALUE	DOCUMENT ID		TECN	COMMENT
0.20 ± 0.08	SARANTSEV	19	DPWA	$\overline{K}N$ multichannel

$\Gamma(\Sigma(1385)\pi)/\Gamma_{total}$ — Γ_5/Γ

VALUE	DOCUMENT ID		TECN	COMMENT
• • • We do not use the following data for averages, fits, limits, etc. • • •				
0.001	[1] KAMANO	15	DPWA	Multichannel

[1] From the preferred solution A in KAMANO 15.

$\Gamma(\Lambda(1405)\pi)/\Gamma_{total}$ — Γ_6/Γ

VALUE	DOCUMENT ID		TECN	COMMENT
0.04 ± 0.02	SARANTSEV	19	DPWA	$\overline{K}N$ multichannel

$\Gamma(\Lambda(1520)\pi)/\Gamma_{total}$ — Γ_7/Γ

VALUE	DOCUMENT ID		TECN	COMMENT
<0.01	SARANTSEV	19	DPWA	$\overline{K}N$ multichannel

$(\Gamma_i\Gamma_f)^{1/2}/\Gamma_{total}$ in $N\overline{K} \to \Sigma(1660) \to \Lambda\pi$ — $(\Gamma_1\Gamma_2)^{1/2}/\Gamma$

VALUE	DOCUMENT ID		TECN	COMMENT
$-0.064^{+0.005}_{-0.003}$	GAO	12	DPWA	$\overline{K}N \to \Lambda\pi$
< 0.04	GOPAL	77	DPWA	$\overline{K}N$ multichannel
$0.12^{+0.12}_{-0.04}$	VANHORN	75	DPWA	$K^-p \to \Lambda\pi^0$
• • • We do not use the following data for averages, fits, limits, etc. • • •				
−0.10 or −0.11	[1] MARTIN	77	DPWA	$\overline{K}N$ multichannel
−0.04 ± 0.02	[2] BAILLON	75	IPWA	$\overline{K}N \to \Lambda\pi$
+0.16 ± 0.01	[3] PONTE	75	DPWA	$K^-p \to \Lambda\pi^0$

[1] The two MARTIN 77 values are from a T-matrix pole and from a Breit-Wigner fit.
[2] From solution 1 of BAILLON 75; not present in solution 2.
[3] From solution 2 of PONTE 75; not present in solution 1.

$(\Gamma_i\Gamma_f)^{1/2}/\Gamma_{total}$ in $N\overline{K} \to \Sigma(1660) \to \Sigma\pi$ — $(\Gamma_1\Gamma_3)^{1/2}/\Gamma$

VALUE	DOCUMENT ID		TECN	COMMENT
−0.13 ± 0.04	[1] KOISO	85	DPWA	$K^-p \to \Sigma\pi$
−0.16 ± 0.03	GOPAL	77	DPWA	$\overline{K}N$ multichannel
−0.11 ± 0.01	KANE	74	DPWA	$K^-p \to \Sigma\pi$
• • • We do not use the following data for averages, fits, limits, etc. • • •				
−0.34 or −0.37	[2] MARTIN	77	DPWA	$\overline{K}N$ multichannel
not seen	HEPP	76B	DPWA	$K^-N \to \Sigma\pi$

[1] The evidence of KOISO 85 is weak.
[2] The two MARTIN 77 values are from a T-matrix pole and from a Breit-Wigner fit.

$\Sigma(1660)$ REFERENCES

ABLIKIM	25AF	JHEP 2502 212	M. Ablikim *et al.*	(BESIII Collab.)
SARANTSEV	19	EPJ A55 180	A.V. Sarantsev *et al.*	(BONN, PNPI)
KAMANO	15	PR C92 025205	H. Kamano *et al.*	(ANL, OSAK)
GAO	12	PR C86 025201	P. Gao, J. Shi, B.S. Zou	(BHEP, BEIJT)
Also		NP A867 41	P. Gao, B.S. Zou, A. Sibirtsev	(BHEP, BEIJT+)
KOISO	85	NP A433 619	H. Koiso *et al.*	(TOKY, MASA)
PDG	82	PL 111B 1	M. Roos *et al.*	(HELS, CIT, CERN)
GOPAL	80	Toronto Conf. 159	G.P. Gopal	(RHEL) IJP
ALSTON-...	78	PR D18 182	M. Alston-Garnjost *et al.*	(LBL, MTHO+) IJP
Also		PRL 38 1007	M. Alston-Garnjost *et al.*	(LBL, MTHO+) IJP
GOPAL	77	NP B119 362	G.P. Gopal *et al.*	(LOIC, RHEL) IJP
MARTIN	77	NP B127 349	B.R. Martin, M.K. Pidcock, R.G. Moorhouse	(LOUC+) IJP
Also		NP B126 266	B.R. Martin, M.K. Pidcock	(LOUC)
Also		NP B126 285	B.R. Martin, M.K. Pidcock	(LOUC) IJP
HEPP	76B	PL 65B 487	V. Hepp *et al.*	(CERN, HEIDH, MPIM) IJP
BAILLON	75	NP B94 39	P.H. Baillon, P.J. Litchfield	(CERN, RHEL) IJP
PONTE	75	PR D12 2597	R.A. Ponte *et al.*	(MASA, TENN, UCR) IJP
VANHORN	75	NP B87 145	A.J. van Horn	(LBL) IJP
Also		NP B87 157	A.J. van Horn	(LBL) IJP
KANE	74	LBL-2452	D.F. Kane	(LBL) IJP

$\Sigma(1670)\ 3/2^-$

$I(J^P) = 1(\frac{3}{2}^-)$ Status: ****

For most results published before 1974 (they are now obsolete), see our 1982 edition Physics Letters **111B** 1 (1982).

Results from production experiments are listed separately in the next entry.

$\Sigma(1670)$ POLE POSITION

REAL PART

VALUE (MeV)	DOCUMENT ID		TECN	COMMENT
1655 to 1675 (≈ 1662) OUR ESTIMATE				
1661 ± 3	SARANTSEV	19	DPWA	$\overline{K}N$ multichannel
1669^{+7}_{-7}	[1] KAMANO	15	DPWA	$\overline{K}N$ multichannel
• • • We do not use the following data for averages, fits, limits, etc. • • •				
1674	ZHANG	13A	DPWA	$\overline{K}N$ multichannel

[1] From the preferred solution A in KAMANO 15.

−2×IMAGINARY PART

VALUE (MeV)	DOCUMENT ID		TECN	COMMENT
45 to 65 (≈ 55) OUR ESTIMATE				
52 ± 6	SARANTSEV	19	DPWA	$\overline{K}N$ multichannel
64^{+10}_{-14}	[1] KAMANO	15	DPWA	$\overline{K}N$ multichannel
• • • We do not use the following data for averages, fits, limits, etc. • • •				
54	ZHANG	13A	DPWA	$\overline{K}N$ multichannel

[1] From the preferred solution A in KAMANO 15.

$\Sigma(1670)$ POLE RESIDUES

The normalized residue is the residue divided by $\Gamma_{pole}/2$.

Normalized residue in $N\overline{K} \to \Sigma(1670) \to N\overline{K}$

MODULUS	PHASE (°)	DOCUMENT ID		TECN	COMMENT
0.10 ±0.02	**−31 ± 12**	SARANTSEV	19	DPWA	$\overline{K}N$ multichannel
• • • We do not use the following data for averages, fits, limits, etc. • • •					
0.129	−20	[1] KAMANO	15	DPWA	$\overline{K}N$ multichannel

[1] From the preferred solution A in KAMANO 15.

Normalized residue in $N\overline{K} \to \Sigma(1670) \to \Sigma\pi$

MODULUS	PHASE (°)	DOCUMENT ID		TECN	COMMENT
0.25 ±0.05	**−25 ± 10**	SARANTSEV	19	DPWA	$\overline{K}N$ multichannel
• • • We do not use the following data for averages, fits, limits, etc. • • •					
0.249	−21	[1] KAMANO	15	DPWA	$\overline{K}N$ multichannel

[1] From the preferred solution A in KAMANO 15.

Normalized residue in $N\overline{K} \to \Sigma(1670) \to \Lambda\pi$

MODULUS	PHASE (°)	DOCUMENT ID		TECN	COMMENT
0.09 ±0.03	**−52 ± 12**	SARANTSEV	19	DPWA	$\overline{K}N$ multichannel
• • • We do not use the following data for averages, fits, limits, etc. • • •					
0.0818	−7	[1] KAMANO	15	DPWA	$\overline{K}N$ multichannel

[1] From the preferred solution A in KAMANO 15.

Normalized residue in $N\overline{K} \to \Sigma(1670) \to \Xi K$

MODULUS	PHASE (°)	DOCUMENT ID		TECN	COMMENT
0.02±0.01	**160 ± 20**	SARANTSEV	19	DPWA	$\overline{K}N$ multichannel

Normalized residue in $N\overline{K} \to \Sigma(1670) \to \Sigma\sigma$

MODULUS	PHASE (°)	DOCUMENT ID		TECN	COMMENT
0.08±0.03	**−25 ± 15**	SARANTSEV	19	DPWA	$\overline{K}N$ multichannel

Normalized residue in $N\overline{K} \to \Sigma(1670) \to \Sigma(1385)\pi$, S-wave

MODULUS	PHASE (°)	DOCUMENT ID		TECN	COMMENT
• • • We do not use the following data for averages, fits, limits, etc. • • •					
0.228	167	[1] KAMANO	15	DPWA	$\overline{K}N$ multichannel

[1] From the preferred solution A in KAMANO 15.

Normalized residue in $N\overline{K} \to \Sigma(1670) \to \Sigma(1385)\pi$, D-wave

MODULUS	PHASE (°)	DOCUMENT ID		TECN	COMMENT
• • • We do not use the following data for averages, fits, limits, etc. • • •					
0.0915	141	KAMANO	15	DPWA	$\overline{K}N$ multichannel

Normalized residue in $N\overline{K} \to \Sigma(1670) \to \Lambda(1405)\pi$

MODULUS	PHASE (°)	DOCUMENT ID		TECN	COMMENT
0.03±0.02	**160 ± 15**	SARANTSEV	19	DPWA	$\overline{K}N$ multichannel

Normalized residue in $N\overline{K} \to \Sigma(1670) \to \Lambda(1520)\pi$, P-wave

MODULUS	PHASE (°)	DOCUMENT ID		TECN	COMMENT
0.04±0.02	**120 ± 20**	SARANTSEV	19	DPWA	$\overline{K}N$ multichannel

Normalized residue in $N\overline{K} \to \Sigma(1670) \to \Lambda(1520)\pi$, F-wave

MODULUS	PHASE (°)	DOCUMENT ID		TECN	COMMENT
0.01±0.01		SARANTSEV	19	DPWA	$\overline{K}N$ multichannel

Normalized residue in $N\overline{K} \to \Sigma(1670) \to \Delta\overline{K}$, S-wave

MODULUS	PHASE (°)	DOCUMENT ID		TECN	COMMENT
0.01±0.01		SARANTSEV	19	DPWA	$\overline{K}N$ multichannel

Normalized residue in $N\overline{K} \to \Sigma(1670) \to N\overline{K}^*(892)$, S=3/2, S-wave

VALUE	DOCUMENT ID		TECN	COMMENT
0.05+-0.03@50+-60	SARANTSEV	19	DPWA	$\overline{K}N$ multichannel

Normalized residue in $N\overline{K} \to \Sigma(1670) \to N\overline{K}^*(892)$, S=3/2, D-wave

MODULUS	PHASE (°)	DOCUMENT ID		TECN	COMMENT
0.01±0.01		SARANTSEV	19	DPWA	$\overline{K}N$ multichannel

Normalized residue in $N\overline{K} \to \Sigma(1670) \to N\overline{K}^*(892)$, S=1/2, D-wave

MODULUS	PHASE (°)	DOCUMENT ID		TECN	COMMENT
0.03±0.02		SARANTSEV	19	DPWA	$\overline{K}N$ multichannel

$\Sigma(1670)$ MASS

VALUE (MeV)	DOCUMENT ID		TECN	COMMENT
1665 to 1685 (≈ 1675) OUR ESTIMATE				
1679.7 ± 3.4 ± 4.3	ABLIKIM	25AF	BES3	$\psi(3686) \to \Lambda\overline{\Sigma}^0\pi^0$ + c.c. (PWA)
1665 ± 3	SARANTSEV	19	DPWA	$\overline{K}N$ multichannel
1678 ± 2	ZHANG	13A	DPWA	$\overline{K}N$ multichannel
1673 ± 1	GAO	12	DPWA	$\overline{K}N \to \Lambda\pi$
1665.1 ± 4.1	KOISO	85	DPWA	$K^-p \to \Sigma\pi$
1682 ± 5	GOPAL	80	DPWA	$\overline{K}N \to \overline{K}N$
1679 ±10	ALSTON-...	78	DPWA	$\overline{K}N \to \overline{K}N$
1670 ± 5	GOPAL	77	DPWA	$\overline{K}N$ multichannel
1670 ± 6	HEPP	76B	DPWA	$K^-N \to \Sigma\pi$
1685 ±20	BAILLON	75	IPWA	$\overline{K}N \to \Lambda\pi$
1659^{+12}_{-5}	VANHORN	75	DPWA	$K^-p \to \Lambda\pi^0$
1670 ± 2	KANE	74	DPWA	$K^-p \to \Sigma\pi$
• • • We do not use the following data for averages, fits, limits, etc. • • •				
1667 or 1668	[1] MARTIN	77	DPWA	$\overline{K}N$ multichannel
1650	DEBELLEFON	76	IPWA	$K^-p \to \Lambda\pi^0$
1671 ± 3	PONTE	75	DPWA	$K^-p \to \Lambda\pi^0$ (sol. 1)
1655 ± 2	PONTE	75	DPWA	$K^-p \to \Lambda\pi^0$ (sol. 2)

[1] The two MARTIN 77 values are from a T-matrix pole and from a Breit-Wigner fit.

$\Sigma(1670)$ WIDTH

VALUE (MeV)	DOCUMENT ID		TECN	COMMENT
40 to 100 (≈ 70) OUR ESTIMATE				
87.0 ± 6.4 ± 8.9	ABLIKIM	25AF	BES3	$\psi(3686) \to \Lambda\overline{\Sigma}^0\pi^0$ + c.c. (PWA)
54 ± 6	SARANTSEV	19	DPWA	$\overline{K}N$ multichannel
55 ± 4	ZHANG	13A	DPWA	$\overline{K}N$ multichannel
52^{+5}_{-2}	GAO	12	DPWA	$\overline{K}N \to \Lambda\pi$
65.0 ± 7.3	KOISO	85	DPWA	$K^-p \to \Sigma\pi$
79 ±10	GOPAL	80	DPWA	$\overline{K}N \to \overline{K}N$
56 ±20	ALSTON-...	78	DPWA	$\overline{K}N \to \overline{K}N$
50 ± 5	GOPAL	77	DPWA	$\overline{K}N$ multichannel
56 ± 3	HEPP	76B	DPWA	$K^-N \to \Sigma\pi$
85 ±25	BAILLON	75	IPWA	$\overline{K}N \to \Lambda\pi$
32 ±11	VANHORN	75	DPWA	$K^-p \to \Lambda\pi^0$
79 ± 6	KANE	74	DPWA	$K^-p \to \Sigma\pi$
• • • We do not use the following data for averages, fits, limits, etc. • • •				
46 or 46	[1] MARTIN	77	DPWA	$\overline{K}N$ multichannel
80	DEBELLEFON	76	IPWA	$K^-p \to \Lambda\pi^0$
44 ±11	PONTE	75	DPWA	$K^-p \to \Lambda\pi^0$ (sol. 1)
76 ± 5	PONTE	75	DPWA	$K^-p \to \Lambda\pi^0$ (sol. 2)

[1] The two MARTIN 77 values are from a T-matrix pole and from a Breit-Wigner fit.

$\Sigma(1670)$ DECAY MODES

	Mode	Fraction (Γ_i/Γ)
Γ_1	$N\overline{K}$	0.06 to 0.12
Γ_2	$\Lambda\pi$	5–15 %
Γ_3	$\Sigma\pi$	30–60 %
Γ_4	$\Lambda\pi\pi$	
Γ_5	$\Sigma\pi\pi$	
Γ_6	$\Sigma\sigma$	(7.0 ±3.0) %
Γ_7	$\Sigma(1385)\pi$	
Γ_8	$\Sigma(1385)\pi$, S-wave	
Γ_9	$\Sigma(1385)\pi$, D-wave	
Γ_{10}	$N\overline{K}^*(892)$, S=1/2, D-wave	
Γ_{11}	$N\overline{K}^*(892)$, S=3/2, S-wave	
Γ_{12}	$N\overline{K}^*(892)$, S=3/2, D-wave	
Γ_{13}	$\Lambda(1405)\pi$	
Γ_{14}	$\Lambda(1520)\pi$	

$\Sigma(1670)$ BRANCHING RATIOS

See "Sign conventions for resonance couplings" in the Note on Λ and Σ Resonances.

$\Gamma(N\overline{K})/\Gamma_{total}$ — Γ_1/Γ

VALUE	DOCUMENT ID		TECN	COMMENT
0.06 to 0.12 OUR ESTIMATE				
0.10 ±0.02	SARANTSEV	19	DPWA	$\overline{K}N$ multichannel
0.062±0.007	ZHANG	13A	DPWA	$\overline{K}N$ multichannel
0.10 ±0.03	GOPAL	80	DPWA	$\overline{K}N \to \overline{K}N$
0.11 ±0.03	ALSTON-...	78	DPWA	$\overline{K}N \to \overline{K}N$
• • • We do not use the following data for averages, fits, limits, etc. • • •				
0.121	[1] KAMANO	15	DPWA	$\overline{K}N$ multichannel
0.08 ±0.03	GOPAL	77	DPWA	See GOPAL 80
0.07 or 0.07	[2] MARTIN	77	DPWA	$\overline{K}N$ multichannel

[1] From the preferred solution A in KAMANO 15.
[2] The two MARTIN 77 values are from a T-matrix pole and from a Breit-Wigner fit.

Int. J. Mod. Phys. A 2026.41. Downloaded from www.worldscientific.com
by UNIVERSITY OF CALIFORNIA @ BERKELEY on 09/16/26. Re-use and distribution is strictly not permitted, except for Open Access articles.

Int. J. Mod. Phys. A 2026.41. Downloaded from www.worldscientific.com
UNIVERSITY OF CALIFORNIA @ BERKELEY on 09/16/26. Re-use and distribution is strictly not permitted, except for Open Access articles.

$\Gamma(\Lambda\pi)/\Gamma_{total}$ — Γ_2/Γ

VALUE	DOCUMENT ID		TECN	COMMENT
0.09 ±0.02	SARANTSEV	19	DPWA	$\overline{K}N$ multichannel
• • • We do not use the following data for averages, fits, limits, etc. • • •				
0.058	[1] KAMANO	15	DPWA	$\overline{K}N$ multichannel

[1] From the preferred solution A in KAMANO 15.

$\Gamma(\Sigma\pi)/\Gamma_{total}$ — Γ_3/Γ

VALUE	DOCUMENT ID		TECN	COMMENT
0.70 ±0.15	SARANTSEV	19	DPWA	$\overline{K}N$ multichannel
• • • We do not use the following data for averages, fits, limits, etc. • • •				
0.465	[1] KAMANO	15	DPWA	$\overline{K}N$ multichannel

[1] From the preferred solution A in KAMANO 15.

$\Gamma(\Lambda\pi\pi)/\Gamma_{total}$ — Γ_4/Γ

VALUE	DOCUMENT ID		TECN	COMMENT
• • • We do not use the following data for averages, fits, limits, etc. • • •				
<0.11	ARMENTEROS	68E	HBC	K^-p (Γ_1=0.09)

$\Gamma(\Sigma\pi\pi)/\Gamma_{total}$ — Γ_5/Γ

VALUE	DOCUMENT ID		TECN	COMMENT
• • • We do not use the following data for averages, fits, limits, etc. • • •				
<0.14	[1] ARMENTEROS	68E	HBC	K^-p, K^-d (Γ_1=0.09)

[1] Ratio only for $\Sigma 2\pi$ system in $I = 1$, which cannot be $\Sigma(1385)$.

$\Gamma(\Sigma\sigma)/\Gamma_{total}$ — Γ_6/Γ

VALUE	DOCUMENT ID		TECN	COMMENT
0.07±0.03	SARANTSEV	19	DPWA	$\overline{K}N$ multichannel

$\Gamma(\Sigma(1385)\pi$, S-wave$)/\Gamma_{total}$ — Γ_8/Γ

VALUE	DOCUMENT ID		TECN	COMMENT
• • • We do not use the following data for averages, fits, limits, etc. • • •				
0.309	[1] KAMANO	15	DPWA	Multichannel

[1] From the preferred solution A in KAMANO 15.

$\Gamma(\Sigma(1385)\pi$, D-wave$)/\Gamma_{total}$ — Γ_9/Γ

VALUE	DOCUMENT ID		TECN	COMMENT
• • • We do not use the following data for averages, fits, limits, etc. • • •				
0.044	[1] KAMANO	15	DPWA	Multichannel

[1] From the preferred solution A in KAMANO 15.

$\Gamma(N\overline{K}^*(892), S=1/2, D$-wave$)/\Gamma_{total}$ — Γ_{10}/Γ

VALUE	DOCUMENT ID		TECN	COMMENT
• • • We do not use the following data for averages, fits, limits, etc. • • •				
0.001	[1] KAMANO	15	DPWA	Multichannel

[1] From the preferred solution A in KAMANO 15.

$\Gamma(N\overline{K}^*(892), S=3/2, S$-wave$)/\Gamma_{total}$ — Γ_{11}/Γ

VALUE	DOCUMENT ID		TECN	COMMENT
• • • We do not use the following data for averages, fits, limits, etc. • • •				
0.002	[1] KAMANO	15	DPWA	Multichannel

[1] From the preferred solution A in KAMANO 15.

$\Gamma(N\overline{K}^*(892), S=3/2, D$-wave$)/\Gamma_{total}$ — Γ_{12}/Γ

VALUE	DOCUMENT ID		TECN	COMMENT
• • • We do not use the following data for averages, fits, limits, etc. • • •				
0.001	[1] KAMANO	15	DPWA	Multichannel

[1] From the preferred solution A in KAMANO 15.

$\Gamma(\Lambda(1405)\pi)/\Gamma_{total}$ — Γ_{13}/Γ

VALUE	DOCUMENT ID		TECN	COMMENT
0.01±0.01	SARANTSEV	19	DPWA	$\overline{K}N$ multichannel
• • • We do not use the following data for averages, fits, limits, etc. • • •				
<0.06	ARMENTEROS	68E	HBC	K^-p, K^-d (Γ_1=0.09)

$\Gamma(\Lambda(1405)\pi)/\Gamma(\Sigma(1385)\pi)$ — Γ_{13}/Γ_7

VALUE	DOCUMENT ID		TECN	COMMENT
0.23±0.08	BRUCKER	70	DBC	$K^-N \to \Sigma\pi\pi$

$(\Gamma_i\Gamma_f)^{1/2}/\Gamma_{total}$ in $N\overline{K} \to \Sigma(1670) \to \Lambda\pi$ — $(\Gamma_1\Gamma_2)^{1/2}/\Gamma$

VALUE	DOCUMENT ID		TECN	COMMENT
+0.08 ±0.01	ZHANG	13A	DPWA	Multichannel
$+0.081^{+0.002}_{-0.004}$	GAO	12	DPWA	$\overline{K}N \to \Lambda\pi$
+0.17 ±0.03	[1] MORRIS	78	DPWA	$K^-n \to \Lambda\pi^-$
+0.13 ±0.02	[1] MORRIS	78	DPWA	$K^-n \to \Lambda\pi^-$
+0.10 ±0.02	GOPAL	77	DPWA	$\overline{K}N$ multichannel
+0.06 ±0.02	BAILLON	75	IPWA	$\overline{K}N \to \Lambda\pi$
+0.09 ±0.02	VANHORN	75	DPWA	$K^-p \to \Lambda\pi^0$
+0.018±0.060	DEVENISH	74B		Fixed-t dispersion rel.
• • • We do not use the following data for averages, fits, limits, etc. • • •				
+0.08 or +0.08	[2] MARTIN	77	DPWA	$\overline{K}N$ multichannel
+0.05	DEBELLEFON	76	IPWA	$K^-p \to \Lambda\pi^0$
+0.08 ±0.01	PONTE	75	DPWA	$K^-p \to \Lambda\pi^0$ (sol. 1)
+0.17 ±0.01	PONTE	75	DPWA	$K^-p \to \Lambda\pi^0$ (sol. 2)

[1] Results are with and without an S_{11} $\Sigma(1620)$ in the fit.
[2] The two MARTIN 77 values are from a T-matrix pole and from a Breit-Wigner fit.

$(\Gamma_i\Gamma_f)^{1/2}/\Gamma_{total}$ in $N\overline{K} \to \Sigma(1670) \to \Sigma\pi$ — $(\Gamma_1\Gamma_3)^{1/2}/\Gamma$

VALUE	DOCUMENT ID		TECN	COMMENT
+0.20±0.01	ZHANG	13A	DPWA	Multichannel
+0.20±0.02	KOISO	85	DPWA	$K^-p \to \Sigma\pi$
+0.21±0.02	GOPAL	77	DPWA	$\overline{K}N$ multichannel
+0.20±0.01	HEPP	76B	DPWA	$K^-N \to \Sigma\pi$
+0.21±0.03	KANE	74	DPWA	$K^-p \to \Sigma\pi$
• • • We do not use the following data for averages, fits, limits, etc. • • •				
+0.18 or +0.17	[1] MARTIN	77	DPWA	$\overline{K}N$ multichannel

[1] The two MARTIN 77 values are from a T-matrix pole and from a Breit-Wigner fit.

$(\Gamma_i\Gamma_f)^{1/2}/\Gamma_{total}$ in $N\overline{K} \to \Sigma(1670) \to \Sigma(1385)\pi$, S-wave — $(\Gamma_1\Gamma_8)^{1/2}/\Gamma$

VALUE	DOCUMENT ID		TECN	COMMENT
+0.11±0.03	PREVOST	74	DPWA	$K^-N \to \Sigma(1385)\pi$
• • • We do not use the following data for averages, fits, limits, etc. • • •				
0.17±0.02	[1] SIMS	68	DBC	$K^-N \to \Lambda\pi\pi$

[1] SIMS 68 uses only cross-section data. Result used as upper limit only.

$\Gamma_i\Gamma_f/\Gamma^2_{total}$ in $N\overline{K} \to \Sigma(1670) \to \Lambda(1405)\pi$ — $\Gamma_1\Gamma_{13}/\Gamma^2$

VALUE	DOCUMENT ID		TECN	COMMENT
0.007±0.002	[1] BRUCKER	70	DBC	$K^-N \to \Sigma\pi\pi$
• • • We do not use the following data for averages, fits, limits, etc. • • •				
<0.03	BERLEY	69	HBC	K^-p 0.6–0.82 GeV/c

[1] Assuming the $\Lambda(1405)\pi$ cross-section bump is due only to $3/2^-$ resonance.

$(\Gamma_i\Gamma_f)^{1/2}/\Gamma_{total}$ in $N\overline{K} \to \Sigma(1670) \to \Lambda(1520)\pi$ — $(\Gamma_1\Gamma_{14})^{1/2}/\Gamma$

VALUE	DOCUMENT ID		TECN	COMMENT
0.081±0.016	[1] CAMERON	77	DPWA	P-wave decay

[1] The CAMERON 77 upper limit on F-wave decay is 0.03.

$\Sigma(1670)$ REFERENCES

ABLIKIM	25AF	JHEP 2502 212	M. Ablikim *et al.*	(BESIII Collab.)
SARANTSEV	19	EPJ A55 180	A.V. Sarantsev *et al.*	(BONN, PNPI)
KAMANO	15	PR C92 025205	H. Kamano *et al.*	(ANL, OSAK)
ZHANG	13A	PR C88 035205	H. Zhang *et al.*	(KSU)
GAO	12	PR C86 025201	P. Gao, J. Shi, B.S. Zou	(BHEP, BEIJT)
Also		NP A867 41	P. Gao, B.S. Zou, A. Sibirtsev	(BHEP, BEIJT+)
KOISO	85	NP A433 619	H. Koiso *et al.*	(TOKY, MASA)
PDG	82	PL 111B 1	M. Roos *et al.*	(HELS, CIT, CERN)
GOPAL	80	Toronto Conf. 159	G.P. Gopal	(RHEL) IJP
ALSTON-...	78	PR D18 182	M. Alston-Garnjost *et al.*	(LBL, MTHO+) IJP
Also		PRL 38 1007	M. Alston-Garnjost *et al.*	(LBL, MTHO+) IJP
MORRIS	78	PR D17 55	W.A. Morris *et al.*	(FSU) IJP
CAMERON	77	NP B131 399	W. Cameron *et al.*	(RHEL, LOIC) IJP
GOPAL	77	NP B119 362	G.P. Gopal *et al.*	(LOIC, RHEL) IJP
MARTIN	77	NP B127 349	B.R. Martin, M.K. Pidcock, R.G. Moorhouse	(LOUC+) IJP
Also		NP B126 266	B.R. Martin, M.K. Pidcock	(LOUC)
Also		NP B126 285	B.R. Martin, M.K. Pidcock	(LOUC) IJP
DEBELLEFON	76	NP B109 129	A. de Bellefon, A. Berthon	(CDEF) IJP
HEPP	76B	PL 65B 487	V. Hepp *et al.*	(CERN, HEIDH, MPIM) IJP
BAILLON	75	NP B94 39	P.H. Baillon, P.J. Litchfield	(CERN, RHEL) IJP
PONTE	75	PR D12 2597	R.A. Ponte *et al.*	(MASA, TENN, UCR) IJP
VANHORN	75	NP B87 145	A.J. van Horn	(LBL) IJP
Also		NP B87 157	A.J. van Horn	(LBL) IJP
DEVENISH	74B	NP B81 330	R.C.E. Devenish, C.D. Froggatt, B.R. Martin	(DESY+)
KANE	74	LBL-2452	D.F. Kane	(LBL) IJP
PREVOST	74	NP B69 246	J. Prevost *et al.*	(SACL, CERN, HEID)
BRUCKER	70	Duke Conf. 155	E.B. Brucker *et al.*	(FSU) I
Hyperon Resonances, 1970				
BERLEY	69	PL 30B 430	D. Berley *et al.*	(BNL)
ARMENTEROS	68E	PL 28B 521	R. Armenteros *et al.*	(CERN, HEID, SACL) I
SIMS	68	PRL 21 1413	W.H. Sims *et al.*	(FSU, TUFTS, BRAN)

$\Sigma(1750)\ 1/2^-$

$I(J^P) = 1(\frac{1}{2}^-)$ Status: ***

For most results published before 1974 (they are now obsolete), see our 1982 edition Physics Letters **111B** 1 (1982).

There is evidence for this state in many partial-wave analyses, but with wide variations in the mass, width, and couplings. The latest analyses indicated significant couplings to $N\overline{K}$ and $\Lambda\pi$, as well as to $\Sigma\eta$ whose threshold is at 1746 MeV (JONES 74).

$\Sigma(1750)$ POLE POSITION

REAL PART

VALUE (MeV)	DOCUMENT ID		TECN	COMMENT
1689±11	SARANTSEV	19	DPWA	$\overline{K}N$ multichannel
• • • We do not use the following data for averages, fits, limits, etc. • • •				
1704^{+3}_{-6}	[1] KAMANO	15	DPWA	$\overline{K}N$ multichannel
1708	ZHANG	13A	DPWA	$\overline{K}N$ multichannel

[1] From the preferred solution A in KAMANO 15. Solution B reports two poles at M = 1551^{+2}_{-9} MeV and 1940^{+2}_{-2} MeV.

−2×IMAGINARY PART

VALUE (MeV)	DOCUMENT ID		TECN	COMMENT
206±18	SARANTSEV	19	DPWA	$\overline{K}N$ multichannel
• • • We do not use the following data for averages, fits, limits, etc. • • •				
86^{+14}_{-4}	[1] KAMANO	15	DPWA	$\overline{K}N$ multichannel
158	ZHANG	13A	DPWA	$\overline{K}N$ multichannel

[1] From the preferred solution A in KAMANO 15. Solution B Reports two poles with Γ = 376^{+12}_{-2} and 172^{+4}_{-4} MeV.

$\Sigma(1750)$ POLE RESIDUES

The normalized residue is the residue divided by $\Gamma_{pole}/2$.

Normalized residue in $N\overline{K} \to \Sigma(1750) \to N\overline{K}$

MODULUS	PHASE (°)	DOCUMENT ID		TECN	COMMENT
0.46 ±0.09	**−144 ± 15**	SARANTSEV	19	DPWA	$\overline{K}N$ multichannel
• • • We do not use the following data for averages, fits, limits, etc. • • •					
0.0982	178	[1] KAMANO	15	DPWA	$\overline{K}N$ multichannel

[1] From the preferred solution A in KAMANO 15.

Normalized residue in $N\overline{K} \to \Sigma(1750) \to \Sigma\pi$

MODULUS	PHASE (°)	DOCUMENT ID		TECN	COMMENT
0.27 ±0.05	**100 ± 18**	SARANTSEV	19	DPWA	$\overline{K}N$ multichannel
• • • We do not use the following data for averages, fits, limits, etc. • • •					
0.192	137	[1] KAMANO	15	DPWA	Multichannel

[1] From the preferred solution A in KAMANO 15.

Normalized residue in $N\overline{K} \to \Sigma(1750) \to \Sigma\eta$

MODULUS	PHASE (°)	DOCUMENT ID		TECN	COMMENT
0.05±0.03		SARANTSEV	19	DPWA	$\overline{K}N$ multichannel

Normalized residue in $N\overline{K} \to \Sigma(1750) \to \Lambda\pi$

MODULUS	PHASE (°)	DOCUMENT ID		TECN	COMMENT
0.26 ±0.06	**115 ± 15**	SARANTSEV	19	DPWA	$\overline{K}N$ multichannel
• • • We do not use the following data for averages, fits, limits, etc. • • •					
0.207	169	[1] KAMANO	15	DPWA	$\overline{K}N$ multichannel

[1] From the preferred solution A in KAMANO 15.

Normalized residue in $N\overline{K} \to \Sigma(1750) \to \Xi K$

MODULUS	PHASE (°)	DOCUMENT ID		TECN	COMMENT
0.02±0.02		SARANTSEV	19	DPWA	$\overline{K}N$ multichannel

Normalized residue in $N\overline{K} \to \Sigma(1750) \to \Sigma(1385)\pi$, D-wave

MODULUS	PHASE (°)	DOCUMENT ID		TECN	COMMENT
0.04 ±0.03		SARANTSEV	19	DPWA	$\overline{K}N$ multichannel
• • • We do not use the following data for averages, fits, limits, etc. • • •					
0.0536	73	[1] KAMANO	15	DPWA	$\overline{K}N$ multichannel

[1] From the preferred solution A in KAMANO 15.

Normalized residue in $N\overline{K} \to \Sigma(1750) \to \Lambda(1520)\pi$

MODULUS	PHASE (°)	DOCUMENT ID		TECN	COMMENT
0.15±0.07	**−25 ± 40**	SARANTSEV	19	DPWA	$\overline{K}N$ multichannel

Normalized residue in $N\overline{K} \to \Sigma(1750) \to N\overline{K}^*(892)$, S=1/2, S-wave

MODULUS	PHASE (°)	DOCUMENT ID		TECN	COMMENT
0.05±0.03	**−100 ± 35**	SARANTSEV	19	DPWA	$\overline{K}N$ multichannel

$\Sigma(1750)$ MASS

VALUE (MeV)	DOCUMENT ID		TECN	COMMENT
1700 to 1800 (≈ 1750) OUR ESTIMATE				
1714.9± 4.2±7.3	ABLIKIM	25AF	BES3	$\psi(3686) \to \Lambda\overline{\Sigma}^0\pi^0$ + c.c. (PWA)
1692 ±11	SARANTSEV	19	DPWA	$\overline{K}N$ multichannel
1739 ± 8	ZHANG	13A	DPWA	$\overline{K}N$ multichannel
1756 ±10	GOPAL	80	DPWA	$\overline{K}N \to \overline{K}N$
1770 ±10	ALSTON-...	78	DPWA	$\overline{K}N \to \overline{K}N$
• • • We do not use the following data for averages, fits, limits, etc. • • •				
1770 ±15	GOPAL	77	DPWA	$\overline{K}N$ multichannel
1800 or 1813	[1] MARTIN	77	DPWA	$\overline{K}N$ multichannel
1715 ±10	[2] CARROLL	76	DPWA	Isospin-1 total σ
1730	DEBELLEFON	76	IPWA	$K^-p \to \Lambda\pi^0$
1780 ±30	BAILLON	75	IPWA	$\overline{K}N \to \Lambda\pi$ (sol. 1)
1700 ±30	BAILLON	75	IPWA	$\overline{K}N \to \Lambda\pi$ (sol. 2)
1697 $^{+20}_{-10}$	VANHORN	75	DPWA	$K^-p \to \Lambda\pi^0$
1785 ±12	CHU	74	DBC	Fits $\sigma(K^-n \to \Sigma^-\eta)$
1760 ± 5	[3] JONES	74	HBC	Fits $\sigma(K^-p \to \Sigma^0\eta)$
1739 ±10	PREVOST	74	DPWA	$K^-N \to \Sigma(1385)\pi$

[1] The two MARTIN 77 values are from a T-matrix pole and from a Breit-Wigner fit.
[2] A total cross-section bump with (J+1/2) Γ_{el} / Γ_{total} = 0.30.
[3] An S-wave Breit-Wigner fit to the threshold cross section with no background and errors statistical only.

$\Sigma(1750)$ WIDTH

VALUE (MeV)	DOCUMENT ID		TECN	COMMENT
100 to 200 (≈ 150) OUR ESTIMATE				
97.2± 9.8±9.7	ABLIKIM	25AF	BES3	$\psi(3686) \to \Lambda\overline{\Sigma}^0\pi^0$ + c.c. (PWA)
208 ±18	SARANTSEV	19	DPWA	$\overline{K}N$ multichannel
182 ±60	ZHANG	13A	DPWA	$\overline{K}N$ multichannel
64 ±10	GOPAL	80	DPWA	$\overline{K}N \to \overline{K}N$
161 ±20	ALSTON-...	78	DPWA	$\overline{K}N \to \overline{K}N$
• • • We do not use the following data for averages, fits, limits, etc. • • •				
60 ±10	GOPAL	77	DPWA	$\overline{K}N$ multichannel
117 or 119	[1] MARTIN	77	DPWA	$\overline{K}N$ multichannel
10	[2] CARROLL	76	DPWA	Isospin-1 total σ
110	DEBELLEFON	76	IPWA	$K^-p \to \Lambda\pi^0$
140 ±30	BAILLON	75	IPWA	$\overline{K}N \to \Lambda\pi$ (sol. 1)
160 ±50	BAILLON	75	IPWA	$\overline{K}N \to \Lambda\pi$ (sol. 2)
66 $^{+14}_{-12}$	VANHORN	75	DPWA	$K^-p \to \Lambda\pi^0$
89 ±33	CHU	74	DBC	Fits $\sigma(K^-n \to \Sigma^-\eta)$
92 ± 7	[3] JONES	74	HBC	Fits $\sigma(K^-p \to \Sigma^0\eta)$
108 ±20	PREVOST	74	DPWA	$K^-N \to \Sigma(1385)\pi$

[1] The two MARTIN 77 values are from a T-matrix pole and from a Breit-Wigner fit.
[2] A total cross-section bump with (J+1/2) Γ_{el} / Γ_{total} = 0.30.
[3] An S-wave Breit-Wigner fit to the threshold cross section with no background and errors statistical only.

$\Sigma(1750)$ DECAY MODES

	Mode	Fraction (Γ_i/Γ)
Γ_1	$N\overline{K}$	0.06 to 0.12
Γ_2	$\Lambda\pi$	(14 ±5) %
Γ_3	$\Sigma\pi$	(16 ±4) %
Γ_4	$\Sigma\eta$	15–55 %
Γ_5	$\Sigma(1385)\pi$, D-wave	< 1 %
Γ_6	$\Lambda(1520)\pi$	(2.0 ±1.0) %
Γ_7	$N\overline{K}^*(892)$, S=1/2	(8 ±4) %
Γ_8	$N\overline{K}^*(892)$, S=3/2, D-wave	

$\Sigma(1750)$ BRANCHING RATIOS

See "Sign conventions for resonance couplings" in the Note on Λ and Σ Resonances.

$\Gamma(N\overline{K})/\Gamma_{total}$ — Γ_1/Γ

VALUE	DOCUMENT ID		TECN	COMMENT
0.06 to 0.12 OUR ESTIMATE				
0.46 ±0.09	SARANTSEV	19	DPWA	$\overline{K}N$ multichannel
0.09 ±0.07	ZHANG	13A	DPWA	Multichannel
0.14 ±0.03	GOPAL	80	DPWA	$\overline{K}N \to \overline{K}N$
0.33 ±0.05	ALSTON-...	78	DPWA	$\overline{K}N \to \overline{K}N$
• • • We do not use the following data for averages, fits, limits, etc. • • •				
0.154	[1] KAMANO	15	DPWA	Multichannel
0.15 ±0.03	GOPAL	77	DPWA	See GOPAL 80
0.06 or 0.05	[2] MARTIN	77	DPWA	$\overline{K}N$ multichannel

[1] From the preferred solution A in KAMANO 15.
[2] The two MARTIN 77 values are from a T-matrix pole and from a Breit-Wigner fit.

$\Gamma(\Lambda\pi)/\Gamma_{total}$ — Γ_2/Γ

VALUE	DOCUMENT ID		TECN	COMMENT
0.14 ±0.05	SARANTSEV	19	DPWA	$\overline{K}N$ multichannel
• • • We do not use the following data for averages, fits, limits, etc. • • •				
0.435	[1] KAMANO	15	DPWA	$\overline{K}N$ multichannel

[1] From the preferred solution A in KAMANO 15.

$\Gamma(\Sigma\pi)/\Gamma_{total}$ — Γ_3/Γ

VALUE	DOCUMENT ID		TECN	COMMENT
0.16 ±0.04	SARANTSEV	19	DPWA	$\overline{K}N$ multichannel
• • • We do not use the following data for averages, fits, limits, etc. • • •				
0.373	[1] KAMANO	15	DPWA	$\overline{K}N$ multichannel

[1] From the preferred solution A in KAMANO 15.

$\Gamma(\Lambda(1520)\pi)/\Gamma_{total}$ — Γ_6/Γ

VALUE	DOCUMENT ID		TECN	COMMENT
0.02±0.01	SARANTSEV	19	DPWA	$\overline{K}N$ multichannel

$\Gamma(\Sigma(1385)\pi, D\text{-wave})/\Gamma_{total}$ — Γ_5/Γ

VALUE	DOCUMENT ID		TECN	COMMENT
<0.01	SARANTSEV	19	DPWA	$\overline{K}N$ multichannel

Int. J. Mod. Phys. A 2026.41. Downloaded from www.worldscientific.com
by UNIVERSITY OF CALIFORNIA @ BERKELEY on 09/16/26. Re-use and distribution is strictly not permitted, except for Open Access articles.

Int. J. Mod. Phys. A 2026.41. Downloaded from www.worldscientific.com
UNIVERSITY OF CALIFORNIA @ BERKELEY on 09/16/26. Re-use and distribution is strictly not permitted, except for Open Access articles.

• • • We do not use the following data for averages, fits, limits, etc. • • •

0.024	[1] KAMANO	15	DPWA	$\overline{K}N$ multichannel

[1] From the preferred solution A in KAMANO 15.

$\Gamma(N\overline{K}^*(892), S=1/2)/\Gamma_{total}$ — Γ_7/Γ

VALUE	DOCUMENT ID		TECN	COMMENT
~ 0	SARANTSEV	19	DPWA	$\overline{K}N$ multichannel
0.08 ±0.04	ZHANG	13A	DPWA	$\overline{K}N$ multichannel

• • • We do not use the following data for averages, fits, limits, etc. • • •

0.004	[1] KAMANO	15	DPWA	$\overline{K}N$ multichannel

[1] From the preferred solution A in KAMANO 15.

$\Gamma(N\overline{K}^*(892), S=3/2, D\text{-wave})/\Gamma_{total}$ — Γ_8/Γ

VALUE	DOCUMENT ID		TECN	COMMENT

• • • We do not use the following data for averages, fits, limits, etc. • • •

0.01	[1] KAMANO	15	DPWA	Multichannel

[1] From the preferred solution A in KAMANO 15.

$(\Gamma_i\Gamma_f)^{1/2}/\Gamma_{total}$ in $N\overline{K}\to\Sigma(1750)\to\Lambda\pi$ — $(\Gamma_1\Gamma_2)^{1/2}/\Gamma$

VALUE	DOCUMENT ID		TECN	COMMENT
+0.10 ±0.04	ZHANG	13A	DPWA	Multichannel
0.04 ±0.03	GOPAL	77	DPWA	$\overline{K}N$ multichannel

• • • We do not use the following data for averages, fits, limits, etc. • • •

−0.10 or −0.09	[1] MARTIN	77	DPWA	$\overline{K}N$ multichannel
−0.12	DEBELLEFON	76	IPWA	$K^-p\to\Lambda\pi^0$
−0.12 ±0.02	BAILLON	75	IPWA	$\overline{K}N\to\Lambda\pi$ (sol. 1)
−0.13 ±0.03	BAILLON	75	IPWA	$\overline{K}N\to\Lambda\pi$ (sol. 2)
−0.13 ±0.04	VANHORN	75	DPWA	$K^-p\to\Lambda\pi^0$
−0.120±0.077	DEVENISH	74B		Fixed-t dispersion rel.

[1] The two MARTIN 77 values are from a T-matrix pole and from a Breit-Wigner fit.

$(\Gamma_i\Gamma_f)^{1/2}/\Gamma_{total}$ in $N\overline{K}\to\Sigma(1750)\to\Sigma\pi$ — $(\Gamma_1\Gamma_3)^{1/2}/\Gamma$

VALUE	DOCUMENT ID		TECN	COMMENT
+0.17±0.07	ZHANG	13A	DPWA	Multichannel
−0.09±0.05	GOPAL	77	DPWA	$\overline{K}N$ multichannel

• • • We do not use the following data for averages, fits, limits, etc. • • •

+0.06 or +0.06	[1] MARTIN	77	DPWA	$\overline{K}N$ multichannel
0.13±0.02	LANGBEIN	72	IPWA	$\overline{K}N$ multichannel

[1] The two MARTIN 77 values are from a T-matrix pole and from a Breit-Wigner fit.

$(\Gamma_i\Gamma_f)^{1/2}/\Gamma_{total}$ in $N\overline{K}\to\Sigma(1750)\to\Sigma\eta$ — $(\Gamma_1\Gamma_4)^{1/2}/\Gamma$

VALUE	DOCUMENT ID		TECN	COMMENT
0.23±0.01	[1] JONES	74	HBC	Fits $\sigma(K^-p\to\Sigma^0\eta)$

• • • We do not use the following data for averages, fits, limits, etc. • • •

seen	CLINE	69	DBC	Threshold bump

[1] An S-wave Breit-Wigner fit to the threshold cross section with no background and errors statistical only.

$(\Gamma_i\Gamma_f)^{1/2}/\Gamma_{total}$ in $N\overline{K}\to\Sigma(1750)\to\Sigma(1385)\pi$, D-wave — $(\Gamma_1\Gamma_5)^{1/2}/\Gamma$

VALUE	DOCUMENT ID		TECN	COMMENT
+0.17±0.07	ZHANG	13A	DPWA	Multichannel
+0.18±0.15	PREVOST	74	DPWA	$K^-N\to\Sigma(1385)\pi$

$(\Gamma_i\Gamma_f)^{1/2}/\Gamma_{total}$ in $N\overline{K}\to\Sigma(1750)\to\Lambda(1520)\pi$ — $(\Gamma_1\Gamma_6)^{1/2}/\Gamma$

VALUE	DOCUMENT ID		TECN	COMMENT

• • • We do not use the following data for averages, fits, limits, etc. • • •

0.032±0.021	CAMERON	77	DPWA	P-wave decay

$\Sigma(1750)$ REFERENCES

ABLIKIM	25AF	JHEP 2502 212	M. Ablikim *et al.*	(BESIII Collab.)
SARANTSEV	19	EPJ A55 180	A.V. Sarantsev *et al.*	(BONN, PNPI)
KAMANO	15	PR C92 025205	H. Kamano *et al.*	(ANL, OSAK)
ZHANG	13A	PR C88 035205	H. Zhang *et al.*	(KSU)
PDG	82	PL 111B 1	M. Roos *et al.*	(HELS, CIT, CERN)
GOPAL	80	Toronto Conf. 159	G.P. Gopal	(RHEL) IJP
ALSTON-...	78	PR D18 182	M. Alston-Garnjost *et al.*	(LBL, MTHO+) IJP
Also		PRL 38 1007	M. Alston-Garnjost *et al.*	(LBL, MTHO+) IJP
CAMERON	77	NP B131 399	W. Cameron *et al.*	(RHEL, LOIC) IJP
GOPAL	77	NP B119 362	G.P. Gopal *et al.*	(LOIC, RHEL) IJP
MARTIN	77	NP B127 349	B.R. Martin, M.K. Pidcock, R.G. Moorhouse	(LOUC+) IJP
Also		NP B126 266	B.R. Martin, M.K. Pidcock	(LOUC)
Also		NP B126 285	B.R. Martin, M.K. Pidcock	(LOUC) IJP
CARROLL	76	PRL 37 806	A.S. Carroll *et al.*	(BNL) I
DEBELLEFON	76	NP B109 129	A. de Bellefon, A. Berthon	(CDEF) IJP
BAILLON	75	NP B94 39	P.H. Baillon, P.J. Litchfield	(CERN, RHEL) IJP
VANHORN	75	NP B87 145	A.J. van Horn	(LBL) IJP
Also		NP B87 157	A.J. van Horn	(LBL) IJP
CHU	74	NC 20A 35	R.Y.L. Chu *et al.*	(PLAT, TUFTS, BRAN) IJP
DEVENISH	74B	NP B81 330	R.C.E. Devenish, C.D. Froggatt, B.R. Martin	(DESY+)
JONES	74	NP B73 141	M.D. Jones	(CHIC) IJP
PREVOST	74	NP B69 246	J. Prevost *et al.*	(SACL, CERN, HEID)
LANGBEIN	72	NP B47 477	W. Langbein, F. Wagner	(MPIM) IJP
CLINE	69	LNC 2 407	D. Cline, R. Laumann, J. Mapp	(WISC)

$\Sigma(1775)\ 5/2^-$

$I(J^P) = 1(\frac{5}{2}^-)$ Status: ****

Discovered by GALTIERI 63, this resonance plays the same role as cornerstone for isospin-1 analyses in this region as the $\Lambda(1820)F_{05}$ does in the isospin-0 channel.

For most results published before 1974 (they are now obsolete), see our 1982 edition Physics Letters **111B** 1 (1982).

$\Sigma(1775)$ POLE POSITION

REAL PART

VALUE (MeV)	DOCUMENT ID		TECN	COMMENT
1760 to 1780 (≈ 1770) OUR ESTIMATE				
1767±4	SARANTSEV	19	DPWA	$\overline{K}N$ multichannel
1767^{+2}_{-2}	[1] KAMANO	15	DPWA	$\overline{K}N$ multichannel

• • • We do not use the following data for averages, fits, limits, etc. • • •

1759	ZHANG	13A	DPWA	$\overline{K}N$ multichannel

[1] From the preferred solution A in KAMANO 15.

−2×IMAGINARY PART

VALUE (MeV)	DOCUMENT ID		TECN	COMMENT
45 to 65 (≈ 55) OUR ESTIMATE				
122±8	SARANTSEV	19	DPWA	$\overline{K}N$ multichannel
128^{+4}_{-2}	[1] KAMANO	15	DPWA	$\overline{K}N$ multichannel

• • • We do not use the following data for averages, fits, limits, etc. • • •

118	ZHANG	13A	DPWA	$\overline{K}N$ multichannel

[1] From the preferred solution A in KAMANO 15.

$\Sigma(1775)$ POLE RESIDUES

The normalized residue is the residue divided by $\Gamma_{pole}/2$.

Normalized residue in $N\overline{K}\to\Sigma(1775)\to N\overline{K}$

MODULUS	PHASE (°)	DOCUMENT ID		TECN	COMMENT
0.44 ±0.09	−17 ± 10	SARANTSEV	19	DPWA	$\overline{K}N$ multichannel

• • • We do not use the following data for averages, fits, limits, etc. • • •

0.371	−32	[1] KAMANO	15	DPWA	$\overline{K}N$ multichannel

[1] From the preferred solution A in KAMANO 15.

Normalized residue in $N\overline{K}\to\Sigma(1775)\to\Sigma\pi$

MODULUS	PHASE (°)	DOCUMENT ID		TECN	COMMENT
0.13 ±0.03	10 ± 12	SARANTSEV	19	DPWA	$\overline{K}N$ multichannel

• • • We do not use the following data for averages, fits, limits, etc. • • •

0.115	−24	[1] KAMANO	15	DPWA	$\overline{K}N$ multichannel

[1] From the preferred solution A in KAMANO 15.

Normalized residue in $N\overline{K}\to\Sigma(1775)\to\Lambda\pi$

MODULUS	PHASE (°)	DOCUMENT ID		TECN	COMMENT
0.47 ±0.10	130 ± 15	SARANTSEV	19	DPWA	$\overline{K}N$ multichannel

• • • We do not use the following data for averages, fits, limits, etc. • • •

0.325	157	[1] KAMANO	15	DPWA	$\overline{K}N$ multichannel

[1] From the preferred solution A in KAMANO 15.

Normalized residue in $N\overline{K}\to\Sigma(1775)\to\Sigma(1385)\pi$, D-wave

MODULUS	PHASE (°)	DOCUMENT ID		TECN	COMMENT

• • • We do not use the following data for averages, fits, limits, etc. • • •

0.391	137	[1] KAMANO	15	DPWA	$\overline{K}N$ multichannel

[1] From the preferred solution A in KAMANO 15.

Normalized residue in $N\overline{K}\to\Sigma(1775)\to\Sigma(1385)\pi$, G-wave

MODULUS	PHASE (°)	DOCUMENT ID		TECN	COMMENT

• • • We do not use the following data for averages, fits, limits, etc. • • •

0.0129	−58	[1] KAMANO	15	DPWA	$\overline{K}N$ multichannel

[1] From the preferred solution A in KAMANO 15.

Normalized residue in $N\overline{K}\to\Sigma(1775)\to N\overline{K}^*(892)$, $S=1/2$, D-wave

MODULUS	PHASE (°)	DOCUMENT ID		TECN	COMMENT
0.04±0.02	−100 ± 60	SARANTSEV	19	DPWA	$\overline{K}N$ multichannel

Normalized residue in $N\overline{K}\to\Sigma(1775)\to N\overline{K}^*(892)$, $S=3/2$, D-wave

MODULUS	PHASE (°)	DOCUMENT ID		TECN	COMMENT
0.09±0.06	10 ± 50	SARANTSEV	19	DPWA	$\overline{K}N$ multichannel

Normalized residue in $N\overline{K}\to\Sigma(1775)\to N\overline{K}^*(892)$, $S=3/2$, G-wave

MODULUS	PHASE (°)	DOCUMENT ID		TECN	COMMENT
0.04±0.02	−100 ± 60	SARANTSEV	19	DPWA	$\overline{K}N$ multichannel

Int. J. Mod. Phys. A 2026.41. Downloaded from www.worldscientific.com
by UNIVERSITY OF CALIFORNIA @ BERKELEY on 09/16/26. Re-use and distribution is strictly not permitted, except for Open Access articles.

Normalized residue in $N\overline{K} \to \Sigma(1775) \to \Xi K$

MODULUS	PHASE (°)	DOCUMENT ID		TECN	COMMENT
0.02±0.01	−90 ± 35	SARANTSEV	19	DPWA	$\overline{K}N$ multichannel

Normalized residue in $N\overline{K} \to \Sigma(1775) \to \Lambda(1520)\pi$, P-wave

MODULUS	PHASE (°)	DOCUMENT ID		TECN	COMMENT
0.09±0.03	10 ± 30	SARANTSEV	19	DPWA	$\overline{K}N$ multichannel

Normalized residue in $N\overline{K} \to \Sigma(1775) \to \Lambda(1520)\pi$, F-wave

VALUE	DOCUMENT ID		TECN	COMMENT
0.01±0.01	SARANTSEV	19	DPWA	$\overline{K}N$ multichannel

Normalized residue in $N\overline{K} \to \Sigma(1775) \to \Delta\overline{K}$, D-wave

VALUE	DOCUMENT ID		TECN	COMMENT
0.02±0.02	SARANTSEV	19	DPWA	$\overline{K}N$ multichannel

$\Sigma(1775)$ MASS

VALUE (MeV)	DOCUMENT ID		TECN	COMMENT
1770 to 1780 (≈ 1775) OUR ESTIMATE				
1776± 4	SARANTSEV	19	DPWA	$\overline{K}N$ multichannel
1778± 1	ZHANG	13A	DPWA	$\overline{K}N$ multichannel
1778± 5	GOPAL	80	DPWA	$\overline{K}N \to \overline{K}N$
1777± 5	ALSTON-...	78	DPWA	$\overline{K}N \to \overline{K}N$
1775±10	BAILLON	75	IPWA	$\overline{K}N \to \Lambda\pi$
1774±10	VANHORN	75	DPWA	$K^-p \to \Lambda\pi^0$
1772± 6	KANE	74	DPWA	$K^-p \to \Sigma\pi$
• • • We do not use the following data for averages, fits, limits, etc. • • •				
1774± 5	GOPAL	77	DPWA	$\overline{K}N$ multichannel
1772 or 1777	[1] MARTIN	77	DPWA	$\overline{K}N$ multichannel
1765	DEBELLEFON	76	IPWA	$K^-p \to \Lambda\pi^0$

[1] The two MARTIN 77 values are from a T-matrix pole and from a Breit-Wigner fit.

$\Sigma(1775)$ WIDTH

VALUE (MeV)	DOCUMENT ID		TECN	COMMENT
105 to 135 (≈ 120) OUR ESTIMATE				
124± 8	SARANTSEV	19	DPWA	$\overline{K}N$ multichannel
131± 3	ZHANG	13A	DPWA	$\overline{K}N$ multichannel
137±10	GOPAL	80	DPWA	$\overline{K}N \to \overline{K}N$
116±10	ALSTON-...	78	DPWA	$\overline{K}N \to \overline{K}N$
125±15	BAILLON	75	IPWA	$\overline{K}N \to \Lambda\pi$
146±18	VANHORN	75	DPWA	$K^-p \to \Lambda\pi^0$
154±10	KANE	74	DPWA	$K^-p \to \Sigma\pi$
• • • We do not use the following data for averages, fits, limits, etc. • • •				
130±10	GOPAL	77	DPWA	$\overline{K}N$ multichannel
102 or 103	[1] MARTIN	77	DPWA	$\overline{K}N$ multichannel
120	DEBELLEFON	76	IPWA	$K^-p \to \Lambda\pi^0$

[1] The two MARTIN 77 values are from a T-matrix pole and from a Breit-Wigner fit.

$\Sigma(1775)$ DECAY MODES

	Mode	Fraction (Γ_i/Γ)
Γ_1	$N\overline{K}$	37–43%
Γ_2	$\Lambda\pi$	14–20%
Γ_3	$\Sigma\pi$	2–5%
Γ_4	$\Sigma(1385)\pi$	8–12%
Γ_5	$\Sigma(1385)\pi$, D-wave	
Γ_6	$\Sigma(1385)\pi$, G-wave	
Γ_7	$\Lambda(1520)\pi$, P-wave	17–23%
Γ_8	$\Sigma\pi\pi$	
Γ_9	$\Delta(1232)\overline{K}$, D-wave	
Γ_{10}	$N\overline{K}^*(892)$, S=1/2	
Γ_{11}	$N\overline{K}^*(892)$, S=1/2, D-wave	
Γ_{12}	$N\overline{K}^*(892)$, S=3/2, D-wave	
Γ_{13}	$N\overline{K}^*(892)$, S=3/2, G-wave	

$\Sigma(1775)$ BRANCHING RATIOS

See "Sign conventions for resonance couplings" in the Note on Λ and Σ Resonances. Also, the errors quoted do not include uncertainties due to the parametrization used in the partial-wave analyses and are thus too small.

$\Gamma(N\overline{K})/\Gamma_{total}$ — Γ_1/Γ

VALUE	DOCUMENT ID		TECN	COMMENT
0.37 to 0.43 OUR ESTIMATE				
0.43 ±0.09	SARANTSEV	19	DPWA	$\overline{K}N$ multichannel
0.40 ±0.01	ZHANG	13A	DPWA	$\overline{K}N$ multichannel
0.40 ±0.02	GOPAL	80	DPWA	$\overline{K}N \to \overline{K}N$
0.37 ±0.03	ALSTON-...	78	DPWA	$\overline{K}N \to \overline{K}N$
• • • We do not use the following data for averages, fits, limits, etc. • • •				
0.402	[1] KAMANO	15	DPWA	Multichannel
0.41 ±0.03	GOPAL	77	DPWA	See GOPAL 80
0.37 or 0.36	[2] MARTIN	77	DPWA	$\overline{K}N$ multichannel

[1] From the preferred solution A in KAMANO 15.
[2] The two MARTIN 77 values are from a T-matrix pole and from a Breit-Wigner fit.

$\Gamma(\Lambda\pi)/\Gamma_{total}$ — Γ_2/Γ

VALUE	DOCUMENT ID		TECN	COMMENT
0.49 ±0.10	SARANTSEV	19	DPWA	$\overline{K}N$ multichannel
• • • We do not use the following data for averages, fits, limits, etc. • • •				
0.244	[1] KAMANO	15	DPWA	$\overline{K}N$ multichannel

[1] From the preferred solution A in KAMANO 15.

$\Gamma(\Lambda\pi)/\Gamma(N\overline{K})$ — Γ_2/Γ_1

VALUE	DOCUMENT ID		TECN	COMMENT
0.33±0.05	UHLIG	67	HBC	K^-p 0.9 GeV/c

$\Gamma(\Sigma\pi)/\Gamma_{total}$ — Γ_3/Γ

VALUE	DOCUMENT ID		TECN	COMMENT
0.035±0.010	SARANTSEV	19	DPWA	$\overline{K}N$ multichannel
• • • We do not use the following data for averages, fits, limits, etc. • • •				
0.042	[1] KAMANO	15	DPWA	$\overline{K}N$ multichannel

[1] From the preferred solution A in KAMANO 15.

$\Gamma(\Sigma(1385)\pi)/\Gamma(N\overline{K})$ — Γ_4/Γ_1

VALUE	DOCUMENT ID		TECN	COMMENT
0.25±0.09	UHLIG	67	HBC	K^-p 0.9 GeV/c

$\Gamma(\Sigma(1385)\pi$, D-wave$)/\Gamma_{total}$ — Γ_5/Γ

VALUE	DOCUMENT ID		TECN	COMMENT
• • • We do not use the following data for averages, fits, limits, etc. • • •				
0.309	[1] KAMANO	15	DPWA	Multichannel

[1] From the preferred solution A in KAMANO 15.

$\Gamma(\Sigma(1385)\pi$, G-wave$)/\Gamma_{total}$ — Γ_6/Γ

VALUE	DOCUMENT ID		TECN	COMMENT
• • • We do not use the following data for averages, fits, limits, etc. • • •				
not seen	[1] KAMANO	15	DPWA	Multichannel

[1] From the preferred solution A in KAMANO 15.

$\Gamma(\Lambda(1520)\pi$, P-wave$)/\Gamma_{total}$ — Γ_7/Γ

VALUE	DOCUMENT ID		TECN	COMMENT
0.02±0.01	SARANTSEV	19	DPWA	$\overline{K}N$ multichannel

$\Gamma(\Lambda(1520)\pi$, P-wave$)/\Gamma(N\overline{K})$ — Γ_7/Γ_1

VALUE	DOCUMENT ID		TECN	COMMENT
0.28±0.05	UHLIG	67	HBC	K^-p 0.9 GeV/c

$\Gamma(\Sigma\pi\pi)/\Gamma_{total}$ — Γ_8/Γ

VALUE	DOCUMENT ID		TECN	COMMENT
• • • We do not use the following data for averages, fits, limits, etc. • • •				
0.12	[1] ARMENTEROS68C		HDBC	$K^-N \to \Sigma\pi\pi$

[1] For about 3/4 of this, the $\Sigma\pi$ system has $I = 0$ and is almost entirely $\Lambda(1520)$. For the rest, the $\Sigma\pi$ has $I = 1$, which is about what is expected from the known $\Sigma(1775) \to \Sigma(1385)\pi$ rate, as seen in $\Lambda\pi\pi$.

$\Gamma(N\overline{K}^*(892)$, S=1/2, D-wave$)/\Gamma_{total}$ — Γ_{11}/Γ

VALUE	DOCUMENT ID		TECN	COMMENT
• • • We do not use the following data for averages, fits, limits, etc. • • •				
not seen	[1] KAMANO	15	DPWA	Multichannel

[1] From the preferred solution A in KAMANO 15.

$\Gamma(N\overline{K}^*(892)$, S=3/2, D-wave$)/\Gamma_{total}$ — Γ_{12}/Γ

VALUE	DOCUMENT ID		TECN	COMMENT
• • • We do not use the following data for averages, fits, limits, etc. • • •				
0.003	[1] KAMANO	15	DPWA	Multichannel

[1] From the preferred solution A in KAMANO 15.

$\Gamma(N\overline{K}^*(892)$, S=3/2, G-wave$)/\Gamma_{total}$ — Γ_{13}/Γ

VALUE	DOCUMENT ID		TECN	COMMENT
• • • We do not use the following data for averages, fits, limits, etc. • • •				
not seen	[1] KAMANO	15	DPWA	Multichannel

[1] From the preferred solution A in KAMANO 15.

$(\Gamma_i\Gamma_f)^{1/2}/\Gamma_{total}$ in $N\overline{K} \to \Sigma(1775) \to \Lambda\pi$ — $(\Gamma_1\Gamma_2)^{1/2}/\Gamma$

VALUE	DOCUMENT ID		TECN	COMMENT
−0.31 ±0.01	ZHANG	13A	DPWA	Multichannel
−0.28 ±0.03	GOPAL	77	DPWA	$\overline{K}N$ multichannel
−0.25 ±0.02	BAILLON	75	IPWA	$\overline{K}N \to \Lambda\pi$
$-0.28\ ^{+0.04}_{-0.05}$	VANHORN	75	DPWA	$K^-p \to \Lambda\pi^0$
−0.259±0.048	DEVENISH	74B		Fixed-t dispersion rel.
• • • We do not use the following data for averages, fits, limits, etc. • • •				
−0.29 or −0.28	[1] MARTIN	77	DPWA	$\overline{K}N$ multichannel
−0.30	DEBELLEFON	76	IPWA	$K^-p \to \Lambda\pi^0$

[1] The two MARTIN 77 values are from a T-matrix pole and from a Breit-Wigner fit.

Int. J. Mod. Phys. A 2026.41. Downloaded from www.worldscientific.com
UNIVERSITY OF CALIFORNIA @ BERKELEY on 09/16/26. Re-use and distribution is strictly not permitted, except for Open Access articles.

$(\Gamma_i\Gamma_f)^{1/2}/\Gamma_{total}$ in $N\overline{K} \to \Sigma(1775) \to \Sigma\pi$ $(\Gamma_1\Gamma_3)^{1/2}/\Gamma$

VALUE	DOCUMENT ID		TECN	COMMENT
$+0.08\pm0.01$	ZHANG	13A	DPWA	Multichannel
$+0.13\pm0.02$	GOPAL	77	DPWA	$\overline{K}N$ multichannel
0.09 ± 0.01	KANE	74	DPWA	$K^-p \to \Sigma\pi$
• • • We do not use the following data for averages, fits, limits, etc. • • •				
$+0.08$ or $+0.08$	[1] MARTIN	77	DPWA	$\overline{K}N$ multichannel

[1] The two MARTIN 77 values are from a T-matrix pole and from a Breit-Wigner fit.

$(\Gamma_i\Gamma_f)^{1/2}/\Gamma_{total}$ in $N\overline{K} \to \Sigma(1775) \to \Sigma(1385)\pi$, D-wave $(\Gamma_1\Gamma_5)^{1/2}/\Gamma$

VALUE	DOCUMENT ID		TECN	COMMENT
$-0.12\ \pm0.01$	ZHANG	13A	DPWA	Multichannel
-0.184 ± 0.011	[1] CAMERON	78	DPWA	$K^-p \to \Sigma(1385)\pi$
$+0.20\ \pm0.02$	PREVOST	74	DPWA	$K^-N \to \Sigma(1385)\pi$
• • • We do not use the following data for averages, fits, limits, etc. • • •				
$0.32\ \pm0.06$	SIMS	68	DBC	$K^-N \to \Lambda\pi\pi$
$0.24\ \pm0.03$	ARMENTEROS	67C	HBC	$K^-p \to \Lambda\pi\pi$

[1] The CAMERON 78 upper limit on G-wave decay is 0.03.

$(\Gamma_i\Gamma_f)^{1/2}/\Gamma_{total}$ in $N\overline{K} \to \Sigma(1775) \to \Lambda(1520)\pi$, P-wave $(\Gamma_1\Gamma_7)^{1/2}/\Gamma$

VALUE	DOCUMENT ID		TECN	COMMENT
$-0.06\ \pm0.01$	ZHANG	13A	DPWA	Multichannel
-0.305 ± 0.010	[1] CAMERON	77	DPWA	$K^-p \to \Lambda(1520)\pi^0$
$0.31\ \pm0.02$	BARLETTA	72	DPWA	$K^-p \to \Lambda(1520)\pi^0$
$0.27\ \pm0.03$	ARMENTEROS	65C	HBC	$K^-p \to \Lambda(1520)\pi^0$

[1] This rate combines P-wave- and F-wave decays. The CAMERON 77 results for the separate P-wave- and F-wave decays are -0.303 ± 0.010 and -0.037 ± 0.014. The published signs have been changed here to be in accord with the baryon-first convention.

$(\Gamma_i\Gamma_f)^{1/2}/\Gamma_{total}$ in $N\overline{K} \to \Sigma(1775) \to \Delta(1232)\overline{K}$, D-wave $(\Gamma_1\Gamma_9)^{1/2}/\Gamma$

VALUE	DOCUMENT ID		TECN	COMMENT
$+0.06\pm0.03$	ZHANG	13A	DPWA	Multichannel

$(\Gamma_i\Gamma_f)^{1/2}/\Gamma_{total}$ in $N\overline{K} \to \Sigma(1775) \to N\overline{K}^*(892)$, $S=1/2$ $(\Gamma_1\Gamma_{10})^{1/2}/\Gamma$

VALUE	DOCUMENT ID		TECN	COMMENT
$+0.04\pm0.01$	ZHANG	13A	DPWA	Multichannel

$(\Gamma_i\Gamma_f)^{1/2}/\Gamma_{total}$ in $N\overline{K} \to \Sigma(1775) \to N\overline{K}^*(892)$, $S=3/2$, D-wave $(\Gamma_1\Gamma_{12})^{1/2}/\Gamma$

VALUE	DOCUMENT ID		TECN	COMMENT
$+0.04\pm0.01$	ZHANG	13A	DPWA	Multichannel

$\Sigma(1775)$ REFERENCES

SARANTSEV	19	EPJ A55 180	A.V. Sarantsev *et al.*	(BONN, PNPI)
KAMANO	15	PR C92 025205	H. Kamano *et al.*	(ANL, OSAK)
ZHANG	13A	PR C88 035205	H. Zhang *et al.*	(KSU)
PDG	82	PL 111B 1	M. Roos *et al.*	(HELS, CIT, CERN)
GOPAL	80	Toronto Conf. 159	G.P. Gopal	(RHEL) IJP
ALSTON-...	78	PR D18 182	M. Alston-Garnjost *et al.*	(LBL, MTHO+) IJP
Also		PRL 38 1007	M. Alston-Garnjost *et al.*	(LBL, MTHO+) IJP
CAMERON	78	NP B143 189	W. Cameron *et al.*	(RHEL, LOIC) IJP
CAMERON	77	NP B131 399	W. Cameron *et al.*	(RHEL, LOIC) IJP
GOPAL	77	NP B119 362	G.P. Gopal *et al.*	(LOIC, RHEL) IJP
MARTIN	77	NP B127 349	B.R. Martin, M.K. Pidcock, R.G. Moorhouse	(LOUC+) IJP
Also		NP B126 266	B.R. Martin, M.K. Pidcock	(LOUC)
Also		NP B126 285	B.R. Martin, M.K. Pidcock	(LOUC) IJP
DEBELLEFON	76	NP B109 129	A. de Bellefon, A. Berthon	(CDEF) IJP
BAILLON	75	NP B94 39	P.H. Baillon, P.J. Litchfield	(CERN, RHEL) IJP
VANHORN	75	NP B87 145	A.J. van Horn	(LBL) IJP
Also		NP B87 157	A.J. van Horn	(LBL) IJP
DEVENISH	74B	NP B81 330	R.C.E. Devenish, C.D. Froggatt, B.R. Martin	(DESY+)
KANE	74	LBL-2452	D.F. Kane	(LBL) IJP
PREVOST	74	NP B69 246	J. Prevost *et al.*	(SACL, CERN, HEID)
BARLETTA	72	NP B40 45	W.A. Barletta	(EFI) IJP
Also		PRL 17 841	S. Fenster *et al.*	(CHIC, ANL, CERN) IJP
ARMENTEROS	68C	NP B8 216	R. Armenteros *et al.*	(CERN, HEID, SACL) I
SIMS	68	PRL 21 1413	W.H. Sims *et al.*	(FSU, TUFTS, BRAN)
ARMENTEROS	67C	ZPHY 202 486	R. Armenteros *et al.*	(CERN, HEID, SACL)
UHLIG	67	PR 155 1448	R.P. Uhlig *et al.*	(UMD, NRL)
ARMENTEROS	65C	PL 19 338	R. Armenteros *et al.*	(CERN, HEID, SACL) IJP
GALTIERI	63	PL 6 296	A. Galtieri, A. Hussain, R. Tripp	(LRL) IJ

$\Sigma(1780)\ 3/2^+$

$I(J^P) = 1(\frac{3}{2}^+)$ Status: *

OMITTED FROM SUMMARY TABLE
was $\Sigma(1730)$

$\Sigma(1780)$ MASS

VALUE (MeV)	DOCUMENT ID		TECN	COMMENT
1730 to 1830 ($\approx$ 1780) OUR ESTIMATE				
1727 ± 27	ZHANG	13A	DPWA	Multichannel
1798 or 1802	[1] MARTIN	77	DPWA	$\overline{K}N$ multichannel
1720 ± 30	[2] BAILLON	75	IPWA	$\overline{K}N \to \Lambda\pi$
1840 ± 10	LANGBEIN	72	IPWA	$\overline{K}N$ multichannel

[1] The two MARTIN 77 values are from a T-matrix pole and from a Breit-Wigner fit.
[2] From solution 1 of BAILLON 75; not present in solution 2.

$\Sigma(1780)$ WIDTH

VALUE (MeV)	DOCUMENT ID		TECN	COMMENT
100 to 300 ($\approx$ 200) OUR ESTIMATE				
276 ± 87	ZHANG	13A	DPWA	Multichannel
93 or 93	[1] MARTIN	77	DPWA	$\overline{K}N$ multichannel
120 ± 30	[2] BAILLON	75	IPWA	$\overline{K}N \to \Lambda\pi$
120 ± 10	LANGBEIN	72	IPWA	$\overline{K}N$ multichannel

[1] The two MARTIN 77 values are from a T-matrix pole and from a Breit-Wigner fit.
[2] From solution 1 of BAILLON 75; not present in solution 2.

$\Sigma(1780)$ DECAY MODES

	Mode	Fraction (Γ_i/Γ)
Γ_1	$N\overline{K}$	(2.0 ± 1.0) %
Γ_2	$\Lambda\pi$	$(70\ \pm17\ )$ %
Γ_3	$\Sigma\pi$	$(12\ \pm6\ )$ %

$\Sigma(1780)$ BRANCHING RATIOS

$\Gamma(N\overline{K})/\Gamma_{total}$ Γ_1/Γ

VALUE	DOCUMENT ID		TECN	COMMENT
0.02±0.01	ZHANG	13A	DPWA	Multichannel

$\Gamma(\Lambda\pi)/\Gamma_{total}$ Γ_2/Γ

VALUE	DOCUMENT ID		TECN	COMMENT
0.70±0.17	ZHANG	13A	DPWA	Multichannel

$\Gamma(\Sigma\pi)/\Gamma_{total}$ Γ_3/Γ

VALUE	DOCUMENT ID		TECN	COMMENT
0.12±0.06	ZHANG	13A	DPWA	Multichannel

$\Sigma(1780)$ REFERENCES

ZHANG	13A	PR C88 035205	H. Zhang *et al.*	(KSU)
MARTIN	77	NP B127 349	B.R. Martin, M.K. Pidcock, R.G. Moorhouse	(LOUC+)
BAILLON	75	NP B94 39	P.H. Baillon, P.J. Litchfield	(CERN, RHEL)
LANGBEIN	72	NP B47 477	W. Langbein, F. Wagner	(MPIM)

$\Sigma(1880)\ 1/2^+$

$I(J^P) = 1(\frac{1}{2}^+)$ Status: **

OMITTED FROM SUMMARY TABLE

A P_{11} resonance is suggested by several partial-wave analyses, but with wide variations in the mass and other parameters. We list here all claims which lie well above the P_{11} $\Sigma(1770)$.

$\Sigma(1880)$ POLE POSITION

REAL PART

VALUE (MeV)	DOCUMENT ID		TECN	COMMENT
• • • We do not use the following data for averages, fits, limits, etc. • • •				
1776	ZHANG	13A	DPWA	Multichannel

$-2\times$IMAGINARY PART

VALUE (MeV)	DOCUMENT ID		TECN	COMMENT
• • • We do not use the following data for averages, fits, limits, etc. • • •				
270	ZHANG	13A	DPWA	Multichannel

$\Sigma(1880)$ MASS

VALUE (MeV)	DOCUMENT ID		TECN	COMMENT
1820 to 1940 ($\approx$ 1880) OUR ESTIMATE				
1821 ± 17	ZHANG	13A	DPWA	Multichannel
1826 ± 20	GOPAL	80	DPWA	$\overline{K}N \to \overline{K}N$
1870 ± 10	CAMERON	78B	DPWA	$K^-p \to N\overline{K}^*$
1847 or 1863	[1] MARTIN	77	DPWA	$\overline{K}N$ multichannel
1960 ± 30	[2] BAILLON	75	IPWA	$\overline{K}N \to \Lambda\pi$
1985 ± 50	VANHORN	75	DPWA	$K^-p \to \Lambda\pi^0$
1898	[3] LEA	73	DPWA	Multichannel K-matrix
~1850	ARMENTEROS	70	IPWA	$\overline{K}N \to \overline{K}N$
1950 ± 50	BARBARO-...	70	DPWA	$K^-N \to \Lambda\pi$
1920 ± 30	LITCHFIELD	70	DPWA	$K^-N \to \Lambda\pi$
1850	BAILEY	69	DPWA	$\overline{K}N \to \overline{K}N$
1882 ± 40	SMART	68	DPWA	$K^-N \to \Lambda\pi$

$\Sigma(1880)$ WIDTH

VALUE (MeV)	DOCUMENT ID		TECN	COMMENT
100 to 300 ($\approx$ 200) OUR ESTIMATE				
300 ± 59	ZHANG	13A	DPWA	Multichannel

86± 15	GOPAL	80	DPWA $\overline{K}N \to \overline{K}N$
80± 10	CAMERON	78B	DPWA $K^- p \to N\overline{K}^*$
216 or 220	[1] MARTIN	77	DPWA $\overline{K}N$ multichannel
260± 40	[2] BAILLON	75	IPWA $\overline{K}N \to \Lambda\pi$
220±140	VANHORN	75	DPWA $K^- p \to \Lambda\pi^0$
222	[3] LEA	73	DPWA Multichannel K-matrix
∼ 30	ARMENTEROS	70	IPWA $\overline{K}N \to \overline{K}N$
200± 50	BARBARO-...	70	DPWA $K^- N \to \Lambda\pi$
170± 40	LITCHFIELD	70	DPWA $K^- N \to \Lambda\pi$
200	BAILEY	69	DPWA $\overline{K}N \to \overline{K}N$
222±150	SMART	68	DPWA $K^- N \to \Lambda\pi$

$\Sigma(1880)$ DECAY MODES

	Mode	Fraction (Γ_i/Γ)
Γ_1	$N\overline{K}$	0.10 to 0.30 (≈ 0.20)
Γ_2	$\Lambda\pi$	
Γ_3	$\Sigma\pi$	
Γ_4	$\Lambda(1520)\pi$, D-wave	(2.0 ±1.0) %
Γ_5	$N\overline{K}^*(892)$, S=1/2, P-wave	
Γ_6	$N\overline{K}^*(892)$, S=3/2, P-wave	
Γ_7	$\Delta(1232)\overline{K}$, P-wave	(39 ±8) %

$\Sigma(1880)$ BRANCHING RATIOS

See "Sign conventions for resonance couplings" in the Note on Λ and Σ Resonances.

$\Gamma(N\overline{K})/\Gamma_{total}$ — Γ_1/Γ

VALUE	DOCUMENT ID		TECN	COMMENT
0.10 to 0.30 (≈ 0.20) OUR ESTIMATE				
0.10±0.03	ZHANG	13A	DPWA	Multichannel
0.06±0.02	GOPAL	80	DPWA	$\overline{K}N \to \overline{K}N$
0.27 or 0.27	[1] MARTIN	77	DPWA	$\overline{K}N$ multichannel
0.31	[3] LEA	73	DPWA	Multichannel K-matrix
0.20	ARMENTEROS	70	IPWA	$\overline{K}N \to \overline{K}N$
0.22	BAILEY	69	DPWA	$\overline{K}N \to \overline{K}N$

$(\Gamma_i\Gamma_f)^{1/2}/\Gamma_{total}$ in $N\overline{K} \to \Sigma(1880) \to \Lambda\pi$ — $(\Gamma_1\Gamma_2)^{1/2}/\Gamma$

VALUE	DOCUMENT ID		TECN	COMMENT
−0.24 or −0.24	[1] MARTIN	77	DPWA	$\overline{K}N$ multichannel
−0.12 ±0.02	[2] BAILLON	75	IPWA	$\overline{K}N \to \Lambda\pi$
$+0.05^{+0.07}_{-0.02}$	VANHORN	75	DPWA	$K^- p \to \Lambda\pi^0$
−0.169±0.119	DEVENISH	74B		Fixed-t dispersion rel.
−0.30	[3] LEA	73	DPWA	Multichannel K-matrix
−0.09 ±0.04	BARBARO-...	70	DPWA	$K^- N \to \Lambda\pi$
−0.14 ±0.03	LITCHFIELD	70	DPWA	$K^- N \to \Lambda\pi$
−0.11 ±0.03	SMART	68	DPWA	$K^- N \to \Lambda\pi$

$(\Gamma_i\Gamma_f)^{1/2}/\Gamma_{total}$ in $N\overline{K} \to \Sigma(1880) \to \Sigma\pi$ — $(\Gamma_1\Gamma_3)^{1/2}/\Gamma$

VALUE	DOCUMENT ID		TECN	COMMENT
+0.30 or +0.29	[1] MARTIN	77	DPWA	$\overline{K}N$ multichannel
not seen	[3] LEA	73	DPWA	Multichannel K-matrix

$\Gamma(\Lambda(1520)\pi, D\text{-wave})/\Gamma_{total}$ — Γ_4/Γ

VALUE	DOCUMENT ID		TECN	COMMENT
0.02±0.01	ZHANG	13A	DPWA	Multichannel

$(\Gamma_i\Gamma_f)^{1/2}/\Gamma_{total}$ in $N\overline{K} \to \Sigma(1880) \to N\overline{K}^*(892)$, S=1/2, P-wave — $(\Gamma_1\Gamma_5)^{1/2}/\Gamma$

VALUE	DOCUMENT ID		TECN	COMMENT
−0.05±0.03	[4] CAMERON	78B	DPWA	$K^- p \to N\overline{K}^*$

$(\Gamma_i\Gamma_f)^{1/2}/\Gamma_{total}$ in $N\overline{K} \to \Sigma(1880) \to N\overline{K}^*(892)$, S=3/2, P-wave — $(\Gamma_1\Gamma_6)^{1/2}/\Gamma$

VALUE	DOCUMENT ID		TECN	COMMENT
+0.11±0.03	CAMERON	78B	DPWA	$K^- p \to N\overline{K}^*$

$\Gamma(\Delta(1232)\overline{K}, P\text{-wave})/\Gamma_{total}$ — Γ_7/Γ

VALUE	DOCUMENT ID		TECN	COMMENT
0.39±0.08	ZHANG	13A	DPWA	Multichannel

$\Sigma(1880)$ FOOTNOTES

[1] The two MARTIN 77 values are from a T-matrix pole and from a Breit-Wigner fit.
[2] From solution 1 of BAILLON 75; not present in solution 2.
[3] Only unconstrained states from table 1 of LEA 73 are listed.
[4] The published sign has been changed to be in accord with the baryon-first convention.

$\Sigma(1880)$ REFERENCES

ZHANG	13A	PR C88 035205	H. Zhang *et al.*	(KSU)
GOPAL	80	Toronto Conf. 159	G.P. Gopal	(RHEL) IJP
CAMERON	78B	NP B146 327	W. Cameron *et al.*	(RHEL, LOIC) IJP
MARTIN	77	NP B127 349	B.R. Martin, M.K. Pidcock, R.G. Moorhouse	(LOUC+) IJP
Also		NP B126 266	B.R. Martin, M.K. Pidcock	(LOUC)
Also		NP B126 285	B.R. Martin, M.K. Pidcock	(LOUC) IJP
BAILLON	75	NP B94 39	P.H. Baillon, P.J. Litchfield	(CERN, RHEL) IJP
VANHORN	75	NP B87 145	A.J. van Horn	(LBL) IJP
Also		NP B87 157	A.J. van Horn	(LBL) IJP
DEVENISH	74B	NP B81 330	R.C.E. Devenish, C.D. Froggatt, B.R. Martin	(DESY+)
LEA	73	NP B56 77	A.T. Lea *et al.*	(RHEL, LOUC, GLAS, AARH) IJP
ARMENTEROS	70	Duke Conf. 123 Hyperon Resonances, 1970	R. Armenteros *et al.*	(CERN, HEID, SACL) IJP
BARBARO-...	70	Duke Conf. 173 Hyperon Resonances, 1970	A. Barbaro-Galtieri	(LRL) IJP
LITCHFIELD	70	NP B22 269	P.J. Litchfield	(RHEL) IJP
BAILEY	69	Thesis UCRL 50617	J.M. Bailey	(LLL) IJP
SMART	68	PR 169 1330	W.M. Smart	(LRL) IJP

$\Sigma(1900)$ $1/2^-$

$I(J^P) = 1(\frac{1}{2}^-)$ Status: ∗∗

OMITTED FROM SUMMARY TABLE

$\Sigma(1900)$ POLE POSITION

REAL PART

VALUE	DOCUMENT ID		TECN	COMMENT
1936±10	SARANTSEV	19	DPWA	$\overline{K}N$ multichannel

−2×IMAGINARY PART

VALUE	DOCUMENT ID		TECN	COMMENT
150±25	SARANTSEV	19	DPWA	$\overline{K}N$ multichannel

$\Sigma(1900)$ POLE RESIDUES

The normalized residue is the residue divided by $\Gamma_{pole}/2$.

Normalized residue in $N\overline{K} \to \Sigma(1900) \to N\overline{K}$

MODULUS	PHASE (°)	DOCUMENT ID		TECN	COMMENT
0.45±0.09	**90 ± 25**	SARANTSEV	19	DPWA	$\overline{K}N$ multichannel

Normalized residue in $N\overline{K} \to \Sigma(1900) \to \Sigma\pi$

MODULUS	PHASE (°)	DOCUMENT ID		TECN	COMMENT
0.38±0.08	**95 ± 20**	SARANTSEV	19	DPWA	$\overline{K}N$ multichannel

Normalized residue in $N\overline{K} \to \Sigma(1900) \to \Sigma\eta$

MODULUS	PHASE (°)	DOCUMENT ID		TECN	COMMENT
0.03±0.01	**20 ± 20**	SARANTSEV	19	DPWA	$\overline{K}N$ multichannel

Normalized residue in $N\overline{K} \to \Sigma(1900) \to \Lambda\pi$

MODULUS	PHASE (°)	DOCUMENT ID		TECN	COMMENT
0.14±0.05	**−160 ± 50**	SARANTSEV	19	DPWA	$\overline{K}N$ multichannel

Normalized residue in $N\overline{K} \to \Sigma(1900) \to \Xi K$

MODULUS	PHASE (°)	DOCUMENT ID		TECN	COMMENT
0.08±0.05	**75 ± 25**	SARANTSEV	19	DPWA	$\overline{K}N$ multichannel

Normalized residue in $N\overline{K} \to \Sigma(1900) \to \Sigma(1385)\pi$

MODULUS	PHASE (°)	DOCUMENT ID		TECN	COMMENT
0.16±0.05	**40 ± 30**	SARANTSEV	19	DPWA	$\overline{K}N$ multichannel

Normalized residue in $N\overline{K} \to \Sigma(1900) \to \Lambda(1520)\pi$

MODULUS	PHASE (°)	DOCUMENT ID		TECN	COMMENT
0.04±0.02	**−25 ± 40**	SARANTSEV	19	DPWA	$\overline{K}N$ multichannel

Normalized residue in $N\overline{K} \to \Sigma(1900) \to \Delta\overline{K}$

MODULUS	PHASE (°)	DOCUMENT ID		TECN	COMMENT
0.11±0.04	**60 ± 30**	SARANTSEV	19	DPWA	$\overline{K}N$ multichannel

Normalized residue in $N\overline{K} \to \Sigma(1900) \to N\overline{K}^*(892)$, S=1/2, S-wave

MODULUS	PHASE (°)	DOCUMENT ID		TECN	COMMENT
0.17±0.06	**50 ± 50**	SARANTSEV	19	DPWA	$\overline{K}N$ multichannel

Normalized residue in $N\overline{K} \to \Sigma(1900) \to N\overline{K}^*(892)$, S=3/2, D-wave

MODULUS	PHASE (°)	DOCUMENT ID		TECN	COMMENT
0.05±0.04		SARANTSEV	19	DPWA	$\overline{K}N$ multichannel

$\Sigma(1900)$ MASS

VALUE (MeV)	DOCUMENT ID		TECN	COMMENT
1900 to 1950 (≈ 1925) OUR ESTIMATE				
1938±12	SARANTSEV	19	DPWA	$\overline{K}N$ multichannel
1900±21	ZHANG	13A	DPWA	$\overline{K}N$ multichannel
1944±15	GOPAL	80	DPWA	$\overline{K}N \to \overline{K}N$
1755 or 1834	[1] MARTIN	77	DPWA	$\overline{K}N$ multichannel
2004±40	VANHORN	75	DPWA	$K^- p \to \Lambda\pi^0$
• • • We do not use the following data for averages, fits, limits, etc. • • •				
1955±15	GOPAL	77	DPWA	$\overline{K}N$ multichannel

[1] The two MARTIN 77 values are from a T-matrix pole and from a Breit-Wigner fit.

Int. J. Mod. Phys. A 2026.41. Downloaded from www.worldscientific.com
by UNIVERSITY OF CALIFORNIA @ BERKELEY on 09/16/26. Re-use and distribution is strictly not permitted, except for Open Access articles.

Int. J. Mod. Phys. A 2026.41. Downloaded from www.worldscientific.com
UNIVERSITY OF CALIFORNIA @ BERKELEY on 09/16/26. Re-use and distribution is strictly not permitted, except for Open Access articles.

$\Sigma(1900)$ WIDTH

VALUE (MeV)	DOCUMENT ID		TECN	COMMENT
140 to 190 (≈ 165) OUR ESTIMATE				
155±30	SARANTSEV	19	DPWA	$\overline{K}N$ multichannel
191±47	ZHANG	13A	DPWA	$\overline{K}N$ multichannel
215±25	GOPAL	80	DPWA	$\overline{K}N \to \overline{K}N$
413 or 450	[1] MARTIN	77	DPWA	$\overline{K}N$ multichannel
116±40	VANHORN	75	DPWA	$K^-p \to \Lambda\pi^0$
• • • We do not use the following data for averages, fits, limits, etc. • • •				
170±40	GOPAL	77	DPWA	$\overline{K}N$ multichannel

[1] The two MARTIN 77 values are from a T-matrix pole and from a Breit-Wigner fit.

$\Sigma(1900)$ DECAY MODES

	Mode	Fraction (Γ_i/Γ)
Γ_1	$N\overline{K}$	0.40 to 0.70 (≈ 0.55)
Γ_2	$\Sigma\pi$	0.10 to 0.40 (≈ 0.25)
Γ_3	$\Sigma\eta$	(1.0 ±1.0) %
Γ_4	$\Lambda\pi$	(6.0 ±2.0) %
Γ_5	ΞK	(3.0 ±2.0) %
Γ_6	$\Sigma(1385)\pi$	(7.0 ±3.0) %
Γ_7	$\Lambda(1520)\pi$	< 1 %
Γ_8	$\Delta\overline{K}$	(2.5 ±1.0) %
Γ_9	$N\overline{K}^*(892)$, S=1/2 , S-wave	(7.0 ±3.0) %
Γ_{10}	$N\overline{K}^*(892)$, S=3/2 , D-wave	< 1 %

$\Sigma(1900)$ BRANCHING RATIOS

$\Gamma(N\overline{K})/\Gamma_{total}$ — Γ_1/Γ

VALUE	DOCUMENT ID		TECN	COMMENT
0.40 to 0.70 (≈ 0.55) OUR ESTIMATE				
0.45±0.09	SARANTSEV	19	DPWA	$\overline{K}N$ multichannel
0.67±0.17	ZHANG	13A	DPWA	$\overline{K}N$ multichannel

$\Gamma(\Sigma\pi)/\Gamma_{total}$ — Γ_2/Γ

VALUE	DOCUMENT ID		TECN	COMMENT
0.10 to 0.40 (≈ 0.25) OUR ESTIMATE				
0.33±0.07	SARANTSEV	19	DPWA	$\overline{K}N$ multichannel
0.10±0.05	ZHANG	13A	DPWA	$\overline{K}N$ multichannel

$\Gamma(\Sigma\eta)/\Gamma_{total}$ — Γ_3/Γ

VALUE	DOCUMENT ID		TECN	COMMENT
0.01±0.01	SARANTSEV	19	DPWA	$\overline{K}N$ multichannel

$\Gamma(\Lambda\pi)/\Gamma_{total}$ — Γ_4/Γ

VALUE	DOCUMENT ID		TECN	COMMENT
0.06±0.02	SARANTSEV	19	DPWA	$\overline{K}N$ multichannel

$\Gamma(\Xi K)/\Gamma_{total}$ — Γ_5/Γ

VALUE	DOCUMENT ID		TECN	COMMENT
0.03±0.02	SARANTSEV	19	DPWA	$\overline{K}N$ multichannel

$\Gamma(\Sigma(1385)\pi)/\Gamma_{total}$ — Γ_6/Γ

VALUE	DOCUMENT ID		TECN	COMMENT
0.07±0.03	SARANTSEV	19	DPWA	$\overline{K}N$ multichannel

$\Gamma(\Lambda(1520)\pi)/\Gamma_{total}$ — Γ_7/Γ

VALUE	DOCUMENT ID		TECN	COMMENT
<0.01	SARANTSEV	19	DPWA	$\overline{K}N$ multichannel

$\Gamma(\Delta\overline{K})/\Gamma_{total}$ — Γ_8/Γ

VALUE	DOCUMENT ID		TECN	COMMENT
0.025±0.010	SARANTSEV	19	DPWA	$\overline{K}N$ multichannel

$\Gamma(N\overline{K}^*(892), S=1/2, S\text{-wave})/\Gamma_{total}$ — Γ_9/Γ

VALUE	DOCUMENT ID		TECN	COMMENT
0.07±0.03	SARANTSEV	19	DPWA	$\overline{K}N$ multichannel

$\Gamma(N\overline{K}^*(892), S=3/2, D\text{-wave})/\Gamma_{total}$ — Γ_{10}/Γ

VALUE	DOCUMENT ID		TECN	COMMENT
<0.01	SARANTSEV	19	DPWA	$\overline{K}N$ multichannel

$\Sigma(1900)$ REFERENCES

SARANTSEV	19	EPJ A55 180	A.V. Sarantsev *et al.*	(BONN, PNPI)
ZHANG	13A	PR C88 035205	H. Zhang *et al.*	(KSU)
GOPAL	80	Toronto Conf. 159	G.P. Gopal	(RHEL)
GOPAL	77	NP B119 362	G.P. Gopal *et al.*	(LOIC, RHEL)
MARTIN	77	NP B127 349	B.R. Martin, M.K. Pidcock, R.G. Moorhouse	(LOUC+)
VANHORN	75	NP B87 145	A.J. van Horn	(LBL)

$\Sigma(1910)\ 3/2^-$

$I(J^P) = 1(\frac{3}{2}^-)$ Status: ***

was $\Sigma(1940)$

For results published before 1974 (they are now obsolete), see our 1982 edition Physics Letters **111B** 1 (1982).

Not all analyses require this state. It is not required by the GOYAL 77 analysis of $K^-n \to (\Sigma\pi)^-$ nor by the GOPAL 80 analysis of $K^-n \to K^-n$. See also HEMINGWAY 75.

$\Sigma(1910)$ POLE RESIDUES

The normalized residue is the residue divided by $\Gamma_{pole}/2$.

Normalized residue in $N\overline{K} \to \Sigma(1910) \to N\overline{K}$

MODULUS	PHASE (°)	DOCUMENT ID		TECN	COMMENT
0.03±0.02	**−95 ± 60**	SARANTSEV	19	DPWA	$\overline{K}N$ multichannel

Normalized residue in $N\overline{K} \to \Sigma(1910) \to \Sigma\pi$

MODULUS	PHASE (°)	DOCUMENT ID		TECN	COMMENT
0.16±0.04	**−160 ± 15**	SARANTSEV	19	DPWA	$\overline{K}N$ multichannel

Normalized residue in $N\overline{K} \to \Sigma(1910) \to \Lambda\pi$

MODULUS	PHASE (°)	DOCUMENT ID		TECN	COMMENT
0.04±0.03	**25 ± 25**	SARANTSEV	19	DPWA	$\overline{K}N$ multichannel

Normalized residue in $N\overline{K} \to \Sigma(1910) \to \Xi\pi$

MODULUS	PHASE (°)	DOCUMENT ID		TECN	COMMENT
0.01±0.01		SARANTSEV	19	DPWA	$\overline{K}N$ multichannel

Normalized residue in $N\overline{K} \to \Sigma(1910) \to \Lambda(1520)\pi$, P-wave

MODULUS	PHASE (°)	DOCUMENT ID		TECN	COMMENT
0.01±0.01		SARANTSEV	19	DPWA	$\overline{K}N$ multichannel

Normalized residue in $N\overline{K} \to \Sigma(1910) \to \Lambda(1520)\pi$, F-wave

MODULUS	PHASE (°)	DOCUMENT ID		TECN	COMMENT
∼ 0		SARANTSEV	19	DPWA	$\overline{K}N$ multichannel

Normalized residue in $N\overline{K} \to \Sigma(1910) \to \Delta\overline{K}$, S-wave

MODULUS	PHASE (°)	DOCUMENT ID		TECN	COMMENT
0.03±0.01	**120 ± 20**	SARANTSEV	19	DPWA	$\overline{K}N$ multichannel

Normalized residue in $N\overline{K} \to \Sigma(1910) \to N\overline{K}^*(892)$, S=3/2, S-wave

MODULUS	PHASE (°)	DOCUMENT ID		TECN	COMMENT
0.03±0.02	**20 ± 35**	SARANTSEV	19	DPWA	$\overline{K}N$ multichannel

Normalized residue in $N\overline{K} \to \Sigma(1910) \to N\overline{K}^*(892)$, S=1/2, D-wave

MODULUS	PHASE (°)	DOCUMENT ID		TECN	COMMENT
0.02±0.01		SARANTSEV	19	DPWA	$\overline{K}N$ multichannel

Normalized residue in $N\overline{K} \to \Sigma(1910) \to N\overline{K}^*(892)$, S=3/2, D-wave

MODULUS	PHASE (°)	DOCUMENT ID		TECN	COMMENT
0.01±0.01		SARANTSEV	19	DPWA	$\overline{K}N$ multichannel

$\Sigma(1910)$ MASS

VALUE (MeV)	DOCUMENT ID		TECN	COMMENT
1870 to 1950 (≈ 1910) OUR ESTIMATE				
1912.1±10.6±33.6	ABLIKIM	25AF	BES3	$\psi(3686) \to \Lambda\overline{\Sigma}^0\pi^0$ + c.c. (PWA)
1878 ±12	SARANTSEV	19	DPWA	$\overline{K}N$ multichannel
1920 ±50	GOPAL	77	DPWA	$\overline{K}N$ multichannel
1950 ±30	BAILLON	75	IPWA	$\overline{K}N \to \Lambda\pi$
1949 $^{+40}_{-60}$	VANHORN	75	DPWA	$K^-p \to \Lambda\pi^0$
1935 ±80	KANE	74	DPWA	$K^-p \to \Sigma\pi$
1940 ±20	LITCHFIELD	74B	DPWA	$K^-p \to \Lambda(1520)\pi^0$
1950 ±20	LITCHFIELD	74C	DPWA	$K^-p \to \Delta(1232)\overline{K}$
• • • We do not use the following data for averages, fits, limits, etc. • • •				
1886 or 1893	[1] MARTIN	77	DPWA	$\overline{K}N$ multichannel
1940	DEBELLEFON	76	IPWA	$K^-p \to \Lambda\pi^0$, F_{17} wave

$\Sigma(1910)$ WIDTH

VALUE (MeV)	DOCUMENT ID		TECN	COMMENT
150 to 300 (≈ 220) OUR ESTIMATE				
225.1±24.5±46.0	ABLIKIM	25AF	BES3	$\psi(3686) \to \Lambda\overline{\Sigma}^0\pi^0$ + c.c. (PWA)
224 ±25	SARANTSEV	19	DPWA	$\overline{K}N$ multichannel
170 ±25	CAMERON	78B	DPWA	$K^-p \to N\overline{K}^*$
300 ±80	GOPAL	77	DPWA	$\overline{K}N$ multichannel
150 ±75	BAILLON	75	IPWA	$\overline{K}N \to \Lambda\pi$

$160\ ^{+70}_{-40}$	VANHORN	75	DPWA	$K^- p \to \Lambda\pi^0$	
330 ± 80	KANE	74	DPWA	$K^- p \to \Sigma\pi$	
60 ± 20	LITCHFIELD	74B	DPWA	$K^- p \to \Lambda(1520)\pi^0$	
$70\ ^{+30}_{-20}$	LITCHFIELD	74C	DPWA	$K^- p \to \Delta(1232)\overline{K}$	
• • • We do not use the following data for averages, fits, limits, etc. • • •					
157 or 159	[1] MARTIN	77	DPWA	$\overline{K}N$ multichannel	

$\Sigma(1910)$ DECAY MODES

	Mode	Fraction (Γ_i/Γ)
Γ_1	$N\overline{K}$	0.01 to 0.05 (≈ 0.02)
Γ_2	$\Lambda\pi$	(6 ± 4) %
Γ_3	$\Sigma\pi$	(86 ± 21) %
Γ_4	ΞK	
Γ_5	$\Sigma(1385)\pi$	seen
Γ_6	$\Sigma(1385)\pi$, S-wave	
Γ_7	$\Lambda(1520)\pi$	seen
Γ_8	$\Lambda(1520)\pi$, P-wave	
Γ_9	$\Lambda(1520)\pi$, F-wave	
Γ_{10}	$\Delta(1232)\overline{K}$	(3.0 ± 1.0) %
Γ_{11}	$\Delta(1232)\overline{K}$, S-wave	
Γ_{12}	$\Delta(1232)\overline{K}$, D-wave	
Γ_{13}	$N\overline{K}^*(892)$	seen
Γ_{14}	$N\overline{K}^*(892)$, S=3/2, S-wave	
Γ_{15}	$N\overline{K}^*(892)$, S=1/2 , D-wave	(1.0 ± 1.0) %
Γ_{16}	$N\overline{K}^*(892)$, S=3/2 , D-wave	

$\Sigma(1910)$ BRANCHING RATIOS

See "Sign conventions for resonance couplings" in the Note on Λ and Σ Resonances.

$\Gamma(N\overline{K})/\Gamma_{total}$ — Γ_1/Γ

VALUE	DOCUMENT ID		TECN	COMMENT
0.01 to 0.05 ($\approx$ 0.02) OUR ESTIMATE				
0.03 ± 0.02	SARANTSEV	19	DPWA	$\overline{K}N$ multichannel
<0.04	GOPAL	77	DPWA	$\overline{K}N$ multichannel
0.14 or 0.13	[1] MARTIN	77	DPWA	$\overline{K}N$ multichannel

$\Gamma(\Lambda\pi)/\Gamma_{total}$ — Γ_2/Γ

VALUE	DOCUMENT ID		TECN	COMMENT
0.06±0.04	SARANTSEV	19	DPWA	$\overline{K}N$ multichannel

$\Gamma(\Sigma\pi)/\Gamma_{total}$ — Γ_3/Γ

VALUE	DOCUMENT ID		TECN	COMMENT
0.86±0.21	SARANTSEV	19	DPWA	$\overline{K}N$ multichannel

$\Gamma(\Xi K)/\Gamma_{total}$ — Γ_4/Γ

VALUE	DOCUMENT ID		TECN	COMMENT
~ 0	SARANTSEV	19	DPWA	$\overline{K}N$ multichannel

$\Gamma(\Lambda(1520)\pi, P\text{-wave})/\Gamma_{total}$ — Γ_8/Γ

VALUE	DOCUMENT ID		TECN	COMMENT
~ 0	SARANTSEV	19	DPWA	$\overline{K}N$ multichannel

$\Gamma(\Lambda(1520)\pi, F\text{-wave})/\Gamma_{total}$ — Γ_9/Γ

VALUE	DOCUMENT ID		TECN	COMMENT
~ 0	SARANTSEV	19	DPWA	$\overline{K}N$ multichannel

$\Gamma(\Delta(1232)\overline{K})/\Gamma_{total}$ — Γ_{10}/Γ

VALUE	DOCUMENT ID		TECN	COMMENT
0.03±0.01	SARANTSEV	19	DPWA	$\overline{K}N$ multichannel

$\Gamma(N\overline{K}^*(892))/\Gamma_{total}$ — Γ_{13}/Γ

VALUE	DOCUMENT ID		TECN	COMMENT
0.03±0.02	SARANTSEV	19	DPWA	$\overline{K}N$ multichannel

$\Gamma(N\overline{K}^*(892), S=1/2, D\text{-wave})/\Gamma_{total}$ — Γ_{15}/Γ

VALUE	DOCUMENT ID		TECN	COMMENT
0.01±0.01	SARANTSEV	19	DPWA	$\overline{K}N$ multichannel

$\Gamma(N\overline{K}^*(892), S=3/2, D\text{-wave})/\Gamma_{total}$ — Γ_{16}/Γ

VALUE	DOCUMENT ID		TECN	COMMENT
~ 0	SARANTSEV	19	DPWA	$\overline{K}N$ multichannel

$(\Gamma_i\Gamma_f)^{1/2}/\Gamma_{total}$ in $N\overline{K} \to \Sigma(1910) \to \Lambda\pi$ — $(\Gamma_1\Gamma_2)^{1/2}/\Gamma$

VALUE	DOCUMENT ID		TECN	COMMENT
-0.06 ± 0.03	GOPAL	77	DPWA	$\overline{K}N$ multichannel
-0.04 ± 0.02	BAILLON	75	IPWA	$\overline{K}N \to \Lambda\pi$
$-0.05\ ^{+0.03}_{-0.02}$	VANHORN	75	DPWA	$K^- p \to \Lambda\pi^0$
-0.153 ± 0.070	DEVENISH	74B		Fixed-t dispersion rel.
• • • We do not use the following data for averages, fits, limits, etc. • • •				
-0.15 or -0.14	[1] MARTIN	77	DPWA	$\overline{K}N$ multichannel

$(\Gamma_i\Gamma_f)^{1/2}/\Gamma_{total}$ in $N\overline{K} \to \Sigma(1910) \to \Sigma\pi$ — $(\Gamma_1\Gamma_3)^{1/2}/\Gamma$

VALUE	DOCUMENT ID		TECN	COMMENT
-0.08 ± 0.04	GOPAL	77	DPWA	$\overline{K}N$ multichannel
-0.14 ± 0.04	KANE	74	DPWA	$K^- p \to \Sigma\pi$
• • • We do not use the following data for averages, fits, limits, etc. • • •				
$+0.16$ or $+0.16$	[1] MARTIN	77	DPWA	$\overline{K}N$ multichannel

$(\Gamma_i\Gamma_f)^{1/2}/\Gamma_{total}$ in $N\overline{K} \to \Sigma(1910) \to \Sigma(1385)\pi$ — $(\Gamma_1\Gamma_5)^{1/2}/\Gamma$

VALUE	DOCUMENT ID		TECN	COMMENT
$+0.066 \pm 0.025$	[2] CAMERON	78	DPWA	$K^- p \to \Sigma(1385)\pi$

$(\Gamma_i\Gamma_f)^{1/2}/\Gamma_{total}$ in $N\overline{K} \to \Sigma(1910) \to \Lambda(1520)\pi$, P-wave — $(\Gamma_1\Gamma_8)^{1/2}/\Gamma$

VALUE	DOCUMENT ID		TECN	COMMENT
< 0.03	CAMERON	77	DPWA	$K^- p \to \Lambda(1520)\pi^0$
-0.11 ± 0.04	LITCHFIELD	74B	DPWA	$K^- p \to \Lambda(1520)\pi^0$

$(\Gamma_i\Gamma_f)^{1/2}/\Gamma_{total}$ in $N\overline{K} \to \Sigma(1910) \to \Lambda(1520)\pi$, F-wave — $(\Gamma_1\Gamma_9)^{1/2}/\Gamma$

VALUE	DOCUMENT ID		TECN	COMMENT
0.062 ± 0.021	CAMERON	77	DPWA	$K^- p \to \Lambda(1520)\pi^0$
-0.08 ± 0.04	LITCHFIELD	74B	DPWA	$K^- p \to \Lambda(1520)\pi^0$

$(\Gamma_i\Gamma_f)^{1/2}/\Gamma_{total}$ in $N\overline{K} \to \Sigma(1910) \to \Delta(1232)\overline{K}$, S-wave — $(\Gamma_1\Gamma_{11})^{1/2}/\Gamma$

VALUE	DOCUMENT ID		TECN	COMMENT
-0.16 ± 0.05	LITCHFIELD	74C	DPWA	$K^- p \to \Delta(1232)\overline{K}$

$(\Gamma_i\Gamma_f)^{1/2}/\Gamma_{total}$ in $N\overline{K} \to \Sigma(1910) \to \Delta(1232)\overline{K}$, D-wave — $(\Gamma_1\Gamma_{12})^{1/2}/\Gamma$

VALUE	DOCUMENT ID		TECN	COMMENT
-0.14 ± 0.05	LITCHFIELD	74C	DPWA	$K^- p \to \Delta(1232)\overline{K}$

$(\Gamma_i\Gamma_f)^{1/2}/\Gamma_{total}$ in $N\overline{K} \to \Sigma(1910) \to N\overline{K}^*(892)$ — $(\Gamma_1\Gamma_{13})^{1/2}/\Gamma$

VALUE	DOCUMENT ID		TECN	COMMENT
-0.09 ± 0.02	[3] CAMERON	78B	DPWA	$K^- p \to N\overline{K}^*$

$\Sigma(1910)$ FOOTNOTES

[1] The two MARTIN 77 values are from a T-matrix pole and from a Breit-Wigner fit.
[2] The published sign has been changed to be in accord with the baryon-first convention.
[3] Upper limits on the D_1 and D_3 waves are each 0.03.

$\Sigma(1910)$ REFERENCES

ABLIKIM	25AF	JHEP 2502 212	M. Ablikim *et al.*	(BESIII Collab.)
SARANTSEV	19	EPJ A55 180	A.V. Sarantsev *et al.*	(BONN, PNPI)
PDG	82	PL 111B 1	M. Roos *et al.*	(HELS, CIT, CERN)
GOPAL	80	Toronto Conf. 159	G.P. Gopal	(RHEL)
CAMERON	78	NP B143 189	W. Cameron *et al.*	(RHEL, LOIC) IJP
CAMERON	78B	NP B146 327	W. Cameron *et al.*	(RHEL, LOIC) IJP
CAMERON	77	NP B131 399	W. Cameron *et al.*	(RHEL, LOIC) IJP
GOPAL	77	NP B119 362	G.P. Gopal *et al.*	(LOIC, RHEL) IJP
GOYAL	77	PR D16 2746	D.P. Goyal, A.V. Sodhi	(DELH)
MARTIN	77	NP B127 349	B.R. Martin, M.K. Pidcock, R.G. Moorhouse	(LOUC+) IJP
Also		NP B126 266	B.R. Martin, M.K. Pidcock	(LOUC)
Also		NP B126 285	B.R. Martin, M.K. Pidcock	(LOUC) IJP
DEBELLEFON	76	NP B109 129	A. de Bellefon, A. Berthon	(CDEF) IJP
BAILLON	75	NP B94 39	P.H. Baillon, P.J. Litchfield	(CERN, RHEL) IJP
HEMINGWAY	75	NP B91 12	R.J. Hemingway *et al.*	(CERN, HEIDH, MPIM) IJP
VANHORN	75	NP B87 145	A.J. van Horn	(LBL) IJP
Also		NP B87 157	A.J. van Horn	(LBL) IJP
DEVENISH	74B	NP B81 330	R.C.E. Devenish, C.D. Froggatt, B.R. Martin	(DESY+)
KANE	74	LBL-2452	D.F. Kane	(LBL) IJP
LITCHFIELD	74B	NP B74 19	P.J. Litchfield *et al.*	(CERN, HEIDH) IJP
LITCHFIELD	74C	NP B74 39	P.J. Litchfield *et al.*	(CERN, HEIDH) IJP

$\Sigma(1915)\ 5/2^+$

$I(J^P) = 1(\frac{5}{2}^+)$ Status: ****

Discovered by COOL 66. For results published before 1974 (they are now obsolete), see our 1982 edition Physics Letters **111B** 1 (1982).

This entry only includes results from partial-wave analyses. Parameters of peaks seen in cross sections and invariant-mass distributions in this region used to be listed in in a separate entry immediately following. They may be found in our 1986 edition Physics Letters **170B** 1 (1986).

$\Sigma(1915)$ POLE POSITION

REAL PART

VALUE (MeV)	DOCUMENT ID		TECN	COMMENT
1885 to 1915 ($\approx$ 1900) OUR ESTIMATE				
1908 ± 7	SARANTSEV	19	DPWA	$\overline{K}N$ multichannel
$1890\ ^{+3}_{-2}$	[1] KAMANO	15	DPWA	$\overline{K}N$ multichannel
• • • We do not use the following data for averages, fits, limits, etc. • • •				
1897	ZHANG	13A	DPWA	$\overline{K}N$ multichannel

[1] From the preferred solution A in KAMANO 15.

Int. J. Mod. Phys. A 2026.41. Downloaded from www.worldscientific.com
by UNIVERSITY OF CALIFORNIA @ BERKELEY on 09/16/26. Re-use and distribution is strictly not permitted, except for Open Access articles.

Int. J. Mod. Phys. A 2026.41. Downloaded from www.worldscientific.com
UNIVERSITY OF CALIFORNIA @ BERKELEY on 09/16/26. Re-use and distribution is strictly not permitted, except for Open Access articles.

−2×IMAGINARY PART

VALUE (MeV)	DOCUMENT ID		TECN	COMMENT
90 to 110 (≈ 100) OUR ESTIMATE				
98±12	SARANTSEV	19	DPWA	$\overline{K}N$ multichannel
97^{+4}_{-6}	[1] KAMANO	15	DPWA	$\overline{K}N$ multichannel
• • • We do not use the following data for averages, fits, limits, etc. • • •				
133	ZHANG	13A	DPWA	$\overline{K}N$ multichannel

[1] From the preferred solution A in KAMANO 15.

$\Sigma(1915)$ POLE RESIDUES

The normalized residue is the residue divided by $\Gamma_{pole}/2$.

Normalized residue in $N\overline{K} \to \Sigma(1915) \to N\overline{K}$

MODULUS	PHASE (°)	DOCUMENT ID		TECN	COMMENT
0.08 ±0.02	**−33 ± 15**	SARANTSEV	19	DPWA	$\overline{K}N$ multichannel
• • • We do not use the following data for averages, fits, limits, etc. • • •					
0.0391	−15	[1] KAMANO	15	DPWA	$\overline{K}N$ multichannel

[1] From the preferred solution A in KAMANO 15.

Normalized residue in $N\overline{K} \to \Sigma(1915) \to \Sigma\pi$

MODULUS	PHASE (°)	DOCUMENT ID		TECN	COMMENT
0.09 ±0.02	**180 ± 12**	SARANTSEV	19	DPWA	$\overline{K}N$ multichannel
• • • We do not use the following data for averages, fits, limits, etc. • • •					
0.157	157	[1] KAMANO	15	DPWA	$\overline{K}N$ multichannel

[1] From the preferred solution A in KAMANO 15.

Normalized residue in $N\overline{K} \to \Sigma(1915) \to \Lambda\pi$

MODULUS	PHASE (°)	DOCUMENT ID		TECN	COMMENT
0.07 ±0.02	**−170 ± 20**	SARANTSEV	19	DPWA	$\overline{K}N$ multichannel
• • • We do not use the following data for averages, fits, limits, etc. • • •					
0.0757	166	[1] KAMANO	15	DPWA	$\overline{K}N$ multichannel

[1] From the preferred solution A in KAMANO 15.

Normalized residue in $N\overline{K} \to \Sigma(1915) \to \Xi K$

MODULUS	PHASE (°)	DOCUMENT ID		TECN	COMMENT
0.02 ±0.01	**−65 ± 35**	SARANTSEV	19	DPWA	$\overline{K}N$ multichannel
• • • We do not use the following data for averages, fits, limits, etc. • • •					
0.002	−88	[1] KAMANO	15	DPWA	$\overline{K}N$ multichannel

[1] From the preferred solution A in KAMANO 15.

Normalized residue in $N\overline{K} \to \Lambda(1915) \to \Sigma(1385)\pi$, P-wave

MODULUS	PHASE (°)	DOCUMENT ID		TECN	COMMENT
0.02 ±0.02		SARANTSEV	19	DPWA	$\overline{K}N$ multichannel
• • • We do not use the following data for averages, fits, limits, etc. • • •					
0.0724	161	[1] KAMANO	15	DPWA	$\overline{K}N$ multichannel

[1] From the preferred solution A in KAMANO 15.

Normalized residue in $N\overline{K} \to \Lambda(1915) \to \Sigma(1385)\pi$, F-wave

MODULUS	PHASE (°)	DOCUMENT ID		TECN	COMMENT
0.05 ±0.03	**−30 ± 50**	SARANTSEV	19	DPWA	$\overline{K}N$ multichannel
• • • We do not use the following data for averages, fits, limits, etc. • • •					
0.0162	−163	[1] KAMANO	15	DPWA	$\overline{K}N$ multichannel

[1] From the preferred solution A in KAMANO 15.

Normalized residue in $N\overline{K} \to \Sigma(1915) \to \Lambda(1520)\pi$, D-wave

MODULUS	PHASE (°)	DOCUMENT ID		TECN	COMMENT
0.08±0.02	**−105 ± 50**	SARANTSEV	19	DPWA	$\overline{K}N$ multichannel

Normalized residue in $N\overline{K} \to \Sigma(1915) \to \Delta\overline{K}$, P-wave

MODULUS	PHASE (°)	DOCUMENT ID		TECN	COMMENT
0.12±0.03	**−10 ± 20**	SARANTSEV	19	DPWA	$\overline{K}N$ multichannel

Normalized residue in $N\overline{K} \to \Sigma(1915) \to \Delta\overline{K}$, F-wave

MODULUS	PHASE (°)	DOCUMENT ID		TECN	COMMENT
0.07±0.02	**−35 ± 25**	SARANTSEV	19	DPWA	$\overline{K}N$ multichannel

Normalized residue in $N\overline{K} \to \Sigma(1915) \to \Lambda(1520)\pi$, G-wave

MODULUS	PHASE (°)	DOCUMENT ID		TECN	COMMENT
0.01±0.01		SARANTSEV	19	DPWA	$\overline{K}N$ multichannel

Normalized residue in $N\overline{K} \to \Sigma(1915) \to N\overline{K}^*(892)$, S=1/2 , F-wave

MODULUS	PHASE (°)	DOCUMENT ID		TECN	COMMENT
0.07 ±0.04	**−60 ± 45**	SARANTSEV	19	DPWA	$\overline{K}N$ multichannel
• • • We do not use the following data for averages, fits, limits, etc. • • •					
0.00476	4	[1] KAMANO	15	DPWA	$\overline{K}N$ multichannel

[1] From the preferred solution A in KAMANO 15.

Normalized residue in $N\overline{K} \to \Sigma(1915) \to N\overline{K}^*(892)$, S=3/2 , P-wave

MODULUS	PHASE (°)	DOCUMENT ID		TECN	COMMENT
• • • We do not use the following data for averages, fits, limits, etc. • • •					
0.0494	51	[1] KAMANO	15	DPWA	$\overline{K}N$ multichannel

[1] From the preferred solution A in KAMANO 15.

Normalized residue in $N\overline{K} \to \Sigma(1915) \to N\overline{K}^*(892)$, S=3/2 , F-wave

MODULUS	PHASE (°)	DOCUMENT ID		TECN	COMMENT
0.07 ±0.03	**−40 ± 45**	SARANTSEV	19	DPWA	$\overline{K}N$ multichannel
• • • We do not use the following data for averages, fits, limits, etc. • • •					
0.000314	16	[1] KAMANO	15	DPWA	$\overline{K}N$ multichannel

[1] From the preferred solution A in KAMANO 15.

$\Sigma(1915)$ MASS

VALUE (MeV)	DOCUMENT ID		TECN	COMMENT
1900 to 1935 (≈ 1915) OUR ESTIMATE				
1918± 6	SARANTSEV	19	DPWA	$\overline{K}N$ multichannel
1920± 7	ZHANG	13A	DPWA	$\overline{K}N$ multichannel
1937±20	ALSTON-...	78	DPWA	$\overline{K}N \to \overline{K}N$
1894± 5	[1] CORDEN	77C		$K^-n \to \Sigma\pi$
1909± 5	[1] CORDEN	77C		$K^-n \to \Sigma\pi$
1920±10	GOPAL	77	DPWA	$\overline{K}N$ multichannel
1920±30	BAILLON	75	IPWA	$\overline{K}N \to \Lambda\pi$
1914±10	HEMINGWAY	75	DPWA	$K^-p \to \overline{K}N$
1920^{+15}_{-20}	VANHORN	75	DPWA	$K^-p \to \Lambda\pi^0$
1920± 5	KANE	74	DPWA	$K^-p \to \Sigma\pi$
• • • We do not use the following data for averages, fits, limits, etc. • • •				
not seen	DECLAIS	77	DPWA	$\overline{K}N \to \overline{K}N$
1925 or 1933	[2] MARTIN	77	DPWA	$\overline{K}N$ multichannel
1900± 4	[3] CORDEN	76	DPWA	$K^-n \to \Lambda\pi^-$
1915	DEBELLEFON	76	IPWA	$K^-p \to \Lambda\pi^0$

[1] The two entries for CORDEN 77C are from two different acceptable solutions.
[2] The two MARTIN 77 values are from a T-matrix pole and from a Breit-Wigner fit.
[3] Preferred solution 3; see CORDEN 76 for other possibilities.

$\Sigma(1915)$ WIDTH

VALUE (MeV)	DOCUMENT ID		TECN	COMMENT
80 to 160 (≈ 120) OUR ESTIMATE				
102±12	SARANTSEV	19	DPWA	$\overline{K}N$ multichannel
149±17	ZHANG	13A	DPWA	Multichannel
161±20	ALSTON-...	78	DPWA	$\overline{K}N \to \overline{K}N$
107±14	[1] CORDEN	77C		$K^-n \to \Sigma\pi$
85±13	[1] CORDEN	77C		$K^-n \to \Sigma\pi$
130±10	GOPAL	77	DPWA	$\overline{K}N$ multichannel
70±20	BAILLON	75	IPWA	$\overline{K}N \to \Lambda\pi$
85±15	HEMINGWAY	75	DPWA	$K^-p \to \overline{K}N$
102±18	VANHORN	75	DPWA	$K^-p \to \Lambda\pi^0$
162±25	KANE	74	DPWA	$K^-p \to \Sigma\pi$
• • • We do not use the following data for averages, fits, limits, etc. • • •				
171 or 173	[2] MARTIN	77	DPWA	$\overline{K}N$ multichannel
75±14	[3] CORDEN	76	DPWA	$K^-n \to \Lambda\pi^-$
60	DEBELLEFON	76	IPWA	$K^-p \to \Lambda\pi^0$

[1] The two entries for CORDEN 77C are from two different acceptable solutions.
[2] The two MARTIN 77 values are from a T-matrix pole and from a Breit-Wigner fit.
[3] Preferred solution 3; see CORDEN 76 for other possibilities.

$\Sigma(1915)$ DECAY MODES

	Mode	Fraction (Γ_i/Γ)
Γ_1	$N\overline{K}$	0.05 to 0.15
Γ_2	$\Lambda\pi$	(6.0 ±2.0) %
Γ_3	$\Sigma\pi$	(10.0 ±2.0) %
Γ_4	ΞK	
Γ_5	$\Sigma(1385)\pi$	
Γ_6	$\Sigma(1385)\pi$, P-wave	(2.0 ±2.0) %
Γ_7	$\Sigma(1385)\pi$, F-wave	(4.0 ±2.0) %
Γ_8	$\Lambda(1520)\pi$, D-wave	(8.0 ±2.0) %
Γ_9	$\Lambda(1520)\pi$, G-wave	
Γ_{10}	$N\overline{K}^*(892)$, S=1/2, F-wave	(5.0 ±3.0) %
Γ_{11}	$N\overline{K}^*(892)$, S=3/2, P-wave	
Γ_{12}	$N\overline{K}^*(892)$, S=3/2, F-wave	(5.0 ±2.0) %
Γ_{13}	$\Delta\overline{K}$, P-wave	(16 ±5) %
Γ_{14}	$\Delta\overline{K}$, F-wave	(5.0 ±3.0) %

Int. J. Mod. Phys. A 2026.41. Downloaded from www.worldscientific.com
by UNIVERSITY OF CALIFORNIA @ BERKELEY on 09/16/26. Re-use and distribution is strictly not permitted, except for Open Access articles.

$\Sigma(1915)$ BRANCHING RATIOS

See "Sign conventions for resonance couplings" in the Note on Λ and Σ Resonances.

$\Gamma(N\overline{K})/\Gamma_{total}$ — Γ_1/Γ

VALUE	DOCUMENT ID		TECN	COMMENT
0.05 to 0.15 OUR ESTIMATE				
0.08 ±0.02	SARANTSEV	19	DPWA	$\overline{K}N$ multichannel
0.026±0.004	ZHANG	13A	DPWA	$\overline{K}N$ multichannel
0.03 ±0.02	[1] GOPAL	80	DPWA	$\overline{K}N \to \overline{K}N$
0.14 ±0.05	ALSTON-...	78	DPWA	$\overline{K}N \to \overline{K}N$
0.11 ±0.04	HEMINGWAY	75	DPWA	$K^-p \to \overline{K}N$
• • • We do not use the following data for averages, fits, limits, etc. • • •				
0.036	[2] KAMANO	15	DPWA	$\overline{K}N$ multichannel
0.05 ±0.03	GOPAL	77	DPWA	See GOPAL 80
0.08 or 0.08	[3] MARTIN	77	DPWA	$\overline{K}N$ multichannel

[1] The mass and width are fixed to the GOPAL 77 values due to the low elasticity.
[2] From the preferred solution A in KAMANO 15.
[3] The two MARTIN 77 values are from a T-matrix pole and from a Breit-Wigner fit.

$\Gamma(\Lambda\pi)/\Gamma_{total}$ — Γ_2/Γ

VALUE	DOCUMENT ID		TECN	COMMENT
0.06 ±0.02	SARANTSEV	19	DPWA	$\overline{K}N$ multichannel
• • • We do not use the following data for averages, fits, limits, etc. • • •				
0.127	[1] KAMANO	15	DPWA	$\overline{K}N$ multichannel

[1] From the preferred solution A in KAMANO 15.

$\Gamma(\Sigma\pi)/\Gamma_{total}$ — Γ_3/Γ

VALUE	DOCUMENT ID		TECN	COMMENT
0.10 ±0.02	SARANTSEV	19	DPWA	$\overline{K}N$ multichannel
• • • We do not use the following data for averages, fits, limits, etc. • • •				
0.678	[1] KAMANO	15	DPWA	$\overline{K}N$ multichannel

[1] From the preferred solution A in KAMANO 15.

$\Gamma(\Xi K)/\Gamma_{total}$ — Γ_4/Γ

VALUE	DOCUMENT ID		TECN	COMMENT
<0.01	SARANTSEV	19	DPWA	$\overline{K}N$ multichannel
• • • We do not use the following data for averages, fits, limits, etc. • • •				
not seen	[1] KAMANO	15	DPWA	Multichannel

[1] From the preferred solution A in KAMANO 15.

$\Gamma(\Sigma(1385)\pi, P\text{-wave})/\Gamma_{total}$ — Γ_6/Γ

VALUE	DOCUMENT ID		TECN	COMMENT
0.02 ±0.02	SARANTSEV	19	DPWA	$\overline{K}N$ multichannel
• • • We do not use the following data for averages, fits, limits, etc. • • •				
0.112	[1] KAMANO	15	DPWA	$\overline{K}N$ multichannel

[1] From the preferred solution A in KAMANO 15.

$\Gamma(\Sigma(1385)\pi, F\text{-wave})/\Gamma_{total}$ — Γ_7/Γ

VALUE	DOCUMENT ID		TECN	COMMENT
0.04 ±0.02	SARANTSEV	19	DPWA	$\overline{K}N$ multichannel
• • • We do not use the following data for averages, fits, limits, etc. • • •				
0.004	[1] KAMANO	15	DPWA	$\overline{K}N$ multichannel

[1] From the preferred solution A in KAMANO 15.

$\Gamma(\Lambda(1520)\pi, D\text{-wave})/\Gamma_{total}$ — Γ_8/Γ

VALUE	DOCUMENT ID		TECN	COMMENT
0.08±0.02	SARANTSEV	19	DPWA	$\overline{K}N$ multichannel

$\Gamma(\Lambda(1520)\pi, G\text{-wave})/\Gamma_{total}$ — Γ_9/Γ

VALUE	DOCUMENT ID		TECN	COMMENT
~ 0	SARANTSEV	19	DPWA	$\overline{K}N$ multichannel

$\Gamma(N\overline{K}^*(892), S=1/2, F\text{-wave})/\Gamma_{total}$ — Γ_{10}/Γ

VALUE	DOCUMENT ID		TECN	COMMENT
0.05 ±0.03	SARANTSEV	19	DPWA	$\overline{K}N$ multichannel
• • • We do not use the following data for averages, fits, limits, etc. • • •				
0.001	[1] KAMANO	15	DPWA	Multichannel

[1] From the preferred solution A in KAMANO 15.

$\Gamma(N\overline{K}^*(892), S=3/2, P\text{-wave})/\Gamma_{total}$ — Γ_{11}/Γ

VALUE	DOCUMENT ID		TECN	COMMENT
• • • We do not use the following data for averages, fits, limits, etc. • • •				
0.042	[1] KAMANO	15	DPWA	Multichannel

[1] From the preferred solution A in KAMANO 15.

$\Gamma(N\overline{K}^*(892), S=3/2, F\text{-wave})/\Gamma_{total}$ — Γ_{12}/Γ

VALUE	DOCUMENT ID		TECN	COMMENT
0.05±0.02	SARANTSEV	19	DPWA	$\overline{K}N$ multichannel
• • • We do not use the following data for averages, fits, limits, etc. • • •				
not seen	[1] KAMANO	15	DPWA	Multichannel

[1] From the preferred solution A in KAMANO 15.

$\Gamma(\Delta\overline{K}, P\text{-wave})/\Gamma_{total}$ — Γ_{13}/Γ

VALUE	DOCUMENT ID		TECN	COMMENT
0.16±0.05	SARANTSEV	19	DPWA	$\overline{K}N$ multichannel

$\Gamma(\Delta\overline{K}, F\text{-wave})/\Gamma_{total}$ — Γ_{14}/Γ

VALUE	DOCUMENT ID		TECN	COMMENT
0.05±0.03	SARANTSEV	19	DPWA	$\overline{K}N$ multichannel

$(\Gamma_i\Gamma_f)^{1/2}/\Gamma_{total}$ in $N\overline{K} \to \Sigma(1915) \to \Lambda\pi$ — $(\Gamma_1\Gamma_2)^{1/2}/\Gamma$

VALUE	DOCUMENT ID		TECN	COMMENT
−0.09 ±0.03	GOPAL	77	DPWA	$\overline{K}N$ multichannel
−0.10 ±0.01	[1] CORDEN	76	DPWA	$K^-n \to \Lambda\pi^-$
−0.06 ±0.02	BAILLON	75	IPWA	$\overline{K}N \to \Lambda\pi$
−0.09 ±0.02	VANHORN	75	DPWA	$K^-p \to \Lambda\pi^0$
−0.087±0.056	DEVENISH	74B		Fixed-t dispersion rel.
• • • We do not use the following data for averages, fits, limits, etc. • • •				
−0.09 or −0.09	[2] MARTIN	77	DPWA	$\overline{K}N$ multichannel
−0.10	DEBELLEFON	76	IPWA	$K^-p \to \Lambda\pi^0$

[1] Preferred solution 3; see CORDEN 76 for other possibilities.
[2] The two MARTIN 77 values are from a T-matrix pole and from a Breit-Wigner fit.

$(\Gamma_i\Gamma_f)^{1/2}/\Gamma_{total}$ in $N\overline{K} \to \Sigma(1915) \to \Sigma\pi$ — $(\Gamma_1\Gamma_3)^{1/2}/\Gamma$

VALUE	DOCUMENT ID		TECN	COMMENT
−0.14±0.01	ZHANG	13A	DPWA	Multichannel
−0.17±0.01	[1] CORDEN	77C		$K^-n \to \Sigma\pi$
−0.15±0.02	[1] CORDEN	77C		$K^-n \to \Sigma\pi$
−0.19±0.03	GOPAL	77	DPWA	$\overline{K}N$ multichannel
−0.16±0.03	KANE	74	DPWA	$K^-p \to \Sigma\pi$
• • • We do not use the following data for averages, fits, limits, etc. • • •				
−0.05 or −0.05	[2] MARTIN	77	DPWA	$\overline{K}N$ multichannel

[1] The two entries for CORDEN 77C are from two different acceptable solutions.
[2] The two MARTIN 77 values are from a T-matrix pole and from a Breit-Wigner fit.

$(\Gamma_i\Gamma_f)^{1/2}/\Gamma_{total}$ in $N\overline{K} \to \Sigma(1915) \to \Sigma(1385)\pi$, P-wave — $(\Gamma_1\Gamma_6)^{1/2}/\Gamma$

VALUE	DOCUMENT ID		TECN	COMMENT
<0.01	CAMERON	78	DPWA	$K^-p \to \Sigma(1385)\pi$

$(\Gamma_i\Gamma_f)^{1/2}/\Gamma_{total}$ in $N\overline{K} \to \Sigma(1915) \to \Sigma(1385)\pi$, F-wave — $(\Gamma_1\Gamma_7)^{1/2}/\Gamma$

VALUE	DOCUMENT ID		TECN	COMMENT
+0.06 ±0.02	ZHANG	13A	DPWA	Multichannel
+0.039±0.009	[1] CAMERON	78	DPWA	$K^-p \to \Sigma(1385)\pi$

[1] The published sign has been changed to be in accord with the baryon-first convention.

$\Sigma(1915)$ REFERENCES

SARANTSEV	19	EPJ A55 180	A.V. Sarantsev *et al.*	(BONN, PNPI)
KAMANO	15	PR C92 025205	H. Kamano *et al.*	(ANL, OSAK)
ZHANG	13A	PR C88 035205	H. Zhang *et al.*	(KSU)
PDG	86	PL 170B 1	M. Aguilar-Benitez *et al.*	(CERN, CIT+)
PDG	82	PL 111B 1	M. Roos *et al.*	(HELS, CIT, CERN)
GOPAL	80	Toronto Conf. 159	G.P. Gopal	(RHEL) IJP
ALSTON-...	78	PR D18 182	M. Alston-Garnjost *et al.*	(LBL, MTHO+) IJP
Also		PRL 38 1007	M. Alston-Garnjost *et al.*	(LBL, MTHO+) IJP
CAMERON	78	NP B143 189	W. Cameron *et al.*	(RHEL, LOIC) IJP
CORDEN	77C	NP B125 61	M.J. Corden *et al.*	(BIRM) IJP
DECLAIS	77	CERN 77-16	Y. Declais *et al.*	(CAEN, CERN) IJP
GOPAL	77	NP B119 362	G.P. Gopal *et al.*	(LOIC, RHEL) IJP
MARTIN	77	NP B127 349	B.R. Martin, M.K. Pidcock, R.G. Moorhouse	(LOUC+) IJP
Also		NP B126 266	B.R. Martin, M.K. Pidcock	(LOUC)
Also		NP B126 285	B.R. Martin, M.K. Pidcock	(LOUC) IJP
CORDEN	76	NP B104 382	M.J. Corden *et al.*	(BIRM) IJP
DEBELLEFON	76	NP B109 129	A. de Bellefon, A. Berthon	(CDEF) IJP
BAILLON	75	NP B94 39	P.H. Baillon, P.J. Litchfield	(CERN, RHEL) IJP
HEMINGWAY	75	NP B91 12	R.J. Hemingway *et al.*	(CERN, HEIDH, MPIM) IJP
VANHORN	75	NP B87 145	A.J. van Horn	(LBL) IJP
Also		NP B87 157	A.J. van Horn	(LBL) IJP
DEVENISH	74B	NP B81 330	R.C.E. Devenish, C.D. Froggatt, B.R. Martin	(DESY+)
KANE	74	LBL-2452	D.F. Kane	(LBL) IJP
COOL	66	PRL 16 1228	R.L. Cool *et al.*	(BNL)

$\Sigma(1940)\ 3/2^+$

$I(J^P) = 1(\frac{3}{2}^+)$ Status: *

OMITTED FROM SUMMARY TABLE

$\Sigma(1940)$ MASS

VALUE (MeV)	DOCUMENT ID		TECN	COMMENT
1920 to 1960 (≈ 1940) OUR ESTIMATE				
1941± 18	ZHANG	13A	DPWA	$\overline{K}N$ multichannel
1925±200	VANHORN	75	DPWA	$K^-p \to \Lambda\pi^0$

$\Sigma(1940)$ WIDTH

VALUE (MeV)	DOCUMENT ID		TECN	COMMENT
100 to 400 (≈ 250) OUR ESTIMATE				
400±49	ZHANG	13A	DPWA	$\overline{K}N$ multichannel
65^{+50}_{-20}	VANHORN	75	DPWA	$K^-p \to \Lambda\pi^0$

Int. J. Mod. Phys. A 2026.41. Downloaded from www.worldscientific.com
UNIVERSITY OF CALIFORNIA @ BERKELEY on 09/16/26. Re-use and distribution is strictly not permitted, except for Open Access articles.

$\Sigma(1940)$ DECAY MODES

	Mode	Fraction (Γ_i/Γ)
Γ_1	$N\overline{K}$	(13.0±2.0) %
Γ_2	$\Sigma\pi$	(4.0±2.0) %
Γ_3	$\Sigma(1385)\pi$, P-wave	(22 ±7) %
Γ_4	$\Lambda(1520)\pi$, S-wave	(5.0±2.0) %

$\Sigma(1940)$ BRANCHING RATIOS

$\Gamma(N\overline{K})/\Gamma_{total}$ — Γ_1/Γ

VALUE	DOCUMENT ID		TECN	COMMENT
0.13±0.02	ZHANG	13A	DPWA	$\overline{K}N$ multichannel

$\Gamma(\Sigma\pi)/\Gamma_{total}$ — Γ_2/Γ

VALUE	DOCUMENT ID		TECN	COMMENT
0.04±0.02	ZHANG	13A	DPWA	$\overline{K}N$ multichannel

$\Gamma(\Sigma(1385)\pi$, P-wave$)/\Gamma_{total}$ — Γ_3/Γ

VALUE	DOCUMENT ID		TECN	COMMENT
0.22±0.07	ZHANG	13A	DPWA	$\overline{K}N$ multichannel

$\Gamma(\Lambda(1520)\pi$, S-wave$)/\Gamma_{total}$ — Γ_4/Γ

VALUE	DOCUMENT ID		TECN	COMMENT
0.05±0.02	ZHANG	13A	DPWA	$\overline{K}N$ multichannel

$\Sigma(1940)$ REFERENCES

ZHANG 13A PR C88 035205 H. Zhang et al. (KSU)
VANHORN 75 NP B87 145 A.J. van Horn (LBL)

$\Sigma(2010)\ 3/2^-$

$I(J^P) = 1(\frac{3}{2}^-)$ Status: *

OMITTED FROM SUMMARY TABLE
was $\Sigma(2000)$

$\Sigma(2010)$ POLE POSITION

REAL PART

VALUE (MeV)	DOCUMENT ID		TECN	COMMENT
1995±12	SARANTSEV	19	DPWA	$\overline{K}N$ multichannel

−2×IMAGINARY PART

VALUE (MeV)	DOCUMENT ID		TECN	COMMENT
175±24	SARANTSEV	19	DPWA	$\overline{K}N$ multichannel

$\Sigma(2010)$ POLE RESIDUES

The normalized residue is the residue divided by $\Gamma_{pole}/2$.

Normalized residue in $N\overline{K} \to \Sigma(2010) \to N\overline{K}$

MODULUS	PHASE (°)	DOCUMENT ID		TECN	COMMENT
0.07±0.03	−115 ± 25	SARANTSEV	19	DPWA	$\overline{K}N$ multichannel

Normalized residue in $N\overline{K} \to \Sigma(2010) \to \Sigma\pi$

MODULUS	PHASE (°)	DOCUMENT ID		TECN	COMMENT
0.04±0.02	130 ± 22	SARANTSEV	19	DPWA	$\overline{K}N$ multichannel

Normalized residue in $N\overline{K} \to \Sigma(2010) \to \Lambda\pi$

MODULUS	PHASE (°)	DOCUMENT ID		TECN	COMMENT
0.06±0.03	170 ± 25	SARANTSEV	19	DPWA	$\overline{K}N$ multichannel

Normalized residue in $N\overline{K} \to \Sigma(2010) \to \Xi K$

MODULUS	PHASE (°)	DOCUMENT ID		TECN	COMMENT
0.04±0.02	−120 ± 45	SARANTSEV	19	DPWA	$\overline{K}N$ multichannel

Normalized residue in $N\overline{K} \to \Sigma(2010) \to \Lambda(1520)\pi$, P-wave

MODULUS	PHASE (°)	DOCUMENT ID		TECN	COMMENT
0.03±0.02	80 ± 35	SARANTSEV	19	DPWA	$\overline{K}N$ multichannel

Normalized residue in $N\overline{K} \to \Sigma(2010) \to \Lambda(1520)\pi$, F-wave

MODULUS	PHASE (°)	DOCUMENT ID		TECN	COMMENT
0.08±0.05	150 ± 65	SARANTSEV	19	DPWA	$\overline{K}N$ multichannel

Normalized residue in $N\overline{K} \to \Sigma(2010) \to \Sigma(1385)\pi$, P-wave

VALUE	DOCUMENT ID		TECN	COMMENT
0.04+-0.02@25+-45	SARANTSEV	19	DPWA	$\overline{K}N$ multichannel

Normalized residue in $N\overline{K} \to \Sigma(2010) \to \Sigma(1385)\pi$, F-wave

VALUE	DOCUMENT ID		TECN	COMMENT
0.02±0.02	SARANTSEV	19	DPWA	$\overline{K}N$ multichannel

Normalized residue in $N\overline{K} \to \Sigma(2010) \to \Delta\overline{K}$, S-wave

MODULUS	PHASE (°)	DOCUMENT ID		TECN	COMMENT
0.08±0.04	0 ± 30	SARANTSEV	19	DPWA	$\overline{K}N$ multichannel

Normalized residue in $N\overline{K} \to \Sigma(2010) \to \Delta\overline{K}$, D-wave

MODULUS	PHASE (°)	DOCUMENT ID		TECN	COMMENT
0.02±0.02		SARANTSEV	19	DPWA	$\overline{K}N$ multichannel

Normalized residue in $N\overline{K} \to \Sigma(2010) \to N\overline{K}^*(892)$, S-wave

VALUE	DOCUMENT ID		TECN	COMMENT
0.12+-0.03@-60+-60	SARANTSEV	19	DPWA	$\overline{K}N$ multichannel

Normalized residue in $N\overline{K} \to \Sigma(2010) \to N\overline{K}^*(892)$, S=1/2 , D-wave

MODULUS	PHASE (°)	DOCUMENT ID		TECN	COMMENT
0.08±0.04	55 ± 60	SARANTSEV	19	DPWA	$\overline{K}N$ multichannel

Normalized residue in $N\overline{K} \to \Sigma(2010) \to N\overline{K}^*(892)$, S=3/2 , D-wave

MODULUS	PHASE (°)	DOCUMENT ID		TECN	COMMENT
0.08±0.04	15 ± 60	SARANTSEV	19	DPWA	$\overline{K}N$ multichannel

$\Sigma(2010)$ MASS

VALUE (MeV)	DOCUMENT ID		TECN	COMMENT
2005 ±14	SARANTSEV	19	DPWA	$\overline{K}N$ multichannel

$\Sigma(2010)$ WIDTH

VALUE (MeV)	DOCUMENT ID		TECN	COMMENT
178±23	SARANTSEV	19	DPWA	$\overline{K}N$ multichannel

$\Sigma(2010)$ DECAY MODES

	Mode	Fraction (Γ_i/Γ)
Γ_1	$N\overline{K}$	(7.0±3.0) %
Γ_2	$\Lambda\pi$	(5.0±2.0) %
Γ_3	$\Sigma\pi$	(3.0±2.0) %
Γ_4	ΞK	(3.0±2.0) %
Γ_5	$\Sigma(1385)\pi$, P-wave	(3.0±2.0) %
Γ_6	$\Sigma(1385)\pi$, F-wave	(2.0±2.0) %
Γ_7	$\Lambda(1520)\pi$, P-wave	(2.0±2.0) %
Γ_8	$\Lambda(1520)\pi$, F-wave	(12 ±6) %
Γ_9	$\Delta\overline{K}$, S-wave	(11 ±5) %
Γ_{10}	$\Delta\overline{K}$, D-wave	(1.0±1.0) %
Γ_{11}	$N\overline{K}^*(892)$, S=1/2, S-wave	(27 ±7) %
Γ_{12}	$N\overline{K}^*(892)$, S=1/2 , D-wave	(13 ±6) %
Γ_{13}	$N\overline{K}^*(892)$, S=3/2, D-wave	(13 ±6) %

$\Sigma(2010)$ BRANCHING RATIOS

See "Sign conventions for resonance couplings" in the Note on Λ and Σ Resonances.

$\Gamma(N\overline{K})/\Gamma_{total}$ — Γ_1/Γ

VALUE	DOCUMENT ID		TECN	COMMENT
0.07±0.03	SARANTSEV	19	DPWA	$\overline{K}N$ multichannel

$\Gamma(\Lambda\pi)/\Gamma_{total}$ — Γ_2/Γ

VALUE	DOCUMENT ID		TECN	COMMENT
0.05±0.02	SARANTSEV	19	DPWA	$\overline{K}N$ multichannel

$\Gamma(\Sigma\pi)/\Gamma_{total}$ — Γ_3/Γ

VALUE	DOCUMENT ID		TECN	COMMENT
0.03±0.02	SARANTSEV	19	DPWA	$\overline{K}N$ multichannel

$\Gamma(\Xi K)/\Gamma_{total}$ — Γ_4/Γ

VALUE	DOCUMENT ID		TECN	COMMENT
0.03±0.02	SARANTSEV	19	DPWA	$\overline{K}N$ multichannel

$\Gamma(\Sigma(1385)\pi$, P-wave$)/\Gamma_{total}$ — Γ_5/Γ

VALUE	DOCUMENT ID		TECN	COMMENT
0.03±0.02	SARANTSEV	19	DPWA	$\overline{K}N$ multichannel

$\Gamma(\Sigma(1385)\pi$, F-wave$)/\Gamma_{total}$ — Γ_6/Γ

VALUE	DOCUMENT ID		TECN	COMMENT
0.02±0.02	SARANTSEV	19	DPWA	$\overline{K}N$ multichannel

$\Gamma(\Lambda(1520)\pi$, P-wave$)/\Gamma_{total}$ — Γ_7/Γ

VALUE	DOCUMENT ID		TECN	COMMENT
0.02±0.02	SARANTSEV	19	DPWA	$\overline{K}N$ multichannel

$\Gamma(\Lambda(1520)\pi$, F-wave$)/\Gamma_{total}$ — Γ_8/Γ

VALUE	DOCUMENT ID		TECN	COMMENT
0.12±0.06	SARANTSEV	19	DPWA	$\overline{K}N$ multichannel

Int. J. Mod. Phys. A 2026.41. Downloaded from www.worldscientific.com
by UNIVERSITY OF CALIFORNIA @ BERKELEY on 09/16/26. Re-use and distribution is strictly not permitted, except for Open Access articles.

$\Gamma(\Delta\overline{K}, S\text{-wave})/\Gamma_{total}$ — Γ_9/Γ

VALUE	DOCUMENT ID		TECN	COMMENT
0.11±0.05	SARANTSEV	19	DPWA	$\overline{K}N$ multichannel

$\Gamma(\Delta\overline{K}, D\text{-wave})/\Gamma_{total}$ — Γ_{10}/Γ

VALUE	DOCUMENT ID		TECN	COMMENT
0.01±0.01	SARANTSEV	19	DPWA	$\overline{K}N$ multichannel

$\Gamma(N\overline{K}^*(892), S=1/2, S\text{-wave})/\Gamma_{total}$ — Γ_{11}/Γ

VALUE	DOCUMENT ID		TECN	COMMENT
0.27±0.07	SARANTSEV	19	DPWA	$\overline{K}N$ multichannel

$\Gamma(N\overline{K}^*(892), S=1/2, D\text{-wave})/\Gamma_{total}$ — Γ_{12}/Γ

VALUE	DOCUMENT ID		TECN	COMMENT
0.13±0.06	SARANTSEV	19	DPWA	$\overline{K}N$ multichannel

$\Gamma(N\overline{K}^*(892), S=3/2, D\text{-wave})/\Gamma_{total}$ — Γ_{13}/Γ

VALUE	DOCUMENT ID		TECN	COMMENT
0.13±0.06	SARANTSEV	19	DPWA	$\overline{K}N$ multichannel

$\Sigma(2010)$ REFERENCES

SARANTSEV 19 EPJ A55 180 A.V. Sarantsev *et al.* (BONN, PNPI)

$\Sigma(2030)\ 7/2^+$

$I(J^P) = 1(\frac{7}{2}^+)$ Status: ****

Discovered by COOL 66 and by WOHL 66. For most results published before 1974 (they are now obsolete), see our 1982 edition Physics Letters **111B** 1 (1982).

This entry only includes results from partial-wave analyses. Parameters of peaks seen in cross sections and invariant-mass distributions around 2030 MeV may be found in our 1984 edition, Reviews of Modern Physics **56** S1 (1984).

$\Sigma(2030)$ POLE POSITION

REAL PART

VALUE (MeV)	DOCUMENT ID		TECN	COMMENT
2010 to 2030 (≈ 2020) OUR ESTIMATE				
2014± 6	SARANTSEV	19	DPWA	$\overline{K}N$ multichannel
2025^{+10}_{-5}	[1] KAMANO	15	DPWA	$\overline{K}N$ multichannel
• • • We do not use the following data for averages, fits, limits, etc. • • •				
1993	ZHANG	13A	DPWA	$\overline{K}N$ multichannel

[1] From the preferred solution A in KAMANO 15.

−2×IMAGINARY PART

VALUE (MeV)	DOCUMENT ID		TECN	COMMENT
130 to 190 (≈ 160) OUR ESTIMATE				
172±12	SARANTSEV	19	DPWA	$\overline{K}N$ multichannel
130^{+6}_{-24}	[1] KAMANO	15	DPWA	$\overline{K}N$ multichannel
• • • We do not use the following data for averages, fits, limits, etc. • • •				
176	ZHANG	13A	DPWA	$\overline{K}N$ multichannel

[1] From the preferred solution A in KAMANO 15.

$\Sigma(2030)$ POLE RESIDUES

The normalized residue is the residue divided by $\Gamma_{pole}/2$.

Normalized residue in $N\overline{K} \to \Sigma(2030) \to N\overline{K}$

MODULUS	PHASE (°)	DOCUMENT ID		TECN	COMMENT
0.20 ±0.04	**−38 ± 8**	SARANTSEV	19	DPWA	$\overline{K}N$ multichannel
• • • We do not use the following data for averages, fits, limits, etc. • • •					
0.220	−38	[1] KAMANO	15	DPWA	$\overline{K}N$ multichannel

[1] From the preferred solution A in KAMANO 15.

Normalized residue in $N\overline{K} \to \Sigma(2030) \to \Sigma\pi$

MODULUS	PHASE (°)	DOCUMENT ID		TECN	COMMENT
0.07 ±0.02	**165 ± 12**	SARANTSEV	19	DPWA	$\overline{K}N$ multichannel
• • • We do not use the following data for averages, fits, limits, etc. • • •					
0.0807	135	[1] KAMANO	15	DPWA	$\overline{K}N$ multichannel

[1] From the preferred solution A in KAMANO 15.

Normalized residue in $N\overline{K} \to \Sigma(2030) \to \Lambda\pi$

MODULUS	PHASE (°)	DOCUMENT ID		TECN	COMMENT
0.18 ±0.04	**−22 ± 12**	SARANTSEV	19	DPWA	$\overline{K}N$ multichannel
• • • We do not use the following data for averages, fits, limits, etc. • • •					
0.138	−24	[1] KAMANO	15	DPWA	$\overline{K}N$ multichannel

[1] From the preferred solution A in KAMANO 15.

Normalized residue in $N\overline{K} \to \Sigma(2030) \to \Xi K$

MODULUS	PHASE (°)	DOCUMENT ID		TECN	COMMENT
0.01 ±0.01		SARANTSEV	19	DPWA	$\overline{K}N$ multichannel
• • • We do not use the following data for averages, fits, limits, etc. • • •					
0.0348	129	[1] KAMANO	15	DPWA	$\overline{K}N$ multichannel

[1] From the preferred solution A in KAMANO 15.

Normalized residue in $N\overline{K} \to \Sigma(2030) \to \Sigma(1385)\pi$, F-wave

MODULUS	PHASE (°)	DOCUMENT ID		TECN	COMMENT
0.04 ±0.03		SARANTSEV	19	DPWA	$\overline{K}N$ multichannel
• • • We do not use the following data for averages, fits, limits, etc. • • •					
0.089	−23	[1] KAMANO	15	DPWA	$\overline{K}N$ multichannel

[1] From the preferred solution A in KAMANO 15.

Normalized residue in $N\overline{K} \to \Sigma(2030) \to \Sigma(1385)\pi$, H-wave

MODULUS	PHASE (°)	DOCUMENT ID		TECN	COMMENT
• • • We do not use the following data for averages, fits, limits, etc. • • •					
0.0245	132	[1] KAMANO	15	DPWA	Multichannel

[1] From the preferred solution A in KAMANO 15.

Normalized residue in $N\overline{K} \to \Sigma(2030) \to \Lambda(1520)\pi$, D-wave

MODULUS	PHASE (°)	DOCUMENT ID		TECN	COMMENT
0.03±0.02	**−100 ± 40**	SARANTSEV	19	DPWA	$\overline{K}N$ multichannel

Normalized residue in $N\overline{K} \to \Sigma(2030) \to \Lambda(1520)\pi$, G-wave

MODULUS	PHASE (°)	DOCUMENT ID		TECN	COMMENT
0.02±0.02		SARANTSEV	19	DPWA	$\overline{K}N$ multichannel

Normalized residue in $N\overline{K} \to \Sigma(2030) \to \Delta\overline{K}$, F-wave

MODULUS	PHASE (°)	DOCUMENT ID		TECN	COMMENT
0.16±0.06	**−130 ± 20**	SARANTSEV	19	DPWA	$\overline{K}N$ multichannel

Normalized residue in $N\overline{K} \to \Sigma(2030) \to \Delta\overline{K}$, H-wave

MODULUS	PHASE (°)	DOCUMENT ID		TECN	COMMENT
0.04±0.02	**−130 ± 35**	SARANTSEV	19	DPWA	$\overline{K}N$ multichannel

Normalized residue in $N\overline{K} \to \Sigma(2030) \to N\overline{K}^*(892)$, $S=1/2$, F-wave

MODULUS	PHASE (°)	DOCUMENT ID		TECN	COMMENT
0.02 ±0.02		SARANTSEV	19	DPWA	$\overline{K}N$ multichannel
• • • We do not use the following data for averages, fits, limits, etc. • • •					
0.193	38	[1] KAMANO	15	DPWA	$\overline{K}N$ multichannel

[1] From the preferred solution A in KAMANO 15.

Normalized residue in $N\overline{K} \to \Sigma(2030) \to N\overline{K}^*(892)$, $S=3/2$, F-wave

MODULUS	PHASE (°)	DOCUMENT ID		TECN	COMMENT
0.16 ±0.09	**−160 ± 40**	SARANTSEV	19	DPWA	$\overline{K}N$ multichannel
• • • We do not use the following data for averages, fits, limits, etc. • • •					
0.320	37	[1] KAMANO	15	DPWA	$\overline{K}N$ multichannel

[1] From the preferred solution A in KAMANO 15.

Normalized residue in $N\overline{K} \to \Sigma(2030) \to N\overline{K}^*(892)$, $S=3/2$, H-wave

MODULUS	PHASE (°)	DOCUMENT ID		TECN	COMMENT
• • • We do not use the following data for averages, fits, limits, etc. • • •					
0.00358	22	[1] KAMANO	15	DPWA	Multichannel

[1] From the preferred solution A in KAMANO 15.

$\Sigma(2030)$ MASS

VALUE (MeV)	DOCUMENT ID		TECN	COMMENT
2025 to 2040 (≈ 2030) OUR ESTIMATE				
2032± 6	SARANTSEV	19	DPWA	$\overline{K}N$ multichannel
2030± 5	ZHANG	13A	DPWA	$\overline{K}N$ multichannel
2036± 5	GOPAL	80	DPWA	$\overline{K}N \to \overline{K}N$
2038±10	CORDEN	77B		$K^-N \to N\overline{K}^*$
2030± 3	[1] CORDEN	76	DPWA	$K^-n \to \Lambda\pi^-$
2035±15	BAILLON	75	IPWA	$\overline{K}N \to \Lambda\pi$
2038±10	HEMINGWAY	75	DPWA	$K^-p \to \overline{K}N$
2042±11	VANHORN	75	DPWA	$K^-p \to \Lambda\pi^0$
2020± 6	KANE	74	DPWA	$K^-p \to \Sigma\pi$
2035±10	LITCHFIELD	74B	DPWA	$K^-p \to \Lambda(1520)\pi^0$
2020±30	LITCHFIELD	74C	DPWA	$K^-p \to \Delta(1232)\overline{K}$
2025±10	LITCHFIELD	74D	DPWA	$K^-p \to \Lambda(1820)\pi^0$
• • • We do not use the following data for averages, fits, limits, etc. • • •				
2040± 5	GOPAL	77	DPWA	$\overline{K}N$ multichannel
2027 to 2057	GOYAL	77	DPWA	$K^-N \to \Sigma\pi$
2030	DEBELLEFON	76	IPWA	$K^-p \to \Lambda\pi^0$

[1] Preferred solution 3; see CORDEN 76 for other possibilities.

Int. J. Mod. Phys. A 2026.41. Downloaded from www.worldscientific.com
UNIVERSITY OF CALIFORNIA @ BERKELEY on 09/16/26. Re-use and distribution is strictly not permitted, except for Open Access articles.

$\Sigma(2030)$ WIDTH

VALUE (MeV)	DOCUMENT ID		TECN	COMMENT
150 to 200 ($\approx$ 180) OUR ESTIMATE				
177±12	SARANTSEV	19	DPWA	$\overline{K}N$ multichannel
207±17	ZHANG	13A	DPWA	$\overline{K}N$ multichannel
172±10	GOPAL	80	DPWA	$\overline{K}N \to \overline{K}N$
137±40	CORDEN	77B		$K^-N \to N\overline{K}^*$
201± 9	[1] CORDEN	76	DPWA	$K^-n \to \Lambda\pi^-$
180±20	BAILLON	75	IPWA	$\overline{K}N \to \Lambda\pi$
172±15	HEMINGWAY	75	DPWA	$K^-p \to \overline{K}N$
178±13	VANHORN	75	DPWA	$K^-p \to \Lambda\pi^0$
111± 5	KANE	74	DPWA	$K^-p \to \Sigma\pi$
160±20	LITCHFIELD	74B	DPWA	$K^-p \to \Lambda(1520)\pi^0$
200±30	LITCHFIELD	74C	DPWA	$K^-p \to \Delta(1232)\overline{K}$
• • • We do not use the following data for averages, fits, limits, etc. • • •				
260	DECLAIS	77	DPWA	$\overline{K}N \to \overline{K}N$
190±10	GOPAL	77	DPWA	$\overline{K}N$ multichannel
126 to 195	GOYAL	77	DPWA	$K^-N \to \Sigma\pi$
160	DEBELLEFON	76	IPWA	$K^-p \to \Lambda\pi^0$
70 to 125	LITCHFIELD	74D	DPWA	$K^-p \to \Lambda(1820)\pi^0$

[1] Preferred solution 3; see CORDEN 76 for other possibilities.

$\Sigma(2030)$ DECAY MODES

	Mode	Fraction (Γ_i/Γ)
Γ_1	$N\overline{K}$	17–23 %
Γ_2	$\Lambda\pi$	17–23 %
Γ_3	$\Sigma\pi$	5–10 %
Γ_4	ΞK	<2 %
Γ_5	$\Sigma(1385)\pi$	5–15 %
Γ_6	$\Sigma(1385)\pi$, F-wave	(1.0±1.0) %
Γ_7	$\Sigma(1385)\pi$, H-wave	
Γ_8	$\Lambda(1520)\pi$	10–20 %
Γ_9	$\Lambda(1520)\pi$, D-wave	
Γ_{10}	$\Lambda(1520)\pi$, G-wave	
Γ_{11}	$\Delta(1232)\overline{K}$	10–20 %
Γ_{12}	$\Delta(1232)\overline{K}$, F-wave	(15 ±5) %
Γ_{13}	$\Delta(1232)\overline{K}$, H-wave	(1.0±1.0) %
Γ_{14}	$N\overline{K}^*(892)$	
Γ_{15}	$N\overline{K}^*(892)$, S=1/2, F-wave	
Γ_{16}	$N\overline{K}^*(892)$, S=3/2, F-wave	(14 ±8) %
Γ_{17}	$N\overline{K}^*(892)$, S=3/2, H-wave	
Γ_{18}	$\Lambda(1820)\pi$, P-wave	

$\Sigma(2030)$ BRANCHING RATIOS

See "Sign conventions for resonance couplings" in the Note on Λ and Σ Resonances.

$\Gamma(N\overline{K})/\Gamma_{total}$ — Γ_1/Γ

VALUE	DOCUMENT ID		TECN	COMMENT
0.17 to 0.23 OUR ESTIMATE				
0.20 ±0.04	SARANTSEV	19	DPWA	$\overline{K}N$ multichannel
0.13 ±0.01	ZHANG	13A	DPWA	$\overline{K}N$ multichannel
0.19 ±0.03	GOPAL	80	DPWA	$\overline{K}N \to \overline{K}N$
0.18 ±0.03	HEMINGWAY	75	DPWA	$K^-p \to \overline{K}N$
• • • We do not use the following data for averages, fits, limits, etc. • • •				
0.269	[1] KAMANO	15	DPWA	Multichannel
0.15	DECLAIS	77	DPWA	$\overline{K}N \to \overline{K}N$
0.24 ±0.02	GOPAL	77	DPWA	See GOPAL 80

[1] From the preferred solution A in KAMANO 15.

$\Gamma(\Lambda\pi)/\Gamma_{total}$ — Γ_2/Γ

VALUE	DOCUMENT ID		TECN	COMMENT
0.17 ±0.04	SARANTSEV	19	DPWA	$\overline{K}N$ multichannel
• • • We do not use the following data for averages, fits, limits, etc. • • •				
0.080	[1] KAMANO	15	DPWA	$\overline{K}N$ multichannel

[1] From the preferred solution A in KAMANO 15.

$\Gamma(\Sigma\pi)/\Gamma_{total}$ — Γ_3/Γ

VALUE	DOCUMENT ID		TECN	COMMENT
0.025±0.008	SARANTSEV	19	DPWA	$\overline{K}N$ multichannel
• • • We do not use the following data for averages, fits, limits, etc. • • •				
0.037	[1] KAMANO	15	DPWA	$\overline{K}N$ multichannel

[1] From the preferred solution A in KAMANO 15.

$\Gamma(\Xi K)/\Gamma_{total}$ — Γ_4/Γ

VALUE	DOCUMENT ID		TECN	COMMENT
<0.01	SARANTSEV	19	DPWA	$\overline{K}N$ multichannel
• • • We do not use the following data for averages, fits, limits, etc. • • •				
0.006	[1] KAMANO	15	DPWA	$\overline{K}N$ multichannel

[1] From the preferred solution A in KAMANO 15.

$\Gamma(\Lambda(1520)\pi, D\text{-wave})/\Gamma_{total}$ — Γ_9/Γ

VALUE	DOCUMENT ID		TECN	COMMENT
~ 0.01	SARANTSEV	19	DPWA	$\overline{K}N$ multichannel

$\Gamma(\Lambda(1520)\pi, G\text{-wave})/\Gamma_{total}$ — Γ_{10}/Γ

VALUE	DOCUMENT ID		TECN	COMMENT
<0.01	SARANTSEV	19	DPWA	$\overline{K}N$ multichannel

$\Gamma(\Sigma(1385)\pi, F\text{-wave})/\Gamma_{total}$ — Γ_6/Γ

VALUE	DOCUMENT ID		TECN	COMMENT
0.01 ±0.01	SARANTSEV	19	DPWA	$\overline{K}N$ multichannel
• • • We do not use the following data for averages, fits, limits, etc. • • •				
0.030	[1] KAMANO	15	DPWA	$\overline{K}N$ multichannel

[1] From the preferred solution A in KAMANO 15.

$\Gamma(\Sigma(1385)\pi, H\text{-wave})/\Gamma_{total}$ — Γ_7/Γ

VALUE	DOCUMENT ID		TECN	COMMENT
• • • We do not use the following data for averages, fits, limits, etc. • • •				
0.003	[1] KAMANO	15	DPWA	Multichannel

[1] From the preferred solution A in KAMANO 15.

$\Gamma(\Delta(1232)\overline{K}, F\text{-wave})/\Gamma_{total}$ — Γ_{12}/Γ

VALUE	DOCUMENT ID		TECN	COMMENT
0.15±0.05	SARANTSEV	19	DPWA	$\overline{K}N$ multichannel

$\Gamma(\Delta(1232)\overline{K}, H\text{-wave})/\Gamma_{total}$ — Γ_{13}/Γ

VALUE	DOCUMENT ID		TECN	COMMENT
0.01±0.01	SARANTSEV	19	DPWA	$\overline{K}N$ multichannel

$\Gamma(N\overline{K}^*(892), S=1/2, F\text{-wave})/\Gamma_{total}$ — Γ_{15}/Γ

VALUE	DOCUMENT ID		TECN	COMMENT
<0.01	SARANTSEV	19	DPWA	$\overline{K}N$ multichannel
• • • We do not use the following data for averages, fits, limits, etc. • • •				
0.154	[1] KAMANO	15	DPWA	$\overline{K}N$ multichannel

[1] From the preferred solution A in KAMANO 15.

$\Gamma(N\overline{K}^*(892), S=3/2, F\text{-wave})/\Gamma_{total}$ — Γ_{16}/Γ

VALUE	DOCUMENT ID		TECN	COMMENT
0.14 ±0.08	SARANTSEV	19	DPWA	$\overline{K}N$ multichannel
• • • We do not use the following data for averages, fits, limits, etc. • • •				
0.422	[1] KAMANO	15	DPWA	$\overline{K}N$ multichannel

[1] From the preferred solution A in KAMANO 15.

$\Gamma(N\overline{K}^*(892), S=3/2, H\text{-wave})/\Gamma_{total}$ — Γ_{17}/Γ

VALUE	DOCUMENT ID		TECN	COMMENT
• • • We do not use the following data for averages, fits, limits, etc. • • •				
not seen	[1] KAMANO	15	DPWA	$\overline{K}N$ multichannel

[1] From the preferred solution A in KAMANO 15.

$(\Gamma_i\Gamma_f)^{1/2}/\Gamma_{total}$ in $N\overline{K} \to \Sigma(2030) \to \Lambda\pi$ — $(\Gamma_1\Gamma_2)^{1/2}/\Gamma$

VALUE	DOCUMENT ID		TECN	COMMENT
+0.15 ±0.01	ZHANG	13A	DPWA	Multichannel
+0.18 ±0.02	GOPAL	77	DPWA	$\overline{K}N$ multichannel
+0.20 ±0.01	[1] CORDEN	76	DPWA	$K^-n \to \Lambda\pi^-$
+0.18 ±0.02	BAILLON	75	IPWA	$\overline{K}N \to \Lambda\pi$
+0.20 ±0.01	VANHORN	75	DPWA	$K^-p \to \Lambda\pi^0$
+0.195±0.053	DEVENISH	74B		Fixed-t dispersion rel.
• • • We do not use the following data for averages, fits, limits, etc. • • •				
0.20	DEBELLEFON	76	IPWA	$K^-p \to \Lambda\pi^0$

[1] Preferred solution 3; see CORDEN 76 for other possibilities.

$(\Gamma_i\Gamma_f)^{1/2}/\Gamma_{total}$ in $N\overline{K} \to \Sigma(2030) \to \Sigma\pi$ — $(\Gamma_1\Gamma_3)^{1/2}/\Gamma$

VALUE	DOCUMENT ID		TECN	COMMENT
−0.08 ±0.01	ZHANG	13A	DPWA	Multichannel
−0.09 ±0.01	[1] CORDEN	77C		$K^-n \to \Sigma\pi$
−0.06 ±0.01	[1] CORDEN	77C		$K^-n \to \Sigma\pi$
−0.15 ±0.03	GOPAL	77	DPWA	$\overline{K}N$ multichannel
−0.10 ±0.01	KANE	74	DPWA	$K^-p \to \Sigma\pi$
• • • We do not use the following data for averages, fits, limits, etc. • • •				
−0.085±0.02	[2] GOYAL	77	DPWA	$K^-N \to \Sigma\pi$

[1] The two entries for CORDEN 77C are from two different acceptable solutions.
[2] This coupling is extracted from unnormalized data.

$(\Gamma_i\Gamma_f)^{1/2}/\Gamma_{total}$ in $N\overline{K} \to \Sigma(2030) \to \Xi K$ — $(\Gamma_1\Gamma_4)^{1/2}/\Gamma$

VALUE	DOCUMENT ID		TECN	COMMENT
0.023	MULLER	69B	DPWA	$K^-p \to \Xi K$
<0.05	BURGUN	68	DPWA	$K^-p \to \Xi K$
<0.05	TRIPP	67	RVUE	$K^-p \to \Xi K$

Int. J. Mod. Phys. A 2026.41. Downloaded from www.worldscientific.com by UNIVERSITY OF CALIFORNIA @ BERKELEY on 09/16/26. Re-use and distribution is strictly not permitted, except for Open Access articles.

$(\Gamma_i\Gamma_f)^{1/2}/\Gamma_{total}$ in $N\overline{K} \to \Sigma(2030) \to \Sigma(1385)\pi$, F-wave $(\Gamma_1\Gamma_6)^{1/2}/\Gamma$

VALUE	DOCUMENT ID		TECN	COMMENT
$+0.16 \pm 0.01$	ZHANG	13A	DPWA	Multichannel
$+0.153 \pm 0.026$	[1] CAMERON	78	DPWA	$K^- p \to \Sigma(1385)\pi$

[1] The published sign has been changed to be in accord with the baryon-first convention.

$(\Gamma_i\Gamma_f)^{1/2}/\Gamma_{total}$ in $N\overline{K} \to \Sigma(2030) \to \Lambda(1520)\pi$, D-wave $(\Gamma_1\Gamma_9)^{1/2}/\Gamma$

VALUE	DOCUMENT ID		TECN	COMMENT
$+0.114 \pm 0.010$	[1] CAMERON	77	DPWA	$K^- p \to \Lambda(1520)\pi^0$
0.14 ± 0.03	LITCHFIELD	74B	DPWA	$K^- p \to \Lambda(1520)\pi^0$
• • • We do not use the following data for averages, fits, limits, etc. • • •				
0.10 ± 0.03	[2] CORDEN	75B	DBC	$K^- n \to N\overline{K}\pi^-$

[1] The published sign has been changed to be in accord with the baryon-first convention.
[2] An upper limit.

$(\Gamma_i\Gamma_f)^{1/2}/\Gamma_{total}$ in $N\overline{K} \to \Sigma(2030) \to \Lambda(1520)\pi$, G-wave $(\Gamma_1\Gamma_{10})^{1/2}/\Gamma$

VALUE	DOCUMENT ID		TECN	COMMENT
$+0.146 \pm 0.010$	[1] CAMERON	77	DPWA	$K^- p \to \Lambda(1520)\pi^0$
0.02 ± 0.02	LITCHFIELD	74B	DPWA	$K^- p \to \Lambda(1520)\pi^0$

[1] The published sign has been changed to be in accord with the baryon-first convention.

$(\Gamma_i\Gamma_f)^{1/2}/\Gamma_{total}$ in $N\overline{K} \to \Sigma(2030) \to \Delta(1232)\overline{K}$, F-wave $(\Gamma_1\Gamma_{12})^{1/2}/\Gamma$

VALUE	DOCUMENT ID		TECN	COMMENT
$+0.12 \pm 0.02$	ZHANG	13A	DPWA	Multichannel
0.16 ± 0.03	LITCHFIELD	74C	DPWA	$K^- p \to \Delta(1232)\overline{K}$
• • • We do not use the following data for averages, fits, limits, etc. • • •				
0.17 ± 0.03	[1] CORDEN	75B	DBC	$K^- n \to N\overline{K}\pi^-$

[1] An upper limit.

$(\Gamma_i\Gamma_f)^{1/2}/\Gamma_{total}$ in $N\overline{K} \to \Sigma(2030) \to \Delta(1232)\overline{K}$, H-wave $(\Gamma_1\Gamma_{13})^{1/2}/\Gamma$

VALUE	DOCUMENT ID		TECN	COMMENT
0.00 ± 0.02	LITCHFIELD	74C	DPWA	$K^- p \to \Delta(1232)\overline{K}$

$(\Gamma_i\Gamma_f)^{1/2}/\Gamma_{total}$ in $N\overline{K} \to \Sigma(2030) \to N\overline{K}^*(892)$, $S=1/2$, F-wave $(\Gamma_1\Gamma_{15})^{1/2}/\Gamma$

VALUE	DOCUMENT ID		TECN	COMMENT
$+0.06 \pm 0.02$	ZHANG	13A	DPWA	Multichannel
$+0.06 \pm 0.03$	[1] CAMERON	78B	DPWA	$K^- p \to N\overline{K}^*$
-0.02 ± 0.01	CORDEN	77B		$K^- d \to N N\overline{K}^*$

[1] The published sign has been changed to be in accord with the baryon-first convention.

$(\Gamma_i\Gamma_f)^{1/2}/\Gamma_{total}$ in $N\overline{K} \to \Sigma(2030) \to N\overline{K}^*(892)$, $S=3/2$, F-wave $(\Gamma_1\Gamma_{16})^{1/2}/\Gamma$

VALUE	DOCUMENT ID		TECN	COMMENT
$+0.05 \pm 0.01$	ZHANG	13A	DPWA	Multichannel
$+0.04 \pm 0.03$	[1] CAMERON	78B	DPWA	$K^- p \to N\overline{K}^*$
-0.12 ± 0.02	CORDEN	77B		$K^- d \to N N\overline{K}^*$

[1] The upper limit on the G_3 wave is 0.03.

$(\Gamma_i\Gamma_f)^{1/2}/\Gamma_{total}$ in $N\overline{K} \to \Sigma(2030) \to \Lambda(1820)\pi$, P-wave $(\Gamma_1\Gamma_{18})^{1/2}/\Gamma$

VALUE	DOCUMENT ID		TECN	COMMENT
0.14 ± 0.02	CORDEN	75B	DBC	$K^- n \to N\overline{K}\pi^-$
0.18 ± 0.04	LITCHFIELD	74D	DPWA	$K^- p \to \Lambda(1820)\pi^0$

$\Sigma(2030)$ REFERENCES

SARANTSEV	19	EPJ A55 180	A.V. Sarantsev *et al.*	(BONN, PNPI)
KAMANO	15	PR C92 025205	H. Kamano *et al.*	(ANL, OSAK)
ZHANG	13A	PR C88 035205	H. Zhang *et al.*	(KSU)
PDG	84	RMP 56 S1	C.G. Wohl *et al.*	(LBL, CIT, CERN)
PDG	82	PL 111B 1	M. Roos *et al.*	(HELS, CIT, CERN)
GOPAL	80	Toronto Conf. 159	G.P. Gopal	(RHEL) IJP
CAMERON	78	NP B143 189	W. Cameron *et al.*	(RHEL, LOIC) IJP
CAMERON	78B	NP B146 327	W. Cameron *et al.*	(RHEL, LOIC) IJP
CAMERON	77	NP B131 399	W. Cameron *et al.*	(RHEL, LOIC) IJP
CORDEN	77B	NP B121 365	M.J. Corden *et al.*	(BIRM) IJP
CORDEN	77C	NP B125 61	M.J. Corden *et al.*	(BIRM) IJP
DECLAIS	77	CERN 77-16	Y. Declais *et al.*	(CAEN, CERN) IJP
GOPAL	77	NP B119 362	G.P. Gopal *et al.*	(LOIC, RHEL) IJP
GOYAL	77	PR D16 2746	D.P. Goyal, A.V. Sodhi	(DELH) IJP
CORDEN	76	NP B104 382	M.J. Corden *et al.*	(BIRM) IJP
DEBELLEFON	76	NP B109 129	A. de Bellefon, A. Berthon	(CDEF) IJP
BAILLON	75	NP B94 39	P.H. Baillon, P.J. Litchfield	(CERN, RHEL) IJP
CORDEN	75B	NP B92 365	M.J. Corden *et al.*	(BIRM) IJP
HEMINGWAY	75	NP B91 12	R.J. Hemingway *et al.*	(CERN, HEIDH, MPIM) IJP
VANHORN	75	NP B87 145	A.J. van Horn	(LBL) IJP
Also		NP B87 157	A.J. van Horn	(LBL) IJP
DEVENISH	74B	NP B81 330	R.C.E. Devenish, C.D. Froggatt, B.R. Martin	(DESY+)
KANE	74	LBL-2452	D.F. Kane	(LBL) IJP
LITCHFIELD	74B	NP B74 19	P.J. Litchfield *et al.*	(CERN, HEIDH) IJP
LITCHFIELD	74C	NP B74 39	P.J. Litchfield *et al.*	(CERN, HEIDH) IJP
LITCHFIELD	74D	NP B74 12	P.J. Litchfield *et al.*	(CERN, HEIDH) IJP
MULLER	69B	Thesis UCRL 19372	R.A. Muller	(LRL)
BURGUN	68	NP B8 447	G. Burgun *et al.*	(SACL, CDEF, RHEL)
TRIPP	67	NP B3 10	R.D. Tripp *et al.*	(LRL, SLAC, CERN+)
COOL	66	PRL 16 1228	R.L. Cool *et al.*	(BNL)
WOHL	66	PRL 17 107	C.G. Wohl, F.T. Solmitz, M.L. Stevenson	(LRL) IJP

$\Sigma(2070)\ 5/2^+$

$I(J^P) = 1(\frac{5}{2}^+)$ Status: *

OMITTED FROM SUMMARY TABLE

This state suggested by BERTHON 70B finds support in GOPAL 80 with new $K^- p$ polarization and $K^- n$ angular distributions. The very broad state seen in KANE 72 is not required in the later (KANE 74) analysis of $\overline{K}N \to \Sigma\pi$.

$\Sigma(2070)$ MASS

VALUE (MeV)	DOCUMENT ID		TECN	COMMENT
2020 to 2100 (≈ 2060) OUR ESTIMATE				
2051 ± 25	GOPAL	80	DPWA	$\overline{K}N \to \overline{K}N$
2070 ± 10	BERTHON	70B	DPWA	$K^- p \to \Sigma\pi$
• • • We do not use the following data for averages, fits, limits, etc. • • •				
2057	KANE	72	DPWA	$K^- p \to \Sigma\pi$

$\Sigma(2070)$ WIDTH

VALUE (MeV)	DOCUMENT ID		TECN	COMMENT
100 to 300 (≈ 200) OUR ESTIMATE				
300 ± 30	GOPAL	80	DPWA	$\overline{K}N \to \overline{K}N$
140 ± 20	BERTHON	70B	DPWA	$K^- p \to \Sigma\pi$
• • • We do not use the following data for averages, fits, limits, etc. • • •				
906	KANE	72	DPWA	$K^- p \to \Sigma\pi$

$\Sigma(2070)$ DECAY MODES

	Mode
Γ_1	$N\overline{K}$
Γ_2	$\Sigma\pi$

$\Sigma(2070)$ BRANCHING RATIOS

See "Sign conventions for resonance couplings" in the Note on Λ and Σ Resonances.

$\Gamma(N\overline{K})/\Gamma_{total}$ Γ_1/Γ

VALUE	DOCUMENT ID		TECN	COMMENT
0.08 ± 0.03	GOPAL	80	DPWA	$\overline{K}N \to \overline{K}N$

$(\Gamma_i\Gamma_f)^{1/2}/\Gamma_{total}$ in $N\overline{K} \to \Sigma(2070) \to \Sigma\pi$ $(\Gamma_1\Gamma_2)^{1/2}/\Gamma$

VALUE	DOCUMENT ID		TECN	COMMENT
0.12 ± 0.02	BERTHON	70B	DPWA	$K^- p \to \Sigma\pi$
• • • We do not use the following data for averages, fits, limits, etc. • • •				
0.104	KANE	72	DPWA	$K^- p \to \Sigma\pi$

$\Sigma(2070)$ REFERENCES

GOPAL	80	Toronto Conf. 159	G.P. Gopal	(RHEL) IJP
KANE	74	LBL-2452	D.F. Kane	(LBL)
KANE	72	PR D5 1583	D.F.J. Kane	(LBL)
BERTHON	70B	NP B24 417	A. Berthon *et al.*	(CDEF, RHEL, SACL) IJP

$\Sigma(2080)\ 3/2^+$

$I(J^P) = 1(\frac{3}{2}^+)$ Status: *

OMITTED FROM SUMMARY TABLE

Suggested by some but not all partial-wave analyses across this region.

$\Sigma(2080)$ MASS

VALUE (MeV)	DOCUMENT ID		TECN	COMMENT
2060 to 2120 (≈ 2090) OUR ESTIMATE				
2091 ± 7	[1] CORDEN	76	DPWA	$K^- n \to \Lambda\pi^-$
2070 to 2120	DEBELLEFON	76	IPWA	$K^- p \to \Lambda\pi^0$
2120 ± 40	BAILLON	75	IPWA	$\overline{K}N \to \Lambda\pi$ (sol. 1)
2140 ± 40	BAILLON	75	IPWA	$\overline{K}N \to \Lambda\pi$ (sol. 2)
2082 ± 4	COX	70	DPWA	See CORDEN 76
2070 ± 30	LITCHFIELD	70	DPWA	$K^- N \to \Lambda\pi$

$\Sigma(2080)$ WIDTH

VALUE (MeV)	DOCUMENT ID		TECN	COMMENT
100 to 240 (≈ 170) OUR ESTIMATE				
186 ± 48	[1] CORDEN	76	DPWA	$K^- n \to \Lambda\pi^-$
100	DEBELLEFON	76	IPWA	$K^- p \to \Lambda\pi^0$
240 ± 50	BAILLON	75	IPWA	$\overline{K}N \to \Lambda\pi$ (sol. 1)
200 ± 50	BAILLON	75	IPWA	$\overline{K}N \to \Lambda\pi$ (sol. 2)
87 ± 20	COX	70	DPWA	See CORDEN 76
250 ± 40	LITCHFIELD	70	DPWA	$K^- N \to \Lambda\pi$

Int. J. Mod. Phys. A 2026.41. Downloaded from www.worldscientific.com
UNIVERSITY OF CALIFORNIA @ BERKELEY on 09/16/26. Re-use and distribution is strictly not permitted, except for Open Access articles.

$\Sigma(2080)$ DECAY MODES

	Mode
Γ_1	$N\overline{K}$
Γ_2	$\Lambda\pi$

$\Sigma(2080)$ BRANCHING RATIOS

See "Sign conventions for resonance couplings" in the Note on Λ and Σ Resonances.

$(\Gamma_i\Gamma_f)^{1/2}/\Gamma_{total}$ in $N\overline{K} \to \Sigma(2080) \to \Lambda\pi$ — **$(\Gamma_1\Gamma_2)^{1/2}/\Gamma$**

VALUE	DOCUMENT ID		TECN	COMMENT
-0.10 ± 0.03	[1] CORDEN	76	DPWA	$K^-n \to \Lambda\pi^-$
-0.10	DEBELLEFON	76	IPWA	$K^-p \to \Lambda\pi^0$
-0.13 ± 0.04	BAILLON	75	IPWA	$\overline{K}N \to \Lambda\pi$ (sol. 1 and 2)
-0.16 ± 0.03	COX	70	DPWA	See CORDEN 76
-0.09 ± 0.03	LITCHFIELD	70	DPWA	$K^-N \to \Lambda\pi$

$\Sigma(2080)$ FOOTNOTES

[1] Preferred solution 3; see CORDEN 76 for other possibilities, including a D_{15} at this mass.

$\Sigma(2080)$ REFERENCES

CORDEN	76	NP B104 382	M.J. Corden *et al.*	(BIRM) IJP
DEBELLEFON	76	NP B109 129	A. de Bellefon, A. Berthon	(CDEF) IJP
Also		NP B90 1	A. de Bellefon *et al.*	(CDEF, SACL) IJP
BAILLON	75	NP B94 39	P.H. Baillon, P.J. Litchfield	(CERN, RHEL) IJP
COX	70	NP B19 61	G.F. Cox *et al.*	(BIRM, EDIN, GLAS, LOIC) IJP
LITCHFIELD	70	NP B22 269	P.J. Litchfield	(RHEL) IJP

$\Sigma(2100)\ 7/2^-$

$I(J^P) = 1(\frac{7}{2}^-)$ Status: $*$

OMITTED FROM SUMMARY TABLE

$\Sigma(2100)$ POLE POSITION

REAL PART

VALUE (MeV)	DOCUMENT ID		TECN	COMMENT
2093±16	SARANTSEV	19	DPWA	$\overline{K}N$ multichannel

$-2\times$IMAGINARY PART

VALUE (MeV)	DOCUMENT ID		TECN	COMMENT
210±35	SARANTSEV	19	DPWA	$\overline{K}N$ multichannel

$\Sigma(2100)$ POLE RESIDUES

Normalized residue in $N\overline{K} \to \Sigma(2100) \to N\overline{K}$

MODULUS	PHASE (°)	DOCUMENT ID		TECN	COMMENT
0.09±0.02	**−110 ± 15**	SARANTSEV	19	DPWA	$\overline{K}N$ multichannel

Normalized residue in $N\overline{K} \to \Sigma(2100) \to \Sigma\pi$

MODULUS	PHASE (°)	DOCUMENT ID		TECN	COMMENT
0.04±0.02	**−50 ± 20**	SARANTSEV	19	DPWA	$\overline{K}N$ multichannel

Normalized residue in $N\overline{K} \to \Sigma(2100) \to \Lambda\pi$

MODULUS	PHASE (°)	DOCUMENT ID		TECN	COMMENT
0.03±0.02	**−100 ± 25**	SARANTSEV	19	DPWA	$\overline{K}N$ multichannel

Normalized residue in $N\overline{K} \to \Sigma(2100) \to \Xi K$

MODULUS	PHASE (°)	DOCUMENT ID		TECN	COMMENT
0.010±0.005	**−120 ± 35**	SARANTSEV	19	DPWA	$\overline{K}N$ multichannel

Normalized residue in $N\overline{K} \to \Sigma(2100) \to \Lambda(1520)\pi$, F-wave

MODULUS	PHASE (°)	DOCUMENT ID		TECN	COMMENT
0.02±0.01	**−100 ± 30**	SARANTSEV	19	DPWA	$\overline{K}N$ multichannel

Normalized residue in $N\overline{K} \to \Sigma(2100) \to \Lambda(1520)\pi$, H-wave

MODULUS	PHASE (°)	DOCUMENT ID		TECN	COMMENT
0.01±0.01		SARANTSEV	19	DPWA	$\overline{K}N$ multichannel

Normalized residue in $N\overline{K} \to \Sigma(2100) \to \Sigma(1385)\pi$, D-wave

MODULUS	PHASE (°)	DOCUMENT ID		TECN	COMMENT
0.10±0.03	**−60 ± 30**	SARANTSEV	19	DPWA	$\overline{K}N$ multichannel

Normalized residue in $N\overline{K} \to \Sigma(2100) \to \Sigma(1385)\pi$, G-wave

MODULUS	PHASE (°)	DOCUMENT ID		TECN	COMMENT
0.03±0.01	**−50 ± 30**	SARANTSEV	19	DPWA	$\overline{K}N$ multichannel

Normalized residue in $N\overline{K} \to \Sigma(2100) \to \Delta\overline{K}$, G-wave

MODULUS	PHASE (°)	DOCUMENT ID		TECN	COMMENT
0.04±0.02	**75 ± 35**	SARANTSEV	19	DPWA	$\overline{K}N$ multichannel

Normalized residue in $N\overline{K} \to \Sigma(2100) \to N\overline{K}^*(892)$, S=3/2, D-wave

MODULUS	PHASE (°)	DOCUMENT ID		TECN	COMMENT
0.08±0.04	**20 ± 50**	SARANTSEV	19	DPWA	$\overline{K}N$ multichannel

$\Sigma(2100)$ MASS

VALUE (MeV)	DOCUMENT ID		TECN	COMMENT
≈ 2100 OUR ESTIMATE				
2146±17	SARANTSEV	19	DPWA	$\overline{K}N$ multichannel
2060±20	BARBARO-...	70	DPWA	$K^-p \to \Lambda\pi^0$
2120±30	BARBARO-...	70	DPWA	$K^-p \to \Sigma\pi$

$\Sigma(2100)$ WIDTH

VALUE (MeV)	DOCUMENT ID		TECN	COMMENT
260±40	SARANTSEV	19	DPWA	$\overline{K}N$ multichannel
70±30	BARBARO-...	70	DPWA	$K^-p \to \Lambda\pi^0$
135±30	BARBARO-...	70	DPWA	$K^-p \to \Sigma\pi$

$\Sigma(2100)$ DECAY MODES

	Mode	Fraction (Γ_i/Γ)
Γ_1	$N\overline{K}$	(8.0±2.0) %
Γ_2	$\Lambda\pi$	(1.5±1.0) %
Γ_3	$\Sigma\pi$	(2.0±1.0) %
Γ_4	ΞK	
Γ_5	$\Sigma(1385)\pi$, D-wave	(12 ±6) %
Γ_6	$\Sigma(1385)\pi$, G-wave	
Γ_7	$\Lambda(1520)\pi$, F-wave	(1.0±1.0) %
Γ_8	$\Lambda(1520)\pi$, H-wave	
Γ_9	$N\overline{K}^*(892)$, S=3/2 , D-wave	(6.0±3.0) %
Γ_{10}	$\Delta\overline{K}$, G-wave	(1.0±1.0) %

$\Sigma(2100)$ BRANCHING RATIOS

See "Sign conventions for resonance couplings" in the Note on Λ and Σ Resonances.

$(\Gamma_i\Gamma_f)^{1/2}/\Gamma_{total}$ in $N\overline{K} \to \Sigma(2100) \to \Lambda\pi$ — **$(\Gamma_1\Gamma_2)^{1/2}/\Gamma$**

VALUE	DOCUMENT ID		TECN	COMMENT
-0.07 ± 0.02	BARBARO-...	70	DPWA	$K^-p \to \Lambda\pi^0$

$(\Gamma_i\Gamma_f)^{1/2}/\Gamma_{total}$ in $N\overline{K} \to \Sigma(2100) \to \Sigma\pi$ — **$(\Gamma_1\Gamma_3)^{1/2}/\Gamma$**

VALUE	DOCUMENT ID		TECN	COMMENT
$+0.13\pm0.02$	BARBARO-...	70	DPWA	$K^-p \to \Sigma\pi$

$\Gamma(N\overline{K})/\Gamma_{total}$ — **Γ_1/Γ**

VALUE	DOCUMENT ID		TECN	COMMENT
0.08±0.02	SARANTSEV	19	DPWA	$\overline{K}N$ multichannel

$\Gamma(\Lambda\pi)/\Gamma_{total}$ — **Γ_2/Γ**

VALUE	DOCUMENT ID		TECN	COMMENT
0.015±0.01	SARANTSEV	19	DPWA	$\overline{K}N$ multichannel

$\Gamma(\Sigma\pi)/\Gamma_{total}$ — **Γ_3/Γ**

VALUE	DOCUMENT ID		TECN	COMMENT
0.02±0.01	SARANTSEV	19	DPWA	$\overline{K}N$ multichannel

$\Gamma(\Xi K)/\Gamma_{total}$ — **Γ_4/Γ**

VALUE	DOCUMENT ID		TECN	COMMENT
<0.01	SARANTSEV	19	DPWA	$\overline{K}N$ multichannel

$\Gamma(\Sigma(1385)\pi$, D-wave$)/\Gamma_{total}$ — **Γ_5/Γ**

VALUE	DOCUMENT ID		TECN	COMMENT
0.12±0.06	SARANTSEV	19	DPWA	$\overline{K}N$ multichannel

$\Gamma(\Sigma(1385)\pi$, G-wave$)/\Gamma_{total}$ — **Γ_6/Γ**

VALUE	DOCUMENT ID		TECN	COMMENT
~ 0.01	SARANTSEV	19	DPWA	$\overline{K}N$ multichannel

$\Gamma(\Lambda(1520)\pi$, F-wave$)/\Gamma_{total}$ — **Γ_7/Γ**

VALUE	DOCUMENT ID		TECN	COMMENT
0.01±0.01	SARANTSEV	19	DPWA	$\overline{K}N$ multichannel

$\Gamma(\Lambda(1520)\pi$, H-wave$)/\Gamma_{total}$ — **Γ_8/Γ**

VALUE	DOCUMENT ID		TECN	COMMENT
~ 0	SARANTSEV	19	DPWA	$\overline{K}N$ multichannel

$\Gamma(N\overline{K}^*(892)$, S=3/2 , D-wave$)/\Gamma_{total}$ — **Γ_9/Γ**

VALUE	DOCUMENT ID		TECN	COMMENT
0.06±0.03	SARANTSEV	19	DPWA	$\overline{K}N$ multichannel

Int. J. Mod. Phys. A 2026.41. Downloaded from www.worldscientific.com
by UNIVERSITY OF CALIFORNIA @ BERKELEY on 09/16/26. Re-use and distribution is strictly not permitted, except for Open Access articles.

$\Gamma(\Delta\overline{K}, G\text{-wave})/\Gamma_{total}$ — Γ_{10}/Γ

VALUE	DOCUMENT ID		TECN	COMMENT
0.01±0.01	SARANTSEV	19	DPWA	$\overline{K}N$ multichannel

$\Sigma(2100)$ REFERENCES

SARANTSEV	19	EPJ A55 180	A.V. Sarantsev *et al.*	(BONN, PNPI)
BARBARO-...	70	Duke Conf. 173 Hyperon Resonances, 1970	A. Barbaro-Galtieri	(LRL) IJP

$\Sigma(2110)\ 1/2^-$

$I(J^P) = 1(\frac{1}{2}^-)$ Status: *

OMITTED FROM SUMMARY TABLE
was $\Sigma(2160)$

$\Sigma(2110)$ POLE POSITION

REAL PART

VALUE (MeV)	DOCUMENT ID		TECN	COMMENT
2158±25	SARANTSEV	19	DPWA	$\overline{K}N$ multichannel

−2×IMAGINARY PART

VALUE (MeV)	DOCUMENT ID		TECN	COMMENT
300^{+300}_{-60}	SARANTSEV	19	DPWA	$\overline{K}N$ multichannel

$\Sigma(2110)$ POLE RESIDUES

Normalized residue in $N\overline{K} \to \Sigma(2110) \to N\overline{K}$

MODULUS	PHASE (°)	DOCUMENT ID		TECN	COMMENT
0.29±0.08	**−20 ± 35**	SARANTSEV	19	DPWA	$\overline{K}N$ multichannel

Normalized residue in $N\overline{K} \to \Sigma(2110) \to \Sigma\pi$

MODULUS	PHASE (°)	DOCUMENT ID		TECN	COMMENT
0.14±0.04	**−5 ± 35**	SARANTSEV	19	DPWA	$\overline{K}N$ multichannel

Normalized residue in $N\overline{K} \to \Sigma(2110) \to \Lambda\pi$

MODULUS	PHASE (°)	DOCUMENT ID		TECN	COMMENT
0.39±0.08	**85 ± 25**	SARANTSEV	19	DPWA	$\overline{K}N$ multichannel

Normalized residue in $N\overline{K} \to \Sigma(2110) \to \Xi K$

MODULUS	PHASE (°)	DOCUMENT ID		TECN	COMMENT
0.05±0.02	**−85 ± 35**	SARANTSEV	19	DPWA	$\overline{K}N$ multichannel

Normalized residue in $N\overline{K} \to \Sigma(2110) \to \Lambda(1520)\pi$

MODULUS	PHASE (°)	DOCUMENT ID		TECN	COMMENT
0.025±0.015		SARANTSEV	19	DPWA	$\overline{K}N$ multichannel

Normalized residue in $N\overline{K} \to \Sigma(2110) \to \Sigma(1385)\pi$

MODULUS	PHASE (°)	DOCUMENT ID		TECN	COMMENT
0.03±0.02		SARANTSEV	19	DPWA	$\overline{K}N$ multichannel

Normalized residue in $N\overline{K} \to \Sigma(2110) \to \Delta\overline{K}$

MODULUS	PHASE (°)	DOCUMENT ID		TECN	COMMENT
0.035±0.02	**−30 ± 40**	SARANTSEV	19	DPWA	$\overline{K}N$ multichannel

Normalized residue in $N\overline{K} \to \Sigma(2110) \to N\overline{K}^*(892)$, S-wave

MODULUS	PHASE (°)	DOCUMENT ID		TECN	COMMENT
0.09±0.03	**−40 ± 50**	SARANTSEV	19	DPWA	$\overline{K}N$ multichannel

Normalized residue in $N\overline{K} \to \Sigma(2110) \to N\overline{K}^*(892)$, D-wave

MODULUS	PHASE (°)	DOCUMENT ID		TECN	COMMENT
0.04±0.03		SARANTSEV	19	DPWA	$\overline{K}N$ multichannel

$\Sigma(2110)$ MASS

VALUE (MeV)	DOCUMENT ID		TECN	COMMENT
2110±50 OUR AVERAGE Error includes scale factor of 3.4.				
2165 ± 23	SARANTSEV	19	DPWA	$\overline{K}N$ multichannel
2060 ± 20	ZHANG	13A	DPWA	$\overline{K}N$ multichannel

$\Sigma(2110)$ WIDTH

VALUE (MeV)	DOCUMENT ID		TECN	COMMENT
310^{+120}_{-50} OUR AVERAGE				
320^{+300}_{-60}	SARANTSEV	19	DPWA	$\overline{K}N$ multichannel
300 ± 134	ZHANG	13A	DPWA	$\overline{K}N$ multichannel

$\Sigma(2110)$ DECAY MODES

	Mode	Fraction (Γ_i/Γ)
Γ_1	$N\overline{K}$	(29 ± 7) %
Γ_2	$\Sigma\pi$	(7.0± 2.0) %
Γ_3	$\Lambda\pi$	(54 ±12) %
Γ_4	$N\overline{K}^*(892)$, S-wave	(3.0± 1.0) %
Γ_5	$N\overline{K}^*(892)$, D-wave	

$\Sigma(2110)$ BRANCHING RATIOS

$\Gamma(N\overline{K})/\Gamma_{total}$ — Γ_1/Γ

VALUE	DOCUMENT ID		TECN	COMMENT
0.29±0.07	SARANTSEV	19	DPWA	$\overline{K}N$ multichannel

$\Gamma(\Sigma\pi)/\Gamma_{total}$ — Γ_2/Γ

VALUE	DOCUMENT ID		TECN	COMMENT
0.07±0.02	SARANTSEV	19	DPWA	$\overline{K}N$ multichannel

$\Gamma(\Lambda\pi)/\Gamma_{total}$ — Γ_3/Γ

VALUE	DOCUMENT ID		TECN	COMMENT
0.54±0.12	SARANTSEV	19	DPWA	$\overline{K}N$ multichannel

$\Gamma(N\overline{K}^*(892), S\text{-wave})/\Gamma_{total}$ — Γ_4/Γ

VALUE	DOCUMENT ID		TECN	COMMENT
0.03±0.01	SARANTSEV	19	DPWA	$\overline{K}N$ multichannel

$\Gamma(N\overline{K}^*(892), D\text{-wave})/\Gamma_{total}$ — Γ_5/Γ

VALUE	DOCUMENT ID		TECN	COMMENT
• • • We do not use the following data for averages, fits, limits, etc. • • •				
∼ 0.01	SARANTSEV	19	DPWA	$\overline{K}N$ multichannel

$\Sigma(2110)$ REFERENCES

SARANTSEV	19	EPJ A55 180	A.V. Sarantsev *et al.*	(BONN, PNPI)
ZHANG	13A	PR C88 035205	H. Zhang *et al.*	(KSU)

$\Sigma(2230)\ 3/2^+$

$I(J^P) = 1(\frac{3}{2}^+)$ Status: *

OMITTED FROM SUMMARY TABLE

$\Sigma(2230)$ POLE POSITION

REAL PART

VALUE (MeV)	DOCUMENT ID		TECN	COMMENT
2234±25	SARANTSEV	19	DPWA	$\overline{K}N$ multichannel

−2×IMAGINARY PART

VALUE (MeV)	DOCUMENT ID		TECN	COMMENT
340±45	SARANTSEV	19	DPWA	$\overline{K}N$ multichannel

$\Sigma(2230)$ POLE RESIDUES

Normalized residue in $N\overline{K} \to \Sigma(2230) \to N\overline{K}$

MODULUS	PHASE (°)	DOCUMENT ID		TECN	COMMENT
0.07±0.02	**25 ± 15**	SARANTSEV	19	DPWA	$\overline{K}N$ multichannel

Normalized residue in $N\overline{K} \to \Sigma(2230) \to \Sigma\pi$

MODULUS	PHASE (°)	DOCUMENT ID		TECN	COMMENT
0.03±0.02	**180 ± 25**	SARANTSEV	19	DPWA	$\overline{K}N$ multichannel

Normalized residue is $N\overline{K} \to \Sigma(2030) \to \Lambda\pi$

MODULUS	PHASE (°)	DOCUMENT ID		TECN	COMMENT
0.11±0.05	**−16 ± 10**	SARANTSEV	19	DPWA	$\overline{K}N$ multichannel

Normalized residue in $N\overline{K} \to \Sigma(2230) \to \Xi K$

MODULUS	PHASE (°)	DOCUMENT ID		TECN	COMMENT
0.04±0.02	**155 ± 20**	SARANTSEV	19	DPWA	$\overline{K}N$ multichannel

Normalized residue in $N\overline{K} \to \Sigma(2230) \to \Lambda(1520)\pi$, S-wave

MODULUS	PHASE (°)	DOCUMENT ID		TECN	COMMENT
0.12±0.05	**−80 ± 25**	SARANTSEV	19	DPWA	$\overline{K}N$ multichannel

Normalized residue in $N\overline{K} \to \Sigma(2230) \to \Lambda(1520)\pi$, D-wave

MODULUS	PHASE (°)	DOCUMENT ID		TECN	COMMENT
0.03±0.02	**160 ± 30**	SARANTSEV	19	DPWA	$\overline{K}N$ multichannel

Normalized residue in $N\overline{K} \to \Sigma(2230) \to \Sigma(1385)\pi$, P-wave

MODULUS	PHASE (°)	DOCUMENT ID		TECN	COMMENT
0.05±0.02	**60 ± 25**	SARANTSEV	19	DPWA	$\overline{K}N$ multichannel

Int. J. Mod. Phys. A 2026.41. Downloaded from www.worldscientific.com
UNIVERSITY OF CALIFORNIA @ BERKELEY on 09/16/26. Re-use and distribution is strictly not permitted, except for Open Access articles.

Normalized residue in $N\overline{K} \to \Sigma(2230) \to \Sigma(1385)\pi$, F-wave

MODULUS	PHASE (°)	DOCUMENT ID		TECN	COMMENT
0.05±0.03	**−70 ± 20**	SARANTSEV	19	DPWA	$\overline{K}N$ multichannel

Normalized residue in $N\overline{K} \to \Sigma(2230) \to \Delta\overline{K}$, P-wave

MODULUS	PHASE (°)	DOCUMENT ID		TECN	COMMENT
0.11±0.04	**60 ± 15**	SARANTSEV	19	DPWA	$\overline{K}N$ multichannel

Normalized residue in $N\overline{K} \to \Sigma(2230) \to \Delta\overline{K}$, F-wave

MODULUS	PHASE (°)	DOCUMENT ID		TECN	COMMENT
0.07±0.03	**90 ± 25**	SARANTSEV	19	DPWA	$\overline{K}N$ multichannel

Normalized residue in $N\overline{K} \to \Sigma(2230) \to N\overline{K}^*(892)$, S=1/2 , P-wave

MODULUS	PHASE (°)	DOCUMENT ID		TECN	COMMENT
0.08±0.04	**40 ± 45**	SARANTSEV	19	DPWA	$\overline{K}N$ multichannel

Normalized residue in $N\overline{K} \to \Sigma(2230) \to N\overline{K}^*(892)$, S=3/2 , P-wave

MODULUS	PHASE (°)	DOCUMENT ID		TECN	COMMENT
0.14±0.03	**−40 ± 45**	SARANTSEV	19	DPWA	$\overline{K}N$ multichannel

Normalized residue in $N\overline{K} \to \Sigma(2230) \to N\overline{K}^*(892)$, S=3/2 , F-wave

MODULUS	PHASE (°)	DOCUMENT ID		TECN	COMMENT
0.05±0.03	**35 ± 30**	SARANTSEV	19	DPWA	$\overline{K}N$ multichannel

$\Sigma(2230)$ MASS

VALUE (MeV)	DOCUMENT ID		TECN	COMMENT
2240±27	SARANTSEV	19	DPWA	$\overline{K}N$ multichannel

$\Sigma(2230)$ WIDTH

VALUE (MeV)	DOCUMENT ID		TECN	COMMENT
345±50	SARANTSEV	19	DPWA	$\overline{K}N$ multichannel

$\Sigma(2230)$ DECAY MODES

	Mode	Fraction (Γ_i/Γ)
Γ_1	$N\overline{K}$	(6.0±2.0) %
Γ_2	$\Sigma\pi$	(2.0±1.0) %
Γ_3	$\Lambda\pi$	(12 ±6) %
Γ_4	ΞK	(2.0±1.0) %
Γ_5	$\Lambda(1520)\pi$, S-wave	(14 ±5) %
Γ_6	$\Lambda(1520)\pi$, D-wave	
Γ_7	$\Sigma(1385)\pi$, P-wave	(4 ±4) %
Γ_8	$\Sigma(1385)\pi$, F-wave	(3.0±2.0) %
Γ_9	$\Delta\overline{K}$, P-wave	(14 ±5) %
Γ_{10}	$\Delta\overline{K}$, F-wave	(8.0±2.0) %
Γ_{11}	$N\overline{K}^*(892)$, S=1/2 , F-wave	(8.0±3.0) %
Γ_{12}	$N\overline{K}^*(892)$, S=3/2 , F-wave	(26 ±5) %

$\Sigma(2230)$ BRANCHING RATIOS

$\Gamma(N\overline{K})/\Gamma_{total}$ — Γ_1/Γ

VALUE	DOCUMENT ID		TECN	COMMENT
0.06±0.02	SARANTSEV	19	DPWA	$\overline{K}N$ multichannel

$\Gamma(\Sigma\pi)/\Gamma_{total}$ — Γ_2/Γ

VALUE	DOCUMENT ID		TECN	COMMENT
0.02±0.01	SARANTSEV	19	DPWA	$\overline{K}N$ multichannel

$\Gamma(\Lambda\pi)/\Gamma_{total}$ — Γ_3/Γ

VALUE	DOCUMENT ID		TECN	COMMENT
0.12±0.06	SARANTSEV	19	DPWA	$\overline{K}N$ multichannel

$\Gamma(\Xi K)/\Gamma_{total}$ — Γ_4/Γ

VALUE	DOCUMENT ID		TECN	COMMENT
0.02±0.01	SARANTSEV	19	DPWA	$\overline{K}N$ multichannel

$\Gamma(\Lambda(1520)\pi$, S-wave$)/\Gamma_{total}$ — Γ_5/Γ

VALUE	DOCUMENT ID		TECN	COMMENT
0.14±0.05	SARANTSEV	19	DPWA	$\overline{K}N$ multichannel

$\Gamma(\Lambda(1520)\pi$, D-wave$)/\Gamma_{total}$ — Γ_6/Γ

VALUE	DOCUMENT ID		TECN	COMMENT
• • • We do not use the following data for averages, fits, limits, etc. • • •				
∼1	SARANTSEV	19	DPWA	$\overline{K}N$ multichannel

$\Gamma(\Sigma(1385)\pi$, P-wave$)/\Gamma_{total}$ — Γ_7/Γ

VALUE	DOCUMENT ID		TECN	COMMENT
0.04±0.04	SARANTSEV	19	DPWA	$\overline{K}N$ multichannel

$\Gamma(\Sigma(1385)\pi$, F-wave$)/\Gamma_{total}$ — Γ_8/Γ

VALUE	DOCUMENT ID		TECN	COMMENT
0.03±0.02	SARANTSEV	19	DPWA	$\overline{K}N$ multichannel

$\Gamma(\Delta\overline{K}$, P-wave$)/\Gamma_{total}$ — Γ_9/Γ

VALUE	DOCUMENT ID		TECN	COMMENT
0.14±0.05	SARANTSEV	19	DPWA	$\overline{K}N$ multichannel

$\Gamma(\Delta\overline{K}$, F-wave$)/\Gamma_{total}$ — Γ_{10}/Γ

VALUE	DOCUMENT ID		TECN	COMMENT
0.08±0.02	SARANTSEV	19	DPWA	$\overline{K}N$ multichannel

$\Gamma(N\overline{K}^*(892)$, S=1/2 , F-wave$)/\Gamma_{total}$ — Γ_{11}/Γ

VALUE	DOCUMENT ID		TECN	COMMENT
0.08±0.03	SARANTSEV	19	DPWA	$\overline{K}N$ multichannel

$\Gamma(N\overline{K}^*(892)$, S=3/2 , F-wave$)/\Gamma_{total}$ — Γ_{12}/Γ

VALUE	DOCUMENT ID		TECN	COMMENT
0.26±0.05	SARANTSEV	19	DPWA	$\overline{K}N$ multichannel

$\Sigma(2230)$ REFERENCES

SARANTSEV 19 EPJ A55 180 A.V. Sarantsev *et al.* (BONN, PNPI)

$\Sigma(2250)$

$I(J^P) = 1(?^?)$ Status: **

OMITTED FROM SUMMARY TABLE

Results from partial-wave analyses are too weak to warrant separating them from the production and cross-section experiments. LASINSKI 71 in $\overline{K}N$ using a Pomeron + resonances model, and DEBELLEFON 76, DEBELLEFON 77, and DEBELLEFON 78 in energy-dependent partial-wave analyses of $\overline{K}N \to \Lambda\pi$, $\Sigma\pi$, and $N\overline{K}$, respectively, suggest two resonances around this mass.

$\Sigma(2250)$ MASS

VALUE (MeV)	DOCUMENT ID		TECN	COMMENT
2210 to 2280 (≈ 2250) OUR ESTIMATE				
2270±50	DEBELLEFON	78	DPWA	D_5 wave
2210±30	DEBELLEFON	78	DPWA	G_9 wave
2275±20	DEBELLEFON	77	DPWA	D_5 wave
2215±20	DEBELLEFON	77	DPWA	G_9 wave
2300±30	[1] DEBELLEFON	75B	HBC	$K^-p \to \Xi^{*0}K^0$
2251^{+30}_{-20}	VANHORN	75	DPWA	$K^-p \to \Lambda\pi^0$, F_5 wave
2280±14	AGUILAR-...	70B	HBC	K^-p 3.9, 4.6 GeV/c
2237±11	BRICMAN	70	CNTR	Total, charge exchange
2255±10	COOL	70	CNTR	K^-p, K^-d total
2250± 7	BUGG	68	CNTR	K^-p, K^-d total
• • • We do not use the following data for averages, fits, limits, etc. • • •				
2260	DEBELLEFON	76	IPWA	D_5 wave
2215	DEBELLEFON	76	IPWA	G_9 wave
2250±20	LU	70	CNTR	$\gamma p \to K^+Y^*$
2245	BLANPIED	65	CNTR	$\gamma p \to K^+Y^*$
2299± 6	BOCK	65	HBC	$\overline{p}p$ 5.7 GeV/c

$\Sigma(2250)$ WIDTH

VALUE (MeV)	DOCUMENT ID		TECN	COMMENT
60 to 150 (≈ 100) OUR ESTIMATE				
120±40	DEBELLEFON	78	DPWA	D_5 wave
80±20	DEBELLEFON	78	DPWA	G_9 wave
70±20	DEBELLEFON	77	DPWA	D_5 wave
60±20	DEBELLEFON	77	DPWA	G_9 wave
130±20	[1] DEBELLEFON	75B	HBC	$K^-p \to \Xi^{*0}K^0$
192±30	VANHORN	75	DPWA	$K^-p \to \Lambda\pi^0$, F_5 wave
100±20	AGUILAR-...	70B	HBC	K^-p 3.9, 4.6 GeV/c
164±50	BRICMAN	70	CNTR	Total, charge exchange
230±20	BUGG	68	CNTR	K^-p, K^-d total
• • • We do not use the following data for averages, fits, limits, etc. • • •				
100	DEBELLEFON	76	IPWA	D_5 wave
140	DEBELLEFON	76	IPWA	G_9 wave
170	COOL	70	CNTR	K^-p, K^-d total
125	LU	70	CNTR	$\gamma p \to K^+Y^*$
150	BLANPIED	65	CNTR	$\gamma p \to K^+Y^*$
21^{+17}_{-21}	BOCK	65	HBC	$\overline{p}p$ 5.7 GeV/c

Int. J. Mod. Phys. A 2026.41. Downloaded from www.worldscientific.com by UNIVERSITY OF CALIFORNIA @ BERKELEY on 09/16/26. Re-use and distribution is strictly not permitted, except for Open Access articles.

$\Sigma(2250)$ DECAY MODES

	Mode	Fraction (Γ_i/Γ)
Γ_1	$N\overline{K}$	<10 %
Γ_2	$\Lambda\pi$	seen
Γ_3	$\Sigma\pi$	seen
Γ_4	$\Xi(1530)K$	

$\Sigma(2250)$ BRANCHING RATIOS

See "Sign conventions for resonance couplings" in the Note on Λ and Σ Resonances.

$\Gamma(N\overline{K})/\Gamma_{total}$ — Γ_1/Γ

VALUE	DOCUMENT ID		TECN	COMMENT
<0.1 OUR ESTIMATE				
0.08±0.02	DEBELLEFON	78	DPWA	D_5 wave
0.02±0.01	DEBELLEFON	78	DPWA	G_9 wave

$(J+\frac{1}{2})\times\Gamma(N\overline{K})/\Gamma_{total}$ — Γ_1/Γ

VALUE	DOCUMENT ID		TECN	COMMENT
• • • We do not use the following data for averages, fits, limits, etc. • • •				
0.16±0.12	BRICMAN	70	CNTR	Total, charge exchange
0.42	COOL	70	CNTR	K^-p, K^-d total
0.47	BUGG	68	CNTR	

$(\Gamma_i\Gamma_f)^{1/2}/\Gamma_{total}$ in $N\overline{K}\to\Sigma(2250)\to\Lambda\pi$ — $(\Gamma_1\Gamma_2)^{1/2}/\Gamma$

VALUE	DOCUMENT ID		TECN	COMMENT
−0.16±0.03	VANHORN	75	DPWA	$K^-p\to\Lambda\pi^0$, F_5 wave
• • • We do not use the following data for averages, fits, limits, etc. • • •				
+0.11	DEBELLEFON	76	IPWA	D_5 wave
−0.10	DEBELLEFON	76	IPWA	G_9 wave
−0.18	BARBARO-...	70	DPWA	$K^-p\to\Lambda\pi^0$, G_9 wave

$(\Gamma_i\Gamma_f)^{1/2}/\Gamma_{total}$ in $N\overline{K}\to\Sigma(2250)\to\Sigma\pi$ — $(\Gamma_1\Gamma_3)^{1/2}/\Gamma$

VALUE	DOCUMENT ID		TECN	COMMENT
+0.06±0.02	DEBELLEFON	77	DPWA	D_5 wave
−0.03±0.02	DEBELLEFON	77	DPWA	G_9 wave
+0.07	BARBARO-...	70	DPWA	$K^-p\to\Sigma\pi$, G_9 wave

$\Gamma(N\overline{K})/\Gamma(\Sigma\pi)$ — Γ_1/Γ_3

VALUE	DOCUMENT ID		TECN	COMMENT
• • • We do not use the following data for averages, fits, limits, etc. • • •				
<0.18	BARNES	69	HBC	1 standard dev. limit

$\Gamma(\Lambda\pi)/\Gamma(\Sigma\pi)$ — Γ_2/Γ_3

VALUE	DOCUMENT ID		TECN	COMMENT
• • • We do not use the following data for averages, fits, limits, etc. • • •				
<0.18	BARNES	69	HBC	1 standard dev. limit

$(\Gamma_i\Gamma_f)^{1/2}/\Gamma_{total}$ in $N\overline{K}\to\Sigma(2250)\to\Xi(1530)K$ — $(\Gamma_1\Gamma_4)^{1/2}/\Gamma$

VALUE	DOCUMENT ID		TECN	COMMENT
0.18±0.04	[1] DEBELLEFON	75B	HBC	$K^-p\to\Xi^{*0}K^0$

$\Sigma(2250)$ FOOTNOTES

[1] Seen in the (initial and final state) D_5 wave. Isospin not determined.

$\Sigma(2250)$ REFERENCES

DEBELLEFON	78	NC 42A 403	A. de Bellefon *et al.*	(CDEF, SACL) IJP
DEBELLEFON	77	NC 37A 175	A. de Bellefon *et al.*	(CDEF, SACL) IJP
DEBELLEFON	76	NP B109 129	A. de Bellefon, A. Berthon	(CDEF) IJP
Also		NP B90 1	A. de Bellefon *et al.*	(CDEF, SACL) IJP
DEBELLEFON	75B	NC 28A 289	A. de Bellefon *et al.*	(CDEF, SACL)
VANHORN	75	NP B87 145	A.J. van Horn	(LBL) IJP
Also		NP B87 157	A.J. van Horn	(LBL) IJP
LASINSKI	71	NP B29 125	T.A. Lasinski	(EFI) IJP
AGUILAR-...	70B	PRL 25 58	M. Aguilar-Benitez *et al.*	(BNL, SYRA)
BARBARO-...	70	Duke Conf. 173 Hyperon Resonances, 1970	A. Barbaro-Galtieri	(LRL) IJP
BRICMAN	70	PL 31B 152	C. Bricman *et al.*	(CERN, CAEN, SACL)
COOL	70	PR D1 1887	R.L. Cool *et al.*	(BNL) I
Also		PRL 16 1228	R.L. Cool *et al.*	(BNL) I
LU	70	PR D2 1846	D.C. Lu *et al.*	(YALE)
BARNES	69	PRL 22 479	V.E. Barnes *et al.*	(BNL, SYRA)
BUGG	68	PR 168 1466	D.V. Bugg *et al.*	(RHEL, BIRM, CAVE) I
BLANPIED	65	PRL 14 741	W.A. Blanpied *et al.*	(YALE, CEA)
BOCK	65	PL 17 166	R.K. Bock *et al.*	(CERN, SACL)

$\Sigma(2455)$ Bumps

$I(J^P) = 1(?^?)$ Status: *

OMITTED FROM SUMMARY TABLE

There is also some slight evidence for Y^* states in this mass region from the reaction $\gamma p\to K^+X$ — see GREENBERG 68.

$\Sigma(2455)$ MASS

VALUE (MeV)	DOCUMENT ID		TECN	COMMENT
≈ 2455 OUR ESTIMATE				
2455±10	ABRAMS	70	CNTR	K^-p, K^-d total
2455± 7	BUGG	68	CNTR	K^-p, K^-d total

$\Sigma(2455)$ WIDTH

VALUE (MeV)	DOCUMENT ID		TECN	COMMENT
140	ABRAMS	70	CNTR	K^-p, K^-d total
100±20	BUGG	68	CNTR	

$\Sigma(2455)$ DECAY MODES

	Mode
Γ_1	$N\overline{K}$

$\Sigma(2455)$ BRANCHING RATIOS

$(J+\frac{1}{2})\times\Gamma(N\overline{K})/\Gamma_{total}$ — Γ_1/Γ

VALUE	DOCUMENT ID		TECN	COMMENT
0.39	ABRAMS	70	CNTR	K^-p, K^-d total
0.05±0.05	[1] BRICMAN	70	CNTR	Total, charge exchange
0.3	BUGG	68	CNTR	

$\Sigma(2455)$ FOOTNOTES

[1] Fit of total cross section given by BRICMAN 70 is poor in this region.

$\Sigma(2455)$ REFERENCES

ABRAMS	70	PR D1 1917	R.J. Abrams *et al.*	(BNL) I
Also		PRL 19 678	R.J. Abrams *et al.*	(BNL)
BRICMAN	70	PL 31B 152	C. Bricman *et al.*	(CERN, CAEN, SACL)
BUGG	68	PR 168 1466	D.V. Bugg *et al.*	(RHEL, BIRM, CAVE) I
GREENBERG	68	PRL 20 221	J.S. Greenberg *et al.*	(YALE)

$\Sigma(2620)$ Bumps

$I(J^P) = 1(?^?)$ Status: *

OMITTED FROM SUMMARY TABLE

$\Sigma(2620)$ MASS

VALUE (MeV)	DOCUMENT ID		TECN	COMMENT
≈ 2620 OUR ESTIMATE				
2542±22	DIBIANCA	75	DBC	$K^-N\to\Xi K\pi$
2620±15	ABRAMS	70	CNTR	K^-p, K^-d total

$\Sigma(2620)$ WIDTH

VALUE (MeV)	DOCUMENT ID		TECN	COMMENT
221±81	DIBIANCA	75	DBC	$K^-N\to\Xi K\pi$
175	ABRAMS	70	CNTR	K^-p, K^-d total

$\Sigma(2620)$ DECAY MODES

	Mode
Γ_1	$N\overline{K}$

$\Sigma(2620)$ BRANCHING RATIOS

$(J+\frac{1}{2})\times\Gamma(N\overline{K})/\Gamma_{total}$ — Γ_1/Γ

VALUE	DOCUMENT ID		TECN	COMMENT
0.32	ABRAMS	70	CNTR	K^-p, K^-d total
0.36±0.12	BRICMAN	70	CNTR	Total, charge exchange

$\Sigma(2620)$ REFERENCES

DIBIANCA	75	NP B98 137	F.A. Dibianca, R.J. Endorf	(CMU)
ABRAMS	70	PR D1 1917	R.J. Abrams *et al.*	(BNL) I
Also		PRL 19 678	R.J. Abrams *et al.*	(BNL)
BRICMAN	70	PL 31B 152	C. Bricman *et al.*	(CERN, CAEN, SACL)

Int. J. Mod. Phys. A 2026.41. Downloaded from www.worldscientific.com
UNIVERSITY OF CALIFORNIA @ BERKELEY on 09/16/26. Re-use and distribution is strictly not permitted, except for Open Access articles.

$\Sigma(3000)$ Bumps

$I(J^P) = 1(?^?)$ Status: *

OMITTED FROM SUMMARY TABLE

Seen as an enhancement in $\Lambda\pi$ and $\overline{K}N$ invariant mass spectra and in the missing mass of neutrals recoiling against a K^0.

$\Sigma(3000)$ MASS

VALUE (MeV)	DOCUMENT ID		TECN	CHG	COMMENT
≈ 3000 OUR ESTIMATE					
3000	EHRLICH	66	HBC	0	$\pi^- p$ 7.91 GeV/c

$\Sigma(3000)$ DECAY MODES

	Mode
Γ_1	$N\overline{K}$
Γ_2	$\Lambda\pi$

$\Sigma(3000)$ REFERENCES

EHRLICH 66 PR 152 1194 R. Ehrlich, W. Selove, H. Yuta (PENN) I

$\Sigma(3170)$ Bumps

$I(J^P) = 1(?^?)$ Status: *

OMITTED FROM SUMMARY TABLE

Seen by AMIRZADEH 79 as a narrow 6.5-standard-deviation enhancement in the reaction $K^- p \to Y^{*+}\pi^-$ using data from independent high statistics bubble chamber experiments at 8.25 and 6.5 GeV/c. The dominant decay modes are multibody, multistrange final states and the production is via isospin-3/2 baryon exchange. Isospin 1 is favored.

Not seen in a $K^- p$ experiment in LASS at 11 GeV/c (ASTON 85B).

$\Sigma(3170)$ MASS (PRODUCTION EXPERIMENTS)

VALUE (MeV)	EVTS	DOCUMENT ID		TECN	COMMENT
≈ 3170 OUR ESTIMATE					
3170±5	35	AMIRZADEH	79	HBC	$K^- p \to Y^{*+}\pi^-$

$\Sigma(3170)$ WIDTH (PRODUCTION EXPERIMENTS)

VALUE (MeV)	EVTS	DOCUMENT ID		TECN	COMMENT
<20	35	[1] AMIRZADEH	79	HBC	$K^- p \to Y^{*+}\pi^-$

$\Sigma(3170)$ DECAY MODES (PRODUCTION EXPERIMENTS)

	Mode	Fraction (Γ_i/Γ)
Γ_1	$\Lambda K\overline{K}\pi$'s	seen
Γ_2	$\Sigma K\overline{K}\pi$'s	seen
Γ_3	$\Xi K\pi$'s	seen

$\Sigma(3170)$ BRANCHING RATIOS (PRODUCTION EXPERIMENTS)

$\Gamma(\Lambda K\overline{K}\pi\text{'s})/\Gamma_{total}$ — Γ_1/Γ

VALUE	DOCUMENT ID		TECN	COMMENT
seen	AMIRZADEH	79	HBC	$K^- p \to Y^{*+}\pi^-$

$\Gamma(\Sigma K\overline{K}\pi\text{'s})/\Gamma_{total}$ — Γ_2/Γ

VALUE	DOCUMENT ID		TECN	COMMENT
seen	AMIRZADEH	79	HBC	$K^- p \to Y^{*+}\pi^-$

$\Gamma(\Xi K\pi\text{'s})/\Gamma_{total}$ — Γ_3/Γ

VALUE	DOCUMENT ID		TECN	COMMENT
seen	AMIRZADEH	79	HBC	$K^- p \to Y^{*+}\pi^-$

$\Sigma(3170)$ FOOTNOTES (PRODUCTION EXPERIMENTS)

[1] Observed width consistent with experimental resolution.

$\Sigma(3170)$ REFERENCES (PRODUCTION EXPERIMENTS)

ASTON 85B PR D32 2270 D. Aston et al. (SLAC, CARL, CNRC, CINC)
AMIRZADEH 79 PL 89B 125 J. Amirzadeh et al. (BIRM, CERN, GLAS+) I
Also Toronto Conf. 263 J.B. Kinson et al. (BIRM, CERN, GLAS+) I

Int. J. Mod. Phys. A 2026.41. Downloaded from www.worldscientific.com
by UNIVERSITY OF CALIFORNIA @ BERKELEY on 09/16/26. Re-use and distribution is strictly not permitted, except for Open Access articles.

Ξ BARYONS
($S = -2$, $I = 1/2$)

$\Xi^0 = uss$, $\Xi^- = dss$

Ξ^0

$I(J^P) = \frac{1}{2}(\frac{1}{2}^+)$ Status: ****

The parity has not actually been measured, but + is of course expected.

Ξ^0 MASS

The fit uses the Ξ^0, Ξ^-, and $\overline{\Xi}^+$ masses and the $\Xi^- - \Xi^0$ mass difference. It assumes that the Ξ^- and $\overline{\Xi}^+$ masses are the same.

VALUE (MeV)	EVTS	DOCUMENT ID		TECN	COMMENT
1314.86±0.20 OUR FIT					
1314.82±0.06±0.20	3120	FANTI	00	NA48	p Be, 450 GeV
• • • We do not use the following data for averages, fits, limits, etc. • • •					
1315.2 ±0.92	49	WILQUET	72	HLBC	
1313.4 ±1.8	1	PALMER	68	HBC	

$m_{\Xi^-} - m_{\Xi^0}$

The fit uses the Ξ^0, Ξ^-, and $\overline{\Xi}^+$ masses and the $\Xi^- - \Xi^0$ mass difference. It assumes that the Ξ^- and $\overline{\Xi}^+$ masses are the same.

VALUE (MeV)	EVTS	DOCUMENT ID		TECN	COMMENT
6.85±0.21 OUR FIT					
6.3 ±0.7 OUR AVERAGE					
6.9 ±2.2	29	LONDON	66	HBC	
6.1 ±0.9	88	PJERROU	65B	HBC	
6.8 ±1.6	23	JAUNEAU	63	FBC	
• • • We do not use the following data for averages, fits, limits, etc. • • •					
6.1 ±1.6	45	CARMONY	64B	HBC	See PJERROU 65B

Ξ^0 MEAN LIFE

VALUE (10^{-10} s)	EVTS	DOCUMENT ID		TECN	COMMENT
2.90±0.09 OUR AVERAGE					
2.83±0.16	6300	[1] ZECH	77	SPEC	Neutral hyperon beam
$2.88^{+0.21}_{-0.19}$	652	BALTAY	74	HBC	1.75 GeV/c K^-p
$2.90^{+0.32}_{-0.27}$	157	[2] MAYEUR	72	HLBC	2.1 GeV/c K^-
$3.07^{+0.22}_{-0.20}$	340	DAUBER	69	HBC	
3.0 ±0.5	80	PJERROU	65B	HBC	
$2.5^{+0.4}_{-0.3}$	101	HUBBARD	64	HBC	
$3.9^{+1.4}_{-0.8}$	24	JAUNEAU	63	FBC	
• • • We do not use the following data for averages, fits, limits, etc. • • •					
$3.5^{+1.0}_{-0.8}$	45	CARMONY	64B	HBC	See PJERROU 65B

[1] The ZECH 77 result is $\tau_{\Xi^0} = [2.77-(\tau_\Lambda - 2.69)] \times 10^{-10}$ s, in which we use $\tau_\Lambda = 2.63 \times 10^{-10}$ s.
[2] The MAYEUR 72 value is modified by the erratum.

Ξ^0 MAGNETIC MOMENT

See the "Quark Model" review.

VALUE (μ_N)	EVTS	DOCUMENT ID		TECN
−1.250±0.014 OUR AVERAGE				
−1.253±0.014	270k	COX	81	SPEC
−1.20 ±0.06	42k	BUNCE	79	SPEC

Ξ^0 DECAY MODES

	Mode	Fraction (Γ_i/Γ)	Scale factor/ Confidence level
Γ_1	$\Lambda\pi^0$	(99.517±0.012) %	S=1.1
Γ_2	$\Lambda\gamma$	(1.24 ±0.07) $\times 10^{-3}$	S=1.3
Γ_3	$\Lambda e^+ e^-$	(7.6 ±0.6) $\times 10^{-6}$	
Γ_4	$\Sigma^0\gamma$	(3.33 ±0.10) $\times 10^{-3}$	
Γ_5	$\Sigma^+ e^- \overline{\nu}_e$	(2.52 ±0.08) $\times 10^{-4}$	
Γ_6	$\Sigma^+ \mu^- \overline{\nu}_\mu$	(2.3 ±0.4) $\times 10^{-6}$	

$\Delta S = \Delta Q$ (SQ) violating modes or $\Delta S = 2$ forbidden ($S2$) modes

Γ_7	$\Sigma^- e^+ \nu_e$	SQ	<	1.6	$\times 10^{-4}$	CL=90%
Γ_8	$\Sigma^- \mu^+ \nu_\mu$	SQ	<	9	$\times 10^{-4}$	CL=90%
Γ_9	$p\pi^-$	$S2$	<	8	$\times 10^{-6}$	CL=90%
Γ_{10}	$p e^- \overline{\nu}_e$	$S2$	<	1.3	$\times 10^{-3}$	
Γ_{11}	$p \mu^- \overline{\nu}_\mu$	$S2$	<	1.3	$\times 10^{-3}$	
Γ_{12}	$K^- e^+$					
Γ_{13}	$K^+ e^-$					

CONSTRAINED FIT INFORMATION

An overall fit to 6 branching ratios uses 12 measurements and one constraint to determine 5 parameters. The overall fit has a $\chi^2 = 10.2$ for 8 degrees of freedom.

The following *off-diagonal* array elements are the correlation coefficients $\langle \delta x_i \delta x_j \rangle / (\delta x_i \cdot \delta x_j)$, in percent, from the fit to the branching fractions, $x_i \equiv \Gamma_i/\Gamma_{total}$. The fit constrains the x_i whose labels appear in this array to sum to one.

	x_1	x_2	x_4	x_5
x_2	−57			
x_4	−82	0		
x_5	−7	0	0	
x_6	0	0	0	0

Ξ^0 BRANCHING RATIOS

$\Gamma(\Lambda\gamma)/\Gamma(\Lambda\pi^0)$ — Γ_2/Γ_1

VALUE (units 10^{-3})	EVTS	DOCUMENT ID		TECN	COMMENT
1.24±0.07 OUR FIT Error includes scale factor of 1.3.					
1.17±0.07 OUR AVERAGE					
1.17±0.05±0.06	672	[1] LAI	04A	NA48	p Be, 450 GeV
1.91±0.34±0.19	31	[2] FANTI	00	NA48	p Be, 450 GeV
1.06±0.12±0.11	116	JAMES	90	SPEC	FNAL hyperons

[1] LAI 04A used our 2002 value of 99.5% for the $\Xi^0 \to \Lambda\pi^0$ branching fraction to get $\Gamma(\Xi^0 \to \Lambda\gamma)/\Gamma_{total} = (1.16 \pm 0.05 \pm 0.06) \times 10^{-3}$. We adjust slightly to go back to what was directly measured.
[2] FANTI 00 used our 1998 value of 99.5% for the $\Xi^0 \to \Lambda\pi^0$ branching fraction to get $\Gamma(\Xi^0 \to \Lambda\gamma)/\Gamma_{total} = (1.90 \pm 0.34 \pm 0.19) \times 10^{-3}$. We adjust slightly to go back to what was directly measured.

$\Gamma(\Lambda\gamma)/\Gamma_{total}$ — Γ_2/Γ

VALUE (units 10^{-3})	EVTS	DOCUMENT ID		TECN	COMMENT
1.24 ±0.07 OUR FIT Error includes scale factor of 1.3.					
1.347±0.066±0.054	0.64k	[1] ABLIKIM	25AL	BES3	$J/\psi \to \Xi^0\overline{\Xi}^0$

[1] Based on 10B J/ψ events.

$\Gamma(\Lambda e^+ e^-)/\Gamma_{total}$ — Γ_3/Γ

VALUE (units 10^{-6})	EVTS	DOCUMENT ID		TECN	COMMENT
7.6±0.4±0.5	397 ± 21	[1] BATLEY	07C	NA48	p Be, 400 GeV

[1] This BATLEY 07C result is consistent with internal bremsstrahlung.

$\Gamma(\Sigma^0\gamma)/\Gamma(\Lambda\pi^0)$ — Γ_4/Γ_1

VALUE (units 10^{-3})	EVTS	DOCUMENT ID		TECN	COMMENT
3.35±0.10 OUR FIT					
3.35±0.10 OUR AVERAGE					
3.34±0.05±0.09	4045	ALAVI-HARATI	01C	KTEV	p nucleus, 800 GeV
3.16±0.76±0.32	17	[1] FANTI	00	NA48	p Be, 450 GeV
3.56±0.42±0.10	85	TEIGE	89	SPEC	FNAL hyperons

[1] FANTI 00 used our 1998 value of 99.5% for the $\Xi^0 \to \Lambda\pi^0$ branching fraction to get $\Gamma(\Xi^0 \to \Sigma^0\gamma)/\Gamma_{total} = (3.14 \pm 0.76 \pm 0.32) \times 10^{-3}$. We adjust slightly to go back to what was directly measured.

$\Gamma(\Sigma^+ e^- \overline{\nu}_e)/\Gamma_{total}$ — Γ_5/Γ

VALUE (units 10^{-4})	EVTS	DOCUMENT ID		TECN	COMMENT
2.52±0.08 OUR FIT					
2.53±0.08 OUR AVERAGE					
2.51±0.03±0.09	6101	BATLEY	07	NA48	p Be, 400 GeV
2.55±0.14±0.10	419	[1] BATLEY	07	NA48	p Be, 400 GeV
2.71±0.22±0.31	176	AFFOLDER	99	KTEV	p nucleus, 800 GeV

[1] This BATLEY 07 result is for $\overline{\Xi}^0 \to \overline{\Sigma}^- e^+ \nu_e$ events.

$\Gamma(\Sigma^+ \mu^- \overline{\nu}_\mu)/\Gamma_{total}$ — Γ_6/Γ

VALUE (units 10^{-6})	EVTS	DOCUMENT ID		TECN	COMMENT
2.3 ±0.4 OUR FIT					
2.17±0.32±0.17	66	[1] BATLEY	13	NA48	p Be, 400 GeV

[1] BATLEY 13 used $\Xi^0 \to \Sigma^+ e^- \overline{\nu}_e$ decay as a normalization mode and its branching fraction value of $(2.51 \pm 0.03 \pm 0.09) \times 10^{-4}$ from BATLEY 07.

Int. J. Mod. Phys. A 2026.41. Downloaded from www.worldscientific.com
UNIVERSITY OF CALIFORNIA @ BERKELEY on 09/16/26. Re-use and distribution is strictly not permitted, except for Open Access articles.

$\Gamma(\Sigma^+\mu^-\overline{\nu}_\mu)/\Gamma(\Sigma^+e^-\overline{\nu}_e)$ — Γ_6/Γ_5

VALUE	EVTS	DOCUMENT ID		TECN	COMMENT
0.0092±0.0015 OUR FIT					
0.018 $^{+0.007}_{-0.005}$ ±0.002	9	ABOUZAID	05	KTEV	p nucleus 800 GeV

$\Gamma(\Sigma^-e^+\nu_e)/\Gamma_{total}$ — Γ_7/Γ

VALUE	CL%	DOCUMENT ID		TECN	COMMENT
<1.6 × 10^{-4}	90	ABLIKIM	23B	BES3	$J/\psi \to \Xi^0\overline{\Xi}^0$

$\Gamma(\Sigma^-e^+\nu_e)/\Gamma(\Lambda\pi^0)$ — Γ_7/Γ_1

Test of $\Delta S = \Delta Q$ rule.

VALUE (units 10^{-3})	CL%	DOCUMENT ID		TECN	COMMENT
• • • We do not use the following data for averages, fits, limits, etc. • • •					
<0.9	90	YEH	74	HBC	Effective denom.=2500
<1.5		DAUBER	69	HBC	
<6		HUBBARD	66	HBC	

$\Gamma(\Sigma^-\mu^+\nu_\mu)/\Gamma(\Lambda\pi^0)$ — Γ_8/Γ_1

Test of $\Delta S = \Delta Q$ rule.

VALUE (units 10^{-3})	CL%	DOCUMENT ID		TECN	COMMENT
<0.9	90	YEH	74	HBC	Effective denom.=2500
• • • We do not use the following data for averages, fits, limits, etc. • • •					
<1.5		DAUBER	69	HBC	
<6		HUBBARD	66	HBC	

$\Gamma(p\pi^-)/\Gamma(\Lambda\pi^0)$ — Γ_9/Γ_1

ΔS=2. Forbidden in first-order weak interaction.

VALUE (units 10^{-6})	CL%	DOCUMENT ID		TECN	COMMENT
< 8.2	90	WHITE	05	HYCP	p Cu, 800 GeV
• • • We do not use the following data for averages, fits, limits, etc. • • •					
< 36	90	GEWENIGER	75	SPEC	
<1800	90	YEH	74	HBC	Effective denom.=1300
< 900		DAUBER	69	HBC	
<5000		HUBBARD	66	HBC	

$\Gamma(pe^-\overline{\nu}_e)/\Gamma(\Lambda\pi^0)$ — Γ_{10}/Γ_1

ΔS=2. Forbidden in first-order weak interaction.

VALUE (units 10^{-3})	CL%	DOCUMENT ID		TECN	COMMENT
<1.3		DAUBER	69	HBC	
• • • We do not use the following data for averages, fits, limits, etc. • • •					
<3.4	90	YEH	74	HBC	Effective denom.=670
<6		HUBBARD	66	HBC	

$\Gamma(p\mu^-\overline{\nu}_\mu)/\Gamma(\Lambda\pi^0)$ — Γ_{11}/Γ_1

ΔS=2. Forbidden in first-order weak interaction.

VALUE (units 10^{-3})	CL%	DOCUMENT ID		TECN	COMMENT
<1.3		DAUBER	69	HBC	
• • • We do not use the following data for averages, fits, limits, etc. • • •					
<3.5	90	YEH	74	HBC	Effective denom.=664
<6		HUBBARD	66	HBC	

$\Gamma(K^-e^+)/\Gamma_{total}$ — Γ_{12}/Γ

VALUE	CL%	DOCUMENT ID		TECN	COMMENT
<3.6 × 10^{-6}	90	[1] ABLIKIM	23AP	BES3	$J/\psi \to \Xi^0\overline{\Xi}^0$

[1] This decay mode violates baryon and lepton number conservation with Δ(B−L) = 0.

$\Gamma(K^+e^-)/\Gamma_{total}$ — Γ_{13}/Γ

VALUE	CL%	DOCUMENT ID		TECN	COMMENT
<1.9 × 10^{-6}	90	[1] ABLIKIM	23AP	BES3	$J/\psi \to \Xi^0\overline{\Xi}^0$

[1] This decay mode violates baryon and lepton number conservation with |Δ(B-L)|=2.

Ξ^0 DECAY PARAMETERS

See the "Note on Baryon Decay Parameters" in the neutron Listings.

$\alpha(\Xi^0)\ \alpha_-(\Lambda)$

This is a product of the $\Xi^0 \to \Lambda\pi^0$ and $\Lambda \to p\pi^-$ asymmetries.

VALUE	EVTS	DOCUMENT ID		TECN	COMMENT
−0.277±0.008 OUR FIT Error includes scale factor of 2.9.					
−0.261±0.006 OUR AVERAGE					
−0.276±0.001±0.035	4M	BATLEY	10B	NA48	p Be, 400 GeV
−0.260±0.004±0.005	300k	HANDLER	82	SPEC	FNAL hyperons
• • • We do not use the following data for averages, fits, limits, etc. • • •					
−0.317±0.027	6075	BUNCE	78	SPEC	FNAL hyperons
−0.35 ±0.06	505	BALTAY	74	HBC	K^-p 1.75 GeV/c
−0.28 ±0.06	739	DAUBER	69	HBC	K^-p 1.7–2.6 GeV/c

α FOR $\Xi^0 \to \Lambda\pi^0$

The PDG 22 average $\alpha(\Xi^0)\alpha_-(\Lambda) = -0.261 \pm 0.006$ divided by the PDG 22 average $\alpha_-(\Lambda) = 0.748 \pm 0.007$ gives $\alpha(\Xi^0) = -0.349 \pm 0.009$.

VALUE	EVTS	DOCUMENT ID		TECN	COMMENT
−0.371 ±0.010 OUR FIT Error includes scale factor of 3.0.					
−0.3750±0.0034±0.0016	327k	ABLIKIM	23AU	BES3	$J/\psi \to \Xi^0\overline{\Xi}^0$
• • • We do not use the following data for averages, fits, limits, etc. • • •					
−0.358 ±0.042 ±0.013	1.9k	ABLIKIM	23AD	BES3	$\psi(2S) \to \Xi^0\overline{\Xi}^0$

α FOR $\overline{\Xi}^0 \to \overline{\Lambda}\pi^0$

VALUE	EVTS	DOCUMENT ID		TECN	COMMENT
0.3790±0.0034±0.0021	327k	ABLIKIM	23AU	BES3	$J/\psi \to \Xi^0\overline{\Xi}^0$
• • • We do not use the following data for averages, fits, limits, etc. • • •					
0.363 ±0.042 ±0.013	1.9k	ABLIKIM	23AD	BES3	$\psi(2S) \to \Xi^0\overline{\Xi}^0$

ϕ ANGLE FOR $\Xi^0 \to \Lambda\pi^0$ — ($\tan\phi = \beta/\gamma$)

VALUE (°)	EVTS	DOCUMENT ID		TECN	COMMENT
0.292± 0.550±0.103	327k	[1] ABLIKIM	23AU	BES3	$J/\psi \to \Xi^0\overline{\Xi}^0$
• • • We do not use the following data for averages, fits, limits, etc. • • •					
1.55 ± 6.70 ±0.63	1.9k	ABLIKIM	23AD	BES3	$\psi(2S) \to \Xi^0\overline{\Xi}^0$
16 ±17	652	BALTAY	74	HBC	1.75 GeV/c K^-p
38 ±19	739	[2] DAUBER	69	HBC	
− 8 ±30	146	[3] BERGE	66	HBC	

[1] Converted from radians to degrees.
[2] DAUBER 69 uses $\alpha_\Lambda = 0.647 \pm 0.020$.
[3] The errors have been multiplied by 1.2 due to approximations used for the Ξ polarization; see DAUBER 69 for a discussion.

ϕ ANGLE FOR $\overline{\Xi}^0 \to \overline{\Lambda}\pi^0$ ($\tan\phi = \beta/\gamma$)

VALUE (°)	EVTS	DOCUMENT ID		TECN	COMMENT
− 0.304±0.556±0.109	327k	ABLIKIM	23AU	BES3	$J/\psi \to \Xi^0\overline{\Xi}^0$
• • • We do not use the following data for averages, fits, limits, etc. • • •					
−10.60 ±6.65 ±0.97	1.9k	ABLIKIM	23AD	BES3	$\psi(2S) \to \Xi^0\overline{\Xi}^0$

$\Delta\phi_{CP}(\Xi^0) = (\phi_{\Xi^0} + \phi_{\overline{\Xi}^0})/2$

VALUE (°)	EVTS	DOCUMENT ID		TECN	COMMENT
−0.006±0.395±0.052	327k	[1] ABLIKIM	23AU	BES3	$J/\psi \to \Xi^0\overline{\Xi}^0$
• • • We do not use the following data for averages, fits, limits, etc. • • •					
−4.53 ±4.70 ±0.57	1.9k	[1] ABLIKIM	23AD	BES3	$\psi(2S) \to \Xi^0\overline{\Xi}^0$

[1] Converted from radians to degrees.

A_{CP} FOR $\Xi^0 \to \Lambda\pi^0$, $\overline{\Xi}^0 \to \overline{\Lambda}\pi^0$

$A_{CP} = (\alpha + \overline{\alpha}) / (\alpha - \overline{\alpha})$

VALUE (units 10^{-3})	EVTS	DOCUMENT ID		TECN	COMMENT
−5.4± 6.5± 3.1	327k	[1] ABLIKIM	23AU	BES3	$J/\psi \to \Xi^0\overline{\Xi}^0$
• • • We do not use the following data for averages, fits, limits, etc. • • •					
−7 ±82 ±25	1.9k	[1] ABLIKIM	23AD	BES3	$\psi(2S) \to \Xi^0\overline{\Xi}^0$

[1] Probing CP symmetry and weak phases with entangled double-strange baryons.

RADIATIVE HYPERON DECAYS

Revised July 2011 by J.D. Jackson (LBNL).

The weak radiative decays of spin-1/2 hyperons, $B_i \to B_f\gamma$, yield information about matrix elements (form factors) similar to that gained from weak hadronic decays. For a polarized spin-1/2 hyperon decaying radiatively via a $\Delta Q = 0$, $\Delta S = 1$ transition, the angular distribution of the direction $\hat{\mathbf{p}}$ of the final spin-1/2 baryon in the hyperon rest frame is

$$\frac{dN}{d\Omega} = \frac{N}{4\pi}\,(1 + \alpha_\gamma\,\mathbf{P}_i\cdot\hat{\mathbf{p}})\ . \qquad (1)$$

Here $\mathbf{P}_i$ is the polarization of the decaying hyperon, and α_γ is the asymmetry parameter. In terms of the form factors $F_1(q^2)$, $F_2(q^2)$, and $G(q^2)$ of the effective hadronic weak electromagnetic vertex,

$$F_1(q^2)\gamma_\lambda + iF_2(q^2)\sigma_{\lambda\mu}q^\mu + G(q^2)\gamma_\lambda\gamma_5\ ,$$

α_γ is

$$\alpha_\gamma = \frac{2\,\mathrm{Re}[G(0)F_M^*(0)]}{|G(0)|^2 + |F_M(0)|^2}\ , \qquad (2)$$

where $F_M = (m_i - m_f)[F_2 - F_1/(m_i + m_f)]$. If the decaying hyperon is unpolarized, the decay baryon has a longitudinal polarization given by $P_f = -\alpha_\gamma$ [1].

The angular distribution for the weak hadronic decay, $B_i \to B_f\pi$, has the same form as Eq. (1), but of course with a different asymmetry parameter, α_π. Now, however, if the decaying hyperon is unpolarized, the decay baryon has a

Int. J. Mod. Phys. A 2026.41. Downloaded from www.worldscientific.com
by UNIVERSITY OF CALIFORNIA @ BERKELEY on 09/16/26. Re-use and distribution is strictly not permitted, except for Open Access articles.

longitudinal polarization given by $P_f = +\alpha_\pi$ [2,3]. The difference of sign is because the spins of the pion and photon are different.

$\Xi^0 \to \Lambda\gamma$ *decay*—The radiative decay $\Xi^0 \to \Lambda\gamma$ of an unpolarized Ξ^0 uses the hadronic decay $\Lambda \to p\pi^-$ as the analyzer. As noted above, the longitudinal polarization of the Λ will be $P_\Lambda = -\alpha_{\Xi\Lambda\gamma}$. Let α_- be the $\Lambda \to p\pi^-$ asymmetry parameter and $\theta_{\Lambda p}$ be the angle, as seen in the Λ rest frame, between the Λ line of flight and the proton momentum. Then the hadronic version of Eq. (1) applied to the $\Lambda \to p\pi^-$ decay gives

$$\frac{dN}{d\cos\theta_{\Lambda p}} = \frac{N}{2}\left(1 - \alpha_{\Xi\Lambda\gamma}\,\alpha_-\cos\theta_{\Lambda p}\right) \qquad (3)$$

for the angular distribution of the proton in the Λ frame. Our current value, from the CERN NA48/1 experiment [4], is $\alpha_{\Xi\Lambda\gamma} = -0.704 \pm 0.019 \pm 0.064$.

$\Xi^0 \to \Sigma^0\gamma$ *decay*—The asymmetry parameter here, $\alpha_{\Xi\Sigma\gamma}$, is measured by following the decay chain $\Xi^0 \to \Sigma^0\gamma$, $\Sigma^0 \to \Lambda\gamma$, $\Lambda \to p\pi^-$. Again, for an unpolarized Ξ^0, the longitudinal polarization of the Σ^0 will be $P_\Sigma = -\alpha_{\Xi\Sigma\gamma}$. In the $\Sigma^0 \to \Lambda\gamma$ decay, a parity-conserving magnetic-dipole transition, the polarization of the Σ^0 is transferred to the Λ, as may be seen as follows. Let $\theta_{\Sigma\Lambda}$ be the angle seen in the Σ^0 rest frame between the Σ^0 line of flight and the Λ momentum. For Σ^0 helicity $+1/2$, the probability amplitudes for positive and negative spin states of the Σ^0 *along the* Λ *momentum* are $\cos(\theta_{\Sigma\Lambda}/2)$ and $\sin(\theta_{\Sigma\Lambda}/2)$. Then the amplitude for a negative helicity photon and a negative helicity Λ is $\cos(\theta_{\Sigma\Lambda}/2)$, while the amplitude for positive helicities for the photon and Λ is $\sin(\theta_{\Sigma\Lambda}/2)$. For Σ^0 helicity $-1/2$, the amplitudes are interchanged. If the Σ^0 has longitudinal polarization P_Σ, the probabilities for Λ helicities $\pm 1/2$ are therefore

$$p(\pm 1/2) = \frac{1}{2}(1 \mp P_\Sigma)\cos^2(\theta_{\Sigma\Lambda}/2) + \frac{1}{2}(1 \pm P_\Sigma)\sin^2(\theta_{\Sigma\Lambda}/2)\ , \qquad (4)$$

and the longitudinal polarization of the Λ is

$$P_\Lambda = -P_\Sigma\cos\theta_{\Sigma\Lambda} = +\alpha_{\Xi\Sigma\gamma}\cos\theta_{\Sigma\Lambda}\ . \qquad (5)$$

Using Eq. (1) for the $\Lambda \to p\pi^-$ decay again, we get for the joint angular distribution of the $\Sigma^0 \to \Lambda\gamma$, $\Lambda \to p\pi^-$ chain,

$$\frac{d^2N}{d\cos\theta_{\Sigma\Lambda}\,d\cos\theta_{\Lambda p}} = \frac{N}{4}\left(1 + \alpha_{\Xi\Sigma\gamma}\cos\theta_{\Sigma\Lambda}\,\alpha_-\cos\theta_{\Lambda p}\right)\ . \qquad (6)$$

Our current average for $\alpha_{\Xi\Sigma\gamma}$ is -0.69 ± 0.06 [4,5].

References

1. R.E. Behrends, Phys. Rev. **111**, 1691 (1958); see Eq. (7) or (8).
2. In ancient times, the signs of the asymmetry term in the angular distributions of radiative and hadronic decays of polarized hyperons were sometimes opposite. For roughly 50 years, however, the overwhelming convention has been to make them the same. The aim, not always achieved, is to remove ambiguities.
3. For the definition of α_π, see the note on "Baryon Decay Parameters" in the Neutron Listings.
4. J.R. Batley *et al.*, Phys. Lett. **B693**, 241 (2010).
5. A. Alavi-Harati *et al.*, Phys. Rev. Lett. **86**, 3239 (2001).

α FOR $\Xi^0 \to \Lambda\gamma$

See the note above on "Radiative Hyperon Decays."

VALUE	EVTS	DOCUMENT ID		TECN	COMMENT
−0.72 ±0.05 OUR AVERAGE					
−0.741±0.062±0.019	0.64k	[1] ABLIKIM	25AL	BES3	$J/\psi \to \Xi^0\overline{\Xi}^0$
−0.704±0.019±0.064	52k	[2] BATLEY	10B	NA48	p Be, 400 GeV
• • • We do not use the following data for averages, fits, limits, etc. • • •					
−0.78 ±0.18 ±0.06	672	LAI	04A	NA48	See BATLEY 10B
−0.43 ±0.44	87	[3] JAMES	90	SPEC	FNAL hyperons

[1] Based on 10B J/ψ events.
[2] BATLEY 10B also measured the $\overline{\Xi}^0 \to \overline{\Lambda}\gamma$ asymmetry to be -0.798 ± 0.064 (no systematic error given) with 4769 events.
[3] The sign has been changed; see the erratum, JAMES 02.

A_{CP} FOR $\Xi^0 \to \Lambda\gamma$, $\overline{\Xi}^0 \to \overline{\Lambda}\gamma$

$A_{CP} = (\alpha + \overline{\alpha}) / (\alpha - \overline{\alpha})$

VALUE	EVTS	DOCUMENT ID		TECN	COMMENT
−0.120±0.084±0.024	0.64k	[1] ABLIKIM	25AL	BES3	$J/\psi \to \Xi^0\overline{\Xi}^0$

[1] Probes *CP* symmetry and weak phases with entangled doubly-strange baryons.

α FOR $\Xi^0 \to \Lambda e^+ e^-$

VALUE	EVTS	DOCUMENT ID		TECN	COMMENT
−0.8±0.2	397 ± 21	[1] BATLEY	07C	NA48	p Be, 400 GeV

[1] This BATLEY 07C result is consistent with the asymmetry α for $\Xi^0 \to \Lambda\gamma$, as expected if the mechanism is internal bremsstrahlung.

α FOR $\Xi^0 \to \Sigma^0\gamma$

See the note above on "Radiative Hyperon Decays."

VALUE	EVTS	DOCUMENT ID		TECN	COMMENT
−0.69 ±0.06 OUR AVERAGE					
−0.729±0.030±0.076	15k	[1] BATLEY	10B	NA48	p Be, 400 GeV
−0.63 ±0.08 ±0.05	4045	ALAVI-HARATI	01C	KTEV	p nucleus, 800 GeV
• • • We do not use the following data for averages, fits, limits, etc. • • •					
+0.20 ±0.32 ±0.05	85	[2] TEIGE	89	SPEC	FNAL hyperons

[1] BATLEY 10B also measured the $\overline{\Xi}^0 \to \overline{\Sigma}^0\gamma$ asymmetry to be -0.786 ± 0.104 (no systematic error given) with 1404 events.
[2] This result has been withdrawn, due to an error. See the erratum, TEIGE 02.

$g_1(0)/f_1(0)$ FOR $\Xi^0 \to \Sigma^+ e^- \overline{\nu}_e$

VALUE	EVTS	DOCUMENT ID		TECN	COMMENT
1.22±0.05 OUR AVERAGE					
1.21±0.05		BATLEY	13	NA48	p Be, 400 GeV
$1.32^{+0.21}_{-0.17}\pm0.05$	487	[1] ALAVI-HARATI	01I	KTEV	p nucleus, 800 GeV
• • • We do not use the following data for averages, fits, limits, etc. • • •					
1.20±0.04±0.03	6520	[2] BATLEY	07	NA48	See BATLEY 13

[1] ALAVI-HARATI 01I assumes here that the second-class current is zero and that the weak-magnetism term takes its exact SU(3) value.
[2] This BATLEY 07 result uses our 2006 value of V_{us} from semileptonic kaon decays as input.

$g_2(0)/f_1(0))$ FOR $\Xi^0 \to \Sigma^+ e^- \overline{\nu}_e$

VALUE	EVTS	DOCUMENT ID		TECN	COMMENT
$\mathbf{-1.7^{+2.1}_{-2.0}\pm0.5}$	487	[1] ALAVI-HARATI	01I	KTEV	p nucleus, 800 GeV

[1] ALAVI-HARATI 01I thus assumes that $g_2 = 0$ in calculating g_1/f_1, above.

$f_2(0)/f_1(0)$ FOR $\Xi^0 \to \Sigma^+ e^- \overline{\nu}_e$

VALUE	EVTS	DOCUMENT ID		TECN	COMMENT
2.0±0.9 OUR AVERAGE					
2.0±1.3		BATLEY	13	NA48	p Be, 400 GeV
2.0±1.2±0.5	487	ALAVI-HARATI	01I	KTEV	p nucleus, 800 GeV

Ξ^0 REFERENCES

ABLIKIM	25AL	SCIB 70 454	M. Ablikim *et al.*	(BESIII Collab.)
ABLIKIM	23AD	PR D108 L011101	M. Ablikim *et al.*	(BESIII Collab.)
ABLIKIM	23AP	PR D108 012006	M. Ablikim *et al.*	(BESIII Collab.)
ABLIKIM	23AU	PR D108 L031106	M. Ablikim *et al.*	(BESIII Collab.)
ABLIKIM	23B	PR D107 012002	M. Ablikim *et al.*	(BESIII Collab.)
PDG	22	PTEP 2022 083C01	R.L. Workman *et al.*	(PDG Collab.)
BATLEY	13	PL B720 105	J.R. Batley *et al.*	(CERN NA48/1 Collab.)
BATLEY	10B	PL B693 241	J.R. Batley *et al.*	(CERN NA48/1 Collab.)
BATLEY	07	PL B645 36	J.R. Batley *et al.*	(CERN NA48/1 Collab.)
BATLEY	07C	PL B650 1	J.R. Batley *et al.*	(CERN NA48 Collab.)
ABOUZAID	05	PRL 95 081801	E. Abouzaid *et al.*	(FNAL KTeV Collab.)
WHITE	05	PRL 94 101804	C.G. White *et al.*	(FNAL HyperCP Collab.)
LAI	04A	PL B584 251	A. Lai *et al.*	(CERN NA48 Collab.)
JAMES	02	PRL 89 169901 (errat.)	C. James *et al.*	(MINN, MICH, WISC, RUTG)
TEIGE	02	PRL 89 169902 (errat.)	S. Teige *et al.*	(RUTG, MICH, MINN)
ALAVI-HARATI	01C	PRL 86 3239	A. Alavi-Harati *et al.*	(FNAL KTeV Collab.)
ALAVI-HARATI	01I	PRL 87 132001	A. Alavi-Harati *et al.*	(FNAL KTeV Collab.)
FANTI	00	EPJ C12 69	V. Fanti *et al.*	(CERN NA48 Collab.)
AFFOLDER	99	PRL 82 3751	A. Affolder *et al.*	(FNAL KTeV Collab.)
JAMES	90	PRL 64 843	C. James *et al.*	(MINN, MICH, WISC, RUTG)
Also		PRL 89 169901 (errat.)	C. James *et al.*	(MINN, MICH, WISC, RUTG)
TEIGE	89	PRL 63 2717	S. Teige *et al.*	(RUTG, MICH, MINN)
HANDLER	82	PR D25 639	R. Handler *et al.*	(WISC, MICH, MINN+)
COX	81	PRL 46 877	P.T. Cox *et al.*	(MICH, WISC, RUTG, MINN+)
BUNCE	79	PL 86B 386	G.R.M. Bunce *et al.*	(BNL, MICH, RUTG+)
BUNCE	78	PR D18 633	G.R.M. Bunce *et al.*	(WISC, MICH, RUTG)
ZECH	77	NP B124 413	G. Zech *et al.*	(SIEG, CERN, DORT, HEIDH)
GEWENIGER	75	PL 57B 193	C. Geweniger *et al.*	(CERN, HEIDH)
BALTAY	74	PR D9 49	C. Baltay *et al.*	(COLU, BING)

YEH	74	PR D10 3545	N. Yeh *et al.*	(BING, COLU)
MAYEUR	72	NP B47 333	C. Mayeur *et al.*	(BRUX, CERN, TUFTS, LOUC)
Also		NP B53 268 (errat.)	C. Mayeur	
WILQUET	72	PL 42B 372	G. Wilquet *et al.*	(BRUX, CERN, TUFTS+)
DAUBER	69	PR 179 1262	P.M. Dauber *et al.*	(LRL)
PALMER	68	PL 26B 323	R.B. Palmer *et al.*	(BNL, SYRA)
BERGE	66	PR 147 945	J.P. Berge *et al.*	(LRL)
HUBBARD	66	Thesis UCRL 11510	J.R. Hubbard	(LRL)
LONDON	66	PR 143 1034	G.W. London *et al.*	(BNL, SYRA)
PJERROU	65B	PRL 14 275	G.M. Pjerrou *et al.*	(UCLA)
Also		Thesis	G.M. Pjerrou	(UCLA)
CARMONY	64B	PRL 12 482	D.D. Carmony *et al.*	(UCLA)
HUBBARD	64	PR 135 B183	J.R. Hubbard *et al.*	(LRL)
JAUNEAU	63	PL 4 49	L. Jauneau *et al.*	(EPOL, CERN, LOUC+)
Also		Siena Conf. 1 1	L. Jauneau *et al.*	(EPOL, CERN, LOUC+)

Ξ^-

$I(J^P) = \frac{1}{2}(\frac{1}{2}^+)$ Status: ****

The parity has not actually been measured, but + is of course expected.

We have omitted some results that have been superseded by later experiments. See our earlier editions.

Ξ^- MASS

The fit uses the Ξ^-, $\overline{\Xi}^+$, and Ξ^0 masses and the $\Xi^- - \overline{\Xi}^+$ mass difference. It assumes that the Ξ^- and $\overline{\Xi}^+$ masses are the same.

VALUE (MeV)	EVTS	DOCUMENT ID		TECN	COMMENT
1321.71 ± 0.07 OUR FIT					
1321.70 ± 0.08 ± 0.05	2478 ± 68	ABDALLAH	06E	DLPH	from Z decays
• • • We do not use the following data for averages, fits, limits, etc. • • •					
1321.46 ± 0.34	632	DIBIANCA	75	DBC	4.9 GeV/c $K^- d$
1321.12 ± 0.41	268	WILQUET	72	HLBC	
1321.87 ± 0.51	195	[1] GOLDWASSER	70	HBC	5.5 GeV/c $K^- p$
1321.67 ± 0.52	6	CHIEN	66	HBC	6.9 GeV/c $\overline{p}p$
1321.4 ± 1.1	299	LONDON	66	HBC	
1321.3 ± 0.4	149	PJERROU	65B	HBC	
1321.1 ± 0.3	241	[2] BADIER	64	HBC	
1321.4 ± 0.4	517	[2] JAUNEAU	63D	FBC	
1321.1 ± 0.65	62	[2] SCHNEIDER	63	HBC	

[1] GOLDWASSER 70 uses $m_\Lambda = 1115.58$ MeV.
[2] These masses have been increased 0.09 MeV because the Λ mass increased.

$\overline{\Xi}^+$ MASS

The fit uses the Ξ^-, $\overline{\Xi}^+$, and Ξ^0 masses and the $\Xi^- - \overline{\Xi}^+$ mass difference. It assumes that the Ξ^- and $\overline{\Xi}^+$ masses are the same.

VALUE (MeV)	EVTS	DOCUMENT ID		TECN	COMMENT
1321.71 ± 0.07 OUR FIT					
1321.73 ± 0.08 ± 0.05	2256 ± 63	ABDALLAH	06E	DLPH	from Z decays
• • • We do not use the following data for averages, fits, limits, etc. • • •					
1321.6 ± 0.8	35	VOTRUBA	72	HBC	10 GeV/c $K^+ p$
1321.2 ± 0.4	34	STONE	70	HBC	
1320.69 ± 0.93	5	CHIEN	66	HBC	6.9 GeV/c $\overline{p}p$

$(m_{\Xi^-} - m_{\overline{\Xi}^+}) / m_{\Xi^-}$

A test of CPT invariance.

VALUE	DOCUMENT ID		TECN	COMMENT
$(-2.5 \pm 8.7) \times 10^{-5}$	ABDALLAH	06E	DLPH	from Z decays

Ξ^- MEAN LIFE

Measurements with an error > 0.2×10^{-10} s or with systematic errors not included have been omitted.

VALUE (10^{-10} s)	EVTS	DOCUMENT ID		TECN	COMMENT
1.639 ± 0.015 OUR AVERAGE					
1.65 ± 0.07 ± 0.12	2478 ± 68	ABDALLAH	06E	DLPH	from Z decays
1.652 ± 0.051	32k	BOURQUIN	84	SPEC	Hyperon beam
1.665 ± 0.065	41k	BOURQUIN	79	SPEC	Hyperon beam
1.609 ± 0.028	4286	HEMINGWAY	78	HBC	4.2 GeV/c $K^- p$
1.67 ± 0.08		DIBIANCA	75	DBC	4.9 GeV/c $K^- d$
1.63 ± 0.03	4303	BALTAY	74	HBC	1.75 GeV/c $K^- p$
$1.73 \pm^{0.08}_{0.07}$	680	MAYEUR	72	HLBC	2.1 GeV/c K^-
1.61 ± 0.04	2610	DAUBER	69	HBC	
1.80 ± 0.16	299	LONDON	66	HBC	
1.70 ± 0.12	246	PJERROU	65B	HBC	
1.69 ± 0.07	794	HUBBARD	64	HBC	
$1.86 \pm^{0.15}_{0.14}$	517	JAUNEAU	63D	FBC	

$\overline{\Xi}^+$ MEAN LIFE

VALUE (10^{-10} s)	EVTS	DOCUMENT ID		TECN	COMMENT
1.70 ± 0.08 ± 0.12	2256 ± 63	ABDALLAH	06E	DLPH	from Z decays
• • • We do not use the following data for averages, fits, limits, etc. • • •					
$1.55 \pm^{0.35}_{0.20}$	35	[1] VOTRUBA	72	HBC	10 GeV/c $K^+ p$
1.6 ± 0.3	34	STONE	70	HBC	
$1.9 \pm^{0.7}_{0.5}$	12	[1] SHEN	67	HBC	
1.51 ± 0.55	5	[1] CHIEN	66	HBC	6.9 GeV/c $\overline{p}p$

[1] The error is statistical only.

$(\tau_{\Xi^-} - \tau_{\overline{\Xi}^+}) / \tau_{\Xi^-}$

A test of CPT invariance.

VALUE	DOCUMENT ID		TECN	COMMENT
−0.01 ± 0.07	ABDALLAH	06E	DLPH	from Z decays

Ξ^- MAGNETIC MOMENT

See the "Quark Model" review.

VALUE (μ_N)	EVTS	DOCUMENT ID		TECN	COMMENT
−0.6507 ± 0.0025 OUR AVERAGE					
−0.6505 ± 0.0025	4.36M	DURYEA	92	SPEC	800 GeV p Be
−0.661 ± 0.036 ± 0.036	44k	TROST	89	SPEC	Ξ^- ~ 250 GeV
−0.69 ± 0.04	218k	RAMEIKA	84	SPEC	400 GeV pBe
• • • We do not use the following data for averages, fits, limits, etc. • • •					
−0.674 ± 0.021 ± 0.020	122k	HO	90	SPEC	See DURYEA 92
−2.1 ± 0.8	2436	COOL	74	OSPK	1.8 GeV/c $K^- p$
−0.1 ± 2.1	2724	BINGHAM	70B	OSPK	1.8 GeV/c $K^- p$

$\overline{\Xi}^+$ MAGNETIC MOMENT

See the "Quark Model" review.

VALUE (μ_N)	EVTS	DOCUMENT ID		TECN	COMMENT
+0.657 ± 0.028 ± 0.020	70k	HO	90	SPEC	800 GeV pBe

$(\mu_{\Xi^-} + \mu_{\overline{\Xi}^+}) / |\mu_{\Xi^-}|$

A test of CPT invariance. We calculate this from the Ξ^- and $\overline{\Xi}^+$ magnetic moments above.

VALUE	DOCUMENT ID
+0.01 ± 0.05 OUR EVALUATION	

Ξ^- DECAY MODES

	Mode		Fraction (Γ_i/Γ)	Confidence level
Γ_1	$\Lambda\pi^-$		(99.887 ± 0.035) %	
Γ_2	$\Sigma^-\gamma$		(1.27 ± 0.23) $\times 10^{-4}$	
Γ_3	$\Lambda e^-\overline{\nu}_e$		(5.63 ± 0.31) $\times 10^{-4}$	
Γ_4	$\Lambda\mu^-\overline{\nu}_\mu$		$(3.5 \pm^{3.5}_{2.2}) \times 10^{-4}$	
Γ_5	$\Sigma^0 e^-\overline{\nu}_e$		(8.7 ± 1.7) $\times 10^{-5}$	
Γ_6	$\Sigma^0\mu^-\overline{\nu}_\mu$		< 8 $\times 10^{-4}$	90%
Γ_7	$\Xi^0 e^-\overline{\nu}_e$		< 2.59 $\times 10^{-4}$	90%
	$\Delta S = 2$ forbidden ($S2$) modes			
Γ_8	$n\pi^-$	$S2$	< 1.9 $\times 10^{-5}$	90%
Γ_9	$n e^-\overline{\nu}_e$	$S2$	< 3.2 $\times 10^{-3}$	90%
Γ_{10}	$n\mu^-\overline{\nu}_\mu$	$S2$	< 1.5 %	90%
Γ_{11}	$p\pi^-\pi^-$	$S2$	< 4 $\times 10^{-4}$	90%
Γ_{12}	$p\pi^- e^-\overline{\nu}_e$	$S2$	< 4 $\times 10^{-4}$	90%
Γ_{13}	$p\pi^-\mu^-\overline{\nu}_\mu$	$S2$	< 4 $\times 10^{-4}$	90%
Γ_{14}	$p\mu^-\mu^-$	L	< 4 $\times 10^{-8}$	90%
Γ_{15}	π^- invisible		not seen	

CONSTRAINED FIT INFORMATION

An overall fit to 4 branching ratios uses 5 measurements and one constraint to determine 5 parameters. The overall fit has a $\chi^2 = 1.0$ for 1 degrees of freedom.

The following *off-diagonal* array elements are the correlation coefficients $\langle \delta x_i \delta x_j \rangle / (\delta x_i \cdot \delta x_j)$, in percent, from the fit to the branching fractions, $x_i \equiv \Gamma_i/\Gamma_{total}$. The fit constrains the x_i whose labels appear in this array to sum to one.

	x_1	x_2	x_3	x_4
x_2	−6			
x_3	−8	0		
x_4	−99	0	−1	
x_5	−5	0	0	0

Int. J. Mod. Phys. A 2026.41. Downloaded from www.worldscientific.com
UNIVERSITY OF CALIFORNIA @ BERKELEY on 09/16/26. Re-use and distribution is strictly not permitted, except for Open Access articles.

Int. J. Mod. Phys. A 2026.41. Downloaded from www.worldscientific.com
by UNIVERSITY OF CALIFORNIA @ BERKELEY on 09/16/26. Re-use and distribution is strictly not permitted, except for Open Access articles.

Ξ^- BRANCHING RATIOS

A number of early results have been omitted.

$\Gamma(\Sigma^-\gamma)/\Gamma(\Lambda\pi^-)$ — Γ_2/Γ_1

VALUE (units 10^{-4})	EVTS	DOCUMENT ID		TECN	COMMENT
1.27±0.24 OUR FIT					
1.27±0.23 OUR AVERAGE					
1.22±0.23±0.06	211	[1] DUBBS	94	E761	Ξ^- 375 GeV
2.27±1.02	9	BIAGI	87B	SPEC	SPS hyperon beam

[1] DUBBS 94 also finds weak evidence that the asymmetry parameter α_γ is positive ($\alpha_\gamma = 1.0 \pm 1.3$).

$\Gamma(\Lambda e^-\overline{\nu}_e)/\Gamma(\Lambda\pi^-)$ — Γ_3/Γ_1

VALUE (units 10^{-3})	EVTS	DOCUMENT ID		TECN	COMMENT
0.564±0.031 OUR FIT					
0.564±0.031	2857	BOURQUIN	83	SPEC	SPS hyperon beam
• • • We do not use the following data for averages, fits, limits, etc. • • •					
0.30 ±0.13	11	THOMPSON	80	ASPK	Hyperon beam

$\Gamma(\Lambda\mu^-\overline{\nu}_\mu)/\Gamma(\Lambda\pi^-)$ — Γ_4/Γ_1

VALUE (units 10^{-3})	CL%	EVTS	DOCUMENT ID		TECN	COMMENT
$0.35^{+0.35}_{-0.22}$ OUR FIT						
0.35±0.35		1	YEH	74	HBC	Effective denom.=2859
• • • We do not use the following data for averages, fits, limits, etc. • • •						
< 2.3	90	0	THOMPSON	80	ASPK	Effective denom.=1017
< 1.3			DAUBER	69	HBC	
<12			BERGE	66	HBC	

$\Gamma(\Sigma^0 e^-\overline{\nu}_e)/\Gamma(\Lambda\pi^-)$ — Γ_5/Γ_1

VALUE (units 10^{-3})	EVTS	DOCUMENT ID		TECN	COMMENT
0.087±0.017 OUR FIT					
0.087±0.017	154	BOURQUIN	83	SPEC	SPS hyperon beam

$[\Gamma(\Lambda e^-\overline{\nu}_e)+\Gamma(\Sigma^0 e^-\overline{\nu}_e)]/\Gamma(\Lambda\pi^-)$ — $(\Gamma_3+\Gamma_5)/\Gamma_1$

VALUE (units 10^{-3})	EVTS	DOCUMENT ID		TECN	COMMENT
• • • We do not use the following data for averages, fits, limits, etc. • • •					
0.651±0.031	3011	[1] BOURQUIN	83	SPEC	SPS hyperon beam
0.68 ±0.22	17	[2] DUCLOS	71	OSPK	

[1] See the separate BOURQUIN 83 values for $\Gamma(\Lambda e^-\overline{\nu}_e)/\Gamma(\Lambda\pi^-)$ and $\Gamma(\Sigma^0 e^-\overline{\nu}_e)/\Gamma(\Lambda\pi^-)$ above.

[2] DUCLOS 71 cannot distinguish Σ^0's from Λ's. The Cabibbo theory predicts the Σ^0 rate is about a factor 6 smaller than the Λ rate.

$\Gamma(\Sigma^0\mu^-\overline{\nu}_\mu)/\Gamma(\Lambda\pi^-)$ — Γ_6/Γ_1

VALUE (units 10^{-3})	CL%	EVTS	DOCUMENT ID		TECN	COMMENT
<0.76	90	0	YEH	74	HBC	Effective denom.=3026
• • • We do not use the following data for averages, fits, limits, etc. • • •						
<5			BERGE	66	HBC	

$\Gamma(\Xi^0 e^-\overline{\nu}_e)/\Gamma_{total}$ — Γ_7/Γ

VALUE	CL%	DOCUMENT ID		TECN	COMMENT
$<2.59\times10^{-4}$	90	ABLIKIM	21AH	BES3	$J/\psi \to \Xi\overline{\Xi}$

$\Gamma(\Xi^0 e^-\overline{\nu}_e)/\Gamma(\Lambda\pi^-)$ — Γ_7/Γ_1

VALUE	CL%	DOCUMENT ID		TECN	COMMENT
• • • We do not use the following data for averages, fits, limits, etc. • • •					
$<2.3\times10^{-3}$	90	YEH	74	HBC	Effective denom.=1000

$\Gamma(n\pi^-)/\Gamma(\Lambda\pi^-)$ — Γ_8/Γ_1

ΔS=2. Forbidden in first-order weak interaction.

VALUE (units 10^{-3})	CL%	EVTS	DOCUMENT ID		TECN	COMMENT
<0.019	90		BIAGI	82B	SPEC	SPS hyperon beam
• • • We do not use the following data for averages, fits, limits, etc. • • •						
<3.0	90	0	YEH	74	HBC	Effective denom.=760
<1.1			DAUBER	69	HBC	
<5.0			FERRO-LUZZI	63	HBC	

$\Gamma(ne^-\overline{\nu}_e)/\Gamma(\Lambda\pi^-)$ — Γ_9/Γ_1

ΔS=2. Forbidden in first-order weak interaction.

VALUE (units 10^{-3})	CL%	EVTS	DOCUMENT ID		TECN	COMMENT
< 3.2	90	0	YEH	74	HBC	Effective denom.=715
• • • We do not use the following data for averages, fits, limits, etc. • • •						
<10	90		BINGHAM	65	RVUE	

$\Gamma(n\mu^-\overline{\nu}_\mu)/\Gamma(\Lambda\pi^-)$ — Γ_{10}/Γ_1

ΔS=2. Forbidden in first-order weak interaction.

VALUE (units 10^{-3})	CL%	EVTS	DOCUMENT ID		TECN	COMMENT
<15.3	90	0	YEH	74	HBC	Effective denom.=150

$\Gamma(p\pi^-\pi^-)/\Gamma(\Lambda\pi^-)$ — Γ_{11}/Γ_1

ΔS=2. Forbidden in first-order weak interaction.

VALUE (units 10^{-4})	CL%	EVTS	DOCUMENT ID		TECN	COMMENT
<3.7	90	0	YEH	74	HBC	Effective denom.=6200

$\Gamma(p\pi^- e^-\overline{\nu}_e)/\Gamma(\Lambda\pi^-)$ — Γ_{12}/Γ_1

ΔS=2. Forbidden in first-order weak interaction.

VALUE (units 10^{-4})	CL%	EVTS	DOCUMENT ID		TECN	COMMENT
<3.7	90	0	YEH	74	HBC	Effective denom.=6200

$\Gamma(p\pi^-\mu^-\overline{\nu}_\mu)/\Gamma(\Lambda\pi^-)$ — Γ_{13}/Γ_1

ΔS=2. Forbidden in first-order weak interaction.

VALUE (units 10^{-4})	CL%	EVTS	DOCUMENT ID		TECN	COMMENT
<3.7	90	0	YEH	74	HBC	Effective denom.=6200

$\Gamma(p\mu^-\mu^-)/\Gamma(\Lambda\pi^-)$ — Γ_{14}/Γ_1

A ΔL=2 decay, forbidden by total lepton number conservation.

VALUE (units 10^{-8})	CL%	DOCUMENT ID		TECN	COMMENT
<4.0	90	RAJARAM	05	HYCP	p Cu, 800 GeV
• • • We do not use the following data for averages, fits, limits, etc. • • •					
$<3.7\times10^4$	90	[1] LITTENBERG	92B	HBC	Uses YEH 74 data

[1] This LITTENBERG 92B limit and the identical YEH 74 limits for the preceding three modes all result from nonobservance of any 3-prong decays of the Ξ^-. One could as well apply the limit to the *sum* of the four modes.

$\Gamma(\pi^-\text{invisible})/\Gamma_{total}$ — Γ_{15}/Γ

VALUE	DOCUMENT ID		TECN	COMMENT
not seen	[1] ABLIKIM	25CQ	BES3	$J/\psi \to \Xi\overline{\Xi}$

[1] ABLIKIM 25CQ reports branching fraction limits ranging from 8×10^{-4} to 5×10^{-5} at 95% CL over the mass range 1.07–1.16 GeV for the invisible particle.

Ξ DECAY PARAMETERS

See the "Note on Baryon Decay Parameters" in the neutron Listings.

$\alpha(\Xi^-)\alpha_-(\Lambda)$

OUR FIT value is obtained from measurements of $\alpha(\Xi^-)$, $\alpha_-(\Lambda)$, and $\alpha(\Xi^-)\alpha_-(\Lambda)$.

VALUE	EVTS	DOCUMENT ID		TECN	COMMENT
−0.288 ±0.005 OUR FIT Error includes scale factor of 2.2.					
−0.294 ±0.005 OUR AVERAGE Error includes scale factor of 1.7. See the ideogram below.					
−0.2963±0.0042	189k	LUK	00	E756	p Be, 800 GeV
−0.2894±0.0073	63k	[1] LUK	00	E756	p Be, 800 GeV
−0.303 ±0.004 ±0.004	192k	RAMEIKA	86	SPEC	400 GeV pBe
−0.257 ±0.020	11k	ASTON	85B	LASS	11 GeV/c K^-p
−0.260 ±0.017	21k	BENSINGER	85	MPS	5 GeV/c K^-p
−0.299 ±0.007	150k	BIAGI	82	SPEC	SPS hyperon beam
−0.315 ±0.026	9046	CLELAND	80C	ASPK	BNL hyperon beam
−0.239 ±0.021	6599	HEMINGWAY	78	HBC	4.2 GeV/c K^-p
−0.243 ±0.025	4303	BALTAY	74	HBC	1.75 GeV/c K^-p
−0.252 ±0.032	2436	COOL	74	OSPK	1.8 GeV/c K^-p
−0.253 ±0.028	2781	DAUBER	69	HBC	

[1] This LUK 00 value is for $\alpha(\overline{\Xi}^+)\ \alpha_+(\overline{\Lambda})$. We assume *CP* conservation here by including it in the average for $\alpha(\Xi^-)\ \alpha_-(\Lambda)$. But see the second data block below for the *CP* test.

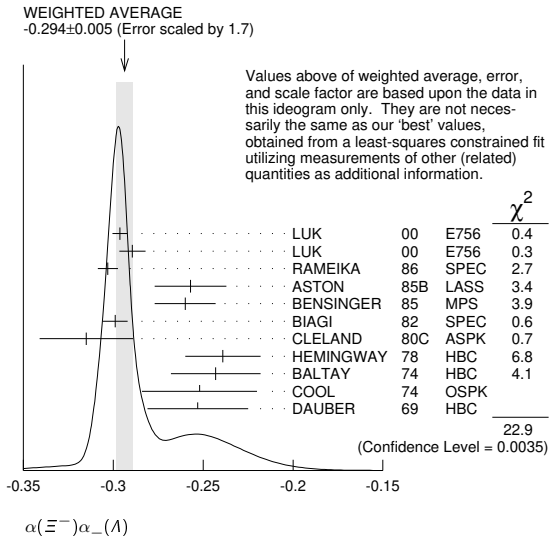

Int. J. Mod. Phys. A 2026.41. Downloaded from www.worldscientific.com
UNIVERSITY OF CALIFORNIA @ BERKELEY on 09/16/26. Re-use and distribution is strictly not permitted, except for Open Access articles.

$\alpha(\Xi^-)$ for $\Xi^- \to \Lambda\pi^-$

OUR FIT value is obtained from measurements of $\alpha(\Xi^-)$, $\alpha_-(\Lambda)$, and $\alpha(\Xi^-)\alpha_-(\Lambda)$.

VALUE	EVTS	DOCUMENT ID		TECN	COMMENT
-0.385 ± 0.008 OUR FIT	Error includes scale factor of 2.4.				
$-0.367\pm0.004^{+0.003}_{-0.004}$	144k	ABLIKIM	24AR	BES3	$J/\psi \to \Xi\overline{\Xi} \to \Lambda\overline{\Lambda}\pi\pi$
• • • We do not use the following data for averages, fits, limits, etc. • • •					
$-0.376\pm0.007\pm0.003$	73k	ABLIKIM	22AD	BES3	$J/\psi \to \Xi\overline{\Xi} \to \Lambda\overline{\Lambda}\pi\pi$
$-0.344\pm0.025\pm0.007$	5.4k	ABLIKIM	22BE	BES3	$\psi(3686) \to \Xi\overline{\Xi} \to \Lambda\overline{\Lambda}\pi\pi$

$\overline{\alpha}(\overline{\Xi}^+)$ for $\overline{\Xi}^+ \to \overline{\Lambda}\pi^+$

VALUE	EVTS	DOCUMENT ID		TECN	COMMENT
$0.374\pm0.004^{+0.003}_{-0.004}$	123k	ABLIKIM	24AR	BES3	$J/\psi \to \Xi\overline{\Xi} \to \Lambda\overline{\Lambda}\pi\pi$
• • • We do not use the following data for averages, fits, limits, etc. • • •					
$0.371\pm0.007\pm0.002$	73k	ABLIKIM	22AD	BES3	$J/\psi \to \Xi\overline{\Xi} \to \Lambda\overline{\Lambda}\pi\pi$
$0.355\pm0.025\pm0.002$	5.4k	ABLIKIM	22BE	BES3	$\psi(3686) \to \Xi\overline{\Xi} \to \Lambda\overline{\Lambda}\pi\pi$

$(\alpha + \overline{\alpha})$ / $(\alpha - \overline{\alpha})$ for $\Xi^- \to \Lambda\pi^-$, $\overline{\Xi}^+ \to \overline{\Lambda}\pi^+$

VALUE (units 10^{-3})	EVTS	DOCUMENT ID		TECN	COMMENT
$-9\pm8^{+7}_{-2}$	267k	ABLIKIM	24AR	BES3	$J/\psi \to \Xi\overline{\Xi} \to \Lambda\overline{\Lambda}\pi\pi$
• • • We do not use the following data for averages, fits, limits, etc. • • •					
$6\pm13\pm6$	73k	ABLIKIM	22AD	BES3	$J/\psi \to \Xi\overline{\Xi} \to \Lambda\overline{\Lambda}\pi\pi$
$-15\pm51\pm10$	5.4k	ABLIKIM	22BE	BES3	$\psi(3686) \to \Xi\overline{\Xi} \to \Lambda\overline{\Lambda}\pi\pi$

$\frac{[\alpha(\Xi^-)\alpha_-(\Lambda)-\overline{\alpha}\overline{\Xi}^+\alpha_+(\overline{\Lambda})]}{[\alpha(\Xi^-)\alpha_-(\Lambda)+\overline{\alpha}\overline{\Xi}^+\alpha_+(\overline{\Lambda})]}$

This is zero if CP is conserved. The α's are the decay-asymmetry parameters for $\Xi^- \to \Lambda\pi^-$ and $\Lambda \to p\pi^-$ and for $\overline{\Xi}^+ \to \overline{\Lambda}\pi^+$ and $\overline{\Lambda} \to \overline{p}\pi^+$.

VALUE (units 10^{-4})	EVTS	DOCUMENT ID		TECN	COMMENT
$0.0\pm5.1\pm4.4$	158M	HOLMSTROM	04	HYCP	p Cu, 800 GeV
• • • We do not use the following data for averages, fits, limits, etc. • • •					
$+120\pm140$	252k	LUK	00	E756	p Be, 800 GeV

ϕ_- ANGLE FOR $\Xi^- \to \Lambda\pi^-$ ($\tan\phi = \beta/\gamma$)

VALUE (°)	EVTS	DOCUMENT ID		TECN	COMMENT
-1.5 ± 0.6 OUR AVERAGE					
$-0.92\pm0.69^{+0.23}_{-0.46}$	144k	[1] ABLIKIM	24AR	BES3	$J/\psi \to \Xi\overline{\Xi} \to \Lambda\overline{\Lambda}\pi\pi$
$-2.39\pm0.64\pm0.64$	144M	[2] HUANG	04	HYCP	p Cu, 800 GeV
$-1.61\pm2.66\pm0.37$	1.35M	[3] CHAKRAVO...	03	E756	p Be, 800 GeV
5 ± 10	11k	ASTON	85B	LASS	K^-p
14.7 ± 16.0	21k	[4] BENSINGER	85	MPS	5 GeV/c K^-p
11 ± 9	4303	BALTAY	74	HBC	1.75 GeV/c K^-p
5 ± 16	2436	COOL	74	OSPK	1.8 GeV/c K^-p
-14 ± 11	2781	DAUBER	69	HBC	Uses $\alpha_\Lambda = 0.647 \pm 0.020$
0 ± 12	1004	[5] BERGE	66	HBC	
• • • We do not use the following data for averages, fits, limits, etc. • • •					
$0.63\pm1.09\pm0.52$	73k	[6] ABLIKIM	22AD	BES3	$J/\psi \to \Xi\overline{\Xi} \to \Lambda\overline{\Lambda}\pi\pi$
$1.32\pm4.24\pm0.17$	5.4k	[7] ABLIKIM	22BE	BES3	$\psi(3686) \to \Xi\overline{\Xi} \to \Lambda\overline{\Lambda}\pi\pi$
-26 ± 30	2724	BINGHAM	70B	OSPK	
0 ± 20.4	364	[5] LONDON	66	HBC	Using α_Λ=0.62
54 ± 30	356	[5] CARMONY	64B	HBC	

[1] Converted from radians to degrees. ABLIKIM 22BE reports a value of $(-1.6\pm1.2^{+0.4}_{-0.8})\times10^{-2}$ radians.
[2] From this result and α_Ξ, HUANG 04 gets $\beta_\Xi = -0.037 \pm 0.011 \pm 0.010$ and $\gamma_\Xi = 0.888 \pm 0.0004 \pm 0.006$. And the strong p–s phase difference for $\Lambda\pi^-$ scattering is $(4.6 \pm 1.4 \pm 1.2)^\circ$.
[3] From this result and α_Ξ, CHAKRAVORTY 03 obtains $\beta_\Xi = -0.025 \pm 0.042 \pm 0.006$ and $\gamma_\Xi = 0.889\pm0.001\pm0.007$. And the strong p–s phase difference for $\Lambda\pi^-$ scattering is $(3.17 \pm 5.28 \pm 0.73)^\circ$.
[4] BENSINGER 85 used $\alpha_\Lambda = 0.642 \pm 0.013$.
[5] The errors have been multiplied by 1.2 due to approximations used for the Ξ polarization; see DAUBER 69 for a discussion.
[6] Converted from radians to degrees. ABLIKIM 22AD reports a value of $(1.1\pm1.9\pm0.9)\times10^{-2}$ radians.
[7] Converted from radians to degrees. ABLIKIM 22BE reports a value of $(2.3\pm7.4\pm0.3)\times10^{-2}$ radians.

ϕ_+ ANGLE FOR $\overline{\Xi}^+ \to \overline{\Lambda}\pi^+$ ($\tan\phi = \beta/\gamma$)

VALUE (°)	EVTS	DOCUMENT ID		TECN	COMMENT
$0.57\pm0.69^{+0.17}_{-0.75}$	123k	[1] ABLIKIM	24AR	BES3	$J/\psi \to \Xi\overline{\Xi} \to \Lambda\overline{\Lambda}\pi\pi$
• • • We do not use the following data for averages, fits, limits, etc. • • •					
$-1.20\pm1.09\pm0.40$	73k	[2] ABLIKIM	22AD	BES3	$J/\psi \to \Xi\overline{\Xi} \to \Lambda\overline{\Lambda}\pi\pi$
$-7.05\pm4.18\pm0.23$	5.4k	[3] ABLIKIM	22BE	BES3	$\psi(3686) \to \Xi\overline{\Xi} \to \Lambda\overline{\Lambda}\pi\pi$

[1] Converted from radians to degrees. ABLIKIM 22BE reports a value of $(1.0\pm1.2^{+0.3}_{-1.3})\times10^{-2}$ radians.
[2] Converted from radians to degrees. ABLIKIM 22AD reports a value of $(-2.1 \pm 1.9 \pm 0.7)\times10^{-2}$ radians.
[3] Converted from radians to degrees. ABLIKIM 22BE reports a value of $(-12.3 \pm 7.3 \pm 0.4)\times10^{-2}$ radians.

$\Delta\phi_{CP} = (\phi_- + \phi_+)/2$

VALUE (°)	EVTS	DOCUMENT ID		TECN	COMMENT
$-0.17\pm0.46^{+0.17}_{-0.40}$	267k	[1] ABLIKIM	24AR	BES3	$J/\psi \to \Xi\overline{\Xi} \to \Lambda\overline{\Lambda}\pi\pi$
• • • We do not use the following data for averages, fits, limits, etc. • • •					
$-0.28\pm0.78\pm0.17$	73k	[2] ABLIKIM	22AD	BES3	$J/\psi \to \Xi\overline{\Xi} \to \Lambda\overline{\Lambda}\pi\pi$
$-2.86\pm2.98\pm0.17$	5.4k	[3] ABLIKIM	22BE	BES3	$\psi(3686) \to \Xi\overline{\Xi} \to \Lambda\overline{\Lambda}\pi\pi$

[1] Converted from radians to degrees. ABLIKIM 22BE reports a value of $(-0.3\pm0.8^{+0.3}_{-0.7})\times10^{-2}$ radians.
[2] Converted from radians to degrees. ABLIKIM 22AD reports a value of $(-0.5 \pm 1.4 \pm 0.3)\times10^{-2}$ radians.
[3] Converted from radians to degrees. ABLIKIM 22BE reports a value of $(-5.0 \pm 5.2 \pm 0.3)\times10^{-2}$ radians.

g_A / g_V FOR $\Xi^- \to \Lambda e^-\overline{\nu}_e$

VALUE	EVTS	DOCUMENT ID		TECN	COMMENT
-0.25 ± 0.05	1992	[1] BOURQUIN	83	SPEC	SPS hyperon beam

[1] BOURQUIN 83 assumes that $g_2 = 0$. Also, the sign has been changed to agree with our conventions, given in the "Note on Baryon Decay Parameters" in the neutron Listings.

Ξ^- REFERENCES

We have omitted some papers that have been superseded by later experiments. See our earlier editions.

ABLIKIM	25CQ	PL B872 140099	M. Ablikim *et al.*	(BESIII Collab.)
ABLIKIM	24AR	PRL 132 101801	M. Ablikim *et al.*	(BESIII Collab.)
ABLIKIM	22AD	NAT 606 64	M. Ablikim *et al.*	(BESIII Collab.)
ABLIKIM	22BE	PR D106 L091101	M. Ablikim *et al.*	(BESIII Collab.)
ABLIKIM	21AH	PR D104 072007	M. Ablikim *et al.*	(BESIII Collab.)
ABDALLAH	06E	PL B639 179	J. Abdallah *et al.*	(DELPHI Collab.)
RAJARAM	05	PRL 94 181801	D. Rajaram *et al.*	(FNAL HyperCP Collab.)
HOLMSTROM	04	PRL 93 262001	T. Holmstrom *et al.*	(FNAL HyperCP Collab.)
HUANG	04	PRL 93 011802	M. Huang *et al.*	(FNAL HyperCP Collab.)
CHAKRAVO...	03	PRL 91 031601	A. Chakravorty *et al.*	(FNAL E756 Collab.)
LUK	00	PRL 85 4860	K.B. Luk *et al.*	(FNAL E756 Collab.)
DUBBS	94	PRL 72 808	T. Dubbs *et al.*	(FNAL E761 Collab.)
DURYEA	92	PRL 68 768	J. Duryea *et al.*	(MINN, FNAL, MICH, RUTG)
LITTENBERG	92B	PR D46 892	L.S. Littenberg, R.E. Shrock	(BNL, STON)
HO	90	PRL 65 1713	P.M. Ho *et al.*	(MICH, FNAL, MINN, RUTG)
Also		PR D44 3402	P.M. Ho *et al.*	(MICH, FNAL, MINN, RUTG)
TROST	89	PR D40 1703	L.H. Trost *et al.*	(FNAL-715 Collab.)
BIAGI	87B	ZPHY C35 143	S.F. Biagi *et al.*	(BRIS, CERN, GEVA+)
RAMEIKA	86	PR D33 3172	R. Rameika *et al.*	(RUTG, MICH, WISC+)
ASTON	85B	PR D32 2270	D. Aston *et al.*	(SLAC, CARL, CNRC, CINC)
BENSINGER	85	NP B252 561	J.R. Bensinger *et al.*	(CHIC, ELMT, FNAL+)
BOURQUIN	84	NP B241 1	M.H. Bourquin *et al.*	(BRIS, GEVA, HEIDP+)
RAMEIKA	84	PRL 52 581	R. Rameika *et al.*	(RUTG, MICH, WISC+)
BOURQUIN	83	ZPHY C21 1	M.H. Bourquin *et al.*	(BRIS, GEVA, HEIDP+)
BIAGI	82	PL 112B 265	S.F. Biagi *et al.*	(BRIS, CAVE, GEVA+)
BIAGI	82B	PL 112B 277	S.F. Biagi *et al.*	(LOQM, GEVA, RL+)
CLELAND	80C	PR D21 12	W.E. Cleland *et al.*	(PITT, BNL)
THOMPSON	80	PR D21 25	J.A. Thompson *et al.*	(PITT, BNL)
BOURQUIN	79	PL 87B 297	M.H. Bourquin *et al.*	(BRIS, GEVA, HEIDP+)
HEMINGWAY	78	NP B142 205	R.J. Hemingway *et al.*	(CERN, ZEEM, NIJM+)
DIBIANCA	75	NP B98 137	F.A. Dibianca, R.J. Endorf	(CMU)
BALTAY	74	PR D9 49	C. Baltay *et al.*	(COLU, BING) J
COOL	74	PR D10 792	R.L. Cool *et al.*	(BNL)
Also		PRL 29 1630	R.L. Cool *et al.*	(BNL)
YEH	74	PR D10 3545	N. Yeh *et al.*	(BING, COLU)
MAYEUR	72	NP B47 333	C. Mayeur *et al.*	(BRUX, CERN, TUFTS, LOUC)
VOTRUBA	72	NP B45 77	M.F. Votruba, A. Safder, T.M. Ratcliffe	(BIRM+)
WILQUET	72	PL 42B 372	G. Wilquet *et al.*	(BRUX, CERN, TUFTS+)
DUCLOS	71	NP B32 493	J. Duclos *et al.*	(CERN)
BINGHAM	70B	PR D1 3010	G.M. Bingham *et al.*	(UCSD, WASH)
GOLDWASSER	70	PR D1 1960	E.L. Goldwasser, P.F. Schultz	(ILL)
STONE	70	PL 32B 515	S.L. Stone *et al.*	(ROCH)
DAUBER	69	PR 179 1262	P.M. Dauber *et al.*	(LRL) J
SHEN	67	PL 25B 443	B.C. Shen, A. Firestone, G. Goldhaber	(UCB+)
BERGE	66	PR 147 945	J.P. Berge *et al.*	(LRL)
CHIEN	66	PR 152 1171	C.Y. Chien *et al.*	(YALE, BNL)
LONDON	66	PR 143 1034	G.W. London *et al.*	(BNL, SYRA)
BINGHAM	65	PRSL 285 202	H.H. Bingham	(CERN)
PJERROU	65B	PRL 14 275	G.M. Pjerrou *et al.*	(UCLA)
Also		Thesis	G.M. Pjerrou	(UCLA)
BADIER	64	Dubna Conf. 1 593	J. Badier *et al.*	(EPOL, SACL, ZEEM)
CARMONY	64B	PRL 12 482	D.D. Carmony *et al.*	(UCLA) J
HUBBARD	64	PR 135 B183	J.R. Hubbard *et al.*	(LRL)
FERRO-LUZZI	63	PR 130 1568	M. Ferro-Luzzi *et al.*	(LRL)
JAUNEAU	63D	Siena Conf. 4	L. Jauneau *et al.*	(EPOL, CERN, LOUC+)
Also		PL 5 261	L. Jauneau *et al.*	(EPOL, CERN, LOUC+)
SCHNEIDER	63	PL 4 360	J. Schneider	(CERN)

Ξ AND Ω RESONANCES

Revised 2025 by V. Crede (FSU), U. Thoma (U. Bonn)

Most of our present knowledge of Ξ and Ω resonances stems from the low-statistics data samples recorded in the 1960s–1980s using K^- beams and in the 1980s and 1990s using hyperon (Σ^-, Ξ^-) beams. This is because (1) they could only be produced as a part of a final state, and so the analysis is more complicated than if direct formation were possible, (2) the production cross sections are small (typically a few μb), and (3) the final states are topologically complicated and difficult to study with electronic techniques. Thus, early information about

Int. J. Mod. Phys. A 2026.41. Downloaded from www.worldscientific.com
by UNIVERSITY OF CALIFORNIA @ BERKELEY on 09/16/26. Re-use and distribution is strictly not permitted, except for Open Access articles.

Ξ resonances came entirely from bubble chamber experiments, where the numbers of events were small, and only in the 1980s did electronic experiments make any significant contributions.

Table 1. Our estimate of the status of the Ξ resonances. Only those with an overall status of *** or **** are included in the Baryon Summary Table.

			Status as seen in —				
Particle	J^P	Overall status	$\Xi\pi$	ΛK	ΣK	$\Xi(1530)\pi$	Other channels
Ξ(1320)	1/2+	****					Decays weakly
Ξ(1530)	3/2+	****	****				
Ξ(1620)		**	**				
Ξ(1690)	1/2−	***	**	***	**		
Ξ(1820)	3/2−	****	**	****	**	**	
Ξ(1950)		***	**	**		*	
Ξ(2030)		***		**	***		
Ξ(2120)		*		*			
Ξ(2250)		**					3-body decays
Ξ(2370)		**					3-body decays
Ξ(2500)		*		*	*		3-body decays

**** Existence is certain, and properties are at least fairly well explored.
*** Existence ranges from very likely to certain, but further confirmation is desirable and/or quantum numbers, branching fractions, *etc.* are not well determined.
** Evidence of existence is only fair.
* Evidence of existence is poor.

In recent years, the two ground states, $\Xi(1320)^-$ and $\Xi(1530)^-$, have been observed in photoproduction by the CLAS Collaboration in the reaction $\gamma p \to K^+K^+\Xi^{(*)}_{\rm miss}$ [1]. New opportunities for studying multi-strange hyperons have also emerged from the high-energy collider experiments, amongst others, Belle, BES III, and LHCb. At these facilities, light-flavor baryon resonances are copiously produced in the decays of heavy baryons containing a charm or bottom quark, or in the decay of heavy-flavor mesons. The available high-statistics data samples provide a rich source for studying multi-strange hyperons. For example, excited Ξ baryons are produced and have been studied in the decay of the charmed Λ_c^+ into $(\Sigma^+K^-)_{\Xi(1690)}\,K^+$ by the Belle Collaboration [2] and into $(\Xi^-\pi^+)_{\Xi^*}\,K^+$ by the BaBar Collaboration [3], but also by Belle in the decay $\Xi_c^+ \to (\Xi^-\pi^+)_{\Xi^*}\,\pi^+$ [4] with high statistical quality. Clear signatures are observed for the decuplet ground state, Ξ(1530), and for the lowest-mass excitations, Ξ(1620) and Ξ(1690). The BES III Collaboration studied Ξ^* production in reactions such as $e^+e^- \to \psi(3686) \to (K^-\Lambda)_{\Xi^*}\bar{\Xi}^+$ and has observed structures associated with the Ξ(1690) and Ξ(1820) resonances [5]. Even a partial wave analysis (PWA) was performed to study the properties of these intermediate state Ξ^* hyperons. However, such studies from $c\bar{c}$ decays are still statistically limited and nothing of significance has been observed for masses beyond 1.9 GeV. Finally, the LHCb Collaboration studied Ξ^* resonances in high-energy pp collisions. The results are based on an analysis of the reaction $\Xi_b \to J/\psi\,(\Lambda K^-)_{\Xi^*}$ and the first observation of Ξ(1690) and Ξ(1820) in the decay of Ξ_b^- was announced [6]. Masses and widths have been determined with improved precision in an amplitude analysis of the $K^-\Lambda$ mass distribution. Large uncertainties in the width of excited Ξ resonances remain. The asignment of the Ξ(1530) to the ground-state decuplet is undisputed and the corresponding $J^P = 3/2^+$ quantum numbers have been experimentally confirmed by the BaBar Collaboration [3]. With few exceptions, experimental analyses and theoretical approaches suggest $J^P = 1/2^-$ and $J^P = 3/2^-$ for Ξ(1690) and Ξ(1820), respectively [7]. All other J^P assignments for Ξ resonances are speculative.

The $\Omega(2012)^- \to \Xi^0 K^-$ $(\Xi^- K^0_S)$ was discovered by Belle in 2018 in the decays of the $b\bar{b}$ mesons $\Upsilon(1S), \Upsilon(2S)$, and $\Upsilon(3S)$ [8]. The ground-state Ω^- is copiously produced in the decay $\Xi_c^0 \to \Omega^- K^-$ and with lower statistics in $\Omega_c^0 \to \Omega^- \pi^+$. Such data samples were used by the BaBar Collaboration for a spin measurement of the Ω^- hyperon [9], for instance. The most recent addition to the family of Ω baryons was reported by the BES III Collaboration in 2025 in the process $e^+e^- \to \Omega(2109)^-\bar{\Omega}^+$ [10].

Reference

1. J. T. Goetz *et al.* [CLAS Collaboration], Phys. Rev. C **98**, 062201 (2018).
2. K. Abe *et al.* [Belle Collaboration], Phys. Lett. B **524**, 33 (2002).
3. B. Aubert *et al.* [BaBar Collaboration], Phys. Rev. D **78**, 034008 (2008).
4. M. Sumihama *et al.* [Belle Collaboration], Phys. Rev. Lett. **122**, 072501 (2019).
5. M. Ablikim *et al.* [BESIII Collaboration], Phys. Rev. D **109**, 072008 (2024).
6. R. Aaij *et al.* [LHCb Collaboration], Sci. Bull. **66**, 1278 (2021).
7. V. Crede and J. Yelton, Rept. Prog. Phys. **87**, 106301 (2024).
8. J. Yelton *et al.* [Belle Collaboration], Phys. Rev. Lett. **121**, 052003 (2018).
9. B. Aubert *et al.* [BaBar Collaboration], Phys. Rev. Lett. **97**, 112001 (2006).
10. M. Ablikim *et al.* [BESIII Collaboration], Phys. Rev. Lett. **134**, 131903 (2025).

Ξ(1530) 3/2+

$I(J^P) = \frac{1}{2}(\frac{3}{2}^+)$ Status: ****

This is the only Ξ resonance whose properties are all reasonably well known. Assuming that the Λ_c^+ has $J^P = 1/2^+$, AUBERT 08AK, in a study of $\Lambda_c^+ \to \Xi^-\pi^+K^+$, finds conclusively that the spin of the $\Xi(1530)^0$ is 3/2. In conjunction with SCHLEIN 63B and BUTTON-SHAFER 66, this proves also that the parity is +.

We use only those determinations of the mass and width that are accompanied by some discussion of systematics and resolution.

Ξ(1530) POLE POSITIONS

$\Xi(1530)^0$ REAL PART

VALUE	DOCUMENT ID	COMMENT
1531.6 ± 0.4	LICHTENBERG74	Using HABIBI 73

$\Xi(1530)^0$ IMAGINARY PART

VALUE	DOCUMENT ID	COMMENT
4.45 ± 0.35	LICHTENBERG74	Using HABIBI 73

$\Xi(1530)^-$ REAL PART

VALUE	DOCUMENT ID	COMMENT
1534.4 ± 1.1	LICHTENBERG74	Using HABIBI 73

Int. J. Mod. Phys. A 2026.41. Downloaded from www.worldscientific.com
UNIVERSITY OF CALIFORNIA @ BERKELEY on 09/16/26. Re-use and distribution is strictly not permitted, except for Open Access articles.

$\Xi(1530)^-$ IMAGINARY PART

VALUE	DOCUMENT ID	COMMENT
$3.9^{+1.75}_{-3.9}$	LICHTENBERG74	Using HABIBI 73

$\Xi(1530)$ MASSES

$\Xi(1530)^0$ MASS

VALUE (MeV)	EVTS	DOCUMENT ID		TECN	COMMENT
1531.80±0.32 OUR FIT Error includes scale factor of 1.3.					
1531.78±0.34 OUR AVERAGE Error includes scale factor of 1.4. See the ideogram below.					
1532.2 ±0.7		DEBELLEFON	75B	HBC	$K^-p \to \Xi^-\overline{K}\pi$
1533 ±1		ROSS	73B	HBC	$K^-p \to \Xi\overline{K}\pi(\pi)$
1531.4 ±0.8	59	BADIER	72	HBC	K^-p 3.95 GeV/c
1532.0 ±0.4	1262	BALTAY	72	HBC	K^-p 1.75 GeV/c
1531.3 ±0.6	324	BORENSTEIN	72	HBC	K^-p 2.2 GeV/c
1532.3 ±0.7	286	KIRSCH	72	HBC	K^-p 2.87 GeV/c
1528.7 ±1.1	76	LONDON	66	HBC	K^-p 2.24 GeV/c
• • • We do not use the following data for averages, fits, limits, etc. • • •					
1532.1 ±0.4	1244	ASTON	85B	LASS	K^-p 11 GeV/c
1532.1 ±0.6	2700	[1] BAUBILLIER	81B	HBC	K^-p 8.25 GeV/c
1530 ±1	450	BIAGI	81	SPEC	SPS hyperon beam
1527 ±6	80	SIXEL	79	HBC	K^-p 10 GeV/c
1535 ±4	100	SIXEL	79	HBC	K^-p 16 GeV/c
1533.6 ±1.4	97	BERTHON	74	HBC	Quasi-2-body σ

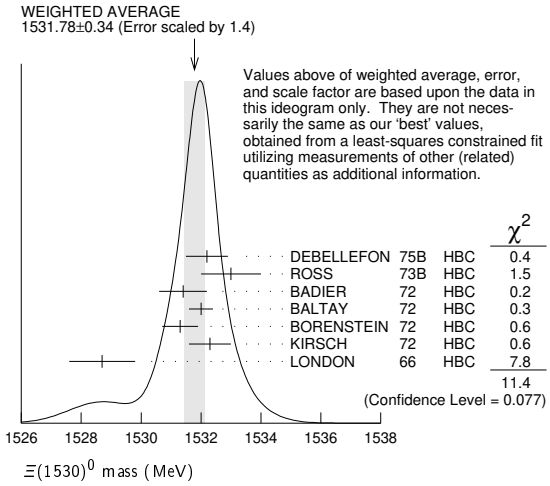

$\Xi(1530)^-$ MASS

VALUE (MeV)	EVTS	DOCUMENT ID		TECN	COMMENT
1535.0±0.6 OUR FIT					
1535.2±0.8 OUR AVERAGE					
1534.5±1.2		DEBELLEFON	75B	HBC	$K^-p \to \Xi^-\overline{K}\pi$
1535.3±2.0		ROSS	73B	HBC	$K^-p \to \Xi\overline{K}\pi(\pi)$
1536.2±1.6	185	KIRSCH	72	HBC	K^-p 2.87 GeV/c
1535.7±3.2	38	LONDON	66	HBC	K^-p 2.24 GeV/c
• • • We do not use the following data for averages, fits, limits, etc. • • •					
1540 ±3	48	BERTHON	74	HBC	Quasi-2-body σ
1534.7±1.1	334	BALTAY	72	HBC	K^-p 1.75 GeV/c

$m_{\Xi(1530)^-} - m_{\Xi(1530)}$

VALUE (MeV)	DOCUMENT ID		TECN	COMMENT
3.2±0.6 OUR FIT				
2.9±0.9 OUR AVERAGE				
2.7±1.0	BALTAY	72	HBC	K^-p 1.75 GeV/c
2.0±3.2	MERRILL	66	HBC	K^-p 1.7–2.7 GeV/c
5.7±3.0	PJERROU	65B	HBC	K^-p 1.8–1.95 GeV/c
• • • We do not use the following data for averages, fits, limits, etc. • • •				
3.9±1.8	[2] KIRSCH	72	HBC	K^-p 2.87 GeV/c
7 ±4	[2] LONDON	66	HBC	K^-p 2.24 GeV/c

$\Xi(1530)$ WIDTHS

$\Xi(1530)^0$ WIDTH

VALUE (MeV)	EVTS	DOCUMENT ID		TECN	COMMENT
9.1±0.5 OUR AVERAGE					
9.5±1.2		DEBELLEFON	75B	HBC	$K^-p \to \Xi^-\overline{K}\pi$
9.1±2.4		ROSS	73B	HBC	$K^-p \to \Xi\overline{K}\pi(\pi)$
11 ±2		BADIER	72	HBC	K^-p 3.95 GeV/c
9.0±0.7		BALTAY	72	HBC	K^-p 1.75 GeV/c
8.4±1.4		BORENSTEIN	72	HBC	$\Xi^-\pi^+$
11.0±1.8		KIRSCH	72	HBC	$\Xi^-\pi^+$
7 ±7		BERGE	66	HBC	K^-p 1.5–1.7 GeV/c
8.5±3.5		LONDON	66	HBC	K^-p 2.24 GeV/c
7 ±2		SCHLEIN	63B	HBC	K^-p 1.8, 1.95 GeV/c
• • • We do not use the following data for averages, fits, limits, etc. • • •					
12.8±1.0	2700	[1] BAUBILLIER	81B	HBC	K^-p 8.25 GeV/c
19 ±6	80	[3] SIXEL	79	HBC	K^-p 10 GeV/c
14 ±5	100	[3] SIXEL	79	HBC	K^-p 16 GeV/c

$\Xi(1530)^-$ WIDTH

VALUE (MeV)	DOCUMENT ID		TECN	COMMENT
$9.9^{+1.7}_{-1.9}$ OUR AVERAGE				
9.6±2.8	DEBELLEFON	75B	HBC	$K^-p \to \Xi^-\overline{K}\pi$
8.3±3.6	ROSS	73B	HBC	$K^-p \to \Xi\overline{K}\pi(\pi)$
$7.8^{+3.5}_{-7.8}$	BALTAY	72	HBC	K^-p 1.75 GeV/c
16.2±4.6	KIRSCH	72	HBC	$\Xi^-\pi^0$, $\Xi^0\pi^-$

$\Xi(1530)$ DECAY MODES

	Mode	Fraction (Γ_i/Γ)	Confidence level
Γ_1	$\Xi\pi$	100 %	
Γ_2	$\Xi\gamma$	<3.7 %	90%

$\Xi(1530)$ BRANCHING RATIOS

$\Gamma(\Xi\gamma)/\Gamma_{total}$ — Γ_2/Γ

VALUE	CL%	DOCUMENT ID		TECN	COMMENT
<0.037	90	ABLIKIM	20	BES3	$J/\psi \to \Xi(1530)^-\overline{\Xi}^+$
• • • We do not use the following data for averages, fits, limits, etc. • • •					
<0.04	90	KALBFLEISCH	75	HBC	K^-p 2.18 GeV/c

$\Xi(1530)$ FOOTNOTES

[1] BAUBILLIER 81B is a fit to the inclusive spectrum. The resolution (5 MeV) is not unfolded.
[2] Redundant with data in the mass Listings.
[3] SIXEL 79 doesn't unfold the experimental resolution of 15 MeV.

$\Xi(1530)$ REFERENCES

ABLIKIM	20	PR D101 012004	M. Ablikim *et al.*	(BESIII Collab.)
AUBERT	08AK	PR D78 034008	B. Aubert *et al.*	(BABAR Collab.)
ASTON	85B	PR D32 2270	D. Aston *et al.*	(SLAC, CARL, CNRC, CINC)
BAUBILLIER	81B	NP B192 1	M. Baubillier *et al.*	(BIRM, CERN, GLAS+)
BIAGI	81	ZPHY C9 305	S.F. Biagi *et al.*	(BRIS, CAVE, GEVA+)
SIXEL	79	NP B159 125	P. Sixel *et al.*	(AACH3, BERL, CERN, LOIC+)
DEBELLEFON	75B	NC 28A 289	A. de Bellefon *et al.*	(CDEF, SACL)
KALBFLEISCH	75	PR D11 987	G.R. Kalbfleisch, R.C. Strand, J.W. Chapman	(BNL+)
BERTHON	74	NC 21A 146	A. Berthon *et al.*	(CDEF, RHEL, SACL+)
LICHTENBERG	74	PR D10 3865	D.B. Lichtenberg	(IND)
Also		Private Comm.	D.B. Lichtenberg	(IND)
HABIBI	73	Thesis Nevis 199	M. Habibi	(COLU)
ROSS	73B	Purdue Conf. 355	R.T. Ross, J.L. Lloyd, D. Radojicic	(OXF)
BADIER	72	NP B37 429	J. Badier *et al.*	(EPOL)
BALTAY	72	PL 42B 129	C. Baltay *et al.*	(COLU, BING)
BORENSTEIN	72	PR D5 1559	S.R. Borenstein *et al.*	(BNL, MICH) I
KIRSCH	72	NP B40 349	L.E. Kirsch *et al.*	(BRAN, UMD, SYRA+) I
BERGE	66	PR 147 945	J.P. Berge *et al.*	(LRL) I
BUTTON-...	66	PR 142 883	J. Button-Shafer *et al.*	(LRL) JP
LONDON	66	PR 143 1034	G.W. London *et al.*	(BNL, SYRA) IJ
MERRILL	66	Thesis UCRL 16455	D.W. Merrill	(LRL) JP
PJERROU	65B	PRL 14 275	G.M. Pjerrou *et al.*	(UCLA)
SCHLEIN	63B	PRL 11 167	P.E. Schlein *et al.*	(UCLA) IJP

OTHER RELATED PAPERS

MAZZUCATO	81	NP B178 1	M. Mazzucato *et al.*	(AMST, CERN, NIJM+)
BRIEFEL	77	PR D16 2706	E. Briefel *et al.*	(BRAN, UMD, SYRA+)
BRIEFEL	75	PR D12 1859	E. Briefel *et al.*	(BRAN, UMD, SYRA+)
HUNGERBU...	74	PR D10 2051	V. Hungerbuhler *et al.*	(YALE, FNAL, BNL+)
BUTTON-...	66	PR 142 883	J. Button-Shafer *et al.*	(LRL) JP

$\Xi(1620)$

$I(J^P) = \frac{1}{2}(?^?)$ Status: **
J, P need confirmation.

OMITTED FROM SUMMARY TABLE

The clearest evidence is a peak in $\Xi^-\pi^+$ seen by SUMIHAMA 19. Older low-statistics experiments (e.g., BORENSTEIN 72 and HASSALL 81) have looked for the state but have not seen any effect.

$\Xi(1620)$ MASS

VALUE (MeV)	EVTS	DOCUMENT ID		TECN	COMMENT
≈1620 OUR ESTIMATE					
$1610.4 \pm 6.0^{+6.1}_{-4.2}$		SUMIHAMA	19	BELL	$\Xi_c^+ \to \Xi(1620)\pi^+$
1624 ± 3	31	BRIEFEL	77	HBC	K^-p 2.87 GeV/c
1633 ±12	34	DEBELLEFON	75B	HBC	$K^-p \to \Xi^-\overline{K}\pi$
1606 ± 6	29	ROSS	72	HBC	K^-p 3.1–3.7 GeV/c

Int. J. Mod. Phys. A 2026.41. Downloaded from www.worldscientific.com
by UNIVERSITY OF CALIFORNIA @ BERKELEY on 09/16/26. Re-use and distribution is strictly not permitted, except for Open Access articles.

$\Xi(1620)$ WIDTH

VALUE (MeV)	EVTS	DOCUMENT ID		TECN	COMMENT
32^{+8}_{-9} OUR AVERAGE		Error includes scale factor of 2.2. See the ideogram below.			
$59.9 \pm 4.8^{+2.8}_{-7.1}$		SUMIHAMA	19	BELL	$\Xi_c^+ \to \Xi(1620)\pi^+$
22.5 ± 7.5	31	[1] BRIEFEL	77	HBC	$K^- p$ 2.87 GeV/c
40 ± 15	34	DEBELLEFON	75B	HBC	$K^- p \to \Xi^- \overline{K} \pi$
21 ± 7	29	ROSS	72	HBC	$K^- p \to \Xi^- \pi^+ K^{*0}(892)$

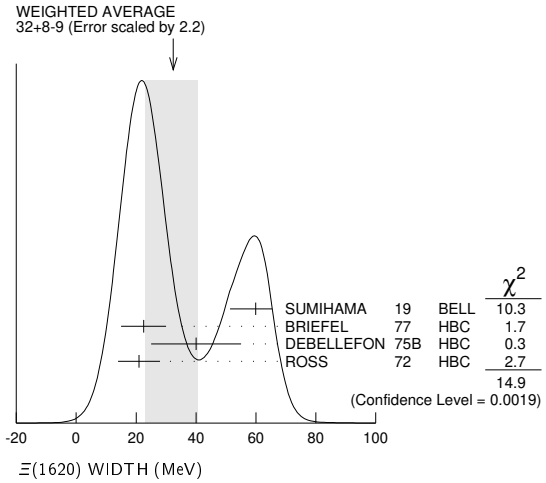

$\Xi(1620)$ DECAY MODES

	Mode
Γ_1	$\Xi\pi$

$\Xi(1620)$ FOOTNOTES

[1] The fit is insensitive to values between 15 and 30 MeV.

$\Xi(1620)$ REFERENCES

SUMIHAMA	19	PRL 122 072501	M. Sumihama *et al.*	(BELLE Collab.)
HASSALL	81	NP B189 397	J.K. Hassall *et al.*	(CAVE, MSU)
BRIEFEL	77	PR D16 2706	E. Briefel *et al.*	(BRAN, UMD, SYRA+)
Also		Duke Conf. 317 Hyperon Resonances, 1970	E. Briefel *et al.*	(BRAN, UMD, SYRA+)
Also		PR D12 1859	E. Briefel *et al.*	(BRAN, UMD, SYRA+)
DEBELLEFON	75B	NC 28A 289	A. de Bellefon *et al.*	(CDEF, SACL)
BORENSTEIN	72	PR D5 1559	S.R. Borenstein *et al.*	(BNL, MICH) I
ROSS	72	PL 38B 177	R.T. Ross *et al.*	(OXF) I

OTHER RELATED PAPERS

HUNGERBU...	74	PR D10 2051	V. Hungerbuhler *et al.*	(YALE, FNAL, BNL+)
SCHMIDT	73	Purdue Conf. 363	P.E. Schmidt	(BRAN)
KALBFLEISCH	70	Duke Conf. 331 Hyperon Resonances 1970	G.R. Kalbfleisch	(BNL) I
APSELL	69	PRL 23 884	S.P. Apsell *et al.*	(BRAN, UMD, SYRA+)
BARTSCH	69	PL 28B 439	J. Bartsch *et al.*	(AACH, BERL, CERN+)

$\Xi(1690)$

$I(J^P) = \frac{1}{2}(?^?)$ Status: ***

AUBERT 08AK, in a study of $\Lambda_c^+ \to \Xi^- \pi^+ K^+$, finds some evidence that the $\Xi(1690)$ has $J^P = 1/2^-$.

DIONISI 78 sees a threshold enhancement in both the neutral and negatively charged $\Sigma\overline{K}$ mass spectra in $K^- p \to (\Sigma\overline{K}) K\pi$ at 4.2 GeV/c. The data from the $\Sigma\overline{K}$ channels alone cannot distinguish between a resonance and a large scattering length. Weaker evidence at the same mass is seen in the corresponding $\Lambda\overline{K}$ channels, and a coupled-channel analysis yields results consistent with a new Ξ.

BIAGI 81 sees an enhancement at 1700 MeV in the diffractively produced ΛK^- system. A peak is also observed in the $\Lambda\overline{K}^0$ mass spectrum at 1660 MeV that is consistent with a 1720 MeV resonance decaying to $\Sigma^0\overline{K}^0$, with the γ from the Σ^0 decay not detected.

BIAGI 87 provides further confirmation of this state in diffractive dissociation of Ξ^- into ΛK^-. The significance claimed is 6.7 standard deviations.

ADAMOVICH 98 sees a peak of 1400 ± 300 events in the $\Xi^-\pi^+$ spectrum produced by 345 GeV/c Σ^--nucleus interactions.

SUMIHAMA 19 observes a peak in the $\Xi^-\pi^+$ spectrum with a significance of 4.0 standard deviations.

$\Xi(1690)$ MASSES

MIXED CHARGES

VALUE (MeV)	DOCUMENT ID
1690±10 OUR ESTIMATE	This is only an educated guess; the error given is larger than the error on the average of the published values.

$\Xi(1690)^0$ MASS

VALUE (MeV)	EVTS	DOCUMENT ID		TECN	COMMENT
1686 ± 4	1400	ADAMOVICH	98	WA89	Σ^- nucleus, 345 GeV/c
1699 ± 5	175	[1] DIONISI	78	HBC	$K^- p$ 4.2 GeV/c
1684 ± 5	183	[2] DIONISI	78	HBC	$K^- p$ 4.2 GeV/c

$\Xi(1690)^-$ MASS

VALUE (MeV)	EVTS	DOCUMENT ID		TECN	COMMENT
$1685^{+3}_{-2} \pm 12$	464	ABLIKIM	24N	PWA	$\psi(3866) \to \Xi(1820)^-\overline{\Xi}^+ \to (K^-\Lambda)\overline{\Xi}^+$
$1691.1 \pm 1.9 \pm 2.0$	104	BIAGI	87	SPEC	Ξ^-Be 116 GeV
1700 ± 10	150	[3] BIAGI	81	SPEC	Ξ^-H 100, 135 GeV
1694 ± 6	45	[4] DIONISI	78	HBC	$K^- p$ 4.2 GeV/c

$\Xi(1690)$ WIDTHS

MIXED CHARGES

VALUE (MeV)	DOCUMENT ID
20±15 OUR ESTIMATE	

$\Xi(1690)^0$ WIDTH

VALUE (MeV)	EVTS	DOCUMENT ID		TECN	COMMENT
10 ± 6	1400	ADAMOVICH	98	WA89	Σ^- nucleus, 345 GeV/c
44 ± 23	175	[1] DIONISI	78	HBC	$K^- p$ 4.2 GeV/c
20 ± 4	183	[2] DIONISI	78	HBC	$K^- p$ 4.2 GeV/c

$\Xi(1690)^-$ WIDTH

VALUE (MeV)	CL%	EVTS	DOCUMENT ID		TECN	COMMENT
< 8	90	104	BIAGI	87	SPEC	Ξ^-Be 116 GeV
47 ± 14		150	[3] BIAGI	81	SPEC	Ξ^-H 100, 135 GeV
26 ± 6		45	[4] DIONISI	78	HBC	$K^- p$ 4.2 GeV/c
• • • We do not use the following data for averages, fits, limits, etc. • • •						
$81^{+10}_{-9} \pm 20$		464	ABLIKIM	24N	PWA	$\psi(3866) \to \Xi(1820)^-\overline{\Xi}^+ \to (K^-\Lambda)\overline{\Xi}^+$

$\Xi(1690)$ DECAY MODES

	Mode	Fraction (Γ_i/Γ)
Γ_1	$\Lambda\overline{K}$	seen
Γ_2	$\Sigma\overline{K}$	seen
Γ_3	$\Xi\pi$	seen
Γ_4	$\Xi^-\pi^+\pi^0$	
Γ_5	$\Xi^-\pi^+\pi^-$	possibly seen
Γ_6	$\Xi(1530)\pi$	

$\Xi(1690)$ BRANCHING RATIOS

$\Gamma(\Lambda\overline{K})/\Gamma_{total}$ — Γ_1/Γ

VALUE	EVTS	DOCUMENT ID		TECN	CHG	COMMENT
seen	104	BIAGI	87	SPEC	–	Ξ^-Be 116 GeV

$\Gamma(\Sigma\overline{K})/\Gamma(\Lambda\overline{K})$ — Γ_2/Γ_1

VALUE	EVTS	DOCUMENT ID		TECN	CHG	COMMENT
0.75 ± 0.39	75	ABE	02C	BELL		$e^+e^- \approx \Upsilon(4S)$
2.7 ± 0.9		DIONISI	78	HBC	0	$K^- p$ 4.2 GeV/c
3.1 ± 1.4		DIONISI	78	HBC	–	$K^- p$ 4.2 GeV/c

$\Gamma(\Xi\pi)/\Gamma(\Sigma\overline{K})$ — Γ_3/Γ_2

VALUE	DOCUMENT ID		TECN	CHG	COMMENT
<0.09	DIONISI	78	HBC	0	$K^- p$ 4.2 GeV/c

$\Gamma(\Xi\pi)/\Gamma_{total}$ — Γ_3/Γ

VALUE	DOCUMENT ID		TECN	COMMENT
seen	ADAMOVICH	98	WA89	Σ^- nucleus, 345 GeV/c

$\Gamma(\Xi^-\pi^+\pi^0)/\Gamma(\Sigma\overline{K})$ — Γ_4/Γ_2

VALUE	DOCUMENT ID		TECN	CHG	COMMENT
<0.04	DIONISI	78	HBC	0	$K^- p$ 4.2 GeV/c

$\Gamma(\Xi^-\pi^+\pi^-)/\Gamma_{total}$ — Γ_5/Γ

VALUE	EVTS	DOCUMENT ID		TECN	CHG	COMMENT
possibly seen	4	BIAGI	87	SPEC	–	Ξ^-Be 116 GeV

Int. J. Mod. Phys. A 2026.41. Downloaded from www.worldscientific.com
UNIVERSITY OF CALIFORNIA @ BERKELEY on 09/16/26. Re-use and distribution is strictly not permitted, except for Open Access articles.

$\Gamma(\Xi^-\pi^+\pi^-)/\Gamma(\Sigma\overline{K})$ — Γ_5/Γ_2

VALUE	DOCUMENT ID		TECN	CHG	COMMENT
<0.03	DIONISI	78	HBC	–	K^-p 4.2 GeV/c

$\Gamma(\Xi(1530)\pi)/\Gamma(\Sigma\overline{K})$ — Γ_6/Γ_2

VALUE	DOCUMENT ID		TECN	CHG	COMMENT
<0.06	DIONISI	78	HBC	–	K^-p 4.2 GeV/c

$\Xi(1690)$ FOOTNOTES

[1] From a fit to the Σ^+K^- spectrum.
[2] From a coupled-channel analysis of the Σ^+K^- and $\Lambda\overline{K}^0$ spectra.
[3] A fit to the inclusive spectrum from $\Xi^-N \to \Lambda K^-X$.
[4] From a coupled-channel analysis of the Σ^0K^- and ΛK^- spectra.

$\Xi(1690)$ REFERENCES

ABLIKIM	24N	PR D109 072008	M. Ablikim *et al.*	(BESIII Collab.)
SUMIHAMA	19	PRL 122 072501	M. Sumihama *et al.*	(BELLE Collab.)
AUBERT	08AK	PR D78 034008	B. Aubert *et al.*	(BABAR Collab.)
ABE	02C	PL B524 33	K. Abe *et al.*	(KEK BELLE Collab.)
ADAMOVICH	98	EPJ C5 621	M.I. Adamovich *et al.*	(CERN WA89 Collab.)
BIAGI	87	ZPHY C34 15	S.F. Biagi *et al.*	(BRIS, CERN, GEVA+) I
BIAGI	81	ZPHY C9 305	S.F. Biagi *et al.*	(BRIS, CAVE, GEVA+)
DIONISI	78	PL 80B 145	C. Dionisi *et al.*	(CERN, AMST, NIJM+) I

$\Xi(1820)\ 3/2^-$

$I(J^P) = \frac{1}{2}(\frac{3}{2}^-)$ Status: ***

The clearest evidence is an 8-standard-deviation peak in ΛK^- seen by GAY 76C. TEODORO 78 favors $J = 3/2$, but cannot make a parity discrimination. BIAGI 87C is consistent with $J = 3/2$ and favors negative parity for this J value.

$\Xi(1820)$ MASS

We only average the measurements that appear to us to be most significant and best determined.

VALUE (MeV)	EVTS	DOCUMENT ID		TECN	CHG	COMMENT
1823 ± 5 OUR ESTIMATE						
1823.2± 1.3 OUR AVERAGE						
$1821^{+2}_{-3} \pm 3$	776	ABLIKIM	24N	PWA	–	$\psi(3866) \to \Xi(1820)^-\overline{\Xi}^+ \to (K^-\Lambda)\overline{\Xi}^+$
1825.5± 4.7±4.7	288	ABLIKIM	20C	BES3	–	$e^+e^- \to \Xi(1820)^-\overline{\Xi}^+$
1819.4± 3.1±2.0	280	[1] BIAGI	87	SPEC	0	Ξ^-Be $\to (\Lambda K^-)$ X
1826 ± 3 ±1	54	BIAGI	87C	SPEC	0	Ξ^-Be $\to (\Lambda\overline{K}^0)$ X
1822 ± 6		JENKINS	83	MPS	–	$K^-p \to K^+$ (MM)
1830 ± 6	300	BIAGI	81	SPEC	–	SPS hyperon beam
1823 ± 2	130	GAY	76C	HBC	–	K^-p 4.2 GeV/c
• • • We do not use the following data for averages, fits, limits, etc. • • •						
1817 ± 3		ADAMOVICH	99B	WA89		Σ^- nucleus, 345 GeV
1797 ±19	74	BRIEFEL	77	HBC	0	K^-p 2.87 GeV/c
1829 ± 9	68	BRIEFEL	77	HBC	−0	$\Xi(1530)\pi$
1860 ±14	39	BRIEFEL	77	HBC	–	$\Sigma^-\overline{K}^0$
1870 ± 9	44	BRIEFEL	77	HBC	0	$\Lambda\overline{K}^0$
1813 ± 4	57	BRIEFEL	77	HBC	–	ΛK^-
1807 ±27		DIBIANCA	75	DBC	−0	$\Xi\pi\pi$, $\Xi^*\pi$
1762 ± 8	28	[2] BADIER	72	HBC	−0	$\Xi\pi$, $\Xi\pi\pi$, YK
1838 ± 5	38	[2] BADIER	72	HBC	−0	$\Xi\pi$, $\Xi\pi\pi$, YK
1830 ±10	25	[3] CRENNELL	70B	DBC	−0	3.6, 3.9 GeV/c
1826 ±12		[4] CRENNELL	70B	DBC	−0	3.6, 3.9 GeV/c
1830 ±10	40	ALITTI	69	HBC	–	Λ, $\Sigma\overline{K}$
1814 ± 4	30	BADIER	65	HBC	0	$\Lambda\overline{K}^0$
1817 ± 7	29	SMITH	65C	HBC	−0	$\Lambda\overline{K}^0$, ΛK^-
1770		HALSTEINSLID	63	FBC	−0	K^-freon 3.5 GeV/c

$\Xi(1820)$ WIDTH

VALUE (MeV)	EVTS	DOCUMENT ID		TECN	CHG	COMMENT
24^{+15}_{-10} OUR ESTIMATE						
24 ± 5 OUR AVERAGE Error includes scale factor of 1.3. See the ideogram below.						
17.0±15.0±7.9	288	ABLIKIM	20C	BES3	–	$e^+e^- \to \Xi(1820)^-\overline{\Xi}^+$
24.6± 5.3	280	[1] BIAGI	87	SPEC	0	Ξ^-Be $\to (\Lambda K^-)$ X
12 ±14 ±1.7	54	BIAGI	87C	SPEC	0	Ξ^-Be $\to (\Lambda\overline{K}^0)$ X
72 ±20	300	BIAGI	81	SPEC	–	SPS hyperon beam
21 ± 7	130	GAY	76C	HBC	–	K^-p 4.2 GeV/c
• • • We do not use the following data for averages, fits, limits, etc. • • •						
$73^{+6}_{-5} \pm 9$	776	ABLIKIM	24N	PWA	–	$\psi(3866) \to \Xi(1820)^-\overline{\Xi}^+ \to (K^-\Lambda)\overline{\Xi}^+$
23 ±13		ADAMOVICH	99B	WA89		Σ^- nucleus, 345 GeV
99 ±57	74	BRIEFEL	77	HBC	0	K^-p 2.87 GeV/c
52 ±34	68	BRIEFEL	77	HBC	−0	$\Xi(1530)\pi$
72 ±17	39	BRIEFEL	77	HBC	–	$\Sigma^-\overline{K}^0$
44 ±11	44	BRIEFEL	77	HBC	0	$\Lambda\overline{K}^0$
26 ±11	57	BRIEFEL	77	HBC	–	ΛK^-
85 ±58		DIBIANCA	75	DBC	−0	$\Xi\pi\pi$, $\Xi^*\pi$
51 ±13		[2] BADIER	72	HBC	−0	Lower mass
58 ±13		[2] BADIER	72	HBC	−0	Higher mass
103^{+38}_{-24}		[3] CRENNELL	70B	DBC	−0	3.6, 3.9 GeV/c
48^{+36}_{-19}		[4] CRENNELL	70B	DBC	−0	3.6, 3.9 GeV/c
55^{+40}_{-20}		ALITTI	69	HBC	–	Λ, $\Sigma\overline{K}$
12 ± 4		BADIER	65	HBC	0	$\Lambda\overline{K}^0$
30 ± 7		SMITH	65B	HBC	−0	$\Lambda\overline{K}$
<80		HALSTEINSLID	63	FBC	−0	K^-freon 3.5 GeV/c

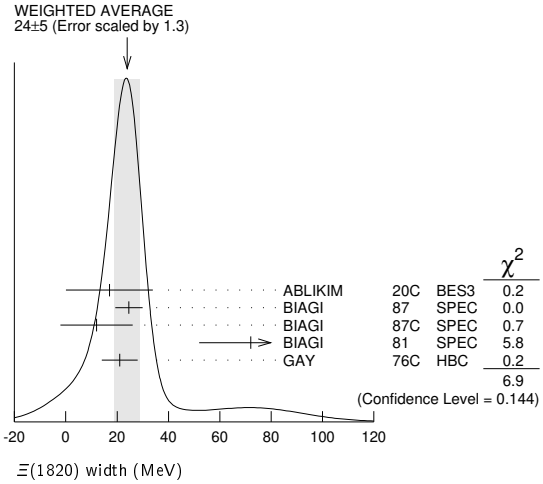

$\Xi(1820)$ DECAY MODES

	Mode	Fraction (Γ_i/Γ)
Γ_1	$\Lambda\overline{K}$	large
Γ_2	$\Sigma\overline{K}$	small
Γ_3	$\Xi\pi$	small
Γ_4	$\Xi(1530)\pi$	small
Γ_5	$\Xi\pi\pi$(not $\Xi(1530)\pi$)	

$\Xi(1820)$ BRANCHING RATIOS

The dominant modes seem to be $\Lambda\overline{K}$ and (perhaps) $\Xi(1530)\pi$, but the branching fractions are very poorly determined.

$\Gamma(\Lambda\overline{K})/\Gamma_{total}$ — Γ_1/Γ

VALUE	DOCUMENT ID		TECN	CHG	COMMENT
0.25±0.05 OUR AVERAGE					
0.24±0.05	ANISOVICH	12A	DPWA		Multichannel
0.30±0.15	ALITTI	69	HBC	–	K^-p 3.9–5 GeV/c

$\Gamma(\Xi\pi)/\Gamma_{total}$ — Γ_3/Γ

VALUE	DOCUMENT ID		TECN	CHG	COMMENT
0.10±0.10	ALITTI	69	HBC	–	K^-p 3.9–5 GeV/c

$\Gamma(\Xi\pi)/\Gamma(\Lambda\overline{K})$ — Γ_3/Γ_1

VALUE	CL%	DOCUMENT ID		TECN	CHG	COMMENT
<0.36	95	GAY	76C	HBC	–	K^-p 4.2 GeV/c
0.20±0.20		BADIER	65	HBC	0	K^-p 3 GeV/c

$\Gamma(\Xi\pi)/\Gamma(\Xi(1530)\pi)$ — Γ_3/Γ_4

VALUE	DOCUMENT ID		TECN	CHG	COMMENT
$1.5^{+0.6}_{-0.4}$	APSELL	70	HBC	0	K^-p 2.87 GeV/c

$\Gamma(\Sigma\overline{K})/\Gamma_{total}$ — Γ_2/Γ

VALUE	DOCUMENT ID		TECN	CHG	COMMENT
0.30±0.15	ALITTI	69	HBC	–	K^-p 3.9–5 GeV/c
• • • We do not use the following data for averages, fits, limits, etc. • • •					
<0.02	TRIPP	67	RVUE		Use SMITH 65C

Int. J. Mod. Phys. A 2026.41. Downloaded from www.worldscientific.com by UNIVERSITY OF CALIFORNIA @ BERKELEY on 09/16/26. Re-use and distribution is strictly not permitted, except for Open Access articles.

$\Gamma(\Sigma\overline{K})/\Gamma(\Lambda\overline{K})$ — Γ_2/Γ_1

VALUE	DOCUMENT ID		TECN	CHG	COMMENT
0.24±0.10	GAY	76C	HBC	–	K^-p 4.2 GeV/c

$\Gamma(\Xi(1530)\pi)/\Gamma_{total}$ — Γ_4/Γ

VALUE	DOCUMENT ID		TECN	CHG	COMMENT
0.30±0.15	ALITTI	69	HBC	–	K^-p 3.9–5 GeV/c
• • • We do not use the following data for averages, fits, limits, etc. • • •					
seen	ASTON	85B	LASS		K^-p 11 GeV/c
not seen	[5] HASSALL	81	HBC		K^-p 6.5 GeV/c
<0.25	[6] DAUBER	69	HBC		K^-p 2.7 GeV/c

$\Gamma(\Xi(1530)\pi)/\Gamma(\Lambda\overline{K})$ — Γ_4/Γ_1

VALUE	DOCUMENT ID		TECN	CHG	COMMENT
0.38±0.27 OUR AVERAGE	Error includes scale factor of 2.3.				
1.0 ±0.3	GAY	76C	HBC	–	K^-p 4.2 GeV/c
0.26±0.13	SMITH	65C	HBC	−0	K^-p 2.45–2.7 GeV/c

$\Gamma(\Xi\pi\pi(\text{not }\Xi(1530)\pi))/\Gamma(\Lambda\overline{K})$ — Γ_5/Γ_1

VALUE	DOCUMENT ID		TECN	CHG	COMMENT
0.30±0.20	BIAGI	87	SPEC	–	Ξ^- Be 116 GeV
• • • We do not use the following data for averages, fits, limits, etc. • • •					
<0.14	[7] BADIER	65	HBC	0	1 st. dev. limit
>0.1	SMITH	65C	HBC	−0	K^-p 2.45–2.7 GeV/c

$\Gamma(\Xi\pi\pi(\text{not }\Xi(1530)\pi))/\Gamma(\Xi(1530)\pi)$ — Γ_5/Γ_4

VALUE	DOCUMENT ID		TECN	CHG	COMMENT
consistent with zero	GAY	76C	HBC	–	K^-p 4.2 GeV/c
• • • We do not use the following data for averages, fits, limits, etc. • • •					
0.3±0.5	[8] APSELL	70	HBC	0	K^-p 2.87 GeV/c

$\Xi(1820)$ FOOTNOTES

[1] BIAGI 87 also sees weak signals in the in the $\Xi^-\pi^+\pi^-$ channel at 1782.6 ± 1.4 MeV (Γ = 6.0 ± 1.5 MeV) and 1831.9 ± 2.8 MeV (Γ = 9.6 ± 9.9 MeV).

[2] BADIER 72 adds all channels and divides the peak into lower and higher mass regions. The data can also be fitted with a single Breit-Wigner of mass 1800 MeV and width 150 MeV.

[3] From a fit to inclusive $\Xi\pi$, $\Xi\pi\pi$, and ΛK^- spectra.

[4] From a fit to inclusive $\Xi\pi$ and $\Xi\pi\pi$ spectra only.

[5] Including $\Xi\pi\pi$.

[6] DAUBER 69 uses in part the same data as SMITH 65C.

[7] For the decay mode $\Xi^-\pi^+\pi^0$ only. This limit includes $\Xi(1530)\pi$.

[8] Or less. Upper limit for the 3-body decay.

$\Xi(1820)$ REFERENCES

ABLIKIM	24N	PR D109 072008	M. Ablikim *et al.*	(BESIII Collab.)
ABLIKIM	20C	PRL 124 032002	M. Ablikim *et al.*	(BESIII Collab.)
ANISOVICH	12A	EPJ A48 15	A.V. Anisovich *et al.*	(BONN, PNPI)
ADAMOVICH	99B	EPJ C11 271	M.I. Adamovich *et al.*	(CERN WA89 Collab.)
BIAGI	87	ZPHY C34 15	S.F. Biagi *et al.*	(BRIS, CERN, GEVA+)
BIAGI	87C	ZPHY C34 175	S.F. Biagi *et al.*	(BRIS, CERN, GEVA+) JP
ASTON	85B	PR D32 2270	D. Aston *et al.*	(SLAC, CARL, CNRC, CINC)
JENKINS	83	PRL 51 951	C.M. Jenkins *et al.*	(FSU, BRAN, LBL+)
BIAGI	81	ZPHY C9 305	S.F. Biagi *et al.*	(BRIS, CAVE, GEVA+)
HASSALL	81	NP B189 397	J.K. Hassall *et al.*	(CAVE, MSU)
TEODORO	78	PL 77B 451	D. Teodoro *et al.*	(AMST, CERN, NIJM+) JP
BRIEFEL	77	PR D16 2706	E. Briefel *et al.*	(BRAN, UMD, SYRA+)
Also		PRL 23 884	S.P. Apsell *et al.*	(BRAN, UMD, SYRA+)
GAY	76C	PL 62B 477	J.B. Gay *et al.*	(AMST, CERN, NIJM) IJ
DIBIANCA	75	NP B98 137	F.A. Dibianca, R.J. Endorf	(CMU)
BADIER	72	NP B37 429	J. Badier *et al.*	(EPOL)
APSELL	70	PRL 24 777	S.P. Apsell *et al.*	(BRAN, UMD, SYRA+) I
CRENNELL	70B	PR D1 847	D.J. Crennell *et al.*	(BNL)
ALITTI	69	PRL 22 79	J. Alitti *et al.*	(BNL, SYRA) I
DAUBER	69	PR 179 1262	P.M. Dauber *et al.*	(LRL)
TRIPP	67	NP B3 10	R.D. Tripp *et al.*	(LRL, SLAC, CERN+)
BADIER	65	PL 16 171	J. Badier *et al.*	(EPOL, SACL, AMST) I
SMITH	65B	Athens Conf. 251	G.A. Smith, J.S. Lindsey	(LRL)
SMITH	65C	PRL 14 25	G.A. Smith *et al.*	(LRL) IJP
HALSTEINSLID	63	Siena Conf. 1 73	A. Halsteinslid *et al.*	(BERG, CERN, EPOL+) I

OTHER RELATED PAPERS

TEODORO	78	PL 77B 451	D. Teodoro *et al.*	(AMST, CERN, NIJM+) JP
BRIEFEL	75	PR D12 1859	E. Briefel *et al.*	(BRAN, UMD, SYRA+)
SCHMIDT	73	Purdue Conf. 363	P.E. Schmidt	(BRAN)
MERRILL	68	PR 167 1202	D.W. Merrill, J. Button-Shafer	(LRL)
SMITH	64	PRL 13 61	G.A. Smith *et al.*	(LRL) IJP

$\Xi(1950)$

$I(J^P) = \frac{1}{2}(?^?)$ Status: ***

We list here everything reported between 1875 and 2000 MeV. The accumulated evidence for a Ξ near 1950 MeV seems strong enough to include a $\Xi(1950)$ in the main Baryon Table, but not much can be said about its properties. In fact, there may be more than one Ξ near this mass.

$\Xi(1950)$ MASS

VALUE (MeV)	EVTS	DOCUMENT ID		TECN	COMMENT
1950±15 OUR ESTIMATE					
1955± 6		ADAMOVICH	99B	WA89	Σ^- nucleus, 345 GeV
1944± 9	129	BIAGI	87	SPEC	Ξ^-Be → $(\Xi^-\pi^+)\pi^-$X
1963± 5±2	63	BIAGI	87C	SPEC	Ξ^-Be → $(\Lambda\overline{K}^0)$ X
1937± 7	150	BIAGI	81	SPEC	SPS hyperon beam
1961±18	139	BRIEFEL	77	HBC	2.87 K^-p → $\Xi^-\pi^+$X
1936±22	44	BRIEFEL	77	HBC	2.87 K^-p → $\Xi^0\pi^-$X
1964±10	56	BRIEFEL	77	HBC	$\Xi(1530)\pi$
1900±12		DIBIANCA	75	DBC	$\Xi\pi$
1952±11	25	ROSS	73C		$(\Xi\pi)^-$
1956± 6	29	BADIER	72	HBC	$\Xi\pi$, $\Xi\pi\pi$, YK
1955±14	21	GOLDWASSER	70	HBC	$\Xi\pi$
1894±18	66	DAUBER	69	HBC	$\Xi\pi$
1930±20	27	ALITTI	68	HBC	$\Xi^-\pi^+$
1933±16	35	BADIER	65	HBC	$\Xi^-\pi^+$

$\Xi(1950)$ WIDTH

VALUE (MeV)	EVTS	DOCUMENT ID		TECN	COMMENT
60±20 OUR ESTIMATE					
68±22		ADAMOVICH	99B	WA89	Σ^- nucleus, 345 GeV
100±31	129	BIAGI	87	SPEC	Ξ^-Be → $(\Xi^-\pi^+)\pi^-$X
25±15±1.2	63	BIAGI	87C	SPEC	Ξ^-Be → $(\Lambda\overline{K}^0)$ X
60± 8	150	BIAGI	81	SPEC	SPS hyperon beam
159±57	139	BRIEFEL	77	HBC	2.87 K^-p → $\Xi^-\pi^+$X
87±26	44	BRIEFEL	77	HBC	2.87 K^-p → $\Xi^0\pi^-$X
60±39	56	BRIEFEL	77	HBC	$\Xi(1530)\pi$
63±78		DIBIANCA	75	DBC	$\Xi\pi$
38±10		ROSS	73C		$(\Xi\pi)^-$
35±11	29	BADIER	72	HBC	$\Xi\pi$, $\Xi\pi\pi$, YK
56±26	21	GOLDWASSER	70	HBC	$\Xi\pi$
98±23	66	DAUBER	69	HBC	$\Xi\pi$
80±40	27	ALITTI	68	HBC	$\Xi^-\pi^+$
140±35	35	BADIER	65	HBC	$\Xi^-\pi^+$

$\Xi(1950)$ DECAY MODES

	Mode	Fraction (Γ_i/Γ)
Γ_1	$\Lambda\overline{K}$	seen
Γ_2	$\Sigma\overline{K}$	possibly seen
Γ_3	$\Xi\pi$	seen
Γ_4	$\Xi(1530)\pi$	
Γ_5	$\Xi\pi\pi$(not $\Xi(1530)\pi$)	

$\Xi(1950)$ BRANCHING RATIOS

$\Gamma(\Sigma\overline{K})/\Gamma(\Lambda\overline{K})$ — Γ_2/Γ_1

VALUE	CL%	EVTS	DOCUMENT ID		TECN	COMMENT
<2.3	90	0	BIAGI	87C	SPEC	Ξ^-Be 116 GeV

$\Gamma(\Sigma\overline{K})/\Gamma_{total}$ — Γ_2/Γ

VALUE	EVTS	DOCUMENT ID		TECN	COMMENT
possibly seen	17	HASSALL	81	HBC	K^-p 6.5 GeV/c

$\Gamma(\Xi\pi)/\Gamma(\Xi(1530)\pi)$ — Γ_3/Γ_4

VALUE	DOCUMENT ID		TECN
$2.8^{+0.7}_{-0.6}$	APSELL	70	HBC

$\Gamma(\Xi\pi\pi(\text{not }\Xi(1530)\pi))/\Gamma(\Xi(1530)\pi)$ — Γ_5/Γ_4

VALUE	DOCUMENT ID		TECN
0.0±0.3	APSELL	70	HBC

$\Xi(1950)$ REFERENCES

ADAMOVICH	99B	EPJ C11 271	M.I. Adamovich *et al.*	(CERN WA89 Collab.)
BIAGI	87	ZPHY C34 15	S.F. Biagi *et al.*	(BRIS, CERN, GEVA+)
BIAGI	87C	ZPHY C34 175	S.F. Biagi *et al.*	(BRIS, CERN, GEVA+)
BIAGI	81	ZPHY C9 305	S.F. Biagi *et al.*	(BRIS, CAVE, GEVA+)
HASSALL	81	NP B189 397	J.K. Hassall *et al.*	(CAVE, MSU)
BRIEFEL	77	PR D16 2706	E. Briefel *et al.*	(BRAN, UMD, SYRA+)
Also		Duke Conf. 317	E. Briefel *et al.*	(BRAN, UMD, SYRA+)
Hyperon Resonances, 1970				
DIBIANCA	75	NP B98 137	F.A. Dibianca, R.J. Endorf	(CMU)
ROSS	73C	Purdue Conf. 345	R.T. Ross, J.L. Lloyd, D. Radojicic	(OXF)
BADIER	72	NP B37 429	J. Badier *et al.*	(EPOL)
APSELL	70	PRL 24 777	S.P. Apsell *et al.*	(BRAN, UMD, SYRA+) I
GOLDWASSER	70	PR D1 1960	E.L. Goldwasser, P.F. Schultz	(ILL)
DAUBER	69	PR 179 1262	P.M. Dauber *et al.*	(LRL) I
ALITTI	68	PRL 21 1119	J. Alitti *et al.*	(BNL, SYRA) I
BADIER	65	PL 16 171	J. Badier *et al.*	(EPOL, SACL, AMST) I

UNIVERSITY OF CALIFORNIA @ BERKELEY on 09/16/26. Re-use and distribution is strictly not permitted, except for Open Access articles.
Int. J. Mod. Phys. A 2026.41. Downloaded from www.worldscientific.com

$\Xi(2030)$

$I(J^P) = \frac{1}{2}(\geq \frac{5}{2}^?)$ Status: ***

The evidence for this state has been much improved by HEMINGWAY 77, who see an eight standard deviation enhancement in $\Sigma\overline{K}$ and a weaker coupling to $\Lambda\overline{K}$. ALITTI 68 and HEMINGWAY 77 observe no signals in the $\Xi\pi\pi$ (or $\Xi(1530)\pi$) channel, in contrast to DIBIANCA 75. The decay $(\Lambda/\Sigma)\overline{K}\pi$ reported by BARTSCH 69 is also not confirmed by HEMINGWAY 77.

A moments analysis of the HEMINGWAY 77 data indicates at a level of three standard deviations that $J \geq 5/2$.

$\Xi(2030)$ MASS

VALUE (MeV)	EVTS	DOCUMENT ID		TECN	CHG	COMMENT
2025 ± 5 OUR ESTIMATE						
2025.1 ± 2.4 OUR AVERAGE Error includes scale factor of 1.3. See the ideogram below.						
2022 ± 7		JENKINS	83	MPS	–	$K^-p \to K^+$ MM
2024 ± 2	200	HEMINGWAY	77	HBC	–	K^-p 4.2 GeV/c
2044 ± 8		DIBIANCA	75	DBC	−0	$\Xi\pi\pi$, $\Xi^*\pi$
2019 ± 7	15	ROSS	73C	HBC	−0	$\Sigma\overline{K}$
2030 ±10	42	ALITTI	69	HBC	–	K^-p 3.9–5 GeV/c
2058 ±17	40	BARTSCH	69	HBC	−0	K^-p 10 GeV/c

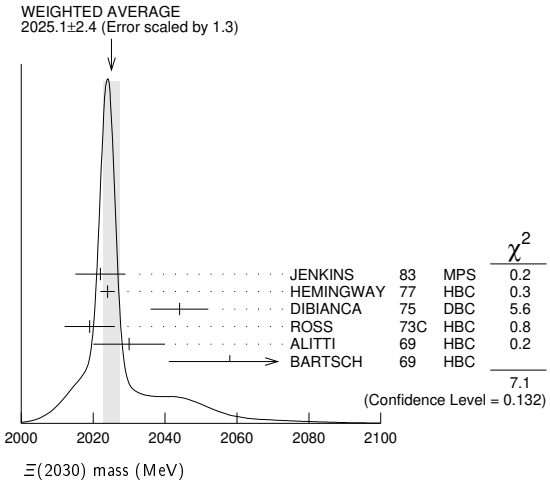

$\Xi(2030)$ WIDTH

VALUE (MeV)	EVTS	DOCUMENT ID		TECN	CHG	COMMENT
20^{+15}_{-5} OUR ESTIMATE						
21 ± 6 OUR AVERAGE Error includes scale factor of 1.3. See the ideogram below.						
16 ± 5	200	HEMINGWAY	77	HBC	–	K^-p 4.2 GeV/c
60 ± 24		DIBIANCA	75	DBC	−0	$\Xi\pi\pi$, $\Xi^*\pi$
33 ± 17	15	ROSS	73C	HBC	−0	$\Sigma\overline{K}$
45^{+40}_{-20}		ALITTI	69	HBC	–	K^-p 3.9–5 GeV/c
57 ± 30		BARTSCH	69	HBC	−0	K^-p 10 GeV/c

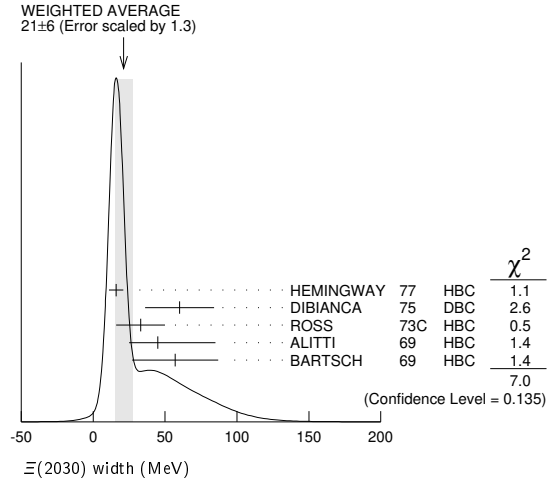

$\Xi(2030)$ DECAY MODES

	Mode	Fraction (Γ_i/Γ)
Γ_1	$\Lambda\overline{K}$	~ 20 %
Γ_2	$\Sigma\overline{K}$	~ 80 %
Γ_3	$\Xi\pi$	small
Γ_4	$\Xi(1530)\pi$	small
Γ_5	$\Xi\pi\pi$(not $\Xi(1530)\pi$)	small
Γ_6	$\Lambda\overline{K}\pi$	small
Γ_7	$\Sigma\overline{K}\pi$	small

$\Xi(2030)$ BRANCHING RATIOS

$\Gamma(\Xi\pi)/[\Gamma(\Lambda\overline{K})+\Gamma(\Sigma\overline{K})+\Gamma(\Xi\pi)+\Gamma(\Xi(1530)\pi)]$ — $\Gamma_3/(\Gamma_1+\Gamma_2+\Gamma_3+\Gamma_4)$

VALUE	DOCUMENT ID		TECN	CHG	COMMENT
• • • We do not use the following data for averages, fits, limits, etc. • • •					
<0.30	ALITTI	69	HBC	–	1 standard dev. limit

$\Gamma(\Xi\pi)/\Gamma(\Sigma\overline{K})$ — Γ_3/Γ_2

VALUE	CL%	DOCUMENT ID		TECN	CHG	COMMENT
<0.19	95	HEMINGWAY	77	HBC	–	K^-p 4.2 GeV/c

$\Gamma(\Lambda\overline{K})/[\Gamma(\Lambda\overline{K})+\Gamma(\Sigma\overline{K})+\Gamma(\Xi\pi)+\Gamma(\Xi(1530)\pi)]$ — $\Gamma_1/(\Gamma_1+\Gamma_2+\Gamma_3+\Gamma_4)$

VALUE	DOCUMENT ID		TECN	CHG	COMMENT
0.25 ± 0.15	ALITTI	69	HBC	–	K^-p 3.9–5 GeV/c

$\Gamma(\Lambda\overline{K})/\Gamma(\Sigma\overline{K})$ — Γ_1/Γ_2

VALUE	DOCUMENT ID		TECN	CHG	COMMENT
0.22 ± 0.09	HEMINGWAY	77	HBC	–	K^-p 4.2 GeV/c

$\Gamma(\Sigma\overline{K})/[\Gamma(\Lambda\overline{K})+\Gamma(\Sigma\overline{K})+\Gamma(\Xi\pi)+\Gamma(\Xi(1530)\pi)]$ — $\Gamma_2/(\Gamma_1+\Gamma_2+\Gamma_3+\Gamma_4)$

VALUE	DOCUMENT ID		TECN	CHG	COMMENT
0.75 ± 0.20	ALITTI	69	HBC	–	K^-p 3.9–5 GeV/c

$\Gamma(\Xi(1530)\pi)/[\Gamma(\Lambda\overline{K})+\Gamma(\Sigma\overline{K})+\Gamma(\Xi\pi)+\Gamma(\Xi(1530)\pi)]$ — $\Gamma_4/(\Gamma_1+\Gamma_2+\Gamma_3+\Gamma_4)$

VALUE	DOCUMENT ID		TECN	CHG	COMMENT
• • • We do not use the following data for averages, fits, limits, etc. • • •					
<0.15	ALITTI	69	HBC	–	1 standard dev. limit

$[\Gamma(\Xi(1530)\pi)+\Gamma(\Xi\pi\pi(\text{not }\Xi(1530)\pi))]/\Gamma(\Sigma\overline{K})$ — $(\Gamma_4+\Gamma_5)/\Gamma_2$

VALUE	CL%	DOCUMENT ID		TECN	CHG	COMMENT
<0.11	95	[1] HEMINGWAY	77	HBC	–	K^-p 4.2 GeV/c

$\Gamma(\Lambda\overline{K}\pi)/\Gamma_{total}$ — Γ_6/Γ

VALUE	DOCUMENT ID		TECN	COMMENT
• • • We do not use the following data for averages, fits, limits, etc. • • •				
seen	BARTSCH	69	HBC	K^-p 10 GeV

$\Gamma(\Lambda\overline{K}\pi)/\Gamma(\Sigma\overline{K})$ — Γ_6/Γ_2

VALUE	CL%	DOCUMENT ID		TECN	CHG	COMMENT
<0.32	95	HEMINGWAY	77	HBC	–	K^-p 4.2 GeV/c

$\Gamma(\Sigma\overline{K}\pi)/\Gamma_{total}$ — Γ_7/Γ

VALUE	DOCUMENT ID		TECN	COMMENT
• • • We do not use the following data for averages, fits, limits, etc. • • •				
seen	BARTSCH	69	HBC	K^-p 10 GeV

$\Gamma(\Sigma\overline{K}\pi)/\Gamma(\Sigma\overline{K})$ — Γ_7/Γ_2

VALUE	CL%	DOCUMENT ID		TECN	CHG	COMMENT
<0.04	95	[2] HEMINGWAY	77	HBC	–	K^-p 4.2 GeV/c

$\Xi(2030)$ FOOTNOTES

[1] For the decay mode $\Xi^-\pi^+\pi^-$ only.
[2] For the decay mode $\Sigma^\pm K^-\pi^\mp$ only.

$\Xi(2030)$ REFERENCES

JENKINS	83	PRL 51 951	C.M. Jenkins *et al.*	(FSU, BRAN, LBL+)
HEMINGWAY	77	PL 68B 197	R.J. Hemingway *et al.*	(AMST, CERN, NIJM+) IJ
Also		PL 62B 477	J.B. Gay *et al.*	(AMST, CERN, NIJM)
DIBIANCA	75	NP B98 137	F.A. Dibianca, R.J. Endorf	(CMU)
ROSS	73C	Purdue Conf. 345	R.T. Ross, J.L. Lloyd, D. Radojicic	(OXF)
ALITTI	69	PRL 22 79	J. Alitti *et al.*	(BNL, SYRA) I
BARTSCH	69	PL 28B 439	J. Bartsch *et al.*	(AACH, BERL, CERN+)
ALITTI	68	PRL 21 1119	J. Alitti *et al.*	(BNL, SYRA)

Int. J. Mod. Phys. A 2026.41. Downloaded from www.worldscientific.com
by UNIVERSITY OF CALIFORNIA @ BERKELEY on 09/16/26. Re-use and distribution is strictly not permitted, except for Open Access articles.

$\Xi(2120)$

$I(J^P) = \frac{1}{2}(?^?)$ Status: *

J, P need confirmation.

OMITTED FROM SUMMARY TABLE

$\Xi(2120)$ MASS

VALUE (MeV)	EVTS	DOCUMENT ID		TECN	COMMENT
≈ 2120 OUR ESTIMATE					
2137±4	18	[1] CHLIAPNIK...	79	HBC	$K^+ p$ 32 GeV/c
2123±7		[2] GAY	76C	HBC	$K^- p$ 4.2 GeV/c

$\Xi(2120)$ WIDTH

VALUE (MeV)	EVTS	DOCUMENT ID		TECN	COMMENT
<20	18	[1] CHLIAPNIK...	79	HBC	$K^+ p$ 32 GeV/c
25±12		[2] GAY	76C	HBC	$K^- p$ 4.2 GeV/c

$\Xi(2120)$ DECAY MODES

	Mode	Fraction (Γ_i/Γ)
Γ_1	$\Lambda\overline{K}$	seen

$\Xi(2120)$ BRANCHING RATIOS

$\Gamma(\Lambda\overline{K})/\Gamma_{total}$ — **Γ_1/Γ**

VALUE	DOCUMENT ID		TECN	COMMENT
seen	[1] CHLIAPNIK...	79	HBC	$K^+ p \to (\overline{\Lambda} K^+)$ X
seen	[2] GAY	76C	HBC	$K^- p$ 4.2 GeV/c

$\Xi(2120)$ FOOTNOTES

[1] CHLIAPNIKOV 79 does not uniquely identify the K^+ in the $(\overline{\Lambda} K^+)$ X final state. It also reports bumps with fewer events at 2240, 2540, and 2830 MeV.

[2] GAY 76C sees a 4-standard deviation signal. However, HEMINGWAY 77, with more events from the same experiment points out that the signal is greatly reduced if a cut is made on the 4-momentum u. This suggests an anomalous production mechanism if the $\Xi(2120)$ is real.

$\Xi(2120)$ REFERENCES

CHLIAPNIK...	79	NP B158 253	P.V. Chliapnikov *et al.*	(CERN, BELG, MONS)
HEMINGWAY	77	PL 68B 197	R.J. Hemingway *et al.*	(AMST, CERN, NIJM+)
GAY	76C	PL 62B 477	J.B. Gay *et al.*	(AMST, CERN, NIJM)

$\Xi(2250)$

$I(J^P) = \frac{1}{2}(?^?)$ Status: **

J, P need confirmation.

OMITTED FROM SUMMARY TABLE

The evidence for this state is mixed. BARTSCH 69 sees a bump of not much statistical significance in $\Lambda\overline{K}\pi$, $\Sigma\overline{K}\pi$, and $\Xi\pi\pi$ mass spectra. GOLDWASSER 70 sees a narrower bump in $\Xi\pi\pi$ at a higher mass. Not seen by HASSALL 81 with 45 events/μb at 6.5 GeV/c. Seen by JENKINS 83. Perhaps seen by BIAGI 87.

$\Xi(2250)$ MASS

VALUE (MeV)	EVTS	DOCUMENT ID		TECN	CHG	COMMENT
≈ 2250 OUR ESTIMATE						
2189± 7	66	BIAGI	87	SPEC	–	$\Xi^- \mathrm{Be} \to (\Xi^- \pi^+ \pi^-)$ X
2214± 5		JENKINS	83	MPS	–	$K^- p \to K^+$ MM
2295±15	18	GOLDWASSER	70	HBC	–	$K^- p$ 5.5 GeV/c
2244±52	35	BARTSCH	69	HBC		$K^- p$ 10 GeV/c

$\Xi(2250)$ WIDTH

VALUE (MeV)	EVTS	DOCUMENT ID		TECN	CHG	COMMENT
46±27	66	BIAGI	87	SPEC	–	$\Xi^- \mathrm{Be} \to (\Xi^- \pi^+ \pi^-)$ X
< 30		GOLDWASSER	70	HBC	–	$K^- p$ 5.5 GeV/c
130±80		BARTSCH	69	HBC		

$\Xi(2250)$ DECAY MODES

	Mode
Γ_1	$\Xi\pi\pi$
Γ_2	$\Lambda\overline{K}\pi$
Γ_3	$\Sigma\overline{K}\pi$

$\Xi(2250)$ REFERENCES

BIAGI	87	ZPHY C34 15	S.F. Biagi *et al.*	(BRIS, CERN, GEVA+)
JENKINS	83	PRL 51 951	C.M. Jenkins *et al.*	(FSU, BRAN, LBL+)
HASSALL	81	NP B189 397	J.K. Hassall *et al.*	(CAVE, MSU)
GOLDWASSER	70	PR D1 1960	E.L. Goldwasser, P.F. Schultz	(ILL)
BARTSCH	69	PL 28B 439	J. Bartsch *et al.*	(AACH, BERL, CERN+)

$\Xi(2370)$

$I(J^P) = \frac{1}{2}(?^?)$ Status: **

J, P need confirmation.

OMITTED FROM SUMMARY TABLE

$\Xi(2370)$ MASS

VALUE (MeV)	EVTS	DOCUMENT ID		TECN	CHG	COMMENT
≈ 2370 OUR ESTIMATE						
2356±10		JENKINS	83	MPS	–	$K^- p \to K^+$ MM
2370	50	HASSALL	81	HBC	−0	$K^- p$ 6.5 GeV/c
2373± 8	94	AMIRZADEH	80	HBC	−0	$K^- p$ 8.25 GeV/c
2392±27		DIBIANCA	75	DBC		$\Xi 2\pi$

$\Xi(2370)$ WIDTH

VALUE (MeV)	EVTS	DOCUMENT ID		TECN	CHG	COMMENT
80	50	HASSALL	81	HBC	−0	$K^- p$ 6.5 GeV/c
80±25	94	AMIRZADEH	80	HBC	−0	$K^- p$ 8.25 GeV/c
75±69		DIBIANCA	75	DBC		$\Xi 2\pi$

$\Xi(2370)$ DECAY MODES

	Mode	Fraction (Γ_i/Γ)
Γ_1	$\Lambda\overline{K}\pi$ Includes $\Gamma_4 + \Gamma_6$.	seen
Γ_2	$\Sigma\overline{K}\pi$ Includes $\Gamma_5 + \Gamma_6$.	seen
Γ_3	$\Omega^- K$	
Γ_4	$\Lambda\overline{K}^*(892)$	
Γ_5	$\Sigma\overline{K}^*(892)$	
Γ_6	$\Sigma(1385)\overline{K}$	

$\Xi(2370)$ BRANCHING RATIOS

$\Gamma(\Lambda\overline{K}\pi)/\Gamma_{total}$ — **Γ_1/Γ**

VALUE	DOCUMENT ID		TECN	CHG	COMMENT
seen	AMIRZADEH	80	HBC	−0	$K^- p$ 8.25 GeV/c

$\Gamma(\Sigma\overline{K}\pi)/\Gamma_{total}$ — **Γ_2/Γ**

VALUE	DOCUMENT ID		TECN	CHG	COMMENT
seen	AMIRZADEH	80	HBC	−0	$K^- p$ 8.25 GeV/c

$[\Gamma(\Lambda\overline{K}\pi) + \Gamma(\Sigma\overline{K}\pi)]/\Gamma_{total}$ — **$(\Gamma_1+\Gamma_2)/\Gamma$**

VALUE	EVTS	DOCUMENT ID		TECN	CHG	COMMENT
seen	50	HASSALL	81	HBC	−0	$K^- p$ 6.5 GeV/c

$\Gamma(\Omega^- K)/\Gamma_{total}$ — **Γ_3/Γ**

VALUE	DOCUMENT ID		TECN	CHG	COMMENT
0.09±0.04	[1] KINSON	80	HBC	–	$K^- p$ 8.25 GeV/c

$[\Gamma(\Lambda\overline{K}^*(892)) + \Gamma(\Sigma\overline{K}^*(892))]/\Gamma_{total}$ — **$(\Gamma_4+\Gamma_5)/\Gamma$**

VALUE	DOCUMENT ID		TECN	CHG	COMMENT
0.22±0.13	[1] KINSON	80	HBC	–	$K^- p$ 8.25 GeV/c

$\Gamma(\Sigma(1385)\overline{K})/\Gamma_{total}$ — **Γ_6/Γ**

VALUE	DOCUMENT ID		TECN	CHG	COMMENT
0.12±0.08	[1] KINSON	80	HBC	–	$K^- p$ 8.25 GeV/c

$\Xi(2370)$ FOOTNOTES

[1] KINSON 80 is a reanalysis of AMIRZADEH 80 with 50% more events.

$\Xi(2370)$ REFERENCES

JENKINS	83	PRL 51 951	C.M. Jenkins *et al.*	(FSU, BRAN, LBL+)
HASSALL	81	NP B189 397	J.K. Hassall *et al.*	(CAVE, MSU)
AMIRZADEH	80	PL 90B 324	J. Amirzadeh *et al.*	(BIRM, CERN, GLAS+) I
KINSON	80	Toronto Conf. 263	J.B. Kinson *et al.*	(BIRM, CERN, GLAS+) I
DIBIANCA	75	NP B98 137	F.A. Dibianca, R.J. Endorf	(CMU)

Int. J. Mod. Phys. A 2026.41. Downloaded from www.worldscientific.com
UNIVERSITY OF CALIFORNIA @ BERKELEY on 09/16/26. Re-use and distribution is strictly not permitted, except for Open Access articles.

Ξ(2500)

$I(J^P) = \frac{1}{2}(?^?)$ Status: *
J, P need confirmation.

OMITTED FROM SUMMARY TABLE

The ALITTI 69 peak might be instead the Ξ(2370) or might be neither the Ξ(2370) nor the Ξ(2500).

Ξ(2500) MASS

VALUE (MeV)	EVTS	DOCUMENT ID		TECN	CHG	COMMENT
≈ 2500 OUR ESTIMATE						
2505±10		JENKINS	83	MPS	−	$K^- p \to K^+$ MM
2430±20	30	ALITTI	69	HBC	−	$K^- p$ 4.6–5 GeV/c
2500±10	45	BARTSCH	69	HBC	−0	$K^- p$ 10 GeV/c

Ξ(2500) WIDTH

VALUE (MeV)	DOCUMENT ID		TECN	CHG
150^{+60}_{-40}	ALITTI	69	HBC	−
59±27	BARTSCH	69	HBC	−0

Ξ(2500) DECAY MODES

	Mode	Fraction (Γ_i/Γ)
Γ_1	$\Xi\pi$	
Γ_2	$\Lambda\overline{K}$	
Γ_3	$\Sigma\overline{K}$	
Γ_4	$\Xi\pi\pi$	seen
Γ_5	$\Xi(1530)\pi$	
Γ_6	$\Lambda\overline{K}\pi + \Sigma\overline{K}\pi$	seen

Ξ(2500) BRANCHING RATIOS

$\Gamma(\Xi\pi)/[\Gamma(\Xi\pi)+\Gamma(\Lambda\overline{K})+\Gamma(\Sigma\overline{K})+\Gamma(\Xi(1530)\pi)]$ — $\Gamma_1/(\Gamma_1+\Gamma_2+\Gamma_3+\Gamma_5)$

VALUE	DOCUMENT ID		TECN	COMMENT
<0.5	ALITTI	69	HBC	1 standard dev. limit

$\Gamma(\Lambda\overline{K})/[\Gamma(\Xi\pi)+\Gamma(\Lambda\overline{K})+\Gamma(\Sigma\overline{K})+\Gamma(\Xi(1530)\pi)]$ — $\Gamma_2/(\Gamma_1+\Gamma_2+\Gamma_3+\Gamma_5)$

VALUE	DOCUMENT ID		TECN	CHG
0.5±0.2	ALITTI	69	HBC	−

$\Gamma(\Sigma\overline{K})/[\Gamma(\Xi\pi)+\Gamma(\Lambda\overline{K})+\Gamma(\Sigma\overline{K})+\Gamma(\Xi(1530)\pi)]$ — $\Gamma_3/(\Gamma_1+\Gamma_2+\Gamma_3+\Gamma_5)$

VALUE	DOCUMENT ID		TECN	CHG
0.5±0.2	ALITTI	69	HBC	−

$\Gamma(\Xi(1530)\pi)/[\Gamma(\Xi\pi)+\Gamma(\Lambda\overline{K})+\Gamma(\Sigma\overline{K})+\Gamma(\Xi(1530)\pi)]$ — $\Gamma_5/(\Gamma_1+\Gamma_2+\Gamma_3+\Gamma_5)$

VALUE	DOCUMENT ID		TECN	COMMENT
<0.2	ALITTI	69	HBC	1 standard dev. limit

$\Gamma(\Xi\pi\pi)/\Gamma_{total}$ — Γ_4/Γ

VALUE	DOCUMENT ID		TECN	CHG
seen	BARTSCH	69	HBC	−0

$[\Gamma(\Lambda\overline{K}\pi)+\Gamma(\Sigma\overline{K}\pi)]/\Gamma_{total}$ — Γ_6/Γ

VALUE	DOCUMENT ID		TECN	CHG
seen	BARTSCH	69	HBC	−0

Ξ(2500) REFERENCES

JENKINS	83	PRL 51 951	C.M. Jenkins *et al.*	(FSU, BRAN, LBL+)
ALITTI	69	PRL 22 79	J. Alitti *et al.*	(BNL, SYRA)I
BARTSCH	69	PL 28B 439	J. Bartsch *et al.*	(AACH, BERL, CERN+)

Int. J. Mod. Phys. A 2026.41. Downloaded from www.worldscientific.com
by UNIVERSITY OF CALIFORNIA @ BERKELEY on 09/16/26. Re-use and distribution is strictly not permitted, except for Open Access articles.

Ω BARYONS
($S = -3$, $I = 0$)

$\Omega^- = sss$

Ω^-

$I(J^P) = 0(\frac{3}{2}^+)$ Status: ****

The unambiguous discovery in both production and decay was by BARNES 64. The quantum numbers follow from the assignment of the particle to the baryon decuplet. DEUTSCHMANN 78 and BAUBILLIER 78 rule out $J = 1/2$ and find consistency with $J = 3/2$. AUBERT,BE 06 finds from the decay angular distributions of $\Xi_c^0 \to \Omega^- K^+$ and $\Omega_c^0 \to \Omega^- K^+$ that $J = 3/2$; this depends on the spins of the Ξ_c^0 and Ω_c^0 being $J = 1/2$, their supposed values. ABLIKIM 21E determines the Ω^- spin to be $J = 3/2$ from the decay angular distributions of the complete decay chain $\psi(3686) \to \Omega^- \overline{\Omega}^+$, with subsequent decays $\Omega^- \to K^- \Lambda$ and $\overline{\Omega}^+ \to K^+ \overline{\Lambda}$.

We have omitted some results that have been superseded by later experiments. See our earlier editions.

Ω^- MASS

The fit assumes the Ω^- and $\overline{\Omega}^+$ masses are the same, and averages them together.

VALUE (MeV)	EVTS	DOCUMENT ID		TECN	COMMENT
1672.45±0.29 OUR FIT					
1672.43±0.32 OUR AVERAGE					
1673 ±1	100	HARTOUNI	85	SPEC	80–280 GeV K_L^0C
1673.0 ±0.8	41	BAUBILLIER	78	HBC	8.25 GeV/c K^-p
1671.7 ±0.6	27	HEMINGWAY	78	HBC	4.2 GeV/c K^-p
1673.4 ±1.7	4	[1] DIBIANCA	75	DBC	4.9 GeV/c K^-d
1673.3 ±1.0	3	PALMER	68	HBC	K^-p 4.6, 5 GeV/c
1671.8 ±0.8	3	SCHULTZ	68	HBC	K^-p 5.5 GeV/c
1674.2 ±1.6	5	SCOTTER	68	HBC	K^-p 6 GeV/c
1672.1 ±1.0	1	[2] FRY	55	EMUL	
• • • We do not use the following data for averages, fits, limits, etc. • • •					
1671.43±0.78	13	[3] DEUTSCH...	73	HBC	K^-p 10 GeV/c
1671.9 ±1.2	6	[3] SPETH	69	HBC	See DEUTSCHMANN 73
1673.0 ±8.0	1	ABRAMS	64	HBC	$\to \Xi^-\pi^0$
1670.6 ±1.0	1	[2] FRY	55B	EMUL	
1615	1	[4] EISENBERG	54	EMUL	

[1] DIBIANCA 75 gives a mass for each event. We quote the average.
[2] The FRY 55 and FRY 55B events were identified as Ω^- by ALVAREZ 73. The masses assume decay to ΛK^- at rest. For FRY 55B, decay from an atomic orbit could Doppler shift the K^- energy and the resulting Ω^- mass by several MeV. This shift is negligible for FRY 55 because the Ω decay is approximately perpendicular to its orbital velocity, as is known because the Λ strikes the nucleus (L.Alvarez, private communication 1973). We have calculated the error assuming that the orbital n is 4 or larger.
[3] Excluded from the average; the Ω^- lifetimes measured by the experiments differ significantly from other measurements.
[4] The EISENBERG 54 mass was calculated for decay in flight. ALVAREZ 73 has shown that the Ω interacted with an Ag nucleus to give $K^- \Xi$Ag.

$\overline{\Omega}^+$ MASS

The fit assumes the Ω^- and $\overline{\Omega}^+$ masses are the same, and averages them together.

VALUE (MeV)	EVTS	DOCUMENT ID		TECN	COMMENT
1672.45±0.29 OUR FIT					
1672.5 ±0.7 OUR AVERAGE					
1672 ±1	72	HARTOUNI	85	SPEC	80–280 GeV K_L^0C
1673.1 ±1.0	1	FIRESTONE	71B	HBC	12 GeV/c K^+d

$(m_{\Omega^-} - m_{\overline{\Omega}^+}) / m_{\Omega^-}$

A test of CPT invariance.

VALUE (units 10^{-5})	DOCUMENT ID		TECN	COMMENT
−1.44±7.98	CHAN	98	E756	p Be, 800 GeV

Ω^- MEAN LIFE

Measurements with an error > 0.1×10^{-10} s have been omitted. The fit assumes the Ω^- and $\overline{\Omega}^+$ mean lives are the same, and averages them together.

VALUE (10^{-10} s)	EVTS	DOCUMENT ID		TECN	COMMENT
0.821±0.011 OUR FIT					
0.821±0.011 OUR AVERAGE					
0.817±0.013±0.018	6934	CHAN	98	E756	p Be, 800 GeV
0.811±0.037	1096	LUK	88	SPEC	pBe 400 GeV
0.823±0.013	12k	BOURQUIN	84	SPEC	SPS hyperon beam
• • • We do not use the following data for averages, fits, limits, etc. • • •					
0.822±0.028	2437	BOURQUIN	79B	SPEC	See BOURQUIN 84

$\overline{\Omega}^+$ MEAN LIFE

The fit assumes the Ω^- and $\overline{\Omega}^+$ mean lives are the same, and averages them together.

VALUE (10^{-10} s)	EVTS	DOCUMENT ID		TECN	COMMENT
0.821±0.011 OUR FIT					
0.823±0.031±0.022	1801	CHAN	98	E756	p Be, 800 GeV

$(\tau_{\Omega^-} - \tau_{\overline{\Omega}^+}) / \tau_{\Omega^-}$

A test of CPT invariance. Our calculation, from the averages in the preceding two data blocks.

VALUE	DOCUMENT ID
0.00±0.05 OUR ESTIMATE	

Ω^- MAGNETIC MOMENT

VALUE (μ_N)	EVTS	DOCUMENT ID		TECN	COMMENT
−2.02 ±0.05 OUR AVERAGE					
−2.024±0.056	235k	WALLACE	95	SPEC	Ω^- 300–550 GeV
−1.94 ±0.17 ±0.14	25k	DIEHL	91	SPEC	Spin-transfer production

Ω^- DECAY MODES

	Mode	Fraction (Γ_i/Γ)	Scale factor/ Confidence level
Γ_1	ΛK^-	(67.7 ±0.7) %	
Γ_2	$\Xi^0\pi^-$	(24.3 ±0.7) %	S=1.5
Γ_3	$\Xi^-\pi^0$	(8.55±0.33) %	
Γ_4	$\Xi^-\pi^+\pi^-$	$(3.7 {}^{+0.7}_{-0.6}) \times 10^{-4}$	
Γ_5	$\Xi(1530)^0\pi^-$	$< 7 \times 10^{-5}$	CL=90%
Γ_6	$\Xi^0 e^- \overline{\nu}_e$	$(5.6 \pm 2.8) \times 10^{-3}$	
Γ_7	$\Xi^-\gamma$	$< 4.6 \times 10^{-4}$	CL=90%
	$\Delta S = 2$ forbidden ($S2$) modes		
Γ_8	$\Lambda\pi^-$ $S2$	$< 2.9 \times 10^{-6}$	CL=90%
Γ_9	$\Sigma^0\pi^-$	$< 5.4 \times 10^{-4}$	CL=90%
Γ_{10}	nK^-	$< 2.4 \times 10^{-4}$	CL=90%

Ω^- BRANCHING RATIOS

The BOURQUIN 84 values (which include results of BOURQUIN 79B, a separate experiment) are much more accurate than any other results, and so the other results have been omitted.

$\Gamma(\Lambda K^-)/\Gamma_{total}$ — Γ_1/Γ

VALUE (%)	EVTS	DOCUMENT ID		TECN	COMMENT
67.7±0.7 OUR AVERAGE					
66.3±0.8±2.0	9.0k	ABLIKIM	23BJ	BES3	$e^+e^- \to \psi(3686) \to \Omega\overline{\Omega}$
67.8±0.7	14k	BOURQUIN	84	SPEC	SPS hyperon beam
• • • We do not use the following data for averages, fits, limits, etc. • • •					
68.6±1.3	1920	BOURQUIN	79B	SPEC	See BOURQUIN 84

$\Gamma(\Xi^0\pi^-)/\Gamma_{total}$ — Γ_2/Γ

VALUE (%)	EVTS	DOCUMENT ID		TECN	COMMENT
24.3 ±0.7 OUR AVERAGE Error includes scale factor of 1.5.					
25.03±0.44±0.53	5.4k	ABLIKIM	23BJ	BES3	$e^+e^- \to \psi(3686) \to \Omega\overline{\Omega}$
23.6 ±0.7	1947	BOURQUIN	84	SPEC	SPS hyperon beam
• • • We do not use the following data for averages, fits, limits, etc. • • •					
23.4 ±1.3	317	BOURQUIN	79B	SPEC	See BOURQUIN 84

$\Gamma(\Xi^-\pi^0)/\Gamma_{total}$ — Γ_3/Γ

VALUE (%)	EVTS	DOCUMENT ID		TECN	COMMENT
8.55±0.33 OUR AVERAGE					
8.43±0.52±0.28	794	ABLIKIM	23BJ	BES3	$e^+e^- \to \psi(3686) \to \Omega\overline{\Omega}$
8.6 ±0.4	759	BOURQUIN	84	SPEC	SPS hyperon beam
• • • We do not use the following data for averages, fits, limits, etc. • • •					
8.0 ±0.8	145	BOURQUIN	79B	SPEC	See BOURQUIN 84

Int. J. Mod. Phys. A 2026.41. Downloaded from www.worldscientific.com
UNIVERSITY OF CALIFORNIA @ BERKELEY on 09/16/26. Re-use and distribution is strictly not permitted, except for Open Access articles.

$\Gamma(\Xi^-\pi^+\pi^-)/\Gamma_{total}$ — Γ_4/Γ

VALUE (units 10^{-4})	EVTS	DOCUMENT ID		TECN	COMMENT
$3.74^{+0.67}_{-0.56}$	100	[5] KAMAEV	10	HYCP	p Cu, 800 GeV
• • • We do not use the following data for averages, fits, limits, etc. • • •					
$4.3^{+3.4}_{-1.3}$	4	BOURQUIN	84	SPEC	SPS hyperon beam

[5] This KAMAEV 10 value uses 76 $\Omega^- \to \Xi^-\pi^+\pi^-$ and 24 $\overline{\Omega}^+ \to \overline{\Xi}^+\pi^-\pi^+$ decays. The Ω^- and $\overline{\Omega}^+$ branching fractions measurements are statistically equal. The errors given combine statistical and systematic contributions. The CP branching-fraction asymmetry, $(\Omega^- - \overline{\Omega}^+)$/sum, is $+0.12 \pm 0.20$.

$\Gamma(\Xi(1530)^0\pi^-)/\Gamma_{total}$ — Γ_5/Γ

VALUE (units 10^{-4})	CL%	EVTS	DOCUMENT ID		TECN	COMMENT
<0.7	90		KAMAEV	10	HYCP	p Cu, 800 GeV
• • • We do not use the following data for averages, fits, limits, etc. • • •						
$6.4^{+5.1}_{-2.0}$		4	[6] BOURQUIN	84	SPEC	SPS hyperon beam

[6] The same 4 events as in the previous mode, with the isospin factor to take into account $\Xi(1530)^0 \to \Xi^0\pi^0$ decays included. BOURQUIN 84 adopted a theoretical assumption that $\Xi(1530)^0\pi^-$ would dominate $\Xi^-\pi^+\pi^-$ decay.

$\Gamma(\Xi^0 e^-\overline{\nu}_e)/\Gamma_{total}$ — Γ_6/Γ

VALUE (units 10^{-3})	EVTS	DOCUMENT ID		TECN	COMMENT
5.6±2.8	14	BOURQUIN	84	SPEC	SPS hyperon beam
• • • We do not use the following data for averages, fits, limits, etc. • • •					
~ 10	3	BOURQUIN	79B	SPEC	See BOURQUIN 84

$\Gamma(\Xi^-\gamma)/\Gamma_{total}$ — Γ_7/Γ

VALUE (units 10^{-4})	CL%	EVTS	DOCUMENT ID		TECN	COMMENT
< 4.6	90	0	ALBUQUERQ...	94	E761	Ω^- 375 GeV
• • • We do not use the following data for averages, fits, limits, etc. • • •						
<22	90	9	BOURQUIN	84	SPEC	SPS hyperon beam
<31	90	0	BOURQUIN	79B	SPEC	See BOURQUIN 84

$\Gamma(\Lambda\pi^-)/\Gamma_{total}$ — Γ_8/Γ

ΔS=2. Forbidden in first-order weak interaction.

VALUE (units 10^{-6})	CL%	DOCUMENT ID		TECN	COMMENT
< 2.9	90	WHITE	05	HYCP	p Cu, 800 GeV
• • • We do not use the following data for averages, fits, limits, etc. • • •					
< 190	90	BOURQUIN	84	SPEC	SPS hyperon beam
<1300	90	BOURQUIN	79B	SPEC	See BOURQUIN 84

$\Gamma(\Sigma^0\pi^-)/\Gamma_{total}$ — Γ_9/Γ

VALUE	CL%	DOCUMENT ID		TECN	COMMENT
$<5.4 \times 10^{-4}$	90	ABLIKIM	24AI	BES3	$e^+e^- \to \psi(3686) \to \Omega\overline{\Omega}$

$\Gamma(nK^-)/\Gamma_{total}$ — Γ_{10}/Γ

VALUE	CL%	DOCUMENT ID		TECN	COMMENT
$<2.4 \times 10^{-4}$	90	ABLIKIM	24AI	BES3	$e^+e^- \to \psi(3686) \to \Omega\overline{\Omega}$

Ω^- DECAY PARAMETERS

$\alpha(\Omega^-)\,\alpha_-(\Lambda)$ FOR $\Omega^- \to \Lambda K^-$

Some early results have been omitted.

VALUE	EVTS	DOCUMENT ID		TECN	COMMENT
0.0115±0.0015 OUR AVERAGE					
0.0133±0.0033±0.0052	960k	[7] CHEN	05	HYCP	p Cu, 800 GeV
0.0114±0.0012±0.0010	4.5M	[7] LU	05A	HYCP	p Cu, 800 GeV
• • • We do not use the following data for averages, fits, limits, etc. • • •					
−0.018 ±0.030	6953	CHAN	98	E756	p Be, 800 GeV
−0.022 ±0.051	1743	LUK	88	SPEC	p Be 400 GeV
−0.016 ±0.018	12k	BOURQUIN	84	SPEC	SPS hyperon beam

[7] The results of CHEN 05 and LU 05A are from different experimental runs.

α FOR $\Omega^- \to \Lambda K^-$

The above average, $\alpha(\Omega^-)\alpha_-(\Lambda) = 0.0115 \pm 0.0015$, divided by our current average $\alpha_-(\Lambda) = 0.748 \pm 0.008$ gives $\alpha(\Omega^-)$:

VALUE	DOCUMENT ID
0.0154±0.0020 OUR EVALUATION	

$\overline{\alpha}$ FOR $\overline{\Omega}^+ \to \overline{\Lambda}K^+$

VALUE	EVTS	DOCUMENT ID		TECN	COMMENT
−0.0181±0.0028±0.0026	1.89M	LU	06	HYCP	p Cu, 800 GeV
• • • We do not use the following data for averages, fits, limits, etc. • • •					
+0.017 ±0.077	1823	CHAN	98	E756	p Be, 800 GeV

$(\alpha + \overline{\alpha})/(\alpha - \overline{\alpha})$ in $\Omega^- \to \Lambda K^-, \overline{\Omega}^+ \to \overline{\Lambda}K^+$

Zero if CP is conserved.

VALUE	DOCUMENT ID		TECN	COMMENT
−0.016±0.092±0.089	[8] LU	06	HYCP	p Cu, 800 GeV

[8] This value uses the results of CHEN 05, LU 05A, and LU 06.

α FOR $\Omega^- \to \Xi^0\pi^-$

VALUE	EVTS	DOCUMENT ID		TECN	COMMENT
+0.09±0.14	1630	BOURQUIN	84	SPEC	SPS hyperon beam

α FOR $\Omega^- \to \Xi^-\pi^0$

VALUE	EVTS	DOCUMENT ID		TECN	COMMENT
+0.05±0.21	614	BOURQUIN	84	SPEC	SPS hyperon beam

Ω^- REFERENCES

We have omitted some papers that have been superseded by later experiments. See our earlier editions.

ABLIKIM	24AI	JHEP 2405 141	M. Ablikim et al.	(BESIII Collab.)
ABLIKIM	23BJ	PR D108 L091101	M. Ablikim et al.	(BESIII Collab.)
ABLIKIM	21E	PRL 126 092002	M. Ablikim et al.	(BESIII Collab.)
KAMAEV	10	PL B693 236	O. Kamaev et al.	(FNAL HyperCP Collab.)
AUBERT,BE	06	PRL 97 112001	B. Aubert et al.	(BABAR Collab.)
LU	06	PRL 96 242001	L.C. Lu et al.	(FNAL HyperCP Collab.)
CHEN	05	PR D71 051102	Y.C. Chen et al.	(FNAL HyperCP Collab.)
LU	05A	PL B617 11	L.C. Lu et al.	(FNAL HyperCP Collab.)
WHITE	05	PRL 94 101804	C.G. White et al.	(FNAL HyperCP Collab.)
CHAN	98	PR D58 072002	A.W. Chan et al.	(FNAL E756 Collab.)
WALLACE	95	PRL 74 3732	N.B. Wallace et al.	(MINN, ARIZ, MICH+)
ALBUQUERQ...	94	PR D50 18	I.F. Albuquerque et al.	(FNAL E761 Collab.)
DIEHL	91	PRL 67 804	H.T. Diehl et al.	(RUTG, FNAL, MICH+)
LUK	88	PR D38 19	K.B. Luk et al.	(RUTG, WISC, MICH, MINN)
HARTOUNI	85	PRL 54 628	E.P. Hartouni et al.	(COLU, ILL, FNAL)
BOURQUIN	84	NP B241 1	M.H. Bourquin et al.	(BRIS, GEVA, HEIDP+)
Also		PL 87B 297	M.H. Bourquin et al.	(BRIS, GEVA, HEIDP+)
BOURQUIN	79B	PL 88B 192	M.H. Bourquin et al.	(BRIS, GEVA, HEIDP+)
BAUBILLIER	78	PL 78B 342	M. Baubillier et al.	(BIRM, CERN, GLAS+) J
DEUTSCH...	78	PL 73B 96	M. Deutschmann et al.	(AACH3, BERL, CERN+) J
HEMINGWAY	78	NP B142 205	R.J. Hemingway et al.	(CERN, ZEEM, NIJM+)
DIBIANCA	75	NP B98 137	F.A. Dibianca, R.J. Endorf	(CMU)
ALVAREZ	73	PR D8 702	L.W. Alvarez	(LBL)
DEUTSCH...	73	NP B61 102	M. Deutschmann et al.	(ABCLV Collab.)
FIRESTONE	71B	PRL 26 410	I. Firestone et al.	(LRL)
SPETH	69	PL 29B 252	R. Speth et al.	(AACH, BERL, CERN, LOIC+)
PALMER	68	PL 26B 323	R.B. Palmer et al.	(BNL, SYRA)
SCHULTZ	68	PR 168 1509	P.F. Schultz et al.	(ILL, ANL, NWES+)
SCOTTER	68	PL 26B 474	D. Scotter et al.	(BIRM, GLAS, LOIC+)
ABRAMS	64	PRL 13 670	G.S. Abrams et al.	(UMD, NRL)
BARNES	64	PRL 12 204	V.E. Barnes et al.	(BNL)
FRY	55	PR 97 1189	W.F. Fry, J. Schneps, M.S. Swami	(WISC)
FRY	55B	NC 2 346	W.F. Fry, J. Schneps, M.S. Swami	(WISC)
EISENBERG	54	PR 96 541	Y. Eisenberg	(CORN)

$\Omega(2012)^-$

$I(J^P) = 0(?^-)$ Status: ***

Seen in Ξ^0K^- and $\Xi^-K^0_S$ decays with a combined significance of 8.3 standard deviations. BELLE results from JIA 19 and JIA 25 are incompatible. JIA 25 claims the older analysis was based on an inaccurate model for decays.

$\Omega(2012)^-$ MASS

VALUE (MeV)	EVTS	DOCUMENT ID		TECN	COMMENT
2012.9 ±0.4 OUR AVERAGE					
2013.35±0.57±0.27	7200	ACHARYA	25C	ALCE	$\Xi\overline{K}$ in pp at 13 TeV
2012.5 ±0.7 ±0.5	844	JIA	25	BELL	In $\Upsilon(1S,2S,3S)$
2012.4 ±0.7 ±0.6	520	YELTON	18A	BELL	In $\Upsilon(1S,2S,3S)$

$\Omega(2012)^-$ WIDTH

VALUE (MeV)	EVTS	DOCUMENT ID		TECN	COMMENT
6.3±2.0 OUR AVERAGE					
6.2±2.1±2.0	7200	ACHARYA	25C	ALCE	$\Xi\overline{K}$ in pp at 13 TeV
$6.4^{+2.5}_{-2.0}$±1.6	520	YELTON	18A	BELL	In $\Upsilon(1S)$, $\Upsilon(2S)$, $\Upsilon(3S)$

$\Omega(2012)^-$ DECAY MODES

	Mode	Fraction (Γ_i/Γ)
Γ_1	ΞK	
Γ_2	Ξ^0K^-	(34^{+17}_{-12}) %
Γ_3	$\Xi^-\overline{K}^0$	(28^{+12}_{-7}) %
Γ_4	$(\Xi\pi)K$	
Γ_5	$\Xi^-\pi^+K^-$	seen

$\Omega(2012)^-$ BRANCHING RATIOS

$\Gamma((\Xi\pi)K)/\Gamma(\Xi K)$ — Γ_4/Γ_1

VALUE	CL%	EVTS	DOCUMENT ID		TECN	COMMENT
0.99 ±0.26±0.06		844	JIA	25	BELL	In $\Upsilon(1S,2S,3S)$
• • • We do not use the following data for averages, fits, limits, etc. • • •						
<0.119	90		JIA	19	BELL	In $\Upsilon(1S,2S,3S)$

$\Gamma(\Xi^0K^-)/\Gamma(\Xi^-\overline{K}^0)$ — Γ_2/Γ_3

VALUE	DOCUMENT ID		TECN	COMMENT
1.2±0.3	YELTON	18A	BELL	In $\Upsilon(1S,2S,3S)$

Int. J. Mod. Phys. A 2026.41. Downloaded from www.worldscientific.com
by UNIVERSITY OF CALIFORNIA @ BERKELEY on 09/16/26. Re-use and distribution is strictly not permitted, except for Open Access articles.

$\Gamma(\Xi^-\overline{K}^0)/\Gamma_{total}$ — Γ_3/Γ

VALUE	DOCUMENT ID		TECN	COMMENT
$0.28^{+0.12}_{-0.07}$	[1] ACHARYA	25C	ALCE	pp at 13 TeV

[1] ACHARYA 25C reports this value as an estimate based on the statistical model.

$\Gamma(\Xi^-\pi^+K^-)/\Gamma(\Xi^0K^-)$ — Γ_5/Γ_2

VALUE	CL%	DOCUMENT ID		TECN	COMMENT
• • • We do not use the following data for averages, fits, limits, etc. • • •					
<0.078	90	JIA	19	BELL	In $\Upsilon(1S,2S,3S)$

$\Gamma(\Xi^-\pi^+K^-)/\Gamma(\Xi^-\overline{K}^0)$ — Γ_5/Γ_3

VALUE	CL%	DOCUMENT ID		TECN	COMMENT
• • • We do not use the following data for averages, fits, limits, etc. • • •					
<0.093	90	JIA	19	BELL	In $\Upsilon(1S,2S,3S)$

$\Omega(2012)^-$ REFERENCES

ACHARYA 25C PR D112 092002 S. Acharya et al. (ALICE Collab.)
JIA 25 PL B860 139224 S. Jia et al. (BELLE Collab.)
JIA 19 PR D100 032006 S. Jia et al. (BELLE Collab.)
YELTON 18A PRL 121 052003 J. Yelton et al. (BELLE Collab.)

$\Omega(2109)^-$

$I(J^P) = 0(?^?)$ Status: *

OMITTED FROM SUMMARY TABLE

ABLIKIM 25C observes a structure around 2.1 GeV with a significance of 4.1 σ in the recoil mass spectrum of the $\overline{\Omega}^+$ in the reaction $e^+e^- \to \Omega^*\overline{\Omega}^+$.

$\Omega(2109)^-$ MASS

VALUE (MeV)	EVTS	DOCUMENT ID		TECN	COMMENT
2108.5±5.2±0.9	53 ± 19	ABLIKIM	25C	BES3	$e^+e^- \to \Omega(2109)^-\overline{\Omega}^+$

$\Omega(2109)^-$ WIDTH

VALUE (MeV)	EVTS	DOCUMENT ID		TECN	COMMENT
18.3±16.4±5.7	53 ± 19	[1] ABLIKIM	25C	BES3	$e^+e^- \to \Omega(2109)^-\overline{\Omega}^+$

[1] ABLIKIM 25C value corresponds to <46.9 MeV at 95% C.L. limit.

$\Omega(2109)^-$ REFERENCES

ABLIKIM 25C PRL 134 131903 M. Ablikim et al. (BESIII Collab.)

$\Omega(2250)^-$

$I(J^P) = 0(?^?)$ Status: ***

$\Omega(2250)^-$ MASS

VALUE (MeV)	EVTS	DOCUMENT ID		TECN	COMMENT
2252± 9 OUR AVERAGE					
2253±13	44	ASTON	87B	LASS	K^-p 11 GeV/c
2251± 9±8	78	BIAGI	86B	SPEC	SPS Ξ^- beam

$\Omega(2250)^-$ WIDTH

VALUE (MeV)	EVTS	DOCUMENT ID		TECN	COMMENT
55±18 OUR AVERAGE					
81±38	44	ASTON	87B	LASS	K^-p 11 GeV/c
48±20	78	BIAGI	86B	SPEC	SPS Ξ^- beam

$\Omega(2250)^-$ DECAY MODES

	Mode	Fraction (Γ_i/Γ)
Γ_1	$\Xi^-\pi^+K^-$	seen
Γ_2	$\Xi(1530)^0K^-$	seen

$\Omega(2250)^-$ BRANCHING RATIOS

$\Gamma(\Xi(1530)^0K^-)/\Gamma(\Xi^-\pi^+K^-)$ — Γ_2/Γ_1

VALUE	EVTS	DOCUMENT ID		TECN	COMMENT
~1.0	44	ASTON	87B	LASS	K^-p 11 GeV/c
0.70±0.20	49	BIAGI	86B	SPEC	Ξ^-Be 116 GeV/c

$\Omega(2250)^-$ REFERENCES

ASTON 87B PL B194 579 D. Aston et al. (SLAC, NAGO, CINC, INUS)
BIAGI 86B ZPHY C31 33 S.F. Biagi et al. (LOQM, GEVA, RAL+)

$\Omega(2380)^-$

Status: **

OMITTED FROM SUMMARY TABLE

$\Omega(2380)^-$ MASS

VALUE (MeV)	EVTS	DOCUMENT ID		TECN	COMMENT
≈ 2380 OUR ESTIMATE					
2384±9±8	45	BIAGI	86B	SPEC	SPS Ξ^- beam

$\Omega(2380)^-$ WIDTH

VALUE (MeV)	EVTS	DOCUMENT ID		TECN	COMMENT
26±23	45	BIAGI	86B	SPEC	SPS Ξ^- beam

$\Omega(2380)^-$ DECAY MODES

	Mode	Fraction (Γ_i/Γ)
Γ_1	$\Xi^-\pi^+K^-$	
Γ_2	$\Xi(1530)^0K^-$	seen
Γ_3	$\Xi^-\overline{K}^*(892)^0$	

$\Omega(2380)^-$ BRANCHING RATIOS

$\Gamma(\Xi(1530)^0K^-)/\Gamma(\Xi^-\pi^+K^-)$ — Γ_2/Γ_1

VALUE	CL%	EVTS	DOCUMENT ID		TECN	COMMENT
<0.44	90	9	BIAGI	86B	SPEC	Ξ^-Be 116 GeV/c

$\Gamma(\Xi^-\overline{K}^*(892)^0)/\Gamma(\Xi^-\pi^+K^-)$ — Γ_3/Γ_1

VALUE	EVTS	DOCUMENT ID		TECN	COMMENT
0.5±0.3	21	BIAGI	86B	SPEC	Ξ^-Be 116 GeV/c

$\Omega(2380)^-$ REFERENCES

BIAGI 86B ZPHY C31 33 S.F. Biagi et al. (LOQM, GEVA, RAL+)

$\Omega(2470)^-$

Status: **

OMITTED FROM SUMMARY TABLE

A peak in the $\Omega^-\pi^+\pi^-$ mass spectrum with a signal significance claimed to be at least 5.5 standard deviations. There is no reason to seriously doubt the existence of this state, but unless the evidence is overwhelming we usually wait for confirmation from a second experiment before elevating peaks to the Summary Table.

$\Omega(2470)^-$ MASS

VALUE (MeV)	EVTS	DOCUMENT ID		TECN	COMMENT
2474±12	59	ASTON	88G	LASS	K^-p 11 GeV/c

$\Omega(2470)^-$ WIDTH

VALUE (MeV)	EVTS	DOCUMENT ID		TECN	COMMENT
72±33	59	ASTON	88G	LASS	K^-p 11 GeV/c

$\Omega(2470)^-$ DECAY MODES

	Mode	Fraction (Γ_i/Γ)
Γ_1	$\Omega^-\pi^+\pi^-$	seen

$\Omega(2470)^-$ BRANCHING RATIOS

$\Gamma(\Omega^-\pi^+\pi^-)/\Gamma_{total}$ — Γ_1/Γ

VALUE	EVTS	DOCUMENT ID		TECN	COMMENT
seen	59	ASTON	88G	LASS	K^-p 11 GeV/c

$\Omega(2470)^-$ REFERENCES

ASTON 88G PL B215 799 D. Aston et al. (SLAC, NAGO, CINC, INUS)

Int. J. Mod. Phys. A 2026.41. Downloaded from www.worldscientific.com
UNIVERSITY OF CALIFORNIA @ BERKELEY on 09/16/26. Re-use and distribution is strictly not permitted, except for Open Access articles.

CHARMED BARYONS ($C = +1$)

$\Lambda_c^+ = udc$, $\Sigma_c^{++} = uuc$, $\Sigma_c^+ = udc$, $\Sigma_c^0 = ddc$,
$\Xi_c^+ = usc$, $\Xi_c^0 = dsc$, $\Omega_c^0 = ssc$

Λ_c^+

$I(J^P) = 0(\frac{1}{2}^+)$ Status: ****

The parity of the Λ_c^+ is defined to be positive (as are the parities of the proton, neutron, and Λ). The quark content is udc. Results of an analysis of $pK^-\pi^+$ decays (JEZABEK 92) are consistent with $J = 1/2$. ABLIKIM 21N determines the Λ_c^+ spin to be $J = 1/2$, from an angular analysis of various 2-body Λ_c^+ decays in $e^+e^- \to \Lambda_c^+\overline{\Lambda}_c^-$.

We have omitted some results that have been superseded by later experiments. The omitted results may be found in earlier editions.

Λ_c^+ MASS

Our value in 2004, 2284.9 ± 0.6 MeV, was the average of the measurements now filed below as "not used." The BABAR measurement is so much better that we use it alone. Note that it is about 2.6 (old) standard deviations above the 2004 value.

The fit also includes Σ_c–Λ_c^+ and Λ_c^{*+}–Λ_c^+ mass-difference measurements, but this doesn't affect the Λ_c^+ mass. The new (in 2006) Λ_c^+ mass simply pushes all those other masses higher.

VALUE (MeV)	EVTS	DOCUMENT ID		TECN	COMMENT
2286.46 ± 0.14 OUR FIT					
2286.46 ± 0.14	4891	[1] AUBERT,B	05S	BABR	$\Lambda K_S^0 K^+$ and $\Sigma^0 K_S^0 K^+$
• • • We do not use the following data for averages, fits, limits, etc. • • •					
2284.7 ± 0.6 ± 0.7	1134	AVERY	91	CLEO	Six modes
2281.7 ± 2.7 ± 2.6	29	ALVAREZ	90B	NA14	$pK^-\pi^+$
2285.8 ± 0.6 ± 1.2	101	BARLAG	89	NA32	$pK^-\pi^+$
2284.7 ± 2.3 ± 0.5	5	AGUILAR-...	88B	LEBC	$pK^-\pi^+$
2283.1 ± 1.7 ± 2.0	628	ALBRECHT	88C	ARG	$pK^-\pi^+$, $p\overline{K}^0$, $\Lambda 3\pi$
2286.2 ± 1.7 ± 0.7	97	ANJOS	88B	E691	$pK^-\pi^+$
2281 ± 3	2	JONES	87	HBC	$pK^-\pi^+$
2283 ± 3	3	BOSETTI	82	HBC	$pK^-\pi^+$
2290 ± 3	1	CALICCHIO	80	HYBR	$pK^-\pi^+$

[1] AUBERT,B 05S uses low-Q $\Lambda K_S^0 K^+$ and $\Sigma^0 K_S^0 K^+$ decays to minimize systematic errors. The error above includes systematic as well as statistical errors. Many cross checks and adjustments to properties of the BABAR detector, as well as the large number of clean events, make this by far the best measurement of the Λ_c^+ mass.

Λ_c^+ MEAN LIFE

Measurements with an error $\geq 100 \times 10^{-15}$ s or with fewer than 20 events have been omitted from the Listings.

VALUE (10^{-15} s)	EVTS	DOCUMENT ID		TECN	COMMENT
202.6 ± 1.0 OUR AVERAGE					
203.20 ± 0.89 ± 0.77	107k	ABUDINEN	23A	BEL2	$\Lambda_c^+ \to pK^-\pi^+$, e^+e^- near $\Upsilon(4S)$
202.1 ± 1.7 ± 0.9	304k	[1] AAIJ	19AG	LHCB	$\Lambda_c^+ \to pK^-\pi^+$
204.6 ± 3.4 ± 2.5	8034	LINK	02C	FOCS	$\Lambda_c^+ \to pK^-\pi^+$
198.1 ± 7.0 ± 5.6	1630	KUSHNIR...	01	SELX	$\Lambda_c^+ \to pK^-\pi^+$
179.6 ± 6.9 ± 4.4	4749	MAHMOOD	01	CLE2	$e^+e^- \approx \Upsilon(4S)$
215 ± 16 ± 8	1340	FRABETTI	93D	E687	γBe, $\Lambda_c^+ \to pK^-\pi^+$
• • • We do not use the following data for averages, fits, limits, etc. • • •					
180 ± 30 ± 30	29	ALVAREZ	90	NA14	γ, $\Lambda_c^+ \to pK^-\pi^+$
200 ± 30 ± 30	90	FRABETTI	90	E687	γBe, $\Lambda_c^+ \to pK^-\pi^+$
196 $^{+23}_{-20}$	101	BARLAG	89	NA32	$pK^-\pi^+$ + c.c.
220 ± 30 ± 20	97	ANJOS	88B	E691	$pK^-\pi^+$ + c.c.

[1] AAIJ 19AG reports [Λ_c^+ MEAN LIFE] / [$D^\pm$ MEAN LIFE] = 0.1956 ± 0.0010 ± 0.0013 which we multiply by our best (shown rounded) value $D^\pm$ MEAN LIFE = (1.033 ± 0.005) × 10^{-12} s. Our first error is their experiment's error and our second error is the systematic error from using our best (shown rounded) value.

Λ_c^+ DECAY MODES

Branching fractions marked with a footnote, e.g. [a], have been corrected for decay modes not observed in the experiments. For example, the submode fraction $\Lambda_c^+ \to p\overline{K}^*(892)^0$ seen in $\Lambda_c^+ \to pK^-\pi^+$ has been multiplied up to include $\overline{K}^*(892)^0 \to \overline{K}^0\pi^0$ decays.

	Mode		Fraction (Γ_i/Γ)	Scale factor / Confidence level
	Hadronic modes with a p or n: $S = -1$ final states			
Γ_1	pK_S^0		(1.63 ± 0.07) %	S=1.1
Γ_2	pK_L^0		(1.67 ± 0.07) %	
Γ_3	$pK^-\pi^+$		(6.37 ± 0.21) %	S=1.2
Γ_4	$p\overline{K}_0^*(700)^0$		(1.9 ± 0.6) × 10^{-3}	
Γ_5	$p\overline{K}^*(892)^0$	[a]	(1.42 ± 0.06) %	
Γ_6	$p\overline{K}_0^*(1430)$		(9.4 ± 1.8) × 10^{-3}	
Γ_7	$\Delta(1232)^{++}K^-$		(1.80 ± 0.08) %	
Γ_8	$\Delta(1600)^{++}K^-$		(2.9 ± 1.0) × 10^{-3}	
Γ_9	$\Delta(1700)^{++}K^-$		(2.5 ± 0.6) × 10^{-3}	
Γ_{10}	$\Lambda(1405)^0\pi^+$		(4.9 ± 1.9) × 10^{-3}	
Γ_{11}	$\Lambda(1520)\pi^+$	[a]	(1.19 ± 0.16) × 10^{-3}	
Γ_{12}	$\Lambda(1600)\pi^+$		(3.3 ± 1.2) × 10^{-3}	
Γ_{13}	$\Lambda(1670)\pi^+$		(7.5 ± 2.1) × 10^{-4}	
Γ_{14}	$\Lambda(1690)\pi^+$		(7.6 ± 2.3) × 10^{-4}	
Γ_{15}	$\Lambda(2000)\pi^+$		(6.1 ± 0.7) × 10^{-3}	
Γ_{16}	$pK^-\pi^+$ nonresonant		(3.5 ± 0.4) %	
Γ_{17}	$pK_S^0\pi^0$		(2.12 ± 0.09) %	S=1.3
Γ_{18}	$pK_L^0\pi^0$		(2.02 ± 0.14) %	
Γ_{19}	$nK_S^0\pi^+$		(1.86 ± 0.09) %	
Γ_{20}	$nK_S^0K^+$		(3.9 $^{+1.7}_{-1.4}$) × 10^{-4}	
Γ_{21}	$nK_S^0\pi^+\pi^0$		(8.5 ± 1.3) × 10^{-3}	
Γ_{22}	$nK^-\pi^+\pi^+$		(1.90 ± 0.12) %	
Γ_{23}	$p\overline{K}^0\eta$		(9.0 ± 0.6) × 10^{-3}	S=1.1
Γ_{24}	$pK_S^0\pi^+\pi^-$		(1.63 ± 0.10) %	S=1.1
Γ_{25}	$pK_L^0\pi^+\pi^-$		(1.69 ± 0.11) %	
Γ_{26}	$pK^-\pi^+\pi^0$		(4.54 ± 0.27) %	S=1.6
Γ_{27}	$pK^*(892)^-\pi^+$	[a]	(1.4 ± 0.5) %	
Γ_{28}	$p(K^-\pi^+)_{\text{nonresonant}}\pi^0$		(4.7 ± 0.8) %	
Γ_{29}	$\Delta(1232)\overline{K}^*(892)$		seen	
Γ_{30}	$pK^-2\pi^+\pi^-$		(1.4 ± 1.0) × 10^{-3}	
Γ_{31}	$pK^-\pi^+2\pi^0$		(1.0 ± 0.5) %	
	Hadronic modes with a p or n: $S = 0$ final states			
Γ_{32}	$p\pi^0$		(1.8 ± 0.4) × 10^{-4}	
Γ_{33}	$n\pi^+$		(6.6 ± 1.3) × 10^{-4}	
Γ_{34}	$p\eta$		(1.49 ± 0.08) × 10^{-3}	
Γ_{35}	$p\eta'$		(4.9 ± 0.9) × 10^{-4}	
Γ_{36}	$p\omega(782)^0$		(9.0 ± 1.0) × 10^{-4}	S=1.2
Γ_{37}	$p\pi^+\pi^-$		(4.69 ± 0.22) × 10^{-3}	
Γ_{38}	$pf_0(980)$	[a]	(3.5 ± 2.3) × 10^{-3}	
Γ_{39}	$p\rho(770)^0$		(1.5 ± 0.4) × 10^{-3}	
Γ_{40}	$n\pi^+\pi^0$		(6.4 ± 0.9) × 10^{-3}	
Γ_{41}	$nK^+\pi^0$		< 7.1 × 10^{-4}	CL=90%
Γ_{42}	$n\pi^+\pi^-\pi^+$		(4.5 ± 0.8) × 10^{-3}	
Γ_{43}	$p2\pi^+2\pi^-$		(2.3 ± 1.5) × 10^{-3}	
Γ_{44}	pK^+K^-		(1.08 ± 0.04) × 10^{-3}	
Γ_{45}	$p\phi$	[a]	(1.06 ± 0.13) × 10^{-3}	S=1.1
Γ_{46}	pK^+K^- non-ϕ		(5.4 ± 1.2) × 10^{-4}	
Γ_{47}	$pK_S^0K_S^0$		(2.41 ± 0.18) × 10^{-4}	
Γ_{48}	$p\phi\pi^0$		(10 ± 4) × 10^{-5}	
Γ_{49}	$pK^+K^-\pi^0$ nonresonant		< 6.3 × 10^{-5}	CL=90%
	Hadronic modes with a hyperon: $S = -1$ final states			
Γ_{50}	$\Lambda\pi^+$		(1.32 ± 0.05) %	S=1.1
Γ_{51}	$\Lambda(1670)\pi^+$, $\Lambda(1670) \to \eta\Lambda$		(3.5 ± 0.5) × 10^{-3}	
Γ_{52}	$\Lambda\pi^+\pi^0$		(7.16 ± 0.33) %	
Γ_{53}	$\Lambda\rho^+$		(4.1 ± 0.5) %	
Γ_{54}	$\Sigma(1385)^+\pi^0$, $\Sigma^+ \to \Lambda\pi^+$		(5.1 ± 0.7) × 10^{-3}	
Γ_{55}	$\Sigma(1385)^0\pi^+$, $\Sigma^0 \to \Lambda\pi^0$		(5.7 ± 0.8) × 10^{-3}	
Γ_{56}	$\Lambda\pi^-2\pi^+$		(3.69 ± 0.26) %	S=1.5
Γ_{57}	$\Sigma(1385)^+\pi^+\pi^-$, $\Sigma^{*+} \to \Lambda\pi^+$		(1.0 ± 0.5) %	
Γ_{58}	$\Sigma(1385)^-2\pi^+$, $\Sigma^{*-} \to \Lambda\pi^-$		(7.8 ± 1.4) × 10^{-3}	
Γ_{59}	$\Lambda\pi^+\rho^0$		(1.5 ± 0.6) %	
Γ_{60}	$\Sigma(1385)^+\rho^0$, $\Sigma^{*+} \to \Lambda\pi^+$		(5 ± 4) × 10^{-3}	
Γ_{61}	$\Lambda\pi^-2\pi^+$ nonresonant		< 1.1 %	CL=90%

Int. J. Mod. Phys. A 2026.41. Downloaded from www.worldscientific.com
by UNIVERSITY OF CALIFORNIA @ BERKELEY on 09/16/26. Re-use and distribution is strictly not permitted, except for Open Access articles.

Γ_{62}	$\Lambda\pi^-\pi^0 2\pi^+$ total		(2.3 ± 0.8) %	
Γ_{63}	$\Lambda\pi^+\omega$	[a]	(1.5 ± 0.5) %	
Γ_{64}	$\Lambda\pi^-\pi^0 2\pi^+$, no η or ω		$< 8 \times 10^{-3}$	CL=90%
Γ_{65}	$\Lambda\pi^+\eta$	[a]	(1.92 ± 0.06) %	
Γ_{66}	$\Sigma(1385)^+\eta$	[a]	$(6.7 \pm 0.6) \times 10^{-3}$	
Γ_{67}	$\Lambda a_0(980)^+$, $a_0^+ \to \pi^+\eta$		(1.04 ± 0.17) %	
Γ_{68}	$\Lambda(1670)\pi^+$, $\Lambda(1670) \to \Lambda\eta$		$(2.7 \pm 0.6) \times 10^{-3}$	
Γ_{69}	$\Lambda K^+\overline{K}^0$		$(5.9 \pm 0.5) \times 10^{-3}$	S=1.2
Γ_{70}	$\Xi(1690)^0 K^+$, $\Xi^{*0} \to \Lambda\overline{K}^0$		$(1.7 \pm 0.4) \times 10^{-3}$	
Γ_{71}	$\Sigma^0\pi^+$		(1.29 ± 0.05) %	S=1.1
Γ_{72}	$\Sigma^0\pi^+\eta$		$(7.6 \pm 0.8) \times 10^{-3}$	
Γ_{73}	$\Sigma^+\pi^0$		(1.27 ± 0.10) %	S=1.1
Γ_{74}	$\Sigma^+\eta$		$(3.4 \pm 0.4) \times 10^{-3}$	
Γ_{75}	$\Sigma^+\eta'$		$(4.2 \pm 0.9) \times 10^{-3}$	
Γ_{76}	$\Sigma^+\pi^+\pi^-$		(4.57 ± 0.18) %	S=1.1
Γ_{77}	$\Sigma^+\rho^0$		< 1.7 %	CL=95%
Γ_{78}	$\Sigma^-2\pi^+$		(1.87 ± 0.18) %	
Γ_{79}	$\Sigma^0\pi^+\pi^0$		(3.6 ± 0.4) %	
Γ_{80}	$\Sigma^+\pi^0\pi^0$		(1.57 ± 0.14) %	
Γ_{81}	$\Sigma^0\pi^-2\pi^+$		(1.13 ± 0.31) %	
Γ_{82}	$\Sigma^+\omega$		(1.72 ± 0.20) %	
Γ_{83}	$\Sigma^-\pi^0 2\pi^+$		(2.1 ± 0.4) %	
Γ_{84}	$\Sigma^0 K_S^0 K^+$		$< 1.28 \times 10^{-3}$	CL=90%
Γ_{85}	$\Sigma^+K^+K^-$		$(3.66 \pm 0.35) \times 10^{-3}$	S=1.1
Γ_{86}	$\Sigma^+K^+K^-$ (non-ϕ)			
Γ_{87}	$\Sigma^+\phi$	[a]	$(4.0 \pm 0.5) \times 10^{-3}$	S=1.1
Γ_{88}	$\Xi(1690)^0 K^+$, $\Xi^{*0} \to \Sigma^+K^-$		$(1.03 \pm 0.25) \times 10^{-3}$	
Γ_{89}	$\Sigma^+K^+K^-$ nonresonant		$< 8 \times 10^{-4}$	CL=90%
Γ_{90}	Ξ^0K^+		$(5.5 \pm 0.7) \times 10^{-3}$	
Γ_{91}	$\Xi^-K^+\pi^+$		$(6.3 \pm 0.5) \times 10^{-3}$	
Γ_{92}	$\Xi^0K^+\pi^0$		$(7.8 \pm 1.7) \times 10^{-3}$	
Γ_{93}	$\Xi^0K_S^0\pi^+$		$(3.7 \pm 0.6) \times 10^{-3}$	
Γ_{94}	$\Xi(1530)^0K^+$		$(4.9 \pm 0.6) \times 10^{-3}$	S=1.1

Hadronic modes with a hyperon: $S = 0$ final states

Γ_{95}	ΛK^+		$(6.54 \pm 0.30) \times 10^{-4}$	
Γ_{96}	$\Lambda K^+\pi^0$		$(1.50 \pm 0.29) \times 10^{-3}$	
Γ_{97}	$\Lambda K_S^0\pi^+$		$(1.73 \pm 0.28) \times 10^{-3}$	
Γ_{98}	$\Lambda K^*(892)K^{*+} \to K_S^0\pi^+$		seen	
Γ_{99}	$\Lambda K^+\pi^+\pi^-$		$(4.2 \pm 1.6) \times 10^{-4}$	
Γ_{100}	Σ^0K^+		$(3.76 \pm 0.31) \times 10^{-4}$	
Γ_{101}	$\Sigma^+K_S^0$		$(4.8 \pm 1.4) \times 10^{-4}$	
Γ_{102}	$\Sigma^0K^+\pi^+\pi^-$		$< 6.5 \times 10^{-4}$	CL=90%
Γ_{103}	$\Sigma^0K^+\pi^0$		$< 5.0 \times 10^{-4}$	CL=90%
Γ_{104}	$\Sigma^+K^+\pi^-$		$(2.05 \pm 0.26) \times 10^{-3}$	
Γ_{105}	$\Sigma^+K^*(892)^0$	[a]	$(3.6 \pm 1.0) \times 10^{-3}$	
Γ_{106}	$\Sigma^+K^+\pi^-\pi^0$		$< 1.1 \times 10^{-3}$	CL=90%
Γ_{107}	$\Sigma^-K^+\pi^+$		$(3.8 \pm 1.2) \times 10^{-4}$	

Doubly Cabibbo-suppressed modes

Γ_{108}	$pK^+\pi^-$		$(1.13 \pm 0.17) \times 10^{-4}$	

Semileptonic modes

Γ_{109}	$\Lambda e^+\nu_e$		(3.56 ± 0.13) %	
Γ_{110}	$\Lambda\pi^+\pi^-e^+\nu_e$		$< 3.9 \times 10^{-4}$	CL=90%
Γ_{111}	$pK^-e^+\nu_e$		$(8.8 \pm 1.8) \times 10^{-4}$	
Γ_{112}	$pK_S^0\pi^-e^+\nu_e$		$< 3.3 \times 10^{-4}$	CL=90%
Γ_{113}	$\Lambda(1520)e^+\nu_e$		$(1.0 \pm 0.5) \times 10^{-3}$	
Γ_{114}	$\Lambda(1405)^0e^+\nu_e$, $\Lambda^0 \to pK^-$		$(4.2 \pm 1.9) \times 10^{-4}$	
Γ_{115}	$\Lambda\mu^+\nu_\mu$		(3.48 ± 0.17) %	

Inclusive modes

Γ_{116}	e^+ anything		(4.06 ± 0.13) %	
Γ_{117}	p anything		(50 ± 16) %	
Γ_{118}	n anything		(32.6 ± 1.6) %	
Γ_{119}	Λ anything		$(38.2 {}^{+2.9}_{-2.4})$ %	
Γ_{120}	K_S^0 anything		(10.90 ± 0.22) %	
Γ_{121}	3prongs		(24 ± 8) %	

$\Delta C = 1$ weak neutral current ($C1$) modes, or Lepton Family number (LF), or Lepton number (L), or Baryon number (B) violating modes

Γ_{122}	pe^+e^-	$C1$	< 5.5	$\times 10^{-6}$	CL=90%
Γ_{123}	$p\mu^+\mu^-$ non-resonant	$C1$	< 2.9	$\times 10^{-8}$	CL=90%
Γ_{124}	$pe^+\mu^-$	LF	< 9.9	$\times 10^{-6}$	CL=90%
Γ_{125}	$pe^-\mu^+$	LF	< 1.9	$\times 10^{-5}$	CL=90%
Γ_{126}	$\overline{p}2e^+$	L,B	< 2.7	$\times 10^{-6}$	CL=90%
Γ_{127}	$\overline{p}2\mu^+$	L,B	< 9.4	$\times 10^{-6}$	CL=90%
Γ_{128}	$\overline{p}e^+\mu^+$	L,B	< 1.6	$\times 10^{-5}$	CL=90%
Γ_{129}	$\Sigma^-\mu^+\mu^+$	L	< 7.0	$\times 10^{-4}$	CL=90%

Radiative modes

Γ_{130}	$\Sigma^+\gamma$		< 2.5	$\times 10^{-4}$	CL=90%

Exotic modes

Γ_{131}	$p\gamma_D$	[b]	< 8.0	$\times 10^{-5}$	CL=90%

[a] This branching fraction includes all the decay modes of the final-state resonance.

[b] Here γ_D stands for a dark photon.

FIT INFORMATION

An overall fit to 56 branching ratios uses 87 measurements to determine 26 parameters. The overall fit has a $\chi^2 = 61.2$ for 61 degrees of freedom.

The following *off-diagonal* array elements are the correlation coefficients $\langle \delta x_i \delta x_j \rangle / (\delta x_i \cdot \delta x_j)$, in percent, from the fit to the branching fractions, $x_i \equiv \Gamma_i/\Gamma_{\text{total}}$.

x_3	32									
x_{17}	28	67								
x_{23}	64	21	18							
x_{24}	26	45	30	17						
x_{26}	32	37	23	21	47					
x_{34}	12	37	25	8	17	14				
x_{35}	5	15	10	3	7	6	6			
x_{36}	8	24	16	5	11	9	9	4		
x_{45}	8	26	17	5	12	10	10	4	17	
x_{50}	37	35	26	24	19	24	13	5	8	9
x_{52}	32	32	26	20	18	20	12	5	8	8
x_{56}	35	17	10	22	30	51	6	3	4	4
x_{65}	12	37	25	8	17	14	14	6	9	10
x_{69}	8	8	6	5	4	5	3	1	2	2
x_{71}	34	23	17	22	16	24	8	3	5	6
x_{73}	26	21	18	17	9	13	8	3	5	5
x_{76}	30	75	50	20	41	42	28	11	18	19
x_{78}	2	5	4	1	2	2	2	1	1	1
x_{81}	7	8	5	4	7	10	3	1	2	2
x_{82}	9	19	13	6	13	17	7	3	5	5
x_{85}	13	31	21	8	17	17	12	5	7	8
x_{87}	10	24	16	6	13	14	9	4	6	6
x_{90}	3	9	6	2	4	3	3	1	2	2
x_{91}	15	18	13	10	9	10	7	3	4	5
x_{94}	1	3	2	1	1	1	1	0	1	1
	x_1	x_3	x_{17}	x_{23}	x_{24}	x_{26}	x_{34}	x_{35}	x_{36}	x_{45}

x_{52}	44									
x_{56}	34	29								
x_{65}	13	12	6							
x_{69}	21	10	7	3						
x_{71}	55	38	34	8	12					
x_{73}	17	20	11	8	4	14				
x_{76}	29	28	24	28	6	20	18			
x_{78}	2	2	1	2	0	1	1	4		
x_{81}	7	6	16	3	1	6	3	7	0	
x_{82}	7	8	11	7	2	6	6	18	1	3
x_{85}	12	12	10	11	3	8	8	42	2	3
x_{87}	9	9	8	9	2	7	6	32	1	2
x_{90}	3	3	2	3	1	2	2	7	0	1
x_{91}	37	17	13	7	8	21	7	14	1	3
x_{94}	1	1	1	1	0	1	1	2	0	0
	x_{50}	x_{52}	x_{56}	x_{65}	x_{69}	x_{71}	x_{73}	x_{76}	x_{78}	x_{81}

x_{85}	7				
x_{87}	6	13			
x_{90}	2	3	2		
x_{91}	4	6	5	2	
x_{94}	1	1	1	0	1
	x_{82}	x_{85}	x_{87}	x_{90}	x_{91}

Int. J. Mod. Phys. A 2026.41. Downloaded from www.worldscientific.com
UNIVERSITY OF CALIFORNIA @ BERKELEY on 09/16/26. Re-use and distribution is strictly not permitted, except for Open Access articles.

Λ_c^+ BRANCHING RATIOS

A few really obsolete results have been omitted.

Hadronic modes with a p: $S = -1$ final states

$\Gamma(pK_S^0)/\Gamma_{total}$ — Γ_1/Γ

VALUE (%)	EVTS	DOCUMENT ID		TECN	COMMENT
1.63±0.07 OUR FIT	Error includes scale factor of 1.1.				
1.52±0.08±0.03	1243	ABLIKIM	16	BES3	$e^+e^- \to \Lambda_c\overline{\Lambda}_c$, 4.599 GeV

$\Gamma(pK_L^0)/\Gamma_{total}$ — Γ_2/Γ

VALUE (%)	EVTS	DOCUMENT ID		TECN	COMMENT
1.67±0.06±0.04	1.6k	[1] ABLIKIM	24CQ	BES3	e^+e^- at 4.600–4.699 GeV

[1] Comparing with the PDG 22 value $B(\Lambda_c^+ \to pK_S^0) = (1.59 \pm 0.07) \times 10^{-2}$, ABLIKIM 24CQ notes the $K_S^0 - K_L^0$ splitting to be -0.025 ± 0.031 in these modes.

$\Gamma(pK_S^0)/\Gamma(pK^-\pi^+)$ — Γ_1/Γ_3

Measurements given as a $\overline{K}^0$ ratio have been divided by 2 to convert to a K_S^0 ratio.

VALUE	EVTS	DOCUMENT ID		TECN	COMMENT
0.255±0.011 OUR FIT	Error includes scale factor of 1.3.				
0.234±0.020 OUR AVERAGE					
0.23 ±0.01 ±0.02	1025	ALAM	98	CLE2	$e^+e^- \approx \Upsilon(4S)$
0.22 ±0.04 ±0.03	133	AVERY	91	CLEO	e^+e^- 10.5 GeV
0.28 ±0.09 ±0.07	45	ANJOS	90	E691	γBe 70–260 GeV
0.31 ±0.08 ±0.02	73	ALBRECHT	88C	ARG	e^+e^- 10 GeV

$\Gamma(pK^-\pi^+)/\Gamma_{total}$ — Γ_3/Γ

VALUE (%)	EVTS	DOCUMENT ID		TECN	COMMENT
6.37±0.21 OUR FIT	Error includes scale factor of 1.2.				
6.3 ±0.5 OUR AVERAGE	Error includes scale factor of 2.0.				
5.84±0.27±0.23	6.3k	ABLIKIM	16	BES3	$e^+e^- \to \Lambda_c\overline{\Lambda}_c$, 4.599 GeV
$6.84\pm0.24^{+0.21}_{-0.27}$	1.4k	[1] ZUPANC	14	BELL	$e^+e^- \to D^{(*)-}\overline{p}\pi^+$ recoil
• • • We do not use the following data for averages, fits, limits, etc. • • •					
5.0 ±1.3		[2] PDG	02		See footnote

[1] This ZUPANC 14 value is the FIRST-EVER model-independent measurement of a Λ_c^+ branching fraction.

[2] See the note by P. Burchat, "Λ_c^+ Branching Fractions," in any edition of the Review from 2002 through 2014 for how this value was obtained. It is now obsolete.

$\Gamma(p\overline{K}_0^*(700)^0)/\Gamma(pK^-\pi^+)$ — Γ_4/Γ_3

VALUE (units 10^{-2})	DOCUMENT ID		TECN	COMMENT
3.02±0.16±0.18±0.92	[1] AAIJ	23Z	LHCB	1.7fb^{-1}, pp at 13 TeV

[1] AAIJ 23Z uses an amplitude analysis of 400k $\Lambda_c \to pK^-\pi^+$ decays, the last uncertainty is due to the amplitude model.

$\Gamma(p\overline{K}^*(892)^0)/\Gamma(pK^-\pi^+)$ — Γ_5/Γ_3

Unseen decay modes of the $\overline{K}^*(892)^0$ are included.

VALUE (units 10^{-2})	EVTS	DOCUMENT ID		TECN	COMMENT
22.3 ± 0.7 OUR AVERAGE					
22.14± 0.23±0.04±0.64		[1] AAIJ	23Z	LHCB	1.7fb^{-1}, pp at 13 TeV
29 ± 4 ±3		[2] AITALA	00	E791	$\pi^- N$, 500 GeV
• • • We do not use the following data for averages, fits, limits, etc. • • •					
$35 \; {}^{+6}_{-7}$ ±3	39	BOZEK	93	NA32	π^-Cu 230 GeV
35 ±11		BARLAG	90D	NA32	See BOZEK 93
42 ±24	12	BASILE	81B	CNTR	$pp \to \Lambda_c^+ e^- X$

[1] AAIJ 23Z uses an amplitude analysis of 400k $\Lambda_c \to pK^-\pi^+$ decays, the last uncertainty is due to the amplitude model.

[2] AITALA 00 makes a coherent 5-dimensional amplitude analysis of 946 ± 38 $\Lambda_c^+ \to pK^-\pi^+$ decays.

$\Gamma(p\overline{K}_0^*(1430))/\Gamma(pK^-\pi^+)$ — Γ_6/Γ_3

VALUE (units 10^{-2})	DOCUMENT ID		TECN	COMMENT
14.7±0.6±0.1±2.7	[1] AAIJ	23Z	LHCB	1.7fb^{-1}, pp at 13 TeV

[1] AAIJ 23Z uses an amplitude analysis of 400k $\Lambda_c \to pK^-\pi^+$ decays, the last uncertainty is due to the amplitude model.

$\Gamma(\Delta(1232)^{++}K^-)/\Gamma(pK^-\pi^+)$ — Γ_7/Γ_3

VALUE (units 10^{-2})	EVTS	DOCUMENT ID		TECN	COMMENT
28.2 ± 0.8 OUR AVERAGE					
28.60± 0.29±0.16±0.76		[1] AAIJ	23Z	LHCB	1.7 fb^{-1}, pp at 13 TeV
18 ± 3 ±3		[2] AITALA	00	E791	$\pi^- N$, 500 GeV
• • • We do not use the following data for averages, fits, limits, etc. • • •					
$12 \; {}^{+4}_{-5}$ ±5	14	BOZEK	93	NA32	π^-Cu 230 GeV
40 ±17	17	BASILE	81B	CNTR	$pp \to \Lambda_c^+ e^- X$

[1] AAIJ 23Z uses an amplitude analysis of 400k $\Lambda_c \to pK^-\pi^+$ decays, the last uncertainty is due to the amplitude model.

[2] AITALA 00 makes a coherent 5-dimensional amplitude analysis of 946 ± 38 $\Lambda_c^+ \to pK^-\pi^+$ decays.

$\Gamma(\Delta(1600)^{++}K^-)/\Gamma(pK^-\pi^+)$ — Γ_8/Γ_3

VALUE (units 10^{-2})	DOCUMENT ID		TECN	COMMENT
4.5±0.3±0.1±1.5	[1] AAIJ	23Z	LHCB	1.7fb^{-1}, pp at 13 TeV

[1] AAIJ 23Z uses an amplitude analysis of 400k $\Lambda_c \to pK^-\pi^+$ decays, the last uncertainty is due to the amplitude model.

$\Gamma(\Delta(1700)^{++}K^-)/\Gamma(pK^-\pi^+)$ — Γ_9/Γ_3

VALUE (units 10^{-2})	DOCUMENT ID		TECN	COMMENT
3.90±0.20±0.07±0.94	[1] AAIJ	23Z	LHCB	1.7fb^{-1}, pp at 13 TeV

[1] AAIJ 23Z uses an amplitude analysis of 400k $\Lambda_c \to pK^-\pi^+$ decays, the last uncertainty is due to the amplitude model.

$\Gamma(\Lambda(1405)^0\pi^+)/\Gamma(pK^-\pi^+)$ — Γ_{10}/Γ_3

VALUE (units 10^{-2})	DOCUMENT ID		TECN	COMMENT
7.7±0.2±0.2±3.0	[1] AAIJ	23Z	LHCB	1.7fb^{-1}, pp at 13 TeV

[1] AAIJ 23Z uses an amplitude analysis of 400k $\Lambda_c \to pK^-\pi^+$ decays, the last uncertainty is due to the amplitude model.

$\Gamma(\Lambda(1520)\pi^+)/\Gamma(pK^-\pi^+)$ — Γ_{11}/Γ_3

Unseen decay modes of the $\Lambda(1520)$ are included.

VALUE (units 10^{-2})	EVTS	DOCUMENT ID		TECN	COMMENT
1.86± 0.09±0.03±0.23		[1] AAIJ	23Z	LHCB	1.7 fb^{-1}, pp at 13 TeV
• • • We do not use the following data for averages, fits, limits, etc. • • •					
34 ± 8 ±5		[2] AITALA	00	E791	$\pi^- N$, 500 GeV
$40 \; {}^{+18}_{-13}$ ±9	12	BOZEK	93	NA32	π^-Cu 230 GeV

[1] AAIJ 23Z uses an amplitude analysis of 400k $\Lambda_c \to pK^-\pi^+$ decays, the last uncertainty is due to the amplitude model.

[2] AITALA 00 makes a coherent 5-dimensional amplitude analysis of 946 ± 38 $\Lambda_c^+ \to pK^-\pi^+$ decays.

$\Gamma(\Lambda(1600)\pi^+)/\Gamma(pK^-\pi^+)$ — Γ_{12}/Γ_3

VALUE (units 10^{-2})	DOCUMENT ID		TECN	COMMENT
5.2±0.2±0.1±1.9	[1] AAIJ	23Z	LHCB	1.7fb^{-1}, pp at 13 TeV

[1] AAIJ 23Z uses an amplitude analysis of 400k $\Lambda_c \to pK^-\pi^+$ decays, the last uncertainty is due to the amplitude model.

$\Gamma(\Lambda(1670)\pi^+)/\Gamma(pK^-\pi^+)$ — Γ_{13}/Γ_3

VALUE (units 10^{-2})	DOCUMENT ID		TECN	COMMENT
1.18±0.06±0.01±0.32	[1] AAIJ	23Z	LHCB	1.7fb^{-1}, pp at 13 TeV

[1] AAIJ 23Z uses an amplitude analysis of 400k $\Lambda_c \to pK^-\pi^+$ decays, the last uncertainty is due to the amplitude model.

$\Gamma(\Lambda(1690)\pi^+)/\Gamma(pK^-\pi^+)$ — Γ_{14}/Γ_3

VALUE (units 10^{-2})	DOCUMENT ID		TECN	COMMENT
1.19±0.09±0.01±0.34	[1] AAIJ	23Z	LHCB	1.7fb^{-1}, pp at 13 TeV

[1] AAIJ 23Z uses an amplitude analysis of 400k $\Lambda_c \to pK^-\pi^+$ decays, the last uncertainty is due to the amplitude model.

$\Gamma(\Lambda(2000)\pi^+)/\Gamma(pK^-\pi^+)$ — Γ_{15}/Γ_3

VALUE (units 10^{-2})	DOCUMENT ID		TECN	COMMENT
9.58±0.27±0.23±0.93	[1] AAIJ	23Z	LHCB	1.7fb^{-1}, pp at 13 TeV

[1] AAIJ 23Z uses an amplitude analysis of 400k $\Lambda_c \to pK^-\pi^+$ decays, the last uncertainty is due to the amplitude model.

$\Gamma(pK^-\pi^+ \text{nonresonant})/\Gamma(pK^-\pi^+)$ — Γ_{16}/Γ_3

VALUE	EVTS	DOCUMENT ID		TECN	COMMENT
0.55±0.06 OUR AVERAGE					
0.55±0.06±0.04		[1] AITALA	00	E791	$\pi^- N$, 500 GeV
$0.56 \; {}^{+0.07}_{-0.09}$ ±0.05	71	BOZEK	93	NA32	π^-Cu 230 GeV

[1] AITALA 00 makes a coherent 5-dimensional amplitude analysis of 946 ± 38 $\Lambda_c^+ \to pK^-\pi^+$ decays.

$\Gamma(pK_S^0\pi^0)/\Gamma_{total}$ — Γ_{17}/Γ

VALUE (%)	EVTS	DOCUMENT ID		TECN	COMMENT
2.12±0.09 OUR FIT	Error includes scale factor of 1.3.				
1.87±0.13±0.05	558	ABLIKIM	16	BES3	$e^+e^- \to \Lambda_c\overline{\Lambda}_c$, 4.599 GeV

$\Gamma(pK_L^0\pi^0)/\Gamma_{total}$ — Γ_{18}/Γ

VALUE (%)	EVTS	DOCUMENT ID		TECN	COMMENT
2.02±0.13±0.05	650	[1] ABLIKIM	24CQ	BES3	e^+e^- at 4.600–4.699 GeV

[1] Comparing with the PDG 22 value $B(\Lambda_c^+ \to pK_S^0\pi^0) = (1.96 \pm 0.12) \times 10^{-2}$, ABLIKIM 24CQ notes the $K_S^0 - K_L^0$ splitting to be 0.015 ± 0.046 in these modes.

$\Gamma(pK_S^0\pi^0)/\Gamma(pK^-\pi^+)$ — Γ_{17}/Γ_3

Measurements given as a $\overline{K}^0$ ratio have been divided by 2 to convert to a K_S^0 ratio.

VALUE	EVTS	DOCUMENT ID		TECN	COMMENT
0.333±0.011 OUR FIT	Error includes scale factor of 1.3.				
0.339±0.009 OUR AVERAGE					
0.339±0.002±0.009	130k	ADACHI	25L	BEL2	e^+e^- at $\Upsilon(nS)$
0.33 ±0.03 ±0.04	774	ALAM	98	CLE2	$e^+e^- \approx \Upsilon(4S)$

Int. J. Mod. Phys. A 2026.41. Downloaded from www.worldscientific.com
by UNIVERSITY OF CALIFORNIA @ BERKELEY on 09/16/26. Re-use and distribution is strictly not permitted, except for Open Access articles.

$\Gamma(nK^0_S\pi^+)/\Gamma_{total}$ — Γ_{19}/Γ

VALUE (%)	EVTS	DOCUMENT ID		TECN	COMMENT
1.86±0.08±0.04	556	ABLIKIM	24BA	BES3	4.5 fb^{-1}, e^+e^- at 4.600–4.699 GeV
• • • We do not use the following data for averages, fits, limits, etc. • • •					
1.82±0.23±0.11	83	[1] ABLIKIM	17H	BES3	e^+e^- at 4.6 GeV

[1] Superseded by ABLIKIM 24BA.

$\Gamma(nK^0_S K^+)/\Gamma_{total}$ — Γ_{20}/Γ

VALUE (units 10^{-4})	EVTS	DOCUMENT ID		TECN	COMMENT
$3.9^{+1.7}_{-1.4}\pm0.3$	9	ABLIKIM	24BA	BES3	4.5 fb^{-1}, e^+e^- at 4.600–4.699 GeV

$\Gamma(nK^0_S\pi^+\pi^0)/\Gamma_{total}$ — Γ_{21}/Γ

VALUE (%)	EVTS	DOCUMENT ID		TECN	COMMENT
0.85±0.13±0.03	98	ABLIKIM	24AX	BES3	4.5 fb^{-1}, e^+e^- at 4.600–4.699 GeV

$\Gamma(nK^-\pi^+\pi^+)/\Gamma_{total}$ — Γ_{22}/Γ

VALUE (%)	EVTS	DOCUMENT ID		TECN	COMMENT
1.90±0.08±0.09	810	ABLIKIM	23A	BES	4.5 fb^{-1}, e^+e^- at 4.600–4.699 GeV

$\Gamma(p\overline{K}^0\eta)/\Gamma_{total}$ — Γ_{23}/Γ

VALUE (%)	EVTS	DOCUMENT ID		TECN	COMMENT
0.90 ±0.06 OR FIT	Error includes scale factor of 1.1.				
0.828±0.168±0.056	42	[1] ABLIKIM	21H	BES3	e^+e^- at 4.6 GeV

[1] ABLIKIM 21H measures $B(\Lambda_c^+ \to pK^0_S\eta) = (0.414 \pm 0.084 \pm 0.028)\%$.

$\Gamma(p\overline{K}^0\eta)/\Gamma(pK^0_S)$ — Γ_{23}/Γ_1

VALUE	EVTS	DOCUMENT ID		TECN	COMMENT
0.550±0.029 OR FIT					
0.546±0.012±0.026	12.6k	[1] LI	23B	BELL	$e^+e^- \to \Upsilon(nS)$

[1] LI 23B measures $B(\Lambda_c^+ \to pK^0_S\eta)/B(\Lambda_c^+ \to pK^0_S) = 0.273 \pm 0.006 \pm 0.013$.

$\Gamma(p\overline{K}^0\eta)/\Gamma(pK^-\pi^+)$ — Γ_{23}/Γ_3

VALUE	EVTS	DOCUMENT ID		TECN	COMMENT
0.140±0.009 OR FIT	Error includes scale factor of 1.1.				
0.25 ±0.04 ±0.04	57	AMMAR	95	CLE2	$e^+e^- \approx \Upsilon(4S)$

$\Gamma(pK^0_S\pi^+\pi^-)/\Gamma_{total}$ — Γ_{24}/Γ

VALUE (%)	EVTS	DOCUMENT ID		TECN	COMMENT
1.63±0.10 OR FIT	Error includes scale factor of 1.1.				
1.53±0.11±0.09	485	ABLIKIM	16	BES3	$e^+e^- \to \Lambda_c\overline{\Lambda}_c$, 4.599 GeV

$\Gamma(pK^0_L\pi^+\pi^-)/\Gamma_{total}$ — Γ_{25}/Γ

VALUE (%)	EVTS	DOCUMENT ID		TECN	COMMENT
1.69±0.10±0.05	650	[1] ABLIKIM	24CQ	BES3	e^+e^- at 4.600–4.699 GeV

[1] Comparing with the PDG 22 value $B(\Lambda_c^+ \to pK^0_S\pi^+\pi^-) = (1.60 \pm 0.11) \times 10^{-2}$, ABLIKIM 24CQ notes the $K^0_S - K^0_L$ splitting to be -0.027 ± 0.048 in these modes.

$\Gamma(pK^0_S\pi^+\pi^-)/\Gamma(pK^-\pi^+)$ — Γ_{24}/Γ_3

Measurements given as a $\overline{K}^0$ ratio have been divided by 2 to convert to a K^0_S ratio.

VALUE	EVTS	DOCUMENT ID		TECN	COMMENT
0.256±0.014 OR FIT	Error includes scale factor of 1.1.				
0.257±0.031 OR AVERAGE					
0.26 ±0.02 ±0.03	985	ALAM	98	CLE2	$e^+e^- \approx \Upsilon(4S)$
0.22 ±0.06 ±0.02	83	AVERY	91	CLEO	e^+e^- 10.5 GeV
0.49 ±0.18 ±0.04	12	BARLAG	90D	NA32	π^- 230 GeV

$\Gamma(pK^-\pi^+\pi^0)/\Gamma_{total}$ — Γ_{26}/Γ

VALUE (%)	EVTS	DOCUMENT ID		TECN	COMMENT
4.54±0.27 OR FIT	Error includes scale factor of 1.6.				
4.53±0.23±0.30	1849	ABLIKIM	16	BES3	$e^+e^- \to \Lambda_c\overline{\Lambda}_c$, 4.599 GeV

$\Gamma(pK^-\pi^+\pi^0)/\Gamma(pK^-\pi^+)$ — Γ_{26}/Γ_3

VALUE	EVTS	DOCUMENT ID		TECN	COMMENT
0.71 ±0.04 OR FIT	Error includes scale factor of 2.4.				
0.685±0.019 OR AVERAGE					
0.685±0.007±0.018	242k	PAL	17	BELL	$e^+e^- \approx \Upsilon(4S), \Upsilon(5S)$
0.67 ±0.04 ±0.11	2.6k	ALAM	98	CLE2	$e^+e^- \approx \Upsilon(4S)$

$\Gamma(pK^*(892)^-\pi^+)/\Gamma(pK^0_S\pi^+\pi^-)$ — Γ_{27}/Γ_{24}

Unseen decay modes of the $K^*(892)^-$ are included.

VALUE	EVTS	DOCUMENT ID		TECN	COMMENT
0.88±0.28	17	ALEEV	94	BIS2	nN 20–70 GeV

$\Gamma(p(K^-\pi^+)_{nonresonant}\pi^0)/\Gamma(pK^-\pi^+)$ — Γ_{28}/Γ_3

VALUE	EVTS	DOCUMENT ID		TECN	COMMENT
0.73±0.12±0.05	67	BOZEK	93	NA32	π^- Cu 230 GeV

$\Gamma(\Delta(1232)\overline{K}^*(892))/\Gamma_{total}$ — Γ_{29}/Γ

VALUE	EVTS	DOCUMENT ID		TECN	COMMENT
seen	35	AMENDOLIA	87	SPEC	γGe-Si

$\Gamma(pK^-2\pi^+\pi^-)/\Gamma(pK^-\pi^+)$ — Γ_{30}/Γ_3

VALUE	DOCUMENT ID		TECN	COMMENT
0.022±0.015	BARLAG	90D	NA32	π^- 230 GeV

$\Gamma(pK^-\pi^+2\pi^0)/\Gamma(pK^-\pi^+)$ — Γ_{31}/Γ_3

VALUE	EVTS	DOCUMENT ID		TECN	COMMENT
0.16±0.07±0.03	15	BOZEK	93	NA32	π^- Cu 230 GeV

Hadronic modes with a p and n: $S = 0$ final states

$\Gamma(p\pi^0)/\Gamma_{total}$ — Γ_{32}/Γ

VALUE (units 10^{-4})	CL%	EVTS	DOCUMENT ID		TECN	COMMENT
• • • We do not use the following data for averages, fits, limits, etc. • • •						
$1.56^{+0.72}_{-0.58}\pm0.20$		9	[1] ABLIKIM	24BB	BES3	Superseded by ABLIKIM 25AS
<2.7	90		ABLIKIM	17Q	BES3	e^+e^- at 4.6 GeV

[1] ABLIKIM 24BB result based on 6.0 fb^{-1} of e^+e^- collisions at 4.600–4.843 GeV.

$\Gamma(p\pi^0)/\Gamma(p\eta)$ — Γ_{32}/Γ_{34}

VALUE	EVTS	DOCUMENT ID		TECN	COMMENT
0.120±0.026±0.007	80	ABLIKIM	25AS	BES3	4.5 fb^{-1}, e^+e^- at 4.600–4.699 GeV

$\Gamma(p\pi^0)/\Gamma(pK^-\pi^+)$ — Γ_{32}/Γ_3

VALUE	CL%	EVTS	DOCUMENT ID		TECN	COMMENT
$<1.273\times10^{-3}$	90	7.7k	[1] LI	21	BELL	e^+e^- at $\Upsilon(nS)$

[1] Uses $B(\pi^0 \to \gamma\gamma) = 0.9882 \pm 0.0003$.

$\Gamma(n\pi^+)/\Gamma_{total}$ — Γ_{33}/Γ

VALUE (units 10^{-4})	EVTS	DOCUMENT ID		TECN	COMMENT
6.6±1.2±0.4	50	ABLIKIM	22S	BES3	e^+e^- at 4.612–4.699 GeV

$\Gamma(p\eta)/\Gamma_{total}$ — Γ_{34}/Γ

Unseen decay modes of the η are included.

VALUE (units 10^{-3})	EVTS	DOCUMENT ID		TECN	COMMENT
1.49±0.08 OR FIT					
1.57±0.11±0.04	507	[1] ABLIKIM	23CB	BES3	4.5 fb^{-1}, e^+e^- at 4.600–4.699 GeV, $\eta \to 2\gamma$, $\pi^+\pi^0\pi^-$
• • • We do not use the following data for averages, fits, limits, etc. • • •					
1.63±0.31±0.11	35	ABLIKIM	24BB	BES3	6.0 fb^{-1}, e^+e^- at 4.600–4.843 GeV, $\eta \to 2\gamma$
1.24±0.28±0.10	52	ABLIKIM	17Q	BES3	$\eta \to 2\gamma$, $\pi^+\pi^0\pi^-$

[1] ABLIKIM 23CB report a significance of 10σ.

$\Gamma(p\eta)/\Gamma(pK^-\pi^+)$ — Γ_{34}/Γ_3

VALUE (units 10^{-2})	EVTS	DOCUMENT ID		TECN	COMMENT
2.34 ±0.12 OR FIT					
2.258±0.077±0.122	7.7k	[1] LI	21	BELL	e^+e^- at $\Upsilon(nS)$

[1] Uses $B(\eta \to \gamma\gamma) = 0.3941 \pm 0.0020$.

$\Gamma(p\eta)/\Gamma(p\phi)$ — Γ_{34}/Γ_{45}

VALUE	DOCUMENT ID		TECN	COMMENT
1.41±0.18 OR FIT				
1.6 ±0.7 ±0.2	[1] AAIJ	24AI	LHCB	pp at 13 TeV

[1] AAIJ 24AI reports $[\Gamma(\Lambda_c^+ \to p\eta)/\Gamma(\Lambda_c^+ \to p\phi)] \times [B(\eta \to \mu^+\mu^-)] / [B(\phi(1020) \to \mu^+\mu^-)] = 0.032 \pm 0.013 \pm 0.004$ which we multiply or divide by our best (shown rounded) values $B(\eta \to \mu^+\mu^-) = (5.8 \pm 0.8) \times 10^{-6}$, $B(\phi(1020) \to \mu^+\mu^-) = (2.86 \pm 0.22) \times 10^{-4}$. Our first error is their experiment's error and our second error is the systematic error from using our best (shown rounded) values.

$\Gamma(p\eta')/\Gamma_{total}$ — Γ_{35}/Γ

VALUE (units 10^{-4})	EVTS	DOCUMENT ID		TECN	COMMENT
4.9 ±0.9 OR FIT					
$5.62^{+2.46}_{-2.04}\pm0.26$	9	[1] ABLIKIM	22AN	BES3	e^+e^- at 4.600–4.699 GeV

[1] Observed with 3.6 σ statistical significance with 4.5 fb^{-1} of e^+e^- collisions between 4.600 and 4.699 GeV. The η' is reconstructed in the two decay modes $\eta' \to \pi^+\pi^-\eta$ and $\eta' \to \pi^+\pi^-\gamma$, with signal yields $4.9^{+3.2}_{-2.6}$ and $4.3^{+2.6}_{-2.2}$ events, respectively.

$\Gamma(p\eta')/\Gamma(pK^-\pi^+)$ — Γ_{35}/Γ_3

VALUE (units 10^{-3})	DOCUMENT ID		TECN	COMMENT
7.7 ±1.4 OR FIT				
7.54±1.32±0.73	LI	22B	BELL	e^+e^- at $\Upsilon(nS)$

$\Gamma(p\omega(782)^0)/\Gamma_{total}$ — Γ_{36}/Γ

VALUE (units 10^{-4})	EVTS	DOCUMENT ID		TECN	COMMENT
9.0±1.0 OR FIT	Error includes scale factor of 1.2.				
11.1±2.0±0.7	234	[1] ABLIKIM	23CB	BES3	$\omega \to \pi^+\pi^-\pi^0$
• • • We do not use the following data for averages, fits, limits, etc. • • •					
9.4±3.2±2.2	13	AAIJ	18N	LHCB	Seen in $\Lambda_c^+ \to p\mu^+\mu^-$

[1] ABLIKIM 23CB report a significance of 5.7σ.

Int. J. Mod. Phys. A 2026.41. Downloaded from www.worldscientific.com
UNIVERSITY OF CALIFORNIA @ BERKELEY on 09/16/26. Re-use and distribution is strictly not permitted, except for Open Access articles.

$\Gamma(p\omega(782)^0)/\Gamma(pK^-\pi^+)$ — Γ_{36}/Γ_3

VALUE (units 10^{-2})	EVTS	DOCUMENT ID		TECN	COMMENT
1.41±0.15 OUR FIT	Error includes scale factor of 1.1.				
1.32±0.12±0.10	1.8k	[1] LI	21E	BELL	e^+e^- at Υ(nS)

[1] LI 21E reconstructs the $\omega(782)$ via $\omega \to \pi^+\pi^-\pi^0$ and $\pi^0 \to \gamma\gamma$.

$\Gamma(p\omega(782)^0)/\Gamma(p\phi)$ — Γ_{36}/Γ_{45}

VALUE	DOCUMENT ID		TECN	COMMENT
0.85±0.13 OUR FIT	Error includes scale factor of 1.1.			
0.93±0.14±0.24	[1] AAIJ	24AI	LHCB	pp at 13 TeV

[1] AAIJ 24AI reports $[\Gamma(\Lambda_c^+ \to p\omega(782)^0)/\Gamma(\Lambda_c^+ \to p\phi)] \times [B(\omega(782) \to \mu^+\mu^-)] / [B(\phi(1020) \to \mu^+\mu^-)] = 0.240 \pm 0.030 \pm 0.018$ which we multiply or divide by our best (shown rounded) values $B(\omega(782) \to \mu^+\mu^-) = (7.4 \pm 1.8) \times 10^{-5}$, $B(\phi(1020) \to \mu^+\mu^-) = (2.86 \pm 0.22) \times 10^{-4}$. Our first error is their experiment's error and our second error is the systematic error from using our best (shown rounded) values.

$\Gamma(p\pi^+\pi^-)/\Gamma(pK^-\pi^+)$ — Γ_{37}/Γ_3

VALUE (units 10^{-2})	EVTS	DOCUMENT ID		TECN	COMMENT
7.35±0.24 OUR AVERAGE	Error includes scale factor of 1.3.				
7.44±0.08±0.18	20k	AAIJ	18V	LHCB	$\Lambda_b^0 \to \Lambda_c^+\mu^- X$
6.70±0.48±0.25	495	ABLIKIM	16U	BES3	e^+e^- at 4.599 GeV
6.9 ±3.6	5	BARLAG	90D	NA32	π^- 230 GeV

$\Gamma(pf_0(980))/\Gamma(pK^-\pi^+)$ — Γ_{38}/Γ_3

Unseen decay modes of the $f_0(980)$ are included.

VALUE	DOCUMENT ID		TECN	COMMENT
0.055±0.036	BARLAG	90D	NA32	π^- 230 GeV

$\Gamma(p\rho(770)^0)/\Gamma(p\phi)$ — Γ_{39}/Γ_{45}

VALUE	DOCUMENT ID		TECN	COMMENT
1.44±0.35±0.14	[1] AAIJ	24AI	LHCB	pp at 13 TeV

[1] AAIJ 24AI reports $[\Gamma(\Lambda_c^+ \to p\rho(770)^0)/\Gamma(\Lambda_c^+ \to p\phi)] \times [B(\rho(770) \to \mu^+\mu^-)] / [B(\phi(1020) \to \mu^+\mu^-)] = 0.229 \pm 0.051 \pm 0.022$ which we multiply or divide by our best (shown rounded) values $B(\rho(770) \to \mu^+\mu^-) = (4.55 \pm 0.28) \times 10^{-5}$, $B(\phi(1020) \to \mu^+\mu^-) = (2.86 \pm 0.22) \times 10^{-4}$. Our first error is their experiment's error and our second error is the systematic error from using our best (shown rounded) values.

$\Gamma(n\pi^+\pi^0)/\Gamma_{total}$ — Γ_{40}/Γ

VALUE (%)	EVTS	DOCUMENT ID		TECN	COMMENT
0.64±0.09±0.02	150	ABLIKIM	23A	BES	4.5 fb^{-1}, e^+e^- at 4.600–4.699 GeV

$\Gamma(nK^+\pi^0)/\Gamma_{total}$ — Γ_{41}/Γ

VALUE	CL%	DOCUMENT ID		TECN	COMMENT
<7.1 × 10^{-4}	90	ABLIKIM	24AW	BES3	6.1 fb^{-1} at e^+e^-, 4.60–4.84 GeV

$\Gamma(n\pi^+\pi^-\pi^+)/\Gamma_{total}$ — Γ_{42}/Γ

VALUE (%)	EVTS	DOCUMENT ID		TECN	COMMENT
0.45±0.07±0.03	120	ABLIKIM	23A	BES	4.5 fb^{-1}, e^+e^- at 4.600–4.699 GeV

$\Gamma(p2\pi^+2\pi^-)/\Gamma(pK^-\pi^+)$ — Γ_{43}/Γ_3

VALUE	DOCUMENT ID		TECN	COMMENT
0.036±0.023	BARLAG	90D	NA32	π^- 230 GeV

$\Gamma(pK^+K^-)/\Gamma(pK^-\pi^+)$ — Γ_{44}/Γ_3

VALUE (units 10^{-2})	EVTS	DOCUMENT ID		TECN	COMMENT
1.70±0.04 OUR AVERAGE					
1.70±0.03±0.03	3.4k	AAIJ	18V	LHCB	$\Lambda_b^0 \to \Lambda_c^+\mu^- X$
1.4 ±0.2 ±0.2	676	ABE	02C	BELL	$e^+e^- \approx \Upsilon(4S)$
3.9 ±0.9 ±0.7	214	ALEXANDER	96C	CLE2	$e^+e^- \approx \Upsilon(4S)$
• • • We do not use the following data for averages, fits, limits, etc. • • •					
9.6 ±2.9 ±1.0	30	FRABETTI	93H	E687	γBe, $\overline{E}_\gamma$ 220 GeV
4.8 ±2.7		BARLAG	90D	NA32	π^- 230 GeV

$\Gamma(p\phi)/\Gamma(pK^-\pi^+)$ — Γ_{45}/Γ_3

Unseen decay modes of the ϕ are included.

VALUE (units 10^{-2})	EVTS	DOCUMENT ID		TECN	COMMENT
1.66±0.20 OUR FIT					
1.70±0.21 OUR AVERAGE					
1.81±0.33±0.13	44	ABLIKIM	16U	BES3	e^+e^- at 4.599 GeV
1.5 ±0.2 ±0.2	345	ABE	02C	BELL	$e^+e^- \approx \Upsilon(4S)$
2.4 ±0.6 ±0.3	54	ALEXANDER	96C	CLE2	$e^+e^- \approx \Upsilon(4S)$
• • • We do not use the following data for averages, fits, limits, etc. • • •					
4.0 ±2.7		BARLAG	90D	NA32	π^- 230 GeV

$\Gamma(pK^+K^-\text{non-}\phi)/\Gamma(pK^-\pi^+)$ — Γ_{46}/Γ_3

VALUE (units 10^{-3})	EVTS	DOCUMENT ID		TECN	COMMENT
8.4 ±1.8 OUR AVERAGE					
9.36±2.22±0.71	38	ABLIKIM	16U	BES3	e^+e^- at 4.599 GeV
7 ±2 ±2	344	ABE	02C	BELL	$e^+e^- \approx \Upsilon(4S)$

$\Gamma(pK^0_SK^0_S)/\Gamma(pK^0_S)$ — Γ_{47}/Γ_1

VALUE (units 10^{-2})	EVTS	DOCUMENT ID		TECN	COMMENT
1.48±0.08±0.04	2.4k	LI	23B	BELL	$e^+e^- \to \Upsilon$(nS)

$\Gamma(p\phi\pi^0)/\Gamma(pK^-\pi^+)$ — Γ_{48}/Γ_3

VALUE (units 10^{-3})	DOCUMENT ID		TECN	COMMENT
1.538±0.641$^{+0.077}_{-0.100}$	PAL	17	BELL	$e^+e^- \approx \Upsilon(4S), \Upsilon(5S)$

$\Gamma(pK^+K^-\pi^0 \text{ nonresonant})/\Gamma_{total}$ — Γ_{49}/Γ

VALUE	CL%	DOCUMENT ID		TECN	COMMENT
<6.3 × 10^{-5}	90	PAL	17	BELL	$e^+e^- \approx \Upsilon(4S), \Upsilon(5S)$

Hadronic modes with a hyperon: $S = -1$ final states

$\Gamma(\Lambda\pi^+)/\Gamma_{total}$ — Γ_{50}/Γ

VALUE (%)	EVTS	DOCUMENT ID		TECN	COMMENT
1.32±0.05 OUR FIT	Error includes scale factor of 1.1.				
1.27±0.06 OUR AVERAGE					
1.31±0.08±0.05	376	ABLIKIM	22S	BES3	e^+e^- at 4.612–4.699 GeV
1.24±0.07±0.03	706	ABLIKIM	16	BES3	$e^+e^- \to \Lambda_c\overline{\Lambda}_c$, 4.599 GeV

$\Gamma(\Lambda\pi^+)/\Gamma(pK^-\pi^+)$ — Γ_{50}/Γ_3

VALUE	EVTS	DOCUMENT ID		TECN	COMMENT
0.207±0.008 OUR FIT	Error includes scale factor of 1.2.				
0.204±0.019 OUR AVERAGE					
0.217±0.013±0.020	750	LINK	05F	FOCS	γ nucleus, $\overline{E}_\gamma \approx 180$ GeV
0.18 ±0.03 ±0.04		ALBRECHT	92	ARG	$e^+e^- \approx 10.4$ GeV
0.18 ±0.03 ±0.03	87	AVERY	91	CLEO	e^+e^- 10.5 GeV

$\Gamma(\Lambda(1670)\pi^+, \Lambda(1670) \to \eta\Lambda)/\Gamma(pK^-\pi^+)$ — Γ_{51}/Γ_3

VALUE (units 10^{-2})	EVTS	DOCUMENT ID		TECN	COMMENT
5.54±0.29±0.73	9.7k	LEE	21A	BELL	$e^+e^- \approx \Upsilon$(nS)

$\Gamma(\Lambda\pi^+\pi^0)/\Gamma_{total}$ — Γ_{52}/Γ

VALUE (%)	EVTS	DOCUMENT ID		TECN	COMMENT
7.16±0.33 OUR FIT					
7.01±0.37±0.19	1497	ABLIKIM	16	BES3	$e^+e^- \to \Lambda_c\overline{\Lambda}_c$, 4.599 GeV

$\Gamma(\Lambda\pi^+\pi^0)/\Gamma(pK^-\pi^+)$ — Γ_{52}/Γ_3

VALUE	EVTS	DOCUMENT ID		TECN	COMMENT
1.12±0.05 OUR FIT	Error includes scale factor of 1.1.				
0.73±0.09±0.16	464	AVERY	94	CLE2	$e^+e^- \approx \Upsilon(3S), \Upsilon(4S)$

$\Gamma(\Lambda\rho^+)/\Gamma(pK^-\pi^+)$ — Γ_{53}/Γ_3

VALUE	CL%	DOCUMENT ID		TECN	COMMENT
• • • We do not use the following data for averages, fits, limits, etc. • • •					
<0.95	95	AVERY	94	CLE2	$e^+e^- \approx \Upsilon(3S), \Upsilon(4S)$

$\Gamma(\Lambda\rho^+)/\Gamma(\Lambda\pi^+\pi^0)$ — Γ_{53}/Γ_{52}

These results are fit fraction from an amplitude / partial wave analysis.

VALUE (units 10^{-2})	EVTS	DOCUMENT ID		TECN	COMMENT
57.2±4.2±4.9	8.9k	ABLIKIM	22BA	BES3	e^+e^- at 4.6–4.7 GeV

$\Gamma(\Sigma(1385)^+\pi^0, \Sigma^+ \to \Lambda\pi^+)/\Gamma(\Lambda\pi^+\pi^0)$ — Γ_{54}/Γ_{52}

These results are fit fraction from an amplitude / partial wave analysis.

VALUE (units 10^{-2})	EVTS	DOCUMENT ID		TECN	COMMENT
7.18±0.60±0.64	8.9k	ABLIKIM	22BA	BES3	e^+e^- at 4.6–4.7 GeV

$\Gamma(\Sigma(1385)^0\pi^+, \Sigma^0 \to \Lambda\pi^0)/\Gamma(\Lambda\pi^+\pi^0)$ — Γ_{55}/Γ_{52}

These results are fit fraction from an amplitude / partial wave analysis.

VALUE (units 10^{-2})	EVTS	DOCUMENT ID		TECN	COMMENT
7.92±0.72±0.80	8.9k	ABLIKIM	22BA	BES3	e^+e^- at 4.6–4.7 GeV

$\Gamma(\Lambda\pi^-2\pi^+)/\Gamma_{total}$ — Γ_{56}/Γ

VALUE (%)	EVTS	DOCUMENT ID		TECN	COMMENT
3.69±0.26 OUR FIT	Error includes scale factor of 1.5.				
3.81±0.24±0.18	609	ABLIKIM	16	BES3	$e^+e^- \to \Lambda_c\overline{\Lambda}_c$, 4.599 GeV

$\Gamma(\Lambda\pi^-2\pi^+)/\Gamma(pK^-\pi^+)$ — Γ_{56}/Γ_3

VALUE	EVTS	DOCUMENT ID		TECN	COMMENT
0.58 ±0.04 OUR FIT	Error includes scale factor of 1.7.				
0.522±0.032 OUR AVERAGE					
0.508±0.024±0.024	1356	LINK	05F	FOCS	γ nucleus, $\overline{E}_\gamma \approx 180$ GeV
0.65 ±0.11 ±0.12	289	AVERY	91	CLEO	e^+e^- 10.5 GeV
0.82 ±0.29 ±0.27	44	ANJOS	90	E691	γBe 70–260 GeV
0.94 ±0.41 ±0.13	10	BARLAG	90D	NA32	π^- 230 GeV
0.61 ±0.16 ±0.04	105	ALBRECHT	88C	ARG	e^+e^- 10 GeV

$\Gamma(\Sigma(1385)^+\pi^+\pi^-, \Sigma^{*+} \to \Lambda\pi^+)/\Gamma(\Lambda\pi^-2\pi^+)$ — Γ_{57}/Γ_{56}

VALUE	DOCUMENT ID		TECN	COMMENT
0.28±0.10±0.08	LINK	05F	FOCS	γ nucleus, $\overline{E}_\gamma \approx 180$ GeV

Int. J. Mod. Phys. A 2026.41. Downloaded from www.worldscientific.com
by UNIVERSITY OF CALIFORNIA @ BERKELEY on 09/16/26. Re-use and distribution is strictly not permitted, except for Open Access articles.

$\Gamma(\Sigma(1385)^-2\pi^+, \Sigma^{*-} \to \Lambda\pi^-)/\Gamma(\Lambda\pi^-2\pi^+)$ — Γ_{58}/Γ_{56}

VALUE	DOCUMENT ID		TECN	COMMENT
0.21±0.03±0.02	LINK	05F	FOCS	γ nucleus, $\overline{E}_\gamma \approx 180$ GeV

$\Gamma(\Lambda\pi^+\rho^0)/\Gamma(\Lambda\pi^-2\pi^+)$ — Γ_{59}/Γ_{56}

VALUE	DOCUMENT ID		TECN	COMMENT
0.40±0.12±0.12	LINK	05F	FOCS	γ nucleus, $\overline{E}_\gamma \approx 180$ GeV

$\Gamma(\Sigma(1385)^+\rho^0, \Sigma^{*+} \to \Lambda\pi^+)/\Gamma(\Lambda\pi^-2\pi^+)$ — Γ_{60}/Γ_{56}

VALUE	DOCUMENT ID		TECN	COMMENT
0.14±0.09±0.07	LINK	05F	FOCS	γ nucleus, $\overline{E}_\gamma \approx 180$ GeV

$\Gamma(\Lambda\pi^-2\pi^+ \text{nonresonant})/\Gamma(\Lambda\pi^-2\pi^+)$ — Γ_{61}/Γ_{56}

VALUE	CL%	DOCUMENT ID		TECN	COMMENT
<0.3	90	LINK	05F	FOCS	γ nucleus, $\overline{E}_\gamma \approx 180$ GeV

$\Gamma(\Lambda\pi^-\pi^0 2\pi^+ \text{total})/\Gamma(pK^-\pi^+)$ — Γ_{62}/Γ_3

VALUE	EVTS	DOCUMENT ID		TECN	COMMENT
0.36±0.09±0.09	50	[1] CRONIN-HEN.	03	CLE3	$e^+e^- \approx \Upsilon(4S)$

[1] CRONIN-HENNESSY 03 finds this channel to be dominantly $\Lambda\eta\pi^+$ and $\Lambda\omega\pi^+$; see below.

$\Gamma(\Lambda\pi^+\omega)/\Gamma(pK^-\pi^+)$ — Γ_{63}/Γ_3

Unseen decay modes of the ω are included.

VALUE	EVTS	DOCUMENT ID		TECN	COMMENT
0.24±0.06±0.06	32	CRONIN-HEN.	03	CLE3	$e^+e^- \approx \Upsilon(4S)$

$\Gamma(\Lambda\pi^-\pi^0 2\pi^+, \text{no } \eta \text{ or } \omega)/\Gamma(pK^-\pi^+)$ — Γ_{64}/Γ_3

VALUE	CL%	DOCUMENT ID		TECN	COMMENT
<0.13	90	CRONIN-HEN.	03	CLE3	$e^+e^- \approx \Upsilon(4S)$

$\Gamma(\Lambda\pi^+\eta)/\Gamma_{\text{total}}$ — Γ_{65}/Γ

VALUE (units 10^{-2})	EVTS	DOCUMENT ID		TECN	COMMENT
1.92±0.06 OUR FIT					
1.94±0.07±0.01	1.3k	ABLIKIM	25AN	BES3	e^+e^-, 4.600–4.843 GeV
• • • We do not use the following data for averages, fits, limits, etc. • • •					
1.84±0.21±0.15	154	ABLIKIM	19Y	BES3	Superseded by ABLIKIM 25AN

$\Gamma(\Lambda\pi^+\eta)/\Gamma(pK^-\pi^+)$ — Γ_{65}/Γ_3

Unseen decay modes of the η are included.

VALUE	EVTS	DOCUMENT ID		TECN	COMMENT
0.301±0.010 OUR FIT					
0.295±0.014 OUR AVERAGE					
0.293±0.003±0.014	51k	LEE	21A	BELL	$e^+e^- \approx \Upsilon(\text{nS})$
0.41 ±0.17 ±0.10	11	CRONIN-HEN.	03	CLE3	$e^+e^- \approx \Upsilon(4S)$
0.35 ±0.05 ±0.06	116	AMMAR	95	CLE2	$e^+e^- \approx \Upsilon(4S)$

$\Gamma(\Sigma(1385)^+\eta)/\Gamma_{\text{total}}$ — Γ_{66}/Γ

VALUE (units 10^{-2})	EVTS	DOCUMENT ID		TECN	COMMENT
• • • We do not use the following data for averages, fits, limits, etc. • • •					
0.91±0.18±0.09	54	ABLIKIM	19Y	BES3	Superseded by ABLIKIM 25AN

$\Gamma(\Sigma(1385)^+\eta)/\Gamma(\Lambda\pi^+\eta)$ — Γ_{66}/Γ_{65}

VALUE	EVTS	DOCUMENT ID		TECN	COMMENT
0.349±0.031±0.006	1.3k	[1,2] ABLIKIM	25AN	BES3	e^+e^-, 4.600–4.843 GeV

[1] ABLIKIM 25AN reports $[\Gamma(\Lambda_c^+ \to \Sigma(1385)^+\eta)/\Gamma(\Lambda_c^+ \to \Lambda\pi^+\eta)] \times [B(\Sigma(1385) \to \Lambda\pi)] = (30.4 \pm 2.6 \pm 0.7) \times 10^{-2}$ which we divide by our best (shown rounded) value $B(\Sigma(1385) \to \Lambda\pi) = (87.0 \pm 1.5) \times 10^{-2}$. Our first error is their experiment's error and our second error is the systematic error from using our best (shown rounded) value.

[2] Amplitude analysis of $\Lambda_c^+ \to \Lambda\pi^+\eta$ with four components.

$\Gamma(\Sigma(1385)^+\eta)/\Gamma(pK^-\pi^+)$ — Γ_{66}/Γ_3

Unseen decay modes of the $\Sigma(1385)^+$ and η are included.

VALUE	EVTS	DOCUMENT ID		TECN	COMMENT
0.190±0.016 OUR AVERAGE					
0.192±0.006±0.016	29k	LEE	21A	BELL	$e^+e^- \approx \Upsilon(\text{nS})$
0.17 ±0.04 ±0.03	54	AMMAR	95	CLE2	$e^+e^- \approx \Upsilon(4S)$

$\Gamma(\Lambda a_0(980)^+, a_0^+ \to \pi^+\eta)/\Gamma(\Lambda\pi^+\eta)$ — Γ_{67}/Γ_{65}

VALUE (units 10^{-2})	EVTS	DOCUMENT ID		TECN	COMMENT
54.0±8.4±2.6	1.3k	[1] ABLIKIM	25AN	BES3	e^+e^-, 4.600–4.843 GeV

[1] Amplitude analysis of $\Lambda_c^+ \to \Lambda\pi^+\eta$ with four components.

$\Gamma(\Lambda(1670)\pi^+, \Lambda(1670) \to \Lambda\eta)/\Gamma(\Lambda\pi^+\eta)$ — Γ_{68}/Γ_{65}

VALUE (units 10^{-2})	EVTS	DOCUMENT ID		TECN	COMMENT
14.1±2.8±1.2	1.3k	[1] ABLIKIM	25AN	BES3	e^+e^-, 4.600–4.843 GeV

[1] Amplitude analysis of $\Lambda_c^+ \to \Lambda\pi^+\eta$ with four components.

$\Gamma(\Lambda K^+\overline{K}^0)/\Gamma_{\text{total}}$ — Γ_{69}/Γ

VALUE (units 10^{-3})	EVTS	DOCUMENT ID		TECN	COMMENT
5.9 ±0.5 OUR FIT Error includes scale factor of 1.2.					
6.14±0.52±0.26		[1] ABLIKIM	25BN	BES3	e^+e^- at 4.600–4.699 GeV
• • • We do not use the following data for averages, fits, limits, etc. • • •					
6.08±0.60±0.32	0.13k	[2] ABLIKIM	25AR	BES3	e^+e^- at 4.600–4.699 GeV, $\Lambda \to p\pi^-$
6.24±0.92±0.30	68	[3] ABLIKIM	25BN	BES3	e^+e^- at 4.600–4.699 GeV, Λ via m^2_{miss}

[1] ABLIKIM 25BN reports $B(\Lambda_c^+ \to \Lambda K^+ K_S^0) = (3.07 \pm 0.26 \pm 0.13) \times 10^{-3}$, which we have multiplied by 2, as a combination of their result with ABLIKIM 25AR, taking into account a small overlap of the two samples.

[2] ABLIKIM 25AR reports $B(\Lambda_c^+ \to \Lambda K^+ K_S^0) = (3.04 \pm 0.30 \pm 0.16) \times 10^{-3}$, which we have multiplied by 2.

[3] ABLIKIM 25BN reports $B(\Lambda_c^+ \to \Lambda K^+ K_S^0) = (3.12 \pm 0.46 \pm 0.15) \times 10^{-3}$, which we have multiplied by 2.

$\Gamma(\Lambda K^+\overline{K}^0)/\Gamma(pK^-\pi^+)$ — Γ_{69}/Γ_3

VALUE	EVTS	DOCUMENT ID		TECN	COMMENT
0.093±0.007 OUR FIT Error includes scale factor of 1.2.					
0.131±0.020 OUR AVERAGE					
0.142±0.018±0.022	251	LINK	05F	FOCS	γ nucleus, $\overline{E}_\gamma \approx 180$ GeV
0.12 ±0.02 ±0.02	59	AMMAR	95	CLE2	$e^+e^- \approx \Upsilon(4S)$

$\Gamma(\Lambda K^+\overline{K}^0)/\Gamma(\Lambda\pi^+)$ — Γ_{69}/Γ_{50}

VALUE	EVTS	DOCUMENT ID		TECN	COMMENT
0.45 ±0.04 OUR FIT Error includes scale factor of 1.2.					
0.395±0.026±0.036	460 ± 30	AUBERT	07U	BABR	$e^+e^- \approx \Upsilon(4S)$

$\Gamma(\Xi(1690)^0 K^+, \Xi^{*0} \to \Lambda\overline{K}^0)/\Gamma(\Lambda K^+\overline{K}^0)$ — Γ_{70}/Γ_{69}

VALUE	EVTS	DOCUMENT ID		TECN	COMMENT
0.28±0.07 OUR AVERAGE					
0.32±0.10±0.04	84±24	LINK	05F	FOCS	γ nucleus, $\overline{E}_\gamma \approx 180$ GeV
0.26±0.08±0.03	93	ABE	02C	BELL	$e^+e^- \approx \Upsilon(4S)$

$\Gamma(\Sigma^0\pi^+)/\Gamma_{\text{total}}$ — Γ_{71}/Γ

VALUE (%)	EVTS	DOCUMENT ID		TECN	COMMENT
1.29±0.05 OUR FIT Error includes scale factor of 1.1.					
1.25±0.07 OUR AVERAGE					
1.22±0.08±0.07	343	ABLIKIM	22S	BES3	e^+e^- at 4.612–4.699 GeV
1.27±0.08±0.03	522	ABLIKIM	16	BES3	$e^+e^- \to \Lambda_c\overline{\Lambda}_c$, 4.599 GeV

$\Gamma(\Sigma^0\pi^+)/\Gamma(pK^-\pi^+)$ — Γ_{71}/Γ_3

VALUE	EVTS	DOCUMENT ID		TECN	COMMENT
0.203±0.009 OUR FIT Error includes scale factor of 1.1.					
0.20 ±0.04 OUR AVERAGE					
0.21 ±0.02 ±0.04	196	AVERY	94	CLE2	$e^+e^- \approx \Upsilon(3S), \Upsilon(4S)$
0.17 ±0.06 ±0.04		ALBRECHT	92	ARG	$e^+e^- \approx 10.4$ GeV

$\Gamma(\Sigma^0\pi^+)/\Gamma(\Lambda\pi^+)$ — Γ_{71}/Γ_{50}

VALUE	EVTS	DOCUMENT ID		TECN	COMMENT
0.98 ±0.04 OUR FIT					
0.98 ±0.05 OUR AVERAGE					
0.977±0.015±0.051	33k	AUBERT	07U	BABR	$e^+e^- \approx \Upsilon(4S)$
1.09 ±0.11 ±0.19	750	LINK	05F	FOCS	γ nucleus, $\overline{E}_\gamma \approx 180$ GeV

$\Gamma(\Sigma^0\pi^+\eta)/\Gamma(pK^-\pi^+)$ — Γ_{72}/Γ_3

VALUE	EVTS	DOCUMENT ID		TECN	COMMENT
0.120±0.006±0.010	17k	LEE	21A	BELL	$e^+e^- \approx \Upsilon(\text{nS})$

$\Gamma(\Sigma^+\pi^0)/\Gamma_{\text{total}}$ — Γ_{73}/Γ

VALUE (%)	EVTS	DOCUMENT ID		TECN	COMMENT
1.27±0.10 OUR FIT Error includes scale factor of 1.1.					
1.18±0.10±0.03	309	ABLIKIM	16	BES3	$e^+e^- \to \Lambda_c\overline{\Lambda}_c$, 4.599 GeV

$\Gamma(\Sigma^+\pi^0)/\Gamma(pK^-\pi^+)$ — Γ_{73}/Γ_3

VALUE	EVTS	DOCUMENT ID		TECN	COMMENT
0.200±0.015 OUR FIT Error includes scale factor of 1.1.					
0.20 ±0.03 ±0.03	93	KUBOTA	93	CLE2	$e^+e^- \approx \Upsilon(4S)$

$\Gamma(\Sigma^+\eta)/\Gamma(pK^-\pi^+)$ — Γ_{74}/Γ_3

Unseen decay modes of the η are included.

VALUE	EVTS	DOCUMENT ID		TECN	COMMENT
0.11±0.03±0.02	26	AMMAR	95	CLE2	$e^+e^- \approx \Upsilon(4S)$

$\Gamma(\Sigma^+\eta)/\Gamma(\Sigma^+\pi^0)$ — Γ_{74}/Γ_{73}

VALUE	EVTS	DOCUMENT ID		TECN	COMMENT
0.267±0.026 OUR AVERAGE					
0.305±0.046±0.007	122	ABLIKIM	25CO	BES3	e^+e^- at 4.600–4.699 GeV
0.25 ±0.03 ±0.01	700	LI	23A	BELL	e^+e^- at/near $\Upsilon(\text{nS})$, n=1,...,5
• • • We do not use the following data for averages, fits, limits, etc. • • •					
0.35 ±0.16 ±0.02	15	[1] ABLIKIM	19X	BES3	Superseded by ABLIKIM 25CO

[1] ABLIKIM 19X report evidence for the observation of the decay $\Lambda_c^+ \to \Sigma^+\eta$ at 2.5σ significance.

Int. J. Mod. Phys. A 2026.41. Downloaded from www.worldscientific.com
UNIVERSITY OF CALIFORNIA @ BERKELEY on 09/16/26. Re-use and distribution is strictly not permitted, except for Open Access articles.

$\Gamma(\Sigma^+\eta')/\Gamma(\Sigma^+\pi^0)$ — Γ_{75}/Γ_{73}

VALUE	EVTS	DOCUMENT ID		TECN	COMMENT
0.33±0.06±0.02	300	LI	23A	BELL	e^+e^- at/near $\Upsilon(nS)$, n=1,...,5

$\Gamma(\Sigma^+\eta')/\Gamma(\Sigma^+\omega)$ — Γ_{75}/Γ_{82}

VALUE	EVTS	DOCUMENT ID		TECN	COMMENT
0.336±0.094±0.037	22	ABLIKIM	25CO	BES3	e^+e^- at 4.600–4.699 GeV
• • • We do not use the following data for averages, fits, limits, etc. • • •					
0.86 ±0.34 ±0.04	13	[1] ABLIKIM	19X	BES3	Superseded by ABLIKIM 25CO

[1] ABLIKIM 19X report evidence for the observation of the decay $\Lambda_c^+ \to \Sigma^+\eta'$ at 3.2σ significance.

$\Gamma(\Sigma^+\pi^+\pi^-)/\Gamma_{total}$ — Γ_{76}/Γ

VALUE (%)	EVTS	DOCUMENT ID		TECN	COMMENT
4.57±0.18 OUR FIT	Error includes scale factor of 1.1.				
4.25±0.24±0.20	1156	ABLIKIM	16	BES3	$e^+e^- \to \Lambda_c\overline{\Lambda}_c$, 4.599 GeV

$\Gamma(\Sigma^+\pi^+\pi^-)/\Gamma(pK^-\pi^+)$ — Γ_{76}/Γ_3

VALUE	EVTS	DOCUMENT ID		TECN	COMMENT
0.716±0.019 OUR FIT					
0.720±0.024 OUR AVERAGE					
0.719±0.003±0.024	2.7M	BERGER	18	BELL	$e^+e^- \approx \Upsilon(4S)$
0.74 ±0.07 ±0.09	487	KUBOTA	93	CLE2	$e^+e^- \approx \Upsilon(4S)$
• • • We do not use the following data for averages, fits, limits, etc. • • •					
0.72 ±0.14	47 ± 9	VAZQUEZ-JA...08		SELX	Σ^- nucleus, 600 GeV
$0.54\ ^{+0.18}_{-0.15}$	11	BARLAG	92	NA32	π^-Cu 230 GeV

$\Gamma(\Sigma^+\rho^0)/\Gamma(pK^-\pi^+)$ — Γ_{77}/Γ_3

VALUE	CL%	DOCUMENT ID		TECN	COMMENT
<0.27	95	KUBOTA	93	CLE2	$e^+e^- \approx \Upsilon(4S)$

$\Gamma(\Sigma^-2\pi^+)/\Gamma_{total}$ — Γ_{78}/Γ

VALUE (%)	EVTS	DOCUMENT ID		TECN	COMMENT
1.87±0.18 OUR FIT					
1.81±0.17±0.09	161	ABLIKIM	17Y	BES3	e^+e^- at 4.6 GeV

$\Gamma(\Sigma^-2\pi^+)/\Gamma(pK^-\pi^+)$ — Γ_{78}/Γ_3

VALUE	EVTS	DOCUMENT ID		TECN	COMMENT
0.294±0.028 OUR FIT					
0.314±0.067	30 ± 6	VAZQUEZ-JA...08		SELX	Σ^- nucleus, 600 GeV

$\Gamma(\Sigma^-2\pi^+)/\Gamma(\Sigma^+\pi^+\pi^-)$ — Γ_{78}/Γ_{76}

VALUE	EVTS	DOCUMENT ID		TECN	COMMENT
0.41±0.04 OUR FIT					
0.53±0.15±0.07	56	FRABETTI	94E	E687	γBe, $\overline{E}_\gamma$ 220 GeV

$\Gamma(\Sigma^0\pi^+\pi^0)/\Gamma(pK^-\pi^+)$ — Γ_{79}/Γ_3

VALUE	EVTS	DOCUMENT ID		TECN	COMMENT
0.56 ±0.05 OUR AVERAGE	Error includes scale factor of 1.5.				
0.575±0.005±0.036	2.7M	BERGER	18	BELL	$e^+e^- \approx \Upsilon(4S)$
0.36 ±0.09 ±0.10	117	AVERY	94	CLE2	$e^+e^- \approx \Upsilon(3S), \Upsilon(4S)$

$\Gamma(\Sigma^+\pi^0\pi^0)/\Gamma(pK^-\pi^+)$ — Γ_{80}/Γ_3

VALUE	EVTS	DOCUMENT ID		TECN	COMMENT
0.247±0.006±0.019	925k	BERGER	18	BELL	$e^+e^- \approx \Upsilon(4S)$

$\Gamma(\Sigma^0\pi^-2\pi^+)/\Gamma(pK^-\pi^+)$ — Γ_{81}/Γ_3

VALUE	EVTS	DOCUMENT ID		TECN	COMMENT
0.18±0.05 OUR FIT					
0.21±0.05±0.05	90	AVERY	94	CLE2	$e^+e^- \approx \Upsilon(3S), \Upsilon(4S)$

$\Gamma(\Sigma^0\pi^-2\pi^+)/\Gamma(\Lambda\pi^-2\pi^+)$ — Γ_{81}/Γ_{56}

VALUE	EVTS	DOCUMENT ID		TECN	COMMENT
0.31±0.08 OUR FIT					
0.26±0.06±0.09	480	LINK	05F	FOCS	γ nucleus, $\overline{E}_\gamma \approx 180$ GeV

$\Gamma(\Sigma^+\omega)/\Gamma_{total}$ — Γ_{82}/Γ

VALUE (%)	EVTS	DOCUMENT ID		TECN	COMMENT
1.72±0.20 OUR FIT					
1.56±0.20±0.07	157	ABLIKIM	16	BES3	$e^+e^- \to \Lambda_c\overline{\Lambda}_c$, 4.599 GeV

$\Gamma(\Sigma^+\omega)/\Gamma(pK^-\pi^+)$ — Γ_{82}/Γ_3

Unseen decay modes of the ω are included.

VALUE	EVTS	DOCUMENT ID		TECN	COMMENT
0.270±0.030 OUR FIT					
0.54 ±0.13 ±0.06	107	KUBOTA	93	CLE2	$e^+e^- \approx \Upsilon(4S)$

$\Gamma(\Sigma^-\pi^02\pi^+)/\Gamma_{total}$ — Γ_{83}/Γ

VALUE (%)	EVTS	DOCUMENT ID		TECN	COMMENT
2.11±0.33±0.14	88	ABLIKIM	17Y	BES3	e^+e^- at 4.6 GeV

$\Gamma(\Sigma^0K^0_SK^+)/\Gamma_{total}$ — Γ_{84}/Γ

VALUE	CL%	DOCUMENT ID		TECN	COMMENT
<1.28 × 10^{-3}	90	ABLIKIM	25BN	BES3	e^+e^- at 4.600–4.699 GeV, Σ^0 via m^2_{miss}

$\Gamma(\Sigma^+K^+K^-)/\Gamma(pK^-\pi^+)$ — Γ_{85}/Γ_3

VALUE	EVTS	DOCUMENT ID		TECN	COMMENT
0.057±0.005 OUR FIT					
0.070±0.011±0.011	59	AVERY	93	CLE2	$e^+e^- \approx 10.5$ GeV

$\Gamma(\Sigma^+K^+K^-)/\Gamma(\Sigma^+\pi^+\pi^-)$ — Γ_{85}/Γ_{76}

VALUE (units 10^{-2})	EVTS	DOCUMENT ID		TECN	COMMENT
8.0 ±0.7 OUR FIT					
7.8 ±0.7 OUR AVERAGE					
8.38±0.93±0.44	110	ABLIKIM	23BY	BES3	e^+e^- at 4.600–4.699 GeV
7.6 ±0.7 ±0.9	246	ABE	02C	BELL	$e^+e^- \approx \Upsilon(4S)$
7.1 ±1.1 ±1.1	103	LINK	02G	FOCS	γ nucleus, ≈ 180 GeV

$\Gamma(\Sigma^+K^+K^-(\text{non-}\phi))/\Gamma(\Sigma^+\pi^+\pi^-)$ — Γ_{86}/Γ_{76}

VALUE	EVTS	DOCUMENT ID		TECN	COMMENT
• • • We do not use the following data for averages, fits, limits, etc. • • •					
4.38±0.79±0.21	75	[1] ABLIKIM	23BY	BES3	e^+e^- at 4.600–4.699 GeV

[1] We do not include this measurement in our average because it is highly correlated to the relative branching fractions $B(\Lambda_c \to \Sigma^+K^+K^-)$ / $B(\Lambda_c \to \Sigma^+\pi^+\pi^-)$ and $B(\Lambda_c \to \Sigma^+\phi)$ / $B(\Lambda_c \to \Sigma^+\pi^+\pi^-)$ measured in the same analysis (which we do use). Although the measurements are done on the same data, ABLIKIM 23BY do not obtain exactly $B(\Lambda_c \to \Sigma^+\phi)\cdot B(\phi \to K^+K^-)$ / $B(\Lambda_c \to \Sigma^+\pi^+\pi^-) + B(\Lambda_c^+ \to \Sigma^+K^+K^-(\text{non-}\phi))$ / $B(\Lambda_c \to \Sigma^+\pi^+\pi^-) = B(\Lambda_c \to \Sigma^+K^+K^-)$ / $B(\Lambda_c \to \Sigma^+\pi^+\pi^-)$.

$\Gamma(\Sigma^+\phi)/\Gamma(pK^-\pi^+)$ — Γ_{87}/Γ_3

Unseen decay modes of the ϕ are included.

VALUE	EVTS	DOCUMENT ID		TECN	COMMENT
0.063±0.007 OUR FIT					
0.069±0.023±0.016	26	AVERY	93	CLE2	$e^+e^- \approx 10.5$ GeV

$\Gamma(\Sigma^+\phi)/\Gamma(\Sigma^+\pi^+\pi^-)$ — Γ_{87}/Γ_{76}

Unseen decay modes of the ϕ are included.

VALUE (units 10^{-2})	EVTS	DOCUMENT ID		TECN	COMMENT
8.8±1.0 OUR FIT					
8.8±1.0 OUR AVERAGE					
9.2±1.8±0.7	119	ABLIKIM	23BY	BES3	e^+e^- at 4.600–4.699 GeV
8.5±1.2±1.2	129	ABE	02C	BELL	$e^+e^- \approx \Upsilon(4S)$
8.7±1.6±0.6	57	LINK	02G	FOCS	γ nucleus, ≈ 180 GeV

$\Gamma(\Xi(1690)^0K^+, \Xi^{*0} \to \Sigma^+K^-)/\Gamma(\Sigma^+\pi^+\pi^-)$ — Γ_{88}/Γ_{76}

VALUE	EVTS	DOCUMENT ID		TECN	COMMENT
0.023±0.005 OUR AVERAGE					
0.023±0.005±0.005	75	ABE	02C	BELL	$e^+e^- \approx \Upsilon(4S)$
0.022±0.006±0.006	34	LINK	02G	FOCS	γ nucleus, ≈ 180 GeV

$\Gamma(\Sigma^+K^+K^-\text{nonresonant})/\Gamma(\Sigma^+\pi^+\pi^-)$ — Γ_{89}/Γ_{76}

VALUE	CL%	DOCUMENT ID		TECN	COMMENT
<0.018	90	ABE	02C	BELL	$e^+e^- \approx \Upsilon(4S)$
• • • We do not use the following data for averages, fits, limits, etc. • • •					
<0.028	90	LINK	02G	FOCS	γ nucleus, ≈ 180 GeV

$\Gamma(\Xi^0K^+)/\Gamma_{total}$ — Γ_{90}/Γ

VALUE (units 10^{-3})	EVTS	DOCUMENT ID		TECN	COMMENT
5.5 ±0.7 OUR FIT					
5.90±0.86±0.39	68	ABLIKIM	18Y	BES3	e^+e^- at 4.6 GeV

$\Gamma(\Xi^0K^+\pi^0)/\Gamma_{total}$ — Γ_{92}/Γ

VALUE (units 10^{-3})	EVTS	DOCUMENT ID		TECN	COMMENT
7.79±1.46±0.95	79	ABLIKIM	24AW	BES3	6.1 fb^{-1} at e^+e^-, 4.60–4.84 GeV

$\Gamma(\Xi^0K^0_S\pi^+)/\Gamma_{total}$ — Γ_{93}/Γ

VALUE (units 10^{-3})	EVTS	DOCUMENT ID		TECN	COMMENT
3.70±0.60±0.21	13	ABLIKIM	25BN	BES3	e^+e^- at 4.600–4.699 GeV, Ξ^0 via m^2_{miss}

$\Gamma(\Xi^0K^+)/\Gamma(pK^-\pi^+)$ — Γ_{90}/Γ_3

VALUE	EVTS	DOCUMENT ID		TECN	COMMENT
0.087±0.011 OUR FIT					
0.078±0.013±0.013	56	AVERY	93	CLE2	$e^+e^- \approx 10.5$ GeV

$\Gamma(\Xi^-K^+\pi^+)/\Gamma_{total}$ — Γ_{91}/Γ

VALUE (units 10^{-3})	EVTS	DOCUMENT ID		TECN	COMMENT
7.74±0.76±0.54	128	ABLIKIM	24AY	BES3	4.5 fb^{-1}, e^+e^- at 4.600–4.699 GeV

Int. J. Mod. Phys. A 2026.41. Downloaded from www.worldscientific.com
by UNIVERSITY OF CALIFORNIA @ BERKELEY on 09/16/26. Re-use and distribution is strictly not permitted, except for Open Access articles.

$\Gamma(\Xi^- K^+ \pi^+)/\Gamma(p K^- \pi^+)$ — Γ_{91}/Γ_3

VALUE	EVTS	DOCUMENT ID		TECN	COMMENT
0.099±0.008 OUR FIT					
0.098±0.021 OUR AVERAGE		Error includes scale factor of 1.3.			See the ideogram below.
0.14 ±0.03 ±0.02	34	ALBRECHT	95B	ARG	$e^+e^- \approx 10.4$ GeV
0.079±0.013±0.014	60	AVERY	93	CLE2	$e^+e^- \approx 10.5$ GeV
0.15 ±0.04 ±0.03	30	AVERY	91	CLEO	e^+e^- 10.5 GeV

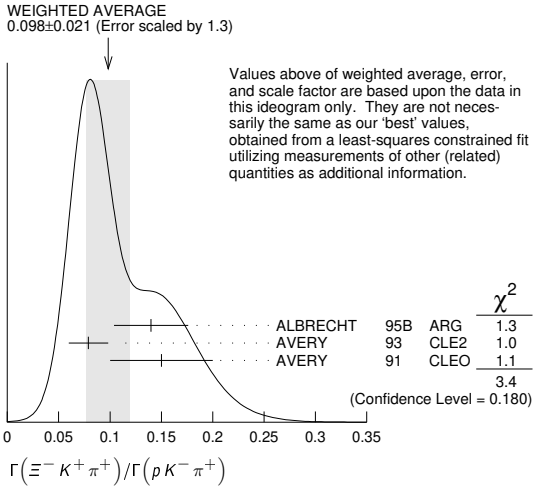

$\Gamma(\Xi^- K^+ \pi^+)/\Gamma(\Lambda \pi^+)$ — Γ_{91}/Γ_{50}

VALUE	EVTS	DOCUMENT ID		TECN	COMMENT
0.48 ±0.04 OUR FIT					
0.480±0.016±0.039	2665 ± 84	AUBERT	07U	BABR	$e^+e^- \approx \Upsilon(4S)$

$\Gamma(\Xi(1530)^0 K^+)/\Gamma_{total}$ — Γ_{94}/Γ

VALUE (units 10^{-3})	EVTS	DOCUMENT ID		TECN	COMMENT
4.9 ±0.6 OUR FIT		Error includes scale factor of 1.1.			
5.4 ±0.6 OUR AVERAGE					
5.99±1.04±0.32		ABLIKIM	24AW	BES3	e^+e^- at 4.60–4.84 GeV, $\Xi(1530) \to \Xi^0\pi^0$
5.03±0.77±0.20	54	ABLIKIM	24AY	BES3	e^+e^- at 4.600–4.699 GeV, $\Xi(1530) \to \Xi^-\pi^+$
• • • We do not use the following data for averages, fits, limits, etc. • • •					
5.02±0.99±0.31	60	ABLIKIM	18Y	BES3	e^+e^- at 4.6 GeV

$\Gamma(\Xi(1530)^0 K^+)/\Gamma(p K^- \pi^+)$ — Γ_{94}/Γ_3

VALUE	EVTS	DOCUMENT ID		TECN	COMMENT
0.077±0.009 OUR FIT					
0.053±0.016±0.010	24	AVERY	93	CLE2	$e^+e^- \approx 10.5$ GeV
• • • We do not use the following data for averages, fits, limits, etc. • • •					
0.05 ±0.02 ±0.01	11	ALBRECHT	95B	ARG	$e^+e^- \approx 10.4$ GeV

Hadronic modes with a hyperon: $S = 0$ final states

$\Gamma(\Lambda K^+)/\Gamma(\Lambda \pi^+)$ — Γ_{95}/Γ_{50}

VALUE (units 10^{-2})	EVTS	DOCUMENT ID		TECN	COMMENT
4.96±0.14 OUR AVERAGE					
5.05±0.13±0.09	11k	LI	23C	BELL	e^+e^- at/near Υ(nS), n=1,...,5
4.78±0.34±0.20		ABLIKIM	22BC	BES3	6.44 fb^{-1}, e^+e^- at 4.599–4.950 GeV
4.4 ±0.4 ±0.3	1.1k	AUBERT	07U	BABR	$e^+e^- \approx \Upsilon(4S)$
• • • We do not use the following data for averages, fits, limits, etc. • • •					
7.4 ±1.0 ±1.2	265	ABE	02C	BELL	$e^+e^- \approx \Upsilon(4S)$

$\Gamma(\Lambda K^+ \pi^+ \pi^-)/\Gamma(\Lambda \pi^+)$ — Γ_{99}/Γ_{50}

VALUE	CL%	DOCUMENT ID		TECN	COMMENT
<4.1 × 10^{-2}	90	AUBERT	07U	BABR	$e^+e^- \approx \Upsilon(4S)$

$\Gamma(\Lambda K^+ \pi^+ \pi^-)/\Gamma(\Lambda \pi^- 2\pi^+)$ — Γ_{99}/Γ_{56}

VALUE (units 10^{-2})	DOCUMENT ID		TECN	COMMENT
1.13±0.41±0.06	ABLIKIM	24AU	BES3	6.4 fb^{-1}, e^+e^- at 4.600–4.950 GeV

$\Gamma(\Lambda K^+ \pi^0)/\Gamma(\Lambda \pi^+ \pi^0)$ — Γ_{96}/Γ_{52}

VALUE (units 10^{-2})	DOCUMENT ID		TECN	COMMENT
2.09±0.39±0.07	ABLIKIM	24AU	BES3	6.4 fb^{-1}, e^+e^- at 4.600–4.950 GeV

$\Gamma(\Lambda K^+ \pi^0)/\Gamma_{total}$ — Γ_{96}/Γ

VALUE	CL%	DOCUMENT ID		TECN	COMMENT
• • • We do not use the following data for averages, fits, limits, etc. • • •					
<2.0 × 10^{-3}	90	ABLIKIM	24AW	BES3	6.1 fb^{-1} at e^+e^-, 4.60–4.84 GeV

$\Gamma(\Lambda K^0_S \pi^+)/\Gamma_{total}$ — Γ_{97}/Γ

VALUE (units 10^{-3})	EVTS	DOCUMENT ID		TECN	COMMENT
1.73±0.26±0.10	0.17k	[1] ABLIKIM	25AR	BES3	e^+e^- at 4.600–4.699 GeV, $\Lambda \to p\pi^-$

[1] ABLIKIM 25AR finds evidence of a $\Lambda_c^+ \to \Lambda K^*(892)^+$ resonant contribution at 4.7σ, and estimates the branching fraction for this intermediate decay under three different interference scenarios.

$\Gamma(\Lambda K^*(892) K^{*+} \to K^0_S \pi^+)/\Gamma_{total}$ — Γ_{98}/Γ

VALUE	EVTS	DOCUMENT ID		TECN	COMMENT
seen	80	[1] ABLIKIM	25AR	BES3	e^+e^- at 4.600–4.699 GeV, $\Lambda \to p\pi^-$

[1] ABLIKIM 25AR finds evidence of a $\Lambda_c^+ \to \Lambda K^*(892)^+$ resonant contribution in $\Lambda_c^+ \to \Lambda K^0_S \pi^+$ at 4.7σ, and estimates the branching fraction for this intermediate decay under three different interference scenarios.

$\Gamma(\Sigma^0 K^+)/\Gamma(\Sigma^0 \pi^+)$ — Γ_{100}/Γ_{71}

VALUE (units 10^{-2})	EVTS	DOCUMENT ID		TECN	COMMENT
2.90±0.21 OUR AVERAGE		Error includes scale factor of 1.4.			See the ideogram below.
2.78±0.15±0.05	2.4k	LI	23C	BELL	e^+e^- at/near Υ(nS), n=1,...,5
3.61±0.73±0.05	43	ABLIKIM	22AK	BES3	e^+e^- at 4.178–4.226 GeV
3.8 ±0.5 ±0.3	366 ± 52	AUBERT	07U	BABR	$e^+e^- \approx \Upsilon(4S)$
5.6 ±1.4 ±0.8	75	ABE	02C	BELL	$e^+e^- \approx \Upsilon(4S)$

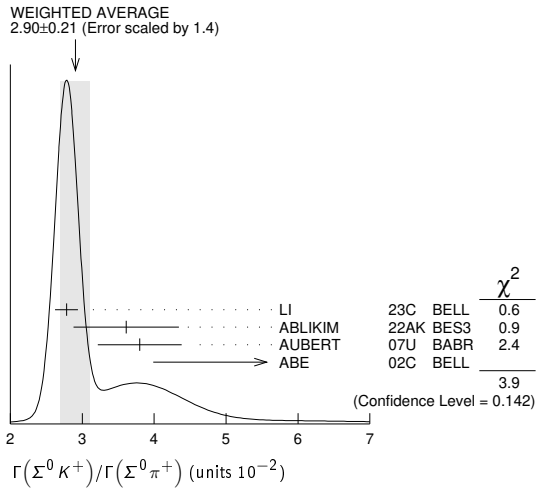

$\Gamma(\Sigma^+ K^0_S)/\Gamma(\Sigma^+ \pi^+ \pi^-)$ — Γ_{101}/Γ_{76}

VALUE (units 10^{-2})	EVTS	DOCUMENT ID		TECN	COMMENT
1.06±0.31±0.04	44	ABLIKIM	22AK	BES3	e^+e^- at 4.178–4.226 GeV

$\Gamma(\Sigma^0 K^+ \pi^0)/\Gamma_{total}$ — Γ_{103}/Γ

VALUE	CL%	DOCUMENT ID		TECN	COMMENT
<5.0 × 10^{-4}	90	[1] ABLIKIM	25BL	BES3	4.5 fb^{-1} e^+e^-, 4.60–4.70 GeV
• • • We do not use the following data for averages, fits, limits, etc. • • •					
<1.8 × 10^{-3}	90	[2] ABLIKIM	24AW	BES3	6.1 fb^{-1} e^+e^-, 4.60–4.84 GeV

[1] Uses a single-tag method.
[2] Uses a double-tag method.

$\Gamma(\Sigma^0 K^+ \pi^+ \pi^-)/\Gamma_{total}$ — Γ_{102}/Γ

VALUE	CL%	DOCUMENT ID		TECN	COMMENT
<6.5 × 10^{-4}	90	ABLIKIM	25BL	BES3	4.5 fb^{-1} e^+e^-, 4.60–4.70 GeV

$\Gamma(\Sigma^0 K^+ \pi^+ \pi^-)/\Gamma(\Sigma^0 \pi^+)$ — Γ_{102}/Γ_{71}

VALUE	CL%	DOCUMENT ID		TECN	COMMENT
<2.0 × 10^{-2}	90	AUBERT	07U	BABR	$e^+e^- \approx \Upsilon(4S)$

$\Gamma(\Sigma^+ K^+ \pi^-)/\Gamma(\Sigma^+ \pi^+ \pi^-)$ — Γ_{104}/Γ_{76}

VALUE (units 10^{-2})	EVTS	DOCUMENT ID		TECN	COMMENT
4.5 ±0.5 OUR AVERAGE					
4.44±0.52±0.25	224	ABLIKIM	23BY	BES3	e^+e^- at 4.600–4.699 GeV
4.7 ±1.1 ±0.8	105	ABE	02C	BELL	$e^+e^- \approx \Upsilon(4S)$

$\Gamma(\Sigma^+ K^*(892)^0)/\Gamma(\Sigma^+ \pi^+ \pi^-)$ — Γ_{105}/Γ_{76}

Unseen decay modes of the $K^*(892)^0$ are included.

VALUE	EVTS	DOCUMENT ID		TECN	COMMENT
0.078±0.018±0.013	49	LINK	02G	FOCS	γ nucleus, ≈ 180 GeV

$\Gamma(\Sigma^+ K^+ \pi^- \pi^0)/\Gamma(\Sigma^+ \pi^+ \pi^-)$ — Γ_{106}/Γ_{76}

VALUE	CL%	DOCUMENT ID		TECN	COMMENT
<2.5 × 10^{-2}	90	ABLIKIM	23BY	BES3	e^+e^- at 4.600–4.699 GeV

Int. J. Mod. Phys. A 2026.41. Downloaded from www.worldscientific.com
UNIVERSITY OF CALIFORNIA @ BERKELEY on 09/16/26. Re-use and distribution is strictly not permitted, except for Open Access articles.

$\Gamma(\Sigma^- K^+ \pi^+)/\Gamma(\Sigma^+ K^*(892)^0)$ — $\Gamma_{107}/\Gamma_{105}$

VALUE	CL%	DOCUMENT ID		TECN	COMMENT
<0.35	90	LINK	02G	FOCS	γ nucleus, ≈ 180 GeV

$\Gamma(\Sigma^- K^+ \pi^+)/\Gamma_{total}$ — Γ_{107}/Γ

VALUE (units 10^{-4})	EVTS	DOCUMENT ID		TECN	COMMENT
3.8±1.2±0.2	12	ABLIKIM	24AY	BES3	4.5 fb^{-1}, e^+e^- at 4.600–4.699 GeV

Doubly Cabibbo-suppressed modes

$\Gamma(pK^+\pi^-)/\Gamma(pK^-\pi^+)$ — Γ_{108}/Γ_3

VALUE (units 10^{-3})	EVTS	DOCUMENT ID		TECN	COMMENT
1.77±0.27 OUR AVERAGE Error includes scale factor of 1.9.					
1.65±0.15±0.05	392	AAIJ	18V	LHCB	$\Lambda_b^0 \to \Lambda_c^+ \mu^- X$
2.35±0.27±0.21	3379	YANG	16	BELL	At or near Υs

Semileptonic modes

$\Gamma(\Lambda e^+ \nu_e)/\Gamma_{total}$ — Γ_{109}/Γ

VALUE (%)	EVTS	DOCUMENT ID		TECN	COMMENT
3.56±0.11±0.07		[1] ABLIKIM	22AT	BES3	4.5 fb^{-1} in e^+e^- at 4.600–4.699 GeV
• • • We do not use the following data for averages, fits, limits, etc. • • •					
3.63±0.38±0.20	104	[2] ABLIKIM	15Y	BES3	567 pb^{-1}, 4.599 GeV

[1] Using Lattice QCD calculations for the form factors yields $|V_{cs}| = 0.936 \pm 0.030$.
[2] Superseded by ABLIKIM 22AT.

$\Gamma(\Lambda e^+ \nu_e)/\Gamma(pK^-\pi^+)$ — Γ_{109}/Γ_3

VALUE	DOCUMENT ID		TECN	COMMENT
• • • We do not use the following data for averages, fits, limits, etc. • • •				
0.43±0.08	[1,2] BERGFELD	94	CLE2	$e^+e^- \approx \Upsilon(4S)$
0.38±0.14	[2,3] ALBRECHT	91G	ARG	$e^+e^- \approx 10.4$ GeV

[1] BERGFELD 94 measures $\sigma(e^+e^- \to \Lambda_c^+ X)\cdot B(\Lambda_c^+ \to \Lambda e^+ \nu_e) = (4.87 \pm 0.28 \pm 0.69)$ pb.
[2] To extract $\Gamma(\Lambda_c^+ \to \Lambda e^+ \nu_e)/\Gamma(\Lambda_c^+ \to pK^-\pi^+)$, we use $\sigma(e^+e^- \to \Lambda_c^+ X)\cdot B(\Lambda_c \to pK^-\pi^+) = (11.2 \pm 1.3)$ pb, which is the weighted average of measurements from ARGUS (ALBRECHT 96E) and CLEO (AVERY 91).
[3] ALBRECHT 91G measures $\sigma(e^+e^- \to \Lambda_c^+ X)\cdot B(\Lambda_c^+ \to \Lambda e^+ \nu_e) = (4.20 \pm 1.28 \pm 0.71)$ pb.

$\Gamma(\Lambda \pi^+ \pi^- e^+ \nu_e)/\Gamma_{total}$ — Γ_{110}/Γ

VALUE	CL%	DOCUMENT ID		TECN	COMMENT
<3.9 × 10^{-4}	90	ABLIKIM	23AB	BES3	4.5 fb^{-1}, e^+e^- at 4.600–4.699 GeV

$\Gamma(pK^- e^+ \nu_e)/\Gamma_{total}$ — Γ_{111}/Γ

VALUE (units 10^{-3})	DOCUMENT ID		TECN	COMMENT
0.88±0.17±0.07	ABLIKIM	22BB	BES	4.5 fb^{-1} in e^+e^- at 4.600–4.699 GeV

$\Gamma(pK^0_S \pi^- e^+ \nu_e)/\Gamma_{total}$ — Γ_{112}/Γ

VALUE	CL%	DOCUMENT ID		TECN	COMMENT
<3.3 × 10^{-4}	90	ABLIKIM	23AB	BES3	4.5 fb^{-1}, e^+e^- at 4.600–4.699 GeV

$\Gamma(\Lambda(1520) e^+ \nu_e)/\Gamma_{total}$ — Γ_{113}/Γ

VALUE (units 10^{-3})	DOCUMENT ID		TECN	COMMENT
1.02±0.52±0.11	[1] ABLIKIM	22BB	BES	4.5 fb^{-1} e^+e^- at 4.600–4.699 GeV

[1] ABLIKIM 22BB reports $B(\Lambda_c^+ \to \Lambda(1520) e^+ \nu_e) \cdot B(\Lambda(1520) \to pK^-) = (2.3 \pm 1.2 \pm 0.2) \times 10^{-4}$, which is divided by the best value for $B(\Lambda(1520) \to pK^-)$ assuming the isospin limit $2 \cdot B(\Lambda(1520) \to pK^-) = B(\Lambda(1520) \to N\overline{K}) = 0.45 \pm 0.01$.

$\Gamma(\Lambda(1405)^0 e^+ \nu_e, \Lambda^0 \to pK^-)/\Gamma_{total}$ — Γ_{114}/Γ

VALUE (units 10^{-3})	DOCUMENT ID		TECN	COMMENT
0.42±0.19±0.04	ABLIKIM	22BB	BES	4.5 fb^{-1} in e^+e^- at 4.600–4.699 GeV

$\Gamma(\Lambda \mu^+ \nu_\mu)/\Gamma_{total}$ — Γ_{115}/Γ

VALUE (%)	EVTS	DOCUMENT ID		TECN	COMMENT
3.48±0.14±0.10	752	ABLIKIM	23AT	BES3	e^+e^- at 4.600–4.699 GeV
• • • We do not use the following data for averages, fits, limits, etc. • • •					
3.49±0.46±0.27	79	[1] ABLIKIM	17D	BES3	e^+e^- at 4.6 GeV

[1] Superseded by ABLIKIM 23AT.

$\Gamma(\Lambda \mu^+ \nu_\mu)/\Gamma(pK^-\pi^+)$ — Γ_{115}/Γ_3

VALUE	DOCUMENT ID		TECN	COMMENT
• • • We do not use the following data for averages, fits, limits, etc. • • •				
0.40±0.09	[1,2] BERGFELD	94	CLE2	$e^+e^- \approx \Upsilon(4S)$
0.35±0.20	[2,3] ALBRECHT	91G	ARG	$e^+e^- \approx 10.4$ GeV

[1] BERGFELD 94 measures $\sigma(e^+e^- \to \Lambda_c^+ X)\cdot B(\Lambda_c^+ \to \Lambda \mu^+ \nu_\mu) = (4.43 \pm 0.51 \pm 0.64)$ pb.
[2] To extract $\Gamma(\Lambda_c^+ \to \Lambda \mu^+ \nu_\mu)/\Gamma(\Lambda_c^+ \to pK^-\pi^+)$, we use $\sigma(e^+e^- \to \Lambda_c^+ X)\cdot B(\Lambda_c \to pK^-\pi^+) = (11.2 \pm 1.3)$ pb, which is the weighted average of measurements from ARGUS (ALBRECHT 96E) and CLEO (AVERY 91).
[3] ALBRECHT 91G measures $\sigma(e^+e^- \to \Lambda_c^+ X)\cdot B(\Lambda_c^+ \to \Lambda \mu^+ \nu_\mu) = (3.91 \pm 2.02 \pm 0.90)$ pb.

$\Gamma(\Lambda \mu^+ \nu_\mu)/\Gamma(\Lambda e^+ \nu_e)$ — $\Gamma_{115}/\Gamma_{109}$

VALUE	DOCUMENT ID		TECN	COMMENT
• • • We do not use the following data for averages, fits, limits, etc. • • •				
0.96±0.16±0.04	[1] ABLIKIM	17D	BES3	e^+e^- at 4.6 GeV

[1] This is the ratio of the ABLIKIM 17D $\Lambda \mu^+ \nu_e$ branching fraction and the ABLIKIM 15Y $\Lambda e^+ \nu_e$ branching fraction (see above), and so is not an independent measurement.

Inclusive modes

$\Gamma(e^+ \text{anything})/\Gamma_{total}$ — Γ_{116}/Γ

VALUE (%)	EVTS	DOCUMENT ID		TECN	COMMENT
4.06±0.10±0.09	4692	ABLIKIM	23AK	BES3	e^+e^- at 4.6–4.698 GeV
• • • We do not use the following data for averages, fits, limits, etc. • • •					
3.95±0.34±0.09	214	[1] ABLIKIM	18AF	BES3	e^+e^- 4.6 GeV

[1] Superseded by ABLIKIM 23AK.

$\Gamma(p \text{ anything})/\Gamma_{total}$ — Γ_{117}/Γ

VALUE	DOCUMENT ID		TECN	COMMENT
0.50±0.08±0.14	[1] CRAWFORD	92	CLEO	e^+e^- 10.5 GeV

[1] This CRAWFORD 92 value includes protons from Λ decay. The value is model dependent, but account is taken of this in the systematic error.

$\Gamma(n \text{ anything})/\Gamma_{total}$ — Γ_{118}/Γ

VALUE (units 10^{-2})	EVTS	DOCUMENT ID		TECN	COMMENT
32.6±1.6 OUR AVERAGE					
32.4±0.7± 1.5	3105	[1] ABLIKIM	23AS	BES3	e^+e^- at 4.6–4.698 GeV
50 ±8 ±14		[2] CRAWFORD	92	CLEO	e^+e^- 10.5 GeV

[1] ABLIKIM 23AS measures the antiparticle decay $\overline{\Lambda}_c^- \to \overline{n}X$.
[2] This CRAWFORD 92 value includes neutrons from Λ decay. The value is model dependent, but account is taken of this in the systematic error.

$\Gamma(\Lambda \text{ anything})/\Gamma_{total}$ — Γ_{119}/Γ

VALUE (%)	EVTS	DOCUMENT ID		TECN	COMMENT
38.2$^{+2.8}_{-2.2}$±0.9	700	ABLIKIM	18E	BES3	e^+e^- at 4.6 GeV

$\Gamma(K^0_S \text{ anything})/\Gamma_{total}$ — Γ_{120}/Γ

VALUE (%)	EVTS	DOCUMENT ID		TECN	COMMENT
10.9±0.2±0.1	4.9k	ABLIKIM	25BH	BES3	e^+e^- at 4.600–4.699 GeV
• • • We do not use the following data for averages, fits, limits, etc. • • •					
9.9±0.6±0.4	478	[1] ABLIKIM	20AJ	BES3	e^+e^- at 4.6 GeV

[1] Superseded by ABLIKIM 25BH.

$\Gamma(3\text{prongs})/\Gamma_{total}$ — Γ_{121}/Γ

VALUE	DOCUMENT ID		TECN	COMMENT
0.24±0.07±0.04	KAYIS-TOPAK.03		CHRS	ν_μ emulsion, $\overline{E}$=27 GeV

Rare or forbidden modes

$\Gamma(pe^+e^-)/\Gamma_{total}$ — Γ_{122}/Γ

A test for the ΔC=1 weak neutral current. Allowed by higher-order electroweak interactions.

VALUE	CL%	EVTS	DOCUMENT ID		TECN	COMMENT
<5.5 × 10^{-6}	90	4.0 ± 7.1	LEES	11G	BABR	$e^+e^- \approx \Upsilon(4S)$

$\Gamma(p\mu^+\mu^- \text{non-resonant})/\Gamma_{total}$ — Γ_{123}/Γ

A test for the ΔC=1 weak neutral current. Allowed by higher-order electroweak interactions.

VALUE	CL%	DOCUMENT ID		TECN	COMMENT
<2.9 × 10^{-8}	90	[1] AAIJ	24AI	LHCB	pp at 13 TeV
• • • We do not use the following data for averages, fits, limits, etc. • • •					
<7.7 × 10^{-8}	90	[2] AAIJ	18N	LHCB	pp at 7,8 TeV
<4.4 × 10^{-5}	90	LEES	11G	BABR	$e^+e^- \approx \Upsilon(4S)$
<3.4 × 10^{-4}	90	KODAMA	95	E653	π^- emulsion 600 GeV

[1] AAIJ 24AI measures $B(\Lambda_c^+ \to p\mu^+\mu^- \text{non-res})/B(\Lambda_c^+ \to p\phi,\ \phi \to \mu^+\mu^-) < 0.09$ (0.10) at 90% (95%) CL corresponding to a limit of 2.9 (3.2) 10^{-8}.
[2] AAIJ 18N measures ratio to $\Lambda_c^+ \to p\phi,\ \phi \to \mu^+\mu^-$.

$\Gamma(pe^+\mu^-)/\Gamma_{total}$ — Γ_{124}/Γ

A test of lepton family-number conservation.

VALUE	CL%	EVTS	DOCUMENT ID		TECN	COMMENT
<9.9 × 10^{-6}	90	−0.7±3.0	LEES	11G	BABR	$e^+e^- \approx \Upsilon(4S)$

$\Gamma(pe^-\mu^+)/\Gamma_{total}$ — Γ_{125}/Γ

A test of lepton family-number conservation.

VALUE	CL%	EVTS	DOCUMENT ID		TECN	COMMENT
<19 × 10^{-6}	90	6.2 ± 4.9	LEES	11G	BABR	$e^+e^- \approx \Upsilon(4S)$

$\Gamma(\overline{p}2e^+)/\Gamma_{total}$ — Γ_{126}/Γ

A test of lepton- and baryon-number conservation.

VALUE	CL%	EVTS	DOCUMENT ID		TECN	COMMENT
<2.7 × 10^{-6}	90	−1.5±4.5	LEES	11G	BABR	$e^+e^- \approx \Upsilon(4S)$

Int. J. Mod. Phys. A 2026.41. Downloaded from www.worldscientific.com
by UNIVERSITY OF CALIFORNIA @ BERKELEY on 09/16/26. Re-use and distribution is strictly not permitted, except for Open Access articles.

$\Gamma(\overline{p}2\mu^+)/\Gamma_{total}$ — Γ_{127}/Γ

A test of lepton- and baryon-number conservation and of lepton family-number conservation.

VALUE	CL%	EVTS	DOCUMENT ID		TECN	COMMENT
$<9.4\times10^{-6}$	90	0.0 ± 2.2	LEES	11G	BABR	$e^+e^-\approx\Upsilon(4S)$

$\Gamma(\overline{p}e^+\mu^+)/\Gamma_{total}$ — Γ_{128}/Γ

A test of lepton- and baryon-number conservation and of lepton family-number conservation.

VALUE	CL%	EVTS	DOCUMENT ID		TECN	COMMENT
$<16\times10^{-6}$	90	10.1 ± 6.8	LEES	11G	BABR	$e^+e^-\approx\Upsilon(4S)$

$\Gamma(\Sigma^-\mu^+\mu^+)/\Gamma_{total}$ — Γ_{129}/Γ

A test of lepton-number conservation.

VALUE	CL%	EVTS	DOCUMENT ID		TECN	COMMENT
$<7.0\times10^{-4}$	90	0	KODAMA	95	E653	π^- emulsion 600 GeV

$\Gamma(\Sigma^+\gamma)/\Gamma_{total}$ — Γ_{130}/Γ

VALUE	CL%	DOCUMENT ID		TECN	COMMENT
$<4.4\times10^{-4}$	90	ABLIKIM	23Z	BES3	e^+e^- at 4.600–4.699 GeV

Radiative modes

$\Gamma(\Sigma^+\gamma)/\Gamma(pK^-\pi^+)$ — Γ_{130}/Γ_3

VALUE	CL%	DOCUMENT ID		TECN	COMMENT
$<4.0\times10^{-3}$	90	LI	23	BELL	$e^+e^-\to\Upsilon(nS)$

Exotic modes

$\Gamma(p\gamma_D)/\Gamma_{total}$ — Γ_{131}/Γ

Here γ_D stands for a dark photon.

VALUE	CL%	DOCUMENT ID		TECN	COMMENT
$<8.0\times10^{-5}$	90	ABLIKIM	22AR	BES	4.5 fb^{-1} e^+e^- at 4.600–4.699 GeV

Λ_c^+ DECAY PARAMETERS

See the review on "Baryon Decay Parameters."

α FOR $\Lambda_c^+\to\Lambda\pi^+$

VALUE	EVTS	DOCUMENT ID		TECN	COMMENT
-0.768 ± 0.015 OUR AVERAGE		Error includes scale factor of 3.4.			
$-0.785\pm0.006\pm0.003$	26k	[1] AAIJ	24AH	LHCB	pp at 13 TeV
$-0.755\pm0.005\pm0.003$	264k	[2] LI	23C	BELL	$e^+e^-\approx\Upsilon(nS)$, n=1,...,5
$-0.80\pm0.11\pm0.02$		ABLIKIM	19AX	BES3	e^+e^- at 4.6 GeV
$-0.78\pm0.16\pm0.19$		LINK	06A	FOCS	γ A, $\overline{E}_\gamma\approx180$ GeV
$-0.94\pm0.21\pm0.12$	414	[3] BISHAI	95	CLE2	$e^+e^-\approx\Upsilon(4S)$
-0.96 ± 0.42		ALBRECHT	92	ARG	$e^+e^-\approx10.4$ GeV
-1.1 ± 0.4	86	AVERY	90B	CLEO	$e^+e^-\approx10.6$ GeV

[1] AAIJ 24AH also reports the measurements of the decay parameters β and γ, the phase difference Δ, the CP asymmetry R_β and the CP average R'_β for $\Lambda_c\to\Lambda\pi$ and its charge-conjugated decay.

[2] LI 23C obtained the value by a fit for the product $\alpha\times\alpha_\Lambda^{avg}$, and dividing by the value $\alpha_\Lambda^{avg}=0.7542\pm0.0026$ reported in ABLIKIM 22AG.

[3] BISHAI 95 actually gives $\alpha=-0.94^{+0.21+0.12}_{-0.06-0.06}$, chopping the errors at the physical limit -1.0. However, for $\alpha\approx-1.0$, some experiments should *get* unphysical values ($\alpha<-1.0$), and for averaging with other measurements such values (or errors that extend below -1.0) should *not* be chopped.

α FOR $\Lambda_c^+\to\Lambda\rho^+$

VALUE	EVTS	DOCUMENT ID		TECN	COMMENT
$-0.763\pm0.053\pm0.045$	8.9k	ABLIKIM	22BA	BES3	e^+e^- at 4.6–4.7 GeV

α FOR $\Lambda_c^+\to\Sigma^+\pi^0$

VALUE	EVTS	DOCUMENT ID		TECN	COMMENT
-0.484 ± 0.027 OUR AVERAGE					
$-0.48\pm0.02\pm0.02$	7k	LI	23A	BELL	e^+e^- at/near $\Upsilon(nS)$, n=1,...,5
$-0.57\pm0.10\pm0.07$		ABLIKIM	19AX	BES3	e^+e^- at 4.6 GeV
$-0.45\pm0.31\pm0.06$	89	BISHAI	95	CLE2	$e^+e^-\approx\Upsilon(4S)$

α FOR $\Lambda_c^+\to\Sigma^+\eta$

VALUE	EVTS	DOCUMENT ID		TECN	COMMENT
$-0.99\pm0.03\pm0.05$	700	LI	23A	BELL	e^+e^- at/near $\Upsilon(nS)$, n=1,...,5

α FOR $\Lambda_c^+\to\Sigma^+\eta'$

VALUE	EVTS	DOCUMENT ID		TECN	COMMENT
$-0.46\pm0.06\pm0.03$	300	LI	23A	BELL	e^+e^- at/near $\Upsilon(nS)$, n=1,...,5

α FOR $\Lambda_c^+\to\Sigma^0\pi^+$

VALUE	EVTS	DOCUMENT ID		TECN	COMMENT
-0.466 ± 0.018 OUR AVERAGE					
$-0.463\pm0.016\pm0.008$	105k	[1] LI	23C	BELL	e^+e^- at/near $\Upsilon(nS)$, n=1,...,5
$-0.73\pm0.17\pm0.07$		ABLIKIM	19AX	BES3	e^+e^- at 4.6 GeV

[1] LI 23C obtained the value by a fit for the product $\alpha\times\alpha_\Lambda^{avg}$, and dividing by the value $\alpha_\Lambda^{avg}=0.7542\pm0.0026$ reported in ABLIKIM 22AG.

α FOR $\Lambda_c^+\to\Sigma(1385)^+\pi^0$

VALUE	EVTS	DOCUMENT ID		TECN	COMMENT
$-0.917\pm0.069\pm0.056$	8.9k	ABLIKIM	22BA	BES3	e^+e^- at 4.6–4.7 GeV

α FOR $\Lambda_c^+\to\Sigma(1385)^0\pi^+$

VALUE	EVTS	DOCUMENT ID		TECN	COMMENT
$-0.789\pm0.098\pm0.056$	8.9k	ABLIKIM	22BA	BES3	e^+e^- at 4.6–4.7 GeV

α FOR $\Lambda_c^+\to\Lambda\ell^+\nu_\ell$

The experiments don't cover the complete (or same incomplete) $M(\Lambda\ell^+)$ range, but we average them together anyway.

VALUE	EVTS	DOCUMENT ID		TECN	COMMENT
-0.875 ± 0.033 OUR AVERAGE					
$-0.94\pm0.07\pm0.03$	752	[1] ABLIKIM	23AT	BES3	e^+e^-, 4.600–4.699 GeV
$-0.86\pm0.03\pm0.02$	3201	[2] HINSON	05	CLEO	$e^+e^-\approx\Upsilon(4S)$
$-0.91\pm0.42\pm0.25$		[3] ALBRECHT	94B	ARG	$e^+e^-\approx10$ GeV
• • • We do not use the following data for averages, fits, limits, etc. • • •					
$-0.82\,^{+0.09}_{-0.06}\,^{+0.06}_{-0.03}$	700	[4] CRAWFORD	95	CLE2	See HINSON 05
$-0.89\,^{+0.17}_{-0.11}\,^{+0.09}_{-0.05}$	350	[5] BERGFELD	94	CLE2	See CRAWFORD 95

[1] ABLIKIM 23AT measures α of $\Lambda_c^+\to\Lambda\mu^+\nu_\mu$ decay over eight q^2 bins from zero to the kinematic endpoint. The value provided here is $\langle\alpha\rangle$, averaged over q^2. The analysis uses form factors extracted from a simultaneous fit to electron and muon mode data.

[2] HINSON 05 measures the form-factor ratio $R\equiv f_2/f_1$ for $\Lambda_c^+\to\Lambda e^+\nu_e$ events to be $-0.31\pm0.05\pm0.04$ and the pole mass to be $2.21\pm0.08\pm0.14$ GeV/c^2, and from these calculates α, averaged over q^2, where $\langle q^2\rangle=0.67$ (GeV/c)^2.

[3] ALBRECHT 94B uses Λe^+ and $\Lambda\mu^+$ events in the mass range $1.85<M(\Lambda\ell^+)<2.20$ GeV.

[4] CRAWFORD 95 measures the form-factor ratio $R\equiv f_2/f_1$ for $\Lambda_c^+\to\Lambda e^+\nu_e$ events to be $-0.25\pm0.14\pm0.08$ and from this calculates α, averaged over q^2, to be the above.

[5] BERGFELD 94 uses Λe^+ events.

α FOR $\Lambda_c^+\to pK_S^0$

VALUE	EVTS	DOCUMENT ID		TECN	COMMENT
$-0.754\pm0.008\pm0.006$	90k	AAIJ	24AH	LHCB	pp at 13 TeV
• • • We do not use the following data for averages, fits, limits, etc. • • •					
$0.18\pm0.43\pm0.14$		ABLIKIM	19AX	BES3	e^+e^- at 4.6 GeV

α FOR $\Lambda_c^+\to\Lambda K^+$

VALUE	EVTS	DOCUMENT ID		TECN	COMMENT
-0.546 ± 0.035 OUR AVERAGE					
$-0.516\pm0.041\pm0.021$	1k	[1] AAIJ	24AH	LHCB	pp at 13 TeV
$-0.585\pm0.049\pm0.018$	11k	[2] LI	23C	BELL	$e^+e^-\approx\Upsilon(nS)$, n=1,...,5

[1] AAIJ 24AH also reports the measurements of the decay parameters β and γ, the phase difference Δ, the CP asymmetry R_β and the CP average R'_β for $\Lambda_c\to\Lambda K$ and its charge-conjugated decay.

[2] LI 23C obtained the value by a fit for the product $\alpha\times\alpha_\Lambda^{avg}$, and dividing by the value $\alpha_\Lambda^{avg}=0.7542\pm0.0026$ reported in ABLIKIM 22AG.

α FOR $\Lambda_c^+\to\Sigma^0K^+$

VALUE	EVTS	DOCUMENT ID		TECN	COMMENT
$-0.54\pm0.18\pm0.09$	2.4k	[1] LI	23C	BELL	e^+e^- at/near $\Upsilon(nS)$, n=1,...,5

[1] LI 23C obtained the value by a fit for the product $\alpha\times\alpha_\Lambda^{avg}$, and dividing by the value $\alpha_\Lambda^{avg}=0.7542\pm0.0026$ reported in ABLIKIM 22AG.

α FOR $\Lambda_c^+\to\Lambda(1405)\pi^+$

The polarization is defined with respect to the daughter baryon momentum in the parent rest frame. See "Baryon Decay Parameters" review.

VALUE	DOCUMENT ID		TECN	COMMENT
$0.58\pm0.05\pm0.01\pm0.28$	[1] AAIJ	23Z	LHCB	1.7fb^{-1}, pp at 13 TeV

[1] AAIJ 23Z uses an amplitude analysis of 400k $\Lambda_c\to pK^-\pi^+$ decays, the last uncertainty is due to the amplitude model. Sign determined per authors; see also AAIJ 23AJ.

α FOR $\Lambda_c^+\to\Lambda(1520)\pi^+$

The polarization is defined with respect to the daughter baryon momentum in the parent rest frame. See "Baryon Decay Parameters" review.

VALUE	DOCUMENT ID		TECN	COMMENT
$0.925\pm0.025\pm0.005\pm0.084$	[1] AAIJ	23Z	LHCB	1.7fb^{-1}, pp at 13 TeV

[1] AAIJ 23Z uses an amplitude analysis of 400k $\Lambda_c\to pK^-\pi^+$ decays, the last uncertainty is due to the amplitude model. Sign determined per authors; see also AAIJ 23AJ.

α FOR $\Lambda_c^+\to\Lambda(1600)\pi^+$

The polarization is defined with respect to the daughter baryon momentum in the parent rest frame. See "Baryon Decay Parameters" review.

VALUE	DOCUMENT ID		TECN	COMMENT
$0.20\pm0.06\pm0.03\pm0.50$	[1] AAIJ	23Z	LHCB	1.7fb^{-1}, pp at 13 TeV

[1] AAIJ 23Z uses an amplitude analysis of 400k $\Lambda_c\to pK^-\pi^+$ decays, the last uncertainty is due to the amplitude model. Sign determined per authors; see also AAIJ 23AJ.

Int. J. Mod. Phys. A 2026.41. Downloaded from www.worldscientific.com
UNIVERSITY OF CALIFORNIA @ BERKELEY on 09/16/26. Re-use and distribution is strictly not permitted, except for Open Access articles.

α FOR $\Lambda_c^+ \to \Lambda(1670)\pi^+$

The polarization is defined with respect to the daughter baryon momentum in the parent rest frame. See "Baryon Decay Parameters" review.

VALUE	DOCUMENT ID		TECN	COMMENT
0.817±0.042±0.006±0.073	[1] AAIJ	23Z	LHCB	1.7fb^{-1}, pp at 13 TeV

[1] AAIJ 23Z uses an amplitude analysis of 400k $\Lambda_c \to pK^-\pi^+$ decays, the last uncertainty is due to the amplitude model. Sign determined per authors; see also AAIJ 23AJ.

α FOR $\Lambda_c^+ \to \Lambda(1690)\pi^+$

The polarization is defined with respect to the daughter baryon momentum in the parent rest frame. See "Baryon Decay Parameters" review.

VALUE	DOCUMENT ID		TECN	COMMENT
0.958±0.020±0.006±0.027	[1] AAIJ	23Z	LHCB	1.7fb^{-1}, pp at 13 TeV

[1] AAIJ 23Z uses an amplitude analysis of 400k $\Lambda_c \to pK^-\pi^+$ decays, the last uncertainty is due to the amplitude model. Sign determined per authors; see also AAIJ 23AJ.

α FOR $\Lambda_c^+ \to \Lambda(2000)\pi^+$

VALUE	DOCUMENT ID		TECN	COMMENT
−0.57±0.03±0.01±0.19	[1] AAIJ	23Z	LHCB	1.7fb^{-1}, pp at 13 TeV

[1] AAIJ 23Z uses an amplitude analysis of 400k $\Lambda_c \to pK^-\pi^+$ decays, the last uncertainty is due to the amplitude model. Sign determined per authors; see also AAIJ 23AJ.

α FOR $\Lambda_c^+ \to \Delta(1232)^{++}K^-$

The polarization is defined with respect to the daughter baryon momentum in the parent rest frame. See "Baryon Decay Parameters" review.

VALUE	DOCUMENT ID		TECN	COMMENT
0.548±0.014±0.004±0.036	[1] AAIJ	23Z	LHCB	1.7fb^{-1}, pp at 13 TeV

[1] AAIJ 23Z uses an amplitude analysis of 400k $\Lambda_c \to pK^-\pi^+$ decays, the last uncertainty is due to the amplitude model. Sign determined per authors; see also AAIJ 23AJ.

α FOR $\Lambda_c^+ \to \Delta(1600)^{++}K^-$

The polarization is defined with respect to the daughter baryon momentum in the parent rest frame. See "Baryon Decay Parameters" review.

VALUE	DOCUMENT ID		TECN	COMMENT
−0.50±0.05±0.01±0.17	[1] AAIJ	23Z	LHCB	1.7fb^{-1}, pp at 13 TeV

[1] AAIJ 23Z uses an amplitude analysis of 400k $\Lambda_c \to pK^-\pi^+$ decays, the last uncertainty is due to the amplitude model. Sign determined per authors; see also AAIJ 23AJ.

α FOR $\Lambda_c^+ \to \Delta(1700)^{++}K^-$

The polarization is defined with respect to the daughter baryon momentum in the parent rest frame. See "Baryon Decay Parameters" review.

VALUE	DOCUMENT ID		TECN	COMMENT
0.216±0.036±0.011±0.075	[1] AAIJ	23Z	LHCB	1.7fb^{-1}, pp at 13 TeV

[1] AAIJ 23Z uses an amplitude analysis of 400k $\Lambda_c \to pK^-\pi^+$ decays, the last uncertainty is due to the amplitude model. Sign determined per authors; see also AAIJ 23AJ.

α FOR $\Lambda_c^+ \to \overline{K}_0^*(700)^0 p$

The polarization is defined with respect to the daughter baryon momentum in the parent rest frame. See "Baryon Decay Parameters" review.

VALUE	DOCUMENT ID		TECN	COMMENT
−0.06±0.66±0.23±0.24	[1] AAIJ	23Z	LHCB	1.7fb^{-1}, pp at 13 TeV

[1] AAIJ 23Z uses an amplitude analysis of 400k $\Lambda_c \to pK^-\pi^+$ decays, the last uncertainty is due to the amplitude model. Sign determined per authors; see also AAIJ 23AJ.

α FOR $\Lambda_c^+ \to \overline{K}_0^*(1430)^0 p$

The polarization is defined with respect to the daughter baryon momentum in the parent rest frame. See "Baryon Decay Parameters" review.

VALUE	DOCUMENT ID		TECN	COMMENT
0.34±0.03±0.01±0.14	[1] AAIJ	23Z	LHCB	1.7fb^{-1}, pp at 13 TeV

[1] AAIJ 23Z uses an amplitude analysis of 400k $\Lambda_c \to pK^-\pi^+$ decays, the last uncertainty is due to the amplitude model. Sign determined per authors; see also AAIJ 23AJ.

α FOR $\Lambda_c^+ \to \Xi^0 K^+$

VALUE	EVTS	DOCUMENT ID		TECN	COMMENT
0.01±0.16±0.03	378	[1] ABLIKIM	24AP	BES3	4.4 fb^{-1}, e^+e^- at 4.60–4.70 GeV

[1] ABLIKIM 24AP report the phase shift between P- and S-wave amplitudes has two solutions, which are $\delta_P - \delta_S = -1.55 \pm 0.25 \pm 0.05$ rad and $1.59 \pm 0.25 \pm 0.05$ rad.

$\Lambda_c^+, \overline{\Lambda}_c^-$ CP-VIOLATING DECAY ASYMMETRIES

$(\alpha+\overline{\alpha})/(\alpha-\overline{\alpha})$ in $\Lambda_c^+ \to \Lambda\pi^+, \overline{\Lambda}_c^- \to \overline{\Lambda}\pi^-$

This is zero if CP is conserved.

VALUE	EVTS	DOCUMENT ID		TECN	COMMENT
0.020±0.016 OUR AVERAGE					
0.020±0.007±0.014	264k	LI	23C	BELL	e^+e^- at/near Υ(nS), n=1,...,5
−0.07 ±0.19 ±0.24		LINK	06A	FOCS	γ A, $E_\gamma \approx$ 180 GeV

$(\alpha+\overline{\alpha})/(\alpha-\overline{\alpha})$ in $\Lambda_c^+ \to \Sigma^0\pi^+, \overline{\Lambda}_c^- \to \overline{\Sigma}^0\pi^-$

VALUE	EVTS	DOCUMENT ID		TECN	COMMENT
−0.023±0.034±0.030	105k	LI	23C	BELL	e^+e^- at/near Υ(nS), n=1,...,5

$(\alpha+\overline{\alpha})/(\alpha-\overline{\alpha})$ in $\Lambda_c^+ \to \Lambda e^+\nu_e, \overline{\Lambda}_c^- \to \overline{\Lambda}e^-\overline{\nu}_e$

This is zero if CP is conserved.

VALUE	DOCUMENT ID		TECN	COMMENT
0.00±0.03±0.02	HINSON	05	CLEO	$e^+e^- \approx \Upsilon(4S)$

$(\alpha+\overline{\alpha})/(\alpha-\overline{\alpha})$ in $\Lambda_c^+ \to \Lambda K^+, \overline{\Lambda}_c^- \to \overline{\Lambda}K^-$

VALUE	EVTS	DOCUMENT ID		TECN	COMMENT
−0.023±0.086±0.071	11k	LI	23C	BELL	e^+e^- at/near Υ(nS), n=1,...,5

$(\alpha+\overline{\alpha})/(\alpha-\overline{\alpha})$ in $\Lambda_c^+ \to \Sigma^0 K^+, \overline{\Lambda}_c^- \to \overline{\Sigma}^0 K^-$

VALUE	EVTS	DOCUMENT ID		TECN	COMMENT
0.08±0.35±0.14	2.4k	LI	23C	BELL	e^+e^- at/near Υ(nS), n=1,...,5

$A_{CP}(\Lambda X)$ in $\Lambda_c \to \Lambda X, \overline{\Lambda}_c \to \overline{\Lambda}X$

VALUE (%)	EVTS	DOCUMENT ID		TECN	COMMENT
$2.1^{+7.0}_{-6.6}\pm1.6$	700	ABLIKIM	18E	BES3	e^+e^- at 4.6 GeV

$A_{CP}(\Lambda K^+)$ in $\Lambda_c \to \Lambda K^+, \overline{\Lambda}_c \to \overline{\Lambda}K^-$

VALUE	EVTS	DOCUMENT ID		TECN	COMMENT
0.021±0.026±0.001	11k	LI	23C	BELL	e^+e^- at/near Υ(nS), n=1,...,5

$A_{CP}(\Sigma^0 K^+)$ in $\Lambda_c \to \Sigma^0 K^+, \overline{\Lambda}_c \to \overline{\Sigma}^0 K^-$

VALUE	EVTS	DOCUMENT ID		TECN	COMMENT
0.025±0.054±0.004	2.4k	LI	23C	BELL	e^+e^- at/near Υ(nS), n=1,...,5

$A_{CP}(p\mu^+\mu^-)$ in $\Lambda_c^+ \to p\mu^+\mu^-, \overline{\Lambda}_c^- \to \overline{p}\mu^+\mu^-$

VALUE (%)	EVTS	DOCUMENT ID		TECN	COMMENT
• • • We do not use the following data for averages, fits, limits, etc. • • •					
−1.1±4.0±0.5	0.78k	[1] AAIJ	25N	LHCB	pp at 13 TeV

[1] AAIJ 25N measures A_{CP} only in the dimuon mass range close to the ϕ resonance, $m_{\mu\mu}$ = 979.46–1059.46 MeV. Also reports, in the same mass range, the CP average and the CP asymmetry of the forward-backward asymmetry in the dimuon system, 3.9 ± 4.0 ± 0.6% and 3.1 ± 4.0 ± 0.4%, respectively.

$\Delta A_{CP} = A_{CP}(\Lambda_c^+ \to pK^+K^-) - A_{CP}(\Lambda_c^+ \to p\pi^+\pi^-)$

VALUE (%)	DOCUMENT ID		TECN	COMMENT
0.30±0.91±0.61	[1] AAIJ	18R	LHCB	pp 7, 8 TeV

[1] AAIJ 18R applies phase-space-dependent weights to the $\Lambda_c^+ \to p\pi^+\pi^-$ sample to align its kinematics with the $\Lambda_c^+ \to pK^+K^-$ sample.

Λ_c^+ REFERENCES

We have omitted some papers that have been superseded by later experiments. The omitted papers may be found in our 1992 edition (Physical Review **D45**, 1 June, Part II) or in earlier editions.

AAIJ	25N	PR D111 L091102	R. Aaij *et al.*	(LHCb Collab.)
ABLIKIM	25AN	PRL 134 021901	M. Ablikim *et al.*	(BESIII Collab.)
ABLIKIM	25AR	PR D111 012014	M. Ablikim *et al.*	(BESIII Collab.)
ABLIKIM	25AS	PR D111 L051101	M. Ablikim *et al.*	(BESIII Collab.)
ABLIKIM	25BH	JHEP 2506 194	M. Ablikim *et al.*	(BESIII Collab.)
ABLIKIM	25BL	CP C49 073001	M. Ablikim *et al.*	(BESIII Collab.)
ABLIKIM	25BN	PR D112 032006	M. Ablikim *et al.*	(BESIII Collab.)
ABLIKIM	25CO	JHEP 2511 067	M. Ablikim *et al.*	(BESIII Collab.)
ADACHI	25L	PR D112 012013	I. Adachi *et al.*	(BELLE and BELLEII Collab.)
AAIJ	24AH	PRL 133 261804	R. Aaij *et al.*	(LHCb Collab.)
AAIJ	24AI	PR D110 052007	R. Aaij *et al.*	(LHCb Collab.)
ABLIKIM	24AP	PRL 132 031801	M. Ablikim *et al.*	(BESIII Collab.)
ABLIKIM	24AU	PR D109 032003	M. Ablikim *et al.*	(BESIII Collab.)
ABLIKIM	24AW	PR D109 052001	M. Ablikim *et al.*	(BESIII Collab.)
ABLIKIM	24AX	PR D109 053005	M. Ablikim *et al.*	(BESIII Collab.)
ABLIKIM	24AY	PR D109 L071103	M. Ablikim *et al.*	(BESIII Collab.)
ABLIKIM	24BA	PR D109 072010	M. Ablikim *et al.*	(BESIII Collab.)
ABLIKIM	24BB	PR D109 L091101	M. Ablikim *et al.*	(BESIII Collab.)
ABLIKIM	24CQ	JHEP 2409 007	M. Ablikim *et al.*	(BESIII Collab.)
AAIJ	23AJ	JHEP 2307 228	R. Aaij *et al.*	(LHCb Collab.)
AAIJ	23Z	PR D108 012023	R. Aaij *et al.*	(LHCb Collab.)
ABLIKIM	23A	CP C47 023001	M. Ablikim *et al.*	(BESIII Collab.)
ABLIKIM	23AB	PL B843 137993	M. Ablikim *et al.*	(BESIII Collab.)
ABLIKIM	23AK	PR D107 052005	M. Ablikim *et al.*	(BESIII Collab.)
ABLIKIM	23AS	PR D108 L031101	M. Ablikim *et al.*	(BESIII Collab.)
ABLIKIM	23AT	PR D108 L031105	M. Ablikim *et al.*	(BESIII Collab.)
ABLIKIM	23BY	JHEP 2309 125	M. Ablikim *et al.*	(BESIII Collab.)
ABLIKIM	23CB	JHEP 2311 137	M. Ablikim *et al.*	(BESIII Collab.)
ABLIKIM	23Z	PR D107 052002	M. Ablikim *et al.*	(BESIII Collab.)
ABUDINEN	23A	PRL 130 071802	F. Abudinen *et al.*	(BELLE II Collab.)
LI	23	PR D107 032001	Y. Li *et al.*	(BELLE Collab.)
LI	23A	PR D107 032003	S.X. Li *et al.*	(BELLE Collab.)
LI	23B	PR D107 032004	L.K. Li *et al.*	(BELLE Collab.)
LI	23C	SCIB 68 583	L.K. Li *et al.*	(BELLE Collab.)
ABLIKIM	22AG	PRL 129 131801	M. Ablikim *et al.*	(BESIII Collab.)
ABLIKIM	22AK	PR D106 052003	M. Ablikim *et al.*	(BESIII Collab.)
ABLIKIM	22AN	PR D106 072002	M. Ablikim *et al.*	(BESIII Collab.)
ABLIKIM	22AR	PR D106 072008	M. Ablikim *et al.*	(BESIII Collab.)
ABLIKIM	22AT	PRL 129 231803	M. Ablikim *et al.*	(BESIII Collab.)
ABLIKIM	22BA	JHEP 2212 033	M. Ablikim *et al.*	(BESIII Collab.)
ABLIKIM	22BB	PR D106 112010	M. Ablikim *et al.*	(BESIII Collab.)
ABLIKIM	22BC	PR D106 L111101	M. Ablikim *et al.*	(BESIII Collab.)
ABLIKIM	22S	PRL 128 142001	M. Ablikim *et al.*	(BESIII Collab.)
LI	22B	JHEP 2203 090	S.X. Li *et al.*	(BELLE Collab.)
PDG	22	PTEP 2022 083C01	R.L. Workman *et al.*	(PDG Collab.)
ABLIKIM	21H	PL B817 136327	M. Ablikim *et al.*	(BESIII Collab.)
ABLIKIM	21N	PR D103 L091101	M. Ablikim *et al.*	(BESIII Collab.) J
LEE	21A	PR D103 052005	J.Y. Lee *et al.*	(BELLE Collab.)
LI	21	PR D103 072004	S.X. Li *et al.*	(BELLE Collab.)
LI	21E	PR D104 072008	S.X. Li *et al.*	(BELLE Collab.)
ABLIKIM	20AJ	EPJ C80 935	M. Ablikim *et al.*	(BESIII Collab.)
AAIJ	19AG	PR D100 032001	R. Aaij *et al.*	(LHCb Collab.)
ABLIKIM	19AX	PR D100 072004	M. Ablikim *et al.*	(BESIII Collab.)
ABLIKIM	19X	CP C43 083002	M. Ablikim *et al.*	(BESIII Collab.)
ABLIKIM	19Y	PR D99 032010	M. Ablikim *et al.*	(BESIII Collab.)
AAIJ	18N	PR D97 091101	R. Aaij *et al.*	(LHCb Collab.)

Int. J. Mod. Phys. A 2026.41. Downloaded from www.worldscientific.com
by UNIVERSITY OF CALIFORNIA @ BERKELEY on 09/16/26. Re-use and distribution is strictly not permitted, except for Open Access articles.

AAIJ	18R	JHEP 1803 182	R. Aaij *et al.*	(LHCb Collab.)
AAIJ	18V	JHEP 1803 043	R. Aaij *et al.*	(LHCb Collab.)
ABLIKIM	18AF	PRL 121 251801	M. Ablikim *et al.*	(BESIII Collab.)
ABLIKIM	18E	PRL 121 062003	M. Ablikim *et al.*	(BESIII Collab.)
ABLIKIM	18Y	PL B783 200	M. Ablikim *et al.*	(BESIII Collab.)
BERGER	18	PR D98 112006	M. Berger *et al.*	(BELLE Collab.)
ABLIKIM	17D	PL B767 42	M. Ablikim *et al.*	(BESIII Collab.)
ABLIKIM	17H	PRL 118 112001	M. Ablikim *et al.*	(BESIII Collab.)
ABLIKIM	17Q	PR D95 111102	M. Ablikim *et al.*	(BESIII Collab.)
ABLIKIM	17Y	PL B772 388	M. Ablikim *et al.*	(BESIII Collab.)
PAL	17	PR D96 051102	B. Pal *et al.*	(BELLE Collab.)
ABLIKIM	16	PRL 116 052001	M. Ablikim *et al.*	(BESIII Collab.)
ABLIKIM	16U	PRL 117 232002	M. Ablikim *et al.*	(BESIII Collab.)
YANG	16	PRL 117 011801	S.B. Yang *et al.*	(BELLE Collab.)
ABLIKIM	15Y	PRL 115 221805	M. Ablikim *et al.*	(BESIII Collab.)
ZUPANC	14	PRL 113 042002	A. Zupanc *et al.*	(BELLE Collab.)
LEES	11G	PR D84 072006	J.P. Lees *et al.*	(BABAR Collab.)
VAZQUEZ-JA...	08	PL B666 299	E. Vazquez-Jauregui *et al.*	(SELEX Collab.)
AUBERT	07U	PR D75 052002	B. Aubert *et al.*	(BABAR Collab.)
LINK	06A	PL B634 165	J.M. Link *et al.*	(FNAL FOCUS Collab.)
AUBERT,B	05S	PR D72 052006	B. Aubert *et al.*	(BABAR Collab.)
HINSON	05	PRL 94 191801	J.W. Hinson *et al.*	(CLEO Collab.)
LINK	05F	PL B624 22	J.M. Link *et al.*	(FNAL FOCUS Collab.)
CRONIN-HEN...	03	PR D67 012001	D. Cronin-Hennessy *et al.*	(CLEO Collab.)
KAYIS-TOPAK...	03	PL B555 156	A. Kayis-Topaksu *et al.*	(CERN CHORUS Collab.)
ABE	02C	PL B524 33	K. Abe *et al.*	(KEK BELLE Collab.)
LINK	02C	PRL 88 161801	J.M. Link *et al.*	(FNAL FOCUS Collab.)
LINK	02G	PL B540 25	J.M. Link *et al.*	(FNAL FOCUS Collab.)
PDG	02	PR D66 010001	K. Hagiwara *et al.*	(PDG Collab.)
KUSHNIR...	01	PRL 86 5243	A. Kushnirenko *et al.*	(FNAL SELEX Collab.)
MAHMOOD	01	PRL 86 2232	A.H. Mahmood *et al.*	(CLEO Collab.)
AITALA	00	PL B471 449	E.M. Aitala *et al.*	(FNAL E791 Collab.)
ALAM	98	PR D57 4467	M.S. Alam *et al.*	(CLEO Collab.)
ALBRECHT	96E	PRPL 276 223	H. Albrecht *et al.*	(ARGUS Collab.)
ALEXANDER	96C	PR D53 1013	J.P. Alexander *et al.*	(CLEO Collab.)
ALBRECHT	95B	PL B342 397	H. Albrecht *et al.*	(ARGUS Collab.)
AMMAR	95	PRL 74 3534	R. Ammar *et al.*	(CLEO Collab.)
BISHAI	95	PL B350 256	M. Bishai *et al.*	(CLEO Collab.)
CRAWFORD	95	PRL 75 624	G. Crawford *et al.*	(CLEO Collab.)
KODAMA	95	PL B345 85	K. Kodama *et al.*	(FNAL E653 Collab.)
ALBRECHT	94B	PL B326 320	H. Albrecht *et al.*	(ARGUS Collab.)
ALEEV	94	PAN 57 1370	A.N. Aleev *et al.*	(Serpukhov BIS-2 Collab.)
		Translated from YF 57 1443.		
AVERY	94	PL B325 257	P. Avery *et al.*	(CLEO Collab.)
BERGFELD	94	PL B323 219	T. Bergfeld *et al.*	(CLEO Collab.)
FRABETTI	94E	PL B328 193	P.L. Frabetti *et al.*	(FNAL E687 Collab.)
AVERY	93	PRL 71 2391	P. Avery *et al.*	(CLEO Collab.)
BOZEK	93	PL B312 247	A. Bozek *et al.*	(CERN NA32 Collab.)
FRABETTI	93D	PRL 70 1755	P.L. Frabetti *et al.*	(FNAL E687 Collab.)
FRABETTI	93H	PL B314 477	P.L. Frabetti *et al.*	(FNAL E687 Collab.)
KUBOTA	93	PRL 71 3255	Y. Kubota *et al.*	(CLEO Collab.)
ALBRECHT	92	PL B274 239	H. Albrecht *et al.*	(ARGUS Collab.)
BARLAG	92	PL B283 465	S. Barlag *et al.*	(ACCMOR Collab.)
CRAWFORD	92	PR D45 752	G. Crawford *et al.*	(CLEO Collab.)
JEZABEK	92	PL B286 175	M. Jezabek, K. Rybicki, R. Rylko	(CRAC)
ALBRECHT	91G	PL B269 234	H. Albrecht *et al.*	(ARGUS Collab.)
AVERY	91	PR D43 3599	P. Avery *et al.*	(CLEO Collab.)
ALVAREZ	90	ZPHY C47 539	M.P. Alvarez *et al.*	(CERN NA14/2 Collab.)
ALVAREZ	90B	PL B246 256	M.P. Alvarez *et al.*	(CERN NA14/2 Collab.)
ANJOS	90	PR D41 801	J.C. Anjos *et al.*	(FNAL E691 Collab.)
AVERY	90B	PRL 65 2842	P. Avery *et al.*	(CLEO Collab.)
BARLAG	90D	ZPHY C48 29	S. Barlag *et al.*	(ACCMOR Collab.)
FRABETTI	90	PL B251 639	P.L. Frabetti *et al.*	(FNAL E687 Collab.)
BARLAG	89	PL B218 374	S. Barlag *et al.*	(ACCMOR Collab.)
AGUILAR-...	88B	ZPHY C40 321	M. Aguilar-Benitez *et al.*	(LEBC-EHS Collab.)
Also		PL B189 254	M. Aguilar-Benitez *et al.*	(LEBC-EHS Collab.)
Also		PL B199 462	M. Aguilar-Benitez *et al.*	(LEBC-EHS Collab.)
Also		SJNP 48 833	M. Begalli *et al.*	(LEBC-EHS Collab.)
		Translated from YAF 48 1310.		
ALBRECHT	88C	PL B207 109	H. Albrecht *et al.*	(ARGUS Collab.)
ANJOS	88B	PRL 60 1379	J.C. Anjos *et al.*	(FNAL E691 Collab.)
AMENDOLIA	87	ZPHY C36 513	S.R. Amendolia *et al.*	(CERN NA1 Collab.)
JONES	87	ZPHY C36 593	G.T. Jones *et al.*	(CERN WA21 Collab.)
BOSETTI	82	PL 109B 234	P.C. Bosetti *et al.*	(AACH3, BONN, CERN+)
BASILE	81B	NC 62A 14	M. Basile *et al.*	(CERN, BGNA, PGIA, FRAS)
CALICCHIO	80	PL 93B 521	M. Calicchio *et al.*	(BARI, BIRM, BRUX+)

OTHER RELATED PAPERS

MIGLIOZZI	99	PL B462 217	P. Migliozzi *et al.*	
DUNIETZ	98	PR D58 094010	I. Dunietz	

$\Lambda_c(2595)^+$

$I(J^P) = 0(\frac{1}{2}^-)$ Status: ***

The $\Lambda_c^+\pi^+\pi^-$ mode is largely, and perhaps entirely, $\Sigma_c\pi$, which is just at threshold; since the Σ_c has $J^P = 1/2^+$, the J^P here is almost certainly $1/2^-$. This result is in accord with the theoretical expectation that this is the charm counterpart of the strange $\Lambda(1405)$.

$\Lambda_c(2595)^+$ MASS

The mass is obtained from the $\Lambda_c(2595)^+$–Λ_c^+ mass-difference measurements below.

VALUE (MeV)	DOCUMENT ID
2592.25±0.28 OUR FIT	

$\Lambda_c(2595)^+ - \Lambda_c^+$ MASS DIFFERENCE

VALUE (MeV)	EVTS	DOCUMENT ID		TECN	COMMENT
305.79±0.24 OUR FIT					
305.79±0.14±0.20	3.5k	AALTONEN	11H	CDF	$p\overline{p}$ at 1.96 TeV
• • • We do not use the following data for averages, fits, limits, etc. • • •					
305.6 ±0.3		[1] BLECHMAN	03		Threshold shift
309.7 ±0.9 ±0.4	19	ALBRECHT	97	ARG	$e^+e^- \approx$ 10 GeV
309.2 ±0.7 ±0.3	14 ± 4.5	FRABETTI	96	E687	γBe, $\overline{E}_\gamma \approx$ 220 GeV
307.5 ±0.4 ±1.0	112 ± 17	EDWARDS	95	CLE2	$e^+e^- \approx$ 10.5 GeV

[1] BLECHMAN 03 finds that a more sophisticated treatment than a simple Breit-Wigner for the proximity of the threshold of the dominant decay, $\Sigma_c(2455)\pi$, lowers the $\Lambda_c(2595)^+ - \Lambda_c^+$ mass difference by 2 or 3 MeV. The analysis of AALTONEN 11H bears this out.

$\Lambda_c(2595)^+$ WIDTH

VALUE (MeV)	EVTS	DOCUMENT ID		TECN	COMMENT
2.59±0.30±0.47	3.5k	[1] AALTONEN	11H	CDF	$p\overline{p}$ at 1.96 TeV
• • • We do not use the following data for averages, fits, limits, etc. • • •					
$2.9\ ^{+2.9}_{-2.1}\ ^{+1.8}_{-1.4}$	19	ALBRECHT	97	ARG	$e^+e^- \approx$ 10 GeV
$3.9\ ^{+1.4}_{-1.2}\ ^{+2.0}_{-1.0}$	112 ± 17	EDWARDS	95	CLE2	$e^+e^- \approx$ 10.5 GeV

[1] AALTONEN 11H treats the three charged modes $\Lambda_c(2595)^+ \to \Sigma_c(2455)^{++}\pi^-$, $\Sigma_c(2455)^+\pi^0$, $\Sigma_c(2455)^0\pi^+$ separately in terms of a common coupling constant h_2 and obtains $h_2^2 = 0.36 \pm 0.08$. From this the width is determined.

$\Lambda_c(2595)^+$ DECAY MODES

$\Lambda_c^+\pi\pi$ and its submode $\Sigma_c(2455)\pi$ — the latter just barely — are the only strong decays allowed for an excited Λ_c^+ having this mass; and the submode seems to dominate.

	Mode		Fraction (Γ_i/Γ)	Confidence level
Γ_1	$\Lambda_c^+\pi^+\pi^-$	[a]	(40±14) %	
Γ_2	$\Sigma_c(2455)^{++}\pi^-$		(15± 6) %	
Γ_3	$\Sigma_c(2455)^0\pi^+$		(15± 6) %	
Γ_4	$\Lambda_c^+\pi^+\pi^-$ 3-body			
Γ_5	$\Lambda_c^+\pi^0\pi^0$	[a]	(60±14) %	
Γ_6	$\Lambda_c^+\pi^0$	[b]	< 140 %	90%
Γ_7	$\Lambda_c^+\gamma$		< 40 %	90%

[a] See AALTONEN 11H, Fig. 8, for the calculated ratio of $\Lambda_c^+\pi^0\pi^0$ and $\Lambda_c^+\pi^+\pi^-$ partial widths as a function of the $\Lambda_c(2595)^+ - \Lambda_c^+$ mass difference. At our value of the mass difference, the predicted ratio is about 4. Using the measured value of $\Lambda_c^+\pi^0\pi^0$ branching fraction and assuming the $\Lambda_c\pi\pi$ branching fractions sum to unity, we derive the $\Lambda_c\pi^+\pi^-$ branching fraction. The derived ratio of the $\Lambda_c\pi^0\pi^0$ to $\Lambda_c\pi^+\pi^-$ partial widths is correspondingly 1.5 ± 0.2.

[b] A test that the isospin is indeed 0, so that the particle is indeed a Λ_c^+.

CONSTRAINED FIT INFORMATION

An overall fit to a branching ratio uses 1 measurements and one constraint to determine 2 parameters. The overall fit has a χ^2 = 0.0 for 0 degrees of freedom.

The following *off-diagonal* array elements are the correlation coefficients $\langle \delta x_i \delta x_j \rangle / (\delta x_i \cdot \delta x_j)$, in percent, from the fit to the branching fractions, $x_i \equiv \Gamma_i/\Gamma_{total}$. The fit constrains the x_i whose labels appear in this array to sum to one.

x_5 | −100
x_1

$\Lambda_c(2595)^+$ BRANCHING RATIOS

$\Gamma(\Lambda_c^+\pi^+\pi^-)/\Gamma_{total}$ — Γ_1/Γ

VALUE	CL%	DOCUMENT ID		TECN	COMMENT
0.41±0.14 OUR FIT					
• • • We do not use the following data for averages, fits, limits, etc. • • •					
<0.85	90	ABLIKIM	24BC	BES3	e^+e^- at 4.918 , 4.950 GeV

$\Gamma(\Sigma_c(2455)^{++}\pi^-)/\Gamma(\Lambda_c^+\pi^+\pi^-)$ — Γ_2/Γ_1

VALUE	DOCUMENT ID		TECN	COMMENT
0.36±0.10 OUR AVERAGE				
0.37±0.12±0.13	ALBRECHT	97	ARG	$e^+e^- \approx$ 10 GeV
0.36±0.09±0.09	EDWARDS	95	CLE2	$e^+e^- \approx$ 10.5 GeV

$\Gamma(\Sigma_c(2455)^0\pi^+)/\Gamma(\Lambda_c^+\pi^+\pi^-)$ — Γ_3/Γ_1

VALUE	DOCUMENT ID		TECN	COMMENT
0.37±0.10 OUR AVERAGE				
0.29±0.10±0.11	ALBRECHT	97	ARG	$e^+e^- \approx$ 10 GeV
0.42±0.09±0.09	EDWARDS	95	CLE2	$e^+e^- \approx$ 10.5 GeV

Int. J. Mod. Phys. A 2026.41. Downloaded from www.worldscientific.com
UNIVERSITY OF CALIFORNIA @ BERKELEY on 09/16/26. Re-use and distribution is strictly not permitted, except for Open Access articles.

$[\Gamma(\Sigma_c(2455)^{++}\pi^-) + \Gamma(\Sigma_c(2455)^0\pi^+)]/\Gamma(\Lambda_c^+\pi^+\pi^-)$ $(\Gamma_2+\Gamma_3)/\Gamma_1$

VALUE	CL%	DOCUMENT ID		TECN	COMMENT
• • • We do not use the following data for averages, fits, limits, etc. • • •					
$0.66^{+0.13}_{-0.16}\pm0.07$		ALBRECHT	97	ARG	$e^+e^-\approx$ 10 GeV
>0.51	90	[1] FRABETTI	96	E687	γBe, $\overline{E}_\gamma\approx$ 220 GeV

[1] The results of FRABETTI 96 are consistent with this ratio being 100%.

$\Gamma(\Lambda_c^+\pi^0\pi^0)/\Gamma_{total}$ Γ_5/Γ

VALUE (%)	EVTS	DOCUMENT ID		TECN	COMMENT
59 ±14 OUR FIT					
59.5±11.1±7.9	95	ABLIKIM	25BJ	BES3	e^+e^- at 4.918, 4.951 GeV

$\Gamma(\Lambda_c^+\pi^0)/\Gamma(\Lambda_c^+\pi^+\pi^-)$ Γ_6/Γ_1

$\Lambda_c^+\pi^0$ decay is forbidden by isospin conservation if this state is in fact a Λ_c.

VALUE	CL%	DOCUMENT ID		TECN	COMMENT
<3.53	90	EDWARDS	95	CLE2	$e^+e^-\approx$ 10.5 GeV

$\Gamma(\Lambda_c^+\gamma)/\Gamma(\Lambda_c^+\pi^+\pi^-)$ Γ_7/Γ_1

VALUE	CL%	DOCUMENT ID		TECN	COMMENT
<0.98	90	EDWARDS	95	CLE2	$e^+e^-\approx$ 10.5 GeV

$\Lambda_c(2595)^+$ REFERENCES

ABLIKIM	25BJ	JHEP 2508 065	M. Ablikim *et al.*	(BESIII Collab.)
ABLIKIM	24BC	PR D109 112007	M. Ablikim *et al.*	(BESIII Collab.)
AALTONEN	11H	PR D84 012003	T. Aaltonen *et al.*	(CDF Collab.)
BLECHMAN	03	PR D67 074033	A.E. Blechman *et al.*	(JHU, FLOR)
ALBRECHT	97	PL B402 207	H. Albrecht *et al.*	(ARGUS Collab.)
FRABETTI	96	PL B365 461	P.L. Frabetti *et al.*	(FNAL E687 Collab.)
EDWARDS	95	PRL 74 3331	K.W. Edwards *et al.*	(CLEO Collab.)

$\Lambda_c(2625)^+$

$I(J^P) = 0(\frac{3}{2}^-)$ Status: ***

The spin-parity has not been measured but is expected to be $3/2^-$: this is presumably the charm counterpart of the strange $\Lambda(1520)$.

$\Lambda_c(2625)^+$ MASS

The mass is obtained from the $\Lambda_c(2625)^+$–Λ_c^+ mass-difference measurements below.

VALUE (MeV)	EVTS	DOCUMENT ID		TECN	COMMENT
2628.00±0.15 OUR FIT					
• • • We do not use the following data for averages, fits, limits, etc. • • •					
2626.6 ±0.5 ±1.5	42 ± 9	ALBRECHT	93F	ARG	See ALBRECHT 97

$\Lambda_c(2625)^+ - \Lambda_c^+$ MASS DIFFERENCE

VALUE (MeV)	EVTS	DOCUMENT ID		TECN	COMMENT
341.54 ±0.05 OUR FIT					
341.54 ±0.05 OUR AVERAGE					
341.518±0.006±0.049	30.3k	WANG	23	BELL	e^+e at/near $\Upsilon(4S)$
341.65 ±0.04 ±0.12	6.2k	AALTONEN	11H	CDF	$p\overline{p}$ at 1.96 TeV
342.1 ±0.5 ±0.5	51	ALBRECHT	97	ARG	$e^+e^-\approx$ 10 GeV
342.2 ±0.2 ±0.5	245	EDWARDS	95	CLE2	$e^+e^-\approx$ 10.5 GeV
340.4 ±0.6 ±0.3	40	FRABETTI	94	E687	γBe, $\overline{E}_\gamma$ = 220 GeV

$\Lambda_c(2625)^+$ WIDTH

VALUE (MeV)	CL%	EVTS	DOCUMENT ID		TECN	COMMENT
<0.52	90	30.3k	WANG	23	BELL	e^+e at/near $\Upsilon(4S)$
• • • We do not use the following data for averages, fits, limits, etc. • • •						
<0.97	90	6.2k	AALTONEN	11H	CDF	$p\overline{p}$ at 1.96 TeV
<1.9	90	245 ± 19	EDWARDS	95	CLE2	$e^+e^-\approx$ 10.5 GeV
<3.2	90		ALBRECHT	93F	ARG	$e^+e^-\approx\Upsilon(4S)$

$\Lambda_c(2625)^+$ DECAY MODES

$\Lambda_c^+\pi\pi$ and its submode $\Sigma(2455)\pi$ are the only strong decays allowed for an excited Λ_c^+ having this mass.

	Mode		Fraction (Γ_i/Γ)	Confidence level
Γ_1	$\Lambda_c^+\pi^+\pi^-$	[a]	(50 ±7) %	
Γ_2	$\Sigma_c(2455)^{++}\pi^-$		(2.6±0.4) %	
Γ_3	$\Sigma_c(2455)^0\pi^+$		(2.6±0.4) %	
Γ_4	$\Lambda_c^+\pi^+\pi^-$ 3-body		seen	
Γ_5	$\Lambda_c^+\pi^0\pi^0$	[a]	(41 ±6) %	
Γ_6	$\Lambda_c^+\pi^0$	[b]	< 50 %	90%
Γ_7	$\Lambda_c^+\gamma$		< 26 %	90%

[a] In the isospin limit, with no other decays, the $\Lambda_c^+\pi^+\pi^-$ branching fraction would be 2/3 and the $\Lambda_c^+\pi^0\pi^0$ branching fraction would be 1/3.

[b] A test that the isospin is indeed 0, so that the particle is indeed a Λ_c^+.

$\Lambda_c(2625)^+$ BRANCHING RATIOS

$\Gamma(\Lambda_c^+\pi^+\pi^-)/\Gamma_{total}$ Γ_1/Γ

VALUE (%)	EVTS	DOCUMENT ID		TECN	COMMENT
50.2±5.7±3.5	70	ABLIKIM	24BC	BES3	e^+e^- at 4.918, 4.950 GeV

$\Gamma(\Sigma_c(2455)^{++}\pi^-)/\Gamma(\Lambda_c^+\pi^+\pi^-)$ Γ_2/Γ_1

VALUE (units 10^{-2})	CL%	EVTS	DOCUMENT ID		TECN	COMMENT
5.13±0.26±0.32		467	[1] WANG	23	BELL	e^+e at/near $\Upsilon(4S)$
• • • We do not use the following data for averages, fits, limits, etc. • • •						
<8	90		EDWARDS	95	CLE2	$e^+e^-\approx$ 10.5 GeV

[1] From a Dalitz plot fit, recovered simultaneously with $\Lambda_c(2625)^+\to\Sigma_c(2455)^0\pi^+$.

$\Gamma(\Sigma_c(2455)^0\pi^+)/\Gamma(\Lambda_c^+\pi^+\pi^-)$ Γ_3/Γ_1

VALUE (units 10^{-2})	CL%	EVTS	DOCUMENT ID		TECN	COMMENT
5.19±0.23±0.40		391	[2] WANG	23	BELL	e^+e at/near $\Upsilon(4S)$
• • • We do not use the following data for averages, fits, limits, etc. • • •						
<7	90		EDWARDS	95	CLE2	$e^+e^-\approx$ 10.5 GeV

[2] From a Dalitz plot fit, recovered simultaneously with $\Lambda_c(2625)^+\to\Sigma_c(2455)^{++}\pi^-$.

$[\Gamma(\Sigma_c(2455)^{++}\pi^-) + \Gamma(\Sigma_c(2455)^0\pi^+)]/\Gamma(\Lambda_c^+\pi^+\pi^-)$ $(\Gamma_2+\Gamma_3)/\Gamma_1$

VALUE	CL%	EVTS	DOCUMENT ID		TECN	COMMENT
• • • We do not use the following data for averages, fits, limits, etc. • • •						
<0.36	90		FRABETTI	94	E687	γBe, $\overline{E}_\gamma$ = 220 GeV
0.46±0.14		21	ALBRECHT	93F	ARG	$e^+e^-\approx\Upsilon(4S)$

$\Gamma(\Lambda_c^+\pi^+\pi^-$ 3-body$)/\Gamma(\Lambda_c^+\pi^+\pi^-)$ Γ_4/Γ_1

VALUE	EVTS	DOCUMENT ID		TECN	COMMENT
• • • We do not use the following data for averages, fits, limits, etc. • • •					
0.54±0.14	16	ALBRECHT	93F	ARG	$e^+e^-\approx\Upsilon(4S)$

$\Gamma(\Lambda_c^+\pi^0\pi^0)/\Gamma_{total}$ Γ_5/Γ

VALUE (%)	EVTS	DOCUMENT ID		TECN	COMMENT
41.0±5.2±3.3	203	ABLIKIM	25BJ	BES3	e^+e^- at 4.918, 4.951 GeV

$\Gamma(\Lambda_c^+\pi^0)/\Gamma(\Lambda_c^+\pi^+\pi^-)$ Γ_6/Γ_1

$\Lambda_c^+\pi^0$ decay is forbidden by isospin conservation if this state is in fact a Λ_c.

VALUE	CL%	DOCUMENT ID		TECN	COMMENT
<0.91	90	EDWARDS	95	CLE2	$e^+e^-\approx$ 10.5 GeV

$\Gamma(\Lambda_c^+\gamma)/\Gamma(\Lambda_c^+\pi^+\pi^-)$ Γ_7/Γ_1

VALUE	CL%	DOCUMENT ID		TECN	COMMENT
<0.52	90	EDWARDS	95	CLE2	$e^+e^-\approx$ 10.5 GeV

$\Lambda_c(2625)^+$ REFERENCES

ABLIKIM	25BJ	JHEP 2508 065	M. Ablikim *et al.*	(BESIII Collab.)
ABLIKIM	24BC	PR D109 112007	M. Ablikim *et al.*	(BESIII Collab.)
WANG	23	PR D107 032008	D. Wang *et al.*	(BELLE Collab.)
AALTONEN	11H	PR D84 012003	T. Aaltonen *et al.*	(CDF Collab.)
ALBRECHT	97	PL B402 207	H. Albrecht *et al.*	(ARGUS Collab.)
EDWARDS	95	PRL 74 3331	K.W. Edwards *et al.*	(CLEO Collab.)
FRABETTI	94	PRL 72 961	P.L. Frabetti *et al.*	(FNAL E687 Collab.)
ALBRECHT	93F	PL B317 227	H. Albrecht *et al.*	(ARGUS Collab.)

$\Lambda_c(2765)^+$ or $\Sigma_c(2765)$

$I(J^P) = ?(?^?)$ Status: *

OMITTED FROM SUMMARY TABLE

A broad, statistically significant peak (997^{+141}_{-129} events) seen in $\Lambda_c^+\pi^+\pi^-$. However, nothing at all is known about its quantum numbers, including whether it is a Λ_c^+ or a Σ_c, or whether the width might be due to overlapping states.

$\Lambda_c(2765)^+$ MASS

The mass is obtained from the $\Lambda_c(2765)^+ - \Lambda_c^+$ mass-difference measurement below.

VALUE (MeV)	DOCUMENT ID
2766.6±2.4 OUR FIT	

Int. J. Mod. Phys. A 2026.41. Downloaded from www.worldscientific.com by UNIVERSITY OF CALIFORNIA @ BERKELEY on 09/16/26. Re-use and distribution is strictly not permitted, except for Open Access articles.

$\Lambda_c(2765)^+ - \Lambda_c^+$ MASS DIFFERENCE

VALUE (MeV)	EVTS	DOCUMENT ID		TECN	COMMENT
480.1±2.4 OUR FIT					
480.1±2.4	997^{+141}_{-129}	ARTUSO	01	CLE2	$e^+e^- \approx \Upsilon(4S)$

$\Lambda_c(2765)^+$ WIDTH

VALUE (MeV)	DOCUMENT ID		TECN	COMMENT
50	ARTUSO	01	CLE2	$e^+e^- \approx \Upsilon(4S)$

$\Lambda_c(2765)^+$ DECAY MODES

	Mode	Fraction (Γ_i/Γ)
Γ_1	$\Lambda_c^+ \pi^+ \pi^-$	seen

$\Lambda_c(2765)^+$ REFERENCES

ARTUSO 01 PRL 86 4479 M. Artuso *et al.* (CLEO Collab.)

$\Lambda_c(2860)^+$

$I(J^P) = 0(\frac{3}{2}^+)$ Status: ***

$\Lambda_c(2860)^+$ MASS

VALUE (MeV)	DOCUMENT ID		TECN	COMMENT
$\mathbf{2856.1^{+2.0}_{-1.7} \pm 0.5^{+1.1}_{-5.6}}$	[1] AAIJ	17S	LHCB	in $\Lambda_b^0 \to D^0 p \pi^-$

[1] The third AAIJ 17S uncertainty comes from modeling the resonant shape of the nearby $\Lambda_c(2880)^+$ and the background (non-resonant) amplitudes.

$\Lambda_c(2860)^+$ WIDTH

VALUE (MeV)	DOCUMENT ID		TECN	COMMENT
$\mathbf{67.6^{+10.1}_{-8.1} \pm 1.4^{+5.9}_{-20.0}}$	[1] AAIJ	17S	LHCB	in $\Lambda_b^0 \to D^0 p \pi^-$

[1] The third AAIJ 17S uncertainty comes from modeling the resonant shape of the nearby $\Lambda_c(2880)^+$ and the background (non-resonant) amplitudes.

$\Lambda_c(2860)^+$ DECAY MODES

	Mode	Fraction (Γ_i/Γ)
Γ_1	$D^0 p$	seen

$\Lambda_c(2860)^+$ BRANCHING RATIOS

$\Gamma(D^0 p)/\Gamma_{total}$ — Γ_1/Γ

VALUE	DOCUMENT ID		TECN	COMMENT
seen	AAIJ	17S	LHCB	in $\Lambda_b^0 \to D^0 p \pi^-$

$\Lambda_c(2860)^+$ REFERENCES

AAIJ 17S JHEP 1705 030 R. Aaij *et al.* (LHCb Collab.) JP

$\Lambda_c(2880)^+$

$I(J^P) = 0(\frac{5}{2}^+)$ Status: ***

A narrow peak seen in $\Lambda_c^+ \pi^+ \pi^-$ and in $p D^0$. It is not seen in $p D^+$, and therefore it is a Λ_c^+ and not a Σ_c.

$\Lambda_c(2880)^+$ MASS

VALUE (MeV)	EVTS	DOCUMENT ID		TECN	COMMENT
2881.63±0.24 OUR FIT					
2881.62±0.24 OUR AVERAGE					
$2881.75 \pm 0.29 \pm 0.07^{+0.14}_{-0.20}$		[1] AAIJ	17S	LHCB	in $\Lambda_b^0 \to D^0 p \pi^-$
2881.9 ±0.1 ±0.5	2.8k	AUBERT	07	BABR	in $p D^0$
2881.2 ±0.2 ±0.4	690	MIZUK	07	BELL	in $\Sigma_c(2455)^{0,++} \pi^\pm$

[1] The third AAIJ 17S uncertainty comes from modeling the resonant shape of the $\Lambda_c(2880)^+$ and the background (non-resonant) amplitudes.

$\Lambda_c(2880)^+ - \Lambda_c^+$ MASS DIFFERENCE

VALUE (MeV)	EVTS	DOCUMENT ID		TECN	COMMENT
595.17±0.28 OUR FIT					
596 ±1 ±2	350	ARTUSO	01	CLE2	in $\Lambda_c^+ \pi^+ \pi^-$

$\Lambda_c(2880)^+$ WIDTH

VALUE (MeV)	CL%	EVTS	DOCUMENT ID		TECN	COMMENT
$\mathbf{5.6^{+0.8}_{-0.6}}$ **OUR AVERAGE**						
$5.43^{+0.77}_{-0.71} \pm 0.29^{+0.81}_{-0.29}$			[2] AAIJ	17S	LHCB	in $\Lambda_b^0 \to D^0 p \pi^-$
5.8 ±1.5 ±1.1		2.8k	AUBERT	07	BABR	in $p D^0$
5.8 ±0.7 ±1.1		690	MIZUK	07	BELL	in $\Sigma_c(2455)^{0,++} \pi^\pm$
• • • We do not use the following data for averages, fits, limits, etc. • • •						
<8		90	ARTUSO	01	CLEO	in $\Lambda_c^+ \pi^+ \pi^-$

[2] AAIJ 17S reports $5.43^{+0.77}_{-0.71} \pm 0.29^{+0.75}_{-0.00}$ MeV value where the third uncertainty comes from modeling the resonant shape of the $\Lambda_c(2880)^+$ and the background (non-resonant) amplitudes. We have combined in quadrature the systematic uncertainties.

$\Lambda_c(2880)^+$ DECAY MODES

	Mode	Fraction (Γ_i/Γ)
Γ_1	$\Lambda_c^+ \pi^+ \pi^-$	seen
Γ_2	$\Sigma_c(2455)^{0,++} \pi^\pm$	seen
Γ_3	$\Sigma_c(2520)^{0,++} \pi^\pm$	seen
Γ_4	$\Lambda_c^+ \eta$	
Γ_5	$p D^0$	seen

$\Lambda_c(2880)^+$ BRANCHING RATIOS

$\Gamma(\Sigma_c(2455)^{0,++}\pi^\pm)/\Gamma(\Lambda_c^+\pi^+\pi^-)$ — Γ_2/Γ_1

VALUE	EVTS	DOCUMENT ID		TECN	COMMENT
0.392±0.031 OUR AVERAGE Error includes scale factor of 1.3.					
0.404±0.021±0.014		MIZUK	07	BELL	in $\Sigma_c(2455)^{0,++} \pi^\pm$
0.31 ±0.06 ±0.03	96	ARTUSO	01	CLE2	$e^+e^- \approx \Upsilon(4S)$

$\Gamma(\Sigma_c(2520)^{0,++}\pi^\pm)/\Gamma(\Lambda_c^+\pi^+\pi^-)$ — Γ_3/Γ_1

VALUE	CL%	DOCUMENT ID		TECN	COMMENT
0.091±0.025±0.010		MIZUK	07	BELL	in $\Sigma_c(2455)^{0,++} \pi^\pm$
• • • We do not use the following data for averages, fits, limits, etc. • • •					
<0.11	90	ARTUSO	01	CLE2	$e^+e^- \approx \Upsilon(4S)$

$\Gamma(\Sigma_c(2520)^{0,++}\pi^\pm)/\Gamma(\Sigma_c(2455)^{0,++}\pi^\pm)$ — Γ_3/Γ_2

VALUE	DOCUMENT ID		TECN	COMMENT
• • • We do not use the following data for averages, fits, limits, etc. • • •				
0.225±0.062±0.025	[3] MIZUK	07	BELL	in $\Sigma_c(2455)^{0,++} \pi^\pm$

[3] This MIZUK 07 ratio is redundant with MIZUK 07 ratios given above.

$\Gamma(\Lambda_c^+\eta)/\Gamma(\Sigma_c(2455)^{0,++}\pi^\pm)$ — Γ_4/Γ_2

VALUE	CL%	DOCUMENT ID		TECN	COMMENT
<0.13	90	LI	24C	BELL	e^+e^- at $\sim \Upsilon(nS)$

$\Gamma(p D^0)/\Gamma(\Sigma_c(2455)^{0,++}\pi^\pm)$ — Γ_5/Γ_2

VALUE	EVTS	DOCUMENT ID		TECN	COMMENT
0.75±0.03±0.07	12k	LI	24C	BELL	e^+e^- at $\sim \Upsilon(nS)$

$\Lambda_c(2880)^+$ REFERENCES

LI 24C PR D110 032021 S.X. Li *et al.* (BELLE Collab.)
AAIJ 17S JHEP 1705 030 R. Aaij *et al.* (LHCb Collab.) JP
AUBERT 07 PRL 98 012001 B. Aubert *et al.* (BABAR Collab.)
MIZUK 07 PRL 98 262001 R. Mizuk *et al.* (BELLE Collab.)
ARTUSO 01 PRL 86 4479 M. Artuso *et al.* (CLEO Collab.)

$\Lambda_c(2910)^+$

$I(J^P) = ?(?^?)$ Status: *

OMITTED FROM SUMMARY TABLE

A candidate heavy quark symmetry doublet partner to the $\Lambda_c(2940)$. Further study is needed to confirm whether this state is an excited Λ_c or Σ_c.

$\Lambda_c(2910)^+$ MASS

VALUE (MeV)	EVTS	DOCUMENT ID		TECN	COMMENT
2913.8±5.6±3.8	150	[1] LI	23E	BELL	$\overline{B}^0 \to \Sigma_c(2455)^{0,++} \pi^\pm \overline{p}$

[1] LI 23E observes evidence for the $\Lambda_c(2910)^+$ at 4.2σ significance.

Int. J. Mod. Phys. A 2026.41. Downloaded from www.worldscientific.com
UNIVERSITY OF CALIFORNIA @ BERKELEY on 09/16/26. Re-use and distribution is strictly not permitted, except for Open Access articles.

$\Lambda_c(2910)^+$ WIDTH

VALUE (MeV)	EVTS	DOCUMENT ID		TECN	COMMENT
51.8±20.0±18.8	150	[1] LI	23E	BELL	$\overline{B}^0 \to \Sigma_c(2455)^{0,++}\pi^\pm\overline{p}$

[1] LI 23E observes evidence for the $\Lambda_c(2910)^+$ at 4.2σ significance.

$\Lambda_c(2910)^+$ DECAY MODES

	Mode	Fraction (Γ_i/Γ)
Γ_1	$\Sigma_c(2455)^0\pi^+$	seen
Γ_2	$\Sigma_c(2455)^{++}\pi^-$	seen

$\Lambda_c(2910)^+$ BRANCHING RATIOS

$\Gamma(\Sigma_c(2455)^0\pi^+)/\Gamma_{total}$ — **Γ_1/Γ**

VALUE	DOCUMENT ID		TECN	COMMENT
seen	LI	23E	BELL	$\overline{B}^0 \to \Sigma_c(2455)^0\pi^+\overline{p}$

$\Gamma(\Sigma_c(2455)^{++}\pi^-)/\Gamma_{total}$ — **Γ_2/Γ**

VALUE	DOCUMENT ID		TECN	COMMENT
seen	LI	23E	BELL	$\overline{B}^0 \to \Sigma_c(2455)^{++}\pi^-\overline{p}$

$\Lambda_c(2910)^+$ REFERENCES

LI 23E PRL 130 031901 Y.B. Li *et al.* (BELLE Collab.)

$\Lambda_c(2940)^+$

$I(J^P) = 0(\frac{3}{2}^-)$ Status: ***

A narrow peak seen in pD^0 and in $\Lambda_c^+\pi^+\pi^-$. It is not seen in pD^+, and therefore it is a Λ_c^+ and not a Σ_c. $J^P = 3/2^-$ is favored, but not certain.

$\Lambda_c(2940)^+$ MASS

VALUE (MeV)	EVTS	DOCUMENT ID		TECN	COMMENT
$2939.6^{+1.3}_{-1.5}$ OUR AVERAGE					
$2944.8^{+3.5}_{-2.5}\pm0.4^{+0.1}_{-4.6}$		[1] AAIJ	17S	LHCB	in $\Lambda_b^0 \to D^0p\pi^-$
$2939.8\pm1.3\pm1.0$	2.2k	AUBERT	07	BABR	in pD^0
$2938.0\pm1.3^{+2.0}_{-4.0}$	220	MIZUK	07	BELL	in $\Sigma_c(2455)^{0,++}\pi^\pm$

[1] The third AAIJ 17S uncertainty comes from modeling the resonant shape of the nearby $\Lambda_c(2880)^+$ and the background (non-resonant) amplitudes.

$\Lambda_c(2940)^+$ WIDTH

VALUE (MeV)	EVTS	DOCUMENT ID		TECN	COMMENT
20^{+6}_{-5} OUR AVERAGE					
$27.7^{+8.2}_{-6.0}\pm0.9^{+5.2}_{-10.4}$		[2] AAIJ	17S	LHCB	in $\Lambda_b^0 \to D^0p\pi^-$
$17.5\pm5.2\pm5.9$	2.2k	AUBERT	07	BABR	in pD^0
$13^{+8}_{-5}{}^{+27}_{-7}$	220	MIZUK	07	BELL	in $\Sigma_c(2455)^{0,++}\pi^\pm$

[2] The third AAIJ 17S uncertainty comes from modeling the resonant shape of the nearby $\Lambda_c(2880)^+$ and the background (non-resonant) amplitudes.

$\Lambda_c(2940)^+$ DECAY MODES

	Mode	Fraction (Γ_i/Γ)
Γ_1	$\Lambda_c\eta$	
Γ_2	pD^0	seen
Γ_3	$\Sigma_c(2455)^{0,++}\pi^\pm$	seen

$\Lambda_c(2940)^+$ BRANCHING RATIOS

$\Gamma(pD^0)/\Gamma_{total}$ — **Γ_2/Γ**

$\Gamma(\Lambda_c\eta)/\Gamma(\Sigma_c(2455)^{0,++}\pi^\pm)$ — **Γ_1/Γ_3**

VALUE	CL%	DOCUMENT ID		TECN	COMMENT
<1.11	90	LI	24C	BELL	e^+e^- at $\sim\Upsilon(nS)$

$\Gamma(pD^0)/\Gamma(\Sigma_c(2455)^{0,++}\pi^\pm)$ — **Γ_2/Γ_3**

VALUE	EVTS	DOCUMENT ID		TECN	COMMENT
3.59±0.21±0.56	16k	LI	24C	BELL	e^+e^- at $\sim\Upsilon(nS)$

$\Lambda_c(2940)^+$ REFERENCES

LI 24C PR D110 032021 S.X. Li *et al.* (BELLE Collab.)
AAIJ 17S JHEP 1705 030 R. Aaij *et al.* (LHCb Collab.) JP
AUBERT 07 PRL 98 012001 B. Aubert *et al.* (BABAR Collab.)
MIZUK 07 PRL 98 262001 R. Mizuk *et al.* (BELLE Collab.)

$\Sigma_c(2455)$

$I(J^P) = 1(\frac{1}{2}^+)$ Status: ****

The angular distribution of $B^- \to \Sigma_c(2455)^0\overline{p}$ favors $J = 1/2$ (as the quark model predicts). $J = 3/2$ is excluded by more than four standard deviations; see AUBERT 08BN.

$\Sigma_c(2455)$ MASSES

The masses are obtained from the mass-difference measurements that follow.

$\Sigma_c(2455)^{++}$ MASS

VALUE (MeV)	DOCUMENT ID
2453.97±0.14 OUR FIT	

$\Sigma_c(2455)^+$ MASS

VALUE (MeV)	DOCUMENT ID
$2452.65^{+0.22}_{-0.16}$ OUR FIT	

$\Sigma_c(2455)^0$ MASS

VALUE (MeV)	DOCUMENT ID
2453.75±0.14 OUR FIT	

$\Sigma_c(2455) - \Lambda_c^+$ MASS DIFFERENCES

$m_{\Sigma_c(2455)^{++}} - m_{\Lambda_c^+}$

VALUE (MeV)	EVTS	DOCUMENT ID		TECN	COMMENT
167.510± 0.017 OUR FIT					
167.510± 0.022 OUR AVERAGE					
167.51 ± 0.01 ±0.02	36k	LEE	14	BELL	e^+e^- at $\Upsilon(4S)$
167.44 ± 0.04 ±0.12	13.8k	AALTONEN	11H	CDF	$p\overline{p}$ at 1.96 TeV
167.4 ± 0.1 ±0.2	2k	ARTUSO	02	CLE2	$e^+e^- \approx \Upsilon(4S)$
167.35 ± 0.19 ±0.12	461	LINK	00C	FOCS	γ A, $\overline{E}_\gamma$ 180 GeV
167.76 ± 0.29 ±0.15	122	AITALA	96B	E791	$\pi^- N$, 500 GeV
167.6 ± 0.6 ±0.6	56	FRABETTI	96	E687	γBe, $\overline{E}_\gamma \approx$ 220 GeV
168.2 ± 0.3 ±0.2	126	CRAWFORD	93	CLE2	$e^+e^- \approx \Upsilon(4S)$
167.8 ± 0.4 ±0.3	54	BOWCOCK	89	CLEO	e^+e^- 10 GeV
168.2 ± 0.5 ±1.6	92	ALBRECHT	88D	ARG	e^+e^- 10 GeV
167.4 ± 0.5 ±2.0	46	DIESBURG	87	SPEC	nA $\sim$ 600 GeV
• • • We do not use the following data for averages, fits, limits, etc. • • •					
167 ± 1	2	JONES	87	HBC	νp in BEBC
166 ± 1	1	BOSETTI	82	HBC	See JONES 87
168 ± 3	6	BALTAY	79	HLBC	ν Ne-H in 15-ft
166 ±15	1	CAZZOLI	75	HBC	νp in BNL 7-ft

$m_{\Sigma_c(2455)^+} - m_{\Lambda_c^+}$

VALUE (MeV)	EVTS	DOCUMENT ID		TECN	COMMENT
$166.19^{+0.16}_{-0.08}$ OUR FIT					
$166.19^{+0.15}_{-0.08}$ OUR AVERAGE					
$166.17\pm0.05^{+0.16}_{-0.07}$		YELTON	21	BELL	e^+e^- at $\Upsilon(nS)$
166.4 ±0.2 ±0.3	661	AMMAR	01	CLE2	$e^+e^- \approx \Upsilon(4S)$
• • • We do not use the following data for averages, fits, limits, etc. • • •					
168.5 ±0.4 ±0.2	111	CRAWFORD	93	CLE2	See AMMAR 01
168 ±3	1	CALICCHIO	80	HBC	νp in BEBC-TST

$m_{\Sigma_c(2455)^0} - m_{\Lambda_c^+}$

VALUE (MeV)	EVTS	DOCUMENT ID		TECN	COMMENT
167.290±0.017 OUR FIT					
167.290±0.022 OUR AVERAGE					
167.29 ±0.01 ±0.02	32k	LEE	14	BELL	e^+e^- at $\Upsilon(4S)$
167.28 ±0.03 ±0.12	15.9k	AALTONEN	11H	CDF	$p\overline{p}$ at 1.96 TeV
167.2 ±0.1 ±0.2	2k	ARTUSO	02	CLE2	$e^+e^- \approx \Upsilon(4S)$
167.38 ±0.21 ±0.13	362	LINK	00C	FOCS	γ A, $\overline{E}_\gamma$ 180 GeV
167.38 ±0.29 ±0.15	143	AITALA	96B	E791	$\pi^- N$, 500 GeV
167.8 ±0.6 ±0.2		ALEEV	96	SPEC	n nucleus, 50 GeV/c
166.6 ±0.5 ±0.6	69	FRABETTI	96	E687	γBe, $\overline{E}_\gamma \approx$ 220 GeV
167.1 ±0.3 ±0.2	124	CRAWFORD	93	CLE2	$e^+e^- \approx \Upsilon(4S)$
168.4 ±1.0 ±0.3	14	ANJOS	89D	E691	γBe 90–260 GeV
• • • We do not use the following data for averages, fits, limits, etc. • • •					
167.9 ±0.5 ±0.3	48	[1] BOWCOCK	89	CLEO	e^+e^- 10 GeV
167.0 ±0.5 ±1.6	70	[1] ALBRECHT	88D	ARG	e^+e^- 10 GeV
178.2 ±0.4 ±2.0	85	[2] DIESBURG	87	SPEC	nA $\sim$ 600 GeV
163 ±2	1	AMMAR	86	EMUL	νA

[1] This result enters the fit through $m_{\Sigma_c^{++}} - m_{\Sigma_c^0}$ given below.

[2] See the note on DIESBURG 87 in the $m_{\Sigma_c^{++}} - m_{\Sigma_c^0}$ section below.

$\Sigma_c(2455)$ MASS DIFFERENCES

$m_{\Sigma_c(2455)^{++}} - m_{\Sigma_c(2455)^0}$

VALUE (MeV)	DOCUMENT ID		TECN	COMMENT
0.220±0.013 OUR FIT				
0.221±0.014 OUR AVERAGE				
0.22 ±0.01 ±0.01	LEE	14	BELL	e^+e^- at $\Upsilon(4S)$
0.2 ±0.1 ±0.1	ARTUSO	02	CLE2	$e^+e^- \approx \Upsilon(4S)$
− 0.03 ±0.28 ±0.11	LINK	00C	FOCS	γ A, $\overline{E}_\gamma$ 180 GeV
0.38 ±0.40 ±0.15	AITALA	96B	E791	$\pi^- N$, 500 GeV
1.1 ±0.4 ±0.1	CRAWFORD	93	CLE2	$e^+e^- \approx \Upsilon(4S)$
− 0.1 ±0.6 ±0.1	BOWCOCK	89	CLEO	e^+e^- 10 GeV
1.2 ±0.7 ±0.3	ALBRECHT	88D	ARG	$e^+e^- \sim$ 10 GeV
• • • We do not use the following data for averages, fits, limits, etc. • • •				
−10.8 ±2.9	[3] DIESBURG	87	SPEC	nA ∼ 600 GeV

[3] DIESBURG 87 is completely incompatible with the other experiments, which is surprising since it agrees with them about $m_{\Sigma_c(2455)^{++}} - m_{\Lambda_c^+}$. We go with the majority here.

$m_{\Sigma_c(2455)^+} - m_{\Sigma_c(2455)^0}$

VALUE (MeV)	DOCUMENT ID		TECN	COMMENT
$-1.10^{+0.16}_{-0.08}$ OUR FIT				
• • • We do not use the following data for averages, fits, limits, etc. • • •				
1.4 ±0.5 ±0.3	CRAWFORD	93	CLE2	See AMMAR 01

$\Sigma_c(2455)$ WIDTHS

$\Sigma_c(2455)^{++}$ WIDTH

VALUE (MeV)	EVTS	DOCUMENT ID		TECN	COMMENT
$1.89^{+0.09}_{-0.18}$ OUR AVERAGE Error includes scale factor of 1.1.					
$1.84 \pm 0.04^{+0.07}_{-0.20}$	36k	LEE	14	BELL	e^+e^- at $\Upsilon(4S)$
2.34±0.13±0.45	13.8k	AALTONEN	11H	CDF	$p\overline{p}$ at 1.96 TeV
2.3 ±0.2 ±0.3	2k	ARTUSO	02	CLE2	$e^+e^- \approx \Upsilon(4S)$
$2.05^{+0.41}_{-0.38} \pm 0.38$	1110	LINK	02	FOCS	γ A, $\overline{E}_\gamma \approx$ 180 GeV

$\Sigma_c(2455)^+$ WIDTH

VALUE (MeV)	CL%	EVTS	DOCUMENT ID		TECN	COMMENT
2.3±0.3±0.3			YELTON	21	BELL	e^+e^- at Υ(nS)
• • • We do not use the following data for averages, fits, limits, etc. • • •						
<4.6	90	661	AMMAR	01	CLE2	$e^+e^- \approx \Upsilon(4S)$

$\Sigma_c(2455)^0$ WIDTH

VALUE (MeV)	EVTS	DOCUMENT ID		TECN	COMMENT
$1.83^{+0.11}_{-0.19}$ OUR AVERAGE Error includes scale factor of 1.2.					
$1.76 \pm 0.04^{+0.09}_{-0.21}$	32k	LEE	14	BELL	e^+e^- at $\Upsilon(4S)$
1.65±0.11±0.49	15.9k	AALTONEN	11H	CDF	$p\overline{p}$ at 1.96 TeV
2.6 ±0.5 ±0.3		AUBERT	08BN	BABR	$B^- \to \overline{p}\Lambda_c^+\pi^-$
2.5 ±0.2 ±0.3	2k	ARTUSO	02	CLE2	$e^+e^- \approx \Upsilon(4S)$
$1.55^{+0.41}_{-0.37} \pm 0.38$	913	LINK	02	FOCS	γ A, $\overline{E}_\gamma \approx$ 180 GeV

$\Sigma_c(2455)$ DECAY MODES

$\Lambda_c^+\pi$ is the only strong decay allowed to a Σ_c having this mass.

	Mode	Fraction (Γ_i/Γ)
Γ_1	$\Lambda_c^+\pi$	≈ 100 %

$\Sigma_c(2455)$ REFERENCES

YELTON	21	PR D104 052003	J. Yelton *et al.*	(BELLE Collab.)
LEE	14	PR D89 091102	S.-H. Lee *et al.*	(BELLE Collab.)
AALTONEN	11H	PR D84 012003	T. Aaltonen *et al.*	(CDF Collab.)
AUBERT	08BN	PR D78 112003	B. Aubert *et al.*	(BABAR Collab.)
ARTUSO	02	PR D65 071101	M. Artuso *et al.*	(CLEO Collab.)
LINK	02	PL B525 205	J.M. Link *et al.*	(FNAL FOCUS Collab.)
AMMAR	01	PRL 86 1167	R. Ammar *et al.*	(CLEO Collab.)
LINK	00C	PL B488 218	J.M. Link *et al.*	(FNAL FOCUS Collab.)
AITALA	96B	PL B379 292	E.M. Aitala *et al.*	(FNAL E791 Collab.)
ALEEV	96	JINRRC 3-77 31	A.N. Aleev *et al.*	(Serpukhov EXCHARM Collab.)
FRABETTI	96	PL B365 461	P.L. Frabetti *et al.*	(FNAL E687 Collab.)
CRAWFORD	93	PRL 71 3259	G. Crawford *et al.*	(CLEO Collab.)
ANJOS	89D	PRL 62 1721	J.C. Anjos *et al.*	(FNAL E691 Collab.)
BOWCOCK	89	PRL 62 1240	T.J.V. Bowcock *et al.*	(CLEO Collab.)
ALBRECHT	88D	PL B211 489	H. Albrecht *et al.*	(ARGUS Collab.)
DIESBURG	87	PRL 59 2711	M. Diesburg *et al.*	(FNAL E400 Collab.)
JONES	87	ZPHY C36 593	G.T. Jones *et al.*	(CERN WA21 Collab.)
AMMAR	86	JETPL 43 515	R. Ammar *et al.*	(ITEP)
		Translated from ZETFP 43 401.		
BOSETTI	82	PL 109B 234	P.C. Bosetti *et al.*	(AACH3, BONN, CERN+)
CALICCHIO	80	PL 93B 521	M. Calicchio *et al.*	(BARI, BIRM, BRUX+)
BALTAY	79	PRL 42 1721	C. Baltay *et al.*	(COLU, BNL) I
CAZZOLI	75	PRL 34 1125	E.G. Cazzoli *et al.*	(BNL)

$\Sigma_c(2520)$

$I(J^P) = 1(\frac{3}{2}^+)$ Status: ***

Seen in the $\Lambda_c^+\pi^\pm$ mass spectrum. The natural assignment is that this is the $J^P = 3/2^+$ excitation of the $\Sigma_c(2455)$, the charm counterpart of the $\Sigma(1385)$, but neither J nor P has been measured.

$\Sigma_c(2520)$ MASSES

The masses are obtained from the mass-difference measurements that follow.

$\Sigma_c(2520)^{++}$ MASS

VALUE (MeV)	EVTS	DOCUMENT ID		TECN	COMMENT
2518.41±0.22 OUR FIT Error includes scale factor of 1.3.					
• • • We do not use the following data for averages, fits, limits, etc. • • •					
2530 ±5 ±5	6	[1] AMMOSOV	93	HLBC	$\nu p \to \mu^- \Sigma_c(2530)^{++}$

[1] AMMOSOV 93 sees a cluster of 6 events and estimates the background to be 1 event.

$\Sigma_c(2520)^+$ MASS

VALUE (MeV)	DOCUMENT ID
$2517.4^{+0.7}_{-0.5}$ OUR FIT	

$\Sigma_c(2520)^0$ MASS

VALUE (MeV)	DOCUMENT ID
2518.48±0.21 OUR FIT Error includes scale factor of 1.2.	

$\Sigma_c(2520)$ MASS DIFFERENCES

$m_{\Sigma_c(2520)^{++}} - m_{\Lambda_c^+}$

VALUE (MeV)	EVTS	DOCUMENT ID		TECN	COMMENT
231.95±0.18 OUR FIT Error includes scale factor of 1.8.					
231.95±0.16 OUR AVERAGE Error includes scale factor of 1.6. See the ideogram below.					
231.99±0.10±0.02	44k	LEE	14	BELL	e^+e^- at $\Upsilon(4S)$
230.73±0.56±0.16	8.8k	AALTONEN	11H	CDF	$p\overline{p}$ at 1.96 TeV
231.5 ±0.4 ±0.3	1.3k	ATHAR	05	CLEO	e^+e^-, 9.4–11.5 GeV
234.5 ±1.1 ±0.8	677	BRANDENB...	97	CLE2	$e^+e^- \approx \Upsilon(4S)$

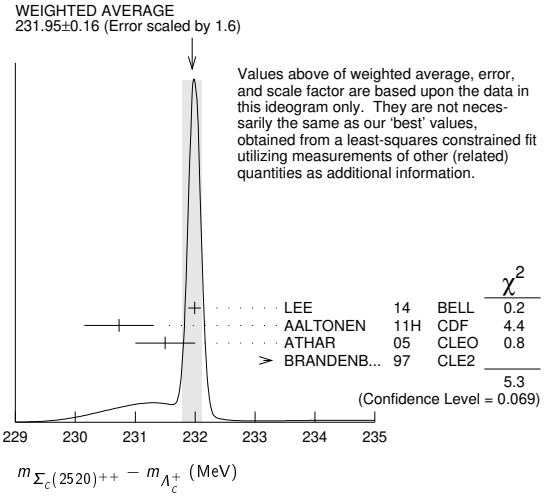

$m_{\Sigma_c(2520)^+} - m_{\Lambda_c^+}$

VALUE (MeV)	EVTS	DOCUMENT ID		TECN	COMMENT
$230.9^{+0.7}_{-0.5}$ OUR FIT					
$230.9^{+0.7}_{-0.5}$ OUR AVERAGE					
$230.9 \pm 0.5^{+0.5}_{-0.1}$		YELTON	21	BELL	e^+e^- at Υ(nS)
231.0±1.1±2.0	327	AMMAR	01	CLE2	$e^+e^- \approx \Upsilon(4S)$

$m_{\Sigma_c(2520)^0} - m_{\Lambda_c^+}$

VALUE (MeV)	EVTS	DOCUMENT ID		TECN	COMMENT
232.02±0.15 OUR FIT Error includes scale factor of 1.4.					
232.02±0.17 OUR AVERAGE Error includes scale factor of 1.5. See the ideogram below.					
231.98±0.11±0.04	41k	LEE	14	BELL	e^+e^- at $\Upsilon(4S)$
232.88±0.43±0.16	9.0k	AALTONEN	11H	CDF	$p\overline{p}$ at 1.96 TeV
231.4 ±0.5 ±0.3	1.3k	ATHAR	05	CLEO	e^+e^-, 9.4–11.5 GeV
232.6 ±1.0 ±0.8	504	BRANDENB...	97	CLE2	$e^+e^- \approx \Upsilon(4S)$

Int. J. Mod. Phys. A 2026.41. Downloaded from www.worldscientific.com
by UNIVERSITY OF CALIFORNIA @ BERKELEY on 09/16/26. Re-use and distribution is strictly not permitted, except for Open Access articles.

UNIVERSITY OF CALIFORNIA @ BERKELEY on 09/16/26. Re-use and distribution is strictly not permitted, except for Open Access articles.
Int. J. Mod. Phys. A 2026.41. Downloaded from www.worldscientific.com

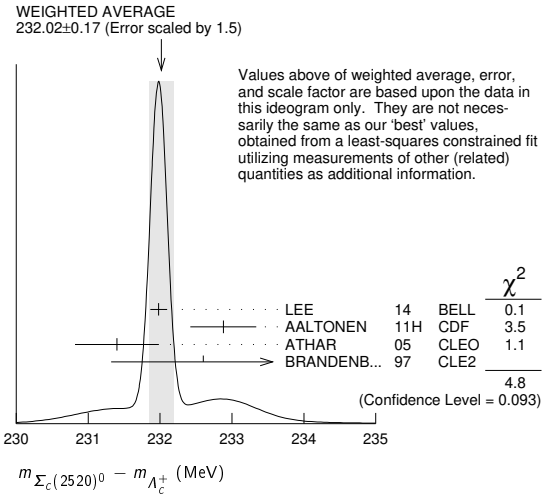

$m_{\Sigma_c(2520)^{++}} - m_{\Sigma_c(2520)^0}$

VALUE (MeV)	EVTS	DOCUMENT ID		TECN	COMMENT
0.01±0.15±0.03	44/41k	LEE	14	BELL	e^+e^- at $\Upsilon(4S)$
• • • We do not use the following data for averages, fits, limits, etc. • • •					
0.1 ±0.8 ±0.3		[2] ATHAR	05	CLEO	e^+e^-, 9.4–11.5 GeV
1.9 ±1.4 ±1.0		[3] BRANDENB...	97	CLE2	$e^+e^- \approx \Upsilon(4S)$

[2] This ATHAR 05 result is redundant with measurements in earlier entries.
[3] This BRANDENBURG 97 result is redundant with measurements in earlier entries.

$\Sigma_c(2520)$ WIDTHS

$\Sigma_c(2520)^{++}$ WIDTH

VALUE (MeV)	EVTS	DOCUMENT ID		TECN	COMMENT
$14.78^{+0.30}_{-0.40}$ OUR AVERAGE					
$14.77\pm0.25^{+0.18}_{-0.30}$	44k	LEE	14	BELL	e^+e^- at $\Upsilon(4S)$
15.03±2.12±1.36	8.8k	AALTONEN	11H	CDF	$p\overline{p}$ at 1.96 TeV
$14.4\ ^{+1.6}_{-1.5}\ \pm1.4$	1.3k	ATHAR	05	CLEO	e^+e^-, 9.4–11.5 GeV
$17.9\ ^{+3.8}_{-3.2}\ \pm4.0$	677	BRANDENB...	97	CLE2	$e^+e^- \approx \Upsilon(4S)$

$\Sigma_c(2520)^+$ WIDTH

VALUE (MeV)	CL%	EVTS	DOCUMENT ID		TECN	COMMENT
$17.2^{+2.3+3.1}_{-2.1-0.7}$			YELTON	21	BELL	e^+e^- at $\Upsilon(nS)$
• • • We do not use the following data for averages, fits, limits, etc. • • •						
<17	90	327	AMMAR	01	CLE2	$e^+e^- \approx \Upsilon(4S)$

$\Sigma_c(2520)^0$ WIDTH

VALUE (MeV)	EVTS	DOCUMENT ID		TECN	COMMENT
$15.3\ ^{+0.4}_{-0.5}$ OUR AVERAGE					
$15.41\pm0.41^{+0.20}_{-0.32}$	41k	LEE	14	BELL	e^+e^- at $\Upsilon(4S)$
12.51±1.82±1.37	9.0k	AALTONEN	11H	CDF	$p\overline{p}$ at 1.96 TeV
$16.6\ ^{+1.9}_{-1.7}\ \pm1.4$	1.3k	ATHAR	05	CLEO	e^+e^-, 9.4–11.5 GeV
$13.0\ ^{+3.7}_{-3.0}\ \pm4.0$	504	BRANDENB...	97	CLE2	$e^+e^- \approx \Upsilon(4S)$

$\Sigma_c(2520)$ DECAY MODES

$\Lambda_c^+\pi$ is the only strong decay allowed to a Σ_c having this mass.

	Mode	Fraction (Γ_i/Γ)
Γ_1	$\Lambda_c^+\pi$	≈ 100 %

$\Sigma_c(2520)$ REFERENCES

YELTON	21	PR D104 052003	J. Yelton *et al.*	(BELLE Collab.)
LEE	14	PR D89 091102	S.-H. Lee *et al.*	(BELLE Collab.)
AALTONEN	11H	PR D84 012003	T. Aaltonen *et al.*	(CDF Collab.)
ATHAR	05	PR D71 051101	S.B. Athar *et al.*	(CLEO Collab.)
AMMAR	01	PRL 86 1167	R. Ammar *et al.*	(CLEO Collab.)
BRANDENB...	97	PRL 78 2304	G. Brandenburg *et al.*	(CLEO Collab.)
AMMOSOV	93	JETPL 58 247	V.V. Ammosov *et al.*	(SERP)
		Translated from ZETFP 58 241.		

$\Sigma_c(2800)$

$I(J^P) = 1(?^?)$ Status: ***

Seen in the $\Lambda_c^+\pi^+$, $\Lambda_c^+\pi^0$, and $\Lambda_c^+\pi^-$ mass spectra.

$\Sigma_c(2800)$ MASSES

The charged ++ and + masses are obtained from the mass-difference measurements that follow. The neutral mass is dominated by the mass-difference measurement, but is pulled up somewhat by the less well-determined but considerably higher direct-mass measurement. It is possible, in fact, that AUBERT 08BN is seeing a different Σ_c.

$\Sigma_c(2800)^{++}$ MASS

VALUE (MeV)	DOCUMENT ID
$2801\ ^{+4}_{-6}$ OUR FIT	

$\Sigma_c(2800)^+$ MASS

VALUE (MeV)	DOCUMENT ID
$2792\ ^{+14}_{-5}$ OUR FIT	

$\Sigma_c(2800)^0$ MASS

VALUE (MeV)	DOCUMENT ID		TECN	COMMENT
$2806\ ^{+5}_{-7}$ OUR FIT Error includes scale factor of 1.3.				
2846±8±10	AUBERT	08BN	BABR	$B^- \to \overline{p}\Lambda_c^+\pi^-$

$\Sigma_c(2800)$ MASS DIFFERENCES

$m_{\Sigma_c(2800)^{++}} - m_{\Lambda_c^+}$

VALUE (MeV)	EVTS	DOCUMENT ID		TECN	COMMENT
$514\ ^{+4}_{-6}$ OUR FIT					
$514.5^{+3.4+2.8}_{-3.1-4.9}$	2810^{+1090}_{-775}	MIZUK	05	BELL	$e^+e^- \approx \Upsilon(4S)$

$m_{\Sigma_c(2800)^+} - m_{\Lambda_c^+}$

VALUE (MeV)	EVTS	DOCUMENT ID		TECN	COMMENT
$505\ ^{+14}_{-5}$ OUR FIT					
$505.4^{+5.8+12.4}_{-4.6-2.0}$	1540^{+1750}_{-1050}	MIZUK	05	BELL	$e^+e^- \approx \Upsilon(4S)$

$m_{\Sigma_c(2800)^0} - m_{\Lambda_c^+}$

VALUE (MeV)	EVTS	DOCUMENT ID		TECN	COMMENT
$519\ ^{+5}_{-7}$ OUR FIT Error includes scale factor of 1.3.					
$515.4^{+3.2+2.1}_{-3.1-6.0}$	2240^{+1300}_{-740}	MIZUK	05	BELL	$e^+e^- \approx \Upsilon(4S)$

$\Sigma_c(2800)$ WIDTHS

$\Sigma_c(2800)^{++}$ WIDTH

VALUE (MeV)	EVTS	DOCUMENT ID		TECN	COMMENT
75^{+18+12}_{-13-11}	2810^{+1090}_{-775}	MIZUK	05	BELL	$e^+e^- \approx \Upsilon(4S)$

$\Sigma_c(2800)^+$ WIDTH

VALUE (MeV)	EVTS	DOCUMENT ID		TECN	COMMENT
62^{+37+52}_{-23-38}	1540^{+1750}_{-1050}	MIZUK	05	BELL	$e^+e^- \approx \Upsilon(4S)$

$\Sigma_c(2800)^0$ WIDTH

VALUE (MeV)	EVTS	DOCUMENT ID		TECN	COMMENT
72^{+22}_{-15} OUR AVERAGE					
$86^{+33}_{-22}\pm12$		AUBERT	08BN	BABR	$B^- \to \overline{p}\Lambda_c^+\pi^-$
61^{+18+22}_{-13-13}	2240^{+1300}_{-740}	MIZUK	05	BELL	$e^+e^- \approx \Upsilon(4S)$

$\Sigma_c(2800)$ DECAY MODES

	Mode	Fraction (Γ_i/Γ)
Γ_1	$\Lambda_c^+\pi$	seen

$\Sigma_c(2800)$ REFERENCES

AUBERT	08BN	PR D78 112003	B. Aubert *et al.*	(BABAR Collab.)
MIZUK	05	PRL 94 122002	R. Mizuk *et al.*	(BELLE Collab.)

Int. J. Mod. Phys. A 2026.41. Downloaded from www.worldscientific.com
by UNIVERSITY OF CALIFORNIA @ BERKELEY on 09/16/26. Re-use and distribution is strictly not permitted, except for Open Access articles.

Ξ_c^+

$I(J^P) = \frac{1}{2}(\frac{1}{2}^+)$ Status: ***

Neither of J or P has actually been measured.

Ξ_c^+ MASS

The fit uses the Ξ_c^+ and Ξ_c^0 mass and mass-difference measurements.

VALUE (MeV)	EVTS	DOCUMENT ID		TECN	COMMENT
2467.79± 0.15 OUR FIT Error includes scale factor of 1.1.					
2467.95± 0.19 OUR AVERAGE					
2467.97± 0.14± 0.17	3.8k	[1] AAIJ	14Z	LHCB	pp at 7, 8 TeV
2468.00± 0.18± 0.51	5.1k	AALTONEN	14B	CDF	$p\overline{p}$ at 1.96 TeV
2468.1 ± 0.4 $^{+0.2}_{-1.4}$	4.9k	[2] LESIAK	05	BELL	e^+e^-, $\Upsilon(4S)$
2465.8 ± 1.9 ± 2.5	90	FRABETTI	98	E687	γ Be, $\overline{E}_\gamma$= 220 GeV
2467.0 ± 1.6 ± 2.0	147	EDWARDS	96	CLE2	$e^+e^- \approx \Upsilon(4S)$
2465.1 ± 3.6 ± 1.9	30	ALBRECHT	90F	ARG	e^+e^- at $\Upsilon(4S)$
2467 ± 3 ± 4	23	ALAM	89	CLEO	e^+e^- 10.6 GeV
2466.5 ± 2.7 ± 1.2	5	BARLAG	89C	ACCM	π^- Cu 230 GeV
• • • We do not use the following data for averages, fits, limits, etc. • • •					
2464.4 ± 2.0 ± 1.4	30	FRABETTI	93B	E687	See FRABETTI 98
2459 ± 5 ±30	56	[3] COTEUS	87	SPEC	nA $\simeq$ 600 GeV
2460 ±25	82	BIAGI	83	SPEC	Σ^-Be 135 GeV

[1] AAIJ 14Z systematic error includes in quadrature the 0.14 MeV uncertainty from the m(Λ_c^+) mass value.

[2] The systematic error was (wrongly) given the other way round in LESIAK 05; see the erratum.

[3] Although COTEUS 87 claims to agree well with BIAGI 83 on the mass and width, there appears to be a discrepancy between the two experiments. BIAGI 83 sees a single peak (stated significance about 6 standard deviations) in the $\Lambda K^-\pi^+\pi^+$ mass spectrum. COTEUS 87 sees *two* peaks in the same spectrum, one at the Ξ_c^+ mass, the other 75 MeV lower. The latter is attributed to $\Xi_c^+ \to \Sigma^0 K^-\pi^+\pi^+ \to (\Lambda\gamma)K^-\pi^+\pi^+$, with the γ unseen. The *combined* significance of the double peak is stated to be 5.5 standard deviations. But the absence of any trace of a lower peak in BIAGI 83 seems to us to throw into question the interpretation of the lower peak of COTEUS 87.

Ξ_c^+ MEAN LIFE

VALUE (10^{-15} s)	EVTS	DOCUMENT ID		TECN	COMMENT
453± 5 OUR AVERAGE					
454± 5± 2	56k	[1] AAIJ	19AG	LHCB	$\Xi_c^+ \to pK^-\pi^+$
503± 47± 18	250	MAHMOOD	02	CLE2	$e^+e^- \approx \Upsilon(4S)$
439± 22± 9	532	LINK	01D	FOCS	γ nucleus, $\overline{E}_\gamma \approx$ 180 GeV
340 $^{+70}_{-50}$ ± 20	56	FRABETTI	98	E687	γ Be, $\overline{E}_\gamma$= 220 GeV
400 $^{+180}_{-120}$ ±100	102	COTEUS	87	SPEC	nA $\simeq$ 600 GeV
480 $^{+210}_{-150}$ $^{+200}_{-100}$	53	BIAGI	85C	SPEC	Σ^-Be 135 GeV
• • • We do not use the following data for averages, fits, limits, etc. • • •					
410 $^{+110}_{-80}$ ± 20	30	FRABETTI	93B	E687	See FRABETTI 98
200 $^{+110}_{-60}$	6	BARLAG	89C	ACCM	π^- (K^-) Cu 230 GeV

[1] AAIJ 19AG reports [Ξ_c^+ MEAN LIFE] / [$D^\pm$ MEAN LIFE] = 0.4392 ± 0.0034 ± 0.0028 which we multiply by our best (shown rounded) value $D^\pm$ MEAN LIFE = (1.033 ± 0.005) × 10^{-12} s. Our first error is their experiment's error and our second error is the systematic error from using our best (shown rounded) value.

Ξ_c^+ DECAY MODES

Branching fractions marked with a footnote, e.g. [a], have been corrected for decay modes not observed in the experiments. For example, the submode fraction $\Xi_c^+ \to \Sigma^+\overline{K}^*(892)^0$ seen in $\Xi_c^+ \to \Sigma^+K^-\pi^+$ has been multiplied up to include $\overline{K}^*(892)^0 \to \overline{K}^0\pi^0$ decays.

	Mode		Fraction (Γ_i/Γ)	Scale factor/ Confidence level
	Cabibbo-favored ($S = -2$) decays			
Γ_1	$p2K_S^0$		(2.5±1.3) × 10^{-3}	
Γ_2	$\Lambda\overline{K}^0\pi^+$		—	
Γ_3	$\Sigma(1385)^+\overline{K}^0$	[a]	(2.9±2.0) %	
Γ_4	$\Lambda K^-2\pi^+$		(9 ±4) × 10^{-3}	
Γ_5	$\Lambda\overline{K}^*(892)^0\pi^+$	[a]	< 5 × 10^{-3}	CL=90%
Γ_6	$\Sigma(1385)^+K^-\pi^+$	[a]	< 6 × 10^{-3}	CL=90%
Γ_7	$\Sigma^+K_S^0$		(1.9±0.9) × 10^{-3}	
Γ_8	$\Sigma^+K^-\pi^+$		(2.7±1.2) %	
Γ_9	$\Sigma^+\overline{K}^*(892)^0$	[a]	(2.3±1.1) %	
Γ_{10}	$\Sigma^0K^-2\pi^+$		(8 ±5) × 10^{-3}	
Γ_{11}	$\Xi^0\pi^+$		(7.2±3.2) × 10^{-3}	
Γ_{12}	$\Xi^-2\pi^+$		(2.9±1.3) %	
Γ_{13}	$\Xi(1530)^0\pi^+$	[a]	< 2.9 × 10^{-3}	CL=90%
Γ_{14}	$\Xi(1620)^0\pi^+$		seen	
Γ_{15}	$\Xi(1690)^0\pi^+$		seen	
Γ_{16}	$\Xi^0\pi^+\pi^0$		(6.7±3.5) %	
Γ_{17}	$\Xi^0\pi^-2\pi^+$		(5.0±2.6) %	
Γ_{18}	$\Xi^0e^+\nu_e$		(7 ±4) %	
Γ_{19}	$\Omega^-K^+\pi^+$		(2.0±1.5) × 10^{-3}	
	Cabibbo-suppressed decays			
Γ_{20}	$pK^-\pi^+$		(6.2±3.0) × 10^{-3}	S=1.5
Γ_{21}	$p\overline{K}^*(892)^0$	[a]	(3.3±1.7) × 10^{-3}	
Γ_{22}	$p\overline{K}_0^*(700)^0$, $\overline{K}_0^*(700)^0 \to K^-\pi^+$		(5 ±4) × 10^{-4}	
Γ_{23}	$p\overline{K}^*(892)^0$, $\overline{K}^* \to K^-\pi^+$		(1.8±0.8) × 10^{-3}	
Γ_{24}	$p\overline{K}_0^*(1430)^0$, $\overline{K}_0^*(1430)^0 \to K^-\pi^+$		(10 ±6) × 10^{-4}	
Γ_{25}	$\Delta(1232)^{++}K^-$, $\Delta(1232)^{++} \to p\pi^+$		(1.1±0.5) × 10^{-3}	
Γ_{26}	$\Delta(1600)^{++}K^-$, $\Delta(1600)^{++} \to p\pi^+$		(2.7±1.5) × 10^{-4}	
Γ_{27}	$\Delta(1700)^{++}K^-$, $\Delta(1700)^{++} \to p\pi^+$		(1.2±0.7) × 10^{-4}	
Γ_{28}	$\Lambda(1405)\pi^+$, $\Lambda(1405) \to pK^-$		(2.0±1.4) × 10^{-4}	
Γ_{29}	$\Lambda(1520)\pi^+$, $\Lambda(1520) \to pK^-$		(1.6±0.8) × 10^{-4}	
Γ_{30}	$\Lambda(1670)\pi^+$, $\Lambda(1670) \to pK^-$		(1.9±0.9) × 10^{-4}	
Γ_{31}	$\Lambda(1820)\pi^+$, $\Lambda(1820) \to pK^-$		(5.1±2.7) × 10^{-5}	
Γ_{32}	$\Lambda(2000)\pi^+$, $\Lambda(2000) \to pK^-$		(4.6±2.3) × 10^{-4}	
Γ_{33}	pK_S^0		(7.1±3.2) × 10^{-4}	
Γ_{34}	$\Lambda\pi^+$		(4.5±2.0) × 10^{-4}	
Γ_{35}	$\Sigma^+\pi^+\pi^-$		(1.4±0.8) %	
Γ_{36}	$\Sigma^-2\pi^+$		(5.1±3.4) × 10^{-3}	
Γ_{37}	$\Sigma^+K^+K^-$		(4.3±2.5) × 10^{-3}	
Γ_{38}	$\Sigma^+\phi$	[a]	< 3.2 × 10^{-3}	CL=90%
Γ_{39}	$\Xi(1690)^0K^+$, $\Xi^0 \to \Sigma^+K^-$		< 1.3 × 10^{-3}	CL=90%
Γ_{40}	$\Sigma^0\pi^+$		(1.2±0.5) × 10^{-3}	
Γ_{41}	Ξ^0K^+		(4.9±2.3) × 10^{-4}	
Γ_{42}	$p\phi(1020)$		(1.2±0.6) × 10^{-4}	

[a] This branching fraction includes all the decay modes of the final-state resonance.

Ξ_c^+ BRANCHING RATIOS

Cabibbo-favored ($S = -2$) decays

$\Gamma(p2K_S^0)/\Gamma(\Xi^-2\pi^+)$ — Γ_1/Γ_{12}

VALUE	EVTS	DOCUMENT ID		TECN	COMMENT
0.087±0.016±0.014	168 ± 27	LESIAK	05	BELL	e^+e^-, $\Upsilon(4S)$

$\Gamma(\Sigma(1385)^+\overline{K}^0)/\Gamma(\Xi^-2\pi^+)$ — Γ_3/Γ_{12}

Unseen decay modes of the $\Sigma(1385)^+$ are included.

VALUE	EVTS	DOCUMENT ID		TECN	COMMENT
1.00±0.49±0.24	20	LINK	03E	FOCS	< 1.72, 90% CL

$\Gamma(\Lambda K^-2\pi^+)/\Gamma(\Xi^-2\pi^+)$ — Γ_4/Γ_{12}

VALUE	EVTS	DOCUMENT ID		TECN	COMMENT
0.323±0.033 OUR AVERAGE					
0.32 ±0.03 ±0.02	1177 ± 55	LESIAK	05	BELL	e^+e^-, $\Upsilon(4S)$
0.28 ±0.06 ±0.06	58	LINK	03E	FOCS	γ nucleus, $\overline{E}_\gamma \approx$ 180 GeV
0.58 ±0.16 ±0.07	61	BERGFELD	96	CLE2	$e^+e^- \approx \Upsilon(4S)$

$\Gamma(\Lambda\overline{K}^*(892)^0\pi^+)/\Gamma(\Lambda K^-2\pi^+)$ — Γ_5/Γ_4

Unseen decay modes of the $\overline{K}^*(892)^0$ are included.

VALUE	CL%	DOCUMENT ID		TECN	COMMENT
<0.5	90	BERGFELD	96	CLE2	$e^+e^- \approx \Upsilon(4S)$

$\Gamma(\Sigma(1385)^+K^-\pi^+)/\Gamma(\Lambda K^-2\pi^+)$ — Γ_6/Γ_4

Unseen decay modes of the $\Sigma(1385)^+$ are included.

VALUE	CL%	DOCUMENT ID		TECN	COMMENT
<0.7	90	BERGFELD	96	CLE2	$e^+e^- \approx \Upsilon(4S)$

$\Gamma(\Sigma^+K_S^0)/\Gamma(\Xi^-2\pi^+)$ — Γ_7/Γ_{12}

VALUE (units 10^{-2})	EVTS	DOCUMENT ID		TECN	COMMENT
6.7±0.7±0.3	0.47k	ADACHI	25T	BEL2	e^+e^- at Υ(nS)

Int. J. Mod. Phys. A 2026.41. Downloaded from www.worldscientific.com
UNIVERSITY OF CALIFORNIA @ BERKELEY on 09/16/26. Re-use and distribution is strictly not permitted, except for Open Access articles.

$\Gamma(\Sigma^+ K^- \pi^+)/\Gamma(\Xi^- 2\pi^+)$ — Γ_8/Γ_{12}

VALUE	EVTS	DOCUMENT ID		TECN	COMMENT
0.94±0.10 OUR AVERAGE					
0.91±0.11±0.04	251	LINK	03E	FOCS	γ nucleus, $\overline{E}_\gamma \approx 180$ GeV
0.92±0.20±0.07		[1] JUN	00	SELX	Σ^- nucleus, 600 GeV
1.18±0.26±0.17	119	BERGFELD	96	CLE2	$e^+e^- \approx \Upsilon(4S)$

[1] This JUN 00 result is redundant with other results given below.

$\Gamma(\Sigma^+ \overline{K}^*(892)^0)/\Gamma(\Xi^- 2\pi^+)$ — Γ_9/Γ_{12}

Unseen decay modes of the $\overline{K}^*(892)^0$ are included.

VALUE	EVTS	DOCUMENT ID		TECN	COMMENT
0.81±0.15 OUR AVERAGE					
0.78±0.16±0.06	119	LINK	03E	FOCS	γ nucleus, $\overline{E}_\gamma \approx 180$ GeV
0.92±0.27±0.14	61	BERGFELD	96	CLE2	$e^+e^- \approx \Upsilon(4S)$

$\Gamma(\Sigma^0 K^- 2\pi^+)/\Gamma(\Lambda K^- 2\pi^+)$ — Γ_{10}/Γ_4

VALUE	EVTS	DOCUMENT ID		TECN	COMMENT
0.84±0.36	47	[1] COTEUS	87	SPEC	$nA \simeq 600$ GeV

[1] See, however, the note on the COTEUS 87 Ξ_c^+ mass measurement.

$\Gamma(\Xi^0 \pi^+)/\Gamma(\Xi^- 2\pi^+)$ — Γ_{11}/Γ_{12}

VALUE	EVTS	DOCUMENT ID		TECN	COMMENT
0.252±0.011 OUR AVERAGE					
0.251±0.005±0.010	4.3k	ADACHI	25T	BEL2	e^+e^- at $\Upsilon(nS)$
0.55 ±0.13 ±0.09	39	EDWARDS	96	CLE2	$e^+e^- \approx \Upsilon(4S)$

$\Gamma(\Xi^- 2\pi^+)/\Gamma_{total}$ — Γ_{12}/Γ

VALUE (units 10^{-2})	EVTS	DOCUMENT ID		TECN	COMMENT
2.86±1.21±0.38	24	[1] LI	19C	BELL	$e^+e^- \approx \Upsilon(4S)$
• • • We do not use the following data for averages, fits, limits, etc. • • •					
seen	131	BERGFELD	96	CLE2	$e^+e^- \approx \Upsilon(4S)$
seen	160	AVERY	95	CLE2	$e^+e^- \approx \Upsilon(4S)$
seen	30	FRABETTI	93B	E687	γBe, $\overline{E}_\gamma = 220$ GeV
seen	30	ALBRECHT	90F	ARG	e^+e^- at $\Upsilon(4S)$
seen	23	ALAM	89	CLEO	e^+e^- 10.6 GeV

[1] LI 19C report a significance of 6.8 σ for the observation of this decay mode, observed in Ξ_c^+ from $\overline{B}^0 \to \overline{\Lambda}_c^- \Xi_c^+$.

$\Gamma(\Xi(1530)^0 \pi^+)/\Gamma(\Xi^- 2\pi^+)$ — Γ_{13}/Γ_{12}

Unseen decay modes of the $\Xi(1530)^0$ are included.

VALUE	CL%	DOCUMENT ID		TECN	COMMENT
<0.1	90	LINK	03E	FOCS	γ nucleus, $\overline{E}_\gamma \approx 180$ GeV
• • • We do not use the following data for averages, fits, limits, etc. • • •					
<0.2	90	BERGFELD	96	CLE2	$e^+e^- \approx \Upsilon(4S)$

$\Gamma(\Xi(1620)^0 \pi^+)/\Gamma_{total}$ — Γ_{14}/Γ

VALUE	DOCUMENT ID		TECN	COMMENT
seen	SUMIHAMA	19	BELL	e^+e^- mostly at $\Upsilon(4S)$

$\Gamma(\Xi(1690)^0 \pi^+)/\Gamma_{total}$ — Γ_{15}/Γ

VALUE	DOCUMENT ID		TECN	COMMENT
seen	SUMIHAMA	19	BELL	e^+e^- mostly at $\Upsilon(4S)$

$\Gamma(\Xi^0 \pi^+ \pi^0)/\Gamma(\Xi^- 2\pi^+)$ — Γ_{16}/Γ_{12}

VALUE	EVTS	DOCUMENT ID		TECN	COMMENT
2.34±0.57±0.37	81	EDWARDS	96	CLE2	$e^+e^- \approx \Upsilon(4S)$

$\Gamma(\Xi(1530)^0 \pi^+)/\Gamma(\Xi^0 \pi^+ \pi^0)$ — Γ_{13}/Γ_{16}

VALUE	CL%	DOCUMENT ID		TECN	COMMENT
• • • We do not use the following data for averages, fits, limits, etc. • • •					
<0.3	90	EDWARDS	96	CLE2	$e^+e^- \approx \Upsilon(4S)$

$\Gamma(\Xi^0 \pi^- 2\pi^+)/\Gamma(\Xi^- 2\pi^+)$ — Γ_{17}/Γ_{12}

VALUE	EVTS	DOCUMENT ID		TECN	COMMENT
1.74±0.42±0.27	57	EDWARDS	96	CLE2	$e^+e^- \approx \Upsilon(4S)$

$\Gamma(\Xi^0 e^+ \nu_e)/\Gamma(\Xi^- 2\pi^+)$ — Γ_{18}/Γ_{12}

VALUE	EVTS	DOCUMENT ID		TECN	COMMENT
$2.3 \pm 0.6^{+0.3}_{-0.6}$	41	ALEXANDER	95B	CLE2	$e^+e^- \approx \Upsilon(4S)$

$\Gamma(\Omega^- K^+ \pi^+)/\Gamma(\Xi^- 2\pi^+)$ — Γ_{19}/Γ_{12}

VALUE	EVTS	DOCUMENT ID		TECN	COMMENT
0.07±0.03±0.03	14	LINK	03E	FOCS	< 0.12, 90% CL

Cabibbo-suppressed decays

$\Gamma(p K^- \pi^+)/\Gamma_{total}$ — Γ_{20}/Γ

VALUE (units 10^{-3})	EVTS	DOCUMENT ID		TECN	COMMENT
6.2 ±3.0 OUR AVERAGE Error includes scale factor of 1.5.					
11.35±0.02±3.87	1.6M	[1] AAIJ	20AH	LHCB	pp at 13 TeV
4.5 ±2.1 ±0.7	24	[2] LI	19C	BELL	$e^+e^- \approx \Upsilon(4S)$

[1] AAIJ 20AH extracts B($\Xi_c^+ \to p K^- \pi^+$) assuming production fraction ratios $f_{\Xi_c^0}/f_{\Lambda_c^+} = (9.7 \pm 0.9 \pm 3.1) \times 10^{-2}$ (from AAIJ 19AB plus heavy quark symmetry arguments) as well as $f_{\Xi_c^0}/f_{\Xi_c^+} = 1.00 \pm 0.01$, and uses the input B($\Lambda_c^+ \to p K^- \pi^+$) = (6.23 ± 0.33) × 10^{-2}. Its correlation with B($\Xi_c^0 \to \Lambda_c^+ \pi^-$), as measured in AAIJ 20AH, is 0.414.

[2] LI 19C report a significance of 4.4 σ for the observation of this decay mode, observed in Ξ_c^+ from $\overline{B}^0 \to \overline{\Lambda}_c^- \Xi_c^+$.

$\Gamma(p K^- \pi^+)/\Gamma(\Xi^- 2\pi^+)$ — Γ_{20}/Γ_{12}

VALUE	EVTS	DOCUMENT ID		TECN	COMMENT
0.21 ±0.04 OUR AVERAGE					
0.194±0.054	47 ± 11	VAZQUEZ-JA...08		SELX	Σ^- nucleus, 600 GeV
0.234±0.047±0.022	202	LINK	01B	FOCS	γ nucleus
• • • We do not use the following data for averages, fits, limits, etc. • • •					
0.20 ±0.04 ±0.02	76	JUN	00	SELX	See VAZQUEZ-JAUREGUI 08

$\Gamma(p \overline{K}^*(892)^0)/\Gamma(p K^- \pi^+)$ — Γ_{21}/Γ_{20}

Unseen decay modes of the $\overline{K}^*(892)^0$ are included.

VALUE	DOCUMENT ID		TECN	COMMENT
0.54±0.09±0.05	LINK	01B	FOCS	γ nucleus

$\Gamma(p \overline{K}_0^*(700)^0, \overline{K}_0^*(700)^0 \to K^- \pi^+)/\Gamma(p K^- \pi^+)$ — Γ_{22}/Γ_{20}

VALUE (units 10^{-2})	EVTS	DOCUMENT ID		TECN	COMMENT
7.4±0.4±0.7±4.8	187k	[1] AAIJ	25AL	LHCB	pp at 7, 8, 13 TeV

[1] Amplitude analysis of 20 resonance modes, the third uncertainty is due to the amplitude model. We report those only those fit fractions that are either large or incompatible with zero at approximately at least 2σ significance, and whose interpretation is not subject to large interference effects.

$\Gamma(p \overline{K}^*(892)^0, \overline{K}^* \to K^- \pi^+)/\Gamma(p K^- \pi^+)$ — Γ_{23}/Γ_{20}

VALUE (units 10^{-2})	EVTS	DOCUMENT ID		TECN	COMMENT
28.61±0.28±0.80±0.82	187k	[1] AAIJ	25AL	LHCB	pp at 7, 8, 13 TeV

[1] Amplitude analysis of 20 resonance modes, the third uncertainty is due to the amplitude model. We report those only those fit fractions that are either large or incompatible with zero at approximately at least 2σ significance, and whose interpretation is not subject to large interference effects.

$\Gamma(p \overline{K}_0^*(1430)^0, \overline{K}_0^*(1430)^0 \to K^- \pi^+)/\Gamma(p K^- \pi^+)$ — Γ_{24}/Γ_{20}

VALUE (units 10^{-2})	EVTS	DOCUMENT ID		TECN	COMMENT
15.6±0.7±1.9±7.1	187k	[1] AAIJ	25AL	LHCB	pp at 7, 8, 13 TeV

[1] Amplitude analysis of 20 resonance modes, the third uncertainty is due to the amplitude model. We report those only those fit fractions that are either large or incompatible with zero at approximately at least 2σ significance, and whose interpretation is not subject to large interference effects.

$\Gamma(\Delta(1232)^{++} K^-, \Delta(1232)^{++} \to p \pi^+)/\Gamma(p K^- \pi^+)$ — Γ_{25}/Γ_{20}

VALUE (units 10^{-2})	EVTS	DOCUMENT ID		TECN	COMMENT
17.2±0.4±0.5±1.3	187k	[1] AAIJ	25AL	LHCB	pp at 7, 8, 13 TeV

[1] Amplitude analysis of 20 resonance modes, the third uncertainty is due to the amplitude model. We report those only those fit fractions that are either large or incompatible with zero at approximately at least 2σ significance, and whose interpretation is not subject to large interference effects.

$\Gamma(\Delta(1600)^{++} K^-, \Delta(1600)^{++} \to p \pi^+)/\Gamma(p K^- \pi^+)$ — Γ_{26}/Γ_{20}

VALUE (units 10^{-2})	EVTS	DOCUMENT ID		TECN	COMMENT
4.31±0.27±0.91±0.96	187k	[1] AAIJ	25AL	LHCB	pp at 7, 8, 13 TeV

[1] Amplitude analysis of 20 resonance modes, the third uncertainty is due to the amplitude model. We report those only those fit fractions that are either large or incompatible with zero at approximately at least 2σ significance, and whose interpretation is not subject to large interference effects.

$\Gamma(\Delta(1700)^{++} K^-, \Delta(1700)^{++} \to p \pi^+)/\Gamma(p K^- \pi^+)$ — Γ_{27}/Γ_{20}

VALUE (units 10^{-2})	EVTS	DOCUMENT ID		TECN	COMMENT
2.01±0.17±0.15±0.44	187k	[1] AAIJ	25AL	LHCB	pp at 7, 8, 13 TeV

[1] Amplitude analysis of 20 resonance modes, the third uncertainty is due to the amplitude model. We report those only those fit fractions that are either large or incompatible with zero at approximately at least 2σ significance, and whose interpretation is not subject to large interference effects.

$\Gamma(\Lambda(1405)\pi^+, \Lambda(1405) \to p K^-)/\Gamma(p K^- \pi^+)$ — Γ_{28}/Γ_{20}

VALUE (units 10^{-2})	EVTS	DOCUMENT ID		TECN	COMMENT
3.3±0.2±0.2±1.5	187k	[1] AAIJ	25AL	LHCB	pp at 7, 8, 13 TeV

[1] Amplitude analysis of 20 resonance modes, the third uncertainty is due to the amplitude model. We report those only those fit fractions that are either large or incompatible with zero at approximately at least 2σ significance, and whose interpretation is not subject to large interference effects.

$\Gamma(\Lambda(1520)\pi^+, \Lambda(1520) \to p K^-)/\Gamma(p K^- \pi^+)$ — Γ_{29}/Γ_{20}

VALUE (units 10^{-2})	EVTS	DOCUMENT ID		TECN	COMMENT
2.64±0.08±0.04±0.11	187k	[1] AAIJ	25AL	LHCB	pp at 7, 8, 13 TeV

[1] Amplitude analysis of 20 resonance modes, the third uncertainty is due to the amplitude model. We report those only those fit fractions that are either large or incompatible with zero at approximately at least 2σ significance, and whose interpretation is not subject to large interference effects.

Int. J. Mod. Phys. A 2026.41. Downloaded from www.worldscientific.com by UNIVERSITY OF CALIFORNIA @ BERKELEY on 09/16/26. Re-use and distribution is strictly not permitted, except for Open Access articles.

$\Gamma(\Lambda(1670)\pi^+, \Lambda(1670) \to pK^-)/\Gamma(pK^-\pi^+)$ — Γ_{30}/Γ_{20}

VALUE (units 10^{-2})	EVTS	DOCUMENT ID		TECN	COMMENT
3.03±0.09±0.11±0.17	187k	[1] AAIJ	25AL	LHCB	pp at 7, 8, 13 TeV

[1] Amplitude analysis of 20 resonance modes, the third uncertainty is due to the amplitude model. We report those only those fit fractions that are either large or incompatible with zero at approximately at least 2σ significance, and whose interpretation is not subject to large interference effects.

$\Gamma(\Lambda(1820)\pi^+, \Lambda(1820) \to pK^-)/\Gamma(pK^-\pi^+)$ — Γ_{31}/Γ_{20}

VALUE (units 10^{-2})	EVTS	DOCUMENT ID		TECN	COMMENT
0.82±0.09±0.08±0.14	187k	[1] AAIJ	25AL	LHCB	pp at 7, 8, 13 TeV

[1] Amplitude analysis of 20 resonance modes, the third uncertainty is due to the amplitude model. We report those only those fit fractions that are either large or incompatible with zero at approximately at least 2σ significance, and whose interpretation is not subject to large interference effects.

$\Gamma(\Lambda(2000)\pi^+, \Lambda(2000) \to pK^-)/\Gamma(pK^-\pi^+)$ — Γ_{32}/Γ_{20}

VALUE (units 10^{-2})	EVTS	DOCUMENT ID		TECN	COMMENT
7.4±0.3±0.8±1.1	187k	[1] AAIJ	25AL	LHCB	pp at 7, 8, 13 TeV

[1] Amplitude analysis of 20 resonance modes, the third uncertainty is due to the amplitude model. We report those only those fit fractions that are either large or incompatible with zero at approximately at least 2σ significance, and whose interpretation is not subject to large interference effects.

$\Gamma(pK_S^0)/\Gamma(\Xi^-2\pi^+)$ — Γ_{33}/Γ_{12}

VALUE (units 10^{-2})	EVTS	DOCUMENT ID		TECN	COMMENT
2.47±0.16±0.07	1.5k	ADACHI	25N	BEL2	e^+e^- at $\Upsilon(nS)$

$\Gamma(\Lambda\pi^+)/\Gamma(\Xi^-2\pi^+)$ — Γ_{34}/Γ_{12}

VALUE (units 10^{-2})	EVTS	DOCUMENT ID		TECN	COMMENT
1.56±0.14±0.09	0.8k	ADACHI	25N	BEL2	e^+e^- at $\Upsilon(nS)$

$\Gamma(\Sigma^+\pi^+\pi^-)/\Gamma(\Xi^-2\pi^+)$ — Γ_{35}/Γ_{12}

VALUE	EVTS	DOCUMENT ID		TECN	COMMENT
0.48±0.20	21 ± 8	VAZQUEZ-JA...	08	SELX	Σ^- nucleus, 600 GeV

$\Gamma(\Sigma^-2\pi^+)/\Gamma(\Xi^-2\pi^+)$ — Γ_{36}/Γ_{12}

VALUE	EVTS	DOCUMENT ID		TECN	COMMENT
0.18±0.09	10 ± 4	VAZQUEZ-JA...	08	SELX	Σ^- nucleus, 600 GeV

$\Gamma(\Sigma^+K^+K^-)/\Gamma(\Sigma^+K^-\pi^+)$ — Γ_{37}/Γ_8

VALUE	EVTS	DOCUMENT ID		TECN	COMMENT
0.16±0.06±0.01	17	LINK	03E	FOCS	γ nucleus, $\overline{E}_\gamma \approx 180$ GeV

$\Gamma(\Sigma^+\phi)/\Gamma(\Sigma^+K^-\pi^+)$ — Γ_{38}/Γ_8

Unseen decay modes of the ϕ are included.

VALUE	CL%	DOCUMENT ID		TECN	COMMENT
<0.12	90	LINK	03E	FOCS	γ nucleus, $\overline{E}_\gamma \approx 180$ GeV

$\Gamma(\Sigma^0\pi^+)/\Gamma(\Xi^-2\pi^+)$ — Γ_{40}/Γ_{12}

VALUE (units 10^{-2})	EVTS	DOCUMENT ID		TECN	COMMENT
4.13±0.26±0.22	0.9k	ADACHI	25N	BEL2	e^+e^- at $\Upsilon(nS)$

$\Gamma(\Xi(1690)^0K^+\times B(\Xi(1690)^0 \to \Sigma^+K^-))/\Gamma(\Sigma^+K^-\pi^+)$ — Γ_{39}/Γ_8

VALUE	CL%	DOCUMENT ID		TECN	COMMENT
<0.05	90	LINK	03E	FOCS	γ nucleus, $\overline{E}_\gamma \approx 180$ GeV

$\Gamma(\Xi^0K^+)/\Gamma(\Xi^-2\pi^+)$ — Γ_{41}/Γ_{12}

VALUE (units 10^{-2})	EVTS	DOCUMENT ID		TECN	COMMENT
1.7±0.3±0.1	0.24k	ADACHI	25T	BEL2	e^+e^- at $\Upsilon(nS)$

$\Gamma(p\phi(1020))/\Gamma(pK^-\pi^+)$ — Γ_{42}/Γ_{20}

VALUE (units 10^{-3})	EVTS	DOCUMENT ID		TECN	COMMENT
19.8±0.7±0.9±0.2	3.4k	[1] AAIJ	19I	LHCB	pp at 8 TeV

[1] The last uncertainty is due to the uncertainty in the $\phi \to K^+K^-$ branching fraction.

Ξ_c^+ REFERENCES

AAIJ	25AL	PR D112 092003	R. Aaij et al.	(LHCb Collab.)
ADACHI	25N	JHEP 2503 061	I. Adachi et al.	(BELLE and BELLE II Collab.)
ADACHI	25T	JHEP 2508 195	I. Adachi et al.	(BELLE and BELLE II Collab.)
AAIJ	20AH	PR D102 071101	R. Aaij et al.	(LHCb Collab.)
AAIJ	19AB	PR D99 052006	R. Aaij et al.	(LHCb Collab.)
AAIJ	19AG	PR D100 032001	R. Aaij et al.	(LHCb Collab.)
AAIJ	19I	JHEP 1904 084	R. Aaij et al.	(LHCb Collab.)
LI	19C	PR D100 031101	Y.B. Li et al.	(BELLE Collab.)
SUMIHAMA	19	PRL 122 072501	M. Sumihama et al.	(BELLE Collab.)
AAIJ	14Z	PRL 113 032001	R. Aaij et al.	(LHCb Collab.)
AALTONEN	14B	PR D89 072014	T. Aaltonen et al.	(CDF Collab.)
VAZQUEZ-JA...	08	PL B666 299	E. Vazquez-Jauregui et al.	(SELEX Collab.)
LESIAK	05	PL B605 237	T. Lesiak et al.	(BELLE Collab.)
Also		PL B617 198 (errat.)	T. Lesiak et al.	(BELLE Collab.)
LINK	03E	PL B571 139	J.M. Link et al.	(FNAL FOCUS Collab.)
MAHMOOD	02	PR D65 031102	A.H. Mahmood et al.	(CLEO Collab.)
LINK	01B	PL B512 277	J.M. Link et al.	(FNAL FOCUS Collab.)
LINK	01D	PL B523 53	J.M. Link et al.	(FNAL FOCUS Collab.)
JUN	00	PRL 84 1857	S.Y. Jun et al.	(FNAL SELEX Collab.)
FRABETTI	98	PL B427 211	P.L. Frabetti et al.	(FNAL E687 Collab.)
BERGFELD	96	PL B365 431	T. Bergfeld et al.	(CLEO Collab.)
EDWARDS	96	PL B373 261	K.W. Edwards et al.	(CLEO Collab.)
ALEXANDER	95B	PRL 74 3113	J. Alexander et al.	(CLEO Collab.)
Also		PRL 75 4155 (errat.)	J. Alexander et al.	(CLEO Collab.)
AVERY	95	PRL 75 4364	P. Avery et al.	(CLEO Collab.)
FRABETTI	93B	PRL 70 1381	P.L. Frabetti et al.	(FNAL E687 Collab.)
ALBRECHT	90F	PL B247 121	H. Albrecht et al.	(ARGUS Collab.)
ALAM	89	PL B226 401	M.S. Alam et al.	(CLEO Collab.)
BARLAG	89C	PL B233 522	S. Barlag et al.	(ACCMOR Collab.)
COTEUS	87	PRL 59 1530	P. Coteus et al.	(FNAL E400 Collab.)
BIAGI	85C	PL 150B 230	S.F. Biagi et al.	(CERN WA62 Collab.)
BIAGI	83	PL 122B 455	S.F. Biagi et al.	(CERN WA62 Collab.)

Ξ_c^0

$I(J^P) = \frac{1}{2}(\frac{1}{2}^+)$ Status: ****

Neither J or P has actually been measured.

Ξ_c^0 MASS

The fit uses the Ξ_c^0 and Ξ_c^+ mass and mass-difference measurements.

VALUE (MeV)	EVTS	DOCUMENT ID		TECN	COMMENT
2470.50±0.25 OUR FIT Error includes scale factor of 1.1.					
$2470.99^{+0.30}_{-0.50}$ OUR AVERAGE					
2470.85±0.24±0.55	3.4k	AALTONEN	14B	CDF	$p\overline{p}$ at 1.96 TeV
2471.0 ±0.3 $^{+0.2}_{-1.4}$	8.6k	[1] LESIAK	05	BELL	e^+e^-, $\Upsilon(4S)$
2470.0 ±2.8 ±2.6	85	FRABETTI	98B	E687	γ Be, $\overline{E}_\gamma = 220$ GeV
2469 ±2 ±3	9	HENDERSON	92B	CLEO	Ω^-K^+
2472.1 ±2.7 ±1.6	54	ALBRECHT	90F	ARG	e^+e^- at $\Upsilon(4S)$
2473.3 ±1.9 ±1.2	4	BARLAG	90	ACCM	$\pi^-(K^-)$ Cu 230 GeV
2472 ±3 ±4	19	ALAM	89	CLEO	e^+e^- 10.6 GeV
• • • We do not use the following data for averages, fits, limits, etc. • • •					
2462.1 ±3.1 ±1.4	42	[2] FRABETTI	93C	E687	See FRABETTI 98B
2471 ±3 ±4	14	AVERY	89	CLEO	See ALAM 89

[1] The systematic error was (wrongly) given the other way round in LESIAK 05.
[2] The FRABETTI 93C mass is well below the other measurements.

$\Xi_c^0 - \Xi_c^+$ MASS DIFFERENCE

VALUE (MeV)	EVTS	DOCUMENT ID		TECN	COMMENT
2.72±0.23 OUR FIT Error includes scale factor of 1.1.					
2.91±0.26 OUR AVERAGE					
2.85±0.30±0.04	5.1/3.4k	AALTONEN	14B	CDF	$p\overline{p}$ at 1.96 TeV
2.9 ±0.5		LESIAK	05	BELL	e^+e^-, $\Upsilon(4S)$
7.0 ±4.5 ±2.2		ALBRECHT	90F	ARG	e^+e^- at $\Upsilon(4S)$
6.8 ±3.3 ±0.5		BARLAG	90	ACCM	$\pi^-(K^-)$ Cu 230 GeV
5 ±4 ±1		ALAM	89	CLEO	$\Xi_c^0 \to \Xi^-\pi^+$, $\Xi_c^+ \to \Xi^-\pi^+\pi^+$

Ξ_c^0 MEAN LIFE

VALUE (10^{-15} s)	EVTS	DOCUMENT ID		TECN	COMMENT
150.0± 1.7 OUR AVERAGE Error includes scale factor of 1.1.					
149.2± 2.5±0.9±0.4	8.3k	[1] AAIJ	25AM	LHCB	$\Xi_b^- \to \Xi_c^0\pi^-$, $\Xi_c^0 \to pK^-K^-\pi^+$
148.0± 2.3±2.2		[2] AAIJ	22Y	LHCB	$pp \to \Xi_c^0 + X$, $\Xi_c^0 \to pK^-K^-\pi^+$
153.4± 2.4±0.7	22k	[3,4] AAIJ	19AG	LHCB	$\Xi_b^- \to \Xi_c^0\mu^-\overline{\nu}_\mu + X$, $\Xi_c^0 \to pK^-K^-\pi^+$
118 $^{+14}_{-12}$ ±5	110	LINK	02H	FOCS	γ nucleus, ≈ 180 GeV
101 $^{+25}_{-17}$ ±5	42	FRABETTI	93C	E687	γBe, $\overline{E}_\gamma = 220$ GeV
82 $^{+59}_{-30}$	4	BARLAG	90	ACCM	$\pi^-(K^-)$ Cu 230 GeV

[1] Uses $B^- \to D^0\pi^-$, $D^0 \to K^-K^+\pi^-\pi^+$ as a normalization mode to minimize the uncertainties associated with the decay time acceptance. The third uncertainty is due to the uncertainty of the D^0 lifetime, which is taken to be 410.3 ± 1.0 fs.
[2] Measured in Ξ_c^0 produced promptly in pp collisions, using $D^0 \to K^+K^-\pi^+\pi^-$ as normalisation mode. AAIJ 22Y reports this lifetime value as $(148.0 \pm 2.3 \pm 2.2 \pm 0.2) \times 10^{-15}$ s where the last uncertainty is due to the uncertainty on the D^0 lifetime value from PDG 20 average, $\tau_{D^0} = (410.1 \pm 1.5)$ fs.
[3] AAIJ 19AG reports [Ξ_c^0 MEAN LIFE] / [$D^\pm$ MEAN LIFE] = 0.1485 ± 0.0017 ± 0.0016 which we multiply by our best (shown rounded) value $D^\pm$ MEAN LIFE = (1.033 ± 0.005) $\times 10^{-12}$ s. Our first error is their experiment's error and our second error is the systematic error from using our best (shown rounded) value.
[4] Measured in Ξ_c^0 produced in semileptonic Ξ_b^- decays.

Int. J. Mod. Phys. A 2026.41. Downloaded from www.worldscientific.com
UNIVERSITY OF CALIFORNIA @ BERKELEY on 09/16/26. Re-use and distribution is strictly not permitted, except for Open Access articles.

Ξ_c^0 DECAY MODES

	Mode	Fraction (Γ_i/Γ)	Confidence level
	Cabibbo-favored decays		
Γ_1	$pK^-K^-\pi^+$	$(4.9 \pm 1.0) \times 10^{-3}$	
Γ_2	$pK^-\overline{K}^*(892)^0$, $\overline{K}^{*0} \to K^-\pi^+$	$(2.0 \pm 0.6) \times 10^{-3}$	
Γ_3	$pK^-K^-\pi^+$ (no $\overline{K}^{*0}$)	$(3.0 \pm 0.8) \times 10^{-3}$	
Γ_4	ΛK_S^0	$(3.2 \pm 0.6) \times 10^{-3}$	
Γ_5	$\Lambda K^-\pi^+$	(1.45 ± 0.28) %	
Γ_6	$\Lambda\overline{K}^*(892)^0$	$(2.6 \pm 0.6) \times 10^{-3}$	
Γ_7	$\Lambda\overline{K}^0\pi^+\pi^-$	seen	
Γ_8	$\Lambda K^-\pi^+\pi^+\pi^-$	seen	
Γ_9	$\Sigma^0 K_S^0$	$(5.4 \pm 1.4) \times 10^{-4}$	
Γ_{10}	Σ^+K^-	$(1.8 \pm 0.4) \times 10^{-3}$	
Γ_{11}	$\Sigma^0\overline{K}^*(892)^0$	$(9.9 \pm 1.9) \times 10^{-3}$	
Γ_{12}	$\Sigma^+K^*(892)^-$	$(4.9 \pm 1.3) \times 10^{-3}$	
Γ_{13}	$\Xi^-\pi^+$	(1.43 ± 0.27) %	
Γ_{14}	$\Xi^-\pi^+\pi^+\pi^-$	(4.8 ± 2.3) %	
Γ_{15}	$\Xi^0\pi^0$	$(6.9 \pm 1.4) \times 10^{-3}$	
Γ_{16}	$\Xi^0\eta$	$(1.6 \pm 0.4) \times 10^{-3}$	
Γ_{17}	$\Xi^0\eta'$	$(1.1 \pm 0.4) \times 10^{-3}$	
Γ_{18}	$\Xi^0K^+K^-$		
Γ_{19}	$\Xi^0\phi$, $\phi \to K^+K^-$	$(5.2 \pm 1.2) \times 10^{-4}$	
Γ_{20}	$\Xi^0K^+K^-$ nonresonant	$(5.6 \pm 1.2) \times 10^{-4}$	
Γ_{21}	Ω^-K^+	$(4.2 \pm 0.9) \times 10^{-3}$	
Γ_{22}	$\Xi^-e^+\nu_e$	(1.06 ± 0.21) %	
Γ_{23}	$\Xi^-\mu^+\nu_\mu$	(1.01 ± 0.21) %	
Γ_{24}	$\Xi^0\gamma$	$< 1.7 \times 10^{-4}$	90%
Γ_{25}	$\Xi^0\mu^+\mu^-$	$< 6 \times 10^{-5}$	90%
Γ_{26}	$\Xi^0e^+e^-$	$< 1.0 \times 10^{-4}$	90%
	Cabibbo-suppressed decays		
Γ_{27}	$\Lambda_c^+\pi^-$	$(5.5 \pm 1.1) \times 10^{-3}$	
Γ_{28}	Ξ^-K^+	$(3.9 \pm 1.1) \times 10^{-4}$	
Γ_{29}	ΛK^+K^- (no ϕ)	$(4.1 \pm 1.3) \times 10^{-4}$	
Γ_{30}	$\Lambda\phi$	$(4.9 \pm 1.3) \times 10^{-4}$	

FIT INFORMATION

An overall fit to 7 branching ratios uses 8 measurements to determine 4 parameters. The overall fit has a $\chi^2 = 1.4$ for 4 degrees of freedom.

The following *off-diagonal* array elements are the correlation coefficients $\langle \delta x_i \delta x_j \rangle / (\delta x_i \cdot \delta x_j)$, in percent, from the fit to the branching fractions, $x_i \equiv \Gamma_i/\Gamma_{total}$.

x_5	64		
x_{13}	86	74	
x_{27}	64	55	75
	x_1	x_5	x_{13}

Ξ_c^0 BRANCHING RATIOS

Cabibbo-favored (S = −2) decays

$\Gamma(pK^-K^-\pi^+)/\Gamma_{total}$ — Γ_1/Γ

VALUE (%)	EVTS	DOCUMENT ID		TECN	COMMENT
0.49±0.10 OUR FIT					
0.58±0.23±0.05	17 ± 5	LI	19A	BELL	e^+e^- at $\Upsilon(4S)$
• • • We do not use the following data for averages, fits, limits, etc. • • •					
seen		AAIJ	25AM	LHCB	pp at 7, 8, 13 TeV

$\Gamma(pK^-K^-\pi^+)/\Gamma(\Xi^-\pi^+)$ — Γ_1/Γ_{13}

VALUE	EVTS	DOCUMENT ID		TECN	COMMENT
0.339±0.035 OUR FIT					
0.34 ±0.04 OUR AVERAGE					
0.33 ±0.03 ±0.03	1908 ± 62	LESIAK	05	BELL	e^+e^-, $\Upsilon(4S)$
0.35 ±0.06 ±0.03	148 ± 18	DANKO	04	CLEO	e^+e^-

$\Gamma(pK^-\overline{K}^*(892)^0, \overline{K}^{*0} \to K^-\pi^+)/\Gamma(\Xi^-\pi^+)$ — Γ_2/Γ_{13}

VALUE	DOCUMENT ID		TECN	COMMENT
0.14±0.03±0.01	DANKO	04	CLEO	e^+e^-

$\Gamma(pK^-K^-\pi^+$ (no $\overline{K}^{*0}$)$)/\Gamma(\Xi^-\pi^+)$ — Γ_3/Γ_{13}

VALUE	DOCUMENT ID		TECN	COMMENT
0.21±0.04±0.02	DANKO	04	CLEO	e^+e^-

$\Gamma(\Lambda K_S^0)/\Gamma(\Xi^-\pi^+)$ — Γ_4/Γ_{13}

VALUE	EVTS	DOCUMENT ID		TECN	COMMENT
0.225±0.013 OUR AVERAGE					
0.229±0.008±0.012	5.6k	LI	21F	BELL	e^+e^- at $\Upsilon(nS)$
0.21 ±0.02 ±0.02	465 ± 37	LESIAK	05	BELL	e^+e^-, $\Upsilon(4S)$

$\Gamma(\Lambda K^-\pi^+)/\Gamma_{total}$ — Γ_5/Γ

VALUE (%)	EVTS	DOCUMENT ID		TECN	COMMENT
1.45±0.28 OUR FIT					
1.17±0.37±0.09	24 ± 6	LI	19A	BELL	e^+e^- at $\Upsilon(4S)$

$\Gamma(\Lambda K^-\pi^+)/\Gamma(\Xi^-\pi^+)$ — Γ_5/Γ_{13}

VALUE	EVTS	DOCUMENT ID		TECN	COMMENT
1.02±0.14 OUR FIT	Error includes scale factor of 1.1.				
1.07±0.12±0.07	2979 ± 211	LESIAK	05	BELL	e^+e^-, $\Upsilon(4S)$

$\Gamma(\Lambda\overline{K}^*(892)^0)/\Gamma(\Xi^-\pi^+)$ — Γ_6/Γ_{13}

VALUE	EVTS	DOCUMENT ID		TECN	COMMENT
0.18±0.02±0.01	4k	JIA	21	BELL	e^+e^- at $\Upsilon(nS)$

$\Gamma(\Lambda\overline{K}^0\pi^+\pi^-)/\Gamma_{total}$ — Γ_7/Γ

VALUE	DOCUMENT ID		TECN	COMMENT
seen	FRABETTI	98B	E687	γ Be, $\overline{E}_\gamma$ = 220 GeV

$\Gamma(\Lambda K^-\pi^+\pi^+\pi^-)/\Gamma_{total}$ — Γ_8/Γ

VALUE	DOCUMENT ID		TECN	COMMENT
seen	FRABETTI	98B	E687	γ Be, $\overline{E}_\gamma$ = 220 GeV

$\Gamma(\Sigma^0 K_S^0)/\Gamma(\Xi^-\pi^+)$ — Γ_9/Γ_{13}

VALUE (units 10^{-2})	EVTS	DOCUMENT ID		TECN	COMMENT
3.8±0.6±0.4	279	LI	21F	BELL	e^+e^- at $\Upsilon(nS)$

$\Gamma(\Sigma^+K^-)/\Gamma(\Xi^-\pi^+)$ — Γ_{10}/Γ_{13}

VALUE (units 10^{-2})	EVTS	DOCUMENT ID		TECN	COMMENT
12.3±0.7±1.0	889	LI	21F	BELL	e^+e^- at $\Upsilon(nS)$

$\Gamma(\Sigma^0\overline{K}^*(892)^0)/\Gamma(\Xi^-\pi^+)$ — Γ_{11}/Γ_{13}

VALUE	EVTS	DOCUMENT ID		TECN	COMMENT
0.69±0.03±0.03	6.3k	JIA	21	BELL	e^+e^- at $\Upsilon(nS)$

$\Gamma(\Sigma^+K^*(892)^-)/\Gamma(\Xi^-\pi^+)$ — Γ_{12}/Γ_{13}

VALUE	EVTS	DOCUMENT ID		TECN	COMMENT
0.34±0.06±0.02	373	JIA	21	BELL	e^+e^- at $\Upsilon(nS)$

$\Gamma(\Xi^-\pi^+)/\Gamma_{total}$ — Γ_{13}/Γ

VALUE (%)	EVTS	DOCUMENT ID		TECN	COMMENT
1.43±0.27 OUR FIT					
1.80±0.50±0.14	45 ± 7	LI	19A	BELL	e^+e^- at $\Upsilon(4S)$

$\Gamma(\Xi^-\pi^+)/\Gamma(\Xi^-\pi^+\pi^+\pi^-)$ — Γ_{13}/Γ_{14}

VALUE	DOCUMENT ID		TECN	COMMENT
0.30±0.12±0.05	ALBRECHT	90F	ARG	e^+e^- at $\Upsilon(4S)$

$\Gamma(\Omega^-K^+)/\Gamma(\Xi^-\pi^+)$ — Γ_{21}/Γ_{13}

VALUE	EVTS	DOCUMENT ID		TECN	COMMENT
0.294±0.018±0.016	650	AUBERT,B	05M	BABR	$e^+e^- \approx \Upsilon(4S)$

$\Gamma(\Xi^0\phi, \phi \to K^+K^-)/\Gamma(\Xi^-\pi^+)$ — Γ_{19}/Γ_{13}

VALUE	EVTS	DOCUMENT ID		TECN	COMMENT
0.036±0.004±0.002	311	[1] MCNEIL	21	BELL	e^+e^- at $\Upsilon(nS)$

[1] MCNEIL 21 assumes an azimuthally symmetric amplitude model to recover resonant and nonresonant contributions to $\Xi_c^0 \to \Xi^0K^+K^-$.

$\Gamma(\Xi^0\pi^0)/\Gamma(\Xi^-\pi^+)$ — Γ_{15}/Γ_{13}

VALUE	EVTS	DOCUMENT ID		TECN	COMMENT
0.48±0.02±0.03	2.2k	[1] ADACHI	24S	BEL2	e^+e^- at $\sim \Upsilon(nS)$

[1] Analysis of Belle and Belle II data samples.

$\Gamma(\Xi^0\eta)/\Gamma(\Xi^-\pi^+)$ — Γ_{16}/Γ_{13}

VALUE	EVTS	DOCUMENT ID		TECN	COMMENT
0.11±0.01±0.01	0.14k	[1] ADACHI	24S	BEL2	e^+e^- at $\sim \Upsilon(nS)$

[1] Analysis of Belle and Belle II data samples.

$\Gamma(\Xi^0\eta')/\Gamma(\Xi^-\pi^+)$ — Γ_{17}/Γ_{13}

VALUE	EVTS	DOCUMENT ID		TECN	COMMENT
0.08±0.02±0.01	31	[1] ADACHI	24S	BEL2	e^+e^- at $\sim \Upsilon(nS)$

[1] Analysis of Belle and Belle II data samples.

$\Gamma(\Xi^0K^+K^-$ nonresonant$)/\Gamma(\Xi^-\pi^+)$ — Γ_{20}/Γ_{13}

VALUE	EVTS	DOCUMENT ID		TECN	COMMENT
0.039±0.004±0.002	311	[1] MCNEIL	21	BELL	e^+e^- at $\Upsilon(nS)$

[1] MCNEIL 21 assumes an azimuthally symmetric amplitude model to recover resonant and nonresonant contributions to $\Xi_c^0 \to \Xi^0K^+K^-$.

Int. J. Mod. Phys. A 2026.41. Downloaded from www.worldscientific.com
by UNIVERSITY OF CALIFORNIA @ BERKELEY on 09/16/26. Re-use and distribution is strictly not permitted, except for Open Access articles.

$\Gamma(\Xi^- e^+ \nu_e)/\Gamma(\Xi^- \pi^+)$ — Γ_{22}/Γ_{13}

VALUE	EVTS	DOCUMENT ID		TECN	COMMENT
0.74 ±0.04 OUR AVERAGE					
0.825±0.094±0.081		ABUALROB	25	ALCE	pp at 13 TeV
0.730±0.021±0.039		[1] LI	21C	BELL	e^+e^- at 10.52, 10.58 GeV
• • • We do not use the following data for averages, fits, limits, etc. • • •					
0.95 ±0.15 ±0.16		[2] ACHARYA	21A	ALCE	Superseded by ABUALROB 25
3.1 ±1.0 $^{+0.3}_{-0.5}$	54	ALEXANDER	95B	CLE2	$e^+e^- \approx \Upsilon(4S)$
0.96 ±0.43 ±0.18	18	[3] ALBRECHT	93B	ARG	$e^+e^- \approx 10.4$ GeV

[1] LI 21C measures ratio $B(\Xi_c^0 \to \Xi^- e^+ \nu_e) / B(\Xi_c^0 \to \Xi^- \mu^+ \nu_\mu) = 1.03 \pm 0.05 \pm 0.07$.

[2] See erratum to ACHARYA 21A, which corrects the previously reported ratio 1.38±0.14±0.22.

[3] This ALBRECHT 93B value is the average of the $(\Xi^- e^+$ anything$)/\Xi^- \pi^+$ and $(\Xi^- \mu^+$ anything$)/\Xi^- \pi^+$ ratios. Here we average it with the $\Xi^- e^+ \nu_e/\Xi^- \pi^+$ ratio.

$\Gamma(\Xi^- e^+ \nu_e)/\Gamma(\Xi^- \mu^+ \nu_\mu)$ — Γ_{22}/Γ_{23}

VALUE	DOCUMENT ID		TECN	COMMENT
• • • We do not use the following data for averages, fits, limits, etc. • • •				
1.03±0.05±0.07	[1] LI	21C	BELL	e^+e^- at 10.52, 10.58 GeV

[1] LI 21C value is not independent from other quoted measurements.

$\Gamma(\Xi^- \mu^+ \nu_\mu)/\Gamma(\Xi^- \pi^+)$ — Γ_{23}/Γ_{13}

VALUE	DOCUMENT ID		TECN	COMMENT
0.708±0.033±0.056	[1] LI	21C	BELL	e^+e^- at 10.52, 10.58 GeV

[1] LI 21C measures ratio $B(\Xi_c^0 \to \Xi^- e^+ \nu_e) / B(\Xi_c^0 \to \Xi^- \mu^+ \nu_\mu) = 1.03 \pm 0.05 \pm 0.07$.

$\Gamma(\Xi^0 \gamma)/\Gamma(\Xi^- \pi^+)$ — Γ_{24}/Γ_{13}

VALUE	CL%	DOCUMENT ID		TECN	COMMENT
$<1.2 \times 10^{-2}$	90	LI	23	BELL	$e^+e^- \to \Upsilon(nS)$

$\Gamma(\Xi^0 \mu^+ \mu^-)/\Gamma(\Xi^- \pi^+)$ — Γ_{25}/Γ_{13}

VALUE	CL%	DOCUMENT ID		TECN	COMMENT
$<4.3 \times 10^{-3}$	90	CUI	24	BELL	980fb^{-1}, e^+e^- at $\Upsilon(4S)$

$\Gamma(\Xi^0 e^+ e^-)/\Gamma(\Xi^- \pi^+)$ — Γ_{26}/Γ_{13}

VALUE	CL%	DOCUMENT ID		TECN	COMMENT
$<6.7 \times 10^{-3}$	90	CUI	24	BELL	980fb^{-1}, e^+e^- at $\Upsilon(4S)$

Cabibbo-suppressed decays

$\Gamma(\Lambda_c^+ \pi^-)/\Gamma_{total}$ — Γ_{27}/Γ

VALUE (units 10^{-3})	EVTS	DOCUMENT ID		TECN	COMMENT
5.5±1.1 OUR FIT					
5.5±0.2±1.8	6.3k	[1] AAIJ	20AH	LHCB	pp at 13 TeV

[1] AAIJ 20AH extracts $B(\Xi_c^0 \to \Lambda_c^+ \pi^-)$ using two different normalization modes: $\Lambda_c^+ \to pK^-\pi^+$ and $\Xi_c^+ \to pK^-\pi^+$. The mean value of both results, taking their correlations into account, is presented as the final result. The measurement assumes production fraction ratios $f_{\Xi_c^0}/f_{\Lambda_c^+} = (9.7 \pm 0.9 \pm 3.1) \times 10^{-2}$ (from AAIJ 19AB plus heavy quark symmetry arguments) as well as $f_{\Xi_c^0}/f_{\Xi_c^+} = 1.00 \pm 0.01$. It further uses the inputs $B(\Lambda_c^+ \to pK^-\pi^+) = (6.23 \pm 0.33) \times 10^{-2}$ and $B(\Xi_c^+ \to pK^-\pi^+) = (4.5 \pm 2.1 \pm 0.7) \times 10^{-3}$ (from LI 19C). Its correlation with $B(\Xi_c^+ \to pK^-\pi^+)$, as measured in AAIJ 20AH, is 0.414.

$\Gamma(\Lambda_c^+ \pi^-)/\Gamma(\Xi^- \pi^+)$ — Γ_{27}/Γ_{13}

VALUE	EVTS	DOCUMENT ID		TECN	COMMENT
0.38±0.05 OUR FIT					
0.38±0.04±0.04	1468	[1] TANG	23	BELL	$e^+e^- \to \Upsilon(nS)$

[1] TANG 23 reports fitted masses $m_{\Lambda_c^+} = 2286.55 \pm 0.03$ MeV and $m_{\Xi_c^0} = 2470.43 \pm 0.06$ MeV.

$\Gamma(\Xi^- K^+)/\Gamma(\Xi^- \pi^+)$ — Γ_{28}/Γ_{13}

VALUE (units 10^{-2})	EVTS	DOCUMENT ID		TECN	COMMENT
2.75±0.51±0.25	314 ± 58	CHISTOV	13	BELL	$e^+e^- \approx \Upsilon(4S)$

$\Gamma(\Lambda K^+ K^- (\text{no}\,\phi))/\Gamma(\Xi^- \pi^+)$ — Γ_{29}/Γ_{13}

VALUE (units 10^{-2})	EVTS	DOCUMENT ID		TECN	COMMENT
2.86±0.61±0.37	510 ± 110	CHISTOV	13	BELL	$e^+e^- \approx \Upsilon(4S)$

$\Gamma(\Lambda\phi)/\Gamma(\Xi^- \pi^+)$ — Γ_{30}/Γ_{13}

VALUE (units 10^{-2})	EVTS	DOCUMENT ID		TECN	COMMENT
3.43±0.58±0.32	316 ± 54	CHISTOV	13	BELL	$e^+e^- \approx \Upsilon(4S)$

Ξ_c^0 DECAY PARAMETERS

See the note on "Baryon Decay Parameters" in the neutron Listings.

α FOR $\Xi_c^0 \to \Xi^- \pi^+$

VALUE	EVTS	DOCUMENT ID		TECN	COMMENT
−0.64±0.05±0.01		LI	21C	BELL	e^+e^- at 10.52, 10.58 GeV
• • • We do not use the following data for averages, fits, limits, etc. • • •					
$-0.56 \pm 0.39 ^{+0.10}_{-0.09}$	138	CHAN	01	CLE2	$e^+e^- \approx \Upsilon(4S)$

α FOR $\overline{\Xi}_c^0 \to \overline{\Xi}^+ \pi^-$

VALUE	DOCUMENT ID		TECN	COMMENT
0.61±0.05±0.01	LI	21C	BELL	e^+e^- at 10.52, 10.58 GeV

α FOR $\Xi_c^0 \to \Lambda \overline{K}^*(892)^0$

VALUE	EVTS	DOCUMENT ID		TECN	COMMENT
0.15±0.22±0.04	4k	[1] JIA	21	BELL	e^+e^- at $\Upsilon(nS)$

[1] JIA 21 measures $\alpha(\Xi_c^0 \to \Lambda \overline{K}^*(892)^0)\ \alpha(\Lambda \to p\pi^-) = 0.115 \pm 0.164 \pm 0.031$, and uses $\alpha(\Lambda \to p\pi^-) = 0.747 \pm 0.010$.

α FOR $\Xi_c^0 \to \Sigma^+ K^*(892)^-$

VALUE	EVTS	DOCUMENT ID		TECN	COMMENT
−0.52±0.30±0.02	373	[1] JIA	21	BELL	e^+e^- at $\Upsilon(nS)$

[1] JIA 21 measures $\alpha(\Xi_c^0 \to \Sigma^+ \overline{K}^*(892)^-)\ \alpha(\Sigma^+ \to p\pi^0) = 0.514 \pm 0.295 \pm 0.012$, and uses $\alpha(\Sigma^+ \to p\pi^0) = -0.980 \pm 0.017$.

α FOR $\Xi_c^0 \to \Xi^0 \pi^0$

VALUE	EVTS	DOCUMENT ID		TECN	COMMENT
−0.90±0.15±0.23	2.2k	[1] ADACHI	24S	BEL2	e^+e^- at $\sim \Upsilon(nS)$

[1] Analysis of Belle and Belle II data samples.

Ξ_c^0 Tests of Baryon Number Violation

τ_{mix}, $\Xi_c^0 - \overline{\Xi}_c^0$ oscillation period

VALUE (10^{-12} s)	DOCUMENT ID		TECN	COMMENT
>1.3	[1] GU	24	BELL	$e^+e^- \to \Upsilon(4S)$

[1] Search for baryon-number violating decay $B^- \to \overline{\Xi}_c^0 \overline{\Lambda}_c^-$, which can be interpreted as a search for $B^- \to \Xi_c^0 \overline{\Lambda}_c^-$ followed by $\Xi_c^0 - \overline{\Xi}_c^0$ baryon-number violating oscillation, from which a bound on the oscillation period τ_{mix} can be inferred, assuming no direct $B^- \to \overline{\Xi}_c^0 \overline{\Lambda}_c^-$ decay.

Ξ_c^0 REFERENCES

AAIJ	25AM	JHEP 2509 157	R. Aaij *et al.*	(LHCb Collab.)
ABUALROB	25	JHEP 2512 038	I.J. Abualrob *et al.*	(ALICE Collab.)
ADACHI	24S	JHEP 2410 045	I. Adachi *et al.*	(BELLE and BELLE II Collab.)
CUI	24	PR D109 052003	J.X.Cui *et al.*	(BELLE Collab.)
GU	24	PRL 133 071802	T. Gu *et al.*	(BELLE Collab.)
LI	23	PR D107 032001	Y. Li *et al.*	(BELLE Collab.)
TANG	23	PR D107 032005	S.S. Tang *et al.*	(BELLE Collab.)
AAIJ	22Y	SCIB 67 479	R. Aaij *et al.*	(LHCb Collab.)
ACHARYA	21A	PRL 127 272001	S. Acharya *et al.*	(ALICE Collab.)
Also		PRL 134 179902 (errat.)	S. Acharya *et al.*	(ALICE Collab.)
JIA	21	JHEP 2106 160	S. Jia *et al.*	(BELLE Collab.)
LI	21C	PRL 127 121803	Y.B. Li *et al.*	(BELLE Collab.)
LI	21F	PR D105 L011102	Y. Li *et al.*	(BELLE Collab.)
MCNEIL	21	PR D103 112002	J.T. McNeil *et al.*	(BELLE Collab.)
AAIJ	20AH	PR D102 071101	R. Aaij *et al.*	(LHCb Collab.)
PDG	20	PTEP 2020 083C01	P.A. Zyla *et al.*	(PDG Collab.)
AAIJ	19AB	PR D99 052006	R. Aaij *et al.*	(LHCb Collab.)
AAIJ	19AG	PR D100 032001	R. Aaij *et al.*	(LHCb Collab.)
LI	19A	PRL 122 082001	Y.B. Li *et al.*	(BELLE Collab.)
LI	19C	PR D100 031101	Y.B. Li *et al.*	(BELLE Collab.)
AALTONEN	14B	PR D89 072014	T. Aaltonen *et al.*	(CDF Collab.)
CHISTOV	13	PR D88 071103	R. Chistov *et al.*	(BELLE Collab.)
AUBERT,B	05M	PRL 95 142003	B. Aubert *et al.*	(BABAR Collab.)
LESIAK	05	PL B605 237	T. Lesiak *et al.*	(BELLE Collab.)
Also		PL B617 198 (errat.)	T. Lesiak *et al.*	(BELLE Collab.)
DANKO	04	PR D69 052004	I. Danko *et al.*	(CLEO Collab.)
LINK	02H	PL B541 211	J.M. Link *et al.*	(FNAL FOCUS Collab.)
CHAN	01	PR D63 111102	S. Chan *et al.*	(CLEO Collab.)
FRABETTI	98B	PL B426 403	P.L. Frabetti *et al.*	(FNAL E687 Collab.)
ALEXANDER	95B	PRL 74 3113	J. Alexander *et al.*	(CLEO Collab.)
Also		PRL 75 4155 (errat.)	J. Alexander *et al.*	(CLEO Collab.)
ALBRECHT	93B	PL B303 368	H. Albrecht *et al.*	(ARGUS Collab.)
FRABETTI	93C	PRL 70 2058	P.L. Frabetti *et al.*	(FNAL E687 Collab.)
HENDERSON	92B	PL B283 161	S. Henderson *et al.*	(CLEO Collab.)
ALBRECHT	90F	PL B247 121	H. Albrecht *et al.*	(ARGUS Collab.)
BARLAG	90	PL B236 495	S. Barlag *et al.*	(ACCMOR Collab.)
ALAM	89	PL B226 401	M.S. Alam *et al.*	(CLEO Collab.)
AVERY	89	PRL 62 863	P. Avery *et al.*	(CLEO Collab.)

$\Xi_c^{\prime +}$

$I(J^P) = \frac{1}{2}(\frac{1}{2}^+)$ Status: ***

The $\Xi_c^{\prime +}$ and $\Xi_c^{\prime 0}$ presumably complete the SU(3) sextet whose other members are the Σ_c^{++}, Σ_c^+, Σ_c^0, and Ω_c^0: see Fig. 5 in the "Quark Model" review. The quantum numbers given above come from this presumption but have not been measured.

$\Xi_c^{\prime +}$ MASS

The mass is obtained from the mass-difference measurement that follows.

VALUE (MeV)	DOCUMENT ID
2578.3±0.4 OUR FIT	

Int. J. Mod. Phys. A 2026.41. Downloaded from www.worldscientific.com
UNIVERSITY OF CALIFORNIA @ BERKELEY on 09/16/26. Re-use and distribution is strictly not permitted, except for Open Access articles.

$\Xi_c'^+ - \Xi_c^+$ MASS DIFFERENCE

VALUE (MeV)	EVTS	DOCUMENT ID		TECN	COMMENT
110.5±0.4 OUR FIT					
110.5±0.1±0.4	7k	YELTON	16	BELL	e^+e^-, Υ regions
• • • We do not use the following data for averages, fits, limits, etc. • • •					
107.8±1.7±2.5	25	JESSOP	99	CLE2	$e^+e^- \approx \Upsilon(4S)$

$\Xi_c'^+ - \Xi_c'^0$ MASS DIFFERENCE

VALUE (MeV)	DOCUMENT ID		TECN	COMMENT
−0.5±0.6 OUR FIT				
• • • We do not use the following data for averages, fits, limits, etc. • • •				
−0.8±0.1±0.5	YELTON	16	BELL	7055 and 11,560 evts

$\Xi_c'^+$ DECAY MODES

The $\Xi_c'^+$–Ξ_c^+ mass difference is too small for any strong decay to occur.

	Mode	Fraction (Γ_i/Γ)
Γ_1	$\Xi_c^+\gamma$	seen

$\Xi_c'^+$ REFERENCES

YELTON	16	PR D94 052011	J. Yelton *et al.*	(BELLE Collab.)
JESSOP	99	PRL 82 492	C.P. Jessop *et al.*	(CLEO Collab.)

$\Xi_c'^0$

$I(J^P) = \frac{1}{2}(\frac{1}{2}^+)$ Status: ***

The $\Xi_c'^0$ and $\Xi_c'^+$ presumably complete the SU(3) sextet whose other members are the Σ_c^{++}, Σ_c^+, Σ_c^0, and Ω_c^0: see Fig. 5 in the "Quark Model" review. The quantum numbers given above come from this presumption but have not been measured.

$\Xi_c'^0$ MASS

The mass is obtained from the mass-difference measurement that follows.

VALUE (MeV)	DOCUMENT ID
2578.8±0.5 OUR FIT	

$\Xi_c'^0 - \Xi_c^0$ MASS DIFFERENCE

VALUE (MeV)	EVTS	DOCUMENT ID		TECN	COMMENT
108.3±0.4 OUR FIT					
108.3±0.1±0.4	11.5k	YELTON	16	BELL	e^+e^-, Υ regions
• • • We do not use the following data for averages, fits, limits, etc. • • •					
107.0±1.4±2.5	28	JESSOP	99	CLE2	$e^+e^- \approx \Upsilon(4S)$

$\Xi_c'^0$ DECAY MODES

The $\Xi_c'^0 - \Xi_c^0$ mass difference is too small for any strong decay to occur.

	Mode	Fraction (Γ_i/Γ)
Γ_1	$\Xi_c^0\gamma$	seen

$\Xi_c'^0$ REFERENCES

YELTON	16	PR D94 052011	J. Yelton *et al.*	(BELLE Collab.)
JESSOP	99	PRL 82 492	C.P. Jessop *et al.*	(CLEO Collab.)

$\Xi_c(2645)$

$I(J^P) = \frac{1}{2}(\frac{3}{2}^+)$ Status: ***

The natural assignment is that this is the $J^P = 3/2^+$ excitation of the Ξ_c in the same SU(4) multiplet as the $\Delta(1232)$, but the quantum numbers have not been measured.

$\Xi_c(2645)$ MASSES

$\Xi_c(2645)^+$ MASS

VALUE (MeV)	EVTS	DOCUMENT ID		TECN	COMMENT
2645.17±0.27 OUR FIT Error includes scale factor of 1.1.					
2645.6 ±0.2 $^{+0.6}_{-0.8}$	578 ± 32	LESIAK	08	BELL	$e^+e^- \approx \Upsilon(4S)$

$\Xi_c(2645)^0$ MASS

VALUE (MeV)	EVTS	DOCUMENT ID		TECN	COMMENT
2646.24±0.18 OUR FIT Error includes scale factor of 1.1.					
2645.7 ±0.2 $^{+0.6}_{-0.7}$	611 ± 32	LESIAK	08	BELL	$e^+e^- \approx \Upsilon(4S)$

$\Xi_c(2645) - \Xi_c$ MASS DIFFERENCES

$m_{\Xi_c(2645)^+} - m_{\Xi_c^0}$

VALUE (MeV)	EVTS	DOCUMENT ID		TECN	COMMENT
174.67±0.09 OUR FIT					
174.66±0.06±0.07	1260	YELTON	16	BELL	e^+e^- in Υ regions
• • • We do not use the following data for averages, fits, limits, etc. • • •					
177.1 ±0.5 ±1.1	47	FRABETTI	98B	E687	γ Be, $\bar{E}_\gamma$ = 220 GeV
174.3 ±0.5 ±1.0	34	GIBBONS	96	CLE2	$e^+e^- \approx \Upsilon(4S)$

$m_{\Xi_c(2645)^0} - m_{\Xi_c^+}$

VALUE (MeV)	EVTS	DOCUMENT ID		TECN	COMMENT
178.45±0.10 OUR FIT					
178.46±0.07±0.07	975	YELTON	16	BELL	e^+e^- in Υ regions
• • • We do not use the following data for averages, fits, limits, etc. • • •					
178.2 ±0.5 ±1.0	55	AVERY	95	CLE2	$e^+e^- \approx \Upsilon(4S)$

$\Xi_c(2645)^+ - \Xi_c(2645)^0$ MASS DIFFERENCE

VALUE (MeV)	DOCUMENT ID		TECN	COMMENT
−1.06±0.27 OUR FIT Error includes scale factor of 1.1.				
• • • We do not use the following data for averages, fits, limits, etc. • • •				
−0.85±0.09±0.49	YELTON	16	BELL	1260 and 975 evts
−0.1 ±0.3 ±0.6	LESIAK	08	BELL	≈ 600 evts each

$\Xi_c(2645)$ WIDTHS

$\Xi_c(2645)^+$ WIDTH

VALUE (MeV)	CL%	EVTS	DOCUMENT ID		TECN	COMMENT
2.14±0.19 OUR AVERAGE Error includes scale factor of 1.1.						
2.06±0.13±0.13		1260	YELTON	16	BELL	e^+e^- in Υ regions
2.6 ±0.2 ±0.4		3.7k	KATO	14	BELL	e^+e^- $\Upsilon(1S)$-$\Upsilon(5S)$
• • • We do not use the following data for averages, fits, limits, etc. • • •						
<3.1	90		GIBBONS	96	CLE2	$e^+e^- \approx \Upsilon(4S)$

$\Xi_c(2645)^0$ WIDTH

VALUE (MeV)	CL%	EVTS	DOCUMENT ID		TECN	COMMENT
2.35±0.18±0.13		975	YELTON	16	BELL	e^+e^- in Υ regions
• • • We do not use the following data for averages, fits, limits, etc. • • •						
<5.5	90	55	AVERY	95	CLE2	$e^+e^- \approx \Upsilon(4S)$

$\Xi_c(2645)$ DECAY MODES

$\Xi_c\pi$ is the only strong decay allowed to a Ξ_c resonance having this mass.

	Mode	Fraction (Γ_i/Γ)
Γ_1	$\Xi_c^0\pi^+$	seen
Γ_2	$\Xi_c^+\pi^-$	seen

$\Xi_c(2645)$ REFERENCES

YELTON	16	PR D94 052011	J. Yelton *et al.*	(BELLE Collab.)
KATO	14	PR D89 052003	Y. Kato *et al.*	(BELLE Collab.)
LESIAK	08	PL B665 9	T. Lesiak *et al.*	(BELLE Collab.)
FRABETTI	98B	PL B426 403	P.L. Frabetti *et al.*	(FNAL E687 Collab.)
GIBBONS	96	PRL 77 810	L.K. Gibbons *et al.*	(CLEO Collab.)
AVERY	95	PRL 75 4364	P. Avery *et al.*	(CLEO Collab.)

$\Xi_c(2790)$

$I(J^P) = \frac{1}{2}(\frac{1}{2}^-)$ Status: ***

Seen in $\Xi_c'\pi$ decays. The simplest assignment, based on the mass, width, and decay mode, is that this belongs in the same SU(4) multiplet as the $\Lambda(1405)$ and the $\Lambda_c(2595)^+$, but the spin and parity have not been measured.

$\Xi_c(2790)$ MASSES

The masses are obtained from the mass-difference measurements that follow.

$\Xi_c(2790)^+$ MASS

VALUE (MeV)	DOCUMENT ID
2792.0±0.5 OUR FIT	

$\Xi_c(2790)^0$ MASS

VALUE (MeV)	DOCUMENT ID
2794.0±0.5 OUR FIT	

Int. J. Mod. Phys. A 2026.41. Downloaded from www.worldscientific.com by UNIVERSITY OF CALIFORNIA @ BERKELEY on 09/16/26. Re-use and distribution is strictly not permitted, except for Open Access articles.

$\Xi_c(2790)$ − Ξ'_c MASS DIFFERENCES

$m_{\Xi_c(2790)^+} - m_{\Xi^0_c}$

VALUE (MeV)	EVTS	DOCUMENT ID		TECN	COMMENT
213.20±0.22 OUR FIT					
213.2 ±0.2 ±0.1		YELTON	16	BELL	2231 and 11,560 evts
• • • We do not use the following data for averages, fits, limits, etc. • • •					
211.2 ±1.3 ±1.0	18	CSORNA	01	CLEO	$e^+e^- \approx \Upsilon(4S)$

$m_{\Xi_c(2790)^0} - m_{\Xi'^+_c}$

VALUE (MeV)	EVTS	DOCUMENT ID		TECN	COMMENT
215.70±0.22 OUR FIT					
215.7 ±0.2 ±0.1		YELTON	16	BELL	1241 and 7055 evts
• • • We do not use the following data for averages, fits, limits, etc. • • •					
216.2 ±1.3 ±1.0	14	CSORNA	01	CLEO	$e^+e^- \approx \Upsilon(4S)$

$\Xi_c(2790)^+$ − $\Xi_c(2790)^0$ MASS DIFFERENCE

VALUE (MeV)	DOCUMENT ID		TECN	COMMENT
−2.0±0.7 OUR FIT				
• • • We do not use the following data for averages, fits, limits, etc. • • •				
−3.3±0.4±0.5	YELTON	16	BELL	2231 and 1241 evts

$\Xi_c(2790)$ WIDTHS

$\Xi_c(2790)^+$ WIDTH

VALUE (MeV)	CL%	EVTS	DOCUMENT ID		TECN	COMMENT
8.9±0.6±0.8		2231	YELTON	16	BELL	e^+e^-, Υ regions
• • • We do not use the following data for averages, fits, limits, etc. • • •						
<15	90		CSORNA	01	CLEO	$e^+e^- \approx \Upsilon(4S)$

$\Xi_c(2790)^0$ WIDTH

VALUE (MeV)	CL%	EVTS	DOCUMENT ID		TECN	COMMENT
10.0±0.7±0.8		1241	YELTON	16	BELL	e^+e^-, Υ regions
• • • We do not use the following data for averages, fits, limits, etc. • • •						
<12	90		CSORNA	01	CLEO	$e^+e^- \approx \Upsilon(4S)$

$\Xi_c(2790)$ DECAY MODES

	Mode	Fraction (Γ_i/Γ)
Γ_1	$\Xi'_c\pi$	seen
Γ_2	$\Xi^0_c\gamma$	
Γ_3	$\Xi^+_c\gamma$	
Γ_4	$\Lambda^+_c K^-$	seen

$\Xi_c(2790)$ BRANCHING RATIOS

$\Gamma(\Xi'_c\pi)/\Gamma_{total}$ — Γ_1/Γ

VALUE	DOCUMENT ID		TECN	COMMENT
seen	YELTON	16	BELL	e^+e^-, Υ regions
seen	CSORNA	01	CLEO	$e^+e^- \approx \Upsilon(4S)$

$\Gamma(\Xi^0_c\gamma)/\Gamma(\Xi'_c\pi)$ — Γ_2/Γ_1

VALUE	EVTS	DOCUMENT ID		TECN	CHG	COMMENT
0.13±0.03±0.02	401	[1] YELTON	20	BELL	0	e^+e^- at $\Upsilon(4S)$

[1] Assumes $B(\Xi'^+_c \to \Xi^+_c\gamma) = 100\%$, noting no strong decay of the Ξ'_c is permitted in the available phase space. YELTON 20 measures $B(\Xi_c(2790)^0 \to \Xi^0_c\gamma)/B(\Xi_c(2790)^0 \to \Xi'^+_c\pi^- \to \Xi^+_c\gamma\pi^-)$.

$\Gamma(\Xi^+_c\gamma)/\Gamma(\Xi'_c\pi)$ — Γ_3/Γ_1

VALUE	CL%	DOCUMENT ID		TECN	CHG	COMMENT
<0.06	90	[1] YELTON	20	BELL	+	e^+e^- at $\Upsilon(4S)$

[1] Assumes $B(\Xi'^0_c \to \Xi^0_c\gamma) = 100\%$, noting no strong decay of the Ξ'_c is permitted in the available phase space. YELTON 20 measures $B(\Xi_c(2790)^+ \to \Xi^+_c\gamma)/B(\Xi_c(2790)^+ \to \Xi'^0_c\pi^+ \to \Xi^0_c\gamma\pi^+)$.

$\Gamma(\Lambda^+_c K^-)/\Gamma_{total}$ — Γ_4/Γ

VALUE	EVTS	DOCUMENT ID		TECN	COMMENT
seen	1.5k	[1] AAIJ	23X	LHCB	$B^- \to \Lambda^+_c\overline{\Lambda}^-_c K^-$

[1] AAIJ 23X observes this decay mode at 3.7σ significance from a study of the $\Lambda^+_c K^-$ system within $B^- \to \Lambda^+_c\overline{\Lambda}^-_c K^-$ decays.

$\Xi_c(2790)$ REFERENCES

AAIJ	23X	PR D108 012020	R. Aaij *et al.*	(LHCb Collab.)
YELTON	20	PR D102 071103	J. Yelton *et al.*	(BELLE Collab.)
YELTON	16	PR D94 052011	J. Yelton *et al.*	(BELLE Collab.)
CSORNA	01	PRL 86 4243	S.E. Csorna *et al.*	(CLEO Collab.)

$\Xi_c(2815)$

$I(J^P) = \frac{1}{2}(\frac{3}{2}^-)$ Status: ***

Seen in both $\Xi'_c\pi$ and $\Xi_c\pi\pi$ decays. The simplest assignment is that this belongs to the same SU(4) multiplet as the $\Lambda(1520)$ and the $\Lambda_c(2625)$, but the spin and parity have not been measured.

$\Xi_c(2815)$ MASSES

The masses are obtained from the mass-difference measurements that follow.

$\Xi_c(2815)^+$ MASS

VALUE (MeV)	EVTS	DOCUMENT ID		TECN	COMMENT
2816.60±0.16 OUR FIT					
2816.65±0.03±0.03±0.23	4.1k	[1] AAIJ	25AI	LHCB	pp at 13 TeV
• • • We do not use the following data for averages, fits, limits, etc. • • •					
2817.0 ±1.2 $^{+0.7}_{-0.8}$	73	LESIAK	08	BELL	$e^+e^- \approx \Upsilon(4S)$

[1] The third uncertainty is due to the Ξ^+_c mass.

$\Xi_c(2815)^0$ MASS

VALUE (MeV)	EVTS	DOCUMENT ID		TECN	COMMENT
2819.85±0.27 OUR FIT Error includes scale factor of 1.1.					
• • • We do not use the following data for averages, fits, limits, etc. • • •					
2820.4 ±1.4 $^{+0.9}_{-1.0}$	48 ± 8	LESIAK	08	BELL	$e^+e^- \approx \Upsilon(4S)$

$\Xi_c(2815)$ − Ξ_c MASS DIFFERENCES

$m_{\Xi_c(2815)^+} - m_{\Xi^+_c}$

VALUE (MeV)	EVTS	DOCUMENT ID		TECN	COMMENT
348.81±0.09 OUR FIT					
348.80±0.08±0.06	941	YELTON	16	BELL	e^+e^-, Υ regions
• • • We do not use the following data for averages, fits, limits, etc. • • •					
348.6 ±0.6 ±1.0	20	ALEXANDER	99B	CLE2	$e^+e^- \approx \Upsilon(4S)$

$m_{\Xi_c(2815)^0} - m_{\Xi^0_c}$

VALUE (MeV)	EVTS	DOCUMENT ID		TECN	COMMENT
349.35±0.11 OUR FIT					
349.35±0.08±0.07	1258	YELTON	16	BELL	e^+e^-, Υ regions
• • • We do not use the following data for averages, fits, limits, etc. • • •					
347.2 ±0.7 ±2.0	9	ALEXANDER	99B	CLE2	$e^+e^- \approx \Upsilon(4S)$

$\Xi_c(2815)^+$ − $\Xi_c(2815)^0$ MASS DIFFERENCE

$m_{\Xi_c(2815)^+} - m_{\Xi_c(2815)^0}$

VALUE (MeV)	DOCUMENT ID		TECN	COMMENT
−3.26±0.27 OUR FIT				
• • • We do not use the following data for averages, fits, limits, etc. • • •				
−3.47±0.12±0.48	YELTON	16	BELL	941 and 1258 evts
−3.4 ±1.9 ±0.9	LESIAK	08	BELL	73 & 48 events

$\Xi_c(2815)$ WIDTHS

$\Xi_c(2815)^+$ WIDTH

VALUE (MeV)	CL%	EVTS	DOCUMENT ID		TECN	COMMENT
2.15±0.15 OUR AVERAGE Error includes scale factor of 1.2.						
2.07±0.08±0.12		4.1k	AAIJ	25AI	LHCB	pp at 13 TeV
2.43±0.20±0.17		941	YELTON	16	BELL	e^+e^-, Υ regions
• • • We do not use the following data for averages, fits, limits, etc. • • •						
<3.5	90		ALEXANDER	99B	CLE2	$e^+e^- \approx \Upsilon(4S)$

$\Xi_c(2815)^0$ WIDTH

VALUE (MeV)	CL%	EVTS	DOCUMENT ID		TECN	COMMENT
2.54±0.18±0.17		1258	YELTON	16	BELL	e^+e^-, Υ regions
• • • We do not use the following data for averages, fits, limits, etc. • • •						
<6.5	90		ALEXANDER	99B	CLE2	$e^+e^- \approx \Upsilon(4S)$

$\Xi_c(2815)$ DECAY MODES

The $\Xi_c\pi\pi$ modes are consistent with being entirely via $\Xi_c(2645)\pi$.

	Mode	Fraction (Γ_i/Γ)
Γ_1	$\Xi'_c\pi$	seen
Γ_2	$\Xi_c(2645)\pi$	seen
Γ_3	$\Xi^+_c\pi^+\pi^-$	seen
Γ_4	$\Xi^0_c\gamma$	seen
Γ_5	$\Xi^+_c\gamma$	

$\Gamma(\Xi'_c\pi)/\Gamma_{total}$ — Γ_1/Γ

VALUE	DOCUMENT ID		TECN	COMMENT
seen	YELTON	16	BELL	e^+e^-, Υ regions
seen	ALEXANDER	99B	CLE2	$e^+e^- \approx \Upsilon(4S)$

Int. J. Mod. Phys. A 2026.41. Downloaded from www.worldscientific.com
UNIVERSITY OF CALIFORNIA @ BERKELEY on 09/16/26. Re-use and distribution is strictly not permitted, except for Open Access articles.

$\Gamma(\Xi_c(2645)\pi)/\Gamma_{total}$ — Γ_2/Γ

VALUE	DOCUMENT ID		TECN	COMMENT
seen	YELTON	16	BELL	e^+e^-, Υ regions
seen	LESIAK	08	BELL	$e^+e^- \approx \Upsilon(4S)$

$\Gamma(\Xi_c^+\pi^+\pi^-)/\Gamma_{total}$ — Γ_3/Γ

VALUE	EVTS	DOCUMENT ID		TECN	COMMENT
seen	4.1k	AAIJ	25AI	LHCB	pp at 13 TeV

$\Gamma(\Xi_c^0\gamma)/\Gamma(\Xi_c(2645)\pi)$ — Γ_4/Γ_2

VALUE	EVTS	DOCUMENT ID		TECN	CHG	COMMENT
0.41±0.05±0.03	222	[1] YELTON	20	BELL	0	e^+e^- at $\Upsilon(4S)$

[1] Assumes $B(\Xi_c(2645)^+ \to \Xi_c^0\pi^+) = 100\%$, which is the only strong decay of the $\Xi_c(2645)$ permitted in the available phase space. YELTON 20 measures $B(\Xi_c(2815)^0 \to \Xi_c^0\gamma)/B(\Xi_c(2815)^0 \to \Xi_c(2645)^+\pi^- \to \Xi_c^0\pi^+\pi^-)$.

$\Gamma(\Xi_c^+\gamma)/\Gamma(\Xi_c(2645)\pi)$ — Γ_5/Γ_2

VALUE	CL%	DOCUMENT ID		TECN	CHG	COMMENT
<0.09	90	[1] YELTON	20	BELL	+	e^+e^- at $\Upsilon(4S)$

[1] Assumes $B(\Xi_c(2645)^0 \to \Xi_c^+\pi^-) = 100\%$, which is the only strong decay of the $\Xi_c(2645)$ permitted in the available phase space. YELTON 20 measures $B(\Xi_c(2815)^+ \to \Xi_c^+\gamma)/B(\Xi_c(2815)^+ \to \Xi_c(2645)^0\pi^+ \to \Xi_c^+\pi^-\pi^+)$.

$\Xi_c(2815)$ REFERENCES

AAIJ	25AI	PRL 135 161901	R. Aaij *et al.*	(LHCb Collab.)
YELTON	20	PR D102 071103	J. Yelton *et al.*	(BELLE Collab.)
YELTON	16	PR D94 052011	J. Yelton *et al.*	(BELLE Collab.)
LESIAK	08	PL B665 9	T. Lesiak *et al.*	(BELLE Collab.)
ALEXANDER	99B	PRL 83 3390	J.P. Alexander *et al.*	(CLEO Collab.)

$\Xi_c(2882)$

$I(J^P) = ?(?^?)$ Status: *

OMITTED FROM SUMMARY TABLE

$\Xi_c(2882)$ MASS

VALUE (MeV)	EVTS	DOCUMENT ID		TECN	COMMENT
2881.8±3.1±8.5	1.5k	[1] AAIJ	23X	LHCB	$B^- \to \Lambda_c^+\overline{\Lambda}_c^- K^-$

[1] AAIJ 23X finds evidence of this state with a local significance of 3.8σ.

$\Xi_c(2882)$ WIDTH

VALUE (MeV)	EVTS	DOCUMENT ID		TECN	COMMENT
12.4±5.3±5.8	1.5k	[1] AAIJ	23X	LHCB	$B^- \to \Lambda_c^+\overline{\Lambda}_c^- K^-$

[1] AAIJ 23X finds evidence of this state with a local significance of 3.8σ.

$\Xi_c(2882)$ DECAY MODES

	Mode	Fraction (Γ_i/Γ)
Γ_1	$\Lambda_c^+ K^-$	seen

$\Xi_c(2882)$ BRANCHING RATIOS

$\Gamma(\Lambda_c^+ K^-)/\Gamma_{total}$ — Γ_1/Γ

VALUE	EVTS	DOCUMENT ID		TECN	COMMENT
seen	1.5k	AAIJ	23X	LHCB	$B^- \to \Lambda_c^+\overline{\Lambda}_c^- K^-$

$\Xi_c(2882)$ REFERENCES

AAIJ	23X	PR D108 012020	R. Aaij *et al.*	(LHCb Collab.)

$\Xi_c(2923)$

$I(J^P) = ?(?^?)$ Status: **

OMITTED FROM SUMMARY TABLE

$\Xi_c(2923)$ MASSES

$\Xi_c(2923)^0$ MASS

VALUE (MeV)	EVTS	DOCUMENT ID		TECN	COMMENT
2923.2 ±0.4 OUR AVERAGE	Error includes scale factor of 1.2.				
2924.5 ±0.4 ±1.1	1.5k	[1] AAIJ	23X	LHCB	$B^- \to \Lambda_c^+\overline{\Lambda}_c^- K^-$
2923.04±0.25±0.24	5.4k	[2] AAIJ	20X	LHCB	pp at 13 TeV

[1] AAIJ 23X studies the $\Lambda_c^+ K^-$ system within $B^- \to \Lambda_c^+\overline{\Lambda}_c^- K^-$ decays.

[2] AAIJ 20X uses a prompt $\Lambda_c^+ K^-$ sample, and reports 2923.04 ± 0.25 ± 0.20 ± 0.14 MeV where the last uncertainty is due to the Λ_c^+ mass.

$\Xi_c(2923)^+$ MASS

VALUE (MeV)	EVTS	DOCUMENT ID		TECN	COMMENT
2922.8±0.3±0.5±0.2	0.74k	[1] AAIJ	25AI	LHCB	pp at 13 TeV

[1] The third uncertainty is due to the Ξ_c^+ mass.

$\Xi_c(2923)$ WIDTHS

$\Xi_c(2923)^0$ WIDTH

VALUE (MeV)	EVTS	DOCUMENT ID		TECN	COMMENT
5.8±1.3 OUR AVERAGE					
4.8±0.9±1.5	1.5k	[1] AAIJ	23X	LHCB	$B^- \to \Lambda_c^+\overline{\Lambda}_c^- K^-$
7.1±0.8±1.8	5.4k	[2] AAIJ	20X	LHCB	pp at 13 TeV

[1] AAIJ 23X studies the $\Lambda_c^+ K^-$ system within $B^- \to \Lambda_c^+\overline{\Lambda}_c^- K^-$ decays.

[2] AAIJ 20X uses a prompt $\Lambda_c^+ K^-$ sample

$\Xi_c(2923)^+$ WIDTH

VALUE (MeV)	EVTS	DOCUMENT ID		TECN	COMMENT
5.3±0.9±1.4	0.74k	AAIJ	25AI	LHCB	pp at 13 TeV

$\Xi_c(2923)$ DECAY MODES

	Mode	Fraction (Γ_i/Γ)
Γ_1	$\Lambda_c^+ K^-$	seen
Γ_2	$\Xi_c^+\pi^+\pi^-$	seen

$\Xi_c(2923)$ BRANCHING RATIOS

$\Gamma(\Lambda_c^+ K^-)/\Gamma_{total}$ — Γ_1/Γ

VALUE	EVTS	DOCUMENT ID		TECN	COMMENT
seen	1.5k	AAIJ	23X	LHCB	$B^- \to \Lambda_c^+\overline{\Lambda}_c^- K^-$
seen	5.4k	AAIJ	20X	LHCB	pp at 13 TeV

$\Gamma(\Xi_c^+\pi^+\pi^-)/\Gamma_{total}$ — Γ_2/Γ

VALUE	EVTS	DOCUMENT ID		TECN	COMMENT
seen	0.74k	[1] AAIJ	25AI	LHCB	pp at 13 TeV

[1] AAIJ 25AI observes the $\Xi_c(2923)^+$ state with over 10σ significance.

$\Xi_c(2923)$ REFERENCES

AAIJ	25AI	PRL 135 161901	R. Aaij *et al.*	(LHCb Collab.)
AAIJ	23X	PR D108 012020	R. Aaij *et al.*	(LHCb Collab.)
AAIJ	20X	PRL 124 222001	R. Aaij *et al.*	(LHCb Collab.)

$\Xi_c(2930)$

$I(J^P) = ?(?^?)$ Status: **

OMITTED FROM SUMMARY TABLE

$\Xi_c(2930)$ MASSES

$\Xi_c(2930)^+$ MASS

VALUE (MeV)	EVTS	DOCUMENT ID		TECN	COMMENT
2942.3±4.4±1.5	21	LI	18D	BELL	e^+e^- at $\Upsilon(4S)$

$\Xi_c(2930)^0$ MASS

VALUE (MeV)	EVTS	DOCUMENT ID		TECN	COMMENT
2938.55±0.30 OUR AVERAGE					
2938.5 ±0.9 ± 2.3	1.5k	[1] AAIJ	23X	LHCB	$B^- \to \Lambda_c^+\overline{\Lambda}_c^- K^-$
2938.55±0.21± 0.22	10.4k	[2] AAIJ	20X	LHCB	pp at 13 TeV
• • • We do not use the following data for averages, fits, limits, etc. • • •					
2928.9 ±3.0 $^{+0.9}_{-12.0}$	61	LI	18A	BELL	e^+e^- at $\Upsilon(4S)$
2931 ±3 ± 5	34	AUBERT	08H	BABR	$\Upsilon(4S) \to B\overline{B}$

[1] AAIJ 23X studies the $\Lambda_c^+ K^-$ system within $B^- \to \Lambda_c^+\overline{\Lambda}_c^- K^-$ decays.

[2] AAIJ 20X uses a prompt $\Lambda_c^+ K^-$ sample and reports 2938.55 ± 0.21 ± 0.17 ± 0.14 MeV where the last uncertainty is due to the Λ_c^+ mass. Observes that the broader resonance at 2930 MeV seen in $B^- \to K^-\Lambda_c^+\overline{\Lambda}_c^-$ by LI 18A and AUBERT 08H resolves into two narrower peaks at approximately 2939 MeV and 2923 MeV.

$\Xi_c(2930)^+ - \Xi_c(2930)^0$ MASS DIFFERENCE

VALUE (MeV)	EVTS	DOCUMENT ID		TECN	COMMENT
• • • We do not use the following data for averages, fits, limits, etc. • • •					
13.4±5.3$^{+1.7}_{-12.1}$	21	[1] LI	18D	BELL	e^+e^- at $\Upsilon(4S)$

[1] This LI 18D value is not independent of the mass measurements.

Int. J. Mod. Phys. A 2026.41. Downloaded from www.worldscientific.com
by UNIVERSITY OF CALIFORNIA @ BERKELEY on 09/16/26. Re-use and distribution is strictly not permitted, except for Open Access articles.

$\Xi_c(2930)$ WIDTHS

$\Xi_c(2930)^+$ WIDTH

VALUE (MeV)	EVTS	DOCUMENT ID		TECN	COMMENT
14.8±8.8±2.5	21	LI	18D	BELL	e^+e^- at $\Upsilon(4S)$

$\Xi_c(2930)^0$ WIDTH

VALUE (MeV)	EVTS	DOCUMENT ID		TECN	COMMENT
10.2±0.8± 1.1	10.4k	[1] AAIJ	20X	LHCB	pp at 13 TeV
• • • We do not use the following data for averages, fits, limits, etc. • • •					
11.0±1.9± 7.5	1.5k	[2] AAIJ	23X	LHCB	$B^- \to \Lambda_c^+ \overline{\Lambda}_c^- K^-$
$19.5 \pm 8.4 ^{+5.9}_{-7.9}$	61	LI	18A	BELL	e^+e^- at $\Upsilon(4S)$
36 ±7 ±11	34	AUBERT	08H	BABR	$\Upsilon(4S) \to B\overline{B}$

[1] AAIJ 20X uses a prompt $\Lambda_c^+ K^-$ sample and observes that the broader resonance at 2930 MeV seen in $B^- \to K^- \Lambda_c^+ \overline{\Lambda}_c^-$ by LI 18A and AUBERT 08H resolves into two narrower peaks at approximately 2939 MeV and 2923 MeV.

[2] AAIJ 23X studies the $\Lambda_c^+ K^-$ system within $B^- \to \Lambda_c^+ \overline{\Lambda}_c^- K^-$ decays.

$\Xi_c(2930)$ DECAY MODES

	Mode	Fraction (Γ_i/Γ)
Γ_1	$\Lambda_c^+ K^-$	seen
Γ_2	$\Lambda_c^+ K_S^0$	seen

$\Xi_c(2930)$ BRANCHING RATIOS

$\Gamma(\Lambda_c^+ K^-)/\Gamma_{total}$ — Γ_1/Γ

VALUE	EVTS	DOCUMENT ID		TECN	COMMENT
seen	1.5k	AAIJ	23X	LHCB	$B^- \to \Lambda_c^+ \overline{\Lambda}_c^- K^-$
seen	10.4k	AAIJ	20X	LHCB	pp at 13 TeV
seen	61	LI	18A	BELL	Significance 5.1 std
seen	34	AUBERT	08H	BABR	e^+e^- at $\Upsilon(4S)$

$\Gamma(\Lambda_c^+ K_S^0)/\Gamma_{total}$ — Γ_2/Γ

VALUE	EVTS	DOCUMENT ID		TECN	COMMENT
seen	21	LI	18D	BELL	Significance 4.1 std

$\Xi_c(2930)$ REFERENCES

AAIJ	23X	PR D108 012020	R. Aaij *et al.*	(LHCb Collab.)
AAIJ	20X	PRL 124 222001	R. Aaij *et al.*	(LHCb Collab.)
LI	18A	EPJ C78 252	Y.B. Li *et al.*	(BELLE Collab.)
LI	18D	EPJ C78 928	Y.B. Li *et al.*	(BELLE Collab.)
AUBERT	08H	PR D77 031101	B. Aubert *et al.*	(BABAR Collab.)

$\Xi_c(2970)$

$I(J^P) = \frac{1}{2}(\frac{1}{2}^+)$ Status: ***

was $\Xi_c(2980)$

$J^P = 1/2^+$ is favored by MOON 21.

$\Xi_c(2970)$ MASSES

$\Xi_c(2970)^+$ MASS

VALUE (MeV)	EVTS	DOCUMENT ID		TECN	COMMENT
2965.2±1.0 OUR FIT Error includes scale factor of 2.9.					
2967.8±1.0 OUR AVERAGE Error includes scale factor of 1.8. See the ideogram below.					
2968.6±0.5±0.6	6.1k	[1] AAIJ	25AI	LHCB	pp at 13 TeV
2966.0±0.8±0.2	0.9k	YELTON	16	BELL	$e^+e^- \to \Upsilon(4S), \Upsilon(5S)$ and continuum
2974.9±1.5±2.1	244 ± 39	KATO	14	BELL	e^+e^- $\Upsilon(1S)$ to $\Upsilon(5S)$
2969.3±2.2±1.7	756 ± 206	AUBERT	08J	BABR	$e^+e^- \approx$ 10.58 GeV
$2967.7 \pm 2.3 ^{+1.1}_{-1.2}$	78 ± 13	LESIAK	08	BELL	$e^+e^- \approx \Upsilon(4S)$
• • • We do not use the following data for averages, fits, limits, etc. • • •					
2978.5±2.1±2.0	405 ± 51	CHISTOV	06	BELL	See KATO 14

[1] AAIJ 25AI reports 2968.6 ± 0.5 ± 0.5 ± 0.2 MeV value where the third uncertainty is due to the Ξ_c^+ mass.

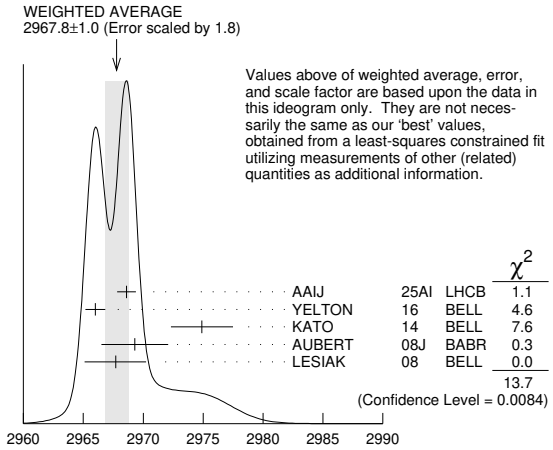

$\Xi_c(2970)^0$ MASS

The evidence is statistically weaker for this charge state.

VALUE (MeV)	EVTS	DOCUMENT ID		TECN	COMMENT
2967.3 ±1.9 OUR FIT Error includes scale factor of 7.2.					
2965.9 ±2.2 OUR AVERAGE Error includes scale factor of 7.4.					
2964.88±0.26±0.20	11.7k	[1] AAIJ	20X	LHCB	pp at 13 TeV
2970.8 ±0.7 ±0.2	1.4k	YELTON	16	BELL	$e^+e^- \to \Upsilon(4S)$, $\Upsilon(5S)$, continuum
2972.9 ±4.4 ±1.6	67 ± 44	AUBERT	08J	BABR	$e^+e^- \approx$ 10.58 GeV
$2965.7 \pm 2.4 ^{+1.1}_{-1.2}$	57 ± 13	LESIAK	08	BELL	$e^+e^- \approx \Upsilon(4S)$
2977.1 ±8.8 ±3.5	42 ± 24	CHISTOV	06	BELL	$e^+e^- \approx \Upsilon(4S)$

[1] AAIJ 20X reports 2964.88 ± 0.26 ± 0.14 ± 0.14 MeV where the last uncertainty is due to the Λ_c^+ mass. Further studies are required to establish whether the narrow resonance at 2965 MeV is a different baryon from the narrow resonance at 2970 MeV seen by YELTON 16.

$\Xi_c(2970) - \Xi_c$ MASS DIFFERENCES

$m_{\Xi_c(2970)^+} - m_{\Xi_c^+}$

VALUE (MeV)	EVTS	DOCUMENT ID		TECN	COMMENT
497.4±1.0 OUR FIT Error includes scale factor of 2.7.					
498.1±0.8±0.2	916	YELTON	16	BELL	e^+e^-, Υ regions

$m_{\Xi_c(2970)^0} - m_{\Xi_c^0}$

VALUE (MeV)	EVTS	DOCUMENT ID		TECN	COMMENT
496.8±1.9 OUR FIT Error includes scale factor of 5.8.					
499.9±0.7±0.2	1.4k	YELTON	16	BELL	e^+e^-, Υ regions

$\Xi_c(2970)^+ - \Xi_c(2970)^0$ MASS DIFFERENCE

VALUE (MeV)	DOCUMENT ID		TECN	COMMENT
−2.1±2.0 OUR FIT Error includes scale factor of 5.4.				
−4.8±0.1±0.5	YELTON	16	BELL	916 and 1443 evts

$\Xi_c(2970)$ WIDTHS

$\Xi_c(2970)^+$ WIDTH

VALUE (MeV)	EVTS	DOCUMENT ID		TECN	COMMENT
$\mathbf{27.2^{+2.8}_{-3.3}}$ **OUR AVERAGE** Error includes scale factor of 1.7. See the ideogram below.					
31.7±1.7±1.9	6.1k	AAIJ	25AI	LHCB	pp at 13 TeV
$28.1 \pm 2.4 ^{+1.0}_{-5.0}$	916	YELTON	16	BELL	e^+e^-, Υ regions
14.8±2.5±4.1	244 ± 39	KATO	14	BELL	e^+e^- $\Upsilon(1S)$ to $\Upsilon(5S)$
27 ±8 ±2	756 ± 206	AUBERT	08J	BABR	$e^+e^- \approx$ 10.58 GeV
18 ±6 ±3	78 ± 13	LESIAK	08	BELL	$e^+e^- \approx \Upsilon(4S)$
• • • We do not use the following data for averages, fits, limits, etc. • • •					
43.5±7.5±7.0	405 ± 51	CHISTOV	06	BELL	See KATO 14

UNIVERSITY OF CALIFORNIA @ BERKELEY on 09/16/26. Re-use and distribution is strictly not permitted, except for Open Access articles.
Int. J. Mod. Phys. A 2026.41. Downloaded from www.worldscientific.com

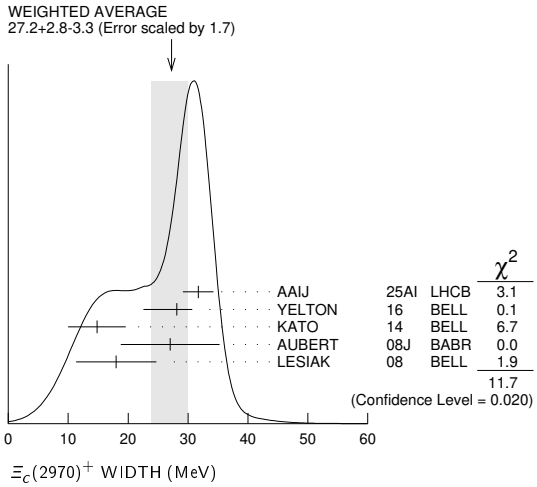

$\Xi_c(2970)^0$ WIDTH

VALUE (MeV)	EVTS	DOCUMENT ID		TECN	COMMENT
$14.1\pm0.9\pm1.3$	11.7k	[1] AAIJ	20X	LHCB	pp at 13 TeV
$30.3\pm2.3^{+1.0}_{-1.8}$	1443	YELTON	16	BELL	e^+e^-, Υ regions
• • • We do not use the following data for averages, fits, limits, etc. • • •					
$31\ \pm7\ \pm8$	67 ± 44	AUBERT	08J	BABR	$e^+e^-\approx$ 10.58 GeV
$15\ \pm6\ \pm3$	57 ± 13	LESIAK	08	BELL	$e^+e^-\approx\Upsilon(4S)$

[1] Further studies are required to establish whether the narrow resonance at 2965 MeV is a different baryon from the narrow resonance at 2970 MeV seen by YELTON 16.

$\Xi_c(2970)$ DECAY MODES

	Mode	Fraction (Γ_i/Γ)
Γ_1	$\Lambda_c^+\overline{K}\pi$	seen
Γ_2	$\Sigma_c(2455)\overline{K}$	seen
Γ_3	$\Lambda_c^+\overline{K}$	not seen
Γ_4	$\Lambda_c^+K^-$	seen
Γ_5	$\Xi_c^+\pi^+\pi^-$	seen
Γ_6	$\Xi_c2\pi$	seen
Γ_7	$\Xi_c'\pi$	seen
Γ_8	$\Xi_c(2645)\pi$	seen

$\Xi_c(2970)$ BRANCHING RATIOS

$\Gamma(\Lambda_c^+\overline{K}\pi)/\Gamma_{total}$ — Γ_1/Γ

VALUE	DOCUMENT ID		TECN	COMMENT
seen	AUBERT	08J	BABR	$e^+e^-\approx\Upsilon(4S)$
seen	CHISTOV	06	BELL	$e^+e^-\approx\Upsilon(4S)$

$\Gamma(\Lambda_c^+K^-)/\Gamma_{total}$ — Γ_4/Γ

VALUE	EVTS	DOCUMENT ID		TECN	COMMENT
seen	11.7k	[1] AAIJ	20X	LHCB	pp at 13 TeV

[1] Further studies are required to establish whether the narrow resonance at 2965 MeV is a different baryon from the narrow resonance at 2970 MeV seen by YELTON 16.

$\Gamma(\Sigma_c(2455)\overline{K})/\Gamma(\Lambda_c^+\overline{K}\pi)$ — Γ_2/Γ_1

VALUE	DOCUMENT ID		TECN	COMMENT
$0.55\pm0.07\pm0.13$	AUBERT	08J	BABR	$e^+e^-\approx\Upsilon(4S)$

$\Gamma(\Xi_c^+\pi^+\pi^-)/\Gamma_{total}$ — Γ_5/Γ

VALUE	EVTS	DOCUMENT ID		TECN	COMMENT
seen	6.1k	AAIJ	25AI	LHCB	pp at 13 TeV

$\Gamma(\Xi_c'\pi)/\Gamma_{total}$ — Γ_7/Γ

VALUE	DOCUMENT ID		TECN	COMMENT
seen	YELTON	16	BELL	e^+e^-, Υ regions

$\Gamma(\Xi_c(2645)\pi)/\Gamma_{total}$ — Γ_8/Γ

VALUE	DOCUMENT ID		TECN	COMMENT
seen	LESIAK	08	BELL	$e^+e^-\approx\Upsilon(4S)$

$\Gamma(\Xi_c'\pi)/\Gamma(\Xi_c(2645)\pi)$ — Γ_7/Γ_8

VALUE	EVTS	DOCUMENT ID		TECN	COMMENT
$1.67\pm0.29^{+0.15}_{-0.09}\pm0.25$	778	[1] MOON	21	BELL	e^+e^- at $\Upsilon(nS)$

[1] Measurement of the ratio of $\Xi_c(2970)^+\to\Xi_c(2645)^0\pi^+$ versus $\Xi_c(2970)^+\to\Xi_c'^0\pi^+$. The last uncertainty is from possible isospin-symmetry-breaking effects. MOON 21 determines from an angular analysis of the $\Xi_c^+\pi^+\pi^-$ final state that the spin of the $\Xi_c(2970)^+$ is strongly compatible with $J=1/2$, assuming domination by the lowest partial wave in $\Xi_c(2970)^+\to\Xi_c(2645)^0\pi^+$. When further combined with the size of this ratio, MOON 21 determines from heavy quark symmetry that the spin-parity of the $\Xi_c(2970)^+$ is favored to be $J^P=1/2^+$, with light degrees of freedom in the 0^+ state.

$\Xi_c(2970)$ REFERENCES

AAIJ	25AI	PRL 135 161901	R. Aaij *et al.*	(LHCb Collab.)
MOON	21	PR D103 L111101	T.J. Moon *et al.*	(BELLE Collab.) JP
AAIJ	20X	PRL 124 222001	R. Aaij *et al.*	(LHCb Collab.)
YELTON	16	PR D94 052011	J. Yelton *et al.*	(BELLE Collab.)
KATO	14	PR D89 052003	Y. Kato *et al.*	(BELLE Collab.)
AUBERT	08J	PR D77 012002	B. Aubert *et al.*	(BABAR Collab.)
LESIAK	08	PL B665 9	T. Lesiak *et al.*	(BELLE Collab.)
CHISTOV	06	PRL 97 162001	R. Chistov *et al.*	(BELLE Collab.)

$\Xi_c(3055)$

$I(J^P)=?(\frac{3}{2}^+)$ Status: ***

AAIJ 25H establishes spin-parity of the $\Xi_c(3055)^+$ and $\Xi_c(3055)^0$ to be $J^P=3/2^+$ at 6.5σ and 3.5σ, respectively, versus other hypotheses.

$\Xi_c(3055)$ MASSES

$\Xi_c(3055)^+$ MASS

VALUE (MeV)	EVTS	DOCUMENT ID		TECN	COMMENT
$3055.2\ \pm0.7$ OUR AVERAGE	Error includes scale factor of 2.4.				
$3054.52\pm0.36\pm0.17$	637	AAIJ	25H	LHCB	$\Xi_b\to\Xi_c(3055)\pi^-$
$3055.9\ \pm0.4$	894	KATO	16	BELL	e^+e^- Υ region
• • • We do not use the following data for averages, fits, limits, etc. • • •					
$3058.1\ \pm1.0\ \pm2.1$	199 ± 46	KATO	14	BELL	See KATO 16
$3054.2\ \pm1.2\ \pm0.5$	218 ± 95	AUBERT	08J	BABR	$e^+e^-\approx$ 10.58 GeV

$\Xi_c(3055)^0$ MASS

VALUE (MeV)	EVTS	DOCUMENT ID		TECN	COMMENT
$3061.00\pm0.80\pm0.23$	232	AAIJ	25H	LHCB	$\Xi_b\to\Xi_c(3055)\pi^-$

$\Xi_c(3055)$ WIDTHS

$\Xi_c(3055)^+$ WIDTH

VALUE (MeV)	EVTS	DOCUMENT ID		TECN	COMMENT
$8.0\ \pm0.8$ OUR AVERAGE					
$8.01\pm0.76\pm\ 0.34$	637	AAIJ	25H	LHCB	$\Xi_b\to\Xi_c(3055)\pi^-$
$7.8\ \pm1.2\ \pm\ 1.5$		KATO	16	BELL	e^+e^- Υ region
• • • We do not use the following data for averages, fits, limits, etc. • • •					
$9.7\ \pm3.4\ \pm\ 3.3$	199 ± 46	KATO	14	BELL	e^+e^- $\Upsilon(1S)$ to $\Upsilon(5S)$
$17\ \ \pm6\ \ \pm11$	218 ± 95	AUBERT	08J	BABR	$e^+e^-\approx$ 10.58 GeV

$\Xi_c(3055)^0$ WIDTH

VALUE (MeV)	EVTS	DOCUMENT ID		TECN	COMMENT
$12.4\pm2.0\pm1.1$	232	AAIJ	25H	LHCB	$\Xi_b\to\Xi_c(3055)\pi^-$

$\Xi_c(3055)$ DECAY MODES

	Mode	Fraction (Γ_i/Γ)
Γ_1	$\Sigma^{++}K^-$	seen
Γ_2	ΛD^+	seen
Γ_3	ΛD^0	seen

$\Xi_c(3055)$ BRANCHING RATIOS

$\Gamma(\Lambda D^+)/\Gamma(\Sigma^{++}K^-)$ — Γ_2/Γ_1

VALUE	DOCUMENT ID		TECN	COMMENT
$5.09\pm1.01\pm0.76$	KATO	16	BELL	721 and 103 evts

$\Gamma(\Lambda D^+)/\Gamma_{total}$ — Γ_2/Γ

VALUE	DOCUMENT ID		TECN	COMMENT
seen	AAIJ	25H	LHCB	$\Xi_b\to\Xi_c(3055)\pi^-$

$\Gamma(\Lambda D^0)/\Gamma_{total}$ — Γ_3/Γ

VALUE	DOCUMENT ID		TECN	COMMENT
seen	AAIJ	25H	LHCB	$\Xi_b\to\Xi_c(3055)\pi^-$

$\Xi_c(3055)$ REFERENCES

AAIJ	25H	PRL 134 081901	R. Aaij *et al.*	(LHCb Collab.) JP
KATO	16	PR D94 032002	Y. Kato *et al.*	(BELLE Collab.)
KATO	14	PR D89 052003	Y. Kato *et al.*	(BELLE Collab.)
AUBERT	08J	PR D77 012002	B. Aubert *et al.*	(BABAR Collab.)

Int. J. Mod. Phys. A 2026.41. Downloaded from www.worldscientific.com by UNIVERSITY OF CALIFORNIA @ BERKELEY on 09/16/26. Re-use and distribution is strictly not permitted, except for Open Access articles.

$\Xi_c(3080)$

$I(J^P) = \frac{1}{2}(?^?)$ Status: ***

$\Xi_c(3080)$ MASSES

$\Xi_c(3080)^+$ MASS

VALUE (MeV)	EVTS	DOCUMENT ID		TECN	COMMENT
3077.2±0.4 OUR AVERAGE					
3076.8±0.7±1.3	0.34k	[1] AAIJ	25AI	LHCB	pp at 13 TeV
3077.9±0.9	596	KATO	16	BELL	e^+e^- Υ region
3077.0±0.4±0.2	403 ± 60	AUBERT	08J	BABR	$e^+e^- \approx$ 10.58 GeV
• • • We do not use the following data for averages, fits, limits, etc. • • •					
3076.9±0.3±0.2	210 ± 30	KATO	14	BELL	See KATO 16
3076.7±0.9±0.5	326 ± 40	CHISTOV	06	BELL	See KATO 14

[1] AAIJ 25AI reports 3076.8 ± 0.7 ± 1.3 ± 0.2 MeV value where the third uncertainty is due to the Ξ_c^+ mass.

$\Xi_c(3080)^0$ MASS

VALUE (MeV)	EVTS	DOCUMENT ID		TECN	COMMENT
3079.9±1.4 OUR AVERAGE Error includes scale factor of 1.3.					
3079.3±1.1±0.2	90 ± 27	AUBERT	08J	BABR	$e^+e^- \approx$ 10.58 GeV
3082.8±1.8±1.5	67 ± 20	CHISTOV	06	BELL	$e^+e^- \approx \Upsilon(4S)$

$\Xi_c(3080)$ WIDTHS

$\Xi_c(3080)^+$ WIDTH

VALUE (MeV)	EVTS	DOCUMENT ID		TECN	COMMENT
3.8±0.9 OUR AVERAGE Error includes scale factor of 1.4. See the ideogram below.					
6.8±2.3±0.9	0.34k	AAIJ	25AI	LHCB	pp at 13 TeV
3.0±0.7±0.4	596	KATO	16	BELL	e^+e^- Υ region
5.5±1.3±0.6	403 ± 60	AUBERT	08J	BABR	$e^+e^- \approx$ 10.58 GeV
• • • We do not use the following data for averages, fits, limits, etc. • • •					
2.4±0.9±1.6	210 ± 30	KATO	14	BELL	See KATO 16
6.2±1.2±0.8	326 ± 40	CHISTOV	06	BELL	See KATO 14

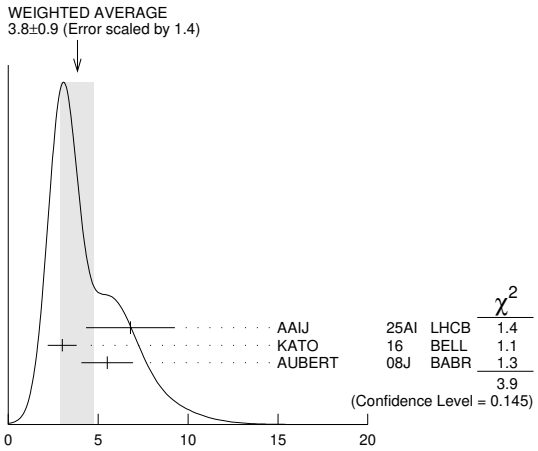

$\Xi_c(3080)^+$ WIDTH (MeV)

$\Xi_c(3080)^0$ WIDTH

VALUE (MeV)	EVTS	DOCUMENT ID		TECN	COMMENT
5.6±2.2 OUR AVERAGE					
5.9±2.3±1.5	90 ± 27	AUBERT	08J	BABR	$e^+e^- \approx$ 10.58 GeV
5.2±3.1±1.8	67 ± 20	CHISTOV	06	BELL	$e^+e^- \approx \Upsilon(4S)$

$\Xi_c(3080)$ DECAY MODES

	Mode	Fraction (Γ_i/Γ)
Γ_1	$\Lambda_c^+ \overline{K} \pi$	seen
Γ_2	$\Xi_c^+ \pi^+ \pi^-$	seen
Γ_3	$\Sigma_c(2455) \overline{K}$	seen
Γ_4	$\Sigma_c(2455)^{++} K^-$	seen
Γ_5	$\Sigma_c(2520)^{++} K^-$	seen
Γ_6	$\Sigma_c(2455) \overline{K} + \Sigma_c(2520) \overline{K}$	seen
Γ_7	$\Lambda_c^+ \overline{K}$	not seen
Γ_8	$\Lambda_c^+ \overline{K} \pi^+ \pi^-$	not seen
Γ_9	ΛD^+	seen

$\Xi_c(3080)$ BRANCHING RATIOS

$\Gamma(\Sigma_c(2455)\overline{K})/\Gamma(\Lambda_c^+ \overline{K} \pi)$ — Γ_3/Γ_1

VALUE	DOCUMENT ID		TECN	COMMENT
0.45±0.06 OUR AVERAGE				
0.45±0.05±0.05	AUBERT	08J	BABR	in $\Lambda_c^+ K^- \pi^+$
0.44±0.12±0.07	AUBERT	08J	BABR	in $\Lambda_c^+ K_S^0 \pi^-$

$\Gamma(\Sigma_c(2520)^{++} K^-)/\Gamma(\Sigma_c(2455)^{++} K^-)$ — Γ_5/Γ_4

VALUE	DOCUMENT ID		TECN	COMMENT
1.07±0.27±0.04	KATO	16	BELL	234 and 176 evts

$[\Gamma(\Sigma_c(2455)\overline{K}) + \Gamma(\Sigma_c(2520)\overline{K})]/\Gamma(\Lambda_c^+ \overline{K} \pi)$ — Γ_6/Γ_1

VALUE	DOCUMENT ID		TECN	COMMENT
0.89±0.12 OUR AVERAGE				
0.95±0.14±0.06	AUBERT	08J	BABR	in $\Lambda_c^+ K^- \pi^+$
0.78±0.21±0.05	AUBERT	08J	BABR	in $\Lambda_c^+ K_S^0 \pi^-$

$\Gamma(\Xi_c^+ \pi^+ \pi^-)/\Gamma_{total}$ — Γ_2/Γ

VALUE	EVTS	DOCUMENT ID		TECN	COMMENT
seen	0.34k	AAIJ	25AI	LHCB	pp at 13 TeV

$\Gamma(\Lambda D^+)/\Gamma(\Sigma_c(2455)^{++} K^-)$ — Γ_9/Γ_4

VALUE	DOCUMENT ID		TECN	COMMENT
1.29±0.30±0.15	KATO	16	BELL	186 and 176 evts

$\Xi_c(3080)$ REFERENCES

AAIJ	25AI	PRL 135 161901	R. Aaij *et al.*	(LHCb Collab.)
KATO	16	PR D94 032002	Y. Kato *et al.*	(BELLE Collab.)
KATO	14	PR D89 052003	Y. Kato *et al.*	(BELLE Collab.)
AUBERT	08J	PR D77 012002	B. Aubert *et al.*	(BABAR Collab.)
CHISTOV	06	PRL 97 162001	R. Chistov *et al.*	(BELLE Collab.)

$\Xi_c(3123)$

$I(J^P) = ?(?^?)$ Status: *

OMITTED FROM SUMMARY TABLE

A peak in the $\Sigma_c(2520)^{++} K^- \to \Lambda_c^+ K^- \pi^+$ mass spectrum with a significance of 3.6 standard deviations. KATO 14 finds no evidence for this state.

$\Xi_c(3123)$ MASSES

$\Xi_c(3123)^+$ MASS

VALUE (MeV)	EVTS	DOCUMENT ID		TECN	COMMENT
3122.9±1.3±0.3	101 ± 35	AUBERT	08J	BABR	$e^+e^- \approx$ 10.58 GeV

$\Xi_c(3123)$ WIDTHS

$\Xi_c(3123)^+$ WIDTH

VALUE (MeV)	EVTS	DOCUMENT ID		TECN	COMMENT
4.4±3.4±1.7	101 ± 35	AUBERT	08J	BABR	$e^+e^- \approx$ 10.58 GeV

$\Xi_c(3123)$ REFERENCES

KATO	14	PR D89 052003	Y. Kato *et al.*	(BELLE Collab.)
AUBERT	08J	PR D77 012002	B. Aubert *et al.*	(BABAR Collab.)

Ω_c^0

$I(J^P) = 0(\frac{1}{2}^+)$ Status: ***

The quantum numbers have not been measured, but are simply assigned in accord with the quark model, in which the Ω_c^0 is the ssc ground state. No absolute branching fractions have been measured.

Ω_c^0 MASS

VALUE (MeV)	EVTS	DOCUMENT ID		TECN	COMMENT
2695.3 ± 0.4 OUR FIT					
2695.3 ± 0.4 OUR AVERAGE					
2695.28± 0.07±0.41	9330	[1] AAIJ	24C	LHCB	5.4fb^{-1}, pp at 13 TeV
2693.6 ± 0.3 $^{+1.8}_{-1.5}$	725	SOLOVIEVA	09	BELL	$\Omega^-\pi^+$ in $e^+e^- \to \Upsilon(4S)$
2694.6 ± 2.6 ±1.9	40	[2] CRONIN-HEN.	01	CLE2	$e^+e^- \approx$ 10.6 GeV
2699.9 ± 1.5 ±2.5	42	[3] FRABETTI	94H	E687	γBe, $\overline{E}_\gamma$= 221 GeV
• • • We do not use the following data for averages, fits, limits, etc. • • •					
2705.9 ± 3.3 ±2.0	10	[4] FRABETTI	93	E687	γBe, $\overline{E}_\gamma$= 221 GeV
2719.0 ± 7.0 ±2.5	11	[5] ALBRECHT	92H	ARG	$e^+e^- \approx$ 10.6 GeV
2740 ±20	3	BIAGI	85B	SPEC	Σ^-Be 135 GeV/c

[1] AAIJ 24C reports this measurements as 2695.28 ± 0.07 ± 0.27 ± 0.30 MeV. The last uncertainty is due to the uncertainty in the Ω^- mass. Also reported is $m_{\Omega_c^0} - m_{\Omega^-}$ = 1022.83 ± 0.07 ± 0.27 MeV.

[2] CRONIN-HENNESSY 01 sees 40.4 ± 9.0 events in a sum over five channels.
[3] FRABETTI 94H claims a signal of 42.5 ± 8.8 $\Sigma^+ K^- K^- \pi^+$ events. The background is about 24 events.
[4] FRABETTI 93 claims a signal of 10.3 ± 3.9 $\Omega^- \pi^+$ events above a background of 5.8 events.
[5] ALBRECHT 92H claims a signal of 11.5 ± 4.3 $\Xi^- K^- \pi^+ \pi^+$ events. The background is about 5 events.

Ω_c^0 MEAN LIFE

VALUE (10^{-15} s)	EVTS	DOCUMENT ID		TECN	COMMENT
274 ±10 OUR AVERAGE					
276.3±19.4± 1.8±0.7	0.36k	[1] AAIJ	25AM	LHCB	$\Omega_b^- \to \Omega_c^0 \pi^-$, $\Omega_c^0 \to p K^- K^- \pi^+$
243 ±48 ±11	88	ABUDINEN	23	BEL2	$e^+ e^- \to \Omega_c^0 + X$, $\Omega_c^0 \to \Omega^- \pi^+$
276.5±13.4± 4.5		[2,3] AAIJ	22Y	LHCB	$pp \to \Omega_c X$, $\Omega_c \to p K^- K^- \pi^+$
268 ±24 ±10	978	[2,4] AAIJ	18J	LHCB	$\Omega_b \to \Omega_c \mu \nu + X$, $\Omega_c \to p K^- K^- \pi^+$
• • • We do not use the following data for averages, fits, limits, etc. • • •					
72 ±11 ±11	64	LINK	03C	FOCS	$\Omega^- \pi^+$, $\Xi^- K^- \pi^+ \pi^+$
55 $^{+13}_{-11}$ $^{+18}_{-23}$	86	ADAMOVICH	95B	WA89	$\Omega^- \pi^- \pi^+ \pi^+$, $\Xi^- K^- \pi^+ \pi^+$
86 $^{+27}_{-20}$ ±28	25	FRABETTI	95D	E687	$\Sigma^+ K^- K^- \pi^+$

[1] Uses $B^- \to D^0 \pi^-$, $D^0 \to K^- K^+ \pi^- \pi^+$ as a normalization mode to minimize the uncertainties associated with the decay time acceptance. The third uncertainty is due to the uncertainty of the D^0 lifetime, which is taken to be 410.3 ± 1.0 fs.
[2] Recent measurements by AAIJ 18J, AAIJ 22Y, and ABUDINEN 23 obtain consistent results that are nearly four times larger than the average result of previous experiments, (69 ± 12) × 10^{-15} s. We go with the more recent results, mostly obtained with much larger data samples, and also note the positive correlation between the measured value and the inverse of the estimated statistical uncertainty in lifetime measurements.
[3] AAIJ 22Y reports this measurement as (276.5 ± 13.4 ± 4.4 ± 0.7) × 10^{-15} s. The last uncertainty is due to the uncertainty on the D^0 lifetime τ_{D^0} = (410.1 ± 1.5) fs from PDG 20. Measured in Ω_c produced promptly in pp collisions, using $D^0 \to K^+ K^- \pi^+ \pi^-$ as normalisation mode.
[4] Measured using Ω_c produced in semileptonic Ω_b decays.

Ω_c^0 DECAY MODES

No absolute branching fractions have been measured. The following are branching *ratios* relative to $\Omega^- \pi^+$.

	Mode	Fraction (Γ_i/Γ)	Confidence level
	Cabibbo-favored ($S = -3$) decays — relative to $\Omega^- \pi^+$		
Γ_1	$\Omega^- \pi^+$	**DEFINED AS 1**	
Γ_2	$\Omega^- \pi^+ \pi^0$	1.80 ±0.33	
Γ_3	$\Omega^- \rho^+$	>1.3	90%
Γ_4	$\Omega^- \pi^- 2\pi^+$	0.31 ±0.05	
Γ_5	$\Omega^- e^+ \nu_e$	1.98 ±0.29	
Γ_6	$\Omega^- \mu^+ \nu_\mu$	1.94 ±0.21	
Γ_7	$\Xi^0 \overline{K}^0$	1.64 ±0.29	
Γ_8	$\Xi^0 K^- \pi^+$	1.20 ±0.18	
Γ_9	$\Xi^0 \overline{K}^{*0}$, $\overline{K}^{*0} \to K^- \pi^+$	0.68 ±0.16	
Γ_{10}	$\Omega(2012)^- \pi^+$, $\Omega(2012)^- \to \Xi^0 K^-$	0.12 ±0.05	
Γ_{11}	$\Xi^- \overline{K}^0 \pi^+$	2.12 ±0.28	
Γ_{12}	$\Omega(2012)^- \pi^+$, $\Omega(2012)^- \to \Xi^- \overline{K}^0$	0.12 ±0.06	
Γ_{13}	$\Xi^- K^- 2\pi^+$	0.63 ±0.09	
Γ_{14}	$\Xi(1530)^0 K^- \pi^+$, $\Xi^{*0} \to \Xi^- \pi^+$	0.21 ±0.06	
Γ_{15}	$\Xi^- \overline{K}^{*0} \pi^+$	0.34 ±0.11	
Γ_{16}	$p K^- K^- \pi^+$	seen	
Γ_{17}	$\Sigma^+ K^- K^- \pi^+$	<0.32	90%
Γ_{18}	$\Lambda \overline{K}^0 \overline{K}^0$	1.72 ±0.35	
	Singly Cabibbo-suppressed modes — relative to $\Omega^- \pi^+$		
Γ_{19}	$\Xi^- \pi^+$	0.161±0.010	
Γ_{20}	$\Omega^- K^+$	0.061±0.006	
	Doubly Cabibbo-suppressed modes — relative to $\Omega^- \pi^+$		
Γ_{21}	$\Xi^- K^+$	<0.07	90%

Ω_c^0 BRANCHING RATIOS

A few early but now obsolete measurements have been omitted. See K.A. Olive, et al. (Particle Data Group), Chinese Physics **C38** 070001 (2014).

$\Gamma(\Omega^- \pi^+ \pi^0)/\Gamma(\Omega^- \pi^+)$ — Γ_2/Γ_1

VALUE	EVTS	DOCUMENT ID		TECN	COMMENT
1.80±0.33 OUR AVERAGE	Error includes scale factor of 1.9.				
2.00±0.17±0.11	403	YELTON	18	BELL	$e^+ e^- \to \Upsilon(4S)$, +higher
1.27±0.31±0.11	64	AUBERT	07AH	BABR	$e^+ e^- \approx \Upsilon(4S)$

$\Gamma(\Omega^- \rho^+)/\Gamma(\Omega^- \pi^+ \pi^0)$ — Γ_3/Γ_2

VALUE	CL%	DOCUMENT ID		TECN	COMMENT
>0.71	90	[1] YELTON	18	BELL	$e^+ e^- \to \Upsilon(4S)$, +higher

[1] This submode fraction is evaluated from a background-subtracted signal in a mass plot. Result ignores interference effects and systematic uncertainties, which YELTON 18 claim are both small.

$\Gamma(\Omega^- \pi^- 2\pi^+)/\Gamma(\Omega^- \pi^+)$ — Γ_4/Γ_1

VALUE	EVTS	DOCUMENT ID		TECN	COMMENT
0.31±0.05 OUR AVERAGE					
0.32±0.05±0.02	108	YELTON	18	BELL	$e^+ e^- \to \Upsilon(4S)$, +higher
0.28±0.09±0.01	25	AUBERT	07AH	BABR	$e^+ e^- \approx \Upsilon(4S)$

$\Gamma(\Omega^- e^+ \nu_e)/\Gamma(\Omega^- \pi^+)$ — Γ_5/Γ_1

VALUE	EVTS	DOCUMENT ID		TECN	COMMENT
1.84±0.32 OUR AVERAGE	Error includes scale factor of 2.3.				
1.12±0.22±0.27	232	[1] ACHARYA	24A	ALCE	pp at 13 TeV
1.98±0.13±0.08		LI	22A	BELL	$e^+ e^-$ at Υ(nS)
• • • We do not use the following data for averages, fits, limits, etc. • • •					
2.4 ±1.1 ±0.2	11	[2] AMMAR	02	CLE2	$e^+ e^- \approx \Upsilon(4S)$

[1] ACHARYA 24A measurement performed over p_T intervals in the range $2 < p_T < 12$ GeV, from which a p_T-independent branching ratio is derived from a weighted average over p_T.
[2] AMMAR 02 reported 0.41 ± 0.19 ± 0.04 for the inverse of this branching fraction.

$\Gamma(\Omega^- \mu^+ \nu_\mu)/\Gamma(\Omega^- \pi^+)$ — Γ_6/Γ_1

VALUE	DOCUMENT ID		TECN	COMMENT
1.94±0.18±0.10	LI	22A	BELL	$e^+ e^-$ at Υ(nS)

$\Gamma(\Omega^- e^+ \nu_e)/\Gamma(\Omega^- \mu^+ \nu_\mu)$ — Γ_5/Γ_6

VALUE	DOCUMENT ID		TECN	COMMENT
1.02±0.10±0.02	LI	22A	BELL	$e^+ e^-$ at Υ(nS)

$\Gamma(\Xi^0 \overline{K}^0)/\Gamma(\Omega^- \pi^+)$ — Γ_7/Γ_1

VALUE	EVTS	DOCUMENT ID		TECN	COMMENT
1.64±0.26±0.12	98	YELTON	18	BELL	$e^+ e^- \to \Upsilon(4S)$, +higher

$\Gamma(\Xi^0 K^- \pi^+)/\Gamma(\Omega^- \pi^+)$ — Γ_8/Γ_1

VALUE	EVTS	DOCUMENT ID		TECN	COMMENT
1.20±0.16±0.08	168	YELTON	18	BELL	$e^+ e^- \to \Upsilon(4S)$, +higher

$\Gamma(\Xi^0 \overline{K}^{*0}, \overline{K}^{*0} \to K^- \pi^+)/\Gamma(\Xi^0 K^- \pi^+)$ — Γ_9/Γ_8

VALUE	EVTS	DOCUMENT ID		TECN	COMMENT
0.57±0.10	95	[1] YELTON	18	BELL	$e^+ e^- \to \Upsilon(4S)$, +higher

[1] This submode fraction is evaluated from a background-subtracted signal in a mass plot. Result ignores interference effects and systematic uncertainties, which YELTON 18 claim are both small.

$\Gamma(\Omega(2012)^- \pi^+, \Omega(2012)^- \to \Xi^0 K^-)/\Gamma(\Xi^0 K^- \pi^+)$ — Γ_{10}/Γ_8

VALUE (units 10^{-2})	EVTS	DOCUMENT ID		TECN	COMMENT
9.6±3.2±1.8	28	[1] LI	21D	BELL	$e^+ e^-$ at Υ(nS)

[1] LI 21D reports the significance of the $\Omega(2012)$ signal is 4.2 σ including systematic uncertainties. Also measures $B(\Omega_c^0 \to \Omega(2012)^- \pi^+, \Omega(2012)^- \to (\overline{K}\Xi)^-)/B(\Omega_c^0 \to \Xi^0 K^- \pi^+) = 0.220 \pm 0.059 \pm 0.035$.

$\Gamma(\Xi^- \overline{K}^0 \pi^+)/\Gamma(\Omega^- \pi^+)$ — Γ_{11}/Γ_1

VALUE	EVTS	DOCUMENT ID		TECN	COMMENT
2.12±0.24±0.14	349	YELTON	18	BELL	$e^+ e^- \to \Upsilon(4S)$, +higher

$\Gamma(\Omega(2012)^- \pi^+, \Omega(2012)^- \to \Xi^- \overline{K}^0)/\Gamma(\Xi^- \overline{K}^0 \pi^+)$ — Γ_{12}/Γ_{11}

VALUE (units 10^{-2})	EVTS	DOCUMENT ID		TECN	COMMENT
5.5±2.8±0.7	18	[1] LI	21D	BELL	$e^+ e^-$ at Υ(nS)

[1] LI 21D reports the significance of the $\Omega(2012)$ signal is 4.2σ including systematic uncertainties. Also measures $B(\Omega_c^0 \to \Omega(2012)^- \pi^+, \Omega(2012)^- \to (\overline{K}\Xi)^-)/B(\Omega_c^0 \to \Xi^0 K^- \pi^+) = 0.220 \pm 0.059 \pm 0.035$.

$\Gamma(\Xi^- K^- 2\pi^+)/\Gamma(\Omega^- \pi^+)$ — Γ_{13}/Γ_1

VALUE	EVTS	DOCUMENT ID		TECN	COMMENT
0.63±0.09 OUR AVERAGE	Error includes scale factor of 1.4.				
0.68±0.07±0.03	278	YELTON	18	BELL	$e^+ e^- \to \Upsilon(4S)$, +higher
0.46±0.13±0.03	45	AUBERT	07AH	BABR	$e^+ e^- \approx \Upsilon(4S)$

Int. J. Mod. Phys. A 2026.41. Downloaded from www.worldscientific.com
UNIVERSITY OF CALIFORNIA @ BERKELEY on 09/16/26. Re-use and distribution is strictly not permitted, except for Open Access articles.

Int. J. Mod. Phys. A 2026.41. Downloaded from www.worldscientific.com by UNIVERSITY OF CALIFORNIA @ BERKELEY on 09/16/26. Re-use and distribution is strictly not permitted, except for Open Access articles.

$\Gamma(\Xi(1530)^0 K^- \pi^+, \Xi^{*0} \to \Xi^- \pi^+)/\Gamma(\Xi^- K^- 2\pi^+)$ — Γ_{14}/Γ_{13}

VALUE	EVTS	DOCUMENT ID		TECN	COMMENT
0.33±0.09	74	[1] YELTON	18	BELL	$e^+e^- \to \Upsilon(4S)$, +higher

[1] This submode fraction is evaluated from a background-subtracted signal in a mass plot. Result ignores interference effects and systematic uncertainties, which YELTON 18 claim are both small.

$\Gamma(\Xi^- \overline{K}^{*0} \pi^+)/\Gamma(\Xi^- K^- 2\pi^+)$ — Γ_{15}/Γ_{13}

VALUE	EVTS	DOCUMENT ID		TECN	COMMENT
0.55±0.16	136	[1] YELTON	18	BELL	$e^+e^- \to \Upsilon(4S)$, +higher

[1] This submode fraction is evaluated from a background-subtracted signal in a mass plot. Result ignores interference effects and systematic uncertainties, which YELTON 18 claim are both small.

$\Gamma(p K^- K^- \pi^+)/\Gamma_{total}$ — Γ_{16}/Γ

VALUE	DOCUMENT ID		TECN	COMMENT
seen	AAIJ	25AM	LHCB	pp at 7, 8, 13 TeV
seen	AAIJ	16O	LHCB	pp at 7, 8 TeV

$\Gamma(\Sigma^+ K^- K^- \pi^+)/\Gamma(\Omega^- \pi^+)$ — Γ_{17}/Γ_1

VALUE	CL%	EVTS	DOCUMENT ID		TECN	COMMENT
<0.32	90	17	YELTON	18	BELL	$e^+e^- \to \Upsilon(4S)$, +higher

$\Gamma(\Lambda \overline{K}^0 \overline{K}^0)/\Gamma(\Omega^- \pi^+)$ — Γ_{18}/Γ_1

VALUE	EVTS	DOCUMENT ID		TECN	COMMENT
1.72±0.32±0.14	95	YELTON	18	BELL	$e^+e^- \to \Upsilon(4S)$, +higher

$\Gamma(\Xi^- \pi^+)/\Gamma(\Omega^- \pi^+)$ — Γ_{19}/Γ_1

VALUE (units 10^{-2})	EVTS	DOCUMENT ID		TECN	COMMENT
16.1 ±1.0 OUR AVERAGE					
15.81±0.87±0.47	2780	[1] AAIJ	24C	LHCB	5.4fb^{-1}, pp at 13 TeV
25.3 ±5.2 ±3.0	208	HAN	23	BELL	$e^+e^- \to \Upsilon(nS)$

[1] AAIJ 24C reports this measurements as (15.81 ± 0.87 ± 0.44 ± 0.16)%. The last uncertainty is due to branching ratios of $\Omega^- \to \Lambda K^-$ and $\Xi^- \to \Lambda \pi^-$ decays taken as external inputs, which are taken to be 67.8 ± 0.7% and 99.887 ± 0.035%, respectively.

$\Gamma(\Omega^- K^+)/\Gamma(\Omega^- \pi^+)$ — Γ_{20}/Γ_1

VALUE (units 10^{-2})	CL%	EVTS	DOCUMENT ID		TECN	COMMENT
6.08±0.51±0.40		425	AAIJ	24C	LHCB	5.4fb^{-1}, pp at 13 TeV
• • • We do not use the following data for averages, fits, limits, etc. • • •						
<29		90	HAN	23	BELL	$e^+e^- \to \Upsilon(nS)$

$\Gamma(\Xi^- K^+)/\Gamma(\Omega^- \pi^+)$ — Γ_{21}/Γ_1

VALUE	CL%	DOCUMENT ID		TECN	COMMENT
<0.070	90	HAN	23	BELL	$e^+e^- \to \Upsilon(nS)$

Ω_c^0 REFERENCES

AAIJ	25AM	JHEP 2509 157	R. Aaij *et al.*	(LHCb Collab.)
AAIJ	24C	PRL 132 081802	R. Aaij *et al.*	(LHCb Collab.)
ACHARYA	24A	PR D110 032014	S. Acharya *et al.*	(ALICE Collab.)
ABUDINEN	23	PR D107 L031103	F. Abudinen *et al.*	(BELLE II Collab.)
HAN	23	JHEP 2301 055	X. Han *et al.*	(BELLE Collab.)
AAIJ	22Y	SCIB 67 479	R. Aaij *et al.*	(LHCb Collab.)
LI	22A	PR D105 L091101	Y.B. Li *et al.*	(BELLE Collab.)
LI	21D	PR D104 052005	Y.B. Li *et al.*	(BELLE Collab.)
PDG	20	PTEP 2020 083C01	P.A. Zyla *et al.*	(PDG Collab.)
AAIJ	18J	PRL 121 092003	R. Aaij *et al.*	(LHCb Collab.)
YELTON	18	PR D97 032001	J. Yelton *et al.*	(BELLE Collab.)
AAIJ	16O	PR D93 092007	R. Aaij *et al.*	(LHCb Collab.)
PDG	14	CP C38 070001	K. Olive *et al.*	(PDG Collab.)
SOLOVIEVA	09	PL B672 1	E. Solovieva *et al.*	(BELLE Collab.)
AUBERT	07AH	PRL 99 062001	B. Aubert *et al.*	(BABAR Collab.)
LINK	03C	PL B561 41	J.M. Link *et al.*	(FNAL FOCUS Collab.)
AMMAR	02	PRL 89 171803	R. Ammar *et al.*	(CLEO Collab.)
CRONIN-HEN...	01	PRL 86 3730	D. Cronin-Hennessy *et al.*	(CLEO Collab.)
ADAMOVICH	95B	PL B358 151	M.I. Adamovich *et al.*	(CERN WA89 Collab.)
FRABETTI	95D	PL B357 678	P.L. Frabetti *et al.*	(FNAL E687 Collab.)
FRABETTI	94H	PL B338 106	P.L. Frabetti *et al.*	(FNAL E687 Collab.)
FRABETTI	93	PL B300 190	P.L. Frabetti *et al.*	(FNAL E687 Collab.)
ALBRECHT	92H	PL B288 367	H. Albrecht *et al.*	(ARGUS Collab.)
BIAGI	85B	ZPHY C28 175	S.F. Biagi *et al.*	(CERN WA62 Collab.)

$\Omega_c(2770)^0$

$I(J^P) = 0(\frac{3}{2}^+)$ Status: ***

The natural assignment is that this goes with the $\Sigma_c(2520)$ and $\Xi_c(2645)$ to complete the lowest mass $J^P = \frac{3}{2}^+$ SU(3) sextet, part of the SU(4) 20-plet that includes the $\Delta(1232)$. But J and P have not been measured.

$\Omega_c(2770)^0$ MASS

The mass is obtained from the mass-difference measurement that follows.

VALUE (MeV)	DOCUMENT ID
2766.0$^{+0.9}_{-1.0}$ OUR FIT	

$\Omega_c(2770)^0 - \Omega_c^0$ MASS DIFFERENCE

VALUE (MeV)	EVTS	DOCUMENT ID		TECN	COMMENT
70.7$^{+0.8}_{-0.9}$ OUR FIT					
70.7$^{+0.8}_{-1.0}$ OUR AVERAGE					
70.7±0.9$^{+0.1}_{-0.9}$	54 ± 9	SOLOVIEVA	09	BELL	$\Omega_c^0\gamma$ in $e^+e^- \to \Upsilon(4S)$
70.8±1.0±1.1	105 ± 22	AUBERT,BE	06I	BABR	$e^+e^- \approx \Upsilon(4S)$

$\Omega_c(2770)^0$ DECAY MODES

The $\Omega_c(2770)^0$–Ω_c^0 mass difference is too small for any strong decay to occur.

	Mode	Fraction (Γ_i/Γ)
Γ_1	$\Omega_c^0\gamma$	presumably 100%

$\Omega_c(2770)^0$ REFERENCES

SOLOVIEVA	09	PL B672 1	E. Solovieva *et al.*	(BELLE Collab.)
AUBERT,BE	06I	PRL 97 232001	B. Aubert *et al.*	(BABAR Collab.)

$\Omega_c(3000)^0$

$I(J^P) = ?(?^?)$ Status: ***

$\Omega_c(3000)^0$ MASS

VALUE (MeV)	EVTS	DOCUMENT ID		TECN	COMMENT
3000.46±0.25 OUR AVERAGE					
3000.44±0.07$^{+0.07}_{-0.13}$±0.23	8.8k	[1] AAIJ	23AS	LHCB	pp at 7, 8, 13 TeV
3000.7 ±1.0 ±0.2	38	YELTON	18B	BELL	e^+e^- at $\Upsilon(4S)$
• • • We do not use the following data for averages, fits, limits, etc. • • •					
2999.2 ±0.9 ±0.9 $^{+0.19}_{-0.22}$	24	[2] AAIJ	21AC	LHCB	pp at 7, 8, 13 TeV
3000.4 ±0.2 ±0.1	1.3k	[3] AAIJ	17AH	LHCB	pp at 7, 8, 13 TeV

[1] The third uncertainty is due to the uncertainty in the Ξ_c^+ mass, taken to be the PDG 22 fit result 2467.71 ± 0.23 MeV.

[2] Measured via $\Omega_b^- \to \Omega_c^{**0}\pi^- \to \Xi_c^+ K^- \pi^-$. The third uncertainty is due to the uncertainty in the Ξ_c^+ mass.

[3] See AAIJ 23AS

$\Omega_c(3000)^0$ WIDTH

VALUE (MeV)	EVTS	DOCUMENT ID		TECN	COMMENT
3.83±0.23$^{+1.59}_{-0.29}$	8.8k	AAIJ	23AS	LHCB	pp at 7, 8, 13 TeV
• • • We do not use the following data for averages, fits, limits, etc. • • •					
4.8 ±2.1 ±2.5	24	AAIJ	21AC	LHCB	pp at 7, 8, 13 TeV
4.5 ±0.6 ±0.3	1.3k	[1] AAIJ	17AH	LHCB	pp at 7, 8, 13 TeV

[1] See AAIJ 23AS.

$\Omega_c(3000)^0$ DECAY MODES

	Mode	Fraction (Γ_i/Γ)
Γ_1	$\Xi_c^+ K^-$	seen

$\Omega_c(3000)^0$ BRANCHING RATIOS

$\Gamma(\Xi_c^+ K^-)/\Gamma_{total}$ — Γ_1/Γ

VALUE	EVTS	DOCUMENT ID		TECN	COMMENT
seen	8.8k	AAIJ	23AS	LHCB	pp at 7, 8, 13 TeV
seen	24	[1] AAIJ	21AC	LHCB	pp at 7, 8, 13 TeV
seen	38	[2] YELTON	18B	BELL	e^+e^- at $\Upsilon(4S)$
• • • We do not use the following data for averages, fits, limits, etc. • • •					
seen	1.3k	[3,4] AAIJ	17AH	LHCB	pp at 7, 8, 13 TeV

[1] AAIJ 21AC report a significance of 6.2 σ.

[2] YELTON 18B report a significance of 3.9 σ

[3] AAIJ 17AH report a significance of 20.4 σ.

[4] See AAIJ 23AS.

$\Omega_c(3000)^0$ REFERENCES

AAIJ	23AS	PRL 131 131902	R. Aaij *et al.*	(LHCb Collab.)
PDG	22	PTEP 2022 083C01	R.L. Workman *et al.*	(PDG Collab.)
AAIJ	21AC	PR D104 L091102	R. Aaij *et al.*	(LHCb Collab.)
YELTON	18B	PR D97 051102	J. Yelton *et al.*	(BELLE Collab.)
AAIJ	17AH	PRL 118 182001	R. Aaij *et al.*	(LHCb Collab.)

Int. J. Mod. Phys. A 2026.41. Downloaded from www.worldscientific.com
UNIVERSITY OF CALIFORNIA @ BERKELEY on 09/16/26. Re-use and distribution is strictly not permitted, except for Open Access articles.

$\Omega_c(3050)^0$

$I(J^P) = ?(?^?)$ Status: ***

AAIJ 21AC rejects $J = 1/2$ hypothesis at 2.2 σ.

$\Omega_c(3050)^0$ MASS

VALUE (MeV)	EVTS	DOCUMENT ID		TECN	COMMENT
3050.17±0.19 OUR AVERAGE					
$3050.18 \pm 0.04^{+0.06}_{-0.07} \pm 0.23$	8.5k	[1] AAIJ	23AS	LHCB	pp at 7, 8, 13 TeV
$3050.1 \pm 0.3 \pm 0.2^{+0.19}_{-0.22}$	33	[2] AAIJ	21AC	LHCB	pp at 7, 8, 13 TeV
$3050.2 \pm 0.4 \pm 0.2$	28	YELTON	18B	BELL	e^+e^- at $\Upsilon(4S)$
• • • We do not use the following data for averages, fits, limits, etc. • • •					
$3050.2 \pm 0.1 \pm 0.1$	970	[3] AAIJ	17AH	LHCB	pp at 7, 8, 13 TeV

[1] The third uncertainty is due to the uncertainty in the Ξ_c^+ mass, taken to be the PDG 22 fit result 2467.71 ± 0.23 MeV.
[2] Measured via $\Omega_b^- \to \Omega_c^{**0}\pi^- \to \Xi_c^+ K^-\pi^-$. The third uncertainty is due to the uncertainty in the Ξ_c^+ mass.
[3] See AAIJ 23AS.

$\Omega_c(3050)^0$ WIDTH

VALUE (MeV)	CL%	EVTS	DOCUMENT ID		TECN	COMMENT
<1.8	95	8.5k	[1] AAIJ	23AS	LHCB	pp at 7, 8, 13 TeV
• • • We do not use the following data for averages, fits, limits, etc. • • •						
<1.6	95	33	AAIJ	21AC	LHCB	pp at 7, 8, 13 TeV
<1.2	95	970	[2] AAIJ	17AH	LHCB	pp at 7, 8, 13 TeV

[1] AAIJ 23AS also report a central value of $0.67 \pm 0.17^{+0.64}_{-0.72}$ MeV.
[2] See AAIJ 23AS.

$\Omega_c(3050)^0$ DECAY MODES

	Mode	Fraction (Γ_i/Γ)
Γ_1	$\Xi_c^+ K^-$	seen

$\Omega_c(3050)^0$ BRANCHING RATIOS

$\Gamma(\Xi_c^+ K^-)/\Gamma_{total}$ — Γ_1/Γ

VALUE	EVTS	DOCUMENT ID		TECN	COMMENT
seen	8.5k	AAIJ	23AS	LHCB	pp at 7, 8, 13 TeV
seen	33	[1] AAIJ	21AC	LHCB	pp at 7, 8, 13 TeV
seen	28	[2] YELTON	18B	BELL	e^+e^- at $\Upsilon(4S)$
• • • We do not use the following data for averages, fits, limits, etc. • • •					
seen	970	[3,4] AAIJ	17AH	LHCB	pp at 7, 8, 13 TeV

[1] AAIJ 21AC report a significance of 9.9 σ.
[2] YELTON 18B report a significance of 4.6 σ
[3] AAIJ 17AH report a significance of 20.4 σ.
[4] See AAIJ 23AS.

$\Omega_c(3050)^0$ REFERENCES

AAIJ	23AS	PRL 131 131902	R. Aaij *et al.*	(LHCb Collab.)
PDG	22	PTEP 2022 083C01	R.L. Workman *et al.*	(PDG Collab.)
AAIJ	21AC	PR D104 L091102	R. Aaij *et al.*	(LHCb Collab.)
YELTON	18B	PR D97 051102	J. Yelton *et al.*	(BELLE Collab.)
AAIJ	17AH	PRL 118 182001	R. Aaij *et al.*	(LHCb Collab.)

$\Omega_c(3065)^0$

$I(J^P) = ?(?^?)$ Status: ***

AAIJ 21AC rejects $J = 1/2$ hypothesis at 3.6 σ.

$\Omega_c(3065)^0$ MASS

VALUE (MeV)	EVTS	DOCUMENT ID		TECN	COMMENT
3065.58±0.21 OUR AVERAGE					
$3065.63 \pm 0.06 \pm 0.06 \pm 0.23$	15k	[1] AAIJ	23AS	LHCB	pp at 7, 8, 13 TeV
$3065.9 \pm 0.4 \pm 0.4^{+0.19}_{-0.22}$	51	[2] AAIJ	21AC	LHCB	pp at 7, 8, 13 TeV
$3064.9 \pm 0.6 \pm 0.2$	82	YELTON	18B	BELL	e^+e^- at $\Upsilon(4S)$
• • • We do not use the following data for averages, fits, limits, etc. • • •					
$3065.6 \pm 0.1 \pm 0.3$	1.74k	[3] AAIJ	17AH	LHCB	pp at 7, 8, 13 TeV

[1] The third uncertainty is due to the uncertainty in the Ξ_c^+ mass, taken to be the PDG 22 fit result 2467.71 ± 0.23 MeV.
[2] Measured via $\Omega_b^- \to \Omega_c^{**0}\pi^- \to \Xi_c^+ K^-\pi^-$. The third uncertainty is due to the uncertainty in the Ξ_c^+ mass.
[3] See AAIJ 23AS.

$\Omega_c(3065)^0$ WIDTH

VALUE (MeV)	EVTS	DOCUMENT ID		TECN	COMMENT
$3.4^{+0.7}_{-0.8}$ OUR AVERAGE Error includes scale factor of 1.7.					
$3.79 \pm 0.20^{+0.38}_{-0.47}$	15k	AAIJ	23AS	LHCB	pp at 7, 8, 13 TeV
$1.7 \pm 1.0 \pm 0.5$	51	AAIJ	21AC	LHCB	pp at 7, 8, 13 TeV
• • • We do not use the following data for averages, fits, limits, etc. • • •					
$3.5 \pm 0.4 \pm 0.2$	1.74k	[1] AAIJ	17AH	LHCB	pp at 7, 8, 13 TeV

[1] See AAIJ 23AS.

$\Omega_c(3065)^0$ DECAY MODES

	Mode	Fraction (Γ_i/Γ)
Γ_1	$\Xi_c^+ K^-$	seen

$\Omega_c(3065)^0$ BRANCHING RATIOS

$\Gamma(\Xi_c^+ K^-)/\Gamma_{total}$ — Γ_1/Γ

VALUE	EVTS	DOCUMENT ID		TECN	COMMENT
seen	15k	AAIJ	23AS	LHCB	pp at 7, 8, 13 TeV
seen	51	[1] AAIJ	21AC	LHCB	pp at 7, 8, 13 TeV
seen	82	YELTON	18B	BELL	e^+e^- at $\Upsilon(4S)$
• • • We do not use the following data for averages, fits, limits, etc. • • •					
seen	1.74k	[2,3] AAIJ	17AH	LHCB	pp at 7, 8, 13 TeV

[1] AAIJ 21AC report a significance of 11.9 σ.
[2] AAIJ 17AH report a significance of 23.9 σ.
[3] See AAIJ 23AS.

$\Omega_c(3065)^0$ REFERENCES

AAIJ	23AS	PRL 131 131902	R. Aaij *et al.*	(LHCb Collab.)
PDG	22	PTEP 2022 083C01	R.L. Workman *et al.*	(PDG Collab.)
AAIJ	21AC	PR D104 L091102	R. Aaij *et al.*	(LHCb Collab.)
YELTON	18B	PR D97 051102	J. Yelton *et al.*	(BELLE Collab.)
AAIJ	17AH	PRL 118 182001	R. Aaij *et al.*	(LHCb Collab.)

$\Omega_c(3090)^0$

$I(J^P) = ?(?^?)$ Status: ***

$\Omega_c(3090)^0$ MASS

VALUE (MeV)	EVTS	DOCUMENT ID		TECN	COMMENT
3090.15±0.26 OUR AVERAGE					
$3090.16 \pm 0.11^{+0.06}_{-0.10} \pm 0.23$	17k	[1] AAIJ	23AS	LHCB	pp at 7, 8, 13 TeV
$3091.0 \pm 1.1 \pm 1.0^{+0.19}_{-0.22}$	41	[2] AAIJ	21AC	LHCB	pp at 7, 8, 13 TeV
$3089.3 \pm 1.2 \pm 0.2$	87	YELTON	18B	BELL	e^+e^- at $\Upsilon(4S)$
• • • We do not use the following data for averages, fits, limits, etc. • • •					
$3090.2 \pm 0.3 \pm 0.5$	2.0k	[3] AAIJ	17AH	LHCB	pp at 7, 8, 13 TeV

[1] The third uncertainty is due to the uncertainty in the Ξ_c^+ mass, taken to be the PDG 22 fit result 2467.71 ± 0.23 MeV.
[2] Measured via $\Omega_b^- \to \Omega_c^{**0}\pi^- \to \Xi_c^+ K^-\pi^-$. The third uncertainty is due to the uncertainty in the Ξ_c^+ mass.
[3] See AAIJ 23AS.

$\Omega_c(3090)^0$ WIDTH

VALUE (MeV)	EVTS	DOCUMENT ID		TECN	COMMENT
$8.48 \pm 0.44^{+0.61}_{-1.62}$	17k	AAIJ	23AS	LHCB	pp at 7, 8, 13 TeV
• • • We do not use the following data for averages, fits, limits, etc. • • •					
$7.4 \pm 3.1 \pm 2.8$	41	AAIJ	21AC	LHCB	pp at 7, 8, 13 TeV
$8.7 \pm 1.0 \pm 0.8$	2.0k	[1] AAIJ	17AH	LHCB	pp at 7, 8, 13 TeV

[1] See AAIJ 23AS.

$\Omega_c(3090)^0$ DECAY MODES

	Mode	Fraction (Γ_i/Γ)
Γ_1	$\Xi_c^+ K^-$	seen

$\Omega_c(3090)^0$ BRANCHING RATIOS

$\Gamma(\Xi_c^+ K^-)/\Gamma_{total}$ — Γ_1/Γ

VALUE	EVTS	DOCUMENT ID		TECN	COMMENT
seen	17k	AAIJ	23AS	LHCB	pp at 7, 8, 13 TeV
seen	41	[1] AAIJ	21AC	LHCB	pp at 7, 8, 13 TeV
seen	87	YELTON	18B	BELL	e^+e^- at $\Upsilon(4S)$
• • • We do not use the following data for averages, fits, limits, etc. • • •					
seen	2.0k	[2,3] AAIJ	17AH	LHCB	pp at 7, 8, 13 TeV

[1] AAIJ 21AC report a significance of 7.8 σ.
[2] AAIJ 17AH report a significance of 21.1 σ.
[3] See AAIJ 23AS.

$\Omega_c(3090)^0$ REFERENCES

AAIJ	23AS	PRL 131 131902	R. Aaij *et al.*	(LHCb Collab.)
PDG	22	PTEP 2022 083C01	R.L. Workman *et al.*	(PDG Collab.)
AAIJ	21AC	PR D104 L091102	R. Aaij *et al.*	(LHCb Collab.)
YELTON	18B	PR D97 051102	J. Yelton *et al.*	(BELLE Collab.)
AAIJ	17AH	PRL 118 182001	R. Aaij *et al.*	(LHCb Collab.)

$\Omega_c(3120)^0$

$I(J^P) = ?(?^?)$ Status: ***

$\Omega_c(3120)^0$ MASS

VALUE (MeV)	EVTS	DOCUMENT ID		TECN	COMMENT
$3118.98 \pm 0.12^{+0.09}_{-0.23} \pm 0.23$	3.7k	[1] AAIJ	23AS	LHCB	pp at 7, 8, 13 TeV
• • • We do not use the following data for averages, fits, limits, etc. • • •					
$3119.1 \pm 0.3 \pm 0.9 \pm 0.3$	480	[2,3] AAIJ	17AH	LHCB	pp at 7, 8, 13 TeV

[1] The third uncertainty is due to the uncertainty in the Ξ_c^+ mass, taken to be the PDG 22 fit result 2467.71 ± 0.23 MeV.
[2] The third error is the uncertainty on the Ξ_c^+ mass. (AAIJ 17AH gave $^{+0.3}_{-0.5}$ MeV here, but as of 2018 it is ±0.3.)
[3] See AAIJ 23AS.

$\Omega_c(3120)^0$ WIDTH

VALUE (MeV)	CL%	EVTS	DOCUMENT ID		TECN	COMMENT
<2.5	95	3.7k	[1] AAIJ	23AS	LHCB	pp at 7, 8, 13 TeV
• • • We do not use the following data for averages, fits, limits, etc. • • •						
<2.6	95	480	[2] AAIJ	17AH	LHCB	pp at 7, 8, 13 TeV

[1] AAIJ 23AS also report a central value of $0.60 \pm 0.63^{+0.90}_{-1.05}$.
[2] See AAIJ 23AS.

$\Omega_c(3120)^0$ DECAY MODES

	Mode	Fraction (Γ_i/Γ)
Γ_1	$\Xi_c^+ K^-$	seen

$\Omega_c(3120)^0$ BRANCHING RATIOS

$\Gamma(\Xi_c^+ K^-)/\Gamma_{total}$ — Γ_1/Γ

VALUE	EVTS	DOCUMENT ID		TECN	COMMENT
seen	3.7k	AAIJ	23AS	LHCB	pp at 7, 8, 13 TeV
• • • We do not use the following data for averages, fits, limits, etc. • • •					
seen	480	[1,2] AAIJ	17AH	LHCB	pp at 7, 8, 13 TeV

[1] AAIJ 17AH report a significance of 10.4 σ.
[2] See AAIJ 23AS.

$\Omega_c(3120)^0$ REFERENCES

AAIJ	23AS	PRL 131 131902	R. Aaij *et al.*	(LHCb Collab.)
PDG	22	PTEP 2022 083C01	R.L. Workman *et al.*	(PDG Collab.)
AAIJ	17AH	PRL 118 182001	R. Aaij *et al.*	(LHCb Collab.)

$\Omega_c(3185)^0$

$I(J^P) = ?(?^?)$ Status: ***

$\Omega_c(3185)^0$ MASS

VALUE (MeV)	EVTS	DOCUMENT ID		TECN	COMMENT
$3185 \pm 1.7^{+7.4}_{-0.9} \pm 0.2$	12k	[1] AAIJ	23AS	LHCB	pp at 7, 8, 13 TeV

[1] The third uncertainty is due to the uncertainty in the Ξ_c^+ mass, taken to be the PDG 22 fit result 2467.71 ± 0.23 MeV.

$\Omega_c(3185)^0$ WIDTH

VALUE (MeV)	EVTS	DOCUMENT ID		TECN	COMMENT
$50 \pm 7^{+10}_{-20}$	12k	AAIJ	23AS	LHCB	pp at 7, 8, 13 TeV

$\Omega_c(3185)^0$ DECAY MODES

	Mode	Fraction (Γ_i/Γ)
Γ_1	$\Xi_c^+ K^-$	seen

$\Omega_c(3185)^0$ BRANCHING RATIOS

$\Gamma(\Xi_c^+ K^-)/\Gamma_{total}$ — Γ_1/Γ

VALUE	EVTS	DOCUMENT ID		TECN	COMMENT
seen	12k	[1] AAIJ	23AS	LHCB	pp at 7, 8, 13 TeV

[1] AAIJ 23AS report a significance of 12σ.

$\Omega_c(3185)^0$ REFERENCES

AAIJ	23AS	PRL 131 131902	R. Aaij *et al.*	(LHCb Collab.)
PDG	22	PTEP 2022 083C01	R.L. Workman *et al.*	(PDG Collab.)

$\Omega_c(3327)^0$

$I(J^P) = ?(?^?)$ Status: ***

$\Omega_c(3327)^0$ MASS

VALUE (MeV)	EVTS	DOCUMENT ID		TECN	COMMENT
$3327.1 \pm 1.2^{+0.1}_{-1.3} \pm 0.2$	4.1k	[1] AAIJ	23AS	LHCB	pp at 7, 8, 13 TeV

[1] The third uncertainty is due to the uncertainty in the Ξ_c^+ mass, taken to be the PDG 22 fit result 2467.71 ± 0.23 MeV.

$\Omega_c(3327)^0$ WIDTH

VALUE (MeV)	EVTS	DOCUMENT ID		TECN	COMMENT
$20 \pm 5^{+13}_{-1}$	4.1k	AAIJ	23AS	LHCB	pp at 7, 8, 13 TeV

$\Omega_c(3327)^0$ DECAY MODES

	Mode	Fraction (Γ_i/Γ)
Γ_1	$\Xi_c^+ K^-$	seen

$\Omega_c(3327)^0$ BRANCHING RATIOS

$\Gamma(\Xi_c^+ K^-)/\Gamma_{total}$ — Γ_1/Γ

VALUE	EVTS	DOCUMENT ID		TECN	COMMENT
seen	4.1k	[1] AAIJ	23AS	LHCB	pp at 7, 8, 13 TeV

[1] AAIJ 23AS report a significance of 10σ.

$\Omega_c(3327)^0$ REFERENCES

AAIJ	23AS	PRL 131 131902	R. Aaij *et al.*	(LHCb Collab.)
PDG	22	PTEP 2022 083C01	R.L. Workman *et al.*	(PDG Collab.)

Int. J. Mod. Phys. A 2026.41. Downloaded from www.worldscientific.com
by UNIVERSITY OF CALIFORNIA @ BERKELEY on 09/16/26. Re-use and distribution is strictly not permitted, except for Open Access articles.

Int. J. Mod. Phys. A 2026.41. Downloaded from www.worldscientific.com
UNIVERSITY OF CALIFORNIA @ BERKELEY on 09/16/26. Re-use and distribution is strictly not permitted, except for Open Access articles.

DOUBLY CHARMED BARYONS ($C = +2$)

$\Xi_{cc}^{++} = ucc$, $\Xi_{cc}^{+} = dcc$, $\Omega_{cc}^{+} = scc$

Ξ_{cc}^{+}

$I(J^P) = ?(?^?)$ Status: *

OMITTED FROM SUMMARY TABLE

Nominally the isospin partner of the Ξ_{cc}^{++} (ccu). While the SELEX experiment (MATTSON 02, OCHERASHVILI 05) claimed an observation of this state, subsequent searches by BABAR (AUBERT,B 06D), Belle (CHISTOV 06, KATO 14), and LHCb (AAIJ 13CD, AAIJ 20AX) did not find any significant signal or evidence for the Ξ_{cc}^{+}. However, AAIJ 21AE reports that its search for $\Xi_{cc}^{+} \to \Xi_c^{+}\pi^+\pi^-$, when combined with a prior search for $\Xi_{cc}^{+} \to \Lambda_c^{+}K^-\pi^+$ decays in AAIJ 20AX, yields a signal at 2.9 σ global significance (4.0 σ local).

Ξ_{cc}^{+} MASS

VALUE (MeV)	EVTS	DOCUMENT ID		TECN	COMMENT
3518.9±0.9 OUR AVERAGE					
3518 ±3	6	[1] OCHERASHVI...05		SELX	Σ^- nucleus ≈ 600 GeV
3519 ±1	16	[2] MATTSON	02	SELX	Σ^- nucleus ≈ 600 GeV
• • • We do not use the following data for averages, fits, limits, etc. • • •					
3623.0±1.4	368 ± 193	[3] AAIJ	21AE	LHCB	pp at 7, 8, 13 TeV

[1] OCHERASHVILI 05 claims "an excess of 5.62 events over ... 1.38 ± 0.13 events" for a significance of 4.8 σ in pD^+K^- events.
[2] MATTSON 02 claims "an excess of 15.9 events over an expected background of 6.1 ± 0.5 events, a statistical significance of 6.3 σ" in the $\Lambda_c^+K^-\pi^+$ invariant-mass spectrum. The probability that the peak is a fluctuation increases from 1.0×10^{-6} to 1.1×10^{-4} when the number of bins searched is considered.
[3] Uncertainties are statistical only. Because of undetermined systematic uncertainties in the extraction of this result it cannot be considered a mass measurement. AAIJ 21AE performs a combined fit to its $\Xi_{cc}^{+} \to \Xi_c^{+}\pi^+\pi^-$ data and the $\Xi_{cc}^{+} \to \Lambda_c^{+}K^-\pi^+$ data from AAIJ 20AX, finding a global significance of 2.9 σ (4.0 σ local).

Ξ_{cc}^{+} MEAN LIFE

VALUE (10^{-15} s)	CL%	DOCUMENT ID		TECN	COMMENT
• • • We do not use the following data for averages, fits, limits, etc. • • •					
<33	90	MATTSON	02	SELX	Σ^- nucleus, ≈ 600 GeV

Ξ_{cc}^{+} DECAY MODES

	Mode	Fraction (Γ_i/Γ)
Γ_1	$\Lambda_c^+K^-\pi^+$	not seen
Γ_2	$\Xi_c^+\pi^+\pi^-$	not seen
Γ_3	pD^+K^-	

$\Gamma(pD^+K^-)/\Gamma(\Lambda_c^+K^-\pi^+)$ — Γ_3/Γ_1

VALUE	EVTS	DOCUMENT ID		TECN	COMMENT
• • • We do not use the following data for averages, fits, limits, etc. • • •					
0.36±0.21	6	OCHERASHVI...05		SELX	Σ^- ≈ 600 GeV

$\Gamma(\Lambda_c^+K^-\pi^+)/\Gamma_{total}$ — Γ_1/Γ

VALUE	DOCUMENT ID		TECN	COMMENT
not seen	[1] AAIJ	20AX	LHCB	pp at 7, 8, 13 TeV

[1] No significant signal is observed in the mass range 3.4–3.8 GeV

$\Gamma(\Xi_c^+\pi^+\pi^-)/\Gamma_{total}$ — Γ_2/Γ

VALUE	CL%	EVTS	DOCUMENT ID		TECN	COMMENT
not seen	95	145 ± 139	[1] AAIJ	21AE	LHCB	pp at 7, 8, 13 TeV

[1] No significant signal is seen in the mass range 3.4–3.8 GeV. AAIJ 21AE performs a combined fit to its $\Xi_{cc}^{+} \to \Xi_c^{+}\pi^+\pi^-$ data and the $\Xi_{cc}^{+} \to \Lambda_c^{+}K^-\pi^+$ data from AAIJ 20AX, finding a global significance of 2.9 σ (4.0 σ local).

Ξ_{cc}^{+} REFERENCES

AAIJ	21AE	JHEP 2112 107	R. Aaij et al.	(LHCb Collab.)
AAIJ	20AX	SCPMA 63 221062	R. Aaij et al.	(LHCb Collab.)
KATO	14	PR D89 052003	Y. Kato et al.	(BELLE Collab.)
AAIJ	13CD	JHEP 1312 090	R. Aaij et al.	(LHCb Collab.)
AUBERT,B	06D	PR D74 011103	B. Aubert et al.	(BABAR Collab.)
CHISTOV	06	PRL 97 162001	R. Chistov et al.	(BELLE Collab.)
OCHERASHVI...05		PL B628 18	A. Ocherashvili et al.	(FNAL SELEX Collab.)
MATTSON	02	PRL 89 112001	M. Mattson et al.	(FNAL SELEX Collab.)

Ξ_{cc}^{++}

$I(J^P) = ?(?^?)$ Status: ***

Ξ_{cc}^{++} MASS

VALUE (MeV)	EVTS	DOCUMENT ID		TECN	COMMENT
3621.55±0.23±0.30	2k	[1] AAIJ	20J	LHCB	pp at 13 TeV
• • • We do not use the following data for averages, fits, limits, etc. • • •					
3620.6 ±1.5 ±0.4 ±0.3	91	[2] AAIJ	18BA	LHCB	pp at 13 TeV
3621.40±0.72±0.27±0.14	313	[3] AAIJ	17BC	LHCB	pp at 13 TeV

[1] AAIJ 20J combines mass measurements 3621.53 ± 0.24 ± 0.29 MeV from $\Xi_{cc}^{++} \to \Lambda_c^+K^-\pi^+\pi^+$ and 3621.95 ± 0.60 ± 0.49 MeV from $\Xi_{cc}^{++} \to \Xi_c^+\pi^+$. Supersedes AAIJ 18BA and AAIJ 17BC.
[2] The third error in AAIJ 18BA value is from the uncertainty of the Ξ_c^+ mass.
[3] The third error in AAIJ 17BC value is from the uncertainty of the Λ_c^+ mass. The width of the signal is 6.6 ± 0.8 MeV, consistent with the experimental resolution.

Ξ_{cc}^{++} MEAN LIFE

VALUE (10^{-15} s)	EVTS	DOCUMENT ID		TECN	COMMENT
$\mathbf{256^{+24}_{-22}\pm14}$	304	AAIJ	18G	LHCB	pp at 13 TeV

Ξ_{cc}^{++} DECAY MODES

	Mode	Fraction (Γ_i/Γ)	Confidence level
Γ_1	$\Lambda_c^+K^-\pi^+\pi^+$	**DEFINED AS 1**	
Γ_2	$\Xi_c^+\pi^+$, $\Xi_c^+ \to pK^-\pi^+$	0.0022±0.0006	
Γ_3	$\Xi_c'^+\pi^+$, $\Xi_c'^+ \to \Xi_c^+\gamma$, $\Xi_c^+ \to pK^-\pi^+$	0.0031±0.0010	
Γ_4	$\Xi_c^0\pi^+\pi^+$, $\Xi_c^0 \to pK^-K^-\pi^+$	0.0067±0.0010	
Γ_5	$D^+pK^-\pi^+$	<0.017	90%

$\Gamma(\Lambda_c^+K^-\pi^+\pi^+)/\Gamma_{total}$ — Γ_1/Γ

VALUE	DOCUMENT ID		TECN	COMMENT
• • • We do not use the following data for averages, fits, limits, etc. • • •				
seen	AAIJ	17BC	LHCB	12 std significance

$\Gamma(\Xi_c^+\pi^+, \Xi_c^+ \to pK^-\pi^+)/\Gamma_{total}$ — Γ_2/Γ

VALUE	EVTS	DOCUMENT ID		TECN	COMMENT
• • • We do not use the following data for averages, fits, limits, etc. • • •					
seen	91	AAIJ	18BA	LHCB	5.9 std significance

$\Gamma(\Xi_c^+\pi^+, \Xi_c^+ \to pK^-\pi^+)/\Gamma(\Lambda_c^+K^-\pi^+\pi^+)$ — Γ_2/Γ_1

VALUE (units 10^{-3})	DOCUMENT ID		TECN	COMMENT
2.2±0.6±0.1	[1] AAIJ	18BA	LHCB	Ratio 91 over 289 events

[1] AAIJ 18BA reports $[\Gamma(\Xi_{cc}^{++} \to \Xi_c^+\pi^+, \Xi_c^+ \to pK^-\pi^+)/\Gamma(\Xi_{cc}^{++} \to \Lambda_c^+K^-\pi^+\pi^+)] / [B(\Lambda_c^+ \to pK^-\pi^+)] = (3.5 \pm 0.9 \pm 0.3) \times 10^{-2}$ which we multiply by our best (shown rounded) value $B(\Lambda_c^+ \to pK^-\pi^+) = (6.37 \pm 0.21) \times 10^{-2}$. Our first error is their experiment's error and our second error is the systematic error from using our best (shown rounded) value.

$\Gamma(\Xi_c'^+\pi^+, \Xi_c'^+ \to \Xi_c^+\gamma, \Xi_c^+ \to pK^-\pi^+)/\Gamma(\Xi_c^+\pi^+, \Xi_c^+ \to pK^-\pi^+)$ — Γ_3/Γ_2

VALUE	EVTS	DOCUMENT ID		TECN	COMMENT
1.41±0.17±0.10	756	[1] AAIJ	22G	LHCB	pp at 13 TeV

[1] The photon in the $\Xi_c'^+ \to \Xi_c^+\gamma$ process is not reconstructed. Analysis uses two disjoint subsamples triggered on and independently from the signal.

$\Gamma(\Xi_c^0\pi^+\pi^+, \Xi_c^0 \to pK^-K^-\pi^+)/\Gamma(\Lambda_c^+K^-\pi^+\pi^+)$ — Γ_4/Γ_1

VALUE (units 10^{-3})	EVTS	DOCUMENT ID		TECN	COMMENT
6.7±1.0±0.2	83	[1] AAIJ	25AO	LHCB	pp at 13 TeV

[1] AAIJ 25AO reports $[\Gamma(\Xi_{cc}^{++} \to \Xi_c^0\pi^+\pi^+, \Xi_c^0 \to pK^-K^-\pi^+)/\Gamma(\Xi_{cc}^{++} \to \Lambda_c^+K^-\pi^+\pi^+)] / [B(\Lambda_c^+ \to pK^-\pi^+)] = 0.105 \pm 0.014 \pm 0.007$ which we multiply by our best (shown rounded) value $B(\Lambda_c^+ \to pK^-\pi^+) = (6.37 \pm 0.21) \times 10^{-2}$. Our first error is their experiment's error and our second error is the systematic error from using our best (shown rounded) value. Dividing further by the less well-known value for $B(\Xi_c^0 \to pK^-K^-\pi^+) = (0.49 \pm 0.10) \times 10^{-2}$, AAIJ 25AO reports $B(\Xi_{cc}^{++} \to \Xi_c^0\pi^+\pi^+)/B(\Xi_{cc}^{++} \to \Lambda_c^+K^-\pi^+\pi^+) = 1.37 \pm 0.18 \pm 0.09 \pm 0.35$ in which the third uncertainty is from the external branching fractions.

$\Gamma(D^+pK^-\pi^+)/\Gamma(\Lambda_c^+K^-\pi^+\pi^+)$ — Γ_5/Γ_1

VALUE	CL%	DOCUMENT ID		TECN	COMMENT
$<1.7 \times 10^{-2}$	90	AAIJ	19AO	LHCB	pp at 13 TeV

Ξ_{cc}^{++} REFERENCES

AAIJ	25AO	JHEP 2510 136	R. Aaij *et al.*	(LHCb Collab.)
AAIJ	22G	JHEP 2205 038	R. Aaij *et al.*	(LHCb Collab.)
AAIJ	20J	JHEP 2002 049	R. Aaij *et al.*	(LHCb Collab.)
AAIJ	19AO	JHEP 1910 124	R. Aaij *et al.*	(LHCb Collab.)
AAIJ	18BA	PRL 121 162002	R. Aaij *et al.*	(LHCb Collab.)
AAIJ	18G	PRL 121 052002	R. Aaij *et al.*	(LHCb Collab.)
AAIJ	17BC	PRL 119 112001	R. Aaij *et al.*	(LHCb Collab.)

Int. J. Mod. Phys. A 2026.41. Downloaded from www.worldscientific.com
by UNIVERSITY OF CALIFORNIA @ BERKELEY on 09/16/26. Re-use and distribution is strictly not permitted, except for Open Access articles.

Int. J. Mod. Phys. A 2026.41. Downloaded from www.worldscientific.com
UNIVERSITY OF CALIFORNIA @ BERKELEY on 09/16/26. Re-use and distribution is strictly not permitted, except for Open Access articles.

BOTTOM BARYONS
($B = -1$)

$\Lambda_b^0 = udb$, $\Sigma_b^0 = udb$, $\Sigma_b^+ = uub$, $\Sigma_b^- = ddb$
$\Xi_b^0 = usb$, $\Xi_b^- = dsb$, $\Omega_b^- = ssb$

Λ_b^0

$I(J^P) = 0(\frac{1}{2}^+)$ Status: ***

In the quark model, a Λ_b^0 is an isospin-0 udb state. The lowest Λ_b^0 ought to have $J^P = 1/2^+$. None of I, J, or P have actually been measured.

Λ_b^0 MASS

$m_{\Lambda_b^0}$

VALUE (MeV)	EVTS	DOCUMENT ID		TECN	COMMENT
5619.57± 0.16 OUR AVERAGE					
5619.34± 0.06± 0.47		[1] AAIJ	24V	LHCB	pp at 13 TeV
5619.62± 0.16± 0.13		[2] AAIJ	17AM	LHCB	pp at 7, 8 TeV
5619.30± 0.34		[3] AAIJ	14AA	LHCB	pp at 7 TeV
5620.15± 0.31± 0.47		[4] AALTONEN	14B	CDF	$p\overline{p}$ at 1.96 TeV
5619.7 ± 0.7 ± 1.1		[4] AAD	13U	ATLS	pp at 7 TeV
5621 ± 4 ± 3		[5] ABE	97B	CDF	$p\overline{p}$ at 1.8 TeV
5668 ± 16 ± 8	4	[6] ABREU	96N	DLPH	$e^+e^- \to Z$
5614 ± 21 ± 4	4	[6] BUSKULIC	96L	ALEP	$e^+e^- \to Z$
• • • We do not use the following data for averages, fits, limits, etc. • • •					
5619.65± 0.17± 0.17		[7] AAIJ	16Y	LHCB	Repl. by AAIJ 17AM
5619.44± 0.13± 0.38		[4] AAIJ	13AV	LHCB	Repl. by AAIJ 17AM
5619.19± 0.70± 0.30		[4] AAIJ	12E	LHCB	Repl. by AAIJ 13AV
5619.7 ± 1.2 ± 1.2		[8] ACOSTA	06	CDF	Repl. by AALTONEN 14B
not seen		[9] ABE	93B	CDF	Repl. by ABE 97B
5640 ± 50 ±30	16	[10] ALBAJAR	91E	UA1	$p\overline{p}$ 630 GeV
5640 $^{+100}_{-210}$	52	BARI	91	SFM	$\Lambda_b^0 \to pD^0\pi^-$
5650 $^{+150}_{-200}$	90	BARI	91	SFM	$\Lambda_b^0 \to \Lambda_c^+\pi^+\pi^-\pi^-$

[1] Uses $\Lambda_b^0 \to \Lambda_c^+ D_s^-$ decays.
[2] Uses $\Lambda_b^0 \to \chi_{c1} p K^-$, $\Lambda_b^0 \to \chi_{c2} p K^-$, $\Lambda_b^0 \to J/\psi\Lambda$, $\Lambda_b^0 \to p\psi(2S)K^-$, $\Lambda_b^0 \to pJ/\psi\pi^+\pi^-K^-$, and $\Lambda_b^0 \to pJ/\psi K^-$ decays.
[3] Uses exclusively reconstructed final states $\Lambda_b^0 \to \Lambda_c^+ D_s^-$, $\Lambda_c^+ D^-$ and $\overline{B}^0 \to D^+ D_s^-$ decays. The uncertainty includes both statistical and systematic contributions.
[4] Uses $\Lambda_b^0 \to J/\psi\Lambda$ fully reconstructed decays.
[5] ABE 97B observed 38 events with a background of 18 ± 1.6 events in the mass range 5.60–5.65 GeV/c^2, a significance of > 3.4 standard deviations.
[6] Uses 4 fully reconstructed Λ_b events.
[7] Uses $\Lambda_b^0 \to p\psi(2S)K^-$, $\Lambda_b^0 \to pJ/\psi\pi^+\pi^-K^-$, and $\Lambda_b^0 \to pJ/\psi K^-$ decays.
[8] Uses exclusively reconstructed final states containing a $J/\psi \to \mu^+\mu^-$ decays.
[9] ABE 93B states that, based on the signal claimed by ALBAJAR 91E, CDF should have found 30 ± 23 $\Lambda_b^0 \to J/\psi(1S)\Lambda$ events. Instead, CDF found not more than 2 events.
[10] ALBAJAR 91E claims 16 ± 5 events above a background of 9 ± 1 events, a significance of about 5 standard deviations.

$m_{\Lambda_b^0} - m_{B^0}$

VALUE (MeV)	DOCUMENT ID		TECN	COMMENT
339.2±1.4±0.1	[1] ACOSTA	06	CDF	$p\overline{p}$ at 1.96 TeV

[1] Uses exclusively reconstructed final states containing $J/\psi \to \mu^+\mu^-$ decays.

$m_{\Lambda_b^0} - m_{B^+}$

VALUE (MeV)	DOCUMENT ID		TECN	COMMENT
339.72±0.28 OUR AVERAGE				
339.72±0.24±0.18	[1] AAIJ	14AA	LHCB	pp at 7 TeV
339.71±0.71±0.09	[2] AAIJ	12E	LHCB	pp at 7 TeV

[1] Uses exclusively reconstructed final states $\Lambda_b^0 \to \Lambda_c^+ D_s^-$, $\Lambda_c^+ D^-$ and $\overline{B}^0 \to D^+ D_s^-$ decays.
[2] Uses exclusively reconstructed final states containing $J/\psi \to \mu^+\mu^-$ decays.

Λ_b^0 MEAN LIFE

See b-baryon Admixture section for data on b-baryon mean life average over species of b-baryon particles.

VALUE (10^{-12} s)	EVTS	DOCUMENT ID		TECN	COMMENT
1.465±0.009 OUR EVALUATION (Produced by HFLAV)					
1.477±0.027±0.009		[1] SIRUNYAN	18BY	CMS	pp at 8 TeV
1.415±0.027±0.006		[2] AAIJ	14E	LHCB	pp at 7 TeV
1.479±0.009±0.010		[3] AAIJ	14U	LHCB	pp at 7, 8 TeV
1.565±0.035±0.020		[2] AALTONEN	14B	CDF	$p\overline{p}$ at 1.96 TeV
1.449±0.036±0.017		[2] AAD	13U	ATLS	pp at 7 TeV
1.503±0.052±0.031		[2] CHATRCHYAN	13AC	CMS	pp at 7 TeV
1.303±0.075±0.035		[2] ABAZOV	12U	D0	$p\overline{p}$ at 1.96 TeV
1.401±0.046±0.035		[4] AALTONEN	10B	CDF	$p\overline{p}$ at 1.96 TeV
• • • We do not use the following data for averages, fits, limits, etc. • • •					
1.482±0.018±0.012		[5] AAIJ	13BB	LHCB	Repl. by AAIJ 14U
1.537±0.045±0.014		[2] AALTONEN	11	CDF	Repl. by AALTONEN 14B
1.218 $^{+0.130}_{-0.115}$ ±0.042		[2] ABAZOV	07S	D0	Repl. by ABAZOV 12U
1.290 $^{+0.119}_{-0.110}$ $^{+0.087}_{-0.091}$		[6] ABAZOV	07U	D0	$p\overline{p}$ at 1.96 TeV
1.593 $^{+0.083}_{-0.078}$ ±0.033		[2] ABULENCIA	07A	CDF	Repl. by AALTONEN 11
1.22 $^{+0.22}_{-0.18}$ ±0.04		[2] ABAZOV	05C	D0	Repl. by ABAZOV 07S
1.11 $^{+0.19}_{-0.18}$ ±0.05		[7] ABREU	99W	DLPH	$e^+e^- \to Z$
1.29 $^{+0.24}_{-0.22}$ ±0.06		[7] ACKERSTAFF	98G	OPAL	$e^+e^- \to Z$
1.21 ±0.11		[7] BARATE	98D	ALEP	$e^+e^- \to Z$
1.32 ±0.15 ±0.07		[8] ABE	96M	CDF	$p\overline{p}$ at 1.8 TeV
1.19 $^{+0.21}_{-0.18}$ $^{+0.07}_{-0.08}$		ABREU	96D	DLPH	Repl. by ABREU 99W
1.27 $^{+0.35}_{-0.29}$ ±0.09		ABREU	95S	DLPH	Repl. by ABREU 99W
1.14 $^{+0.22}_{-0.19}$ ±0.07	69	AKERS	95K	OPAL	Repl. by ACKERSTAFF 98G
1.02 $^{+0.23}_{-0.18}$ ±0.06	44	BUSKULIC	95L	ALEP	Repl. by BARATE 98D

[1] Measured using $\Lambda_b^0 \to J/\psi\Lambda$ decays.
[2] Measured mean life using fully reconstructed $\Lambda_b^0 \to J/\psi\Lambda$ decays.
[3] Used $\Lambda_b^0 \to J/\psi p K^-$ decays.
[4] Measured mean life using fully reconstructed $\Lambda_b^0 \to \Lambda_c^+\pi^-$ decays.
[5] Measured the lifetime ratio of decays $\Lambda_b^0 \to J/\psi p K^-$ to $B^0 \to J/\psi\pi^+K^-$ to be 0.976 ± 0.012 ± 0.006 with τ_{B^0} = 1.519 ± 0.007 ps.
[6] Measured using semileptonic decays $\Lambda_b^0 \to \Lambda_c^+\mu\nu X$ and $\Lambda_c^+ \to K_S^0 p$.
[7] Measured using $\Lambda_c\ell^-$ and $\Lambda\ell^+\ell^-$.
[8] Excess $\Lambda_c\ell^-$, decay lengths.

$\tau_{\Lambda_b^0}/\tau_{\overline{\Lambda}_b^0}$

VALUE	DOCUMENT ID		TECN	COMMENT
0.940±0.035±0.006	[1] AAIJ	14E	LHCB	pp at 7 TeV

[1] Measured using $\Lambda_b^0 \to J/\psi\Lambda$ decays.

$\tau_{\Lambda_b^0}/\tau_{B^0}$ MEAN LIFE RATIO

$\tau_{\Lambda_b^0}/\tau_{B^0}$ (direct measurements)

VALUE	DOCUMENT ID		TECN	COMMENT
0.970±0.006 OUR EVALUATION (Produced by HFLAV)				
0.970±0.009 OUR AVERAGE Error includes scale factor of 1.4. See the ideogram below.				
0.978±0.018±0.006	[1] SIRUNYAN	18BY	CMS	pp at 8 TeV
0.929±0.018±0.004	[1] AAIJ	14E	LHCB	pp at 7 TeV
0.974±0.006±0.004	[2] AAIJ	14U	LHCB	pp at 7, 8 TeV
0.960±0.025±0.016	[3] AAD	13U	ATLS	pp at 7 TeV
0.864±0.052±0.033	[4,5] ABAZOV	12U	D0	$p\overline{p}$ at 1.96 TeV
1.020±0.030±0.008	[4] AALTONEN	11	CDF	$p\overline{p}$ at 1.96 TeV
• • • We do not use the following data for averages, fits, limits, etc. • • •				
0.976±0.012±0.006	[6] AAIJ	13BB	LHCB	Repl. by AAIJ 14U
0.811 $^{+0.096}_{-0.087}$ ±0.034	[4,5] ABAZOV	07S	D0	Repl. by ABAZOV 12U
1.041±0.057	[7] ABULENCIA	07A	CDF	Repl. by AALTONEN 11
0.87 $^{+0.17}_{-0.14}$ ±0.03	[7] ABAZOV	05C	D0	Repl. by ABAZOV 07S

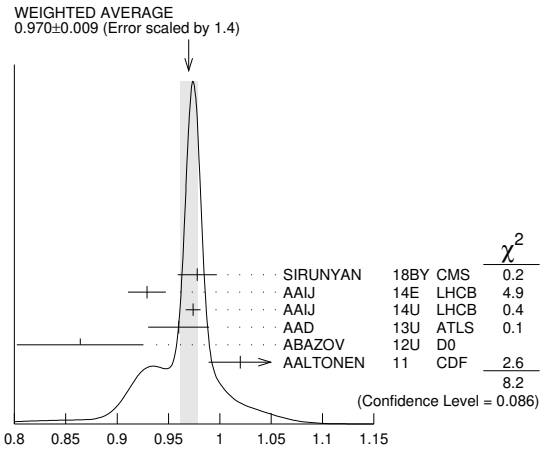

[1] Measured using $\Lambda_b^0 \to J/\psi\Lambda$ and $B^0 \to J/\psi K^*(892)^0$ decays.
[2] Used $\Lambda_b^0 \to J/\psi p K^-$ and $B^0 \to J/\psi K^*(892)^0$ decays.
[3] Measured with $\Lambda_b^0 \to J/\psi(\mu^+\mu^-)\,\Lambda^0(p\pi^-)$ decays.
[4] Uses fully reconstructed $\Lambda_b \to J/\psi\Lambda$ decays.
[5] Uses $B^0 \to J/\psi K_S^0$ decays for denominator.
[6] Measures $1/\tau_{\Lambda_b^0} - 1/\tau_{B^0}$ and uses $\tau_{B^0} = 1.519 \pm 0.007$ ps to extract lifetime ratio.
[7] Measured mean life ratio using fully reconstructed decays.

Λ_b^0 DECAY MODES

The branching fractions B(b-baryon $\to \Lambda\ell^-\overline{\nu}_\ell$anything) and B($\Lambda_b^0 \to \Lambda_c^+\ell^-\overline{\nu}_\ell$anything) are not pure measurements because the underlying measured products of these with B($b \to b$-baryon) were used to determine B($b \to b$-baryon), as described in the note "Production and Decay of b-Flavored Hadrons."

For inclusive branching fractions, *e.g.*, $\Lambda_b \to \overline{\Lambda}_c$anything, the values usually are multiplicities, not branching fractions. They can be greater than one.

	Mode		Fraction (Γ_i/Γ)	Scale factor/ Confidence level
Γ_1	$J/\psi(1S)\Lambda$		$(3.0 \pm 0.8) \times 10^{-4}$	
Γ_2	$J/\psi(1S)\Lambda\phi$		$(1.2 \pm 0.4) \times 10^{-5}$	
Γ_3	$\psi(2S)\Lambda$		$(1.5 \pm 0.4) \times 10^{-4}$	
Γ_4	$pD^0\pi^-$		$(6.4 \pm 0.6) \times 10^{-4}$	
Γ_5	$\Lambda_c(2860)^+\pi^-,\ \Lambda_c^+ \to D^0 p$			
Γ_6	$\Lambda_c(2880)^+\pi^-,\ \Lambda_c^+ \to D^0 p$			
Γ_7	$\Lambda_c(2940)^+\pi^-,\ \Lambda_c^+ \to D^0 p$			
Γ_8	$pD^+\pi^-\pi^-$		$(2.8 \pm 0.4) \times 10^{-4}$	
Γ_9	$pD^*(2010)^+\pi^-\pi^-$		$(5.3 \pm 1.0) \times 10^{-4}$	
Γ_{10}	pD^0K^-		$(4.6 \pm 0.8) \times 10^{-5}$	
Γ_{11}	$pDK^-,\ D \to K^-\pi^+$			
Γ_{12}	$pDK^-,\ D \to K^+\pi^-$			
Γ_{13}	$pJ/\psi\pi^-$		$(2.6\ ^{+0.5}_{-0.4}) \times 10^{-5}$	
Γ_{14}	$p\pi^- J/\psi,\ J/\psi \to \mu^+\mu^-$		$(1.6 \pm 0.8) \times 10^{-6}$	
Γ_{15}	$pJ/\psi K^-$		$(3.2\ ^{+0.6}_{-0.5}) \times 10^{-4}$	
Γ_{16}	$J/\psi\Xi^-K^+$		$(3.6 \pm 1.1) \times 10^{-6}$	
Γ_{17}	$p\eta_c(1S)K^-$		$(1.06 \pm 0.26) \times 10^{-4}$	
Γ_{18}	$P_{c\overline{c}}(4312)^+K^-,\ P_{c\overline{c}}^+ \to p\eta_c(1S)$		$< 2.5 \times 10^{-5}$	CL=95%
Γ_{19}	$P_{c\overline{c}}(4380)^+K^-,\ P_{c\overline{c}}^+ \to pJ/\psi$	[a]	$(2.7 \pm 1.4) \times 10^{-5}$	
Γ_{20}	$P_c(4450)^+K^-,\ P_c \to pJ/\psi$	[a]	$(1.3 \pm 0.4) \times 10^{-5}$	
Γ_{21}	$\chi_{c1}(1P)pK^-$		$(7.7\ ^{+1.5}_{-1.3}) \times 10^{-5}$	
Γ_{22}	$\chi_{c1}(1P)p\pi^-$		$(5.1\ ^{+1.3}_{-1.2}) \times 10^{-6}$	
Γ_{23}	$\chi_{c2}(1P)pK^-$		$(8.0\ ^{+1.7}_{-1.4}) \times 10^{-5}$	
Γ_{24}	$\chi_{c2}(1P)p\pi^-$		$(4.8 \pm 1.9) \times 10^{-6}$	
Γ_{25}	$pJ/\psi(1S)\pi^+\pi^-K^-$		$(6.6\ ^{+1.3}_{-1.1}) \times 10^{-5}$	
Γ_{26}	$p\psi(2S)K^-$		$(6.6\ ^{+1.2}_{-1.0}) \times 10^{-5}$	
Γ_{27}	$\chi_{c1}(3872)pK^-$		$(2.8 \pm 1.2) \times 10^{-5}$	
Γ_{28}	$\chi_{c1}(3872)\Lambda(1520)$		$(1.6 \pm 0.8) \times 10^{-5}$	
Γ_{29}	$\psi(2S)p\pi^-$		$(7.5\ ^{+1.6}_{-1.4}) \times 10^{-6}$	
Γ_{30}	$p\overline{K}^0\pi^-$		$(1.95 \pm 0.34) \times 10^{-5}$	S=1.9
Γ_{31}	pK^0K^-		$(1.22 \pm 0.23) \times 10^{-6}$	
Γ_{32}	$\Lambda_c^+\pi^-$		$(4.9 \pm 0.4) \times 10^{-3}$	S=1.2
Γ_{33}	$\Lambda_c^+K^-$		$(3.56 \pm 0.28) \times 10^{-4}$	S=1.2
Γ_{34}	$\Lambda_c^+a_1(1260)^-$		seen	
Γ_{35}	$\Lambda_c^+D^-$		$(4.6 \pm 0.6) \times 10^{-4}$	
Γ_{36}	$\Lambda_c^+D_s^-$		(1.10 ± 0.10) %	
Γ_{37}	$\Lambda_c^+D_s^{*-}$		(1.83 ± 0.18) %	
Γ_{38}	$\Lambda_c^+D_s^-K^+K^-$		$(1.55 \pm 0.28) \times 10^{-4}$	
Γ_{39}	$P_{c\overline{c}s}(4459)K^+K^-,\ P_{c\overline{c}s}(4459) \to \Lambda_c^+D_s^-$		$< 2.6 \times 10^{-5}$	CL=90%
Γ_{40}	$P_{c\overline{c}s}(4338)K^+K^-,\ P_{c\overline{c}s}(4338) \to \Lambda_c^+D_s^-$		$< 1.6 \times 10^{-5}$	CL=90%
Γ_{41}	$\Lambda_c^+\overline{D}^0K^-$		$(2.13 \pm 0.20) \times 10^{-3}$	
Γ_{42}	$\Lambda_c^+\overline{D}^{*0}K^-$		$(6.6 \pm 0.7) \times 10^{-3}$	
Γ_{43}	$\Lambda_c^+\pi^+\pi^-\pi^-$		$(7.6 \pm 1.1) \times 10^{-3}$	S=1.1
Γ_{44}	$\Lambda_c(2595)^+\pi^-,\ \Lambda_c(2595)^+ \to \Lambda_c^+\pi^+\pi^-$		$(3.4 \pm 1.4) \times 10^{-4}$	
Γ_{45}	$\Lambda_c(2625)^+\pi^-,\ \Lambda_c(2625)^+ \to \Lambda_c^+\pi^+\pi^-$		$(3.3 \pm 1.3) \times 10^{-4}$	
Γ_{46}	$\Sigma_c(2455)^0\pi^+\pi^-,\ \Sigma_c^0 \to \Lambda_c^+\pi^-$		$(5.7 \pm 2.2) \times 10^{-4}$	
Γ_{47}	$\Sigma_c(2455)^{++}\pi^-\pi^-,\ \Sigma_c^{++} \to \Lambda_c^+\pi^+$		$(3.2 \pm 1.5) \times 10^{-4}$	
Γ_{48}	$\Sigma_c(2455)^{++}D^-K^-$		$(6.0 \pm 0.8) \times 10^{-4}$	
Γ_{49}	$\Sigma_c(2455)^{++}D^{*-}K^-$		$(1.36 \pm 0.23) \times 10^{-3}$	
Γ_{50}	$\Sigma_c(2520)^{++}D^-K^-$		$(2.8 \pm 0.5) \times 10^{-4}$	
Γ_{51}	$\Sigma_c(2520)^{++}D^{*-}K^-$		$(5.4 \pm 1.1) \times 10^{-4}$	
Γ_{52}	$\Lambda_c^+K^+K^-\pi^-$		$(1.02 \pm 0.11) \times 10^{-3}$	
Γ_{53}	$\Lambda_c^+p\overline{p}\pi^-$		$(2.63 \pm 0.27) \times 10^{-4}$	
Γ_{54}	$\Sigma_c(2455)^0p\overline{p},\ \Sigma_c^0 \to \Lambda_c^+\pi^-$		$(2.3 \pm 0.5) \times 10^{-5}$	
Γ_{55}	$\Sigma_c(2520)^0p\overline{p},\ \Sigma_c(2520)^0 \to \Lambda_c^+\pi^-$		$(3.1 \pm 0.7) \times 10^{-5}$	
Γ_{56}	$\Lambda K^0 2\pi^+2\pi^-$			
Γ_{57}	$\Lambda_c^+\ell^-\overline{\nu}_\ell$anything	[b]	(10.9 ± 2.2) %	
Γ_{58}	$\Lambda_c^+\ell^-\overline{\nu}_\ell$		$(6.2\ ^{+1.4}_{-1.3})$ %	
Γ_{59}	$\Lambda_c^+\tau^-\overline{\nu}_\tau$		(1.9 ± 0.5) %	
Γ_{60}	$\Lambda_c^+\pi^+\pi^-\ell^-\overline{\nu}_\ell$		(5.6 ± 3.1) %	
Γ_{61}	$\Lambda_c(2595)^+\ell^-\overline{\nu}_\ell$		$(7.9\ ^{+4.0}_{-3.5}) \times 10^{-3}$	
Γ_{62}	$\Lambda_c(2625)^+\ell^-\overline{\nu}_\ell$		$(1.3\ ^{+0.6}_{-0.5})$ %	
Γ_{63}	$\Sigma_c(2455)^0\pi^+\ell^-\overline{\nu}_\ell$			
Γ_{64}	$\Sigma_c(2455)^{++}\pi^-\ell^-\overline{\nu}_\ell$			
Γ_{65}	ph^-	[c]	$< 2.3 \times 10^{-5}$	CL=90%
Γ_{66}	$p\pi^-$		$(4.6 \pm 0.8) \times 10^{-6}$	
Γ_{67}	pK^-		$(5.5 \pm 1.0) \times 10^{-6}$	
Γ_{68}	pD_s^-		$(1.25 \pm 0.13) \times 10^{-5}$	
Γ_{69}	$p\mu^-\overline{\nu}_\mu$		$(4.1 \pm 1.0) \times 10^{-4}$	
Γ_{70}	$\Lambda\mu^+\mu^-$		$(1.08 \pm 0.28) \times 10^{-6}$	
Γ_{71}	$p\pi^-\mu^+\mu^-$		$(6.9 \pm 2.5) \times 10^{-8}$	
Γ_{72}	$pK^-e^+e^-$		$(3.1 \pm 0.6) \times 10^{-7}$	
Γ_{73}	$pK^-\mu^+\mu^-$		$(2.6\ ^{+0.5}_{-0.4}) \times 10^{-7}$	
Γ_{74}	$\Lambda(1520)^0\mu^+\mu^-$			
Γ_{75}	$\Lambda\gamma$		$(7.1 \pm 1.7) \times 10^{-6}$	
Γ_{76}	$\overline{p}K^-\gamma$			
Γ_{77}	$\Lambda(1405)^0\gamma$			
Γ_{78}	$\Lambda(1520)^0\gamma$			
Γ_{79}	$\Lambda(1600)^0\gamma$			
Γ_{80}	$\Lambda(1670)^0\gamma$			
Γ_{81}	$\Lambda(1690)^0\gamma$			
Γ_{82}	$\Lambda(1800)^0\gamma$			
Γ_{83}	$\Lambda(1810)^0\gamma$			
Γ_{84}	$\Lambda(1820)^0\gamma$			
Γ_{85}	$\Lambda(1830)^0\gamma$			
Γ_{86}	$\Lambda(1890)^0\gamma$			
Γ_{87}	$\Lambda(2100)^0\gamma$			
Γ_{88}	$\Lambda(2110)^0\gamma$			
Γ_{89}	$\Lambda(2530)^0\gamma$			
Γ_{90}	$(\overline{p}K^-)$ nonresonantγ			
Γ_{91}	$\Lambda\eta$		$(9\ ^{+7}_{-5}) \times 10^{-6}$	
Γ_{92}	$\Lambda\eta'(958)$		$< 3.1 \times 10^{-6}$	CL=90%
Γ_{93}	$\Lambda\pi^+\pi^-$		$(6.4 \pm 0.9) \times 10^{-6}$	
Γ_{94}	$\Lambda K^+\pi^-$		$(5.5 \pm 0.7) \times 10^{-6}$	
Γ_{95}	ΛK^+K^-		$(1.29 \pm 0.12) \times 10^{-5}$	
Γ_{96}	ΛD^+D^-		$(1.24 \pm 0.35) \times 10^{-4}$	
Γ_{97}	$\Lambda\phi$		$(9.8 \pm 2.6) \times 10^{-6}$	
Γ_{98}	$p\pi^-\pi^+\pi^-$		$(2.13 \pm 0.21) \times 10^{-5}$	
Γ_{99}	$pK^-K^+\pi^-$		$(4.1 \pm 0.6) \times 10^{-6}$	
Γ_{100}	$pK^-\pi^+\pi^-$		$(5.1 \pm 0.5) \times 10^{-5}$	
Γ_{101}	$pK^-K^+K^-$		$(1.28 \pm 0.13) \times 10^{-5}$	

[a] P_c^+ is a pentaquark-charmonium state.
[b] Not a pure measurement. See note at head of Λ_b^0 Decay Modes.
[c] Here h^- means π^- or K^-.

Int. J. Mod. Phys. A 2026.41. Downloaded from www.worldscientific.com
by UNIVERSITY OF CALIFORNIA @ BERKELEY on 09/16/26. Re-use and distribution is strictly not permitted, except for Open Access articles.

Int. J. Mod. Phys. A 2026.41. Downloaded from www.worldscientific.com
UNIVERSITY OF CALIFORNIA @ BERKELEY on 09/16/26. Re-use and distribution is strictly not permitted, except for Open Access articles.

FIT INFORMATION

An overall fit to 14 branching ratios uses 18 measurements to determine 9 parameters. The overall fit has a $\chi^2 = 11.7$ for 9 degrees of freedom.

The following *off-diagonal* array elements are the correlation coefficients $\langle \delta x_i \delta x_j \rangle / (\delta x_i \cdot \delta x_j)$, in percent, from the fit to the branching fractions, $x_i \equiv \Gamma_i/\Gamma_{\rm total}$.

x_3	99							
x_{16}	89	88						
x_{32}	0	0	0					
x_{33}	0	0	0	92				
x_{43}	0	0	0	46	43			
x_{58}	0	0	0	13	12	6		
x_{66}	0	0	0	0	0	0	0	
x_{67}	0	0	0	0	0	0	0	82
	x_1	x_3	x_{16}	x_{32}	x_{33}	x_{43}	x_{58}	x_{66}

Λ_b^0 BRANCHING RATIOS

$\Gamma(J/\psi(1S)\Lambda)/\Gamma_{\rm total}$ — Γ_1/Γ

VALUE (units 10^{-4})	EVTS	DOCUMENT ID		TECN	COMMENT
3.0± 0.8 OUR FIT					
3.0± 0.8 OUR AVERAGE					
3.0± 0.4± 0.7		[1] ABAZOV	11O	D0	$p\overline{p}$ at 1.96 TeV
2.4± 1.2± 0.6		[2] ABE	97B	CDF	$p\overline{p}$ at 1.8 TeV
• • • We do not use the following data for averages, fits, limits, etc. • • •					
91 ±55 ±21	16	[3] ALBAJAR	91E	UA1	$p\overline{p}$ at 630 GeV

[1] ABAZOV 11O reports $[\Gamma(\Lambda_b^0 \to J/\psi(1S)\Lambda)/\Gamma_{\rm total}] \times [B(\overline{b} \to b\text{-baryon at } p\overline{p})] = (6.01 \pm 0.60 \pm 0.58 \pm 0.28) \times 10^{-5}$ which we divide by our best (shown rounded) value $B(\overline{b} \to b\text{-baryon at } p\overline{p}) = (19.8 \pm 4.6) \times 10^{-2}$. Our first error is their experiment's error and our second error is the systematic error from using our best (shown rounded) value.

[2] ABE 97B reports $[\Gamma(\Lambda_b^0 \to J/\psi(1S)\Lambda)/\Gamma_{\rm total}] \times [B(\overline{b} \to b\text{-baryon at } p\overline{p})] = (4.7 \pm 2.3 \pm 0.2) \times 10^{-5}$ which we divide by our best (shown rounded) value $B(\overline{b} \to b\text{-baryon at } p\overline{p}) = (19.8 \pm 4.6) \times 10^{-2}$. Our first error is their experiment's error and our second error is the systematic error from using our best (shown rounded) value.

[3] ALBAJAR 91E reports $[\Gamma(\Lambda_b^0 \to J/\psi(1S)\Lambda)/\Gamma_{\rm total}] \times [B(\overline{b} \to b\text{-baryon at } p\overline{p})] = (18 \pm 6 \pm 9) \times 10^{-4}$ which we divide by our best (shown rounded) value $B(\overline{b} \to b\text{-baryon at } p\overline{p}) = (19.8 \pm 4.6) \times 10^{-2}$. Our first error is their experiment's error and our second error is the systematic error from using our best (shown rounded) value.

$\Gamma(J/\psi(1S)\Lambda\phi)/\Gamma(\psi(2S)\Lambda)$ — Γ_2/Γ_3

VALUE (units 10^{-2})	DOCUMENT ID		TECN	COMMENT
8.26±0.90±0.69	SIRUNYAN	20H	CMS	pp at 13 TeV

$\Gamma(\psi(2S)\Lambda)/\Gamma(J/\psi(1S)\Lambda)$ — Γ_3/Γ_1

VALUE	DOCUMENT ID		TECN	COMMENT
0.506±0.023 OUR FIT				
0.508±0.023 OUR AVERAGE				
0.513±0.023±0.019	[1] AAIJ	19F	LHCB	pp at 7, 8 TeV
0.50 ±0.03 ±0.02	[2] AAD	15CH	ATLS	pp at 8 TeV

[1] AAIJ 19F uses $B(J/\psi \to \mu^+\mu^-) = (5.961 \pm 0.033) \times 10^{-2}$ and $B(\psi(2S) \to e^+e^-) = (7.93 \pm 0.17) \times 10^{-3}$ from PDG 18 with assumption of lepton universality. AAIJ 19F reports this result as $0.513 \pm 0.023 \pm 0.016 \pm 0.011$, where the last uncertainty is the contribution due to the external input of branching fractions used in the analysis.

[2] AAD 15CH uses $B(J/\psi \to \mu^+\mu^-) = (5.961 \pm 0.033) \times 10^{-2}$ and $B(\psi(2S) \to \mu^+\mu^-) = (7.89 \pm 0.17) \times 10^{-3}$ from PDG 14 with assumption of lepton universality.

$\Gamma(pD^0\pi^-)/\Gamma_{\rm total}$ — Γ_4/Γ

VALUE	EVTS	DOCUMENT ID		TECN	COMMENT
• • • We do not use the following data for averages, fits, limits, etc. • • •					
seen	52	BARI	91	SFM	$D^0 \to K^-\pi^+$
seen		BASILE	81	SFM	$D^0 \to K^-\pi^+$

$\Gamma(\Lambda_c(2860)^+\pi^-, \Lambda_c^+ \to D^0p)/\Gamma(\Lambda_c(2880)^+\pi^-, \Lambda_c^+ \to D^0p)$ — Γ_5/Γ_6

VALUE	DOCUMENT ID		TECN	COMMENT
$4.54^{+0.51+0.21}_{-0.39-0.59}$	AAIJ	17S	LHCB	pp at 7, 8 TeV

$\Gamma(\Lambda_c(2940)^+\pi^-, \Lambda_c^+ \to D^0p)/\Gamma(\Lambda_c(2880)^+\pi^-, \Lambda_c^+ \to D^0p)$ — Γ_7/Γ_6

VALUE	DOCUMENT ID		TECN	COMMENT
$0.83^{+0.31+0.18}_{-0.10-0.43}$	AAIJ	17S	LHCB	pp at 7, 8 TeV

$\Gamma(pD^+\pi^-\pi^-)/\Gamma(\Lambda_c^+\pi^+\pi^-\pi^-)$ — Γ_8/Γ_{43}

VALUE (%)	DOCUMENT ID		TECN	COMMENT
3.66±0.18±0.13	[1] AAIJ	22R	LHCB	pp at 7 and 8 TeV

[1] AAIJ 22R reports $[\Gamma(\Lambda_b^0 \to pD^+\pi^-\pi^-)/\Gamma(\Lambda_b^0 \to \Lambda_c^+\pi^+\pi^-\pi^-)] \times [B(D^+ \to K^-2\pi^+)] / [B(\Lambda_c^+ \to pK^-\pi^+)] = 5.35 \pm 0.21 \pm 0.16$ % which we multiply or divide by our best (shown rounded) values $B(D^+ \to K^-2\pi^+) = (9.31 \pm 0.14) \times 10^{-2}$, $B(\Lambda_c^+ \to pK^-\pi^+) = (6.37 \pm 0.21) \times 10^{-2}$. Our first error is their experiment's error and our second error is the systematic error from using our best (shown rounded) values.

$\Gamma(pD^*(2010)^+\pi^-\pi^-)/\Gamma(pD^+\pi^-\pi^-)$ — Γ_9/Γ_8

VALUE	DOCUMENT ID		TECN	COMMENT
1.90±0.19	[1] AAIJ	22R	LHCB	pp at 7 and 8 TeV

[1] AAIJ 22R uses partial reconstruction of $pD^+\pi^-\pi^-$ final state.

$\Gamma(pD^0K^-)/\Gamma(pD^0\pi^-)$ — Γ_{10}/Γ_4

VALUE (units 10^{-2})	DOCUMENT ID		TECN	COMMENT
$7.3 \pm 0.8^{+0.5}_{-0.6}$	AAIJ	14H	LHCB	pp at 7 TeV

$\Gamma(pDK^-, D \to K^-\pi^+)/\Gamma(pDK^-, D \to K^+\pi^-)$ — Γ_{11}/Γ_{12}

VALUE	DOCUMENT ID		TECN	COMMENT
$7.1 \pm 0.8^{+0.4}_{-0.3}$	[1] AAIJ	21AD	LHCB	pp at 7, 8, 13 TeV

[1] Measured in the full phase space.

$\Gamma(pJ/\psi\pi^-)/\Gamma(pJ/\psi K^-)$ — Γ_{13}/Γ_{15}

VALUE (units 10^{-2})	DOCUMENT ID		TECN	COMMENT
8.24±0.25±0.42	AAIJ	14K	LHCB	pp at 7, 8 TeV

$\Gamma(pJ/\psi K^-)/\Gamma_{\rm total}$ — Γ_{15}/Γ

VALUE (units 10^{-4})	DOCUMENT ID		TECN	COMMENT
$3.17 \pm 0.04^{+0.57}_{-0.45}$	[1] AAIJ	16A	LHCB	pp at 7, 8 TeV

[1] AAIJ 16A reported the measurement of $(3.17 \pm 0.04 \pm 0.07 \pm 0.34^{+0.45}_{-0.28}) \times 10^{-4}$ where the first uncertainty is statistical, the second is systematic, the third is due to the branching fraction of $B^0 \to J/\psi K^*(892)^0$, and the fourth is due to the knowledge of f_{Λ_b}/f_d. We combined in quadrature second to fourth uncertainties to a total systematic uncertainty.

$\Gamma(J/\psi\Xi^-K^+)/\Gamma(J/\psi(1S)\Lambda)$ — Γ_{16}/Γ_1

VALUE (units 10^{-2})	DOCUMENT ID		TECN	COMMENT
1.21±0.16 OUR FIT				
1.17±0.14±0.08	AAIJ	25AA	LHCB	pp at 13 TeV

$\Gamma(J/\psi\Xi^-K^+)/\Gamma(\psi(2S)\Lambda)$ — Γ_{16}/Γ_3

VALUE (units 10^{-2})	DOCUMENT ID		TECN	COMMENT
2.38±0.33 OUR FIT				
3.39±1.19±0.03	[1] HAYRAPETY...24BA		CMS	pp at 13 TeV

[1] HAYRAPETYAN 24BA reports $(3.38 \pm 1.02 \pm 0.61 \pm 0.03) \times 10^{-2}$ from a measurement of $[\Gamma(\Lambda_b^0 \to J/\psi\Xi^-K^+)/\Gamma(\Lambda_b^0 \to \psi(2S)\Lambda)] \times [B(\Xi^- \to \Lambda\pi^-)] / [B(\psi(2S) \to J/\psi(1S)\pi^+\pi^-)]$ assuming $B(\Xi^- \to \Lambda\pi^-) = (99.887 \pm 0.035) \times 10^{-2}$, $B(\psi(2S) \to J/\psi(1S)\pi^+\pi^-) = (34.68 \pm 0.30) \times 10^{-2}$, which we rescale to our best (shown rounded) values $B(\Xi^- \to \Lambda\pi^-) = (99.887 \pm 0.035) \times 10^{-2}$, $B(\psi(2S) \to J/\psi(1S)\pi^+\pi^-) = (34.78 \pm 0.33) \times 10^{-2}$. Our first error is their experiment's error and our second error is the systematic error from using our best (shown rounded) values.

$\Gamma(p\eta_c(1S)K^-)/\Gamma(pJ/\psi K^-)$ — Γ_{17}/Γ_{15}

VALUE	DOCUMENT ID		TECN	COMMENT
0.333±0.050±0.037	[1] AAIJ	20AK	LHCB	pp at 13 TeV

[1] AAIJ 20AK reported the measurement of $0.333 \pm 0.050 \pm 0.019 \pm 0.032$, where the last uncertainty is due uncertainties of the used branching fractions of $J/\psi \to p\overline{p}$ and $\eta_c \to p\overline{p}$ decays. We combined in quadrature the systematic uncertainties.

$\Gamma(P_{c\overline{c}}(4312)^+K^-, P_{c\overline{c}}^+ \to p\eta_c(1S))/\Gamma(p\eta_c(1S)K^-)$ — Γ_{18}/Γ_{17}

VALUE	CL%	DOCUMENT ID		TECN	COMMENT
<0.24	95	AAIJ	20AK	LHCB	pp at 13 TeV

$\Gamma(P_{c\overline{c}}(4380)^+K^-, P_{c\overline{c}}^+ \to pJ/\psi)/\Gamma_{\rm total}$ — Γ_{19}/Γ

P_c^+ is a pentaquark-charmonium state.

VALUE (units 10^{-5})	DOCUMENT ID		TECN	COMMENT
$2.66 \pm 0.22^{+1.41}_{-1.38}$	[1] AAIJ	16A	LHCB	pp at 7, 8 TeV

[1] AAIJ 16 total systematic includes the uncertainties on $f(P_c^+)$ and $B(\Lambda_b \to pJ/\psi K^-)$.

$\Gamma(P_c(4450)^+K^-, P_c \to pJ/\psi)/\Gamma_{\rm total}$ — Γ_{20}/Γ

P_c^+ is a pentaquark-charmonium state.

VALUE (units 10^{-5})	DOCUMENT ID		TECN	COMMENT
$1.30 \pm 0.16^{+0.42}_{-0.39}$	[1] AAIJ	16A	LHCB	pp at 7, 8 TeV

[1] AAIJ 16 total systematic includes the uncertainties on $f(P_c^+)$ and $B(\Lambda_b \to pJ/\psi K^-)$.

$\Gamma(\chi_{c1}(1P)pK^-)/\Gamma(pJ/\psi K^-)$ — Γ_{21}/Γ_{15}

VALUE	DOCUMENT ID		TECN	COMMENT
0.242±0.014±0.016	[1] AAIJ	17AM	LHCB	pp at 7, 8 TeV

[1] AAIJ 17AM reports $0.242 \pm 0.014 \pm 0.016$ from a measurement of $[\Gamma(\Lambda_b^0 \to \chi_{c1}(1P)pK^-)/\Gamma(\Lambda_b^0 \to pJ/\psi K^-)] \times [B(\chi_{c1}(1P) \to \gamma J/\psi(1S))]$ assuming $B(\chi_{c1}(1P) \to \gamma J/\psi(1S)) = (33.9 \pm 1.2) \times 10^{-2}$.

Int. J. Mod. Phys. A 2026.41. Downloaded from www.worldscientific.com
by UNIVERSITY OF CALIFORNIA @ BERKELEY on 09/16/26. Re-use and distribution is strictly not permitted, except for Open Access articles.

$\Gamma(\chi_{c1}(1P)p\pi^-)/\Gamma(\chi_{c1}(1P)pK^-)$ — Γ_{22}/Γ_{21}

VALUE (units 10^{-2})	DOCUMENT ID		TECN	COMMENT
6.59±1.01±0.22	AAIJ	21R	LHCB	pp at 13 TeV

$\Gamma(\chi_{c2}(1P)pK^-)/\Gamma(pJ/\psi K^-)$ — Γ_{23}/Γ_{15}

VALUE	DOCUMENT ID		TECN	COMMENT
0.251±0.025±0.010	[1] AAIJ	17AM	LHCB	pp at 7, 8 TeV

[1] AAIJ 17AM reports 0.248 ± 0.02 ± 0.017 from a measurement of $[\Gamma(\Lambda_b^0 \to \chi_{c2}(1P)pK^-)/\Gamma(\Lambda_b^0 \to pJ/\psi K^-)] \times [B(\chi_{c2}(1P) \to \gamma J/\psi(1S))]$ assuming $B(\chi_{c2}(1P) \to \gamma J/\psi(1S)) = (19.2 \pm 0.7) \times 10^{-2}$, which we rescale to our best (shown rounded) value $B(\chi_{c2}(1P) \to \gamma J/\psi(1S)) = (19.0 \pm 0.8) \times 10^{-2}$. Our first error is their experiment's error and our second error is the systematic error from using our best (shown rounded) value.

$\Gamma(\chi_{c2}(1P)pK^-)/\Gamma(\chi_{c1}(1P)pK^-)$ — Γ_{23}/Γ_{21}

VALUE	DOCUMENT ID		TECN	COMMENT
1.06±0.05±0.04±0.04	[1] AAIJ	21R	LHCB	pp at 13 TeV

[1] The first uncertainty is statistical, the second is systematic and the third is related to the uncertainties in the branching fractions of the $\chi_{cJ} \to J/\psi\gamma$ decays.

$\Gamma(\chi_{c2}(1P)p\pi^-)/\Gamma(\chi_{c1}(1P)p\pi^-)$ — Γ_{24}/Γ_{22}

VALUE	DOCUMENT ID		TECN	COMMENT
0.95±0.30±0.04±0.04	[1] AAIJ	21R	LHCB	pp at 13 TeV

[1] Evidence for the $\Lambda_b^0 \to \chi_{c2}p\pi^-$ decay is obtained with a significance of 3.5 standard deviations. The first uncertainty is statistical, the second is systematic and the third is related to the uncertainties in the branching fractions of the $\chi_{cJ} \to J/\psi\gamma$ decays.

$\Gamma(pJ/\psi(1S)\pi^+\pi^-K^-)/\Gamma(pJ/\psi K^-)$ — Γ_{25}/Γ_{15}

VALUE	DOCUMENT ID		TECN	COMMENT
0.2086±0.0096±0.0134	[1] AAIJ	16Y	LHCB	pp at 7, 8 TeV

[1] Excludes $\psi(2S) \to J/\psi\pi^+\pi^-$.

$\Gamma(p\psi(2S)K^-)/\Gamma(pJ/\psi K^-)$ — Γ_{26}/Γ_{15}

VALUE	DOCUMENT ID		TECN	COMMENT
0.2070±0.0076±0.0059	[1] AAIJ	16Y	LHCB	pp at 7, 8 TeV

[1] AAIJ 16Y reports a measurement of 0.2070 ± 0.0076 ± 0.0046 ± 0.0037 where the third uncertainty is due to the knowledge of J/ψ and $\psi(2S)$ branching fractions. We have combined both systematic uncertainties in quadrature.

$\Gamma(\chi_{c1}(3872)pK^-)/\Gamma(p\psi(2S)K^-)$ — Γ_{27}/Γ_{26}

VALUE	DOCUMENT ID		TECN	COMMENT
0.43±0.09±0.14	[1] AAIJ	19AN	LHCB	pp at 7, 8, 13 TeV

[1] AAIJ 19AN reports $[\Gamma(\Lambda_b^0 \to \chi_{c1}(3872)pK^-)/\Gamma(\Lambda_b^0 \to p\psi(2S)K^-)] \times [B(\chi_{c1}(3872) \to \pi^+\pi^-J/\psi(1S))] / [B(\psi(2S) \to J/\psi(1S)\pi^+\pi^-)] = (5.4 \pm 1.1 \pm 0.2) \times 10^{-2}$ which we multiply or divide by our best (shown rounded) values $B(\chi_{c1}(3872) \to \pi^+\pi^-J/\psi(1S)) = (4.3 \pm 1.4) \times 10^{-2}$, $B(\psi(2S) \to J/\psi(1S)\pi^+\pi^-) = (34.78 \pm 0.33) \times 10^{-2}$. Our first error is their experiment's error and our second error is the systematic error from using our best (shown rounded) values.

$\Gamma(\chi_{c1}(3872)\Lambda(1520))/\Gamma(\chi_{c1}(3872)pK^-)$ — Γ_{28}/Γ_{27}

VALUE	DOCUMENT ID		TECN	COMMENT
0.58±0.15	AAIJ	19AN	LHCB	pp at 7, 8, 13 TeV

$\Gamma(\psi(2S)p\pi^-)/\Gamma(p\psi(2S)K^-)$ — Γ_{29}/Γ_{26}

VALUE (%)	DOCUMENT ID		TECN	COMMENT
11.4±1.3±0.2	AAIJ	18AF	LHCB	pp at 7, 8, 13 TeV

$\Gamma(p\overline{K}^0\pi^-)/\Gamma_{total}$ — Γ_{30}/Γ

VALUE (units 10^{-5})	DOCUMENT ID		TECN	COMMENT
1.95 ±0.34 OUR AVERAGE	Error includes scale factor of 1.9.			
2.124±0.042±0.198	[1] AAIJ	25AP	LHCB	pp at 7, 8, 13 TeV
1.26 ±0.19 ±0.36	[2] AAIJ	14Q	LHCB	pp at 7 TeV

[1] Measured relative to $\Lambda_b^0 \to \Lambda_c^+\pi^-$, $\Lambda_c^+ \to pK_S^0$. The last error includes both systematic and the uncertainties on $B(\Lambda_b^0 \to \Lambda_c^+\pi^-, \Lambda_c^+ \to pK_S^0)$.

[2] Used the normalizing mode branching fraction value of $B(B^0 \to K^0\pi^+\pi^-) = (4.96 \pm 0.20) \times 10^{-5}$.

$\Gamma(pK^0K^-)/\Gamma_{total}$ — Γ_{31}/Γ

VALUE (units 10^{-6})	CL%	DOCUMENT ID		TECN	COMMENT
1.22±0.16±0.17		[1] AAIJ	25AP	LHCB	pp at 7, 8, 13 TeV
• • • We do not use the following data for averages, fits, limits, etc. • • •					
<3.5	90	AAIJ	14Q	LHCB	Repl. by AAIJ 25AP

[1] Measured relative to $\Lambda_b^0 \to \Lambda_c^+K^-$, $\Lambda_c^+ \to pK_S^0$. The last error includes both systematic and the uncertainties on $B(\Lambda_b^0 \to \Lambda_c^+K^-, \Lambda_c^+ \to pK_S^0)$.

$\Gamma(\Lambda_c^+\pi^-)/\Gamma_{total}$ — Γ_{32}/Γ

VALUE (units 10^{-3})	EVTS	DOCUMENT ID		TECN	COMMENT
4.9 ±0.4 OUR FIT	Error includes scale factor of 1.2.				
4.8 ±0.5 OUR AVERAGE	Error includes scale factor of 1.5.				
$4.60^{+0.31}_{-0.30} \pm 0.14$		[1] AAIJ	14I	LHCB	pp at 7 TeV
5.97±0.28±0.81		[2] AAIJ	14Q	LHCB	pp at 7 TeV
8.8 ±2.8 ±1.5		[3] ABULENCIA	07B	CDF	$p\overline{p}$ at 1.96 TeV
• • • We do not use the following data for averages, fits, limits, etc. • • •					
seen	3	ABREU	96N	DLPH	$\Lambda_c^+ \to pK^-\pi^+$
seen	4	BUSKULIC	96L	ALEP	$\Lambda_c^+ \to pK^-\pi^+$, $p\overline{K}^0$, $\Lambda\pi^+\pi^+\pi^-$

[1] AAIJ 14I reports $(4.30 \pm 0.03^{+0.12}_{-0.11} \pm 0.26 \pm 0.21) \times 10^{-3}$ from a measurement of $[\Gamma(\Lambda_b^0 \to \Lambda_c^+\pi^-)/\Gamma_{total}] \times [B(B^0 \to D^-\pi^+)]$ assuming $B(B^0 \to D^-\pi^+) = (2.68 \pm 0.13) \times 10^{-3}$, which we rescale to our best (shown rounded) value $B(B^0 \to D^-\pi^+) = (2.51 \pm 0.08) \times 10^{-3}$. Our first error is their experiment's error and our second error is the systematic error from using our best (shown rounded) value. Uses information on f_{baryon}/f_d from measurement in semileptonic decays by the same authors.

[2] Obtained using the branching fraction of $\Lambda_c^+ \to pK^-\pi^+$ decay.

[3] The result is obtained from $(f_{baryon}/f_d)\,(B(\Lambda_b^0 \to \Lambda_c^+\pi^-)/B(\overline{B}^0 \to D^+\pi^-)) = 0.82 \pm 0.08 \pm 0.11 \pm 0.22$, assuming $f_{baryon}/f_d = 0.25 \pm 0.04$ and $B(\overline{B}^0 \to D^+\pi^-) = (2.68 \pm 0.13) \times 10^{-3}$.

$\Gamma(pD^0\pi^-)/\Gamma(\Lambda_c^+\pi^-)$ — Γ_4/Γ_{32}

VALUE	DOCUMENT ID		TECN	COMMENT
0.131±0.007±0.004	[1] AAIJ	14H	LHCB	pp at 7 TeV

[1] AAIJ 14H reports $[\Gamma(\Lambda_b^0 \to pD^0\pi^-)/\Gamma(\Lambda_b^0 \to \Lambda_c^+\pi^-)] \times [B(D^0 \to K^-\pi^+)] / [B(\Lambda_c^+ \to pK^-\pi^+)] = (8.06 \pm 0.23 \pm 0.35) \times 10^{-2}$ which we multiply or divide by our best (shown rounded) values $B(D^0 \to K^-\pi^+) = (3.936 \pm 0.030) \times 10^{-2}$, $B(\Lambda_c^+ \to pK^-\pi^+) = (6.37 \pm 0.21) \times 10^{-2}$. Our first error is their experiment's error and our second error is the systematic error from using our best (shown rounded) values.

$\Gamma(\Lambda_c^+K^-)/\Gamma_{total}$ — Γ_{33}/Γ

VALUE (units 10^{-4})	DOCUMENT ID		TECN	COMMENT
3.56±0.28 OUR FIT	Error includes scale factor of 1.2.			
3.55±0.44±0.50	[1] AAIJ	14Q	LHCB	pp at 7 TeV

[1] Obtained using the branching fraction of $\Lambda_c^+ \to pK^-\pi^+$ decay.

$\Gamma(\Lambda_c^+K^-)/\Gamma(\Lambda_c^+\pi^-)$ — Γ_{33}/Γ_{32}

VALUE (units 10^{-2})	DOCUMENT ID		TECN	COMMENT
7.31±0.22 OUR FIT				
7.31±0.16±0.16	AAIJ	14H	LHCB	pp at 7 TeV

$\Gamma(\Lambda_c^+a_1(1260)^-)/\Gamma_{total}$ — Γ_{34}/Γ

VALUE	EVTS	DOCUMENT ID		TECN	COMMENT
seen	1	ABREU	96N	DLPH	$\Lambda_c^+ \to pK^-\pi^+$, $a_1^- \to \rho^0\pi^- \to \pi^+\pi^-\pi^-$

$\Gamma(\Lambda_c^+D_s^-)/\Gamma_{total}$ — Γ_{36}/Γ

VALUE (units 10^{-2})	DOCUMENT ID		TECN	COMMENT
1.1±0.1	[1] AAIJ	14AA	LHCB	pp at 7 TeV

[1] Uses $B(\overline{B}^0 \to D^+D_s^-) = (7.2 \pm 0.8) \times 10^{-3}$ and their measured $B(\Lambda_b^0 \to \Lambda_c^+\pi^-))/B(\overline{B}^0 \to D^+\pi^-)$ values.

$\Gamma(\Lambda_c^+D^-)/\Gamma(\Lambda_c^+D_s^-)$ — Γ_{35}/Γ_{36}

VALUE	DOCUMENT ID		TECN	COMMENT
0.042±0.003±0.003	AAIJ	14AA	LHCB	pp at 7 TeV

$\Gamma(\Lambda_c^+D_s^{*-})/\Gamma(\Lambda_c^+D_s^-)$ — Γ_{37}/Γ_{36}

VALUE	DOCUMENT ID		TECN	COMMENT
$1.668 \pm 0.022^{+0.061}_{-0.055}$	AAIJ	24X	LHCB	pp at 13 TeV

$\Gamma(\Lambda_c^+D_s^-K^+K^-)/\Gamma(\Lambda_c^+D_s^-)$ — Γ_{38}/Γ_{36}

VALUE (units 10^{-2})	DOCUMENT ID		TECN	COMMENT
1.41±0.19±0.12	AAIJ	25AK	LHCB	pp at 13 TeV

$\Gamma(P_{c\overline{c}s}(4459)K^+K^-,\ P_{c\overline{c}s}(4459) \to \Lambda_c^+D_s^-)/\Gamma(\Lambda_c^+D_s^-K^+K^-)$ — Γ_{39}/Γ_{38}

VALUE	CL%	DOCUMENT ID		TECN	COMMENT
<0.17	90	AAIJ	25AK	LHCB	pp at 13 TeV

$\Gamma(P_{c\overline{c}s}(4338)K^+K^-,\ P_{c\overline{c}s}(4338) \to \Lambda_c^+D_s^-)/\Gamma(\Lambda_c^+D_s^-K^+K^-)$ — Γ_{40}/Γ_{38}

VALUE	CL%	DOCUMENT ID		TECN	COMMENT
<0.10	90	AAIJ	25AK	LHCB	pp at 13 TeV

$\Gamma(\Lambda_c^+\overline{D}^0K^-)/\Gamma(\Lambda_c^+D_s^-)$ — Γ_{41}/Γ_{36}

VALUE	DOCUMENT ID		TECN	COMMENT
0.194±0.004±0.003	[1] AAIJ	24X	LHCB	pp at 13 TeV

[1] AAIJ 24X reports $[\Gamma(\Lambda_b^0 \to \Lambda_c^+\overline{D}^0K^-)/\Gamma(\Lambda_b^0 \to \Lambda_c^+D_s^-)] \times [B(D^0 \to K^-\pi^+)] / [B(D_s^+ \to K^+K^-\pi^+)] = 0.1400^{+0.0026}_{-0.0025}{}^{+0.0012}_{-0.0013}$ which we multiply or divide by our best (shown rounded) values $B(D^0 \to K^-\pi^+) = (3.936 \pm 0.030) \times 10^{-2}$, $B(D_s^+ \to K^+K^-\pi^+) = (5.45 \pm 0.08) \times 10^{-2}$. Our first error is their experiment's error and our second error is the systematic error from using our best (shown rounded) values.

Int. J. Mod. Phys. A 2026.41. Downloaded from www.worldscientific.com
UNIVERSITY OF CALIFORNIA @ BERKELEY on 09/16/26. Re-use and distribution is strictly not permitted, except for Open Access articles.

$\Gamma(\Lambda_c^+ \overline{D}^{*0} K^-)/\Gamma(\Lambda_c^+ D_s^-)$ — Γ_{42}/Γ_{36}

VALUE	DOCUMENT ID		TECN	COMMENT
0.598±0.025±0.010	[1] AAIJ	24X	LHCB	pp at 13 TeV

[1] AAIJ 24X reports $[\Gamma(\Lambda_b^0 \to \Lambda_c^+ \overline{D}^{*0} K^-)/\Gamma(\Lambda_b^0 \to \Lambda_c^+ D_s^-)] \times [B(D^0 \to K^-\pi^+)] / [B(D_s^+ \to K^+K^-\pi^+)] = 0.432^{+0.013}_{-0.012} \pm 0.013$ which we multiply or divide by our best (shown rounded) values $B(D^0 \to K^-\pi^+) = (3.936 \pm 0.030) \times 10^{-2}$, $B(D_s^+ \to K^+K^-\pi^+) = (5.45 \pm 0.08) \times 10^{-2}$. Our first error is their experiment's error and our second error is the systematic error from using our best (shown rounded) values.

$\Gamma(\Lambda_c^+ \overline{D}^{*0} K^-)/\Gamma(\Lambda_c^+ \overline{D}^0 K^-)$ — Γ_{42}/Γ_{41}

VALUE	DOCUMENT ID		TECN	COMMENT
• • • We do not use the following data for averages, fits, limits, etc. • • •				
$3.09^{+0.11}_{-0.10}{}^{+0.09}_{-0.10}$	AAIJ	24X	LHCB	pp at 13 TeV

$\Gamma(\Lambda_c^+ \pi^+\pi^-\pi^-)/\Gamma_{total}$ — Γ_{43}/Γ

VALUE (units 10^{-3})	EVTS	DOCUMENT ID		TECN	COMMENT
7.6±1.1 OUR FIT Error includes scale factor of 1.1.					
$14.8^{+3.8}_{-3.1}\pm1.1$		[1] AALTONEN	12A	CDF	$p\overline{p}$ at 1.96 TeV
• • • We do not use the following data for averages, fits, limits, etc. • • •					
seen	90	BARI	91	SFM	$\Lambda_c^+ \to pK^-\pi^+$

[1] AALTONEN 12A reports $[\Gamma(\Lambda_b^0 \to \Lambda_c^+\pi^+\pi^-\pi^-)/\Gamma_{total}] / [B(\Lambda_b^0 \to \Lambda_c^+\pi^-)] = 3.04 \pm 0.33^{+0.70}_{-0.55}$ which we multiply by our best (shown rounded) value $B(\Lambda_b^0 \to \Lambda_c^+\pi^-) = (4.9 \pm 0.4) \times 10^{-3}$. Our first error is their experiment's error and our second error is the systematic error from using our best (shown rounded) value.

$\Gamma(\Lambda_c^+ \pi^+\pi^-\pi^-)/\Gamma(\Lambda_c^+ \pi^-)$ — Γ_{43}/Γ_{32}

VALUE	DOCUMENT ID		TECN	COMMENT
1.57±0.21 OUR FIT				
1.43±0.16±0.13	AAIJ	11E	LHCB	pp at 7 TeV

$\Gamma(\Lambda_c(2595)^+\pi^-, \Lambda_c(2595)^+ \to \Lambda_c^+\pi^+\pi^-)/\Gamma(\Lambda_c^+\pi^+\pi^-\pi^-)$ — Γ_{44}/Γ_{43}

VALUE (units 10^{-2})	DOCUMENT ID		TECN	COMMENT
$\mathbf{4.4\pm1.7^{+0.6}_{-0.4}}$	AAIJ	11E	LHCB	pp at 7 TeV

$\Gamma(\Lambda_c(2625)^+\pi^-, \Lambda_c(2625)^+ \to \Lambda_c^+\pi^+\pi^-)/\Gamma(\Lambda_c^+\pi^+\pi^-\pi^-)$ — Γ_{45}/Γ_{43}

VALUE (units 10^{-2})	DOCUMENT ID		TECN	COMMENT
4.3±1.5±0.4	AAIJ	11E	LHCB	pp at 7 TeV

$\Gamma(\Sigma_c(2455)^0\pi^+\pi^-, \Sigma_c^0 \to \Lambda_c^+\pi^-)/\Gamma(\Lambda_c^+\pi^+\pi^-\pi^-)$ — Γ_{46}/Γ_{43}

VALUE (units 10^{-2})	DOCUMENT ID		TECN	COMMENT
7.4±2.4±1.2	AAIJ	11E	LHCB	pp at 7 TeV

$\Gamma(\Sigma_c(2455)^{++}\pi^-\pi^-, \Sigma_c^{++} \to \Lambda_c^+\pi^+)/\Gamma(\Lambda_c^+\pi^+\pi^-\pi^-)$ — Γ_{47}/Γ_{43}

VALUE (units 10^{-2})	DOCUMENT ID		TECN	COMMENT
4.2±1.8±0.7	AAIJ	11E	LHCB	pp at 7 TeV

$\Gamma(\Sigma_c(2455)^{++} D^- K^-)/\Gamma(\Lambda_c^+ \overline{D}^0 K^-)$ — Γ_{48}/Γ_{41}

VALUE	DOCUMENT ID		TECN	COMMENT
0.282±0.016±0.017	[1] AAIJ	24Y	LHCB	pp at 13 TeV

[1] AAIJ 24Y uses $\Sigma_c(2455)^{++} \to \Lambda_c^+\pi^+$, $D^- \to K^+\pi^-\pi^-$ and $\overline{D}^0 \to K^+\pi^-$, analyzing an integrated luminosity of 6 fb^{-1}.

$\Gamma(\Sigma_c(2455)^{++} D^{*-} K^-)/\Gamma(\Sigma_c(2455)^{++} D^- K^-)$ — Γ_{49}/Γ_{48}

VALUE	DOCUMENT ID		TECN	COMMENT
2.261±0.202±0.137	[1] AAIJ	24Y	LHCB	pp at 13 TeV

[1] AAIJ 24Y uses $\Sigma_c(2455)^{++} \to \Lambda_c^+\pi^+$ and $D^- \to K^+\pi^-\pi^-$, analyzing an integrated luminosity of 6 fb^{-1}.

$\Gamma(\Sigma_c(2520)^{++} D^- K^-)/\Gamma(\Sigma_c(2455)^{++} D^- K^-)$ — Γ_{50}/Γ_{48}

VALUE	DOCUMENT ID		TECN	COMMENT
0.460±0.052±0.028	[1] AAIJ	24Y	LHCB	pp at 13 TeV

[1] AAIJ 24Y uses $\Sigma_c(2455)^{++} \to \Lambda_c^+\pi^+$, $\Sigma_c(2520)^{++} \to \Lambda_c^+\pi^+$, and $D^- \to K^+\pi^-\pi^-$, analyzing an integrated luminosity of 6 fb^{-1}.

$\Gamma(\Sigma_c(2520)^{++} D^{*-} K^-)/\Gamma(\Sigma_c(2455)^{++} D^- K^-)$ — Γ_{51}/Γ_{48}

VALUE	DOCUMENT ID		TECN	COMMENT
0.896±0.137±0.068	[1] AAIJ	24Y	LHCB	pp at 13 TeV

[1] AAIJ 24Y uses $\Sigma_c(2455)^{++} \to \Lambda_c^+\pi^+$, $\Sigma_c(2520)^{++} \to \Lambda_c^+\pi^+$, and $D^- \to K^+\pi^-\pi^-$ analyzing an integrated luminosity of 6 fb^{-1}.

$\Gamma(\Lambda_c^+ K^+K^-\pi^-)/\Gamma(\Lambda_c^+ D_s^-)$ — Γ_{52}/Γ_{36}

VALUE (units 10^{-2})	DOCUMENT ID		TECN	COMMENT
9.26±0.29±0.53	[1] AAIJ	21B	LHCB	pp at 7 and 8 TeV

[1] AAIJ 21B systematic uncertainty includes the contribution from the $D_s^- \to K^+K^-\pi^-$ branching fraction.

$\Gamma(\Lambda_c^+ p\overline{p}\pi^-)/\Gamma(\Lambda_c^+ \pi^-)$ — Γ_{53}/Γ_{32}

VALUE (units 10^{-2})	DOCUMENT ID		TECN	COMMENT
5.40±0.23±0.32	AAIJ	18AW	LHCB	pp at 7 and 8 TeV

$\Gamma(\Sigma_c(2455)^0 p\overline{p}, \Sigma_c^0 \to \Lambda_c^+\pi^-)/\Gamma(\Lambda_c^+ p\overline{p}\pi^-)$ — Γ_{54}/Γ_{53}

VALUE (units 10^{-2})	DOCUMENT ID		TECN	COMMENT
8.9±1.5±0.6	AAIJ	18AW	LHCB	pp at 7 and 8 TeV

$\Gamma(\Sigma_c(2520)^0 p\overline{p}, \Sigma_c(2520)^0 \to \Lambda_c^+\pi^-)/\Gamma(\Lambda_c^+ p\overline{p}\pi^-)$ — Γ_{55}/Γ_{53}

VALUE	DOCUMENT ID		TECN	COMMENT
0.119±0.020±0.014	AAIJ	18AW	LHCB	pp at 7 and 8 TeV

$\Gamma(\Lambda K^0 2\pi^+2\pi^-)/\Gamma_{total}$ — Γ_{56}/Γ

VALUE	EVTS	DOCUMENT ID		TECN	COMMENT
• • • We do not use the following data for averages, fits, limits, etc. • • •					
seen	4	[1] ARENTON	86	FMPS	$\Lambda K_S^0 2\pi^+2\pi^-$

[1] See the footnote to the ARENTON 86 mass value.

$\Gamma(\Lambda_c^+ \ell^-\overline{\nu}_\ell \text{anything})/\Gamma_{total}$ — Γ_{57}/Γ

The values and averages in this section serve only to show what values result if one assumes our $B(b \to b\text{-baryon})$. They cannot be thought of as measurements since the underlying product branching fractions were also used to determine $B(b \to b\text{-baryon})$ as described in the note on "Production and Decay of b-Flavored Hadrons."

VALUE	EVTS	DOCUMENT ID		TECN	COMMENT
0.109±0.022 OUR AVERAGE					
0.102±0.019±0.013		[1] BARATE	98D	ALEP	$e^+e^- \to Z$
$0.14^{+0.05}_{-0.04}\pm0.02$	29	[2] ABREU	95S	DLPH	$e^+e^- \to Z$
• • • We do not use the following data for averages, fits, limits, etc. • • •					
0.090±0.022±0.012	55	[3] BUSKULIC	95L	ALEP	Repl. by BARATE 98D
0.18 ±0.07 ±0.02	21	[4] BUSKULIC	92E	ALEP	$\Lambda_c^+ \to pK^-\pi^+$

[1] BARATE 98D reports $[\Gamma(\Lambda_b^0 \to \Lambda_c^+\ell^-\overline{\nu}_\ell \text{anything})/\Gamma_{total}] \times [B(\overline{b} \to b\text{-baryon at } Z)] = 0.0086 \pm 0.0007 \pm 0.0014$ which we divide by our best (shown rounded) value $B(\overline{b} \to b\text{-baryon at } Z) = (8.4 \pm 1.1) \times 10^{-2}$. Our first error is their experiment's error and our second error is the systematic error from using our best (shown rounded) value. Measured using $\Lambda_c\ell^-$ and $\Lambda\ell^+\ell^-$.

[2] ABREU 95S reports $[\Gamma(\Lambda_b^0 \to \Lambda_c^+\ell^-\overline{\nu}_\ell \text{anything})/\Gamma_{total}] \times [B(\overline{b} \to b\text{-baryon at } Z)] = 0.0118 \pm 0.0026^{+0.0031}_{-0.0021}$ which we divide by our best (shown rounded) value $B(\overline{b} \to b\text{-baryon at } Z) = (8.4 \pm 1.1) \times 10^{-2}$. Our first error is their experiment's error and our second error is the systematic error from using our best (shown rounded) value.

[3] BUSKULIC 95L reports $[\Gamma(\Lambda_b^0 \to \Lambda_c^+\ell^-\overline{\nu}_\ell \text{anything})/\Gamma_{total}] \times [B(\overline{b} \to b\text{-baryon at } Z)] = 0.00755 \pm 0.0014 \pm 0.0012$ which we divide by our best (shown rounded) value $B(\overline{b} \to b\text{-baryon at } Z) = (8.4 \pm 1.1) \times 10^{-2}$. Our first error is their experiment's error and our second error is the systematic error from using our best (shown rounded) value.

[4] BUSKULIC 92E reports $[\Gamma(\Lambda_b^0 \to \Lambda_c^+\ell^-\overline{\nu}_\ell \text{anything})/\Gamma_{total}] \times [B(\overline{b} \to b\text{-baryon at } Z)] = 0.015 \pm 0.0035 \pm 0.0045$ which we divide by our best (shown rounded) value $B(\overline{b} \to b\text{-baryon at } Z) = (8.4 \pm 1.1) \times 10^{-2}$. Our first error is their experiment's error and our second error is the systematic error from using our best (shown rounded) value. Superseded by BUSKULIC 95L.

$\Gamma(\Lambda_c^+ \ell^-\overline{\nu}_\ell)/\Gamma_{total}$ — Γ_{58}/Γ

VALUE	DOCUMENT ID		TECN	COMMENT
$\mathbf{0.062^{+0.014}_{-0.013}}$ **OUR FIT**				
$\mathbf{0.050^{+0.011}_{-0.008}{}^{+0.016}_{-0.012}}$	[1] ABDALLAH	04A	DLPH	$e^+e^- \to Z^0$

[1] Derived from a combined likelihood and event rate fit to the distribution of the Isgur-Wise variable and using HQET. The slope of the form factor is measured to be $\rho^2 = 2.03 \pm 0.46^{+0.72}_{-1.00}$.

$\Gamma(\Lambda_c^+ \ell^-\overline{\nu}_\ell)/\Gamma(\Lambda_c^+ \pi^-)$ — Γ_{58}/Γ_{32}

VALUE	DOCUMENT ID		TECN	COMMENT
$\mathbf{12.8^{+3.0}_{-2.7}}$ **OUR FIT**				
$\mathbf{16.6\pm3.0^{+2.8}_{-3.6}}$	AALTONEN	09E	CDF	$p\overline{p}$ at 1.96 TeV

$\Gamma(\Lambda_c^+ \tau^-\overline{\nu}_\tau)/\Gamma(\Lambda_c^+ \pi^+\pi^-\pi^-)$ — Γ_{59}/Γ_{43}

VALUE	DOCUMENT ID		TECN	COMMENT
2.46±0.27±0.40	[1] AAIJ	22K	LHCB	pp at 7, 8 TeV

[1] Uses $\tau^- \to \pi^-\pi^+\pi^-(\pi^0)\nu_\tau$ decays.

$\Gamma(\Lambda_c^+ \pi^+\pi^-\ell^-\overline{\nu}_\ell)/\Gamma_{total}$ — Γ_{60}/Γ

VALUE	DOCUMENT ID		TECN	COMMENT
$\mathbf{0.056^{+0.031}_{-0.030}}$	[1] ABDALLAH	04A	DLPH	$e^+e^- \to Z^0$

[1] Derived from the fraction of $\Gamma(\Lambda_b^0 \to \Lambda_c^+\ell^-\overline{\nu}_\ell) / (\Gamma(\Lambda_b^0 \to \Lambda_c^+\ell^-\overline{\nu}_\ell) + \Gamma(\Lambda_b^0 \to \Lambda_c^+\pi^+\pi^-\ell^-\overline{\nu}_\ell)) = 0.47^{+0.10}_{-0.08}{}^{+0.07}_{-0.06}$.

$\Gamma(\Lambda_c^+ \ell^-\overline{\nu}_\ell)/[\Gamma(\Lambda_c^+ \ell^-\overline{\nu}_\ell) + \Gamma(\Lambda_c^+ \pi^+\pi^-\ell^-\overline{\nu}_\ell)]$ — $\Gamma_{58}/(\Gamma_{58}+\Gamma_{60})$

VALUE	DOCUMENT ID		TECN	COMMENT
$\mathbf{0.47^{+0.10}_{-0.08}{}^{+0.07}_{-0.06}}$	ABDALLAH	04A	DLPH	$e^+e^- \to Z^0$

Int. J. Mod. Phys. A 2026.41. Downloaded from www.worldscientific.com
by UNIVERSITY OF CALIFORNIA @ BERKELEY on 09/16/26. Re-use and distribution is strictly not permitted, except for Open Access articles.

$\Gamma(\Lambda_c(2595)^+\ell^-\overline{\nu}_\ell)/\Gamma(\Lambda_c^+\ell^-\overline{\nu}_\ell)$ — Γ_{61}/Γ_{58}

VALUE	DOCUMENT ID		TECN	COMMENT
$0.126\pm0.033^{+0.047}_{-0.038}$	[1] AALTONEN	09E	CDF	$p\overline{p}$ at 1.96 TeV

[1] AALTONEN 09E assumes isospin conservation for $\Lambda_c(2595) \to \Lambda_c\pi^+\pi^+$ and $\Lambda_c(2595) \to \Lambda_c\pi^0\pi^0$. Significant isospin violation from thresholds in $\Lambda_c(2595) \to \Sigma_c(2455)\pi \to \Lambda_c\pi\pi$ may alter the recovered ratio.

$\Gamma(\Lambda_c(2625)^+\ell^-\overline{\nu}_\ell)/\Gamma(\Lambda_c^+\ell^-\overline{\nu}_\ell)$ — Γ_{62}/Γ_{58}

VALUE	DOCUMENT ID		TECN	COMMENT
$0.210\pm0.042^{+0.071}_{-0.050}$	AALTONEN	09E	CDF	$p\overline{p}$ at 1.96 TeV

$[\frac{1}{2}\Gamma(\Sigma_c(2455)^0\pi^+\ell^-\overline{\nu}_\ell) + \frac{1}{2}\Gamma(\Sigma_c(2455)^{++}\pi^-\ell^-\overline{\nu}_\ell)]/\Gamma(\Lambda_c^+\ell^-\overline{\nu}_\ell)$ — $(\frac{1}{2}\Gamma_{63}+\frac{1}{2}\Gamma_{64})/\Gamma_{58}$

VALUE	DOCUMENT ID		TECN	COMMENT
$0.054\pm0.022^{+0.021}_{-0.018}$	AALTONEN	09E	CDF	$p\overline{p}$ at 1.96 TeV

$\Gamma(p h^-)/\Gamma_{total}$ — Γ_{65}/Γ

VALUE	CL%	DOCUMENT ID		TECN	COMMENT
$<2.3\times10^{-5}$	90	[1] ACOSTA	05O	CDF	$p\overline{p}$ at 1.96 TeV

[1] Assumes f_Λ / f_d = 0.25, and equal momentum distribution for Λ_b and B mesons.

$\Gamma(p\pi^-)/\Gamma_{total}$ — Γ_{66}/Γ

VALUE (units 10^{-6})	CL%	DOCUMENT ID		TECN	COMMENT
4.6±0.8 OUR FIT					
4.1±0.9±0.5		[1] AALTONEN	09C	CDF	$p\overline{p}$ at 1.96 TeV
• • • We do not use the following data for averages, fits, limits, etc. • • •					
<50	90	[2] BUSKULIC	96V	ALEP	$e^+e^- \to Z$

[1] AALTONEN 09C reports $[\Gamma(\Lambda_b^0 \to p\pi^-)/\Gamma_{total}]$ / $[B(B^0 \to K^+\pi^-)] \times [B(\overline{b} \to b\text{-baryon at } Z)]$ / $[B(\overline{b} \to B^0 \text{ at } Z)] = 0.042 \pm 0.007 \pm 0.006$ which we multiply or divide by our best (shown rounded) values $B(B^0 \to K^+\pi^-) = (2.00 \pm 0.04)\times10^{-5}$, $B(\overline{b} \to b\text{-baryon at } Z) = (8.4 \pm 1.1)\times10^{-2}$, $B(\overline{b} \to B^0 \text{ at } Z) = (40.8 \pm 0.7)\times10^{-2}$. Our first error is their experiment's error and our second error is the systematic error from using our best (shown rounded) values.

[2] BUSKULIC 96V assumes PDG 96 production fractions for B^0, B^+, B_s, b baryons.

$\Gamma(pK^-)/\Gamma_{total}$ — Γ_{67}/Γ

VALUE (units 10^{-6})	CL%	DOCUMENT ID		TECN	COMMENT
5.5±1.0 OUR FIT					
6.4±1.2±0.9		[1] AALTONEN	09C	CDF	$p\overline{p}$ at 1.96 TeV
• • • We do not use the following data for averages, fits, limits, etc. • • •					
<360	90	[2] ADAM	96D	DLPH	$e^+e^- \to Z$
< 50	90	[3] BUSKULIC	96V	ALEP	$e^+e^- \to Z$

[1] AALTONEN 09C reports $[\Gamma(\Lambda_b^0 \to pK^-)/\Gamma_{total}]$ / $[B(B^0 \to K^+\pi^-)] \times [B(\overline{b} \to b\text{-baryon at } Z)]$ / $[B(\overline{b} \to B^0 \text{ at } Z)] = 0.066 \pm 0.009 \pm 0.008$ which we multiply or divide by our best (shown rounded) values $B(B^0 \to K^+\pi^-) = (2.00 \pm 0.04)\times10^{-5}$, $B(\overline{b} \to b\text{-baryon at } Z) = (8.4 \pm 1.1)\times10^{-2}$, $B(\overline{b} \to B^0 \text{ at } Z) = (40.8 \pm 0.7)\times10^{-2}$. Our first error is their experiment's error and our second error is the systematic error from using our best (shown rounded) values.

[2] ADAM 96D assumes $f_{B^0} = f_{B^-} = 0.39$ and $f_{B_s} = 0.12$.

[3] BUSKULIC 96V assumes PDG 96 production fractions for B^0, B^+, B_s, b baryons.

$\Gamma(p\pi^-)/\Gamma(pK^-)$ — Γ_{66}/Γ_{67}

VALUE	DOCUMENT ID		TECN	COMMENT
0.84±0.09 OUR FIT				
0.86±0.08±0.05	AAIJ	12AR	LHCB	pp at 7 TeV

$\Gamma(pD_s^-)/\Gamma_{total}$ — Γ_{68}/Γ

VALUE	CL%	DOCUMENT ID		TECN	COMMENT
• • • We do not use the following data for averages, fits, limits, etc. • • •					
$<4.8\times10^{-4}$	90	AAIJ	14Q	LHCB	pp at 7 TeV

$\Gamma(pD_s^-)/\Gamma(\Lambda_c^+\pi^-)$ — Γ_{68}/Γ_{32}

VALUE (units 10^{-3})	DOCUMENT ID		TECN	COMMENT
2.56±0.10±0.15	[1] AAIJ	23K	LHCB	pp at 13 TeV

[1] AAIJ 23K reports this measurement as $(2.56 \pm 0.10 \pm 0.05 \pm 0.14)\times10^{-3}$ where the last uncertainty is due to the branching fractions $B(D_s^- \to K^-K^+\pi^-)$ and $B(\Lambda_c^+ \to pK^-\pi^+)$ uncertainties.

$\Gamma(p\mu^-\overline{\nu}_\mu)/\Gamma_{total}$ — Γ_{69}/Γ

VALUE (units 10^{-4})	DOCUMENT ID		TECN	COMMENT
4.1±1.0	[1] AAIJ	15BG	LHCB	pp at 8 TeV

[1] The ratio of $B(\Lambda_b^0 \to p\mu^-\overline{\nu}_\mu)$ to $B(\Lambda_b^0 \to \Lambda_c^+\mu^-\overline{\nu}_\mu)$ is measured within a restricted q^2 region. Combined with theoretical calculations of the form factors and the previously measured value of $|V_{cb}|$, the first $|V_{ub}| = (3.27 \pm 0.15 \pm 0.16 \pm 0.06)\times10^{-3}$ measurement from the Λ_b decay is obtained, consistent with the exclusively measured world averages.

$\Gamma(p\mu^-\overline{\nu}_\mu)/\Gamma(\Lambda_c^+\ell^-\overline{\nu}_\ell)$ — Γ_{69}/Γ_{58}

VALUE (units 10^{-2})	DOCUMENT ID		TECN	COMMENT
• • • We do not use the following data for averages, fits, limits, etc. • • •				
$1.0\pm0.04\pm0.08$	[1] AAIJ	15BG	LHCB	pp at 8 TeV

[1] This measurement is a ratio of $\Gamma(\Lambda_b^0 \to p\mu^-\overline{\nu}_\mu)[q^2 > 15 \text{ GeV}/c^2]$ to $\Gamma(\Lambda_b^0 \to \Lambda_c^+\mu^-\overline{\nu}_\mu)[q^2 > 7 \text{ GeV}/c^2]$ within a restricted q^2 region. Combined with theoretical calculations of the form factors and the previously measured value of $|V_{cb}|$, the first $|V_{ub}| = (3.27 \pm 0.15 \pm 0.16 \pm 0.06)\times10^{-3}$ measurement from the Λ_b decay is obtained, consistent with the exclusively measured world averages.

$\Gamma(\Lambda\mu^+\mu^-)/\Gamma_{total}$ — Γ_{70}/Γ

VALUE (units 10^{-7})	DOCUMENT ID		TECN	COMMENT
10.8±2.8 OUR AVERAGE				
$9.6\pm1.6\pm2.5$	[1] AAIJ	13AJ	LHCB	pp at 7 TeV
$17.3\pm4.2\pm5.5$	AALTONEN	11AI	CDF	$p\overline{p}$ at 1.96 TeV

[1] Uses $B(\Lambda_b^0 \to J/\psi\Lambda) = (6.2 \pm 1.4)\times10^{-4}$. This measurement comes from the sum of the differential rates in q^2 regions excluding those corresponding to J/ψ and $\psi(2S)$ ([8.68,10.09] and [12.86, 14.18] GeV$^2/c^4$).

$\Gamma(p\pi^-\mu^+\mu^-)/\Gamma_{total}$ — Γ_{71}/Γ

VALUE (units 10^{-8})	DOCUMENT ID		TECN	COMMENT
$6.9\pm1.9^{+1.7}_{-1.5}$	[1] AAIJ	17P	LHCB	pp at 7, 8 TeV

[1] Excludes J/ψ and $\psi(2S)$ decays to $\mu^+\mu^-$.

$\Gamma(p\pi^-\mu^+\mu^-)/\Gamma(p\pi^-J/\psi,\ J/\psi \to \mu^+\mu^-)$ — Γ_{71}/Γ_{14}

VALUE (units 10^{-2})	DOCUMENT ID		TECN	COMMENT
4.4±1.2±0.7	[1] AAIJ	17P	LHCB	pp at 7, 8 TeV

[1] The $p\pi^-\mu^+\mu^-$ mode excludes J/ψ and $\psi(2S)$ decays to $\mu^+\mu^-$.

$\Gamma(pK^-e^+e^-)/\Gamma_{total}$ — Γ_{72}/Γ

VALUE (units 10^{-6})	DOCUMENT ID		TECN	COMMENT
$0.310\pm0.040^{+0.054}_{-0.047}$	[1,2] AAIJ	20M	LHCB	pp at 7, 8, 13 TeV

[1] Measured over $0.1 < q^2 < 6.0$ GeV/c^2, and $m_{pK} < 2.6$ GeV/c^2.

[2] The first uncertainty is the statistical uncertainty and the second is the combination of all systematic uncertainties including those related to the normalization of $\Lambda_b^0 \to J/\psi pK^-$.

$\Gamma(pK^-\mu^+\mu^-)/\Gamma_{total}$ — Γ_{73}/Γ

VALUE (units 10^{-6})	DOCUMENT ID		TECN	COMMENT
$0.265\pm0.014^{+0.049}_{-0.039}$	[1,2] AAIJ	20M	LHCB	pp at 7, 8, 13 TeV

[1] Measured over $0.1 < q^2 < 6.0$ GeV/c^2, and $m_{pK} < 2.6$ GeV/c^2.

[2] The first uncertainty is the statistical uncertainty and the second is the combination of all systematic uncertainties including those related to the normalization of $\Lambda_b^0 \to J/\psi pK^-$.

$\Gamma(pK^-\mu^+\mu^-)/\Gamma(pK^-e^+e^-)$ — Γ_{73}/Γ_{72}

VALUE	DOCUMENT ID		TECN	COMMENT
$0.86^{+0.14}_{-0.11}\pm0.05$	[1] AAIJ	20M	LHCB	pp at 7, 8, 13 TeV

[1] Measured over $0.1 < q^2 < 6.0$ GeV/c^2, and $m_{pK} < 2.6$ GeV/c^2.

$\Gamma(pK^-e^+e^-)/\Gamma(pJ/\psi K^-)$ — Γ_{72}/Γ_{15}

VALUE (units 10^{-4})	DOCUMENT ID		TECN	COMMENT
$9.8^{+1.4}_{-1.3}\pm0.8$	[1] AAIJ	20M	LHCB	pp at 7, 8, 13 TeV

[1] Measured over $0.1 < q^2 < 6.0$ GeV/c^2, and $m_{pK} < 2.6$ GeV/c^2.

$\Gamma(pK^-\mu^+\mu^-)/\Gamma(pJ/\psi K^-)$ — Γ_{73}/Γ_{15}

VALUE (units 10^{-4})	DOCUMENT ID		TECN	COMMENT
8.4±0.4±0.4	[1] AAIJ	20M	LHCB	pp at 7, 8, 13 TeV

[1] Measured over $0.1 < q^2 < 6.0$ GeV/c^2, and $m_{pK} < 2.6$ GeV/c^2.

$\Gamma(\Lambda\gamma)/\Gamma_{total}$ — Γ_{75}/Γ

VALUE (units 10^{-6})	CL%	DOCUMENT ID		TECN	COMMENT
7.1±1.5±0.9		[1] AAIJ	19Z	LHCB	pp at 13 TeV
• • • We do not use the following data for averages, fits, limits, etc. • • •					
<1300	90	ACOSTA	02G	CDF	$p\overline{p}$ at 1.8 TeV

[1] AAIJ 19Z normalized to $B^0 \to K^{*0}\gamma$ and used an integrated luminosity of 1.7 fb^{-1}.

$\Gamma(\Lambda(1405)^0\gamma)/\Gamma(\overline{p}K^-\gamma)$ — Γ_{77}/Γ_{76}

VALUE (units 10^{-2})	DOCUMENT ID		TECN	COMMENT
$3.5^{+0.3}_{-0.4}{}^{+1.9}_{-0.3}$	[1] AAIJ	24P	LHCB	pp at 7, 8, 13 TeV

[1] AAIJ 24P employs a Dalitz plot analysis of $\Lambda_b^0 \to \overline{p}K^-\gamma$ decays.

Int. J. Mod. Phys. A 2026.41. Downloaded from www.worldscientific.com
UNIVERSITY OF CALIFORNIA @ BERKELEY on 09/16/26. Re-use and distribution is strictly not permitted, except for Open Access articles.

$\Gamma(\Lambda(1520)^0\gamma)/\Gamma(\overline{p}K^-\gamma)$ — Γ_{78}/Γ_{76}

VALUE (units 10^{-2})	DOCUMENT ID		TECN	COMMENT
$10.4^{+0.4}_{-0.2}{}^{+2.2}_{-1.2}$	[1] AAIJ	24P	LHCB	pp at 7, 8, 13 TeV

[1] AAIJ 24P employs a Dalitz plot analysis of $\Lambda_b^0 \to \overline{p}K^-\gamma$ decays.

$\Gamma(\Lambda(1600)^0\gamma)/\Gamma(\overline{p}K^-\gamma)$ — Γ_{79}/Γ_{76}

VALUE (units 10^{-2})	DOCUMENT ID		TECN	COMMENT
$15.6^{+0.6}_{-0.9}{}^{+4.3}_{-4.6}$	[1] AAIJ	24P	LHCB	pp at 7, 8, 13 TeV

[1] AAIJ 24P employs a Dalitz plot analysis of $\Lambda_b^0 \to \overline{p}K^-\gamma$ decays.

$\Gamma(\Lambda(1670)^0\gamma)/\Gamma(\overline{p}K^-\gamma)$ — Γ_{80}/Γ_{76}

VALUE (units 10^{-2})	DOCUMENT ID		TECN	COMMENT
$1.3\pm0.2^{+1.3}_{-0.2}$	[1] AAIJ	24P	LHCB	pp at 7, 8, 13 TeV

[1] AAIJ 24P employs a Dalitz plot analysis of $\Lambda_b^0 \to \overline{p}K^-\gamma$ decays.

$\Gamma(\Lambda(1690)^0\gamma)/\Gamma(\overline{p}K^-\gamma)$ — Γ_{81}/Γ_{76}

VALUE (units 10^{-2})	DOCUMENT ID		TECN	COMMENT
$7.7^{+0.4}_{-0.8}{}^{+6.2}_{-0.2}$	[1] AAIJ	24P	LHCB	pp at 7, 8, 13 TeV

[1] AAIJ 24P employs a Dalitz plot analysis of $\Lambda_b^0 \to \overline{p}K^-\gamma$ decays.

$\Gamma(\Lambda(1800)^0\gamma)/\Gamma(\overline{p}K^-\gamma)$ — Γ_{82}/Γ_{76}

VALUE (units 10^{-2})	DOCUMENT ID		TECN	COMMENT
$18.3^{+1.3}_{-1.6}{}^{+3.2}_{-6.2}$	[1] AAIJ	24P	LHCB	pp at 7, 8, 13 TeV

[1] AAIJ 24P employs a Dalitz plot analysis of $\Lambda_b^0 \to \overline{p}K^-\gamma$ decays.

$\Gamma(\Lambda(1810)^0\gamma)/\Gamma(\overline{p}K^-\gamma)$ — Γ_{83}/Γ_{76}

VALUE (units 10^{-2})	DOCUMENT ID		TECN	COMMENT
$0.1^{+0.9}_{-0.4}{}^{+4.8}_{-0.7}$	[1] AAIJ	24P	LHCB	pp at 7, 8, 13 TeV

[1] AAIJ 24P employs a Dalitz plot analysis of $\Lambda_b^0 \to \overline{p}K^-\gamma$ decays.

$\Gamma(\Lambda(1820)^0\gamma)/\Gamma(\overline{p}K^-\gamma)$ — Γ_{84}/Γ_{76}

VALUE (units 10^{-2})	DOCUMENT ID		TECN	COMMENT
$8.3^{+0.4}_{-0.7}{}^{+1.0}_{-5.7}$	[1] AAIJ	24P	LHCB	pp at 7, 8, 13 TeV

[1] AAIJ 24P employs a Dalitz plot analysis of $\Lambda_b^0 \to \overline{p}K^-\gamma$ decays.

$\Gamma(\Lambda(1830)^0\gamma)/\Gamma(\overline{p}K^-\gamma)$ — Γ_{85}/Γ_{76}

VALUE	DOCUMENT ID		TECN	COMMENT
$(0.3\pm0.4^{+1.6}_{-0.9})\times10^{-2}$	[1] AAIJ	24P	LHCB	pp at 7, 8, 13 TeV

[1] AAIJ 24P employs a Dalitz plot analysis of $\Lambda_b^0 \to \overline{p}K^-\gamma$ decays.

$\Gamma(\Lambda(1890)^0\gamma)/\Gamma(\overline{p}K^-\gamma)$ — Γ_{86}/Γ_{76}

VALUE (units 10^{-2})	DOCUMENT ID		TECN	COMMENT
$11.2^{+0.7}_{-0.6}{}^{+4.6}_{-4.9}$	[1] AAIJ	24P	LHCB	pp at 7, 8, 13 TeV

[1] AAIJ 24P employs a Dalitz plot analysis of $\Lambda_b^0 \to \overline{p}K^-\gamma$ decays.

$\Gamma(\Lambda(2100)^0\gamma)/\Gamma(\overline{p}K^-\gamma)$ — Γ_{87}/Γ_{76}

VALUE (units 10^{-2})	DOCUMENT ID		TECN	COMMENT
$7.3\pm0.5^{+1.4}_{-2.9}$	[1] AAIJ	24P	LHCB	pp at 7, 8, 13 TeV

[1] AAIJ 24P employs a Dalitz plot analysis of $\Lambda_b^0 \to \overline{p}K^-\gamma$ decays.

$\Gamma(\Lambda(2110)^0\gamma)/\Gamma(\overline{p}K^-\gamma)$ — Γ_{88}/Γ_{76}

VALUE (units 10^{-2})	DOCUMENT ID		TECN	COMMENT
$6.5^{+0.6}_{-0.7}{}^{+6.3}_{-0.2}$	[1] AAIJ	24P	LHCB	pp at 7, 8, 13 TeV

[1] AAIJ 24P employs a Dalitz plot analysis of $\Lambda_b^0 \to \overline{p}K^-\gamma$ decays.

$\Gamma(\Lambda(2530)^0\gamma)/\Gamma(\overline{p}K^-\gamma)$ — Γ_{89}/Γ_{76}

VALUE (units 10^{-2})	DOCUMENT ID		TECN	COMMENT
$1.0^{+0.2}_{-0.1}{}^{+0.8}_{-0.1}$	[1] AAIJ	24P	LHCB	pp at 7, 8, 13 TeV

[1] AAIJ 24P employs a Dalitz plot analysis of $\Lambda_b^0 \to \overline{p}K^-\gamma$ decays.

$\Gamma((\overline{p}K^-)\ \text{nonresonant}\gamma)/\Gamma(\overline{p}K^-\gamma)$ — Γ_{90}/Γ_{76}

VALUE (units 10^{-2})	DOCUMENT ID		TECN	COMMENT
$2.8^{+0.5}_{-0.4}{}^{+2.4}_{-1.3}$	[1] AAIJ	24P	LHCB	pp at 7, 8, 13 TeV

[1] AAIJ 24P employs a Dalitz plot analysis of $\Lambda_b^0 \to \overline{p}K^-\gamma$ decays.

$\Gamma(\Lambda\eta)/\Gamma_{total}$ — Γ_{91}/Γ

VALUE (units 10^{-6})	DOCUMENT ID		TECN	COMMENT
$9^{+7}_{-5}\pm1$	[1] AAIJ	15AH	LHCB	pp at 7, 8 TeV

[1] AAIJ 15AH reports $[\Gamma(\Lambda_b^0 \to \Lambda\eta)/\Gamma_{total}]$ / $[B(B^0 \to \eta' K^0)] = 0.142^{+0.11}_{-0.08}$ which we multiply by our best (shown rounded) value $B(B^0 \to \eta' K^0) = (6.6\pm0.4)\times10^{-5}$. Our first error is their experiment's error and our second error is the systematic error from using our best (shown rounded) value. The single uncertainty quoted with the original measurement combines in quadrature statistical and systematic uncertainties.

$\Gamma(\Lambda\eta'(958))/\Gamma_{total}$ — Γ_{92}/Γ

VALUE	CL%	DOCUMENT ID		TECN	COMMENT
$<3.1\times10^{-6}$	90	[1] AAIJ	15AH	LHCB	pp at 7, 8 TeV

[1] AAIJ 15AH reports $[\Gamma(\Lambda_b^0 \to \Lambda\eta'(958))/\Gamma_{total}]$ / $[B(B^0 \to \eta' K^0)] < 0.047$ which we multiply by our best (shown rounded) value $B(B^0 \to \eta' K^0) = 6.6\times10^{-5}$.

$\Gamma(\Lambda\pi^+\pi^-)/\Gamma_{total}$ — Γ_{93}/Γ

VALUE (units 10^{-6})	DOCUMENT ID		TECN	COMMENT
$6.4\pm0.7\pm0.5$	[1] AAIJ	25J	LHCB	pp at 7, 8, 13 TeV

[1] AAIJ 25J reports $(5.3\pm0.4\pm0.7)\times10^{-6}$ from a measurement of $[\Gamma(\Lambda_b^0 \to \Lambda\pi^+\pi^-)/\Gamma_{total}]$ / $[B(\Lambda_b^0 \to \Lambda_c^+\pi^-)]$ / $[B(\Lambda_c^+ \to \Lambda\pi^+)]$ assuming $B(\Lambda_b^0 \to \Lambda_c^+\pi^-) = (4.30\pm0.36)\times10^{-3}$, $B(\Lambda_c^+ \to \Lambda\pi^+) = (1.24\pm0.08)\times10^{-2}$, which we rescale to our best (shown rounded) values $B(\Lambda_b^0 \to \Lambda_c^+\pi^-) = (4.9\pm0.4)\times10^{-3}$, $B(\Lambda_c^+ \to \Lambda\pi^+) = (1.32\pm0.05)\times10^{-2}$. Our first error is their experiment's error and our second error is the systematic error from using our best (shown rounded) values.

$\Gamma(\Lambda\pi^+\pi^-)/\Gamma(\Lambda_c^+\pi^-)$ — Γ_{93}/Γ_{32}

VALUE (units 10^{-4})	DOCUMENT ID		TECN	COMMENT
$9.6\pm3.8\pm0.3$	[1] AAIJ	16W	LHCB	pp at 7, 8 TeV

[1] AAIJ 16W reports $[\Gamma(\Lambda_b^0 \to \Lambda\pi^+\pi^-)/\Gamma(\Lambda_b^0 \to \Lambda_c^+\pi^-)]$ / $[B(\Lambda_c^+ \to \Lambda\pi^+)] = (7.3\pm1.9\pm2.2)\times10^{-2}$ which we multiply by our best (shown rounded) value $B(\Lambda_c^+ \to \Lambda\pi^+) = (1.32\pm0.05)\times10^{-2}$. Our first error is their experiment's error and our second error is the systematic error from using our best (shown rounded) value.

$\Gamma(\Lambda K^+\pi^-)/\Gamma_{total}$ — Γ_{94}/Γ

VALUE (units 10^{-6})	DOCUMENT ID		TECN	COMMENT
$5.5\pm0.5^{+0.5}_{-0.4}$	[1] AAIJ	25J	LHCB	pp at 7, 8, 13 TeV

[1] AAIJ 25J reports $(4.6\pm0.2\pm0.6)\times10^{-6}$ from a measurement of $[\Gamma(\Lambda_b^0 \to \Lambda K^+\pi^-)/\Gamma_{total}]$ / $[B(\Lambda_b^0 \to \Lambda_c^+\pi^-)]$ / $[B(\Lambda_c^+ \to \Lambda\pi^+)]$ assuming $B(\Lambda_b^0 \to \Lambda_c^+\pi^-) = (4.30\pm0.36)\times10^{-3}$, $B(\Lambda_c^+ \to \Lambda\pi^+) = (1.24\pm0.08)\times10^{-2}$, which we rescale to our best (shown rounded) values $B(\Lambda_b^0 \to \Lambda_c^+\pi^-) = (4.9\pm0.4)\times10^{-3}$, $B(\Lambda_c^+ \to \Lambda\pi^+) = (1.32\pm0.05)\times10^{-2}$. Our first error is their experiment's error and our second error is the systematic error from using our best (shown rounded) values.

$\Gamma(\Lambda K^+\pi^-)/\Gamma(\Lambda_c^+\pi^-)$ — Γ_{94}/Γ_{32}

VALUE (units 10^{-4})	DOCUMENT ID		TECN	COMMENT
$11.7\pm2.3\pm0.4$	[1] AAIJ	16W	LHCB	pp at 7, 8 TeV

[1] AAIJ 16W reports $[\Gamma(\Lambda_b^0 \to \Lambda K^+\pi^-)/\Gamma(\Lambda_b^0 \to \Lambda_c^+\pi^-)]$ / $[B(\Lambda_c^+ \to \Lambda\pi^+)] = (8.9\pm1.2\pm1.3)\times10^{-2}$ which we multiply by our best (shown rounded) value $B(\Lambda_c^+ \to \Lambda\pi^+) = (1.32\pm0.05)\times10^{-2}$. Our first error is their experiment's error and our second error is the systematic error from using our best (shown rounded) value.

$\Gamma(\Lambda K^+K^-)/\Gamma_{total}$ — Γ_{95}/Γ

VALUE (units 10^{-6})	DOCUMENT ID		TECN	COMMENT
$12.9\pm0.6^{+1.1}_{-1.0}$	[1] AAIJ	25J	LHCB	pp at 7, 8, 13 TeV

[1] AAIJ 25J reports $(10.7\pm0.3\pm1.2)\times10^{-6}$ from a measurement of $[\Gamma(\Lambda_b^0 \to \Lambda K^+K^-)/\Gamma_{total}]$ / $[B(\Lambda_b^0 \to \Lambda_c^+\pi^-)]$ / $[B(\Lambda_c^+ \to \Lambda\pi^+)]$ assuming $B(\Lambda_b^0 \to \Lambda_c^+\pi^-) = (4.30\pm0.36)\times10^{-3}$, $B(\Lambda_c^+ \to \Lambda\pi^+) = (1.24\pm0.08)\times10^{-2}$, which we rescale to our best (shown rounded) values $B(\Lambda_b^0 \to \Lambda_c^+\pi^-) = (4.9\pm0.4)\times10^{-3}$, $B(\Lambda_c^+ \to \Lambda\pi^+) = (1.32\pm0.05)\times10^{-2}$. Our first error is their experiment's error and our second error is the systematic error from using our best (shown rounded) values.

$\Gamma(\Lambda K^+K^-)/\Gamma(\Lambda_c^+\pi^-)$ — Γ_{95}/Γ_{32}

VALUE (units 10^{-3})	DOCUMENT ID		TECN	COMMENT
$3.33\pm0.35\pm0.12$	[1] AAIJ	16W	LHCB	pp at 7, 8 TeV

[1] AAIJ 16W reports $[\Gamma(\Lambda_b^0 \to \Lambda K^+K^-)/\Gamma(\Lambda_b^0 \to \Lambda_c^+\pi^-)]$ / $[B(\Lambda_c^+ \to \Lambda\pi^+)] = (25.3\pm1.9\pm1.9)\times10^{-2}$ which we multiply by our best (shown rounded) value $B(\Lambda_c^+ \to \Lambda\pi^+) = (1.32\pm0.05)\times10^{-2}$. Our first error is their experiment's error and our second error is the systematic error from using our best (shown rounded) value.

$\Gamma(\Lambda D^+D^-)/\Gamma_{total}$ — Γ_{96}/Γ

VALUE (units 10^{-4})	DOCUMENT ID		TECN	COMMENT
$1.24\pm0.15\pm0.32$	[1] AAIJ	24R	LHCB	pp at 13 TeV

[1] AAIJ 24R reports $(1.24 \pm 0.15 \pm 0.10 \pm 0.28 \pm 0.11) \times 10^{-4}$ from a measurement of $[\Gamma(\Lambda_b^0 \to \Lambda D^+ D^-)/\Gamma_{total}]$ / $[B(B^0 \to D^- D^+ K^0)]$ assuming $B(B^0 \to D^- D^+ K^0) = (7.5 \pm 1.7) \times 10^{-4}$. The first error is statistical, the second experimental systematic, the third due to the B^0 branching fraction, and the fourth due to the cross-section ratio of Λ_b^0 to B^0 of 0.541 ± 0.048.

$\Gamma(\Lambda\phi)/\Gamma_{total}$ — Γ_{97}/Γ

VALUE (units 10^{-6})	DOCUMENT ID		TECN	COMMENT
$9.8 \pm 2.1^{+1.6}_{-1.5}$	[1] AAIJ	16J	LHCB	pp at 7, 8 TeV

[1] AAIJ 16J reports $[\Gamma(\Lambda_b^0 \to \Lambda\phi)/\Gamma_{total}]$ / $[B(B^0 \to K^0\phi)] \times [B(\overline{b} \to b\text{-baryon at } Z)]$ / $[B(\overline{b} \to B^0 \text{ at } Z)] = 0.275 \pm 0.055 \pm 0.020$ which we multiply or divide by our best (shown rounded) values $B(B^0 \to K^0\phi) = (7.3 \pm 0.7) \times 10^{-6}$, $B(\overline{b} \to b\text{-baryon at } Z) = (8.4 \pm 1.1) \times 10^{-2}$, $B(\overline{b} \to B^0 \text{ at } Z) = (40.8 \pm 0.7) \times 10^{-2}$. Our first error is their experiment's error and our second error is the systematic error from using our best (shown rounded) values.

$\Gamma(p\pi^-\pi^+\pi^-)/\Gamma(\Lambda_c^+\pi^-)$ — Γ_{98}/Γ_{32}

VALUE (units 10^{-3})	DOCUMENT ID		TECN	COMMENT
$4.37 \pm 0.24^{+0.14}_{-0.15}$	[1] AAIJ	18Q	LHCB	pp at 7, 8 TeV

[1] AAIJ 18Q reports $[\Gamma(\Lambda_b^0 \to p\pi^-\pi^+\pi^-)/\Gamma(\Lambda_b^0 \to \Lambda_c^+\pi^-)]$ / $[B(\Lambda_c^+ \to pK^-\pi^+)] = (6.85 \pm 0.19 \pm 0.08 \pm 0.32) \times 10^{-2}$ which we multiply by our best (shown rounded) value $B(\Lambda_c^+ \to pK^-\pi^+) = (6.37 \pm 0.21) \times 10^{-2}$. Our first error is their experiment's error and our second error is the systematic error from using our best (shown rounded) value.

$\Gamma(pK^-K^+\pi^-)/\Gamma(\Lambda_c^+\pi^-)$ — Γ_{99}/Γ_{32}

VALUE (units 10^{-3})	DOCUMENT ID		TECN	COMMENT
$0.84 \pm 0.10 \pm 0.03$	[1] AAIJ	18Q	LHCB	pp at 7, 8 TeV

[1] AAIJ 18Q reports $[\Gamma(\Lambda_b^0 \to pK^-K^+\pi^-)/\Gamma(\Lambda_b^0 \to \Lambda_c^+\pi^-)]$ / $[B(\Lambda_c^+ \to pK^-\pi^+)] = (1.32 \pm 0.09 \pm 0.09 \pm 0.10) \times 10^{-2}$ which we multiply by our best (shown rounded) value $B(\Lambda_c^+ \to pK^-\pi^+) = (6.37 \pm 0.21) \times 10^{-2}$. Our first error is their experiment's error and our second error is the systematic error from using our best (shown rounded) value.

$\Gamma(pK^-\pi^+\pi^-)/\Gamma(\Lambda_c^+\pi^-)$ — Γ_{100}/Γ_{32}

VALUE (units 10^{-3})	DOCUMENT ID		TECN	COMMENT
$10.5 \pm 0.5^{+0.3}_{-0.4}$	[1] AAIJ	18Q	LHCB	pp at 7, 8 TeV

[1] AAIJ 18Q reports $[\Gamma(\Lambda_b^0 \to pK^-\pi^+\pi^-)/\Gamma(\Lambda_b^0 \to \Lambda_c^+\pi^-)]$ / $[B(\Lambda_c^+ \to pK^-\pi^+)] = (16.4 \pm 0.3 \pm 0.2 \pm 0.7) \times 10^{-2}$ which we multiply by our best (shown rounded) value $B(\Lambda_c^+ \to pK^-\pi^+) = (6.37 \pm 0.21) \times 10^{-2}$. Our first error is their experiment's error and our second error is the systematic error from using our best (shown rounded) value.

$\Gamma(pK^-K^+K^-)/\Gamma(\Lambda_c^+\pi^-)$ — Γ_{101}/Γ_{32}

VALUE (units 10^{-3})	DOCUMENT ID		TECN	COMMENT
$2.62 \pm 0.15 \pm 0.09$	[1] AAIJ	18Q	LHCB	pp at 7, 8 TeV

[1] AAIJ 18Q reports $[\Gamma(\Lambda_b^0 \to pK^-K^+K^-)/\Gamma(\Lambda_b^0 \to \Lambda_c^+\pi^-)]$ / $[B(\Lambda_c^+ \to pK^-\pi^+)] = (4.11 \pm 0.12 \pm 0.06 \pm 0.19) \times 10^{-2}$ which we multiply by our best (shown rounded) value $B(\Lambda_c^+ \to pK^-\pi^+) = (6.37 \pm 0.21) \times 10^{-2}$. Our first error is their experiment's error and our second error is the systematic error from using our best (shown rounded) value.

PARTIAL BRANCHING FRACTIONS

$B(\Lambda_b \to \Lambda\mu^+\mu^-)$ ($q^2 < 2.0$ GeV$^2/c^4$)

VALUE (units 10^{-7})	DOCUMENT ID		TECN	COMMENT
0.71 ± 0.27 OUR AVERAGE				
$0.72^{+0.24}_{-0.22} \pm 0.14$	[1] AAIJ	15AE	LHCB	pp at 7, 8 TeV
$0.15 \pm 2.01 \pm 0.05$	AALTONEN	11AI	CDF	$p\overline{p}$ at 1.96 TeV
• • • We do not use the following data for averages, fits, limits, etc. • • •				
$0.56 \pm 0.76 \pm 0.80$	[2] AAIJ	13AJ	LHCB	Repl. by AAIJ 15AE

[1] AAIJ 15AE measurement covers $0.1 < q^2 < 2.0$ GeV$^2/c^4$.
[2] Uses $B(\Lambda_b^0 \to J/\psi\Lambda) = (6.2 \pm 1.4) \times 10^{-4}$.

$B(\Lambda_b \to \Lambda\mu^+\mu^-)$ ($2.0 < q^2 < 4.3$ GeV$^2/c^4$)

VALUE (units 10^{-7})	DOCUMENT ID		TECN	COMMENT
$0.28^{+0.28}_{-0.21}$ OUR AVERAGE				
$0.253^{+0.276}_{-0.207} \pm 0.046$	[1] AAIJ	15AE	LHCB	pp at 7, 8 TeV
$1.8 \pm 1.7 \pm 0.6$	AALTONEN	11AI	CDF	$p\overline{p}$ at 1.96 TeV
• • • We do not use the following data for averages, fits, limits, etc. • • •				
$0.71 \pm 0.60 \pm 0.23$	[2] AAIJ	13AJ	LHCB	Repl. by AAIJ 15AE

[1] AAIJ 15AE measurement covers $2.0 < q^2 < 4.0$ GeV$^2/c^4$.
[2] Uses $B(\Lambda_b^0 \to J/\psi\Lambda) = (6.2 \pm 1.4) \times 10^{-4}$.

$B(\Lambda_b \to \Lambda\mu^+\mu^-)$ ($q^2 < 4.3$ GeV$^2/c^4$)

VALUE (units 10^{-7})	DOCUMENT ID		TECN	COMMENT
$2.7 \pm 2.5 \pm 0.9$	AALTONEN	11AI	CDF	$p\overline{p}$ at 1.96 TeV

$B(\Lambda_b \to \Lambda\mu^+\mu^-)$ ($4.0 < q^2 < 6.0$ GeV$^2/c^4$)

VALUE (units 10^{-7})	DOCUMENT ID		TECN	COMMENT
$0.04^{+0.18}_{-0.00} \pm 0.02$	AAIJ	15AE	LHCB	pp at 7, 8 TeV

$B(\Lambda_b \to \Lambda\mu^+\mu^-)$ ($1.0 < q^2 < 6.0$ GeV$^2/c^4$)

VALUE (units 10^{-7})	DOCUMENT ID		TECN	COMMENT
$0.47^{+0.31}_{-0.27}$ OUR AVERAGE				
$0.45^{+0.30}_{-0.25} \pm 0.10$	[1] AAIJ	15AE	LHCB	pp at 7 and 8 TeV
$1.3 \pm 2.1 \pm 0.4$	AALTONEN	11AI	CDF	$p\overline{p}$ at 1.96 TeV

[1] AAIJ 15AE measurement covers $1.1 < q^2 < 6.0$ GeV$^2/c^4$.

$B(\Lambda_b \to \Lambda\mu^+\mu^-)$ ($6.0 < q^2 < 8.0$ GeV$^2/c^4$)

VALUE (units 10^{-7})	DOCUMENT ID		TECN	COMMENT
$0.50^{+0.24}_{-0.22} \pm 0.10$	AAIJ	15AE	LHCB	pp at 7, 8 TeV

$B(\Lambda_b \to \Lambda\mu^+\mu^-)$ ($4.3 < q^2 < 8.68$ GeV$^2/c^4$)

VALUE (units 10^{-7})	DOCUMENT ID		TECN	COMMENT
0.5 ± 0.7 OUR AVERAGE				
$0.66 \pm 0.74 \pm 0.18$	[1] AAIJ	13AJ	LHCB	pp at 7 TeV
$-0.2 \pm 1.6 \pm 0.1$	AALTONEN	11AI	CDF	$p\overline{p}$ at 1.96 TeV

[1] Uses $B(\Lambda_b^0 \to J/\psi\Lambda) = (6.2 \pm 1.4) \times 10^{-4}$.

$B(\Lambda_b \to \Lambda\mu^+\mu^-)$ ($10.09 < q^2 < 12.86$ GeV$^2/c^4$)

VALUE (units 10^{-7})	DOCUMENT ID		TECN	COMMENT
2.2 ± 0.6 OUR AVERAGE				
$2.08^{+0.42}_{-0.39} \pm 0.42$	[1] AAIJ	15AE	LHCB	pp at 7, 8 TeV
$3.0 \pm 1.5 \pm 1.0$	AALTONEN	11AI	CDF	$p\overline{p}$ at 1.96 TeV
• • • We do not use the following data for averages, fits, limits, etc. • • •				
$1.55 \pm 0.58 \pm 0.55$	[2] AAIJ	13AJ	LHCB	Repl. by AAIJ 15AE

[1] AAIJ 15AE measurement covers $11.0 < q^2 < 12.5$ GeV$^2/c^4$.
[2] Uses $B(\Lambda_b^0 \to J/\psi\Lambda) = (6.2 \pm 1.4) \times 10^{-4}$.

$B(\Lambda_b \to \Lambda\mu^+\mu^-)$ ($14.18 < q^2 < 16.0$ GeV$^2/c^4$)

VALUE (units 10^{-7})	DOCUMENT ID		TECN	COMMENT
1.7 ± 0.5 OUR AVERAGE Error includes scale factor of 1.1.				
$2.04^{+0.35}_{-0.33} \pm 0.42$	[1] AAIJ	15AE	LHCB	pp at 7, 8 TeV
$1.0 \pm 0.7 \pm 0.3$	AALTONEN	11AI	CDF	$p\overline{p}$ at 1.96 TeV
• • • We do not use the following data for averages, fits, limits, etc. • • •				
$1.44 \pm 0.44 \pm 0.42$	[2] AAIJ	13AJ	LHCB	Repl. by AAIJ 15AE

[1] AAIJ 15AE measurement covers $15.0 < q^2 < 16.0$ GeV$^2/c^4$.
[2] Uses $B(\Lambda_b^0 \to J/\psi\Lambda) = (6.2 \pm 1.4) \times 10^{-4}$.

$B(\Lambda_b \to \Lambda\mu^+\mu^-)$ ($16.0 < q^2$ GeV$^2/c^4$)

VALUE (units 10^{-7})	DOCUMENT ID		TECN	COMMENT
$7.0 \pm 1.9 \pm 2.2$	AALTONEN	11AI	CDF	$p\overline{p}$ at 1.96 TeV
• • • We do not use the following data for averages, fits, limits, etc. • • •				
$4.73 \pm 0.77 \pm 1.25$	[1,2] AAIJ	13AJ	LHCB	Repl. by AAIJ 15AE

[1] Uses $B(\Lambda_b^0 \to J/\psi\Lambda) = (6.2 \pm 1.4) \times 10^{-4}$.
[2] Requires $16.00 < q^2 < 20.30$ GeV$^2/c^4$.

$B(\Lambda_b \to \Lambda\mu^+\mu^-)$ ($18.0 < q^2 < 20.0$ GeV$^2/c^4$)

VALUE (units 10^{-7})	DOCUMENT ID		TECN	COMMENT
$2.44 \pm 0.28 \pm 0.50$	AAIJ	15AE	LHCB	pp at 7, 8 TeV

$B(\Lambda_b \to \Lambda\mu^+\mu^-)$ ($15.0 < q^2 < 20.0$ GeV$^2/c^4$)

VALUE (units 10^{-7})	DOCUMENT ID		TECN	COMMENT
$6.00 \pm 0.45 \pm 1.25$	AAIJ	15AE	LHCB	pp at 7, 8 TeV

$B(\Lambda_b \to \Lambda(1520)^0\mu^+\mu^-)$ ($1.1 < q^2 < 6.0$ GeV$^2/c^4$)

VALUE (units 10^{-8})	DOCUMENT ID		TECN	COMMENT
$9.56 \pm 1.13 \pm 0.78 \pm 1.81$	[1] AAIJ	23BB	LHCB	pp at 7, 8, 13 TeV

[1] Uses $B(\Lambda_b \to J/\psi p K^-) = (3.2 \pm 0.6) \times 10^{-4}$. The last uncertainty is due to uncertainties of $B(\Lambda_b^0 \to p K^- J/\psi)$ and $B(J/\psi \to \mu^+\mu^-)$ values.

$B(\Lambda_b \to \Lambda(1520)^0\mu^+\mu^-)$ ($15.0 < q^2 < 17.0$ GeV$^2/c^4$)

VALUE (units 10^{-8})	DOCUMENT ID		TECN	COMMENT
$1.14 \pm 0.48 \pm 0.26 \pm 0.22$	[1] AAIJ	23BB	LHCB	pp at 7, 8, 13 TeV

[1] Uses $B(\Lambda_b \to J/\psi p K^-) = (3.2 \pm 0.6) \times 10^{-4}$. The last uncertainty is due to uncertainties of $B(\Lambda_b^0 \to p K^- J/\psi)$ and $B(J/\psi \to \mu^+\mu^-)$ values.

Int. J. Mod. Phys. A 2026.41. Downloaded from www.worldscientific.com
by UNIVERSITY OF CALIFORNIA @ BERKELEY on 09/16/26. Re-use and distribution is strictly not permitted, except for Open Access articles.

Int. J. Mod. Phys. A 2026.41. Downloaded from www.worldscientific.com
UNIVERSITY OF CALIFORNIA @ BERKELEY on 09/16/26. Re-use and distribution is strictly not permitted, except for Open Access articles.

CP VIOLATION

A_{CP} is defined as

$$A_{CP} = \frac{B(\Lambda_b^0 \to f) - B(\overline{\Lambda}_b^0 \to \overline{f})}{B(\Lambda_b^0 \to f) + B(\overline{\Lambda}_b^0 \to \overline{f})},$$

the *CP*-violation asymmetry of exclusive Λ_b^0 and $\overline{\Lambda}_b^0$ decay.

$A_{CP}(\Lambda_b \to p\pi^-)$

VALUE (units 10^{-2})	DOCUMENT ID		TECN	COMMENT
0.3± 0.9 OUR AVERAGE				
0.2± 0.8±0.4	AAIJ	25O	LHCB	pp at 7, 8, 13 TeV
6 ± 7 ±3	AALTONEN	14P	CDF	$p\overline{p}$ at 1.96 TeV
• • • We do not use the following data for averages, fits, limits, etc. • • •				
−3.5± 1.7±2.0	AAIJ	18AX	LHCB	Repl. by AAIJ 25O
3 ±17 ±5	AALTONEN	11N	CDF	Repl. by AALTONEN 14P

$A_{CP}(\Lambda_b \to pK^-)$

VALUE (units 10^{-2})	DOCUMENT ID		TECN	COMMENT
− 1.2± 0.8 OUR AVERAGE				
− 1.1± 0.7±0.4	AAIJ	25O	LHCB	pp at 7, 8, 13 TeV
−10 ± 8 ±4	AALTONEN	14P	CDF	$p\overline{p}$ at 1.96 TeV
• • • We do not use the following data for averages, fits, limits, etc. • • •				
− 2.0± 1.3±1.9	AAIJ	18AX	LHCB	Repl. by AAIJ 25O
37 ±17 ±3	AALTONEN	11N	CDF	Repl. by AALTONEN 14P

$A_{CP}(\Lambda_b \to DpK^-)$

VALUE	DOCUMENT ID		TECN	COMMENT
$0.12 \pm 0.09^{+0.02}_{-0.03}$	[1] AAIJ	21AD	LHCB	pp at 7, 8, 13 TeV

[1] A_{CP} is measured from $(B(\Lambda_b^0 \to [K^+\pi^-]_D pK^-) - B(\overline{\Lambda}_b^0 \to [K^-\pi^+]_D \overline{p}K^+))/(B(\Lambda_b^0 \to [K^+\pi^-]_D pK^-) + B(\overline{\Lambda}_b^0 \to [K^-\pi^+]_D \overline{p}K^+))$ in the full phase space.

$A_{CP}(\Lambda_b^0 \to \Lambda_c^+\pi^-)$

VALUE	DOCUMENT ID		TECN	COMMENT
0.007±0.008±0.005	[1] AAIJ	24AH	LHCB	pp at 7, 8, 13 TeV

[1] Analyzes the angular distribution of $\Lambda_b^0 \to \Lambda_c^+\pi^-$.

$A_{CP}(\Lambda_b^0 \to \Lambda_c^+K^-)$

VALUE	DOCUMENT ID		TECN	COMMENT
−0.032±0.029±0.006	[1] AAIJ	24AH	LHCB	pp at 7, 8, 13 TeV

[1] Analyzes the angular distribution of $\Lambda_b^0 \to \Lambda_c^+K^-$.

$\Delta A_{CP}(pK^-/\pi^-)$

$\Delta A_{CP} \equiv A_{CP}(pK^-) - A_{CP}(p\pi^-)$

VALUE	DOCUMENT ID		TECN	COMMENT
0.014±0.022±0.010	AAIJ	18AX	LHCB	pp at 7 and 8 TeV

$A_{CP}(\Lambda_b \to p\overline{K}^0\pi^-)$

VALUE	DOCUMENT ID		TECN	COMMENT
0.039±0.021 OUR AVERAGE				
0.034±0.019±0.009	AAIJ	25AP	LHCB	pp at 7, 8, 13 TeV
0.22 ±0.13 ±0.03	AAIJ	14Q	LHCB	pp at 7 TeV

$A_{CP}(\Lambda_b \to p\overline{K}^0K^-)$

VALUE	DOCUMENT ID		TECN	COMMENT
0.02±0.13±0.09	AAIJ	25AP	LHCB	pp at 7, 8, 13 TeV

$\Delta A_{CP}(J/\psi p\pi^-/K^-)$

$\Delta A_{CP} \equiv A_{CP}(J/\psi p\pi^-) - A_{CP}(J/\psi pK^-)$

VALUE (units 10^{-2})	DOCUMENT ID		TECN	COMMENT
5.7±2.4±1.2	AAIJ	14K	LHCB	pp at 7, 8 TeV

$A_{CP}(\Lambda_b \to \Lambda\pi^+\pi^-)$

VALUE	DOCUMENT ID		TECN	COMMENT
−0.013±0.053±0.018	[1] AAIJ	25J	LHCB	pp at 7, 8, 13 TeV

[1] Measured relative to $\Lambda_b^0 \to \Lambda_c^+\pi^-$ decay.

$A_{CP}(\Lambda_b \to \Lambda K^+\pi^-)$

VALUE	DOCUMENT ID		TECN	COMMENT
−0.118±0.045±0.021	[1] AAIJ	25J	LHCB	pp at 7, 8, 13 TeV
• • • We do not use the following data for averages, fits, limits, etc. • • •				
−0.53 ±0.23 ±0.11	[1] AAIJ	16W	LHCB	Repl. by AAIJ 25J

[1] Measured relative to $\Lambda_b^0 \to \Lambda_c^+\pi^-$ decay.

$A_{CP}(\Lambda_b \to \Lambda K^+K^-)$

VALUE	DOCUMENT ID		TECN	COMMENT
0.083±0.023±0.016	[1] AAIJ	25J	LHCB	pp at 7, 8, 13 TeV
• • • We do not use the following data for averages, fits, limits, etc. • • •				
−0.28 ±0.10 ±0.07	[1] AAIJ	16W	LHCB	Repl. by AAIJ 25J

[1] Measured relative to $\Lambda_b^0 \to \Lambda_c^+\pi^-$ decay.

$\Delta A_{CP}(\Lambda_b^0 \to pK^-\mu^+\mu^-)$

$\Delta A_{CP} \equiv A_{CP}(pK^-\mu^+\mu^-) - A_{CP}(pK^-J/\psi)$

VALUE (units 10^{-2})	DOCUMENT ID		TECN	COMMENT
−3.5±5.0±0.2	AAIJ	17T	LHCB	pp at 7, 8 TeV

$\Delta A_{CP}(\Lambda_b^0 \to p\pi^-\pi^+\pi^-)$

$\Delta A_{CP} \equiv A_{CP}(\Lambda_b^0 \to p\pi^-\pi^+\pi^-) - A_{CP}(\Lambda_b^0 \to (\Lambda_c^+ \to p\pi^-\pi^+)\pi^-)$

VALUE (units 10^{-2})	DOCUMENT ID		TECN	COMMENT
1.1±2.5±0.6	[1] AAIJ	19AH	LHCB	pp at 7 and 8 TeV

[1] Full phase space.

$\Delta A_{CP}(\Lambda_b^0 \to (p\pi^-\pi^+\pi^-)_{LBM})$

$\Delta A_{CP} \equiv A_{CP}(\Lambda_b^0 \to (p\pi^-\pi^+\pi^-)_{LBM}) - A_{CP}(\Lambda_b^0 \to (\Lambda_c^+ \to p\pi^-\pi^+)\pi^-)$. Two-body low invariant-mass region (LBM): $m(p\pi^-) < 2000$MeV and $m(\pi^+\pi^-) < 1640$ MeV.

VALUE (units 10^{-2})	DOCUMENT ID		TECN	COMMENT
3.7±4.1±0.5	[1] AAIJ	19AH	LHCB	pp at 7 and 8 TeV

[1] Measurement done with $m(p\pi^-) < 2000$ MeV/c^2 and $m(\pi^+\pi^-) < 1640$ MeV/c^2.

$\Delta A_{CP}(\Lambda_b^0 \to pa_1(1260)^-)$

$\Delta A_{CP} \equiv A_{CP}(\Lambda_b^0 \to pa_1(1260)^-) - A_{CP}(\Lambda_b^0 \to (\Lambda_c^+ \to p\pi^-\pi^+)\pi^-)$. $419 < m(\pi^+\pi^-\pi^+) < 1500$ MeV.

VALUE (units 10^{-2})	DOCUMENT ID		TECN	COMMENT
−1.5±4.2±0.6	AAIJ	19AH	LHCB	pp at 7 and 8 TeV

$\Delta A_{CP}(\Lambda_b^0 \to N(1520)^0\rho(770)^0)$

$\Delta A_{CP} \equiv A_{CP}(\Lambda_b^0 \to N(1520)^0\rho(770)^0) - A_{CP}(\Lambda_b^0 \to (\Lambda_c^+ \to p\pi^-\pi^+)\pi^-)$. $1078 < m(p\pi^-) < 1800$ MeV and $m(\pi^+\pi^-) < 1100$ MeV.

VALUE (units 10^{-2})	DOCUMENT ID		TECN	COMMENT
2.0±4.9±0.4	AAIJ	19AH	LHCB	pp at 7 and 8 TeV

$\Delta A_{CP}(\Lambda_b^0 \to \Delta(1232)^{++}\pi^-\pi^-)$

$\Delta A_{CP} \equiv A_{CP}(\Lambda_b^0 \to \Delta(1232)^{++}\pi^-\pi^-) - A_{CP}(\Lambda_b^0 \to (\Lambda_c^+ \to p\pi^-\pi^+)\pi^-)$. $1078 < m(p\pi^+) < 1432$ MeV.

VALUE (units 10^{-2})	DOCUMENT ID		TECN	COMMENT
0.1±3.2±0.6	AAIJ	19AH	LHCB	pp at 7 and 8 TeV

$\Delta A_{CP}(\Lambda_b^0 \to pK^-\pi^+\pi^-)$

$\Delta A_{CP} \equiv A_{CP}(\Lambda_b^0 \to pK^-\pi^+\pi^-) - A_{CP}(\Lambda_b^0 \to (\Lambda_c^+ \to pK^-\pi^+)\pi^-)$

VALUE (units 10^{-2})	DOCUMENT ID		TECN	COMMENT
2.45±0.46±0.10	[1] AAIJ	25AB	LHCB	pp at 7, 8, 13 TeV
• • • We do not use the following data for averages, fits, limits, etc. • • •				
3.2 ±1.1 ±0.6	[2] AAIJ	19AH	LHCB	Repl. by AAIJ 25AB

[1] AAIJ 25AB provides also measurements in parts of the phase-space.
[2] Full phase space.

$\Delta A_{CP}(\Lambda_b^0 \to (pK^-\pi^+\pi^-)_{LBM})$

$\Delta A_{CP} \equiv A_{CP}(\Lambda_b^0 \to (pK^-\pi^+\pi^-)_{LBM}) - A_{CP}(\Lambda_b^0 \to (\Lambda_c^+ \to pK^-\pi^+)\pi^-)$. Two-body low invariant-mass region (LBM): $m(pK^-) < 2000$ MeV and $m(\pi^+\pi^-) < 1640$ MeV.

VALUE (units 10^{-2})	DOCUMENT ID		TECN	COMMENT
3.5±1.5±0.5	[1] AAIJ	19AH	LHCB	pp at 7 and 8 TeV

[1] Measurement done with $m(pK^-) < 2000$ MeV/c^2 and $m(\pi^+\pi^-) < 1640$ MeV/c^2.

$\Delta A_{CP}(\Lambda_b^0 \to N(1520)^0K^*(892)^0)$

$\Delta A_{CP} \equiv A_{CP}(\Lambda_b^0 \to N(1520)^0K^*(892)^0) - A_{CP}(\Lambda_b^0 \to (\Lambda_c^+ \to pK^-\pi^+)\pi^-)$. $1078 < m(p\pi^-) < 1800$ MeV and $750 < m(\pi^+K^-) < 1100$ MeV.

VALUE (units 10^{-2})	DOCUMENT ID		TECN	COMMENT
5.5±2.5±0.5	AAIJ	19AH	LHCB	pp at 7 and 8 TeV

$\Delta A_{CP}(\Lambda_b^0 \to \Lambda(1520)\rho(770)^0)$

$\Delta A_{CP} \equiv A_{CP}(\Lambda_b^0 \to \Lambda(1520)\rho(770)^0) - A_{CP}(\Lambda_b^0 \to (\Lambda_c^+ \to pK^-\pi^+)\pi^-)$. $1460 < m(pK^-) < 1580$ MeV and $m(\pi^+\pi^-) < 1100$ MeV.

VALUE (units 10^{-2})	DOCUMENT ID		TECN	COMMENT
0.6±6.0±0.5	AAIJ	19AH	LHCB	pp at 7 and 8 TeV

$\Delta A_{CP}(\Lambda_b^0 \to \Delta(1232)^{++}K^-\pi^-)$

$\Delta A_{CP} \equiv A_{CP}(\Lambda_b^0 \to \Delta(1232)^{++}K^-\pi^-) - A_{CP}(\Lambda_b^0 \to (\Lambda_c^+ \to pK^-\pi^+)\pi^-)$. $1078 < m(p\pi^+) < 1432$ MeV.

VALUE (units 10^{-2})	DOCUMENT ID		TECN	COMMENT
4.4±2.6±0.6	AAIJ	19AH	LHCB	pp at 7 and 8 TeV

$\Delta A_{CP}(\Lambda_b^0 \to pK_1(1410)^-)$

$\Delta A_{CP} \equiv A_{CP}(\Lambda_b^0 \to pK_1(1410)^-) - A_{CP}(\Lambda_b^0 \to (\Lambda_c^+ \to pK^-\pi^+)\pi^-)$. $1200 < m(K^-\pi^+\pi^-) < 1600$ MeV.

VALUE (units 10^{-2})	DOCUMENT ID		TECN	COMMENT
4.7±3.5±0.8	AAIJ	19AH	LHCB	pp at 7 and 8 TeV

Int. J. Mod. Phys. A 2026.41. Downloaded from www.worldscientific.com
by UNIVERSITY OF CALIFORNIA @ BERKELEY on 09/16/26. Re-use and distribution is strictly not permitted, except for Open Access articles.

$\Delta A_{CP}(\Lambda_b^0 \to p K^- K^+ \pi^-)$

$\Delta A_{CP} \equiv A_{CP}(\Lambda_b^0 \to p K^- K^+ \pi^-) - A_{CP}(\Lambda_b^0 \to (\Lambda_c^+ \to p \pi^- \pi^+) \pi^-)$

VALUE (units 10^{-2})	DOCUMENT ID		TECN	COMMENT
−6.9±4.9±0.8	[1] AAIJ	19AH	LHCB	pp at 7 and 8 TeV

[1] Full phase space.

$\Delta A_{CP}(\Lambda_b^0 \to p K^- K^+ K^-)$

$\Delta A_{CP} \equiv A_{CP}(\Lambda_b^0 \to p K^- K^+ K^-) - A_{CP}(\Lambda_b^0 \to (\Lambda_c^+ \to p K^- \pi^+) \pi^-)$

VALUE (units 10^{-2})	DOCUMENT ID		TECN	COMMENT
0.2±1.8±0.6	[1] AAIJ	19AH	LHCB	pp at 7 and 8 TeV

[1] Full phase space.

$\Delta A_{CP}(\Lambda_b^0 \to \Lambda(1520)\phi(1020))$

$\Delta A_{CP} \equiv A_{CP}(\Lambda_b^0 \to \Lambda(1520)\phi(1020)) - A_{CP}(\Lambda_b^0 \to (\Lambda_c^+ \to p K^- \pi^+) \pi^-)$. $1460 < m(p K^-) < 1600$ MeV and $1005 < m(K^+ K^-) < 1040$ MeV.

VALUE (units 10^{-2})	DOCUMENT ID		TECN	COMMENT
4.3±5.6±0.4	AAIJ	19AH	LHCB	pp at 7 and 8 TeV

$\Delta A_{CP}(\Lambda_b^0 \to (p K^-)_{highmass}\, \phi(1020))$

$\Delta A_{CP} \equiv A_{CP}(\Lambda_b^0 \to (p K^-)_{highmass}\, \phi(1020)) - A_{CP}(\Lambda_b^0 \to (\Lambda_c p K^- \pi^+) \pi^-)$. $m(p K^-) > 1600$ MeV and $1005 < m(K^+ K^-) < 1040$ MeV.

VALUE (units 10^{-2})	DOCUMENT ID		TECN	COMMENT
−0.7±3.3±0.7	[1] AAIJ	19AH	LHCB	pp at 7 and 8 TeV

[1] Measurement done with $m(p K^-) > 1600$ MeV/c^2.

$\Delta A_{CP}(\Lambda_b^0 \to (p K^- K^+ K^-)_{LBM})$

$\Delta A_{CP} \equiv A_{CP}(\Lambda_b^0 \to (p K^- K^+ K^-)_{LBM}) - A_{CP}(\Lambda_b^0 \to (\Lambda_c^+ \to p K^- \pi^+) \pi^-)$. Two-body low invariant-mass region (LBM): $m(p K^-) < 2000$ MeVand $m(K^+ K^-) < 1675$ MeV.

VALUE (units 10^{-2})	DOCUMENT ID		TECN	COMMENT
2.7±2.3±0.6	[1] AAIJ	19AH	LHCB	pp at 7 and 8 TeV

[1] Measurement done with $m(p K^-) < 2000$ MeV/c^2 and $m(K^+ K^-) < 1675$ MeV/c^2.

CP AND *T* VIOLATION PARAMETERS

Measured values of the triple-product asymmetry parameters, odd under time-reversal, are defined as $A_{c(s)}(\Lambda/\phi) = (N^+_{c(s)} - N^-_{c(s)}) / (\text{sum})$ where $N^+_{c(s)}$, $N^-_{c(s)}$ are the number of Λ or ϕ candidates for which the $\cos(\Phi)$ and $\sin(\Phi)$ observables are positive and negative, respectively. Angles $\cos(\Phi)$ and $\sin(\Phi)$ are defined as in LEITNER 07.

$A_c(\Lambda)$

VALUE	DOCUMENT ID		TECN	COMMENT
−0.22±0.12±0.06	AAIJ	16J	LHCB	pp at 7, 8 TeV

$A_s(\Lambda)$

VALUE	DOCUMENT ID		TECN	COMMENT
0.13±0.12±0.05	AAIJ	16J	LHCB	pp at 7, 8 TeV

$A_c(\phi)$

VALUE	DOCUMENT ID		TECN	COMMENT
−0.01±0.12±0.03	AAIJ	16J	LHCB	pp at 7, 8 TeV

$A_s(\phi)$

VALUE	DOCUMENT ID		TECN	COMMENT
−0.07±0.12±0.01	AAIJ	16J	LHCB	pp at 7, 8 TeV

$a_{CP}(\Lambda_b^0 \to p \pi^- \pi^+ \pi^-)$

Observable calculated as half of the difference between triple products for Λ_b^0 and $\overline{\Lambda}_b^0$, which is sensitive to *CP* violation.

VALUE (%)	DOCUMENT ID		TECN	COMMENT
−0.7 ±0.7 ±0.2	[1] AAIJ	20AB	LHCB	pp at 7, 8, 13 TeV
• • • We do not use the following data for averages, fits, limits, etc. • • •				
1.15 ±1.45 ±0.32	[2] AAIJ	17H	LHCB	Repl. by AAIJ 20AB

[1] Used both triple product asymmetries and the unbinned energy test method.
[2] Measured over full phase space of the decay.

$a_{CP}(\Lambda_b^0 \to p K^- \pi^+ \pi^-)$

Observable calculated as half of the difference between triple products for Λ_b^0 and $\overline{\Lambda}_b^0$, which is sensitive to *CP* violation.

VALUE (%)	DOCUMENT ID		TECN	COMMENT
−0.81±0.84±0.31	[1] AAIJ	18AG	LHCB	pp at 7, 8 TeV

[1] Measured over full phase space of the decay.

$a_{CP}(\Lambda_b^0 \to p K^- K^+ \pi^-)$

Observable calculated as half of the difference between triple products for Λ_b^0 and $\overline{\Lambda}_b^0$, which is sensitive to *CP* violation.

VALUE (%)	DOCUMENT ID		TECN	COMMENT
−0.93±4.54±0.42	[1] AAIJ	17H	LHCB	pp at 7, 8 TeV

[1] Measured over full phase space of the decay.

$a_{CP}(\Lambda_b^0 \to p K^- K^+ K^-)$

Observable calculated as half of the difference between triple products for Λ_b^0 and $\overline{\Lambda}_b^0$, which is sensitive to *CP* violation.

VALUE (%)	DOCUMENT ID		TECN	COMMENT
1.12±1.51±0.32	[1] AAIJ	18AG	LHCB	pp at 7, 8 TeV

[1] Measured over full phase space of the decay.

$a_{CP}(\Lambda_b^0 \to p K^- \mu^+ \mu^-)$

VALUE (%)	DOCUMENT ID		TECN	COMMENT
1.2±5.0±0.7	AAIJ	17T	LHCB	pp at 7, 8 TeV

P VIOLATION PARAMETERS

Observables calculated as average of the triple products for Λ_b^0 and $\overline{\Lambda}_b^0$, which is sensitive to parity violation.

$a_P(\Lambda_b^0 \to p \pi^- \pi^+ \pi^-)$

VALUE (%)	DOCUMENT ID		TECN	COMMENT
−4.0 ±0.7 ±0.2	[1] AAIJ	20AB	LHCB	pp at 7, 8, 13 TeV
• • • We do not use the following data for averages, fits, limits, etc. • • •				
−3.71 ±1.45 ±0.32	[2] AAIJ	17H	LHCB	Repl. by AAIJ 20AB

[1] Used both triple product asymmetries and the unbinned energy test method.
[2] Measured over full phase space of the decay.

$a_P(\Lambda_b^0 \to p K^- \pi^+ \pi^-)$

VALUE (%)	DOCUMENT ID		TECN	COMMENT
−0.60±0.84±0.31	[1] AAIJ	18AG	LHCB	pp at 7, 8 TeV

[1] Measured over full phase space of the decay.

$a_P(\Lambda_b^0 \to p K^- K^+ \pi^-)$

VALUE (%)	DOCUMENT ID		TECN	COMMENT
3.62±4.54±0.42	[1] AAIJ	17H	LHCB	pp at 7, 8 TeV

[1] Measured over full phase space of the decay.

$a_P(\Lambda_b^0 \to p K^- K^+ K^-)$

VALUE (%)	DOCUMENT ID		TECN	COMMENT
−1.56±1.51±0.32	[1] AAIJ	18AG	LHCB	pp at 7, 8 TeV

[1] Measured over full phase space of the decay.

$a_P(\Lambda_b^0 \to p K^- \mu^+ \mu^-)$

VALUE (%)	DOCUMENT ID		TECN	COMMENT
−4.8±5.0±0.7	AAIJ	17T	LHCB	pp at 7, 8 TeV

Λ_b^0 DECAY PARAMETERS

See the note on "Baryon Decay Parameters" in the neutron Listings.

α decay parameter for $\Lambda_b \to J/\psi \Lambda$

VALUE	DOCUMENT ID		TECN	COMMENT
−0.017±0.026 OUR AVERAGE				
$-0.022^{+0.027}_{-0.026}$	[1] AAIJ	20O	LHCB	pp at 7, 8, 13 TeV
−0.14 ±0.14 ±0.10	[2] SIRUNYAN	18R	CMS	pp at 7, 8 TeV
0.30 ±0.16 ±0.06	[3] AAD	14L	ATLS	pp at 7 TeV
• • • We do not use the following data for averages, fits, limits, etc. • • •				
0.05 ±0.17 ±0.07	[4] AAIJ	13AG	LHCB	Repl. by AAIJ 20O

[1] Extracted using a Bayesian analysis. The most probable value is given as −0.022, with a 68% credibility interval [-0.048, 0.005]. Transverse polarizations of Λ_b^0 of −0.004 (68% credibility interval [-0.064, 0.051]), 0.001 (68% credibility interval [-0.035, 0.045]), and 0.032 (68% credibility interval [-0.011, 0.065]) are also reported at 7 TeV, 8 TeV and 13 TeV, respectively. Note that both statistical and systematic uncertainties are included.
[2] An angular analysis of $\Lambda_b \to J/\psi \Lambda$ decay is performed. Note that the sign of α in CMS definition is the opposite to that used by AAIJ 13AG and AAD 14L. Λ_b transverse production polarization of 0.00 ± 0.06 ± 0.06 is also reported, as well as squares of the helicity amplitudes.
[3] An angular analysis of $\Lambda_b \to J/\psi \Lambda$ decay is performed and magnitudes of all helicity amplitudes are also reported.
[4] An angular analysis of $\Lambda_b \to J/\psi \Lambda$ decay is performed and a Λ_b transverse production polarization of 0.06 ± 0.07 ± 0.02 is also reported.

CP-averaged α decay parameter for $\Lambda_b^0 \to \Lambda_c^+ \pi^-$

VALUE	DOCUMENT ID		TECN	COMMENT
−1.003±0.008±0.005	[1] AAIJ	24AH	LHCB	pp at 7, 8, 13 TeV

[1] Analyzes the angular distribution of $\Lambda_b^0 \to \Lambda_c^+ \pi^-$.

CP-averaged α decay parameter for $\Lambda_b^0 \to \Lambda_c^+ K^-$

VALUE	DOCUMENT ID		TECN	COMMENT
−0.964±0.028±0.015	[1] AAIJ	24AH	LHCB	pp at 7, 8, 13 TeV

[1] Analyzes the angular distribution of $\Lambda_b^0 \to \Lambda_c^+ K^-$.

α_γ decay parameter for $\Lambda_b \to \Lambda\gamma$

Measures asymmetry between left- and right-handed photons in the decay.

VALUE	DOCUMENT ID		TECN	COMMENT
$\mathbf{0.82^{+0.17+0.04}_{-0.26-0.13}}$	[1] AAIJ	22M	LHCB	pp at 13 TeV

[1] AAIJ 22M provides a combined measurement as well as measured $\alpha_\gamma^- = 1.26 \pm 0.42 \pm 0.20$ and $\alpha_\gamma^+ = 0.55 \pm 0.32 \pm 0.16$ for Λ_b^0 and $\overline{\Lambda}_b^0$ separately.

Int. J. Mod. Phys. A 2026.41. Downloaded from www.worldscientific.com
UNIVERSITY OF CALIFORNIA @ BERKELEY on 09/16/26. Re-use and distribution is strictly not permitted, except for Open Access articles.

$f_L(\mu\mu)$ longitudinal polarization fraction in $\Lambda_b \to \Lambda\mu^+\mu^-$

VALUE	DOCUMENT ID		TECN	COMMENT
$\mathbf{0.61^{+0.11}_{-0.14} \pm 0.03}$	[1] AAIJ	15AE	LHCB	pp at 7, 8 TeV

[1] AAIJ 15AE measurement covers $15.0 < q^2 < 20.0$ GeV^2/c^4.

FORWARD-BACKWARD ASYMMETRIES

The forward-backward assymmetry is defined as $A_{FB}(\Lambda_b^0)$ = [N(F) − N(B)] / [N(F) + N(B)], where the forward (F) direction corresponds to a particle (Λ_b^0 or Λ_b^-) sharing valence quark flavors with a beam particle with the same sign of rapidity.

$A_{FB}(\Lambda_b^0 \to J/\psi\Lambda)$

VALUE	DOCUMENT ID		TECN	COMMENT
$\mathbf{0.04 \pm 0.07 \pm 0.02}$	[1] ABAZOV	15I	D0	pp at 1.96 TeV

[1] The measured asymmetry integrated over rapidity y in the range of $0.1 < |y| < 2.0$.

$A_{FB}^{\ell}(\mu\mu)$ in $\Lambda_b \to \Lambda\mu^+\mu^-$

VALUE	DOCUMENT ID		TECN	COMMENT
$\mathbf{-0.39 \pm 0.04 \pm 0.01}$	[1] AAIJ	18AP	LHCB	pp at 7, 8, 13 TeV
• • • We do not use the following data for averages, fits, limits, etc. • • •				
$-0.05 \pm 0.09 \pm 0.03$	[2] AAIJ	15AE	LHCB	Repl. by AAIJ 18AP.

[1] The measurement covers $15.0 < q^2 < 20.0$ GeV^2/c^4.
[2] AAIJ 15AE measurement covers $15.0 < q^2 < 20.0$ GeV^2/c^4.

$\Delta(A_{FB}^{\ell}(\mu\mu))$ in $\Lambda_b \to \Lambda\mu^+\mu^-$

Difference of asymmetries $A_{FB}^{\ell}(\mu\mu)$ in $\Lambda_b \to \Lambda\mu^+\mu^-$ between Λ_b and $\overline{\Lambda}_b$ decays

VALUE	DOCUMENT ID		TECN	COMMENT
$\mathbf{-0.05 \pm 0.09 \pm 0.03}$	AAIJ	18AO	LHCB	pp at 7, 8 TeV

$A_{FB}^{h}(p\pi)$ in $\Lambda_b \to \Lambda(p\pi)\mu^+\mu^-$

VALUE	DOCUMENT ID		TECN	COMMENT
$\mathbf{-0.30 \pm 0.05 \pm 0.02}$	[1] AAIJ	18AP	LHCB	pp at 7, 8, 13 TeV
• • • We do not use the following data for averages, fits, limits, etc. • • •				
$-0.29 \pm 0.07 \pm 0.03$	[2] AAIJ	15AE	LHCB	Repl. by AAIJ 18AP.

[1] The measurement covers $15.0 < q^2 < 20.0$ GeV^2/c^4.
[2] AAIJ 15AE measurement covers $15.0 < q^2 < 20.0$ GeV^2/c^4.

$A_{FB}^{\ell h}$ in $\Lambda_b \to \Lambda\mu^+\mu^-$

VALUE	DOCUMENT ID		TECN	COMMENT
$\mathbf{0.25 \pm 0.04 \pm 0.01}$	[1] AAIJ	18AP	LHCB	pp at 7, 8, 13 TeV

[1] The measurement covers $15.0 < q^2 < 20.0$ GeV^2/c^4.

$\Lambda_b^0 - \overline{\Lambda}_b^0$ Production Asymmetry

$$A_P(\Lambda_b^0) = [\sigma(\Lambda_b^0) - \sigma(\overline{\Lambda}_b^0)] / [\sigma(\Lambda_b^0) + \sigma(\overline{\Lambda}_b^0)]$$

$A_P(\Lambda_b^0)$

VALUE (units 10^{-2})	DOCUMENT ID		TECN	COMMENT
1.4 ±0.4 OUR AVERAGE	Error includes scale factor of 1.8.			
1.92 ± 0.35	[1] AAIJ	21AJ	LHCB	pp at 7 TeV
1.09 ± 0.29	[1] AAIJ	21AJ	LHCB	pp at 8 TeV
$-0.11 \pm 2.53 \pm 1.08$	[2] AAIJ	17BF	LHCB	pp at 7 TeV
$3.44 \pm 1.61 \pm 0.76$	[2] AAIJ	17BF	LHCB	pp at 8 TeV

[1] Integrated over the kinematic range $2 < p_T < 27$ GeV/c and $2.15 < y < 4.10$.
[2] Indirect determination in kinematic range $2 < p_T < 30$ GeV/c and $2.1 < \eta < 4.5$ from production asymmetries of B^+, B^0 and B_s^0.

Λ_b^0 REFERENCES

AAIJ	25AA	EPJ C85 812	R. Aaij et al.	(LHCb Collab.)
AAIJ	25AB	NAT 643 1223	R. Aaij et al.	(LHCb Collab.)
AAIJ	25AK	PR D112 052013	R. Aaij et al.	(LHCb Collab.)
AAIJ	25AP	JHEP 2510 169	R. Aaij et al.	(LHCb Collab.)
AAIJ	25J	PRL 134 101802	R. Aaij et al.	(LHCb Collab.)
AAIJ	25O	PR D111 092004	R. Aaij et al.	(LHCb Collab.)
AAIJ	24AH	PRL 133 261804	R. Aaij et al.	(LHCb Collab.)
AAIJ	24P	JHEP 2406 098	R. Aaij et al.	(LHCb Collab.)
AAIJ	24R	JHEP 2407 140	R. Aaij et al.	(LHCb Collab.)
AAIJ	24V	EPJ C84 237	R. Aaij et al.	(LHCb Collab.)
AAIJ	24X	EPJ C84 575	R. Aaij et al.	(LHCb Collab.)
AAIJ	24Y	PR D110 L031104	R. Aaij et al.	(LHCb Collab.)
HAYRAPETY...	24BA	EPJ C84 1062	A. Hayrapetyan et al.	(CMS Collab.)
AAIJ	23BB	PRL 131 151801	R. Aaij et al.	(LHCb Collab.)
AAIJ	23K	JHEP 2307 075	R. Aaij et al.	(LHCb Collab.)
AAIJ	22K	PRL 128 191803	R. Aaij et al.	(LHCb Collab.)
AAIJ	22M	PR D105 L051104	R. Aaij et al.	(LHCb Collab.)
AAIJ	22R	JHEP 2203 153	R. Aaij et al.	(LHCb Collab.)
AAIJ	21AD	PR D104 112008	R. Aaij et al.	(LHCb Collab.)
AAIJ	21AJ	JHEP 2110 060	R. Aaij et al.	(LHCb Collab.)
AAIJ	21B	PL B815 136172	R. Aaij et al.	(LHCb Collab.)
AAIJ	21R	JHEP 2105 095	R. Aaij et al.	(LHCb Collab.)
AAIJ	20AB	PR D102 051101	R. Aaij et al.	(LHCb Collab.)
AAIJ	20AK	PR D102 112012	R. Aaij et al.	(LHCb Collab.)
AAIJ	20M	JHEP 2005 040	R. Aaij et al.	(LHCb Collab.)
AAIJ	20O	JHEP 2006 110	R. Aaij et al.	(LHCb Collab.)
SIRUNYAN	20H	PL B802 135203	A.M. Sirunyan et al.	(CMS Collab.)
AAIJ	19AH	EPJ C79 745	R. Aaij et al.	(LHCb Collab.)
AAIJ	19AN	JHEP 1909 028	R. Aaij et al.	(LHCb Collab.)
AAIJ	19F	JHEP 1903 126	R. Aaij et al.	(LHCb Collab.)
AAIJ	19Z	PRL 123 031801	R. Aaij et al.	(LHCb Collab.)
AAIJ	18AF	JHEP 1808 131	R. Aaij et al.	(LHCb Collab.)
AAIJ	18AG	JHEP 1808 039	R. Aaij et al.	(LHCb Collab.)
AAIJ	18AO	JHEP 1809 145 (errat.)	R. Aaij et al.	(LHCb Collab.)
AAIJ	18AP	JHEP 1809 146	R. Aaij et al.	(LHCb Collab.)
AAIJ	18AW	PL B784 101	R. Aaij et al.	(LHCb Collab.)
AAIJ	18AX	PL B787 124	R. Aaij et al.	(LHCb Collab.)
AAIJ	18Q	JHEP 1802 098	R. Aaij et al.	(LHCb Collab.)
PDG	18	PR D98 030001	M. Tanabashi et al.	(PDG Collab.)
SIRUNYAN	18BY	EPJ C78 457	A.M. Sirunyan et al.	(CMS Collab.)
SIRUNYAN	18R	PR D97 072010	A.M. Sirunyan et al.	(CMS Collab.)
AAIJ	17AM	PRL 119 062001	R. Aaij et al.	(LHCb Collab.)
AAIJ	17BF	PL B774 139	R. Aaij et al.	(LHCb Collab.)
AAIJ	17H	NATP 13 391	R. Aaij et al.	(LHCb Collab.)
AAIJ	17P	JHEP 1704 029	R. Aaij et al.	(LHCb Collab.)
AAIJ	17S	JHEP 1705 030	R. Aaij et al.	(LHCb Collab.)
AAIJ	17T	JHEP 1706 108	R. Aaij et al.	(LHCb Collab.)
AAIJ	16	JHEP 1601 012	R. Aaij et al.	(LHCb Collab.)
AAIJ	16A	CP C40 011001	R. Aaij et al.	(LHCb Collab.)
AAIJ	16J	PL B759 282	R. Aaij et al.	(LHCb Collab.)
AAIJ	16W	JHEP 1605 081	R. Aaij et al.	(LHCb Collab.)
AAIJ	16Y	JHEP 1605 132	R. Aaij et al.	(LHCb Collab.)
AAD	15CH	PL B751 63	G. Aad et al.	(ATLAS Collab.)
AAIJ	15AE	JHEP 1506 115	R. Aaji et al.	(LHCb Collab.)
Also		JHEP 1809 145 (errat.)	R. Aaij et al.	(LHCb Collab.)
AAIJ	15AH	JHEP 1509 006	R. Aaij et al.	(LHCb Collab.)
AAIJ	15BG	NATP 11 743	R. Aaij et al.	(LHCb Collab.)
ABAZOV	15I	PR D91 072008	V.M. Abazov et al.	(D0 Collab.)
AAD	14L	PR D89 092009	G. Aad et al.	(ATLAS Collab.)
AAIJ	14AA	PRL 112 202001	R. Aaij et al.	(LHCb Collab.)
AAIJ	14E	JHEP 1404 114	R. Aaij et al.	(LHCb Collab.)
AAIJ	14H	PR D89 032001	R. Aaij et al.	(LHCb Collab.)
AAIJ	14I	JHEP 1408 143	R. Aaij et al.	(LHCb Collab.)
AAIJ	14K	JHEP 1407 103	R. Aaij et al.	(LHCb Collab.)
AAIJ	14Q	JHEP 1404 087	R. Aaij et al.	(LHCb Collab.)
AAIJ	14U	PL B734 122	R. Aaij et al.	(LHCb Collab.)
AALTONEN	14B	PR D89 072014	T. Aaltonen et al.	(CDF Collab.)
AALTONEN	14P	PRL 113 242001	T. Aaltonen et al.	(CDF Collab.)
PDG	14	CP C38 070001	K. Olive et al.	(PDG Collab.)
AAD	13U	PR D87 032002	G. Aad et al.	(ATLAS Collab.)
AAIJ	13AG	PL B724 27	R. Aaij et al.	(LHCb Collab.)
AAIJ	13AJ	PL B725 25	R. Aaij et al.	(LHCb Collab.)
AAIJ	13AV	PRL 110 182001	R. Aaij et al.	(LHCb Collab.)
AAIJ	13BB	PRL 111 102003	R. Aaij et al.	(LHCb Collab.)
CHATRCHYAN	13AC	JHEP 1307 163	S. Chatrchyan et al.	(CMS Collab.)
AAIJ	12AR	JHEP 1210 037	R. Aaij et al.	(LHCb Collab.)
AAIJ	12E	PL B708 241	R. Aaij et al.	(LHCb Collab.)
AALTONEN	12A	PR D85 032003	T. Aaltonen et al.	(CDF Collab.)
ABAZOV	12U	PR D85 112003	V.M. Abazov et al.	(D0 Collab.)
AAIJ	11E	PR D84 092001	R. Aaij et al.	(LHCb Collab.)
Also		PR D85 039904 (errat.)	R. Aaij et al.	(LHCb Collab.)
AALTONEN	11	PRL 106 121804	T. Aaltonen et al.	(CDF Collab.)
AALTONEN	11AI	PRL 107 201802	T. Aaltonen et al.	(CDF Collab.)
AALTONEN	11N	PRL 106 181802	T. Aaltonen et al.	(CDF Collab.)
ABAZOV	11O	PR D84 031102	V.M. Abazov et al.	(D0 Collab.)
AALTONEN	10B	PRL 104 102002	T. Aaltonen et al.	(CDF Collab.)
AALTONEN	09C	PRL 103 031801	T. Aaltonen et al.	(CDF Collab.)
AALTONEN	09E	PR D79 032001	T. Aaltonen et al.	(CDF Collab.)
ABAZOV	07S	PRL 99 142001	V.M. Abazov et al.	(D0 Collab.)
ABAZOV	07U	PRL 99 182001	V.M. Abazov et al.	(D0 Collab.)
ABULENCIA	07A	PRL 98 122001	A. Abulencia et al.	(FNAL CDF Collab.)
ABULENCIA	07B	PRL 98 122002	A. Abulencia et al.	(FNAL CDF Collab.)
LEITNER	07	NPBPS 174 169	O. Leitner, Z.J. Ajaltouni	
ACOSTA	06	PRL 96 202001	D. Acosta et al.	(CDF Collab.)
ABAZOV	05C	PRL 94 102001	V.M. Abazov et al.	(D0 Collab.)
ACOSTA	05O	PR D72 051104	D. Acosta et al.	(CDF Collab.)
ABDALLAH	04A	PL B585 63	J. Abdallah et al.	(DELPHI Collab.)
ACOSTA	02G	PR D66 112002	D. Acosta et al.	(CDF Collab.)
ABREU	99W	EPJ C10 185	P. Abreu et al.	(DELPHI Collab.)
ACKERSTAFF	98G	PL B426 161	K. Ackerstaff et al.	(OPAL Collab.)
BARATE	98D	EPJ C2 197	R. Barate et al.	(ALEPH Collab.)
ABE	97B	PR D55 1142	F. Abe et al.	(CDF Collab.)
ABE	96M	PRL 77 1439	F. Abe et al.	(CDF Collab.)
ABREU	96D	ZPHY C71 199	P. Abreu et al.	(DELPHI Collab.)
ABREU	96N	PL B374 351	P. Abreu et al.	(DELPHI Collab.)
ADAM	96D	ZPHY C72 207	W. Adam et al.	(DELPHI Collab.)
BUSKULIC	96L	PL B380 442	D. Buskulic et al.	(ALEPH Collab.)
BUSKULIC	96V	PL B384 471	D. Buskulic et al.	(ALEPH Collab.)
PDG	96	PR D54 1	R. M. Barnett et al.	(PDG Collab.)
ABREU	95S	ZPHY C68 375	P. Abreu et al.	(DELPHI Collab.)
AKERS	95K	PL B353 402	R. Akers et al.	(OPAL Collab.)
BUSKULIC	95L	PL B357 685	D. Buskulic et al.	(ALEPH Collab.)
ABE	93B	PR D47 2639	F. Abe et al.	(CDF Collab.)
BUSKULIC	92E	PL B294 145	D. Buskulic et al.	(ALEPH Collab.)
ALBAJAR	91E	PL B273 540	C. Albajar et al.	(UA1 Collab.)
BARI	91	NC 104A 1787	G. Bari et al.	(CERN R422 Collab.)
ARENTON	86	NP B274 707	M.W. Arenton et al.	(ARIZ, NDAM, VAND)
BASILE	81	LNC 31 97	M. Basile et al.	(CERN R415 Collab.)

$\Lambda_b(5912)^0$

$J^P = \frac{1}{2}^-$ Status: ***

Quantum numbers are based on quark model expectations.

$\Lambda_b(5912)^0$ MASS

VALUE (MeV)	DOCUMENT ID		TECN	COMMENT
5912.16±0.16 OUR AVERAGE				
$5912.16 \pm 0.03 \pm 0.16$	[1] AAIJ	20Q	LHCB	pp at 7, 8, 13 TeV
$5912.29 \pm 0.12 \pm 0.16$	[2] SIRUNYAN	20K	CMS	pp at 13 TeV
• • • We do not use the following data for averages, fits, limits, etc. • • •				
$5912.17 \pm 0.13 \pm 0.16$	[3,4] AAIJ	12AL	LHCB	Repl. by AAIJ 20Q

[1] AAIJ 20Q measures $m(\Lambda_b(5912)^0) - m(\Lambda_b^0) = 292.589 \pm 0.029 \pm 0.010$ MeV. We have adjusted the measurement to our best value of $m(\Lambda_b^0) = 5619.57 \pm 0.16$ MeV. Our first error is their experiment's error and our second error is the systematic error from using our best values.
[2] SIRUNYAN 20K measures $m(\Lambda_b(5912)^0) - m(\Lambda_b^0) = 292.72 \pm 0.12 \pm 0.01$ MeV. We have adjusted the measurement to our best value of $m(\Lambda_b^0) = 5619.57 \pm 0.16$ MeV. Our first error is their experiment's error and our second error is the systematic error from using our best values.

[3] Observed in $\Lambda_b(5912)^0 \to \Lambda_b^0 \pi^+ \pi^-$ decays with 17.6 ± 4.8 candidates with a significance of 5.2 sigma.

[4] AAIJ 12AL measures $m(\Lambda_b(5912)^0) - m(\Lambda_b^0) = 292.60 \pm 0.12 \pm 0.04$ MeV. We have adjusted the measurement to our best value of $m(\Lambda_b^0) = 5619.57 \pm 0.16$ MeV. Our first error is their experiment's error and our second error is the systematic error from using our best values.

$\Lambda_b(5912)^0$ WIDTH

VALUE (MeV)	CL%	DOCUMENT ID		TECN	COMMENT
<0.25	90	AAIJ	20Q	LHCB	pp at 7, 8, 13 TeV
• • • We do not use the following data for averages, fits, limits, etc. • • •					
<0.66	90	AAIJ	12AL	LHCB	Repl. by AAIJ 20Q

$\Lambda_b(5912)^0$ DECAY MODES

	Mode	Fraction (Γ_i/Γ)
Γ_1	$\Lambda_b^0 \pi^+ \pi^-$	seen

$\Lambda_b(5912)^0$ BRANCHING RATIOS

$\Gamma(\Lambda_b^0 \pi^+ \pi^-)/\Gamma_{total}$ — Γ_1/Γ

VALUE	DOCUMENT ID		TECN	COMMENT
seen	AAIJ	20Q	LHCB	pp at 7, 8, 13 TeV
seen	SIRUNYAN	20K	CMS	pp at 13 TeV
seen	AAIJ	12AL	LHCB	pp at 7 TeV

$\Lambda_b(5912)^0$ REFERENCES

AAIJ	20Q	JHEP 2006 136	R. Aaij *et al.*	(LHCb Collab.)
SIRUNYAN	20K	PL B803 135345	A.M. Sirunyan *et al.*	(CMS Collab.)
AAIJ	12AL	PRL 109 172003	R. Aaij *et al.*	(LHCb Collab.)

$\Lambda_b(5920)^0$

$J^P = \frac{3}{2}^-$ Status: ***

Quantum numbers are based on quark model expectations.

$\Lambda_b(5920)^0$ MASS

VALUE (MeV)	DOCUMENT ID		TECN	COMMENT
5920.07±0.16 OUR AVERAGE				
5920.06±0.02±0.16	[1] AAIJ	20Q	LHCB	pp at 7, 8, 13 TeV
5920.13±0.07±0.16	[2] SIRUNYAN	20K	CMS	pp at 13 TeV
• • • We do not use the following data for averages, fits, limits, etc. • • •				
5919.4 ±0.5 ±0.2	[3,4] AALTONEN	13V	CDF	$p\overline{p}$ at 1.96 TeV
5919.97±0.09±0.16	[5,6] AAIJ	12AL	LHCB	Repl. by AAIJ 20Q

[1] AAIJ 20Q measures $m(\Lambda_b(5920)^0) - m(\Lambda_b^0) = 300.492 \pm 0.019 \pm 0.010$ MeV. We have adjusted the measurement to our best value of $m(\Lambda_b^0) = 5619.57 \pm 0.16$ MeV. Our first error is their experiment's error and our second error is the systematic error from using our best values.

[2] SIRUNYAN 20K measures $m(\Lambda_b(5920)^0) - m(\Lambda_b^0) = 300.56 \pm 0.07 \pm 0.01$ MeV. We have adjusted the measurement to our best value of $m(\Lambda_b^0) = 5619.57 \pm 0.16$ MeV. Our first error is their experiment's error and our second error is the systematic error from using our best values.

[3] Measured in $\Lambda_b(5920)^0 \to \Lambda_b^0 \pi^+ \pi^-$ decays with $17.3^{+5.3}_{-4.6}$ events, with a significance of 3.5 sigma.

[4] AALTONEN 13V measures $m(\Lambda_b(5920)^0) - m(\Lambda_b^0) - 2m(\pi) = 20.68 \pm 0.35 \pm 0.30$ MeV. We have adjusted the measurement to our best values of $m(\Lambda_b^0) = 5619.57 \pm 0.16$ MeV and $m(\pi) = 139.57039 \pm 0.00018$ MeV. Our first error is their experiment's error and our second error is the systematic error from using our best values.

[5] Observed in $\Lambda_b(5920)^0 \to \Lambda_b^0 \pi^+ \pi^-$ decays with 52.5 ± 8.1 candidates with a significance of 10.2 sigma.

[6] AAIJ 12AL measures $m(\Lambda_b(5920)^0) - m(\Lambda_b^0) = 300.40 \pm 0.08 \pm 0.04$ MeV. We have adjusted the measurement to our best value of $m(\Lambda_b^0) = 5619.57 \pm 0.16$ MeV. Our first error is their experiment's error and our second error is the systematic error from using our best values.

$\Lambda_b(5920)^0$ WIDTH

VALUE (MeV)	CL%	DOCUMENT ID		TECN	COMMENT
<0.19	90	AAIJ	20Q	LHCB	pp at 7, 8, 13 TeV
• • • We do not use the following data for averages, fits, limits, etc. • • •					
<0.63	90	AAIJ	12AL	LHCB	Repl. by AAIJ 20Q

$\Lambda_b(5920)^0$ DECAY MODES

	Mode	Fraction (Γ_i/Γ)
Γ_1	$\Lambda_b^0 \pi^+ \pi^-$	seen

$\Lambda_b(5920)^0$ BRANCHING RATIOS

$\Gamma(\Lambda_b^0 \pi^+ \pi^-)/\Gamma_{total}$ — Γ_1/Γ

VALUE	DOCUMENT ID		TECN	COMMENT
seen	AAIJ	20Q	LHCB	pp at 7, 8, 13 TeV
seen	SIRUNYAN	20K	LHCB	pp at 13 TeV
seen	AALTONEN	13V	CDF	$p\overline{p}$ at 1.96 TeV
seen	AAIJ	12AL	LHCB	pp at 7 TeV

$\Lambda_b(5920)^0$ REFERENCES

AAIJ	20Q	JHEP 2006 136	R. Aaij *et al.*	(LHCb Collab.)
SIRUNYAN	20K	PL B803 135345	A.M. Sirunyan *et al.*	(CMS Collab.)
AALTONEN	13V	PR D88 071101	T. Aaltonen *et al.*	(CDF Collab.)
AAIJ	12AL	PRL 109 172003	R. Aaij *et al.*	(LHCb Collab.)

$\Lambda_b(6070)^0$

$J^P = \frac{1}{2}^+$ Status: ***

Quantum numbers are based on quark model expectations.

$\Lambda_b(6070)^0$ MASS

VALUE (MeV)	DOCUMENT ID		TECN	COMMENT
6072.3±2.9±0.2	[1] AAIJ	20Q	LHCB	pp at 7, 8, 13 TeV

[1] AAIJ 20Q measures $m(\Lambda_b(6070)^0) - m(\Lambda_b^0) = 452.7 \pm 2.9 \pm 0.5$ MeV. We have adjusted the measurement to our best value of $m(\Lambda_b^0) = 5619.57 \pm 0.16$ MeV. Our first error is their experiment's error and our second error is the systematic error from using our best values.

$\Lambda_b(6070)^0$ WIDTH

VALUE (MeV)	DOCUMENT ID		TECN	COMMENT
72±11±2	AAIJ	20Q	LHCB	pp at 7, 8, 13 TeV

$\Lambda_b(6070)^0$ DECAY MODES

	Mode	Fraction (Γ_i/Γ)
Γ_1	$\Lambda_b^0 \pi^+ \pi^-$	seen

$\Lambda_b(6070)^0$ BRANCHING RATIOS

$\Gamma(\Lambda_b^0 \pi^+ \pi^-)/\Gamma_{total}$ — Γ_1/Γ

VALUE	DOCUMENT ID		TECN	COMMENT
seen	AAIJ	20Q	LHCB	pp at 7, 8, 13 TeV

$\Lambda_b(6070)^0$ REFERENCES

AAIJ	20Q	JHEP 2006 136	R. Aaij *et al.*	(LHCb Collab.)

$\Lambda_b(6146)^0$

$J^P = \frac{3}{2}^+$ Status: ***

Quantum numbers are based on quark model expectations.

$\Lambda_b(6146)^0$ MASS

$\Lambda_b(6146)^0$ MASS

VALUE (MeV)	DOCUMENT ID		TECN	COMMENT
6146.2 ±0.4 OUR AVERAGE				
6146.5 ±2.1 ±0.2	[1] SIRUNYAN	20K	CMS	pp at 13 TeV
6146.17±0.33±0.27	[2] AAIJ	19AJ	LHCB	pp at 7, 8, 13 TeV

[1] SIRUNYAN 20K measures $m(\Lambda_b(6146)^0) - m(\Lambda_b^0) = 526.9 \pm 1.9 \pm 0.8$ MeV. We have adjusted the measurement to our best value of $m(\Lambda_b^0) = 5619.57 \pm 0.16$ MeV. Our first error is their experiment's error and our second error is the systematic error from using our best values.

[2] Observed in $\Lambda_b^0 \pi^+ \pi^-$ mode.

$m_{\Lambda_b(6146)^0} - m_{\Lambda_b^0}$

VALUE (MeV)	DOCUMENT ID		TECN	COMMENT
526.55±0.33±0.10	[1] AAIJ	19AJ	LHCB	pp at 7, 8, 13 TeV

[1] Observed in $\Lambda_b^0 \pi^+ \pi^-$ mode.

$\Lambda_b(6146)^0$ WIDTH

VALUE (MeV)	DOCUMENT ID		TECN	COMMENT
2.9±1.3±0.3	[1] AAIJ	19AJ	LHCB	pp at 7, 8, 13 TeV

[1] Observed in $\Lambda_b^0 \pi^+ \pi^-$ mode.

Int. J. Mod. Phys. A 2026.41. Downloaded from www.worldscientific.com
by UNIVERSITY OF CALIFORNIA @ BERKELEY on 09/16/26. Re-use and distribution is strictly not permitted, except for Open Access articles.

Int. J. Mod. Phys. A 2026.41. Downloaded from www.worldscientific.com
UNIVERSITY OF CALIFORNIA @ BERKELEY on 09/16/26. Re-use and distribution is strictly not permitted, except for Open Access articles.

$\Lambda_b(6146)^0$ DECAY MODES

	Mode	Fraction (Γ_i/Γ)
Γ_1	$\Lambda_b^0 \pi^+ \pi^-$	seen

$\Lambda_b(6146)^0$ BRANCHING RATIOS

$\Gamma(\Lambda_b^0 \pi^+ \pi^-)/\Gamma_{total}$ — Γ_1/Γ

VALUE	DOCUMENT ID		TECN	COMMENT
seen	SIRUNYAN	20K	LHCB	pp at 13 TeV
seen	AAIJ	19AJ	LHCB	pp at 7, 8, 13 TeV

$\Lambda_b(6146)^0$ REFERENCES

SIRUNYAN 20K PL B803 135345 A.M. Sirunyan *et al.* (CMS Collab.)
AAIJ 19AJ PRL 123 152001 R. Aaij *et al.* (LHCb Collab.)

$\Lambda_b(6152)^0$

$J^P = \frac{5}{2}^+$ Status: ***

Quantum numbers are based on quark model expectations.

$\Lambda_b(6152)^0$ MASS

$\Lambda_b(6152)^0$ MASS

VALUE (MeV)	DOCUMENT ID		TECN	COMMENT
6152.5 ±0.4 OUR AVERAGE				
6152.7 ±1.2 ±0.2	[1] SIRUNYAN	20K	CMS	pp at 13 TeV
6152.51±0.26±0.27	[2] AAIJ	19AJ	LHCB	pp at 7, 8, 13 TeV

[1] SIRUNYAN 20K measures $m(\Lambda_b(6152)^0) - m(\Lambda_b^0) = 533.1 \pm 1.1 \pm 0.4$ MeV. We have adjusted the measurement to our best value of $m(\Lambda_b^0) = 5619.57 \pm 0.16$ MeV. Our first error is their experiment's error and our second error is the systematic error from using our best values.
[2] Observed in $\Lambda_b^0 \pi^+ \pi^-$ mode.

$m_{\Lambda_b(6152)^0} - m_{\Lambda_b^0}$

VALUE (MeV)	DOCUMENT ID		TECN	COMMENT
532.89±0.26±0.10	[1] AAIJ	19AJ	LHCB	pp at 7, 8, 13 TeV

[1] Observed in $\Lambda_b^0 \pi^+ \pi^-$ mode.

$m_{\Lambda_b(6152)^0} - m_{\Lambda_b(6146)^0}$

VALUE (MeV)	DOCUMENT ID		TECN	COMMENT
6.34±0.32±0.02	AAIJ	19AJ	LHCB	pp at 7, 8, 13 TeV

$\Lambda_b(6152)^0$ WIDTH

VALUE (MeV)	DOCUMENT ID		TECN	COMMENT
2.1±0.8±0.3	[1] AAIJ	19AJ	LHCB	pp at 7, 8, 13 TeV

[1] Observed in $\Lambda_b^0 \pi^+ \pi^-$ mode.

$\Lambda_b(6152)^0$ DECAY MODES

	Mode	Fraction (Γ_i/Γ)
Γ_1	$\Lambda_b^0 \pi^+ \pi^-$	seen

$\Lambda_b(6152)^0$ BRANCHING RATIOS

$\Gamma(\Lambda_b^0 \pi^+ \pi^-)/\Gamma_{total}$ — Γ_1/Γ

VALUE	DOCUMENT ID		TECN	COMMENT
seen	SIRUNYAN	20K	LHCB	pp at 13 TeV
seen	AAIJ	19AJ	LHCB	pp at 7, 8, 13 TeV

$\Lambda_b(6152)^0$ REFERENCES

SIRUNYAN 20K PL B803 135345 A.M. Sirunyan *et al.* (CMS Collab.)
AAIJ 19AJ PRL 123 152001 R. Aaij *et al.* (LHCb Collab.)

Σ_b

$I(J^P) = 1(\frac{1}{2}^+)$ Status: ***
I, J, P need confirmation.

In the quark model Σ_b^+, Σ_b^0, Σ_b^- are an isotriplet (uub, udb, ddb) state. The lowest Σ_b ought to have $J^P = 1/2^+$. None of I, J, or P have actually been measured.

Σ_b MASS

Σ_b^+ MASS

VALUE (MeV)	DOCUMENT ID		TECN	COMMENT
5810.56±0.25 OUR AVERAGE				
5810.55±0.11±0.23	[1] AAIJ	19A	LHCB	pp at 7, 8 TeV
5811.3 $^{+0.9}_{-0.8}$ ±1.7	[2] AALTONEN	12F	CDF	$p\overline{p}$ at 1.96 TeV
• • • We do not use the following data for averages, fits, limits, etc. • • •				
5807.8 $^{+2.0}_{-2.2}$ ±1.7	[3] AALTONEN	07K	CDF	Repl. by AALTONEN 12F

[1] Measured using fully reconstructed $\Lambda_b^0 \to \Lambda_c^+ \pi^-$ and $\Lambda_c^+ \to p K^- \pi^+$ decays.
[2] Measured using fully reconstructed $\Lambda_b^0 \to \Lambda_c^+ \pi^-$ and $\Lambda_c^+ \to K^- \pi^+$ decays.
[3] Observed four $\Lambda_b^0 \pi^\pm$ resonances in the fully reconstructed decay mode $\Lambda_b^0 \to \Lambda_c^+ \pi^-$, where $\Lambda_c^+ \to p K^- \pi^+$.

Σ_b^- MASS

VALUE (MeV)	DOCUMENT ID		TECN	COMMENT
5815.64±0.27 OUR AVERAGE				
5815.64±0.14±0.24	[1] AAIJ	19A	LHCB	pp at 7, 8 TeV
5815.5 $^{+0.6}_{-0.5}$ ±1.7	[2] AALTONEN	12F	CDF	$p\overline{p}$ at 1.96 TeV
• • • We do not use the following data for averages, fits, limits, etc. • • •				
5815.2 ±1.0 ±1.7	[3] AALTONEN	07K	CDF	Repl. by AALTONEN 12F

[1] Measured using fully reconstructed $\Lambda_b^0 \to \Lambda_c^+ \pi^-$ and $\Lambda_c^+ \to p K^- \pi^+$ decays.
[2] Measured using fully reconstructed $\Lambda_b^0 \to \Lambda_c^+ \pi^-$ and $\Lambda_c^+ \to K^- \pi^+$ decays.
[3] Observed four $\Lambda_b^0 \pi^\pm$ resonances in the fully reconstructed decay mode $\Lambda_b^0 \to \Lambda_c^+ \pi^-$, where $\Lambda_c^+ \to p K^- \pi^+$.

$m_{\Sigma_b^+} - m_{\Sigma_b^-}$

VALUE (MeV)	DOCUMENT ID		TECN	COMMENT
−5.06±0.18 OUR AVERAGE				
−5.09±0.18±0.01	[1] AAIJ	19A	LHCB	pp at 7, 8 TeV
−4.2 $^{+1.1}_{-1.0}$ ±0.1	[2] AALTONEN	12F	CDF	$p\overline{p}$ at 1.96 TeV

[1] Measured using fully reconstructed $\Lambda_b^0 \to \Lambda_c^+ \pi^-$ and $\Lambda_c^+ \to p K^- \pi^+$ decays.
[2] Measured using fully reconstructed $\Lambda_b^0 \to \Lambda_c^+ \pi^-$ and $\Lambda_c^+ \to K^- \pi^+$ decays.

Σ_b WIDTH

Σ_b^+ WIDTH

VALUE (MeV)	DOCUMENT ID		TECN	COMMENT
5.0 ±0.5 OUR AVERAGE				
4.83±0.31±0.37	[1] AAIJ	19A	LHCB	pp at 7, 8 TeV
9.7 $^{+3.8}_{-2.8}$ $^{+1.2}_{-1.1}$	[2] AALTONEN	12F	CDF	$p\overline{p}$ at 1.96 TeV

[1] Measured using fully reconstructed $\Lambda_b^0 \to \Lambda_c^+ \pi^-$ and $\Lambda_c^+ \to p K^- \pi^+$ decays.
[2] Measured using fully reconstructed $\Lambda_b^0 \to \Lambda_c^+ \pi^-$ and $\Lambda_c^+ \to K^- \pi^+$ decays.

Σ_b^- WIDTH

VALUE (MeV)	DOCUMENT ID		TECN	COMMENT
5.3 ±0.5 OUR AVERAGE				
5.33±0.42±0.37	[1] AAIJ	19A	LHCB	pp at 7, 8 TeV
4.9 $^{+3.1}_{-2.1}$ ±1.1	[2] AALTONEN	12F	CDF	$p\overline{p}$ at 1.96 TeV

[1] Measured using fully reconstructed $\Lambda_b^0 \to \Lambda_c^+ \pi^-$ and $\Lambda_c^+ \to p K^- \pi^+$ decays.
[2] Measured using fully reconstructed $\Lambda_b^0 \to \Lambda_c^+ \pi^-$ and $\Lambda_c^+ \to K^- \pi^+$ decays.

Σ_b DECAY MODES

	Mode	Fraction (Γ_i/Γ)
Γ_1	$\Lambda_b^0 \pi$	dominant

Σ_b BRANCHING RATIOS

$\Gamma(\Lambda_b^0 \pi)/\Gamma_{total}$ — Γ_1/Γ

VALUE	DOCUMENT ID		TECN	COMMENT
dominant	AALTONEN	07K	CDF	$p\overline{p}$ at 1.96 TeV

Σ_b REFERENCES

AAIJ 19A PRL 122 012001 R. Aaij *et al.* (LHCb Collab.)
AALTONEN 12F PR D85 092011 T. Aaltonen *et al.* (CDF Collab.)
AALTONEN 07K PRL 99 202001 T. Aaltonen *et al.* (CDF Collab.)

Int. J. Mod. Phys. A 2026.41. Downloaded from www.worldscientific.com by UNIVERSITY OF CALIFORNIA @ BERKELEY on 09/16/26. Re-use and distribution is strictly not permitted, except for Open Access articles.

Σ_b^*

$I(J^P) = 1(\frac{3}{2}^+)$ Status: ***

I, J, P need confirmation.

I, J, P need confirmation. Quantum numbers shown are quark-model predictions.

Σ_b^* MASS

Σ_b^{*+} MASS

VALUE (MeV)	DOCUMENT ID		TECN	COMMENT
5830.32±0.27 OUR AVERAGE				
5830.28±0.14±0.24	[1] AAIJ	19A	LHCB	pp at 7, 8 TeV
5832.1 ±0.7 $^{+1.7}_{-1.8}$	[2] AALTONEN	12F	CDF	$p\overline{p}$ at 1.96 TeV

[1] Measured using fully reconstructed $\Lambda_b^0 \to \Lambda_c^+\pi^-$ and $\Lambda_c^+ \to pK^-\pi^+$ decays.
[2] Measured using fully reconstructed $\Lambda_b^0 \to \Lambda_c^+\pi^-$ and $\Lambda_c^+ \to K^-\pi^+$ decays.

Σ_b^{*-} MASS

VALUE (MeV)	DOCUMENT ID		TECN	COMMENT
5834.74±0.30 OUR AVERAGE				
5834.73±0.17±0.25	[1] AAIJ	19A	LHCB	pp at 7, 8 TeV
5835.1 ±0.6 $^{+1.7}_{-1.8}$	[2] AALTONEN	12F	CDF	$p\overline{p}$ at 1.96 TeV

[1] Measured using fully reconstructed $\Lambda_b^0 \to \Lambda_c^+\pi^-$ and $\Lambda_c^+ \to pK^-\pi^+$ decays.
[2] Measured using fully reconstructed $\Lambda_b^0 \to \Lambda_c^+\pi^-$ and $\Lambda_c^+ \to K^-\pi^+$ decays.

$m_{\Sigma_b^{*+}} - m_{\Sigma_b^{*-}}$

VALUE (MeV)	DOCUMENT ID		TECN	COMMENT
−4.37±0.33 OUR AVERAGE Error includes scale factor of 1.6.				
−4.45±0.22±0.01	[1] AAIJ	19A	LHCB	pp at 7, 8 TeV
−3.0 $^{+1.0}_{-0.9}$ ±0.1	[2] AALTONEN	12F	CDF	$p\overline{p}$ at 1.96 TeV

[1] Measured using fully reconstructed $\Lambda_b^0 \to \Lambda_c^+\pi^-$ and $\Lambda_c^+ \to pK^-\pi^+$ decays.
[2] Measured using fully reconstructed $\Lambda_b^0 \to \Lambda_c^+\pi^-$ and $\Lambda_c^+ \to K^-\pi^+$ decays.

$m_{\Sigma_b^{*+}} - m_{\Sigma_b^+}$

VALUE	DOCUMENT ID		TECN	COMMENT
19.73±0.18±0.01	[1] AAIJ	19A	LHCB	pp at 7, 8 TeV

[1] Measured using fully reconstructed $\Lambda_b^0 \to \Lambda_c^+\pi^-$ and $\Lambda_c^+ \to pK^-\pi^+$ decays.

$m_{\Sigma_b^{*-}} - m_{\Sigma_b^-}$

VALUE	DOCUMENT ID		TECN	COMMENT
19.09±0.22±0.02	[1] AAIJ	19A	LHCB	pp at 7, 8 TeV

[1] Measured using fully reconstructed $\Lambda_b^0 \to \Lambda_c^+\pi^-$ and $\Lambda_c^+ \to pK^-\pi^+$ decays.

Σ_b^* WIDTH

Σ_b^{*+} WIDTH

VALUE (MeV)	DOCUMENT ID		TECN	COMMENT
9.4 ±0.5 OUR AVERAGE				
9.34±0.47±0.26	[1] AAIJ	19A	LHCB	pp at 7, 8 TeV
11.5 $^{+2.7}_{-2.2}$ $^{+1.0}_{-1.5}$	[2] AALTONEN	12F	CDF	$p\overline{p}$ at 1.96 TeV

[1] Measured using fully reconstructed $\Lambda_b^0 \to \Lambda_c^+\pi^-$ and $\Lambda_c^+ \to pK^-\pi^+$ decays.
[2] Measured using fully reconstructed $\Lambda_b^0 \to \Lambda_c^+\pi^-$ and $\Lambda_c^+ \to K^-\pi^+$ decays.

Σ_b^{*-} WIDTH

VALUE (MeV)	DOCUMENT ID		TECN	COMMENT
10.4 ±0.8 OUR AVERAGE Error includes scale factor of 1.3.				
10.68±0.60±0.33	[1] AAIJ	19A	LHCB	pp at 7, 8 TeV
7.5 $^{+2.2}_{-1.8}$ $^{+0.9}_{-1.4}$	[2] AALTONEN	12F	CDF	$p\overline{p}$ at 1.96 TeV

[1] Measured using fully reconstructed $\Lambda_b^0 \to \Lambda_c^+\pi^-$ and $\Lambda_c^+ \to pK^-\pi^+$ decays.
[2] Measured using fully reconstructed $\Lambda_b^0 \to \Lambda_c^+\pi^-$ and $\Lambda_c^+ \to K^-\pi^+$ decays.

$m_{\Sigma_b^*} - m_{\Sigma_b}$

VALUE (MeV)	DOCUMENT ID		TECN	COMMENT
21.2$^{+2.0}_{-1.9}$$^{+0.4}_{-0.3}$	[1] AALTONEN	07K	CDF	$p\overline{p}$ at 1.96 TeV

[1] Observed four $\Lambda_b^0\pi^\pm$ resonances in the fully reconstructed decay mode $\Lambda_b^0 \to \Lambda_c^+\pi^-$, where $\Lambda_c^+ \to pK^-\pi^+$. Assumes $m_{\Sigma_b^{*+}} - m_{\Sigma_b^+} = m_{\Sigma_b^{*-}} - m_{\Sigma_b^-}$

Σ_b^* DECAY MODES

	Mode	Fraction (Γ_i/Γ)
Γ_1	$\Lambda_b^0\pi$	dominant

Σ_b^* BRANCHING RATIOS

$\Gamma(\Lambda_b^0\pi)/\Gamma_{total}$ — Γ_1/Γ

VALUE	DOCUMENT ID		TECN	COMMENT
dominant	AALTONEN	07K	CDF	$p\overline{p}$ at 1.96 TeV

Σ_b^* REFERENCES

AAIJ 19A PRL 122 012001 R. Aaij et al. (LHCb Collab.)
AALTONEN 12F PR D85 092011 T. Aaltonen et al. (CDF Collab.)
AALTONEN 07K PRL 99 202001 T. Aaltonen et al. (CDF Collab.)

$\Sigma_b(6097)^+$

$J^P = ?^?$ Status: ***

$\Sigma_b(6097)^+$ MASS

VALUE (MeV)	DOCUMENT ID		TECN	COMMENT
6095.8±1.7±0.4	[1] AAIJ	19A	LHCB	pp at 7, 8 TeV

[1] Measured using fully reconstructed $\Lambda_b^0 \to \Lambda_c^+\pi^-$ and $\Lambda_c^+ \to pK^-\pi^+$ decays.

$m_{\Sigma_b(6097)^\pm} - m_{\Sigma_b(6097)^-}$

VALUE	DOCUMENT ID		TECN	COMMENT
-2.2 +-2.4 +-0.3 MeV	[1] AAIJ	19A	LHCB	pp at 7, 8 TeV

[1] Measured using fully reconstructed $\Lambda_b^0 \to \Lambda_c^+\pi^-$ and $\Lambda_c^+ \to pK^-\pi^+$ decays.

$\Sigma_b(6097)^+$ WIDTH

VALUE (MeV)	DOCUMENT ID		TECN	COMMENT
31.0±5.5±0.7	[1] AAIJ	19A	LHCB	pp at 7, 8 TeV

[1] Measured using fully reconstructed $\Lambda_b^0 \to \Lambda_c^+\pi^-$ and $\Lambda_c^+ \to pK^-\pi^+$ decays.

$\Sigma_b(6097)^+$ DECAY MODES

	Mode	Fraction (Γ_i/Γ)
Γ_1	$\Lambda_b\pi^+ \times B(b \to \Sigma_b(6097)^+)$	seen

$\Sigma_b(6097)^+$ BRANCHING RATIOS

$\Gamma(\Lambda_b\pi^+ \times B(b \to \Sigma_b(6097)^+))/\Gamma_{total}$ — Γ_1/Γ

VALUE	DOCUMENT ID		TECN	COMMENT
seen	AAIJ	19A	LHCB	pp at 7, 8 TeV

$\Sigma_b(6097)^+$ REFERENCES

AAIJ 19A PRL 122 012001 R. Aaij et al. (LHCb Collab.)

$\Sigma_b(6097)^-$

$J^P = ?^?$ Status: ***

$\Sigma_b(6097)^-$ MASS

VALUE (MeV)	DOCUMENT ID		TECN	COMMENT
6098.0±1.7±0.5	[1] AAIJ	19A	LHCB	pp at 7, 8 TeV

[1] Measured using fully reconstructed $\Lambda_b^0 \to \Lambda_c^+\pi^-$ and $\Lambda_c^+ \to pK^-\pi^+$ decays.

$\Sigma_b(6097)^-$ WIDTH

VALUE (MeV)	DOCUMENT ID		TECN	COMMENT
28.9±4.2±0.9	[1] AAIJ	19A	LHCB	pp at 7, 8 TeV

[1] Measured using fully reconstructed $\Lambda_b^0 \to \Lambda_c^+\pi^-$ and $\Lambda_c^+ \to pK^-\pi^+$ decays.

$\Sigma_b(6097)^-$ DECAY MODES

	Mode	Fraction (Γ_i/Γ)
Γ_1	$\Lambda_b\pi^- \times B(b \to \Sigma_b(6097)^-)$	seen

$\Sigma_b(6097)^-$ BRANCHING RATIOS

$\Gamma(\Lambda_b\pi^- \times B(b \to \Sigma_b(6097)^-))/\Gamma_{total}$ — Γ_1/Γ

VALUE	DOCUMENT ID		TECN	COMMENT
seen	AAIJ	19A	LHCB	pp at 7, 8 TeV

$\Sigma_b(6097)^-$ REFERENCES

AAIJ 19A PRL 122 012001 R. Aaij et al. (LHCb Collab.)

Int. J. Mod. Phys. A 2026.41. Downloaded from www.worldscientific.com
UNIVERSITY OF CALIFORNIA @ BERKELEY on 09/16/26. Re-use and distribution is strictly not permitted, except for Open Access articles.

Ξ_b^-

$I(J^P) = \frac{1}{2}(\frac{1}{2}^+)$ Status: ***
I, J, P need confirmation.

In the quark model, Ξ_b^0 and Ξ_b^- are an isodoublet (usb, dsb) state; the lowest Ξ_b^0 and Ξ_b^- ought to have $J^P = 1/2^+$. None of I, J, or P have actually been measured.

Ξ_b^- MASS

Ξ_b^- MASS

VALUE (MeV)	DOCUMENT ID		TECN	COMMENT
5797.0 ± 0.4 OUR AVERAGE	Error includes scale factor of 1.4. See the ideogram below.			
5797.02 ± 0.63 ± 0.57	[1] AAIJ	24V	LHCB	pp at 13 TeV
5796.70 ± 0.39 ± 0.23	AAIJ	19AB	LHCB	pp at 7, 8 and 13 TeV
5797.72 ± 0.46 ± 0.31	[2] AAIJ	14BJ	LHCB	pp at 7, 8 TeV
5793.4 ± 1.8 ± 0.7	[3] AALTONEN	14B	CDF	$p\overline{p}$ at 1.96 TeV
5774 ±11 ±15	[4] ABAZOV	07K	D0	$p\overline{p}$ at 1.96 TeV
• • • We do not use the following data for averages, fits, limits, etc. • • •				
5795.8 ± 0.9 ± 0.4	[5] AAIJ	13AV	LHCB	Repl. by AAIJ 19AB
5796.7 ± 5.1 ± 1.4	[6] AALTONEN	11X	CDF	Repl. by AALTONEN 14B
5790.9 ± 2.6 ± 0.8	[7] AALTONEN	09AP	CDF	Repl. by AALTONEN 14B
5792.9 ± 2.5 ± 1.7	[8] AALTONEN	07A	CDF	Repl. by AALTONEN 09AP

[1] Uses $\Xi_b^- \to \Xi_c^0 D_s^-$ decays.
[2] Reconstructed in $\Xi_b^- \to \Xi_c^0 \pi^-$, $\Xi_c^0 \to p K^- K^- \pi^+$ decays. Reference Λ_b^0 mass 5619.30 ± 0.34 MeV from AAIJ 14AA.
[3] Uses $\Xi_b^- \to J/\psi \Xi^-$ and $\Xi_c^0 \pi^-$ decays.
[4] Observed in $\Xi_b^- \to J/\psi \Xi^-$ decays with $15.2 \pm 4.4 {}^{+1.9}_{-0.4}$ candidates, a significance of 5.5 sigma.
[5] Measured in $\Xi_b^- \to J/\psi \Xi^-$ decays.
[6] Measured in $\Xi_b^- \to \Xi_c^0 \pi^-$ with $25.8 {}^{+5.5}_{-5.2}$ candidates.
[7] Measured in $\Xi_b^- \to J/\psi \Xi^-$ decays with $66 {}^{+14}_{-9}$ candidates.
[8] Observed in $\Xi_b^- \to J/\psi \Xi^-$ decays with 17.5 ± 4.3 candidates, a significance of 7.7 sigma.

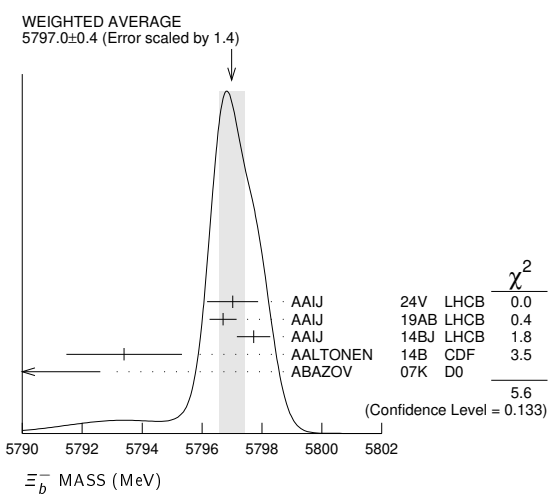

$m_{\Xi_b^-} - m_{\Lambda_b^0}$

VALUE (MeV)	DOCUMENT ID		TECN	COMMENT
177.48±0.24 OUR AVERAGE	Error includes scale factor of 1.1.			
177.68±0.63±0.33	[1] AAIJ	24V	LHCB	pp at 13 TeV
177.71±0.24±0.16	[2] AAIJ	21	LHCB	pp at 7, 8, 13 TeV
177.08±0.47±0.16	[3] AAIJ	17BE	LHCB	pp at 7, 8 TeV
176.2 ±0.9 ±0.1	[4] AAIJ	13AV	LHCB	pp at 7 TeV
• • • We do not use the following data for averages, fits, limits, etc. • • •				
177.73±0.33±0.14	[5] AAIJ	17BE	LHCB	pp at 7, 8 TeV
178.36±0.46±0.16	[2,6] AAIJ	14BJ	LHCB	Repl. by AAIJ 2021

[1] Uses $\Xi_b^- \to \Xi_c^0 D_s^-$ and $\Lambda_b^0 \to \Lambda_c^+ D_s^-$ decays.
[2] Reconstructed in $\Xi_b^- \to \Xi_c^0 \pi^-$, $\Xi_c^0 \to p K^- K^- \pi^+$ decays.Reference decays $\Lambda_b^0 \to \Lambda_c^+ \pi^-$ were used.
[3] Reconstructed in $\Xi_b^- \to J/\psi \Lambda K^-$ decays. Reference decays $\Lambda_b^0 \to J/\psi \Lambda$ were used.
[4] Reconstructed in $\Xi_b^- \to J/\psi \Xi^-$ decays.
[5] Combination of the original statistically independent measurements of AAIJ 17BE and AAIJ 14BJ taking into account correlation between systematic uncertainties.
[6] Combined with AAIJ 17BE.

$m_{\Xi_b^-} - m_{\Xi_b^0}$

VALUE (MeV)	DOCUMENT ID		TECN	COMMENT
5.9 ±0.5 OUR AVERAGE				
5.90±0.87±0.32	[1] AAIJ	24V	LHCB	pp at 13 TeV
5.92±0.60±0.23	[2] AAIJ	14BJ	LHCB	pp at 7, 8 TeV
3.1 ±5.6 ±1.3	[3] AALTONEN	11X	CDF	$p\overline{p}$ at 1.96 TeV

[1] Uses $\Xi_b^- \to \Xi_c^0 D_s^-$ and $\Xi_b^0 \to \Xi_c^+ D_s^-$ decays.
[2] Reconstructed in $\Xi_b^- \to \Xi_c^0 \pi^-$, $\Xi_c^0 \to p K^- K^- \pi^+$ decays. Uses $m(\Xi_b^0) - m(\Lambda_b^0) = 172.44 \pm 0.39 \pm 0.17$ MeV from AAIJ 14Z.
[3] Derived from measurements in $\Xi_b^0 \to \Xi_c^+ \pi^-$ and $\Xi_b^- \to J/\psi \Xi^-$ from AALTONEN 09AP taking correlated systematic uncertainties into account.

Ξ_b^- MEAN LIFE

"OUR EVALUATION" is an average using rescaled values of the data listed below. The average and rescaling were performed by the Heavy Flavor Averaging Group (HFLAV) and are described at https://hflav.web.cern.ch/. The averaging/rescaling procedure takes into account correlations between the measurements and asymmetric lifetime errors.

Ξ_b^- MEAN LIFE

VALUE (10^{-12} s)	DOCUMENT ID		TECN	COMMENT
1.575±0.021 OUR EVALUATION	(Produced by HFLAV)			
1.570±0.023 OUR AVERAGE				
1.578±0.018±0.015	[1,2] AAIJ	24AJ	LHCB	pp at 7, 8, 13 TeV
1.55 ${}^{+0.10}_{-0.09}$ ±0.03	[3] AAIJ	14T	LHCB	pp at 7, 8 TeV
1.32 ±0.14 ±0.02	AALTONEN	14B	CDF	$p\overline{p}$ at 1.96 TeV
• • • We do not use the following data for averages, fits, limits, etc. • • •				
1.575±0.019±0.014	[1] AAIJ	24AJ	LHCB	pp at 13 TeV
1.599±0.041±0.022	[4] AAIJ	14BJ	LHCB	pp at 7, 8 TeV
1.56 ${}^{+0.27}_{-0.25}$ ±0.02	[5] AALTONEN	09AP	CDF	Repl. by AALTONEN 14B

[1] Reconstructed in $\Xi_b^- \to \Xi_c^0 \pi^-$, $\Xi_c^0 \to p K^- K^- \pi^+$ decays. Reference Λ_b^0 lifetime 1.464 ± 0.010 ps from PDG 22.
[2] Supersedes AAIJ 14BJ and AAIJ 24AJ.
[3] Measured in $\Xi_b^- \to J/\psi \Xi^-$ decays.
[4] Reconstructed in $\Xi_b^- \to \Xi_c^0 \pi^-$, $\Xi_c^0 \to p K^- K^- \pi^+$ decays. Reference Λ_b^0 lifetime 1.479 ± 0.009 ± 0.010 ps from AAIJ 14U.
[5] Measured in $\Xi_b^- \to J/\psi \Xi^-$ decays with $66 {}^{+14}_{-9}$ candidates.

MEAN LIFE RATIOS

$\tau_{\Xi_b^-} / \tau_{\Lambda_b^0}$ mean life ratio

VALUE	DOCUMENT ID		TECN	COMMENT
1.078±0.012±0.007	[1,2] AAIJ	24AJ	LHCB	pp at 7, 8, 13 TeV
• • • We do not use the following data for averages, fits, limits, etc. • • •				
1.076±0.013±0.006	[1] AAIJ	24AJ	LHCB	pp at 13 TeV
1.089±0.026±0.011	[1] AAIJ	14BJ	LHCB	pp at 7, 8 TeV

[1] Reconstructed in $\Xi_b^- \to \Xi_c^0 \pi^-$, $\Xi_c^0 \to p K^- K^- \pi^+$ decays. Used $\Lambda_b^0 \to \Lambda_c^+ \pi^-$ for normalization.
[2] Supersedes AAIJ 14BJ and AAIJ 24AJ.

$\tau_{\Xi_b^-} / \tau_{\Xi_b^0}$ mean life ratio

VALUE	DOCUMENT ID		TECN	COMMENT
1.083±0.032±0.016	[1] AAIJ	14BJ	LHCB	pp at 7, 8 TeV

[1] Reconstructed in $\Xi_b^- \to \Xi_c^0 \pi^-$, $\Xi_c^0 \to p K^- K^- \pi^+$ decays. Uses Ξ_b^0 measurements from AAIJ 14Z.

Ξ_b^- DECAY MODES

	Mode	Fraction (Γ_i/Γ)	Confidence level
Γ_1	$J/\psi \Xi^- \times B(b \to \Xi_b^-)$	$(1.0 \pm 0.4) \times 10^{-5}$	
Γ_2	$J/\psi \Lambda K^- \times B(b \to \Xi_b^-)$	$(2.3 \pm 0.7) \times 10^{-6}$	
Γ_3	$p K^- K^- \times B(b \to \Xi_b^-)$	$(3.7 \pm 0.8) \times 10^{-8}$	
Γ_4	$p K^- K^-$	$(2.3 \pm 0.9) \times 10^{-6}$	
Γ_5	$p \pi^- \pi^-$	$< 1.3 \times 10^{-6}$	90%
Γ_6	$p K^- \pi^-$	$(2.3 \pm 1.1) \times 10^{-6}$	
Γ_7	$\Lambda_b^0 \pi^- \times B(b \to \Xi_b^-)/B(b \to \Lambda_b^0)$	$(7.0 \pm 0.9) \times 10^{-4}$	
Γ_8	$\Xi_c^0 \pi^-$	seen	
Γ_9	$\Xi_c^0 D_s^- \times B(b \to \Xi_b^-)/B(b \to \Lambda_b^0)$	$(1.9 \pm 0.5) \times 10^{-3}$	
Γ_{10}	$\Sigma(1385) K^-$	$(2.6 \pm 2.3) \times 10^{-7}$	
Γ_{11}	$\Lambda(1405) K^-$	$(1.9 \pm 1.2) \times 10^{-7}$	
Γ_{12}	$\Lambda(1520) K^-$	$(7.6 \pm 3.2) \times 10^{-7}$	
Γ_{13}	$\Lambda(1670) K^-$	$(4.5 \pm 2.3) \times 10^{-7}$	
Γ_{14}	$\Sigma(1775) K^-$	$(2.2 \pm 1.5) \times 10^{-7}$	
Γ_{15}	$\Sigma(1915) K^-$	$(2.6 \pm 2.5) \times 10^{-7}$	
Γ_{16}	$\Lambda_c^+ K^- \pi^-$		
Γ_{17}	$\Lambda_c^+ K^- K^-$		
Γ_{18}	$\Lambda_c^+ \pi^- \pi^-$		
Γ_{19}	$J/\psi \Xi^-$	seen	
Γ_{20}	$\psi(2S) \Xi^-$	seen	
Γ_{21}	$\Xi^- \gamma$	$< 1.3 \times 10^{-4}$	95%

Int. J. Mod. Phys. A 2026.41. Downloaded from www.worldscientific.com
by UNIVERSITY OF CALIFORNIA @ BERKELEY on 09/16/26. Re-use and distribution is strictly not permitted, except for Open Access articles.

Ξ_b^- BRANCHING RATIOS

$\Gamma(J/\psi\Xi^- \times B(b \to \Xi_b^-))/\Gamma_{total}$ — Γ_1/Γ

VALUE (units 10^{-4})	DOCUMENT ID		TECN	COMMENT
0.10 ±0.04 OUR AVERAGE				
$0.098^{+0.023}_{-0.016}\pm0.035$	[1] AALTONEN	09AP	CDF	$p\overline{p}$ at 1.96 TeV
0.16 ±0.07 ±0.06	[2] ABAZOV	07K	D0	$p\overline{p}$ at 1.96 TeV

[1] AALTONEN 09AP reports $[\Gamma(\Xi_b^- \to J/\psi\Xi^- \times B(b \to \Xi_b^-))/\Gamma_{total}]$ / $[B(\Lambda_b^0 \to J/\psi(1S)\Lambda)]$ / $[B(\overline{b} \to b\text{-baryon at } p\overline{p})] = 0.167^{+0.037}_{-0.025} \pm 0.012$ which we multiply by our best (shown rounded) values $B(\Lambda_b^0 \to J/\psi(1S)\Lambda) = (3.0 \pm 0.8) \times 10^{-4}$, $B(\overline{b} \to b\text{-baryon at } p\overline{p}) = (19.8 \pm 4.6) \times 10^{-2}$. Our first error is their experiment's error and our second error is the systematic error from using our best (shown rounded) values.

[2] ABAZOV 07K reports $[\Gamma(\Xi_b^- \to J/\psi\Xi^- \times B(b \to \Xi_b^-))/\Gamma_{total}]$ / $[B(\Lambda_b^0 \to J/\psi(1S)\Lambda)]$ / $[B(\overline{b} \to b\text{-baryon at } p\overline{p})] = 0.28 \pm 0.09^{+0.09}_{-0.08}$ which we multiply by our best (shown rounded) values $B(\Lambda_b^0 \to J/\psi(1S)\Lambda) = (3.0 \pm 0.8) \times 10^{-4}$, $B(\overline{b} \to b\text{-baryon at } p\overline{p}) = (19.8 \pm 4.6) \times 10^{-2}$. Our first error is their experiment's error and our second error is the systematic error from using our best (shown rounded) values.

$\Gamma(J/\psi\Lambda K^- \times B(b \to \Xi_b^-))/\Gamma_{total}$ — Γ_2/Γ

VALUE (units 10^{-6})	DOCUMENT ID		TECN	COMMENT
2.3±0.2±0.6	[1,2] AAIJ	17BE	LHCB	pp at 7 and 8 TeV

[1] AAIJ 17BE reports $[\Gamma(\Xi_b^- \to J/\psi\Lambda K^- \times B(b \to \Xi_b^-))/\Gamma_{total}]$ / $[B(\Lambda_b^0 \to J/\psi(1S)\Lambda)]$ / $[B(\overline{b} \to b\text{-baryon at } pp)] = (4.19 \pm 0.29 \pm 0.15) \times 10^{-2}$ which we multiply by our best (shown rounded) values $B(\Lambda_b^0 \to J/\psi(1S)\Lambda) = (3.0 \pm 0.8) \times 10^{-4}$, $B(\overline{b} \to b\text{-baryon at } pp) = (18.7 \pm 1.1) \times 10^{-2}$. Our first error is their experiment's error and our second error is the systematic error from using our best (shown rounded) values.

[2] Integrated over the b-baryon transverse momentum $p_T < 25$ GeV and rapidity $2.0 < y < 4.5$.

$\Gamma(pK^-K^- \times B(b \to \Xi_b^-))/\Gamma_{total}$ — Γ_3/Γ

VALUE (units 10^{-8})	DOCUMENT ID		TECN	COMMENT
3.7±0.8±0.2	[1] AAIJ	17F	LHCB	pp at 7, 8 TeV

[1] AAIJ 17F reports $[\Gamma(\Xi_b \to pK^-K^- \times B(\overline{b} \to \Xi_b))/\Gamma_{total}]$ / $[B(B^+ \to K^+K^-K^+)]$ / $[B(\overline{b} \to B^+ \text{ at } Z)] = (2.65 \pm 0.35 \pm 0.47) \times 10^{-3}$ which we multiply by our best (shown rounded) values $B(B^+ \to K^+K^-K^+) = (3.40 \pm 0.14) \times 10^{-5}$, $B(\overline{b} \to B^+ \text{ at } Z) = (40.8 \pm 0.7) \times 10^{-2}$. Our first error is their experiment's error and our second error is the systematic error from using our best (shown rounded) values.

$\Gamma(pK^-K^-)/\Gamma_{total}$ — Γ_4/Γ

VALUE (units 10^{-6})	DOCUMENT ID		TECN	COMMENT
2.3±0.9	[1,2] AAIJ	21AH	LHCB	pp at 7, 8, 13 TeV

[1] Obtained using the ratio of fragmentation and branching fractions relative to the $B^- \to K^+K^-K^-$ decay.

[2] The ratio of $f_{\Xi_b^-}/f_{\Lambda_b^0}$ was used as input obtained from AAIJ 19AB.

$\Gamma(p\pi^-\pi^-)/\Gamma(pK^-K^-)$ — Γ_5/Γ_4

VALUE	CL%	DOCUMENT ID		TECN	COMMENT
<0.56	90	[1] AAIJ	17F	LHCB	pp at 7, 8 TeV

[1] Measures the ratio as 0.28 ± 0.16 ± 0.13.

$\Gamma(pK^-\pi^-)/\Gamma(pK^-K^-)$ — Γ_6/Γ_4

VALUE	DOCUMENT ID		TECN	COMMENT
0.98±0.27±0.09	AAIJ	17F	LHCB	pp at 7, 8 TeV

$\Gamma(\Lambda_b^0\pi^- \times B(b \to \Xi_b^-)/B(b \to \Lambda_b^0))/\Gamma_{total}$ — Γ_7/Γ

VALUE (units 10^{-4})	DOCUMENT ID		TECN	COMMENT
7.0±0.9 OUR AVERAGE				
7.3±0.8±0.6	[1] AAIJ	23AV	LHCB	pp at 13 TeV
$5.7\pm1.8^{+0.8}_{-0.9}$	[2] AAIJ	15BA	LHCB	pp at 7, 8 TeV

[1] Measured in the decay chain of $\Xi_b^- \to \Lambda_b^0\pi^-$, $\Lambda_b^0 \to \Lambda_c^+\pi^-$ and $\Lambda_b^0 \to \Lambda_c^+\pi^-\pi^+\pi^-$, with $\Lambda_c^+ \to pK^-\pi^+$.

[2] A signal is reported with a significance of 3.2 standard deviations in the decay chain of $\Xi_b^- \to \Lambda_b^0\pi^-$, $\Lambda_b^0 \to \Lambda_c^+\pi^-$, and $\Lambda_c^+ \to pK^-\pi^+$.

$\Gamma(\Xi_c^0\pi^-)/\Gamma_{total}$ — Γ_8/Γ

VALUE	DOCUMENT ID		TECN	COMMENT
seen	AAIJ	16O	LHCB	pp at 7, 8 TeV

$\Gamma(\Xi_c^0 D_s^- \times B(b \to \Xi_b^-)/B(b \to \Lambda_b^0))/\Gamma_{total}$ — Γ_9/Γ

VALUE (units 10^{-3})	DOCUMENT ID		TECN	COMMENT
1.9±0.5±0.2	[1] AAIJ	24V	LHCB	pp at 13 TeV

[1] AAIJ 24V reports $[\Gamma(\Xi_b^- \to \Xi_c^0 D_s^- \times B(b \to \Xi_b^-)/B(b \to \Lambda_b^0))/\Gamma_{total}]$ / $[B(\Lambda_b^0 \to \Lambda_c^+ D_s^-)] = (16.9 \pm 1.3 \pm 4.4) \times 10^{-2}$ which we multiply by our best (shown rounded) value $B(\Lambda_b^0 \to \Lambda_c^+ D_s^-) = (1.10 \pm 0.10) \times 10^{-2}$. Our first error is their experiment's error and our second error is the systematic error from using our best (shown rounded) value.

$\Gamma(\Sigma(1385)K^-)/\Gamma_{total}$ — Γ_{10}/Γ

VALUE (units 10^{-6})	DOCUMENT ID		TECN	COMMENT
0.26±0.11±0.20	[1,2] AAIJ	21AH	LHCB	pp at 7, 8 and 13 TeV

[1] Obtained from an amplitude analysis of quasi-two-body contributions to the $\Xi_b^- \to RK^-$ decay, with $R \to pK^-$.

[2] The ratio of $f_{\Xi_b^-}/f_{\Lambda_b^0}$ was used as input obtained from AAIJ 19AB.

$\Gamma(\Lambda(1405)K^-)/\Gamma_{total}$ — Γ_{11}/Γ

VALUE (units 10^{-6})	DOCUMENT ID		TECN	COMMENT
0.19±0.06±0.10	[1,2] AAIJ	21AH	LHCB	pp at 7, 8 and 13 TeV

[1] Obtained from an amplitude analysis of quasi-two-body contributions to the $\Xi_b^- \to RK^-$ decay, with $R \to pK^-$.

[2] The ratio of $f_{\Xi_b^-}/f_{\Lambda_b^0}$ was used as input obtained from AAIJ 19AB.

$\Gamma(\Lambda(1520)K^-)/\Gamma_{total}$ — Γ_{12}/Γ

VALUE (units 10^{-6})	DOCUMENT ID		TECN	COMMENT
0.76±0.09±0.31	[1,2] AAIJ	21AH	LHCB	pp at 7, 8 and 13 TeV

[1] Obtained from an amplitude analysis of quasi-two-body contributions to the $\Xi_b^- \to RK^-$ decay, with $R \to pK^-$.

[2] The ratio of $f_{\Xi_b^-}/f_{\Lambda_b^0}$ was used as input obtained from AAIJ 19AB.

$\Gamma(\Lambda(1670)K^-)/\Gamma_{total}$ — Γ_{13}/Γ

VALUE (units 10^{-6})	DOCUMENT ID		TECN	COMMENT
0.45±0.07±0.22	[1,2] AAIJ	21AH	LHCB	pp at 7, 8 and 13 TeV

[1] Obtained from an amplitude analysis of quasi-two-body contributions to the $\Xi_b^- \to RK^-$ decay, with $R \to pK^-$.

[2] The ratio of $f_{\Xi_b^-}/f_{\Lambda_b^0}$ was used as input obtained from AAIJ 19AB.

$\Gamma(\Sigma(1775)K^-)/\Gamma_{total}$ — Γ_{14}/Γ

VALUE (units 10^{-6})	DOCUMENT ID		TECN	COMMENT
0.22±0.08±0.13	[1,2] AAIJ	21AH	LHCB	pp at 7, 8 and 13 TeV

[1] Obtained from an amplitude analysis of quasi-two-body contributions to the $\Xi_b^- \to RK^-$ decay, with $R \to pK^-$.

[2] The ratio of $f_{\Xi_b^-}/f_{\Lambda_b^0}$ was used as input obtained from AAIJ 19AB.

$\Gamma(\Sigma(1915)K^-)/\Gamma_{total}$ — Γ_{15}/Γ

VALUE (units 10^{-6})	DOCUMENT ID		TECN	COMMENT
0.26±0.09±0.23	[1,2] AAIJ	21AH	LHCB	pp at 7, 8 and 13 TeV

[1] Obtained from an amplitude analysis of quasi-two-body contributions to the $\Xi_b^- \to RK^-$ decay, with $R \to pK^-$.

[2] The ratio of $f_{\Xi_b^-}/f_{\Lambda_b^0}$ was used as input obtained from AAIJ 19AB.

$\Gamma(\Lambda_c^+K^-K^-)/\Gamma(\Lambda_c^+K^-\pi^-)$ — Γ_{17}/Γ_{16}

VALUE (units 10^{-2})	DOCUMENT ID		TECN	COMMENT
4.5±1.1±0.5	AAIJ	24T	LHCB	pp at 7, 8, 13 TeV

$\Gamma(\Lambda_c^+\pi^-\pi^-)/\Gamma(\Lambda_c^+K^-\pi^-)$ — Γ_{18}/Γ_{16}

VALUE	DOCUMENT ID		TECN	COMMENT
$<6.5 \times 10^{-2}$	AAIJ	24T	LHCB	pp at 7, 8, 13 TeV

$\Gamma(\psi(2S)\Xi^-)/\Gamma(J/\psi\Xi^-)$ — Γ_{20}/Γ_{19}

VALUE	DOCUMENT ID		TECN	COMMENT
$0.84^{+0.21}_{-0.19}\pm0.10\pm0.02$	[1] HAYRAPETY...24R		CMS	pp at 13 TeV

[1] HAYRAPETYAN 24R value last uncertainty comes from the uncertainties in the branching fractions of the charmonium states.

$\Gamma(\Xi^-\gamma)/\Gamma_{total}$ — Γ_{21}/Γ

VALUE	CL%	DOCUMENT ID		TECN	COMMENT
$<1.3 \times 10^{-4}$	95	[1] AAIJ	22F	LHCB	pp at 13 TeV

[1] Used $\Xi_b^- \to \Xi^- J/\psi$ as normalization and an integrated luminosity of 5.4 fb^{-1}.

P VIOLATION ASYMMETRY

$A_P(\Xi_b)$, $\Xi_b^- - \Xi_b^+$ production asymmetry

$A_P(\Xi_b) = [\sigma(\Xi_b^-) - \sigma(\Xi_b^+)]/[\sigma(\Xi_b^-) + \sigma(\Xi_b^+)]$

VALUE (units 10^{-2})	DOCUMENT ID		TECN	COMMENT
−2 ±4 OUR AVERAGE				
1.1±5.6±1.9	[1,2] AAIJ	19AB	LHCB	pp at 7 and 8 TeV
−3.9±4.9±2.5	[1,2] AAIJ	19AB	LHCB	pp at 13 TeV

[1] Baryon kinematic range $p_T < 20$ GeV/c and $2 < \eta < 6$.

[2] Measured using previous measurements of $A_P(\Lambda_b)$ in AAIJ 17BF.

Int. J. Mod. Phys. A 2026.41. Downloaded from www.worldscientific.com
UNIVERSITY OF CALIFORNIA @ BERKELEY on 09/16/26. Re-use and distribution is strictly not permitted, except for Open Access articles.

CP VIOLATION in Ξ_b deays

$A_{CP}(\Xi_b) = [B(\Xi_b^- \to f) - B(\Xi_b^+ \to \overline{f})]/\text{Sum}$

$A_{CP}(\Xi_b^- \to \Sigma(1385) K^-)$

VALUE (units 10^{-2})	DOCUMENT ID		TECN	COMMENT
−27±34±73	AAIJ	21AH	LHCB	pp at 7, 8, 13 TeV

$A_{CP}(\Xi_b^- \to \Lambda(1405) K^-)$

VALUE (units 10^{-2})	DOCUMENT ID		TECN	COMMENT
−1±24±32	AAIJ	21AH	LHCB	pp at 7, 8, 13 TeV

$A_{CP}(\Xi_b^- \to \Lambda(1520) K^-)$

VALUE (units 10^{-2})	DOCUMENT ID		TECN	COMMENT
−5±9±8	AAIJ	21AH	LHCB	pp at 7, 8, 13 TeV

$A_{CP}(\Xi_b^- \to \Lambda(1670) K^-)$

VALUE (units 10^{-2})	DOCUMENT ID		TECN	COMMENT
3±14±10	AAIJ	21AH	LHCB	pp at 7, 8, 13 TeV

$A_{CP}(\Xi_b^- \to \Sigma(1775) K^-)$

VALUE (units 10^{-2})	DOCUMENT ID		TECN	COMMENT
−47±26±14	AAIJ	21AH	LHCB	pp at 7, 8, 13 TeV

$A_{CP}(\Xi_b^- \to \Sigma(1915) K^-)$

VALUE (units 10^{-2})	DOCUMENT ID		TECN	COMMENT
11±26±22	AAIJ	21AH	LHCB	pp at 7, 8, 13 TeV

Ξ_b^- REFERENCES

AAIJ	24AJ	PR D110 072002	R. Aaij et al.	(LHCb Collab.)
AAIJ	24T	JHEP 2408 132	R. Aaij	(LHCb Collab.)
AAIJ	24V	EPJ C84 237	R. Aaij et al.	(LHCb Collab.)
HAYRAPETY...	24R	PR D110 012002	A. Hayrapetyan et al.	(CMS Collab.)
AAIJ	23AV	PR D108 072002	R. Aaij et al.	(LHCb Collab.)
AAIJ	22F	JHEP 2201 069	R. Aaij et al.	(LHCb Collab.)
PDG	22	PTEP 2022 083C01	R.L. Workman et al.	(PDG Collab.)
AAIJ	21	PR D103 012004	R. Aaij et al.	(LHCb Collab.)
AAIJ	21AH	PR D104 052010	R. Aaij et al.	(LHCb Collab.)
AAIJ	19AB	PR D99 052006	R. Aaij et al.	(LHCb Collab.)
AAIJ	17BE	PL B772 265	R. Aaij et al.	(LHCb Collab.)
AAIJ	17BF	PL B774 139	R. Aaij et al.	(LHCb Collab.)
AAIJ	17F	PRL 118 071801	R. Aaij et al.	(LHCb Collab.)
AAIJ	16O	PR D93 092007	R. Aaij et al.	(LHCb Collab.)
AAIJ	15BA	PRL 115 241801	R. Aaij et al.	(LHCb Collab.)
AAIJ	14AA	PRL 112 202001	R. Aaij et al.	(LHCb Collab.)
AAIJ	14BJ	PRL 113 242002	R. Aaij et al.	(LHCb Collab.)
AAIJ	14T	PL B736 154	R. Aaij et al.	(LHCb Collab.)
AAIJ	14U	PL B734 122	R. Aaij et al.	(LHCb Collab.)
AAIJ	14Z	PRL 113 032001	R. Aaij et al.	(LHCb Collab.)
AALTONEN	14B	PR D89 072014	T. Aaltonen et al.	(CDF Collab.)
AAIJ	13AV	PRL 110 182001	R. Aaij et al.	(LHCb Collab.)
AALTONEN	11X	PRL 107 102001	T. Aaltonen et al.	(CDF Collab.)
AALTONEN	09AP	PR D80 072003	T. Aaltonen et al.	(CDF Collab.)
AALTONEN	07A	PRL 99 052002	T. Aaltonen et al.	(CDF Collab.)
ABAZOV	07K	PRL 99 052001	V.M. Abazov et al.	(D0 Collab.)

Ξ_b^0

$I(J^P) = \frac{1}{2}(\frac{1}{2}^+)$ Status: ***
I, J, P need confirmation.

In the quark model, Ξ_b^0 and Ξ_b^- are an isodoublet (usb, dsb) state; the lowest Ξ_b^0 and Ξ_b^- ought to have $J^P = 1/2^+$. None of I, J, or P have actually been measured.

Ξ_b^0 MASS

Ξ_b^0 MASS

VALUE (MeV)	DOCUMENT ID		TECN	COMMENT
5791.7 ±0.4 OUR AVERAGE				
5791.12±0.60±0.51	[1] AAIJ	24V	LHCB	pp at 13 TeV
5794.3 ±2.4 ±0.7	AAIJ	14H	LHCB	pp at 7 TeV
5791.80±0.39±0.31	[2] AAIJ	14Z	LHCB	pp at 7, 8 TeV
5788.7 ±4.3 ±1.4	[3] AALTONEN	14B	CDF	$p\overline{p}$ at 1.96 TeV
• • • We do not use the following data for averages, fits, limits, etc. • • •				
5787.8 ±5.0 ±1.3	[4] AALTONEN	11X	CDF	Repl. by AALTONEN 14B

[1] Uses $\Xi_b^0 \to \Xi_c^+ D_s^-$ decays.
[2] Uses $\Xi_b^0 \to \Xi_c^+ \pi^-$ and $\Xi_c^+ \to pK^-\pi^+$ decays. The measurement comes from the mass difference of Ξ_b^0 and Λ_b^0.
[3] Uses $\Xi_b^0 \to \Xi_c^+ \pi^-$ decays.
[4] Measured in $\Xi_b^0 \to \Xi_c^+ \pi^-$ with $25.3^{+5.6}_{-5.4}$ candidates.

$m_{\Xi_b^0} - m_{\Lambda_b^0}$

VALUE (MeV)	DOCUMENT ID		TECN	COMMENT
172.3 ±0.4 OUR AVERAGE				
171.78±0.60±0.33	[1] AAIJ	24V	LHCB	pp at 13 TeV
174.8 ±2.4 ±0.5	AAIJ	14H	LHCB	pp at 7 TeV
172.44±0.39±0.17	[2] AAIJ	14Z	LHCB	pp at 7, 8 TeV

[1] Uses $\Xi_b^0 \to \Xi_c^+ D_s^-$ and $\Lambda_b^0 \to \Lambda_c^+ D_s^-$ decays.
[2] Uses $\Xi_b^0 \to \Xi_c^+ \pi^-$ and $\Xi_c^+ \to pK^-\pi^+$ decays.

Ξ_b^0 MEAN LIFE

"OUR EVALUATION" is an average using rescaled values of the data listed below. The average and rescaling were performed by the Heavy Flavor Averaging Group (HFLAV) and are described at https://hflav.web.cern.ch/. The averaging/rescaling procedure takes into account correlations between the measurements and asymmetric lifetime errors.

Ξ_b^0 MEAN LIFE

VALUE (10^{-12} s)	DOCUMENT ID		TECN	COMMENT
1.472±0.016 OUR EVALUATION	(Produced by HFLAV)			
1.475±0.012±0.012	[1] AAIJ	25AJ	LHCB	pp at 7, 8, 13 TeV
• • • We do not use the following data for averages, fits, limits, etc. • • •				
1.473±0.014±0.013	[1] AAIJ	25AJ	LHCB	pp at 13 TeV
1.477±0.026±0.019	[1] AAIJ	14Z	LHCB	pp at 7, 8 TeV

[1] Uses $\Xi_b^0 \to \Xi_c^+ \pi^-$, $\Xi_c^+ \to pK^-\pi^+$ decays. The measurement comes from the value of relative lifetimes of Ξ_b^0 to Λ_b^0.

τ_{mix} (1/2π) times the $\Xi_b^0 - \overline{\Xi}_b^0$ oscillation period

VALUE (s)	DOCUMENT ID		TECN	COMMENT
$>13 \times 10^{-12}$	[1] AAIJ	17BH	LHCB	pp at 7, 8 TeV

[1] Uses Ξ_b^{*-} and $\Xi_b^{\prime -}$ decays to $\Xi_b^0 \pi^-$, where $\Xi_b^0 \to \Xi_c^+ \pi^-$, $\Xi_c^+ \to pK^-\pi^+$.

Ξ_b^0 DECAY MODES

	Mode	Fraction (Γ_i/Γ)	Confidence level
Γ_1	$pD^0K^- \times B(b \to \Xi_b^0)$	$(1.7 \pm 0.6) \times 10^{-6}$	
Γ_2	$p\overline{K}^0\pi^- \times B(b \to \Xi_b^0)/B(\overline{b} \to B^0)$	$< 1.6 \times 10^{-6}$	90%
Γ_3	$p\overline{K}^0\pi^-$	$< 5.6 \times 10^{-6}$	90%
Γ_4	$pK^0K^- \times B(b \to \Xi_b^0)/B(\overline{b} \to B^0)$	$< 1.1 \times 10^{-6}$	90%
Γ_5	$p\overline{K}^0K^-$	$(7.8 \pm 3.3) \times 10^{-6}$	
Γ_6	$\Lambda\pi^+\pi^- \times B(b \to \Xi_b^0)/B(b \to \Lambda_b^0)$	$< 1.7 \times 10^{-6}$	90%
Γ_7	$\Lambda K^-\pi^+ \times B(b \to \Xi_b^0)/B(b \to \Lambda_b^0)$	$< 8 \times 10^{-7}$	90%
Γ_8	$\Lambda K^+K^- \times B(b \to \Xi_b^0)/B(b \to \Lambda_b^0)$	$< 3 \times 10^{-7}$	90%
Γ_9	$\Lambda\pi^+\pi^-$	$(1.3 \pm 0.6) \times 10^{-5}$	
Γ_{10}	$\Lambda K^-\pi^+$	$(1.3 \pm 0.5) \times 10^{-5}$	
Γ_{11}	ΛK^+K^-	$< 3.4 \times 10^{-6}$	95%
Γ_{12}	$J/\psi\Lambda$	seen	
Γ_{13}	$J/\psi\Xi^0$	seen	
Γ_{14}	$J/\psi\Xi^-\pi^+ \times B(b \to \Xi_b^0)$	$(1.2 \pm 0.5) \times 10^{-6}$	
Γ_{15}	$\Xi_c^+ D_s^- \times B(b \to \Xi_b^0)/B(b \to \Lambda_b^0)$	$(1.7 \pm 0.9) \times 10^{-3}$	
Γ_{16}	$\Lambda_c^+ K^- \times B(b \to \Xi_b^0)$	$(6 \pm 4) \times 10^{-7}$	
Γ_{17}	$pK^-\pi^+\pi^- \times B(b \to \Xi_b^0)/B(b \to \Lambda_b^0)$	$(1.9 \pm 0.4) \times 10^{-6}$	
Γ_{18}	$pK^-K^-\pi^+ \times B(b \to \Xi_b^0)/B(b \to \Lambda_b^0)$	$(1.74 \pm 0.31) \times 10^{-6}$	
Γ_{19}	$pK^-K^+K^- \times B(b \to \Xi_b^0)/B(b \to \Lambda_b^0)$	$(1.8 \pm 1.0) \times 10^{-7}$	

Ξ_b^0 BRANCHING RATIOS

$\Gamma(pD^0K^- \times B(b \to \Xi_b^0))/\Gamma_{total}$ — Γ_1/Γ

VALUE (units 10^{-6})	DOCUMENT ID		TECN	COMMENT
1.7±0.4±0.4	[1] AAIJ	14H	LHCB	pp at 7 TeV

[1] AAIJ 14H reports $[\Gamma(\Xi_b \to pD^0K^- \times B(\overline{b} \to \Xi_b))/\Gamma_{total}] / [B(\overline{b} \to b\text{-baryon at } Z)] / [B(\Lambda_b^0 \to pD^0K^-)] = 0.44 \pm 0.09 \pm 0.06$ which we multiply by our best (shown rounded) values $B(\overline{b} \to b\text{-baryon at } Z) = (8.4 \pm 1.1) \times 10^{-2}$, $B(\Lambda_b^0 \to pD^0K^-) = (4.6 \pm 0.8) \times 10^{-5}$. Our first error is their experiment's error and our second error is the systematic error from using our best (shown rounded) values.

$\Gamma(p\overline{K}^0\pi^- \times B(b \to \Xi_b^0)/B(\overline{b} \to B^0))/\Gamma_{total}$ — Γ_2/Γ

VALUE	CL%	DOCUMENT ID		TECN	COMMENT
$<1.6 \times 10^{-6}$	90	AAIJ	14Q	LHCB	pp at 7 TeV

$\Gamma(p\overline{K}^0\pi^-)/\Gamma_{total}$ — Γ_3/Γ

VALUE	CL%	DOCUMENT ID		TECN	COMMENT
$<5.6 \times 10^{-6}$	90	[1] AAIJ	25AP	LHCB	pp at 7, 8, 13 TeV

[1] Measured relative to $\Lambda_b^0 \to \Lambda_c^+ \pi^-$, $\Lambda_c^+ \to p K_S^0$. The last error includes systematic, the uncertainties on $B(\Lambda_b^0 \to \Lambda_c^+ \pi^-$, $\Lambda_c^+ \to p K_S^0)$, and the ratio of $f_{\Xi_b^0}/f_{\Lambda_b^0}$ obtained from AAIJ 19AB by assuming SU(3) flavor symmetry.

$\Gamma(p K^0 K^- \times B(b \to \Xi_b^0)/B(\overline{b} \to B^0))/\Gamma_{total}$ — Γ_4/Γ

VALUE	CL%	DOCUMENT ID		TECN	COMMENT
$<1.1 \times 10^{-6}$	90	AAIJ	14Q	LHCB	pp at 7 TeV

$\Gamma(p \overline{K}^0 K^-)/\Gamma_{total}$ — Γ_5/Γ

VALUE (units 10^{-6})	DOCUMENT ID		TECN	COMMENT
$7.8 \pm 1.2 \pm 3.1$	[1] AAIJ	25AP	LHCB	pp at 7, 8, 13 TeV

[1] Measured relative to $\Lambda_b^0 \to \Lambda_c^+ K^-$, $\Lambda_c^+ \to p K_S^0$. The last error includes systematic, the uncertainties on $B(\Lambda_b^0 \to \Lambda_c^+ K^-$, $\Lambda_c^+ \to p K_S^0)$, and the ratio of $f_{\Xi_b^0}/f_{\Lambda_b^0}$ obtained from AAIJ 19AB by assuming SU(3) flavor symmetry.

$\Gamma(\Lambda \pi^+ \pi^- \times B(b \to \Xi_b^0)/B(b \to \Lambda_b^0))/\Gamma_{total}$ — Γ_6/Γ

VALUE	CL%	DOCUMENT ID		TECN	COMMENT
$<1.7 \times 10^{-6}$	90	AAIJ	16W	LHCB	pp at 7, 8 TeV

$\Gamma(\Lambda K^- \pi^+ \times B(b \to \Xi_b^0)/B(b \to \Lambda_b^0))/\Gamma_{total}$ — Γ_7/Γ

VALUE	CL%	DOCUMENT ID		TECN	COMMENT
$<0.8 \times 10^{-6}$	90	AAIJ	16W	LHCB	pp at 7, 8 TeV

$\Gamma(\Lambda K^+ K^- \times B(b \to \Xi_b^0)/B(b \to \Lambda_b^0))/\Gamma_{total}$ — Γ_8/Γ

VALUE	CL%	DOCUMENT ID		TECN	COMMENT
$<0.3 \times 10^{-6}$	90	AAIJ	16W	LHCB	pp at 7, 8 TeV

$\Gamma(\Lambda \pi^+ \pi^-)/\Gamma_{total}$ — Γ_9/Γ

VALUE (units 10^{-6})	DOCUMENT ID		TECN	COMMENT
$13 \pm 6 \pm 1$	[1] AAIJ	25J	LHCB	pp at 7, 8, 13 TeV

[1] AAIJ 25J reports $(11.0 \pm 2.6 \pm 4.1) \times 10^{-6}$ from a measurement of $[\Gamma(\Xi_b^0 \to \Lambda \pi^+ \pi^-)/\Gamma_{total}]$ / $[B(\Lambda_b^0 \to \Lambda_c^+ \pi^-)]$ / $[B(\Lambda_c^+ \to \Lambda \pi^+)]$ assuming $B(\Lambda_b^0 \to \Lambda_c^+ \pi^-) = (4.30 \pm 0.36) \times 10^{-3}$, $B(\Lambda_c^+ \to \Lambda \pi^+) = (1.24 \pm 0.08) \times 10^{-2}$, which we rescale to our best (shown rounded) values $B(\Lambda_b^0 \to \Lambda_c^+ \pi^-) = (4.9 \pm 0.4) \times 10^{-3}$, $B(\Lambda_c^+ \to \Lambda \pi^+) = (1.32 \pm 0.05) \times 10^{-2}$. Our first error is their experiment's error and our second error is the systematic error from using our best (shown rounded) values.

$\Gamma(\Lambda K^- \pi^+)/\Gamma_{total}$ — Γ_{10}/Γ

VALUE (units 10^{-6})	DOCUMENT ID		TECN	COMMENT
$13 \pm 5 \pm 1$	[1] AAIJ	25J	LHCB	pp at 7, 8, 13 TeV

[1] AAIJ 25J reports $(10.4 \pm 1.4 \pm 3.7) \times 10^{-6}$ from a measurement of $[\Gamma(\Xi_b^0 \to \Lambda K^- \pi^+)/\Gamma_{total}]$ / $[B(\Lambda_b^0 \to \Lambda_c^+ \pi^-)]$ / $[B(\Lambda_c^+ \to \Lambda \pi^+)]$ assuming $B(\Lambda_b^0 \to \Lambda_c^+ \pi^-) = (4.30 \pm 0.36) \times 10^{-3}$, $B(\Lambda_c^+ \to \Lambda \pi^+) = (1.24 \pm 0.08) \times 10^{-2}$, which we rescale to our best (shown rounded) values $B(\Lambda_b^0 \to \Lambda_c^+ \pi^-) = (4.9 \pm 0.4) \times 10^{-3}$, $B(\Lambda_c^+ \to \Lambda \pi^+) = (1.32 \pm 0.05) \times 10^{-2}$. Our first error is their experiment's error and our second error is the systematic error from using our best (shown rounded) values.

$\Gamma(\Lambda K^+ K^-)/\Gamma_{total}$ — Γ_{11}/Γ

VALUE	CL%	DOCUMENT ID		TECN	COMMENT
$<3.4 \times 10^{-6}$	95	[1] AAIJ	25J	LHCB	pp at 7, 8, 13 TeV

[1] AAIJ 25J reports $< 2.8 \times 10^{-6}$ from a measurement of $[\Gamma(\Xi_b^0 \to \Lambda K^+ K^-)/\Gamma_{total}]$ / $[B(\Lambda_b^0 \to \Lambda_c^+ \pi^-)]$ / $[B(\Lambda_c^+ \to \Lambda \pi^+)]$ assuming $B(\Lambda_b^0 \to \Lambda_c^+ \pi^-) = (4.30 \pm 0.36) \times 10^{-3}$, $B(\Lambda_c^+ \to \Lambda \pi^+) = (1.24 \pm 0.08) \times 10^{-2}$, which we rescale to our best (shown rounded) values $B(\Lambda_b^0 \to \Lambda_c^+ \pi^-) = 4.9 \times 10^{-3}$, $B(\Lambda_c^+ \to \Lambda \pi^+) = 1.32 \times 10^{-2}$.

$\Gamma(J/\psi \Lambda)/\Gamma(J/\psi \Xi^0)$ — Γ_{12}/Γ_{13}

VALUE (units 10^{-3})	DOCUMENT ID		TECN	COMMENT
$8.2 \pm 2.1 \pm 0.9$	[1] AAIJ	20U	LHCB	pp at 7, 8 and 13 TeV

[1] The Cabibbo suppressed $\Xi_b \to J/\psi \Lambda$ decay is observed for the first time.

$\Gamma(J/\psi \Xi^- \pi^+ \times B(b \to \Xi_b^0))/\Gamma_{total}$ — Γ_{14}/Γ

VALUE (units 10^{-5})	DOCUMENT ID		TECN	COMMENT
$0.12 \pm 0.02 \pm 0.05$	[1] AAIJ	25AA	LHCB	pp at 13 TeV

[1] AAIJ 25AA reports $[\Gamma(\Xi_b^0 \to J/\psi \Xi^- \pi^+ \times B(b \to \Xi_b^0))/\Gamma_{total}]$ / $[B(\Xi_b^- \to J/\psi \Xi^- \times B(b \to \Xi_b^-))] = (11.9 \pm 1.4 \pm 0.6) \times 10^{-2}$ which we multiply by our best (shown rounded) value $B(\Xi_b^- \to J/\psi \Xi^- \times B(b \to \Xi_b^-)) = (1.0 \pm 0.4) \times 10^{-5}$. Our first error is their experiment's error and our second error is the systematic error from using our best (shown rounded) value.

$\Gamma(\Xi_c^+ D_s^- \times B(b \to \Xi_b^0)/B(b \to \Lambda_b^0))/\Gamma_{total}$ — Γ_{15}/Γ

VALUE (units 10^{-3})	DOCUMENT ID		TECN	COMMENT
$1.7 \pm 0.9 \pm 0.2$	[1] AAIJ	24V	LHCB	pp at 13 TeV

[1] AAIJ 24V reports $[\Gamma(\Xi_b^0 \to \Xi_c^+ D_s^- \times B(b \to \Xi_b^0)/B(b \to \Lambda_b^0))/\Gamma_{total}]$ / $[B(\Lambda_b^0 \to \Lambda_c^+ D_s^-)] = (15.8 \pm 1.1 \pm 7.7) \times 10^{-2}$ which we multiply by our best (shown rounded) value $B(\Lambda_b^0 \to \Lambda_c^+ D_s^-) = (1.10 \pm 0.10) \times 10^{-2}$. Our first error is their experiment's error and our second error is the systematic error from using our best (shown rounded) value.

$\Gamma(\Lambda_c^+ K^- \times B(b \to \Xi_b^0))/\Gamma(p D^0 K^- \times B(b \to \Xi_b^0))$ — Γ_{16}/Γ_1

VALUE	DOCUMENT ID		TECN	COMMENT
$0.35 \pm 0.19 \pm 0.01$	[1] AAIJ	14H	LHCB	pp at 7 TeV

[1] AAIJ 14H reports $[\Gamma(\Xi_b \to \Lambda_c^+ K^- \times B(\overline{b} \to \Xi_b))/\Gamma(\Xi_b \to p D^0 K^- \times B(\overline{b} \to \Xi_b))] \times [B(\Lambda_c^+ \to p K^- \pi^+)]$ / $[B(D^0 \to K^- \pi^+)] = 0.57 \pm 0.22 \pm 0.21$ which we multiply or divide by our best (shown rounded) values $B(\Lambda_c^+ \to p K^- \pi^+) = (6.37 \pm 0.21) \times 10^{-2}$, $B(D^0 \to K^- \pi^+) = (3.936 \pm 0.030) \times 10^{-2}$. Our first error is their experiment's error and our second error is the systematic error from using our best (shown rounded) values.

$\Gamma(p K^- \pi^+ \pi^- \times B(b \to \Xi_b^0)/B(b \to \Lambda_b^0))/\Gamma_{total}$ — Γ_{17}/Γ

VALUE (units 10^{-6})	DOCUMENT ID		TECN	COMMENT
$1.9 \pm 0.4 \pm 0.2$	[1] AAIJ	18Q	LHCB	pp at 7, 8 TeV

[1] AAIJ 18Q reports $[\Gamma(\Xi_b \to p K^- \pi^+ \pi^- \times B(b \to \Xi_b^0)/B(b \to \Lambda_b^0))/\Gamma_{total}]$ / $[B(\Lambda_c^+ \to p K^- \pi^+)]$ / $[B(\Lambda_b^0 \to \Lambda_c^+ \pi^-)] = (6.2 \pm 0.8 \pm 0.2 \pm 0.8) \times 10^{-3}$ which we multiply by our best (shown rounded) values $B(\Lambda_c^+ \to p K^- \pi^+) = (6.37 \pm 0.21) \times 10^{-2}$, $B(\Lambda_b^0 \to \Lambda_c^+ \pi^-) = (4.9 \pm 0.4) \times 10^{-3}$. Our first error is their experiment's error and our second error is the systematic error from using our best (shown rounded) values.

$\Gamma(p K^- K^- \pi^+ \times B(b \to \Xi_b^0)/B(b \to \Lambda_b^0))/\Gamma_{total}$ — Γ_{18}/Γ

VALUE (units 10^{-6})	DOCUMENT ID		TECN	COMMENT
$1.74 \pm 0.27 \pm 0.14$	[1] AAIJ	18Q	LHCB	pp at 7, 8 TeV

[1] AAIJ 18Q reports $[\Gamma(\Xi_b \to p K^- K^- \pi^+ \times B(b \to \Xi_b^0)/B(b \to \Lambda_b^0))/\Gamma_{total}]$ / $[B(\Lambda_c^+ \to p K^- \pi^+)]$ / $[B(\Lambda_b^0 \to \Lambda_c^+ \pi^-)] = (5.6 \pm 0.6 \pm 0.4 \pm 0.5) \times 10^{-3}$ which we multiply by our best (shown rounded) values $B(\Lambda_c^+ \to p K^- \pi^+) = (6.37 \pm 0.21) \times 10^{-2}$, $B(\Lambda_b^0 \to \Lambda_c^+ \pi^-) = (4.9 \pm 0.4) \times 10^{-3}$. Our first error is their experiment's error and our second error is the systematic error from using our best (shown rounded) values.

$\Gamma(p K^- K^+ K^- \times B(b \to \Xi_b^0)/B(b \to \Lambda_b^0))/\Gamma_{total}$ — Γ_{19}/Γ

VALUE (units 10^{-6})	DOCUMENT ID		TECN	COMMENT
$0.18 \pm 0.10 \pm 0.01$	[1,2] AAIJ	18Q	LHCB	pp at 7, 8 TeV

[1] AAIJ 18Q reports $[\Gamma(\Xi_b \to p K^- K^+ K^- \times B(b \to \Xi_b^0)/B(b \to \Lambda_b^0))/\Gamma_{total}]$ / $[B(\Lambda_c^+ \to p K^- \pi^+)]$ / $[B(\Lambda_b^0 \to \Lambda_c^+ \pi^-)] = (0.57 \pm 0.28 \pm 0.08 \pm 0.10) \times 10^{-3}$ which we multiply by our best (shown rounded) values $B(\Lambda_c^+ \to p K^- \pi^+) = (6.37 \pm 0.21) \times 10^{-2}$, $B(\Lambda_b^0 \to \Lambda_c^+ \pi^-) = (4.9 \pm 0.4) \times 10^{-3}$. Our first error is their experiment's error and our second error is the systematic error from using our best (shown rounded) values.

[2] AAIJ 18Q sees excess with a significance of 2.3σ. Using $B(\Lambda_b^0 \to \Lambda_c^+ \pi^-) = (0.430 \pm 0.036) \times 10^{-2}$ and $B(\Lambda_c^+ \to p K^- \pi^+) = (6.46 \pm 0.24) \times 10^{-2}$ the authors set two sided limit [0.11–0.25] at 90% C.L.

P AND *CP* VIOLATION ASYMMETRIES

$a_P(\Xi_b^0 \to p K^- K^- \pi^+)$

Observable calculated as average of the triple products for Ξ_b^0 and $\overline{\Xi}_b^0$, which is sensitive to parity violation.

VALUE (%)	DOCUMENT ID		TECN	COMMENT
$-3.04 \pm 5.19 \pm 0.36$	[1] AAIJ	18AG	LHCB	pp at 7, 8 TeV

[1] Measured over full phase space of the decay.

$a_{CP}(\Xi_b^0 \to p K^- K^- \pi^+)$

Observable calculated as half of the difference between triple products for Ξ_b^0 and $\overline{\Xi}_b^0$, which is sensitive to *CP* violation.

VALUE (%)	DOCUMENT ID		TECN	COMMENT
$-3.58 \pm 5.19 \pm 0.36$	[1] AAIJ	18AG	LHCB	pp at 7, 8 TeV

[1] Measured over full phase space of the decay.

$\Delta A_{CP}(\Xi_b^0 \to p K^- \pi^+ \pi^-)$

$$\Delta A_{CP} \equiv A_{CP}(\Xi_b^0 \to p K^- \pi^+ \pi^-) - A_{CP}(\Xi_b^0 \to (\Xi_c^+ \to p K^- \pi^+) \pi^-)$$

VALUE (units 10^{-2})	DOCUMENT ID		TECN	COMMENT
$-17 \pm 11 \pm 1$	[1] AAIJ	19AH	LHCB	pp at 7 and 8 TeV

[1] Full phase space.

$\Delta A_{CP}(\Xi_b^0 \to p K^- \pi^+ K^-)$

$$\Delta A_{CP} \equiv A_{CP}(\Xi_b^0 \to p K^- \pi^+ K^-) - A_{CP}(\Xi_b^0 \to (\Xi_c^+ \to p K^- \pi^+) \pi^-)$$

VALUE (units 10^{-2})	DOCUMENT ID		TECN	COMMENT
$-6.8 \pm 8.0 \pm 0.8$	[1] AAIJ	19AH	LHCB	pp at 7 and 8 TeV

[1] Full phase space.

$A_{CP}(\Xi_b^0 \to p \overline{K}^0 K^-)$

VALUE	DOCUMENT ID		TECN	COMMENT
$0.22 \pm 0.15 \pm 0.11$	AAIJ	25AP	LHCB	pp at 7, 8, 13 TeV

$A_{CP}(\Xi_b^0 \to \Lambda K^- \pi^+)$

VALUE	DOCUMENT ID		TECN	COMMENT
$0.27 \pm 0.12 \pm 0.05$	[1] AAIJ	25J	LHCB	pp at 7, 8, 13 TeV

[1] Measured relative to $\Lambda_b^0 \to \Lambda_c^+ \pi^-$ decay.

Int. J. Mod. Phys. A 2026.41. Downloaded from www.worldscientific.com
by UNIVERSITY OF CALIFORNIA @ BERKELEY on 09/16/26. Re-use and distribution is strictly not permitted, except for Open Access articles.

Int. J. Mod. Phys. A 2026.41. Downloaded from www.worldscientific.com
UNIVERSITY OF CALIFORNIA @ BERKELEY on 09/16/26. Re-use and distribution is strictly not permitted, except for Open Access articles.

Ξ_b^0 REFERENCES

AAIJ	25AA	EPJ C85 812	R. Aaij *et al.*	(LHCb Collab.)
AAIJ	25AJ	PR D112 052012	R. Aaij *et al.*	(LHCb Collab.)
AAIJ	25AP	JHEP 2510 169	R. Aaij *et al.*	(LHCb Collab.)
AAIJ	25J	PRL 134 111802	R. Aaij *et al.*	(LHCb Collab.)
AAIJ	24V	EPJ C84 237	R. Aaij *et al.*	(LHCb Collab.)
AAIJ	20U	PRL 124 111802	R. Aaij *et al.*	(LHCb Collab.)
AAIJ	19AB	PR D99 052006	R. Aaij *et al.*	(LHCb Collab.)
AAIJ	19AH	EPJ C79 745	R. Aaij *et al.*	(LHCb Collab.)
AAIJ	18AG	JHEP 1808 039	R. Aaij *et al.*	(LHCb Collab.)
AAIJ	18Q	JHEP 1802 098	R. Aaij *et al.*	(LHCb Collab.)
AAIJ	17BH	PRL 119 181807	R. Aaij *et al.*	(LHCb Collab.)
AAIJ	16W	JHEP 1605 081	R. Aaij *et al.*	(LHCb Collab.)
AAIJ	14H	PR D89 032001	R. Aaij *et al.*	(LHCb Collab.)
AAIJ	14Q	JHEP 1404 087	R. Aaij *et al.*	(LHCb Collab.)
AAIJ	14Z	PRL 113 032001	R. Aaij *et al.*	(LHCb Collab.)
AALTONEN	14B	PR D89 072014	T. Aaltonen *et al.*	(CDF Collab.)
AALTONEN	11X	PRL 107 102001	T. Aaltonen *et al.*	(CDF Collab.)

$\Xi_b'(5935)^-$

$J^P = \frac{1}{2}^+$ Status: ***

$\Xi_b'(5935)^-$ MASS

VALUE (MeV)	DOCUMENT ID		TECN	COMMENT
5934.9 ±0.4 OUR AVERAGE				
5934.89±0.01±0.41	[1,2] AAIJ	23AU	LHCB	pp at 7, 8, 13 TeV
5934.88±0.02±0.41	[1,3] AAIJ	15H	LHCB	pp at 7, 8 TeV

[1] Observed in $\Xi_b^0\pi^-$ channel with $\Xi_b^0 \to \Xi_c^+\pi^-$ and $\Xi_c^+ \to pK^-\pi^+$.

[2] AAIJ 23AU measures $m(\Xi_b'(5935)^-) - m(\Xi_b^0) - m(\pi^-) = 3.66 \pm 0.01 \pm 0.00$ MeV. We have adjusted the measurement to our best values of $m(\Xi_b^0) = 5791.7 \pm 0.4$ MeV, $m(\pi^-) = 139.57039 \pm 0.00018$ MeV. Our first error is their experiment's error and our second error is the systematic error from using our best values.

[3] AAIJ 15H measures $m(\Xi_b'(5935)^-) - m(\Xi_b^0) - m(\pi^-) = 3.653 \pm 0.018 \pm 0.006$ MeV. We have adjusted the measurement to our best values of $m(\Xi_b^0) = 5791.7 \pm 0.4$ MeV, $m(\pi^-) = 139.57039 \pm 0.00018$ MeV. Our first error is their experiment's error and our second error is the systematic error from using our best values.

$\Xi_b'(5935)^-$ WIDTH

VALUE (MeV)	CL%	DOCUMENT ID		TECN	COMMENT
0.03±0.01±0.03		[1] AAIJ	23AU	LHCB	pp at 7, 8, 13 TeV
• • • We do not use the following data for averages, fits, limits, etc. • • •					
<0.08	95	[1] AAIJ	15H	LHCB	pp at 7, 8 TeV

[1] Observed in $\Xi_b^0\pi^-$ channel with $\Xi_b^0 \to \Xi_c^+\pi^-$ and $\Xi_c^+ \to pK^-\pi^+$.

$\Xi_b'(5935)^-$ DECAY MODES

	Mode	Fraction (Γ_i/Γ)
Γ_1	$\Xi_b^0\pi^- \times B(\overline{b} \to \Xi_b'(5935)^-)/B(\overline{b} \to \Xi_b^0)$	(11.8±1.8) %

$\Xi_b'(5935)^-$ BRANCHING RATIOS

$\Gamma(\Xi_b^0\pi^- \times B(\overline{b} \to \Xi_b'(5935)^-)/B(\overline{b} \to \Xi_b^0))/\Gamma_{total}$ — Γ_1/Γ

VALUE	DOCUMENT ID		TECN	COMMENT
0.118±0.017±0.007	[1] AAIJ	15H	LHCB	pp at 7, 8 TeV

[1] Observed in $\Xi_b^0\pi^-$ channel with $\Xi_b^0 \to \Xi_c^+\pi^-$ and $\Xi_c^+ \to pK^-\pi^+$.

$\Xi_b'(5935)^-$ REFERENCES

AAIJ	23AU	PRL 131 171901	R. Aaij *et al.*	(LHCb Collab.)
AAIJ	15H	PRL 114 062004	R. Aaij *et al.*	(LHCb Collab.)

$\Xi_b(5945)^0$

$J^P = \frac{3}{2}^+$ Status: ***

Quantum numbers are based on quark model expectations.

$\Xi_b(5945)^0$ MASS

VALUE (MeV)	DOCUMENT ID		TECN	COMMENT
5952.3 ±0.6 OUR AVERAGE				
5952.4 ±0.1 ±0.6	[1] HAYRAPETY...	24R	CMS	pp at 13 TeV
5952.35±0.02±0.58	[2,3] AAIJ	23AU	LHCB	pp at 7, 8, 13 TeV
5952.3 ±0.1 ±0.6	[4] AAIJ	16AE	LHCB	pp at 7, 8 TeV
5951.4 ±0.8 ±0.6	[5] CHATRCHYAN	12S	CMS	pp at 7 TeV, 5.3 fb^{-1}

[1] HAYRAPETYAN 24R measures $m(\Xi_b(4945)^0) - m(\Xi_b^-) - m(\pi^\pm) = 15.810 \pm 0.077 \pm 0.052$ MeV. We have adjusted the measurement to our best values of $m(\Xi_b^-) = 5797.0 \pm 0.6$ MeV, $m(\pi^+) = 139.57039 \pm 0.00018$ MeV. Our first error is their experiment's error and our second error is the systematic error from using our best values.

[2] Measured using $\Xi_b(5945)^0 \to \Xi_b^-\pi^+$, $\Xi_b^- \to \Xi_c^0\pi^-$, $\Xi_c^0 \to pK^-K^-\pi^+$ decays.

[3] AAIJ 23AU measures $m(\Xi_b(5945)^0) - m(\Xi_b^-) - m(\pi^+) = 15.80 \pm 0.02 \pm 0.01$ MeV. We have adjusted the measurement to our best values of $m(\Xi_b^-) = 5797.0 \pm 0.6$ MeV, $m(\pi^+) = 139.57039 \pm 0.00018$ MeV. Our first error is their experiment's error and our second error is the systematic error from using our best values.

[4] AAIJ 16AE measures $m(\Xi_b(5945)^0) - m(\Xi_b^-) - m(\pi^+) = 15.727 \pm 0.068 \pm 0.023$ MeV. We have adjusted the measurement to our best values of $m(\Xi_b^-) = 5797.0 \pm 0.6$ MeV, $m(\pi^+) = 139.57039 \pm 0.00018$ MeV. Our first error is their experiment's error and our second error is the systematic error from using our best values.

[5] CHATRCHYAN 12S measures $m(\Xi_b(5945)^0) - m(\Xi_b^-) - m(\pi^+) = 14.84 \pm 0.74 \pm 0.28$ MeV. We have adjusted the measurement to our best values of $m(\Xi_b^-) = 5797.0 \pm 0.6$ MeV, $m(\pi^+) = 139.57039 \pm 0.00018$ MeV. Our first error is their experiment's error and our second error is the systematic error from using our best values.

$\Xi_b(5945)^0$ WIDTH

VALUE (MeV)	DOCUMENT ID		TECN	COMMENT
0.87±0.07 OUR AVERAGE				
$0.87^{+0.22}_{-0.20} \pm 0.16$	HAYRAPETY...	24R	CMS	pp at 13 TeV
0.87±0.06±0.05	[1] AAIJ	23AU	LHCB	pp at 7, 8, 13 TeV
• • • We do not use the following data for averages, fits, limits, etc. • • •				
0.90±0.16±0.08	[1] AAIJ	16AE	LHCB	pp at 7, 8 TeV
2.1 ±1.7	[2] CHATRCHYAN	12S	CMS	pp at 7 TeV, 5.3 fb^{-1}

[1] Measured using $\Xi_b(5945)^0 \to \Xi_b^-\pi^+$, $\Xi_b^- \to \Xi_c^0\pi^-$, $\Xi_c^0 \to pK^-K^-\pi^+$ decays.

[2] Systematic uncertainty not evaluated.

$\Xi_b(5945)^0$ DECAY MODES

	Mode	Fraction (Γ_i/Γ)
Γ_1	$\Xi_b^-\pi^+$	seen

$\Xi_b(5945)^0$ BRANCHING RATIOS

$\Gamma(\Xi_b^-\pi^+)/\Gamma_{total}$ — Γ_1/Γ

VALUE	DOCUMENT ID		TECN	COMMENT
seen	[1] HAYRAPETY...	24R	CMS	pp at 13 TeV
seen	AAIJ	16AE	ATLS	pp at 7, 8 TeV
seen	CHATRCHYAN	12S	CMS	pp at 7 TeV, 5.3 fb^{-1}

[1] HAYRAPETYAN 24R measures $B(\Xi_b(5945)^0 \to \Xi_b^-\pi^+) \times B(b \to \Xi_b(5945)^0X)$ / $B(b \to \Xi_b^-X) = 0.22 \pm 0.02 \pm 0.02$.

$\Xi_b(5945)^0$ REFERENCES

HAYRAPETY...	24R	PR D110 012002	A. Hayrapetyan *et al.*	(CMS Collab.)
AAIJ	23AU	PRL 131 171901	R. Aaij *et al.*	(LHCb Collab.)
AAIJ	16AE	JHEP 1605 161	R. Aaij *et al.*	(LHCb Collab.)
CHATRCHYAN	12S	PRL 108 252002	S. Chatrchyan *et al.*	(CMS Collab.)

$\Xi_b(5955)^-$

$J^P = \frac{3}{2}^+$ Status: ***

$\Xi_b(5955)^-$ MASS

VALUE (MeV)	DOCUMENT ID		TECN	COMMENT
5955.5 ±0.4 OUR AVERAGE				
5955.50±0.03±0.41	[1,2] AAIJ	23AU	LHCB	pp at 7, 8, 13 TeV
5955.2 ±0.1 ±0.4	[1,3] AAIJ	15H	LHCB	pp at 7, 8 TeV

[1] Observed in $\Xi_b^0\pi^-$ channel with $\Xi_b^0 \to \Xi_c^+\pi^-$ and $\Xi_c^+ \to pK^-\pi^+$.

[2] AAIJ 23AU measures $m(\Xi_b(5955)^-) - m(\Xi_b^0) - m(\pi^-) = 24.27 \pm 0.03 \pm 0.01$ MeV. We have adjusted the measurement to our best values of $m(\Xi_b^0) = 5791.7 \pm 0.4$ MeV, $m(\pi^-) = 139.57039 \pm 0.00018$ MeV. Our first error is their experiment's error and our second error is the systematic error from using our best values.

[3] AAIJ 15H measures $m(\Xi_b(5955)^-) - m(\Xi_b^0) - m(\pi^-) = 24.96 \pm 0.12 \pm 0.06$ MeV. We have adjusted the measurement to our best values of $m(\Xi_b^0) = 5791.7 \pm 0.4$ MeV, $m(\pi^-) = 139.57039 \pm 0.00018$ MeV. Our first error is their experiment's error and our second error is the systematic error from using our best values.

$\Xi_b(5955)^-$ WIDTH

VALUE (MeV)	DOCUMENT ID		TECN	COMMENT
1.43±0.08±0.08	[1] AAIJ	23AU	LHCB	pp at 7, 8, 13 TeV
• • • We do not use the following data for averages, fits, limits, etc. • • •				
1.65±0.31±0.10	[1] AAIJ	15H	LHCB	pp at 7, 8 TeV

[1] Observed in $\Xi_b^0\pi^-$ channel with $\Xi_b^0 \to \Xi_c^+\pi^-$ and $\Xi_c^+ \to pK^-\pi^+$.

Int. J. Mod. Phys. A 2026.41. Downloaded from www.worldscientific.com by UNIVERSITY OF CALIFORNIA @ BERKELEY on 09/16/26. Re-use and distribution is strictly not permitted, except for Open Access articles.

$\Xi_b(5955)^-$ DECAY MODES

	Mode	Fraction (Γ_i/Γ)
Γ_1	$\Xi_b^0\pi^- \times B(\overline{b} \to \Xi_b^*(5955)^-)/B(\overline{b} \to \Xi_b^0)$	(20.7 ± 3.5) %

$\Xi_b(5955)^-$ BRANCHING RATIOS

$\Gamma(\Xi_b^0\pi^- \times B(\overline{b} \to \Xi_b^*(5955)^-)/B(\overline{b} \to \Xi_b^0))/\Gamma_{total}$ — Γ_1/Γ

VALUE	DOCUMENT ID		TECN	COMMENT
0.207±0.032±0.015	[1] AAIJ	15H	LHCB	pp at 7, 8 TeV

[1] Observed in $\Xi_b^0\pi^-$ channel with $\Xi_b^0 \to \Xi_c^+\pi^-$ and $\Xi_c^+ \to pK^-\pi^+$.

$\Xi_b(5955)^-$ REFERENCES

AAIJ	23AU	PRL 131 171901	R. Aaij *et al.*	(LHCb Collab.)
AAIJ	15H	PRL 114 062004	R. Aaij *et al.*	(LHCb Collab.)

$\Xi_b(6087)^0$

$I(J^P) = \frac{1}{2}(?^?)$ Status: ***

$\Xi_b(6087)^0$ MASS

VALUE (MeV)	DOCUMENT ID		TECN	COMMENT
6087.0±0.2±0.4	[1,2] AAIJ	23AU	LHCB	pp at 7, 8, 13 TeV

[1] Observed in $\Xi_b^0\pi^+\pi^-$ channel with $\Xi_b^0 \to \Xi_c^+\pi^-$ and $\Xi_b^0 \to \Xi_c^+\pi^-\pi^+\pi^-$ and $\Xi_c^+ \to pK^-\pi^+$. Measured as mass difference, listed separately.

[2] AAIJ 23AU measures $m(\Xi_b(6087)^0) - m(\Xi_b^0) - 2m(\pi^\pm) = 16.20 \pm 0.20 \pm 0.06$ MeV. We have adjusted the measurement to our best values of $m(\Xi_b^0) = 5791.7 \pm 0.4$ MeV, $m(\pi^\pm) = 139.57039 \pm 0.00018$ MeV. Our first error is their experiment's error and our second error is the systematic error from using our best values.

$\Xi_b(6087)^0$ WIDTH

VALUE (MeV)	DOCUMENT ID		TECN	COMMENT
2.43±0.51±0.10	[1] AAIJ	23AU	LHCB	pp at 7, 8, 13 TeV

[1] Observed in $\Xi_b^0\pi^+\pi^-$ channel with $\Xi_b^0 \to \Xi_c^+\pi^-$ and $\Xi_b^0 \to \Xi_c^+\pi^-\pi^+\pi^-$ and $\Xi_c^+ \to pK^-\pi^+$

$\Xi_b(6087)^0$ DECAY MODES

	Mode	Fraction (Γ_i/Γ)
Γ_1	$\Xi_b^0\pi^+\pi^-$	seen

$\Xi_b(6087)^0$ BRANCHING RATIOS

$\Gamma(\Xi_b^0\pi^+\pi^-)/\Gamma_{total}$ — Γ_1/Γ

VALUE	DOCUMENT ID		TECN	COMMENT
seen	AAIJ	23AU	LHCB	pp at 7, 8, 13 TeV

$\Xi_b(6087)^0$ REFERENCES

AAIJ	23AU	PRL 131 171901	R. Aaij *et al.*	(LHCb Collab.)

$\Xi_b(6095)^0$

$I(J^P) = \frac{1}{2}(?^?)$ Status: ***

$\Xi_b(6095)^0$ MASS

VALUE (MeV)	DOCUMENT ID		TECN	COMMENT
6095.1±0.2±0.4	[1,2] AAIJ	23AU	LHCB	pp at 7, 8, 13 TeV

[1] Observed in $\Xi_b^0\pi^+\pi^-$ channel with $\Xi_b^0 \to \Xi_c^+\pi^-$ and $\Xi_b^0 \to \Xi_c^+\pi^-\pi^+\pi^-$ and $\Xi_c^+ \to pK^-\pi^+$. Measured as mass difference, listed separately.

[2] AAIJ 23AU measures $m(\Xi_b(6095)^0) - m(\Xi_b^0) - 2m(\pi^\pm) = 24.32 \pm 0.15 \pm 0.03$ MeV. We have adjusted the measurement to our best values of $m(\Xi_b^0) = 5791.7 \pm 0.4$ MeV, $m(\pi^\pm) = 139.57039 \pm 0.00018$ MeV. Our first error is their experiment's error and our second error is the systematic error from using our best values.

$\Xi_b(6095)^0$ WIDTH

VALUE (MeV)	DOCUMENT ID		TECN	COMMENT
0.50±0.33±0.11	[1] AAIJ	23AU	LHCB	pp at 7, 8, 13 TeV

[1] Observed in $\Xi_b^0\pi^+\pi^-$ channel with $\Xi_b^0 \to \Xi_c^+\pi^-$ and $\Xi_b^0 \to \Xi_c^+\pi^-\pi^+\pi^-$ and $\Xi_c^+ \to pK^-\pi^+$

$\Xi_b(6095)^0$ DECAY MODES

	Mode	Fraction (Γ_i/Γ)
Γ_1	$\Xi_b^0\pi^+\pi^-$	seen

$\Xi_b(6095)^0$ BRANCHING RATIOS

$\Gamma(\Xi_b^0\pi^+\pi^-)/\Gamma_{total}$ — Γ_1/Γ

VALUE	DOCUMENT ID		TECN	COMMENT
seen	AAIJ	23AU	LHCB	pp at 7, 8, 13 TeV

$\Xi_b(6095)^0$ REFERENCES

AAIJ	23AU	PRL 131 171901	R. Aaij *et al.*	(LHCb Collab.)

$\Xi_b(6100)^-$

$J^P = \frac{3}{2}^-$ Status: ***

J, P need confirmation.

$\Xi_b(6100)^-$ MASS

VALUE (MeV)	DOCUMENT ID		TECN	COMMENT
6099.8±0.4 OUR AVERAGE				
6099.7±0.1±0.4	[1,2] AAIJ	23AU	LHCB	pp at 7, 8, 13 TeV
6100.3±0.2±0.4	[3,4] SIRUNYAN	21F	CMS	pp at 13 TeV

[1] Observed in $\Xi_b^-\pi^+\pi^-$ channel with $\Xi_b^- \to \Xi_c^0\pi^-$ and $\Xi_b^- \to \Xi_c^0\pi^-\pi^+\pi^-$ and $\Xi_c^0 \to pK^-K^-\pi^+$.

[2] AAIJ 23AU measures $m(\Xi_b(6100)^-) - m(\Xi_b^-) - 2m(\pi^\pm) = 23.60 \pm 0.11 \pm 0.12$ MeV. We have adjusted the measurement to our best values of $m(\Xi_b^-) = 5797.0 \pm 0.4$ MeV, $m(\pi^\pm) = 139.57039 \pm 0.00018$ MeV. Our first error is their experiment's error and our second error is the systematic error from using our best values.

[3] Observed in $\Xi_b(6100)^- \to \Xi_b^-\pi^+\pi^-$ decays.

[4] SIRUNYAN 21F measures $m(\Xi_b(6100)^-) - m(\Xi_b^-) - 2m(\pi^\pm) = 24.14 \pm 0.22 \pm 0.09$ MeV. We have adjusted the measurement to our best values of $m(\Xi_b^-) = 5797.0 \pm 0.4$ MeV, $m(\pi^\pm) = 139.57039 \pm 0.00018$ MeV. Our first error is their experiment's error and our second error is the systematic error from using our best values.

$\Xi_b(6100)^-$ WIDTH

VALUE (MeV)	CL%	DOCUMENT ID		TECN	COMMENT
0.94±0.30±0.08		[1] AAIJ	23AU	LHCB	pp at 7, 8, 13 TeV
• • • We do not use the following data for averages, fits, limits, etc. • • •					
<1.9	95	[2] SIRUNYAN	21F	CMS	pp at 13 TeV

[1] Observed in $\Xi_b^-\pi^+\pi^-$ channel with $\Xi_b^- \to \Xi_c^0\pi^-$ and $\Xi_b^- \to \Xi_c^0\pi^-\pi^+\pi^-$ and $\Xi_c^0 \to pK^-K^-\pi^+$

[2] Observed in $\Xi_b(6100)^- \to \Xi_b^-\pi^+\pi^-$ decays.

$\Xi_b(6100)^-$ DECAY MODES

	Mode	Fraction (Γ_i/Γ)
Γ_1	$\Xi_b^-\pi^+\pi^-$	seen

$\Xi_b(6100)^-$ BRANCHING RATIOS

$\Gamma(\Xi_b^-\pi^+\pi^-)/\Gamma_{total}$ — Γ_1/Γ

VALUE	EVTS	DOCUMENT ID		TECN	COMMENT
seen		AAIJ	23AU	LHCB	pp at 7, 8, 13 TeV
seen	60	SIRUNYAN	21F	CMS	pp at 13 TeV

$\Xi_b(6100)^-$ REFERENCES

AAIJ	23AU	PRL 131 171901	R. Aaij *et al.*	(LHCb Collab.)
SIRUNYAN	21F	PRL 126 252003	A.M. Sirunyan *et al.*	(CMS Collab.)

$\Xi_b(6227)^-$

$J^P = ?^?$ Status: ***

$\Xi_b(6227)^-$ MASS

VALUE (MeV)	DOCUMENT ID		TECN	COMMENT
6227.9±0.9±0.2	[1] AAIJ	21	LHCB	pp at 7, 8, 13 TeV
• • • We do not use the following data for averages, fits, limits, etc. • • •				
6226.9±2.0±0.4	[2,3] AAIJ	18H	LHCB	Repl. by AAIJ 2021

[1] AAIJ 21 measures $m(\Xi_b(6227)^-) - m(\Lambda_b^0) = 608.3 \pm 0.8 \pm 0.4$ MeV. We have adjusted the measurement to our best value of $m(\Lambda_b^0) = 5619.57 \pm 0.16$ MeV. Our first error is

Int. J. Mod. Phys. A 2026.41. Downloaded from www.worldscientific.com
UNIVERSITY OF CALIFORNIA @ BERKELEY on 09/16/26. Re-use and distribution is strictly not permitted, except for Open Access articles.

their experiment's error and our second error is the systematic error from using our best values.
[2] Uses $\Lambda_b^0 K^-$ and $\Xi_b^0 \pi^-$ modes.
[3] Measures mass difference $m(\Xi_b(6227)^-) - m(\Lambda_b^0) = 607.3 \pm 2.0 \pm 0.3$ MeV and uses $m(\Lambda_b^0) = 5619.58 \pm 0.17$ MeV.

$\Xi_b(6227)^-$ WIDTH

VALUE (MeV)	DOCUMENT ID		TECN	COMMENT
19.9±2.1±1.5	[1] AAIJ	21	LHCB	pp at 7, 8, 13 TeV
• • • We do not use the following data for averages, fits, limits, etc. • • •				
18.1±5.4±1.8	[2] AAIJ	18H	LHCB	Repl. by AAIJ 2021

[1] Uses $\Lambda_b^0 K^-$ decays.
[2] Uses $\Lambda_b^0 K^-$ and $\Xi_b^0 \pi^-$ modes.

$\Xi_b(6227)^-$ DECAY MODES

	Mode	Fraction (Γ_i/Γ)	Scale factor
Γ_1	$\Lambda_b^0 K^- \times$ B($b \to \Xi_b(6227)$)/B($b \to \Lambda_b^0$)	$(3.20 \pm 0.35) \times 10^{-3}$	
Γ_2	$\Xi_b^0 \pi^- \times$ B($b \to \Xi_b(6227)$)/B($b \to \Xi_b^0$)	(2.8 ±1.1) %	1.8

$\Xi_b(6227)^-$ BRANCHING RATIOS

$\Gamma(\Lambda_b^0 K^- \times B(b \to \Xi_b(6227))/B(b \to \Lambda_b^0))/\Gamma_{total}$ — **Γ_1/Γ**

VALUE (units 10^{-3})	DOCUMENT ID		TECN	COMMENT
3.20±0.35 OUR AVERAGE				
3.0 ±0.3 ±0.4	AAIJ	18H	LHCB	pp at 7, 8 TeV
3.4 ±0.3 ±0.4	AAIJ	18H	LHCB	pp at 13 TeV

$\Gamma(\Xi_b^0 \pi^- \times B(b \to \Xi_b(6227))/B(b \to \Xi_b^0))/\Gamma_{total}$ — **Γ_2/Γ**

VALUE (units 10^{-3})	DOCUMENT ID		TECN	COMMENT
28±11 OUR AVERAGE Error includes scale factor of 1.8.				
47±10±7	AAIJ	18H	LHCB	pp at 7, 8 TeV
22± 6±3	AAIJ	18H	LHCB	pp at 13 TeV

$\Xi_b(6227)^-$ REFERENCES

AAIJ 21 PR D103 012004 R. Aaij et al. (LHCb Collab.)
AAIJ 18H PRL 121 072002 R. Aaij et al. (LHCb Collab.)

$\Xi_b(6227)^0$

$J^P = ?^?$ Status: ***

$\Xi_b(6227)^0$ MASS

VALUE (MeV)	DOCUMENT ID		TECN	COMMENT
$6226.8^{+1.4}_{-1.5} \pm 0.6$	[1,2] AAIJ	21	LHCB	pp at 7, 8, 13 TeV

[1] AAIJ 21 measures $m(\Xi_b(6227)^0) - m(\Xi_b^-) = 429.8^{+1.4}_{-1.5} \pm 0.3$ MeV. We have adjusted the measurement to our best value of $m(\Xi_b^-) = 5797.0 \pm 0.6$ MeV. Our first error is their experiment's error and our second error is the systematic error from using our best values.
[2] Uses $\Xi_b^- \pi^+$ decays.

$\Xi_b(6227)^0$ WIDTH

VALUE (MeV)	DOCUMENT ID		TECN	COMMENT
$18.6^{+5.0}_{-4.1} \pm 1.4$	[1] AAIJ	21	LHCB	pp at 7, 8, 13 TeV

[1] Uses $\Xi_b^- \pi^+$ decays.

$\Xi_b(6227)^0$ DECAY MODES

	Mode	Fraction (Γ_i/Γ)
Γ_1	$\Xi_b^- \pi^+ \times$ B($b \to \Xi_b(6227)^0$)/B($b \to \Xi_b^-$)	(4.5±0.9) %

$\Xi_b(6227)^0$ BRANCHING RATIOS

$\Gamma(\Xi_b^- \pi^+ \times B(b \to \Xi_b(6227)^0)/B(b \to \Xi_b^-))/\Gamma_{total}$ — **Γ_1/Γ**

VALUE (%)	DOCUMENT ID		TECN	COMMENT
4.5±0.8±0.4	AAIJ	21	LHCB	pp at 7, 8, 13 TeV

$\Xi_b(6227)^0$ REFERENCES

AAIJ 21 PR D103 012004 R. Aaij et al. (LHCb Collab.)

$\Xi_b(6327)^0$

$J^P = ?^?$ Status: ***

$\Xi_b(6327)^0$ MASS

VALUE (MeV)	DOCUMENT ID		TECN	COMMENT
$6327.28^{+0.23}_{-0.21} \pm 0.27$	AAIJ	22I	LHCB	pp at 13 TeV

$\Xi_b(6327)^0$ WIDTH

VALUE (MeV)	CL%	DOCUMENT ID		TECN	COMMENT
<2.56	95	AAIJ	22I	LHCB	pp at 13 TeV

$\Xi_b(6327)^0$ DECAY MODES

	Mode	Fraction (Γ_i/Γ)
Γ_1	$\Lambda_b^0 K^- \pi^+$	seen

$\Xi_b(6327)^0$ BRANCHING RATIOS

$\Gamma(\Lambda_b^0 K^- \pi^+)/\Gamma_{total}$ — **Γ_1/Γ**

VALUE	DOCUMENT ID		TECN	COMMENT
seen	AAIJ	22I	LHCB	pp at 13 TeV

$\Xi_b(6327)^0$ REFERENCES

AAIJ 22I PRL 128 162001 R. Aaij et al. (LHCb Collab.)

$\Xi_b(6333)^0$

$J^P = ?^?$ Status: ***

$\Xi_b(6333)^0$ MASS

VALUE (MeV)	DOCUMENT ID		TECN	COMMENT
$6332.69^{+0.17}_{-0.18} \pm 0.22$	AAIJ	22I	LHCB	pp at 13 TeV

$\Xi_b(6333)^0$ WIDTH

VALUE (MeV)	CL%	DOCUMENT ID		TECN	COMMENT
<1.92	95	AAIJ	22I	LHCB	pp at 13 TeV

$\Xi_b(6333)^0$ DECAY MODES

	Mode	Fraction (Γ_i/Γ)
Γ_1	$\Lambda_b^0 K^- \pi^+$	seen

$\Xi_b(6333)^0$ BRANCHING RATIOS

$\Gamma(\Lambda_b^0 K^- \pi^+)/\Gamma_{total}$ — **Γ_1/Γ**

VALUE	DOCUMENT ID		TECN	COMMENT
seen	AAIJ	22I	LHCB	pp at 13 TeV

$\Xi_b(6333)^0$ REFERENCES

AAIJ 22I PRL 128 162001 R. Aaij et al. (LHCb Collab.)

Ξ_{bc}^0

$J^P = \frac{1}{2}^+$

OMITTED FROM SUMMARY TABLE

Ξ_{bc}^0 DECAY MODES

	Mode	Fraction (Γ_i/Γ)	Confidence level
Γ_1	$D^0 p K^- \times$ B($b \to \Xi_{bc}^0$)/B($b \to \Lambda_b$)	$<1.4 \times 10^{-5}$	95%

Ξ_{bc}^0 BRANCHING RATIOS

$\Gamma(D^0 p K^- \times B(b \to \Xi_{bc}^0)/B(b \to \Lambda_b))/\Gamma_{total}$ — **Γ_1/Γ**

VALUE	CL%	DOCUMENT ID		TECN	COMMENT
$<1.4 \times 10^{-5}$	95	[1,2] AAIJ	20AM	LHCB	pp at 13 TeV

[1] AAIJ 20AM reports upper limits for $[\Gamma(\Xi^0_{bc} \to D^0 p K^- \times B(b \to \Xi^0_{bc}) / B(b \to \Lambda_b))/\Gamma_{total}] / [B(\Lambda^0_b \to p D^0 K^-)] < 3.0 \times 10^{-1}$–$1.7 \times 10^{-2}$ for the considered Ξ^0_{bc} mass and lifetime hypotheses ranging from 6.7 to 7.2 GeV and from 100 to 500 fs. We use the 3.0×10^{-1} limit for the quoted result.

[2] AAIJ 20AM reports $[\Gamma(\Xi^0_{bc} \to D^0 p K^- \times B(b \to \Xi^0_{bc}) / B(b \to \Lambda_b))/\Gamma_{total}] / [B(\Lambda^0_b \to p D^0 K^-)] < 3.0 \times 10^{-1}$ which we multiply by our best (shown rounded) value $B(\Lambda^0_b \to p D^0 K^-) = 4.6 \times 10^{-5}$.

Ξ^0_{bc} REFERENCES

AAIJ 20AM JHEP 2011 095 R. Aaij et al. (LHCb Collab.)

Ω^-_b

$I(J^P) = 0(\frac{1}{2}^+)$ Status: ***

I, J, P need confirmation.

In the quark model Ω^-_b is ssb ground state. None of its quantum numbers has been measured.

Ω^-_b MASS

VALUE (MeV)	DOCUMENT ID		TECN	COMMENT
6045.8 ± 0.8 OUR AVERAGE				
6045.7 ± 0.5 ± 0.6	[1] AAIJ	23BD	LHCB	pp at 7, 8, 13 TeV
6047.5 ± 3.8 ± 0.6	[2] AALTONEN	14B	CDF	$p\overline{p}$ at 1.96 TeV
• • • We do not use the following data for averages, fits, limits, etc. • • •				
6045.9 ± 0.5 ± 0.6	[3] AAIJ	23BD	LHCB	pp at 7, 8, 13 TeV
6044.30 ± 1.20 ± 1.12	[4] AAIJ	21AC	LHCB	Repl. by AAIJ 23BD
6045.1 ± 3.2 ± 0.8	[5] AAIJ	16O	LHCB	Repl. by AAIJ 23BD
6046.0 ± 2.2 ± 0.5	[6] AAIJ	13AV	LHCB	Repl. by AAIJ 23BD
6054.4 ± 6.8 ± 0.9	[7] AALTONEN	09AP	CDF	Repl. by AALTONEN 14B
6165 ±10 ±13	[8] ABAZOV	08AL	D0	$p\overline{p}$ at 1.96 TeV

[1] Combines measurement using $\Omega^-_b \to J/\psi\Omega^-$ decays with results from AAIJ 16O and AAIJ 21AC taking into account correlations amongst systematic uncertainties. Uses Ξ^-_b mass 5797.33 ± 0.24 ± 029 MeV from AAIJ 21.

[2] Uses $\Omega^-_b \to J/\psi\Omega^-$ and $\Omega^0_c\pi^-$ decays, with the first evidence for $\Omega^-_b \to \Omega^0_c\pi^-$ at 3.3 σ significance.

[3] Uses $\Omega^-_b \to J/\psi\Omega^-$ decays.

[4] Uses $\Omega^-_b \to \Xi^+_c K^-\pi^-$ and $\Xi^+_c \to p K^-\pi^+$ decays. Reports the value of 6044.3 ± 1.2 ± $1.1^{+0.19}_{-0.22}$ MeV where the last uncertainty is due to the mass of Ξ^+_c. We have combined the two systematic uncertainties in quadrature.

[5] Reconstructed in $\Omega^-_b \to \Omega^0_c\pi^-$, $\Omega^0_c \to p K^- K^-\pi^+$ decays. Reference Ξ^-_b mass 5797.72 ± 0.6 MeV from AAIJ 14B.

[6] Measured in $\Omega^-_b \to J/\psi\Omega^-$ with 19 ± 5 events.

[7] Observed in $\Omega^-_b \to J/\psi\Omega^-$ decays with 16^{+6}_{-4} candidates, a significance of 5.5 sigma from a combined mass-lifetime fit.

[8] Observed in $\Omega^-_b \to J/\psi\Omega^-$ decays with 17.8 ± 4.9 ± 0.8 candidates, a significance of 5.4 sigma.

$m_{\Omega^-_b} - m_{\Lambda^0_b}$

VALUE (MeV)	DOCUMENT ID		TECN	COMMENT
426.4±2.2±0.4	AAIJ	13AV	LHCB	pp at 7 TeV

$m_{\Omega^-_b} - m_{\Xi^-_b}$

VALUE (MeV)	DOCUMENT ID		TECN	COMMENT
248.50±0.51±0.37	[1] AAIJ	23BD	LHCB	pp at 7, 8, 13 TeV
• • • We do not use the following data for averages, fits, limits, etc. • • •				
248.54±0.51±0.38	[2] AAIJ	23BD	LHCB	pp at 7, 8, 13 TeV
247.3 ±3.2 ±0.5	[3] AAIJ	16O	LHCB	Repl. by AAIJ 23BD

[1] Uses $\Omega^-_b \to J/\psi\Omega$ decays combined with the result from AAIJ 16O obtained using $\Omega^-_b \to \Omega^0_c\pi^-$, $\Omega^0_c \to p K^- K^-\pi^+$ and $\Xi^-_b \to \Xi^0_c\pi^-$, $\Xi^0_c \to p K^- K^-\pi^+$ decays taking into account correlation of systematic uncertainties.

[2] Uses $\Omega^-_b \to J/\psi\Omega$ decays.

[3] Uses $\Omega^-_b \to \Omega^0_c\pi^-$, $\Omega^0_c \to p K^- K^-\pi^+$ and $\Xi^-_b \to \Xi^0_c\pi^-$, $\Xi^0_c \to p K^- K^-\pi^+$ decays.

Ω_b MEAN LIFE

VALUE (10^{-12} s)	DOCUMENT ID		TECN	COMMENT
1.64±0.16 OUR EVALUATION	(Produced by HFLAV)			
$1.65^{+0.18}_{-0.16}$ OUR AVERAGE				
1.78±0.26±0.05±0.06	[1] AAIJ	16O	LHCB	pp at 7, 8 TeV
$1.54^{+0.26}_{-0.21}$±0.05	[2] AAIJ	14T	LHCB	pp at 7, 8 TeV
$1.66^{+0.53}_{-0.40}$±0.02	[2] AALTONEN	14B	CDF	$p\overline{p}$ at 1.96 TeV
• • • We do not use the following data for averages, fits, limits, etc. • • •				
$1.13^{+0.53}_{-0.40}$±0.02	[3] AALTONEN	09AP	CDF	Repl. by AALTONEN 14B

[1] Measured in $\Omega^-_b \to \Omega^0_c\pi^-$, $\Omega^0_c \to p K^- K^-\pi^+$ decays relative to $\Xi^-_b \to \Xi^0_c\pi^-$, $\Xi^0_c \to p K^- K^-\pi^+$ decays with reference Ξ^-_b mean life 1.599 ± 0.06 ps from AAIJ 14B.

[2] Measured in $\Omega^-_b \to J/\psi\Omega^-$ decays.

[3] Observed in $\Omega^-_b \to J/\psi\Omega^-$ decays with 16^{+6}_{-4} candidates, a significance of 5.5 sigma from a combined mass-lifetime fit.

$\tau(\Omega^-_b)/\tau(\Xi^-_b)$ mean life ratio

VALUE	DOCUMENT ID		TECN	COMMENT
1.11±0.16±0.03	[1] AAIJ	16O	LHCB	pp at 7, 8 TeV

[1] Uses $\Omega^-_b \to \Omega^0_c\pi^-$, $\Omega^0_c \to p K^- K^-\pi^+$ and $\Xi^-_b \to \Xi^0_c\pi^-$, $\Xi^0_c \to p K^- K^-\pi^+$ decays.

Ω^-_b DECAY MODES

	Mode	Fraction (Γ_i/Γ)	Scale factor/ Confidence level
Γ_1	$J/\psi\Omega^- \times B(b \to \Omega_b)$	$(1.5 \pm 0.5) \times 10^{-6}$	S=1.1
Γ_2	$p K^- K^- \times B(\overline{b} \to \Omega_b)$	$< 2.3 \times 10^{-9}$	CL=90%
Γ_3	$p\pi^-\pi^- \times B(\overline{b} \to \Omega_b)$	$< 1.5 \times 10^{-8}$	CL=90%
Γ_4	$p K^-\pi^- \times B(\overline{b} \to \Omega_b)$	$< 7 \times 10^{-9}$	CL=90%
Γ_5	$\Omega^0_c\pi^-$	seen	
Γ_6	$\Omega^0_c\pi^-$, $\Omega^0_c \to p K^- K^-\pi^+$	seen	
Γ_7	$\Xi^+_c K^-\pi^-$	seen	
Γ_8	$\Lambda^+_c K^- K^-$		
Γ_9	$\Lambda^+_c K^-\pi^-$		
Γ_{10}	$\Lambda^+_c\pi^-\pi^-$		

Ω^-_b BRANCHING RATIOS

$\Gamma(J/\psi\Omega^- \times B(b \to \Omega_b))/\Gamma_{total}$ — Γ_1/Γ

VALUE (units 10^{-6})	DOCUMENT ID		TECN	COMMENT
1.5±0.5 OUR AVERAGE Error includes scale factor of 1.1.				
1.2±0.1±0.5	[1,2] AAIJ	23BD	LHCB	pp at 13 TeV
$2.6^{+1.0}_{-0.7}$±0.9	[3] AALTONEN	09AP	CDF	$p\overline{p}$ at 1.96 TeV
8 ±4 ±2	[4] ABAZOV	08AL	D0	$p\overline{p}$ at 1.96 TeV

[1] AAIJ 23BD reports $[\Gamma(\Omega^-_b \to J/\psi\Omega^- \times B(b \to \Omega_b))/\Gamma_{total}] / [B(\Xi^-_b \to J/\psi\Xi^- \times B(b \to \Xi^-_b))] = 0.120 \pm 0.008 \pm 0.008$ which we multiply by our best (shown rounded) value $B(\Xi^-_b \to J/\psi\Xi^- \times B(b \to \Xi^-_b)) = (1.0 \pm 0.4) \times 10^{-5}$. Our first error is their experiment's error and our second error is the systematic error from using our best (shown rounded) value.

[2] Reconstructing beauty baryons in the kinematic region $2 < \eta < 6$ and $p_T < 20$ GeV/c with their decays to a J/ψ meson and a hyperon.

[3] AALTONEN 09AP reports $[\Gamma(\Omega^-_b \to J/\psi\Omega^- \times B(b \to \Omega_b))/\Gamma_{total}] / [B(\Lambda^0_b \to J/\psi(1S)\Lambda)] / [B(\overline{b} \to b\text{-baryon at } p\overline{p})] = 0.045^{+0.017}_{-0.012} \pm 0.004$ which we multiply by our best (shown rounded) values $B(\Lambda^0_b \to J/\psi(1S)\Lambda) = (3.0 \pm 0.8) \times 10^{-4}$, $B(\overline{b} \to b\text{-baryon at } p\overline{p}) = (19.8 \pm 4.6) \times 10^{-2}$. Our first error is their experiment's error and our second error is the systematic error from using our best (shown rounded) values.

[4] ABAZOV 08AL reports $[\Gamma(\Omega^-_b \to J/\psi\Omega^- \times B(b \to \Omega_b))/\Gamma_{total}] / [B(\Xi_b \to J/\psi\Xi^- \times B(b \to \Xi^-_b))] = 0.80 \pm 0.32^{+0.14}_{-0.22}$ which we multiply by our best (shown rounded) value $B(\Xi_b \to J/\psi\Xi^- \times B(b \to \Xi^-_b)) = (1.02^{+0.26}_{-0.21}) \times 10^{-5}$. Our first error is their experiment's error and our second error is the systematic error from using our best (shown rounded) value.

$\Gamma(p K^- K^- \times B(\overline{b} \to \Omega_b))/\Gamma_{total}$ — Γ_2/Γ

VALUE (units 10^{-5})	CL%	DOCUMENT ID		TECN	COMMENT
$<2.3 \times 10^{-4}$	90	[1] AAIJ	21AH	LHCB	pp at 7, 8, 13 TeV
• • • We do not use the following data for averages, fits, limits, etc. • • •					
$<2.5 \times 10^{-4}$	90	[2] AAIJ	17F	LHCB	pp at 7, 8 TeV

[1] AAIJ 21AH reports $[\Gamma(\Omega^-_b \to p K^- K^- \times B(\overline{b} \to \Omega_b))/\Gamma_{total}] / [B(\Xi^-_b \to p K^- K^- \times B(b \to \Xi^-_b))] < 62 \times 10^{-3}$ which we multiply by our best (shown rounded) value $B(\Xi^-_b \to p K^- K^- \times B(b \to \Xi^-_b)) = 3.7 \times 10^{-8}$.

[2] AAIJ 17F reports $[\Gamma(\Omega^-_b \to p K^- K^- \times B(\overline{b} \to \Omega_b))/\Gamma_{total}] / [B(B^+ \to K^+ K^- K^+)] / [B(\overline{b} \to B^+ \text{ at } Z)] < 18 \times 10^{-5}$ which we multiply by our best (shown rounded) values $B(B^+ \to K^+ K^- K^+) = 3.40 \times 10^{-5}$, $B(\overline{b} \to B^+ \text{ at } Z) = 40.8 \times 10^{-2}$.

$\Gamma(p\pi^-\pi^- \times B(\overline{b} \to \Omega_b))/\Gamma_{total}$ — Γ_3/Γ

VALUE (units 10^{-5})	CL%	DOCUMENT ID		TECN	COMMENT
$<1.5 \times 10^{-3}$	90	[1] AAIJ	17F	LHCB	pp at 7, 8 TeV

[1] AAIJ 17F reports $[\Gamma(\Omega^-_b \to p\pi^-\pi^- \times B(\overline{b} \to \Omega_b))/\Gamma_{total}] / [B(B^+ \to K^+ K^- K^+)] / [B(\overline{b} \to B^+ \text{ at } Z)] < 109 \times 10^{-5}$ which we multiply by our best (shown rounded) values $B(B^+ \to K^+ K^- K^+) = 3.40 \times 10^{-5}$, $B(\overline{b} \to B^+ \text{ at } Z) = 40.8 \times 10^{-2}$.

Int. J. Mod. Phys. A 2026.41. Downloaded from www.worldscientific.com
by UNIVERSITY OF CALIFORNIA @ BERKELEY on 09/16/26. Re-use and distribution is strictly not permitted, except for Open Access articles.

Int. J. Mod. Phys. A 2026.41. Downloaded from www.worldscientific.com
UNIVERSITY OF CALIFORNIA @ BERKELEY on 09/16/26. Re-use and distribution is strictly not permitted, except for Open Access articles.

$\Gamma(pK^-\pi^-\times B(\bar{b}\to\Omega_b))/\Gamma_{total}$ — Γ_4/Γ

VALUE (units 10^{-5})	CL%	DOCUMENT ID		TECN	COMMENT
<7 × 10⁻⁴	90	[1] AAIJ	17F	LHCB	pp at 7, 8 TeV

[1] AAIJ 17F reports $[\Gamma(\Omega_b^- \to pK^-\pi^-\times B(\bar{b}\to\Omega_b))/\Gamma_{total}]$ / $[B(B^+\to K^+K^-K^+)]$ / $[B(\bar{b}\to B^+ \text{ at } Z)] < 51\times10^{-5}$ which we multiply by our best (shown rounded) values $B(B^+\to K^+K^-K^+) = 3.40\times10^{-5}$, $B(\bar{b}\to B^+ \text{ at } Z) = 40.8\times10^{-2}$.

$\Gamma(\Omega_c^0\pi^-)/\Gamma_{total}$ — Γ_5/Γ

VALUE	DOCUMENT ID		TECN	COMMENT
seen	AAIJ	16O	LHCB	pp at 7, 8 TeV

$\Gamma(\Xi_c^+K^-\pi^-)/\Gamma(\Omega_c^0\pi^-,\ \Omega_c^0\to pK^-K^-\pi^+)$ — Γ_7/Γ_6

VALUE (units 10^2)	DOCUMENT ID		TECN	COMMENT
2.2±0.2±1.0	[1] AAIJ	21AC	LHCB	pp at 7, 8, 13 TeV

[1] AAIJ 21AC reports $[\Gamma(\Omega_b^-\to\Xi_c^+K^-\pi^-)/\Gamma(\Omega_b^-\to\Omega_c^0\pi^-,\ \Omega_c^0\to pK^-K^-\pi^+)]\times[B(\Xi_c^+\to pK^-\pi^+)] = 1.35\pm0.11\pm0.05$ which we divide by our best (shown rounded) value $B(\Xi_c^+\to pK^-\pi^+) = (6.2\pm3.0)\times10^{-3}$. Our first error is their experiment's error and our second error is the systematic error from using our best (shown rounded) value.

$\Gamma(\Lambda_c^+K^-\pi^-)/\Gamma(\Lambda_c^+K^-K^-)$ — Γ_9/Γ_8

VALUE	DOCUMENT ID		TECN	COMMENT
<0.56	AAIJ	24T	LHCB	pp at 7, 8, 13 TeV

$\Gamma(\Lambda_c^+\pi^-\pi^-)/\Gamma(\Lambda_c^+K^-K^-)$ — Γ_{10}/Γ_8

VALUE	DOCUMENT ID		TECN	COMMENT
<0.37	AAIJ	24T	LHCB	pp at 7, 8, 13 TeV

Ω_b^- REFERENCES

AAIJ	24T	JHEP 2408 132	R. Aaij	(LHCb Collab.)
AAIJ	23BD	PR D108 052008	R. Aaij *et al.*	(LHCb Collab.)
AAIJ	21	PR D103 012004	R. Aaij *et al.*	(LHCb Collab.)
AAIJ	21AC	PR D104 L091102	R. Aaij *et al.*	(LHCb Collab.)
AAIJ	21AH	PR D104 052010	R. Aaij *et al.*	(LHCb Collab.)
AAIJ	17F	PRL 118 071801	R. Aaij *et al.*	(LHCb Collab.)
AAIJ	16O	PR D93 092007	R. Aaij *et al.*	(LHCb Collab.)
AAIJ	14B	PL B728 234	R. Aaij *et al.*	(LHCb Collab.)
AAIJ	14T	PL B736 154	R. Aaij *et al.*	(LHCb Collab.)
AALTONEN	14B	PR D89 072014	T. Aaltonen *et al.*	(CDF Collab.)
AAIJ	13AV	PRL 110 182001	R. Aaij *et al.*	(LHCb Collab.)
AALTONEN	09AP	PR D80 072003	T. Aaltonen *et al.*	(CDF Collab.)
ABAZOV	08AL	PRL 101 232002	V.M. Abazov *et al.*	(D0 Collab.)

$\Omega_b(6316)^-$

$I(J^P) = ?(?^?)$ Status: ***
I, J, P need confirmation.

$\Omega_b(6316)^-$ MASS

VALUE (MeV)	DOCUMENT ID		TECN	COMMENT
6315.6±0.3±0.5	[1] AAIJ	20T	LHCB	pp at 7, 8, 13 TeV

[1] AAIJ 20T measures $m(\Omega_b(6316)^-)-m(\Xi_b^0) = 523.74\pm0.31\pm0.07$ MeV. We have adjusted the measurement to our best values of $m(\Xi_b^0) = 5791.9\pm0.5$ MeV. Our first error is their experiment's error and our second error is the systematic error from using our best values.

$\Omega_b(6316)^-$ WIDTH

VALUE (MeV)	CL%	DOCUMENT ID		TECN	COMMENT
<4.2	95	AAIJ	20T	LHCB	pp at 7, 8, 13 TeV

$\Omega_b(6316)^-$ DECAY MODES

	Mode	Fraction (Γ_i/Γ)
Γ_1	$\Xi_b^0K^-$	seen

$\Omega_b(6316)^-$ BRANCHING RATIOS

$\Gamma(\Xi_b^0K^-)/\Gamma_{total}$ — Γ_1/Γ

VALUE	DOCUMENT ID		TECN	COMMENT
seen	[1] AAIJ	20T	LHCB	pp at 7, 8, 13 TeV

[1] AAIJ 20T establishes the decay at 2.1 σ significance level.

$\Omega_b(6316)^-$ REFERENCES

AAIJ	20T	PRL 124 082002	R. Aaij *et al.*	(LHCb Collab.)

$\Omega_b(6330)^-$

$I(J^P) = ?(?^?)$ Status: ***
I, J, P need confirmation.

$\Omega_b(6330)^-$ MASS

VALUE (MeV)	DOCUMENT ID		TECN	COMMENT
6330.3±0.3±0.5	[1] AAIJ	20T	LHCB	pp at 7, 8, 13 TeV

[1] AAIJ 20T measures $m(\Omega_b(6330)^-)-m(\Xi_b^0) = 538.40\pm0.28\pm0.07$ MeV. We have adjusted the measurement to our best values of $m(\Xi_b^0) = 5791.9\pm0.5$ MeV. Our first error is their experiment's error and our second error is the systematic error from using our best values.

$\Omega_b(6330)^-$ WIDTH

VALUE (MeV)	CL%	DOCUMENT ID		TECN	COMMENT
<4.7	95	AAIJ	20T	LHCB	pp at 7, 8, 13 TeV

$\Omega_b(6330)^-$ DECAY MODES

	Mode	Fraction (Γ_i/Γ)
Γ_1	$\Xi_b^0K^-$	seen

$\Omega_b(6330)^-$ BRANCHING RATIOS

$\Gamma(\Xi_b^0K^-)/\Gamma_{total}$ — Γ_1/Γ

VALUE	DOCUMENT ID		TECN	COMMENT
seen	[1] AAIJ	20T	LHCB	pp at 7, 8, 13 TeV

[1] AAIJ 20T establishes the decay at 2.6 σ significance level.

$\Omega_b(6330)^-$ REFERENCES

AAIJ	20T	PRL 124 082002	R. Aaij *et al.*	(LHCb Collab.)

$\Omega_b(6340)^-$

$I(J^P) = ?(?^?)$ Status: ***
I, J, P need confirmation.

$\Omega_b(6340)^-$ MASS

VALUE (MeV)	DOCUMENT ID		TECN	COMMENT
6339.7±0.3±0.5	[1] AAIJ	20T	LHCB	pp at 7, 8, 13 TeV

[1] AAIJ 20T measures $m(\Omega_b(6340)^-)-m(\Xi_b^0) = 547.81\pm0.26\pm0.05$ MeV. We have adjusted the measurement to our best values of $m(\Xi_b^0) = 5791.9\pm0.5$ MeV. Our first error is their experiment's error and our second error is the systematic error from using our best values.

$\Omega_b(6340)^-$ WIDTH

VALUE (MeV)	CL%	DOCUMENT ID		TECN	COMMENT
<1.8	95	AAIJ	20T	LHCB	pp at 7, 8, 13 TeV

$\Omega_b(6340)^-$ DECAY MODES

	Mode	Fraction (Γ_i/Γ)
Γ_1	$\Xi_b^0K^-$	seen

$\Omega_b(6340)^-$ BRANCHING RATIOS

$\Gamma(\Xi_b^0K^-)/\Gamma_{total}$ — Γ_1/Γ

VALUE	DOCUMENT ID		TECN	COMMENT
seen	AAIJ	20T	LHCB	pp at 7, 8, 13 TeV

$\Omega_b(6340)^-$ REFERENCES

AAIJ	20T	PRL 124 082002	R. Aaij *et al.*	(LHCb Collab.)

$\Omega_b(6350)^-$

$I(J^P) = ?(?^?)$ Status: ***
I, J, P need confirmation.

$\Omega_b(6350)^-$ MASS

VALUE (MeV)	DOCUMENT ID		TECN	COMMENT
6349.8±0.4±0.5	[1] AAIJ	20T	LHCB	pp at 7, 8, 13 TeV

[1] AAIJ 20T measures $m(\Omega_b(6350)^-)-m(\Xi_b^0) = 557.98\pm0.35\pm0.05$ MeV. We have adjusted the measurement to our best values of $m(\Xi_b^0) = 5791.9\pm0.5$ MeV. Our first

Int. J. Mod. Phys. A 2026.41. Downloaded from www.worldscientific.com
by UNIVERSITY OF CALIFORNIA @ BERKELEY on 09/16/26. Re-use and distribution is strictly not permitted, except for Open Access articles.

error is their experiment's error and our second error is the systematic error from using our best values.

$\Omega_b(6350)^-$ WIDTH

VALUE (MeV)	CL%	DOCUMENT ID		TECN	COMMENT
<3.2	95	AAIJ	20T	LHCB	pp at 7, 8, 13 TeV

$\Omega_b(6350)^-$ DECAY MODES

	Mode	Fraction (Γ_i/Γ)
Γ_1	$\Xi_b^0 K^-$	seen

$\Omega_b(6350)^-$ BRANCHING RATIOS

$\Gamma(\Xi_b^0 K^-)/\Gamma_{total}$ — Γ_1/Γ

VALUE	DOCUMENT ID		TECN	COMMENT
seen	AAIJ	20T	LHCB	pp at 7, 8, 13 TeV

$\Omega_b(6350)^-$ REFERENCES

AAIJ 20T PRL 124 082002 R. Aaij *et al.* (LHCb Collab.)

b-baryon ADMIXTURE (Λ_b, Ξ_b, Ω_b)

b-baryon ADMIXTURE MEAN LIFE

Each measurement of the b-baryon mean life is an average over an admixture of various b baryons which decay weakly. Different techniques emphasize different admixtures of produced particles, which could result in a different b-baryon mean life. More b-baryon flavor specific channels are not included in the measurement.

VALUE (10^{-12} s)	EVTS	DOCUMENT ID		TECN	COMMENT
• • • We do not use the following data for averages, fits, limits, etc. • • •					
$1.218^{+0.130}_{-0.115}\pm0.042$		[1] ABAZOV	07S	D0	Repl. by ABAZOV 12U
$1.22^{+0.22}_{-0.18}\pm0.04$		[1] ABAZOV	05C	D0	Repl. by ABAZOV 07S
$1.16\pm0.20\pm0.08$		[2] ABREU	99W	DLPH	$e^+e^-\to Z$
$1.19\pm0.14\pm0.07$		[3] ABREU	99W	DLPH	$e^+e^-\to Z$
$1.14\pm0.08\pm0.04$		[4] ABREU	99W	DLPH	$e^+e^-\to Z$
$1.11^{+0.19}_{-0.18}\pm0.05$		[5] ABREU	99W	DLPH	$e^+e^-\to Z$
$1.29^{+0.24}_{-0.22}\pm0.06$		[5] ACKERSTAFF	98G	OPAL	$e^+e^-\to Z$
$1.20\pm0.08\pm0.06$		[6] BARATE	98D	ALEP	$e^+e^-\to Z$
1.21 ± 0.11		[5] BARATE	98D	ALEP	$e^+e^-\to Z$
$1.32\pm0.15\pm0.07$		[7] ABE	96M	CDF	$p\overline{p}$ at 1.8 TeV
$1.46^{+0.22}_{-0.21}{}^{+0.07}_{-0.09}$		ABREU	96D	DLPH	Repl. by ABREU 99W
$1.10^{+0.19}_{-0.17}\pm0.09$		[5] ABREU	96D	DLPH	$e^+e^-\to Z$
$1.16\pm0.11\pm0.06$		[5] AKERS	96	OPAL	$e^+e^-\to Z$
$1.27^{+0.35}_{-0.29}\pm0.09$		ABREU	95S	DLPH	Repl. by ABREU 99W
$1.05^{+0.12}_{-0.11}\pm0.09$	290	BUSKULIC	95L	ALEP	Repl. by BARATE 98D
$1.04^{+0.48}_{-0.38}\pm0.10$	11	[8] ABREU	93F	DLPH	Excess $\Lambda\mu^-$, decay lengths
$1.05^{+0.23}_{-0.20}\pm0.08$	157	[9] AKERS	93	OPAL	Excess $\Lambda\ell^-$, decay lengths
$1.12^{+0.32}_{-0.29}\pm0.16$	101	[10] BUSKULIC	92I	ALEP	Excess $\Lambda\ell^-$, impact parameters

[1] Measured mean life using fully reconstructed $\Lambda_b^0\to J/\psi\Lambda$ decays.
[2] Measured using $\Lambda\ell^-$ decay length.
[3] Measured using $p\ell^-$ decay length.
[4] This ABREU 99W result is the combined result of the $\Lambda\ell^-$, $p\ell^-$, and excess $\Lambda\mu^-$ impact parameter measurements.
[5] Measured using $\Lambda_c\ell^-$ and $\Lambda\ell^+\ell^-$.
[6] Measured using the excess of $\Lambda\ell^-$, lepton impact parameter.
[7] Measured using $\Lambda_c\ell^-$.
[8] ABREU 93F superseded by ABREU 96D.
[9] AKERS 93 superseded by AKERS 96.
[10] BUSKULIC 92I superseded by BUSKULIC 95L.

b-baryon ADMIXTURE DECAY MODES (Λ_b, Ξ_b, Ω_b)

These branching fractions are actually an average over weakly decaying b-baryons weighted by their production rates at the LHC, LEP, and Tevatron, branching ratios, and detection efficiencies. They scale with the b-baryon production fraction B($b\to$ b-baryon).

The branching fractions B(b-baryon $\to\Lambda\ell^-\overline{\nu}_\ell$ anything) and B($\Lambda_b^0\to\Lambda_c^+\ell^-\overline{\nu}_\ell$ anything) are not pure measurements because the underlying measured products of these with B($b\to$ b-baryon) were used to determine B($b\to$ b-baryon), as described in the note "Production and Decay of b-Flavored Hadrons."

For inclusive branching fractions, *e.g.*, $B\to D^\pm$ anything, the values usually are multiplicities, not branching fractions. They can be greater than one.

	Mode	Fraction (Γ_i/Γ)	Scale factor
Γ_1	$p\mu^-\overline{\nu}$ anything	$(5.8^{+2.3}_{-2.0})$ %	
Γ_2	$p\ell\overline{\nu}_\ell$ anything	(5.6 ± 1.2) %	
Γ_3	p anything	(70 ± 22) %	
Γ_4	$\Lambda\ell^-\overline{\nu}_\ell$ anything	(3.8 ± 0.6) %	
Γ_5	$\Lambda\ell^+\nu_\ell$ anything	(3.2 ± 0.8) %	
Γ_6	Λ anything	(39 ± 7) %	
Γ_7	$\Xi^-\ell^-\overline{\nu}_\ell$ anything	$(4.6\pm1.4)\times10^{-3}$	1.2

b-baryon ADMIXTURE (Λ_b, Ξ_b, Ω_b) BRANCHING RATIOS

$\Gamma(p\mu^-\overline{\nu}\text{anything})/\Gamma_{total}$ — Γ_1/Γ

VALUE (%)	EVTS	DOCUMENT ID		TECN	COMMENT
$\mathbf{5.8^{+2.2}_{-1.9}\pm0.8}$	125	[1] ABREU	95S	DLPH	$e^+e^-\to Z$

[1] ABREU 95S reports $[\Gamma(b\text{-baryon}\to p\mu^-\overline{\nu}\text{anything})/\Gamma_{total}]\times[B(\overline{b}\to b\text{-baryon at }Z)] = 0.0049\pm0.0011^{+0.0015}_{-0.0011}$ which we divide by our best (shown rounded) value $B(\overline{b}\to b\text{-baryon at }Z) = (8.4\pm1.1)\times10^{-2}$. Our first error is their experiment's error and our second error is the systematic error from using our best (shown rounded) value.

$\Gamma(p\ell\overline{\nu}_\ell\text{anything})/\Gamma_{total}$ — Γ_2/Γ

VALUE (%)	DOCUMENT ID		TECN	COMMENT
5.6±0.9±0.7	[1] BARATE	98V	ALEP	$e^+e^-\to Z$

[1] BARATE 98V reports $[\Gamma(b\text{-baryon}\to p\ell\overline{\nu}_\ell\text{anything})/\Gamma_{total}]\times[B(\overline{b}\to b\text{-baryon at }Z)] = (4.72\pm0.66\pm0.44)\times10^{-3}$ which we divide by our best (shown rounded) value $B(\overline{b}\to b\text{-baryon at }Z) = (8.4\pm1.1)\times10^{-2}$. Our first error is their experiment's error and our second error is the systematic error from using our best (shown rounded) value.

$\Gamma(p\ell\overline{\nu}_\ell\text{anything})/\Gamma(p\text{anything})$ — Γ_2/Γ_3

VALUE (%)	DOCUMENT ID		TECN	COMMENT
8.0±1.2±1.4	BARATE	98V	ALEP	$e^+e^-\to Z$

$\Gamma(\Lambda\ell^-\overline{\nu}_\ell\text{anything})/\Gamma_{total}$ — Γ_4/Γ

The values and averages in this section serve only to show what values result if one assumes our B($b\to$ b-baryon). They cannot be thought of as measurements since the underlying product branching fractions were also used to determine B($b\to$ b-baryon) as described in the note on "Production and Decay of b-Flavored Hadrons."

VALUE (%)	EVTS	DOCUMENT ID		TECN	COMMENT
3.8±0.6 OUR AVERAGE					
3.9±0.5±0.5		[1] BARATE	98D	ALEP	$e^+e^-\to Z$
3.5±0.4±0.5		[2] AKERS	96	OPAL	Excess of $\Lambda\ell^-$ over $\Lambda\ell^+$
3.6±0.9±0.5	262	[3] ABREU	95S	DLPH	Excess of $\Lambda\ell^-$ over $\Lambda\ell^+$
7.3±1.4±1.0	290	[4] BUSKULIC	95L	ALEP	Excess of $\Lambda\ell^-$ over $\Lambda\ell^+$
• • • We do not use the following data for averages, fits, limits, etc. • • •					
seen	157	[5] AKERS	93	OPAL	Excess of $\Lambda\ell^-$ over $\Lambda\ell^+$
8.3±2.5±1.1	101	[6] BUSKULIC	92I	ALEP	Excess of $\Lambda\ell^-$ over $\Lambda\ell^+$

[1] BARATE 98D reports $[\Gamma(b\text{-baryon}\to\Lambda\ell^-\overline{\nu}_\ell\text{anything})/\Gamma_{total}]\times[B(\overline{b}\to b\text{-baryon at }Z)] = 0.00326\pm0.00016\pm0.00039$ which we divide by our best (shown rounded) value $B(\overline{b}\to b\text{-baryon at }Z) = (8.4\pm1.1)\times10^{-2}$. Our first error is their experiment's error and our second error is the systematic error from using our best (shown rounded) value. Measured using the excess of $\Lambda\ell^-$, lepton impact parameter.
[2] AKERS 96 reports $[\Gamma(b\text{-baryon}\to\Lambda\ell^-\overline{\nu}_\ell\text{anything})/\Gamma_{total}]\times[B(\overline{b}\to b\text{-baryon at }Z)] = 0.00291\pm0.00023\pm0.00025$ which we divide by our best (shown rounded) value $B(\overline{b}\to b\text{-baryon at }Z) = (8.4\pm1.1)\times10^{-2}$. Our first error is their experiment's error and our second error is the systematic error from using our best (shown rounded) value.
[3] ABREU 95S reports $[\Gamma(b\text{-baryon}\to\Lambda\ell^-\overline{\nu}_\ell\text{anything})/\Gamma_{total}]\times[B(\overline{b}\to b\text{-baryon at }Z)] = 0.0030\pm0.0006\pm0.0004$ which we divide by our best (shown rounded) value $B(\overline{b}\to b\text{-baryon at }Z) = (8.4\pm1.1)\times10^{-2}$. Our first error is their experiment's error and our second error is the systematic error from using our best (shown rounded) value.
[4] BUSKULIC 95L reports $[\Gamma(b\text{-baryon}\to\Lambda\ell^-\overline{\nu}_\ell\text{anything})/\Gamma_{total}]\times[B(\overline{b}\to b\text{-baryon at }Z)] = 0.0061\pm0.0006\pm0.0010$ which we divide by our best (shown rounded) value $B(\overline{b}\to b\text{-baryon at }Z) = (8.4\pm1.1)\times10^{-2}$. Our first error is their experiment's error and our second error is the systematic error from using our best (shown rounded) value.
[5] AKERS 93 superseded by AKERS 96.

[6] BUSKULIC 92I reports [$\Gamma(b\text{-baryon} \to \Lambda \ell^- \overline{\nu}_\ell \text{anything})/\Gamma_{total}$] × [B($\overline{b} \to b$-baryon at Z)] = 0.0070 ± 0.0010 ± 0.0018 which we divide by our best (shown rounded) value B($\overline{b} \to b$-baryon at Z) = (8.4 ± 1.1) × 10^{-2}. Our first error is their experiment's error and our second error is the systematic error from using our best (shown rounded) value. Superseded by BUSKULIC 95L.

$\Gamma(\Lambda \ell^+ \nu_\ell \text{anything})/\Gamma(\Lambda \text{anything})$ — Γ_5/Γ_6

VALUE (units 10^{-2})	DOCUMENT ID		TECN	COMMENT
8.0±1.2±0.8	ABBIENDI	99L	OPAL	$e^+e^- \to Z$
• • • We do not use the following data for averages, fits, limits, etc. • • •				
7.0±1.2±0.7	ACKERSTAFF	97N	OPAL	Repl. by ABBIENDI 99L

$\Gamma(\Lambda \text{anything})/\Gamma_{total}$ — Γ_6/Γ

VALUE (%)	DOCUMENT ID		TECN	COMMENT
39± 7 OUR AVERAGE				
42± 6±5	[1] ABBIENDI	99L	OPAL	$e^+e^- \to Z$
27^{+15}_{-9}±3	[2] ABREU	95C	DLPH	$e^+e^- \to Z$
• • • We do not use the following data for averages, fits, limits, etc. • • •				
47± 7±6	[3] ACKERSTAFF	97N	OPAL	Repl. by ABBIENDI 99L

[1] ABBIENDI 99L reports [$\Gamma(b\text{-baryon} \to \Lambda \text{anything})/\Gamma_{total}$] × [B($\overline{b} \to b$-baryon at Z)] = 0.035 ± 0.0032 ± 0.0035 which we divide by our best (shown rounded) value B($\overline{b} \to b$-baryon at Z) = (8.4 ± 1.1) × 10^{-2}. Our first error is their experiment's error and our second error is the systematic error from using our best (shown rounded) value.

[2] ABREU 95C reports $0.28^{+0.17}_{-0.12}$ from a measurement of [$\Gamma(b\text{-baryon} \to \Lambda \text{anything})/\Gamma_{total}$] × [B($\overline{b} \to b$-baryon at Z)] assuming B($\overline{b} \to b$-baryon at Z) = 0.08 ± 0.02, which we rescale to our best (shown rounded) value B($\overline{b} \to b$-baryon at Z) = (8.4 ± 1.1) × 10^{-2}. Our first error is their experiment's error and our second error is the systematic error from using our best (shown rounded) value.

[3] ACKERSTAFF 97N reports [$\Gamma(b\text{-baryon} \to \Lambda \text{anything})/\Gamma_{total}$] × [B($\overline{b} \to b$-baryon at Z)] = 0.0393 ± 0.0046 ± 0.0037 which we divide by our best (shown rounded) value B($\overline{b} \to b$-baryon at Z) = (8.4 ± 1.1) × 10^{-2}. Our first error is their experiment's error and our second error is the systematic error from using our best (shown rounded) value.

$\Gamma(\Xi^- \ell^- \overline{\nu}_\ell \text{anything})/\Gamma_{total}$ — Γ_7/Γ

VALUE (units 10^{-3})	DOCUMENT ID		TECN	COMMENT
4.6±1.4 OUR AVERAGE	Error includes scale factor of 1.2.			
3.6±1.2±0.5	[1] ABDALLAH	05C	DLPH	$e^+e^- \to Z^0$
6.4±1.6±0.8	[2] BUSKULIC	96T	ALEP	Excess $\Xi^- \ell^-$ over $\Xi^- \ell^+$
• • • We do not use the following data for averages, fits, limits, etc. • • •				
7.0±2.8±0.9	[3] ABREU	95V	DLPH	Repl. by ABDALLAH 05C

[1] ABDALLAH 05C reports [$\Gamma(b\text{-baryon} \to \Xi^- \ell^- \overline{\nu}_\ell \text{anything})/\Gamma_{total}$] × [B($\overline{b} \to b$-baryon at Z)] = (3.0 ± 1.0 ± 0.3) × 10^{-4} which we divide by our best (shown rounded) value B($\overline{b} \to b$-baryon at Z) = (8.4 ± 1.1) × 10^{-2}. Our first error is their experiment's error and our second error is the systematic error from using our best (shown rounded) value.

[2] BUSKULIC 96T reports [$\Gamma(b\text{-baryon} \to \Xi^- \ell^- \overline{\nu}_\ell \text{anything})/\Gamma_{total}$] × [B($\overline{b} \to b$-baryon at Z)] = (5.4 ± 1.1 ± 0.8) × 10^{-4} which we divide by our best (shown rounded) value B($\overline{b} \to b$-baryon at Z) = (8.4 ± 1.1) × 10^{-2}. Our first error is their experiment's error and our second error is the systematic error from using our best (shown rounded) value.

[3] ABREU 95V reports [$\Gamma(b\text{-baryon} \to \Xi^- \ell^- \overline{\nu}_\ell \text{anything})/\Gamma_{total}$] × [B($\overline{b} \to b$-baryon at Z)] = (5.9 ± 2.1 ± 1.0) × 10^{-4} which we divide by our best (shown rounded) value B($\overline{b} \to b$-baryon at Z) = (8.4 ± 1.1) × 10^{-2}. Our first error is their experiment's error and our second error is the systematic error from using our best (shown rounded) value.

b-baryon ADMIXTURE (Λ_b, Ξ_b, Ω_b) REFERENCES

ABAZOV	12U	PR D85 112003	V.M. Abazov et al.	(D0 Collab.)
ABAZOV	07S	PRL 99 142001	V.M. Abazov et al.	(D0 Collab.)
ABAZOV	05C	PRL 94 102001	V.M. Abazov et al.	(D0 Collab.)
ABDALLAH	05C	EPJ C44 299	J. Abdallah et al.	(DELPHI Collab.)
ABBIENDI	99L	EPJ C9 1	G. Abbiendi et al.	(OPAL Collab.)
ABREU	99W	EPJ C10 185	P. Abreu et al.	(DELPHI Collab.)
ACKERSTAFF	98G	PL B426 161	K. Ackerstaff et al.	(OPAL Collab.)
BARATE	98D	EPJ C2 197	R. Barate et al.	(ALEPH Collab.)
BARATE	98V	EPJ C5 205	R. Barate et al.	(ALEPH Collab.)
ACKERSTAFF	97N	ZPHY C74 423	K. Ackerstaff et al.	(OPAL Collab.)
ABE	96M	PRL 77 1439	F. Abe et al.	(CDF Collab.)
ABREU	96D	ZPHY C71 199	P. Abreu et al.	(DELPHI Collab.)
AKERS	96	ZPHY C69 195	R. Akers et al.	(OPAL Collab.)
BUSKULIC	96T	PL B384 449	D. Buskulic et al.	(ALEPH Collab.)
ABREU	95C	PL B347 447	P. Abreu et al.	(DELPHI Collab.)
ABREU	95S	ZPHY C68 375	P. Abreu et al.	(DELPHI Collab.)
ABREU	95V	ZPHY C68 541	P. Abreu et al.	(DELPHI Collab.)
BUSKULIC	95L	PL B357 685	D. Buskulic et al.	(ALEPH Collab.)
ABREU	93F	PL B311 379	P. Abreu et al.	(DELPHI Collab.)
AKERS	93	PL B316 435	R. Akers et al.	(OPAL Collab.)
BUSKULIC	92I	PL B297 449	D. Buskulic et al.	(ALEPH Collab.)

Int. J. Mod. Phys. A 2026.41. Downloaded from www.worldscientific.com
UNIVERSITY OF CALIFORNIA @ BERKELEY on 09/16/26. Re-use and distribution is strictly not permitted, except for Open Access articles.

Int. J. Mod. Phys. A 2026.41. Downloaded from www.worldscientific.com by UNIVERSITY OF CALIFORNIA @ BERKELEY on 09/16/26. Re-use and distribution is strictly not permitted, except for Open Access articles.

EXOTIC BARYONS

See the related review(s):

Pentaquarks

$P_{c\overline{c}}(4312)^+$

$I(J^P) = \frac{1}{2}(?^?)$ Status: *

OMITTED FROM SUMMARY TABLE

Was $P_c(4312)^+$.

$P_{c\overline{c}}(4312)^+$ MASS

VALUE (MeV)	DOCUMENT ID		TECN	COMMENT
$4311.9 \pm 0.7^{+6.8}_{-0.6}$	AAIJ	19W	LHCB	pp at 7, 8, 13 TeV

$P_{c\overline{c}}(4312)^+$ WIDTH

VALUE (MeV)	DOCUMENT ID		TECN	COMMENT
$9.8 \pm 2.7^{+3.7}_{-4.5}$	AAIJ	19W	LHCB	pp at 7, 8, 13 TeV

$P_{c\overline{c}}(4312)^+$ DECAY MODES

	Mode	Fraction (Γ_i/Γ)
Γ_1	$J/\psi p$	seen
Γ_2	$\Lambda_c^+ \overline{D}^0$	not seen
Γ_3	$\Lambda_c^+ \pi^+ D^-$	not seen
Γ_4	$\overline{\Lambda}_c^- \pi^+ D^+$	[a] not seen

[a] Searched for the charge conjugate mode from $\overline{P}^-_{c\overline{c}}$ decays.

$P_{c\overline{c}}(4312)^+$ BRANCHING RATIOS

$\Gamma(J/\psi p)/\Gamma_{total}$ — Γ_1/Γ

VALUE	EVTS	DOCUMENT ID		TECN	COMMENT
seen	246k	[1] AAIJ	19W	LHCB	pp at 7, 8, 13 TeV
• • • We do not use the following data for averages, fits, limits, etc. • • •					
not seen	797	[2] AAIJ	22H	LHCB	pp at 7, 8, 13 TeV

[1] Amplitude analysis of $\Lambda_b^0 \to J/\psi p K^-$.

[2] Amplitude analysis of $B_s^0 \to J/\psi p \overline{p}$. AAIJ 22H finds evidence at just over 3 σ for a $J/\psi p$ structure at $4337^{+7}_{-4} \pm 2$ MeV.

$\Gamma(\Lambda_c^+ \overline{D}^0)/\Gamma_{total}$ — Γ_2/Γ

VALUE	DOCUMENT ID		TECN	COMMENT
not seen	AAIJ	24Z	LHCB	pp, 5.7 fb^{-1} at 13 TeV

$\Gamma(\Lambda_c^+ \pi^+ D^-)/\Gamma_{total}$ — Γ_3/Γ

VALUE	DOCUMENT ID		TECN	COMMENT
not seen	AAIJ	24Z	LHCB	pp, 5.7 fb^{-1} at 13 TeV

$\Gamma(\overline{\Lambda}_c^- \pi^+ D^+)/\Gamma_{total}$ — Γ_4/Γ

VALUE	DOCUMENT ID		TECN	COMMENT
not seen	AAIJ	24Z	LHCB	$\overline{P}^-_{c\overline{c}} \to \Lambda_c^+ \pi^- D^-$

$P_{c\overline{c}}(4312)^+$ REFERENCES

AAIJ 24Z PR D110 032001 R. Aaij *et al.* (LHCb Collab.)
AAIJ 22H PRL 128 062001 R. Aaij *et al.* (LHCb Collab.)
AAIJ 19W PRL 122 222001 R. Aaij *et al.* (LHCb Collab.)

$P_{c\overline{c}s}(4338)^0$

$I(J^P) = 0(\frac{1}{2}^-)$ Status: *

AAIJ 23Q determines that spin-parity $J^P = 1/2^-$ is preferred, while spin-parity $J^P = 1/2^+$ is excluded at a 90% confidence level and spin $J = 3/2$ hypotheses are discarded.

$P_{c\overline{c}s}(4338)^0$ MASS

VALUE (MeV)	EVTS	DOCUMENT ID		TECN	COMMENT
$4338.2 \pm 0.7 \pm 0.4$	4.4k	AAIJ	23Q	LHCB	$B^- \to J/\psi \Lambda \overline{p}$

$P_{c\overline{c}s}(4338)^0$ WIDTH

VALUE (MeV)	EVTS	DOCUMENT ID		TECN	COMMENT
$7.0 \pm 1.2 \pm 1.3$	4.4k	AAIJ	23Q	LHCB	$B^- \to J/\psi \Lambda \overline{p}$

$P_{c\overline{c}s}(4338)^0$ DECAY MODES

	Mode	Fraction (Γ_i/Γ)
Γ_1	$J/\psi \Lambda$	seen
Γ_2	$\Lambda_c^+ D_s^-$	not seen

$P_{c\overline{c}s}(4338)^0$ BRANCHING RATIOS

$\Gamma(J/\psi \Lambda)/\Gamma_{total}$ — Γ_1/Γ

VALUE	EVTS	DOCUMENT ID		TECN	COMMENT
seen	4.4k	AAIJ	23Q	LHCB	$B^- \to J/\psi \Lambda \overline{p}$

$\Gamma(\Lambda_c^+ D_s^-)/\Gamma_{total}$ — Γ_2/Γ

VALUE	DOCUMENT ID		TECN	COMMENT
not seen	[1] AAIJ	25AK	LHCB	pp at 13 TeV

[1] An analysis of $\Lambda_b^0 \to \Lambda_c^+ D_s^- K^+ K^-$ decays, AAIJ 25AK reports $B(\Lambda_b^0 \to P_{c\overline{c}s}(4338)^0 K^+ K^-, P_{c\overline{c}s} \to \Lambda_c^+ D_s^-) / B(\Lambda_b^0 \to \Lambda_c^+ D_s^- K^+ K^-) < 0.12$ at 95% CL.

$P_{c\overline{c}s}(4338)^0$ REFERENCES

AAIJ 25AK PR D112 052013 R. Aaij *et al.* (LHCb Collab.)
AAIJ 23Q PRL 131 031901 R. Aaij *et al.* (LHCb Collab.) JP

$P_{c\overline{c}}(4380)^+$

$I(J^P) = \frac{1}{2}(?^?)$ Status: *

OMITTED FROM SUMMARY TABLE

Was $P_c(4380)^+$.

A resonance seen in $\Lambda_b^0 \to P_c^+ K^-$, then $P_c \to J/\psi p$, with a significance of 9 standard deviations. The $J/\psi p$ quark content is $uudc\overline{c}$, a pentaquark. See also the $P_c(4450)^+$. In the best amplitude fit, the two states have opposite parity, one having $J = 3/2$, the other $J = 5/2$.

Extraction of the pentaquark signals requires some understanding of the dominant $K^- p$ background. AAIJ 15P used a model-dependent approach. AAIJ 16AG reanalyzed the data making minimal assumptions about the $K^- p$ background, and thus confirmed the strong significance of the pentaquark signals.

$P_{c\overline{c}}(4380)^+$ MASS

VALUE (MeV)	DOCUMENT ID		TECN	COMMENT
$4380 \pm 8 \pm 29$	AAIJ	15P	LHCB	pp at 7, 8 TeV

$P_{c\overline{c}}(4380)^+$ WIDTH

VALUE (MeV)	DOCUMENT ID		TECN	COMMENT
$205 \pm 18 \pm 86$	AAIJ	15P	LHCB	pp at 7, 8 TeV

$P_{c\overline{c}}(4380)^+$ DECAY MODES

	Mode	Fraction (Γ_i/Γ)
Γ_1	$J/\psi p$	seen

Int. J. Mod. Phys. A 2026.41. Downloaded from www.worldscientific.com
UNIVERSITY OF CALIFORNIA @ BERKELEY on 09/16/26. Re-use and distribution is strictly not permitted, except for Open Access articles.

$P_{c\overline{c}}(4380)^+$ BRANCHING RATIOS

$\Gamma(J/\psi p)/\Gamma_{total}$ — Γ_1/Γ

VALUE	DOCUMENT ID		TECN	COMMENT
seen	AAIJ	15P	LHCB	pp at 7, 8 TeV

$P_{c\overline{c}}(4380)^+$ REFERENCES

AAIJ	16AG	PRL 117 082002	R. Aaij *et al.*	(LHCb Collab.)
AAIJ	15P	PRL 115 072001	R. Aaij *et al.*	(LHCb Collab.)

$P_{c\overline{c}}(4440)^+$

$I(J^P) = \frac{1}{2}(?^?)$ Status: *

OMITTED FROM SUMMARY TABLE
Was $P_c(4440)^+$.

$P_{c\overline{c}}(4440)^+$ MASS

VALUE (MeV)	DOCUMENT ID		TECN	COMMENT
$4440.3 \pm 1.3^{+4.1}_{-4.7}$	AAIJ	19W	LHCB	pp at 7, 8, 13 TeV

$P_{c\overline{c}}(4440)^+$ WIDTH

VALUE (MeV)	DOCUMENT ID		TECN	COMMENT
$20.6 \pm 4.9^{+8.7}_{-10.1}$	AAIJ	19W	LHCB	pp at 7, 8, 13 TeV

$P_{c\overline{c}}(4440)^+$ DECAY MODES

	Mode	Fraction (Γ_i/Γ)
Γ_1	$J/\psi p$	seen
Γ_2	$\Lambda_c^+ \overline{D}^0$	not seen
Γ_3	$\Lambda_c^+ \pi^+ D^-$	not seen
Γ_4	$\Sigma_c(2455)^{++} D^-$	not seen
Γ_5	$\Sigma_c(2520)^{++} D^-$	not seen
Γ_6	$\overline{\Lambda}_c^- \pi^+ D^+$	[a] not seen
Γ_7	$\overline{\Sigma}_c(2455)^0 D^+$	[a] not seen
Γ_8	$\overline{\Sigma}_c(2520)^0 D^+$	[a] not seen
Γ_9	$\Lambda_c^+ \pi^+ D^{*-}$	not seen
Γ_{10}	$\overline{\Lambda}_c^- \pi^+ D^{*+}$	[a] not seen

[a] Searched for the charge conjugate mode from $\overline{P}^-_{c\overline{c}}$ decays.

$P_{c\overline{c}}(4440)^+$ BRANCHING RATIOS

$\Gamma(J/\psi p)/\Gamma_{total}$ — Γ_1/Γ

VALUE	DOCUMENT ID		TECN	COMMENT
seen	[1] POPOV	21	D0	$p\overline{p}$ at 1.96 TeV
seen	AAIJ	19W	LHCB	pp at 7, 8, 13 TeV

[1] Search for J/ψ inclusive production in association with a charged particle, assumed to be a proton. POPOV 21 observes a resonant signal consistent with a superposition of the $P_{c\overline{c}}(4440)^+$ and $P_{c\overline{c}}(4457)^+$, using masses and widths measured by AAIJ 19W, at significance of 3σ.

$\Gamma(\Lambda_c^+ \overline{D}^0)/\Gamma_{total}$ — Γ_2/Γ

VALUE	DOCUMENT ID		TECN	COMMENT
not seen	AAIJ	24Z	LHCB	pp, 5.7 fb^{-1} at 13 TeV

$\Gamma(\Lambda_c^+ \pi^+ D^-)/\Gamma_{total}$ — Γ_3/Γ

VALUE	DOCUMENT ID		TECN	COMMENT
not seen	AAIJ	24Z	LHCB	pp, 5.7 fb^{-1} at 13 TeV

$\Gamma(\Sigma_c(2455)^{++} D^-)/\Gamma_{total}$ — Γ_4/Γ

VALUE	DOCUMENT ID		TECN	COMMENT
not seen	AAIJ	24Z	LHCB	pp, 5.7 fb^{-1} at 13 TeV

$\Gamma(\Sigma_c(2520)^{++} D^-)/\Gamma_{total}$ — Γ_5/Γ

VALUE	DOCUMENT ID		TECN	COMMENT
not seen	AAIJ	24Z	LHCB	pp, 5.7 fb^{-1} at 13 TeV

$\Gamma(\overline{\Lambda}_c^- \pi^+ D^+)/\Gamma_{total}$ — Γ_6/Γ

VALUE	DOCUMENT ID		TECN	COMMENT
not seen	AAIJ	24Z	LHCB	$\overline{P}^-_{c\overline{c}} \to \Lambda_c^+ \pi^- D^-$

$\Gamma(\overline{\Sigma}_c(2455)^0 D^+)/\Gamma_{total}$ — Γ_7/Γ

VALUE	DOCUMENT ID		TECN	COMMENT
not seen	AAIJ	24Z	LHCB	$\overline{P}^-_{c\overline{c}} \to \Sigma_c(2455)^0 D^-$

$\Gamma(\overline{\Sigma}_c(2520)^0 D^+)/\Gamma_{total}$ — Γ_8/Γ

VALUE	DOCUMENT ID		TECN	COMMENT
not seen	AAIJ	24Z	LHCB	$\overline{P}^-_{c\overline{c}} \to \Sigma_c(2520)^0 D^-$

$\Gamma(\Lambda_c^+ \pi^+ D^{*-})/\Gamma_{total}$ — Γ_9/Γ

VALUE	DOCUMENT ID		TECN	COMMENT
not seen	AAIJ	24Z	LHCB	pp, 5.7 fb^{-1} at 13 TeV

$\Gamma(\overline{\Lambda}_c^- \pi^+ D^{*+})/\Gamma_{total}$ — Γ_{10}/Γ

VALUE	DOCUMENT ID		TECN	COMMENT
not seen	AAIJ	24Z	LHCB	$\overline{P}^-_{c\overline{c}} \to \Lambda_c^+ \pi^- D^{*-}$

$P_{c\overline{c}}(4440)^+$ REFERENCES

AAIJ	24Z	PR D110 032001	R. Aaij *et al.*	(LHCb Collab.)
POPOV	21	PAN 83 1383	A.V. Popov *et al.*	(D0 Collab.)
AAIJ	19W	PRL 122 222001	R. Aaij *et al.*	(LHCb Collab.)

$P_{c\overline{c}}(4457)^+$

$I(J^P) = \frac{1}{2}(?^?)$ Status: *

OMITTED FROM SUMMARY TABLE
was $P_c(4450)$

A resonance seen in $\Lambda_b^0 \to P_c^+ K^-$, then $P_c \to J/\psi p$, with a significance of 12 standard deviations. The $J/\psi p$ quark content is $uudc\overline{c}$, a pentaquark. See also the $P_{c\overline{c}}(4380)^+$. In the best amplitude fit, the two states have opposite parity, one having $J = 3/2$, the other $J = 5/2$.

Extraction of the pentaquark signals requires some understanding of the dominant $K^- p$ background. AAIJ 15P used a model-dependent approach. AAIJ 16AG reanalyzed the data making minimal assumptions about the $K^- p$ background, and thus confirmed the strong significance of the pentaquark signals.

$P_{c\overline{c}}(4457)^+$ MASS

VALUE (MeV)	DOCUMENT ID		TECN	COMMENT
$4457.3 \pm 0.6^{+4.1}_{-1.7}$	AAIJ	19W	LHCB	pp at 7, 8, 13 TeV
• • • We do not use the following data for averages, fits, limits, etc. • • •				
$4449.8 \pm 1.7 \pm 2.5$	[1] AAIJ	15P	LHCB	Repl. by AAIJ 19W

[1] Considering $P_{c\overline{c}}(4440)$ and $P_{c\overline{c}}(4457)$ as a single resonance.

$P_{c\overline{c}}(4457)^+$ WIDTH

VALUE (MeV)	DOCUMENT ID		TECN	COMMENT
$6.4 \pm 2.0^{+5.7}_{-1.9}$	AAIJ	19W	LHCB	pp at 7, 8, 13 TeV
• • • We do not use the following data for averages, fits, limits, etc. • • •				
$39 \pm 5 \pm 19$	[1] AAIJ	15P	LHCB	Repl. by AAIJ 19W

[1] Considering $P_{c\overline{c}}(4440)$ and $P_{c\overline{c}}(4457)$ as a single resonance.

$P_{c\overline{c}}(4457)^+$ DECAY MODES

	Mode	Fraction (Γ_i/Γ)
Γ_1	$J/\psi p$	seen
Γ_2	$\Lambda_c^+ \overline{D}^0$	not seen
Γ_3	$\Lambda_c^+ \pi^+ D^-$	not seen
Γ_4	$\Sigma_c(2455)^{++} D^-$	not seen
Γ_5	$\Sigma_c(2520)^{++} D^-$	not seen
Γ_6	$\overline{\Lambda}_c^- \pi^+ D^+$	[a] not seen
Γ_7	$\overline{\Sigma}_c(2455)^0 D^+$	[a] not seen
Γ_8	$\overline{\Sigma}_c(2520)^0 D^+$	[a] not seen
Γ_9	$\Lambda_c^+ \pi^+ D^{*-}$	not seen
Γ_{10}	$\overline{\Lambda}_c^- \pi^+ D^{*+}$	[a] not seen

[a] Searched for the charge conjugate mode from $\overline{P}^-_{c\overline{c}}$ decays.

$P_{c\overline{c}}(4457)^+$ BRANCHING RATIOS

$\Gamma(J/\psi p)/\Gamma_{total}$ — Γ_1/Γ

VALUE	DOCUMENT ID		TECN	COMMENT
seen	[1] POPOV	21	D0	$p\overline{p}$ at 1.96 TeV
seen	AAIJ	19W	LHCB	pp at 7, 8, 13 TeV
seen	AAIJ	15P	LHCB	pp at 7, 8 TeV

[1] Search for J/ψ inclusive production in association with a charged particle, assumed to be a proton. POPOV 21 observes a resonant signal consistent with a superposition of the $P_{c\overline{c}}(4440)^+$ and $P_{c\overline{c}}(4457)^+$, using masses and widths measured by AAIJ 19W, at significance of 3σ.

Int. J. Mod. Phys. A 2026.41. Downloaded from www.worldscientific.com
by UNIVERSITY OF CALIFORNIA @ BERKELEY on 09/16/26. Re-use and distribution is strictly not permitted, except for Open Access articles.

$\Gamma(\Lambda_c^+ \overline{D}^0)/\Gamma_{total}$ — Γ_2/Γ

VALUE	DOCUMENT ID		TECN	COMMENT
not seen	AAIJ	24z	LHCB	pp, 5.7 fb^{-1} at 13 TeV

$\Gamma(\Lambda_c^+ \pi^+ D^-)/\Gamma_{total}$ — Γ_3/Γ

VALUE	DOCUMENT ID		TECN	COMMENT
not seen	AAIJ	24z	LHCB	pp, 5.7 fb^{-1} at 13 TeV

$\Gamma(\Sigma_c(2455)^{++} D^-)/\Gamma_{total}$ — Γ_4/Γ

VALUE	DOCUMENT ID		TECN	COMMENT
not seen	AAIJ	24z	LHCB	pp, 5.7 fb^{-1} at 13 TeV

$\Gamma(\Sigma_c(2520)^{++} D^-)/\Gamma_{total}$ — Γ_5/Γ

VALUE	DOCUMENT ID		TECN	COMMENT
not seen	AAIJ	24z	LHCB	pp, 5.7 fb^{-1} at 13 TeV

$\Gamma(\overline{\Lambda}_c^- \pi^+ D^+)/\Gamma_{total}$ — Γ_6/Γ

VALUE	DOCUMENT ID		TECN	COMMENT
not seen	AAIJ	24z	LHCB	$\overline{P}^-_{c\overline{c}} \to \Lambda_c^+ \pi^- D^-$

$\Gamma(\overline{\Sigma}_c(2455)^0 D^+)/\Gamma_{total}$ — Γ_7/Γ

VALUE	DOCUMENT ID		TECN	COMMENT
not seen	AAIJ	24z	LHCB	$\overline{P}^-_{c\overline{c}} \to \Sigma_c(2455)^0 D^-$

$\Gamma(\overline{\Sigma}_c(2520)^0 D^+)/\Gamma_{total}$ — Γ_8/Γ

VALUE	DOCUMENT ID		TECN	COMMENT
not seen	AAIJ	24z	LHCB	$\overline{P}^-_{c\overline{c}} \to \Sigma_c(2520)^0 D^-$

$\Gamma(\Lambda_c^+ \pi^+ D^{*-})/\Gamma_{total}$ — Γ_9/Γ

VALUE	DOCUMENT ID		TECN	COMMENT
not seen	AAIJ	24z	LHCB	pp, 5.7 fb^{-1} at 13 TeV

$\Gamma(\overline{\Lambda}_c^- \pi^+ D^{*+})/\Gamma_{total}$ — Γ_{10}/Γ

VALUE	DOCUMENT ID		TECN	COMMENT
not seen	AAIJ	24z	LHCB	$\overline{P}^-_{c\overline{c}} \to \Lambda_c^+ \pi^- D^{*-}$

$P_{c\overline{c}}(4457)^+$ REFERENCES

AAIJ	24Z	PR D110 032001	R. Aaij *et al.*	(LHCb Collab.)
POPOV	21	PAN 83 1383	A.V. Popov *et al.*	(D0 Collab.)
AAIJ	19W	PRL 122 222001	R. Aaij *et al.*	(LHCb Collab.)
AAIJ	16AG	PRL 117 082002	R. Aaij *et al.*	(LHCb Collab.)
AAIJ	15P	PRL 115 072001	R. Aaij *et al.*	(LHCb Collab.)

$P_{c\overline{c}s}(4459)^0$

$I(J^P) = 0(?^?)$ Status: *

OMITTED FROM SUMMARY TABLE

$P_{c\overline{c}s}(4459)^0$ MASS

VALUE (MeV)	EVTS	DOCUMENT ID		TECN	COMMENT
$4466\ ^{+6}_{-5}$ OUR AVERAGE Error includes scale factor of 1.8.					
$4471.7 \pm 4.8 \pm 0.6$	21	[1] ADACHI	25A	BELL	$\Upsilon(1S/2S) \to J/\psi\Lambda$ incl.
$4458.8 \pm 2.9\ ^{+4.7}_{-1.1}$	1.8k	[2] AAIJ	21AO	LHCB	$\Xi_b^- \to J/\psi\Lambda K^-$

[1] ADACHI 25A sees evidence for the $P_{c\overline{c}s}(4459)$ at 2.8σ global significance.
[2] AAIJ 21AO sees evidence for the $P_{c\overline{c}s}(4459)$ at 3.1σ global significance.

$P_{c\overline{c}s}(4459)^0$ WIDTH

VALUE (MeV)	EVTS	DOCUMENT ID		TECN	COMMENT
$19\ ^{+8}_{-7}$ OUR AVERAGE					
$22 \pm 13 \pm 3$	21	[1] ADACHI	25A	BELL	$\Upsilon(1S/2S) \to J/\psi\Lambda$ incl.
$17.3 \pm 6.5\ ^{+8.0}_{-5.7}$	1.8k	[2] AAIJ	21AO	LHCB	$\Xi_b^- \to J/\psi\Lambda K^-$

[1] ADACHI 25A sees evidence for the $P_{c\overline{c}s}(4459)$ at 2.8σ global significance.
[2] AAIJ 21AO sees evidence for the $P_{c\overline{c}s}(4459)$ at 3.1σ global significance

$P_{c\overline{c}s}(4459)^0$ DECAY MODES

	Mode	Fraction (Γ_i/Γ)
Γ_1	$J/\psi\Lambda$	seen
Γ_2	$\Lambda_c^+ D_s^-$	not seen

$P_{c\overline{c}s}(4459)^0$ BRANCHING RATIOS

$\Gamma(J/\psi\Lambda)/\Gamma_{total}$ — Γ_1/Γ

VALUE	EVTS	DOCUMENT ID		TECN	COMMENT
seen	21	[1] ADACHI	25A	BELL	$\Upsilon(1S/2S) \to J/\psi\Lambda$ incl.
seen	1.8k	[2] AAIJ	21AO	LHCB	$\Xi_b^- \to J/\psi\Lambda K^-$

[1] ADACHI 25A sees evidence for the $P_{c\overline{c}s}(4459)$ at 2.8σ global significance.
[2] AAIJ 21AO sees evidence for the $P_{c\overline{c}s}(4459)$ at 3.1σ global significance.

$\Gamma(\Lambda_c^+ D_s^-)/\Gamma_{total}$ — Γ_2/Γ

VALUE	DOCUMENT ID		TECN	COMMENT
not seen	[1] AAIJ	25AK	LHCB	pp at 13 TeV

[1] An analysis of $\Lambda_b^0 \to \Lambda_c^+ D_s^- K^+ K^-$ decays, AAIJ 25AK reports $B(\Lambda_b^0 \to P_{c\overline{c}s}(4459)^0 K^+ K^-,\ P_{c\overline{c}s} \to \Lambda_c^+ D_s^-) / B(\Lambda_b^0 \to \Lambda_c^+ D_s^- K^+ K^-) < 0.20$ at 95% CL.

$P_{c\overline{c}s}(4459)^0$ REFERENCES

AAIJ	25AK	PR D112 052013	R. Aaij *et al.*	(LHCb Collab.)
ADACHI	25A	PRL 135 041901	I. Adachi *et al.*	(BELLE and BELLE II Collab.)
AAIJ	21AO	SCIB 66 1278	R. Aaij *et al.*	(LHCb Collab.)

Int. J. Mod. Phys. A 2026.41. Downloaded from www.worldscientific.com
UNIVERSITY OF CALIFORNIA @ BERKELEY on 09/16/26. Re-use and distribution is strictly not permitted, except for Open Access articles.

Int. J. Mod. Phys. A 2026.41. Downloaded from www.worldscientific.com
by UNIVERSITY OF CALIFORNIA @ BERKELEY on 09/16/26. Re-use and distribution is strictly not permitted, except for Open Access articles.

MISCELLANEOUS SEARCHES

Magnetic Monopole Searches 2429
Supersymmetric Particle Searches 2432
Technicolor 2493
Quark and Lepton Compositeness 2494
Extra Dimensions 2499
WIMP and Dark Matter Searches 2505
Other Particle Searches 2523

SEARCHES IN OTHER SECTIONS

Neutral Higgs Bosons, Searches for 1300
Charged Higgs Bosons ($H^{\pm}$ and $H^{\pm\pm}$), Searches for 1313
New Heavy Bosons 1317
Axions (A^0) and Other Very Light Bosons 1338
Heavy Charged Lepton Searches 1403
Double-β Decay 1416
Heavy Neutral Leptons, Searches for 1440
b' (Fourth Generation) Quark 1477
t' (Fourth Generation) Quark 1480
Free Quark Searches 1482

Related Reviews in Volume 1

84. Extra dimensions (rev.) 1067
85. W'-boson searches (rev.) 1076
86. Z'-boson searches (rev.) 1080
87. Supersymmetry: theory (rev.) 1086
88. Supersymmetry: experiment (rev.) 1108
89. Axions and other similar particles (rev.) 1130
90. Quark and lepton compositeness, searches for (rev.) . . 1150
91. Dynamical electroweak symmetry breaking: implications of the H^0 (rev.) 1156
92. Grand unified theories (rev.) 1171
93. Leptoquarks (rev.) 1189
94. Magnetic monopoles (rev.) 1194

Int. J. Mod. Phys. A 2026.41. Downloaded from www.worldscientific.com
by UNIVERSITY OF CALIFORNIA @ BERKELEY on 09/16/26. Re-use and distribution is strictly not permitted, except for Open Access articles.

Int. J. Mod. Phys. A 2026.41. Downloaded from www.worldscientific.com
by UNIVERSITY OF CALIFORNIA @ BERKELEY on 09/16/26. Re-use and distribution is strictly not permitted, except for Open Access articles.

SEARCHES not in other sections

Magnetic Monopole Searches

See the related review(s):
Magnetic Monopoles

Monopole Production Cross Section — Accelerator Searches

X-SECT (cm^2)	MASS (GeV)	CHG (g)	ENERGY (GeV)	BEAM	DOCUMENT ID		TECN
<1.45E-30	60	1	5360	PbPb	[1] AAD	25B	ATLS
<1E-39-1E-35		1–10	13000	pp	[2] ACHARYA	25	MOED
	0–80	1–50	2760	PbPb	[3] ACHARYA	24	INDU
<4 E-41	200–4000	1–2	13000	pp	[4] AAD	23CO	ATLS
<4 E-38	590–1000	1–4	8000	pp	[5] ACHARYA	22A	INDU
<2 E-29	0–70	1–3	5020	PbPb	[6] ACHARYA	22B	INDU
<3 E-38	750–1910	1–5	13000	pp	[7] ACHARYA	21	INDU
<1.3E−40	200–4000	1	13000	pp	[8] AAD	20G	ATLS
<5.6E−40	500–4000	2	13000	pp	[8] AAD	20G	ATLS
	200–5000	2	13000	pp	[9] ACHARYA	19B	INDU
	200–5000	1	13000	pp	[10] ACHARYA	18A	INDU
<2.5E−37	200–6000	1	13000	pp	[11] ACHARYA	17	INDU
<2E−37	200–6000	2	13000	pp	[11] ACHARYA	17	INDU
<4E−37	200–5000	3	13000	pp	[11] ACHARYA	17	INDU
<1.5E−36	400–4000	4	13000	pp	[11] ACHARYA	17	INDU
<7E−36	1000–3000	5	13000	pp	[11] ACHARYA	17	INDU
<5E−40	200–2500	0.5–2.0	8000	pp	[12] AAD	16AB	ATLS
<2E−37	100–3500	1	8000	pp	[13] ACHARYA	16	INDU
<2E−37	100–3500	2	8000	pp	[13] ACHARYA	16	INDU
<6E−37	500–3000	3	8000	pp	[13] ACHARYA	16	INDU
<7E−36	1000–2000	4	8000	pp	[13] ACHARYA	16	INDU
<1.6E−38	200–1200	1	7000	pp	[14] AAD	12CS	ATLS
<5E−38	45–102	1	206	e^+e^-	[15] ABBIENDI	08	OPAL
<0.2E−36	200–700	1	1960	$p\overline{p}$	[16] ABULENCIA	06K	CNTR
< 2.E−36		1	300	e^+p	[17,18] AKTAS	05A	INDU
< 0.2 E−36		2	300	e^+p	[17,18] AKTAS	05A	INDU
< 0.09E−36		3	300	e^+p	[17,18] AKTAS	05A	INDU
< 0.05E−36		≥ 6	300	e^+p	[17,18] AKTAS	05A	INDU
< 2.E−36		1	300	e^+p	[17,19] AKTAS	05A	INDU
< 0.2E−36		2	300	e^+p	[17,19] AKTAS	05A	INDU
< 0.07E−36		3	300	e^+p	[17,19] AKTAS	05A	INDU
< 0.06E−36		≥ 6	300	e^+p	[17,19] AKTAS	05A	INDU
< 0.6E−36	>265	1	1800	$p\overline{p}$	[20] KALBFLEISCH	04	INDU
< 0.2E−36	>355	2	1800	$p\overline{p}$	[20] KALBFLEISCH	04	INDU
< 0.07E−36	>410	3	1800	$p\overline{p}$	[20] KALBFLEISCH	04	INDU
< 0.2E−36	>375	6	1800	$p\overline{p}$	[20] KALBFLEISCH	04	INDU
< 0.7E−36	>295	1	1800	$p\overline{p}$	[21,22] KALBFLEISCH	00	INDU
< 7.8E−36	>260	2	1800	$p\overline{p}$	[21,22] KALBFLEISCH	00	INDU
< 2.3E−36	>325	3	1800	$p\overline{p}$	[21,23] KALBFLEISCH	00	INDU
< 0.11E−36	>420	6	1800	$p\overline{p}$	[21,23] KALBFLEISCH	00	INDU
<0.65E−33	<3.3	≥ 2	11A	^{197}Au	[24,25] HE	97	
<1.90E−33	<8.1	≥ 2	160A	^{208}Pb	[24,25] HE	97	
<3.E−37	<45.0	1.0	88–94	e^+e^-	PINFOLD	93	PLAS
<3.E−37	<41.6	2.0	88–94	e^+e^-	PINFOLD	93	PLAS
<7.E−35	<44.9	0.2–1.0	89–93	e^+e^-	KINOSHITA	92	PLAS
<2.E−34	<850	≥ 0.5	1800	$p\overline{p}$	BERTANI	90	PLAS
<1.2E−33	<800	≥ 1	1800	$p\overline{p}$	PRICE	90	PLAS
<1.E−37	<29	1	50–61	e^+e^-	KINOSHITA	89	PLAS
<1.E−37	<18	2	50–61	e^+e^-	KINOSHITA	89	PLAS
<1.E−38	<17	<1	35	e^+e^-	BRAUNSCH...	88B	CNTR
<8.E−37	<24	1	50–52	e^+e^-	KINOSHITA	88	PLAS
<1.3E−35	<22	2	50–52	e^+e^-	KINOSHITA	88	PLAS
<9.E−37	<4	<0.15	10.6	e^+e^-	GENTILE	87	CLEO
<3.E−32	<800	≥ 1	1800	$p\overline{p}$	PRICE	87	PLAS
<3.E−38		<3	29	e^+e^-	FRYBERGER	84	PLAS
<1.E−31		1,3	540	$p\overline{p}$	AUBERT	83B	PLAS
<4.E−38	<10	<6	34	e^+e^-	MUSSET	83	PLAS
<8.E−36	<20		52	pp	[26] DELL	82	CNTR
<9.E−37	<30	<3	29	e^+e^-	KINOSHITA	82	PLAS
<1.E−37	<20	<24	63	pp	CARRIGAN	78	CNTR
<1.E−37	<30	<3	56	pp	HOFFMANN	78	PLAS
			62	pp	[26] DELL	76	SPRK
<4.E−33			300	p	[26] STEVENS	76B	SPRK
<1.E−40	<5	<2	70	p	[27] ZRELOV	76	CNTR
<2.E−30			300	n	[26] BURKE	75	OSPK
<1.E−38			8	ν	[28] CARRIGAN	75	HLBC
<5.E−43	<12	<10	400	p	EBERHARD	75B	INDU
<2.E−36	<30	<3	60	pp	GIACOMELLI	75	PLAS
<5.E−42	<13	<24	400	p	CARRIGAN	74	CNTR
<6.E−42	<12	<24	300	p	CARRIGAN	73	CNTR
<2.E−36		1	0.001	γ	[27] BARTLETT	72	CNTR
<1.E−41	<5		70	p	GUREVICH	72	EMUL
<1.E−40	<3	<2	28	p	AMALDI	63	EMUL
<2.E−40	<3	<2	30	p	PURCELL	63	CNTR
<1.E−35	<3	<4	28	p	FIDECARO	61	CNTR
<2.E−35	<1	1	6	p	BRADNER	59	EMUL

[1] AAD 25B searches are made for monopoles produced in ultra-peripheral PbPb collisions. Model-dependent mass exclusions between 20–150 GeV are made. Limit given at the mass of 60 GeV.

[2] ACHARYA 25 present cross section and mass limits presented for a suite of searches covering charges between 1 and 10 Dirac charges and interpreted within various model scenarios.

[3] ACHARYA 24 search for monopoles produced by the Schwinger mechanism. Results are model dependent.

[4] AAD 23CO limits given for monopoles pair produced via a Drell-Yan or photon-fusion mechanism. Spins 1/2 and 0 are considered. The quoted limit is representative of the lowest values that were achieved.

[5] ACHARYA 22A give limits for monopoles pair-produced via a Drell-Yan production. Spins 0, 1/2, and 1 are considered. The cross section limit is representative of the lowest values that were achieved. The experiment used a combination of nuclear track detectors to look evidence of passing monopoles and a SQUID magnetometer to look for stopped monopoles.

[6] ACHARYA 22B achieved limits on monopole (point-like included) production via the Schwinger mechanism in Pb-Pb collisions at 5.02 TeV centre-of-mass energy per nucleon pair. The upper cross section limit value quoted here is representative of the lowest values achieved.

[7] ACHARYA 21 search for dyons at LHC. Using a production model limits (we report the lowest) are set for dyons with magnetic charge up to 5 gD, electric charges up to 200 e and spins 0, 1/2, 1. The corresponding mass limits for magnetic monopoles are in the range 870–2040 GeV for magnetic charges in the same range.

[8] AAD 20G give limits for Drell-Yan production with spin-0 and spin-1/2 monopoles. The above limit is for spin = 0 at mass = 3 TeV.

[9] ACHARYA 19B limits both β-dependent and β-independent on monopoles with spins 0, 1/2, and 1 and with magnetic charges ranging from one to five times the Dirac charge in mass ranges between 200 GeV and 5000 GeV.

[10] ACHARYA 18A provide limits on monopoles with spins 0, 1/2, and 1 and with magnetic charges ranging from two to five times the Dirac charge.

[11] The search was sensitive to monopoles which had stopped in aluminium trapping volumes. Monopoles with spins 0 and 1/2 were considered; mass-dependent spin 1/2 monopole limits are quoted here.

[12] AAD 16AB model-independent 95% CL limits estimated using a fiducial region of approximately constant acceptance. Limits are mass-dependent.

[13] ACHARYA 16 limits at 95% CL estimated using a Drell-Yan-like production mechanism for scalar monopoles.

[14] AAD 12CS searched for monopoles as highly ionising objects. The cross section limits are based on an assumed Drell Yan-like production process for spin 1/2 monopoles. The limits are mass- and scenario-dependent.

[15] ABBIENDI 08 assume production of spin 1/2 monopoles with effective charge $g\beta$ (n=1), via $e^+e^- \rightarrow \gamma^* \rightarrow M\overline{M}$, so that the cross section is proportional to $(1 + \cos^2\theta)$. There is no z information for such highly saturated tracks, so a parabolic track in the jet chamber is projected onto the xy plane. Charge per hit in the chamber produces a clean separation of signal and background.

[16] ABULENCIA 06K searches for high-ionizing signals in CDF central outer tracker and time-of-flight detector. For Drell-Yan $M\overline{M}$ production, the cross section limit implies $M > 360$ GeV at 95% CL.

[17] AKTAS 05A model-dependent limits as a function of monopole mass shown for arbitrary mass of 60 GeV. Based on search for stopped monopoles in the H1 Al beam pipe.

[18] AKTAS 05A limits with assumed elastic spin 0 monopole pair production.

[19] AKTAS 05A limits with assumed inelastic spin 1/2 monopole pair production.

[20] KALBFLEISCH 04 reports searches for stopped magnetic monopoles in Be, Al, and Pb samples obtained from discarded material from the upgrading of DØ and CDF. A large-aperture warm-bore cryogenic detector was used. The approach was an extension of the methods of KALBFLEISCH 00. Cross section results moderately model dependent; interpretation as a mass lower limit depends on possibly invalid perturbation expansion.

[21] KALBFLEISCH 00 used an induction method to search for stopped monopoles in pieces of the DØ (FNAL) beryllium beam pipe and in extensions to the drift chamber aluminum support cylinder. Results are model dependent.

[22] KALBFLEISCH 00 result is for aluminum.

[23] KALBFLEISCH 00 result is for beryllium.

[24] HE 97 used a lead target and barium phosphate glass detectors. Cross-section limits are well below those predicted via the Drell-Yan mechanism.

[25] This work has also been reinterpreted in the framework of monopole production via the thermal Schwinger process (GOULD 17); this gives rise to lower mass limits.

[26] Multiphoton events.

[27] Cherenkov radiation polarization.

[28] Re-examines CERN neutrino experiments.

Monopole Production — Other Accelerator Searches

MASS (GeV)	CHG (g)	SPIN	ENERGY (GeV)	BEAM	DOCUMENT ID		TECN
> 610	≥ 1	0	1800	$p\overline{p}$	[1] ABBOTT	98K	D0
> 870	≥ 1	1/2	1800	$p\overline{p}$	[1] ABBOTT	98K	D0
>1580	≥ 1	1	1800	$p\overline{p}$	[1] ABBOTT	98K	D0
> 510			88–94	e^+e^-	[2] ACCIARRI	95C	L3

[1] ABBOTT 98K search for heavy pointlike Dirac monopoles via central production of a pair of photons with high transverse energies.

[2] ACCIARRI 95C finds a limit $B(Z \rightarrow \gamma\gamma\gamma) < 0.8 \times 10^{-5}$ (which is possible via a monopole loop) at 95% CL and sets the mass limit via a cross section model.

Int. J. Mod. Phys. A 2026.41. Downloaded from www.worldscientific.com
by UNIVERSITY OF CALIFORNIA @ BERKELEY on 09/16/26. Re-use and distribution is strictly not permitted, except for Open Access articles.

Monopole Flux — Cosmic Ray Searches

"Caty" in the charge column indicates a search for monopole-catalyzed nucleon decay.

FLUX ($cm^{-2}sr^{-1}s^{-1}$)	MASS (GeV)	CHG (g)	COMMENTS ($\beta = v/c$)	DOCUMENT ID		TECN
<2E-19		1	0.86< β <0.995	[1] ABBASI	22	ICCB
<7E-18		1	β >0.55	[2] ALBERT	22C	ANTR
<2E-14	>5E8		6E-4< β <5E-3	[3] ACERO	21	NOVA
<1E-17		Caty	1E-5 < β <1E-3	[4] GAPONENKO	21	BAIK
<1.5E−18		1	β >0.6	[5] ALBERT	17	ANTR
<2.5E−21		1	1E8< γ <1E13	[6] AAB	16	AUGE
<1.55E-18			β >0.51	[7] AARTSEN	16B	ICCB
<1E-17		Caty	1E-3< β <1E-2	[8] AARTSEN	14	ICCB
<3E-18		1	β >0.8	[9] ABBASI	13	ICCB
<1.3E-17		1	β >0.625	[10] ADRIAN-MAR..	12A	ANTR
<6E-28	<1E17	Caty	1E-5< β <0.04	[11] UENO	12	SKAM
<1E-19		1	γ >1E10	[12] DETRIXHE	11	ANIT
<3.8E-17		1	β >0.76	[9] ABBASI	10A	ICCB
<1.3E−15	1E4<M<5E13	1	β >0.05	[13] BALESTRA	08	PLAS
<0.65E−15	>5E13	1	β >0.05	[13] BALESTRA	08	PLAS
<1E−18		1	γ >1 E8	[12] HOGAN	08	RICE
<1.4E−16		**1**	**1.1E−4 < β <0.99**	[14] AMBROSIO	02B	MCRO
<3E−16		Caty	1.1E−4 < β <5E−3	[15] AMBROSIO	02C	MCRO
<1.5E−15		1	5E−3 < β < 0.99	[16] AMBROSIO	02D	MCRO
<1E−15		1	1.1×10^{-4}–0.1	[17] AMBROSIO	97	MCRO
<5.6E−15		1	(0.18–3.0)E−3	[18] AHLEN	94	MCRO
<2.7E−15		Caty	$\beta \sim 1 \times 10^{-3}$	[19] BECKER-SZ...	94	IMB
<8.7E−15		1	>2.E−3	THRON	92	SOUD
<4.4E−12		1	all β	GARDNER	91	INDU
<7.2E−13		1	all β	HUBER	91	INDU
<3.7E−15	>E12	1	β=1.E−4	[20] ORITO	91	PLAS
<3.2E−16	>E10	1	β > 0.05	[20] ORITO	91	PLAS
<3.2E−16	>E10–E12	2, 3		[20] ORITO	91	PLAS
<3.8E−13		1	all β	BERMON	90	INDU
<5.E−16		Caty	β <1.E−3	[19] BEZRUKOV	90	CHER
<1.8E−14		1	β >1.1E−4	[21] BUCKLAND	90	HEPT
<1E−18			3.E−4 < β <1.5E−3	[22] GHOSH	90	MICA
<7.2E−13		1	all β	HUBER	90	INDU
<5.E−12	>E7	1	3.E−4 < β <5.E−3	BARISH	87	CNTR
<1.E−13		Caty	1.E−5 < β <1	[19] BARTELT	87	SOUD
<1.E−10		1	all β	EBISU	87	INDU
<2.E−13			1.E−4 < β <6.E−4	MASEK	87	HEPT
<2.E−14			4.E−5 < β <2.E−4	NAKAMURA	87	PLAS
<2.E−14			1.E−3 < β <1	NAKAMURA	87	PLAS
<5.E−14			9.E−4 < β <1.E−2	SHEPKO	87	CNTR
<2.E−13			4.E−4 < β <1	TSUKAMOTO	87	CNTR
<5.E−14		1	all β	[23] CAPLIN	86	INDU
<5.E−12		1		CROMAR	86	INDU
<1.E−13		1	7.E−4 < β	HARA	86	CNTR
<7.E−11		1	all β	INCANDELA	86	INDU
<1.E−18			4.E−4 < β <1.E−3	[22] PRICE	86	MICA
<5.E−12		1		BERMON	85	INDU
<6.E−12		1		CAPLIN	85	INDU
<6.E−10		1		EBISU	85	INDU
<3.E−15		Caty	5.E−5 ≤ β ≤ 1.E−3	[19] KAJITA	85	KAMI
<2.E−21		Caty	β <1.E−3	[19,24] KAJITA	85	KAMI
<3.E−15		Caty	1.E−3 < β <1.E−1	[19] PARK	85B	CNTR
<5.E−12		1	1.E−4 < β <1	BATTISTONI	84	NUSX
<7.E−12		1		INCANDELA	84	INDU
<7.E−13		1	3.E−4 < β	[21] KAJINO	84	CNTR
<2.E−12		1	3.E−4 < β <1.E−1	KAJINO	84B	CNTR
<6.E−13		1	5.E−4 < β <1	KAWAGOE	84	CNTR
<2.E−14			1.E−3 < β	[19] KRISHNA...	84	CNTR
<4.E−13		1	6.E−4 < β <2.E−3	LISS	84	CNTR
<1.E−16			3.E−4 < β <1.E−3	[22] PRICE	84	MICA
<1.E−13		1	1.E−4 < β	PRICE	84B	PLAS
<4.E−13		1	6.E−4 < β <2.E−3	TARLE	84	CNTR
				[25] ANDERSON	83	EMUL
<4.E−13		1	1.E−2 < β <1.E−3	BARTELT	83B	CNTR
<1.E−12		1	7.E−3 < β <1	BARWICK	83	PLAS
<3.E−13		1	1.E−3 < β <4.E−1	BONARELLI	83	CNTR
<3.E−12		Caty	5.E−4 < β <5.E−2	[19] BOSETTI	83	CNTR
<4.E−11		1		CABRERA	83	INDU
<5.E−15		1	1.E−2 < β <1	DOKE	83	PLAS
<8.E−15		Caty	1.E−4 < β <1.E−1	[19] ERREDE	83	IMB
<5.E−12		1	1.E−4 < β <3.E−2	GROOM	83	CNTR
<2.E−12			6.E−4 < β <1	MASHIMO	83	CNTR
<1.E−13		1	β=3.E−3	ALEXEYEV	82	CNTR
<2.E−12		1	7.E−3 < β <6.E−1	BONARELLI	82	CNTR
6.E−10		1	all β	[26] CABRERA	82	INDU
<2.E−11			1.E−2 < β <1.E−1	MASHIMO	82	CNTR
<2.E−15			concentrator	BARTLETT	81	PLAS
<1.E−13	>1		1.E−3 < β	KINOSHITA	81B	PLAS
<5.E−11	<E17		3.E−4 < β <1.E−3	ULLMAN	81	CNTR
<2.E−11			concentrator	BARTLETT	78	PLAS
1.E−1	>200	2		[27] PRICE	75	PLAS
<2.E−13		>2		FLEISCHER	71	PLAS
<1.E−19		>2	obsidian, mica	FLEISCHER	69C	PLAS
<5.E−15	<15	<3	concentrator	CARITHERS	66	ELEC
<2.E−11		<1–3	concentrator	MALKUS	51	EMUL

[1] ABBASI 22 search was based on Cherenkov light detection in an array of optical modules in the Antarctic ice cap. Limits are speed-dependent.

[2] ALBERT 22C search for magnetic monopoles using data taken with the ANTARES neutrino telescope over a period of 10 years. No signal observed. Velocity dependent upper limits set on the flux of magnetic monopoles.

[3] ACERO 21 employ NOvA experiment to set reported 90% CL upper limit on the cosmic monopoles flux for velocity $6 \times 10^{-4} < \beta < 5 \times 10^{-3}$ and mass $> 5 \times 10^{8}$ GeV.

[4] GAPONENKO 21 use data of NT200 two-year operation at Baikal to give speed-dependent limits for different assumed catalysis cross sections. Reported limit is for $\sigma = 10$ mb.

[5] ALBERT 17 limits were estimated using a Cherenkov light in an array of optical modules under the Mediterranean Sea. The limits are for MM masses between 10^{10} and 10^{14} GeV. The limits are speed-dependent.

[6] AAB 16 search was made with a set of telescopes sampling the longitudinal profile of fluorescence light emitted by extensive air showers. Limits are speed dependent.

[7] AARTSEN 16B was based on a Cherenkov signature in an array of optical modules which were sunk in the Antarctic ice cap. Limits are speed-dependent.

[8] Beyond the monopole speed, the limits of AARTSEN 14 depend on the catalysis cross section (σ) which corresponds to the monopole radiating $\tilde{l}$ times the light per track length compared to the Cherenkov light from a single electrically charged, relativistic particle. The values quoted here correspond to $\sigma = 1$ barn or $\tilde{l} = 30$.

[9] ABBASI 13 and ABBASI 10A were based on a Cherenkov signature in an array of optical modules which were sunk in the Antarctic ice cap. Limits are speed-dependent.

[10] ADRIAN-MARTINEZ 12A measurements were based on a Cherenkov signature in an underwater telescope in the Western Mediterranean Sea. Limits are speed-dependent.

[11] The limits from UENO 12 depend on the monopole speed and are also sensitive to assumed values of monopole mass and the catalysis cross section.

[12] HOGAN 08 and DETRIXHE 11 limits on relativistic monopoles are based on nonobservation of radio Cherenkov signals at the South Pole. Limits are speed-dependent.

[13] BALESTRA 08 exposed of nuclear track detector modules totaling 400 m^2 for 4 years at the Chacaltaya Laboratory (5230 m) in search for intermediate-mass monopoles with $\beta >$ 0.05. The analysis is mainly based on three CR39 modules. For $M > 5 \times 10^{13}$ GeV there can be upward-going monopoles as well, hence the flux limit is half that obtained for less massive monopoles. Previous experiments (e.g. MACRO and OHYA (ORITO 91)) had set limits only for $M > 1 \times 10^{9}$ GeV.

[14] AMBROSIO 02B direct search final result for $m \geq 10^{17}$ GeV, based upon 4.2 to 9.5 years of running, depending upon the subsystem. Limit with CR39 track-etch detector extends the limit from β=4×10^{-5} (3×10^{-16} cm^{-2} sr^{-1} s^{-1}) to β= 1×10^{-4} (2.1×10^{-16} cm^{-2} sr^{-1} s^{-1}). Limit curve in paper is piecewise continuous due to different detection techniques for different β ranges.

[15] AMBROSIO 02C limit for catalysis of nucleon decay with catalysis cross section of $\approx$ 1 mb. The flux limit increases by $\sim$ 3 at the higher β limit, and increases to 1×10^{-14} cm^{-2} sr^{-1} s^{-1} if the catalysis cross section is 0.01 mb. Based upon 71193 hr of data with the streamer detector, with an acceptance of 4250 m^2 sr.

[16] AMBROSIO 02D result for "more than two years of data." Ionization search using several subsystems. Limit curve as a function of β not given. Included in AMBROSIO 02B.

[17] AMBROSIO 97 global MACRO 90%CL is 0.78×10^{-15} at β=1.1×10^{-4}, goes through a minimum at 0.61×10^{-15} near β=(1.1–2.7) $\times 10^{-3}$, then rises to 0.84×10^{-15} at β=0.1. The global limit in this region is below the Parker bound at 10^{-15}. Less stringent limits are established for $4 \times 10^{-5} < \beta < 1 \times 10^{-4}$. Limits set by various triggers and different subdetectors are given in the paper. All limits assume a catalysis cross section smaller than a few mb.

[18] AHLEN 94 limit for dyons extends down to β=0.9E−4 and a limit of 1.3E−14 extends to β = 0.8E−4. Also see comment by PRICE 94 and reply of BARISH 94. One loophole in the AHLEN 94 result is that in the case of monopoles catalyzing nucleon decay, relativistic particles could veto the events. See AMBROSIO 97 for additional results.

[19] Catalysis of nucleon decay; sensitive to assumed catalysis cross section.

[20] ORITO 91 limits are functions of velocity. Lowest limits are given here.

[21] Used DKMPR mechanism and Penning effect.

[22] Assumes monopole attaches fermion nucleus.

[23] Limit from combining data of CAPLIN 86, BERMON 85, INCANDELA 84, and CABRERA 83. For a discussion of controversy about CAPLIN 86 observed event, see GUY 87. Also see SCHOUTEN 87.

[24] Based on lack of high- energy solar neutrinos from catalysis in the sun.

[25] Anomalous long-range α (^{4}He) tracks.

[26] CABRERA 82 candidate event has single Dirac charge within ±5%.

[27] ALVAREZ 75, FLEISCHER 75, and FRIEDLANDER 75 explain as fragmenting nucleus. EBERHARD 75 and ROSS 76 discuss conflict with other experiments. HAGSTROM 77 reinterprets as antinucleus. PRICE 78 reassesses.

Monopole Flux — Astrophysics

FLUX ($cm^{-2}sr^{-1}s^{-1}$)	MASS (GeV)	CHG (g)	COMMENTS ($\beta = v/c$)	DOCUMENT ID		TECN
$< 3 \times 10^{-21}$	$< 10^{18}$	1	Parker	[1] KOBAYASHI	23A	COSM
$< 1.3 \times 10^{-20}$			faint white dwarf	[2] FREESE	99	ASTR
$< 1 \times 10^{-16}$	10^{17}	1	galactic field	[3] ADAMS	93	COSM
$< 1 \times 10^{-23}$			Jovian planets	[2] ARAFUNE	85	ASTR
$< 1 \times 10^{-16}$	10^{15}		solar trapping	BRACCI	85B	ASTR
$< 1 \times 10^{-18}$		1		[2] HARVEY	84	COSM
$< 3 \times 10^{-23}$			neutron stars	KOLB	84	ASTR
$< 7 \times 10^{-22}$			pulsars	[2] FREESE	83B	ASTR
$< 1 \times 10^{-18}$	$< 10^{18}$	1	intergalactic field	[2] REPHAELI	83	COSM
$< 1 \times 10^{-23}$			neutron stars	[2] DIMOPOUL...	82	COSM
$< 5 \times 10^{-22}$			neutron stars	[2] KOLB	82	COSM
$< 5 \times 10^{-15}$	$> 10^{21}$		galactic halo	SALPETER	82	COSM
$< 1 \times 10^{-12}$	10^{19}	1	β=3×10^{-3}	[4] TURNER	82	COSM
$< 1 \times 10^{-16}$		1	galactic field	PARKER	70	COSM

[1] KOBAYASHI 23A found Parker-type bounds on magnetic monopoles with arbitrary magnetic charge based on the survival of galactic, seed, and primordial magnetic fields.

Int. J. Mod. Phys. A 2026.41. Downloaded from www.worldscientific.com
by UNIVERSITY OF CALIFORNIA @ BERKELEY on 09/16/26. Re-use and distribution is strictly not permitted, except for Open Access articles.

Bounds are between 3×10^{-21} and 10^{-5} $cm^{-2}sr^{-1}s^{-1}$ for masses $< 10^{18}$ GeV. Reported bound is the most stringent one.

[2] Catalysis of nucleon decay.

[3] ADAMS 93 limit based on "survival and growth of a small galactic seed field" is 10^{-16} $(m/10^{17}$ GeV$)$ $cm^{-2}s^{-1}sr^{-1}$. Above 10^{17} GeV, limit 10^{-16} $(10^{17}$ GeV$/m)$ $cm^{-2}s^{-1}sr^{-1}$ (from requirement that monopole density does not overclose the universe) is more stringent.

[4] Re-evaluates PARKER 70 limit for GUT monopoles.

Monopole Density — Matter Searches

DENSITY	CHG (g)	MATERIAL	DOCUMENT ID		TECN
<9.8E−5/gram	≥ 1	Polar rock	BENDTZ	13	INDU
<6.9E−6/gram	>1/3	Meteorites and other	JEON	95	INDU
<2.E−7/gram	>0.6	Fe ore	[1] EBISU	87	INDU
<4.6E−6/gram	> 0.5	deep schist	KOVALIK	86	INDU
<1.6E−6/gram	> 0.5	manganese nodules	[2] KOVALIK	86	INDU
<1.3E−6/gram	> 0.5	seawater	KOVALIK	86	INDU
>1.E+14/gram	>1/3	iron aerosols	MIKHAILOV	83	SPEC
<6.E−4/gram		air, seawater	CARRIGAN	76	CNTR
<5.E−1/gram	>0.04	11 materials	CABRERA	75	INDU
<2.E−4/gram	>0.05	moon rock	ROSS	73	INDU
<6.E−7/gram	<140	seawater	KOLM	71	CNTR
<1.E−2/gram	<120	manganese nodules	FLEISCHER	69	PLAS
<1.E−4/gram	>0	manganese	FLEISCHER	69B	PLAS
<2.E−3/gram	<1–3	magnetite, meteor	GOTO	63	EMUL
<2.E−2/gram		meteorite	PETUKHOV	63	CNTR

[1] Mass 1×10^{14}–1×10^{17} GeV.

[2] KOVALIK 86 examined 498 kg of schist from two sites which exhibited clear mineralogical evidence of having been buried at least 20 km deep and held below the Curie temperature.

Monopole Density — Astrophysics

DENSITY	CHG (g)	MATERIAL	DOCUMENT ID		TECN
<1.E−9/gram	1	sun, catalysis	[1] ARAFUNE	83	COSM
<6.E−33/nucl	1	moon wake	SCHATTEN	83	ELEC
<2.E−28/nucl		earth heat	CARRIGAN	80	COSM
<2.E−4/prot		42cm absorption	BRODERICK	79	COSM
<2.E−13/m^3		moon wake	SCHATTEN	70	ELEC

[1] Catalysis of nucleon decay.

REFERENCES FOR Magnetic Monopole Searches

AAD	25B	PRL 134 061803	G. Aad *et al.*	(ATLAS Collab.)
ACHARYA	25	PRL 134 071802	B. Acharya *et al.*	(MoEDAL Collab.)
ACHARYA	24	PRL 133 071803	B. Acharya *et al.*	(MoEDAL Collab.)
AAD	23CO	JHEP 2311 112	G. Aad *et al.*	(ATLAS Collab.)
KOBAYASHI	23A	PR D108 083005	T. Kobayashi, D. Perri	(SISSA)
ABBASI	22	PRL 128 051101	R. Abbasi *et al.*	(IceCube Collab.)
ACHARYA	22A	EPJ C82 694	B. Acharya *et al.*	(MoEDAL Collab.)
ACHARYA	22B	NAT 602 63	B. Acharya *et al.*	(MoEDAL Collab.)
ALBERT	22C	JHEAP 34 1	A. Albert *et al.*	(ANTARES Collab.)
ACERO	21	PR D103 012007	M.A. Acero *et al.*	(NOvA Collab.)
ACHARYA	21	PRL 126 071801	B. Acharya *et al.*	(MoEDAL Collab.)
GAPONENKO	21	PAN 84 287	O.N. Gaponenko	(ASCI)
AAD	20G	PRL 124 031802	G. Add *et al.*	(ATLAS Collab.)
ACHARYA	19B	PRL 123 021802	B. Acharya *et al.*	(MoEDAL Collab.)
ACHARYA	18A	PL B782 510	B. Acharya *et al.*	(MoEDAL Collab.)
ACHARYA	17	PRL 118 061801	B. Acharya *et al.*	(MoEDAL Collab.)
ALBERT	17	JHEP 1707 054	A. Albert *et al.*	(ANTARES Collab.)
GOULD	17	PRL 119 241601	O. Gould, A. Rajantie	
AAB	16	PR D94 082002	A. Aab *et al.*	(Pierre Auger Collab.)
AAD	16AB	PR D93 052009	G. Aad *et al.*	(ATLAS Collab.)
AARTSEN	16B	EPJ C76 133	M.G. Aartsen *et al.*	(IceCube Collab.)
ACHARYA	16	JHEP 1608 067	B. Acharya *et al.*	(MoEDAL Collab.)
AARTSEN	14	EPJ C74 2938	M.G. Aartsen *et al.*	(IceCube Collab.)
Also		EPJ C79 124 (errat.)	M.G. Aartsen *et al.*	(IceCube Collab.)
ABBASI	13	PR D87 022001	R. Abbasi *et al.*	(IceCube Collab.)
BENDTZ	13	PRL 110 121803	K. Bendtz *et al.*	
AAD	12CS	PRL 109 261803	G. Aad *et al.*	(ATLAS Collab.)
ADRIAN-MAR...	12A	ASP 35 634	S. Adrian-Martinez *et al.*	(ANTARES Collab.)
UENO	12	ASP 36 131	K. Ueno *et al.*	(Super-Kamiokande Collab.)
DETRIXHE	11	PR D83 023513	M. Detrixhe *et al.*	(ANITA Collab.)
ABBASI	10A	EPJ C69 361	R. Abbasi *et al.*	(IceCube Collab.)
ABBIENDI	08	PL B663 37	G. Abbiendi *et al.*	(OPAL Collab.)
BALESTRA	08	EPJ C55 57	S. Balestra *et al.*	(SLIM Collab.)
HOGAN	08	PR D78 075031	D.P. Hogan *et al.*	(KANS, NEBR, DELA)
ABULENCIA	06K	PRL 96 201801	A. Abulencia *et al.*	(CDF Collab.)
AKTAS	05A	EPJ C41 133	A. Aktas *et al.*	(H1 Collab.)
KALBFLEISCH	04	PR D69 052002	G.R. Kalbfleisch *et al.*	(OKLA)
AMBROSIO	02B	EPJ C25 511	M. Ambrosio *et al.*	(MACRO Collab.)
AMBROSIO	02C	EPJ C26 163	M. Ambrosio *et al.*	(MACRO Collab.)
AMBROSIO	02D	ASP 18 27	M. Ambrosio *et al.*	(MACRO Collab.)
KALBFLEISCH	00	PRL 85 5292	G.R. Kalbfleisch *et al.*	
FREESE	99	PR D59 063007	K. Freese, E. Krasteva	
ABBOTT	98K	PRL 81 524	B. Abbott *et al.*	(D0 Collab.)
AMBROSIO	97	PL B406 249	M. Ambrosio *et al.*	(MACRO Collab.)
HE	97	PRL 79 3134	Y.D. He	(UCB)
ACCIARRI	95C	PL B345 609	M. Acciarri *et al.*	(L3 Collab.)
JEON	95	PRL 75 1443	H. Jeon, M.J. Longo	(MICH)
Also		PRL 76 159 (errat.)	H. Jeon, M.J. Longo	
AHLEN	94	PRL 72 608	S.P. Ahlen *et al.*	(MACRO Collab.)
BARISH	94	PRL 73 1306	B.C. Barish, G. Giacomelli, J.T. Hong	(CIT+)
BECKER-SZ...	94	PR D49 2169	R.A. Becker-Szendy *et al.*	(IMB Collab.)
PRICE	94	PRL 73 1305	P.B. Price	(UCB)
ADAMS	93	PRL 70 2511	F.C. Adams *et al.*	(MICH, FNAL)
PINFOLD	93	PL B316 407	J.L. Pinfold *et al.*	(ALBE, HARV, MONT+)
KINOSHITA	92	PR D46 881	K. Kinoshita *et al.*	(HARV, BGNA, REHO)
THRON	92	PR D46 4846	J.L. Thron *et al.*	(SOUDAN-2 Collab.)
GARDNER	91	PR D44 622	R.D. Gardner *et al.*	(STAN)
HUBER	91	PR D44 636	M.E. Huber *et al.*	(STAN)
ORITO	91	PRL 66 1951	S. Orito *et al.*	(ICEPP, WASCR, NIHO, ICRR)
BERMON	90	PRL 64 839	S. Bermon *et al.*	(IBM, BNL)
BERTANI	90	EPL 12 613	M. Bertani *et al.*	(BGNA, INFN)
BEZRUKOV	90	SJNP 52 54	L.B. Bezrukov *et al.*	(INRM)
		Translated from YAF 52 86.		
BUCKLAND	90	PR D41 2726	K.N. Buckland *et al.*	(UCSD)
GHOSH	90	EPL 12 25	D.C. Ghosh, S. Chatterjea	(JADA)
HUBER	90	PRL 64 835	M.E. Huber *et al.*	(STAN)
PRICE	90	PRL 65 149	P.B. Price, J. Guiru, K. Kinoshita	(UCB, HARV)
KINOSHITA	89	PL B228 543	K. Kinoshita *et al.*	(HARV, TISA, KEK+)
BRAUNSCH...	88B	ZPHY C38 543	R. Braunschweig *et al.*	(TASSO Collab.)
KINOSHITA	88	PRL 60 1610	K. Kinoshita *et al.*	(HARV, TISA, KEK+)
BARISH	87	PR D36 2641	B.C. Barish, G. Liu, C. Lane	(CIT)
BARTELT	87	PR D36 1990	J.E. Bartelt *et al.*	(Soudan Collab.)
Also		PR D40 1701 (errat.)	J.E. Bartelt *et al.*	(Soudan Collab.)
EBISU	87	PR D36 3359	T. Ebisu, T. Watanabe	(KOBE)
Also		JP G11 883	T. Ebisu, T. Watanabe	(KOBE)
GENTILE	87	PR D35 1081	T. Gentile *et al.*	(CLEO Collab.)
GUY	87	NAT 325 463	J. Guy	(LOIC)
MASEK	87	PR D35 2758	G.E. Masek *et al.*	(UCSD)
NAKAMURA	87	PL B183 395	S. Nakamura *et al.*	(INUS, WASCR, NIHO)
PRICE	87	PRL 59 2523	P.B. Price, R. Guoxiao, K. Kinoshita	(UCB, HARV)
SCHOUTEN	87	JP E20 850	J.C. Schouten *et al.*	(LOIC)
SHEPKO	87	PR D35 2917	M.J. Shepko *et al.*	(TAMU)
TSUKAMOTO	87	EPL 3 39	T. Tsukamoto *et al.*	(ICRR)
CAPLIN	86	NAT 321 402	A.D. Caplin *et al.*	(LOIC)
Also		JP E20 850	J.C. Schouten *et al.*	(LOIC)
Also		NAT 325 463	J. Guy	(LOIC)
CROMAR	86	PRL 56 2561	M.W. Cromar, A.F. Clark, F.R. Fickett	(NBSB)
HARA	86	PRL 56 553	T. Hara *et al.*	(ICRR, KYOT, KEK, KOBE+)
INCANDELA	86	PR D34 2637	J. Incandela *et al.*	(CHIC, FNAL, MICH)
KOVALIK	86	PR A33 1183	J.M. Kovalik, J.L. Kirschvink	(CIT)
PRICE	86	PRL 56 1226	P.B. Price, M.H. Salamon	(UCB)
ARAFUNE	85	PR D32 2586	J. Arafune, M. Fukugita, S. Yanagita	(ICRR, KYOTU+)
BERMON	85	PRL 55 1850	S. Bermon *et al.*	(IBM)
BRACCI	85B	NP B258 726	L. Bracci, G. Fiorentini, G. Mezzorani	(PISA+)
Also		LNC 42 123	L. Bracci, G. Fiorentini	(PISA)
CAPLIN	85	NAT 317 234	A.D. Caplin *et al.*	(LOIC)
EBISU	85	JP G11 883	T. Ebisu, T. Watanabe	(KOBE)
KAJITA	85	JPSJ 54 4065	T. Kajita *et al.*	(ICRR, KEK, NIIG)
PARK	85B	NP B252 261	H.S. Park *et al.*	(IMB Collab.)
BATTISTONI	84	PL 133B 454	G. Battistoni *et al.*	(NUSEX Collab.)
FRYBERGER	84	PR D29 1524	D. Fryberger *et al.*	(SLAC, UCB)
HARVEY	84	NP B236 255	J.A. Harvey	(PRIN)
INCANDELA	84	PRL 53 2067	J. Incandela *et al.*	(CHIC, FNAL, MICH)
KAJINO	84	PRL 52 1373	F. Kajino *et al.*	(ICRR)
KAJINO	84B	JP G10 447	F. Kajino *et al.*	(ICRR)
KAWAGOE	84	LNC 41 315	K. Kawagoe *et al.*	(TOKY)
KOLB	84	APJ 286 702	E.W. Kolb, M.S. Turner	(FNAL, CHIC)
KRISHNA...	84	PL 142B 99	M.R. Krishnaswamy *et al.*	(TATA, OSKC+)
LISS	84	PR D30 884	T.M. Liss, S.P. Ahlen, G. Tarle	(UCB, IND+)
PRICE	84	PRL 52 1265	P.B. Price *et al.*	(ROMA, UCB, IND+)
PRICE	84B	PL 140B 112	P.B. Price	(CERN)
TARLE	84	PRL 52 90	G. Tarle, S.P. Ahlen, T.M. Liss	(UCB, MICH+)
ANDERSON	83	PR D28 2308	S.N. Anderson *et al.*	(WASH)
ARAFUNE	83	PL 133B 380	J. Arafune, M. Fukugita	(ICRR, KYOTU)
AUBERT	83B	PL 120B 465	B. Aubert *et al.*	(CERN, LAPP)
BARTELT	83B	PRL 50 655	J.E. Bartelt *et al.*	(MINN, ANL)
BARWICK	83	PR D28 2338	S.W. Barwick, K. Kinoshita, P.B. Price	(UCB)
BONARELLI	83	PL 126B 137	R. Bonarelli, P. Capiluppi, I. d'Antone	(BGNA)
BOSETTI	83	PL 133B 265	P.C. Bosetti *et al.*	(AACH3, HAWA, TOKY)
CABRERA	83	PRL 51 1933	B. Cabrera *et al.*	(STAN)
DOKE	83	PL 129B 370	T. Doke *et al.*	(WASU, RIKK, TTAM, RIKEN)
ERREDE	83	PRL 51 245	S.M. Errede *et al.*	(IMB Collab.)
FREESE	83B	PRL 51 1625	K. Freese, M.S. Turner, D.N. Schramm	(CHIC)
GROOM	83	PRL 50 573	D.E. Groom *et al.*	(UTAH, STAN)
MASHIMO	83	PL 128B 327	T. Mashimo *et al.*	(ICEPP)
MIKHAILOV	83	PL 130B 331	V.F. Mikhailov	(KAZA)
MUSSET	83	PL 128B 333	P. Musset, M. Price, E. Lohrmann	(CERN, HAMB)
REPHAELI	83	PL 121B 115	Y. Rephaeli, M.S. Turner	(CHIC)
SCHATTEN	83	PR D27 1525	K.H. Schatten	(NASA)
ALEXEYEV	82	LNC 35 413	E.N. Alekseev *et al.*	(INRM)
BONARELLI	82	PL 112B 100	R. Bonarelli *et al.*	(BGNA)
CABRERA	82	PRL 48 1378	B. Cabrera	(STAN)
DELL	82	NP B209 45	G.F. Dell *et al.*	(BNL, ADEL, ROMA)
DIMOPOUL...	82	PL 119B 320	S. Dimopoulos, J. Preskill, F. Wilczek	(HARV+)
KINOSHITA	82	PRL 48 77	K. Kinoshita, P.B. Price, D. Fryberger	(UCB+)
KOLB	82	PRL 49 1373	E.W. Kolb, S.A. Colgate, J.A. Harvey	(LASL, PRIN)
MASHIMO	82	JPSJ 51 3067	T. Mashimo, K. Kawagoe, M. Koshiba	(INUS)
SALPETER	82	PRL 49 1114	E.E. Salpeter, S.L. Shapiro, I. Wasserman	(CORN)
TURNER	82	PR D26 1296	M.S. Turner, E.N. Parker, T.J. Bogdan	(CHIC)
BARTLETT	81	PR D24 612	D.F. Bartlett *et al.*	(COLO, GESC)
KINOSHITA	81B	PR D24 1707	K. Kinoshita, P.B. Price	(UCB)
ULLMAN	81	PRL 47 289	J.D. Ullman	(LEHM, BNL)
CARRIGAN	80	NAT 288 348	R.A. Carrigan	(FNAL)
BRODERICK	79	PR D19 1046	J.J. Broderick *et al.*	(VPI)
BARTLETT	78	PR D18 2253	D.F. Bartlett, D. Soo, M.G. White	(COLO, PRIN)
CARRIGAN	78	PR D17 1754	R.A. Carrigan, B.P. Strauss, G. Giacomelli	(FNAL+)
HOFFMANN	78	LNC 23 357	H. Hoffmann *et al.*	(CERN, ROMA)
PRICE	78	PR D18 1382	P.B. Price *et al.*	(UCB, HOUS)
HAGSTROM	77	PRL 38 729	R. Hagstrom	(LBL)
CARRIGAN	76	PR D13 1823	R.A. Carrigan, F.A. Nezrick, B.P. Strauss	(FNAL)
DELL	76	LNC 15 269	G.F. Dell *et al.*	(CERN, BNL, ROMA, ADEL)
ROSS	76	LBL-4665	R.R. Ross	(LBL)
STEVENS	76B	PR D14 2207	D.M. Stevens *et al.*	(VPI, BNL)
ZRELOV	76	CZJP B26 1306	V.P. Zrelov *et al.*	(JINR)
ALVAREZ	75	LBL-4260	L.W. Alvarez	(LBL)
BURKE	75	PL 60B 113	D.L. Burke *et al.*	(MICH)
CABRERA	75	Thesis	B. Cabrera	(STAN)
CARRIGAN	75	NP B91 279	R.A. Carrigan, F.A. Nezrick	(FNAL)
Also		PR D3 56	R.A. Carrigan, F.A. Nezrick	(FNAL)
EBERHARD	75	PR D11 3099	P.H. Eberhard *et al.*	(LBL, MPIM)
EBERHARD	75B	LBL-4289	P.H. Eberhard	(LBL)
FLEISCHER	75	PRL 35 1412	R.L. Fleischer, R.N.F. Walker	(GESC, WUSL)
FRIEDLANDER	75	PRL 35 1167	M.W. Friedlander	(WUSL)
GIACOMELLI	75	NC 28A 21	G. Giacomelli *et al.*	(BGNA, CERN, SACL+)
PRICE	75	PRL 35 487	P.B. Price *et al.*	(UCB, HOUS)
CARRIGAN	74	PR D10 3867	R.A. Carrigan, F.A. Nezrick, B.P. Strauss	(FNAL)
CARRIGAN	73	PR D8 3717	R.A. Carrigan, F.A. Nezrick, B.P. Strauss	(FNAL)
ROSS	73	PR D8 698	R.R. Ross *et al.*	(LBL, SLAC)
Also		PR D4 3260	P.H. Eberhard *et al.*	(LBL, SLAC)
Also		SCI 167 701	L.W. Alvarez *et al.*	(LBL, SLAC)
BARTLETT	72	PR D6 1817	D.F. Bartlett, M.D. Lahana	(COLO)
GUREVICH	72	PL 38B 549	I.I. Gurevich *et al.*	(KIAE, NOVO, SERP)
Also		JETP 34 917	L.M. Barkov, I.I. Gurevich, M.S. Zolotorev	(KIAE+)
		Translated from ZETF 61 1721.		
Also		PL 31B 394	I.I. Gurevich *et al.*	(KIAE, NOVO, SERP)
FLEISCHER	71	PR D4 24	R.L. Fleischer *et al.*	(GESC)
KOLM	71	PR D4 1285	H.H. Kolm, F. Villa, A. Odian	(MIT, SLAC)
PARKER	70	APJ 160 383	E.N. Parker	(CHIC)
SCHATTEN	70	PR D1 2245	K.H. Schatten	(NASA)
FLEISCHER	69	PR 177 2029	R.L. Fleischer *et al.*	(GESC, FSU)
FLEISCHER	69B	PR 184 1393	R.L. Fleischer *et al.*	(GESC, UNCS, GSCO)

FLEISCHER	69C	PR 184 1398	R.L. Fleischer, P.B. Price, R.T. Woods	(GESC)
Also		JAP 41 958	R.L. Fleischer *et al.*	(GESC)
CARITHERS	66	PR 149 1070	W.C.J. Carithers, R.J. Stefanski, R.K. Adair	
AMALDI	63	NC 28 773	E. Amaldi *et al.*	(ROMA, UCSD, CERN)
GOTO	63	PR 132 387	E. Goto, H.H. Kolm, K.W. Ford	(TOKY, MIT, BRAN)
PETUKHOV	63	NP 49 87	V.A. Petukhov, M.N. Yakimenko	(LEBD)
PURCELL	63	PR 129 2326	E.M. Purcell *et al.*	(HARV, BNL)
FIDECARO	61	NC 22 657	M. Fidecaro, G. Finocchiaro, G. Giacomelli	(CERN)
BRADNER	59	PR 114 603	H. Bradner, W.M. Isbell	(LBL)
MALKUS	51	PR 83 899	W.V.R. Malkus	(CHIC)

OTHER RELATED PAPERS

GROOM	86	PRPL 140 323	D.E. Groom	(UTAH)
Review				

Supersymmetric Particle Searches

The exclusion of particle masses within a mass range (m_1, m_2) will be denoted with the notation "none m_1–m_2" in the VALUE column of the following Listings. The latest unpublished results are described in the "Supersymmetry: Experiment" review.

See the related review(s):
Supersymmetry, Part I (Theory)
Supersymmetry, Part II (Experiment)

CONTENTS:

$\widetilde{\chi}^0_1$ (Lightest Neutralino) mass limit
– Accelerator limits for stable $\widetilde{\chi}^0_1$
– Bounds on $\widetilde{\chi}^0_1$ from dark matter searches
– $\widetilde{\chi}^0_1$-p elastic cross section
Spin-dependent interactions
Spin-independent interactions
– Other bounds on $\widetilde{\chi}^0_1$ from astrophysics and cosmology
– Unstable $\widetilde{\chi}^0_1$ (Lightest Neutralino) mass limit
$\widetilde{\chi}^0_2$, $\widetilde{\chi}^0_3$, $\widetilde{\chi}^0_4$ (Neutralinos) mass limits
$\widetilde{\chi}^\pm_1$, $\widetilde{\chi}^\pm_2$ (Charginos) mass limits
Long-lived $\widetilde{\chi}^\pm$ (Chargino) mass limit
$\widetilde{\nu}$ (Sneutrino) mass limit
Charged sleptons
– R-parity conserving $\widetilde{e}$ (Selectron) mass limit
– R-partiy violating $\widetilde{e}$ (Selectron) mass limit
– R-parity conserving $\widetilde{\mu}$ (Smuon) mass limit
– R-parity violating $\widetilde{\mu}$ (Smuon) mass limit
– R-parity conserving $\widetilde{\tau}$ (Stau) mass limit
– R-parity violating $\widetilde{\tau}$ (Stau) mass limit
– Long-lived $\widetilde{\ell}$ (Slepton) mass limit
$\widetilde{q}$ (Squark) mass limit
– R-parity conserving $\widetilde{q}$ (Squark) mass limit
– R-parity violating $\widetilde{q}$ (Squark) mass limit
Long-lived $\widetilde{q}$ (Squark) mass limit
$\widetilde{b}$ (Sbottom) mass limit
– R-parity conserving $\widetilde{b}$ (Sbottom) mass limit
– R-parity violating $\widetilde{b}$ (Sbottom) mass limit
$\widetilde{t}$ (Stop) mass limit
– R-parity conserving $\widetilde{t}$ (Stop) mass limit
– R-parity violating $\widetilde{t}$ (Stop) mass limit
Heavy $\widetilde{g}$ (Gluino) mass limit
– R-parity conserving heavy $\widetilde{g}$ (Gluino) mass limit
– R-parity violating heavy $\widetilde{g}$ (Gluino) mass limit
Long-lived $\widetilde{g}$ (Gluino) mass limit
Light $\widetilde{G}$ (Gravitino) mass limits from collider experiments
Supersymmetry miscellaneous results

The results shown below, unless stated otherwise, are based on the Minimal Supersymmetric Standard Model (MSSM), as described in the Note on Supersymmetry. Unless otherwise indicated, this includes the assumption of common gaugino and scalar masses at the scale of Grand Unification (GUT), and use of the resulting relations in the spectrum and decay branching ratios. Unless otherwise indicated, it is also assumed that R-parity (R) is conserved and that:

1) The $\widetilde{\chi}^0_1$ is the lighest supersymmetric particle (LSP),
2) $m_{\widetilde{f}_L} = m_{\widetilde{f}_R}$, where $\widetilde{f}_{L,R}$ refer to the scalar partners of left- and right-handed fermions.

Limits involving different assumptions are identified in the Comments or in the Footnotes, in particular also the many simplified models, see definitions below. We summarize here the notations used in this Chapter to characterize some of the most common deviations from the MSSM (for further details, see the Note on Supersymmetry).

Theories with R-parity violation (RPV) are characterized by a superpotential of the form: $\lambda_{ijk} L_i L_j e^c_k + \lambda'_{ijk} L_i Q_j d^c_k + \lambda''_{ijk} u^c_i d^c_j d^c_k$, where i, j, k are generation indices. The presence of any of these couplings is often identified in the following by the symbols $LL\overline{E}$, $LQ\overline{D}$, and $\overline{UDD}$. Mass limits in the presence of RPV will often refer to "direct" and "indirect" decays. Direct refers to RPV decays of the particle in consideration. Indirect refers to cases where RPV appears in the decays of the LSP. The LSP need not be the $\widetilde{\chi}^0_1$.

In several models, most notably in theories with so-called Gauge Mediated Supersymmetry Breaking (GMSB), the gravitino ($\widetilde{G}$) is the LSP. It is usually much lighter than any other massive particle in the spectrum, and $m_{\widetilde{G}}$ is then neglected in all decay processes involving gravitinos. In these scenarios, particles other than the neutralino are sometimes considered as the next-to-lighest supersymmetric particle (NLSP), and are assumed to decay to their even-R partner plus $\widetilde{G}$. If the lifetime is short enough for the decay to take place within the detector, $\widetilde{G}$ is assumed to be undetected and to give rise to missing energy ($\not{E}$) or missing transverse energy ($\not{E}_T$) signatures.

When needed, specific assumptions on the eigenstate content of $\widetilde{\chi}^0$ and $\widetilde{\chi}^\pm$ states are indicated, using the notation $\widetilde{\gamma}$ (photino), $\widetilde{H}$ (higgsino), $\widetilde{W}$ (wino), and $\widetilde{Z}$ (zino) to signal that the limit of pure states was used. The term gaugino is also used, to generically indicate wino-like charginos and zino-like neutralinos.

In the listings we have made use of the following abbreviations for simplified models employed by the experimental collaborations in supersymmetry searches published in the past year.

WARNING: Experimental lower mass limits determined within simplified models are to be treated with extreme care as they might not be directly applicable to realistic models. This is outlined in detail in the publications and we recommend consulting them before using bounds. For example, branching ratios, typically fixed to specific values in simplified models, can vary substantially in more elaborate models.

Simplified Models Table

Tglu1A: gluino pair production with $\tilde{g} \to q\bar{q}\tilde{\chi}^0_1$.

Tglu1B: gluino pair production with $\tilde{g} \to qq'\tilde{\chi}^\pm_1$, $\tilde{\chi}^\pm_1 \to W^\pm\tilde{\chi}^0_1$.

Tglu1C: gluino pair production with a 2/3 probability of having a $\tilde{g} \to qq'\tilde{\chi}^\pm_1$, $\tilde{\chi}^\pm_1 \to W^\pm\tilde{\chi}^0_1$ decay and a 1/3 probability of having a $\tilde{g} \to qq\tilde{\chi}^0_2$, $\tilde{\chi}^0_2 \to Z^\pm\tilde{\chi}^0_1$ decay.

Tglu1D: gluino pair production with one gluino decaying to $q\bar{q}'\tilde{\chi}^\pm_1$ with $\tilde{\chi}^\pm_1 \to W^\pm + \tilde{G}$, and the other gluino decaying to $q\bar{q}\tilde{\chi}^0_1$ with $\tilde{\chi}^0_1 \to \gamma + \tilde{G}$.

Tglu1E: gluino pair production with $\tilde{g} \to qq'\tilde{\chi}^\pm_1$, $\tilde{\chi}^\pm_1 \to W^\pm\tilde{\chi}^0_2$ and $\tilde{\chi}^0_2 \to Z^\pm\tilde{\chi}^0_1$ where $m_{\tilde{\chi}^\pm_1} = (m_{\tilde{g}} + m_{\tilde{\chi}^0_1})/2$, $m_{\tilde{\chi}^0_2} = (m_{\tilde{\chi}^\pm_1} + m_{\tilde{\chi}^0_1})/2$.

Tglu1F: gluino pair production with $\tilde{g} \to qq'\tilde{\chi}^\pm_1$ or $\tilde{g} \to qq\tilde{\chi}^0_2$ with equal branching ratios, where $\tilde{\chi}^\pm_1$ decays through an intermediate scalar tau lepton or sneutrino to $\tau\nu\tilde{\chi}^0_1$ and where $\tilde{\chi}^0_2$ decays through an intermediate scalar tau lepton or sneutrino to $\tau^+\tau^-\tilde{\chi}^0_1$ or $\nu\bar{\nu}\tilde{\chi}^0_1$; the mass hierarchy is such that $m_{\tilde{\chi}^\pm_1} \sim m_{\tilde{\chi}^0_2} = (m_{\tilde{g}} + m_{\tilde{\chi}^0_1})/2$ and $m_{\tilde{\tau},\tilde{\nu}} = (m_{\tilde{\chi}^\pm_1} + m_{\tilde{\chi}^0_1})/2$.

Int. J. Mod. Phys. A 2026.41. Downloaded from www.worldscientific.com
by UNIVERSITY OF CALIFORNIA @ BERKELEY on 09/16/26. Re-use and distribution is strictly not permitted, except for Open Access articles.

Int. J. Mod. Phys. A 2026.41. Downloaded from www.worldscientific.com
by UNIVERSITY OF CALIFORNIA @ BERKELEY on 09/16/26. Re-use and distribution is strictly not permitted, except for Open Access articles.

Tglu1G: gluino pair production with $\tilde{g} \to q\bar{q}\tilde{\chi}_2^0$, and $\tilde{\chi}_2^0$ decaying through an intermediate slepton or sneutrino to $l^+l^-\tilde{\chi}_1^0$ or $\nu\bar{\nu}\tilde{\chi}_1^0$ where $m_{\tilde{\chi}_2^0} = (m_{\tilde{g}} + m_{\tilde{\chi}_1^0})/2$ and $m_{\tilde{\ell},\tilde{\nu}} = (m_{\tilde{\chi}_2^0} + m_{\tilde{\chi}_1^0})/2$.

Tglu1H: gluino pair production with $\tilde{g} \to q\bar{q}\tilde{\chi}_2^0$, and $\tilde{\chi}_2^0 \to \tilde{\chi}_1^0 Z^{0(*)}$.

Tglu1I: gluino pair production with $\tilde{g} \to q\bar{q}\tilde{\chi}_2^0$, and $\tilde{\chi}_2^0 \to \tilde{\chi}_1^0 H$.

Tglu1J: gluino pair production with $\tilde{g} \to q\bar{q}\tilde{\chi}_2^0$, and $\mathrm{BR}(\tilde{\chi}_2^0 \to \tilde{\chi}_1^0 Z^{0(*)}) = \mathrm{BR}(\tilde{\chi}_2^0 \to \tilde{\chi}_1^0 H) = 0.5$.

Tglu1LL gluino pair production where $\tilde{g} \to q\bar{q}\tilde{\chi}_1^0$ happens with 1/3 probability and $\tilde{g} \to q\bar{q}\tilde{\chi}_1^\pm$ happens with 2/3 probability. The $\tilde{\chi}_1^\pm$ is assumed to be few hundreds of MeV heavier than the $\tilde{\chi}_1^0$, and decays to $\tilde{\chi}_1^0$ via a pion.

Tglu2A: gluino pair production with $\tilde{g} \to b\bar{b}\tilde{\chi}_1^0$.

Tglu3A: gluino pair production with $\tilde{g} \to t\bar{t}\tilde{\chi}_1^0$.

Tglu3B: gluino pair production with $\tilde{g} \to t\bar{\tilde{t}}$ where $\tilde{t}$ decays exclusively to $t\tilde{\chi}_1^0$.

Tglu3C: gluino pair production with $\tilde{g} \to t\bar{\tilde{t}}$ where $\tilde{t}$ decays exclusively to $c\tilde{\chi}_1^0$.

Tglu3D: gluino pair production with $\tilde{g} \to t\bar{b}\tilde{\chi}_1^\pm$ with $\tilde{\chi}_1^\pm \to W^\pm\tilde{\chi}_1^0$.

Tglu3E: gluino pair production where the gluino decays 25% of the time through $\tilde{g} \to t\bar{t}\tilde{\chi}_1^0$, 25% of the time through $\tilde{g} \to b\bar{b}\tilde{\chi}_1^0$ and 50% of the time through $\tilde{g} \to t\bar{b}\tilde{\chi}_1^\pm$ with $\tilde{\chi}_1^\pm \to W^\pm\tilde{\chi}_1^0$.

Tglu3F: gluino pair production with wino-like couplings to electroweakinos, that is: $\tilde{g} \to t\bar{t}\tilde{\chi}_{1,2}^0$ with BR 17%, $\tilde{g} \to b\bar{b}\tilde{\chi}_{1,2}^0$ with BR 17%, $\tilde{g} \to t\bar{t}\tilde{\chi}_1^\pm$ with BR 66%.

Tglu3G: gluino pair production with higgsino-like couplings to electroweakinos, that is: $\tilde{g} \to t\bar{t}\tilde{\chi}_{1,2}^0$ with BR 50%, $\tilde{g} \to t\bar{t}\tilde{\chi}_1^\pm$ with BR 50%.

Tglu4A: gluino pair production with one gluino decaying to $q\bar{q}'\tilde{\chi}_1^\pm$ with $\tilde{\chi}_1^\pm \to W^\pm + \tilde{G}$, and the other gluino decaying to $q\bar{q}\tilde{\chi}_1^0$ with $\tilde{\chi}_1^0 \to \gamma + \tilde{G}$.

Tglu4B: gluino pair production with gluinos decaying to $q\bar{q}\tilde{\chi}_1^0$ and $\tilde{\chi}_1^0 \to \gamma + \tilde{G}$.

Tglu4C: gluino pair production with gluinos decaying to $\tilde{g} \to q\bar{q}\tilde{\chi}_1^0$ and $\tilde{\chi}_1^0 \to Z + \tilde{G}$.

Tglu4D: gluino pair production with $\tilde{g} \to q\bar{q}\tilde{\chi}_1^0$ where the $\tilde{\chi}_1^0$ decays with equal probability to $\tilde{\chi}_1^0 \to \gamma + \tilde{G}$ or to $\tilde{\chi}_1^0 \to H + \tilde{G}$.

Tglu4E: gluino pair production with $\tilde{g} \to b\bar{b}\tilde{\chi}_1^0$ where the $\tilde{\chi}_1^0$ decays with equal probability to $\tilde{\chi}_1^0 \to \gamma + \tilde{G}$ or to $\tilde{\chi}_1^0 \to Z + \tilde{G}$.

Tglu4F: gluino pair production with $\tilde{g} \to t\bar{t}\tilde{\chi}_1^0$ where the $\tilde{\chi}_1^0$ decays with equal probability to $\tilde{\chi}_1^0 \to \gamma + \tilde{G}$ or to $\tilde{\chi}_1^0 \to Z + \tilde{G}$.

Tglu4G: gluino pair production with $\tilde{g} \to qq\tilde{\chi}_1^0$ where the $\tilde{\chi}_1^0$ decays with equal probability to $\tilde{\chi}_1^0 \to \gamma + \tilde{G}$ or to $\tilde{\chi}_1^0 \to Z + \tilde{G}$.

Tglu1RPV: gluino pair production with $\tilde{g} \to uds$ via RPV coupling λ''_{112}.

Tglu2RPV: gluino pair production with $\tilde{g} \to (tbd, tbs)$ via RPV coupling λ''_{313} or λ''_{323}.

Tsqk1: squark pair production with $\tilde{q} \to q\tilde{\chi}_1^0$.

Tsqk1LL squark pair production where $\tilde{q} \to q\tilde{\chi}_1^0$ and $\tilde{q} \to q\tilde{\chi}_1^\pm$ each happen with 50% probability. The $\tilde{\chi}_1^\pm$ is assumed to be few hundreds of MeV heavier than the $\tilde{\chi}_1^0$, and decays to $\tilde{\chi}_1^0$ via a pion.

Tsqk2: squark pair production with $\tilde{q} \to q\tilde{\chi}_2^0$ and $\tilde{\chi}_2^0 \to Z + \tilde{\chi}_1^0$.

Tsqk2A: squark pair production with $\tilde{q} \to q\tilde{\chi}_2^0$, where one of the $\tilde{\chi}_2^0 \to Z^{(*)}\tilde{\chi}_1^0 \to f\bar{f}\tilde{\chi}_1^0$ and the other $\tilde{\chi}_2^0 \to \tilde{\ell}\ell^+ \to \ell^+\ell^-\tilde{\chi}_1^0$.

Tsqk3: squark pair production with $\tilde{q} \to q'\tilde{\chi}_1^\pm$, $\tilde{\chi}_1^\pm \to W^\pm\tilde{\chi}_1^0$ (like Tglu1B but for squarks)

Tsqk4: squark pair production with squarks decaying to $q\tilde{\chi}_1^0$ and $\tilde{\chi}_1^0 \to \gamma + \tilde{G}$.

Tsqk4A: squark pair production with one squark decaying to $q\tilde{\chi}_1^\pm$ with $\tilde{\chi}_1^\pm \to W^\pm + \tilde{G}$, and the other squark decaying to $q\tilde{\chi}_1^0$ with $\tilde{\chi}_1^0 \to \gamma + \tilde{G}$.

Tsqk4B: squark pair production with squarks decaying to $q\tilde{\chi}_1^0$ and $\tilde{\chi}_1^0 \to \gamma + \tilde{G}$.

Tsqk5: squark pair production with four-fold mass degeneracy ($m_{\tilde{u}_L} = m_{\tilde{d}_L} = m_{\tilde{c}_L} = m_{\tilde{s}_L}$), with $\tilde{q}_L \to q'\tilde{\chi}_1^\pm$ or $\tilde{q}_L \to q\tilde{\chi}_2^0$ with equal branching ratios, where $\tilde{\chi}_1^\pm \to \tau\nu\tilde{\chi}_1^0$ and $\tilde{\chi}_2^0 \to \tau^+\tau^-\tilde{\chi}_1^0$ or $\nu\bar{\nu}\tilde{\chi}_1^0$; the mass hierarchy is such that $m_{\tilde{\chi}_1^\pm} \sim m_{\tilde{\chi}_2^0} = (m_{\tilde{q}_L} + m_{\tilde{\chi}_1^0})/2$ and $m_{\tilde{\tau},\tilde{\nu}} = (m_{\tilde{\chi}_1^\pm} + m_{\tilde{\chi}_1^0})/2$.

Tsqk1RPV: squark pair production with squarks decaying to $q\tilde{\chi}_1^0$ and $\tilde{\chi}_1^0 \to u_i d_j d_k$ via λ''_{ijk}.

Tsqk2RPV: squark pair production with squarks decaying to $q\tilde{\chi}_1^0$ and $\tilde{\chi}_1^0 \to (\ell_i u_j d_k, \nu_i d_j d_k)$ via λ'_{ijk}.

Tsqk3RPV: squark pair production with squarks decaying to $q\tilde{\chi}_1^0$ and $\tilde{\chi}_1^0 \to (\ell_i \nu_j \ell_k, \nu_i \ell_j \ell_k)$ via λ_{ijk}.

Tstop1: stop pair production with $\tilde{t} \to t\tilde{\chi}_1^0$.

Tstop1LL stop pair production where $\tilde{t} \to t\tilde{\chi}_1^0$ and $\tilde{t} \to b\tilde{\chi}_1^\pm$ each happen with 50% probability. The $\tilde{\chi}_1^\pm$ is assumed to be few hundreds of MeV heavier than the $\tilde{\chi}_1^0$, and decays to $\tilde{\chi}_1^0$ via a pion.

Tstop2: stop pair production with $\tilde{t} \to b\tilde{\chi}_1^\pm$ with $\tilde{\chi}_1^\pm \to W^\pm\tilde{\chi}_1^0$.

Tstop3: stop pair production with the subsequent four-body decay $\tilde{t} \to bff'\tilde{\chi}_1^0$ where f represents a lepton or a quark.

Tstop4: stop pair production with $\tilde{t} \to c\tilde{\chi}_1^0$.

Tstop5: stop pair production with $\tilde{t} \to b\bar{\nu}\tilde{\tau}$ with $\tilde{\tau} \to \tau\tilde{G}$.

Tstop6: stop pair production with $\tilde{t} \to t + \tilde{\chi}_2^0$, where $\tilde{\chi}_2^0 \to Z + \tilde{\chi}_1^0$ or $H + \tilde{\chi}_1^0$ each with BR 50%.

Tstop6RPV: stop pair production with $\tilde{t} \to t\tilde{\chi}_1^0$, $\tilde{\chi}_1^0 \to qqq$ via RPV coupling λ''_{abc}, with $a, b, c \in \{1, 2\}$.

Tstop7: stop pair production with $\tilde{t}_2 \to \tilde{t}_1 + H/Z$, where $\tilde{t}_1 \to t + \tilde{\chi}_1^0$.

Tstop8: stop pair production with equal probability of the stop decaying via $\tilde{t} \to t\tilde{\chi}_1^0$ or via $\tilde{t} \to b\tilde{\chi}_1^\pm$ with $\tilde{\chi}_1^\pm \to W^\pm\tilde{\chi}_1^0$.

Tstop9: stop pair production with equal probability of the stop decaying via $\tilde{t} \to c\tilde{\chi}_1^0$ or via the four-body decay $\tilde{t} \to bff'\tilde{\chi}_1^0$ where f represents a lepton or a quark.

Tstop10: stop pair production with $\tilde{t} \to b\tilde{\chi}_1^\pm$ and $\tilde{\chi}_1^\pm \to W^{\pm *}\tilde{\chi}_1^0 \to (f\bar{f}') + \tilde{\chi}_1^0$ with a virtual W-boson.

Tstop11: stop pair production with $\tilde{t} \to b\tilde{\chi}_1^\pm$ with $\tilde{\chi}_1^\pm$ decaying through an intermediate slepton to $l\nu\tilde{\chi}_1^0$

Tstop12: stop pair production with $\tilde{t} \to t\tilde{\chi}_1^0$ and $\tilde{\chi}_1^0 \to \gamma + \tilde{G}$

Tstop13: stop pair production with $\tilde{t} \to t\tilde{\chi}_1^0$ where the $\tilde{\chi}_1^0$ can decay with equal probability to $\tilde{\chi}_1^0 \to \gamma + \tilde{G}$ or to $\tilde{\chi}_1^0 \to Z + \tilde{G}$.

Tstop14: stop pair production with wino-like couplings to electroweakinos, that is: $\tilde{t} \to t\tilde{\chi}_{1,2}^0$ with BR 33%, $\tilde{g} \to b\tilde{\chi}_1^\pm$ with BR 67%.

Tstop15: stop pair production with higgsino-like couplings to electroweakinos, that is: $\tilde{t} \to t\tilde{\chi}_{1,2}^0$ with BR 50%, $\tilde{g} \to b\tilde{\chi}_1^\pm$ with BR 50%.

Tstop16: stop pair production with $\tilde{t} \to b\tilde{\chi}_1^\pm$, followed either by $\tilde{\chi}_1^\pm \to \nu_\tau\tilde{\tau}_1$ and $\tilde{\tau}_1 \to \tau\tilde{\chi}_1^0$, or by $\tilde{\chi}_1^\pm \to \tau\tilde{\nu}_\tau$ and $\tilde{\nu}_\tau \to \nu\tilde{\chi}_1^0$, each with BR 50%.

Tstop1RPV: stop pair production with $\tilde{t} \to \bar{b}\bar{s}$ via RPV coupling λ''_{323}.

Tstop2RPV: stop pair production with $\tilde{t} \to b\ell$, via RPV coupling λ'_{i33}.

Tstop3RPV: stop pair production with $\tilde{t} \to q\mu$, via RPV coupling λ'_{23k}.

Tstop4RPV: stop pair production with $\tilde{t} \to b\tilde{\chi}_1^\pm$, $\tilde{\chi}_1^\pm \to bbs$ via RPV coupling λ''_{323}.

Tstop5RPV: stop pair production with $\tilde{t} \to t\tilde{\chi}_{1,2}^0$, $\tilde{\chi}_{1,2}^0 \to tbs$ via RPV coupling λ''_{323}.

Tsbot1: sbottom pair production with $\tilde{b} \to b\tilde{\chi}_1^0$.

Tsbot2: sbottom pair production with $\tilde{b} \to t\chi_1^-$, $\chi_1^- \to W^-\tilde{\chi}_1^0$.

Tsbot3: sbottom pair production with $\tilde{b} \to b\tilde{\chi}_2^0$, where one of the $\tilde{\chi}_2^0 \to Z^{(*)}\tilde{\chi}_1^0 \to f\bar{f}\tilde{\chi}_1^0$ and the other $\tilde{\chi}_2^0 \to \tilde{\ell}\ell^+ \to \ell^+\ell^-\tilde{\chi}_1^0$.

Tsbot4: sbottom pair production with $\tilde{b} \to b\tilde{\chi}_2^0$, with $\tilde{\chi}_2^0 \to H\tilde{\chi}_1^0$

Tchi1chi1A: electroweak pair and associated production of nearly mass-degenerate charginos $\tilde{\chi}_1^\pm$ and neutralinos $\tilde{\chi}_1^0$, where $\tilde{\chi}_1^\pm$ decays to $\tilde{\chi}_1^0$ plus soft radiation, and where one of the $\tilde{\chi}_1^0$ decays to $\gamma + \tilde{G}$ while the other one decays to $Z/H + \tilde{G}$ (with equal probability).

Tchi1chi1B: electroweak pair production of charginos $\tilde{\chi}_1^\pm$, where $\tilde{\chi}_1^\pm$ decays through an intermediate slepton or sneutrino to $l\nu\tilde{\chi}_1^0$ and where the slepton or sneutrino mass is 5%, 25%, 50%, 75% and 95% of the $\tilde{\chi}_1^\pm$ mass.

Tchi1chi1C: electroweak pair production of charginos $\tilde{\chi}_1^\pm$, where $\tilde{\chi}_1^\pm$ decays through an intermediate slepton or sneutrino to $l\nu\tilde{\chi}_1^0$ and where $m_{\tilde{\ell},\tilde{\nu}} = (m_{\tilde{\chi}_1^\pm} + m_{\tilde{\chi}_1^0})/2$.

Tchi1chi1D: electroweak associated pair production of charginos $\tilde{\chi}_1^\pm$, where $\tilde{\chi}_1^\pm$ decays through an intermediate scalar tau lepton or sneutrino to $\tau\nu\tilde{\chi}_1^0$ and where $m_{\tilde{\tau}}, m_{\tilde{\nu}} = (m_{\tilde{\chi}_1^\pm} + m_{\tilde{\chi}_1^0})/2$.

Tchi1chi1F: electroweak pair and associated production of nearly mass-degenerate charginos $\tilde{\chi}_1^\pm$ and neutralinos $\tilde{\chi}_1^0$ (*i.e.* $\tilde{\chi}_1^\pm\tilde{\chi}_1^\pm$ and $\tilde{\chi}_1^\pm\tilde{\chi}_1^0$ production) where the $\tilde{\chi}_1^\pm$ decays exclusively to $\tilde{\chi}_1^0$ plus soft radiation and the $\tilde{\chi}_1^0$ decays to $\gamma/Z + \tilde{G}$.

Tchi1chi1G: electroweak pair production of charginos $\tilde{\chi}_1^\pm$, which are nearly mass-degenerate with neutralinos $\tilde{\chi}_1^0$. The $\tilde{\chi}_1^\pm$ decays either

Int. J. Mod. Phys. A 2026.41. Downloaded from www.worldscientific.com
by UNIVERSITY OF CALIFORNIA @ BERKELEY on 09/16/26. Re-use and distribution is strictly not permitted, except for Open Access articles.

to $W^{\pm} + \tilde{G}$, or to $\tilde{\chi}_1^0$ plus soft radiation. The $\tilde{\chi}_1^0$ decays exclusively to $\gamma + \tilde{G}$.

Tchi1chi1H: electroweak pair production of charginos $\tilde{\chi}_1^{\pm}$, with $\tilde{\chi}_1^{\pm} \to W^{\pm} + \tilde{\chi}_1^0$ and $W^{\pm} \to \ell^{\pm} + \nu$.

Tchi1chi1I: electroweak pair production of charginos $\tilde{\chi}_1^{\pm}$ with $\tilde{\chi}_1^{\pm} \to W^{\pm}\tilde{\chi}_1^0$ and $W^{\pm} \to q\bar{q}'$.

Tchi1n1A: electroweak associated production of mass-degenerate charginos $\tilde{\chi}_1^{\pm}$ and neutralinos $\tilde{\chi}_1^0$, where $\tilde{\chi}_1^{\pm}$ decays exclusively to $W^{\pm} + \tilde{G}$ and $\tilde{\chi}_1^0$ decays exclusively to $\gamma + \tilde{G}$.

Tchi1n2A: electroweak associated production of mass-degenerate charginos $\tilde{\chi}_1^{\pm}$ and neutralinos $\tilde{\chi}_2^0$, where $\tilde{\chi}_1^{\pm}$ decays through an intermediate slepton or sneutrino to $l\nu\tilde{\chi}_1^0$ and where $\tilde{\chi}_2^0$ decays through an intermediate slepton or sneutrino to $l^+l^-\tilde{\chi}_1^0$ or $\nu\bar{\nu}\tilde{\chi}_1^0$.

Tchi1n2B: electroweak associated production of mass-degenerate charginos $\tilde{\chi}_1^{\pm}$ and neutralinos $\tilde{\chi}_2^0$, where $\tilde{\chi}_1^{\pm}$ decays through an intermediate slepton or sneutrino to $l\nu\tilde{\chi}_1^0$ and where $\tilde{\chi}_2^0$ decays through an intermediate slepton or sneutrino to $l^+l^-\tilde{\chi}_1^0$ or $\nu\bar{\nu}\tilde{\chi}_1^0$ and where the slepton or sneutrino mass is 5%, 25%, 50%, 75% and 95% of the $\tilde{\chi}_1^{\pm}$ mass.

Tchi1n2C: electroweak associated production of mass-degenerate charginos $\tilde{\chi}_1^{\pm}$ and neutralinos $\tilde{\chi}_2^0$, where $\tilde{\chi}_1^{\pm}$ decays through an intermediate slepton or sneutrino to $l\nu\tilde{\chi}_1^0$ and where $\tilde{\chi}_2^0$ decays through an intermediate slepton or sneutrino to $l^+l^-\tilde{\chi}_1^0$ or $\nu\bar{\nu}\tilde{\chi}_1^0$ and where $m_{\tilde{\ell},\tilde{\nu}} = (m_{\tilde{\chi}_1^{\pm}} + m_{\tilde{\chi}_1^0})/2$.

Tchi1n2D: electroweak associated production of mass-degenerate charginos $\tilde{\chi}_1^{\pm}$ and neutralinos $\tilde{\chi}_2^0$, where $\tilde{\chi}_1^{\pm}$ decays through an intermediate scalar tau lepton or sneutrino to $\tau\nu\tilde{\chi}_1^0$ and where $\tilde{\chi}_2^0$ decays through an intermediate scalar tau lepton or sneutrino to $\tau^+\tau^-\tilde{\chi}_1^0$ or $\nu\bar{\nu}\tilde{\chi}_1^0$ and where $m_{\tilde{\tau},\tilde{\nu}} = (m_{\tilde{\chi}_1^{\pm}} + m_{\tilde{\chi}_1^0})/2$.

Tchi1n2E: electroweak associated production of mass-degenerate charginos $\tilde{\chi}_1^{\pm}$ and neutralinos $\tilde{\chi}_2^0$, where $\tilde{\chi}_1^{\pm} \to W^{\pm} + \tilde{\chi}_1^0$ and $\tilde{\chi}_2^0 \to H + \tilde{\chi}_1^0$.

Tchi1n2F: electroweak associated production of mass-degenerate wino-like charginos $\tilde{\chi}_1^{\pm}$ and neutralinos $\tilde{\chi}_2^0$, where $\tilde{\chi}_1^{\pm}$ decays through an intermediate $W^{\pm *}$ to $l\nu\tilde{\chi}_1^0$ and where $\tilde{\chi}_2^0$ decays through an intermediate Z^* to $l^+l^-\tilde{\chi}_1^0$ or $\nu\bar{\nu}\tilde{\chi}_1^0$.

Tchi1n2Fa: electroweak associated production of mass-degenerate wino-like charginos $\tilde{\chi}_1^{\pm}$ and neutralinos $\tilde{\chi}_2^0$, where $\tilde{\chi}_1^{\pm}$ decays through an intermediate $W^{\pm *}$ to $q\bar{q}\tilde{\chi}_1^0$ and where $\tilde{\chi}_2^0$ decays through an intermediate Z^* to $l^+l^-\tilde{\chi}_1^0$ or $\nu\bar{\nu}\tilde{\chi}_1^0$.

Tchi1n2Fb: electroweak associated production of mass-degenerate wino-like charginos $\tilde{\chi}_1^{\pm}$ and neutralinos $\tilde{\chi}_2^0$, where $\tilde{\chi}_1^{\pm}$ decays through an intermediate $W^{(*)}$ to $q\bar{q}\tilde{\chi}_1^0$ and where $\tilde{\chi}_2^0$ decays through an intermediate $Z^{(*)}$ to $q\bar{q}\tilde{\chi}_1^0$.

Tchi1n2Fc: electroweak associated production of mass-degenerate wino-like charginos $\tilde{\chi}_1^{\pm}$ and neutralinos $\tilde{\chi}_2^0$, where $\tilde{\chi}_1^{\pm}$ decays through an intermediate $W^{(*)}$ to $q\bar{q}\tilde{\chi}_1^0$ and where $\tilde{\chi}_2^0$ decays through an intermediate $H^{(*)}$ to $q\bar{q}\tilde{\chi}_1^0$.

Tchi1n2G: electroweak associated production of Higgsino-like charginos $\tilde{\chi}_1^{\pm}$ and neutralinos $\tilde{\chi}_2^0$, and electroweak associated production of $\tilde{\chi}_2^0$ and $\tilde{\chi}_1^0$, where $m_{\tilde{\chi}_1^{\pm}} = (m_{\tilde{\chi}_2^0} + m_{\tilde{\chi}_1^0})/2$ and where $\tilde{\chi}_1^{\pm}$ decays through an intermediate $W^{\pm *}$ to $q\bar{q}\tilde{\chi}_1^0$ and where $\tilde{\chi}_2^0$ decays through an intermediate Z^* to $l^+l^-\tilde{\chi}_1^0$.

Tchi1n2Ga: electroweak associated production of Higgsino-like charginos $\tilde{\chi}_1^{\pm}$ and neutralinos $\tilde{\chi}_2^0$, and electroweak associated production of $\tilde{\chi}_2^0$ and $\tilde{\chi}_1^0$, where $m_{\tilde{\chi}_1^{\pm}} = (m_{\tilde{\chi}_2^0} + m_{\tilde{\chi}_1^0})/2$ and where $\tilde{\chi}_1^{\pm}$ decays through an intermediate $W^{\pm *}$ to $l\nu\tilde{\chi}_1^0$ and where $\tilde{\chi}_2^0$ decays through an intermediate Z^* to $l^+l^-\tilde{\chi}_1^0$.

Tchi1n2H: electroweak associated production of mass-degenerate charginos $\tilde{\chi}_1^{\pm}$ and neutralinos $\tilde{\chi}_2^0$, where $\tilde{\chi}_1^{\pm}$ decays through an intermediate slepton or sneutrino to $l\nu\tilde{\chi}_1^0$ and where $\tilde{\chi}_2^0$ decays through an intermediate scalar tau lepton or sneutrino to $\tau^+\tau^-\tilde{\chi}_1^0$ or $\nu\bar{\nu}\tilde{\chi}_1^0$.

Tchi1n2I: electroweak associated production of mass-degenerate charginos $\tilde{\chi}_1^{\pm}$ and neutralinos $\tilde{\chi}_2^0$, where $\tilde{\chi}_1^{\pm}$ decays to $W^{\pm} + \tilde{\chi}_1^0$ and where $\tilde{\chi}_2^0$ decays 50% of the time to $Z + \tilde{\chi}_1^0$ and 50% of the time to $H + \tilde{\chi}_1^0$.

1n12_GGM: in the framework of General Gauge Mediation (GGM): electroweak pair and associated production of nearly mass-degenerate charginos $\tilde{\chi}_1^{\pm}$ and neutralinos $\tilde{\chi}_1^0$, $\tilde{\chi}_2^0$ (*i.e.* $\tilde{\chi}_1^{\pm}\tilde{\chi}_1^{\pm}$, $\tilde{\chi}_1^{\pm}\tilde{\chi}_1^0$ and $\tilde{\chi}_1^{\pm}\tilde{\chi}_2^0$ production) where the $\tilde{\chi}_1^{\pm}$ decays exclusively to $W^{\pm} + \tilde{G}$, the $\tilde{\chi}_2^0$ decays to $Z/H + \tilde{G}$ and the $\tilde{\chi}_1^0$ decays to $\gamma/Z + \tilde{G}$. The branching ratios depend on the composition of the gauge eigenstates of the neutralinos in the GGM scenario.

TwinoLSPBL: Electroweak pair production of wino-like $\tilde{\chi}_1^{\pm}$ and $\tilde{\chi}_1^0$ (i.e. $\tilde{\chi}_1^{\pm}\tilde{\chi}_1^{\pm}$ and $\tilde{\chi}_1^0\tilde{\chi}_1^0$). The $\tilde{\chi}_1^{\pm}$ can decay via bi-linear RPV into $Z\ell$, $H\ell$ or $W\nu$; the $\tilde{\chi}_1^0$ can decay into $Z\nu$, $H\nu$ or $W\ell$.

Tn1n1A: electroweak pair and associated production of nearly mass-degenerate Higgsino-like charginos $\tilde{\chi}_1^{\pm}$ and neutralinos $\tilde{\chi}_1^0$ and $\tilde{\chi}_2^0$, where $\tilde{\chi}_1^{\pm}$ and $\tilde{\chi}_2^0$ decay to $\tilde{\chi}_1^0$ plus soft radiation and where both of the $\tilde{\chi}_1^0$ decay to $H + \tilde{G}$.

Tn1n1B: electroweak pair and associated production of nearly mass-degenerate Higgsino-like charginos $\tilde{\chi}_1^{\pm}$ and neutralinos $\tilde{\chi}_1^0$ and $\tilde{\chi}_2^0$, where $\tilde{\chi}_1^{\pm}$ and $\tilde{\chi}_2^0$ decay to $\tilde{\chi}_1^0$ plus soft radiation and where the $\tilde{\chi}_1^0$ decays 50% of the time to $H + \tilde{G}$ and 50 % of the time to $Z + \tilde{G}$.

Tn1n1C: electroweak pair and associated production of nearly mass-degenerate Higgsino-like charginos $\tilde{\chi}_1^{\pm}$ and neutralinos $\tilde{\chi}_1^0$ and $\tilde{\chi}_2^0$, where $\tilde{\chi}_1^{\pm}$ and $\tilde{\chi}_2^0$ decay to $\tilde{\chi}_1^0$ plus soft radiation and where both of the $\tilde{\chi}_1^0$ decay to $Z + \tilde{G}$.

Tn1n1D: electroweak pair and associated production of nearly mass-degenerate Higgsino-like charginos $\tilde{\chi}_1^{\pm}$ and neutralinos $\tilde{\chi}_1^0$, $\tilde{\chi}_2^0$.

Tn1n1E: electroweak pair and associated production of nearly mass-degenerate wino-like charginos $\tilde{\chi}_1^{\pm}$ and neutralinos $\tilde{\chi}_1^0$.

Tn1n2A: electroweak associated production of nearly mass-degenerate neutralinos $\tilde{\chi}_1^0$ and $\tilde{\chi}_2^0$, where the $\tilde{\chi}_2^0$ always decays to $\gamma + \tilde{G}$ and $\tilde{\chi}_1^0$ 50% of the time to $H + \tilde{G}$ and 50 % of the time to $Z + \tilde{G}$.

Tn2n3A: electroweak associated production of mass-degenerate neutralinos $\tilde{\chi}_2^0$ and $\tilde{\chi}_3^0$, where $\tilde{\chi}_2^0$ and $\tilde{\chi}_3^0$ decay through intermediate sleptons to $l^+l^-\tilde{\chi}_1^0$ and where the slepton mass is 5%, 25%, 50%, 75% and 95% of the $\tilde{\chi}_2^0$ mass.

Tn2n3B: electroweak associated production of mass-degenerate neutralinos $\tilde{\chi}_2^0$ and $\tilde{\chi}_3^0$, where $\tilde{\chi}_2^0$ and $\tilde{\chi}_3^0$ decay through intermediate sleptons to $l^+l^-\tilde{\chi}_1^0$ and where $m_{\tilde{\ell}} = (m_{\tilde{\chi}_2^0} + m_{\tilde{\chi}_1^0})/2$.

TWinoBinoA: electroweak pair production of mass-degenerate wino-like doublet $(\tilde{\chi}_2^0, \tilde{\chi}_1^{\pm})$ (including all pair-production mechanisms) decaying into a bino singlet $(\tilde{\chi}_1^0)$. Decays happen via Standard Model bosons, assumed to decay via hadrons.

TWinoHinoA: electroweak pair production of mass-degenerate wino-like doublet $(\tilde{\chi}_3^0, \tilde{\chi}_2^{\pm})$ (including all possible pair-production mechanisms) decaying into a quasi-mass-degenerate Higgsino triplet $(\tilde{\chi}_1^0, \tilde{\chi}_2^0, \tilde{\chi}_1^{\pm})$. Decays happen via Standard Model bosons, assumed to decay via hadrons.

THinoBinoA: electroweak pair production of quasi-mass-degenerate higgsino-like triplet $(\tilde{\chi}_2^0, \tilde{\chi}_3^0, \tilde{\chi}_1^{\pm})$ (including all possible pair-production mechanisms) decaying into a bino singlet $(\tilde{\chi}_1^0)$. Decays happen via Standard Model bosons, assumed to decay via hadrons.

THinoWinoA: electroweak pair production of quasi-mass-degenerate higgsino-like triplet $(\tilde{\chi}_2^0, \tilde{\chi}_2^0, \tilde{\chi}_2^{\pm})$ (including all possible pair-production mechanisms) decaying into a mass-degenerate wino doublet $(\tilde{\chi}_1^0, \tilde{\chi}_1^{\pm})$. Decays happen via Standard Model bosons, assumed to decay via hadrons.

$\tilde{\chi}_1^0$ (Lightest Neutralino) mass limit

$\tilde{\chi}_1^0$ is often assumed to be the lightest supersymmetric particle (LSP). See also the $\tilde{\chi}_2^0$, $\tilde{\chi}_3^0$, $\tilde{\chi}_4^0$ section below.

We have divided the $\tilde{\chi}_1^0$ listings below into five sections:

1) Accelerator limits for stable $\tilde{\chi}_1^0$,
2) Bounds on $\tilde{\chi}_1^0$ from dark matter searches,
3) $\tilde{\chi}_1^0 - p$ elastic cross section (spin-dependent, spin-independent interactions),
4) Other bounds on $\tilde{\chi}_1^0$ from astrophysics and cosmology, and
5) Unstable $\tilde{\chi}_1^0$ (Lightest Neutralino) mass limit.

Accelerator limits for stable $\tilde{\chi}_1^0$

Unless otherwise stated, results in this section assume spectra, production rates, decay modes, and branching ratios as evaluated in the MSSM, with gaugino and sfermion mass unification at the GUT scale. These papers

Int. J. Mod. Phys. A 2026.41. Downloaded from www.worldscientific.com
by UNIVERSITY OF CALIFORNIA @ BERKELEY on 09/16/26. Re-use and distribution is strictly not permitted, except for Open Access articles.

generally study production of $\widetilde{\chi}^0_i \widetilde{\chi}^0_j$ ($i \geq 1$, $j \geq 2$), $\widetilde{\chi}^+_1 \widetilde{\chi}^-_1$, and (in the case of hadronic collisions) $\widetilde{\chi}^+_1 \widetilde{\chi}^0_2$ pairs. The mass limits on $\widetilde{\chi}^0_1$ are either direct, or follow indirectly from the constraints set by the non-observation of $\widetilde{\chi}^\pm_1$ and $\widetilde{\chi}^0_2$ states on the gaugino and higgsino MSSM parameters M_2 and μ. In some cases, information is used from the nonobservation of slepton decays.

Obsolete limits obtained from e^+e^- collisions up to $\sqrt{s}$=184 GeV have been removed from this compilation and can be found in the 2000 Edition (The European Physical Journal **C15** 1 (2000)) of this Review. $\Delta m = m_{\widetilde{\chi}^0_2} - m_{\widetilde{\chi}^0_1}$.

VALUE (GeV)	CL%	DOCUMENT ID		TECN	COMMENT
>850	95	[1] AAD	24Z	ATLS	2 same-sign/3ℓ + jets, Tglu1E, $m_{\widetilde{g}}$=1000 GeV
none 0.5–4.29	95	[2] LEES	23C	BABR	B + charged track, RPV $B \to \widetilde{\chi}^0_1 p$, λ''_{113} of order 10^{-7}–10^{-6}
>150	95	[3] AAD	22E	ATLS	$t\widetilde{\mu}_L$ production, RPV, $\widetilde{\mu}_L \to \mu\widetilde{\chi}^0_1$, λ'_{231} = 1, 200 GeV < $m_{\widetilde{\mu}_L}$ < 600 GeV.
none 125–175	95	[4] TUMASYAN	22S	CMS	2 same-sign e or μ, 3 or 4 leptons, Tn1n1A, $m_{\widetilde{G}}$ = 1 GeV
none 125–415	95	[4] TUMASYAN	22S	CMS	2 same-sign e or μ, 3 or 4 leptons, Tn1n1B, $m_{\widetilde{G}}$ = 1 GeV
none 100–625	95	[4] TUMASYAN	22S	CMS	2 same-sign e or μ, 3 or 4 leptons, Tn1n1C, $m_{\widetilde{G}}$ = 1 GeV
none 175–1025	95	[5] TUMASYAN	22V	CMS	3, 4 b-tag jets or 2 large-radius jets, $\not{E}_T$; Tn1n1A; $m_{\widetilde{G}}$=1 GeV
none 450–930	95	[6] AAD	21AX	ATLS	jets + large-R jets + $\not{E}_T$, Tn1n1C
none 200–320	95	[7] AAD	21BF	ATLS	$\ell^\pm$ + b-jets + many jets, Tn1n1D, RPV, λ''_{323} electroweakino decay, degenerate Higgsino triplet
none 200–370	95	[7] AAD	21BF	ATLS	$\ell^\pm$ + b-jets + many jets, Tn1n1E, RPV, λ''_{323} electroweakino decay, degenerate Wino doublet
		[8] DREINER	09	THEO	
> 40	95	[9] ABBIENDI	04H	OPAL	all tanβ, Δm >5 GeV, m_0 >500 GeV, A_0 = 0
> 42.4	95	[10] HEISTER	04	ALEP	all tanβ, all Δm, all m_0
> 39.2	95	[11] ABDALLAH	03M	DLPH	all tanβ, $m_{\widetilde{\nu}}$ >500 GeV
> 46	95	[12] ABDALLAH	03M	DLPH	all tanβ, all Δm, all m_0
> 32.5	95	[13] ACCIARRI	00D	L3	tanβ > 0.7, Δm > 3 GeV, all m_0
• • • We do not use the following data for averages, fits, limits, etc. • • •					
		[14] AAD	14K	ATLS	
> 24		[15] CALIBBI	13		thermal relic abundance, MSSM particle content

[1] AAD 24Z searched in 139 fb^{-1} of pp collisions at $\sqrt{s}$ = 13 TeV for events with exactly two same-sign leptons or at least three leptons. Several signal regions, including a $\not{E}_T$ selection targeting RPC models, and selections based on b-jet multiplicities, targeting RPV models, are considered. No significant excess over the Standard Model expectation is found. Exclusion limits at 95% C.L. are set on the gluino or squark mass, in multi-step RPC decays via charginos, neutralinos or sleptons into quarks, leptons and neutralinos, or RPV decays of either the neutralino LSP or directly the stop produced in $\widetilde{g} \to t\,\widetilde{t}$ into quarks. See their Fig. 7.

[2] LEES 23C search in 398 fb^{-1} of e^+e^- annihilations at 10.58 GeV for SUSY in events with a tagged B meson and one and only one charged track that must be consistent with the hypothesis of being a proton. The results are interpreted in an RPV SUSY model, where a neutralino is produced in the decay of a B meson into a neutralino and a proton with the RPV coupling λ''_{113}. A branching fraction upper limit is determined for the λ''_{113} coupling, divided by the relevant squark mass squared as a function of the neutralino mass, see their figure 6. They also search for a new dark sector antibaryon that could be produced in decays of B mesons.

[3] AAD 22E searched in 139 fb^{-1} of pp collisions at $\sqrt{s}$ = 13 TeV for supersymmetry by measuring the yield asymmetry between events containing $e^-\mu^+$ and those containing $e^+\mu^-$. This was found in agreement with the standard model prediction of 1. Limits are set on the RPV production of $t\widetilde{\mu}_L$ events with $\widetilde{\mu}_L \to \mu\widetilde{\chi}^0_1$ for various values of λ'_{231}, see their figures 6 and 7.

[4] TUMASYAN 22S searched in 137 fb^{-1} of pp collisions at $\sqrt{s}$ = 13 TeV for evidence of electroweakino pair production in events with three or four leptons, with up to two hadronically decaying τ leptons, or two same-sign light leptons (e or μ). No significant excess above the Standard Model expectations is observed. Limits are set on the mass of $\widetilde{\chi}^0_2$ and $\widetilde{\chi}^\pm_1$ in the models Tchi1n2B (in flavory-democratic and tau-enriched or -dominated scenarios), Tchi1n2E, Tchi1n2F, see their Figures 16–20, and on the mass of the higgsino-triplet $\widetilde{\chi}^0_2$, $\widetilde{\chi}^\pm_1$, and $\widetilde{\chi}^0_1$ in the models Tn1n1A, Tn1n1B, and Tn1n1C, see their Figure 21.

[5] TUMASYAN 22V searched in 137 fb^{-1} of pp collisions at $\sqrt{s}$ = 13 TeV for evidence of electroweakino pair production with decay to two Higgs bosons H, with $H \to b\overline{b}$, resulting either in 4 resolved b-jets or two large-radius jets, and large $\not{E}_T$. No significant excess above the Standard Model expectations is observed. Limits are set on the mass of $\widetilde{\chi}^0_2$ and $\widetilde{\chi}^\pm_1$ in the models Tn1n1A, see their Figures 11 and 12, or in a model where higgsino-like nearly mass degenerate $\widetilde{\chi}^0_2$ and $\widetilde{\chi}^0_3$ are pair produced and each decay to H and a bino-like $\widetilde{\chi}^0_1$, see their Figure 13. Limits are also set on the gluino mass in the model Tglu1I, see their Figure 14.

[6] AAD 21AX searched in 139 fb^{-1} of pp collisions at $\sqrt{s}$ = 13 TeV for pair production of electroweakinos decaying to the LSP via the emission of Standard Model bosons (Higgs, W, Z) decaying into hadrons. The final state in all cases characterised by the presence of $\not{E}_T$, jets, and large-R jets tagged according to the boson of interest. Different assumptions (Higgsino, Wino, Bino) are made for the pair produced electroweakinos and for the LSP multiplet. No significant excess above the Standard Model predictions is observed. Limits are set on the electroweakino masses as a function of the model parameters (in particular $m_{\widetilde{\chi}^0_1}$). See Fig. 16.

[7] AAD 21BF searched in 139 fb^{-1} of pp collisions at $\sqrt{s}$ = 13 TeV for pair production of gluinos, stops, electroweakinos decaying RPV either directly or indirectly via the LSP. The final state in all cases is one or two leptons, many jets (up to fifteen) and b-jets. Different models with different branching fractions of the gluino or stop follow from the assumptions on the nature of the electroweakinos. No significant excess above the Standard Model predictions is observed. Limits are set on the *gluino*, $\widetilde{t}_1$, electroweakino masses as a function of the $\widetilde{\chi}^0_1$ mass in several scenarios of gluino, stop and electroweakino pair production.

[8] DREINER 09 show that in the general MSSM with non-universal gaugino masses there exists no model-independent laboratory bound on the mass of the lightest neutralino. An essentially massless χ^0_1 is allowed by the experimental and observational data, imposing some constraints on other MSSM parameters, including M_2, μ and the slepton and squark masses.

[9] ABBIENDI 04H search for charginos and neutralinos in events with acoplanar leptons+jets and multi-jet final states in the 192–209 GeV data, combined with the results on leptonic final states from ABBIENDI 04. The results hold for a scan over the parameter space covering the region $0 < M_2 < 5000$ GeV, $-1000 < \mu < 1000$ GeV and tanβ from 1 to 40. This limit supersedes ABBIENDI 00H.

[10] HEISTER 04 data collected up to 209 GeV. Updates earlier analysis of selectrons from HEISTER 02E, includes a new analysis of charginos and neutralinos decaying into stau and uses results on charginos with initial state radiation from HEISTER 02J. The limit is based on the direct search for charginos and neutralinos, the constraints from the slepton search and the Higgs mass limits from HEISTER 02 using a top mass of 175 GeV, interpreted in a framework with universal gaugino and sfermion masses. Assuming the mixing in the stau sector to be negligible, the limit improves to 43.1 GeV. Under the assumption of MSUGRA with unification of the Higgs and sfermion masses, the limit improves to 50 GeV, and reaches 53 GeV for A_0 = 0. These limits include and update the results of BARATE 01.

[11] ABDALLAH 03M uses data from $\sqrt{s}$ = 192–208 GeV. A limit on the mass of $\widetilde{\chi}^0_1$ is derived from direct searches for neutralinos combined with the chargino search. Neutralinos are searched in the production of $\widetilde{\chi}^0_1\widetilde{\chi}^0_2$, $\widetilde{\chi}^0_1\widetilde{\chi}^0_3$, as well as $\widetilde{\chi}^0_2\widetilde{\chi}^0_3$ and $\widetilde{\chi}^0_2\widetilde{\chi}^0_4$ giving rise to cascade decays, and $\widetilde{\chi}^0_1\widetilde{\chi}^0_2$ and $\widetilde{\chi}^0_1\widetilde{\chi}^0_2$, followed by the decay $\widetilde{\chi}^0_2 \to \widetilde{\tau}\tau$. The results hold for the parameter space defined by values of M_2 < 1 TeV, $|\mu| \leq 2$ TeV with the $\widetilde{\chi}^0_1$ as LSP. The limit is obtained for tanβ = 1 and large m_0, where $\widetilde{\chi}^0_2\widetilde{\chi}^0_4$ and chargino pair production are important. If the constraint from Higgs searches is also imposed, the limit improves to 49.0 GeV in the m_h^{max} scenario with m_t=174.3 GeV. These limits update the results of ABREU 00J.

[12] ABDALLAH 03M uses data from $\sqrt{s}$ = 192–208 GeV. An indirect limit on the mass of $\widetilde{\chi}^0_1$ is derived by constraining the MSSM parameter space by the results from direct searches for neutralinos (including cascade decays and $\widetilde{\tau}\tau$ final states), for charginos (for all Δm_+) and for sleptons, stop and sbottom. The results hold for the full parameter space defined by values of M_2 < 1 TeV, $|\mu| \leq 2$ TeV with the $\widetilde{\chi}^0_1$ as LSP. Constraints from the Higgs search in the m_h^{max} scenario assuming m_t=174.3 GeV are included. The limit is obtained for tan$\beta \geq$ 5 when stau mixing leads to mass degeneracy between $\widetilde{\tau}_1$ and $\widetilde{\chi}^0_1$ and the limit is based on $\widetilde{\chi}^0_2$ production followed by its decay to $\widetilde{\tau}_1\tau$. In the pathological scenario where m_0 and $|\mu|$ are large, so that the $\widetilde{\chi}^0_2$ production cross section is negligible, and where there is mixing in the stau sector but not in stop nor sbottom, the limit is based on charginos with soft decay products and an ISR photon. The limit then degrades to 39 GeV. See Figs. 40–42 for the dependence of the limit on tanβ and $m_{\widetilde{\nu}}$. These limits update the results of ABREU 00W.

[13] ACCIARRI 00D data collected at $\sqrt{s}$=189 GeV. The results hold over the full parameter space defined by $0.7 \leq$ tan$\beta \leq 60$, $0 \leq M_2 \leq 2$ TeV, $m_0 \leq 500$ GeV, $|\mu| \leq 2$ TeV The minimum mass limit is reached for tanβ=1 and large m_0. The results of slepton searches from ACCIARRI 99W are used to help set constraints in the region of small m_0. The limit improves to 48 GeV for $m_0 \gtrsim 200$ GeV and tan$\beta \gtrsim 10$. See their Figs. 6–8 for the tanβ and m_0 dependence of the limits. Updates ACCIARRI 98F.

[14] AAD 14K sets limits on the χ-nucleon spin-dependent and spin-independent cross sections out to m_χ = 10 TeV.

[15] CALIBBI 13 use the fact that if the relic abundance of $\widetilde{\chi}^0_1$ does not overclose the universe, scalar lepton and Higgsino masses must be relatively small. Using 8 TeV ATLAS constraints on the scalar tau mass and on invisible Higgs decays, they estimate a lower bound for the $\widetilde{\chi}^0_1$ mass.

Bounds on $\widetilde{\chi}^0_1$ from dark matter searches

These papers generally exclude regions in the $M_2 - \mu$ parameter plane assuming that $\widetilde{\chi}^0_1$ is the dominant form of dark matter in the galactic halo. These limits are based on the lack of detection in laboratory experiments, telescopes, or by the absence of a signal in underground neutrino detectors. The latter signal is expected if $\widetilde{\chi}^0_1$ accumulates in the Sun or the Earth and annihilates into high-energy ν's.

VALUE	DOCUMENT ID		TECN
• • • We do not use the following data for averages, fits, limits, etc. • • •			
	[1] ABBASI	25A	ICCB
	[2] MCDANIEL	24	FLAT
	[3] ABBASI	23A	ICCB
	[4] ABE	23B	MGIC
	[5] ALBERT	23	HAWC
	[6] CHENG	23A	FLAT
	[7] FOSTER	23	FLAT
	[8] GUO	23A	ICCB
	[9] LAVIS	23	MEER

Int. J. Mod. Phys. A 2026.41. Downloaded from www.worldscientific.com
by UNIVERSITY OF CALIFORNIA @ BERKELEY on 09/16/26. Re-use and distribution is strictly not permitted, except for Open Access articles.

[10] ABBASI 22B ICCB
[11] ABDALLA 22 HESS
[12] ABDALLAH 21 HESS
[13] ABAZAJIAN 20 FLAT
[14] ABDALLAH 20 HESS
[15] ABE 20G SKAM
[16] ALBERT 20 HAWC
[17] ALBERT 20A ANTR
[18] ALBERT 20C ANIC
[19] ALVAREZ 20 FLAT
[20] HOOF 20 FLAT
[21] DI-MAURO 19 FLAT
[22] JOHNSON 19 FLAT
[23] LI 19D FLAT
[24] AHNEN 18 MGIC
[25] ALBERT 18B HAWC
[26] ALBERT 18C HAWC
[27] AARTSEN 17A ICCB
[28] AARTSEN 17C ICCB
[29] ARCHAMBAU..17 VRTS
[30] ADRIAN-MAR..16 ANTR
[31] AHNEN 16 MGFL
[32] AVRORIN 16 BAIK
[33] CIRELLI 16 THEO
[33] LEITE 16 THEO
[34] ACKERMANN 15 FLAT
[35] ACKERMANN 15A FLAT
[36] ACKERMANN 15B FLAT
[37] BUCKLEY 15 THEO
[38] CHOI 15 SKAM
[39] ALEKSIC 14 MGIC
[40] AVRORIN 14 BAIK
[41] AARTSEN 13C ICCB
[42] BERGSTROM 13 COSM
[43] BOLIEV 13 BAKS
[42] JIN 13 ASTR
[42] KOPP 13 COSM
[44] ACKERMANN 10 FLAT
[45] ACHTERBERG 06 AMND
[46] ACKERMANN 06 AMND
[47] DEBOER 06 RVUE
[48] DESAI 04 SKAM
[48] AMBROSIO 99 MCRO
[49] LOSECCO 95 RVUE
[50] MORI 93 KAMI
[51] BOTTINO 92 COSM
[52] BOTTINO 91 RVUE
[53] GELMINI 91 COSM
[54] KAMIONKOW..91 RVUE
[55] MORI 91B KAMI
none 4–15 GeV [56] OLIVE 88 COSM

[1] ABBASI 25A is based on 10 years of data collected with IceCube. They looked for interactions of ν's resulting from neutralino annihilations in the Earth over a background of atmospheric neutrinos and set 90% CL limits on the spin independent neutralino-proton cross section for neutralino masses in the range 10–10000 GeV. This updates AARTSEN 17.

[2] MCDANIEL 24 uses 14 years of Fermi-LAT data from Milky Way Dwarf Spheroidals to constrain dark matter annihilation cross sections.

[3] ABBASI 23A sets limits on the dark matter annihilation cross section from searches of monochromatic neutrinos produced in the galactic center. They set a limit on the annihilation cross section for dark matter with masses between 10–40000 GeV annihilating in the Galactic center assuming an NFW profile. The limit is of order 10×10^{-24} cm^{3}s^{-1} in the $\nu_e\overline{\nu}_e$ channel.

[4] ABE 23B sets limits on the dark matter annihilation cross section from line-like features in TeV gamma-rays in the direction of the Galactic center using the MAGIC stereoscopic telescope.

[5] ALBERT 23 uses gamma-ray observation of the Galactic halo to constrain the dark matter annihilation cross section for annihilations for masses between 10–100 TeV.

[6] CHENG 23A uses 13 years of Fermi-LAT data and 5 years of DAMPE data to constrain dark matter annihilation in the Galactic halo from searches of gamma-ray spectral lines.

[7] FOSTER 23 sets limits on the dark matter annihilation cross section from monochromatic gamma-rays in the inner Milky Way using 14 years of data from Fermi-LAT.

[8] GUO 23A sets limits on the dark matter annihilation cross section from 10 years of IceCube muon-track data from 18 dwarf speroidal galaxies.

[9] LAVIS 23 uses a statistical analysis of the radio flux densities within galaxy clusters in data from the MeerKAT Galaxy Cluster Legacy Survey to constrain dark matter annihilations for masses less than 1 TeV.

[10] ABBASI 22B presents 7 years of data from a search of neutrinos from dark matter annihilations in the sun using the DeepCore sub-array of IceCube. Annihilation cross section limits applies to dark matter masses between 5–100 GeV.

[11] ABDALLA 22 uses gamma-ray observations in the Galactic center to constrain the dark matter annihilation cross section for annihilations into WW and $\tau\tau$ for dark matter masses between 200 GeV to 70 TeV. This updates ABDALLAH 18.

[12] ABDALLAH 21 places constraints on the dark matter annihilation cross section for annihilations into gamma-rays from the dwarf irregular galaxy WLM for masses between 0.15 to 10 TeV.

[13] ABAZAJIAN 20 sets constraints on the dark matter annihilation from gamma-ray searches from Fermi LAT observations of the Galactic center.

[14] ABDALLAH 20 places constraints on the dark matter annihilation cross section for annihilations into gamma-rays from Milky Way dwarf galaxy satellites for masses between 0.2 to 40 TeV.

[15] ABE 20G is based on SuperKamiokande data taken from 1996 to 2016 searching for neutrinos produced from dark matter annihilations in the galactic center or halo. They place constraints on the dark matter-nucleon scattering cross section for dark matter masses between 1 GeV and 10 TeV.

[16] ALBERT 20 sets limits on the annihilation cross section of dark matter with mass between 1 and 100 TeV from gamma-ray observations of the local dwarf spheroidal galaxies.

[17] ALBERT 20A set limits on the dark matter annihilation cross section from neutrinos observations in the Galactic center using 11 years of ANTARES data.

[18] ALBERT 20C set limits on the dark matter annihilation cross section from neutrinos observations in the Galactic center combining Antares and IceCube data.

[19] ALVAREZ 20 set limits on the dark matter annihilation from gamma-ray searches from Fermi LAT observations in the directions of dwarf spheroidal galaxies.

[20] HOOF 20 set limits on the dark matter annihilation from gamma-ray searches from Fermi LAT observations in the directions of dwarf spheroidal galaxies.

[21] DI-MAURO 19 sets limits on the dark matter annihilation from gamma-ray searches in M31 and M33 galaxies using Fermi LAT data.

[22] JOHNSON 19 sets limits on p-wave dark matter annihilations in the galactic center using Fermi data.

[23] LI 19D sets limits on dark matter annihilation cross sections searching for line-like signals in the all-sky Fermi data.

[24] AHNEN 18 uses observations of the dwarf satellite galaxy Ursa Major II to obtain upper limits on annihilation cross sections for dark matter in various channels for masses between 0.1–100 TeV.

[25] ALBERT 18B sets limits on the annihilation cross section of dark matter with mass between 1 and 100 TeV from gamma-ray observations of the Andromeda galaxy.

[26] ALBERT 18C sets limits on the spin-dependent coupling of dark matter to protons from dark matter annihilation in the Sun.

[27] AARTSEN 17A is based on data collected during 532 days of livetime with the IceCube 86-string detector including the DeepCore sub-array. They looked for interactions of ν's from neutralino annihilations in the Sun over a background of atmospheric neutrinos and set 90% CL limits on the spin dependent neutralino-proton cross section for neutralino masses in the range 10–10000 GeV. This updates AARTSEN 16C.

[28] AARTSEN 17C is based on 1005 days of running with the IceCube detector. They set a limit on the annihilation cross section for dark matter with masses between 10–1000 GeV annihilating in the Galactic center assuming an NFW profile. The limit is of 1.2×10^{23} cm^{3}s^{-1} in the $\tau^+\tau^-$ channel. Supercedes AARTSEN 15E.

[29] ARCHAMBAULT 17 performs a joint statistical analysis of four dwarf galaxies with VERITAS looking for gamma-ray emission from neutralino annihilation. They set limits on the neutralino annihilation cross section.

[30] ADRIAN-MARTINEZ 16 is based on data from the ANTARES neutrino telescope. They looked for interactions of ν's from neutralino annihilations in the Sun over a background of atmospheric neutrinos and set 90% CL limits on the muon neutrino flux. They also obtain limits on the spin dependent and spin independent neutralino-proton cross section for neutralino masses in the range 50 to 5,000 GeV. This updates ADRIAN-MARTINEZ 13.

[31] AHNEN 16 combines 158 hours of Segue 1 observations with MAGIC with 6 year observations of 15 dwarf satellite galaxies by Fermi-LAT to set limits on annihilation cross sections for dark matter masses between 10 GeV and 100 TeV.

[32] AVRORIN 16 is based on 2.76 years with Lake Baikal neutrino telescope. They derive 90% upper limits on the annihilation cross section from dark matter annihilations in the Galactic center.

[33] CIRELLI 16 and LEITE 16 derive bounds on the annihilation cross section from radio observations.

[34] ACKERMANN 15 is based on 5.8 years of data with Fermi-LAT and search for monochromatic gamma-rays in the energy range of 0.2–500 GeV from dark matter annihilations. This updates ACKERMANN 13A.

[35] ACKERMANN 15A is based on 50 months of data with Fermi-LAT and search for dark matter annihilation signals in the isotropic gamma-ray background as well as galactic subhalos in the energy range of a few GeV to a few tens of TeV.

[36] ACKERMANN 15B is based on 6 years of data with Fermi-LAT observations of Milky Way dwarf spheroidal galaxies. Set limits on the annihilation cross section from $m_\chi =$ 2 GeV to 10 TeV. This updates ACKERMANN 14.

[37] BUCKLEY 15 is based on 5 years of Fermi-LAT data searching for dark matter annihilation signals from Large Magellanic Cloud.

[38] CHOI 15 is based on 3903 days of SuperKamiokande data searching for neutrinos produced from dark matter annihilations in the sun. They place constraints on the dark matter-nucleon scattering cross section for dark matter masses between 4–200 GeV.

[39] ALEKSIC 14 is based on almost 160 hours of observations of Segue 1 satellite dwarf galaxy using the MAGIC telescopes between 2011 and 2013. Sets limits on the annihilation cross section out to $m_\chi = 10$ TeV.

[40] AVRORIN 14 is based on almost 2.76 years with Lake Baikal neutrino telescope. They derive 90% upper limits on the fluxes of muons and muon neutrinos from dark matter annihilations in the Sun.

[41] AARTSEN 13C is based on data collected during 339.8 effective days with the IceCube 59-string detector. They looked for interactions of ν_μ's from neutralino annihilations in nearby galaxies and galaxy clusters. They obtain limits on the neutralino annihilation cross section for neutralino masses in the range 30–100, 000 GeV.

[42] BERGSTROM 13, JIN 13, and KOPP 13 derive limits on the mass and annihilation cross section using AMS-02 data. JIN 13 also sets a limit on the lifetime of the dark matter particle.

[43] BOLIEV 13 is based on data collected during 24.12 years of live time with the Bakson Underground Scintillator Telescope. They looked for interactions of ν_μ's from neutralino annihilations in the Sun over a background of atmospheric neutrinos and set 90% CL limits on the muon flux. They also obtain limits on the spin dependent and spin independent neutralino-proton cross section for neutralino masses in the range 10–1000 GeV.

[44] ACKERMANN 10 place upper limits on the annihilation cross section with $b\overline{b}$ or $\mu^+\mu^-$ final states.

[45] ACHTERBERG 06 is based on data collected during 421.9 effective days with the AMANDA detector. They looked for interactions of ν_μs from the centre of the Earth over a background of atmospheric neutrinos and set 90 % CL limits on the muon flux. Their limit is compared with the muon flux expected from neutralino annihilations into W^+W^- and $b\overline{b}$ at the centre of the Earth for MSSM parameters compatible with the relic dark matter density, see their Fig. 7.

[46] ACKERMANN 06 is based on data collected during 143.7 days with the AMANDA-II detector. They looked for interactions of ν_μs from the Sun over a background of atmospheric neutrinos and set 90 % CL limits on the muon flux. Their limit is compared

Int. J. Mod. Phys. A 2026.41. Downloaded from www.worldscientific.com
by UNIVERSITY OF CALIFORNIA @ BERKELEY on 09/16/26. Re-use and distribution is strictly not permitted, except for Open Access articles.

with the muon flux expected from neutralino annihilations into $W^+ W^-$ in the Sun for SUSY model parameters compatible with the relic dark matter density, see their Fig. 3.

[47] DEBOER 06 interpret an excess of diffuse Galactic gamma rays observed with the EGRET satellite as originating from π^0 decays from the annihilation of neutralinos into quark jets. They analyze the corresponding parameter space in a supergravity inspired MSSM model with radiative electroweak symmetry breaking, see their Fig. 3 for the preferred region in the $(m_0, m_{1/2})$ plane of a scenario with large $\tan\beta$.

[48] AMBROSIO 99 and DESAI 04 set new neutrino flux limits which can be used to limit the parameter space in supersymmetric models based on neutralino annihilation in the Sun and the Earth.

[49] LOSECCO 95 reanalyzed the IMB data and places lower limit on $m_{\tilde{\chi}^0_1}$ of 18 GeV if the LSP is a photino and 10 GeV if the LSP is a higgsino based on LSP annihilation in the sun producing high-energy neutrinos and the limits on neutrino fluxes from the IMB detector.

[50] MORI 93 excludes some region in M_2–μ parameter space depending on $\tan\beta$ and lightest scalar Higgs mass for neutralino dark matter $m_{\tilde{\chi}^0} > m_W$, using limits on upgoing muons produced by energetic neutrinos from neutralino annihilation in the Sun and the Earth.

[51] BOTTINO 92 excludes some region M_2-μ parameter space assuming that the lightest neutralino is the dark matter, using upgoing muons at Kamiokande, direct searches by Ge detectors, and by LEP experiments. The analysis includes top radiative corrections on Higgs parameters and employs two different hypotheses for nucleon-Higgs coupling. Effects of rescaling in the local neutralino density according to the neutralino relic abundance are taken into account.

[52] BOTTINO 91 excluded a region in $M_2 - \mu$ plane using upgoing muon data from Kamioka experiment, assuming that the dark matter surrounding us is composed of neutralinos and that the Higgs boson is not too heavy.

[53] GELMINI 91 exclude a region in $M_2 - \mu$ plane using dark matter searches.

[54] KAMIONKOWSKI 91 excludes a region in the M_2–μ plane using IMB limit on upgoing muons originated by energetic neutrinos from neutralino annihilation in the sun, assuming that the dark matter is composed of neutralinos and that $m_{H^0_1} \lesssim 50$ GeV. See Fig. 8 in the paper.

[55] MORI 91B exclude a part of the region in the M_2–μ plane with $m_{\tilde{\chi}^0_1} \lesssim 80$ GeV using a limit on upgoing muons originated by energetic neutrinos from neutralino annihilation in the earth, assuming that the dark matter surrounding us is composed of neutralinos and that $m_{H^0_1} \lesssim 80$ GeV.

[56] OLIVE 88 result assumes that photinos make up the dark matter in the galactic halo. Limit is based on annihilations in the sun and is due to an absence of high energy neutrinos detected in underground experiments. The limit is model dependent.

$\tilde{\chi}^0_1$-p elastic cross section

Experimental results on the $\tilde{\chi}^0_1$-p elastic cross section are evaluated at $m_{\tilde{\chi}^0_1}$=100 GeV. The experimental results on the cross section are often mass dependent. Therefore, the mass and cross section results are also given where the limit is strongest, when appropriate. Results are quoted separately for spin-dependent interactions (based on an effective 4-Fermi Lagrangian of the form $\overline{\chi}\gamma^\mu\gamma^5\chi\overline{q}\gamma_\mu\gamma^5 q$) and spin-independent interactions ($\overline{\chi}\chi\overline{q}q$). For calculational details see GRIEST 88B, ELLIS 88D, BARBIERI 89C, DREES 93B, ARNOWITT 96, BERGSTROM 96, and BAER 97 in addition to the theory papers listed in the Tables. For a description of the theoretical assumptions and experimental techniques underlying most of the listed papers, see the review on "Dark matter" in this "Review of Particle Physics," and references therein. Most of the following papers use galactic halo and nuclear interaction assumptions from (LEWIN 96).

Spin-dependent interactions

VALUE (pb)	CL%	DOCUMENT ID		TECN	COMMENT
• • • We do not use the following data for averages, fits, limits, etc. • • •					
$< 1.5 \times 10^{-5}$	90	[1] AALBERS	25	LZ	Xe
$< 2.0 \times 10^{-4}$	90	[2] APRILE	25B	XENT	Xe
$< 1 \times 10^{-4}$	90	[3] BO	25	PNDX	Xe
$< 4 \times 10^{-5}$	90	[4] AMOLE	19	PICO	C_3F_8
$< 5 \times 10^{-4}$	90	[5] APRILE	19A	XE1T	Xe
$< 8 \times 10^{-4}$	90	[6] AKERIB	17A	LUX	Xe
< 0.28	90	[7] BATTAT	17	DRFT	CS_2; CF_4
< 0.027	90	[8] BEHNKE	17	PICA	C_4F_{10}
$< 5 \times 10^{-4}$	90	[9] AMOLE	16	PICO	CF_3I
$< 6.8 \times 10^{-3}$	90	[10] APRILE	16B	X100	Xe
$< 6.3 \times 10^{-3}$	90	[11] FELIZARDO	14	SMPL	C_2ClF_5
< 0.01	90	[12] AKIMOV	12	ZEP3	Xe
$< 7 \times 10^{-3}$		[13] BEHNKE	12	COUP	CF_3I
$< 8.5 \times 10^{-3}$		[14] FELIZARDO	12	SMPL	C_2ClF_5
< 0.016	90	[15] KIM	12	KIMS	CsI
5×10^{-10} to 10^{-5}	95	[16] BUCHMUEL...	11B	THEO	
< 1	90	[17] ANGLE	08A	XE10	Xe
< 0.055		[18] BEDNYAKOV	08	HDMS	Ge
< 0.33	90	[19] BEHNKE	08	COUP	CF_3I
< 5		[20] AKERIB	06	CDMS	Ge
< 2		[21] SHIMIZU	06A	CNTR	CaF_2
< 0.4		[22] ALNER	05	NAIA	NaI Spin Dep.
< 2		[23] BARNABE-HE..	05	PICA	C
2×10^{-11} to 1×10^{-4}		[24] ELLIS	04	THEO	$\mu > 0$
< 0.8		[25] AHMED	03	NAIA	NaI Spin Dep.
< 40		[26] TAKEDA	03	BOLO	NaF Spin Dep.
< 10		[27] ANGLOHER	02	CRES	Saphire
8×10^{-7} to 2×10^{-5}		[28] ELLIS	01C	THEO	$\tan\beta \leq 10$
< 3.8		[29] BERNABEI	00D	DAMA	Xe
< 0.8		SPOONER	00	UKDM	NaI
< 4.8		[30] BELLI	99C	DAMA	F
< 100		[31] OOTANI	99	BOLO	LiF
< 0.6		BERNABEI	98C	DAMA	Xe
< 5		[30] BERNABEI	97	DAMA	F

[1] The strongest upper limit is 9.8×10^{-6} pb at 40 GeV. The limit for scattering on neutrons is 5.3×10^{-7} pb at 100 GeV and is 3.7×10^{-7} pb at 46 GeV. This updates AALBERS 23.

[2] The strongest upper limit is 8.5×10^{-5} pb at 30 GeV. The limit for scattering on neutrons is 6.7×10^{-6} pb at 100 GeV and is 2.8×10^{-6} pb at 30 GeV. This updates APRILE 23A.

[3] The strongest upper limit is 7.7×10^{-5} pb at a WIMP mass of 40 GeV. The limit for scattering on neutrons is 4×10^{-6} pb at 100 GeV and is 2.7×10^{-6} pb at 40 GeV. The corresponding plots are found in the supplementary material on the journal webpage. This updates HUANG 22.

[4] The strongest limit is $< 3.2 \times 10^{-5}$ pb at $m_\chi = 25$ GeV. This updates AMOLE 17.

[5] The strongest limit is $< 2 \times 10^{-4}$ pb at $m_\chi = 30$ GeV. For scatterings on neutrons, the strongest limit is $< 6.3 \times 10^{-6}$ at $m_\chi = 30$ GeV.

[6] The strongest limit is 5×10^{-4} pb at $m_\chi = 35$ GeV. The limit for scattering on neutrons is 3×10^{-5} pb at 100 GeV and is 1.6×10^{-5} pb at 35 GeV. This updates AKERIB 16A.

[7] Directional recoil detector. This updates DAW 12.

[8] This result updates ARCHAMBAULT 12. The strongest limit is 0.013 pb at $m_\chi = 20$ GeV.

[9] The strongest limit is 5×10^{-4} pb at $m_\chi = 80$ GeV.

[10] The strongest limit is 5.2×10^{-3} pb at 50 GeV. The limit for scattering on neutrons is 2.8×10^{-4} pb at 100 GeV and the strongest limit is 2.0×10^{-4} pb at 50 GeV. This updates APRILE 13.

[11] The strongest limit is 0.0043 pb and occurs at $m_\chi = 35$ GeV. FELIZARDO 14 also presents limits for the scattering on neutrons. At $m_\chi = 100$ GeV, the upper limit is 0.13 pb and the strongest limit is 0.066 pb at $m_\chi = 35$ GeV.

[12] This result updates LEBEDENKO 09A. The strongest limit is 8×10^{-3} pb at $m_\chi = 50$ GeV. Limit applies to the neutralino neutron elastic cross section.

[13] The strongest limit is 6×10^{-3} at $m_\chi = 60$ GeV.

[14] The strongest limit is 5.7×10^{-3} at $m_\chi = 35$ GeV.

[15] This result updates LEE 07A. The strongest limit is at $m_\chi = 80$ GeV.

[16] Predictions for the spin-dependent elastic cross section based on a frequentist approach to electroweak observables in the framework of $N = 1$ supergravity models with radiative breaking of the electroweak gauge symmetry.

[17] The strongest limit is 0.6 pb and occurs at m_χ= 30 GeV. The limit for scattering on neutrons is 0.01 pb at m_χ= 100 GeV, and the strongest limit is 0.0045 pb at m_χ= 30 GeV.

[18] Limit applies to neutron elastic cross section.

[19] The strongest upper limit is 0.25 pb and occurs at $m_\chi \simeq 40$ GeV.

[20] The strongest upper limit is 4 pb and occurs at $m_\chi \simeq 60$ GeV. The limit on the neutron spin-dependent elastic cross section is 0.07 pb. This latter limit is improved in AHMED 09, where a limit of 0.02 pb is obtained at $m_\chi = 100$ GeV. The strongest limit in AHMED 09 is 0.018 pb and occurs at $m_\chi = 60$ GeV.

[21] The strongest upper limit is 1.2 pb and occurs at $m_\chi \simeq 40$ GeV. The limit on the neutron spin-dependent cross section is 35 pb.

[22] The strongest upper limit is 0.35 pb and occurs at $m_\chi \simeq 60$ GeV.

[23] The strongest upper limit is 1.2 pb and occurs $m_\chi \simeq 30$ GeV.

[24] ELLIS 04 calculates the χp elastic scattering cross section in the framework of N=1 supergravity models with radiative breaking of the electroweak gauge symmetry, but without universal scalar masses. In the case of universal squark and slepton masses, but non-universal Higgs masses, the limit becomes 2×10^{-4}, see ELLIS 03E.

[25] The strongest upper limit is 0.75 pb and occurs at $m_\chi \approx 70$ GeV.

[26] The strongest upper limit is 30 pb and occurs at $m_\chi \approx 20$ GeV.

[27] The strongest upper limit is 8 pb and occurs at $m_\chi \simeq 30$ GeV.

[28] ELLIS 01C calculates the χ-p elastic scattering cross section in the framework of N=1 supergravity models with radiative breaking of the electroweak gauge symmetry. In models with nonuniversal Higgs masses, the upper limit to the cross section is 6×10^{-4}.

[29] The strongest upper limit is 3 pb and occurs at $m_\chi \simeq 60$ GeV. The limits are for inelastic scattering $X^0 + {}^{129}Xe \rightarrow X^0 + {}^{129}Xe^*$ (39.58 keV).

[30] The strongest upper limit is 4.4 pb and occurs at $m_\chi \simeq 60$ GeV.

[31] The strongest upper limit is about 35 pb and occurs at $m_\chi \simeq 15$ GeV.

Spin-independent interactions

VALUE (pb)	CL%	DOCUMENT ID		TECN	COMMENT
• • • We do not use the following data for averages, fits, limits, etc. • • •					
$< 3.5 \times 10^{-12}$	90	[1] AALBERS	25	LZ	Xe
$< 3.9 \times 10^{-11}$	90	[2] APRILE	25B	XENT	Xe
$< 3 \times 10^{-11}$	90	[3] BO	25	PNDX	Xe
$< 9 \times 10^{-8}$	90	[4] YU	25	C100	NaI
$< 1.6 \times 10^{-8}$	90	[5] ABE	23E	XMAS	Xe
$< 5 \times 10^{-10}$	90	[6] WANG	20G	PNDX	Xe
$< 3.9 \times 10^{-9}$	90	[7] AJAJ	19	DEAP	Ar
$< 2 \times 10^{-8}$	90	[8] AMOLE	19	PICO	C_3F_8
$< 1.14 \times 10^{-8}$	90	[9] AGNES	18A	DS50	Ar
$< 1.6 \times 10^{-8}$	90	[10] AGNESE	18A	CDMS	Ge
$< 9 \times 10^{-11}$	90	[11] APRILE	18	XE1T	Xe
$< 1.8 \times 10^{-10}$	90	[12] AKERIB	17	LUX	Xe
$< 1.5 \times 10^{-9}$	90	[13] APRILE	16B	X100	Xe
$< 1.5 \times 10^{-9}$	90	[14] AKERIB	14	LUX	Xe
10^{-11}–10^{-7}	95	[15] BUCHMUEL...	14A	THEO	

$< 4.6 \times 10^{-6}$	90	[16] FELIZARDO	14	SMPL C_2ClF_5
10^{-11}–10^{-8}	95	[17] ROSZKOWSKI	14	THEO
$< 2.2 \times 10^{-6}$	90	[18] AGNESE	13	CDMS Si
$< 5 \times 10^{-8}$	90	[19] AKIMOV	12	ZEP3 Xe
1.6×10^{-6}; 3.7×10^{-5}		[20] ANGLOHER	12	CRES $CaWO_4$
3×10^{-12} to 3×10^{-9}	95	[21] BECHTLE	12	THEO
$< 1.6 \times 10^{-7}$		[22] BEHNKE	12	COUP CF_3I
$< 2.3 \times 10^{-7}$	90	[23] KIM	12	KIMS CsI
$< 3.3 \times 10^{-8}$	90	[24] AHMED	11A	Ge
$< 4.4 \times 10^{-8}$	90	[25] ARMENGAUD	11	EDE2 Ge
$< 1 \times 10^{-7}$	90	[26] ANGLE	08	XE10 Xe
$< 1 \times 10^{-6}$	90	BENETTI	08	WARP Ar
$< 7.5 \times 10^{-7}$	90	[27] ALNER	07A	ZEP2 Xe
$< 2 \times 10^{-7}$		[28] AKERIB	06A	CDMS Ge
$<90 \times 10^{-7}$		ALNER	05	NAIA NaI Spin Indep.
$<12 \times 10^{-7}$		[29] ALNER	05A	ZEPL
$<14 \times 10^{-7}$		SANGLARD	05	EDEL Ge
$< 4 \times 10^{-7}$		[30] AKERIB	04	CDMS Ge
2×10^{-11} to 1.5×10^{-7}	95	[31] BALTZ	04	THEO
2×10^{-11} to 8×10^{-6}		[32,33] ELLIS	04	THEO $\mu > 0$
$< 5 \times 10^{-8}$		[34] PIERCE	04A	THEO
$< 2 \times 10^{-5}$		[35] AHMED	03	NAIA NaI Spin Indep.
$< 3 \times 10^{-6}$		[36] AKERIB	03	CDMS Ge
2×10^{-13} to 2×10^{-7}		[37] BAER	03A	THEO
$< 1.4 \times 10^{-5}$		[38] KLAPDOR-K...	03	HDMS Ge
$< 6 \times 10^{-6}$		[39] ABRAMS	02	CDMS Ge
1×10^{-12} to 7×10^{-6}		[32] KIM	02B	THEO
$< 3 \times 10^{-5}$		[40] MORALES	02B	CSME Ge
$< 1 \times 10^{-5}$		[41] MORALES	02C	IGEX Ge
$< 1 \times 10^{-6}$		BALTZ	01	THEO
$< 3 \times 10^{-5}$		[42] BAUDIS	01	HDMS Ge
$< 7 \times 10^{-6}$		[43] BOTTINO	01	THEO
$< 1 \times 10^{-8}$		[44] CORSETTI	01	THEO $\tan\beta \leq 25$
5×10^{-10} to 1.5×10^{-8}		[45] ELLIS	01C	THEO $\tan\beta \leq 10$
$< 4 \times 10^{-6}$		[44] GOMEZ	01	THEO
2×10^{-10} to 1×10^{-7}		[44] LAHANAS	01	THEO
$< 3 \times 10^{-6}$		ABUSAIDI	00	CDMS Ge, Si
$< 6 \times 10^{-7}$		[46] ACCOMANDO	00	THEO
		[47] BERNABEI	00	DAMA NaI
2.5×10^{-9} to 3.5×10^{-8}		[48] FENG	00	THEO $\tan\beta$=10
$< 1.5 \times 10^{-5}$		MORALES	00	IGEX Ge
$< 4 \times 10^{-5}$		SPOONER	00	UKDM NaI
$< 7 \times 10^{-6}$		BAUDIS	99	HDMO ^{76}Ge
$< 7 \times 10^{-6}$		BERNABEI	98C	DAMA Xe

[1] The strongest upper limit is 2.2×10^{-12} pb at 40 GeV. This updates AALBERS 23.

[2] The strongest upper limit is 1.7×10^{-11} pb at 30 GeV. This updates APRILE 23A.

[3] The strongest limit is 1.6×10^{-11} pb at $m_\chi = 40$ GeV. This updates MENG 21B.

[4] The strongest limit is 7×10^{-8} at m = 85 GeV. This updates ADHIKARI 18.

[5] ABE 23E strongest upper limit is 1.4×10^{-8} pb at 60 GeV. Updates ABE 19.

[6] WANG 20G strongest limit is 2.2×10^{-10} pb at 30 GeV using 132 ton-day full exposure of PandaX-II. This updates CUI 17A, though the results here provide weaker constraints.

[7] This updates AMAUDRUZ 18.

[8] This updates AMOLE 16.

[9] The strongest limit is 1.09×10^{-8} pb at $m_\chi = 126$ GeV. This updates AGNES 15.

[10] The strongest limit is 1.0×10^{-8} pb at $m_\chi = 46$ GeV. This updates AGNESE 15B.

[11] Based on 278.8 days of data collection. The strongest limit is 4.1×10^{-11} pb at $m_\chi = 30$ GeV. This updates APRILE 17G.

[12] AKERIB 17. The strongest limit is 1.1×10^{-10} pb at 50 GeV. This updates AKERIB 16.

[13] The strongest limit is 1.1×10^{-9} pb at 50 GeV. This updates APRILE 12.

[14] The strongest upper limit is 7.6×10^{-10} at $m_\chi = 33$ GeV.

[15] Predictions for the spin-independent elastic cross section based on a frequentist approach to electroweak observables in the framework of $N = 1$ supergravity models with radiative breaking of the electroweak gauge symmetry using the 20 fb^{-1} 8 TeV and the 5 fb^{-1} 7 TeV LHC data and the LUX data.

[16] The strongest limit is 3.6×10^{-6} pb and occurs at $m_\chi = 35$ GeV. Felizardo 2014 updates Felizardo 2012.

[17] Predictions for the spin-independent elastic cross section based on a Bayesian approach to electroweak observables in the framework of $N = 1$ supergravity models with radiative breaking of the electroweak gauge symmetry using the 20 fb^{-1} LHC data and LUX.

[18] AGNESE 13 presents 90% CL limits on the elastic cross section for masses in the range 7–100 GeV using the Si based detector. The strongest upper limit is 1.8×10^{-6} pb at $m_\chi = 50$ GeV. This limit is improved to 7×10^{-7} pb in AGNESE 13A.

[19] This result updates LEBEDENKO 09. The strongest limit is 3.9×10^{-8} pb at $m_\chi = 52$ GeV.

[20] ANGLOHER 12 presents results of 730 kg days from the CRESST-II dark matter detector. They find two maxima in the likelihood function corresponding to best fit WIMP masses of 25.3 and 11.6 GeV with elastic cross sections of 1.6×10^{-6} and 3.7×10^{-5} pb respectively, see their Table 4. The statistical significance is more than 4σ. ANGLOHER 12 updates ANGLOHER 09

[21] Predictions for the spin-independent elastic cross section based on a frequentist approach to electroweak observables in the framework of $N = 1$ supergravity models with radiative breaking of the electroweak gauge symmetry using the 5 fb^{-1} LHC data and XENON100.

[22] The strongest limit is 1.4×10^{-7} at $m_\chi = 60$ GeV.

[23] This result updates LEE 07A. The strongest limit is 2.1×10^{-7} at $m_\chi = 70$ GeV.

[24] AHMED 11A gives combined results from CDMS and EDELWEISS. The strongest limit is at $m_\chi = 90$ GeV.

[25] ARMENGAUD 11 updates result of ARMENGAUD 10. Strongest limit at $m_\chi = 85$ GeV.

[26] The strongest upper limit is 5.1×10^{-8} pb and occurs at $m_\chi \simeq 30$ GeV. The values quoted here are based on the analysis performed in ANGLE 08 with the update from SORENSEN 09.

[27] The strongest upper limit is 6.6×10^{-7} pb and occurs at $m_\chi \simeq 65$ GeV.

[28] AKERIB 06A updates the results of AKERIB 05. The strongest upper limit is 1.6×10^{-7} pb and occurs at $m_\chi \approx 60$ GeV.

[29] The strongest upper limit is also close to 1.0×10^{-6} pb and occurs at $m_\chi \simeq 70$ GeV. BENOIT 06 claim that the discrimination power of ZEPLIN-I measurement (ALNER 05A) is not reliable enough to obtain a limit better than 1×10^{-3} pb. However, SMITH 06 do not agree with the criticisms of BENOIT 06.

[30] AKERIB 04 is incompatible with BERNABEI 00 most likely value, under the assumption of standard WIMP-halo interactions. The strongest upper limit is 4×10^{-7} pb and occurs at $m_\chi \simeq 60$ GeV.

[31] Predictions for the spin-independent elastic cross section in the framework of $N = 1$ supergravity models with radiative breaking of the electroweak gauge symmetry.

[32] KIM 02 and ELLIS 04 calculate the χp elastic scattering cross section in the framework of N=1 supergravity models with radiative breaking of the electroweak gauge symmetry, but without universal scalar masses.

[33] In the case of universal squark and slepton masses, but non-universal Higgs masses, the limit becomes 2×10^{-6} (2×10^{-11} when constraint from the BNL $g-2$ experiment are included), see ELLIS 03E. ELLIS 05 display the sensitivity of the elastic scattering cross section to the π-Nucleon Σ term.

[34] PIERCE 04A calculates the χp elastic scattering cross section in the framework of models with very heavy scalar masses. See Fig. 2 of the paper.

[35] The strongest upper limit is 1.8×10^{-5} pb and occurs at $m_\chi \approx 80$ GeV.

[36] Under the assumption of standard WIMP-halo interactions, Akerib 03 is incompatible with BERNABEI 00 most likely value at the 99.98% CL. See Fig. 4.

[37] BAER 03A calculates the χp elastic scattering cross section in several models including the framework of N=1 supergravity models with radiative breaking of the electroweak gauge symmetry.

[38] The strongest upper limit is 7×10^{-6} pb and occurs at $m_\chi \simeq 30$ GeV.

[39] ABRAMS 02 is incompatible with the DAMA most likely value at the 99.9% CL. The strongest upper limit is 3×10^{-6} pb and occurs at $m_\chi \simeq 30$ GeV.

[40] The strongest upper limit is 2×10^{-5} pb and occurs at $m_\chi \simeq 40$ GeV.

[41] The strongest upper limit is 7×10^{-6} pb and occurs at $m_\chi \simeq 46$ GeV.

[42] The strongest upper limit is 1.8×10^{-5} pb and occurs at $m_\chi \simeq 32$ GeV

[43] BOTTINO 01 calculates the χ-p elastic scattering cross section in the framework of the following supersymmetric models: N=1 supergravity with the radiative breaking of the electroweak gauge symmetry, N=1 supergravity with nonuniversal scalar masses and an effective MSSM model at the electroweak scale.

[44] Calculates the χ-p elastic scattering cross section in the framework of N=1 supergravity models with radiative breaking of the electroweak gauge symmetry.

[45] ELLIS 01C calculates the χ-p elastic scattering cross section in the framework of N=1 supergravity models with radiative breaking of the electroweak gauge symmetry. ELLIS 02B find a range 2×10^{-8}–1.5×10^{-7} at $\tan\beta$=50. In models with nonuniversal Higgs masses, the upper limit to the cross section is 4×10^{-7}.

[46] ACCOMANDO 00 calculate the χ-p elastic scattering cross section in the framework of minimal N=1 supergravity models with radiative breaking of the electroweak gauge symmetry. The limit is relaxed by at least an order of magnitude when models with nonuniversal scalar masses are considered. A subset of the authors in ARNOWITT 02 updated the limit to $< 9 \times 10^{-8}$ ($\tan\beta < 55$).

[47] BERNABEI 00 search for annual modulation of the WIMP signal. The data favor the hypothesis of annual modulation at 4σ and are consistent, for a particular model framework quoted there, with m_{χ^0}=44^{+12}_{-9} GeV and a spin-independent χ^0-proton cross section of $(5.4 \pm 1.0) \times 10^{-6}$ pb. See also BERNABEI 01 and BERNABEI 00C.

[48] FENG 00 calculate the χ-p elastic scattering cross section in the framework of N=1 supergravity models with radiative breaking of the electroweak gauge symmetry with a particular emphasis on focus point models. At $\tan\beta$=50, the range is 8×10^{-8}–4×10^{-7}.

Other bounds on $\widetilde{\chi}^0_1$ from astrophysics and cosmology

Most of these papers generally exclude regions in the $M_2 - \mu$ parameter plane by requiring that the $\widetilde{\chi}^0_1$ contribution to the overall cosmological density is less than some maximal value to avoid overclosure of the Universe. Those not based on the cosmological density are indicated. Many of these papers also include LEP and/or other bounds.

VALUE	DOCUMENT ID		TECN	COMMENT
>46 GeV	[1] ELLIS	00	RVUE	
• • • We do not use the following data for averages, fits, limits, etc. • • •				
	[2] ATHRON	17B	COSM	
	[3] BECHTLE	16	COSM	
	[4] BAGNASCHI	15	COSM	
	[5] BUCHMUEL...	14	COSM	
	[6] BUCHMUEL...	14A	COSM	
	[7] ROSZKOWSKI	14	COSM	
	[8] CABRERA	13	COSM	
	[9] ELLIS	13B	COSM	
	[8] STREGE	13	COSM	
	[5] AKULA	12	COSM	
	[5] ARBEY	12A	COSM	
	[5] BAER	12	COSM	
	[10] BALAZS	12	COSM	
	[11] BECHTLE	12	COSM	
	[12] BESKIDT	12	COSM	
> 18 GeV	[13] BOTTINO	12	COSM	
	[5] BUCHMUEL...	12	COSM	
	[5] CAO	12A	COSM	

Int. J. Mod. Phys. A 2026.41. Downloaded from www.worldscientific.com
by UNIVERSITY OF CALIFORNIA @ BERKELEY on 09/16/26. Re-use and distribution is strictly not permitted, except for Open Access articles.

Int. J. Mod. Phys. A 2026.41. Downloaded from www.worldscientific.com
by UNIVERSITY OF CALIFORNIA @ BERKELEY on 09/16/26. Re-use and distribution is strictly not permitted, except for Open Access articles.

	[5] ELLIS	12B	COSM	
	[14] FENG	12B	COSM	
	[5] KADASTIK	12	COSM	
	[10] STREGE	12	COSM	
	[15] BUCHMUEL...	11	COSM	
	[16] ROSZKOWSKI	11	COSM	
	[17] ELLIS	10	COSM	
	[18] BUCHMUEL...	09	COSM	
	[19] DREINER	09	THEO	
	[20] BUCHMUEL...	08	COSM	
	[16] ELLIS	08	COSM	
	[21] CALIBBI	07	COSM	
	[22] ELLIS	07	COSM	
	[23] ALLANACH	06	COSM	
	[24] DE-AUSTRI	06	COSM	
	[16] BAER	05	COSM	
	[25] BALTZ	04	COSM	
> 6 GeV	[13,26] BELANGER	04	THEO	
	[27] ELLIS	04B	COSM	
	[28] PIERCE	04A	COSM	
	[29] BAER	03	COSM	
ef¿ 6 GeV	[13] BOTTINO	03	COSM	
	[29] CHATTOPAD...	03	COSM	
	[30] ELLIS	03	COSM	
	[16] ELLIS	03B	COSM	
	[29] ELLIS	03C	COSM	
	[29] LAHANAS	03	COSM	
	[31] LAHANAS	02	COSM	
	[32] BARGER	01C	COSM	
	[33] ELLIS	01B	COSM	
	[30] BOEHM	00B	COSM	
	[34] FENG	00	COSM	
< 600 GeV	[35] ELLIS	98B	COSM	
	[36] EDSJO	97	COSM	Co-annihilation
	[37] BAER	96	COSM	
	[16] BEREZINSKY	95	COSM	
	[38] FALK	95	COSM	*CP*-violating phases
	[39] DREES	93	COSM	Minimal supergravity
	[40] FALK	93	COSM	Sfermion mixing
	[39] KELLEY	93	COSM	Minimal supergravity
	[41] MIZUTA	93	COSM	Co-annihilation
	[42] LOPEZ	92	COSM	Minimal supergravity, m_0=A=0
	[43] MCDONALD	92	COSM	
	[44] GRIEST	91	COSM	
	[45] NOJIRI	91	COSM	Minimal supergravity
	[46] OLIVE	91	COSM	
	[47] ROSZKOWSKI	91	COSM	
	[48] GRIEST	90	COSM	
	[46] OLIVE	89	COSM	
none 100 eV – 15 GeV	SREDNICKI	88	COSM	$\widetilde{\gamma}$; $m_{\widetilde{f}}$=100 GeV
none 100 eV–5 GeV	ELLIS	84	COSM	$\widetilde{\gamma}$; for $m_{\widetilde{f}}$=100 GeV
	GOLDBERG	83	COSM	$\widetilde{\gamma}$
	[49] KRAUSS	83	COSM	$\widetilde{\gamma}$
	VYSOTSKII	83	COSM	$\widetilde{\gamma}$

[1] ELLIS 00 updates ELLIS 98. Uses LEP e^+e^- data at $\sqrt{s}$=202 and 204 GeV to improve bound on neutralino mass to 51 GeV when scalar mass universality is assumed and 46 GeV when Higgs mass universality is relaxed. Limits on tanβ improve to > 2.7 (μ > 0), > 2.2 (μ < 0) when scalar mass universality is assumed and > 1.9 (both signs of μ) when Higgs mass universality is relaxed.

[2] ATHRON 17B places constraints on the SUSY parameter space in the framework of N = 1 supergravity models with radiative breaking of the electroweak gauge symmetry using all Run I and the 13 fb^{-1} 13 TeV Run II LHC searches and other experimental data.

[3] BECHTLE 16 places constraints on the SUSY parameter space in the framework of N = 1 supergravity models with radiative breaking of the electroweak gauge symmetry using all Run I LHC searches.

[4] BAGNASCHI 15 places constraints on the SUSY parameter space in the framework of N = 1 supergravity models with radiative breaking of the electroweak gauge symmetry using all Run I LHC searches.

[5] Implications of the LHC result on the Higgs mass and on the SUSY parameter space in the framework of N = 1 supergravity models with radiative breaking of the electroweak gauge symmetry.

[6] BUCHMUELLER 14A places constraints on the SUSY parameter space in the framework of N = 1 supergravity models with radiative breaking of the electroweak gauge symmetry using indirect experimental searches using the 20 fb^{-1} 8 TeV and the 5 fb^{-1} 7 TeV LHC and the LUX data.

[7] ROSZKOWSKI 14 places constraints on the SUSY parameter space in the framework of N = 1 supergravity models with radiative breaking of the electroweak gauge symmetry using Bayesian statistics and indirect experimental searches using the 20 fb^{-1} LHC and the LUX data.

[8] CABRERA 13 and STREGE 13 place constraints on the SUSY parameter space in the framework of N = 1 supergravity models with radiative breaking of the electroweak gauge symmetry with and without non-universal Higgs masses using the 5.8 fb^{-1}, $\sqrt{s}$ = 7 TeV ATLAS supersymmetry searches and XENON100 results.

[9] ELLIS 13B place constraints on the SUSY parameter space in the framework of N = 1 supergravity models with radiative breaking of the electroweak gauge symmetry with and without Higgs mass universality. Models with universality below the GUT scale are also considered.

[10] BALAZS 12 and STREGE 12 place constraints on the SUSY parameter space in the framework of N = 1 supergravity models with radiative breaking of the electroweak gauge symmetry using the 1 fb^{-1} LHC supersymmetry searches, the 5 fb^{-1} Higgs mass constraints, both with $\sqrt{s}$ = 7 TeV, and XENON100 results.

[11] BECHTLE 12 places constraints on the SUSY parameter space in the framework of N = 1 supergravity models with radiative breaking of the electroweak gauge symmetry using indirect experimental searches, using the 5 fb^{-1} LHC and XENON100 data.

[12] BESKIDT 12 places constraints on the SUSY parameter space in the framework of N = 1 supergravity models with radiative breaking of the electroweak gauge symmetry using indirect experimental searches, the 5 fb^{-1} LHC and the XENON100 data.

[13] BELANGER 04 and BOTTINO 12 (see also BOTTINO 03, BOTTINO 03A and BOTTINO 04) do not assume gaugino or scalar mass unification.

[14] FENG 12B places constraints on the SUSY parameter space in the framework of N = 1 supergravity models with radiative breaking of the electroweak gauge symmetry and large sfermion masses using the 1 fb^{-1} LHC supersymmetry searches, the 5 fb^{-1} LHC Higgs mass constraints both with $\sqrt{s}$ = 7 TeV, and XENON100 results.

[15] BUCHMUELLER 11 places constraints on the SUSY parameter space in the framework of N = 1 supergravity models with radiative breaking of the electroweak gauge symmetry using indirect experimental searches and including supersymmetry breaking relations between A and B parameters.

[16] Places constraints on the SUSY parameter space in the framework of N=1 supergravity models with radiative breaking of the electroweak gauge symmetry but non-Universal Higgs masses.

[17] ELLIS 10 places constraints on the SUSY parameter space in the framework of N = 1 supergravity models with radiative breaking of the electroweak gauge symmetry with universality above the GUT scale.

[18] BUCHMUELLER 09 places constraints on the SUSY parameter space in the framework of N = 1 supergravity models with radiative breaking of the electroweak gauge symmetry using indirect experimental searches.

[19] DREINER 09 show that in the general MSSM with non-universal gaugino masses there exists no model-independent laboratory bound on the mass of the lightest neutralino. An essentially massless χ^0_1 is allowed by the experimental and observational data, imposing some constraints on other MSSM parameters, including M_2, μ and the slepton and squark masses.

[20] BUCHMUELLER 08 places constraints on the SUSY parameter space in the framework of N = 1 supergravity models with radiative breaking of the electroweak gauge symmetry using indirect experimental searches.

[21] CALIBBI 07 places constraints on the SUSY parameter space in the framework of N = 1 supergravity models with radiative breaking of the electroweak gauge symmetry with universality above the GUT scale including the effects of right-handed neutrinos.

[22] ELLIS 07 places constraints on the SUSY parameter space in the framework of N = 1 supergravity models with radiative breaking of the electroweak gauge symmetry with universality below the GUT scale.

[23] ALLANACH 06 places constraints on the SUSY parameter space in the framework of N = 1 supergravity models with radiative breaking of the electroweak gauge symmetry.

[24] DE-AUSTRI 06 places constraints on the SUSY parameter space in the framework of N = 1 supergravity models with radiative breaking of the electroweak gauge symmetry.

[25] BALTZ 04 places constraints on the SUSY parameter space in the framework of N = 1 supergravity models with radiative breaking of the electroweak gauge symmetry.

[26] Limit assumes a pseudo scalar mass < 200 GeV. For larger pseudo scalar masses, m_χ > 18(29) GeV for tanβ = 50(10). Bounds from WMAP, $(g-2)_\mu$, $b \to s\gamma$, LEP.

[27] ELLIS 04B places constraints on the SUSY parameter space in the framework of N=1 supergravity models with radiative breaking of the electroweak gauge symmetry including supersymmetry breaking relations between A and B parameters. See also ELLIS 03D.

[28] PIERCE 04A places constraints on the SUSY parameter space in the framework of models with very heavy scalar masses.

[29] BAER 03, CHATTOPADHYAY 03, ELLIS 03C and LAHANAS 03 place constraints on the SUSY parameter space in the framework of N=1 supergravity models with radiative breaking of the electroweak gauge symmetry based on WMAP results for the cold dark matter density.

[30] BOEHM 00B and ELLIS 03 place constraints on the SUSY parameter space in the framework of minimal N=1 supergravity models with radiative breaking of the electroweak gauge symmetry. Includes the effect of χ-$\tilde{t}$ co-annihilations.

[31] LAHANAS 02 places constraints on the SUSY parameter space in the framework of minimal N=1 supergravity models with radiative breaking of the electroweak gauge symmetry. Focuses on the role of pseudo-scalar Higgs exchange.

[32] BARGER 01C use the cosmic relic density inferred from recent CMB measurements to constrain the parameter space in the framework of minimal N=1 supergravity models with radiative breaking of the electroweak gauge symmetry.

[33] ELLIS 01B places constraints on the SUSY parameter space in the framework of minimal N=1 supergravity models with radiative breaking of the electroweak gauge symmetry. Focuses on models with large tanβ.

[34] FENG 00 explores cosmologically allowed regions of MSSM parameter space with multi-TeV masses.

[35] ELLIS 98B assumes a universal scalar mass and radiative supersymmetry breaking with universal gaugino masses. The upper limit to the LSP mass is increased due to the inclusion of $\chi - \widetilde{\tau}_R$ coannihilations.

[36] EDSJO 97 included all coannihilation processes between neutralinos and charginos for any neutralino mass and composition.

[37] Notes the location of the neutralino Z resonance and h resonance annihilation corridors in minimal supergravity models with radiative electroweak breaking.

[38] Mass of the bino (=LSP) is limited to $m_{\widetilde{B}} \lesssim$ 350 GeV for m_t = 174 GeV.

[39] DREES 93, KELLEY 93 compute the cosmic relic density of the LSP in the framework of minimal N=1 supergravity models with radiative breaking of the electroweak gauge symmetry.

[40] FALK 93 relax the upper limit to the LSP mass by considering sfermion mixing in the MSSM.

[41] MIZUTA 93 include coannihilations to compute the relic density of Higgsino dark matter.

[42] LOPEZ 92 calculate the relic LSP density in a minimal SUSY GUT model.

[43] MCDONALD 92 calculate the relic LSP density in the MSSM including exact tree-level annihilation cross sections for all two-body final states.

[44] GRIEST 91 improve relic density calculations to account for coannihilations, pole effects, and threshold effects.

[45] NOJIRI 91 uses minimal supergravity mass relations between squarks and sleptons to narrow cosmologically allowed parameter space.

Int. J. Mod. Phys. A 2026.41. Downloaded from www.worldscientific.com
by UNIVERSITY OF CALIFORNIA @ BERKELEY on 09/16/26. Re-use and distribution is strictly not permitted, except for Open Access articles.

[46] Mass of the bino (=LSP) is limited to $m_{\widetilde{B}} \lesssim 350$ GeV for $m_t \leq 200$ GeV. Mass of the higgsino (=LSP) is limited to $m_{\widetilde{H}} \lesssim 1$ TeV for $m_t \leq 200$ GeV.

[47] ROSZKOWSKI 91 calculates LSP relic density in mixed gaugino/higgsino region.

[48] Mass of the bino (=LSP) is limited to $m_{\widetilde{B}} \lesssim 550$ GeV. Mass of the higgsino (=LSP) is limited to $m_{\widetilde{H}} \lesssim 3.2$ TeV.

[49] KRAUSS 83 finds $m_{\widetilde{\gamma}}$ not 30 eV to 2.5 GeV. KRAUSS 83 takes into account the gravitino decay. Find that limits depend strongly on reheated temperature. For example a new allowed region $m_{\widetilde{\gamma}}$ = 4–20 MeV exists if $m_{\text{gravitino}}$ <40 TeV. See figure 2.

Unstable $\widetilde{\chi}^0_1$ (Lightest Neutralino) mass limit

Unless otherwise stated, results in this section assume spectra and production rates as evaluated in the MSSM. Unless otherwise stated, the goldstino or gravitino mass $m_{\widetilde{G}}$ is assumed to be negligible relative to all other masses. In the following, $\widetilde{G}$ is assumed to be undetected and to give rise to a missing energy ($\not{E}$) signature.

Some earlier papers are now obsolete and have been omitted. They were last listed in our PDG 14 edition: K. Olive, *et al.* (Particle Data Group), Chinese Physics **C38** 070001 (2014) (http://pdg.lbl.gov).

VALUE (GeV)	CL%	DOCUMENT ID		TECN	COMMENT
>1170	95	[1] AAD	25BJ	ATLS	Wino pair-production, RPV λ'_{333}, $\widetilde{\chi}^0_1 \to b t \tau$, $b b \nu$ (BR 50% each) and $\widetilde{\chi}^\pm_1 \to b b \tau$, $b t \nu$ (BR 50% each)
> 880	95	[1] AAD	25BJ	ATLS	Higgsino pair-production, RPV λ'_{333}, $\widetilde{\chi}^0 \to b t \tau$, $b b \nu$ (BR 50% each) and $\widetilde{\chi}^\pm_1 \to b b \tau$, $b t \nu$ (BR 50% each)
> 320	95	[2] AAD	24AX	ATLS	2γ+$2b$-jets, Tn1n1A, $m_{\widetilde{G}}$ = 1 MeV
> 130	95	[2] AAD	24AX	ATLS	2γ+$2b$-jets, Tn1n1B-like , $h \to \gamma\gamma$, $h/Z \to b b$, B($\widetilde{\chi}^0_1 \to h \widetilde{G}$) = 36%, $m_{\widetilde{G}}$ = 1 MeV
none 130–940	95	[3] AAD	24U	ATLS	$\geq$ 3 b-jets + $\not{E}_T$, Tn1n1A, $m_{\widetilde{G}}$ = 1 MeV
none 70–75, 95–112	95	[4] HAYRAPETY...	24AP	CMS	2 large-radius jets, $\widetilde{\chi}^0_1$ pair production with RPV $\widetilde{\chi}^0_1 \to q q q$
> 840	95	[5] HAYRAPETY...	24N	CMS	Combination, Tn1n1A
> 760	95	[5] HAYRAPETY...	24N	CMS	Combination, Tn1n1B
>1025	95	[5] HAYRAPETY...	24N	CMS	Combination, Tn1n1C
> 900	95	[6] AAD	23AE	ATLS	2 SFOS ℓ, jets, $\not{E}_T$, Tn1n1C, $m_{\widetilde{\chi}^0_1}$ = 1 GeV
> 365	95	[7] AAD	23AM	ATLS	long-lived $\widetilde{\chi}^0_1$, displaced diphoton vertex, Tn1n1A, τ = 2 ns
> 605	95	[7] AAD	23AM	ATLS	long-lived $\widetilde{\chi}^0_1$, displaced diphoton vertex, Tn1n1B, τ = 2 ns
> 705	95	[7] AAD	23AM	ATLS	long-lived $\widetilde{\chi}^0_1$, displaced diphoton vertex, Tn1n1C, τ = 2 ns
> 440	95	[8] AAD	23CP	ATLS	2 same-sign or 3 ℓ, Tn1n1D, bRPV higgsino decays to νW, ℓW
>1180	95	[9] TUMASYAN	23AO	CMS	long-lived $\widetilde{\chi}^0_1$, $\geq$ 2 trackless delayed jets + $\not{E}_T$, Tn1n1B, cτ = 0.5 m
> 990	95	[9] TUMASYAN	23AO	CMS	long-lived $\widetilde{\chi}^0_1$, $\geq$ 2 trackless delayed jets + $\not{E}_T$, Tn1n1B, cτ = 3 m
> 540	95	[10] AAD	21Y	ATLS	$\geq 4\ell$, Tchi1n12-GGM, $\widetilde{\chi}^0_1 \to Z \widetilde{G}$
none 7–50	95	[11] AAIJ	21V	LHCB	$e^\pm \mu^\mp$, RPV $\widetilde{\chi}^0_1 \to e^\pm \mu^\mp \nu$, 2 ps < τ < 50 ps
>1100	95	[12] SIRUNYAN	21AF	CMS	long-lived $\widetilde{\chi}^0_1$, RPV $\widetilde{\chi}^0_1 \to tbs$, λ''_{323} coupling, 0.6 mm < cτ < 70 mm
> 800	95	[13] SIRUNYAN	21M	CMS	$\ell^\pm \ell^\mp + \not{E}_T$, Tn1n1C
> 650	95	[13] SIRUNYAN	21M	CMS	$\ell^\pm \ell^\mp + \not{E}_T$, Tn1n1B
> 380	95	[14] AAD	20AN	ATLS	$2\gamma + \not{E}_T$,Tn1n1A, GMSB
> 525	95	[15] SIRUNYAN	19CA	CMS	$\widetilde{\chi}^0_1 \to \gamma \widetilde{G}$, GMSB, SPS8, c$\tau$=1 m
> 290	95	[16] SIRUNYAN	19CI	CMS	$\geq$ 1 H ($\to \gamma\gamma$) + jets + $\not{E}_T$, Tn1n1A, GMSB
> 230	95	[16] SIRUNYAN	19CI	CMS	$\geq$ 1 H ($\to \gamma\gamma$) + jets + $\not{E}_T$, Tn1n1B , GMSB
> 930	95	[17] SIRUNYAN	19K	CMS	γ + lepton + $\not{E}_T$, Tchi1n1A
none 130–230, 290–880	95	[18] AABOUD	18CK	ATLS	$2H$ ($\to b b$)+$\not{E}_T$,Tn1n1A, GMSB
> 295	95	[19] AABOUD	18Z	ATLS	$\geq 4\ell$, GMSB, Tn1n1C
> 180	95	[20] SIRUNYAN	18AO	CMS	$\ell^\pm \ell^\pm$ or $\geq 3\ell$, Tn1n1A
> 260	95	[20] SIRUNYAN	18AO	CMS	$\ell^\pm \ell^\pm$ or $\geq 3\ell$, Tn1n1B
> 450	95	[20] SIRUNYAN	18AO	CMS	$\ell^\pm \ell^\pm$ or $\geq 3\ell$, Tn1n1C
> 750	95	[21] SIRUNYAN	18AP	CMS	Combination of searches, GMSB, Tn1n1A
> 650	95	[21] SIRUNYAN	18AP	CMS	Combination of searches, GMSB, Tn1n1B
> 690	95	[21] SIRUNYAN	18AP	CMS	Combination of searches, GMSB, Tn1n1C
> 500	95	[22] SIRUNYAN	18AR	CMS	$\ell^\pm \ell^\mp$+ jets +$\not{E}_T$, GMSB, Tn1n1B
> 650	95	[22] SIRUNYAN	18AR	CMS	$\ell^\pm \ell^\mp$+ jets +$\not{E}_T$, GMSB, Tn1n1C
none 230–770	95	[23] SIRUNYAN	18O	CMS	2 H ($\to b b$) + $\not{E}_T$, Tn1n1A, GMSB
> 205	95	[24] SIRUNYAN	18X	CMS	$\geq$ 1 H ($\to \gamma\gamma$) + jets + $\not{E}_T$, Tn1n1A, GMSB
> 130	95	[24] SIRUNYAN	18X	CMS	$\geq$ 1 H ($\to \gamma\gamma$) + jets + $\not{E}_T$, Tn1n1B , GMSB
> 380	95	[25] KHACHATRY...	14L	CMS	$\widetilde{\chi}^0_1 \to Z \widetilde{G}$ simplified models, GMSB, RPV
• • • We do not use the following data for averages, fits, limits, etc. • • •					
		[26] AAD	20D		$\widetilde{q} \to q \widetilde{\chi}^0_1$, $\widetilde{\chi}^0_1 \to \ell\ell\nu$, RPV, λ_{121} or $\lambda_{122} \neq 0$
none 300–1000	95	[27] AABOUD	19G	ATLS	$\widetilde{\chi}^0_1 \to Z \widetilde{G}$ from gluinos as in Tglu1A, GMSB, depending on cτ
		[28] AAIJ	17Z		displaced vertex with associated μ
		[29] KHACHATRY...	16BX	CMS	$\geq 3\ell^\pm$, RPV, λ or λ' couplings, wino- or higgsino-like neutralinos
		[30] AAD	14BH	ATLS	$2\gamma + \not{E}_T$, GMSB, SPS8
		[31] AAD	13AP	ATLS	$2\gamma + \not{E}_T$, GMSB, SPS8
none 220–380	95	[32] AAD	13Q	ATLS	$\gamma + b + \not{E}_T$, higgsino-like neutralino, GMSB
		[33] AAD	13R	ATLS	$\widetilde{\chi}^0_1 \to \mu j j$, RPV, $\lambda'_{211} \neq 0$
		[34] AALTONEN	13I	CDF	$\widetilde{\chi}^0_1 \to \gamma \widetilde{G}$, $\not{E}_T$, GMSB
> 220	95	[35] CHATRCHYAN	13AH	CMS	$\widetilde{\chi}^0_1 \to \gamma \widetilde{G}$, GMSB, SPS8, c$\tau$ < 500 mm
		[36] AAD	12CP	ATLS	$2\gamma + \not{E}_T$, GMSB
		[37] AAD	12CT	ATLS	$\geq 4\ell^\pm$, RPV
		[38] AAD	12R	ATLS	$\widetilde{\chi}^0_1 \to \mu j j$, RPV, $\lambda'_{211} \neq 0$
		[39] ABAZOV	12AD	D0	$\widetilde{\chi}^0_1 \widetilde{\chi}^0_1 \to \gamma Z \widetilde{G} \widetilde{G}$, GMSB
		[40] CHATRCHYAN	12BK	CMS	$2\gamma + \not{E}_T$, GMSB
		[41] CHATRCHYAN	11B	CMS	$\widetilde{W}^0 \to \gamma \widetilde{G}$, $\widetilde{W}^\pm \to \ell^\pm \widetilde{G}$, GMSB
> 149	95	[42] AALTONEN	10	CDF	$p\overline{p} \to \widetilde{\chi}\widetilde{\chi}$, $\widetilde{\chi}$=$\widetilde{\chi}^0_2$, $\widetilde{\chi}^\pm_1$, $\widetilde{\chi}^0_1 \to \gamma \widetilde{G}$, GMSB
> 175	95	[43] ABAZOV	10P	D0	$\widetilde{\chi}^0_1 \to \gamma \widetilde{G}$, GMSB
> 125	95	[44] ABAZOV	08F	D0	$p\overline{p} \to \widetilde{\chi}\widetilde{\chi}$, $\widetilde{\chi}$=$\widetilde{\chi}^0_2$, $\widetilde{\chi}^\pm_1$, $\widetilde{\chi}^0_1 \to \gamma \widetilde{G}$, GMSB
		[45] ABULENCIA	07H	CDF	RPV, $LL\overline{E}$
> 96.8	95	[46] ABBIENDI	06B	OPAL	$e^+ e^- \to \widetilde{B} \widetilde{B}$, ($\widetilde{B} \to \widetilde{G} \gamma$)
		[47] ABDALLAH	05B	DLPH	$e^+ e^- \to \widetilde{G} \widetilde{\chi}^0_1$, ($\widetilde{\chi}^0_1 \to \widetilde{G} \gamma$)
> 96	95	[48] ABDALLAH	05B	DLPH	$e^+ e^- \to \widetilde{B} \widetilde{B}$, ($\widetilde{B} \to \widetilde{G} \gamma$)

[1] AAD 25BJ searched in 140 fb^{-1} of pp collisions at $\sqrt{s}$ = 13 TeV for an excess of 0-lepton events with at least one hadronically decaying τ and at least 3 b-jet. The search is performed by training a neural network to separate a signal of vector-like leptons from the Standard Model background. No significant excess above the Standard Model expectations is observed. Limits are set also in a model of SUSY, where members of either a higgsino LSP triplet or a wino LSP doublet are produced, and decay via a RPV λ'_{333} coupling to b, t quarks and τ, ν_τ leptons, see their Figs. 13 and 14.

[2] AAD 24AX searched in 139 fb^{-1} of pp collisions at $\sqrt{s}$ = 13 TeV for evidence of higgsino pair production in events with two photons and two b-tagged jets. No significant excess above the Standard Model expectations is observed. Limits are set in the model Tn1n1A, see their Fig. 5, and in a model similar to Tn1n1B, but with variable branching ratios of $\widetilde{\chi}^0_1 \to h \widetilde{G}$ and $\widetilde{\chi}^0_1 \to Z \widetilde{G}$, to reflect the dependency on the neutralino mixing matrix, see their Fig. 6.

[3] AAD 24U searched in 126–139 fb^{-1} of pp collisions at $\sqrt{s}$ = 13 TeV for evidence of higgsino pair production in events with $\geq$ 3 b-tagged jets and $\not{E}_T$. No significant excess above the Standard Model expectations is observed. Limits are set in the model Tn1n1A, see their Fig. 12, which also contains upper limits on the branching ratio, reaching as low as 14% for a higgsino mass of 400 GeV. Model-independent limits are also set on the visible cross section for new physics processes.

[4] HAYRAPETYAN 24AP searched in 128 fb^{-1} of pp collisions at $\sqrt{s}$ = 13 TeV for evidence of pair-produced multijet signatures probing fully hadronic final states. No significant excess above the Standard Model expectations is observed. Limits are set in three RPV SUSY models: higgsino pair production with decay to merged trijets, stop pair production with decay to merged dijets, and pair-produced gluinos decaying to resolved trijets, see their Fig. 4.

[5] HAYRAPETYAN 24N searched in up to 137 fb^{-1} of pp collisions at $\sqrt{s}$ = 13 TeV for evidence of wino-like chargino-neutralino pairs, Higgsino-like neutralino pair production in a gauge-mediated SUSY breaking inspired scenario, a Higgsino-bino interpretation, and slepton pair production in a combination of a number of previously reported searches for SUSY in different final states. No significant excess above the Standard Model expectations is observed. Limits are set on the $\widetilde{\chi}^\pm_1$ mass in the wino-bino models Tchi1n2E1, Tchi1n2E, and Tchi1n2l, see their Fig. 11, and on the $\widetilde{\chi}^0_1$ in the higgsino-like GMSB models Tn1n1A, Tn1n1B, and Tn1n1C, see their Fig. 13. In addition, Fig. 14 shows the mass exclusion limit as a function of the branching fraction to the H boson. Limits are also set in a Higgsino-bino interpretation as in THinoBinoA, but also including leptonic decays, see their Fig. 15. Limits are also set on slepton ($\widetilde{e}$, $\widetilde{\mu}$) production with the decay $\widetilde{\ell} \to \ell \widetilde{\chi}^0_1$, see their Fig. 16.

[6] AAD 23AE searched in 139 fb^{-1} of pp collisions at $\sqrt{s}$ = 13 TeV for events with 2 ℓ with same flavour and opposite sign, plus jets and $\not{E}_T$, defining signal region with the dilepton invariant mass both on- and off-shell with respect to the Z boson. No significant excess above the Standard Model predictions is observed. Limits are set on models of strong and electroweak production. In this case, limits are placed on production of mass-degenerate, higgsino triplet NLSP with $\widetilde{\chi}^0_1 \to Z \widetilde{G}$ in a GGM-like scenario, see figure 15.

[7] AAD 23AM searched in 139 fb^{-1} of pp collisions at $\sqrt{s}$ = 13 TeV for events containing electron/photon pairs with invariant mass compatible with h/Z and originating from a common displaced vertex. No significant excess above the Standard Model predictions is observed. Limits are set on a model where members of a nearly degenerate higgsino triplet are pair-produced, yielding long-lived $\widetilde{\chi}^0_1$ followed by $\widetilde{\chi}^0_1 \to h/Z \widetilde{G}$. Limits are set on $m_{\widetilde{\chi}^0_1}$ as a function of its lifetime and of the B($\widetilde{\chi}^0_1 \to h \widetilde{G}$) assuming B($\widetilde{\chi}^0_1 \to h \widetilde{G}$) + B($\widetilde{\chi}^0_1 \to Z \widetilde{G}$) = 1, see Figure 10.

Int. J. Mod. Phys. A 2026.41. Downloaded from www.worldscientific.com by UNIVERSITY OF CALIFORNIA @ BERKELEY on 09/16/26. Re-use and distribution is strictly not permitted, except for Open Access articles.

[8] AAD 23CP searched in 139 fb^{-1} of pp collisions at $\sqrt{s}$ = 13 TeV for events with 2 ℓ with same charge or 3 ℓ plus at least one jet and $\not{E}_T$, defining signal region based on 'stransverse mass' of the dilepton system, $\not{E}_T$ significance and effective mass. No significant excess above the Standard Model predictions is observed. Limits are set on the mass of a mass-degenerate higgsino triplet decaying into a lepton (neutral or charged) and a W via a bilinear RPV coupling, see figure 14.

[9] TUMASYAN 23AO searched in 138 fb^{-1} of pp collisions at $\sqrt{s}$ = 13 TeV for evidence of neutralino-chargino production in events with nearly trackless and out-of-time jets that are used to identify decays of long-lived particles. No significant excess above the Standard Model expectations is observed. Limits are set on the mass of the long-lived $\widetilde{\chi}^0_1$ in the model Tn1n1B, see their figures 8–10.

[10] AAD 21Y searched in 139 fb^{-1} of pp collisions at $\sqrt{s}$ = 13 TeV for supersymmetry in events with four or more leptons (electrons, muons and tau-leptons). No significant excess above the Standard Model expectations is observed. Limits are set on Tchi1n12-GGM, and RPV models similar to Tchi1n2l, Tglu1A (with $q = u, d, s, c, b$, with equal branching fractions), and $\widetilde{\ell}_L/\widetilde{\nu} \rightarrow \ell/\nu\widetilde{\chi}^0_1$ (mass-degenerate $\widetilde{\ell}_L$ and $\widetilde{\nu}$ of all 3 generations), all with $\widetilde{\chi}^0_1 \rightarrow \ell^\pm\ell^\mp\nu$ via λ_{12k} or λ_{i33} (where $i,k \in 1,2$), see their Figure 11.

[11] AAIJ 21V searched in 5.38 fb^{-1} of pp collisions at $\sqrt{s}$ = 13 TeV for long-lived particles (LLP) decaying to $e^\pm\mu^\mp\nu$. The LLP can be a $\widetilde{\chi}^0_1$ in RPV SUSY, or a right-handed neutrino, and can be produced in pairs, in the decay of the Higgs boson, or from charged current processes. No significant excess above the Standard Model expectations is observed. Limits are set on the cross section times branching ratio for all three production mechanisms, see their Figures 6–8.

[12] SIRUNYAN 21AF searched in 140 fb^{-1} of pp collisions at $\sqrt{s}$ = 13 TeV for supersymmetry in events with with two displaced vertices from long-lived particles decaying into multijet or dijet final states. No significant excess above the Standard Model expectations is observed. Limits are set on the gluino mass in the simplified model Tglu2RPV with λ''_{323} coupling, on the $\widetilde{\chi}^0_1$ mass in an RPV model with $\widetilde{\chi}^0_1$ pair production and the RPV decay $\widetilde{\chi}^0_1 \rightarrow tbs$ with λ''_{323} coupling and on the $\widetilde{t}$ mass in an RPV model with top squark pair production and the RPV decay $\widetilde{t} \rightarrow \overline{d}_i\,\overline{d}_j$ with λ''_{3ij} coupling, see their Figure 7.

[13] SIRUNYAN 21M searched in 137 fb^{-1} of pp collisions at $\sqrt{s}$ = 13 TeV for supersymmetry in events with two opposite-sign same-flavor leptons (electrons, muons) and $\not{E}_T$. No significant excess above the Standard Model expectations is observed. Limits are set on the gluino mass in the simplified model Tglu4C, see their Figure 10, on the $\widetilde{\chi}^0_2$ and $\widetilde{\chi}^\pm_1$ mass in Tchi1n2Fa, see their Figure 11, on the $\widetilde{\chi}^0_1$ mass in Tn1n1C and Tn1n1B for $m_{\widetilde{\chi}^0_2} = m_{\widetilde{\chi}^\pm_1} = m_{\widetilde{\chi}^0_1}$, see their Figure 12. Limits are also set on the light squark mass for the simplified model Tsqk2A, on the sbottom mass in Tsbot3, see their Figure 13, and on the slepton mass in direct electroweak pair production of mass-degenerate left- and right-handed sleptons (selectrons and smuons), see their Figure 14.

[14] AAD 20AN searched in 139 fb^{-1} of pp collisions at $\sqrt{s}$ = 13 TeV for events with two photons and missing transverse momentum. Events are further categorised in terms of lepton or jet multiplicity. No significant excess over the expected background is observed. Limits at 95% C.L. are set on the Higgsino mass in the T1n1n1A simplified model, see their Figure 11.

[15] SIRUNYAN 19CA searched in 77.4 fb^{-1} of pp collisions at $\sqrt{s}$ = 13 TeV for events containing delayed photons in both single and diphoton plus $\not{E}_T$ final states. No excess is observed above the background expected from Standard Model processes. The results are used to set 95% C.L. exclusion limits in the context of GMSB, using the SPS8 benchmark model. For neutralino proper decay lengths of 0.1, 1, 10, and 100 m, masses up to about 320, 525, 360, and 215 GeV are excluded, respectively. See their Fig. 5. The searches involve the simplified models Tglu1D, Tglu4A,B,C, Tsqk4,4A,4B.

[16] SIRUNYAN 19CI searched in 77.5 fb^{-1} of pp collisions at $\sqrt{s}$ = 13 TeV for events with one or more high-momentum Higgs bosons, decaying to pairs of photons, jets and $\not{E}_T$. No significant excess above the Standard Model expectations is observed. Limits are set on the sbottom mass in the Tsbot4 simplified model, see Figure 3, and on the wino mass in the Tchi1n2E simplified model, see their Figure 4. Limits are also set on the higgsino mass in the Tn1n1A and Tn1n1B simplified models, see their Figure 5.

[17] SIRUNYAN 19K searched in 35.9 fb^{-1} of pp collisions at $\sqrt{s}$ = 13 TeV for events with a photon, an electron or muon, and large $\not{E}_T$. No significant excess above the Standard Model expectations is observed. In the framework of GMSB, limits are set on the chargino and neutralino mass in the Tchi1n1A simplified model, see their Figure 6. Limits are also set on the gluino mass in the Tglu4A simplified model, and on the squark mass in the Tsqk4A simplified model, see their Figure 7.

[18] AABOUD 18CK searched for events with at least 3 b-jets and large missing transverse energy in two datasets of pp collisions at $\sqrt{s}$ = 13 TeV of 36.1 fb^{-1} and 24.3 fb^{-1} depending on the trigger requirements. The analyses aimed to reconstruct two Higgs bosons decaying to pairs of b-quarks. No significant excess above the Standard Model expectations is observed. Limits are set on the Higgsino mass in the Tn1n1A simplified model, see their Figure 15(a). Constraints are also presented as a function of the BR of Higgsino decaying into an higgs boson and a gravitino, see their Figure 15(b).

[19] AABOUD 18Z searched in 36.1 fb^{-1} of pp collisions at $\sqrt{s}$ = 13 TeV for events containing four or more charged leptons (electrons, muons and up to two hadronically decaying taus). No significant deviation from the expected SM background is observed. Limits are set on the Higgsino mass in simplified models of general gauge mediated supersymmetry Tn1n1A/Tn1n1B/Tn1n1C, see their Figure 9. Limits are also set on the wino, slepton, sneutrino and gluino mass in a simplified model of NLSP pair production with R-parity violating decays of the LSP via λ_{12k} or λ_{i33} to charged leptons, see their Figures 7, 8.

[20] SIRUNYAN 18AO searched in 35.9 fb^{-1} of pp collisions at $\sqrt{s}$ = 13 TeV for direct electroweak production of charginos and neutralinos in events with either two or more leptons (electrons or muons) of the same electric charge, or with three or more leptons, which can include up to two hadronically decaying tau leptons. No significant excess above the Standard Model expectations is observed. Limits are set on the chargino/neutralino mass in the Tchi1n2A, Tchi1n2H, Tchi1n2D, Tchi1n2E and Tchi1n2F simplified models, see their Figures 14, 15, 16, 17 and 18. Limits are also set on the higgsino mass in the Tn1n1A, Tn1n1B and Tn1n1C simplified models, see their Figure 19.

[21] SIRUNYAN 18AP searched in 35.9 fb^{-1} of pp collisions at $\sqrt{s}$ = 13 TeV for direct electroweak production of charginos and neutralinos by combining a number of previous and new searches. No significant excess above the Standard Model expectations is observed. Limits are set on the chargino/neutralino mass in the Tchi1n2E, Tchi1n2F and Tchi1n2l simplified models, see their Figures 7, 8, 9 an 10. Limits are also set on the higgsino mass in the Tn1n1A, Tn1n1B and Tn1n1C simplified models, see their Figure 11, 12, 13 and 14.

[22] SIRUNYAN 18AR searched in 35.9 fb^{-1} of pp collisions at $\sqrt{s}$ = 13 TeV for events containing two opposite-charge, same-flavour leptons (electrons or muons), jets and $\not{E}_T$. No significant excess above the Standard Model expectations is observed. Limits are set on the gluino mass in the Tglu4C simplified model, see their Figure 7. Limits are also set on the chargino/neutralino mass in the Tchi1n2F simplified models, see their Figure 8, and on the higgsino mass in the Tn1n1B and Tn1n1C simplified models, see their Figure 9. Finally, limits are set on the sbottom mass in the Tsbot3 simplified model, see their Figure 10.

[23] SIRUNYAN 18O searched in 35.9 fb^{-1} of pp collisions at $\sqrt{s}$ = 13 TeV for events with two Higgs bosons, decaying to pairs of b-quarks, and large $\not{E}_T$. No significant excess above the Standard Model expectations is observed. Limits are set on the Higgsino mass in the T1n1n1A simplified model, see their Figure 9.

[24] SIRUNYAN 18X searched in 35.9 fb^{-1} of pp collisions at $\sqrt{s}$ = 13 TeV for events with one or more high-momentum Higgs bosons, decaying to pairs of photons, jets and $\not{E}_T$. The razor variables (M_R and R^2) are used to categorise the events. No significant excess above the Standard Model expectations is observed. Limits are set on the sbottom mass in the Tsbot4 simplified model and on the wino mass in the Tchi1n2E simplified model, see their Figure 5. Limits are also set on the higgsino mass in the Tn1n1A and Tn1n1B simplified models, see their Figure 6.

[25] KHACHATRYAN 14L searched in 19.5 fb^{-1} of pp collisions at $\sqrt{s}$ = 8 TeV for evidence of direct pair production of neutralinos with Higgs or Z-bosons in the decay chain, leading to HH, HZ and ZZ final states with missing transverse energy. The decays of 16–20. a Higgs boson to a b-quark pair, to a photon pair, and to final states with leptons are considered in conjunction with hadronic and leptonic decay modes of the Z and W bosons. No significant excesses over the expected SM backgrounds are observed. The results are interpreted in the context of GMSB simplified models where the decays $\widetilde{\chi}^0_1 \rightarrow H\widetilde{G}$ or $\widetilde{\chi}^0_1 \rightarrow Z\widetilde{G}$ take place either 100% or 50% of the time, see Figs. 16–20.

[26] AAD 20D searched in 32.8 fb^{-1} of pp collisions at $\sqrt{s}$ = 13 TeV for events containing an oppositely charge lepton pair (ee, $\mu\mu$ or $e\mu$) coming from long-lived neutralinos decaying through the R-parity-violating decay $\widetilde{\chi}^0_1 \rightarrow \ell\ell\nu$ with $\lambda_{121} \neq 0$ or $\lambda_{122} \neq 0$. No excess over the expected background is observed. Limits are derived for decay lengths of the neutralino between 1 mm and 10 m in a scenario where a squark-antisquark pair is produced, with the squark decaying to a quark and a $\widetilde{\chi}^0_1$, with either $\widetilde{\chi}^0_1 \rightarrow ee\nu/e\mu\nu$ ($\lambda_{121} \neq 0$) or $\widetilde{\chi}^0_1 \rightarrow e\mu\nu/\mu\mu\nu$ ($\lambda_{122} \neq 0$), see their Figures 4 and 5.

[27] AABOUD 19G searched in 32.9 fb^{-1} of pp collisions at $\sqrt{s}$ = 13 TeV for evidence of neutralinos decaying into a Z-boson and a gravitino, in events characterized by the presence of dimuon vertices with displacements from the pp interaction point in the range of 1400 cm. Neutralinos are assumed to be produced in the decay chain of gluinos as in Tglu1A models. No significant excess is observed in the number of vertices relative to the predicted background. In GGM with a gluino mass of 1100 GeV, neutralino masses in the range 300–1000 GeV are excluded for certain values of $c\tau$, see their Figure 7.

[28] AAIJ 17Z searched in 1 fb^{-1} of pp collisions at $\sqrt{s}$ = 7 TeV and in 2 fb^{-1} of pp collisions at $\sqrt{s}$ = 8 TeV for events containing a displaced vertex with one associated high transverse momentum μ. No excess is observed above the background expected from Standard Model processes. The results are used to set 95% C.L. upper limits on the cross section times branching fractions of pair-produced neutralinos decaying non-promptly into a muon and two quarks. Long-lived particles in a mass range 23–198 GeV are considered, see their Fig. 5 and Fig. 6.

[29] KHACHATRYAN 16BX searched in 19.5 fb^{-1} of pp collisions at $\sqrt{s}$ = 8 TeV for events containing 3 or more leptons coming from the electroweak production of wino- or higgsino-like neutralinos, assuming non-zero R-parity-violating leptonic couplings λ_{122}, λ_{123}, and λ_{233} or semileptonic couplings λ'_{131}, λ'_{233}, λ'_{331}, and λ'_{333}. No excess over the expected background is observed and limits are derived on the neutralino mass, see Figs. 24 and 25.

[30] AAD 14BH searched in 20.3 fb^{-1} of pp collisions at $\sqrt{s}$ = 8 TeV for events containing non-pointing photons in a diphoton plus missing transverse energy final state. No excess is observed above the background expected from Standard Model processes. The results are used to set 95% C.L. exclusion limits in the contact of gauge-mediated supersymmetric breaking models, with the lightest neutralino being the next-to-lightest supersymmetric particle and decaying with a lifetime in the range from 0.25 ns to about 100 ns into a photon and a gravitino. For limits on the NLSP lifetime versus Λ plane, for the SPS8 model, see their Fig. 7.

[31] AAD 13AP searched in 4.8 fb^{-1} of pp collisions at $\sqrt{s}$ = 7 TeV for events containing non-pointing photons in a diphoton plus missing transverse energy final state. No excess is observed above the background expected from Standard Model processes. The results are used to set 95% C.L. exclusion limits in the context of gauge-mediated supersymmetric breaking models, with the lightest neutralino being the next-to-lightest supersymmetric particle and decaying with a lifetime in excess of 0.25 ns into a photon and a gravitino. For limits in the NLSP lifetime versus Λ plane, for the SPS8 model, see their Fig. 8.

[32] AAD 13Q searched in 4.7 fb^{-1} of pp collisions at $\sqrt{s}$ = 7 TeV for events containing a high-p_T isolated photon, at least one jet identified as originating from a bottom quark, and high missing transverse momentum. Such signatures may originate from supersymmetric models with gauge-mediated supersymmetry breaking in events in which one of a pair of higgsino-like neutralinos decays into a photon and a gravitino while the other decays into a Higgs boson and a gravitino. No significant excess above the expected background was found and limits were set on the neutralino mass in a generalized GMSB model (GGM) with a higgsino-like neutralino NLSP, see their Fig. 4. Intermediate neutralino masses between 220 and 380 GeV are excluded at 95% C.L, regardless of the squark and gluino masses, purely on the basis of the expected weak production.

[33] AAD 13R looked in 4.4 fb^{-1} of pp collisions at $\sqrt{s}$ = 7 TeV for events containing new, heavy particles that decay at a significant distance from their production point into a final state containing a high-momentum muon and charged hadrons. No excess over the expected background is observed and limits are placed on the production cross-section of neutralinos via squarks for various $m_{\widetilde{q}}$, $m_{\widetilde{\chi}^0_1}$ in an R-parity violating scenario with $\lambda'_{211} \neq 0$, as a function of the neutralino lifetime, see their Fig. 6.

[34] AALTONEN 13I searched in 6.3 fb^{-1} of $p\overline{p}$ collisions at $\sqrt{s}$ = 1.96 TeV for events containing $\not{E}_T$ and a delayed photon that arrives late in the detector relative to the time expected from prompt production. No evidence of delayed photon production is observed.

[35] CHATRCHYAN 13AH searched in 4.9 fb^{-1} of pp collisions at $\sqrt{s}$ = 7 TeV for events containing $\not{E}_T$ and a delayed photon that arrives late in the detector relative to the time expected from prompt production. No significant excess above the expected background was found and limits were set on the pair production of $\widetilde{\chi}^0_1$ depending on the neutralino proper decay length, see Fig. 8. Supersedes CHATRCHYAN 12BK.

Int. J. Mod. Phys. A 2026.41. Downloaded from www.worldscientific.com
by UNIVERSITY OF CALIFORNIA @ BERKELEY on 09/16/26. Re-use and distribution is strictly not permitted, except for Open Access articles.

[36] AAD 12CP searched in 4.8 fb^{-1} of pp collisions at $\sqrt{s}$ = 7 TeV for events with two photons and large $\not{E}_T$ due to $\widetilde{\chi}^0_1 \rightarrow \gamma \widetilde{G}$ decays in a GMSB framework. No significant excess above the expected background was found and limits were set on the neutralino mass in a generalized GMSB model (GGM) with a bino-like neutralino NLSP, see Figs. 6 and 7. The other sparticle masses were decoupled, tanβ = 2 and $c\tau_{NLSP}$ < 0.1 mm. Also, in the framework of the SPS8 model, limits are presented in Fig. 8.

[37] AAD 12CT searched in 4.7 fb^{-1} of pp collisions at $\sqrt{s}$ = 7 TeV for events containing four or more leptons (electrons or muons) and either moderate values of missing transverse momentum or large effective mass. No significant excess is found in the data. Limits are presented in a simplified model of R-parity violating supersymmetry in which charginos are pair-produced and then decay into a W-boson and a $\widetilde{\chi}^0_1$, which in turn decays through an RPV coupling into two charged leptons ($e^\pm e^\mp$ or $\mu^\pm \mu^\mp$) and a neutrino. In this model, limits are set on the neutralino mass as a function of the chargino mass, see Fig. 3a. Limits are also set in an R-parity violating mSUGRA model, see Fig. 3b.

[38] AAD 12R looked in 33 pb^{-1} of pp collisions at $\sqrt{s}$ = 7 TeV for events containing new, heavy particles that decay at a significant distance from their production point into a final state containing a high-momentum muon and charged hadrons. No excess over the expected background is observed and limits are placed on the production cross-section of neutralinos via squarks for various ($m_{\widetilde{q}}$, $m_{\widetilde{\chi}^0_1}$) in an R-parity violating scenario with $\lambda'_{211} \neq 0$, as a function of the neutralino lifetime, see their Fig. 8. Superseded by AAD 13R.

[39] ABAZOV 12AD looked in 6.2 fb^{-1} of pp collisions at $\sqrt{s}$ = 1.96 TeV for events with a photon, a Z-boson, and large $\not{E}_T$ in the final state. This topology corresponds to a GMSB model where pairs of neutralino NLSPs are either pair produced promptly or from decays of other supersymmetric particles and then decay to either $Z\widetilde{G}$ or $\gamma\widetilde{G}$. No significant excess over the SM expectation is observed and a limit at 95% C.L. on the cross section is derived as a function of the effective SUSY breaking scale Λ, see Fig. 3. Assuming N_{mes} = 2, M_{mes} = 3 Λ, tanβ = 3, μ = 0.75 M_1, and C_{grav} = 1, the model is excluded at 95% C.L. for values of Λ < 87 TeV.

[40] CHATRCHYAN 12BK searched in 2.23 fb^{-1} of pp collisions at $\sqrt{s}$ = 7 TeV for events with two photons and large $\not{E}_T$ due to $\widetilde{\chi}^0_1 \rightarrow \gamma\widetilde{G}$ decays in a GMSB framework. No significant excess above the expected background was found and limits were set on the pair production of $\widetilde{\chi}^0_1$ depending on the neutralino lifetime, see Fig. 6.

[41] CHATRCHYAN 11B looked in 35 pb^{-1} of pp collisions at $\sqrt{s}$=7 TeV for events with an isolated lepton (e or μ), a photon and $\not{E}_T$ which may arise in a generalized gauge mediated model from the decay of Wino-like NLSPs. No evidence for an excess over the expected background is observed. Limits are derived in the plane of squark/gluino mass versus Wino mass (see Fig. 4). Mass degeneracy of the produced squarks and gluinos is assumed.

[42] AALTONEN 10 searched in 2.6 fb^{-1} of $p\overline{p}$ collisions at $\sqrt{s}$ = 1.96 TeV for diphoton events with large $\not{E}_T$. They may originate from the production of $\widetilde{\chi}^\pm$ in pairs or associated to a $\widetilde{\chi}^0_2$, decaying into $\widetilde{\chi}^0_1$ which itself decays in GMSB to $\gamma\widetilde{G}$. There is no excess of events beyond expectation. An upper limit on the cross section is calculated in the GMSB model as a function of the $\widetilde{\chi}^0_1$ mass and lifetime, see their Fig. 2. A limit is derived on the $\widetilde{\chi}^0_1$ mass of 149 GeV for $\tau_{\widetilde{\chi}^0_1} \ll 1$ ns, which improves the results of previous searches.

[43] ABAZOV 10P looked in 6.3 fb^{-1} of $p\overline{p}$ collisions at $\sqrt{s}$ = 1.96 TeV for events with at least two isolated γs and large $\not{E}_T$. These could be the signature of $\widetilde{\chi}^0_2$ and $\widetilde{\chi}^\pm_1$ production, decaying to $\widetilde{\chi}^0_1$ and finally $\widetilde{\chi}^0_1 \rightarrow \gamma\widetilde{G}$ in a GMSB framework. No significant excess over the SM expectation is observed, and a limit at 95% C.L. on the cross section is derived for N_{mes} = 1, tanβ = 15 and μ > 0, see their Fig. 2. This allows them to set a limit on the effective SUSY breaking scale Λ > 124 TeV, from which the excluded $\widetilde{\chi}^0_1$ mass range is obtained.

[44] ABAZOV 08F looked in 1.1 fb^{-1} of $p\overline{p}$ collisions at $\sqrt{s}$ = 1.96 TeV for diphoton events with large $\not{E}_T$. They may originate from the production of $\widetilde{\chi}^\pm$ in pairs or associated to a $\widetilde{\chi}^0_2$, decaying to a $\widetilde{\chi}^0_1$ which itself decays promptly in GMSB to $\widetilde{\chi}^0_1 \rightarrow \gamma\widetilde{G}$. No significant excess was found compared to the background expectation. A limit is derived on the masses of SUSY particles in the GMSB framework for $M = 2\Lambda$, N = 1, tanβ = 15 and μ > 0, see Figure 2. It also excludes Λ < 91.5 TeV. Supersedes the results of ABAZOV 05A. Superseded by ABAZOV 10P.

[45] ABULENCIA 07H searched in 346 pb^{-1} of $p\overline{p}$ collisions at $\sqrt{s}$ = 1.96 TeV for events with at least three leptons (e or μ) from the decay of $\widetilde{\chi}^0_1$ via $LL\overline{E}$ couplings. The results are consistent with the hypothesis of no signal. Upper limits on the cross-section are extracted and a limit is derived in the framework of mSUGRA on the masses of $\widetilde{\chi}^0_1$ and $\widetilde{\chi}^\pm_1$, see e.g. their Fig. 3 and Tab. II.

[46] ABBIENDI 06B use 600 pb^{-1} of data from $\sqrt{s}$ = 189–209 GeV. They look for events with diphotons + $\not{E}$ final states originating from prompt decays of pair-produced neutralinos in a GMSB scenario with $\widetilde{\chi}^0_1$ NLSP. Limits on the cross-section are computed as a function of m($\widetilde{\chi}^0_1$), see their Fig. 14. The limit on the $\widetilde{\chi}^0_1$ mass is for a pure Bino state assuming a prompt decay, with lifetimes up to 10^{-9}s. Supersedes the results of ABBIENDI 04N.

[47] ABDALLAH 05B use data from $\sqrt{s}$ = 180–209 GeV. They look for events with single photons + $\not{E}$ final states. Limits are computed in the plane (m($\widetilde{G}$) , m($\widetilde{\chi}^0_1$)), shown in their Fig. 9b for a pure Bino state in the GMSB framework and in Fig. 9c for a no-scale supergravity model. Supersedes the results of ABREU 00Z.

[48] ABDALLAH 05B use data from $\sqrt{s}$ = 130–209 GeV. They look for events with diphotons + $\not{E}$ final states and single photons not pointing to the vertex, expected in GMSB when the $\widetilde{\chi}^0_1$ is the NLSP. Limits are computed in the plane (m($\widetilde{G}$), m($\widetilde{\chi}^0_1$)), see their Fig. 10. The lower limit is derived on the $\widetilde{\chi}^0_1$ mass for a pure Bino state assuming a prompt decay and $m_{\widetilde{e}_R} = m_{\widetilde{e}_L} = 2\, m_{\widetilde{\chi}^0_1}$. It improves to 100 GeV for $m_{\widetilde{e}_R} = m_{\widetilde{e}_L} = 1.1\, m_{\widetilde{\chi}^0_1}$. and the limit in the plane (m($\widetilde{\chi}^0_1$), m($\widetilde{e}_R$)) is shown in Fig. 10b. For long-lived neutralinos, cross-section limits are displayed in their Fig 11. Supersedes the results of ABREU 00Z.

$\widetilde{\chi}^0_2$, $\widetilde{\chi}^0_3$, $\widetilde{\chi}^0_4$ (Neutralinos) mass limits

Neutralinos are unknown mixtures of photinos, z-inos, and neutral higgsinos (the supersymmetric partners of photons and of Z and Higgs bosons). The limits here apply only to $\widetilde{\chi}^0_2$, $\widetilde{\chi}^0_3$, and $\widetilde{\chi}^0_4$. $\widetilde{\chi}^0_1$ is the lightest supersymmetric particle (LSP); see $\widetilde{\chi}^0_1$ Mass Limits. It is not possible to quote rigorous mass limits because they are extremely model dependent; i.e. they depend on branching ratios of various $\widetilde{\chi}^0$ decay modes, on the masses of decay products ($\widetilde{e}$, $\widetilde{\gamma}$, $\widetilde{q}$, $\widetilde{g}$), and on the $\widetilde{e}$ mass exchanged in $e^+e^- \rightarrow \widetilde{\chi}^0_i \widetilde{\chi}^0_j$. Limits arise either from direct searches, or from the MSSM constraints set on the gaugino and higgsino mass parameters M_2 and μ through searches for lighter charginos and neutralinos. Often limits are given as contour plots in the $m_{\widetilde{\chi}^0} - m_{\widetilde{e}}$ plane vs other parameters. When specific assumptions are made, e.g, the neutralino is a pure photino ($\widetilde{\gamma}$), pure z-ino ($\widetilde{Z}$), or pure neutral higgsino ($\widetilde{H}^0$), the neutralinos will be labelled as such.

Limits obtained from e^+e^- collisions at energies up to 136 GeV, as well as other limits from different techniques, are now superseded and have not been included in this compilation. They can be found in the 1998 Edition (The European Physical Journal **C3** 1 (1998)) of this Review. Some later papers are now obsolete and have been omitted. They were last listed in our PDG 14 edition: K. Olive, *et al.* (Particle Data Group), Chinese Physics **C38** 070001 (2014) (http://pdg.lbl.gov).

VALUE (GeV)	CL%	DOCUMENT ID		TECN	COMMENT
> 880	95	[1] AAD	25BJ	ATLAS	Higgsino pair-production, RPV λ'_{333}, $\widetilde{\chi}^0 \rightarrow b t \tau$, $b b \nu$ (BR 50% each) and $\widetilde{\chi}^\pm_1 \rightarrow b b \tau$, $b t \nu$ (BR 50% each)
> 325	95	[2] CHEKHOVSKY	25M	CMS	$\geq$ 1 ISR jet + (in-)visible decay products, wino-like $\widetilde{\chi}^0_2 \widetilde{\chi}^\pm_1$ prod. with $\widetilde{\chi}^0_2 \rightarrow Z\widetilde{\chi}^0_1$, $\widetilde{\chi}^\pm_1 \rightarrow W\widetilde{\chi}^0_1$, $m_{\widetilde{\chi}^0_2}$ - $m_{\widetilde{\chi}^0_1}$ = 50 GeV
> 175	95	[2] CHEKHOVSKY	25M	CMS	$\geq$ 1 ISR jet + (in-)visible decay products, higgsino-like $\widetilde{\chi}^0_2 \widetilde{\chi}^\pm_1$ prod.,$\widetilde{\chi}^0_2 \rightarrow Z\widetilde{\chi}^0_1$, $\widetilde{\chi}^\pm_1 \rightarrow W\widetilde{\chi}^0_1$, $m_{\widetilde{\chi}^0_2} - m_{\widetilde{\chi}^0_1}$ = 10 GeV
> 300	95	[2] CHEKHOVSKY	25M	CMS	$\geq$ 1 ISR jet + X, wino-like $\widetilde{\chi}^0_2 \widetilde{\chi}^\pm_1$ prod. with $\widetilde{\chi}^0_2 \rightarrow Z\widetilde{\chi}^0_1$, $\widetilde{\chi}^\pm_1 \rightarrow W\widetilde{\chi}^0_1$, 8 < $m_{\widetilde{\chi}^0_2} - m_{\widetilde{\chi}^0_1}$ < 65 GeV
> 163	95	[2] CHEKHOVSKY	25M	CMS	$\geq$ 1 ISR jet + X, higgsino-like $\widetilde{\chi}^0_2 \widetilde{\chi}^\pm_1$ prod. with $\widetilde{\chi}^0_2 \rightarrow Z\widetilde{\chi}^0_1$, $\widetilde{\chi}^\pm_1 \rightarrow W\widetilde{\chi}^0_1$, 3 < $m_{\widetilde{\chi}^0_2} - m_{\widetilde{\chi}^0_1}$ < 50 GeV
> 375	95	[3] HAYRAPETY...	25AH	CMS	3 ℓ (μ or e) + $\geq$ 2 jets, RPV Tchi1n2E with $\widetilde{\chi}^0_1 \rightarrow u d s$ or $\widetilde{\chi}^0_1 \rightarrow u d b$, $m_{\widetilde{\chi}^0_1}$ = 275 GeV
> 280	95	[3] HAYRAPETY...	25AH	CMS	3 ℓ (μ or e) + $\geq$ 2 jets, RPV Tchi1n2E with $\widetilde{\chi}^0_1 \rightarrow u d s$ or $\widetilde{\chi}^0_1 \rightarrow u d b$, $m_{\widetilde{\chi}^0_1}$ = 180 GeV
>1170	95	[4] AAD	24AJ	ATLAS	2 hadronic τ+$\not{E}_T$, Tchi1n2D, $m_{\widetilde{\chi}^0_1}$ = 1 GeV
none 130–330	95	[4] AAD	24AJ	ATLAS	2 hadronic τ+$\not{E}_T$, Tchi1n2E, $m_{\widetilde{\chi}^0_1}$ = 1 GeV
> 170	95	[5] AAD	24G	ATLAS	1-4 jets + $\not{E}_T$ + displaced low-p_t track, Tn1n1D, Δm ($\widetilde{\chi}^\pm_1$, $\widetilde{\chi}^0_1$) = 0.6 GeV
>1000	95	[6] AAD	24I	ATLAS	combination, wino-like Tchi1n2E, $m_{\widetilde{\chi}^0_1}$ < 200 GeV
>1000	95	[6] AAD	24I	ATLAS	combination, wino-like $pp \rightarrow \widetilde{\chi}^0_2 \widetilde{\chi}^\pm_1$, $\widetilde{\chi}^\pm_1 \rightarrow W\widetilde{\chi}^0_1$ and $\widetilde{\chi}^\pm_2 \rightarrow Z\widetilde{\chi}^0_1$, $m_{\widetilde{\chi}^0_1}$ < 170 GeV
> 850	95	[6] AAD	24I	ATLAS	combination, Tn1n1D, $\widetilde{\chi}^0_1 \rightarrow Z\widetilde{G}$ or $\widetilde{\chi}^0_1 \rightarrow h\widetilde{G}$, independent of B($\widetilde{\chi}^0_1 \rightarrow h\widetilde{G}$)
> 875	95	[7] HAYRAPETY...	24N	CMS	Combination, Tchi1n2E1, $m_{\widetilde{\chi}^0_1}$ < 50 GeV
> 990	95	[7] HAYRAPETY...	24N	CMS	Combination, Tchi1n2E, $m_{\widetilde{\chi}^0_1}$ < 50 GeV
> 875	95	[7] HAYRAPETY...	24N	CMS	Combination, Tchi1n2l, $m_{\widetilde{\chi}^0_1}$ < 50 GeV
none 225–800	95	[7] HAYRAPETY...	24N	CMS	Comb., THinoBinoA, $m_{\widetilde{\chi}^0_1}$ < 50 GeV
> 820	95	[8] AAD	23AE	ATLAS	2 SFOS ℓ, jets, $\not{E}_T$, Tchi1n2Fa, $m_{\widetilde{\chi}^0_1}$ = 1 GeV
none 260–420	95	[9] AAD	23CI	ATLAS	1ℓ + jets + $\not{E}_T$, Tchi1n2J, $m_{\widetilde{\chi}^0_1}$ = 0 GeV
> 230	95	[10] AAD	23CI	ATLAS	1ℓ + jets + $\not{E}_T$, Tchi1n2E, $m_{\widetilde{\chi}^0_2} - m_{\widetilde{\chi}^0_1}$ = 133 GeV
> 450	95	[10] AAD	23CI	ATLAS	1ℓ + jets + $\not{E}_T$, Tchi1n2E, $m_{\widetilde{\chi}^0_2} - m_{\widetilde{\chi}^0_1}$ = 260 GeV

Int. J. Mod. Phys. A 2026.41. Downloaded from www.worldscientific.com
by UNIVERSITY OF CALIFORNIA @ BERKELEY on 09/16/26. Re-use and distribution is strictly not permitted, except for Open Access articles.

> 525	95	[11] AAD	23CP	ATLS	2 same-sign ℓ, Tchi1n2E, wino-bino, $m_{\widetilde{\chi}^0_1}$= 1 GeV
none 200–250	95	[11] AAD	23CP	ATLS	2 same-sign ℓ, Tchi1n2F, wino-bino, $m_{\widetilde{\chi}^0_1}$= 1 GeV
none 200–585	95	[12] AAD	23CR	ATLS	RPV, 2 same-sign, 3, 4 ℓ, 1, 2 b-jets, higgsino production with $\widetilde{\chi} \rightarrow b + \ell/\nu + t/b$ via λ'_{i33} coupling
none 200–670	95	[12] AAD	23CR	ATLS	RPV, 2 same-sign, 3, 4 ℓ, 1, 2 b-jets, wino production with $\widetilde{\chi} \rightarrow b + \ell/\nu + t/b$ via λ'_{i33} coupling
>1050	95	[13] HAYRAPETY...	23E	CMS	γ + jets + $\not{E}_T$, Tchi1chi1A
> 450	95	[13] HAYRAPETY...	23E	CMS	γ + jets + $\not{E}_T$, Tn1n2A
none 290–670	95	[14] TUMASYAN	23B	CMS	2 AK8 jets + 2–6 AK4 jets + $\not{E}_T$, Tchi1chi1l, $m_{\widetilde{\chi}^0_1}$ = 1 GeV
none 230–760	95	[14] TUMASYAN	23B	CMS	2 AK8 jets + 2–6 AK4 jets + $\not{E}_T$, Tchi1n2Fb, $m_{\widetilde{\chi}^0_1}$ = 1 GeV
none 240–970	95	[14] TUMASYAN	23B	CMS	2 AK8 jets + 2–6 AK4 jets + $\not{E}_T$, Tchi1n2Fc, $m_{\widetilde{\chi}^0_1}$ = 1 GeV
none 300–650	95	[14] TUMASYAN	23B	CMS	2 AK8 jets + 2–6 AK4 jets + $\not{E}_T$, THinoBinoA, $m_{\widetilde{\chi}^0_1}$ = 1 GeV
> 275	95	[15] TUMASYAN	22Q	CMS	2 or 3 ℓ (soft), $\not{E}_T$; Tchi1n2F, wino-bino,$m_{\widetilde{\chi}^0_2}-m_{\widetilde{\chi}^0_1}$=10 GeV
> 205	95	[15] TUMASYAN	22Q	CMS	2 or 3 ℓ (soft), $\not{E}_T$; higgsino model with $\widetilde{\chi}^0_2\,\widetilde{\chi}^\pm_1$ and $\widetilde{\chi}^0_2\,\widetilde{\chi}^0_1$ prod., $m_{\widetilde{\chi}^0_2}-m_{\widetilde{\chi}^0_1}$ = 7.5 GeV
> 150	95	[15] TUMASYAN	22Q	CMS	2 or 3 ℓ (soft), $\not{E}_T$; higgsino model with $\widetilde{\chi}^0_2\,\widetilde{\chi}^\pm_1$ and $\widetilde{\chi}^0_2\,\widetilde{\chi}^0_1$ prod., $m_{\widetilde{\chi}^0_2}-m_{\widetilde{\chi}^0_1}$ = 3 GeV
>1450	95	[16] TUMASYAN	22S	CMS	2 same-sign e or μ, 3 or 4 leptons, Tchi1n2B (flavor-democratic), $m_{\widetilde{\ell}} = 1/2(m_{\widetilde{\chi}^\pm_1}+m_{\widetilde{\chi}^0_1})$, $m_{\widetilde{\chi}^0_1}$ = 850 GeV
>1360	95	[16] TUMASYAN	22S	CMS	2 same-sign e or μ, 3 or 4 leptons, Tchi1n2B (flavor-democratic), $m_{\widetilde{\ell}} = 1/2(m_{\widetilde{\chi}^\pm_1}+m_{\widetilde{\chi}^0_1})$, $m_{\widetilde{\chi}^0_1}$ = 0 GeV
>1290	95	[16] TUMASYAN	22S	CMS	2 same-sign e or μ, 3 or 4 leptons, Tchi1n2B (flavor-democratic), $m_{\widetilde{\ell}} = 0.05m_{\widetilde{\chi}^\pm_1}+0.95m_{\widetilde{\chi}^0_1}$, $m_{\widetilde{\chi}^0_1}$ = 0 GeV
>1440	95	[16] TUMASYAN	22S	CMS	2 same-sign e or μ, 3 or 4 leptons, Tchi1n2B (flavor-democratic), $m_{\widetilde{\ell}} = 0.95m_{\widetilde{\chi}^\pm_1}+0.05m_{\widetilde{\chi}^0_1}$, $m_{\widetilde{\chi}^0_1}$ = 0 GeV
>1140	95	[16] TUMASYAN	22S	CMS	2 same-sign e or μ, 3 or 4 leptons, Tchi1n2B (lepton in $\widetilde{\chi}^\pm_1$ decay is τ), $m_{\widetilde{\ell}} = 1/2(m_{\widetilde{\chi}^\pm_1}+m_{\widetilde{\chi}^0_1})$, $m_{\widetilde{\chi}^0_1}$ = 0 GeV
>1110	95	[16] TUMASYAN	22S	CMS	2 same-sign e or μ, 3 or 4 leptons, Tchi1n2B (lepton in $\widetilde{\chi}^\pm_1$ decay is τ), $m_{\widetilde{\ell}} = 0.05m_{\widetilde{\chi}^\pm_1}+0.95m_{\widetilde{\chi}^0_1}$, $m_{\widetilde{\chi}^0_1}$ = 0 GeV
>1140	95	[16] TUMASYAN	22S	CMS	2 same-sign e or μ, 3 or 4 leptons, Tchi1n2B (lepton in $\widetilde{\chi}^\pm_1$ decay is τ), $m_{\widetilde{\ell}} = 0.95m_{\widetilde{\chi}^\pm_1}+0.05m_{\widetilde{\chi}^0_1}$, $m_{\widetilde{\chi}^0_1}$ = 0 GeV
> 980	95	[16] TUMASYAN	22S	CMS	2 same-sign e or μ, 3 or 4 leptons, Tchi1n2B (leptons in $\widetilde{\chi}^\pm_1$ and $\widetilde{\chi}^0_2$ decays are τ), $m_{\widetilde{\ell}} = 1/2(m_{\widetilde{\chi}^\pm_1}+m_{\widetilde{\chi}^0_1})$, $m_{\widetilde{\chi}^0_1}$ = 0 GeV
> 905	95	[16] TUMASYAN	22S	CMS	2 same-sign e or μ, 3 or 4 leptons, Tchi1n2B (leptons in $\widetilde{\chi}^\pm_1$ and $\widetilde{\chi}^0_2$ decays are τ), $m_{\widetilde{\ell}} = 0.05m_{\widetilde{\chi}^\pm_1}+0.95m_{\widetilde{\chi}^0_1}$, $m_{\widetilde{\chi}^0_1}$ = 0 GeV
> 875	95	[16] TUMASYAN	22S	CMS	2 same-sign e or μ, 3 or 4 leptons, Tchi1n2B (leptons in $\widetilde{\chi}^\pm_1$ and $\widetilde{\chi}^0_2$ decays are τ), $m_{\widetilde{\ell}} = 0.95m_{\widetilde{\chi}^\pm_1}+0.05m_{\widetilde{\chi}^0_1}$, $m_{\widetilde{\chi}^0_1}$ = 0 GeV
> 650	95	[16] TUMASYAN	22S	CMS	2 same-sign e or μ, 3 or 4 leptons, Tchi1n2F, $m_{\widetilde{\chi}^0_1}$ = 0 GeV
> 260	95	[16] TUMASYAN	22S	CMS	2 same-sign e or μ, 3 or 4 leptons, Tchi1n2E, $m_{\widetilde{\chi}^0_1}$ = 0 GeV
none 265–305	95	[17] TUMASYAN	22V	CMS	3, 4 b-tagged or 2 large-radius jets, $\not{E}_T$; higgsino $\widetilde{\chi}^0_2\,\widetilde{\chi}^0_3$ prod. with $\widetilde{\chi}^0_{2,3} \rightarrow H\widetilde{\chi}^0_1$; $m_{\widetilde{\chi}^0_1}$ = 1 GeV
> 640	95	[18] AAD	21BG	ATLS	3ℓ+ $\not{E}_T$, Tchi1n2F, wino cross section, $m_{\widetilde{\chi}^0_1}$ = 0 GeV
> 300	95	[18] AAD	21BG	ATLS	3ℓ+ $\not{E}_T$, Tchi1n2F, wino cross section, $m_{\widetilde{\chi}^0_2} - m_{\widetilde{\chi}^0_1} = m_Z$
> 240	95	[18] AAD	21BG	ATLS	3ℓ+ $\not{E}_T$, Tchi1n2F, wino cross section, $m_{\widetilde{\chi}^0_2}-m_{\widetilde{\chi}^0_1}$= 10 GeV
> 195	95	[18] AAD	21BG	ATLS	3ℓ+ $\not{E}_T$, Tchi1n2Ga, higgsino cross section, $m_{\widetilde{\chi}^0_2}-m_{\widetilde{\chi}^0_1}$= 10 GeV
> 190	95	[18] AAD	21BG	ATLS	3ℓ+ $\not{E}_T$, Tchi1n2E, wino cross section, $m_{\widetilde{\chi}^0_1}$ = 0 GeV
>1600	95	[19] AAD	21Y	ATLS	$\geq$ 4ℓ, RPV Tchi1n2l with $\widetilde{\chi}^0_1 \rightarrow \ell^\pm\ell^\mp\nu$, $\lambda_{12k} \neq 0$, $m_{\widetilde{\chi}^0_1}$ = 1200 GeV
>1100	95	[19] AAD	21Y	ATLS	$\geq$ 4ℓ, RPV Tchi1n2l with $\widetilde{\chi}^0_1 \rightarrow \ell^\pm\ell^\mp\nu$, $\lambda_{i33} \neq 0$, $m_{\widetilde{\chi}^0_1}$ = 1000 GeV
> 750	95	[20] SIRUNYAN	21M	CMS	$\ell^\pm\ell^\mp + \not{E}_T$, Tchi1n2Fa , $m_{\widetilde{\chi}^0_1}$ < 100 GeV
none 400–820	95	[21] TUMASYAN	21C	CMS	1 $\ell^\pm$ + 2b-jets + $\not{E}_T$, Tchi1n2E, $\widetilde{\chi}^0_1$ = 200 GeV
none 160–820	95	[21] TUMASYAN	21C	CMS	1 $\ell^\pm$ + 2b-jets + $\not{E}_T$, Tchi1n2E, $\widetilde{\chi}^0_1$ = 0 GeV
> 380	95	[22] AAD	20AN	ATLS	2γ + $\not{E}_T$,Tn1n1A, GMSB
> 193	95	[23] AAD	20I	ATLS	2ℓ (soft), jets, $\not{E}_T$; Tchi1n2Ga, higgsino, $m_{\widetilde{\chi}^0_2}-m_{\widetilde{\chi}^0_1}$=9.3 GeV
> 240	95	[24] AAD	20I	ATLS	2ℓ (soft), jets, $\not{E}_T$; Tchi1n2Fa, wino, $m_{\widetilde{\chi}^0_2} - m_{\widetilde{\chi}^0_1}$ = 7 GeV
> 345	95	[25] AAD	20K	ATLS	3ℓ+$\not{E}_T$, Tchi1n2F, $m_{\widetilde{\chi}^0_1}$ = 0 GeV
> 740	95	[26] AAD	20R	ATLS	1ℓ + 2b-jets + $\not{E}_T$, Tchi1n2E, $m_{\widetilde{\chi}^0_1}$ = 0 GeV
> 290	95	[27] SIRUNYAN	20AU	CMS	soft τ + jet + $\not{E}_T$, Tchi1n2D, wino, $m_{\widetilde{\chi}^\pm_1} - m_{\widetilde{\chi}^0_1}$ = 50 GeV
> 680	95	[28] AABOUD	19AU	ATL	0, 1, 2 or more ℓ, H ($\rightarrow \gamma\gamma$, bb, WW^*, ZZ^*, $\tau\tau$) (various searches), Tchi1n2E, $m_{\widetilde{\chi}^0_1}$=0 GeV
> 112	95	[29] SIRUNYAN	19BU	CMS	$pp \rightarrow \widetilde{\chi}^+_1\,\widetilde{\chi}^0_2$ + 2 jets, $\widetilde{\chi}^0_2 \rightarrow \ell^+\ell^-\widetilde{\chi}^0_1$, heavy sleptons, $m_{\widetilde{\chi}^0_2} - m_{\widetilde{\chi}^0_1}$ = 1 GeV, $m_{\widetilde{\chi}^0_2} = m_{\widetilde{\chi}^+_1}$
> 215	95	[29] SIRUNYAN	19BU	CMS	$pp \rightarrow \widetilde{\chi}^+_1\,\widetilde{\chi}^0_2$ + 2 jets, $\widetilde{\chi}^0_2 \rightarrow \ell^+\ell^-\widetilde{\chi}^0_1$, heavy sleptons, $m_{\widetilde{\chi}^0_2} - m_{\widetilde{\chi}^0_1}$ = 30 GeV, $m_{\widetilde{\chi}^0_2} = m_{\widetilde{\chi}^+_1}$
> 760	95	[30] AABOUD	18AY	ATLS	2τ+$\not{E}_T$, Tchi1n2D and $\widetilde{\tau}_L$-only, $m_{\widetilde{\chi}^0_1}$ = 0 GeV
>1125	95	[31] AABOUD	18BT	ATLS	2,3ℓ+$\not{E}_T$, Tchi1n2C, $m_{\widetilde{\chi}^0_1}$=0 GeV
> 580	95	[32] AABOUD	18BT	ATLS	2,3ℓ+$\not{E}_T$, Tchi1n2F, $m_{\widetilde{\chi}^0_1}$=0 GeV
none 130–230, 290–880	95	[33] AABOUD	18CK	ATLS	2H ($\rightarrow bb$)+$\not{E}_T$,Tn1n1A, GMSB
none 220–600	95	[34] AABOUD	18CO	ATLS	2,3ℓ + $\not{E}_T$, recursive jigsaw, Tchi1n2F, $m_{\widetilde{\chi}^0_1}$ = 0 GeV
> 145	95	[35] AABOUD	18R	ATLS	2ℓ (soft) + $\not{E}_T$, Tchi1n2G, higgsino, $m_{\widetilde{\chi}^0_2} - m_{\widetilde{\chi}^0_1}$ = 5 GeV
> 175	95	[36] AABOUD	18R	ATLS	2ℓ (soft) + $\not{E}_T$, Tchi1n2F, wino, $m_{\widetilde{\chi}^0_2} - m_{\widetilde{\chi}^0_1}$ = 10 GeV
>1060	95	[37] AABOUD	18U	ATLS	2 γ + $\not{E}_T$, GGM,Tchi1chi1A, any NLSP mass
> 167	95	[38] SIRUNYAN	18AJ	CMS	2ℓ (soft) + $\not{E}_T$, Tchi1n2G, higgsino, $m_{\widetilde{\chi}^0_2} - m_{\widetilde{\chi}^0_1}$ = 15 GeV
> 710	95	[39] SIRUNYAN	18DP	CMS	2τ+$\not{E}_T$, Tchi1n2D, $m_{\widetilde{\chi}^0_1}$ = 0 GeV
none 220–490	95	[40] SIRUNYAN	17AW	CMS	1ℓ+ 2 b-jets + $\not{E}_T$, Tchi1n2E, $m_{\widetilde{\chi}^0_1}$ = 0 GeV
> 600	95	[41] AAD	16AA	ATLS	3,4ℓ + $\not{E}_T$, Tn2n3A, $m_{\widetilde{\chi}^0_1}$=0GeV
> 670	95	[41] AAD	16AA	ATLS	3,4ℓ+$\not{E}_T$,Tn2n3B,$m_{\widetilde{\chi}^0_1}$ < 200GeV
> 250	95	[42] AAD	15BA	ATLS	$m_{\widetilde{\chi}^\pm_1} = m_{\widetilde{\chi}^0_2}$, $m_{\widetilde{\chi}^0_1}$ = 0 GeV
> 380	95	[43] AAD	14H	ATLS	$\widetilde{\chi}^\pm_1\,\widetilde{\chi}^0_2 \rightarrow \tau^\pm\nu\widetilde{\chi}^0_1\tau^\pm\tau^\mp\widetilde{\chi}^0_1$, simplified model, $m_{\widetilde{\chi}^\pm_1} = m_{\widetilde{\chi}^0_2}$, $m_{\widetilde{\chi}^0_1}$ = 0 GeV

> 700	95	[43] AAD	14H	ATLAS	$\widetilde{\chi}_1^\pm \widetilde{\chi}_2^0 \rightarrow \ell^\pm \nu \widetilde{\chi}_1^0 \ell^\pm \ell^\mp \widetilde{\chi}_1^0$, simplified model, $m_{\widetilde{\chi}_1^\pm} = m_{\widetilde{\chi}_2^0}$, $m_{\widetilde{\chi}_1^0} = 0$ GeV
> 345	95	[43] AAD	14H	ATLAS	$\widetilde{\chi}_1^\pm \widetilde{\chi}_2^0 \rightarrow W \widetilde{\chi}_1^0 Z \widetilde{\chi}_1^0$, simplified model, $m_{\widetilde{\chi}_1^\pm} = m_{\widetilde{\chi}_2^0}$, $m_{\widetilde{\chi}_1^0} = 0$ GeV
> 148	95	[43] AAD	14H	ATLAS	$\widetilde{\chi}_1^\pm \widetilde{\chi}_2^0 \rightarrow W \widetilde{\chi}_1^0 H \widetilde{\chi}_1^0$, simplified model, $m_{\widetilde{\chi}_1^\pm} = m_{\widetilde{\chi}_2^0}$, $m_{\widetilde{\chi}_1^0} = 0$ GeV
> 620	95	[44] AAD	14X	ATLAS	$\geq 4\ell^\pm$, $\widetilde{\chi}_{2,3}^0 \rightarrow \ell^\pm \ell^\mp \widetilde{\chi}_1^0$, $m_{\widetilde{\chi}_1^0} = 0$ GeV
		[45] AAD	13	ATLAS	$3\ell^\pm + \not{E}_T$, pMSSM, SMS
		[46] CHATRCHYAN	12BJ	CMS	$\geq 2\ \ell$, jets $+ \not{E}_T$, $pp \rightarrow \widetilde{\chi}_1^\pm \widetilde{\chi}_2^0$
> 62.4	95	[47] ABREU	00W	DLPH	$\widetilde{\chi}_2^0$, $1 \leq \tan\beta \leq 40$, all Δm, all m_0
> 99.9	95	[47] ABREU	00W	DLPH	$\widetilde{\chi}_3^0$, $1 \leq \tan\beta \leq 40$, all Δm, all m_0
> 116.0	95	[47] ABREU	00W	DLPH	$\widetilde{\chi}_4^0$, $1 \leq \tan\beta \leq 40$, all Δm, all m_0
• • • We do not use the following data for averages, fits, limits, etc. • • •					
> 310	95	[48] AAD	20AN	ATLAS	$2\gamma + \not{E}_T$, Tchi1n2E, $m_{\widetilde{\chi}_1^0}$=0 GeV
none 180–355	95	[49] AAD	14G	ATLAS	$\widetilde{\chi}_1^\pm \widetilde{\chi}_2^0 \rightarrow W \widetilde{\chi}_1^0 Z \widetilde{\chi}_1^0$, simplified model, $m_{\widetilde{\chi}_1^\pm} = m_{\widetilde{\chi}_2^0}$, $m_{\widetilde{\chi}_1^0} = 0$ GeV
		[50] KHACHATRY...	14I	CMS	$\widetilde{\chi}_2^0 \rightarrow (Z,\ H) \widetilde{\chi}_1^0\ \widetilde{\ell}\ell$, simplified model
		[51] AAD	12AS	ATLAS	$3\ell^\pm + \not{E}_T$, pMSSM
		[52] AAD	12T	ATLAS	$\ell^\pm \ell^\pm + \not{E}_T$, $pp \rightarrow \widetilde{\chi}_1^\pm \widetilde{\chi}_2^0$

[1] AAD 25BJ searched in 140 fb^{-1} of pp collisions at $\sqrt{s} = 13$ TeV for an excess of 0-lepton events with at least one hadronically decaying τ and at least 3 b-jet. The search is performed by training a neural network to separate a signal of vector-like leptons from the Standard Model background. No significant excess above the Standard Model expectations is observed. Limits are set also in a model of SUSY, where members of either a higgsino LSP triplet or a wino LSP doublet are produced, and decay via a RPV λ'_{333} coupling to b, t quarks and τ, ν_τ leptons, see their Figs. 13 and 14.

[2] CHEKHOVSKY 25M searched in 138 fb^{-1} of pp collisions at $\sqrt{s} = 13$ TeV for evidence of SUSY models with compressed mass spectra in events with a high transverse momentum system from initial-state-radiation jets recoiling against a potential sparticle system with significant missing transverse momentum. These events are further categorized based on their lepton multiplicity, jet multiplicity, number of b-tagged jets, and kinematic variables sensitive to the sparticle masses and mass splittings. No significant excess above the Standard Model expectations is observed. The results are interpreted in models of top squark, electroweakino and slepton pair production. Limits are set for top squark pair production in the models Tstop1 and Tstop2, see their figure 25, and in Tstop4, see their figure 26. The results are also interpreted in models describing the production of mass-degenerate $\widetilde{\chi}_2^0$ and $\widetilde{\chi}_1^\pm$ with decays $\widetilde{\chi}_2^0 \rightarrow Z \widetilde{\chi}_1^0$ and $\widetilde{\chi}_1^\pm \rightarrow W \widetilde{\chi}_1^0$, applying both a wino-like and higgsino-like $\widetilde{\chi}_1^\pm \widetilde{\chi}_2^0$ production cross section, see their figure 27. Limits are also set for wino-like $\widetilde{\chi}_1^\pm$ pair production, either with $\widetilde{\chi}_1^\pm \rightarrow W \widetilde{\chi}_1^0$ or in the model Tchi1chi1C. This paper also addresses direct slepton production, taking into account pure right-handed, pure left-handed and combined production of either selectrons, smuons, or mass-degenerate sleptons of the first and second generation, see their figures 30 and 31.

[3] HAYRAPETYAN 25AH searched in 138 fb^{-1} of pp collisions at $\sqrt{s} = 13$ TeV for new physics in jet multiplicity patterns in three-lepton events with and without b quarks. No significant excess above the Standard Model expectations is observed. The results are interpreted in a model similar to Tchi1n2E, but with additional prompt hadronic R-parity violating decay of $\widetilde{\chi}_1^0$ to three quarks, either as $\widetilde{\chi}_1^0 \rightarrow uds$ or $\widetilde{\chi}_1^0 \rightarrow udb$, see their figure 3.

[4] AAD 24AJ searched in 139 fb^{-1} of pp collisions at $\sqrt{s} = 13$ TeV for evidence of direct stau pair production, or electroweakino pair production with decay via an intermediate stau, in events with two taus decaying hadronically (including a same-charge channel), no b-jets and moderate $\not{E}_T$, using a BDT for the direct stau search and a more traditional cut-and-count selection for the electroweakino search. No significant excess above the Standard Model expectations is observed. Limits are set in models of direct stau production $\widetilde{\tau} \rightarrow \tau \widetilde{\chi}_1^0$, $\widetilde{\tau}_L$, $\widetilde{\tau}_R$ or degenerate production. Limits are also set in models of pair production of charginos (Tchichi1D) or of charginos and neutralinos (Tchi1n2D) followed by the decay via intermediate staus, or (for the latter) via Wh (Tchi1n2E). See their figures 12, 14 and 16.

[5] AAD 24G searched in 140 fb^{-1} of pp collisions at $\sqrt{s} = 13$ TeV for evidence of higgsino pair production in events with low-momentum mildly displaced tracks. No significant excess above the Standard Model expectations is observed. Limits are set in the model Tn1n1D, see their Fig. 3, assuming that the $\widetilde{\chi}_1^\pm$ has a flight length of about 0.11 mm from the pp interaction point and decays to $\widetilde{\chi}_1^0$ and a charged particle (usually a soft pion) that is measured as low-momentum track.

[6] AAD 24I provides a statistical combination of the results of a number of analyses targeting electroweak production performed using 139 fb^{-1} of pp collisions at $\sqrt{s} = 13$ TeV. The combination was used to set limits on the pair-produced particle masses as a function of the LSP mass for wino-like $\widetilde{\chi}_1^\pm \widetilde{\chi}_1^\pm$ followed by $\widetilde{\chi}_1^\pm \rightarrow W \widetilde{\chi}_1^0$, wino-like $\widetilde{\chi}_2^0 \widetilde{\chi}_1^\pm$ followed by $\widetilde{\chi}_1^\pm \rightarrow W \widetilde{\chi}_1^0$ and either $\widetilde{\chi}_2^0 \rightarrow Z \widetilde{\chi}_1^0$ or $\widetilde{\chi}_2^0 \rightarrow h \widetilde{\chi}_1^0$, or a GGM-like model with a full higgsino triplet decaying to a gravitino. See their Fig. 2.

[7] HAYRAPETYAN 24N searched in up to 137 fb^{-1} of pp collisions at $\sqrt{s} = 13$ TeV for evidence of wino-like chargino-neutralino pairs, Higgsino-like neutralino pair production in a gauge-mediated SUSY breaking inspired scenario, a Higgsino-bino interpretation, and slepton pair production in a combination of a number of previously reported searches for SUSY in different final states. No significant excess above the Standard Model expectations is observed. Limits are set on the $\widetilde{\chi}_1^\pm$ mass in the wino-bino models Tchi1n2E1, Tchi1n2E, and Tchi1n2l, see their Fig. 11, and on the $\widetilde{\chi}_1^0$ in the higgsino-like GMSB models Tn1n1A, Tn1n1B, and Tn1n1C, see their Fig. 13. In addition, Fig. 14 shows the mass exclusion limit as a function of the branching fraction to the H boson. Limits are also set in a Higgsino-bino interpretation as in THinoBinoA, but also including leptonic decays, see their Fig. 15. Limits are also set on slepton ($\widetilde{e}$, $\widetilde{\mu}$) production with the decay $\widetilde{\ell} \rightarrow \ell \widetilde{\chi}_1^0$, see their Fig. 16.

[8] AAD 23AE searched in 139 fb^{-1} of pp collisions at $\sqrt{s} = 13$ TeV for events with 2 ℓ with same flavour and opposite sign, plus jets and $\not{E}_T$, defining signal region with the dilepton invariant mass both on- and off-shell with respect to the Z boson. No significant excess above the Standard Model predictions is observed. Limits are set on models of strong and electroweak production. For electroweak production, limits are placed on production of mass-degenerate, wino-like $\widetilde{\chi}_2^0 \widetilde{\chi}_1$ with $\widetilde{\chi}_2^0 \rightarrow Z \widetilde{\chi}_1^0$ and $\widetilde{\chi}_1 \rightarrow W \widetilde{\chi}_1^0$, see figure 15.

[9] AAD 23CI searched in 139 fb^{-1} of pp collisions for events containing 1 ℓ (e or μ), jets, and $\not{E}_T$. Final states consistent with the production of a diboson system plus $\not{E}_T$ were identified also by making use of large-R jet tagging techniques. No excess on top of the Standard Model background was observed. Limits were set on the production of $\widetilde{\chi}_1^\pm \widetilde{\chi}_2^0$ and $\widetilde{\chi}_1^\pm \widetilde{\chi}_1^\pm$ (assuming wino cross sections) decaying to $WZ \widetilde{\chi}_1^0 \widetilde{\chi}_1^0$ or $WW \widetilde{\chi}_1^0 \widetilde{\chi}_1^0$. See their figure 9.

[10] AAD 23CI searched in 139 fb^{-1} of pp collisions for events containing 1 ℓ (e or μ), jets, and $\not{E}_T$. Final states consistent with the production of a boson + Higgs system plus $\not{E}_T$ were identified via a BDT. No excess on top of the Standard Model background was observed. Limits were set on the production of degenerate $\widetilde{\chi}_1^\pm \widetilde{\chi}_2^0$ (assuming wino cross sections) decaying into $Wh \widetilde{\chi}_1^0 \widetilde{\chi}_1^0$. See their figure 10.

[11] AAD 23CP searched in 139 fb^{-1} of pp collisions at $\sqrt{s} = 13$ TeV for events with 2 ℓ with same charge plus at least one jet and $\not{E}_T$, defining signal region based on 'stransverse mass' of the dilepton system, $\not{E}_T$ significance and effective mass. No significant excess above the Standard Model predictions is observed. Limits are set on the mass of mass-degenerate $\widetilde{\chi}_1^\pm$ and $\widetilde{\chi}_2^0$ for the wino-like production of $\widetilde{\chi}_1^\pm \widetilde{\chi}_2^0$ followed by the decay into either $WZ \widetilde{\chi}_1^0 \widetilde{\chi}_1^0$ or $Wh \widetilde{\chi}_1^0 \widetilde{\chi}_1^0$, see figure 13.

[12] AAD 23CR searched in 139 fb^{-1} of pp collisions at $\sqrt{s} = 13$ TeV for RPV SUSY in final states with multiple leptons and b-tagged jets. No significant excess above the Standard Model expectations is observed. Limits are set on the production of electroweakinos (wino or higgsino) that decay via RPV coupling λ'_{i33} to a charged lepton or a neutrino, a b quark, and an additional t or b quark, see their figure 16. A second model addresses direct $\widetilde{\mu}_{L,R}$ production and decay to a muon and a bino-like neutralino, which decays in the same way as in the first model, see their figure 17.

[13] HAYRAPETYAN 23E searched in 137 fb^{-1} of pp collisions at $\sqrt{s} = 13$ TeV for evidence of gluino, top squark and electroweakino pair production in events with at least one photon, multiple jets, and large $\not{E}_T$. No significant excess above the Standard Model expectations is observed. Limits are set in models for strong production, Tglu4D, Tglu4E, Tglu4F and Tstop13, see their figure 9. They also interpret the results in the models for electroweak production, shown in their figure 10. Tchi1n1A assumes wino-like $\widetilde{\chi}_1^\pm \widetilde{\chi}_1^0$ production, while Tchi1chi1A assumes higgsino-like cross sections and includes $\widetilde{\chi}_1^\pm \widetilde{\chi}_1^\pm$, $\widetilde{\chi}_1^0 \widetilde{\chi}_2^0$ and $\widetilde{\chi}_{1,2}^0 \widetilde{\chi}_1^\pm$ production. For $\widetilde{\chi}_1^0 \widetilde{\chi}_2^0$ alone no mass point can be excluded in the model Tchi1chi1A, but in another model for $\widetilde{\chi}_1^0 \widetilde{\chi}_2^0$ production, Tn1n2A.

[14] TUMASYAN 23B searched in 137 fb^{-1} of pp collisions at $\sqrt{s} = 13$ TeV for evidence of electroweakino pair production with decays including hadronically decaying bosons, WW, WZ, WH, or ZH, identified with a DNN classifying large-area (AK8) jets. No significant excess above the Standard Model expectations is observed. Limits are set on the mass of the nearly mass degenerate wino-like $\widetilde{\chi}_2^0$ and $\widetilde{\chi}_1^\pm$ in the models Tchi1chi1l , Tchi1n2Fb, and Tchi1n2Fc, see their figure 4. They also consider a model that contains both $\widetilde{\chi}_2^0 \widetilde{\chi}_1^\pm$ and $\widetilde{\chi}_1^\pm \widetilde{\chi}_1^\pm$ production, see their figure 5 (upper). Results are also interpreted in the model THinoBinoA with nearly mass-degenerate higgsino-like $\widetilde{\chi}_3^0$, $\widetilde{\chi}_2^0$, $\widetilde{\chi}_1^\pm$, and a lighter bino-like $\widetilde{\chi}_1^0$, see their figure 5 (lower).

[15] TUMASYAN 22Q searched in up to 137 fb^{-1} of pp collisions at $\sqrt{s} = 13$ TeV for evidence of electroweakino and top squark pair production with a small mass difference between the produced supersymmetric particles and the lightest neutralino in events with two or three low-momentum leptons and missing transverse momentum. No significant excess above the Standard Model expectations is observed. Limits are set on the mass of $\widetilde{\chi}_2^0$ and $\widetilde{\chi}_1^\pm$ in the model Tchi1n2F, see their Figure 8. Limits are also set in a higgsino simplified model with both $\widetilde{\chi}_2^0 \widetilde{\chi}_1^\pm$ and $\widetilde{\chi}_2^0 \widetilde{\chi}_1^0$ production, where $\widetilde{\chi}_2^0 \rightarrow Z \widetilde{\chi}_1^0$ and $m_{\widetilde{\chi}_1^\pm} = 1/2(m_{\widetilde{\chi}_2^0} + m_{\widetilde{\chi}_1^0})$. A model inspired by the pMSSM is used for further interpretations in the case of a higgsino LSP, see their Figure 9. Limits are also set on the mass of the top squark in the models Tstop2 and Tstop3, see their Figure 10.

[16] TUMASYAN 22S searched in 137 fb^{-1} of pp collisions at $\sqrt{s} = 13$ TeV for evidence of electroweakino pair production in events with three or four leptons, with up to two hadronically decaying τ leptons, or two same-sign light leptons (e or μ). No significant excess above the Standard Model expectations is observed. Limits are set on the mass of $\widetilde{\chi}_2^0$ and $\widetilde{\chi}_1^\pm$ in the models Tchi1n2B (in flavory-democratic and tau-enriched or -dominated scenarios), Tchi1n2E, Tchi1n2F, see their Figures 16–20, and on the mass of the higgsino-triplet $\widetilde{\chi}_2^0$, $\widetilde{\chi}_1^\pm$, and $\widetilde{\chi}_1^0$ in the models Tn1n1A, Tn1n1B, and Tn1n1C, see their Figure 21.

[17] TUMASYAN 22V searched in 137 fb^{-1} of pp collisions at $\sqrt{s} = 13$ TeV for evidence of electroweakino pair production with decay to two Higgs bosons H, with $H \rightarrow b\overline{b}$, resulting either in 4 resolved b-jets or two large-radius jets, and large $\not{E}_T$. No significant excess above the Standard Model expectations is observed. Limits are set on the mass of $\widetilde{\chi}_2^0$ and $\widetilde{\chi}_1^\pm$ in the models Tn1n1A, see their Figures 11 and 12, or in a model where higgsino-like nearly mass degenerate $\widetilde{\chi}_2^0$ and $\widetilde{\chi}_3^0$ are pair produced and each decay to H and a bino-like $\widetilde{\chi}_1^0$, see their Figure 13. Limits are also set on the gluino mass in the model Tglu1l, see their Figure 14.

Int. J. Mod. Phys. A 2026.41. Downloaded from www.worldscientific.com
by UNIVERSITY OF CALIFORNIA @ BERKELEY on 09/16/26. Re-use and distribution is strictly not permitted, except for Open Access articles.

Int. J. Mod. Phys. A 2026.41. Downloaded from www.worldscientific.com
by UNIVERSITY OF CALIFORNIA @ BERKELEY on 09/16/26. Re-use and distribution is strictly not permitted, except for Open Access articles.

[18] AAD 21BG searched in 139 fb^{-1} of pp collisions at $\sqrt{s}$ = 13 TeV for pair production $\widetilde{\chi}^0_2\widetilde{\chi}^\pm_1$ in final states with three leptons, with and without assuming the presence of a $Z \rightarrow \ell\ell$ decay. No significant excess above the Standard Model predictions is observed. Limits are set on the $\widetilde{\chi}^0_2$ and $\widetilde{\chi}^\pm_1$ mass in Tchi1n2E, Tchi1n2F and Tchi1n2Ga. See their Fig. 16.

[19] AAD 21Y searched in 139 fb^{-1} of pp collisions at $\sqrt{s}$ = 13 TeV for supersymmetry in events with four or more leptons (electrons, muons and tau-leptons). No significant excess above the Standard Model expectations is observed. Limits are set on Tchi1n12-GGM, and RPV models similar to Tchi1n2l, Tglu1A (with $q = u, d, s, c, b$, with equal branching fractions), and $\widetilde{\ell}_L/\widetilde{\nu} \rightarrow \ell/\nu\widetilde{\chi}^0_1$ (mass-degenerate $\widetilde{\ell}_L$ and $\widetilde{\nu}$ of all 3 generations), all with $\widetilde{\chi}^0_1 \rightarrow \ell^\pm\ell^\mp\nu$ via λ_{12k} or λ_{i33} (where $i,k \in 1,2$), see their Figure 11.

[20] SIRUNYAN 21M searched in 137 fb^{-1} of pp collisions at $\sqrt{s}$ = 13 TeV for supersymmetry in events with two opposite-sign same-flavor leptons (electrons, muons) and $\not{E}_T$. No significant excess above the Standard Model expectations is observed. Limits are set on the gluino mass in the simplified model Tglu4C, see their Figure 10, on the $\widetilde{\chi}^0_2$ and $\widetilde{\chi}^\pm_1$ mass in Tchi1n2Fa, see their Figure 11, on the $\widetilde{\chi}^0_1$ mass in Tn1n1C and Tn1n1B for $m_{\widetilde{\chi}^0_2}=m_{\widetilde{\chi}^\pm_1}=m_{\widetilde{\chi}^0_1}$, see their Figure 12. Limits are also set on the light squark mass for the simplified model Tsqk2A, on the sbottom mass in Tsbot3, see their Figure 13, and on the slepton mass in direct electroweak pair production of mass-degenerate left- and right-handed sleptons (selectrons and smuons), see their Figure 14.

[21] TUMASYAN 21C searched in 137 fb^{-1} of pp collisions at $\sqrt{s}$ = 13 TeV for supersymmetry in events with with one lepton, a Higgs boson decaying to a pair of bottom quarks, and large $\not{E}_T$. No significant excess above the Standard Model expectations is observed. Lower limits are set on the masses of $\widetilde{\chi}^0_2$ and $\widetilde{\chi}^\pm_1$ in the simplified model Tchi1n2E, see their Figure 6.

[22] AAD 20AN searched in 139 fb^{-1} of pp collisions at $\sqrt{s}$ = 13 TeV for events with two photons and missing transverse momentum. Events are further categorised in terms of lepton or jet multiplicity. No significant excess over the expected background is observed. Limits at 95% C.L. are set on the Higgsino mass in the T1n1n1A simplified model, see their Figure 11.

[23] AAD 20I reported on ATLAS searches for electroweak production in models with compressed mass spectra as Tchi1n2Ga. A dataset of pp collisions at $\sqrt{s}$ = 13 TeV corresponding to an integrated luminosity of 139 fb^{-1} was used. Events with $\not{E}_T$, two same-flavour, opposite-charge, low-transverse-momentum leptons, and jets from initial-state radiation or characteristic of vector-boson fusion production are selected. Constraints at 95% C.L. are placed in Higgsino models on the mass of the $\widetilde{\chi}^0_2$ (the $\widetilde{\chi}^\pm_1$ mass is halfway between the $\widetilde{\chi}^0_2$ and $\widetilde{\chi}^0_1$ masses) at 193 GeV for a mass splitting between $\widetilde{\chi}^0_2$ and $\widetilde{\chi}^0_1$ of 9.3 GeV and extend down to a mass splitting of 2.4 GeV at the LEP chargino mass limit. See their Fig. 14(a).

[24] AAD 20I reported on ATLAS searches for electroweak production in models with compressed mass spectra as Tchi1n2Fa. A dataset of pp collisions at $\sqrt{s}$ = 13 TeV corresponding to an integrated luminosity of 139 fb^{-1} was used. Events with $\not{E}_T$, two same-flavour, opposite-charge, low-transverse-momentum leptons, and jets from initial-state radiation or characteristic of vector-boson fusion production are selected. Constraints at 95% C.L. are placed in Wino-Bino models on the mass of the $\widetilde{\chi}^0_2$ (degenerate with $\widetilde{\chi}^\pm_1$) at 240 GeV for a mass splitting between $\widetilde{\chi}^0_2$ and $\widetilde{\chi}^0_1$ of 7 GeV and extend down to a mass splitting of 1.5 GeV at the LEP chargino mass limit of 92.4 GeV. See their Fig. 14(b,c).

[25] AAD 20K reported on a search for electroweak production in models with mass splittings near the electroweak scale as Tchi1n2F and exploiting three-lepton final state events with an emulated recursive jigsaw reconstruction method. The analysis uses a dataset of pp collisions at $\sqrt{s}$ = 13 TeV corresponding to an integrated luminosity of 139 fb^{-1}. Exclusion limits at 95% C.L. are derived on next-to-lightest neutralinos and charginos with masses up to 345 GeV for a massless lightest neutralino, see their Fig. 7.

[26] AAD 20R searched for electroweak production in the model Tchi1n2E, selecting events with a pair of b-tagged jets consistent with those from a Higgs boson decay, either an electron or a muon from the W boson decay and $\not{E}_T$. The analysis uses a dataset of pp collisions at $\sqrt{s}$ = 13 TeV corresponding to an integrated luminosity of 139 fb^{-1}. Exclusion limits at 95% C.L. are derived on next-to-lightest neutralinos and charginos with masses up to 740 GeV for a massless lightest neutralino, assuming pure wino cross-sections. See their Fig. 6.

[27] SIRUNYAN 20AU searched in 77.2 fb^{-1} of pp collisions at $\sqrt{s}$ = 13 TeV for events containing one soft, hadronically decaying tau lepton, one energetic jet from initial-state radiation, and large $\not{E}_T$. No excess over the expected background is observed. Limits are derived on the wino mass in the Tchi1n2D simplified model, see their Figure 2.

[28] AABOUD 19AU searched in 36.1 fb^{-1} of pp collisions at $\sqrt{s}$ = 13 TeV for direct electroweak production of charginos and next-to-lightest neutralinos decaying into lightest neutralinos and a W and a Higgs boson, respectively. Fully hadronic, semileptonic, diphoton, and multilepton (electrons, muons) final states with missing transverse momentum are considered in this search. Observations are consistent with the Standard Model expectations, and 95% confidence-level limits of up to 680 GeV on the chargino/next-to-lightest neutralino masses are set (Tchi1n2E model). See their Figure 14 for an overlay of exclusion contours from all searches.

[29] SIRUNYAN 19BU searched for pair production of gauginos via vector boson fusion assuming the gaugino spectrum is compressed, in 35.9 fb^{-1} of pp collisions at $\sqrt{s}$ = 13 TeV. The final states explored included zero leptons plus two jets, one lepton plus two jets, and one hadronic tau plus two jets. A similar bound is obtained in the light slepton limit.

[30] AABOUD 18AY searched in 36.1 fb^{-1} of pp collisions at $\sqrt{s}$ = 13 TeV for direct electroweak production of charginos and neutralinos as in Tchi1n2D models, in events characterised by the presence of at least two hadronically decaying tau leptons and large missing transverse energy. No significant deviation from the expected SM background is observed. Assuming decays via intermediate $\widetilde{\tau}_L$ and $m_{\widetilde{\chi}^\pm_1} = m_{\widetilde{\chi}^0_2}$, the observed limits rule out $\widetilde{\chi}^0_2$ masses up to 760 GeV for a massless $\widetilde{\chi}^0_1$. See their Fig.7 (right). Interpretations are also provided in Fig 8 (bottom) for different assumptions on the ratio between $m_{\widetilde{\tau}}$ and $m_{\widetilde{\chi}^0_2} + m_{\widetilde{\chi}^0_1}$.

[31] AABOUD 18BT searched in 36.1 fb^{-1} of pp collisions at $\sqrt{s}$ = 13 TeV for direct electroweak production of charginos, chargino and next-to-lightest neutralinos and sleptons in events with two or three leptons (electrons or muons), with or without jets, and large missing transverse energy. No significant excess above the Standard Model expectations is observed. Limits are set on the next-to-lightest neutralino mass up to 1100 GeV for massless $\widetilde{\chi}^0_1$ in the Tchi1n2C simplified model exploiting the 3ℓ signature, see their Figure 8(c).

[32] AABOUD 18BT searched in 36.1 fb^{-1} of pp collisions at $\sqrt{s}$ = 13 TeV for direct electroweak production of charginos, chargino and next-to-lightest neutralinos and sleptons in events with two or three leptons (electrons or muons), with or without jets, and large missing transverse energy. No significant excess above the Standard Model expectations is observed. Limits are set on the next-to-lightest neutralino mass up to 580 GeV for massless $\widetilde{\chi}^0_1$ in the Tchi1n2F simplified model exploiting the 2ℓ+2 jets and 3ℓ signatures, see their Figure 8(d).

[33] AABOUD 18CK searched for events with at least 3 b-jets and large missing transverse energy in two datasets of pp collisions at $\sqrt{s}$ = 13 TeV of 36.1 fb^{-1} and 24.3 fb^{-1} depending on the trigger requirements. The analyses aimed to reconstruct two Higgs bosons decaying to pairs of b-quarks. No significant excess above the Standard Model expectations is observed. Limits are set on the Higgsino mass in the T1n1n1A simplified model, see their Figure 15(a). Constraints are also presented as a function of the BR of Higgsino decaying into an higgs boson and a gravitino, see their Figure 15(b).

[34] AABOUD 18CO searched in 36.1 fb^{-1} of pp collisions at $\sqrt{s}$ = 13 TeV for direct electroweak production of mass-degenerate charginos and next-to-lightest neutralinos in events with two or three leptons (electrons or muons), with or without jets, and large missing transverse energy. The search channels are based on recursive jigsaw reconstruction. Limits are set on the next-to-lightest neutralinos mass up to 600 GeV for massless neutralinos in the Tchi1n2F simplified model exploiting the statistical combination of 2ℓ+2 jets and 3ℓ channels. Next-to-lightest neutralinos masses below 220 GeV are not excluded due to an excess of events above the SM prediction in the dedicated regions. See their Figure 13(d).

[35] AABOUD 18R searched in 36.1 fb^{-1} of pp collisions at $\sqrt{s}$ = 13 TeV for electroweak production in scenarios with compressed mass spectra in final states with two low-momentum leptons and missing transverse momentum. The data are found to be consistent with the SM prediction. Results are interpreted in Tchi1n2G higgsino models, and $\widetilde{\chi}^0_2$ masses are excluded up to 145 GeV for $m_{\widetilde{\chi}^0_2} - m_{\widetilde{\chi}^0_1}$ = 5 GeV. The exclusion limits extend down to mass splittings of 2.5 GeV, see their Fig. 10 (top). Results are also interpreted in terms of exclusion bounds on the production cross-sections for the NUHM2 scenario as a function of the universal gaugino mass $m_{1/2}$ and $m_{\widetilde{\chi}^0_2} - m_{\widetilde{\chi}^0_1}$, see their Fig. 12.

[36] AABOUD 18R searched in 36.1 fb^{-1} of pp collisions at $\sqrt{s}$ = 13 TeV for electroweak production in scenarios with compressed mass spectra in final states with two low-momentum leptons and missing transverse momentum. The data are found to be consistent with the SM prediction. Results are interpreted in Tchi1n2F wino models, and $\widetilde{\chi}^0_2$ masses are excluded up to 175 GeV for $m_{\widetilde{\chi}^0_2} - m_{\widetilde{\chi}^0_1}$ = 10 GeV. The exclusion limits extend down to mass splittings of 2 GeV, see their Fig. 10 (bottom). Results are also interpreted in terms of exclusion bounds on the production cross-sections for the NUHM2 scenario as a function of the universal gaugino mass $m_{1/2}$ and $m_{\widetilde{\chi}^0_2} - m_{\widetilde{\chi}^0_1}$, see their Fig. 12.

[37] AABOUD 18U searched in 36.1 fb^{-1} of pp collisions at $\sqrt{s}$ = 13 TeV in events with at least one isolated photon, possibly jets and significant transverse momentum targeting generalised models of gauge-mediated SUSY breaking. No significant excess of events is observed above the SM prediction. Results of the diphoton channel are interpreted in terms of lower limits on the masses of gauginos Tchi1chi1A models, which reach as high as 1.3 TeV. Gaugino masses below 1060 GeV are excluded for any NLSP mass, see their Fig. 10.

[38] SIRUNYAN 18AJ searched in 35.9 fb^{-1} of pp collisions at $\sqrt{s}$ = 13 TeV for events containing two low-momentum, oppositely charged leptons (electrons or muons) and $\not{E}_T$. No excess over the expected background is observed. Limits are derived on the wino mass in the Tchi1n2F simplified model, see their Figure 5. Limits are also set on the stop mass in the Tstop10 simplified model, see their Figure 6. Finally, limits are set on the Higgsino mass in the Tchi1n2G simplified model, see Figure 8 and in the pMSSM, see Figure 7.

[39] SIRUNYAN 18DP searched in 35.9 fb^{-1} of pp collisions at $\sqrt{s}$ = 13 TeV for direct electroweak production of charginos and neutralinos or of chargino pairs in events with a tau lepton pair and significant missing transverse momentum. Both hadronic and leptonic decay modes are considered for the tau lepton. No significant excess above the Standard Model expectations is observed. Limits are set on the chargino mass in the Tchi1chi1D and Tchi1n2 simplified models, see their Figures 14 and 15. Also, excluded stau pair production cross sections are shown in Figures 11, 12, and 13.

[40] SIRUNYAN 17AW searched in 35.9 fb^{-1} of pp collisions at $\sqrt{s}$ = 13 TeV for events with a charged lepton (electron or muon), two jets identified as originating from a b-quark, and large $\not{E}_T$. No significant excess above the Standard Model expectations is observed. Limits are set on the mass of the chargino and the next-to-lightest neutralino in the Tchi1n2E simplified model, see their Figure 6.

[41] AAD 16AA summarized and extended ATLAS searches for electroweak supersymmetry in final states containing several charged leptons, $\not{E}_T$, with or without hadronic jets, in 20 fb^{-1} of pp collisions at $\sqrt{s}$ = 8 TeV. The paper reports the results of new interpretations and statistical combinations of previously published analyses, as well as new analyses. Exclusion limits at 95% C.L. are set on mass-degenerate $\widetilde{\chi}^0_2$ and $\widetilde{\chi}^0_3$ masses in the Tn2n3A and Tn2n3B simplified models. See their Fig. 15.

[42] AAD 15BA searched in 20.3 fb^{-1} of pp collisions at $\sqrt{s}$ = 8 TeV for electroweak production of charginos and neutralinos decaying to a final state containing a W boson and a 125 GeV Higgs boson, plus missing transverse momentum. No excess beyond the Standard Model expectation is observed. Exclusion limits are derived in simplified models of direct chargino and next-to-lightest neutralino production, with the decays $\widetilde{\chi}^\pm_1 \rightarrow W^\pm\widetilde{\chi}^0_1$ and $\widetilde{\chi}^0_2 \rightarrow H\widetilde{\chi}^0_1$ having 100% branching fraction, see Fig. 8. A combination of the multiple final states for the Higgs decay yields the best limits (Fig. 8d).

[43] AAD 14H searched in 20.3 fb^{-1} of pp collisions at $\sqrt{s}$ = 8 TeV for electroweak production of charginos and neutralinos decaying to a final sate with three leptons and missing transverse momentum. No excess beyond the Standard Model expectation is observed. Exclusion limits are derived in simplified models of direct chargino and next-to-lightest neutralino production, with decays to the lightest neutralino via either all three generations of leptons, staus only, gauge bosons, or Higgs bosons, see Fig. 7. An interpretation in the pMSSM is also given, see Fig. 8.

[44] AAD 14X searched in 20.3 fb^{-1} of pp collisions at $\sqrt{s}$ = 8 TeV for events with at least four leptons (electrons, muons, taus) in the final state. No significant excess above the Standard Model expectations is observed. Limits are set on the neutralino mass in an R-parity conserving simplified model where the decay $\widetilde{\chi}^0_{2,3} \rightarrow \ell^\pm\ell^\mp\widetilde{\chi}^0_1$ takes place with a branching ratio of 100%, see Fig. 10.

[45] AAD 13 searched in 4.7 fb^{-1} of pp collisions at $\sqrt{s}$ = 7 TeV for charginos and neutralinos decaying to a final state with three leptons (e and μ) and missing transverse energy. No excess beyond the Standard Model expectation is observed. Exclusion limits are derived in the phenomenological MSSM, see Fig. 2 and 3, and in simplified models, see Fig. 4. For the simplified models with intermediate slepton decays, degenerate $\widetilde{\chi}^{\pm}_1$ and $\widetilde{\chi}^0_2$ masses up to 500 GeV are excluded at 95% C.L. for very large mass differences with the $\widetilde{\chi}^0_1$. Supersedes AAD 12AS.

[46] CHATRCHYAN 12BJ searched in 4.98 fb^{-1} of pp collisions at $\sqrt{s}$ = 7 TeV for direct electroweak production of charginos and neutralinos in events with at least two leptons, jets and missing transverse momentum. No significant excesses over the expected SM backgrounds are observed and 95% C.L. limits on the production cross section of $\widetilde{\chi}^{\pm}_1\widetilde{\chi}^0_2$ pair production were set in a number of simplified models, see Figs. 7 to 12. Most limits are for exactly 3 jets.

[47] ABREU 00W combines data collected at $\sqrt{s}$=189 GeV with results from lower energies. The mass limit is obtained by constraining the MSSM parameter space with gaugino and sfermion mass universality at the GUT scale, using the results of negative direct searches for neutralinos (including cascade decays and $\widetilde{\tau}\tau$ final states) from ABREU 01, for charginos from ABREU 00J and ABREU 00T (for all Δm_+), and for charged sleptons from ABREU 01B. The results hold for the full parameter space defined by all values of M_2 and $|\mu| \leq 2$ TeV with the $\widetilde{\chi}^0_1$ as LSP.

[48] AAD 20AN searched in 139 fb^{-1} of pp collisions at $\sqrt{s}$ = 13 TeV for events with two photons and missing transverse momentum. Events are further categorised in terms of lepton or jet multiplicity. No significant excess over the expected background is observed. Limits at 95% C.L. are derived in Tchi1n2E simplified models. Next-to-lightest neutralinos and charginos with masses up to 310 GeV for a massless lightest neutralino are excluded. See their Fig. 10.

[49] AAD 14G searched in 20.3 fb^{-1} of pp collisions at $\sqrt{s}$ = 8 TeV for electroweak production of chargino-neutralino pairs, decaying to a final sate with two leptons (e and μ) and missing transverse momentum. No excess beyond the Standard Model expectation is observed. Exclusion limits are derived in simplified models of chargino and next-to-lightest neutralino production, with decays to the lightest neutralino via gauge bosons, see Fig. 7. An interpretation in the pMSSM is also given, see Fig. 10.

[50] KHACHATRYAN 14I searched in 19.5 fb^{-1} of pp collisions at $\sqrt{s}$ = 8 TeV for electroweak production of charginos and neutralinos decaying to a final state with three leptons (e or μ) and missing transverse momentum, or with a Z-boson, dijets and missing transverse momentum. No excess beyond the Standard Model expectation is observed. Exclusion limits are derived in simplified models, see Figs. 12–16.

[51] AAD 12AS searched in 2.06 fb^{-1} of pp collisions at $\sqrt{s}$ = 7 TeV for charginos and neutralinos decaying to a final state with three leptons (e and μ) and missing transverse energy. No excess beyond the Standard Model expectation is observed. Exclusion limits are derived in the phenomenological MSSM, see Fig. 2 (top), and in simplified models, see Fig. 2 (bottom).

[52] AAD 12T looked in 1 fb^{-1} of pp collisions at $\sqrt{s}$ = 7 TeV for the production of supersymmetric particles decaying into final states with missing transverse momentum and exactly two isolated leptons (e or μ). Same-sign dilepton events were separately studied. Additionally, in opposite-sign events, a search was made for an excess of same-flavor over different-flavor lepton pairs. No excess over the expected background is observed and limits are placed on the effective production cross section of opposite-sign dilepton events with $\not{E}_T$ > 250 GeV and on same-sign dilepton events with $\not{E}_T$ > 100 GeV. The latter limit is interpreted in a simplified electroweak gaugino production model.

$\widetilde{\chi}^{\pm}_1, \widetilde{\chi}^{\pm}_2$ (Charginos) mass limits

Charginos are unknown mixtures of w-inos and charged higgsinos (the supersymmetric partners of W and Higgs bosons). A lower mass limit for the lightest chargino ($\widetilde{\chi}^{\pm}_1$) of approximately 45 GeV, independent of the field composition and of the decay mode, has been obtained by the LEP experiments from the analysis of the Z width and decays. These results, as well as other now superseded limits from e^+e^- collisions at energies below 136 GeV, and from hadronic collisions, can be found in the 1998 Edition (The European Physical Journal **C3** 1 (1998)) of this Review.

Unless otherwise stated, results in this section assume spectra, production rates, decay modes and branching ratios as evaluated in the MSSM, with gaugino and sfermion mass unification at the GUT scale. These papers generally study production of $\widetilde{\chi}^0_1\widetilde{\chi}^0_2$, $\widetilde{\chi}^+_1\widetilde{\chi}^-_1$ and (in the case of hadronic collisions) $\widetilde{\chi}^{\pm}_1\widetilde{\chi}^0_2$ pairs, including the effects of cascade decays. The mass limits on $\widetilde{\chi}^{\pm}_1$ are either direct, or follow indirectly from the constraints set by the non-observation of $\widetilde{\chi}^0_2$ states on the gaugino and higgsino MSSM parameters M_2 and μ. For generic values of the MSSM parameters, limits from high-energy e^+e^- collisions coincide with the highest value of the mass allowed by phase-space, namely $m_{\widetilde{\chi}^{\pm}_1} \lesssim \sqrt{s}/2$. The still unpublished combination of the results of the four LEP collaborations from the 2000 run of LEP2 at $\sqrt{s}$ up to $\simeq$ 209 GeV yields a lower mass limit of 103.5 GeV valid for general MSSM models. The limits become however weaker in certain regions of the MSSM parameter space where the detection efficiencies or production cross sections are suppressed. For example, this may happen when: (i) the mass differences $\Delta m_+ = m_{\widetilde{\chi}^{\pm}_1} - m_{\widetilde{\chi}^0_1}$ or $\Delta m_\nu = m_{\widetilde{\chi}^{\pm}_1} - m_{\widetilde{\nu}}$ are very small, and the detection efficiency is reduced; (ii) the electron sneutrino mass is small, and the $\widetilde{\chi}^{\pm}_1$ production rate is suppressed due to a destructive interference between s and t channel exchange diagrams. The regions of MSSM parameter space where the following limits are valid are indicated in the comment lines or in the footnotes.

Some earlier papers are now obsolete and have been omitted. They were last listed in our PDG 14 edition: K. Olive, *et al.* (Particle Data Group), Chinese Physics **C38** 070001 (2014) (http://pdg.lbl.gov).

VALUE (GeV)	CL%	DOCUMENT ID		TECN	COMMENT
>1170	95	[1] AAD	25BJ	ATLS	Wino pair-production, RPV λ'_{333}, $\widetilde{\chi}^0_1 \to b t \tau$, $b b \nu$ (BR 50% each) and $\widetilde{\chi}^{\pm}_1 \to b b \tau$, $b t \nu$ (BR 50% each)
> 880	95	[1] AAD	25BJ	ATLS	Higgsino pair-production, RPV λ'_{333}, $\widetilde{\chi}^0 \to b t \tau$, $b b \nu$ (BR 50% each) and $\widetilde{\chi}^{\pm}_1 \to b b \tau$, $b t \nu$ (BR 50% each)
> 380	95	[2] AAD	25M	ATLS	displaced 2ℓ; $\widetilde{\chi}^{\pm}_1$ pair production; $\widetilde{\chi}^{\pm}_1 \to W \widetilde{\chi}^0_1$; $\tau_{\widetilde{\chi}^0_1}$ = 0.3 ns, $m_{\widetilde{\chi}^{\pm}_1} - m_{\widetilde{\chi}^0_1}$ = 40 GeV
> 325	95	[3] CHEKHOVSKY	25M	CMS	$\geq$ 1 ISR jet + (in-)visible decay products X, wino-like $\widetilde{\chi}^0_2\widetilde{\chi}^{\pm}_1$ prod. with $\widetilde{\chi}^0_2 \to Z \widetilde{\chi}^0_1$, $\widetilde{\chi}^{\pm}_1 \to W \widetilde{\chi}^0_1$, $m_{\widetilde{\chi}^{\pm}_1}$ - $m_{\widetilde{\chi}^0_1}$ = 50 GeV
> 175	95	[3] CHEKHOVSKY	25M	CMS	$\geq$ 1 ISR jet + (in-)visible decay products, higgsino-like $\widetilde{\chi}^0_2\widetilde{\chi}^{\pm}_1$ prod. with $\widetilde{\chi}^0_2 \to Z \widetilde{\chi}^0_1$, $\widetilde{\chi}^{\pm}_1 \to W \widetilde{\chi}^0_1$, $m_{\widetilde{\chi}^{\pm}_1}$ - $m_{\widetilde{\chi}^0_1}$ = 10 GeV
> 300	95	[3] CHEKHOVSKY	25M	CMS	$\geq$ 1 ISR jet + X, wino-like $\widetilde{\chi}^0_2\widetilde{\chi}^{\pm}_1$ prod. with $\widetilde{\chi}^0_2 \to Z \widetilde{\chi}^0_1$, $\widetilde{\chi}^{\pm}_1 \to W \widetilde{\chi}^0_1$, 8 < $m_{\widetilde{\chi}^{\pm}_1} - m_{\widetilde{\chi}^0_1}$ < 65 GeV
> 163	95	[3] CHEKHOVSKY	25M	CMS	$\geq$ 1 ISR jet + X, higgsino-like $\widetilde{\chi}^0_2\widetilde{\chi}^{\pm}_1$ prod. with $\widetilde{\chi}^0_2 \to Z \widetilde{\chi}^0_1$, $\widetilde{\chi}^{\pm}_1 \to W \widetilde{\chi}^0_1$, 3 < $m_{\widetilde{\chi}^{\pm}_1} - m_{\widetilde{\chi}^0_1}$ < 50 GeV
> 200	95	[3] CHEKHOVSKY	25M	CMS	$\geq$ 1 ISR jet + (in-)visible decay products X, wino-like $\widetilde{\chi}^{\pm}_1$ pair production with $\widetilde{\chi}^{\pm}_1 \to W \widetilde{\chi}^0_1$, $m_{\widetilde{\chi}^{\pm}_1} - m_{\widetilde{\chi}^0_1}$ = 5 GeV
> 120	95	[3] CHEKHOVSKY	25M	CMS	$\geq$ 1 ISR jet + (in-)visible decay products X, wino-like $\widetilde{\chi}^{\pm}_1$ pair production with $\widetilde{\chi}^{\pm}_1 \to W \widetilde{\chi}^0_1$, $m_{\widetilde{\chi}^{\pm}_1} - m_{\widetilde{\chi}^0_1}$ > 5 GeV
> 490	95	[3] CHEKHOVSKY	25M	CMS	$\geq$ 1 ISR jet + (in-)visible decay products X, wino-like Tchi1chi1C, $m_{\widetilde{\chi}^{\pm}_1} - m_{\widetilde{\chi}^0_1}$ = 55 GeV
> 375	95	[4] HAYRAPETY...	25AH	CMS	3 ℓ (μ or e) + $\geq$ 2 jets, RPV Tchi1n2E with $\widetilde{\chi}^0_1 \to u d s$ or $\widetilde{\chi}^0_1 \to u d b$, $m_{\widetilde{\chi}^0_1}$ = 275 GeV
> 280	95	[4] HAYRAPETY...	25AH	CMS	3 ℓ (μ or e) + $\geq$ 2 jets, RPV Tchi1n2E with $\widetilde{\chi}^0_1 \to u d s$ or $\widetilde{\chi}^0_1 \to u d b$, $m_{\widetilde{\chi}^0_1}$ = 180 GeV
none 150–970	95	[5] AAD	24AJ	ATLS	2 hadronic τ+$\not{E}_T$, Tchi1chi1D, $m_{\widetilde{\chi}^0_1}$ = 1 GeV
>1170	95	[5] AAD	24AJ	ATLS	2 hadronic τ+$\not{E}_T$, Tchi1n2D, $m_{\widetilde{\chi}^0_1}$ = 1 GeV
none 130–330	95	[5] AAD	24AJ	ATLS	2 hadronic τ+$\not{E}_T$, Tchi1n2E, $m_{\widetilde{\chi}^0_1}$ = 1 GeV
> 117	95	[6] AAD	24CE	ATLS	0-lepton, 2 jets, large rapidity gap, Tchi1n2F, $m_{\widetilde{\chi}^0_2} = m_{\widetilde{\chi}^{\pm}_1} = m_{\widetilde{\chi}^0_1}$ + 1 GeV
> 170	95	[7] AAD	24G	ATLS	1-4 jets + $\not{E}_T$ + displaced low-p_t track, Tn1n1D, Δm ($\widetilde{\chi}^{\pm}_1$, $\widetilde{\chi}^0_1$) = 0.6 GeV
> 780	95	[8] AAD	24I	ATLS	combination, wino-like $pp \to \widetilde{\chi}^{\pm}_1\widetilde{\chi}^{\pm}_1$, $\widetilde{\chi}^{\pm}_1 \to W \widetilde{\chi}^0_1$, $m_{\widetilde{\chi}^0_1}$ = 0
>1000	95	[8] AAD	24I	ATLS	combination, wino-like $pp \to \widetilde{\chi}^0_2\widetilde{\chi}^{\pm}_1$, $\widetilde{\chi}^{\pm}_1 \to W \widetilde{\chi}^0_1$ and $\widetilde{\chi}^{\pm}_2 \to Z \widetilde{\chi}^0_1$, $m_{\widetilde{\chi}^0_1}$ < 170 GeV
>1000	95	[8] AAD	24I	ATLS	combination, wino-like Tchi1n2E, $m_{\widetilde{\chi}^0_1}$ < 200 GeV
> 850	95	[8] AAD	24I	ATLS	combination, Tn1n1D, $\widetilde{\chi}^0_1 \to Z \widetilde{G}$ or $\widetilde{\chi}^0_1 \to h \widetilde{G}$, independent of B($\widetilde{\chi}^0_1 \to h \widetilde{G}$)
> 650	95	[9] HAYRAPETY...	24M	CMS	$\geq$ 1 disappearing track+ $\not{E}_T$, pure wino $\widetilde{\chi}^0_1$ model, Δm ($\widetilde{\chi}^{\pm}_1$, $\widetilde{\chi}^0_1$) = 0.16 GeV

Int. J. Mod. Phys. A 2026.41. Downloaded from www.worldscientific.com
by UNIVERSITY OF CALIFORNIA @ BERKELEY on 09/16/26. Re-use and distribution is strictly not permitted, except for Open Access articles.

Int. J. Mod. Phys. A 2026.41. Downloaded from www.worldscientific.com
by UNIVERSITY OF CALIFORNIA @ BERKELEY on 09/16/26. Re-use and distribution is strictly not permitted, except for Open Access articles.

> 190	95	[9] HAYRAPETY...	24M	CMS	$\geq$ 1 disappearing track+ $\not{E}_T$, pure higgsino $\widetilde{\chi}^0_1$ model, Δm ($\widetilde{\chi}^\pm_1$, $\widetilde{\chi}^0_1$) = 0.3 GeV
> 875	95	[10] HAYRAPETY...	24N	CMS	Combination, Tchi1n2E1, $m_{\widetilde{\chi}^0_1}$ < 50 GeV
> 990	95	[10] HAYRAPETY...	24N	CMS	Combination, Tchi1n2E, $m_{\widetilde{\chi}^0_1}$ < 50 GeV
> 875	95	[10] HAYRAPETY...	24N	CMS	Combination, Tchi1n2l, $m_{\widetilde{\chi}^0_1}$ < 50 GeV
none 225–800	95	[10] HAYRAPETY...	24N	CMS	Combination, THinoBinoA, $m_{\widetilde{\chi}^0_1}$ < 50 GeV
> 820	95	[11] AAD	23AE	ATLS	2 SFOS ℓ, jets, $\not{E}_T$, Tchi1n2Fa, $m_{\widetilde{\chi}^0_1}$ = 1 GeV
none 260–420	95	[12] AAD	23CI	ATLS	1ℓ + jets + $\not{E}_T$, Tchi1n2J, $m_{\widetilde{\chi}^0_1}$ = 0 GeV
none 260–520	95	[12] AAD	23CI	ATLS	1ℓ + jets + $\not{E}_T$, Tchi1chi1J, $m_{\widetilde{\chi}^0_1}$ = 0 GeV
> 230	95	[13] AAD	23CI	ATLS	1ℓ + jets + $\not{E}_T$, Tchi1n2E, $m_{\widetilde{\chi}^0_2} - m_{\widetilde{\chi}^0_1}$ = 133 GeV
> 450	95	[13] AAD	23CI	ATLS	1ℓ + jets + $\not{E}_T$, Tchi1n2E, $m_{\widetilde{\chi}^0_2} - m_{\widetilde{\chi}^0_1}$ = 260 GeV
none 200–250	95	[14] AAD	23CP	ATLS	2 same-sign ℓ, Tchi1n2F, wino-bino, $m_{\widetilde{\chi}^0_1}$= 1 GeV
> 525	95	[14] AAD	23CP	ATLS	2 same-sign ℓ, Tchi1n2E, wino-bino, $m_{\widetilde{\chi}^0_1}$= 1 GeV
none 200–585	95	[15] AAD	23CR	ATLS	RPV, 2 same-sign, 3, 4 ℓ, 1, 2 b-jets, higgsino production with $\widetilde{\chi} \rightarrow b + \ell/\nu + t/b$ via λ'_{i33} coupling
none 200–670	95	[15] AAD	23CR	ATLS	RPV, 2 same-sign, 3, 4 ℓ, 1, 2 b-jets, wino production with $\widetilde{\chi} \rightarrow b + \ell/\nu + t/b$ via λ'_{i33} coupling
> 150	95	[16] AAD	23M	ATLS	2ℓ, Tchi1chi1H, $m_{\widetilde{\chi}^\pm_1} - m_{\widetilde{\chi}^0_1}$ > 110 GeV
> 104	95	[16] AAD	23M	ATLS	2ℓ, Tchi1chi1H, $m_{\widetilde{\chi}^\pm_1} - m_{\widetilde{\chi}^0_1}$ > 90 GeV
>1230	95	[17] HAYRAPETY...	23E	CMS	γ + jets + $\not{E}_T$, Tchi1n1A
>1050	95	[17] HAYRAPETY...	23E	CMS	γ + jets + $\not{E}_T$, Tchi1chi1A
none 290–670	95	[18] TUMASYAN	23B	CMS	2 AK8 jets + 2–6 AK4 jets + $\not{E}_T$, Tchi1chi1l, $m_{\widetilde{\chi}^0_1}$ = 1 GeV
none 230–760	95	[18] TUMASYAN	23B	CMS	2 AK8 jets + 2–6 AK4 jets + $\not{E}_T$, Tchi1n2Fb, $m_{\widetilde{\chi}^0_1}$ = 1 GeV
none 240–970	95	[18] TUMASYAN	23B	CMS	2 AK8 jets + 2–6 AK4 jets + $\not{E}_T$, Tchi1n2Fc, $m_{\widetilde{\chi}^0_1}$ = 1 GeV
none 300–650	95	[18] TUMASYAN	23B	CMS	2 AK8 jets + 2–6 AK4 jets +$\not{E}_T$, THinoBinoA, $m_{\widetilde{\chi}^0_1}$ = 1 GeV
> 275	95	[19] TUMASYAN	22Q	CMS	2 or 3 ℓ (soft), $\not{E}_T$; Tchi1n2F, wino-bino, $m_{\widetilde{\chi}^0_2} - m_{\widetilde{\chi}^0_1}$= 10 GeV
> 205	95	[19] TUMASYAN	22Q	CMS	2 or 3 ℓ (soft), $\not{E}_T$; higgsino model with $\widetilde{\chi}^0_2\,\widetilde{\chi}^\pm_1$ and $\widetilde{\chi}^0_2\,\widetilde{\chi}^0_1$ prod., $m_{\widetilde{\chi}^0_2} - m_{\widetilde{\chi}^0_1}$ = 7.5 GeV
> 150	95	[19] TUMASYAN	22Q	CMS	2 or 3 ℓ (soft), $\not{E}_T$; higgsino model with $\widetilde{\chi}^0_2\,\widetilde{\chi}^\pm_1$ and $\widetilde{\chi}^0_2\,\widetilde{\chi}^0_1$ prod., $m_{\widetilde{\chi}^0_2} - m_{\widetilde{\chi}^0_1}$ = 3 GeV
>1450	95	[20] TUMASYAN	22S	CMS	2 same-sign e or μ, 3 or 4 leptons, Tchi1n2B (flavor-democratic), $m_{\widetilde{\ell}} = 1/2(m_{\widetilde{\chi}^\pm_1} + m_{\widetilde{\chi}^0_1})$, $m_{\widetilde{\chi}^0_1}$ = 850 GeV
>1360	95	[20] TUMASYAN	22S	CMS	2 same-sign e or μ, 3 or 4 leptons, Tchi1n2B (flavor-democratic), $m_{\widetilde{\ell}} = 1/2(m_{\widetilde{\chi}^\pm_1} + m_{\widetilde{\chi}^0_1})$, $m_{\widetilde{\chi}^0_1}$ = 0 GeV
>1290	95	[20] TUMASYAN	22S	CMS	2 same-sign e or μ, 3 or 4 leptons, Tchi1n2B (flavor-democratic), $m_{\widetilde{\ell}} = 0.05 m_{\widetilde{\chi}^\pm_1} + 0.95 m_{\widetilde{\chi}^0_1}$, $m_{\widetilde{\chi}^0_1}$ = 0 GeV
>1440	95	[20] TUMASYAN	22S	CMS	2 same-sign e or μ, 3 or 4 leptons, Tchi1n2B (flavor-democratic), $m_{\widetilde{\ell}} = 0.95 m_{\widetilde{\chi}^\pm_1} + 0.05 m_{\widetilde{\chi}^0_1}$, $m_{\widetilde{\chi}^0_1}$ = 0 GeV
>1140	95	[20] TUMASYAN	22S	CMS	2 same-sign e or μ, 3 or 4 leptons, Tchi1n2B (lepton in $\widetilde{\chi}^\pm_1$ decay is τ), $m_{\widetilde{\ell}} = 1/2(m_{\widetilde{\chi}^\pm_1} + m_{\widetilde{\chi}^0_1})$, $m_{\widetilde{\chi}^0_1}$ = 0 GeV
>1110	95	[20] TUMASYAN	22S	CMS	2 same-sign e or μ, 3 or 4 leptons, Tchi1n2B (lepton in $\widetilde{\chi}^\pm_1$ decay is τ), $m_{\widetilde{\ell}} = 0.05 m_{\widetilde{\chi}^\pm_1} + 0.95 m_{\widetilde{\chi}^0_1}$, $m_{\widetilde{\chi}^0_1}$ = 0 GeV
>1140	95	[20] TUMASYAN	22S	CMS	2 same-sign e or μ, 3 or 4 leptons, Tchi1n2B (lepton in $\widetilde{\chi}^\pm_1$ decay is τ), $m_{\widetilde{\ell}} = 0.95 m_{\widetilde{\chi}^\pm_1} + 0.05 m_{\widetilde{\chi}^0_1}$, $m_{\widetilde{\chi}^0_1}$ = 0 GeV
> 980	95	[20] TUMASYAN	22S	CMS	2 same-sign e or μ, 3 or 4 leptons, Tchi1n2B (leptons in $\widetilde{\chi}^\pm_1$ and $\widetilde{\chi}^0_2$ decays are τ), $m_{\widetilde{\ell}} = 1/2(m_{\widetilde{\chi}^\pm_1} + m_{\widetilde{\chi}^0_1})$, $m_{\widetilde{\chi}^0_1}$ = 0 GeV
> 905	95	[20] TUMASYAN	22S	CMS	2 same-sign e or μ, 3 or 4 leptons, Tchi1n2B (leptons in $\widetilde{\chi}^\pm_1$ and $\widetilde{\chi}^0_2$ decays are τ), $m_{\widetilde{\ell}} = 0.05 m_{\widetilde{\chi}^\pm_1} + 0.95 m_{\widetilde{\chi}^0_1}$, $m_{\widetilde{\chi}^0_1}$ = 0 GeV
> 875	95	[20] TUMASYAN	22S	CMS	2 same-sign e or μ, 3 or 4 leptons, Tchi1n2B (leptons in $\widetilde{\chi}^\pm_1$ and $\widetilde{\chi}^0_2$ decays are τ), $m_{\widetilde{\ell}} = 0.95 m_{\widetilde{\chi}^\pm_1} + 0.05 m_{\widetilde{\chi}^0_1}$, $m_{\widetilde{\chi}^0_1}$ = 0 GeV
> 650	95	[20] TUMASYAN	22S	CMS	2 same-sign e or μ, 3 or 4 leptons, Tchi1n2F, $m_{\widetilde{\chi}^0_1}$ = 0 GeV
> 260	95	[20] TUMASYAN	22S	CMS	2 same-sign e or μ, 3 or 4 leptons, Tchi1n2E, $m_{\widetilde{\chi}^0_1}$ = 0 GeV
>1080	95	[21] AAD	21AX	ATLS	jets + large-R jets + $\not{E}_T$, TWinoBinoA, nearly independent of B($\widetilde{\chi}^0_2 \rightarrow Z\widetilde{\chi}^0_1$), $m_{\widetilde{\chi}^0_1}$ = 0 GeV
>1060	95	[21] AAD	21AX	ATLS	jets + large-R jets + $\not{E}_T$, TWinoHinoA, tan β = 10, μ > 0, $m_{\widetilde{\chi}^0_1}$ = 0 GeV
> 900	95	[21] AAD	21AX	ATLS	jets + large-R jets + $\not{E}_T$, THinoBinoA, nearly independent of B($\widetilde{\chi}^0_2 \rightarrow Z\widetilde{\chi}^0_1$), $m_{\widetilde{\chi}^0_1}$ = 0 GeV
> 900	95	[21] AAD	21AX	ATLS	jets + large-R jets + $\not{E}_T$, THinoWinoA, tan β = 10, μ > 0, $m_{\widetilde{\chi}^0_1}$ = 0 GeV
>1060	95	[21] AAD	21AX	ATLS	jets + large-R jets + $\not{E}_T$, Tchi1n2E, full hadronic final state, $m_{\widetilde{\chi}^0_1}$ = 0 GeV
> 960	95	[21] AAD	21AX	ATLS	jets + large-R jets + $\not{E}_T$, Tchi1n2Fb, $m_{\widetilde{\chi}^0_1}$ = 0 GeV
none 620–740	95	[21] AAD	21AX	ATLS	jets + large-R jets + $\not{E}_T$, Tchi1chi1l, $m_{\widetilde{\chi}^0_1}$ = 0 GeV
> 640	95	[22] AAD	21BG	ATLS	3ℓ+ $\not{E}_T$, Tchi1n2F, wino cross section, $m_{\widetilde{\chi}^0_1}$ = 0 GeV
> 300	95	[22] AAD	21BG	ATLS	3ℓ+ $\not{E}_T$, Tchi1n2F, wino cross section, $m_{\widetilde{\chi}^0_2} - m_{\widetilde{\chi}^0_1} = m_Z$
> 240	95	[22] AAD	21BG	ATLS	3ℓ+ $\not{E}_T$, Tchi1n2F, wino cross section, $m_{\widetilde{\chi}^0_2} - m_{\widetilde{\chi}^0_1}$ = 10 GeV
> 190	95	[22] AAD	21BG	ATLS	3ℓ+ $\not{E}_T$, Tchi1n2E, wino cross section, $m_{\widetilde{\chi}^0_1}$ = 0 GeV
>1100	95	[23] AAD	21E	ATLS	3ℓ, $Z\ell$ resonances, TwinoL-SPBL, RPV, B($\widetilde{\chi}^\pm_1 \rightarrow Z e$) = B($\widetilde{\chi}^0_1 \rightarrow Z\nu$) = 1
>1050	95	[23] AAD	21E	ATLS	3ℓ, $Z\ell$ resonances, TwinoL-SPBL, RPV, B($\widetilde{\chi}^\pm_1 \rightarrow Z\mu$) = B($\widetilde{\chi}^0_1 \rightarrow Z\nu$) = 1
> 625	95	[23] AAD	21E	ATLS	3ℓ, $Z\ell$ resonances, TwinoL-SPBL, RPV, B($\widetilde{\chi}^\pm_1 \rightarrow Z\tau$) = B($\widetilde{\chi}^0_1 \rightarrow Z\nu$) = 1
> 975	95	[23] AAD	21E	ATLS	3ℓ, $Z\ell$ resonances, TwinoL-SPBL, RPV, B($\widetilde{\chi}^\pm_1 \rightarrow Z\ell$) = B($\widetilde{\chi}^0_1 \rightarrow Z\nu$) = 1 and ℓ = e,μ,τ
>1600	95	[24] AAD	21Y	ATLS	$\geq$ 4ℓ, RPV Tchi1n2l with $\widetilde{\chi}^0_1 \rightarrow \ell^\pm\ell^\mp\nu$, $\lambda_{12k} \neq 0$, $m_{\widetilde{\chi}^0_1}$ = 1200 GeV
>1100	95	[24] AAD	21Y	ATLS	$\geq$ 4ℓ, RPV Tchi1n2l with $\widetilde{\chi}^0_1 \rightarrow \ell^\pm\ell^\mp\nu$, $\lambda_{i33} \neq 0$, $m_{\widetilde{\chi}^0_1}$ = 1000 GeV

Int. J. Mod. Phys. A 2026.41. Downloaded from www.worldscientific.com
by UNIVERSITY OF CALIFORNIA @ BERKELEY on 09/16/26. Re-use and distribution is strictly not permitted, except for Open Access articles.

> 750	95	[25] SIRUNYAN	21M	CMS	$\ell^\pm\ell^\mp + \not{E}_T$, Tchi1n2Fa, $m_{\widetilde{\chi}^0_1} <$ 100 GeV
none 400–820	95	[26] TUMASYAN	21C	CMS	1 $\ell^\pm$ + 2b-jets + $\not{E}_T$, Tchi1n2E, $\widetilde{\chi}^0_1 = 200$ GeV
none 160–820	95	[26] TUMASYAN	21C	CMS	1 $\ell^\pm$ + 2b-jets + $\not{E}_T$, Tchi1n2E, $\widetilde{\chi}^0_1 = 0$ GeV
> 380	95	[27] AAD	20AN	ATLS	2γ + $\not{E}_T$,Tn1n1A, GMSB
> 240	95	[28] AAD	20I	ATLS	2ℓ (soft), jets, $\not{E}_T$; Tchi1n2Fa, wino, $m_{\widetilde{\chi}^\pm_1} - m_{\widetilde{\chi}^0_1} = 7$ GeV
> 345	95	[29] AAD	20K	ATLS	3ℓ+$\not{E}_T$, Tchi1n2F, $m_{\widetilde{\chi}^0_1} = 0$ GeV
> 420	95	[30] AAD	20O	ATLS	2ℓ+$\not{E}_T$, Tchi1chi1H, $m_{\widetilde{\chi}^0_1}$=0 GeV
>1000	95	[31] AAD	20O	ATLS	2ℓ+$\not{E}_T$, Tchi1chi1C, $m_{\widetilde{\chi}^0_1}$=0 GeV
> 740	95	[32] AAD	20R	ATLS	1ℓ + 2b-jets + $\not{E}_T$, Tchi1n2E, $m_{\widetilde{\chi}^0_1} = 0$ GeV
> 290	95	[33] SIRUNYAN	20AU	CMS	soft τ + jet + $\not{E}_T$, Tchi1n2D, wino, $m_{\widetilde{\chi}^\pm_1} - m_{\widetilde{\chi}^0_1} = 50$ GeV
>1050	95	[34] SIRUNYAN	20B	CMS	$\geq 1\gamma + \not{E}_T$, Tchi1chi1F, $\widetilde{\chi}^0_1 \rightarrow \gamma\widetilde{G}$
> 825	95	[34] SIRUNYAN	20B	CMS	$\geq 1\gamma + \not{E}_T$, Tchi1chi1G, $\widetilde{\chi}^\pm_1 \rightarrow \widetilde{\chi}^0_1$ + soft
> 840	95	[34] SIRUNYAN	20B	CMS	$\geq 1\gamma + \not{E}_T$, Tchi1n12-GGM, 120 GeV $< m_{\widetilde{\chi}^0_1} <$ 720 GeV
> 680	95	[35] AABOUD	19AU	ATL	0, 1, 2 or more ℓ, H ($\rightarrow \gamma\gamma$, bb, WW^*, ZZ^*,$\tau\tau$) (various searches), Tchi1n2E, $m_{\widetilde{\chi}^0_1}$=0 GeV
> 112	95	[36] SIRUNYAN	19BU	CMS	$pp \rightarrow \widetilde{\chi}^+_1\widetilde{\chi}^0_2$+2 jets, $\widetilde{\chi}^+_1 \rightarrow \ell^+\nu\widetilde{\chi}^0_1$, heavy sleptons, $m_{\widetilde{\chi}^+_1} - m_{\widetilde{\chi}^0_1} = 1$ GeV, $m_{\widetilde{\chi}^+_1} = m_{\widetilde{\chi}^0_2}$
> 215	95	[36] SIRUNYAN	19BU	CMS	$pp \rightarrow \widetilde{\chi}^+_1\widetilde{\chi}^0_2$ + 2 jets, $\widetilde{\chi}^+_1 \rightarrow \ell^+\nu\widetilde{\chi}^0_1$, heavy sleptons, $m_{\widetilde{\chi}^+_1} - m_{\widetilde{\chi}^0_1} = 30$ GeV, $m_{\widetilde{\chi}^+_1} = m_{\widetilde{\chi}^0_2}$
> 235	95	[37] SIRUNYAN	19CI	CMS	≥ 1 H ($\rightarrow \gamma\gamma$) + jets + $\not{E}_T$, Tchi1n2E, $m_{\widetilde{\chi}^0_1} = 1$ GeV
> 930	95	[38] SIRUNYAN	19K	CMS	γ + lepton + $\not{E}_T$, Tchi1n1A
> 630	95	[39] AABOUD	18AY	ATLS	2τ+$\not{E}_T$, Tchi1chi1D and $\widetilde{\tau}_L$-only, $m_{\widetilde{\chi}^0_1} = 0$ GeV
> 760	95	[40] AABOUD	18AY	ATLS	2τ+$\not{E}_T$, Tchi1n2D and $\widetilde{\tau}_L$-only, $m_{\widetilde{\chi}^0_1} = 0$ GeV
> 740	95	[41] AABOUD	18BT	ATLS	2ℓ+$\not{E}_T$, Tchi1chi1C, $m_{\widetilde{\chi}^0_1}$=0 GeV
>1125	95	[42] AABOUD	18BT	ATLS	2,3ℓ+$\not{E}_T$, Tchi1n2C, $m_{\widetilde{\chi}^0_1}$=0 GeV
> 580	95	[43] AABOUD	18BT	ATLS	2,3ℓ+$\not{E}_T$, Tchi1n2F, $m_{\widetilde{\chi}^0_1}$=0 GeV
none 130–230, 290–880	95	[44] AABOUD	18CK	ATLS	2H ($\rightarrow bb$)+$\not{E}_T$,Tn1n1A, GMSB
none 220–600	95	[45] AABOUD	18CO	ATLS	2,3ℓ + $\not{E}_T$, recursive jigsaw, Tchi1n2F, $m_{\widetilde{\chi}^0_1} = 0$ GeV
> 175	95	[46] AABOUD	18R	ATLS	2ℓ (soft) + $\not{E}_T$, Tchi1n2F, wino, $m_{\widetilde{\chi}^\pm_1} - m_{\widetilde{\chi}^0_1} = 10$ GeV
> 145	95	[47] AABOUD	18R	ATLS	2ℓ (soft) + $\not{E}_T$, Tchi1n2G, higgsino, $m_{\widetilde{\chi}^\pm_1} - m_{\widetilde{\chi}^0_1} = 5$ GeV
>1060	95	[48] AABOUD	18U	ATLS	2γ + $\not{E}_T$, GGM, Tchi1chi1A, any NLSP mass
>1400	95	[49] AABOUD	18Z	ATLS	$\geq 4\ell$, RPV, $\lambda_{12k} \neq 0$, $m_{\widetilde{\chi}^0_1} >$ 500 GeV
>1320	95	[49] AABOUD	18Z	ATLS	$\geq 4\ell$, RPV, $\lambda_{12k} \neq 0$, $m_{\widetilde{\chi}^0_1} >$ 50 GeV
> 980	95	[49] AABOUD	18Z	ATLS	$\geq 4\ell$, RPV, $\lambda_{i33} \neq 0$, 400 GeV $< m_{\widetilde{\chi}^0_1} <$ 700 GeV
> 980	95	[50] SIRUNYAN	18AA	CMS	$\geq 1\gamma + \not{E}_T$, GGM, wino-like $\widetilde{\chi}^0_2\widetilde{\chi}^\pm_1$ pair production, nearly degenerate wino and bino masses
> 780	95	[50] SIRUNYAN	18AA	CMS	$\geq 1\gamma + \not{E}_T$, Tchi1n1A
> 950	95	[50] SIRUNYAN	18AA	CMS	$\geq 1\gamma + \not{E}_T$, Tchi1chi1A
> 230	95	[51] SIRUNYAN	18AJ	CMS	2ℓ (soft) + $\not{E}_T$, Tchi1n2F, wino, $m_{\widetilde{\chi}^0_2} - m_{\widetilde{\chi}^0_1} = 20$ GeV
>1150	95	[52] SIRUNYAN	18AO	CMS	$\ell^\pm\ell^\pm$ or $\geq 3\ell$, Tchi1n2A, $m_{\widetilde{\ell}} = m_{\widetilde{\nu}} = m_{\widetilde{\chi}^0_1}$+ 0.5 ($m_{\widetilde{\chi}^\pm_1} - m_{\widetilde{\chi}^0_1}$), $m_{\widetilde{\chi}^0_1} = 0$ GeV
>1120	95	[52] SIRUNYAN	18AO	CMS	$\ell^\pm\ell^\pm$ or $\geq 3\ell$, Tchi1n2A, $m_{\widetilde{\ell}} = m_{\widetilde{\nu}} = m_{\widetilde{\chi}^0_1}$+ 0.05 ($m_{\widetilde{\chi}^\pm_1} - m_{\widetilde{\chi}^0_1}$), $m_{\widetilde{\chi}^0_1} = 0$ GeV
>1050	95	[52] SIRUNYAN	18AO	CMS	$\ell^\pm\ell^\pm$ or $\geq 3\ell$, Tchi1n2A, $m_{\widetilde{\ell}} = m_{\widetilde{\nu}} = m_{\widetilde{\chi}^0_1}$+ 0.95 ($m_{\widetilde{\chi}^\pm_1} - m_{\widetilde{\chi}^0_1}$), $m_{\widetilde{\chi}^0_1} = 0$ GeV
>1080	95	[52] SIRUNYAN	18AO	CMS	$\ell^\pm\ell^\pm$ or $\geq 3\ell$, Tchi1n2H, $m_{\widetilde{\ell}} = m_{\widetilde{\chi}^0_1}$+ 0.5 ($m_{\widetilde{\chi}^\pm_1} - m_{\widetilde{\chi}^0_1}$), $m_{\widetilde{\chi}^0_1} = 0$ GeV
>1030	95	[52] SIRUNYAN	18AO	CMS	$\ell^\pm\ell^\pm$ or $\geq 3\ell$, Tchi1n2H, $m_{\widetilde{\ell}} = m_{\widetilde{\chi}^0_1}$+ 0.05 ($m_{\widetilde{\chi}^\pm_1} - m_{\widetilde{\chi}^0_1}$), $m_{\widetilde{\chi}^0_1} = 0$ GeV
>1050	95	[52] SIRUNYAN	18AO	CMS	$\ell^\pm\ell^\pm$ or $\geq 3\ell$, Tchi1n2H, $m_{\widetilde{\ell}} = m_{\widetilde{\chi}^0_1}$+ 0.95 ($m_{\widetilde{\chi}^\pm_1} - m_{\widetilde{\chi}^0_1}$), $m_{\widetilde{\chi}^0_1} = 0$ GeV
> 625	95	[52] SIRUNYAN	18AO	CMS	$\ell^\pm\ell^\pm$ or $\geq 3\ell$, Tchi1n2D, $m_{\widetilde{\tau}} = m_{\widetilde{\chi}^0_1}$+ 0.5 ($m_{\widetilde{\chi}^\pm_1} - m_{\widetilde{\chi}^0_1}$), $m_{\widetilde{\chi}^0_1} = 0$ GeV
> 180	95	[52] SIRUNYAN	18AO	CMS	$\ell^\pm\ell^\pm$ or $\geq 3\ell$, Tchi1n2E, $m_{\widetilde{\chi}^0_1}$ = 0 GeV
> 450	95	[52] SIRUNYAN	18AO	CMS	$\ell^\pm\ell^\pm$ or $\geq 3\ell$, Tchi1n2F, $m_{\widetilde{\chi}^0_1}$ = 0 GeV
> 480	95	[53] SIRUNYAN	18AP	CMS	Combination of searches, Tchi1n2E, $m_{\widetilde{\chi}^0_1} = 0$ GeV
> 650	95	[53] SIRUNYAN	18AP	CMS	Combination of searches, Tchi1n2F, $m_{\widetilde{\chi}^0_1} = 0$ GeV
> 535	95	[53] SIRUNYAN	18AP	CMS	Combination of searches, Tchi1n2l, $m_{\widetilde{\chi}^0_1} = 0$ GeV
none 160–610	95	[54] SIRUNYAN	18AR	CMS	$\ell^\pm\ell^\mp$ + jets + $\not{E}_T$, Tchi1n2F, $m_{\widetilde{\chi}^0_1} = 0$ GeV
none 170–200	95	[55] SIRUNYAN	18DN	CMS	$\ell^\pm\ell^\mp$, Tchi1chi1E, $m_{\widetilde{\chi}^0_1} = 1$ GeV
> 810	95	[55] SIRUNYAN	18DN	CMS	$\ell^\pm\ell^\mp$, Tchi1chi1C, $m_{\widetilde{\chi}^0_1} = 0$ GeV
> 630	95	[56] SIRUNYAN	18DP	CMS	2τ+$\not{E}_T$, Tchi1chi1D,$m_{\widetilde{\chi}^0_1}$=0 GeV
> 710	95	[56] SIRUNYAN	18DP	CMS	2τ+$\not{E}_T$, Tchi1n2D, $m_{\widetilde{\chi}^0_1} = 0$ GeV
> 170	95	[57] SIRUNYAN	18X	CMS	≥ 1 H ($\rightarrow \gamma\gamma$) + jets + $\not{E}_T$, Tchi1n2E, $m_{\widetilde{\chi}^0_1} <$ 25 GeV
> 420	95	[58] KHACHATRY...	17L	CMS	2τ+$\not{E}_T$, Tchi1chi1C and $\widetilde{\tau}$-only, $m_{\widetilde{\chi}^0_1}$=0 GeV
none 220–490	95	[59] SIRUNYAN	17AW	CMS	1ℓ + 2b-jets + $\not{E}_T$, Tchi1n2E, $m_{\widetilde{\chi}^0_1} = 0$ GeV
> 500	95	[60] AAD	16AA	ATLS	2$\ell^\pm$+$\not{E}_T$,Tchi1chi1B,$m_{\widetilde{\chi}^0_1}$=0 GeV
> 220	95	[60] AAD	16AA	ATLS	2$\ell^\pm$+$\not{E}_T$, Tchi1chi1C, low Δm for $\widetilde{\chi}^\pm_1$, $\widetilde{\chi}^0_1$
> 700	95	[61] AAD	16AA	ATLS	3,4ℓ+$\not{E}_T$,Tchi1n2B, $m_{\widetilde{\chi}^0_1}$=0 GeV
> 700	95	[61] AAD	16AA	ATLS	3,4ℓ+$\not{E}_T$, Tchi1n2C, $m_{\widetilde{\ell}} = m_{\widetilde{\chi}^0_1}$+ 0.5 (or 0.95) ($m_{\widetilde{\chi}^\pm_1} - m_{\widetilde{\chi}^0_1}$)
> 400	95	[61] AAD	16AA	ATLS	2 hadronic τ+$\not{E}_T$ & 3ℓ+$\not{E}_T$ combination,Tchi1n2D,$m_{\widetilde{\chi}^0_1}$=0 GeV
> 540	95	[62] KHACHATRY...	16R	CMS	$\geq 1\gamma + 1$ e or $\mu + \not{E}_T$, Tchi1n1A
> 250	95	[63] AAD	15BA	ATLS	$m_{\widetilde{\chi}^\pm_1} = m_{\widetilde{\chi}^0_2}$, $m_{\widetilde{\chi}^0_1} = 0$ GeV
> 590	95	[64] AAD	15CA	ATLS	$\geq 2\ \gamma + \not{E}_T$, GGM, bino-like NLSP, any NLSP mass
none 124–361	95	[64] AAD	15CA	ATLS	$\geq 1\ \gamma$ + e,μ + $\not{E}_T$, GGM, wino-like NLSP
> 700	95	[65] AAD	14H	ATLS	$\widetilde{\chi}^\pm_1\widetilde{\chi}^0_2 \rightarrow \ell^\pm\nu\widetilde{\chi}^0_1\ell^\pm\ell^\mp\widetilde{\chi}^0_1$, simplified model, $m_{\widetilde{\chi}^\pm_1} = m_{\widetilde{\chi}^0_2}$, $m_{\widetilde{\chi}^0_1} = 0$ GeV
> 345	95	[65] AAD	14H	ATLS	$\widetilde{\chi}^\pm_1\widetilde{\chi}^0_2 \rightarrow W\widetilde{\chi}^0_1 Z\widetilde{\chi}^0_1$, simplified model, $m_{\widetilde{\chi}^\pm_1} = m_{\widetilde{\chi}^0_2}$, $m_{\widetilde{\chi}^0_1} =$ 0 GeV
> 148	95	[65] AAD	14H	ATLS	$\widetilde{\chi}^\pm_1\widetilde{\chi}^0_2 \rightarrow W\widetilde{\chi}^0_1 H\widetilde{\chi}^0_1$, simplified model, $m_{\widetilde{\chi}^\pm_1} = m_{\widetilde{\chi}^0_2}$, $m_{\widetilde{\chi}^0_1} =$ 0 GeV

Int. J. Mod. Phys. A 2026.41. Downloaded from www.worldscientific.com
by UNIVERSITY OF CALIFORNIA @ BERKELEY on 09/16/26. Re-use and distribution is strictly not permitted, except for Open Access articles.

$>$ 380	95	[65] AAD	14H	ATLAS	$\widetilde{\chi}^{\pm}_1\widetilde{\chi}^0_2 \rightarrow \tau^{\pm}\nu\widetilde{\chi}^0_1\tau^{\pm}\tau^{\mp}\widetilde{\chi}^0_1$, simplified model, $m_{\widetilde{\chi}^{\pm}_1} = m_{\widetilde{\chi}^0_2}$, $m_{\widetilde{\chi}^0_1} = 0$ GeV	
$>$ 750	95	[66] AAD	14X	ATLAS	RPV, $\geq 4\ell^{\pm}$, $\widetilde{\chi}^{\pm}_1 \rightarrow W^{(*)\pm}\widetilde{\chi}^0_1$, $\widetilde{\chi}^0_1 \rightarrow \ell^{\pm}\ell^{\mp}\nu$	
$>$ 210	95	[67] KHACHATRY...14L		CMS	$\widetilde{\chi}^0_2 \rightarrow H\widetilde{\chi}^0_1$ and $\widetilde{\chi}^{\pm}_1 \rightarrow W^{\pm}\widetilde{\chi}^0_1$ simplified models, $m_{\widetilde{\chi}^0_2} = m_{\widetilde{\chi}^{\pm}_1}$, $m_{\widetilde{\chi}^0_1} = 0$ GeV	
		[68] AAD	13	ATLAS	$3\ell^{\pm} + \not{E}_T$, pMSSM, SMS	
		[69] AAD	13B	ATLAS	$2\ell^{\pm} + \not{E}_T$, pMSSM, SMS	
$>$ 540	95	[70] AAD	12CT	ATLAS	$\geq 4\ell^{\pm}$, RPV, $m_{\widetilde{\chi}^0_1} > 300$ GeV	
		[71] CHATRCHYAN	12BJ	CMS	$\geq 2\ \ell$, jets $+ \not{E}_T$, $pp \rightarrow \widetilde{\chi}^{\pm}_1\widetilde{\chi}^0_2$	
$>$ 94	95	[72] ABDALLAH	03M	DLPH	$\widetilde{\chi}^{\pm}_1$, $\tan\beta \leq 40$, $\Delta m_+ > 3$ GeV,all m_0	
• • • We do not use the following data for averages, fits, limits, etc. • • •						
$>$ 310	95	[73] AAD	20AN	ATLAS	$2\gamma + \not{E}_T$, Tchi1n2E, $m_{\widetilde{\chi}^0_1}$=0 GeV	
$>$ 570	95	[74] KHACHATRY...16AA		CMS	$\geq 1\gamma$ + jets $+ \not{E}_T$, Tchi1chi1A	
$>$ 680	95	[74] KHACHATRY...16AA		CMS	$\geq 1\gamma$ + jets $+ \not{E}_T$, Tchi1n1A	
$>$ 710	95	[74] KHACHATRY...16AA		CMS	$\geq 1\gamma$ + jets $+ \not{E}_T$, GGM, $\widetilde{\chi}^0_2\widetilde{\chi}^{\pm}_1$ pair production, wino-like NLSP	
$>$1000	95	[75] KHACHATRY...16R		CMS	$\geq 1\gamma + 1\ e$ or $\mu + \not{E}_T$, Tglu1F, $m_{\widetilde{\chi}^{\pm}_1} = m_{\widetilde{\chi}^0_2} > 200$ GeV	
$>$ 307	95	[76] KHACHATRY...16Y		CMS	1,2 soft $\ell^{\pm}$+jets+$\not{E}_T$, Tchi1n2A, $m_{\widetilde{\chi}^{\pm}_1} - m_{\widetilde{\chi}^0_1}$=20 GeV	
$>$ 410	95	[77] AAD	14AV	ATLAS	$\geq 2\ \tau + \not{E}_T$, direct $\widetilde{\chi}^{\pm}_1\widetilde{\chi}^0_2$, $\widetilde{\chi}^{\pm}_1\widetilde{\chi}^{\mp}_1$ production, $m_{\widetilde{\chi}^0_2} = m_{\widetilde{\chi}^{\pm}_1}$, $m_{\widetilde{\chi}^0_1} = 0$ GeV	
$>$ 345	95	[78] AAD	14AV	ATLAS	$\geq 2\ \tau + \not{E}_T$, direct $\widetilde{\chi}^{\pm}_1\widetilde{\chi}^{\mp}_1$ production, $m_{\widetilde{\chi}^0_1} = 0$ GeV	
none 100–105, 120–135, 145–160	95	[79] AAD	14G	ATLAS	$\widetilde{\chi}^{\pm}_1\widetilde{\chi}^{\mp}_1 \rightarrow W^+\widetilde{\chi}^0_1 W^-\widetilde{\chi}^0_1$, simplified model, $m_{\widetilde{\chi}^0_1} = 0$ GeV	
none 140–465	95	[79] AAD	14G	ATLAS	$\widetilde{\chi}^{\pm}_1\widetilde{\chi}^{\mp}_1 \rightarrow \ell^+\nu\widetilde{\chi}^0_1\ell^-\overline{\nu}\widetilde{\chi}^0_1$, simplified model, $m_{\widetilde{\chi}^0_1} = 0$ GeV	
none 180–355	95	[79] AAD	14G	ATLAS	$\widetilde{\chi}^{\pm}_1\widetilde{\chi}^0_2 \rightarrow W\widetilde{\chi}^0_1 Z\widetilde{\chi}^0_1$, simplified model, $m_{\widetilde{\chi}^{\pm}_1} = m_{\widetilde{\chi}^0_2}$, $m_{\widetilde{\chi}^0_1} = 0$ GeV	
$>$ 168	95	[80] AALTONEN	14	CDF	$3\ell^{\pm} + \not{E}_T$, $\widetilde{\chi}^{\pm}_1 \rightarrow \ell\nu\widetilde{\chi}^0_1$, mSUGRA with m_0=60 GeV	
		[81] KHACHATRY...14I		CMS	$\widetilde{\chi}^{\pm}_1 \rightarrow W\widetilde{\chi}^0_1$, $\ell\widetilde{\nu}$, $\widetilde{\ell}\nu$, simplified model	
		[82] AALTONEN	13Q	CDF	$\widetilde{\chi}^{\pm}_1 \rightarrow \tau X$, simplified gravity- and gauge-mediated models	
		[83] AAD	12AS	ATLAS	$3\ell^{\pm} + \not{E}_T$, pMSSM	
		[84] AAD	12T	ATLAS	$\ell^{\pm}\ell^{\mp} + \not{E}_T$, $\ell^{\pm}\ell^{\pm} + \not{E}_T$, $pp \rightarrow \widetilde{\chi}^{\pm}_1\widetilde{\chi}^0_2$	
		[85] CHATRCHYAN	11B	CMS	$\widetilde{W}^0 \rightarrow \gamma\widetilde{G}$,$\widetilde{W}^{\pm} \rightarrow \ell^{\pm}\widetilde{G}$,GMSB	
$>$ 163	95	[86] CHATRCHYAN	11V	CMS	$\tan\beta$=3, m_0=60 GeV, A_0=0, $\mu > 0$	

[1] AAD 25BJ searched in 140 fb^{-1} of pp collisions at $\sqrt{s}$ = 13 TeV for an excess of 0-lepton events with at least one hadronically decaying τ and at least 3 b-jet. The search is performed by training a neural network to separate a signal of vector-like leptons from the Standard Model background. No significant excess above the Standard Model expectations is observed. Limits are set also in a model of SUSY, where members of either a higgsino LSP triplet or a wino LSP doublet are produced, and decay via a RPV λ'_{333} coupling to b, t quarks and τ, ν_τ leptons, see their Figs. 13 and 14.

[2] AAD 25M searched for an excess of displaced leptons (e or μ) in pp collisions (140 fb^{-1} at $\sqrt{s}$ = 13 TeV and 56.3 at fb^{-1} at $\sqrt{s}$ = 13.6 TeV). The models considered were long-lived slepton (electron or muon) pair production followed by $\widetilde{\ell} \rightarrow \ell\widetilde{G}$, and long-lived chargino pair production in a dark sector model, followed by $\widetilde{\chi}^{\pm}_1 \rightarrow \widetilde{\chi}^0_1 W$. Displaced leptons were reconstructed thanks to an improved large radius tracking and to the pointing capabilities of the electromagnetic calorimeter. Two different analyses (ABCD and EM-BDT) are combined to obtain limits on $\widetilde{e}$ pair production, while the ABCD analysis only is used for $\widetilde{\mu}$, $\widetilde{\tau}$ and $\widetilde{\chi}^{\pm}_1$ pair production. No significant excess of events is observed over the background prediction. 95% CL limits are extracted in the lifetime vs mass plane, see their figures 6 and 8.

[3] CHEKHOVSKY 25M searched in 138 fb^{-1} of pp collisions at $\sqrt{s}$ = 13 TeV for evidence of SUSY models with compressed mass spectra in events with a high transverse momentum system from initial-state-radiation jets recoiling against a potential sparticle system with significant missing transverse momentum. These events are further categorized based on their lepton multiplicity, jet multiplicity, number of b-tagged jets, and kinematic variables sensitive to the sparticle masses and mass splittings. No significant excess above the Standard Model expectations is observed. The results are interpreted in models of top squark, electroweakino and slepton pair production. Limits are set for top squark pair production in the models Tstop1 and Tstop2, see their figure 25, and in Tstop4, see their figure 26. The results are also interpreted in models describing the production of mass-degenerate $\widetilde{\chi}^0_2$ and $\widetilde{\chi}^{\pm}_1$ with decays $\widetilde{\chi}^0_2 \rightarrow Z\widetilde{\chi}^0_1$ and $\widetilde{\chi}^{\pm}_1 \rightarrow W\widetilde{\chi}^0_1$, applying both a wino-like and higgsino-like $\widetilde{\chi}^{\pm}_1\widetilde{\chi}^0_2$ production cross section, see their figure 27. Limits are also set for wino-like $\widetilde{\chi}^{\pm}_1$ pair production, either with $\widetilde{\chi}^{\pm}_1 \rightarrow W\widetilde{\chi}^0_1$ or in the model Tchi1chi1C. This paper also addresses direct slepton production, taking into account pure right-handed, pure left-handed and combined production of either selectrons, smuons, or mass-degenerate sleptons of the first and second generation, see their figures 30 and 31.

[4] HAYRAPETYAN 25AH searched in 138 fb^{-1} of pp collisions at $\sqrt{s}$ = 13 TeV for new physics in jet multiplicity patterns in three-lepton events with and without b quarks. No significant excess above the Standard Model expectations is observed. The results are interpreted in a model similar to Tchi1n2E, but with additional prompt hadronic R-parity violating decay of $\widetilde{\chi}^0_1$ to three quarks, either as $\widetilde{\chi}^0_1 \rightarrow uds$ or $\widetilde{\chi}^0_1 \rightarrow udb$, see their figure 3.

[5] AAD 24AJ searched in 139 fb^{-1} of pp collisions at $\sqrt{s}$ = 13 TeV for evidence of direct stau pair production, or electroweakino pair production with decay via an intermediate stau, in events with two taus decaying hadronically (including a same-charge channel), no b-jets and moderate $\not{E}_T$, using a BDT for the direct stau search and a more traditional cut-and-count selection for the electroweakino search. No significant excess above the Standard Model expectations is observed. Limits are set in models of direct stau production $\widetilde{\tau} \rightarrow \tau\widetilde{\chi}^0_1$, $\widetilde{\tau}_L$, $\widetilde{\tau}_R$ or degenerate production. Limits are also set in models of pair production of charginos (Tchichi1D) or of charginos and neutralinos (Tchi1n2D) followed by the decay via intermediate staus, or (for the latter) via Wh (Tchi1n2E). See their figures 12, 14 and 16.

[6] AAD 24CE searched for VBF production of a wino pair almost mass-degenerate with a bino-like LSP, in events with two jets with a large rapidity gap between them and no leptons in 140 fb^{-1} of pp collisions. Care was taken into including interference effects between VBF QCD and electroweak diagrams for the cross section estimate. A BDT was trained based on the two jet kinematics and the missing transverse momentum. Results are interpreted in a scenario where wino-like degenerate charginos and neutralinos are pair produced and decay into a nearly degenerate bino-like neutralino LSP, see their Figure 8.

[7] AAD 24G searched in 140 fb^{-1} of pp collisions at $\sqrt{s}$ = 13 TeV for evidence of higgsino pair production in events with low-momentum mildly displaced tracks. No significant excess above the Standard Model expectations is observed. Limits are set in the model Tn1n1D, see their Fig. 3, assuming that the $\widetilde{\chi}^{\pm}_1$ has a flight length of about 0.11 mm from the pp interaction point and decays to $\widetilde{\chi}^0_1$ and a charged particle (usually a soft pion) that is measured as low-momentum track.

[8] AAD 24I provides a statistical combination of the results of a number of analyses targeting electroweak production performed using 139 fb^{-1} of pp collisions at $\sqrt{s}$ = 13 TeV. The combination was used to set limits on the pair-produced particle masses as a function of the LSP mass for wino-like $\widetilde{\chi}^{\pm}_1\widetilde{\chi}^{\pm}_1$ followed by $\widetilde{\chi}^{\pm}_1 \rightarrow W\widetilde{\chi}^0_1$, wino-like $\widetilde{\chi}^0_2\widetilde{\chi}^{\pm}_1$ followed by $\widetilde{\chi}^{\pm}_1 \rightarrow W\widetilde{\chi}^0_1$ and either $\widetilde{\chi}^0_2 \rightarrow Z\widetilde{\chi}^0_1$ or $\widetilde{\chi}^0_2 \rightarrow h\widetilde{\chi}^0_1$, or a GGM-like model with a full higgsino triplet decaying to a gravitino. See their Fig. 2.

[9] HAYRAPETYAN 24M searched in 137 fb^{-1} of pp collisions at $\sqrt{s}$ = 13 TeV for evidence of wino- and Higgsino-like charginos in final states with one or more disappearing tracks from the decay $\widetilde{\chi}^{\pm}_1 \rightarrow \pi^{\pm}\widetilde{\chi}^0_1$ where the soft pion is not reconstructed, $\not{E}_T$, and varying numbers of jets, b-tagged jets, electrons, and muons. No significant excess above the Standard Model expectations is observed. Limits are set on the $\widetilde{b}$ mass in the model Tbot1LL for various proper decay lengths $c\tau$ of the $\widetilde{\chi}^{\pm}_1$ as well as on the $\widetilde{t}$ mass in the model Tstop1LL, see their Fig. 10. Limits are also set in the model Tglu1LL, see their Fig. 11. In addition, limits are set in specific pure wino as well as pure higgsino dark matter models, in which the relationships among the electroweakino masses, the $\widetilde{\chi}^{\pm}_1$ lifetime, and the $\widetilde{\chi}^{\pm}_1$ decay width are constrained by radiative corrections that account for a large difference between the LSP mass and the SUSY-breaking scale, see their Fig. 12.

[10] HAYRAPETYAN 24N searched in up to 137 fb^{-1} of pp collisions at $\sqrt{s}$ = 13 TeV for evidence of wino-like chargino-neutralino pairs, Higgsino-like neutralino pair production in a gauge-mediated SUSY breaking inspired scenario, a Higgsino-bino interpretation, and slepton pair production in a combination of a number of previously reported searches for SUSY in different final states. No significant excess above the Standard Model expectations is observed. Limits are set on the $\widetilde{\chi}^{\pm}_1$ mass in the wino-bino models Tchi1n2E1, Tchi1n2E, and Tchi1n2l, see their Fig. 11, and on the $\widetilde{\chi}^0_1$ in the higgsino-like GMSB models Tn1n1A, Tn1n1B, and Tn1n1C, see their Fig. 13. In addition, Fig. 14 shows the mass exclusion limit as a function of the branching fraction to the H boson. Limits are also set in a Higgsino-bino interpretation as in THinoBinoA, but also including leptonic decays, see their Fig. 15. Limits are also set on slepton ($\widetilde{e}$, $\widetilde{\mu}$) production with the decay $\widetilde{\ell} \rightarrow \ell\widetilde{\chi}^0_1$, see their Fig. 16.

[11] AAD 23AE searched in 139 fb^{-1} of pp collisions at $\sqrt{s}$ = 13 TeV for events with 2 ℓ with same flavour and opposite sign, plus jets and $\not{E}_T$, defining signal region with the dilepton invariant mass both on- and off-shell with respect to the Z boson. No significant excess above the Standard Model predictions is observed. Limits are set on models of strong and electroweak production. For electroweak production, limits are placed on production of mass-degenerate, wino-like $\widetilde{\chi}^0_2\ \widetilde{\chi}_1$ with $\widetilde{\chi}^0_2 \rightarrow Z\widetilde{\chi}^0_1$ and $\widetilde{\chi}_1 \rightarrow W\widetilde{\chi}^0_1$, see figure 15.

[12] AAD 23CI searched in 139 fb^{-1} of pp collisions for events containing 1 ℓ (e or μ), jets, and $\not{E}_T$. Final states consistent with the production of a diboson system plus $\not{E}_T$ were identified also by making use of large-R jet tagging techniques. No excess on top of the Standard Model background was observed. Limits were set on the production of $\widetilde{\chi}^{\pm}_1\widetilde{\chi}^0_2$ and $\widetilde{\chi}^{\pm}_1\widetilde{\chi}^{\pm}_1$ (assuming wino cross sections) decaying to $WZ\widetilde{\chi}^0_1\widetilde{\chi}^0_1$ or $WW\widetilde{\chi}^0_1\widetilde{\chi}^0_1$. See their figure 9.

[13] AAD 23CI searched in 139 fb^{-1} of pp collisions for events containing 1 ℓ (e or μ), jets, and $\not{E}_T$. Final states consistent with the production of a boson + Higgs system plus $\not{E}_T$ were identified via a BDT. No excess on top of the Standard Model background was

Int. J. Mod. Phys. A 2026.41. Downloaded from www.worldscientific.com
by UNIVERSITY OF CALIFORNIA @ BERKELEY on 09/16/26. Re-use and distribution is strictly not permitted, except for Open Access articles.

observed. Limits were set on the production of degenerate $\widetilde{\chi}_1^{\pm}\widetilde{\chi}_2^0$ (assuming wino cross sections) decaying into $Wh\widetilde{\chi}_1^0\widetilde{\chi}_1^0$. See their figure 10.

[14] AAD 23CP searched in 139 fb^{-1} of pp collisions at $\sqrt{s}$ = 13 TeV for events with 2 ℓ with same charge plus at least one jet and $\not{E}_T$, defining signal region based on 'stransverse mass' of the dilepton system, $\not{E}_T$ significance and effective mass. No significant excess above the Standard Model predictions is observed. Limits are set on the mass of mass-degenerate $\widetilde{\chi}_1^{\pm}$ and $\widetilde{\chi}_2^0$ for the wino-like production of $\widetilde{\chi}_1^{\pm}\widetilde{\chi}_2^0$ followed by the decay into either $WZ\widetilde{\chi}_1^0\widetilde{\chi}_1^0$ or $Wh\widetilde{\chi}_1^0\widetilde{\chi}_1^0$, see figure 13.

[15] AAD 23CR searched in 139 fb^{-1} of pp collisions at $\sqrt{s}$ = 13 TeV for RPV SUSY in final states with multiple leptons and b-tagged jets. No significant excess above the Standard Model expectations is observed. Limits are set on the production of electroweakinos (wino or higgsino) that decay via RPV coupling λ'_{i33} to a charged lepton or a neutrino, a b quark, and an additional t or b quark, see their figure 16. A second model addresses direct $\widetilde{\mu}_{L,R}$ production and decay to a muon and a bino-like neutralino, which decays in the same way as in the first model, see their figure 17.

[16] AAD 23M searched in 139 fb^{-1} of pp collisions at $\sqrt{s}$ = 13 TeV for $\widetilde{\chi}_1^{\pm}$ pair production, followed by $\widetilde{\chi}_1^{\pm} \rightarrow W^{\pm}\widetilde{\chi}_1^0 \rightarrow \ell^{\pm}\nu\widetilde{\chi}_1^0$ in events with two leptons. The focus is on models where $m_{\widetilde{\chi}_1^{\pm}} - m_{\widetilde{\chi}_1^0}$ is close to the W mass. No significant excess above the Standard Model predictions is observed. Limits are set on the $\widetilde{\chi}_1^{\pm}$ mass as a function of $m_{\widetilde{\chi}_1^0}$, see Figure 9.

[17] HAYRAPETYAN 23E searched in 137 fb^{-1} of pp collisions at $\sqrt{s}$ = 13 TeV for evidence of gluino, top squark and electroweakino pair production in events with at least one photon, multiple jets, and large $\not{E}_T$. No significant excess above the Standard Model expectations is observed. Limits are set in models for strong production, Tglu4D, Tglu4E, Tglu4F and Tstop13, see their figure 9. They also interpret the results in the models for electroweak production, shown in their figure 10. Tchi1n1A assumes wino-like $\widetilde{\chi}_1^{\pm}\widetilde{\chi}_1^0$ production, while Tchi1chi1A assumes higgsino-like cross sections and includes $\widetilde{\chi}_1^{\pm}\widetilde{\chi}_1^{\pm}$, $\widetilde{\chi}_1^0\widetilde{\chi}_2^0$ and $\widetilde{\chi}_{1,2}^0\widetilde{\chi}_1^{\pm}$ production. For $\widetilde{\chi}_1^0\widetilde{\chi}_2^0$ alone no mass point can be excluded in the model Tchi1chi1A, but in another model for $\widetilde{\chi}_1^0\widetilde{\chi}_2^0$ production, Tn1n2A.

[18] TUMASYAN 23B searched in 137 fb^{-1} of pp collisions at $\sqrt{s}$ = 13 TeV for evidence of electroweakino pair production with decays including hadronically decaying bosons, WW, WZ, WH, or ZH, identified with a DNN classifying large-area (AK8) jets. No significant excess above the Standard Model expectations is observed. Limits are set on the mass of the nearly mass degenerate wino-like $\widetilde{\chi}_2^0$ and $\widetilde{\chi}_1^{\pm}$ in the models Tchi1chi1l , Tchi1n2Fb, and Tchi1n2Fc, see their figure 4. They also consider a model that contains both $\widetilde{\chi}_2^0\widetilde{\chi}_1^{\pm}$ and $\widetilde{\chi}_1^{\pm}\widetilde{\chi}_1^{\pm}$ production, see their figure 5 (upper). Results are also interpreted in the model THinoBinoA with nearly mass-degenerate higgsino-like $\widetilde{\chi}_3^0$, $\widetilde{\chi}_2^0$, $\widetilde{\chi}_1^{\pm}$, and a lighter bino-like $\widetilde{\chi}_1^0$, see their figure 5 (lower).

[19] TUMASYAN 22Q searched in up to 137 fb^{-1} of pp collisions at $\sqrt{s}$ = 13 TeV for evidence of electroweakino and top squark pair production with a small mass difference between the produced supersymmetric particles and the lightest neutralino in events with two or three low-momentum leptons and missing transverse momentum. No significant excess above the Standard Model expectations is observed. Limits are set on the mass of $\widetilde{\chi}_2^0$ and $\widetilde{\chi}_1^{\pm}$ in the model Tchi1n2F, see their Figure 8. Limits are also set in a higgsino simplified model with both $\widetilde{\chi}_2^0\widetilde{\chi}_1^{\pm}$ and $\widetilde{\chi}_2^0\widetilde{\chi}_1^0$ production, where $\widetilde{\chi}_2^0 \rightarrow Z\widetilde{\chi}_1^0$ and $m_{\widetilde{\chi}_1^{\pm}} = 1/2(m_{\widetilde{\chi}_2^0} + m_{\widetilde{\chi}_1^0})$. A model inspired by the pMSSM is used for further interpretations in the case of a higgsino LSP, see their Figure 9. Limits are also set on the mass of the top squark in the models Tstop2 and Tstop3, see their Figure 10.

[20] TUMASYAN 22S searched in 137 fb^{-1} of pp collisions at $\sqrt{s}$ = 13 TeV for evidence of electroweakino pair production in events with three or four leptons, with up to two hadronically decaying τ leptons, or two same-sign light leptons (e or μ). No significant excess above the Standard Model expectations is observed. Limits are set on the mass of $\widetilde{\chi}_2^0$ and $\widetilde{\chi}_1^{\pm}$ in the models Tchi1n2B (in flavory-democratic and tau-enriched or -dominated scenarios), Tchi1n2E, Tchi1n2F, see their Figures 16–20, and on the mass of the higgsino-triplet $\widetilde{\chi}_2^0$, $\widetilde{\chi}_1^{\pm}$, and $\widetilde{\chi}_1^0$ in the models Tn1n1A, Tn1n1B, and Tn1n1C, see their Figure 21.

[21] AAD 21AX searched in 139 fb^{-1} of pp collisions at $\sqrt{s}$ = 13 TeV for pair production of electroweakinos decaying to the LSP via the emission of Standard Model bosons (Higgs, W, Z) decaying into hadrons. The final state in all cases characterised by the presence of $\not{E}_T$, jets, and large-R jets tagged according to the boson of interest. Different assumptions (Higgsino, Wino, Bino) are made for the pair produced electroweakinos and for the LSP multiplet. No significant excess above the Standard Model predictions is observed. Limits are set on the electroweakino masses as a function of the model parameters (in particular $m_{\widetilde{\chi}_1^0}$). See Figs. 12, 14, 15.

[22] AAD 21BG searched in 139 fb^{-1} of pp collisions at $\sqrt{s}$ = 13 TeV for pair production $\widetilde{\chi}_2^0\widetilde{\chi}_1^{\pm}$ in final states with three leptons, with and without assuming the presence of a $Z \rightarrow \ell\ell$ decay. No significant excess above the Standard Model predictions is observed. Limits are set on the $\widetilde{\chi}_2^0$ and $\widetilde{\chi}_1^{\pm}$ mass in Tchi1n2E, Tchi1n2F and Tchi1n2Ga. See their Fig. 16.

[23] AAD 21E searched in 139 fb^{-1} of pp collisions at $\sqrt{s}$ = 13 TeV for production of wino-like $\widetilde{\chi}_1^{\pm}\widetilde{\chi}_1^{\pm}$ and $\widetilde{\chi}_1^{\pm}\widetilde{\chi}_1^0$, followed by the RPV decay of $\widetilde{\chi}_1^{\pm}$ into $Z\ell$, $H\ell$ or $W\nu$ and of $\widetilde{\chi}_1^0$ into $Z\nu$, $H\nu$ or $W\ell$, in events with three leptons, looking for $Z\ell$ resonances. No significant excess above the Standard Model predictions is observed. Limits are set on the common $m_{\widetilde{\chi}_1^{\pm}}/m_{\widetilde{\chi}_1^0}$ mass in the TwinoLSPRPV simplified model, as a function of the common $\widetilde{\chi}_1^{\pm}/\widetilde{\chi}_1^0$ branching fraction to a Z boson. See Figure 9.

[24] AAD 21Y searched in 139 fb^{-1} of pp collisions at $\sqrt{s}$ = 13 TeV for supersymmetry in events with four or more leptons (electrons, muons and tau-leptons). No significant excess above the Standard Model expectations is observed. Limits are set on Tchi1n12-GGM, and RPV models similar to Tchi1n2l, Tglu1A (with $q = u, d, s, c, b$, with equal branching fractions), and $\widetilde{\ell}_L/\widetilde{\nu} \rightarrow \ell/\nu\widetilde{\chi}_1^0$ (mass-degenerate $\widetilde{\ell}_L$ and $\widetilde{\nu}$ of all 3 generations), all with $\widetilde{\chi}_1^0 \rightarrow \ell^{\pm}\ell^{\mp}\nu$ via λ_{12k} or λ_{i33} (where $i,k \in 1,2$), see their Figure 11.

[25] SIRUNYAN 21M searched in 137 fb^{-1} of pp collisions at $\sqrt{s}$ = 13 TeV for supersymmetry in events with two opposite-sign same-flavor leptons (electrons, muons) and $\not{E}_T$. No significant excess above the Standard Model expectations is observed. Limits are set on the gluino mass in the simplified model Tglu4C, see their Figure 10, on the $\widetilde{\chi}_2^0$ and $\widetilde{\chi}_1^{\pm}$ mass in Tchi1n2Fa, see their Figure 11, on the $\widetilde{\chi}_1^0$ mass in Tn1n1C and Tn1n1B for $m_{\widetilde{\chi}_2^0} = m_{\widetilde{\chi}_1^{\pm}} = m_{\widetilde{\chi}_1^0}$, see their Figure 12. Limits are also set on the light squark mass for the simplified model Tsqk2A, on the sbottom mass in Tsbot3, see their Figure 13, and on the slepton mass in direct electroweak pair production of mass-degenerate left- and right-handed sleptons (selectrons and smuons), see their Figure 14.

[26] TUMASYAN 21C searched in 137 fb^{-1} of pp collisions at $\sqrt{s}$ = 13 TeV for supersymmetry in events with with one lepton, a Higgs boson decaying to a pair of bottom quarks, and large $\not{E}_T$. No significant excess above the Standard Model expectations is observed. Lower limits are set on the masses of $\widetilde{\chi}_2^0$ and $\widetilde{\chi}_1^{\pm}$ in the simplified model Tchi1n2E, see their Figure 6.

[27] AAD 20AN searched in 139 fb^{-1} of pp collisions at $\sqrt{s}$ = 13 TeV for events with two photons and missing transverse momentum. Events are further categorised in terms of lepton or jet multiplicity. No significant excess over the expected background is observed. Limits at 95% C.L. are set on the Higgsino mass in the T1n1n1A simplified model, see their Figure 11.

[28] AAD 20I reported on ATLAS searches for electroweak production in models with compressed mass spectra as Tchi1n2Fa. A dataset of pp collisions at $\sqrt{s}$ = 13 TeV corresponding to an integrated luminosity of 139 fb^{-1} was used. Events with $\not{E}_T$, two same-flavour, opposite-charge, low-transverse-momentum leptons, and jets from initial-state radiation or characteristic of vector-boson fusion production are selected. Constraints at 95% C.L. are placed on the mass of the $\widetilde{\chi}_1^{\pm}$ (degenerate with $\widetilde{\chi}_2^0$) at 240 GeV for a mass splitting between $\widetilde{\chi}_1^{\pm}$ and $\widetilde{\chi}_1^0$ of 7 GeV and extend down to a mass splitting of 1.5 GeV at the LEP chargino mass limit of 92.4 GeV. See their Fig. 14(b,c).

[29] AAD 20K reported on a search for electroweak production in models with mass splittings near the electroweak scale as Tchi1n2F and exploiting three-lepton final state events with an emulated recursive jigsaw reconstruction method. The analysis uses a dataset of pp collisions at $\sqrt{s}$ = 13 TeV corresponding to an integrated luminosity of 139 fb^{-1}. Exclusion limits at 95% C.L. are derived on next-to-lightest neutralinos and charginos with masses up to 345 GeV for a massless lightest neutralino, see their Fig. 7.

[30] AAD 20O reported on a search for electroweak production in models with charginos and sleptons decaying into final states with exactly two oppositely charged leptons and missing transverse momentum. A dataset of pp collisions at $\sqrt{s}$ = 13 TeV corresponding to an integrated luminosity of 139 fb^{-1} was used. Exclusion limits at 95% C.L. are derived on $m_{\widetilde{\chi}_1^{\pm}}$ decaying according to the Tchi1chi1H simplified model. Chargino masses up to 420 GeV are excluded for a massless lightest neutralino, see their Fig. 7(a).

[31] AAD 20O reported on a search for electroweak production in models with charginos and sleptons decaying into final states with exactly two oppositely charged leptons and missing transverse momentum. A dataset of pp collisions at $\sqrt{s}$ = 13 TeV corresponding to an integrated luminosity of 139 fb^{-1} was used. Exclusion limits at 95% C.L. are derived on $m_{\widetilde{\chi}_1^{\pm}}$ decaying according to the Tchi1chi1C simplified model. Chargino masses up to 1000 GeV are excluded for a massless lightest neutralino, see their Fig. 7(b).

[32] AAD 20R searched for electroweak production in the model Tchi1n2E, selecting events with a pair of b-tagged jets consistent with those from a Higgs boson decay, either an electron or a muon from the W boson decay and $\not{E}_T$. The analysis uses a dataset of pp collisions at $\sqrt{s}$ = 13 TeV corresponding to an integrated luminosity of 139 fb^{-1}. Exclusion limits at 95% C.L. are derived on next-to-lightest neutralinos and charginos with masses up to 740 GeV for a massless lightest neutralino, assuming pure wino cross-sections. See their Fig. 6.

[33] SIRUNYAN 20AU searched in 77.2 fb^{-1} of pp collisions at $\sqrt{s}$ = 13 TeV for events containing one soft, hadronically decaying tau lepton, one energetic jet from initial-state radiation, and large $\not{E}_T$. No excess over the expected background is observed. Limits are derived on the wino mass in the Tchi1n2D simplified model, see their Figure 2.

[34] SIRUNYAN 20B searched in 35.9 fb^{-1} of pp collisions at $\sqrt{s}$ = 13 TeV for events with at least one photon and large $\not{E}_T$. No significant excess above the Standard Model expectations is observed. Limits are set on chargino masses in a general gauge-mediated SUSY breaking (GGM) scenario Tchi1n12-GGM, see Figure 4. Limits are also set on the NLSP mass in the Tchi1chi1F and Tchi1chi1G simplified models, see their Figure 5. Finally, limits are set on the gluino mass in the Tglu4A simplified model, see Figure 6.

[35] AABOUD 19AU searched in 36.1 fb^{-1} of pp collisions at $\sqrt{s}$ = 13 TeV for direct electroweak production of charginos and next-to-lightest neutralinos decaying into lightest neutralinos and a W, and a Higgs boson, respectively. Fully hadronic, semileptonic, diphoton, and multilepton (electrons, muons) final states with missing transverse momentum are considered in this search. Observations are consistent with the Standard Model expectations, and 95% confidence-level limits of up to 680 GeV on the chargino/next-to-lightest neutralino masses are set (Tchi1n2E model). See their Figure 14 for an overlay of exclusion contours from all searches.

[36] SIRUNYAN 19BU searched for pair production of gauginos via vector boson fusion assuming the gaugino spectrum is compressed, in 35.9 fb^{-1} of pp collisions at $\sqrt{s}$ = 13 TeV. The final states explored included zero leptons plus two jets, one lepton plus two jets, and one hadronic tau plus two jets. A similar bound is obtained in the light slepton limit.

[37] SIRUNYAN 19CI searched in 77.5 fb^{-1} of pp collisions at $\sqrt{s}$ = 13 TeV for events with one or more high-momentum Higgs bosons, decaying to pairs of photons, jets and $\not{E}_T$. No significant excess above the Standard Model expectations is observed. Limits are set on the sbottom mass in the Tsbot4 simplified model, see Figure 3, and on the wino mass in the Tchi1n2E simplified model, see their Figure 4. Limits are also set on the higgsino mass in the Tn1n1A and Tn1n1B simplified models, see their Figure 5.

[38] SIRUNYAN 19K searched in 35.9 fb^{-1} of pp collisions at $\sqrt{s}$ = 13 TeV for events with a photon, an electron or muon, and large $\not{E}_T$. No significant excess above the Standard Model expectations is observed. In the framework of GMSB, limits are set on the chargino and neutralino mass in the Tchi1n1A simplified model, see their Figure 6. Limits are also set on the gluino mass in the Tglu4A simplified model, and on the squark mass in the Tsqk4A simplified model, see their Figure 7.

[39] AABOUD 18AY searched in 36.1 fb^{-1} of pp collisions at $\sqrt{s}$ = 13 TeV for direct electroweak production of charginos as in Tchi1chi1D models in events characterised by the presence of at least two hadronically decaying tau leptons and large missing transverse energy. No significant deviation from the expected SM background is observed. In the Tchi1chi1D model, assuming decays via intermediate $\widetilde{\tau}_L$, the observed limits rule out $\widetilde{\chi}_1^{\pm}$ masses up to 630 GeV for a massless $\widetilde{\chi}_1^0$. See their Fig.7 (left). Interpretations are

Int. J. Mod. Phys. A 2026.41. Downloaded from www.worldscientific.com by UNIVERSITY OF CALIFORNIA @ BERKELEY on 09/16/26. Re-use and distribution is strictly not permitted, except for Open Access articles.

also provided in Fig 8 (top) for different assumptions on the ratio between $m_{\widetilde{\tau}}$ and $m_{\widetilde{\chi}_1^\pm} + m_{\widetilde{\chi}_1^0}$.

[40] AABOUD 18AY searched in 36.1 fb^{-1} of pp collisions at $\sqrt{s}$ = 13 TeV for direct electroweak production of charginos and neutralinos as in Tchi1n2D models, in events characterised by the presence of at least two hadronically decaying tau leptons and large missing transverse energy. No significant deviation from the expected SM background is observed. Assuming decays via intermediate $\widetilde{\tau}_L$ and $m_{\widetilde{\chi}_1^\pm} = m_{\widetilde{\chi}_2^0}$, the observed limits rule out $\widetilde{\chi}_1^\pm$ masses up to 760 GeV for a massless $\widetilde{\chi}_1^0$. See their Fig.7 (right). Interpretations are also provided in Fig 8 (bottom) for different assumptions on the ratio between $m_{\widetilde{\tau}}$ and $m_{\widetilde{\chi}_1^\pm} + m_{\widetilde{\chi}_1^0}$.

[41] AABOUD 18BT searched in 36.1 fb^{-1} of pp collisions at $\sqrt{s}$ = 13 TeV for direct electroweak production of charginos, chargino and next-to-lightest neutralinos and sleptons in events with two or three leptons (electrons or muons), with or without jets and large missing transverse energy. No significant excess above the Standard Model expectations is observed. Limits are set on the chargino mass up to 750 GeV for massless neutralinos in the Tchi1chi1C simplified model exploiting $2\ell + 0$ jets signatures, see their Figure 8(a).

[42] AABOUD 18BT searched in 36.1 fb^{-1} of pp collisions at $\sqrt{s}$ = 13 TeV for direct electroweak production of charginos, chargino and next-to-lightest neutralinos and sleptons in events with two or three leptons (electrons or muons), with or without jets, and large missing transverse energy. No significant excess above the Standard Model expectations is observed. Limits are set on the chargino mass up to 1100 GeV for massless neutralinos in the Tchi1n2C simplified model exploiting 3ℓ signature, see their Figure 8(c).

[43] AABOUD 18BT searched in 36.1 fb^{-1} of pp collisions at $\sqrt{s}$ = 13 TeV for direct electroweak production of charginos, chargino and next-to-lightest neutralinos and sleptons in events with two or three leptons (electrons or muons), with or without jets, and large missing transverse energy. No significant excess above the Standard Model expectations is observed. Limits are set on the chargino mass up to 580 GeV for massless neutralinos in the Tchi1n2F simplified model exploiting 2ℓ+2 jets and 3ℓ signatures, see their Figure 8(d).

[44] AABOUD 18CK searched for events with at least 3 b-jets and large missing transverse energy in two datasets of pp collisions at $\sqrt{s}$ = 13 TeV of 36.1 fb^{-1} and 24.3 fb^{-1} depending on the trigger requirements. The analyses aimed to reconstruct two Higgs bosons decaying to pairs of b-quarks. No significant excess above the Standard Model expectations is observed. Limits are set on the Higgsino mass in the T1n1n1A simplified model, see their Figure 15(a). Constraints are also presented as a function of the BR of Higgsino decaying into an higgs boson and a gravitino, see their Figure 15(b).

[45] AABOUD 18CO searched in 36.1 fb^{-1} of pp collisions at $\sqrt{s}$ = 13 TeV for direct electroweak production of mass-degenerate charginos and next-to-lightest neutralinos in events with two or three leptons (electrons or muons), with or without jets, and large missing transverse energy. The search channels are based on recursive jigsaw reconstruction. Limits are set on the chargino mass up to 600 GeV for massless neutralinos in the Tchi1n2F simplified model exploiting the statistical combination of 2ℓ+2 jets and 3ℓ channels. Chargino masses below 220 GeV are not excluded due to an excess of events above the SM prediction in the dedicated regions. See their Figure 13(d).

[46] AABOUD 18R searched in 36.1 fb^{-1} of pp collisions at $\sqrt{s}$ = 13 TeV for electroweak production in scenarios with compressed mass spectra in final states with two low-momentum leptons and missing transverse momentum. The data are found to be consistent with the SM prediction. Results are interpreted in Tchi1n2G wino models and $\widetilde{\chi}_1^\pm$ masses are excluded up to 175 GeV for $m_{\widetilde{\chi}_1^\pm} - m_{\widetilde{\chi}_1^0} = 10$ GeV. The exclusion limits extend down to mass splittings of 2 GeV, see their Fig. 10 (bottom).

[47] AABOUD 18R searched in 36.1 fb^{-1} of pp collisions at $\sqrt{s}$ = 13 TeV for electroweak production in scenarios with compressed mass spectra in final states with two low-momentum leptons and missing transverse momentum. The data are found to be consistent with the SM prediction. Results are interpreted in Tchi1n2G higgsino models and $\widetilde{\chi}_1^\pm$ masses are excluded up to 145 GeV for $m_{\widetilde{\chi}_1^\pm}$ - $m_{\widetilde{\chi}_1^0}$ = 5 GeV. The exclusion limits extend down to mass splittings of 2.5 GeV, see their Fig. 10 (top).

[48] AABOUD 18U searched in 36.1 fb^{-1} of pp collisions at $\sqrt{s}$ = 13 TeV in events with at least one isolated photon, possibly jets and significant transverse momentum targeting generalised models of gauge-mediated SUSY breaking. No significant excess of events is observed above the SM prediction. Results of the diphoton channel are interpreted in terms of lower limits on the masses of gauginos Tchi1chi1A models, which reach as high as 1.3 TeV. Gaugino masses below 1060 GeV are excluded for any NLSP mass, see their Fig. 10.

[49] AABOUD 18Z searched in 36.1 fb^{-1} of pp collisions at $\sqrt{s}$ = 13 TeV for events containing four or more charged leptons (electrons, muons and up to two hadronically decaying taus). No significant deviation from the expected SM background is observed. Limits are set on the Higgsino mass in simplified models of general gauge mediated supersymmetry Tn1n1A/Tn1n1B/Tn1n1C, see their Figure 9. Limits are also set on the wino, slepton, sneutrino and gluino mass in a simplified model of NLSP pair production with R-parity violating decays of the LSP via λ_{12k} or λ_{i33} to charged leptons, see their Figures 7, 8.

[50] SIRUNYAN 18AA searched in 35.9 fb^{-1} of pp collisions at $\sqrt{s}$ = 13 TeV for events with at least one photon and large $\not{E}_T$. No significant excess above the Standard Model expectations is observed. Limits are set on wino masses in a general gauge-mediated SUSY breaking (GGM) scenario with bino-like $\widetilde{\chi}_1^0$ and wino-like $\widetilde{\chi}_1^\pm$ and $\widetilde{\chi}_2^0$, see Figure 7. Limits are also set on the NLSP mass in the Tchi1n1A and Tchi1chi1A simplified models, see their Figure 8. Finally, limits are set on the gluino mass in the Tglu4A and Tglu4B simplified models, see their Figure 9, and on the squark mass in the Tskq4A and Tsqk4B simplified models, see their Figure 10.

[51] SIRUNYAN 18AJ searched in 35.9 fb^{-1} of pp collisions at $\sqrt{s}$ = 13 TeV for events containing two low-momentum, oppositely charged leptons (electrons or muons) and $\not{E}_T$. No excess over the expected background is observed. Limits are derived on the wino mass in the Tchi1n2F simplified model, see their Figure 5. Limits are also set on the stop mass in the Tstop10 simplified model, see their Figure 6. Finally, limits are set on the Higgsino mass in the Tchi1n2G simplified model, see Figure 8 and in the pMSSM, see Figure 7.

[52] SIRUNYAN 18AO searched in 35.9 fb^{-1} of pp collisions at $\sqrt{s}$ = 13 TeV for direct electroweak production of charginos and neutralinos in events with either two or more leptons (electrons or muons) of the same electric charge, or with three or more leptons, which can include up to two hadronically decaying tau leptons. No significant excess above the Standard Model expectations is observed. Limits are set on the chargino/neutralino mass in the Tchi1n2A, Tchi1n2H, Tchi1n2D, Tchi1n2E and Tchi1n2F simplified models, see their Figures 14, 15, 16, 17 and 18. Limits are also set on the higgsino mass in the Tn1n1A, Tn1n1B and Tn1n1C simplified models, see their Figure 19.

[53] SIRUNYAN 18AP searched in 35.9 fb^{-1} of pp collisions at $\sqrt{s}$ = 13 TeV for direct electroweak production of charginos and neutralinos by combining a number of previous and new searches. No significant excess above the Standard Model expectations is observed. Limits are set on the chargino/neutralino mass in the Tchi1n2E, Tchi1n2F and Tchi1n2l simplified models, see their Figures 7, 8, 9 an 10. Limits are also set on the higgsino mass in the Tn1n1A, Tn1n1B and Tn1n1C simplified models, see their Figure 11, 12, 13 and 14.

[54] SIRUNYAN 18AR searched in 35.9 fb^{-1} of pp collisions at $\sqrt{s}$ = 13 TeV for events containing two opposite-charge, same-flavour leptons (electrons or muons), jets and $\not{E}_T$. No significant excess above the Standard Model expectations is observed. Limits are set on the gluino mass in the Tglu4C simplified model, see their Figure 7. Limits are also set on the chargino/neutralino mass in the Tchi1n2F simplified models, see their Figure 8, and on the higgsino mass in the Tn1n1B and Tn1n1C simplified models, see their Figure 9. Finally, limits are set on the sbottom mass in the Tsbot3 simplified model, see their Figure 10.

[55] SIRUNYAN 18DN searched in 35.9 fb^{-1} of pp collisions at $\sqrt{s}$ = 13 TeV for direct electroweak production of charginos and for pair production of top squarks in events with two leptons (electrons or muons) of the opposite electric charge. No significant excess above the Standard Model expectations is observed. Limits are set on the chargino mass in the Tchi1chi1C and Tchi1chi1E simplified models, see their Figure 8. Limits are also set on the stop mass in the Tstop1 and Tstop2 simplified models, see their Figure 9.

[56] SIRUNYAN 18DP searched in 35.9 fb^{-1} of pp collisions at $\sqrt{s}$ = 13 TeV for direct electroweak production of charginos and neutralinos or of chargino pairs in events with a tau lepton pair and significant missing transverse momentum. Both hadronic and leptonic decay modes are considered for the tau lepton. No significant excess above the Standard Model expectations is observed. Limits are set on the chargino mass in the Tchi1chi1D and Tchi1n2 simplified models, see their Figures 14 and 15. Also, excluded stau pair production cross sections are shown in Figures 11, 12, and 13.

[57] SIRUNYAN 18X searched in 35.9 fb^{-1} of pp collisions at $\sqrt{s}$ = 13 TeV for events with one or more high-momentum Higgs bosons, decaying to pairs of photons, jets and $\not{E}_T$. The razor variables (M_R and R^2) are used to categorise the events. No significant excess above the Standard Model expectations is observed. Limits are set on the sbottom mass in the Tsbot4 simplified model and on the wino mass in the Tchi1n2E simplified model, see their Figure 5. Limits are also set on the higgsino mass in the Tn1n1A and Tn1n1B simplified models, see their Figure 6.

[58] KHACHATRYAN 17L searched in about 19 fb^{-1} of pp collisions at $\sqrt{s}$ = 8 TeV for events with two τ (at least one decaying hadronically) and $\not{E}_T$. In the Tchi1chi1C model, assuming decays via intermediate $\widetilde{\tau}$ or $\widetilde{\nu}_\tau$ with equivalent mass, the observed limits rule out $\widetilde{\chi}_1^\pm$ masses up to 420 GeV for a massless $\widetilde{\chi}_1^0$. See their Fig.5.

[59] SIRUNYAN 17AW searched in 35.9 fb^{-1} of pp collisions at $\sqrt{s}$ = 13 TeV for events with a charged lepton (electron or muon), two jets identified as originating from a b-quark, and large $\not{E}_T$. No significant excess above the Standard Model expectations is observed. Limits are set on the mass of the chargino and the next-to-lightest neutralino in the Tchi1n2E simplified model, see their Figure 6.

[60] AAD 16AA summarized and extended ATLAS searches for electroweak supersymmetry in final states containing several charged leptons, $\not{E}_T$, with or without hadronic jets, in 20 fb^{-1} of pp collisions at $\sqrt{s}$ = 8 TeV. The paper reports the results of new interpretations and statistical combinations of previously published analyses, as well as new analyses. Exclusion limits at 95% C.L. are set on the $\widetilde{\chi}_1^\pm$ mass in the Tchi1chi1B and Tchi1chi1C simplified models. See their Fig. 13.

[61] AAD 16AA summarized and extended ATLAS searches for electroweak supersymmetry in final states containing several charged leptons, $\not{E}_T$, with or without hadronic jets, in 20 fb^{-1} of pp collisions at $\sqrt{s}$ = 8 TeV. The paper reports the results of new interpretations and statistical combinations of previously published analyses, as well as new analyses. Exclusion limits at 95% C.L. are set on mass-degenerate $\widetilde{\chi}_1^\pm$ and $\widetilde{\chi}_2^0$ masses in the Tchi1n2B, Tchi1n2C, and Tchi1n2D simplified models. See their Figs. 16, 17, and 18. Interpretations in phenomenological-MSSM, two-parameter Non Universal Higgs Masses (NUHM2), and gauge-mediated symmetry breaking (GMSB) models are also given in their Figs. 20, 21 and 22.

[62] KHACHATRYAN 16R searched in 19.7 fb^{-1} of pp collisions at $\sqrt{s}$ = 8 TeV for events with one or more photons, one electron or muon, and $\not{E}_T$. No significant excess above the Standard Model expectations is observed. Limits are set on wino masses in a general gauge-mediated SUSY breaking model (GGM), for a wino-like neutralino NLSP scenario, see Fig. 5. Limits are also set in the Tglu1D and Tchi1n1A simplified models, see Fig. 6. The Tchi1n1A limit is reduced to 340 GeV for a branching ratio reduced by the weak mixing angle.

[63] AAD 15BA searched in 20.3 fb^{-1} of pp collisions at $\sqrt{s}$ = 8 TeV for electroweak production of charginos and neutralinos decaying to a final state containing a W boson and a 125 GeV Higgs boson, plus missing transverse momentum. No excess beyond the Standard Model expectation is observed. Exclusion limits are derived in simplified models of direct chargino and next-to-lightest neutralino production, with the decays $\widetilde{\chi}_1^\pm \rightarrow W^\pm\widetilde{\chi}_1^0$ and $\widetilde{\chi}_2^0 \rightarrow H\widetilde{\chi}_1^0$ having 100% branching fraction, see Fig. 8. A combination of the multiple final states for the Higgs decay yields the best limits (Fig. 8d).

[64] AAD 15CA searched in 20.3 fb^{-1} of pp collisions at $\sqrt{s}$ = 8 TeV for events with one or more photons and $\not{E}_T$, with or without leptons (e, μ). No significant excess above the Standard Model expectations is observed. Limits are set on wino masses in the general gauge-mediated SUSY breaking model (GGM), for wino-like NLSP, see Fig. 9, 12

[65] AAD 14H searched in 20.3 fb^{-1} of pp collisions at $\sqrt{s}$ = 8 TeV for electroweak production of charginos and neutralinos decaying to a final sate with three leptons and missing transverse momentum. No excess beyond the Standard Model expectation is observed. Exclusion limits are derived in simplified models of direct chargino and next-to-lightest neutralino production, with decays to the lightest neutralino via either all three generations of leptons, staus only, gauge bosons, or Higgs bosons, see Fig. 7. An interpretation in the pMSSM is also given, see Fig. 8.

[66] AAD 14X searched in 20.3 fb^{-1} of pp collisions at $\sqrt{s}$ = 8 TeV for events with at least four leptons (electrons, muons, taus) in the final state. No significant excess above the Standard Model expectations is observed. Limits are set on the wino-like chargino mass in an R-parity violating simplified model where the decay $\widetilde{\chi}_1^\pm \rightarrow W^{(*)\pm}\widetilde{\chi}_1^0$, with $\widetilde{\chi}_1^0 \rightarrow \ell^\pm\ell^\mp\nu$, takes place with a branching ratio of 100%, see Fig. 8.

[67] KHACHATRYAN 14L searched in 19.5 fb^{-1} of pp collisions at $\sqrt{s}$ = 8 TeV for evidence of chargino-neutralino $\widetilde{\chi}_1^\pm\widetilde{\chi}_2^0$ pair production with Higgs or W-bosons in the decay chain,

Int. J. Mod. Phys. A 2026.41. Downloaded from www.worldscientific.com
by UNIVERSITY OF CALIFORNIA @ BERKELEY on 09/16/26. Re-use and distribution is strictly not permitted, except for Open Access articles.

leading to HW final states with missing transverse energy. The decays of a Higgs boson to a photon pair are considered in conjunction with hadronic and leptonic decay modes of the W bosons. No significant excesses over the expected SM backgrounds are observed. The results are interpreted in the context of simplified models where the decays $\widetilde{\chi}^0_2 \rightarrow H\widetilde{\chi}^0_1$ and $\widetilde{\chi}^\pm_1 \rightarrow W^\pm\widetilde{\chi}^0_1$ take place 100% of the time, see Figs. 22–23.

[68] AAD 13 searched in 4.7 fb^{-1} of pp collisions at $\sqrt{s}$ = 7 TeV for charginos and neutralinos decaying to a final state with three leptons (e and μ) and missing transverse energy. No excess beyond the Standard Model expectation is observed. Exclusion limits are derived in the phenomenological MSSM, see Fig. 2 and 3, and in simplified models, see Fig. 4. For the simplified models with intermediate slepton decays, degenerate $\widetilde{\chi}^\pm_1$ and $\widetilde{\chi}^0_2$ masses up to 500 GeV are excluded at 95% C.L. for very large mass differences with the $\widetilde{\chi}^0_1$. Supersedes AAD 12AS.

[69] AAD 13B searched in 4.7 fb^{-1} of pp collisions at $\sqrt{s}$ = 7 TeV for gauginos decaying to a final state with two leptons (e and μ) and missing transverse energy. No excess beyond the Standard Model expectation is observed. Limits are derived in a simplified model of wino-like chargino pair production, where the chargino always decays to the lightest neutralino via an intermediate on-shell charged slepton, see Fig. 2(b). Chargino masses between 110 and 340 GeV are excluded at 95% C.L. for $m_{\widetilde{\chi}^0_1}$ = 10 GeV. Exclusion limits are also derived in the phenomenological MSSM, see Fig. 3.

[70] AAD 12CT searched in 4.7 fb^{-1} of pp collisions at $\sqrt{s}$ = 7 TeV for events containing four or more leptons (electrons or muons) and either moderate values of missing transverse momentum or large effective mass. No significant excess is found in the data. Limits are presented in a simplified model of R-parity violating supersymmetry in which charginos are pair-produced and then decay into a W-boson and a $\widetilde{\chi}^0_1$, which in turn decays through an RPV coupling into two charged leptons ($e^\pm e^\mp$ or $e^\pm\mu^\mp$) and a neutrino. In this model, chargino masses up to 540 GeV are excluded at 95% C.L. for $m_{\widetilde{\chi}^0_1}$ above 300 GeV, see Fig. 3a. The limit deteriorates for lighter $\widetilde{\chi}^0_1$. Limits are also set in an R-parity violating mSUGRA model, see Fig. 3b.

[71] CHATRCHYAN 12BJ searched in 4.98 fb^{-1} of pp collisions at $\sqrt{s}$ = 7 TeV for direct electroweak production of charginos and neutralinos in events with at least two leptons, jets and missing transverse momentum. No significant excesses over the expected SM backgrounds are observed and 95% C.L. limits on the production cross section of $\widetilde{\chi}^\pm_1\widetilde{\chi}^0_2$ pair production were set in a number of simplified models, see Figs. 7 to 12.

[72] ABDALLAH 03M uses data from $\sqrt{s}$ = 192–208 GeV to obtain limits in the framework of the MSSM with gaugino and sfermion mass universality at the GUT scale. An indirect limit on the mass of charginos is derived by constraining the MSSM parameter space by the results from direct searches for neutralinos (including cascade decays), for charginos and for sleptons. These limits are valid for values of $M_2 < 1$ TeV, $|\mu| \leq 2$ TeV with the $\widetilde{\chi}^0_1$ as LSP. Constraints from the Higgs search in the m_h^{max} scenario assuming m_t= 174.3 GeV are included. The quoted limit applies if there is no mixing in the third family or when $m_{\widetilde{\tau}_1} - m_{\widetilde{\chi}^0_1} > 6$ GeV. If mixing is included the limit degrades to 90 GeV. See Fig. 43 for the mass limits as a function of tanβ. These limits update the results of ABREU 00W.

[73] AAD 20AN searched in 139 fb^{-1} of pp collisions at $\sqrt{s}$ = 13 TeV for events with two photons and missing transverse momentum. Events are further categorised in terms of lepton or jet multiplicity. No significant excess over the expected background is observed. Limits at 95% C.L. are derived in Tchi1n2E simplified models. Next-to-lightest neutralinos and charginos with masses up to 310 GeV for a massless lightest neutralino are excluded. See their Fig. 10.

[74] KHACHATRYAN 16AA searched in 7.4 fb^{-1} of pp collisions at $\sqrt{s}$ = 8 TeV for events with one or more photons, hadronic jets and $\not{E}_T$. No significant excess above the Standard Model expectations is observed. Limits are set on wino masses in the general gauge-mediated SUSY breaking model (GGM), for a wino-like neutralino NLSP scenario and with the wino mass fixed at 10 GeV above the bino mass, see Fig. 4. Limits are also set in the Tchi1chi1A and Tchi1n1A simplified models, see Fig. 3.

[75] KHACHATRYAN 16R searched in 19.7 fb^{-1} of pp collisions at $\sqrt{s}$ = 8 TeV for events with one or more photons, one electron or muon, and $\not{E}_T$. No significant excess above the Standard Model expectations is observed. Limits are also set in the Tglu1F simplified model, see Fig. 6.

[76] KHACHATRYAN 16Y searched in 19.7 fb^{-1} of pp collisions at $\sqrt{s}$ = 8 TeV for events with one or two soft isolated leptons, hadronic jets, and $\not{E}_T$. No significant excess above the Standard Model expectations is observed. Limits are set on the $\widetilde{\chi}^\pm_1$ mass (which is degenerate with the $\widetilde{\chi}^0_2$) in the Tchi1n2A simplified model, see Fig. 4.

[77] AAD 14AV searched in 20.3 fb^{-1} of pp collisions at $\sqrt{s}$ = 8 TeV for the direct production of charginos, neutralinos and staus in events containing at last two hadronically decaying τ-leptons, large missing transverse momentum and low jet activity. The quoted limit was derived for direct $\widetilde{\chi}^\pm_1\widetilde{\chi}^0_2$ and $\widetilde{\chi}^\pm_1\widetilde{\chi}^\mp_1$ production with $\widetilde{\chi}^0_2 \rightarrow \widetilde{\tau}\tau \rightarrow \tau\tau\widetilde{\chi}^0_1$ and $\widetilde{\chi}^\pm_1 \rightarrow \widetilde{\tau}\nu(\widetilde{\nu}_\tau\tau) \rightarrow \tau\nu\widetilde{\chi}^0_1$, $m_{\widetilde{\chi}^0_2} = m_{\widetilde{\chi}^\pm_1}$, $m_{\widetilde{\tau}}$ = 0.5 ($m_{\widetilde{\chi}^\pm_1} + m_{\widetilde{\chi}^0_1}$), $m_{\widetilde{\chi}^0_1}$ = 0 GeV. No excess over the expected SM background is observed. Exclusion limits are set in simplified models of $\widetilde{\chi}^\pm_1\widetilde{\chi}^\mp_1$ and $\widetilde{\chi}^\pm_1\widetilde{\chi}^0_2$ pair production, see their Figure 7. Upper limits on the cross section and signal strength for direct di-stau production are derived, see Figures 8 and 9. Also, limits are derived in a pMSSM model where the only light slepton is the $\widetilde{\tau}_R$, see Figure 10.

[78] AAD 14AV searched in 20.3 fb^{-1} of pp collisions at $\sqrt{s}$ = 8 TeV for the direct production of charginos, neutralinos and staus in events containing at last two hadronically decaying τ-leptons, large missing transverse momentum and low jet activity. The quoted limit was derived for direct $\widetilde{\chi}^\pm_1\widetilde{\chi}^\mp_1$ production with $\widetilde{\chi}^\pm_1 \rightarrow \widetilde{\tau}\nu(\widetilde{\nu}_\tau\tau) \rightarrow \tau\nu\widetilde{\chi}^0_1$, $m_{\widetilde{\tau}}$ = 0.5 ($m_{\widetilde{\chi}^\pm_1} + m_{\widetilde{\chi}^0_1}$), $m_{\widetilde{\chi}^0_1}$ = 0 GeV. No excess over the expected SM background is observed. Exclusion limits are set in simplified models of $\widetilde{\chi}^\pm_1\widetilde{\chi}^\mp_1$ and $\widetilde{\chi}^\pm_1\widetilde{\chi}^0_2$ pair production, see their Figure 7. Upper limits on the cross section and signal strength for direct di-stau production are derived, see Figures 8 and 9. Also, limits are derived in a pMSSM model where the only light slepton is the $\widetilde{\tau}_R$, see Figure 10.

[79] AAD 14G searched in 20.3 fb^{-1} of pp collisions at $\sqrt{s}$ = 8 TeV for electroweak production of chargino pairs, or chargino-neutralino pairs, decaying to a final state with two leptons (e and μ) and missing transverse momentum. No excess beyond the Standard Model expectation is observed. Exclusion limits are derived in simplified models of chargino pair production, with chargino decays to the lightest neutralino via either sleptons or gauge bosons, see Fig 5.; or in simplified models of chargino and next-to-lightest neutralino production, with decays to the lightest neutralino via gauge bosons, see Fig. 7. An interpretation in the pMSSM is also given, see Fig. 10.

[80] AALTONEN 14 searched in 5.8 fb^{-1} of $p\overline{p}$ collisions at $\sqrt{s}$ = 1.96 TeV for evidence of chargino and next-to-lightest neutralino associated production in final states consisting of three leptons (electrons, muons or taus) and large missing transverse momentum. The results are consistent with the Standard Model predictions within 1.85 σ. Limits on the chargino mass are derived in an mSUGRA model with m_0 = 60 GeV, tanβ = 3, A_0 = 0 and μ >0, see their Fig. 2.

[81] KHACHATRYAN 14I searched in 19.5 fb^{-1} of pp collisions at $\sqrt{s}$ = 8 TeV for electroweak production of chargino pairs decaying to a final state with opposite-sign lepton pairs (e or μ) and missing transverse momentum. No excess beyond the Standard Model expectation is observed. Exclusion limits are derived in simplified models, see Fig. 18.

[82] AALTONEN 13Q searched in 6.0 fb^{-1} of $p\overline{p}$ collisions at $\sqrt{s}$ = 1.96 TeV for evidence of chargino-neutralino associated production in like-sign dilepton final states. One lepton is identified as the hadronic decay of a tau lepton, while the other is an electron or muon. Good agreement with the Standard Model predictions is observed and limits are set on the chargino-neutralino cross section for simplified gravity- and gauge-mediated models, see their Figs. 2 and 3.

[83] AAD 12AS searched in 2.06 fb^{-1} of pp collisions at $\sqrt{s}$ = 7 TeV for charginos and neutralinos decaying to a final state with three leptons (e and μ) and missing transverse energy. No excess beyond the Standard Model expectation is observed. Exclusion limits are derived in the phenomenological MSSM, see Fig. 2 (top), and in simplified models, see Fig. 2 (bottom).

[84] AAD 12T looked in 1 fb^{-1} of pp collisions at $\sqrt{s}$ = 7 TeV for the production of supersymmetric particles decaying into final states with missing transverse momentum and exactly two isolated leptons (e or μ). Opposite-sign and same-sign dilepton events were separately studied. Additionally, in opposite-sign events, a search was made for an excess of same-flavor over different-flavor lepton pairs. No excess over the expected background is observed and limits are placed on the effective production cross section of opposite-sign dilepton events with $\not{E}_T$ > 250 GeV and on same-sign dilepton events with $\not{E}_T$ > 100 GeV. The latter limit is interpreted in a simplified electroweak gaugino production model as a lower chargino mass limit.

[85] CHATRCHYAN 11B looked in 35 pb^{-1} of pp collisions at $\sqrt{s}$=7 TeV for events with an isolated lepton (e or μ), a photon and $\not{E}_T$ which may arise in a generalized gauge mediated model from the decay of Wino-like NLSPs. No evidence for an excess over the expected background is observed. Limits are derived in the plane of squark/gluino mass versus Wino mass (see Fig. 4). Mass degeneracy of the produced squarks and gluinos is assumed.

[86] CHATRCHYAN 11V looked in 35 pb^{-1} of pp collisions at $\sqrt{s}$ = 7 TeV for events with $\geq$ 3 isolated leptons (e, μ or τ), with or without jets and $\not{E}_T$. No evidence for an excess over the expected background is observed. Limits are derived in the CMSSM (m_0, $m_{1/2}$) plane for tanβ = 3 (see Fig. 5).

Long-lived $\widetilde{\chi}^\pm$ (Chargino) mass limit

Limits on charginos which leave the detector before decaying.

VALUE (GeV)	CL%	DOCUMENT ID		TECN	COMMENT
>1300	95	[1] AAD	25AE	ATLS	$\widetilde{\chi}^\pm \rightarrow \widetilde{\chi}^0_1\pi^\pm$, wino LSP, stable, $\tau_{\widetilde{\chi}^\pm_1}$ > 100 ns
>1050	95	[2] AAD	23G	ATLS	$\widetilde{\chi}^\pm \rightarrow \widetilde{\chi}^0_1\pi^\pm$, wino LSP,$\tau$=20 ns
>1050	95	[2] AAD	23G	ATLS	$\widetilde{\chi}^\pm \rightarrow \widetilde{\chi}^0_1\pi^\pm$, wino LSP, stable
> 660	95	[3] AAD	22U	ATLS	$\widetilde{\chi}^\pm \rightarrow \widetilde{\chi}^0_1\pi^\pm$, wino LSP, AMSB, tan$\beta$ = 5, μ > 0, τ = 0.2 ns
> 860	95	[3] AAD	22U	ATLS	$\widetilde{\chi}^\pm \rightarrow \widetilde{\chi}^0_1\pi^\pm$, wino LSP, AMSB, tan$\beta$ = 5, μ > 0, τ = 1.5 ns
> 220	95	[3] AAD	22U	ATLS	$\widetilde{\chi}^\pm \rightarrow \widetilde{\chi}^0_1\pi^\pm$, higgsino LSP, τ=0.04 ns
> 710	95	[3] AAD	22U	ATLS	$\widetilde{\chi}^\pm \rightarrow \widetilde{\chi}^0_1\pi^\pm$, higgsino LSP, τ=1 ns
> 884	95	[4] SIRUNYAN	20N	CMS	$\widetilde{\chi}^\pm \rightarrow \widetilde{\chi}^0_1\pi^\pm$, wino LSP, AMSB, tan$\beta$ = 5, μ > 0, τ = 3 ns
> 474	95	[4] SIRUNYAN	20N	CMS	$\widetilde{\chi}^\pm \rightarrow \widetilde{\chi}^0_1\pi^\pm$, wino LSP, AMSB, tan$\beta$ = 5, μ > 0, τ = 0.2 ns
> 750	95	[4] SIRUNYAN	20N	CMS	$\widetilde{\chi}^\pm \rightarrow \widetilde{\chi}^0_1\pi^\pm$, higgsino LSP, AMSB, tanβ=5, μ >0,τ=3ns
> 175	95	[4] SIRUNYAN	20N	CMS	$\widetilde{\chi}^\pm \rightarrow \widetilde{\chi}^0_1\pi^\pm$, higgsino LSP, AMSB, tanβ=5,μ >0,τ=0.05ns
>1090	95	[5] AABOUD	19AT	ATLS	long-lived $\widetilde{\chi}^\pm_1$ mAMSB
> 460	95	[6] AABOUD	18AS	ATLS	$\widetilde{\chi}^\pm \rightarrow \widetilde{\chi}^0_1\pi^\pm$, lifetime 0.2 ns, $m_{\widetilde{\chi}^\pm} - m_{\widetilde{\chi}^0_1}$ = 160 MeV
> 715	95	[7] SIRUNYAN	18BR	CMS	$\widetilde{\chi}^\pm \rightarrow \widetilde{\chi}^0_1\pi^\pm$, AMSB, tan$\beta$ = 5 and μ > 0, τ = 3 ns
> 695	95	[7] SIRUNYAN	18BR	CMS	$\widetilde{\chi}^\pm \rightarrow \widetilde{\chi}^0_1\pi^\pm$, AMSB, tan$\beta$ = 5 and μ > 0, τ = 7 ns
> 505	95	[7] SIRUNYAN	18BR	CMS	$\widetilde{\chi}^\pm \rightarrow \widetilde{\chi}^0_1\pi^\pm$, AMSB, tan$\beta$ = 5, μ > 0, 0.5 ns > τ > 60 ns
> 620	95	[8] AAD	15AE	ATLS	stable $\widetilde{\chi}^\pm$
> 534	95	[9] AAD	15BM	ATLS	stable $\widetilde{\chi}^\pm$
> 239	95	[9] AAD	15BM	ATLS	$\widetilde{\chi}^\pm \rightarrow \widetilde{\chi}^0_1\pi^\pm$, lifetime 1 ns, $m_{\widetilde{\chi}^\pm} - m_{\widetilde{\chi}^0_1}$ = 0.14 GeV
> 482	95	[9] AAD	15BM	ATLS	$\widetilde{\chi}^\pm \rightarrow \widetilde{\chi}^0_1\pi^\pm$, lifetime 15 ns, $m_{\widetilde{\chi}^\pm} - m_{\widetilde{\chi}^0_1}$ = 0.14 GeV
> 103	95	[10] AAD	13H	ATLS	long-lived $\widetilde{\chi}^\pm \rightarrow \widetilde{\chi}^0_1\pi^\pm$, mAMSB, $\Delta m_{\widetilde{\chi}^0_1}$ = 160 MeV
> 92	95	[11] AAD	12BJ	ATLS	long-lived $\widetilde{\chi}^\pm \rightarrow \pi^\pm\widetilde{\chi}^0_1$, mAMSB
> 171	95	[12] ABAZOV	09M	D0	$\widetilde{H}$
> 102	95	[13] ABBIENDI	03L	OPAL	$m_{\widetilde{\nu}}$ >500 GeV
none 2–93.0	95	[14] ABREU	00T	DLPH	$\widetilde{H}^\pm$ or $m_{\widetilde{\nu}} > m_{\widetilde{\chi}^\pm}$

Int. J. Mod. Phys. A 2026.41. Downloaded from www.worldscientific.com
by UNIVERSITY OF CALIFORNIA @ BERKELEY on 09/16/26. Re-use and distribution is strictly not permitted, except for Open Access articles.

• • • We do not use the following data for averages, fits, limits, etc. • • •

> 260	95	[15] KHACHATRY...15AB	CMS		$\widetilde{\chi}^{\pm}_1 \rightarrow \widetilde{\chi}^0_1 \pi^{\pm}$, $\tau_{\widetilde{\chi}^{\pm}_1}$=0.2ns, AMSB
> 800	95	[16] KHACHATRY...15AO	CMS		long-lived $\widetilde{\chi}^{\pm}_1$, mAMSB, τ >100ns
> 100	95	[16] KHACHATRY...15AO	CMS		long-lived $\widetilde{\chi}^{\pm}_1$, mAMSB, τ > 3 ns
		[17] KHACHATRY...15W	CMS		long-lived $\widetilde{\chi}^0$, $\widetilde{q} \rightarrow q\widetilde{\chi}^0$, $\widetilde{\chi}^0 \rightarrow \ell^+\ell^-\nu$, RPV
> 270	95	[18] AAD	13BD	ATLS	disappearing-track signature, AMSB
> 278	95	[19] ABAZOV	13B	D0	long-lived $\widetilde{\chi}^{\pm}$, gaugino-like
> 244	95	[19] ABAZOV	13B	D0	long-lived $\widetilde{\chi}^{\pm}$, higgsino-like

[1] AAD 25AE searched for massive, charged long-lived particles in 140 fb^{-1} of pp collisions at $\sqrt{s}$ = 13 TeV. Two analyses are conducted: one looking for a single track, with high specific ionisation losses in the pixel detector and long time of flight to the hadron calorimeter, and one looking for two tracks, both with high specific ionisation in the pixel detector. No excess above the expected background is found. Limits are set in scenarios of long-lived R-hadrons (gluino) production, chargino production or stau pair production, see their figures 13 and 14.

[2] AAD 23G searched in 139 fb^{-1} of pp collisions at $\sqrt{s}$ = 13 TeV for chargino/neutralino pair production (wino-like LSP) in events with high-pt tracks with large ionisation in the pixel detector. No significant excess above the Standard Model predictions is observed. Limits are set on the chargino mass as a function of its lifetime, see Figure 19.

[3] AAD 22U searched for the signature of disappearing track from a long-lived chargino in 139 fb^{-1} of pp collisions at $\sqrt{s}$ = 13 TeV. Long-lived charginos decay into quasi-degenerate neutralino emitting a low-momentum particle whose identification is not attempted. The signal is identified by requiring short tracklets in the four pixel layers with no continuation in the SCT (strip) detector. The main background from fake tracklets is estimated directly with the data. No significant excess above the background prediction is found. The results are interpreted in an AMSB scenario (wino LSP), on $pp \rightarrow \widetilde{\chi}^{\pm}\widetilde{\chi}^{\pm}$ and $pp \rightarrow \widetilde{\chi}^{\pm}\widetilde{\chi}^0_1$, assuming B($\widetilde{\chi}^{\pm} \rightarrow \widetilde{\chi}^0_1\pi^{\pm}$) = 100%, see their figure 7. Results are also interpreted in a higgsino-LSP model, with $pp \rightarrow \widetilde{\chi}^{\pm}\widetilde{\chi}^{\mp}$, and $pp \rightarrow \widetilde{\chi}^{\pm}\widetilde{\chi}^0_{1,2}$, assuming B($\widetilde{\chi}^{\pm} \rightarrow \widetilde{\chi}^0_1\pi^{\pm}$) = 95.5%, B($\widetilde{\chi}^{\pm} \rightarrow \widetilde{\chi}^0_1 e^{\pm}$) = 3%, B($\widetilde{\chi}^{\pm} \rightarrow \widetilde{\chi}^0_1\mu^{\pm}$) = 1.5%, see their figure 8. Finally, results are interpreted in a simplified model of gluino pair production, with $pp \rightarrow \widetilde{g}\widetilde{g}$ and B($\widetilde{g} \rightarrow qq\widetilde{\chi}^0_1$) = B($\widetilde{g} \rightarrow qq\widetilde{\chi}^+$) = B($\widetilde{g} \rightarrow qq\widetilde{\chi}^-$) = 1/3, see their figure 9.

[4] SIRUNYAN 20N searched in 101 fb^{-1} of pp collisions at $\sqrt{s}$ = 13 TeV for direct electroweak production of long-lived charginos in events containing isolated tracks with missing hits in the outer layer of the silicon tracker and little or no associated calorimetric energy deposits (disappearing tracks). No significant excess above the Standard Model expectations is observed. In an AMSB context and assuming a wino LSP, limits are set on the cross section of direct chargino production through $pp \rightarrow \widetilde{\chi}^{\pm}\widetilde{\chi}^{\mp}$ and $pp \rightarrow \widetilde{\chi}^{\pm}\widetilde{\chi}^0_1$, assuming B($\widetilde{\chi}^{\pm} \rightarrow \widetilde{\chi}^0_1\pi^{\pm}$) = 100%, as a function of the chargino mass and mean proper lifetime, see Figure 2. In the case of a Higgsino LSP, limits are set on the cross section of direct chargino production through $pp \rightarrow \widetilde{\chi}^{\pm}\widetilde{\chi}^{\mp}$ and $pp \rightarrow \widetilde{\chi}^{\pm}\widetilde{\chi}^0_{1,2}$, assuming B($\widetilde{\chi}^{\pm} \rightarrow \widetilde{\chi}^0_1\pi^{\pm}$) = 95.5%, B($\widetilde{\chi}^{\pm} \rightarrow \widetilde{\chi}^0_1 e^{\pm}$) = 3%, B($\widetilde{\chi}^{\pm} \rightarrow \widetilde{\chi}^0_1\mu^{\pm}$) = 1.5%, as a function of the chargino mass and mean proper lifetime, see Figure 3.

[5] AABOUD 19AT searched in 36.1 fb^{-1} of pp collisions at $\sqrt{s}$ = 13 TeV for metastable R-hadrons. Multiple search strategies for a wide range of lifetimes, corresponding to path lengths of a few meters, are defined. No significant deviations from the expected Standard Model background are observed. Results are interpreted in terms of direct electroweak production of long-lived charginos in the context of mAMSB scenarios. Chargino masses are excluded at 95% C.L. below 1090 GeV. See their Figure 10 (right).

[6] AABOUD 18AS searched in 36.1 fb^{-1} of pp collisions at $\sqrt{s}$ = 13 TeV for direct electroweak production of long-lived charginos in the context of AMSB or phenomenological MSSM scenarios with wino-like LSP. Events with a disappearing track due to a low-momentum pion accompanied by at least one jet with high transverse momentum from initial-state radiation are considered. No significant excess above the Standard Model expectations is observed. Exclusion limits are set at 95% confidence level on the mass of charginos for different chargino lifetimes. For a pure wino with a lifetime of about 0.2 ns, corresponding to a mass-splitting between the charged and neutral wino of around 160 MeV, chargino masses up to 460 GeV are excluded, see their Fig. 8.

[7] SIRUNYAN 18BR searched in 38.4 fb^{-1} of pp collisions at $\sqrt{s}$ = 13 TeV for direct electroweak production of long-lived charginos in events containing isolated tracks with missing hits in the outer layer of the silicon tracker and little or no associated calorimetric energy deposits (disappearing tracks). No significant excess above the Standard Model expectations is observed. In an AMSB context, limits are set on the cross section of direct chargino production through $pp \rightarrow \widetilde{\chi}^{\pm}\widetilde{\chi}^{\mp}$ and $pp \rightarrow \widetilde{\chi}^{\pm}\widetilde{\chi}^0_1$, assuming BR($\widetilde{\chi}^{\pm} \rightarrow \widetilde{\chi}^0_1\pi^{\pm}$) = 100%, as a function of the chargino mass and mean proper lifetime, see Figures 3, 4 and 5.

[8] AAD 15AE searched in 19.1 fb^{-1} of pp collisions at $\sqrt{s}$ = 8 TeV for heavy long-lived charged particles, measured through their specific ionization energy loss in the ATLAS pixel detector or their time-of-flight in the ALTAS muon system. In the absence of an excess of events above the expected backgrounds, limits are set on stable charginos, see Fig. 10.

[9] AAD 15BM searched in 18.4 fb^{-1} of pp collisions at $\sqrt{s}$ = 8 TeV for stable and metastable non-relativistic charged particles through their anomalous specific ionization energy loss in the ATLAS pixel detector. In absence of an excess of events above the expected backgrounds, limits are set on stable charginos (see Table 5) and on metastable charginos decaying to $\widetilde{\chi}^0_1\pi^{\pm}$, see Fig. 11.

[10] AAD 13H searched in 4.7 fb^{-1} of pp collisions at $\sqrt{s}$ = 7 TeV for direct electroweak production of long-lived charginos in the context of AMSB scenarios. The search is based on the signature of a high-momentum isolated track with few associated hits in the outer part of the tracking system, arising from a chargino decay into a neutralino and a low-momentum pion. The p_T spectrum of the tracks was found to be consistent with the SM expectations. Constraints on the lifetime and the production cross section were obtained, see Fig. 6. In the minimal AMSB framework with tanβ = 5, and μ > 0, a chargino having a mass below 103 (85) GeV for a chargino-neutralino mass splitting $\Delta m_{\widetilde{\chi}^0_1}$ of 160 (170) MeV is excluded at the 95% C.L. See Fig. 7 for more precise bounds.

[11] AAD 12BJ looked in 1.02 fb^{-1} of pp collisions at $\sqrt{s}$ = 7 TeV for signatures of decaying charginos resulting in isolated tracks with few associated hits in the outer region of the tracking system. The p_T spectrum of the tracks was found to be consistent with the SM expectations. Constraints on the lifetime and the production cross section were obtained. In the minimal AMSB framework with $m_{3/2}$ < 32 TeV, m_0 < 1.5 TeV, tanβ = 5, and μ > 0, a chargino having a mass below 92 GeV and a lifetime between 0.5 ns and 2 ns is excluded at the 95% C.L. See their Fig. 8 for more precise bounds.

[12] ABAZOV 09M searched in 1.1 fb^{-1} of $p\overline{p}$ collisions at $\sqrt{s}$ = 1.96 TeV for events with direct production of a pair of charged massive stable particles identified by their TOF. The number of the observed events is consistent with the predicted background. The data are used to constrain the production cross section as a function of the $\widetilde{\chi}^{\pm}_1$ mass, see their Fig. 2. The quoted limit improves to 206 GeV for gaugino-like charginos.

[13] ABBIENDI 03L used e^+e^- data at $\sqrt{s}$ = 130–209 GeV to select events with two high momentum tracks with anomalous dE/dx. The excluded cross section is compared to the theoretical expectation as a function of the heavy particle mass in their Fig. 3. The bounds are valid for colorless fermions with lifetime longer than 10^{-6} s. Supersedes the results from ACKERSTAFF 98P.

[14] ABREU 00T searches for the production of heavy stable charged particles, identified by their ionization or Cherenkov radiation, using data from $\sqrt{s}$= 130 to 189 GeV. These limits include and update the results of ABREU 98P.

[15] KHACHATRYAN 15AB searched in 19.5 fb^{-1} of pp collisions at $\sqrt{s}$ = 8 TeV for events containing tracks with little or no associated calorimeter energy deposits and with missing hits in the outer layers of the tracking system (disappearing-track signature). Such disappearing tracks can result from the decay of charginos that are nearly mass degenerate with the lightest neutralino. The number of observed events is in agreement with the background expectation. Limits are set on the cross section of electroweak chargino production in terms of the chargino mass and mean proper lifetime, see Fig. 4. In the minimal AMSB model, a chargino mass below 260 GeV is excluded at 95% C.L., see their Fig. 5.

[16] KHACHATRYAN 15O searched in 18.8 fb^{-1} of pp collisions at $\sqrt{s}$ = 8 TeV for evidence of long-lived charginos in the context of AMSB and pMSSM scenarios. The results are based on a previously published search for heavy stable charged particles at 7 and 8 TeV. In the minimal AMSB framework with tanβ = 5 and μ > 0, constraints on the chargino mass and lifetime were placed, see Fig. 5. Charginos with a mass below 800 (100) GeV are excluded at the 95% C.L. for lifetimes above 100 ns (3 ns). Constraints are also placed on the pMSSM parameter space, see Fig. 3.

[17] KHACHATRYAN 15W searched in up to 20.5 fb^{-1} of pp collisions at $\sqrt{s}$ = 8 TeV for evidence of long-lived neutralinos produced through $\widetilde{q}$-pair production, with $\widetilde{q} \rightarrow q\widetilde{\chi}^0$ and $\widetilde{\chi}^0 \rightarrow \ell^+\ell^-\nu$ (RPV: λ_{121}, $\lambda_{122} \neq 0$). 95% C.L. exclusion limits on cross section times branching ratio are set as a function of mean proper decay length of the neutralino, see Figs. 6 and 9.

[18] AAD 13BD searched in 20.3 fb^{-1} of pp collisions at $\sqrt{s}$ = 8 TeV for events containing tracks with no associated hits in the outer region of the tracking system resulting from the decay of charginos that are nearly mass degenerate with the lightest neutralino, as is often the case in AMSB scenarios. No significant excess above the background expectation is observed for candidate tracks with large transverse momentum. Constraints on chargino properties are obtained and in the minimal AMSB model, a chargino mass below 270 GeV is excluded at 95% C.L., see their Fig. 7.

[19] ABAZOV 13B looked in 6.3 fb^{-1} of $p\overline{p}$ collisions at $\sqrt{s}$ = 1.96 TeV for charged massive long-lived particles in events with muon-like particles that have both speed and ionization energy loss inconsistent with muons produced in beam collisions. In the absence of an excess, limits are set at 95% C.L. on gaugino- and higgsino-like charginos, see their Table 20 and Fig. 23.

$\widetilde{\nu}$ (Sneutrino) mass limit

The limits may depend on the number, $N(\widetilde{\nu})$, of sneutrinos assumed to be degenerate in mass. Only $\widetilde{\nu}_L$ (not $\widetilde{\nu}_R$) is assumed to exist. It is possible that $\widetilde{\nu}$ could be the lightest supersymmetric particle (LSP).

We report here, but do not include in the Listings, the limits obtained from the fit of the final results obtained by the LEP Collaborations on the invisible width of the Z boson ($\Delta\Gamma_{\rm inv.}$ < 2.0 MeV, LEP-SLC 06): $m_{\widetilde{\nu}}$ > 43.7 GeV ($N(\widetilde{\nu})$=1) and $m_{\widetilde{\nu}}$ > 44.7 GeV ($N(\widetilde{\nu})$=3) .

Some earlier papers are now obsolete and have been omitted. They were last listed in our PDG 14 edition: K. Olive, *et al.* (Particle Data Group), Chinese Physics **C38** 070001 (2014) (http://pdg.lbl.gov).

VALUE (GeV)	CL%	DOCUMENT ID		TECN	COMMENT
> 450	95	[1] AAD	25L	ATLS	3ℓ; $\widetilde{\ell} \rightarrow \ell\widetilde{\chi}^0_3$; $\widetilde{\chi}^0_3 \rightarrow Z/h/W + \widetilde{\chi}$; ℓ=e,μ,ν_e,ν_μ; $\widetilde{\chi}$ higgsino; $m_{\widetilde{\chi}^0_3}$=170 GeV; $m_{\widetilde{\chi}}$=100 GeV
> 410	95	[1] AAD	25L	ATLS	3ℓ; $\widetilde{\ell} \rightarrow \ell\widetilde{\chi}^0_3$; $\widetilde{\chi}^0_3 \rightarrow Z/h/W + \widetilde{\chi}$; ℓ=e,ν_e; $\widetilde{\chi}$ higgsino; $m_{\widetilde{\chi}^0_3}$=170 GeV; $m_{\widetilde{\chi}}$=100 GeV
> 340	95	[1] AAD	25L	ATLS	3ℓ; $\widetilde{\ell} \rightarrow \ell\widetilde{\chi}^0_3$; $\widetilde{\chi}^0_3 \rightarrow Z/h/W + \widetilde{\chi}$; ℓ=μ,ν_μ; $\widetilde{\chi}$ higgsino; $m_{\widetilde{\chi}^0_3}$=180 GeV; $m_{\widetilde{\chi}}$=100 GeV
>3900	95	[2] AAD	23CB	ATLS	RPV, $\widetilde{\nu}_\tau \rightarrow e\mu$, $\lambda_{312} = \lambda_{321}$ = 0.07, λ'_{311} = 0.11
>2800	95	[2] AAD	23CB	ATLS	RPV, $\widetilde{\nu}_\tau \rightarrow e\tau$, λ_{313} = 0.07, λ'_{311} = 0.11
>2700	95	[2] AAD	23CB	ATLS	RPV, $\widetilde{\nu}_\tau \rightarrow \mu\tau$, λ_{323} = 0.07, λ'_{311} = 0.11
>4200	95	[3] TUMASYAN	23H	CMS	$1e + 1\mu$, RPV $\nu_\tau \rightarrow e\mu$, λ=λ' = 0.1
>3700	95	[3] TUMASYAN	23H	CMS	$1e + 1\tau$, RPV $\nu_\tau \rightarrow e\tau$, λ= λ' = 0.1
>3600	95	[3] TUMASYAN	23H	CMS	$1\mu + 1\tau$, RPV $\nu_\tau \rightarrow \mu\tau$, λ= λ' = 0.1
>2200	95	[3] TUMASYAN	23H	CMS	$1e + 1\mu$, RPV $\nu_\tau \rightarrow e\mu$, λ= λ' = 0.01
>1600	95	[3] TUMASYAN	23H	CMS	$1e + 1\tau$, RPV $\nu_\tau \rightarrow e\tau$, λ= λ' = 0.01
>1600	95	[3] TUMASYAN	23H	CMS	$1\mu + 1\tau$, RPV $\nu_\tau \rightarrow \mu\tau$, λ= λ' = 0.01

>3400	95	[4] AABOUD	18CM	ATLS	RPV, $\widetilde{\nu}_\tau \rightarrow e\mu$, $\lambda_{312} = \lambda_{321} = 0.07$, $\lambda'_{311} = 0.11$
>2900	95	[5] AABOUD	18CM	ATLS	RPV, $\widetilde{\nu}_\tau \rightarrow e\tau$, $\lambda_{313} = \lambda_{331} = 0.07$, $\lambda'_{311} = 0.11$
>2600	95	[6] AABOUD	18CM	ATLS	RPV, $\widetilde{\nu}_\tau \rightarrow \mu\tau$, $\lambda_{323} = \lambda_{332} = 0.07$, $\lambda'_{311} = 0.11$
>1060	95	[7] AABOUD	18Z	ATLS	RPV, $\geq 4\ell$, $\lambda_{12k} \neq 0$, $m_{\widetilde{\chi}^0_1} =$ 600 GeV (mass-degenerate left-handed sleptons and sneutrinos of all 3 generations)
> 780	95	[7] AABOUD	18Z	ATLS	RPV, $\geq 4\ell$, $\lambda_{i33} \neq 0$, $m_{\widetilde{\chi}^0_1} =$ 300 GeV (mass-degenerate left-handed sleptons and sneutrinos of all 3 generations)
>1700	95	[8] SIRUNYAN	18AT	CMS	RPV, $\widetilde{\nu}_\tau \rightarrow e\mu$, $\lambda_{132} = \lambda_{231} = \lambda'_{311} = 0.01$
>3800	95	[8] SIRUNYAN	18AT	CMS	RPV, $\widetilde{\nu}_\tau \rightarrow e\mu$, $\lambda_{132} = \lambda_{231} = \lambda'_{311} = 0.1$
>2300	95	[9] AABOUD	16P	ATLS	RPV, $\widetilde{\nu}_\tau \rightarrow e\mu$, $\lambda'_{311} = 0.11$
>2200	95	[9] AABOUD	16P	ATLS	RPV, $\widetilde{\nu}_\tau \rightarrow e\tau$, $\lambda'_{311} = 0.11$
>1900	95	[9] AABOUD	16P	ATLS	RPV, $\widetilde{\nu}_\tau \rightarrow \mu\tau$, $\lambda'_{311} = 0.11$
> 400	95	[10] AAD	14X	ATLS	RPV, $\geq 4\ell^\pm$, $\widetilde{\nu} \rightarrow \nu\widetilde{\chi}^0_1$, $\widetilde{\chi}^0_1 \rightarrow \ell^\pm\ell^\mp\nu$
		[11] AAD	11Z	ATLS	RPV, $\widetilde{\nu}_\tau \rightarrow e\mu$
> 94	95	[12] ABDALLAH	03M	DLPH	$1 \leq \tan\beta \leq 40$, $m_{\widetilde{e}_R} - m_{\widetilde{\chi}^0_1} > 10$ GeV
> 84	95	[13] HEISTER	02N	ALEP	$\widetilde{\nu}_e$, any Δm
> 41	95	[14] DECAMP	92	ALEP	$\Gamma(Z \rightarrow$ invisible$)$; $N(\widetilde{\nu})$=3, model independent
• • • We do not use the following data for averages, fits, limits, etc. • • •					
		[15] SIRUNYAN	19AO		RPV, $\mu^\pm\mu^\pm + \geq$ 2jets, $\lambda'_{211} \neq 0$, $\widetilde{\nu}_\mu \rightarrow \mu\widetilde{\chi}^\pm_1$, $\widetilde{\chi}^\pm_1 \rightarrow \mu q\overline{q}q\overline{q}$
>1280	95	[16] KHACHATRY...	16BE	CMS	RPV, $\widetilde{\nu}_\tau \rightarrow e\mu$, $\lambda_{132} = \lambda_{231} = \lambda'_{311} = 0.01$
>2300	95	[16] KHACHATRY...	16BE	CMS	RPV, $\widetilde{\nu}_\tau \rightarrow e\mu$, $\lambda_{132} = \lambda_{231} = 0.07$, $\lambda'_{311} = 0.11$
>2000	95	[17] AAD	15O	ATLS	RPV $(e\mu)$, $\widetilde{\nu}_\tau$, $\lambda'_{311} = 0.11$, $\lambda_{i3k} = 0.07$
>1700	95	[17] AAD	15O	ATLS	RPV $(\tau\mu, e\tau)$, $\widetilde{\nu}_\tau$, $\lambda'_{311} = 0.11$, $\lambda_{i3k} = 0.07$
		[18] AAD	13AI	ATLS	RPV, $\widetilde{\nu}_\tau \rightarrow e\mu, e\tau, \mu\tau$
		[19] AAD	11H	ATLS	RPV, $\widetilde{\nu}_\tau \rightarrow e\mu$
		[20] AALTONEN	10Z	CDF	RPV, $\widetilde{\nu}_\tau \rightarrow e\mu, e\tau, \mu\tau$
		[21] ABAZOV	10M	D0	RPV, $\widetilde{\nu}_\tau \rightarrow e\mu$
> 95	95	[22] ABDALLAH	04H	DLPH	AMSB, $\mu > 0$
> 37.1	95	[23] ADRIANI	93M	L3	$\Gamma(Z \rightarrow$ invisible$)$; $N(\widetilde{\nu})$=1
> 36	95	ABREU	91F	DLPH	$\Gamma(Z \rightarrow$ invisible$)$; $N(\widetilde{\nu})$=1
> 31.2	95	[24] ALEXANDER	91F	OPAL	$\Gamma(Z \rightarrow$ invisible$)$; $N(\widetilde{\nu})$=1

[1] AAD 25L searched for an excess of three-lepton events in 140 fb^{-1} of pp collisions at $\sqrt{s}$ = 13 TeV. The search targets scenarios connected with potential anomalous muon magnetic moment: pair-produced sleptons (either charged or neutral) are assumed to decay to a bino-like $\widetilde{\chi}^0_3$, decaying to a mass-degenerate higgsino triplet LSP via the emission of a W, Z or h boson (with branching ratio 50%, 25% and 25% respectively). Three sets of signal regions are defined (with a SFOS pair on- and off-shell of the Z boson, and with three SS leptons). No significant excess is observed over the background prediction. 95% CL limits are extracted assuming degenerete $\widetilde{e}_L$, $\widetilde{\nu}_e$, $\widetilde{\mu}_L$, $\widetilde{\nu}_\mu$, degenerete $\widetilde{e}_L$, $\widetilde{\nu}_e$, and degenerete $\widetilde{\mu}_L$, $\widetilde{\nu}_\mu$, see their figures 15, 16a, and 16b.

[2] AAD 23CB searched in 139 fb^{-1} of pp collisions at $\sqrt{s}$ = 13 TeV for heavy particles decaying into an $e\mu$, $e\tau$, $\mu\tau$ final state. No significant deviation from the expected SM background is observed. Limits are set on the mass of a stau neutrino with R-parity-violating couplings, with decays $\widetilde{\nu}_\tau \rightarrow e\mu$, $\widetilde{\nu}_\tau \rightarrow e\tau$, $\widetilde{\nu}_\tau \rightarrow \mu\tau$, see figures 4b, 5b, 6b.

[3] TUMASYAN 23H searched in 138 fb^{-1} of pp collisions at $\sqrt{s}$ = 13 TeV for evidence of resonant $\widetilde{\nu}_\tau$ production in events with two charged leptons, $e\mu$, $e\tau$, or $\mu\tau$. No significant excess above the Standard Model expectations is observed. Limits are set on the mass of $\widetilde{\nu}_\tau$ in an RPV model for resonant sneutrino production, where all RPV couplings vanish, except for those that are connected to the production and decay of the $\widetilde{\nu}_\tau$, considering a SUSY mass hierarchy with $\widetilde{\nu}_\tau$ as the LSP. The $\widetilde{\nu}_\tau$ is produced resonantly through λ'_{311} coupling, and decays via λ_{i3k} coupling to two leptons, see their figure 3 for couplings of 0.1 and 0.01. Exclusion limits are also shown in the plane of $\widetilde{\nu}_\tau$ mass and λ' coupling, for four values of λ couplings, see their figure 6. In addition, limits are set on heavy Z' gauge bosons with lepton flavor violating decays, see their figure 4, and on nonresonant quantum black hole production in models with extra spatial dimensions, see their figure 5. Model-independent upper limits on the product of the cross section, the branching fraction, acceptance, and efficiency are given as well, see their figure 7.

[4] AABOUD 18CM searched in 36.1 fb^{-1} of pp collisions at $\sqrt{s}$ = 13 TeV for heavy particles decaying into an $e\mu$, $e\tau$, $\mu\tau$ final state. No significant deviation from the expected SM background is observed. Limits are set on the mass of a stau neutrino with R-parity-violating couplings. For $\widetilde{\nu}_\tau \rightarrow e\mu$, masses below 3.4 TeV are excluded at 95% CL, see their Figure 4(b). Upper limits on the RPV couplings $|\lambda_{312}|$ versus $|\lambda'_{311}|$ are also performed, see their Figure 8(a-b).

[5] AABOUD 18CM searched in 36.1 fb^{-1} of pp collisions at $\sqrt{s}$ = 13 TeV for heavy particles decaying into an $e\mu$, $e\tau$, $\mu\tau$ final state. No significant deviation from the expected SM background is observed. Limits are set on the mass of a stau neutrino with R-parity-violating couplings. For $\widetilde{\nu}_\tau \rightarrow e\tau$, masses below 2.9 TeV are excluded at 95% CL, see their Figure 5(b). Upper limits on the RPV couplings $|\lambda_{313}|$ versus $|\lambda'_{311}|$ are also performed, see their Figure 8(c).

[6] AABOUD 18CM searched in 36.1 fb^{-1} of pp collisions at $\sqrt{s}$ = 13 TeV for heavy particles decaying into an $e\mu$, $e\tau$, $\mu\tau$ final state. No significant deviation from the expected SM background is observed. Limits are set on the mass of a stau neutrino with R-parity-violating couplings. For $\widetilde{\nu}_\tau \rightarrow \mu\tau$, masses below 2.6 TeV are excluded at 95% CL, see their Figure 6(b). Upper limits on the RPV couplings $|\lambda_{323}|$ versus $|\lambda'_{311}|$ are also performed, see their Figure 8(d).

[7] AABOUD 18Z searched in 36.1 fb^{-1} of pp collisions at $\sqrt{s}$ = 13 TeV for events containing four or more charged leptons (electrons, muons and up to two hadronically decaying taus). No significant deviation from the expected SM background is observed. Limits are set on the Higgsino mass in simplified models of general gauge mediated supersymmetry Tn1n1A/Tn1n1B/Tn1n1C, see their Figure 9. Limits are also set on the wino, slepton, sneutrino and gluino mass in a simplified model of NLSP pair production with R-parity violating decays of the LSP via λ_{12k} or λ_{i33} to charged leptons, see their Figures 7, 8.

[8] SIRUNYAN 18AT searched in 35.9 fb^{-1} of pp collisions at $\sqrt{s}$ = 13 TeV for heavy resonances decaying into $e\mu$ final states. No significant excess above the Standard Model expectation is observed and 95% C.L. exclusions are placed on the cross section times branching ratio for the R-parity-violating production and decay of a supersymmetric tau sneutrino, see their Fig. 3.

[9] AABOUD 16P searched in 3.2 fb^{-1} of pp collisions at $\sqrt{s}$ = 13 TeV for events with different flavour dilepton pairs ($e\mu$, $e\tau$, $\mu\tau$) from the production of $\widetilde{\nu}_\tau$ via an RPV λ'_{311} coupling and followed by a decay via $\lambda_{312} = \lambda_{321} = 0.07$ for $e + \mu$, via $\lambda_{313} = \lambda_{331} = 0.07$ for $e + \tau$ and via $\lambda_{323} = \lambda_{332} = 0.07$ for $\mu + \tau$. No evidence for a dilepton resonance over the SM expectation is observed, and limits are derived on $m_{\widetilde{\nu}}$ at 95% CL, see their Figs. 2(b), 3(b), 4(b), and Table 3.

[10] AAD 14X searched in 20.3 fb^{-1} of pp collisions at $\sqrt{s}$ = 8 TeV for events with at least four leptons (electrons, muons, taus) in the final state. No significant excess above the Standard Model expectations is observed. Limits are set on the sneutrino mass in an R-parity violating simplified model where the decay $\widetilde{\nu} \rightarrow \nu\widetilde{\chi}^0_1$, with $\widetilde{\chi}^0_1 \rightarrow \ell^\pm\ell^\mp\nu$, takes place with a branching ratio of 100%, see Fig. 9.

[11] AAD 11Z looked in 1.07 fb^{-1} of pp collisions at $\sqrt{s}$ = 7 TeV for events with one electron and one muon of opposite charge from the production of $\widetilde{\nu}_\tau$ via an RPV λ'_{311} coupling and followed by a decay via λ_{312} into $e + \mu$. No evidence for an (e, μ) resonance over the SM expectation is observed, and a limit is derived in the plane of λ'_{311} versus $m_{\widetilde{\nu}}$ for three values of λ_{312}, see their Fig. 2. Masses $m_{\widetilde{\nu}} < 1.32$ (1.45) TeV are excluded for $\lambda'_{311} = 0.10$ and $\lambda_{312} = 0.05$ ($\lambda'_{311} = 0.11$ and $\lambda_{312} = 0.07$).

[12] ABDALLAH 03M uses data from $\sqrt{s}$ = 192–208 GeV to obtain limits in the framework of the MSSM with gaugino and sfermion mass universality at the GUT scale. An indirect limit on the mass is derived by constraining the MSSM parameter space by the results from direct searches for neutralinos (including cascade decays) and for sleptons. These limits are valid for values of $M_2 < 1$ TeV, $|\mu| \leq 1$ TeV with the $\widetilde{\chi}^0_1$ as LSP. The quoted limit is obtained when there is no mixing in the third family. See Fig. 43 for the mass limits as a function of $\tan\beta$. These limits update the results of ABREU 00W.

[13] HEISTER 02N derives a bound on $m_{\widetilde{\nu}_e}$ by exploiting the mass relation between the $\widetilde{\nu}_e$ and $\widetilde{e}$, based on the assumption of universal GUT scale gaugino and scalar masses $m_{1/2}$ and m_0 and the search described in the $\widetilde{e}$ section. In the MSUGRA framework with radiative electroweak symmetry breaking, the limit improves to $m_{\widetilde{\nu}_e} > 130$ GeV, assuming a trilinear coupling A_0=0 at the GUT scale. See Figs. 5 and 7 for the dependence of the limits on $\tan\beta$.

[14] DECAMP 92 limit is from $\Gamma(\text{invisible})/\Gamma(\ell\ell) = 5.91 \pm 0.15$ ($N_\nu = 2.97 \pm 0.07$).

[15] SIRUNYAN 19AO searched in 35.9 fb^{-1} of pp collisions at $\sqrt{s}$ = 13 TeV for events containing two same-sign muons and at last two jets, originating from resonant production of second-generation sleptons ($\widetilde{\mu}_L$, $\widetilde{\nu}_\mu$) via the R-parity violating coupling λ'_{211} to quarks. No significant excess above the Standard Model expectations is observed. Upper limits on cross sections are derived in the context of two simplified models, see their Figure 4. The cross section limits are translated into limits on λ'_{211} for a modified CMSSM, see their Figure 5.

[16] KHACHATRYAN 16BE searched in 19.7 fb^{-1} of pp collisions at $\sqrt{s}$ = 8 TeV for evidence of narrow resonances decaying into $e\mu$ final states. No significant excess above the Standard Model expectation is observed and 95% C.L. exclusions are placed on the cross section times branching ratio for the production of an R-parity-violating supersymmetric tau sneutrino, see their Fig. 3.

[17] AAD 15O searched in 20.3 fb^{-1} of pp collisions at $\sqrt{s}$ = 8 TeV for evidence of heavy particles decaying into $e\mu$, $e\tau$ or $\mu\tau$ final states. No significant excess above the Standard Model expectation is observed, and 95% C.L. exclusions are placed on the cross section times branching ratio for the production of an R-parity-violating supersymmetric tau sneutrino, applicable to any sneutrino flavour, see their Fig. 2.

[18] AAD 13AI searched in 4.6 fb^{-1} of pp collisions at $\sqrt{s}$ = 7 TeV for evidence of heavy particles decaying into $e\mu$, $e\tau$ or $\mu\tau$ final states. No significant excess above the Standard Model expectation is observed, and 95% C.L. exclusions are placed on the cross section times branching ratio for the production of an R-parity-violating supersymmetric tau sneutrino, see their Fig. 2. For couplings $\lambda'_{311} = 0.10$ and $\lambda_{i3k} = 0.05$, the lower limits on the $\widetilde{\nu}_\tau$ mass are 1610, 1110, 1100 GeV in the $e\mu$, $e\tau$, and $\mu\tau$ channels, respectively.

[19] AAD 11H looked in 35 pb^{-1} of pp collisions at $\sqrt{s}$ = 7 TeV for events with one electron and one muon of opposite charge from the production of $\widetilde{\nu}_\tau$ via an RPV λ'_{311} coupling and followed by a decay via λ_{312} into $e + \mu$. No evidence for an excess over the SM expectation is observed, and a limit is derived in the plane of λ'_{311} versus $m_{\widetilde{\nu}}$ for several values of λ_{312}, see their Fig. 2. Superseded by AAD 11Z.

[20] AALTONEN 10Z searched in 1 fb^{-1} of $p\overline{p}$ collisions at $\sqrt{s}$ = 1.96 TeV for events from the production $d\overline{d} \rightarrow \widetilde{\nu}_\tau$ with the subsequent decays $\widetilde{\nu}_\tau \rightarrow e\mu$, $\mu\tau$, $e\tau$ in the MSSM framework with RPV. Two isolated leptons of different flavor and opposite charges are required, with τs identified by their hadronic decay. No statistically significant excesses are observed over the SM background. Upper limits on λ'^2_{311} times the branching ratio are listed in their Table III for various $\widetilde{\nu}_\tau$ masses. Limits on the cross section times branching ratio for $\lambda'_{311} = 0.10$ and $\lambda_{i3k} = 0.05$, displayed in Fig. 2, are used to set limits on the $\widetilde{\nu}_\tau$ mass of 558 GeV for the $e\mu$, 441 GeV for the $\mu\tau$ and 442 GeV for the $e\tau$ channels.

Int. J. Mod. Phys. A 2026.41. Downloaded from www.worldscientific.com
by UNIVERSITY OF CALIFORNIA @ BERKELEY on 09/16/26. Re-use and distribution is strictly not permitted, except for Open Access articles.

Int. J. Mod. Phys. A 2026.41. Downloaded from www.worldscientific.com
by UNIVERSITY OF CALIFORNIA @ BERKELEY on 09/16/26. Re-use and distribution is strictly not permitted, except for Open Access articles.

[21] ABAZOV 10M looked in 5.3 fb^{-1} of $p\overline{p}$ collisions at $\sqrt{s}$ = 1.96 TeV for events with exactly one pair of high p_T isolated $e\mu$ and a veto against hard jets. No evidence for an excess over the SM expectation is observed, and a limit at 95% C.L. on the cross section times branching ratio is derived, see their Fig. 3. These limits are translated into limits on couplings as a function of $m_{\widetilde{\nu}_\tau}$ as shown on their Fig. 4. As an example, for $m_{\widetilde{\nu}_\tau}$ = 100 GeV and $\lambda_{312} \leq 0.07$, couplings $\lambda'_{311} > 7.7 \times 10^{-4}$ are excluded.

[22] ABDALLAH 04H use data from LEP 1 and $\sqrt{s}$ = 192–208 GeV. They re-use results or re-analyze the data from ABDALLAH 03M to put limits on the parameter space of anomaly-mediated supersymmetry breaking (AMSB), which is scanned in the region $1 < m_{3/2} < 50$ TeV, $0 < m_0 < 1000$ GeV, $1.5 < \tan\beta < 35$, both signs of μ. The constraints are obtained from the searches for mass degenerate chargino and neutralino, for SM-like and invisible Higgs, for leptonically decaying charginos and from the limit on non-SM Z width of 3.2 MeV. The limit is for m_t = 174.3 GeV (see Table 2 for other m_t values). The limit improves to 114 GeV for $\mu < 0$.

[23] ADRIANI 93M limit from $\Delta\Gamma(Z)$(invisible)< 16.2 MeV.

[24] ALEXANDER 91F limit is for one species of $\widetilde{\nu}$ and is derived from Γ(invisible, new)/$\Gamma(\ell\ell)$ < 0.38.

Charged sleptons

This section contains limits on charged scalar leptons ($\widetilde{\ell}$, with ℓ=e,μ,τ). Studies of width and decays of the Z boson (use is made here of $\Delta\Gamma_{\rm inv}$ < 2.0 MeV, LEP 00) conclusively rule out $m_{\widetilde{\ell}_R}$ < 40 GeV (41 GeV for $\widetilde{\ell}_L$) , independently of decay modes, for each individual slepton. The limits improve to 43 GeV (43.5 GeV for $\widetilde{\ell}_L$) assuming all 3 flavors to be degenerate. Limits on higher mass sleptons depend on model assumptions and on the mass splitting Δm= $m_{\widetilde{\ell}} - m_{\widetilde{\chi}^0_1}$. The mass and composition of $\widetilde{\chi}^0_1$ may affect the selectron production rate in e^+e^- collisions through t-channel exchange diagrams. Production rates are also affected by the potentially large mixing angle of the lightest mass eigenstate $\widetilde{\ell}_1$=$\widetilde{\ell}_R$ sinθ_ℓ + $\widetilde{\ell}_L$ cosθ_ℓ. It is generally assumed that only $\widetilde{\tau}$ may have significant mixing. The coupling to the Z vanishes for θ_ℓ=0.82. In the high-energy limit of e^+e^- collisions the interference between γ and Z exchange leads to a minimal cross section for θ_ℓ=0.91, a value which is sometimes used in the following entries relative to data taken at LEP2. When limits on $m_{\widetilde{\ell}_R}$ are quoted, it is understood that limits on $m_{\widetilde{\ell}_L}$ are usually at least as strong.

Possibly open decays involving gauginos other than $\widetilde{\chi}^0_1$ will affect the detection efficiencies. Unless otherwise stated, the limits presented here result from the study of $\widetilde{\ell}^+\widetilde{\ell}^-$ production, with production rates and decay properties derived from the MSSM. Limits made obsolete by the recent analyses of e^+e^- collisions at high energies can be found in previous Editions of this Review.

For decays with final state gravitinos ($\widetilde{G}$), $m_{\widetilde{G}}$ is assumed to be negligible relative to all other masses.

R-parity conserving $\widetilde{e}$ (Selectron) mass limit

Some earlier papers are now obsolete and have been omitted. They were last listed in our PDG 14 edition: K. Olive, *et al.* (Particle Data Group), Chinese Physics **C38** 070001 (2014) (http://pdg.lbl.gov).

VALUE (GeV)	CL%	DOCUMENT ID		TECN	COMMENT
>215	95	[1] AAD	25AH	ATLS	2ℓ, $\widetilde{\ell}$ pair production, $m_{\widetilde{e}_L}$ = $m_{\widetilde{e}_R}$, $m_{\widetilde{e}} - m_{\widetilde{\chi}^0_1}$ = 5 GeV
>450	95	[2] AAD	25L	ATLS	3ℓ; $\widetilde{\ell} \to \ell\widetilde{\chi}^0_3$; $\widetilde{\chi}^0_3 \to Z/h/W + \widetilde{\chi}$; ℓ=e,μ,ν_e,ν_μ; $\widetilde{\chi}$ higgsino; $m_{\widetilde{\chi}^0_3}$=170 GeV; $m_{\widetilde{\chi}}$=100 GeV
>410	95	[2] AAD	25L	ATLS	3ℓ; $\widetilde{\ell} \to \ell\widetilde{\chi}^0_3$; $\widetilde{\chi}^0_3 \to Z/h/W + \widetilde{\chi}$; ℓ=e,ν_e; $\widetilde{\chi}$ higgsino; $m_{\widetilde{\chi}^0_3}$=170 GeV; $m_{\widetilde{\chi}}$=100 GeV
>740	95	[3] AAD	25M	ATLS	displaced 2ℓ; $\widetilde{e}$ pair production; $\widetilde{e} \to e\widetilde{G}$; $\tau_{\widetilde{e}}$ = 0.3 ns
>160	95	[4] CHEKHOVSKY	25M	CMS	$\geq$ 1 ISR jet + (in-)visible decay products, $\widetilde{e}_R$ pair production, $\widetilde{e}_R \to e\widetilde{\chi}^0_1$, $m_{\widetilde{e}_R} - m_{\widetilde{\chi}^0_1}$ = 5 GeV
>230	95	[4] CHEKHOVSKY	25M	CMS	$\geq$ 1 ISR jet + (in-)visible decay products, $\widetilde{e}_L$ pair production, $\widetilde{e}_L \to e\widetilde{\chi}^0_1$, $m_{\widetilde{e}_L} - m_{\widetilde{\chi}^0_1}$ = 5 GeV
>250	95	[4] CHEKHOVSKY	25M	CMS	$\geq$ 1 ISR jet + (in-)visible decay products, $\widetilde{e}_{R,L}$ pair production, $\widetilde{e}_{R,L} \to e\widetilde{\chi}^0_1$, $m_{\widetilde{e}_{R,L}} - m_{\widetilde{\chi}^0_1}$ = 5 GeV
none 130–700	95	[5] HAYRAPETY...	24N	CMS	Combination, $\widetilde{e} \to e\widetilde{\chi}^0_1$, $m_{\widetilde{\chi}^0_1}$ < 50 GeV
>215	95	[5] HAYRAPETY...	24N	CMS	Combination, $\widetilde{e} \to e\widetilde{\chi}^0_1$, Δm ($\widetilde{\chi}^\pm_1$, $\widetilde{\chi}^0_1$) = 5 GeV
>270	95	[6] AAD	23M	ATLS	2ℓ, $\widetilde{\ell}$ pair production, $m_{\widetilde{e}_L}$ = $m_{\widetilde{e}_R}$, $m_{\widetilde{\chi}^0_1}$ = 0 GeV
> 90	95	[6] AAD	23M	ATLS	2ℓ, $\widetilde{\ell}$ pair production, $m_{\widetilde{e}_L}$ = $m_{\widetilde{e}_R}$, $m_{\widetilde{e}} - m_{\widetilde{\chi}^0_1}$ = 26 GeV
>700	95	[7] SIRUNYAN	21M	CMS	$\ell^\pm\ell^\mp + \not{E}_T$, $m_{\widetilde{\ell}_R} = m_{\widetilde{\ell}_L}$ and $\widetilde{\ell}$=$\widetilde{e}$, $\widetilde{\mu}$, $m_{\widetilde{\chi}^0_1}$ = 0 GeV
>700	95	[8] AAD	20O	ATLS	2ℓ+$\not{E}_T$, $m_{\widetilde{\ell}_R} = m_{\widetilde{\ell}_L}$ and $\widetilde{\ell}$=$\widetilde{e}$, $\widetilde{\mu}$, $m_{\widetilde{\chi}^0_1}$=0 GeV
>250	95	[9] SIRUNYAN	19AW	CMS	$\ell^\pm\ell^\mp + \not{E}_T$, $\widetilde{e}_R$, $m_{\widetilde{\chi}^0_1}$ = 0 GeV
>310	95	[9] SIRUNYAN	19AW	CMS	$\ell^\pm\ell^\mp + \not{E}_T$, $\widetilde{e}_L$, $m_{\widetilde{\chi}^0_1}$ = 0 GeV
>350	95	[9] SIRUNYAN	19AW	CMS	$\ell^\pm\ell^\mp + \not{E}_T$, $m_{\widetilde{e}_R} = m_{\widetilde{e}_L}$, $m_{\widetilde{\chi}^0_1}$ = 0 GeV
>290	95	[9] SIRUNYAN	19AW	CMS	$\ell^\pm\ell^\mp + \not{E}_T$, $\widetilde{\ell}_R$ and $\widetilde{\ell}$=$\widetilde{e}$, $\widetilde{\mu}$, $m_{\widetilde{\chi}^0_1}$ = 0 GeV
>400	95	[9] SIRUNYAN	19AW	CMS	$\ell^\pm\ell^\mp + \not{E}_T$, $\widetilde{\ell}_L$ and $\widetilde{\ell}$=$\widetilde{e}$, $\widetilde{\mu}$, $m_{\widetilde{\chi}^0_1}$ = 0 GeV
>450	95	[9] SIRUNYAN	19AW	CMS	$\ell^\pm\ell^\mp + \not{E}_T$, $m_{\widetilde{\ell}_R} = m_{\widetilde{\ell}_L}$ and $\widetilde{\ell}$=$\widetilde{e}$, $\widetilde{\mu}$, $m_{\widetilde{\chi}^0_1}$ = 0 GeV
>500	95	[10] AABOUD	18BT	ATLS	$2\ell + \not{E}_T$, $m_{\widetilde{\ell}_R} = m_{\widetilde{\ell}_L}$ and $\widetilde{\ell}$=$\widetilde{e}$, $\widetilde{\mu}$, $\widetilde{\tau}$, with $m_{\widetilde{\chi}^0_1}$ = 0 GeV
>190	95	[11] AABOUD	18R	ATLS	2ℓ (soft) + $\not{E}_T$, $m_{\widetilde{e}} = m_{\widetilde{\mu}}$, $m_{\widetilde{e}} - m_{\widetilde{\chi}^0_1}$ = 5 GeV
		[12] CHATRCHYAN	14R	CMS	$\geq 3\ell^\pm$, $\widetilde{\ell} \to \ell^\pm\tau^\mp\tau^\mp\widetilde{G}$ simplified model, GMSB, stau (N)NLSP scenario
		[13] AAD	13B	ATLS	$2\ell^\pm + \not{E}_T$, SMS, pMSSM
> 97.5		[14] ABBIENDI	04	OPAL	$\widetilde{e}_R$,Δm > 11 GeV, $\lvert\mu\rvert$ >100 GeV, tanβ=1.5
> 94.4		[15] ACHARD	04	L3	$\widetilde{e}_R$,Δm > 10 GeV, $\lvert\mu\rvert$ >200 GeV, tan$\beta \geq$ 2
> 71.3		[15] ACHARD	04	L3	$\widetilde{e}_R$, all Δm
none 30–94	95	[16] ABDALLAH	03M	DLPH	Δm >15 GeV, $\widetilde{e}^+_R\widetilde{e}^-_R$
> 94	95	[17] ABDALLAH	03M	DLPH	$\widetilde{e}_R$,1 $\leq$ tan$\beta \leq$ 40, Δm >10 GeV
> 95	95	[18] HEISTER	02E	ALEP	Δm > 15 GeV, $\widetilde{e}^+_R\widetilde{e}^-_R$
> 73	95	[19] HEISTER	02N	ALEP	$\widetilde{e}_R$, any Δm
>107	95	[19] HEISTER	02N	ALEP	$\widetilde{e}_L$, any Δm
• • • We do not use the following data for averages, fits, limits, etc. • • •					
>101	95	[20] AAD	20I	ATLS	2ℓ (soft), jets, $\not{E}_T$, $\widetilde{e}_R$ only, $m_{\widetilde{e}_R} - m_{\widetilde{\chi}^0_1}$ = 7.5 GeV
>169	95	[21] AAD	20I	ATLS	2ℓ (soft), jets, $\not{E}_T$, $\widetilde{e}_L$ only, $m_{\widetilde{e}_L} - m_{\widetilde{\chi}^0_1}$ = 7.1 GeV
none 90–325	95	[22] AAD	14G	ATLS	$\widetilde{\ell}\widetilde{\ell} \to \ell^+\widetilde{\chi}^0_1\ell^-\widetilde{\chi}^0_1$, simplified model, $m_{\widetilde{\ell}_L} = m_{\widetilde{\ell}_R}$, $m_{\widetilde{\chi}^0_1}$ = 0 GeV
		[23] KHACHATRY...	14I	CMS	$\widetilde{\ell} \to \ell\widetilde{\chi}^0_1$, simplified model

[1] AAD 25AH searched for an excess in same-flavour dilepton production events in 140 fb^{-1} of pp collisions at $\sqrt{s}$ = 13 TeV using a BDT selection optimised on simplified models including sleptons and neutralinos with $m_{\widetilde{e}} - m_{\widetilde{\chi}^0_1} < m_W$: pair-produced sleptons decay to a lepton and a neutralino. Several signal regions are defined, depending on the BDT score. Despite some local excess at the level of 2.4 σ, the data agree with the background prediction. 95% CL limits are extracted a s a function of $m_{\widetilde{e}} - m_{\widetilde{\chi}^0_1}$, see their figure 13.

[2] AAD 25L searched for an excess of three-lepton events in 140 fb^{-1} of pp collisions at $\sqrt{s}$ = 13 TeV. The search targets scenarios connected with potential anomalous muon magnetic moment: pair-produced sleptons (either charged or neutral) are assumed to decay to a bino-like $\widetilde{\chi}^0_3$, decaying to a mass-degenerate higgsino triplet LSP via the emission of a W, Z or h boson (with branching ratio 50%, 25% and 25% respectively). Three sets of signal regions are defined (with a SFOS pair on- and off-shell of the Z boson, and with three SS leptons). No significant excess is observed over the background prediction. 95% CL limits are extracted assuming degenerete $\widetilde{e}_L$, $\widetilde{\nu}_e$, $\widetilde{\mu}_L$, $\widetilde{\nu}_\mu$, degenerate $\widetilde{e}_L$, $\widetilde{\nu}_e$, and degenerete $\widetilde{\mu}_L$, $\widetilde{\nu}_\mu$, see their figures 15, 16a, and 16b.

[3] AAD 25M searched for an excess of displaced leptons (e or μ) in pp collisions (140 fb^{-1} at $\sqrt{s}$ = 13 TeV and 56.3 at fb^{-1} at $\sqrt{s}$ = 13.6 TeV). The models considered were long-lived slepton (electron or muon) pair production followed by $\widetilde{\ell} \to \ell\widetilde{G}$, and long-lived chargino pair production in a dark sector model, followed by $\widetilde{\chi}^\pm_1 \to \widetilde{\chi}^0_1 W$. Displaced leptons were reconstructed thanks to an improved large radius tracking and to the pointing capabilities of the electromagnetic calorimeter. Two different analyses (ABCD and EM-BDT) are combined to obtain limits on $\widetilde{e}$ pair production, while the ABCD analysis only is used for $\widetilde{\mu}$, $\widetilde{\tau}$ and $\widetilde{\chi}^\pm_1$ pair production. No significant excess of events is observed over the background prediction. 95% CL limits are extracted in the lifetime vs mass plane, see their figures 6 and 8.

Int. J. Mod. Phys. A 2026.41. Downloaded from www.worldscientific.com
by UNIVERSITY OF CALIFORNIA @ BERKELEY on 09/16/26. Re-use and distribution is strictly not permitted, except for Open Access articles.

[4] CHEKHOVSKY 25M searched in 138 fb^{-1} of pp collisions at $\sqrt{s}$ = 13 TeV for evidence of SUSY models with compressed mass spectra in events with a high transverse momentum system from initial-state-radiation jets recoiling against a potential sparticle system with significant missing transverse momentum. These events are further categorized based on their lepton multiplicity, jet multiplicity, number of b-tagged jets, and kinematic variables sensitive to the sparticle masses and mass splittings. No significant excess above the Standard Model expectations is observed. The results are interpreted in models of top squark, electroweakino and slepton pair production. Limits are set for top squark pair production in the models Tstop1 and Tstop2, see their figure 25, and in Tstop4, see their figure 26. The results are also interpreted in models describing the production of mass-degenerate $\widetilde{\chi}^0_2$ and $\widetilde{\chi}^\pm_1$ with decays $\widetilde{\chi}^0_2 \rightarrow Z\widetilde{\chi}^0_1$ and $\widetilde{\chi}^\pm_1 \rightarrow W\widetilde{\chi}^0_1$, applying both a wino-like and higgsino-like $\widetilde{\chi}^\pm_1\widetilde{\chi}^0_2$ production cross section, see their figure 27. Limits are also set for wino-like $\widetilde{\chi}^\pm_1$ pair production, either with $\widetilde{\chi}^\pm_1 \rightarrow W\widetilde{\chi}^0_1$ or in the model Tchi1chi1C. This paper also addresses direct slepton production, taking into account pure right-handed, pure left-handed and combined production of either selectrons, smuons, or mass-degenerate sleptons of the first and second generation, see their figures 30 and 31.

[5] HAYRAPETYAN 24N searched in up to 137 fb^{-1} of pp collisions at $\sqrt{s}$ = 13 TeV for evidence of wino-like chargino-neutralino pairs, Higgsino-like neutralino pair production in a gauge-mediated SUSY breaking inspired scenario, a Higgsino-bino interpretation, and slepton pair production in a combination of a number of previously reported searches for SUSY in different final states. No significant excess above the Standard Model expectations is observed. Limits are set on the $\widetilde{\chi}^\pm_1$ mass in the wino-bino models Tchi1n2E1, Tchi1n2E, and Tchi1n2l, see their Fig. 11, and on the $\widetilde{\chi}^0_1$ in the higgsino-like GMSB models Tn1n1A, Tn1n1B, and Tn1n1C, see their Fig. 13. In addition, Fig. 14 shows the mass exclusion limit as a function of the branching fraction to the H boson. Limits are also set in a Higgsino-bino interpretation as in THinoBinoA, but also including leptonic decays, see their Fig. 15. Limits are also set on slepton ($\widetilde{e}$, $\widetilde{\mu}$) production with the decay $\widetilde{\ell} \rightarrow \ell\widetilde{\chi}^0_1$, see their Fig. 16.

[6] AAD 23M searched in 139 fb^{-1} of pp collisions at $\sqrt{s}$ = 13 TeV for $\widetilde{\ell}^\pm$ pair production, followed by $\widetilde{\ell}^\pm \rightarrow \ell^\pm\widetilde{\chi}^0_1$ in events with two leptons. The focus is on models where $m_{\widetilde{\ell}^\pm} - m_{\widetilde{\chi}^0_1}$ is close to the W mass. No significant excess above the Standard Model predictions is observed. Limits were set on the $\widetilde{\ell}$ mass (assuming $\widetilde{e} - \widetilde{\mu}$ and $L - R$ degeneracy), as a function of $m_{\widetilde{\chi}^0_1}$, see Figure 6. Limits were also derived for single $\widetilde{e}$ or $\widetilde{\mu}$, and for L and R independently, see Figure 7.

[7] SIRUNYAN 21M searched in 137 fb^{-1} of pp collisions at $\sqrt{s}$ = 13 TeV for supersymmetry in events with two opposite-sign same-flavor leptons (electrons, muons) and $\not{E}_T$. No significant excess above the Standard Model expectations is observed. Limits are set on the gluino mass in the simplified model Tglu4C, see their Figure 10, on the $\widetilde{\chi}^0_2$ and $\widetilde{\chi}^\pm_1$ mass in Tchi1n2Fa, see their Figure 11, on the $\widetilde{\chi}^0_1$ mass in Tn1n1C and Tn1n1B for $m_{\widetilde{\chi}^0_2}$=$m_{\widetilde{\chi}^\pm_1}$=$m_{\widetilde{\chi}^0_1}$, see their Figure 12. Limits are also set on the light squark mass for the simplified model Tsqk2A, on the sbottom mass in Tsbot3, see their Figure 13, and on the slepton mass in direct electroweak pair production of mass-degenerate left- and right-handed sleptons (selectrons and smuons), see their Figure 14.

[8] AAD 20O reported on a search for electroweak production in models with charginos and sleptons decaying into final states with exactly two oppositely charged leptons and missing transverse momentum. A dataset of pp collisions at $\sqrt{s}$ = 13 TeV corresponding to an integrated luminosity of 139 fb^{-1} was used. Light-flavour sleptons $\widetilde{e}$ and $\widetilde{\mu}$ are constrained at 95% C.L. to have masses above 700 GeV for massless lightest neutralino, see their Fig. 7(c). Exclusion limits are also set for selectrons and smuons separately, considering either right- or left-handed components, by including only the di-electron and di-muon same-flavour signal regions defined in the search, see their Fig. 8.

[9] SIRUNYAN 19AW searched in 35.9 fb^{-1} of pp collisions at $\sqrt{s}$ = 13 TeV for direct electroweak pair production of selectrons or smuons in events with two leptons (electrons or muons) of the opposite electric charge and same flavour, no jets and large $\not{E}_T$. No significant excess above the Standard Model expectations is observed. Limits are set on the selectron mass assuming left-handed, right-handed or both left- and right-handed (mass degenerate) production, see their Figure 6. Similarly, limits are set on the smuon mass, see their Figure 7. Limits are also set on slepton masses under the assumption that the selectron and smuon are mass degenerate, see their Figure 5.

[10] AABOUD 18BT searched in 36.1 fb^{-1} of pp collisions at $\sqrt{s}$ = 13 TeV for direct electroweak production of charginos, chargino and next-to-lightest neutralinos and sleptons in events with two or three leptons (electrons or muons), with or without jets, and large missing transverse energy. No significant excess above the Standard Model expectations is observed. Limits are set on the slepton mass up to 500 GeV for massless $\widetilde{\chi}^0_1$, assuming degeneracy of $\widetilde{e}$, $\widetilde{\mu}$, and $\widetilde{\tau}$ and exploiting the 2ℓ signature, see their Figure 8(b).

[11] AABOUD 18R searched in 36.1 fb^{-1} of pp collisions at $\sqrt{s}$ = 13 TeV for electroweak production in scenarios with compressed mass spectra in final states with two low-momentum leptons and missing transverse momentum. The data are found to be consistent with the SM prediction. Results are interpreted in slepton pair production models with a fourfold degeneracy assumed in selectron and smuon masses. The $\widetilde{e}$ masses are excluded up to 190 GeV for $m_{\widetilde{e}} - m_{\widetilde{\chi}^0_1}$ = 5 GeV. The exclusion limits extend down to mass splittings of 1 GeV, see their Fig. 11.

[12] CHATRCHYAN 14R searched in 19.5 fb^{-1} of pp collisions at $\sqrt{s}$ = 8 TeV for events with at least three leptons (electrons, muons, taus) in the final state. No significant excess above the Standard Model expectations is observed. Limits are set on the slepton mass in a stau (N)NLSP simplified model (GMSB) where the decay $\widetilde{\ell} \rightarrow \ell^\pm\tau^\pm\tau^\mp\widetilde{G}$ takes place with a branching ratio of 100%, see Fig. 8.

[13] AAD 13B searched in 4.7 fb^{-1} of pp collisions at $\sqrt{s}$ = 7 TeV for sleptons decaying to a final state with two leptons (e and μ) and missing transverse energy. No excess beyond the Standard Model expectation is observed. Limits are derived in a simplified model of direct left-handed slepton pair production, where left-handed slepton masses between 85 and 195 GeV are excluded at 95% C.L. for $m_{\widetilde{\chi}^0_1}$ = 20 GeV. See also Fig. 2(a). Exclusion limits are also derived in the phenomenological MSSM, see Fig. 3.

[14] ABBIENDI 04 search for $\widetilde{e}_R\widetilde{e}_R$ production in acoplanar di-electron final states in the 183–208 GeV data. See Fig. 13 for the dependence of the limits on $m_{\widetilde{\chi}^0_1}$ and for the limit at tanβ=35 This limit supersedes ABBIENDI 00G.

[15] ACHARD 04 search for $\widetilde{e}_R\widetilde{e}_L$ and $\widetilde{e}_R\widetilde{e}_R$ production in single- and acoplanar di-electron final states in the 192–209 GeV data. Absolute limits on $m_{\widetilde{e}_R}$ are derived from a scan over the MSSM parameter space with universal GUT scale gaugino and scalar masses $m_{1/2}$ and m_0, $1 \leq \tan\beta \leq 60$ and $-2 \leq \mu \leq 2$ TeV. See Fig. 4 for the dependence of the limits on $m_{\widetilde{\chi}^0_1}$. This limit supersedes ACCIARRI 99W.

[16] ABDALLAH 03M looked for acoplanar dielectron $+\not{E}$ final states at $\sqrt{s}$ = 189–208 GeV. The limit assumes μ=$-$200 GeV and tanβ=1.5 in the calculation of the production cross section and B($\widetilde{e} \rightarrow e\widetilde{\chi}^0_1$). See Fig. 15 for limits in the ($m_{\widetilde{e}_R}$, $m_{\widetilde{\chi}^0_1}$) plane. These limits include and update the results of ABREU 01

[17] ABDALLAH 03M uses data from $\sqrt{s}$ = 192–208 GeV to obtain limits in the framework of the MSSM with gaugino and sfermion mass universality at the GUT scale. An indirect limit on the mass is derived by constraining the MSSM parameter space by the results from direct searches for neutralinos (including cascade decays) and for sleptons. These limits are valid for values of M_2 <1 TeV, $|\mu| \leq 1$ TeV with the $\widetilde{\chi}^0_1$ as LSP. The quoted limit is obtained when there is no mixing in the third family. See Fig. 43 for the mass limits as a function of tanβ. These limits update the results of ABREU 00W.

[18] HEISTER 02E looked for acoplanar dielectron $+\not{E}_T$ final states from e^+e^- interactions between 183 and 209 GeV. The mass limit assumes $\mu < -200$ GeV and tanβ=2 for the production cross section and B($\widetilde{e} \rightarrow e\widetilde{\chi}^0_1$)=1. See their Fig. 4 for the dependence of the limit on Δm. These limits include and update the results of BARATE 01.

[19] HEISTER 02N search for $\widetilde{e}_R\widetilde{e}_L$ and $\widetilde{e}_R\widetilde{e}_R$ production in single- and acoplanar di-electron final states in the 183–208 GeV data. Absolute limits on $m_{\widetilde{e}_R}$ are derived from a scan over the MSSM parameter space with universal GUT scale gaugino and scalar masses $m_{1/2}$ and m_0, $1 \leq \tan\beta \leq 50$ and $-10 \leq \mu \leq 10$ TeV. The region of small $|\mu|$, where cascade decays are important, is covered by a search for $\widetilde{\chi}^0_1\widetilde{\chi}^0_3$ in final states with leptons and possibly photons. Limits on $m_{\widetilde{e}_L}$ are derived by exploiting the mass relation between the $\widetilde{e}_L$ and $\widetilde{e}_R$, based on universal m_0 and $m_{1/2}$. When the constraint from the mass limit of the lightest Higgs from HEISTER 02 is included, the bounds improve to $m_{\widetilde{e}_R}$ >77(75) GeV and $m_{\widetilde{e}_L}$ >115(115) GeV for a top mass of 175(180) GeV. In the MSUGRA framework with radiative electroweak symmetry breaking, the limits improve further to $m_{\widetilde{e}_R}$ >95 GeV and $m_{\widetilde{e}_L}$ >152 GeV, assuming a trilinear coupling A_0=0 at the GUT scale. See Figs. 4, 5, 7 for the dependence of the limits on tanβ.

[20] AAD 20I reported on ATLAS searches for slepton pair production in models with compressed mass spectra. A dataset of pp collisions at $\sqrt{s}$ = 13 TeV corresponding to an integrated luminosity of 139 fb^{-1} was used. Events with $\not{E}_T$, two same-flavour, opposite-charge, low-transverse-momentum leptons, and jets from initial-state radiation or characteristic of vector-boson fusion production are selected. Light-flavour sleptons $\widetilde{e}$ and $\widetilde{\mu}$ are constrained at 95% C.L. to have masses above 251 GeV for a mass splitting slepton$-\widetilde{\chi}^0_1$ of 10 GeV, with constraints extending down to mass splittings of 550 MeV at the LEP slepton limits (73 GeV), see their Fig. 16(a). If only selectrons are considered, and $\widetilde{e} = \widetilde{e}_R$, masses below 101 GeV are excluded for mass splitting $\widetilde{e}_R$, $\widetilde{\chi}^0_1$ of 7.5 GeV. See their Fig. 16(b).

[21] AAD 20I reported on ATLAS searches for slepton pair production in models with compressed mass spectra. A dataset of pp collisions at $\sqrt{s}$ = 13 TeV corresponding to an integrated luminosity of 139 fb^{-1} was used. Events with $\not{E}_T$, two same-flavour, opposite-charge, low-transverse-momentum leptons, and jets from initial-state radiation or characteristic of vector-boson fusion production are selected. Light-flavour sleptons $\widetilde{e}$ and $\widetilde{\mu}$ are constrained at 95% C.L. to have masses above 251 GeV for a mass splitting slepton$-\widetilde{\chi}^0_1$ of 10 GeV, with constraints extending down to mass splittings of 550 MeV at the LEP slepton limits (73 GeV). See their Fig. 16(a). If only selectron are considered, and $\widetilde{e} = \widetilde{e}_L$, masses below 169 GeV are excluded for mass splitting $\widetilde{e}_L$, $\widetilde{\chi}^0_1$ of 7.1 GeV. See their Fig. 16(b).

[22] AAD 14G searched in 20.3 fb^{-1} of pp collisions at $\sqrt{s}$ = 8 TeV for electroweak production of slepton pairs, decaying to a final sate with two leptons (e and μ) and missing transverse momentum. No excess beyond the Standard Model expectation is observed. Exclusion limits are derived in simplified models of slepton pair production, see Fig. 8. An interpretation in the pMSSM is also given, see Fig. 10.

[23] KHACHATRYAN 14I searched in 19.5 fb^{-1} of pp collisions at $\sqrt{s}$ = 8 TeV for electroweak production of slepton pairs decaying to a final state with opposite-sign lepton pairs (e or μ) and missing transverse momentum. No excess beyond the Standard Model expectation is observed. Exclusion limits are derived in simplified models, see Fig. 18.

R-partiy violating $\widetilde{e}$ (Selectron) mass limit

Some earlier papers are now obsolete and have been omitted. They were last listed in our PDG 14 edition: K. Olive, *et al.* (Particle Data Group), Chinese Physics **C38** 070001 (2014) (http://pdg.lbl.gov).

VALUE (GeV)	CL%	DOCUMENT ID		TECN	COMMENT
>1200	95	[1] AAD	21Y	ATLS	$\geq 4\ell$, $\lambda_{12k} \neq 0$, $m_{\widetilde{\chi}^0_1}$ = 900 GeV (mass-degenerate $\widetilde{\ell}_L$ and $\widetilde{\nu}$ of all 3 generations)
> 870	95	[1] AAD	21Y	ATLS	$\geq 4\ell$, $\lambda_{i33} \neq 0$, $m_{\widetilde{\chi}^0_1}$ = 450 GeV (mass-degenerate $\widetilde{\ell}_L$ and $\widetilde{\nu}$ of all 3 generations)
>1065	95	[2] AABOUD	18Z	ATLS	$\geq 4\ell$, $\lambda_{12k} \neq 0$, $m_{\widetilde{\chi}^0_1}$ = 600 GeV (mass-degenerate left-handed sleptons and sneutrinos of all 3 generations)
> 780	95	[2] AABOUD	18Z	ATLS	$\geq 4\ell$, $\lambda_{i33} \neq 0$, $m_{\widetilde{\chi}^0_1}$ = 300 GeV (mass-degenerate left-handed sleptons and sneutrinos of all 3 generations)
> 410	95	[3] AAD	14X	ATLS	$\geq 4\ell^\pm$, $\widetilde{\ell} \rightarrow l\widetilde{\chi}^0_1$, $\widetilde{\chi}^0_1 \rightarrow \ell^\pm\ell^\mp\nu$
• • • We do not use the following data for averages, fits, limits, etc. • • •					
> 89	95	[4] ABBIENDI	04F	OPAL	$\widetilde{e}_L$
> 92	95	[5] ABDALLAH	04M	DLPH	$\widetilde{e}_R$, indirect, Δm >5 GeV

[1] AAD 21Y searched in 139 fb^{-1} of pp collisions at $\sqrt{s}$ = 13 TeV for supersymmetry in events with four or more leptons (electrons, muons and tau-leptons). No significant excess above the Standard Model expectations is observed. Limits are set on Tchi1n12-GGM, and RPV models similar to Tchi1n2l, Tglu1A (with q = u, d, s, c, b, with

Int. J. Mod. Phys. A 2026.41. Downloaded from www.worldscientific.com by UNIVERSITY OF CALIFORNIA @ BERKELEY on 09/16/26. Re-use and distribution is strictly not permitted, except for Open Access articles.

equal branching fractions), and $\widetilde{\ell}_L/\widetilde{\nu} \rightarrow \ell/\nu\widetilde{\chi}^0_1$ (mass-degenerate $\widetilde{\ell}_L$ and $\widetilde{\nu}$ of all 3 generations), all with $\widetilde{\chi}^0_1 \rightarrow \ell^\pm\ell^\mp\nu$ via λ_{12k} or λ_{i33} (where $i,k \in 1,2$), see their Figure 11.

[2] AABOUD 18Z searched in 36.1 fb^{-1} of pp collisions at $\sqrt{s} = 13$ TeV for events containing four or more charged leptons (electrons, muons and up to two hadronically decaying taus). No significant deviation from the expected SM background is observed. Limits are set on the Higgsino mass in simplified models of general gauge mediated supersymmetry Tn1n1A/Tn1n1B/Tn1n1C, see their Figure 9. Limits are also set on the wino, slepton, sneutrino and gluino mass in a simplified model of NLSP pair production with R-parity violating decays of the LSP via λ_{12k} or λ_{i33} to charged leptons, see their Figures 7, 8.

[3] AAD 14X searched in 20.3 fb^{-1} of pp collisions at $\sqrt{s} = 8$ TeV for events with at least four leptons (electrons, muons, taus) in the final state. No significant excess above the Standard Model expectations is observed. Limits are set on the slepton mass in an R-parity violating simplified model where the decay $\widetilde{\ell} \rightarrow \ell\widetilde{\chi}^0_1$, with $\widetilde{\chi}^0_1 \rightarrow \ell^\pm\ell^\mp\nu$, takes place with a branching ratio of 100%, see Fig. 9.

[4] ABBIENDI 04F use data from $\sqrt{s} = 189$–209 GeV. They derive limits on sparticle masses under the assumption of RPV with $LL\overline{E}$ or $LQ\overline{D}$ couplings. The results are valid for $\tan\beta = 1.5$, $\mu = -200$ GeV, with, in addition, $\Delta m > 5$ GeV for indirect decays via $LQ\overline{D}$. The limit quoted applies to direct decays via $LL\overline{E}$ or $LQ\overline{D}$ couplings. For indirect decays, the limits on the $\widetilde{e}_R$ mass are respectively 99 and 92 GeV for $LL\overline{E}$ and $LQ\overline{D}$ couplings and $m_{\widetilde{\chi}^0} = 10$ GeV and degrade slightly for larger $\widetilde{\chi}^0_1$ mass. Supersedes the results of ABBIENDI 00.

[5] ABDALLAH 04M use data from $\sqrt{s} = 192$–208 GeV to derive limits on sparticle masses under the assumption of RPV with $LL\overline{E}$ or $\overline{UDD}$ couplings. The results are valid for $\mu = -200$ GeV, $\tan\beta = 1.5$, $\Delta m > 5$ GeV and assuming a BR of 1 for the given decay. The limit quoted is for indirect $\overline{UDD}$ decays using the neutralino constraint of 39.5 GeV for $LL\overline{E}$ and of 38.0 GeV for $\overline{UDD}$ couplings, also derived in ABDALLAH 04M. For indirect decays via $LL\overline{E}$ the limit improves to 95 GeV if the constraint from the neutralino is used and to 94 GeV if it is not used. For indirect decays via $\overline{UDD}$ couplings it remains unchanged when the neutralino constraint is not used. Supersedes the result of ABREU 00U.

R-parity conserving $\widetilde{\mu}$ (Smuon) mass limit

VALUE (GeV)	CL%	DOCUMENT ID		TECN	COMMENT
>235	95	[1] AAD	25AH	ATLAS	2ℓ, $\widetilde{\ell}$ pair production, $m_{\widetilde{\mu}_L} = m_{\widetilde{\mu}_R}$, $m_{\widetilde{\mu}} - m_{\widetilde{\chi}^0_1} = 5$ GeV
>450	95	[2] AAD	25L	ATLAS	3ℓ; $\widetilde{\ell} \rightarrow \ell\widetilde{\chi}^0_3$; $\widetilde{\chi}^0_3 \rightarrow Z/h/W + \widetilde{\chi}$; $\ell = e,\mu,\nu_e,\nu_\mu$; $\widetilde{\chi}$ higgsino; $m_{\widetilde{\chi}^0_3}$=170 GeV; $m_{\widetilde{\chi}}$=100 GeV
>340	95	[2] AAD	25L	ATLAS	3ℓ; $\widetilde{\ell} \rightarrow \ell\widetilde{\chi}^0_3$; $\widetilde{\chi}^0_3 \rightarrow Z/h/W + \widetilde{\chi}$; $\ell = \mu,\nu_\mu$; $\widetilde{\chi}$ higgsino; $m_{\widetilde{\chi}^0_3}$=180 GeV; $m_{\widetilde{\chi}}$=100 GeV
>830	95	[3] AAD	25M	ATLAS	displaced 2ℓ; $\widetilde{\mu}$ pair production; $\widetilde{\mu} \rightarrow \mu\widetilde{G}$; $\tau_{\widetilde{\mu}} = 0.3$ ns
>145	95	[4] CHEKHOVSKY	25M	CMS	≥ 1 ISR jet + (in-)visible decay products, $\widetilde{\mu}_R$ pair production, $\widetilde{\mu}_R \rightarrow \mu\widetilde{\chi}^0_1$, $m_{\widetilde{\mu}_R} - m_{\widetilde{\chi}^0_1} = 5$ GeV
>195	95	[4] CHEKHOVSKY	25M	CMS	≥ 1 ISR jet + (in-)visible decay products, $\widetilde{\mu}_L$ pair production, $\widetilde{\mu}_L \rightarrow \mu\widetilde{\chi}^0_1$, $m_{\widetilde{\mu}_L} - m_{\widetilde{\chi}^0_1} = 5$ GeV
>240	95	[4] CHEKHOVSKY	25M	CMS	≥ 1 ISR jet + (in-)visible decay products, $\widetilde{\mu}_{R,L}$ pair production, $\widetilde{\mu}_{R,L} \rightarrow \mu\widetilde{\chi}^0_1$, $m_{\widetilde{\mu}_{R,L}} - m_{\widetilde{\chi}^0_1} = 5$ GeV
none 130–700	95	[5] HAYRAPETY...	24N	CMS	Combination, $\widetilde{\mu} \rightarrow \mu\widetilde{\chi}^0_1$, $m_{\widetilde{\chi}^0_1} < 50$ GeV
>215	95	[5] HAYRAPETY...	24N	CMS	Combination, $\widetilde{\mu} \rightarrow \mu\widetilde{\chi}^0_1$, Δm $(\widetilde{\chi}^\pm_1, \widetilde{\chi}^0_1) = 5$ GeV
none 220–460	95	[6] AAD	23CR	ATLAS	2 same-sign, 3, 4 ℓ, 1, 2 b-jets, $\widetilde{\mu}_{L,R}$ pair production with $\widetilde{\mu}_{L,R} \rightarrow \mu\widetilde{\chi}^0_1$, $\widetilde{\chi}^0_1 \rightarrow b + \ell/\nu + t/b$ via λ'_{i33} coupling
>240	95	[7] AAD	23M	ATLAS	2ℓ, $\widetilde{\ell}$ pair production, $m_{\widetilde{\mu}_L} = m_{\widetilde{\mu}_R}$, $m_{\widetilde{\chi}^0_1} = 0$ GeV
> 90	95	[7] AAD	23M	ATLAS	2ℓ, $\widetilde{\ell}$ pair production, $m_{\widetilde{\mu}_L} = m_{\widetilde{\mu}_R}$, $m_{\widetilde{\mu}} - m_{\widetilde{\chi}^0_1} = 32$ GeV
>700	95	[8] SIRUNYAN	21M	CMS	$\ell^\pm\ell^\mp + \not{E}_T$, $m_{\widetilde{\ell}_R} = m_{\widetilde{\ell}_L}$ and $\widetilde{\ell}$=$\widetilde{e}$, $\widetilde{\mu}$, $m_{\widetilde{\chi}^0_1} = 0$ GeV
>150	95	[9] AAD	20I	ATLAS	2ℓ (soft), jets, $\not{E}_T$, $\widetilde{\mu}_R$ only, $m_{\widetilde{\mu}_R} - m_{\widetilde{\chi}^0_1} = 8.2$ GeV
>216	95	[10] AAD	20I	ATLAS	2ℓ (soft), jets, $\not{E}_T$, $\widetilde{\mu}_L$ only, $m_{\widetilde{\mu}_L} - m_{\widetilde{\chi}^0_1} = 10$ GeV
>700	95	[11] AAD	20O	ATLAS	2ℓ+$\not{E}_T$, $m_{\widetilde{\ell}_R} = m_{\widetilde{\ell}_L}$ and $\widetilde{\ell}$=$\widetilde{e}$, $\widetilde{\mu}$, $m_{\widetilde{\chi}^0_1}$=0 GeV
>210	95	[12] SIRUNYAN	19AW	CMS	$\ell^\pm\ell^\mp + \not{E}_T$, $\widetilde{\mu}_R$, $m_{\widetilde{\chi}^0_1} = 0$ GeV
>280	95	[12] SIRUNYAN	19AW	CMS	$\ell^\pm\ell^\mp + \not{E}_T$, $\widetilde{\mu}_L$, $m_{\widetilde{\chi}^0_1} = 0$ GeV
>290	95	[12] SIRUNYAN	19AW	CMS	$\ell^\pm\ell^\mp + \not{E}_T$, $\widetilde{\ell}_R$ and $\widetilde{\ell}$=$\widetilde{e}$, $\widetilde{\mu}$, $m_{\widetilde{\chi}^0_1} = 0$ GeV
>400	95	[12] SIRUNYAN	19AW	CMS	$\ell^\pm\ell^\mp + \not{E}_T$, $\widetilde{\ell}_L$ and $\widetilde{\ell}$=$\widetilde{e}$, $\widetilde{\mu}$, $m_{\widetilde{\chi}^0_1} = 0$ GeV
>450	95	[12] SIRUNYAN	19AW	CMS	$\ell^\pm\ell^\mp + \not{E}_T$, $m_{\widetilde{\ell}_R} = m_{\widetilde{\ell}_L}$ and $\widetilde{\ell}$=$\widetilde{e}$, $\widetilde{\mu}$, $m_{\widetilde{\chi}^0_1} = 0$ GeV
>310	95	[12] SIRUNYAN	19AW	CMS	$\ell^\pm\ell^\mp + \not{E}_T$, $m_{\widetilde{\mu}_R} = m_{\widetilde{\mu}_L}$, $m_{\widetilde{\chi}^0_1} = 0$ GeV
>190	95	[13] AABOUD	18R	ATLAS	2ℓ (soft) + $\not{E}_T$, $m_{\widetilde{e}} = m_{\widetilde{\mu}}$, $m_{\widetilde{\mu}} - m_{\widetilde{\chi}^0_1} = 5$ GeV
		[14] CHATRCHYAN	14R	CMS	$\geq 3\ell^\pm$, $\widetilde{\ell} \rightarrow \ell^\pm\tau^\mp\tau^\mp\widetilde{G}$ simplified model, GMSB, stau (N)NLSP scenario
		[15] AAD	13B	ATLAS	$2\ell^\pm + \not{E}_T$, SMS, pMSSM
> 91.0		[16] ABBIENDI	04	OPAL	Δm >3 GeV, $\widetilde{\mu}^+_R\widetilde{\mu}^-_R$, $\lvert\mu\rvert$ >100 GeV, $\tan\beta$=1.5
> 86.7		[17] ACHARD	04	L3	Δm >10 GeV, $\widetilde{\mu}^+_R\widetilde{\mu}^-_R$, $\lvert\mu\rvert$ >200 GeV, $\tan\beta \geq 2$
none 30–88	95	[18] ABDALLAH	03M	DLPH	Δm >5 GeV, $\widetilde{\mu}^+_R\widetilde{\mu}^-_R$
> 94	95	[19] ABDALLAH	03M	DLPH	$\widetilde{\mu}_R$,1 $\leq \tan\beta \leq$ 40, Δm >10 GeV
> 88	95	[20] HEISTER	02E	ALEP	$\Delta m > 15$ GeV, $\widetilde{\mu}^+_R\widetilde{\mu}^-_R$
• • • We do not use the following data for averages, fits, limits, etc. • • •					
>500	95	[21] AABOUD	18BT	ATLAS	$2\ell + \not{E}_T$, $m_{\widetilde{\ell}_R} = m_{\widetilde{\ell}_L}$ and $\widetilde{\ell}$=$\widetilde{e}$, $\widetilde{\mu}$, $\widetilde{\tau}$, with $m_{\widetilde{\chi}^0_1} = 0$ GeV
none 90–325	95	[22] AAD	14G	ATLAS	$\widetilde{\ell}\widetilde{\ell} \rightarrow \ell^+\widetilde{\chi}^0_1\ell^-\widetilde{\chi}^0_1$, simplified model, $m_{\widetilde{\ell}_L} = m_{\widetilde{\ell}_R}$, $m_{\widetilde{\chi}^0_1} = 0$ GeV
		[23] KHACHATRY...	14I	CMS	$\widetilde{\ell} \rightarrow \ell\widetilde{\chi}^0_1$, simplified model
> 80	95	[24] ABREU	00V	DLPH	$\widetilde{\mu}_R\widetilde{\mu}_R$ ($\widetilde{\mu}_R \rightarrow \mu\widetilde{G}$), $m_{\widetilde{G}}$ >8 eV

[1] AAD 25AH searched for an excess in same-flavour dilepton production events in 140 fb^{-1} of pp collisions at $\sqrt{s} = 13$ TeV using a BDT selection optimised on simplified models including sleptons and neutralinos with $m_{\widetilde{\mu}} - m_{\widetilde{\chi}^0_1} < m_W$: pair-produced sleptons decay to a lepton and a neutralino. Several signal regions are defined, depending on the BDT score. Despite some local excess at the level of 2.4 σ, the data agree with the background prediction. 95% CL limits are extracted a s a function of $m_{\widetilde{\mu}} - m_{\widetilde{\chi}^0_1}$, see their figure 13.

[2] AAD 25L searched for an excess of three-lepton events in 140 fb^{-1} of pp collisions at $\sqrt{s} = 13$ TeV. The search targets scenarios connected with potential anomalous muon magnetic moment: pair-produced sleptons (either charged or neutral) are assumed to decay to a bino-like $\widetilde{\chi}^0_3$, decaying to a mass-degenerate higgsino triplet LSP via the emission of a W, Z or h boson (with branching ratio 50%, 25% and 25% respectively). Three sets of signal regions are defined (with a SFOS pair on- and off-shell of the Z boson, and with three SS leptons). No significant excess is observed over the background prediction. 95% CL limits are extracted assuming degenerete $\widetilde{e}_L$, $\widetilde{\nu}_e$, $\widetilde{\mu}_L$, $\widetilde{\nu}_\mu$, degenerete $\widetilde{e}_L$, $\widetilde{\nu}_e$, and degenerete $\widetilde{\mu}_L$, $\widetilde{\nu}_\mu$, see their figures 15, 16a, and 16b.

[3] AAD 25M searched for an excess of displaced leptons (e or μ) in pp collisions (140 fb^{-1} at $\sqrt{s} = 13$ TeV and 56.3 at fb^{-1} at $\sqrt{s} = 13.6$ TeV). The models considered were long-lived slepton (electron or muon) pair production followed by $\widetilde{\ell} \rightarrow \ell\widetilde{G}$, and long-lived chargino pair production in a dark sector model, followed by $\widetilde{\chi}^\pm_1 \rightarrow \widetilde{\chi}^0_1 W$. Displaced leptons were reconstructed thanks to an improved large radius tracking and to the pointing capabilities of the electromagnetic calorimeter. Two different analyses (ABCD and EM-BDT) are combined to obtain limits on $\widetilde{e}$ pair production, while the ABCD analysis only is used for $\widetilde{\mu}$, $\widetilde{\tau}$ and $\widetilde{\chi}^\pm_1$ pair production. No significant excess of events is observed over the background prediction. 95% CL limits are extracted in the lifetime vs mass plane, see their figures 6 and 8.

[4] CHEKHOVSKY 25M searched in 138 fb^{-1} of pp collisions at $\sqrt{s} = 13$ TeV for evidence of SUSY models with compressed mass spectra in events with a high transverse momentum system from initial-state-radiation jets recoiling against a potential sparticle system with significant missing transverse momentum. These events are further categorized based on their lepton multiplicity, jet multiplicity, number of b-tagged jets, and kinematic variables sensitive to the sparticle masses and mass splittings. No significant excess above the Standard Model expectations is observed. The results are interpreted in models of top squark, electroweakino and slepton pair production. Limits are set for top squark pair production in the models Tstop1 and Tstop2, see their figure 25, and in Tstop4, see their figure 26. The results are also interpreted in models describing the production of mass-degenerate $\widetilde{\chi}^0_2$ and $\widetilde{\chi}^\pm_1$ with decays $\widetilde{\chi}^0_2 \rightarrow Z\widetilde{\chi}^0_1$ and $\widetilde{\chi}^\pm_1 \rightarrow W\widetilde{\chi}^0_1$, applying both a wino-like and higgsino-like $\widetilde{\chi}^\pm_1\widetilde{\chi}^0_2$ production cross section, see their figure 27. Limits are also set for wino-like $\widetilde{\chi}^\pm_1$ pair production, either with $\widetilde{\chi}^\pm_1 \rightarrow W\widetilde{\chi}^0_1$ or in the model Tchi1chi1C. This paper also addresses direct slepton production, taking into account pure right-handed, pure left-handed and combined production of either selectrons, smuons, or mass-degenerate sleptons of the first and second generation, see their figures 30 and 31.

Int. J. Mod. Phys. A 2026.41. Downloaded from www.worldscientific.com
by UNIVERSITY OF CALIFORNIA @ BERKELEY on 09/16/26. Re-use and distribution is strictly not permitted, except for Open Access articles.

[5] HAYRAPETYAN 24N searched in up to 137 fb^{-1} of pp collisions at $\sqrt{s}$ = 13 TeV for evidence of wino-like chargino-neutralino pairs, Higgsino-like neutralino pair production in a gauge-mediated SUSY breaking inspired scenario, a Higgsino-bino interpretation, and slepton pair production in a combination of a number of previously reported searches for SUSY in different final states. No significant excess above the Standard Model expectations is observed. Limits are set on the $\widetilde{\chi}^{\pm}_1$ mass in the wino-bino models Tchi1n2E1, Tchi1n2E, and Tchi1n2l, see their Fig. 11, and on the $\widetilde{\chi}^0_1$ in the higgsino-like GMSB models Tn1n1A, Tn1n1B, and Tn1n1C, see their Fig. 13. In addition, Fig. 14 shows the mass exclusion limit as a function of the branching fraction to the H boson. Limits are also set in a Higgsino-bino interpretation as in THinoBinoA, but also including leptonic decays, see their Fig. 15. Limits are also set on slepton ($\widetilde{e}$, $\widetilde{\mu}$) production with the decay $\widetilde{\ell} \rightarrow \ell\widetilde{\chi}^0_1$, see their Fig. 16.

[6] AAD 23CR searched in 139 fb^{-1} of pp collisions at $\sqrt{s}$ = 13 TeV for RPV SUSY in final states with multiple leptons and b-tagged jets. No significant excess above the Standard Model expectations is observed. Limits are set on the production of electroweakinos (wino or higgsino) that decay via RPV coupling λ'_{i33} to a charged lepton or a neutrino, a b quark, and an additional t or b quark, see their figure 16. A second model addresses direct $\widetilde{\mu}_{L,R}$ production and decay to a muon and a bino-like neutralino, which decays in the same way as in the first model, see their figure 17.

[7] AAD 23M searched in 139 fb^{-1} of pp collisions at $\sqrt{s}$ = 13 TeV for $\widetilde{\ell}^{\pm}$ pair production, followed by $\widetilde{\ell}^{\pm} \rightarrow \ell^{\pm}\widetilde{\chi}^0_1$ in events with two leptons. The focus is on models where $m_{\widetilde{\ell}^{\pm}} - m_{\widetilde{\chi}^0_1}$ is close to the W mass. No significant excess above the Standard Model predictions is observed. Limits were set on the $\widetilde{\ell}$ mass (assuming $\widetilde{e} - \widetilde{\mu}$ and $L - R$ degeneracy), as a function of $m_{\widetilde{\chi}^0_1}$, see Figure 6. Limits were also derived for single $\widetilde{e}$ or $\widetilde{\mu}$, and for L and R independently, see Figure 7.

[8] SIRUNYAN 21M searched in 137 fb^{-1} of pp collisions at $\sqrt{s}$ = 13 TeV for supersymmetry in events with two opposite-sign same-flavor leptons (electrons, muons) and $\not{E}_T$. No significant excess above the Standard Model expectations is observed. Limits are set on the gluino mass in the simplified model Tglu4C, see their Figure 10, on the $\widetilde{\chi}^0_2$ and $\widetilde{\chi}^{\pm}_1$ mass in Tchi1n2Fa, see their Figure 11, on the $\widetilde{\chi}^0_1$ mass in Tn1n1C and Tn1n1B for $m_{\widetilde{\chi}^0_2}$=$m_{\widetilde{\chi}^{\pm}_1}$=$m_{\widetilde{\chi}^0_1}$, see their Figure 12. Limits are also set on the light squark mass for the simplified model Tsqk2A, on the sbottom mass in Tsbot3, see their Figure 13, and on the slepton mass in direct electroweak pair production of mass-degenerate left- and right-handed sleptons (selectrons and smuons), see their Figure 14.

[9] AAD 20I reported on ATLAS searches for slepton pair production in models with compressed mass spectra. A dataset of pp collisions at $\sqrt{s}$ = 13 TeV corresponding to an integrated luminosity of 139 fb^{-1} was used. Events with $\not{E}_T$, two same-flavour, opposite-charge, low-transverse-momentum leptons, and jets from initial-state radiation or characteristic of vector-boson fusion production are selected. Light-flavour sleptons $\widetilde{e}$ and $\widetilde{\mu}$ are constrained at 95% C.L. to have masses above 251 GeV for a mass splitting slepton$-\widetilde{\chi}^0_1$ of 10 GeV, with constraints extending down to mass splittings of 550 MeV at the LEP slepton limits (73 GeV). See their Fig. 16(a). If only smuon are considered, and $\widetilde{\mu} = \widetilde{\mu}_R$, masses below 150 GeV are excluded for mass splitting $\widetilde{\mu}_R$, $\widetilde{\chi}^0_1$ of 8.2 GeV. See their Fig. 16(b).

[10] AAD 20I reported on ATLAS searches for slepton pair production in models with compressed mass spectra. A dataset of pp collisions at $\sqrt{s}$ = 13 TeV corresponding to an integrated luminosity of 139 fb^{-1} was used. Events with $\not{E}_T$, two same-flavour, opposite-charge, low-transverse-momentum leptons, and jets from initial-state radiation or characteristic of vector-boson fusion production are selected. Light-flavour sleptons $\widetilde{e}$ and $\widetilde{\mu}$ are constrained at 95% C.L. to have masses above 251 GeV for a mass splitting slepton$-\widetilde{\chi}^0_1$ of 10 GeV, with constraints extending down to mass splittings of 550 MeV at the LEP slepton limits (73 GeV). See their Fig. 16(a). If only smuon are considered, and $\widetilde{\mu} = \widetilde{\mu}_L$, masses below 216 GeV are excluded for mass splitting $\widetilde{\mu}_L$, $\widetilde{\chi}^0_1$ of 10 GeV. See their Fig. 16(b).

[11] AAD 20O reported on a search for electroweak production in models with charginos and sleptons decaying into final states with exactly two oppositely charged leptons and missing transverse momentum. A dataset of pp collisions at $\sqrt{s}$ = 13 TeV corresponding to an integrated luminosity of 139 fb^{-1} was used. Light-flavour sleptons $\widetilde{e}$ and $\widetilde{\mu}$ are constrained at 95% C.L. to have masses above 700 GeV for massless lightest neutralino, see their Fig. 7(c). Exclusion limits are also set for selectrons and smuons separately, considering either right- or left-handed components, by including only the di-electron and di-muon same-flavour signal regions defined in the search, see their Fig. 8.

[12] SIRUNYAN 19AW searched in 35.9 fb^{-1} of pp collisions at $\sqrt{s}$ = 13 TeV for direct electroweak pair production of selectrons or smuons in events with two leptons (electrons or muons) of the opposite electric charge and same flavour, no jets and large $\not{E}_T$. No significant excess above the Standard Model expectations is observed. Limits are set on the selectron mass assuming left-handed, right-handed or both left- and right-handed (mass degenerate) production, see their Figure 6. Similarly, limits are set on the smuon mass, see their Figure 7. Limits are also set on slepton masses under the assumption that the selectron and smuon are mass degenerate, see their Figure 5.

[13] AABOUD 18R searched in 36.1 fb^{-1} of pp collisions at $\sqrt{s}$ = 13 TeV for electroweak production in scenarios with compressed mass spectra in final states with two low-momentum leptons and missing transverse momentum. The data are found to be consistent with the SM prediction. Results are interpreted in slepton pair production models with a fourfold degeneracy assumed in selectron and smuon masses. The $\widetilde{\mu}$ masses are excluded up to 190 GeV for $m_{\widetilde{\mu}} - m_{\widetilde{\chi}^0_1}$ = 5 GeV. The exclusion limits extend down to mass splittings of 1 GeV, see their Fig. 11.

[14] CHATRCHYAN 14R searched in 19.5 fb^{-1} of pp collisions at $\sqrt{s}$ = 8 TeV for events with at least three leptons (electrons, muons, taus) in the final state. No significant excess above the Standard Model expectations is observed. Limits are set on the slepton mass in a stau (N)NLSP simplified model (GMSB) where the decay $\widetilde{\ell} \rightarrow \ell^{\pm}\tau^{\pm}\tau^{\mp}\widetilde{G}$ takes place with a branching ratio of 100%, see Fig. 8.

[15] AAD 13B searched in 4.7 fb^{-1} of pp collisions at $\sqrt{s}$ = 7 TeV for sleptons decaying to a final state with two leptons (e and μ) and missing transverse energy. No excess beyond the Standard Model expectation is observed. Limits are derived in a simplified model of direct left-handed slepton pair production, where left-handed slepton masses between 85 and 195 GeV are excluded at 95% C.L. for $m_{\widetilde{\chi}^0_1}$ = 20 GeV. See also Fig. 2(a). Exclusion limits are also derived in the phenomenological MSSM, see Fig. 3.

[16] ABBIENDI 04 search for $\widetilde{\mu}_R\widetilde{\mu}_R$ production in acoplanar di-muon final states in the 183–208 GeV data. See Fig. 14 for the dependence of the limits on $m_{\widetilde{\chi}^0_1}$ and for the limit at tanβ=35. Under the assumption of 100% branching ratio for $\widetilde{\mu}_R \rightarrow \mu\widetilde{\chi}^0_1$, the limit improves to 94.0 GeV for $\Delta m > 4$ GeV. See Fig. 11 for the dependence of the limits on $m_{\widetilde{\chi}^0_1}$ at several values of the branching ratio. This limit supersedes ABBIENDI 00G.

[17] ACHARD 04 search for $\widetilde{\mu}_R\widetilde{\mu}_R$ production in acoplanar di-muon final states in the 192–209 GeV data. Limits on $m_{\widetilde{\mu}_R}$ are derived from a scan over the MSSM parameter space with universal GUT scale gaugino and scalar masses $m_{1/2}$ and m_0, $1 \leq$ tan$\beta \leq 60$ and $-2 \leq \mu \leq 2$ TeV. See Fig. 4 for the dependence of the limits on $m_{\widetilde{\chi}^0_1}$. This limit supersedes ACCIARRI 99W.

[18] ABDALLAH 03M looked for acoplanar dimuon $+\not{E}$ final states at $\sqrt{s}$ = 189–208 GeV. The limit assumes B($\widetilde{\mu} \rightarrow \mu\widetilde{\chi}^0_1$) = 100%. See Fig. 16 for limits on the ($m_{\widetilde{\mu}_R}$, $m_{\widetilde{\chi}^0_1}$) plane. These limits include and update the results of ABREU 01.

[19] ABDALLAH 03M uses data from $\sqrt{s}$ = 192–208 GeV to obtain limits in the framework of the MSSM with gaugino and sfermion mass universality at the GUT scale. An indirect limit on the mass is derived by constraining the MSSM parameter space by the results from direct searches for neutralinos (including cascade decays) and for sleptons. These limits are valid for values of $M_2 < 1$ TeV, $|\mu| \leq 1$ TeV with the $\widetilde{\chi}^0_1$ as LSP. The quoted limit is obtained when there is no mixing in the third family. See Fig. 43 for the mass limits as a function of tanβ. These limits update the results of ABREU 00W.

[20] HEISTER 02E looked for acoplanar dimuon $+\not{E}_T$ final states from e^+e^- interactions between 183 and 209 GeV. The mass limit assumes B($\widetilde{\mu} \rightarrow \mu\widetilde{\chi}^0_1$)=1. See their Fig. 4 for the dependence of the limit on Δm. These limits include and update the results of BARATE 01.

[21] AABOUD 18BT searched in 36.1 fb^{-1} of pp collisions at $\sqrt{s}$ = 13 TeV for direct electroweak production of charginos, chargino and next-to-lightest neutralinos and sleptons in events with two or three leptons (electrons or muons), with or without jets, and large missing transverse energy. No significant excess above the Standard Model expectations is observed. Limits are set on the slepton mass up to 500 GeV for massless $\widetilde{\chi}^0_1$, assuming degeneracy of $\widetilde{e}$, $\widetilde{\mu}$, and $\widetilde{\tau}$ and exploiting the 2ℓ signature, see their Figure 8(b).

[22] AAD 14G searched in 20.3 fb^{-1} of pp collisions at $\sqrt{s}$ = 8 TeV for electroweak production of slepton pairs, decaying to a final sate with two leptons (e and μ) and missing transverse momentum. No excess beyond the Standard Model expectation is observed. Exclusion limits are derived in simplified models of slepton pair production, see Fig. 8. An interpretation in the pMSSM is also given, see Fig. 10.

[23] KHACHATRYAN 14I searched in 19.5 fb^{-1} of pp collisions at $\sqrt{s}$ = 8 TeV for electroweak production of slepton pairs decaying to a final state with opposite-sign lepton pairs (e or μ) and missing transverse momentum. No excess beyond the Standard Model expectation is observed. Exclusion limits are derived in simplified models, see Fig. 18.

[24] ABREU 00V use data from $\sqrt{s}$= 130–189 GeV to search for tracks with large impact parameter or visible decay vertices. Limits are obtained as function of $m_{\widetilde{G}}$, after combining these results with the search for slepton pair production in the SUGRA framework from ABREU 01 to cover prompt decays and on stable particle searches from ABREU 00Q. For limits at different $m_{\widetilde{G}}$, see their Fig. 12.

R-parity violating $\widetilde{\mu}$ (Smuon) mass limit

VALUE (GeV)	CL%	DOCUMENT ID		TECN	COMMENT
none 120–645	95	[1] AAD	22E	ATLS	$t\widetilde{\mu}_L$ production, RPV, $\widetilde{\mu}_L \rightarrow \mu\widetilde{\chi}^0_1$, λ'_{231} = 1, $m_{\widetilde{\chi}^0_1}$=0 GeV.
>1200	95	[2] AAD	21Y	ATLS	$\geq 4\ell$, $\lambda_{12k} \neq 0$, $m_{\widetilde{\chi}^0_1}$ = 900 GeV (mass-degenerate $\widetilde{\ell}_L$ and $\widetilde{\nu}$ of all 3 generations)
> 870	95	[2] AAD	21Y	ATLS	$\geq 4\ell$, $\lambda_{i33} \neq 0$, $m_{\widetilde{\chi}^0_1}$ = 450 GeV (mass-degenerate $\widetilde{\ell}_L$ and $\widetilde{\nu}$ of all 3 generations)
> 780	95	[3] AABOUD	18Z	ATLS	$\geq 4\ell$, $\lambda_{j33} \neq 0$, $m_{\widetilde{\chi}^0_1}$=300 GeV (mass-degenerate left-handed sleptons and sneutrinos of all 3 generations)
>1060	95	[3] AABOUD	18Z	ATLS	$\geq 4\ell$, $\lambda_{12k} \neq 0$, $m_{\widetilde{\chi}^0_1}$=600 GeV (mass-degenerate left-handed sleptons and sneutrinos of all 3 generations)
> 410	95	[4] AAD	14X	ATLS	RPV, $\geq 4\ell^{\pm}$, $\widetilde{\ell} \rightarrow \ell\widetilde{\chi}^0_1$, $\widetilde{\chi}^0_1 \rightarrow \ell^{\pm}\ell^{\mp}\nu$
• • • We do not use the following data for averages, fits, limits, etc. • • •					
		[5] SIRUNYAN	19AO		$\mu^{\pm}\mu^{\pm}$ + $\geq$ 2jets, $\lambda'_{211} \neq 0$, $\widetilde{\mu}_L \rightarrow \mu\widetilde{\chi}^0_1$, $\widetilde{\chi}^0_1 \rightarrow \mu q\overline{q}$
> 87	95	[6] ABDALLAH	04M	DLPH	RPV, $\widetilde{\mu}_R$, indirect, Δm >5 GeV
> 81	95	[7] HEISTER	03G	ALEP	RPV, $\widetilde{\mu}_L$

[1] AAD 22E searched in 139 fb^{-1} of pp collisions at $\sqrt{s}$ = 13 TeV for supersymmetry by measuring the yield asymmetry between events containing $e^-\mu^+$ and those containing $e^+\mu^-$. This was found in agreement with the standard model prediction of 1. Limits are set on the RPV production of $t\widetilde{\mu}_L$ events with $\widetilde{\mu}_L \rightarrow \mu\widetilde{\chi}^0_1$ for various values of λ'_{231}, see their figures 6 and 7.

[2] AAD 21Y searched in 139 fb^{-1} of pp collisions at $\sqrt{s}$ = 13 TeV for supersymmetry in events with four or more leptons (electrons, muons and tau-leptons). No significant excess above the Standard Model expectations is observed. Limits are set on Tchi1n12-GGM, and RPV models similar to Tchi1n2l, Tglu1A (with q = u, d, s, c, b, with equal branching fractions), and $\widetilde{\ell}_L/\widetilde{\nu} \rightarrow \ell/\nu\widetilde{\chi}^0_1$ (mass-degenerate $\widetilde{\ell}_L$ and $\widetilde{\nu}$ of all 3 generations), all with $\widetilde{\chi}^0_1 \rightarrow \ell^{\pm}\ell^{\mp}\nu$ via λ_{12k} or λ_{i33} (where $i,k \in 1,2$), see their Figure 11.

[3] AABOUD 18Z searched in 36.1 fb^{-1} of pp collisions at $\sqrt{s}$ = 13 TeV for events containing four or more charged leptons (electrons, muons and up to two hadronically decaying taus). No significant deviation from the expected SM background is observed. Limits are set on the Higgsino mass in simplified models of general gauge mediated supersymmetry Tn1n1A/Tn1n1B/Tn1n1C, see their Figure 9. Limits are also set on the wino, slepton,

Int. J. Mod. Phys. A 2026.41. Downloaded from www.worldscientific.com by UNIVERSITY OF CALIFORNIA @ BERKELEY on 09/16/26. Re-use and distribution is strictly not permitted, except for Open Access articles.

sneutrino and gluino mass in a simplified model of NLSP pair production with R-parity violating decays of the LSP via λ_{12k} or λ_{i33} to charged leptons, see their Figures 7, 8.

[4] AAD 14X searched in 20.3 fb^{-1} of pp collisions at $\sqrt{s}$ = 8 TeV for events with at least four leptons (electrons, muons, taus) in the final state. No significant excess above the Standard Model expectations is observed. Limits are set on the slepton mass in an R-parity violating simplified model where the decay $\tilde{\ell} \rightarrow \ell\tilde{\chi}^0_1$, with $\tilde{\chi}^0_1 \rightarrow \ell^{\pm}\ell^{\mp}\nu$, takes place with a branching ratio of 100%, see Fig. 9.

[5] SIRUNYAN 19AO searched in 35.9 fb^{-1} of pp collisions at $\sqrt{s}$ = 13 TeV for events containing two same-sign muons and at last two jets, originating from resonant production of second-generation sleptons ($\tilde{\mu}_L$, $\tilde{\nu}_\mu$) via the R-parity violating coupling λ'_{211} to quarks. No significant excess above the Standard Model expectations is observed. Upper limits on cross sections are derived in the context of two simplified models, see their Figure 4. The cross section limits are translated into limits on λ'_{211} for a modified CMSSM, see their Figure 5.

[6] ABDALLAH 04M use data from $\sqrt{s}$ = 192–208 GeV to derive limits on sparticle masses under the assumption of RPV with $LL\overline{E}$ or $\overline{UDD}$ couplings. The results are valid for μ = −200 GeV, tanβ = 1.5, Δm > 5 GeV and assuming a BR of 1 for the given decay. The limit quoted is for indirect $\overline{UDD}$ decays using the neutralino constraint of 39.5 GeV for $LL\overline{E}$ and of 38.0 GeV for $\overline{UDD}$ couplings, also derived in ABDALLAH 04M. For indirect decays via $LL\overline{E}$ the limit improves to 90 GeV if the constraint from the neutralino is used and remains at 87 GeV if it is not used. For indirect decays via $\overline{UDD}$ couplings it degrades to 85 GeV when the neutralino constraint is not used. Supersedes the result of ABREU 00U.

[7] HEISTER 03G searches for the production of smuons in the case of RPV prompt decays with $LL\overline{E}$, $LQ\overline{D}$ or $\overline{UDD}$ couplings at $\sqrt{s}$ = 189–209 GeV. The search is performed for direct and indirect decays, assuming one coupling at a time to be non-zero. The limit holds for direct decays mediated by RPV $LQ\overline{D}$ couplings and improves to 90 GeV for indirect decays (for Δm > 10 GeV). Limits are also given for $LL\overline{E}$ direct ($m_{\tilde{\mu}R}$ > 87 GeV) and indirect decays ($m_{\tilde{\mu}R}$ > 96 GeV for $m(\tilde{\chi}^0_1)$ > 23 GeV from BARATE 98S) and for $\overline{UDD}$ indirect decays ($m_{\tilde{\mu}R}$ > 85 GeV for Δm > 10 GeV). Supersedes the results from BARATE 01B.

R-parity conserving $\tilde{\tau}$ (Stau) mass limit

Some earlier papers are now obsolete and have been omitted. They were last listed in our PDG 14 edition: K. Olive, *et al.* (Particle Data Group), Chinese Physics **C38** 070001 (2014) (http://pdg.lbl.gov).

VALUE (GeV)	CL%	DOCUMENT ID		TECN	COMMENT
>440	95	[1] AAD	25M	ATLS	displaced 2ℓ; $\tilde{\tau}$ pair production; $\tilde{\tau} \rightarrow \tau\tilde{G}$; $\tau_{\tilde{\tau}}$ = 0.3 ns
>500	95	[2] AAD	24AJ	ATLS	2 hadronic $\tau + \not{E}_T$, $\tilde{\tau}_{R,L} \rightarrow \tau\tilde{\chi}^0_1$, $m_{\tilde{\chi}^0_1}$ = 1 GeV
none 80–425	95	[2] AAD	24AJ	ATLS	2 hadronic $\tau + \not{E}_T$, $\tilde{\tau}_L \rightarrow \tau\tilde{\chi}^0_1$, $m_{\tilde{\chi}^0_1}$ = 1 GeV
none 100–350	95	[2] AAD	24AJ	ATLS	2 hadronic $\tau + \not{E}_T$, $\tilde{\tau}_R \rightarrow \tau\tilde{\chi}^0_1$, $m_{\tilde{\chi}^0_1}$ = 1 GeV
>400	95	[3] TUMASYAN	23AG	CMS	2 hadronic $\tau + \not{E}_T$, $\tilde{\tau}_{R,L} \rightarrow \tau\tilde{\chi}^0_1$, $m_{\tilde{\chi}^0_1}$ = 1 GeV
none 115–340	95	[3] TUMASYAN	23AG	CMS	2 hadronic $\tau + \not{E}_T$, $\tilde{\tau}_L \rightarrow \tau\tilde{\chi}^0_1$, $m_{\tilde{\chi}^0_1}$ = 1 GeV
none 120–390	95	[4] AAD	20H		2 hadronic $\tau + \not{E}_T$, $\tilde{\tau}_{R/L} \rightarrow \tau\tilde{\chi}^0_1$, $m_{\tilde{\chi}^0_1}$ = 0 GeV
none 90–150	95	[5] SIRUNYAN	20P	CMS	2 $\tau+\not{E}_T$, $\tau_h\tau_h$ and $\ell\tau_h$, $m_{\tilde{\tau}_R}$=$m_{\tilde{\tau}_L}$, $m_{\tilde{\chi}^0_1}$ = 1 GeV
> 85.2		[6] ABBIENDI	04	OPAL	Δm > 6 GeV, θ_τ=π/2, $\lvert\mu\rvert$ > 100 GeV, tanβ=1.5
> 78.3		[7] ACHARD	04	L3	Δm > 15 GeV, θ_τ=π/2, $\lvert\mu\rvert$ >200 GeV,tan$\beta \geq$ 2
> 81.9	95	[8] ABDALLAH	03M	DLPH	Δm >15 GeV, all θ_τ
> 79	95	[9] HEISTER	02E	ALEP	Δm > 15 GeV, θ_τ=π/2
> 76	95	[9] HEISTER	02E	ALEP	Δm > 15 GeV, θ_τ=0.91
• • • We do not use the following data for averages, fits, limits, etc. • • •					
>500	95	[10] AABOUD	18BT	ATLS	2ℓ+$\not{E}_T$, $m_{\tilde{\ell}_R}$=$m_{\tilde{\ell}_L}$, $\tilde{\ell}$=$\tilde{e}$, $\tilde{\mu}$, $\tilde{\tau}$, $m_{\tilde{\chi}^0_1}$ = 0 GeV
		[11] KHACHATRY...	17L	CMS	2 $\tau+\not{E}_T$, $\tilde{\tau}_L \rightarrow \tau\tilde{\chi}^0_1$, $m_{\tilde{\chi}^0_1}$ = 0 GeV
none 109	95	[12] AAD	16AA	ATLS	2 hadronic $\tau + \not{E}_T$, $\tilde{\tau}_{R/L} \rightarrow \tau\tilde{\chi}^0_1$, $m_{\tilde{\chi}^0_1}$ = 0 GeV
		[13] AAD	12AF	ATLS	2τ + jets + $\not{E}_T$, GMSB
		[14] AAD	12AG	ATLS	$\geq$ 1τ_h + jets + $\not{E}_T$, GMSB
		[15] AAD	12CM	ATLS	$\geq$1τ + jets + $\not{E}_T$, GMSB
> 87.4	95	[16] ABBIENDI	06B	OPAL	$\tilde{\tau}_R \rightarrow \tau\tilde{G}$, all $\tau(\tilde{\tau}_R)$
> 68	95	[17] ABDALLAH	04H	DLPH	AMSB, μ > 0
none m_τ− 26.3	95	[8] ABDALLAH	03M	DLPH	Δm >m_τ, all θ_τ

[1] AAD 25M searched for an excess of displaced leptons (e or μ) in pp collisions (140 fb^{-1} at $\sqrt{s}$ = 13 TeV and 56.3 at fb^{-1} at $\sqrt{s}$ = 13.6 TeV). The models considered were long-lived slepton (electron or muon) pair production followed by $\tilde{\ell} \rightarrow \ell\tilde{G}$, and long-lived chargino pair production in a dark sector model, followed by $\tilde{\chi}^{\pm}_1 \rightarrow \tilde{\chi}^0_1 W$. Displaced leptons were reconstructed thanks to an improved large radius tracking and to the pointing capabilities of the electromagnetic calorimeter. Two different analyses (ABCD and EM-BDT) are combined to obtain limits on $\tilde{e}$ pair production, while the ABCD analysis only is used for $\tilde{\mu}$, $\tilde{\tau}$ and $\tilde{\chi}^{\pm}_1$ pair production. No significant excess of events is observed over the background prediction. 95% CL limits are extracted in the lifetime vs mass plane, see their figures 6 and 8.

[2] AAD 24AJ searched in 139 fb^{-1} of pp collisions at $\sqrt{s}$ = 13 TeV for evidence of direct stau pair production, or electroweakino pair production with decay via an intermediate stau, in events with two taus decaying hadronically (including a same-charge channel), no b-jets and moderate $\not{E}_T$, using a BDT for the direct stau search and a more traditional cut-and-count selection for the electroweakino search. No significant excess above the Standard Model expectations is observed. Limits are set in models of direct stau production $\tilde{\tau} \rightarrow \tau\tilde{\chi}^0_1$, $\tilde{\tau}_L$, $\tilde{\tau}_R$ or degenerate production. Limits are also set in models of pair production of charginos (Tchichi1D) or of charginos and neutralinos (Tchi1n2D) followed by the decay via intermediate staus, or (for the latter) via Wh (Tchi1n2E). See their figures 12, 14 and 16.

[3] TUMASYAN 23AG searched in 138 fb^{-1} of pp collisions at $\sqrt{s}$ = 13 TeV for or direct pair production of tau sleptons in events with two hadronically decaying tau leptons. No significant excess above the Standard Model expectations is observed. Limits are set on the mass of the tau slepton in models with $\tilde{\tau} \rightarrow \tau\tilde{\chi}^0_1$ for mass-degenerate, pure left-handed and pure right-handed tau sleptons, see their figures 4–7. Limits are also set for the maximally mixed scenario with long-lived tau sleptons and $\tilde{\tau}$ lifetimes of 0.01 mm to 2.5 mm, see their figure 8.

[4] AAD 20H presented ATLAS searches for direct production for $\tilde{\tau}$ in final states with two hadronically decaying leptons and $\not{E}_T$. The analysis uses a dataset of pp collisions at $\sqrt{s}$ = 13 TeV corresponding to an integrated luminosity of 139 fb^{-1}. Exclusion limits at 95% C.L. are derived in scenarios of direct production of $\tilde{\tau}$ pairs with each $\tilde{\tau}$ decaying into a τ and the lightest neutralino $\tilde{\chi}^0_1$ in simplified models where the $\tilde{\tau}_R$ and $\tilde{\tau}_L$ mass eigenstates are degenerate. Stau masses from 120GeV to 390GeV are excluded for a massless lightest neutralino, see their Fig. 7(a). If $\tilde{\tau}_L$-only pair production is considered, the exclusion region extends between 155 GeV to 310 GeV, see their Fig. 7(b).

[5] SIRUNYAN 20P searched in 77.2 fb^{-1} of pp collisions at $\sqrt{s}$ = 13 TeV for direct pair production of tau sleptons in events with a tau lepton pair and significant missing transverse momentum. Final states with two double hadronic decay of the tau leptons are considered, as well as where one of the tau leptons decays into an electron or a muon. No significant excess above the Standard Model expectations is observed. Limits are set on the stau mass in a simplified models where two tau sleptons are pair produced and decay to a tau lepton and the lightest neutralino, assuming either only left-handed stau production, see Figure 8, or assuming degenerate left- and right-handed stau production, see Figure 9.

[6] ABBIENDI 04 search for $\tilde{\tau}\tilde{\tau}$ production in acoplanar di-tau final states in the 183–208 GeV data. See Fig. 15 for the dependence of the limits on $m_{\tilde{\chi}^0_1}$ and for the limit at tanβ=35. Under the assumption of 100% branching ratio for $\tilde{\tau}_R \rightarrow \tau\tilde{\chi}^0_1$, the limit improves to 89.8 GeV for Δm > 8 GeV. See Fig. 12 for the dependence of the limits on $m_{\tilde{\chi}^0_1}$ at several values of the branching ratio and for their dependence on θ_τ. This limit supersedes ABBIENDI 00G.

[7] ACHARD 04 search for $\tilde{\tau}\tilde{\tau}$ production in acoplanar di-tau final states in the 192–209 GeV data. Limits on $m_{\tilde{\tau}_R}$ are derived from a scan over the MSSM parameter space with universal GUT scale gaugino and scalar masses $m_{1/2}$ and m_0, 1 $\leq$ tan$\beta \leq$ 60 and −2 $\leq \mu \leq$ 2 TeV. See Fig. 4 for the dependence of the limits on $m_{\tilde{\chi}^0_1}$.

[8] ABDALLAH 03M looked for acoplanar ditaus +$\not{E}$ final states at $\sqrt{s}$ = 130–208 GeV. A dedicated search was made for low mass $\tilde{\tau}$s decoupling from the Z^0. The limit assumes B($\tilde{\tau} \rightarrow \tau\tilde{\chi}^0_1$) = 100%. See Fig. 20 for limits on the ($m_{\tilde{\tau}}$,$m_{\tilde{\chi}^0_1}$) plane and as function of the $\tilde{\chi}^0_1$ mass and of the branching ratio. The limit in the low-mass region improves to 29.6 and 31.1 GeV for $\tilde{\tau}_R$ and $\tilde{\tau}_L$, respectively, at $\Delta m > m_\tau$. The limit in the high-mass region improves to 84.7 GeV for $\tilde{\tau}_R$ and Δm > 15 GeV. These limits include and update the results of ABREU 01.

[9] HEISTER 02E looked for acoplanar ditau + $\not{E}_T$ final states from e^+e^- interactions between 183 and 209 GeV. The mass limit assumes B($\tilde{\tau} \rightarrow \tau\tilde{\chi}^0_1$)=1. See their Fig. 4 for the dependence of the limit on Δm. These limits include and update the results of BARATE 01.

[10] AABOUD 18BT searched in 36.1 fb^{-1} of pp collisions at $\sqrt{s}$ = 13 TeV for direct electroweak production of charginos, chargino and next-to-lightest neutralinos and sleptons in events with two or three leptons (electrons or muons), with or without jets, and large missing transverse energy. No significant excess above the Standard Model expectations is observed. Limits are set on the slepton mass up to 500 GeV for massless $\tilde{\chi}^0_1$, assuming degeneracy of $\tilde{e}$, $\tilde{\mu}$, and $\tilde{\tau}$ and exploiting the 2ℓ signature, see their Figure 8(b).

[11] KHACHATRYAN 17L searched in about 19 fb^{-1} of pp collisions at $\sqrt{s}$ = 8 TeV for events with two τ (at least one decaying hadronically) and $\not{E}_T$. Results were interpreted to set constraints on the cross section for production of $\tilde{\tau}_L$ pairs for $m_{\tilde{\chi}^0_1}$=1 GeV. No mass constraints are set, see their Fig. 7.

[12] AAD 16AA summarized and extended ATLAS searches for electroweak supersymmetry in final states containing several charged leptons, $\not{E}_T$, with or without hadronic jets, in 20 fb^{-1} of pp collisions at $\sqrt{s}$ = 8 TeV. The paper reports 95% C.L. exclusion limits on the cross-section for production of $\tilde{\tau}_R$ and $\tilde{\tau}_L$ pairs for various $m_{\tilde{\chi}^0_1}$, using the 2 hadronic $\tau + \not{E}_T$ analysis. The $m_{\tilde{\tau}_{R/L}}$ = 109 GeV is excluded for $m_{\tilde{\chi}^0_1}$ = 0 GeV, with the constraints being stronger for $\tilde{\tau}_R$. See their Fig. 12.

[13] AAD 12AF searched in 2 fb^{-1} of pp collisions at $\sqrt{s}$ = 7 TeV for events with two tau leptons, jets and large $\not{E}_T$ in a GMSB framework. No significant excess above the expected background was found and an upper limit on the visible cross section for new phenomena is set. A 95% C.L. lower limit of 32 TeV on the mGMSB breaking scale Λ is set for M_{mess} = 250 TeV, N_S = 3, μ > 0 and C_{grav} = 1, independent of tanβ.

[14] AAD 12AG searched in 2.05 fb^{-1} of pp collisions at $\sqrt{s}$ = 7 TeV for events with at least one hadronically decaying tau lepton, jets, and large $\not{E}_T$ in a GMSB framework. No significant excess above the expected background was found and an upper limit on

Int. J. Mod. Phys. A 2026.41. Downloaded from www.worldscientific.com
by UNIVERSITY OF CALIFORNIA @ BERKELEY on 09/16/26. Re-use and distribution is strictly not permitted, except for Open Access articles.

the visible cross section for new phenomena is set. A 95% C.L. lower limit of 30 TeV on the mGMSB breaking scale Λ is set for M_{mess} = 250 TeV, N_5 = 3, μ > 0 and C_{grav} = 1, independent of tanβ. For large values of tanβ, the limit on Λ increases to 43 TeV.

[15] AAD 12CM searched in 4.7 fb^{-1} of pp collisions at $\sqrt{s}$=7 TeV for events with at least one tau lepton, zero or one additional light lepton (e/μ) jets, and large $\not{E}_T$ in a GMSB framework. No significant excess above the expected background was found and an upper limit on the visible cross section for new phenomena is set. A 95% C. L. lower limit of 54 TeV on the mGMSB breaking scale Λ is set for M_{mess} = 250 TeV, N_5 = 3, μ > 0 and C_{grav} = 1, for tanβ > 20. Here the $\widetilde{\tau}_1$ is the NLSP.

[16] ABBIENDI 06B use 600 pb^{-1} of data from $\sqrt{s}$ = 189–209 GeV. They look for events from pair-produced staus in a GMSB scenario with $\widetilde{\tau}$ NLSP including prompt $\widetilde{\tau}$ decays to ditaus + $\not{E}$ final states, large impact parameters, kinked tracks and heavy stable charged particles. Limits on the cross-section are computed as a function of m($\widetilde{\tau}$) and the lifetime, see their Fig. 7. The limit is compared to the $\sigma \cdot BR^2$ from a scan over the GMSB parameter space.

[17] ABDALLAH 04H use data from LEP 1 and $\sqrt{s}$ = 192–208 GeV. They re-use results or re-analyze the data from ABDALLAH 03M to put limits on the parameter space of anomaly-mediated supersymmetry breaking (AMSB), which is scanned in the region 1< $m_{3/2}$ <50 TeV, 0< m_0 <1000 GeV, 1.5<tanβ <35, both signs of μ. The constraints are obtained from the searches for mass degenerate chargino and neutralino, for SM-like and invisible Higgs, for leptonically decaying charginos and from the limit on non-SM Z width of 3.2 MeV. The limit is for m_t = 174.3 GeV (see Table 2 for other m_t values). The limit improves to 75 GeV for μ < 0.

R-parity violating $\widetilde{\tau}$ (Stau) mass limit

Some earlier papers are now obsolete and have been omitted. They were last listed in our PDG 14 edition: K. Olive, *et al.* (Particle Data Group), Chinese Physics **C38** 070001 (2014) (http://pdg.lbl.gov).

VALUE (GeV)	CL%	DOCUMENT ID		TECN	COMMENT
>1200	95	[1] AAD	21Y	ATLS	$\geq 4\ell$, $\lambda_{12k} \neq 0$, $m_{\widetilde{\chi}^0_1}$ = 900 GeV (mass-degenerate $\widetilde{\ell}_L$ and $\widetilde{\nu}$ of all 3 generations)
> 870	95	[1] AAD	21Y	ATLS	$\geq 4\ell$, $\lambda_{i33} \neq 0$, $m_{\widetilde{\chi}^0_1}$ = 450 GeV (mass-degenerate $\widetilde{\ell}_L$ and $\widetilde{\nu}$ of all 3 generations)
>1060	95	[2] AABOUD	18Z	ATLS	$\geq 4\ell$, $\lambda_{12k} \neq 0$, $m_{\widetilde{\chi}^0_1}$ = 600 GeV (mass-degenerate left-handed sleptons and sneutrinos of all 3 generations)
> 780	95	[2] AABOUD	18Z	ATLS	$\geq 4\ell$, $\lambda_{i33} \neq 0$, $m_{\widetilde{\chi}^0_1}$ = 300 GeV (mass-degenerate left-handed sleptons and sneutrinos of all 3 generations)
> 90	95	[3] ABDALLAH	04M	DLPH	$\widetilde{\tau}_R$, indirect, Δm >5 GeV
• • • We do not use the following data for averages, fits, limits, etc. • • •					
> 74	95	[4] ABBIENDI	04F	OPAL	$\widetilde{\tau}_L$

[1] AAD 21Y searched in 139 fb^{-1} of pp collisions at $\sqrt{s}$ = 13 TeV for supersymmetry in events with four or more leptons (electrons, muons and tau-leptons). No significant excess above the Standard Model expectations is observed. Limits are set on Tchi1n12-GGM, and RPV models similar to Tchi1n2l, Tglu1A (with q = u, d, s, c, b, with equal branching fractions), and $\widetilde{\ell}_L/\widetilde{\nu} \rightarrow \ell/\nu\widetilde{\chi}^0_1$ (mass-degenerate $\widetilde{\ell}_L$ and $\widetilde{\nu}$ of all 3 generations), all with $\widetilde{\chi}^0_1 \rightarrow \ell^{\pm}\ell^{\mp}\nu$ via λ_{12k} or λ_{i33} (where $i,k \in 1,2$), see their Figure 11.

[2] AABOUD 18Z searched in 36.1 fb^{-1} of pp collisions at $\sqrt{s}$ = 13 TeV for events containing four or more charged leptons (electrons, muons and up to two hadronically decaying taus). No significant deviation from the expected SM background is observed. Limits are set on the Higgsino mass in simplified models of general gauge mediated supersymmetry Tn1n1A/Tn1n1B/Tn1n1C, see their Figure 9. Limits are also set on the wino, slepton, sneutrino and gluino mass in a simplified model of NLSP pair production with R-parity violating decays of the LSP via λ_{12k} or λ_{i33} to charged leptons, see their Figures 7, 8.

[3] ABDALLAH 04M use data from $\sqrt{s}$ = 192–208 GeV to derive limits on sparticle masses under the assumption of RPV with $LL\overline{E}$ couplings. The results are valid for μ = −200 GeV, tanβ = 1.5, Δm > 5 GeV and assuming a BR of 1 for the given decay. The limit quoted is for indirect decays using the neutralino constraint of 39.5 GeV, also derived in ABDALLAH 04M. For indirect decays via $LL\overline{E}$ the limit decreases to 86 GeV if the constraint from the neutralino is not used. Supersedes the result of ABREU 00U.

[4] ABBIENDI 04F use data from $\sqrt{s}$ = 189–209 GeV. They derive limits on sparticle masses under the assumption of RPV with $LL\overline{E}$ or $LQ\overline{D}$ couplings. The results are valid for tanβ = 1.5, μ = −200 GeV, with, in addition, Δm > 5 GeV for indirect decays via $LQ\overline{D}$. The limit quoted applies to direct decays with $LL\overline{E}$ couplings and improves to 75 GeV for $LQ\overline{D}$ couplings. The limit on the $\widetilde{\tau}_R$ mass for indirect decays is 92 GeV for $LL\overline{E}$ couplings at $m_{\widetilde{\chi}^0}$ = 10 GeV and no exclusion is obtained for $LQ\overline{D}$ couplings. Supersedes the results of ABBIENDI 00.

Long-lived $\widetilde{\ell}$ (Slepton) mass limit

Limits on scalar leptons which leave detector before decaying. Limits from Z decays are independent of lepton flavor. Limits from continuum e^+e^- annihilation are also independent of flavor for smuons and staus. Selectron limits from e^+e^- collisions in the continuum depend on MSSM parameters because of the additional neutralino exchange contribution.

VALUE (GeV)	CL%	DOCUMENT ID		TECN	COMMENT
>460	95	[1] AAD	25AE	ATLS	direct $\widetilde{\tau}$ pair, $\widetilde{\tau} \rightarrow \tau\widetilde{G}$, stable
>580	95	[1] AAD	25AE	ATLS	direct $\widetilde{\tau}$ pair, $\widetilde{\tau} \rightarrow \tau\widetilde{G}$,$\tau_{\widetilde{\tau}}$=30 ns
none 300–690	95	[2] HAYRAPETY...	25V	CMS	large dE/dx in Si tracker, det.-stable $\widetilde{\tau}_{L,R}$, $m_{\widetilde{\tau}_L} = m_{\widetilde{\tau}_R}$
>520	95	[3] AAD	23BQ	ATLS	2ℓ slightly displaced, long-lived $\widetilde{\mu},\widetilde{\mu} \rightarrow \mu\widetilde{G}$, $m_{\widetilde{\mu}_R} = m_{\widetilde{\mu}_L}$, $\tau_{\widetilde{\mu}}$ = 10 ps
>190	95	[3] AAD	23BQ	ATLS	2ℓ slightly displaced, long-lived $\widetilde{\mu},\widetilde{\mu} \rightarrow \mu\widetilde{G}$, $m_{\widetilde{\mu}_R} = m_{\widetilde{\mu}_L}$, $\tau_{\widetilde{\mu}}$ = 1 ps
none 220–360	95	[4] AAD	23G	ATLS	direct $\widetilde{\tau}$ pair, $\widetilde{\tau} \rightarrow \tau\widetilde{G}$, τ= 10 ns
none 150–220	95	[5] TUMASYAN	23AG	CMS	2 hadronic $\tau + \not{E}_T$, $\widetilde{\tau} \rightarrow \tau\widetilde{\chi}^0_1$, maximally mixed scenario with cτ = 0.1 mm, $m_{\widetilde{\chi}^0_1}$ = 1 GeV
>610	95	[6] TUMASYAN	22AF	CMS	2ℓ displaced, long-lived $\widetilde{e},\widetilde{e} \rightarrow e\widetilde{G}$, $m_{\widetilde{e}_R} = m_{\widetilde{e}_L}$, c$\tau$ = 0.7 cm
>610	95	[6] TUMASYAN	22AF	CMS	2ℓ displaced, long-lived $\widetilde{\mu},\widetilde{\mu} \rightarrow \mu\widetilde{G}$, $m_{\widetilde{\mu}_R} = m_{\widetilde{\mu}_L}$, c$\tau$ = 3 cm
>405	95	[6] TUMASYAN	22AF	CMS	2ℓ displaced, long-lived $\widetilde{\tau},\widetilde{\tau} \rightarrow \tau\widetilde{G}$, $m_{\widetilde{\tau}_R} = m_{\widetilde{\tau}_L}$, c$\tau$ = 2 cm
>270	95	[6] TUMASYAN	22AF	CMS	2ℓ displaced, long-lived $\widetilde{\ell},\widetilde{\ell} \rightarrow \ell\widetilde{G}$, $m_{\widetilde{\ell}_R} = m_{\widetilde{\ell}_L}$, $m_{\widetilde{e}} = m_{\widetilde{\mu}} = m_{\widetilde{\tau}}$, 0.005 cm < c$\tau$ < 265 cm
>680	95	[6] TUMASYAN	22AF	CMS	2ℓ displaced, long-lived $\widetilde{\ell},\widetilde{\ell} \rightarrow \ell\widetilde{G}$, $m_{\widetilde{\ell}_R} = m_{\widetilde{\ell}_L}$, $m_{\widetilde{e}} = m_{\widetilde{\mu}} = m_{\widetilde{\tau}}$, c$\tau$ = 2 cm
>720	95	[7] AAD	21AL	ATLS	2ℓ displaced, long-lived $\widetilde{e},\widetilde{e} \rightarrow e\widetilde{G}$, $m_{\widetilde{e}_R} = m_{\widetilde{e}_L}$, $\tau_{\widetilde{e}}$ = 0.1 ns
>680	95	[7] AAD	21AL	ATLS	2ℓ displaced, long-lived $\widetilde{\mu},\widetilde{\mu} \rightarrow \mu\widetilde{G}$, $m_{\widetilde{\mu}_R} = m_{\widetilde{\mu}_L}$, $\tau_{\widetilde{\mu}}$ = 0.1 ns
>340	95	[7] AAD	21AL	ATLS	2ℓ displaced, long-lived $\widetilde{\tau},\widetilde{\tau} \rightarrow \tau\widetilde{G}$, mixing sin$\theta_{\widetilde{\tau}}$ = 0.95, $\tau_{\widetilde{\tau}}$ = 0.1 ns
>820	95	[7] AAD	21AL	ATLS	2ℓ displaced, long-lived $\widetilde{\ell},\widetilde{\ell} \rightarrow \ell\widetilde{G}$, $m_{\widetilde{\ell}_R} = m_{\widetilde{\ell}_L}$, $m_{\widetilde{e}} = m_{\widetilde{\mu}} = m_{\widetilde{\tau}}$, $\tau_{\widetilde{\ell}}$ = 0.1 ns
>430	95	[8] AABOUD	19AT	ATLS	long-lived $\widetilde{\tau}$, GMSB
>490	95	[9] KHACHATRY...	16BW	CMS	long-lived $\widetilde{\tau}$ from inclusive production, mGMSB SPS line 7 scenario
>240	95	[9] KHACHATRY...	16BW	CMS	long-lived $\widetilde{\tau}$ from direct pair production, mGMSB SPS line 7 scenario
>440	95	[10] AAD	15AE	ATLS	mGMSB, M_{mess} = 250 TeV, N_5 = 3, μ > 0, C_{grav} = 5000, tanβ = 10
>385	95	[10] AAD	15AE	ATLS	mGMSB, M_{mess} = 250 TeV, N_5 = 3, μ > 0, C_{grav} = 5000, tanβ = 50
>286	95	[10] AAD	15AE	ATLS	direct $\widetilde{\tau}$ production
none 124–309	95	[11] AAIJ	15BD	LHCB	long-lived $\widetilde{\tau}$, mGMSB, SPS7
> 98	95	[12] ABBIENDI	03L	OPAL	$\widetilde{\mu}_R$, $\widetilde{\tau}_R$
none 2–87.5	95	[13] ABREU	00Q	DLPH	$\widetilde{\mu}_R$, $\widetilde{\tau}_R$
> 81.2	95	[14] ACCIARRI	99H	L3	$\widetilde{\mu}_R$, $\widetilde{\tau}_R$
> 81	95	[15] BARATE	98K	ALEP	$\widetilde{\mu}_R$, $\widetilde{\tau}_R$
• • • We do not use the following data for averages, fits, limits, etc. • • •					
>300	95	[16] AAD	13AA	ATLS	long-lived $\widetilde{\tau}$, GMSB, tanβ = 5–20
		[17] ABAZOV	13B	D0	long-lived $\widetilde{\tau}$, 100 <$m_{\widetilde{\tau}}$ <300 GeV
>339	95	[18,19] CHATRCHYAN	13AB	CMS	long-lived $\widetilde{\tau}$, direct $\widetilde{\tau}_1$ pair prod., minimal GMSB, SPS line 7
>500	95	[18,20] CHATRCHYAN	13AB	CMS	long-lived $\widetilde{\tau}$, $\widetilde{\tau}_1$ from direct pair prod. and from decay of heavier SUSY particles, minimal GMSB, SPS line 7
>314	95	[21] CHATRCHYAN	12L	CMS	long-lived $\widetilde{\tau}$, $\widetilde{\tau}_1$ from decay of heavier SUSY particles, minimal GMSB, SPS line 7
>136	95	[22] AAD	11P	ATLS	stable $\widetilde{\tau}$, GMSB scenario, tanβ=5

[1] AAD 25AE searched for massive, charged long-lived particles in 140 fb^{-1} of pp collisions at $\sqrt{s}$ = 13 TeV. Two analyses are conducted: one looking for a single track, with high specific ionisation losses in the pixel detector and long time of flight to the hadron calorimeter, and one looking for two tracks, both with high specific ionisation in the pixel detector. No excess above the expected background is found. Limits are set in scenarios of long-lived R-hadrons (gluino) production, chargino production or stau pair production, see their figures 13 and 14.

[2] HAYRAPETYAN 25V searched in 101 fb^{-1} of pp collisions at $\sqrt{s}$ = 13 TeV for heavy, long-lived, charged particles with large ionization energy loss within the silicon tracker of the CMS experiment. No significant excess above the Standard Model expectations is observed. Limits are set on the pair production of gluino R-hadrons, top squark R-hadrons, and detector-stable $\widetilde{\tau}_{R,L}$, see their figure 6. Limits are also set in a model predicting a pair of single- and double-charged τ' fermions from a Z' boson decay, see their figure 7.

[3] AAD 23BQ searched in 139 fb^{-1} of pp collisions at $\sqrt{s}$ = 13 TeV for pair production of long-lived $\widetilde{\mu}$ in events with muons with impact parameters in the millimeter range. No significant excess above the Standard Model predictions is observed. Limits are set on $m_{\widetilde{\mu}}$ as a function of the $\widetilde{\mu}$ lifetime, assuming the $\widetilde{\mu} \rightarrow \mu\widetilde{G}$ decay and mass-degenerate $\widetilde{\mu}_L$ and $\widetilde{\mu}_R$. See Figure 4.

[4] AAD 23G searched in 139 fb^{-1} of pp collisions at $\sqrt{s}$ = 13 TeV for stau pair production in events with high-pt tracks with large ionisation in the pixel detector. No significant excess above the Standard Model predictions is observed. Limits are set on the stau mass as a function of its lifetime, see Figure 19.

[5] TUMASYAN 23AG searched in 138 fb^{-1} of pp collisions at $\sqrt{s}$ = 13 TeV for or direct pair production of tau sleptons in events with two hadronically decaying tau leptons. No significant excess above the Standard Model expectations is observed. Limits are set for the maximally mixed scenario with long-lived tau sleptons and $\widetilde{\tau}$ lifetimes of 0.01 mm

Int. J. Mod. Phys. A 2026.41. Downloaded from www.worldscientific.com
by UNIVERSITY OF CALIFORNIA @ BERKELEY on 09/16/26. Re-use and distribution is strictly not permitted, except for Open Access articles.

to 2.5 mm, see their figure 8. Limits are also set on the mass of the tau slepton in models with $\widetilde{\tau} \rightarrow \tau \widetilde{\chi}^0_1$ for mass-degenerate, pure left-handed and pure right-handed tau sleptons, see their figures 4–7.

[6] TUMASYAN 22AF searched for evidence of new long-lived particles decaying to leptons in pp collisions at $\sqrt{s}$ = 13 TeV, corresponding to 118 (113) fb^{-1} in the ee channel ($e\mu$ and $\mu\mu$) channels. The leptons are required to have transverse impact parameter values between 0.01 and 10 cm and are not required to form a common vertex. No significant excess above the Standard Model expectations is observed. Limits are set on the mass of the top squark in RPV models with top squark pair production and $\widetilde{t} \rightarrow b\overline{\ell}$ and $\widetilde{t} \rightarrow d\overline{\ell}$, see their Figure 4, which contains a wider range of lifetime limits. Limits are also set on a gauge-mediated SUSY breaking model, where the next-to-lightest SUSY particle is a slepton and the lightest SUSY particle a gravitino $\widetilde{G}$, see their Figure 5, which also contains a wider range of lifetime limits. Limits are also set in a model that produces BSM Higgs bosons (H) with a mass of 125 GeV through gluongluon fusion, where the H decays to two long-lived scalars S, each of which decays to two oppositely charged and same-flavor leptons.

[7] AAD 21AL searched in 139 fb^{-1} of pp collisions at $\sqrt{s}$ = 13 TeV for pair production of long-lived sleptons in events with highly displaced leptons. No significant excess above the Standard Model predictions is observed. Limits are set on $m_{\widetilde{e}}$, $m_{\widetilde{\mu}}$, $m_{\widetilde{\tau}}$ as a function of the slepton lifetime, assuming the $\widetilde{\ell} \rightarrow \ell \widetilde{G}$ decay and mass-degenerate $\widetilde{\ell}_L$ and $\widetilde{\ell}_R$. See Figures 2.

[8] AABOUD 19AT searched in 36.1 fb^{-1} of pp collisions at $\sqrt{s}$ = 13 TeV for metastable and stable R-hadrons. Multiple search strategies for a wide range of lifetimes, corresponding to path lengths of a few meters, are defined. No significant deviations from the expected Standard Model background are observed. Results are interpreted in terms of exclusion limits on long-lived stau in the context of GMSB models. Lower limits on the mass for direct production of staus are set at 430 GeV, see their Fig. 10 (left).

[9] KHACHATRYAN 16BW searched in 2.5 fb^{-1} of pp collisions at $\sqrt{s}$ = 13 TeV for events with heavy stable charged particles, identified by their anomalously high energy deposits in the silicon tracker and/or long time-of-flight measurements by the muon system. No evidence for an excess over the expected background is observed. Limits are derived for pair production of tau sleptons as a function of mass, depending on their direct or inclusive production in a minimal GMSB scenario along the Snowmass Points and Slopes (SPS) line 7, see Fig. 4 and Table 7.

[10] AAD 15AE searched in 19.1 fb^{-1} of pp collisions at $\sqrt{s}$ = 8 TeV for heavy long-lived charged particles, measured through their specific ionization energy loss in the ATLAS pixel detector or their time-of-flight in the ALTAS muon system. In the absence of an excess of events above the expected backgrounds, limits are set on stable $\widetilde{\tau}$ sleptons in various scenarios, see Figs. 5-7.

[11] AAIJ 15BD searched in 3.0 fb^{-1} of pp collisions at $\sqrt{s}$ = 7 and 8 TeV for evidence of Drell-Yan pair production of long-lived $\widetilde{\tau}$ particles. No evidence for such particles is observed and 95% C.L. upper limits on the cross section of $\widetilde{\tau}$ pair production are derived, see Fig. 7. In the mGMSB, assuming the SPS7 benchmark scenario $\widetilde{\tau}$ masses between 124 and 309 GeV are excluded at 95% C.L.

[12] ABBIENDI 03L used e^+e^- data at $\sqrt{s}$ = 130–209 GeV to select events with two high momentum tracks with anomalous dE/dx. The excluded cross section is compared to the theoretical expectation as a function of the heavy particle mass in their Fig. 3. The limit improves to 98.5 GeV for $\widetilde{\mu}_L$ and $\widetilde{\tau}_L$. The bounds are valid for colorless spin 0 particles with lifetimes longer than 10^{-6} s. Supersedes the results from ACKERSTAFF 98P.

[13] ABREU 00Q searches for the production of pairs of heavy, charged stable particles in e^+e^- annihilation at $\sqrt{s}$= 130–189 GeV. The upper bound improves to 88 GeV for $\widetilde{\mu}_L$, $\widetilde{\tau}_L$. These limits include and update the results of ABREU 98P.

[14] ACCIARRI 99H searched for production of pairs of back-to-back heavy charged particles at $\sqrt{s}$=130–183 GeV. The upper bound improves to 82.2 GeV for $\widetilde{\mu}_L$, $\widetilde{\tau}_L$.

[15] The BARATE 98K mass limit improves to 82 GeV for $\widetilde{\mu}_L$,$\widetilde{\tau}_L$. Data collected at $\sqrt{s}$=161–184 GeV.

[16] AAD 13AA searched in 4.7 fb^{-1} of pp collisions at $\sqrt{s}$ = 7 TeV for events containing long-lived massive particles in a GMSB framework. No significant excess above the expected background was found. A 95% C.L. lower limit of 300 GeV is placed on long-lived $\widetilde{\tau}$'s in the GMSB model with M_{mess} = 250 TeV, N_S = 3, μ > 0, for tanβ = 5–20. The lower limit on the GMSB breaking scale Λ was found to be 99–110 TeV, for tanβ values between 5 and 40, see Fig. 4 (top). Also, directly produced long-lived sleptons, or sleptons decaying to long-lived ones, are excluded at 95% C.L. up to a $\widetilde{\tau}$ mass of 278 GeV for models with slepton splittings smaller than 50 GeV.

[17] ABAZOV 13B looked in 6.3 fb^{-1} of $p\overline{p}$ collisions at $\sqrt{s}$ = 1.96 TeV for charged massive long-lived particles in events with muon-like particles that have both speed and ionization energy loss inconsistent with muons produced in beam collisions. In the absence of an excess, limits are set at 95% C.L. on the production cross section of stau leptons in the mass range 100–300 GeV, see their Table 20 and Fig. 23.

[18] CHATRCHYAN 13AB looked in 5.0 fb^{-1} of pp collisions at $\sqrt{s}$ = 7 TeV and in 18.8 fb^{-1} of pp collisions at $\sqrt{s}$ = 8 TeV for events with heavy stable particles, identified by their anomalous dE/dx in the tracker or additionally requiring that it be identified as muon in the muon chambers, from pair production of $\widetilde{\tau}_1$'s. No evidence for an excess over the expected background is observed. Supersedes CHATRCHYAN 12L.

[19] CHATRCHYAN 13AB limits are derived for pair production of $\widetilde{\tau}_1$ as a function of mass in minimal GMSB scenarios along the Snowmass Points and Slopes (SPS) line 7 (see Fig. 8 and Table 7). The limit given here is valid for direct pair $\widetilde{\tau}_1$ production.

[20] CHATRCHYAN 13AB limits are derived for the production of $\widetilde{\tau}_1$ as a function of mass in minimal GMSB scenarios along the Snowmass Points and Slopes (SPS) line 7 (see Fig. 8 and Table 7). The limit given here is valid for the production of $\widetilde{\tau}_1$ from both direct pair production and from the decay of heavier supersymmetric particles.

[21] CHATRCHYAN 12L looked in 5.0 fb^{-1} of pp collisions at $\sqrt{s}$ = 7 TeV for events with heavy stable particles, identified by their anomalous dE/dx in the tracker or additionally requiring that it be identified as muon in the muon chambers, from pair production of $\widetilde{\tau}_1$'s. No evidence for an excess over the expected background is observed. Limits are derived for the production of $\widetilde{\tau}_1$ as a function of mass in minimal GMSB scenarios along the Snowmass Points and Slopes (SPS) line 7 (see Fig. 3). The limit given here is valid for the production of $\widetilde{\tau}_1$ in the decay of heavier supersymmetric particles.

[22] AAD 11P looked in 37 pb^{-1} of pp collisions at $\sqrt{s}$ = 7 TeV for events with two heavy stable particles, reconstructed in the Inner tracker and the Muon System and identified by their time of flight in the Muon System. No evidence for an excess over the SM expectation is observed. Limits on the mass are derived, see Fig. 3, for $\widetilde{\tau}$ in a GMSB scenario and for sleptons produced by electroweak processes only, in which case the limit degrades to 110 GeV.

$\widetilde{q}$ (Squark) mass limit

For $m_{\widetilde{q}}$ > 60–70 GeV, it is expected that squarks would undergo a cascade decay via a number of neutralinos and/or charginos rather than undergo a direct decay to photinos as assumed by some papers. Limits obtained when direct decay is assumed are usually higher than limits when cascade decays are included.

Limits from e^+e^- collisions depend on the mixing angle of the lightest mass eigenstate $\widetilde{q}_1$=$\widetilde{q}_R$sinθ_q+$\widetilde{q}_L$cosθ_q. It is usually assumed that only the sbottom and stop squarks have non-trivial mixing angles (see the stop and sbottom sections). Here, unless otherwise noted, squarks are always taken to be either left/right degenerate, or purely of left or right type. Data from Z decays have set squark mass limits above 40 GeV, in the case of $\widetilde{q} \rightarrow q\widetilde{\chi}_1$ decays if Δm=$m_{\widetilde{q}} - m_{\widetilde{\chi}^0_1} \gtrsim$ 5 GeV. For smaller values of Δm, current constraints on the invisible width of the Z ($\Delta\Gamma_{\rm inv}$ < 2.0 MeV, LEP 00) exclude $m_{\widetilde{u}_{L,R}}$ <44 GeV, $m_{\widetilde{d}_R}$ <33 GeV, $m_{\widetilde{d}_L}$ <44 GeV and, assuming all squarks degenerate, $m_{\widetilde{q}}$ <45 GeV.

Some earlier papers are now obsolete and have been omitted. They were last listed in our PDG 14 edition: K. Olive, *et al.* (Particle Data Group), Chinese Physics **C38** 070001 (2014) (http://pdg.lbl.gov).

R-parity conserving $\widetilde{q}$ (Squark) mass limit

VALUE (GeV)	CL%	DOCUMENT ID		TECN	COMMENT
>1700	95	[1] AAD	25BM	ATLS	1 or 2 $\tau + \not{E}_T$, Tsqk5, $m_{\widetilde{u}_L} = m_{\widetilde{d}_L} = m_{\widetilde{c}_L} = m_{\widetilde{s}_L}$, $m_{\widetilde{\chi}^0_1}$ = 100 GeV
>1260	95	[2] AAD	24Z	ATLS	2 same-sign/3ℓ + jets, like Tglu1E but for squarks, $m_{\widetilde{\chi}^0_1}$ = 100 GeV
>1700	95	[2] AAD	24Z	ATLS	2 same-sign/3ℓ + jets, like Tglu1G but for squarks, $m_{\widetilde{\chi}^0_1}$ = 100 GeV
>1850	95	[3] HAYRAPETY...	24Q	CMS	$\geq$ 2 γ + $\geq$ 4 jets, stealth SUSY, 500 GeV < $m_{\widetilde{\chi}^0_1}$ < 1300 GeV
>1550	95	[4] AAD	23AE	ATLS	2 SFOS ℓ, jets, $\not{E}_T$, Tsqk2, $m_{\widetilde{\chi}^0_2}$ = $(m_{\widetilde{q}} + m_{\widetilde{\chi}^0_1})/2$, , $m_{\widetilde{\chi}^0_1}$ = 100 GeV
none 1200–2500	95	[5] TUMASYAN	23X	CMS	2 AK8 jets + 1 AK4 jet, $\widetilde{q} \rightarrow q\widetilde{\chi}^0_2$ and $\widetilde{\chi}^0_2 \rightarrow H_1\widetilde{\chi}^0_S$, 40 < m_{H_1} < 120 GeV
>1400	95	[6] AAD	21AK	ATLS	$\ell^\pm$ + jets + $\not{E}_T$, Tsqk3, 4 degenerate light $\widetilde{q}_\ell$, $m_{\widetilde{\chi}^\pm_1}$ = $(m_{\widetilde{q}} + m_{\widetilde{\chi}^0_1})/2$, $m_{\widetilde{\chi}^0_1}$ < 200 GeV
>1040	95	[6] AAD	21AK	ATLS	$\ell^\pm$ + jets + $\not{E}_T$, Tsqk3, 1 light $\widetilde{q}_\ell$, $m_{\widetilde{\chi}^\pm_1} = (m_{\widetilde{q}} + m_{\widetilde{\chi}^0_1})/2$, $m_{\widetilde{\chi}^0_1}$ < 200 GeV
> 925	95	[7] AAD	21F	ATLS	$\geq$ 1 jet + $\not{E}_T$, Tsqk1, $m_{\widetilde{q}}-m_{\widetilde{\chi}^0_1}$ = 5 GeV
> 550	95	[7] AAD	21F	ATLS	$\geq$ 1 jet + $\not{E}_T$, Tstop3, $m_{\widetilde{t}}-m_{\widetilde{\chi}^0_1}$ = 5 GeV
> 550	95	[7] AAD	21F	ATLS	$\geq$ 1 jet + $\not{E}_T$, Tstop4, $m_{\widetilde{t}}-m_{\widetilde{\chi}^0_1}$ = 5 GeV
> 545	95	[7] AAD	21F	ATLS	$\geq$ 1 jet + $\not{E}_T$, Tsbot1, $m_{\widetilde{b}}-m_{\widetilde{\chi}^0_1}$ = 5 GeV
>1850	95	[8] AAD	21L	ATLS	jets + $\not{E}_T$, Tsqk1, 8 degenerate $\widetilde{q}$, $m_{\widetilde{\chi}^0_1}$ = 0 GeV
>1220	95	[8] AAD	21L	ATLS	jets + $\not{E}_T$, Tsqk1, 1 non-degenerate $\widetilde{q}$, $m_{\widetilde{\chi}^0_1}$ = 0 GeV
>1310	95	[8] AAD	21L	ATLS	jets + $\not{E}_T$, Tsqk3, 4 degenerate $\widetilde{q}_l$, $m_{\widetilde{\chi}^\pm_1} = (m_{\widetilde{q}} + m_{\widetilde{\chi}^0_1})/2$, $m_{\widetilde{\chi}^0_1}$ = 0 GeV
>3000	95	[8] AAD	21L	ATLS	jets + $\not{E}_T$, combined $\widetilde{g}\widetilde{g}$, $\widetilde{g}\ \widetilde{q}$, $\widetilde{q}\widetilde{q}$ production, $\widetilde{g} \rightarrow qq'\widetilde{\chi}^0_1$, $\widetilde{q} \rightarrow q\widetilde{\chi}^0_1$, $m_{\widetilde{q}} = m_{\widetilde{g}}$, $m_{\widetilde{\chi}^0_1}$ = 0 GeV
>1800	95	[9] SIRUNYAN	21M	CMS	$\ell^\pm\ell^\mp + \not{E}_T$, Tsqk2A, $m_{\widetilde{\chi}^0_2}$ = 1500 GeV, $m_{\widetilde{\chi}^0_1}$ = 100 GeV
>1590	95	[10] SIRUNYAN	19AG	CMS	2γ +$\not{E}_T$, Tsqk4B, 500 GeV <$m_{\widetilde{\chi}^0_1}$ < 1500 GeV
>1130	95	[11] SIRUNYAN	19CH	CMS	jets+$\not{E}_T$, Tsqk1, 1 light flavour, $m_{\widetilde{\chi}^0_1}$ = 0 GeV
>1630	95	[11] SIRUNYAN	19CH	CMS	jets+$\not{E}_T$, Tsqk1, 8 degenerate light flavours, $m_{\widetilde{\chi}^0_1}$ = 0 GeV
>1430	95	[12] SIRUNYAN	19K	CMS	$\gamma + \ell + \not{E}_T$, Tsqk4A, $m_{\widetilde{\chi}^0_1}$ = 1200 GeV

>1200	95	[13] AABOUD	18BJ	ATLS	$\ell^\pm\ell^\mp$ + jets + $\not{E}_T$, Tsqk2, $m_{\widetilde{\chi}^0_1}$ = 1 GeV, any $m_{\widetilde{\chi}^0_2}$
> 850	95	[14] AABOUD	18BV	ATLS	c-jets+$\not{E}_T$, Tsqk1 (charm only), $m_{\widetilde{\chi}^0_1}$ = 0 GeV
> 710	95	[15] AABOUD	18I	ATLS	≥ 1 jets+$\not{E}_T$, Tsqk1, $m_{\widetilde{q}} \sim m_{\widetilde{\chi}^0_1}$
>1820	95	[16] AABOUD	18U	ATLS	2 γ + $\not{E}_T$, GGM, Tsqk4B, any NLSP mass
>1550	95	[17] AABOUD	18V	ATLS	jets+$\not{E}_T$, Tsqk1, $m_{\widetilde{\chi}^0_1}$ = 0 GeV
>1150	95	[18] AABOUD	18V	ATLS	jets+$\not{E}_T$, Tsqk3, $m_{\widetilde{\chi}^\pm_1}$ = 0.5 ($m_{\widetilde{q}}$ + $m_{\widetilde{\chi}^0_1}$), $m_{\widetilde{\chi}^0_1}$ = 0 GeV
>1650	95	[19] SIRUNYAN	18AA	CMS	≥ 1γ + $\not{E}_T$, Tsqk4A
>1750	95	[19] SIRUNYAN	18AA	CMS	≥ 1γ + $\not{E}_T$, Tsqk4B
> 675	95	[20] SIRUNYAN	18AY	CMS	jets+$\not{E}_T$, Tsqk1, 1 light flavor state, $m_{\widetilde{\chi}^0_1}$ = 0 GeV
>1320	95	[20] SIRUNYAN	18AY	CMS	jets+$\not{E}_T$,Tsqk1,8 degenerate light flavor states, $m_{\widetilde{\chi}^0_1}$ = 0 GeV
>1220	95	[21] AABOUD	17AR	ATLS	1ℓ+jets+$\not{E}_T$, Tsqk3, $m_{\widetilde{\chi}^0_1}$ = 0 GeV
>1000	95	[22] AABOUD	17N	ATLS	2 same-flavour, opposite-sign ℓ + jets + $\not{E}_T$, Tsqk2, $m_{\widetilde{\chi}^0_1}$ = 0 GeV
>1150	95	[23] KHACHATRY...	17P	CMS	1 or more jets+$\not{E}_T$, Tsqk1, 4(flavor) x 2(isospin) = 8 mass degenerate states, $m_{\widetilde{\chi}^0_1}$ = 0 GeV
> 575	95	[23] KHACHATRY...	17P	CMS	1 or more jets+$\not{E}_T$, Tsqk1, one light flavor state, $m_{\widetilde{\chi}^0_1}$ = 0 GeV
>1370	95	[24] KHACHATRY...	17V	CMS	2 γ + $\not{E}_T$, GGM, Tsqk4, any NLSP mass
>1600	95	[25] SIRUNYAN	17AY	CMS	γ + jets+$\not{E}_T$, Tsqk4B, $m_{\widetilde{\chi}^0_1}$ = 0 GeV
>1370	95	[25] SIRUNYAN	17AY	CMS	γ + jets+$\not{E}_T$, Tsqk4A, $m_{\widetilde{\chi}^0_1}$ = 0 GeV
>1050	95	[26] SIRUNYAN	17AZ	CMS	≥ 1 jets+$\not{E}_T$, Tsqk1, single light flavor state, $m_{\widetilde{\chi}^0_1}$ = 0 GeV
>1550	95	[26] SIRUNYAN	17AZ	CMS	≥ 1 jets+$\not{E}_T$, Tsqk1, 4(flavor) x 2(isospin) = 8 degenerate mass states, $m_{\widetilde{\chi}^0_1}$ = 0 GeV
>1390	95	[27] SIRUNYAN	17P	CMS	jets+$\not{E}_T$, Tsqk1, 4(flavor) x 2(isospin) = 8 degenerate mass states, $m_{\widetilde{\chi}^0_1}$ = 0 GeV
> 950	95	[27] SIRUNYAN	17P	CMS	jets+$\not{E}_T$, Tsqk1, one light flavor state, $m_{\widetilde{\chi}^0_1}$ = 0 GeV
> 608	95	[28] AABOUD	16D	ATLS	≥ 1 jet + $\not{E}_T$, Tsqk1, $m_{\widetilde{q}}-m_{\widetilde{\chi}^0_1}$ = 5 GeV
>1030	95	[29] AABOUD	16N	ATLS	≥ 2 jets + $\not{E}_T$, Tsqk1, $m_{\widetilde{\chi}^0_1}$ = 0 GeV
> 600	95	[30] KHACHATRY...	16BS	CMS	jets + $\not{E}_T$, Tsqk1, single light squark, $m_{\widetilde{\chi}^0_1}$ = 0 GeV
>1260	95	[30] KHACHATRY...	16BS	CMS	jets + $\not{E}_T$, Tsqk1, 8 degenerate light squarks, $m_{\widetilde{\chi}^0_1}$ = 0 GeV
> 850	95	[31] AAD	15BV	ATLS	jets + $\not{E}_T$, $\widetilde{q} \rightarrow q\widetilde{\chi}^0_1$, $m_{\widetilde{\chi}^0_1}$ = 100 GeV
> 250	95	[32] AAD	15CS	ATLS	photon + $\not{E}_T$, $pp \rightarrow \widetilde{q}\widetilde{q}^*\gamma$, $\widetilde{q} \rightarrow q\widetilde{\chi}^0_1$, $m_{\widetilde{q}} - m_{\widetilde{\chi}^0_1} = m_c$
> 490	95	[33] AAD	15K	ATLS	$\widetilde{c} \rightarrow c\widetilde{\chi}^0_1$, $m_{\widetilde{\chi}^0_1}$ < 200 GeV
> 875	95	[34] KHACHATRY...	15AF	CMS	$\widetilde{q} \rightarrow q\widetilde{\chi}^0_1$, simplified model, 8 degenerate light $\widetilde{q}$, $m_{\widetilde{\chi}^0_1}$ = 0
> 520	95	[34] KHACHATRY...	15AF	CMS	$\widetilde{q} \rightarrow q\widetilde{\chi}^0_1$, simplified model, single light squark, $m_{\widetilde{\chi}^0_1}$ = 0
>1450	95	[34] KHACHATRY...	15AF	CMS	CMSSM, tanβ = 30, $A_0 = -2\max(m_0, m_{1/2})$, μ > 0
> 850	95	[35] AAD	14AE	ATLS	jets + $\not{E}_T$, $\widetilde{q} \rightarrow q\widetilde{\chi}^0_1$ simplified model, mass degenerate first and second generation squarks, $m_{\widetilde{\chi}^0_1}$ = 0 GeV
> 440	95	[35] AAD	14AE	ATLS	jets + $\not{E}_T$, $\widetilde{q} \rightarrow q\widetilde{\chi}^0_1$ simplified model, single light-flavour squark, $m_{\widetilde{\chi}^0_1}$ = 0 GeV
>1700	95	[35] AAD	14AE	ATLS	jets + $\not{E}_T$, mSUGRA/CMSSM, $m_{\widetilde{q}} = m_{\widetilde{g}}$
> 800	95	[36] CHATRCHYAN	14AH	CMS	jets + $\not{E}_T$, $\widetilde{q} \rightarrow q\widetilde{\chi}^0_1$ simplified model, $m_{\widetilde{\chi}^0_1}$ = 50 GeV
> 780	95	[37] CHATRCHYAN	14I	CMS	multijets + $\not{E}_T$, $\widetilde{q} \rightarrow q\widetilde{\chi}^0_1$ simplified model, $m_{\widetilde{\chi}^0_1}$ < 200 GeV
>1360	95	[38] AAD	13L	ATLS	jets + $\not{E}_T$, CMSSM, $m_{\widetilde{g}} = m_{\widetilde{q}}$
>1200	95	[39] AAD	13Q	ATLS	γ+b+$\not{E}_T$,higgsino-like neutralino, $m_{\widetilde{\chi}^0_1}$ > 220 GeV, GMSB
		[40] CHATRCHYAN	13	CMS	$\ell^\pm\ell^\mp$ + jets + $\not{E}_T$, CMSSM
>1250	95	[41] CHATRCHYAN	13G	CMS	0,1,2, ≥ 3 b-jets + $\not{E}_T$, CMSSM, $m_{\widetilde{q}} = m_{\widetilde{g}}$
>1430	95	[42] CHATRCHYAN	13H	CMS	2γ + ≥ 4 jets + low $\not{E}_T$, stealth SUSY model
> 750	95	[43] CHATRCHYAN	13T	CMS	jets + $\not{E}_T$, $\widetilde{q} \rightarrow q\widetilde{\chi}^0_1$ simplified model, $m_{\widetilde{\chi}^0_1}$= 0 GeV
> 820	95	[44] AAD	12AX	ATLS	ℓ +jets +$\not{E}_T$, CMSSM, $m_{\widetilde{q}}$=$m_{\widetilde{g}}$
>1200	95	[45] AAD	12CJ	ATLS	$\ell^\pm$+jets+$\not{E}_T$, CMSSM, $m_{\widetilde{q}}$=$m_{\widetilde{g}}$
> 870	95	[46] AAD	12CP	ATLS	2γ +$\not{E}_T$, GMSB, bino NLSP, $m_{\widetilde{\chi}^0_1}$ > 50 GeV
> 950	95	[47] AAD	12W	ATLS	jets + $\not{E}_T$, CMSSM, $m_{\widetilde{q}} = m_{\widetilde{g}}$
		[48] CHATRCHYAN	12	CMS	e, μ, jets, razor, CMSSM
> 760	95	[49] CHATRCHYAN	12AE	CMS	jets + $\not{E}_T$, $\widetilde{q} \rightarrow q\widetilde{\chi}^0_1$, $m_{\widetilde{\chi}^0_1}$ < 200 GeV
>1110	95	[50] CHATRCHYAN	12AT	CMS	jets + $\not{E}_T$, CMSSM
>1180	95	[50] CHATRCHYAN	12AT	CMS	jets + $\not{E}_T$, CMSSM, $m_{\widetilde{q}}$=$m_{\widetilde{g}}$
• • • We do not use the following data for averages, fits, limits, etc. • • •					
>1080	95	[51] AABOUD	18V	ATLS	jets+$\not{E}_T$, Tsqk5, $(m_{\widetilde{\chi}^0_2}-m_{\widetilde{\chi}^0_1})/(m_{\widetilde{q}}-m_{\widetilde{\chi}^0_1})$ < 0.95, $m_{\widetilde{\chi}^0_1}$ = 60 GeV
> 300	95	[52] KHACHATRY...	16BT	CMS	19-parameter pMSSM model, global Bayesian analysis, flat prior
		[53] AAD	15AI	ATLS	$\ell^\pm$ + jets + $\not{E}_T$
>1650	95	[31] AAD	15BV	ATLS	jets + $\not{E}_T$, $m_{\widetilde{g}} = m_{\widetilde{q}}$, $m_{\widetilde{\chi}^0_1}$ = 1 GeV
> 790	95	[31] AAD	15BV	ATLS	jets + $\not{E}_T$, $\widetilde{q} \rightarrow qW\widetilde{\chi}^0_1$, $m_{\widetilde{\chi}^0_1}$ = 100 GeV
> 820	95	[31] AAD	15BV	ATLS	2 or 3 leptons + jets, $\widetilde{q}$ decays via sleptons, $m_{\widetilde{\chi}^0_1}$ = 100 GeV
> 850	95	[31] AAD	15BV	ATLS	τ, $\widetilde{q}$ decays via staus, $m_{\widetilde{\chi}^0_1}$ = 50 GeV
> 700	95	[54] KHACHATRY...	15AR	CMS	$\widetilde{q} \rightarrow q\widetilde{\chi}^0_1$, $\widetilde{\chi}^0_1 \rightarrow \widetilde{S}g$, $\widetilde{S} \rightarrow S\widetilde{G}$, $S \rightarrow gg$, $m_{\widetilde{S}}$ = 100 GeV, m_S = 90 GeV
> 550	95	[54] KHACHATRY...	15AR	CMS	$\ell^\pm$, $\widetilde{q} \rightarrow q\widetilde{\chi}^\pm_1$, $\widetilde{\chi}^\pm_1 \rightarrow \widetilde{S}W^\pm$, $\widetilde{S} \rightarrow S\widetilde{G}$, $S \rightarrow gg$, $m_{\widetilde{S}}$ = 100 GeV, m_S = 90 GeV
>1500	95	[55] KHACHATRY...	15AZ	CMS	≥ 2 γ, ≥ 1 jet, (Razor), bino-like NLSP, $m_{\widetilde{\chi}^0_1}$ = 375 GeV
>1000	95	[55] KHACHATRY...	15AZ	CMS	≥ 1 γ, ≥ 2 jet, wino-like NLSP, $m_{\widetilde{\chi}^0_1}$ = 375 GeV
> 670	95	[56] AAD	14E	ATLS	$\ell^\pm\ell^\pm(\ell^\mp)$ + jets, $\widetilde{q} \rightarrow q'\widetilde{\chi}^\pm_1$, $\widetilde{\chi}^\pm_1 \rightarrow W^{(*)\pm}\widetilde{\chi}^0_2$, $\widetilde{\chi}^0_2 \rightarrow Z^{(*)}\widetilde{\chi}^0_1$ simplified model, $m_{\widetilde{\chi}^0_1}$ < 300 GeV
> 780	95	[56] AAD	14E	ATLS	$\ell^\pm\ell^\pm(\ell^\mp)$ + jets, $\widetilde{q} \rightarrow q'\widetilde{\chi}^\pm_1/\widetilde{\chi}^0_2$, $\widetilde{\chi}^\pm_1 \rightarrow \ell^\pm\nu\widetilde{\chi}^0_1$, $\widetilde{\chi}^0_2 \rightarrow \ell^\pm\ell^\mp(\nu\nu)\widetilde{\chi}^0_1$ simplified model
> 700	95	[57] CHATRCHYAN	13AO	CMS	$\ell^\pm\ell^\mp$ + jets + $\not{E}_T$, CMSSM, m_0 < 700 GeV
>1350	95	[58] CHATRCHYAN	13AV	CMS	jets (+ leptons) + $\not{E}_T$, CMSSM, $m_{\widetilde{g}} = m_{\widetilde{q}}$
> 800	95	[59] CHATRCHYAN	13W	CMS	≥ 1 photons + jets + $\not{E}_T$, GGM, wino-like NLSP, $m_{\widetilde{\chi}^0_1}$ = 375 GeV
>1000	95	[59] CHATRCHYAN	13W	CMS	≥ 2 photons + jets + $\not{E}_T$, GGM, bino-like NLSP, $m_{\widetilde{\chi}^0_1}$ = 375 GeV
> 340	95	[60] DREINER	12A	THEO	$m_{\widetilde{q}} \sim m_{\widetilde{\chi}^0_1}$
> 650	95	[61] DREINER	12A	THEO	$m_{\widetilde{q}} = m_{\widetilde{g}} \sim m_{\widetilde{\chi}^0_1}$

[1] AAD 25BM searched in 140 fb^{-1} (at $\sqrt{s}$ = 13 TeV) and 58.6 fb^{-1} (at $\sqrt{s}$ = 13.6 TeV) of pp collisions for an excess of events with taus and $\not{E}_T$. Several signal regions are defined requiring one τ and no other leptons, one τ and one e or μ, or two τ, and then using both a BDT or a cut-and-count analysis to target scenarios with different kinematic regimes. No significant excess over the Standard Model expectation is found. Exclusion limits at 95% C.L. are set on the gluino or squark mass, assuming that the squark (other intermediate or pair-produced) decays to intermediate wino-like $\widetilde{\chi}^\pm_1$ or $\widetilde{\chi}^0_2$, which, in turn, decays to the $\widetilde{\chi}^0_1$ LSP via staus or tau sneutrinos, as in model Tglu1F for gluinos (and similar for squarks). See their Figs. 13 and 14.

Int. J. Mod. Phys. A 2026.41. Downloaded from www.worldscientific.com
by UNIVERSITY OF CALIFORNIA @ BERKELEY on 09/16/26. Re-use and distribution is strictly not permitted, except for Open Access articles.

Int. J. Mod. Phys. A 2026.41. Downloaded from www.worldscientific.com by UNIVERSITY OF CALIFORNIA @ BERKELEY on 09/16/26. Re-use and distribution is strictly not permitted, except for Open Access articles.

[2] AAD 24Z searched in 139 fb^{-1} of pp collisions at $\sqrt{s}$ = 13 TeV for events with exactly two same-sign leptons or at least three leptons. Several signal regions, including a $\not{E}_T$ selection targeting RPC models, and selections based on b-jet multiplicities, targeting RPV models, are considered. No significant excess over the Standard Model expectation is found. Exclusion limits at 95% C.L. are set on the gluino or squark mass, in multi-step RPC decays via charginos, neutralinos or sleptons into quarks, leptons and neutralinos, or RPV decays of either the neutralino LSP or the stop produced in $\widetilde{g} \rightarrow t\,\widetilde{t}$ into quarks. See their Fig. 7.

[3] HAYRAPETYAN 24Q searched in 138 fb^{-1} of pp collisions at $\sqrt{s}$ = 13 TeV for evidence of stealth supersymmetry in final states with two photons and jets, and low $\not{E}_T$. No significant excess above the Standard Model expectations is observed. The investigated models include a singlet scalar boson S, and its SUSY fermion $\widetilde{S}$. In the investigated models, either gluinos or squarks are pair produced and each decay to a $\widetilde{\chi}^0_1$ and a gluon or squark, respectively, followed by the decays $\widetilde{\chi}^0_1 \rightarrow \gamma\widetilde{S}$, $\widetilde{S} \rightarrow \widetilde{G}\,S$ and $S \rightarrow gg$. Limits are set on the $\widetilde{g}$ and the $\widetilde{q}$ mass, see their Fig. 4.

[4] AAD 23AE searched in 139 fb^{-1} of pp collisions at $\sqrt{s}$ = 13 TeV for events with 2 ℓ with same flavour and opposite sign, plus jets and $\not{E}_T$, defining signal region with the dilepton invariant mass both on- and off-shell with respect to the Z boson. No significant excess above the Standard Model predictions is observed. Limits are set on models of strong and electroweak production. In this case, limits are placed on the mass of pair-produced squarks, assuming a scenario like in Tsqk2, see figure 16.

[5] TUMASYAN 23X searched in 138 fb^{-1} of pp collisions at $\sqrt{s}$ = 13 TeV for squark pair production with cascade decays to CP-even singlet-like Higgs bosons (H_1), leading to final states with small missing transverse momentum. This search targets H_1 decays to $b\overline{b}$-pairs that are reconstructed in large-area (AK8) jets. No significant excess above the Standard Model expectations is observed. Limits are set in the next-to-minimal supersymmetric extension of the SM, where a singlino of small mass leads to squark and gluino cascade decays that can predominantly end in a highly Lorentz-boosted singlet-like H_1 and a singlino-like neutralino $\widetilde{\chi}^0_S$ of small transverse momentum. The eight first- and second-generation squarks are assumed mass-degenerate, and the gluino mass is set at 1% larger.

[6] AAD 21AK searched in 139 fb^{-1} of pp collisions at $\sqrt{s}$ = 13 TeV for pair production of gluinos and squarks in events with a single isolated electron or muon, originating from the decay of a W boson, multiple jets and significant $\not{E}_T$. No significant excess above the Standard Model expectations is observed. Limits are set on the gluino mass in the Tglu1B simplified model and on the squark mass in the Tsqk3 simplified model, see their Figure 8.

[7] AAD 21F searched in 139 fb^{-1} of pp collisions at $\sqrt{s}$ = 13 TeV for pair production of squarks in events with a high-p_T jet and $\not{E}_T$. No significant excess above the Standard Model predictions is observed. Limits are set on the $\widetilde{t}$ mass in the Tstop3 and Tstop4, on the $\widetilde{b}$ mass in the Tsbot1, and on the $\widetilde{q}$ mass in the Tsqk1 simplified model (four-flavour, two chirality states degeneracy).

[8] AAD 21L searched in 139 fb^{-1} of pp collisions at $\sqrt{s}$ = 13 TeV for pair production of gluinos and squarks in events with jets, large missing transverse momentum but no electrons or muons. No significant excess above the Standard Model expectations is observed. Limits are set on the gluino mass in the Tglu1A and Tglu1B simplified models, on the squark mass in the Tsqk1 and Tsqk3 simplified models and in a simplified model for gluino-squark production, see their Figures 13-17.

[9] SIRUNYAN 21M searched in 137 fb^{-1} of pp collisions at $\sqrt{s}$ = 13 TeV for supersymmetry in events with two opposite-sign same-flavor leptons (electrons, muons) and $\not{E}_T$. No significant excess above the Standard Model expectations is observed. Limits are set on the gluino mass in the simplified model Tglu4C, see their Figure 10, on the $\widetilde{\chi}^0_2$ and $\widetilde{\chi}^\pm_1$ mass in Tchi1n2Fa, see their Figure 11, on the $\widetilde{\chi}^0_1$ mass in Tn1n1C and Tn1n1B for $m_{\widetilde{\chi}^0_2} = m_{\widetilde{\chi}^\pm_1} = m_{\widetilde{\chi}^0_1}$, see their Figure 12. Limits are also set on the light squark mass for the simplified model Tsqk2A, on the sbottom mass in Tsbot3, see their Figure 13, and on the slepton mass in direct electroweak pair production of mass-degenerate left- and right-handed sleptons (selectrons and smuons), see their Figure 14.

[10] SIRUNYAN 19AG searched in 35.9 fb^{-1} of pp collisions at $\sqrt{s}$ = 13 TeV for events with two photons and large $\not{E}_T$. No significant excess above the Standard Model expectations is observed. Limits are set on the gluino mass in the Tglu4B simplified model and on the squark mass in the Tsqk4B simplified model, see their Figure 3.

[11] SIRUNYAN 19CH searched in 137 fb^{-1} of pp collisions at $\sqrt{s}$ = 13 TeV for events containing multiple jets and large $\not{E}_T$. No significant excess above the Standard Model expectations is observed. Limits are set on the gluino mass in the Tglu1A, Tglu1C, Tglu2A and Tglu3A simplified models, see their Figure 13. Limits are also set on squark, sbottom and stop masses in the Tsqk1, Tsbot1, Tstop1 simplified models, see their Figure 14.

[12] SIRUNYAN 19K searched in 35.9 fb^{-1} of pp collisions at $\sqrt{s}$ = 13 TeV for events with a photon, an electron or muon, and large $\not{E}_T$. No significant excess above the Standard Model expectations is observed. In the framework of GMSB, limits are set on the chargino and neutralino mass in the Tchi1n1A simplified model, see their Figure 6. Limits are also set on the gluino mass in the Tglu4A simplified model, and on the squark mass in the Tsqk4A simplified model, see their Figure 7.

[13] AABOUD 18BJ searched in 36.1 fb^{-1} of pp collisions at $\sqrt{s}$ = 13 TeV in events with two opposite-sign charged leptons (electrons and muons), jets and missing transverse momentum, with various requirements to be sensitive to signals with different kinematic endpoint values in the dilepton invariant mass distribution. The data are found to be consistent with the SM expectation. Results are interpreted in the Tsqk2 model in case of $m_{\widetilde{\chi}^0_1}$ = 1 GeV: for any $m_{\widetilde{\chi}^0_2}$, squark masses below 1200 GeV are excluded, see their Fig. 14(b).

[14] AABOUD 18BV searched in 36.1 fb^{-1} of pp collisions at $\sqrt{s}$ = 13 TeV for events with at least one jet identified as c-jet, large missing transverse energy and no leptons. Good agreement is observed between the number of events in data and Standard Model predictions. The results are translated into exclusion limits in Tsqk1 models considering only $\widetilde{c}_1$. In scenarios with massless neutralinos, scharm masses below 850 GeV are excluded. If the differences of the $\widetilde{c}_1$ and $\widetilde{\chi}^0_1$ masses is below 100 GeV, scharm masses below 500 GeV are excluded. See their Fig.6 and Fig.7.

[15] AABOUD 18I searched in 36.1 fb^{-1} of pp collisions at $\sqrt{s}$ = 13 TeV for events with at least one jet with a transverse momentum above 250 GeV and no leptons. Good agreement is observed between the number of events in data and Standard Model predictions. The results are translated into exclusion limits in Tsqk1 models. In the compressed scenario with similar squark and neutralino masses, squark masses below 710 GeV are excluded. See their Fig.10(b).

[16] AABOUD 18U searched in 36.1 fb^{-1} of pp collisions at $\sqrt{s}$ = 13 TeV in events with at least one isolated photon, possibly jets and significant transverse momentum targeting generalised models of gauge-mediated SUSY breaking. No significant excess of events is observed above the SM prediction. Results are interpreted in terms of lower limits on the masses of squark in Tsqk4B models. Masses below 1820 GeV are excluded for any NLSP mass, see their Fig. 9.

[17] AABOUD 18V searched in 36.1 fb^{-1} of pp collisions at $\sqrt{s}$ = 13 TeV in events with no charged leptons, jets and missing transverse momentum. The data are found to be consistent with the SM expectation. Results are interpreted in the Tsqk1 model: squark masses below 1550 GeV are excluded for massless LSP, see their Fig. 13(a).

[18] AABOUD 18V searched in 36.1 fb^{-1} of pp collisions at $\sqrt{s}$ = 13 TeV in events with no charged leptons, jets and missing transverse momentum. The data are found to be consistent with the SM expectation. Results are interpreted in the Tsqk3 model. Assuming that $m_{\widetilde{\chi}^\pm_1} = 0.5\ (m_{\widetilde{q}} + m_{\widetilde{\chi}^0_1})$, squark masses below 1150 GeV are excluded for massless LSP, see their Fig. 14(a). Exclusions are also shown assuming $m_{\widetilde{\chi}^0_1}$ = 60 GeV, see their Fig. 14(b).

[19] SIRUNYAN 18AA searched in 35.9 fb^{-1} of pp collisions at $\sqrt{s}$ = 13 TeV for events with at least one photon and large $\not{E}_T$. No significant excess above the Standard Model expectations is observed. Limits are set on wino masses in a general gauge-mediated SUSY breaking (GGM) scenario with bino-like $\widetilde{\chi}^0_1$ and wino-like $\widetilde{\chi}^\pm_1$ and $\widetilde{\chi}^0_2$, see Figure 7. Limits are also set on the NLSP mass in the Tchi1n1A and Tchi1chi1A simplified models, see their Figure 8. Finally, limits are set on the gluino mass in the Tglu4A and Tglu4B simplified models, see their Figure 9, and on the squark mass in the Tskq4A and Tsqk4B simplified models, see their Figure 10.

[20] SIRUNYAN 18AY searched in 35.9 fb^{-1} of pp collisions at $\sqrt{s}$ = 13 TeV for events containing one or more jets and significant $\not{E}_T$. No significant excess above the Standard Model expectations is observed. Limits are set on the gluino mass in the Tglu1A, Tglu2A and Tglu3A simplified models, see their Figure 3. Limits are also set on squark, sbottom and stop masses in the Tsqk1, Tsbot1, Tstop1 and Tstop4 simplified models, see their Figure 3. Finally, limits are set on long-lived gluino masses in a Tglu1A simplified model where the gluino is metastable or long-lived with proper decay lengths in the range 10^{-3} mm $< c\tau < 10^5$ mm, see their Figure 4.

[21] AABOUD 17AR searched in 36.1 fb^{-1} of pp collisions at $\sqrt{s}$ = 13 TeV for events with one isolated lepton, at least two jets and large missing transverse momentum. No significant excess above the Standard Model expectations is observed. Limits up to 1.25 TeV are set on the 1st and 2nd generation squark masses in Tsqk3 simplified models, with $x = (m_{\widetilde{\chi}^\pm_1} - m_{\widetilde{\chi}^0_1})\ /\ (m_{\widetilde{q}} - m_{\widetilde{\chi}^0_1}) = 1/2$. Similar limits are obtained for variable x and fixed neutralino mass, $m_{\widetilde{\chi}^0_1}$ = 60 GeV. See their Figure 13.

[22] AABOUD 17N searched in 14.7 fb^{-1} of pp collisions at $\sqrt{s}$ = 13 TeV for events with 2 same-flavour, opposite-sign leptons (electrons or muons), jets and large missing transverse momentum. The results are interpreted as 95% C.L. limits in Tsqk2 models, assuming $m_{\widetilde{\chi}^0_1}$ = 0 GeV and $m_{\widetilde{\chi}^0_2}$ = 600 GeV. See their Fig. 12 for exclusion limits as a function of $m_{\widetilde{\chi}^0_2}$.

[23] KHACHATRYAN 17P searched in 2.3 fb^{-1} of pp collisions at $\sqrt{s}$ = 13 TeV for events with one or more jets and large $\not{E}_T$. No significant excess above the Standard Model expectations is observed. Limits are set on the gluino mass in the Tglu1A, Tglu2A, Tglu3A, Tglu3B, Tglu3C and Tglu3D simplified models, see their Figures 7 and 8. Limits are also set on the squark mass in the Tsqk1 simplified model, see their Fig. 7, and on the sbottom mass in the Tsbot1 simplified model, see Fig. 8. Finally, limits are set on the stop mass in the Tstop1, Tstop3, Tstop4, Tstop6 and Tstop7 simplified models, see Fig. 8.

[24] KHACHATRYAN 17V searched in 2.3 fb^{-1} of pp collisions at $\sqrt{s}$ = 13 TeV for events with two photons and large $\not{E}_T$. No significant excess above the Standard Model expectations is observed. Limits are set on the gluino and squark mass in the context of general gauge mediation models Tglu4B and Tsqk4, see their Fig. 4.

[25] SIRUNYAN 17AY searched in 35.9 fb^{-1} of pp collisions at $\sqrt{s}$ = 13 TeV for events with at least one photon, jets and large $\not{E}_T$. No significant excess above the Standard Model expectations is observed. Limits are set on the gluino mass in the Tglu4A and Tglu4B simplified models, and on the squark mass in the Tskq4A and Tsqk4B simplified models, see their Figure 6.

[26] SIRUNYAN 17AZ searched in 35.9 fb^{-1} of pp collisions at $\sqrt{s}$ = 13 TeV for events with one or more jets and large $\not{E}_T$. No significant excess above the Standard Model expectations is observed. Limits are set on the gluino mass in the Tglu1A, Tglu2A, Tglu3A simplified models, see their Figures 6. Limits are also set on the squark mass in the Tsqk1 simplified model (for single light squark and for 8 degenerate light squarks), on the sbottom mass in the Tsbot1 simplified model and on the stop mass in the Tstop1 simplified model, see their Fig. 7. Finally, limits are set on the stop mass in the Tstop2, Tstop4 and Tstop8 simplified models, see Fig. 8.

[27] SIRUNYAN 17P searched in 35.9 fb^{-1} of pp collisions at $\sqrt{s}$ = 13 TeV for events with multiple jets and large $\not{E}_T$. No significant excess above the Standard Model expectations is observed. Limits are set on the gluino mass in the Tglu1A, Tglu1C, Tglu2A, Tglu3A and Tglu3D simplified models, see their Fig. 12. Limits are also set on the squark mass in the Tsqk1 simplified model, on the stop mass in the Tstop1 simplified model, and on the sbottom mass in the Tsbot1 simplified model, see Fig. 13.

[28] AABOUD 16D searched in 3.2 fb^{-1} of pp collisions at $\sqrt{s}$ = 13 TeV for events with an energetic jet and large missing transverse momentum. The results are interpreted as 95% C.L. limits on masses of first and second generation squarks decaying into a quark and the lightest neutralino in scenarios with $m_{\widetilde{q}} - m_{\widetilde{\chi}^0_1} < 25$ GeV. See their Fig. 6.

[29] AABOUD 16N searched in 3.2 fb^{-1} of pp collisions at $\sqrt{s}$ = 13 TeV for events containing hadronic jets, large $\not{E}_T$, and no electrons or muons. No significant excess above the Standard Model expectations is observed. First- and second-generation squark masses below 1030 GeV are excluded at the 95% C.L. decaying to quarks and a massless lightest neutralino. See their Fig. 7a.

[30] KHACHATRYAN 16BS searched in 2.3 fb^{-1} of pp collisions at $\sqrt{s}$ = 13 TeV for events with at least one energetic jet , no isolated leptons, and significant $\not{E}_T$, using the transverse mass variable M_{T2} to discriminate between signal and background processes. No significant excess above the Standard Model expectations is observed. Limits are set on the squark mass in the Tskq1 simplified model, both in the assumption of a single light squark and of 8 degenerate squarks, see Fig. 11 and Table 3.

[31] AAD 15BV summarized and extended ATLAS searches for gluinos and first- and second-generation squarks in final states containing jets and missing transverse momentum, with or without leptons or b-jets in the $\sqrt{s}$ = 8 TeV data set collected in 2012. The paper reports the results of new interpretations and statistical combinations of previously

Int. J. Mod. Phys. A 2026.41. Downloaded from www.worldscientific.com
by UNIVERSITY OF CALIFORNIA @ BERKELEY on 09/16/26. Re-use and distribution is strictly not permitted, except for Open Access articles.

published analyses, as well as new analyses. Exclusion limits at 95% C.L. are set on the squark mass in several R-parity conserving models. See their Figs. 9, 11, 18, 22, 24, 27, 28.

[32] AAD 15CS searched in 20.3 fb^{-1} of pp collisions at $\sqrt{s}$ = 8 TeV for evidence of pair production of squarks, decaying into a quark and a neutralino, where a photon was radiated either from an initial-state quark, from an intermediate squark, or from a final-state quark. No evidence was found for an excess above the expected level of Standard Model background and a 95% C.L. exclusion limit was set on the squark mass as a function of the squark-neutralino mass difference, see Fig. 19.

[33] AAD 15K searched in 20.3 fb^{-1} of pp collisions at $\sqrt{s}$ = 8 TeV for events containing at least two jets, where the two leading jets are each identified as originating from c-quarks, and large missing transverse momentum. No excess of events above the expected level of Standard Model background was found. Exclusion limits at 95% C.L. are set on the mass of superpartners of charm quarks ($\tilde{c}$). Assuming that the decay $\tilde{c} \rightarrow c\tilde{\chi}^0_1$ takes place 100% of the time, a scalar charm mass below 490 GeV is excluded for $m_{\tilde{\chi}^0_1} < 200$ GeV. For more details, see their Fig. 2.

[34] KHACHATRYAN 15AF searched in 19.5 fb^{-1} of pp collisions at $\sqrt{s}$ = 8 TeV for events with at least two energetic jets and significant $\not{E}_T$, using the transverse mass variable M_{T2} to discriminate between signal and background processes. No significant excess above the Standard Model expectations is observed. Limits are set on the squark mass in simplified models where the decay $\tilde{q} \rightarrow q\tilde{\chi}^0_1$ takes place with a branching ratio of 100%, both for the case of a single light squark or 8 degenerate squarks, see Fig. 12. See also Table 5. Exclusions in the CMSSM, assuming tanβ = 30, $A_0 = -2$ max(m_0, $m_{1/2}$) and $\mu > 0$, are also presented, see Fig. 15.

[35] AAD 14AE searched in 20.3 fb^{-1} of pp collisions at $\sqrt{s}$ = 8 TeV for strongly produced supersymmetric particles in events containing jets and large missing transverse momentum, and no electrons or muons. No excess over the expected SM background is observed. Exclusion limits are derived in simplified models containing squarks that decay via $\tilde{q} \rightarrow q\tilde{\chi}^0_1$, where either a single light state or two degenerate generations of squarks are assumed, see Fig. 10.

[36] CHATRCHYAN 14AH searched in 4.7 fb^{-1} of pp collisions at $\sqrt{s}$ = 7 TeV for events with at least two energetic jets and significant $\not{E}_T$, using the razor variables (M_R and R^2) to discriminate between signal and background processes. No significant excess above the Standard Model expectations is observed. Limits are set on squark masses in simplified models where the decay $\tilde{q} \rightarrow q\tilde{\chi}^0_1$ takes place with a branching ratio of 100%, see Fig. 28. Exclusions in the CMSSM, assuming tanβ = 10, A_0 = 0 and $\mu > 0$, are also presented, see Fig. 26.

[37] CHATRCHYAN 14I searched in 19.5 fb^{-1} of pp collisions at $\sqrt{s}$ = 8 TeV for events containing multijets and large $\not{E}_T$. No excess over the expected SM background is observed. Exclusion limits are derived in simplified models containing squarks that decay via $\tilde{q} \rightarrow q\tilde{\chi}^0_1$, where either a single light state or two degenerate generations of squarks are assumed, see Fig. 7a.

[38] AAD 13L searched in 4.7 fb^{-1} of pp collisions at $\sqrt{s}$ = 7 TeV for the production of squarks and gluinos in events containing jets, missing transverse momentum and no high-p_T electrons or muons. No excess over the expected SM background is observed. In mSUGRA/CMSSM models with tanβ = 10, A_0 = 0 and $\mu > 0$, squarks and gluinos of equal mass are excluded for masses below 1360 GeV at 95% C.L. In a simplified model containing only squarks of the first two generations, a gluino octet and a massless neutralino, squark masses below 1320 GeV are excluded at 95% C.L. for gluino masses below 2 TeV. See Figures 10–15 for more precise bounds.

[39] AAD 13Q searched in 4.7 fb^{-1} of pp collisions at $\sqrt{s}$ = 7 TeV for events containing a high-p_T isolated photon, at least one jet identified as originating from a bottom quark, and high missing transverse momentum. Such signatures may originate from supersymmetric models with gauge-mediated supersymmetry breaking in events in which one of a pair of higgsino-like neutralinos decays into a photon and a gravitino while the other decays into a Higgs boson and a gravitino. No significant excess above the expected background was found and limits were set on the squark mass as a function of the neutralino mass in a generalized GMSB model (GGM) with a higgsino-like neutralino NLSP, see their Fig. 4. For neutralino masses greater than 220 GeV, squark masses below 1020 GeV are excluded at 95% C.L.

[40] CHATRCHYAN 13 looked in 4.98 fb^{-1} of pp collisions at $\sqrt{s}$ = 7 TeV for events with two opposite-sign leptons (e, μ, τ), jets and missing transverse energy. No excess beyond the Standard Model expectation is observed. Exclusion limits are derived in the mSUGRA/CMSSM model with tanβ = 10, A_0 = 0 and $\mu > 0$, see Fig. 6.

[41] CHATRCHYAN 13G searched in 4.98 fb^{-1} of pp collisions at $\sqrt{s}$ = 7 TeV for the production of squarks and gluinos in events containing 0,1,2, $\geq$ 3 b-jets, missing transverse momentum and no electrons or muons. No excess over the expected SM background is observed. In mSUGRA/CMSSM models with tanβ = 10, A_0 = 0, and $\mu > 0$, squarks and gluinos of equal mass are excluded for masses below 1250 GeV at 95% C.L. Exclusions are also derived in various simplified models, see Fig. 7.

[42] CHATRCHYAN 13H searched in 4.96 fb^{-1} of pp collisions at $\sqrt{s}$ = 7 TeV for events with two photons, $\geq$ 4 jets and low $\not{E}_T$ due to $\tilde{q} \rightarrow \gamma\tilde{\chi}^0_1$ decays in a stealth SUSY framework, where the $\tilde{\chi}^0_1$ decays through a singlino ($\tilde{S}$) intermediate state to $\gamma S \tilde{G}$, with the singlet state S decaying to two jets. No significant excess above the expected background was found and limits were set in a particular R-parity conserving stealth SUSY model. The model assumes $m_{\tilde{\chi}^0_1} = 0.5\ m_{\tilde{q}}$, $m_{\tilde{S}}$ = 100 GeV and m_S = 90 GeV. Under these assumptions, squark masses less than 1430 GeV were excluded at the 95% C.L.

[43] CHATRCHYAN 13T searched in 11.7 fb^{-1} of pp collisions at $\sqrt{s}$ = 8 TeV for events with at least two energetic jets and significant $\not{E}_T$, using the α_T variable to discriminate between processes with genuine and misreconstructed $\not{E}_T$. No significant excess above the Standard Model expectations is observed. Limits are set on squark masses in simplified models where the decay $\tilde{q} \rightarrow q\tilde{\chi}^0_1$ takes place with a branching ratio of 100%, assuming an eightfold degeneracy of the masses of the first two generation squarks, see Fig. 8 and Table 9. Also limits in the case of a single light squark are given.

[44] AAD 12AX searched in 1.04 fb^{-1} of pp collisions at $\sqrt{s}$ = 7 TeV for supersymmetry in events containing jets, missing transverse momentum and one isolated electron or muon. No excess over the expected SM background is observed and model-independent limits are set on the cross section of new physics contributions to the signal regions. In mSUGRA/CMSSM models with tanβ = 10, A_0 = 0 and $\mu > 0$, squarks and gluinos of equal mass are excluded for masses below 820 GeV at 95% C.L. Limits are also set on simplified models for squark production and decay via an intermediate chargino and on supersymmetric models with bilinear R-parity violation. Supersedes AAD 11G.

[45] AAD 12CJ searched in 4.7 fb^{-1} of pp collisions at $\sqrt{s}$ = 7 TeV for events containing one or more isolated leptons (electrons or muons), jets and $\not{E}_T$. The observations are in good agreement with the SM expectations and exclusion limits have been set in number of SUSY models. In the mSUGRA/CMSSM model with tanβ = 10, A_0 = 0, and $\mu > 0$, 95% C.L. exclusion limits have been derived for $m_{\tilde{q}} < 1200$ GeV, assuming equal squark and gluino masses. In minimal GMSB, values of the effective SUSY breaking scale $\Lambda <$ 50 TeV are excluded at 95% C.L. for tanβ < 45. Also exclusion limits in a number of simplified models have been presented, see Figs. 10 and 12.

[46] AAD 12CP searched in 4.8 fb^{-1} of pp collisions at $\sqrt{s}$ = 7 TeV for events with two photons and large $\not{E}_T$ due to $\tilde{\chi}^0_1 \rightarrow \gamma\tilde{G}$ decays in a GMSB framework. No significant excess above the expected background was found and limits were set on the squark mass as a function of the neutralino mass in a generalized GMSB model (GGM) with a bino-like neutralino NLSP. The other sparticle masses were decoupled, tanβ = 2 and $c\tau_{NLSP}$ < 0.1 mm. Also, in the framework of the SPS8 model, a 95% C.L. lower limit was set on the breaking scale Λ of 196 TeV.

[47] AAD 12W searched in 1.04 fb^{-1} of pp collisions at $\sqrt{s}$ = 7 TeV for the production of squarks and gluinos in events containing jets, missing transverse momentum and no electrons or muons. No excess over the expected SM background is observed. In mSUGRA/CMSSM models with tanβ = 10, A_0 = 0 and $\mu > 0$, squarks and gluinos of equal mass are excluded for masses below 950 GeV at 95% C.L. In a simplified model containing only squarks of the first two generations, a gluino octet and a massless neutralino, squark masses below 875 GeV are excluded at 95% C.L.

[48] CHATRCHYAN 12 looked in 35 pb^{-1} of pp collisions at $\sqrt{s}$ = 7 TeV for events with e and/or μ and/or jets, a large total transverse energy, and $\not{E}_T$. The event selection is based on the dimensionless razor variable R, related to the $\not{E}_T$ and M_R, an indicator of the heavy particle mass scale. No evidence for an excess over the expected background is observed. Limits are derived in the CMSSM (m_0, $m_{1/2}$) plane for tanβ = 3, 10 and 50 (see Fig. 7 and 8). Limits are also obtained for Simplified Model Spectra.

[49] CHATRCHYAN 12AE searched in 4.98 fb^{-1} of pp collisions at $\sqrt{s}$ = 7 TeV for events with at least three jets and large missing transverse momentum. No significant excesses over the expected SM backgrounds are observed and 95% C.L. limits on the production cross section of squarks in a scenario where $\tilde{q} \rightarrow q\tilde{\chi}^0_1$ with a 100% branching ratio, see Fig. 3. For $m_{\tilde{\chi}^0_1} < 200$ GeV, values of $m_{\tilde{q}}$ below 760 GeV are excluded at 95% C.L. Also limits in the CMSSM are presented, see Fig. 2.

[50] CHATRCHYAN 12AT searched in 4.73 fb^{-1} of pp collisions at $\sqrt{s}$ = 7 TeV for the production of squarks and gluinos in events containing jets, missing transverse momentum and no electrons or muons. No excess over the expected SM background is observed. In mSUGRA/CMSSM models with tanβ = 10, A_0 = 0 and $\mu > 0$, squarks with masses below 1110 GeV are excluded at 95% C.L. Squarks and gluinos of equal mass are excluded for masses below 1180 GeV at 95% C.L. Exclusions are also derived in various simplified models, see Fig. 6.

[51] AABOUD 18V searched in 36.1 fb^{-1} of pp collisions at $\sqrt{s}$ = 13 TeV in events with no charged leptons, jets and missing transverse momentum. The data are found to be consistent with the SM expectation. Results are interpreted in the Tsqk5 model. Squark masses below 1100 GeV are excluded if $(m_{\tilde{\chi}^0_2} - m_{\tilde{\chi}^0_1})/(m_{\tilde{q}} - m_{\tilde{\chi}^0_1}) < 0.95$ and $m_{\tilde{\chi}^0_1}$ = 60 GeV, see their Fig. 16(a).

[52] KHACHATRYAN 16BT performed a global Bayesian analysis of a wide range of CMS results obtained with data samples corresponding to 5.0 fb^{-1} of pp collisions at $\sqrt{s}$ = 7 TeV and in 19.5 fb^{-1} of pp collisions at $\sqrt{s}$ = 8 TeV. The set of searches considered, both individually and in combination, includes those with all-hadronic final states, same-sign and opposite-sign dileptons, and multi-lepton final states. An interpretation was given in a scan of the 19-parameter pMSSM. No scan points with a gluino mass less than 500 GeV survived and 98% of models with a squark mass less than 300 GeV were excluded.

[53] AAD 15AI searched in 20 fb^{-1} of pp collisions at $\sqrt{s}$ = 8 TeV for events containing at least one isolated lepton (electron or muon), jets, and large missing transverse momentum. No excess of events above the expected level of Standard Model background was found. Exclusion limits at 95% C.L. are set on the squark masses in the CMSSM/mSUGRA, see Fig. 15, in the NUHMG, see Fig. 16, and in various simplified models, see Figs. 19–21.

[54] KHACHATRYAN 15AR searched in 19.7 of fb^{-1} of pp collisions at $\sqrt{s}$ = 8 TeV for events containing jets, either a charged lepton or a photon, and low missing transverse momentum. No significant excess above the Standard Model expectations is observed. Limits are set on the squark mass in a stealth SUSY model where the decays $\tilde{q} \rightarrow q\tilde{\chi}^{\pm}_1$, $\tilde{\chi}^{\pm}_1 \rightarrow \tilde{S}W^{\pm}$, $\tilde{S} \rightarrow S\tilde{G}$ and $S \rightarrow gg$, with $m_{\tilde{S}}$ = 100 GeV and m_S = 90 GeV, take place with a branching ratio of 100%. See Fig. 6 for γ or Fig. 7 for $\ell^{\pm}$ analyses.

[55] KHACHATRYAN 15AZ searched in 19.7 fb^{-1} of pp collisions at $\sqrt{s}$ = 8 TeV for events with either at least one photon, hadronic jets and $\not{E}_T$ (single photon channel) or with at least two photons and at least one jet and using the razor variables. No significant excess above the Standard Model expectations is observed. Limits are set on gluino masses in the general gauge-mediated SUSY breaking model (GGM), for both a bino-like and wino-like neutralino NLSP scenario, see Fig. 8 and 9.

[56] AAD 14E searched in 20.3 fb^{-1} of pp collisions at $\sqrt{s}$ = 8 TeV for strongly produced supersymmetric particles in events containing jets and two same-sign leptons or three leptons. The search also utilises jets originating from b-quarks, missing transverse momentum and other variables. No excess over the expected SM background is observed. Exclusion limits are derived in simplified models containing gluinos and squarks, see Figures 5 and 6. In the $\tilde{q} \rightarrow q'\tilde{\chi}^{\pm}_1$, $\tilde{\chi}^{\pm}_1 \rightarrow W^{(*)\pm}\tilde{\chi}^0_2$, $\tilde{\chi}^0_2 \rightarrow Z^{(*)}\tilde{\chi}^0_1$ simplified model, the following assumptions have been made: $m_{\tilde{\chi}^{\pm}_1} = 0.5\ m_{\tilde{\chi}^0_1} + m_{\tilde{g}}$, $m_{\tilde{\chi}^0_2} = 0.5\ (m_{\tilde{\chi}^0_1} + m_{\tilde{\chi}^{\pm}_1})$. In the $\tilde{q} \rightarrow q'\tilde{\chi}^{\pm}_1$ or $\tilde{q} \rightarrow q'\tilde{\chi}^0_2$, $\tilde{\chi}^{\pm}_1 \rightarrow \ell^{\pm}\nu\tilde{\chi}^0_1$ or $\tilde{\chi}^0_2 \rightarrow \ell^{\pm}\ell^{\mp}(\nu\nu)\tilde{\chi}^0_1$ simplified model, the following assumptions have been made: $m_{\tilde{\chi}^{\pm}_1} = m_{\tilde{\chi}^0_2} = 0.5\ (m_{\tilde{\chi}^0_1} + m_{\tilde{q}})$, $m_{\tilde{\chi}^0_1} < 460$ GeV. Limits are also derived in the mSUGRA/CMSSM, bRPV and GMSB models, see their Fig. 8.

[57] CHATRCHYAN 13AO searched in 4.98 fb^{-1} of pp collisions at $\sqrt{s}$ = 7 TeV for events with two opposite-sign isolated leptons accompanied by hadronic jets and $\not{E}_T$. No significant excesses over the expected SM backgrounds are observed and 95% C.L. exclusion limits are derived in the mSUGRA/CMSSM model with tanβ = 10, A_0 = 0 and $\mu > 0$, see Fig. 8.

[58] CHATRCHYAN 13AV searched in 4.7 fb^{-1} of pp collisions at $\sqrt{s}$ = 7 TeV for new heavy particle pairs decaying into jets (possibly b-tagged), leptons and $\not{E}_T$ using the Razor variables. No significant excesses over the expected SM backgrounds are observed

Int. J. Mod. Phys. A 2026.41. Downloaded from www.worldscientific.com
by UNIVERSITY OF CALIFORNIA @ BERKELEY on 09/16/26. Re-use and distribution is strictly not permitted, except for Open Access articles.

and 95% C.L. exclusion limits are derived in the mSUGRA/CMSSM model with $\tan\beta = 10$, $A_0 = 0$ and $\mu > 0$, see Fig. 3. The results are also interpreted in various simplified models, see Fig. 4.

[59] CHATRCHYAN 13W searched in 4.93 fb^{-1} of pp collisions at $\sqrt{s} = 7$ TeV for events with one or more photons, hadronic jets and $\not{E}_T$. No significant excess above the Standard Model expectations is observed. Limits are set on squark masses in the general gauge-mediated SUSY breaking model (GGM), for both a wino-like and bino-like neutralino NLSP scenario, see Fig. 5.

[60] DREINER 12A reassesses constraints from CMS (at 7 TeV, $\sim$ 4.4 fb^{-1}) under the assumption that the fist and second generation squarks and the lightest SUSY particle are quasi-degenerate in mass (compressed spectrum).

[61] DREINER 12A reassesses constraints from CMS (at 7 TeV, $\sim$ 4.4 fb^{-1}) under the assumption that the first and second generation squarks, the gluino, and the lightest SUSY particle are quasi-degenerate in mass (compressed spectrum).

R-parity violating $\widetilde{q}$ (Squark) mass limit

VALUE (GeV)	CL%	DOCUMENT ID		TECN	COMMENT
>1600	95	[1] HAYRAPETY...24Y		CMS	$\mu^+\mu^-$ from displaced vertex, Tsqk3RPV, 0.7 mm $< c\tau <$ 4cm, $m_{\widetilde{\chi}^0_1} = 50$ GeV
>1600	95	[1] HAYRAPETY...24Y		CMS	$\mu^+\mu^-$ from displaced vertex, Tsqk3RPV, 0.07 mm $< c\tau <$ 2 m, $m_{\widetilde{\chi}^0_1} = 500$ GeV
none 100–720	95	[2] SIRUNYAN	18EA	CMS	2 large jets with four-parton substructure, $\widetilde{q} \to q\,4q$
>1600	95	[3] KHACHATRY...16BX		CMS	$\widetilde{q} \to q\widetilde{\chi}^0_1$, $\widetilde{\chi}^0_1 \to \ell\ell\nu$, λ_{121} or $\lambda_{122} \neq 0$, $m_{\widetilde{g}} = 2400$ GeV
>1000	95	[4] AAD	15CB	ATLS	jets, $\widetilde{q} \to q\widetilde{\chi}^0_1$, $\widetilde{\chi}^0_1 \to \ell q q$, $m_{\widetilde{\chi}^0_1} = 108$ GeV and 2.5 $<$ $c\tau_{\widetilde{\chi}^0_1} < 200$ mm
		[5] AAD	12AX	ATLS	ℓ +jets $+\not{E}_T$, CMSSM, $m_{\widetilde{q}}$=$m_{\widetilde{g}}$
		[6] CHATRCHYAN	12AL	CMS	$\geq 3\ell^\pm$

[1] HAYRAPETYAN 24Y searched in 36.6 fb^{-1} of pp collisions at $\sqrt{s} = 13.6$ TeV for evidence of R-parity violating (RPV) SUSY in events with a pair of oppositely charged muons originating from a secondary vertex spatially separated from the pp interaction point by distances ranging from several hundred μm to several meters. No significant excess above the Standard Model expectations is observed. Limits are set in the model Tsqk3RPV on the lifetime of the $\widetilde{\chi}^0_1$ for several values of the $\widetilde{q}$ mass, see their Fig. 16. Limits are also interpreted in the framework of a hidden Abelian Higgs model, in which the Higgs boson decays to a pair of long-lived dark photons, see their Figs. 14 and 15.

[2] SIRUNYAN 18EA searched in 38.2 fb^{-1} of pp collisions at $\sqrt{s} = 13$ TeV for the pair production of resonances, each decaying to at least four quarks. Reconstructed particles are clustered into two large jets of similar mass, each consistent with four-parton substructure. No statistically significant excess over the Standard Model expectation is observed. Limits are set on the squark and gluino mass in RPV supersymmetry models where squarks (gluinos) decay, through intermediate higgsinos, to four (five) quarks, see their Figure 4.

[3] KHACHATRYAN 16BX searched in 19.5 fb^{-1} of pp collisions at $\sqrt{s} = 8$ TeV for events containing 4 leptons coming from R-parity-violating decays of $\widetilde{\chi}^0_1 \to \ell\ell\nu$ with $\lambda_{121} \neq 0$ or $\lambda_{122} \neq 0$. No excess over the expected background is observed. Limits are derived on the gluino, squark and stop masses, see Fig. 23.

[4] AAD 15CB searched for events containing at least one long-lived particle that decays at a significant distance from its production point (displaced vertex, DV) into two leptons or into five or more charged particles in 20.3 fb^{-1} of pp collisions at $\sqrt{s} = 8$ TeV. The dilepton signature is characterised by DV formed from at least two lepton candidates. Four different final states were considered for the multitrack signature, in which the DV must be accompanied by a high-transverse momentum muon or electron candidate that originates from the DV, jets or missing transverse momentum. No events were observed in any of the signal regions. Results were interpreted in SUSY scenarios involving R-parity violation, split supersymmetry, and gauge mediation. See their Fig. 14–20.

[5] AAD 12AX searched in 1.04 fb^{-1} of pp collisions at $\sqrt{s} = 7$ TeV for supersymmetry in events containing jets, missing transverse momentum and one isolated electron or muon. No excess over the expected SM background is observed and model-independent limits are set on the cross section of new physics contributions to the signal regions. In mSUGRA/CMSSM models with $\tan\beta = 10$, $A_0 = 0$ and $\mu > 0$, squarks and gluinos of equal mass are excluded for masses below 820 GeV at 95% C.L. Limits are also set on simplified models for squark production and decay via an intermediate chargino and on supersymmetric models with bilinear R-parity violation. Supersedes AAD 11G.

[6] CHATRCHYAN 12AL looked in 4.98 fb^{-1} of pp collisions at $\sqrt{s} = 7$ TeV for anomalous production of events with three or more isolated leptons. Limits on squark and gluino masses are set in RPV SUSY models with leptonic $LL\overline{E}$ couplings, $\lambda_{123} > 0.05$, and hadronic $\overline{UDD}$ couplings, $\lambda''_{112} > 0.05$, see their Fig. 5. In the $\overline{UDD}$ case the leptons arise from supersymmetric cascade decays. A very specific supersymmetric spectrum is assumed. All decays are prompt.

Long-lived $\widetilde{q}$ (Squark) mass limit

The following are bounds on long-lived scalar quarks, assumed to hadronise into hadrons with lifetime long enough to escape the detector prior to a possible decay. Limits may depend on the mixing angle of mass eigenstates: $\widetilde{q}_1 = \widetilde{q}_L \cos\theta_q + \widetilde{q}_R \sin\theta_q$. The coupling to the Z^0 boson vanishes for up-type squarks when θ_u=0.98, and for down type squarks when θ_d=1.17.

VALUE (GeV)	CL%	DOCUMENT ID		TECN	COMMENT
>1470	95	[1] HAYRAPETY...25V		CMS	large dE/dx in Si tracker, $\widetilde{t}$ R-hadrons
>1250	95	[2] AABOUD	19AT	ATLS	$\widetilde{b}$ R-hadrons
>1340	95	[3] AABOUD	19AT	ATLS	$\widetilde{t}$ R-hadrons
>1600	95	[4] SIRUNYAN	19BH	CMS	long-lived $\widetilde{t}$, RPV, $\widetilde{t} \to \overline{d}\,\overline{d}$, 10 mm $< c\tau <$ 110 mm
>1350	95	[4] SIRUNYAN	19BH	CMS	long-lived $\widetilde{t}$, RPV, $\widetilde{t} \to b\ell$, 7 mm $< c\tau <$ 110 mm
> 805	95	[5] AABOUD	16B	ATLS	$\widetilde{b}$ R-hadrons
> 890	95	[6] AABOUD	16B	ATLS	$\widetilde{t}$ R-hadrons
>1040	95	[7] KHACHATRY...16BW		CMS	$\widetilde{t}$ R-hadrons, cloud interaction model
>1000	95	[7] KHACHATRY...16BW		CMS	$\widetilde{t}$ R-hadrons, charge-suppressed interaction model
> 845	95	[8] AAD	15AE	ATLS	$\widetilde{b}$ R-hadron, stable, Regge model
> 900	95	[8] AAD	15AE	ATLS	$\widetilde{t}$ R-hadron, stable, Regge model
>1500	95	[8] AAD	15AE	ATLS	$\widetilde{g}$ decaying to 300 GeV stable sleptons, LeptoSUSY model
> 751	95	[9] AAD	15BM	ATLS	$\widetilde{b}$ R-hadron, stable, Regge model
> 766	95	[9] AAD	15BM	ATLS	$\widetilde{t}$ R-hadron, stable, Regge model
> 525	95	[10] KHACHATRY...15AK		CMS	$\widetilde{t}$ R-hadrons, 10 μs$< \tau <$1000 s
> 470	95	[10] KHACHATRY...15AK		CMS	$\widetilde{t}$ R-hadrons, 1 μs$< \tau <$1000 s
• • • We do not use the following data for averages, fits, limits, etc. • • •					
> 683	95	[11] AAD	13AA	ATLS	$\widetilde{t}$, R-hadrons, generic interaction model
> 612	95	[12] AAD	13AA	ATLS	$\widetilde{b}$, R-hadrons, generic interaction model
> 344	95	[13] AAD	13BC	ATLS	R-hadrons, $\widetilde{t} \to b\widetilde{\chi}^0_1$, Regge model, lifetime between 10^{-5} and 10^3 s, $m_{\widetilde{\chi}^0_1} = 100$ GeV
> 379	95	[14] AAD	13BC	ATLS	R-hadrons, $\widetilde{t} \to t\widetilde{\chi}^0_1$, Regge model, lifetime between 10^{-5} and 10^3 s, $m_{\widetilde{\chi}^0_1} = 100$ GeV
> 935	95	[15] CHATRCHYAN	13AB	CMS	long-lived $\widetilde{t}$ forming R-hadrons, cloud interaction model

[1] HAYRAPETYAN 25V searched in 101 fb^{-1} of pp collisions at $\sqrt{s} = 13$ TeV for heavy, long-lived, charged particles with large ionization energy loss within the silicon tracker of the CMS experiment. No significant excess above the Standard Model expectations is observed. Limits are set on the pair production of gluino R-hadrons, top squark R-hadrons, and detector-stable $\widetilde{\tau}_{R,L}$, see their figure 6. Limits are also set in a model predicting a pair of single- and double-charged τ' fermions from a Z' boson decay, see their figure 7.

[2] AABOUD 19AT searched in 36.1 fb^{-1} of pp collisions at $\sqrt{s} = 13$ TeV for metastable and stable R-hadrons. Multiple search strategies for a wide range of lifetimes, corresponding to path lengths of a few meters, are defined. No significant deviations from the expected Standard Model background are observed. Sbottom R-hadrons are excluded at 95% C.L. for masses below 1250 GeV. Less stringent constraints are achieved with the muon-spectrometer agnostic analysis. See their Figure 9 (bottom-left).

[3] AABOUD 19AT searched in 36.1 fb^{-1} of pp collisions at $\sqrt{s} = 13$ TeV for metastable and stable R-hadrons. Multiple search strategies for a wide range of lifetimes, corresponding to path lengths of a few meters, are defined. No significant deviations from the expected Standard Model background are observed. Stop R-hadrons are excluded at 95% C.L. for masses below 1340 GeV. Similar constraints are achieved with the muon-spectrometer agnostic analysis. See their Figure 9 (bottom-right).

[4] SIRUNYAN 19BH searched in 35.9 fb^{-1} of pp collisions at $\sqrt{s} = 13$ TeV for long-lived particles decaying into jets, with each long-lived particle having a decay vertex well displaced from the production vertex. The selected events are found to be consistent with standard model predictions. Limits are set on the gluino mass in a GMSB model where the gluino is decaying via $\widetilde{g} \to g\widetilde{G}$, see their Figure 4 and in an RPV model of supersymmetry where the gluino is decaying via $\widetilde{g} \to \widetilde{t}\overline{b}\overline{s}$, see their Figures 5. Limits are also set on the stop mass in two RPV models, see their Figure 6 (for $\widetilde{t} \to b\ell$ decays) and Figure 7 (for $\widetilde{t} \to \overline{d}\,\overline{d}$ decays).

[5] AABOUD 16B searched in 3.2 fb^{-1} of pp collisions at $\sqrt{s} = 13$ TeV for long-lived R-hadrons using observables related to large ionization losses and slow propagation velocities, which are signatures of heavy charged particles traveling significantly slower than the speed of light. Exclusion limits at 95% C.L. are set on the long-lived sbottom masses exceeding 805 GeV. See their Fig. 5.

[6] AABOUD 16B searched in 3.2 fb^{-1} of pp collisions at $\sqrt{s} = 13$ TeV for long-lived R-hadrons using observables related to large ionization losses and slow propagation velocities, which are signatures of heavy charged particles traveling significantly slower than the speed of light. Exclusion limits at 95% C.L. are set on the long-lived stop masses exceeding 890 GeV. See their Fig. 5.

[7] KHACHATRYAN 16BW searched in 2.5 fb^{-1} of pp collisions at $\sqrt{s} = 13$ TeV for events with heavy stable charged particles, identified by their anomalously high energy deposits in the silicon tracker and/or long time-of-flight measurements by the muon system. No evidence for an excess over the expected background is observed. Limits are derived for pair production of top squarks as a function of mass, depending on the interaction model, see Fig. 4 and Table 7.

[8] AAD 15AE searched in 19.1 fb^{-1} of pp collisions at $\sqrt{s} = 8$ TeV for heavy long-lived charged particles, measured through their specific ionization energy loss in the ATLAS pixel detector or their time-of-flight in the ALTAS muon system. In the absence of an excess of events above the expected backgrounds, limits are set R-hadrons in various scenarios, see Fig. 11. Limits are also set in LeptoSUSY models where the gluino decays to stable 300 GeV leptons, see Fig. 9.

[9] AAD 15BM searched in 18.4 fb^{-1} of pp collisions at $\sqrt{s} = 8$ TeV for stable and metastable non-relativistic charged particles through their anomalous specific ionization energy loss in the ATLAS pixel detector. In absence of an excess of events above the expected backgrounds, limits are set on stable bottom and top squark R-hadrons, see Table 5.

[10] KHACHATRYAN 15AK looked in a data set corresponding to fb^{-1} of pp collisions at $\sqrt{s} = 8$ TeV, and a search interval corresponding to 281 h of trigger lifetime, for long-lived particles that have stopped in the CMS detector. No evidence for an excess over the expected background in a cloud interaction model is observed. Assuming the decay $\widetilde{t} \to t\widetilde{\chi}^0_1$ and lifetimes between 1 μ and 1000 s, limits are derived on $\widetilde{t}$ production as a function of $m_{\widetilde{\chi}^0_1}$, see Figs. 4 and 7. The exclusions require that $m_{\widetilde{\chi}^0_1}$ is kinematically consistent with the minimum values of the jet energy thresholds used.

[11] AAD 13AA searched in 4.7 fb^{-1} of pp collisions at $\sqrt{s} = 7$ TeV for events containing colored long-lived particles that hadronize forming R-hadrons. No significant excess above the expected background was found. Long-lived R-hadrons containing a $\widetilde{t}$ are excluded for masses up to 683 GeV at 95% C.L in a general interaction model. Also, limits independent of the fraction of R-hadrons that arrive charged in the muon system were derived, see Fig. 6.

Int. J. Mod. Phys. A 2026.41. Downloaded from www.worldscientific.com
by UNIVERSITY OF CALIFORNIA @ BERKELEY on 09/16/26. Re-use and distribution is strictly not permitted, except for Open Access articles.

[12] AAD 13AA searched in 4.7 fb^{-1} of pp collisions at $\sqrt{s}$ = 7 TeV for events containing colored long-lived particles that hadronize forming R-hadrons. No significant excess above the expected background was found. Long-lived R-hadrons containing a $\tilde{b}$ are excluded for masses up to 612 GeV at 95% C.L in a general interaction model. Also, limits independent of the fraction of R-hadrons that arrive charged in the muon system were derived, see Fig. 6.

[13] AAD 13BC searched in 5.0 fb^{-1} of pp collisions at $\sqrt{s}$ = 7 TeV and in 22.9 fb^{-1} of pp collisions at $\sqrt{s}$ = 8 TeV for bottom squark R-hadrons that have come to rest within the ATLAS calorimeter and decay at some later time to hadronic jets and a neutralino. In absence of an excess of events above the expected backgrounds, limits are set on sbottom masses for the decay $\tilde{b} \rightarrow b\tilde{\chi}^0_1$, for different lifetimes, and for a neutralino mass of 100 GeV, see their Table 6 and Fig 10.

[14] AAD 13BC searched in 5.0 fb^{-1} of pp collisions at $\sqrt{s}$ = 7 TeV and in 22.9 fb^{-1} of pp collisions at $\sqrt{s}$ = 8 TeV for bottom squark R-hadrons that have come to rest within the ATLAS calorimeter and decay at some later time to hadronic jets and a neutralino. In absence of an excess of events above the expected backgrounds, limits are set on stop masses for the decay $\tilde{t} \rightarrow t\tilde{\chi}^0_1$, for different lifetimes, and for a neutralino mass of 100 GeV, see their Table 6 and Fig 10.

[15] CHATRCHYAN 13AB looked in 5.0 fb^{-1} of pp collisions at $\sqrt{s}$ = 7 TeV and in 18.8 fb^{-1} of pp collisions at $\sqrt{s}$ = 8 TeV for events with heavy stable particles, identified by their anomalous dE/dx in the tracker or additionally requiring that it be identified as muon in the muon chambers, from pair production of $\tilde{t}_1$'s. No evidence for an excess over the expected background is observed. Limits are derived for pair production of stops as a function of mass in the cloud interaction model (see Fig. 8 and Table 6). In the charge-suppressed model, the limit decreases to 818 GeV.

$\tilde{b}$ (Sbottom) mass limit

Limits in e^+e^- depend on the mixing angle of the mass eigenstate $\tilde{b}_1 = \tilde{b}_L \cos\theta_b + \tilde{b}_R \sin\theta_b$. Coupling to the Z vanishes for $\theta_b \sim 1.17$. As a consequence, no absolute constraint in the mass region $\lesssim$40 GeV is available in the literature at this time from e^+e^- collisions. In the Listings below, we use $\Delta m = m_{\tilde{b}_1} - m_{\tilde{\chi}^0_1}$.

Some earlier papers are now obsolete and have been omitted. They were last listed in our PDG 14 edition: K. Olive, *et al.* (Particle Data Group), Chinese Physics **C38** 070001 (2014) (http://pdg.lbl.gov).

R-parity conserving $\tilde{b}$ (Sbottom) mass limit

VALUE (GeV)	CL%	DOCUMENT ID		TECN	COMMENT
>1490	95	[1] HAYRAPETY...24M		CMS	$\geq$ 1 disappearing track+ $\not{E}_T$, $m_{\tilde{\chi}^\pm_1} \simeq m_{\tilde{\chi}^0_1}$ = 200 GeV, $c\tau(\tilde{\chi}^\pm_1)$ = 10 cm
>1540	95	[1] HAYRAPETY...24M		CMS	$\geq$ 1 disappearing track+ $\not{E}_T$, $m_{\tilde{\chi}^\pm_1} \simeq m_{\tilde{\chi}^0_1}$ = 1000 GeV, $c\tau(\tilde{\chi}^\pm_1)$ = 200 cm
> 850	95	[2] AAD	21AM	ATLAS	$\tau^\pm$'s + b-jets + $\not{E}_T$, Tsbot4, $m_{\tilde{\chi}^0_2} - m_{\tilde{\chi}^0_1}$ = 130 GeV, $m_{\tilde{\chi}^0_2}$ < 180 GeV
>1270	95	[3] AAD	21S	ATLAS	b-jets + $\not{E}_T$, Tsbot1, $m_{\tilde{\chi}^0_1}$=0 GeV
> 660	95	[3] AAD	21S	ATLAS	b-jets + $\not{E}_T$, Tsbot1,$m_{\tilde{b}_1} - m_{\tilde{\chi}^0_1}$ = 10 GeV
>1600	95	[4] SIRUNYAN	21M	CMS	$\ell^\pm\ell^\mp$ + $\not{E}_T$, Tsbot3, $m_{\tilde{\chi}^0_2}$ = 1500 GeV, $m_{\tilde{\chi}^0_1}$ = 100 GeV
> 750	95	[5] AAD	20V	ATLAS	same-sign $\ell^\pm\ell^\pm$ + jets, Tsbot2, $m_{\tilde{\chi}^\pm_1} = m_{\tilde{\chi}^0_1}$ + 100 GeV, $m_{\tilde{\chi}^0_1} \sim$ 50 GeV
> 850	95	[6] SIRUNYAN	20T	CMS	same-sign $\ell^\pm\ell^\pm$ or $\geq 3\ell^\pm$ + jets, Tsbot2, $m_{\tilde{\chi}^\pm_1}$ < 800 GeV, $m_{\tilde{\chi}^0_1}$ = 50 GeV
>1500	95	[7] AAD	19H	ATLAS	$\geq$ 3 b-jets + $\not{E}_T$, Tsbot4, $\geq$ 1 $h(\rightarrow b\overline{b})$, $m_{\tilde{\chi}^0_1}$ = 60 GeV
>1300	95	[8] AAD	19H	ATLAS	$\geq$ 3 b-jets+$\not{E}_T$, Tsbot4, $\geq 1h(\rightarrow b\overline{b})$, $m_{\tilde{\chi}^0_2} = m_{\tilde{\chi}^0_1}$ +130 GeV
>1220	95	[9] SIRUNYAN	19CH	CMS	jets+$\not{E}_T$, Tsbot1, $m_{\tilde{\chi}^0_1}$ = 0 GeV
> 530	95	[10] SIRUNYAN	19CI	CMS	≥ 1 H $(\rightarrow \gamma\gamma)$ + jets + $\not{E}_T$, Tsbot4, $m_{\tilde{\chi}^0_2} = m_{\tilde{\chi}^0_1}$ + 130 GeV, $m_{\tilde{\chi}^0_1}$ = 1 GeV
> 430	95	[11] AABOUD	18I	ATLAS	$\geq$ 1 jets+$\not{E}_T$, Tsbot1, $m_{\tilde{b}} - m_{\tilde{\chi}^0_1} \sim m_b$
> 840	95	[12] SIRUNYAN	18AL	CMS	$\geq 3\ell^\pm$ + jets + $\not{E}_T$, Tsbot2, $m_{\tilde{\chi}^0_1}$ = 50 GeV
> 975	95	[13] SIRUNYAN	18AR	CMS	$\ell^\pm\ell^\mp$ + jets + $\not{E}_T$, Tsbot3, $m_{\tilde{\ell}} = (m_{\tilde{\chi}^0_2} + m_{\tilde{\chi}^0_1})/2$, $m_{\tilde{\chi}^0_1}$= 100 GeV
>1060	95	[14] SIRUNYAN	18AY	CMS	jets+$\not{E}_T$, Tsbot1, $m_{\tilde{\chi}^0_1}$ = 0 GeV
>1230	95	[15] SIRUNYAN	18B	CMS	jets+$\not{E}_T$, Tsbot1, $m_{\tilde{\chi}^0_1}$ = 0 GeV
> 420	95	[16] SIRUNYAN	18X	CMS	≥ 1 H $(\rightarrow \gamma\gamma)$ + jets + $\not{E}_T$, Tsbot4, $m_{\tilde{\chi}^0_2} = m_{\tilde{\chi}^0_1}$ + 130 GeV, $m_{\tilde{\chi}^0_1}$ < 225 GeV
> 700	95	[17] AABOUD	17AJ	ATLS	same-sign $\ell^\pm\ell^\pm$ / 3 ℓ + jets + $\not{E}_T$, Tsbot2, $m_{\tilde{\chi}^0_1}$ = 0 GeV
> 950	95	[18] AABOUD	17AX	ATLS	2 b-jets+$\not{E}_T$, Tsbot1, $m_{\tilde{\chi}^0_1}$ = 0 GeV
> 880	95	[19] AABOUD	17AX	ATLS	2 b-jets + $\not{E}_T$, mixture Tsbot1 and Tsbot2 BR=50%, $m_{\tilde{\chi}^0_1}$ = 0 GeV, $m_{\tilde{\chi}^\pm_1} - m_{\tilde{\chi}^0_1}$ = 1 GeV
> 315	95	[20] KHACHATRY...17A		CMS	2 VBF jets + $\not{E}_T$, Tsbot1, $m_{\tilde{b}} - m_{\tilde{\chi}^0_1}$ = 5 GeV
> 450	95	[21] KHACHATRY...17AW		CMS	$\geq 3\ell^\pm$, 2 jets, Tsbot2, $m_{\tilde{\chi}^0_1}$ = 50 GeV, $m_{\tilde{\chi}^\pm_1}$ = 200 GeV
> 800	95	[22] KHACHATRY...17P		CMS	1 or more jets+$\not{E}_T$, Tsbot1, $m_{\tilde{\chi}^0_1}$ = 0 GeV
>1175	95	[23] SIRUNYAN	17AZ	CMS	$\geq$ 1 jets+$\not{E}_T$, Tsbot1, $m_{\tilde{\chi}^0_1}$ = 0 GeV
> 890	95	[24] SIRUNYAN	17K	CMS	jets+$\not{E}_T$, Tsbot1, $m_{\tilde{\chi}^0_1}$ = 0 GeV
> 810	95	[25] SIRUNYAN	17S	CMS	same-sign $\ell^\pm\ell^\pm$ + jets + $\not{E}_T$, Tsbot2, $m_{\tilde{\chi}^0_1}$ = 50 GeV, $m_{\tilde{\chi}^\pm_1}$ = 100 GeV
> 323	95	[26] AABOUD	16D	ATLS	$\geq$ 1 jet + $\not{E}_T$, Tsbot1, $m_{\tilde{b}_1} - m_{\tilde{\chi}^0_1}$ = 5 GeV
> 840	95	[27] AABOUD	16Q	ATLS	2 b-jets + $\not{E}_T$, Tsbot1, $m_{\tilde{\chi}^0_1}$ = 100 GeV
> 540	95	[28] AAD	16BB	ATLS	2 same-sign/3ℓ + jets + $\not{E}_T$, Tsbot2, $m_{\tilde{\chi}^0_1}$ < 55 GeV
> 680	95	[29] KHACHATRY...16BJ		CMS	same-sign $\ell^\pm\ell^\pm$, Tsbot2, $m_{\tilde{\chi}^\pm_1}$ < 550 GeV, $m_{\tilde{\chi}^0_1}$ = 50 GeV
> 500	95	[29] KHACHATRY...16BJ		CMS	same-sign $\ell^\pm\ell^\pm$, Tsbot2, $m_{\tilde{b}} - m_{\tilde{\chi}^\pm_1}$ <100 GeV, $m_{\tilde{\chi}^0_1}$=50 GeV
> 880	95	[30] KHACHATRY...16BS		CMS	jets + $\not{E}_T$, Tsbot1, $m_{\tilde{\chi}^0_1}$ = 0 GeV
> 550	95	[31] KHACHATRY...16BY		CMS	opposite-sign $\ell^\pm\ell^\pm$, Tsbot3, $m_{\tilde{\chi}^0_1}$ = 100 GeV
> 600	95	[32] AAD	15CJ	ATLS	$\tilde{b} \rightarrow b\tilde{\chi}^0_1$, $m_{\tilde{\chi}^0_1}$ < 250 GeV
> 440	95	[32] AAD	15CJ	ATLS	$\tilde{b} \rightarrow t\tilde{\chi}^\pm_1$, $\tilde{\chi}^\pm_1 \rightarrow W^{(*)}\tilde{\chi}^0_1$, $m_{\tilde{\chi}^0_1}$ = 60 GeV, $m_{\tilde{b}} - m_{\tilde{\chi}^\pm_1}$ < m_t
none 300–650	95	[32] AAD	15CJ	ATLS	$\tilde{b} \rightarrow \tilde{b}b\tilde{\chi}^0_2$, $\tilde{\chi}^0_2 \rightarrow h\tilde{\chi}^0_1$, $m_{\tilde{\chi}^0_1}$ = 60 GeV, $m_{\tilde{\chi}^0_2}$ > 250 GeV
> 640	95	[33] KHACHATRY...15AF		CMS	$\tilde{b} \rightarrow b\tilde{\chi}^0_1$, $m_{\tilde{\chi}^0_1}$ = 0
> 650	95	[34] KHACHATRY...15AH		CMS	$\tilde{b} \rightarrow b\tilde{\chi}^0_1$, $m_{\tilde{\chi}^0_1}$ = 0
> 250	95	[34] KHACHATRY...15AH		CMS	$\tilde{b} \rightarrow b\tilde{\chi}^0_1$, $m_{\tilde{b}} - m_{\tilde{\chi}^0_1}$ < 10 GeV
> 570	95	[35] KHACHATRY...15I		CMS	$\tilde{b} \rightarrow t\tilde{\chi}^\pm_1$, $\tilde{\chi}^\pm_1 \rightarrow W^\pm\tilde{\chi}^0_1$, $m_{\tilde{\chi}^0_1}$ =50 GeV, 150<$m_{\tilde{\chi}^\pm_1}$ <300 GeV
> 255	95	[36] AAD	14T	ATLS	$\tilde{b}_1 \rightarrow b\tilde{\chi}^0_1$, $m_{\tilde{b}_1} - m_{\tilde{\chi}^0_1} \approx m_b$
> 400	95	[37] CHATRCHYAN	14AH	CMS	jets + $\not{E}_T$, $\tilde{b} \rightarrow b\tilde{\chi}^0_1$ simplified model, $m_{\tilde{\chi}^0_1}$ = 50 GeV
		[38] CHATRCHYAN	14R	CMS	$\geq 3\ell^\pm$, $\tilde{b} \rightarrow t\tilde{\chi}^\pm_1$, $\tilde{\chi}^\pm_1 \rightarrow W^\pm\tilde{\chi}^0_1$ simplified model, $m_{\tilde{\chi}^0_1}$ = 50 GeV
• • • We do not use the following data for averages, fits, limits, etc. • • •					
		[39] KHACHATRY...15AD		CMS	$\ell^\pm\ell^\mp$ + jets + $\not{E}_T$, $\tilde{b} \rightarrow b\ell^\pm\ell^\mp\tilde{\chi}^0_1$
none 340–600	95	[40] AAD	14AX	ATLS	$\geq$ 3 b-jets + $\not{E}_T$, $\tilde{b} \rightarrow b\tilde{\chi}^0_2$ simplified model with $\tilde{\chi}^0_2 \rightarrow h\tilde{\chi}^0_1$, $m_{\tilde{\chi}^0_1}$=60 GeV, $m_{\tilde{\chi}^0_2}$=300 GeV
> 440	95	[41] AAD	14E	ATLS	$\ell^\pm\ell^\pm(\ell^\mp)$ + jets, $\tilde{b}_1 \rightarrow t\tilde{\chi}^\pm_1$ with $\tilde{\chi}^\pm_1 \rightarrow W^{(*)\pm}\tilde{\chi}^0_1$ simplified model, $m_{\tilde{\chi}^\pm_1} = 2\, m_{\tilde{\chi}^0_1}$
> 500	95	[42] CHATRCHYAN	14H	CMS	same-sign $\ell^\pm\ell^\pm$, $\tilde{b} \rightarrow t\tilde{\chi}^\pm_1$, $\tilde{\chi}^\pm_1 \rightarrow W^\pm\tilde{\chi}^0_1$ simplified model, $m_{\tilde{\chi}^\pm_1}$ = 2 GeV, $m_{\tilde{\chi}^0_1}$ = 100 GeV
> 620	95	[43] AAD	13AU	ATLS	2 b-jets + $\not{E}_T$, $\tilde{b}_1 \rightarrow b\tilde{\chi}^0_1$, $m_{\tilde{\chi}^0_1}$ < 120 GeV
> 550	95	[44] CHATRCHYAN	13AT	CMS	jets + $\not{E}_T$, $\tilde{b} \rightarrow b\tilde{\chi}^0_1$ simplified model, $m_{\tilde{\chi}^0_1}$= 50 GeV

> 600	95	[45] CHATRCHYAN 13T	CMS	jets + $\not{E}_T$, $\tilde{b} \to b\tilde{\chi}^0_1$ simplified model, $m_{\tilde{\chi}^0_1}$ = 0 GeV
> 450	95	[46] CHATRCHYAN 13V	CMS	same-sign $\ell^\pm\ell^\pm$ + $\geq$ 2 b-jets, $\tilde{b} \to t\tilde{\chi}^\pm_1$, $\tilde{\chi}^\pm_1 \to W^\pm\tilde{\chi}^0_1$ simplified model, $m_{\tilde{\chi}^0_1}$ = 50 GeV
> 390		[47] AAD 12AN	ATLS	$\tilde{b}_1 \to b\tilde{\chi}^0_1$, simplified model, $m_{\tilde{\chi}^0_1}$ < 60 GeV
		[48] CHATRCHYAN 12AI	CMS	$\ell^\pm\ell^\pm$ + b-jets + $\not{E}_T$
> 410	95	[49] CHATRCHYAN 12BO	CMS	$\tilde{b}_1 \to b\tilde{\chi}^0_1$, simplified model, $m_{\tilde{\chi}^0_1}$ = 50 GeV
> 294	95	[50] AAD 11K	ATLS	stable $\tilde{b}$
		[51] AAD 11O	ATLS	$\tilde{g} \to \tilde{b}_1 b$, $\tilde{b}_1 \to b\tilde{\chi}^0_1$, $m_{\tilde{\chi}^0_1}$=60 GeV
		[52] CHATRCHYAN 11D	CMS	$\tilde{b},\tilde{t} \to b$
> 230	95	[53] AALTONEN 10R	CDF	$\tilde{b}_1 \to b\tilde{\chi}^0_1$, $m_{\tilde{\chi}^0_1}$ < 70 GeV
> 247	95	[54] ABAZOV 10L	D0	$\tilde{b}_1 \to b\tilde{\chi}^0_1$, $m_{\tilde{\chi}^0_1}$ = 0 GeV

[1] HAYRAPETYAN 24M searched in 137 fb^{-1} of pp collisions at $\sqrt{s}$ = 13 TeV for evidence of wino- and Higgsino-like charginos in final states with one or more disappearing tracks from the decay $\tilde{\chi}^\pm_1 \to \pi^\pm\tilde{\chi}^0_1$ where the soft pion is not reconstructed, $\not{E}_T$, and varying numbers of jets, b-tagged jets, electrons, and muons. No significant excess above the Standard Model expectations is observed. Limits are set on the $\tilde{b}$ mass in the model Tbot1LL for various proper decay lengths cτ of the $\tilde{\chi}^\pm_1$ as well as on the $\tilde{t}$ mass in the model Tstop1LL, see their Fig. 10. Limits are also set in the model Tglu1LL, see their Fig. 11. In addition, limits are set in specific pure wino as well as pure higgsino dark matter models, in which the relationships among the electroweakino masses, the $\tilde{\chi}^\pm_1$ lifetime, and the $\tilde{\chi}^\pm_1$ decay width are constrained by radiative corrections that account for a large difference between the LSP mass and the SUSY-breaking scale, see their Fig. 12.

[2] AAD 21AM searched in 139 fb^{-1} of pp collisions at $\sqrt{s}$ = 13 TeV for pair production of bottom squarks in events with hadronically decaying $\tau^\pm$-leptons, b-tagged jets, and large $\not{E}_T$. No significant excess above the Standard Model expectations is observed. Limits are set on the bottom squark mass in the Tsbot4 simplified model, assuming $m_{\tilde{\chi}^0_2} - m_{\tilde{\chi}^0_1}$ = 130 GeV, see their Figure 8.

[3] AAD 21S searched in 139 fb^{-1} of pp collisions at $\sqrt{s}$ = 13 TeV for pair production of sbottoms, LQ or dark matter in events with b-jets and $\not{E}_T$, also using dedicated secondary-vertex-finding techniques. No significant excess above the Standard Model predictions is observed. Limits are set on $m_{\tilde{b}_1}$ in the Tsbot1 simplified model, on the LQ masses depending on the BR in $b\nu$, on scalar and pseudoscalar dark matter mediator masses. See Figures 8, 9, 10.

[4] SIRUNYAN 21M searched in 137 fb^{-1} of pp collisions at $\sqrt{s}$ = 13 TeV for supersymmetry in events with two opposite-sign same-flavor leptons (electrons, muons) and $\not{E}_T$. No significant excess above the Standard Model expectations is observed. Limits are set on the gluino mass in the simplified model Tglu4C, see their Figure 10, on the $\tilde{\chi}^0_2$ and $\tilde{\chi}^\pm_1$ mass in Tchi1n2Fa, see their Figure 11, on the $\tilde{\chi}^0_1$ mass in Tn1n1C and Tn1n1B for $m_{\tilde{\chi}^0_2}$=$m_{\tilde{\chi}^\pm_1}$=$m_{\tilde{\chi}^0_1}$, see their Figure 12. Limits are also set on the light squark mass for the simplified model Tsqk2A, on the sbottom mass in Tsbot3, see their Figure 13, and on the slepton mass in direct electroweak pair production of mass-degenerate left- and right-handed sleptons (selectrons and smuons), see their Figure 14.

[5] AAD 20V searched in 139 fb^{-1} of pp collisions at $\sqrt{s}$ = 13 TeV for events with two same-sign charged leptons (electrons or muons) and jets. No significant excess above the Standard Model expectations is observed. Exclusion limits at 95% C.L. are set on the bottom squark masses in the Tsbot2 simplified model for $m_{\tilde{\chi}^\pm_1} = m_{\tilde{\chi}^0_1}$ + 100 GeV, see their Fig. 8(a).

[6] SIRUNYAN 20T searched in 137 fb^{-1} of pp collisions at $\sqrt{s}$ = 13 TeV for events with at least two jets, and two isolated same-sign or three or more charged leptons (electrons or muons). No significant excess above the Standard Model expectations is observed. Limits are set on the gluino mass in the Tglu3A, Tglu3B, Tglu3C and Tglu3D simplified models, see their Figure 7, and in the Tglu1C and Tglu1B simplified models, see their Figures 8 and 9. Limits are also set on the sbottom mass in the Tsbot2 simplified model, see their Figure 10, and on the stop mass in the Tstop7 simplified model, see their Figure 11. Finally, limits are set on the gluino mass in RPV simplified models where the gluino decays either via $\tilde{g} \to q q \overline{q} \overline{q}$ + $e/\mu/\tau$ or via $\tilde{g} \to t b s$, see Figure 12.

[7] AAD 19H searched in 139 fb^{-1} of pp collisions at $\sqrt{s}$ = 13 TeV for events with no charged leptons, three or more b-jets, and large $\not{E}_T$. Higgs boson candidates are reconstructed as b-jet pairs. No significant excess above the Standard Model expectations is observed. Limits up to 1500 GeV are set on the sbottom mass in the Tsbot4 simplified model, see Figure 8(a), for fixed $m_{\tilde{\chi}^0_1}$ = 60 GeV and for $m_{\tilde{\chi}^0_2}$ up to 1200 GeV.

[8] AAD 19H searched in 139 fb^{-1} of pp collisions at $\sqrt{s}$ = 13 TeV for events with no charged leptons, three or more b-jets, and large $\not{E}_T$. Higgs boson candidates are reconstructed as b-jet pairs. No significant excess above the Standard Model expectations is observed. Limits up to 1300 GeV are set on the sbottom mass in the Tsbot4 simplified model, see Figure 8(b), for $m_{\tilde{\chi}^0_2} = m_{\tilde{\chi}^0_1}$ + 130 GeV and $m_{\tilde{\chi}^0_2}$ from 200 to 750 GeV.

[9] SIRUNYAN 19CH searched in 137 fb^{-1} of pp collisions at $\sqrt{s}$ = 13 TeV for events containing multiple jets and large $\not{E}_T$. No significant excess above the Standard Model expectations is observed. Limits are set on the gluino mass in the Tglu1A, Tglu1C, Tglu2A and Tglu3A simplified models, see their Figure 13. Limits are also set on squark, sbottom and stop masses in the Tsqk1, Tsbot1, Tstop1 simplified models, see their Figure 14.

[10] SIRUNYAN 19CI searched in 77.5 fb^{-1} of pp collisions at $\sqrt{s}$ = 13 TeV for events with one or more high-momentum Higgs bosons, decaying to pairs of photons, jets and $\not{E}_T$. No significant excess above the Standard Model expectations is observed. Limits are set on the sbottom mass in the Tsbot4 simplified model, see Figure 3, and on the wino mass in the Tchi1n2E simplified model, see their Figure 4. Limits are also set on the higgsino mass in the Tn1n1A and Tn1n1B simplified models, see their Figure 5.

[11] AABOUD 18I searched in 36.1 fb^{-1} of pp collisions at $\sqrt{s}$ = 13 TeV for events with at least one jet with a transverse momentum above 250 GeV and no leptons. Good agreement is observed between the number of events in data and Standard Model predictions. The results are translated into exclusion limits in Tsbot1 models. In the compressed scenario with sbottom and neutralino masses differing by m_b, sbottom masses below 430 GeV are excluded. For $m_{\tilde{\chi}^0_1}$ = 0 they exclude sbottom masses up to 610 GeV. See their Fig.10(a).

[12] SIRUNYAN 18AL searched in 35.9 fb^{-1} of pp collisions at $\sqrt{s}$ = 13 TeV for events with at least three charged leptons, in any combination of electrons and muons, jets and significant $\not{E}_T$. No significant excess above the Standard Model expectations is observed. Limits are set on the gluino mass in the Tglu3A and Tglu1C simplified models, see their Figure 5. Limits are also set on the sbottom mass in the Tsbot2 simplified model, see their Figure 6, and on the stop mass in the Tstop7 simplified model, see their Figure 7.

[13] SIRUNYAN 18AR searched in 35.9 fb^{-1} of pp collisions at $\sqrt{s}$ = 13 TeV for events containing two opposite-charge, same-flavour leptons (electrons or muons), jets and $\not{E}_T$. No significant excess above the Standard Model expectations is observed. Limits are set on the gluino mass in the Tglu4C simplified model, see their Figure 7. Limits are also set on the chargino/neutralino mass in the Tchi1n2F simplified model, see their Figure 8, and on the neutralino mass in the Tn1n1B and Tn1n1C simplified models, see their Figure 9. Finally, limits are set on the sbottom mass in the Tsbot3 simplified model, see their Figure 10.

[14] SIRUNYAN 18AY searched in 35.9 fb^{-1} of pp collisions at $\sqrt{s}$ = 13 TeV for events containing one or more jets and significant $\not{E}_T$. No significant excess above the Standard Model expectations is observed. Limits are set on the gluino mass in the Tglu1A, Tglu2A and Tglu3A simplified models, see their Figure 3. Limits are also set on squark, sbottom and stop masses in the Tsqk1, Tsbot1, Tstop1 and Tstop4 simplified models, see their Figure 3. Finally, limits are set on long-lived gluino masses in a Tglu1A simplified model where the gluino is metastable or long-lived with proper decay lengths in the range 10^{-3} mm < cτ < 10^5 mm, see their Figure 4.

[15] SIRUNYAN 18B searched in 35.9 fb^{-1} of pp collisions at $\sqrt{s}$ = 13 TeV for the pair production of third-generation squarks in events with jets and large $\not{E}_T$. No significant excess above the Standard Model expectations is observed. Limits are set on the sbottom mass in the Tsbot1 simplified model, see their Figure 5, and on the stop mass in the Tstop4 simplified model, see their Figure 6.

[16] SIRUNYAN 18X searched in 35.9 fb^{-1} of pp collisions at $\sqrt{s}$ = 13 TeV for events with one or more high-momentum Higgs bosons, decaying to pairs of photons, jets and $\not{E}_T$. The razor variables (M_R and R^2) are used to categorise the events. No significant excess above the Standard Model expectations is observed. Limits are set on the sbottom mass in the Tsbot4 simplified model and on the wino mass in the Tchi1n2E simplified model, see their Figure 5. Limits are also set on the higgsino mass in the Tn1n1A and Tn1n1B simplified models, see their Figure 6.

[17] AABOUD 17AJ searched in 36.1 fb^{-1} of pp collisions at $\sqrt{s}$ = 13 TeV for events with two same-sign or three leptons, jets and large missing transverse momentum. No significant excess above the Standard Model expectations is observed. Limits up to 700 GeV are set on the bottom squark mass in Tsbot2 simplified models assuming $m_{\tilde{\chi}^0_1}$ = 0 GeV. See their Figure 4(d).

[18] AABOUD 17AX searched in 36 fb^{-1} of pp collisions at $\sqrt{s}$ = 13 TeV for events containing two jets identified as originating from b-quarks and large missing transverse momentum. No excess of events above the expected level of Standard Model background was found. Exclusion limits at 95% C.L. are set on the masses of bottom squarks. In the Tsbot1 simplified model, a $\tilde{b}_1$ mass below 950 GeV is excluded for $m_{\tilde{\chi}^0_1}$ = 0 (<420) GeV. See their Fig. 7(a).

[19] AABOUD 17AX searched in 36 fb^{-1} of pp collisions at $\sqrt{s}$ = 13 TeV for events containing two jets identified as originating from b-quarks and large missing transverse momentum, with or without leptons. No excess of events above the expected level of Standard Model background was found. Exclusion limits at 95% C.L. are set on the masses of bottom squarks. Assuming 50% BR for Tsbot1 and Tsbot2 simplified models, a $\tilde{b}_1$ mass below 880 (860) GeV is excluded for $m_{\tilde{\chi}^0_1}$ = 0 (<250) GeV. See their Fig. 7(b).

[20] KHACHATRYAN 17A searched in 18.5 fb^{-1} of pp collisions at $\sqrt{s}$ = 8 TeV for events with two forward jets, produced through vector boson fusion, and missing transverse momentum. No significant excess above the Standard Model expectations is observed. A limit is set on sbottom masses in the Tsbot1 simplified model, see Fig. 3.

[21] KHACHATRYAN 17AW searched in 2.3 fb^{-1} of pp collisions at $\sqrt{s}$ = 13 TeV for events with at least three charged leptons, in any combination of electrons and muons, and significant $\not{E}_T$. No significant excess above the Standard Model expectations is observed. Limits are set on the gluino mass in the Tglu3A and Tglu1C simplified models, and on the sbottom mass in the Tsbot2 simplified model, see their Figure 4.

[22] KHACHATRYAN 17P searched in 2.3 fb^{-1} of pp collisions at $\sqrt{s}$ = 13 TeV for events with one or more jets and large $\not{E}_T$. No significant excess above the Standard Model expectations is observed. Limits are set on the gluino mass in the Tglu1A, Tglu2A, Tglu3A, Tglu3B, Tglu3C and Tglu3D simplified models, see their Figures 7 and 8. Limits are also set on the squark mass in the Tsqk1 simplified model, see their Fig. 7, and on the sbottom mass in the Tsbot1 simplified model, see Fig. 8. Finally, limits are set on the stop mass in the Tstop1, Tstop3, Tstop4, Tstop6 and Tstop7 simplified models, see Fig. 8.

[23] SIRUNYAN 17AZ searched in 35.9 fb^{-1} of pp collisions at $\sqrt{s}$ = 13 TeV for events with one or more jets and large $\not{E}_T$. No significant excess above the Standard Model expectations is observed. Limits are set on the gluino mass in the Tglu1A, Tglu2A, Tglu3A simplified models, see their Figures 6. Limits are also set on the squark mass in the Tsqk1 simplified model (for single light squark and for 8 degenerate light squarks), on the sbottom mass in the Tsbot1 simplified model and on the stop mass in the Tstop1 simplified model, see their Fig. 7. Finally, limits are set on the stop mass in the Tstop2, Tstop4 and Tstop8 simplified models, see Fig. 8.

[24] SIRUNYAN 17K searched in 2.3 fb^{-1} of pp collisions at $\sqrt{s}$ = 13 TeV for direct production of stop or sbottom pairs in events with multiple jets and significant $\not{E}_T$. A second search also requires an isolated lepton and is combined with the all-hadronic search. No significant excess above the Standard Model expectations is observed. Limits are set on the stop mass in the Tstop1, Tstop8 and Tstop4 simplified models, see their Figures 7, 8 and 9 (for the Tstop4 limits, only the results of the all-hadronic search are used). Limits are also set on the sbottom mass in the Tsbot1 simplified model, see Fig. 10 (also here, only the results of the all-hadronic search are used).

[25] SIRUNYAN 17S searched in 35.9 fb^{-1} of pp collisions at $\sqrt{s}$ = 13 TeV for events with two isolated same-sign leptons, jets, and large $\not{E}_T$. No significant excess above the Standard Model expectations is observed. Limits are set on the mass of the gluino mass

Int. J. Mod. Phys. A 2026.41. Downloaded from www.worldscientific.com
by UNIVERSITY OF CALIFORNIA @ BERKELEY on 09/16/26. Re-use and distribution is strictly not permitted, except for Open Access articles.

Int. J. Mod. Phys. A 2026.41. Downloaded from www.worldscientific.com
by UNIVERSITY OF CALIFORNIA @ BERKELEY on 09/16/26. Re-use and distribution is strictly not permitted, except for Open Access articles.

in the Tglu3A, Tglu3B, Tglu3C, Tglu3D and Tglu1B simplified models, see their Figures 5 and 6, and on the sbottom mass in the Tsbot2 simplified model, see their Figure 6.

[26] AABOUD 16D searched in 3.2 fb^{-1} of pp collisions at $\sqrt{s}$ = 13 TeV for events with an energetic jet and large missing transverse momentum. The results are interpreted as 95%C.L. limits on mass of sbottom decaying into a b-quark and the lightest neutralino in scenarios with $m_{\widetilde{b}_1} - m_{\widetilde{\chi}^0_1}$ between 5 and 20 GeV. See their Fig. 6.

[27] AABOUD 16Q searched in 3.2 fb^{-1} of pp collisions at $\sqrt{s}$ = 13 TeV for events containing two jets identified as originating from b-quarks and large missing transverse momentum. No excess of events above the expected level of Standard Model background was found. Exclusion limits at 95% C.L. are set on the masses of third-generation squarks. Assuming that the decay $\widetilde{b}_1 \rightarrow b\widetilde{\chi}^0_1$ (Tsbot1) takes place 100% of the time, a $\widetilde{b}_1$ mass below 840 (800) GeV is excluded for $m_{\widetilde{\chi}^0_1} < 100$ (360) GeV. Differences in mass above 100 GeV between the $\widetilde{b}_1$ and the $\widetilde{\chi}^0_1$ are excluded up to a $\widetilde{b}_1$ mass of 500 GeV. For more details, see their Fig. 4.

[28] AAD 16BB searched in 3.2 fb^{-1} of pp collisions at $\sqrt{s}$ = 13 TeV for events with exactly two same-sign leptons or at least three leptons, multiple hadronic jets, b-jets, and $\not{E}_T$. No significant excess over the Standard Model expectation is found. Exclusion limits at 95% C.L. are set on the sbottom mass for the Tsbot2 model, assuming $m_{\widetilde{\chi}^\pm_1} = m_{\widetilde{\chi}^0_1}$ + 100 GeV. See their Fig. 4c.

[29] KHACHATRYAN 16BJ searched in 2.3 fb^{-1} of pp collisions at $\sqrt{s}$ = 13 TeV for events with two isolated same-sign dileptons and jets in the final state. No significant excess above the Standard Model expectations is observed. Limits are set on the sbottom mass in the Tsbot2 simplified model, see Fig. 6.

[30] KHACHATRYAN 16BS searched in 2.3 fb^{-1} of pp collisions at $\sqrt{s}$ = 13 TeV for events with at least one energetic jet , no isolated leptons, and significant $\not{E}_T$, using the transverse mass variable M_{T2} to discriminate between signal and background processes. No significant excess above the Standard Model expectations is observed. Limits are set on the sbottom mass in the Tsbot1 simplified model, see Fig. 11 and Table 3.

[31] KHACHATRYAN 16BY searched in 2.3 fb^{-1} of pp collisions at $\sqrt{s}$ = 13 TeV for events with two opposite-sign, same-flavour leptons, jets, and missing transverse momentum. No significant excess above the Standard Model expectations is observed. Limits are set on the gluino mass in the Tglu4C simplified model, see Fig. 4, and on sbottom masses in the Tsbot3 simplified model, see Fig. 5.

[32] AAD 15CJ searched in 20 fb^{-1} of pp collisions at $\sqrt{s}$ = 8 TeV for evidence of third generation squarks by combining a large number of searches covering various final states. Limits on the sbottom mass are shown, either assuming the $\widetilde{b} \rightarrow b\widetilde{\chi}^0_1$ decay, see Fig. 11, or assuming the $\widetilde{b} \rightarrow t\widetilde{\chi}^\pm_1$ decay, with $\widetilde{\chi}^\pm_1 \rightarrow W^{(*)}\widetilde{\chi}^0_1$, see Fig. 12a, or assuming the $\widetilde{b} \rightarrow b\widetilde{\chi}^0_2$ decay, with $\widetilde{\chi}^0_2 \rightarrow h\widetilde{\chi}^0_1$, see Fig. 12b. Interpretations in the pMSSM are also discussed, see Figures 13–15.

[33] KHACHATRYAN 15AF searched in 19.5 fb^{-1} of pp collisions at $\sqrt{s}$ = 8 TeV for events with at least two energetic jets and significant $\not{E}_T$, using the transverse mass variable M_{T2} to discriminate between signal and background processes. No significant excess above the Standard Model expectations is observed. Limits are set on the sbottom mass in simplified models where the decay $\widetilde{b} \rightarrow b\widetilde{\chi}^0_1$ takes place with a branching ratio of 100%, see Fig. 12. See also Table 5. Exclusions in the CMSSM, assuming tanβ = 30, $A_0 = -2$ max(m_0, $m_{1/2}$) and $\mu > 0$, are also presented, see Fig. 15.

[34] KHACHATRYAN 15AH searched in 19.4 or 19.7 fb^{-1} of pp collisions at $\sqrt{s}$ = 8 TeV for events containing either a fully reconstructed top quark, or events containing dijets requiring one or both jets to originate from b-quarks, or events containing a mono-jet. No significant excess above the Standard Model expectations is observed. Limits are set on the sbottom mass in simplified models where the decay $\widetilde{b} \rightarrow b\widetilde{\chi}^0_1$ takes place with a branching ratio of 100%, see Fig. 12. Limits are also set in a simplified model where the decay $\widetilde{b} \rightarrow c\widetilde{\chi}^0_1$ takes place with a branching ratio of 100%, see Fig. 12.

[35] KHACHATRYAN 15I searched in 19.5 fb^{-1} of pp collisions at $\sqrt{s}$ = 8 TeV for events in which b-jets and four W-bosons are produced. Five individual search channels are combined (fully hadronic, single lepton, same-sign dilepton, opposite-sign dilepton, multilepton). No significant excess above the Standard Model expectations is observed. Limits are set on the sbottom mass in a simplified model where the decay $\widetilde{b} \rightarrow t\widetilde{\chi}^\pm_1$, with $\widetilde{\chi}^\pm_1 \rightarrow W^\pm\widetilde{\chi}^0_1$, takes place with a branching ratio of 100%, see Fig. 7.

[36] AAD 14T searched in 20.3 fb^{-1} of pp collisions at $\sqrt{s}$ = 8 TeV for monojet-like events. No excess of events above the expected level of Standard Model background was found. Exclusion limits at 95% C.L. are set on the masses of third-generation squarks in simplified models which assume that the decay $\widetilde{b}_1 \rightarrow b\widetilde{\chi}^0_1$ takes place 100% of the time, see Fig. 12.

[37] CHATRCHYAN 14AH searched in 4.7 fb^{-1} of pp collisions at $\sqrt{s}$ = 7 TeV for events with at least two energetic jets and significant $\not{E}_T$, using the razor variables (M_R and R^2) to discriminate between signal and background processes. A second analysis requires at least one of the jets to be originating from a b-quark. No significant excess above the Standard Model expectations is observed. Limits are set on sbottom masses in simplified models where the decay $\widetilde{b} \rightarrow b\widetilde{\chi}^0_1$ takes place with a branching ratio of 100%, see Figs. 28 and 29. Exclusions in the CMSSM, assuming tanβ = 10, A_0 = 0 and μ >0, are also presented, see Fig. 26.

[38] CHATRCHYAN 14R searched in 19.5 fb^{-1} of pp collisions at $\sqrt{s}$ = 8 TeV for events with at least three leptons (electrons, muons, taus) in the final state. No significant excess above the Standard Model expectations is observed. Limits are set on the gluino mass in a simplified model where the decay $\widetilde{b} \rightarrow t\widetilde{\chi}^\pm_1$, with $\widetilde{\chi}^\pm_1 \rightarrow W^\pm\widetilde{\chi}^0_1$, takes place with a branching ratio of 100%, see Fig. 11.

[39] KHACHATRYAN 15AD searched in 19.4 fb^{-1} of pp collisions at $\sqrt{s}$ = 8 TeV for events with two opposite-sign same flavor isolated leptons featuring either a kinematic edge, or a peak at the Z-boson mass, in the invariant mass spectrum. No evidence for a statistically significant excess over the expected SM backgrounds is observed and 95% C.L. exclusion limits are derived in a simplified model of sbottom pair production where the sbottom decays into a b-quark, two opposite-sign dileptons and a neutralino LSP, through an intermediate state containing either an off-shell Z-boson or a slepton, see Fig. 8.

[40] AAD 14AX searched in 20.1 fb^{-1} of pp collisions at $\sqrt{s}$ = 8 TeV for the strong production of supersymmetric particles in events containing either zero or at last one high-p_T lepton, large missing transverse momentum, high jet multiplicity and at least three jets identified as originating from b-quarks. No excess over the expected SM background is observed. Limits are derived in mSUGRA/CMSSM models with tanβ = 30, A_0 = $-2\ m_0$ and μ > 0, see their Fig. 14. Also, exclusion limits are set in simplified models containing scalar bottom quarks, where the decay $\widetilde{b} \rightarrow b\widetilde{\chi}^0_2$ and $\widetilde{\chi}^0_2 \rightarrow h\widetilde{\chi}^0_1$ takes place with a branching ratio of 100%, see their Figures 11.

[41] AAD 14E searched in 20.3 fb^{-1} of pp collisions at $\sqrt{s}$ = 8 TeV for strongly produced supersymmetric particles in events containing jets and two same-sign leptons or three leptons. The search also utilises jets originating from b-quarks, missing transverse momentum and other variables. No excess over the expected SM background is observed. Exclusion limits are derived in simplified models containing bottom, see Fig. 7. Limits are also derived in the mSUGRA/CMSSM, bRPV and GMSB models, see their Fig. 8.

[42] CHATRCHYAN 14H searched in 19.5 fb^{-1} of pp collisions at $\sqrt{s}$ = 8 TeV for events with two isolated same-sign dileptons and jets in the final state. No significant excess above the Standard Model expectations is observed. Limits are set on the sbottom mass in a simplified models where the decay $\widetilde{b} \rightarrow t\widetilde{\chi}^\pm_1$, $\widetilde{\chi}^\pm_1 \rightarrow W^\pm\widetilde{\chi}^0_1$ takes place with a branching ratio of 100%, with varying mass of the $\widetilde{\chi}^\pm_1$, for $m_{\widetilde{\chi}^0_1}$ = 50 GeV, see Fig. 6.

[43] AAD 13AU searched in 20.1 fb^{-1} of pp collisions at $\sqrt{s}$ = 8 TeV for events containing two jets identified as originating from b-quarks and large missing transverse momentum. No excess of events above the expected level of Standard Model background was found. Exclusion limits at 95% C.L. are set on the masses of third-generation squarks. Assuming that the decay $\widetilde{b}_1 \rightarrow b\widetilde{\chi}^0_1$ takes place 100% of the time, a $\widetilde{b}_1$ mass below 620 GeV is excluded for $m_{\widetilde{\chi}^0_1} < 120$ GeV. For more details, see their Fig. 5.

[44] CHATRCHYAN 13AT provides interpretations of various searches for supersymmetry by the CMS experiment based on 4.73–4.98 fb^{-1} of pp collisions at $\sqrt{s}$ = 7 TeV in the framework of simplified models. Limits are set on the sbottom mass in a simplified models where sbottom quarks are pair-produced and the decay $\widetilde{b} \rightarrow b\widetilde{\chi}^0_1$ takes place with a branching ratio of 100%, see Fig. 4.

[45] CHATRCHYAN 13T searched in 11.7 fb^{-1} of pp collisions at $\sqrt{s}$ = 8 TeV for events with at least two energetic jets and significant $\not{E}_T$, using the α_T variable to discriminate between processes with genuine and misreconstructed $\not{E}_T$. No significant excess above the Standard Model expectations is observed. Limits are set on sbottom masses in simplified models where the decay $\widetilde{b} \rightarrow b\widetilde{\chi}^0_1$ takes place with a branching ratio of 100%, see Fig. 8 and Table 9.

[46] CHATRCHYAN 13V searched in 10.5 fb^{-1} of pp collisions at $\sqrt{s}$ = 8 TeV for events with two isolated same-sign dileptons and at least two b-jets in the final state. No significant excess above the Standard Model expectations is observed. Limits are set on the bottom mass in a simplified models where the decay $\widetilde{b} \rightarrow t\widetilde{\chi}^\pm_1$, $\widetilde{\chi}^\pm_1 \rightarrow W^\pm\widetilde{\chi}^0_1$ takes place with a branching ratio of 100%, with varying mass of the $\widetilde{\chi}^\pm_1$, for $m_{\widetilde{\chi}^0_1}$ = 50 GeV, see Fig. 4.

[47] AAD 12AN searched in 2.05 fb^{-1} of pp collisions at $\sqrt{s}$ = 7 TeV for scalar bottom quarks in events with large missing transverse momentum and two b-jets in the final state. The data are found to be consistent with the Standard Model expectations. Limits are set in an R-parity conserving minimal supersymmetric scenario, assuming B($\widetilde{b}_1 \rightarrow b\widetilde{\chi}^0_1$) = 100%, see their Fig. 2.

[48] CHATRCHYAN 12AI looked in 4.98 fb^{-1} of pp collisions at $\sqrt{s}$ = 7 TeV for events with two same-sign leptons (e, μ), but not necessarily same flavor, at least 2 b-jets and missing transverse energy. No excess beyond the Standard Model expectation is observed. Exclusion limits are derived in a simplified model for sbottom pair production, where the sbottom decays through $\widetilde{b}_1 \rightarrow t\widetilde{\chi}_1 W$, see Fig. 8.

[49] CHATRCHYAN 12BO searched in 4.7 fb^{-1} of pp collisions at $\sqrt{s}$ = 7 TeV for scalar bottom quarks in events with large missing transverse momentum and two b-jets in the final state. The data are found to be consistent with the Standard Model expectations. Limits are set in an R-parity conserving minimal supersymmetric scenario, assuming B($\widetilde{b}_1 \rightarrow b\widetilde{\chi}^0_1$) = 100%, see their Fig. 2.

[50] AAD 11K looked in 34 pb^{-1} of pp collisions at $\sqrt{s}$ = 7 TeV for events with heavy stable particles, identified by their anomalous dE/dx in the tracker or time of flight in the tile calorimeter, from pair production of $\widetilde{b}$. No evidence for an excess over the SM expectation is observed and limits on the mass are derived for pair production of sbottom, see Fig. 4.

[51] AAD 11O looked in 35 pb^{-1} of pp collisions at $\sqrt{s}$ = 7 TeV for events with jets, of which at least one is a b-jet, and $\not{E}_T$. No excess above the Standard Model was found. Limits are derived in the ($m_{\widetilde{g}}$, $m_{\widetilde{b}_1}$) plane (see Fig. 2) under the assumption of 100% branching ratios and $\widetilde{b}_1$ being the lightest squark. The quoted limit is valid for $m_{\widetilde{b}_1}$ < 500 GeV. A similar approach for $\widetilde{t}_1$ as the lightest squark with $\widetilde{g} \rightarrow \widetilde{t}_1 t$ and $\widetilde{t}_1 \rightarrow b\widetilde{\chi}^\pm_1$ with 100% branching ratios leads to a gluino mass limit of 520 GeV for 130 < $m_{\widetilde{t}_1}$ < 300 GeV. Limits are also derived in the CMSSM (m_0, $m_{1/2}$) plane for tanβ = 40, see Fig. 4, and in scenarios based on the gauge group SO(10).

[52] CHATRCHYAN 11D looked in 35 pb^{-1} of pp collisions at $\sqrt{s}$ = 7 TeV for events with $\geq$ 2 jets, at least one of which is b-tagged, and $\not{E}_T$, where the b-jets are decay products of $\widetilde{t}$ or $\widetilde{b}$. No evidence for an excess over the expected background is observed. Limits are derived in the CMSSM (m_0, $m_{1/2}$) plane for tanβ = 50 (see Fig. 2).

[53] AALTONEN 10R searched in 2.65 fb^{-1} of $p\overline{p}$ collisions at $\sqrt{s}$ = 1.96 TeV for events with $\not{E}_T$ and exactly two jets, at least one of which is b-tagged. The results are in agreement with the SM prediction, and a limit on the cross section of 0.1 pb is obtained for the range of masses 80 < $m_{\widetilde{b}_1}$ < 280 GeV assuming that the sbottom decays exclusively to $b\widetilde{\chi}^0_1$. The excluded mass region in the framework of conserved R_p is shown in a plane of ($m_{\widetilde{b}_1}$, $m_{\widetilde{\chi}^0_1}$), see their Fig.2.

[54] ABAZOV 10L looked in 5.2 fb^{-1} of $p\overline{p}$ collisions at $\sqrt{s}$ = 1.96 TeV for events with at least 2 b-jets and $\not{E}_T$ from the production of $\widetilde{b}_1\widetilde{b}_1$. No evidence for an excess over the SM expectation is observed, and a limit on the cross section is derived under the assumption of 100% branching ratio. The excluded mass region in the framework of conserved R_p is shown in a plane of ($m_{\widetilde{b}_1}$,$m_{\widetilde{\chi}^0_1}$), see their Fig. 3b. The exclusion also extends to $m_{\widetilde{\chi}^0_1}$ = 110 GeV for 160< $m_{\widetilde{b}_1}$ < 200 GeV.

Int. J. Mod. Phys. A 2026.41. Downloaded from www.worldscientific.com
by UNIVERSITY OF CALIFORNIA @ BERKELEY on 09/16/26. Re-use and distribution is strictly not permitted, except for Open Access articles.

R-parity violating $\tilde{b}$ (Sbottom) mass limit

VALUE (GeV)	CL%	DOCUMENT ID		TECN	COMMENT
>307	95	[1] KHACHATRY...16BX		CMS	RPV, $\tilde{b} \to t\,d$ or $t\,s$, λ''_{332} or λ''_{331} coupling
• • • We do not use the following data for averages, fits, limits, etc. • • •					
		[2] AAD	14E	ATLAS	$\ell^\pm \ell^\pm (\ell^\mp)$ + jets, $\tilde{b}_1 \to t\,\tilde{\chi}^\pm_1$ with $\tilde{\chi}^\pm_1 \to W^{(*)\pm}\tilde{\chi}^0_1$ simplified model, $m_{\tilde{\chi}^\pm_1} = 2\,m_{\tilde{\chi}^0_1}$

[1] KHACHATRYAN 16BX searched in 19.5 fb^{-1} of pp collisions at $\sqrt{s} = 8$ TeV for events containing 2 leptons coming from R-parity-violating decays of supersymmetric particles. No excess over the expected background is observed. Limits are derived on the sbottom mass, assuming the RPV $\tilde{b} \to t\,d$ or $\tilde{b} \to t\,s$ decay, see Fig. 15.

[2] AAD 14E searched in 20.3 fb^{-1} of pp collisions at $\sqrt{s} = 8$ TeV for strongly produced supersymmetric particles in events containing jets and two same-sign leptons or three leptons. The search also utilises jets originating from b-quarks, missing transverse momentum and other variables. No excess over the expected SM background is observed. Exclusion limits are derived in simplified models containing bottom, see Fig. 7. Limits are also derived in the mSUGRA/CMSSM, bRPV and GMSB models, see their Fig. 8.

$\tilde{t}$ (Stop) mass limit

Limits depend on the decay mode. In e^+e^- collisions they also depend on the mixing angle of the mass eigenstate $\tilde{t}_1 = \tilde{t}_L \cos\theta_t + \tilde{t}_R \sin\theta_t$. The coupling to the Z vanishes when $\theta_t = 0.98$. In the Listings below, we use $\Delta m \equiv m_{\tilde{t}_1} - m_{\tilde{\chi}^0_1}$ or $\Delta m \equiv m_{\tilde{t}_1} - m_{\tilde{\nu}}$, depending on relevant decay mode. See also bounds in "$\tilde{q}$ (Squark) MASS LIMIT."

Some earlier papers are now obsolete and have been omitted. They were last listed in our PDG 14 edition: K. Olive, *et al.* (Particle Data Group), Chinese Physics **C38** 070001 (2014) (http://pdg.lbl.gov).

R-parity conserving $\tilde{t}$ (Stop) mass limit

VALUE (GeV)	CL%	DOCUMENT ID		TECN	COMMENT
900	95	[1] AAD	25V	ATLAS	$\geq$ 2 c-jets + $\not{E}_T$, Tstop4, $m_{\tilde{\chi}^0_1}$ = 0 GeV
> 780	95	[2] CHEKHOVSKY	25M	CMS	$\geq$ 1 ISR jet + (in-)visible decay products, Tstop1, $m_{\tilde{t}} - m_{\tilde{\chi}^0_1}$ = 150 GeV
> 750	95	[2] CHEKHOVSKY	25M	CMS	$\geq$ 1 ISR jet + (in-)visible decay products, Tstop1, 60 < $m_{\tilde{t}} - m_{\tilde{\chi}^0_1}$ < 175 GeV
> 620	95	[2] CHEKHOVSKY	25M	CMS	$\geq$ 1 ISR jet + (in-)visible decay products, Tstop2, 50 < $m_{\tilde{t}} - m_{\tilde{\chi}^0_1}$ < 90 GeV
> 550	95	[2] CHEKHOVSKY	25M	CMS	$\geq$ 1 ISR jet + (in-)visible decay products, Tstop2, 35 < $m_{\tilde{t}} - m_{\tilde{\chi}^0_1}$ < 140 GeV
> 660	95	[2] CHEKHOVSKY	25M	CMS	$\geq$ 1 ISR jet + (in-)visible decay products, Tstop4, $m_{\tilde{t}} - m_{\tilde{\chi}^0_1}$ = 20 GeV
> 520	95	[2] CHEKHOVSKY	25M	CMS	$\geq$ 1 ISR jet + (in-)visible decay products, Tstop4, 10 < $m_{\tilde{t}} - m_{\tilde{\chi}^0_1}$ < 60 GeV
> 980	95	[3] AAD	24AC	ATLAS	1ℓ + jets + $\not{E}_T$, Tstop1, $m_{\tilde{\chi}^0_1}$ = 600 GeV
> 685	95	[3] AAD	24AC	ATLAS	1ℓ + jets + $\not{E}_T$, Tstop1, $m_{\tilde{t}_1} - m_{\tilde{\chi}^0_1} = m_t$
> 800	95	[4] AAD	24AO	ATLAS	jets + $\not{E}_T$ + c-jets, like Tstop9 but extended to on-shell $\tilde{t} \to t\,\tilde{\chi}^0_1$ decays, $m_{\tilde{\chi}^0_1}$ = 0, B($\tilde{t} \to t\,\tilde{\chi}^0_1$) = 50%
>1500	95	[5] HAYRAPETY...	24M	CMS	$\geq$ 1 disappearing track+ $\not{E}_T$, $m_{\tilde{\chi}^\pm_1} \simeq m_{\tilde{\chi}^0_1}$ = 200 GeV, $c\tau(\tilde{\chi}^\pm_1)$ = 10 cm
>1590	95	[5] HAYRAPETY...	24M	CMS	$\geq$ 1 disappearing track+ $\not{E}_T$, $m_{\tilde{\chi}^\pm_1} \simeq m_{\tilde{\chi}^0_1}$ = 1050 GeV, $c\tau(\tilde{\chi}^\pm_1)$ = 200 cm
>1430	95	[6] HAYRAPETY...	23E	CMS	γ + jets + $\not{E}_T$, Tstop13, $m_{\tilde{\chi}^0_1}$ = 1170 GeV
>1150	95	[7] TUMASYAN	23AB	CMS	$\geq$ 1 $\tau^\pm$ + $\not{E}_T$, Tstop16, $m_{\tilde{\chi}^0_1}$ = 1 GeV
> 480	95	[8] TUMASYAN	23K	CMS	1 high-p_t jet, 1 low-p_t e or μ, Tstop3, $m_{\tilde{t}} - m_{\tilde{\chi}^0_1}$ = 10 GeV
> 700	95	[8] TUMASYAN	23K	CMS	1 high-p_t jet, 1 low-p_t e or μ, Tstop3, $m_{\tilde{t}} - m_{\tilde{\chi}^0_1}$ = 80 GeV
> 480	95	[9] TUMASYAN	22Q	CMS	2 or 3 ℓ (soft), $\not{E}_T$; Tstop2, $m_{\tilde{t}} - m_{\tilde{\chi}^0_1}$ = 30 GeV
> 540	95	[9] TUMASYAN	22Q	CMS	2 or 3 ℓ (soft), $\not{E}_T$; Tstop3, $m_{\tilde{t}} - m_{\tilde{\chi}^0_1}$ = 30 GeV
>1400	95	[10] AAD	21AW	ATLAS	$\tau^\pm$ + jets + b-jets + $\not{E}_T$, Tstop5, $m_{\tilde{t}_1}$ = 1200 GeV
>1200	95	[11] AAD	21O	ATLAS	$\ell^\pm$ + jet + $\not{E}_T$, Tstop1, $m_{\tilde{\chi}^0_1}$ = 0 GeV
> 710	95	[11] AAD	21O	ATLAS	$\ell^\pm$ + jet + $\not{E}_T$, Tstop1, $m_{\tilde{\chi}^0_1}$ = 580 GeV
> 640	95	[11] AAD	21O	ATLAS	$\ell^\pm$ + jet + $\not{E}_T$, Tstop3, $m_{\tilde{\chi}^0_1}$ = 580 GeV
>1000	95	[12] AAD	21P	ATLAS	$\ell^\pm \ell^\mp$ + jets + $\not{E}_T$, Tstop1, $m_{\tilde{\chi}^0_1}$ = 0 GeV
> 600	95	[12] AAD	21P	ATLAS	$\ell^\pm \ell^\mp$ + jets + $\not{E}_T$, Tstop2, $m_{\tilde{\chi}^0_1}$ = 500 GeV
> 550	95	[12] AAD	21P	ATLAS	$\ell^\pm \ell^\mp$ + jets + $\not{E}_T$, Tstop3, $m_{\tilde{\chi}^0_1}$ = 500 GeV
>1310	95	[13] SIRUNYAN	21AD	CMS	jets + $\not{E}_T$, Tstop1, $m_{\tilde{\chi}^0_1}$ < 300 GeV
>1170	95	[13] SIRUNYAN	21AD	CMS	jets + $\not{E}_T$, Tstop2, $m_{\tilde{\chi}^\pm_1} = (m_{\tilde{t}} + m_{\tilde{\chi}^0_1})/2$, $m_{\tilde{\chi}^0_1}$ < 100 GeV
>1150	95	[13] SIRUNYAN	21AD	CMS	jets + $\not{E}_T$, Tstop1 (50%) or Tstop2 (50%), $m_{\tilde{\chi}^\pm_1} - m_{\tilde{\chi}^0_1}$ = 5 GeV, $m_{\tilde{\chi}^0_1}$ = 100 GeV
> 640	95	[13] SIRUNYAN	21AD	CMS	jets + $\not{E}_T$, Tstop3, $m_{\tilde{t}} - m_{\tilde{\chi}^0_1}$ = 50 GeV
> 620	95	[13] SIRUNYAN	21AD	CMS	jets + $\not{E}_T$, Tstop3, 10 GeV < $m_{\tilde{t}} - m_{\tilde{\chi}^0_1}$ < 60 GeV
> 740	95	[13] SIRUNYAN	21AD	CMS	jets + $\not{E}_T$, Tstop2, $m_{\tilde{t}} - m_{\tilde{\chi}^0_1}$ = 80 GeV
> 720	95	[13] SIRUNYAN	21AD	CMS	jets + $\not{E}_T$, Tstop2, 40 GeV < $m_{\tilde{t}} - m_{\tilde{\chi}^0_1}$ < 80 GeV
> 595	95	[13] SIRUNYAN	21AD	CMS	jets + $\not{E}_T$, Tstop2, $m_{\tilde{t}} - m_{\tilde{\chi}^0_1}$ = 10 GeV
> 630	95	[13] SIRUNYAN	21AD	CMS	jets + $\not{E}_T$, Tstop4, $m_{\tilde{t}} - m_{\tilde{\chi}^0_1}$ = 20 GeV
none 200–920	95	[14] SIRUNYAN	21B	CMS	$\ell^\pm \ell^\mp$ + b-jets + $\not{E}_T$, Tstop1, $m_{\tilde{\chi}^0_1}$ = 0 GeV
none 250–810		[14] SIRUNYAN	21B	CMS	$\ell^\pm \ell^\mp$ + b-jets + $\not{E}_T$, Tstop2, $m_{\tilde{\chi}^\pm_1} = (m_{\tilde{t}} + m_{\tilde{\chi}^0_1})/2$, $m_{\tilde{\chi}^0_1}$ = 0 GeV
>1300	95	[14] SIRUNYAN	21B	CMS	$\ell^\pm \ell^\mp$+b-jets+$\not{E}_T$, Tstop11, $m_{\tilde{\chi}^\pm_1}$=$(m_{\tilde{t}} + m_{\tilde{\chi}^0_1})/2$, $m_{\tilde{\ell}} = (m_{\tilde{\chi}^\pm_1} - m_{\tilde{\chi}^0_1})/2 + m_{\tilde{\chi}^0_1}$, $m_{\tilde{\chi}^0_1}$ = 0
none 400–1180	95	[14] SIRUNYAN	21B	CMS	$\ell^\pm \ell^\mp$+b-jets+$\not{E}_T$, Tstop11, $m_{\tilde{\chi}^\pm_1}$=$(m_{\tilde{t}} + m_{\tilde{\chi}^0_1})/2$, $m_{\tilde{\ell}} = 0.05\,(m_{\tilde{\chi}^\pm_1} - m_{\tilde{\chi}^0_1}) + m_{\tilde{\chi}^0_1}$, $m_{\tilde{\chi}^0_1}$ =0
>1400	95	[14] SIRUNYAN	21B	CMS	$\ell^\pm \ell^\mp$+b-jets+$\not{E}_T$, Tstop11, $m_{\tilde{\chi}^\pm_1}$=$(m_{\tilde{t}} + m_{\tilde{\chi}^0_1})/2$, $m_{\tilde{\ell}} = 0.95\,(m_{\tilde{\chi}^\pm_1} - m_{\tilde{\chi}^0_1}) + m_{\tilde{\chi}^0_1}$, $m_{\tilde{\chi}^0_1}$ =0
>1325	95	[15] TUMASYAN	21I	CMS	$\geq$ 2 jets + $\not{E}_T$ + 0,1,2 ℓ, Tstop1, $m_{\tilde{\chi}^0_1}$ = 0 GeV
>1150	95	[15] TUMASYAN	21I	CMS	$\geq$ 2 jets + $\not{E}_T$ + 0,1,2 ℓ, Tstop1, $m_{\tilde{\chi}^0_1}$ = 700 GeV
>1260	95	[15] TUMASYAN	21I	CMS	$\geq$ 2 jets + $\not{E}_T$ + 0,1,2 ℓ, Tstop2, $m_{\tilde{\chi}^0_1}$ = 0 GeV
>1000	95	[15] TUMASYAN	21I	CMS	$\geq$ 2 jets + $\not{E}_T$ + 0,1,2 ℓ, Tstop2, $m_{\tilde{\chi}^0_1}$ <575 GeV
>1175	95	[15] TUMASYAN	21I	CMS	$\geq$ 2 jets + $\not{E}_T$ + 0,1,2 ℓ, Tstop1 (50%) or Tstop2 (50%), $m_{\tilde{\chi}^0_1}$ = 0 GeV
>1000	95	[15] TUMASYAN	21I	CMS	$\geq$ 2 jets + $\not{E}_T$ + 0,1,2 ℓ, Tstop1 (50%) or Tstop2 (50%), $\tilde{\chi}^0_1$ = 570 GeV
none 145–295	95	[15] TUMASYAN	21I	CMS	$\ell^\pm \ell^\mp$ + jets + $\not{E}_T$, Tstop1, $\lvert m_{\tilde{t}} - m_{\tilde{\chi}^0_1} - 175\text{ GeV}\rvert$ < 30 GeV
none, 170–230	95	[16] AABOUD	20	ATLAS	$e^\pm \mu^\mp$ + $\geq$ 1b-jet, Tstop1, $m_{\tilde{\chi}^0_1}$ = 0.5 GeV
none, 170–220	95	[16] AABOUD	20	ATLAS	$e^\pm \mu^\mp$ + $\geq$ 1b-jet, Tstop1, $m_{\tilde{\chi}^0_1}$ < 62 GeV
>1220	95	[17] AAD	20AS	ATLAS	$\ell^\pm \ell^\mp$ or 2 b-jets and $\not{E}_T$, Tstop6, $m_{\tilde{\chi}^0_2}$=900 GeV

Int. J. Mod. Phys. A 2026.41. Downloaded from www.worldscientific.com
by UNIVERSITY OF CALIFORNIA @ BERKELEY on 09/16/26. Re-use and distribution is strictly not permitted, except for Open Access articles.

> 860	95	[18] AAD	20AS	ATLS	$\ell^\pm\ell^\mp$ or 2 b-jets and $\not{E}_T$, $\tilde{t}_2$ with $\tilde{t}_2 \to \tilde{t}_1 Z$, $\tilde{t}_1 \to b f f' \tilde{\chi}^0_1$, $\Delta m(\tilde{t}_1, \tilde{\chi}^0_1) = 40$ GeV
none 400–1250	95	[19] AAD	20S	ATLS	jets+$\not{E}_T$, Tstop1, $m_{\tilde{\chi}^0_1}$=0 GeV
none 300–660	95	[20] AAD	20S	ATLS	jets+$\not{E}_T$, Tstop3, $m_{\tilde{\chi}^0_1}$=0 GeV
> 765	95	[21] AAD	20V	ATLS	same-sign $\ell^\pm\ell^\pm$ + jets, $\tilde{t}_1 \to t\tilde{\chi}^0_2$, $\tilde{\chi}^0_2 \to \tilde{\chi}^\pm_1 W$, $\tilde{\chi}^\pm_1 \to \tilde{\chi}^0_1 W$, $m_{\tilde{\chi}^\pm_1} \sim m_{\tilde{\chi}^0_1}$
>1200	95	[22] SIRUNYAN	20AH	CMS	$\ell^\pm$ + jet + $\not{E}_T$, Tstop1, $m_{\tilde{\chi}^0_1}$ = 0 GeV
>1175	95	[22] SIRUNYAN	20AH	CMS	$\ell^\pm$ + jet + $\not{E}_T$, Tstop1, $m_{\tilde{\chi}^0_1}$ < 425 GeV
none 230–1140	95	[22] SIRUNYAN	20AH	CMS	$\ell^\pm$ + jet + $\not{E}_T$, Tstop2, $m_{\tilde{\chi}^\pm_1} = (m_{\tilde{t}} + m_{\tilde{\chi}^0_1})/2$, $m_{\tilde{\chi}^0_1}$ = 0 GeV
>1100	95	[22] SIRUNYAN	20AH	CMS	$\ell^\pm$ + jet + $\not{E}_T$, Tstop2, $m_{\tilde{\chi}^\pm_1} = (m_{\tilde{t}} + m_{\tilde{\chi}^0_1})/2$, 50 < $m_{\tilde{\chi}^0_1}$ < 425 GeV
>1070	95	[22] SIRUNYAN	20AH	CMS	$\ell^\pm$ + jet + $\not{E}_T$, Tstop8, $m_{\tilde{\chi}^\pm_1} - m_{\tilde{\chi}^0_1}$ = 5 GeV, $m_{\tilde{\chi}^0_1}$ = 0 GeV
>1050	95	[22] SIRUNYAN	20AH	CMS	$\ell^\pm$ + jet + $\not{E}_T$, Tstop8, $m_{\tilde{\chi}^\pm_1} - m_{\tilde{\chi}^0_1}$ = 5 GeV, $m_{\tilde{\chi}^0_1}$ < 350 GeV
> 730	95	[23] SIRUNYAN	20T	CMS	same-sign $\ell^\pm\ell^\pm$ or $\geq 3\ell^\pm$ + jets, Tstop7, $m_{\tilde{t}_1} - m_{\tilde{\chi}^0_1}$ = 175 GeV, $m_{\tilde{t}_1}$ = 200 GeV, $B(\tilde{t}_2 \to \tilde{t}_1 H)$ = 100%
> 890	95	[23] SIRUNYAN	20T	CMS	same-sign $\ell^\pm\ell^\pm$ or $\geq 3\ell^\pm$ + jets, Tstop7, $m_{\tilde{t}_1} - m_{\tilde{\chi}^0_1}$ = 175 GeV, $m_{\tilde{t}_1}$ = 200 GeV, $B(\tilde{t}_2 \to \tilde{t}_1 Z)$ = 100%
> 760	95	[23] SIRUNYAN	20T	CMS	same-sign $\ell^\pm\ell^\pm$ or $\geq 3\ell^\pm$ + jets, Tstop7, $m_{\tilde{t}_1} - m_{\tilde{\chi}^0_1}$ = 175 GeV, $m_{\tilde{t}_1}$ = 200 GeV, $B(\tilde{t}_2 \to \tilde{t}_1 Z) = B(\tilde{t}_2 \to \tilde{t}_1 H)$ = 50%
>1100	95	[24] SIRUNYAN	20U	CMS	$\tau^\pm\tau^\mp$ + b-jets + $\not{E}_T$, Tstop11, $m_{\tilde{\chi}^\pm_1} = 0.5\ (m_{\tilde{t}} + m_{\tilde{\chi}^0_1})$, $m_{\tilde{\tau}} = 0.5\ m_{\tilde{\chi}^\pm_1}$, $m_{\tilde{\chi}^0_1}$ = 0
>1110	95	[25] SIRUNYAN	19AU	CMS	γ + jets + b-jets + $\not{E}_T$, Tstop13, $m_{\tilde{\chi}^0_1}$ = 1 GeV
>1230	95	[25] SIRUNYAN	19AU	CMS	γ + jets + b-jets + $\not{E}_T$, Tstop13, $m_{\tilde{\chi}^0_1}$ = 800 GeV
>1190	95	[26] SIRUNYAN	19CH	CMS	jets+$\not{E}_T$, Tstop1, $m_{\tilde{\chi}^0_1}$= 0 GeV
>1140	95	[27] SIRUNYAN	19S	CMS	1 or 2 ℓ + jets + $\not{E}_T$, Tstop1, $m_{\tilde{\chi}^0_1}$ < 200 GeV
> 208	95	[28] SIRUNYAN	19U	CMS	$e^\pm\mu^\mp$ + $\geq 1b$-jet, Tstop1, $m_{\tilde{t}_1} - m_{\tilde{\chi}^0_1}$= 175 GeV
> 235	95	[28] SIRUNYAN	19U	CMS	$e^\pm\mu^\mp$ + $\geq 1b$-jet, Tstop1, $m_{\tilde{t}_1} - m_{\tilde{\chi}^0_1}$= 182.5 GeV
> 242	95	[28] SIRUNYAN	19U	CMS	$e^\pm\mu^\mp$ + $\geq 1b$-jet, Tstop1, $m_{\tilde{t}_1} - m_{\tilde{\chi}^0_1}$= 167.5 GeV
> 940	95	[29] AABOUD	18AQ	ATLS	1ℓ+jets+$\not{E}_T$, Tstop1, $m_{\tilde{\chi}^0_1}$ = 0 GeV
> 270	95	[30] AABOUD	18AQ	ATLS	1ℓ+jets+$\not{E}_T$, Tstop3, $m_{\tilde{t}} - m_{\tilde{\chi}^0_1}$ = 20 GeV
> 840	95	[31] AABOUD	18AQ	ATLS	1ℓ+jets+$\not{E}_T$, Tstop2, $m_{\tilde{t}} - m_{\tilde{\chi}^\pm_1}$ = 10 GeV
> 500	95	[32] AABOUD	18BV	ATLS	c-jets+$\not{E}_T$, Tstop4, $m_{\tilde{t}} - m_{\tilde{\chi}^0_1}$ < 100 GeV
> 850	95	[33] AABOUD	18BV	ATLS	c-jets+$\not{E}_T$, Tstop4, $m_{\tilde{\chi}^0_1}$ = 0 GeV
> 390	95	[34] AABOUD	18I	ATLS	≥ 1 jets+$\not{E}_T$, Tstop3, $m_{\tilde{t}} \sim m_{\tilde{\chi}^0_1}$
> 430	95	[35] AABOUD	18I	ATLS	≥ 1 jets+$\not{E}_T$, Tstop4, $m_{\tilde{t}} - m_{\tilde{\chi}^0_1}$ = 5 GeV
>1160	95	[36] AABOUD	18Y	ATLS	2ℓ (≥ 1 hadronic τ) + b-jets + $\not{E}_T$, Tstop5, $m_{\tilde{\tau}} \sim 800$ GeV
> 450	95	[37] SIRUNYAN	18AJ	CMS	2ℓ (soft) + $\not{E}_T$, Tstop10, $m_{\tilde{\chi}^\pm_1} = (m_{\tilde{t}} + m_{\tilde{\chi}^0_1})/2$, $m_{\tilde{t}_1} - m_{\tilde{\chi}^0_1}$ = 40 GeV
> 720	95	[38] SIRUNYAN	18AL	CMS	$\geq 3\ell^\pm$ + jets + $\not{E}_T$, Tstop7, $m_{\tilde{t}_1} - m_{\tilde{\chi}^0_1}$ = 175 GeV, $m_{\tilde{t}_1}$ = 200 GeV, $BR(\tilde{t}_2 \to \tilde{t}_1 H)$ = 100%
> 780	95	[38] SIRUNYAN	18AL	CMS	$\geq 3\ell^\pm$ + jets + $\not{E}_T$, Tstop7, $m_{\tilde{t}_1} - m_{\tilde{\chi}^0_1}$ = 175 GeV, $m_{\tilde{t}_1}$ = 200 GeV, $BR(\tilde{t}_2 \to \tilde{t}_1 Z)$ = 100%
> 710	95	[38] SIRUNYAN	18AL	CMS	$\geq 3\ell^\pm$ + jets + $\not{E}_T$, Tstop7, $m_{\tilde{t}_1} - m_{\tilde{\chi}^0_1}$ = 175 GeV, $m_{\tilde{t}_1}$ = 200 GeV, $BR(\tilde{t}_2 \to \tilde{t}_1 Z) = BR(\tilde{t}_2 \to \tilde{t}_1 H)$ = 50%
> 730	95	[39] SIRUNYAN	18AN	CMS	1 or 2 $\gamma + \ell$ + jets, GGM, Tstop12, $m_{\tilde{\chi}^0_1}$ = 150 GeV
> 650	95	[39] SIRUNYAN	18AN	CMS	1 or 2 $\gamma + \ell$ + jets, GGM, Tstop12, $m_{\tilde{\chi}^0_1}$ = 500 GeV
>1000	95	[40] SIRUNYAN	18AY	CMS	jets+$\not{E}_T$, Tstop1, $m_{\tilde{\chi}^0_1}$=0 GeV
> 500	95	[40] SIRUNYAN	18AY	CMS	jets+$\not{E}_T$,Tstop4,$m_{\tilde{\chi}^0_1}$=420 GeV
> 510	95	[41] SIRUNYAN	18B	CMS	jets+$\not{E}_T$, Tstop4, $m_{\tilde{t}} - m_{\tilde{\chi}^0_1}$ = 10 GeV
> 800	95	[42] SIRUNYAN	18C	CMS	$\ell^\pm\ell^\mp$ + b-jets + $\not{E}_T$, Tstop1, $m_{\tilde{\chi}^0_1}$ = 0
> 750	95	[42] SIRUNYAN	18C	CMS	$\ell^\pm\ell^\mp$ + b-jets + $\not{E}_T$, Tstop2, $m_{\tilde{\chi}^\pm_1} = (m_{\tilde{t}} + m_{\tilde{\chi}^0_1})/2$, $m_{\tilde{\chi}^0_1}$ = 0
>1050	95	[42] SIRUNYAN	18C	CMS	Combination of all-hadronic, 1 $\ell^\pm$ and $\ell^\pm\ell^\mp$ searches, Tstop1, $m_{\tilde{\chi}^0_1}$ = 0
>1000	95	[42] SIRUNYAN	18C	CMS	Combination of all-hadronic, 1 $\ell^\pm$ and $\ell^\pm\ell^\mp$ searches, Tstop2, $m_{\tilde{\chi}^\pm_1} = (m_{\tilde{t}} + m_{\tilde{\chi}^0_1})/2$, $m_{\tilde{\chi}^0_1}$ = 0
>1200	95	[42] SIRUNYAN	18C	CMS	$\ell^\pm\ell^\mp$ + b-jets + $\not{E}_T$, Tstop11, $m_{\tilde{\chi}^\pm_1} = 0.5\ (m_{\tilde{t}} + m_{\tilde{\chi}^0_1})$, $m_{\tilde{\ell}} = 0.5\ m_{\tilde{\chi}^\pm_1}$, $m_{\tilde{\chi}^0_1}$ = 0
>1300	95	[42] SIRUNYAN	18C	CMS	$\ell^\pm\ell^\mp$ + b-jets + $\not{E}_T$, Tstop11, $m_{\tilde{\chi}^\pm_1} = 0.5\ (m_{\tilde{t}} + m_{\tilde{\chi}^0_1})$, $m_{\tilde{\ell}} = 0.95\ m_{\tilde{\chi}^\pm_1}$, $m_{\tilde{\chi}^0_1}$ = 0
none 460–1060	95	[42] SIRUNYAN	18C	CMS	$\ell^\pm\ell^\mp$ + b-jets + $\not{E}_T$, Tstop11, $m_{\tilde{\chi}^\pm_1} = 0.5\ (m_{\tilde{t}} + m_{\tilde{\chi}^0_1})$, $m_{\tilde{\ell}} = 0.05\ m_{\tilde{\chi}^\pm_1}$, $m_{\tilde{\chi}^0_1}$ = 0
>1020	95	[43] SIRUNYAN	18D	CMS	top quark (hadronically decaying) + jets + $\not{E}_T$, Tstop1, $m_{\tilde{\chi}^0_1}$ = 0 GeV
> 420	95	[44] SIRUNYAN	18DI	CMS	$\ell^\pm$ + jet + $\not{E}_T$, Tstop3, $m_{\tilde{t}_1} - m_{\tilde{\chi}^0_1}$ = 10 GeV
> 560	95	[44] SIRUNYAN	18DI	CMS	$\ell^\pm$ + jet + $\not{E}_T$, Tstop3, $m_{\tilde{t}_1} - m_{\tilde{\chi}^0_1}$ = 80 GeV
> 540	95	[44] SIRUNYAN	18DI	CMS	$\ell^\pm$, Tstop10, $m_{\tilde{\chi}^\pm_1} = (m_{\tilde{t}} + m_{\tilde{\chi}^0_1})/2$, $m_{\tilde{t}_1} - m_{\tilde{\chi}^0_1}$ = 40 GeV
> 590	95	[44] SIRUNYAN	18DI	CMS	Combination of all-hadronic and 1 $\ell^\pm$ searches, Tstop3, $m_{\tilde{t}_1} - m_{\tilde{\chi}^0_1}$ = 30 GeV
> 670	95	[44] SIRUNYAN	18DI	CMS	Combination of all-hadronic and 1 $\ell^\pm$ searches, Tstop10, $m_{\tilde{\chi}^\pm_1} = (m_{\tilde{t}} + m_{\tilde{\chi}^0_1})/2$, $m_{\tilde{t}_1} - m_{\tilde{\chi}^0_1}$ = 60 GeV
> 450	95	[45] SIRUNYAN	18DN	CMS	$\ell^\pm\ell^\mp$, Tstop1, $m_{\tilde{t}_1} - m_{\tilde{\chi}^0_1} = m_W$
none 225–325	95	[45] SIRUNYAN	18DN	CMS	$\ell^\pm\ell^\mp$, Tstop2, $m_{\tilde{\chi}^\pm_1} = (m_{\tilde{t}} + m_{\tilde{\chi}^0_1})/2$, $m_{\tilde{t}} - m_{\tilde{\chi}^0_1} = 2\ m_W$
none 210–690	95	[45] SIRUNYAN	18DN	CMS	$\ell^\pm\ell^\mp$, Tstop1, $m_{\tilde{\chi}^0_1}$ = 0 GeV
none 250–600	95	[45] SIRUNYAN	18DN	CMS	$\ell^\pm\ell^\mp$, Tstop2, $m_{\tilde{\chi}^\pm_1} = (m_{\tilde{t}} + m_{\tilde{\chi}^0_1})/2$, $m_{\tilde{\chi}^0_1}$ = 0 GeV
> 700	95	[46] AABOUD	17AJ	ATLS	same-sign $\ell^\pm\ell^\pm$ / 3 ℓ + jets + $\not{E}_T$, Tstop11, $m_{\tilde{\chi}^0_2} = m_{\tilde{\chi}^0_1}$ + 100 GeV

See key on page 1227

> 880	95	[47] AABOUD	17AX	ATLS	b-jets+$\not{E}_T$, mixture Tstop1 and Tstop2 with BR=50%, $m_{\widetilde{\chi}^0_1}$ = 0 GeV, $m_{\widetilde{\chi}^\pm_1}$ - $m_{\widetilde{\chi}^0_1}$ = 1 GeV
none 250–1000	95	[48] AABOUD	17AY	ATLS	jets+$\not{E}_T$, Tstop1, $m_{\widetilde{\chi}^0_1}$ = 0 GeV
none 450–850	95	[49] AABOUD	17AY	ATLS	jets+$\not{E}_T$, mixture of Tstop1 and Tstop2 with BR=50%, $m_{\widetilde{\chi}^\pm_1} - m_{\widetilde{\chi}^0_1}$ = 1 GeV
> 720	95	[50] AABOUD	17BE	ATLS	$\ell^\pm\ell^\mp + \not{E}_T$, Tstop1, $m_{\widetilde{\chi}^0_1}$ = 0 GeV
> 400	95	[51] AABOUD	17BE	ATLS	$\ell^\pm\ell^\mp + \not{E}_T$, Tstop3, $m_{\widetilde{t}_1} - m_{\widetilde{\chi}^0_1}$ = 40 GeV
> 430	95	[52] AABOUD	17BE	ATLS	$\ell^\pm\ell^\mp + \not{E}_T$, Tstop1 (offshell t), $m_{\widetilde{t}_1} - m_{\widetilde{\chi}^0_1} \sim m_W$
> 700	95	[53] AABOUD	17BE	ATLS	$\ell^\pm\ell^\mp + \not{E}_T$, Tstop2, $m_{\widetilde{t}_1} - m_{\widetilde{\chi}^\pm_1}$ = 10 GeV, $m_{\widetilde{\chi}^0_1}$ = 0 GeV
> 750	95	[54] KHACHATRY...	17	CMS	jets+$\not{E}_T$,Tstop1,$m_{\widetilde{\chi}^0_1}$=100GeV
none 250–740	95	[55] KHACHATRY...	17AD	CMS	jets+b-jets+$\not{E}_T$, Tstop1, $m_{\widetilde{\chi}^0_1}$ = 0 GeV
> 610	95	[56] KHACHATRY...	17AD	CMS	jets+b-jets+$\not{E}_T$, mixture Tstop1 and Tstop2 with BR=50%, $m_{\widetilde{\chi}^0_1}$ = 60 GeV
> 590	95	[57] KHACHATRY...	17P	CMS	1 or more jets+$\not{E}_T$, Tstop8, $m_{\widetilde{\chi}^\pm_1} - m_{\widetilde{\chi}^0_1}$ = 5 GeV, $m_{\widetilde{\chi}^0_1}$ = 100 GeV
none 280–640	95	[57] KHACHATRY...	17P	CMS	1 or more jets+$\not{E}_T$, Tstop1, $m_{\widetilde{\chi}^0_1}$ = 0 GeV
> 350	95	[57] KHACHATRY...	17P	CMS	1 or more jets+$\not{E}_T$, Tstop4, 10 GeV < $m_{\widetilde{t}_1} - m_{\widetilde{\chi}^0_1}$ < 80 GeV
> 280	95	[57] KHACHATRY...	17P	CMS	1 or more jets+$\not{E}_T$, Tstop3, 10 GeV < $m_{\widetilde{t}_1} - m_{\widetilde{\chi}^0_1}$ < 80 GeV
> 320	95	[57] KHACHATRY...	17P	CMS	1 or more jets+$\not{E}_T$, Tstop9, 10 GeV < $m_{\widetilde{t}_1} - m_{\widetilde{\chi}^0_1}$ < 80 GeV
> 240	95	[58] KHACHATRY...	17S	CMS	jets+$\not{E}_T$, Tstop4, $m_{\widetilde{t}} - m_{\widetilde{\chi}^0_1}$ = 10 GeV
> 225	95	[59] KHACHATRY...	17S	CMS	jets+$\not{E}_T$, Tstop3, $m_{\widetilde{t}} - m_{\widetilde{\chi}^0_1}$ = 10 GeV
> 325	95	[60] KHACHATRY...	17S	CMS	jets+$\not{E}_T$, Tstop2, $m_{\widetilde{\chi}^\pm_1}$ = 0.25 $m_{\widetilde{t}}$ + 0.75 $m_{\widetilde{\chi}^0_1}$, $m_{\widetilde{\chi}^0_1}$ = 225 GeV
> 400	95	[61] KHACHATRY...	17S	CMS	jets+$\not{E}_T$, Tstop2, $m_{\widetilde{\chi}^\pm_1}$ = 0.75 $m_{\widetilde{t}}$ + 0.25 $m_{\widetilde{\chi}^0_1}$, $m_{\widetilde{\chi}^0_1}$ = 0 GeV
> 500	95	[62] KHACHATRY...	17S	CMS	jets+$\not{E}_T$, Tstop1, $m_{\widetilde{\chi}^0_1}$ = 0 GeV
>1120	95	[63] SIRUNYAN	17AS	CMS	1ℓ+jets+$\not{E}_T$, Tstop1, $m_{\widetilde{\chi}^0_1}$ = 0 GeV
>1000	95	[63] SIRUNYAN	17AS	CMS	1ℓ+jets+$\not{E}_T$, Tstop2, $m_{\widetilde{\chi}^\pm_1}$ = $(m_{\widetilde{t}} + m_{\widetilde{\chi}^0_1})/2$, $m_{\widetilde{\chi}^0_1}$ = 0 GeV
> 980	95	[63] SIRUNYAN	17AS	CMS	1ℓ+jets+$\not{E}_T$, Tstop8, $m_{\widetilde{\chi}^\pm_1} - m_{\widetilde{\chi}^0_1}$ = 5 GeV, $m_{\widetilde{\chi}^0_1}$ = 0 GeV
>1040	95	[64] SIRUNYAN	17AT	CMS	jets+$\not{E}_T$, Tstop1, $m_{\widetilde{\chi}^0_1}$ = 0 GeV
> 750	95	[64] SIRUNYAN	17AT	CMS	jets+$\not{E}_T$, Tstop2, $m_{\widetilde{\chi}^\pm_1}$ = $(m_{\widetilde{t}} + m_{\widetilde{\chi}^0_1})/2$, $m_{\widetilde{\chi}^0_1}$ = 0 GeV
> 940	95	[64] SIRUNYAN	17AT	CMS	jets+$\not{E}_T$, Tstop8, $m_{\widetilde{\chi}^\pm_1} - m_{\widetilde{\chi}^0_1}$ = 5 GeV, $m_{\widetilde{\chi}^0_1}$ = 100 GeV
> 540	95	[64] SIRUNYAN	17AT	CMS	jets+$\not{E}_T$, Tstop3, 10 GeV < $m_{\widetilde{t}_1} - m_{\widetilde{\chi}^0_1}$ < 80 GeV
> 480	95	[64] SIRUNYAN	17AT	CMS	jets+$\not{E}_T$, Tstop4, 10 GeV < $m_{\widetilde{t}_1} - m_{\widetilde{\chi}^0_1}$ < 80 GeV
> 530	95	[64] SIRUNYAN	17AT	CMS	jets+$\not{E}_T$, Tstop10, $m_{\widetilde{\chi}^\pm_1}$ = $(m_{\widetilde{t}} + m_{\widetilde{\chi}^0_1})/2$, 10 GeV < $m_{\widetilde{t}_1} - m_{\widetilde{\chi}^0_1}$ < 80 GeV
>1070	95	[65] SIRUNYAN	17AZ	CMS	≥ 1 jets+$\not{E}_T$, Tstop1, $m_{\widetilde{\chi}^0_1}$ = 0 GeV
> 900	95	[65] SIRUNYAN	17AZ	CMS	≥ 1 jets+$\not{E}_T$, Tstop2, $m_{\widetilde{\chi}^\pm_1}$ = $(m_{\widetilde{t}} + m_{\widetilde{\chi}^0_1})/2$, $m_{\widetilde{\chi}^0_1}$ = 0 GeV
>1020	95	[65] SIRUNYAN	17AZ	CMS	≥ 1jets+$\not{E}_T$, Tstop8, $m_{\widetilde{\chi}^\pm_1} - m_{\widetilde{\chi}^0_1}$ = 5 GeV, $m_{\widetilde{\chi}^0_1}$ = 100 GeV
> 540	95	[65] SIRUNYAN	17AZ	CMS	≥ 1 jets+$\not{E}_T$, Tstop4, 10 GeV < $m_{\widetilde{t}_1} - m_{\widetilde{\chi}^0_1}$ < 80 GeV
none 280–830	95	[66] SIRUNYAN	17K	CMS	0, 1 $\ell^\pm$+jets+$\not{E}_T$ (combination), Tstop1, $m_{\widetilde{\chi}^0_1}$ = 0 GeV
> 700	95	[66] SIRUNYAN	17K	CMS	0, 1 $\ell^\pm$+jets+$\not{E}_T$ (combination), Tstop8, $m_{\widetilde{\chi}^\pm_1} - m_{\widetilde{\chi}^0_1}$ = 5 GeV, $m_{\widetilde{\chi}^0_1}$ = 100 GeV
> 160	95	[66] SIRUNYAN	17K	CMS	jets+$\not{E}_T$, Tstop4, 10 < $m_{\widetilde{t}} - m_{\widetilde{\chi}^0_1}$ < 80 GeV
none 230–960	95	[67] SIRUNYAN	17P	CMS	jets+$\not{E}_T$, Tstop1, $m_{\widetilde{\chi}^0_1}$ = 0 GeV
> 990	95	[67] SIRUNYAN	17P	CMS	jets+$\not{E}_T$, Tsbot1, $m_{\widetilde{\chi}^0_1}$ = 0 GeV
> 323	95	[68] AABOUD	16D	ATLS	≥ 1 jet + $\not{E}_T$, Tstop4, $m_{\widetilde{t}_1} - m_{\widetilde{\chi}^0_1}$ = 5 GeV
none, 745–780	95	[69] AABOUD	16J	ATLS	1 $\ell^\pm$ + ≥ 4 jets + $\not{E}_T$, Tstop1, $m_{\widetilde{\chi}^0_1}$ = 0 GeV
> 490–650	95	[70] AAD	16AY	ATLS	2ℓ (including hadronic τ) + $\not{E}_T$, Tstop5, 87 GeV< $m_{\widetilde{\tau}} < m_{\widetilde{t}_1}$
> 700	95	[71] KHACHATRY...	16AV	CMS	1 or 2 $\ell^\pm$+jets+b-jets+$\not{E}_T$, Tstop1, $m_{\widetilde{\chi}^0_1}$ < 250 GeV
> 700	95	[71] KHACHATRY...	16AV	CMS	1 or 2 $\ell^\pm$+jets+b-jets $\not{E}_T$, Tstop2, $m_{\widetilde{\chi}^0_1}$ = 0 GeV, $m_{\widetilde{\chi}^\pm_1}$ = 0.75 $m_{\widetilde{t}_1}$ + 0.25 $m_{\widetilde{\chi}^0_1}$
> 775	95	[72] KHACHATRY...	16BK	CMS	jets+$\not{E}_T$,Tstop1,$m_{\widetilde{\chi}^0_1}$ <200GeV
> 620	95	[72] KHACHATRY...	16BK	CMS	jets+$\not{E}_T$, Tstop2, $m_{\widetilde{\chi}^0_1}$=0 GeV
> 800	95	[73] KHACHATRY...	16BS	CMS	jets+$\not{E}_T$, Tstop1, $m_{\widetilde{\chi}^0_1}$=0 GeV
> 316	95	[74] KHACHATRY...	16Y	CMS	1 or 2 soft $\ell^\pm$ + jets + $\not{E}_T$, Tstop3,$m_{\widetilde{t}} - m_{\widetilde{\chi}^0_1}$=25 GeV
> 250	95	[75] AAD	15CJ	ATLS	B($\widetilde{t} \to c\widetilde{\chi}^0_1$)+B($\widetilde{t} \to b f f' \widetilde{\chi}^0_1$) = 1, $m_{\widetilde{t}} - m_{\widetilde{\chi}^0_1}$ = 10 GeV
> 270	95	[75] AAD	15CJ	ATLS	$\widetilde{t} \to c\widetilde{\chi}^0_1$, $m_{\widetilde{t}} - m_{\widetilde{\chi}^0_1}$=80 GeV
none, 200–700	95	[75] AAD	15CJ	ATLS	$\widetilde{t} \to t\widetilde{\chi}^0_1$, $m_{\widetilde{\chi}^0_1}$ = 0
> 500	95	[75] AAD	15CJ	ATLS	B($\widetilde{t} \to t\widetilde{\chi}^0_1$) + B($\widetilde{t} \to b\widetilde{\chi}^\pm_1$) = 1, $\widetilde{\chi}^\pm_1 \to W^{(*)}\widetilde{\chi}^0_1$, $m_{\widetilde{\chi}^\pm_1}$ = $2m_{\widetilde{\chi}^0_1}$, $m_{\widetilde{\chi}^0_1}$ < 160 GeV
> 600	95	[75] AAD	15CJ	ATLS	$\widetilde{t}_2 \to Z\widetilde{t}_1$, $m_{\widetilde{t}_1} - m_{\widetilde{\chi}^0_1}$ = 180 GeV, $m_{\widetilde{\chi}^0_1}$ = 0
> 600	95	[75] AAD	15CJ	ATLS	$\widetilde{t}_2 \to h\widetilde{t}_1$, $m_{\widetilde{t}_1} - m_{\widetilde{\chi}^0_1}$ = 180 GeV, $m_{\widetilde{\chi}^0_1}$ = 0
none, 172.5–191	95	[76] AAD	15J	ATLS	$\widetilde{t} \to t\widetilde{\chi}^0_1$, $m_{\widetilde{\chi}^0_1}$ = 1 GeV
> 450	95	[77] KHACHATRY...	15AF	CMS	$\widetilde{t} \to t\widetilde{\chi}^0_1$, $m_{\widetilde{\chi}^0_1}$ = 0, $m_{\widetilde{t}} > m_t + m_{\widetilde{\chi}^0_1}$
> 560	95	[78] KHACHATRY...	15AH	CMS	$\widetilde{t} \to t\widetilde{\chi}^0_1$, $m_{\widetilde{\chi}^0_1}$ = 0, $m_{\widetilde{t}} > m_t + m_{\widetilde{\chi}^0_1}$
> 250	95	[79] KHACHATRY...	15AH	CMS	$\widetilde{t} \to c\widetilde{\chi}^0_1$, $m_{\widetilde{t}} - m_{\widetilde{\chi}^0_1}$ <10 GeV
> 730	95	[80] KHACHATRY...	15X	CMS	$\widetilde{t} \to t\widetilde{\chi}^0_1$, $m_{\widetilde{\chi}^0_1}$ = 100 GeV, $m_{\widetilde{t}} > m_t + m_{\widetilde{\chi}^0_1}$
none 400–645	95	[80] KHACHATRY...	15X	CMS	$\widetilde{t} \to t\widetilde{\chi}^0_1$ or $\widetilde{t} \to b\widetilde{\chi}^\pm_1$, $m_{\widetilde{\chi}^0_1}$ = 100 GeV, $m_{\widetilde{\chi}^\pm_1} - m_{\widetilde{\chi}^0_1}$ = 5 GeV
none 270–645	95	[81] AAD	14AJ	ATLS	≥ 4 jets + $\not{E}_T$, $\widetilde{t}_1 \to t\widetilde{\chi}^0_1$, $m_{\widetilde{\chi}^0_1}$ < 30 GeV
none 250–550	95	[81] AAD	14AJ	ATLS	≥ 4 jets + $\not{E}_T$, B($\widetilde{t}_1 \to b\widetilde{\chi}^\pm_1$) = 50 %, $m_{\widetilde{\chi}^\pm_1}$ = 2 $m_{\widetilde{\chi}^0_1}$, $m_{\widetilde{\chi}^0_1}$ < 60 GeV
none 210–640	95	[82] AAD	14BD	ATLS	$\ell^\pm$ + jets + $\not{E}_T$, $\widetilde{t}_1 \to t\widetilde{\chi}^0_1$, $m_{\widetilde{\chi}^0_1}$ = 0 GeV
> 500	95	[82] AAD	14BD	ATLS	$\ell^\pm$ + jets + $\not{E}_T$, $\widetilde{t}_1 \to b\widetilde{\chi}^\pm_1$, $m_{\widetilde{\chi}^\pm_1}$ = 2 $m_{\widetilde{\chi}^0_1}$, 100 GeV < $m_{\widetilde{\chi}^0_1}$ < 150 GeV
none 150–445	95	[83] AAD	14F	ATLS	$\ell^\pm\ell^\mp$ final state, $\widetilde{t}_1 \to b\widetilde{\chi}^\pm_1$, $m_{\widetilde{t}_1} - m_{\widetilde{\chi}^\pm_1}$ = 10 GeV, $m_{\widetilde{\chi}^0_1}$ = 1 GeV

Int. J. Mod. Phys. A 2026.41. Downloaded from www.worldscientific.com
by UNIVERSITY OF CALIFORNIA @ BERKELEY on 09/16/26. Re-use and distribution is strictly not permitted, except for Open Access articles.

none 215–530	95	[83] AAD	14F	ATLS	$\ell^\pm\ell^\mp$ final state, $\widetilde{t}_1 \to t\widetilde{\chi}^0_1$, $m_{\widetilde{\chi}^0_1} = 1$ GeV
> 270	95	[84] AAD	14T	ATLS	$\widetilde{t}_1 \to c\widetilde{\chi}^0_1$, $m_{\widetilde{\chi}^0_1} = 200$ GeV
> 240	95	[84] AAD	14T	ATLS	$\widetilde{t}_1 \to c\widetilde{\chi}^0_1$, $m_{\widetilde{t}_1} - m_{\widetilde{\chi}^0_1} < 85$ GeV
> 255	95	[84] AAD	14T	ATLS	$\widetilde{t}_1 \to b f f' \widetilde{\chi}^0_1$, $m_{\widetilde{t}_1} - m_{\widetilde{\chi}^0_1} \approx m_b$
> 400	95	[85] CHATRCHYAN	14AH	CMS	jets + $\not{E}_T$, $\widetilde{t} \to t\widetilde{\chi}^0_1$ simplified model, $m_{\widetilde{\chi}^0_1} = 50$ GeV
		[86] CHATRCHYAN	14R	CMS	$\geq 3\ell^\pm$, $\widetilde{t} \to (b\widetilde{\chi}^\pm_1/t\widetilde{\chi}^0_1)$, $\widetilde{\chi}^\pm_1 \to (q q'/\ell\nu)\widetilde{\chi}^0_1$, $\widetilde{\chi}^0_1 \to (H/Z)\widetilde{G}$, GMSB, natural higgsino NLSP scenario
• • • We do not use the following data for averages, fits, limits, etc. • • •					
> 850	95	[87] AABOUD	17AF	ATLS	2ℓ+jets+b-jets+$\not{E}_T$, Tstop6, $m_{\widetilde{\chi}^0_1} = 0$
> 800	95	[88] AABOUD	17AF	ATLS	2ℓ+jets+b-jets+$\not{E}_T$, Tstop7 with 100% decays via Z, $m_{\widetilde{\chi}^0_1} = 50$ GeV
> 880	95	[89] AABOUD	17AF	ATLS	2ℓ+jets+b-jets+$\not{E}_T$, Tstop7 with 100% decays via higgs, $m_{\widetilde{\chi}^0_1} = 50$ GeV
		[90] AABOUD	17AY	ATLS	jets+$\not{E}_T$, pMSSM-inspired
> 230		ROLBIECKI	15	THEO	WW xsection, $\widetilde{t}_1 \to bW\widetilde{\chi}^0_1$, $m_{\widetilde{t}_1} \simeq m_b + m_W + m_{\widetilde{\chi}^0_1}$
> 600	95	[91] AAD	14B	ATLS	Z+b $\not{E}_T$, $\widetilde{t}_2 \to Z\widetilde{t}_1$, $\widetilde{t}_1 \to t\widetilde{\chi}^0_1$, $m_{\widetilde{\chi}^0_1} < 200$ GeV
> 540	95	[91] AAD	14B	ATLS	Z+b $\not{E}_T$, $\widetilde{t}_1 \to t\widetilde{\chi}^0_1$, $\widetilde{\chi}^0_1 \to Z\widetilde{G}$, natural GMSB, 100 GeV $< m_{\widetilde{\chi}^0_1} < m_{\widetilde{t}_1} - 10$ GeV
> 360	95	[92] CHATRCHYAN	14U	CMS	$\widetilde{t}_1 \to b\widetilde{\chi}^\pm_1 r$, $\widetilde{\chi}^\pm_1 \to f f' \widetilde{\chi}^0_1$, $\widetilde{\chi}^0_1 \to H\widetilde{G}$ simplified model, $m_{\widetilde{\chi}^\pm_1} - m_{\widetilde{\chi}^0_1} = 5$ GeV,GMSB
> 215	95	CZAKON	14		$\widetilde{t} \to t\chi^0_1$, $m_{\chi^0_1} < 10$ GeV
		[93] KHACHATRY...	14C	CMS	$\widetilde{t}_2 \to H\widetilde{t}_1$ or $\widetilde{t}_2 \to Z\widetilde{t}_1$ simplified model

[1] AAD 25V searched in 139fb^{-1} of pp collisions at $\sqrt{s} = 13$ TeV for evidence of pair-produced charm or top squarks, each decaying into a charm quark and the $\widetilde{\chi}^0_1$. No significant excess above the Standard Model expectations is observed. Limits are set in two RPC SUSY models resulting in a final state with two charm quarks and missing transverse momentum, either in the decay of pair produced top squarks (Tstop4) or of pair-produced charm squarks, see their figure 8. Limits are also shown for a varying branching fraction of the top squark decay either into a top or charm quark and a $\widetilde{\chi}^0_1$ as two-dimensional projections in the plane of the squark mass and assumed branching fraction, shown in figure 9. Limits are also set for up-type scalar leptoquarks coupled to first- or second-generation leptons, see their figure 10.

[2] CHEKHOVSKY 25M searched in 138 fb^{-1} of pp collisions at $\sqrt{s} = 13$ TeV for evidence of SUSY models with compressed mass spectra in events with a high transverse momentum system from initial-state-radiation jets recoiling against a potential sparticle system with significant missing transverse momentum. These events are further categorized based on their lepton multiplicity, jet multiplicity, number of b-tagged jets, and kinematic variables sensitive to the sparticle masses and mass splittings. No significant excess above the Standard Model expectations is observed. The results are interpreted in models of top squark, electroweakino and slepton pair production. Limits are set for top squark pair production in the models Tstop1 and Tstop2, see their Figure 25, and in Tstop4, see their Figure 26. The results are also interpreted in models describing the production of mass-degenerate $\widetilde{\chi}^0_2$ and $\widetilde{\chi}^\pm_1$ with decays $\widetilde{\chi}^0_2 \to Z\widetilde{\chi}^0_1$ and $\widetilde{\chi}^\pm_1 \to W\widetilde{\chi}^0_1$, applying both a wino-like and higgsino-like $\widetilde{\chi}^\pm_1\widetilde{\chi}^0_2$ production cross section, see their Figure 27. Limits are also set for wino-like $\widetilde{\chi}^\pm_1$ pair production, either with $\widetilde{\chi}^\pm_1 \to W\widetilde{\chi}^0_1$ or in the model Tchi1chi1C. This paper also addresses direct slepton production, taking into account pure right-handed, pure left-handed and combined production of either selectrons, smuons, or mass-degenerate sleptons of the first and second generation, see their Figures 30 and 31.

[3] AAD 24AC searched in 140 fb^{-1} of pp collisions at $\sqrt{s} = 13$ TeV for evidence of stop pair production in events with one lepton, multiple jets, and large $\not{E}_T$, using a neural network for the top system reconstruction. The stop analysis is optimised for scenarios with $m_{\widetilde{t}_1} - m_{\widetilde{\chi}^0_1} \sim m_t$. No significant excess above the Standard Model expectations is observed. Limits are set in models for stop pair production, Tstop1 (with the t possibly off-shell), see their figures 10 and 11.

[4] AAD 24AO searched in 139 fb^{-1} of pp collisions at $\sqrt{s} = 13$ TeV for evidence of stop pair production in events with no leptons, jets, b- and c-jets, and large $\not{E}_T$. The search analysis is optimized for events where a top quark and a c quarks are produced in the decay of the stops. No significant excess above the Standard Model expectations is observed. Limits are set on models for stop pair production with equal branching ratio for $\widetilde{t} \to t\widetilde{\chi}^0_1$ and $\widetilde{t} \to c\widetilde{\chi}^0_1$, Tstop9 (but also investigating large mass gaps between $\widetilde{t}$ and $\widetilde{\chi}^0_1$). See their figures 9 and 10.

[5] HAYRAPETYAN 24M searched in 137 fb^{-1} of pp collisions at $\sqrt{s} = 13$ TeV for evidence of wino- and Higgsino-like charginos in final states with one or more disappearing tracks from the decay $\widetilde{\chi}^\pm_1 \to \pi^\pm\widetilde{\chi}^0_1$ where the soft pion is not reconstructed, $\not{E}_T$, and varying numbers of jets, b-tagged jets, electrons, and muons. No significant excess above the Standard Model expectations is observed. Limits are set on the $\widetilde{b}$ mass in the model Tbot1LL for various proper decay lengths $c\tau$ of the $\widetilde{\chi}^\pm_1$ as well as on the $\widetilde{t}$ mass in the model Tstop1LL, see their Fig. 10. Limits are also set in the model Tglu1LL, see their Fig. 11. In addition, limits are set in specific pure wino as well as pure higgsino dark matter models, in which the relationships among the electroweakino masses, the $\widetilde{\chi}^\pm_1$ lifetime, and the $\widetilde{\chi}^\pm_1$ decay width are constrained by radiative corrections that account for a large difference between the LSP mass and the SUSY-breaking scale, see their Fig. 12.

[6] HAYRAPETYAN 23E searched in 137 fb^{-1} of pp collisions at $\sqrt{s} = 13$ TeV for evidence of gluino, top squark and electroweakino pair production in events with at least one photon, multiple jets, and large $\not{E}_T$. No significant excess above the Standard Model expectations is observed. Limits are set in models for strong production, Tglu4D, Tglu4E, Tglu4F and Tstop13, see their figure 9. They also interpret the results in the models for electroweak production, shown in their figure 10. Tchi1n1A assumes wino-like $\widetilde{\chi}^\pm_1\widetilde{\chi}^0_1$ production, while Tchi1chi1A assumes higgsino-like cross sections and includes $\widetilde{\chi}^\pm_1\widetilde{\chi}^\pm_1$, $\widetilde{\chi}^0_1\widetilde{\chi}^0_2$ and $\widetilde{\chi}^0_{1,2}\widetilde{\chi}^\pm_1$ production. For $\widetilde{\chi}^0_1\widetilde{\chi}^0_2$ alone no mass point can be excluded in the model Tchi1chi1A, but in another model for $\widetilde{\chi}^0_1\widetilde{\chi}^0_2$ production, Tn1n2A.

[7] TUMASYAN 23AB searched in 138 fb^{-1} of pp collisions at $\sqrt{s} = 13$ TeV for evidence of top squark pair production in a final state with at least one hadronically decaying tau lepton and large missing transverse momentum. No significant excess above the Standard Model expectations is observed. Limits are set on the mass of $\widetilde{t}$ for the model Tstop16, see their Figure 9. The exclusion limits are not very sensitive to the choice of the $\widetilde{\tau}$ mass parameter, chosen between $0.25 < (m_{\widetilde{\tau}^\pm_1} - m_{\widetilde{\chi}^0_1})/(m_{\widetilde{\chi}^\pm_1} - m_{\widetilde{\chi}^0_1}) < 0.75$ because of the complementary nature of the signal diagrams.

[8] TUMASYAN 23K searched in 138 fb^{-1} of pp collisions at $\sqrt{s} = 13$ TeV for evidence of top squark pair production in events with a high-momentum jet, an electron or muon with low transverse momentum, and significant $\not{E}_T$. No significant excess above the Standard Model expectations is observed. Limits are set on the top squark mass in the simplified model Tstop3 for 10 GeV $< m_{\widetilde{t}} - m_{\widetilde{\chi}^0_1} < 80$ GeV, see their Figure 10.

[9] TUMASYAN 22Q searched in up to 137 fb^{-1} of pp collisions at $\sqrt{s} = 13$ TeV for evidence of electroweakino and top squark pair production with a small mass difference between the produced supersymmetric particles and the lightest neutralino in events with two or three low-momentum leptons and missing transverse momentum. No significant excess above the Standard Model expectations is observed. Limits are set on the mass of $\widetilde{\chi}^0_2$ and $\widetilde{\chi}^\pm_1$ in the model Tchi1n2F, see their Figure 8. Limits are also set in a higgsino simplified model with both $\widetilde{\chi}^0_2\widetilde{\chi}^\pm_1$ and $\widetilde{\chi}^0_2\widetilde{\chi}^0_1$ production, where $\widetilde{\chi}^0_2 \to Z\widetilde{\chi}^0_1$ and $m_{\widetilde{\chi}^\pm_1} = 1/2(m_{\widetilde{\chi}^0_2} + m_{\widetilde{\chi}^0_1})$. A model inspired by the pMSSM is used for further interpretations in the case of a higgsino LSP, see their Figure 9. Limits are also set on the mass of the top squark in the models Tstop2 and Tstop3, see their Figure 10.

[10] AAD 21AW searched in 139 fb^{-1} of pp collisions at $\sqrt{s} = 13$ TeV for pair production of stops in events with one or two hadronically decaying τ leptons, jets, b-jets and $\not{E}_T$. No significant excess above the Standard Model predictions is observed. Limits are set on the $\widetilde{t}_1$ mass as a function of the $\widetilde{\tau}_1$ in the Tstop5 scenario. See their Fig. 8.

[11] AAD 21O searched in 139 fb^{-1} of pp collisions at $\sqrt{s} = 13$ TeV for pair production of top squarks in events with one electron or muon, jets, and large missing transverse momentum. No significant excess above the Standard Model expectations is observed. Limits are set on the top squark mass in the Tstop1 and Tstop3 simplified models and dark matter models, see their Figures 13, 14 and 15.

[12] AAD 21P searched in 139 fb^{-1} of pp collisions at $\sqrt{s} = 13$ TeV for pair production of top squarks in events with two opposite-sign leptons, jets, and large missing transverse momentum. No significant excess above the Standard Model expectations is observed. Limits are set on the top squark mass in the Tstop1, Tstop2, and Tstop3 simplified models, see their Figures 14.

[13] SIRUNYAN 21AD searched in 137 fb^{-1} of pp collisions at $\sqrt{s} = 13$ TeV for supersymmetry in events with multiple jets, no leptons, and large $\not{E}_T$. No significant excess above the Standard Model expectations is observed. Limits are set on the top squark mass in the simplified models Tstop1, Tstop2 with $m_{\widetilde{\chi}^\pm_1} = (m_{\widetilde{t}} + m_{\widetilde{\chi}^0_1})/2$, and a 50:50 mixture of these with $m_{\widetilde{\chi}^\pm_1} - m_{\widetilde{\chi}^0_1} = 5$ GeV, see their Figure 8. Limits are also set on the top squark mass for 10 GeV $< m_{\widetilde{t}} - m_{\widetilde{\chi}^\pm_1} < 80$ GeV in the simplified models Tstop2, Tstop 3, and Tstop4, see their Figure 9. For indirect top squark production, limits are set on the gluino mass in the simplified models Tglu3A, Tglu3C with $m_{\widetilde{t}} - m_{\widetilde{\chi}^0_1} = 20$ GeV, and Tglu3D with $m_{\widetilde{\chi}^\pm_1} - m_{\widetilde{\chi}^0_1} = 5$ GeV, see their Figure 10.

[14] SIRUNYAN 21B searched in 137 fb^{-1} of pp collisions at $\sqrt{s} = 13$ TeV for the pair production of top squarks in events with two oppositely charged leptons (electrons or muons), jets identified as originating from a b-quark and significant $\not{E}_T$. No significant excess above the Standard Model expectations is observed. Limits are set on the stop mass in the Tstop1, Tstop2 and Tstop11 simplified models, see their Figures 6 and 7.

[15] TUMASYAN 21I searched in 137 fb^{-1} of pp collisions at $\sqrt{s} = 13$ TeV for evidence of top squarks in events with at least two jets and large $\not{E}_T$, categorized into events with 0, 1, or 2 leptons. No significant excess above the Standard Model expectations is observed. Limits are set on the top squark mass in the simplified model Tstop1 in the top corridor $\left|m_{\widetilde{t}} - m_{\widetilde{\chi}^0_1} - 175\text{ GeV}\right| < 30$ GeV using dilepton events, see their Figure 7. Limits are also set for a combination of earlier searches with 0, 1, and 2 leptons in the models Tstop1, Tstop2 and a 50:50 mixture of these models, see their Figure 9. The results are interpreted in an alternative signal model of dark matter production via a spin-0 mediator in association with a top quark pair as well.

[16] AABOUD 20 searched in 36.1 fb^{-1} of pp collisions at $\sqrt{s} = 13$ TeV for events containing one electron-muon pair with opposite charge. The search targets a region of parameter space where the kinematics of top squark pair production and top quark pair production is very similar and makes use of the double-differential angular distributions of the leptons. No excess above the Standard Model expectations is observed. Limits are set on the stop mass in the Tstop1 model, see Figures 16 and 17.

Int. J. Mod. Phys. A 2026.41. Downloaded from www.worldscientific.com
by UNIVERSITY OF CALIFORNIA @ BERKELEY on 09/16/26. Re-use and distribution is strictly not permitted, except for Open Access articles.

Int. J. Mod. Phys. A 2026.41. Downloaded from www.worldscientific.com by UNIVERSITY OF CALIFORNIA @ BERKELEY on 09/16/26. Re-use and distribution is strictly not permitted, except for Open Access articles.

[17] AAD 20AS searched in 139 fb^{-1} of pp collisions at $\sqrt{s}$ = 13 TeV for evidence of top squarks in events containing either a pair of jets consistent with SM Higgs boson decay into b-quarks or a same-flavour opposite-sign dilepton pair with an invariant mass consistent with a Z boson. No significant excess over the expected background is observed. Limits at 95% C.L. are set in Tstop6 simplified model. Assuming $m_{\widetilde{\chi}^0_1}$ = 0 GeV, $\widetilde{t}_1$ masses up to 1220 GeV are excluded for $m_{\widetilde{\chi}^0_2}$ around 900 GeV. Limits reduce down to $\widetilde{t}_1$ masses up to 900 GeV for $m_{\widetilde{\chi}^0_2}$=130 GeV. See their Fig. 10. Limits are presented also in case of B($\widetilde{\chi}^0_2 \rightarrow \widetilde{\chi}^0_1 h$) = 0 and 1, see their Fig. 11.

[18] AAD 20AS searched in 139 fb^{-1} of pp collisions at $\sqrt{s}$ = 13 TeV for evidence of top squarks in events containing either a pair of jets consistent with SM Higgs boson decay into b-quarks or a same-flavour opposite-sign dilepton pair with an invariant mass consistent with a Z boson. No significant excess over the expected background is observed. Limits at 95% C.L. are set in simplified model featuring $\widetilde{t}_2$ pair production, $\widetilde{t}_2 \rightarrow \widetilde{t}_1 Z$ and $\widetilde{t}_1 \rightarrow b f f' \widetilde{\chi}^0_1$. Assuming $m_{\widetilde{\chi}^0_1}$ = 300 GeV, and a mass difference between $\widetilde{t}_1$ and $\widetilde{\chi}^0_1$ of 40 GeV, $\widetilde{t}_2$ masses up to 860 GeV are excluded. See their Fig. 12.

[19] AAD 20s searched in 139 fb^{-1} of pp collisions at $\sqrt{s}$ = 13 TeV for events containing multiple jets and large $\not{E}_T$. No significant excess above the Standard Model expectations is observed. Exclusion limits at 95% C.L. are set on top squark masses in the Tstop1 model up to 1250 GeV for lightest neutralino masses below 200 GeV. Additional constraints are set in the case where $m_{\widetilde{t}} - m_{\widetilde{\chi}^0_1} \sim m_t$ for which top squark masses in the range 300–630 GeV are excluded. See their Fig. 13.

[20] AAD 20s searched in 139 fb^{-1} of pp collisions at $\sqrt{s}$ = 13 TeV for events containing multiple jets and large $\not{E}_T$. No significant excess above the Standard Model expectations is observed. Exclusion limits at 95% C.L. are set on top squark masses in the Tstop3 model in the range 300–660 GeV. In case $m_{\widetilde{t}} - m_{\widetilde{\chi}^0_1} \sim$ 5 GeV or above, $m_{\widetilde{t}}$ below 500 GeV are excluded. See their Fig. 13(b).

[21] AAD 20V searched in 139 fb^{-1} of pp collisions at $\sqrt{s}$ = 13 TeV for events with two same-sign charged leptons (electrons or muons) and jets. No significant excess above the Standard Model expectations is observed. Exclusion limits at 95% C.L. are set on the top squark mass up to 765 GeV assuming $\widetilde{t}_1 \rightarrow t\widetilde{\chi}^0_2$ with $\widetilde{\chi}^0_2 \rightarrow \widetilde{\chi}^\pm_1 W$ and $\widetilde{\chi}^\pm_1 \rightarrow \widetilde{\chi}^0_1 W$. Masses of the charginos and lightest neutralinos are set as $m_{\widetilde{\chi}^0_1} = m_{\widetilde{t}_1} - 275$ GeV, $m_{\widetilde{\chi}^0_2} = m_{\widetilde{\chi}^0_1}$ + 100 GeV and $m_{\widetilde{\chi}^\pm_1} \sim m_{\widetilde{\chi}^0_1}$. See their Fig. 8(b).

[22] SIRUNYAN 20AH searched in 137 fb^{-1} of pp collisions at $\sqrt{s}$ = 13 TeV for pair production of top squarks in events with a single isolated electron or muon, multiple jets and large $\not{E}_T$. No significant excess above the Standard Model expectations is observed. Limits are set on the stop mass in the Tstop1, Tstop2 and Tstop8 simplified models, see Figures 6, 7 and 8, respectively.

[23] SIRUNYAN 20T searched in 137 fb^{-1} of pp collisions at $\sqrt{s}$ = 13 TeV for events with at least two jets, and two isolated same-sign or three or more charged leptons (electrons or muons). No significant excess above the Standard Model expectations is observed. Limits are set on the gluino mass in the Tglu3A, Tglu3B, Tglu3C and Tglu3D simplified models, see their Figure 7, and in the Tglu1C and Tglu1B simplified models, see their Figures 8 and 9. Limits are also set on the sbottom mass in the Tsbot2 simplified model, see their Figure 10, and on the stop mass in the Tstop7 simplified model, see their Figure 11. Finally, limits are set on the gluino mass in RPV simplified models where the gluino decays either via $\widetilde{g} \rightarrow q q \overline{q} \overline{q} + e/\mu/\tau$ or via $\widetilde{g} \rightarrow t b s$, see Figure 12.

[24] SIRUNYAN 20U searched in 77.2 fb^{-1} of pp collisions at $\sqrt{s}$ = 13 TeV for the pair production of top squarks in events with two hadronically decaying taus, jets identified as originating from a b-quark and large $\not{E}_T$. No significant excess above the Standard Model expectations is observed. Limits are set on the stop mass in the Tstop11 simplified model assuming the final state leptons are taus. Different values of the scalar tau mass are considered; the impact on the lower bound is negligible.

[25] SIRUNYAN 19AU searched in 35.9 fb^{-1} of pp collisions at $\sqrt{s}$ = 13 TeV for events with at last one photon, jets, some of which are identified as originating from b-quarks, and large $\not{E}_T$. No significant excess above the Standard Model expectations is observed. In the framework of GMSB, limits are set on the gluino mass in the Tglu4C, Tglu4D and Tglu4E simplified models, and on the top squark mass in the Tstop13 simplified model, see their Figure 5.

[26] SIRUNYAN 19CH searched in 137 fb^{-1} of pp collisions at $\sqrt{s}$ = 13 TeV for events containing multiple jets and large $\not{E}_T$. No significant excess above the Standard Model expectations is observed. Limits are set on the gluino mass in the Tglu1A, Tglu1C, Tglu2A and Tglu3A simplified models, see their Figure 13. Limits are also set on squark, sbottom and stop masses in the Tsqk1, Tsbot1, Tstop1 simplified models, see their Figure 14.

[27] SIRUNYAN 19S searched in 35.9 fb^{-1} of pp collisions at $\sqrt{s}$ = 13 TeV for events with zero or one charged leptons, jets and $\not{E}_T$. The razor variables (M_R and R^2) are used to categorize the events. No significant excess above the Standard Model expectations is observed. Limits are set on the gluino mass in the Tglu3A and Tglu3C simplified models, see Figures 22 and 23, and on the stop mass in the Tstop1 simplified model, see their Figure 24.

[28] SIRUNYAN 19U searched in 35.9 fb^{-1} of pp collisions at $\sqrt{s}$ = 13 TeV for events containing one electron-muon pair with opposite charge. The search targets a region of parameter space where the kinematics of top squark pair production and top quark pair production is very similar, due to the mass difference between the top squark and the neutralino being close to the top quark mass. No excess above the Standard Model expectations is observed. Limits are set on the stop mass in the Tstop1 model, with $m_{\widetilde{t}_1} - m_{\widetilde{\chi}^0_1}$ close to m_t, see Figure 5.

[29] AABOUD 18AQ searched in 36.1 fb^{-1} of pp collisions at $\sqrt{s}$ = 13 TeV for top squark pair production in final states with one isolated electron or muon, several energetic jets, and missing transverse momentum. No significant excess over the Standard Model prediction is observed. In case of Tstop1 models, top squark masses up to 940 GeV are excluded assuming $m_{\widetilde{\chi}^0_1}$ = 0 GeV, see their Fig. 20. If the top quark is not on-shell (3-body) decay, exclusions up to 500 GeV are obtained for $m_{\widetilde{\chi}^0_1}$ = 300 GeV. Exclusions as a function of $m_{\widetilde{t}_1} - m_{\widetilde{\chi}^0_1}$ are given in their Fig. 21.

[30] AABOUD 18AQ searched in 36.1 fb^{-1} of pp collisions at $\sqrt{s}$ = 13 TeV for top squark pair production in final states with one isolated electron or muon, several energetic jets, and missing transverse momentum. No significant excess over the Standard Model prediction is observed. In case of Tstop3 models (4-body), top squark masses up to 370 GeV are excluded for $m_{\widetilde{t}} - m_{\widetilde{\chi}^0_1}$ as low as 20 GeV. Top squark masses below 195 GeV are excluded for all $m_{\widetilde{\chi}^0_1}$, see their Fig. 20 and Fig. 21.

[31] AABOUD 18AQ searched in 36.1 fb^{-1} of pp collisions at $\sqrt{s}$ = 13 TeV for top squark pair production in final states with one isolated electron or muon, several energetic jets, and missing transverse momentum. No significant excess over the Standard Model prediction is observed. In case of Tstop2 models, top squark masses up to 840 GeV are excluded for $m_{\widetilde{t}} - m_{\widetilde{\chi}^\pm_1}$ = 10 GeV. See their Fig. 23. Exclusion limits for this decay mode are presented also in the context of Higgsino-LSP phenomenological MSSM models, where $m_{\widetilde{\chi}^\pm_1} - m_{\widetilde{\chi}^0_1}$ = 5 GeV, see their Fig 26.

[32] AABOUD 18BV searched in 36.1 fb^{-1} of pp collisions at $\sqrt{s}$ = 13 TeV for events with at least one jet identified as c-jet, large missing transverse energy and no leptons. Good agreement is observed between the number of events in data and Standard Model predictions. The results are translated into exclusion limits in Tstop4 models. In scenarios with differences of the stop and neutralino masses below 100 GeV, stop masses below 500 GeV are excluded. See their Fig.6 and Fig.7.

[33] AABOUD 18BV searched in 36.1 fb^{-1} of pp collisions at $\sqrt{s}$ = 13 TeV for events with at least one jet identified as c-jet, large missing transverse energy and no leptons. Good agreement is observed between the number of events in data and Standard Model predictions. The results are translated into exclusion limits in Tstop1 models. In scenarios with massless neutralinos, top squark masses below 850 GeV are excluded. See their Fig.6.

[34] AABOUD 18I searched in 36.1 fb^{-1} of pp collisions at $\sqrt{s}$ = 13 TeV for events with at least one jet with a transverse momentum above 250 GeV and no leptons. Good agreement is observed between the number of events in data and Standard Model predictions. The results are translated into exclusion limits in Tstop3 models. Stop masses below 390 GeV are excluded for $m_{\widetilde{t}} - m_{\widetilde{\chi}^0_1} = m_b$. See their Fig.9(b).

[35] AABOUD 18I searched in 36.1 fb^{-1} of pp collisions at $\sqrt{s}$ = 13 TeV for events with at least one jet with a transverse momentum above 250 GeV and no leptons. Good agreement is observed between the number of events in data and Standard Model predictions. The results are translated into exclusion limits in Tstop4 models. In scenarios with differences of the stop and neutralino masses around 5 GeV, stop masses below 430 GeV are excluded. See their Fig.9(a).

[36] AABOUD 18Y searched in 36.1 fb^{-1} of pp collisions at $\sqrt{s}$ = 13 TeV for direct pair production of top squarks in final states with two tau leptons, b-jets, and missing transverse momentum. At least one hadronic τ is required. No significant deviation from the SM predictions is observed in the data. The analysis results are interpreted in Tstop5 models with a nearly massless gravitino. Top squark masses up to 1.16 TeV and tau slepton masses up to 1 TeV are excluded, see their Fig 7.

[37] SIRUNYAN 18AJ searched in 35.9 fb^{-1} of pp collisions at $\sqrt{s}$ = 13 TeV for events containing two low-momentum, oppositely charged leptons (electrons or muons) and $\not{E}_T$. No excess over the expected background is observed. Limits are derived on the wino mass in the Tchi1n2F simplified model, see their Figure 5. Limits are also set on the stop mass in the Tstop10 simplified model, see their Figure 6. Finally, limits are set on the Higgsino mass in the Tchi1n2G simplified model, see Figure 8 and in the pMSSM, see Figure 7.

[38] SIRUNYAN 18AL searched in 35.9 fb^{-1} of pp collisions at $\sqrt{s}$ = 13 TeV for events with at least three charged leptons, in any combination of electrons and muons, jets and significant $\not{E}_T$. No significant excess above the Standard Model expectations is observed. Limits are set on the gluino mass in the Tglu3A and Tglu1C simplified models, see their Figure 5. Limits are also set on the sbottom mass in the Tsbot2 simplified model, see their Figure 6, and on the stop mass in the Tstop7 simplified model, see their Figure 7.

[39] SIRUNYAN 18AN searched in 19.7 fb^{-1} of pp collisions at $\sqrt{s}$ = 8 TeV for events containing one or two photons and a pair of top quarks from the decay of a pair of top squark in a natural gauge-mediated scenario. The final state consists of a lepton (electron or muon), jets and one or two photons. No significant excess above the Standard Model expectations is observed. Limits are set on the stop mass in the Tstop12 simplified model, see their Figure 6.

[40] SIRUNYAN 18AY searched in 35.9 fb^{-1} of pp collisions at $\sqrt{s}$ = 13 TeV for events containing one or more jets and significant $\not{E}_T$. No significant excess above the Standard Model expectations is observed. Limits are set on the gluino mass in the Tglu1A, Tglu2A and Tglu3A simplified models, see their Figure 3. Limits are also set on squark, sbottom and stop masses in the Tsqk1, Tsbot1, Tstop1 and Tstop4 simplified models, see their Figure 3. Finally, limits are set on long-lived gluino masses in a Tglu1A simplified model where the gluino is metastable or long-lived with proper decay lengths in the range 10^{-3} mm $< c\tau < 10^5$ mm, see their Figure 4.

[41] SIRUNYAN 18B searched in 35.9 fb^{-1} of pp collisions at $\sqrt{s}$ = 13 TeV for the pair production of third-generation squarks in events with jets and large $\not{E}_T$. No significant excess above the Standard Model expectations is observed. Limits are set on the sbottom mass in the Tsbot1 simplified model, see their Figure 5, and on the stop mass in the Tstop4 simplified model, see their Figure 6.

[42] SIRUNYAN 18C searched in 35.9 fb^{-1} of pp collisions at $\sqrt{s}$ = 13 TeV for the pair production of top squarks in events with two oppositely charged leptons (electrons or muons), jets identified as originating from a b-quark and large $\not{E}_T$. No significant excess above the Standard Model expectations is observed. Limits are set on the stop mass in the Tstop1, Tstop2 and Tstop11 simplified models, see their Figures 11 and 12. The Tstop1 and Tstop2 results are combined with complementary searches in the all-hadronic and single lepton channels, see their Figures 13 and 14.

[43] SIRUNYAN 18D searched in 35.9 fb^{-1} of pp collisions at $\sqrt{s}$ = 13 TeV for events containing identified hadronically decaying top quarks, no leptons, and $\not{E}_T$. No significant excess above the Standard Model expectations is observed. Limits are set on the stop mass in the Tstop1 simplified model, see their Figure 8, and on the gluino mass in the Tglu3A, Tglu3B, Tglu3C and Tglu3E simplified models, see their Figure 9.

[44] SIRUNYAN 18DI searched in 35.9 fb^{-1} of pp collisions at $\sqrt{s}$ = 13 TeV for pair production of top squarks in events with a low transverse momentum lepton (electron or muon), a high-momentum jet and significant missing transverse momentum. No significant excess above the Standard Model expectations is observed. Limits are set on the stop mass in the Tstop3 and Tstop10 simplified models, see their Figures 7 and 8. A combination of this search with the all-hadronic search is presented in Figure 9.

[45] SIRUNYAN 18DN searched in 35.9 fb^{-1} of pp collisions at $\sqrt{s}$ = 13 TeV for direct electroweak production of charginos and for pair production of top squarks in events with two leptons (electrons or muons) of the opposite electric charge. No significant excess above the Standard Model expectations is observed. Limits are set on the chargino mass in the Tchi1chi1C and Tchi1chi1E simplified models, see their Figure 8. Limits are also set on the stop mass in the Tstop1 and Tstop2 simplified models, see their Figure 9.

Int. J. Mod. Phys. A 2026.41. Downloaded from www.worldscientific.com
by UNIVERSITY OF CALIFORNIA @ BERKELEY on 09/16/26. Re-use and distribution is strictly not permitted, except for Open Access articles.

[46] AABOUD 17AJ searched in 36.1 fb^{-1} of pp collisions at $\sqrt{s}$ = 13 TeV for events with two same-sign or three leptons, jets and large missing transverse momentum. No significant excess above the Standard Model expectations is observed. Limits up to 700 GeV are set on the top squark mass in Tstop11 simplified models, assuming $m_{\widetilde{\chi}^0_1} = m_{\widetilde{t}} - 275$ GeV and $m_{\widetilde{\chi}^0_2} = m_{\widetilde{\chi}^0_1} + 100$ GeV. See their Figure 4(e).

[47] AABOUD 17AX searched in 36 fb^{-1} of pp collisions at $\sqrt{s}$ = 13 TeV for events containing two jets identified as originating from b-quarks and large missing transverse momentum, with or without leptons. No excess of events above the expected level of Standard Model background was found. Exclusion limits at 95% C.L. are set on the masses of top squarks. Assuming 50% BR for Tstop1 and Tstop2 simplified models, a $\widetilde{t}_1$ mass below 880 (860) GeV is excluded for $m_{\widetilde{\chi}^0_1} = 0$ (<250) GeV. See their Fig. 7(b).

[48] AABOUD 17AY searched in 36.1 fb^{-1} of pp collisions at $\sqrt{s}$ = 13 TeV for events with at least four jets and large missing transverse momentum. No significant excess above the Standard Model expectations is observed. Limits in the range 250–1000 GeV are set on the top squark mass in Tstop1 simplified models. For the first time, additional constraints are set for the region $m_{\widetilde{t}_1} \sim m_t + m_{\widetilde{\chi}^0_1}$, with exclusion of the $\widetilde{t}_1$ mass range 235–590 GeV. See their Figure 8.

[49] AABOUD 17AY searched in 36.1 fb^{-1} of pp collisions at $\sqrt{s}$ = 13 TeV for events with at least four jets and large missing transverse momentum. No significant excess above the Standard Model expectations is observed. Limits in the range 450–850 GeV are set on the top squark mass in a mixture of Tstop1 and Tstop2 simplified models with BR=50% and assuming $m_{\widetilde{\chi}^\pm_1} - m_{\widetilde{\chi}^0_1} = 1$ GeV and $m_{\chi^0_1} < 240$ GeV. Constraints are given for various values of the BR. See their Figure 9.

[50] AABOUD 17BE searched in 36.1 fb^{-1} of pp collisions at $\sqrt{s}$ = 13 TeV for events with two opposite-charge leptons (electrons and muons) and large missing transverse momentum. No significant excess above the Standard Model expectations is observed. Limits up to 720 GeV are set on the top squark mass in Tstop1 simplified models, assuming massless neutralinos. See their Figure 9 (2-body area).

[51] AABOUD 17BE searched in 36.1 fb^{-1} of pp collisions at $\sqrt{s}$ = 13 TeV for events with two opposite-charge leptons (electrons and muons) and large missing transverse momentum. No significant excess above the Standard Model expectations is observed. Limits up to 400 GeV are set on the top squark mass in Tstop3 simplified models, assuming $m_{\widetilde{t}_1} - m_{\widetilde{\chi}^0_1}$ = 40 GeV. See their Figure 9 (4-body area).

[52] AABOUD 17BE searched in 36.1 fb^{-1} of pp collisions at $\sqrt{s}$ = 13 TeV for events with two opposite-charge leptons (electrons and muons) and large missing transverse momentum. No significant excess above the Standard Model expectations is observed. Limits up to 430 GeV are set on the top squark mass in Tstop1 simplified models where top quarks are offshell, assuming $m_{\widetilde{t}_1} - m_{\widetilde{\chi}^0_1}$ close to the W mass. See their Figure 9 (3-body area).

[53] AABOUD 17BE searched in 36.1 fb^{-1} of pp collisions at $\sqrt{s}$ = 13 TeV for events with two opposite-charge leptons (electrons and muons) and large missing transverse momentum. No significant excess above the Standard Model expectations is observed. Limits up to 700 GeV are set on the top squark mass in Tstop2 simplified models, assuming $m_{\widetilde{t}_1} - m_{\widetilde{\chi}^\pm_1} = 10$ GeV and massless neutralinos. See their Figure 10.

[54] KHACHATRYAN 17 searched in 2.3 fb^{-1} of pp collisions at $\sqrt{s}$ = 13 TeV for events containing four or more jets, no more than one lepton, and missing transverse momentum, using the razor variables (M_R and R^2) to discriminate between signal and background processes. No evidence for an excess over the expected background is observed. Limits are derived on the stop mass in the Tstop1 simplified model, see Fig. 17.

[55] KHACHATRYAN 17AD searched in 2.3 fb^{-1} of pp collisions at $\sqrt{s}$ = 13 TeV for events containing at least four jets (including b-jets), missing transverse momentum and tagged top quarks. No evidence for an excess over the expected background is observed. Top squark masses in the range 250–740 GeV and neutralino masses up to 240 GeV are excluded at 95% C.L. See Fig. 12.

[56] KHACHATRYAN 17AD searched in 2.3 fb^{-1} of pp collisions at $\sqrt{s}$ = 13 TeV for events containing at least four jets (including b-jets), missing transverse momentum and tagged top quarks. No evidence for an excess over the expected background is observed. Limits are derived on the $\widetilde{t}$ mass in simplified models that are a mixture of Tstop1 and Tstop2 with branching fractions 50% for each of the two decay modes: top squark masses of up to 610 GeV and neutralino masses up to 190 GeV are excluded at 95% C.L. The $\widetilde{\chi}^\pm_1$ and the $\widetilde{\chi}^0_1$ are assumed to be nearly degenerate in mass, with a 5 GeV difference between their masses. See Fig. 12.

[57] KHACHATRYAN 17P searched in 2.3 fb^{-1} of pp collisions at $\sqrt{s}$ = 13 TeV for events with one or more jets and large $\not{E}_T$. No significant excess above the Standard Model expectations is observed. Limits are set on the gluino mass in the Tglu1A, Tglu2A, Tglu3A, Tglu3B, Tglu3C and Tglu3D simplified models, see their Figures 7 and 8. Limits are also set on the squark mass in the Tsqk1 simplified model, see their Fig. 7, and on the sbottom mass in the Tsbot1 simplified model, see Fig. 8. Finally, limits are set on the stop mass in the Tstop1, Tstop3, Tstop4, Tstop6 and Tstop7 simplified models, see Fig. 8.

[58] KHACHATRYAN 17S searched in 18.5 fb^{-1} of pp collisions at $\sqrt{s}$ = 8 TeV for events containing multiple jets and missing transverse momentum, using the α_T variable to discriminate between signal and background processes. No evidence for an excess over the expected background is observed. Limits are derived on the stop mass in the Tstop4 model: for $\Delta m = m_{\widetilde{t}} - m_{\widetilde{\chi}^0_1}$ equal to 10 and 80 GeV, masses of stop below 240 and 260 GeV are excluded, respectively. See their Fig.3.

[59] KHACHATRYAN 17S searched in 18.5 fb^{-1} of pp collisions at $\sqrt{s}$ = 8 TeV for events containing multiple jets and missing transverse momentum, using the α_T variable to discriminate between signal and background processes. No evidence for an excess over the expected background is observed. Limits are derived on the stop mass in the Tstop3 model: for $\Delta m = m_{\widetilde{t}} - m_{\widetilde{\chi}^0_1}$ equal to 10 and 80 GeV, masses of stop below 225 and 130 GeV are excluded, respectively. See their Fig.3.

[60] KHACHATRYAN 17S searched in 18.5 fb^{-1} of pp collisions at $\sqrt{s}$ = 8 TeV for events containing multiple jets and missing transverse momentum, using the α_T variable to discriminate between signal and background processes. No evidence for an excess over the expected background is observed. Limits are derived on the stop mass in the Tstop2 model: assuming $m_{\widetilde{\chi}^\pm_1} = 0.25\ m_{\widetilde{t}} + 0.75\ m_{\widetilde{\chi}^0_1}$, masses of stop up to 325 GeV and masses of the neutralino up to 225 GeV are excluded. See their Fig.3.

[61] KHACHATRYAN 17S searched in 18.5 fb^{-1} of pp collisions at $\sqrt{s}$ = 8 TeV for events containing multiple jets and missing transverse momentum, using the α_T variable to discriminate between signal and background processes. No evidence for an excess over the expected background is observed. Limits are derived on the stop mass in the Tstop2 model: assuming $m_{\widetilde{\chi}^\pm_1} = 0.75\ m_{\widetilde{t}} + 0.25\ m_{\widetilde{\chi}^0_1}$, masses of stop up to 400 GeV are excluded for low neutralino masses. See their Fig.3.

[62] KHACHATRYAN 17S searched in 18.5 fb^{-1} of pp collisions at $\sqrt{s}$ = 8 TeV for events containing multiple jets and missing transverse momentum, using the α_T variable to discriminate between signal and background processes. No evidence for an excess over the expected background is observed. Limits are derived on the stop mass in the Tstop1 model: assuming masses of stop up to 500 GeV and masses of the neutralino up to 105 GeV are excluded. See their Fig.3.

[63] SIRUNYAN 17AS searched in 35.9 fb^{-1} of pp collisions at $\sqrt{s}$ = 13 TeV for events with a single lepton (electron or muon), jets, and large $\not{E}_T$. No significant excess above the Standard Model expectations is observed. Limits are set on the stop mass in the Tstop1, Tstop2 and Tstop8 simplified models, see their Figures 5, 6 and 7.

[64] SIRUNYAN 17AT searched in 35.9 fb^{-1} of pp collisions at $\sqrt{s}$ = 13 TeV for direct production of top squarks in events with jets and large $\not{E}_T$. No significant excess above the Standard Model expectations is observed. Limits are set on the stop mass in the Tstop1, Tstop2 , Tstop3, Tstop4, Tstop8 and Tstop10 simplified models, see their Figures 9 to 14.

[65] SIRUNYAN 17AZ searched in 35.9 fb^{-1} of pp collisions at $\sqrt{s}$ = 13 TeV for events with one or more jets and large $\not{E}_T$. No significant excess above the Standard Model expectations is observed. Limits are set on the gluino mass in the Tglu1A, Tglu2A, Tglu3A simplified models, see their Figures 6. Limits are also set on the squark mass in the Tsqk1 simplified model (for single light squark and for 8 degenerate light squarks), on the sbottom mass in the Tsbot1 simplified model and on the stop mass in the Tstop1 simplified model, see their Fig. 7. Finally, limits are set on the stop mass in the Tstop2, Tstop4 and Tstop8 simplified models, see Fig. 8.

[66] SIRUNYAN 17K searched in 2.3 fb^{-1} of pp collisions at $\sqrt{s}$ = 13 TeV for direct production of stop or sbottom pairs in events with multiple jets and significant $\not{E}_T$. A second search also requires an isolated lepton and is combined with the all-hadronic search. No significant excess above the Standard Model expectations is observed. Limits are set on the stop mass in the Tstop1, Tstop8 and Tstop4 simplified models, see their Figures 7, 8 and 9 (for the Tstop4 limits, only the results of the all-hadronic search are used). Limits are also set on the sbottom mass in the Tsbot1 simplified model, see Fig. 10 (also here, only the results of the all-hadronic search are used).

[67] SIRUNYAN 17P searched in 35.9 fb^{-1} of pp collisions at $\sqrt{s}$ = 13 TeV for events with multiple jets and large $\not{E}_T$. No significant excess above the Standard Model expectations is observed. Limits are set on the gluino mass in the Tglu1A, Tglu1C, Tglu2A, Tglu3A and Tglu3D simplified models, see their Fig. 12. Limits are also set on the squark mass in the Tsqk1 simplified model, on the stop mass in the Tstop1 simplified model, and on the sbottom mass in the Tsbot1 simplified model, see Fig. 13.

[68] AABOUD 16D searched in 3.2 fb^{-1} of pp collisions at $\sqrt{s}$ = 13 TeV in events with an energetic jet and large missing transverse momentum. The results are interpreted as 95% C.L. limits on mass of stop decaying into a charm-quark and the lightest neutralino in scenarios with $m_{\widetilde{t}_1} - m_{\widetilde{\chi}^0_1}$ between 5 and 20 GeV. See their Fig. 5.

[69] AABOUD 16J searched in 3.2 fb^{-1} of pp collisions at $\sqrt{s}$ = 13 TeV in final states with one isolated electron or muon, jets, and missing transverse momentum. For the direct stop pair production model where the stop decays via top and lightest neutralino, the results exclude at 95% C.L. stop masses between 745 GeV and 780 GeV for a massless $\widetilde{\chi}^0_1$. See their Fig. 8.

[70] AAD 16AY searched in 20 fb^{-1} of pp collisions at $\sqrt{s}$ = 8 TeV for events with either two hadronically decaying tau leptons, one hadronically decaying tau and one light lepton, or two light leptons. No significant excess over the Standard Model expectation is found. Exclusion limits at 95% C.L. on the mass of top squarks decaying via $\widetilde{\tau}$ to a nearly massless gravitino are placed depending on $m_{\widetilde{\tau}}$ which is ranging from the 87 GeV LEP limit to $m_{\widetilde{t}_1}$. See their Figs. 9 and 10.

[71] KHACHATRYAN 16AV searched in 19.7 fb^{-1} of pp collisions at $\sqrt{s}$ = 8 TeV for events with one or two isolated leptons, hadronic jets, b-jets and $\not{E}_T$. No significant excess above the Standard Model expectations is observed. Limits are set on the stop mass in the Tstop1 and Tstop2 simplified models, see Fig. 11.

[72] KHACHATRYAN 16BK searched in 18.9 fb^{-1} of pp collisions at $\sqrt{s}$ = 8 TeV for events with hadronic jets and $\not{E}_T$. No significant excess above the Standard Model expectations is observed. Limits are set on the stop mass in the Tstop1 and Tstop2 simplified models, see Fig. 16.

[73] KHACHATRYAN 16BS searched in 2.3 fb^{-1} of pp collisions at $\sqrt{s}$ = 13 TeV for events with at least one energetic jet , no isolated leptons, and significant $\not{E}_T$, using the transverse mass variable M_{T2} to discriminate between signal and background processes. No significant excess above the Standard Model expectations is observed. Limits are set on the stop mass in the Tstop1 simplified model, see Fig. 11 and Table 3.

[74] KHACHATRYAN 16Y searched in 19.7 fb^{-1} of pp collisions at $\sqrt{s}$ = 8 TeV for events with one or two soft isolated leptons, hadronic jets, and $\not{E}_T$. No significant excess above the Standard Model expectations is observed. Limits are set on the stop mass in the Tstop3 simplified model, see Fig. 3.

[75] AAD 15CJ searched in 20 fb^{-1} of pp collisions at $\sqrt{s}$ = 8 TeV for evidence of third generation squarks by combining a large number of searches covering various final states. Stop decays with and without charginos in the decay chain are considered and summaries of all ATLAS Run 1 searches for direct stop production can be found in Fig. 4 (no intermediate charginos) and Fig. 7 (intermediate charginos). Limits are set on stop masses in compressed mass regions regions, with B($\widetilde{t} \rightarrow c\widetilde{\chi}^0_1$) + B($\widetilde{t} \rightarrow bff'\widetilde{\chi}^0_1$) = 1, see Fig. 5. Limits are also set on stop masses assuming that both the decay $\widetilde{t} \rightarrow t\widetilde{\chi}^0_1$ and $\widetilde{t} \rightarrow b\widetilde{\chi}^\pm_1$ are possible, with both their branching rations summing up to 1, assuming $\widetilde{\chi}^\pm_1 \rightarrow W^{(*)}\widetilde{\chi}^0_1$ and $m_{\widetilde{\chi}^\pm_1} = 2\ m_{\widetilde{\chi}^0_1}$, see Fig. 6. Limits on the mass of the next-to-lightest stop $\widetilde{t}_2$, decaying either to $Z\widetilde{t}_1$, $h\widetilde{t}_1$ or $t\widetilde{\chi}^0_1$, are also presented, see Figs. 9 and 10.Interpretations in the pMSSM are also discussed, see Figs 13–15.

[76] AAD 15J interpreted the measurement of spin correlations in $t\overline{t}$ production using 20.3 fb^{-1} of pp collisions at $\sqrt{s}$ = 8 TeV in exclusion limits on the pair production of light $\widetilde{t}_1$ squarks with masses similar to the top quark mass. The $\widetilde{t}_1$ is assumed to decay through $\widetilde{t}_1 \rightarrow t\widetilde{\chi}^0_1$ with predominantly right-handed top and a 100% branching ratio. The data are found to be consistent with the Standard Model expectations and masses between the top quark mass and 191 GeV are excluded, see their Fig. 2

[77] KHACHATRYAN 15AF searched in 19.5 fb^{-1} of pp collisions at $\sqrt{s}$ = 8 TeV for events with at least two energetic jets and significant $\not{E}_T$, using the transverse mass variable

Int. J. Mod. Phys. A 2026.41. Downloaded from www.worldscientific.com
by UNIVERSITY OF CALIFORNIA @ BERKELEY on 09/16/26. Re-use and distribution is strictly not permitted, except for Open Access articles.

M_{T2} to discriminate between signal and background processes. No significant excess above the Standard Model expectations is observed. Limits are set on the stop mass in simplified models where the decay $\tilde{t} \rightarrow t\tilde{\chi}^0_1$ takes place with a branching ratio of 100%, see Fig. 12. See also Table 5. Exclusions in the CMSSM, assuming $\tan\beta = 30$, $A_0 = -2\max(m_0, m_{1/2})$ and $\mu > 0$, are also presented, see Fig. 15.

[78] KHACHATRYAN 15AH searched in 19.4 or 19.7 fb^{-1} of pp collisions at $\sqrt{s} = 8$ TeV for events containing either a fully reconstructed top quark, or events containing dijets requiring one or both jets to originate from b-quarks, or events containing a mono-jet. No significant excess above the Standard Model expectations is observed. Limits are set on the stop mass in simplified models where the decay $\tilde{t} \rightarrow t\tilde{\chi}^0_1$ takes place with a branching ratio of 100%, see Fig. 9. Limits are also set in simplified models where the decays $\tilde{t} \rightarrow t\tilde{\chi}^0_1$ and $\tilde{t} \rightarrow b\tilde{\chi}^\pm_1$, with $m_{\tilde{\chi}^\pm_1} - m_{\tilde{\chi}^0_1} = 5$ GeV, each take place with a branching ratio of 50%, see Fig. 10, or with other fractions, see Fig. 11. Finally, limits are set in a simplified model where the decay $\tilde{t} \rightarrow c\tilde{\chi}^0_1$ takes place with a branching ratio of 100%, see Figs. 9, 10 and 11.

[79] KHACHATRYAN 15AH searched in 19.4 or 19.7 fb^{-1} of pp collisions at $\sqrt{s} = 8$ TeV for events containing either a fully reconstructed top quark, or events containing dijets requiring one or both jets to originate from b-quarks, or events containing a mono-jet. No significant excess above the Standard Model expectations is observed. Limits are set on the stop mass in simplified models where the decay $\tilde{t} \rightarrow t\tilde{\chi}^0_1$ takes place with a branching ratio of 100%, see Fig. 9. Limits are also set in simplified models where the decays $\tilde{t} \rightarrow t\tilde{\chi}^0_1$ and $\tilde{t} \rightarrow b\tilde{\chi}^\pm_1$, with $m_{\tilde{\chi}^\pm_1} - m_{\tilde{\chi}^0_1} = 5$ GeV, each take place with a branching ratio of 50%, see Fig. 10, or with other fractions, see Fig. 11. Finally, limits are set in a simplified model where the decay $\tilde{t} \rightarrow c\tilde{\chi}^0_1$ takes place with a branching ratio of 100%, see Figs. 9, 10, and 11.

[80] KHACHATRYAN 15X searched in 19.3 fb^{-1} of pp collisions at $\sqrt{s} = 8$ TeV for events with at least two energetic jets, at least one of which is required to originate from a b quark, possibly a lepton, and significant $\not{E}_T$, using the razor variables (M_R and R^2) to discriminate between signal and background processes. No significant excess above the Standard Model expectations is observed. Limits are set on the stop mass in simplified models where the decay $\tilde{t} \rightarrow t\tilde{\chi}^0_1$ and the decay $\tilde{t} \rightarrow b\tilde{\chi}^\pm_1$, with $m_{\tilde{\chi}^\pm_1} - m_{\tilde{\chi}^0_1} = 5$ GeV, take place with branching ratios varying between 0 and 100%, see Figs. 15, 16 and 17.

[81] AAD 14AJ searched in 20.1 fb^{-1} of pp collisions at $\sqrt{s} = 8$ TeV for events containing four or more jets and large missing transverse momentum. No excess of events above the expected level of Standard Model background was found. Exclusion limits at 95% C.L. are set on the masses of third-generation squarks in simplified models which either assume that the decay $\tilde{t}_1 \rightarrow t\tilde{\chi}^0_1$ takes place 100% of the time, see Fig. 8, or that this decay takes place 50% of the time, while the decay $\tilde{t}_1 \rightarrow b\tilde{\chi}^\pm_1$ takes place the other 50% of the time, see Fig. 9.

[82] AAD 14BD searched in 20 fb^{-1} of pp collisions at $\sqrt{s} = 8$ TeV for events containing one isolated lepton, jets and large missing transverse momentum. No excess of events above the expected level of Standard Model background was found. Exclusion limits at 95% C.L. are set on the masses of third-generation squarks in simplified models which either assume that the decay $\tilde{t}_1 \rightarrow t\tilde{\chi}^0_1$ takes place 100% of the time, see Fig. 15, or the decay $\tilde{t}_1 \rightarrow b\tilde{\chi}^\pm_1$ takes place 100% of the time, see Fig. 16–22. For the mixed decay scenario, see Fig. 23.

[83] AAD 14F searched in 20.3 fb^{-1} of pp collisions at $\sqrt{s} = 8$ TeV for events containing two leptons (e or μ), and possibly jets and missing transverse momentum. No excess of events above the expected level of Standard Model background was found. Exclusion limits at 95% C.L. are set on the masses of third-generation squarks in simplified models which either assume that the decay $\tilde{t}_1 \rightarrow b\tilde{\chi}^\pm_1$ takes place 100% of the time, see Figs. 14–17 and 20, or that the decay $\tilde{t}_1 \rightarrow t\tilde{\chi}^0_1$ takes place 100% of the time, see Figs. 18 and 19.

[84] AAD 14T searched in 20.3 fb^{-1} of pp collisions at $\sqrt{s} = 8$ TeV for monojet-like and c-tagged events. No excess of events above the expected level of Standard Model background was found. Exclusion limits at 95% C.L. are set on the masses of third-generation squarks in simplified models which assume that the decay $\tilde{t}_1 \rightarrow c\tilde{\chi}^0_1$ takes place 100% of the time, see Fig. 9 and 10. The results of the monojet-like analysis are also interpreted in terms of stop pair production in the four-body decay $\tilde{t}_1 \rightarrow b f f' \tilde{\chi}^0_1$, see Fig. 11.

[85] CHATRCHYAN 14AH searched in 4.7 fb^{-1} of pp collisions at $\sqrt{s} = 7$ TeV for events with at least two energetic jets and significant $\not{E}_T$, using the razor variables (M_R and R^2) to discriminate between signal and background processes. A second analysis requires at least one of the jets to be originating from a b-quark. No significant excess above the Standard Model expectations is observed. Limits are set on sbottom masses in simplified models where the decay $\tilde{t} \rightarrow t\tilde{\chi}^0_1$ takes place with a branching ratio of 100%, see Figs. 28 and 29. Exclusions in the CMSSM, assuming $\tan\beta = 10$, $A_0 = 0$ and $\mu > 0$, are also presented, see Fig. 26.

[86] CHATRCHYAN 14R searched in 19.5 fb^{-1} of pp collisions at $\sqrt{s} = 8$ TeV for events with at least three leptons (electrons, muons, taus) in the final state. No significant excess above the Standard Model expectations is observed. Limits are set on the stop mass in a natural higgsino NLSP simplified model (GMSB) where the decay $\tilde{t} \rightarrow b\tilde{\chi}^\pm_1$, with $\tilde{\chi}^\pm_1 \rightarrow (q q'/\ell\nu) H,\ Z\tilde{G}$, takes place with a branching ratio of 100% (the particles between brackets have a soft p_T spectrum), see Figs. 4–6.

[87] AABOUD 17AF searched in 36 fb^{-1} of pp collisions at $\sqrt{s} = 13$ TeV for evidence of top squarks in events containing 2 leptons, jets, b-jets and $\not{E}_T$. In Tstop6 model, assuming $m_{\tilde{\chi}^0_1} = 0$ GeV, $\tilde{t}_1$ masses up to 850 GeV are excluded for $m_{\tilde{\chi}^0_2} > 200$ GeV.

[88] AABOUD 17AF searched in 36 fb^{-1} of pp collisions at $\sqrt{s} = 13$ TeV for evidence of $\tilde{t}_2$ in events containing 2 leptons, jets, b-jets and $\not{E}_T$. In Tstop7 model, assuming $m_{\tilde{\chi}^0_1} =$ 50 GeV and 100% decays via Z boson, $\tilde{t}_2$ masses up to 800 GeV are excluded. Exclusion limits are also shown as a function of the $\tilde{t}_2$ branching ratios in their Figure 7.

[89] AABOUD 17AF searched in 36 fb^{-1} of pp collisions at $\sqrt{s} = 13$ TeV for evidence of $\tilde{t}_2$ in events containing 2 leptons, jets, b-jets and $\not{E}_T$. In Tstop7 model, assuming $m_{\tilde{\chi}^0_1}$ = 50 GeV and 100% decays via higgs boson, $\tilde{t}_2$ masses up to 880 GeV are excluded. Exclusion limits are also shown as a function of the $\tilde{t}_2$ branching ratios in their Figure 7.

[90] AABOUD 17AY searched in 36.1 fb^{-1} of pp collisions at $\sqrt{s} = 13$ TeV for events with at least four jets and large missing transverse momentum. No significant excess above the Standard Model expectations is observed. Limits are set on the top squark mass assuming three pMSSM-inspired models. The first one, referred to as Higgsino LSP model, assumes $m_{\tilde{\chi}^\pm_1} - m_{\tilde{\chi}^0_1} = 5$ GeV and $m_{\tilde{\chi}^0_2} - m_{\tilde{\chi}^0_1} = 10$ GeV, with a mixture of decay modes as in Tstop1, Tstop2 and Tstop6. See their Figure 10. The second and third models are referred to as Wino NLSP and well-tempered pMSSM models, respectively. See their Figure 11 and Figure 12, and text for details on assumptions.

[91] AAD 14B searched in 20.3 fb^{-1} of pp collisions at $\sqrt{s} = 8$ TeV for events containing a Z boson, with or without additional leptons, plus jets originating from b-quarks and significant missing transverse momentum. No excess over the expected SM background is observed. Limits are derived in simplified models featuring $\tilde{t}_2$ production, with $\tilde{t}_2 \rightarrow Z\tilde{t}_1$, $\tilde{t}_1 \rightarrow t\tilde{\chi}^0_1$ with a 100% branching ratio, see Fig. 4, and in the framework of natural GMSB, see Fig. 6.

[92] CHATRCHYAN 14U searched in 19.7 fb^{-1} of pp collisions at $\sqrt{s} = 8$ TeV for evidence of direct pair production of top squarks, with Higgs bosons in the decay chain. The search is performed using a selection of events containing two Higgs bosons, each decaying to a photon pair, missing transverse energy and possibly b-quark jets. No significant excesses over the expected SM backgrounds are observed. The results are interpreted in the context of a "natural SUSY" simplified model where the decays $\tilde{t}_1 \rightarrow b\tilde{\chi}^\pm_1$, with $\tilde{\chi}^\pm_1 \rightarrow f f' \tilde{\chi}^0_1$, and $\tilde{\chi}^0_1 \rightarrow H\tilde{G}$, all happen with 100% branching ratio, see Fig. 4.

[93] KHACHATRYAN 14C searched in 19.5 fb^{-1} of pp collisions at $\sqrt{s} = 8$ TeV for evidence of direct pair production of top squarks, with Higgs or Z-bosons in the decay chain. The search is performed using a selection of events containing leptons and b-quark jets. No significant excesses over the expected SM backgrounds are observed. The results are interpreted in the context of a simplified model with pair production of a heavier top-squark mass eigenstate $\tilde{t}_2$ decaying to a lighter top-squark eigenstate $\tilde{t}_1$ via either $\tilde{t}_2 \rightarrow H\tilde{t}_1$ or $\tilde{t}_2 \rightarrow Z\tilde{t}_1$, followed in both cases by $\tilde{t}_1 \rightarrow t\tilde{\chi}^0_1$. The interpretation is performed in the region where the mass difference between the $\tilde{t}_1$ and $\tilde{\chi}^0_1$ is approximately equal to the top-quark mass, which is not probed by searches for direct $\tilde{t}_1$ pair production, see Figs. 5 and 6. The analysis excludes top squarks with masses $m_{\tilde{t}_2} < 575$ GeV and $m_{\tilde{t}_1} < 400$ GeV at 95% C.L.

R-parity violating $\tilde{t}$ (Stop) mass limit

VALUE (GeV)	CL%	DOCUMENT ID		TECN	COMMENT
> 700	95	[1] CHEKHOVSKY	25K	CMS	0,1,2 μ or e, ≥ 6 jets, Tstop6RPV
> 930	95	[1] CHEKHOVSKY	25K	CMS	0,1,2 μ or e, ≥ 6 jets, stealth model SYY
>1900	95	[2] AAD	24BT	ATLS	$\tilde{t} \rightarrow be$, prompt, Tstop2RPV.
>1800	95	[2] AAD	24BT	ATLS	$\tilde{t} \rightarrow b\mu$, prompt, Tstop2RPV.
> 800	95	[2] AAD	24BT	ATLS	$\tilde{t} \rightarrow b\tau$, prompt, Tstop2RPV.
none 70–200	95	[3] HAYRAPETY...	24AP	CMS	2 large-radius jets, $\tilde{t}$ pair production with RPV $\tilde{t} \rightarrow qq$
none 500–520, 580–770	95	[4] TUMASYAN	23L	CMS	4 jets with dijet masses > 350 GeV, Tstop1aRPV
>1500	95	[5] TUMASYAN	22AF	CMS	long-lived $\tilde{t}$, $\tilde{t} \rightarrow b\overline{\ell}$, $c\tau = 2$ cm
>1500	95	[5] TUMASYAN	22AF	CMS	long-lived $\tilde{t}$, $\tilde{t} \rightarrow d\overline{\ell}$, $c\tau = 2$ cm
> 460	95	[5] TUMASYAN	22AF	CMS	long-lived $\tilde{t}$, $\tilde{t} \rightarrow b\overline{\ell}$, 0.01cm $< c\tau <$ 1000 cm
> 460	95	[5] TUMASYAN	22AF	CMS	long-lived $\tilde{t}$, $\tilde{t} \rightarrow d\overline{\ell}$, 0.01cm $< c\tau <$ 1000 cm
>1100	95	[6] AAD	21BF	ATLS	$\ell^\pm$ + b-jets + many jets, Tstop14, λ''_{323} electroweakino decay, 500 GeV $< m_{\tilde{\chi}^0_1} <$ 800 GeV
>1150	95	[6] AAD	21BF	ATLS	$\ell^\pm$ + b-jets + many jets, Tstop15, λ''_{323} electroweakino decay, 600 GeV $< m_{\tilde{\chi}^0_1} <$ 900 GeV
>1300	95	[6] AAD	21BF	ATLS	$\ell^\pm$ + b-jets + many jets, Tstop1, λ''_{323}, electroweakino decay, 500 GeV $< m_{\tilde{\chi}^0_1} <$ 1000 GeV
>1600	95	[7] SIRUNYAN	21AF	CMS	long-lived $\tilde{t}$, $\tilde{t} \rightarrow \overline{d}\overline{d}$, λ''_{3i3} coupling, 0.4 mm $< c\tau <$ 80 mm
>1600	95	[8] SIRUNYAN	21U	CMS	long-lived $\tilde{t}$, $\tilde{t} \rightarrow b\overline{\ell}$, 5 $< c\tau <$ 240 mm
>1600	95	[8] SIRUNYAN	21U	CMS	long-lived $\tilde{t}$, $\tilde{t} \rightarrow d\overline{\ell}$, λ'_{x31} coupling, 3 $< c\tau <$ 360 mm
>1600	95	[8] SIRUNYAN	21U	CMS	long-lived $\tilde{t}$, $\tilde{t} \rightarrow \overline{d}\overline{d}$, η''_{311} coupling, 2 $< c\tau <$ 1320 mm
> 670	95	[9] SIRUNYAN	21V	CMS	$\ell^\pm$ + ≥ 7 jets, Tstop1 with $\tilde{\chi}^0_1 \rightarrow qqq$, λ''_{abc} coupling, $a,b,c \in 1,2$
> 870	95	[9] SIRUNYAN	21V	CMS	$\ell^\pm$ + ≥ 7 jets, stealth SYY model
>1700	95	[10] AAD	20M	ATLS	$\tilde{t} \rightarrow q\mu$, long-lived, Tstop3RPV, $\tau = 0.1$ ns
>1150	95	[11] SIRUNYAN	19BI	ATLS	$\tilde{t} \rightarrow b\mu$, long-lived, Tstop2RPV, $c\tau = 0.1$ cm
>1100	95	[12] SIRUNYAN	19BJ	CMS	$\tilde{t} \rightarrow be$, Tstop2RPV, prompt
none 100–410	95	[13] AABOUD	18BB	ATLS	4 jets, Tstop1RPV with $\tilde{t} \rightarrow ds$, λ''_{312} coupling
none 100–470, 480–610	95	[14] AABOUD	18BB	ATLS	4 jets, Tstop1RPV, λ''_{323} coupling

Int. J. Mod. Phys. A 2026.41. Downloaded from www.worldscientific.com
by UNIVERSITY OF CALIFORNIA @ BERKELEY on 09/16/26. Re-use and distribution is strictly not permitted, except for Open Access articles.

$\geq$ 600–1500	95	[15] AABOUD	18P	ATLS	2ℓ + b-jets, Tstop2RPV, depending on λ'_{i33} coupling (i = 1, 2, 3)
>1130	95	[16] SIRUNYAN	18AD	CMS	$\widetilde{t} \rightarrow b\ell$, long-lived, $c\tau$ = 70–100 mm
> 550	95	[16] SIRUNYAN	18AD	CMS	$\widetilde{t} \rightarrow b\ell$, long-lived, $c\tau$ = 1–1000 mm
>1400	95	[17] SIRUNYAN	18DV	CMS	long-lived $\widetilde{t}$, $\widetilde{t} \rightarrow \overline{d}\overline{d}$, 0.6 mm < $c\tau$ < 80 mm
none 80–520	95	[18] SIRUNYAN	18DY	CMS	2, 4 jets, Tstop3RPV, λ''_{312} coupling
none 80–270, 285–340, 400–525	95	[18] SIRUNYAN	18DY	CMS	2 , 4 jets, Tstop1RPV, λ''_{323} coupling
>1200	95	[19] AABOUD	17AI	ATLS	$\geq 1\ell$+ $\geq$ 8 jets, Tstop1 with $\widetilde{\chi}^0_1 \rightarrow tbs$, λ''_{323} coupling, $m_{\widetilde{\chi}^0_1}$=500 GeV
none, 100–315	95	[20] AAD	16AM	ATLS	2 large-radius jets, Tstop1RPV
none, 200–350	95	[21] KHACHATRY...	15L	CMS	$\widetilde{t} \rightarrow qq$, $\lambda''_{312} \neq 0$
none, 200–385	95	[21] KHACHATRY...	15L	CMS	$\widetilde{t} \rightarrow qb$, $\lambda''_{323} \neq 0$
> 740	95	[22] KHACHATRY...	14T	CMS	τ + b-jets, $LQ\overline{D}$, $\lambda'_{333} \neq 0$, $\widetilde{t} \rightarrow \tau b$ simplified model
> 580	95	[22] KHACHATRY...	14T	CMS	τ + b-jets, $LQ\overline{D}$, $\lambda'_{3jk} \neq 0$ ($j \neq$ =3), $\widetilde{t} \rightarrow \widetilde{\chi}^{\pm} b$, $\widetilde{\chi}^{\pm} \rightarrow qq\tau^{\pm}$ simplified model
• • • We do not use the following data for averages, fits, limits, etc. • • •					
> 770	95	[23] AAD	21B	ATLS	$\geq$ 8 jets, $\geq$ 5 b-jets,Tstop4RPV
> 890	95	[24] KHACHATRY...	16AC	CMS	e^+e^-+ $\geq$ 5 jets; $\widetilde{t} \rightarrow b\widetilde{\chi}^{\pm}_1$; $\widetilde{\chi}^{\pm}_1 \rightarrow \ell^{\pm}jj$, λ'_{ijk}
>1000	95	[24] KHACHATRY...	16AC	CMS	$\mu^+\mu^-$+ $\geq$ 5 jets; $\widetilde{t} \rightarrow b\widetilde{\chi}^{\pm}_1$; $\widetilde{\chi}^{\pm}_1 \rightarrow \ell^{\pm}jj$, λ'_{ijk}
> 950	95	[25] KHACHATRY...	16BX	CMS	$\widetilde{t} \rightarrow t\widetilde{\chi}^0_1$, $\widetilde{\chi}^0_1 \rightarrow \ell\ell\nu$, λ_{121} or $\lambda_{122} \neq 0$
> 790	95	[26] KHACHATRY...	15E	CMS	$\widetilde{t}_1 \rightarrow b\ell$, $c\tau$ = 2 cm

[1] CHEKHOVSKY 25K searched in 138 fb^{-1} of pp collisions at $\sqrt{s}$ = 13 TeV for evidence of top squark pair production in events with 0, 1, or 2 electrons or muons and at least six jets. No significant excess above the Standard Model expectations is observed. Limits are set in the frameworks of RPV and stealth SUSY models, see their figure 7. In the RPV model Tstop6RPV, each top squark decays to a top quark and a neutralino $\widetilde{\chi}^0_1$, followed by an RPV decay of the $\widetilde{\chi}^0_1$ to three light-flavor jets. The stealth SUSY model $SY\overline{Y}$ assumes a new hidden sector containing a scalar particle S with even R-parity and its superpartner $\widetilde{S}$, both of which are singlets under all SM interactions. SUSY is approximately conserved in the hidden sector for this model, resulting in nearly mass-degenerate $\widetilde{S}$ and S masses. The stealth sector couples in this model through a gauge singlet MSSM operator $Y\overline{Y}$ within the SU(5) GUT group. In this model, the top squark decays as follows: $\widetilde{t} \rightarrow g\widetilde{S}$, with $\widetilde{S} \rightarrow gg\widetilde{G}$.

[2] AAD 24BT searched in 140 fb^{-1} of pp collisions at $\sqrt{s}$ = 13 TeV for pair production of stops decaying RPV to a lepton and a b-quark. The final state consists of two resonant $\ell - b$ pairs. No excess over the SM prediction is observed. Limits are set on the mass of the $\widetilde{t}$ assuming decays in a single lepton flavour, or into the three lepton flavours with BR of 1/3, see their Figure 9. Limits are also extracted as a function of the branching fraction into each lepton flavour, assuming that the $\widetilde{t}$ decays only via $\widetilde{t} \rightarrow b\ell$, see their Figure 8.

[3] HAYRAPETYAN 24AP searched in 128 fb^{-1} of pp collisions at $\sqrt{s}$ = 13 TeV for evidence of pair-produced multijet signatures probing fully hadronic final states. No significant excess above the Standard Model expectations is observed. Limits are set in three RPV SUSY models: higgsino pair production with decay to merged trijets, stop pair production with decay to merged dijets, and pair-produced gluinos decaying to resolved trijets, see their Fig. 4.

[4] TUMASYAN 23L searched in 138 fb^{-1} of pp collisions at $\sqrt{s}$ = 13 TeV for pairs of dijet resonances with the same mass in final states with at least four jets, for the case where the four-jet production proceeds via an intermediate resonant state and for nonresonant production. No significant excess above the Standard Model expectations is observed. Limits are set in the nonresonant search on the top squark mass in the simplified model Tstop1aRPV with λ_{312} coupling, assuming B(ds) = 1, see their figure 12. Limits are also set on resonant pair production of dijet resonances via high mass intermediate states and compared to a signal model of diquarks that decay into pairs of vector-like quarks, see their figures 10 and 11.

[5] TUMASYAN 22AF searched for evidence of new long-lived particles decaying to leptons in pp collisions at $\sqrt{s}$ = 13 TeV, corresponding to 118 (113) fb^{-1} in the ee channel ($e\mu$ and $\mu\mu$) channels. The leptons are required to have transverse impact parameter values between 0.01 and 10 cm and are not required to form a common vertex. No significant excess above the Standard Model expectations is observed. Limits are set on the mass of the top squark in RPV models with top squark pair production and $\widetilde{t} \rightarrow b\overline{\ell}$ and $\widetilde{t} \rightarrow d\overline{\ell}$, see their Figure 4, which contains a wider range of lifetime limits. Limits are also set on a gauge-mediated SUSY breaking model, where the next-to-lightest SUSY particle is a slepton and the lightest SUSY particle a gravitino $\widetilde{G}$, see their Figure 5, which also contains a wider range of lifetime limits. Limits are also set in a model that produces BSM Higgs bosons (H) with a mass of 125 GeV through gluongluon fusion, where the H decays to two long-lived scalars S, each of which decays to two oppositely charged and same-flavor leptons.

[6] AAD 21BF searched in 139 fb^{-1} of pp collisions at $\sqrt{s}$ = 13 TeV for pair production of gluinos, stops, electroweakinos decaying RPV either directly or indirectly via the LSP. The final state in all cases is one or two leptons, many jets (up to fifteen) and b-jets. Different models with different branching fractions of the gluino or stop follow from the assumptions on the nature of the electroweakinos. No significant excess above the Standard Model predictions is observed. Limits are set on the $gluino$, $\widetilde{t}_1$, electroweakino masses as a function of the $\widetilde{\chi}^0_1$ mass in several scenarios of gluino, stop and electroweakino pair production.

[7] SIRUNYAN 21AF searched in 140 fb^{-1} of pp collisions at $\sqrt{s}$ = 13 TeV for supersymmetry in events with with two displaced vertices from long-lived particles decaying into multijet or dijet final states. No significant excess above the Standard Model expectations is observed. Limits are set on the gluino mass in the simplified model Tglu2RPV with λ''_{323} coupling, on the $\widetilde{\chi}^0_1$ mass in an RPV model with $\widetilde{\chi}^0_1$ pair production and the RPV decay $\widetilde{\chi}^0_1 \rightarrow tbs$ with λ''_{323} coupling and on the $\widetilde{t}$ mass in an RPV model with top squark pair production and the RPV decay $\widetilde{t} \rightarrow \overline{d}_i\overline{d}_j$ with λ''_{3ij} coupling, see their Figure 7.

[8] SIRUNYAN 21U searched in 132 fb^{-1} of pp collisions at $\sqrt{s}$ = 13 TeV for supersymmetry in events with displaced tracks and displaced vertices associated with a dijet system. No significant excess above the Standard Model expectations is observed. Limits are set on long-lived gluinos in an RPC GMSB SUSY model of gluino pair production, with $\widetilde{g} \rightarrow g\widetilde{G}$, see their Figure 9, in Tglu1A in a mini-split model, see their Figure 10, and in an RPV model of gluino pair production, with $\widetilde{g} \rightarrow tbs$ with coupling λ''_{323}, see their Figure 11. Limits are also set on long-lived top squarks in Tstop2RPV, see their Figure 12, in an RPV model with $\widetilde{t} \rightarrow d\overline{\ell}$ and λ'_{x31} coupling, see their Figure 13, and in a dynamical RPV model with $\widetilde{t} \rightarrow \overline{d}\overline{d}$ via a nonholomorphic RPV coupling η''_{311}, see their Figure 14. The best mass limit is achieved in all cases at $c\tau$ = 30 mm.

[9] SIRUNYAN 21V searched in 137 fb^{-1} of pp collisions at $\sqrt{s}$ = 13 TeV for supersymmetry in events with one charged lepton ($e^{\pm}$ or $\mu^{\pm}$) and $\geq$ 7 jets. No significant excess above the Standard Model expectations is observed. Limits are set on an RPV SUSY model like Tstop1 with the additional decay $\widetilde{\chi}^0_1 \rightarrow qqq$ with coupling λ''_{abc}, with $a,b,c \in$ 1,2, and on a stealth SUSY model called SYY, with one scalar particle S with even R-parity and its superpartner $\widetilde{S}$, both singlets under all SM interactions, and with a portal mediated by loop interactions involving a new vectorlike messenger field (Y), where pair produced top squarks decay as $\widetilde{t} \rightarrow tg\widetilde{S}$, and $\widetilde{S} \rightarrow \widetilde{G}S$, and $S \rightarrow gg$, see their Figure 6 and 7.

[10] AAD 20M searched for long-lived particles decaying into hadrons and at least one muon in events containing a displaced muon track and a displaced vertex. The analysis uses a dataset of pp collisions at $\sqrt{s}$ = 13 TeV corresponding to an integrated luminosity of 136 fb^{-1}. Using the Tstop3RPV simplified model, top squarks with masses up to 1.7 TeV are excluded for a lifetime of 0.1 ns, and masses below 1.3 TeV are excluded for lifetimes between 0.01 ns and 30 ns, see their Fig. 7. The dependence on the RPV coupling λ_{23k} multiplied by cosθ_t, with θ_t the mixing angle between the left- and right-handed $\widetilde{t}$ squarks, is also shown, see their Fig. 7.

[11] SIRUNYAN 19BI searched in 35.9 fb^{-1} of pp collisions at $\sqrt{s}$ = 13 TeV in final states with two muons and two jets, or with one muon, two jets, and missing transverse momentum. Limits are set in a model of pair-produced, prompt or long-lived top squarks with R-parity violating decays to a b-quark and a lepton (Tstop2RPV), branching fraction of $\widetilde{t} \rightarrow b\mu$ equal to 1/3 and $c\tau$ between 0.1 cm and 10 cm in the case of long-lived top squarks. See their Fig. 10.

[12] SIRUNYAN 19BJ searched in 35.9 fb^{-1} of pp collisions at $\sqrt{s}$ = 13 TeV in final states with two electrons and two jets, or with one electron, two jets, and missing transverse momentum. Limits are set in a model of pair-produced, prompt top squarks with R-parity violating decays to a b-quark and a lepton (Tstop2RPV), assuming branching fraction of $\widetilde{t} \rightarrow be$ equal to 1/3 and $c\tau$ = 0 cm. See their Fig.10.

[13] AABOUD 18BB searched in 36.7 fb^{-1} of pp collisions at $\sqrt{s}$ = 13 TeV for massive colored resonances which are pair-produced and decay into two jets. No significant deviation from the background prediction is observed. Results are interpreted in a SUSY simplified model as Tstop1RPV with $\widetilde{t} \rightarrow ds$. Top squarks with masses in the range 100–410 GeV are excluded, see their Figure 9(a). The λ''_{312} coupling is assumed to be sufficiently large for the decays to be prompt, but small enough to neglect the single-top-squark resonant production through RPV couplings.

[14] AABOUD 18BB searched in 36.7 fb^{-1} of pp collisions at $\sqrt{s}$ = 13 TeV for massive coloured resonances which are pair-produced and decay into two jets. No significant deviation from the background prediction is observed. Results are interpreted in Tstop1RPV. Top squarks with masses in the range 100–470 GeV or 480–610 GeV are excluded, see their Figure 9(b). The λ''_{323} coupling is assumed to be sufficiently large for the decays to be prompt, but small enough to neglect the single-top-squark resonant production through RPV couplings.

[15] AABOUD 18P searched in 36.1 fb^{-1} of pp collisions at $\sqrt{s}$ = 13 TeV for pair-produced top squarks that decay through RPV λ'_{i33} (i = 1, 2, 3) couplings to a final state with two leptons and two jets, at least one of which is identified as a b-jet. No significant excess is observed over the SM background. In the Tstop2RPV model, lower limits on the top squark masses between 600 and 1500 GeV are set depending on the branching fraction to be, $b\mu$, and $b\tau$ final states. See their Figs 6 and 7.

[16] SIRUNYAN 18AD searched in 2.6 fb^{-1} of pp collisions at $\sqrt{s}$ = 13 TeV for long-lived particles by exploiting the multiplicity of displaced jets to search for the presence of signal decays occurring at distances between 1 and 1000 mm. Limits are set in a model of pair-produced, long-lived top squarks with R-parity violating decays to a b-quark and a lepton, see their Figure 3.

[17] SIRUNYAN 18DV searched in 38.5 fb^{-1} of pp collisions at $\sqrt{s}$ = 13 TeV for long-lived particles in events with multiple jets and two displaced vertices composed of many tracks. No events with two well-separated high-track-multiplicity vertices were observed. Limits are set on the stop and the gluino mass in RPV models of supersymmetry where the stop (gluino) is decaying solely into dijet (multijet) final states, see their Figures 6 and 7.

[18] SIRUNYAN 18DY searched in 35.9 fb^{-1} of pp collisions at $\sqrt{s}$ = 13 TeV for the pair production of resonances, each decaying to two quarks. The search is conducted separately in a boosted (two-jet) and resolved (four-jet) jet topology. The mass spectra are found to be consistent with the Standard Model expectations. Limits are set on the stop mass in the Tstop3RPV and Tstop1RPV simplified models, see their Figure 11.

[19] AABOUD 17AI searched in 36.1 fb^{-1} of pp collisions at $\sqrt{s}$ = 13 TeV for events with one or more isolated lepton, at least eight jets, either zero or many b-jets, for evidence of R-parity violating decays of the top squark. No significant excess above the Standard Model expectations is observed. Limits up to 1.25 (1.10) TeV are set on the top squark mass in R-parity-violating supersymmetry models where $\widetilde{t}_1$ decays for a bino LSP as: $\widetilde{t} \rightarrow t\widetilde{\chi}^0_1$ and for a higgsino LSP as $\widetilde{t} \rightarrow t\widetilde{\chi}^0_{1,2}/b\widetilde{\chi}^+_1$. These is followed by the decays through the non-zero λ''_{323} coupling $\widetilde{\chi}^0_{1,2} \rightarrow tbs$, $\widetilde{\chi}^{\pm}_1 \rightarrow bbs$. See their Figure 10 and text for details on model assumptions.

[20] AAD 16AM searched in 17.4 fb^{-1} of pp collisions at $\sqrt{s}$ = 8 TeV for events containing two large-radius hadronic jets. No deviation from the background prediction is observed. Top squarks with masses between 100 and 315 GeV are excluded at 95% C.L. in the

Int. J. Mod. Phys. A 2026.41. Downloaded from www.worldscientific.com
by UNIVERSITY OF CALIFORNIA @ BERKELEY on 09/16/26. Re-use and distribution is strictly not permitted, except for Open Access articles.

hypothesis that they both decay via R-parity violating coupling λ''_{323} to b- and s-quarks. See their Fig. 10.

[21] KHACHATRYAN 15L searched in 19.4 fb^{-1} of pp collisions at $\sqrt{s}$ = 8 TeV for pair production of heavy resonances decaying to pairs of jets in four jet events. No significant excess above the Standard Model expectations is observed. Limits are set on the stop mass in R-parity-violating supersymmetry models where $\widetilde{t} \rightarrow qq$ ($\lambda''_{312} \neq 0$), see Fig. 6 (top) and $\widetilde{t} \rightarrow qb$ ($\lambda''_{323} \neq 0$), see Fig. 6 (bottom).

[22] KHACHATRYAN 14T searched in 19.7 fb^{-1} of pp collisions at $\sqrt{s}$ = 8 TeV for events with τ-leptons and b-quark jets, possibly with extra light-flavour jets. No excess above the Standard Model expectations is observed. Limits are set on stop masses in RPV SUSY models with $LQ\overline{D}$ couplings, in two simplified models. In the first model, the decay $\widetilde{t} \rightarrow \tau b$ is considered, with $\lambda'_{333} \neq 0$, see Fig. 3. In the second model, the decay $\widetilde{t} \rightarrow \widetilde{\chi}^{\pm} b$, with the subsequent decay $\widetilde{\chi}^{\pm} \rightarrow qq\tau^{\pm}$ is considered, with $\lambda'_{3jk} \neq 0$ and the mass splitting between the top squark and the charging chosen to be 100 GeV, see Fig. 4.

[23] AAD 21B searched in 139 fb^{-1} of pp collisions at $\sqrt{s}$ = 13 TeV for events with at least eight jets and at least 5 b-jets, for evidence of R-parity violating decays of the top squark. No significant excess above the Standard Model expectations is observed. Limits up to 950 GeV are set on the top squark mass in Tstop4RPV simplified model. See their Figure 7 for more detailed mass bounds.

[24] KHACHATRYAN 16AC searched in 19.7 fb^{-1} of pp collisions at $\sqrt{s}$ = 8 TeV for events with low missing transverse momentum, two oppositely charged electrons or muons, and at least five jets, at least one of which is a b-jet, for evidence of R-parity violating, charging-mediated decays of the top squark. No significant excess above the Standard Model expectations is observed. Limits are set on the stop mass in R-parity-violating supersymmetry models where $\widetilde{t} \rightarrow b\widetilde{\chi}^{\pm}_1$ with $\widetilde{\chi}^{\pm}_1 \rightarrow \ell^{\pm} jj$, $\lambda'_{ijk} \neq 0$ ($i,j,k \leq 2$), and with $m_{\widetilde{t}} - m_{\widetilde{\chi}^{\pm}_1}$ = 100 GeV, see Fig. 3.

[25] KHACHATRYAN 16BX searched in 19.5 fb^{-1} of pp collisions at $\sqrt{s}$ = 8 TeV for events containing 4 leptons coming from R-parity-violating decays of $\widetilde{\chi}^0_1 \rightarrow \ell\ell\nu$ with $\lambda_{121} \neq 0$ or $\lambda_{122} \neq 0$. No excess over the expected background is observed. Limits are derived on the gluino, squark and stop masses, see Fig. 23.

[26] KHACHATRYAN 15E searched for long-lived particles decaying to leptons in 19.7 fb^{-1} of pp collisions at $\sqrt{s}$ = 8 TeV. Events were selected with an electron and muon with opposite charges and each with transverse impact parameter values between 0.02 and 2 cm. Limits are set on SUSY benchmark models with pair production of top squarks decaying into an $e\mu$ final state via RPV interactions. See their Fig. 2

Heavy $\widetilde{g}$ (Gluino) mass limit

For $m_{\widetilde{g}}$ > 60–70 GeV, it is expected that gluinos would undergo a cascade decay via a number of neutralinos and/or charginos rather than undergo a direct decay to photinos as assumed by some papers. Limits obtained when direct decay is assumed are usually higher than limits when cascade decays are included.

Some earlier papers are now obsolete and have been omitted. They were last listed in our PDG 14 edition: K. Olive, *et al.* (Particle Data Group), Chinese Physics **C38** 070001 (2014) (http://pdg.lbl.gov).

R-parity conserving heavy $\widetilde{g}$ (Gluino) mass limit

VALUE (GeV)	CL%	DOCUMENT ID		TECN	COMMENT
>2250	95	[1] AAD	25BM	ATLS	1 or 2 τ + $\not{E}_T$, Tglu1F, $m_{\widetilde{\chi}^0_1}$ = 100 GeV
>2000	95	[2] AAD	24Z	ATLS	2 same-sign/3ℓ + jets, Tglu1E, $m_{\widetilde{\chi}^0_1}$ < 700 GeV
>2300	95	[2] AAD	24Z	ATLS	2 same-sign/3ℓ + jets, Tglu1G, $m_{\widetilde{\chi}^0_1}$ = 100 GeV
>2200	95	[2] AAD	24Z	ATLS	2 same-sign/3ℓ + jets, Tglu1A, RPV, with $\widetilde{\chi}^0_1 \rightarrow \ell qq$, 300 GeV <$m_{\widetilde{\chi}^0_1}$ < 2000 GeV
>1650	95	[2] AAD	24Z	ATLS	2 same-sign/3ℓ + jets, Tglu2RPV ($\widetilde{g} \rightarrow \widetilde{t}t$, $\widetilde{t} \rightarrow bd$), $m_{\widetilde{t}}$ < 1400 GeV
>2300	95	[3] HAYRAPETY...24M		CMS	$\geq$ 1 disappearing track+ $\not{E}_T$, $m_{\widetilde{\chi}^{\pm}_1} \simeq m_{\widetilde{\chi}^0_1}$ = 1500 GeV, c$\tau(\widetilde{\chi}^{\pm}_1)$ = 200 cm
>2120	95	[3] HAYRAPETY...24M		CMS	$\geq$ 1 disappearing track+ $\not{E}_T$, $m_{\widetilde{\chi}^{\pm}_1} \simeq m_{\widetilde{\chi}^0_1}$ = 250 GeV, c$\tau(\widetilde{\chi}^{\pm}_1)$ = 10 cm
>1800	95	[4] HAYRAPETY...24P		CMS	$\geq$ 1 displ. vertex + $\not{E}_T$, split SUSY, cτ = 1–100 mm, Δm ($\widetilde{g}$, $\widetilde{\chi}^0_1$) = 100 GeV
>1600	95	[4] HAYRAPETY...24P		CMS	$\geq$ 1 displ. vertex + $\not{E}_T$, split SUSY, cτ = 1–30 mm, Δm ($\widetilde{g}$, $\widetilde{\chi}^0_1$) > 50 GeV
>2240	95	[4] HAYRAPETY...24P		CMS	$\geq$ 1 displ. vertex + $\not{E}_T$, GMSB SUSY, $\widetilde{g} \rightarrow g\widetilde{G}$, c$\tau$ = 0.3–100 mm
>2150	95	[5] HAYRAPETY...24Q		CMS	$\geq$ 2 γ + $\geq$ 4 jets, stealth SUSY, 600 GeV < $m_{\widetilde{\chi}^0_1}$ < 1200 GeV
>2200	95	[6] AAD	23AB	ATLS	$\geq$ 1 γ + jets + $\not{E}_T$, GGM-like, Tglu4D, $\widetilde{\chi}^0_1$ NLSP, $m_{\widetilde{\chi}^0_1}$ > 300 GeV
>2200	95	[6] AAD	23AB	ATLS	$\geq$ 1 γ + jets + $\not{E}_T$, GGM-like, Tglu4G, $\widetilde{\chi}^0_1$ NLSP, $m_{\widetilde{\chi}^0_1}$ > 350 GeV
>2250	95	[7] AAD	23AE	ATLS	2 SFOS ℓ, jets, $\not{E}_T$, Tglu1G, $m_{\widetilde{\chi}^0_1}$ = 100 GeV
>1950	95	[8] AAD	23AE	ATLS	2 SFOS ℓ, jets, $\not{E}_T$, Tglu1H, $m_{\widetilde{\chi}^0_2} = (m_{\widetilde{g}} + m_{\widetilde{\chi}^0_1})/2$, , $m_{\widetilde{\chi}^0_1}$ = 100 GeV
>2440	95	[9] AAD	23AL	ATLS	At least 3 b-tagged jets, 0 or 1 lepton, Tglu3B, $m_{\widetilde{\chi}^0_1}$ = 1 GeV
>2350	95	[9] AAD	23AL	ATLS	At least 3 b-tagged jets, 0 or 1 lepton, Tglu2A, $m_{\widetilde{\chi}^0_1}$ = 1 GeV
>2050	95	[10] AAD	23AL	ATLS	At least 3 b-tagged jets, 0 or 1 lepton, Tglu3E, $m_{\widetilde{\chi}^{\pm}_1} - m_{\widetilde{\chi}^0_1}$ = 2 GeV, $m_{\widetilde{\chi}^0_1}$ = 1 GeV
>2320	95	[11] HAYRAPETY...23E		CMS	γ + jets + $\not{E}_T$, Tglu4E, $m_{\widetilde{\chi}^0_1}$ = 1700 GeV
>2375	95	[11] HAYRAPETY...23E		CMS	γ + jets + $\not{E}_T$, Tglu4D, $m_{\widetilde{\chi}^0_1}$ = 1700 GeV
>2260	95	[11] HAYRAPETY...23E		CMS	γ + jets + $\not{E}_T$, Tglu4F, $m_{\widetilde{\chi}^0_1}$ = 1700 GeV
>2120	95	[12] TUMASYAN	23AY	CMS	$\ell^{\pm}$ + $\geq$ 6 jets + $\geq$ 1 b-jet, Tglu3A, $m_{\widetilde{\chi}^0_1}$ = 0 GeV
>2050	95	[12] TUMASYAN	23AY	CMS	$\ell^{\pm}$ + $\geq$ 5 jets, 0 b-jets, Tglu1B, $m_{\widetilde{\chi}^0_1}$ = 0 GeV, $m_{\widetilde{\chi}^{\pm}_1} = 0.5(m_{\widetilde{g}} + m_{\widetilde{\chi}^0_1})$
>2200	95	[13] AAD	22U	ATLS	$\widetilde{g} \rightarrow qq\widetilde{\chi}^0_1$, $qq\widetilde{\chi}^{\pm}$, $m_{\widetilde{\chi}^{\pm}}$ = 1000 GeV, $\tau(\widetilde{\chi}^{\pm})$ = 1 ns
>2330	95	[14] TUMASYAN	22V	CMS	3 or 4 b-tagged jets or 2 large-radius jets, $\not{E}_T$; Tglu1I; $m_{\widetilde{\chi}^0_1}$ = 1 GeV
>2200	95	[15] AAD	21AK	ATLS	$\ell^{\pm}$ + jets + $\not{E}_T$, Tglu1B, $m_{\widetilde{\chi}^{\pm}_1} = (m_{\widetilde{g}} + m_{\widetilde{\chi}^0_1})/2$, $m_{\widetilde{\chi}^0_1}$ < 400 GeV
none 1300–2050	95	[15] AAD	21AK	ATLS	$\ell^{\pm}$ + jets + $\not{E}_T$, Tglu1B, $m_{\widetilde{\chi}^{\pm}_1} = (m_{\widetilde{g}} + m_{\widetilde{\chi}^0_1})/2$, $m_{\widetilde{\chi}^0_1}$ < 1000 GeV
>2300	95	[16] AAD	21L	ATLS	jets + $\not{E}_T$, Tglu1A, $m_{\widetilde{\chi}^0_1}$ < 200 GeV
>3000	95	[16] AAD	21L	ATLS	jets + $\not{E}_T$, combined $\widetilde{g}\widetilde{g}$, $\widetilde{g}\,\widetilde{q}$, $\widetilde{q}\widetilde{q}$ production, $\widetilde{g} \rightarrow qq'\widetilde{\chi}^0_1$, $\widetilde{q} \rightarrow q\widetilde{\chi}^0_1$, $m_{\widetilde{q}} = m_{\widetilde{g}}$, $m_{\widetilde{\chi}^0_1}$ = 0 GeV
>2200	95	[16] AAD	21L	ATLS	jets + $\not{E}_T$, Tglu1B, $m_{\widetilde{\chi}^0_1}$ = 0 GeV
>1400	95	[17] AAD	21X	ATLS	jets in empty bunch crossings, Tglu1A, long-lived R-hadron, $m_{\widetilde{\chi}^0_1}$ = 100 GeV, 10^{-5} s < $\tau_{R-hadron}$ < 10^3 s
> 870	95	[17] AAD	21X	ATLS	jets in empty bunch crossings, Tglu1A, long-lived R-hadron, $m_{\widetilde{g}} - m_{\widetilde{\chi}^0_1}$ = 100 GeV, 10^{-5} s < $\tau_{R-hadron}$ < 10^3 s
>2260	95	[18] SIRUNYAN	21AD	CMS	jets + $\not{E}_T$, Tglu3A, $m_{\widetilde{\chi}^0_1}$ < 1050 GeV
>2150	95	[18] SIRUNYAN	21AD	CMS	jets + $\not{E}_T$, Tglu3C, $m_{\widetilde{\chi}^0_1}$ = 600 GeV, $m_{\widetilde{t}} - m_{\widetilde{\chi}^0_1}$ = 20 GeV
>2250	95	[18] SIRUNYAN	21AD	CMS	jets + $\not{E}_T$, Tglu3D, $m_{\widetilde{\chi}^0_1}$ = 700 GeV, $m_{\widetilde{\chi}^{\pm}_1} - m_{\widetilde{\chi}^0_1}$ = 5 GeV
>1870	95	[19] SIRUNYAN	21M	CMS	$\ell^{\pm}\ell^{\mp}$ + $\not{E}_T$, Tglu4C, $m_{\widetilde{\chi}^0_1}$ = 1100 GeV
>1980	95	[20] AAD	20AL	ATLS	8 or more jets + $\not{E}_T$, Tglu1E, $m_{\widetilde{\chi}^0_1}$ = 100 GeV
>1820	95	[20] AAD	20AL	ATLS	8 or more jets + $\not{E}_T$, Tglu3A, $m_{\widetilde{\chi}^0_1}$ = 100 GeV
>1600	95	[21] AAD	20V	ATLS	same-sign $\ell^{\pm}\ell^{\pm}$ + jets, Tglu1E, $m_{\widetilde{\chi}^0_1}$ = 100 GeV
>1975	95	[22] SIRUNYAN	20B	CMS	$\geq$ 1γ + $\not{E}_T$, Tglu4A, BR($\widetilde{g} \rightarrow qq\widetilde{\chi}^{\pm}_1$)=0.5, $m_{\widetilde{\chi}^0_1} \simeq m_{\widetilde{g}}$
>1920	95	[23] SIRUNYAN	20BJ	CMS	jets+$\not{E}_T$, Tglu1H, $m_{\widetilde{g}} - m_{\widetilde{\chi}^0_2}$ = 50 GeV, $m_{\widetilde{\chi}^0_1}$ = 1 GeV
>2150	95	[24] SIRUNYAN	20E	CMS	1ℓ+jets, Tglu3A, $m_{\widetilde{\chi}^0_1}$ <700 GeV
>2050	95	[24] SIRUNYAN	20E	CMS	1ℓ+jets, Tglu3A, $m_{\widetilde{\chi}^0_1}$ <1100GeV

>1650	95	[24] SIRUNYAN	20E	CMS	1ℓ + jets, Tglu3C, $m_{\widetilde{t}_1} - m_{\widetilde{\chi}^0_1}$ = 175 GeV, $m_{\widetilde{\chi}^0_1}$ < 1150 GeV
>1700	95	[25] SIRUNYAN	20T	CMS	same-sign $\ell^\pm\ell^\pm$ or $\geq 3\ell^\pm$ + jets, Tglu3A, $m_{\widetilde{\chi}^0_1}$ = 0 GeV
>1610	95	[25] SIRUNYAN	20T	CMS	same-sign $\ell^\pm\ell^\pm$ or $\geq 3\ell^\pm$ + jets, Tglu3B, $m_{\widetilde{t}_1} - m_{\widetilde{\chi}^0_1}$ = 175 GeV, $m_{\widetilde{\chi}^0_1}$ = 0 GeV
>1300	95	[25] SIRUNYAN	20T	CMS	same-sign $\ell^\pm\ell^\pm$ or $\geq 3\ell^\pm$ + jets, Tglu3C, $m_{\widetilde{t}_1} - m_{\widetilde{\chi}^0_1}$ = 20 GeV, $m_{\widetilde{\chi}^0_1}$ = 0 GeV
>1500	95	[25] SIRUNYAN	20T	CMS	same-sign $\ell^\pm\ell^\pm$ or $\geq 3\ell^\pm$ + jets, Tglu3D, $m_{\widetilde{\chi}^\pm_1} = m_{\widetilde{\chi}^0_1}$ + 5 GeV, $m_{\widetilde{\chi}^0_1}$ = 0 GeV
>1350	95	[25] SIRUNYAN	20T	CMS	same-sign $\ell^\pm\ell^\pm$ or $\geq 3\ell^\pm$ + jets, Tglu1C, $m_{\widetilde{\chi}^0_2} = m_{\widetilde{\chi}^\pm_1} = (m_{\widetilde{g}} + m_{\widetilde{\chi}^0_1})/2$, $m_{\widetilde{\chi}^0_1}$ = 0 GeV
>1250	95	[25] SIRUNYAN	20T	CMS	same-sign $\ell^\pm\ell^\pm$ or $\geq 3\ell^\pm$ + jets, Tglu1C, $m_{\widetilde{\chi}^0_2} = m_{\widetilde{\chi}^\pm_1} = m_{\widetilde{\chi}^0_1}$+20 GeV, $m_{\widetilde{\chi}^0_1}$=0 GeV
>1425	95	[25] SIRUNYAN	20T	CMS	same-sign $\ell^\pm\ell^\pm$ or $\geq 3\ell^\pm$ + jets, Tglu1B, $m_{\widetilde{\chi}^\pm_1} = (m_{\widetilde{g}} + m_{\widetilde{\chi}^0_1})/2$, $m_{\widetilde{\chi}^0_1}$ = 0 GeV
>1425	95	[25] SIRUNYAN	20T	CMS	same-sign $\ell^\pm\ell^\pm$ or $\geq 3\ell^\pm$ + jets, Tglu1B, $m_{\widetilde{\chi}^\pm_1} = m_{\widetilde{\chi}^0_1}$ + 20 GeV, $m_{\widetilde{\chi}^0_1}$ = 0 GeV
>2000	95	[26] AABOUD	19I	ATL	$\geq$ 2 jets + 1 or 2 τ + $\not{E}_T$, Tglu1F, $m_{\widetilde{\chi}^0_1}$ = 100 GeV
>1860	95	[27] SIRUNYAN	19AG	CMS	2γ +$\not{E}_T$, Tglu4B, 500 GeV <$m_{\widetilde{\chi}^0_1}$ < 1500 GeV
>1920	95	[28] SIRUNYAN	19AU	CMS	γ +jets + b-jets + $\not{E}_T$, Tglu4D, $m_{\widetilde{\chi}^0_1}$ = 127 GeV
>1950	95	[28] SIRUNYAN	19AU	CMS	γ + jets + b-jets + $\not{E}_T$, Tglu4E, $m_{\widetilde{\chi}^0_1}$ = 1 GeV
>1800	95	[28] SIRUNYAN	19AU	CMS	γ + jets + b-jets + $\not{E}_T$, Tglu4F, $m_{\widetilde{\chi}^0_1}$ = 1 GeV
>2090	95	[28] SIRUNYAN	19AU	CMS	γ + jets + b-jets + $\not{E}_T$, Tglu4D, $m_{\widetilde{\chi}^0_1}$ = 1200 GeV
>2120	95	[28] SIRUNYAN	19AU	CMS	γ + jets + b-jets + $\not{E}_T$, Tglu4E, $m_{\widetilde{\chi}^0_1}$ = 1200 GeV
>1970	95	[28] SIRUNYAN	19AU	CMS	γ + jets + b-jets + $\not{E}_T$, Tglu4F, $m_{\widetilde{\chi}^0_1}$ = 1200 GeV
>1700	95	[29] SIRUNYAN	19CE	CMS	2 jets, Stealth SUSY, Tglu1A and $\widetilde{\chi}^0_1 \rightarrow \widetilde{S}\,\gamma\,(\widetilde{S} \rightarrow S\,\widetilde{G})$, $m_{\widetilde{\chi}^0_1}$ = 200 GeV
>2000	95	[30] SIRUNYAN	19CH	CMS	jets+$\not{E}_T$, Tglu1A, $m_{\widetilde{\chi}^0_1}$ = 0 GeV
>2030	95	[30] SIRUNYAN	19CH	CMS	jets+$\not{E}_T$, Tglu1C, $m_{\widetilde{\chi}^\pm_1}$=$m_{\widetilde{\chi}^0_2}$= 0.5($m_{\widetilde{g}}$+$m_{\widetilde{\chi}^0_1}$), $m_{\widetilde{\chi}^0_1}$ = 0 GeV
>2270	95	[30] SIRUNYAN	19CH	CMS	jets+$\not{E}_T$, Tglu2A, $m_{\widetilde{\chi}^0_1}$ = 0 GeV
>2180	95	[30] SIRUNYAN	19CH	CMS	jets+$\not{E}_T$, Tglu3A, $m_{\widetilde{\chi}^0_1}$ = 0 GeV
>1750	95	[31] SIRUNYAN	19K	CMS	γ+ℓ+$\not{E}_T$, Tglu4A, $m_{\widetilde{\chi}^0_1}$ = 1500 GeV
>2000	95	[32] SIRUNYAN	19S	CMS	1 or 2 ℓ + jets + $\not{E}_T$, Tglu3A, $m_{\widetilde{\chi}^0_1}$ < 700 GeV
>1900	95	[32] SIRUNYAN	19S	CMS	1 or 2 ℓ + jets + $\not{E}_T$, Tglu3C, 150 GeV < $m_{\widetilde{\chi}^0_1}$ < 950 GeV
>1970	95	[33] AABOUD	18AR	ATLS	jets+ $\geq$ 3b-jets+$\not{E}_T$, Tglu3A, $m_{\widetilde{\chi}^0_1}$ < 300 GeV
>1920	95	[34] AABOUD	18AR	ATLS	jets+ $\geq$ 3b-jets+$\not{E}_T$, Tglu2A, $m_{\widetilde{\chi}^0_1}$ < 600 GeV
>1650	95	[35] AABOUD	18AS	ATLS	$\geq$ 4 jets and disappearing tracks from $\widetilde{\chi}^\pm \rightarrow \widetilde{\chi}^0_1\pi^\pm$, modified Tglu1A or Tglu1B, $\widetilde{\chi}^\pm$ lifetime 0.2 ns, $m_{\widetilde{\chi}^\pm}$ = 460 GeV
>1850	95	[36] AABOUD	18BJ	ATLS	$\ell^\pm\ell^\mp$ + jets + $\not{E}_T$, Tglu1G, $m_{\widetilde{\chi}^0_1}$ = 100 GeV
>1650	95	[37] AABOUD	18BJ	ATLS	$\ell^\pm\ell^\mp$ + jets + $\not{E}_T$, Tglu1H, $m_{\widetilde{\chi}^0_1}$ = 100 GeV
>2150	95	[38] AABOUD	18U	ATLS	2 γ + $\not{E}_T$, GGM, Tglu4B, any NLSP mass
>1600	95	[39] AABOUD	18U	ATLS	γ + jets + $\not{E}_T$, GGM higgsino-bino, mix of Tglu4B and Tglu4C, any NLSP mass
>2030	95	[40] AABOUD	18V	ATLS	jets+$\not{E}_T$, Tglu1A, $m_{\widetilde{\chi}^0_1}$ = 0 GeV
>1980	95	[41] AABOUD	18V	ATLS	jets+$\not{E}_T$, Tglu1B, $m_{\widetilde{\chi}^\pm_1}$=0.5($m_{\widetilde{g}}$+$m_{\widetilde{\chi}^0_1}$), $m_{\widetilde{\chi}^0_1}$ = 0 GeV
>1750	95	[42] AABOUD	18V	ATLS	jets+$\not{E}_T$, Tglu1C, $m_{\widetilde{\chi}^0_1}$ = 1 GeV, any $m_{\widetilde{\chi}^0_2}$ > 100 GeV
>2000	95	[43] SIRUNYAN	18AA	CMS	$\geq 1\gamma$ + $\not{E}_T$, Tglu4A
>2100	95	[43] SIRUNYAN	18AA	CMS	$\geq 1\gamma$ + $\not{E}_T$, Tglu4B
>1800	95	[44] SIRUNYAN	18AC	CMS	1ℓ+jets, Tglu3A, $m_{\widetilde{\chi}^0_1}$ <650 GeV
>1700	95	[44] SIRUNYAN	18AC	CMS	1ℓ+jets, Tglu3A,$m_{\widetilde{\chi}^0_1}$ <1040 GeV
>1900	95	[44] SIRUNYAN	18AC	CMS	1ℓ + jets, Tglu1B, $m_{\widetilde{\chi}^\pm_1} = (m_{\widetilde{g}} + m_{\widetilde{\chi}^0_1})/2$, $m_{\widetilde{\chi}^0_1}$ < 300 GeV
>1250	95	[44] SIRUNYAN	18AC	CMS	1ℓ + jets, Tglu1B, $m_{\widetilde{\chi}^\pm_1} = (m_{\widetilde{g}} + m_{\widetilde{\chi}^0_1})/2$, $m_{\widetilde{\chi}^0_1}$ < 950 GeV
>1610	95	[45] SIRUNYAN	18AL	CMS	$\geq 3\ell^\pm$ + jets + $\not{E}_T$, Tglu3A, $m_{\widetilde{\chi}^0_1}$ = 0 GeV
>1160	95	[45] SIRUNYAN	18AL	CMS	$\geq 3\ell^\pm$ + jets + $\not{E}_T$, Tglu1C, $m_{\widetilde{\chi}^0_2} = m_{\widetilde{\chi}^\pm_1} = (m_{\widetilde{g}} + m_{\widetilde{\chi}^0_1})/2$, $m_{\widetilde{\chi}^0_1}$ = 0 GeV
>1500	95	[46] SIRUNYAN	18AR	CMS	$\ell^\pm\ell^\mp$ + jets + $\not{E}_T$, GMSB, Tglu4C, $m_{\widetilde{\chi}^0_1}$ = 100 GeV
>1770	95	[46] SIRUNYAN	18AR	CMS	$\ell^\pm\ell^\mp$ + jets + $\not{E}_T$, GMSB, Tglu4C, $m_{\widetilde{\chi}^0_1}$ = 1400 GeV
>1625	95	[47] SIRUNYAN	18AY	CMS	jets+$\not{E}_T$, Tglu1A, $m_{\widetilde{\chi}^0_1}$ = 0 GeV
>1825	95	[47] SIRUNYAN	18AY	CMS	jets+$\not{E}_T$, Tglu2A, $m_{\widetilde{\chi}^0_1}$ = 0 GeV
>1625	95	[47] SIRUNYAN	18AY	CMS	jets+$\not{E}_T$, Tglu3A, $m_{\widetilde{\chi}^0_1}$ = 0 GeV
>2040	95	[48] SIRUNYAN	18D	CMS	top quark (hadronically decaying) + jets + $\not{E}_T$, Tglu3A, $m_{\widetilde{\chi}^0_1}$ = 0 GeV
>1930	95	[48] SIRUNYAN	18D	CMS	top quark (hadronically decaying) + jets + $\not{E}_T$, Tglu3B, $m_{\widetilde{t}_1} - m_{\widetilde{\chi}^0_1}$ = 175 GeV, $m_{\widetilde{\chi}^0_1}$ = 200 GeV
>1690	95	[48] SIRUNYAN	18D	CMS	top quark (hadronically decaying) + jets + $\not{E}_T$, Tglu3C, $m_{\widetilde{t}_1} - m_{\widetilde{\chi}^0_1}$ = 20 GeV, $m_{\widetilde{\chi}^0_1}$ = 0 GeV
>1990	95	[48] SIRUNYAN	18D	CMS	top quark (hadronically decaying) + jets + $\not{E}_T$, Tglu3E, $m_{\widetilde{\chi}^\pm_1} = m_{\widetilde{\chi}^0_1}$ + 5 GeV, $m_{\widetilde{\chi}^0_1}$ = 100 GeV
>2010	95	[49] SIRUNYAN	18M	CMS	$\geq 1\ H\ (\rightarrow\ bb)$ + $\not{E}_T$, Tglu1I
>1825	95	[49] SIRUNYAN	18M	CMS	$\geq 1\ H\ (\rightarrow\ bb)$ + $\not{E}_T$, Tglu1J
>1750	95	[50] AABOUD	17AJ	ATLS	same-sign $\ell^\pm\ell^\pm$ / 3 ℓ + jets + $\not{E}_T$, Tglu3A, $m_{\widetilde{\chi}^0_1}$ = 100 GeV
>1570	95	[51] AABOUD	17AJ	ATLS	same-sign $\ell^\pm\ell^\pm$ / 3 ℓ + jets + $\not{E}_T$, Tglu1E, $m_{\widetilde{\chi}^0_1}$ = 100 GeV
>1860	95	[52] AABOUD	17AJ	ATLS	same-sign $\ell^\pm\ell^\pm$ / 3 ℓ + jets + $\not{E}_T$, Tglu1G, $m_{\widetilde{\chi}^0_1}$ = 200 GeV
>2100	95	[53] AABOUD	17AR	ATLS	1ℓ+jets+$\not{E}_T$, Tglu1B, $m_{\widetilde{\chi}^0_1}$ = 0 GeV
>1740	95	[54] AABOUD	17AR	ATLS	1ℓ+jets+$\not{E}_T$, Tglu1E, $m_{\widetilde{\chi}^0_1}$ = 0 GeV
>1800	95	[55] AABOUD	17AY	ATLS	jets+$\not{E}_T$, Tglu3A, $m_{\widetilde{t}_1} - m_{\widetilde{\chi}^0_1}$ = 5 GeV
>1800	95	[56] AABOUD	17AZ	ATLS	$\geq$ 7 jets+$\not{E}_T$, large R-jets and/or b-jets, Tglu1E, $m_{\widetilde{\chi}^0_1}$ = 100 GeV
>1540	95	[57] AABOUD	17AZ	ATLS	$\geq$ 7 jets+$\not{E}_T$, large R-jets and/or b-jets, Tglu3A, $m_{\widetilde{\chi}^0_1}$ = 0 GeV
>1340	95	[58] AABOUD	17N	ATLS	2 same-flavor, opposite-sign ℓ + jets + $\not{E}_T$, Tglu1H, $m_{\widetilde{\chi}^0_1}$ = 0 GeV
>1310	95	[59] AABOUD	17N	ATLS	2 same-flavor, opposite-sign ℓ + jets + $\not{E}_T$, Tglu1H, $m_{\widetilde{\chi}^0_2}$ = ($m_{\widetilde{g}}$+$m_{\widetilde{\chi}^0_1}$)/2, $m_{\widetilde{\chi}^0_1}$ < 400 GeV
>1700	95	[60] AABOUD	17N	ATLS	2 same-flavor, opposite-sign ℓ + jets + $\not{E}_T$, Tglu1G, $m_{\widetilde{\chi}^0_1}$ ~ 1 GeV
>1400	95	[61] KHACHATRY...17		CMS	jets+$\not{E}_T$,Tglu1A,$m_{\widetilde{\chi}^0_1}$=200GeV
>1650	95	[61] KHACHATRY...17		CMS	jets+$\not{E}_T$,Tglu2A,$m_{\widetilde{\chi}^0_1}$=200 GeV
>1600	95	[61] KHACHATRY...17		CMS	jets+$\not{E}_T$,Tglu3A,$m_{\widetilde{\chi}^0_1}$=200GeV

Int. J. Mod. Phys. A 2026.41. Downloaded from www.worldscientific.com
by UNIVERSITY OF CALIFORNIA @ BERKELEY on 09/16/26. Re-use and distribution is strictly not permitted, except for Open Access articles.

Int. J. Mod. Phys. A 2026.41. Downloaded from www.worldscientific.com
by UNIVERSITY OF CALIFORNIA @ BERKELEY on 09/16/26. Re-use and distribution is strictly not permitted, except for Open Access articles.

>1550	95	[62] KHACHATRY...17AD	CMS	jets+b-jets+$\not{E}_T$, Tglu3A, $m_{\widetilde{\chi}^0_1}$ = 0 GeV
>1450	95	[63] KHACHATRY...17AD	CMS	jets+b-jets+$\not{E}_T$, Tglu3C, 200 < $m_{\widetilde{\chi}^0_1}$ < 400 GeV
>1570	95	[64] KHACHATRY...17AS	CMS	1ℓ, Tglu3A, $m_{\widetilde{\chi}^0_1}$ < 600 GeV
>1500	95	[64] KHACHATRY...17AS	CMS	1ℓ, Tglu3A, $m_{\widetilde{\chi}^0_1}$ < 775 GeV
>1400	95	[64] KHACHATRY...17AS	CMS	1ℓ, Tglu1B, $m_{\widetilde{\chi}^\pm_1}$ = ($m_{\widetilde{g}}$ + $m_{\widetilde{\chi}^0_1}$)/2, $m_{\widetilde{\chi}^0_1}$ < 725 GeV
none 1050–1350	95	[64] KHACHATRY...17AS	CMS	1ℓ, Tglu1B, $m_{\widetilde{\chi}^\pm_1}$ = ($m_{\widetilde{g}}$ + $m_{\widetilde{\chi}^0_1}$)/2, $m_{\widetilde{\chi}^0_1}$ < 850 GeV
>1175	95	[65] KHACHATRY...17AW	CMS	$\geq 3\ell^\pm$, 2 jets, Tglu3A, $m_{\widetilde{\chi}^0_1}$ = 0 GeV
> 825	95	[65] KHACHATRY...17AW	CMS	$\geq 3\ell^\pm$, 2 jets, Tglu1C, $m_{\widetilde{\chi}^\pm_1}$ = ($m_{\widetilde{g}}$ + $m_{\widetilde{\chi}^0_1}$)/2, $m_{\widetilde{\chi}^0_1}$ = 0 GeV
>1350	95	[66] KHACHATRY...17P	CMS	1 or more jets+$\not{E}_T$, Tglu1A, $m_{\widetilde{\chi}^0_1}$ = 0 GeV
>1545	95	[66] KHACHATRY...17P	CMS	1 or more jets+$\not{E}_T$, Tglu2A, $m_{\widetilde{\chi}^0_1}$ = 0 GeV
>1120	95	[66] KHACHATRY...17P	CMS	1 or more jets+$\not{E}_T$, Tglu3A, $m_{\widetilde{\chi}^0_1}$ = 0 GeV
>1300	95	[66] KHACHATRY...17P	CMS	1 or more jets+$\not{E}_T$, Tglu3D, $m_{\widetilde{\chi}^\pm_1}$ = $m_{\widetilde{\chi}^0_1}$ + 5 GeV, $m_{\widetilde{\chi}^0_1}$ = 100 GeV
> 780	95	[66] KHACHATRY...17P	CMS	1 or more jets+$\not{E}_T$, Tglu3B, $m_{\widetilde{t}_1}$ − $m_{\widetilde{\chi}^0_1}$ = 175 GeV, $m_{\widetilde{\chi}^0_1}$ = 50 GeV
> 790	95	[66] KHACHATRY...17P	CMS	1 or more jets+$\not{E}_T$, Tglu3C, $m_{\widetilde{t}_1}$ − $m_{\widetilde{\chi}^0_1}$ = 20 GeV, $m_{\widetilde{\chi}^0_1}$ = 0 GeV
>1650	95	[67] KHACHATRY...17V	CMS	2 γ + $\not{E}_T$, GGM, Tglu4B, any NLSP mass
>1900	95	[68] SIRUNYAN 17AF	CMS	1ℓ+jets+b-jets+$\not{E}_T$, Tglu3A, $m_{\widetilde{\chi}^0_1}$ = 0 GeV
>1600	95	[68] SIRUNYAN 17AF	CMS	1ℓ+jets+b-jets+$\not{E}_T$, Tglu3B, $m_{\widetilde{t}_1}$ − $m_{\widetilde{\chi}^0_1}$ = 175 GeV, $m_{\widetilde{\chi}^0_1}$ = 50 GeV
>1800	95	[69] SIRUNYAN 17AY	CMS	γ + jets+$\not{E}_T$, Tglu4B, $m_{\widetilde{\chi}^0_1}$ = 0 GeV
>1600	95	[69] SIRUNYAN 17AY	CMS	γ + jets+$\not{E}_T$, Tglu4A, $m_{\widetilde{\chi}^0_1}$ = 0 GeV
>1860	95	[70] SIRUNYAN 17AZ	CMS	$\geq$ 1 jets + $\not{E}_T$, Tglu1A, $m_{\widetilde{\chi}^0_1}$ = 0 GeV
>2025	95	[70] SIRUNYAN 17AZ	CMS	$\geq$ 1 jets+$\not{E}_T$, Tglu2A, $m_{\widetilde{\chi}^0_1}$ = 0 GeV
>1900	95	[70] SIRUNYAN 17AZ	CMS	$\geq$ 1 jets+$\not{E}_T$, Tglu3A, $m_{\widetilde{\chi}^0_1}$ = 0 GeV
>1825	95	[71] SIRUNYAN 17P	CMS	jets+$\not{E}_T$, Tglu1A, $m_{\widetilde{\chi}^0_1}$ = 0 GeV
>1950	95	[71] SIRUNYAN 17P	CMS	jets+$\not{E}_T$, Tglu2A, $m_{\widetilde{\chi}^0_1}$ = 0 GeV
>1960	95	[71] SIRUNYAN 17P	CMS	jets+$\not{E}_T$, Tglu3A, $m_{\widetilde{\chi}^0_1}$ = 0 GeV
>1800	95	[71] SIRUNYAN 17P	CMS	jets+$\not{E}_T$, Tglu1C, $m_{\widetilde{\chi}^\pm_1}$ = $m_{\widetilde{\chi}^0_2}$ = ($m_{\widetilde{g}}$+$m_{\widetilde{\chi}^0_1}$)/2, $m_{\widetilde{\chi}^0_1}$ = 0 GeV
>1870	95	[71] SIRUNYAN 17P	CMS	jets+$\not{E}_T$, Tglu3D, $m_{\widetilde{\chi}^\pm_1}$ = $m_{\widetilde{\chi}^0_1}$ + 5 GeV, $m_{\widetilde{\chi}^0_1}$ = 1000 GeV
>1520	95	[72] SIRUNYAN 17S	CMS	same-sign $\ell^\pm\ell^\pm$ + jets + $\not{E}_T$, Tglu3A, $m_{\widetilde{\chi}^0_1}$ = 0 GeV
>1200	95	[72] SIRUNYAN 17S	CMS	same-sign $\ell^\pm\ell^\pm$ + jets + $\not{E}_T$, Tglu3D, $m_{\widetilde{\chi}^\pm_1}$ = $m_{\widetilde{\chi}^0_1}$ + 5 GeV, $m_{\widetilde{\chi}^0_1}$ = 100 GeV
>1370	95	[72] SIRUNYAN 17S	CMS	same-sign $\ell^\pm\ell^\pm$ + jets + $\not{E}_T$, Tglu3B, $m_{\widetilde{t}_1}$ − $m_{\widetilde{\chi}^0_1}$ = 175 GeV, $m_{\widetilde{\chi}^0_1}$ = 50 GeV
>1180	95	[72] SIRUNYAN 17S	CMS	same-sign $\ell^\pm\ell^\pm$ + jets + $\not{E}_T$, Tglu3C, $m_{\widetilde{t}_1}$ − $m_{\widetilde{\chi}^0_1}$ = 20 GeV, $m_{\widetilde{\chi}^0_1}$ = 0 GeV
>1280	95	[72] SIRUNYAN 17S	CMS	same-sign $\ell^\pm\ell^\pm$ + jets + $\not{E}_T$, Tglu1B, $m_{\widetilde{\chi}^\pm_1}$ = ($m_{\widetilde{g}}$ + $m_{\widetilde{\chi}^0_1}$)/2, $m_{\widetilde{\chi}^0_1}$ = 0 GeV
>1300	95	[72] SIRUNYAN 17S	CMS	same-sign $\ell^\pm\ell^\pm$ + jets + $\not{E}_T$, Tglu1B, $m_{\widetilde{t}_1}$ − $m_{\widetilde{\chi}^0_1}$ = 20 GeV, $m_{\widetilde{\chi}^0_1}$ = 100 GeV
>1570	95	[73] AABOUD 16AC	ATLS	$\geq$ 2 jets + 1 or 2 τ + $\not{E}_T$, Tglu1F, $m_{\widetilde{\chi}^0_1}$ = 100 GeV
>1460	95	[74] AABOUD 16J	ATLS	1 $\ell^\pm$ + $\geq$ 4 jets + $\not{E}_T$, Tglu3C, $m_{\widetilde{t}_1}$ − $m_{\widetilde{\chi}^0_1}$ = 5 GeV
>1650	95	[75] AABOUD 16M	ATLS	2 γ + $\not{E}_T$, Tglu1D, any NLSP mass
>1510	95	[76] AABOUD 16N	ATLS	$\geq$ 4 jets + $\not{E}_T$, Tglu1A, $m_{\widetilde{\chi}^0_1}$ = 0 GeV
>1500	95	[77] AABOUD 16N	ATLS	$\geq$ 4 jets + $\not{E}_T$, Tglu1B, $m_{\widetilde{\chi}^\pm_1}$ = ($m_{\widetilde{g}}$+$m_{\widetilde{\chi}^0_1}$)/2, $m_{\widetilde{\chi}^0_1}$=200GeV
>1780	95	[78] AAD 16AD	ATLS	0ℓ, $\geq$ 3 b-jets + $\not{E}_T$, Tglu2A, $m_{\widetilde{\chi}^0_1}$ < 800 GeV
>1760	95	[79] AAD 16AD	ATLS	1ℓ, $\geq$ 3 b-jets + $\not{E}_T$, Tglu3A, $m_{\widetilde{\chi}^0_1}$ < 700 GeV
>1300	95	[80] AAD 16BB	ATLS	2 same-sign/3ℓ + jets + $\not{E}_T$, Tglu1D, $m_{\widetilde{\chi}^0_1}$ < 600 GeV
>1100	95	[80] AAD 16BB	ATLS	2 same-sign/3ℓ + jets + $\not{E}_T$, Tglu1E, $m_{\widetilde{\chi}^0_1}$ < 300 GeV
>1200	95	[80] AAD 16BB	ATLS	2 same-sign /3ℓ + jets + $\not{E}_T$, Tglu3A, $m_{\widetilde{\chi}^0_1}$ < 600 GeV
>1600		[81] AAD 16BG	ATLS	1ℓ, $\geq$ 4 jets, $\not{E}_T$, Tglu1B, $m_{\widetilde{\chi}^\pm_1}$= ($m_{\widetilde{g}}$ + $m_{\widetilde{\chi}^0_1}$)/2, $m_{\widetilde{\chi}^0_1}$= 100 GeV
>1400	95	[82] AAD 16V	ATLS	$\geq$ 7 to $\geq$ 10 jets + $\not{E}_T$, Tglu1E, $m_{\widetilde{\chi}^0_1}$ < 200 GeV
>1400	95	[82] AAD 16V	ATLS	$\geq$ 7 to $\geq$ 10 jets + $\not{E}_T$, pMSSM M_1 = 60 GeV, M_2 = 3 TeV, tanβ=10, μ < 0
>1100	95	[83] KHACHATRY...16AM	CMS	boosted W+b, Tglu3C, $m_{\widetilde{t}_1}$ − $m_{\widetilde{\chi}^0_1}$ <80GeV,$m_{\widetilde{\chi}^0_1}$ <400GeV
> 700	95	[83] KHACHATRY...16AM	CMS	boosted W+b, Tglu3B, $m_{\widetilde{t}_1}$ − $m_{\widetilde{\chi}^0_1}$=175 GeV, $m_{\widetilde{\chi}^0_1}$=0 GeV
>1050	95	[84] KHACHATRY...16BJ	CMS	same-sign $\ell^\pm\ell^\pm$, Tglu3A, $m_{\widetilde{\chi}^0_1}$ < 800 GeV
>1300	95	[84] KHACHATRY...16BJ	CMS	same-sign $\ell^\pm\ell^\pm$,Tglu3A,$m_{\widetilde{\chi}^0_1}$=0
>1140	95	[84] KHACHATRY...16BJ	CMS	same-sign $\ell^\pm\ell^\pm$, Tglu3B, $m_{\widetilde{t}}$ − $m_{\widetilde{\chi}^0_1}$ = 20 GeV, $m_{\widetilde{\chi}^0_1}$ = 0
> 850	95	[84] KHACHATRY...16BJ	CMS	same-sign $\ell^\pm\ell^\pm$, Tglu3B, $m_{\widetilde{t}}$− $m_{\widetilde{\chi}^0_1}$=20 GeV,$m_{\widetilde{\chi}^0_1}$ <700 GeV
> 950	95	[84] KHACHATRY...16BJ	CMS	same-sign $\ell^\pm\ell^\pm$, Tglu3D, $m_{\widetilde{\chi}^\pm_1}$ = $m_{\widetilde{\chi}^0_1}$ + 5 GeV
>1100	95	[84] KHACHATRY...16BJ	CMS	same-sign $\ell^\pm\ell^\pm$,Tglu1B,$m_{\widetilde{\chi}^\pm_1}$= 0.5($m_{\widetilde{g}}$+$m_{\widetilde{\chi}^0_1}$),$m_{\widetilde{\chi}^0_1}$ <400GeV
> 830	95	[84] KHACHATRY...16BJ	CMS	same-sign $\ell^\pm\ell^\pm$,Tglu1B,$m_{\widetilde{\chi}^\pm_1}$= 0.5($m_{\widetilde{g}}$+$m_{\widetilde{\chi}^0_1}$),$m_{\widetilde{\chi}^0_1}$ <700GeV
>1300	95	[84] KHACHATRY...16BJ	CMS	same-sign $\ell^\pm\ell^\pm$, Tglu3B, $m_{\widetilde{t}}$ − $m_{\widetilde{\chi}^0_1}$ = m_t, $m_{\widetilde{\chi}^0_1}$ = 0
>1050	95	[84] KHACHATRY...16BJ	CMS	same-sign $\ell^\pm\ell^\pm$, Tglu3B, $m_{\widetilde{t}}$ − $m_{\widetilde{\chi}^0_1}$ = m_t, $m_{\widetilde{\chi}^0_1}$ < 800 GeV
>1725	95	[85] KHACHATRY...16BS	CMS	jets + $\not{E}_T$, Tglu1A, $m_{\widetilde{\chi}^0_1}$ = 0
>1750	95	[85] KHACHATRY...16BS	CMS	jets + $\not{E}_T$, Tglu2A, $m_{\widetilde{\chi}^0_1}$ = 0
>1550	95	[85] KHACHATRY...16BS	CMS	jets + $\not{E}_T$, Tglu3A, $m_{\widetilde{\chi}^0_1}$ = 0
>1280	95	[86] KHACHATRY...16BY	CMS	opposite-sign $\ell^\pm\ell^\pm$, Tglu4C, $m_{\widetilde{\chi}^0_1}$ = 1000 GeV
>1030	95	[86] KHACHATRY...16BY	CMS	opposite-sign $\ell^\pm\ell^\pm$, Tglu4C, $m_{\widetilde{\chi}^0_1}$ = 0 GeV
>1440	95	[87] KHACHATRY...16V	CMS	jets + $\not{E}_T$, Tglu1A, $m_{\widetilde{\chi}^0_1}$ = 0
>1600	95	[87] KHACHATRY...16V	CMS	jets + $\not{E}_T$, Tglu2A, $m_{\widetilde{\chi}^0_1}$ = 0
>1550	95	[87] KHACHATRY...16V	CMS	jets + $\not{E}_T$, Tglu3A, $m_{\widetilde{\chi}^0_1}$ = 0
>1450	95	[87] KHACHATRY...16V	CMS	jets + $\not{E}_T$, Tglu1C, $m_{\widetilde{\chi}^0_1}$ = 0
> 820	95	[88] AAD 15BG	ATLS	GGM, $\widetilde{g} \rightarrow q\bar{q}Z\widetilde{G}$, tan$\beta$ = 30, μ > 600 GeV
> 850	95	[88] AAD 15BG	ATLS	GGM, $\widetilde{g} \rightarrow q\bar{q}Z\widetilde{G}$, tan$\beta$ = 1.5, μ > 450 GeV
>1150	95	[89] AAD 15BV	ATLS	general RPC $\widetilde{g}$ decays, $m_{\widetilde{\chi}^0_1}$ < 100 GeV
> 700	95	[90] AAD 15BX	ATLS	$\widetilde{g} \rightarrow X\widetilde{\chi}^0_1$, independent of $m_{\widetilde{\chi}^0_1}$
>1290	95	[91] AAD 15CA	ATLS	$\geq$ 2 γ + $\not{E}_T$, GGM, bino-like NLSP, any NLSP mass

Int. J. Mod. Phys. A 2026.41. Downloaded from www.worldscientific.com
by UNIVERSITY OF CALIFORNIA @ BERKELEY on 09/16/26. Re-use and distribution is strictly not permitted, except for Open Access articles.

>1260	95	[91] AAD	15CA	ATLS	$\geq 1\ \gamma + b$-jets $+ \not{E}_T$, GGM, higgsino-bino admix. NLSP and $\mu < 0$, m(NLSP)>450 GeV
>1140	95	[91] AAD	15CA	ATLS	$\geq 1\ \gamma$ + jets $+ \not{E}_T$, GGM, higgsino-bino admixture NLSP, all $\mu > 0$
>1225	95	[92] KHACHATRY...	15AF	CMS	$\tilde{g} \rightarrow q\overline{q}\tilde{\chi}^0_1$, $m_{\tilde{\chi}^0_1} = 0$
>1300	95	[92] KHACHATRY...	15AF	CMS	$\tilde{g} \rightarrow b\overline{b}\tilde{\chi}^0_1$, $m_{\tilde{\chi}^0_1} = 0$
>1225	95	[92] KHACHATRY...	15AF	CMS	$\tilde{g} \rightarrow t\overline{t}\tilde{\chi}^0_1$, $m_{\tilde{\chi}^0_1} = 0$
>1550	95	[92] KHACHATRY...	15AF	CMS	CMSSM, $\tan\beta$=30, $m_{\tilde{g}}$=$m_{\tilde{q}}$, A_0=$-2\max(m_0,m_{1/2})$, $\mu > 0$
>1150	95	[92] KHACHATRY...	15AF	CMS	CMSSM, $\tan\beta$=30, A_0=$-2\max(m_0,m_{1/2})$, $\mu > 0$
>1280	95	[93] KHACHATRY...	15I	CMS	$\tilde{g} \rightarrow t\overline{t}\tilde{\chi}^0_1$, $m_{\tilde{\chi}^0_1} = 0$
>1310	95	[94] KHACHATRY...	15X	CMS	$\tilde{g} \rightarrow b\overline{b}\tilde{\chi}^0_1$, $m_{\tilde{\chi}^0_1} = 100$ GeV
>1175	95	[94] KHACHATRY...	15X	CMS	$\tilde{g} \rightarrow t\overline{t}\tilde{\chi}^0_1$, $m_{\tilde{\chi}^0_1} = 100$ GeV
>1330	95	[95] AAD	14AE	ATLS	jets $+ \not{E}_T$, $\tilde{g} \rightarrow q\overline{q}\tilde{\chi}^0_1$ simplified model, $m_{\tilde{\chi}^0_1} = 0$ GeV
>1700	95	[95] AAD	14AE	ATLS	jets $+ \not{E}_T$, mSUGRA/CMSSM, $m_{\tilde{q}} = m_{\tilde{g}}$
>1090	95	[96] AAD	14AG	ATLS	τ + jets $+ \not{E}_T$, natural Gauge Mediation
>1600	95	[96] AAD	14AG	ATLS	τ + jets $+ \not{E}_T$, mGMSB, M_{mess} = 250 GeV, $N_5 = 3$, $\mu > 0$, $C_{grav} = 1$
> 640	95	[97] AAD	14X	ATLS	$\geq 4\ell^{\pm}$, $\tilde{g} \rightarrow q\overline{q}\tilde{\chi}^0_1$, $\tilde{\chi}^0_1 \rightarrow \ell^{\pm}\ell^{\mp}\tilde{G}$, $\tan\beta = 30$, GGM
>1000	95	[98] CHATRCHYAN	14AH	CMS	jets $+ \not{E}_T$, $\tilde{g} \rightarrow q\overline{q}\tilde{\chi}^0_1$ simplified model, $m_{\tilde{\chi}^0_1} = 50$ GeV
>1350	95	[98] CHATRCHYAN	14AH	CMS	jets $+ \not{E}_T$, CMSSM, $m_{\tilde{g}} = m_{\tilde{q}}$
>1000	95	[99] CHATRCHYAN	14AH	CMS	jets $+ \not{E}_T$, $\tilde{g} \rightarrow b\overline{b}\tilde{\chi}^0_1$ simplified model, $m_{\tilde{\chi}^0_1} = 50$ GeV
>1000	95	[100] CHATRCHYAN	14AH	CMS	jets $+ \not{E}_T$, $\tilde{g} \rightarrow t\overline{t}\tilde{\chi}^0_1$ simplified model, $m_{\tilde{\chi}^0_1} = 50$ GeV
>1160	95	[101] CHATRCHYAN	14I	CMS	jets $+ \not{E}_T$, $\tilde{g} \rightarrow q\overline{q}\tilde{\chi}^0_1$ simplified model, $m_{\tilde{\chi}^0_1} < 100$ GeV
>1130	95	[101] CHATRCHYAN	14I	CMS	multijets $+ \not{E}_T$, $\tilde{g} \rightarrow t\overline{t}\tilde{\chi}^0_1$ simplified model, $m_{\tilde{\chi}^0_1} < 100$ GeV
>1210	95	[101] CHATRCHYAN	14I	CMS	multijets $+ \not{E}_T$, $\tilde{g} \rightarrow q\overline{q}W/Z\tilde{\chi}^0_1$ simplified model, $m_{\tilde{\chi}^0_1} < 100$ GeV
>1260	95	[102] CHATRCHYAN	14N	CMS	$1\ell^{\pm}$ + jets + $\geq 2b$-jets, $\tilde{g} \rightarrow t\overline{t}\tilde{\chi}^0_1$ simplified model, $m_{\tilde{\chi}^0_1}$=0 GeV, $m_{\tilde{t}} > m_{\tilde{g}}$
		[103] CHATRCHYAN	14R	CMS	$\geq 3\ell^{\pm}$, $(\tilde{g}/\tilde{q}) \rightarrow q\ell^{\pm}\ell^{\mp}\tilde{G}$ simplified model, GMSB, slepton co-NLSP scenario
		[104] CHATRCHYAN	14R	CMS	$\geq 3\ell^{\pm}$, $\tilde{g} \rightarrow t\overline{t}\tilde{\chi}^0_1$ simplified model
• • • We do not use the following data for averages, fits, limits, etc. • • •					
>1500	95	[105] AABOUD	18BJ	ATLS	$\ell^{\pm}\ell^{\mp}$ + jets $+ \not{E}_T$, Tglu1H, $m_{\tilde{\chi}^0_1} = 1$ GeV, any $m_{\tilde{\chi}^0_2}$
>1770	95	[106] AABOUD	18V	ATLS	jets$+\not{E}_T$, Tglu1C-like, 1/2 BR per decay mode, any $m_{\tilde{\chi}^0_2}-m_{\tilde{\chi}^0_1}$, $m_{\tilde{\chi}^0_1} = 60$ GeV
>1600	95	[107] AABOUD	17AZ	ATLS	≥ 7 jets$+\not{E}_T$, large R-jets and/or b-jets, pMSSM, $m_{\tilde{\chi}^{\pm}_1} = 200$ GeV
>1600	95	[108] KHACHATRY...	16AY	CMS	$1\ell^{\pm}$ + jets + b-jets $+ \not{E}_T$, Tglu3A, $m_{\tilde{\chi}^0_1} = 0$ GeV
> 500	95	[109] KHACHATRY...	16BT	CMS	19-parameter pMSSM model, global Bayesian analysis, flat prior
		[110] AAD	15AB	ATLS	$\tilde{g} \rightarrow \tilde{S}g$, $c\tau = 1$ m, $\tilde{S} \rightarrow S\tilde{G}$ and $S \rightarrow gg$, BR = 100%
		[111] AAD	15AI	ATLS	$\ell^{\pm}$ + jets $+ \not{E}_T$
>1600	95	[89] AAD	15BV	ATLS	pMSSM, M_1 = 60 GeV, $m_{\tilde{q}} < 1500$ GeV
>1280	95	[89] AAD	15BV	ATLS	mSUGRA, $m_0 > 2$ TeV
>1100	95	[89] AAD	15BV	ATLS	via $\tilde{\tau}$, natural GMSB, all $m_{\tilde{\tau}}$
>1330	95	[89] AAD	15BV	ATLS	jets $+ \not{E}_T$, $\tilde{g} \rightarrow q\overline{q}\tilde{\chi}^0_1$, $m_{\tilde{\chi}^0_1} = 1$ GeV
>1500	95	[89] AAD	15BV	ATLS	jets $+ \not{E}_T$, $\tilde{g} \rightarrow \tilde{q}q$, $\tilde{q} \rightarrow q\tilde{\chi}^0_1$, $m_{\tilde{\chi}^0_1} = 1$ GeV
>1650	95	[89] AAD	15BV	ATLS	jets $+ \not{E}_T$, $m_{\tilde{g}} = m_{\tilde{q}}$, $m_{\tilde{\chi}^0_1} = 1$ GeV
> 850	95	[89] AAD	15BV	ATLS	jets $+ \not{E}_T$, $\tilde{g} \rightarrow g\tilde{\chi}^0_1$, $m_{\tilde{\chi}^0_1} < 550$ GeV
>1270	95	[89] AAD	15BV	ATLS	jets $+ \not{E}_T$, $\tilde{g} \rightarrow q\overline{q}W\tilde{\chi}^0_1$, $m_{\tilde{\chi}^0_1} = 100$ GeV
>1150	95	[89] AAD	15BV	ATLS	jets $+ \ell^{\pm}\ell^{\pm}$, $\tilde{g} \rightarrow q\overline{q}WZ\tilde{\chi}^0_1$, $m_{\tilde{\chi}^0_1} = 100$ GeV
>1320	95	[89] AAD	15BV	ATLS	jets $+ \ell^{\pm}\ell^{\pm}$, $\tilde{g}$ decays via sleptons, $m_{\tilde{\chi}^0_1} = 100$ GeV
>1220	95	[89] AAD	15BV	ATLS	τ, $\tilde{q}$ decays via staus, $m_{\tilde{\chi}^0_1} = 100$ GeV
>1310	95	[89] AAD	15BV	ATLS	b-jets, $\tilde{g} \rightarrow t\overline{t}\tilde{\chi}^0_1$, $m_{\tilde{\chi}^0_1} < 400$ GeV
>1220	95	[89] AAD	15BV	ATLS	b-jets, $\tilde{g} \rightarrow \tilde{t}_1 t$ and $\tilde{t}_1 \rightarrow t\tilde{\chi}^0_1$, $m_{T_1} < 1000$ GeV
>1180	95	[89] AAD	15BV	ATLS	b-jets, $\tilde{g} \rightarrow \tilde{t}_1 t$ and $\tilde{t}_1 \rightarrow b\tilde{\chi}^{\pm}_1$, $m_{T_1} < 1000$ GeV, $m_{\tilde{\chi}^0_1} = 60$ GeV
>1260	95	[89] AAD	15BV	ATLS	b-jets, $\tilde{g} \rightarrow \tilde{t}_1 t$ and $\tilde{g} \rightarrow c\tilde{\chi}^0_1$
>1200	95	[89] AAD	15BV	ATLS	b-jets, $\tilde{g} \rightarrow \tilde{b}_1 b$ and $\tilde{b}_1 \rightarrow b\tilde{\chi}^0_1$, $m_{\tilde{b}_1} < 1000$ GeV
>1250	95	[89] AAD	15BV	ATLS	b-jets, $\tilde{g} \rightarrow b\overline{b}\tilde{\chi}^0_1$, $m_{\tilde{\chi}^0_1} < 400$ GeV
none, 750–1250	95	[89] AAD	15BV	ATLS	b-jets, $\tilde{g}$ decay via offshell $\tilde{t}_1$ and $\tilde{b}_1$, $m_{\tilde{\chi}^0_1} < 500$ GeV
>1100	95	[112] AAD	15CB	ATLS	jets, $\tilde{g} \rightarrow qq\tilde{\chi}^0_1$, $\tilde{\chi}^0_1 \rightarrow Z\tilde{G}$, GGM, $m_{\tilde{\chi}^0_1} = 400$ GeV and $3 < c\tau_{\tilde{\chi}^0_1} < 500$ mm
>1400	95	[112] AAD	15CB	ATLS	jets or $\not{E}_T$, $\tilde{g} \rightarrow qq\tilde{\chi}^0_1$, Split SUSY, $m_{\tilde{\chi}^0_1} = 100$ GeV and $15 < c\tau < 300$ mm
>1500	95	[112] AAD	15CB	ATLS	$\not{E}_T$, $\tilde{g} \rightarrow qq\tilde{\chi}^0_1$, Split SUSY, $m_{\tilde{\chi}^0_1} = 100$ GeV and $20 < c\tau < 250$ mm
		[113] KHACHATRY...	15AD	CMS	$\ell^{\pm}\ell^{\mp}$ + jets $+ \not{E}_T$, GMSB, $\tilde{g} \rightarrow q\overline{q}Z\tilde{G}$
>1300	95	[114] KHACHATRY...	15AZ	CMS	$\geq 2\ \gamma$, ≥ 1 jet, (Razor), bino-like NLSP, $m_{\tilde{\chi}^0_1} = 375$ GeV
> 800	95	[114] KHACHATRY...	15AZ	CMS	$\geq 1\ \gamma$, ≥ 2 jet, wino-like NLSP, $m_{\tilde{\chi}^0_1} = 375$ GeV
>1280	95	[115] AAD	14AX	ATLS	$\geq 3\ b$-jets $+ \not{E}_T$, CMSSM
>1250	95	[115] AAD	14AX	ATLS	$\geq 3\ b$-jets $+ \not{E}_T$, $\tilde{g} \rightarrow \tilde{b}_1 b\tilde{\chi}^0_1$ simplified model, $\tilde{b}_1 \rightarrow b\tilde{\chi}^0_1$, $m_{\tilde{\chi}^0_1} = 60$ GeV, $m_{\tilde{b}_1} < 900$ GeV
>1190	95	[115] AAD	14AX	ATLS	$\geq 3\ b$-jets $+ \not{E}_T$, $\tilde{g} \rightarrow \tilde{t}_1 t\tilde{\chi}^0_1$ simplified model, $\tilde{t}_1 \rightarrow t\tilde{\chi}^0_1$, $m_{\tilde{\chi}^0_1} = 60$ GeV, $m_{\tilde{t}_1} < 1000$ GeV
>1180	95	[115] AAD	14AX	ATLS	$\geq 3\ b$-jets $+ \not{E}_T$, $\tilde{g} \rightarrow \tilde{t}_1 t\tilde{\chi}^0_1$ simplified model, $\tilde{t}_1 \rightarrow b\tilde{\chi}^{\pm}_1$, $m_{\tilde{\chi}^{\pm}_1}$=2$m_{\tilde{\chi}^0_1}$, $m_{\tilde{\chi}^0_1}$=60 GeV, $m_{\tilde{t}_1}$<1000 GeV
>1250	95	[115] AAD	14AX	ATLS	$\geq 3\ b$-jets $+ \not{E}_T$, $\tilde{g} \rightarrow b\overline{b}\tilde{\chi}^0_1$ simplified model, $m_{\tilde{\chi}^0_1} < 400$ GeV
>1340	95	[115] AAD	14AX	ATLS	$\geq 3\ b$-jets $+ \not{E}_T$, $\tilde{g} \rightarrow t\overline{t}\tilde{\chi}^0_1$ simplified model, $m_{\tilde{\chi}^0_1} < 400$ GeV
>1300	95	[115] AAD	14AX	ATLS	$\geq 3\ b$-jets $+ \not{E}_T$, $\tilde{g} \rightarrow t\overline{b}\tilde{\chi}^{\pm}_1$ simplified model, $\tilde{\chi}^{\pm}_1 \rightarrow f f'\tilde{\chi}^0_1$, $m_{\tilde{\chi}^{\pm}_1}-m_{\tilde{\chi}^0_1} = 2$ GeV, $m_{\tilde{\chi}^0_1} < 300$ GeV
> 950	95	[116] AAD	14E	ATLS	$\ell^{\pm}\ell^{\pm}(\ell^{\mp})$ + jets, $\tilde{g} \rightarrow t\overline{t}\tilde{\chi}^0_1$ simplified model
>1000	95	[116] AAD	14E	ATLS	$\ell^{\pm}\ell^{\pm}(\ell^{\mp})$ + jets, $\tilde{g} \rightarrow t\tilde{t}_1$ with $\tilde{t}_1 \rightarrow b\tilde{\chi}^{\pm}_1$ simplified model, $m_{\tilde{t}_1} < 200$ GeV, $m_{\tilde{\chi}^{\pm}_1} = 118$ GeV, $m_{\tilde{\chi}^0_1} = 60$ GeV
> 640	95	[116] AAD	14E	ATLS	$\ell^{\pm}\ell^{\pm}(\ell^{\mp})$ + jets, $\tilde{g} \rightarrow t\tilde{t}_1$ with $\tilde{t}_1 \rightarrow c\tilde{\chi}^0_1$ simplified model, $m_{\tilde{t}_1} = m_{\tilde{\chi}^0_1} + 20$ GeV
> 860	95	[116] AAD	14E	ATLS	$\ell^{\pm}\ell^{\pm}(\ell^{\mp})$ + jets, $\tilde{g} \rightarrow qq'\tilde{\chi}^{\pm}_1$, $\tilde{\chi}^{\pm}_1 \rightarrow W^{(*)\pm}\tilde{\chi}^0_1$ simplified model, $m_{\tilde{\chi}^{\pm}_1} = 2\ m_{\tilde{\chi}^0_1}$, $m_{\tilde{\chi}^0_1} < 400$ GeV

>1040	95	[116] AAD	14E	ATLS	$\ell^\pm\ell^\pm(\ell^\mp)$ + jets, $\widetilde{g} \rightarrow q q' \widetilde{\chi}_1^\pm$, $\widetilde{\chi}_1^\pm \rightarrow W^{(*)\pm}\widetilde{\chi}_2^0$, $\widetilde{\chi}_2^0 \rightarrow Z^{(*)}\widetilde{\chi}_1^0$ simplified model, $m_{\widetilde{\chi}_1^0} < 520$ GeV
>1200	95	[116] AAD	14E	ATLS	$\ell^\pm\ell^\pm(\ell^\mp)$ + jets, $\widetilde{g} \rightarrow q q' \widetilde{\chi}_1^\pm/\widetilde{\chi}_2^0$, $\widetilde{\chi}_1^\pm \rightarrow \ell^\pm\nu\widetilde{\chi}_1^0$, $\widetilde{\chi}_2^0 \rightarrow \ell^\pm\ell^\mp(\nu\nu)\widetilde{\chi}_1^0$ simplified model
>1050	95	[117] CHATRCHYAN	14H	CMS	same-sign $\ell^\pm\ell^\pm$, $\widetilde{g} \rightarrow t\overline{t}\widetilde{\chi}_1^0$ simplified model, massless $\widetilde{\chi}_1^0$
> 900	95	[118] CHATRCHYAN	14H	CMS	same-sign $\ell^\pm\ell^\pm$, $\widetilde{g} \rightarrow q q' \widetilde{\chi}_1^\pm$, $\widetilde{\chi}_1^\pm \rightarrow W^\pm\widetilde{\chi}_1^0$ simplified model, $m_{\widetilde{\chi}_1^\pm} = 0.5\ m_{\widetilde{g}}$, massless $\widetilde{\chi}_1^0$
>1050	95	[119] CHATRCHYAN	14H	CMS	same-sign $\ell^\pm\ell^\pm$, $\widetilde{g} \rightarrow b\overline{t}\widetilde{\chi}_1^\pm$, $\widetilde{\chi}_1^\pm \rightarrow W^\pm\widetilde{\chi}_1^0$ simplified model, $m_{\widetilde{\chi}_1^\pm} = 300$ GeV, $m_{\widetilde{\chi}_1^0} = 50$ GeV

[1] AAD 25BM searched in 140 fb^{-1} (at $\sqrt{s}$ = 13 TeV) and 58.6 fb^{-1} (at $\sqrt{s}$ = 13.6 TeV) of pp collisions for an excess of events with taus and $\not{E}_T$. Several signal regions are defined requiring one τ and no other leptons, one τ and one e or μ, or two τ, and then using both a BDT or a cut-and-count analysis to target scenarios with different kinematic regimes. No significant excess over the Standard Model expectation is found. Exclusion limits at 95% C.L. are set on the gluino or squark mass, assuming that the squark (other intermediate or pair-produced) decays to intermediate wino-like $\widetilde{\chi}_1^\pm$ or $\widetilde{\chi}_2^0$, which, in turn, decays to the $\widetilde{\chi}_1^0$ LSP via staus or tau sneutrinos, as in model Tglu1F for gluinos (and similar for squarks). See their Figs. 13 and 14.

[2] AAD 24Z searched in 139 fb^{-1} of pp collisions at $\sqrt{s}$ = 13 TeV for events with exactly two same-sign leptons or at least three leptons. Several signal regions, including a $\not{E}_T$ selection targeting RPC models, and selections based on b-jet multiplicities, targeting RPV models, are considered. No significant excess over the Standard Model expectation is found. Exclusion limits at 95% C.L. are set on the gluino or squark mass, in multi-step RPC decays via charginos, neutralinos or sleptons into quarks, leptons and neutralinos, or RPV decays of either the neutralino LSP or the stop produced in $\widetilde{g} \rightarrow t\overline{t}$ into quarks. See their Fig. 7.

[3] HAYRAPETYAN 24M searched in 137 fb^{-1} of pp collisions at $\sqrt{s}$ = 13 TeV for evidence of wino- and Higgsino-like charginos in final states with one or more disappearing tracks from the decay $\widetilde{\chi}_1^\pm \rightarrow \pi^\pm\widetilde{\chi}_1^0$ where the soft pion is not reconstructed, $\not{E}_T$, and varying numbers of jets, b-tagged jets, electrons, and muons. No significant excess above the Standard Model expectations is observed. Limits are set on the $\widetilde{b}$ mass in the model Tbot1LL for various proper decay lengths cτ of the $\widetilde{\chi}_1^\pm$ as well as on the $\widetilde{t}$ mass in the model Tstop1LL, see their Fig. 10. Limits are also set in the model Tglu1LL, see their Fig. 11. In addition, limits are set in specific pure wino as well as pure higgsino dark matter models, in which the relationships among the electroweakino masses, the $\widetilde{\chi}_1^\pm$ lifetime, and the $\widetilde{\chi}_1^\pm$ decay width are constrained by radiative corrections that account for a large difference between the LSP mass and the SUSY-breaking scale, see their Fig. 12.

[4] HAYRAPETYAN 24P searched in 137 fb^{-1} of pp collisions at $\sqrt{s}$ = 13 TeV for evidence of gluino pair production in events with long-lived particles with mean proper decay lengths between 0.1 and 1000 mm, whose decay products produce a final state with at least one displaced vertex and large $\not{E}_T$. No significant excess above the Standard Model expectations is observed. Limits are set on the $\widetilde{g}$ mass in a model for split SUSY, shown in Fig. 8, where the SUSY breaking scale is assumed to be $\gg 10^6$ TeV, and all scalar masses are set to that scale, except for a single, fine-tuned, Higgs boson mass. The decay is as in the model Tglu1A, but the $\widetilde{g}$ is long-lived because of its decay through a high-mass, virtual squark. Limits are also set in a GMSB model, where the pair-produced $\widetilde{g}$ decays to a gluon and a nearly massless gravitino $\widetilde{G}$, see their Fig. 9.

[5] HAYRAPETYAN 24Q searched in 138 fb^{-1} of pp collisions at $\sqrt{s}$ = 13 TeV for evidence of stealth supersymmetry in final states with two photons and jets, and low $\not{E}_T$. No significant excess above the Standard Model expectations is observed. The investigated models include a singlet scalar boson S, and its SUSY fermion $\widetilde{S}$. In the investigated models, either gluinos or squarks are pair produced and then each decay to a $\widetilde{\chi}_1^0$ and a gluon or squark, respectively, followed by the decays $\widetilde{\chi}_1^0 \rightarrow \gamma\widetilde{S}$, $\widetilde{S} \rightarrow \widetilde{G}S$ and $S \rightarrow gg$. Limits are set on the $\widetilde{g}$ and the $\widetilde{q}$ mass, see their Fig. 4.

[6] AAD 23AB searched in 139 fb^{-1} of pp collisions at $\sqrt{s}$ = 13 TeV for an excess of events with one photon, jets and $\not{E}_T$. No significant excess above the Standard Model predictions is observed. Limits are set on the mass of pair produced gluinos decaying to $\widetilde{g} \rightarrow q q\widetilde{\chi}_1^0$ followed by $\widetilde{\chi}_1^0 \rightarrow \gamma\widetilde{G}$ or $\widetilde{\chi}_1^0 \rightarrow X\widetilde{G}$ with equal probability, see Figure 4. X can be Z (left figure) or h (right figure).

[7] AAD 23AE searched in 139 fb^{-1} of pp collisions at $\sqrt{s}$ = 13 TeV for events with 2 ℓ with same flavour and opposite sign, plus jets and $\not{E}_T$, defining signal region with the dilepton invariant mass both on- and off-shell with respect to the Z boson. No significant excess above the Standard Model predictions is observed. Limits are set on models of strong and electroweak production. In this case, limits are placed on the mass of pair-produced gluinos, assuming a scenario like in Tglu1G, see figure 16.

[8] AAD 23AE searched in 139 fb^{-1} of pp collisions at $\sqrt{s}$ = 13 TeV for events with 2 ℓ with same flavour and opposite sign, plus jets and $\not{E}_T$, defining signal region with the dilepton invariant mass both on- and off-shell with respect to the Z boson. No significant excess above the Standard Model predictions is observed. Limits are set on models of strong and electroweak production. In this case, limits are placed on the gluino mass assuming gluino pair production, assuming a scenario like in Tglu1H, see figure 16.

[9] AAD 23AL searched in 139 fb^{-1} of pp collisions at $\sqrt{s}$ = 13 TeV for events with 0 or 1 lepton and at least three b-tagged jets. No significant excess above the Standard Model prediction is observed. Results are interpreted in terms of gluino pair production followed by the decay of gluinos into off-shell third generation squarks, yielding final states with top and bottom quarks, and missing transverse momentum from a $\widetilde{\chi}_1^0$ LSP. Limits are set on the mass of the gluino as a function of the $\widetilde{\chi}_1^0$ assuming B($\widetilde{g} \rightarrow \widetilde{t}t$) = 100% or B($\widetilde{g} \rightarrow \widetilde{b}b$) = 100%, see figure 10.

[10] AAD 23AL searched in 139 fb^{-1} of pp collisions at $\sqrt{s}$ = 13 TeV for events with 0 or 1 lepton and at least three b-tagged jets. No significant excess above the Standard Model prediction is observed. Results are interpreted in terms of gluino pair production followed by the decay of gluinos into off-shell third generation squarks, yielding final states with top and bottom quarks, and missing transverse momentum from a $\widetilde{\chi}_1^0$ LSP. Limits are set on the mass of the gluino as a function of $m_{\widetilde{\chi}_1^0}$, assuming B($\widetilde{g} \rightarrow \widetilde{t}t$) + B($\widetilde{g} \rightarrow \widetilde{b}b$) + B($\widetilde{g} \rightarrow tb\widetilde{\chi}_1^\pm$) = 100%, and $m_{\widetilde{\chi}_1^\pm} - m_{\widetilde{\chi}_1^0} = 2$ GeV, see figures 11–13.

[11] HAYRAPETYAN 23E searched in 137 fb^{-1} of pp collisions at $\sqrt{s}$ = 13 TeV for evidence of gluino, top squark and electroweakino pair production in events with at least one photon, multiple jets, and large $\not{E}_T$. No significant excess above the Standard Model expectations is observed. Limits are set in models for strong production, Tglu4D, Tglu4E, Tglu4F and Tstop13, see their figure 9. They also interpret the results in the models for electroweak production, shown in their figure 10. Tchi1n1A assumes wino-like $\widetilde{\chi}_1^\pm\widetilde{\chi}_1^0$ production, while Tchi1chi1A assumes higgsino-like cross sections and includes $\widetilde{\chi}_1^\pm\widetilde{\chi}_1^\pm$, $\widetilde{\chi}_1^0\widetilde{\chi}_2^0$ and $\widetilde{\chi}_{1,2}^0\widetilde{\chi}_1^\pm$ production. For $\widetilde{\chi}_1^0\widetilde{\chi}_2^0$ alone no mass point can be excluded in the model Tchi1chi1A, but in another model for $\widetilde{\chi}_1^0\widetilde{\chi}_2^0$ production, Tn1n2A.

[12] TUMASYAN 23AY searched in 138 fb^{-1} of pp collisions at $\sqrt{s}$ = 13 TeV for evidence of gluino pair production in events with a single electron or muon and multiple hadronic jets. No significant excess above the Standard Model expectations is observed. Limits are set in the models Tglu3A and Tglu1B, see their figure 11. For Tglu1B, the chargino mass is set to $m_{\widetilde{\chi}_1^\pm} = 0.5\ (m_{\widetilde{g}} + m_{\widetilde{\chi}_1^0})$.

[13] AAD 22U searched for the signature of disappearing track from a long-lived chargino in 139 fb^{-1} of pp collisions at $\sqrt{s}$ = 13 TeV. Long-lived charginos decay into quasi-degenerate neutralino emitting a low-momentum particle whose identification is not attempted. The signal is identified by requiring short tracklets in the four pixel layers with no continuation in the SCT (strip) detector. The main background from fake tracklets is estimated directly with the data. No significant excess above the background prediction is found. The results are interpreted in an AMSB scenario (win LSP), on $pp \rightarrow \widetilde{\chi}^\pm\widetilde{\chi}^\pm$ and $pp \rightarrow \widetilde{\chi}^\pm\widetilde{\chi}_1^0$, assuming B($\widetilde{\chi}^\pm \rightarrow \widetilde{\chi}_1^0\pi^\pm$) = 100%, see their figure 7. Results are also interpreted in a higgsino-LSP model, with $pp \rightarrow \widetilde{\chi}^\pm\widetilde{\chi}^\mp$, and $pp \rightarrow \widetilde{\chi}^\pm\widetilde{\chi}_{1,2}^0$, assuming B($\widetilde{\chi}^\pm \rightarrow \widetilde{\chi}_1^0\pi^\pm$) = 95.5%, B($\widetilde{\chi}^\pm \rightarrow \widetilde{\chi}_1^0 e^\pm$) = 3%, B($\widetilde{\chi}^\pm \rightarrow \widetilde{\chi}_1^0\mu^\pm$) = 1.5%, see their figure 8. Finally, results are interpreted in a simplified model of gluino pair production, with $pp \rightarrow \widetilde{g}\widetilde{g}$ and B($\widetilde{g} \rightarrow q q\widetilde{\chi}_1^0$) = B($\widetilde{g} \rightarrow q q\widetilde{\chi}^+$) = B($\widetilde{g} \rightarrow q q\widetilde{\chi}^-$) = 1/3, see their figure 9.

[14] TUMASYAN 22V searched in 137 fb^{-1} of pp collisions at $\sqrt{s}$ = 13 TeV for evidence of electroweakino pair production with decay to two Higgs bosons H, with $H \rightarrow b\overline{b}$, resulting either in 4 resolved b-jets or two large-radius jets, and large $\not{E}_T$. No significant excess above the Standard Model expectations is observed. Limits are set on the mass of $\widetilde{\chi}_2^0$ and $\widetilde{\chi}_1^\pm$ in the models Tn1n1A, see their Figures 11 and 12, or in a model where higgsino-like nearly mass degenerate $\widetilde{\chi}_2^0$ and $\widetilde{\chi}_3^0$ are pair produced and each decay to H and a bino-like $\widetilde{\chi}_1^0$, see their Figure 13. Limits are also set on the gluino mass in the model Tglu1l, see their Figure 14.

[15] AAD 21AK searched in 139 fb^{-1} of pp collisions at $\sqrt{s}$ = 13 TeV for pair production of gluinos and squarks in events with a single isolated electron or muon, originating from the decay of a W boson, multiple jets and significant $\not{E}_T$. No significant excess above the Standard Model expectations is observed. Limits are set on the gluino mass in the Tglu1B simplified model and on the squark mass in the Tsqk3 simplified model, see their Figure 8.

[16] AAD 21L searched in 139 fb^{-1} of pp collisions at $\sqrt{s}$ = 13 TeV for pair production of gluinos and squarks in events with jets, large missing transverse momentum but no electrons or muons. No significant excess above the Standard Model expectations is observed. Limits are set on the gluino mass in the Tglu1A and Tglu1B simplified models, on the squark mass in the Tsqk1 and Tsqk3 simplified models and in a simplified model for gluino-squark production, see their Figures 13-17.

[17] AAD 21X searched in 139 fb^{-1} of pp collisions at $\sqrt{s}$ = 13 TeV for the decay of long-lived R-hadrons stopped by the calorimeter, producing high-momentum jets resulting in large out-of-time energy deposits in the calorimeters. These decays are detected using data collected during periods in the LHC bunch structure when collisions are absent. No significant excess above the predicted background is observed. Limits are set on the R-hadron mass in the Tglu1A simplified model ad a function of the R-hadron lifetime, for different $m_{\widetilde{\chi}_1^0}$. See Figures 9, 10.

[18] SIRUNYAN 21AD searched in 137 fb^{-1} of pp collisions at $\sqrt{s}$ = 13 TeV for supersymmetry in events with multiple jets, no leptons, and large $\not{E}_T$. No significant excess above the Standard Model expectations is observed. Limits are set on the top squark mass in the simplified models Tstop1, Tstop2 with $m_{\widetilde{\chi}_1^\pm} = (m_{\widetilde{t}} + m_{\widetilde{\chi}_1^0})/2$, and a 50:50 mixture of these with $m_{\widetilde{\chi}_1^\pm} - m_{\widetilde{\chi}_1^0} = 5$ GeV, see their Figure 8. Limits are also set on the top squark mass for 10 GeV $< m_{\widetilde{t}} - m_{\widetilde{\chi}_1^\pm} <$ 80 GeV in the simplified models Tstop2, Tstop 3, and Tstop4, see their Figure 9. For indirect top squark production, limits are set on the gluino mass in the simplified models Tglu3A, Tglu3C with $m_{\widetilde{t}} - m_{\widetilde{\chi}_1^0} = 20$ GeV, and Tglu3D with $m_{\widetilde{\chi}_1^\pm} - m_{\widetilde{\chi}_1^0} = 5$ GeV, see their Figure 10.

[19] SIRUNYAN 21M searched in 137 fb^{-1} of pp collisions at $\sqrt{s}$ = 13 TeV for supersymmetry in events with two opposite-sign same-flavor leptons (electrons, muons) and $\not{E}_T$. No significant excess above the Standard Model expectations is observed. Limits are set on the gluino mass in the simplified model Tglu4C, see their Figure 10, on the $\widetilde{\chi}_2^0$ and $\widetilde{\chi}_1^\pm$ mass in Tchi1n2Fa, see their Figure 11, on the $\widetilde{\chi}_1^0$ mass in Tn1n1C and Tn1n1B for $m_{\widetilde{\chi}_2^0} = m_{\widetilde{\chi}_1^\pm} = m_{\widetilde{\chi}_1^0}$, see their Figure 12. Limits are also set on the light squark mass for the simplified model Tsqk2A, on the sbottom mass in Tsbot3, see their Figure 13, and on the slepton mass in direct electroweak pair production of mass-degenerate left- and right-handed sleptons (selectrons and smuons), see their Figure 14.

[20] AAD 20AL searched in 139 fb^{-1} of pp collisions at $\sqrt{s}$ = 13 TeV for events with 8 or more jets and moderate missing transverse momentum. The selection makes requirements

Int. J. Mod. Phys. A 2026.41. Downloaded from www.worldscientific.com
by UNIVERSITY OF CALIFORNIA @ BERKELEY on 09/16/26. Re-use and distribution is strictly not permitted, except for Open Access articles.

Int. J. Mod. Phys. A 2026.41. Downloaded from www.worldscientific.com
by UNIVERSITY OF CALIFORNIA @ BERKELEY on 09/16/26. Re-use and distribution is strictly not permitted, except for Open Access articles.

according to the number of b-tagged jets and the scalar sum of masses of large-radius jets. No significant excess above the Standard Model expectations is observed. Limits up to about 2 TeV are set on the gluino mass in Tglu1E simplified model. Limits up to about 1.8 TeV are set on the gluino mass in Tglu3A simplified model. See their Fig. 10(a).

[21] AAD 20V searched in 139 fb^{-1} of pp collisions at $\sqrt{s}$ = 13 TeV in final states with same-sign charged leptons (electrons or muons) and jets. No significant excess over the Standard Model expectation is observed. In the Tglu1E model, considering off-shell intermediate W and Z bosons in the decay chains, gluino masses are excluded at 95% C.L. up to 1600 GeV for neutralino masses of 100 GeV or above (up to 1000 GeV). See their Fig. 7(a).

[22] SIRUNYAN 20B searched in 35.9 fb^{-1} of pp collisions at $\sqrt{s}$ = 13 TeV for events with at least one photon and large $\not{E}_T$. No significant excess above the Standard Model expectations is observed. Limits are set on chargino masses in a general gauge-mediated SUSY breaking (GGM) scenario Tchi1n12-GGM, see Figure 4. Limits are also set on the NLSP mass in the Tchi1chi1F and Tchi1chi1G simplified models, see their Figure 5. Finally, limits are set on the gluino mass in the Tglu4A simplified model, see Figure 6.

[23] SIRUNYAN 20BJ searched in 137 fb^{-1} of pp collisions at $\sqrt{s}$ = 13 TeV for events containing two hadronically decaying, highly energetic Z bosons and large $\not{E}_T$. No significant excess above the Standard Model expectations is observed. Limits are set on the gluino mass in the Tglu1H simplified model, see their Figure 9.

[24] SIRUNYAN 20E searched in 137 fb^{-1} of pp collisions at $\sqrt{s}$ = 13 TeV for events with a single electron or muon and multiple jets, including at least one identified as originating from a b-quark, and large $\not{E}_T$. No significant excess above the Standard Model expectations is observed. Limits are set on the gluino mass in the Tglu3A simplified model, see their Fig. 10, and the Tglu3C simplified model, see their Fig. 11.

[25] SIRUNYAN 20T searched in 137 fb^{-1} of pp collisions at $\sqrt{s}$ = 13 TeV for events with at least two jets, and two isolated same-sign or three or more charged leptons (electrons or muons). No significant excess above the Standard Model expectations is observed. Limits are set on the gluino mass in the Tglu3A, Tglu3B, Tglu3C and Tglu3D simplified models, see their Figure 7, and in the Tglu1C and Tglu1B simplified models, see their Figures 8 and 9. Limits are also set on the sbottom mass in the Tsbot2 simplified model, see their Figure 10, and on the stop mass in the Tstop7 simplified model, see their Figure 11. Finally, limits are set on the gluino mass in RPV simplified models where the gluino decays either via $\tilde{g} \rightarrow q q \bar{q} \bar{q} + e/\mu/\tau$ or via $\tilde{g} \rightarrow t b s$, see Figure 12.

[26] AABOUD 19I searched in 36.1 fb^{-1} of pp collisions at $\sqrt{s}$ = 13 TeV in final states with hadronic jets, 1 or two hadronically decaying τ and $\not{E}_T$. In Tglu1F, gluino masses are excluded at 95% C.L. up to 2000 GeV for neutralino masses of 100 GeV or below. Neutralino masses up to 1000 GeV are excluded for all gluino masses below 1400 GeV. See their Fig. 9. Limits are also presented in the context of Gauge-Mediated Symmetry Breaking models: in this case, values of Λ below 110 TeV are excluded at the 95% CL for all values of $\tan\beta$ in the range $2 < \tan\beta < 60$, see their Fig 10.

[27] SIRUNYAN 19AG searched in 35.9 fb^{-1} of pp collisions at $\sqrt{s}$ = 13 TeV for events with two photons and large $\not{E}_T$. No significant excess above the Standard Model expectations is observed. Limits are set on the gluino mass in the Tglu4B simplified model and on the squark mass in the Tsqk4B simplified model, see their Figure 3.

[28] SIRUNYAN 19AU searched in 35.9 fb^{-1} of pp collisions at $\sqrt{s}$ = 13 TeV for events with at last one photon, jets, some of which are identified as originating from b-quarks, and large $\not{E}_T$. No significant excess above the Standard Model expectations is observed. In the framework of GMSB, limits are set on the gluino mass in the Tglu4C, Tglu4D and Tglu4E simplified models, and on the top squark mass in the Tstop13 simplified model, see their Figure 5.

[29] SIRUNYAN 19CE searched in 35.9 fb^{-1} of pp collisions at $\sqrt{s}$ = 13 TeV for new particles decaying to a photon and two gluons in events with at least three large-radius jets of which two have substructure and are composed of a photon and two gluons. No statistically significant excess is observed above the SM background expectation. Upper limits at 95% confidence level on the cross section for gluino pair production are set, using a simplified Tglu1A-like stealth SUSY model. Gluino masses up to 1500-1700 GeV are excluded, depending on the neutralino mass, with the highest exclusion set for $m_{\widetilde{\chi}_1^0}$ = 200 GeV. See their Fig 4.

[30] SIRUNYAN 19CH searched in 137 fb^{-1} of pp collisions at $\sqrt{s}$ = 13 TeV for events containing multiple jets and large $\not{E}_T$. No significant excess above the Standard Model expectations is observed. Limits are set on the gluino mass in the Tglu1A, Tglu1C, Tglu2A and Tglu3A simplified models, see their Figure 13. Limits are also set on squark, sbottom and stop masses in the Tsqk1, Tsbot1, Tstop1 simplified models, see their Figure 14.

[31] SIRUNYAN 19K searched in 35.9 fb^{-1} of pp collisions at $\sqrt{s}$ = 13 TeV for events with a photon, an electron or muon, and large $\not{E}_T$. No significant excess above the Standard Model expectations is observed. In the framework of GMSB, limits are set on the chargino and neutralino mass in the Tchi1n1A simplified model, see their Figure 6. Limits are also set on the gluino mass in the Tglu4A simplified model, and on the squark mass in the Tsqk4A simplified model, see their Figure 7.

[32] SIRUNYAN 19S searched in 35.9 fb^{-1} of pp collisions at $\sqrt{s}$ = 13 TeV for events with zero or one charged leptons, jets and $\not{E}_T$. The razor variables (M_R and R^2) are used to categorize the events. No significant excess above the Standard Model expectations is observed. Limits are set on the gluino mass in the Tglu3A and Tglu3C simplified models, see Figures 22 and 23, and on the stop mass in the Tstop1 simplified model, see their Figure 24.

[33] AABOUD 18AR searched in 36.1 fb^{-1} of pp collisions at $\sqrt{s}$ = 13 TeV for gluino pair production in events containing large missing transverse momentum and several energetic jets, at least three of which must be identified as originating from b-quarks. No excess is found above the predicted background. In Tglu3A models, gluino masses of less than 1.97 TeV are excluded for $m_{\widetilde{\chi}_1^0}$ below 300 GeV, see their Fig. 10(a). Interpretations are also provided for scenarios where Tglu3A modes mix with Tglu2A and Tglu3D, see their Fig 11.

[34] AABOUD 18AR searched in 36.1 fb^{-1} of pp collisions at $\sqrt{s}$ = 13 TeV for gluino pair production in events containing large missing transverse momentum and several energetic jets, at least three of which must be identified as originating from b-quarks. No excess is found above the predicted background. In Tglu2A models, gluino masses of less than 1.92 TeV are excluded for $m_{\widetilde{\chi}_1^0}$ below 600 GeV, see their Fig. 10(b). Interpretations are also provided for scenarios where Tglu2A modes mix with Tglu3A and Tglu3D, see their Fig 11.

[35] AABOUD 18AS searched for in 36.1 fb^{-1} of pp collisions at $\sqrt{s}$ = 13 TeV for gluino pair production in the context of AMSB or phenomenological MSSM scenarios with wino-like LSP and long-lived charginos. Events with a disappearing track due to a low-momentum pion accompanied by at least four jets are considered. No significant excess above the Standard Model expectations is observed. Exclusion limits are set at 95% confidence level on the mass of gluinos for different chargino lifetimes. Gluino masses up to 1.65 TeV are excluded assuming a chargino mass of 460 GeV and lifetime of 0.2 ns, corresponding to a mass-splitting between the charged and neutral wino of around 160 MeV. See their Fig. 9.

[36] AABOUD 18BJ searched in 36.1 fb^{-1} of pp collisions at $\sqrt{s}$ = 13 TeV in events with two opposite-sign charged leptons (electrons and muons), jets and missing transverse momentum, with various requirements to be sensitive to signals with different kinematic endpoint values in the dilepton invariant mass distribution. The data are found to be consistent with the SM expectation. Results are interpreted in the Tglu1G model: gluino masses below 1850 GeV are excluded for $m_{\widetilde{\chi}_1^0}$ = 100 GeV, see their Fig. 12(a).

[37] AABOUD 18BJ searched in 36.1 fb^{-1} of pp collisions at $\sqrt{s}$ = 13 TeV in events with two opposite-sign charged leptons (electrons and muons), jets and missing transverse momentum, with various requirements to be sensitive to signals with different kinematic endpoint values in the dilepton invariant mass distribution. The data are found to be consistent with the SM expectation. Results are interpreted in the Tglu1H model: gluino masses below 1650 GeV are excluded for $m_{\widetilde{\chi}_1^0}$ = 100 GeV, see their Fig. 13(a).

[38] AABOUD 18U searched in 36.1 fb^{-1} of pp collisions at $\sqrt{s}$ = 13 TeV in events with at least one isolated photon, possibly jets and significant transverse momentum targeting generalised models of gauge-mediated SUSY breaking. No significant excess of events is observed above the SM prediction. Results for the di-photon channel are interpreted in terms of lower limits on the masses of gluinos in Tglu4B models, which reach as high as 2.3 TeV. Gluinos with masses below 2.15 TeV are excluded for any NLSP mass, see their Fig. 8.

[39] AABOUD 18U searched in 36.1 fb^{-1} of pp collisions at $\sqrt{s}$ = 13 TeV in events with at least one isolated photon, possibly jets and significant transverse momentum targeting generalised models of gauge-mediated SUSY breaking. No significant excess of events is observed above the SM prediction. Results of the γ + jets + $\not{E}_T$ channel are interpreted in terms of lower limits on the masses of gluinos in GGM higgsino-bino models (mix of Tglu4B and Tglu4C), which reach as high as 2050 GeV. Gluino masses below 1600 GeV are excluded for any NLSP mass provided that $m_{\widetilde{g}} - m_{\widetilde{\chi}_1^0} > 50$ GeV. See their Fig. 11.

[40] AABOUD 18V searched in 36.1 fb^{-1} of pp collisions at $\sqrt{s}$ = 13 TeV in events with no charged leptons, jets and missing transverse momentum. The data are found to be consistent with the SM expectation. Results are interpreted in the Tglu1A model: gluino masses below 2030 GeV are excluded for massless LSP, see their Fig. 13(b).

[41] AABOUD 18V searched in 36.1 fb^{-1} of pp collisions at $\sqrt{s}$ = 13 TeV in events with no charged leptons, jets and missing transverse momentum. The data are found to be consistent with the SM expectation. Results are interpreted in the Tglu1B model. Assuming that $m_{\widetilde{\chi}_1^\pm} = 0.5\ (m_{\widetilde{g}} + m_{\widetilde{\chi}_1^0})$, gluino masses below 1980 GeV are excluded for massless LSP, see their Fig. 14(c). Exclusions are also shown assuming $m_{\widetilde{\chi}_1^0}$ = 60 GeV, see their Fig. 14(d).

[42] AABOUD 18V searched in 36.1 fb^{-1} of pp collisions at $\sqrt{s}$ = 13 TeV in events with no charged leptons, jets and missing transverse momentum. The data are found to be consistent with the SM expectation. Results are interpreted in the Tglu1E model: gluino masses below 1750 GeV are excluded for $m_{\widetilde{\chi}_1^0}$ = 1 GeV and any $m_{\widetilde{\chi}_2^0}$ above 100 GeV, see their Fig. 15. Gluino mass exclusion up to 2 TeV is found for $m_{\widetilde{\chi}_2^0}$ = 1 TeV.

[43] SIRUNYAN 18AA searched in 35.9 fb^{-1} of pp collisions at $\sqrt{s}$ = 13 TeV for events with at least one photon and large $\not{E}_T$. No significant excess above the Standard Model expectations is observed. Limits are set on wino masses in a general gauge-mediated SUSY breaking (GGM) scenario with bino-like $\widetilde{\chi}_1^0$ and wino-like $\widetilde{\chi}_1^\pm$ and $\widetilde{\chi}_2^0$, see Figure 7. Limits are also set on the NLSP mass in the Tchi1n1A and Tchi1chi1A simplified models, see their Figure 8. Finally, limits are set on the gluino mass in the Tglu4A and Tglu4B simplified models, see their Figure 9, and on the squark mass in the Tsqk4A and Tsqk4B simplified models, see their Figure 10.

[44] SIRUNYAN 18AC searched in 35.9 fb^{-1} of pp collisions at $\sqrt{s}$ = 13 TeV for events with a single electron or muon and multiple jets. No significant excess above the Standard Model expectations is observed. Limits are set on the gluino mass in the Tglu3A and Tglu1B simplified models, see their Figure 5.

[45] SIRUNYAN 18AL searched in 35.9 fb^{-1} of pp collisions at $\sqrt{s}$ = 13 TeV for events with at least three charged leptons, in any combination of electrons and muons, jets and significant $\not{E}_T$. No significant excess above the Standard Model expectations is observed. Limits are set on the gluino mass in the Tglu3A and Tglu1C simplified models, see their Figure 5. Limits are also set on the sbottom mass in the Tsbot2 simplified model, see their Figure 6, and on the stop mass in the Tstop7 simplified model, see their Figure 7.

[46] SIRUNYAN 18AR searched in 35.9 fb^{-1} of pp collisions at $\sqrt{s}$ = 13 TeV for events containing two opposite-charge, same-flavour leptons (electrons or muons), jets and $\not{E}_T$. No significant excess above the Standard Model expectations is observed. Limits are set on the gluino mass in the Tglu4C simplified model, see their Figure 7. Limits are also set on the chargino/neutralino mass in the Tchi1n2F simplified models, see their Figure 8, and on the higgsino mass in the Tn1n1B and Tn1n1C simplified models, see their Figure 9. Finally, limits are set on the sbottom mass in the Tsbot3 simplified model, see their Figure 10.

[47] SIRUNYAN 18AY searched in 35.9 fb^{-1} of pp collisions at $\sqrt{s}$ = 13 TeV for events containing one or more jets and significant $\not{E}_T$. No significant excess above the Standard Model expectations is observed. Limits are set on the gluino mass in the Tglu1A, Tglu2A and Tglu3A simplified models, see their Figure 3. Limits are also set on squark, sbottom and stop masses in the Tsqk1, Tsbot1, Tstop1 and Tstop4 simplified models, see their Figure 3. Finally, limits are set on long-lived gluino masses in a Tglu1A simplified model where the gluino is metastable or long-lived with proper decay lengths in the range 10^{-3} mm $< c\tau < 10^5$ mm, see their Figure 4.

[48] SIRUNYAN 18D searched in 35.9 fb^{-1} of pp collisions at $\sqrt{s}$ = 13 TeV for events containing identified hadronically decaying top quarks, no leptons, and $\not{E}_T$. No significant excess above the Standard Model expectations is observed. Limits are set on the stop mass in the Tstop1 simplified model, see their Figure 8, and on the gluino mass in the Tglu3A, Tglu3B, Tglu3C and Tglu3E simplified models, see their Figure 9.

[49] SIRUNYAN 18M searched in 35.9 fb^{-1} of pp collisions at $\sqrt{s}$ = 13 TeV for events with one or more high-momentum Higgs bosons, decaying to pairs of b-quarks, and large $\not{E}_T$. No significant excess above the Standard Model expectations is observed. Limits are set on the gluino mass in the Tglu1I and Tglu1J simplified models, see their Figure 3.

[50] AABOUD 17AJ searched in 36.1 fb^{-1} of pp collisions at $\sqrt{s}$ = 13 TeV for events with two same-sign or three leptons, jets and large missing transverse momentum. No significant excess above the Standard Model expectations is observed. Limits up to 1.75 TeV are

Int. J. Mod. Phys. A 2026.41. Downloaded from www.worldscientific.com by UNIVERSITY OF CALIFORNIA @ BERKELEY on 09/16/26. Re-use and distribution is strictly not permitted, except for Open Access articles.

set on the gluino mass in Tglu3A simplified models in case of off-shell top squarks and for $m_{\widetilde{\chi}^0_1} = 100$ GeV. See their Figure 4(a).

[51] AABOUD 17AJ searched in 36.1 fb^{-1} of pp collisions at $\sqrt{s} = 13$ TeV for events with two same-sign or three leptons, jets and large missing transverse momentum. No significant excess above the Standard Model expectations is observed. Limits up to 1.57 TeV are set on the gluino mass in Tglu1E simplified models (2-step models) for $m_{\widetilde{\chi}^0_1} = 100$ GeV. See their Figure 4(b).

[52] AABOUD 17AJ searched in 36.1 fb^{-1} of pp collisions at $\sqrt{s} = 13$ TeV for events with two same-sign or three leptons, jets and large missing transverse momentum. No significant excess above the Standard Model expectations is observed. Limits up to 1.86 TeV are set on the gluino mass in Tglu1G simplified models for $m_{\widetilde{\chi}^0_1} = 200$ GeV. See their Figure 4(c).

[53] AABOUD 17AR searched in 36.1 fb^{-1} of pp collisions at $\sqrt{s} = 13$ TeV for events with one isolated lepton, at least two jets and large missing transverse momentum. No significant excess above the Standard Model expectations is observed. Limits up to 2.1 TeV are set on the gluino mass in Tglu1B simplified models, with $x = (m_{\widetilde{\chi}^\pm_1} - m_{\widetilde{\chi}^0_1}) / (m_{\widetilde{g}} - m_{\widetilde{\chi}^0_1}) = 1/2$. Similar limits are obtained for variable x and fixed neutralino mass, $m_{\widetilde{\chi}^0_1} = 60$ GeV. See their Figure 13.

[54] AABOUD 17AR searched in 36.1 fb^{-1} of pp collisions at $\sqrt{s} = 13$ TeV for events with one isolated lepton, at least two jets and large missing transverse momentum. No significant excess above the Standard Model expectations is observed. Limits up to 1.74 TeV are set on the gluino mass in Tglu1E simplified model. Limits up to 1.7 TeV are also set on pMSSM models leading to similar signal event topologies. See their Figure 13.

[55] AABOUD 17AY searched in 36.1 fb^{-1} of pp collisions at $\sqrt{s} = 13$ TeV for events with at least four jets and large missing transverse momentum. No significant excess above the Standard Model expectations is observed. Limits up to 1.8 TeV are set on the gluino mass in Tglu3A simplified models assuming $m_{\widetilde{t}_1} - m_{\widetilde{\chi}^0_1} = 5$ GeV. See their Figure 13.

[56] AABOUD 17AZ searched in 36.1 fb^{-1} of pp collisions at $\sqrt{s} = 13$ TeV for events with at least seven jets and large missing transverse momentum. Selected events are further classified based on the presence of large R-jets or b-jets and no leptons. No significant excess above the Standard Model expectations is observed. Limits up to 1.8 TeV are set on the gluino mass in Tglu1E simplified models. See their Figure 6b.

[57] AABOUD 17AZ searched in 36.1 fb^{-1} of pp collisions at $\sqrt{s} = 13$ TeV for events with at least seven jets and large missing transverse momentum. Selected events are further classified based on the presence of large R-jets or b-jets and no leptons. No significant excess above the Standard Model expectations is observed. Limits up to 1.54 TeV are set on the gluino mass in Tglu3A simplified models. See their Figure 7a.

[58] AABOUD 17N searched in 14.7 fb^{-1} of pp collisions at $\sqrt{s} = 13$ TeV in final states with 2 same-flavor, opposite-sign leptons (electrons or muons), jets and large missing transverse momentum. In Tglu1J models, gluino masses are excluded at 95% C.L. up to 1300 GeV for $m_{\widetilde{\chi}^0_1} = 0$ GeV and $m_{\widetilde{\chi}^0_2} = 1100$ GeV. See their Fig. 12 for exclusion limits as a function of $m_{\widetilde{\chi}^0_2}$. Limits are also presented assuming $m_{\widetilde{\chi}^0_2} = m_{\widetilde{\chi}^0_1} + 100$ GeV, see their Fig. 13.

[59] AABOUD 17N searched in 14.7 fb^{-1} of pp collisions at $\sqrt{s} = 13$ TeV in final states with 2 same-flavor, opposite-sign leptons (electrons or muons), jets and large missing transverse momentum. In Tglu1H models, gluino masses are excluded at 95% C.L. up to 1310 GeV for $m_{\widetilde{\chi}^0_1} < 400$ GeV and assuming $m_{\widetilde{\chi}^0_2} = (m_{\widetilde{g}} + m_{\widetilde{\chi}^0_1})/2$. See their Fig. 15.

[60] AABOUD 17N searched in 14.7 fb^{-1} of pp collisions at $\sqrt{s} = 13$ TeV in final states with 2 same-flavor, opposite-sign leptons (electrons or muons), jets and large missing transverse momentum. In Tglu1G models, gluino masses are excluded at 95% C.L. up to 1700 GeV for small $m_{\widetilde{\chi}^0_1}$. The results probe kinematic endpoints as small as $m_{\widetilde{\chi}^0_2} - m_{\widetilde{\chi}^0_1} = (m_{\widetilde{g}} - m_{\widetilde{\chi}^0_1})/2 = 50$ GeV. See their Fig. 14.

[61] KHACHATRYAN 17 searched in 2.3 fb^{-1} of pp collisions at $\sqrt{s} = 13$ TeV for events containing four or more jets, no more than one lepton, and missing transverse momentum, using the razor variables (M_R and R^2) to discriminate between signal and background processes. No evidence for an excess over the expected background is observed. Limits are derived on the gluino mass in the Tglu1A, Tglu2A and Tglu3A simplified models, see Figs. 16 and 17. Also, assuming gluinos decay only via three-body processes involving third-generation quarks plus a neutralino/chargino, and assuming $m_{\widetilde{\chi}^\pm_1} = m_{\widetilde{\chi}^0_1} + 5$ GeV, a branching ratio-independent limit on the gluino mass is given, see Fig. 16.

[62] KHACHATRYAN 17AD searched in 2.3 fb^{-1} of pp collisions at $\sqrt{s} = 13$ TeV for events containing at least four jets (including b-jets), missing transverse momentum and tagged top quarks. No evidence for an excess over the expected background is observed. Gluino masses up to 1550 GeV and neutralino masses up to 900 GeV are excluded at 95% C.L. See Fig. 13.

[63] KHACHATRYAN 17AD searched in 2.3 fb^{-1} of pp collisions at $\sqrt{s} = 13$ TeV for events containing at least four jets (including b-jets), missing transverse momentum and tagged top quarks. No evidence for an excess over the expected background is observed. Gluino masses up to 1450 GeV and neutralino masses up to 820 GeV are excluded at 95% C.L. See Fig. 13.

[64] KHACHATRYAN 17AS searched in 2.3 fb^{-1} of pp collisions at $\sqrt{s} = 13$ TeV for events with a single electron or muon and multiple jets. No significant excess above the Standard Model expectations is observed. Limits are set on the gluino mass in the Tglu3A and Tglu1B simplified models, see their Fig. 7.

[65] KHACHATRYAN 17AW searched in 2.3 fb^{-1} of pp collisions at $\sqrt{s} = 13$ TeV for events with at least three charged leptons, in any combination of electrons and muons, and significant $\not{E}_T$. No significant excess above the Standard Model expectations is observed. Limits are set on the gluino mass in the Tglu3A and Tglu1C simplified models, and on the sbottom mass in the Tsbot2 simplified model, see their Figure 4.

[66] KHACHATRYAN 17P searched in 2.3 fb^{-1} of pp collisions at $\sqrt{s} = 13$ TeV for events with one or more jets and large $\not{E}_T$. No significant excess above the Standard Model expectations is observed. Limits are set on the gluino mass in the Tglu1A, Tglu2A, Tglu3A, Tglu3B, Tglu3C and Tglu3D simplified models, see their Figures 7 and 8. Limits are also set on the squark mass in the Tsqk1 simplified model, see their Fig. 7, and on the sbottom mass in the Tsbot1 simplified model, see Fig. 8. Finally, limits are set on the stop mass in the Tstop1, Tstop3, Tstop4, Tstop6 and Tstop7 simplified models, see Fig. 8.

[67] KHACHATRYAN 17V searched in 2.3 fb^{-1} of pp collisions at $\sqrt{s} = 13$ TeV for events with two photons and large $\not{E}_T$. No significant excess above the Standard Model expectations is observed. Limits are set on the gluino and squark mass in the context of general gauge mediation models Tglu4B and Tsqk4, see their Fig. 4.

[68] SIRUNYAN 17AF searched in 35.9 fb^{-1} of pp collisions at $\sqrt{s} = 13$ TeV for events with a single lepton (electron or muon), jets, including at least one jet originating from a b-quark, and large $\not{E}_T$. No significant excess above the Standard Model expectations is observed. Limits are set on the gluino mass in the Tglu3A and Tglu3B simplified models, see their Figure 2.

[69] SIRUNYAN 17AY searched in 35.9 fb^{-1} of pp collisions at $\sqrt{s} = 13$ TeV for events with at least one photon, jets and large $\not{E}_T$. No significant excess above the Standard Model expectations is observed. Limits are set on the gluino mass in the Tglu4A and Tglu4B simplified models, and on the squark mass in the Tskq4A and Tsqk4B simplified models, see their Figure 6.

[70] SIRUNYAN 17AZ searched in 35.9 fb^{-1} of pp collisions at $\sqrt{s} = 13$ TeV for events with one or more jets and large $\not{E}_T$. No significant excess above the Standard Model expectations is observed. Limits are set on the gluino mass in the Tglu1A, Tglu2A, Tglu3A simplified models, see their Figures 6. Limits are also set on the squark mass in the Tsqk1 simplified model (for single light squark and for 8 degenerate light squarks), on the sbottom mass in the Tsbot1 simplified model and on the stop mass in the Tstop1 simplified model, see their Fig. 7. Finally, limits are set on the stop mass in the Tstop2, Tstop4 and Tstop8 simplified models, see Fig. 8.

[71] SIRUNYAN 17P searched in 35.9 fb^{-1} of pp collisions at $\sqrt{s} = 13$ TeV for events with multiple jets and large $\not{E}_T$. No significant excess above the Standard Model expectations is observed. Limits are set on the gluino mass in the Tglu1A, Tglu1C, Tglu2A, Tglu3A and Tglu3D simplified models, see their Fig. 12. Limits are also set on the squark mass in the Tsqk1 simplified model, on the stop mass in the Tstop1 simplified model, and on the sbottom mass in the Tsbot1 simplified model, see Fig. 13.

[72] SIRUNYAN 17S searched in 35.9 fb^{-1} of pp collisions at $\sqrt{s} = 13$ TeV for events with two isolated same-sign leptons, jets, and large $\not{E}_T$. No significant excess above the Standard Model expectations is observed. Limits are set on the mass of the gluino mass in the Tglu3A, Tglu3B, Tglu3C, Tglu3D and Tglu1B simplified models, see their Figures 5 and 6, and on the sbottom mass in the Tsbot2 simplified model, see their Figure 6.

[73] AABOUD 16AC searched in 3.2 fb^{-1} of pp collisions at $\sqrt{s} = 13$ TeV in final states with hadronic jets, 1 or two hadronically decaying τ and $\not{E}_T$. In Tglu1F, gluino masses are excluded at 95% C.L. up to 1570 GeV for neutralino masses of 100 GeV or below. Neutralino masses up to 700 GeV are excluded for all gluino masses between 800 GeV and 1500 GeV, while the strongest neutralino-mass exclusion of 750 GeV is achieved for gluino masses around 1400 GeV. See their Fig. 8. Limits are also presented in the context of Gauge-Mediated Symmetry Breaking models: in this case, values of Λ below 92 TeV are excluded at the 95% CL, corresponding to gluino masses below 2000 GeV. See their Fig. 9.

[74] AABOUD 16J searched in 3.2 fb^{-1} of pp collisions at $\sqrt{s} = 13$ TeV in final states with one isolated electron or muon, hadronic jets, and $\not{E}_T$. Gluino-mediated pair production of stops with a nearly mass-degenerate stop and neutralino are targeted and gluino masses are excluded at 95% C.L. up to 1460 GeV. A 100% of stops decaying via charm + neutralino is assumed. The results are also valid in case of 4-body decays $\widetilde{t}_1 \to f f' b \widetilde{\chi}^0_1$. See their Fig. 8.

[75] AABOUD 16M searched in 3.2 fb^{-1} of pp collisions at $\sqrt{s} = 13$ TeV for events with two photons, hadronic jets and $\not{E}_T$. No significant excess above the Standard Model expectations is observed. Exclusion limits at 95% C.L. are set on gluino masses in the general gauge-mediated SUSY breaking model (GGM), for bino-like NLSP. See their Fig. 3.

[76] AABOUD 16N searched in 3.2 fb^{-1} of pp collisions at $\sqrt{s} = 13$ TeV for events containing hadronic jets, large $\not{E}_T$, and no electrons or muons. No significant excess above the Standard Model expectations is observed. Gluino masses below 1510 GeV are excluded at the 95% C.L. in a simplified model with only gluinos and the lightest neutralino. See their Fig. 7b.

[77] AABOUD 16N searched in 3.2 fb^{-1} of pp collisions at $\sqrt{s} = 13$ TeV for events containing hadronic jets, large $\not{E}_T$, and no electrons or muons. No significant excess above the Standard Model expectations is observed. Gluino masses below 1500 GeV are excluded at the 95% C.L. in a simplified model with gluinos decaying via an intermediate $\widetilde{\chi}^\pm_1$ to two quarks, a W boson and a $\widetilde{\chi}^0_1$, for $m_{\widetilde{\chi}^0_1} = 200$ GeV. See their Fig 8.

[78] AAD 16AD searched in 3.2 fb^{-1} of pp collisions at $\sqrt{s} = 13$ TeV for events containing several energetic jets, of which at least three must be identified as b-jets, large $\not{E}_T$ and no electrons or muons. No significant excess above the Standard Model expectations is observed. For $\widetilde{\chi}^0_1$ below 800 GeV, gluino masses below 1780 GeV are excluded at 95% C.L. for gluinos decaying via bottom squarks. See their Fig. 7a.

[79] AAD 16AD searched in 3.2 fb^{-1} of pp collisions at $\sqrt{s} = 13$ TeV for events containing several energetic jets, of which at least three must be identified as b-jets, large $\not{E}_T$ and one electron or muon. Large-radius jets with a high mass are also used to identify highly boosted top quarks. No significant excess above the Standard Model expectations is observed. For $\widetilde{\chi}^0_1$ below 700 GeV, gluino masses below 1760 GeV are excluded at 95% C.L. for gluinos decaying via top squarks. See their Fig. 7b.

[80] AAD 16BB searched in 3.2 fb^{-1} of pp collisions at $\sqrt{s} = 13$ TeV for events with exactly two same-sign leptons or at least three leptons, multiple hadronic jets, b-jets, and $\not{E}_T$. No significant excess over the Standard Model expectation is found. Exclusion limits at 95% C.L. are set on the gluino mass in various simplified models (Tglu1D, Tglu1E, Tglu3A). See their Figs. 4.a, 4.b, and 4.d.

[81] AAD 16BG searched in 3.2 fb^{-1} of pp collisions at $\sqrt{s} = 13$ TeV in final states with one isolated electron or muon, hadronic jets, and $\not{E}_T$. The data agree with the SM background expectation in the six signal selections defined in the search, and the largest deviation is a 2.1 standard deviation excess. Gluinos are excluded at 95% C.L. up to 1600 GeV assuming they decay via the lightest chargino to the lightest neutralino as in the model Tglu1B for $m_{\widetilde{\chi}^0_1}$=100 GeV, assuming $m_{\widetilde{\chi}^\pm_1}$=$(m_{\widetilde{g}} + m_{\widetilde{\chi}^0_1})/2$. See their Fig. 6.

[82] AAD 16V searched in 3.2 fb^{-1} of pp collisions at $\sqrt{s} = 13$ TeV for events with $\not{E}_T$ various hadronic jet multiplicities from ≥ 7 to ≥ 10 and with various b-jet multiplicity requirements. No significant excess over the Standard Model expectation is found. Exclusion limits at 95% C.L. are set on the gluino mass in one simplified model (Tglu1E) and a pMSSM-inspired model. See their Fig. 5.

[83] KHACHATRYAN 16AM searched in 19.7 fb^{-1} of pp collisions at $\sqrt{s} = 8$ TeV for events with highly boosted W-bosons and b-jets, using the razor variables (M_R and R^2) to discriminate between signal and background processes. No significant excess above the

Int. J. Mod. Phys. A 2026.41. Downloaded from www.worldscientific.com
by UNIVERSITY OF CALIFORNIA @ BERKELEY on 09/16/26. Re-use and distribution is strictly not permitted, except for Open Access articles.

Standard Model expectations is observed. Limits are set on the gluino mass in the Tglu3C and Tglu3B simplified models, see Fig. 12.

[84] KHACHATRYAN 16BJ searched in 2.3 fb^{-1} of pp collisions at $\sqrt{s}$ = 13 TeV for events with two isolated same-sign dileptons and jets in the final state. No significant excess above the Standard Model expectations is observed. Limits are set on the gluino mass in the following simplified models: Tglu3A and Tglu3D, see Fig. 4, Tglu3B and Tglu3C, see Fig. 5, and Tglu1B, see Fig. 7.

[85] KHACHATRYAN 16BS searched in 2.3 fb^{-1} of pp collisions at $\sqrt{s}$ = 13 TeV for events with at least one energetic jet , no isolated leptons, and significant $\not{E}_T$, using the transverse mass variable M_{T2} to discriminate between signal and background processes. No significant excess above the Standard Model expectations is observed. Limits are set on the gluino mass in the Tglu1A, Tglu2A and Tglu3A simplified models, see Fig. 10 and Table 3.

[86] KHACHATRYAN 16BY searched in 2.3 fb^{-1} of pp collisions at $\sqrt{s}$ = 13 TeV for events with two opposite-sign, same-flavour leptons, jets, and missing transverse momentum. No significant excess above the Standard Model expectations is observed. Limits are set on the gluino mass in the Tglu4C simplified model, see Fig. 4, and on sbottom masses in the Tsbot3 simplified model, see Fig. 5.

[87] KHACHATRYAN 16V searched in 2.3 fb^{-1} of pp collisions at $\sqrt{s}$ = 13 TeV for events with at least four energetic jets and significant $\not{E}_T$, no identified isolated electron or muon or charged track. No significant excess above the Standard Model expectations is observed. Limits are set on the gluino mass in the Tglu1A, Tglu1C, Tglu2A, and Tglu3A simplified models, see Fig. 8.

[88] AAD 15BG searched in 20.3 fb^{-1} of pp collisions at $\sqrt{s}$ = 8 TeV for events with jets, missing E_T, and two opposite-sign same flavor isolated leptons featuring either a kinematic edge, or a peak at the Z-boson mass, in the invariant mass spectrum. No evidence for a statistically significant excess over the expected SM backgrounds are observed and 95% C.L. exclusion limits are derived in a GGM simplified model of gluino pair production where the gluino decays into quarks, a Z-boson, and a massless gravitino LSP, see Fig. 12. Also, limits are set in simplified models with slepton/sneutrino intermediate states, see Fig. 13.

[89] AAD 15BV summarized and extended ATLAS searches for gluinos and first- and second-generation squarks in final states containing jets and missing transverse momentum, with or without leptons or b-jets in the $\sqrt{s}$ =8 TeV data set collected in 2012. The paper reports the results of new interpretations and statistical combinations of previously published analyses, as well as new analyses. Exclusion limits at 95% C.L. are set on the gluino mass in several R-parity conserving models, leading to a generalized constraint on gluino masses exceeding 1150 GeV for lightest supersymmetric particle masses below 100 GeV. See their Figs. 10, 19, 20, 21, 23, 25, 26, 29-37.

[90] AAD 15BX interpreted the results of a wide range of ATLAS direct searches for supersymmetry, during the first run of the LHC using the $\sqrt{s}$ =7 TeV and $\sqrt{s}$ = 8 TeV data set collected in 2012, within the wider framework of the phenomenological MSSM (pMSSM). The integrated luminosity was up to 20.3 fb^{-1}. From an initial random sampling of 500 million pMSSM points, generated from the 19-parameter pMSSM, a total of 310,327 model points with $\widetilde{\chi}^0_1$ LSP were selected each of which satisfies constraints from previous collider searches, precision measurements, cold dark matter energy density measurements and direct dark matter searches. The impact of the ATLAS Run 1 searches on this space was presented, considering the fraction of model points surviving, after projection into two-dimensional spaces of sparticle masses. Good complementarity is observed between different ATLAS analyses, with almost all showing regions of unique sensitivity. ATLAS searches have good sensitivity at LSP mass below 800 GeV.

[91] AAD 15CA searched in 20.3 fb^{-1} of pp collisions at $\sqrt{s}$ = 8 TeV for events with one or more photons, hadronic jets or b-jets and $\not{E}_T$. No significant excess above the Standard Model expectations is observed. Limits are set on gluino masses in the general gauge-mediated SUSY breaking model (GGM), for bino-like or higgsino-bino admixtures NLSP, see Fig. 8, 10, 11

[92] KHACHATRYAN 15AF searched in 19.5 fb^{-1} of pp collisions at $\sqrt{s}$ = 8 TeV for events with at least two energetic jets and significant $\not{E}_T$, using the transverse mass variable M_{T2} to discriminate between signal and background processes. No significant excess above the Standard Model expectations is observed. Limits are set on the gluino mass in simplified models where the decay $\widetilde{g} \rightarrow q\overline{q}\widetilde{\chi}^0_1$ takes place with a branching ratio of 100%, see Fig. 13(a), or where the decay $\widetilde{g} \rightarrow b\overline{b}\widetilde{\chi}^0_1$ takes place with a branching ratio of 100%, see Fig. 13(b), or where the decay $\widetilde{g} \rightarrow t\overline{t}\widetilde{\chi}^0_1$ takes place with a branching ratio of 100%, see Fig. 13(c). See also Table 5. Exclusions in the CMSSM, assuming tanβ = 30, $A_0 = -2$ max(m_0, $m_{1/2}$) and $\mu > 0$, are also presented, see Fig. 15.

[93] KHACHATRYAN 15I searched in 19.5 fb^{-1} of pp collisions at $\sqrt{s}$ = 8 TeV for events in which b-jets and four W-bosons are produced. Five individual search channels are combined (fully hadronic, single lepton, same-sign dilepton, opposite-sign dilepton, multilepton). No significant excess above the Standard Model expectations is observed. Limits are set on the gluino mass in a simplified model where the decay $\widetilde{g} \rightarrow t\overline{t}\widetilde{\chi}^0_1$ takes place with a branching ratio of 100%, see Fig. 5. Also a simplified model with gluinos decaying into on-shell top squarks is considered, see Fig. 6.

[94] KHACHATRYAN 15X searched in 19.3fb^{-1} of pp collisions at $\sqrt{s}$ = 8 TeV for events with at least two energetic jets, at least one of which is required to originate from a b quark, and significant $\not{E}_T$, using the razor variables (M_R) and R^2) to discriminate between signal and background processes. No significant excess above the Standard Model expectations is observed. Limits are set on the gluino mass in simplified models where the decay $\widetilde{g} \rightarrow b\overline{b}\widetilde{\chi}^0_1$ and the decay $\widetilde{g} \rightarrow t\overline{t}\widetilde{\chi}^0_1$ take place with branching ratios varying between 0, 50 and 100%, see Figs. 13 and 14.

[95] AAD 14AE searched in 20.3 fb^{-1} of pp collisions at $\sqrt{s}$ = 8 TeV for strongly produced supersymmetric particles in events containing jets and large missing transverse momentum, and no electrons or muons. No excess over the expected SM background is observed. Exclusion limits are derived in simplified models containing gluinos and squarks, see Figures 5, 6 and 7. Limits are also derived in the mSUGRA/CMSSM with parameters tanβ = 30, $A_0 = -2\ m_0$ and $\mu > 0$, see their Fig. 8.

[96] AAD 14AG searched in 20.3 fb^{-1} of pp collisions at $\sqrt{s}$ = 8 TeV for events containing one hadronically decaying τ-lepton, zero or one additional light leptons (electrons or muons), jets and large missing transverse momentum. No excess of events above the expected level of Standard Model background was found. Exclusion limits at 95% C.L. are set in several SUSY scenarios. For an interpretation in the minimal GMSB model, see their Fig. 8. For an interpretation in the mSUGRA/CMSSM with parameters tanβ = 30, $A_0 = -2\ m_0$ and $\mu > 0$, see their Fig. 9. For an interpretation in the framework of natural Gauge Mediation, see Fig. 10. For an interpretation in the bRPV scenario, see their Fig. 11.

[97] AAD 14X searched in 20.3 fb^{-1} of pp collisions at $\sqrt{s}$ = 8 TeV for events with at least four leptons (electrons, muons, taus) in the final state. No significant excess above the Standard Model expectations is observed. Limits are set on the gluino mass in a general gauge-mediation model (GGM) where the decay $\widetilde{g} \rightarrow q\overline{q}\widetilde{\chi}^0_1$, with $\widetilde{\chi}^0_1 \rightarrow \ell^{\pm}\ell^{\mp}\widetilde{G}$, takes place with a branching ratio of 100%, for two choices of tanβ = 1.5 and 30, see Fig. 11. Also some constraints on the higgsino mass parameter μ are discussed.

[98] CHATRCHYAN 14AH searched in 4.7 fb^{-1} of pp collisions at $\sqrt{s}$ = 7 TeV for events with at least two energetic jets and significant $\not{E}_T$, using the razor variables (M_R and R^2) to discriminate between signal and background processes. No significant excess above the Standard Model expectations is observed. Limits are set on sbottom masses in simplified models where the decay $\widetilde{g} \rightarrow q\overline{q}\widetilde{\chi}^0_1$ takes place with a branching ratio of 100%, see Fig. 28. Exclusions in the CMSSM, assuming tanβ = 10, $A_0 = 0$ and $\mu > 0$, are also presented, see Fig. 26.

[99] CHATRCHYAN 14AH searched in 4.7 fb^{-1} of pp collisions at $\sqrt{s}$ = 7 TeV for events with at least two energetic jets and significant $\not{E}_T$, using the razor variables (M_R and R^2) to discriminate between signal and background processes. A second analysis requires at least one of the jets to be originating from a b-quark. No significant excess above the Standard Model expectations is observed. Limits are set on sbottom masses in simplified models where the decay $\widetilde{g} \rightarrow b\overline{b}\widetilde{\chi}^0_1$ takes place with a branching ratio of 100%, see Figs. 28 and 29. Exclusions in the CMSSM, assuming tanβ = 10, $A_0 = 0$ and $\mu > 0$, are also presented, see Fig. 26.

[100] CHATRCHYAN 14AH searched in 4.7 fb^{-1} of pp collisions at $\sqrt{s}$ = 7 TeV for events with at least two energetic jets and significant $\not{E}_T$, using the razor variables (M_R and R^2) to discriminate between signal and background processes. A second analysis requires at least one of the jets to be originating from a b-quark. No significant excess above the Standard Model expectations is observed. Limits are set on sbottom masses in simplified models where the decay $\widetilde{g} \rightarrow t\overline{t}\widetilde{\chi}^0_1$ takes place with a branching ratio of 100%, see Figs. 28 and 29. Exclusions in the CMSSM, assuming tanβ = 10, $A_0 = 0$ and μ >0, are also presented, see Fig. 26.

[101] CHATRCHYAN 14I searched in 19.5 fb^{-1} of pp collisions at $\sqrt{s}$ = 8 TeV for events containing multijets and large $\not{E}_T$. No excess over the expected SM background is observed. Exclusion limits are derived in simplified models containing gluinos that decay via $\widetilde{g} \rightarrow q\overline{q}\widetilde{\chi}^0_1$ with a 100% branching ratio, see Fig. 7b, or via $\widetilde{g} \rightarrow t\overline{t}\widetilde{\chi}^0_1$ with a 100% branching ratio, see Fig. 7c, or via $\widetilde{g} \rightarrow q\overline{q}W/Z\widetilde{\chi}^0_1$, see Fig. 7d.

[102] CHATRCHYAN 14N searched in 19.3 fb^{-1} of pp collisions at $\sqrt{s}$ = 8 TeV for events containing a single isolated electron or muon and multiple jets, at least two of which are identified as originating from a b-quark. No significant excesses over the expected SM backgrounds are observed. The results are interpreted in three simplified models of gluino pair production with subsequent decay into virtual or on-shell top squarks, where each of the top squarks decays in turn into a top quark and a $\widetilde{\chi}^0_1$, see Fig. 4. The models differ in which masses are allowed to vary.

[103] CHATRCHYAN 14R searched in 19.5 fb^{-1} of pp collisions at $\sqrt{s}$ = 8 TeV for events with at least three leptons (electrons, muons, taus) in the final state. No significant excess above the Standard Model expectations is observed. Limits are set on the gluino mass in a slepton co-NLSP simplified model (GMSB) where the decay $\widetilde{g} \rightarrow q\ell^{\pm}\ell^{\mp}\widetilde{G}$ takes place with a branching ratio of 100%, see Fig. 8.

[104] CHATRCHYAN 14R searched in 19.5 fb^{-1} of pp collisions at $\sqrt{s}$ = 8 TeV for events with at least three leptons (electrons, muons, taus) in the final state. No significant excess above the Standard Model expectations is observed. Limits are set on the gluino mass in a simplified model where the decay $\widetilde{g} \rightarrow t\overline{t}\widetilde{\chi}^0_1$ takes place with a branching ratio of 100%, see Fig. 11.

[105] AABOUD 18BJ searched in 36.1 fb^{-1} of pp collisions at $\sqrt{s}$ = 13 TeV in events with two opposite-sign charged leptons (electrons and muons), jets and missing transverse momentum, with various requirements to be sensitive to signals with different kinematic endpoint values in the dilepton invariant mass distribution. The data are found to be consistent with the SM expectation. Results are interpreted in the Tglu1H model in case of $m_{\widetilde{\chi}^0_1}$ = 1 GeV: for any $m_{\widetilde{\chi}^0_2}$, gluino masses below 1500 GeV are excluded, see their Fig. 14(a).

[106] AABOUD 18V searched in 36.1 fb^{-1} of pp collisions at $\sqrt{s}$ = 13 TeV in events with no charged leptons, jets and missing transverse momentum. The data are found to be consistent with the SM expectation. Results are interpreted in a Tglu1C-like model, assuming 50% BR for each gluino decay mode. Gluino masses below 1770 GeV are excluded for any $m_{\widetilde{\chi}^0_2} - m_{\widetilde{\chi}^0_1}$ and $m_{\widetilde{\chi}^0_1}$ = 60 GeV, see their Fig. 16(b).

[107] AABOUD 17AZ searched in 36.1 fb^{-1} of pp collisions at $\sqrt{s}$ = 13 TeV for events with at least seven jets and large missing transverse momentum. Selected events are further classified based on the presence of large R-jets or b-jets and no leptons. No significant excess above the Standard Model expectations is observed. Limits are set for pMSSM models with M_1 = 60 GeV, tan(β) = 10, $\mu < 0$ varying the soft-breaking parameters M_3 and μ. Gluino masses up to 1600 GeV are excluded for $m_{\widetilde{\chi}^{\pm}_1}$ = 200 GeV. See their Figure 6a and text for details on the model.

[108] KHACHATRYAN 16AY searched in 2.3 fb^{-1} of pp collisions at $\sqrt{s}$ = 13 TeV for events with one isolated high transverse momentum lepton (e or μ), hadronic jets of which at least one is identified as coming from a b-quark, and large $\not{E}_T$. No significant excess above the Standard Model expectations is observed. Limits are set on the gluino mass in the Tglu3A simplified model, see Fig. 10, and in the Tglu3B model, see Fig. 11.

[109] KHACHATRYAN 16BT performed a global Bayesian analysis of a wide range of CMS results obtained with data samples corresponding to 5.0 fb^{-1} of pp collisions at $\sqrt{s}$ = 7 TeV and in 19.5 fb^{-1} of pp collisions at $\sqrt{s}$ = 8 TeV. The set of searches considered, both individually and in combination, includes those with all-hadronic final states, same-sign and opposite-sign dileptons, and multi-lepton final states. An interpretation was given in a scan of the 19-parameter pMSSM. No scan points with a gluino mass less than 500 GeV survived and 98% of models with a squark mass less than 300 GeV were excluded.

[110] AAD 15AB searched for the decay of neutral, weakly interacting, long-lived particles in 20.3 fb^{-1} of pp collisions at $\sqrt{s}$ = 8 TeV. Signal events require at least two reconstructed vertices possibly originating from long-lived particles decaying to jets in the inner tracking detector and muon spectrometer. No significant excess of events over the expected background was found. Results were interpreted in Stealth SUSY benchmark models where a pair of gluinos decay to long-lived singlinos, $\widetilde{S}$, which in turn each decay to a low-mass gravitino and a pair of jets. The 95% confidence-level limits are set on the cross section $\times$ branching ratio for the decay $\widetilde{g} \rightarrow \widetilde{S}g$, as a function of the singlino proper lifetime (cτ). See their Fig. 10(f)

Int. J. Mod. Phys. A 2026.41. Downloaded from www.worldscientific.com
by UNIVERSITY OF CALIFORNIA @ BERKELEY on 09/16/26. Re-use and distribution is strictly not permitted, except for Open Access articles.

[111] AAD 15AI searched in 20 fb^{-1} of pp collisions at $\sqrt{s}$ = 8 TeV for events containing at least one isolated lepton (electron or muon), jets, and large missing transverse momentum. No excess of events above the expected level of Standard Model background was found. Exclusion limits at 95% C.L. are set on the gluino mass in the CMSSM/mSUGRA, see Fig. 15, in the NUHMG, see Fig. 16, and in various simplified models, see Figs. 18–22.

[112] AAD 15CB searched for events containing at least one long-lived particle that decays at a significant distance from its production point (displaced vertex, DV) into two leptons or into five or more charged particles in 20.3 fb^{-1} of pp collisions at $\sqrt{s}$ = 8 TeV. The dilepton signature is characterised by DV formed from at least two lepton candidates. Four different final states were considered for the multitrak signature, in which the DV must be accompanied by a high-transverse momentum muon or electron candidate that originates from the DV, jets or missing transverse momentum. No events were observed in any of the signal regions. Results were interpreted in SUSY scenarios involving R-parity violation, split supersymmetry, and gauge mediation. See their Fig. 12–20.

[113] KHACHATRYAN 15AD searched in 19.4 fb^{-1} of pp collisions at $\sqrt{s}$ = 8 TeV for events with two opposite-sign same flavor isolated leptons featuring either a kinematic edge, or a peak at the Z-boson mass, in the invariant mass spectrum. No evidence for a statistically significant excess over the expected SM backgrounds is observed and 95% C.L. exclusion limits are derived in a simplified model of gluino pair production where the gluino decays into quarks, a Z-boson, and a massless gravitino LSP, see Fig. 9.

[114] KHACHATRYAN 15AZ searched in 19.7 fb^{-1} of pp collisions at $\sqrt{s}$ = 8 TeV for events with either at least one photon, hadronic jets and $\not{E}_T$ (single photon channel) or with at least two photons and at least one jet and using the razor variables. No significant excess above the Standard Model expectations is observed. Limits are set on gluino masses in the general gauge-mediated SUSY breaking model (GGM), for both a bino-like and wino-like neutralino NLSP scenario, see Fig. 8 and 9.

[115] AAD 14AX searched in 20.1 fb^{-1} of pp collisions at $\sqrt{s}$ = 8 TeV for the strong production of supersymmetric particles in events containing either zero or at last one high high-p_T lepton, large missing transverse momentum, high jet multiplicity and at least three jets identified as originating from b-quarks. No excess over the expected SM background is observed. Limits are derived in mSUGRA/CMSSM models with $\tan\beta$ = 30, $A_0 = -2m_0$ and $\mu > 0$, see their Fig. 14. Also, exclusion limits in simplified models containing gluinos and scalar top and bottom quarks are set, see their Figures 12, 13.

[116] AAD 14E searched in 20.3 fb^{-1} of pp collisions at $\sqrt{s}$ = 8 TeV for strongly produced supersymmetric particles in events containing jets and two same-sign leptons or three leptons. The search also utilises jets originating from b-quarks, missing transverse momentum and other variables. No excess over the expected SM background is observed. Exclusion limits are derived in simplified models containing gluinos and squarks, see Figures 5 and 6. In the $\tilde{g} \rightarrow qq'\tilde{\chi}_1^{\pm}$, $\tilde{\chi}_1^{\pm} \rightarrow W^{(*)\pm}\tilde{\chi}_2^0$, $\tilde{\chi}_2^0 \rightarrow Z^{(*)}\tilde{\chi}_1^0$ simplified model, the following assumptions have been made: $m_{\tilde{\chi}_1^{\pm}} = 0.5\ m_{\tilde{\chi}_1^0} + m_{\tilde{g}}$, $m_{\tilde{\chi}_2^0} = 0.5\ (m_{\tilde{\chi}_1^0} + m_{\tilde{\chi}_1^{\pm}})$, $m_{\tilde{\chi}_1^0} < 520$ GeV. In the $\tilde{g} \rightarrow qq'\tilde{\chi}_1^{\pm}$, $\tilde{\chi}_1^{\pm} \rightarrow \ell^{\pm}\nu\tilde{\chi}_1^0$ or $\tilde{g} \rightarrow qq'\tilde{\chi}_2^0$, $\tilde{\chi}_2^0 \rightarrow \ell^{\pm}\ell^{\mp}(\nu\nu)\tilde{\chi}_1^0$ simplified model, the following assumptions have been made: $m_{\tilde{\chi}_1^{\pm}} = m_{\tilde{\chi}_2^0} = 0.5\ (m_{\tilde{\chi}_1^0} + m_{\tilde{g}})$, $m_{\tilde{\chi}_1^0} < 660$ GeV. Limits are also derived in the mSUGRA/CMSSM, bRPV and GMSB models, see their Fig. 8.

[117] CHATRCHYAN 14H searched in 19.5 fb^{-1} of pp collisions at $\sqrt{s}$ = 8 TeV for events with two isolated same-sign dileptons and jets in the final state. No significant excess above the Standard Model expectations is observed. Limits are set on the gluino mass in simplified models where the decay $\tilde{g} \rightarrow t\bar{t}\tilde{\chi}_1^0$ takes place with a branching ratio of 100%, or where the decay $\tilde{g} \rightarrow \tilde{t}t$, $\tilde{t} \rightarrow t\tilde{\chi}_1^0$ takes place with a branching ratio of 100%, with varying mass of the $\tilde{\chi}_1^0$, or where the decay $\tilde{g} \rightarrow \tilde{b}b$, $\tilde{b} \rightarrow t\tilde{\chi}_1^{\pm}$, $\tilde{\chi}_1^{\pm} \rightarrow W^{\pm}\tilde{\chi}_1^0$ takes place with a branching ratio of 100%, with varying mass of the $\tilde{\chi}_1^{\pm}$, see Fig. 5.

[118] CHATRCHYAN 14H searched in 19.5 fb^{-1} of pp collisions at $\sqrt{s}$ = 8 TeV for events with two isolated same-sign dileptons and jets in the final state. No significant excess above the Standard Model expectations is observed. Limits are set on the gluino mass in simplified models where the decay $\tilde{g} \rightarrow qq'\tilde{\chi}_1^{\pm}$, $\tilde{\chi}_1^{\pm} \rightarrow W^{\pm}\tilde{\chi}_1^0$ takes place with a branching ratio of 100%, with varying mass of the $\tilde{\chi}_1^{\pm}$ and $\tilde{\chi}_1^0$, see Fig. 7.

[119] CHATRCHYAN 14H searched in 19.5 fb^{-1} of pp collisions at $\sqrt{s}$ = 8 TeV for events with two isolated same-sign dileptons and jets in the final state. No significant excess above the Standard Model expectations is observed. Limits are set on the gluino mass in simplified models where the decay $\tilde{g} \rightarrow b\bar{t}\tilde{\chi}_1^{\pm}$, $\tilde{\chi}_1^{\pm} \rightarrow W^{\pm}\tilde{\chi}_1^0$ takes place with a branching ratio of 100%, for two choices of $m_{\tilde{\chi}_1^{\pm}}$ and fixed $m_{\tilde{\chi}_1^0}$, see Fig. 6.

R-parity violating heavy $\tilde{g}$ (Gluino) mass limit

VALUE (GeV)	CL%	DOCUMENT ID		TECN	COMMENT
>1720	95	[1] AAD	24AF	ATLS	jets + b-jets, Tglu1RPV, $\tilde{g} \rightarrow qqq$
>1760	95	[1] AAD	24AF	ATLS	jets + b-jets, Tglu1RPV, $\tilde{g} \rightarrow qqb$
>2230	95	[1] AAD	24AF	ATLS	jets + b-jets, Tglu1A, $\tilde{\chi}_1^0 \rightarrow qqq$, $m_{\tilde{\chi}_1^0}$ = 1300 GeV
>2330	95	[1] AAD	24AF	ATLS	jets + b-jets, Tglu1A, $\tilde{\chi}_1^0 \rightarrow qqb$, $m_{\tilde{\chi}_1^0}$ = 1400 GeV
>2200	95	[2] AAD	21BF	ATLS	$\ell^{\pm}$ + b-jets + many jets, Tglu3F, λ''_{323} electroweakino decay, 500 GeV < $m_{\tilde{\chi}_1^0}$ < 1600 GeV
>2250	95	[2] AAD	21BF	ATLS	$\ell^{\pm}$ + b-jets + many jets, Tglu3G, λ''_{323} electroweakino decay, 600 GeV < $m_{\tilde{\chi}_1^0}$ < 1600 GeV
>2200	95	[2] AAD	21BF	ATLS	$\ell^{\pm}$ + b-jets + many jets, Tglu3B, λ''_{323} electroweakino decay, 600 GeV < $m_{\tilde{\chi}_1^0}$ < 1600 GeV
>1800	95	[2] AAD	21BF	ATLS	$\ell^{\pm}$ + b-jets + many jets, Tglu3B, λ''_{323}, $\tilde{t}$ decay, $m_{\tilde{t}}$ < 1200 GeV
>2200	95	[2] AAD	21BF	ATLS	$\ell^{\pm}$ + b-jets + many jets, Tglu1A, λ', $\tilde{\chi}_1^0$ decay with equal probability into e, μ, ν_e, ν_μ, 400 GeV < $m_{\tilde{\chi}_1^0}$ < 1700 GeV
>2500	95	[3] AAD	21Y	ATLS	$\geq 4\ell$, Tglu1A with $\tilde{\chi}_1^0 \rightarrow \ell^{\pm}\ell^{\mp}\nu$, $\lambda_{12k} \neq 0$, $m_{\tilde{\chi}_1^0}$ = 2200 GeV
>1900	95	[3] AAD	21Y	ATLS	$\geq 4\ell$, Tglu1A with $\tilde{\chi}_1^0 \rightarrow \ell^{\pm}\ell^{\mp}\nu$, $\lambda_{i33} \neq 0$, $m_{\tilde{\chi}_1^0}$ = 1550 GeV
>1600	95	[4] AAD	20AL	ATLS	8 or more jets+$\not{E}_T$, Tglu2RPV
>1600	95	[5] AAD	20V	ATLS	same-sign $\ell^{\pm}\ell^{\pm}$ + jets, $\tilde{g} \rightarrow tbd$ simplified model
>2150	95	[6] SIRUNYAN	20T	CMS	same-sign $\ell^{\pm}\ell^{\pm}$ or $\geq 3\ell^{\pm}$ + jets, $\tilde{g} \rightarrow qq\bar{q}\bar{q}$ + $e/\mu/\tau$ simplified model
>1725	95	[6] SIRUNYAN	20T	CMS	same-sign $\ell^{\pm}\ell^{\pm}$ or $\geq 3\ell^{\pm}$+jets, $\tilde{g} \rightarrow tbs$ simplified model
>1500	95	[7] SIRUNYAN	19F	CMS	$\tilde{g} \rightarrow jjj$
>2260	95	[8] AABOUD	18Z	ATLS	$\geq 4\ell$, $\lambda_{12k} \neq 0$, $m_{\tilde{\chi}_1^0}$ > 1000 GeV
>1650	95	[8] AABOUD	18Z	ATLS	$\geq 4\ell$, $\lambda_{i33} \neq 0$, $m_{\tilde{\chi}_1^0}$ > 500 GeV
>1610	95	[9] SIRUNYAN	18AK	CMS	$\tilde{g} \rightarrow tbs$, λ''_{332} coupling
>1690	95	[10] SIRUNYAN	18D	CMS	top quark (hadronically decaying) + jets + $\not{E}_T$, Tglu3C, $m_{\tilde{t}_1} - m_{\tilde{\chi}_1^0}$ = 20 GeV, $m_{\tilde{\chi}_1^0}$ = 0 GeV
none 100–1410	95	[11] SIRUNYAN	18EA	CMS	2 large jets with four-parton substructure, $\tilde{g} \rightarrow 5q$
>2100	95	[12] AABOUD	17AI	ATLS	$\geq 1\ell$+ $\geq$ 8 jets, Tglu3A and $\tilde{\chi}_1^0 \rightarrow uds$, λ''_{112} coupling, $m_{\tilde{\chi}_1^0}$=1000 GeV
>1650	95	[13] AABOUD	17AI	ATLS	$\geq 1\ell$+ $\geq$ 8 jets, $\tilde{g} \rightarrow t\tilde{t}$, $\tilde{t} \rightarrow bs$, λ''_{323} coupling, $m_{\tilde{t}}$=1000 GeV
>1800	95	[14] AABOUD	17AI	ATLS	$\geq 1\ell$+ $\geq$ 8 jets, Tglu1A and $\tilde{\chi}_1^0 \rightarrow qql$, λ' coupling, $m_{\tilde{\chi}_1^0}$=1000 GeV
>1800	95	[15] AABOUD	17AJ	ATLS	same-sign $\ell^{\pm}\ell^{\pm}$ / 3 ℓ + jets + $\not{E}_T$, Tglu3A, λ''_{112} coupling, $m_{\tilde{\chi}_1^0}$ = 50 GeV
>1750	95	[16] AABOUD	17AJ	ATLS	same-sign $\ell^{\pm}\ell^{\pm}$ / 3 ℓ + jets + $\not{E}_T$, Tglu1A and $\tilde{\chi}_1^0 \rightarrow qq\ell$, λ' coupling
>1450	95	[17] AABOUD	17AJ	ATLS	same-sign $\ell^{\pm}\ell^{\pm}$ / 3 ℓ + jets + $\not{E}_T$, $\tilde{g} \rightarrow t\tilde{t}_1$ and $\tilde{t}_1 \rightarrow sd$, λ''_{321} coupling
>1450	95	[18] AABOUD	17AJ	ATLS	same-sign $\ell^{\pm}\ell^{\pm}$ / 3 ℓ + jets + $\not{E}_T$, $\tilde{g} \rightarrow t\tilde{t}_1$ and $\tilde{t}_1 \rightarrow bd$, λ''_{313} coupling
> 400	95	[19] AABOUD	17AJ	ATLS	same-sign $\ell^{\pm}\ell^{\pm}$ / 3 ℓ + jets + $\not{E}_T$, $\tilde{d}_R \rightarrow tb(ts)$, λ''_{313} (λ''_{321}) coupling
none 625–1375	95	[20] AABOUD	17AZ	ATLS	$\geq$ 7 jets+$\not{E}_T$, large R-jets and/or b-jets, $\tilde{g} \rightarrow t\tilde{t}_1$ and $\tilde{t}_1 \rightarrow bs$, λ''_{323} coupling
none 600–650	95	[21] KHACHATRY...	17Y	CMS	$\tilde{g} \rightarrow qqqqq$, λ''_{212} coupling, $m_{\tilde{q}}$ = 100 GeV
none 600–1030	95	[21] KHACHATRY...	17Y	CMS	$\tilde{g} \rightarrow qqqqq$, λ''_{212} coupling, $m_{\tilde{q}}$ = 900 GeV
none 600–650	95	[21] KHACHATRY...	17Y	CMS	$\tilde{g} \rightarrow qqqqb$, λ''_{213} coupling, $m_{\tilde{q}}$ = 100 GeV
none 600–1080	95	[21] KHACHATRY...	17Y	CMS	$\tilde{g} \rightarrow qqqqb$, λ''_{213} coupling, $m_{\tilde{q}}$ = 900 GeV
none 600–680	95	[21] KHACHATRY...	17Y	CMS	$\tilde{g} \rightarrow qqqbb$, λ''_{212} coupling, $m_{\tilde{q}}$ = 100 GeV
none 600–1080	95	[21] KHACHATRY...	17Y	CMS	$\tilde{g} \rightarrow qqqbb$, λ''_{212} coupling, $m_{\tilde{q}}$ = 900 GeV
none 600–650	95	[21] KHACHATRY...	17Y	CMS	$\tilde{g} \rightarrow qqbbb$, λ''_{213} coupling, $m_{\tilde{q}}$ = 100 GeV
none 600–1100	95	[21] KHACHATRY...	17Y	CMS	$\tilde{g} \rightarrow qqbbb$, λ''_{213} coupling, $m_{\tilde{q}}$ = 900 GeV
>1050	95	[22] KHACHATRY...	16BJ	CMS	same-sign $\ell^{\pm}\ell^{\pm}$, Tglu3A, $m_{\tilde{\chi}_1^0}$ < 800 GeV
>1140	95	[22] KHACHATRY...	16BJ	CMS	same-sign $\ell^{\pm}\ell^{\pm}$, Tglu3B, $m_{\tilde{t}} - m_{\tilde{\chi}_1^0}$ = 20 GeV, $m_{\tilde{\chi}_1^0}$ = 0

>1030	95	[23] KHACHATRY...16BX	CMS	$\widetilde{g} \rightarrow t b s$, λ''_{332} coupling
>1150	95	[24] AAD 15BV	ATLAS	general RPC $\widetilde{g}$ decays, $m_{\widetilde{\chi}^0_1} <$ 100 GeV
>1350	95	[25] AAD 14X	ATLAS	$\geq 4\ell^{\pm}$, $\widetilde{g} \rightarrow q\overline{q}\widetilde{\chi}^0_1$, $\widetilde{\chi}^0_1 \rightarrow \ell^{\pm}\ell^{\mp}\nu$
> 650	95	[26] CHATRCHYAN 14P	CMS	$\widetilde{g} \rightarrow jjj$
none 200–835	95	[26] CHATRCHYAN 14P	CMS	$\widetilde{g} \rightarrow bjj$
• • • We do not use the following data for averages, fits, limits, etc. • • •				
>1875	95	[27] AABOUD 18CF	ATLAS	jets and large R-jets, Tglu2RPV and $\widetilde{\chi}^0_1 \rightarrow qqq$, λ'' coupling, $m_{\widetilde{\chi}^0_1}$=1000 GeV
>1400	95	[28] KHACHATRY...16BX	CMS	$\widetilde{g} \rightarrow q q \widetilde{\chi}^0_1$, $\widetilde{\chi}^0_1 \rightarrow \ell\ell\nu$, λ_{121} or $\lambda_{122} \neq 0$, $m_{\widetilde{\chi}^0_1} > 400$ GeV
>1600	95	[24] AAD 15BV	ATLAS	pMSSM, M_1 = 60 GeV, $m_{\widetilde{q}} <$ 1500 GeV
>1280	95	[24] AAD 15BV	ATLAS	mSUGRA, m_0 > 2 TeV
>1100	95	[24] AAD 15BV	ATLAS	via $\widetilde{\tau}$, natural GMSB, all $m_{\widetilde{\tau}}$
>1220	95	[24] AAD 15BV	ATLAS	b-jets, $\widetilde{g} \rightarrow \widetilde{t}_1 t$ and $\widetilde{t}_1 \rightarrow t\widetilde{\chi}^0_1$, $m_{\widetilde{T}_1} <$ 1000 GeV
>1180	95	[24] AAD 15BV	ATLAS	b-jets, $\widetilde{g} \rightarrow \widetilde{t}_1 t$ and $\widetilde{t}_1 \rightarrow b\widetilde{\chi}^{\pm}_1$, $m_{\widetilde{T}_1} <$ 1000 GeV, $m_{\widetilde{\chi}^0_1}$ = 60 GeV
> 880	95	[24] AAD 15BV	ATLAS	jets, $\widetilde{g} \rightarrow \widetilde{t}_1 t$ and $\widetilde{t}_1 \rightarrow s b$, $400 < m_{\widetilde{t}_1} <$ 1000 GeV
		[29] AAD 15CB	ATLAS	ℓ, $\widetilde{g} \rightarrow (e/\mu) q q$, benchmark gluino, neutralino masses
> 600	95	[29] AAD 15CB	ATLAS	$\ell\ell/Z$, $\widetilde{g} \rightarrow (ee/\mu\mu/e\mu) q q$, $m_{\widetilde{\chi}^0_1}$ = 400 GeV and $0.7 < c\tau_{\widetilde{\chi}^0_1} < 3 \times 10^5$ mm
>1000	95	[30] AAD 15X	ATLAS	$\geq$ 10 jets, $\widetilde{g} \rightarrow q\overline{q}\widetilde{\chi}^0_1$, $\widetilde{\chi}^0_1 \rightarrow qqq$, $m_{\widetilde{\chi}^0_1}$=500 GeV
> 917	95	[30] AAD 15X	ATLAS	$\geq$ 6,7 jets, $\widetilde{g} \rightarrow qqq$, (light-quark, λ'' couplings)
> 929	95	[30] AAD 15X	ATLAS	$\geq$ 6,7 jets, $\widetilde{g} \rightarrow qqq$, (b-quark, λ'' couplings)
>1180	95	[31] AAD 14AX	ATLAS	$\geq$ 3 b-jets + $\not{E}_T$, $\widetilde{g} \rightarrow \widetilde{t}_1 t \widetilde{\chi}^0_1$ simplified model, $\widetilde{t}_1 \rightarrow b\widetilde{\chi}^{\pm}_1$, $m_{\widetilde{\chi}^{\pm}_1}$=2$m_{\widetilde{\chi}^0_1}$, $m_{\widetilde{\chi}^0_1}$=60 GeV, $m_{\widetilde{t}_1}$ <1000 GeV
> 850	95	[32] AAD 14E	ATLAS	$\ell^{\pm}\ell^{\pm}(\ell^{\mp})$ + jets, $\widetilde{g} \rightarrow t\widetilde{t}_1$ with $\widetilde{t}_1 \rightarrow b s$ simplified model
> 900	95	[33] CHATRCHYAN 14H	CMS	same-sign $\ell^{\pm}\ell^{\pm}$, $\widetilde{g} \rightarrow t b s$ simplified model

[1] AAD 24AF searched in 140 fb^{-1} of pp collisions at $\sqrt{s}$ = 13 TeV for evidence of gluino pair production followed by direct RPV gluino decays into three jets or $\widetilde{g} \rightarrow q q \widetilde{\chi}^0_1$ followed by the decay of $\widetilde{\chi}^0_1$ into three jets. No excess above the Standard Model prediction is observed, and the results are interpreted in models with non-vanishing λ''_{112} or λ''_{113}, Tglu1RPV and Tglu1A with $\widetilde{\chi}^0_1$ RPV decay, see their Figures 9 and 10.

[2] AAD 21BF searched in 139 fb^{-1} of pp collisions at $\sqrt{s}$ = 13 TeV for pair production of gluinos, stops, electroweakinos decaying RPV either directly or indirectly via the LSP. The final state in all cases is one or two leptons, many jets (up to fifteen) and b-jets. Different models with different branching fractions of the gluino or stop follow from the assumptions on the nature of the electroweakinos. No significant excess above the Standard Model predictions is observed. Limits are set on the *gluino*, $\widetilde{t}_1$, electroweakino masses as a function of the $\widetilde{\chi}^0_1$ mass in several scenarios of gluino, stop and electroweakino pair production.

[3] AAD 21Y searched in 139 fb^{-1} of pp collisions at $\sqrt{s}$ = 13 TeV for supersymmetry in events with four or more leptons (electrons, muons and tau-leptons). No significant excess above the Standard Model expectations is observed. Limits are set on Tchi1n12-GGM, and RPV models similar to Tchi1n2l, Tglu1A (with q = u, d, s, c, b, with equal branching fractions), and $\widetilde{\ell}_L/\widetilde{\nu} \rightarrow \ell/\nu\widetilde{\chi}^0_1$ (mass-degenerate $\widetilde{\ell}_L$ and $\widetilde{\nu}$ of all 3 generations), all with $\widetilde{\chi}^0_1 \rightarrow \ell^{\pm}\ell^{\mp}\nu$ via λ_{12k} or λ_{i33} (where $i,k \in 1,2$), see their Figure 11.

[4] AAD 20AL searched in 139 fb^{-1} of pp collisions at $\sqrt{s}$ = 13 TeV for events with 8 or more jets and moderate missing transverse momentum. The selection makes requirements according to the number of b-tagged jets and the scalar sum of masses of large-radius jets. No significant excess above the Standard Model expectations is observed. Exclusion limits at 95% C.L. are set on the gluino mass in RPV simplified models where the gluino decays via $\widetilde{g} \rightarrow t b d$ or $\widetilde{g} \rightarrow t b s$. They extend up to almost 1.6 TeV for a $\widetilde{t}_1$ mass of 900 GeV. See their Fig. 10(c).

[5] AAD 20V searched in 139 fb^{-1} of pp collisions at $\sqrt{s}$ = 13 TeV for events with two same-sign charged leptons (electrons or muons) and jets. No significant excess above the Standard Model expectations is observed. Exclusion limits at 95% C.L. are set on the gluino mass in RPV simplified models where the gluino decays via $\widetilde{g} \rightarrow t b d$, see Figure 7(b).

[6] SIRUNYAN 20T searched in 137 fb^{-1} of pp collisions at $\sqrt{s}$ = 13 TeV for events with at least two jets, and two isolated same-sign or three or more charged leptons (electrons or muons). No significant excess above the Standard Model expectations is observed. Limits are set on the gluino mass in the Tglu3A, Tglu3B, Tglu3C and Tglu3D simplified models, see their Figure 7, and in the Tglu1C and Tglu1B simplified models, see their Figures 8 and 9. Limits are also set on the sbottom mass in the Tsbot2 simplified model, see their Figure 10, and on the stop mass in the Tstop7 simplified model, see their Figure 11. Finally, limits are set on the gluino mass in RPV simplified models where the gluino decays either via $\widetilde{g} \rightarrow q q \overline{q}\overline{q} + e/\mu/\tau$ or via $\widetilde{g} \rightarrow t b s$, see Figure 12.

[7] SIRUNYAN 19F searched in 35.9 fb^{-1} of pp collisions at $\sqrt{s}$ = 13 TeV for three-jet resonances produced in the decay of a gluino in R-parity violating supersymmetric models. The mass range from 200 to 2000GeV is explored in four separate mass regions. The observations show agreement with standard model expectations. The results are interpreted within the framework of R-parity violating SUSY, where pair-produced gluinos decay to a six quark final state. Gluino masses below 1500GeV are excluded at 95% C.L. See their Fig.5.

[8] AABOUD 18Z searched in 36.1 fb^{-1} of pp collisions at $\sqrt{s}$ = 13 TeV for events containing four or more charged leptons (electrons, muons and up to two hadronically decaying taus). No significant deviation from the expected SM background is observed. Limits are set on the Higgsino mass in simplified models of general gauge mediated supersymmetry Tn1n1A/Tn1n1B/Tn1n1C, see their Figure 9. Limits are also set on the wino, slepton, sneutrino and gluino mass in a simplified model of NLSP pair production with R-parity violating decays of the LSP via λ_{12k} or λ_{i33} to charged leptons, see their Figures 7, 8.

[9] SIRUNYAN 18AK searched in 35.9 fb^{-1} of pp collisions at $\sqrt{s}$ = 13 TeV for events containing a single lepton, large jet and b-quark jet multiplicities, coming from R-parity-violating decays of gluinos. No excess over the expected background is observed. Limits are derived on the gluino mass, assuming the RPV $\widetilde{g} \rightarrow t b s$ decay, see their Figure 9.

[10] SIRUNYAN 18D searched in 35.9 fb^{-1} of pp collisions at $\sqrt{s}$ = 13 TeV for events containing identified hadronically decaying top quarks, no leptons, and $\not{E}_T$. No significant excess above the Standard Model expectations is observed. Limits are set on the stop mass in the Tstop1 simplified model, see their Figure 8, and on the gluino mass in the Tglu3A, Tglu3B, Tglu3C and Tglu3E simplified models, see their Figure 9.

[11] SIRUNYAN 18EA searched in 38.2 fb^{-1} of pp collisions at $\sqrt{s}$ = 13 TeV for the pair production of resonances, each decaying to at least four quarks. Reconstructed particles are clustered into two large jets of similar mass, each consistent with four-parton substructure. No statistically significant excess over the Standard Model expectation is observed. Limits are set on the squark and gluino mass in RPV supersymmetry models where squarks (gluinos) decay, through intermediate higgsinos, to four (five) quarks, see their Figure 4.

[12] AABOUD 17AI searched in 36.1 fb^{-1} of pp collisions at $\sqrt{s}$ = 13 TeV for events with one or more isolated lepton, at least eight jets, either zero or many b-jets, for evidence of R-parity violating decays of the gluino. No significant excess above the Standard Model expectations is observed. Limits up to 2.1 TeV are set on the gluino mass in R-parity-violating supersymmetry models as Tglu3A with LSP decay through the non-zero λ''_{112} coupling as $\widetilde{\chi}^0_1 \rightarrow u d s$. See their Figure 9.

[13] AABOUD 17AI searched in 36.1 fb^{-1} of pp collisions at $\sqrt{s}$ = 13 TeV for events with one or more isolated lepton, at least eight jets, either zero or many b-jets, for evidence of R-parity violating decays of the gluino. No significant excess above the Standard Model expectations is observed. Limits up to 1.65 TeV are set on the gluino mass in R-parity-violating supersymmetry models with $\widetilde{g} \rightarrow t\widetilde{t}$, $\widetilde{t} \rightarrow b s$ through the non-zero λ''_{323} coupling. See their Figure 9.

[14] AABOUD 17AI searched in 36.1 fb^{-1} of pp collisions at $\sqrt{s}$ = 13 TeV for events with one or more isolated lepton, at least eight jets, either zero or many b-jets, for evidence of R-parity violating decays of the gluino. No significant excess above the Standard Model expectations is observed. Limits up to 1.8 TeV are set on the gluino mass in R-parity-violating supersymmetry models as Tglu1A with the LSP decay through the non-zero λ' coupling as $\widetilde{\chi}^0_1 \rightarrow q q \ell$. See their Figure 9.

[15] AABOUD 17AJ searched in 36.1 fb^{-1} of pp collisions at $\sqrt{s}$ = 13 TeV for events with two same-sign or three leptons, jets and large missing transverse momentum. No significant excess above the Standard Model expectations is observed. Limits up to 1.8 TeV are set on the gluino mass in R-parity-violating supersymmetry models as Tglu3A with LSP decaying through the non-zero λ''_{112} coupling as $\widetilde{\chi}^0_1 \rightarrow u d s$. See their Figure 5(d).

[16] AABOUD 17AJ searched in 36.1 fb^{-1} of pp collisions at $\sqrt{s}$ = 13 TeV for events with two same-sign or three leptons, jets and large missing transverse momentum. No significant excess above the Standard Model expectations is observed. Limits up to 1.75 TeV are set on the gluino mass in R-parity-violating supersymmetry models as Tglu1A with LSP decaying through the non-zero λ' coupling as $\widetilde{\chi}^0_1 \rightarrow q q \ell$. See their Figure 5(c).

[17] AABOUD 17AJ searched in 36.1 fb^{-1} of pp collisions at $\sqrt{s}$ = 13 TeV for events with two same-sign or three leptons, jets and large missing transverse momentum. No significant excess above the Standard Model expectations is observed. Limits up to 1.45 TeV are set on the gluino mass in R-parity-violating supersymmetry models where $\widetilde{g} \rightarrow t\widetilde{t}_1$ and $\widetilde{t}_1 \rightarrow s d$ through the non-zero λ''_{321} coupling. See their Figure 5(b).

[18] AABOUD 17AJ searched in 36.1 fb^{-1} of pp collisions at $\sqrt{s}$ = 13 TeV for events with two same-sign or three leptons, jets and large missing transverse momentum. No significant excess above the Standard Model expectations is observed. Limits up to 1.45 TeV are set on the gluino mass in R-parity-violating supersymmetry models where $\widetilde{g} \rightarrow t\widetilde{t}_1$ and $\widetilde{t}_1 \rightarrow b d$ through the non-zero λ''_{313} coupling. See their Figure 5(a).

[19] AABOUD 17AJ searched in 36.1 fb^{-1} of pp collisions at $\sqrt{s}$ = 13 TeV for events with two same-sign or three leptons, jets and large missing transverse momentum. No significant excess above the Standard Model expectations is observed. Limits up to 400 GeV are set on the down type squark ($\widetilde{d}_R$ mass in R-parity-violating supersymmetry models where $\widetilde{d}_R \rightarrow t b$ through the non-zero λ''_{313} coupling or $\widetilde{d}_R \rightarrow t s$ through the non-zero λ''_{321}. See their Figure 5(e) and 5(f).

[20] AABOUD 17AZ searched in 36.1 fb^{-1} of pp collisions at $\sqrt{s}$ = 13 TeV for events with at least seven jets and large missing transverse momentum. Selected events are further classified based on the presence of large R-jets or b-jets and no leptons. No significant excess above the Standard Model expectations is observed. Limits are set for R-parity violating decays of the gluino assuming $\widetilde{g} \rightarrow t\widetilde{t}_1$ and $\widetilde{t}_1 \rightarrow b s$ through the non-zero λ''_{323} couplings. The range 625–1375 GeV is excluded for $m_{\widetilde{t}_1}$ = 400 GeV. See their Figure 7b.

[21] KHACHATRYAN 17Y searched in 19.7 fb^{-1} of pp collisions at $\sqrt{s}$ = 8 TeV for events containing at least 8 or 10 jets, possibly b-tagged, coming from R-parity-violating decays of supersymmetric particles. No excess over the expected background is observed. Limits are derived on the gluino mass, assuming various RPV decay modes, see Fig. 7.

[22] KHACHATRYAN 16BJ searched in 2.3 fb^{-1} of pp collisions at $\sqrt{s}$ = 13 TeV for events with two isolated same-sign dileptons and jets in the final state. No significant excess above the Standard Model expectations is observed. Limits are set on the gluino mass in the following simplified models: Tglu3A and Tglu3D, see Fig. 4, Tglu3B and Tglu3C, see Fig. 5, and Tglu1B, see Fig. 7.

Int. J. Mod. Phys. A 2026.41. Downloaded from www.worldscientific.com
by UNIVERSITY OF CALIFORNIA @ BERKELEY on 09/16/26. Re-use and distribution is strictly not permitted, except for Open Access articles.

Int. J. Mod. Phys. A 2026.41. Downloaded from www.worldscientific.com
by UNIVERSITY OF CALIFORNIA @ BERKELEY on 09/16/26. Re-use and distribution is strictly not permitted, except for Open Access articles.

[23] KHACHATRYAN 16BX searched in 19.5 fb^{-1} of pp collisions at $\sqrt{s}$ = 8 TeV for events containing 0 or 1 leptons and b-tagged jets, coming from R-parity-violating decays of supersymmetric particles. No excess over the expected background is observed. Limits are derived on the gluino mass, assuming the RPV $\widetilde{g} \rightarrow t\,b\,s$ decay, see Fig. 7 and 10.

[24] AAD 15BV summarized and extended ATLAS searches for gluinos and first- and second-generation squarks in final states containing jets and missing transverse momentum, with or without leptons or b-jets in the $\sqrt{s}$ =8 TeV data set collected in 2012. The paper reports the results of new interpretations and statistical combinations of previously published analyses, as well as new analyses. Exclusion limits at 95% C.L. are set on the gluino mass in several R-parity conserving models, leading to a generalized constraint on gluino masses exceeding 1150 GeV for lightest supersymmetric particle masses below 100 GeV. See their Figs. 10, 19, 20, 21, 23, 25, 26, 29-37.

[25] AAD 14X searched in 20.3 fb^{-1} of pp collisions at $\sqrt{s}$ = 8 TeV for events with at least four leptons (electrons, muons, taus) in the final state. No significant excess above the Standard Model expectations is observed. Limits are set on the gluino mass in an R-parity violating simplified model where the decay $\widetilde{g} \rightarrow q\overline{q}\widetilde{\chi}^0_1$, with $\widetilde{\chi}^0_1 \rightarrow \ell^\pm\ell^\mp\nu$, takes place with a branching ratio of 100%, see Fig. 8.

[26] CHATRCHYAN 14P searched in 19.4 fb^{-1} of pp collisions at $\sqrt{s}$ = 8 TeV for three-jet resonances produced in the decay of a gluino in R-parity violating supersymmetric models. No excess over the expected SM background is observed. Assuming a 100% branching ratio for the gluino decay into three light-flavour jets, limits are set on the cross section of gluino pair production, see Fig. 7, and gluino masses below 650 GeV are excluded at 95% C.L. Assuming a 100% branching ratio for the gluino decaying to one b-quark jet and two light-flavour jets, gluino masses between 200 GeV and 835 GeV are excluded at 95% C L.

[27] AABOUD 18CF searched in 36.1 fb^{-1} of pp collisions at $\sqrt{s}$ = 13 TeV for events with several jets, possibly b-jets, and large-radius jets for evidence of R-parity violating decays of the gluino. No significant excess above the Standard Model expectations is observed. Limits between 1000 and 1875 GeV are set on the gluino mass in R-parity-violating supersymmetry models as Tglu2RPV with the LSP decay through the non-zero λ'' coupling as $\widetilde{\chi}^0_1 \rightarrow q\,q\,q$. The most stringent limit is obtained for $m_{\widetilde{\chi}^0_1}$ = 1000 GeV, the weakest for $m_{\widetilde{\chi}^0_1}$ = 50 GeV. See their Figure 7(b). Figure 7(a) presents results for gluinos directly decaying into 3 quarks, Tglu1RPV.

[28] KHACHATRYAN 16BX searched in 19.5 fb^{-1} of pp collisions at $\sqrt{s}$ = 8 TeV for events containing 4 leptons coming from R-parity-violating decays of $\widetilde{\chi}^0_1 \rightarrow \ell\ell\nu$ with $\lambda_{121} \neq 0$ or $\lambda_{122} \neq 0$. No excess over the expected background is observed. Limits are derived on the gluino, squark and stop masses, see Fig. 23.

[29] AAD 15CB searched for events containing at least one long-lived particle that decays at a significant distance from its production point (displaced vertex, DV) into two leptons or into five or more charged particles in 20.3 fb^{-1} of pp collisions at $\sqrt{s}$ = 8 TeV. The dilepton signature is characterised by DV formed from at least two lepton candidates. Four different final states were considered for the multitrak signature, in which the DV must be accompanied by a high-transverse momentum muon or electron candidate that originates from the DV, jets or missing transverse momentum. No events were observed in any of the signal regions. Results were interpreted in SUSY scenarios involving R-parity violation, split supersymmetry, and gauge mediation. See their Fig. 12–20.

[30] AAD 15X searched in 20.3 fb^{-1} of pp collisions at $\sqrt{s}$ = 8 TeV for events containing large number of jets, no requirements on missing transverse momentum and no isolated electrons or muons. The sensitivity of the search is enhanced by considering the number of b-tagged jets and the scalar sum of masses of large-radius jets in an event. No evidence was found for excesses above the expected level of Standard Model background. Exclusion limits at 95% C.L. are set on the gluino mass assuming the gluino decays to various quark flavors, and for various neutralino masses. See their Fig. 11–16.

[31] AAD 14AX searched in 20.1 fb^{-1} of pp collisions at $\sqrt{s}$ = 8 TeV for the strong production of supersymmetric particles in events containing either zero or at last one high-p_T lepton, large missing transverse momentum, high jet multiplicity and at least three jets identified as originating from b-quarks. No excess over the expected SM background is observed. Limits are derived in mSUGRA/CMSSM models with tanβ = 30, $A_0 = -2m_0$ and $\mu > 0$, see their Fig. 14. Also, exclusion limits in simplified models containing gluinos and scalar top and bottom quarks are set, see their Figures 12, 13.

[32] AAD 14E searched in 20.3 fb^{-1} of pp collisions at $\sqrt{s}$ = 8 TeV for strongly produced supersymmetric particles in events containing jets and two same-sign leptons or three leptons. The search also utilises jets originating from b-quarks, missing transverse momentum and other variables. No excess over the expected SM background is observed. Exclusion limits are derived in simplified models containing gluinos and squarks, see Figures 5 and 6. In the $\widetilde{g} \rightarrow q\,q'\widetilde{\chi}^\pm_1$, $\widetilde{\chi}^\pm_1 \rightarrow W^{(*)\pm}\widetilde{\chi}^0_2$, $\widetilde{\chi}^0_2 \rightarrow Z^{(*)}\widetilde{\chi}^0_1$ simplified model, the following assumptions have been made: $m_{\widetilde{\chi}^\pm_1} = 0.5\ m_{\widetilde{\chi}^0_1} + m_{\widetilde{g}}$, $m_{\widetilde{\chi}^0_2} = 0.5\ (m_{\widetilde{\chi}^0_1} + m_{\widetilde{\chi}^\pm_1})$, $m_{\widetilde{\chi}^0_1} < 520$ GeV. In the $\widetilde{g} \rightarrow q\,q'\widetilde{\chi}^\pm_1$, $\widetilde{\chi}^\pm_1 \rightarrow \ell^\pm\nu\widetilde{\chi}^0_1$ or $\widetilde{g} \rightarrow q\,q'\widetilde{\chi}^0_2$, $\widetilde{\chi}^0_2 \rightarrow \ell^\pm\ell^\mp(\nu\nu)\widetilde{\chi}^0_1$ simplified model, the following assumptions have been made: $m_{\widetilde{\chi}^\pm_1} = m_{\widetilde{\chi}^0_2} = 0.5\ (m_{\widetilde{\chi}^0_1} + m_{\widetilde{g}})$, $m_{\widetilde{\chi}^0_1} < 660$ GeV. Limits are also derived in the mSUGRA/CMSSM, bRPV and GMSB models, see their Fig. 8.

[33] CHATRCHYAN 14H searched in 19.5 fb^{-1} of pp collisions at $\sqrt{s}$ = 8 TeV for events with two isolated same-sign dileptons and jets in the final state. No significant excess above the Standard Model expectations is observed. Limits are set on the gluino mass in simplified models where the R-parity violating decay $\widetilde{g} \rightarrow t\,b\,s$ takes place with a branching ratio of 100%, see Fig. 8.

Long-lived $\widetilde{g}$ (Gluino) mass limit

Limits on light gluinos ($m_{\widetilde{g}}$ < 5 GeV) were last listed in our PDG 14 edition: K. Olive, *et al.* (Particle Data Group), Chinese Physics **C38** 070001 (2014) (http://pdg.lbl.gov).

VALUE (GeV)	CL%	DOCUMENT ID		TECN	COMMENT
>2200	95	[1] AAD	25AE	ATLS	R-hadrons, Tglu1A, τ > 10 ns, $m_{\widetilde{\chi}^0_1}$ = 100 GeV
>2080	95	[2] HAYRAPETY...	25V	CMS	large dE/dx in Si tracker, gluino R-hadrons
none 70–1700	95	[3] HAYRAPETY...	24AP	CMS	≥ 6 jets $\widetilde{g}$ pair production with RPV $\widetilde{g} \rightarrow q\,q\,q$
>2050	95	[4] AAD	23G	ATLS	R-hadrons, Tglu1A, stable, $m_{\widetilde{\chi}^0_1}$ = 100 GeV
>2270	95	[4] AAD	23G	ATLS	R-hadrons, Tglu1A, τ = 20 ns, $m_{\widetilde{\chi}^0_1}$ = 100 GeV
>2050	95	[4] AAD	23G	ATLS	R-hadrons, Tglu1A, stable, $m_{\widetilde{g}} - m_{\widetilde{\chi}^0_1}$ = 30 GeV
>2050	95	[4] AAD	23G	ATLS	R-hadrons, Tglu1A, τ = 20 ns, $m_{\widetilde{g}} - m_{\widetilde{\chi}^0_1}$ = 30 GeV
>2500	95	[5] SIRUNYAN	21AF	CMS	long-lived $\widetilde{g}$, Tglu2RPV , λ''_{323} coupling, 0.6 mm < cτ < 90 mm
>2450	95	[6] SIRUNYAN	21U	CMS	long-lived $\widetilde{g}$, $pp \rightarrow \widetilde{g}\widetilde{g}$, $\widetilde{g} \rightarrow g\widetilde{G}$, GMSB, 6 < c$\tau$ < 550 mm
>2500	95	[6] SIRUNYAN	21U	CMS	long-lived $\widetilde{g}$, $pp \rightarrow \widetilde{g}\widetilde{g}$, $\widetilde{g} \rightarrow q\overline{q}\widetilde{\chi}^0_1$, mini-split, $m_{\widetilde{\chi}^0_1}$ =100 GeV, 7 < cτ < 360 mm
>2500	95	[6] SIRUNYAN	21U	CMS	long-lived $\widetilde{g}$, $pp \rightarrow \widetilde{g}\widetilde{g}$, $\widetilde{g} \rightarrow t\,b\,s$, λ''_{323} coupling, 3 < cτ < 1000 mm
>1980	95	[7] AABOUD	19AT	ATLS	R-hadrons, Tglu1A, metastable
>2060	95	[8] AABOUD	19C	ATLS	R-hadrons, Tglu1A, $\tau \geq 10$ ns, $m_{\widetilde{\chi}^0_1}$ = 100 GeV
>1890	95	[8] AABOUD	19C	ATLS	R-hadrons, Tglu1A, stable
>2400	95	[9] SIRUNYAN	19BH	CMS	long-lived $\widetilde{g}$, RPV, $\widetilde{g} \rightarrow \overline{t}\,\overline{b}\,\overline{s}$, 10 mm < c$\tau$ < 250 mm
>2300	95	[9] SIRUNYAN	19BH	CMS	long-lived $\widetilde{g}$, GMSB, $\widetilde{g} \rightarrow g\widetilde{G}$, 20 mm < c$\tau$ < 110 mm
>2100	95	[10] SIRUNYAN	19BT	CMS	long-lived $\widetilde{g}$, GMSB, $\widetilde{g} \rightarrow g\widetilde{G}$, 0.3 m < c$\tau$ < 30 m
>2500	95	[10] SIRUNYAN	19BT	CMS	long-lived $\widetilde{g}$, GMSB, $\widetilde{g} \rightarrow g\widetilde{G}$, c$\tau$ = 1 m
>1900	95	[10] SIRUNYAN	19BT	CMS	long-lived $\widetilde{g}$, GMSB, $\widetilde{g} \rightarrow g\widetilde{G}$, c$\tau$ = 100 m
>2370	95	[11] AABOUD	18S	ATLS	displaced vertex + $\not{E}_T$, long-lived Tglu1A, $m_{\widetilde{\chi}^0_1}$ = 100 GeV, and τ=0.17 ns
>1600	95	[12] SIRUNYAN	18AY	CMS	jets+$\not{E}_T$, Tglu1A, cτ < 0.1 mm, $m_{\widetilde{\chi}^0_1}$ = 100 GeV
>1750	95	[12] SIRUNYAN	18AY	CMS	jets+$\not{E}_T$, Tglu1A, cτ = 1 mm, $m_{\widetilde{\chi}^0_1}$ = 100 GeV
>1640	95	[12] SIRUNYAN	18AY	CMS	jets+$\not{E}_T$, Tglu1A, cτ = 10 mm, $m_{\widetilde{\chi}^0_1}$ = 100 GeV
>1490	95	[12] SIRUNYAN	18AY	CMS	jets+$\not{E}_T$, Tglu1A, cτ = 100 mm, $m_{\widetilde{\chi}^0_1}$ = 100 GeV
>1300	95	[12] SIRUNYAN	18AY	CMS	jets+$\not{E}_T$, Tglu1A, cτ = 1 m, $m_{\widetilde{\chi}^0_1}$ = 100 GeV
> 960	95	[12] SIRUNYAN	18AY	CMS	jets+$\not{E}_T$, Tglu1A, cτ = 10 m, $m_{\widetilde{\chi}^0_1}$ = 100 GeV
> 900	95	[12] SIRUNYAN	18AY	CMS	jets+$\not{E}_T$, Tglu1A, cτ = 100 m, $m_{\widetilde{\chi}^0_1}$ = 100 GeV
>2200	95	[13] SIRUNYAN	18DV	CMS	long-lived $\widetilde{g}$, RPV, $\widetilde{g} \rightarrow \overline{t}\,\overline{b}\,\overline{s}$, 0.6 mm < c$\tau$ < 80 mm
>1000	95	[14] KHACHATRY...	17AR	CMS	long-lived $\widetilde{g}$, RPV, $\widetilde{g} \rightarrow t\,\overline{b}\,\overline{s}$, c$\tau$ = 0.3 mm
>1300	95	[14] KHACHATRY...	17AR	CMS	long-lived $\widetilde{g}$, RPV, $\widetilde{g} \rightarrow t\,\overline{b}\,\overline{s}$, c$\tau$ = 1.0 mm
>1400	95	[14] KHACHATRY...	17AR	CMS	long-lived $\widetilde{g}$, RPV, $\widetilde{g} \rightarrow t\,\overline{b}\,\overline{s}$, 2 mm < c$\tau$ < 30 mm
>1580	95	[15] AABOUD	16B	ATLS	long-lived R-hadrons
> 740–1590	95	[16] AABOUD	16C	ATLS	R-hadrons, Tglu1A, $\tau \geq 0.4$ ns, $m_{\widetilde{\chi}^0_1}$ = 100 GeV
>1570	95	[16] AABOUD	16C	ATLS	R-hadrons, Tglu1A, stable
>1610	95	[17] KHACHATRY...	16BW	CMS	long-lived $\widetilde{g}$ forming R-hadrons, f = 0.1, cloud interaction model
>1580	95	[17] KHACHATRY...	16BW	CMS	long-lived $\widetilde{g}$ forming R-hadrons, f = 0.1, charge-suppressed interaction model
>1520	95	[17] KHACHATRY...	16BW	CMS	long-lived $\widetilde{g}$ forming R-hadrons, f = 0.5, cloud interaction model
>1540	95	[17] KHACHATRY...	16BW	CMS	long-lived $\widetilde{g}$ forming R-hadrons, f = 0.5, charge-suppressed interaction model
>1270	95	[18] AAD	15AE	ATLS	$\widetilde{g}$ R-hadron, generic R-hadron model
>1360	95	[18] AAD	15AE	ATLS	$\widetilde{g}$ decaying to 300 GeV stable sleptons, LeptoSUSY model
>1115	95	[19] AAD	15BM	ATLS	$\widetilde{g}$ R-hadron, stable
>1185	95	[19] AAD	15BM	ATLS	$\widetilde{g} \rightarrow (g\,/\,q\overline{q})\widetilde{\chi}^0_1$, lifetime 10 ns, $m_{\widetilde{\chi}^0_1}$ = 100 GeV

>1099	95	[19] AAD	15BM	ATLS	$\widetilde{g} \rightarrow (g/q\overline{q})\widetilde{\chi}^0_1$, lifetime 10 ns, $m_{\widetilde{g}} - m_{\widetilde{\chi}^0_1} = 100$ GeV
>1182	95	[19] AAD	15BM	ATLS	$\widetilde{g} \rightarrow t\overline{t}\widetilde{\chi}^0_1$, lifetime 10 ns, $m_{\widetilde{\chi}^0_1} = 100$ GeV
>1157	95	[19] AAD	15BM	ATLS	$\widetilde{g} \rightarrow t\overline{t}\widetilde{\chi}^0_1$, lifetime 10 ns, $m_{\widetilde{g}} - m_{\widetilde{\chi}^0_1} = 480$ GeV
> 869	95	[19] AAD	15BM	ATLS	$\widetilde{g} \rightarrow (g/q\overline{q})\widetilde{\chi}^0_1$, lifetime 1 ns, $m_{\widetilde{\chi}^0_1} = 100$ GeV
> 821	95	[19] AAD	15BM	ATLS	$\widetilde{g} \rightarrow (g/q\overline{q})\widetilde{\chi}^0_1$, lifetime 1 ns, $m_{\widetilde{g}} - m_{\widetilde{\chi}^0_1} = 100$ GeV
> 836	95	[19] AAD	15BM	ATLS	$\widetilde{g} \rightarrow t\overline{t}\widetilde{\chi}^0_1$, lifetime 1 ns, $m_{\widetilde{\chi}^0_1} = 100$ GeV
> 836	95	[19] AAD	15BM	ATLS	$\widetilde{g} \rightarrow t\overline{t}\widetilde{\chi}^0_1$, lifetime 10 ns, $m_{\widetilde{g}} - m_{\widetilde{\chi}^0_1} = 480$ GeV
>1000	95	[20] KHACHATRY...	15AK	CMS	$\widetilde{g}$ R-hadrons, 10 μs< τ <1000 s
> 880	95	[20] KHACHATRY...	15AK	CMS	$\widetilde{g}$ R-hadrons, 1 μs< τ <1000 s
• • • We do not use the following data for averages, fits, limits, etc. • • •					
> 985	95	[21] AAD	13AA	ATLS	$\widetilde{g}$, R-hadrons, generic interaction model
> 832	95	[22] AAD	13BC	ATLS	R-hadrons, $\widetilde{g} \rightarrow g/q\overline{q}\widetilde{\chi}^0_1$, generic R-hadron model, lifetime between 10^{-5} and 10^3 s, $m_{\widetilde{\chi}^0_1} = 100$ GeV
>1322	95	[23] CHATRCHYAN	13AB	CMS	long-lived $\widetilde{g}$ forming R-hadrons, f = 0.1, cloud interaction model
none 200–341	95	[24] AAD	12P	ATLS	long-lived $\widetilde{g} \rightarrow g\widetilde{\chi}^0_1$, $m_{\widetilde{\chi}^0_1} =$ 100 GeV
> 640	95	[25] CHATRCHYAN	12AN	CMS	long-lived $\widetilde{g} \rightarrow g\widetilde{\chi}^0_1$
>1098	95	[26] CHATRCHYAN	12L	CMS	long-lived $\widetilde{g}$ forming R-hadrons, f = 0.1
> 586	95	[27] AAD	11K	ATLS	stable $\widetilde{g}$
> 544	95	[28] AAD	11P	ATLS	stable $\widetilde{g}$, GMSB scenario, tanβ=5
> 370	95	[29] KHACHATRY...	11	CMS	long lived $\widetilde{g}$
> 398	95	[30] KHACHATRY...	11C	CMS	stable $\widetilde{g}$

[1] AAD 25AE searched for massive, charged long-lived particles in 140 fb^{-1} of pp collisions at $\sqrt{s}$ = 13 TeV. Two analyses are conducted: one looking for a single track, with high specific ionisation losses in the pixel detector and long time of flight to the hadron calorimeter, and one looking for two tracks, both with high specific ionisation in the pixel detector. No excess above the expected background is found. Limits are set in scenarios of long-lived R-hadrons (gluino) production, chargino production or stau pair production, see their figures 13 and 14.

[2] HAYRAPETYAN 25V searched in 101 fb^{-1} of pp collisions at $\sqrt{s}$ = 13 TeV for heavy, long-lived, charged particles with large ionization energy loss within the silicon tracker of the CMS experiment. No significant excess above the Standard Model expectations is observed. Limits are set on the pair production of gluino R-hadrons, top squark R-hadrons, and detector-stable $\widetilde{\tau}_{R,L}$, see their figure 6. Limits are also set in a model predicting a pair of single- and double-charged τ' fermions from a Z' boson decay, see their figure 7.

[3] HAYRAPETYAN 24AP searched in 128 fb^{-1} of pp collisions at $\sqrt{s}$ = 13 TeV for evidence of pair-produced multijet signatures probing fully hadronic final states. No significant excess above the Standard Model expectations is observed. Limits are set in three RPV SUSY models: higgsino pair production with decay to merged trijets, stop pair production with decay to merged dijets, and pair-produced gluinos decaying to resolved trijets, see their Fig. 4.

[4] AAD 23G searched in 139 fb^{-1} of pp collisions at $\sqrt{s}$ = 13 TeV for R-hadron pair production in events with high-pt tracks with large ionisation in the pixel detector. No significant excess above the Standard Model predictions is observed. Limits are set on the R-hadron mass for different masses of the LSP and for different R-hadron lifetimes, see Figure 18.

[5] SIRUNYAN 21AF searched in 140 fb^{-1} of pp collisions at $\sqrt{s}$ = 13 TeV for supersymmetry in events with with two displaced vertices from long-lived particles decaying into multijet or dijet final states. No significant excess above the Standard Model expectations is observed. Limits are set on the gluino mass in the simplified model Tglu2RPV with λ''_{323} coupling, on the $\widetilde{\chi}^0_1$ mass in an RPV model with $\widetilde{\chi}^0_1$ pair production and the RPV decay $\widetilde{\chi}^0_1 \rightarrow tbs$ with λ''_{323} coupling and on the $\widetilde{t}$ mass in an RPV model with top squark pair production and the RPV decay $\widetilde{t} \rightarrow \overline{d}_i\overline{d}_j$ with λ''_{3ij} coupling, see their Figure 7.

[6] SIRUNYAN 21U searched in 132 fb^{-1} of pp collisions at $\sqrt{s}$ = 13 TeV for supersymmetry in events with displaced tracks and displaced vertices associated with a dijet system. No significant excess above the Standard Model expectations is observed. Limits are set on long-lived gluinos in an RPC GMSB SUSY model of gluino pair production, with $\widetilde{g} \rightarrow g\widetilde{G}$, see their Figure 9, in Tglu1A in a mini-split model, see their Figure 10, and in an RPV model of gluino pair production, with $\widetilde{g} \rightarrow tbs$ with coupling λ''_{323}, see their Figure 11. Limits are also set on long-lived top squarks in Tstop2RPV, see their Figure 12, in an RPV model with $\widetilde{t} \rightarrow d\overline{t}$ and λ'_{x31} coupling, see their Figure 13, and in a dynamical RPV model with $\widetilde{t} \rightarrow \overline{d}\overline{d}$ via a nonholomorphic RPV coupling η''_{311}, see their Figure 14. The best mass limit is achieved in all cases at cτ = 30 mm.

[7] AABOUD 19AT searched in 36.1 fb^{-1} of pp collisions at $\sqrt{s}$ = 13 TeV for metastable and stable R-hadrons. Multiple search strategies for a wide range of lifetimes, corresponding to path lengths of a few meters, are defined. No significant deviations from the expected Standard Model background are observed. Gluino R-hadrons with lifetimes of the order of 50 ns are excluded at 95% C.L. for masses below 1980 GeV using the muon-spectrometer agnostic analysis. Using the full-detector search, the observed lower limits on the mass are 2000 GeV. See their Figure 9 (top).

[8] AABOUD 19C searched in 36.1 fb^{-1} of pp collisions at $\sqrt{s}$ = 13 TeV for metastable and stable R-hadrons arising as excesses in the mass distribution of reconstructed tracks with high transverse momentum and large dE/dx. Gluino R-hadrons with lifetimes above 10 ns are excluded at 95% C.L. with lower mass limit range between 1000 GeV and 2060 GeV, see their Figure 5(a). Masses smaller than 1290 GeV are excluded for a lifetime of 1 ns, see their Figure 6. In the case of stable R-hadrons, the lower mass limit is 1890 GeV, see their Figure 5(b).

[9] SIRUNYAN 19BH searched in 35.9 fb^{-1} of pp collisions at $\sqrt{s}$ = 13 TeV for long-lived particles decaying into jets, with each long-lived particle having a decay vertex well displaced from the production vertex. The selected events are found to be consistent with standard model predictions. Limits are set on the gluino mass in a GMSB model where the gluino is decaying via $\widetilde{g} \rightarrow g\widetilde{G}$, see their Figure 4 and in an RPV model of supersymmetry where the gluino is decaying via $\widetilde{g} \rightarrow \overline{t}\overline{b}\overline{s}$, see their Figures 5. Limits are also set on the stop mass in two RPV models, see their Figure 6 (for $\widetilde{t} \rightarrow b\ell$ decays) and Figure 7 (for $\widetilde{t} \rightarrow \overline{d}\overline{d}$ decays).

[10] SIRUNYAN 19BT searched in 137 fb^{-1} of pp collisions at $\sqrt{s}$ = 13 TeV for long-lived particles decaying to displaced, nonprompt jets and missing transverse momentum. Candidate signal events are identified using the timing capabilities of the CMS electromagnetic calorimeter. The results of the search are found to be consistent with the background predictions. Limits are set on the gluino mass in a GMSB model where long-lived gluinos are pair produced and decaying via $\widetilde{g} \rightarrow g\widetilde{G}$, see their Figures 4 and 5.

[11] AABOUD 18S searched in 32.8 fb^{-1} of pp collisions at $\sqrt{s}$ = 13 TeV for long-lived gluinos in final states with large missing transverse momentum and at least one high-mass displaced vertex with five or more tracks. The observed yield is consistent with the expected background. Exclusion limits are derived for Tglu1A models predicting the existence of long-lived gluinos reaching roughly m($\widetilde{g}$) = 2000 GeV to 2370 GeV for m($\widetilde{\chi}^0_1$) = 100 GeV and gluino lifetimes between 0.02 and 10 ns, see their Fig. 8. Limits are presented also as a function of the lifetime (for a fixed gluino-neutralino mass difference of 100 GeV) and of the gluino and neutralino masses (for a fixed lifetime of 1 ns). See their Fig. 9 and 10 respectively.

[12] SIRUNYAN 18AY searched in 35.9 fb^{-1} of pp collisions at $\sqrt{s}$ = 13 TeV for events containing one or more jets and significant $\not{E}_T$. No significant excess above the Standard Model expectations is observed. Limits are set on the gluino mass in the Tglu1A, Tglu2A and Tglu3A simplified models, see their Figure 3. Limits are also set on squark, sbottom and stop masses in the Tsqk1, Tsbot1, Tstop1 and Tstop4 simplified models, see their Figure 3. Finally, limits are set on long-lived gluino masses in a Tglu1A simplified model where the gluino is metastable or long-lived with proper decay lengths in the range 10^{-3} mm $< c\tau < 10^5$ mm, see their Figure 4.

[13] SIRUNYAN 18DV searched in 38.5 fb^{-1} of pp collisions at $\sqrt{s}$ = 13 TeV for long-lived particles in events with multiple jets and two displaced vertices composed of many tracks. No events with two well-separated high-track-multiplicity vertices were observed. Limits are set on the stop and the gluino mass in RPV models of supersymmetry where the stop (gluino) is decaying solely into dijet (multijet) final states, see their Figures 6 and 7.

[14] KHACHATRYAN 17AR searched in 17.6 fb^{-1} of pp collisions at $\sqrt{s}$ = 8 TeV for R-parity-violating SUSY in which long-lived neutralinos or gluinos decay into multijet final states. No significant excess above the Standard Model expectations is observed. Limits are set on the gluino mass for a range of mean proper decay lengths (cτ), see their Fig. 7. The upper limits on the production cross section times branching ratio squared (Fig. 7) are also applicable to long-lived neutralinos.

[15] AABOUD 16B searched in 3.2 fb^{-1} of pp collisions at $\sqrt{s}$ = 13 TeV for long-lived R-hadrons using observables related to large ionization losses and slow propagation velocities, which are signatures of heavy charged particles traveling significantly slower than the speed of light. Exclusion limits at 95% C.L. are set on the long-lived gluino masses exceeding 1580 GeV. See their Fig. 5.

[16] AABOUD 16C searched in 3.2 fb^{-1} of pp collisions at $\sqrt{s}$ = 13 TeV for long-lived and stable R-hadrons identified by anomalous specific ionization energy loss in the ATLAS Pixel detector. Gluino R-hadrons with lifetimes above 0.4 ns are excluded at 95% C.L. with lower mass limit range between 740 GeV and 1590 GeV. In the case of stable R-hadrons, the lower mass limit is 1570 GeV. See their Figs. 5 and 6.

[17] KHACHATRYAN 16BW searched in 2.5 fb^{-1} of pp collisions at $\sqrt{s}$ = 13 TeV for events with heavy stable charged particles, identified by their anomalously high energy deposits in the silicon tracker and/or long time-of-flight measurements by the muon system. No evidence for an excess over the expected background is observed. Limits are derived for pair production of gluinos as a function of mass, depending on the interaction model and on the fraction f, of produced gluinos hadronizing into a $\widetilde{g}$ - gluon state, see Fig. 4 and Table 7.

[18] AAD 15AE searched in 19.1 fb^{-1} of pp collisions at $\sqrt{s}$ = 8 TeV for heavy long-lived charged particles, measured through their specific ionization energy loss in the ATLAS pixel detector or their time-of-flight in the ALTAS muon system. In the absence of an excess of events above the expected backgrounds, limits are set R-hadrons in various scenarios, see Fig. 11. Limits are also set in LeptoSUSY models where the gluino decays to stable 300 GeV leptons, see Fig. 9.

[19] AAD 15BM searched in 18.4 fb^{-1} of pp collisions at $\sqrt{s}$ = 8 TeV for stable and metastable non-relativistic charged particles through their anomalous specific ionization energy loss in the ATLAS pixel detector. In absence of an excess of events above the expected backgrounds, limits are set within a generic R-hadron model, on stable gluino R-hadrons (see Table 5) and on metastable gluino R-hadrons decaying to $(g/q\overline{q})$ plus a light $\widetilde{\chi}^0_1$ (see Fig. 7) and decaying to $t\overline{t}$ plus a light $\widetilde{\chi}^0_1$ (see Fig. 9).

[20] KHACHATRYAN 15AK looked in a data set corresponding to 18.6 fb^{-1} of pp collisions at $\sqrt{s}$ = 8 TeV, and a search interval corresponding to 281 h of trigger lifetime, for long-lived particles that have stopped in the CMS detector. No evidence for an excess over the expected background in a cloud interaction model is observed. Assuming the decay $\widetilde{g} \rightarrow g\widetilde{\chi}^0_1$ and lifetimes between 1 μ and 1000 s, limits are derived on $\widetilde{g}$ production as a function of $m_{\widetilde{\chi}^0_1}$, see Figs. 4 and 6. The exclusions require that $m_{\widetilde{\chi}^0_1}$ is kinematically consistent with the minimum values of the jet energy thresholds used.

[21] AAD 13AA searched in 4.7 fb^{-1} of pp collisions at $\sqrt{s}$ = 7 TeV for events containing colored long-lived particles that hadronize forming R-hadrons. No significant excess above the expected background was found. Long-lived R-hadrons containing a $\widetilde{g}$ are excluded for masses up to 985 GeV at 95% C.L in a general interaction model. Also, limits independent of the fraction of R-hadrons that arrive charged in the muon system were derived, see Fig. 6.

[22] AAD 13BC searched in 5.0 fb^{-1} of pp collisions at $\sqrt{s}$ = 7 TeV and in 22.9 fb^{-1} of pp collisions at $\sqrt{s}$ = 8 TeV for bottom squark R-hadrons that have come to rest within the

Int. J. Mod. Phys. A 2026.41. Downloaded from www.worldscientific.com
by UNIVERSITY OF CALIFORNIA @ BERKELEY on 09/16/26. Re-use and distribution is strictly not permitted, except for Open Access articles.

Int. J. Mod. Phys. A 2026.41. Downloaded from www.worldscientific.com by UNIVERSITY OF CALIFORNIA @ BERKELEY on 09/16/26. Re-use and distribution is strictly not permitted, except for Open Access articles.

ATLAS calorimeter and decay at some later time to hadronic jets and a neutralino. In absence of an excess of events above the expected backgrounds, limits are set on gluino masses for different decays, lifetimes, and neutralino masses, see their Table 6 and Fig. 10.

[23] CHATRCHYAN 13AB looked in 5.0 fb^{-1} of pp collisions at $\sqrt{s}$ = 7 TeV and in 18.8 fb^{-1} of pp collisions at $\sqrt{s}$ = 8 TeV for events with heavy stable particles, identified by their anomalous dE/dx in the tracker or additionally requiring that it be identified as muon in the muon chambers, from pair production of $\widetilde{g}$'s. No evidence for an excess over the expected background is observed. Limits are derived for pair production of gluinos as a function of mass (see Fig. 8 and Table 5), depending on the fraction, f, of formation of $\widetilde{g}$–g (R-gluonball) states. The quoted limit is for f = 0.1, while for f = 0.5 it degrades to 1276 GeV. In the conservative scenario where every hadronic interaction causes it to become neutral, the limit decreases to 928 GeV for f = 0.1.

[24] AAD 12P looked in 31 pb^{-1} of pp collisions at $\sqrt{s}$ = 7 TeV for events with pair production of long-lived gluinos. The hadronization of the gluinos leads to R-hadrons which may stop inside the detector and later decay via $\widetilde{g} \rightarrow g\widetilde{\chi}^0_1$ during gaps between the proton bunches. No significant excess over the expected background is observed. From a counting experiment, a limit at 95% C.L. on the cross section as a function of $m_{\widetilde{g}}$ is derived for $m_{\widetilde{\chi}^0_1}$ = 100 GeV, see Fig. 4. The limit is valid for lifetimes between 10^{-5} and 10^3 seconds and assumes the *Generic* matter interaction model for the production cross section.

[25] CHATRCHYAN 12AN looked in 4.0 fb^{-1} of pp collisions at $\sqrt{s}$ = 7 TeV for events with pair production of long-lived gluinos. The hadronization of the gluinos leads to R-hadrons which may stop inside the detector and later decay via $\widetilde{g} \rightarrow g\widetilde{\chi}^0_1$ during gaps between the proton bunches. No significant excess over the expected background is observed. From a counting experiment, a limit at 95% C.L. on the cross section as a function of $m_{\widetilde{g}}$ is derived, see Fig. 3. The mass limit is valid for lifetimes between 10^{-5} and 10^3 seconds, for what they call "the daughter gluon energy E_g >" 100 GeV and assuming the *cloud* interaction model for R-hadrons. Supersedes KHACHATRYAN 11.

[26] CHATRCHYAN 12L looked in 5.0 fb^{-1} of pp collisions at $\sqrt{s}$ = 7 TeV for events with heavy stable particles, identified by their anomalous dE/dx in the tracker or additionally requiring that it be identified as muon in the muon chambers, from pair production of $\widetilde{g}$'s. No evidence for an excess over the expected background is observed. Limits are derived for pair production of gluinos as a function of mass (see Fig. 3), depending on the fraction, f, of formation of $\widetilde{g}$–g (R-glueball) states. The quoted limit is for f = 0.1, while for f = 0.5 it degrades to 1046 GeV. In the conservative scenario where every hadronic interaction causes it to become neutral, the limit decreases to 928 GeV for f=0.1. Supersedes KHACHATRYAN 11C.

[27] AAD 11K looked in 34 pb^{-1} of pp collisions at $\sqrt{s}$ = 7 TeV for events with heavy stable particles, identified by their anomalous dE/dx in the tracker or time of flight in the tile calorimeter, from pair production of $\widetilde{g}$. No evidence for an excess over the SM expectation is observed. Limits are derived for pair production of gluinos as a function of mass (see Fig. 4), for a fraction, f = 10%, of formation of $\widetilde{g} - g$ (R-gluonball). If instead of a phase space driven approach for the hadronic scattering of the R-hadrons, a triple-Regge model or a bag-model is used, the limit degrades to 566 and 562 GeV, respectively.

[28] AAD 11P looked in 37 pb^{-1} of pp collisions at $\sqrt{s}$ = 7 TeV for events with heavy stable particles, reconstructed and identified by their time of flight in the Muon System. There is no requirement on their observation in the tracker to increase the sensitivity to cases where gluinos have a large fraction, f, of formation of neutral $\widetilde{g} - g$ (R-gluonball). No evidence for an excess over the SM expectation is observed. Limits are derived as a function of mass (see Fig. 4), for f=0.1. For fractions f = 0.5 and 1.0 the limit degrades to 537 and 530 GeV, respectively.

[29] KHACHATRYAN 11 looked in 10 pb^{-1} of pp collisions at $\sqrt{s}$ = 7 TeV for events with pair production of long-lived gluinos. The hadronization of the gluinos leads to R-hadrons which may stop inside the detector and later decay via $\widetilde{g} \rightarrow g\widetilde{\chi}^0_1$ during gaps between the proton bunches. No significant excess over the expected background is observed. From a counting experiment, a limit at 95% C.L. on the cross section times branching ratio is derived for $m_{\widetilde{g}} - m_{\widetilde{\chi}^0_1} > 100$ GeV, see their Fig. 2. Assuming 100% branching ratio, lifetimes between 75 ns and 3×10^5 s are excluded for $m_{\widetilde{g}}$ = 300 GeV. The $\widetilde{g}$ mass exclusion is obtained with the same assumptions for lifetimes between 10 μs and 1000 s, but shows some dependence on the model for R-hadron interactions with matter, illustrated in Fig. 3. From a time-profile analysis, the mass exclusion is 382 GeV for a lifetime of 10 μs under the same assumptions as above.

[30] KHACHATRYAN 11C looked in 3.1 pb^{-1} of pp collisions at $\sqrt{s}$ = 7 TeV for events with heavy stable particles, identified by their anomalous dE/dx in the tracker or additionally requiring that it be identified as muon in the muon chambers, from pair production of $\widetilde{g}$. No evidence for an excess over the expected background is observed. Limits are derived for pair production of gluinos as a function of mass (see Fig. 3), depending on the fraction, f, of formation of $\widetilde{g} - g$ (R-gluonball). The quoted limit is for f=0.1, while for f=0.5 it degrades to 357 GeV. In the conservative scenario where every hadronic interaction causes it to become neutral, the limit decreases to 311 GeV for f=0.1.

Light $\widetilde{G}$ (Gravitino) mass limits from collider experiments

The following are bounds on light ($\ll$ 1 eV) gravitino indirectly inferred from its coupling to matter suppressed by the gravitino decay constant.

Unless otherwise stated, all limits assume that other supersymmetric particles besides the gravitino are too heavy to be produced. The gravitino is assumed to be undetected and to give rise to a missing energy ($\not{E}$) signature.

Some earlier papers are now obsolete and have been omitted. They were last listed in our PDG 14 edition: K. Olive, *et al.* (Particle Data Group), Chinese Physics **C38** 070001 (2014) (http://pdg.lbl.gov).

VALUE (eV)	CL%	DOCUMENT ID		TECN	COMMENT
• • • We do not use the following data for averages, fits, limits, etc. • • •					
$> 3.5 \times 10^{-4}$	95	[1] AAD	15BH	ATLS	jet + $\not{E}_T$, $pp \rightarrow (\widetilde{q}/\widetilde{g})\widetilde{G}$, $m_{\widetilde{q}} = m_{\widetilde{g}}$ = 500 GeV
$> 3 \times 10^{-4}$	95	[1] AAD	15BH	ATLS	jet + $\not{E}_T$, $pp \rightarrow (\widetilde{q}/\widetilde{g})\widetilde{G}$, $m_{\widetilde{q}} = m_{\widetilde{g}}$ = 1000 GeV
$> 2 \times 10^{-4}$	95	[1] AAD	15BH	ATLS	jet + $\not{E}_T$, $pp \rightarrow (\widetilde{q}/\widetilde{g})\widetilde{G}$, $m_{\widetilde{q}} = m_{\widetilde{g}}$ = 1500 GeV
$> 1.09 \times 10^{-5}$	95	[2] ABDALLAH	05B	DLPH	$e^+e^- \rightarrow \widetilde{G}\widetilde{G}\gamma$
$> 1.35 \times 10^{-5}$	95	[3] ACHARD	04E	L3	$e^+e^- \rightarrow \widetilde{G}\widetilde{G}\gamma$
$> 1.3 \times 10^{-5}$		[4] HEISTER	03C	ALEP	$e^+e^- \rightarrow \widetilde{G}\widetilde{G}\gamma$
$>11.7 \times 10^{-6}$	95	[5] ACOSTA	02H	CDF	$p\overline{p} \rightarrow \widetilde{G}\widetilde{G}\gamma$
$> 8.7 \times 10^{-6}$	95	[6] ABBIENDI,G	00D	OPAL	$e^+e^- \rightarrow \widetilde{G}\widetilde{G}\gamma$

[1] AAD 15BH searched in 20.3 fb^{-1} of pp collisions at $\sqrt{s}$ = 8 TeV for associated production of a light gravitino and a squark or gluino. The squark (gluino) is assumed to decay exclusively to a quark (gluon) and a gravitino. No evidence was found for an excess above the expected level of Standard Model background and 95% C.L. lower limits were set on the gravitino mass as a function of the squark/gluino mass, both in the case of degenerate and non-degenerate squark/gluino masses, see Figs. 14 and 15.

[2] ABDALLAH 05B use data from $\sqrt{s}$ = 180–208 GeV. They look for events with a single photon + $\not{E}$ final states from which a cross section limit of $\sigma < 0.18$ pb at 208 GeV is obtained, allowing a limit on the mass to be set. Supersedes the results of ABREU 00Z.

[3] ACHARD 04E use data from $\sqrt{s}$ = 189–209 GeV. They look for events with a single photon + $\not{E}$ final states from which a limit on the Gravitino mass is set corresponding to $\sqrt{F}$ > 238 GeV. Supersedes the results of ACCIARRI 99R.

[4] HEISTER 03C use the data from $\sqrt{s}$ = 189–209 GeV to search for $\gamma\not{E}_T$ final states.

[5] ACOSTA 02H looked in 87 pb^{-1} of $p\overline{p}$ collisions at $\sqrt{s}$=1.8 TeV for events with a high-E_T photon and $\not{E}_T$. They compared the data with a GMSB model where the final state could arise from $q\overline{q} \rightarrow \widetilde{G}\widetilde{G}\gamma$. Since the cross section for this process scales as $1/|F|^4$, a limit at 95% CL is derived on $|F|^{1/2}$ > 221 GeV. A model independent limit for the above topology is also given in the paper.

[6] ABBIENDI,G 00D searches for $\gamma\not{E}$ final states from $\sqrt{s}$=189 GeV.

Supersymmetry miscellaneous results

Results that do not appear under other headings or that make nonminimal assumptions.

Some earlier papers are now obsolete and have been omitted. They were last listed in our PDG 14 edition: K. Olive, *et al.* (Particle Data Group), Chinese Physics **C38** 070001 (2014) (http://pdg.lbl.gov).

VALUE	CL%	DOCUMENT ID		TECN	COMMENT
• • • We do not use the following data for averages, fits, limits, etc. • • •					
		[1] AAD	24AH	ATLS	pMSSM search
		[2] AAD	20C	ATLS	habemus MSSM, m_A–tanβ plane
none 450–1400	95	[3] AAD	20L	ATLS	heavy neutral Higgs bosons, hMSSM, m_A–tanβ plane
>65	95	[4] AABOUD	16AF	ATLS	selected ATLAS searches on EWK sector
none 0–2	95	[5] AAD	16AG	ATLS	dark photon, γ_d, in SUSY- and Higgs-portal models
		[6] AAD	13P	ATLS	dark γ, hidden valley
		[7] AALTONEN	12AB	CDF	hidden-valley Higgs
none 100–185	95	[8] AAD	11AA	ATLS	scalar gluons
		[9] CHATRCHYAN	11E	CMS	$\mu\mu$ resonances
		[10] ABAZOV	10N	D0	γ_D, hidden valley

[1] AAD 24AH combined a number of ATLAS analyses to use them and interpret in a series of models derived from a flat-prior scan to pMSSM parameter space. Limits are provided in terms of fraction of models excluded as a function of one or two parameters, while marginalising over the others.

[2] AAD 20C uses a statistical combination of six final states $b\overline{b}b\overline{b}$, $b\overline{b}WW$, $b\overline{b}\tau\tau$, $WWWW$, $b\overline{b}\gamma\gamma$, and $WW\gamma\gamma$ to search for non-resonant and resonant production of Higgs boson pairs. The search uses 36.1 fb^{-1} of pp collisions data at $\sqrt{s}$ = 13 TeV. Constraints in the habemus Minimal Supersymmetric Standard Model in the (m_A, tanβ) parameter space are placed, see their Figure 7(b).

[3] AAD 20L used 27.8 fb^{-1} of pp collision data at $\sqrt{s}$ = 13 TeV to search for heavy neutral Higgs bosons produced in association with at least one b-quark and decaying into a pair of b-quarks. The data are compatible with SM expectations, yielding no significant excess of events in the mass range 450–1400 GeV, see their Fig. 11. Exclusion limits at 95% C.L. were derived in hMSSM scenarios as a function of m_A and tanβ, see their Fig. 9 and 10.

[4] AABOUD 16AF uses a selection of searches by ATLAS for the electroweak production of SUSY particles studying resulting constraints on dark matter candidates. They use 20 fb^{-1} of pp collisions at $\sqrt{s}$ = 8 TeV. A likelihood-driven scan of an effective model focusing on the gaugino-higgsino and Higgs sector of the pMSSM is performed. The ATLAS searches impact models where $m_{\chi^0_1}$ < 65 GeV, excluding 86% of them. See their Figs. 2, 4, and 6.

[5] AAD 16AG searches for prompt lepton-jets using 20 fb^{-1} of pp collisions at $\sqrt{s}$ = 8 TeV collected with the ATLAS detector. Lepton-jets are expected from decays of low-mass dark photons in SUSY-portal and Higgs-portal models. No significant excess of events is observed and 95% CL upper limits are computed on the production cross section times branching ratio for two prompt lepton-jets in models predicting 2 or 4 γ_d via SUSY-portal topologies, for γ_d mass values between 0 and 2 GeV. See their Figs 9 and 10. The results are also interpreted in terms of a 90% CL exclusion region in kinetic mixing and dark-photon mass parameter space. See their Fig. 13.

[6] AAD 13P searched in 5 fb^{-1} of pp collisions at $\sqrt{s}$ = 7 TeV for single lepton-jets with at least four muons; pairs of lepton-jets, each with two or more muons; and pairs of lepton-jets with two or more electrons. All of these could be signatures of Hidden Valley supersymmetric models. No statistically significant deviations from the Standard Model expectations are found. 95% C.L. limits are placed on the production cross section times branching ratio of dark photons for several parameter sets of a Hidden Valley model.

[7] AALTONEN 12AB looked in 5.1 fb^{-1} of $p\overline{p}$ collisions at $\sqrt{s}$ = 1.96 TeV for anomalous production of multiple low-energy leptons in association with a W or Z boson. Such events may occur in hidden valley models in which a supersymmetric Higgs boson is produced in association with a W or Z boson, with $H \rightarrow \widetilde{\chi}^0_1\widetilde{\chi}^0_1$ pair and with the $\widetilde{\chi}^0_1$ further decaying into a dark photon (γ_D) and the unobservable lightest SUSY particle of the hidden sector. As the γ_D is expected to be light, it may decay into a lepton pair.

No significant excess over the SM expectation is observed and a limit at 95% C.L. is set on the cross section for a benchmark model of supersymmetric hidden-valley Higgs production.

[8] AAD 11AA looked in 34 pb^{-1} of pp collisions at $\sqrt{s}$ = 7 TeV for events with ≥ 4 jets originating from pair production of scalar gluons, each decaying to two gluons. No two-jet resonances are observed over the SM background. Limits are derived on the cross section times branching ratio (see Fig. 3). Assuming 100% branching ratio for the decay to two gluons, the quoted exclusion range is obtained, except for a 5 GeV mass window around 140 GeV.

[9] CHATRCHYAN 11E looked in 35 pb^{-1} of pp collisions at $\sqrt{s}$ = 7 TeV for events with collimated μ pairs (leptonic jets) from the decay of hidden sector states. No evidence for new resonance production is found. Limits are derived and compared to various SUSY models (see Fig. 4) where the LSP, either the $\widetilde{\chi}^0_1$ or a $\widetilde{q}$, decays to dark sector particles.

[10] ABAZOV 10N looked in 5.8 fb^{-1} of $p\overline{p}$ collisions at $\sqrt{s}$ = 1.96 TeV for events from hidden valley models in which a $\widetilde{\chi}^0_1$ decays into a dark photon, γ_D, and the unobservable lightest SUSY particle of the hidden sector. As the γ_D is expected to be light, it may decay into a tightly collimated lepton pair, called lepton jet. They searched for events with $\not{E}_T$ and two isolated lepton jets observable by an opposite charged lepton pair ee, $e\mu$ or $\mu\mu$. No significant excess over the SM expectation is observed, and a limit at 95% C.L. on the cross section times branching ratio is derived, see their Table I. They also examined the invariant mass of the lepton jets for a narrow resonance, see their Fig. 4, but found no evidence for a signal.

REFERENCES FOR Supersymmetric Particle Searches

AAD	25AE	JHEP 2507 140	G. Aad *et al.*	(ATLAS Collab.)
AAD	25AH	JHEP 2508 053	G. Aad *et al.*	(ATLAS Collab.)
AAD	25BJ	EPJ C85 1335	G. Aad *et al.*	(ATLAS Collab.)
AAD	25BM	EPJ C85 1437	G. Aad *et al.*	(ATLAS Collab.)
AAD	25L	PR D112 012005	G. Aad *et al.*	(ATLAS Collab.)
AAD	25M	PR D112 012016	G. Aad *et al.*	(ATLAS Collab.)
AAD	25V	JHEP 2502 193	G.Aad *et al.*	(ATLAS Collab.)
AALBERS	25	PRL 135 011802	J. Aalbers *et al.*	(LZ Collab.)
ABBASI	25A	EPJ C85 490	R. Abbasi *et al.*	(IceCube Collab.)
APRILE	25B	PRL 135 221003	E. Aprile *et al.*	(XENONnT Collab.)
BO	25	PRL 134 011805	Z. Bo *et al.*	(PandaX-4T Collab.)
CHEKHOVSKY	25K	JHEP 2510 236	V. Chekhovsky *et al.*	(CMS Collab.)
CHEKHOVSKY	25M	PR D112 112023	V. Chekhovsky *et al.*	(CMS Collab.)
HAYRAPETY...	25AH	PRL 135 231804	A. Hayrapetyan *et al.*	(CMS Collab.)
HAYRAPETY...	25V	JHEP 2504 109	A. Hayrapetyan *et al.*	(CMS Collab.)
YU	25	PRL 135 231001	G.H. Yu *et al.*	(COSINE-100 Collab.)
AAD	24AC	JHEP 2403 139	G. Aad *et al.*	(ATLAS Collab.)
AAD	24AF	JHEP 2405 003	G. Aad *et al.*	(ATLAS Collab.)
AAD	24AH	JHEP 2405 106	G. Aad *et al.*	(ATLAS Collab.)
AAD	24AJ	JHEP 2405 150	G. Aad *et al.*	(ATLAS Collab.)
AAD	24AO	JHEP 2407 250	G. Aad *et al.*	(ATLAS Collab.)
AAD	24AX	PL B856 138938	G. Aad *et al.*	(ATLAS Collab.)
AAD	24BT	PR D110 092004	G. Aad *et al.*	(ATLAS Collab.)
AAD	24CE	JHEP 2412 116	G. Aad *et al.*	(ATLAS Collab.)
AAD	24G	PRL 132 221801	G. Aad *et al.*	(ATLAS Collab.)
AAD	24I	PRL 133 031802	G. Aad *et al.*	(ATLAS Collab.)
AAD	24U	PR D109 112011	G. Aad *et al.*	(ATLAS Collab.)
AAD	24Z	JHEP 2402 107	G. Aad *et al.*	(ATLAS Collab.)
HAYRAPETY...	24AP	PRL 133 201803	A. Hayrapetyan *et al.*	(CMS Collab.)
HAYRAPETY...	24M	PR D109 072007	A. Hayrapetyan *et al.*	(CMS Collab.)
HAYRAPETY...	24N	PR D109 112001	A. Hayrapetyan *et al.*	(CMS Collab.)
HAYRAPETY...	24P	PR D109 112005	A. Hayrapetyan *et al.*	(CMS Collab.)
HAYRAPETY...	24Q	PR D109 112009	A. Hayrapetyan *et al.*	(CMS Collab.)
HAYRAPETY...	24Y	JHEP 2405 047	A. Hayrapetyan *et al.*	(CMS Collab.)
MCDANIEL	24	PR D109 063024	A. McDaniel *et al.*	(CLEMS, NASA, TURIN+)
AAD	23AB	JHEP 2307 021	G. Aad *et al.*	(ATLAS Collab.)
AAD	23AE	EPJ C83 515	G. Aad *et al.*	(ATLAS Collab.)
AAD	23AL	EPJ C83 561	G. Aad *et al.*	(ATLAS Collab.)
AAD	23AM	PR D108 012012	G. Aad *et al.*	(ATLAS Collab.)
AAD	23BQ	PL B846 138172	G. Aad *et al.*	(ATLAS Collab.)
AAD	23CB	JHEP 2310 082	G. Aad *et al.*	(ATLAS Collab.)
AAD	23CI	JHEP 2312 167	G. Aad *et al.*	(ATLAS Collab.)
AAD	23CP	JHEP 2311 150	G. Aad *et al.*	(ATLAS Collab.)
AAD	23CR	JHEP 2312 081	G. Aad *et al.*	(ATLAS Collab.)
AAD	23G	JHEP 2306 158	G. Aad *et al.*	(ATLAS Collab.)
AAD	23M	JHEP 2306 031	G. Aad *et al.*	(ATLAS Collab.)
AALBERS	23	PRL 131 041002	J. Aalbers *et al.*	(LZ Collab.)
ABBASI	23A	PR D108 102004	R. Abbasi *et al.*	(IceCube Collab.)
ABE	23B	PRL 130 061002	H. Abe *et al.*	(MAGIC Collab.)
ABE	23E	PR D108 083022	K. Abe *et al.*	(XMASS-I Collab.)
ALBERT	23	JCAP 2312 038	A. Albert *et al.*	(HAWC Collab.)
APRILE	23A	PRL 131 041003	E. Aprile *et al.*	(XENONnT Collab.)
CHENG	23A	PR D108 063015	J.-G. Cheng, Y.-F. Liang, E.-W. Liang	
FOSTER	23	PR D107 103047	J.W. Foster *et al.*	(MIT, UCB, LBL+)
GUO	23A	PR D108 043001	X.-K. Guo *et al.*	
HAYRAPETY...	23E	JHEP 2310 046	A. Hayrapetyan *et al.*	(CMS Collab.)
LAVIS	23	PR D108 123536	N. Lavis *et al.*	(WITW, RHODE)
LEES	23C	PRL 131 201801	J.P. Lees *et al.*	(BABAR Collab.)
TUMASYAN	23AB	JHEP 2307 110	A. Tumasyan *et al.*	(CMS Collab.)
TUMASYAN	23AG	PR D108 012011	A. Tumasyan *et al.*	(CMS Collab.)
TUMASYAN	23AO	JHEP 2307 210	A. Tumasyan *et al.*	(CMS Collab.)
TUMASYAN	23AY	JHEP 2309 149	A. Tumasyan *et al.*	(CMS Collab.)
TUMASYAN	23B	PL B842 137460	A. Tumasyan *et al.*	(CMS Collab.)
TUMASYAN	23H	JHEP 2305 227	A. Tumasyan *et al.*	(CMS Collab.)
TUMASYAN	23K	JHEP 2306 060	A. Tumasyan *et al.*	(CMS Collab.)
TUMASYAN	23L	JHEP 2307 161	A. Tumasyan *et al.*	(CMS Collab.)
Also		JHEP 2505 113 (errat.)	A. Tumasyan *et al.*	(CMS Collab.)
TUMASYAN	23X	EPJ C83 571	A. Tumasyan *et al.*	(CMS Collab.)
AAD	22E	PL B830 137106	G. Aad *et al.*	(ATLAS Collab.)
AAD	22U	EPJ C82 606	G. Aad *et al.*	(ATLAS Collab.)
ABBASI	22B	PR D105 062004	R. Abbasi *et al.*	(IceCube Collab.)
ABDALLA	22	PRL 129 111101	H. Abdalla *et al.*	(H.E.S.S. Collab.)
HUANG	22	PL B834 137487	Z. Huang *et al.*	(PandaX-4T Collab.)
TUMASYAN	22AF	EPJ C82 153	A. Tumasyan *et al.*	(CMS Collab.)
TUMASYAN	22Q	JHEP 2204 091	A. Tumasyan *et al.*	(CMS Collab.)
TUMASYAN	22S	JHEP 2204 147	A. Tumasyan *et al.*	(CMS Collab.)
TUMASYAN	22V	JHEP 2205 014	A. Tumasyan *et al.*	(CMS Collab.)
AAD	21AK	EPJ C81 600	G. Aad *et al.*	(ATLAS Collab.)
AAD	21AL	PRL 127 051802	G. Aad *et al.*	(ATLAS Collab.)
AAD	21AM	PR D104 032014	G. Aad *et al.*	(ATLAS Collab.)
AAD	21AW	PR D104 112005	G. Aad *et al.*	(ATLAS Collab.)
AAD	21AX	PR D104 112010	G. Aad *et al.*	(ATLAS Collab.)
AAD	21B	EPJ C81 11	G. Aad *et al.*	(ATLAS Collab.)
Also		EPJ C81 249 (errat.)	G. Aad *et al.*	(ATLAS Collab.)
AAD	21BF	EPJ C81 1023	G. Aad *et al.*	(ATLAS Collab.)
AAD	21BG	EPJ C81 1118	G. Aad *et al.*	(ATLAS Collab.)
AAD	21E	PR D103 112003	G. Aad *et al.*	(ATLAS Collab.)
AAD	21F	PR D103 112006	G. Aad *et al.*	(ATLAS Collab.)
AAD	21L	JHEP 2102 143	G. Aad *et al.*	(ATLAS Collab.)
AAD	21O	JHEP 2104 174	G. Aad *et al.*	(ATLAS Collab.)
AAD	21P	JHEP 2104 165	G. Aad *et al.*	(ATLAS Collab.)
AAD	21S	JHEP 2105 093	G. Aad *et al.*	(ATLAS Collab.)
AAD	21X	JHEP 2107 173	G. Aad *et al.*	(ATLAS Collab.)
AAD	21Y	JHEP 2107 167	G. Aad *et al.*	(ATLAS Collab.)
AAIJ	21V	EPJ C81 261	R. Aaij *et al.*	(LHCb Collab.)
ABDALLAH	21	PR D103 102002	H. Abdallah *et al.*	(H.E.S.S. Collab.)
MENG	21B	PRL 127 261802	Y. Meng *et al.*	(PandaX-4T Collab.)
SIRUNYAN	21AD	PR D104 052001	A.M. Sirunyan *et al.*	(CMS Collab.)
SIRUNYAN	21AF	PR D104 052011	A.M. Sirunyan *et al.*	(CMS Collab.)
SIRUNYAN	21B	EPJ C81 3	A.M. Sirunyan *et al.*	(CMS Collab.)
SIRUNYAN	21M	JHEP 2104 123	A.M. Sirunyan *et al.*	(CMS Collab.)
SIRUNYAN	21U	PR D104 012015	A.M. Sirunyan *et al.*	(CMS Collab.)
SIRUNYAN	21V	PR D104 032006	A.M. Sirunyan *et al.*	(CMS Collab.)
TUMASYAN	21C	JHEP 2110 045	A. Tumasyan *et al.*	(CMS Collab.)
TUMASYAN	21I	EPJ C81 970	A. Tumasyan *et al.*	(CMS Collab.)
AABOUD	20	EPJ C80 754	M. Aaboud *et al.*	(ATLAS Collab.)
AAD	20AL	JHEP 2010 062	G. Aad *et al.*	(ATLAS Collab.)
AAD	20AN	JHEP 2010 005	G. Aad *et al.*	(ATLAS Collab.)
AAD	20AS	EPJ C80 1080	G. Aad *et al.*	(ATLAS Collab.)
AAD	20C	PL B800 135103	G. Aad *et al.*	(ATLAS Collab.)
AAD	20D	PL B801 135114	G. Aad *et al.*	(ATLAS Collab.)
AAD	20H	PR D101 032009	G. Aad *et al.*	(ATLAS Collab.)
AAD	20I	PR D101 052005	G. Aad *et al.*	(ATLAS Collab.)
AAD	20K	PR D101 072001	G. Aad *et al.*	(ATLAS Collab.)
AAD	20L	PR D102 032004	G. Aad *et al.*	(ATLAS Collab.)
AAD	20M	PR D102 032006	G. Aad *et al.*	(ATLAS Collab.)
AAD	20O	EPJ C80 123	G. Aad *et al.*	(ATLAS Collab.)
AAD	20R	EPJ C80 691	G. Aad *et al.*	(ATLAS Collab.)
AAD	20S	EPJ C80 737	G. Aad *et al.*	(ATLAS Collab.)
AAD	20V	JHEP 2006 046	G. Aad *et al.*	(ATLAS Collab.)
ABAZAJIAN	20	PR D102 043012	K.N. Abazajian *et al.*	(UCI, VPI, TOKY+)
ABDALLAH	20	PR D102 062001	H. Abdallah *et al.*	(H.E.S.S. Collab.)
ABE	20G	PR D102 072002	K. Abe *et al.*	(Super-Kamiokande Collab.)
ALBERT	20	PR D101 103001	A. Albert *et al.*	(HAWC Collab.)
ALBERT	20A	PL B805 135439	A. Albert *et al.*	(ANTARES Collab.)
ALBERT	20C	PR D102 082002	A. Albert *et al.*	(ANTARES and IceCube Collab.)
ALVAREZ	20	JCAP 2009 004	A. Alvarez *et al.*	
HOOF	20	JCAP 2002 012	S. Hoof, A. Geringer-Sameth, R. Trotta	(GOET+)
SIRUNYAN	20AH	JHEP 2005 032	A.M. Sirunyan *et al.*	(CMS Collab.)
SIRUNYAN	20AU	PRL 124 041803	A.M. Sirunyan *et al.*	(CMS Collab.)
SIRUNYAN	20B	PL B801 135183	A.M. Sirunyan *et al.*	(CMS Collab.)
SIRUNYAN	20BJ	JHEP 2009 149	A.M. Sirunyan *et al.*	(CMS Collab.)
SIRUNYAN	20E	PR D101 052010	A.M. Sirunyan *et al.*	(CMS Collab.)
SIRUNYAN	20N	PL B806 135502	A.M. Sirunyan *et al.*	(CMS Collab.)
SIRUNYAN	20P	EPJ C80 189	A.M. Sirunyan *et al.*	(CMS Collab.)
SIRUNYAN	20T	EPJ C80 752	A.M. Sirunyan *et al.*	(CMS Collab.)
SIRUNYAN	20U	JHEP 2002 015	A.M. Sirunyan *et al.*	(CMS Collab.)
WANG	20G	CP C44 125001	Q. Wang *et al.*	(PandaX-II Collab.)
AABOUD	19AT	PR D99 092007	M. Aaboud *et al.*	(ATLAS Collab.)
AABOUD	19AU	PR D100 012006	M. Aaboud *et al.*	(ATLAS Collab.)
AABOUD	19C	PL B788 96	M. Aaboud *et al.*	(ATLAS Collab.)
AABOUD	19G	PR D99 012001	M. Aaboud *et al.*	(ATLAS Collab.)
AABOUD	19I	PR D99 012009	M. Aaboud *et al.*	(ATLAS Collab.)
AAD	19H	JHEP 1912 060	G. Aad *et al.*	(ATLAS Collab.)
ABE	19	PL B789 45	K. Abe *et al.*	(XMASS Collab.)
AJAJ	19	PR D100 022004	R. Ajaj *et al.*	(DEAP-3600 Collab.)
AMOLE	19	PR D100 022001	C. Amole *et al.*	(PICO Collab.)
APRILE	19A	PRL 122 141301	E. Aprile *et al.*	(XENON1T Collab.)
DI-MAURO	19	PR D99 123027	M. Di Mauro *et al.*	
JOHNSON	19	PR D99 103007	C. Johnson *et al.*	
LI	19D	PR D99 123519	S. Li *et al.*	
SIRUNYAN	19AG	JHEP 1906 143	A.M. Sirunyan *et al.*	(CMS Collab.)
SIRUNYAN	19AO	EPJ C79 305	A.M. Sirunyan *et al.*	(CMS Collab.)
SIRUNYAN	19AU	EPJ C79 444	A.M. Sirunyan *et al.*	(CMS Collab.)
SIRUNYAN	19AW	PL B790 140	A.M. Sirunyan *et al.*	(CMS Collab.)
SIRUNYAN	19BH	PR D99 032011	A.M. Sirunyan *et al.*	(CMS Collab.)
SIRUNYAN	19BI	PR D99 032014	A.M. Sirunyan *et al.*	(CMS Collab.)
SIRUNYAN	19BJ	PR D99 052002	A.M. Sirunyan *et al.*	(CMS Collab.)
SIRUNYAN	19BT	PL B797 134876	A.M. Sirunyan *et al.*	(CMS Collab.)
SIRUNYAN	19BU	JHEP 1908 150	A.M. Sirunyan *et al.*	(CMS Collab.)
SIRUNYAN	19CA	PR D100 112003	A.M. Sirunyan *et al.*	(CMS Collab.)
SIRUNYAN	19CE	PRL 123 241801	A.M. Sirunyan *et al.*	(CMS Collab.)
SIRUNYAN	19CH	JHEP 1910 244	A.M. Sirunyan *et al.*	(CMS Collab.)
SIRUNYAN	19CI	JHEP 1911 109	A.M. Sirunyan *et al.*	(CMS Collab.)
SIRUNYAN	19F	PR D99 012010	A.M. Sirunyan *et al.*	(CMS Collab.)
SIRUNYAN	19K	JHEP 1901 154	A.M. Sirunyan *et al.*	(CMS Collab.)
SIRUNYAN	19S	JHEP 1903 031	A.M. Sirunyan *et al.*	(CMS Collab.)
SIRUNYAN	19U	JHEP 1903 101	A.M. Sirunyan *et al.*	(CMS Collab.)
AABOUD	18AQ	JHEP 1806 108	M. Aaboud *et al.*	(ATLAS Collab.)
AABOUD	18AR	JHEP 1806 107	M. Aaboud *et al.*	(ATLAS Collab.)
AABOUD	18AS	JHEP 1806 022	M. Aaboud *et al.*	(ATLAS Collab.)
AABOUD	18AY	EPJ C78 154	M. Aaboud *et al.*	(ATLAS Collab.)
AABOUD	18BB	EPJ C78 250	M. Aaboud *et al.*	(ATLAS Collab.)
AABOUD	18BJ	EPJ C78 625	M. Aaboud *et al.*	(ATLAS Collab.)
AABOUD	18BT	EPJ C78 995	M. Aaboud *et al.*	(ATLAS Collab.)
AABOUD	18BV	JHEP 1809 050	M. Aaboud *et al.*	(ATLAS Collab.)
AABOUD	18CF	PL B785 136	M. Aaboud *et al.*	(ATLAS Collab.)
AABOUD	18CK	PR D98 092002	M. Aaboud *et al.*	(ATLAS Collab.)
AABOUD	18CM	PR D98 092008	M. Aaboud *et al.*	(ATLAS Collab.)
AABOUD	18CO	PR D98 092012	M. Aaboud *et al.*	(ATLAS Collab.)
AABOUD	18I	JHEP 1801 126	M. Aaboud *et al.*	(ATLAS Collab.)
AABOUD	18P	PR D97 032003	M. Aaboud *et al.*	(ATLAS Collab.)
AABOUD	18R	PR D97 052010	M. Aaboud *et al.*	(ATLAS Collab.)
AABOUD	18S	PR D97 052012	M. Aaboud *et al.*	(ATLAS Collab.)
AABOUD	18U	PR D97 092006	M. Aaboud *et al.*	(ATLAS Collab.)
AABOUD	18V	PR D97 112001	M. Aaboud *et al.*	(ATLAS Collab.)
AABOUD	18Y	PR D98 032008	M. Aaboud *et al.*	(ATLAS Collab.)
AABOUD	18Z	PR D98 032009	M. Aaboud *et al.*	(ATLAS Collab.)
ABDALLAH	18	PRL 120 201101	H. Abdallah *et al.*	(H.E.S.S. Collab.)
ADHIKARI	18	NAT 564 83	G. Adhikari *et al.*	(COSINE-100 Collab.)
AGNES	18A	PR D98 102006	P. Agnes *et al.*	(DarkSide-50 Collab.)
AGNESE	18A	PRL 120 061802	R. Agnese *et al.*	(SuperCDMS Collab.)
AHNEN	18	JCAP 1803 009	M.L. Ahnen *et al.*	(MAGIC Collab.)
ALBERT	18B	JCAP 1806 043	A. Albert *et al.*	(HAWC Collab.)
ALBERT	18C	PR D98 123012	A. Albert *et al.*	(HAWC Collab.)
AMAUDRUZ	18	PRL 121 071801	P.A. Amaudruz *et al.*	(DEAP-3600 Collab.)
APRILE	18	PRL 121 111302	E. Aprile *et al.*	(XENON1T Collab.)
SIRUNYAN	18AA	PL B780 118	A.M. Sirunyan *et al.*	(CMS Collab.)
SIRUNYAN	18AC	PL B780 384	A.M. Sirunyan *et al.*	(CMS Collab.)
SIRUNYAN	18AD	PL B780 432	A.M. Sirunyan *et al.*	(CMS Collab.)
SIRUNYAN	18AJ	PL B782 440	A.M. Sirunyan *et al.*	(CMS Collab.)
SIRUNYAN	18AK	PL B783 114	A.M. Sirunyan *et al.*	(CMS Collab.)
SIRUNYAN	18AL	JHEP 1802 067	A.M. Sirunyan *et al.*	(CMS Collab.)
SIRUNYAN	18AN	JHEP 1803 167	A.M. Sirunyan *et al.*	(CMS Collab.)
SIRUNYAN	18AO	JHEP 1803 166	A.M. Sirunyan *et al.*	(CMS Collab.)
SIRUNYAN	18AP	JHEP 1803 160	A.M. Sirunyan *et al.*	(CMS Collab.)
SIRUNYAN	18AR	JHEP 1803 076	A.M. Sirunyan *et al.*	(CMS Collab.)
SIRUNYAN	18AT	JHEP 1804 073	A.M. Sirunyan *et al.*	(CMS Collab.)
SIRUNYAN	18AY	JHEP 1805 025	A.M. Sirunyan *et al.*	(CMS Collab.)
SIRUNYAN	18B	PL B778 263	A.M. Sirunyan *et al.*	(CMS Collab.)
SIRUNYAN	18BR	JHEP 1808 016	A.M. Sirunyan *et al.*	(CMS Collab.)
SIRUNYAN	18C	PR D97 032009	A.M. Sirunyan *et al.*	(CMS Collab.)

Int. J. Mod. Phys. A 2026.41. Downloaded from www.worldscientific.com
by UNIVERSITY OF CALIFORNIA @ BERKELEY on 09/16/26. Re-use and distribution is strictly not permitted, except for Open Access articles.

Int. J. Mod. Phys. A 2026.41. Downloaded from www.worldscientific.com
by UNIVERSITY OF CALIFORNIA @ BERKELEY on 09/16/26. Re-use and distribution is strictly not permitted, except for Open Access articles.

SIRUNYAN 18D PR D97 012007 A.M. Sirunyan *et al.* (CMS Collab.)
SIRUNYAN 18DI JHEP 1809 065 A.M. Sirunyan *et al.* (CMS Collab.)
SIRUNYAN 18DN JHEP 1811 079 A.M. Sirunyan *et al.* (CMS Collab.)
SIRUNYAN 18DP JHEP 1811 151 A.M. Sirunyan *et al.* (CMS Collab.)
SIRUNYAN 18DV PR D98 092011 A.M. Sirunyan *et al.* (CMS Collab.)
SIRUNYAN 18DY PR D98 112014 A.M. Sirunyan *et al.* (CMS Collab.)
SIRUNYAN 18EA PRL 121 141802 A.M. Sirunyan *et al.* (CMS Collab.)
SIRUNYAN 18M PRL 120 241801 A.M. Sirunyan *et al.* (CMS Collab.)
SIRUNYAN 18O PR D97 032007 A.M. Sirunyan *et al.* (CMS Collab.)
SIRUNYAN 18X PL B779 166 A.M. Sirunyan *et al.* (CMS Collab.)
AABOUD 17AF JHEP 1708 006 M. Aaboud *et al.* (ATLAS Collab.)
AABOUD 17AI JHEP 1709 088 M. Aaboud *et al.* (ATLAS Collab.)
AABOUD 17AJ JHEP 1709 084 M. Aaboud *et al.* (ATLAS Collab.)
Also JHEP 1908 121 (errat.) M. Aaboud *et al.* (ATLAS Collab.)
AABOUD 17AR PR D96 112010 M. Aaboud *et al.* (ATLAS Collab.)
AABOUD 17AX JHEP 1711 195 M. Aaboud *et al.* (ATLAS Collab.)
AABOUD 17AY JHEP 1712 085 M. Aaboud *et al.* (ATLAS Collab.)
AABOUD 17AZ JHEP 1712 034 M. Aaboud *et al.* (ATLAS Collab.)
AABOUD 17BE EPJ C77 898 M. Aaboud *et al.* (ATLAS Collab.)
AABOUD 17N EPJ C77 144 M. Aaboud *et al.* (ATLAS Collab.)
AAIJ 17Z EPJ C77 224 R. Aaij *et al.* (LHCb Collab.)
AARTSEN 17 EPJ C77 82 M.G. Aartsen *et al.* (IceCube Collab.)
AARTSEN 17A EPJ C77 146 M.G. Aartsen *et al.* (IceCube Collab.)
Also EPJ C79 214 (errat.) M.G. Aartsen *et al.* (IceCube Collab.)
AARTSEN 17C EPJ C77 627 M.G. Aartsen *et al.* (IceCube Collab.)
AKERIB 17 PRL 118 021303 D.S. Akerib *et al.* (LUX Collab.)
AKERIB 17A PRL 118 251302 D.S. Akerib *et al.* (LUX Collab.)
AMOLE 17 PRL 118 251301 C. Amole *et al.* (PICO Collab.)
APRILE 17G PRL 119 181301 E. Aprile *et al.* (XENON Collab.)
ARCHAMBAU... 17 PR D95 082001 S. Archambault *et al.* (VERITAS Collab.)
ATHRON 17B EPJ C77 824 P. Athron *et al.* (GAMBIT Collab.)
BATTAT 17 ASP 91 65 J.B.R. Battat *et al.* (DRIFT-IId Collab.)
BEHNKE 17 ASP 90 85 E. Behnke *et al.* (PICASSO Collab.)
CUI 17A PRL 119 181302 X. Cui *et al.* (PandaX-II Collab.)
KHACHATRY... 17 PR D95 012003 V. Khachatryan *et al.* (CMS Collab.)
KHACHATRY... 17A PRL 118 021802 V. Khachatryan *et al.* (CMS Collab.)
KHACHATRY... 17AD PR D96 012004 V. Khachatryan *et al.* (CMS Collab.)
KHACHATRY... 17AR PR D95 012009 V. Khachatryan *et al.* (CMS Collab.)
KHACHATRY... 17AS PR D95 012011 V. Khachatryan *et al.* (CMS Collab.)
KHACHATRY... 17AW EPJ C77 635 V. Khachatryan *et al.* (CMS Collab.)
KHACHATRY... 17L JHEP 1704 018 V. Khachatryan *et al.* (CMS Collab.)
KHACHATRY... 17P EPJ C77 294 V. Khachatryan *et al.* (CMS Collab.)
KHACHATRY... 17S PL B767 403 V. Khachatryan *et al.* (CMS Collab.)
KHACHATRY... 17V PL B769 391 V. Khachatryan *et al.* (CMS Collab.)
KHACHATRY... 17Y PL B770 257 V. Khachatryan *et al.* (CMS Collab.)
SIRUNYAN 17AF PRL 119 151802 A.M. Sirunyan *et al.* (CMS Collab.)
SIRUNYAN 17AS JHEP 1710 019 A.M. Sirunyan *et al.* (CMS Collab.)
SIRUNYAN 17AT JHEP 1710 005 A.M. Sirunyan *et al.* (CMS Collab.)
SIRUNYAN 17AW JHEP 1711 029 A.M. Sirunyan *et al.* (CMS Collab.)
SIRUNYAN 17AY JHEP 1712 142 A.M. Sirunyan *et al.* (CMS Collab.)
SIRUNYAN 17AZ EPJ C77 710 A.M. Sirunyan *et al.* (CMS Collab.)
SIRUNYAN 17K EPJ C77 327 A.M. Sirunyan *et al.* (CMS Collab.)
SIRUNYAN 17P PR D96 032003 A.M. Sirunyan *et al.* (CMS Collab.)
SIRUNYAN 17S EPJ C77 578 A.M. Sirunyan *et al.* (CMS Collab.)
AABOUD 16AC EPJ C76 683 M. Aaboud *et al.* (ATLAS Collab.)
AABOUD 16AF JHEP 1609 175 M. Aaboud *et al.* (ATLAS Collab.)
AABOUD 16B PL B760 647 M. Aaboud *et al.* (ATLAS Collab.)
AABOUD 16C PR D93 112015 M. Aaboud *et al.* (ATLAS Collab.)
AABOUD 16D PR D94 032005 M. Aaboud *et al.* (ATLAS Collab.)
AABOUD 16J PR D94 052009 M. Aaboud *et al.* (ATLAS Collab.)
AABOUD 16M EPJ C76 517 M. Aaboud *et al.* (ATLAS Collab.)
AABOUD 16N EPJ C76 392 M. Aaboud *et al.* (ATLAS Collab.)
AABOUD 16P EPJ C76 541 M. Aaboud *et al.* (ATLAS Collab.)
AABOUD 16Q EPJ C76 547 M. Aaboud *et al.* (ATLAS Collab.)
AAD 16AA PR D93 052002 G. Aad *et al.* (ATLAS Collab.)
AAD 16AD PR D94 032003 G. Aad *et al.* (ATLAS Collab.)
AAD 16AG JHEP 1602 062 G. Aad *et al.* (ATLAS Collab.)
AAD 16AM JHEP 1606 067 G. Aad *et al.* (ATLAS Collab.)
AAD 16AY EPJ C76 81 G. Aad *et al.* (ATLAS Collab.)
AAD 16BB EPJ C76 259 G. Aad *et al.* (ATLAS Collab.)
AAD 16BG EPJ C76 565 G. Aad *et al.* (ATLAS Collab.)
AAD 16V PL B757 334 G. Aad *et al.* (ATLAS Collab.)
AARTSEN 16C JCAP 1604 022 M.G. Aartsen *et al.* (IceCube Collab.)
ADRIAN-MAR... 16 PL B759 69 S. Adrian-Martinez *et al.* (ANTARES Collab.)
AHNEN 16 JCAP 1602 039 M.L. Ahnen *et al.* (MAGIC and Fermi-LAT Collab.)
AKERIB 16 PRL 116 161301 D.S. Akerib *et al.* (LUX Collab.)
AKERIB 16A PRL 116 161302 D.S. Akerib *et al.* (LUX Collab.)
AMOLE 16 PR D93 052014 C. Amole *et al.* (PICO Collab.)
APRILE 16B PR D94 122001 E. Aprile *et al.* (XENON100 Collab.)
AVRORIN 16 ASP 81 12 A.D. Avrorin *et al.* (BAIKAL Collab.)
BECHTLE 16 EPJ C76 96 P. Bechtle *et al.*
CIRELLI 16 JCAP 1607 041 M. Cirelli, M. Taoso (LPNHE, MADE)
KHACHATRY... 16AA PL B759 479 V. Khachatryan *et al.* (CMS Collab.)
KHACHATRY... 16AC PL B760 178 V. Khachatryan *et al.* (CMS Collab.)
KHACHATRY... 16AM PR D93 092009 V. Khachatryan *et al.* (CMS Collab.)
KHACHATRY... 16AV JHEP 1607 027 V. Khachatryan *et al.* (CMS Collab.)
KHACHATRY... 16AY JHEP 1608 122 V. Khachatryan *et al.* (CMS Collab.)
KHACHATRY... 16BE EPJ C76 317 V. Khachatryan *et al.* (CMS Collab.)
KHACHATRY... 16BJ EPJ C76 439 V. Khachatryan *et al.* (CMS Collab.)
KHACHATRY... 16BK EPJ C76 460 V. Khachatryan *et al.* (CMS Collab.)
KHACHATRY... 16BS JHEP 1610 006 V. Khachatryan *et al.* (CMS Collab.)
KHACHATRY... 16BT JHEP 1610 129 V. Khachatryan *et al.* (CMS Collab.)
KHACHATRY... 16BW PR D94 112004 V. Khachatryan *et al.* (CMS Collab.)
KHACHATRY... 16BX PR D94 112009 V. Khachatryan *et al.* (CMS Collab.)
KHACHATRY... 16BY JHEP 1612 013 V. Khachatryan *et al.* (CMS Collab.)
KHACHATRY... 16R PL B757 6 V. Khachatryan *et al.* (CMS Collab.)
KHACHATRY... 16V PL B758 152 V. Khachatryan *et al.* (CMS Collab.)
KHACHATRY... 16Y PL B759 9 V. Khachatryan *et al.* (CMS Collab.)
LEITE 16 JCAP 1611 021 N. Leite *et al.*
AAD 15AB PR D92 012010 G. Aad *et al.* (ATLAS Collab.)
AAD 15AE JHEP 1501 068 G. Aad *et al.* (ATLAS Collab.)
AAD 15AI JHEP 1504 116 G. Aad *et al.* (ATLAS Collab.)
AAD 15BA EPJ C75 208 G. Aad *et al.* (ATLAS Collab.)
AAD 15BG EPJ C75 318 G. Aad *et al.* (ATLAS Collab.)
Also EPJ C75 463 G. Aad *et al.* (ATLAS Collab.)
AAD 15BH EPJ C75 299 G. Aad *et al.* (ATLAS Collab.)
Also EPJ C75 408 (errat.) G. Aad *et al.* (ATLAS Collab.)
AAD 15BM EPJ C75 407 G. Aad *et al.* (ATLAS Collab.)
AAD 15BV JHEP 1510 054 G. Aad *et al.* (ATLAS Collab.)
AAD 15BX JHEP 1510 134 G. Aad *et al.* (ATLAS Collab.)
AAD 15CA PR D92 072001 G. Aad *et al.* (ATLAS Collab.)
AAD 15CB PR D92 072004 G. Aad *et al.* (ATLAS Collab.)
AAD 15CJ EPJ C75 510 G. Aad (ATLAS Collab.)
AAD 15CS PR D91 012008 G. Aad *et al.* (ATLAS Collab.)
Also PR D92 059903 (errat.) G. Aad *et al.* (ATLAS Collab.)
AAD 15J PRL 114 142001 G. Aad *et al.* (ATLAS Collab.)
AAD 15K PRL 114 161801 G. Aad *et al.* (ATLAS Collab.)
AAD 15O PRL 115 031801 G. Aad *et al.* (ATLAS Collab.)
AAD 15X PR D91 112016 G. Aad *et al.* (ATLAS Collab.)
AAIJ 15BD EPJ C75 595 R. Aaij *et al.* (LHCb Collab.)
AARTSEN 15E EPJ C75 492 M.G. Aartsen *et al.* (IceCube Collab.)
ACKERMANN 15 PR D91 122002 M. Ackermann *et al.* (Fermi-LAT Collab.)
ACKERMANN 15A JCAP 1509 008 M. Ackermann *et al.* (Fermi-LAT Collab.)
ACKERMANN 15B PRL 115 231301 M. Ackermann *et al.* (Fermi-LAT Collab.)
AGNES 15 PL B743 456 P. Agnes *et al.* (DarkSide-50 Collab.)
AGNESE 15B PR D92 072003 R. Agnese *et al.* (SuperCDMS Collab.)
BAGNASCHI 15 EPJ C75 500 E.A. Bagnaschi *et al.*
BUCKLEY 15 PR D91 102001 M.R. Buckley *et al.*
CHOI 15 PRL 114 141301 K. Choi *et al.* (Super-Kamiokande Collab.)
KHACHATRY... 15AB JHEP 1501 096 V. Khachatryan *et al.* (CMS Collab.)
KHACHATRY... 15AD JHEP 1504 124 V. Khachatryan *et al.* (CMS Collab.)
KHACHATRY... 15AF JHEP 1505 078 V. Khachatryan *et al.* (CMS Collab.)
KHACHATRY... 15AH JHEP 1506 116 V. Khachatryan *et al.* (CMS Collab.)
KHACHATRY... 15AK EPJ C75 151 V. Khachatryan *et al.* (CMS Collab.)
KHACHATRY... 15AO EPJ C75 325 V. Khachatryan *et al.* (CMS Collab.)
KHACHATRY... 15AR PL B743 503 V. Khachatryan *et al.* (CMS Collab.)
KHACHATRY... 15AZ PR D92 072006 V. Khachatryan *et al.* (CMS Collab.)
KHACHATRY... 15E PRL 114 061801 V. Khachatryan *et al.* (CMS Collab.)
KHACHATRY... 15I PL B745 5 V. Khachatryan *et al.* (CMS Collab.)
KHACHATRY... 15L PL B747 98 V. Khachatryan *et al.* (CMS Collab.)
KHACHATRY... 15O PL B748 255 V. Khachatryan *et al.* (CMS Collab.)
KHACHATRY... 15W PR D91 052012 V. Khachatryan *et al.* (CMS Collab.)
KHACHATRY... 15X PR D91 052018 V. Khachatryan *et al.* (CMS Collab.)
ROLBIECKI 15 PL B750 247 K. Rolbiecki, J. Tattersall (MADE, HEID)
AAD 14AE JHEP 1409 176 G. Aad *et al.* (ATLAS Collab.)
AAD 14AG JHEP 1409 103 G. Aad *et al.* (ATLAS Collab.)
AAD 14AJ JHEP 1409 015 G. Aad *et al.* (ATLAS Collab.)
AAD 14AV JHEP 1410 096 G. Aad *et al.* (ATLAS Collab.)
AAD 14AX JHEP 1410 024 G. Aad *et al.* (ATLAS Collab.)
AAD 14B EPJ C74 2883 G. Aad *et al.* (ATLAS Collab.)
AAD 14BD JHEP 1411 118 G. Aad *et al.* (ATLAS Collab.)
AAD 14BH PR D90 112005 G. Aad *et al.* (ATLAS Collab.)
AAD 14E JHEP 1406 035 G. Aad *et al.* (ATLAS Collab.)
AAD 14F JHEP 1406 124 G. Aad *et al.* (ATLAS Collab.)
AAD 14G JHEP 1405 071 G. Aad *et al.* (ATLAS Collab.)
AAD 14H JHEP 1404 169 G. Aad *et al.* (ATLAS Collab.)
AAD 14K PR D90 012004 G. Aad *et al.* (ATLAS Collab.)
AAD 14T PR D90 052008 G. Aad *et al.* (ATLAS Collab.)
AAD 14X PR D90 052001 G. Aad *et al.* (ATLAS Collab.)
AALTONEN 14 PR D90 012011 T. Aaltonen *et al.* (CDF Collab.)
ACKERMANN 14 PR D89 042001 M. Ackermann *et al.* (Fermi-LAT Collab.)
AKERIB 14 PRL 112 091303 D.S. Akerib *et al.* (LUX Collab.)
ALEKSIC 14 JCAP 1402 008 J. Aleksic *et al.* (MAGIC Collab.)
AVRORIN 14 ASP 62 12 A.D. Avrorin *et al.* (BAIKAL Collab.)
BUCHMUEL... 14 EPJ C74 2809 O. Buchmueller *et al.*
BUCHMUEL... 14A EPJ C74 2922 O. Buchmueller *et al.*
CHATRCHYAN 14AH PR D90 112001 S. Chatrchyan *et al.* (CMS Collab.)
CHATRCHYAN 14H JHEP 1401 163 S. Chatrchyan *et al.* (CMS Collab.)
CHATRCHYAN 14I JHEP 1406 055 S. Chatrchyan *et al.* (CMS Collab.)
CHATRCHYAN 14N PL B733 328 S. Chatrchyan *et al.* (CMS Collab.)
CHATRCHYAN 14P PL B730 193 S. Chatrchyan *et al.* (CMS Collab.)
CHATRCHYAN 14R PR D90 032006 S. Chatrchyan *et al.* (CMS Collab.)
CHATRCHYAN 14U PRL 112 161802 S. Chatrchyan *et al.* (CMS Collab.)
CZAKON 14 PRL 113 201803 M. Czakon *et al.* (AACH, CAMB, UCB, LBL+)
FELIZARDO 14 PR D89 072013 M. Felizardo *et al.* (SIMPLE Collab.)
KHACHATRY... 14C PL B736 371 V. Khachatryan *et al.* (CMS Collab.)
KHACHATRY... 14I EPJ C74 3036 V. Khachatryan *et al.* (CMS Collab.)
KHACHATRY... 14L PR D90 092007 V. Khachatryan *et al.* (CMS Collab.)
KHACHATRY... 14T PL B739 229 V. Khachatryan *et al.* (CMS Collab.)
PDG 14 CP C38 070001 K. Olive *et al.* (PDG Collab.)
ROSZKOWSKI 14 JHEP 1408 067 L. Roszkowski, E.M. Sessolo, A.J. Williams (WINR)
AAD 13 PL B718 841 G. Aad *et al.* (ATLAS Collab.)
AAD 13AA PL B720 277 G. Aad *et al.* (ATLAS Collab.)
AAD 13AI PL B723 15 G. Aad *et al.* (ATLAS Collab.)
AAD 13AP PR D88 012001 G. Aad *et al.* (ATLAS Collab.)
AAD 13AU JHEP 1310 189 G. Aad *et al.* (ATLAS Collab.)
AAD 13B PL B718 879 G. Aad *et al.* (ATLAS Collab.)
AAD 13BC PR D88 112003 G. Aad *et al.* (ATLAS Collab.)
AAD 13BD PR D88 112006 G. Aad *et al.* (ATLAS Collab.)
AAD 13H JHEP 1301 131 G. Aad *et al.* (ATLAS Collab.)
AAD 13L PR D87 012008 G. Aad *et al.* (ATLAS Collab.)
AAD 13P PL B719 299 G. Aad *et al.* (ATLAS Collab.)
AAD 13Q PL B719 261 G. Aad *et al.* (ATLAS Collab.)
AAD 13R PL B719 280 G. Aad *et al.* (ATLAS Collab.)
AALTONEN 13I PR D88 031103 T. Aaltonen *et al.* (CDF Collab.)
AALTONEN 13Q PRL 110 201802 T. Aaltonen *et al.* (CDF Collab.)
AARTSEN 13C PR D88 122001 M.G. Aartsen *et al.* (IceCube Collab.)
ABAZOV 13B PR D87 052011 V.M. Abazov *et al.* (D0 Collab.)
ACKERMANN 13A PR D88 082002 M. Ackermann *et al.* (Fermi-LAT Collab.)
ADRIAN-MAR... 13 JCAP 1311 032 S. Adrian-Martinez *et al.* (ANTARES Collab.)
AGNESE 13 PR D88 031104 R. Agnese *et al.* (CDMS Collab.)
AGNESE 13A PRL 111 251301 R. Agnese *et al.* (CDMS Collab.)
APRILE 13 PRL 111 021301 E. Aprile *et al.* (XENON100 Collab.)
BERGSTROM 13 PRL 111 171101 L. Bergstrom *et al.*
BOLIEV 13 JCAP 1309 019 M. Boliev *et al.*
CABRERA 13 JHEP 1307 182 M. Cabrera, J. Casas, R. de Austri
CALIBBI 13 JHEP 1310 132 L. Calibbi *et al.*
CHATRCHYAN 13 PL B718 815 S. Chatrchyan *et al.* (CMS Collab.)
CHATRCHYAN 13AB JHEP 1307 122 S. Chatrchyan *et al.* (CMS Collab.)
Also JHEP 2211 149 (errat.) S. Chatrchyan *et al.* (CMS Collab.)
CHATRCHYAN 13AH PL B722 273 S. Chatrchyan *et al.* (CMS Collab.)
CHATRCHYAN 13AO PR D87 072001 S. Chatrchyan *et al.* (CMS Collab.)
CHATRCHYAN 13AT PR D88 052017 S. Chatrchyan *et al.* (CMS Collab.)
CHATRCHYAN 13AV PRL 111 081802 S. Chatrchyan *et al.* (CMS Collab.)
CHATRCHYAN 13G JHEP 1301 077 S. Chatrchyan *et al.* (CMS Collab.)
CHATRCHYAN 13H PL B719 42 S. Chatrchyan *et al.* (CMS Collab.)
CHATRCHYAN 13T EPJ C73 2568 S. Chatrchyan *et al.* (CMS Collab.)
CHATRCHYAN 13V JHEP 1303 037 S. Chatrchyan *et al.* (CMS Collab.)
Also JHEP 1307 041 (errat.) S. Chatrchyan *et al.* (CMS Collab.)
CHATRCHYAN 13W JHEP 1303 111 S. Chatrchyan *et al.* (CMS Collab.)
ELLIS 13B EPJ C73 2403 J. Ellis *et al.*
JIN 13 JCAP 1311 026 H.-B. Jin, Y.-L. Wu, Y.-F. Zhou
KOPP 13 PR D88 076013 J. Kopp
STREGE 13 JCAP 1304 013 C. Strege *et al.*
AAD 12AF PL B714 180 G. Aad *et al.* (ATLAS Collab.)
AAD 12AG PL B714 197 G. Aad *et al.* (ATLAS Collab.)
AAD 12AN PRL 108 181802 G. Aad *et al.* (ATLAS Collab.)
AAD 12AS PRL 108 261804 G. Aad *et al.* (ATLAS Collab.)
AAD 12AX PR D85 012006 G. Aad *et al.* (ATLAS Collab.)
Also PR D87 099903 (errat.) G. Aad *et al.* (ATLAS Collab.)
AAD 12BJ EPJ C72 1993 G. Aad *et al.* (ATLAS Collab.)
AAD 12CJ PR D86 092002 G. Aad *et al.* (ATLAS Collab.)
AAD 12CM EPJ C72 2215 G. Aad *et al.* (ATLAS Collab.)
AAD 12CP PL B718 411 G. Aad *et al.* (ATLAS Collab.)
AAD 12CT JHEP 1212 124 G. Aad *et al.* (ATLAS Collab.)
AAD 12P EPJ C72 1965 G. Aad *et al.* (ATLAS Collab.)
AAD 12R PL B707 478 G. Aad *et al.* (ATLAS Collab.)
AAD 12T PL B709 137 G. Aad *et al.* (ATLAS Collab.)
AAD 12W PL B710 67 G. Aad *et al.* (ATLAS Collab.)
AALTONEN 12AB PR D85 092001 T. Aaltonen *et al.* (CDF Collab.)
ABAZOV 12AD PR D86 071701 V.M. Abazov *et al.* (D0 Collab.)
AKIMOV 12 PL B709 14 D.Yu. Akimov *et al.* (ZEPLIN-III Collab.)
AKULA 12 PR D85 075001 S. Akula *et al.* (NEAS, MICH)
ANGLOHER 12 EPJ C72 1971 G. Angloher *et al.* (CRESST-II Collab.)

Int. J. Mod. Phys. A 2026.41. Downloaded from www.worldscientific.com
by UNIVERSITY OF CALIFORNIA @ BERKELEY on 09/16/26. Re-use and distribution is strictly not permitted, except for Open Access articles.

APRILE	12	PRL 109 181301	E. Aprile *et al.*	(XENON100 Collab.)
ARBEY	12A	PL B708 162	A. Arbey *et al.*	
ARCHAMBAU...	12	PL B711 153	S. Archambault *et al.*	(PICASSO Collab.)
BAER	12	JHEP 1205 091	H. Baer, V. Barger, A. Mustafayev	(OKLA, WISC+)
BALAZS	12	EPJ C73 2563	C. Balazs *et al.*	
BECHTLE	12	JHEP 1206 098	P. Bechtle *et al.*	
BEHNKE	12	PR D86 052001	E. Behnke *et al.*	(COUPP Collab.)
Also		PR D90 079902 (errat.)	E. Behnke *et al.*	(COUPP Collab.)
BESKIDT	12	EPJ C72 2166	C. Beskidt *et al.*	(KARLE, JINR, ITEP)
BOTTINO	12	PR D85 095013	A. Bottino, N. Fornengo, S. Scopel	(TORI, SOGA)
BUCHMUEL...	12	EPJ C72 2020	O. Buchmueller *et al.*	
CAO	12A	PL B710 665	J. Cao *et al.*	
CHATRCHYAN	12	PR D85 012004	S. Chatrchyan *et al.*	(CMS Collab.)
CHATRCHYAN	12AE	PRL 109 171803	S. Chatrchyan *et al.*	(CMS Collab.)
CHATRCHYAN	12AI	JHEP 1208 110	S. Chatrchyan *et al.*	(CMS Collab.)
CHATRCHYAN	12AL	JHEP 1206 169	S. Chatrchyan *et al.*	(CMS Collab.)
CHATRCHYAN	12AN	JHEP 1208 026	S. Chatrchyan *et al.*	(CMS Collab.)
CHATRCHYAN	12AT	JHEP 1210 018	S. Chatrchyan *et al.*	(CMS Collab.)
CHATRCHYAN	12BJ	JHEP 1211 147	S. Chatrchyan *et al.*	(CMS Collab.)
CHATRCHYAN	12BK	JHEP 1211 172	S. Chatrchyan *et al.*	(CMS Collab.)
CHATRCHYAN	12BO	JHEP 1212 055	S. Chatrchyan *et al.*	(CMS Collab.)
CHATRCHYAN	12L	PL B713 408	S. Chatrchyan *et al.*	(CMS Collab.)
DAW	12	ASP 35 397	E. Daw *et al.*	(DRIFT-IId Collab.)
DREINER	12A	EPL 99 61001	H.K. Dreiner, M. Kramer, J. Tattersall	(BONN+)
ELLIS	12B	EPJ C72 2005	J. Ellis, K. Olive	
FELIZARDO	12	PRL 108 201302	M. Felizardo *et al.*	(SIMPLE Collab.)
FENG	12B	PR D85 075007	J. Feng, K. Matchev, D. Sanford	
KADASTIK	12	JHEP 1205 061	M. Kadastik *et al.*	
KIM	12	PRL 108 181301	S.C. Kim *et al.*	(KIMS Collab.)
STREGE	12	JCAP 1203 030	C. Strege *et al.*	(LOIC, AMST, MADU, GRAN+)
AAD	11AA	EPJ C71 1828	G. Aad *et al.*	(ATLAS Collab.)
AAD	11G	PRL 106 131802	G. Aad *et al.*	(ATLAS Collab.)
AAD	11H	PRL 106 251801	G. Aad *et al.*	(ATLAS Collab.)
AAD	11K	PL B701 1	G. Aad *et al.*	(ATLAS Collab.)
AAD	11O	PL B701 398	G. Aad *et al.*	(ATLAS Collab.)
AAD	11P	PL B703 428	G. Aad *et al.*	(ATLAS Collab.)
AAD	11Z	EPJ C71 1809	G. Aad *et al.*	(ATLAS Collab.)
AHMED	11A	PR D84 011102	Z. Ahmed *et al.*	(CDMS and EDELWEISS Collabs.)
ARMENGAUD	11	PL B702 329	E. Armengaud *et al.*	(EDELWEISS-II Collab.)
BUCHMUEL...	11	EPJ C71 1583	O. Buchmueller *et al.*	
BUCHMUEL...	11B	EPJ C71 1722	O. Buchmueller *et al.*	
CHATRCHYAN	11B	JHEP 1106 093	S. Chatrchyan *et al.*	(CMS Collab.)
CHATRCHYAN	11D	JHEP 1107 113	S. Chatrchyan *et al.*	(CMS Collab.)
CHATRCHYAN	11E	JHEP 1107 098	S. Chatrchyan *et al.*	(CMS Collab.)
CHATRCHYAN	11V	PL B704 411	S. Chatrchyan *et al.*	(CMS Collab.)
KHACHATRY...	11	PRL 106 011801	V. Khachatryan *et al.*	(CMS Collab.)
KHACHATRY...	11C	JHEP 1103 024	V. Khachatryan *et al.*	(CMS Collab.)
ROSZKOWSKI	11	PR D83 015014	L. Roszkowski *et al.*	
AALTONEN	10	PRL 104 011801	T. Aaltonen *et al.*	(CDF Collab.)
AALTONEN	10R	PRL 105 081802	T. Aaltonen *et al.*	(CDF Collab.)
AALTONEN	10Z	PRL 105 191801	T. Aaltonen *et al.*	(CDF Collab.)
ABAZOV	10L	PL B693 95	V.M. Abazov *et al.*	(D0 Collab.)
ABAZOV	10M	PRL 105 191802	V.M. Abazov *et al.*	(D0 Collab.)
ABAZOV	10N	PRL 105 211802	V.M. Abazov *et al.*	(D0 Collab.)
ABAZOV	10P	PRL 105 221802	V.M. Abazov *et al.*	(D0 Collab.)
ACKERMANN	10	JCAP 1005 025	M. Ackermann	(Fermi-LAT Collab.)
ARMENGAUD	10	PL B687 294	E. Armengaud *et al.*	(EDELWEISS-II Collab.)
ELLIS	10	EPJ C69 201	J. Ellis, A. Mustafayev, K. Olive	
ABAZOV	09M	PRL 102 161802	V.M. Abazov *et al.*	(D0 Collab.)
AHMED	09	PRL 102 011301	Z. Ahmed *et al.*	(CDMS Collab.)
ANGLOHER	09	ASP 31 270	G. Angloher *et al.*	(CRESST Collab.)
BUCHMUEL...	09	EPJ C64 391	O. Buchmueller *et al.*	(LOIC, FNAL, CERN+)
DREINER	09	EPJ C62 547	H. Dreiner *et al.*	
LEBEDENKO	09	PR D80 052010	V.N. Lebedenko *et al.*	(ZEPLIN-III Collab.)
LEBEDENKO	09A	PRL 103 151302	V.N. Lebedenko *et al.*	(ZEPLIN-III Collab.)
SORENSEN	09	NIM A601 339	P. Sorensen *et al.*	(XENON10 Collab.)
ABAZOV	08F	PL B659 856	V.M. Abazov *et al.*	(D0 Collab.)
ANGLE	08	PRL 100 021303	J. Angle *et al.*	(XENON10 Collab.)
ANGLE	08A	PRL 101 091301	J. Angle *et al.*	(XENON10 Collab.)
BEDNYAKOV	08	PAN 71 111	V.A. Bednyakov, H.P. Klapdor-Kleingrothaus, I.V. Krivosheina	
		Translated from YAF 71 112.		
BEHNKE	08	SCI 319 933	E. Behnke	(COUPP Collab.)
BENETTI	08	ASP 28 495	P. Benetti *et al.*	(WARP Collab.)
BUCHMUEL...	08	JHEP 0809 117	O. Buchmueller *et al.*	
ELLIS	08	PR D78 075012	J. Ellis, K. Olive, P. Sandick	(CERN, MINN)
ABULENCIA	07H	PRL 98 131804	A. Abulencia *et al.*	(CDF Collab.)
ALNER	07A	ASP 28 287	G.J. Alner *et al.*	(ZEPLIN-II Collab.)
CALIBBI	07	JHEP 0709 081	L. Calibbi *et al.*	
ELLIS	07	JHEP 0706 079	J. Ellis, K. Olive, P. Sandick	(CERN, MINN)
LEE	07A	PRL 99 091301	H.S. Lee *et al.*	(KIMS Collab.)
ABBIENDI	06B	EPJ C46 307	G. Abbiendi *et al.*	(OPAL Collab.)
ACHTERBERG	06	ASP 26 129	A. Achterberg *et al.*	(AMANDA Collab.)
ACKERMANN	06	ASP 24 459	M. Ackermann *et al.*	(AMANDA Collab.)
AKERIB	06	PR D73 011102	D.S. Akerib *et al.*	(CDMS Collab.)
AKERIB	06A	PRL 96 011302	D.S. Akerib *et al.*	(CDMS Collab.)
ALLANACH	06	PR D73 015013	B.C. Allanach *et al.*	
BENOIT	06	PL B637 156	A. Benoit *et al.*	
DE-AUSTRI	06	JHEP 0605 002	R.R. de Austri, R. Trotta, L. Roszkowski	
DEBOER	06	PL B636 13	W. de Boer *et al.*	
LEP-SLC	06	PRPL 427 257	ALEPH, DELPHI, L3, OPAL, SLD and working groups	
SHIMIZU	06A	PL B633 195	Y. Shimizu *et al.*	
SMITH	06	PL B642 567	N.J.T. Smith, A.S. Murphy, T.J. Summer	
ABAZOV	05A	PRL 94 041801	V.M. Abazov *et al.*	(D0 Collab.)
ABDALLAH	05B	EPJ C38 395	J. Abdallah *et al.*	(DELPHI Collab.)
AKERIB	05	PR D72 052009	D.S. Akerib *et al.*	(CDMS Collab.)
ALNER	05	PL B616 17	G.J. Alner *et al.*	(UK Dark Matter Collab.)
ALNER	05A	ASP 23 444	G.J. Alner *et al.*	(UK Dark Matter Collab.)
BAER	05	JHEP 0507 065	H. Baer *et al.*	(FSU, MSU, HAWA)
BARNABE-HE...	05	PL B624 186	M. Barnabe-Heider *et al.*	(PICASSO Collab.)
ELLIS	05	PR D71 095007	J. Ellis *et al.*	
SANGLARD	05	PR D71 122002	V. Sanglard *et al.*	(EDELWEISS Collab.)
ABBIENDI	04	EPJ C32 453	G. Abbiendi *et al.*	(OPAL Collab.)
ABBIENDI	04F	EPJ C33 149	G. Abbiendi *et al.*	(OPAL Collab.)
ABBIENDI	04H	EPJ C35 1	G. Abbiendi *et al.*	(OPAL Collab.)
ABBIENDI	04N	PL B602 167	G. Abbiendi *et al.*	(OPAL Collab.)
ABDALLAH	04H	EPJ C34 145	J. Abdallah *et al.*	(DELPHI Collab.)
ABDALLAH	04M	EPJ C36 1	J. Abdallah *et al.*	(DELPHI Collab.)
Also		EPJ C37 129 (errat.)	J. Abdallah *et al.*	(DELPHI Collab.)
ACHARD	04	PL B580 37	P. Achard *et al.*	(L3 Collab.)
ACHARD	04E	PL B587 16	P. Achard *et al.*	(L3 Collab.)
AKERIB	04	PRL 93 211301	D.S. Akerib *et al.*	(CDMS II Collab.)
BALTZ	04	JHEP 0410 052	E. Baltz, P. Gondolo	
BELANGER	04	JHEP 0403 012	G. Belanger *et al.*	
BOTTINO	04	PR D69 037302	A. Bottino *et al.*	
DESAI	04	PR D70 083523	S. Desai *et al.*	(Super-Kamiokande Collab.)
ELLIS	04	PR D69 015005	J. Ellis *et al.*	
ELLIS	04B	PR D70 055005	J. Ellis *et al.*	
HEISTER	04	PL B583 247	A. Heister *et al.*	(ALEPH Collab.)
PIERCE	04A	PR D70 075006	A. Pierce	
ABBIENDI	03L	PL B572 8	G. Abbiendi *et al.*	(OPAL Collab.)
ABDALLAH	03M	EPJ C31 421	J. Abdallah *et al.*	(DELPHI Collab.)
AHMED	03	ASP 19 691	B. Ahmed *et al.*	(UK Dark Matter Collab.)
AKERIB	03	PR D68 082002	D.S. Akerib *et al.*	(CDMS Collab.)
BAER	03	JCAP 0305 006	H. Baer, C. Balazs	
BAER	03A	JCAP 0309 007	H. Baer *et al.*	
BOTTINO	03	PR D68 043506	A. Bottino *et al.*	
BOTTINO	03A	PR D67 063519	A. Bottino, N. Fornengo, S. Scopel	
CHATTOPAD...	03	PR D68 035005	U. Chattopadhyay, A. Corsetti, P. Nath	
ELLIS	03	ASP 18 395	J. Ellis, K.A. Olive, Y. Santoso	
ELLIS	03B	NP B652 259	J. Ellis *et al.*	
ELLIS	03C	PL B565 176	J. Ellis *et al.*	
ELLIS	03D	PL B573 162	J. Ellis *et al.*	
ELLIS	03E	PR D67 123502	J. Ellis *et al.*	
HEISTER	03C	EPJ C28 1	A. Heister *et al.*	(ALEPH Collab.)
HEISTER	03G	EPJ C31 1	A. Heister *et al.*	(ALEPH Collab.)
KLAPDOR-K...	03	ASP 18 525	H.V. Klapdor-Kleingrothaus *et al.*	
LAHANAS	03	PL B568 55	A. Lahanas, D. Nanopoulos	
TAKEDA	03	PL B572 145	A. Takeda *et al.*	
ABRAMS	02	PR D66 122003	D. Abrams *et al.*	(CDMS Collab.)
ACOSTA	02H	PRL 89 281801	D. Acosta *et al.*	(CDF Collab.)
ANGLOHER	02	ASP 18 43	G. Angloher *et al.*	(CRESST Collab.)
ARNOWITT	02	hep-ph/0211417	R. Arnowitt, B. Dutta	
ELLIS	02B	PL B532 318	J. Ellis, A. Ferstl, K.A. Olive	
HEISTER	02	PL B526 191	A. Heister *et al.*	(ALEPH Collab.)
HEISTER	02E	PL B526 206	A. Heister *et al.*	(ALEPH Collab.)
HEISTER	02J	PL B533 223	A. Heister *et al.*	(ALEPH Collab.)
HEISTER	02N	PL B544 73	A. Heister *et al.*	(ALEPH Collab.)
KIM	02	PL B527 18	H.B. Kim *et al.*	
KIM	02B	JHEP 0212 034	Y.G. Kim *et al.*	
LAHANAS	02	EPJ C23 185	A. Lahanas, V.C. Spanos	
MORALES	02B	ASP 16 325	A. Morales *et al.*	(COSME Collab.)
MORALES	02C	PL B532 8	A. Morales *et al.*	(IGEX Collab.)
ABREU	01	EPJ C19 29	P. Abreu *et al.*	(DELPHI Collab.)
ABREU	01B	EPJ C19 201	P. Abreu *et al.*	(DELPHI Collab.)
BALTZ	01	PRL 86 5004	E. Baltz, P. Gondolo	
BARATE	01	PL B499 67	R. Barate *et al.*	(ALEPH Collab.)
BARATE	01B	EPJ C19 415	R. Barate *et al.*	(ALEPH Collab.)
BARGER	01C	PL B518 117	V. Barger, C. Kao	
BAUDIS	01	PR D63 022001	L. Baudis *et al.*	(Heidelberg-Moscow Collab.)
BERNABEI	01	PL B509 197	R. Bernabei *et al.*	(DAMA Collab.)
BOTTINO	01	PR D63 125003	A. Bottino *et al.*	
CORSETTI	01	PR D64 125010	A. Corsetti, P. Nath	
ELLIS	01B	PL B510 236	J. Ellis *et al.*	
ELLIS	01C	PR D63 065016	J. Ellis, A. Ferstl, K.A. Olive	
GOMEZ	01	PL B512 252	M.E. Gomez, J.D. Vergados	
LAHANAS	01	PL B518 94	A. Lahanas, D.V. Nanopoulos, V. Spanos	
ABBIENDI	00	EPJ C12 1	G. Abbiendi *et al.*	(OPAL Collab.)
ABBIENDI	00G	EPJ C14 51	G. Abbiendi *et al.*	(OPAL Collab.)
ABBIENDI	00H	EPJ C14 187	G. Abbiendi *et al.*	(OPAL Collab.)
Also		EPJ C16 707 (errat.)	G. Abbiendi *et al.*	(OPAL Collab.)
ABBIENDI,G	00D	EPJ C18 253	G. Abbiendi *et al.*	(OPAL Collab.)
ABREU	00J	PL B479 129	P. Abreu *et al.*	(DELPHI Collab.)
ABREU	00Q	PL B478 65	P. Abreu *et al.*	(DELPHI Collab.)
ABREU	00T	PL B485 95	P. Abreu *et al.*	(DELPHI Collab.)
ABREU	00U	PL B487 36	P. Abreu *et al.*	(DELPHI Collab.)
ABREU	00V	EPJ C16 211	P. Abreu *et al.*	(DELPHI Collab.)
ABREU	00W	PL B489 38	P. Abreu *et al.*	(DELPHI Collab.)
ABREU	00Z	EPJ C17 53	P. Abreu *et al.*	(DELPHI Collab.)
ABUSAIDI	00	PRL 84 5699	R. Abusaidi *et al.*	(CDMS Collab.)
ACCIARRI	00D	PL B472 420	M. Acciarri *et al.*	(L3 Collab.)
ACCOMANDO	00	NP B585 124	E. Accomando *et al.*	
BERNABEI	00	PL B480 23	R. Bernabei *et al.*	(DAMA Collab.)
BERNABEI	00C	EPJ C18 283	R. Bernabei *et al.*	(DAMA Collab.)
BERNABEI	00D	NJP 2 15	R. Bernabei *et al.*	(DAMA Collab.)
BOEHM	00B	PR D62 035012	C. Boehm, A. Djouadi, M. Drees	
ELLIS	00	PR D62 075010	J. Ellis *et al.*	
FENG	00	PL B482 388	J.L. Feng, K.T. Matchev, F. Wilczek	
LEP	00	CERN-EP-2000-016	LEP Collabs.	(ALEPH, DELPHI, L3, OPAL, SLD+)
MORALES	00	PL B489 268	A. Morales *et al.*	(IGEX Collab.)
PDG	00	EPJ C15 1	D.E. Groom *et al.*	(PDG Collab.)
SPOONER	00	PL B473 330	N.J.C. Spooner *et al.*	(UK Dark Matter Col.)
ACCIARRI	99H	PL B456 283	M. Acciarri *et al.*	(L3 Collab.)
ACCIARRI	99R	PL B470 268	M. Acciarri *et al.*	(L3 Collab.)
ACCIARRI	99W	PL B471 280	M. Acciarri *et al.*	(L3 Collab.)
AMBROSIO	99	PR D60 082002	M. Ambrosio *et al.*	(Macro Collab.)
BAUDIS	99	PR D59 022001	L. Baudis *et al.*	(Heidelberg-Moscow Collab.)
BELLI	99C	NP B563 97	P. Belli *et al.*	(DAMA Collab.)
OOTANI	99	PL B461 371	W. Ootani *et al.*	
ABREU	98P	PL B444 491	P. Abreu *et al.*	(DELPHI Collab.)
ACCIARRI	98F	EPJ C4 207	M. Acciarri *et al.*	(L3 Collab.)
ACKERSTAFF	98P	PL B433 195	K. Ackerstaff *et al.*	(OPAL Collab.)
BARATE	98K	PL B433 176	R. Barate *et al.*	(ALEPH Collab.)
BARATE	98S	EPJ C4 433	R. Barate *et al.*	(ALEPH Collab.)
BERNABEI	98C	PL B436 379	R. Bernabei *et al.*	(DAMA Collab.)
ELLIS	98	PR D58 095002	J. Ellis *et al.*	
ELLIS	98B	PL B444 367	J. Ellis, T. Falk, K. Olive	
PDG	98	EPJ C3 1	C. Caso *et al.*	(PDG Collab.)
BAER	97	PR D57 567	H. Baer, M. Brhlik	
BERNABEI	97	ASP 7 73	R. Bernabei *et al.*	(DAMA Collab.)
EDSJO	97	PR D56 1879	J. Edsjo, P. Gondolo	
ARNOWITT	96	PR D54 2374	R. Arnowitt, P. Nath	
BAER	96	PR D53 597	H. Baer, M. Brhlik	
BERGSTROM	96	ASP 5 263	L. Bergstrom, P. Gondolo	
LEWIN	96	ASP 6 87	J.D. Lewin, P.F. Smith	
BEREZINSKY	95	ASP 5 1	V. Berezinsky *et al.*	
FALK	95	PL B354 99	T. Falk, K.A. Olive, M. Srednicki	(MINN, UCSB)
LOSECCO	95	PL B342 392	J.M. LoSecco	(NDAM)
ADRIANI	93M	PRPL 236 1	O. Adriani *et al.*	(L3 Collab.)
DREES	93	PR D47 376	M. Drees, M.M. Nojiri	(DESY, SLAC)
DREES	93B	PR D48 3483	M. Drees, M.M. Nojiri	
FALK	93	PL B318 354	T. Falk *et al.*	(UCB, UCSB, MINN)
KELLEY	93	PR D47 2461	S. Kelley *et al.*	(TAMU, ALAH)
MIZUTA	93	PL B298 120	S. Mizuta, M. Yamaguchi	(TOHO)
MORI	93	PR D48 5505	M. Mori *et al.*	(KEK, NIIG, TOKY, TOKA+)
BOTTINO	92	MPL A7 733	A. Bottino *et al.*	(TORI, ZARA)
Also		PL B265 57	A. Bottino *et al.*	(TORI, INFN)
DECAMP	92	PRPL 216 253	D. Decamp *et al.*	(ALEPH Collab.)
LOPEZ	92	NP B370 445	J.L. Lopez, D.V. Nanopoulos, K.J. Yuan	(TAMU)
MCDONALD	92	PL B283 80	J. McDonald, K.A. Olive, M. Srednicki	(LISB+)
ABREU	91F	NP B367 511	P. Abreu *et al.*	(DELPHI Collab.)
ALEXANDER	91F	ZPHY C52 175	G. Alexander *et al.*	(OPAL Collab.)
BOTTINO	91	PL B265 57	A. Bottino *et al.*	(TORI, INFN)
GELMINI	91	NP B351 623	G.B. Gelmini, P. Gondolo, E. Roulet	(UCLA, TRST)
GRIEST	91	PR D43 3191	K. Griest, D. Seckel	
KAMIONKOW...	91	PR D44 3021	M. Kamionkowski	(CHIC, FNAL)
MORI	91B	PL B270 89	M. Mori *et al.*	(Kamiokande Collab.)
NOJIRI	91	PL B261 76	M.M. Nojiri	(KEK)
OLIVE	91	NP B355 208	K.A. Olive, M. Srednicki	(MINN, UCSB)
ROSZKOWSKI	91	PL B262 59	L. Roszkowski	(CERN)
GRIEST	90	PR D41 3565	K. Griest, M. Kamionkowski, M.S. Turner	(UCB+)
BARBIERI	89C	NP B313 725	R. Barbieri, M. Frigeni, G. Giudice	
OLIVE	89	PL B230 78	K.A. Olive, M. Srednicki	(MINN, UCSB)
ELLIS	88D	NP B307 883	J. Ellis, R. Flores	
GRIEST	88B	PR D38 2357	K. Griest	

Int. J. Mod. Phys. A 2026.41. Downloaded from www.worldscientific.com
by UNIVERSITY OF CALIFORNIA @ BERKELEY on 09/16/26. Re-use and distribution is strictly not permitted, except for Open Access articles.

OLIVE	88	PL B205 553	K.A. Olive, M. Srednicki	(MINN, UCSB)
SREDNICKI	88	NP B310 693	M. Srednicki, R. Watkins, K.A. Olive	(MINN, UCSB)
ELLIS	84	NP B238 453	J. Ellis *et al.*	(CERN)
GOLDBERG	83	PRL 50 1419	H. Goldberg	(NEAS)
KRAUSS	83	NP B227 556	L.M. Krauss	(HARV)
VYSOTSKII	83	SJNP 37 948	M.I. Vysotsky	(ITEP)
		Translated from YAF 37 1597.		

Technicolor

See the related review(s):

Dynamical Electroweak Symmetry Breaking: Implications of the H^0

The latest unpublished results are described in "Dynamical Electroweak Symmetry Breaking" review.

MASS LIMITS for Resonances in Models of Dynamical Electroweak Symmetry Breaking

VALUE (GeV)	CL%	DOCUMENT ID		TECN	COMMENT
• • • We do not use the following data for averages, fits, limits, etc. • • •					
>3900	95	[1] AAD	20AM	ATLS	top-color Z'
		[2] AAD	20W	ATLS	$\rho_T \to W\pi_T \to \ell\nu q\overline{q}$
		[3] AAD	16W	ATLS	color octet vector resonance
>2400	95	[4] KHACHATRY...	16E	CMS	top-color Z'
		[5] AAD	15AB	ATLS	$h \to \pi_V\pi_V$
>1800	95	[6] AAD	15AO	ATLS	top-color Z'
		[7] AAD	15BB	ATLS	$pp \to \rho_T/a_{1T} \to Wh$ or Zh
		[8] AAD	15Q	ATLS	$h \to \pi_V\pi_V$
		[9] AAIJ	15AN	LHCB	$h \to \pi_V\pi_V$
>1140	95	[10] KHACHATRY...	15C	CMS	$\rho_T \to WZ$
		[11] KHACHATRY...	15W	CMS	$H \to \pi_V\pi_V$
none 200–700, 750–890	95	[12] AAD	14AT	ATLS	$pp \to \omega_T \to Z\gamma$
none 275–960	95	[12] AAD	14AT	ATLS	$pp \to a_T \to W\gamma$
		[13] AAD	14V	ATLS	color singlet techni-vector
> 703		[14] AAD	13AN	ATLS	$pp \to a_T \to W\gamma$
> 494		[15] AAD	13AN	ATLS	$pp \to \omega_T \to Z\gamma$
none 500–1740	95	[16] AAD	13AQ	ATLS	top-color Z'
>1300	95	[17] CHATRCHYAN	13AP	CMS	top-color Z'
>2100	95	[16] CHATRCHYAN	13BM	CMS	top-color Z'
		[18] BAAK	12	RVUE	QCD-like technicolor
none 167–687	95	[19] CHATRCHYAN	12AF	CMS	$\rho_T \to WZ$
> 805	95	[16] AALTONEN	11AD	CDF	top-color Z'
> 805	95	[16] AALTONEN	11AE	CDF	top-color Z'
		[20] CHIVUKULA	11	RVUE	top-Higgs
		[21] CHIVUKULA	11A	RVUE	techini-π
		[22] AALTONEN	10I	CDF	$p\overline{p} \to \rho_T/\omega_T \to W\pi_T$
none 208–408	95	[23] ABAZOV	10A	D0	$\rho_T \to WZ$
		[24] ABAZOV	07I	D0	$p\overline{p} \to \rho_T/\omega_T \to W\pi_T$
> 280	95	[25] ABULENCIA	05A	CDF	$\rho_T \to e^+e^-, \mu^+\mu^-$
		[26] CHEKANOV	02B	ZEUS	color octet techni-π
> 207	95	[27] ABAZOV	01B	D0	$\rho_T \to e^+e^-$
none 90–206.7	95	[28] ABDALLAH	01	DLPH	$e^+e^- \to \rho_T$
		[29] AFFOLDER	00F	CDF	color-singlet techni-ρ, $\rho_T \to W\pi_T, 2\pi_T$
> 600	95	[30] AFFOLDER	00K	CDF	color-octet techni-ρ, $\rho_{T8} \to 2\pi_{LQ}$
none 350–440	95	[31] ABE	99F	CDF	color-octet techni-ρ, $\rho_{T8} \to \overline{b}b$
		[32] ABE	99N	CDF	techni-ω, $\omega_T \to \gamma\overline{b}b$
none 260–480	95	[33] ABE	97G	CDF	color-octet techni-ρ, $\rho_{T8} \to$ 2jets

[1] AAD 20AM search for a top-color Z' decaying to $t\overline{t}$ in pp collisions at $\sqrt{s}$ = 13 TeV. The quoted limit is for $\Gamma_{Z'}/M_{Z'}$ = 0.01. The limit becomes $M_{Z'}$ > 4700 GeV for $\Gamma_{Z'}/M_{Z'}$ = 0.03.

[2] AAD 20W search for techni-ρ decaying to $\pi_T W$ in pp collisions at $\sqrt{s}$ = 13 TeV. See their Fig. 5a for limits on $\sigma \cdot B$.

[3] AAD 16W search for color octet vector resonance decaying to bB in pp collisions at $\sqrt{s}$ = 8 TeV. The vector like quark B is assumed to decay to bH. See their Fig.3 and Fig.4 for limits on $\sigma \cdot B$.

[4] KHACHATRYAN 16E search for top-color Z' decaying to $t\overline{t}$. The quoted limit is for $\Gamma_{Z'}/m_{Z'}$ = 0.012. Also exclude $m_{Z'}$ < 2.9 TeV for wider topcolor Z' with $\Gamma_{Z'}/m_{Z'}$ = 0.1.

[5] AAD 15AB search for long-lived hidden valley π_V particles which are produced in pairs by the decay of a scalar boson. π_V is assumed to decay into dijets. See their Fig. 10 for the limit on σB.

[6] AAD 15AO search for top-color Z' decaying to $t\overline{t}$. The quoted limit is for $\Gamma_{Z'}/m_{Z'}$ = 0.012.

[7] AAD 15BB search for minimal walking technicolor (MWT) isotriplet vector and axial-vector resonances decaying to Wh or Zh. See their Fig. 3 for the exclusion limit in the MWT parameter space.

[8] AAD 15Q search for long-lived hidden valley π_V particles which are produced in pairs by the decay of scalar boson. π_V is assumed to decay into dijets. See their Fig. 5 and Fig. 6 for the limit on σB.

[9] AAIJ 15AN search for long-lived hidden valley π_V particles which are produced in pairs by the decay of scalar boson with a mass of 120GeV. π_V is assumed to decay into dijets. See their Fig. 4 for the limit on σB.

[10] KHACHATRYAN 15C search for a vector techni-resonance decaying to WZ. The limit assumes M_{π_T} = (3/4) M_{ρ_T} − 25 GeV. See their Fig.3 for the limit in $M_{\pi_T} - M_{\rho_T}$ plane of the low scale technicolor model.

[11] KHACHATRYAN 15W search for long-lived hidden valley π_V particles which are produced in pairs in the decay of heavy higgs boson H. π_V is assumed to decay into $\ell^+\ell^-$. See their Fig. 7 and Fig. 8 for the limits on σB.

[12] AAD 14AT search for techni-ω and techni-a resonances decaying to $V\gamma$ with $V = W(\to \ell\nu)$ or $Z(\to \ell^+\ell^-)$.

[13] AAD 14V search for vector techni-resonances decaying into electron or muon pairs in pp collisions at $\sqrt{s}$ = 8 TeV. See their table IX for exclusion limits with various assumptions.

[14] AAD 13AN search for vector techni-resonance a_T decaying into $W\gamma$.

[15] AAD 13AN search for vector techni-resonance ω_T decaying into $Z\gamma$.

[16] Search for top-color Z' decaying to $t\overline{t}$. The quoted limit is for $\Gamma_{Z'}/m_{Z'}$ = 0.012.

[17] CHATRCHYAN 13AP search for top-color leptophobic Z' decaying to $t\overline{t}$. The quoted limit is for $\Gamma_{Z'}/m_{Z'}$ = 0.012.

[18] BAAK 12 give electroweak oblique parameter constraints on the QCD-like technicolor models. See their Fig. 28.

[19] CHATRCHYAN 12AF search for a vector techni-resonance decaying to WZ. The limit assumes M_{π_T} = (3/4) M_{ρ_T} − 25 GeV. See their Fig. 3 for the limit in $M_{\pi_T} - M_{\rho_T}$ plane of the low scale technicolor model.

[20] Using the LHC limit on the Higgs boson production cross section, CHIVUKULA 11 obtain a limit on the top-Higgs mass > 300 GeV at 95% CL assuming 150 GeV top-pion mass.

[21] Using the LHC limit on the Higgs boson production cross section, CHIVUKULA 11A obtain a limit on the techinipion mass ruling out the region 110 GeV < m_P < $2m_t$. Existence of color techni-fermions, top-color mechanism, and $N_{TC} \geq$ 3 are assumed.

[22] AALTONEN 10I search for the vector techni-resonances (ρ_T, ω_T) decaying into $W\pi_T$ with $W \to \ell\nu$ and $\pi_T \to b\overline{b}$, $b\overline{c}$, or $b\overline{u}$. See their Fig. 3 for the exclusion plot in $M_{\pi_T} - M_{\rho_T}$ plane.

[23] ABAZOV 10A search for a vector techni-resonance decaying into WZ. The limit assumes $M_{\rho_T} < M_{\pi_T} + M_W$.

[24] ABAZOV 07I search for the vector techni-resonances (ρ_T, ω_T) decaying into $W\pi_T$ with $W \to e\nu$ and $\pi_T \to b\overline{b}$ or $b\overline{c}$. See their Fig. 2 for the exclusion plot in $M_{\pi_T} - M_{\rho_T}$ plane.

[25] ABULENCIA 05A search for resonances decaying to electron or muon pairs in $p\overline{p}$ collisions. at $\sqrt{s}$ = 1.96 TeV. The limit assumes Technicolor-scale mass parameters $M_V = M_A$ = 500 GeV.

[26] CHEKANOV 02B search for color octet techni-π P decaying into dijets in ep collisions. See their Fig. 5 for the limit on $\sigma(ep \to ePX)\cdot B(P \to 2j)$.

[27] ABAZOV 01B searches for vector techni-resonances (ρ_T,ω_T) decaying to e^+e^-. The limit assumes $M_{\rho_T} = M_{\omega_T} < M_{\pi_T} + M_W$.

[28] The limit is independent of the π_T mass. See their Fig. 9 and Fig. 10 for the exclusion plot in the $M_{\rho_T} - M_{\pi_T}$ plane. ABDALLAH 01 limit on the techni-pion mass is M_{π_T} > 79.8 GeV for N_D=2, assuming its point-like coupling to gauge bosons.

[29] AFFOLDER 00F search for ρ_T decaying into $W\pi_T$ or $\pi_T\pi_T$ with $W \to \ell\nu$ and $\pi_T \to \overline{b}b$, $\overline{b}c$. See Fig. 1 in the above Note on "Dynamical Electroweak Symmetry Breaking" for the exclusion plot in the $M_{\rho_T} - M_{\pi_T}$ plane.

[30] AFFOLDER 00K search for the ρ_{T8} decaying into $\pi_{LQ}\pi_{LQ}$ with $\pi_{LQ} \to b\nu$. For $\pi_{LQ} \to c\nu$, the limit is $M_{\rho_{T8}}$ >510 GeV. See their Fig. 2 and Fig. 3 for the exclusion plot in the $M_{\rho_{T8}} - M_{\pi_{LQ}}$ plane.

[31] ABE 99F search for a new particle X decaying into $b\overline{b}$ in $p\overline{p}$ collisions at E_{cm}= 1.8 TeV. See Fig. 7 in the above Note on "Dynamical Electroweak Symmetry Breaking" for the upper limit on $\sigma(p\overline{p} \to X)\times B(X \to b\overline{b})$. ABE 99F also exclude top gluons of width Γ=0.3M in the mass interval 280 <M< 670 GeV, of width Γ=0.5M in the mass interval 340 <M< 640 GeV, and of width Γ=0.7M in the mass interval 375 <M< 560 GeV.

[32] ABE 99N search for the techni-ω decaying into $\gamma\pi_T$. The technipion is assumed to decay $\pi_T \to b\overline{b}$. See Fig. 2 in the above Note on "Dynamical Electroweak Symmetry Breaking" for the exclusion plot in the $M_{\omega_T} - M_{\pi_T}$ plane.

[33] ABE 97G search for a new particle X decaying into dijets in $p\overline{p}$ collisions at E_{cm}= 1.8 TeV. See Fig. 5 in the above Note on "Dynamical Electroweak Symmetry Breaking" for the upper limit on $\sigma(p\overline{p} \to X)\times B(X \to 2j)$.

REFERENCES FOR Technicolor

AAD	20AM	JHEP 2010 061	G. Aad *et al.*	(ATLAS Collab.)
AAD	20W	JHEP 2006 151	G. Aad *et al.*	(ATLAS Collab.)
AAD	16W	PL B758 249	G. Aad *et al.*	(ATLAS Collab.)
KHACHATRY...	16E	PR D93 012001	V. Khachatryan *et al.*	(CMS Collab.)
AAD	15AB	PR D92 012010	G. Aad *et al.*	(ATLAS Collab.)
AAD	15AO	JHEP 1508 148	G. Aad *et al.*	(ATLAS Collab.)
AAD	15BB	EPJ C75 263	G. Aad *et al.*	(ATLAS Collab.)
AAD	15Q	PL B743 15	G. Aad *et al.*	(ATLAS Collab.)
AAIJ	15AN	EPJ C75 152	R. Aaij *et al.*	(LHCb Collab.)
KHACHATRY...	15C	PL B740 83	V. Khachatryan *et al.*	(CMS Collab.)
KHACHATRY...	15W	PR D91 052012	V. Khachatryan *et al.*	(CMS Collab.)
AAD	14AT	PL B738 428	G. Aad *et al.*	(ATLAS Collab.)
AAD	14V	PR D90 052005	G. Aad *et al.*	(ATLAS Collab.)
AAD	13AN	PR D87 112003	G. Aad *et al.*	(ATLAS Collab.)
Also		PR D91 119901 (errat.)	G. Aad *et al.*	(ATLAS Collab.)
AAD	13AQ	PR D88 012004	G. Aad *et al.*	(ATLAS Collab.)
CHATRCHYAN	13AP	PR D87 072002	S. Chatrchyan *et al.*	(CMS Collab.)
CHATRCHYAN	13BM	PRL 111 211804	S. Chatrchyan *et al.*	(CMS Collab.)
Also		PRL 112 119903 (errat.)	S. Chatrchyan *et al.*	(CMS Collab.)
BAAK	12	EPJ C72 2003	M. Baak *et al.*	(Gfitter Group)
CHATRCHYAN	12AF	PRL 109 141801	S. Chatrchyan *et al.*	(CMS Collab.)
AALTONEN	11AD	PR D84 072003	T. Aaltonen *et al.*	(CDF Collab.)
AALTONEN	11AE	PR D84 072004	T. Aaltonen *et al.*	(CDF Collab.)
CHIVUKULA	11	PR D84 095022	R.S. Chivukula *et al.*	
CHIVUKULA	11A	PR D84 115025	R. S. Chivukula *et al.*	
AALTONEN	10I	PRL 104 111802	T. Aaltonen *et al.*	(CDF Collab.)
ABAZOV	10A	PRL 104 061801	V.M. Abazov *et al.*	(D0 Collab.)
ABAZOV	07I	PRL 98 221801	V.M. Abazov *et al.*	(D0 Collab.)
ABULENCIA	05A	PRL 95 252001	A. Abulencia *et al.*	(CDF Collab.)

CHEKANOV	02B	PL B531 9	S. Chekanov *et al.*	(ZEUS Collab.)
ABAZOV	01B	PRL 87 061802	V.M. Abazov *et al.*	(D0 Collab.)
ABDALLAH	01	EPJ C22 17	J. Abdallah *et al.*	(DELPHI Collab.)
AFFOLDER	00F	PRL 84 1110	T. Affolder *et al.*	(CDF Collab.)
AFFOLDER	00K	PRL 85 2056	T. Affolder *et al.*	(CDF Collab.)
ABE	99F	PRL 82 2038	F. Abe *et al.*	(CDF Collab.)
ABE	99N	PRL 83 3124	F. Abe *et al.*	(CDF Collab.)
ABE	97G	PR D55 5263	F. Abe *et al.*	(CDF Collab.)

Quark and Lepton Compositeness, Searches for

The latest unpublished results are described in the "Quark and Lepton Compositeness" review.

See the related review(s):

Searches for Quark and Lepton Compositeness

CONTENTS:

Scale Limits for Contact Interactions: $\Lambda(eeee)$
Scale Limits for Contact Interactions: $\Lambda(ee\mu\mu)$
Scale Limits for Contact Interactions: $\Lambda(ee\tau\tau)$
Scale Limits for Contact Interactions: $\Lambda(\ell\ell\ell\ell)$
Scale Limits for Contact Interactions: $\Lambda(eeqq)$
Scale Limits for Contact Interactions: $\Lambda(\mu\mu qq)$
Scale Limits for Contact Interactions: $\Lambda(\ell\nu\ell\nu)$
Scale Limits for Contact Interactions: $\Lambda(e\nu qq)$
Scale Limits for Contact Interactions: $\Lambda(qqqq)$
Scale Limits for Contact Interactions: $\Lambda(\nu\nu qq)$
Mass Limits for Excited e (e^*)
— Limits for Excited e (e^*) from Pair Production
— Limits for Excited e (e^*) from Single Production
— Limits for Excited e (e^*) from $e^+e^- \to \gamma\gamma$
— Indirect Limits for Excited e (e^*)
Mass Limits for Excited μ (μ^*)
— Limits for Excited μ (μ^*) from Pair Production
— Limits for Excited μ (μ^*) from Single Production
— Indirect Limits for Excited μ (μ^*)
Mass Limits for Excited τ (τ^*)
— Limits for Excited τ (τ^*) from Pair Production
— Limits for Excited τ (τ^*) from Single Production
Mass Limits for Excited Neutrino (ν^*)
— Limits for Excited ν (ν^*) from Pair Production
— Limits for Excited ν (ν^*) from Single Production
Mass Limits for Excited q (q^*)
— Limits for Excited q (q^*) from Pair Production
— Limits for Excited q (q^*) from Single Production
Mass Limits for Color Sextet Quarks (q_6)
Mass Limits for Color Octet Charged Leptons (ℓ_8)
Mass Limits for Color Octet Neutrinos (ν_8)
Mass Limits for W_8 (Color Octet W Boson)

SCALE LIMITS for Contact Interactions: $\Lambda(eeee)$

Limits are for $\Lambda^{\pm}_{LL}$ only. For other cases, see each reference.

Λ^+_{LL}(TeV)	Λ^-_{LL}(TeV)	CL%	DOCUMENT ID		TECN	COMMENT
>8.3	**>10.3**	95	[1] BOURILKOV	01	RVUE	E_{cm}= 192–208 GeV
• • • We do not use the following data for averages, fits, limits, etc. • • •						
>4.5	>7.0	95	[2] SCHAEL	07A	ALEP	E_{cm}= 189–209 GeV
>5.3	>6.8	95	ABDALLAH	06C	DLPH	E_{cm}= 130–207 GeV
>4.7	>6.1	95	[3] ABBIENDI	04G	OPAL	E_{cm}= 130–207 GeV
>4.3	>4.9	95	ACCIARRI	00P	L3	E_{cm}= 130–189 GeV

[1] A combined analysis of the data from ALEPH, DELPHI, L3, and OPAL.
[2] SCHAEL 07A limits are from R_c, Q^{depl}_{FB}, and hadronic cross section measurements.
[3] ABBIENDI 04G limits are from $e^+e^- \to e^+e^-$ cross section at $\sqrt{s}$ = 130–207 GeV.

SCALE LIMITS for Contact Interactions: $\Lambda(ee\mu\mu)$

Limits are for $\Lambda^{\pm}_{LL}$ only. For other cases, see each reference.

Λ^+_{LL}(TeV)	Λ^-_{LL}(TeV)	CL%	DOCUMENT ID		TECN	COMMENT
>6.6	**>9.5**	95	[1] SCHAEL	07A	ALEP	E_{cm}= 189–209 GeV
> 8.5	>3.8	95	ACCIARRI	00P	L3	E_{cm}= 130–189 GeV
• • • We do not use the following data for averages, fits, limits, etc. • • •						
>7.3	>7.6	95	ABDALLAH	06C	DLPH	E_{cm}= 130–207 GeV
>8.1	>7.3	95	[2] ABBIENDI	04G	OPAL	E_{cm}= 130–207 GeV

[1] SCHAEL 07A limits are from R_c, Q^{depl}_{FB}, and hadronic cross section measurements.
[2] ABBIENDI 04G limits are from $e^+e^- \to \mu\mu$ cross section at $\sqrt{s}$ = 130–207 GeV.

SCALE LIMITS for Contact Interactions: $\Lambda(ee\tau\tau)$

Limits are for $\Lambda^{\pm}_{LL}$ only. For other cases, see each reference.

Λ^+_{LL}(TeV)	Λ^-_{LL}(TeV)	CL%	DOCUMENT ID		TECN	COMMENT
>7.9	>5.8	95	[1] SCHAEL	07A	ALEP	E_{cm}= 189–209 GeV
>7.9	>4.6	95	ABDALLAH	06C	DLPH	E_{cm}= 130–207 GeV
>4.9	**>7.2**	95	[2] ABBIENDI	04G	OPAL	E_{cm}= 130–207 GeV
• • • We do not use the following data for averages, fits, limits, etc. • • •						
>5.4	>4.7	95	ACCIARRI	00P	L3	E_{cm}= 130–189 GeV

[1] SCHAEL 07A limits are from R_c, Q^{depl}_{FB}, and hadronic cross section measurements.
[2] ABBIENDI 04G limits are from $e^+e^- \to \tau\tau$ cross section at $\sqrt{s}$ = 130–207 GeV.

SCALE LIMITS for Contact Interactions: $\Lambda(\ell\ell\ell\ell)$

Lepton universality assumed. Limits are for $\Lambda^{\pm}_{LL}$ only. For other cases, see each reference.

Λ^+_{LL}(TeV)	Λ^-_{LL}(TeV)	CL%	DOCUMENT ID		TECN	COMMENT
>7.9	**> 10.3**	95	[1] SCHAEL	07A	ALEP	E_{cm}= 189–209 GeV
>9.1	>8.2	95	ABDALLAH	06C	DLPH	E_{cm}= 130–207 GeV
• • • We do not use the following data for averages, fits, limits, etc. • • •						
>7.7	>9.5	95	[2] ABBIENDI	04G	OPAL	E_{cm}= 130–207 GeV
			[3] BABICH	03	RVUE	
>9.0	>5.2	95	ACCIARRI	00P	L3	E_{cm}= 130–189 GeV

[1] SCHAEL 07A limits are from R_c, Q^{depl}_{FB}, and hadronic cross section measurements.
[2] ABBIENDI 04G limits are from $e^+e^- \to \ell^+\ell^-$ cross section at $\sqrt{s}$ = 130–207 GeV.
[3] BABICH 03 obtain a bound -0.175 TeV^{-2} $<1/\Lambda^2_{LL} < 0.095$ TeV^{-2} (95%CL) in a model independent analysis allowing all of Λ_{LL}, Λ_{LR}, Λ_{RL}, Λ_{RR} to coexist.

SCALE LIMITS for Contact Interactions: $\Lambda(eeqq)$

Limits are for $\Lambda^{\pm}_{LL}$ only. For other cases, see each reference.

Λ^+_{LL}(TeV)	Λ^-_{LL}(TeV)	CL%	DOCUMENT ID		TECN	COMMENT
>24	**>37**	95	[1] AABOUD	17AT	ATLS	$(eeqq)$
> 8.4	**>10.2**	95	[2] ABDALLAH	09	DLPH	$(eebb)$
> 9.4	**>5.6**	95	[3] SCHAEL	07A	ALEP	$(eecc)$
> 9.4	>4.9	95	[2] SCHAEL	07A	ALEP	$(eebb)$
>23.3	**>12.5**	95	[4] CHEUNG	01B	RVUE	$(eeuu)$
>11.1	**>26.4**	95	[4] CHEUNG	01B	RVUE	$(eedd)$
• • • We do not use the following data for averages, fits, limits, etc. • • •						
> 7.1	>7.1	95	[5] AAD	21AU	ATLS	$(eebs)$
>23.5	>26.1	95	[6] AAD	21Q	ATLS	$(eeqq)$
>19.5	>24.0	95	[7] SIRUNYAN	21N	CMS	$(eeqq)$
>23.5	>26.1	95	[8] AAD	20AP	ATLS	$(eeqq)$
> 4.5	>12.8	95	[9] ABRAMOWICZ	19	ZEUS	$(eeqq)$
>16.8	>23.9	95	[10] SIRUNYAN	19AC	CMS	$(eeqq)$
>15.5	>19.5	95	[11] AABOUD	16U	ATLS	$(eeqq)$
>13.5	>18.3	95	[12] KHACHATRY...	15AE	CMS	$(eeqq)$
>16.4	>20.7	95	[13] AAD	14BE	ATLS	$(eeqq)$
> 9.5	>12.1	95	[14] AAD	13E	ATLS	$(eeqq)$
>10.1	>9.4	95	[15] AAD	12AB	ATLS	$(eeqq)$
> 4.2	>4.0	95	[16] AARON	11C	H1	$(eeqq)$
> 3.8	>3.8	95	[17] ABDALLAH	11	DLPH	$(eetc)$
>12.9	>7.2	95	[18] SCHAEL	07A	ALEP	$(eeqq)$
> 3.7	>5.9	95	[19] ABULENCIA	06L	CDF	$(eeqq)$

[1] AABOUD 17AT limits are from pp collisions at $\sqrt{s}$ = 13 TeV. The quoted limit uses a uniform positive prior in $1/\Lambda^2$.
[2] ABDALLAH 09 and SCHAEL 07A limits are from R_b, A^b_{FB}.
[3] SCHAEL 07A limits are from R_c, Q^{depl}_{FB}, and hadronic cross section measurements.
[4] CHEUNG 01B is an update of BARGER 98E.
[5] AAD 21AU search for new phenomena in final states with e^+e^- and one or no b-tagged jets in pp collisions at $\sqrt{s}$ = 13 TeV. The quoted limits assume $g^2_* = 4\pi$.
[6] AAD 21Q limits are from pp collisions at $\sqrt{s}$ = 13 TeV. A frequentist statistical framework is used to remove the prior dependence.
[7] SIRUNYAN 21N limits are from e^+e^- mass distribution in pp collisions at $\sqrt{s}$ = 13 TeV.
[8] AAD 20AP limits are from e^+e^- mass distribution in pp collisions at $\sqrt{s}$ = 13 TeV.
[9] ABRAMOWICZ 19 limits are from Q^2 spectrum measurements of $e^{\pm}p \to e^{\pm}X$.
[10] SIRUNYAN 19AC limits are from e^+e^- mass distribution in pp collisions at $\sqrt{s}$ = 13 TeV.
[11] AABOUD 16U limits are from pp collisions at $\sqrt{s}$ = 13 TeV. The quoted limit uses a uniform positive prior in $1/\Lambda^2$.
[12] KHACHATRYAN 15AE limit is from e^+e^- mass distribution in pp collisions at E_{cm} = 8 TeV.
[13] AAD 14BE limits are from pp collisions at $\sqrt{s}$ = 8 TeV. The quoted limit uses a uniform positive prior in $1/\Lambda^2$.
[14] AAD 13E limis are from e^+e^- mass distribution in pp collisions at E_{cm} = 7 TeV.
[15] AAD 12AB limis are from e^+e^- mass distribution in pp collisions at E_{cm} = 7 TeV.
[16] AARON 11C limits are from Q^2 spectrum measurements of $e^{\pm}p \to e^{\pm}X$.
[17] ABDALLAH 11 limit is from $e^+e^- \to t\overline{c}$ cross section. $\Lambda_{LL} = \Lambda_{LR} = \Lambda_{RL} = \Lambda_{RR}$ is assumed.
[18] SCHAEL 07A limit assumes quark flavor universality of the contact interactions.
[19] ABULENCIA 06L limits are from $p\overline{p}$ collisions at $\sqrt{s}$ = 1.96 TeV.

Int. J. Mod. Phys. A 2026.41. Downloaded from www.worldscientific.com
by UNIVERSITY OF CALIFORNIA @ BERKELEY on 09/16/26. Re-use and distribution is strictly not permitted, except for Open Access articles.

Int. J. Mod. Phys. A 2026.41. Downloaded from www.worldscientific.com
by UNIVERSITY OF CALIFORNIA @ BERKELEY on 09/16/26. Re-use and distribution is strictly not permitted, except for Open Access articles.

SCALE LIMITS for Contact Interactions: $\Lambda(\mu\mu qq)$

Λ^+_{LL}(TeV)	Λ^-_{LL}(TeV)	CL%	DOCUMENT ID		TECN	COMMENT
>23.3	**>40.0**	95	[1] SIRUNYAN	21N	CMS	$(\mu\mu qq)$
• • • We do not use the following data for averages, fits, limits, etc. • • •						
> 8.5	>8.5	95	[2] AAD	21AU	ATLS	$(\mu\mu bs)$
>22.3	>32.7	95	[3] AAD	21Q	ATLS	$(\mu\mu qq)$
>22.3	>32.7	95	[4] AAD	20AP	ATLS	$(\mu\mu qq)$
>20.4	>30.4	95	[5] SIRUNYAN	19AC	CMS	$(\mu\mu qq)$
>20	>30	95	[6] AABOUD	17AT	ATLS	$(\mu\mu qq)$
>15.8	>21.8	95	[7] AABOUD	16U	ATLS	$(\mu\mu qq)$
>12.0	>15.2	95	[8] KHACHATRY...	15AE	CMS	$(\mu\mu qq)$
>12.5	>16.7	95	[9] AAD	14BE	ATLS	$(\mu\mu qq)$
> 9.6	>12.9	95	[10] AAD	13E	ATLS	$(\mu\mu qq)$ (isosinglet)
> 9.5	>13.1	95	[11] CHATRCHYAN	13K	CMS	$(\mu\mu qq)$ (isosinglet)
> 8.0	>7.0	95	[12] AAD	12AB	ATLS	$(\mu\mu qq)$ (isosinglet)

[1] SIRUNYAN 21N limits are from $\mu^+\mu^-$ mass distribution in pp collisions at $\sqrt{s} = 13$ TeV.

[2] AAD 21AU search for new phenomena in final states with $\mu^+\mu^-$ and one or no b-tagged jets in pp collisions at $\sqrt{s} = 13$ TeV. The quoted limits assume $g_*^2 = 4\pi$.

[3] AAD 21Q limits are from pp collisions at $\sqrt{s} = 13$ TeV. A frequentist statistical framework is used to remove the prior dependence.

[4] AAD 20AP limits are from $\mu^+\mu^-$ mass distribution in pp collisions at $\sqrt{s} = 13$ TeV.

[5] SIRUNYAN 19AC limits are from $\mu^+\mu^-$ mass distribution in pp collisions at $\sqrt{s} = 13$ TeV.

[6] AABOUD 17AT limits are from pp collisions at $\sqrt{s} = 13$ TeV. The quoted limit uses a uniform positive prior in $1/\Lambda^2$.

[7] AABOUD 16U limits are from pp collisions at $\sqrt{s} = 13$ TeV. The quoted limit uses a uniform positive prior in $1/\Lambda^2$.

[8] KHACHATRYAN 15AE limit is from $\mu^+\mu^-$ mass distribution in pp collisions at $E_{cm} = 8$ TeV.

[9] AAD 14BE limits are from pp collisions at $\sqrt{s} = 8$ TeV. The quoted limit uses a uniform positive prior in $1/\Lambda^2$.

[10] AAD 13E limis are from $\mu^+\mu^-$ mass distribution in pp collisions at $E_{cm} = 7$ TeV.

[11] CHATRCHYAN 13K limis are from $\mu^+\mu^-$ mass distribution in pp collisions at $E_{cm} = 7$ TeV.

[12] AAD 12AB limis are from $\mu^+\mu^-$ mass distribution in pp collisions at $E_{cm} = 7$ TeV.

SCALE LIMITS for Contact Interactions: $\Lambda(\ell\nu\ell\nu)$

VALUE (TeV)	CL%	DOCUMENT ID		TECN	COMMENT
>3.10	90	[1] JODIDIO	86	SPEC	$\Lambda^{\pm}_{LR}(\nu_\mu \nu_e \mu e)$
• • • We do not use the following data for averages, fits, limits, etc. • • •					
>3.8		[2] DIAZCRUZ	94	RVUE	$\Lambda^+_{LL}(\tau\nu_\tau e\nu_e)$
>8.1		[2] DIAZCRUZ	94	RVUE	$\Lambda^-_{LL}(\tau\nu_\tau e\nu_e)$
>4.1		[3] DIAZCRUZ	94	RVUE	$\Lambda^+_{LL}(\tau\nu_\tau \mu\nu_\mu)$
>6.5		[3] DIAZCRUZ	94	RVUE	$\Lambda^-_{LL}(\tau\nu_\tau \mu\nu_\mu)$

[1] JODIDIO 86 limit is from $\mu^+ \to \overline{\nu}_\mu e^+ \nu_e$. Chirality invariant interactions $L = (g^2/\Lambda^2)$ $[\eta_{LL}\ (\overline{\nu}_{\mu L}\gamma^\alpha\mu_L)\ (\overline{e}_L\gamma_\alpha\nu_{eL}) + \eta_{LR}\ (\overline{\nu}_{\mu L}\gamma^\alpha\nu_{eL}\ (\overline{e}_R\gamma_\alpha\mu_R)]$ with $g^2/4\pi = 1$ and $(\eta_{LL},\eta_{LR}) = (0,\pm1)$ are taken. No limits are given for $\Lambda^{\pm}_{LL}$ with $(\eta_{LL},\eta_{LR}) = (\pm1,0)$. For more general constraints with right-handed neutrinos and chirality nonconserving contact interactions, see their text.

[2] DIAZCRUZ 94 limits are from $\Gamma(\tau \to e\nu\nu)$ and assume flavor-dependent contact interactions with $\Lambda(\tau\nu_\tau e\nu_e) \ll \Lambda(\mu\nu_\mu e\nu_e)$.

[3] DIAZCRUZ 94 limits are from $\Gamma(\tau \to \mu\nu\nu)$ and assume flavor-dependent contact interactions with $\Lambda(\tau\nu_\tau \mu\nu_\mu) \ll \Lambda(\mu\nu_\mu e\nu_e)$.

SCALE LIMITS for Contact Interactions: $\Lambda(e\nu qq)$

VALUE (TeV)	CL%	DOCUMENT ID		TECN
>2.81	95	[1] AFFOLDER	01I	CDF

[1] AFFOLDER 00I bound is for a scalar interaction $\overline{q}_R\, q_L\, \overline{\nu} e_L$.

SCALE LIMITS for Contact Interactions: $\Lambda(qqqq)$

Λ^+_{LL}(TeV)	Λ^-_{LL}(TeV)	CL%	DOCUMENT ID		TECN	COMMENT
>13.1 none 17.4–29.5	**>21.8**	95	[1] AABOUD	17AK	ATLS	pp dijet angl.
• • • We do not use the following data for averages, fits, limits, etc. • • •						
			[2] AABOUD	18AV	ATLS	$pp \to t\overline{t}t\overline{t}$
>12.8	>17.5	95	[3] SIRUNYAN	18DD	CMS	pp dijet angl.
>11.5	>14.7	95	[4] SIRUNYAN	17F	CMS	pp dijet angl.
>12.0	>17.5	95	[5] AAD	16S	ATLS	pp dijet angl.
			[6] AAD	15AR	ATLS	$pp \to t\overline{t}t\overline{t}$
			[7] AAD	15BY	ATLS	$pp \to t\overline{t}t\overline{t}$
> 8.1	>12.0	95	[8] AAD	15L	ATLS	pp dijet angl.
> 9.0	>11.7	95	[9] KHACHATRY...	15J	CMS	pp dijet angl.
> 5		95	[10] FABBRICHESI	14	RVUE	$q\overline{q}t\overline{t}$

[1] AABOUD 17AK limit is from dijet angular distribution in pp collisions at $\sqrt{s} = 13$ TeV. u, d, and s quarks are assumed to be composite.

[2] AABOUD 18AV obtain limit on t_R compositeness $2\pi/\Lambda^2_{RR} < 1.6$ TeV^{-2} at 95% CL from $t\overline{t}t\overline{t}$ production in the pp collisions at $E_{cm} = 13$ TeV.

[3] SIRUNYAN 18DD limit is from dijet angular distribution in pp collisions at $\sqrt{s} = 13$ TeV.

[4] SIRUNYAN 17F limit is from dijet angular cross sections in pp collisions at $E_{cm} = 13$ TeV. All quarks are assumed to be composite.

[5] AAD 16S limit is from dijet angular selections in pp collisions at $E_{cm} = 13$ TeV. u, d, and s quarks are assumed to be composite.

[6] AAD 15AR obtain limit on the t_R compositeness $2\pi/\Lambda^2_{RR} < 6.6$ TeV^{-2} at 95% CL from the $t\overline{t}t\overline{t}$ production in the pp collisions at $E_{cm} = 8$ TeV.

[7] AAD 15BY obtain limit on the t_R compositeness $2\pi/\Lambda^2_{RR} < 15.1$ TeV^{-2} at 95% CL from the $t\overline{t}t\overline{t}$ production in the pp collisions at $E_{cm} = 8$ TeV.

[8] AAD 15L limit is from dijet angular distribution in pp collisions at $E_{cm} = 8$ TeV. u, d, and s quarks are assumed to be composite.

[9] KHACHATRYAN 15J limit is from dijet angular distribution in pp collisions at $E_{cm} = 8$ TeV. u, d, s, c, and b quarks are assumed to be composite.

[10] FABBRICHESI 14 obtain bounds on chromoelectric and chromomagnetic form factors of the top-quark using $pp \to t\overline{t}$ and $p\overline{p} \to t\overline{t}$ cross sections. The quoted limit on the $q\overline{q}t\overline{t}$ contact interaction is derived from their bound on the chromoelectric form factor.

SCALE LIMITS for Contact Interactions: $\Lambda(\nu\nu qq)$

Limits are for $\Lambda^{\pm}_{LL}$ only. For other cases, see each reference.

Λ^+_{LL}(TeV)	Λ^-_{LL}(TeV)	CL%	DOCUMENT ID		TECN	COMMENT
>2.23	>2.13	95	[1] AAD	24AC	ATLS	$t\overline{t}\nu\overline{\nu}$
>5.0	**>5.4**	95	[2] MCFARLAND	98	CCFR	νN scattering

[1] AAD 24AC limit is from the measurement of the $t\overline{t}$ production cross section with large missing $\not{E}_T$ in pp collisions at $\sqrt{s} = 13$ TeV.

[2] MCFARLAND 98 assumed a flavor universal interaction. Neutrinos were mostly of muon type.

MASS LIMITS for Excited e (e^*)

Most e^+e^- experiments assume one-photon or Z exchange. The limits from some e^+e^- experiments which depend on λ have assumed transition couplings which are chirality violating ($\eta_L = \eta_R$). However they can be interpreted as limits for chirality-conserving interactions after multiplying the coupling value λ by $\sqrt{2}$; see Note.

Excited leptons have the same quantum numbers as other ortholeptons. See also the searches for ortholeptons in the "Searches for Heavy Leptons" section.

Limits for Excited e (e^*) from Pair Production

These limits are obtained from $e^+e^- \to e^{*+}e^{*-}$ and thus rely only on the (electroweak) charge of e^*. Form factor effects are ignored unless noted. For the case of limits from Z decay, the e^* coupling is assumed to be of sequential type. Possible t channel contribution from transition magnetic coupling is neglected. All limits assume a dominant $e^* \to e\gamma$ decay except the limits from $\Gamma(Z)$.

For limits prior to 1987, see our 1992 edition (Physical Review **D45** S1 (1992)).

VALUE (GeV)	CL%	DOCUMENT ID		TECN	COMMENT
>103.2	95	[1] ABBIENDI	02G	OPAL	$e^+e^- \to e^*e^*$ Homodoublet type
• • • We do not use the following data for averages, fits, limits, etc. • • •					
>102.8	95	[2] ACHARD	03B	L3	$e^+e^- \to e^*e^*$ Homodoublet type

[1] From e^+e^- collisions at $\sqrt{s} = 183$–209 GeV. $f = f'$ is assumed.

[2] From e^+e^- collisions at $\sqrt{s} = 189$–209 GeV. $f = f'$ is assumed. ACHARD 03B also obtain limit for $f = -f'$: $m_{e^*} > 96.6$ GeV.

Limits for Excited e (e^*) from Single Production

ATLAS and CMS limits are from $q\overline{q} \to ee^*$. Other limits are from $e^+e^- \to e^*e$, $W \to e^*\nu$, or $ep \to e^*X$ and depend on transition magnetic coupling between e and e^*. All limits assume $e^* \to e\gamma$ decay except as noted. Limits from LEP, UA2, and H1 are for chiral coupling, whereas all other limits are for nonchiral coupling, $\eta_L = \eta_R = 1$. In most papers, the limit is expressed in the form of an excluded region in the λ–m_{e^*} plane. See the original papers. For limits prior to 1987, see our PDG 92 edition (Physical Review **D45** S1 (1992)).

VALUE (GeV)	CL%	DOCUMENT ID		TECN	COMMENT
>5600	95	[1] SIRUNYAN	20AJ	CMS	$pp \to ee^*X$
• • • We do not use the following data for averages, fits, limits, etc. • • •					
>4800	95	[2] AABOUD	19AZ	ATLS	$pp \to ee^*X$
>3900	95	[3] SIRUNYAN	19Z	CMS	$pp \to ee^*X$
>2450	95	[4] KHACHATRY...	16AQ	CMS	$pp \to ee^*X$
>3000	95	[5] AAD	15AP	ATLS	$pp \to e^{(*)}e^*X$
>2200	95	[6] AAD	13BB	ATLS	$pp \to ee^*X$
>1900	95	[7] CHATRCHYAN	13AE	CMS	$pp \to ee^*X$
>1870	95	[8] AAD	12AZ	ATLS	$pp \to e^{(*)}e^*X$

[1] SIRUNYAN 20AJ search for e^* production in $2e2j$ final states in pp collisions at $\sqrt{s} = 13$ TeV. The quoted limit assumes $\Lambda = m_{e^*}$, $f = f' = 1$. The contact interaction is included. See their Fig.11 for exclusion limits in m_{e^*}–Λ plane.

[2] AABOUD 19AZ search for single e^* production in pp collisions at $\sqrt{s} = 13$ TeV. The limit quoted above is from $e^* \to eq\overline{q}$ and $e^* \to \nu W$ decays assuming $f = f' = 1$ and $m_{e^*} = \Lambda$. The contact interaction is included in e^* production and decay amplitudes. See their Fig.6 for exclusion limits in $m_{e^*} - \Lambda$ plane.

[3] SIRUNYAN 19Z search for e^* production in $\ell\ell\gamma$ final states in pp collisions at $\sqrt{s} = 13$ TeV. The quoted limit assumes $\Lambda = m_{e^*}$, $f = f' = 1$. The contact interaction is included in the e^* production and decay amplitudes.

[4] KHACHATRYAN 16AQ search for single e^* production in pp collisions at $\sqrt{s}$ = 8 TeV. The limit above is from the $e^* \to e\gamma$ search channel assuming $f = f' = 1$, $m_{e^*} = \Lambda$. See their Table 7 for limits in other search channels or with different assumptions.

[5] AAD 15AP search for e^* production in evens with three or more charged leptons in pp collisions at $\sqrt{s}$ = 8 TeV. The quoted limit assumes $\Lambda = m_{e^*}$, $f = f' = 1$. The contact interaction is included in the e^* production and decay amplitudes.

[6] AAD 13BB search for single e^* production in pp collisions with $e^* \to e\gamma$ decay. $f = f' = 1$, and e^* production via contact interaction with $\Lambda = m_{e^*}$ are assumed.

[7] CHATRCHYAN 13AE search for single e^* production in pp collisions with $e^* \to e\gamma$ decay. $f = f' = 1$, and e^* production via contact interaction with $\Lambda = m_{e^*}$ are assumed.

[8] AAD 12AZ search for e^* production via four-fermion contact interaction in pp collisions with $e^* \to e\gamma$ decay. The quoted limit assumes $\Lambda = m_{e^*}$. See their Fig. 8 for the exclusion plot in the mass-coupling plane.

Limits for Excited e (e^*) from $e^+e^- \to \gamma\gamma$

These limits are derived from indirect effects due to e^* exchange in the t channel and depend on transition magnetic coupling between e and e^*. All limits are for $\lambda_\gamma = 1$. All limits except ABE 89J and ACHARD 02D are for nonchiral coupling with $\eta_L = \eta_R = 1$. We choose the chiral coupling limit as the best limit and list it in the Summary Table.

For limits prior to 1987, see our 1992 edition (Physical Review **D45** S1 (1992)).

VALUE (GeV)	CL%	DOCUMENT ID		TECN	COMMENT
>356	95	[1] ABDALLAH	04N	DLPH	$\sqrt{s}$= 161–208 GeV
• • • We do not use the following data for averages, fits, limits, etc. • • •					
>310	95	ACHARD	02D	L3	$\sqrt{s}$= 192–209 GeV

[1] ABDALLAH 04N also obtain a limit on the excited electron mass with $e e^*$ chiral coupling, $m_{e^*} > 295$ GeV at 95% CL.

Indirect Limits for Excited e (e^*)

These limits make use of loop effects involving e^* and are therefore subject to theoretical uncertainty.

VALUE (GeV)	DOCUMENT ID		TECN	COMMENT
• • • We do not use the following data for averages, fits, limits, etc. • • •				
	[1] DORENBOS...	89	CHRM	$\overline{\nu}_\mu e \to \overline{\nu}_\mu e$, $\nu_\mu e \to \nu_\mu e$
	[2] GRIFOLS	86	THEO	$\nu_\mu e \to \nu_\mu e$
	[3] RENARD	82	THEO	$g-2$ of electron

[1] DORENBOSCH 89 obtain the limit $\lambda_\gamma^2 \Lambda_{cut}^2 / m_{e^*}^2 < 2.6$ (95% CL), where Λ_{cut} is the cutoff scale, based on the one-loop calculation by GRIFOLS 86. If one assumes that Λ_{cut} = 1 TeV and $\lambda_\gamma = 1$, one obtains $m_{e^*} > 620$ GeV. However, one generally expects $\lambda_\gamma \approx m_{e^*}/\Lambda_{cut}$ in composite models.

[2] GRIFOLS 86 uses $\nu_\mu e \to \nu_\mu e$ and $\overline{\nu}_\mu e \to \overline{\nu}_\mu e$ data from CHARM Collaboration to derive mass limits which depend on the scale of compositeness.

[3] RENARD 82 derived from $g-2$ data limits on mass and couplings of e^* and μ^*. See figures 2 and 3 of the paper.

MASS LIMITS for Excited μ (μ^*)

Limits for Excited μ (μ^*) from Pair Production

These limits are obtained from $e^+e^- \to \mu^{*+}\mu^{*-}$ and thus rely only on the (electroweak) charge of μ^*. Form factor effects are ignored unless noted. For the case of limits from Z decay, the μ^* coupling is assumed to be of sequential type. All limits assume a dominant $\mu^* \to \mu\gamma$ decay except the limits from $\Gamma(Z)$.

For limits prior to 1987, see our 1992 edition (Physical Review **D45** S1 (1992)).

VALUE (GeV)	CL%	DOCUMENT ID		TECN	COMMENT
>103.2	95	[1] ABBIENDI	02G	OPAL	$e^+e^- \to \mu^*\mu^*$ Homodoublet type
• • • We do not use the following data for averages, fits, limits, etc. • • •					
>102.8	95	[2] ACHARD	03B	L3	$e^+e^- \to \mu^*\mu^*$ Homodoublet type

[1] From e^+e^- collisions at $\sqrt{s}$ = 183–209 GeV. $f = f'$ is assumed.

[2] From e^+e^- collisions at $\sqrt{s}$ = 189–209 GeV. $f = f'$ is assumed. ACHARD 03B also obtain limit for $f = -f'$: $m_{\mu^*} > 96.6$ GeV.

Limits for Excited μ (μ^*) from Single Production

ATLAS and CMS limits are from $q\overline{q} \to \mu^*\mu$. Other limits are from $e^+e^- \to \mu^*\mu$ and depend on transition magnetic coupling between μ and μ^*. All limits assume $\mu^* \to \mu\gamma$ decay. Limits from LEP are for chiral coupling, whereas all other limits are for nonchiral coupling, $\eta_L = \eta_R = 1$. In most papers, the limit is expressed in the form of an excluded region in the λ–m_{μ^*} plane. See the original papers. For limits prior to 1987, see our PDG 92 edition (Physical Review **D45** S1 (1992)).

VALUE (GeV)	CL%	DOCUMENT ID		TECN	COMMENT
>5700	95	[1] SIRUNYAN	20AJ	CMS	$pp \to \mu\mu^* X$
• • • We do not use the following data for averages, fits, limits, etc. • • •					
>3800	95	[2] SIRUNYAN	19Z	CMS	$pp \to \mu\mu^* X$
>2800	95	[3] AAD	16BM	ATLS	$pp \to \mu\mu^* X$
>2470	95	[4] KHACHATRY...	16AQ	CMS	$pp \to \mu\mu^* X$
>3000	95	[5] AAD	15AP	ATLS	$pp \to \mu^{(*)}\mu^* X$
>2200	95	[6] AAD	13BB	ATLS	$pp \to \mu\mu^* X$
>1900	95	[7] CHATRCHYAN	13AE	CMS	$pp \to \mu\mu^* X$
>1750	95	[8] AAD	12AZ	ATLS	$pp \to \mu^{(*)}\mu^* X$

[1] SIRUNYAN 20AJ search for μ^* production in $2\mu 2j$ final states in pp collisions at $\sqrt{s}$ = 13 TeV. The quoted limit assumes $\Lambda = m_{\mu^*}$, $f = f' = 1$. The contact interaction is included. See their Fig.11 for exclusion limits in m_{μ^*}–Λ plane.

[2] SIRUNYAN 19Z search for μ^* production in $\ell\ell\gamma$ final states in pp collisions at $\sqrt{s}$ = 13 TeV. The quoted limit assumes $\Lambda = m_{\mu^*}$, $f = f' = 1$. The contact interaction is included in the μ^* production and decay amplitudes.

[3] AAD 16BM search for μ^* production in $\mu\mu jj$ events in pp collisions at $\sqrt{s}$ = 8 TeV. Both the production and decay are assumed to occur via a contact interaction with $\Lambda = m_{\mu^*}$.

[4] KHACHATRYAN 16AQ search for single μ^* production in pp collisions at $\sqrt{s}$ = 8 TeV. The limit above is from the $\mu^* \to \mu\gamma$ search channel assuming $f = f' = 1$, $m_{\mu^*} = \Lambda$. See their Table 7 for limits in other search channels or with different assumptions.

[5] AAD 15AP search for μ^* production in evens with three or more charged leptons in pp collisions at $\sqrt{s}$ = 8 TeV. The quoted limit assumes $\Lambda = m_{\mu^*}$, $f = f' = 1$. The contact interaction is included in the μ^* production and decay amplitudes.

[6] AAD 13BB search for single μ^* production in pp collisions with $\mu^* \to \mu\gamma$ decay. $f = f' = 1$, and μ^* production via contact interaction with $\Lambda = m_{\mu^*}$ are assumed.

[7] CHATRCHYAN 13AE search for single μ^* production in pp collisions with $\mu^* \to \mu\gamma$ decay. $f = f' = 1$, and μ^* production via contact interaction with $\Lambda = m_{\mu^*}$ are assumed.

[8] AAD 12AZ search for μ^* production via four-fermion contact interaction in pp collisions with $\mu^* \to \mu\gamma$ decay. The quoted limit assumes $\Lambda = m_{\mu^*}$. See their Fig. 8 for the exclusion plot in the mass-coupling plane.

Indirect Limits for Excited μ (μ^*)

These limits make use of loop effects involving μ^* and are therefore subject to theoretical uncertainty.

VALUE (GeV)	DOCUMENT ID		TECN	COMMENT
• • • We do not use the following data for averages, fits, limits, etc. • • •				
	[1] RENARD	82	THEO	$g-2$ of muon

[1] RENARD 82 derived from $g-2$ data limits on mass and couplings of e^* and μ^*. See figures 2 and 3 of the paper.

MASS LIMITS for Excited τ (τ^*)

Limits for Excited τ (τ^*) from Pair Production

Except for CHEKHOVSKY 25E, these limits are obtained from $e^+e^- \to \tau^{*+}\tau^{*-}$ and thus rely only on the (electroweak) charge of τ^*. Form factor effects are ignored unless noted. For the case of limits from Z decay, the τ^* coupling is assumed to be of sequential type. All limits assume a dominant $\tau^* \to \tau\gamma$ decay except the limits from $\Gamma(Z)$. For limits prior to 1987, see our PDG 92 edition (Physical Review **D45** S1 (1992)).

VALUE (GeV)	CL%	DOCUMENT ID		TECN	COMMENT
>103.2	95	[1] ABBIENDI	02G	OPAL	$e^+e^- \to \tau^*\tau^*$ Homodoublet type
• • • We do not use the following data for averages, fits, limits, etc. • • •					
		[2] CHEKHOVSKY	25E	CMS	$\tau' \to \tau a_\tau$, $a_\tau \to \gamma\gamma$
>102.8	95	[3] ACHARD	03B	L3	$e^+e^- \to \tau^*\tau^*$ Homodoublet type

[1] From e^+e^- collisions at $\sqrt{s}$ = 183–209 GeV. $f = f'$ is assumed.

[2] CHEKHOVSKY 25E search for pair production of vector-like τ' in pp collisions at $\sqrt{s}$ = 13 TeV. τ' is assumed to be an $SU(2)_W$ singlet decaying to τ and light pseudoscalar a_τ decaying to $\gamma\gamma$. See their Fig. 5 for limits on σ.

[3] From e^+e^- collisions at $\sqrt{s}$ = 189–209 GeV. $f = f'$ is assumed. ACHARD 03B also obtain limit for $f = -f'$: $m_{\tau^*} > 96.6$ GeV.

Limits for Excited τ (τ^*) from Single Production

ATLAS and CMS limits are from $q\overline{q} \to \tau^*\tau$ including contact interactions. Other limits are from $e^+e^- \to \tau^*\tau$ and depend on transition magnetic coupling between τ and τ^*. All limits assume $\tau^* \to \tau\gamma$ decay. Limits from LEP are for chiral coupling, whereas all other limits are for nonchiral coupling, $\eta_L = \eta_R = 1$. In most papers, the limit is expressed in the form of an excluded region in the λ–m_{τ^*} plane. See the original papers.

VALUE (GeV)	CL%	DOCUMENT ID		TECN	COMMENT
>4700	95	[1] HAYRAPETY...	25Y	CMS	$pp \to \tau\tau^*$
• • • We do not use the following data for averages, fits, limits, etc. • • •					
>4600	95	[2] AAD	23BJ	ATLS	$pp \to \tau\tau^*$
>2500	95	[3] AAD	15AP	ATLS	$pp \to \tau^{(*)}\tau^* X$
> 180	95	[4] ACHARD	03B	L3	$e^+e^- \to \tau\tau^*$
> 185	95	[5] ABBIENDI	02G	OPAL	$e^+e^- \to \tau\tau^*$

[1] HAYRAPETYAN 25Y search for τ^* produced in association with τ via a contact interaction and decaying into $\tau\gamma$. The limit quoted above assumes $f = f' = 1$ and $\Lambda = m_{\tau^*}$.

[2] AAD 23BJ search for τ^* produced in association with τ and decaying into $\tau q\overline{q}$ via a contact interaction with $g^2_{contact} = (4\pi)^2$. The limit quoted above assumes $\Lambda = m_{\tau^*}$.

[3] AAD 15AP search for τ^* production in events with three or more charged leptons in pp collisions at $\sqrt{s}$ = 8 TeV. The quoted limit assumes $\Lambda = m_{\tau^*}$, $f = f' = 1$. The contact interaction is included in the τ^* production and decay amplitudes.

[4] ACHARD 03B result is from e^+e^- collisions at $\sqrt{s}$ = 189–209 GeV. $f = f' = \Lambda/m_{\tau^*}$ is assumed. See their Fig. 4 for the exclusion plot in the mass-coupling plane.

[5] ABBIENDI 02G result is from e^+e^- collisions at $\sqrt{s}$ = 183–209 GeV. $f = f' = \Lambda/m_{\tau^*}$ is assumed for τ^* coupling. See their Fig. 4c for the exclusion limit in the mass-coupling plane.

Int. J. Mod. Phys. A 2026.41. Downloaded from www.worldscientific.com
by UNIVERSITY OF CALIFORNIA @ BERKELEY on 09/16/26. Re-use and distribution is strictly not permitted, except for Open Access articles.

Int. J. Mod. Phys. A 2026.41. Downloaded from www.worldscientific.com
by UNIVERSITY OF CALIFORNIA @ BERKELEY on 09/16/26. Re-use and distribution is strictly not permitted, except for Open Access articles.

MASS LIMITS for Excited Neutrino (ν^*)

Limits for Excited ν (ν^*) from Pair Production

These limits are obtained from $e^+e^- \to \nu^*\nu^*$ and thus rely only on the (electroweak) charge of ν^*. Form factor effects are ignored unless noted. The ν^* coupling is assumed to be of sequential type unless otherwise noted. All limits assume a dominant $\nu^* \to \nu\gamma$ decay except the limits from $\Gamma(Z)$.

VALUE (GeV)	CL%	DOCUMENT ID		TECN	COMMENT
>1600	95	[1] AAD	15AP	ATLS	$pp \to \nu^*\nu^* X$
• • • We do not use the following data for averages, fits, limits, etc. • • •					
		[2] ABBIENDI	04N	OPAL	
> 102.6	95	[3] ACHARD	03B	L3	$e^+e^- \to \nu^*\nu^*$ Homodoublet type

[1] AAD 15AP search for ν^* pair production in evens with three or more charged leptons in pp collisions at $\sqrt{s}$ = 8 TeV. The quoted limit assumes $\Lambda = m_{\nu^*}$, $f = f' = 1$. The contact interaction is included in the ν^* production and decay amplitudes.

[2] From e^+e^- collisions at $\sqrt{s}$ = 192–209 GeV, ABBIENDI 04N obtain limit on $\sigma(e^+e^- \to \nu^*\nu^*)$ $B^2(\nu^* \to \nu\gamma)$. See their Fig.2. The limit ranges from 20 to 45 fb for m_{ν^*} > 45 GeV.

[3] From e^+e^- collisions at $\sqrt{s}$ = 189–209 GeV. $f = -f'$ is assumed. ACHARD 03B also obtain limit for $f = f'$: $m_{\nu^*_e}$ > 101.7 GeV, $m_{\nu^*_\mu}$ > 101.8 GeV, and $m_{\nu^*_\tau}$ > 92.9 GeV. See their Fig. 4 for the exclusion plot in the mass-coupling plane.

Limits for Excited ν (ν^*) from Single Production

These limits are from $e^+e^- \to \nu\nu^*$, $Z \to \nu\nu^*$, or $ep \to \nu^* X$ and depend on transition magnetic coupling between ν/e and ν^*. Assumptions about ν^* decay mode are given in footnotes.

VALUE (GeV)	CL%	DOCUMENT ID		TECN	COMMENT
> 213	95	[1] AARON	08	H1	$ep \to \nu^* X$
• • • We do not use the following data for averages, fits, limits, etc. • • •					
>6000	95	[2] TUMASYAN	23AL	CMS	$pp \to \ell\nu^* \to \ell\ell qq$, $\ell = e$
> 190	95	[3] ACHARD	03B	L3	$e^+e^- \to \nu\nu^*$
none 50–150	95	[4] ADLOFF	02	H1	$ep \to \nu^* X$
> 158	95	[5] CHEKANOV	02D	ZEUS	$ep \to \nu^* X$

[1] AARON 08 search for single ν^* production in ep collisions with the decays $\nu^* \to \nu\gamma$, νZ, eW. The quoted limit assumes $f = -f' = \Lambda/m_{\nu^*}$. See their Fig. 3 and Fig. 4 for the exclusion plots in the mass-coupling plane.

[2] TUMASYAN 23AL search for Majorana excited neutrino ν^* produced and decaying via gauge and contact interactions. The limit quoted above is for $\ell = e$ with $\Lambda = M_{\nu^*}$. The limit becomes M_{ν^*} > 6.1 TeV for $\ell = \mu$.

[3] ACHARD 03B result is from e^+e^- collisions at $\sqrt{s}$ = 189–209 GeV. The quoted limit is for ν^*_e. $f = -f' = \Lambda/m_{\nu^*}$ is assumed. See their Fig. 4 for the exclusion plot in the mass-coupling plane.

[4] ADLOFF 02 search for single ν^* production in ep collisions with the decays $\nu^* \to \nu\gamma$, νZ, eW. The quoted limit assumes $f = -f' = \Lambda/m_{\nu^*}$. See their Fig. 1 for the exclusion plots in the mass-coupling plane.

[5] CHEKANOV 02D search for single ν^* production in ep collisions with the decays $\nu^* \to \nu\gamma$, νZ, eW. $f = -f' = \Lambda/m_{\nu^*}$ is assumed for the e^* coupling. CHEKANOV 02D also obtain limit for $f = f' = \Lambda/m_{\nu^*}$: m_{ν^*} >135 GeV. See their Fig. 5c and Fig. 5d for the exclusion plot in the mass-coupling plane.

MASS LIMITS for Excited q (q^*)

Limits for Excited q (q^*) from Pair Production

Limits from CDF and CMS are from q^*q^* production via strong interactions. Other limits are mostly obtained from $e^+e^- \to q^*\overline{q}^*$ and thus rely only on the (electroweak) charge of the q^*. Form factor effects are ignored unless noted. Assumptions about the q^* decay are given in the comments and footnotes.

VALUE (GeV)	CL%	DOCUMENT ID		TECN	COMMENT
• • • We do not use the following data for averages, fits, limits, etc. • • •					
>1050	95	[1] HAYRAPETY...	25AA	CMS	$t^* \to tg$
>1700	95	[2] HAYRAPETY...	25AA	CMS	$pp \to t^*_{3/2}\overline{t}^*_{3/2} \to t\overline{t}gg$
none 700–1200	95	[3] SIRUNYAN	18V	CMS	$pp \to t^*_{3/2}\overline{t}^*_{3/2} \to t\overline{t}gg$
> 338	95	[4] AALTONEN	10H	CDF	$q^* \to tW^-$
		[5] BARATE	98U	ALEP	$Z \to q^*q^*$
> 45.6	95	[6] ADRIANI	93M	L3	u or d type, $Z \to q^*q^*$
> 41.7	95	[7] BARDADIN-...	92	RVUE	u-type, $\Gamma(Z)$
> 44.7	95	[7] BARDADIN-...	92	RVUE	d-type, $\Gamma(Z)$
> 40.6	95	[8] DECAMP	92	ALEP	u-type, $\Gamma(Z)$
> 44.2	95	[8] DECAMP	92	ALEP	d-type, $\Gamma(Z)$
> 45	95	[9] DECAMP	92	ALEP	u or d type, $Z \to q^*q^*$
> 45	95	[8] ABREU	91F	DLPH	u-type, $\Gamma(Z)$
> 45	95	[8] ABREU	91F	DLPH	d-type, $\Gamma(Z)$

[1] HAYRAPETYAN 25AA search for pair production of vector-like t^* in pp collisions at $\sqrt{s}$ = 13 TeV. t^* is assumed to be an $SU(2)_W$ singlet decaying to tg. See their Fig. 7 for limits on $\sigma \cdot B^2$.

[2] HAYRAPETYAN 25AA search for pair production of spin 3/2 excited top quark $t^*_{3/2}$ in pp collisions at $\sqrt{s}$ = 13 TeV. See their Fig. 8 for limits on $\sigma \cdot B^2$.

[3] SIRUNYAN 18V search for pair production of spin 3/2 excited top quarks. $B(t^*_{3/2} \to tg) = 1$ is assumed.

[4] AALTONEN 10H obtain limits on the q^*q^* production cross section in $p\overline{p}$ collisions. See their Fig. 3.

[5] BARATE 98U obtain limits on the form factor. See their Fig. 16 for limits in mass-form factor plane.

[6] ADRIANI 93M limit is valid for $B(q^* \to qg)$> 0.25 (0.17) for up (down) type.

[7] BARDADIN-OTWINOWSKA 92 limit based on $\Delta\Gamma(Z)$<36 MeV.

[8] These limits are independent of decay modes.

[9] Limit is for $B(q^* \to qg)+B(q^* \to q\gamma)$=1.

Limits for Excited q (q^*) from Single Production

These limits are from $e^+e^- \to q^*\overline{q}$, $p\overline{p} \to q^*X$, or $pp \to q^*X$ and depend on transition magnetic couplings between q and q^*. Assumptions about q^* decay mode are given in the footnotes and comments.

VALUE (GeV)	CL%	DOCUMENT ID		TECN	COMMENT
>6700 (CL = 95%) OUR LIMIT					
none 1800–2500	95	[1] TUMASYAN	23AF	CMS	$pp \to b^*X$, $b^* \to bg$
none 1000–6000	95	[2] TUMASYAN	23BC	CMS	$pp \to q^*X$, $q^* \to q\gamma$
none 1000–2200	95	[3] TUMASYAN	23BC	CMS	$pp \to b^*X$, $b^* \to b\gamma$
none 2000–6700	95	[4] AAD	20T	ATLS	$pp \to q^*X$, $q^* \to qg$
none 1250–3200	95	[4] AAD	20T	ATLS	$pp \to b^*X$, $b^* \to bg$, $b\gamma$, bZ, tW
none 1800–6300	95	[5] SIRUNYAN	20AI	CMS	$pp \to q^*X$, $q^* \to qg$
none 1500–2600	95	[6] AABOUD	18AB	ATLS	$pp \to b^*X$, $b^* \to bg$
none 1500–5300	95	[7] AABOUD	18BA	ATLS	$pp \to q^*X$, $q^* \to q\gamma$
none 1000–5500	95	[8] SIRUNYAN	18AG	CMS	$pp \to q^*X$, $q^* \to q\gamma$
none 1000–1800	95	[9] SIRUNYAN	18AG	CMS	$pp \to b^*X$, $b^* \to b\gamma$
none 600–6000	95	[10] SIRUNYAN	18BO	CMS	$pp \to q^*X$, $q^* \to qg$
none 1200–5000	95	[11] SIRUNYAN	18P	CMS	$pp \to q^*X$, $q^* \to qW$
none 1200–4700	95	[11] SIRUNYAN	18P	CMS	$pp \to q^*X$, $q^* \to qZ$
>6000	95	[12] AABOUD	17AK	ATLS	$pp \to q^*X$, $q^* \to qg$
• • • We do not use the following data for averages, fits, limits, etc. • • •					
		[13] HAYRAPETY...	24G	CMS	$pp \to q^*X$, $q^* \to qY$, $Y \to q\overline{q}$
none 700–3000	95	[14] TUMASYAN	22O	CMS	$pp \to b^*X$, $b^* \to tW$
>2600	95	[15] SIRUNYAN	21AG	CMS	$pp \to b^*X$, $b^* \to tW$
none 600–5400	95	[16] KHACHATRY...	17W	CMS	$pp \to q^*X$, $q^* \to qg$
none 1100–2100	95	[17] AABOUD	16	ATLS	$pp \to b^*X$, $b^* \to bg$
>1500	95	[18] AAD	16AH	ATLS	$pp \to b^*X$, $b^* \to tW$
>4400	95	[19] AAD	16AI	ATLS	$pp \to q^*X$, $q^* \to q\gamma$
		[20] AAD	16AV	ATLS	$pp \to q^*X$, $q^* \to Wb$
>5200	95	[21] AAD	16S	ATLS	$pp \to q^*X$, $q^* \to qg$
>1390	95	[22] KHACHATRY...	16I	CMS	$pp \to b^*X$, $b^* \to tW$
>5000	95	[23] KHACHATRY...	16K	CMS	$pp \to q^*X$, $q^* \to qg$
none 500–1600	95	[24] KHACHATRY...	16L	CMS	$pp \to q^*X$, $q^* \to qg$
>4060	95	[25] AAD	15V	ATLS	$pp \to q^*X$, $q^* \to qg$
>3500	95	[26] KHACHATRY...	15V	CMS	$pp \to q^*X$, $q^* \to qg$
>3500	95	[27] AAD	14A	ATLS	$pp \to q^*X$, $q^* \to q\gamma$
>3200	95	[28] KHACHATRY...	14	CMS	$pp \to q^*X$, $q^* \to qW$
>2900	95	[29] KHACHATRY...	14	CMS	$pp \to q^*X$, $q^* \to qZ$
none 700–3500	95	[30] KHACHATRY...	14J	CMS	$pp \to q^*X$, $q^* \to q\gamma$
>2380	95	[31] CHATRCHYAN	13AJ	CMS	$pp \to q^*X$, $q^* \to qW$
>2150	95	[32] CHATRCHYAN	13AJ	CMS	$pp \to q^*X$, $q^* \to qZ$

[1] TUMASYAN 23AF limit quoted above assumes $bg \to b^*$ production. The limit becomes m_{b^*} > 4 TeV if contact interaction is included in the b^* production cross section. See their Fig. 5 for limits on $\sigma \cdot B$.

[2] TUMASYAN 23BC search for excited light flavor quark q^* in pp collisions at $\sqrt{s}$ = 13 TeV. f = 1.0 is assumed.

[3] TUMASYAN 23BC search for excited b quark b^* in pp collisions at $\sqrt{s}$ = 13 TeV. b^* production via gauge interactions and f = 1.0 are assumed. The limit becomes m_{b^*} > 3.8TeV if contact interaction is included in the b^* production cross section.

[4] AAD 20T search for resonances decaying into dijets in pp collisions at $\sqrt{s}$ = 13 TeV. Assume $\Lambda = m_{q^*}$, $f_s = f = f' = 1$.

[5] SIRUNYAN 20AI search for resonances decaying into dijets in pp collisions at $\sqrt{s}$ = 13 TeV. Assume $\Lambda = m_{q^*}$, $f_s = f = f' = 1$.

[6] AABOUD 18AB assume $\Lambda = m_{b^*}$, $f_s = f = f' = 1$. The contact interactions are not included in b^* production and decay amplitudes.

[7] AABOUD 18BA search for first-generation excited quarks (u^* and d^*) with degenerate mass, assuming $\Lambda = m_{q^*}$, $f_s = f = f' = 1$. The contact interactions are not included in q^* production and decay amplitudes.

[8] SIRUNYAN 18AG search for first-generation excited quarks (u^* and d^*) with degenerate mass, assuming $\Lambda = m_{q^*}$, $f_s = f = f' = 1$.

[9] SIRUNYAN 18AG search for excited b quark assuming $\Lambda = m_{q^*}$, $f_s = f = f' = 1$.

[10] SIRUNYAN 18BO assume $\Lambda = m_{q^*}$, $f_s = f = f' = 1$. The contact interactions are not included in q^* production and decay amplitudes.

[11] SIRUNYAN 18P use the hadronic decay of W or Z, assuming $\Lambda = m_{q^*}$, $f_s = f = f' = 1$.

[12] AABOUD 17AK assume $\Lambda = m_{q^*}$, $f_s = f = f' = 1$. The contact interactions are not included in q^* production and decay amplitudes. Only the decay of $q^* \to gu$ and $q^* \to gd$ is simulated as the benchmark signals in the analysis.

[13] HAYRAPETYAN 24G search for singly produced narrow resonances decaying to jjj in pp collisions at $\sqrt{s}$ = 13 TeV. See their Fig. 3 for limits on $\sigma \cdot B$.

[14] TUMASYAN 22O search for b^* decaying to tW in pp collisions at $\sqrt{s}$ = 13 TeV. The limit quoted above assumes $\kappa^b_L = g_L = 1$, $\kappa^b_R = g_R = 0$. The limit becomes m_{b^*} >

Int. J. Mod. Phys. A 2026.41. Downloaded from www.worldscientific.com
by UNIVERSITY OF CALIFORNIA @ BERKELEY on 09/16/26. Re-use and distribution is strictly not permitted, except for Open Access articles.

3.0 TeV (>3.2 TeV) if we assume $\kappa_L^b = g_L = 0$, $\kappa_R^b = g_R = 1$ ($\kappa_L^b = g_L = 1$, $\kappa_R^b = g_R = 1$). See their Fig. 3 for limits on $\sigma \cdot B$.

[15] SIRUNYAN 21AG search for b^* decaying to tW in pp collisions at $\sqrt{s} = 13$ TeV. The limit quoted above assumes $\kappa_L^b = g_L = 1$, $\kappa_R^b = g_R = 0$. The limit becomes $m_{b^*} >$ 2.8 TeV (> 3.1 TeV) if we assume $\kappa_L^b = g_L = 0$, $\kappa_R^b = g_R = 1$ ($\kappa_L^b = g_L = \kappa_R^b = g_R = 1$). See their Fig. 5 for limits on $\sigma \cdot B$.

[16] KHACHATRYAN 17W assume $\Lambda = m_{q^*}$, $f_s = f = f' = 1$. The contact interactions are not included in q^* production and decay amplitudes.

[17] AABOUD 16 assume $\Lambda = m_{b^*}$, $f_s = f = f' = 1$. The contact interactions are not included in the b^* production and decay amplitudes.

[18] AAD 16AH search for b^* decaying to tW in pp collisions at $\sqrt{s} = 8$ TeV. $f_g = f_L = f_R = 1$ are assumed. See their Fig. 12b for limits on $\sigma \cdot B$.

[19] AAD 16AI assume $\Lambda = m_{q^*}$, $f_s = f = f' = 1$.

[20] AAD 16AV search for single production of vector-like quarks decaying to Wb in pp collisions. See their Fig. 8 for the limits on couplings and mixings.

[21] AAD 16S assume $\Lambda = m_{q^*}$, $f_s = f = f' = 1$. The contact interactions are not included in q^* production and decay amplitudes.

[22] KHACHATRYAN 16I search for b^* decaying to tW in pp collisions at $\sqrt{s} = 8$ TeV. $\kappa_L^b = g_L = 1$, $\kappa_R^b = g_R = 0$ are assumed. See their Fig. 8 for limits on $\sigma \cdot B$.

[23] KHACHATRYAN 16K assume $\Lambda = m_{q^*}$, $f_s = f = f' = 1$. The contact interactions are not included in q^* production and decay amplitudes.

[24] KHACHATRYAN 16L search for resonances decaying to dijets in pp collisions at $\sqrt{s} =$ 8 TeV using the data scouting technique which increases the sensitivity to the low mass resonances.

[25] AAD 15V assume $\Lambda = m_{q^*}$, $f_s = f = f' = 1$. The contact interactions are not included in q^* production and decay amplitudes.

[26] KHACHATRYAN 15V assume $\Lambda = m_{q^*}$, $f_s = f = f' = 1$. The contact interactions are not included in q^* production and decay amplitudes.

[27] AAD 14A assume $\Lambda = m_{q^*}$, $f_s = f = f' = 1$.

[28] KHACHATRYAN 14 use the hadronic decay of W, assuming $\Lambda = m_{q^*}$, $f_s = f = f' = 1$.

[29] KHACHATRYAN 14 use the hadronic decay of Z, assuming $\Lambda = m_{q^*}$, $f_s = f = f' = 1$.

[30] KHACHATRYAN 14J assume $f_s = f = f' = \Lambda / m_{q^*}$.

[31] CHATRCHYAN 13AJ use the hadronic decay of W.

[32] CHATRCHYAN 13AJ use the hadronic decay of Z.

MASS LIMITS for Color Sextet Quarks (q_6)

VALUE (GeV)	CL%		DOCUMENT ID		TECN	COMMENT
>84	95	[1]	ABE	89D	CDF	$p\overline{p} \rightarrow q_6 \overline{q}_6$

[1] ABE 89D look for pair production of unit-charged particles which leave the detector before decaying. In the above limit the color sextet quark is assumed to fragment into a unit-charged or neutral hadron with equal probability and to have long enough lifetime not to decay within the detector. A limit of 121 GeV is obtained for a color decuplet.

MASS LIMITS for Color Octet Charged Leptons (ℓ_8)

$\lambda \equiv m_{\ell_8}/\Lambda$

VALUE (GeV)	CL%		DOCUMENT ID		TECN	COMMENT
>86	95	[1]	ABE	89D	CDF	Stable ℓ_8: $p\overline{p} \rightarrow \ell_8 \overline{\ell}_8$
• • • We do not use the following data for averages, fits, limits, etc. • • •						
		[2]	ABT	93	H1	e_8: $ep \rightarrow e_8 X$

[1] ABE 89D look for pair production of unit-charged particles which leave the detector before decaying. In the above limit the color octet lepton is assumed to fragment into a unit-charged or neutral hadron with equal probability and to have long enough lifetime not to decay within the detector. The limit improves to 99 GeV if it always fragments into a unit-charged hadron.

[2] ABT 93 search for e_8 production via e-gluon fusion in ep collisions with $e_8 \rightarrow eg$. See their Fig. 3 for exclusion plot in the m_{e_8}–Λ plane for $m_{e_8} = 35$–220 GeV.

MASS LIMITS for Color Octet Neutrinos (ν_8)

$\lambda \equiv m_{\ell_8}/\Lambda$

VALUE (GeV)	CL%		DOCUMENT ID		TECN	COMMENT
>110	90	[1]	BARGER	89	RVUE	ν_8: $p\overline{p} \rightarrow \nu_8 \overline{\nu}_8$
• • • We do not use the following data for averages, fits, limits, etc. • • •						
none 3.8–29.8	95	[2]	KIM	90	AMY	ν_8: $e^+e^- \rightarrow$ acoplanar jets
none 9–21.9	95	[3]	BARTEL	87B	JADE	ν_8: $e^+e^- \rightarrow$ acoplanar jets

[1] BARGER 89 used ABE 89B limit for events with large missing transverse momentum. Two-body decay $\nu_8 \rightarrow \nu g$ is assumed.

[2] KIM 90 is at $E_{cm} = 50$–60.8 GeV. The same assumptions as in BARTEL 87B are used.

[3] BARTEL 87B is at $E_{cm} = 46.3$–46.78 GeV. The limit assumes the ν_8 pair production cross section to be eight times larger than that of the corresponding heavy neutrino pair production. This assumption is not valid in general for the weak couplings, and the limit can be sensitive to its $SU(2)_L \times U(1)_Y$ quantum numbers.

MASS LIMITS for W_8 (Color Octet W Boson)

VALUE (GeV)	DOCUMENT ID		TECN	COMMENT
• • • We do not use the following data for averages, fits, limits, etc. • • •				
	[1] ALBAJAR	89	UA1	$p\overline{p} \rightarrow W_8 X$, $W_8 \rightarrow Wg$

[1] ALBAJAR 89 give $\sigma(W_8 \rightarrow W + \text{jet})/\sigma(W) < 0.019$ (90% CL) for $m_{W_8} > 220$ GeV.

REFERENCES FOR Searches for Quark and Lepton Compositeness

CHEKHOVSKY	25E	JHEP 2508 156	V. Chekhovsky *et al.*	(CMS Collab.)
HAYRAPETY...	25AA	EPJ C85 342	A. Hayrapetyan *et al.*	(CMS Collab.)
HAYRAPETY...	25Y	JHEP 2506 006	A. Hayrapetyan	(CMS Collab.)
AAD	24AC	JHEP 2403 139	G. Aad *et al.*	(ATLAS Collab.)
HAYRAPETY...	24G	PRL 133 011801	A. Hayrapetyan *et al.*	(CMS Collab.)
AAD	23BJ	JHEP 2306 199	G. Aad *et al.*	(ATLAS Collab.)
TUMASYAN	23AF	PR D108 012009	A. Tumasyan *et al.*	(CMS Collab.)
TUMASYAN	23AL	PL B843 137803	A. Tumasyan *et al.*	(CMS Collab.)
TUMASYAN	23BC	JHEP 2312 189	A. Tumasyan *et al.*	(CMS Collab.)
TUMASYAN	22O	JHEP 2204 048	A. Tumasyan *et al.*	(CMS Collab.)
AAD	21AU	PRL 127 141801	G. Aad *et al.*	(ATLAS Collab.)
AAD	21Q	JHEP 2104 142	G. Aad *et al.*	(ATLAS Collab.)
SIRUNYAN	21AG	JHEP 2112 106	A.M. Sirunyan *et al.*	(CMS Collab.)
SIRUNYAN	21N	JHEP 2107 208	A.M. Sirunyan *et al.*	(CMS Collab.)
AAD	20AP	JHEP 2011 005	G. Aad *et al.*	(ATLAS Collab.)
AAD	20T	JHEP 2003 145	G. Aad *et al.*	(ATLAS Collab.)
SIRUNYAN	20AI	JHEP 2005 033	A.M. Sirunyan *et al.*	(CMS Collab.)
SIRUNYAN	20AJ	JHEP 2005 052	A.M. Sirunyan *et al.*	(CMS Collab.)
AABOUD	19AZ	EPJ C79 803	M. Aaboud *et al.*	(ATLAS Collab.)
ABRAMOWICZ	19	PR D99 092006	H. Abramowicz *et al.*	(ZEUS Collab.)
SIRUNYAN	19AC	JHEP 1904 114	A.M. Sirunyan *et al.*	(CMS Collab.)
SIRUNYAN	19Z	JHEP 1904 015	A.M. Sirunyan *et al.*	(CMS Collab.)
AABOUD	18AB	PR D98 032016	M. Aaboud *et al.*	(ATLAS Collab.)
AABOUD	18AV	JHEP 1807 089	M. Aaboud *et al.*	(ATLAS Collab.)
AABOUD	18BA	EPJ C78 102	M. Aaboud *et al.*	(ATLAS Collab.)
SIRUNYAN	18AG	PL B781 390	A.M. Sirunyan *et al.*	(CMS Collab.)
SIRUNYAN	18BO	JHEP 1808 130	A.M. Sirunyan *et al.*	(CMS Collab.)
SIRUNYAN	18DD	EPJ C78 789	A.M. Sirunyan *et al.*	(CMS Collab.)
SIRUNYAN	18P	PR D97 072006	A.M. Sirunyan *et al.*	(CMS Collab.)
SIRUNYAN	18V	PL B778 349	A.M. Sirunyan *et al.*	(CMS Collab.)
AABOUD	17AK	PR D96 052004	M. Aaboud *et al.*	(ATLAS Collab.)
AABOUD	17AT	JHEP 1710 182	M. Aaboud *et al.*	(ATLAS Collab.)
KHACHATRY...	17W	PL B769 520	V. Khachatryan *et al.*	(CMS Collab.)
SIRUNYAN	17F	JHEP 1707 013	A.M. Sirunyan *et al.*	(CMS Collab.)
AABOUD	16	PL B759 229	M. Aaboud *et al.*	(ATLAS Collab.)
AABOUD	16U	PL B761 372	M. Aaboud *et al.*	(ATLAS Collab.)
AAD	16AH	JHEP 1602 110	G. Aad *et al.*	(ATLAS Collab.)
AAD	16AI	JHEP 1603 041	G. Aad *et al.*	(ATLAS Collab.)
AAD	16AV	EPJ C76 442	G. Aad *et al.*	(ATLAS Collab.)
AAD	16BM	NJP 18 073021	G. Aad *et al.*	(ATLAS Collab.)
AAD	16S	PL B754 302	G. Aad *et al.*	(ATLAS Collab.)
KHACHATRY...	16AQ	JHEP 1603 125	V. Khachatryan *et al.*	(CMS Collab.)
KHACHATRY...	16I	JHEP 1601 166	V. Khachatryan *et al.*	(CMS Collab.)
KHACHATRY...	16K	PRL 116 071801	V. Khachatryan *et al.*	(CMS Collab.)
KHACHATRY...	16L	PRL 117 031802	V. Khachatryan *et al.*	(CMS Collab.)
AAD	15AP	JHEP 1508 138	G. Aad *et al.*	(ATLAS Collab.)
AAD	15AR	JHEP 1508 105	G. Aad *et al.*	(ATLAS Collab.)
AAD	15BY	JHEP 1510 150	G. Aad *et al.*	(ATLAS Collab.)
AAD	15L	PRL 114 221802	G. Aad *et al.*	(ATLAS Collab.)
AAD	15V	PR D91 052007	G. Aad *et al.*	(ATLAS Collab.)
KHACHATRY...	15AE	JHEP 1504 025	V. Khachatryan *et al.*	(CMS Collab.)
KHACHATRY...	15J	PL B746 79	V. Khachatryan *et al.*	(CMS Collab.)
KHACHATRY...	15V	PR D91 052009	V. Khachatryan *et al.*	(CMS Collab.)
AAD	14A	PL B728 562	G. Aad *et al.*	(ATLAS Collab.)
AAD	14BE	EPJ C74 3134	G. Aad *et al.*	(ATLAS Collab.)
FABBRICHESI	14	PR D89 074028	M. Fabbrichesi, M. Pinamonti, A. Tonero	
KHACHATRY...	14	JHEP 1408 173	V. Khachatryan *et al.*	(CMS Collab.)
KHACHATRY...	14J	PL B738 274	V. Khachatryan *et al.*	(CMS Collab.)
AAD	13BB	NJP 15 093011	G. Aad *et al.*	(ATLAS Collab.)
AAD	13E	PR D87 015010	G. Aad *et al.*	(ATLAS Collab.)
CHATRCHYAN	13AE	PL B720 309	S. Chatrchyan *et al.*	(CMS Collab.)
CHATRCHYAN	13AJ	PL B723 280	S. Chatrchyan *et al.*	(CMS Collab.)
CHATRCHYAN	13K	PR D87 032001	S. Chatrchyan *et al.*	(CMS Collab.)
AAD	12AB	PL B712 40	G. Aad *et al.*	(ATLAS Collab.)
AAD	12AZ	PR D85 072003	G. Aad *et al.*	(ATLAS Collab.)
AARON	11C	PL B705 52	F. D. Aaron *et al.*	(H1 Collab.)
ABDALLAH	11	EPJ C71 1555	J. Abdallah *et al.*	(DELPHI Collab.)
AALTONEN	10H	PRL 104 091801	T. Aaltonen *et al.*	(CDF Collab.)
ABDALLAH	09	EPJ C60 1	J. Abdallah *et al.*	(DELPHI Collab.)
AARON	08	PL B663 382	F.D. Aaron *et al.*	(H1 Collab.)
SCHAEL	07A	EPJ C49 411	S. Schael *et al.*	(ALEPH Collab.)
ABDALLAH	06C	EPJ C45 589	J. Abdallah *et al.*	(DELPHI Collab.)
ABULENCIA	06L	PRL 96 211801	A. Abulencia *et al.*	(CDF Collab.)
ABBIENDI	04G	EPJ C33 173	G. Abbiendi *et al.*	(OPAL Collab.)
ABBIENDI	04N	PL B602 167	G. Abbiendi *et al.*	(OPAL Collab.)
ABDALLAH	04N	EPJ C37 405	J. Abdallah *et al.*	(DELPHI Collab.)
ACHARD	03B	PL B568 23	P. Achard *et al.*	(L3 Collab.)
BABICH	03	EPJ C29 103	A.A. Babich *et al.*	
ABBIENDI	02G	PL B544 57	G. Abbiendi *et al.*	(OPAL Collab.)
ACHARD	02D	PL B531 28	P. Achard *et al.*	(L3 Collab.)
ADLOFF	02	PL B525 9	C. Adloff *et al.*	(H1 Collab.)
CHEKANOV	02D	PL B549 32	S. Chekanov *et al.*	(ZEUS Collab.)
AFFOLDER	01I	PRL 87 231803	T. Affolder *et al.*	(CDF Collab.)
BOURILKOV	01	PR D64 071701	D. Bourilkov	
CHEUNG	01B	PL B517 167	K. Cheung	
ACCIARRI	00P	PL B489 81	M. Acciarri *et al.*	(L3 Collab.)
AFFOLDER	00I	PR D62 012004	T. Affolder *et al.*	(CDF Collab.)
BARATE	98U	EPJ C4 571	R. Barate *et al.*	(ALEPH Collab.)
BARGER	98E	PR D57 391	V. Barger *et al.*	
MCFARLAND	98	EPJ C1 509	K.S. McFarland *et al.*	(CCFR/NuTeV Collab.)
DIAZCRUZ	94	PR D49 2149	J.L. Diaz Cruz, O.A. Sampayo	(CINV)
ABT	93	NP B396 3	I. Abt *et al.*	(H1 Collab.)
ADRIANI	93M	PRPL 236 1	O. Adriani *et al.*	(L3 Collab.)
BARDADIN-...	92	ZPHY C55 163	M. Bardadin-Otwinowska	(CLER)
DECAMP	92	PRPL 216 253	D. Decamp *et al.*	(ALEPH Collab.)
PDG	92	PR D45 S1	K. Hikasa *et al.*	(KEK, LBL, BOST+)
ABREU	91F	NP B367 511	P. Abreu *et al.*	(DELPHI Collab.)
KIM	90	PL B240 243	G.N. Kim *et al.*	(AMY Collab.)
ABE	89B	PRL 62 1825	F. Abe *et al.*	(CDF Collab.)
ABE	89D	PRL 63 1447	F. Abe *et al.*	(CDF Collab.)
ABE	89J	ZPHY C45 175	K. Abe *et al.*	(VENUS Collab.)
ALBAJAR	89	ZPHY C44 15	C. Albajar *et al.*	(UA1 Collab.)
BARGER	89	PL B220 464	V. Barger *et al.*	(WISC, KEK)
DORENBOS...	89	ZPHY C41 567	J. Dorenbosch *et al.*	(CHARM Collab.)
BARTEL	87B	ZPHY C36 15	W. Bartel *et al.*	(JADE Collab.)
GRIFOLS	86	PL 168B 264	J.A. Grifols, S. Peris	(BARC)
JODIDIO	86	PR D34 1967	A. Jodidio *et al.*	(LBL, NWES, TRIU)
Also		PR D37 237 (errat.)	A. Jodidio *et al.*	(LBL, NWES, TRIU)
RENARD	82	PL 116B 264	F.M. Renard	(CERN)

Int. J. Mod. Phys. A 2026.41. Downloaded from www.worldscientific.com
by UNIVERSITY OF CALIFORNIA @ BERKELEY on 09/16/26. Re-use and distribution is strictly not permitted, except for Open Access articles.

Extra Dimensions

For explanation of terms used and discussion of significant model dependence of following limits, see the "Extra Dimensions" review. Footnotes describe originally quoted limit. δ indicates the number of extra dimensions.

Limits not encoded here are summarized in the "Extra Dimensions" review, where the latest unpublished results are also described.

See the related review(s):

Extra Dimensions

CONTENTS:

Limits on R from Deviations in Gravitational Force Law
Limits on R from On-Shell Production of Gravitons: $\delta = 2$
Mass Limits on M_{TT}
Limits on $1/R = M_c$
Limits on Kaluza-Klein Gravitons in Warped Extra Dimensions
Limits on Kaluza-Klein Gluons in Warped Extra Dimensions
Black Hole Production Limits
– Semiclassical Black Holes
– Quantum Black Holes

Limits on R from Deviations in Gravitational Force Law

This section includes limits on the size of extra dimensions from deviations in the Newtonian ($1/r^2$) gravitational force law at short distances. Deviations are parametrized by a gravitational potential of the form $V = -(G\ m\ m'/r)\ [1 + \alpha \exp(-r/R)]$. For δ toroidal extra dimensions of equal size, $\alpha = 8\delta/3$. Quoted bounds are for $\delta = 2$ unless otherwise noted.

VALUE (μm)	CL%	DOCUMENT ID		TECN	COMMENT
• • • We do not use the following data for averages, fits, limits, etc. • • •					
		[1] FIORILLO	25		Neutron star
		[2] BLAKEMORE	21		Optical levitation
		[3] HEACOCK	21		Neutron scattering
		[4] LEE	20		Torsion pendulum
$<$ 37	95	[5] TAN	20A		Torsion pendulum
		[6] BERGE	18	MICR	Space accelerometer
		[7] FAYET	18A	MICR	Space accelerometer
		[8] KLIMCHITSK...	17A		Torsion oscillator
		[9] XU	13		Nuclei properties
		[10] BEZERRA	11		Torsion oscillator
		[11] SUSHKOV	11		Torsion pendulum
		[12] BEZERRA	10		Microcantilever
		[13] MASUDA	09		Torsion pendulum
		[14] GERACI	08		Microcantilever
		[15] TRENKEL	08		Newton's constant
		[16] DECCA	07A		Torsion oscillator
$<$ 37	95	[17] KAPNER	07		Torsion pendulum
$<$ 47	95	[18] TU	07		Torsion pendulum
		[19] SMULLIN	05		Microcantilever
$<$130	95	[20] HOYLE	04		Torsion pendulum
		[21] CHIAVERINI	03		Microcantilever
$\lesssim$200	95	[22] LONG	03		Microcantilever
$<$190	95	[23] HOYLE	01		Torsion pendulum
		[24] HOSKINS	85		Torsion pendulum

[1] FIORILLO 25 use neutron star cooling to search for new forces probing a range of $|\alpha| \simeq 4\times10^{10}$–$1\times10^{19}$ and length scales $R \simeq 1$–1×10^{-6} μm. See their Fig. 1 for details on the bound.

[2] BLAKEMORE 21 obtain constraints on non-Newtonian forces with strengths $|\alpha| \gtrsim 10^8$ and length scales $R > 10$ μm. See their Fig. 4 for more details including comparison with previous searches.

[3] HEACOCK 21 obtain constraints on non-Newtonian forces with strengths $10^{18} \lesssim |\alpha| \lesssim 10^{25}$ and length scales $R \simeq$ 0.02–10 nm. See their Figure 3 for more details. This improves the results of HADDOCK 18. These constraints do not place limits on the size of extra flat dimensions.

[4] LEE 20 search for new forces probing a range of $|\alpha| \simeq 0.1$–10^5 and length scales $R \simeq$ 7–90 μm. For $\delta = 1$ the bound on R is 30 μm. See their Fig. 5 for details on the bound.

[5] TAN 20A search for new forces probing a range of $|\alpha| \simeq 4\times10^{-3}$–$1\times10^2$ and length scales $R \simeq$ 40–350 μm. See their Fig. 6 for details on the bound.

[6] BERGE 18 uses results from the MICROSCOPE experiment to obtain constraints on non-Newtonian forces with strengths $10^{-11} \lesssim |\alpha| \lesssim 10^{-7}$ and length scales $R \gtrsim 10^5$ m. See their Figure 1 for more details. These constraints do not place limits on the size of extra flat dimensions.

[7] FAYET 18A uses results from the MICROSCOPE experiment to obtain constraints on an EP-violating force possibly arising from a new U(1) gauge boson. For $R \gtrsim 10^7$ m the limits are $|\alpha| \lesssim$ a few 10^{-13} to a few 10^{-11} depending on the coupling, corresponding to $|\epsilon| \lesssim 10^{-24}$ for the coupling of the new spin-1 or spin-0 mediator. These constraints do not place limits on the size of extra flat dimensions. This extends the results of FAYET 18.

[8] KLIMCHITSKAYA 17A uses an experiment that measures the difference of Casimir forces to obtain bounds on non-Newtonian forces with strengths $|\alpha| \simeq 10^5$–10^{17} and length scales $R = 0.03$–10 μm. See their Fig. 3. These constraints do not place limits on the size of extra flat dimensions.

[9] XU 13 obtain constraints on non-Newtonian forces with strengths $|\alpha| \simeq 10^{34}$–10^{36} and length scales $R \simeq 1$–10 fm. See their Fig. 4 for more details. These constraints do not place limits on the size of extra flat dimensions.

[10] BEZERRA 11 obtain constraints on non-Newtonian forces with strengths $10^{11} \lesssim |\alpha| \lesssim 10^{18}$ and length scales $R = 30$–1260 nm. See their Fig. 2 for more details. These constraints do not place limits on the size of extra flat dimensions.

[11] SUSHKOV 11 obtain improved limits on non-Newtonian forces with strengths $10^7 \lesssim |\alpha| \lesssim 10^{11}$ and length scales 0.4 μm $< R < 4$ μm (95% CL). See their Fig. 2. These bounds do not place limits on the size of extra flat dimensions. However, a model dependent bound of $M_* > 70$ TeV is obtained assuming gauge bosons that couple to baryon number also propagate in $(4 + \delta)$ dimensions.

[12] BEZERRA 10 obtain improved constraints on non-Newtonian forces with strengths $10^{19} \lesssim |\alpha| \lesssim 10^{29}$ and length scales $R = 1.6$–14 nm (95% CL). See their Fig. 1. This bound does not place limits on the size of extra flat dimensions.

[13] MASUDA 09 obtain improved constraints on non-Newtonian forces with strengths $10^9 \lesssim |\alpha| \lesssim 10^{11}$ and length scales $R = 1.0$–2.9 μm (95% CL). See their Fig. 3. This bound does not place limits on the size of extra flat dimensions.

[14] GERACI 08 obtain improved constraints on non-Newtonian forces with strengths $|\alpha| >$ 14,000 and length scales $R = 5$–15 μm. See their Fig. 9. This bound does not place limits on the size of extra flat dimensions.

[15] TRENKEL 08 uses two independent measurements of Newton's constant G to constrain new forces with strength $|\alpha| \simeq 10^{-4}$ and length scales $R = 0.02$–1 m. See their Fig. 1. This bound does not place limits on the size of extra flat dimensions.

[16] DECCA 07A search for new forces and obtain bounds in the region with strengths $|\alpha| \simeq 10^{13}$–10^{18} and length scales $R = 20$–86 nm. See their Fig. 6. This bound does not place limits on the size of extra flat dimensions.

[17] KAPNER 07 search for new forces, probing a range of $|\alpha| \simeq 10^{-3}$–10^5 and length scales $R \simeq 10$–1000 μm. For $\delta = 1$ the bound on R is 44 μm. For $\delta = 2$, the bound is expressed in terms of M_*, here translated to a bound on the radius. See their Fig. 6 for details on the bound.

[18] TU 07 search for new forces probing a range of $|\alpha| \simeq 10^{-1}$–10^5 and length scales $R \simeq$ 20–1000 μm. For $\delta = 1$ the bound on R is 53 μm. See their Fig. 3 for details on the bound.

[19] SMULLIN 05 search for new forces, and obtain bounds in the region with strengths $\alpha \simeq 10^3$–10^8 and length scales $R = 6$–20 μm. See their Figs. 1 and 16 for details on the bound. This work does not place limits on the size of extra flat dimensions.

[20] HOYLE 04 search for new forces, probing α down to 10^{-2} and distances down to 10μm. Quoted bound on R is for $\delta = 2$. For $\delta = 1$, bound goes to 160 μm. See their Fig. 34 for details on the bound.

[21] CHIAVERINI 03 search for new forces, probing α above 10^4 and λ down to 3μm, finding no signal. See their Fig. 4 for details on the bound. This bound does not place limits on the size of extra flat dimensions.

[22] LONG 03 search for new forces, probing α down to 3, and distances down to about 10μm. See their Fig. 4 for details on the bound.

[23] HOYLE 01 search for new forces, probing α down to 10^{-2} and distances down to 20μm. See their Fig. 4 for details on the bound. The quoted bound is for $\alpha \geq 3$.

[24] HOSKINS 85 search for new forces, probing distances down to 4 mm. See their Fig. 13 for details on the bound. This bound does not place limits on the size of extra flat dimensions.

Limits on R from On-Shell Production of Gravitons: $\delta = 2$

This section includes limits on on-shell production of gravitons in collider and astrophysical processes. Bounds quoted are on R, the assumed common radius of the flat extra dimensions, for $\delta = 2$ extra dimensions. Studies often quote bounds in terms of derived parameter; experiments are actually sensitive to the masses of the KK gravitons: $m_{\vec{n}} = |\vec{n}|/R$. See the Review on "Extra Dimensions" for details. Bounds are given in μm for $\delta = 2$.

VALUE (μm)	CL%	DOCUMENT ID		TECN	COMMENT
$<$ 3.8	95	[1] AAD	21F	ATLS	$pp \to jG$
$<$ 0.00016	95	[2] HANNESTAD	03		Neutron star heating
• • • We do not use the following data for averages, fits, limits, etc. • • •					
$<$ 56	95	[3] SIRUNYAN	21A	CMS	$pp \to ZG$
$<$ 4.1	95	[4] TUMASYAN	21D	CMS	$pp \to jG$
		[5] SIRUNYAN	17AQ	CMS	$pp \to \gamma G$
$<$ 90	95	[6] AABOUD	16F	ATLS	$pp \to \gamma G$
		[7] KHACHATRY...	16N	CMS	$pp \to \gamma G$
		[8] AAD	15CS	ATLS	$pp \to \gamma G$
$<$ 127	95	[9] AAD	13C	ATLS	$pp \to \gamma G$
$<$ 34.4	95	[10] AAD	13D	ATLS	$pp \to jj$
$<$ 0.0087	95	[11] AJELLO	12	FLAT	Neutron star γ sources
$<$ 245	95	[12] AALTONEN	08AC	CDF	$p\overline{p} \to \gamma G, jG$
$<$ 615	95	[13] ABAZOV	08S	D0	$p\overline{p} \to \gamma G$
$<$ 0.916	95	[14] DAS	08		Supernova cooling
$<$ 350	95	[15] ABULENCIA,A	06	CDF	$p\overline{p} \to jG$
$<$ 270	95	[16] ABDALLAH	05B	DLPH	$e^+e^- \to \gamma G$
$<$ 210	95	[17] ACHARD	04E	L3	$e^+e^- \to \gamma G$
$<$ 480	95	[18] ACOSTA	04C	CDF	$\overline{p}p \to jG$
$<$ 0.00038	95	[19] CASSE	04		Neutron star γ sources
$<$ 610	95	[20] ABAZOV	03	D0	$\overline{p}p \to jG$
$<$ 0.96	95	[21] HANNESTAD	03		Supernova cooling
$<$ 0.096	95	[22] HANNESTAD	03		Diffuse γ background
$<$ 0.051	95	[23] HANNESTAD	03		Neutron star γ sources
$<$ 300	95	[24] HEISTER	03C	ALEP	$e^+e^- \to \gamma G$
		[25] FAIRBAIRN	01		Cosmology
$<$ 0.66	95	[26] HANHART	01		Supernova cooling
		[27] CASSISI	00		Red giants
$<$1300	95	[28] ACCIARRI	99S	L3	$e^+e^- \to ZG$

[1] AAD 21F search for $pp \to jG$, using 139 fb^{-1} of data at $\sqrt{s} = 13$ TeV to place lower limits on M_D for two to six extra dimensions (see their Table X), from which this bound on R is derived. This limit supersedes that in AABOUD 18I.

[2] HANNESTAD 03 obtain a limit on R from the heating of old neutron stars by the surrounding cloud of trapped KK gravitons. Limits for all $\delta \leq 7$ are given in their Tables V and VI. These limits supersede those in HANNESTAD 02.

[3] SIRUNYAN 21A search for $pp \rightarrow ZG$, using 137 fb^{-1} of data at $\sqrt{s} = 13$ TeV to place lower limits on M_D for two to seven extra dimensions (see their Figure 12), from which this bound on R is derived. These limits supersede those obtained in SIRUNYAN 18BV.

[4] TUMASYAN 21D search for $pp \rightarrow jG$, using 137 fb^{-1} of data at $\sqrt{s} = 13$ TeV to place lower limits on M_D for two to seven extra dimensions (see their Table 3), from which this bound on R is derived. This limit supersedes that in SIRUNYAN 18S.

[5] SIRUNYAN 17AQ search for $pp \rightarrow \gamma G$, using 12.9 fb^{-1} of data at $\sqrt{s} = 13$ TeV to place limits on M_D for three to six extra dimensions (see their Table 3).

[6] AABOUD 16F search for $pp \rightarrow \gamma G$, using 3.2 fb^{-1} of data at $\sqrt{s} = 13$ TeV to place limits on M_D for two to six extra dimensions (see their Figure 9), from which this bound on R is derived.

[7] KHACHATRYAN 16N search for $pp \rightarrow \gamma G$, using 19.6 fb^{-1} of data at $\sqrt{s} = 8$ TeV to place limits on M_D for three to six extra dimensions (see their Table 5).

[8] AAD 15CS search for $pp \rightarrow \gamma G$, using 20.3 fb^{-1} of data at $\sqrt{s} = 8$ TeV to place lower limits on M_D for two to six extra dimensions (see their Fig. 18).

[9] AAD 13C search for $pp \rightarrow \gamma G$, using 4.6 fb^{-1} of data at $\sqrt{s} = 7$ TeV to place bounds on M_D for two to six extra dimensions, from which this bound on R is derived.

[10] AAD 13D search for the dijet decay of quantum black holes in 4.8 fb^{-1} of data produced in pp collisions at $\sqrt{s} = 7$ TeV to place bounds on M_D for two to seven extra dimensions, from which these bounds on R are derived. Limits on M_D for all $\delta \leq 7$ are given in their Table 3.

[11] AJELLO 12 obtain a limit on R from the gamma-ray emission of point γ sources that arise from the photon decay of KK gravitons which are gravitationally bound around neutron stars. Limits for all $\delta \leq 7$ are given in their Table 7.

[12] AALTONEN 08AC search for $p\overline{p} \rightarrow \gamma G$ and $p\overline{p} \rightarrow jG$ at $\sqrt{s} = 1.96$ TeV with 2.0 fb^{-1} and 1.1 fb^{-1} respectively, in order to place bounds on the fundamental scale and size of the extra dimensions. See their Table III for limits on all $\delta \leq 6$.

[13] ABAZOV 08S search for $p\overline{p} \rightarrow \gamma G$, using 1 fb^{-1} of data at $\sqrt{s} = 1.96$ TeV to place bounds on M_D for two to eight extra dimensions, from which these bounds on R are derived. See their paper for intermediate values of δ.

[14] DAS 08 obtain a limit on R from Kaluza-Klein graviton cooling of SN1987A due to plasmon-plasmon annihilation.

[15] ABULENCIA,A 06 search for $p\overline{p} \rightarrow jG$ using 368 pb^{-1} of data at $\sqrt{s} = 1.96$ TeV. See their Table II for bounds for all $\delta \leq 6$.

[16] ABDALLAH 05B search for $e^+e^- \rightarrow \gamma G$ at $\sqrt{s} = 180$–209 GeV to place bounds on the size of extra dimensions and the fundamental scale. Limits for all $\delta \leq 6$ are given in their Table 6. These limits supersede those in ABREU 00Z.

[17] ACHARD 04E search for $e^+e^- \rightarrow \gamma G$ at $\sqrt{s} = 189$–209 GeV to place bounds on the size of extra dimensions and the fundamental scale. See their Table 8 for limits with $\delta \leq 8$. These limits supersede those in ACCIARRI 99R.

[18] ACOSTA 04C search for $\overline{p}p \rightarrow jG$ at $\sqrt{s} = 1.8$ TeV to place bounds on the size of extra dimensions and the fundamental scale. See their paper for bounds on $\delta = 4, 6$.

[19] CASSE 04 obtain a limit on R from the gamma-ray emission of point γ sources that arises from the photon decay of gravitons around newly born neutron stars, applying the technique of HANNESTAD 03 to neutron stars in the galactic bulge. Limits for all $\delta \leq 7$ are given in their Table I.

[20] ABAZOV 03 search for $p\overline{p} \rightarrow jG$ at $\sqrt{s}$=1.8 TeV to place bounds on M_D for 2 to 7 extra dimensions, from which these bounds on R are derived. See their paper for bounds on intermediate values of δ. We quote results without the approximate NLO scaling introduced in the paper.

[21] HANNESTAD 03 obtain a limit on R from graviton cooling of supernova SN1987a. Limits for all $\delta \leq 7$ are given in their Tables V and VI.

[22] HANNESTAD 03 obtain a limit on R from gravitons emitted in supernovae and which subsequently decay, contaminating the diffuse cosmic γ background. Limits for all $\delta \leq 7$ are given in their Tables V and VI. These limits supersede those in HANNESTAD 02.

[23] HANNESTAD 03 obtain a limit on R from gravitons emitted in two recent supernovae and which subsequently decay, creating point γ sources. Limits for all $\delta \leq 7$ are given in their Tables V and VI. These limits are corrected in the published erratum.

[24] HEISTER 03C use the process $e^+e^- \rightarrow \gamma G$ at $\sqrt{s} = 189$–209 GeV to place bounds on the size of extra dimensions and the scale of gravity. See their Table 4 for limits with $\delta \leq 6$ for derived limits on M_D.

[25] FAIRBAIRN 01 obtains bounds on R from over production of KK gravitons in the early universe. Bounds are quoted in paper in terms of fundamental scale of gravity. Bounds depend strongly on temperature of QCD phase transition and range from R< 0.13 μm to 0.001 μm for δ=2; bounds for δ=3,4 can be derived from Table 1 in the paper.

[26] HANHART 01 obtain bounds on R from limits on graviton cooling of supernova SN 1987a using numerical simulations of proto-neutron star neutrino emission.

[27] CASSISI 00 obtain rough bounds on M_D (and thus R) from red giant cooling for δ=2,3. See their paper for details.

[28] ACCIARRI 99S search for $e^+e^- \rightarrow ZG$ at $\sqrt{s}$=189 GeV. Limits on the gravity scale are found in their Table 2, for $\delta \leq 4$.

Mass Limits on M_{TT}

This section includes limits on the cut-off mass scale, M_{TT}, of dimension-8 operators from KK graviton exchange in models of large extra dimensions. Ambiguities in the UV-divergent summation are absorbed into the parameter λ, which is taken to be $\lambda = \pm 1$ in the following analyses. Bounds for $\lambda = -1$ are shown in parenthesis after the bound for $\lambda = +1$, if appropriate. Different papers use slightly different definitions of the mass scale. The definition used here is related to another popular convention by $M_{TT}^4 = (2/\pi)\ \Lambda_T^4$, as discussed in the above Review on "Extra Dimensions."

VALUE (TeV)		CL%	DOCUMENT ID		TECN	COMMENT
> 9.02		95	[1] SIRUNYAN	18DD	CMS	$pp \rightarrow$ dijet, ang. distrib.
>20.6	**(> 15.7)**	95	[2] GIUDICE	03	RVUE	Dim-6 operators
• • • We do not use the following data for averages, fits, limits, etc. • • •						
> 8.3	(>7.1)	95	[3] HAYRAPETY...	24AJ	CMS	$pp \rightarrow \gamma\gamma$
> 6.7		95	[4] SIRUNYAN	21N	CMS	$pp \rightarrow e^+e^-, \mu^+\mu^-$
> 6.9		95	[5] SIRUNYAN	19AC	CMS	$pp \rightarrow e^+e^-, \mu^+\mu^-, \gamma\gamma$
> 6.5		95	[6] AABOUD	17AP	ATLS	$pp \rightarrow \gamma\gamma$
> 3.8		95	[7] AAD	14BE	ATLS	$pp \rightarrow e^+e^-, \mu^+\mu^-$
> 3.2		95	[8] AAD	13E	ATLS	$pp \rightarrow e^+e^-, \mu^+\mu^-, \gamma\gamma$
			[9] BAAK	12	RVUE	Electroweak
> 0.90	(>0.92)	95	[10] AARON	11C	H1	$e^\pm p \rightarrow e^\pm X$
> 1.48		95	[11] ABAZOV	09AE	D0	$p\overline{p} \rightarrow$ dijet, ang. distrib.
> 1.45		95	[12] ABAZOV	09D	D0	$p\overline{p} \rightarrow e^+e^-, \gamma\gamma$
> 1.1	(> 1.0)	95	[13] SCHAEL	07A	ALEP	$e^+e^- \rightarrow e^+e^-$
> 0.898	(> 0.998)	95	[14] ABDALLAH	06C	DLPH	$e^+e^- \rightarrow \ell^+\ell^-$
> 0.853	(> 0.939)	95	[15] GERDES	06		$p\overline{p} \rightarrow e^+e^-, \gamma\gamma$
> 0.96	(> 0.93)	95	[16] ABAZOV	05V	D0	$p\overline{p} \rightarrow \mu^+\mu^-$
> 0.78	(> 0.79)	95	[17] CHEKANOV	04B	ZEUS	$e^\pm p \rightarrow e^\pm X$
> 0.805	(> 0.956)	95	[18] ABBIENDI	03D	OPAL	$e^+e^- \rightarrow \gamma\gamma$
> 0.7	(> 0.7)	95	[19] ACHARD	03D	L3	$e^+e^- \rightarrow ZZ$
> 0.82	(> 0.78)	95	[20] ADLOFF	03	H1	$e^\pm p \rightarrow e^\pm X$
> 1.28	(> 1.25)	95	[21] GIUDICE	03	RVUE	
> 0.80	(> 0.85)	95	[22] HEISTER	03C	ALEP	$e^+e^- \rightarrow \gamma\gamma$
> 0.84	(> 0.99)	95	[23] ACHARD	02D	L3	$e^+e^- \rightarrow \gamma\gamma$
> 1.2	(> 1.1)	95	[24] ABBOTT	01	D0	$p\overline{p} \rightarrow e^+e^-, \gamma\gamma$
> 0.60	(> 0.63)	95	[25] ABBIENDI	00R	OPAL	$e^+e^- \rightarrow \mu^+\mu^-$
> 0.63	(> 0.50)	95	[25] ABBIENDI	00R	OPAL	$e^+e^- \rightarrow \tau^+\tau^-$
> 0.68	(> 0.61)	95	[25] ABBIENDI	00R	OPAL	$e^+e^- \rightarrow \mu^+\mu^-, \tau^+\tau^-$
			[26] ABREU	00A	DLPH	$e^+e^- \rightarrow \gamma\gamma$
> 0.680	(> 0.542)	95	[27] ABREU	00S	DLPH	$e^+e^- \rightarrow \mu^+\mu^-, \tau^+\tau^-$
> 15–28		99.7	[28] CHANG	00B	RVUE	Electroweak
> 0.98		95	[29] CHEUNG	00	RVUE	$e^+e^- \rightarrow \gamma\gamma$
> 0.29–0.38		95	[30] GRAESSER	00	RVUE	$(g-2)_\mu$
> 0.50–1.1		95	[31] HAN	00	RVUE	Electroweak
> 2.0	(> 2.0)	95	[32] MATHEWS	00	RVUE	$\overline{p}p \rightarrow jj$
> 1.0	(> 1.1)	95	[33] MELE	00	RVUE	$e^+e^- \rightarrow VV$
			[34] ABBIENDI	99P	OPAL	
			[35] ACCIARRI	99M	L3	
			[36] ACCIARRI	99S	L3	
> 1.412	(> 1.077)	95	[37] BOURILKOV	99		$e^+e^- \rightarrow e^+e^-$

[1] SIRUNYAN 18DD use dijet angular distributions in 35.9 fb^{-1} of data from pp collisions at $\sqrt{s} = 13$ TeV to place a lower bound on Λ_T, here converted to M_{TT}. This updates the results of SIRUNYAN 17F.

[2] GIUDICE 03 place bounds on Λ_6, the coefficient of the gravitationally-induced dimension-6 operator $(2\pi\lambda/\Lambda_6^2)(\sum \overline{f}\gamma_\mu\gamma^5 f)(\sum \overline{f}\gamma^\mu\gamma^5 f)$, using data from a variety of experiments. Results are quoted for $\lambda = \pm 1$ and are independent of δ.

[3] HAYRAPETYAN 24AJ use 138 fb^{-1} of data from pp collisions at $\sqrt{s} = 13$ TeV to place lower limits on M_{TT} (equivalent to their M_S). This updates the results of SIRUNYAN 18DU.

[4] SIRUNYAN 21N use 137 (140) fb^{-1} of data from pp collisions at $\sqrt{s} = 13$ TeV in the dielectron (dimuon) channels to place a lower limit on Λ_T, here converted to M_{TT}. Bounds on individual channels can be found in their Table 7.

[5] SIRUNYAN 19AC use 35.9 (36.3) fb^{-1} of data from pp collisions at $\sqrt{s} = 13$ TeV in the dielectron (dimuon) channels to place a lower limit on Λ_T, here converted to M_{TT}. The dielectron and dimuon channels are combined with previous results in the diphoton channel to set the best limit. Bounds on individual channels and different priors can be found in their Table 2. This updates the results in KHACHATRYAN 15AE.

[6] AABOUD 17AP use 36.7 fb^{-1} of data from pp collisions at $\sqrt{s} = 13$ TeV to place lower limits on M_{TT} (equivalent to their M_S). This updates the results of AAD 13AS.

[7] AAD 14BE use 20 fb^{-1} of data from pp collisions at $\sqrt{s} = 8$ TeV in the dilepton channel to place lower limits on M_{TT} (equivalent to their M_S).

[8] AAD 13E use 4.9 and 5.0 fb^{-1} of data from pp collisions at $\sqrt{s} = 7$ TeV in the dielectron and dimuon channels, respectively, to place lower limits on M_{TT} (equivalent to their M_S). The dielectron and dimuon channels are combined with previous results in the diphoton channel to set the best limit. Bounds on individual channels and different priors can be found in their Table VIII.

[9] BAAK 12 use electroweak precision observables to place bounds on the ratio Λ_T/M_D as a function of M_D. See their Fig. 22 for constraints with a Higgs mass of 120 GeV.

[10] AARON 11C search for deviations in the differential cross section of $e^\pm p \rightarrow e^\pm X$ in 446 pb^{-1} of data taken at $\sqrt{s} = 301$ and 319 GeV to place a bound on M_{TT}.

[11] ABAZOV 09AE use dijet angular distributions in 0.7 fb^{-1} of data from $p\overline{p}$ collisions at $\sqrt{s} = 1.96$ TeV to place lower bounds on Λ_T (equivalent to their M_S), here converted to M_{TT}.

[12] ABAZOV 09D use 1.05 fb^{-1} of data from $p\overline{p}$ collisions at $\sqrt{s} = 1.96$ TeV to place lower bounds on Λ_T (equivalent to their M_s), here converted to M_{TT}.

[13] SCHAEL 07A use e^+e^- collisions at $\sqrt{s} = 189$–209 GeV to place lower limits on Λ_T, here converted to limits on M_{TT}.

[14] ABDALLAH 06C use e^+e^- collisions at $\sqrt{s} \sim 130$–207 GeV to place lower limits on M_{TT}, which is equivalent to their definition of M_s. Bound shown includes all possible final state leptons, $\ell = e, \mu, \tau$. Bounds on individual leptonic final states can be found in their Table 31.

[15] GERDES 06 use 100 to 110 pb^{-1} of data from $p\overline{p}$ collisions at $\sqrt{s} = 1.8$ TeV, as recorded by the CDF Collaboration during Run I of the Tevatron. Bound shown includes a K-factor of 1.3. Bounds on individual e^+e^- and $\gamma\gamma$ final states are found in their Table I.

[16] ABAZOV 05V use 246 pb^{-1} of data from $p\overline{p}$ collisions at $\sqrt{s} = 1.96$ TeV to search for deviations in the differential cross section to $\mu^+\mu^-$ from graviton exchange.

[17] CHEKANOV 04B search for deviations in the differential cross section of $e^\pm p \rightarrow e^\pm X$ with 130 pb^{-1} of combined data and Q^2 values up to 40,000 GeV^2 to place a bound on M_{TT}.

[18] ABBIENDI 03D use e^+e^- collisions at $\sqrt{s}$=181–209 GeV to place bounds on the ultraviolet scale M_{TT}, which is equivalent to their definition of M_s.

[19] ACHARD 03D look for deviations in the cross section for $e^+e^- \rightarrow ZZ$ from $\sqrt{s} =$ 200–209 GeV to place a bound on M_{TT}.

[20] ADLOFF 03 search for deviations in the differential cross section of $e^\pm p \rightarrow e^\pm X$ at $\sqrt{s}$=301 and 319 GeV to place bounds on M_{TT}.

Int. J. Mod. Phys. A 2026.41. Downloaded from www.worldscientific.com
by UNIVERSITY OF CALIFORNIA @ BERKELEY on 09/16/26. Re-use and distribution is strictly not permitted, except for Open Access articles.

Int. J. Mod. Phys. A 2026.41. Downloaded from www.worldscientific.com
by UNIVERSITY OF CALIFORNIA @ BERKELEY on 09/16/26. Re-use and distribution is strictly not permitted, except for Open Access articles.

[21] GIUDICE 03 review existing experimental bounds on M_{TT} and derive a combined limit.

[22] HEISTER 03C use e^+e^- collisions at $\sqrt{s}$= 189–209 GeV to place bounds on the scale of dim-8 gravitational interactions. Their $M_s^{\pm}$ is equivalent to our M_{TT} with $\lambda=\pm1$.

[23] ACHARD 02 search for s-channel graviton exchange effects in $e^+e^- \rightarrow \gamma\gamma$ at E_{cm} = 192–209 GeV.

[24] ABBOTT 01 search for variations in differential cross sections to e^+e^- and $\gamma\gamma$ final states at the Tevatron.

[25] ABBIENDI 00R uses e^+e^- collisions at $\sqrt{s}$= 189 GeV.

[26] ABREU 00A search for s-channel graviton exchange effects in $e^+e^- \rightarrow \gamma\gamma$ at E_{cm}= 189–202 GeV.

[27] ABREU 00S uses e^+e^- collisions at $\sqrt{s}$=183 and 189 GeV. Bounds on μ and τ individual final states given in paper.

[28] CHANG 00B derive 3σ limit on M_{TT} of (28,19,15) TeV for δ=(2,4,6) respectively assuming the presence of a torsional coupling in the gravitational action. Highly model dependent.

[29] CHEUNG 00 obtains limits from anomalous diphoton production at OPAL due to graviton exchange. Original limit for δ=4. However, unknown UV theory renders δ dependence unreliable. Original paper works in HLZ convention.

[30] GRAESSER 00 obtains a bound from graviton contributions to $g-2$ of the muon through loops of 0.29 TeV for δ=2 and 0.38 TeV for δ=4,6. Limits scale as $\lambda^{1/2}$. However calculational scheme not well-defined without specification of high-scale theory. See the "Extra Dimensions Review."

[31] HAN 00 calculates corrections to gauge boson self-energies from KK graviton loops and constrain them using S and T. Bounds on M_{TT} range from 0.5 TeV (δ=6) to 1.1 TeV (δ=2); see text. Limits have strong dependence, $\lambda^{\delta+2}$, on unknown λ coefficient.

[32] MATHEWS 00 search for evidence of graviton exchange in CDF and DØ dijet production data. See their Table 2 for slightly stronger δ-dependent bounds. Limits expressed in terms of $\widetilde{M}_S^4 = M_{TT}^4/8$.

[33] MELE 00 obtains bound from KK graviton contributions to $e^+e^- \rightarrow VV$ (V=γ,W,Z) at LEP. Authors use Hewett conventions.

[34] ABBIENDI 99P search for s-channel graviton exchange effects in $e^+e^- \rightarrow \gamma\gamma$ at E_{cm}=189 GeV. The limits $G_+ > 660$ GeV and $G_- > 634$ GeV are obtained from combined E_{cm}=183 and 189 GeV data, where $G_{\pm}$ is a scale related to the fundamental gravity scale.

[35] ACCIARRI 99M search for the reaction $e^+e^- \rightarrow \gamma G$ and s-channel graviton exchange effects in $e^+e^- \rightarrow \gamma\gamma$, W^+W^-, ZZ, e^+e^-, $\mu^+\mu^-$, $\tau^+\tau^-$, $q\overline{q}$ at E_{cm}=183 GeV. Limits on the gravity scale are listed in their Tables 1 and 2.

[36] ACCIARRI 99S search for the reaction $e^+e^- \rightarrow ZG$ and s-channel graviton exchange effects in $e^+e^- \rightarrow \gamma\gamma$, W^+W^-, ZZ, e^+e^-, $\mu^+\mu^-$, $\tau^+\tau^-$, $q\overline{q}$ at E_{cm}=189 GeV. Limits on the gravity scale are listed in their Tables 1 and 2.

[37] BOURILKOV 99 performs global analysis of LEP data on e^+e^- collisions at $\sqrt{s}$=183 and 189 GeV. Bound is on Λ_T.

Limits on $1/R = M_c$

This section includes limits on $1/R = M_c$, the compactification scale in models with one TeV-sized extra dimension, due to exchange of Standard Model KK excitations. Bounds assume fermions are not in the bulk, unless stated otherwise. See the "Extra Dimensions" review for discussion of model dependence.

VALUE (TeV)	CL%	DOCUMENT ID		TECN	COMMENT
>4.16	95	[1] AAD	12CC	ATLS	$pp \rightarrow \ell\overline{\ell}$
>6.1		[2] BARBIERI	04	RVUE	Electroweak
• • • We do not use the following data for averages, fits, limits, etc. • • •					
		[3] FLORES	23	RVUE	minimal universal extra dims
		[4] AVNISH	21	RVUE	$pp \rightarrow$ multijet
		[5] AABOUD	18AV	ATLS	$pp \rightarrow t\overline{t}t\overline{t}$
		[6] AABOUD	18CE	ATLS	$pp \rightarrow t\overline{t}t\overline{t}$
>3.8	95	[7] ACCOMANDO	15	RVUE	Electroweak
>3.40	95	[8] KHACHATRY...	15T	CMS	$pp \rightarrow \ell X$
		[9] CHATRCHYAN	13AQ	CMS	$pp \rightarrow \ell X$
>1.38	95	[10] CHATRCHYAN	13W	CMS	$pp \rightarrow \gamma\gamma$, δ=6, M_D=5 TeV
>0.715	95	[11] EDELHAUSER	13	RVUE	$pp \rightarrow \ell\overline{\ell} + X$
>1.40	95	[12] AAD	12CP	ATLS	$pp \rightarrow \gamma\gamma$, δ=6, M_D=5 TeV
>1.23	95	[13] AAD	12X	ATLS	$pp \rightarrow \gamma\gamma$, δ=6, M_D=5 TeV
>0.26	95	[14] ABAZOV	12M	D0	$p\overline{p} \rightarrow \mu\mu$
>0.75	95	[15] BAAK	12	RVUE	Electroweak
		[16] FLACKE	12	RVUE	Electroweak
>0.43	95	[17] NISHIWAKI	12	RVUE	$H \rightarrow WW, \gamma\gamma$
>0.729	95	[18] AAD	11F	ATLS	$pp \rightarrow \gamma\gamma$, δ=6, M_D=5 TeV
>0.961	95	[19] AAD	11X	ATLS	$pp \rightarrow \gamma\gamma$, δ=6, M_D=5 TeV
>0.477	95	[20] ABAZOV	10P	D0	$p\overline{p} \rightarrow \gamma\gamma$, δ=6, M_D=5 TeV
>1.59	95	[21] ABAZOV	09AE	D0	$p\overline{p} \rightarrow$ dijet, angular dist.
>0.6	95	[22] HAISCH	07	RVUE	$\overline{B} \rightarrow X_s\gamma$
>0.6	90	[23] GOGOLADZE	06	RVUE	Electroweak
>3.3	95	[24] CORNET	00	RVUE	Electroweak
> 3.3–3.8	95	[25] RIZZO	00	RVUE	Electroweak

[1] AAD 12CC use 4.9 and 5.0 fb^{-1} of data from pp collisions at $\sqrt{s}$ = 7 TeV in the dielectron and dimuon channels, respectively, to place a lower bound on the mass of the lightest KK Z/γ boson (equivalent to $1/R = M_c$). The limit quoted here assumes a flat prior corresponding to when the pure Z/γ KK cross section term dominates. See their Section 15 for more details.

[2] BARBIERI 04 use electroweak precision observables to place a lower bound on the compactification scale $1/R$. Both the gauge bosons and the Higgs boson are assumed to propagate in the bulk.

[3] FLORES 23 use a number of 13 TeV Run 2 searches at the LHC to place constraints on the compactification scale $1/R$ and cutoff scale Λ in the minimal universal extra dimension model with Standard Model fields propagating in the bulk (see their Fig.6).

[4] AVNISH 21 perform a study on the ATLAS collaboration search for multiple jets plus missing transverse energy from pp collisions at $\sqrt{s}$ = 13 TeV and integrated luminosity of 139 fb^{-1}, to place constraints on the compactification scale and cutoff scale Λ in universal extra dimension models with Standard Model fields propagating in the bulk.

[5] AABOUD 18AV use 36.1 fb^{-1} of data from pp collisions at $\sqrt{s}$ = 13 TeV in final states with multiple b-jets, to place a lower bound on the compactification scale in a model with two universal extra dimensions. Assuming the radii of the two extra dimensions are equal, a lower limit of 1.8 TeV for the Kaluza-Klein mass is obtained.

[6] AABOUD 18CE use 36.1 fb^{-1} of data from pp collisions at $\sqrt{s}$ = 13 TeV in final states with same-charge leptons and b-jets, to place a lower bound on the compactification scale in a model with two universal extra dimensions. Assuming the radii of the two extra dimensions are equal, a lower limit of 1.45 TeV for the Kaluza-Klein mass is obtained.

[7] ACCOMANDO 15 use electroweak precision observables to place a lower bound on the compactification scale $1/R$. See their Fig. 2 for the bound as a function of sinβ, which parametrizes the VEV contribution from brane and bulk Higgs fields. The quoted value is for the minimum bound which occurs at sinβ = 0.45.

[8] KHACHATRYAN 15T use 19.7 fb^{-1} of data from pp collisions at $\sqrt{s}$ = 8 TeV to place a lower bound on the compactification scale $1/R$.

[9] CHATRCHYAN 13AQ use 5.0 fb^{-1} of data from pp collisions at $\sqrt{s}$ = 7 TeV and a further 3.7 fb^{-1} of data at $\sqrt{s}$ = 8 TeV to place a lower bound on the compactification scale $1/R$, in models with universal extra dimensions and Standard Model fields propagating in the bulk. See their Fig. 5 for the bound as a function of the universal bulk fermion mass parameter μ.

[10] CHATRCHYAN 13W use diphoton events with large missing transverse momentum in 4.93 fb^{-1} of data produced from pp collisions at $\sqrt{s}$ = 7 TeV to place a lower bound on the compactification scale in a universal extra dimension model with gravitational decays. The bound assumes that the cutoff scale Λ, for the radiative corrections to the Kaluza-Klein masses, satisfies Λ/M_c = 20. The model parameters are chosen such that the decay $\gamma^* \rightarrow G\gamma$ occurs with an appreciable branching fraction.

[11] EDELHAUSER 13 use 19.6 and 20.6 fb^{-1} of data from pp collisions at $\sqrt{s}$ = 8 TeV analyzed by the CMS Collaboration in the dielectron and dimuon channels, respectively, to place a lower bound on the mass of the second lightest Kaluza-Klein Z/γ boson (converted to a limit on $1/R = M_c$). The bound assumes Standard Model fields propagating in the bulk and that the cutoff scale Λ, for the radiative corrections to the Kaluza-Klein masses, satisfies Λ/M_c = 20.

[12] AAD 12CP use diphoton events with large missing transverse momentum in 4.8 fb^{-1} of data produced from pp collisions at $\sqrt{s}$ = 7 TeV to place a lower bound on the compactification scale in a universal extra dimension model with gravitational decays. The bound assumes that the cutoff scale Λ, for the radiative corrections to the Kaluza-Klein masses, satisfies Λ/M_c = 20. The model parameters are chosen such that the decay $\gamma^* \rightarrow G\gamma$ occurs with an appreciable branching fraction.

[13] AAD 12X use diphoton events with large missing transverse momentum in 1.07 fb^{-1} of data produced from pp collisions at $\sqrt{s}$ = 7 TeV to place a lower bound on the compactification scale in a universal extra dimension model with gravitational decays. The bound assumes that the cutoff scale Λ, for the radiative corrections to the Kaluza-Klein masses, satisfies Λ/M_c = 20. The model parameters are chosen such that the decay $\gamma^* \rightarrow G\gamma$ occurs with an appreciable branching fraction.

[14] ABAZOV 12M use same-sign dimuon events in 7.3 fb^{-1} of data from $p\overline{p}$ collisions at $\sqrt{s}$ = 1.96 TeV to place a lower bound on the compactification scale $1/R$, in models with universal extra dimensions where all Standard Model fields propagate in the bulk.

[15] BAAK 12 use electroweak precision observables to place a lower bound on the compactification scale $1/R$, in models with universal extra dimensions and Standard Model fields propagating in the bulk. Bound assumes a 125 GeV Higgs mass. See their Fig. 25 for the bound as a function of the Higgs mass.

[16] FLACKE 12 use electroweak precision observables to place a lower bound on the compactification scale $1/R$, in models with universal extra dimensions and Standard Model fields propagating in the bulk. See their Fig. 1 for the bound as a function of the universal bulk fermion mass parameter μ.

[17] NISHIWAKI 12 use up to 2 fb^{-1} of data from the ATLAS and CMS experiments that constrains the production cross section of a Higgs-like particle to place a lower bound on the compactification scale $1/R$ in universal extra dimension models. The quoted bound assumes Standard Model fields propagating in the bulk and a 125 GeV Higgs mass. See their Fig. 1 for the bound as a function of the Higgs mass.

[18] AAD 11F use diphoton events with large missing transverse energy in 3.1 pb^{-1} of data produced from pp collisions at $\sqrt{s}$ = 7 TeV to place a lower bound on the compactification scale in a universal extra dimension model with gravitational decays. The bound assumes that the cutoff scale Λ, for the radiative corrections to the Kaluza-Klein masses, satisfies Λ/M_c = 20. The model parameters are chosen such that the decay $\gamma^* \rightarrow G\gamma$ occurs with an appreciable branching fraction.

[19] AAD 11X use diphoton events with large missing transverse energy in 36 pb^{-1} of data produced from pp collisions at $\sqrt{s}$ = 7 TeV to place a lower bound on the compactification scale in a universal extra dimension model with gravitational decays. The bound assumes that the cutoff scale Λ, for the radiative corrections to the Kaluza-Klein masses, satisfies Λ/M_c = 20. The model parameters are chosen such that the decay $\gamma^* \rightarrow G\gamma$ occurs with an appreciable branching fraction.

[20] ABAZOV 10P use diphoton events with large missing transverse energy in 6.3 fb^{-1} of data produced from $p\overline{p}$ collisions at $\sqrt{s}$ = 1.96 TeV to place a lower bound on the compactification scale in a universal extra dimension model with gravitational decays. The bound assumes that the cutoff scale Λ, for the radiative corrections to the Kaluza-Klein masses, satisfies Λ/M_c=20. The model parameters are chosen such that the decay $\gamma^* \rightarrow G\gamma$ occurs with an appreciable branching fraction.

[21] ABAZOV 09AE use dijet angular distributions in 0.7 fb^{-1} of data from $p\overline{p}$ collisions at $\sqrt{s}$ = 1.96 TeV to place a lower bound on the compactification scale.

[22] HAISCH 07 use inclusive $\overline{B}$-meson decays to place a Higgs mass independent bound on the compactification scale $1/R$ in the minimal universal extra dimension model.

[23] GOGOLADZE 06 use electroweak precision observables to place a lower bound on the compactification scale in models with universal extra dimensions. Bound assumes a 115 GeV Higgs mass. See their Fig. 3 for the bound as a function of the Higgs mass.

[24] CORNET 00 translates a bound on the coefficient of the 4-fermion operator $(\overline{\ell}\gamma_\mu\tau^a\ell)(\overline{\ell}\gamma^\mu\tau^a\ell)$ derived by Hagiwara and Matsumoto into a limit on the mass scale of KK W bosons.

[25] RIZZO 00 obtains limits from global electroweak fits in models with a Higgs in the bulk (3.8 TeV) or on the standard brane (3.3 TeV).

Int. J. Mod. Phys. A 2026.41. Downloaded from www.worldscientific.com
by UNIVERSITY OF CALIFORNIA @ BERKELEY on 09/16/26. Re-use and distribution is strictly not permitted, except for Open Access articles.

Limits on Kaluza-Klein Gravitons in Warped Extra Dimensions

This section places limits on the mass of the first Kaluza-Klein (KK) excitation of the graviton in the warped extra dimension model of Randall and Sundrum. Bounds in parenthesis assume Standard Model fields propagate in the bulk. Experimental bounds depend strongly on the warp parameter, k. See the "Extra Dimensions" review for a full discussion.

Here we list limits for the value of the warp parameter $k/\overline{M}_P = 0.1$.

VALUE (TeV)	CL%	DOCUMENT ID		TECN	COMMENT
>4.78	95	[1] SIRUNYAN	21N	CMS	$pp \to G \to e^+e^-, \mu^+\mu^-$
• • • We do not use the following data for averages, fits, limits, etc. • • •					
		[2] TUMASYAN	25	CMS	$pp \to G \to HH$
		[3] HAYRAPETY...	24AE	CMS	$pp \to G \to HH$
>4.8	95	[4] HAYRAPETY...	24AJ	CMS	$pp \to G \to \gamma\gamma$
		[5] TUMASYAN	24B	CMS	$pp \to G \to HH$
		[6] TUMASYAN	23AP	CMS	$pp \to G \to WW,\ ZZ$
		[7] AAD	22F	ATLS	$pp \to G \to HH$
		[8] TUMASYAN	22D	CMS	$pp \to G \to WW$
		[9] TUMASYAN	22J	CMS	$pp \to G \to ZZ$
		[10] TUMASYAN	22R	CMS	$pp \to G \to ZZ$
		[11] TUMASYAN	22U	CMS	$pp \to G \to HH$
		[12] AAD	21AF	ATLS	$pp \to G \to ZZ$
>4.5	95	[13] AAD	21AY	ATLS	$pp \to G \to \gamma\gamma$
		[14] AAD	20AT	ATLS	$pp \to G \to WW,\ ZZ$
		[15] AAD	20C	ATLS	$pp \to G \to HH$
		[16] AAD	20T	ATLS	$pp \to G \to b\overline{b}$
>2.6	95	[17] SIRUNYAN	20AI	CMS	$pp \to G \to jj$
		[18] SIRUNYAN	20F	CMS	$pp \to G \to HH$
		[19] AABOUD	19O	ATLS	$pp \to G \to HH$
		[20] AAD	19D	ATLS	$pp \to G \to WW,\ ZZ$
		[21] SIRUNYAN	19BE	CMS	$pp \to G \to HH$
		[22] AABOUD	18BI	ATLS	$pp \to G \to t\overline{t}$
		[23] AABOUD	18CJ	ATLS	$pp \to G \to VV, VH, \ell\overline{\ell}$
		[24] AABOUD	18CQ	ATLS	$pp \to G \to HH$
		[25] AABOUD	18CW	ATLS	$pp \to G \to HH$
		[26] SIRUNYAN	18AS	CMS	$pp \to G \to ZZ$
		[27] SIRUNYAN	18I	CMS	$pp \to G \to b\overline{b}$
		[28] AAD	16R	ATLS	$pp \to G \to WW, ZZ$
		[29] AAD	15AZ	ATLS	$pp \to G \to WW$
		[30] AAD	15CP	ATLS	$pp \to G \to WW, ZZ$
>2.68	95	[31] AAD	14V	ATLS	$pp \to G \to e^+e^-, \mu^+\mu^-$
>1.23 (>0.84)	95	[32] AAD	13A	ATLS	$pp \to G \to WW$
>0.94 (>0.71)	95	[33] AAD	13AO	ATLS	$pp \to G \to WW$
>2.23	95	[34] AAD	13AS	ATLS	$pp \to \gamma\gamma, e^+e^-, \mu^+\mu^-$
>0.845	95	[35] AAD	12AD	ATLS	$pp \to G \to ZZ$
		[36] AALTONEN	12V	CDF	$p\overline{p} \to G \to ZZ$
		[37] BAAK	12	RVUE	Electroweak
		[38] AALTONEN	11G	CDF	$p\overline{p} \to G \to ZZ$
>1.058	95	[39] AALTONEN	11R	CDF	$p\overline{p} \to G \to e^+e^-, \gamma\gamma$
>0.754	95	[40] ABAZOV	11H	D0	$p\overline{p} \to G \to WW$
>0.607		[41] AALTONEN	10N	CDF	$p\overline{p} \to G \to WW$
>1.05		[42] ABAZOV	10F	D0	$p\overline{p} \to G \to e^+e^-,\ \gamma\gamma$
		[43] AALTONEN	08S	CDF	$p\overline{p} \to G \to ZZ$
>0.90		[44] ABAZOV	08J	D0	$p\overline{p} \to G \to e^+e^-, \gamma\gamma$
		[45] AALTONEN	07G	CDF	$p\overline{p} \to G \to \gamma\gamma$
>0.889		[46] AALTONEN	07H	CDF	$p\overline{p} \to G \to e\overline{e}$
>0.785		[47] ABAZOV	05N	D0	$p\overline{p} \to G \to \ell\ell, \gamma\gamma$
>0.71		[48] ABULENCIA	05A	CDF	$p\overline{p} \to G \to \ell\overline{\ell}$

[1] SIRUNYAN 21N use 137 (140) fb^{-1} of data from pp collisions at $\sqrt{s} = 13$ TeV to search for dilepton resonances in the dielectron (dimuon) channel. See Table 6 for other limits with warp parameter values $k/\overline{M}_P = 0.01$ and 0.05. This updates the results of SIRUNYAN 18BB.

[2] TUMASYAN 25 use 138 fb^{-1} of data from pp collisions at $\sqrt{s} = 13$ TeV to search for Higgs boson pair production in the $b\overline{b}b\overline{b}$ final state. See their Figure 5 for limits on the cross section times branching fraction as a function of the KK graviton mass, corresponding to $k/\overline{M}_P = 0.5$. This updates the results of SIRUNYAN 18AF and SIRUNYAN 18CW.

[3] HAYRAPETYAN 24AE use 138 fb^{-1} of data from pp collisions at $\sqrt{s} = 13$ TeV to search for Higgs boson pair production in the $b\overline{b}WW$ final state. See their Figure 19 for limits on the cross section times branching fraction as a function of the KK graviton mass for $k/\overline{M}_P = 0.3$, 0.5 and 1.

[4] HAYRAPETYAN 24AJ use 138 fb^{-1} of data from pp collisions at $\sqrt{s} = 13$ TeV, in the diphoton channel to place a lower limit on the mass of the lightest KK graviton. See their paper for limits with other warp parameter values $k/\overline{M}_P = 0.01$ and 0.2. This updates the results of SIRUNYAN 18DU.

[5] TUMASYAN 24B use 138 fb^{-1} of data from pp collisions at $\sqrt{s} = 13$ TeV to search for Higgs boson pair production in the $\gamma\gamma b\overline{b}$ final state. See their Figure 6 for limits on the cross section times branching fraction as a function of the KK graviton mass assuming $k/\overline{M}_P = 0.5$ and 1. This updates the result of SIRUNYAN 19.

[6] TUMASYAN 23AP use 138 fb^{-1} of data from pp collisions at $\sqrt{s} = 13$ TeV to search for WW, ZZ diboson resonances in $q\overline{q}q\overline{q}$ final states. See their Figure 7 for the limit on the cross section times branching fraction as a function of the KK graviton mass. Assuming $k/\overline{M}_P = 0.5$, a graviton mass is excluded below 1400 GeV. This updates the result of SIRUNYAN 20Q.

[7] AAD 22F use 126–139 fb^{-1} of data from pp collisions at $\sqrt{s} = 13$ TeV to search for Higgs boson pair production in the $b\overline{b}b\overline{b}$ final state. See their Figure 14 for limits on the cross section times branching fraction as a function of the KK graviton mass. Assuming $k/\overline{M}_P = 1$, gravitons in the mass range 298–1460 GeV are excluded. This updates the results of AABOUD 19A.

[8] TUMASYAN 22D use 137 fb^{-1} of data from pp collisions at $\sqrt{s} = 13$ TeV to search for WW resonances in $\ell\nu qq$ final states ($\ell = e, \mu$). See their Figure 6 for the limit on the KK graviton mass as a function of the cross section times branching fraction, including theoretical values for $k/\overline{M}_P = 0.5$. This updates the results of SIRUNYAN 18AX.

[9] TUMASYAN 22J use 137 fb^{-1} of data from pp collisions at $\sqrt{s} = 13$ TeV to search for ZZ resonances in the $\nu\overline{\nu}q\overline{q}$ final state. See their Figure 10 for the limit on the KK graviton mass as a function of the cross section times branching fraction, assuming $k/\overline{M}_P = 0.5$. This updates the result of SIRUNYAN 18BK.

[10] TUMASYAN 22R use 138 fb^{-1} of data from pp collisions at $\sqrt{s} = 13$ TeV to search for ZZ resonances in $2\ell 2q$ final states ($\ell = e, \mu$). See their Figure 8 for the limit on the KK graviton mass as a function of the cross section times branching fraction. Assuming $k/\overline{M}_P = 0.5$, a graviton mass is excluded below 1200 GeV. This updates the result of SIRUNYAN 18DJ.

[11] TUMASYAN 22U use 138 fb^{-1} of data from pp collisions at $\sqrt{s} = 13$ TeV to search for Higgs boson pair production in the $b\overline{b}q\overline{q}'\ell\nu$, $b\overline{b}\ell\nu\ell\nu$ and $b\overline{b}\ell\nu\nu\ell\nu\nu$ final states ($\ell = e, \mu$). See their Figure 7 for limits on the cross section times branching fraction as a function of the KK graviton mass, including theoretical values for $k/\overline{M}_P = 0.3$ and 0.5. This updates the results of SIRUNYAN 19CF and SIRUNYAN 18F.

[12] AAD 21AF use 139 fb^{-1} of data from pp collisions at $\sqrt{s} = 13$ TeV to search for ZZ resonances in the $\ell\ell\ell\ell$ and $\ell\ell\nu\overline{\nu}$ final states (ℓ=e, μ). See their Figure 8 for the limit on the cross section times branching fraction as a function of the KK graviton mass, including theoretical values for $k/\overline{M}_P = 1$. This updates the results of AAD 15AU and AABOUD 18BF.

[13] AAD 21AY use 139 fb^{-1} of data from pp collisions at $\sqrt{s} = 13$ TeV in the diphoton channel to place a lower limit on the mass of the lightest KK graviton. This updates the results of AABOUD 17AP.

[14] AAD 20AT use 139 fb^{-1} of data from pp collisions at $\sqrt{s} = 13$ TeV to search for diboson resonances in semileptonic final states ($\ell\nu qq$,$\ell\ell qq$, $\nu\nu qq$). See their Figure 15 for the limit on the cross section times branching fraction as a function of the KK graviton mass. Lower limits on the graviton mass are also given for $k/\overline{M}_P = 1$. This updates the results of AABOUD 18AK and AABOUD 18AL.

[15] AAD 20C use 36.1 fb^{-1} of data from pp collisions at $\sqrt{s} = 13$ TeV to search for Higgs boson pair production in the $b\overline{b}b\overline{b}$, $b\overline{b}W^+W^-$, and $b\overline{b}\tau^+\tau^-$ final states. See their Figure 5(b)(c) for limits on the cross section as a function of the KK graviton mass. In the case of $k/\overline{M}_P = 1$ and 2, gravitons are excluded in the mass range 260–3000 GeV and 260–1760 GeV, respectively.

[16] AAD 20T use 139 fb^{-1} of data from pp collisions at $\sqrt{s} = 13$ TeV to search for narrow resonances decaying to bottom quark pairs. See their Figure 7 for the limit on the product of the cross section, branching fraction, acceptance and b-tagging efficiency as a function of the KK graviton mass. In the case of $k/\overline{M}_P = 0.2$, KK gravitons in the mass range 1.25–2.8 TeV are excluded.

[17] SIRUNYAN 20AI use 137 fb^{-1} of data from pp collisions at $\sqrt{s} = 13$ TeV to search for dijet resonances. See their Figure 6 for the limit on the product of the cross section, branching fraction and acceptance as a function of the KK graviton mass. This updates the results of SIRUNYAN 18BO.

[18] SIRUNYAN 20F use 35.9 fb^{-1} of data from pp collisions at $\sqrt{s} = 13$ TeV to search for Higgs boson pair production in the $b\overline{b}ZZ$ final state. See their Figure 4 for limits on the cross section times branching fraction as a function of the KK graviton mass, and Figure 5 for limits as a function of $k/\overline{M}_P$.

[19] AABOUD 19O use 36.1 fb^{-1} of data from pp collisions at $\sqrt{s} = 13$ TeV to search for Higgs boson pair production in the $b\overline{b}WW$ final state. See their Figure 12 for limits on the cross section times branching fraction as a function of the KK graviton mass for $k/\overline{M}_P = 1$ and $k/\overline{M}_P = 2$.

[20] AAD 19D use 139 fb^{-1} of data from pp collisions at $\sqrt{s} = 13$ TeV to search for diboson resonances in the all-hadronic final state. See their Figure 9(b) for the limit on the cross section times branching fraction as a function of the KK graviton mass, including theoretical values for $k/\overline{M}_P = 1$. This updates the results of AABOUD 18F.

[21] SIRUNYAN 19BE use 35.9 fb^{-1} of data from pp collisions at $\sqrt{s} = 13$ TeV to search for Higgs boson pair production by combining the results from four final states: $b\overline{b}\gamma\gamma$, $b\overline{b}\tau\overline{\tau}$, $b\overline{b}b\overline{b}$, and $b\overline{b}VV$. See their Figure 7 for limits on the cross section times branching fraction as a function of the KK graviton mass.

[22] AABOUD 18BI use 36.1 fb^{-1} of data from pp collisions at $\sqrt{s} = 13$ TeV to search for top-quark pairs decaying into the lepton-plus jets topology. See their Figure 16 for the limit on the KK graviton mass as a function of the cross section times branching fraction, including theoretical values for $k/\overline{M}_P = 1$.

[23] AABOUD 18CJ combine the searches for heavy resonances decaying into bosonic and leptonic final states from 36.1 fb^{-1} of pp collision data at $\sqrt{s} = 13$ TeV. The lower limit on the KK graviton mass, with $k/\overline{M}_P = 1$, is 2.3 TeV.

[24] AABOUD 18CQ use 36.1 fb^{-1} of data from pp collisions at $\sqrt{s} = 13$ TeV to search for Higgs boson pair production in the $b\overline{b}\tau^+\tau^-$ final state. See their Figure 2 for limits on the cross section times branching fraction as a function of the KK graviton mass. Assuming $k/\overline{M}_P = 1$, gravitons in the mass range 325–885 GeV are excluded.

[25] AABOUD 18CW use 36.1 fb^{-1} of data from pp collisions at $\sqrt{s} = 13$ TeV to search for Higgs boson pair production in the $\gamma\gamma b\overline{b}$ final state. See their Figure 7 for limits on the cross section times branching fraction as a function of the KK graviton mass.

[26] SIRUNYAN 18AS use 35.9 fb^{-1} of data from pp collisions at $\sqrt{s} = 13$ TeV to search for ZZ resonances in the $\ell\ell\nu\overline{\nu}$ final state (ℓ=e, μ). See their Figure 5 for the limit on the KK graviton mass as a function of the cross section times branching fraction, including theoretical values for $k/\overline{M}_P = 0.1$, 0.5, and 1.0.

[27] SIRUNYAN 18I use 19.7 fb^{-1} of data from pp collisions at $\sqrt{s} = 8$ TeV to search for narrow resonances decaying to bottom quark pairs. See their Figure 3 for the limit on the KK graviton mass as a function of the cross section times branching fraction in the mass range of 325–1200 GeV.

[28] AAD 16R use 20.3 fb^{-1} of data from pp collisions at $\sqrt{s} = 8$ TeV to place a lower bound on the mass of the lightest KK graviton. See their Figure 4 for the limit on the KK graviton mass as a function of the cross section times branching fraction.

[29] AAD 15AZ use 20.3 fb^{-1} of data from pp collisions at $\sqrt{s} = 8$ TeV to place a lower bound on the mass of the lightest KK graviton. See their Figure 2 for limits on the KK graviton mass as a function of the cross section times branching ratio.

[30] AAD 15CP use 20.3 fb^{-1} of data from pp collisions at $\sqrt{s} = 8$ TeV to place a lower bound on the mass of the lightest KK graviton. See their Figures 6b and 6c for the limit on the KK graviton mass as a function of the cross section times branching fraction.

[31] AAD 14V use 20.3 (20.5) fb^{-1} of data from pp collisions at $\sqrt{s} = 8$ TeV in the dielectron (dimuon) channels to place a lower bound on the mass of the lightest KK graviton. This updates the results of AAD 12CC .

[32] AAD 13A use 4.7 fb^{-1} of data from pp collisions at $\sqrt{s} = 7$ TeV in the $\ell\nu\ell\nu$ channel, to place a lower bound on the mass of the lightest KK graviton.

Int. J. Mod. Phys. A 2026.41. Downloaded from www.worldscientific.com by UNIVERSITY OF CALIFORNIA @ BERKELEY on 09/16/26. Re-use and distribution is strictly not permitted, except for Open Access articles.

[33] AAD 13AO use 4.7 fb^{-1} of data from pp collisions at $\sqrt{s}$ = 7 TeV in the $\ell\nu jj$ channel, to place a lower bound on the mass of the lightest KK graviton.

[34] AAD 13AS use 4.9 fb^{-1} of data from pp collisions at $\sqrt{s}$ = 7 TeV in the diphoton channel to place lower limits on the mass of the lightest KK graviton. The diphoton channel is combined with previous results in the dielectron and dimuon channels to set the best limit. See their Table 2 for warp parameter values $k/\overline{M}_P$ between 0.01 and 0.1. This updates the results of AAD 12Y .

[35] AAD 12AD use 1.02 fb^{-1} of data from pp collisions at $\sqrt{s}$ = 7 TeV to search for KK gravitons in a warped extra dimension decaying to ZZ dibosons in the $lljj$ and $llll$ channels (ℓ=e, μ). The limit is quoted for the combined $lljj + llll$ channels. See their Figure 5 for limits on the cross section $\sigma(G \rightarrow ZZ)$ as a function of the graviton mass.

[36] AALTONEN 12V use 6 fb^{-1} of data from $p\overline{p}$ collisions at $\sqrt{s}$ = 1.96 TeV to search for KK gravitons in a warped extra dimension decaying to ZZ dibosons in the $lljj$ and $llll$ channels (ℓ=e, μ). It provides improved limits over the previous analysis in AALTONEN 11G. See their Figure 16 for limits from all channels combined on the cross section times branching ratio $\sigma(p\overline{p} \rightarrow G^* \rightarrow ZZ)$ as a function of the graviton mass.

[37] BAAK 12 use electroweak precision observables to place a lower bound on the compactification scale $k\,e^{-\pi kR}$, assuming Standard Model fields propagate in the bulk and the Higgs is confined to the IR brane. See their Fig. 27 for more details.

[38] AALTONEN 11G use 2.5–2.9 fb^{-1} of data from $p\overline{p}$ collisions at $\sqrt{s}$ = 1.96 TeV to search for KK gravitons in a warped extra dimension decaying to ZZ dibosons via the $eeee$, $ee\mu\mu$, $\mu\mu\mu\mu$, $eejj$, and $\mu\mu jj$ channels. See their Fig. 20 for limits on the cross section $\sigma(G \rightarrow ZZ)$ as a function of the graviton mass.

[39] AALTONEN 11R uses 5.7 fb^{-1} of data from $p\overline{p}$ collisions at $\sqrt{s}$ = 1.96 TeV in the dielectron channel to place a lower bound on the mass of the lightest graviton. It provides combined limits with the diphoton channel analysis of AALTONEN 11U. For warp parameter values $k/\overline{M}_P$ between 0.01 to 0.1 the lower limit on the mass of the lightest graviton is between 612 and 1058 GeV. See their Table I for more details.

[40] ABAZOV 11H use 5.4 fb^{-1} of data from $p\overline{p}$ collisions at $\sqrt{s}$ = 1.96 TeV to place a lower bound on the mass of the lightest graviton. Their 95% C.L. exclusion limit does not include masses less than 300 GeV.

[41] AALTONEN 10N use 2.9 fb^{-1} of data from $p\overline{p}$ collisions at $\sqrt{s}$ = 1.96 TeV to place a lower bound on the mass of the lightest graviton.

[42] ABAZOV 10F use 5.4 fb^{-1} of data from $p\overline{p}$ collisions at $\sqrt{s}$ = 1.96 TeV to place a lower bound on the mass of the lightest graviton. For warp parameter values of $k/\overline{M}_P$ between 0.01 and 0.1 the lower limit on the mass of the lightest graviton is between 560 and 1050 GeV. See their Fig. 3 for more details.

[43] AALTONEN 08S use $p\overline{p}$ collisions at $\sqrt{s}$ = 1.96 TeV to search for KK gravitons in warped extra dimensions. They search for graviton resonances decaying to four electrons via two Z bosons using 1.1 fb^{-1} of data. See their Fig. 8 for limits on $\sigma \cdot$ B$(G \rightarrow ZZ)$ versus the graviton mass.

[44] ABAZOV 08J use $p\overline{p}$ collisions at $\sqrt{s}$ = 1.96 TeV to search for KK gravitons in warped extra dimensions. They search for graviton resonances decaying to electrons and photons using 1 fb^{-1} of data. For warp parameter values of $k/\overline{M}_P$ between 0.01 and 0.1 the lower limit on the mass of the lightest excitation is between 300 and 900 GeV. See their Fig. 4 for more details.

[45] AALTONEN 07G use $p\overline{p}$ collisions at $\sqrt{s}$ = 1.96 TeV to search for KK gravitons in warped extra dimensions. They search for graviton resonances decaying to photons using 1.2 fb^{-1} of data. For warp parameter values of $k/\overline{M}_P$ = 0.1, 0.05, and 0.01 the bounds on the graviton mass are 850, 694, and 230 GeV, respectively. See their Fig. 3 for more details. See also AALTONEN 07H.

[46] AALTONEN 07H use $p\overline{p}$ collisions at $\sqrt{s}$ = 1.96 TeV to search for KK gravitons in warped extra dimensions. They search for graviton resonances decaying to electrons using 1.3 fb^{-1} of data. For a warp parameter value of $k/\overline{M}_P$ = 0.1 the bound on the graviton mass is 807 GeV. See their Fig. 4 for more details. A combined analysis with the diphoton data of AALTONEN 07G yields for $k/\overline{M}_P$ = 0.1 a graviton mass lower bound of 889 GeV.

[47] ABAZOV 05N use $p\overline{p}$ collisions at $\sqrt{s}$ = 1.96 TeV to search for KK gravitons in warped extra dimensions. They search for graviton resonances decaying to muons, electrons or photons, using 260 pb^{-1} of data. For warp parameter values of $k/\overline{M}_P$ = 0.1, 0.05, and 0.01, the bounds on the graviton mass are 785, 650 and 250 GeV respectively. See their Fig. 3 for more details.

[48] ABULENCIA 05A use $p\overline{p}$ collisions at $\sqrt{s}$ = 1.96 TeV to search for KK gravitons in warped extra dimensions. They search for graviton resonances decaying to muons or electrons, using 200 pb^{-1} of data. For warp parameter values of $k/\overline{M}_P$ = 0.1, 0.05, and 0.01, the bounds on the graviton mass are 710, 510 and 170 GeV respectively.

Limits on Kaluza-Klein Gluons in Warped Extra Dimensions

This section places limits on the mass of the first Kaluza-Klein (KK) excitation of the gluon in warped extra dimension models with Standard Model fields propagating in the bulk. Bounds are given for a specific benchmark model with Γ/m = 15.3% where Γ is the width and m the mass of the KK gluon. See the "Extra Dimensions" review for more discussion.

VALUE (TeV)	CL%	DOCUMENT ID		TECN	COMMENT
>3.8	95	[1] AABOUD	18BI	ATLS	$g_{KK} \rightarrow t\overline{t} \rightarrow \ell j$
• • • We do not use the following data for averages, fits, limits, etc. • • •					
		[2] HAYRAPETY...	25T	CMS	$g_{KK} \rightarrow gR,\ R \rightarrow WW$
		[3] HAYRAPETY...	24G	CMS	$g_{KK} \rightarrow Rj \rightarrow jjj$
		[4] AABOUD	19AS	ATLS	$g_{KK} \rightarrow t\overline{t} \rightarrow jj$
		[5] SIRUNYAN	19AL	CMS	$g_{KK} \rightarrow tT$
>2.5	95	[6] CHATRCHYAN	13BM	CMS	$g_{KK} \rightarrow t\overline{t}$
		[7] CHEN	13A		$\overline{B} \rightarrow X_s\gamma$
>1.5	95	[8] AAD	12BV	ATLS	$g_{KK} \rightarrow t\overline{t} \rightarrow \ell j$

[1] AABOUD 18BI use 36.1 fb^{-1} of data from pp collisions at $\sqrt{s}$ = 13 TeV. This result updates AAD 13AQ.

[2] HAYRAPETYAN 25T use 138 fb^{-1} of data from pp collisions at $\sqrt{s}$ = 13 TeV to place limits on a KK gluon decaying to W bosons via a spin-0 radion, R. See their Figure 6 for limits on the cross section times branching fraction as a function of the KK gluon and radion mass.

[3] HAYRAPETYAN 24G use 138 fb^{-1} of data from pp collisions at $\sqrt{s}$ = 13 TeV to place limits on a KK gluon decaying to gluons via a spin-0 radion, R. See their Figure 3 for limits on the cross section times branching fraction as a function of the KK gluon mass and various values of the radion mass. This updates the results of TUMASYAN 22C.

[4] AABOUD 19AS use 36.1 fb^{-1} of data from pp collisions at $\sqrt{s}$ = 13 TeV. An upper bound of 3.4 TeV is placed on the KK gluon mass for Γ/m = 30%.

[5] SIRUNYAN 19AL use 35.9 fb^{-1} of data from pp collisions at $\sqrt{s}$ = 13 TeV to place limits on a KK gluon decaying to a top quark and a heavy vector-like fermion, T. KK gluon masses between 1.5 and 2.3 TeV and between 2.0 and 2.4 TeV are excluded for T masses of 1.2 and 1.5 TeV, respectively.

[6] CHATRCHYAN 13BM use 19.7 fb^{-1} of data from pp collisions at $\sqrt{s}$ = 8 TeV. Bound is for a width of approximately 15–20% of the KK gluon mass.

[7] CHEN 13A place limits on the KK mass scale for a specific warped model with custodial symmetry and bulk fermions. See their Figures 4 and 5.

[8] AAD 12BV use 2.05 fb^{-1} of data from pp collisions at $\sqrt{s}$ = 7 TeV.

Black Hole Production Limits

Semiclassical Black Holes

VALUE (GeV)	DOCUMENT ID		TECN	COMMENT
• • • We do not use the following data for averages, fits, limits, etc. • • •				
	[1] SIRUNYAN	18DA	CMS	$pp \rightarrow$ multijet
	[2] AAD	16N	ATLS	$pp \rightarrow$ multijet
	[3] AAD	16O	ATLS	$pp \rightarrow \ell + (\ell\ell/\ell j/jj)$
	[4] AAD	13AW	ATLS	$pp \rightarrow \mu\mu$

[1] SIRUNYAN 18DA use 35.9 fb^{-1} of data from pp collisions at $\sqrt{s}$ = 13 TeV to search for semiclassical black holes decaying to multijet final states. No excess of events above the expected level of standard model background was observed. Exclusions at 95% CL are set on the mass threshold for black hole production as a function of the higher-dimensional Planck scale for rotating and nonrotating black holes under several model assumptions (ADD, 2, 4, 6 extra dimensions model) in the 7.1–10.3 TeV range. These limits supersede those in SIRUNYAN 17CP.

[2] AAD 16N use 3.6 fb^{-1} of data from pp collisions at $\sqrt{s}$ = 13 TeV to search for semiclassical black hole decays to multijet final states. No excess of events above the expected level of Standard Model background was observed. Exclusion contours at 95% C.L. are set on the mass threshold for black hole production versus higher-dimensional Planck scale for rotating black holes (ADD, 6 extra dimensions model).

[3] AAD 16O use 3.2 fb^{-1} of data from pp collisions at $\sqrt{s}$ = 13 TeV to search for semiclassical black hole decays to high-mass final states with leptons and jets. No excess of events above the expected level of Standard Model background was observed. Exclusion contours at 95% C.L. are set on the mass threshold for black hole production versus higher-dimensional Planck scale for rotating black holes (ADD, 2 to 6 extra dimensions).

[4] AAD 13AW use 20.3 fb^{-1} of data from pp collisions at $\sqrt{s}$ = 8 TeV to search for semiclassical black hole decays to like-sign dimuon final states using large track multiplicity. No excess of events above the expected level of Standard Model background was observed. Exclusion contours at 95% C.L. are set on the mass threshold for black hole production versus higher-dimensional Planck scale in various extra dimensions, rotating and non-rotating models.

Quantum Black Holes

VALUE (GeV)	DOCUMENT ID		TECN	COMMENT
• • • We do not use the following data for averages, fits, limits, etc. • • •				
	[1] AAD	24S	ATLS	$pp \rightarrow \ell j$
	[2] AAD	23CB	ATLS	$pp \rightarrow e\mu,\ e\tau,\ \mu\tau$
	[3] TUMASYAN	23AW	CMS	$pp \rightarrow \tau\nu$
	[4] TUMASYAN	23BC	CMS	$pp \rightarrow \gamma j$
	[5] TUMASYAN	23H	CMS	$pp \rightarrow e\mu,\ e\tau,\ \mu\tau$
	[6] AAD	20T	ATLS	$pp \rightarrow jj$
	[7] AABOUD	18BA	ATLS	$pp \rightarrow \gamma j$
	[8] SIRUNYAN	18AT	CMS	$pp \rightarrow e\mu$
	[9] SIRUNYAN	18DD	CMS	$pp \rightarrow$ dijet, ang. distrib.
	[10] SIRUNYAN	17CP	CMS	$pp \rightarrow jj$
	[11] KHACHATRY...	16BE	CMS	$pp \rightarrow e\mu$
	[12] KHACHATRY...	15V	CMS	$pp \rightarrow jj$
	[13] AAD	14V	ATLS	$pp \rightarrow ee,\ \mu\mu$
	[14] CHATRCHYAN	13A	CMS	$pp \rightarrow jj$

[1] AAD 24S use 140 fb^{-1} of data from pp collisions at $\sqrt{s}$ = 13 TeV to search for quantum black hole decays to final states with high-invariant-mass lepton + jet. No excess of events above the expected level of Standard Model background was observed. Exclusion limits at 95% C.L. are set on mass thresholds for black hole production in an ADD (6 extra dimensions) model and the Randall-Sundrum (one extra dimension) model. The resulting lower mass threshold limits in the ADD (RS) models are 9.2 (6.8) TeV. The ADD limit supersedes that in AAD 14AL.

[2] AAD 23CB use 139 fb^{-1} of data from pp collisions at $\sqrt{s}$ = 13 TeV to search for quantum black hole decays with different-flavor high-mass dilepton final states. No excess of events above the expected level of Standard Model background was observed. Exclusion limits at 95% C.L. are set on mass thresholds for black hole production in ADD (6 extra dimensions) and RS1 models. Assuming the black hole mass threshold is equal to the higher-dimensional Planck scale, mass thresholds below 5.9 (3.8), 5.2 (3.0), and 5.1 (3.0) TeV are excluded in the $e\mu$, $e\tau$ and $\mu\tau$ channels for the ADD (RS1) models, respectively. These limits supersede those in AABOUD 18CM.

[3] TUMASYAN 23AW use 138 fb^{-1} of data from pp collisions at $\sqrt{s}$ = 13 TeV to search for quantum black hole decays in the tau lepton plus missing transverse momentum final state. Assuming the black hole mass threshold is equal to the higher-dimensional Planck scale, threshold masses below 6.6 TeV are excluded in the ADD model with four extra dimensions (see their Figure 8).

[4] TUMASYAN 23BC use 138 fb^{-1} of data from pp collisions at $\sqrt{s}$ = 13 TeV to search for quantum black hole decays to final states with a photon and a jet. No excess of events above the expected level of Standard Model background was observed. Exclusion limits at 95% C.L. are set on mass thresholds for black hole production in ADD (6 extra dimensions) and RS1 models. Assuming the black hole mass threshold is equal to the higher-dimensional Planck scale, mass thresholds below 7.5 TeV and 5.2 TeV are excluded for the ADD and RS1 models, respectively (see their Figure 9).

[5] TUMASYAN 23H use 138 fb^{-1} of data from pp collisions at $\sqrt{s}$ = 13 TeV to search for quantum black hole decays with different-flavor high-mass dilepton final states. No excess of events above the expected level of Standard Model background was observed.

Exclusion limits at 95% C.L. are set on mass thresholds for black hole production in the ADD model (with 4 extra dimensions). Assuming the black hole mass threshold is equal to the higher-dimensional Planck scale, mass thresholds below 5.6, 5.2, and 5.0 TeV are excluded in the $e\mu$, $e\tau$ and $\mu\tau$ channels, respectively.

[6] AAD 20T use 139 fb^{-1} of data from pp collisions at $\sqrt{s}$ = 13 TeV to search for quantum black hole decays to final states with dijets. No excess of events above the expected level of Standard Model background was observed. Exclusion limits at 95% C.L. are set on mass thresholds for black hole production in an ADD (6 extra dimensions) model. Assuming the black hole mass threshold is equal to the higher-dimensional Planck scale, mass thresholds below 9.4 TeV are excluded. This limit supersedes AABOUD 17AK.

[7] AABOUD 18BA use 36.7 fb^{-1} of data from pp collisions at $\sqrt{s}$ = 13 TeV to search for quantum black hole decays to final states with a photon and a jet. No excess of events above the expected level of Standard Model background was observed. Exclusion limits at 95% C.L. are set on mass thresholds for black hole production in ADD (6 extra dimensions) and RS1 models. Assuming the black hole mass threshold is equal to the Planck scale, mass thresholds below 7.1 TeV and 4.4 TeV are excluded for the ADD and RS1 models, respectively. These limits supersede those in AAD 16AI.

[8] SIRUNYAN 18AT use 35.9 fb^{-1} of data from pp collisions at $\sqrt{s}$ = 13 TeV to search for quantum black hole decays to $e\mu$ final states. In Figure 4, lower mass limits of 5.3, 5.5 and 5.6 TeV are placed in a model with 4, 5 and 6 extra dimensions, respectively, and a lower mass limit of 3.6 TeV is found for a single warped dimension.

[9] SIRUNYAN 18DD use 35.9 fb^{-1} of data from pp collisions at $\sqrt{s}$ = 13 TeV to search for quantum black hole decays in dijet angular distributions. A lower mass limit of 5.9 (8.2) TeV is placed in the RS (ADD) model with one (six) extra dimension(s).

[10] SIRUNYAN 17CP use 2.3 fb^{-1} of data from pp collisions at $\sqrt{s}$ = 13 TeV to search for quantum black holes decaying to dijet final states. No excess of events above the expected level of standard model background was observed. Limits on the quantum black hole mass threshold are set as a function of the higher-dimensional Planck scale, under the assumption that the mass threshold must exceed the above Planck scale. Depending on the model, mass thresholds in the range up to 5.1–9.0 TeV are excluded.

[11] KHACHATRYAN 16BE use 19.7 fb^{-1} of data from pp collisions at $\sqrt{s}$ = 8 TeV to search for quantum black holes undergoing lepton flavor violating decay to the $e\mu$ final state. No excess of events above the expected level of standard model background was observed. Exclusion limits at 95% CL are set on mass thresholds for black hole production in the ADD (2–6 flat extra dimensions), RS1 (1 warped extra dimension), and a model with a Planck scale at the TeV scale from a renormalization of the gravitational constant (no extra dimensions). Limits on the black hole mass threshold are set assuming that it is equal to the higher-dimensional Planck scale. Mass thresholds for quantum black holes in the range up to 3.15–3.63 TeV are excluded in the ADD model. In the RS1 model, mass thresholds below 2.81 TeV are excluded in the PDG convention for the Schwarzschild radius. In the model with no extra dimensions, mass thresholds below 1.99 TeV are excluded.

[12] KHACHATRYAN 15V use 19.7 fb^{-1} of data from pp collisions at $\sqrt{s}$ = 8 TeV to search for quantum black holes decaying to dijet final states. No excess of events above the expected level of standard model background was observed. Exclusion limits at 95% CL are set on mass thresholds for black hole production in the ADD (2–6 flat extra dimensions) and RS1 (1 warped extra dimension) model. Limits on the black hole mass threshold are set as a function of the higher-dimensional Planck scale, under the assumption that the mass threshold must exceed the above Planck scale. Depending on the model, mass thresholds in the range up to 5.0–6.3 TeV are excluded. This paper supersedes CHATRCHYAN 13AD.

[13] AAD 14V use 20.3 (20.5) fb^{-1} of data in the dielectron (dimuon) channels from pp collisions at $\sqrt{s}$ = 8 TeV to search for quantum black hole decays involving high-mass dilepton resonances. No excess of events above the expected level of Standard Model background was observed. Exclusion limits at 95% C.L. are set on mass thresholds for black hole production in ADD (6 extra dimensions) and RS1 models. Assuming the black hole mass threshold is equal to the higher-dimensional Planck scale, mass thresholds below 3.65 TeV and 2.24 TeV are excluded for the ADD and RS1 models, respectively.

[14] CHATRCHYAN 13A use 5 fb^{-1} of data from pp collisions at $\sqrt{s}$ = 7 TeV to search for quantum black holes decaying to dijet final states. No excess of events above the expected level of standard model background was observed. Exclusion limits at 95% CL are set on mass thresholds for black hole production in the ADD (2–6 flat extra dimensions) and RS (1 warped extra dimension) model. Limits on the black hole mass threshold are set as a function of the higher-dimensional Planck scale, under assumption that the mass threshold must exceed the above Planck scale. Depending on the model, mass thresholds in the range up to 4.0–5.3 TeV are excluded.

REFERENCES FOR Extra Dimensions

FIORILLO	25	PRL 135 211003	D.F.G. Fiorillo *et al.*	(DESY, INFNP, SYDN+)
HAYRAPETY...	25T	JHEP 2502 199	A. Hayrapetyan *et al.*	(CMS Collab.)
TUMASYAN	25	JHEP 2502 040	A. Tumasyan *et al.*	(CMS Collab.)
AAD	24S	PR D109 032010	G. Aad *et al.*	(ATLAS Collab.)
HAYRAPETY...	24AE	JHEP 2407 293	A. Hayrapetyan *et al.*	(CMS Collab.)
HAYRAPETY...	24AJ	JHEP 2408 215	A. Hayrapetyan *et al.*	(CMS Collab.)
HAYRAPETY...	24G	PRL 133 011801	A. Hayrapetyan *et al.*	(CMS Collab.)
TUMASYAN	24B	JHEP 2405 316	A. Tumasyan *et al.*	(CMS Collab.)
AAD	23CB	JHEP 2310 082	G. Aad *et al.*	(ATLAS Collab.)
FLORES	23	IJMP A38 2350002	M.M. Flores *et al.*	(WITS, WARS, NIP-UPD+)
TUMASYAN	23AP	PL B844 137813	A. Tumasyan *et al.*	(CMS Collab.)
TUMASYAN	23AW	JHEP 2309 051	A. Tumasyan *et al.*	(CMS Collab.)
TUMASYAN	23BC	JHEP 2312 189	A. Tumasyan *et al.*	(CMS Collab.)
TUMASYAN	23H	JHEP 2305 227	A. Tumasyan *et al.*	(CMS Collab.)
AAD	22F	PR D105 092002	G. Aad *et al.*	(ATLAS Collab.)
TUMASYAN	22C	PL B832 137263	A. Tumasyan *et al.*	(CMS Collab.)
TUMASYAN	22D	PR D105 032008	A. Tumasyan *et al.*	(CMS Collab.)
TUMASYAN	22J	PR D106 012004	A. Tumasyan *et al.*	(CMS Collab.)
TUMASYAN	22R	JHEP 2204 087	A. Tumasyan *et al.*	(CMS Collab.)
TUMASYAN	22U	JHEP 2205 005	A. Tumasyan *et al.*	(CMS Collab.)
AAD	21AF	EPJ C81 332	G. Aad *et al.*	(ATLAS Collab.)
AAD	21AY	PL B822 136651	G. Aad *et al.*	(ATLAS Collab.)
AAD	21F	PR D103 112006	G. Aad *et al.*	(ATLAS Collab.)
AVNISH	21	PR D103 115011	Avnish *et al.*	
BLAKEMORE	21	PR D104 L061101	C.P. Blakemore *et al.*	(STAN)
HEACOCK	21	SCI 373 1239	B. Heacock *et al.*	(NIST, RIKEN, NAGO+)
SIRUNYAN	21A	EPJ C81 13	A.M. Sirunyan *et al.*	(CMS Collab.)
Also		EPJ C81 333 (errat.)	A.M. Sirunyan *et al.*	(CMS Collab.)
SIRUNYAN	21N	JHEP 2107 208	A.M. Sirunyan *et al.*	(CMS Collab.)
TUMASYAN	21D	JHEP 2111 153	A. Tumasyan *et al.*	(CMS Collab.)
AAD	20AT	EPJ C80 1165	G. Aad *et al.*	(ATLAS Collab.)
AAD	20C	PL B800 135103	G. Aad *et al.*	(ATLAS Collab.)
AAD	20T	JHEP 2003 145	G. Aad *et al.*	(ATLAS Collab.)
LEE	20	PRL 124 101101	J.G. Lee *et al.*	(WASH)
SIRUNYAN	20AI	JHEP 2005 033	A.M. Sirunyan *et al.*	(CMS Collab.)
SIRUNYAN	20F	PR D102 032003	A.M. Sirunyan *et al.*	(CMS Collab.)
SIRUNYAN	20Q	EPJ C80 237	A.M. Sirunyan *et al.*	(CMS Collab.)
TAN	20A	PRL 124 051301	W.-H. Tan *et al.*	
AABOUD	19A	JHEP 1901 030	M. Aaboud *et al.*	(ATLAS Collab.)
AABOUD	19AS	PR D99 092004	M. Aaboud *et al.*	(ATLAS Collab.)
AABOUD	19O	JHEP 1904 092	M. Aaboud *et al.*	(ATLAS Collab.)
AAD	19D	JHEP 1909 091	G. Aad *et al.*	(ATLAS Collab.)
Also		JHEP 2006 042 (errat.)	G. Aad *et al.*	(ATLAS Collab.)
SIRUNYAN	19	PL B788 7	A.M. Sirunyan *et al.*	(CMS Collab.)
SIRUNYAN	19AC	JHEP 1904 114	A.M. Sirunyan *et al.*	(CMS Collab.)
SIRUNYAN	19AL	EPJ C79 208	A.M. Sirunyan *et al.*	(CMS Collab.)
SIRUNYAN	19BE	PRL 122 121803	A.M. Sirunyan *et al.*	(CMS Collab.)
SIRUNYAN	19CF	JHEP 1910 125	A.M. Sirunyan *et al.*	(CMS Collab.)
AABOUD	18AK	JHEP 1803 042	M. Aaboud *et al.*	(ATLAS Collab.)
AABOUD	18AL	JHEP 1803 009	M. Aaboud *et al.*	(ATLAS Collab.)
AABOUD	18AV	JHEP 1807 089	M. Aaboud *et al.*	(ATLAS Collab.)
AABOUD	18BA	EPJ C78 102	M. Aaboud *et al.*	(ATLAS Collab.)
AABOUD	18BF	EPJ C78 293	M. Aaboud *et al.*	(ATLAS Collab.)
AABOUD	18BI	EPJ C78 565	M. Aaboud *et al.*	(ATLAS Collab.)
AABOUD	18CE	JHEP 1812 039	M. Aaboud *et al.*	(ATLAS Collab.)
AABOUD	18CJ	PR D98 052008	M. Aaboud *et al.*	(ATLAS Collab.)
AABOUD	18CM	PR D98 092008	M. Aaboud *et al.*	(ATLAS Collab.)
AABOUD	18CQ	PRL 121 191801	M. Aaboud *et al.*	(ATLAS Collab.)
AABOUD	18CW	JHEP 1811 040	M. Aaboud *et al.*	(ATLAS Collab.)
AABOUD	18F	PL B777 91	M. Aaboud *et al.*	(ATLAS Collab.)
AABOUD	18I	JHEP 1801 126	M. Aaboud *et al.*	(ATLAS Collab.)
BERGE	18	PRL 120 141101	J. Berge *et al.*	(MICROSCOPE Collab.)
FAYET	18	PR D97 055039	P. Fayet	(EPOL)
FAYET	18A	PR D99 055043	P. Fayet	(ENSP, EPOL)
HADDOCK	18	PR D97 062002	C. Haddock *et al.*	(NAGO, KEK, OSAK+)
SIRUNYAN	18AF	PL B781 244	A.M. Sirunyan *et al.*	(CMS Collab.)
SIRUNYAN	18AS	JHEP 1803 003	A.M. Sirunyan *et al.*	(CMS Collab.)
SIRUNYAN	18AT	JHEP 1804 073	A.M. Sirunyan *et al.*	(CMS Collab.)
SIRUNYAN	18AX	JHEP 1805 088	A.M. Sirunyan *et al.*	(CMS Collab.)
SIRUNYAN	18BB	JHEP 1806 120	A.M. Sirunyan *et al.*	(CMS Collab.)
SIRUNYAN	18BK	JHEP 1807 075	A.M. Sirunyan *et al.*	(CMS Collab.)
SIRUNYAN	18BO	JHEP 1808 130	A.M. Sirunyan *et al.*	(CMS Collab.)
SIRUNYAN	18BV	EPJ C78 291	A.M. Sirunyan *et al.*	(CMS Collab.)
SIRUNYAN	18CW	JHEP 1808 152	A.M. Sirunyan *et al.*	(CMS Collab.)
SIRUNYAN	18DA	JHEP 1811 042	A.M. Sirunyan *et al.*	(CMS Collab.)
SIRUNYAN	18DD	EPJ C78 789	A.M. Sirunyan *et al.*	(CMS Collab.)
SIRUNYAN	18DJ	JHEP 1809 101	A.M. Sirunyan *et al.*	(CMS Collab.)
SIRUNYAN	18DU	PR D98 092001	A.M. Sirunyan *et al.*	(CMS Collab.)
SIRUNYAN	18F	JHEP 1801 054	A.M. Sirunyan *et al.*	(CMS Collab.)
SIRUNYAN	18I	PRL 120 201801	A.M. Sirunyan *et al.*	(CMS Collab.)
SIRUNYAN	18S	PR D97 092005	A.M. Sirunyan *et al.*	(CMS Collab.)
AABOUD	17AK	PR D96 052004	M. Aaboud *et al.*	(ATLAS Collab.)
AABOUD	17AP	PL B775 105	M. Aaboud *et al.*	(ATLAS Collab.)
KLIMCHITSK...	17A	PR D95 123013	G.L. Klimchitskaya, V.M. Mostepanenko	
SIRUNYAN	17AQ	JHEP 1710 073	A.M. Sirunyan *et al.*	(CMS Collab.)
SIRUNYAN	17CP	PL B774 279	A.M. Sirunyan *et al.*	(CMS Collab.)
SIRUNYAN	17F	JHEP 1707 013	A.M. Sirunyan *et al.*	(CMS Collab.)
AABOUD	16F	JHEP 1606 059	M. Aaboud *et al.*	(ATLAS Collab.)
AAD	16AI	JHEP 1603 041	G. Aad *et al.*	(ATLAS Collab.)
AAD	16N	JHEP 1603 026	G. Aad *et al.*	(ATLAS Collab.)
AAD	16O	PL B760 520	G. Aad *et al.*	(ATLAS Collab.)
AAD	16R	PL B755 285	G. Aad *et al.*	(ATLAS Collab.)
KHACHATRY...	16BE	EPJ C76 317	V. Khachatryan *et al.*	(CMS Collab.)
KHACHATRY...	16N	PL B755 102	V. Khachatryan *et al.*	(CMS Collab.)
AAD	15AU	EPJ C75 69	G. Aad *et al.*	(ATLAS Collab.)
AAD	15AZ	EPJ C75 209	G. Aad *et al.*	(ATLAS Collab.)
Also		EPJ C75 370 (errat.)	G. Aad *et al.*	(ATLAS Collab.)
AAD	15CP	JHEP 1512 055	G. Aad *et al.*	(ATLAS Collab.)
AAD	15CS	PR D91 012008	G. Aad *et al.*	(ATLAS Collab.)
Also		PR D92 059903 (errat.)	G. Aad *et al.*	(ATLAS Collab.)
ACCOMANDO	15	MPL A30 1540010	E. Accomando	(SHMP)
KHACHATRY...	15AE	JHEP 1504 025	V. Khachatryan *et al.*	(CMS Collab.)
KHACHATRY...	15T	PR D91 092005	V. Khachatryan *et al.*	(CMS Collab.)
KHACHATRY...	15V	PR D91 052009	V. Khachatryan *et al.*	(CMS Collab.)
AAD	14AL	PRL 112 091804	G. Aad *et al.*	(ATLAS Collab.)
AAD	14BE	EPJ C74 3134	G. Aad *et al.*	(ATLAS Collab.)
AAD	14V	PR D90 052005	G. Aad *et al.*	(ATLAS Collab.)
AAD	13A	PL B718 860	G. Aad *et al.*	(ATLAS Collab.)
AAD	13AO	PR D87 112006	G. Aad *et al.*	(ATLAS Collab.)
AAD	13AQ	PR D88 012004	G. Aad *et al.*	(ATLAS Collab.)
AAD	13AS	NJP 15 043007	G. Aad *et al.*	(ATLAS Collab.)
AAD	13AW	PR D88 072001	G. Aad *et al.*	(ATLAS Collab.)
AAD	13C	PRL 110 011802	G. Aad *et al.*	(ATLAS Collab.)
AAD	13D	JHEP 1301 029	G. Aad *et al.*	(ATLAS Collab.)
AAD	13E	PR D87 015010	G. Aad *et al.*	(ATLAS Collab.)
CHATRCHYAN	13A	JHEP 1301 013	S. Chatrchyan *et al.*	(CMS Collab.)
CHATRCHYAN	13AD	JHEP 1307 178	S. Chatrchyan *et al.*	(CMS Collab.)
CHATRCHYAN	13AQ	PR D87 072005	S. Chatrchyan *et al.*	(CMS Collab.)
CHATRCHYAN	13BM	PRL 111 211804	S. Chatrchyan *et al.*	(CMS Collab.)
Also		PRL 112 119903 (errat.)	S. Chatrchyan *et al.*	(CMS Collab.)
CHATRCHYAN	13W	JHEP 1303 111	S. Chatrchyan *et al.*	(CMS Collab.)
CHEN	13A	CP C37 063102	J-B. Chen *et al.*	(DALI)
EDELHAUSER	13	JHEP 1308 091	L. Edelhauser, T. Flacke, M. Kramer	(AACH, KAIST)
XU	13	JP G40 035107	J. Xu *et al.*	
AAD	12AD	PL B712 331	G. Aad *et al.*	(ATLAS Collab.)
AAD	12BV	JHEP 1209 041	G. Aad *et al.*	(ATLAS Collab.)
AAD	12CC	JHEP 1211 138	G. Aad *et al.*	(ATLAS Collab.)
AAD	12CP	PL B718 411	G. Aad *et al.*	(ATLAS Collab.)
AAD	12X	PL B710 519	G. Aad *et al.*	(ATLAS Collab.)
AAD	12Y	PL B710 538	G. Aad *et al.*	(ATLAS Collab.)
AALTONEN	12V	PR D85 012008	T. Aaltonen *et al.*	(CDF Collab.)
ABAZOV	12M	PRL 108 131802	V.M. Abazov *et al.*	(D0 Collab.)
AJELLO	12	JCAP 1202 012	M. Ajello *et al.*	(Fermi-LAT Collab.)
BAAK	12	EPJ C72 2003	M. Baak *et al.*	(Gfitter Group)
FLACKE	12	PR D85 126007	T. Flacke, C. Pasold	(WURZ)
NISHIWAKI	12	PL B707 506	K. Nishiwaki *et al.*	(KOBE, OSAK)
AAD	11F	PRL 106 121803	G. Aad *et al.*	(ATLAS Collab.)
AAD	11X	EPJ C71 1744	G. Aad *et al.*	(ATLAS Collab.)
AALTONEN	11G	PR D83 112008	T. Aaltonen *et al.*	(CDF Collab.)
AALTONEN	11R	PRL 107 051801	T. Aaltonen *et al.*	(CDF Collab.)
AALTONEN	11U	PR D83 011102	T. Aaltonen *et al.*	(CDF Collab.)
AARON	11C	PL B705 52	F. D. Aaron *et al.*	(H1 Collab.)
ABAZOV	11H	PRL 107 011801	V.M. Abazov *et al.*	(D0 Collab.)
BEZERRA	11	PR D83 075004	V.B. Bezerra *et al.*	
SUSHKOV	11	PRL 107 171101	A.O. Sushkov *et al.*	
AALTONEN	10N	PRL 104 241801	T. Aaltonen *et al.*	(CDF Collab.)
ABAZOV	10F	PRL 104 241802	V.M. Abazov *et al.*	(D0 Collab.)
ABAZOV	10P	PRL 105 221802	V.M. Abazov *et al.*	(D0 Collab.)
BEZERRA	10	PR D81 055003	V.B. Bezerra *et al.*	
ABAZOV	09AE	PRL 103 191803	V.M. Abazov *et al.*	(D0 Collab.)
ABAZOV	09D	PRL 102 051601	V.M. Abazov *et al.*	(D0 Collab.)
MASUDA	09	PRL 102 171101	M. Masuda, M. Sasaki	(ICRR)
AALTONEN	08AC	PRL 101 181602	T. Aaltonen *et al.*	(CDF Collab.)
AALTONEN	08S	PR D78 012008	T. Aaltonen *et al.*	(CDF Collab.)
ABAZOV	08J	PRL 100 091802	V.M. Abazov *et al.*	(D0 Collab.)
ABAZOV	08S	PRL 101 011601	V.M. Abazov *et al.*	(D0 Collab.)
DAS	08	PR D78 063011	P.K. Das, V.H.S. Kumar, P.K. Suresh	
GERACI	08	PR D78 022002	A.A. Geraci *et al.*	(STAN)
TRENKEL	08	PR D77 122001	C. Trenkel	

Int. J. Mod. Phys. A 2026.41. Downloaded from www.worldscientific.com
by UNIVERSITY OF CALIFORNIA @ BERKELEY on 09/16/26. Re-use and distribution is strictly not permitted, except for Open Access articles.

AALTONEN	07G	PRL 99 171801	T. Aaltonen *et al.*	(CDF Collab.)
AALTONEN	07H	PRL 99 171802	T. Aaltonen *et al.*	(CDF Collab.)
DECCA	07A	EPJ C51 963	R.S. Decca *et al.*	
HAISCH	07	PR D76 034014	U. Haisch, A. Weiler	
KAPNER	07	PRL 98 021101	D.J. Kapner *et al.*	
SCHAEL	07A	EPJ C49 411	S. Schael *et al.*	(ALEPH Collab.)
TU	07	PRL 98 201101	L.-C. Tu *et al.*	
ABDALLAH	06C	EPJ C45 589	J. Abdallah *et al.*	(DELPHI Collab.)
ABULENCIA,A	06	PRL 97 171802	A. Abulencia *et al.*	(CDF Collab.)
GERDES	06	PR D73 112008	D. Gerdes *et al.*	
GOGOLADZE	06	PR D74 093012	I. Gogoladze, C. Macesanu	
ABAZOV	05N	PRL 95 091801	V.M. Abazov *et al.*	(D0 Collab.)
ABAZOV	05V	PRL 95 161602	V.M. Abazov *et al.*	(D0 Collab.)
ABDALLAH	05B	EPJ C38 395	J. Abdallah *et al.*	(DELPHI Collab.)
ABULENCIA	05A	PRL 95 252001	A. Abulencia *et al.*	(CDF Collab.)
SMULLIN	05	PR D72 122001	S.J. Smullin *et al.*	
ACHARD	04E	PL B587 16	P. Achard *et al.*	(L3 Collab.)
ACOSTA	04C	PRL 92 121802	D. Acosta *et al.*	(CDF Collab.)
BARBIERI	04	NP B703 127	R. Barbieri *et al.*	
CASSE	04	PRL 92 111102	M. Casse *et al.*	
CHEKANOV	04B	PL B591 23	S. Chekanov *et al.*	(ZEUS Collab.)
HOYLE	04	PR D70 042004	C.D. Hoyle *et al.*	(WASH)
ABAZOV	03	PRL 90 251802	V.M. Abazov *et al.*	(D0 Collab.)
ABBIENDI	03D	EPJ C26 331	G. Abbiendi *et al.*	(OPAL Collab.)
ACHARD	03D	PL B572 133	P. Achard *et al.*	(L3 Collab.)
ADLOFF	03	PL B568 35	C. Adloff *et al.*	(H1 Collab.)
CHIAVERINI	03	PRL 90 151101	J. Chiaverini *et al.*	
GIUDICE	03	NP B663 377	G.F. Giudice, A. Strumia	
HANNESTAD	03	PR D67 125008	S. Hannestad, G.G. Raffelt	
Also		PR D69 029901(errat.)	S. Hannestad, G.G. Raffelt	
HEISTER	03C	EPJ C28 1	A. Heister *et al.*	(ALEPH Collab.)
LONG	03	NAT 421 922	J.C. Long *et al.*	
ACHARD	02	PL B524 65	P. Achard *et al.*	(L3 Collab.)
ACHARD	02D	PL B531 28	P. Achard *et al.*	(L3 Collab.)
HANNESTAD	02	PRL 88 071301	S. Hannestad, G. Raffelt	
ABBOTT	01	PRL 86 1156	B. Abbott *et al.*	(D0 Collab.)
FAIRBAIRN	01	PL B508 335	M. Fairbairn	
HANHART	01	PL B509 1	C. Hanhart *et al.*	
HOYLE	01	PRL 86 1418	C.D. Hoyle *et al.*	
ABBIENDI	00R	EPJ C13 553	G. Abbiendi *et al.*	(OPAL Collab.)
ABREU	00A	PL B491 67	P. Abreu *et al.*	(DELPHI Collab.)
ABREU	00S	PL B485 45	P. Abreu *et al.*	(DELPHI Collab.)
ABREU	00Z	EPJ C17 53	P. Abreu *et al.*	(DELPHI Collab.)
CASSISI	00	PL B481 323	S. Cassisi *et al.*	
CHANG	00B	PRL 85 3765	L.N. Chang *et al.*	
CHEUNG	00	PR D61 015005	K. Cheung	
CORNET	00	PR D61 037701	F. Cornet, M. Relano, J. Rico	
GRAESSER	00	PR D61 074019	M.L. Graesser	
HAN	00	PR D62 125018	T. Han, D. Marfatia, R.-J. Zhang	
MATHEWS	00	JHEP 0007 008	P. Mathews, S. Raychaudhuri, K. Sridhar	
MELE	00	PR D61 117901	S. Mele, E. Sanchez	
RIZZO	00	PR D61 016007	T.G. Rizzo, J.D. Wells	
ABBIENDI	99P	PL B465 303	G. Abbiendi *et al.*	(OPAL Collab.)
ACCIARRI	99M	PL B464 135	M. Acciarri *et al.*	(L3 Collab.)
ACCIARRI	99R	PL B470 268	M. Acciarri *et al.*	(L3 Collab.)
ACCIARRI	99S	PL B470 281	M. Acciarri *et al.*	(L3 Collab.)
BOURILKOV	99	JHEP 9908 006	D. Bourilkov	
HOSKINS	85	PR D32 3084	J.K. Hoskins *et al.*	

WIMP and Dark Matter Searches

We omit papers on CHAMP's, millicharged particles, and other exotic particles.

GALACTIC WIMP SEARCHES

These limits are for weakly-interacting stable particles that may constitute the invisible mass in the galaxy. Unless otherwise noted, a local mass density of 0.3 GeV/cm^3 is assumed; see each paper for velocity distribution assumptions. In the papers the limit is given as a function of the X^0 mass. Here we list limits only for typical mass values of sub-GeV, GeV, 20 GeV, 100 GeV, and 1 TeV. Specific limits on supersymmetric dark matter particles may be found in the Supersymmetry section.

Spin-Independent Cross Section Limits for Dark Matter Particle (X^0) on Nucleon

For m_{X^0} in GeV range

We provide here limits fo m_{X^0} < 5 GeV

VALUE (pb)	CL%	DOCUMENT ID		TECN	COMMENT
• • • We do not use the following data for averages, fits, limits, etc. • • •					
<5000	90	[1] AALBERS	25A	LZ	cosmic ray boosted DM
		[2] ADAMS	25	PICO	fermionic DM absorption
< 2.5×10^{-9}	90	[3] APRILE	25	XENT	light DM search
< 2×10^{-3}	90	[4] APRILE	25A	XENT	light DM search
< 4×10^{4}	90	[5] BUI	25	TESS	light DM search
< 1.1×10^{-7}	90	[6] ZHANG	25B	PNDX	wimp search
< 3×10^{3}	90	[7] ANGLOHER	24	CRES	light WIMP via diamond
< 1×10^{4}	90	[8] ANGLOHER	24B	CRES	low mass DM search
< 3×10^{-3}	90	[9] AALBERS	23A	LZ	SI scatter on Xe
< 4×10^{-7}	90	[10] AGNES	23	DS50	LDM search via Migdal
< 6×10^{-7}	90	[11] AGNES	23B	DS50	LDM scatter on nucleons
< 0.5	90	[12] ALBAKRY	23	SCDM	LDM via Migdal
< 1	95	[13] AMBROSONE	23		DM distortion of CR spectra
< 70	90	[14] ANGLOHER	23	CRES	LDM search
< 8×10^{-8}	90	[15] LI	23F	PNDX	SI light DM limits
< 5×10^{-10}	90	[16] MA	23A	PNDX	LDM search
< 10	90	[17] ADHIKARI	22B	C100	sub-GeV WIMP via SI coupling/Migdal effect
< 1.4×10^{4}	90	[18] ARMENGAUD	22	EDEL	GeV-scale DM on Ge via Migdal effect
< 5×10^{5}	90	[19] CUI	22	PNDX	sub-GeV boosted DM
< 6.5×10^{6}	90	[20] XU	22	CDEX	sub-GeV DM
< 2×10^{-7}	95	[21] AKERIB	21A	LUX	low mass WIMPs
< 5×10^{6}	90	[22] ALKHATIB	21	SCDM	light DM
< 1×10^{8}	95	[23] ANDRIAMIR...	21A		sub-GeV DM on nucleon
< 1×10^{-8}	90	[24] APRILE	21	XE1T	GeV scale DM
< 8×10^{-4}	90	[25] AGUILAR-AR...	20C	DMIC	WIMP SI scatter on Si
< 8×10^{-4}	90	[26] AKERIB	20A	LUX	GeV-scale WIMP search
< 1×10^{-2}	90	[27] ABDELHAME...	19A	CRES	$CaWO_4$
< 5.4×10^{-6}	90	[28] AGNESE	19A	SCDM	GeV-scale WIMPs on Ge
< 1	90	[29] AKERIB	19	LUX	light DM on Xe via Migdal/brem effect
< 1×10^{-6}	90	[30] AMOLE	19	PICO	C_3F_8
< 1.6×10^{-3}	90	[31] APRILE	19C	XE1T	DM on Xe
< 1×10^{-7}	90	[32] APRILE	19D	XE1T	DM on Xe
< 0.1	90	[33] ARMENGAUD	19	EDEL	GeV-scale WIMPs on Ge
< 1.6×10^{3}	90	[34] KOBAYASHI	19	XMAS	annual modulation Xe
< 7×10^{2}	90	[35] LIU	19B	CDEX	Ge; sub-GeV DM via Migdal
< 7×10^{-7}	90	[36] AGNES	18	DS50	GeV-scale WIMPs on Ar
< 1.5×10^{-5}	95	[37] AGNESE	18	SCDM	GeV-scale WIMPs on Ge
< 2×10^{-8}	90	[38] APRILE	18	XE1T	Xe, SI
< 4.5×10^{-3}	90	[39] ARNAUD	18	NEWS	low mass WIMP, Ne
< 8×10^{-6}	90	[40] JIANG	18	CDEX	GeV-scale WIMPs on Ge
< 3×10^{-5}	90	[41] YANG	18	CDEX	WIMPs on Ge
< 1×10^{-6}	90	[42] AKERIB	17	LUX	Xe
< 1×10^{2}	90	[43] ANGLOHER	17A	CRES	GeV-scale WIMPs
< 7×10^{-5}	90	[44] ANGLOHER	16	CRES	$CaWO_4$
< 3×10^{-5}	90	[45] APRILE	16	X100	Xe
< 4.3×10^{-4}	90	[46] ARMENGAUD	16	EDE3	GeV-scale WIMPs on Ge
< 7×10^{-5}	90	[47] HEHN	16	EDE3	SI WIMP on Ge
< 6×10^{-5}	90	[48] ZHAO	16	CDEX	GeV-scale WIMPs on Ge
< 1×10^{-4}	90	[49] AMOLE	15	PICO	C_3F_8
< 8×10^{-5}	90	[50] XIAO	15	PNDX	WIMPs on Xe
< 3×10^{-5}	90	[51] AGNESE	14	SCDM	GeV-scale WIMPs
< 1×10^{-3}	90	[52] AKERIB	14	LUX	WIMP on Xe
< 9×10^{-4}	90	[53] LI	13B	TEXO	WIMPs on Ge
< 3×10^{-4}	90	[54] ARCHAMBAU...	12	PICA	C_4F_{10}
< 2×10^{-4}	90	[55] AALSETH	11	CGNT	GeV WIMPs on Ge
< 5×10^{-4}	90	[56] AHMED	11B	CDM2	GeV-scale WIMPs on Ge
< 8×10^{-5}	90	[57] ANGLE	11	XE10	Xe
< 5×10^{-4}	90	[58] AKERIB	10	CDM2	WIMPs on Ge/Si

[1] AALBERS 25A search for sub-GeV cosmic-ray boosted wimps at LZ. No signal observed. Limits placed in m(DM): 1×10^{-4}–1 GeV range vs. σ^{SI} plane. Quoted limit for m(DM) = 1 MeV.

[2] ADAMS 25 report on fermionic DM in MeV range search via DM absorption at PICO-60. No signal observed. Limits placed on absorption cross section for EFT operator O_4 vs. m(DM) .

[3] APRILE 25 report light DM search near edge of neutrino fog using XENONnT. No signal observed. Require $\sigma^{SI}(\chi N) < 2.5 \times 10^{-9}$ pb for m(χ) = 6 GeV.

[4] APRILE 25A search for light MeV-scale DM using XENONnT. No signal observed. Limits placed in various planes. Quoted limit for Halo light DM with heavy mediator Fig. 5b with m(χ) = 1 GeV.

[5] BUI 25 report search for light DM via phonons in TESSERACT detector. No signal observed. Limits placed in m(χ) vs. σ^{SI} plane for MeV-scale DM. Quoted limit is for m(χ) = 87 MeV.

[6] ZHANG 25B search for light GeV-scale wimps using run 0 and run 1 PandaX-4T data. No signal observed. Quoted limit is for m(χ) = 3 GeV.

[7] ANGLOHER 24 search for spin-independent light WIMP (mass between 0.16 and 6 GeV) scatter on diamond target. No signal observed. Limits placed in σ^{SI} vs mass plane for sub-GeV WIMPs. Quoted limit is for m(WIMP) = 0.2 GeV.

[8] ANGLOHER 24B search for low mass m(wimp) $\sim$ 100 MeV. No signal observed. Limits placed in cross section vs. mass plane. Quoted limit for m(wimp) = 100 MeV.

[9] AALBERS 23A search for *e* recoil events from GeV scale WIMP scatter on Xe. No signal observed. Limits placed on 6 different models including $\sigma^{SI} < 3 \times 10^{-3}$ for m(χ) $\sim$ 1 GeV via Migdal scattering.

[10] AGNES 23 for for light DM via *e* recoil/Migdal effect. No signal observed. $\sigma^{SI}(\chi N) < 4 \times 10^{-7}$ pb for m(χ) = 3 GeV.

[11] AGNES 23B search for GeV-scale DM scatter on nucleons in Ar. No signal observed. Limit $\sigma^{SI}(\chi N) < 6 \times 10^{-7}$ pb for m(χ) = 3 GeV.

[12] ALBAKRY 23 search for light DM via Migdal effect. No signal observed. Allow σ^{SI} < 0.5 pb for m(χ)=1 GeV (see e.g. Fig. 7).

[13] AMBROSONE 23 derive limits on $\sigma(\chi p)$ due to possible DM distortion of cosmic ray spectra in starburst galaxies. Limits placed in σ vs. mass (10^{-3}–10 MeV) plane, the most stringent given above being at 1 keV.

[14] ANGLOHER 23 search for light DM using Si target. No signal observed. Require σ^{SI} < 70 pb for m(χ) = 0.3 GeV (see e.g. Fig. 5).

[15] LI 23F searches for SI light DM scatter from Xe. No signal observed. The quoted limit for m(χ) = 4 GeV.

[16] MA 23A search for GeV-scale DM using PandaX-4T. No signal observed. $\sigma(\chi p) < 5 \times 10^{-10}$ pb for m(χ) = 10 GeV.

[17] ADHIKARI 22B search for sub-GeV WIMPs via SI and SD detection; no signal detected; limits placed in m(χ) vs. σ plane for m(χ): 0.2–3 GeV; quoted limit is for m(χ) = 1 GeV.

[18] ARMENGAUD 22 search for GeV-scale DM scatter on Ge at EDELWEISS via Migdal effect; no signal observed; limits placed in $\sigma^{SI}(\chi N)$ vs. m(DM) plane; quoted limit is for m(DM) = 100 MeV.

[19] CUI 22 search for sub-GeV boosted DM at PandaX-II at CJPL; no signal detected; limits set in $\sigma^{SI}(\chi p)$ vs. m(χ) plane; quoted limit for m(χ) = 0.1 GeV.

Int. J. Mod. Phys. A 2026.41. Downloaded from www.worldscientific.com
by UNIVERSITY OF CALIFORNIA @ BERKELEY on 09/16/26. Re-use and distribution is strictly not permitted, except for Open Access articles.

Int. J. Mod. Phys. A 2026.41. Downloaded from www.worldscientific.com
by UNIVERSITY OF CALIFORNIA @ BERKELEY on 09/16/26. Re-use and distribution is strictly not permitted, except for Open Access articles.

[20] XU 22 search for sub-GeV boosted DM in CDEX; no signal observed; limits placed in $\sigma(\chi N)$ vs. m(DM) plane; quoted limit is for m(DM) = 0.1 GeV.

[21] AKERIB 21A present new technique for low mass WIMP detection. Require $\sigma^{SI}(p\chi) < 2 \times 10^{-7}$ pb for m(WIMP) 10 GeV.

[22] ALKHATIB 21 search for light DM using SuperCDMS; require $\sigma^{SI}(p\chi) < 5 \times 10^{6}$ for m(DM) = 0.1 GeV.

[23] ANDRIAMIRADO 21A search for upscattered (boosted) sub-GeV DM interacting with proton in PROSPECT detector. No signal observed. Limits placed in $\sigma(\chi N)$ vs. m(DM) plane for m(DM) $\sim$ 1 keV − 0.5 GeV. The listed limit is for m(DM) = 1 keV.

[24] APRILE 21 search for low recoil energy GeV-scale DM in XENON1T with 1.6 keV threshold. No signal in 0.6 t y exposure. Limits placed in $\sigma^{SI}(\chi N)$ vs. m(DM) plane for m(DM) between 3–12 GeV. The listed limit is for m(DM) = 5 GeV.

[25] AGUILAR-AREVALO 20C search for WIMP SI scatter on Si using DAMIC at SNOLab; some excess; limits placed in σ vs m(DM) for m(DM) in 1.2–10 GeV; quoted limit for m(WIMP) = 2 GeV.

[26] AKERIB 20A search for GeV-scale WIMPs via WIMP-nucleon scatter with single photon emission; no signal; limits placed in m(WIMP) vs σ^{SI} plane: for example $\sigma^{SI}(\chi n) < 8 \times 10^{-4}$ pb for m(WIMP) = 2.5 GeV.

[27] ABDELHAMEED 19A search for GeV scale dark matter SI scatter on $CaWO_4$; no signal, limits placed in σ vs. mass plane for m(DM) $\sim$ 0.1–10 GeV. The listed limit is for m(DM) = 1 GeV.

[28] AGNESE 19A search for 1.5–10 GeV WIMP scatter on Ge in CDMSlite dataset. Limits set in a likelihood analysis. No signal was observed. Limit reported for m(χ) = 5 GeV.

[29] AKERIB 19 search for 0.4–5 GeV DM using bremsstrahlung photons and "Migdal" electrons; 1.4×10^{4} kg d exposure of liquid Xe; constraint $\sigma^{SI}(\chi N) < 1$ pb for m(χ) = 5 GeV in light scalar mediator model.

[30] AMOLE 19 search for SI WIMP scatter on C_3F_8 in PICO-60 bubble chamber; no signal: set limit for spin independent coupling $\sigma^{SI}(\chi N) < 1 \times 10^{-6}$ pb for m(χ) = 5 GeV.

[31] APRILE 19C search for light DM scatter on Xe via atomic excitation, ionization (Migdal effect) or bremsstrahlung; no signal, limits placed in σ vs. m(DM) plane for m(DM) $\sim$ 0.085–2 GeV. The listed limit is for m(DM) = 1 GeV.

[32] APRILE 19D search for light DM scatter on Xe via ionization to probe SI, SD, and χe cross sections; with 22 t d exposure, limits placed in various σ vs. m(DM) planes. Quoted limit is for m(DM) = 5 GeV.

[33] ARMENGAUD 19search for GeV scale WIMP scatter on Ge; limits placed in $\sigma^{SI}(\chi N)$ vs. m(χ) plane for m(χ) $\sim$ 0.045–10 GeV; quoted limit is for m(χ) = 5 GeV.

[34] KOBAYASHI 19 search for sub-GeV WIMP annual modulation in Xe via brems; no signal; limits placed in $\sigma^{SI}(\chi N)$ vs. m(χ) plane for m $\sim$ 0.3–1 GeV; quoted limit is for m(χ) = 0.5 GeV.

[35] LIU 19B seach for sub-GeV DM using Migdal effect on Ge at CDEX-IB; no signal, require $\sigma^{SI}(\chi N) < 7 \times 10^{2}$ pb for m(χ) = 0.1 GeV.

[36] AGNES 18 search for 1.8–20 GeV WIMP SI scatter on Ar; quoted limit is for m(χ) = 5 GeV.

[37] AGNESE 18 search for GeV scale WIMPs using CDMSlite; limits placed in $\sigma^{SI}(\chi N)$ vs. m(χ) plane for m $\sim$ 1.5–20 GeV; quoted limit is for m(χ) = 5 GeV.

[38] APRILE 18 search for WIMP scatter on 1 t yr Xe; no signal, limits set in $\sigma(\chi N)$ vs. m(χ) plane for m(χ) $\sim$ 6–1000 GeV; quoted limit is for m = 6 GeV.

[39] ARNAUD 18 search for low mass WIMP scatter on Ne via SPC at NEWS-G; limits set in $\sigma^{SI}(\chi N)$ vs. m(χ) plane for m $\sim$ 0.5–20 GeV; quoted limit is for m = 5 GeV.

[40] JIANG 18 search for GeV scale WIMP scatter on Ge; limits placed in $\sigma^{SI}(\chi N)$ vs. m(χ) plane for m(χ) $\sim$ 3–10 GeV; quoted limit is for m(χ) = 5 GeV.

[41] YANG 18 search for WIMP scatter on Ge; limits placed in $\sigma^{SI}(\chi N)$ vs. m(χ) plane for m(χ) $\sim$ 2–10 GeV; quoted limit is for m(χ) = 5 GeV.

[42] AKERIB 17 search for WIMP scatter on Xe; limits placed in $\sigma^{SI}(\chi N)$ vs. m(χ) plane for m(χ) $\sim$ 5–1×10^{5} GeV; quoted limit is for m(χ) = 5 GeV.

[43] ANGLOHER 17A search for GeV scale WIMP scatter on Al_2O_3 crystal; limits placed in $\sigma^{SI}(\chi N)$ vs. m(χ) plane for m(χ) $\sim$ 0.15–10 GeV; quoted limit is for m(χ) = 5 GeV.

[44] ANGLOHER 16 search for GeV scale WIMP scatter on $CaWO_4$; limits placed in $\sigma^{SI}(\chi N)$ vs. m(χ) plane for m(χ) $\sim$ 0.5–30 GeV; quoted limit is for m(χ) = 5 GeV.

[45] APRILE 16 search for low mass WIMPs via ionization at XENON100; limits placed in $\sigma^{SI}(\chi N)$ vs m(χ) plane for m $\sim$ 3.5–20 GeV; quoted limit is for m(χ) = 5 GeV.

[46] ARMENGAUD 16 search for GeV scale WIMP scatter on Ge; limits placed in $\sigma^{SI}(\chi N)$ vs. m(χ) plane for m(χ) $\sim$ 4–30 GeV; quoted limit is for m(χ) = 5 GeV.

[47] HEHN 16 search for low mass WIMPs via SI scatter on Ge target using profile likelihood analysis; limits placed in $\sigma^{SI}(\chi N)$ vs. m(χ) plane for m(χ) $\sim$ 4–30 GeV; quoted limit is for m(χ) = 5 GeV.

[48] ZHAO 16 search for GeV-scale WIMP scatter on Ge; limits placed in $\sigma^{SI}(\chi N)$ vs. m(χ) plane for m(χ) $\sim$ 4–30 GeV; quoted limit is for m(χ) = 5 GeV.

[49] AMOLE 15 search for WIMP scatter on C_3F_8 in PICO-2L; limits placed in $\sigma^{SI}(\chi N)$ vs. m(χ) plane for m(χ) $\sim$ 4–25 GeV; quoted limit is for m(χ) = 5 GeV.

[50] XIAO 15 search for WIMP scatter on Xe with PandaX-I; limits placed in $\sigma^{SI}(\chi N)$ vs. m(χ) plane for m(χ) $\sim$ 5–100 GeV; quoted limit is for m(χ) = 5 GeV.

[51] AGNESE 14 search for GeV scale WIMPs SI scatter at SuperCDMS; no signal, limits placed in $\sigma^{SI}(\chi N)$ vs. m(χ) plane for m(χ) $\sim$ 3.5–30 GeV; quoted limit is for m(χ) = 5 GeV.

[52] AKERIB 14 search for WIMP scatter on Xe; limits placed in $\sigma^{SI}(\chi N)$ vs. m(χ) plane for m(χ) $\sim$ 5–5000 GeV. Limit given for m(χ) = 5 GeV.

[53] LI 13B search for WIMP scatter on Ge; limits placed in $\sigma^{SI}(\chi N)$ vs. m(χ) plane for m(χ) $\sim$ 4–100 GeV; quoted limit is for m(χ) = 5 GeV.

[54] ARCHAMBAULT 12 search for low mass WIMP scatter on C_4F_{10}; limits set in $\sigma^{SI}(\chi N)$ vs. m(χ) plane for m $\sim$ 4–12 GeV; quoted limit is for m = 5 GeV.

[55] AALSETH 11 search for GeV-scale SI WIMP scatter on Ge; limits placed on $\sigma^{SI}(\chi N)$ for m(χ) $\sim$ 3.5–100 GeV; quoted limit is for m(χ) = 5 GeV.

[56] AHMED 11B search for GeV scale WIMP scatter on Ge in CDMS II; limits placed in $\sigma^{SD}(\chi n)$ vs. m(χ) plane for m $\sim$ 4–12 GeV.

[57] ANGLE 11 search for GeV scale WIMPs in Xenon-10; limits placed in $\sigma^{SI}(\chi N)$ vs. m(χ) plane for m(χ) $\sim$ 4–20 GeV; quoted limit is for m(χ) = 5 GeV.

[58] AKERIB 10 search for WIMP scatter on Ge/Si in CDMS II; limits place in $\sigma_{SI}(\chi N)$ vs. m(χ) plane for m $\sim$ 3–100 GeV. Limit given for m(DM) = 5 GeV.

For m_{χ^0} = 20 GeV

For limits from χ^0 annihilation in the Sun, the assumed annihilation final state is shown in parenthesis in the comment.

VALUE (pb)	CL%	DOCUMENT ID		TECN	COMMENT
• • • We do not use the following data for averages, fits, limits, etc. • • •					
$<3 \times 10^{-12}$	90	[1] AALBERS	25	LZ	SI wimp DM search
$<2 \times 10^{-11}$	90	[2] APRILE	25B	XENT	wimp search
$<3 \times 10^{-11}$	90	[3] BO	25	PNDX	wimp search
$<2 \times 10^{-4}$	90	[4] DAS	25	INDX	DM search
$<8 \times 10^{5}$	95	[5] UMEMOTO	25	NIT	directional nano-imaging DM search
$<1 \times 10^{-6}$	90	[6] YU	25	C100	wimp search
$<3 \times 10^{-3}$	90	[7] ANGLOHER	24A	COSN	WIMP search
$<1 \times 10^{-11}$	90	[8] AALBERS	23	LZ	SI scatter on Xe
$<2 \times 10^{-7}$	90	[9] ABE	23E	XMAS	WIMP search
$<4 \times 10^{-11}$	90	[10] APRILE	23A	XENT	Si WIMP search
$<5 \times 10^{-11}$	90	[11] MENG	21B	PNDX	Xe WIMP search
$<5 \times 10^{-5}$		[12] FELIZARDO	20	SMPL	C_2ClF_5
$<2.2 \times 10^{-10}$	90	[13] WANG	20G	PNDX	Xe TPC
		[14] ANGLOHER	19	CRES	$CaWO_4$
$<7 \times 10^{-5}$	90	[15] KIM	19A	KIMS	NaI
$<3 \times 10^{-7}$	90	[16] KOBAYASHI	19	XMAS	SI WIMP on Xe
		[17] SEONG	19	BELL	$\Upsilon \to \gamma A$, $A \to \chi\chi$
$<3.5 \times 10^{-5}$	90	[18] YANG	19	CDEX	annual modulation Ge
$<2 \times 10^{-7}$	90	[19] ABE	18C	XMAS	X^0- Xe modulation
$<1.44 \times 10^{-5}$	90	[20] ADHIKARI	18	C100	NaI
$<3 \times 10^{-7}$	90	[21] AGNES	18	DS50	X^0-Ar
$<5 \times 10^{-6}$	95	[22] AGNESE	18	SCDM	Ge
$<4 \times 10^{-8}$	90	[23] AGNESE	18A	SCDM	Ge
$<6 \times 10^{-11}$	90	[24] APRILE	18	XE1T	Xe, SI
$<4.5 \times 10^{-3}$	90	[25] ARNAUD	18	NEWS	GeV WIMPs on Ne
$<2 \times 10^{-6}$	90	[26] AARTSEN	17	ICCB	ν, earth
$<2 \times 10^{-10}$	90	[27] AKERIB	17	LUX	Xe
$<1 \times 10^{-3}$	90	[28] BARBOSA-D...	17	ICCB	NaI
$<1.7 \times 10^{-10}$	90	[29] CUI	17A	PNDX	WIMPs on Xe
$<7.3 \times 10^{-7}$	90	AGNES	16	DS50	Ar
$<1 \times 10^{-5}$	90	[30] AGNESE	16	CDMS	Ge
$<2 \times 10^{-4}$	90	[31] AGUILAR-AR...	16	DMIC	Si CCDs
$<4.5 \times 10^{-5}$	90	[32] ANGLOHER	16	CRES	$CaWO_4$
$<2 \times 10^{-6}$	90	[33] APRILE	16	X100	Xe
$<9.4 \times 10^{-8}$	90	[34] ARMENGAUD	16	EDE3	Ge
$<1.0 \times 10^{-7}$	90	[35] HEHN	16	EDE3	Ge
$<5 \times 10^{-6}$	90	[36] ZHAO	16	CDEX	Ge
$<1 \times 10^{-5}$	90	AGNES	15	DS50	Ar
$<1.5 \times 10^{-6}$	90	[37] AGNESE	15A	CDM2	Ge
$<1.5 \times 10^{-7}$	90	[38] AGNESE	15B	CDM2	Ge
$<2 \times 10^{-6}$	90	[39] AMOLE	15	PICO	C_3F_8
$<1.2 \times 10^{-5}$	90	CHOI	15	SKAM	H, solar ν ($b\overline{b}$)
$<1.19 \times 10^{-6}$	90	CHOI	15	SKAM	H, solar ν ($\tau^+\tau^-$)
$<2 \times 10^{-8}$	90	[40] XIAO	15	PNDX	Xe
$<2.0 \times 10^{-7}$	90	[41] AGNESE	14	SCDM	Ge
$<3.7 \times 10^{-5}$	90	[42] AGNESE	14A	SCDM	Ge
$<1 \times 10^{-9}$	90	[43] AKERIB	14	LUX	Xe
$<2 \times 10^{-6}$	90	[44] ANGLOHER	14	CRES	$CaWO_4$
$<5 \times 10^{-6}$	90	FELIZARDO	14	SMPL	C_2ClF_5
$<8 \times 10^{-6}$	90	[45] LEE	14A	KIMS	CsI
$<2 \times 10^{-4}$	90	[46] LIU	14A	CDEX	Ge
$<1 \times 10^{-5}$	90	[47] YUE	14	CDEX	Ge
$<1.08 \times 10^{-4}$	90	[48] AARTSEN	13	ICCB	H, solar ν ($\tau^+\tau^-$)
$<1.5 \times 10^{-5}$	90	[49] ABE	13B	XMAS	Xe
$<3.1 \times 10^{-6}$	90	[50] AGNESE	13	CDM2	Si
$<3.4 \times 10^{-6}$	90	[51] AGNESE	13A	CDM2	Si
$<2.2 \times 10^{-6}$	90	[52] AGNESE	13A	CDM2	Si
		[53] BERNABEI	13A	DAMA	NaI modulation
$<1.2 \times 10^{-4}$	90	[54] LI	13B	TEXO	Ge
		[55] ZHAO	13	CDEX	Ge
$<1.2 \times 10^{-7}$	90	AKIMOV	12	ZEP3	Xe
		[56] ANGLOHER	12	CRES	$CaWO_4$
$<8 \times 10^{-6}$	90	[57] ANGLOHER	12	CRES	$CaWO_4$
$<7 \times 10^{-9}$	90	[58] APRILE	12	X100	Xe
$<7 \times 10^{-7}$	90	[59] ARMENGAUD	12	EDE2	Ge
		[60] BARRETO	12	DMIC	CCD
$<2 \times 10^{-6}$	90	BEHNKE	12	COUP	CF_3I
$<7 \times 10^{-6}$		[61] FELIZARDO	12	SMPL	C_2ClF_5
$<1.5 \times 10^{-6}$	90	KIM	12	KIMS	CsI
$<5 \times 10^{-5}$	90	[62] AALSETH	11	CGNT	Ge
		[63] AALSETH	11A	CGNT	Ge
$<5 \times 10^{-7}$	90	[64] AHMED	11	CDM2	Ge, inelastic
$<2.7 \times 10^{-7}$	90	[65] AHMED	11A	RVUE	Ge
$<3 \times 10^{-6}$	90	[66] ANGLE	11	XE10	Xe
$<7 \times 10^{-8}$	90	[67] APRILE	11	X100	Xe
		[68] APRILE	11A	X100	Xe, inelastic
$<2 \times 10^{-8}$	90	[58] APRILE	11B	X100	Xe
		[69] HORN	11	ZEP3	Xe
$<2 \times 10^{-7}$	90	AHMED	10	CDM2	Ge

<1	$\times 10^{-5}$	90	[70] AKERIB	10	CDM2	Si, Ge, low threshold
<1	$\times 10^{-7}$	90	APRILE	10	X100	Xe
<2	$\times 10^{-6}$	90	ARMENGAUD	10	EDE2	Ge
<4	$\times 10^{-5}$	90	FELIZARDO	10	SMPL	C_2ClF_3
<1.5	$\times 10^{-7}$	90	[71] AHMED	09	CDM2	Ge
<2	$\times 10^{-4}$	90	[72] LIN	09	TEXO	Ge
			[73] AALSETH	08	CGNT	Ge

[1] AALBERS 25 report search for SI WIMP interaction at LZ using 4.2 ton-years exposure. No signal observed. Limits placed in m(DM) vs. $\sigma^{SI}(\chi N)$ plane.

[2] APRILE 25B search for wimps using 3.1 ton-years of data. No signal observed. Limits placed in σ^{SI} vs m(χ) plane.

[3] BO 25 search for wimp dark matter with PandaX-4T. No signal detected. Limits placed in $\sigma^{SI}(\chi N)$ vs. m(χ) plane.

[4] DAS 25 report WIMP DM search with InDEx detector. No signal observed. Limits placed in σ vs. m plane.

[5] UMEMOTO 25 report on directional DM search using nano-imaging tracking (NIT) emulsion device. No signal observed. Limits placed in $\sigma^{SI}(\chi N)$ vs. m(χ) plane.

[6] YU 25 report on COSINE-100 wimp search in 3-year data. No signal observed. Limits placed in σ^{SI} vs m(χ) plane.

[7] ANGLOHER 24A search for WIMP scatter on NaI target. No signal observed. Limits placed in σ^{SI} vs m plane.

[8] AALBERS 23 present first limits for WIMP scatter on Xe. $\sigma^{SI}(\chi p) < 1 \times 10^{-11}$ pb for m(χ) = 20 GeV.

[9] ABE 23E search for WIMP scatter on Xe in XMASS. No signal observed. Require $\sigma^{SI} < 2 \times 10^{-7}$ pb for m(χ) = 20 GeV.

[10] APRILE 23A present first results from Xe-nton SI WIMP search. No signal observed. Quoted limit is for m(χ) = 20 GeV.

[11] MENG 21B search for SI WIMP interaction with 3.7 t Xe and 0.63 t yr exposure. No signal observed. Limits placed in m(DM) vs. σ^{SI} plane.

[12] FELIZARDO 20 presents 2014 SIMPLE bounds on WIMP DM using C_2ClF_5 target.

[13] WANG 20G search for SI WIMP scatter on Xe with 132 t d exposure of PANDAX-II.

[14] ANGLOHER 19 search for low mass WIMP scatter on $CaWO_4$; no signal; limits placed on Wilson coefficients for m(χ) = 0.6–60 GeV.

[15] KIM 19A search for WIMP scatter in NaI KIMS experiment; no signal: require $\sigma^{SI}(\chi n) < 7 \times 10^{-5}$ pb for m(χ) = 20 GeV.

[16] KOBAYASHI 19 search for WIMP scatter in XMASS single-phase liquid Xe detector; no signal; require $\sigma^{SI}(\chi N) < 3 \times 10^{-7}$ pb for m(χ) = 20 GeV.

[17] SEONG 19 search for $\Upsilon \rightarrow \gamma A$, $A \rightarrow \chi\chi$ via CP-odd Higgs; no signal; limits on BF set; model dependent conversion to WIMP-nucleon scattering cross section limits $\sigma^{SI} < 10^{-36}$ cm^2 for m(χ) = 0.01–1 GeV.

[18] YANG 19 search for low mass wimps via annual modulation in Ge; no signal; require $\sigma^{SI}(\chi N) < 3.5 \times 10^{-5}$ pb for m(χ) = 20 GeV.

[19] ABE 18C search for WIMP annual modulation signal for m(WIMP): 6–20 GeV; limits set on SI WIMP-nucleon cross section: see Fig. 6.

[20] ADHIKARI 18 search for WIMP scatter on NaI; no signal; require $\sigma^{SI} < 1.44 \times 10^{-5}$ pb for m(WIMP) = 20 GeV; inconsistent with DAMA/LIBRA result.

[21] AGNES 18 search low mass m(WIMP): 1.8–20 GeV scatter on Ar; limits on SI WIMP-nucleon cross section set in Fig. 8.

[22] AGNESE 18 give limits for $\sigma^{SI}(\chi N)$ for m(WIMP) between 1.5 and 20 GeV using CDMSlite mode data.

[23] AGNESE 18A search for WIMP scatter on Ge at SuperCDMS; 1 event, consistent with expected background; set limit in $\sigma^{SI}(\chi N)$ vs. m(χ) plane for m $\sim$ 10–250 GeV.

[24] APRILE 18 search for WIMP scatter on 1 t yr Xe; no signal, limits placed in $\sigma^{SI}(\chi N)$ vs. m(χ) plane for m(χ) $\sim$ 6–1000 GeV.

[25] ARNAUD 18 search for low mass WIMP scatter on Ne via SPC at NEWS-G; limits set in $\sigma^{SI}(\chi N)$ vs. m(χ) plane for m $\sim$ 0.5–20 GeV.

[26] AARTSEN 17 obtain σ(SI) $< 6 \times 10^{-6}$ pb for m(wimp) = 20 GeV from ν from earth.

[27] AKERIB 17 search for WIMP scatter on Xe; limits placed in $\sigma^{SI}(\chi N)$ vs. m(χ) plane for m(χ) $\sim$ 5–1 $\times 10^5$ GeV.

[28] BARBOSA-DE-SOUZA 17 search for annual modulation of WIMP scatter on NaI using an exposure of 61 kg yr of DM-Ice17 for recoil energy in the 4–20 keV range (DAMA found modulation for recoil energy $<$ 5 keV). No modulation seen. Sensitivity insufficient to distinguish DAMA signal from null.

[29] CUI 17A search for SI WIMP scatter; limits placed in $\sigma^{SI}(\chi N)$ vs. m(χ) plane for m $\sim$ 10–1 $\times 10^4$ GeV using 54 ton-day exposure of Xe.

[30] AGNESE 16 CDMSlite excludes low mass WIMPs 1.6–5.5 GeV and SI scattering cross section depending on m(WIMP); see Fig. 4.

[31] AGUILAR-AREVALO 16 search low mass 1–10 GeV WIMP scatter on Si CCDs; set limits Fig. 11.

[32] ANGLOHER 16 search for GeV scale WIMP scatter on $CaWO_4$; limits placed in $\sigma^{SI}(\chi N)$ vs. m(χ) plane for m(χ) $\sim$ 0.5–30 GeV.

[33] APRILE 16 search for low mass WIMPs via ionization at XENON100; limits placed in $\sigma^{SI}(\chi N)$ vs m(χ) plane for m $\sim$ 3.5–20 GeV.

[34] ARMENGAUD 16 search for GeV scale WIMP scatter on Ge; limits placed in $\sigma^{SI}(\chi N)$ vs. m(χ) plane for m(χ) $\sim$ 4–30 GeV.

[35] HEHN 16 search for low mass WIMPs via SI scatter on Ge target using profile likelihood analysis; limits placed in $\sigma^{SI}(\chi N)$ vs. m(χ) plane for m(χ) $\sim$ 4–30 GeV.

[36] ZHAO 16 search for GeV-scale WIMP scatter on Ge; limits placed in $\sigma^{SI}(\chi N)$ vs. m(χ) plane for m(χ) $\sim$ 4–30 GeV.

[37] AGNESE 15A reanalyse AHMED 11B low threshold data. See their Fig. 12 (left) for improved limits extending down to 5 GeV.

[38] AGNESE 15B reanalyse AHMED 10 data.

[39] See their Fig. 7 for limits extending down to 4 GeV.

[40] XIAO 15 search for WIMP scatter on Xe with PandaX-I; limits placed in $\sigma^{SI}(\chi N)$ vs. m(χ) plane for m(χ) $\sim$ 5–100 GeV.

[41] This limit value is provided by the authors. See their Fig. 4 for limits extending down to $m_{X^0} = 3.5$ GeV.

[42] This limit value is provided by the authors. AGNESE 14A result is from CDMSlite mode operation with enhanced sensitivity to low mass m_{X^0}. See their Fig. 3 for limits extending down to $m_{X^0} = 3.5$ GeV (see also Fig. 4 in AGNESE 14).

[43] See their Fig. 5 for limits extending down to $m_{X^0} = 5.5$ GeV.

[44] See their Fig. 5 for limits extending down to $m_{X^0} = 1$ GeV.

[45] See their Fig. 5 for limits extending down to $m_{X^0} = 5$ GeV.

[46] LIU 14A result is based on prototype CDEX-0 detector. See their Fig. 13 for limits extending down to $m_{X^0} = 2$ GeV.

[47] See their Fig. 4 for limits extending down to $m_{X^0} = 4.5$ GeV.

[48] AARTSEN 13 search for neutrinos from the Sun arising from the pair annihilation of X^0 trapped by the sun in data taken between June 2010 and May 2011.

[49] See their Fig. 8 for limits extending down to $m_{X^0} = 7$ GeV.

[50] This limit value is provided by the authors. AGNESE 13 use data taken between Oct. 2006 and July 2007. See their Fig. 4 for limits extending down to $m_{X^0} = 7$ GeV.

[51] This limit value is provided by the authors. AGNESE 13A use data taken between July 2007 and Sep. 2008. Three candidate events are seen. Assuming these events are real, the best fit parameters are $m_{X^0} = 8.6$ GeV and $\sigma = 1.9 \times 10^{-5}$ pb.

[52] This limit value is provided by the authors. Limit from combined data of AGNESE 13 and AGNESE 13A. See their Fig. 4 for limits extending down to $m_{X^0} = 5.5$ GeV.

[53] BERNABEI 13A search for annual modulation of counting rate in the 2–6 keV recoil energy interval, in a 14 yr live time exposure of 1.33 t yr. Find a modulation of 0.0112 $\pm$ 0.0012 counts/(day kg keV) with 9.3 sigma C.L. Find period and phase in agreement with expectations from DM particles.

[54] LI 13B search for WIMP scatter on Ge; limits placed in $\sigma^{SI}(\chi N)$ vs. m(χ) plane for m(χ) $\sim$ 4–100 GeV.

[55] See their Fig. 5 for limits for m_{X^0} = 4–12 GeV.

[56] ANGLOHER 12 observe excess events above the expected background which are consistent with X^0 with mass $\sim$ 25 GeV (or 12 GeV) and spin-independent X^0-nucleon cross section of 2×10^{-6} pb (or 4×10^{-5} pb).

[57] Reanalysis of ANGLOHER 09 data with all three nuclides. See also BROWN 12.

[58] See also APRILE 14A.

[59] See their Fig. 4 for limits extending down to $m_{X^0} = 7$ GeV.

[60] See their Fig. 13 for cross section limits for m_{X^0} between 1.2 and 10 GeV.

[61] See also DAHL 12 for a criticism.

[62] See their Fig. 4 for limits extending to $m_{X^0} = 3.5$ GeV.

[63] AALSETH 11A find indications of annual modulation of the data, the energy spectrum being compatible with X^0 mass around 8 GeV. See also AALSETH 13.

[64] AHMED 11 search for X^0 inelastic scattering. See their Fig. 8–10 for limits. The inelastic cross section reduces to the elastic cross section at the limit of zero mass splitting (Fig. 8, left).

[65] AHMED 11A combine CDMS II and EDELWEISS data.

[66] ANGLE 11 show limits down to $m_{X^0} = 4$ GeV on Fig. 3.

[67] APRILE 11 reanalyze APRILE 10 data.

[68] APRILE 11A search for X^0 inelastic scattering. See their Fig. 2 and 3 for limits. See also APRILE 14A.

[69] HORN 11 perform detector calibration by neutrons. Earlier results are only marginally affected.

[70] See their Fig. 10 and 12 for limits extending to X^0 mass of 1 GeV.

[71] Superseded by AHMED 10.

[72] See their Fig. 6(a) for cross section limits for m_{X^0} extending down to 2 GeV.

[73] See their Fig. 2 for cross section limits for m_{X^0} between 4 and 10 GeV.

For m_{X^0} = 100 GeV

For limits from X^0 annihilation in the Sun, the assumed annihilation final state is shown in parenthesis in the comment.

VALUE (pb)	CL%	DOCUMENT ID		TECN	COMMENT
• • • We do not use the following data for averages, fits, limits, etc. • • •					
$<3 \times 10^{-12}$	90	[1] AALBERS	25	LZ	SI wimp DM search
$<3.9 \times 10^{-11}$	90	[2] APRILE	25B	XENT	wimp search
$<3 \times 10^{-11}$	90	[3] BO	25	PNDX	wimp search
$<1 \times 10^{5}$	95	[4] UMEMOTO	25	NIT	directional nano-imaging DM search
$<8 \times 10^{-8}$	90	[5] YU	25	C100	wimp search
$<1 \times 10^{-3}$	90	[6] ANGLOHER	24A	COSN	WIMP search
$<2.5 \times 10^{-11}$	90	[7] AALBERS	23	LZ	SI scatter on Xe
$<2 \times 10^{-8}$	90	[8] ABE	23E	XMAS	WIMP search
$<6 \times 10^{-11}$	90	[9] APRILE	23A	XENT	SI WIMP search
$<6 \times 10^{-11}$	90	[10] MENG	21B	PNDX	Xe WIMP search
		[11] ADHIKARI	20	DEAP	Ar
$<5 \times 10^{-5}$		[12] FELIZARDO	20	SMPL	W
$<4.2 \times 10^{-10}$	90	[13] WANG	20G	PNDX	Xe TPC
$<4 \times 10^{-8}$	90	[14] ABE	19	XMAS	Xe
$<3.9 \times 10^{-9}$	90	[15] AJAJ	19	DEAP	Ar
$<2.3 \times 10^{-6}$	90	[16] ADHIKARI	18	C100	NaI
$<1.14 \times 10^{-8}$	90	[17] AGNES	18A	DS50	Ar
$<2 \times 10^{-8}$	90	[18] AGNESE	18A	CDMS	Ge
$<1.2 \times 10^{-8}$	90	[19] AMAUDRUZ	18	DEAP	Ar
$<9.12 \times 10^{-11}$	90	[20] APRILE	18	XE1T	Xe
		[21] REN	18	PNDX	SIDM at PDX-II
$<1.7 \times 10^{-10}$	90	[22] AKERIB	17	LUX	Xe
$<1.2 \times 10^{-10}$	90	[23] APRILE	17G	XE1T	Xe
$<1.2 \times 10^{-10}$	90	[24] CUI	17A	PNDX	Xe
$<2.0 \times 10^{-8}$	90	AGNES	16	DS50	Ar
$<1 \times 10^{-9}$	90	[25] AKERIB	16	LUX	Xe
$<1 \times 10^{-9}$	90	[26] APRILE	16B	X100	Xe
$<2 \times 10^{-8}$	90	[27] TAN	16	PNDX	Xe

Int. J. Mod. Phys. A 2026.41. Downloaded from www.worldscientific.com
by UNIVERSITY OF CALIFORNIA @ BERKELEY on 09/16/26. Re-use and distribution is strictly not permitted, except for Open Access articles.

Int. J. Mod. Phys. A 2026.41. Downloaded from www.worldscientific.com
by UNIVERSITY OF CALIFORNIA @ BERKELEY on 09/16/26. Re-use and distribution is strictly not permitted, except for Open Access articles.

<4	$\times 10^{-10}$	90	[28] TAN	16B	PNDX	Xe
<6	$\times 10^{-8}$	90	AGNES	15	DS50	Ar
<4	$\times 10^{-8}$	90	[29] AGNESE	15B	CDM2	Ge
<7.13	$\times 10^{-6}$	90	CHOI	15	SKAM	H, solar ν ($b\overline{b}$)
<6.26	$\times 10^{-7}$	90	CHOI	15	SKAM	H, solar ν ($W^+ W^-$)
<2.76	$\times 10^{-7}$	90	CHOI	15	SKAM	H, solar ν ($\tau^+ \tau^-$)
<1.5	$\times 10^{-8}$	90	[30] XIAO	15	PNDX	Xe
<1	$\times 10^{-9}$	90	AKERIB	14	LUX	Xe
<4.0	$\times 10^{-6}$	90	[31] AVRORIN	14	BAIK	H, solar ν ($W^+ W^-$)
<1.0	$\times 10^{-4}$	90	[31] AVRORIN	14	BAIK	H, solar ν ($b\overline{b}$)
<1.6	$\times 10^{-6}$	90	[31] AVRORIN	14	BAIK	H, solar ν ($\tau^+ \tau^-$)
<5	$\times 10^{-6}$	90	FELIZARDO	14	SMPL	C_2ClF_5
<6.01	$\times 10^{-7}$	90	[32] AARTSEN	13	ICCB	H, solar ν ($W^+ W^-$)
<3.30	$\times 10^{-5}$	90	[32] AARTSEN	13	ICCB	H, solar ν ($b\overline{b}$)
<1.9	$\times 10^{-6}$	90	[33] ADRIAN-MAR.	13	ANTR	H, solar ν ($W^+ W^-$)
<1.2	$\times 10^{-4}$	90	[33] ADRIAN-MAR.	13	ANTR	H, solar ν ($b\overline{b}$)
<7.6	$\times 10^{-7}$	90	[33] ADRIAN-MAR.	13	ANTR	H, solar ν ($\tau^+ \tau^-$)
<2	$\times 10^{-6}$	90	[34] AGNESE	13	CDM2	Si
<1.6	$\times 10^{-6}$	90	[35] BOLIEV	13	BAKS	H, solar ν ($W^+ W^-$)
<1.9	$\times 10^{-5}$	90	[35] BOLIEV	13	BAKS	H, solar ν ($b\overline{b}$)
<7.1	$\times 10^{-7}$	90	[35] BOLIEV	13	BAKS	H, solar ν ($\tau^+ \tau^-$)
<3.2	$\times 10^{-4}$	90	[36] LI	13B	TEXO	WIMPs on Ge
<1.67	$\times 10^{-6}$	90	[37] ABBASI	12	ICCB	H, solar ν ($W^+ W^-$)
<1.07	$\times 10^{-4}$	90	[37] ABBASI	12	ICCB	H, solar ν ($b\overline{b}$)
<4	$\times 10^{-8}$	90	AKIMOV	12	ZEP3	Xe
<1.4	$\times 10^{-6}$	90	[38] ANGLOHER	12	CRES	$CaWO_4$
<3	$\times 10^{-9}$	90	[39] APRILE	12	X100	Xe
<3	$\times 10^{-7}$	90	BEHNKE	12	COUP	CF_3I
<7	$\times 10^{-6}$		FELIZARDO	12	SMPL	C_2ClF_5
<2.5	$\times 10^{-7}$	90	[40] KIM	12	KIMS	CsI
<2	$\times 10^{-4}$	90	AALSETH	11	CGNT	Ge
			[41] AHMED	11	CDM2	Ge, inelastic
<3.3	$\times 10^{-8}$	90	[42] AHMED	11A	RVUE	Ge
			[43] AJELLO	11	FLAT	
<3	$\times 10^{-8}$	90	[44] APRILE	11	X100	Xe
			[45] APRILE	11A	X100	Xe, inelastic
<1	$\times 10^{-8}$	90	[39] APRILE	11B	X100	Xe
<5	$\times 10^{-8}$	90	[46] ARMENGAUD	11	EDE2	Ge
			[47] HORN	11	ZEP3	Xe
<4	$\times 10^{-8}$	90	AHMED	10	CDM2	Ge
<9	$\times 10^{-6}$	90	AKERIB	10	CDM2	Si, Ge, low threshold
			[48] AKIMOV	10	ZEP3	Xe, inelastic
<5	$\times 10^{-8}$	90	APRILE	10	X100	Xe
<1	$\times 10^{-7}$	90	ARMENGAUD	10	EDE2	Ge
<3	$\times 10^{-5}$	90	FELIZARDO	10	SMPL	C_2ClF_3
<5	$\times 10^{-8}$	90	[49] AHMED	09	CDM2	Ge
			[50] ANGLE	09	XE10	Xe, inelastic
<3	$\times 10^{-4}$	90	LIN	09	TEXO	Ge
			[51] GIULIANI	05	RVUE	

[1] AALBERS 25 search for WIMP DM using 4.2 ton-year LZ exposure. No signal observed. Limits placed in m(DM) vs. $\sigma^{SI}(\chi N)$ plane.

[2] APRILE 25B search for wimps using 3.1 ton-years of data. No signal observed. Limits placed in σ^{SI} vs m(χ) plane.

[3] BO 25 search for wimp dark matter with PandaX-4T. No signal detected. Limits placed in $\sigma^{SI}(\chi N)$ vs. m(χ) plane.

[4] UMEMOTO 25 use directional DM search in nano-imaging tracking (NIT) emulsion device. No signal observed. Limits placed in $\sigma^{SI}(\chi N)$ vs. m(χ) plane.

[5] YU 25 report on COSINE-100 wimp search in 3-year data. No signal observed. Limits placed in σ^{SI} vs m(χ) plane.

[6] ANGLOHER 24A search for WIMP scatter on NaI target. No signal observed. Limits placed in σ^{SI} vs m plane.

[7] AALBERS 23 present first LZ limits on SI WIMP-nucleon scatter from Xe. $\sigma^{SI}(\chi p) < 2.5 \times 10^{-11}$ pb for m(χ) = 100 GeV.

[8] ABE 23E search for WIMP scatter on Xe in XMASS. No signal observed. Require $\sigma^{SI} < 2 \times 10^{-7}$ pb for m(χ) = 100 GeV.

[9] APRILE 23A present first results from Xe-nton SI WIMP search. No signal observed. Quoted limit is for m(χ) = 100 GeV.

[10] MENG 21B search for SI WIMP interaction with 3.7 t Xe and 0.63 t yr exposure. No signal observed. Limits placed in m(DM) vs. σ^{SI} plane.

[11] ADHIKARI 20 search for SI WIMP scatter from Ar in AJAJ 19 data. No signal observed. Limits placed on σ^p vs. m(WIMP) for various assumed operators and models.

[12] FELIZARDO 20 presents 2014 SIMPLE bounds on WIMP DM using C_2ClF_5 target.

[13] WANG 20G search for SI WIMP scatter on Xe with 132 t d exposure of PANDAX-II.

[14] ABE 19 search for SI DD in single phase Xe; no signal; require $\sigma^{SI}(\chi p) < 4 \times 10^{-8}$ pb for m(χ) $\sim$ 100 GeV.

[15] AJAJ 19 search for SI WIMP-nucleon scatter with 758 tonne day exposure of single phase liquid Ar; no signal: require $\sigma^{SI}(\chi N) < 3.9 \times 10^{-9}$ pb for m(χ) = 100 GeV.

[16] ADHIKARI 18 search for WIMP scatter on NaI;limit set $\sigma^{SI}(\chi p) < 2.3 \times 10^{-6}$ pb for m(χ) = 100 GeV.

[17] AGNES 18A search for WIMP scatter on 46.4 kg Ar; no signal; require $\sigma^{SI}(\chi N) < 1.14 \times 10^{-8}$ pb for m(χ) = 100 GeV.

[18] AGNESE 18A set limit $\sigma^{SI}(\chi N) < 2 \times 10^{-8}$ pb for m(WIMP) = 100 GeV.

[19] AMAUDRUZ 18 search for WIMP scatter on Ar with DEAP-3600; limits set: $\sigma^{SI}(\chi p) < 1.2 \times 10^{-8}$ pb for m(WIMP) = 100 GeV.

[20] APRILE 18 search for WIMP scatter on 1.3 t liquid Xe; no signal; require $\sigma^{SI}(\chi p) < 9.12 \times 10^{-11}$ pb for m(χ) = 100 GeV.

[21] REN 18 search for self-interacting DM at Panda-X-II with a total exposure of 54 ton day; limits set in m(DM) vs. m(mediator) plane.

[22] AKERIB 17 exclude SI cross section > 1.7×10^{-10} pb for m(WIMP) = 100 GeV. Uses complete LUX data set.

[23] APRILE 17G set limit $\sigma^{SI}(\chi p) < 1.2\ 10^{-10}$ pb for m(WIMP) = 100 GeV using 1 ton fiducial mass Xe TPC. Exposure is 34.2 live days.

[24] CUI 17A search for SI WIMP scatter; limits placed in $\sigma^{SI}(\chi N)$ vs. m(χ) plane for m $\sim$ 10–1 $\times 10^4$ GeV using 54 ton-day exposure of Xe.

[25] AKERIB 16 re-analysis of 2013 data exclude SI cross section > 1×10^{-9} pb for m(WIMP) = 100 GeV on Xe target.

[26] APRILE 16B combined 447 live days using Xe target exclude σ(SI) > 1.1×10^{-9} pb for m(WIMP) = 50 GeV.

[27] TAN 16 search for WIMP scatter off Xe target; see SI exclusion plot Fig. 6.

[28] TAN 16B search for WIMP-p scatter off Xe target; see Fig. 5 for SI exclusion.

[29] AGNESE 15B reanalyse AHMED 10 data.

[30] XIAO 15 search for WIMP scatter on Xe with PandaX-I; limits placed in $\sigma^{SI}(\chi N)$ vs. m(χ) plane for m(χ) $\sim$ 5–100 GeV.

[31] AVRORIN 14 search for neutrinos from the Sun arising from the pair annihilation of X^0 trapped by the Sun in data taken between 1998 and 2003. See their Table 1 for limits assuming annihilation into neutrino pairs.

[32] AARTSEN 13 search for neutrinos from the Sun arising from the pair annihilation of X^0 trapped by the sun in data taken between June 2010 and May 2011.

[33] ADRIAN-MARTINEZ 13 search for neutrinos from the Sun arising from the pair annihilation of X^0 trapped by the sun in data taken between Jan. 2007 and Dec. 2008.

[34] AGNESE 13 use data taken between Oct. 2006 and July 2007.

[35] BOLIEV 13 search for neutrinos from the Sun arising from the pair annihilation of X^0 trapped by the sun in data taken from 1978 to 2009. See also SUVOROVA 13 for an older analysis of the same data.

[36] LI 13B search for WIMP scatter on Ge; limits placed in $\sigma^{SI}(\chi N)$ vs. m(χ) plane for m(χ) $\sim$ 4–100 GeV.

[37] ABBASI 12 search for neutrinos from the Sun arising from the pair annihilation of X^0 trapped by the Sun. The amount of X^0 depends on the X^0-proton cross section.

[38] Reanalysis of ANGLOHER 09 data with all three nuclides. See also BROWN 12.

[39] See also APRILE 14A.

[40] See their Fig. 6 for a limit on inelastically scattering X^0 for m_{X^0} = 70 GeV.

[41] AHMED 11 search for X^0 inelastic scattering. See their Fig. 8–10 for limits.

[42] AHMED 11A combine CDMS and EDELWEISS data.

[43] AJELLO 11 search for $e^{\pm}$ flux from X^0 annihilations in the Sun. Models in which X^0 annihilates into an intermediate long-lived weakly interacting particles or X^0 scatters inelastically are constrained. See their Fig. 6–8 for limits.

[44] APRILE 11 reanalyze APRILE 10 data.

[45] APRILE 11A search for X^0 inelastic scattering. See their Fig. 2 and 3 for limits. See also APRILE 14A.

[46] Supersedes ARMENGAUD 10. A limit on inelastic cross section is also given.

[47] HORN 11 perform detector calibration by neutrons. Earlier results are only marginally affected.

[48] AKIMOV 10 give cross section limits for inelastically scattering dark matter. See their Fig. 4.

[49] Superseded by AHMED 10.

[50] ANGLE 09 search for X^0 inelastic scattering. See their Fig. 4 for limits.

[51] GIULIANI 05 analyzes the spin-independent X^0-nucleon cross section limits with both isoscalar and isovector couplings. See their Fig. 3 and 4 for limits on the couplings.

For m_{X^0} = 1 TeV

For limits from X^0 annihilation in the Sun, the assumed annihilation final state is shown in parenthesis in the comment.

VALUE (pb)	CL%	DOCUMENT ID		TECN	COMMENT
• • • We do not use the following data for averages, fits, limits, etc. • • •					
<3 $\times 10^{-11}$	90	[1] AALBERS	25	LZ	SI wimp DM search
<3.7 $\times 10^{-10}$	90	[2] APRILE	25B	XENT	wimp search
<2 $\times 10^{-10}$	90	[3] BO	25	PNDX	wimp search
<6 $\times 10^{-7}$	90	[4] YU	25	C100	wimp search
<4 $\times 10^{-3}$	90	[5] ANGLOHER	24A	COSN	WIMP search
<2.8 $\times 10^{-10}$	90	[6] AALBERS	23	LZ	SI scatter on Xe
<1 $\times 10^{-7}$	90	[7] ABE	23E	XMAS	WIMP search
<5 $\times 10^{-10}$	90	[8] MENG	21B	PNDX	Xe WIMP search
		[9] ADHIKARI	20	DEAP	Ar
<4 $\times 10^{-9}$	90	[10] WANG	20G	PNDX	Xe TPC
<3 $\times 10^{-6}$	90	[11] YAGUNA	19		Ar; I-spin viol DM
<3.8 $\times 10^{-8}$	90	[12] AGNES	18A	DS50	Ar
<8.24 $\times 10^{-10}$	90	[13] APRILE	18	XE1T	Xe
<2 $\times 10^{-9}$	90	[14] AKERIB	17	LUX	Xe
<0.3	90	[15] CHEN	17E	PNDX	$\chi N \rightarrow \chi^* \rightarrow \chi\gamma$
<1.2 $\times 10^{-9}$	90	[16] CUI	17A	PNDX	SI WIMPs on Xe
<8.6 $\times 10^{-8}$	90	AGNES	16	DS50	Ar
<2 $\times 10^{-7}$	90	AGNES	15	DS50	Ar
<2 $\times 10^{-7}$	90	[17] AGNESE	15B	CDM2	Ge
<1 $\times 10^{-8}$	90	AKERIB	14	LUX	Xe
<2.2 $\times 10^{-6}$	90	[18] AVRORIN	14	BAIK	H, solar ν ($W^+ W^-$)
<5.5 $\times 10^{-5}$	90	[18] AVRORIN	14	BAIK	H, solar ν ($b\overline{b}$)
<6.8 $\times 10^{-7}$	90	[18] AVRORIN	14	BAIK	H, solar ν ($\tau^+ \tau^-$)
<3.46 $\times 10^{-7}$	90	[19] AARTSEN	13	ICCB	H, solar ν ($W^+ W^-$)
<7.75 $\times 10^{-6}$	90	[19] AARTSEN	13	ICCB	H, solar ν ($b\overline{b}$)
<6.9 $\times 10^{-7}$	90	[20] ADRIAN-MAR.	13	ANTR	H, solar ν ($W^+ W^-$)
<1.5 $\times 10^{-5}$	90	[20] ADRIAN-MAR.	13	ANTR	H, solar ν ($b\overline{b}$)
<1.8 $\times 10^{-7}$	90	[20] ADRIAN-MAR.	13	ANTR	H, solar ν ($\tau^+ \tau^-$)

Int. J. Mod. Phys. A 2026.41. Downloaded from www.worldscientific.com
by UNIVERSITY OF CALIFORNIA @ BERKELEY on 09/16/26. Re-use and distribution is strictly not permitted, except for Open Access articles.

$<4.3 \times 10^{-6}$	90	[21] BOLIEV	13	BAKS	H, solar ν ($W^+ W^-$)
$<3.4 \times 10^{-5}$	90	[21] BOLIEV	13	BAKS	H, solar ν ($b\overline{b}$)
$<1.2 \times 10^{-6}$	90	[21] BOLIEV	13	BAKS	H, solar ν ($\tau^+\tau^-$)
$<2.12 \times 10^{-7}$	90	[22] ABBASI	12	ICCB	H, solar ν ($W^+ W^-$)
$<6.56 \times 10^{-6}$	90	[22] ABBASI	12	ICCB	H, solar ν ($b\overline{b}$)
$<4 \times 10^{-7}$	90	AKIMOV	12	ZEP3	Xe
$<1.1 \times 10^{-5}$	90	[23] ANGLOHER	12	CRES	$CaWO_4$
$<2 \times 10^{-8}$	90	[24] APRILE	12	X100	Xe
$<2 \times 10^{-6}$	90	BEHNKE	12	COUP	CF_3I
$<4 \times 10^{-6}$		FELIZARDO	12	SMPL	C_2ClF_5
$<1.5 \times 10^{-6}$	90	KIM	12	KIMS	CsI
		[25] AHMED	11	CDM2	Ge, inelastic
$<1.5 \times 10^{-7}$	90	[26] AHMED	11A	RVUE	Ge
$<2 \times 10^{-7}$	90	[27] APRILE	11	X100	Xe
$<8 \times 10^{-8}$	90	[24] APRILE	11B	X100	Xe
$<2 \times 10^{-7}$	90	[28] ARMENGAUD	11	EDE2	Ge
		[29] HORN	11	ZEP3	Xe
$<2 \times 10^{-7}$	90	AHMED	10	CDM2	Ge
$<4 \times 10^{-7}$	90	APRILE	10	X100	Xe
$<6 \times 10^{-7}$	90	ARMENGAUD	10	EDE2	Ge
$<3.5 \times 10^{-7}$	90	[30] AHMED	09	CDM2	Ge

[1] AALBERS 25 report on SI WIMP search using 4.2 ton-years LZ exposure. No signal observed. Limits placed in m(DM) vs. $\sigma^{SI}(\chi N)$ plane.

[2] APRILE 25B search for wimps using 3.1 ton-years of data. No signal observed. Limits placed in σ^{SI} vs m(χ) plane.

[3] BO 25 search for wimp dark matter with PandaX-4T. No signal detected. Limits placed in $\sigma^{SI}(\chi N)$ vs. m(χ) plane.

[4] YU 25 report on COSINE-100 wimp search in 3-year data. No signal observed. Limits placed in σ^{SI} vs m(χ) plane.

[5] ANGLOHER 24A search for WIMP scatter on NaI target. No signal observed. Limits placed in σ^{SI} vs m plane.

[6] AALBERS 23 give first LZ limits on WIMP-nucleon scatter from Xe. $\sigma^{SI} < 2.8\times10^{-10}$ pb for m(χ) = 1 TeV.

[7] ABE 23E search for WIMP scatter on Xe in XMASS. No signal observed. Require $\sigma^{SI} < 2\times10^{-7}$ pb for m(χ) = 1000 GeV.

[8] MENG 21B search for SI WIMP interaction with 3.7 t Xe and 0.63 t yr exposure. No signal observed. Limits placed in m(DM) vs. σ^{SI} plane.

[9] ADHIKARI 20 search for SI WIMP scatter from Ar in AJAJ 19 data. No signal observed. Limits placed on σ^p vs. m(WIMP) for various assumed operators and models.

[10] WANG 20G search for SI WIMP scatter on Xe with 132 t d exposure of PANDAX-II.

[11] YAGUNA 19 recasts DEAP-3600 single-phase liquid argon results in limit for isospin violating DM; for $f_n/f_p = -0.69$, requires $\sigma^{SI}(\chi p) < 3\times10^{-6}$ pb for m(χ) = 1 TeV.

[12] AGNES 18A search for WIMP scatter on 46.4 kg Ar; no signal; require $\sigma^{SI}(\chi N) < 3.8\times10^{-8}$ pb for m(χ) = 1 TeV.

[13] APRILE 18 search for WIMP scatter on 1.3 t Xe; no signal seen; require $\sigma^{SI}(\chi p) < 8.24\times10^{-10}$ pb for m(χ) = 1 TeV.

[14] AKERIB 17 search for WIMP scatter on Xe using complete LUX data set; limits placed in $\sigma^{SI}(\chi N)$ vs. m(χ) plane for m(χ) $\sim$ 5–1 $\times 10^5$ GeV.

[15] CHEN 17E search for inelastic WIMP scatter on Xe; require $\sigma^{SI}(\chi N) < 0.3$ pb for m(χ) = 1 TeV and (mass difference) = 300 keV.

[16] CUI 17A search for WIMP scatter using 54 ton-day exposure of Xe; limits placed in $\sigma^{SI}(\chi N)$ vs. m(χ) plane for m $\sim$ 10–1 $\times 10^4$ GeV.

[17] AGNESE 15B reanalyse AHMED 10 data.

[18] AVRORIN 14 search for neutrinos from the Sun arising from the pair annihilation of X^0 trapped by the Sun in data taken between 1998 and 2003. See their Table 1 for limits assuming annihilation into neutrino pairs.

[19] AARTSEN 13 search for neutrinos from the Sun arising from the pair annihilation of X^0 trapped by the sun in data taken between June 2010 and May 2011.

[20] ADRIAN-MARTINEZ 13 search for neutrinos from the Sun arising from the pair annihilation of X^0 trapped by the sun in data taken between Jan. 2007 and Dec. 2008.

[21] BOLIEV 13 search for neutrinos from the Sun arising from the pair annihilation of X^0 trapped by the sun in data taken from 1978 to 2009. See also SUVOROVA 13 for an older analysis of the same data.

[22] ABBASI 12 search for neutrinos from the Sun arising from the pair annihilation of X^0 trapped by the Sun. The amount of X^0 depends on the X^0-proton cross section.

[23] Reanalysis of ANGLOHER 09 data with all three nuclides. See also BROWN 12.

[24] See also APRILE 14A.

[25] AHMED 11 search for X^0 inelastic scattering. See their Fig. 8–10 for limits.

[26] AHMED 11A combine CDMS and EDELWEISS data.

[27] APRILE 11 reanalyze APRILE 10 data.

[28] Supersedes ARMENGAUD 10. A limit on inelastic cross section is also given.

[29] HORN 11 perform detector calibration by neutrons. Earlier results are only marginally affected.

[30] Superseded by AHMED 10.

For Super-heavy dark matter ($m_{X^0} > 10^{10}$ GeV)

VALUE	DOCUMENT ID		TECN	COMMENT
• • • We do not use the following data for averages, fits, limits, etc. • • •				
	[1] AALBERS	24A	LZ	ultraheavy DM
	[2] ABREU	23	AUGE	DM decay to photons
	[3] ACEVEDO	23		DM tracks in ancient mica

[1] AALBERS 24A search for ultraheavy dark matter in range 10×10^8–10×10^{17} GeV via multiple scatter. No signal observed. Limits placed in σ^{SI} vs m plane for two different nuclear scaling possibilities.

[2] ABREU 23 search for superheavy DM X decay to $q\overline{q}$ pairs via instanton, then to γs. No signal detected. Exclude m(X) $> 3\times10^{13}$ GeV for dark gauge coupling $\alpha_X = 0.09$.

[3] ACEVEDO 23 re-examine data from ancient mica to place limits on superheavy DM in the mass range 10^7–10^{25} GeV. See Fig. 3 for σ^{SI} and σ^{SD} limits.

Spin-Dependent Cross Section Limits for Dark Matter Particle (X^0) on Proton

For m_{X^0} in GeV range

We provide here limits for $m_{X^0} < 5$ GeV

VALUE (pb)	CL%	DOCUMENT ID		TECN	COMMENT
• • • We do not use the following data for averages, fits, limits, etc. • • •					
		[1] ADAMS	25	PICO	fermionic DM absorption
< 30.9	90	[2] ARORA	25	NEWS	light DM search
< 5	90	[3] YU	25	C100	wimp search
< 0.56	90	[4] ZHANG	25B	PNDX	wimp search
$< 1 \times 10^9$	90	[5] ANGLOHER	24B	CRES	low mass wimp search
$< 1 \times 10^4$	90	[6] AALBERS	23A	LZ	SD scatter on Xe
$< 2 \times 10^5$	90	[7] ADHIKARI	22B	C100	sub-GeV WIMP via SD coupling/Migdal effect
$< 9 \times 10^4$	90	[8] ANGLOHER	22	CRES	SD limit using Li
< 40	90	[9] ANGLOHER	22A	CRES	SD limit using Li and Al
$< 8 \times 10^4$	90	[10] ABDELHAME..	20A	CRES	$LiAlO_2$
$< 1 \times 10^6$	95	[11] ABDELHAME..	19	CRES	GeV-scale WIMPs on Li
$< 3 \times 10^{-4}$	90	[12] AMOLE	19	PICO	C_3F_8
$< 1.7 \times 10^4$	90	[13] APRILE	19C	XE1T	light DM on Xe via Migdal/brem effect
$< 8 \times 10^6$	90	[14] ARMENGAUD	19	EDEL	GeV-scale WIMPs on Ge
< 70	90	[15] XIA	19A	PNDX	SD WIMP on Xe
<100	90	[16] AGNESE	18	SCDM	GeV-scale WIMPs on Ge
< 1	90	[17] AKERIB	17A	LUX	Xe
< 0.6	90	[18] FU	17	PNDX	SD WIMP on Xe
< 0.2	90	[19] AMOLE	15	PICO	C_3F_8
$< 1.6 \times 10^{-1}$	90	[20] ARCHAMBAU..	12	PICA	^{19}F

[1] ADAMS 25 report on fermionic DM in MeV range search via nuclear absorption at PICO-60. No signal observed. Limits placed on m(DM) vs. absorption cross section for EFT operator O_4.

[2] ARORA 25 report search for light DM at NEWS-G. No signal observed. Limits placed in $\sigma^{SD}(\chi p)$ vs m(χ) plane. Quoted limit is for m(χ) = 0.76 GeV.

[3] YU 25 report on COSINE-100 wimp search in 3-year data. No signal observed. Limits placed in $\sigma^{SD}(\chi p)$ vs m(χ) plane. Quoted limit for m(χ) = 3 GeV.

[4] ZHANG 25B search for light GeV-scale wimps using run 0 and run 1 PandaX-4T data. No signal observed. Quoted limit is for m(χ) = 3 GeV.

[5] ANGLOHER 24B search for low mass wimps. No signal observed. Limits placed in σ vs. m plane. Quoted limit for m = 100 MeV.

[6] AALBERS 23A search for GeV-scale WIMP scatter on Xe. No signal observed. Limits placed in $\sigma^{SD}(\chi p)$ vs. m(χ) plane. Quoted limit is for m(χ) = 1 GeV via Migdal scattering.

[7] ADHIKARI 22B search for sub-GeV WIMPs via SI and SD detection; no signal detected; limits placed in m(χ) vs. σ plane for m(χ): 0.2–3 GeV; quoted limit is for SD m(χ) = 1 GeV.

[8] ANGLOHER 22 search for SD WIMP-proton scatter from Li target; no signal detected; limits placed in σ vs. m(WIMP) plane; limit quoted for m(WIMP) = 1 GeV.

[9] ANGLOHER 22A search for spin-dependent DM scatter on Li and Al for m(DM) $\sim$ 0.2–6 GeV; no signal observed; limits set in $\sigma(\chi p)$ vs. m(DM) plane; quoted limit is for m(DM) = 1 GeV.

[10] ABDELHAMEED 20A use $LiAlO_2$ target in CRESST to search for SD WIMP scatter on p; no signal; quoted limit is for m(DM) = 1 GeV.

[11] ABDELHAMEED 19 search for SD WIMP scatter on ^{7}Li; limits placed on $\sigma^{SD}(\chi p)$ for m(χ) $\sim$ 0.8–20 GeV; quoted limit is for m(χ) = 1 GeV.

[12] AMOLE 19 search for SD WIMP scatter on C_3F_8 in PICO-60 bubble chamber; no signal: set limit for spin dependent coupling $\sigma^{SD}(\chi p) < 2\times10^{-4}$ pb for m(χ) = 5 GeV.

[13] APRILE 19C search for light DM on Xe via Migdal/brem effect; no signal, require $\sigma^{SD}(\chi p) < 1.7\times10^4$ pb for m(χ) = 1 GeV.

[14] ARMENGAUD 19 search for GeV scale WIMP scatter on Ge; limits placed in $\sigma^{SD}(\chi p)$ vs. m(χ) plane for m(χ) $\sim$ 0.5–10 GeV; quoted limit is for m(χ) = 5 GeV.

[15] XIA 19A search for WIMP scatter on Xe in PandaX-II; limits placed in $\sigma^{SD}(\chi p)$ vs. m(χ) plane for m(χ) $\sim$ 5–1 $\times 10^5$ GeV; quoted limit is for m(χ) = 5 GeV.

[16] AGNESE 18 search for GeV scale WIMPs with CDMSlite; limits placed in $\sigma^{SD}(\chi p)$ vs. m(χ) plane for m(χ) $\sim$ 1.5–20 GeV; quoted limit is for m(χ) = 5 GeV.

[17] AKERIB 17A search for SD WIMP scatter on Xe using 129.5 kg yr exposure; limits placed in $\sigma^{SD}(\chi p)$ vs. m(χ) plane for m(χ) $\sim$ 6–1 $\times 10^5$ GeV.

[18] FU 17 search for SD WIMP scatter on Xe; limits set in $\sigma^{SD}(\chi p)$ vs. m(χ) plane for m(χ) $\sim$ 4–1 $\times 10^3$ GeV.; quoted limit is for m(χ) = 5 GeV.

[19] AMOLE 15 search for WIMP scatter on C_3F_8 in PICO-2L; limits placed in $\sigma^{SD}(\chi p)$ vs. m(χ) plane for m(χ) $\sim$ 4–1 $\times 10^4$ GeV; quoted limit is for m(χ) = 5 GeV.

[20] ARCHAMBAULT 12 search for SD WIMP scatter in ^{19}F with PICASSO; limits set in $\sigma^{SD}(\chi p)$ vs. m(χ) plane for m $\sim$ 4–500 GeV; quoted limit is for m(χ) = 5 GeV.

For $m_{X^0} = 20$ GeV

For limits from X^0 annihilation in the Sun, the assumed annihilation final state is shown in parenthesis in the comment.

VALUE (pb)	CL%	DOCUMENT ID		TECN	COMMENT
• • • We do not use the following data for averages, fits, limits, etc. • • •					
< 0.1	90	[1] DAS	25	INDX	DM search
$< 6 \times 10^{-5}$	90	[2] AALBERS	23	LZ	SD scatter on Xe
$< 3.5 \times 10^{-5}$	90	[3] ABBASI	22B	ICCB	IceCube SD limit
$< 1.5 \times 10^5$	90	[4] ANGLOHER	22	CRES	SD limit using Li
$< 2 \times 10^{-4}$	90	[5] HUANG	22	PNDX	SD DM limits
$< 9 \times 10^{-5}$	90	[6] AARTSEN	20C	ICCB	SD WIMP on p
$< 2 \times 10^5$	90	[7] ABDELHAME..	20A	CRES	$LiAlO_2$
$< 5 \times 10^{-3}$		[8] FELIZARDO	20	SMPL	WIMPs via SIMPLE
$< 3 \times 10^5$	95	[9] ABDELHAME..	19	CRES	^{7}Li

Int. J. Mod. Phys. A 2026.41. Downloaded from www.worldscientific.com
by UNIVERSITY OF CALIFORNIA @ BERKELEY on 09/16/26. Re-use and distribution is strictly not permitted, except for Open Access articles.

$< 2.5 \times 10^{-5}$	90	[10] AMOLE	19	PICO	C_3F_8
$< 2.5 \times 10^{-4}$	90	[11] APRILE	19A	XE1T	Xe, SD
$< 1 \times 10^{-3}$	90	[12] XIA	19A	PNDX	SD WIMP on Xe
< 30	95	[13] AGNESE	18	SCDM	Ge
$< 1 \times 10^{-3}$	90	[14] AKERIB	17A	LUX	Xe
$< 1.32 \times 10^{-2}$	90	[15] BEHNKE	17	PICA	C_4F_{10}
$< 2 \times 10^{-3}$	90	[16] FU	17	PNDX	SD WIMP on Xe
$< 5 \times 10^{-4}$	90	[17] AMOLE	16A	PICO	C_3F_8
$< 2 \times 10^{-6}$	90	[18] KHACHATRY...	16AJ	CMS	8 TeV $pp \rightarrow Z+\not{E}_T$; $Z \rightarrow \ell\overline{\ell}$
$< 1.2 \times 10^{-3}$	90	AMOLE	15	PICO	C_3F_8
$< 1.43 \times 10^{-3}$	90	CHOI	15	SKAM	H, solar ν ($b\overline{b}$)
$< 1.42 \times 10^{-4}$	90	CHOI	15	SKAM	H, solar ν ($\tau^+\tau^-$)
$< 5 \times 10^{-3}$	90	FELIZARDO	14	SMPL	C_2ClF_5
$< 1.29 \times 10^{-2}$	90	[19] AARTSEN	13	ICCB	H, solar ν ($\tau^+\tau^-$)
$< 3.17 \times 10^{-2}$	90	[20] APRILE	13	X100	Xe
$< 3 \times 10^{-2}$	90	[21] ARCHAMBAU..	12	PICA	F (C_4F_{10})
$< 6 \times 10^{-2}$	90	BEHNKE	12	COUP	CF_3I
< 20	90	DAW	12	DRFT	F (CF_4)
$< 7 \times 10^{-3}$		FELIZARDO	12	SMPL	C_2ClF_5
< 0.15	90	KIM	12	KIMS	CsI
$< 1 \times 10^5$	90	[22] AHLEN	11	DMTP	F (CF_4)
< 0.1	90	[22] BEHNKE	11	COUP	CF_3I
$< 1.5 \times 10^{-2}$	90	[23] TANAKA	11	SKAM	H, solar ν ($b\overline{b}$)
< 0.2	90	ARCHAMBAU..	09	PICA	F
< 4	90	LEBEDENKO	09A	ZEP3	Xe
< 0.6	90	ANGLE	08A	XE10	Xe
<100	90	ALNER	07	ZEP2	Xe
< 1	90	LEE	07A	KIMS	CsI
< 20	90	[24] AKERIB	06	CDMS	^{73}Ge, ^{29}Si
< 2	90	SHIMIZU	06A	CNTR	F (CaF_2)
< 0.5	90	ALNER	05	NAIA	NaI
< 1.5	90	BARNABE-HE..	05	PICA	F (C_4F_{10})
< 1.5	90	GIRARD	05	SMPL	F (C_2ClF_5)
< 35	90	MIUCHI	03	BOLO	LiF
< 30	90	TAKEDA	03	BOLO	NaF

[1] DAS 25 search for WIMP DM with InDEx detector. No signal observed. Limits placed in σ vs. m plane.

[2] AALBERS 23 yield first SD LZ limits on WIMP-p scatter using Xe. $\sigma^{SD}(\chi p) < 6 \times 10^{-5}$ pb for m(χ) = 20 GeV.

[3] ABBASI 22B search for WIMP annihilation to $b\overline{b}$, $\tau\overline{\tau}$, $\nu\overline{\nu}$ in Sun with 7 years data; no signal; limits set in m(χ) vs. $\sigma^{SD}(\chi p)$ plane for m(χ): 10–100 GeV; quoted limit for $\nu\overline{\nu}$ channel.

[4] ANGLOHER 22 search for SD WIMP-proton scatter from Li target; no signal detected; limits placed in σ vs. m(WIMP) plane.

[5] HUANG 22 search for SD DM scatter on Xe; no signal observed; limits placed in $\sigma(\chi n)$ vs. m(DM) plane; quoted limit is for m(DM) = 20 GeV.

[6] AARTSEN 20C place combined IceCube and Pico-60 velocity-independent limits on spin-dependent WIMP-p scatter $\sigma^{SD}(\chi p) <$ 9–5 pb for m(WIMP) = 20 GeV assuming dominant annihilation to $\tau\overline{\tau}$.

[7] ABDELHAMEED 20A use $LiAlO_2$ target in CRESST to search for spin-dependent WIMP scatter on p; limits set for m(WIMP): 0.3–30 GeV in Fig. 8. Quoted limit is for M(WIMP) = 30 GeV.

[8] FELIZARDO 20 presents 2014 SIMPLE bounds on WIMP DM using C_2ClF_5 target.

[9] ABDELHAMEED 19 uses Li_2MoO_4 target to set limit for spin dependent coupling $\sigma^{SD}(\chi p) < 3. \times 10^5$ pb for m(χ) = 20 GeV.

[10] AMOLE 19 search for SD WIMP scatter on C_3F_8 in PICO-60 bubble chamber; no signal: set limit for spin dependent coupling $\sigma^{SD}(\chi p) < 2.5 \times 10^{-5}$ pb for m(χ) = 20 GeV.

[11] APRILE 19A search for SD WIMP scatter on 1 t yr Xe; no signal, limits placed in $\sigma^{SD}(\chi p)$ vs. m(χ) plane for m $\sim$ 6–1000 GeV.

[12] XIA 19A search for WIMP scatter on Xe in PandaX-II; limits placed in $\sigma^{SD}(\chi p)$ vs. m(χ) plane for m(χ) $\sim$ 5–1 $\times 10^5$ GeV.

[13] AGNESE 18 give limits for $\sigma^{SD}(p\chi)$ for m(WIMP) between 1.5 and 20 GeV using CDMSlite mode data.

[14] AKERIB 17A search for SD WIMP scatter on Xe using 129.5 kg yr exposure; limits placed in $\sigma^{SD}(\chi p)$ vs. m(χ) plane for m(χ) $\sim$ 6–1 $\times 10^5$ GeV.

[15] BEHNKE 17 show final Picasso results based on 231.4 kg d exposure at SNOLab for WIMP scatter on C_4F_{10} search via superheated droplet; require σ(SD) $< 1.32 \times 10^{-2}$ pb for m(WIMP) = 20 GeV.

[16] FU 17 search for SD WIMP scatter on Xe; limits set in $\sigma^{SD}(\chi p)$ vs. m(χ) plane for m(χ) $\sim$ 4–1 $\times 10^3$ GeV.

[17] AMOLE 16A require SD WIMP-p scattering $< 5 \times 10^{-4}$ pb for m(WIMP) = 20 GeV; bubbles from C_3F_8 target.

[18] KHACHATRYAN 16AJ require SD WIMP-p $< 2 \times 10^{-6}$ pb for m(WIMP) = 20 GeV from $pp \rightarrow Z + \not{E}_T$; $Z \rightarrow \ell\overline{\ell}$ signal.

[19] AARTSEN 13 search for neutrinos from the Sun arising from the pair annihilation of X^0 trapped by the sun in data taken between June 2010 and May 2011.

[20] The value has been provided by the authors. APRILE 13 note that the proton limits on Xe are highly sensitive to the theoretical model used. See also APRILE 14A.

[21] ARCHAMBAULT 12 search for WIMP scatter on C_4F_{10}; limits set in $\sigma^{SD}(\chi p)$ vs. m(χ) plane for m $\sim$ 4–500 GeV.

[22] Use a direction-sensitive detector.

[23] TANAKA 11 search for neutrinos from the Sun arising from the pair annihilation of X^0 trapped by the Sun. The amount of X^0 depends on the X^0-proton cross section.

[24] See also AKERIB 05.

For m_{X^0} = 100 GeV

For limits from X^0 annihilation in the Sun, the assumed annihilation final state is shown in parenthesis in the comment.

VALUE (pb)	CL%	DOCUMENT ID		TECN	COMMENT
• • • We do not use the following data for averages, fits, limits, etc. • • •					
$< 1.5 \times 10^{-4}$	90	[1] AALBERS	23	LZ	SD scatter on Xe
< 1	90	[2] ADHIKARI	23C	C100	SD WIMP scatter on I
< 25.7	90	[3] SHIMADA	23	NAGE	directional WIMP search
$< 2.5 \times 10^{-5}$	90	[4] ABBASI	22B	ICCB	IceCube SD limit
$< 2 \times 10^{-4}$	90	[5] HUANG	22	PNDX	SD DM limits
< 50	90	[6] IKEDA	21	NAGE	directional gas TPC
$< 3.34 \times 10^{-4}$	90	[7] AARTSEN	20C	ICCB	SD WIMP on p
$< 6.5 \times 10^{-3}$		[8] FELIZARDO	20	SMPL	WIMPs via SIMPLE
$< 4 \times 10^{-5}$	90	[9] AMOLE	19	PICO	C_3F_8
$< 4 \times 10^{-4}$	90	[10] APRILE	19A	XE1T	Xe, SD
$< 8 \times 10^{-4}$	90	[11] XIA	19A	PNDX	SD WIMP on Xe
$< 8 \times 10^{-4}$	90	[12] AKERIB	17A	LUX	Xe
$< 5 \times 10^{-5}$	90	[13] AMOLE	17	PICO	C_3F_8
$< 3.3 \times 10^{-2}$	90	[14] APRILE	17A	X100	Xe inelastic
$< 2.8 \times 10^{-1}$	90	[15] BATTAT	17	DRFT	CS_2
$< 1.5 \times 10^{-3}$	90	[16] FU	17	PNDX	Xe
< 0.553–0.019	95	[17] AABOUD	16D	ATLS	$pp \rightarrow j + \not{E}_T$
$< 1 \times 10^{-5}$	90	[18] AABOUD	16F	ATLS	$pp \rightarrow \gamma + \not{E}_T$
$< 1 \times 10^{-4}$	90	[19] AARTSEN	16C	ICCB	solar ν (W^+W^-)
$< 2 \times 10^{-4}$	90	[20] ADRIAN-MAR..	16	ANTR	solar ν (WW, $b\overline{b}$, $\tau\overline{\tau}$)
$< 3 \times 10^{-3}$	90	[21] AKERIB	16A	LUX	Xe
$< 5 \times 10^{-4}$	90	[22] AMOLE	16	PICO	CF_3I
$< 1.5 \times 10^{-3}$	90	AMOLE	15	PICO	C_3F_8
$< 3.19 \times 10^{-3}$	90	CHOI	15	SKAM	H, solar ν ($b\overline{b}$)
$< 2.80 \times 10^{-4}$	90	CHOI	15	SKAM	H, solar ν (W^+W^-)
$< 1.24 \times 10^{-4}$	90	CHOI	15	SKAM	H, solar ν ($\tau^+\tau^-$)
$< 8 \times 10^2$	90	[23] NAKAMURA	15	NAGE	CF_4
$< 1.7 \times 10^{-3}$	90	[24] AVRORIN	14	BAIK	H, solar ν (W^+W^-)
$< 4.5 \times 10^{-2}$	90	[24] AVRORIN	14	BAIK	H, solar ν ($b\overline{b}$)
$< 7.1 \times 10^{-4}$	90	[24] AVRORIN	14	BAIK	H, solar ν ($\tau^+\tau^-$)
$< 6 \times 10^{-3}$	90	FELIZARDO	14	SMPL	C_2ClF_5
$< 2.68 \times 10^{-4}$	90	[25] AARTSEN	13	ICCB	H, solar ν (W^+W^-)
$< 1.47 \times 10^{-2}$	90	[25] AARTSEN	13	ICCB	H, solar ν ($b\overline{b}$)
$< 8.5 \times 10^{-4}$	90	[26] ADRIAN-MAR..	13	ANTR	H, solar ν (W^+W^-)
$< 5.5 \times 10^{-2}$	90	[26] ADRIAN-MAR..	13	ANTR	H, solar ν ($b\overline{b}$)
$< 3.4 \times 10^{-4}$	90	[26] ADRIAN-MAR..	13	ANTR	H, solar ν ($\tau^+\tau^-$)
$< 1.00 \times 10^{-2}$	90	[27] APRILE	13	X100	Xe
$< 7.1 \times 10^{-4}$	90	[28] BOLIEV	13	BAKS	H, solar ν (W^+W^-)
$< 8.4 \times 10^{-3}$	90	[28] BOLIEV	13	BAKS	H, solar ν ($b\overline{b}$)
$< 3.1 \times 10^{-4}$	90	[28] BOLIEV	13	BAKS	H, solar ν ($\tau^+\tau^-$)
$< 7.07 \times 10^{-4}$	90	[29] ABBASI	12	ICCB	H, solar ν (W^+W^-)
$< 4.53 \times 10^{-2}$	90	[29] ABBASI	12	ICCB	H, solar ν ($b\overline{b}$)
$< 7 \times 10^{-2}$	90	[30] ARCHAMBAU..	12	PICA	F (C_4F_{10})
$< 1 \times 10^{-2}$	90	BEHNKE	12	COUP	CF_3I
< 1.8	90	DAW	12	DRFT	F (CF_4)
$< 9 \times 10^{-3}$		FELIZARDO	12	SMPL	C_2ClF_5
$< 2 \times 10^{-2}$	90	KIM	12	KIMS	CsI
$< 2 \times 10^3$	90	[23] AHLEN	11	DMTP	F (CF_4)
$< 7 \times 10^{-2}$	90	BEHNKE	11	COUP	CF_3I
$< 2.7 \times 10^{-4}$	90	[31] TANAKA	11	SKAM	H, solar ν (W^+W^-)
$< 4.5 \times 10^{-3}$	90	[31] TANAKA	11	SKAM	H, solar ν ($b\overline{b}$)
		[32] FELIZARDO	10	SMPL	C_2ClF_3
$< 6 \times 10^3$	90	[23] MIUCHI	10	NAGE	CF_4
< 0.4	90	ARCHAMBAU..	09	PICA	F
< 0.8	90	LEBEDENKO	09A	ZEP3	Xe
< 1.0	90	ANGLE	08A	XE10	Xe
< 15	90	ALNER	07	ZEP2	Xe
< 0.2	90	LEE	07A	KIMS	CsI
$< 1 \times 10^4$	90	[23] MIUCHI	07	NAGE	F (CF_4)
< 5	90	[33] AKERIB	06	CDMS	^{73}Ge, ^{29}Si
< 2	90	SHIMIZU	06A	CNTR	F (CaF_2)
< 0.3	90	ALNER	05	NAIA	NaI
< 2	90	BARNABE-HE..	05	PICA	F (C_4F_{10})
<100	90	BENOIT	05	EDEL	^{73}Ge
< 1.5	90	GIRARD	05	SMPL	F (C_2ClF_5)
< 0.7		[34] GIULIANI	05A	RVUE	
		[35] GIULIANI	04	RVUE	
		[36] GIULIANI	04A	RVUE	
< 35	90	MIUCHI	03	BOLO	LiF
< 40	90	TAKEDA	03	BOLO	NaF

[1] AALBERS 23 yield first SD LZ limits on WIMP-p scatter using Xe. $\sigma^{SD}(\chi p) < 1.5 \times 10^{-4}$ pb for m(χ) = 100 GeV.

[2] ADHIKARI 23C search for SD WIMP scatter on I. No signal observed. Require $\sigma^{SD}(\chi p) < 1$ pb for m(χ) = 100 GeV.

[3] SHIMADA 23 search for WIMPs in NEWAGE directional detector. No signal observed. Limits placed in $\sigma^{SD}(\chi p)$ vs. mass plane. Quoted limit for m(χ) = 150 GeV.

[4] ABBASI 22B search for WIMP annihilation to $b\overline{b}$, $\tau\overline{\tau}$, $\nu\overline{\nu}$ in Sun with 7 years data; no signal; limits set in m(χ) vs. $\sigma^{SD}(\chi p)$ plane for m(χ): 10–100 GeV; quoted limit for $\nu\overline{\nu}$ channel.

Int. J. Mod. Phys. A 2026.41. Downloaded from www.worldscientific.com by UNIVERSITY OF CALIFORNIA @ BERKELEY on 09/16/26. Re-use and distribution is strictly not permitted, except for Open Access articles.

[5] HUANG 22 search for SD DM scatter on Xe; no signal observed; limits placed in $\sigma(\chi n)$ vs. m(DM) plane; quoted limit is for m(DM) = 100 GeV.

[6] IKEDA 21 use direction sensitive TPC NEWAGE to search for SD WIMPs. No signal observed. Limits set in $\sigma^{SD}(\chi p)$ vs. m plane; $\sigma^{SD}(\chi p) < 50$ pb for m(DM) = 100 GeV.

[7] AARTSEN 20C place combined IceCube and Pico-60 velocity-independent limits on spin-dependent WIMP-p scatter $\sigma^{SD}(\chi p) < 3.34 \times 10^{-4}$ pb for m(WIMP) = 100 GeV assuming dominant annihilation to $\tau\overline{\tau}$.

[8] FELIZARDO 20 presents 2014 SIMPLE bounds on WIMP DM using C_2ClF_5 target.

[9] AMOLE 19 search for SD WIMP scatter on C_3F_8 in PICO-60 bubble chamber; no signal: set limit for spin dependent coupling $\sigma^{SD}(\chi p) < 4 \times 10^{-5}$ pb for m(χ) = 100 GeV.

[10] APRILE 19A search for SD WIMP scatter on 1 t yr Xe; no signal, limits placed in $\sigma^{SD}(\chi p)$ vs. m(χ) plane for m $\sim$ 6–1000 GeV.

[11] XIA 19A search for WIMP scatter on Xe in PandaX-II; limits placed in $\sigma^{SD}(\chi p)$ vs. m(χ) plane for m(χ) $\sim$ 5–1 $\times 10^5$ GeV.

[12] AKERIB 17A search for SD WIMP scatter on Xe using 129.5 kg yr exposure; limits placed in $\sigma^{SD}(\chi p)$ vs. m(χ) plane for m(χ) $\sim$ 6–1 $\times 10^5$ GeV.

[13] AMOLE 17 require σ(WIMP-p)^{SD} $< 5 \times 10^{-5}$ pb for m(WIMP) = 100 GeV using PICO-60 1167 kg-days exposure at SNOLab.

[14] APRILE 17A require require σ(WIMP-p)(inelastic)^{SD} $< 3.3 \times 10^{-2}$ pb for m(WIMP) = 100 GeV, based on 7640 kg day exposure at LNGS.

[15] BATTAT 17 use directional detection of CS_2 ions to require σ(SD) $< 2.8 \times 10^{-1}$ pb for 100 GeV WIMP with a 55 days exposure at the Boulby Underground Science Facility.

[16] FU 17 from a 33000 kg d exposure at CJPL, PANDAX II derive for m(DM) = 100 GeV, σ^{SD}(WIMP-p) $< 2 \times 10^{-3}$ pb.

[17] AABOUD 16D use ATLAS 13 TeV 3.2 fb^{-1} of data to search for monojet plus missing E_T; agree with SM rates; present limits on large extra dimensions, compressed SUSY spectra and wimp pair production.

[18] AABOUD 16F search for monophoton plus missing E_T events at ATLAS with 13 Tev and 3.2 fb^{-1}; signal agrees with SM background; place limits on SD WIMP-proton scattering vs. mediator mass and large extra dimension models.

[19] AARTSEN 16C search for high energy ν from WIMP annihilation in solar core; limits set on SD WIMP-p scattering (Fig. 8).

[20] ADRIAN-MARTINEZ 16 search for WIMP annihilation into ν from solar core; exclude SD cross section < few 10^{-4} depending on m(WIMP).

[21] AKERIB 16A using 2013 data exclude SD WIMP-proton scattering $> 3 \times 10^{-3}$ pb for m(WIMP) = 100 GeV.

[22] AMOLE 16 use bubble technique on CF_3I target to exclude SD WIMP-p scattering $> 5 \times 10^{-4}$ pb for m(WIMP) = 100 GeV.

[23] Use a direction-sensitive detector.

[24] AVRORIN 14 search for neutrinos from the Sun arising from the pair annihilation of X^0 trapped by the Sun in data taken between 1998 and 2003. See their Table 1 for limits assuming annihilation into neutrino pairs.

[25] AARTSEN 13 search for neutrinos from the Sun arising from the pair annihilation of X^0 trapped by the sun in data taken between June 2010 and May 2011.

[26] ADRIAN-MARTINEZ 13 search for neutrinos from the Sun arising from the pair annihilation of X^0 trapped by the sun in data taken between Jan. 2007 and Dec. 2008.

[27] The value has been provided by the authors. APRILE 13 note that the proton limits on Xe are highly sensitive to the theoretical model used. See also APRILE 14A.

[28] BOLIEV 13 search for neutrinos from the Sun arising from the pair annihilation of X^0 trapped by the sun in data taken from 1978 to 2009. See also SUVOROVA 13 for an older analysis of the same data.

[29] ABBASI 12 search for neutrinos from the Sun arising from the pair annihilation of X^0 trapped by the Sun. The amount of X^0 depends on the X^0-proton cross section.

[30] ARCHAMBAULT 12 search for WIMP scatter on C_4F_{10}; limits set in $\sigma^{SD}(\chi p)$ vs. m(χ) plane for m $\sim$ 4–500 GeV.

[31] TANAKA 11 search for neutrinos from the Sun arising from the pair annihilation of X^0 trapped by the Sun. The amount of X^0 depends on the X^0-proton cross section.

[32] See their Fig. 3 for limits on spin-dependent proton couplings for X^0 mass of 50 GeV.

[33] See also AKERIB 05.

[34] GIULIANI 05A analyze available data and give combined limits.

[35] GIULIANI 04 reanalyze COLLAR 00 data and give limits for spin-dependent X^0-proton coupling.

[36] GIULIANI 04A give limits for spin-dependent X^0-proton couplings from existing data.

For m_{X^0} = 1 TeV

For limits from X^0 annihilation in the Sun, the assumed annihilation final state is shown in parenthesis in the comment.

VALUE (pb)	CL%	DOCUMENT ID		TECN	COMMENT
• • • We do not use the following data for averages, fits, limits, etc. • • •					
$< 1.5 \times 10^{-3}$	90	[1] AALBERS	23	LZ	SD scatter on Xe
< 0.2	90	[2] ADHIKARI	23C	C100	SD WIMP scatter on I
$< 1.2 \times 10^{-3}$	90	[3] HUANG	22	PNDX	SD DM limits
<200	90	[4] IKEDA	21	NAGE	directional gas TPC
$< 4.81 \times 10^{-3}$	90	[5] AARTSEN	20C	ICCB	SD WIMP on p
$< 3 \times 10^{-4}$	90	[6] AMOLE	19	PICO	C_3F_8
$< 4 \times 10^{-3}$	90	[7] APRILE	19A	XE1T	Xe, SD
$< 5 \times 10^{-3}$	90	[8] XIA	19A	PNDX	SD WIMP on Xe
		[9] ALBERT	18C	HAWC	DM annihilation in Sun to long-lived mediator
$< 2.05 \times 10^{-5}$	90	[10] AARTSEN	17A	ICCB	ν, sun
$< 7 \times 10^{-3}$	90	[11] AKERIB	17A	LUX	Xe
$< 2 \times 10^{-2}$	90	[12] FU	17	PNDX	SD WIMP on Xe
		[13] ADRIAN-MAR..	16B	ANTR	solar μ from WIMP annih.
$< 1 \times 10^{-2}$	90	AMOLE	15	PICO	C_3F_8
$< 1.5 \times 10^3$	90	NAKAMURA	15	NAGE	CF_4
$< 2.7 \times 10^{-3}$	90	[14] AVRORIN	14	BAIK	H, solar ν (W^+W^-)
$< 6.9 \times 10^{-2}$	90	[14] AVRORIN	14	BAIK	H, solar ν ($b\overline{b}$)
$< 8.4 \times 10^{-4}$	90	[14] AVRORIN	14	BAIK	H, solar ν ($\tau^+\tau^-$)
$< 4.48 \times 10^{-4}$	90	[15] AARTSEN	13	ICCB	H, solar ν (W^+W^-)
$< 1.00 \times 10^{-2}$	90	[15] AARTSEN	13	ICCB	H, solar ν ($b\overline{b}$)
$< 8.9 \times 10^{-4}$	90	[16] ADRIAN-MAR..	13	ANTR	H, solar ν (W^+W^-)
$< 2.0 \times 10^{-2}$	90	[16] ADRIAN-MAR..	13	ANTR	H, solar ν ($b\overline{b}$)
$< 2.3 \times 10^{-4}$	90	[16] ADRIAN-MAR..	13	ANTR	H, solar ν ($\tau^+\tau^-$)
$< 7.57 \times 10^{-2}$	90	[17] APRILE	13	X100	Xe
$< 5.4 \times 10^{-3}$	90	[18] BOLIEV	13	BAKS	H, solar ν (W^+W^-)
$< 4.2 \times 10^{-2}$	90	[18] BOLIEV	13	BAKS	H, solar ν ($b\overline{b}$)
$< 1.5 \times 10^{-3}$	90	[18] BOLIEV	13	BAKS	H, solar ν ($\tau^+\tau^-$)
$< 2.50 \times 10^{-4}$	90	[19] ABBASI	12	ICCB	H, solar ν (W^+W^-)
$< 7.86 \times 10^{-3}$	90	[19] ABBASI	12	ICCB	H, solar ν ($b\overline{b}$)
$< 8 \times 10^{-2}$	90	BEHNKE	12	COUP	CF_3I
< 8	90	DAW	12	DRFT	F (CF_4)
$< 6 \times 10^{-2}$		FELIZARDO	12	SMPL	C_2ClF_5
$< 8 \times 10^{-2}$	90	KIM	12	KIMS	CsI
$< 8 \times 10^3$	90	[20] AHLEN	11	DMTP	F (CF_4)
< 0.4	90	BEHNKE	11	COUP	CF_3I
$< 2 \times 10^{-3}$	90	[21] TANAKA	11	SKAM	H, solar ν ($b\overline{b}$)
$< 2 \times 10^{-2}$	90	[21] TANAKA	11	SKAM	H, solar ν (W^+W^-)
$< 1 \times 10^{-3}$	90	[22] ABBASI	10	ICCB	KK dark matter
$< 2 \times 10^4$	90	[20] MIUCHI	10	NAGE	CF_4
$< 8.7 \times 10^{-4}$	90	ABBASI	09B	ICCB	H, solar ν (W^+W^-)
$< 2.2 \times 10^{-2}$	90	ABBASI	09B	ICCB	H, solar ν ($b\overline{b}$)
< 3	90	ARCHAMBAU..	09	PICA	F
< 6	90	LEBEDENKO	09A	ZEP3	Xe
< 9	90	ANGLE	08A	XE10	Xe
<100	90	ALNER	07	ZEP2	Xe
< 0.8	90	LEE	07A	KIMS	CsI
$< 4 \times 10^4$	90	[20] MIUCHI	07	NAGE	F (CF_4)
< 30	90	[23] AKERIB	06	CDMS	^{73}Ge, ^{29}Si
< 1.5	90	ALNER	05	NAIA	NaI
< 15	90	BARNABE-HE..	05	PICA	F (C_4F_{10})
<600	90	BENOIT	05	EDEL	^{73}Ge
< 10	90	GIRARD	05	SMPL	F (C_2ClF_5)
<260	90	MIUCHI	03	BOLO	LiF
<150	90	TAKEDA	03	BOLO	NaF

[1] AALBERS 23 yield first SD LZ limits on WIMP-p scatter using Xe. $\sigma^{SD}(\chi p) < 2 \times 10^{-3}$ pb for m(χ) = 1 TeV.

[2] ADHIKARI 23C search for SD WIMP scatter on I. No signal observed. Require $\sigma^{SD}(\chi p) < 0.2$ pb for m(χ) = 1 TeV.

[3] HUANG 22 search for SD DM scatter on Xe; no signal observed; limits placed in $\sigma(\chi n)$ vs. m(DM) plane; quoted limit is for m(DM) = 1 TeV.

[4] IKEDA 21 use direction sensitive TPC NEWAGE to search for SD WIMPs. No signal observed. Limits set in $\sigma^{SD}(\chi p)$ vs. m plane; $\sigma^{SD}(\chi p) < 200$ pb for m(DM) = 1000 GeV.

[5] AARTSEN 20C place combined IceCube and Pico-60 velocity-independent limits on spin-dependent WIMP-p scatter $\sigma^{SD}(\chi p) < 3 \times 10^{-3}$ pb for m(WIMP) = 1 TeV assuming dominant annihilation to WW.

[6] AMOLE 19 search for SD WIMP scatter on C_3F_8 in PICO-60 bubble chamber; no signal: set limit for spin dependent coupling $\sigma^{SD}(\chi p) < 3 \times 10^{-4}$ pb for m(χ) = 1000 GeV.

[7] APRILE 19A search for SD WIMP scatter on 1 t yr Xe; no signal, limits placed in $\sigma^{SD}(\chi p)$ vs. m(χ) plane for m $\sim$ 6–1000 GeV.

[8] XIA 19A search for WIMP scatter on Xe in PandaX-II; limits placed in $\sigma^{SD}(\chi p)$ vs. m(χ) plane for m(χ) $\sim$ 5–1 $\times 10^5$ GeV.

[9] ALBERT 18C search for DM annihilation in Sun to long-lived mediator (LLM) which decays outside Sun, for DM masses above 1 TeV; assuming LLM, limits set on $\sigma^{SD}(\chi p)$.

[10] AARTSEN 17A search for neutrinos from solar WIMP annihilation into $\tau^+\tau^-$ in 532 days of live time.

[11] AKERIB 17A search for SD WIMP scatter on Xe using 129.5 kg yr exposure; limits placed in $\sigma^{SD}(\chi p)$ vs. m(χ) plane for m(χ) $\sim$ 6–1 $\times 10^5$ GeV.

[12] FU 17 search for SD WIMP scatter on Xe; limits set in $\sigma^{SD}(\chi p)$ vs. m(χ) plane for m(χ) $\sim$ 4–1 $\times 10^3$ GeV.

[13] ADRIAN-MARTINEZ 16B search for secluded DM via WIMP annihilation in solar core into light mediator which later decays to μ or ν; limits presented in Figures 3 and 4.

[14] AVRORIN 14 search for neutrinos from the Sun arising from the pair annihilation of X^0 trapped by the Sun in data taken between 1998 and 2003. See their Table 1 for limits assuming annihilation into neutrino pairs.

[15] AARTSEN 13 search for neutrinos from the Sun arising from the pair annihilation of X^0 trapped by the sun in data taken between June 2010 and May 2011.

[16] ADRIAN-MARTINEZ 13 search for neutrinos from the Sun arising from the pair annihilation of X^0 trapped by the sun in data taken between Jan. 2007 and Dec. 2008.

[17] The value has been provided by the authors. APRILE 13 note that the proton limits on Xe are highly sensitive to the theoretical model used. See also APRILE 14A.

[18] BOLIEV 13 search for neutrinos from the Sun arising from the pair annihilation of X^0 trapped by the sun in data taken from 1978 to 2009. See also SUVOROVA 13 for an older analysis of the same data.

[19] ABBASI 12 search for neutrinos from the Sun arising from the pair annihilation of X^0 trapped by the Sun. The amount of X^0 depends on the X^0-proton cross section.

[20] Use a direction-sensitive detector.

[21] TANAKA 11 search for neutrinos from the Sun arising from the pair annihilation of X^0 trapped by the Sun. The amount of X^0 depends on the X^0-proton cross section.

[22] ABBASI 10 search for ν_μ from annihilations of Kaluza-Klein photon dark matter in the Sun.

[23] See also AKERIB 05.

Int. J. Mod. Phys. A 2026.41. Downloaded from www.worldscientific.com
by UNIVERSITY OF CALIFORNIA @ BERKELEY on 09/16/26. Re-use and distribution is strictly not permitted, except for Open Access articles.

Spin-Dependent Cross Section Limits for Dark Matter Particle (X^0) on Neutron

For m_{X^0} in GeV range

We provide here limits fo m_{X^0} < 5 GeV

VALUE (pb)	CL%	DOCUMENT ID		TECN	COMMENT
• • • We do not use the following data for averages, fits, limits, etc. • • •					
$< 4 \times 10^{-4}$	90	[1] APRILE	25	XENT	light DM search
$< 1.6 \times 10^{-2}$	90	[2] ZHANG	25B	PNDX	wimp search
$< 1 \times 10^{10}$	90	[3] ANGLOHER	24B	CRES	low mass DM search
$< 1 \times 10^{2}$	90	[4] AALBERS	23A	LZ	SD scatter on Xe
$< 1 \times 10^{6}$	90	[5] ANGLOHER	22	CRES	SD limit using Li
<570	90	[6] ANGLOHER	22A	CRES	SD limit using Li and Al
$< 1 \times 10^{8}$	90	[7] ABDELHAME..	20A	CRES	$LiAlO_2$
$< 1 \times 10^{10}$	95	[8] ABDELHAME..	19	CRES	SD low mass DM on Li
$< 2.3 \times 10^{2}$	90	[9] APRILE	19C	XE1T	light DM on Xe via Migdal/brem effect
$< 1 \times 10^{-2}$	90	[10] APRILE	19D	XE1T	light DM on Xe via ionization
$< 4 \times 10^{4}$	90	[11] ARMENGAUD	19	EDEL	GeV-scale WIMPs on Ge
$< 8 \times 10^{-2}$	90	[12] XIA	19A	PNDX	SD WIMP on Xe
< 3	90	[13] AGNESE	18	SCDM	GeV-scale WIMPs on Ge
< 3	90	[14] JIANG	18	CDEX	GeV-scale WIMPs on Ge
< 10	90	[15] YANG	18	CDEX	WIMPs on Ge
$< 1 \times 10^{-1}$	90	[16] AKERIB	17A	LUX	Xe
< 0.1	90	[17] FU	17	PNDX	SD WIMP on Xe
< 20	90	[18] ZHAO	16	CDEX	GeV-scale WIMPs on Ge
<150	90	[19] AHMED	11B	CDM2	GeV-scale WIMPs on Ge

[1] APRILE 25 report GeV-scale DM search near edge of neutrino fog using XENONnT. No signal observed. Limits set in $\sigma^{SD}(\chi N)$ vs. m(χ) plane. Quoted limit is for m(χ) = 6 GeV.
[2] ZHANG 25B search for light GeV-scale wimps using run 0 and run 1 PandaX-4T data. No signal observed. Quoted limit is for m(χ) = 3 GeV.
[3] ANGLOHER 24B search for low mass wimps. No signal observed. Limits placed in σ vs. m plane. Quoted limit for m = 100 MeV.
[4] AALBERS 23A search for GeV-scale WIMP scatter on Xe. No signal observed. Limits placed in $\sigma^{SD}(\chi n)$ vs. m(χ) plane. Quoted limit is for m(χ) = 1 GeV via Migdal scattering.
[5] ANGLOHER 22 search for SD WIMP scatter on Li target; no signal detected; limits placed on WIMP-neutron SD scatter versus m(WIMP); limit quoted for m(WIMP) = 1 GeV.
[6] ANGLOHER 22A search for spin-dependent DM scatter on Li and Al for m(DM) ~ 0.2–6 GeV; no signal observed; limits set in $\sigma(\chi n)$ vs. m(DM) plane; quoted limit is for m(DM) = 1 GeV.
[7] ABDELHAMEED 20A use $LiAlO_2$ target in CRESST to search for SD WIMP scatter; no signal; quoted limit is for m(DM) = 1 GeV.
[8] ABDELHAMEED 19 search for GeV-scale WIMP SD scatter on ^{7}Li crystal; set limit $\sigma^{SD}(\chi n)$ for m(χ) ~ 0.8–20 GeV; quoted limit for m(χ) = 1 GeV.
[9] APRILE 19C search for light DM on Xe via Migdal/bremsstrahlung effect; no signal, require $\sigma^{SD}(\chi n)$ <230 pb for m(χ) = 1 GeV.
[10] APRILE 19D search for light DM scatter on Xe via ionization; no signal, limits placed in σ vs. m(DM) ~ 3–6 GeV; quoted limit is for m(DM) = 5 GeV.
[11] ARMENGAUD 19 search for GeV scale WIMP scatter on Ge; limits placed in $\sigma^{SD}(\chi n)$ vs. m(χ) plane for m(χ) ~ 0.5–10 GeV; quoted limit is for m(χ) = 5 GeV.
[12] XIA 19A search for WIMP scatter on Xe in PandaX-II; limits placed in $\sigma^{SD}(\chi n)$ vs. m(χ) plane for m(χ) ~ 5–1 × 10^5 GeV; quoted limit is for m(χ) = 5 GeV.
[13] AGNESE 18 search for GeV scale WIMPs scatter at CDMSlite; limits placed in $\sigma^{SD}(\chi n)$ vs. m(χ) plane for m ~ 1.5–20 GeV; quoted limit is for m(χ) = 5 GeV.
[14] JIANG 18 search for GeV scale WIMP scatter on Ge; limits placed in $\sigma^{SD}(\chi n)$ vs. m(χ) plane for m(χ) ~ 3–10 GeV; quoted limit is for m(χ) = 5 GeV.
[15] YANG 18 search for WIMP scatter on Ge; limits placed in $\sigma^{SD}(\chi n)$ vs. m(χ) plane for m(χ) ~ 2–10 GeV; quoted limit is for m(χ) = 5 GeV.
[16] AKERIB 17A search for SD WIMP scatter on Xe with 129.5 kg yr exposure; limits placed in $\sigma^{SD}(\chi n)$ vs. m(χ) plane for m(χ) ~ 5–1 × 10^5 GeV; quoted limit is for m(χ) = 5 GeV.
[17] FU 17 search for SD WIMP scatter on Xe; limits set in $\sigma^{SD}(\chi n)$ vs. m(χ) plane for m(χ) ~ 4–1 × 10^3 GeV.; quoted limit is for m(χ) = 5 GeV.
[18] ZHAO 16 search for GeV-scale WIMP scatter on Ge; limits placed in $\sigma^{SD}(\chi n)$ vs. m(χ) plane for m(χ) ~ 4–30 GeV; quoted limit is for m(χ) = 5 GeV.
[19] AHMED 11B search for GeV scale WIMP scatter on Ge in CDMS II; limits placed in $\sigma^{SD}(\chi n)$ vs. m(χ) plane for m ~ 4–12 GeV. Limit given for m(χ) = 5 GeV.

For m_{X^0} = 20 GeV

VALUE (pb)	CL%	DOCUMENT ID		TECN	COMMENT
• • • We do not use the following data for averages, fits, limits, etc. • • •					
$< 2 \times 10^{-6}$	90	[1] AALBERS	23	LZ	SD scatter on Xe
$< 5 \times 10^{6}$	90	[2] ANGLOHER	22	CRES	SD limit using Li
$< 7 \times 10^{-6}$	90	[3] HUANG	22	PNDX	SD DM limits
$< 5 \times 10^{7}$	90	[4] ABDELHAME..	20A	CRES	$LiAlO_2$
$< 1 \times 10^{-1}$		[5] FELIZARDO	20	SMPL	WIMPs via SIMPLE
$< 8 \times 10^{-6}$	90	[6] APRILE	19A	XE1T	Xe, SD
$< 3 \times 10^{-5}$	90	[7] XIA	19A	PNDX	SD WIMP on Xe
< 1.5	95	[8] AGNESE	18	SCDM	Ge
$< 2.5 \times 10^{-5}$	90	[9] AKERIB	17A	LUX	Xe
$< 7 \times 10^{-5}$	90	[10] FU	17	PNDX	SD WIMP on Xe
< 2	90	[11] ZHAO	16	CDEX	GeV-scale WIMPs on Ge
< 0.09	90	FELIZARDO	14	SMPL	C_2ClF_5
< 8	90	[12] UCHIDA	14	XMAS	^{129}Xe, inelastic
$< 1.13 \times 10^{-3}$	90	[13] APRILE	13	X100	Xe
< 0.02	90	AKIMOV	12	ZEP3	Xe
< 0.06	90	AHMED	09	CDM2	Ge
< 0.04	90	LEBEDENKO	09A	ZEP3	Xe
< 50		[14] LIN	09	TEXO	Ge
$< 6 \times 10^{-3}$	90	ANGLE	08A	XE10	Xe
< 0.5	90	ALNER	07	ZEP2	Xe
< 25	90	LEE	07A	KIMS	CsI
< 0.3	90	[15] AKERIB	06	CDMS	^{73}Ge, ^{29}Si
< 30	90	SHIMIZU	06A	CNTR	F (CaF_2)
< 60	90	ALNER	05	NaIA	NaI
< 20	90	BARNABE-HE..	05	PICA	F (C_4F_{10})
< 10	90	BENOIT	05	EDEL	^{73}Ge
< 4	90	KLAPDOR-K...	05	HDMS	^{73}Ge (enriched)
<600	90	TAKEDA	03	BOLO	NaF

[1] AALBERS 23 yield first LZ limits on SD WIMP-n scatter using Xe. $\sigma^{SD}(\chi n)$< 2×10^{-6} pb for m(χ) = 20 GeV.
[2] ANGLOHER 22 search for SD WIMP-neutron scatter from Li target; no signal detected; limits placed in σ vs. m(WIMP) plane.
[3] HUANG 22 search for SD DM scatter on Xe; no signal observed; limits placed in $\sigma(\chi n)$ vs. m(DM) plane; quoted limit is for m(DM) = 20 GeV.
[4] ABDELHAMEED 20A use $LiAlO_2$ target in CRESST to search for SD WIMP scatter on n; limits placed for m(WIMP): 0.3–30 GeV in Fig. 8. Quoted limit is for M(WIMP) = 30 GeV.
[5] FELIZARDO 20 presents 2014 SIMPLE bounds on WIMP DM using C_2ClF_5 target.
[6] APRILE 19A search for SD WIMP scatter on 1 t yr Xe; no signal: limits placed in $\sigma^{SD}(\chi n)$ vs. m(χ) plane for m ~ 6–1000 GeV.
[7] XIA 19A search for WIMP scatter on Xe in PandaX-II; limits placed in $\sigma^{SD}(\chi n)$ vs. m(χ) plane for m(χ) ~ 5–1 × 10^5 GeV.
[8] AGNESE 18 give limits for $\sigma^{SD}(n\chi)$ for m(WIMP) between 1.5 and 20 GeV using CDMSlite mode data.
[9] AKERIB 17A search for SD WIMP scatter on Xe with 129.5 kg yr exposure; limits placed in $\sigma^{SD}(\chi n)$ vs. m(χ) plane for m(χ) ~ 5–1 × 10^5 GeV.
[10] FU 17 search for SD WIMP scatter on Xe; limits set in $\sigma^{SD}(\chi n)$ vs. m(χ) plane for m(χ) ~ 4–1 × 10^3 GeV.
[11] ZHAO 16 search for GeV-scale WIMP scatter on Ge; limits placed in $\sigma^{SD}(\chi n)$ vs. m(χ) plane for m(χ) ~ 4–30 GeV.
[12] Derived limit from search for inelastic scattering $X^0 + {}^{129}Xe \rightarrow X^0 + {}^{129}Xe^*$(39.58 keV).
[13] The value has been provided by the authors. See also APRILE 14A.
[14] See their Fig. 6(b) for cross section limits for m_{X^0} extending down to 2 GeV.
[15] See also AKERIB 05.

For m_{X^0} = 100 GeV

VALUE (pb)	CL%	DOCUMENT ID		TECN	COMMENT
• • • We do not use the following data for averages, fits, limits, etc. • • •					
$< 5 \times 10^{-6}$	90	[1] AALBERS	23	LZ	SD scatter on Xe
$< 1 \times 10^{-5}$	90	[2] HUANG	22	PNDX	SD DM limits
$< 1.5 \times 10^{-1}$		[3] FELIZARDO	20	SMPL	WIMPs via SIMPLE
$< 1.5 \times 10^{-5}$	90	[4] APRILE	19A	XE1T	Xe, SD
$< 4 \times 10^{-3}$	90	[5] SUZUKI	19	XMAS	^{129}Xe, inelastic
$< 2 \times 10^{-5}$	90	[6] XIA	19A	PNDX	SD WIMP on Xe
$< 2.5 \times 10^{-5}$	90	[7] AKERIB	17A	LUX	Xe
$< 7 \times 10^{-5}$	90	[8] FU	17	PNDX	SD WIMP on Xe
< 0.1	90	FELIZARDO	14	SMPL	C_2ClF_5
< 0.05	90	[9] UCHIDA	14	XMAS	^{129}Xe, inelastic
$< 4.68 \times 10^{-4}$	90	[10] APRILE	13	X100	Xe
< 0.01	90	AKIMOV	12	ZEP3	Xe
		[11] FELIZARDO	10	SMPL	C_2ClF_3
< 0.02	90	AHMED	09	CDM2	Ge
< 0.01	90	LEBEDENKO	09A	ZEP3	Xe
<100	90	LIN	09	TEXO	Ge
< 0.01	90	ANGLE	08A	XE10	Xe
< 0.05	90	[12] BEDNYAKOV	08	RVUE	Ge
< 0.08	90	ALNER	07	ZEP2	Xe
< 6	90	LEE	07A	KIMS	CsI
< 0.07	90	[13] AKERIB	06	CDMS	^{73}Ge, ^{29}Si
< 30	90	SHIMIZU	06A	CNTR	F (CaF_2)
< 10	90	ALNER	05	NaIA	NaI
< 30	90	BARNABE-HE..	05	PICA	F (C_4F_{10})
< 0.7	90	BENOIT	05	EDEL	^{73}Ge
< 0.2		[14] GIULIANI	05A	RVUE	
< 1.5	90	KLAPDOR-K...	05	HDMS	^{73}Ge (enriched)
		[15] GIULIANI	04	RVUE	
		[16] GIULIANI	04A	RVUE	
		[17] MIUCHI	03	BOLO	LiF
<800	90	TAKEDA	03	BOLO	NaF

[1] AALBERS 23 yield first LZ limits on SD WIMP-n scatter using Xe. $\sigma(\chi n) < 5 \times 10^{-6}$ pb for m(χ) = 100 GeV.
[2] HUANG 22 search for SD DM scatter on Xe; no signal observed; limits placed in $\sigma(\chi n)$ vs. m(DM) plane; quoted limit is for m(DM) = 100 GeV.
[3] FELIZARDO 20 presents 2014 SIMPLE bounds on WIMP DM using C_2ClF_5 target.
[4] APRILE 19A search for SD WIMP scatter on 1 t yr Xe; no signal, limits placed in $\sigma^{SD}(\chi n)$ vs. m(χ) plane for m ~ 6–1000 GeV.
[5] SUZUKI 19 search in single phase liquid xenon detector for inelastic scattering $X^0 + {}^{129}Xe \rightarrow X^0 + {}^{129}Xe^*$ (39.58 keV) ; no signal: require $\sigma(\chi n)^{SD} < 4 \times 10^{-3}$ pb for m(χ) = 100 GeV.

Int. J. Mod. Phys. A 2026.41. Downloaded from www.worldscientific.com by UNIVERSITY OF CALIFORNIA @ BERKELEY on 09/16/26. Re-use and distribution is strictly not permitted, except for Open Access articles.

[6] XIA 19A search for WIMP scatter on Xe in PandaX-II; limits placed in $\sigma^{SD}(\chi n)$ vs. m(χ) plane for m(χ) $\sim$ 5–1 $\times 10^5$ GeV.
[7] AKERIB 17A search for SD WIMP scatter on Xe with 129.5 kg yr exposure; limits placed in $\sigma^{SD}(\chi n)$ vs. m(χ) plane for m(χ) $\sim$ 5–1 $\times 10^5$ GeV.
[8] FU 17 search for SD WIMP scatter on Xe; limits set in $\sigma^{SD}(\chi n)$ vs. m(χ) plane for m(χ) $\sim$ 4–1 $\times 10^3$ GeV.
[9] UCHIDA 14 derived limit from search for inelastic scattering $X^0 + {}^{129}$Xe $\rightarrow X^0 + {}^{129}$Xe(39.58 keV).
[10] The value has been provided by the authors. See also APRILE 14A.
[11] See their Fig. 3 for limits on spin-dependent neutron couplings for X^0 mass of 50 GeV.
[12] BEDNYAKOV 08 reanalyze KLAPDOR-KLEINGROTHAUS 05 and BAUDIS 01 data.
[13] See also AKERIB 05.
[14] GIULIANI 05A analyze available data and give combined limits.
[15] GIULIANI 04 reanalyze COLLAR 00 data and give limits for spin-dependent X^0-neutron coupling.
[16] GIULIANI 04A give limits for spin-dependent X^0-neutron couplings from existing data.
[17] MIUCHI 03 give model-independent limit for spin-dependent X^0-proton and neutron cross sections. See their Fig. 5.

For m_{X^0} = 1 TeV

VALUE (pb)	CL%	DOCUMENT ID		TECN	COMMENT
• • • We do not use the following data for averages, fits, limits, etc. • • •					
$< 5 \times 10^{-5}$	90	[1] AALBERS	23	LZ	SD scatter on Xe
$< 6 \times 10^{-5}$	90	[2] HUANG	22	PNDX	SD DM limits
$< 7 \times 10^{-1}$		[3] FELIZARDO	20	SMPL	WIMPs via SIMPLE
$< 1.2 \times 10^{-4}$	90	[4] APRILE	19A	XE1T	Xe, SD
$< 2 \times 10^{-4}$	90	[5] XIA	19A	PNDX	Xe
$< 2.5 \times 10^{-4}$	90	[6] AKERIB	17A	LUX	Xe
$< 4 \times 10^{-4}$	90	[7] FU	17	PNDX	SD WIMP on Xe
< 0.07	90	FELIZARDO	14	SMPL	C_2ClF_5
< 0.2	90	[8] UCHIDA	14	XMAS	^{129}Xe, inelastic
$< 3.64 \times 10^{-3}$	90	[9] APRILE	13	X100	Xe
< 0.08	90	AKIMOV	12	ZEP3	Xe
< 0.2	90	AHMED	09	CDM2	Ge
< 0.1	90	LEBEDENKO	09A	ZEP3	Xe
< 0.1	90	ANGLE	08A	XE10	Xe
< 0.25	90	[10] BEDNYAKOV	08	RVUE	Ge
< 0.6	90	ALNER	07	ZEP2	Xe
< 30	90	LEE	07A	KIMS	CsI
< 0.5	90	[11] AKERIB	06	CDMS	^{73}Ge, ^{29}Si
< 40	90	ALNER	05	NAIA	NaI
<200	90	BARNABE-HE..	05	PICA	F (C_4F_{10})
< 4	90	BENOIT	05	EDEL	^{73}Ge
< 10	90	KLAPDOR-K...	05	HDMS	^{73}Ge (enriched)
$< 4 \times 10^3$	90	TAKEDA	03	BOLO	NaF

[1] AALBERS 23 yield first LZ SD limits on WIMP-n scatter on Xe. $\sigma^{SD}(\chi n) < 5 \times 10^{-5}$ pb for m(χ) = 1 TeV.
[2] HUANG 22 search for SD DM scatter on Xe; no signal observed; limits placed in $\sigma(\chi n)$ vs. m(DM) plane; quoted limit is for m(DM) = 1 TeV.
[3] FELIZARDO 20 presents 2014 SIMPLE bounds on WIMP DM using C_2ClF_5 target.
[4] APRILE 19A search for SD WIMP scatter on 1 t yr Xe; no signal, limits placed in $\sigma^{SD}(\chi n)$ vs. m(χ) plane for m $\sim$ 6–1000 GeV.
[5] XIA 19A search for WIMP scatter on Xe in PandaX-II; limits placed in $\sigma^{SD}(\chi n)$ vs. m(χ) plane for m(χ) $\sim$ 5–1 $\times 10^5$ GeV.
[6] AKERIB 17A search for SD WIMP scatter on Xe with 129.5 kg yr exposure; limits placed in $\sigma^{SD}(\chi n)$ vs. m(χ) plane for m(χ) $\sim$ 5–1 $\times 10^5$ GeV.
[7] FU 17 search for SD WIMP scatter on Xe; limits set in $\sigma^{SD}(\chi n)$ vs. m(χ) plane for m(χ) $\sim$ 4–1 $\times 10^3$ GeV.
[8] Derived limit from search for inelastic scattering $X^0 + {}^{129}$Xe* $\rightarrow X^0 + {}^{129}$Xe*(39.58 keV).
[9] The value has been provided by the authors. See also APRILE 14A.
[10] BEDNYAKOV 08 reanalyze KLAPDOR-KLEINGROTHAUS 05 and BAUDIS 01 data.
[11] See also AKERIB 05.

Cross-Section Limits for Dark Matter Particles (X^0) on electron

For m_{X^0} in GeV range

We provide here limits fo m_{X^0} < 5 GeV

VALUE (pb)	CL%	DOCUMENT ID		TECN	COMMENT
• • • We do not use the following data for averages, fits, limits, etc. • • •					
		[1] ADARI	25	SENS	MeV-scale DM
$< 7 \times 10^{-3}$	90	[2] AGGARWAL	25A	DMIC	MeV-scale DM search
< 70	90	[3] ALBAKRY	25	SCDM	MeV-scale DM
		[4] BAUDIS	25	QRDL	nanowire MeV-scale DM
$< 3 \times 10^2$	90	[5] BLOCH	25	SENS	MeV-scale DM
< 31.7	90	[6] CHOI	25	NEON	light DM search
		[7] DU	25	JWST	strongly interacting DM
$< 4 \times 10^5$	90	[8] LIANG	25		reanalysis of SENSEI DM search using plasmon
$< 5 \times 10^{-3}$	90	[9] SHEN	25	PNDX	solar boosted DM
		[10] ZHANG	25B	PNDX	wimp search
		[11] SHANG	24	PNDX	boosted keV-scale DM
		[12] ZHANG	24A	CDEX	accelerated DM scatter on e in semiconductor
		[13] ZHANG	24E	CDEX	evaporating PBH DM
$< 3 \times 10^{-3}$	90	[14] AGNES	23A	DS50	LDM scatter on e
< 0.3	90	[15] ARNQUIST	23A	DAMC	LDM search via CCDs
$< 2 \times 10^{-5}$	90	[16] LI	23F	PNDX	light DM limits
		[17] AGOSTINI	22A	GERD	search for superWIMPs
<1000	90	[18] APRILE	22	XE1T	WIMP-e scatter
		[19] BATTAGLIERI	22	BDX	light DM from beam dump
$< 2 \times 10^{-9}$	95	[20] BOSE	22		DM-e limits from solar γs
< 100		[21] GHOSH	22		boosted DM-e/DM-ν scatter
		[22] HOCHBERG	22	SNSP	superconducting nanowire search for light DM
		[23] ZHANG	22A	CDEX	light DM search on e in Ge
< 10	90	[24] CHENG	21	PNDX	MeV-scale DM on e
		[25] AKERIB	20	LUX	mirror DM with Xe
$< 8.7 \times 10^2$	90	[26] AMARAL	20	SCDM	light DM scatter on e in Si
		[27] APRILE	20	XE1T	excess keV electron recoil in Xe
< 100	90	[28] ARNAUD	20	EDEL	MeV DM scatter on e in Ge
< 0.6	90	[29] BARAK	20	SENS	MeV scale DM scatter from e in Si
$< 2 \times 10^6$	90	[30] ABRAMOFF	19	SENS	WIMP-e scatter on Si
		[31] AGUILAR-AR...	19A	DMIC	MeV scale DM scatter on e in Si
$< 1 \times 10^{-4}$	90	[32] APRILE	19D	XE1T	ionizing light DM on Xe
$< 9 \times 10^{-3}$	90	[33] AGNES	18B	DS50	Ar
$< 1 \times 10^4$	90	[34] AGNESE	18B	SCDM	$e\chi$ scatter
$< 5 \times 10^3$	90	[35] CRISLER	18	SENS	Si CCD
		[36] APRILE	17	X100	Xe, annual modulation

[1] ADARI 25 search for MeV-scale DM using SENSEI at SNOLab. No signal observed. Limits placed in σ_e vs. mass plane for light and heavy mediator models.
[2] AGGARWAL 25A search for MeV-scale DM scattering on e at DAMIC-M. No signal observed. Limits placed in m(DM) vs. σ_e plane for light and heavy mediator models. Quoted limit is for m(DM) = 10 MeV for heavy mediator model with $F_{DM} = 1$.
[3] ALBAKRY 25 report on search for MeV-scale DM using HVeV detectors at SuperCDMS. No signal observed. Limits placed in various planes for different DM hypotheses. Quoted limit is for σ_e for light WIMP interacting via heavy mediator with $F_{DM} = 1$ and m(DM) = 10 MeV.
[4] BAUDIS 25 search for MeV-scale DM via microwire-based superconducting nanowire single-photon detector (SNSPD) as a target and sensor for dark matter scattering and absorption in QROCODILE experiment. No signal observed. Limits placed in m(DM): 1–5000 MeV vs. σ plane for MeV-scale dark photon scattering from e or nucleon via light or heavy mediator.
[5] BLOCH 25 report search for MeV-scale DM at SENSEI at SnoLab. No signal observed. Limits place in σ_e vs. m(χ) plane. Quoted limit is for m(χ) = 1 MeV assuming light mediator.
[6] CHOI 25 search for keV range DM produced from dark photon decay in NEON experiment. No signal observed. Limits placed in σ_e vs. m(χ) plane. Quoted limit is for m(χ) = 100 keV.
[7] DU 25 place bounds on strongly interacting DM scatter on e using JWST images. No signal observed. Limits placed in σ_e vs. m plane for assumed light mediator and fraction DM abundance.
[8] LIANG 25 reexamine SENSEI data using plasmon effect and considers that DM can be boosted scattering with cosmic rays.They place new limits on sub-MeV DM in m(χ) vs. σ_e plane for light and heavy mediator. Quoted limit is from SENSEI light mediator reanalysis with m(χ) = 0.01 MeV.
[9] SHEN 25 search for MeV-scale solar boosted DM scatter on e. No signal observed. Limits placed in σ_e vs m(χ) plane. Quoted limit is for m(χ) = 1 MeV.
[10] ZHANG 25B search for light GeV-scale wimps using run 0 and run 1 PandaX-4T data. No signal observed. Limits placed on σ_e vs. m(χ) depending on assumed light/heavy mediator model.
[11] SHANG 24 report on search for electron cosmic-ray boosted DM in keV range or below with PandaX-4T. No signal observed. Limits plotted in $\sigma(\chi e)$ vs m plane for m $\sim$ 10^{-2}–10^3 keV.
[12] ZHANG 24A examine detection of accelerated MeV-scale DM on e in Ge semiconductor. Limits placed in σ_e vs. m plane depending on various mediator assumptions.
[13] ZHANG 24E search for dark matter from evaporating primordial black holes (PBH) scattering on electrons in Ge with CDEX10 experiment conducted in the China Jinping Underground Laboratory. No signal observed. Limits placed in $\sigma(\chi e)$ vs. m(χ) and other planes for assumed PBH mass and fractional abundance.
[14] AGNES 23A search for MeV-scale DM scatter from e using Ar. No signal observed. $\sigma(\chi e) < 3 \times 10^{-3}$ pb for m(χ) = 30 MeV.
[15] ARNQUIST 23A search for LDM scatter on e using CCDs. No signal observed. Require $\sigma(\chi e) <$ 0.3 pb for m(χ) = 10 MeV and $F_{DM} = 1$ (Fig. 3b).
[16] LI 23F search for light DM in MeV range via scatter from e. No signal observed. Limits set. The quoted limit is for m(χ) = 0.2 GeV with $F_{DM} = 1$.
[17] AGOSTINI 22 search for superWIMP particles using GERDA detector; no signal observed; limits placed in mass vs coupling plane for m(DM) 0.06–1 MeV.
[18] APRILE 22 place new limits on WIMP-e scatter for dark photon and various multipole moments vs. WIMP mass for various DM models; quoted limit for m(WIMP) = 1 GeV in light mediator model.
[19] BATTAGLIERI 22 search for light MeV scale DM particles produced in JLAB beam dump; no signal observed; limits set in kinetic mixing vs. m(DM) plane for m(DM) $\sim$ 1–200 MeV .
[20] BOSE 22 theoretically derive limits on WIMP-e scatter from solar gamma rays using data of Fermi-LAT; limit quoted for m(WIMP) = 5 GeV.
[21] GHOSH 22 derive limits on sub-GeV boosted DM scatter from e or ν using SuperK/XENON1T data; quoted limit for m(χ) = 1 MeV.
[22] HOCHBERG 22 search for sub-eV or sub-MeV scale DM scatter/absorption on e in superconducting nanowire; no signal observed; limits set in m(DM) vs. cross section plane for sub-MeV-scale DM and in m(DM) vs. kinetic mixing plane for sub-eV-scale DM.
[23] ZHANG 22A search for DM scatter on e using CDEX-10; no signal observed; limits placed on $\sigma(\chi e)$ vs. m(DM) plane for m(DM) $\sim$ 0.07–10 GeV for various simplified models.
[24] CHENG 21 search for MeV-scale DM scatter from e in PANDAX-II. No signal detected. Limits set in $\sigma(\chi e)$ vs. m(DM) plane for two choices of form factors; $\sigma(\chi e) < 10$ pb for m(χ) = 10 MeV and $F_{DM} = 1$.

Int. J. Mod. Phys. A 2026.41. Downloaded from www.worldscientific.com
by UNIVERSITY OF CALIFORNIA @ BERKELEY on 09/16/26. Re-use and distribution is strictly not permitted, except for Open Access articles.

[25] AKERIB 20 search for mirror DM with LUX 95 d × 118 kg data for mirror e scatter from Xe; no signal, limits placed in kinetic mixing parameter vs. mirror e temperature T ∼ 0.1–0.9 keV plane.
[26] AMARAL 20 search SuperCDMS data for low mass DM scatter from e in Si; no signal; quoted limit $\sigma_e < 8.7 \times 10^2$ pb for m(DM) = 10 MeV with form factor $F_{DM} = 1$.
[27] APRILE 20 report excess at electron recoil around 2–3 keV in Xe; data compared to unforeseen tritium background, and various signal models (bosonic DM, solar axion, and neutrino magnetic moment).
[28] ARNAUD 20 search for MeV DM scattering from e in Ge; no signal; quoted limit is for m(DM) = 10 MeV with form factor $F_{DM} = 1$.
[29] BARAK 20 report search for MeV scale DM scatter from e in Si; limits placed in σ_e vs. m(DM) plane; quoted limit is for m(DM) = 10 MeV and form factor $F_{DM} = 1$.
[30] ABRAMOFF 19 search for MeV-scale WIMP scatter from Si skipper-CCD; limits placed on $\sigma(\chi e)$ for m(χ) ∼ 0.5–100 MeV depending on DM form factors. Limit given for m(DM) = 1 MeV.
[31] AGUILAR-AREVALO 19A search for MeV scale DM scatter from e in Si CCDs at SNOLAB; no signal, limits placed in σ(e) vs. m(DM) plane for m(DM) ∼ 0.6–100 MeV.
[32] APRILE 19D search for light DM scatter on Xe via ionization; no signal, limits placed in σ on nucleus vs. m(DM) plane for m(DM) ∼ 0.02–10 GeV; quoted limit is for m(DM) = 0.2 GeV.
[33] AGNES 18B search for MeV scale WIMP scatter from e in Ar; no signal, limits set in σ_e vs. m(χ) plane for m ∼ 20–1000 MeV and two choices of form factor F(DM); quoted limit for m(χ) = 100 MeV and F = 1.
[34] AGNESE 18B search for $e\chi$ scatter in SuperCDMS; limits placed in $\sigma(e\chi)$ vs. m(χ) plane for m ∼ 0.3–1 × 10^4 MeV for two assumed form factors and also in m(dark photon) vs. kinetic mixing plane. Limit given for m(χ) = 1 GeV and F=1.
[35] CRISLER 18 search for $\chi e \rightarrow \chi e$ scatter in Si CCD; place limits on MeV DM in σ_e vs. m(χ) plane for m ∼ 0.5–1000 MeV for different form factors; quoted limit is for F(DM) = 1 and m(χ) = 10 MeV.
[36] APRILE 17 search for WIMP-e annual modulation signal for recoil energy in the 2.0–5.8 keV interval using 4 years data with Xe. No significant effect seen.

Cross-Section Limits for Dark Matter Particles (X^0) on Nuclei

For m_{X^0} in GeV range

We provide here limits fo $m_{X^0} < 5$ GeV

VALUE (pb)	CL%	DOCUMENT ID		TECN	COMMENT
• • • We do not use the following data for averages, fits, limits, etc. • • •					
$<1 \times 10^{-5}$	90	[1] NIE	25	CDEX	GeV DM search
		[2] AKIMOV	22	COHR	DM mediators

[1] NIE 25 report search for GeV-scale DM in CDEX-10 experiment. No signal observed. Limits placed on $\sigma(\chi N)$ vs. m(χ) for mediator masses of 1 MeV and 1 GeV. Quoted limit is for m(χ) = 4 GeV with m(mediator) = 1 GeV.
[2] AKIMOV 22 use COHERENT CsI(Na) detector to search for sub GeV DM particles produced by the Spallation Neutron Source. No signal observed. Limits placed in mediator mass vs. coupling plane for leptophobic DM models.

For m_{X^0} = 20 GeV

VALUE (nb)	CL%	DOCUMENT ID		TECN	COMMENT
• • • We do not use the following data for averages, fits, limits, etc. • • •					
< 0.03	90	[1] UCHIDA	14	XMAS	^{129}Xe, inelastic
< 0.08	90	[2] ANGLOHER	02	CRES	Al
		[3] BENOIT	00	EDEL	Ge
< 0.04	95	[4] KLIMENKO	98	CNTR	^{73}Ge, inel.
< 0.8		ALESSAND...	96	CNTR	O
< 6		ALESSAND...	96	CNTR	Te
< 0.02	90	[5] BELLI	96	CNTR	^{129}Xe, inel.
		[6] BELLI	96C	CNTR	^{129}Xe
< 4 × 10^{-3}	90	[7] BERNABEI	96	CNTR	Na
< 0.3	90	[7] BERNABEI	96	CNTR	I
< 0.2	95	[8] SARSA	96	CNTR	Na
< 0.015	90	[9] SMITH	96	CNTR	Na
< 0.05	95	[10] GARCIA	95	CNTR	Natural Ge
< 0.1	95	QUENBY	95	CNTR	Na
<90	90	[11] SNOWDEN-...	95	MICA	^{16}O
< 4 × 10^3	90	[11] SNOWDEN-...	95	MICA	^{39}K
< 0.7	90	BACCI	92	CNTR	Na
< 0.12	90	[12] REUSSER	91	CNTR	Natural Ge
< 0.06	95	CALDWELL	88	CNTR	Natural Ge

[1] UCHIDA 14 limit is for inelastic scattering $X^0 + {}^{129}\text{Xe}^* \rightarrow X^0 + {}^{129}\text{Xe}^*$ (39.58 keV).
[2] ANGLOHER 02 limit is for spin-dependent WIMP-Aluminum cross section.
[3] BENOIT 00 find four event categories in Ge detectors and suggest that low-energy surface nuclear recoils can explain anomalous events reported by UKDMC and Saclay NaI experiments.
[4] KLIMENKO 98 limit is for inelastic scattering $X^0\,{}^{73}\text{Ge} \rightarrow X^0\,{}^{73}\text{Ge}^*$ (13.26 keV).
[5] BELLI 96 limit for inelastic scattering $X^0\,{}^{129}\text{Xe} \rightarrow X^0\,{}^{129}\text{Xe}^*$(39.58 keV).
[6] BELLI 96C use background subtraction and obtain $\sigma < 150$ pb (< 1.5 fb) (90% CL) for spin-dependent (independent) X^0-proton cross section. The confidence level is from R. Bernabei, private communication, May 20, 1999.
[7] BERNABEI 96 use pulse shape discrimination to enhance the possible signal. The limit here is from R. Bernabei, private communication, September 19, 1997.
[8] SARSA 96 search for annual modulation of WIMP signal. See SARSA 97 for details of the analysis. The limit here is from M.L. Sarsa, private communication, May 26, 1997.
[9] SMITH 96 use pulse shape discrimination to enhance the possible signal. A dark matter density of 0.4 GeV cm^{-3} is assumed.
[10] GARCIA 95 limit is from the event rate. A weaker limit is obtained from searches for diurnal and annual modulation.
[11] SNOWDEN-IFFT 95 look for recoil tracks in an ancient mica crystal. Similar limits are also given for ^{27}Al and ^{28}Si. See COLLAR 96 and SNOWDEN-IFFT 96 for discussion on potential backgrounds.
[12] REUSSER 91 limit here is changed from published (0.04) after reanalysis by authors. J.L. Vuilleumier, private communication, March 29, 1996.

For m_{X^0} = 100 GeV

VALUE (nb)	CL%	DOCUMENT ID		TECN	COMMENT
• • • We do not use the following data for averages, fits, limits, etc. • • •					
< 3.3 × 10^{-6}	90	[1] APRILE	21A	XE1T	^{129}Xe, inelastic
< 3 × 10^{-3}	90	[2] UCHIDA	14	XMAS	^{129}Xe, inelastic
< 0.3	90	[3] ANGLOHER	02	CRES	Al
		[4] BELLI	02	RVUE	
		[5] BERNABEI	02C	DAMA	
		[6] GREEN	02	RVUE	
		[7] ULLIO	01	RVUE	
		[8] BENOIT	00	EDEL	Ge
< 4 × 10^{-3}	90	[9] BERNABEI	00D		^{129}Xe, inelastic
		[10] AMBROSIO	99	MCRO	
		[11] BRHLIK	99	RVUE	
< 8 × 10^{-3}	95	[12] KLIMENKO	98	CNTR	^{73}Ge, inelastic
< 0.08	95	[13] KLIMENKO	98	CNTR	^{73}Ge, inelastic
< 4		ALESSAND...	96	CNTR	O
<25		ALESSAND...	96	CNTR	Te
< 6 × 10^{-3}	90	[14] BELLI	96	CNTR	^{129}Xe, inelastic
		[15] BELLI	96C	CNTR	^{129}Xe
< 1 × 10^{-3}	90	[16] BERNABEI	96	CNTR	Na
< 0.3	90	[16] BERNABEI	96	CNTR	I
< 0.7	95	[17] SARSA	96	CNTR	Na
< 0.03	90	[18] SMITH	96	CNTR	Na
< 0.8	90	[18] SMITH	96	CNTR	I
< 0.35	95	[19] GARCIA	95	CNTR	Natural Ge
< 0.6	95	QUENBY	95	CNTR	Na
< 3	95	QUENBY	95	CNTR	I
< 1.5 × 10^2	90	[20] SNOWDEN-...	95	MICA	^{16}O
< 4 × 10^2	90	[20] SNOWDEN-...	95	MICA	^{39}K
< 0.08	90	[21] BECK	94	CNTR	^{76}Ge
< 2.5	90	BACCI	92	CNTR	Na
< 3	90	BACCI	92	CNTR	I
< 0.9	90	[22] REUSSER	91	CNTR	Natural Ge
< 0.7	95	CALDWELL	88	CNTR	Natural Ge

[1] APRILE 21A search for inelastic DM scatter off ^{129}Xe nuclei with 0.83 t yr exposure. No signal obseved. Limits placed in $\sigma(\chi\text{Xe})$ vs. m(DM) plane for WIMP mass between 20 GeV and 10 TeV.
[2] UCHIDA 14 limit is for inelastic scattering $X^0 + {}^{129}\text{Xe}^* \rightarrow X^0 + {}^{129}\text{Xe}^*$(39.58 keV).
[3] ANGLOHER 02 limit is for spin-dependent WIMP-Aluminum cross section.
[4] BELLI 02 discuss dependence of the extracted WIMP cross section on the assumptions of the galactic halo structure.
[5] BERNABEI 02C analyze the DAMA data in the scenario in which X^0 scatters into a slightly heavier state as discussed by SMITH 01.
[6] GREEN 02 discusses dependence of extracted WIMP cross section limits on the assumptions of the galactic halo structure.
[7] ULLIO 01 disfavor the possibility that the BERNABEI 99 signal is due to spin-dependent WIMP coupling.
[8] BENOIT 00 find four event categories in Ge detectors and suggest that low-energy surface nuclear recoils can explain anomalous events reported by UKDMC and Saclay NaI experiments.
[9] BERNABEI 00D limit is for inelastic scattering $X^0\,{}^{129}\text{Xe} \rightarrow X^0\,{}^{129}\text{Xe}$ (39.58 keV).
[10] AMBROSIO 99 search for upgoing muon events induced by neutrinos originating from WIMP annihilations in the Sun and Earth.
[11] BRHLIK 99 discuss the effect of astrophysical uncertainties on the WIMP interpretation of the BERNABEI 99 signal.
[12] KLIMENKO 98 limit is for inelastic scattering $X^0\,{}^{73}\text{Ge} \rightarrow X^0\,{}^{73}\text{Ge}^*$ (13.26 keV).
[13] KLIMENKO 98 limit is for inelastic scattering $X^0\,{}^{73}\text{Ge} \rightarrow X^0\,{}^{73}\text{Ge}^*$ (66.73 keV).
[14] BELLI 96 limit for inelastic scattering $X^0\,{}^{129}\text{Xe} \rightarrow X^0\,{}^{129}\text{Xe}^*$(39.58 keV).
[15] BELLI 96C use background subtraction and obtain $\sigma < 0.35$ pb (< 0.15 fb) (90% CL) for spin-dependent (independent) X^0-proton cross section. The confidence level is from R. Bernabei, private communication, May 20, 1999.
[16] BERNABEI 96 use pulse shape discrimination to enhance the possible signal. The limit here is from R. Bernabei, private communication, September 19, 1997.
[17] SARSA 96 search for annual modulation of WIMP signal. See SARSA 97 for details of the analysis. The limit here is from M.L. Sarsa, private communication, May 26, 1997.
[18] SMITH 96 use pulse shape discrimination to enhance the possible signal. A dark matter density of 0.4 GeV cm^{-3} is assumed.
[19] GARCIA 95 limit is from the event rate. A weaker limit is obtained from searches for diurnal and annual modulation.
[20] SNOWDEN-IFFT 95 look for recoil tracks in an ancient mica crystal. Similar limits are also given for ^{27}Al and ^{28}Si. See COLLAR 96 and SNOWDEN-IFFT 96 for discussion on potential backgrounds.
[21] BECK 94 uses enriched ^{76}Ge (86% purity).
[22] REUSSER 91 limit here is changed from published (0.3) after reanalysis by authors. J.L. Vuilleumier, private communication, March 29, 1996.

For m_{X^0} = 1 TeV

VALUE (nb)	CL%	DOCUMENT ID		TECN	COMMENT
• • • We do not use the following data for averages, fits, limits, etc. • • •					
< 0.03	90	[1] UCHIDA	14	XMAS	^{129}Xe, inelastic
< 3	90	[2] ANGLOHER	02	CRES	Al
		[3] BENOIT	00	EDEL	Ge
		[4] BERNABEI	99D	CNTR	SIMP
		[5] DERBIN	99	CNTR	SIMP
< 0.06	95	[6] KLIMENKO	98	CNTR	^{73}Ge, inel.
< 0.4	95	[7] KLIMENKO	98	CNTR	^{73}Ge, inel.
< 40		ALESSAND...	96	CNTR	O

Int. J. Mod. Phys. A 2026.41. Downloaded from www.worldscientific.com
by UNIVERSITY OF CALIFORNIA @ BERKELEY on 09/16/26. Re-use and distribution is strictly not permitted, except for Open Access articles.

<700		ALESSAND...	96	CNTR	Te
< 0.05	90	[8] BELLI	96	CNTR	^{129}Xe, inel.
< 1.5	90	[9] BELLI	96	CNTR	^{129}Xe, inel.
		[10] BELLI	96C	CNTR	^{129}Xe
< 0.01	90	[11] BERNABEI	96	CNTR	Na
< 9	90	[11] BERNABEI	96	CNTR	I
< 7	95	[12] SARSA	96	CNTR	Na
< 0.3	90	[13] SMITH	96	CNTR	Na
< 6	90	[13] SMITH	96	CNTR	I
< 6	95	[14] GARCIA	95	CNTR	Natural Ge
< 8	95	QUENBY	95	CNTR	Na
< 50	95	QUENBY	95	CNTR	I
<700	90	[15] SNOWDEN-...	95	MICA	^{16}O
< 1 $\times 10^3$	90	[15] SNOWDEN-...	95	MICA	^{39}K
< 0.8	90	[16] BECK	94	CNTR	^{76}Ge
< 30	90	BACCI	92	CNTR	Na
< 30	90	BACCI	92	CNTR	I
< 15	90	[17] REUSSER	91	CNTR	Natural Ge
< 6	95	CALDWELL	88	CNTR	Natural Ge

[1] UCHIDA 14 limit is for inelastic scattering $X^0 + {}^{129}\mathrm{Xe}^* \rightarrow X^0 + {}^{129}\mathrm{Xe}^*$ (39.58 keV).

[2] ANGLOHER 02 limit is for spin-dependent WIMP-Aluminum cross section.

[3] BENOIT 00 find four event categories in Ge detectors and suggest that low-energy surface nuclear recoils can explain anomalous events reported by UKDMC and Saclay NaI experiments.

[4] BERNABEI 99D search for SIMPs (Strongly Interacting Massive Particles) in the mass range 10^3–10^{16} GeV. See their Fig. 3 for cross-section limits.

[5] DERBIN 99 search for SIMPs (Strongly Interacting Massive Particles) in the mass range 10^2–10^{14} GeV. See their Fig. 3 for cross-section limits.

[6] KLIMENKO 98 limit is for inelastic scattering $X^0\ {}^{73}\mathrm{Ge} \rightarrow X^0\ {}^{73}\mathrm{Ge}^*$ (13.26 keV).

[7] KLIMENKO 98 limit is for inelastic scattering $X^0\ {}^{73}\mathrm{Ge} \rightarrow X^0\ {}^{73}\mathrm{Ge}^*$ (66.73 keV).

[8] BELLI 96 limit for inelastic scattering $X^0\ {}^{129}\mathrm{Xe} \rightarrow X^0\ {}^{129}\mathrm{Xe}^*$(39.58 keV).

[9] BELLI 96 limit for inelastic scattering $X^0\ {}^{129}\mathrm{Xe} \rightarrow X^0\ {}^{129}\mathrm{Xe}^*$(236.14 keV).

[10] BELLI 96C use background subtraction and obtain $\sigma < 0.7$ pb (< 0.7 fb) (90% CL) for spin-dependent (independent) X^0-proton cross section. The confidence level is from R. Bernabei, private communication, May 20, 1999.

[11] BERNABEI 96 use pulse shape discrimination to enhance the possible signal. The limit here is from R. Bernabei, private communication, September 19, 1997.

[12] SARSA 96 search for annual modulation of WIMP signal. See SARSA 97 for details of the analysis. The limit here is from M.L. Sarsa, private communication, May 26, 1997.

[13] SMITH 96 use pulse shape discrimination to enhance the possible signal. A dark matter density of 0.4 GeV cm^{-3} is assumed.

[14] GARCIA 95 limit is from the event rate. A weaker limit is obtained from searches for diurnal and annual modulation.

[15] SNOWDEN-IFFT 95 look for recoil tracks in an ancient mica crystal. Similar limits are also given for ^{27}Al and ^{28}Si. See COLLAR 96 and SNOWDEN-IFFT 96 for discussion on potential backgrounds.

[16] BECK 94 uses enriched ^{76}Ge (86% purity).

[17] REUSSER 91 limit here is changed from published (5) after reanalysis by authors. J.L. Vuilleumier, private communication, March 29, 1996.

Miscellaneous Results from Underground Dark Matter Searches

VALUE	CL%	DOCUMENT ID		TECN	COMMENT
• • • We do not use the following data for averages, fits, limits, etc. • • •					
		[1] AGNES	25	DS50	MeV-scale boosted DM from PBHs
		[2] AMARE	25	ANAI	annual modulation in NaI
		[3] BERGHAUS	25	ICCB	ultra-heavy decaying DM
		[4] CARLIN	25	ANAI	Cosine-100/Anais annual modulation
		[5] LIANG	25A	CDEX	inelastic DM search
		[6] NING	25B	PNDX	leptonic mediator DM search
		[7] WANG	25A	CDEX	boosted DM search
		[8] ABE	24A	KLNZ	WIMP-nuclei bound states
		[9] AGNES	24	DS50	search for annual modulation
		[10] ARNQUIST	24A	DAMC	ultralight DM
		[11] ABE	23A	SKAM	boosted DM limits
		[12] ADAMS	23	PICO	inelastic DM search
		[13] ADHIKARI	23B	C100	BDM/heavy photon DM
		[14] AL-KHARUSI	23	EXO2	UDM search
		[15] APRILE	23	XE1T	Planck scale DM search
		[16] HUANG	23	PNDX	scalar DM via dark mediator decay
		[17] NING	23A	PNDX	boosted LDM
		[18] ADHIKARI	22	DEAP	Planck scale DM multiple scatter on Ar
		[19] ADHIKARI	22D	NAI	COSINE-100 annual modulation DM search
		[20] DAI	22A	CDEX	MeV scale exotic DM
		[21] GU	22	PNDX	absorption of fermion DM
		[22] ZHANG	22	PNDX	light DM search
		[23] AKERIB	21B	LUX	limits on WIMP EFT couplings
		[24] AMARE	21	ANAI	annual modulation on NaI
		[25] WANG	21K	CDEX	DM effective operator limits
		[26] AGOSTINI	20	HPGE	keV-MeV scale super-WIMP absorption in Ge
		[27] ANDRIANAV...	20	FUNK	hidden photon DM search
		[28] CLARK	20		superheavy MIMP DM
		[29] ABRAMOFF	19	SENS	MeV DM e-Si; dark photon Si absorption
		[30] ADHIKARI	19	C100	annual modulation NaI
		[31] AMARE	19	ANAI	annual modulation NaI
$<6.4 \times 10^{-10}$	90	[32] APRILE	19	XE1T	π (Xe)
		[33] BRINGMANN	19		cosmic ray DM
		[34] BRUNE	19		Majoran DM
		[35] CHOI	19	THEO	290 TeV IceCube ν
		[36] HA	19	C100	inelastic boosted dark γ
		[37] KLOPF	19		$n \rightarrow \chi e^+ e^-$
		[38] AARTSEN	18D	ICCB	relic WIMP $\chi \rightarrow \nu X$
		[39] ABE	18F	XMAS	$A' e \rightarrow A' e$
		[40] AGNES	18B	DS50	Ar
		[41] AGNESE	18B	SCDM	MeV DM e-Si; dark photon Si absorption
		[42] AKERIB	18A	LUX	Xe
		[43] ARMENGAUD	18	EDE3	Ge
		[44] KACHULIS	18	SKAM	boosted DM on e
$<1 \times 10^{-12}$	90	[45] AGUILAR-AR...	17	DMIC	γ' on Si
		[46] APRILE	17	X100	Xe
		[47] APRILE	17D	X100	Xe
		[48] APRILE	17H	X100	keV bosonic DM search
		[49] APRILE	17K	X100	$\chi N \rightarrow \chi^* \rightarrow \chi\gamma$
$<4 \times 10^{-3}$	90	[50] ANGLOHER	16A	CRES	$CaWO_4$
		[51] APRILE	15	X100	Event rate modulation
		[52] APRILE	15A	X100	Electron scattering

[1] AGNES 25 report on search for MeV-scale boosted dark matter arising form primordial black hole (PBH) evaporation using DarkSide-50 detector with a 12202 ± 180 kg·d exposure. No signal observed. Limits depend on PBH mass and abundance: see Fig. 4 in m(χ) vs. σ^{SI} plane.

[2] AMARE 25 reports on annual modulation modulation search in NaI target at ANAIS-112 in the Canfranc underground laboratory. No signal observed. Results incompatible with DAMA/LIBRA results at 4σ.

[3] BERGHAUS 25 derive limits on ultra-heavy decaying DM in m(DM): 10^{10}–10^{16} GeV range. Limits placed in lifetime τ vs. mass plane for various assumed decay modes from gamma ray searches at Fermi-LAT and neutrino searches at IceCube.

[4] CARLIN 25 reports combined Cosine-100 and Anais-112 annual modulation for DM scatter on NaI. No annual modulation found. Incompatible with DAMA/LIBRA results at 4.7σ.

[5] LIANG 25A report on inelastic WIMP search using CDEX-IB. No signal observed. Limits placed in σ^{SI} vs. δ (mass difference) plane for various inelastic wimp mass values m(χ), see Fig. 8.

[6] NING 25B search for leptonic-mediator dark matter at PandaX-4T. No signal observed. Limits placed in mediator mass m(ϕ) vs. DM mass m(χ) plane for both Dirac and Majorana DM particles with coupling $\lambda = 1$.

[7] WANG 25A report on search for boosted dark matter at CDEX-10. No signal observed. Exclusion limits presented for boosted DM model in m(χ) vs. non-relativistic effective field theory (NREFT) operator couplings for various NREFT operators.

[8] ABE 24A report Kamland-Zen search for de-excitation of WIMP DM bound to nucleus due to small mass splitting with charged WIMP partner. No signal observed. Limits placed in several parameter planes such as charged WIMP decay width vs. mass splitting (e.g. Fig. 7).

[9] AGNES 24 search for annual modulation signal from wimp interactions in Ar. No signal observed.

[10] ARNQUIST 24A report DAMIC-M search for MeV-scale DM scatter on e via mediator. No signal observed. Limits placed in σ(e) vs m plane.

[11] ABE 23A search for boosted sub-GeV DM using 0.37 Mt·y exposure of SuperK data. No signal observed. Model dependent limits set, see Fig. 3 corrected in ABE 23G erratum.

[12] ADAMS 23 search for inelastic DM scatter in fluorocarbons. No signal observed. Limits placed in σ vs. m(χ) mass splitting plane.

[13] ADHIKARI 23B search for boosted heavy photon DM in MeV range using Cosine-100. No signal observed. Limits placed in coupling vs. mass plane for masses 1–100 MeV.

[14] AL-KHARUSI 23 search for absorption of MeV-scale DM with 234.1 kg·y exposure of ^{136}Xe, triggering beta decay. No signal observed. Limit placed in cross section vs. mass plane for m(χ) = 1.7–11.6 MeV (see Fig. 5).

[15] APRILE 23 search for multiple scatter events from Planck scale-DM particles. No signal observed. Limits set on σ^{SI} and σ^{SD} on n and p.

[16] HUANG 23 search for MeV-scale scalar DM interacting via GeV-scale dark mediator. Limits placed on cross section vs. mass plane.

[17] NING 23A search for boosted LDM arising from η decays which are produced in CR events with 0.63 t·y exposure. No signal observed. Limits placed in $\sigma(\chi N)$ vs. m(χ) plane for various mediator models and branching fraction assumptions (see Fig. 2).

[18] ADHIKARI 22 search for multiple scatter of Planck scale DM on Ar using DEAP detector. No signal observed. Limits placed in mass vs. cross section plane for m(DM): 10^7–10^{19} GeV.

[19] ADHIKARI 22D report search for annual modulation signal of DM in a 173 kg·yr exposure of NaI; result consistent with both the modulation amplitude reported by DAMA/LIBRA and no-modulation .

[20] DAI 22A search for MeV-scale exotic DM interaction with Ge; no signal observed; limits set in m(DM) vs. cross section plane for m(DM) ∼ 5–60 MeV in simplified model.

[21] GU 22 use PANDAX to search for absorption of fermionic DM in MeV range in Xe; no signal observed; limits set in m(DM) vs. cross section plane for m(DM) ∼ 30–125 MeV.

[22] ZHANG 22 search for light DM scatter on e; no signal observed; limits placed in $\sigma \cdot v$ vs. m(DM) plane for m(DM) ∼ 10–180 keV.

[23] AKERIB 21B place limits on 15 WIMP non-relativistic EFT couplings for m(DM): 10–4000 GeV using 3.14 kg d exposure.

[24] AMARE 21 search for WIMP annual modulation signal on NaI target in the Canfranc Underground Laboratory (LSC). With an effective exposure of 313.95 kg y, and a sensitivity of 2.5 σ no signal is observed. Incompatible with DAMA/LIBRA at 3.3 σ level.

[25] WANG 21K use CDEX detector to search for WIMP dark matter scatter on Ge; no signal observed; limits placed on 14 non-relativistic effective operators along with WIMP-pion coupling for m(WIMP) ∼ 3–20 GeV.

Int. J. Mod. Phys. A 2026.41. Downloaded from www.worldscientific.com
by UNIVERSITY OF CALIFORNIA @ BERKELEY on 09/16/26. Re-use and distribution is strictly not permitted, except for Open Access articles.

[26] AGOSTINI 20 search for keV–MeV scale super-WIMP absorption in Ge in GERDA; no signal; limits placed on keV–MeV scale bosonic superWIMPs in coupling vs. mass plane.
[27] ANDRIANAVALOMAHEFA 20 search for hidden photon DM in eV range; place limits in m(DM) vs ln(χ) plane: exclude coupling $\chi \lesssim 1 \times 10^{-12}$ for m(DM) $\sim$ 2.5–7 eV.
[28] CLARK 20 use Majorana and Xe-1-ton data to constrain superheavy multply interacting dark matter (MIMP) in range m$\sim 10^8$–10^{17} GeV depending on interaction cross section.
[29] ABRAMOFF 19 search for MeV scale DM via DM$-e$ scattering and dark photon DM via absorption in Si; limits set in coupling vs. m(χ) plane and on dark photon in m(A) vs. kinetic mixing parameter plane.
[30] ADHIKARI 19 search for annual modulation signal from WIMP scatter on NaI with 1.7 yr exposure; result consistent with both DAMA/LIBRA and null hypothesis.
[31] AMARE 19 is ANAIS-112 search for WIMP scatter annual modulation on NaI; 157.55 kg yr exposure; result compatible with null hypothesis; confirm goal of reaching sensitivity at 3σ to DAMA/LIBRA result in 5 years.
[32] APRILE 19 search for WIMP-pion scattering in Xe; no signal: require $\sigma(\chi\pi) < 6.4 \times 10^{-10}$ pb for m(χ) = 30 GeV.
[33] BRINGMANN 19 derive theoretically limits on GeV and sub-GeV mass dark matter, in its high energy component generated by interaction with cosmic rays; place limits on σ^{SI} and $\sigma^{SD} < 10^5$ pb.
[34] BRUNE 19 examine possibility of Majoron dark matter; limits placed on Majoron mass vs. coupling from SN1987a and ν-less double beta decay.
[35] CHOI 19 from multimessenger observation finds limit on $\sigma(\nu\chi)$/m(DM) $< 5.1 \times 10^{-23}$ cm^2/GeV based on 290 TeV IceCube neutrino event.
[36] HA 19 search for inelastic boosted MeV scale dark photon using COSINE-100 data; limits placed in m vs. epsilon plane for various mediators.
[37] KLOPF 19 search for DM via $n \to \chi e^+ e^-$; no signal: limits placed in branching fraction vs. m($e^+ e^-$) plane.
[38] AARTSEN 18D search for long-lived DM particles decaying $\chi \to \nu X$; no excess seen; for DM masses above 10 TeV, excluding lifetimes shorter than 10^{28} s.
[39] ABE 18F search for keV mass ALPs and hidden photons (HP) scatter on electrons; limits set on mass vs. coupling.
[40] AGNES 18B search for MeV-scale DM scatter on electrons in Ar; no signal; require $\sigma(\chi e) < 9 \times 10^{-3}$ pb for DM form factor F(DM) = 1 and < 300 pb for F(DM) proportional to 1/q^2 for m(χ) = 100 MeV.
[41] AGNESE 18B search for MeV scale DM via DM-e scattering and dark photon DM via absorption in Si; limits set on MeV DM in coupling vs. m(χ) plane and on dark photon in m(A') vs. kinetic mixing plane.
[42] AKERIB 18A search for annual and diurnal modulation of DM scattering rate on electrons for recoil energy between 2 and 6 keVee; no signal found.
[43] ARMENGAUD 18 search for ALP from the Sun and galactic bosonic DM, interacting in Ge; no signal; limits set for 0.8–500 keV DM particles.
[44] KACHULIS 18 search for an excess of elastically scattered electrons above the atmospheric neutrino background in Super-K; limits placed for simple annihilation or decay in the Sun or galactic center producing "boosted" dark matter.
[45] AGUILAR-AREVALO 17 search for hidden photon DM scatter on Si target CCD; limit kinetic mixing $\kappa < 1 \times 10^{-12}$ for m = 10 eV.
[46] APRILE 17 search for WIMP-e annual modulation signal for recoil energy in the 2.0–5.8 keV interval using 4 years data with Xe. No significant effect seen.
[47] APRILE 17D set limits on 14 WIMP-nucleon different interaction operators. No deviations found using 225 live days in the 6.6–240 keV recoil energy range.
[48] APRILE 17H search for keV bosonic DM via $e\chi \to e$, looking for electronic recoils with 224.6 live days of data and 34 kg of LXe. Limits set on $\chi e e$ coupling for m(χ) = 8–125 keV.
[49] APRILE 17K search for magnetic inelastic DM via $\chi N \to \chi^* \to \chi\gamma$. Limits set in DM magnetic moment vs. mass splitting plane for two DM masses corresponding to the DAMA/LIBRA best fit values.
[50] ANGLOHER 16A require q^2 dependent scattering $< 8 \times 10^{-3}$ pb for asymmetric DM m(WIMP) = 3 GeV on $CaWO_4$ target. It uses a local dark matter density of 0.38 GeV/cm^3.
[51] APRILE 15 search for periodic variation of electronic recoil event rate in the data between Feb. 2011 and Mar. 2012. No significant modulation is found for periods up to 500 days.
[52] APRILE 15A search for X^0 scattering off electrons. See their Fig. 4 for limits on cross section through axial-vector coupling for m_{X^0} between 0.6 GeV and 1 TeV. For m_{X^0} = 2 GeV, $\sigma < 60$ pb (90%CL) is obtained.

X^0 Annihilation Cross Section

Limits are on σv for X^0 pair annihilation for the X^0 mass specified in the footnote when needed.

VALUE (cm^{3}s^{-1})	CL%	DOCUMENT ID		TECN	COMMENT
• • • We do not use the following data for averages, fits, limits, etc. • • •					
		[1] ABBASI	25A	ICCB	WIMP annihilation to ν_μ in center of earth
$<1.9 \times 10^{-24}$	95	[2] ABE	25A	MGIC	search for branon DM
$<2.5 \times 10^{-24}$	90	[3] AIELLO	25B	KM3N	DM to ν search
$<1 \times 10^{-26}$	95	[4] CRNOGORC...	25	FLAT	DM annihilation from cusps in galactic clusters
		[5] FERNANDEZ...	25	FLAT	wimp annihilation in stellar streams
$<4 \times 10^{-34}$	95	[6] ZAKHAROV	25	NUST	keV-scale DM annihilation to X-rays
$<2 \times 10^{-24}$	95	[7] ACHARYYA	24	VRTS	TeV-scale wimp annihilation
$<2 \times 10^{-22}$	95	[8] CAO	24	LHAS	superheavy WIMP annihilation
		[9] CHOLIS	24		γ-ray background
		[10] CRNOGORC...	24		Ursa-Major III DM annihilation
		[11] DE-LA-TORR...	24		WIMP annihilation to gammas
$<6.4 \times 10^{-26}$		[12] MANNA	24		wimp annihilation to gammas from galaxy clusters
$<2 \times 10^{-26}$	95	[13] MCDANIEL	24	FLAT	combined WIMP annihilation in dwarf spheroidals
$<2 \times 10^{-26}$	95	[14] MCDANIEL	24	FLAT	combined Fermi-LAT dwarf spheroidal constraints
		[15] SONG	24	FLAT	heavy WIMPs
		[16] SONG	24A	FLAT	heavy WIMP annihilation in galaxy clusters
$<1 \times 10^{-33}$	95	[17] ZAKHAROV	24A		keV-scale DM annihilation
$<1 \times 10^{-24}$	90	[18] ABBASI	23A	ICCB	WIMP annihilation to ν's
$<1 \times 10^{-22}$	90	[19] ABBASI	23B	ICCB	PeV WIMP annihilation
$<5 \times 10^{-28}$	95	[20] ABE	23B	MGIC	Wimp annihilation to γ
		[21] ALBERT	23	HAWC	WIMP annihilation to γ in galactic halo
		[22] CHENG	23A		Fermi-LAT and DAMPE combined γ line search
$<2 \times 10^{-25}$	95	[23] FOSTER	23	FLAT	DM annihilation to gamma line
		[24] GUO	23	FAST	DM annihilation in dwarf spheroidal galaxy
		[25] GUO	23A		WIMP annihilation in dwarf spheroidal galaxies
$<2 \times 10^{-26}$	95	[26] LAVIS	23		$b\overline{b}$ + 2HDM+S, m<1000 GeV
$<1.2 \times 10^{-26}$	95	[27] ABDALLA	22	HESS	DM annihilation to gamma rays
		[28] ALBERT	22A	ANTR	PeV-scale DM search
$<1 \times 10^{-27}$		[29] CHAN	22		DM annihilation from Omega Centauri X-rays
$<3 \times 10^{-26}$		[30] EGOROV	22		DM annihilation to radio waves from M31
		[31] MANCONI	22		polarized synchrotron emission from DM annihilation via Planck
$<5 \times 10^{-24}$	95	[32] ABDALLAH	21	HESS	WIMP annihilation in dwarf irregular galaxy
		[33] CIRELLI	21		light DM annihilation producing X-rays
		[34] JOHN	21		cosmic positron spectra limits on leptophilic DM
$<2.5 \times 10^{-27}$	95	[35] ABAZAJIAN	20	FLAT	γ from galactic center
		[36] ABDALLAH	20	HESS	WIMP annihilation in dwarf satellite galaxies
$<1.2 \times 10^{-24}$	90	[37] ABE	20G	SKAM	WIMP annihilation to neutrinos
$<2.2 \times 10^{-24}$	95	[38] ALBERT	20	HAWC	WIMP annihilation to γ
$<5 \times 10^{-24}$	90	[39] ALBERT	20A	ANTR	WIMP annihilation to νs in galactic center
$<1 \times 10^{-23}$	90	[40] ALBERT	20C	ANTR	Antares/IceCube search for WIMP annihilation to νs
$<8 \times 10^{-26}$		[41] ALVAREZ	20	FLAT	dwarf spheroidal; J-distribution
$<2 \times 10^{-26}$	90	[42] HOOF	20	FLAT	WIMP annihilation to γ
		[43] MAZZIOTTA	20	FLAT	DM annihilation in Sun to γ
		[44] ABEYSEKARA	19	HAWC	DM annihilation to γs within galactic substructure
$<0.8 \times 10^{-22}$	95	[45] ALBERT	19B	HAWC	annihilation/decay to γ in M31
$<4 \times 10^{-26}$	95	[46] CHEUNG	19	EDGS	$\chi\chi \to e^+ e^-$ and $b\overline{b}$
$<7 \times 10^{-27}$	95	[47] DI-MAURO	19	FLAT	Fermi-LAT M31 and M33
		[48] JOHNSON	19	FLAT	P-wave DM; Fermi-LAT
$<2 \times 10^{-26}$	95	[49] LI	19D	FLAT	$\chi\chi \to \gamma$
$<1 \times 10^{-32}$		[50] NG	19		sterile ν decay/annihilation
		[51] QUEIROZ	19		semi-annihilating DM
$<4 \times 10^{-28}$	95	[52] ABDALLAH	18	HESS	$X^0 X^0 \to \gamma X$; galactic halo
$<1 \times 10^{-23}$	95	[53] AHNEN	18	MGIC	$X^0 X^0 \to \gamma X$; Ursa Major II
$<1 \times 10^{-22}$	95	[54] ALBERT	18B	HAWC	$X^0 X^0 \to \gamma X$; Andromeda
$<1 \times 10^{-26}$	95	[55] CHANG	18A		$\chi\chi \to b\overline{b} \to \gamma$
		[56] LISANTI	18	THEO	Fermi, γ; galaxy groups
		[57] MAZZIOTTA	18	FLAT	Fermi-LAT CRE data
$<1.2 \times 10^{-23}$	95	[58] AARTSEN	17C	ICCB	$\chi\chi \to$ neutrinos
$<1 \times 10^{-23}$	90	[59] ALBERT	17A	ANTR	ν, DM annihilation
$<1.32 \times 10^{-25}$	95	[60] ARCHAMBAU..	17	VRTS	γ dwarf galaxies
$<7 \times 10^{-21}$	90	[61] AVRORIN	17	BAIK	cosmic ν
$<1 \times 10^{-28}$		[62] BOUDAUD	17		MeV DM to $e^+ e^-$
		[63] AARTSEN	16D	ICCB	ν, galactic center
$<6 \times 10^{-26}$	95	[64] ABDALLAH	16	HESS	Central Galactic Halo
$<1 \times 10^{-27}$	95	[65] ABDALLAH	16A	HESS	WIMP+WIMP $\to \gamma\gamma$; galactic center
$<3 \times 10^{-26}$	95	[66] AHNEN	16	MGFL	Satellite galaxy, m(WIMP)=100 GeV
$<1.9 \times 10^{-21}$	90	[67] AVRORIN	16	BAIK	νs from galactic center
$<3 \times 10^{-26}$	95	[68] CAPUTO	16	FLAT	small Magellanic cloud
$<1 \times 10^{-25}$	95	[69] FORNASA	16	FLAT	Fermi-LAT γ-ray anisotropy
$<5 \times 10^{-27}$		[70] LEITE	16		WIMP, radio
$<2 \times 10^{-26}$	95	[71] LI	16	FLAT	dwarf galaxies
$<1 \times 10^{-25}$	95	[72] LI	16A	FLAT	Fermi-LAT; M31
$<1 \times 10^{-26}$		[73] LIANG	16	FLAT	Fermi-LAT, gamma line
$<1 \times 10^{-25}$	95	[74] LU	16	FLAT	Fermi-LAT and AMS-02
$<1 \times 10^{-23}$	95	[75] SHIRASAKI	16	FLAT	extra galactic
		[76] AARTSEN	15C	ICCB	ν, Galactic halo
		[77] AARTSEN	15E	ICCB	ν, Galactic center
		[78] ABRAMOWSKI	15	HESS	Galactic center
		[79] ACKERMANN	15	FLAT	monochromatic γ
		[80] ACKERMANN	15A	FLAT	isotropic γ background
		[81] ACKERMANN	15B	FLAT	Satellite galaxy
		[82] ADRIAN-MAR..	15	ANTR	ν, Galactic center
$<2.90 \times 10^{-26}$	95	[83,84] ACKERMANN	14	FLAT	Satellite galaxy, m = 10 GeV
$<1.84 \times 10^{-25}$	95	[83,85] ACKERMANN	14	FLAT	Satellite galaxy, m = 100 GeV
$<1.75 \times 10^{-24}$	95	[83,85] ACKERMANN	14	FLAT	Satellite galaxy, m = 1 TeV
$<4.52 \times 10^{-24}$	95	[86] ALEKSIC	14	MGIC	Segue 1, m = 1.35 TeV
		[87] AARTSEN	13C	ICCB	Galaxies

Int. J. Mod. Phys. A 2026.41. Downloaded from www.worldscientific.com
by UNIVERSITY OF CALIFORNIA @ BERKELEY on 09/16/26. Re-use and distribution is strictly not permitted, except for Open Access articles.

			[88] ABRAMOWSKI	13	HESS	Central Galactic Halo
			[89] ACKERMANN	13A	FLAT	Galaxy
			[90] ABRAMOWSKI	12	HESS	Fornax Cluster
			[91] ACKERMANN	12	FLAT	Galaxy
			[92] ACKERMANN	12	FLAT	Galaxy
			[93] ALIU	12	VRTS	Segue 1
<1	$\times 10^{-22}$	90	[94] ABBASI	11C	ICCB	Galactic halo, m=1 TeV
<3	$\times 10^{-25}$	95	[95] ABRAMOWSKI	11	HESS	Near Galactic center, m=1 TeV
<1	$\times 10^{-26}$	95	[96] ACKERMANN	11	FLAT	Satellite galaxy, m=10 GeV
<1	$\times 10^{-25}$	95	[96] ACKERMANN	11	FLAT	Satellite galaxy, m=100 GeV
<1	$\times 10^{-24}$	95	[96] ACKERMANN	11	FLAT	Satellite galaxy, m=1 TeV

[1] ABBASI 25A search for WIMP annihilation to ν_μ in center of earth. No signal observed. Limits placed in mass vs. σ^{SI} plane for various WIMP-WIMP annihilation channels.

[2] ABE 25A search for branon DM annihilation to γ-rays in dwarf spheroidals. No signal observed. Limits placed in m(branon) vs. $\langle\sigma\cdot v\rangle$ plane. The quoted limit is for m(branon) = 1.5 TeV.

[3] AIELLO 25B search for ν from DM annihilation in galactic center and sun with KM3NeT. No signal observed. Limits placed in various planes for different DM annihilation channels. Quoted limit is for DM annihilation to ν (direct channel, no intermediate states) in galactic center which limits $\langle\sigma\cdot v\rangle$ for m(DM) = 1 TeV.

[4] CRNOGORCEVIC 25 examine DM annihilation from cusps in galactic clusters. No signal observed. Results depend on galactic cluster DM profile. Quoted limit comes from m(χ) = 100 GeV for annihilation into $b\overline{b}$ and excludes claimed DM annihilation signal from Milky Way center.

[5] FERNANDEZ-SUAREZ 25 search for gamma ray signal in Fermi-LAT data arising from wimp annihilation in stellar streams. No signal observed. Limits placed in $\langle\sigma\cdot v\rangle$ vs. m(χ) plane for different annihilation final states.

[6] ZAKHAROV 25 report search for keV-scale DM annihilation to x-rays using 11 years NuSTAR data. No signal observed. Limts placed on $\langle\sigma\cdot v\rangle$. Quoted limit is for m($\chi$) = 10 keV.

[7] ACHARYYA 24 search for TeV-scale wimp annihilation in dwarf spheroidals. No signal observed. Limits placed on $\langle\sigma\cdot v\rangle$ vs. m(wimp) in various annihilation channels. Quoted limit for $\chi\chi \rightarrow W W$.

[8] CAO 24 search for superheavy WIMP annihilation in dwarf spheroidals to $b\overline{b}$ or $\tau\overline{\tau}$. No signal observed. Limits set in $\langle\sigma\cdot v\rangle$ vs. m(WIMP) plane. Quoted limit for $b\overline{b}$ with m(WIMP) = 1 TeV.

[9] CHOLIS 24 derive limits on wimp annihilation contribution to Fermi-LAT observation of isotropic gamma ray background. Limits set in $\langle\sigma\cdot v\rangle$ vs m plane for various $\chi\chi$ annihilation channel.

[10] CRNOGORCEVIC 24 interpret published Fermi-LAT data aimed at Ursa-Major III to derive limits on WIMP annihilation in high J-factor dwarf spheroidal. Fermi-LAT limits are recast in $\langle\sigma\cdot v\rangle$ vs m plane depend on J and on assumed annihilation channel.

[11] DE-LA-TORRE-LUQUE 24 analyze 15 years Fermi-LAT data for m(WIMP) 10–300 GeV annihilation to photons. No signal observed. Limits placed in $\langle\sigma\cdot v\rangle$ vs m plane for several models motivated by galactic center excess.

[12] MANNA 24 analyze SPT-SZ survay for 1–300 GeV gamma rays from wimp annihilation in galaxy clusters. Some slight signals observed in conflict with dwarf spheroidal searches. Limits in $\langle\sigma\cdot v\rangle$ vs m plane; quoted limit is for m(wimp) = 10 GeV in $b\overline{b}$ annihilation channel.

[13] MCDANIEL 24 combined 14.3 years Fermi-LAT data from multiple dwarf spheroidals to gain updated bounds on WIMP annihilation rates with some 2σ excesses claimed. Reported limit is for 100 GeV WIMP mass.

[14] MCDANIEL 24 perform combined 14 year Fermi-LAT analysis of gammas from dwarf spheroidals. New limits obtained from Fig. 6. Quoted value for m(WIMP) = 100 GeV in $b\overline{b}$ and $\tau\overline{\tau}$ annihilation channels.

[15] SONG 24 use Fermi-LAT data to constrain heavy 10^3–10^{11} GeV DM annihilation and decay. Limits placed in $\langle\sigma\cdot v\rangle$ vs. m and lifetime vs. m planes.

[16] SONG 24A examine Fermi-LAT gamma ray data from superheavy WIMP annihilation/decay in galaxy clusters. Limits placed in $\langle\sigma\cdot v\rangle$ vs m and lifetime vs m planes for a variety of annihilation/decay modes.

[17] ZAKHAROV 24A derive limits DM annihilation to X-rays in the 4–15 keV particle mass range via SRG/ART-XC telescope. Limits placed in $\langle\sigma\cdot v\rangle$ vs m plane. Quoted limit is from MW halo for m = 10 keV, see Fig. 10.

[18] ABBASI 23A search for WIMP-WIMP annihilation to ν's. No signal observed. Require $\langle\sigma\cdot v\rangle < 10^{-24}$ cm^3/s for m(χ) $\sim$ 10–10 $\times 10^4$ GeV for various halo profiles.

[19] ABBASI 23B search for PeV-scale WIMP-WIMP annihilation to μ or b pairs. No signal observed. Require $\langle\sigma\cdot v\rangle < 10^{-22}$ cm^3/s for $\chi\chi \rightarrow b\overline{b}$ with m(χ) about 1 PeV or $\langle\sigma\cdot v\rangle < 10^{-23}$ cm^3/s for $\chi\chi \rightarrow \mu^+\mu^-$ with m(χ) about 1 PeV.

[20] ABE 23B search for WMP-WIMP annihilation to γ in GC. No signal observed. Require $\langle\sigma\cdot v\rangle < 5\times 10^{-28}$ cm^3/s for m(χ) = 1 TeV or $\langle\sigma\cdot v\rangle < 1\times 10^{-25}$ cm^3/s for m(χ) = 100 TeV.

[21] ALBERT 23 search for WIMP pair annihilation to γ in galactic halo. No signal observed. Limits placed in $\langle\sigma\cdot v\rangle$ vs. mass (10–100 TeV) plane for various annihilation channels.

[22] CHENG 23A provide updated combined Fermi-LAT/DAMPE search for gamma line from WIMP annihilation. No signal observed. Limits placed in $\langle\sigma\cdot v\rangle$ vs. mass (6–200 GeV) plane for various halo profiles.

[23] FOSTER 23 search for gamma ray line in Fermi-LAT data. No signal observed. Limits placed in $\langle\sigma\cdot v\rangle$ vs. m(χ) plane. For Higgsino DM limit see Fig. 12.

[24] GUO 23 search with Five-hundred-meter Aperture Spherical Radio Telescope for synchrotron emission radio signal of DM annihilation from dwarf spheroidal galaxy. No signal observed. Limits set in $\langle\sigma\cdot v\rangle$ vs. m(χ) plane for various annihilation final states.

[25] GUO 23A search in public IceCube data for DM annihilation to neutrinos. No signal observed. Limits placed in $\langle\sigma\cdot v\rangle$ vs m(χ) plane for various annihilation assumptions.

[26] LAVIS 23 search for 2HDM+S DM and generic spectra using MeerKAT. No signal observed. Limits placed in $\langle\sigma\cdot v\rangle$ vs. mass (10–1000 GeV) plane for various annihilation channels.

[27] ABDALLA 22 search for WIMP annihilation in galactic center to gamma rays using HESS; no signal observed; limits set in mass vs $\langle\sigma\cdot v\rangle$ plane for dominant annihilation to $W W$ or $\tau\overline{\tau}$. Limit here for $\tau\overline{\tau}$ channel 0.7 TeV mass.

[28] ALBERT 22A search for secluded PeV-scale DM annihilation to four final states; no signal detected; limits placed in $\langle\sigma\cdot v\rangle$ vs. m(χ) plane for m(χ): 6–6000 TeV for m(mediator) = 50, 250, and 1000 GeV.

[29] CHAN 22 derive a variety of limits on DM annihilation to various channels resulting in X-rays from dwarf galaxy Omega Centauri. Limits are very dependent on assumed DM density and diffusion coefficient. Quoted limit is for m(WIMP) = 100 GeV annihilating to $W W$ with parameters as in Fig. 4.

[30] EGOROV 22 derives limits on DM annihilation to $b\overline{b}$ or $\tau\overline{\tau}$ via radio signals from M31; quoted limit from $b\overline{b}$ channel with LOFAR telescope as main data source, using parameters as in Fig. 10 (green curve) for m(χ) = 100 GeV.

[31] MANCONI 22 use polarized synchrotron emission data from Planck to constrain WIMP annihilation cross section in Galaxy; limits set in $\langle\sigma\cdot v\rangle$ vs. m(DM) plane.

[32] ABDALLAH 21 search for WIMP-WIMP annihilation into 2 monoenergetic γ rays in WLM dwarf irregular galaxy using HESS data. No signal. Limits placed in $\langle\sigma\cdot v\rangle$ vs. m(WIMP) plane for a mass of 370 GeV.

[33] CIRELLI 21 derive limits on light DM annihilation to ee, $\mu\mu$, $\pi\pi$ that then produce X-rays using data published by INTEGRAL telescope. Limits placed in $\langle\sigma\cdot v\rangle$ vs. m(DM) plane for m(DM) = 1–5000 MeV.

[34] JOHN 21 derive limits on leptophilic DM annihilating to positrons by comparing expected spectra to AMS-02 data. The range m(DM): 60–300 GeV appears excluded for this type of model, see Fig. 3.

[35] ABAZAJIAN 20 derive new limits on WIMP annihilation in galactic center (GC): $\langle\sigma\cdot v\rangle < 2.5\times 10^{-27}$ cm^3/s for m(WIMP) = 50 GeV: seems to rule out WIMP explanation for GC γ excess, favouring an astrophysics origin.

[36] ABDALLAH 20 search for WIMP annihilation in newly discovered by DES dwarf satellite galaxies using HESS; limits placed in $\langle\sigma\cdot v\rangle$ vs. m(DM) plane depending on annihilation channel and which dwarf satellite.

[37] ABE 20G search Super-Kamiokande data for WIMP annihilation to neutrinos in galactic center/halo; no signal; limits placed in $\langle\sigma\cdot v\rangle$ vs. m(DM) plane depending on annihilation channel and m(WIMP). Reported limit for annihilation to $\nu\overline{\nu}$ at 1 GeV.

[38] ALBERT 20 search for TeV-scale WIMP annihilation to $\gamma\gamma$ in dwarf spheroidal galaxies; no signal; limits placed in $\sigma\cdot v$ vs m(WIMP) plane: e.g. $\sigma\cdot v < 2.2\times 10^{-24}$ cm^3/s for m(WIMP) = 1 TeV.

[39] ALBERT 20A search for WIMP annihilation to ν in galactic center using Antares; limits placed in $\sigma\cdot$ v vs m(WIMP) plane e.g. $\sigma\cdot$ v $< 5\times 10^{-24}$ cm^3/s for m(WIMP) = 1 TeV assuming annihilation dominantly to $\tau\overline{\tau}$.

[40] ALBERT 20C report combined Antares + IceCube search for WIMP annihilation to $\tau\overline{\tau}$; for NFW halo profile report $\sigma\cdot v < 1\times 10^{-23}$ cm^3/s for m(WIMP) = 100 GeV.

[41] ALVAREZ 20 use profiling over J-factor distributions and background to derive new limits on $\sigma\cdot$ v; e.g. $\sigma\cdot$ v $< 8\times 10^{-26}$ cm^3/s for m(WIMP) = 100 GeV.

[42] HOOF 20 examine γ rays from 27 dwarf spheroidals using Fermi-LAT data; place limits in $\sigma\cdot$ v vs m(WIMP) plane using profile likelihood and marginalized posterior techniques for DM annihilation to $\tau\overline{\tau}$ and $b\overline{b}$; quoted limit uses first technique and $b\overline{b}$ channel for m(WIMP) = 100 GeV; results rule out WIMP explanation of galactic center excess.

[43] MAZZIOTTA 20 use Fermi-LAT pointed-at-Sun data to search for DM annihilation in the Sun to long-lived mediators decaying into gamma rays, i.e. $\chi\chi \rightarrow \phi\phi \rightarrow 4\gamma$. Limits placed on the SI and SD DM-nucleon cross sections in the σ–DM mass plane for DM masses in the range 3 GeV – 1.8 TeV. Limits are evaluated in both cases of equilibrium and non-equilibrium.

[44] ABEYSEKARA 19 search for γs from DM annihilation in galactic substructures with HAWC; no signal, limits placed in J$\langle\sigma\cdot v\rangle$ vs. declination plane for m(DM) $\sim$ 1–108 TeV.

[45] ALBERT 19B search for DM signal from M31 galaxy in μ, τ, t, b, W channels using HAWC for m(DM) $\sim$ 1–100 TeV; no signal, limits placed in $\langle\sigma\cdot v\rangle$ vs. m(DM) plane.

[46] CHEUNG 19 derive model-dependent bounds on $\langle\sigma\cdot v\rangle$ from EDGES data: $< 4\times 10^{-26}$ cm^3/s for e^+e^- and $b\overline{b}$ for m(χ) = 100 GeV (including boost factor).

[47] DI-MAURO 19 place limits on WIMP annihilation via Fermi-LAT observation of M31 and M33 galaxies: $\langle\sigma\cdot v\rangle < 7\times 10^{-27}$cm^3/s for m($\chi$) = 20 GeV from M31.

[48] JOHNSON 19 search for γ-rays, 10–600 GeV energy, from P-wave annihilating DM around SgrA* BH using Fermi-LAT; limits set for various models.

[49] LI 19D search for $\chi\chi \rightarrow \gamma$ in Fermi-LAT data; no signal, require $\langle\sigma\cdot v\rangle < 2\times 10^{-26}$ cm^3/s for m(χ) = 100 GeV.

[50] NG 19 search for X-ray line from sterile ν decay/annihilation using NuStar M-31; no signal: limits placed in m(ν) vs mixing angle and $\langle\sigma\cdot v\rangle$ vs m(ν).

[51] QUEIROZ 19 examine $\chi\chi \rightarrow \chi SM$ semi-annihilation of DM reaction; limits placed for various assumed SM particles in $\langle\sigma\cdot v\rangle$ vs. m(χ) plane.

[52] ABDALLAH 18 search for WIMP WIMP $\rightarrow \gamma X$ in central galactic halo, 10 years of data; limits placed in $\langle\sigma\cdot v\rangle$ vs. m(WIMP) plane for m(WIMP): 0.3–70 TeV.

[53] AHNEN 18 search for WIMP WIMP$\rightarrow \gamma X$ from Ursa Major II; limits set in $\langle\sigma\cdot v\rangle$ vs. m(WIMP) plane for $b\overline{b}$, W^+W^-, $\tau^+\tau^-$, and $\mu^+\mu^-$ annihilation modes.

[54] ALBERT 18B search for TeV-scale WIMPs with WIMP WIMP $\rightarrow \gamma X$ in Andromeda galaxy using HAWC Observatory; limits set in $\langle\sigma\cdot v\rangle$ vs m(WIMP) plane.

[55] CHANG 18A examine $\chi\chi \rightarrow b\overline{b} \rightarrow \gamma$ using Fermi Pass 8 data; no signal; require $\langle\sigma\cdot v\rangle < 10^{-26}$ cm^3/s for m(χ) = 50 GeV.

[56] LISANTI 18 examine Fermi Pass 8 γ-ray data from galaxy groups; report m(WMP) > 30 GeV for annihilation in $b\overline{b}$ channel.

[57] MAZZIOTTA 18 examine Fermi-LAT electron and positron spectra searching for features originating from DM particles annihilation into e^+e^- pairs, from 45 GeV to 2 TeV; no signal found, limits are obtained.

[58] AARTSEN 17C use 1005 days of IceCube data to search for $\chi\chi \rightarrow$ neutrinos via various annihilation channels. Limits set.

[59] ALBERT 17A search for DM annihilation to ν using ANTARES data from 2007–2015. No signal. Limits set in $\langle\sigma\cdot v\rangle$ vs. m(DM) plane for m(DM) $\sim$ 10–10 $\times 10^5$ GeV. The listed limit is for m(DM) = 100 TeV.

[60] ARCHAMBAULT 17 set limits for WIMP mass between 100 GeV and 1 TeV on $\langle\sigma\cdot v\rangle$ for W^+W^-, ZZ, $b\overline{b}$, $s\overline{s}$, $u\overline{u}$, $d\overline{d}$, $t\overline{t}$, e^+e^-, gg, $c\overline{c}$, hh, $\gamma\gamma$, $\mu^+\mu^-$,$\tau^+\tau^-$ annihilation channels.

[61] AVRORIN 17 find upper limits for the annhilation cross section in various channels for DM particle mass between 30 GeV and 10 TeV. Strongest upper limits coming from the two neutrino channel require $\langle\sigma\cdot v\rangle < 6\times 10^{-20}$ cm^3/s in dwarf galaxies and $\langle\sigma\cdot v\rangle < 7\times 10^{-21}$ cm^3/s in LMC for 5 TeV WIMP mass.

[62] BOUDAUD 17 use data from the spacecraft Voyager 1, beyond the heliopause, and from AMS02 on $\chi\chi \rightarrow e^+e^-$ to require $\langle\sigma\cdot v\rangle < 1.\times 10^{-28}$ cm^3/s for m(χ) = 10 MeV.

Int. J. Mod. Phys. A 2026.41. Downloaded from www.worldscientific.com
by UNIVERSITY OF CALIFORNIA @ BERKELEY on 09/16/26. Re-use and distribution is strictly not permitted, except for Open Access articles.

[63] AARTSEN 16D search for GeV ν from WIMP annihilation in galaxy; limits set on $\langle\sigma\cdot v\rangle$ in Fig. 6, 7.

[64] ABDALLAH 16 require $\langle\sigma\cdot v\rangle < 6\times10^{-26}$ cm^3/s for m(WIMP) = 1.5 TeV from 254 hours observation (WW channel) and $< 2\times10^{-26}$ cm^3/s for m(WIMP) = 1.0 TeV in $\tau^+\tau^-$ channel.

[65] ABDALLAH 16A search for line spectra from WIMP + WIMP $\rightarrow \gamma\gamma$ in 18 hr HESS data; rule out previous 130 GeV WIMP hint from Fermi-LAT data.

[66] AHNEN 16 require $\langle\sigma\cdot v\rangle < 3\times10^{-26}$ cm^3/s for m(WIMP) = 100 GeV (WW channel).

[67] AVRORIN 16 require $\langle$s.v$\rangle < 1.91\times10^{-21}$ cm^3/s from WIMP annihilation to ν via WW channel for m(WIMP) = 1 TeV.

[68] CAPUTO 16 place limits on WIMPs from annihilation to gamma rays in Small Magellanic Cloud using Fermi-LaT data: $\langle\sigma\cdot v\rangle < 3\times10^{-26}$cm^3/s for m(WIMP) = 10 GeV.

[69] FORNASA 16 use anisotropies in the γ-ray diffuse emission detected by Fermi-LAT to bound $\langle\sigma\cdot v\rangle < 10^{-25}$cm^3/s for m(WIMP) = 100 GeV in $b\overline{b}$ channel: see Fig. 28. The limit is driven by dark-matter subhalos in the Milky Way and it refers to their Most Constraining Scenario.

[70] LEITE 16 constrain WIMP annihilation via search for radio emissions from Smith cloud; $\langle\sigma\cdot v\rangle < 5\times10^{-27}$cm^3/s in ee channel for m(WIMP) = 5 GeV.

[71] LI 16 re-analyze Fermi-LAT data on 8 dwarf spheroidals; set limit $\langle\sigma\cdot v\rangle < 2\times10^{-26}$ cm^3/s for m(WIMP) = 100 GeV in $b\overline{b}$ mode with substructures included.

[72] LI 16A constrain $\langle\sigma\cdot v\rangle < 10^{-25}$cm^3/s in $b\overline{b}$ channel for m(WIMP) = 100 GeV using Fermi-LAT data from M31; see Fig. 6.

[73] LIANG 16 search dwarf spheroidal galaxies, Large Magellanic Cloud, and Small Magellanic Cloud for γ-line in Fermi-LAT data.

[74] LU 16 re-analyze Fermi-LAT and AMS-02 data; require $\langle\sigma\cdot v\rangle < 10^{-25}$cm^3/s for m_m(WIMP) = 1 TeV in $b\overline{b}$ channel.

[75] SHIRASAKI 16 re-anayze Fermi-LAT extra-galactic data; require $\langle\sigma\cdot v\rangle < 10^{-23}$cm^3/s for m(WIMP) = 1 TeV in $b\overline{b}$ channel; see Fig. 8.

[76] AARTSEN 15C search for neutrinos from X^0 annihilation in the Galactic halo. See their Figs. 16 and 17, and Table 5 for limits on $\sigma\cdot$v for X^0 mass between 100 GeV and 100 TeV.

[77] AARTSEN 15E search for neutrinos from X^0 annihilation in the Galactic center. See their Figs. 7 and 9, and Table 3 for limits on $\sigma\cdot$v for X^0 mass between 30 GeV and 10 TeV.

[78] ABRAMOWSKI 15 search for γ from X^0 annihilation in the Galactic center. See their Fig. 4 for limits on $\sigma\cdot$v for X^0 mass between 250 GeV and 10 TeV.

[79] ACKERMANN 15 search for monochromatic γ from X^0 annihilation in the Galactic halo. See their Fig. 8 and Tables 2–4 for limits on $\sigma\cdot$v for X^0 mass between 0.2 GeV and 500 GeV.

[80] ACKERMANN 15A search for γ from X^0 annihilation (both Galactic and extragalactic) in the isotropic γ background. See their Fig. 7 for limits on $\sigma\cdot$v for X^0 mass between 10 GeV and 30 TeV.

[81] ACKERMANN 15B search for γ from X^0 annihilation in 15 dwarf spheroidal satellite galaxies of the Milky Way. See their Figs. 1 and 2 for limits on $\sigma\cdot$v for X^0 mass between 2 GeV and 10 TeV.

[82] ADRIAN-MARTINEZ 15 search for neutrinos from X^0 annihilation in the Galactic center. See their Figs. 10 and 11 and Tables 1 and 2 for limits on $\sigma\cdot$v for X^0 mass between 25 GeV and 10 TeV.

[83] ACKERMANN 14 search for γ from X^0 annihilation in 25 dwarf spheroidal satellite galaxies of the Milky Way. See their Tables II–VII for limits assuming annihilation into e^+e^-, $\mu^+\mu^-$, $\tau^+\tau^-$, $u\overline{u}$, $b\overline{b}$, and W^+W^-, for X^0 mass ranging from 2 GeV to 10 TeV.

[84] Limit assuming X^0 pair annihilation into $b\overline{b}$.

[85] Limit assuming X^0 pair annihilation into W^+W^-.

[86] ALEKSIC 14 search for γ from X^0 annihilation in the dwarf spheroidal galaxy Segue 1. The listed limit assumes annihilation into W^+W^-. See their Figs. 6, 7, and 16 for limits on $\sigma\cdot$v for annihilation channels $\mu^+\mu^-$, $\tau^+\tau^-$, $b\overline{b}$, $t\overline{t}$, $\gamma\gamma$, γZ, W^+W^-, ZZ for X^0 mass between 10^2 and 10^4 GeV.

[87] AARTSEN 13C search for neutrinos from X^0 annihilation in nearby galaxies and galaxy clusters. See their Figs. 5–7 for limits on $\sigma\cdot$v for $X^0X^0 \rightarrow \nu\overline{\nu}$, $\mu^+\mu^-$, $\tau^+\tau^-$, and W^+W^- for X^0 mass between 300 GeV and 100 TeV.

[88] ABRAMOWSKI 13 search for monochromatic γ from X^0 annihilation in the Milky Way halo in the central region. Limit on $\sigma\cdot$v between 10^{-28} and 10^{-25} cm^3 s^{-1} (95% CL) is obtained for X^0 mass between 500 GeV and 20 TeV for $X^0X^0 \rightarrow \gamma\gamma$. X^0 density distribution in the Galaxy by Einasto is assumed. See their Fig. 4.

[89] ACKERMANN 13A search for monochromatic γ from X^0 annihilation in the Milky Way. Limit on $\sigma\cdot$v for the process $X^0X^0 \rightarrow \gamma\gamma$ in the range 10^{-29}–10^{-27} cm^3 s^{-1} (95% CL) is obtained for X^0 mass between 5 and 300 GeV. The limit depends slightly on the assumed density profile of X^0 in the Galaxy. See their Tables VII–X and Fig.10. Supersedes ACKERMANN 12.

[90] ABRAMOWSKI 12 search for γ's from X^0 annihilation in the Fornax galaxy cluster. See their Fig. 7 for limits on $\sigma\cdot$v for X^0 mass between 0.1 and 100 TeV for the annihilation channels $\tau^+\tau^-$, $b\overline{b}$, and W^+W^-.

[91] ACKERMANN 12 search for monochromatic γ from X^0 annihilation in the Milky Way. Limit on $\sigma\cdot$v in the range 10^{-28}–10^{-26} cm^{3}s^{-1} (95% CL) is obtained for X^0 mass between 7 and 200 GeV if X^0 annihilates into $\gamma\gamma$. The limit depends slightly on the assumed density profile of X^0 in the Galaxy. See their Table III and Fig. 15.

[92] ACKERMANN 12 search for γ from X^0 annihilation in the Milky Way in the diffuse γ background. Limit on $\sigma\cdot$v of 10^{-24} cm^{3}s^{-1} or larger is obtained for X^0 mass between 5 GeV and 10 TeV for various annihilation channels including W^+W^-, $b\overline{b}$, gg, e^+e^-, $\mu^+\mu^-$, $\tau^+\tau^-$. The limit depends slightly on the assumed density profile of X^0 in the Galaxy. See their Figs. 17–20.

[93] ALIU 12 search for γ's from X^0 annihilation in the dwarf spheroidal galaxy Segue 1. Limit on $\sigma\cdot$v in the range 10^{-24}–10^{-20} cm^{3}s^{-1} (95% CL) is obtained for X^0 mass between 10 GeV and 2 TeV for annihilation channels e^+e^-, $\mu^+\mu^-$, $\tau^+\tau^-$, $b\overline{b}$, and W^+W^-. See their Fig. 3.

[94] ABBASI 11C search for ν_μ from X^0 annihilation in the outer halo of the Milky Way. The limit assumes annihilation into $\nu\nu$. See their Fig. 9 for limits with other annihilation channels.

[95] ABRAMOWSKI 11 search for γ from X^0 annihilation near the Galactic center. The limit assumes Einasto DM density profile.

[96] ACKERMANN 11 search for γ from X^0 annihilation in ten dwarf spheroidal satellite galaxies of the Milky Way. The limit for m = 10 GeV assumes annihilation into $b\overline{b}$, the others W^+W^-. See their Fig. 2 for limits with other final states. See also GERINGER-SAMETH 11 for a different analysis of the same data.

Dark Matter Particle (X^0) Production in Hadron Collisions

Searches for X^0 production in association with observable particles (γ, jets, ...) in high energy hadron collisions. If a specific form of effective interaction Lagrangian is assumed, the limits may be translated into limits on X^0-nucleon scattering cross section.

VALUE	DOCUMENT ID		TECN	COMMENT
• • • We do not use the following data for averages, fits, limits, etc. • • •				
	[1] AAD	25BA	ATLS	dark Higgs, DM search
	[2] AAD	25C	ATLS	DM in association with dark Higgs
	[3] CHEKHOVSKY	25D	CMS	DM search with top
	[4] CHEKHOVSKY	25H	CMS	single top + DM
	[5] HAYRAPETY...	25P	CMS	DM in 2HDM+a
	[6] AAD	24AC	ATLS	$t\overline{t}$ + mediator
	[7] AAD	24AC	ATLS	$t\overline{t}$ + mediator
	[8] AAD	24AH	ATLS	SUSY pMSSM search
	[9] AAD	24AK	ATLS	t + MET search
	[10] AAD	24CD	ATLS	hadronic W/Z + MET search
	[11] HAYRAPETY...	24B	CMS	inelastic DM search
	[12] HAYRAPETY...	24W	CMS	dark matter/dark Higgs
	[13] AAD	23A	ATLS	$H \rightarrow$ invisible search
	[14] AAD	23AF	ATLS	$\overline{t}t$ + $H \rightarrow$ invisible search
	[15] AAD	23AJ	ATLS	extended 2HDM search
	[16] AAD	23BX	ATLS	Ha, $a \rightarrow$ DM search
	[17] AAD	23W	ATLS	dark Higgs model
	[18] AKIMOV	23	COHR	LDM search at SNS
	[19] LIN	23C	KOTO	$\chi \rightarrow \gamma\gamma$ from K^0_L decay
	[20] AAD	22D	ATLS	Z+H with $H \rightarrow$ DM
	[21] AAD	22P	ATLS	$H \rightarrow \chi\chi$ search via VBF
	[22] AGUILAR-AR...	22A	CCM	p dump search for MeV-scale DM
	[23] TUMASYAN	22AA	CMS	$Z' \rightarrow$ DM search
	[24] TUMASYAN	22AG	CMS	strongly interacting DM search
	[25] TUMASYAN	22G	CMS	DM search via VBF to Higgs
	[26] AAD	21AZ	ATLS	DM search in $H\,\not{E}_T \rightarrow \gamma\gamma\,\not{E}_T$
	[27] AAD	21BB	ATLS	DM search in $H\,\not{E}_T \rightarrow b\overline{b}\,\not{E}_T$
	[28] AAD	21D	ATLS	Dark Higgs
	[29] AAD	21F	ATLS	jet + missing momentum
	[30] AAD	21K	ATLS	photon + DM
	[31] AAD	21O	ATLS	ℓ + jets + $\not{E}_T$ to search for t-pairs + DM
	[32] AAD	21P	ATLS	$\ell^+\ell^-$ + jets + $\not{E}_T$
	[33] AAD	21S	ATLS	b-jets + $\not{E}_T$
	[34] SIRUNYAN	21A	CMS	$pp \rightarrow Z\chi\chi$; $Z \rightarrow \ell\overline{\ell}$
	[35] TUMASYAN	21D	CMS	DM search in jets + $\not{E}_T$
	[36] SIRUNYAN	20X	CMS	$pp \rightarrow Z' \rightarrow A(Z')h \rightarrow h + \not{E}_T$
	[37] AABOUD	19AA	ATLS	multi-channel BSM search
	[38] AABOUD	19AI	ATLS	$H \rightarrow \chi\chi$
	[39] AABOUD	19AL	ATLS	$H \rightarrow \chi\chi$
	[40] AABOUD	19Q	ATLS	single t+$\not{E}_T$
	[41] AABOUD	19V	ATLS	review mediator based DM searches
	[42] BANERJEE	19	NA64	$eN \rightarrow eN$+$\not{E}$
	[43] SIRUNYAN	19AN	CMS	$H\chi\chi \rightarrow b\overline{b}\,\not{E}_T$
	[44] SIRUNYAN	19BC	CMS	LQ LQ $\rightarrow \mu j\,\not{E}_T$
	[45] SIRUNYAN	19BO	CMS	$VV \rightarrow Hqq$; $H \rightarrow$ DM
	[46] SIRUNYAN	19C	CMS	$pp \rightarrow t\overline{t}\chi\chi$
	[47] SIRUNYAN	19O	CMS	$pp \rightarrow \gamma\,\not{E}_T$
	[48] SIRUNYAN	19X	CMS	$pp \rightarrow t\overline{t} + \not{p}_T$; $pp \rightarrow t(\overline{t}) + \not{p}_T$
	[49] AABOUD	18	ATLS	$pp \rightarrow Z\chi\chi$; $Z \rightarrow \ell\ell$
	[50] AABOUD	18A	ATLS	$pp \rightarrow t\overline{t}\,\not{E}_T$; $pp \rightarrow b\overline{b}\,\not{E}_T$
	[51] AABOUD	18CA	ATLS	$pp \rightarrow V\chi\chi$; $V \rightarrow jj$
	[52] AABOUD	18I	ATLS	$pp \rightarrow$ jet(s) + $\not{E}_T$
	[53] AGUILAR-AR...	18B	MBNE	$pN \rightarrow \chi X$, $\chi = e$, π, or N
	[54] KHACHATRY...	18	CMS	$pp \rightarrow Z(\ell\ell) + \not{E}_T$
	[55] SIRUNYAN	18BF	CMS	$pp \rightarrow t\,\not{E}_T$
	[56] SIRUNYAN	18BO	CMS	dijet resonance search
	[57] SIRUNYAN	18BV	CMS	$pp \rightarrow Z\,\not{E}_T$
	[58] SIRUNYAN	18C	CMS	$pp \rightarrow t\overline{t}\,\not{E}_T$
	[59] SIRUNYAN	18CU	CMS	$pp \rightarrow Z\,\not{E}_T$
	[60] SIRUNYAN	18DH	CMS	$pp \rightarrow \chi\chi h$; $h \rightarrow \gamma\gamma$ or $\tau\overline{\tau}$
	[61] SIRUNYAN	18S	CMS	$pp \rightarrow$ jets $\not{E}_T$
	[62] AABOUD	17A	ATLS	pp ($H \rightarrow b\overline{b}$ + WIMP pair)
	[63] AABOUD	17AM	ATLS	$pp \rightarrow Z' \rightarrow Ah \rightarrow h(b\overline{b}) + \not{E}_T$
	[64] AABOUD	17AQ	ATLS	$pp \rightarrow h(\gamma\gamma) + \not{E}_T$
	[65] AABOUD	17BD	ATLS	$pp \rightarrow$ jet(s) + $\not{E}_T$
	[66] AABOUD	17R	ATLS	$pp \rightarrow \gamma\not{E}_T$
	[67] AGUILAR-AR...	17A	MBNE	$pN \rightarrow \chi\chi X$; $\chi N \rightarrow \chi N$
	[68] BANERJEE	17	NA64	$eN \rightarrow eN\gamma'$
	[69] KHACHATRY...	17A	CMS	forward jets + $\not{E}_T$
	[70] KHACHATRY...	17F	CMS	$H \rightarrow$ invisibles
	[71] SIRUNYAN	17	CMS	$Z + \not{E}_T$

Int. J. Mod. Phys. A 2026.41. Downloaded from www.worldscientific.com
by UNIVERSITY OF CALIFORNIA @ BERKELEY on 09/16/26. Re-use and distribution is strictly not permitted, except for Open Access articles.

[72] SIRUNYAN	17AP	CMS	$pp \to Z' \to Ah \to h + \not{E}_T$
[73] SIRUNYAN	17AQ	CMS	$pp \to \gamma + \not{E}_T$
[74] SIRUNYAN	17BB	CMS	$pp \to t\overline{t}+\not{E}_T$; $pp \to b\overline{b}+\not{E}_T$
[75] SIRUNYAN	17G	CMS	$pp \to j + \not{E}_T$
[76] SIRUNYAN	17U	CMS	$pp \to Z\chi\chi$; $Z \to \ell\overline{\ell}$
[77] AABOUD	16AD	ATLS	(W or $Z \to$ jets) + $\not{E}_T$
[78] AAD	16AF	ATLS	$VV \to$ forward jets $+\not{E}_T$
[79] AAD	16AG	ATLS	ℓ + jets
[80] AAD	16M	ATLS	$pp \to H + \not{E}_T$, $H \to b\overline{b}$
[81] KHACHATRY...	16BZ	CMS	jet(s) + $\not{E}_T$
[82] KHACHATRY...	16CA	CMS	jets + $\not{E}_T$
[83] KHACHATRY...	16N	CMS	$pp \to \gamma + \not{E}_T$
[84] AAD	15AS	ATLS	$b\ (\overline{b}) + \not{E}_T$, $t\overline{t} + \not{E}_T$
[85] AAD	15BH	ATLS	jet + $\not{E}_T$
[86] AAD	15CF	ATLS	$H + \not{E}_T$
[87] AAD	15CS	ATLS	$\gamma + \not{E}_T$
[88] KHACHATRY...	15AG	CMS	$t\overline{t} + \not{E}_T$
[89] KHACHATRY...	15AL	CMS	jet + $\not{E}_T$
[90] KHACHATRY...	15T	CMS	$\ell + \not{E}_T$
[91] AAD	14AI	ATLS	$W + \not{E}_T$
[92] AAD	14BK	ATLS	$W, Z + \not{E}_T$
[93] AAD	14K	ATLS	$Z + \not{E}_T$
[94] AAD	14O	ATLS	$Z + \not{E}_T$
[95] AAD	13AD	ATLS	jet + $\not{E}_T$
[96] AAD	13C	ATLS	$\gamma + \not{E}_T$
[97] AALTONEN	12K	CDF	$t + \not{E}_T$
[98] AALTONEN	12M	CDF	jet + $\not{E}_T$
[99] CHATRCHYAN	12AP	CMS	jet + $\not{E}_T$
[100] CHATRCHYAN	12T	CMS	$\gamma + \not{E}_T$

[1] AAD 25BA reports search for dark Higgs s with dark matter ($\chi\chi$) produced via Z' leading to 3–4 b-jets plus $\not{E}_T$ with 140 fb^{-1} in Run 2. No signal observed. Limits placed in m(s) vs. m(Z') plane.

[2] AAD 25C reports search for dark matter $\chi\chi$ produced in association with dark Higgs s decaying to $b\overline{b}$ with 140 fb^{-1}. No signal observed. Limits placed in m(Z') vs m(s) and other planes for three different dark Higgs scenarios.

[3] CHEKHOVSKY 25D report on search for DM production in association with top quarks. Slight excess of events observed. Limits placed depend on assumed mediator mass and assuming m(χ) = 1 GeV. Limits also placed on ALP simplified model.

[4] CHEKHOVSKY 25H search for dark matter $\chi\chi$ plus single top production via flavor-changing mediator boson M in 138 fb^{-1}. No signal observed. Limits placed in m(M) vs m(χ) plane for flavor-changing mediator model.

[5] HAYRAPETYAN 25P search for DM χ production in association with $b\overline{b}$ at CMS with 138 fb^{-1}. No signal observed. Limits placed in m(χ) vs m(a) and other planes for various choices of 2HDM+a model parameters.

[6] AAD 24AC search for $t\overline{t}$ + mediator, where mediator decays to dark matter, within 140 fb^{-1} of data. No signal observed. Limits placed in σ vs m(mediator) plane.

[7] AAD 24AC search for $t\overline{t}$+MET signal at $\sqrt{s}$=13 TeV and 139 fb^{-1}. No signal observed. Assume DM mediator model coupling to $t\overline{t}$ and limits placed in various m(DM), m(mediator), coupling planes.

[8] AAD 24AH search for SUSY in pMSSM model. No signal observed. Several regions of DM-allowed parameters space now ruled out.

[9] AAD 24AK search for top + MET in various simplified models including mediator decaying to DM. No signal observed. Limits placed in various parameter space planes.

[10] AAD 24CD search for hadronically-decaying W/Z plus MET events in 140 fb^{-1} at 13 TeV. No signal observed. Limits placed in m(χ) vs. mediator mass plane for simplified dark matter model.

[11] HAYRAPETYAN 24B search for inelastic DM production where heavier state decays to displaced muons. No signal observed. Limits placed in signal strength vs mass plane for various choices of mass gap.

[12] HAYRAPETYAN 24W search for dark matter via dark Higgs decay in WW + MET events. No signal observed. Limits placed in m(χ) vs m(mediator) or m(s) plane where s is dark Higgs.

[13] AAD 23A search for $H \to$ invisible. No signal observed. Results interpreted in terms of several DM Higgs portal simplified models.

[14] AAD 23AF search for $\overline{t}t + H \to$ invisible with 139 fb^{-1} of data. No signal observed. Limits placed on branching fractions of H decays etc. for various DM mediator models. Result also included in AAD 23A.

[15] AAD 23AJ search for $tW\chi\chi$ production in mediator-extended 2HDM with 139 fb^{-1} of data. No signal observed. Limits placed in m(H) vs. m(mediator) and tan(β) vs. m(H) planes.

[16] AAD 23BX search for $A \to Ha$ production where $H \to \tau\overline{\tau}$ and $a \to \chi\chi$. No signal observed. Limits placed on 2HDM+a model.

[17] AAD 23W search for DM in dark Higgs model via $WW\chi\chi$ final state with 139 fb^{-1} of data. No signal detected. Limits set in m(dark Higgs) vs. m(Z') plane.

[18] AKIMOV 23 search for light DM via COHERENT CsI detector at SNS. No signal observed. For scalar DM model, limits set for m(χ) = 1–300 MeV. Limit of $\sigma(\chi N) < 1 \times 10^1$ pb set at peak sensitivity m(χ) = 25 MeV.

[19] LIN 23C search for $\chi \to \gamma\gamma$ decay where $p \to \chi\chi$ at KOTO. No signal observed. Limits placed on K^0_L branching fraction.

[20] AAD 22D search for Z+H production with $Z \to l\overline{l}$ and $H \to \chi\chi$ with 139 fb^{-1} at 13 TeV; no signal found; limits placed in various simplified models depending on Higgs portal and DM mediator.

[21] AAD 22P search for H production via VBF with $H \to \chi\chi$ with 139 fb^{-1} at 13 TeV; no signal found; limits placed for various Higgs DM portal simplified models.

[22] AGUILAR-AREVALO 22A report search for MeV vector portal and leptophobic DM via scatter on liquid Ar at the Lujan stopped pion source at LANL; no signal detected; limits placed on vector portal and leptophobic DM vs. m(χ): 1–40 MeV.

[23] TUMASYAN 22AA search for Z' decay to dark quarks with 138 fb^{-1} at 13 TeV; no signal observed; limits exclude a wide range of strongly coupled hidden sector models.

[24] TUMASYAN 22AG search for strongly interacting dark matter production via scalar mediator, with SIMP decay to trackless jets with 16.1 fb^{-1} at 13 TeV; no signal detected; limits placed in mass vs. cross section plane for simplified models.

[25] TUMASYAN 22G search for VBF production of Higgs with $H \to \chi\chi$ with 101 fb^{-1} at 13 TeV, combined with earlier searches, in total 19.7 fb^{-1} at 8 TeV and 140 fb^{-1} at 13 TeV are used; no signal detected; limits placed in mass vs. cross section plane for various Higgs portal simplified models.

[26] AAD 21AZ search for DM in $H\not{E}_T \to \gamma\gamma\not{E}_T$ events with 139 fb^{-1} at 13 TeV. No signal observed. Limits placed for several simplified models.

[27] AAD 21BB search for DM in $H\not{E}_T \to b\overline{b}\not{E}_T$ events with 139 fb^{-1} at 13 TeV. No signal observed. Limits placed for several simplified models.

[28] AAD 21D search for $VV + \chi\chi$, $V \to q\overline{q}$ with 139 fb^{-1} at 13 TeV LHC. No signal detected. Limits placed in dark Higgs boson mass vs. m(Z') plane. Here VV stand for $W^{\pm}W^{\mp}$, ZZ.

[29] AAD 21F search for monojet recoiling against invisibles with 139 fb^{-1} at 13 TeV LHC. No signal detected. Limits placed in various simplified dark matter models.

[30] AAD 21K search for a photon recoiling against dark matter with 139 fb^{-1} at 13 TeV LHC. No signal detected. Limits placed on parameter space of various simplified models.

[31] AAD 21O search for ℓ + jets + $\not{E}_T$ to search for t-pairs + DM particles with 139 fb^{-1} at LHC 13 TeV LHC. No signal detected. Limits placed in the cross-section vs. mediator mass plane, assuming light DM states.

[32] AAD 21P search for $\ell^+\ell^-$ + jets + $\not{E}_T$ in context of various BSM models with 139 fb^{-1} at 13 TeV LHC. No signal observed. Limits placed in parameter space of dark matter models and SUSY.

[33] AAD 21S search for b-jets + $\not{E}_T$ signal from BSM/DM models with 139 fb^{-1} at 13 TeV LHC. No signal observed. Limits placed on parameter space of DM models.

[34] SIRUNYAN 21A search for DM production in association with leptonically decaying Z boson in 137 fb^{-1} at 13 TeV; no signal; limits set in large variety of simplified DM models.

[35] TUMASYAN 21D search for DM and other exotica at CMS in jets + $\not{E}_T$ events with 137 fb^{-1} at 13 TeV. No signal observed. Limits placed for a variety of simplified models.

[36] SIRUNYAN 20X search for DM in $pp \to Z' \to A(Z')h \to h + \not{E}_T$ in CMS at 13 TeV with 35.9 fb^{-1}; no signal; limits placed in σ^{SI} vs. m(χ), and σ, m(A) and tanβ vs m(Z') for considered DM models.

[37] AABOUD 19AA searches for BSM physics in more than 700 event classes with more than 10^5 regions at 13 TeV with 3.2 fb^{-1}; no significant signal.

[38] AABOUD 19AI searches for vector boson fusion $pp \to Hqq$, $H \to$ invisible at 13 TeV with 36.1 fb^{-1}; no signal: require B($H \to$ invisible) < 0.37 (0.28 expected).

[39] AABOUD 19AL perform search in three different channels for $H \to \chi\chi$ at 7, 8 and 13 TeV; combined result BF($H \to$ invisible) < 0.26 (0.17 expected).

[40] AABOUD 19Q search for single $t + \not{E}_T$ at 13 TeV with 36.1 fb^{-1} of data; no signal; limits set in σ or coupling vs. mass plane for simplified models.

[41] AABOUD 19V review ATLAS results from 7, 8 and 13 TeV searches for mediator-based DM and DE scalar which couples to gravity; no signal: limits set for large variety of simplified models.

[42] BANERJEE 19 search for dark photon via $eN \to eN+\not{E}$ in NA64; no signal, limits placed in kinetic mixing ϵ vs. m(DM) plane for m(DM) $\sim$ 0.001–1 GeV.

[43] SIRUNYAN 19AN search at 13 TeV with 35.9 fb^{-1} for $pp \to H\chi\chi \to b\overline{b}\not{E}_T$; no signal: limits set in the context of a 2HDM + pseudoscalar (a) model and a baryonic Z' model.

[44] SIRUNYAN 19BC search for DM via LeptoQuark pair annihilation LQ LQ $\to \mu j\chi\chi \to \mu j\not{E}_T$ with 77.4 fb^{-1}, 13 TeV; no signal: limits placed in m(χ) vs. m(LQ) plane. Model dependent limits on DM mass up to 600 GeV depending on m(LQ) placed.

[45] SIRUNYAN 19BO search for vector boson fusion $VV \to qqH$ with $H \to \chi\chi$ at 13 TeV with 38.2 fb^{-1}; no signal: limits placed for several models. Also search for $H \to$ invisible at 7, 8, and 13 TeV; no signal: limit placed on BF < 0.19.

[46] SIRUNYAN 19C search for DM via $pp \to t\overline{t}\chi\chi$ at 13 TeV, 35.9 fb^{-1}; no signal; limits placed on coupling vs. mediator mass for various simplified models.

[47] SIRUNYAN 19O search for $pp \to \gamma$ at 13 TeV with 35.9 fb^{-1}; no signal: limits placed on parameters of various models.

[48] SIRUNYAN 19X search for $pp \to t\overline{t}\not{E}_T$ and $pp \to t\not{E}_T$ + ... at 13 TeV with 35.9 fb^{-1}; no signal: limits placed on χ production σ for various simplified models with m(χ) = 1 GeV.

[49] AABOUD 18 search for $pp \to Z + \not{E}_T$ with $Z \to \ell\ell$ at 13 TeV with 36.1 fb^{-1} of data. Limits set for simplified models.

[50] AABOUD 18A search for $pp \to t\overline{t}\not{E}_T$ or $pp \to b\overline{b}\not{E}_T$ at 13 TeV, 36.1 fb^{-1} of data. Limits set for simplified models.

[51] AABOUD 18CA search for $pp \to V\chi\chi$ with $V \to jj$ at 13 TeV, 36.1 fb^{-1}. No signal observed. Limits set in m(DM) vs m(mediator) simplified model plane.

[52] AABOUD 18I search for $pp \to j + \not{E}_T$ at 13 TeV with 36.1 fb^{-1} of data. Limits set for simplified models with pair-produced weakly interacting dark-matter candidates.

[53] AGUILAR-AREVALO 18B search for WIMP production in MiniBooNE p beam dump; no signal; limits set for m(χ) $\sim$ 5–50 MeV in vector portal DM model.

[54] KHACHATRYAN 18 search for $pp \to Z(\ell\ell) + \not{E}_T$. No signal observed. Llimits set on effective dark matter interactions and other exotic physics models.

[55] SIRUNYAN 18BF search for $pp \to t\not{E}_T$ at 13 TeV and 36 fb^{-1}; no signal; limits placed on DM models involving a flavor changing neutral current, scalar resonance decaying to top quark and DM.

[56] SIRUNYAN 18BO search for high mass dijet resonances at 13 TeV and 36 fb^{-1}; no signal: limits placed on various models, including simplified DM models involving a spin = 1 Z' mediator.

[57] SIRUNYAN 18BV search for $pp \to Z\not{E}_T$ at 13 TeV; no signal, limits placed for various exotic physics models including DM.

[58] SIRUNYAN 18C search for new physics in $pp \to$ final states with two oppositely charged leptons at 13 TeV with 35.9 fb^{-1}. Limits placed on m(mediator) and top squark for various simplified models.

[59] SIRUNYAN 18CU search for $pp \to Z\not{E}_T$ at 13 TeV and 2.3 fb^{-1}. No signal observed. Limits placed for various exotic models including DM.

[60] SIRUNYAN 18DH search for $pp \to \chi\chi h$; $h \to \gamma\gamma$ or $\tau\overline{\tau}$ at 13 TeV, 35.9 fb^{-1}; no signal; limits placed on massive boson mediator Z' in the context of Z'+2HDM and baryonic Z' models. Limits also cast in terms of spin-independent WIMP-nucleon cross section for masses 1–200 GeV.

Int. J. Mod. Phys. A 2026.41. Downloaded from www.worldscientific.com
by UNIVERSITY OF CALIFORNIA @ BERKELEY on 09/16/26. Re-use and distribution is strictly not permitted, except for Open Access articles.

[61] SIRUNYAN 18S search for $pp \to$ jets $\not{E}_T$ at 13 TeV; no signal: limits placed on simplified dark matter models, on the branching ratio of the Higgs boson to invisible particles, and on several other exotic physics models including fermion portal DM.

[62] AABOUD 17A search for $H \to b\overline{b} + \not{E}_T$. See Fig. 4b for limits set on VB mediator vs WIMP mass.

[63] AABOUD 17AM search for $pp \to Z' \to Ah \to h(b\overline{b}) + \not{E}_T$ at 13 TeV. Limits set in m(Z') vs. m(A) plane and on the visible cross section of $h(b\overline{b}) + \not{E}_T$ events in bins of $\not{E}_T$.

[64] AABOUD 17AQ search for WIMP in $pp \to h(\gamma\gamma) + \not{E}_T$ in 36.1 fb^{-1} of data. Limits on the visible cross section are also provided. Model dependent limits on spin independent DM - Nucleon cross-section are also presented, which are more stringent than those from direct searches for DM mass smaller than 2.5 GeV.

[65] AABOUD 17BD search for $pp \to$ jet(s) $+ \not{E}_T$ at 13 TeV with 3.2 fb^{-1} of data. Limits set for simplified models. Observables corrected for detector effects can be used to constrain other models.

[66] AABOUD 17R, for an axial vector mediator in the s-channel, excludes m(mediator) $<$ 750–1200 GeV for m(DM) $<$ 230–480 GeV, depending on the couplings.

[67] AGUILAR-AREVALO 17A search for DM produced in 8 GeV proton collisions with steel beam dump followed by DM-nucleon scattering in MiniBooNE detector. Limit placed on DM cross section parameter $Y < 2 \times 10^{-8}$ for $\alpha_D = 0.5$ and for $0.01 < m(\mathrm{DM}) < 0.3$ GeV.

[68] BANERJEE 17 search for dark photon invisible decay via $e\,N$ scattering; exclude m(γ') $<$ 100 MeV as an explanation of (g_μ−2) muon anomaly.

[69] KHACHATRYAN 17A search for WIMPs in forward jets $+ \not{E}_T$ channel with 18.5 fb^{-1} at 8 TeV; limits set in effective theory model, Fig. 3.

[70] KHACHATRYAN 17F search for $H \to$ invisibles in pp collisions at 7, 8, and 13 TeV; place limits on Higgs portal DM.

[71] SIRUNYAN 17 search for $pp \to Z + \not{E}_T$ with 2.3 fb^{-1} at 13 TeV; no signal seen; limits placed on WIMPs and unparticles.

[72] SIRUNYAN 17AP search for $pp \to Z' \to Ah \to h + \not{E}_T$ with $h \to b\overline{b}$ or $\gamma\gamma$ and $A \to \chi\chi$ with 2.3 fb^{-1} at 13 TeV. Limits set in m(Z') vs. m(A) plane.

[73] SIRUNYAN 17AQ search for $pp \to \gamma + \not{E}_T$ at 13 TeV with 12.9 fb^{-1}. Limits derived for simplified DM models, effective electroweak-DM interaction and Extra Dimensions models.

[74] SIRUNYAN 17BB search for WIMPs via $pp \to t\overline{t}+\not{E}_T$, $pp \to b\overline{b}+\not{E}_T$ at 13 TeV with 2.2 fb^{-1}. Limits derived for various simplified models.

[75] SIRUNYAN 17G search for $pp \to j + \not{E}_T$ with 12.9 fb^{-1} at 13 TeV; limits placed on WIMP mass/mediators in DM simplified models.

[76] SIRUNYAN 17U search for WIMPs/unparticles via $pp \to Z\chi\chi$, $Z \to \ell\overline{\ell}$ at 13 TeV with 2.3 fb^{-1}. Limits derived for various simplified models.

[77] AABOUD 16AD place limits on VVXX effective theory via search for hadronic W or Z plus WIMP pair production. See Fig. 5.

[78] AAD 16AF search for $VV \to (H \to$ WIMP pair$)$ + forward jets with 20.3 fb^{-1} at 8 TeV; set limits in Higgs portal model, Fig. 8.

[79] AAD 16AG search for lepton jets with 20.3 fb^{-1} of data at 8 TeV; Fig. 13 excludes dark photons around 0.1–1 GeV for kinetic mixing 10^{-6}–10^{-2}.

[80] AAD 16M search with 20.3 fb^{-1} of data at 8 TeV pp collisions; limits placed on EFT model (Fig. 7) and simplified Z' model (Fig. 6).

[81] KHACHATRYAN 16BZ search for jet(s) $+ \not{E}_T$ in 19.7 fb^{-1} at 8 TeV; limits set for variety of simplified models.

[82] KHACHATRYAN 16CA search for WIMPs via jet(s) $+ \not{E}_T$ using razor variable; require mediator scale > 1 TeV for various effective theories.

[83] KHACHATRYAN 16N search for γ + WIMPs in 19.6 fb^{-1} at 8 TeV; limits set on SI and SD WIMP-p scattering in Fig. 3.

[84] AAD 15AS search for events with one or more bottom quark and missing E_T, and also events with a top quark pair and missing E_T in pp collisions at $E_{\rm cm}$ = 8 TeV with L = 20.3 fb^{-1}. See their Figs. 5 and 6 for translated limits on X^0-nucleon cross section for m = 1–700 GeV.

[85] AAD 15BH search for events with a jet and missing E_T in pp collisions at $E_{\rm cm}$ = 8 TeV with L = 20.3 fb^{-1}. See their Fig. 12 for translated limits on X^0-nucleon cross section for m = 1–1200 GeV.

[86] AAD 15CF search for events with a H^0 ($\to \gamma\gamma$) and missing E_T in pp collisions at $E_{\rm cm}$ = 8 TeV with L = 20.3 fb^{-1}. See paper for limits on the strength of some contact interactions containing X^0 and the Higgs fields.

[87] AAD 15CS search for events with a photon and missing E_T in pp collisions at $E_{\rm cm}$ = 8 TeV with L = 20.3 fb^{-1}. See their Fig. 13 (see also erratum) for translated limits on X^0-nucleon cross section for m = 1–1000 GeV.

[88] KHACHATRYAN 15AG search for events with a top quark pair and missing E_T in pp collisions at $E_{\rm cm}$ = 8 TeV with L = 19.7 fb^{-1}. See their Fig. 8 for translated limits on X^0-nucleon cross section for m = 1–200 GeV.

[89] KHACHATRYAN 15AL search for events with a jet and missing E_T in pp collisions at $E_{\rm cm}$ = 8 TeV with L = 19.7 fb^{-1}. See their Fig. 5 and Tables 4–6 for translated limits on X^0-nucleon cross section for m = 1–1000 GeV.

[90] KHACHATRYAN 15T search for events with a lepton and missing E_T in pp collisions at $E_{\rm cm}$ = 8 TeV with L = 19.7 fb^{-1}. See their Fig. 17 for translated limits on X^0-proton cross section for m = 1–1000 GeV.

[91] AAD 14AI search for events with a W and missing E_T in pp collisions at $E_{\rm cm}$ = 8 TeV with L = 20.3 fb^{-1}. See their Fig. 4 for translated limits on X^0–nucleon cross section for m = 1–1500 GeV.

[92] AAD 14BK search for hadronically decaying W, Z in association with $\not{E}_T$ in 20.3 fb^{-1} at 8 TeV pp collisions. Fig. 5 presents exclusion results for SI and SD scattering cross section. In addition, cross section limits on the anomalous production of W or Z bosons with large missing transverse momentum are also set in two fiducial regions.

[93] AAD 14K search for events with a Z and missing E_T in pp collisions at $E_{\rm cm}$ = 8 TeV with L = 20.3 fb^{-1}. See their Fig. 5 and 6 for translated limits on X^0–nucleon cross section for m = 1–10^3 GeV.

[94] AAD 14O search for ZH^0 production with H^0 decaying to invisible final states. See their Fig. 4 for translated limits on X^0–nucleon cross section for m = 1–60 GeV in Higgs-portal X^0 scenario.

[95] AAD 13AD search for events with a jet and missing E_T in pp collisions at $E_{\rm cm}$ = 7 TeV with L = 4.7 fb^{-1}. See their Figs. 5 and 6 for translated limits on X^0-nucleon cross section for m = 1–1300 GeV.

[96] AAD 13C search for events with a photon and missing E_T in pp collisions at $E_{\rm cm}$ = 7 TeV with L = 4.6 fb^{-1}. See their Fig. 3 for translated limits on X^0-nucleon cross section for m = 1–1000 GeV.

[97] AALTONEN 12K search for events with a top quark and missing E_T in $p\overline{p}$ collisions at $E_{\rm cm}$ = 1.96 TeV with L = 7.7 fb^{-1}. Upper limits on $\sigma(tX^0)$ in the range 0.4–2 pb (95% CL) is given for m_{X^0} = 0–150 GeV.

[98] AALTONEN 12M search for events with a jet and missing E_T in $p\overline{p}$ collisions at $E_{\rm cm}$ = 1.96 TeV with L = 6.7 fb^{-1}. Upper limits on the cross section in the range 2–10 pb (90% CL) is given for m_{X^0} = 1–300 GeV. See their Fig. 2 for translated limits on X^0-nucleon cross section.

[99] CHATRCHYAN 12AP search for events with a jet and missing E_T in pp collisions at $E_{\rm cm}$ = 7 TeV with L = 5.0 fb^{-1}. See their Fig. 4 for translated limits on X^0-nucleon cross section for m_{X^0} = 0.1–1000 GeV.

[100] CHATRCHYAN 12T search for events with a photon and missing E_T in pp collisions at $E_{\rm cm}$ = 7 TeV with L = 5.0 fb^{-1}. Upper limits on the cross section in the range 13–15 fb (90% CL) is given for m_{X^0} = 1–1000 GeV. See their Fig. 2 for translated limits on X^0-nucleon cross section.

Dark Matter Particle (X^0) Production in e^+e^- Collisions

Model dependent limits on dark matter parameters.

VALUE	DOCUMENT ID	TECN	COMMENT
• • • We do not use the following data for averages, fits, limits, etc. • • •			
	[1] ADACHI 25U	BEL2	inelastic DM in association with dark photon and dark Higgs

[1] ADACHI 25U report on search for inelastic dark matter wimps produced in e^+e^- collisions in association with dark photon and dark Higgs. No signal observed. Limits placed on GeV-scale DM in m(h') vs. mixing angle and m(χ) vs. kinetic mixing planes.

REFERENCES FOR WIMP and Dark Matter Searches

AAD	25BA	JHEP 2509 067	G. Aad et al.	(ATLAS Collab.)
AAD	25C	PRL 134 121801	G. Aad et al.	(ATLAS Collab.)
AALBERS	25	PRL 135 011802	J. Aalbers et al.	(LZ Collab.)
AALBERS	25A	PRL 134 241801	J. Aalbers et al.	(LZ Collab.)
ABBASI	25A	EPJ C85 490	R. Abbasi et al.	(IceCube Collab.)
ABE	25A	JCAP 2503 020	S. Abe et al.	(MAGIC Collab.)
ADACHI	25U	PRL 135 131801	I. Adachi et al.	(BELLE II Collab.)
ADAMS	25	PRL 135 011001	E. Adams et al.	(PICO Collab.)
ADARI	25	PRL 134 011804	P. Adari et al.	(SENSEI Collab.)
AGGARWAL	25A	PRL 135 071002	L. Aggarwal et al.	(DAMIC Collab.)
AGNES	25	PR D112 123058	P. Agnes et al.	(DarkSide-50 Collab.)
AIELLO	25B	JCAP 2503 058	S. Aiello et al.	(KM3Net Collab.)
ALBAKRY	25	PR D111 012006	M.F. Albakry et al.	(SuperCDMS Collab.)
AMARE	25	PRL 135 051001	J. Amare et al.	(ANAIS Collab.)
APRILE	25	PRL 134 111802	E. Aprile et al.	(XENONnT Collab.)
APRILE	25A	PRL 134 161004	E. Aprile et al.	(XENONnT Collab.)
APRILE	25B	PRL 135 221003	E. Aprile et al.	(XENONnT Collab.)
ARORA	25	PRL 134 141002	M. Arora et al.	(NEWS-G Collab.)
BAUDIS	25	PRL 135 081002	L. Baudis et al.	(QROCODILE Collab.)
BERGHAUS	25	JCAP 2507 067	K. Berghaus, D. Hooper, E. Simon	(CIT, WISC+)
BLOCH	25	PRL 134 161002	I. Bloch et al.	(SENSEI Collab.)
BO	25	PRL 134 011805	Z. Bo et al.	(PandaX-4T Collab.)
BUI	25	PRL 135 161002	T.K. Bui et al.	(TESSERACT Collab.)
CARLIN	25	PRL 135 121002	N. Carlin et al.	(COSINE-100, ANAIS Collabs.)
CHEKHOVSKY	25D	JHEP 2508 085	V. Chekhovsky et al.	(CMS Collab.)
CHEKHOVSKY	25H	JHEP 2509 141	V. Chekhovsky et al.	(CMS Collab.)
CHOI	25	PRL 134 021802	J. Choi et al.	(NEON Collab.)
CRNOGORC...	25	PR D112 103001	M. Crnogorcevic et al.	
DAS	25	PR D112 042003	S. Das et al.	(InDEx Collab.)
DU	25	PRL 135 051002	P. Du et al.	(RUTG, STON, NASA)
FERNANDEZ...	25	JCAP 2509 003	C. Fernandez-Suarez, M.A. Sanchez-Conde	(MADU)
HAYRAPETY...	25P	JHEP 2502 050	A. Hayrapetyan et al.	(CMS Collab.)
LIANG	25	PRL 134 071001	Z.L. Liang et al.	
LIANG	25A	PR D112 112025	Y.F. Liang et al.	(CDEX Collab.)
NIE	25	CP C49 043002	Q-Y. Nie et al.	(CDEX Collab.)
NING	25B	PL B864 139389	X. Ning et al.	(PandaX-4T Collab.)
SHEN	25	PRL 134 161003	G. Shen et al.	(PandaX-4T Collab.)
UMEMOTO	25	JCAP 2502 012	A. Umemoto et al.	(NEWSdm Collab.)
WANG	25A	PR D112 092011	J.Z. Wang et al.	(CDEX-10 Collab.)
YU	25	PRL 135 231001	G.H. Yu et al.	(COSINE-100 Collab.)
ZAKHAROV	25	PR D112 103037	E.I. Zakharov et al.	(NuSTAR Collab.)
ZHANG	25B	PRL 135 211001	M. Zhang et al.	(PandaX-4T Collab.)
AAD	24AC	JHEP 2403 139	G. Aad et al.	(ATLAS Collab.)
AAD	24AH	JHEP 2405 106	G. Aad et al.	(ATLAS Collab.)
AAD	24AK	JHEP 2405 263	G. Aad et al.	(ATLAS Collab.)
AAD	24CD	JHEP 2411 126	G. Aad et al.	(ATLAS Collab.)
AALBERS	24A	PR D109 112010	J. Aalbers et al.	(LZ Collab.)
ABE	24A	PL B855 138846	S. Abe et al.	(KamLAND-Zen Collab.)
ACHARYYA	24	PR D110 063034	A. Acharyya et al.	(VERITAS Collab.)
AGNES	24	PR D110 102006	P. Agnes et al.	(DarkSide-50 Collab.)
ANGLOHER	24	EPJ C84 324	G. Angloher et al.	(CRESST Collab.)
ANGLOHER	24A	PR D110 043010	G. Angloher et al.	(COSINUS Collab.)
ANGLOHER	24B	PR D110 083038	G. Angloher et al.	(CRESST-III Collab.)
ARNQUIST	24A	PRL 132 101006	I.J. Arnquist et al.	(DAMIC Collab.)
CAO	24	PRL 133 061001	Z. Cao et al.	(LHAASO Collab.)
CHOLIS	24	PR D110 103032	I. Cholis, I. Krommydas	(OAKU, ROCH)
CRNOGORC...	24	PR D109 083018	M. Crnogorcevic, T. Linden	(STOH)
DE-LA-TORR...	24	PR D109 L041301	P. De La Torre Luque, J. Smirnov, T. Linden	(STOH+)
HAYRAPETY...	24B	PRL 132 041802	A. Hayrapetyan et al.	(CMS Collab.)
HAYRAPETY...	24W	JHEP 2403 134	A. Hayrapetyan et al.	(CMS Collab.)
MANNA	24	JCAP 2410 023	S. Manna, S. Desai	(INIT)
MCDANIEL	24	PR D109 063024	A. McDaniel et al.	(CLEMS, NASA, TURIN+)
SHANG	24	PRL 133 101805	X. Shang et al.	(PandaX-4T Collab.)
SONG	24	JCAP 2405 087	D. Song, N. Hiroshima, K. Murase	(KYOT, YOKO+)
SONG	24A	JCAP 2403 024	D. Song, K. Murase, A. Kheirandish	(KYOT, PSU+)
ZAKHAROV	24A	PR D110 123026	E.I. Zakharov et al.	(SRG-ART-XC/IKI RAS)
ZHANG	24A	PRL 132 171001	Z.Y. Zhang et al.	(CDEX Collab.)
ZHANG	24E	SCPMA 67 101011	Z.H. Zhang et al.	(CDEX Collab.)
AAD	23A	PL B842 137963	G. Aad et al.	(ATLAS Collab.)
AAD	23AF	EPJ C83 503	G. Aad et al.	(ATLAS Collab.)
AAD	23AJ	EPJ C83 603	G. Aad et al.	(ATLAS Collab.)
AAD	23BX	JHEP 2309 189	G. Aad et al.	(ATLAS Collab.)
AAD	23W	JHEP 2307 116	G. Aad et al.	(ATLAS Collab.)
AALBERS	23	PRL 131 041002	J. Aalbers et al.	(LZ Collab.)

Int. J. Mod. Phys. A 2026.41. Downloaded from www.worldscientific.com
by UNIVERSITY OF CALIFORNIA @ BERKELEY on 09/16/26. Re-use and distribution is strictly not permitted, except for Open Access articles.

AALBERS	23A	PR D108 072006	J. Aalbers *et al.*	(LZ Collab.)
ABBASI	23A	PR D108 102004	R. Abbasi *et al.*	(IceCube Collab.)
ABBASI	23B	JCAP 2310 003	R. Abbasi *et al.*	(IceCube Collab.)
ABE	23A	PRL 130 031802	K. Abe *et al.*	(Super-Kamiokande Collab.)
Also		PRL 131 159903 (errat.)	K. Abe *et al.*	(Super-Kamiokande Collab.)
ABE	23B	PRL 130 061002	H. Abe *et al.*	(MAGIC Collab.)
ABE	23E	PR D108 083022	K. Abe *et al.*	(XMASS-I Collab.)
ABE	23G	PRL 131 159903 (errat.)	K. Abe *et al.*	(Super-Kamiokande Collab.)
ABREU	23	PRL 130 061001	P. Abreu *et al.*	(Pierre Auger Collab.)
ACEVEDO	23	JCAP 2311 085	J.F. Acevedo, J. Bramante, A. Goodman	(QUKI+)
ADAMS	23	PR D108 062003	E. Adams *et al.*	(PICO Collab.)
ADHIKARI	23B	PRL 131 201802	G. Adhikari *et al.*	(COSINE-100 Collab.)
ADHIKARI	23C	PR D108 092006	G. Adhikari *et al.*	(COSINE-100 Collab.)
AGNES	23	PRL 130 101001	P. Agnes *et al.*	(DarkSide-50 Collab.)
AGNES	23A	PRL 130 101002	P. Agnes *et al.*	(DarkSide-50 Collab.)
AGNES	23B	PR D107 063001	P. Agnes *et al.*	(DarkSide-50 Collab.)
AKIMOV	23	PRL 130 051803	D. Akimov *et al.*	(COHERENT Collab.)
ALBAKRY	23	PR D107 112013	M.F. Albakry *et al.*	(SuperCDMS Collab.)
ALBERT	23	JCAP 2312 038	A. Albert *et al.*	(HAWC Collab.)
AL-KHARUSI	23	PR D107 012007	S. Al Kharusi *et al.*	(EXO-200 Collab.)
AMBROSONE	23	PRL 131 111003	A. Ambrosone *et al.*	
ANGLOHER	23	PR D107 122003	G. Angloher *et al.*	(CRESST-III Collab.)
APRILE	23	PRL 130 261002	E. Aprile *et al.*	(XENON1T Collab.)
APRILE	23A	PRL 131 041003	E. Aprile *et al.*	(XENONnT Collab.)
ARNQUIST	23A	PRL 130 171003	I.J. Arnquist *et al.*	(DAMIC Collab.)
CHENG	23A	PR D108 063015	J.-G. Cheng, Y.-F. Liang, E.-W. Liang	
FOSTER	23	PR D107 103047	J.W. Foster *et al.*	(MIT, UCB, LBL+)
GUO	23	PR D107 103011	W.-Q. Guo *et al.*	
GUO	23A	PR D108 043001	X.-K. Guo *et al.*	
HUANG	23	PRL 131 191002	D. Huang *et al.*	(PandaX-4T Collab.)
LAVIS	23	PR D108 123536	N. Lavis *et al.*	(WITW, RHODE)
LI	23F	PRL 130 261001	S. Li *et al.*	(PandaX-4T Collab.)
LIN	23C	PRL 130 111801	C. Lin *et al.*	(KOTO Collab.)
MA	23A	PRL 130 021802	W. Ma *et al.*	(PandaX-4T Collab.)
NING	23A	PRL 131 041001	X. Ning *et al.*	(PandaX-4T Collab.)
SHIMADA	23	PTEP 2023 103F01	T. Shimada *et al.*	(NEWAGE Collab.)
AAD	22D	PL B829 137066	G. Aad *et al.*	(ATLAS Collab.)
AAD	22P	JHEP 2208 104	G. Aad *et al.*	(ATLAS Collab.)
ABBASI	22B	PR D105 062004	R. Abbasi *et al.*	(IceCube Collab.)
ABDALLA	22	PRL 129 111101	H. Abdalla *et al.*	(H.E.S.S. Collab.)
ADHIKARI	22	PRL 128 011801	P. Adhikari *et al.*	(DEAP Collab.)
ADHIKARI	22B	PR D105 042006	G. Adhikari *et al.*	(COSINE-100 Collab.)
ADHIKARI	22D	PR D106 052005	G. Adhikari *et al.*	(COSINE-100 Collab.)
AGOSTINI	22	JCAP 2212 012	M. Agostini *et al.*	(GERDA Collab.)
AGOSTINI	22A	PRL 129 089901	M. Agostini *et al.*	(GERDA Collab.)
AGUILAR-AR...	22A	PR D106 012001	A.A. Aguilar-Arevalo *et al.*	(CCM Collab.)
AKIMOV	22	PR D106 052004	D. Akimov *et al.*	(COHERENT Collab.)
ALBERT	22A	JCAP 2206 028	A. Albert *et al.*	(ANTARES Collab.)
ANGLOHER	22	EPJ C82 207	G. Angloher *et al.*	(CRESST Collab.)
ANGLOHER	22A	PR D106 092008	G. Angloher *et al.*	(CRESST-III Collab.)
APRILE	22	PR D106 022001	E. Aprile *et al.*	(XENON1T Collab.)
Also		PR D110 109903 (errat.)	E. Aprile *et al.*	(XENON1T Collab.)
ARMENGAUD	22	PR D106 062004	E. Armengaud *et al.*	(EDELWEISS Collab.)
BATTAGLIERI	22	PR D106 072011	M. Battaglieri *et al.*	(BDX-MINI Collab.)
BOSE	22	PR D105 123013	D. Bose, T.N. Maity, T.S. Ray	
CHAN	22	PR D105 123006	M.H. Chan, C.M. Lee	
CUI	22	PRL 128 171801	X. Cui *et al.*	(PandaX-II Collab.)
DAI	22A	PRL 129 221802	W.H. Dai *et al.*	(CDEX Collab.)
EGOROV	22	PR D106 023023	A.E. Egorov	(LEBD)
GHOSH	22	PR D105 103029	D. Ghosh, A. Guha, D. Sachdeva	
GU	22	PRL 129 161803	L. Gu *et al.*	(PandaX-4T Collab.)
HOCHBERG	22	PR D106 112005	Y. Hochberg *et al.*	(SNSPD Collab.)
HUANG	22	PL B834 137487	Z. Huang *et al.*	(PandaX-4T Collab.)
MANCONI	22	PRL 129 111103	S. Manconi, A. Cuoco, J. Lesgourgues	
TUMASYAN	22AA	JHEP 2206 156	A. Tumasyan *et al.*	(CMS Collab.)
TUMASYAN	22AG	EPJ C82 213	A. Tumasyan *et al.*	(CMS Collab.)
TUMASYAN	22G	PR D105 092007	A. Tumasyan *et al.*	(CMS Collab.)
XU	22	PR D106 052008	R. Xu *et al.*	(CDEX Collab.)
ZHANG	22	PRL 129 161804	D. Zhang *et al.*	(PandaX-4T Collab.)
ZHANG	22A	PRL 129 221301	Z.Y. Zhang *et al.*	(CDEX Collab.)
AAD	21AZ	JHEP 2110 013	G. Aad *et al.*	(ATLAS Collab.)
AAD	21BB	JHEP 2111 209	G. Aad *et al.*	(ATLAS Collab.)
AAD	21D	PRL 126 121802	G. Aad *et al.*	(ATLAS Collab.)
AAD	21F	PR D103 112006	G. Aad *et al.*	(ATLAS Collab.)
AAD	21K	JHEP 2102 226	G. Aad *et al.*	(ATLAS Collab.)
AAD	21O	JHEP 2104 174	G. Aad *et al.*	(ATLAS Collab.)
AAD	21P	JHEP 2104 165	G. Aad *et al.*	(ATLAS Collab.)
AAD	21S	JHEP 2105 093	G. Aad *et al.*	(ATLAS Collab.)
ABDALLAH	21	PR D103 102002	H. Abdallah *et al.*	(H.E.S.S. Collab.)
AKERIB	21A	PR D104 012011	D.S. Akerib *et al.*	(LUX Collab.)
AKERIB	21B	PR D104 062005	D.S. Akerib *et al.*	(LUX Collab.)
ALKHATIB	21	PRL 127 061801	I. Alkhatib *et al.*	(SuperCDMS Collab.)
AMARE	21	PR D103 102005	J. Amare *et al.*	(ANAIS Collab.)
ANDRIAMIR...	21A	PR D104 012009	M. Andriamirado *et al.*	(PROSPECT Collab.)
APRILE	21	PRL 126 091301	E. Aprile *et al.*	(XENON1T Collab.)
APRILE	21A	PR D103 063028	E. Aprile *et al.*	(XENON1T Collab.)
CHENG	21	PRL 126 211803	C. Cheng *et al.*	(PandaX-II Collab.)
CIRELLI	21	PR D103 063022	M. Cirelli *et al.*	
IKEDA	21	PTEP 2021 063F01	T. Ikeda *et al.*	(NEWAGE Collab.)
JOHN	21	JCAP 2112 007	I. John, T. Linden	(STOH)
MENG	21B	PRL 127 261802	Y. Meng *et al.*	(PandaX-4T Collab.)
SIRUNYAN	21A	EPJ C81 13	A.M. Sirunyan *et al.*	(CMS Collab.)
Also		EPJ C81 333 (errat.)	A.M. Sirunyan *et al.*	(CMS Collab.)
TUMASYAN	21D	JHEP 2111 153	A. Tumasyan *et al.*	(CMS Collab.)
WANG	21K	SCPMA 64 281011	Y. Wang *et al.*	(CDEX Collab.)
AARTSEN	20C	EPJ C80 819	M.G. Aartsen *et al.*	(IceCube, PICO Collabs)
ABAZAJIAN	20	PR D102 043012	K.N. Abazajian *et al.*	(UCI, VPI, TOKY+)
ABDALLAH	20	PR D102 062001	H. Abdallah *et al.*	(H.E.S.S. Collab.)
ABDELHAME...	20A	EPJ C80 834	A.H. Abdelhameed *et al.*	(CRESST Collab.)
ABE	20G	PR D102 072002	K. Abe *et al.*	(Super-Kamiokande Collab.)
ADHIKARI	20	PR D102 082001	P. Adhikari *et al.*	(DEAP-3600 Collab.)
AGOSTINI	20	PRL 125 011801	M. Agostini *et al.*	(GERDA Collab.)
AGUILAR-AR...	20C	PRL 125 241803	A. Aguilar-Arevalo	(DAMIC Collab.)
AKERIB	20	PR D101 012003	D.S. Akerib *et al.*	(LUX Collab.)
AKERIB	20A	PR D101 042001	D.S. Akerib *et al.*	(LUX Collab.)
ALBERT	20	PR D101 103001	A. Albert *et al.*	(HAWC Collab.)
ALBERT	20A	PL B805 135439	A. Albert *et al.*	(ANTARES Collab.)
ALBERT	20C	PR D102 082002	A. Albert *et al.*	(ANTARES and IceCube Collab.)
ALVAREZ	20	JCAP 2009 004	A. Alvarez *et al.*	
AMARAL	20	PR D102 091101	D.W. Amaral *et al.*	(SuperCDMS Collab.)
ANDRIANAV...	20	PR D102 042001	A. Andrianavalomahefa *et al.*	(FUNK Collab.)
APRILE	20	PR D102 072004	E. Aprile *et al.*	(XENON Collab.)
ARNAUD	20	PRL 125 141301	Q. Arnaud *et al.*	(EDELWEISS Collab.)
BARAK	20	PRL 125 171802	L. Barak *et al.*	(SENSEI Collab.)
CLARK	20	PR D102 123026	M. Clark *et al.*	(PURD)
Also		PR D104 129903 (errat.)	M. Clark *et al.*	
FELIZARDO	20	IJMP A35 2030005	M. Felizardo	(SIMPLE Collab.)
HOOF	20	JCAP 2002 012	S. Hoof, A. Geringer-Sameth, R. Trotta	(GOET+)
MAZZIOTTA	20	PR D102 022003	M.N. Mazziotta *et al.*	
SIRUNYAN	20X	JHEP 2003 025	A.M. Sirunyan *et al.*	(CMS Collab.)
WANG	20G	CP C44 125001	Q. Wang *et al.*	(PandaX-II Collab.)
AABOUD	19AA	EPJ C79 120	M. Aaboud *et al.*	(ATLAS Collab.)
AABOUD	19AI	PL B793 499	M. Aaboud *et al.*	(ATLAS Collab.)
AABOUD	19AL	PRL 122 231801	M. Aaboud *et al.*	(ATLAS Collab.)
AABOUD	19Q	JHEP 1905 041	M. Aaboud *et al.*	(ATLAS Collab.)
AABOUD	19V	JHEP 1905 142	M. Aaboud *et al.*	(ATLAS Collab.)
ABDELHAME...	19	EPJ C79 630	A.H. Abdelhameed *et al.*	(CRESST Collab.)
ABDELHAME...	19A	PR D100 102002	A.H. Abdelhameed *et al.*	(CRESST Collab.)
ABE	19	PL B789 45	K. Abe *et al.*	(XMASS Collab.)
ABEYSEKARA	19	JCAP 1907 022	A.U. Abeysekara *et al.*	(HAWC Collab.)
ABRAMOFF	19	PRL 122 161801	O. Abramoff *et al.*	(SENSEI Collab.)
ADHIKARI	19	PRL 123 031302	G. Adhikari *et al.*	(COSINE-100 Collab.)
AGNESE	19A	PR D99 062001	R. Agnese *et al.*	(CDMS Collab.)
AGUILAR-AR...	19A	PRL 123 181802	A. Aguilar-Arevalo *et al.*	(DAMIC Collab.)
AJAJ	19	PR D100 022004	R. Ajaj *et al.*	(DEAP-3600 Collab.)
AKERIB	19	PRL 122 131301	D.S. Akerib *et al.*	(LUX Collab.)
ALBERT	19B	JCAP 1904 E01	A. Albert *et al.*	(HAWC Collab.)
AMARE	19	PRL 123 031301	J. Amare *et al.*	(ANAIS Collab.)
AMOLE	19	PR D100 022001	C. Amole *et al.*	(PICO Collab.)
ANGLOHER	19	EPJ C79 43	G. Angloher *et al.*	(CRESST-II Collab.)
APRILE	19	PRL 122 071301	E. Aprile *et al.*	(XENON1T Collab.)
APRILE	19A	PRL 122 141301	E. Aprile *et al.*	(XENON1T Collab.)
APRILE	19C	PRL 123 241803	E. Aprile *et al.*	(XENON1T Collab.)
APRILE	19D	PRL 123 251801	E. Aprile *et al.*	(XENON1T Collab.)
ARMENGAUD	19	PR D99 082003	E. Armengaud *et al.*	(EDELWEISS Collab.)
BANERJEE	19	PRL 123 121801	D. Banerjee *et al.*	(NA64 Collab.)
BRINGMANN	19	PRL 122 171801	T. Bringmann, M. Pospelov	(OSLO, VICT)
BRUNE	19	PR D99 096005	T. Brune, H. Pas	(DORT)
CHEUNG	19	PL B789 137	K. Cheung *et al.*	
CHOI	19	PR D99 083018	K.-Y. Choi, J. Kim, C. Rott	(SUNG)
DI-MAURO	19	PR D99 123027	M. Di Mauro *et al.*	
HA	19	PRL 122 131802	C. Ha *et al.*	(COSINE-100 Collab.)
JOHNSON	19	PR D99 103007	C. Johnson *et al.*	
KIM	19A	JHEP 1903 194	K.W. Kim *et al.*	(KIMS Collab.)
KLOPF	19	PRL 122 222503	M. Klopf *et al.*	(PERKEO II Collab.)
KOBAYASHI	19	PL B795 308	M. Kobayashi *et al.*	(XMASS Collab.)
LI	19D	PR D99 123519	S. Li *et al.*	
LIU	19B	PRL 123 161301	Z.Z. Liu *et al.*	(CDEX Collab.)
NG	19	PR D99 083005	K.C.Y. Ng *et al.*	
QUEIROZ	19	JCAP 1904 048	F.S. Queiroz, C. Siqueira	
SEONG	19	PRL 122 011801	I.S. Seong *et al.*	(BELLE Collab.)
SIRUNYAN	19AN	EPJ C79 280	A.M. Sirunyan *et al.*	(CMS Collab.)
SIRUNYAN	19BC	PL B795 76	A.M. Sirunyan *et al.*	(CMS Collab.)
SIRUNYAN	19BO	PL B793 520	A.M. Sirunyan *et al.*	(CMS Collab.)
SIRUNYAN	19C	PRL 122 011803	A.M. Sirunyan *et al.*	(CMS Collab.)
SIRUNYAN	19O	JHEP 1902 074	A.M. Sirunyan *et al.*	(CMS Collab.)
SIRUNYAN	19X	JHEP 1903 141	A.M. Sirunyan *et al.*	(CMS Collab.)
SUZUKI	19	ASP 110 1	T. Suzuki *et al.*	(XMASS Collab.)
XIA	19A	PL B792 193	J. Xia *et al.*	(PandaX-II Collab.)
YAGUNA	19	JCAP 1904 041	C. Yaguna	
YANG	19	PRL 123 221301	L.T. Yang *et al.*	(CDEX Collab.)
AABOUD	18	PL B776 318	M. Aaboud *et al.*	(ATLAS Collab.)
AABOUD	18A	EPJ C78 18	M. Aaboud *et al.*	(ATLAS Collab.)
AABOUD	18CA	JHEP 1810 180	M. Aaboud *et al.*	(ATLAS Collab.)
AABOUD	18I	JHEP 1801 126	M. Aaboud *et al.*	(ATLAS Collab.)
AARTSEN	18D	EPJ C78 831	M.G. Aartsen *et al.*	(IceCube Collab.)
ABDALLAH	18	PRL 120 201101	H. Abdallah *et al.*	(H.E.S.S. Collab.)
ABE	18C	PR D97 102006	K. Abe *et al.*	(XMASS Collab.)
ABE	18F	PL B787 153	K. Abe *et al.*	(XMASS Collab.)
ADHIKARI	18	NAT 564 83	G. Adhikari *et al.*	(COSINE-100 Collab.)
AGNES	18	PRL 121 081307	P. Agnes *et al.*	(DarkSide-50 Collab.)
AGNES	18A	PR D98 102006	P. Agnes *et al.*	(DarkSide-50 Collab.)
AGNES	18B	PRL 121 111303	P. Agnes *et al.*	(DarkSide-50 Collab.)
AGNESE	18	PR D97 022002	R. Agnese *et al.*	(SuperCDMS Collab.)
AGNESE	18A	PRL 120 061802	R. Agnese *et al.*	(SuperCDMS Collab.)
AGNESE	18B	PRL 121 051301	R. Agnese *et al.*	(SuperCDMS Collab.)
Also		PRL 122 069901 (errat.)	R. Agnese *et al.*	(SuperCDMS Collab.)
AGUILAR-AR...	18B	PR D98 112004	A.A. Aguilar-Arevalo	(MiniBooNE Collab.)
AHNEN	18	JCAP 1803 009	M.L. Ahnen *et al.*	(MAGIC Collab.)
AKERIB	18A	PR D98 062005	D.S. Akerib *et al.*	(LUX Collab.)
ALBERT	18B	JCAP 1806 043	A. Albert *et al.*	(HAWC Collab.)
ALBERT	18C	PR D98 123012	A. Albert *et al.*	(HAWC Collab.)
AMAUDRUZ	18	PRL 121 071801	P.A. Amaudruz *et al.*	(DEAP-3600 Collab.)
APRILE	18	PRL 121 111302	E. Aprile *et al.*	(XENON1T Collab.)
ARMENGAUD	18	PR D98 082004	E. Armengaud *et al.*	(EDELWEISS-III Collab.)
ARNAUD	18	ASP 97 54	Q. Arnaud *et al.*	(NEWS-G Collab.)
CHANG	18A	PR D98 123004	L.J. Chang, M. Lisanti, S. Mishra-Sharma	(PRIN)
CRISLER	18	PRL 121 061803	M. Crisler *et al.*	(SENSEI Collab.)
JIANG	18	PRL 120 241301	H. Jiang *et al.*	(CDEX Collab.)
KACHULIS	18	PRL 120 221301	C. Kachulis *et al.*	(Super-Kamiokande Collab.)
KHACHATRY...	18	PR D97 099903	V. Khachatryan *et al.*	(CMS Collab.)
LISANTI	18	PRL 120 101101	M. Lisanti *et al.*	(PRIN, MIT, MICH)
MAZZIOTTA	18	PR D98 022006	M. Mazziotta *et al.*	(Fermi-LAT Collab.)
REN	18	PRL 121 021304	X. Ren *et al.*	(PandaX-II Collab.)
SIRUNYAN	18BF	JHEP 1806 027	A.M. Sirunyan *et al.*	(CMS Collab.)
SIRUNYAN	18BO	JHEP 1808 130	A.M. Sirunyan *et al.*	(CMS Collab.)
SIRUNYAN	18BV	EPJ C78 291	A.M. Sirunyan *et al.*	(CMS Collab.)
SIRUNYAN	18C	PR D97 032009	A.M. Sirunyan *et al.*	(CMS Collab.)
SIRUNYAN	18CU	JHEP 1801 056	A.M. Sirunyan *et al.*	(CMS Collab.)
SIRUNYAN	18DH	JHEP 1809 046	A.M. Sirunyan *et al.*	(CMS Collab.)
SIRUNYAN	18S	PR D97 092005	A.M. Sirunyan *et al.*	(CMS Collab.)
YANG	18	CP C42 023002	L.T. Yang *et al.*	(CDEX Collab.)
AABOUD	17A	PL B765 11	M. Aaboud *et al.*	(ATLAS Collab.)
AABOUD	17AM	PRL 119 181804	M. Aaboud *et al.*	(ATLAS Collab.)
AABOUD	17AQ	PR D96 112004	M. Aaboud *et al.*	(ATLAS Collab.)
AABOUD	17BD	EPJ C77 765	M. Aaboud *et al.*	(ATLAS Collab.)
AABOUD	17R	EPJ C77 393	M. Aaboud *et al.*	(ATLAS Collab.)
AARTSEN	17	EPJ C77 82	M.G. Aartsen *et al.*	(IceCube Collab.)
AARTSEN	17A	EPJ C77 146	M.G. Aartsen *et al.*	(IceCube Collab.)
Also		EPJ C79 214 (errat.)	M.G. Aartsen *et al.*	(IceCube Collab.)
AARTSEN	17C	EPJ C77 627	M.G. Aartsen *et al.*	(IceCube Collab.)
AGUILAR-AR...	17	PRL 118 141803	A. Aguilar-Arevalo *et al.*	(DAMIC Collab.)
AGUILAR-AR...	17A	PRL 118 221803	A.A. Aguilar-Arevalo *et al.*	(MiniBooNE Collab.)
AKERIB	17	PRL 118 021303	D.S. Akerib *et al.*	(LUX Collab.)
AKERIB	17A	PRL 118 251302	D.S. Akerib *et al.*	(LUX Collab.)
ALBERT	17A	PL B769 249	A. Albert *et al.*	(ANTARES Collab.)
Also		PL B796 253 (errat.)	A. Albert *et al.*	(ANTARES Collab.)
AMOLE	17	PRL 118 251301	C. Amole *et al.*	(PICO Collab.)
ANGLOHER	17A	EPJ C77 637	G. Angloher *et al.*	(CRESST Collab.)
APRILE	17	PRL 118 101101	E. Aprile *et al.*	(XENON100 Collab.)
APRILE	17A	PR D96 022008	E. Aprile *et al.*	(XENON100 Collab.)
APRILE	17D	PR D96 042004	E. Aprile *et al.*	(XENON100 Collab.)
APRILE	17G	PRL 119 181301	E. Aprile *et al.*	(XENON Collab.)
APRILE	17H	PR D96 122002	E. Aprile *et al.*	(XENON100 Collab.)
APRILE	17K	JCAP 1710 039	E. Aprile *et al.*	(XENON100 Collab.)
ARCHAMBAU...	17	PR D95 082001	S. Archambault *et al.*	(VERITAS Collab.)
AVRORIN	17	JETP 125 80	A.D. Avrorin *et al.*	(BAIKAL Collab.)
BANERJEE	17	PRL 118 011802	D. Banerjee *et al.*	(NA64 Collab.)
BARBOSA-D...	17	PR D95 032006	E. Barbosa de Souza *et al.*	(DM17 Collab.)
BATTAT	17	ASP 91 65	J.B.R. Battat *et al.*	(DRIFT-IId Collab.)
BEHNKE	17	ASP 90 85	E. Behnke *et al.*	(PICASSO Collab.)
BOUDAUD	17	PRL 119 021103	M. Boudaud, J. Lavalle, P. Salati	
CHEN	17E	PR D96 102007	X. Chen *et al.*	(PandaX-II Collab.)
CUI	17A	PRL 119 181302	X. Cui *et al.*	(PandaX-II Collab.)

Int. J. Mod. Phys. A 2026.41. Downloaded from www.worldscientific.com
by UNIVERSITY OF CALIFORNIA @ BERKELEY on 09/16/26. Re-use and distribution is strictly not permitted, except for Open Access articles.

FU	17	PRL 118 071301	C. Fu *et al.*	(PandaX-II Collab.)
Also		PRL 120 049902 (errat.)	C. Fu *et al.*	(PandaX-II Collab.)
KHACHATRY...	17A	PRL 118 021802	V. Khachatryan *et al.*	(CMS Collab.)
KHACHATRY...	17F	JHEP 1702 135	V. Khachatryan *et al.*	(CMS Collab.)
SIRUNYAN	17	JHEP 1703 061	A.M. Sirunyan *et al.*	(CMS Collab.)
SIRUNYAN	17AP	JHEP 1710 180	A.M. Sirunyan *et al.*	(CMS Collab.)
SIRUNYAN	17AQ	JHEP 1710 073	A.M. Sirunyan *et al.*	(CMS Collab.)
SIRUNYAN	17BB	EPJ C77 845	A.M. Sirunyan *et al.*	(CMS Collab.)
SIRUNYAN	17G	JHEP 1707 014	A.M. Sirunyan *et al.*	(CMS Collab.)
SIRUNYAN	17U	JHEP 1709 106	A.M. Sirunyan *et al.*	(CMS Collab.)
AABOUD	16AD	PL B763 251	M. Aaboud *et al.*	(ATLAS Collab.)
AABOUD	16D	PR D94 032005	M. Aaboud *et al.*	(ATLAS Collab.)
AABOUD	16F	JHEP 1606 059	M. Aaboud *et al.*	(ATLAS Collab.)
AAD	16AF	JHEP 1601 172	G. Aad *et al.*	(ATLAS Collab.)
AAD	16AG	JHEP 1602 062	G. Aad *et al.*	(ATLAS Collab.)
AAD	16M	PR D93 072007	G. Aad *et al.*	(ATLAS Collab.)
AARTSEN	16C	JCAP 1604 022	M.G. Aartsen *et al.*	(IceCube Collab.)
AARTSEN	16D	EPJ C76 531	M.G. Aartsen *et al.*	(IceCube Collab.)
ABDALLAH	16	PRL 117 111301	H. Abdallah *et al.*	(H.E.S.S. Collab.)
ABDALLAH	16A	PRL 117 151302	H. Abdallah *et al.*	(H.E.S.S. Collab.)
ADRIAN-MAR...	16	PL B759 69	S. Adrian-Martinez *et al.*	(ANTARES Collab.)
ADRIAN-MAR...	16B	JCAP 1605 016	S. Adrian-Martinez *et al.*	(ANTARES Collab.)
AGNES	16	PR D93 081101	P. Agnes *et al.*	(DarkSide-50 Collab.)
AGNESE	16	PRL 116 071301	R. Agnese *et al.*	(SuperCDMS Collab.)
AGUILAR-AR...	16	PR D94 082006	A. Aguilar-Arevalo *et al.*	(DAMIC Collab.)
AHNEN	16	JCAP 1602 039	M.L. Ahnen *et al.*	(MAGIC and Fermi-LAT Collab.)
AKERIB	16	PRL 116 161301	D.S. Akerib *et al.*	(LUX Collab.)
AKERIB	16A	PRL 116 161302	D.S. Akerib *et al.*	(LUX Collab.)
AMOLE	16	PR D93 052014	C. Amole *et al.*	(PICO Collab.)
AMOLE	16A	PR D93 061101	C. Amole *et al.*	(PICO Collab.)
ANGLOHER	16	EPJ C76 25	G. Angloher *et al.*	(CRESST-II Collab.)
ANGLOHER	16A	PRL 117 021303	G. Angloher *et al.*	(CRESST-II Collab.)
APRILE	16	PR D94 092001	E. Aprile *et al.*	(XENON100 Collab.)
APRILE	16B	PR D94 122001	E. Aprile *et al.*	(XENON100 Collab.)
ARMENGAUD	16	JCAP 1605 019	E. Armengaud *et al.*	(EDELWEISS-III Collab.)
AVRORIN	16	ASP 81 12	A.D. Avrorin *et al.*	(BAIKAL Collab.)
CAPUTO	16	PR D93 062004	R. Caputo *et al.*	
FORNASA	16	PR D94 123005	M. Fornasa *et al.*	(Fermi-LAT Collab.)
HEHN	16	EPJ C76 548	L. Hehn *et al.*	(EDELWEISS-III Collab.)
KHACHATRY...	16AJ	PR D93 052011	V. Khachatryan *et al.*	(CMS Collab.)
KHACHATRY...	16BZ	JHEP 1612 083	V. Khachatryan *et al.*	(CMS Collab.)
Also		JHEP 1708 035 (errat.)	V. Khachatryan *et al.*	(CMS Collab.)
KHACHATRY...	16CA	JHEP 1612 088	V. Khachatryan *et al.*	(CMS Collab.)
KHACHATRY...	16N	PL B755 102	V. Khachatryan *et al.*	(CMS Collab.)
LEITE	16	JCAP 1611 021	N. Leite *et al.*	
LI	16	PR D93 043518	S. Li *et al.*	
LI	16A	JCAP 1612 028	Z. Li *et al.*	
LIANG	16	PR D94 103502	Y.-F. Liang *et al.*	
LU	16	PR D93 103517	B-Q. Lu, H-S. Zong	
SHIRASAKI	16	PR D94 063522	M. Shirasaki *et al.*	
TAN	16	PR D93 122009	T.H. Tan *et al.*	(PandaX Collab.)
TAN	16B	PRL 117 121303	A. Tan *et al.*	(PandaX Collab.)
ZHAO	16	PR D93 092003	W. Zhao *et al.*	(CDEX Collab.)
AAD	15AS	EPJ C75 92	G. Aad *et al.*	(ATLAS Collab.)
AAD	15BH	EPJ C75 299	G. Aad *et al.*	(ATLAS Collab.)
Also		EPJ C75 408 (errat.)	G. Aad *et al.*	(ATLAS Collab.)
AAD	15CF	PRL 115 131801	G. Aad *et al.*	(ATLAS Collab.)
AAD	15CS	PR D91 012008	G. Aad *et al.*	(ATLAS Collab.)
Also		PR D92 059903 (errat.)	G. Aad *et al.*	(ATLAS Collab.)
AARTSEN	15C	EPJ C75 20	M.G. Aartsen *et al.*	(IceCube Collab.)
AARTSEN	15E	EPJ C75 492	M.G. Aartsen *et al.*	(IceCube Collab.)
ABRAMOWSKI	15	PRL 114 081301	A. Abramowski *et al.*	(H.E.S.S. Collab.)
ACKERMANN	15	PR D91 122002	M. Ackermann *et al.*	(Fermi-LAT Collab.)
ACKERMANN	15A	JCAP 1509 008	M. Ackermann *et al.*	(Fermi-LAT Collab.)
ACKERMANN	15B	PRL 115 231301	M. Ackermann *et al.*	(Fermi-LAT Collab.)
ADRIAN-MAR...	15	JCAP 1510 068	S. Adrian-Martinez *et al.*	(ANTARES Collab.)
AGNES	15	PL B743 456	P. Agnes *et al.*	(DarkSide-50 Collab.)
AGNESE	15A	PR D91 052021	R. Agnese *et al.*	(SuperCDMS Collab.)
AGNESE	15B	PR D92 072003	R. Agnese *et al.*	(SuperCDMS Collab.)
AMOLE	15	PRL 114 231302	C. Amole *et al.*	(PICO Collab.)
APRILE	15	PRL 115 091302	E. Aprile *et al.*	(XENON Collab.)
APRILE	15A	SCI 349 851	E. Aprile *et al.*	(XENON Collab.)
CHOI	15	PRL 114 141301	K. Choi *et al.*	(Super-Kamiokande Collab.)
KHACHATRY...	15AG	JHEP 1506 121	V. Khachatryan *et al.*	(CMS Collab.)
KHACHATRY...	15AL	EPJ C75 235	V. Khachatryan *et al.*	(CMS Collab.)
KHACHATRY...	15T	PR D91 092005	V. Khachatryan *et al.*	(CMS Collab.)
NAKAMURA	15	PTEP 2015 4 043F01	K. Nakamura *et al.*	(NEWAGE Collab.)
XIAO	15	PR D92 052004	X. Xiao *et al.*	(PandaX Collab.)
AAD	14AI	JHEP 1409 037	G. Aad *et al.*	(ATLAS Collab.)
AAD	14BK	PRL 112 041802	G. Aad *et al.*	(ATLAS Collab.)
AAD	14K	PR D90 012004	G. Aad *et al.*	(ATLAS Collab.)
AAD	14O	PRL 112 201802	G. Aad *et al.*	(ATLAS Collab.)
ACKERMANN	14	PR D89 042001	M. Ackermann *et al.*	(Fermi-LAT Collab.)
AGNESE	14	PRL 112 241302	R. Agnese *et al.*	(SuperCDMS Collab.)
AGNESE	14A	PRL 112 041302	R. Agnese *et al.*	(SuperCDMS Collab.)
AKERIB	14	PRL 112 091303	D.S. Akerib *et al.*	(LUX Collab.)
ALEKSIC	14	JCAP 1402 008	J. Aleksic *et al.*	(MAGIC Collab.)
ANGLOHER	14	EPJ C74 3184	G. Angloher *et al.*	(CRESST-II Collab.)
APRILE	14A	ASP 54 11	E. Aprile *et al.*	(XENON100 Collab.)
AVRORIN	14	ASP 62 12	A.D. Avrorin *et al.*	(BAIKAL Collab.)
FELIZARDO	14	PR D89 072013	M. Felizardo *et al.*	(SIMPLE Collab.)
LEE	14A	PR D90 052006	H.S. Lee *et al.*	(KIMS Collab.)
LIU	14A	PR D90 032003	S.K. Liu *et al.*	(CDEX Collab.)
UCHIDA	14	PTEP 2014 063C01	H. Uchida *et al.*	(XMASS Collab.)
YUE	14	PR D90 091701	Q. Yue *et al.*	(CDEX Collab.)
AAD	13AD	JHEP 1304 075	G. Aad *et al.*	(ATLAS Collab.)
AAD	13C	PRL 110 011802	G. Aad *et al.*	(ATLAS Collab.)
AALSETH	13	PR D88 012002	C.E. Aalseth *et al.*	(CoGeNT Collab.)
AARTSEN	13	PRL 110 131302	M.G. Aartsen *et al.*	(IceCube Collab.)
AARTSEN	13C	PR D88 122001	M.G. Aartsen *et al.*	(IceCube Collab.)
ABE	13B	PL B719 78	K. Abe *et al.*	(XMASS Collab.)
ABRAMOWSKI	13	PRL 110 041301	A. Abramowski *et al.*	(H.E.S.S. Collab.)
ACKERMANN	13A	PR D88 082002	M. Ackermann *et al.*	(Fermi-LAT Collab.)
ADRIAN-MAR...	13	JCAP 1311 032	S. Adrian-Martinez *et al.*	(ANTARES Collab.)
AGNESE	13	PR D88 031104	R. Agnese *et al.*	(CDMS Collab.)
AGNESE	13A	PRL 111 251301	R. Agnese *et al.*	(CDMS Collab.)
APRILE	13	PRL 111 021301	E. Aprile *et al.*	(XENON100 Collab.)
BERNABEI	13A	EPJ C73 2648	R. Bernabei *et al.*	(DAMA Collab.)
BOLIEV	13	JCAP 1309 019	M. Boliev *et al.*	
LI	13B	PRL 110 261301	H.B. Li *et al.*	(TEXONO Collab.)
SUVOROVA	13	PAN 76 1367	O.V. Suvorova *et al.*	(INRM)
		Translated from YAF 76 1433.		
ZHAO	13	PR D88 052004	W. Zhao *et al.*	(CDEX Collab.)
AALTONEN	12K	PRL 108 201802	T. Aaltonen *et al.*	(CDF Collab.)
AALTONEN	12M	PRL 108 211804	T. Aaltonen *et al.*	(CDF Collab.)
ABBASI	12	PR D85 042002	R. Abbasi *et al.*	(IceCube Collab.)
ABRAMOWSKI	12	APJ 750 123	A. Abramowski *et al.*	(H.E.S.S. Collab.)
ACKERMANN	12	PR D86 022002	M. Ackermann *et al.*	(Fermi-LAT Collab.)
AKIMOV	12	PL B709 14	D.Yu. Akimov *et al.*	(ZEPLIN-III Collab.)
ALIU	12	PR D85 062001	E. Aliu *et al.*	(VERITAS Collab.)
ANGLOHER	12	EPJ C72 1971	G. Angloher *et al.*	(CRESST-II Collab.)
APRILE	12	PRL 109 181301	E. Aprile *et al.*	(XENON100 Collab.)
ARCHAMBAU...	12	PL B711 153	S. Archambault *et al.*	(PICASSO Collab.)
ARMENGAUD	12	PR D86 051701	E. Armengaud *et al.*	(EDELWEISS Collab.)
BARRETO	12	PL B711 264	J. Barreto *et al.*	(DAMIC Collab.)
BEHNKE	12	PR D86 052001	E. Behnke *et al.*	(COUPP Collab.)
Also		PR D90 079902 (errat.)	E. Behnke *et al.*	(COUPP Collab.)
BROWN	12	PR D85 021301	A. Brown *et al.*	(OXF)
CHATRCHYAN	12AP	JHEP 1209 094	S. Chatrchyan *et al.*	(CMS Collab.)
CHATRCHYAN	12T	PRL 108 261803	S. Chatrchyan *et al.*	(CMS Collab.)
DAHL	12	PRL 108 259001	C.E. Dahl, J. Hall, W.H. Lippincott	(CHIC, FNAL)
DAW	12	ASP 35 397	E. Daw *et al.*	(DRIFT-IId Collab.)
FELIZARDO	12	PRL 108 201302	M. Felizardo *et al.*	(SIMPLE Collab.)
KIM	12	PRL 108 181301	S.C. Kim *et al.*	(KIMS Collab.)
AALSETH	11	PRL 106 131301	C.E. Aalseth *et al.*	(CoGeNT Collab.)
AALSETH	11A	PRL 107 141301	C.E. Aalseth *et al.*	(CoGeNT Collab.)
ABBASI	11C	PR D84 022004	R. Abbasi *et al.*	(IceCube Collab.)
ABRAMOWSKI	11	PRL 106 161301	A. Abramowski *et al.*	(H.E.S.S. Collab.)
ACKERMANN	11	PRL 107 241302	M. Ackermann *et al.*	(Fermi-LAT Collab.)
AHLEN	11	PL B695 124	S. Ahlen *et al.*	(DMTPC Collab.)
AHMED	11	PR D83 112002	Z. Ahmed *et al.*	(CDMS Collab.)
AHMED	11A	PR D84 011102	Z. Ahmed *et al.*	(CDMS and EDELWEISS Collabs.)
AHMED	11B	PRL 106 131302	Z. Ahmed *et al.*	(CDMS Collab.)
AJELLO	11	PR D84 032007	M. Ajello *et al.*	(Fermi-LAT Collab.)
ANGLE	11	PRL 107 051301	J. Angle *et al.*	(XENON10 Collab.)
Also		PRL 110 249901 (errat.)	J. Angle *et al.*	(XENON10 Collab.)
APRILE	11	PR D84 052003	E. Aprile *et al.*	(XENON100 Collab.)
APRILE	11A	PR D84 061101	E. Aprile *et al.*	(XENON100 Collab.)
APRILE	11B	PRL 107 131302	E. Aprile *et al.*	(XENON100 Collab.)
ARMENGAUD	11	PL B702 329	E. Armengaud *et al.*	(EDELWEISS-II Collab.)
BEHNKE	11	PRL 106 021303	E. Behnke *et al.*	(COUPP Collab.)
GERINGER-SA...	11	PRL 107 241303	A. Geringer-Sameth, S.M. Koushiappas	
HORN	11	PL B705 471	M. Horn *et al.*	(ZEPLIN-III Collab.)
TANAKA	11	APJ 742 78	T. Tanaka *et al.*	(Super-Kamiokande Collab.)
ABBASI	10	PR D81 057101	R. Abbasi *et al.*	(IceCube Collab.)
AHMED	10	SCI 327 1619	Z. Ahmed *et al.*	(CDMS II Collab.)
AKERIB	10	PR D82 122004	D.S. Akerib *et al.*	(CDMS II Collab.)
AKIMOV	10	PL B692 180	D.Yu. Akimov *et al.*	(ZEPLIN-III Collab.)
APRILE	10	PRL 105 131302	E. Aprile *et al.*	(XENON100 Collab.)
ARMENGAUD	10	PL B687 294	E. Armengaud *et al.*	(EDELWEISS-II Collab.)
FELIZARDO	10	PRL 105 211301	M. Felizardo *et al.*	(The SIMPLE Collab.)
MIUCHI	10	PL B686 11	K. Miuchi *et al.*	(NEWAGE Collab.)
ABBASI	09B	PRL 102 201302	R. Abbasi *et al.*	(IceCube Collab.)
AHMED	09	PRL 102 011301	Z. Ahmed *et al.*	(CDMS Collab.)
ANGLE	09	PR D80 115005	J. Angle *et al.*	(XENON10 Collab.)
ANGLOHER	09	ASP 31 270	G. Angloher *et al.*	(CRESST Collab.)
ARCHAMBAU...	09	PL B682 185	S. Archambault *et al.*	(PICASSO Collab.)
LEBEDENKO	09A	PRL 103 151302	V.N. Lebedenko *et al.*	(ZEPLIN-III Collab.)
LIN	09	PR D79 061101	S.T. Lin *et al.*	(TEXONO Collab.)
AALSETH	08	PRL 101 251301	C.E. Aalseth *et al.*	(CoGeNT Collab.)
Also		PRL 102 109903 (errat.)	C.E. Aalseth *et al.*	(CoGeNT Collab.)
ANGLE	08A	PRL 101 091301	J. Angle *et al.*	(XENON10 Collab.)
BEDNYAKOV	08	PAN 71 111	V.A. Bednyakov, H.P. Klapdor-Kleingrothaus, I.V. Krivosheina	
		Translated from YAF 71 112.		
ALNER	07	PL B653 161	G.J. Alner *et al.*	(ZEPLIN-II Collab.)
LEE	07A	PRL 99 091301	H.S. Lee *et al.*	(KIMS Collab.)
MIUCHI	07	PL B654 58	K. Miuchi *et al.*	
AKERIB	06	PR D73 011102	D.S. Akerib *et al.*	(CDMS Collab.)
SHIMIZU	06A	PL B633 195	Y. Shimizu *et al.*	
AKERIB	05	PR D72 052009	D.S. Akerib *et al.*	(CDMS Collab.)
ALNER	05	PL B616 17	G.J. Alner *et al.*	(UK Dark Matter Collab.)
BARNABE-HE...	05	PL B624 186	M. Barnabe-Heider *et al.*	(PICASSO Collab.)
BENOIT	05	PL B616 25	A. Benoit *et al.*	(EDELWEISS Collab.)
GIRARD	05	PL B621 233	T.A. Girard *et al.*	(SIMPLE Collab.)
GIULIANI	05	PRL 95 101301	F. Giuliani	
GIULIANI	05A	PR D71 123503	F. Giuliani, T.A. Girard	
KLAPDOR-K...	05	PL B609 226	H.V. Klapdor-Kleingrothaus, I.V. Krivosheina, C. Tomei	
GIULIANI	04	PL B588 151	F. Giuliani, T.A. Girard	
GIULIANI	04A	PRL 93 161301	F. Giuliani	
MIUCHI	03	ASP 19 135	K. Miuchi *et al.*	
TAKEDA	03	PL B572 145	A. Takeda *et al.*	
ANGLOHER	02	ASP 18 43	G. Angloher *et al.*	(CRESST Collab.)
BELLI	02	PR D66 043503	P. Belli *et al.*	
BERNABEI	02C	EPJ C23 61	R. Bernabei *et al.*	(DAMA Collab.)
GREEN	02	PR D66 083003	A.M. Green	
BAUDIS	01	PR D63 022001	L. Baudis *et al.*	(Heidelberg-Moscow Collab.)
SMITH	01	PR D64 043502	D. Smith, N. Weiner	
ULLIO	01	JHEP 0107 044	P. Ullio, M. Kamionkowski, P. Vogel	
BENOIT	00	PL B479 8	A. Benoit *et al.*	(EDELWEISS Collab.)
BERNABEI	00D	NJP 2 15	R. Bernabei *et al.*	(DAMA Collab.)
COLLAR	00	PRL 85 3083	J.I. Collar *et al.*	(SIMPLE Collab.)
AMBROSIO	99	PR D60 082002	M. Ambrosio *et al.*	(Macro Collab.)
BERNABEI	99	PL B450 448	R. Bernabei *et al.*	(DAMA Collab.)
BERNABEI	99D	PRL 83 4918	R. Bernabei *et al.*	(DAMA Collab.)
BRHLIK	99	PL B464 303	M. Brhlik, L. Roszkowski	
DERBIN	99	PAN 62 1886	A.V. Derbin *et al.*	
		Translated from YAF 62 2034.		
KLIMENKO	98	JETPL 67 875	A.A. Klimenko *et al.*	
		Translated from ZETFP 67 835.		
SARSA	97	PR D56 1856	M.L. Sarsa *et al.*	(ZARA)
ALESSAND...	96	PL B384 316	A. Alessandrello *et al.*	(MILA, MILAI, SASSO)
BELLI	96	PL B387 222	P. Belli *et al.*	(DAMA Collab.)
Also		PL B389 783 (errat.)	P. Belli *et al.*	(DAMA Collab.)
BELLI	96C	NC C19 537	P. Belli *et al.*	(DAMA Collab.)
BERNABEI	96	PL B389 757	R. Bernabei *et al.*	(DAMA Collab.)
COLLAR	96	PRL 76 331	J.I. Collar	(SCUC)
SARSA	96	PL B386 458	M.L. Sarsa *et al.*	(ZARA)
Also		PR D56 1856	M.L. Sarsa *et al.*	(ZARA)
SMITH	96	PL B379 299	P.F. Smith *et al.*	(RAL, SHEF, LOIC+)
SNOWDEN-...	96	PRL 76 332	D.P. Snowden-Ifft, E.S. Freeman, P.B. Price	(UCB)
GARCIA	95	PR D51 1458	E. Garcia *et al.*	(ZARA, SCUC, PNL)
QUENBY	95	PL B351 70	J.J. Quenby *et al.*	(LOIC, RAL, SHEF+)
SNOWDEN-...	95	PRL 74 4133	D.P. Snowden-Ifft, E.S. Freeman, P.B. Price	(UCB)
Also		PRL 76 331	J.I. Collar	(SCUC)
Also		PRL 76 332	D.P. Snowden-Ifft, E.S. Freeman, P.B. Price	(UCB)
BECK	94	PL B336 141	M. Beck *et al.*	(MPIK, KIAE, SASSO)
BACCI	92	PL B293 460	C. Bacci *et al.*	(Beijing-Roma-Saclay Collab.)
REUSSER	91	PL B255 143	D. Reusser *et al.*	(NEUC, CIT, PSI)
CALDWELL	88	PRL 61 510	D.O. Caldwell *et al.*	(UCSB, UCB, LBL)

Int. J. Mod. Phys. A 2026.41. Downloaded from www.worldscientific.com
by UNIVERSITY OF CALIFORNIA @ BERKELEY on 09/16/26. Re-use and distribution is strictly not permitted, except for Open Access articles.

Other Particle Searches

OMITTED FROM SUMMARY TABLE

OTHER PARTICLE SEARCHES

Revised February 2018 by K. Hikasa (Tohoku University).

We collect here those searches which do not appear in any other search categories. These are listed in the following order:

- Concentration of stable particles in matter
- General new physics searches
- Limits on jet-jet resonance in hadron collisions
- Limits on neutral particle production at accelerators
- Limits on charged particles in e^+e^- collisions
- Limits on charged particles in hadron reactions
- Limits on charged particles in cosmic rays
- Searches for quantum black hole production

Note that searches appear in separate sections elsewhere for Higgs bosons (and technipions), other heavy bosons (including W_R, W', Z', leptoquarks, axigluons), axions (including pseudo-Goldstone bosons, Majorons, familons), WIMPs, heavy leptons, heavy neutrinos, free quarks, monopoles, supersymmetric particles, and compositeness.

We no longer list for limits on tachyons and centauros. See our 1994 edition for these limits.

CONCENTRATION OF STABLE PARTICLES IN MATTER

Concentration of Heavy (Charge +1) Stable Particles in Matter

VALUE	CL%	DOCUMENT ID		TECN	COMMENT
• • • We do not use the following data for averages, fits, limits, etc. • • •					
$<4\times10^{-17}$	95	[1] YAMAGATA	93	SPEC	Deep sea water, M=5–1600m_p
$<6\times10^{-15}$	95	[2] VERKERK	92	SPEC	Water, M= 10^5 to 3×10^7 GeV
$<7\times10^{-15}$	95	[2] VERKERK	92	SPEC	Water, M= 10^4, 6×10^7 GeV
$<9\times10^{-15}$	95	[2] VERKERK	92	SPEC	Water, M= 10^8 GeV
$<3\times10^{-23}$	90	[3] HEMMICK	90	SPEC	Water, M = 1000m_p
$<2\times10^{-21}$	90	[3] HEMMICK	90	SPEC	Water, M = 5000m_p
$<3\times10^{-20}$	90	[3] HEMMICK	90	SPEC	Water, M = 10000m_p
$<1.\times10^{-29}$		SMITH	82B	SPEC	Water, M=30–400m_p
$<2.\times10^{-28}$		SMITH	82B	SPEC	Water, M=12–1000m_p
$<1.\times10^{-14}$		SMITH	82B	SPEC	Water, M >1000 m_p
$<(0.2–1.)\times10^{-21}$		SMITH	79	SPEC	Water, M=6–350 m_p

[1] YAMAGATA 93 used deep sea water at 4000 m since the concentration is enhanced in deep sea due to gravity.

[2] VERKERK 92 looked for heavy isotopes in sea water and put a bound on concentration of stable charged massive particle in sea water. The above bound can be translated into into a bound on charged dark matter particle (5×10^6 GeV), assuming the local density, ρ=0.3 GeV/cm^3, and the mean velocity $\langle v\rangle$=300 km/s.

[3] See HEMMICK 90 Fig. 7 for other masses 100–10000 m_p.

Concentration of Heavy Stable Particles Bound to Nuclei

VALUE	CL%	DOCUMENT ID		TECN	COMMENT
• • • We do not use the following data for averages, fits, limits, etc. • • •					
$<2\times10^{-17}$/nucleon	95	[1] AFEK	21		millicharged particle search
$<1.2\times10^{-11}$	95	[2] JAVORSEK	01	SPEC	Au, M= 3 GeV
$<6.9\times10^{-10}$	95	[2] JAVORSEK	01	SPEC	Au, M= 144 GeV
$<1\times10^{-11}$	95	[3] JAVORSEK	01B	SPEC	Au, M= 188 GeV
$<1\times10^{-8}$	95	[3] JAVORSEK	01B	SPEC	Au, M= 1669 GeV
$<6\times10^{-9}$	95	[3] JAVORSEK	01B	SPEC	Fe, M= 188 GeV
$<1\times10^{-8}$	95	[3] JAVORSEK	01B	SPEC	Fe, M= 647 GeV
$<4\times10^{-20}$	90	[4] HEMMICK	90	SPEC	C, M = 100m_p
$<8\times10^{-20}$	90	[4] HEMMICK	90	SPEC	C, M = 1000m_p
$<2\times10^{-16}$	90	[4] HEMMICK	90	SPEC	C, M = 10000m_p
$<6\times10^{-13}$	90	[4] HEMMICK	90	SPEC	Li, M = 1000m_p
$<1\times10^{-11}$	90	[4] HEMMICK	90	SPEC	Be, M = 1000m_p
$<6\times10^{-14}$	90	[4] HEMMICK	90	SPEC	B, M = 1000m_p
$<4\times10^{-17}$	90	[4] HEMMICK	90	SPEC	O, M = 1000m_p
$<4\times10^{-15}$	90	[4] HEMMICK	90	SPEC	F, M = 1000m_p
$<1.5\times10^{-13}$/nucleon	68	[5] NORMAN	89	SPEC	^{206}PbX^-
$<1.2\times10^{-12}$/nucleon	68	[5] NORMAN	87	SPEC	^{56,58}FeX^-

[1] AFEK 21 search for millicharged particles bound to matter using an optomechanical device. No signal was observed. Limits placed in the abundance vs. charge plane (Fig. 3). This is translated to the mass versus charge plane by requiring bound states to be stable.

[2] JAVORSEK 01 search for (neutral) SIMPs (strongly interacting massive particles) bound to Au nuclei. Here M is the effective SIMP mass.

[3] JAVORSEK 01B search for (neutral) SIMPs (strongly interacting massive particles) bound to Au and Fe nuclei from various origins with exposures on the earth's surface, in a satellite, heavy ion collisions, etc. Here M is the mass of the anomalous nucleus. See also JAVORSEK 02.

[4] See HEMMICK 90 Fig. 7 for other masses 100–10000 m_p.

[5] Bound valid up to $m_{X^-}\sim$ 100 TeV.

GENERAL NEW PHYSICS SEARCHES

This subsection lists some of the search experiments which look for general signatures characteristic of new physics, independent of the framework of a specific model.

The observed events are compatible with Standard Model expectation, unless noted otherwise.

VALUE	DOCUMENT ID		TECN	COMMENT
• • • We do not use the following data for averages, fits, limits, etc. • • •				
	[1] HAYRAPETY...	24AO	CMS	soft unclustered energy search
	[2] ALKHATIB	21A	SCDM	fractionally charged relics
	[3] AGUILAR-AR...	20B	CONN	ν elastic scatter on nuclei
	[4] FEDDERKE	20		CHAMPs from white dwarfs
	[5] SIRUNYAN	20A	CMS	SUSY/LQ search with mT2 or long-lived charged particles
	[6] ALCANTARA	19		Auger, superheavy DM
	[7] PORAYKO	18	PPTA	pulsar timing fuzzy DM search
	[8] AAD	15AT	ATLS	$t+\not{E}_T$
	[9] KHACHATRY...	15F	CMS	$t+\not{E}_T$
	[10] AALTONEN	14J	CDF	W + 2 jets
	[11] AAD	13A	ATLS	$WW\to\ell\nu\ell'\nu$
	[12] AAD	13C	ATLS	$\gamma+\not{E}_T$
	[13] AALTONEN	13I	CDF	Delayed $\gamma+\not{E}_T$
	[14] CHATRCHYAN	13	CMS	$\ell^+\ell^-$ + jets + $\not{E}_T$
	[15] AAD	12C	ATLS	$t\bar{t}+\not{E}_T$
	[16] AALTONEN	12M	CDF	jet + $\not{E}_T$
	[17] CHATRCHYAN	12AP	CMS	jet + $\not{E}_T$
	[18] CHATRCHYAN	12Q	CMS	Z + jets + $\not{E}_T$
	[19] CHATRCHYAN	12T	CMS	$\gamma+\not{E}_T$
	[20] AAD	11S	ATLS	jet + $\not{E}_T$
	[21] AALTONEN	11AF	CDF	$\ell^\pm\ell^\pm$
	[22] CHATRCHYAN	11C	CMS	$\ell^+\ell^-$ + jets + $\not{E}_T$
	[23] CHATRCHYAN	11U	CMS	jet + $\not{E}_T$
	[24] AALTONEN	10AF	CDF	$\gamma\gamma+\ell$, $\not{E}_T$
	[25] AALTONEN	09AF	CDF	$\ell\gamma b\not{E}_T$
	[26] AALTONEN	09G	CDF	$\ell\ell\ell\not{E}_T$

[1] HAYRAPETYAN 24AO report on search for soft unclustered energy deposits. No signal observed. Limits placed in mediator mass vs. decay temperature plane.

[2] ALKHATIB 21A search for lightly ionizing fractionally charged relics scattering from Ge. No signal observed. Limits plotted in fractional charge f vs. vertical intensity plane for m $\sim$ 5 MeV to 100 TeV.

[3] AGUILAR-AREVALO 20B search for light BSM mediator effect on ν elastic scatter on nuclei; no signal; limits placed in m(mediator) vs. coupling plane for two models of MeV-scale mediators.

[4] FEDDERKE 20 place limits on cosmic relic charged massive particles (CHAMPs) due to their capture and subsequent disruption of old white dwarf stars; limits placed in the m(CHAMP) vs. relic density parameter plane.

[5] SIRUNYAN 20A search for SUSY and LQ production using mT2 or presence of long-lived charged particle; no signal, limits placed in various mass planes for different BSM scenarios and various assumed lifetimes.

[6] ALCANTARA 19 place limits on m(WIMPzilla=X) vs lifetime from upper bound on ultra high energy cosmic rays at Auger experiment: e.g. $\tau(X)<4\times10^{22}$ yr for m(X) = 10^{16} GeV.

[7] PORAYKO 18 search for deviations in the residuals of pulsar timing data using PPTA. No signal observed. Limits set on fuzzy DM with $3\times10^{-24}<$ m(DM) $<2\times10^{-22}$ eV.

[8] AAD 15AT search for events with a top quark and mssing E_T in pp collisions at $E_{\rm cm}$ = 8 TeV with L = 20.3 fb^{-1}.

[9] KHACHATRYAN 15F search for events with a top quark and mssing E_T in pp collisions at $E_{\rm cm}$ = 8 TeV with L = 19.7 fb^{-1}.

[10] AALTONEN 14J examine events with a W and two jets in $p\bar{p}$ collisions at $E_{\rm cm}$ = 1.96 TeV with L = 8.9 fb^{-1}. Invariant mass distributions of the two jets are consistent with the Standard Model expectation.

[11] AAD 13A search for resonant WW production in pp collisions at $E_{\rm cm}$ = 7 TeV with L = 4.7 fb^{-1}.

[12] AAD 13C search for events with a photon and missing $\not{E}_T$ in pp collisions at $E_{\rm cm}$ = 7 TeV with L = 4.6 fb^{-1}.

[13] AALTONEN 13I search for events with a photon and missing E_T, where the photon is detected after the expected timing, in $p\bar{p}$ collisions at $E_{\rm cm}$ = 1.96 TeV with L = 6.3 fb^{-1}. The data are consistent with the Standard Model expectation.

[14] CHATRCHYAN 13 search for events with an opposite-sign lepton pair, jets, and missing E_T in pp collisions at $E_{\rm cm}$ = 7 TeV with L = 4.98 fb^{-1}.

[15] AAD 12C search for events with a $t\bar{t}$ pair and missing $\not{E}_T$ in pp collisions at $E_{\rm cm}$ = 7 TeV with L = 1.04 fb^{-1}.

[16] AALTONEN 12M search for events with a jet and missing E_T in $p\overline{p}$ collisions at E_{cm} = 1.96 TeV with L = 6.7 fb^{-1}.
[17] CHATRCHYAN 12AP search for events with a jet and missing E_T in pp collisions at E_{cm} = 7 TeV with L = 5.0 fb^{-1}.
[18] CHATRCHYAN 12Q search for events with a Z, jets, and missing $\not{E}_T$ in pp collisions at E_{cm} = 7 TeV with L = 4.98 fb^{-1}.
[19] CHATRCHYAN 12T search for events with a photon and missing $\not{E}_T$ in pp collisions at E_{cm} = 7 TeV with L = 5.0 fb^{-1}.
[20] AAD 11S search for events with one jet and missing E_T in pp collisions at E_{cm} = 7 TeV with L = 33 pb^{-1}.
[21] AALTONEN 11AF search for high-p_T like-sign dileptons in $p\overline{p}$ collisions at E_{cm} = 1.96 TeV with L = 6.1 fb^{-1}.
[22] CHATRCHYAN 11C search for events with an opposite-sign lepton pair, jets, and missing E_T in pp collisions at E_{cm} = 7 TeV with L = 34 pb^{-1}.
[23] CHATRCHYAN 11U search for events with one jet and missing E_T in pp collisions at E_{cm} = 7 TeV with L = 36 pb^{-1}.
[24] AALTONEN 10AF search for $\gamma\gamma$ events with e, μ, τ, or missing E_T in $p\overline{p}$ collisions at E_{cm} = 1.96 TeV with L = 1.1–2.0 fb^{-1}.
[25] AALTONEN 09AF search for $\ell\gamma b$ events with missing E_T in $p\overline{p}$ collisions at E_{cm} = 1.96 TeV with L = 1.9 fb^{-1}. The observed events are compatible with Standard Model expectation including $t\overline{t}\gamma$ production.
[26] AALTONEN 09G search for $\mu\mu\mu$ and $\mu\mu e$ events with missing E_T in $p\overline{p}$ collisions at E_{cm} = 1.96 TeV with L = 976 pb^{-1}.

LIMITS ON JET-JET RESONANCES

Heavy Particle Production Cross Section

Limits are for a particle decaying to two hadronic jets.

Units(pb)	CL%	Mass(GeV)	DOCUMENT ID		TECN	COMMENT
• • • We do not use the following data for averages, fits, limits, etc. • • •						
			[1] AAD	25AX	ATLS	BSM dijet search
			[2] AAD	25AZ	ATLS	dijet search
			[3] HAYRAPETY...	24G	CMS	trijet resonance search
			[4] TUMASYAN	23L	CMS	dijet resonance in 4-jet events
			[5] AAD	20AD	ATLS	pp at 13 TeV, dijet resonance
			[6] AAD	20T	ATLS	dijet resonance search
			[7] AAD	20W	ATLS	dijet resonance plus lepton
			[8] SIRUNYAN	20AI	CMS	dijet resonance search
			[9] AABOUD	19AJ	ATLS	$pp \to \gamma X$, $X \to jj$
			[10] SIRUNYAN	19B	CMS	$pp \to jA$, $A \to b\overline{b}$
			[11] SIRUNYAN	19CD	CMS	$pp \to Z'\gamma$, $Z' \to jj$
			[12] AABOUD	18AD	ATLS	$pp \to Y \to HX \to (bb) + (qq)$
			[13] AABOUD	18CK	ATLS	$pp \to bbb + \not{E}_T$
			[14] AABOUD	18CL	ATLS	$pp \to$ vector-like quarks
			[15] AABOUD	18N	ATLS	$pp \to jj$ resonance
			[16] SIRUNYAN	18DJ	CMS	$pp \to ZZ$ or $WZ \to \ell\overline{\ell}jj$
			[17] SIRUNYAN	18DY	CMS	$pp \to RR$; $R \to jj$
			[18] KHACHATRY...	17W	CMS	$pp \to jj$ resonance
			[19] KHACHATRY...	17Y	CMS	$pp \to$ (8–10) $j+\not{E}_T$
			[20] SIRUNYAN	17F	CMS	$pp \to jj$ angular distribution
			[21] AABOUD	16	ATLS	$pp \to b$ + jet
			[22] AAD	16N	ATLS	$pp \to$ 3 high E_T jets
			[23] AAD	16S	ATLS	$pp \to jj$ resonance
			[24] KHACHATRY...	16K	CMS	$pp \to jj$ resonance
			[25] KHACHATRY...	16L	CMS	$pp \to jj$ resonance
			[26] AAD	13D	ATLS	7 TeV $pp \to$ 2 jets
			[27] AALTONEN	13R	CDF	1.96 TeV $p\overline{p} \to$ 4 jets
			[28] CHATRCHYAN	13A	CMS	7 TeV $pp \to$ 2 jets
			[29] CHATRCHYAN	13A	CMS	7 TeV $pp \to b\overline{b}X$
			[30] AAD	12S	ATLS	7 TeV $pp \to$ 2 jets
			[31] CHATRCHYAN	12BL	CMS	7 TeV $pp \to t\overline{t}X$
			[32] AAD	11AG	ATLS	7 TeV $pp \to$ 2 jets
			[33] AALTONEN	11M	CDF	1.96 TeV $p\overline{p} \to W+$ 2 jets
			[34] ABAZOV	11I	D0	1.96 TeV $p\overline{p} \to W+$ 2 jets
			[35] AAD	10	ATLS	7 TeV $pp \to$ 2 jets
			[36] KHACHATRY...	10	CMS	7 TeV $pp \to$ 2 jets
			[37] ABE	99F	CDF	1.8 TeV $p\overline{p} \to b\overline{b}+$ anything
			[38] ABE	97G	CDF	1.8 TeV $p\overline{p} \to$ 2 jets
<2603	95	200	[39] ABE	93G	CDF	1.8 TeV $p\overline{p} \to$ 2 jets
< 44	95	400	[39] ABE	93G	CDF	1.8 TeV $p\overline{p} \to$ 2 jets
< 7	95	600	[39] ABE	93G	CDF	1.8 TeV $p\overline{p} \to$ 2 jets

[1] AAD 25AX report on search for BSM dijet events via $pp \to A \to BC$ using various signal regions and new physics models. Results from Fig. 6 place upper bounds on new physics expected cross sections for different models and signal regions.
[2] AAD 25AZ report on ATLAS dijet resonance search with 132 fb^{-1} using the trigger-level analysis. No signal observed. Limits are set on leptophobic Z' model in m(Z') vs coupling plane.
[3] HAYRAPETYAN 24G search for trijet resonance at CMS with 138 fb^{-1} of data at 13 TeV. No signal observed. Limits placed on various models vs mass(resonance).
[4] TUMASYAN 23L search for dijet resonance in 4-jet events with 138 fb^{-1} fb of data. There are two events in the tails of the distributions, each with a four-jet mass of 8 TeV and an average dijet mass of 2 TeV, resulting in local and global significances of 3.9 and 1.6 standard deviations, respectively, if interpreted as a signal. Limits set for simplified diquark model.
[5] AAD 20AD search for weakly supervised dijet resonance in ATLAS with 139 fb^{-1} at 13 TeV; no signal; various limits placed depending on kinematics and production cross section.
[6] AAD 20T search for dijet resonance with or without b-jets at 13 TeV and 139 fb^{-1}; no signal; limits placed in $\sigma \cdot$ BF vs mass plane for various BSM models.
[7] AAD 20W search for dijet resonance plus lepton with ATLAS at 13 TeV and 139 fb^{-1}; no signal; limits placed in $\sigma \cdot$ BF vs. mass plane for various BSM models.
[8] SIRUNYAN 20AI search for dijet resonance in CMS at 13 TeV with 137 fb^{-1}; no signal; limits set in σ vs. mass plane for various BSM models.
[9] AABOUD 19AJ search for low mass dijet resonance in $pp \to \gamma X$, $X \to jj$ at 13 TeV with 79.8 fb^{-1} of data; no signal found; limits placed on Z' model in coupling vs. m(Z') plane.
[10] SIRUNYAN 19B search for low mass resonance $pp \to jA$, $A \to b\overline{b}$ at 13 TeV using 35.9 fb^{-1}; no signal; exclude resonances 50–350 GeV depending on production and decay.
[11] SIRUNYAN 19CD search for $pp \to Z'\gamma$, $Z' \to jj$ with fat jet (jj); no signal, limits placed in m(Z') vs. coupling plane for Z' masses from 10 to 125 GeV.
[12] AABOUD 18AD search for new heavy particle $Y \to HX \to (bb) + (qq)$. No signal observed. Limits set on m(Y) vs. m(X) in the ranges of m(Y) in 1–4 TeV and m(X) in 50–1000 GeV.
[13] AABOUD 18CK search for SUSY Higgsinos in gauge-mediation via $pp \to bbb + \not{E}_T$ at 13 TeV using two complementary analyses with 24.3/36.1 fb^{-1}; no signal is found and Higgsinos with masses between 130 and 230 GeV and between 290 and 880 GeV are excluded at the 95% confidence level.
[14] AABOUD 18CL search for $pp \to$ vector-like quarks $\to$ jets at 13 TeV with 36 fb^{-1}; no signal seen; limits set on various VLQ scenarios. For pure $B \to Hb$ or $T \to Ht$, set the mass limit m > 1010 GeV.
[15] AABOUD 18N search for dijet resonance at Atlas with 13 TeV and 29.3 fb^{-1}; limits set on m(Z') in the mass range of 450–1800 GeV.
[16] SIRUNYAN 18DJ search for $pp \to ZZ$ or $WZ \to \ell\overline{\ell}jj$ resonance at 13 TeV, 35.9 fb^{-1}; no signal; limits set in the 400–4500 GeV mass range, exclusion of W' up to 2270 GeV in the HVT model A, and up to 2330 GeV for HVT model B. WED bulk graviton exclusion up to 925 GeV.
[17] SIRUNYAN 18DY search for $pp \to RR$; $R \to jj$ two dijet resonances at 13 TeV 35.9 fb^{-1}; no signal; limits placed on RPV top-squark pair production.
[18] KHACHATRYAN 17W search for dijet resonance in 12.9 fb^{-1} data at 13 TeV; see Fig. 2 for limits on axigluons, diquarks, dark matter mediators etc.
[19] KHACHATRYAN 17Y search for $pp \to$ (8–10) j in 19.7 fb^{-1} at 8 TeV. No signal seen. Limits set on colorons, axigluons, RPV, and SUSY.
[20] SIRUNYAN 17F measure $pp \to jj$ angular distribution in 2.6 fb^{-1} at 13 TeV; limits set on LEDs and quantum black holes.
[21] AABOUD 16 search for resonant dijets including one or two b-jets with 3.2 fb^{-1} at 13 TeV; exclude excited b^* quark from 1.1–2.1 TeV; exclude leptophilic Z' with SM couplings from 1.1–1.5 TeV.
[22] AAD 16N search for $\geq$ 3 jets with 3.6 fb^{-1} at 13 TeV; limits placed on micro black holes (Fig. 10) and string balls (Fig. 11).
[23] AAD 16S search for high mass jet-jet resonance with 3.6 fb^{-1} at 13 TeV; exclude portions of excited quarks, W', Z' and contact interaction parameter space.
[24] KHACHATRYAN 16K search for dijet resonance in 2.4 fb^{-1} data at 13 TeV; see Fig. 3 for limits on axigluons, diquarks etc.
[25] KHACHATRYAN 16L use data scouting technique to search for jj resonance on 18.8 fb^{-1} of data at 8 TeV. Limits on the coupling of a leptophobic Z' to quarks are set, improving on the results by other experiments in the mass range between 500–800 GeV.
[26] AAD 13D search for dijet resonances in pp collisions at E_{cm} = 7 TeV with L = 4.8 fb^{-1}. The observed events are compatible with Standard Model expectation. See their Fig. 6 and Table 2 for limits on resonance cross section in the range m = 1.0–4.0 TeV.
[27] AALTONEN 13R search for production of a pair of jet-jet resonances in $p\overline{p}$ collisions at E_{cm} = 1.96 TeV with L = 6.6 fb^{-1}. See their Fig. 5 and Tables I, II for cross section limits.
[28] CHATRCHYAN 13A search for qq, qg, and gg resonances in pp collisions at E_{cm} = 7 TeV with L = 4.8 fb^{-1}. See their Fig. 3 and Table 1 for limits on resonance cross section in the range m = 1.0–4.3 TeV.
[29] CHATRCHYAN 13A search for $b\overline{b}$ resonances in pp collisions at E_{cm} = 7 TeV with L = 4.8 fb^{-1}. See their Fig. 8 and Table 4 for limits on resonance cross section in the range m = 1.0–4.0 TeV.
[30] AAD 12S search for dijet resonances in pp collisions at E_{cm} = 7 TeV with L = 1.0 fb^{-1}. See their Fig. 3 and Table 2 for limits on resonance cross section in the range m = 0.9–4.0 TeV.
[31] CHATRCHYAN 12BL search for $t\overline{t}$ resonances in pp collisions at E_{cm} = 7 TeV with L = 4.4 fb^{-1}. See their Fig. 4 for limits on resonance cross section in the range m = 0.5–3.0 TeV.
[32] AAD 11AG search for dijet resonances in pp collisions at E_{cm} = 7 TeV with L = 36 pb^{-1}. Limits on number of events for m = 0.6–4 TeV are given in their Table 3.
[33] AALTONEN 11M find a peak in two jet invariant mass distribution around 140 GeV in W + 2 jet events in $p\overline{p}$ collisions at E_{cm} = 1.96 TeV with L = 4.3 fb^{-1}.
[34] ABAZOV 11I search for two-jet resonances in W + 2 jet events in $p\overline{p}$ collisions at E_{cm} = 1.96 TeV with L = 4.3 fb^{-1} and give limits σ < (2.6–1.3) pb (95% CL) for m = 110–170 GeV. The result is incompatible with AALTONEN 11M.
[35] AAD 10 search for narrow dijet resonances in pp collisions at E_{cm} = 7 TeV with L = 315 nb^{-1}. Limits on the cross section in the range 10–10^3 pb is given for m = 0.3–1.7 TeV.
[36] KHACHATRYAN 10 search for narrow dijet resonances in pp collisions at E_{cm} = 7 TeV with L = 2.9 pb^{-1}. Limits on the cross section in the range 1–300 pb is given for m = 0.5–2.6 TeV separately in the final states qq, qg, and gg.
[37] ABE 99F search for narrow $b\overline{b}$ resonances in $p\overline{p}$ collisions at E_{cm}=1.8 TeV. Limits on $\sigma(p\overline{p} \to X+$ anything)$\times$B($X \to b\overline{b}$) in the range 3–10^3 pb (95%CL) are given for m_X=200–750 GeV. See their Table I.
[38] ABE 97G search for narrow dijet resonances in $p\overline{p}$ collisions with 106 pb^{-1} of data at E_{cm} = 1.8 TeV. Limits on $\sigma(p\overline{p} \to X+$ anything)$\cdot$B($X \to jj$) in the range 10^4–10^{-1} pb (95%CL) are given for dijet mass m=200–1150 GeV with both jets having $|\eta| < 2.0$ and the dijet system having $|\cos\theta^*| < 0.67$. See their Table I for the list of limits. Supersedes ABE 93G.
[39] ABE 93G give cross section times branching ratio into light (d, u, s, c, b) quarks for Γ = 0.02 M. Their Table II gives limits for M = 200–900 GeV and Γ = (0.02–0.2) M.

Int. J. Mod. Phys. A 2026.41. Downloaded from www.worldscientific.com
by UNIVERSITY OF CALIFORNIA @ BERKELEY on 09/16/26. Re-use and distribution is strictly not permitted, except for Open Access articles.

Int. J. Mod. Phys. A 2026.41. Downloaded from www.worldscientific.com by UNIVERSITY OF CALIFORNIA @ BERKELEY on 09/16/26. Re-use and distribution is strictly not permitted, except for Open Access articles.

LIMITS ON NEUTRAL PARTICLE PRODUCTION

Production Cross Section of Radiatively-Decaying Neutral Particle

VALUE (pb)	CL%	DOCUMENT ID		TECN	COMMENT
• • • We do not use the following data for averages, fits, limits, etc. • • •					
		[1] AAD	24AT	ATLS	$h \to$ ALPs search
		[2] ALBERT	18C	HAWC	γ from Sun
		[3] KHACHATRY...	17D	CMS	$Z\gamma$ resonance
<0.0008	95	[4] AAD	16AI	ATLS	$pp \to \gamma$ + jet
		[5] KHACHATRY...	16M	CMS	$pp \to \gamma\gamma$ resonance
$<(0.043–0.17)$	95	[6] ABBIENDI	00D	OPAL	$e^+e^- \to X^0Y^0$, $X^0 \to Y^0\gamma$
$<(0.05–0.8)$	95	[7] ABBIENDI	00D	OPAL	$e^+e^- \to X^0X^0$, $X^0 \to Y^0\gamma$
$<(2.5–0.5)$	95	[8] ACKERSTAFF	97B	OPAL	$e^+e^- \to X^0Y^0$, $X^0 \to Y^0\gamma$
$<(1.6–0.9)$	95	[9] ACKERSTAFF	97B	OPAL	$e^+e^- \to X^0X^0$, $X^0 \to Y^0\gamma$

[1] AAD 24AT search for $h \to$ ALPs with ALP $\to \gamma\gamma$. No signal observed. Limits placed in BF(h) vs. m(ALP) plane.

[2] ALBERT 18C search for WIMP annihilation in Sun to long-lived, radiatively decaying mediator; no signal; limits set on $\sigma^{SD}(\chi p)$ assuming long-lived mediator.

[3] KHACHATRYAN 17D search for new scalar resonance decaying to $Z\gamma$ with $Z \to e^+e^-$, $\mu^+\mu^-$ in pp collisions at 8 and 13 TeV; no signal seen.

[4] AAD 16AI search for excited quarks (EQ) and quantum black holes (QBH) in 3.2 fb^{-1} at 13 TeV of data; exclude EQ below 4.4 TeV and QBH below 3.8 (6.2) TeV for RS1 (ADD) models. The visible cross section limit was obtained for 5 TeV resonance with $\sigma_G/M_G = 2\%$.

[5] KHACHATRYAN 16M search for $\gamma\gamma$ resonance using 19.7 fb^{-1} at 8 TeV and 3.3 fb^{-1} at 13 Tev; slight excess at 750 GeV noted; limit set on RS graviton.

[6] ABBIENDI 00D associated production limit is for m_{X^0}= 90–188 GeV, m_{Y^0}=0 at E_{cm}=189 GeV. See also their Fig. 9.

[7] ABBIENDI 00D pair production limit is for m_{X^0} = 45–94 GeV, m_{Y^0}=0 at E_{cm}=189 GeV. See also their Fig. 12.

[8] ACKERSTAFF 97B associated production limit is for m_{X^0} = 80–160 GeV, m_{Y^0}=0 from 10.0 pb^{-1} at E_{cm} = 161 GeV. See their Fig. 3(a).

[9] ACKERSTAFF 97B pair production limit is for m_{X^0} = 40–80 GeV, m_{Y^0}=0 from 10.0 pb^{-1} at E_{cm} = 161 GeV. See their Fig. 3(b).

Heavy Particle Production Cross Section

VALUE (cm^2/N)	CL%	DOCUMENT ID		TECN	COMMENT
• • • We do not use the following data for averages, fits, limits, etc. • • •					
		[1] AFANACIEV	25	MEG	X17 nuclear emission
		[2] ALRAHMAN	25	ICAR	LLP decay to dimuons
		[3] HAYRAPETY...	25O	CMS	heavy neutral lepton search
		[4] AAD	24AE	ATLS	heavy vector triplet search
		[5] AAD	24BV	ATLS	VBF di-Higgs to $4b$ events
		[6] AAD	24CD	ATLS	hadronic W/Z + MET
		[7] AAD	24E	ATLS	resonance search
		[8] AAD	24S	ATLS	QBH via lepton + jet
		[9] HAYRAPETY...	24AB	CMS	heavy neutral lepton search
		[10] HAYRAPETY...	24AC	CMS	heavy neutrino from B-decay
		[11] HAYRAPETY...	24AZ	CMS	four-muon events search
		[12] AAD	23P	ATLS	exotica search in association with $h \to \gamma\gamma$
		[13] TUMASYAN	23BC	CMS	γ-jet resonance search
		[14] TUMASYAN	23BF	CMS	$pp + \gamma/Z + X$ search
		[15] TUMASYAN	22AG	CMS	SIMP search
		[16] AAD	21F	ATLS	monojet search
		[17] AAIJ	20AL	LHCB	pp at 13 TeV, dimuon resonance
		[18] SIRUNYAN	20AY	CMS	$\Upsilon(1S)\mu^+\mu^-$ decay states
		[19] SIRUNYAN	20Z	CMS	multilepton BSM search, 13 TeV
		[20] AABOUD	19H	ATLS	di-photon-jet resonance
		[21] AABOUD	19V	ATLS	review, mediator-based DM
		[22] SIRUNYAN	19O	CMS	$pp \to \gamma \not{E}_T$
		[23] AABOUD	18CJ	ATLS	$pp \to VV/\ell\ell/\ell\nu$, $V = W,Z,h$
		[24] AABOUD	18CM	ATLS	$pp \to e\mu/e\tau/\mu\tau$
		[25] AAIJ	18AJ	LHCB	$pp \to A' \to \mu^+\mu^-$; dark photon
		[26] BANERJEE	18	NA64	$eZ \to eZX(A')$
		[27] BANERJEE	18A	NA64	$eZ \to eZA'$, $A' \to \chi\chi$
		[28] MARSICANO	18	E137	$e^+e^- \to A'(\gamma)$ visible decay
		[29] SIRUNYAN	18BB	CMS	$pp \to Z' \to \ell^+\ell^-$ at 13 TeV
		[30] SIRUNYAN	18DA	CMS	$pp \to$ Black Hole, string ball, sphaleron
		[31] SIRUNYAN	18DD	CMS	$pp \to jj$
		[32] SIRUNYAN	18DR	CMS	$pp \to b\mu\overline{\mu}$
		[33] SIRUNYAN	18DU	CMS	$pp \to \gamma\gamma$
		[34] SIRUNYAN	18ED	CMS	$pp \to V \to Wh$; $h \to b\overline{b}$; $W \to \ell\nu$
		[35] AABOUD	17B	ATLS	WH, ZH resonance
		[36] AAIJ	17BR	LHCB	$pp \to \pi_V\pi_V$, $\pi_V \to jj$
		[37] AAD	16O	ATLS	ℓ + (ℓs or jets)
		[38] AAD	16R	ATLS	WW, WZ, ZZ resonance
		[39] KRASZNAHO...	16		$p\,^7\mathrm{Li} \to {}^8\mathrm{Be} \to X(17)N$, $X(17) \to e^+e^-$
		[40] LEES	15E	BABR	e^+e^- collisions
		[41] ADAMS	97B	KTEV	m= 1.2–5 GeV
$<10^{-36}$–10^{-33}	90	[42] GALLAS	95	TOF	m= 0.5–20 GeV
$<(4–0.3)\times10^{-31}$	95	[43] AKESSON	91	CNTR	m = 0–5 GeV
$<2 \times10^{-36}$	90	[44] BADIER	86	BDMP	$\tau = (0.05–1.)\times10^{-8}$s
$<2.5\times10^{-35}$		[45] GUSTAFSON	76	CNTR	$\tau > 10^{-7}$ s

[1] AFANACIEV 25 report on search for ^{8}Be* emission of $X \to e^+e^-$ at MEG-II. No signal observed. Limits placed in m(e^+e^-) vs. branching fraction plane.

[2] ALRAHMAN 25 report on search for neutral long-lived particle (S) produced from K decay but decaying $S \to \mu^+\mu^-$ at ICARUS experiment at Fermilab. No signal observed. Limits placed in mass vs.coupling plane for axion and Higgs portal models.

[3] HAYRAPETYAN 25O search for long-lived heavy neutral leptons at CMS with 138 fb^{-1}using displaced lepton plus jet. No signal observed. Limits placed in lepton mixing angle vs mass plane for masses in the range of 1.0–16.5 GeV.

[4] AAD 24AE search for heavy vector triplet production with decay to boson pairs. No signal was observed. Limits placed in σ vs m plane. Limits also placed in various two-dimensional coupling planes (g_F, g_H, g_ℓ, g_ℓ(3rd Gen), g_q, g_q(3rd Gen), g_q(1st/2nd Gen)).

[5] AAD 24BV search for VBF di-Higgs production with decay to boosted $4b$ state. No signal observed. Limits placed in mass vs. cross section plane for various simplified models.

[6] AAD 24CD search for hadronically-decaying W/Z + MET events from new physics with 140 fb^{-1} at 13 TeV. No signal observed. Limits placed on various simplified new physics models.

[7] AAD 24E uses a new resonance search technique for two-body decays into any pair of ℓ, b, and jet with 140 fb^{-1} of data. No signal was observed. Limits placed in σ vs mass plane for various decay modes.

[8] AAD 24S search for quantum black hole (QBH) decay to lepton + jet in 140 fb^{-1} of data. No signal observed. Limits placed in $\sigma\cdot$BF vs mass plane for ADD and RS models.

[9] HAYRAPETYAN 24AB search for heavy neutral leptons N at CMS with 138 fb^{-1} of data. No signal observed. Limits placed in mixing angle vs m(N) plane.

[10] HAYRAPETYAN 24AC search for heavy long-lived neutrino N produced in B-decays in 41.6 fb^{-1} of data. No signal observed. Limits placed in mixing angle vs m(N) plane.

[11] HAYRAPETYAN 24AZ search for various new bosons via production and decay to four muon states with 41.5 and 59.7 fb^{-1} of data at 13 TeV. No signal observed. Limits placed usually in mass vs. cross section plane for a variety of new physics simplified models.

[12] AAD 23P search in 22 channels for exotica produced in association with $h \to \gamma\gamma$ in 139 fb^{-1} of data. No signal observed. Limits placed on production cross section in various channels.

[13] TUMASYAN 23BC search for γ-jet resonance at CMS with 138 fb^{-1} of data. No signal observed. Limits placed on quantum black hole and excited quark models.

[14] TUMASYAN 23BF search for $pp \to pp + \gamma/Z + X$ search where X is missing particle using CMS-TOTEM with 37.2 fb^{-1} of data. No signal observed. Limits placed on σ vs. m plane.

[15] TUMASYAN 22AG search for strongly interacting neutral massive particles via trackless jets with 16.1 fb^{-1} at 13 TeV; no signal detected; limits placed in mass vs. cross section plane for various simplified models.

[16] AAD 21F search for hard monojet production at ATLAS with 139 $^{-1}$ of 13 TeV data. No signal observed. Limits placed on invisible production cross-section recoiling against ISR and interpreted in variety of BSM models.

[17] AAIJ 20AL search for dimuon resonance from promptly decaying X particle. No signal detected. Limits placed on m(X) up to 60 GeV depending on mixing in 2HDM.

[18] SIRUNYAN 20AY measured $\Upsilon(1S)$ pair production cross section and searched for new states decaying into $\Upsilon(1S)\mu^+\mu^-$ at CMS with 13 TeV with 35.9 fb^{-1}. No signal is found and limits are set in $\sigma\cdot$BF vs. mass plane for tetra-b-quarks with masses between 17.5 and 19 GeV and for generic search for narrow resonances with mass between 16.5 and 27 GeV.

[19] SIRUNYAN 20Z search for BSM physics via multilepton production with CMS at 13 TeV with 137 fb^{-1}; no signal is found and limits are set on type-III seesaw and other BSM models.

[20] AABOUD 19H searches for di-photon-jet resonance at 13 TeV and 36.7 fb^{-1} of data; no signal found and limits placed on $\sigma\cdot$BR vs. mass plane for various simplified models.

[21] AABOUD 19V review ATLAS searches for mediator-based DM at 7, 8, and 13 TeV with up to 37 fb^{-1} of data; no signal found and limits set for wide variety of simplified models of dark matter.

[22] SIRUNYAN 19O search for $pp \to \gamma \not{E}_T$ at 13 TeV with 36.1 fb^{-1}; no signal found and limits set for various simplified models.

[23] AABOUD 18CJ make multichannel search for $pp \to VV/\ell\ell/\ell\nu$, $V = W,Z,h$ at 13 TeV, 36.1 fb^{-1}; no signal found; limits placed for several BSM models.

[24] AABOUD 18CM search for lepton-flavor violating resonance in $pp \to e\mu/e\tau/\mu\tau$ at 13 TeV, 36.1 fb^{-1}; no signal is found and limits placed for various BSM models.

[25] AAIJ 18AJ search for prompt and delayed dark photon decay $A' \to \mu^+\mu^-$ at LHCb detector using 1.6 fb^{-1} of pp collisions at 13 TeV; limits on m(A') vs. kinetic mixing are set.

[26] BANERJEE 18 search for dark photon A'/16.7 MeV boson X at NA64 via $eZ \to eZX(A')$; no signal found and limits set on the X-e^- coupling ϵ_e in the range $1.3\times10^{-4} \le \epsilon_e \le 4.2\times10^{-4}$ excluding part of the allowed parameter space.

[27] BANERJEE 18A search for invisibly decaying dark photons in $eZ \to eZA'$, $A' \to$ invisible; no signal found and limits set on mixing for m(A') $<$ 1 GeV.

[28] MARSICANO 18 search for dark photon $e^+e^- \to A'(\gamma)$ visible decay in SLAC E137 e beam dump data. No signal observed and limits set in ϵ coupling vs m(A') plane, see their figure 7.

[29] SIRUNYAN 18BB search for high mass dilepton resonance; no signal found and exclude portions of p-space of Z', KK graviton models.

[30] SIRUNYAN 18DA search for $pp \to$ Black Hole, string ball, sphaleron via high multiplicity events at 13 TeV, 35.9 fb^{-1}; no signal, require e.g. m(BH) $>$ 10.1 TeV.

Int. J. Mod. Phys. A 2026.41. Downloaded from www.worldscientific.com
by UNIVERSITY OF CALIFORNIA @ BERKELEY on 09/16/26. Re-use and distribution is strictly not permitted, except for Open Access articles.

[31] SIRUNYAN 18DD search for $pp \to jj$ deviations in dijet angular distribution. No signal observed. Set limits on large extra dimensions, black holes and DM mediators e.g. m(BH) > 5.9–8.2 TeV.

[32] SIRUNYAN 18DR search for dimuon resonance in $pp \to b\mu\overline{\mu}$ at 8 and 13 TeV. Slight excess seen at m($\mu\overline{\mu}$) ~ 28 GeV in some channels.

[33] SIRUNYAN 18DU search for high mass diphoton resonance in $pp \to \gamma\gamma$ at 13 TeV using 35.9 fb^{-1}; no signal; limits placed on RS Graviton, LED, and clockwork.

[34] SIRUNYAN 18ED search for $pp \to V \to Wh$; $h \to b\overline{b}$; $W \to \ell\nu$ at 13 TeV with 35.9 fb^{-1}; no signal; limits set on m(W') > 2.9 TeV.

[35] AABOUD 17B exclude m(W', Z') < 1.49–2.31 TeV depending on the couplings and W'/Z' degeneracy assumptions via WH, ZH search in pp collisions at 13 TeV with 3.2 fb^{-1} of data.

[36] AAIJ 17BR search for long-lived hidden valley pions from Higgs decay. Limits are set on the signal strength as a function of the mass and lifetime of the long-lived particle in their Fig. 4 and Tab. 4.

[37] AAD 16O search for high E_T ℓ + (ℓs or jets) with 3.2 fb^{-1} at 13 TeV; exclude micro black holes mass < 8 TeV (Fig. 3) for models with two extra dimensions.

[38] AAD 16R search for WW, WZ, ZZ resonance in 20.3 fb^{-1} at 8 TeV data; limits placed on massive RS graviton (Fig. 4).

[39] KRASZNAHORKAY 16 report pLi → Be → $e\overline{e}N$ 5σ resonance at 16.7 MeV– possible evidence for nuclear interference or new light boson. However, such nuclear interference was ruled out already by ZANG 17.

[40] LEES 15E search for long-lived neutral particles produced in e^+e^- collisions in the Upsilon region, which decays into e^+e^-, $\mu^+\mu^-$, $e^\pm\mu^\mp$, $\pi^+\pi^-$, K^+K^-, or $\pi^\pm K^\mp$. See their Fig. 2 for cross section limits.

[41] ADAMS 97B search for a hadron-like neutral particle produced in pN interactions, which decays into a ρ^0 and a weakly interacting massive particle. Upper limits are given for the ratio to K_L production for the mass range 1.2–5 GeV and lifetime 10^{-9}–10^{-4} s. See also our Light Gluino Section.

[42] GALLAS 95 limit is for a weakly interacting neutral particle produced in 800 GeV/c pN interactions decaying with a lifetime of 10^{-4}–10^{-8} s. See their Figs. 8 and 9. Similar limits are obtained for a stable particle with interaction cross section 10^{-29}–10^{-33} cm^2. See Fig. 10.

[43] AKESSON 91 limit is from weakly interacting neutral long-lived particles produced in pN reaction at 450 GeV/c performed at CERN SPS. Bourquin-Gaillard formula is used as the production model. The above limit is for $\tau > 10^{-7}$ s. For $\tau > 10^{-9}$ s, $\sigma < 10^{-30}$ cm^{-2}/nucleon is obtained.

[44] BADIER 86 looked for long-lived particles at 300 GeV π^- beam dump. The limit applies for nonstrongly interacting neutral or charged particles with mass >2 GeV. The limit applies for particle modes, $\mu^+\pi^-$, $\mu^+\mu^-$, $\pi^+\pi^-$X, $\pi^+\pi^-\pi^\pm$ etc. See their figure 5 for the contours of limits in the mass-τ plane for each mode.

[45] GUSTAFSON 76 is a 300 GeV FNAL experiment looking for heavy (m >2 GeV) long-lived neutral hadrons in the M4 neutral beam. The above typical value is for m = 3 GeV and assumes an interaction cross section of 1 mb. Values as a function of mass and interaction cross section are given in figure 2.

Production of New Penetrating Non-ν Like States in Beam Dump

VALUE	DOCUMENT ID		TECN	COMMENT
• • • We do not use the following data for averages, fits, limits, etc. • • •				
	[1] ANDREEV	24	NA64	mu + E(missing) search
	[2] ABRATENKO	22A	MCBN	search for LLPs
	[3] ANDREEV	22A	NA64	new boson X in $eZ \to eZX$
	[4] ANDREEV	21	NA64	new boson X in $eZ \to eZX$
	[5] LOSECCO	81	CALO	28 GeV protons

[1] ANDREEV 24 search for $\mu \to \mu$ + E(missing). No signal observed. Limits placed on Z' models and DM models.

[2] ABRATENKO 22A search for LLPs from kaon decay in MicroBooNE absorber; no signal observed; limits placed for heavy neutral leptons (HNLs) and Higgs portal scalars (HPSs) in the MeV mass range.

[3] ANDREEV 22A search for new light B-L gauge boson $Z' \to \nu\overline{\nu}$ in electron beam dump at NA64; no signal observed; limits set in m(Z') vs coupling plane for m(Z') ~ 10^{-6}–1 GeV.

[4] ANDREEV 21 search for new invisibly decaying boson X in $eZ \to eZX$ at NA64. No signal observed. Limits set in coupling vs. m(X) plane for m(X) ~ 10^{-3} to 1 GeV.

[5] No excess neutral-current events leads to σ(production) × σ(interaction)×acceptance < 2.26×10^{-71} cm^4/nucleon^2 (CL = 90%) for light neutrals. Acceptance depends on models (0.1 to 4. × 10^{-4}).

LIMITS ON CHARGED PARTICLES IN e^+e^-

Heavy Particle Production Cross Section in e^+e^-

Ratio to $\sigma(e^+e^- \to \mu^+\mu^-)$ unless noted. See also entries in Free Quark Search and Magnetic Monopole Searches.

VALUE	CL%	DOCUMENT ID		TECN	COMMENT
• • • We do not use the following data for averages, fits, limits, etc. • • •					
		[1] BOSSI	25	PADM	X17 search
		[2] ADACHI	23K	BELL	search for LLP in B decays
		[3] KILE	18	ALEP	$e^+e^- \to$ 4 jets
<1 × 10^{-3}	90	[4] ABLIKIM	17AA	BES3	$e^+e^- \to \ell\overline{\ell}\gamma$
		[5] ACKERSTAFF	98P	OPAL	Q=1,2/3, m=45–89.5 GeV
		[6] ABREU	97D	DLPH	Q=1,2/3, m=45–84 GeV
		[7] BARATE	97K	ALEP	Q=1, m=45–85 GeV
<2 × 10^{-5}	95	[8] AKERS	95R	OPAL	Q=1, m= 5–45 GeV
<1 × 10^{-5}	95	[8] AKERS	95R	OPAL	Q=2, m= 5–45 GeV
<2 × 10^{-3}	90	[9] BUSKULIC	93C	ALEP	Q=1, m=32–72 GeV
<(10^{-2}–1)	95	[10] ADACHI	90C	TOPZ	Q=1, m=1–16, 18–27 GeV
<7 × 10^{-2}	90	[11] ADACHI	90E	TOPZ	Q = 1, m = 5–25 GeV
<1.6 × 10^{-2}	95	[12] KINOSHITA	82	PLAS	Q=3–180, m <14.5 GeV
<5.0 × 10^{-2}	90	[13] BARTEL	80	JADE	Q=(3,4,5)/3 2–12 GeV

[1] BOSSI 25 search for 17 MeV resonance in $e^+e^- \to e^+e^-$ and $\gamma\gamma$ at PADME at Frascati experiment. No signal observed. Limits are placed above approximately 4×10^{-4} exclusion at 90% CL in mass vs. coupling plane in vicinity of 17 MeV. The most significant deviation is found at 16.90 MeV, corresponding to a global significance of approximately 2 standard deviations over the null hypothesis expectation.

[2] ADACHI 23K search for spin-0 LLP called S in B decays. No signal observed. Limits placed in branching fraction vs. m(S) plane.

[3] KILE 18 investigate archived ALEPH $e^+e^- \to$ 4 jets data and see 4–5 σ excess at 110 GeV.

[4] ABLIKIM 17AA search for dark photon $A \to \ell\overline{\ell}$ at 3.773 GeV with 2.93 fb^{-1}. Limits are set in ϵ vs m(A) plane.

[5] ACKERSTAFF 98P search for pair production of long-lived charged particles at E_{cm} between 130 and 183 GeV and give limits σ <(0.05–0.2) pb (95%CL) for spin-0 and spin-1/2 particles with m=45–89.5 GeV, charge 1 and 2/3. The limit is translated to the cross section at E_{cm}=183 GeV with the s dependence described in the paper. See their Figs. 2–4.

[6] ABREU 97D search for pair production of long-lived particles and give limits σ <(0.4–2.3) pb (95%CL) for various center-of-mass energies E_{cm}=130–136, 161, and 172 GeV, assuming an almost flat production distribution in cosθ.

[7] BARATE 97K search for pair production of long-lived charged particles at E_{cm} = 130, 136, 161, and 172 GeV and give limits σ <(0.2–0.4) pb (95%CL) for spin-0 and spin-1/2 particles with m=45–85 GeV. The limit is translated to the cross section at E_{cm}=172 GeV with the E_{cm} dependence described in the paper. See their Figs. 2 and 3 for limits on J = 1/2 and J = 0 cases.

[8] AKERS 95R is a CERN-LEP experiment with W_{cm} ~ m_Z. The limit is for the production of a stable particle in multihadron events normalized to $\sigma(e^+e^- \to$ hadrons). Constant phase space distribution is assumed. See their Fig. 3 for bounds for Q = ±2/3, ±4/3.

[9] BUSKULIC 93C is a CERN-LEP experiment with W_{cm} = m_Z. The limit is for a pair or single production of heavy particles with unusual ionization loss in TPC. See their Fig. 5 and Table 1.

[10] ADACHI 90C is a KEK-TRISTAN experiment with W_{cm} = 52–60 GeV. The limit is for pair production of a scalar or spin-1/2 particle. See Figs. 3 and 4.

[11] ADACHI 90E is KEK-TRISTAN experiment with W_{cm} = 52–61.4 GeV. The above limit is for inclusive production cross section normalized to $\sigma(e^+e^- \to \mu^+\mu^-)\cdot\beta(3-\beta^2)/2$, where $\beta = (1 - 4m^2/W_{cm}^2)^{1/2}$. See the paper for the assumption about the production mechanism.

[12] KINOSHITA 82 is SLAC PEP experiment at W_{cm} = 29 GeV using lexan and ^{39}Cr plastic sheets sensitive to highly ionizing particles.

[13] BARTEL 80 is DESY-PETRA experiment with W_{cm} = 27–35 GeV. Above limit is for inclusive pair production and ranges between 1. × 10^{-1} and 1. × 10^{-2} depending on mass and production momentum distributions. (See their figures 9, 10, 11).

Branching Fraction of Z^0 to a Pair of Stable Charged Heavy Fermions

VALUE	CL%	DOCUMENT ID		TECN	COMMENT
• • • We do not use the following data for averages, fits, limits, etc. • • •					
<5 × 10^{-6}	95	[1] AKERS	95R	OPAL	m= 40.4–45.6 GeV
<1 × 10^{-3}	95	AKRAWY	90O	OPAL	m = 29–40 GeV

[1] AKERS 95R give the 95% CL limit $\sigma(X\overline{X})/\sigma(\mu\mu) < 1.8\times10^{-4}$ for the pair production of singly- or doubly-charged stable particles. The limit applies for the mass range 40.4–45.6 GeV for $X^\pm$ and < 45.6 GeV for $X^{\pm\pm}$. See the paper for bounds for Q = ±2/3, ±4/3.

LIMITS ON CHARGED PARTICLES IN HADRONIC REACTIONS

MASS LIMITS for Long-Lived Charged Heavy Fermions

Limits are for spin 1/2 particles with no color and SU(2)$_L$ charge. The electric charge Q of the particle (in the unit of e) is therefore equal to its weak hypercharge. Pair production by Drell-Yan like γ and Z exchange is assumed to derive the limits.

VALUE (GeV)	CL%	DOCUMENT ID		TECN	COMMENT
• • • We do not use the following data for averages, fits, limits, etc. • • •					
		[1] HAYRAPETY...	25D	CMS	fractionally charged particles
		[2] BARAK	24	SENS	millicharged particles
		[3] HAYRAPETY...	24AD	CMS	emerging dark jet
		[4] AAD	23BT	ATLS	multi-charged LLP
		[5] SIRUNYAN	20N	CMS	disappearing track LLP
>660	95	[6] AAD	15BJ	ATLS	$\|Q\|$ = 2
>200	95	[7] CHATRCHYAN	13AB	CMS	$\|Q\|$ = 1/3
>480	95	[7] CHATRCHYAN	13AB	CMS	$\|Q\|$ = 2/3
>574	95	[7] CHATRCHYAN	13AB	CMS	$\|Q\|$ = 1
>685	95	[7] CHATRCHYAN	13AB	CMS	$\|Q\|$ = 2
>140	95	[8] CHATRCHYAN	13AR	CMS	$\|Q\|$ = 1/3
>310	95	[8] CHATRCHYAN	13AR	CMS	$\|Q\|$ = 2/3

[1] HAYRAPETYAN 25D search for pair production of long-lived fractionally charged particles at CMS with 138 fb^{-1}. No signal detected. Limits placed in charge vs mass plane with charges Q = (0.3–0.9)e and mass up to 640 GeV.

[2] BARAK 24 search for milli-charged particle production in p-graphite collisions using skipper CCDs. No signal was observed. Limits at 95% placed in charge vs. mass plane in a wide range of masses in the MeV range.

[3] HAYRAPETYAN 24AD search for emerging dark jets from dark mediator pair production in 138 fb^{-1} of data at 13 TeV. No signal observed. Limits placed in the dark $\tau(\pi_d)$ vs m(mediator) plane.

[4] AAD 23BT search for multi-charged long-lived particles with ATLAS detector using 139 fb^{-1}. No signal observed. Limits placed on LLP mass vs. charge plane.

[5] SIRUNYAN 20N search for LLPs using disappearing track signature at CMS at 13 TeV with 101 fb^{-1}; no signal; limits placed on long-lived winos and higgsinos from SUSY depending on mass and lifetime: e.g. at 95% CL, for a purely higgsino neutralino, m(chargino) > 750 (175) GeV for τ = 3 (0.05) ns, and for a purely wino neutralino, m(chargino) > 884 (474) GeV for τ = 3 (0.2) ns.

[6] AAD 15BJ use 20.3 fb^{-1} of pp collisions at E_{cm} = 8 TeV. See paper for limits for $|Q|$ = 3, 4, 5, 6.

[7] CHATRCHYAN 13AB use 5.0 fb^{-1} of pp collisions at E_{cm} = 7 TeV and 18.8 fb^{-1} at E_{cm} = 8 TeV. See paper for limits for $|Q|$ = 3, 4,. . ., 8.

[8] CHATRCHYAN 13AR use 5.0 fb^{-1} of pp collisions at E_{cm} = 7 TeV.

Int. J. Mod. Phys. A 2026.41. Downloaded from www.worldscientific.com
by UNIVERSITY OF CALIFORNIA @ BERKELEY on 09/16/26. Re-use and distribution is strictly not permitted, except for Open Access articles.

Heavy Particle Production Cross Section

VALUE (nb)	CL%	DOCUMENT ID		TECN	COMMENT
• • • We do not use the following data for averages, fits, limits, etc. • • •					
		[1] AAD	25AA	ATLS	vector-like lepton search
		[2] AAD	24AK	ATLS	top + MET search
		[3] AAD	24B	ATLS	non-resonant jet search
		[4] AAD	24CM	ATLS	dark meson $\rightarrow$ t/b search
		[5] AAD	22G	ATLS	vector-like matter search
		[6] TUMASYAN	22H	CMS	search for new matter via multileptons
		[7] SIRUNYAN	21T	CMS	model independent search
		[8] SIRUNYAN	20C	CMS	$4t$ search via multileptons
		[9] AABOUD	19AA	ATLS	BSM search
		[10] AABOUD	19Q	ATLS	single top +MET
		[11] AABOUD	17D	ATLS	anomalous $WWjj$, $WZjj$
		[12] AABOUD	17L	ATLS	m>870 GeV, $Z(\rightarrow \nu\nu)tX$
		[13] SIRUNYAN	17B	CMS	tH
		[14] SIRUNYAN	17C	CMS	Z + (t or b)
		[15] SIRUNYAN	17J	CMS	$X_{5/3} \rightarrow tW$
		[16] AAIJ	15BD	LHCB	m=124–309 GeV
		[17] AAD	13AH	ATLS	$\lvert q\rvert$=(2–6)e, m=50–600 GeV
$<1.2 \times 10^{-3}$	95	[18] AAD	11I	ATLS	$\lvert q\rvert$=10e, m=0.2–1 TeV
$<1.0 \times 10^{-5}$	95	[19,20] AALTONEN	09Z	CDF	m>100 GeV, noncolored
$<4.8 \times 10^{-5}$	95	[19,21] AALTONEN	09Z	CDF	m>100 GeV, colored
$< 0.31–0.04 \times 10^{-3}$	95	[22] ABAZOV	09M	D0	pair production
<0.19	95	[23] AKTAS	04C	H1	m=3–10 GeV
<0.05	95	[24] ABE	92J	CDF	m=50–200 GeV
<30–130		[25] CARROLL	78	SPEC	m=2–2.5 GeV
<100		[26] LEIPUNER	73	CNTR	m=3–11 GeV

[1] AAD 25AA search for vector-like lepton (VLL) pair production at ATLAS with 140 fb^{-1} of data. No signal observed. Limits placed on VLL mass for singlet and doublet models with mxing to e or μ. The resulting mass lower limits are 1220 GeV (1270 GeV) and 320 GeV (400 GeV) for vector-like electrons (muons) in the doublet and singlet scenarios, respectively.

[2] AAD 24AK search for single top + MET in 140 fb^{-1} fb of data. No signal observed. Limits placed in various planes such as σ vs m(mediator) for assumed simplified models.

[3] AAD 24B search for non-resonant jets +MET at $\sqrt{s}$ = 13 TeV with 139 fb^{-1}. No excess observed. Limits placed on dark sector model mediator mass and coupling.

[4] AAD 24CM search for new dark mesons decaying to t/b states with 140 fb^{-1} at 13 TeV. No signal observed. Limits placed in mass vs. σ plane for various new physics simplified models.

[5] AAD 22G search for single vector-like quark T with $T \rightarrow th$ in all hadronic mode with 139 fb^{-1} at 13 TeV; no signal observed; limits placed in mass vs. coupling plane.

[6] TUMASYAN 22H search for new states of matter via non-resonant mutilepton production based on a luminosity of 138 fb^{-1}; no signal observed; limits placed on vector-like leptons, leptoquarks, and new fermions from type-III seesaw model.

[7] SIRUNYAN 21T perform model unspecific search for deviations from SM with CMS at 13 TeV with 35.9^{-1} fb data in numerous signature channels. No deviations from SM found.

[8] SIRUNYAN 20C search for four top-quark production with decay to multileptons at CMS at 13 TeV with 137 fb^{-1}; no signal is found and limits are placed on the Higgs boson oblique parameter in the effective field theory framework (EFT) and the model parameters (tanβ).

[9] AABOUD 19AA search for BSM physics at 13 TeV with 3.2 fb^{-1} in $> 10^5$ regions of $>$ 700 event classes; no significant signal found.

[10] AABOUD 19Q search for single top+MET events at 13 TeV with 36.1 fb^{-1} of data; no signal found and limits set in σ or coupling vs. mass plane for variety of simplified models including DM and vector-like top quark T.

[11] AABOUD 17D search for $WWjj$, $WZjj$ in pp collisions at 8 TeV with 3.2 fb^{-1}; set limits on anomalous couplings.

[12] AABOUD 17L search for the pair production of heavy vector-like T quarks in the $Z(\rightarrow \nu\nu)tX$ final state.

[13] SIRUNYAN 17B search for vector-like quark $pp \rightarrow TX \rightarrow tHX$ in 2.3 fb^{-1} at 13 TeV; no signal seen; limits placed.

[14] SIRUNYAN 17C search for vector-like quark $pp \rightarrow TX \rightarrow Z$ + (t or b) in 2.3 fb^{-1} at 13 TeV; no signal seen; limits placed.

[15] SIRUNYAN 17J search for $pp \rightarrow X_{5/3}X_{5/3} \rightarrow tWtW$ with 2.3 fb^{-1} at 13 TeV. No signal seen: m(X) > 1020 (990) GeV for RH (LH) new charge 5/3 quark.

[16] AAIJ 15BD search for production of long-lived particles in pp collisions at E_{cm} = 7 and 8 TeV. See their Table 6 for cross section limits.

[17] AAD 13AH search for production of long-lived particles with $\lvert q\rvert$=(2–6)e in pp collisions at E_{cm} = 7 TeV with 4.4 fb^{-1}. See their Fig. 8 for cross section limits.

[18] AAD 11I search for production of highly ionizing massive particles in pp collisions at E_{cm} = 7 TeV with L = 3.1 pb^{-1}. See their Table 5 for similar limits for $\lvert q\rvert$ = 6e and 17e, Table 6 for limits on pair production cross section.

[19] AALTONEN 09Z search for long-lived charged particles in $p\overline{p}$ collisions at E_{cm} = 1.96 TeV with L = 1.0 fb^{-1}. The limits are on production cross section for a particle of mass above 100 GeV in the region $\lvert\eta\rvert \lesssim 0.7$, $p_T > 40$ GeV, and $0.4 < \beta < 1.0$.

[20] Limit for weakly interacting charge-1 particle.

[21] Limit for up-quark like particle.

[22] ABAZOV 09M search for pair production of long-lived charged particles in $p\overline{p}$ collisions at E_{cm} = 1.96 TeV with L = 1.1 fb^{-1}. Limit on the cross section of (0.31–0.04) pb (95% CL) is given for the mass range of 60–300 GeV, assuming the kinematics of stau pair production.

[23] AKTAS 04C look for charged particle photoproduction at HERA with mean c.m. energy of 200 GeV.

[24] ABE 92J look for pair production of unit-charged particles which leave detector before decaying. Limit shown here is for m=50 GeV. See their Fig. 5 for different charges and stronger limits for higher mass.

[25] CARROLL 78 look for neutral, $S = -2$ dihyperon resonance in $pp \rightarrow 2K^+X$. Cross section varies within above limits over mass range and p_{lab} = 5.1–5.9 GeV/c.

[26] LEIPUNER 73 is an NAL 300 GeV p experiment. Would have detected particles with lifetime greater than 200 ns.

Heavy Particle Production Differential Cross Section

VALUE (cm^{2}sr^{-1}GeV^{-1})	CL%	DOCUMENT ID		TECN	CHG	COMMENT
• • • We do not use the following data for averages, fits, limits, etc. • • •						
		[1] AAD	25N	ATLS		semi-visible jet search
		[2] HAYRAPETY...	23F	CMS		top $\rightarrow \ell$s via EFT ops.
$<2.6 \times 10^{-36}$	90	[3] BALDIN	76	CNTR	−	Q= 1, m=2.1–9.4 GeV
$<2.2 \times 10^{-33}$	90	[4] ALBROW	75	SPEC	±	Q= ±1, m=4–15 GeV
$<1.1 \times 10^{-33}$	90	[4] ALBROW	75	SPEC	±	Q= ±2, m=6–27 GeV
$<8. \times 10^{-35}$	90	[5] JOVANOV...	75	CNTR	±	m=15–26 GeV
$<1.5 \times 10^{-34}$	90	[5] JOVANOV...	75	CNTR	±	Q= ±2, m=3–10 GeV
$<6. \times 10^{-35}$	90	[5] JOVANOV...	75	CNTR	±	Q= ±2, m=10–26 GeV
$<1. \times 10^{-31}$	90	[6] APPEL	74	CNTR	±	m=3.2–7.2 GeV
$<5.8 \times 10^{-34}$	90	[7] ALPER	73	SPEC	±	m=1.5–24 GeV
$<1.2 \times 10^{-35}$	90	[8] ANTIPOV	71B	CNTR	−	Q=−, m=2.2–2.8
$<2.4 \times 10^{-35}$	90	[9] ANTIPOV	71C	CNTR	−	Q=−, m=1.2–1.7, 2.1–4
$<2.4 \times 10^{-35}$	90	BINON	69	CNTR	−	Q=−, m=1–1.8 GeV
$<1.5 \times 10^{-36}$		[10] DORFAN	65	CNTR		Be target m=3–7 GeV
$<3.0 \times 10^{-36}$		[10] DORFAN	65	CNTR		Fe target m=3–7 GeV

[1] AAD 25N search for semi-visible jets arising from dark sector particle production via Z'. No signal observed. Limits placed in m(Z') vs. R, the fraction of invisible particles in a jet.

[2] HAYRAPETYAN 23F search for anomalous top $\rightarrow$ leptons decay via effective operators. No signal observed. Limits placed on EFT operators.

[3] BALDIN 76 is a 70 GeV Serpukhov experiment. Value is per Al nucleus at θ = 0. For other charges in range −0.5 to −3.0, CL = 90% limit is $(2.6 \times 10^{-36})/\lvert$(charge)$\rvert$ for mass range (2.1–9.4 GeV) $\times \lvert$(charge)$\rvert$. Assumes stable particle interacting with matter as do antiprotons.

[4] ALBROW 75 is a CERN ISR experiment with E_{cm} = 53 GeV. θ = 40 mr. See figure 5 for mass ranges up to 35 GeV.

[5] JOVANOVICH 75 is a CERN ISR 26+26 and 15+15 GeV pp experiment. Figure 4 covers ranges Q = 1/3 to 2 and m = 3 to 26 GeV. Value is per GeV momentum.

[6] APPEL 74 is NAL 300 GeV pW experiment. Studies forward production of heavy (up to 24 GeV) charged particles with momenta 24–200 GeV (−charge) and 40–150 GeV (+charge). Above typical value is for 75 GeV and is per GeV momentum per nucleon.

[7] ALPER 73 is CERN ISR 26+26 GeV pp experiment. p >0.9 GeV, 0.2 < β <0.65.

[8] ANTIPOV 71B is from same 70 GeV p experiment as ANTIPOV 71C and BINON 69.

[9] ANTIPOV 71C limit inferred from flux ratio. 70 GeV p experiment.

[10] DORFAN 65 is a 30 GeV/c p experiment at BNL. Units are per GeV momentum per nucleon.

Long-Lived Heavy Particle Invariant Cross Section

VALUE (cm^2/GeV^2/N)	CL%	DOCUMENT ID		TECN	CHG	COMMENT
• • • We do not use the following data for averages, fits, limits, etc. • • •						
$< 5–700 \times 10^{-35}$	90	[1] BERNSTEIN	88	CNTR		
$< 5–700 \times 10^{-37}$	90	[1] BERNSTEIN	88	CNTR		
$<2.5 \times 10^{-36}$	90	[2] THRON	85	CNTR	−	Q= 1, m=4–12 GeV
$<1. \times 10^{-35}$	90	[2] THRON	85	CNTR	+	Q= 1, m=4–12 GeV
$<6. \times 10^{-33}$	90	[3] ARMITAGE	79	SPEC		m=1.87 GeV
$<1.5 \times 10^{-33}$	90	[3] ARMITAGE	79	SPEC		m=1.5–3.0 GeV
		[4] BOZZOLI	79	CNTR	±	Q = (2/3, 1, 4/3, 2)
$<1.1 \times 10^{-37}$	90	[5] CUTTS	78	CNTR		m=4–10 GeV
$<3.0 \times 10^{-37}$	90	[6] VIDAL	78	CNTR		m=4.5–6 GeV

[1] BERNSTEIN 88 limits apply at x = 0.2 and p_T = 0. Mass and lifetime dependence of limits are shown in the regions: m = 1.5–7.5 GeV and $\tau = 10^{-8}$–2×10^{-6} s. First number is for hadrons; second is for weakly interacting particles.

[2] THRON 85 is FNAL 400 GeV proton experiment. Mass determined from measured velocity and momentum. Limits are for $\tau > 3 \times 10^{-9}$ s.

[3] ARMITAGE 79 is CERN-ISR experiment at E_{cm} = 53 GeV. Value is for x = 0.1 and p_T = 0.15. Observed particles at m = 1.87 GeV are found all consistent with being antideuterons.

[4] BOZZOLI 79 is CERN-SPS 200 GeV pN experiment. Looks for particle with τ larger than 10^{-8} s. See their figure 11–18 for production cross-section upper limits vs mass.

[5] CUTTS 78 is pBe experiment at FNAL sensitive to particles of $\tau > 5 \times 10^{-8}$ s. Value is for −0.3 <x <0 and p_T = 0.175.

[6] VIDAL 78 is FNAL 400 GeV proton experiment. Value is for x = 0 and p_T = 0. Puts lifetime limit of $< 5 \times 10^{-8}$ s on particle in this mass range.

Long-Lived Heavy Particle Production (σ(Heavy Particle) / $\sigma(\pi)$)

VALUE	EVTS	DOCUMENT ID		TECN	CHG	COMMENT
• • • We do not use the following data for averages, fits, limits, etc. • • •						
$<10^{-8}$		[1] NAKAMURA	89	SPEC	±	Q= (−5/3,±2)
	0	[2] BUSSIERE	80	CNTR	±	Q= (2/3,1,4/3,2)

[1] NAKAMURA 89 is KEK experiment with 12 GeV protons on Pt target. The limit applies for mass $\lesssim$ 1.6 GeV and lifetime $\gtrsim 10^{-7}$ s.

[2] BUSSIERE 80 is CERN-SPS experiment with 200–240 GeV protons on Be and Al target. See their figures 6 and 7 for cross-section ratio vs mass.

Production and Capture of Long-Lived Massive Particles

VALUE (10^{-36} cm^2)	DOCUMENT ID		TECN	COMMENT
• • • We do not use the following data for averages, fits, limits, etc. • • •				
	[1] ACHARYA	25	MOED	monople and HECO search
	[2] AAD	21X	ATLS	search for captured LLPs
	[3] ACHARYA	21	INDU	dyons production, capture

<20 to 800	[4] ALEKSEEV	76	ELEC	τ=5 ms to 1 day
<200 to 2000	[4] ALEKSEEV	76B	ELEC	τ=100 ms to 1 day
<1.4 to 9	[5] FRANKEL	75	CNTR	τ=50 ms to 10 hours
<0.1 to 9	[6] FRANKEL	74	CNTR	τ=1 to 1000 hours

[1] ACHARYA 25 search for monoples and high electric charge objects (HECOs) with the MoEDAL detector at LHC. No signal observed. Limits placed in mass vs. cross section plane for a Drell-Yan production model.

[2] AAD 21X search for LLPs which come to rest in ATLAS detector to deposit energy between collisions. No signal observed in 111 fb^{-1} of data. Limits placed in lifetime vs. mass place assuming model with gluino hadrons: e.g. m > 1.4 TeV for $\tau \sim 10^{-5}$ to 10^3 sec.

[3] ACHARYA 21 search for dyons (carrying electric and magnetic charge) and monopoles via production and capture in 6.46 fb^{-1} of 13 TeV LHC data. No signal observed. Limits placed in mass vs. magnetic charge plane.

[4] ALEKSEEV 76 and ALEKSEEV 76B are 61–70 GeV p Serpukhov experiment. Cross section is per Pb nucleus.

[5] FRANKEL 75 is extension of FRANKEL 74.

[6] FRANKEL 74 looks for particles produced in thick Al targets by 300–400 GeV/c protons.

Long-Lived Particle (LLP) Search at Hadron Collisions

Limits are for cross section times branching ratio.

VALUE (fb)	CL%	DOCUMENT ID		TECN	COMMENT
• • • We do not use the following data for averages, fits, limits, etc. • • •					
		[1] AAD	25AE	ATLS	heavy charged LLP search
		[2] AAD	25AY	ATLS	LLP search
		[3] AAD	25M	ATLS	LLP search
		[4] ABRAHAM	25	FASR	long-lived ALPs
		[5] ALCOTT	25		milliQan search for milli-charged particles
		[6] CHEKHOVSKY	25E	CMS	VLL decay to long-lived boson
		[7] HAYRAPETY...	25V	CMS	long-lived HIP search
		[8] AAD	24AS	ATLS	long-lived dark photon search
		[9] AAD	24BN	ATLS	hadronic LLP search
		[10] AAD	24BZ	ATLS	LLP + lepton/jet search
		[11] ABREU	24	FASR	dark photon decay to $e^+ e^-$
		[12] HAYRAPETY...	24AI	CMS	LLP search
		[13] HAYRAPETY...	24M	CMS	long-lived SUSY
		[14] HAYRAPETY...	24P	CMS	LLP from SUSY search
		[15] HAYRAPETY...	24S	CMS	long-lived HNL search
		[16] HAYRAPETY...	24Y	CMS	LLP $\rightarrow$ dimuon search
		[17] AAD	23AM	ATLS	LLP higgsino search
		[18] AAD	23AR	ATLS	LLP search via displaced γ
		[19] AAD	23BQ	ATLS	displaced dimuon search
		[20] AAD	23CO	ATLS	highly ionizing LLP/monopole
		[21] AAD	23G	ATLS	heavy highly ionizing LLP search
		[22] AAD	23I	ATLS	light LLP via collimated decays
		[23] TUMASYAN	23AO	CMS	LLP search via trackless jets
		[24] TUMASYAN	23G	CMS	LLP search via displaced dimuons
		[25] AAD	22H	ATLS	LLP search with μ spectrometer
		[26] AAD	22K	ATLS	LLP search via displaced jets in the calorimeter
		[27] AAD	22U	ATLS	LLP/chargino search via tracklet
		[28] AAIJ	22U	LHCB	LLP semileptonic decay to muon
		[29] ACHARYA	22A	MOED	monopoles/HECOs at LHC
		[30] TUMASYAN	22AD	CMS	heavy neutral lepton LLP search
		[31] TUMASYAN	22AF	CMS	LLP search via displaced lepton tracks
		[32] TUMASYAN	22M	CMS	LLP search via ZH production
		[33] TUMASYAN	22N	CMS	LLP search via dimuons
		[34] AAD	21AL	ATLS	charged LLPs search
		[35] AAD	21BA	ATLS	LLP from higgs decay search
		[36] AAIJ	21V	LHCB	LLP $\rightarrow$ $e\mu\nu$ search
		[37] SIRUNYAN	21AF	CMS	LLP search via displaced jets
< 0.07	95	[38] SIRUNYAN	21U	CMS	LLP search via displaced jets
		[39] TUMASYAN	21	CMS	LLP endcap muon detector searches
		[40] AAD	20D	ATLS	$pp \rightarrow$ LLPs at 13 TeV
		[41] AAD	20J	ATLS	scalar boson decay to LLPs
		[42] AAD	20M	ATLS	LLP top squark decay to μ
		[43] AAD	20P	ATLS	LLP dark photon search
		[44] AAIJ	20AL	LHCB	pp dimuon resonance
		[45] BALL	20		LLP milli-charged particles at LHC
		[46] AABOUD	19AE	ATLS	pp at 13 TeV
		[47] AABOUD	19AK	ATLS	$pp \rightarrow \Phi \rightarrow Z Z_d$
		[48] AABOUD	19AM	ATLS	DY multi-charged LLP production
		[49] AABOUD	19AO	ATLS	LLP via displaced jets
		[50] AABOUD	19AT	ATLS	heavy, charged LLPs
		[51] AABOUD	19G	ATLS	LLP decay to $\mu^+ \mu^-$
		[52] SIRUNYAN	19BH	CMS	LLP via displaced jets
		[53] SIRUNYAN	19BT	CMS	LLP via displaced jets+MET
		[54] SIRUNYAN	19CA	CMS	LLP $\rightarrow$ γ search
		[55] SIRUNYAN	19Q	CMS	$pp \rightarrow j$ + displaced dark quark jet
		[56] SIRUNYAN	18AW	CMS	Long-lived particle search
		[57] AAIJ	16AR	LHCB	$H \rightarrow XX$ LLPs
		[58] KHACHATRY...	16BW	CMS	direct production: HSCPs
<2000	90	[59] BADIER	86	BDMP	$\tau = (0.05–1.) \times 10^{-8}$s

[1] AAD 25AE search for heavy long-lived particles in ATLAS detector. No signal observed. Limits placed in mass vs. lifetime plane for several R-parity violating SUSY models.

[2] AAD 25AY report on long-lived particle (LLP) search at ATLAS with 140 fb^{-1} of pp collisions data at $\sqrt{s}$ = 13 TeV. No signal observed. Limits set on cross-section times LLP branching fraction to hadronic jets with decay in the proper decay length ($c\tau$) range between 0.1–100 m, depending on particle masses from production point for Higgs portal model, baryogenesis model and ALP model.

[3] AAD 25M searches for long-lived sleptons and charginos decaying to displaced leptons in ATLAS Run 2 and a subset of Run 3 data. No signal observed. Limits placed in m(LLP) vs. lifetime τ plane for different LLP hypotheses.

[4] ABRAHAM 25 report search for LLPs produced at LHC but undergo delayed decays to multi-photon final states downstream at FASER detector. 1 event observed. Limits placed in mass vs. coupling plane for a variety of BSM models, including ALPs.

[5] ALCOTT 25 use displaced milliQan detector to search for millicharged particles at CMS with 124.7 fb^{-1} of data at LHC. No signal observed. Limits placed in milli-charge vs. mass plane.

[6] CHEKHOVSKY 25E report on CMS search for vector-like lepton pair production with decay to long-lived boson a which decays to $\gamma\gamma$ in muon chamber. No signal observed. Limits placed in m(VLL) vs τ_a plane.

[7] HAYRAPETYAN 25V search for multi-charged long-lived particles (R-hadrons and other exotica) at CMS with 101 fb^{-1}. No signal observed. Limits placed on production cross section vs. mass.

[8] AAD 24AS search for long-lived dark photons (DP) produced from dark sector. No signal observed. Limits placed in portal coupling vs m(DP) plane.

[9] AAD 24BN report on ATLAS search for hadronically-decaying long-lived particles that decay in the tracking detector. No signal was observed. Limits placed in $c\tau$ vs cross section or branching fraction plane for various simplified new physics models.

[10] AAD 24BZ search for long-lived particle decaying to jets in hadronic calorimeter in association with lepton/jet. No signal observed. Limits placed in $c\tau$ vs. cross section plane for various simplified new physics models.

[11] ABREU 24 report FASER search for long-lived dark photon A' decay to $e^+ e^-$ with 27 fb^{-1}. No signal observed. Limits placed in m(A') vs. kinetic mixing plane and also for a B-L extended gauge model.

[12] HAYRAPETYAN 24AI search for long-lived particles (LLPs) using a Muon Detector Shower with a high hit multiplicity in the muon chambers with 138 fb^{-1} of data at 13 TeV. No signal was observed. Limits placed in Higgs BF vs. $c\tau$ (lifetime) plane.

[13] HAYRAPETYAN 24M search for long-lived charginos in SUSY decays with 138 fb^{-1} of data at 13 TeV. No signal observed. Limits placed in mass vs mass difference plane for various simplified models.

[14] HAYRAPETYAN 24P search for long-lived particles in SUSY models via displaced vertices with 138 fb^{-1} of data at 13 TeV. No signal observed. Limits set in split SUSY and gauge mediated SUSY breaking models.

[15] HAYRAPETYAN 24S search for long-lived heavy neutral lepton decaying in muon chambers with 138 fb^{-1} of data at 13 TeV. No signal observed. Limits placed in mass vs. mixing angle plane.

[16] HAYRAPETYAN 24Y search for displaced dimuons in CMS with 36 fb^{-1} of data at 13.6 TeV. No signal observed. Limits placed for various models inclduing Abelian dark Higgs and RPV SUSY.

[17] AAD 23AM search for long-lived higgsinos from gauge-mediation which decay to Z or H. No signal observed. Limits placed in $c\tau$ vs m(χ) plane for various simplified models.

[18] AAD 23AR search for long-lived particles via decay to displaced γ with 139 fb^{-1} of data. No signal observed. Limits placed in m vs. τ and BF vs. τ planes for gauge-mediated SUSY model.

[19] AAD 23BQ search for displaced dimuon events in ATLAS detector. No signal observed. Limits placed in smuon lifetime vs. mass plane for long-lived smuon model.

[20] AAD 23CO search for monopoles and high-electric-charge LLPs in ATLAS with 139 fb^{-1} of data. No signal observed. Limits placed in mass vs. charge plane.

[21] AAD 23G search for heavy highly ionizing long-lived particles with 139 fb^{-1} of data. No signal observed. Limits placed in m vs. τ plane for several SUSY models.

[22] AAD 23I search for light long-lived particles decaying to collimated decay products (e.g. dileptons). No signal observed. Limits placed in BF vs. τ plane.

[23] TUMASYAN 23AO search for trackless jets from LLP production at CMS. No signal observed. Limits placed for SUSY model with long-lived neutralino in m(χ) vs. $c\tau$ plane.

[24] TUMASYAN 23G search for LLP decaying to displaced dimuons at CM with 97.6 fb^{-1} fb of data. No signal observed. Limits placed in $c\tau$ vs. m plane for hidden Abelian Higgs simplified model.

[25] AAD 22H search for scalar mediator decay to two LLPs which decay in muon chambers with 139 fb^{-1} at 13 TeV; no signal detected; limits placed on various simplified models.

[26] AAD 22K search for LLP pair production via scalar mediator with LLP decay in hadron calorimeter; no signal detected; limits placed for various simplified models.

[27] AAD 22U search for chargino LLP via disappearing tracks; no signal observed; limits placed in m(chargino) vs lifetime plane for cases of higgsino- or wino-like chargino.

[28] AAIJ 22U reports search for LLP production at LHCB with 5.4 fb^{-1} at 13 TeV followed by semileptonic decay to muon; no signal detected; limits placed in mass or lifetime vs. cross section plane for several simplified models.

[29] ACHARYA 22A report search for monople and HECO production via DY at 8 TeV LHC with 2.2 fb^{-1} with MoEDAL detector; no signal detected; limits placed in mass vs. cross section plane for various electric/magnetic charge scenarios.

[30] TUMASYAN 22AD search for heavy neutral lepton which decays as LLP to trilepton state with 138 fb^{-1} at 13 TeV; no signal detected; limits placed in mass vs. coupling plane.

[31] TUMASYAN 22AF search for LLPs via displaced lepton vertices. The analysis is performed with an integrated luminosity of 118 (113) fb^{-1} when analyzing the ee ($e\mu$, $\mu\mu$) channel; no signal detected; limits placed for a variety of simplified models.

[32] TUMASYAN 22M search in 117 fb^{-1} of 13 TeV data for ZH production with $H \rightarrow SS$ where S is a LLP; no signal observed; limits placed in decay length vs. branching fraction plane.

[33] TUMASYAN 22N search in 101 fb^{-1} of 13 TeV data for LLP production via decay to dimuons; no signal observed; limits placed on mass vs. coupling or lifetime for a variety of simplified models.

[34] AAD 21AL reports on ATLAS search for long-lived charged particles with 139 fb^{-1} at 13 TeV. No signal observed. Limits placed in lifetime vs. mass plane: e.g. for τ(LLP) $\sim$ 0.1 ns, m(selectron) > 720 GeV.

[35] AAD 21BA search for long-lived particles from ZH production ($H \rightarrow b\overline{b}$) with 2 displaced vertices in 139 fb^{-1} of data at 13 TeV. No signal detected. Limits placed in branching fraction vs. lifetime plane.

Int. J. Mod. Phys. A 2026.41. Downloaded from www.worldscientific.com
by UNIVERSITY OF CALIFORNIA @ BERKELEY on 09/16/26. Re-use and distribution is strictly not permitted, except for Open Access articles.

Int. J. Mod. Phys. A 2026.41. Downloaded from www.worldscientific.com by UNIVERSITY OF CALIFORNIA @ BERKELEY on 09/16/26. Re-use and distribution is strictly not permitted, except for Open Access articles.

[36] AAIJ 21V search for $pp \to$ LLP + LLP with LLP$\to e\mu\nu$ in the lifetime range between 2 and 50 ps at LHCb with 5.4 fb^{-1} at 13 TeV. No signal observed. Limits placed in LLP cross section vs. mass or lifetime plane for m(LLP) $\sim$ 7 to 50 GeV.

[37] SIRUNYAN 21AF search for LLPs at CMS via jets with 2 displaced vertices in 140 fb^{-1} of data at 13 TeV. No signal observed. Limits placed for RPV SUSY models in which a long-lived neutralino or gluino decays into a multijet final state with top, bottom, and strange quarks.

[38] SIRUNYAN 21U search for long-lived particles (LLPs) via displaced jets at CMS with LHC13 and 132 fb^{-1}. No signal detected. Limits placed on simplified model production of LLP $X \to q\overline{q}$ with $\sigma < 0.07$ fb for m(X) $>$ 500 GeV and $c\tau \sim$ 2 to 250 mm.

[39] TUMASYAN 21 search for long-lived particles in CMS muon endcap detector in 137 fb^{-1} of data at 13 TeV. No signal detected. Limits are placed depending on the branching fraction of Higgs boson to LLP decaying to dd, bb, and $\tau^+\tau^-$, depending on proper decay length, and LLP masses.

[40] AAD 20D search for opposite-sign dileptons originating from long-lived particles in pp collisions at 13 Tev with 32.8 fb^{-1}; limits placed in squark cross section vs. $c\tau$ plane for RPV SUSY.

[41] AAD 20J search for scalar boson decay to two long-lived particles; no signal; limits placed in BF vs $c\tau$ plane for various mass hypotheses. This search is also combined with other ATLAS displaced-jet searches.

[42] AAD 20M search for long-lived top-squarks decay to μ and hadrons; no signal; limits placed in cross section vs. mass and mass vs. lifetime planes.

[43] AAD 20P search for long-lived dark photons produced from the decay of a scalar boson, with each dark photon decaying into displaced collimated leptons or light hadrons at 13 TeV with 36 fb^{-1}; no signal; limits placed in $\sigma \cdot$BF vs. $c\tau$ and other planes.

[44] AAIJ 20AL search for long-lived $X \to \mu^+\mu^-$ decays in 5.1 fb^{-1} of LHCb data at 13 TeV; no signal; limits placed on m(X) up to 3 GeV depending on kinetic mixing.

[45] BALL 20 search for long-lived milli-charged particles produced at LHC; limits placed in charge vs. mass plane (Fig. 8).

[46] AABOUD 19AE search for long-lived particles via displaced jets using 10.8 fb^{-1} or 33.0 fb^{-1} data (depending on a trigger) at 13 TeV; no signal found and limits set in branching ratio vs. decay length plane.

[47] AABOUD 19AK searches for long-lived particle Z_d via $pp \to \Phi \to Z Z_d$ at 13 TeV with 36.1 fb^{-1}; no signal found and limits set in $\sigma\times$BR vs. lifetime plane for simplified model.

[48] AABOUD 19AM search for Drell-Yan (DY) production of long-lived multi-charge particles at 13 TeV with 36.1 fb^{-1} of data; no signal found and exclude 50 GeV $<$ m(LLMCP) $<$ 980–1220 GeV for electric charge |q| = (2–7)e.

[49] AABOUD 19AO search for neutral long-lived particles producing displaced jets at 13 TeV with 36.1 fb^{-1} of data; no signal found and exclude regions of $\sigma \cdot$BR vs. lifetime plane for various models.

[50] AABOUD 19AT search for heavy, charged long-lived particles at 13 TeV with 36.1 fb^{-1}; no signal found and upper limits set on masses of various hypothetical particles.

[51] AABOUD 19G search for long-lived particle with decay to $\mu^+\mu^-$ at 13 TeV with 32.9 fb^{-1}; no signal found and limits set in combinations of lifetime, mass and coupling planes for various simplified models.

[52] SIRUNYAN 19BH search for long-lived SUSY particles via displaced jets at 13 TeV with 35.9 fb^{-1}; no signal found and limits placed in mass vs lifetime plane for various hypothetical models.

[53] SIRUNYAN 19BT search for displaced jet(s)+$\not{E}_T$ at 13 TeV with 137 fb^{-1}; no signal found and limits placed in mass vs lifetime plane for gauge mediated SUSY breaking models.

[54] SIRUNYAN 19CA search for gluino/squark decay to long-lived neutralino, decay to γ in GMSB; no signal, limits placed in m(χ) vs. lifetime plane for SPS8 GMSB benchmark point.

[55] SIRUNYAN 19Q search for $pp \to j$ + displaced jet via dark quark with 13 TeV at 16.1 fb^{-1}; no signal found and limits set in mass vs lifetime plane for dark quark/dark pion model.

[56] SIRUNYAN 18AW search for very long lived particles (LLPs) decaying hadronically or to $\mu\overline{\mu}$ in CMS detector; none seen/limits set on lifetime vs. cross section.

[57] AAIJ 16AR search for long lived particles from $H \to XX$ with displaced X decay vertex using 0.62 fb^{-1} at 7 TeV; limits set in Fig. 7.

[58] KHACHATRYAN 16BW search for heavy stable charged particles via ToF with 2.5 fb^{-1} at 13 TeV; require stable m(gluinoball) $>$ 1610 GeV.

[59] BADIER 86 looked for long-lived particles at 300 GeV π^- beam dump. The limit applies for nonstrongly interacting neutral or charged particles with mass $>$2 GeV. The limit applies for particle modes, $\mu^+\pi^-$, $\mu^+\mu^-$, $\pi^+\pi^-$X, $\pi^+\pi^-\pi^\pm$ etc. See their figure 5 for the contours of limits in the mass-τ plane for each mode.

Long-Lived Heavy Particle Cross Section

VALUE (pb/sr)	CL%	DOCUMENT ID		TECN	COMMENT
• • • We do not use the following data for averages, fits, limits, etc. • • •					
$<$34	95	[1] RAM	94	SPEC	1015$<m_{X^{++}}<$1085 MeV
$<$75	95	[1] RAM	94	SPEC	920$<m_{X^{++}}<$1025 MeV

[1] RAM 94 search for a long-lived doubly-charged fermion X^{++} with mass between m_N and m_N+m_π and baryon number +1 in the reaction $pp \to X^{++}n$. No candidate is found. The limit is for the cross section at 15° scattering angle at 460 MeV incident energy and applies for $\tau(X^{++}) \gg 0.1$ μs.

LIMITS ON CHARGED PARTICLES IN COSMIC RAYS

Heavy Particle Flux in Cosmic Rays

VALUE (cm^{-2}sr^{-1}s^{-1})	CL%	EVTS	DOCUMENT ID		TECN	COMMENT
• • • We do not use the following data for averages, fits, limits, etc. • • •						
		0	[1] AALBERS	25B	LZ	milli-charged particles from CRs
$< 6.2 \times 10^{-10}$	90	0	[2] ALEMANNO	22	DAMP	fractionally charged particles in space
			[3] CAO	22		superheavy DM $\to$ γ rays
			[4] ALVIS	18	MAJD	Fractionally charged
$< 1 \times 10^{-8}$	90		[5] AGNESE	15	CDM2	$Q = 1/6$
$\sim 6 \times 10^{-9}$		2	[6] SAITO	90		$Q \simeq 14$, $m \simeq 370 m_p$
$< 1.4 \times 10^{-12}$	90	0	[7] MINCER	85	CALO	$m \geq 1$ TeV
			[8] SAKUYAMA	83B	PLAS	$m \sim 1$ TeV
$< 1.7 \times 10^{-11}$	99	0	[9] BHAT	82	CC	
$< 1. \times 10^{-9}$	90	0	[10] MARINI	82	CNTR	Q= 1, $m \sim 4.5 m_p$
$2. \times 10^{-9}$		3	[11] YOCK	81	SPRK	Q= 1, $m \sim 4.5 m_p$
		3	[11] YOCK	81	SPRK	Fractionally charged
3.0×10^{-9}		3	[12] YOCK	80	SPRK	$m \sim 4.5$ m_p
$(4 \pm 1) \times 10^{-11}$		3	GOODMAN	79	ELEC	$m \geq 5$ GeV
$< 1.3 \times 10^{-9}$	90		[13] BHAT	78	CNTR	$m >$1 GeV
$< 1.0 \times 10^{-9}$		0	BRIATORE	76	ELEC	
$< 7. \times 10^{-10}$	90	0	YOCK	75	ELEC	$Q >7e$ or $< -7e$
$> 6. \times 10^{-9}$		5	[14] YOCK	74	CNTR	$m >$6 GeV
$< 3.0 \times 10^{-8}$		0	DARDO	72	CNTR	
$< 1.5 \times 10^{-9}$		0	TONWAR	72	CNTR	$m >$10 GeV
$< 3.0 \times 10^{-10}$		0	BJORNBOE	68	CNTR	$m >$5 GeV
$< 5.0 \times 10^{-11}$	90	0	JONES	67	ELEC	m=5–15 GeV

[1] AALBERS 25B report results of search for milli-charged particles which are produced in cosmic rays but detected at LZ. No signal observed. Limits placed in mass vs. fractional charge plane.

[2] ALEMANNO 22 search for flux of fractionally charged particles (FCPs) in space; no signal observed; limits set in flux vs charge plane for mass as low as GeV.

[3] CAO 22 search for superheavy DM decaying to gamma rays; no signal observed; limits placed in mass vs. lifetime plane for m $\sim 10^5$–10^9 GeV for DM decays to $b\overline{b}$ or $\tau\overline{\tau}$.

[4] ALVIS 18 search for fractional charged flux of cosmic matter at Majorana demonstrator; no signal observed and limits are set on the flux of lightly ionizing particles for charge as low as e/1000.

[5] See AGNESE 15 Fig. 6 for limits extending down to Q = 1/200.

[6] SAITO 90 candidates carry about 450 MeV/nucleon. Cannot be accounted for by conventional backgrounds. Consistent with strange quark matter hypothesis.

[7] MINCER 85 is high statistics study of calorimeter signals delayed by 20–200 ns. Calibration with AGS beam shows they can be accounted for by rare fluctuations in signals from low-energy hadrons in the shower. Claim that previous delayed signals including BJORNBOE 68, DARDO 72, BHAT 82, SAKUYAMA 83B below may be due to this fake effect.

[8] SAKUYAMA 83B analyzed 6000 extended air shower events. Increase of delayed particles and change of lateral distribution above 10^{17} eV may indicate production of very heavy parent at top of atmosphere.

[9] BHAT 82 observed 12 events with delay $> 2.\times10^{-8}$ s and with more than 40 particles. 1 eV has good hadron shower. However all events are delayed in only one of two detectors in cloud chamber, and could not be due to strongly interacting massive particle.

[10] MARINI 82 applied PEP-counter for TOF. Above limit is for velocity = 0.54 of light. Limit is inconsistent with YOCK 80 YOCK 81 events if isotropic dependence on zenith angle is assumed.

[11] YOCK 81 saw another 3 events with $Q = \pm1$ and m about $4.5m_p$ as well as 2 events with $m > 5.3m_p$, $Q = \pm0.75 \pm 0.05$ and $m > 2.8m_p$, $Q = \pm0.70 \pm 0.05$ and 1 event with $m = (9.3 \pm 3.)m_p$, $Q = \pm0.89 \pm 0.06$ as possible heavy candidates.

[12] YOCK 80 events are with charge exactly or approximately equal to unity.

[13] BHAT 78 is at Kolar gold fields. Limit is for $\tau > 10^{-6}$ s.

[14] YOCK 74 events could be tritons.

Superheavy Particle (Quark Matter) Flux in Cosmic Rays

VALUE (cm^{-2}sr^{-1}s^{-1})	CL%	DOCUMENT ID		TECN	COMMENT
• • • We do not use the following data for averages, fits, limits, etc. • • •					
		[1] ADRIANI	15	PMLA	$4 < m < 1.2 \times 10^5$ m_p
$<5 \times 10^{-16}$	90	[2] AMBROSIO	00B	MCRO	$m > 5 \times 10^{14}$ GeV
$<1.8 \times 10^{-12}$	90	[3] ASTONE	93	CNTR	$m \geq 1.5 \times 10^{-13}$gram
$<1.1 \times 10^{-14}$	90	[4] AHLEN	92	MCRO	$10^{-10} < m < 0.1$ gram
$<2.2 \times 10^{-14}$	90	[5] NAKAMURA	91	PLAS	$m > 10^{11}$ GeV
$<6.4 \times 10^{-16}$	90	[6] ORITO	91	PLAS	$m > 10^{12}$ GeV
$<2.0 \times 10^{-11}$	90	[7] LIU	88	BOLO	$m > 1.5 \times 10^{-13}$ gram
$<4.7 \times 10^{-12}$	90	[8] BARISH	87	CNTR	$1.4 \times 10^8 < m < 10^{12}$ GeV
$<3.2 \times 10^{-11}$	90	[9] NAKAMURA	85	CNTR	$m > 1.5 \times 10^{-13}$gram
$<3.5 \times 10^{-11}$	90	[10] ULLMAN	81	CNTR	Planck-mass 10^{19}GeV
$<7. \times 10^{-11}$	90	[10] ULLMAN	81	CNTR	$m \leq 10^{16}$ GeV

[1] ADRIANI 15 search for relatively light quark matter with charge $Z = 1$–8. See their Figs. 2 and 3 for flux upper limits.

[2] AMBROSIO 00B searched for quark matter ("nuclearites") in the velocity range (10^{-5}–1) c. The listed limit is for 2×10^{-3} c.

[3] ASTONE 93 searched for quark matter ("nuclearites") in the velocity range (10^{-3}–1) c. Their Table 1 gives a compilation of searches for nuclearites.

[4] AHLEN 92 searched for quark matter ("nuclearites"). The bound applies to velocity $< 2.5 \times 10^{-3}$ c. See their Fig. 3 for other velocity/c and heavier mass range.

[5] NAKAMURA 91 searched for quark matter in the velocity range (4×10^{-5}–1) c.

[6] ORITO 91 searched for quark matter. The limit is for the velocity range (10^{-4}–10^{-3}) c.

[7] LIU 88 searched for quark matter ("nuclearites") in the velocity range (2.5×10^{-3}–1)c. A less stringent limit of 5.8×10^{-11} applies for (1–2.5) $\times 10^{-3}c$.

[8] BARISH 87 searched for quark matter ("nuclearites") in the velocity range (2.7×10^{-4}–5×10^{-3})c.

[9] NAKAMURA 85 at KEK searched for quark-matter. These might be lumps of strange quark matter with roughly equal numbers of u, d, s quarks. These lumps or nuclearites were assumed to have velocity of (10^{-4}–10^{-3}) c.

[10] ULLMAN 81 is sensitive for heavy slow singly charge particle reaching earth with vertical velocity 100–350 km/s.

Highly Ionizing Particle Flux

VALUE ($m^{-2}yr^{-1}$)	CL%	EVTS	DOCUMENT ID		TECN	COMMENT
• • • We do not use the following data for averages, fits, limits, etc. • • •						
<0.4	95	0	KINOSHITA	81B	PLAS	Z/β 30–100

SEARCHES FOR BLACK HOLE PRODUCTION

VALUE	DOCUMENT ID		TECN	COMMENT
• • • We do not use the following data for averages, fits, limits, etc. • • •				
not seen	[1] AABOUD	16P	ATLS	13 TeV $pp \to e\mu, e\tau, \mu\tau$
	[2] AAD	15AN	ATLS	8 TeV $pp \to$ multijets
	[3] AAD	14A	ATLS	8 TeV $pp \to \gamma +$ jet
	[4] AAD	14AL	ATLS	8 TeV $pp \to \ell +$ jet
	[5] AAD	14C	ATLS	8 TeV $pp \to \ell + (\ell$ or jets)
	[6] AAD	13D	ATLS	7 TeV $pp \to 2$ jets
	[7] CHATRCHYAN	13A	CMS	7 TeV $pp \to 2$ jets
	[8] CHATRCHYAN	13AD	CMS	8 TeV $pp \to$ multijets
	[9] AAD	12AK	ATLS	7 TeV $pp \to \ell + (\ell$ or jets)
	[10] CHATRCHYAN	12W	CMS	7 TeV $pp \to$ multijets
	[11] AAD	11AG	ATLS	7 TeV $pp \to 2$ jets

[1] AABOUD 16P set limits on quantum BH production in n = 6 ADD or n = 1 RS models.

[2] AAD 15AN search for black hole or string ball formation followed by its decay to multijet final states, in pp collisions at $E_{cm} = 8$ TeV with $L = 20.3$ fb^{-1}. See their Figs. 6–8 for limits.

[3] AAD 14A search for quantum black hole formation followed by its decay to a γ and a jet, in pp collisions at $E_{cm} = 8$ TeV with $L = 20$ fb^{-1}. See their Fig. 3 for limits.

[4] AAD 14AL search for quantum black hole formation followed by its decay to a lepton and a jet, in pp collisions at $E_{cm} = 8$ TeV with $L = 20.3$ fb^{-1}. See their Fig. 2 for limits.

[5] AAD 14C search for microscopic (semiclassical) black hole formation followed by its decay to final states with a lepton and ≥ 2 (leptons or jets), in pp collisions at $E_{cm} = 8$ TeV with $L = 20.3$ fb^{-1}. See their Figures 8–11, Tables 7, 8 for limits.

[6] AAD 13D search for quantum black hole formation followed by its decay to two jets, in pp collisions at $E_{cm} = 7$ TeV with $L = 4.8$ fb^{-1}. See their Fig. 8 and Table 3 for limits.

[7] CHATRCHYAN 13A search for quantum black hole formation followed by its decay to two jets, in pp collisions at $E_{cm} = 7$ TeV with $L = 5$ fb^{-1}. See their Figs. 5 and 6 for limits.

[8] CHATRCHYAN 13AD search for microscopic (semiclassical) black hole formation followed by its evapolation to multiparticle final states, in multijet (including γ, ℓ) events in pp collisions at $E_{cm} = 8$ TeV with $L = 12$ fb^{-1}. See their Figs. 5–7 for limits.

[9] AAD 12AK search for microscopic (semiclassical) black hole formation followed by its decay to final states with a lepton and ≥ 2 (leptons or jets), in pp collisions at $E_{cm} = 7$ TeV with $L = 1.04$ fb^{-1}. See their Fig. 4 and 5 for limits.

[10] CHATRCHYAN 12W search for microscopic (semiclassical) black hole formation followed by its evapolation to multiparticle final states, in multijet (including γ, ℓ) events in pp collisions at $E_{cm} = 7$ TeV with $L = 4.7$ fb^{-1}. See their Figs. 5–8 for limits.

[11] AAD 11AG search for quantum black hole formation followed by its decay to two jets, in pp collisions at $E_{cm} = 7$ TeV with L = 36 pb^{-1}. See their Fig. 11 and Table 4 for limits.

REFERENCES FOR Other Particle Searches

AAD	25AA	JHEP 2505 075	G. Aad et al.	(ATLAS Collab.)
AAD	25AE	JHEP 2507 140	G. Aad et al.	(ATLAS Collab.)
AAD	25AX	PR D112 072009	G. Aad et al.	(ATLAS Collab.)
AAD	25AY	PR D112 092001	G. Aad et al.	(ATLAS Collab.)
AAD	25AZ	PR D112 092015	G. Aad et al.	(ATLAS Collab.)
AAD	25M	PR D112 012016	G. Aad et al.	(ATLAS Collab.)
AAD	25N	PR D112 012021	G. Aad et al.	(ATLAS Collab.)
AALBERS	25B	PRL 134 241802	J. Aalbers et al.	(LZ Collab.)
ABRAHAM	25	JHEP 2501 199	R. Abraham et al.	(FASER Collab.)
ACHARYA	25	PRL 134 071802	B. Acharya et al.	(MoEDAL Collab.)
AFANACIEV	25	EPJ C85 763	K. Afanaciev et al.	(MEG II Collab.)
ALCOTT	25	PRL 135 121802	S. Alcott et al.	(milliQan Collab.)
ALRAHMAN	25	PRL 134 151801	F.A. Alrahman et al.	(ICARUS Collab.)
BOSSI	25	JHEP 2511 007	F. Bossi et al.	(PADME Collab.)
CHEKHOVSKY	25E	JHEP 2508 156	V. Chekhovsky et al.	(CMS Collab.)
HAYRAPETY...	25D	PRL 134 131802	A. Hayrapetyan et al.	(CMS Collab.)
HAYRAPETY...	25O	JHEP 2502 036	A. Hayrapetyan et al.	(CMS Collab.)
HAYRAPETY...	25V	JHEP 2504 109	A. Hayrapetyan et al.	(CMS Collab.)
AAD	24AE	JHEP 2404 118	G. Aad et al.	(ATLAS Collab.)
AAD	24AK	JHEP 2405 263	G. Aad et al.	(ATLAS Collab.)
AAD	24AS	EPJ C84 719	G. Aad et al.	(ATLAS Collab.)
AAD	24AT	EPJ C84 742	G. Aad et al.	(ATLAS Collab.)
AAD	24B	PL B848 138324	G. Aad et al.	(ATLAS Collab.)
AAD	24BN	PRL 133 161803	G. Aad et al.	(ATLAS Collab.)
AAD	24BV	PL B858 139007	G. Aad et al.	(ATLAS Collab.)
AAD	24BZ	JHEP 2411 036	G. Aad et al.	(ATLAS Collab.)
Also		JHEP 2511 061 (errat.)	G. Aad et al.	(ATLAS Collab.)
AAD	24CD	JHEP 2411 126	G. Aad et al.	(ATLAS Collab.)
AAD	24CM	JHEP 2409 005	G. Aad et al.	(ATLAS Collab.)
AAD	24E	PRL 132 081801	G. Aad et al.	(ATLAS Collab.)
AAD	24S	PR D109 032010	G. Aad et al.	(ATLAS Collab.)
ABREU	24	PL B848 138378	H. Abreu et al.	(FASER Collab.)
ANDREEV	24	PRL 132 211803	Yu.M. Andreev et al.	(NA64 Collab.)
BARAK	24	PRL 133 071801	L. Barak et al.	(SENSEI Collab., +)
HAYRAPETY...	24AB	JHEP 2406 123	A. Hayrapetyan et al.	(CMS Collab.)
HAYRAPETY...	24AC	JHEP 2406 183	A. Hayrapetyan et al.	(CMS Collab.)
HAYRAPETY...	24AD	JHEP 2407 142	A. Hayrapetyan et al.	(CMS Collab.)
HAYRAPETY...	24AI	PR D110 032007	A. Hayrapetyan et al.	(CMS Collab.)
HAYRAPETY...	24AO	PRL 133 191902	A. Hayrapetyan et al.	(CMS Collab.)
HAYRAPETY...	24AZ	JHEP 2412 172	A. Hayrapetyan et al.	(CMS Collab.)
HAYRAPETY...	24G	PRL 133 011801	A. Hayrapetyan et al.	(CMS Collab.)
HAYRAPETY...	24M	PR D109 072007	A. Hayrapetyan et al.	(CMS Collab.)
HAYRAPETY...	24P	PR D109 112005	A. Hayrapetyan et al.	(CMS Collab.)
HAYRAPETY...	24S	PR D110 012004	A. Hayrapetyan et al.	(CMS Collab.)
HAYRAPETY...	24Y	JHEP 2405 047	A. Hayrapetyan et al.	(CMS Collab.)
AAD	23AM	PR D108 012012	G. Aad et al.	(ATLAS Collab.)
AAD	23AR	PR D108 032016	G. Aad et al.	(ATLAS Collab.)
AAD	23BQ	PL B846 138172	G. Aad et al.	(ATLAS Collab.)
AAD	23BT	PL B847 138316	G. Aad et al.	(ATLAS Collab.)
AAD	23CO	JHEP 2311 112	G. Aad et al.	(ATLAS Collab.)
AAD	23G	JHEP 2306 158	G. Aad et al.	(ATLAS Collab.)
AAD	23I	JHEP 2306 153	G. Aad et al.	(ATLAS Collab.)
AAD	23P	JHEP 2307 176	G. Aad et al.	(ATLAS Collab.)
ADACHI	23K	PR D108 L111104	I. Adachi et al.	(BELLE II Collab.)
HAYRAPETY...	23F	JHEP 2312 068	A. Hayrapetyan et al.	(CMS Collab.)
TUMASYAN	23AO	JHEP 2307 210	A. Tumasyan et al.	(CMS Collab.)
TUMASYAN	23BC	JHEP 2312 189	A. Tumasyan et al.	(CMS Collab.)
TUMASYAN	23BF	EPJ C83 827	A. Tumasyan et al.	(CMS Collab.)
TUMASYAN	23G	JHEP 2305 228	A. Tumasyan et al.	(CMS Collab.)
TUMASYAN	23L	JHEP 2307 161	A. Tumasyan et al.	(CMS Collab.)
Also		JHEP 2505 113 (errat.)	A. Tumasyan et al.	(CMS Collab.)
AAD	22G	PR D105 092012	G. Aad et al.	(ATLAS Collab.)
AAD	22H	PR D106 032005	G. Aad et al.	(ATLAS Collab.)
AAD	22K	JHEP 2206 005	G. Aad et al.	(ATLAS Collab.)
AAD	22U	EPJ C82 606	G. Aad et al.	(ATLAS Collab.)
AAIJ	22U	EPJ C82 373	R. Aaij et al.	(LHCb Collab.)
ABRATENKO	22A	PR D106 092006	P. Abratenko et al.	(MicroBooNE Collab.)
ACHARYA	22A	EPJ C82 694	B. Acharya et al.	(MoEDAL Collab.)
ALEMANNO	22	PR D106 063026	F. Alemanno et al.	(DAMPE Collab.)
ANDREEV	22A	PRL 129 161801	Yu.M. Andreev et al.	(NA64 Collab.)
CAO	22	PRL 129 261103	Z. Cao et al.	(LHAASO Collab.)
TUMASYAN	22AD	JHEP 2207 081	A. Tumasyan et al.	(CMS Collab.)
TUMASYAN	22AF	EPJ C82 153	A. Tumasyan et al.	(CMS Collab.)
TUMASYAN	22AG	EPJ C82 213	A. Tumasyan et al.	(CMS Collab.)
TUMASYAN	22H	PR D105 112007	A. Tumasyan et al.	(CMS Collab.)
TUMASYAN	22M	JHEP 2203 160	A. Tumasyan et al.	(CMS Collab.)
TUMASYAN	22N	JHEP 2204 062	A. Tumasyan et al.	(CMS Collab.)
AAD	21AL	PRL 127 051802	G. Aad et al.	(ATLAS Collab.)
AAD	21BA	JHEP 2111 229	G. Aad et al.	(ATLAS Collab.)
AAD	21F	PR D103 112006	G. Aad et al.	(ATLAS Collab.)
AAD	21X	JHEP 2107 173	G. Aad et al.	(ATLAS Collab.)
AAIJ	21V	EPJ C81 261	R. Aaij et al.	(LHCb Collab.)
ACHARYA	21	PRL 126 071801	B. Acharya et al.	(MoEDAL Collab.)
AFEK	21	PR D104 012004	G. Afek et al.	(YALE)
ALKHATIB	21A	PRL 127 081802	I. Alkhatib et al.	(SuperCDMS Collab.)
ANDREEV	21	PRL 126 211802	Yu.M. Andreev et al.	(NA64 Collab.)
SIRUNYAN	21AF	PR D104 052011	A.M. Sirunyan et al.	(CMS Collab.)
SIRUNYAN	21T	EPJ C81 629	A.M. Sirunyan et al.	(CMS Collab.)
SIRUNYAN	21U	PR D104 012015	A.M. Sirunyan et al.	(CMS Collab.)
TUMASYAN	21	PRL 127 261804	A. Tumasyan et al.	(CMS Collab.)
AAD	20AD	PRL 125 131801	G. Aad et al.	(ATLAS Collab.)
AAD	20D	PL B801 135114	G. Aad et al.	(ATLAS Collab.)
AAD	20J	PR D101 052013	G. Aad et al.	(ATLAS Collab.)
AAD	20M	PR D102 032006	G. Aad et al.	(ATLAS Collab.)
AAD	20P	EPJ C80 450	G. Aad et al.	(ATLAS Collab.)
AAD	20T	JHEP 2003 145	G. Aad et al.	(ATLAS Collab.)
AAD	20W	JHEP 2006 151	G. Aad et al.	(ATLAS Collab.)
AAIJ	20AL	JHEP 2010 156	R. Aaij et al.	(LHCb Collab.)
AGUILAR-AR...	20B	JHEP 2004 054	A. Aguilar-Arevalo et al.	(CONNIE Collab.)
BALL	20	PR D102 032002	A.H. Ball et al.	(milliQan)
FEDDERKE	20	PR D101 115021	M.A. Fedderke, P.W. Graham, S. Rajendran	(STAN+)
SIRUNYAN	20A	EPJ C80 3	A.M. Sirunyan et al.	(CMS Collab.)
SIRUNYAN	20AI	JHEP 2005 033	A.M. Sirunyan et al.	(CMS Collab.)
SIRUNYAN	20AY	PL B808 135578	A.M. Sirunyan et al.	(CMS Collab.)
SIRUNYAN	20C	EPJ C80 75	A.M. Sirunyan et al.	(CMS Collab.)
SIRUNYAN	20N	PL B806 135502	A.M. Sirunyan et al.	(CMS Collab.)
SIRUNYAN	20Z	JHEP 2003 051	A.M. Sirunyan et al.	(CMS Collab.)
AABOUD	19AA	EPJ C79 120	M. Aaboud et al.	(ATLAS Collab.)
AABOUD	19AE	EPJ C79 481	M. Aaboud et al.	(ATLAS Collab.)
AABOUD	19AJ	PL B795 56	M. Aaboud et al.	(ATLAS Collab.)
AABOUD	19AK	PRL 122 151801	M. Aaboud et al.	(ATLAS Collab.)
AABOUD	19AM	PR D99 052003	M. Aaboud et al.	(ATLAS Collab.)
AABOUD	19AO	PR D99 052005	M. Aaboud et al.	(ATLAS Collab.)
AABOUD	19AT	PR D99 092007	M. Aaboud et al.	(ATLAS Collab.)
AABOUD	19G	PR D99 012001	M. Aaboud et al.	(ATLAS Collab.)
AABOUD	19H	PR D99 012008	M. Aaboud et al.	(ATLAS Collab.)
AABOUD	19Q	JHEP 1905 041	M. Aaboud et al.	(ATLAS Collab.)
AABOUD	19V	JHEP 1905 142	M. Aaboud et al.	(ATLAS Collab.)
ALCANTARA	19	PR D99 103016	E. Alcantara, L.A. Anchordoqui, J.F. Soriano	
SIRUNYAN	19B	PR D99 012005	A.M. Sirunyan et al.	(CMS Collab.)
SIRUNYAN	19BH	PR D99 032011	A.M. Sirunyan et al.	(CMS Collab.)
SIRUNYAN	19BT	PL B797 134876	A.M. Sirunyan et al.	(CMS Collab.)
SIRUNYAN	19CA	PR D100 112003	A.M. Sirunyan et al.	(CMS Collab.)
SIRUNYAN	19CD	PRL 123 231803	A.M. Sirunyan et al.	(CMS Collab.)
SIRUNYAN	19O	JHEP 1902 074	A.M. Sirunyan et al.	(CMS Collab.)
SIRUNYAN	19Q	JHEP 1902 179	A.M. Sirunyan et al.	(CMS Collab.)
AABOUD	18AD	PL B779 24	M. Aaboud et al.	(ATLAS Collab.)
AABOUD	18CJ	PR D98 052008	M. Aaboud et al.	(ATLAS Collab.)
AABOUD	18CK	PR D98 092002	M. Aaboud et al.	(ATLAS Collab.)
AABOUD	18CL	PR D98 092005	M. Aaboud et al.	(ATLAS Collab.)
AABOUD	18CM	PR D98 092008	M. Aaboud et al.	(ATLAS Collab.)
AABOUD	18N	PRL 121 081801	M. Aaboud et al.	(ATLAS Collab.)
AAIJ	18AJ	PRL 120 061801	R. Aaij et al.	(LHCb Collab.)
ALBERT	18C	PR D98 123012	A. Albert et al.	(HAWC Collab.)
ALVIS	18	PRL 120 211804	S.I. Alvis et al.	(MAJORANA Collab.)
BANERJEE	18	PRL 120 231802	D. Banerjee et al.	(NA64 Collab.)
BANERJEE	18A	PR D97 072002	D. Banerjee et al.	(NA64 Collab.)
KILE	18	JHEP 1810 116	J. Kile, J. von Wimmersperg-Toeller	(LISBT)
MARSICANO	18	PR D98 015031	L. Marsicano et al.	
PORAYKO	18	PR D98 102002	N.K. Porayako et al.	(PPTA Collab.)
SIRUNYAN	18AW	JHEP 1805 127	A.M. Sirunyan et al.	(CMS Collab.)
SIRUNYAN	18BB	JHEP 1806 120	A.M. Sirunyan et al.	(CMS Collab.)
SIRUNYAN	18DA	JHEP 1811 042	A.M. Sirunyan et al.	(CMS Collab.)
SIRUNYAN	18DD	EPJ C78 789	A.M. Sirunyan et al.	(CMS Collab.)
SIRUNYAN	18DJ	JHEP 1809 101	A.M. Sirunyan et al.	(CMS Collab.)
SIRUNYAN	18DR	JHEP 1811 161	A.M. Sirunyan et al.	(CMS Collab.)
SIRUNYAN	18DU	PR D98 092001	A.M. Sirunyan et al.	(CMS Collab.)
SIRUNYAN	18DY	PR D98 112014	A.M. Sirunyan et al.	(CMS Collab.)
SIRUNYAN	18ED	JHEP 1811 172	A.M. Sirunyan et al.	(CMS Collab.)
AABOUD	17B	PL B765 32	M. Aaboud et al.	(ATLAS Collab.)
AABOUD	17D	PR D95 032001	M. Aaboud et al.	(ATLAS Collab.)
AABOUD	17L	JHEP 1708 052	M. Aaboud et al.	(ATLAS Collab.)
AAIJ	17BR	EPJ C77 812	R. Aaij et al.	(LHCb Collab.)
ABLIKIM	17AA	PL B774 252	M. Ablikim et al.	(BESIII Collab.)
KHACHATRY...	17D	JHEP 1701 076	V. Khachatryan et al.	(CMS Collab.)
KHACHATRY...	17W	PL B769 520	V. Khachatryan et al.	(CMS Collab.)
KHACHATRY...	17Y	PL B770 257	V. Khachatryan et al.	(CMS Collab.)
SIRUNYAN	17B	JHEP 1704 136	A.M. Sirunyan et al.	(CMS Collab.)
SIRUNYAN	17C	JHEP 1705 029	A.M. Sirunyan et al.	(CMS Collab.)
SIRUNYAN	17F	JHEP 1707 013	A.M. Sirunyan et al.	(CMS Collab.)
SIRUNYAN	17J	JHEP 1708 073	A.M. Sirunyan et al.	(CMS Collab.)
ZANG	17	PL B773 159	X. Zang, G.A. Miller	(WASH)
AABOUD	16	PL B759 229	M. Aaboud et al.	(ATLAS Collab.)
AABOUD	16P	EPJ C76 541	M. Aaboud et al.	(ATLAS Collab.)
AAD	16AI	JHEP 1603 041	G. Aad et al.	(ATLAS Collab.)
AAD	16N	JHEP 1603 026	G. Aad et al.	(ATLAS Collab.)
AAD	16O	PL B760 520	G. Aad et al.	(ATLAS Collab.)
AAD	16R	PL B755 285	G. Aad et al.	(ATLAS Collab.)
AAD	16S	PL B754 302	G. Aad et al.	(ATLAS Collab.)
AAIJ	16AR	EPJ C76 664	R. Aaij et al.	(LHCb Collab.)

Int. J. Mod. Phys. A 2026.41. Downloaded from www.worldscientific.com
by UNIVERSITY OF CALIFORNIA @ BERKELEY on 09/16/26. Re-use and distribution is strictly not permitted, except for Open Access articles.

Int. J. Mod. Phys. A 2026.41. Downloaded from www.worldscientific.com
by UNIVERSITY OF CALIFORNIA @ BERKELEY on 09/16/26. Re-use and distribution is strictly not permitted, except for Open Access articles.

KHACHATRY...	16BW	PR D94 112004	V. Khachatryan *et al.*	(CMS Collab.)
KHACHATRY...	16K	PRL 116 071801	V. Khachatryan *et al.*	(CMS Collab.)
KHACHATRY...	16L	PRL 117 031802	V. Khachatryan *et al.*	(CMS Collab.)
KHACHATRY...	16M	PRL 117 051802	V. Khachatryan *et al.*	(CMS Collab.)
KRASZNAHO...	16	PRL 116 042501	A.J. Krasznahorkay *et al.*	(HINR, ANIK+)
AAD	15AN	JHEP 1507 032	G. Aad *et al.*	(ATLAS Collab.)
AAD	15AT	EPJ C75 79	G. Aad *et al.*	(ATLAS Collab.)
AAD	15BJ	EPJ C75 362	G. Aad *et al.*	(ATLAS Collab.)
AAIJ	15BD	EPJ C75 595	R. Aaij *et al.*	(LHCb Collab.)
ADRIANI	15	PRL 115 111101	O. Adriani *et al.*	(PAMELA Collab.)
AGNESE	15	PRL 114 111302	R. Agnese *et al.*	(CDMS Collab.)
KHACHATRY...	15F	PRL 114 101801	V. Khachatryan *et al.*	(CMS Collab.)
LEES	15E	PRL 114 171801	J.P. Lees *et al.*	(BABAR Collab.)
AAD	14A	PL B728 562	G. Aad *et al.*	(ATLAS Collab.)
AAD	14AL	PRL 112 091804	G. Aad *et al.*	(ATLAS Collab.)
AAD	14C	JHEP 1408 103	G. Aad *et al.*	(ATLAS Collab.)
AALTONEN	14J	PR D89 092001	T. Aaltonen *et al.*	(CDF Collab.)
AAD	13A	PL B718 860	G. Aad *et al.*	(ATLAS Collab.)
AAD	13AH	PL B722 305	G. Aad *et al.*	(ATLAS Collab.)
AAD	13C	PRL 110 011802	G. Aad *et al.*	(ATLAS Collab.)
AAD	13D	JHEP 1301 029	G. Aad *et al.*	(ATLAS Collab.)
AALTONEN	13I	PR D88 031103	T. Aaltonen *et al.*	(CDF Collab.)
AALTONEN	13R	PRL 111 031802	T. Aaltonen *et al.*	(CDF Collab.)
CHATRCHYAN	13	PL B718 815	S. Chatrchyan *et al.*	(CMS Collab.)
CHATRCHYAN	13A	JHEP 1301 013	S. Chatrchyan *et al.*	(CMS Collab.)
CHATRCHYAN	13AB	JHEP 1307 122	S. Chatrchyan *et al.*	(CMS Collab.)
Also		JHEP 2211 149 (errat.)	S. Chatrchyan *et al.*	(CMS Collab.)
CHATRCHYAN	13AD	JHEP 1307 178	S. Chatrchyan *et al.*	(CMS Collab.)
CHATRCHYAN	13AR	PR D87 092008	S. Chatrchyan *et al.*	(CMS Collab.)
Also		PR D106 099903 (errat.)	S. Chatrchyan *et al.*	(CMS Collab.)
AAD	12AK	PL B716 122	G. Aad *et al.*	(ATLAS Collab.)
AAD	12C	PRL 108 041805	G. Aad *et al.*	(ATLAS Collab.)
AAD	12S	PL B708 37	G. Aad *et al.*	(ATLAS Collab.)
AALTONEN	12M	PRL 108 211804	T. Aaltonen *et al.*	(CDF Collab.)
CHATRCHYAN	12AP	JHEP 1209 094	S. Chatrchyan *et al.*	(CMS Collab.)
CHATRCHYAN	12BL	JHEP 1212 015	S. Chatrchyan *et al.*	(CMS Collab.)
CHATRCHYAN	12Q	PL B716 260	S. Chatrchyan *et al.*	(CMS Collab.)
CHATRCHYAN	12T	PRL 108 261803	S. Chatrchyan *et al.*	(CMS Collab.)
CHATRCHYAN	12W	JHEP 1204 061	S. Chatrchyan *et al.*	(CMS Collab.)
AAD	11AG	NJP 13 053044	G. Aad *et al.*	(ATLAS Collab.)
AAD	11I	PL B698 353	G. Aad *et al.*	(ATLAS Collab.)
AAD	11S	PL B705 294	G. Aad *et al.*	(ATLAS Collab.)
AALTONEN	11AF	PRL 107 181801	T. Aaltonen *et al.*	(CDF Collab.)
AALTONEN	11M	PRL 106 171801	T. Aaltonen *et al.*	(CDF Collab.)
ABAZOV	11I	PRL 107 011804	V.M. Abazov *et al.*	(D0 Collab.)
CHATRCHYAN	11C	JHEP 1106 026	S. Chatychyan *et al.*	(CMS Collab.)
CHATRCHYAN	11U	PRL 107 201804	S. Chatychyan *et al.*	(CMS Collab.)
AAD	10	PRL 105 161801	G. Aad *et al.*	(ATLAS Collab.)
AALTONEN	10AF	PR D82 052005	T. Aaltonen *et al.*	(CDF Collab.)
KHACHATRY...	10	PRL 105 211801	V. Khachatryan *et al.*	(CMS Collab.)
Also		PRL 106 029902	V. Khachatryan *et al.*	(CMS Collab.)
AALTONEN	09AF	PR D80 011102	T. Aaltonen *et al.*	(CDF Collab.)
AALTONEN	09G	PR D79 052004	T. Aaltonen *et al.*	(CDF Collab.)
AALTONEN	09Z	PRL 103 021802	T. Aaltonen *et al.*	(CDF Collab.)
ABAZOV	09M	PRL 102 161802	V.M. Abazov *et al.*	(D0 Collab.)
AKTAS	04C	EPJ C36 413	A. Atkas *et al.*	(H1 Collab.)
JAVORSEK	02	PR D65 072003	D. Javorsek II *et al.*	
JAVORSEK	01	PR D64 012005	D. Javorsek II *et al.*	
JAVORSEK	01B	PRL 87 231804	D. Javorsek II *et al.*	
ABBIENDI	00D	EPJ C13 197	G. Abbiendi *et al.*	(OPAL Collab.)
AMBROSIO	00B	EPJ C13 453	M. Ambrosio *et al.*	(MACRO Collab.)
ABE	99F	PRL 82 2038	F. Abe *et al.*	(CDF Collab.)
ACKERSTAFF	98P	PL B433 195	K. Ackerstaff *et al.*	(OPAL Collab.)
ABE	97G	PR D55 5263	F. Abe *et al.*	(CDF Collab.)
ABREU	97D	PL B396 315	P. Abreu *et al.*	(DELPHI Collab.)
ACKERSTAFF	97B	PL B391 210	K. Ackerstaff *et al.*	(OPAL Collab.)
ADAMS	97B	PRL 79 4083	J. Adams *et al.*	(FNAL KTeV Collab.)
BARATE	97K	PL B405 379	R. Barate *et al.*	(ALEPH Collab.)
AKERS	95R	ZPHY C67 203	R. Akers *et al.*	(OPAL Collab.)
GALLAS	95	PR D52 6	E. Gallas *et al.*	(MSU, FNAL, MIT, FLOR)
RAM	94	PR D49 3120	S. Ram *et al.*	(TELA, TRIU)
ABE	93G	PRL 71 2542	F. Abe *et al.*	(CDF Collab.)
ASTONE	93	PR D47 4770	P. Astone *et al.*	(ROMA, ROMAI, CATA, FRAS)
BUSKULIC	93C	PL B303 198	D. Buskulic *et al.*	(ALEPH Collab.)
YAMAGATA	93	PR D47 1231	T. Yamagata, Y. Takamori, H. Utsunomiya	(KONAN)
ABE	92J	PR D46 1889	F. Abe *et al.*	(CDF Collab.)
AHLEN	92	PRL 69 1860	S.P. Ahlen *et al.*	(MACRO Collab.)
VERKERK	92	PRL 68 1116	P. Verkerk *et al.*	(ENSP, SACL, PAST)
AKESSON	91	ZPHY C52 219	T. Akesson *et al.*	(HELIOS Collab.)
NAKAMURA	91	PL B263 529	S. Nakamura *et al.*	
ORITO	91	PRL 66 1951	S. Orito *et al.*	(ICEPP, WASCR, NIHO, ICRR)
ADACHI	90C	PL B244 352	I. Adachi *et al.*	(TOPAZ Collab.)
ADACHI	90E	PL B249 336	I. Adachi *et al.*	(TOPAZ Collab.)
AKRAWY	90O	PL B252 290	M.Z. Akrawy *et al.*	(OPAL Collab.)
HEMMICK	90	PR D41 2074	T.K. Hemmick *et al.*	(ROCH, MICH, OHIO+)
SAITO	90	PRL 65 2094	T. Saito *et al.*	(ICRR, KOBE)
NAKAMURA	89	PR D39 1261	T.T. Nakamura *et al.*	(KYOT, TMTC)
NORMAN	89	PR D39 2499	E.B. Norman *et al.*	(LBL)
BERNSTEIN	88	PR D37 3103	R.M. Bernstein *et al.*	(STAN, WISC)
LIU	88	PRL 61 271	G. Liu, B. Barish	
BARISH	87	PR D36 2641	B.C. Barish, G. Liu, C. Lane	(CIT)
NORMAN	87	PRL 58 1403	E.B. Norman, S.B. Gazes, D.A. Bennett	(LBL)
BADIER	86	ZPHY C31 21	J. Badier *et al.*	(NA3 Collab.)
MINCER	85	PR D32 541	A. Mincer *et al.*	(UMD, GMAS, NSF)
NAKAMURA	85	PL 161B 417	K. Nakamura *et al.*	(KEK, INUS)
THRON	85	PR D31 451	J.L. Thron *et al.*	(YALE, FNAL, IOWA)
SAKUYAMA	83B	LNC 37 17	H. Sakuyama, N. Suzuki	(MEIS)
Also		LNC 36 389	H. Sakuyama, K. Watanabe	(MEIS)
Also		NC 78A 147	H. Sakuyama, K. Watanabe	(MEIS)
Also		NC 6C 371	H. Sakuyama, K. Watanabe	(MEIS)
BHAT	82	PR D25 2820	P.N. Bhat *et al.*	(TATA)
KINOSHITA	82	PRL 48 77	K. Kinoshita, P.B. Price, D. Fryberger	(UCB+)
MARINI	82	PR D26 1777	A. Marini *et al.*	(FRAS, LBL, NWES, STAN+)
SMITH	82B	NP B206 333	P.F. Smith *et al.*	(RAL)
KINOSHITA	81B	PR D24 1707	K. Kinoshita, P.B. Price	(UCB)
LOSECCO	81	PL 102B 209	J.M. LoSecco *et al.*	(MICH, PENN, BNL)
ULLMAN	81	PRL 47 289	J.D. Ullman	(LEHM, BNL)
YOCK	81	PR D23 1207	P.C.M. Yock	(AUCK)
BARTEL	80	ZPHY C6 295	W. Bartel *et al.*	(JADE Collab.)
BUSSIERE	80	NP B174 1	A. Bussiere *et al.*	(BGNA, SACL, LAPP)
YOCK	80	PR D22 61	P.C.M. Yock	(AUCK)
ARMITAGE	79	NP B150 87	J.C.M. Armitage *et al.*	(CERN, DARE, FOM+)
BOZZOLI	79	NP B159 363	W. Bozzoli *et al.*	(BGNA, LAPP, SACL+)
GOODMAN	79	PR D19 2572	J.A. Goodman *et al.*	(UMD)
SMITH	79	NP B149 525	P.F. Smith, J.R.J. Bennett	(RHEL)
BHAT	78	PRAM 10 115	P.N. Bhat, P.V. Ramana Murthy	(TATA)
CARROLL	78	PRL 41 777	A.S. Carroll *et al.*	(BNL, PRIN)
CUTTS	78	PRL 41 363	D. Cutts *et al.*	(BROW, FNAL, ILL, BARI+)
VIDAL	78	PL 77B 344	R.A. Vidal *et al.*	(COLU, FNAL, STON+)
ALEKSEEV	76	SJNP 22 531	G.D. Alekseev *et al.*	(JINR)
		Translated from YAF 22 1021.		
ALEKSEEV	76B	SJNP 23 633	G.D. Alekseev *et al.*	(JINR)
		Translated from YAF 23 1190.		
BALDIN	76	SJNP 22 264	B.Y. Baldin *et al.*	(JINR)
		Translated from YAF 22 512.		
BRIATORE	76	NC 31A 553	L. Briatore *et al.*	(LCGT, FRAS, FREIB)
GUSTAFSON	76	PRL 37 474	H.R. Gustafson *et al.*	(MICH)
ALBROW	75	NP B97 189	M.G. Albrow *et al.*	(CERN, DARE, FOM+)
FRANKEL	75	PR D12 2561	S. Frankel *et al.*	(PENN, FNAL)
JOVANOV...	75	PL 56B 105	J.V. Jovanovich *et al.*	(MANI, AACH, CERN+)
YOCK	75	NP B86 216	P.C.M. Yock	(AUCK, SLAC)
APPEL	74	PRL 32 428	J.A. Appel *et al.*	(COLU, FNAL)
FRANKEL	74	PR D9 1932	S. Frankel *et al.*	(PENN, FNAL)
YOCK	74	NP B76 175	P.C.M. Yock	(AUCK)
ALPER	73	PL 46B 265	B. Alper *et al.*	(CERN, LIVP, LUND, BOHR+)
LEIPUNER	73	PRL 31 1226	L.B. Leipuner *et al.*	(BNL, YALE)
DARDO	72	NC 9A 319	M. Dardo *et al.*	(TORI)
TONWAR	72	JP A5 569	S.C. Tonwar, S. Naranan, B.V. Sreekantan	(TATA)
ANTIPOV	71B	NP B31 235	Y.M. Antipov *et al.*	(SERP)
ANTIPOV	71C	PL 34B 164	Y.M. Antipov *et al.*	(SERP)
BINON	69	PL 30B 510	F.G. Binon *et al.*	(SERP)
BJORNBOE	68	NC B53 241	J. Bjornboe *et al.*	(BOHR, TATA, BERN+)
JONES	67	PR 164 1584	L.W. Jones	(MICH, WISC, LBL, UCLA, MINN+)
DORFAN	65	PRL 14 999	D.E. Dorfan *et al.*	(COLU)

Int. J. Mod. Phys. A 2026.41. Downloaded from www.worldscientific.com
by UNIVERSITY OF CALIFORNIA @ BERKELEY on 09/16/26. Re-use and distribution is strictly not permitted, except for Open Access articles.